

Contents of Volume

Number 1	
Preparation of thin carbon nanotubes by catalytic pyrolysis on a support E G Rakov	1
Progress in the studies of oxidation of dihydropyridines and their analogues A I Matern, V N Charushin, O N Chupakhin	23
Radical chemistry of iron carbonyls Yu A Belousov	41
Methods for investigation of the free volume in polymers Yu P Yampolskii	59
Determination of biologically active phenols and polyphenols in various objects by chromatographic techniques M V Kochetova, E N Semenistaya, O G Larionov, A A Revina	79
The mechanism of electronic excitation in the bacterial bioluminescent reaction E V Nemtseva, N S Kudryasheva	91
Number 2	
Crystal chemistry and features of the structure formation of mercury oxo- and chalcogenides S A Magarill, N V Pervukhina, S V Borisov, N A Pal'chik	101
Sonochemical synthesis of inorganic materials A Y Baranchikov, V K Ivanov, Yu D Tretyakov	133
Oxidative catalysis on high-temperature ionic melts Yu S Chekryshkin, T A Rozdyalovskaya, A A Fedorov, G V Lisichkin	153
The use of tetrazolium salts in inorganic analysis K B Gavazov, A N Dimitrov, V D Lekova	169
Gold nanoparticles: preparation, functionalisation and applications in biochemistry and immunochemistry L A Dykman, V A Bogatyrev	181
Number 3	
1,2,3,4,5-Pentathiepin and 1,2,3,4,5-pentathiepanes L S Konstantinova, S A Amelichev, O A Rakitin	195
Thermodynamics and mechanisms of the formation of supramolecules and supramolecular assemblies of s, p, d and f elements: problems and prospects A Yu Tsivadze, G V Ionova, V K Mikhalko, Yu N Kostrubov	213
Physicochemical properties of plasma-solution systems and prospects for their use in technology A G Zakharov, A I Maksimov, Yu V Titova	235
Post-metallocene catalysts for olefin polymerisation K P Bryliakov	253

RNA bulges as targets for selective cleavage by metal ions and organic compounds I L Kuznetsova, M A Zenkova, V V Vlassov	279
Number 4	
Synthesis, structures and reactivity of polyhalo[60]fullerenes A A Goryunkov, N S Ovchinnikova, I V Trushkov, M A Yurovskaya	289
The chemistry of indoloindoles Sh A Samsoniya, M V Trapaidze	313
Synthesis of arylenephosphamacrocycles using tri- and pentavalent phosphorus compounds E E Nifantsev, P V Slitikov, E N Rasadkina	327
Detonation-synthesis nanodiamonds: synthesis, structure, properties and applications V Yu Dolmatov	339
Ion-selective electrodes in medicinal drug determination S V Kharitonov	361
Number 5	
Microwave-assisted synthesis of individual and multicomponent oxides A S Vanetsev, Yu D Tretyakov	397
Ionics of nanoheterogeneous materials N F Uvarov	415
Nanotechnologies. Properties and applications of nanostructured materials A A Rempel	435
Multifunctional nanostructured films E A Levashov, D V Shtansky	463
Long-range surface forces and their role in the progress L B Boinovich	471
Number 6	
Chemical research at the Siberian Branch of the Russian Academy of Sciences V N Parmon	489
Quantum beats in radical pairs V A Bagryansky, V I Borovkov, Yu N Molin	493
Acetylene: new prospects of classical reactions B A Trofimov, N K Gusarova	507
Chalcogenide clusters of Group 5–7 metals V E Fedorov, Yu V Mironov, N G Naumov, M N Sokolov, V P Fedin	529
Modern trends in the development of surface science as applied to catalysis. The elucidation of the structure–activity relationships in heterogeneous catalysts V I Bukhtiyarov	553
Multinuclear magnetic resonance imaging as a multifunctional tool for the investigation of the properties of materials, transport processes and catalytic reactions I V Koptug, A A Lysova, K V Kovtunov, V V Zhivonitko, A V Khomichev, R Z Sagdeev	583

Number 7	
Spin chemistry of enzymatic processes M S Afanasyeva, P A Purtov, M B Taraban, T V Leshina	599
Advances in the development of new catalysts for ethylene and α-olefin polymerisation S S Ivanchev	617
Unsteady catalytic processes and sorption-catalytic technologies A N Zagoruiko	639
Plant metabolites of the Siberian flora. Chemical transformations and the scope of practical application E E Shults, V A Raldugin, K P Volcho, N F Salakhutdinov, G A Tolstikov	655
Methods for the synthesis of polycyclic nitramines S V Sysolyatin, G V Sakovich, V N Surmachev	673
Non-symmetrically substituted phthalocyanines: synthesis and structure modification A Yu Tolbin, L G Tomilova, N S Zefirov	681
Number 8	
Bibliometric analysis of the journal Uspekhi Khimii (Russian Chemical Reviews) I V Zibareva, T N Teplova, O M Nefedov	693
Pulsed EPR in the method of spin labels and probes S A Dzuba	699
The formation of [5,6]- and [6,6]-open fulleroid structures M V Reinov, M A Yurovskaya	715
Processes for obtaining linear block copolymers T B Zheltonozhskaya, S V Fedorchuk, V G Syromyatnikov	731
Rigid aromatic dendrimers M S Rajadurai, Z B Shifrina, N V Kuchkina, A L Rusanov, K Müllen	767
Number 9	
Synthesis of azomethine macrocycles by condensation of dicarbonyl compounds with diamines without using metal ions as template agents N E Borisova, M D Reshetova, Yu A Ustynyuk	785
Hypervalent silicon-containing organosilicon derivatives of nitrogen heterocycles M G Voronkov, O M Trofimova, Yu I Bolgova, N F Chernov	825
Chemistry of metallasiloxanes. Current trends and new concepts M M Levitsky, B G Zavin, A N Bilyachenko	847
Kinetics of 'blue' flames in the gas-phase oxidation and combustion of hydrocarbons and their derivatives V Ya Basevich, S M Frolov	867
Number 10	
Chemical functionalisation of polychloroarenes A A Vasil'ev, A S Burukin, S G Zlotin	885
Outer-sphere association of calixarenes and other macrocyclic ligands with metal complexes as the basis for the design of molecular devices A R Mustafina, V V Skripacheva, A I Kononov	917

Spectroscopy and kinetics of germylene and digermene reactions photogenerated in the condensed phase V F Plyusnin, M V Kaletina, T V Leshina	931
Chirospecific analysis of plant volatiles A V Tkachev	951
Physicochemical methods for enhancing oil recovery from oil fields L K Altunina, V A Kuvshinov	971
Number 11	
Electronic mechanisms of molecular oxygen activation B F Minaev	989
Nanomaterials for sensors V E Bochenkov, G B Sergeev	1013
The chemistry of combustion of organophosphorus compounds O P Korobeinichev, V M Shvartsberg, A G Shmakov	1023
Non-metallocene rare-earth organometallic derivatives: synthesis, structure and application in the catalysis of transformations of unsaturated substrates A A Trifonov	1051
Synthesis of polymers with protogenic groups by polymer-analogous transformations A L Rusanov, E A Solodova, E G Bulycheva, M Abadie, V Voitekunas	1073
Number 12	
Investigation of matrix-isolated species: spectroscopy and molecular modelling A V Nemukhin, L Yu Khriachtchev, B L Grigorenko, A V Bochenkova, M Räsänen	1085
Gas phase reaction kinetics at very low temperatures: recent advances on carbon chemistry using the CRESU technique A Canosa	1093
Tunnelling chemical reactions of hydrogen isotopes in quantum solids V V Khmelenko, E P Bernard, S R Vasiliev, D M Lee	1107
Competitive cryochemical reactions of transition metal atoms, clusters and nanosized particles T I Shabatina, J Mascetti, J S Ogden, G B Sergeev	1123
Study of photochemical transformations of organic azides by matrix isolation techniques and quantum chemistry N P Gritsan	1139

Preparation of thin carbon nanotubes by catalytic pyrolysis on a support

E G Rakov

Contents

I. Introduction	1
II. Versions of catalytic pyrolysis	2
III. Pyrolysis with supported catalysts	2
IV. Conclusion	15

Abstract. The preparation of single-walled, double-walled and thin multi-walled nanotubes by hydrocarbon pyrolysis or carbon monoxide catalytic decomposition is considered. The versions of methods, reagents and catalysts are described systematically. The kinetics and mechanisms of processes are characterised. Trends in the development of methods for nanotube synthesis are shown: the increasing role of pyrolytic methods as compared with the graphite sublimation. The advantages of thin multi-walled nanotubes over single-walled ones are noted. Some unsolved problems are formulated. The bibliography includes 485 references.

I. Introduction

Carbon nanotubes (CNTs) and nanofibres (CNFs) belong to materials that attract the keenest attention of scientists and technologists all over the world (*e.g.*, see Refs 1–10).

In recent summarising publications,^{11–16} the methods of preparation of these materials are divided into two main groups, where the first group includes the graphite sublimation followed by desublimation and the second group comprises hydrocarbon pyrolysis and decomposition of carbon oxides (monoxide and suboxides). The other methods such as electrolysis, chemical reduction of certain organic derivatives with alkali and alkaline-earth metals, chlorination of metal carbides or thermal exfoliation play far less important roles.

Two current trends in the development of synthetic methods and the application of carbon nanotubes and nanofibres are observed. One of them reflects the increasing interest in pyrolytic methods of CNT or CNF preparation, while the second concerns revision of the role and significance of single-walled CNTs (SWCNTs).

Indeed, pyrolytic methods do not require such high temperatures as sublimation, are amenable to scaleup and easier to control, provide means for the effective organisation of continuous processes and are more diversified and versatile. As regards the number of versions, these methods far surpass the electro-arc and laser-oven sublimation of graphite. A potential advantage of certain pyrolytic methods is that in addition to CNTs they allow one to produce hydrogen free of CO, which is very important for

the development of hydrogen energetics¹⁷ and chemical syntheses.¹⁸

Initially, the potential of pyrolytic methods was believed to be restricted to the synthesis of multi-walled CNTs (MWCNTs); however, it is already clear that this is wrong and these methods can be applied for the SWCNT production. Dai *et al.*¹⁹ (1996),[†] were the first to demonstrate the possibility of the SWCNT synthesis by the catalytic pyrolysis of hydrocarbons, while the conditions for the synthesis of high-quality SWCNTs were found as early as in 1998.^{23,24}

The second trend reflects the fact that the opinion that SWCNTs have higher properties than MWCNTs has been shaken. Indeed, double-walled CNTs (DWCNTs) were the first to be appreciated as promising industrial materials.^{25,26} Particularly, DWCNTs were shown to surpass SWCNTs in mechanical properties.²⁷ In addition, DWCNTs exhibit the higher thermal stability, thermal and electric conductivity as compared with SWCNTs.²⁸ SWCNTs start coalescing at ~1200 °C, whereas DWCNTs coalesce above 2000 °C. DWCNT-based nanopaper exhibits higher characteristics than a paper made of SWCNTs.²⁹

The inevitable topological defects typical of all CNTs have a weaker effect on the DWCNT properties as compared with SWCNTs. Covalent addition of chemical groups to the surface drastically changes the electronic properties of SWCNTs and in certain cases makes their functionalisation (and, hence, their solubilisation and the possibility of using aqueous colloid solutions of SWCNT for purification, production of composites, *etc.*) extremely unwanted. In the DWCNT case, the groups are added to the external wall and have virtually no effect on the electronic properties of the internal wall.

Next, a concept of ‘thin MWCNTs’ (from here on; denoted as t-MWCNTs) has been formulated. These tubes gradually came to occupy a special place among other filamentous carbon nanomaterials. Tubes with diameters not exceeding 10 nm are classified as t-MWCNTs,^{30–34} although certain authors place the upper limit of diameters at 5 nm. Tubes that contain from 2 to 8–10 walls fall into this category.

Incidentally, the first industrial production of CNTs organised by ‘Hyperion Catalysis’ (USA) in the mid-1980s was based on the hydrocarbon pyrolysis and allowed the production of t-MWCNTs with diameters of 8–10 nm. Later, other countries have also organised the pilot production of CNTs and CNFs by pyrolysis. In 2004, a pilot-line production of carbon nanotubes

E G Rakov D I Mendelev University of Chemical Technology of Russia, Miusskaya pl. 9, 125047 Moscow, Russian Federation.
Fax (7-495) 490 75 23, tel. (7-495) 490 75 24, e-mail: rakov@rctu.ru; nanotube@mail.ru

Received 11 May 2006

Uspekhi Khimii 76 (1) 3–26 (2007); translated by T Ya Safonova

[†] The first syntheses of MWCNTs from hydrocarbons were carried out several years earlier,^{20,21} while their synthesis from CO was carried out more than 100 years ago, in the end of the XIXth century.²²

was organised in Tambov based on the works from the D I Mendeleev University of Chemical Technology of Russia.

Certain versions of pyrolytic methods of the CNT synthesis resemble those of chemical vapour deposition (CVD) which are widely used in the production of coatings of pyrolytic graphite, diamond and diamond-like carbon and are characterised by certain versatility. Indeed, they have their drawbacks, particularly, those associated with the necessity of strict control over the synthetic conditions aimed at the production of pure and uniform CNTs.

Several reviews were devoted to the pyrolytic methods (*e.g.*, see the recently published reviews^{35–42}); a survey that summarises studies on the plasma-enhanced pyrolysis has appeared.¹⁶ However, the majority of these reviews did not dwell into the synthesis of thin CNTs (one exception is a paper³⁷ entirely devoted to SWCNTs) and did not include the most of recent data. The present review summarises studies devoted to the synthesis of thin CNTs, which were carried out in the past 4–5 years. The attention is focused on bimetallic catalysts. For the first time, an attempt is undertaken to generalise the data on the kinetics of CNT formation. Certain potentials of pyrolytic techniques are demonstrated by the example of MWCNT synthesis.

II. Versions of catalytic pyrolysis

Pyrolysis is the transformation of organic substances on heating, which can proceed *via* many routes to ultimately yield elemental carbon. The process is carried out under different conditions, namely, the temperature of the process may vary from nearly ambient to above 1000 °C, while the pressure may be both below and above the atmospheric pressure. Solid (polyethylene, *etc.*) and liquid (supercritical toluene) substances and also aqueous and non-aqueous solutions undergo the pyrolysis to evolve carbon. Pyrolysis of gases and vapours is very close to the CVD processes (although it may differ from such processes⁴³), while the pyrolysis of aqueous solutions resembles the hydrothermal synthesis.

The CNT synthesis under hydrothermal conditions involves the introduction of organic precursors (polyethylene, ethylene glycol, *etc.*) and metal catalysts^{44,45} into the system. The process is carried out at 700–800 °C and a pressure of 60–100 MPa. It was employed for the production of only MWCNTs with the number of walls from 5 to 100 and more. The inner diameter of such MWCNT was 20–1300 nm.

MWCNTs were also synthesised by the pyrolysis of a ferrocene solution in toluene under supercritical conditions at 600 °C and a pressure of ~12.4 MPa (MWCNTs or CNFs were obtained).^{46,47} Resistive heating of the Si substrate covered with a thin Fe film up to 500–1000 °C in certain organic solvents (methanol, ethanol) also yielded CNTs.⁴⁸ Pyrolysis of organic substances in a gel matrix can be carried out at surprisingly low temperatures (300 °C).⁴⁹ The catalytic pyrolysis of liquid hydrocarbons under the conditions of supersonically induced cavitation stands somewhat apart from the above methods. This synthesis was first carried out to produce CNTs in 1999 as the pyrolysis of *o*-dichlorobenzene in the presence of ZnCl₂. Its new version was described recently.^{50,51}

The methods of catalytic pyrolysis of gases are divided into the following two groups according to the way of catalyst loading:

- pyrolysis with a supported catalyst;
- pyrolysis with a ‘volatile’ catalyst.

Based on this, two groups of processes performed under different condition are distinguished. In both cases, to minimise the non-catalytic decomposition of gaseous monoatomic and heteroatomic hydrocarbons, their pyrolysis is recommended to be carried out at a reduced total pressure in the system and a low partial pressure of the main reagent.

SWCNTs can also be prepared by the pyrolysis without a catalyst.^{52,53}

III. Pyrolysis with supported catalysts

1. Versions and specific features of processes

Pyrolysis on a supported catalyst has several versions and offers the widest opportunities. The pyrolysis with powder catalysts and the pyrolysis on smooth (flat) or relief (patterned) substrates can be assigned to its major versions.

The general possibilities may include the production of long CNTs, CNTs of a given diameter, CNTs of definite shapes, doped CNTs, CNTs with the diameter- and length-varying compositions and CNT-containing composites.

On smooth or patterned substrates, it is possible to prepare CNTs oriented in a definite way or various structures formed by CNTs, where oriented CNTs or their structures can occupy relatively wide areas.

The simplest and most frequently applied method is the pyrolysis with powder catalysts. The overwhelming majority of CNT syntheses were carried out in set-ups that represented a heated horizontal reactor in the central zone of which a combustion boat with a weighed portion of the catalyst was placed. The starting hydrocarbons were fed into the reactor. Upon the end of the process, the boat contents were taken out and the CNTs formed were washed from the catalyst remainders with acids and other reagents.

The large-scale pyrolysis with powder catalysts was performed in reactors of the following three types: reactors with stirred (mobile), suspended, and filter beds.⁵⁴ Horizontal vibroreactors used in the synthesis of carbon nanofibres pertain to the first-type reactors.^{55,56} Rotating tube reactors^{38,57} and screw-conveyer type reactors were also used. Suspended-bed reactors include vertical reactors⁵⁸ and reactors with fluidised beds.¹¹ The latter are most popular. They are intended to be used in the preparation of SWCNTs in the CoMoCAT (formed from the words Co – Mo-catalyst) processes^{43,59,60} and also in the pyrolysis of C₂H₂,⁶¹ C₂H₄–H₂ mixtures⁶² and CH₄.⁶³

Long (several mm or cm) CNTs and their bundles were prepared.^{64–74} Such tubes can be used later in the CNT ‘cloning’ (the growth of SWCNTs with identical geometry and structure),⁷⁵ for example, in a cycle shown in Fig. 1. For this purpose, an array of open-end SWCNTs was synthesised, then, the catalyst particles were deposited on their ends and the pyrolysis was repeated. The scheme of ‘cloning’ may be more complicated. Thus the catalyst particles were attached to shortened and functionalised SWCNTs in solution, which was followed by the deposition of tubes onto the substrate. The process resembles the epitaxial growth of single crystals.⁷⁵

Carbon nanotubes of equal lengths are used most often for growing arrays of identically oriented tubes (‘forest’) on smooth substrates. The use of calibrated catalyst particles allows one to synthesise CNTs of definite diameters. In this way, SWCNTs with diameters of 1.45 ± 0.50 nm (Refs 76 and 77) and 1.3 ± 0.4 nm

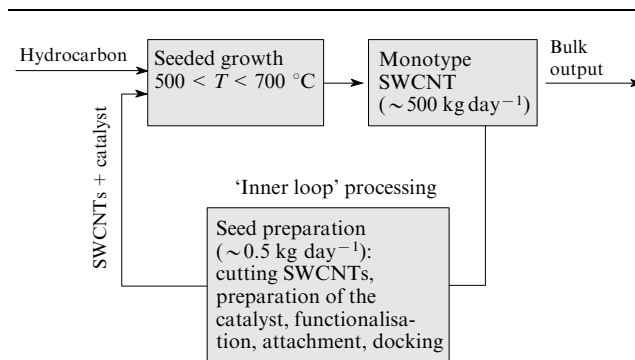


Figure 1. Block diagram of commercial production of SWCNTs of a definite diameter and desired morphology (chirality); [http://www.hydrogen.energy.gov/pdfs/review05/stp_37_smallley.pdf].

(Ref. 78) and also t-MWCNTs with diameters of 4–6 nm were prepared.⁷⁹ The use of the MSM-41 molecular sieves made it possible to control the SWCNT diameter within 0.5–0.8 nm with an accuracy of 0.05 nm.^{80–82} By varying the concentrations of added thiophene in the CH₄ pyrolysis it is possible to control the SWCNT diameter within 0.88–1.18 nm.⁸³ The chemical treatment of zeolites allowed varying the diameter of the void in their crystal structure thus changing the size of catalyst particles incorporated into this void and the diameter of resulting t-MWCNTs.⁸⁴ When MWCNTs are synthesised on flat substrates with deposited catalysts, it is possible to regulate the diameter of tubes and their density on the substrate by varying the intensity of the catalytic film pretreatment in the NH₃ plasma.⁸⁵ Morphology and diameters of CNTs can be changed as a result of changes in the catalyst composition, for instance, by the addition of Co to the Ni/Al₂O₃ catalyst.⁸⁶

Pyrolyses on flat and patterned substrates have their peculiarities, making possible the preparation of oriented CNTs and CNT structures. The oriented CNT packing is possible in the cases of pyrolysis in electric field (the majority of papers describe the MWCNT preparation)^{2, 87–96} and magnetic-field orientation of catalyst particles,⁹⁷ as well as in a directed gas stream^{66, 69–71, 98–100} and at a definite position of the substrate with respect to the gravity vector.¹⁰¹

The growth of oriented CNT was observed² in electric fields with the strength of $\sim 1 \text{ V } \mu\text{m}^{-1}$. Somewhat weaker fields ($0.4 \text{ V } \mu\text{m}^{-1}$) were used in the formation of SWCNT bridges as long as 25 μm between the electrodes.⁹¹ The induced dipole moment was $\sim 10^6 \text{ D}$ for $\sim 1 \mu\text{m}$ -long CNTs in a field of $1 \text{ V } \mu\text{m}^{-1}$.

The most perfect packing of CNTs on a substrate in electric field requires the optimisation of the electrode shape and the elimination of van der Waals interactions between the tubes. Periodic changes in the electrode position and in the direction of the constant electric field during the CNT growth allow one to change the CNT morphology, *viz.*, form bended and zigzag tubes.^{102–104} For CNTs to continue their growth upon a change in the electrode position, the carbon capping that passivates the catalyst particles should be etched away.

A method of SWCNT orientation (aligning), which involved the deposition of Al₂O₃ islets, has been developed.^{93, 105} In this process, the tubes grow perpendicular to the boundary due to the appearance of a space charge. The deposition of a local thin SiO₂ coating on the catalyst film allowed CNTs aligned along the silicon substrate to be grown.¹⁰⁶

Orientation under the effect of the gas flow made it possible to form networks of crossed SWCNTs (in a two-step process)^{66, 69} as well as more complex structures based on 1-cm long tubes.⁷⁰ The best results were achieved at rapid heating of the substrate. Here, a 'kite' mechanism was assumed to operate, *i.e.*, the temperatures of the substrate and the gas increased at different rates, which gave rise to upward convection flows. It is these flows that lift up the ends of growing SWCNTs from the substrate.⁷¹

CNT deposition on silicon, quartz or sapphire single-crystal substrates can also be accompanied by the CNT orientation, which resembled the epitaxial orientation. The growth of oriented SWCNTs coordinated with the surface orientation of silicon single crystals was first observed by Su *et al.*¹⁰⁷ (later, analogous studies were performed with sapphire^{108–112}). It was shown that when ferritin clusters were used as the catalyst and sapphire served as the substrate, the formed SWCNT deposits were ordered on the A and R faces of sapphire and disordered on its M and C faces. Such behaviour was attributed to the different packing of Al atoms on different faces. Sapphire is widely employed as the substrate material in microelectronics; hence, the further development of studies in this direction can lead to the appearance of a new integral circuit technology.

The oriented deposition of CNTs also occurs along atomic steps of vicinal faces of α -Al₂O₃.^{108, 113} The directed growth of

SWCNTs was also observed on the Y-cut of a quartz single crystal.¹¹⁴

As compared with the CNT deposition on flat or powder substrates, the method of growing of arrays of oriented CNTs in Al₂O₃ matrices with cylindrical pores arranged perpendicularly to the external surface was used less often. The vast majority of studies that employed this method were aimed at the MWCNT preparation.^{115–118} Mesoporous silicates were used for the same purposes.^{119, 120} On the other hand, the use of AlPO₄ single crystals,^{121–126} molecular sieves MSM-41 (Refs 80–82 and 127–129) and ordered films of mesoporous SiO₂ (Ref. 130) made it possible to prepare SWCNTs. Zeolites (see Section III.5) and porous silicon served as the matrices in the SWCNT growth. In Al₂O₃ matrices with crossed pores, branched CNTs were synthesised.¹³¹

The method of preparation of a CNT 'forest' described by Dai² is more popular. Catalyst particles of the given size and density were deposited onto inert substrates thus providing the tube growth in only one direction. This allowed SWCNTs to be grown on different substrates in the pyrolysis of ethanol,^{131–135} methane,¹³⁶ ethylene⁶⁷ and mixtures of different gases.

The use of photolithography, methods of substrate profiling or other methods in the deposition of patterns of catalyst particles on substrates made it possible to grow 'columns', 'towers', 'rods', 'tubes' and other CNT structures aligned perpendicularly to the surface. The growth of individual SWCNTs on the patterns formed by photolithographic or microprinting techniques is very promising.^{12, 23, 130, 136}

The preparation of structures of the 'power-line' type, namely, submicron Si or SiO₂ columns with CNT-connected vertices was a remarkable achievement.^{2, 12, 136–141} To synthesise such structures, catalyst particles were preliminarily deposited on column vertices. The formation of 'wires' was explained by swaying of the growing CNTs.

Patterned growth of CNTs on 100 (Refs 142–144) and 150 mm Si wafers [<http://www.elecdesign.com/Articles/Index.Cfm?AD=1&ArticleID=2462>] was documented.

The pyrolytic method of CNT preparation can be employed in the formation of two- and three-dimensional structures.^{145–147} A procedure of preparation of 'pellets' from CNTs aligned in parallel and transplantation them onto any substrate chosen has been developed (Fig. 2).¹⁴⁸

The catalytic pyrolysis allows, in principle, a process similar to the chemical deposition with infiltration to be carried out. Particularly, attempts were undertaken to prepare carbon–carbon composites built of carbon fibres and CNTs.¹⁴⁹

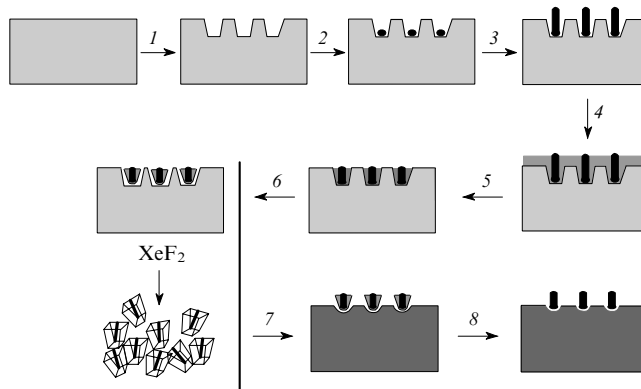


Figure 2. Sequence of operations in the preparation and packing of 'pellets' with CNTs (nanopelleting processes).

(1) Etching trenches, (2) filling trenches with the catalyst, (3) CNT growth, (4) spin casting⁴² an epoxy polymer, (5) planarising and polishing the outer layer to create isolated pellets with uniform-length CNTs, (6) withdrawal of pellets, (7) transplantation of pellets onto a new substrate, (8) etching in the O₂ plasma to remove the polymer.

In the pyrolytic synthesis, the yield of particular CNT types (SWCNTs or DWCNTs) can reach 90%–95% (e.g., see Ref. 150). However, the realisation of the above-described ‘cloning’ of tubes would be the most remarkable achievement.⁷⁵

Tube doping (with nitrogen, boron, *etc.*) was employed, as a rule, only in the production of MWCNTs or carbon nanofibres,^{151, 152} although examples are known where SWCNTs^{52, 153, 154} and even DWCNTs¹⁵⁵ were doped with nitrogen.

The synthesis of CNTs with a composition varying along their lengths or diameters was achieved by changing the growth conditions, particularly, the starting gas composition. Thus CNTs covered with one or several concentric coatings with different compositions were grown.

Pyrolytic methods for the preparation of composites of a ceramic matrix filled with CNTs were actively developed in France.^{156–166} The CNT synthesis was carried out on solid oxide solutions or spinels. In the course of their reduction, solid solutions and compounds based on Al_2O_3 or MgO with formulas of $\text{Mg}_{1-x}\text{M}_x\text{O}$ ($\text{M} = \text{Co}, \text{Ni}$) or $\text{Mg}_{1-x}\text{M}_x\text{Al}_2\text{O}_4$ ($\text{M} = \text{Fe}, \text{Co}, \text{Ni}; x \ll 1$) evolved Fe, Co or Ni nanoparticles which served as the catalysts of the CNT growth. Mixtures of SWCNTs with t-MWCNTs,^{167, 168} SWCNTs with DWCNTs,^{169, 170} DWCNTs,^{159, 160, 171} and also DWCNTs with triple-walled CNTs¹⁷² were prepared from the $\text{CH}_4\text{--H}_2$ gas mixture with appropriately chosen concentrations of Fe, Co or Ni (x values). Oxides CaO , Cr_2O_3 , La_2O_3 , *etc.* can also serve as the matrices.

The catalytic pyrolysis of the $\text{CH}_4\text{--H}_2$ mixture also allowed the formation of a composite film containing MgO and SWCNTs.¹⁷³ A composite containing long CNTs, Fe and ZrC was prepared by the pyrolysis of hydrocarbons on a Zr–Fe film.¹⁷⁴ A composite of SWCNTs and nanocrystalline Al was obtained.¹⁷⁵

Actually, any process of hydrocarbon pyrolysis or CO decomposition on powder catalysts can be modified to produce composites.

2. Methods of enhancement of pyrolytic processes

Several methods of enhancement of catalytic pyrolysis were described, namely, thermal, plasma, hot-filament, and laser enhancement.

There are two versions of thermal enhancement, *viz.*, heating of the substrate (either directly or through the reactor walls) and heating of gaseous hydrocarbons by their partial combustion. In the second version, which is used very rarely, the substrate covered with catalyst is placed into a certain zone of flame. Heating of the substrate was used more often. As a rule, the heating is performed through the reactor walls; however, resistive heating of the substrate was described (the use of Joule heat) in which the reactor walls remain cold^{176, 177} and also heating of the substrate using high-frequency current.^{178, 179} To decrease the temperature of the process¹⁸⁰ and the velocity of the gas flow,¹⁸¹ reduced pressure was used. Thus the pyrolysis of pure C_2H_4 at a pressure of 100 Pa made it possible to build SWCNT and t-MWCNT bridges between the electrodes of nitrided Ta.¹⁸²

The pyrolysis activated by different types of gas discharges, namely, arc, microwave, corona, glow, high-frequency (with frequency from several kHz to several and even tens MHz) was also carried out at reduced pressure.⁴¹ Two types of these processes are distinguished, *viz.*, in which the substrate is placed either immediately into the flame discharge zone or outside of it and it is the gases that are subjected to activation, while the substrate has a relatively low temperature. An example of the use of a plasma source at a distance from the substrate was described.¹⁸³ The elimination of the direct action of microwave plasma on the substrate favours the increase in the CNT growth rate.¹⁸⁴

The plasma enhancement allows one to carry out syntheses at low temperatures of the substrate. Thus MWCNTs were prepared from CH_4 with addition of small amounts of O_2 under the action

of high-frequency plasma at the substrate temperature of 350 °C¹⁸⁵ and also from a $\text{CH}_4\text{--H}_2$ mixture under the action of inductively coupled plasma at the substrate temperature of 200 °C.¹⁸⁶ This can be associated with the fact that charged species formed in plasma can change the mechanism of chemical reactions.

Presumably, the advantages of plasma enhancement over thermal enhancement are that the former allows the effective decomposition of starting hydrocarbons and a strict control over the concentration of reactive species; the drawbacks include the somewhat higher disordering of the product structure.¹⁸⁷

Plasma enhancement was used most often in the MWCNT synthesis.^{16, 41, 188–190} At the same time, the formation of SWCNTs and t-MWCNTs was reported. The microwave discharge plasma was used most extensively. Thus on a Fe catalyst, SWCNTs and DWCNTs with the packing density of $\sim 10^{12}\text{--}10^{13}\text{ cm}^{-2}$ were formed from a $\text{C}_2\text{H}_2\text{--NH}_3$ mixture,¹⁹¹ t-MWCNTs with diameters of 3–20 nm were prepared from a $\text{CH}_4\text{--CO}_2$ mixture,¹⁹² SWCNTs or t-MWCNTs were obtained from a $\text{CH}_4\text{--H}_2$ mixture [http://www.nsti.org/Nanotech2005/Showabstract.html?absno=273] and MWCNTs were formed from a $\text{CH}_4\text{--NH}_3\text{--H}_2$ mixture.¹⁹³ The MWCNT diameter was regulated by varying the size of catalyst particles on the substrate. This could be achieved, for example, by changing the thickness of the deposited metal-catalyst film.^{189, 194–197} A method of preparation of a SWCNT ‘forest’ under the action of point-arc microwave¹⁹⁸ or ‘diffusion’^{199–201} plasmas was described.

An interesting feature of SWCNTs formed in the CH_4 pyrolysis activated by high-frequency discharge is the domination of tubes with semiconductor characteristics.^{183, 202}

For the first time, in the plasma generated at the electron cyclotron resonance, SWCNTs or DWCNTs were grown directly on silicon substrates, which were not preoxidised.²⁰³

The hot-filament activated pyrolysis, *i.e.*, activated by an incandescent tungsten wire heated with Joule heat up to ~ 2000 °C, is a purely laboratory method. This process is easily organised (Fig. 3). Such activation can be accompanied by the formation of plasma, provided a certain potential difference is applied between the cathode and the tungsten wire, which allows SWCNTs to be grown. The tubes were deposited onto low-melting substrates.^{79, 204–206}

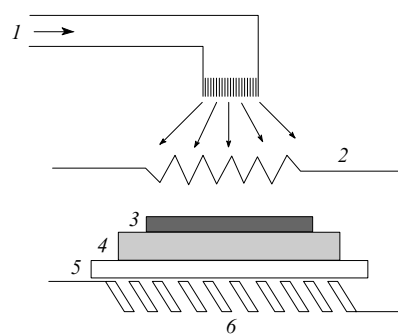


Figure 3. Illustration of CNT preparation in hot-filament activated pyrolysis.

(1) Gas mixture inlet, (2) hot tungsten spiral wire, (3) catalyst, (4) cathode, (5) substrate, (6) substrate heater.

Three types of laser activation are known. In the first method, a directed laser beam locally heats one or another substrate area (SWCNTs were obtained this way).^{207, 208} In the second method, by employing an appropriate frequency of laser radiation, one can selectively activate gases subjected to the pyrolysis or decomposition. Finally, laser beams can be used for heating of diathermic gases by adding to them substances capable of selective absorption of laser radiation.²⁰⁹

A specific feature of pyrolytic processes is that the CNT growth is accompanied by incorporation of only active metal particles²¹⁰ into CNT hollows, whereas the inert substrate (*e.g.*, oxide, see Section III.5) remains outside the tubes. This is the result of the effect of catalysts on the formation of tubes.

3. Starting compounds

The set of starting compounds used in the production of SWCNTs and t-MWCNTs is much more limited as compared with the production of MWCNTs or CNFs. Among hydrocarbons, methane is the most suitable for this purpose (Refs 23, 24, 27, 28, 83, 87, 92, 101, 105, 107, 114, 136, 141, 173, 185, 211–254). This hydrocarbon is thermally more stable as compared with others; this is why its catalytic pyrolysis produces smaller amounts of amorphous carbon impurities. Dilution with hydrogen, which is the main gaseous product of pyrolysis, inhibits the non-catalytic pyrolysis of methane even at relatively high temperatures.^{74, 106, 142, 143, 156–172, 186, 189, 199–201, 233, 246, 255–262} In the plasma-enhanced CVD, the dilution with hydrogen is of vital importance; here, mixtures containing as little as 2 vol.% – 6 vol.% CH₄ (*e.g.*, see Ref. 197) are often used. Dilution with inert gases also has a positive effect. The introduction of small amounts of C₂H₄ into the CH₄–H₂ mixture is a common practice.^{88, 94, 109}

In addition to methane, unsaturated hydrocarbons, particularly, ethylene (Refs 67, 75, 176, 180, 182, 219, 240, 262–270), acetylene (Refs 61, 79, 84, 89, 182, 209, 215, 271–299) and propylene,³⁰⁰ were pyrolysed to form SWCNTs, DWCNTs and t-MWCNTs. Mixtures of unsaturated hydrocarbons with methane^{31, 64, 301–304} and benzene^{227, 305} were also used.

As regards the CNT yield and purity, cyclic hydrocarbons, particularly, cyclohexane, naphthalene and anthracene, do not surpass methane.³⁰⁵ This is also true for benzene.

Mixtures C₂H₂–NH₃ proved to be efficient in the synthesis of CNFs,^{41, 306} MWCNTs,^{41, 188, 283, 307, 308} t-MWCNTs^{195, 196} and SWCNTs¹⁹¹ in plasma. The role of NH₃ in the MWCNT preparation consists of the maintenance of the active surface state of catalytic particles due to the removal of amorphous carbon,³⁰⁹ which accounts for the appearance of HCN in the gas^{308, 310} or the increase in the concentration of hydrogen atoms.¹⁹³ The synthesised CNTs contained up to 10 at.% of nitrogen.¹⁸⁸

The difference between the pyrolysis of C₂H₂ and the pyrolysis of other hydrocarbons is that the former process is highly exothermic. The catalytic synthesis of a CNT ‘forest’ was carried out using C₂H₂ molecular beams.²⁹⁴ In the initial stages, before the thickness of the layer of products reached 50 µm, SWCNTs with diameters of ~1 nm were preferentially formed, which was followed by the growth of SWCNTs with larger diameters and DWCNTs.

In the last 3–4 years, keen attention was paid to the use of ethanol as the starting compound in the CNT synthesis. It was assumed that OH radicals remove amorphous carbon admixtures to yield much purer SWCNTs as compared with cases where other reagents were used. This line of research was actively explored by Japanese scientists of the Maruyama group.^{132, 134, 135, 177, 311–320} Analogous syntheses were carried out by other scientific groups.^{66, 72, 75, 78, 178, 179, 321–327} Low partial vapour pressures (0.7–1.4 kPa or 5–10 Torr) and a temperature of 800 °C were commonly used. Ethanol pyrolysis on a Fe–Co/SiO₂ catalyst selectively produced DWCNTs.³²⁶

The introduction of OH radicals into the gas phase can also be accomplished by the addition of O₂ (Refs 185 and 187) or H₂O vapours.⁶⁷ Presumably, the higher yields and formation rates of MWCNTs in the CH₄ pyrolysis on the oxide catalysts that were not subjected to preliminary reduction as compared with reduced catalysts were also attributed to the effect of H₂O vapours evolved in the oxide reduction during the pyrolysis.²⁴⁴

Single-walled CNTs were prepared from vapours of methanol³²³ and mixtures CH₃OH + H₂ and CH₃OH + Ar.⁷¹

The rate of MWCNT formation from methanol was substantially lower as compared with ethanol.³²⁸ A synthesis of SWCNTs was carried out from methanol and propan-2-ol in a set-up with a hot filament.³²⁹ Low SWCNT yields were obtained from camphor³³⁰ and its analogues, namely, camphorquinone, norcamphor, norbornane, fenchone. These experiments did not reveal any beneficial effect of oxygen on the yield and quality of tubes.³³¹

A matrix synthesis of SWCNTs was carried out using tripropylamine.^{121, 125, 332} A mixture of SWCNTs and MWCNTs was isolated after the acetonitrile pyrolysis.³³³ The synthesis of CNTs (with a fraction of t-MWCNTs) from associated gas was described.^{236, 334}

In recent years, the CNT synthesis by the thermal decomposition of carbon monoxide was actively developed (Refs 19, 43, 59, 60, 68, 80–82, 127–129, 263, 335–349). The equilibrium of CO decomposition is such that the solid product yield decreases with an increase in the temperature. This makes the choice of conditions that suppress the formation of amorphous carbon much easier. An increase in the pressure substantially increased the yield of SWCNTs and made them more uniform in the diameter.¹²⁸ The addition of H₂ was observed to have a positive effect on the rate of CNT formation^{69, 71, 335, 342} and, in the case of Co/MgO catalysts, the tube diameter was observed to decrease with the decrease in the Co concentration.³⁴² This method allowed one to prepare both ordinary^{339–341} and long SWCNTs.³⁴⁴

A large-scale production of SWCNTs *via* the catalytic decomposition of CO was proposed based on the aforementioned CoMoCAT process (Fig. 4). The reaction is carried out at 700–950 °C and a pressure of ~0.5 MPa (5 atm). Stable operation of the set-up requires a low degree of CO decomposition in the reaction zone; this is why the set-up provides the CO recycling after the recovery of CO₂ formed. It was shown that the lower the temperature of the process the smaller the average diameter of SWCNTs formed, *i.e.*, the diameter approached 0.8 nm at 750 °C, 1.0 nm at 850 °C and 1.2 nm at 950 °C. The catalyst selectivity with respect to SWCNTs (the SWCNT fraction in the total CNT mass) was 80%–90%. The fraction of semiconductor CNTs in the total amount of tubes was 57%.

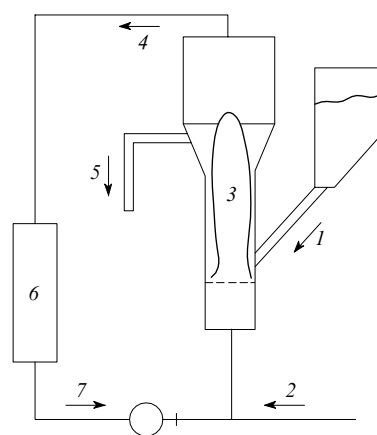


Figure 4. A principal scheme of the CoMoCAT process.

(1) Catalyst load slot, (2) fresh CO feed line, (3) fluidised catalyst bed, (4) outlet of reaction gases, (5) product output, (6) CO₂ trap, (7) inlet of recycled CO; [http://www.ou.edu/engineering/nanotube/comocat.html].

4. Catalysts

Among individual metals, Fe, Co and Ni exhibit the highest catalytic activity in the pyrolytic synthesis of CNTs. It is a wide opinion that the characteristics of metal–carbon systems are of the prime importance for the catalytic activity of metals in the pyrolysis.

In a review,⁴¹ the catalysts used in the preparation of various filamentous carbon nanoparticles on substrates were tabulated and the original literature references (more than 60) were cited; however, only three of references are devoted to the synthesis of SWCNTs. This is why the present survey shows a new list of catalysts as applied to the synthesis of SWCNTs, DWCNTs and t-MWCNTs.

The preparation of SWCNTs, DWCNTs and t-MWCNTs involves most often the use of bimetallic catalysts, *i.e.*, active metals.³⁵⁰ They exhibit enhanced activity, selectivity and thermal stability and are less susceptible to poisoning. Such catalysts allow the diameter and purity of CNTs obtained to be controlled within certain limits.

The major metal catalysts, namely, Fe, Co or Ni, are often supplemented with molybdenum compounds (Tables 1 and 2). Molybdenum as such, its oxides and certain other compounds also exhibit catalytic properties in the pyrolysis of hydrocarbons and the decomposition of CO; however, in the CNT synthesis, their

effect is either weak or they impair the morphology of the solid products of the pyrolysis. In place of CNTs, non-tubular CNFs or wide-diameter CNTs are often formed. At the same time, the use of Mo as a promoting additive favours the decrease in the CNT diameter, the increase in the total yield of solid products and the decrease in the amount of admixed CNFs. Particularly, it is assumed that the addition of Mo to the Co/MgO system gives rise to small Co clusters that are formed due to the decomposition of CoMoO₄ and provide sites for the CNT growth.²⁸⁸

Table 1 shows examples of the use of binary powder catalysts Co–Mo on different substrates in the heat-activated pyrolytic synthesis of SWCNTs, DWCNTs, t-MWCNTs and CNFs. The data in Table 1 may be supplemented by the results on disproportionation of undiluted CO on the Co–Mo/SiO catalyst.³³⁶ It was shown that this catalyst changes its chemical composition in the course of CNT formation. As reported in numerous publications, binary powder catalysts based on Co–Mo make it possible to synthesise SWCNTs from various carbon-containing precursors.

Table 1. Composition and application conditions of binary powder catalysts Co–Mo/support (A) in the heat-activated CNT synthesis.

A	Co : Mo : A /mol (Co : Mo)	Process conditions			Products	Ref.
		starting compounds	<i>T</i> /°C	<i>p</i> /atm		
MgO	(0–5) : (5–0) : 95	CH ₄ (20%)–H ₂	1000	1.0	t-MWCNTs, CNFs	34
MgO	5 : 1 : 94	CH ₄ (20%)–H ₂	1000	1.0	t-MWCNTs, CNFs	32
MgO	2.5 : 2.5 : 95.0 ^a	C ₂ H ₂ (10%)–H ₂	800	1.0	SWCNTs	288
MgO	(1 : 4)	CO (100%)	700	1.0	SWCNTs	351
MgO	(1 : (2–30))	CH ₄ (97%)–H ₂	1000	1.0	t-MWCNTs	352
MgO	1.0 : 0.1 : 20.0	CH ₄ (9%)–Ar	800–850	1.0	DWCNTs	239
SiO ₂	0.5 : 1.5 : 98.0 ^a	CO (100%)	750	5.0	SWCNTs	60
SiO ₂	2 : 4 : 94	CO (100%)	700	1.0	SWCNTs	59, 337
SiO ₂ (see ^b)	(1.0 : 3.5)	CO (100%)	850	1.0	SWCNTs	343
SiO ₂	(2 : 1)–(1 : 4)	CO (20% or 50%)–He	700, 800	(1.0)	SWCNTs	337
SiO ₂	~0.5 : 1.5 : 98.0 ^a	CO (100%)	700–950	1–10	SWCNTs	43, 345
SBA-16	(1.0 : (0.3–1.0))	C ₂ H ₅ OH–Ar (see ^c)	850	1.0	SWCNTs	66
Zeol or Al ₂ O ₃	(0–5) : (5–0) : 95 ^a	C ₂ H ₂ (9%)–N ₂	700	1.0	t-MWCNTs	353
Al ₂ O ₃	1 : 4 : 50 ^a	CH ₄ (50%)–Ar	550–850	1.0	MWCNTs	244

^a Mass ratio. ^b Catalysts with Na additives were also tested. ^c The partial pressure of ethanol vapours was 0.0155 atm.

Table 2. Composition and application conditions of binary powder catalysts Fe–Mo/support (A) at thermal activation and atmospheric pressure.

A	Fe : Mo : A /mol (Fe : Mo)	Process conditions		Products	Ref.
		starting compounds	<i>T</i> /°C		
MgO	10.0 : 2.5 : 87.5	CH ₄ –C ₂ H ₄ –H ₂	900	t-MWCNTs	31
MgO	(1.0–2.0) : (0.05–0.10) : 13.0	CH ₄ (20%)–H ₂ (N ₂)	1000	SWCNTs	241
MgO	(0.5–2.0) : (0.05–0.2) : 11	C ₂ H ₂ (1%–13%)–Ar	850–950	SWCNTs	296
MgO	1.0 : 0.1 : 11.0 ^a	C ₂ H ₂ (2%)–Ar	800–950	SWCNTs	287
MgO	1.0 : 0.1 : 12.0 ^a	C ₆ H ₁₄ –Ar	900	DWCNTs	354
Al ₂ O ₃	9 : 1 : 90	C ₂ H ₄ (0.06%)–Ar–H ₂ (0.03%)	850	SWCNTs + DWCNTs	263
Al ₂ O ₃	1.00 : 0.16 : 10.00	CH ₄	900	t-MWCNTs ^b	355
Al ₂ O ₃	1.00 : 0.16 : 10.00	CH ₄ (50%)–H ₂	950	SWCNTs ^b	355
Al ₂ O ₃	1.00 : 0.17 : 10.00	CH ₄ (60%)–H ₂ (see ^c)	700–900	SWCNTs	181
Al ₂ O ₃	1.00 : 0.25 : 10.00	CH ₄ (20%)–H ₂	1000	SWCNTs	356
Al ₂ O ₃	1.0 : 0.1 : 13.0	CH ₄ (17%)–Ar	950	SWCNTs + DWCNTs	232
Al ₂ O ₃	(5 : 1) ^a	CH ₄ (10%)–Ar	680–900	SWCNTs	220
Al ₂ O ₃	1.00 : 0.17 : 16.00	CH ₄	900	SWCNTs	213
Al ₂ O ₃	1.00 : 0.16 : 16.00	CH ₄	850–1000	SWCNTs	215
Al ₂ O ₃	(6 : 1)	CH ₄ (2.2%–35.2%)–Ar (see ^d)	680–850	SWCNTs	223
Al ₂ O ₃	9 : 1 : 90	CO (1.18 atm)	700–850	SWCNTs (+ DWCNTs)	263
SiO ₂ + Al ₂ O ₃	1.0 : 0.17 : (16.00 + 16.00)	CH ₄	900	SWCNTs	213

^a Mass ratio. ^b Depending on the catalyst synthesis conditions, MWCNTs and CNFs can be obtained. ^c The total pressure was 0.13 atm. ^d The total pressure was 0.79 atm.

Table 3. Composition and application conditions of binary powder catalysts $M-M'/A$ ($M, M' = \text{Fe, Co or Ni}$; A is support).

$M-M'/A$	$M:M':A$ /mol ($M:M'$)	Process conditions			Enhancement method	Products	Ref.
		starting compounds	$T/^{\circ}\text{C}$	p/atm			
Fe–Co/Zeol (or Al_2O_3)	(0–5):(5–0):95 ^a	C_2H_2 (9%)– N_2	700	1.0	thermal	t-MWCNTs, MWCNTs	353
Fe–Co/ MgAl_2O_4	6.5:3.5:90.0 ^b	CH_4 (18%)– H_2	700–1070	1.0	"	t-MWCNTs, CNFs	359
Fe–Co/ MgAl_2O_4	(0–0.1):(0.1–0):0.9	CH_4 (18%)– H_2	1070	1.0	"	SWCNTs, DWCNTs	170
Fe–Co/ MgAl_2O_4	80 ^c	CH_4 – H_2	1070	1.0	"	SWCNTs, t-MWCNTs	167
Fe–Co/ Al_2O_3 (see ^d)	2.5:2.5:95.0 ^a	C_2H_4 (27%)– N_2	1080	1.0	"	SWCNTs	264
Fe–Co/Zeol	2.5:2.5:95.0 ^a	$\text{C}_2\text{H}_5\text{OH}$ –Ar	700–800	6.6×10^{-3}	"	SWCNTs	311
Fe–Co/Zeol	2.5:2.5:95.0 ^a	$\text{C}_2\text{H}_5\text{OH}$	850	1.3×10^{-4}	plasma	SWCNTs	177
Fe–Co/Zeol	2.5:2.5:95.0 ^a	$\text{C}_2\text{H}_5\text{OH}$	800	0.013	thermal	SWCNTs	313
Fe–Co/Zeol	2.5:2.5:95.0 ^a	$\text{C}_2\text{H}_5\text{OH}$ –Ar	800	6.6×10^{-3}	"	SWCNTs	316
Fe–Co/Zeol	2.5:2.5:95.0 ^a	$\text{C}_2\text{H}_5\text{OH}$ –Ar– H_2	800	6.6×10^{-3}	"	SWCNTs	315
Fe–Co/Zeol	2.5:2.5:95.0 ^a	$\text{C}_2\text{H}_5\text{OH}$ –Ar	900–1000	1.0	"	SWCNTs	178, 179
Fe–Co/Zeol	2.5:2.5:95.0 ^a	$\text{C}_2\text{H}_5\text{OH}$	900	0.05–0.08	hot filament	SWCNTs	360
Fe–Co/ MgO	(10–0):(0–10) ^c	$\text{C}_2\text{H}_5\text{OH}$, CH_3OH	450–950	$(6.6–13.1) \times 10^{-3}$	thermal	SWCNTs	323
Fe–Co/Zeol	(1:1)	C_2H_2 (0.4%–1.6%)–Ar	900	1.0	"	DWCNTs	280
Fe–Ni/ MgAl_2O_4	6.5:3.5:90.0 ^b	CH_4 (18%)– H_2	700–1070	1.0	"	t-MWCNTs, CNFs	359
Fe–Ni/ MgAl_2O_4	80 ^c	CH_4 (18%)– H_2	1070	1.0	"	SWCNTs, t-MWCNTs	167
Co–Ni/ MgAl_2O_4	80 ^c	CH_4 (18%)– H_2	1070	1.0	"	SWCNTs, t-MWCNTs	167
Co–Ni/ SiO_2 (Al_2O_3)	(1:1)	CH_4	1000	1.25	"	SWCNTs	23

^a Mass ratio. ^b Ratio Fe:Co:Mg or Fe:Ni:Mg. ^c Content of MgAl_2O_4 /mol. ^d Good results were also obtained for the Fe–Co–Ni/ Al_2O_3 catalyst. ^e The MgO content was about 97 mass %; Si and SiO_2 supports were also used.

sors. Moreover, after certain changes in the conditions, even DWCNTs, t-MWCNTs and CNFs can be isolated. In the pyrolysis of CH_4 – H_2 mixtures, the highest yield was achieved for the molecular ratio $\text{Co}:\text{Mo} = 1:3$.^{34,357}

In addition to studies cited in Table 2, the use of the Fe–Mo/ MgO catalyst in the synthesis of DWCNTs from CH_4 – H_2 deserves mention.³⁵⁸

As follows from Tables 1 and 2, the lowest temperature of the SWCNT synthesis is 680 $^{\circ}\text{C}$ [e.g., from CH_4 with a catalyst based on Fe and Mo oxides deposited on Al_2O_3 at the mass ratio $\text{Fe}:\text{Mo} = 5:1$ (Ref. 220)];[†] however, such tubes are conventionally obtained at temperatures not lower than 800 $^{\circ}\text{C}$.

The pyrolytic synthesis of CNTs employs Fe–Co, Fe–Ni and Co–Ni catalysts on different substrates (Table 3). In addition to

[†] Iron oxides are inactive under these conditions but can be activated by pre-reduction with a He– H_2 (10%) mixture.

catalysts shown in Table 3, Fe–Co/ MgO (preparation of DWCNTs in the CH_4 pyrolysis),²⁴⁵ Fe–Co/Zeol (SWCNTs, C_2H_2)²⁷⁸ and Fe–Co/ SiO_2 (DWCNTs, $\text{C}_2\text{H}_5\text{OH}$)³²⁶ were described. The use of the Ni–Mo composition was also mentioned.³⁶¹

Besides Mo, the additions of platinum metals, e.g., Ru,²¹³ Pt^{71,317} and also compounds of tungsten,^{280,345} vanadium,³⁵³ chromium²⁸⁰ and manganese²⁸⁰ was used in the preparation of bimetallic catalysts based on Fe, Co or Ni. It was shown that the Co–Mo catalyst is more efficient than Co–Pt³¹⁷ and the Co–Ni catalyst is more efficient than Co–V, Co–Cr and Co–Mn.²⁸⁰

A series of iron-based catalysts with different additives were tested,³⁵⁹ namely, Fe–Cr/ Al_2O_3 , Fe–Ni/ Al_2O_3 , Fe–Ru/ Al_2O_3 , Fe–Cr/ Cr_2O_3 , Fe–Co–Ni/ Cr_2O_3 , Fe–Co–Ni/ MgO and Fe–Co–Ni/ MgAl_2O_4 .

In addition to binary powder catalysts based on Fe, Co or Ni, more complex catalysts and supported binary catalysts were also

Table 4. Composition and application conditions of multilayer catalysts sputtered on flat and patterned substrates in the heat-activated pyrolysis (the sequence of layers begins with the external layer).

$M-M'-M''$ or $M-M'$	Layer thickness for M, M' and M'' /nm	Process conditions				Products	Ref.
		substrate	starting compounds	$T/^{\circ}\text{C}$	p/atm		
Mo–Fe–Al	0.2, 1.0, 10	Si	C_2H_2 (0.3%)–Ar (83.0%)– H_2 (16.7%)	600–1100	1.0	SWCNTs, DWCNTs	282
Mo–Fe–Al	0.2, 1.0, 10	Si	C_2H_2	1000	$(0.7–2.7) \times 10^{-3}$	SWCNTs	289
Mo–Fe–Al	0.2, 1.0, 10	Si	C_2H_2	700–1000	2.5×10^{-3}	SWCNTs	290
Mo–Fe–Al	0.2, 1.0, 10	Si	C_2H_2 – H_2 –Ar	535–900	1.0	t-MWCNTs	298
Mo–Fe–Al	2, 1, 20	see ^a	CH_4 –Ar	950	1.0	SWCNTs, t-MWCNTs, MWCNTs	237
Mo–Fe–Al	(0–0.2), (0–0.2), 10 ^b	Si	C_2H_2	730	1.0	t-MWCNTs	362
(Fe, Ni, Co)–Al	(1–10), (10–1) ^d	glass	CO (6%)– H_2	550	1.0	t-MWCNTs	363, 364
Ni–Al	1, (2–10)	SiO_2/Si	CH_4	800	0.13	SWCNTs	365
Co–Pt	2, 10	SiO_2/Si	$\text{C}_2\text{H}_5\text{OH}$ (4.7%)–Ar	not specified	2.6×10^{-3}	SWCNTs	321

^a 15 Substrates of different compositions were tested. ^b The best properties were observed for $\text{Mo}_{0.06}\text{Fe}_{0.94}$ with the total layer thickness of 0.5–2.0 nm.

^c Simultaneous sputtering was carried out. ^d The limits of layer thickness variation are shown.

Table 5. Composition of catalysts deposited on substrates from the gas phase or from solutions and suspensions and the conditions of their use in the heat-activated pyrolysis.

M – M'	Pyrolysis conditions				Ref.
	substrate	starting compounds	$T/^{\circ}\text{C}$	p/atm	
Co–Mo	Si or SiO ₂	C ₂ H ₅ OH	600–850	1.3×10^{-2} , 2.6×10^{-2}	312, 314, 320
Co–Mo ^a	SiO ₂	C ₂ H ₅ OH	800	0.9×10^{-2}	132
Co–Mo	Si ₂	C ₂ H ₅ OH	800	1.3×10^{-2}	134, 135
Co–Mo ^b	SiO ₂	C ₂ H ₅ OH	800	not specified	317
Co–Mo	SiO ₂	C ₂ H ₅ OH	800	1.3×10^{-2}	133
Co–Mo	SiO ₂	C ₂ H ₅ OH	800	1.3×10^{-2}	318
Fe–Mo–Al ₂ O ₃	SiO ₂ /Si	CH ₄	900, 1000	1.0	24, 212, 214, 369 ^d
Fe–Mo–Al ₂ O ₃	SiO ₂ /Si	CH ₄ –H ₂	900	1.0	142
Fe–Mo ^c	Si or SiO ₂	CH ₄	900	1.0	218
Fe–Mo	SiO ₂ /Si	CO (80%)–H ₂	900	1.0	98, 99
Fe–Mo	Al ₂ O ₃ /Si	CH ₄	900	1.0	370
Fe–Mo	Al ₂ O ₃ /Si	CH ₄	900	1.0	107
Fe–Mo–Al ₂ O ₃	SiO ₂ /Si	CH ₄ –H ₂	950	1.0	230
Fe–Mo	SiO ₂ /Si ^e	CO–H ₂	950	1.0	339
Fe–Mo	Si ₃ N ₄ (see ^f)	CH ₄ (50%)–H ₂	950	1.1	257
Fe–Mo–MgO	SiO ₂	CH ₄ –H ₂	950	1.0	173
Fe–Mo–Al ₂ O ₃	Cr/Au/SiO ₂ /Si	CH ₄ –H ₂	900	1.0	65

^a Thickness of the layer on the substrate was 1–2 nm. ^b Particles measuring 10 ± 1 nm were deposited. ^c A promoting catalyst deposited as a powder was also used. ^d In this work,³⁶⁹ the deposition was carried out onto Si tips. ^e Substrates of Al₂O₃ and MgO were also tested. ^f The substrate was hydrophilised in the O₂ plasma.

used (Table 4). The synthesis of CNTs from CO on Co–Mo films deposited on quartz³⁴⁴ and also by plasma-enhanced pyrolysis on the Al₂O₃ (thickness 0.7 nm)–Fe (0.5 nm)–Al₂O₃ (5.0 nm) film sputtered on silicon^{198, 348} was described.

The studies by a group of Japanese scientists on the pyrolysis of hydrocarbons on sputtered Fe catalysts deserve mention.^{366–368} In particular, they have shown that the CNT diameter can be regulated by varying the thickness of the sputtered catalyst film.

In certain cases, the catalysts were applied onto substrates by the methods simpler than sputtering, *viz.*, by dipping in solutions or suspensions, chemical vapour deposition, *etc.* Table 5 shows the examples of CNT syntheses on such catalysts.

A two-step mechanism was proposed³⁷¹ to explain the effect of bimetallic catalysts in the formation of SWCNTs. The role of the second metal, *e.g.*, Mo, may consist of the promotion of the formation of an intermediate CNT precursor. This promoter can be spatially separated from the main metal on which CNTs are formed. For instance, a ‘conditioning’ catalyst or ‘pre-catalyst’ placed immediately in the gas stream fed into the pyrolysis reactor was observed to substantially increase the CNT yield.^{28, 29, 249, 372} It was found that the ‘pre-catalyst’ favours the formation of small amounts of C₆H₆ from CH₄.

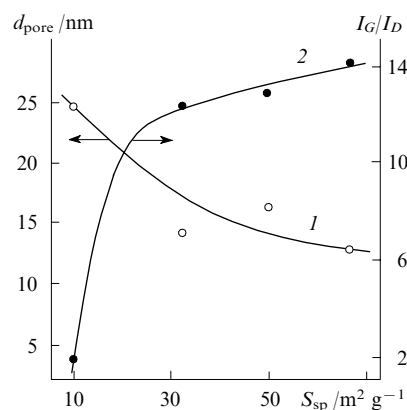
5. Catalyst supports and substrates

In powder catalyst composition, an inert support separates the active metal particles preventing their aggregation. In the preliminary stages of the preparation of compositions, due to the formation of solid solutions, the support favours more uniform distribution of catalyst precursors. This is why attention is focused on the choice of supports and the selection of the composition. A combinatory method for the selection of the composition of catalysts for the synthesis of MWCNTs,^{373, 374} t-MWCNTs³⁷⁴ and SWCNTs^{375, 376} was described.

Based on a large number of examples, the relationship between the diameters of a CNT formed and a catalyst particle was studied and these diameters were shown to be similar.^{79, 277, 322} For instance, it was assumed that the size of metal particles should be limited to 3 nm.³¹⁹ At the same time, it was shown that SWCNTs with diameters of 1.45 ± 0.50 nm grow on uniform Ni particles with diameters of 4.7 ± 1.4 nm,^{76, 77} tubes with diameters

of 1.3 ± 0.4 nm grow on Fe particles with diameters of 1.7 ± 0.6 nm^{78, 377} and CNTs with diameters of 1–2 nm grow of Fe particles with diameters of ~ 5 –14 nm.²⁶⁰ The experimental results have not yet been brought in complete agreement with one another. It was shown³⁷⁶ that the ratio of diameters of a catalyst particle and a SWCNT approached 1.6; however, in the MWCNT preparation (diameter 27–57 nm), a considerably smaller ratio of diameters, namely, 1.2–1.4, was observed.³⁷⁸

Testing of various powder catalyst supports has shown that MgO surpasses SiO₂, ZrO₂, Al₂O₃, CaO, *etc.* in the stability and the SWCNT yields reached.²²⁷ For powder MgO with mesopores of a certain size ($d = 12$ –16 nm), the specific surface area (S_{sp}) of the powder is related to the SWCNT purity, as evidenced by the changes in the intensities of G- and D-modes in the Raman spectra of tubes (Fig. 5). At the same time, no unambiguous relationship between S_{sp} of the support and CNT characteristics was revealed, *viz.*, on a SiO₂ support with the pore diameter of 7.2 nm, no

**Figure 5.** Effect of the specific surface area of MgO powder prepared by different methods on (1) the average size of powder pores and (2) the ratio of intensities of G and D modes in the Raman spectra of SWCNTs synthesised.

Points correspond to experimental data.

Table 6. Properties of catalyst supports and the pyrolysis products of the CH₄–Ar mixture at 850 °C (reproduced with permission of the Royal Chemical Society).

Material	$S_{sp}/m^2\text{ g}^{-1}$	d_{pore}/nm	RBM peak ^a	I_G/I_D
SiO ₂	446	7.2	absent	—
CaO	4.8	38	"	—
ZrO ₂	102	22	"	—
Al ₂ O ₃	155	15	present	2.3

^a RBM is the radial breathing mode that characterises the presence of SWCNTs.

SWCNTs or t-MWCNTs were formed at all even if S_{sp} of the support was as large as 446 m² g^{−1} (Table 6).

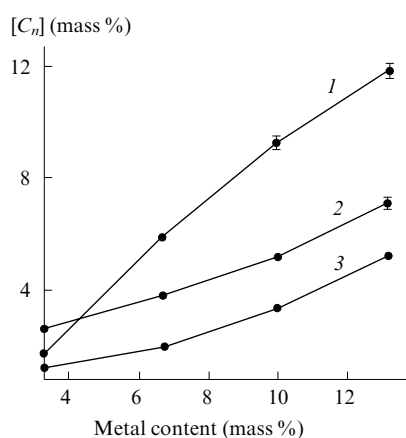
The increase in the active metal content in the catalyst entailed the increase in the deposit yield (Fig. 6)¹⁵⁶ but impaired the CNT quality, as follows from the S_{sp} of the carbon product (Fig. 7).¹⁵⁶

For sputtered catalysts, the chemical composition of the substrate surfaces affects the CNT formation. Thus on hydrogenated silicon substrates, the formation of tube nuclei occurred easier than on oxidised substrates or those treated with tetramethylammonium hydroxide.²⁰⁵ A buffer layer (Al₂O₃, TiO₂, etc.) between the substrate (Si) and the active metal (Fe) is not less significant, because it can determine the chemical composition of the catalyst.^{379,380} For example, under similar conditions, iron deposited on an Al₂O₃ layer exists as FeO and can catalyse the formation of SWCNTs, DWCNTs and t-MWCNTs, whereas in an iron layer deposited on TiN and TiO₂ layers, iron is present in the metal form and causes the growth of thick MWCNTs with more than 20 layers.^{379,380}

To prepare t-MWCNTs with diameters of less than 10 nm on metal electrodes, it was recommended to sputter a silicon interlayer between the metal electrode and the catalyst particles.³⁸¹

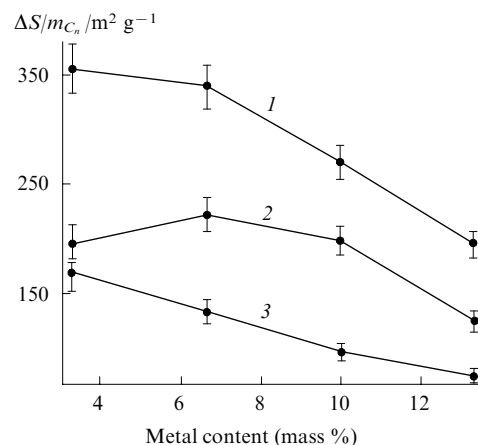
By changing the composition and thickness of sputtered layers, one can regulate the CNT density on the substrate.³⁸² The results of a systematic study²³⁷ point to the strong effect of the substrate on the morphology and quality of CNTs formed (Table 7).

The different effects of substrates on the CNT growth were attributed^{237,383} to the different roughness of their surfaces. The surface roughness affects the S_{sp} value, the density of defects and, as a consequence, the size of catalyst particles. Rough supports should be preferred. In the case of powder catalysts, the important

**Figure 6.** Effect of the content of transition metals in a powder catalyst on the carbon yield in the deposit.¹⁵⁶

(1) Fe, (2) Co, (3) Ni.

(Reproduced with permission of Prof. Rao and the Materials Research Society.)

**Figure 7.** Effect of the content of transition metals in a powder catalyst on the quality of CNTs obtained (the ratio of the carbon deposit specific surface area to the deposit mass).¹⁵⁶

(1) Co, (2) Ni, (3) Fe.

(Reproduced with permission of Prof. Rao and the Materials Research Society.)

Table 7. Characteristics of CNTs prepared on the Mo(thickness 2 nm)–Fe(1 nm)–Al(20 nm) catalyst (reproduced with permission of the Elsevier Publishers).²³⁷

Substrate	I_G/I_D	Diameters of SWCNTs /nm	Diameters of MWCNTs /nm
Deposited Al ₂ O ₃	16.0	1.5–3.5	—
SiC	6.0	1.4–2.2	~ 9
Si(001)	4.1	1.3–3.75	5.4–20
Quartz	4.1	1.5–2.4	5.0–13.6
Sapphire	3.2	1.7–2.7	9.0–24
Si/SiO ₂	1.7	1.2–4.3	7.5–18
MgO	1.4	2.3–4.3	11.0–27.7
Porous Si	1.4	≤ 5.0	5.6–7.4
Aerogel (80%)	1.4	—	5.9–15.7
Aerogel (50%)	1.2	—	7.1–19.9
Aerogel (30%)	1.1	—	9.4–20.8
Fused SiO ₂	1.1	—	5.5–12.5
Etched Si(001)	1.0	—	6.3–10.4
Plasma SiO ₂	1.0	—	5.6–25.9
Si/Si	0.99	—	6.1–22.4

role was assigned²³⁸ to the interaction of the metal with the support.

For the plasma-enhanced catalytic pyrolysis of hydrocarbons, the substrate can become the source of radicals, *i.e.*, take part in chemical reactions and also be sputtered with the transfer of the substrate material to the CNF surface.⁴¹

To obtain SWCNTs with small diameters (0.4–0.5 nm), AlPO₄-5 molecular sieves were used.³⁸⁴ The pore size in the Co-substituted molecular sieves MSM-41 and, therefore, the SWCNT diameter could be regulated by varying the composition of liquid matrices in the sieve preparation.⁸¹

An unordinary substrate, namely, uniform SiO₂ microspheres with diameters from 300 to 700 nm was used in the synthesis of SWCNTs.²⁵¹ After the application of Fe particles on these spheres (the spheres were impregnated with a FeCl₃ solution), the CH₄ pyrolysis at 900 °C produced SWCNTs that formed ‘nanoclaws’ patterns on the spheres.

6. Methods of synthesis of catalysts

In the preparation of catalysts for the synthesis of SWCNTs, DWCNTs and t-MWCNTs, it is necessary to produce active-phase particles with sizes not exceeding 3–5 nm.^{76–79, 319, 377, 385} The methods of preparation of such catalysts are less abundant as compared with those used in the synthesis of ordinary MWCNTs and CNFs. The co-deposition of hydroxides, impregnation of fine-grain or mesoporous supports with metal salt solutions followed by the salt decomposition and the reduction of metals with hydrogen, and also the reduction of metallates, the method of ‘wet combustion’ and the sol–gel process were used in the catalyst preparation. Ion exchange processes were employed much more rarely.^{272, 386}

In particular, the co-deposition was used in the synthesis of catalysts deposited on MgO²²⁸ and Al₂O₃.³³⁴

Metal salt solutions were utilised in the impregnation of zeolites^{84, 177, 178, 267, 271, 272, 311, 316, 353, 360} (including the thermally stable Ti-containing zeolite TS-1),²⁸⁰ molecular sieve MSM-41,^{80, 127, 128, 387} MgO,^{227, 228, 231, 256, 288, 323, 354} silica gel,^{59, 60, 63, 264, 337, 343} Al₂O₃ powder and foam (Refs 19, 23, 24, 30, 223, 232, 263, 264, 353), Mg₂(OH)₂CO₃ (Ref. 333) and powders of different compositions.²²⁷ Catalysts were prepared by the hydrolysis of tetraethylorthosilicate in the presence of Al₂O₃ nanoparticles followed by impregnation.²¹³ An aerogel of Al₂O₃ impregnated with Fe and Mo salts proved its worth in the production of SWCNTs from carbon monoxide.³⁴⁰ Impregnation is conventionally carried out under conditions of ultrasonic activation. Salt melts can also be used for the impregnation.⁶³ The impregnation is carried out together with thermal decomposition and reduction of metals.

The reduction of solid solutions M_xMg_{1-x}Al₂O₄ (M = Fe, Fe–Co, Fe–Ni),^{158, 159, 169, 358} Fe_xMg_{1-x}O (Refs 159, 388, 389) and Co_xMg_{1-x}O,^{159, 168, 216, 390} Fe_xAl_{2-x}O₃ (Refs 159, 162, 255, 391 and 392) and also solid solutions of Co in MSM-41,^{80, 81, 127, 128, 388, 393–395} compounds FeLaO₃ (Ref. 396) and NiLa₂O₄ (Refs 397 and 398) was carried out. A linear correlation between the diameter of Fe particles formed in the reduction of Fe_{0.3}Al_{1.7}O₃ and the specific surface of the catalyst was revealed.³⁹¹ The reduction of solid solutions can also occur immediately in the course of pyrolysis.³⁹⁹

The method of ‘wet combustion’ consists of the preparation of a homogeneous aqueous solution of metal nitrates and an organic reducing agent, its rapid heating (an open vessel with the solution is placed into a heated furnace), evaporation of water and spontaneous ignition of the residue.⁴⁰⁰ Thus the reaction of Fe and Mg nitrates with citric acid yielded a highly efficient catalyst for the synthesis of t-MWCNTs, namely, Fe–Mo/MgO (Mo salts were also added to the starting mixture).³¹ The syntheses of a Co/MgO catalyst that involved the use of urea²¹⁶ and citric acid^{342, 401} were described. This method was also used in the synthesis of the following catalysts: Ni/MgO,^{402–404} Co–Mo/MgO (with the use of citric acid),³⁵² Fe–Mo/Al₂O₃ [with the use of poly(ethylene glycol) (PEG)],³⁵⁶ Fe–Mo/MgO²⁴¹ and Fe–Co/MgO (with the use of urea).^{169, 170}

The CNT quality and yields on catalysts prepared in such a way were largely determined by the treatment of the combustion product. In the presence of excess of a reducing agent, the catalyst contained carbon black admixtures, which were removed by annealing in air. In the Co/MgO synthesis, the annealing of the reaction products of Co and Mg nitrates with an organic reducing agent resulted in the formation of a solid solution Co_xMg_{1-x}O, which was difficult to reduce in the H₂ or CO medium (especially for low Co contents) and which proved inefficient in the synthesis of MWCNTs from CO.³⁴² A much more efficient catalyst was synthesised in the preliminary reduction of the uncalcined primary product in H₂. However, it is Co_xMg_{1-x}O from which Co particles necessary for the SWCNT production were formed.²⁸⁸

Active bimetallic catalysts based on alumogel were prepared by the sol–gel method.^{215, 233, 340, 355}

The catalysts were applied on flat or patterned substrates by sputtering (*e.g.*, magnetron), aerosol deposition, the ‘drop’ method, spin-coating of liquid compositions followed by thermal treatment (drying, calcination, reduction), pneumatic spraying of solutions or suspensions,²⁵⁸ microprinting. A method of dipping of the substrate into a solution followed by its withdrawal at a certain rate^{133, 318} (*e.g.*, at 4 cm min^{−1}) was also employed. This method is also suitable for the deposition of catalysts on fibres or wires.

The ‘drop’ method is very simple;⁷⁴ however, it can be applied only in laboratory syntheses. Spinning is more efficient and was used, *e.g.*, in the large-scale production of cantilevers with CNTs³⁶⁹ and in the growth of large CNT arrays.¹⁴² Particles of Al₂O₃ (Ref. 142) and polysiloxane solutions are sometimes added to the composition to be deposited.²⁶⁰ This method allows one to prepare size-uniform Fe₂O₃ particles that are used in the synthesis of SWCNTs with diameters around 1 nm.⁴⁰⁵

A unique version of the spinning method was used.²²⁸ A homogenised ethanolic solution of Mg and Fe nitrates and PEG was spread over the substrate, which rotated at 3500 rpm. After evaporation of ethanol, the substrate was placed into a furnace heated to 600 °C.

In the evaporation method, a block co-polymer is often added to the starting solution.¹⁷³ Dilute (0.01 mass %) ethanolic solutions of metal nitrates are commonly used.^{133, 134} Thus a solution of Fe(NO₃)₃·9 H₂O in propan-2-ol was utilised.²⁶⁸ Immersion of the substrate for a certain time into an aqueous FeCl₃ solution with preliminarily added NH₂OH·HCl was described.³⁰³

Nanosize catalyst particles can be prepared by the thermal decomposition of salts. Such particles are stored in organic solvents and deposited by spin-coating.²⁸⁶ Monodispersed particles Fe–Mo with diameters of 3–14 nm were formed in the thermal decomposition of carbonyls of these metals in a medium of long-chain carboxylic acids or amines.³⁷⁰ Iron particles of different diameters were synthesised by the thermal decomposition of Fe(CO)₅ solutions in dioctyl ether in the presence of oleic, lauric or caprylic acids.²¹⁹ Nickel formate, which forms uniform nickel particles upon decomposition, is a good precursor of Ni catalysts.^{222, 406} A catalyst based on Fe particles was prepared by the plasma treatment of Fe(C₇H₁₅COO)₃ deposited on the substrate by spin-coating.⁴⁰⁷ The methods based on the thermal decomposition of compounds containing metal clusters deserve special mention, *e.g.*, [H_xPMo₁₂O₄₀][−][H₄Mo₇₂Fe₃₀·(CH₃COO)₁₅O₂₅₄(H₂O)₉₈]·60 H₂O (contains 84 Mo atoms and 30 Fe atoms), Na₂[{Mo^{VI}(Mo^{VI})₅]₁₂{Mo^VFe^{III}}(CH₃COO)₂₀·O₂₅₈(H₂O)₈₄]·150 H₂O (78 Mo + 24 Fe), [(Mo^{VI})Mo^V·O₂₁(H₂O)₆]₁₂[Fe^{III}(H₂O)₂]₃₀]·150 H₂O (72 Mo + 30 Fe) and their analogues [http://www.hydrogen.energy.gov/pdfs/review05/stp_35_liu.pdf].

A procedure that involves the co-deposition of salts of two metals in the course of slow evaporation followed by thermal decomposition was used.²⁵⁵

The inverse micelle method^{304, 408–410} is usually combined with the deposition of a colloid solution by dipping, spinning or pneumatic spraying.

Very small (1–2 nm) individual catalyst particles of the same size may be supported with the use of ferritin, apoferritin^{2, 114, 226, 411–413} and ferritin-like proteins⁴¹⁴ or dendrimers.³⁰²

When annealed in an inert medium, thin metal films sputtered over flat substrates are transformed into islets or nanosize particles. The sputtering was performed using a magnetron,^{194, 195} by electron- or ion-beam evaporation²⁸² and the laser ablation of the target.³¹⁷ Usually, the thickness of the deposited film did not exceed several atomic monolayers, for example, corresponded to 5 × 10¹⁵ atoms per cm² (Ref. 92). According to a publication,¹⁴⁰ the sputtering and annealing of a Co-catalyst film with a thickness of 0.5–1.0 nm resulted in the formation of cobalt particles measuring 3–7 nm that favoured the growth of a dense ‘forest’ of SWCNTs. The results obtained in the plasma-enhanced pyrolysis of a mixture of NH₃ and C₂H₂ (Ref. 415) are quite demon-

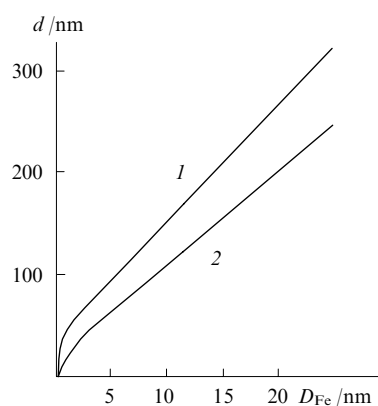


Figure 8. Dependence of (1) the average diameter of islets formed in film annealing and (2) the average diameter of filiform carbon particles grown on islets on the initial thickness of the sputtered Fe film (D_{Fe}) (according to Wang *et al.*⁴¹⁶)

strative (Fig. 8, Ref. 416). The pyrolysis products synthesised under similar conditions differed not only in the diameter but also in the morphology, namely, SWCNTs, DWCNTs, t-MWCNTs, MWCNTs and, finally, CNFs were obtained.

In the preparation of MWCNTs, it was found that on a catalyst islet, several (up to 7–8) tubes could be grown with diameters much smaller (2–3-fold) than the islet diameter.⁴¹⁷ Moreover, the smaller the diameter of the islet the smaller number of tubes can grow; this is why the elucidated feature does not always hold for t-MWCNTs.

A procedure that allows the determination of the optimum thickness of a layered film in few experiments has been developed.³⁶² Combinatory methods were proposed for the determination and optimisation of the deposition conditions.^{319, 418, 419} Thermodynamic conditions for the transition of films (5-, 10- and 20-nm thick) into particles were considered.¹⁸⁹ According to thermodynamic calculations, in the case of Ni, the radius of a particle formed exceeded the thickness of the deposited film by a factor of 1.5.⁴²⁰

The deposition can be performed through masks to promote the growth of CNTs on definite areas on the substrate and their organisation into one or another type of structures (*e.g.*, see Refs 2, 136 and 291). Ordered arrays of SiO₂ microspheres can serve as a sort of masks in the preparation of individual SWCNTs or their bundles.³⁴¹ Polymeric spheres with diameters from 1 to 125 μm can also be used.^{421, 422}

Organometallic polymers deposited on the substrate as thin films can serve as the precursors of catalysts. Particularly, a polyferrocenylsilane block copolymer was used in the synthesis of SWCNTs.⁴²³

The synthesis of CNTs on catalysts deposited by the microprinting technique is of special interest (Fig. 9). In microprinting, polymethylsiloxane stamps are commonly used.^{87, 137, 372} This method is relatively simple and versatile; it allows one to prepare a considerable number of copies on relatively wide (more than 1 cm^2) areas with the resolution varying from below 100 nm to above 1 μm . The catalyst deposition involves the use of 'ink', *i.e.*, alcohol (ethanol, isopropyl alcohol) solutions of metal nitrates, *e.g.*, Fe(NO₃)₃·9H₂O containing Al₂O₃ or SiO₂ particles and MoO₂Cl₂ or MoO₂(acac)₂ additives.^{87, 137, 372} (The details can be found in numerous publications, *e.g.*, Refs 23, 99, 130, 138, 230, 257, 275, 273, 375, 424 and 425.) By changing the concentration of the applied solution and the pyrolysis temperature, it is possible to regulate the CNT diameter.²⁷⁵ A gel catalyst was used in the synthesis of t-MWCNTs.⁴²⁶

The deposition of Fe nanoparticles of the same size (1.7 ± 0.6 nm) on the substrate surface with the accuracy of their positioning of ± 5 nm was described.³⁷⁷ An organometallic com-

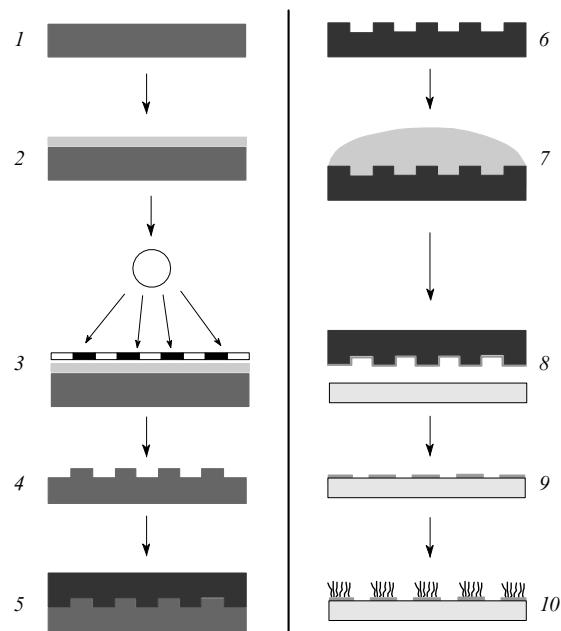


Figure 9. Sequence of steps in the production of stamps, microprinting and CNT growth.

(1) Substrate, (2) substrate with resist, (3) exposure with the use of a mask, (4) etched structure, (5) elastomer casting, (6) elastomer stamp, (7) inking of the stamp, (8) microprinting on the new substrate, (9) printed pattern, (10) growth of CNTs.

pound mixed with the resist served as the catalyst precursor. The diameter of SWCNTs formed was 1.3 ± 0.4 nm.

The positional packing of SWCNTs on a substrate can sometimes be carried out by an unexpected method. For instance, it was found that lithographically deposited islets of Pb(Zr_{0.5}Ti_{0.5})O₃ are capable of sorbing the Fe–Mo catalyst particles and initiating the local growth of tubes.²²⁵ In this case, the stronger sorption of catalyst particles could be associated with the porous structure of islets. In the pyrolytic synthesis of CNTs on quartz or oxidised silicon surfaces, the localisation of tubes involves the creation of active sites by mechanically damaging the substrate (scratching).⁴²⁷

Studies devoted to the initial stages of CNT growth in the hot-filament activated pyrolysis demonstrated⁴²⁸ the important role of the catalyst pre-treatment stage in the preparation of finer particles.

MWCNTs can be used as the substrate.⁴¹³

7. Mechanism and kinetics

The catalytic growth of CNTs proceeds by the following three macroscopic mechanisms: base growth, tip growth and branched growth mechanisms.

In the base growth mechanism, a catalyst particle remains on the substrate. In the tip growth mechanism, the particle is detached from the substrate and removed from it as the CNT grows and the tube tip moves away from the substrate or the catalyst support. The branched growth can be a version of either base or tip growth mechanisms and is typical of MWCNT growth. In the first case, the catalyst particle is split to form a dendrite structure;⁴²⁹ in the second case, octopus-like structures are formed. Sometimes, branched MWCNTs grow from a single catalyst particle.⁴³⁰ The base and tip growth scenarios can occur simultaneously to form products with different morphology.^{29, 431} In many experiments, catalyst particles were observed to change their shape and size in the course of the process or to be in continuous or impulsive motion.

The base growth mechanism is typical of the preparation of SWCNTs, where the scheme of transformation of carbon or carbon-containing substances is described by a sequence vapour–liquid–solid.⁴³²

The rate of this process depends on several factors (seven factors have been proposed²⁹⁶), among which two most important factors can be outlined. First, the rate is determined by several reactions that occur both on the catalyst surface and in the gas phase. Precisely this factor was used for explaining the effect of the aforementioned ‘pre-catalyst’ (conditioning catalyst) on the formation rate and yield of SWCNTs.²⁴⁹ An equally bright example of the effect of gas-phase reactions on the overall process of CNT formation is the experimental fact that the length of a thin-film catalyst sample can affect the rate of the process.²⁷⁰ Thus, on a Mo–Fe/Al₂O₃ sample with the film dimensions of 1 × 1 cm, no CNTs were formed from CH₄, whereas the growth of a CNT ‘forest’ was observed on a sample of 1 × 15 cm. Moreover, the process strongly depends on the gas flow rate and the position of the substrate in the path of gases in the reaction zone.

Second, the rate is determined by the size of catalyst particles. In addition, it is important that the changes in the conditions of the process can cause changes in the CNT morphology.

On the surfaces of formed CNTs, secondary processes can occur. Thus the tubes can become thicker due to the deposition of amorphous carbon, polyaromatic compounds or graphitised particles on their walls; moreover, the increase in the temperature and the duration of the process results in the active growth of such deposits and substantially increases the CNT diameter.

This is why the catalytic pyrolysis differs substantially from the processes of chemical vapour deposition, although these processes are often confused in the literature. The optimum conditions for the CNT synthesis are developed in those cases where the temperature is sufficiently high for the rapid growth of tubes but too low for the formation amorphous carbon and other undesired forms.

The pyrolysis proceeds at different conditions on a powder catalyst, on a substrate with the catalyst deposit (the formation of ‘forest’) and on porous membranes of the Al₂O₃ type. Thus on a substrate, the secondary processes can be suppressed by building a ‘shelter’ over the catalyst particles.²⁷⁰

Table 8 shows the experimentally measured rates of the linear growth of CNTs under different conditions. As follows from these data, the rates vary in a very wide range, viz., from 0.2 to

660 $\mu\text{m min}^{-1}$ [for the MWCNT growth, the rate was found to vary in the ranges of 60–600 $\mu\text{m min}^{-1}$ (Ref. 436) and 0.4–50 $\mu\text{m min}^{-1}$ (Ref. 298)]. This entailed no changes in the kinetics of formation of SWCNTs and MWCNTs. It is noteworthy that some studies^{67,437} described the synthesis of high-quality SWCNTs that grew at a very high rate. The authors of those studies have explained this fact by the effect of small amounts of H₂O vapour that favour the prolongation of the catalyst service life. Still higher growth rates of SWCNTs with diameters of 4–6 nm (480 $\mu\text{m min}^{-1}$) were observed in the decomposition of CO at 880 °C.^{68,349} Ultralong SWCNTs were grown at a rate of 660 $\mu\text{m min}^{-1}$.⁷² Ultimately, at 700 °C the record-breaking rate of the MWCNT growth from C₂H₂, namely, 6000 $\mu\text{m min}^{-1}$ was reached (although in the 1st second).²⁹²

It should be noted that very high rates of MWCNT growth (60–600 $\mu\text{m min}^{-1}$) were observed at rather low pressures.⁴³⁶ The interpretation of these results requires their refinement.

So far, it is difficult to explain the wide deviations in the linear rates of tube growth found in different studies and relate the linear growth rates to the catalyst efficiency (a relative amount of CNTs formed before complete poisoning of the catalyst).

As seen in Fig. 10, the rate of CNT growth in the plasma-enhanced pyrolysis is associated with their diameter, the latter being determined by the thickness of the deposited metal-catalyst

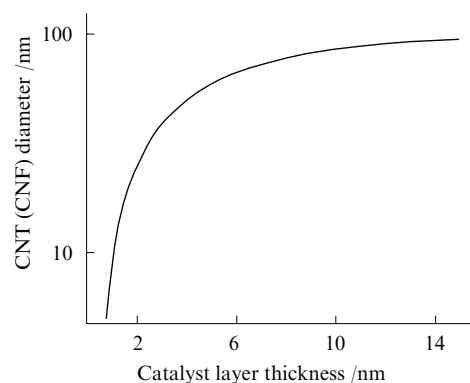


Figure 10. Effect of the average outer diameter of CNTs and CNFs on the thickness of sputtered Fe, Co or Ni films during the plasma pyrolysis.

Table 8. Linear growth rate of CNTs.

Reagent	Catalyst	$T/^{\circ}\text{C}$	p/atm	Enhancement method	Morphology	Diameter /nm	Growth rate / $\mu\text{m min}^{-1}$	Ref.
CH ₄	NiO _x	700	1.0	plasma	MWCNTs	50–80	0.2	433
CH ₄ + H ₂	Fe–Ti	600	0.1	"	t-MWCNTs	~ 5	~ 10	197
CH ₄	Fe	700	2.6×10^{-2}	"	MWCNTs	~ 20	5.4–16.8	184
C ₂ H ₂	Fe	750–950	1.0	thermal	MWCNTs	30–130	0.5–2.0	434
C ₂ H ₂	Fe	750	(1.0)	"	MWCNTs	10–15	20	291
C ₂ H ₂	Fe–Mo	730	1.0	"	SWCNTs + MWCNTs	1–20	> 17	362
C ₂ H ₂	Ni	480	$(2.6–13.0) \times 10^{-5}$	"	MWCNTs	not specified	2.1–2.4	293
C ₂ H ₂	Ni	480	$\leq 1.3 \times 10^{-5}$	"	SWCNTs	3.5	0.4–0.5	293
C ₂ H ₂ + Ar + H ₂	Fe–Mo	535–600	(1.0)	"	t-MWCNTs	not specified	12–30	298
C ₂ H ₂ + Ar + H ₂	Fe–Mo	700	(1.0)	"	DWCNTs + SWCNTs	not specified	13.2	298
C ₂ H ₂	Co–Ni	800–900	1.0	"	MWCNTs	~ 200	0.5	273
C ₂ H ₄	Ni(Fe; Ni–Fe)	850–1000	3.2×10^{-4}	plasma	MWCNTs	10–50	0.25	176
C ₂ H ₄ (see ^a)	Fe	750	1.0	thermal	SWCNTs	1–3	250	67
C ₂ H ₅ OH	Co–Mo	800	1.3×10^{-2}	"	SWCNTs	1.0–2.0	0.3	134
C ₂ H ₅ OH	Fe	900	(1.0)	"	SWCNTs	1.3–2.2	660	72
B ₂ H ₆ + CH ₄ + N ₂ + H ₂	–	600–650	0.02	plasma	nanofibres ^b	50–400	0.17	435

^a 1 vol.%–13 vol.% C₂H₄ in a mixture Ar (He)–40 vol.% H₂ in the presence of additions of 0.0175 mass % H₂O vapours. ^b Nanofibres of boron carbonitride.

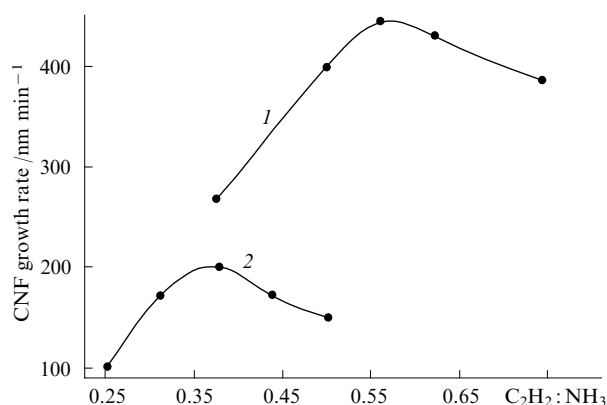


Figure 11. Effect of the gas mixture composition and the set-up geometry on the CNF formation rate during the plasma pyrolysis. Nozzle diameter: (1) 1 mm and (2) 5 mm. [Reproduced with permission of the Elsevier Publishers according to V I Merkulov, A V Melechko, M A Guillorn, D H Lowndes, M L Simpson *Chem. Phys. Lett.* **361** 492 (2002).]

film.¹⁹⁵ In the C₂H₂–NH₃ mixture, the growth rate of nanofibres depended on the set-up design (the distance between the plasma source and the substrate) and on the reactant ratio (Fig. 11).⁴¹

The temperature of the SWCNT growth also depends on the diameter of catalyst particles. Thus, for Fe particles measuring 10–30 nm, tubes were formed at 900–950 °C, whereas for the 5-nm particles, the tubes started to form at 780 °C.¹⁹⁵

Only few papers show the classical kinetic parameters of processes involved in the pyrolysis of organic substances to yield CNTs. Thus the activation energy (E_a) was assessed as 71–73 kJ mol⁻¹ (Ref. 438) for the methane pyrolysis on a Ni/La₂O₃ catalyst to yield CNFs and as 95–98 kJ mol⁻¹ (Ref. 244) for the same process on a Co–Mo/Al₂O₃ catalyst to form MWCNTs with diameters of 10–30 nm. At the same time, E_a of the formation of a pyrolytic carbon deposit on a Fe catalyst at 500–600 °C was much higher being equal to 150 kJ mol⁻¹ (Refs 439 and 440). It was noted that the latter value is close to the E_a of the Fe₃C formation equal to 158 kJ mol⁻¹.

The formation of SWCNTs in the CH₄ pyrolysis on different catalysts at 900 °C has two periods, namely, a short period of a fast mass increase and a long period of a relatively slow mass gain.³⁰¹ The catalyst Fe–Mo/Al₂O₃–SiO₂, which was prepared by gelation of a SiO₂ sol in the presence of Al₂O₃ nanoparticles followed by impregnation of the calcined gel with Fe and Mo salts (the molar ratio of 1.00:0.17), proved to be the best for this reaction. Among all catalysts studied, this one has the largest specific surface area (S_{sp} = 196 m² g⁻¹) and the greatest pore volume (0.79 ml g⁻¹).

The results obtained by Choi *et al.*³⁰² were processed by Vinciguerra *et al.*⁴⁴¹ They described the reaction rate in terms of the extrusion-diffusion model and derived an empiric equation that adequately describes the experimental data but contains no standard kinetic parameters.

Our calculations based on experimental data obtained²⁵⁵ have shown that the reaction order in CH₄ changed from 1.24 to 1.77 being in average 1.45. It seems that the deviation of the reaction order from unity is associated with the increase in the contribution of non-catalytic decomposition of CH₄ with the increase in its partial pressure. The formal reaction order of the pyrolysis to yield CNFs was also shown⁴³⁸ to depend on the temperature and to increase from 1.05 at 600 °C to 1.3 at 700 °C. According to the results of another study,⁴³⁹ the order of this reaction is equal to 1.

A threshold value of CH₄ partial pressure (0.4 atm at 850 °C) above which the rate of the catalytic pyrolysis to yield SWCNTs becomes independent of the partial pressure was observed.²³³

Presumably, such behaviour is associated with the transition of the process into the region where the rate is limited by the surface or volume diffusion. It cannot be ruled out that the thermodynamic restrictions may also affect the reaction rate.

The kinetics of catalytic pyrolysis of CH₄ and C₂H₂ was also discussed by Nagy *et al.*²⁴³

Pulsed hydrocarbon feeding is one of the ways for the improvement of CNT purity and yield in the catalytic pyrolysis.^{235, 368} However, this can also decrease the average rate of the process; hence, this method requires optimisation.

Somewhat different mechanisms are typical of the acetylene pyrolysis. The use of an interesting method of ‘marks’ allowed the kinetic parameters of the MWCNT growth to be determined in the pyrolysis of C₂H₂ on Fe islets.²⁹⁷ It was shown that after a short interruption of the pyrolysis process due to the C₂H₂ feeding cutoff (by replacing it by Ar) followed by the resumption of the process on the grown tubes (‘forest’), clear boundaries (marks) were left which could characterise the growth rate if one took into account the duration of individual growth stages. The position of ‘marks’ and the length of grown segments were determined using a scanning electron or optical microscope. As a result, it was found that the activation energy of the process was 159 ± 5 kJ mol⁻¹ in the temperature range of 873–953 K (the partial pressure used in the calculation of the E_a value was not shown²⁹⁷) and the reaction order in C₂H₂ was unity for the C₂H₂ partial pressure of 2–10 kPa and a temperature of 953 K. The linear rate of CNT growth reached 20 μm min⁻¹. The E_a value of the MWCNT growth from C₂H₂ on a Fe catalyst at 800–1100 °C was 125 kJ mol⁻¹.⁴⁴²

The obtained E_a values made it possible to abandon the earlier assumptions that the process is limited by the carbon diffusion in a liquid or quasiliquid catalyst particle (a solution of carbon in a metal),⁴⁴³ because E_a of this process should be substantially lower than the found values. It was assumed that a surface reaction at the gas–catalyst interface is the limiting stage of this process. At the same time, the experimentally observed involvement of the liquid phase in this process cannot be denied.^{444, 445}

Yet another, optical method was used for measuring the growth rate of the MWCNT ‘forest’ in the C₂H₂ pyrolysis.^{298, 446} A multilayer film Mo(0.2 nm)–Fe(1 nm)–Al(10 nm) on Si served as the catalyst, the gas mixture contained 0.25% C₂H₂, 16.62% H₂ and 83.13% Ar. It was shown that with the increase in the temperature from 535 to 900 °C, thinner CNTs were formed, *viz.*, 6–10-walled CNTs were mainly formed at 575 °C, DWCNTs predominated at 725 °C and the fraction of SWCNTs increased at higher temperatures. The highest growth rate (~12 μm min⁻¹) was observed at 700–730 °C; the effective E_a of this process in the low-temperature region was ~2 eV (~190 kJ mol⁻¹). Under isothermal conditions, the pyrolysis occurred with deceleration. With the increase in the C₂H₂ concentration, this deceleration was more pronounced and the CNT growth stopped at a smaller ultimate length of tubes (the ‘forest’ height).

A simplified mechanism of C₂H₂ pyrolysis on a Fe catalyst involves the C₂H₂ dissociation on the Fe surface, the dissolution of carbon in the near-surface disordered ‘fused’ Fe layer and the diffusion of C atoms in this layer to the CNT formation site (with the diffusion coefficient that at 1000 K exceeds the diffusion coefficient in solid Fe by 3 orders of magnitude). CNTs grow until the near-surface carbon-containing layer is distributed throughout the surface of Fe particles. The equations that adequately describe the experimental results were derived.

Yet another method, laser diffraction was proposed⁴⁴⁷ for measuring the kinetic parameters of the CNT ‘forest’ growth. The results obtained⁴⁴⁷ point to the exponential increase in the CNT length in time. According to the field emission characteristics,⁴⁴⁸ the growth rate of MWCNTs in the electric field measured at a low pressure (less than 10⁻² mbar) was in the range of 60–600 μm min⁻¹. With the increase in the C₂H₂ partial pressure, the MWCNT growth rate increased.⁴⁴⁸

The addition of H_2 reduced the amount of amorphous carbon, favoured the decrease in the MWCNT diameter and increased the linear growth rate 1.85-fold.²⁷⁶

The growth rate of the CNT 'forest' from a mixture of C_2H_2 and NH_3 (the volume ratio 1:3, temperature 700 °C, total pressure ~ 0.2 kPa, or ~ 2 Torr) on a Ni catalyst increased in the initial plasma-enhanced stages, reached its maximum ($6.5\text{--}8.5\ \mu\text{m min}^{-1}$) and began to decrease upon reaching the CNT length of $\sim 2\ \mu\text{m}$.⁴⁴⁹ Such kinetics of the process is associated with the mechanism of the CNT growth that involves the surface diffusion. Presumably, the process decelerates when the tube length exceeds the diffusion path.

The formation of the MWCNT 'forest' in the plasma-enhanced process can proceed at the substrate temperature of 120 °C.^{283,450} The E_a value at 120–527 °C turned out to be very low ($22\ \text{kJ mol}^{-1}$) as compared with the value typical of the heat-activated process ($116.4\ \text{kJ mol}^{-1}$).⁴⁵¹ This means that the process is limited by the surface diffusion of carbon over Ni particles. This mechanism can operate on Fe, Ni and Co catalysts in the pyrolysis of not only C_2H_2 , but also CH_4 .⁴⁵² It should be noted that a comparatively low E_a value ($37\ \text{kJ mol}^{-1}$) was also found for the SWCNT formation at 1050–1200 °C under conditions of the laser-oven sublimation, which was associated with the following mechanism: vapour–liquid–solid.⁴⁵³

The MWCNT formation was observed *in situ* using transmission electron microscopy,^{292,293} which allowed the researchers to propose a realistic growth model. The tubes grow on individual faces of a Ni particle and with the highest rate on its (100) face. Catalyst particles rotate or are fused and recrystallised; hence, the growth direction can change.

The kinetics of ethylene pyrolysis was less thoroughly studied than that for methane; however, it is known that the rate of this reaction can be very high.^{67,437} The catalyst efficiency (the amount of CNTs formed per catalyst mass unit before its complete poisoning) in a process described by Japanese authors was $500\ \text{g g}^{-1}$, which exceeded the catalyst efficiency in the HiPco process (thermal decomposition of CO in the presence of volatile Fe carbonyl as a catalyst precursor) by two orders of magnitude. At the same time, the product contained less than 0.013% Fe.

The increase in the pyrolysis temperature narrows the region of C_2H_4 partial pressures at which SWCNTs are formed (Fig. 12).¹⁸⁰

The relative rate of the ethanol reaction with metal clusters depends on the metal nature and the cluster size (Fig. 13).

Many studies^{454–474} were devoted to the simulation of CNT formation; however, most of them dealt with high-temperature methods, namely, the graphite sublimation in an electric arc and in

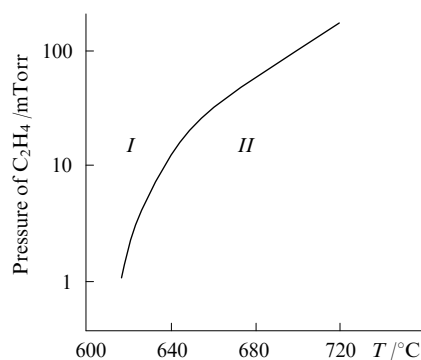


Figure 12. Effect of the pyrolysis conditions on the morphology of CNTs formed.¹⁸⁰

(I) A region in which no SWCNTs could be obtained, (II) a region of SWCNT formation. (Reproduced with permission of the American Chemical Society.)

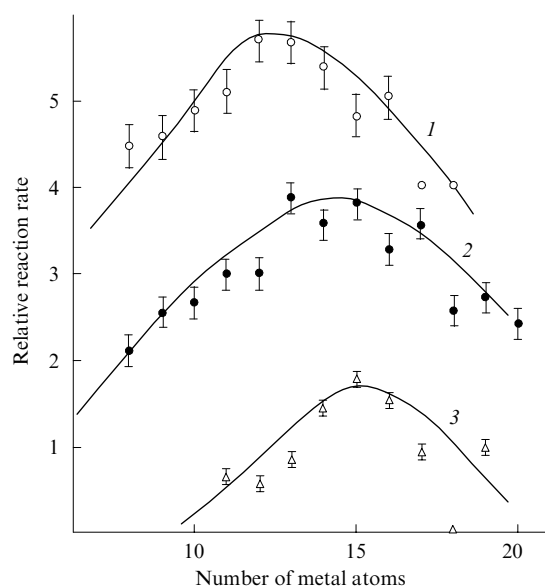


Figure 13. Relative reaction rate of ethanol vapours with clusters of (1) Fe, (2) Co and (3) Ni [http://www.photon.t.u-tokyo.ac.jp/~maruyama/papers/04/Inoue_JCP.pdf].

laser radiation. Particularly, a process in which mobile Ni atoms located on the tip of a growing CNT play the active role was considered.⁴⁵⁴ Later,⁴⁵⁶ a basically different mechanism of the effect of Ni atoms was substantiated and an attempt was undertaken to resolve the contradictions between these mechanisms.

A relationship between the Fe cluster size, the CNT diameter and the number of CNT walls was demonstrated.^{455,463} The processes of heat and mass transfer were considered as applied to the tip mechanism of CNT growth.⁴⁶⁹

The theoretical analysis of the catalytic pyrolysis of CH_4 mixed with H_2 arrived at the assumption that this method of SWCNT synthesis is a very difficult task.⁴⁷⁴ As follows from the experimental data mentioned above, this conclusion should be corrected. Nonetheless, a model that takes into account not only the chemical stages of the process but its hydrodynamics and the heat transfer has been developed.⁴⁷⁵ The authors of this model cited numerous publications and estimated the kinetic parameters for 47 gas-phase reactions, 19 reactions on powder Co catalysts and 15 surface reactions resulting in amorphous carbon, which may be useful for further calculations.

A thermodynamic model of the formation of MWCNTs with diameters of 5–35 nm in the C_2H_2 pyrolysis (this reaction releases a great amount of heat) assumes the presence of gradients of temperature and carbon concentration on a catalyst particle.⁴⁷⁰ It was shown that the growth rate should be inversely proportional to the CNT diameter (d). This corresponds to experimental results,⁴³⁴ although it was shown earlier⁴⁷⁶ that for CNFs the rate is inversely proportional to $d^{0.5}$.

The formation of a liquid external layer on a catalyst particle and its effect on the SWCNT formation was discussed.⁴⁷⁷ The SWCNT growth proceeds until the catalyst particle, which represents an eutectic metal–carbon mixture, remains liquid and stops when the catalyst becomes solid.

Presumably,⁴⁷⁸ the key stage in the CNT synthesis is the formation of tube nuclei. In this case, the SWCNT growth is possible only on liquid catalyst particles.

The choice of the catalyst affects its specific efficiency. Thus under equal conditions, the alumogel-supported catalyst exhibited the selective efficiency with respect to SWCNTs at least 5-times higher ($6\ \text{g g}^{-1}$) than a catalyst of the same composition prepared by impregnation of Al_2O_3 .²¹⁵ The efficiency of ordinary

catalysts in the SWCNT formation was ~ 40 mass % (or 0.40 g g^{-1}).²¹³ The catalyst efficiency in the CoMoCAT process was $\sim 0.25 \text{ g g}^{-1}$. The Fe–Mo/MgO catalyst exhibited the highest efficiency in the synthesis of t-MWCNTs (3000 mass %, or 30 g g^{-1}).²⁸

It was noted⁴³⁴ that the increase in the pyrolysis temperature accelerates the growth of MWCNTs in their length, and their average diameter increases. The hydrocarbon partial pressure affects both the pyrolysis rate and the morphology of CNTs prepared. The MWCNT diameter changes with variations in the total pressure in the system.⁴⁷⁹ The length and the diameter of growing SWCNTs can be controlled by changing the duration of the process or by adding a promoter.⁸³ The effect of the temperature and the hydrocarbon partial pressure on the CNT morphology was also studied by the other researchers.⁴⁸⁰ By the example of the $\text{C}_2\text{H}_2\text{--NH}_3$ mixture, it was shown that the decrease in the pressure favours the transition from bamboo-like nanofibres to cylindrical MWCNTs.⁴⁸¹

The catalytic decomposition of carbon oxide decelerates in time,³⁴⁰ and the product yield is proportional to $t^{0.5}$. The rate of MWCNT formation from the CO--H_2 mixture and the tube quality depended on the medium in which the catalyst based on the sputtered Fe–Co–Ni alloy was pre-treated.³⁶⁴ Thus catalysts pre-treated in vacuum demonstrated poorer properties than the catalysts treated in Ar or N_2 . After heating in these gases, the linear rate of MWCNT growth at 580°C was about $0.4 \mu\text{m min}^{-1}$, whereas after heating in vacuum the growth rate was ten times lower.

According to calculations,³⁴⁶ in the CO decomposition, SWCNTs can grow by the adsorption of molecules on the open ends of tubes; catalysts favour the formation of nanotube nuclei.³⁴⁶

IV. Conclusion

While this review was in the stage of preparation for publication, several new publications have appeared that deserve mention. These are the materials of the 7th International Conference on Scientific Application of Nanotubes,⁴⁸² two Russian books^{483, 484} and a monograph⁴⁸⁵ in English.

The 7th International Conference on Scientific Application of Nanotubes in which only one participant from Russia took part confirmed in a certain sense the trend mentioned in the beginning of this review. Thus analysing the posters presented in the Session devoted to the CNT synthesis, Professor A Windle (Cambridge University) noted that the majority of the 76 reports presented were devoted to the catalytic pyrolysis. Moreover, the majority of reports dealt with supported catalysts and heat-activated processes. Among metal catalysts, attention was focused on Fe, followed by Co and Mo; the main substrates were SiO_2 and Al_2O_3 , while the starting compounds included $\text{C}_2\text{H}_5\text{OH}$, CH_4 , C_2H_4 and CO (shown in the order of decreasing citation frequency). The latter factor was apparently associated with the domination of scientists from Japan who focus their attention on the ethanol pyrolysis.

Windle has formulated the following ‘five questions of science to answer:

1. Does surface of metal particle catalyse: (a) decomposition of hydrocarbon, (b) decomposition of further metal precursor?
2. What is metallurgy of nano particles? (a) Melting point, surface melting, internal pressure, (b) carbon solubility (as function of radius), (c) phase diagram with carbon (modelling + experiment).
3. Does a region of metal particles have to remain free of a graphene coating? If it doesn't, is that a killer?
4. What determines rate of growth? (a) Diffusion rate in metal (surface), (b) supply of carbon to particle, (c) shape changes due to flow of small (not necessarily molten) particles, (d) interface modifiers such as sulphur, (e) do we have a reliable E_a yet?

5. What determines type and size of nanotube? (a) Metal particle diameter and/or composition, (b) temperature, (c) feed-stock, (d) what is the difference in growth mechanism between (say) a double wall tube and an 8ish layer multi-wall tube of similar diameter?’

Two Russian books are written from absolutely different standpoints and contain complementary information, *viz.*, the monograph⁴⁸³ is largely devoted to the quantum chemistry of carbon nanotubes, a subject absent in the textbook.⁴⁸⁴ At the same time, the classification of nanotubes, their properties, synthesis and applications are described more comprehensively in the textbook⁴⁸⁴ with substantial attention paid to pyrolytic methods.

The textbook⁴⁸⁴ mentions the following most important challenges (some of them are beyond the frames of the present review):

- elucidation and mathematical description of the mechanism of formation of CNTs with different morphology and structure under different conditions;
- determination of the functional relationship between the kinetics of CNT formation and their morphology and structure;
- the search for the methods for regulation and control over the CNT morphology and structure during their syntheses;
- elaboration of methods for deep and selective as well as local functionalisation of CNTs;
- elucidation of mechanisms of the behaviour of CNTs with different morphology and structure in colloid solutions;
- determination of the influence of CNTs and modified CNTs on organisms.

According to the aforementioned book,⁴⁸⁴ the most important unsolved technological problems include the following directions:

- development of a process for efficient industrial production of CNTs with the same morphology and structure;
- development of a process for CNT isolation (grading) with respect to morphology, structure and size, that allows scaleup;
- elaboration of methods for preparation of stable dispersions of individual CNTs in aqueous and organic media;
- the search for the methods of introduction of individual CNTs into polymeric, ceramic, and metal matrices and preparation of CNT composites;
- development of methods for the production of macro-materials from CNTs, especially, macrofibres and nanopaper with the oriented packing of individual tubes;
- development of methods of commercial production of functional devices with CNTs, namely, electron emitters, transistors, sensors, actuators, *etc.*

The third book,⁴⁸⁵ which has an intriguing title, is destined, according to its summary and contents, for a learned reader and embraces both the main information on the subject, the latest achievements and potential application fields.

In the conclusion, I would like to express my gratitude to I V Anoshkin for making it possible for me to get acquaintance with the materials of the 7th International Conference on Scientific Application of Nanotubes, to Nguyen Tran Hung for his help in the preparation of this review and also to all colleagues who have sent me copies of their papers.

References

1. C N R Rao, B C Satishkumar, A Govindaraj, M Nath *Phys. Chem. Chem. Phys.* **2** 78 (2001)
2. H Dai *Acc. Chem. Res.* **35** 1035 (2002)
3. M Terrones *Annu. Rev. Mater. Res.* **33** 419 (2003)
4. L Dai, A Patil, X Gong, Z Guo, L Liu, Y Liu, D Zhu *Phys. Chem. Chem. Phys.* **4** 1150 (2003)
5. P Petit, A Loiseau *C. R. Phys.* **4** 967 (2003)
6. *The Wondrous World of Carbon Nanotubes* (Eindhoven: Eindhoven University of Technology, 2003)
7. A V Krestinin *Ros. Khim. Zh.* **48** (5) 21 (2004)
8. M Meyyappan *Carbon Nanotubes: Science and Applications* (Boca Raton, FL: CRC Press, 2004)

9. S Reich, C Thomsen, J Maultzsch *Carbon Nanotubes: Basic Concepts and Physical Properties* (Berlin: Wiley, 2004)
10. E G Rakov, in *Nanomaterials Handbook* (Ed. Yu Gogotsi) (Boca Raton, FL: CRC Press, 2006) p. 103
11. C E Baddour, C Briens *Int. J. Chem. React. Eng.* **3** R3 (2005)
12. H Dai, in *Carbon Nanotubes: Synthesis, Structure, Properties and Applications (Topics in Applied Physics Series)* Vol. 80 (Eds M S Dresselhaus, G Dresselhaus, Ph Avouris) (Berlin: Springer, 2001) p. 29
13. C T Kingston, B Simard *Anal. Lett.* **36** 3119 (2003)
14. Y Ando, X Zhao, T Sugai, M Kumar *Mater. Today* **7** 22 (2004)
15. C R C Viveckchand, L M Cele, F L Deepak, A J Raju, A Govindaraj *Chem. Phys. Lett.* **386** 313 (2004)
16. M Meyyappan, L Delzeit, A Cassell, D Hash *Plasma Sources Sci. Technol.* **12** 205 (2003)
17. R Aiello, J E Fiscus, H-C zur Loye, M D Amiridis *Appl. Catal. A* **192** 227 (2000)
18. A Meier, V A Kirillov, G G Kuvshinov, Yu I Mogilnykh, A Weidenkaff, A Steinfeld *J. Phys. IV* **9** (P3) 393 (1999)
19. H J Dai, A G Rinzler, P Nikolaev, A Thess, D T Colbert, R E Smalley *Chem. Phys. Lett.* **260** 471 (1996)
20. M J Yacaman, M N Yosida, L Rendon, J G Santiesteban *Appl. Phys. Lett.* **62** 202 (1993)
21. V Ivanov, J B Nagy, Ph Lambin, A Lukas, X B Zhang, X F Zhang, D Bernaerts, G Van Tendeloo, S Amelinckx, J Van Landuyt *Chem. Phys. Lett.* **223** 329 (1994)
22. V B Felonov *Poristy Uglerod* (Porous Carbon) (Novosibirsk: Institute of Catalysis, RAS, 1995)
23. J Kong, A M Cassell, H J Dai *Chem. Phys. Lett.* **292** 567 (1998)
24. J Kong, H Soh, A M Cassell, C F Quate, H J Dai *Nature (London)* **395** 878 (1998)
25. A Charlier, E McRae, R Heyd, M F Charlier, D Moretti *Carbon* **37** 1779 (1999)
26. A V Belikov, Yu E Lozovik, A G Nikolaev, A M Popov *Chem. Phys. Lett.* **385** 72 (2004)
27. Y Li, K Wang, J Wei, Z Gu, Z Wang, J Luo, D Wu *Carbon* **43** 31 (2005)
28. Y A Kim, H Muramatsu, T Hayashi, M Endo, M Terrones, M S Dresselhaus *Chem. Phys. Lett.* **398** 87 (2004)
29. H Muramatsu, T Hayashi, Y A Kim, D Shimamoto, Y J Kim, K Tantrakarn, M Endo, M Terrones, M S Dresselhaus *Chem. Phys. Lett.* **414** 444 (2005)
30. J Cumings, W Mickelson, A Zettl *Solid State Commun.* **126** 359 (2003)
31. H J Jeong, K K Kim, S Y Jeong, M H Park, C W Yang, Y H Lee *J. Phys. Chem. B* **108** 17695 (2004)
32. E G Rakov, D A Grishin, Yu V Gavrilov, E V Rakova, A G Nasibulin, Kh Dzhan, E I Kauppinen *Zh. Fiz. Khim.* **78** 2204 (2004)^a
33. D Y Kim, C-M Yang, Y S Park, K K Kim, S Y Jeong, J H Han, Y H Lee *Chem. Phys. Lett.* **413** 135 (2005)
34. D A Grishin, Yu V Gavrilov, F G Nasibulin, Kh Dzhan, E I Kauppinen, S S Bukalov, L A Mikhailitsyn, E G Rakov *Poverkhnost. Rentgen. Sinkhrotron. Neitron. Issled.* (12) 52 (2005)
35. E G Rakov *Ros. Khim. Zh.* **48** (5) 12 (2004)
36. K B K Teo, C Singh, M Chhowalla, W I Milne, in *Encyclopedia of Nanoscience and Nanotechnology* Vol. 1 (Valencia, CA: Am. Sci. Publ., 2004) p. 665
37. A Moisala, A G Nasibulin, E I Kauppinen *J. Phys.: Condens. Matter* **15** S3011 (2003)
38. J W Seo, E Couteau, P Umek, K Hernadi, P Marcoux, B Lukic, Cs Mikó, M Milas, R Gaál, L Forró *New J. Phys.* **5** 120 (2003)
39. M Meyyappan, in *Encyclopedia of Nanoscience and Nanotechnology* Vol. 1 (Valencia, CA: Am. Sci. Publ., 2004) p. 581
40. P V Fursikov, B P Tarasov *Mezhdun. Zh. Altern. Energ. Ekol.* (10) 24 (2004)^b
41. A V Melechko, V I Merkulov, T E McKnight, M A Guillorn, K L Klein, D N Lowndes, M L Simpson *J. Appl. Phys.* **97** 041301 (2005)
42. Ç Öncel, Y Yürüm *Fullerenes, Nanotubes, Carbon Nanostruct.* **14** 17 (2006)
43. D E Resasco, W E Alvarez, F Pompeo, L Balzano, J E Herrera, B Kitiyanan, A Borgna *J. Nanopart. Res.* **4** 131 (2002)
44. Y Gogotsi, J A Libera *J. Mater. Res.* **15** 2591 (2000)
45. J Libera, Y Gogotsi *Carbon* **39** 1307 (2001)
46. D C Lee, F V Mikulec, B A Korgel *J. Am. Chem. Soc.* **126** 4951 (2004)
47. D C Lee, B A Korgel *Mol. Simul.* **31** 637 (2005)
48. Y F Zhang, M N Gamo, C Y Xiao, T Ando *Physica B* **323** 293 (2002)
49. L Ji, J Lin, H C Zeng *Chem. Mater.* **12** 3466 (2000)
50. S-H Jeong, J-H Ko, J-P Park, W Park *J. Am. Chem. Soc.* **126** 15982 (2004)
51. C Srinivasan *Curr. Sci.* **80** 12 (2005)
52. G Keskar, R Rao, J Luo, J Hudson, J Chen, A M Rao *Chem. Phys. Lett.* **412** 269 (2005)
53. T Uchino, K N Bourdakos, P Ashburn, C H de Groot, M E Kiziroglou, D C Smith, in *The 6th International Conference on Science Application of Nanotubes (Abstracts of Reports)*, Gothenburg, Sweden, 2005 p. 83
54. K B K Teo, R G Lacerda, M H Yang, A S Teh, L A W Robinson, S H Dalal, N L Rupasinghe, M Chhowalla, S B Lee, D A Jefferson, D G Hasko, G A J Amaratunga, W L Milne, P Legagneux, L Gangloff, E Minoux, J P Schnell, D Pribat *IEE Proc. — Circuits Devices Syst.* **151** 443 (2004)
55. B C Liu, M Z Qu, Z L Yu *Chin. Chem. Lett.* **12** 1135 (2001)
56. E G Rakov, S N Blinov, I G Ivanov, E V Rakova, N G Digurov *Zh. Prikl. Khim.* **77** 193 (2004)^c
57. E Couteau, K Hernadi, J W Seo, L Thiên-Nga, C Mikó, R Gaál, L Forró *Chem. Phys. Lett.* **378** 9 (2003)
58. A R Harutyunyan, in *The 6th International Conference on Science Application of Nanotubes (Abstracts of Reports)*, Gothenburg, Sweden, 2005 p. 42
59. B Kitiyanan, W E Alvarez, J H Harwell, D E Resasco *Chem. Phys. Lett.* **317** 497 (2000)
60. S M Bachilo, L Balzano, J E Herrera, F Pompeo, D E Resasco, R B Weisman *J. Am. Chem. Soc.* **125** 11186 (2003)
61. Ph Mauron, Ch Emmenegger, P Sudan, P Wenger, S Rentsch, A Züttel *Diamond Relat. Mater.* **12** 780 (2003)
62. D Venegoni, P Serp, R Feurer, Y Kihn, C Vahlas, P Kalck *Carbon* **40** 1799 (2002)
63. Y-L Li, I A Kinloch, M S P Shafer, J Geng, B Johnson, A H Windle *Chem. Phys. Lett.* **384** 98 (2004)
64. W Kim, H C Choi, M Shim, Y Li, D Wang, H Dai *Nano Lett.* **2** 703 (2002)
65. Z Yu, S Li, P J Burke *Chem. Mater.* **16** 3414 (2004)
66. L Huang, X Cui, B White, S P O'Brien *J. Phys. Chem. B* **108** 16451 (2004)
67. K Hata, D N Futoba, K Mizuno, T Namai, M Yumura, S Iijima *Science* **306** 1362 (2004)
68. P Queipo, A G Nasibulin, U Tapper, D Gonzalez, K Grigoras, H Jiang, E I Kauppinen, in *The 6th International Conference on Science Application of Nanotubes (Abstracts of Reports)*, Gothenburg, Sweden, 2005 p. 47
69. S Huang, X Cai, J Liu *J. Am. Chem. Soc.* **125** 5636 (2004)
70. S Huang, B Maynor, X Cai, J Liu *Adv. Mater.* **15** 1651 (2003)
71. S Huang, M Woodson, R Smalley, J Liu *Nano Lett.* **4** 1025 (2004)
72. L X Zheng, M J O'Connell, S K Doorn, X Z Liao, Y H Zhao, E A Akhadov, M A Hoffbauer, B J Roop, Q X Jia, R C Dye, D E Peterson, S M Huang, J Liu, Y T Zhu *Nat. Mater.* **3** 673 (2004)
73. S K Doorn, L Zheng, M J O'Connell, Y Zhu, S Huang, J Liu *J. Phys. Chem. B* **109** 3751 (2005)
74. B H Hong, J Y Lee, T Beetz, Y Zhu, P Kim, K S Kim *J. Am. Chem. Soc.* **127** 15336 (2005)
75. Y Wang, M J Kim, H Shan, C Kittrell, H Fan, L M Ericson, W-F Hwang, S Arepalli, R H Hauge, R E Smalley *Nano Lett.* **5** 997 (2005)
76. M Paillet, V Jourdain, P Poncharal, J-I Sauvajol, A Zahab *J. Phys. Chem. B* **108** 17112 (2004)
77. M Paillet, V Jourdain, P Poncharal, J-I Sauvajol, A Zahab, J C Meyer, S Roth, N Cordente, C Amiens, B Chaudret *Diamond Relat. Mater.* **14** 1426 (2005)
78. *NEC J. Adv. Technol.* **1** 370 (2004)
79. S Sato, A Kawabata, M Nihei, Y Awano *Chem. Phys. Lett.* **382** 361 (2003)

80. D Ciuparu, Y Chen, S Lim, G L Haller, L Pfefferle *J. Phys. Chem. B* **108** 503 (2004)
81. D Ciuparu, Y Chen, S Lim, Y Yang, G L Haller, L Pfefferle *J. Phys. Chem. B* **108** 15565 (2004)
82. D Ciuparu, P Haider, M Fernández-García, Y Chen, S Lim, G L Haller, L Pfefferle *J. Phys. Chem. B* **109** 16332 (2005)
83. X Li, J Zhang, H Lia, Z Liu, in *The 8th International Conference on Electronic Materials, IUMRS-ICEM, 2002, Xi'an, China, 2002* p. 48
84. A Zhang, C Li, S Bao, Q Xu *Microporous Mesoporous Mater.* **29** 383 (1999)
85. S Wang, P Wang, O Zhou *Diamond Relat. Mater.* **15** 361 (2006)
86. Y Yang, H Xu, W Li *Nanotechnology* **16** 129 (2005)
87. Y Zhang, A Chang, J Cao, Q Wang, W Kim, Y Li, N Morris, E Yenilmez, J Kong, H Dai *Appl. Phys. Lett.* **79** 3155 (2001)
88. A Ural, Y Li, H Dai *Appl. Phys. Lett.* **81** 3464 (2002)
89. T Ono, H Miyashita, M Esashi *Nanotechnology* **13** 62 (2002)
90. T Ono, E Oesterschulze, G Georgiev, A Georgieva, R Kassing *Nanotechnology* **14** 37 (2003)
91. L Delzeit, R Stevens, C Nguyen, M Meyyappan *Int. J. Nanosci.* **1** 197 (2002)
92. H B Peng, T G Ristorph, G M Schurmann, G M King, J Yoon, V Narayanamurti, J A Golovchenko *Appl. Phys. Lett.* **83** 4238 (2003)
93. Y Hanein, D H Cobden, I Radu *Nanotechnology* **15** 473 (2004)
94. A Nojeh, A Ural, R F Pease, H Dai *J. Vac. Sci. Technol., B* **22** 3421 (2004)
95. M Maeda, C-K Hyon, T Kamimura, A Kojima, K Sakamoto, K Matsumoto *Jpn. J. Appl. Phys.* **44** 1585 (2005)
96. E Joselevich, C M Lieber *Nano Lett.* **2** 1137 (2002)
97. K-H Lee, J-M Cho, W Sigmund *Appl. Phys. Lett.* **82** 448 (2003)
98. S Huang, X Cai, C Du, J Liu *J. Phys. Chem. B* **107** 13251 (2003)
99. S Huang, Q Fu, L An, J Liu *Phys. Chem. Chem. Phys.* **6** 1077 (2004)
100. H Xin, A T Wooley *Nano Lett.* **4** 1481 (2004)
101. S Zhu, C-H Su, J C Cochrane, S Lehoczy, A Burger *J. Cryst. Growth* **234** 584 (2002)
102. J F AuBuchon, L-H Chen, A I Gapin, D-W Kim, C Daraio, S Jin *Nano Lett.* **4** 1781 (2004)
103. L-H Chen, J F AuBuchon, A Gapin, C Daraio, P Bandaru, S Jin, D W Kim, I K Yoo, C M Wang *Appl. Phys. Lett.* **85** 5373 (2000)
104. J F AuBuchon, L-H Chen, S Jin *J. Phys. Chem. B* **109** 6044 (2005)
105. I Radu, Y Hanein, D H Cobden *Nanotechnology* **15** 473 (2001)
106. W Y Lee, C H Weng, Z Y Juang, J F Lai, K C Leou, C H Tsai *Diamond Relat. Mater.* **14** 1852 (2005)
107. M Su, Y Li, B Maynor, A Buldum, J P Lu, J Liu *J. Phys. Chem. B* **104** 6505 (2000)
108. A Ismach, L Segev, E Wachtel, E Joselevich *Angew. Chem., Int. Ed.* **43** 6140 (2004)
109. S Han, X Liu, C Zhu *J. Am. Chem. Soc.* **127** 5294 (2002)
110. H Ago, K Nakamura, K-i Ikeda, N Uehara, N Ishigami, M Tsui *Chem. Phys. Lett.* **408** 433 (2005)
111. X Liu, S Han, C Zhou *Nano Lett.* **6** 34 (2006)
112. M Yudasaka, Y Kasuya, F Jing, M Zhang, S Iijima *J. Nanosci. Nanotechnol.* **4** 428 (2004)
113. E Joselevich, A Ismach, L Segev, E Wachtel, in *The 6th International Conference on Science Application of Nanotubes (Abstracts of Reports)*, Gothenburg, Sweden, 2005 p. 150
114. C Kocbas, S-H Hur, A Gaur, M A Meitl, M Shim, J A Rogers *Small* **1** 1 (2005)
115. P Ciambelly, D Sannino, M Sarno, A Fonseca, J B Nagy *J. Nanosci. Nanotechnol.* **4** 779 (2004)
116. O-J Lee, S-K Hwang, S-H Jeong, P S Lee, K-H Lee *Synth. Met.* **148** 263 (2005)
117. R Krishnan, H Q Nguyen, C V Thompson, W K Choi, Y L Foo *Nanotechnology* **16** 841 (2005)
118. N Kouklin *Appl. Phys. Lett.* **87** 203105 (2005)
119. W Z Li, S S Xie, L X Qian, B H Chang, B S Zou, W Y Zhou, R A Zhao, G Wang *Science* **274** 1701 (1996)
120. M Urbán, Z Kónya, D Méhn, J Zhu, I Kirichi *J. Nanosci. Nanotechnol.* **3** 111 (2003)
121. Z K Tang, H D Sun, J Wang *Appl. Phys. Lett.* **73** 2287 (1998)
122. Z K Tang, H D Sun, J Wang, J Chen, G Li *J. Korean Phys. Soc.* **34** (Suppl.) S7 (1999)
123. Z K Tang, H D Sun, J Wang *Physica (Amsterdam)* **279** 200 (2000)
124. H D Sun, Z K Tang, J N Wang *J. Magn. Magn. Mater.* **198–199** 255 (1999)
125. H D Sun, Z K Tang, J Chen, G Li *Appl. Phys. A* **69** 381 (1999)
126. F Zheng, L Liang, Y Gao, J H Sakamoto, C L Aardahl *Nano Lett.* **2** 729 (2002)
127. Y Chen, D Ciuparu, S Lim, Y Yang, G L Haller, L Pfefferle *J. Catal.* **225** 453 (2004)
128. Y Chen, D Ciuparu, S Lim, Y Yang, G L Haller, L Pfefferle *J. Catal.* **226** 351 (2004)
129. S Lim, D Ciuparu, Y Chen, L Pfefferle, G L Haller *J. Phys. Chem. B* **108** 20095 (2004)
130. L Huang, S J Wind, S P O'Brien *Nano Lett.* **3** 299 (2003)
131. G W Meng, Y J Jung, A Cao, R Vajtai, P M Ajayan *Proc. R. Soc. London, Ser. A* **102** 7074 (2005)
132. Y Murakami, S Chiashi, Y Miyauchi, M Hu, M Ogura, T Okubo, S Maruyama *Chem. Phys. Lett.* **385** 298 (2004)
133. M Hu, Y Murakami, M Ogura, S Maruyama, T Okubo *J. Catal.* **225** 230 (2004)
134. E Einarsson, T Edamura, Y Murakami, Y Igarashi, S Maruyama *Therm. Sci. Eng.* **12** 77 (2004)
135. S Maruyama, E Einarsson, Y Murakami, T Edamura *Chem. Phys. Lett.* **403** 320 (2005)
136. H Dai *Surf. Sci.* **500** 218 (2002)
137. A Cassell, N Franklin, T Tomblor, E Chan, J Han, H Dai *J. Am. Chem. Soc.* **121** 7975 (1999)
138. H Dai, J Kong, C Zhou, N Franklin, T Tomblor, A Cassell, S Fan, M Chapline *J. Phys. Chem. B* **103** 11246 (1999)
139. Y Homma, Y Kobayashi, T Ogino *Appl. Phys. Lett.* **81** 2261 (2002)
140. Y J Jung, Y Homma, T Ogino, Y Kobayashi, D Takagi, B Wei, R Vajtai, P M Ajayan *J. Phys. Chem. B* **107** 6859 (2003)
141. Y Homma, Y Kobayashi, T Ogino *NTT Tech. Rev.* **2** (2) 28 (2004)
142. N R Franklin, Y Li, R J Chen, A Javey, H Dai *Appl. Phys. Lett.* **79** 4571 (2001)
143. N R Franklin, Q Wang, T W Tomblor, A Javey, M Shim, H Dai *Appl. Phys. Lett.* **81** 913 (2002)
144. J-C P Gabriel *Mater. Res. Soc. Symp. Proc.* **776** Q12.7.1 (2003)
145. Z Chen, J Merikhi, I Koehler, P K Bachmann *Diamond Relat. Mater.* **15** 104 (2006)
146. B Q Wei, R Vajtai, Y Jung, J Ward, R Zhang, G Ramanath, P M Ajayan *Nature (London)* **416** 495 (2002)
147. R Vajtai, B Q Wei, P M Ajayan *Philos. Trans.: Math., Phys. Eng. Sci.* **362** 2143 (2004)
148. T A El-Aguizy, J-h Jeong, Y-B Jeon, W Z Li, Z F Ren, S-G Kim *Appl. Phys. Lett.* **85** 5995 (2004)
149. E T Thostenson, W Z Li, D Z Wang, Z F Ren, T W Chou *J. Appl. Phys.* **91** 6034 (2002)
150. M Ritschel, K Bartsch, A Leonhardt, A Graff, C Tischner, T Mühl, J Fink *Highlights* **23** (2000)
151. Y T Lee, N S Kim, S Y Bae, J Park, S-C Yu, H Ryu, H J Lee *J. Phys. Chem. B* **107** 12958 (2003)
152. R Ma, D Golberg, Y Bando, T Sasaki *Philos. Trans.: Math., Phys. Eng. Sci.* **362** 2161 (2004)
153. A H Nevidomskyy, G Csányi, M C Payne *Phys. Rev. Lett.* **91** 105502 (2003)
154. C P Ewels, M Glerup *J. Nanosci. Nanotechnol.* **5** 1345 (2005)
155. S Y Kim, J Lee, C W Na, J Park, K Seo, B Kim *Chem. Phys. Lett.* **413** 300 (2005)
156. A Govindaraj, E Flahaut, Ch Laurent, A Peigney, A Rousset, C N R Rao *J. Mater. Res.* **14** 2567 (1999)
157. Ch Laurent, A Peigney, E Flahaut, A Rousset *Mater. Res. Bull.* **35** 661 (2000)
158. Ch Laurent, A Peigney, E Flahaut, R Bacsa, A Rousset, in *Science and Application of Nanotubes* (Eds D Tománek, R Enbody) (New York: Kluwer Academic, Plenum, 2000) p. 151
159. A Peigney, Ch Laurent, E Flahaut, A Rousset *Ceram. Int.* **26** 677 (2000)

160. E Flahaut, A Peigney, Ch Laurent, Ch Marlière, F Chastel, A Rousset *Acta Mater.* **48** 3803 (2000)
161. P Coquay, E De Grave, R E Vanderberghe, C Dauwe, E Flahaut, Ch Laurent, A Peigney, A Rousset *Acta Mater.* **48** 3015 (2000)
162. A Peigney, P Coquay, E Flahaut, R E Vanderberghe, E De Grave, Ch Laurent *J. Phys. Chem. B* **105** 9699 (2001)
163. A Peigney, E Flahaut, Ch Laurent, F Chastel, A Rousset *Chem. Phys. Lett.* **352** 20 (2002)
164. E Flahaut, R Bacsá, A Peigney, Ch Laurent *Chem. Commun.* 1442 (2003)
165. E Flahaut, A Peigney, Ch Laurent *J. Nanosci. Nanotechnol.* **3** 151 (2003)
166. A Cordier, E Flahaut, C Viazzi, Ch Laurent, A Peigney *J. Mater. Chem.* **15** 4041 (2005)
167. E Flahaut, A Govindaraj, A Peigney, Ch Laurent, A Rousset, C N R Rao *Chem. Phys. Lett.* **300** 236 (1999)
168. E Flahaut, A Peigney, Ch Laurent, A Rousset *J. Mater. Chem.* **10** 249 (2000)
169. P Coquay, A Peigney, E De Grave, E Flahaut, R E Vanderberghe, Ch Laurent *J. Phys. Chem. B* **109** 17813 (2005)
170. P Coquay, E Flahaut, E De Grave, A Peigney, R E Vanderberghe, Ch Laurent *J. Phys. Chem. B* **109** 17825 (2005)
171. R R Bacsá, E Flahaut, Ch Laurent, A Peigney, S Aloni, P Puech, W S Bacsá *New J. Phys.* **5** 131 (2003)
172. E Flahaut, Ch Laurent, A Peigney *Carbon* **43** 375 (2003)
173. C S Du, N Pan *Nanotechnology* **15** 227 (2004)
174. L Huang, S P Lau, Y B Zhang, B K Tay, Y Q Fu *Nanotechnology* **15** 663 (2004)
175. Y Tang, H Cong, R Zhong, H-M Cheng *Carbon* **42** 3260 (2004)
176. O Englander, D Christensen, L Li *Appl. Phys. Lett.* **82** 4797 (2003)
177. S Chiaschi, Y Murakami, Y Miyauchi, S Maruyama *Chem. Phys. Lett.* **386** 89 (2004)
178. A Okamoto, H Shinohara *Carbon* **43** 431 (2005)
179. A Okamoto, H Shinohara *R&D Rev. Toyota CRDL* **40** (1) 22 (2005)
180. H Liao, J H Hafner *J. Phys. Chem. B* **108** 6941 (2004)
181. R Zhang, R K Tsui, J Tresek, A M Rawlett, I Amlani, T Hopson *J. Phys. Chem. B* **107** 3137 (2003)
182. T Ikuno, M Katayama, N Yamauchi, W Wongwiriyan, S Honda, K Oura, R Hobara, S Hasegawa *Jpn. J. Appl. Phys.* **43** 860 (2004)
183. Y Li, D Mann, M Rolandi, W Kim, A Ural, S Hung, A Javey, J Cao, D Wang, E Yenilmez, Q Wang, J F Gibson, Y Nishi, H Dai *Nano Lett.* **4** 317 (2004)
184. H Kinoshita, I Kume, H Sakai, M Tagawa, N Ohmae *Carbon* **42** 2753 (2004)
185. T Ikuno, S-i Honda, K Kamada, K Oura, M Katayama *J. Appl. Phys.* **97** 104329 (2005)
186. K-Y Lee, M Katayama, S-i Honda, T Kuzuoka, T Miyake, Y Terao, J-G Lee, H Mori, T Hirao, K Oura *Jpn. J. Appl. Phys.* **42** L804 (2003)
187. G Zhang, D Mann, L Zhang, A Javey, Y Li, E Yenilmez, Q Wang, J P McVittie, Y Nishi, J Gibbons, H Dai *Proc. Natl. Acad. Sci. USA* **102** 16141 (2005)
188. K B K Teo, M Chhowalla, G A J Amaratunga, W I Milne, G Pirio, P Legagneux, F Wyczisk, J Oliver, D Pribat *J. Vac. Sci. Technol., B* **20** 116 (2002)
189. Y B Zhu, W L Wang, K J Liao, Y Ma *Diamond Relat. Mater.* **12** 1862 (2003)
190. K Bartsch, A Leonhardt *Carbon* **42** 1731 (2004)
191. Y Y Wang, S Gupta, R J Nemanich *Appl. Phys. Lett.* **85** 2601 (2004)
192. M Chen, C-M Chen, H-S Koo, C-F Chen *Diamond Relat. Mater.* **12** 1829 (2003)
193. Y S Woo, D Y Jeon, I T Han, N S Lee, J E Jung, J M Kim *Diamond Relat. Mater.* **11** 59 (2002)
194. M Chhowalla, K B K Teo, C Ducati, N L Rupasinghe, G A J Amaratunga, A C Ferrari, D Roy, J Robertson, W I Milne *J. Appl. Phys.* **90** 5308 (2001)
195. S Hofmann, M Cantoro, B Kleinsorge, C Casiraghi, A Parvez, J Robertson, C Ducati *J. Appl. Phys.* **98** 034308 (2005)
196. S Hofmann, G Csanyi, A C Ferrari, C Ducati, M Cantoro, B Kleinsorge, M C Payne, J Robertson, in *The 6th International Conference on Science Application of Nanotubes (Abstracts of Reports)*, Gothenburg, Sweden, 2005 p. 91
197. S Kishimoto, Y Kojima, Y Ohno, T Sugai, H Shinohara, T Mizutani *Jpn. J. Appl. Phys.* **44** 1554 (2005)
198. G Zhong, T Iwasaki, K Honda, Y Furukawa, I Ohdomari, H Kwarada *Jpn. J. Appl. Phys.* **44** 1558 (2005)
199. T Kato, G-H Jeong, T Hirata, R Hatakeyama, K Tohji, K Motomiya *Chem. Phys. Lett.* **381** 422 (2003)
200. T Kato, G-H Jeong, T Hirata, R Hatakeyama, K Tohji *Jpn. J. Appl. Phys.* **43** L 1278 (2004)
201. T Kato, T Hirata, R Hatakeyama, K Tohji, in *The 6th International Conference on Science Application of Nanotubes (Abstracts of Reports)*, Gothenburg, Sweden, 2005 p. 57
202. Y Li, S Peng, D Mann, J Cao, R Tu, K J Cho, H Dai *J. Phys. Chem. B* **109** 6968 (2005)
203. A Gohier, S Point, A Djouadi, A Granier, T Minea, in *The 6th International Conference on Science Application of Nanotubes (Abstracts of Reports)*, Gothenburg, Sweden, 2005 p. 116
204. A H Mahan, J L Alleman, M J Heben, P A Parilla, K M Jones, A C Dillon *Appl. Phys. Lett.* **81** 4061 (2002)
205. L T T Tuyen, P N Minh, E Roduner, P T D Chi, T Ono, H Miyashita, P H Khoi, M Esashi *Chem. Phys. Lett.* **415** 333 (2005)
206. S Orlanducci, A Fiori, E Tamburri, V Sessa, M L Terranova, M Rossi *Cryst. Res. Technol.* **40** 928 (2005)
207. Y Fujiwara, K Maehashi, Y Ohno, K Inoue, K Matsumoto *Jpn. J. Appl. Phys.* **44** 1581 (2005)
208. Y Fujiwara, K Maehashi, Y Ohno, K Inoue, K Matsumoto, in *The 6th International Conference on Science Application of Nanotubes (Abstracts of Reports)*, Gothenburg, Sweden, 2005 p. 60
209. R Alexandrescu, A Crunteanu, R-E Morjan, I Morjan, F Rohmund, L K L Falk, G Ledoux, F Huisken *Infrared Phys. Technol.* **44** 43 (2003)
210. B Chen, P Wu *Carbon* **43** 3172 (2005)
211. H Hongo, M Yudasaka, T Ichihashi, F Niney, S Iijima *Chem. Phys. Lett.* **361** 349 (2002)
212. J Kong, C Zhou, A Morpurgo, H T Soh, C F Quate, C Marcus, H Dai *Appl. Phys. A* **69** 305 (1999)
213. A M Cassell, J A Raymakers, J Kong, H Dai *J. Phys. Chem. B* **103** 6484 (1999)
214. H T Soh, C F Quate, A F Morpurgo, C F Marcus, J Kong, H Dai *Appl. Phys. Lett.* **75** 627 (1999)
215. M Su, Bo Zheng, J Lie *Chem. Phys. Lett.* **322** 321 (2000)
216. R R Bacsá, Ch Laurent, A Peigney, W S Bacsá, Th Vaugien, A Rousset *Chem. Phys. Lett.* **323** 566 (2000)
217. J-F Colomer, J-M Benoit, C Stephan, S Lefrant, G Van Tendeloo, J B Nagy *Chem. Phys. Lett.* **345** 11 (2001)
218. L An, J M Owens, L E McNeil, J Liu *J. Am. Chem. Soc.* **124** 13688 (2002)
219. C L Cheung, A Kurtz, H Park, C M Lieber *J. Phys. Chem. B* **106** 2429 (2002)
220. A Harutyunyan, B Pradhan, U Kim, G Chen, P C Eklund *Nano Lett.* **2** 525 (2002)
221. W C Ren, F Li, J Chen, S Bai, H-M Cheng *Chem. Phys. Lett.* **359** 196 (2002)
222. J Geng, C Singh, D S Shepard, M S P Shafer, B F G Johnson, A H Windle *Chem. Commun.* 2666 (2002)
223. G L Hornyak, L Grigorian, A C Dillon, P A Parilla, K M Jones, M J Heben *J. Phys. Chem. B* **106** 2821 (2002)
224. L Delzeit, C Nguyen, R Stevens, M Meyyappan *Nanotechnology* **13** 280 (2002)
225. S Matsumoto, L Pan, H Tokumoto, Y Nakayama *Physica B, Condens. Matter* **323** 275 (2002)
226. Y Zhang, Y Li, D Wang, H Dai *Appl. Phys. A* **74** 325 (2002)
227. Q Li, H Yan, Y Cheng, J Zhang, Z Liu *J. Mater. Chem.* **12** 1179 (2002)
228. H Yan, Q Li, Z Liu *Carbon* **40** 2693 (2002)
229. Y J Yoon, J C Bae, H K Baik, S J Cho, S-J Lee, K M Song, N S Myung *Physica B, Condens. Matter* **323** 318 (2002)

230. C Jiang, J Zhao, H A Therese, M Friedrich, A Mews *J. Phys. Chem. B* **107** 8742 (2003)
231. W Z Li, J G Wen, M Sennett, Z F Ren *Chem. Phys. Lett.* **368** 299 (2003)
232. B C Liu, S C Lyu, Y J Lee, S K Choi, S J Eum, C W Yang, C Y Park, C J Lee *Chem. Phys. Lett.* **373** 475 (2003)
233. W Liu, W Cai, L Tao, X Li, Z Yao *J. Mater. Sci.* **38** 3051 (2003)
234. F Li, S G Chou, W Ren, J A Gardecki, A K Swan, M S Ünlü, B B Goldberg, H-M Cheng, M S Dresselhaus *J. Mater. Res.* **18** 1251 (2003)
235. Q Li, H Yan, J Zhang, Z Liu *Carbon* **41** 2876 (2003)
236. W Qian, T Liu, F Wei, Z Wang, H Yu *Carbon* **41** 846 (2003)
237. J W Ward, B Q Wei, P M Ajayan *Chem. Phys. Lett.* **376** 717 (2003)
238. H Ago, K Nakamura, N Uehara, M Tsui *J. Phys. Chem. B* **108** 18908 (2004)
239. H C Choi, S Y Kim, W S Jang, S Y Bae, J Park, K L Kim, K Kim *Chem. Phys. Lett.* **399** 255 (2004)
240. J-F Colomer, L Henrard, P Launios, G Van Tendeloo, A A Lukas, Ph Lambin *Chem. Commun.* 2592 (2004)
241. Y Li, X Zhang, L Shen, J Luo, X Tao, F Liu, G Xu, Y Wang, H J Geise, G Van Tendeloo *Chem. Phys. Lett.* **398** 276 (2004)
242. L W Liu, J H Fang, L Lu, Y J Ma, Z Zhang, H F Fang, A Z Jin, C Z Gu *J. Phys. Chem. B* **108** 18460 (2004)
243. J B Nagy, G Bister, A Fonseca, D Mghn, I Kirichi, Z E Horvth, L P Bird *J. Nanosci. Nanotechnol.* **4** 326 (2004)
244. W Qian, T Liu, F Wei, Z Wang, Y Li *Appl. Catal. A* **258** 121 (2004)
245. B C Liu, B Yu, M X Zhang *Chem. Phys. Lett.* **407** 232 (2005)
246. Z Zhong, F Chen, X Xiong, H Soon, J Lin, K L Tan *J. Nanosci. Nanotechnol.* **4** 183 (2004)
247. H Ago, S Imamura, T Okazaki, T Saito, M Yumura, M Tsui *J. Phys. Chem. B* **109** 10035 (2005)
248. H Muramatsu, T Hayashi, Y A Kim, M Endo, M Terrones, M S Dresselhaus *J. Nanosci. Nanotechnol.* **5** 404 (2005)
249. M Endo, H Muramatsu, T Hayashi, Y A Kim, M Terrones, M S Dresselhaus *Nature (London)* **433** 476 (2005)
250. D Takagi, Y Homma, S Suzuki, Y Kobayashi *Jpn. J. Appl. Phys.* **44** 1564 (2005)
251. W Zhou, Y Zhang, X Li, S Yuan, Z Jin, J Xu, Y Li *J. Phys. Chem. B* **109** 6963 (2005)
252. E F Mosavi, M M Akbarnejad, G Abolhamid, A M Rashidi, in *The 6th International Conference on Science Application of Nanotubes (Abstracts of Reports)*, Gothenburg, Sweden, 2005 p. 71
253. Q Zhang, H Yu, G Luo, W Qian, F Wei, in *The 6th International Conference on Science Application of Nanotubes (Abstracts of Reports)*, Gothenburg, Sweden, 2005 p. 74
254. Z E Horváth, L P Biró, G Van Tendeloo, C Tondeur, G Bister, N Pierard, A Fonseca, J B Nagy *Solid State Phenom.* **94** 271 (2003)
255. A Peigney, Ch Laurent, A Rousset *J. Mater. Chem.* **9** 1167 (1999)
256. J-F Colomer, C Stephan, S Lefrant, G Van Tendeloo, I Willems, Z Kónya, A Fonseca, Ch Laurent, J B Nagy *Chem. Phys. Lett.* **317** 83 (2000)
257. G Gu, G Philipp, X Wu, M Burghard, A M Bittner, S Roth *Adv. Funct. Mater.* **11** 295 (2001)
258. H Allouche, M Monthieux, R L Jacobsen *Carbon* **41** 2897 (2003)
259. J-F Colomer, L Henrard, G Van Tendeloo, A Lukas, P Lambin *J. Mater. Chem.* **14** 603 (2004)
260. M J Pender, L A Sowards, B Maruyama, R A Vaia, M O Stone *Chem. Mater.* **16** 2544 (2004)
261. C H Hsu, C-F Chen, C-C Chen, S-Y Chan *Diamond Relat. Mater.* **14** 739 (2005)
262. D L Ma, C H Tsai, in *The 6th International Conference on Science Application of Nanotubes (Abstracts of Reports)*, Gothenburg, Sweden, 2005 p. 110
263. J Hafner, M Bronikowski, B Azamian, P Nikolaev, A Rinzler, D Colbert, K Smith, R E Smalley *Chem. Phys. Lett.* **296** 195 (1998)
264. J-F Colomer, G Bister, I Willems, Z Kónya, A Fonseca, G Van Tendeloo, J B Nagy *Chem. Commun.* 1343 (1999)
265. C L Cheung, J H Hafner, T W Odom, K Kim, C M Lieber *Appl. Phys. Lett.* **76** 3136 (2000)
266. C L Cheung, J H Hafner, C M Lieber *Proc. Natl. Acad. Sci. USA* **97** 3809 (2000)
267. C Park, M A Keane *Langmuir* **17** 8386 (2001)
268. J H Hafner, C-L Cheung, T H Oosterkamp, C M Lieber *J. Phys. Chem. B* **105** 743 (2001)
269. A J Hart, A H Slocum, in *The 6th International Conference on Science Application of Nanotubes (Abstracts of Reports)*, Gothenburg, Sweden, 2005 p. 64
270. A J Hart, A H Slocum, in *The 6th International Conference on Science Application of Nanotubes (Abstracts of Reports)*, Gothenburg, Sweden, 2005 p. 65
271. V Ivanov, A Fonseca, J B Nagy, A Lukas, P Lambin, D Bernaerts, X B Zhang *Carbon* **33** 1727 (1995)
272. A Fonseca, K Hernadi, P Piedigrosso, J-F Colomer, K Mukhopadhyay, R Doome, S Lazarescu, L P Biro, Ph Lambin, P A Thiry, D Bernaerts, J B Nagy *Appl. Phys. A* **67** 11 (1998)
273. C J Lee, D W Kim, T J Lee, Y C Choi, Y S Park, Y H Lee, W B Choi, N S Lee, G-S Park, J M Kim *Chem. Phys. Lett.* **312** 461 (1999)
274. Y H Mo, A K M F Kibria, K S Nahm *Synth. Met.* **122** 443 (2001)
275. C Klinke, J-M Bonard, K Kern *Surf. Sci.* **492** 195 (2001)
276. L Dong, J Jiao, S Foxley, D W Tuggle, C L Mosher, G H Grathoff *J. Nanosci. Nanotechnol.* **2** 155 (2002)
277. O A Nerushev, R-E Morjan, D I Ostrovskii, M Sveningsson, M Jönsson, F Rohmund, E E B Campbell *Physica B, Condens. Matter* **323** 51 (2002)
278. A Okamoto, T Kawakubo, T Hiraoka, T Okazaki, T Sugai, H Shinohara *Mol. Cryst. Liq. Cryst.* **387** 317 (2002)
279. I Willems, Z Kónya, A Fonseca, J B Nagy *Appl. Catal. A* **229** 229 (2002)
280. T Hiraoka, T Kawakubo, J Kimura, R Taniguchi, A Okamoto, T Okazaki, T Sugai, Y Ozeki, M Yoshikawa, H Shinohara *Chem. Phys. Lett.* **382** 679 (2003)
281. Y Huh, J Y Lee, J Cheon, Y K Hong, J Y Koo, T Y Koo, T J Lee, C J Lee *J. Mater. Chem.* **13** 2297 (2003)
282. H Cui, G Eres, J Y Howe, A Puzetzy, M Varela, D B Geohegan, D H Lowndes *Chem. Phys. Lett.* **374** 222 (2003)
283. S Hofmann, C Ducati, B Kleinsorge, J Robertson *Appl. Phys. Lett.* **83** 4661 (2003)
284. H J Jeong, K H An, S C Lim, M-S Park, J-S Chang, S-E Park, S J Eum, C W Yang, C-Y Park, Y H Lee *Chem. Phys. Lett.* **380** 263 (2003)
285. P N López, I R Ramos, A G Ruiz *Carbon* **41** 2509 (2003)
286. S N Zaretskiy, Y-K Hong, D H Ha, J-H Yoon, J Cheon, J-Y Koo *Chem. Phys. Lett.* **372** 300 (2003)
287. B C Liu, S C Lyu, S I Jung, H K Kang, C-W Yang, J W Park, C Y Park, C J Lee *Chem. Phys. Lett.* **383** 104 (2004)
288. Md Shajahan, Y H Mo, A K M Fazle Kibria, M J Kim, K S Nahm *Carbon* **42** 2245 (2004)
289. R G Lacerda, A S Teh, M H Yang, K B K Teo, N L Rupesinghe, S H Dalal, K K K Koziol, D Roy, G A J Amaratunga, W I Milne, M Chhowalla, D G Hasco, F Wyczisk, P Legagneux *Appl. Phys. Lett.* **84** 269 (2004)
290. R G Lacerda, K B K Teo, A S Teh, M H Yang, S H Dalal, D A Jefferson, J H Durrell, N L Rupesinghe, D Roy, G A J Amaratunga, W I Milne, F Wyczisk, P Legagneux, M Chhowalla *J. Appl. Phys.* **96** 4456 (2004)
291. G S Duesberg, A P Graham, F Kreupl, M Liebau, R Seidel, E Unger, W Hoenlein *Diamond Relat. Mater.* **13** 354 (2004)
292. O Suekane, T Nagasaka, K Kiyotaki, T Nosaka, Y Nakayama *Jpn. J. Appl. Phys.* **43** L1214 (2004)
293. R Sharma, P Rez, M M J Treacy, S J Stuart *J. Electron Microsc.* **54** 231 (2005)
294. G Eres, A A Puzetzy, D B Geohegan, C M Rouleau, H Cui, in *The 6th International Conference on Science Application of Nanotubes (Abstracts of Reports)*, Gothenburg, Sweden, 2005 p. 135

295. I I Khodos, Yu A Kasumov, V N Matveev, V T Volkov, A Yu Kasumov, in *The 6th International Conference on Science Application of Nanotubes (Abstracts of Reports)*, Gothenburg, Sweden, 2005 p. 53
296. A Kukovecz, D Méhn, E Nemes-Nagy, R Szabó, I Kiricsi *Carbon* **43** 2842 (2005)
297. K Liu, K Jiang, C Feng, Z Chen, S Fan *Carbon* **43** 2850 (2005)
298. A A Puzetzy, D B Geohegan, S Jesse, I N Ivanov, G Eres *Appl. Phys. A* **81** 223 (2005)
299. D Kondo, S Sato, Y Awano, in *The 6th International Conference on Science Application of Nanotubes (Abstracts of Reports)*, Gothenburg, Sweden, 2005 p. 77
300. R Sharma, Z Iqbal *Appl. Phys. Lett.* **84** 990 (2004)
301. A Javey, Q Wang, A Ural, Y Li, H Dai *Nano Lett.* **2** 929 (2002)
302. H C Choi, W Kim, D Wang, H Dai *J. Phys. Chem. B* **106** 12361 (2002)
303. H C Choi, S Kundaria, D Wang, A Ajavey, Q Wang, M Roland, H Dai *Nano Lett.* **3** 157 (2003)
304. Q Fu, S Huang, J Liu *J. Phys. Chem. B* **108** 6124 (2004)
305. Q Li, H Yan, J Zhang, Z Liu *Carbon* **42** 829 (2004)
306. Y Yao, L K L Falk, R E Morjan, O A Nerushev, E E B Campbell *J. Microsc.* **219** 69 (2005)
307. C Bower, W Zhu, S Jin, O Zhou *Appl. Phys. Lett.* **77** 830 (2000)
308. D B Hash, M S Bell, K B K Teo, B A Cruden, W I Milne, M Meyyappan *Nanotechnology* **16** 925 (2005)
309. Z Y Juang, J F Lai, C H Weng, J H Lee, H J Lai, T S Lai, C H Tsai *Diamond Relat. Mater.* **13** 2140 (2004)
310. M S Bell, R G Lacerda, K B K Teo, N L Rupasinghe, G A J Amaratunga, W I Milne, M Chhowalla *Appl. Phys. Lett.* **85** 1137 (2004)
311. S Maruyama, R Kojima, Y Miyauchi, S Chiashi, M Kohno *Chem. Phys. Lett.* **360** 229 (2002)
312. Y Murakami, Y Miyauchi, S Chiashi, S Maruyama *Chem. Phys. Lett.* **377** 49 (2003)
313. Y Murakami, Y Miyauchi, S Chiashi, S Maruyama *Chem. Phys. Lett.* **374** 53 (2003)
314. Y Murakami, S Chiashi, Y Miyauchi, S Maruyama *Jpn. J. Appl. Phys.* **43** 1221 (2004)
315. S Maruyama, Y Murakami, Y Shibuta, Y Miyauchi, S Chiashi *J. Nanosci. Nanotechnol.* **4** 360 (2004)
316. H Igarashi, H Murakami, Y Murakami, S Maruyama, N Nakashima *Chem. Phys. Lett.* **392** 529 (2004)
317. M Kohno, T Orii, M Hirasawa, T Seto, Y Murakami, S Chiashi, Y Miyauchi, S Maruyama *Appl. Phys. A* **79** 787 (2004)
318. S Yamashita, Y Inoue, S Maruyama, Y Murakami, H Yaguchi, M Jablonski, S Y Set *Opt. Lett.* **29** 1581 (2004)
319. S Noda, Y Tsuji, Y Murakami, S Maruyama *Appl. Phys. Lett.* **86** 173106 (2005)
320. Y Ohno, Y Kurokawa, S Kishimoto, T Mizutani, T Shimada, M Ishida, T Okazaki, H Shinohara, Y Murakami, S Murayama, A Sakai, K Hiraga *Appl. Phys. Lett.* **86** 023109 (2005)
321. Y Ohno, S Iwatsu, T Hiraoka, T Okazaki, S Kishimoto, K Maezawa, H Shinohara, T Mizutani *Jpn. J. Appl. Phys.* **42** 4116 (2003)
322. S Inoue, Y Kikuchi *Chem. Phys. Lett.* **410** 209 (2005)
323. H E Unalan, M Chhowalla *Nanotechnology* **16** 2153 (2005)
324. H E Unalan, M Chhowalla *Mater. Res. Soc. Symp. Proc.* **858** HH1.5.1 (2005)
325. S Filatov, G Kuchinski, in *The 7th Biennial International Workshop on Fullerene Atomic Clusters IWFAC'2005 (Abstracts of Reports)*, St. Petersburg, 2005 p. 219
326. P Ramesh, T Okazaki, R Taniguchi, T Sugai, K Sato, Y Ozeki, H Shinohara *J. Phys. Chem. B* **109** 1141 (2005)
327. H Yang, P Mercier, S C Wang, D L Akins *Chem. Phys. Lett.* **416** 18 (2005)
328. K B Kouravelou, S V Sotirchos *Rev. Adv. Mater. Sci.* **10** 243 (2005)
329. T Okazaki, H Shinohara *Chem. Phys. Lett.* **376** 606 (2003)
330. M Kumar, Y Ando *Diamond Relat. Mater.* **12** 1845 (2003)
331. R J Andrews, C F Smith, A J Alexander *Carbon* **44** 341 (2006)
332. L-C Qin, X Zhao, K Hirahara, Y Miyamoto, Y Ando, S Iijima *Nature (London)* **408** 50 (2000)
333. H Yan, Q Li, J Zhang, Z Liu, in *The 8th International Conference on Electronic Materials, IUMRS-ICEM, 2002, Xi'an, China, 2002* p. 1
334. W Qian, H Yu, F Wei, Q F Zhang, Z Wang *Carbon* **40** 2968 (2002)
335. P Pinheiro, M C Schouler, P Gadelle, M Mermoux, E Dooryhée *Carbon* **38** 1469 (2000)
336. J E Herrera, L Balzano, A Borgna, W E Alvarez, D E Resasco *J. Catal.* **204** 129 (2001)
337. W E Alvarez, B Kitiyanan, A Borgna, D E Resasco *Carbon* **39** 547 (2001)
338. J H Han, S H Choi, T Y Lee, J B Yoo, C Y Park, T W Jeong, H J Kim, Y J Park, I T Han, J N Heo, C S Lee, J H Lee, S G Yu, W K Yi, J M Kim *Physica B, Condens. Matter* **323** 182 (2002)
339. B Zheng, C Lu, G Gu, A Makarovski, G Finkelstein, J Liu *Nano Lett.* **2** 895 (2002)
340. B Zheng, Y Li, J Liu *Appl. Phys. A* **74** 345 (2002)
341. A Lan, Z Iqbal, M Libera, H Grebel *Appl. Phys. Lett.* **81** 433 (2002)
342. J P Pinheiro, M C Schouler, P Gadelle *Carbon* **41** 2949 (2003)
343. J E Herrera, D E Resasco *J. Catal.* **221** 354 (2004)
344. Y T Zhu, G W Egeland, Y Li, Q X Jia, J Gallegos, A Serquis, X Z Liao, D E Peterson, R C Dye, B J Roop, M A Hoffbauer *J. Nanosci. Nanotechnol.* **4** 189 (2004)
345. D E Resasco, J E Herrera, L Balzano *J. Nanosci. Nanotechnol.* **4** 398 (2004)
346. K Seo, C Kim, B Kim, Y H Lee, K Song *J. Phys. Chem. B* **108** 4308 (2004)
347. Y Chen, D Ciuparu, Y Yang, S Lim, C Wang, G L Haller, L D Pfefferle *Nanotechnology* **16** S476 (2005)
348. G F Zhong, T Iwasaki, K Honda, Y Furukawa, I Ohdomari, H Kawarada *Chem. Vap. Deposition* **11** 127 (2005)
349. P Queipo, A G Nasibulin, P V Pikhitsa, H Jiang, E I Kauppinen, in *The 6th International Conference on Science Application of Nanotubes (Abstracts of Reports)*, Gothenburg, Sweden, 2005 p. 48
350. T Guo, in *Nanotechnology in Catalysis* Vol. 1 (Eds B Zhou, S Hermans, G A Somorjai) (Berlin: Springer, 2004) p. 137; <http://nanofast.ucdavis.edu/Publications/Ch7.pdf>
351. K H Park, M Chhowalla, Z Iqbal, F Sesti *J. Biol. Chem.* **278** 50212 (2003)
352. M Pérez-Mendoza, C Valés, W K Maser, M T Martínez, A M Benito *Nanotechnology* **16** S224 (2005)
353. I Willems, Z Kónya, J-F Colomer, G Van Tendeloo, N Nagaraju, A Fonseca, J B Nagy *Chem. Phys. Lett.* **317** 71 (2000)
354. S C Lyu, B C Liu, S H Lee, C Y Park, H K Kang, C-W Yang, C J Lee *J. Phys. Chem. B* **108** 2192 (2004)
355. D Méhn, A Fonseca, G Bister, J B Nagy *Chem. Phys. Lett.* **393** 378 (2004)
356. L Shen, X Zhang, Y Li, X Yang, J Luo, G Xu *Nanotechnology* **15** 337 (2004)
357. S Tang, Z Zhong, Z Xiong, L Sun, L Liu, J Lin, Z X Shen, K L Tan *Chem. Phys. Lett.* **350** 19 (2001)
358. G Y Xiong, Y Suda, D Z Wang, J Y Huang, Z F Ren *Nanotechnology* **16** 532 (2005)
359. P Coquay, Ch Laurent, A Peigney, O Quénard, E De Grave, R E Vanderberghe *Hyperfine Interact.* **130** 275 (2000)
360. T Sugai, T Okazaki, H Yoshida, H Shinohara *New J. Phys.* **6** 21 (2004)
361. Y Li, X B Zhang, X Y Tao, J M Xu, W Z Huang, J H Luo, Z Q Luo, T Li, F Liu, Y Bao, H J Geise *Carbon* **43** 295 (2005)
362. H M Christen, A A Puzetzy, H Cui, K Belay, P H Fleming, D B Geohegan, D H Lowndes *Nano Lett.* **4** 1939 (2004)
363. I T Han, B K Kim, H J Kim, M Yang, Y W Jin, S J Jung, N Lee, S K Kim, J M Kim *Chem. Phys. Lett.* **400** 139 (2004)
364. I T Han, H J Kim, Y J Park, Y W Jin, J E Jung, J M Kim, B K Kim, N Lee, S K Kim *Jpn. J. Appl. Phys.* **43** 3631 (2004)
365. R Y Zhang, I Amlani, J Baker, J Tresek, R K Tsui *Nano Lett.* **3** 731 (2003)
366. S Honda, Y-G Baek, K-Y Lee, T Ikuno, T Kuzuoka, J-T Ryu, S Ohkura, M Katayama, K Aoki, T Hirao, K Oura *Thin Solid Films* **464–465** 290 (2004)

367. W Wongwiriyan, M Katayama, T Ikuno, N Yamauchi, T Mizuta, T Murakami, S-i Honda, K Oura, K Kisoda, H Harima *Jpn. J. Appl. Phys.* **44** 457 (2005)
368. K-Y Lee, S-i Honda, M Katayama, T Miyake, K Himura, K Oura, J-G Lee, H Mori, T Hiro *J. Vac. Sci. Technol., B* **23** 1450 (2005)
369. E Yenilmez, Q Wang, R J Chen, D Wang, H Dai *Appl. Phys. Lett.* **80** 2225 (2002)
370. Y Li, J Liu, Y Wang, Z L Wang *Chem. Mater.* **13** 1008 (2001)
371. W-Q Deng, X Xu, W A Goddard III *Nano Lett.* **4** 2331 (2004)
372. N Franklin, H Dai *Adv. Mater.* **12** 890 (2000)
373. A M Cassell, S Verma, L Delzeit, M Meyyappan, J Han *Langmuir* **17** 260 (2001)
374. I A Kinloch, M S P Shaffer, Y M Lam, A H Windle *Carbon* **42** 101 (2004)
375. B Chen, G Parker II, J Han, M Meyyappan, A M Cassell *Chem. Mater.* **14** 1891 (2002)
376. A G Nasibulin, P V Pikhitsa, H Jiang, E I Kauppinen *Carbon* **43** 2251 (2005)
377. M Ishida, H Hongo, F Nihey, Y Ochiai *Jpn. J. Appl. Phys.* **43** L1356 (2004)
378. H-N Lin, Y-H Chang, J-H Yen, J-H Hsu, I-C Leu, M-H Hon *Chem. Phys. Lett.* **399** 422 (2004)
379. T de los Arcos, M G Garnier, P Oelhafen, D Mathys, J W Seo, C Domingo, J V García-Ramos, S Sánchez-Cortés *Carbon* **42** 187 (2004)
380. T de los Arcos, M G Garnier, J W Seo, P Oelhafen, V Thommen, D Mathys *J. Phys. Chem. B* **108** 7728 (2004)
381. M S Kabir, R E Morjan, O A Nerushev, P Lundgren, S Bengtsson, P Enokson, E E B Campbell *Nanotechnology* **16** 458 (2005)
382. L Delzeit, B Chen, A Cassell, R Stevens, C Nguyen, M Meyyappan *Chem. Phys. Lett.* **348** 368 (2001)
383. I K Song, W J Yu, Y S Cho, G S Choi, D Kim *Nanotechnology* **15** 590 (2004)
384. P Launois, R Morel, D Le Bolloc'h, P A Albouy, Z K Tang, G Li, J Chen *Solid State Commun.* **116** 99 (2000)
385. Y Li, W Kim, Y Zhang, M Roland, D Wang, H Dai *J. Phys. Chem. B* **105** 11424 (2001)
386. L F Sun, S S Xie, J M Mao, Z W Pan, B H Chang, W Y Zhou, G Wang, L X Qian *Appl. Phys. Lett.* **76** 828 (2000)
387. Y Chen, D Ciuparu, S Lim, G L Haller, L D Pfefferle *Carbon* **44** 67 (2006)
388. P Coquay, E De Grave, A Peigney, R E Vanderberghe, Ch Laurent *J. Phys. Chem. B* **106** 13186 (2002)
389. P Coquay, A Peigney, E De Grave, R E Vanderberghe, Ch Laurent *J. Phys. Chem. B* **106** 13199 (2002)
390. J-F Colomer, L Henrard, E Flahaut, G Van Tendeloo, A A Lukas, Ph Lambin *Nano Lett.* **3** 685 (2003)
391. X Devaux, Sh Laurent, A Rousset, in *Nanostructured Materials* Vol. 2 (New York: Pergamon Press, 1993) p. 339
392. A Peigney, Ch Laurent, F Dobigeon, A Rousset *J. Mater. Res.* **12** 613 (1997)
393. S Lim, D Ciuparu, C Pak, F Dobek, Y Chen, D Harding, L Pfefferle, G Haller *J. Phys. Chem. B* **107** 11048 (2003)
394. S Lim, D Ciuparu, Y Chen, Y Yang, L Pfefferle, G L Haller *J. Phys. Chem. B* **109** 2285 (2005)
395. S Lim, Y Yang, D Ciuparu, C Wang, Y Chen, L Pfefferle, G L Haller *Top. Catal.* **34** 31 (2005)
396. B C Liu, S H Tang, Z L Liu, B L Zhang, T Chen, S Y Zhang *Chem. Phys. Lett.* **357** 297 (2002)
397. Q Liang, Q Li, B L Zhang, Z L Yu *Chin. Chem. Lett.* **11** 559 (2000)
398. Q Liang, L Z Gao, Q Li, S H Tang, B C Liu, Z L Yu *Carbon* **39** 897 (2001)
399. S Delpeux, K Szostak, E Frackowiak, S Bonnamy, F Béguin *J. Nanosci. Nanotechnol.* **2** 481 (2002)
400. K C Patil, S T Aruna, T Mimani *Curr. Opin. Solid State Mater. Sci.* **6** 507 (2002)
401. Y Soneda, K Szostak, S Delpeux, S Bonnamy, F Béguin *AIP Conf. Proc.* **591** (1) 199 (2001)
402. P Chen, H B Zhang, G D Lin, Q Hong, K R Tsai *Carbon* **35** 1495 (1997)
403. P Chen, X Wu, J Lin, K L Tan *Carbon* **38** 139 (2000)
404. L Chen, X Sun, Y Liu, Y Li *Appl. Catal. A* **265** 123 (2004)
405. Y Kobayashi, H Nakashima, D Tanigaki, Y Homma *Thin Solid Films* **464–465** 289 (2004)
406. J Geng, H Li, V B Golovko, D S Shephard, D A Jefferson, B F G Johnson, S Hofmann, B Kleinsorge, J Robertson, C Ducati *J. Phys. Chem. B* **108** 18446 (2004)
407. H-F Cheng, Y Chou, K-S Liu, C-H Tsai, I-N Lin *Physica B, Condens. Matter* **323** 308 (2002)
408. H Ago, T Komatsu, S Ohshima, Y Kuriki, M Yumura *Appl. Phys. Lett.* **77** 79 (2000)
409. H Ago, K Murata, M Yumura, J Yotani, S Uemura *Appl. Phys. Lett.* **82** 811 (2003)
410. H Ago, J Qi, K Tsukagoshi, K Murata, S Ohshima, Y Aoyagi, M Yumura *J. Electroanal. Chem.* **559** 25 (2003)
411. Y Zhou, A Gaur, S-H Hur, C Kocabas, M A Meitl, M Shim, J A Rogers *Nano Lett.* **4** 2031 (2004)
412. C Klinke, E Delvigne, J V Barth, K Kern *J. Phys. Chem. B* **109** 21677 (2005)
413. M Yoshimura, K Tanaka, K Ueda *Jpn. J. Appl. Phys.* **44** 1562 (2005)
414. R M Kramer, L A Sowards, M J Pender, M O Stone, R R Naik *Langmuir* **21** 8466 (2005)
415. Y Y Wang, G Y Tang, F A M Koeck, B Brown, J M Garguilo, R J Nemanich *Diamond Relat. Mater.* **13** 1287 (2004)
416. Y Y Wang, S Gupta, R J Nemanich, Z J Liu, L C Qin *J. Appl. Phys.* **98** 014312 (2005)
417. K B K Teo, S-B Lee, M Chhowalla, V Semet, Vu Thien Binh, O Groening, M Castignolles, A Loiseau, G Pirio, P Legagneux, D Pribat, D G Hasko, H Ahmed, G A J Amaratunga, W I Milne *Nanotechnology* **14** 204 (2003)
418. H M Christen, I Ohkubo, C M Rouleau, G E Jellison, A A Poretzky, D B Geohegan, D H Lowndes *Meas. Sci. Technol.* **16** 21 (2005)
419. C J Tailor, R E Cavicchi, C B Montgomery, S Turner *Nanotechnology* **15** 62 (2004)
420. Q Jiang, Y W Wang, J C Li *Appl. Surf. Sci.* **152** 156 (1999)
421. K Kempa, B Kimball, J Rybczynski, Z P Huang, P F Wu, D Steeves, M Sennett, M Giersig, D V G L N Rao, D L Carnahan, D Z Wang, J Y Lao, W Z Li, Z F Ren *Nano Lett.* **3** 13 (2003)
422. Z P Huang, D L Carnahan, J Rybczynski, M Giersig, M Sennett, D Z Wang, J G Wen, K Kempa, Z F Ren *Appl. Phys. Lett.* **82** 460 (2003)
423. S Lastella, Y J Jung, H Yang, R Vajtai, P M Ajayan, C Y Ryu, D A Rider, I Manners *J. Mater. Chem.* **14** 1791 (2004)
424. H Kind, J-M Bonard *Adv. Mater.* **11** 1285 (1999)
425. H Yokomichi, F Sakai, M Ichihara, N Kishimoto *Physica B, Condens. Matter* **323** 311 (2002)
426. H Kind, J-M Bonard, L Forrd, K Kern, K Hernadi, L-O Nilsson, L Schlappach *Langmuir* **16** 6877 (2000)
427. Y Chen, J Yu *Appl. Phys. Lett.* **87** 033103 (2005)
428. T Hayashi, Y A Kim, T Matoba, M Esaka, K Nishimura, M Endo, M S Dresselhaus *Nano Lett.* **3** 887 (2003)
429. S-H Tsai, C-T Shiu, S-H Lai, H-C Shih *Carbon* **40** 1597 (2002)
430. J-M Ting, R-M Liu *Carbon* **41** 601 (2003)
431. H Yu, Q Zhang, F Wei, W Qian, G Luo *Carbon* **41** 2855 (2003)
432. J Gavillet, A Loiseau, C Journet, F Williams, F Ducastelle, J-C Charlier *Phys. Rev. Lett.* **87** 275504 (2001)
433. J-H Huang, H-N Lin, C-C Chuang, H-W Lai, J-H Hsu *Diamond Relat. Mater.* **14** 744 (2005)
434. C J Lee, J Park, Y Huh, J Y Lee *Chem. Phys. Lett.* **343** 33 (2001)
435. X D Bai, J D Guo, J Yu, E G Wang, J Yuan, W Zhou *Appl. Phys. Lett.* **76** 2624 (2000)
436. J-M Bonard, M Croci, F Conus, T Stöckli, A Chatelain *Appl. Phys. Lett.* **81** 2836 (2002)
437. D N Futaba, K Hata, T Yamada, K Mizuno, M Yumura, S Iijima *Phys. Rev. Lett.* **95** 056104 (2005)
438. E G Rakov, I G Ivanov, S N Blinov, N V Kazakov, V V Skudin, N G Diguurov, A K Bogdanovich *Fullerenes, Nanotubes, Carbon Nanostruct.* **12** 29 (2004)
439. U Narkiewicz, W Arabczyk, W Konicki, I Kucharewicz *Rev. Adv. Mater. Sci.* **8** 53 (2004)

440. U Narkiewicz, W Arabczyk, W Konicki *Fullerenes, Nanotubes, Carbon Nanostruct.* **13** (Suppl. 1) 99 (2005)
 441. V Vinciguerra, F Buonocore, G Panzera, L Occhipinti *Nanotechnology* **14** 655 (2003)
 442. Y T Lee, J Park, Y S Choi, H Ryu, H J Lee *J. Phys. Chem. B* **106** 7614 (2002)
 443. E F Kukovitsky, S G L'vov, N A Sainov *Chem. Phys. Lett.* **317** 65 (2000)
 444. S Helveg, C Lopez-Cartes, J Sehested, P L Hansen, B S Clausen, J R Rostrup-Nielsen, F Abild-Pedersen, J K Nørskov *Nature (London)* **427** 426 (2004)
 445. T Ichihashi, J Fujita, M Ishida, Y Ochiai *Phys. Rev. Lett.* **92** 215702 (2004)
 446. D B Geohegan, A A Puzos, I N Ivanov, S Jesse, G Eres, J Y Howe *Appl. Phys. Lett.* **83** 1851 (2003)
 447. L M Dell'Acqua-Bellavitis, J D Ballard, P M Ajayan, R W Siegel *Nano Lett.* **4** 1613 (2004)
 448. J-M Bonard, M Croci, C Klinke, F Conus, I Afraoui, T Stöckli, A Chatelain *Phys. Rev. B* **67** 085412 (2003)
 449. D-H Kim, H-S Jang, C-D Kim, D-S Cho, H-S Yang, H-D Kang, B-K Min, H-R Lee *Nano Lett.* **3** 863 (2003)
 450. S Hofmann, B Kleinsorge, C Ducati, J Robertson *New J. Phys.* **5** 153 (2003)
 451. C Ducati, I Alexandrou, M Chhowalla, G A J Amarutunga, J Robertson *J. Appl. Phys.* **92** 3299 (2002)
 452. S Hofmann, G Csányi, A C Ferrari, M C Paine, J Robertson *Phys. Rev. Lett.* **95** 036101 (2005)
 453. A Gorbunov, O Jost, W Pompe, A Graff *Carbon* **40** 113 (2002)
 454. Y H Lee, S G Kim, D Tománek *Phys. Rev. Lett.* **78** 2393 (1997)
 455. S B Sinnott, R Andrews, D Qian, A M Rao, Z Mao, E C Dickey, F Derbyshire *Chem. Phys. Lett.* **315** 25 (1999)
 456. A N Andriotis, M Menon, G Froudakis *Phys. Rev. Lett.* **85** 3193 (2000)
 457. S Maruyama, Y Shibuta *Mol. Cryst. Liq. Cryst.* **387** 87 (2002)
 458. H Kanzow, P Bernier, A Ding *Appl. Phys. A* **74** 411 (2002)
 459. O A Louchev, Y Sato, H Kanda *Appl. Phys. Lett.* **80** 2752 (2002)
 460. O A Louchev, Y Sato, H Kanda *Phys. Rev. E* **66** 011601 (2002)
 461. O A Louchev, T Laude, Y Sato, H Kanda *J. Chem. Phys.* **118** 7622 (2003)
 462. Y Shibuta, S Maruyama *Heat Transfer — Asian Res.* **32** 690 (2003)
 463. F Ding, A Rosén, K Bolton *J. Chem. Phys.* **121** 2775 (2004)
 464. F Ding, K Bolton, A Rosén *J. Vac. Sci. Technol., A* **22** 1471 (2004)
 465. F Ding, A Rosén, K Bolton *Phys. Rev. B* **70** 075416 (2004)
 466. F Ding, A Rosén, K Bolton *Chem. Phys. Lett.* **393** 309 (2004)
 467. F Ding, A Rosén, K Bolton *Carbon* **43** 2215 (2005)
 468. O A Louchev, H Kanda, A Rosén, K Bolton *J. Chem. Phys.* **121** 446 (2004)
 469. S Pannala, R F Wood *J. Nanosci. Nanotechnol.* **4** 463 (2004)
 470. C Klinke, J-M Bonard, K Kern *Phys. Rev. B* **71** 035403 (2005)
 471. J-Y Raty, F Gygi, G Galli *Phys. Rev. Lett.* **95** 096103 (2005)
 472. F Ding, K Bolton, A Rosén *J. Phys. Chem. B* **108** 17369 (2004)
 473. J Zhao, A Martinez-Limia, P B Balbuena *Nanotechnology* **16** S575 (2005)
 474. M Grujicic, G Gao, B Gersten *Mater. Sci. Eng. B* **94** 247 (2002)
 475. M Grujicic, G Gao, B Gersten *Appl. Surf. Sci.* **191** 223 (2002)
 476. R T K Baker, M A Barber, P S Harris, F S Feter, R J Waite *J. Catal.* **26** 51 (1972)
 477. F Larouche, O Smiljanic, X Sun, B L Stansfield *Carbon* **43** 986 (2005)
 478. V L Kuznetsov, A N Usoltseva, A L Chuvilin, E D Obratsova, J-M Bonard *Phys. Rev. B* **64** 235401 (2001)
 479. C H Lin, S H Lee, C M Hsu, C T Kuo *Diamond Relat. Mater.* **13** 2147 (2004)
 480. O Jost, A Gorbunov, X Liu, W Pompe, J Fink *J. Nanosci. Nanotechnol.* **4** 433 (2004)
 481. W Z Li, J G Wen, Y Tu, Z F Ren *Appl. Phys. A* **73** 259 (2001)
 482. *Nanotube 2006. The 7th International Conference on Scientific Application of Nanotubes (Book of Abstracts), Nagano, Japan, 2006*
 483. P N D'yachkov *Uglerodnye Nanotrubki: Stroenie, Svoistva, Primeneniya* (Carbon Nanotubes: Structure, Properties, Applications) (Moscow: BINOM, Laboratoriya Znanii, 2006)
 484. E G Rakov *Nanotrubki i Fullereny (Uchebnoe Posobie) (Novaya Universitetskaya Biblioteka)* [Nanotubes and Fullerenes (Textbook) (New University Library)] (Moscow: Logos, 2006)
 485. A Loiseau (Ed.) *Understanding Carbon Nanotubes* (Berlin: Springer, 2006)
- ^a — *Russ. J. Phys. Chem. (Engl. Transl.)*
^b — *Int. Sci. J. Alternative Energy Ecology (Engl. Transl.)*
^c — *Russ. J. Appl. Chem. (Engl. Transl.)*

Progress in the studies of oxidation of dihydropyridines and their analogues

A I Matern, V N Charushin, O N Chupakhin

Contents

I. Introduction	23
II. Hydride transfer mechanisms in oxidation of dihydropyridines	24
III. Three-dimensional structures of dihydropyridines and stereospecificity of hydride transfer	32
IV. Molecular devices based on dihydropyridines	35

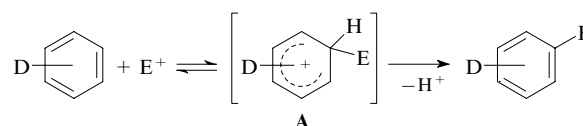
Abstract. Published data on oxidation of dihydropyridines and on the mechanisms and the role of hydride shifts in bioorganic chemistry, enantioselective synthesis and supramolecular chemistry are generalised. The bibliography includes 218 references.

I. Introduction

Almost two hundred years ago, the German chemist Schorlemmer defined organic chemistry as the chemistry of hydrocarbons and their derivatives, from which it follows that the nature of C–H bonds and the conditions of their formation and cleavage are important subjects of chemical investigation.

Actually, many processes associated with the formation of new chemical bonds involve the attack of various reagents, such as electrophiles, nucleophiles, radicals, carbenes and other active species, on the C–H fragment. Radical reagents cause C(sp³)–H bond homolysis, carbenes are inserted into C(sp³ or sp²)–H bonds, whereas the attack of electrophilic or nucleophilic species, which generally occurs on the carbon atoms of C(sp²)–H, ends in the transformation of the substrate molecule into σ^H adducts containing the C(sp³) fragment (a geminal unit). It should be noted that the hydrogen atom elimination is preceded by the formation of σ^H adducts and the latter process radically changes the C–H bond character.

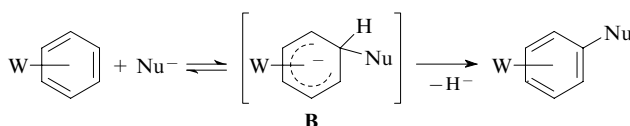
Electrophilic aromatic substitution of hydrogen is a typical example of this transformation. This is a well-developed approach to structural modifications of arenes, which has come into common use as an industrial method for the synthesis of various aromatic compounds.



D is an electron-donating group and E is an electrophile.

Electrophilic aromatic substitution reactions are based on the ease of C(sp³)–H bond cleavage in cationic arene onium σ^H complexes **A** with restoration of aromaticity of the system, which is the driving force for the process.

The nucleophilic attack on aromatic carbon atoms gives rise to anionic σ^H adducts **B**. For many years, the difficulties associated with elimination of the hydride ion from these adducts have limited the development of studies on nucleophilic aromatic substitution of hydrogen (S_N^H). However, investigations performed in the last decades substantially extended knowledge of the synthetic potential of this important approach, which is nowadays used in both oxidative and elimination (*ipso* substitution) modifications.^{1–20}



W is an electron-withdrawing group and Nu is a nucleophile.

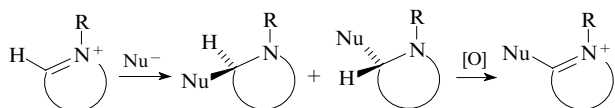
Since the publication of the first review on S_N^H reactions in 1976,⁹ extensive data on amination, arylation, alkylation, cyana-tion, hetarylation and other analogous reactions, which enable the direct introduction of fragments of various nucleophiles into activated aromatic compounds of carbo- or heterocyclic series, have been accumulated in the literature. The conditions of the formation of anionic σ^H adducts (as the first step of S_N^H reactions)^{1–3, 10–19} and the characteristic features of their spatial structures, dissociation and isomerisation were revealed. The asymmetric induction in the new bond formation in nucleophiles containing the unsubstituted carbon atom was examined for a series of azinium salts.²⁰

A I Matern Urals State Technical University, ul. Mira 19, 620002 Ekaterinburg, Russian Federation. Fax (7-343) 374 04 58, tel. (7-343) 374 39 05, e-mail decan@htf.ustu.ru

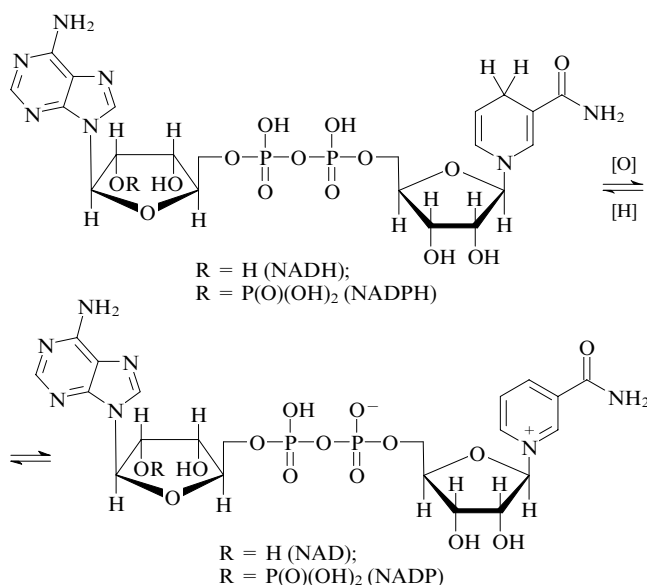
V N Charushin, O N Chupakhin I Ya Postovsky Institute of Organic Synthesis, Urals Branch of the Russian Academy of Sciences, ul. S Kovalevskoi 22, 620219 Ekaterinburg, Russian Federation. Fax/tel. (7-343) 374 11 89, e-mail: charushin@ios.uran.ru (V N Charushin), tel. (7-343) 375 45 01, e-mail: chupakhin@ios.uran.ru (O N Chupakhin)

Received 25 May 2006

Uspekhi Khimii 76 (1) 27–45 (2007); translated by T N Safonova



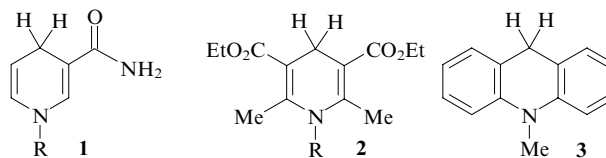
The mechanism of abstraction of 'hydride-labile hydrogen' [†] (the second step of S_N^H reactions) from dihydropyridines is of fundamental importance for organic and bioorganic chemistry and has been the subject of numerous studies and discussions for almost three decades.^{21–28} The importance of knowledge of this mechanism is not only of theoretical interest. The characteristic features of transformations of dihydropyridines and the hydride transfer mechanism are at the basis of important processes in living nature involving nicotinamide adenine dinucleotides and their phosphates (NADH ⇌ NAD, NADPH ⇌ NADP), which are the main components of metabolism and cell energy supply.^{21–23, 28–32}



The mechanism of hydride-labile hydrogen transfer has come under discussion almost immediately after the publication of pioneering studies on oxidation of compounds containing such hydrogen atoms. Kosower²¹ explained an increased attention to this problem by the fact that the choice between the electron transfer and hydride ion transfer is critical to establishing the oxidation mechanism of pyridine nucleotides. Two fundamentally different mechanisms are considered: the one-step (concerted) and stepwise (redox, single-electron transfer, SET) mechanisms. In the latter case, the electron and hydrogen transfer or the two-electron–proton transfer are distinguished. Biochemists have long considered NADH as a source and a component in the electron transport chain, while organic chemists engaged in studies of model chemical compounds are actively debating the nature of hydride transfer.

In the last two decades, the main approaches to investigation of hydride-labile hydrogen transfer and to the choice of NADH models were developed. 1,4-Dihydropyridine derivatives, such as dihydronicotinamides **1**, Hantzsch esters **2** and *N*-methylacridane (10-methyl-9,10-dihydroacridine, AcrH₂, **3**), are most often used as models because these compounds are structurally similar to pyridine-dependent dehydrogenases and their spatial structures and electronic properties can be varied over a wide range, thus influencing the hydride ion mobility.

[†] The term 'hydride-labile hydrogen' is used to designate H[−] that can be eliminated as either a proton and two electrons or a hydrogen atom and an electron, and the hydride shift is used in reference to the transfer of these species.



R = Alk, Ar.

Nowadays, authoritative research groups concerned with the problem of hydride shift in such compounds work in different countries. A considerable contribution to the development of knowledge of the mechanism and characteristic features of oxidation of dihydropyridines was made by the research teams headed by Kosower and Chipman in USA, Stradyn and Duburs in Latvia, Bruice and Moiroux in France, Colter in Canada, Ohno and Fukuzumi in Japan, Cheng and Zhu in China, Hilgeroth in Germany, Beletskaya and Pozharskii in Russia, *etc.* For example, the group headed by Prof. Ohno investigated the characteristic features and stereoselectivity of reduction of various unsaturated systems by dihydronicotinamides, and the results of these studies were published in hundreds of articles. The group headed by Prof. Fukuzumi, who is a recognised expert in the field of investigation of single-electron transfer processes in chemistry and biology and one of the editors of the five-volume encyclopedia *Electron Transfer in Chemistry* published in 2001, has a comparable number of publications on hydride migrations in dihydro derivatives of pyridine and acridine.

The review of the literature demonstrates that the oxidation mechanism of dihydropyridines and the use of these compounds as a 'redox arm' (electron carriers) have attracted considerable interest in the last 5–10 years. This is confirmed by an increase in the number of investigations on the design of qualitatively new materials and processes based on these compounds. The extensive development of biotechnology, nanotechnology and materials sciences and the progress in the field of coordination and supramolecular chemistry facilitated investigations of the hydride shift mechanism. The acquired knowledge of the pathways of redox transformations of nicotinamide adenine dinucleotides was useful in the preparation of antioxidants, free-radical process inhibitors and corrosion inhibitors, in the enantioselective synthesis and asymmetric cleavage, in medicine and biochemistry, in the design of enzyme reactors, bioelectrochemical systems, organic conductors, molecular devices, *etc.*

The present review covers the main directions and trends of the development of knowledge of the hydride transfer mechanism in the series of dihydropyridines and their analogues discussed in the literature in the last two decades. This period of studies of hydride transfer reactions is characterised by development of new methods for initiation and catalysis of oxidation processes, the extension of the range of physicochemical methods and the combined application of various analytical methods.

II. Hydride transfer mechanisms in oxidation of dihydropyridines

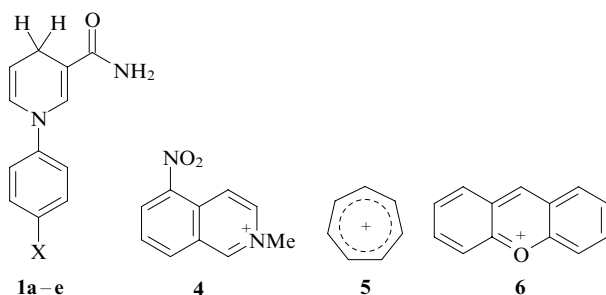
1. Study of the properties of dihydropyridines by theoretical and kinetic methods

A combination of kinetic and calculation methods for studying oxidation of dihydropyridines is a main line of investigation of the hydride transfer mechanism. The development of the single-electron concept in organic chemistry,^{32,33} the progress in investigation of redox processes^{34–36} and the elaboration of the theory of single-electron transfer [‡] (Marcus theory)^{36–39} gave impetus to studies, in which experimental results were compared with the calculated energies of hydride transfer reactions and steps of this process.^{40–42}

[‡] This theory relates the driving force for redox reactions, *i.e.*, the energy differences of the reagents and reactions products, to their rates.

Nowadays, various methods are available for quantitative and qualitative estimation of the 'hydride activity' of dihydropyridines taking into account the energy, magnetic, chemical and structural criteria.^{1,6,23} For example, a comparison of the energy profiles of the hydride and hydrogen transfer reactions and of the proton and two-electron transfer led to different conclusions about the possible mechanisms of the process.^{43–46} It was noted that in the single-electron transfer mechanism, the electron and proton transfer occurs between different reaction centres, which is energetically unfavourable. The solvent effect and reorganisation of the solvent in transition states for both the one-step and stepwise oxidation mechanisms were discussed. A comparison of the calculated and experimental data demonstrated that enzymatic reactions are characterised by the one-step hydride transfer, whereas the proton and two-electron transfer occurs in solutions of model compounds. Analogous conclusions were drawn after calculations by the Marcus equation, which relates the reaction rate constants to the standard free energy changes, for the hydride transfer between NADH and NAD analogues.⁴⁷

The Gibbs free energy changes and the Brønsted and Hammett coefficients were calculated for oxidation of 1-aryl-1,4-dihydronicotinamides **1a–e** by 5-nitroisoquinolinium (**4**), tropylium (**5**) and xanthylium (**6**) cations.⁴⁸ It appeared that the one-step hydride transfer is most probable for isoquinolinium cation **4**, whereas the initial electron transfer (the single-electron transfer mechanism) is more probable for the tropylium and xanthylium cations.



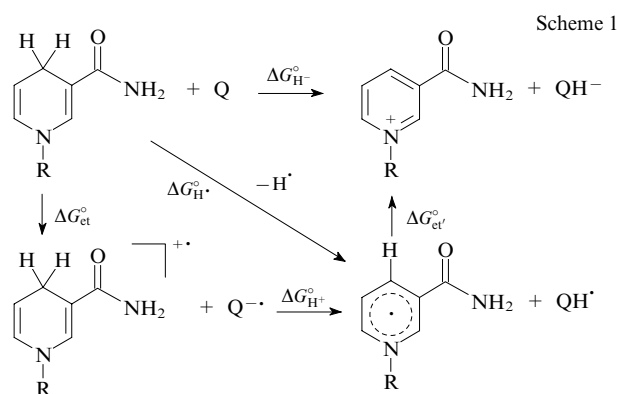
X = OMe (**a**), Me (**b**), H (**c**), Cl (**d**), Br (**e**).

Analysis of the kinetic data, including the isotope effects, and calculations of the activation parameters of oxidation of 1,4-dihydropyridines (Hantzsch esters) and benzylidenemalononitriles suggested the one-step hydride transfer mechanism for these processes.⁴⁹ Based on the estimation of the influence of the structural factors of substituents on the hydride mobility and the direct detection of radical species, it was concluded that the hydrogen abstraction in reduction of radicals and radical ions by a series of 4-substituted 1,4-dihydropyridines occurs by the single-electron transfer mechanism.⁵⁰

Lu *et al.*⁵¹ believed that considerable differences between the expected and real kinetic isotope effects, the difference between the energy profiles of the one-step and stepwise hydride transfer reactions and the detection of intermediates in the reaction of 10-methyl-9,10-dihydroacridine (**3**) with the 1-benzyl-3-cyanoquinolinium ion (see below) do not rule out the possibility of hydride tunnelling.

Based on the energy profiles of the hydride transfer from 1-benzyl-1,4-dihydronicotinamide (BNAH, **1f**) to *p*-benzoquinone derivatives calculated thermodynamically, the stepwise mechanism of electron and proton abstraction according to the electron–proton–electron (EPE) scheme was assumed.^{52,53} It was noted that the Gibbs free energy changes for the single-electron transfer between dihydro adducts and electron acceptors correlate well with the rate constants and the primary kinetic isotope effects.

For the reactions of quinones (Q) with dihydropyridines PyH₂ (including 1-benzyl-1,4-dihydronicotinamide), the Gibbs free energy changes (ΔG°) for different steps of the mobile hydrogen



transfer (Scheme 1), such as the transfer of the first (et) and second (et') electrons and the proton, hydrogen and hydride abstraction, were calculated⁵⁴ according to Eqns (1)–(5), respectively.

$$\frac{\Delta G_{\text{et}}^\circ}{F} = E^\circ(\text{PyH}^{+\bullet}/\text{PyH}_2) - E^\circ(\text{Q}/\text{Q}^-), \quad (1)$$

$$\frac{\Delta G_{\text{et}'}^\circ}{F} = E^\circ(\text{PyH}^{+\bullet}/\text{PyH}^{\bullet}) - E^\circ(\text{QH}^\bullet/\text{QH}^-), \quad (2)$$

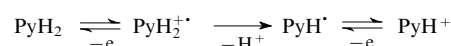
$$\Delta G_{\text{H}^+}^\circ = 2.3 RT[\text{p}K_a(\text{PyH}^{+\bullet}/\text{PyH}^{\bullet}) - \text{p}K_a(\text{QH}^\bullet/\text{QH}^-)], \quad (3)$$

$$\Delta G_{\text{H}^\bullet}^\circ = \Delta G_{\text{et}}^\circ + \Delta G_{\text{H}^+}^\circ, \quad (4)$$

$$\Delta G_{\text{H}^-}^\circ = \Delta G_{\text{et}}^\circ + \Delta G_{\text{H}^+}^\circ + \Delta G_{\text{et}'}^\circ, \quad (5)$$

where F is the Faraday constant and E° is the redox potential.

As a result, it was established that the energy barriers of the one-step hydride transfer for dihydronicotinamide are higher than those for the stepwise transfer. A comparison of the calculated and experimental primary kinetic isotope effects and the influence of the magnesium(II) concentration on the hydride transfer rate and the redox potentials of the reactants led to the conclusion that the reaction proceeds by the single-electron transfer mechanism:



The question about the possibility of homolytic and heterolytic C–H bond cleavage in oxidation of the main NADH models, *viz.*, compounds **1a–g**, **2a,b** and **3**, by perchlorate of the *N,N,N',N'*-tetramethyl-*p*-phenylenediamine radical cation (TMPA^{•+}) was considered by Chinese researchers⁵⁵ with the use of thermodynamic calculations and data from cyclic voltammetry and calorimetric measurements.^{55,56}

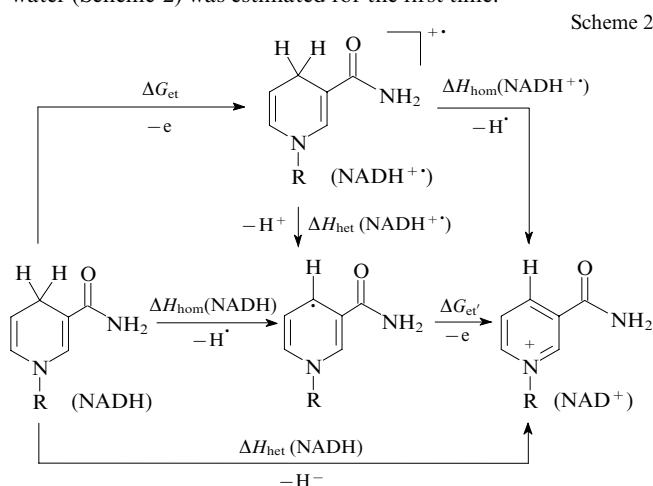


R = 4-XC₆H₄ [X = OMe (**a**), Me (**b**), H (**c**), Cl (**d**), Br (**e**), F₃C (**g**)], PhCH₂ (**f**)

The heterolytic and homolytic C–H bond dissociation energies in an organic solvent (acetonitrile) are 64.2–81.1 and 67.9–73.7 kcal mol^{−1} (for neutral forms of NADH models) and 4.1–9.7 and 31.4–43.5 kcal mol^{−1} (for radical cations), respectively. The energy differences of the heterolytic C–H bond cleavage for BNAH and AcrH₂ are respectively smaller (by 3.62 kcal mol^{−1}) and larger (by 7.4 kcal mol^{−1}) than the corresponding energy of the homolytic process, whereas the analogous values for compound **2a** are similar (69.3 and 69.4 kcal mol^{−1}).

Consequently, the hydride transfer in dihydropyridines **1** should occur more readily than the hydrogen abstraction. An opposite situation is observed for dihydroacridine **3**, whereas both situations are equally probable for Hantzsch esters **2**. The data for the radical cations (for all 10 models, the homolytic C–H bond dissociation energies are 23.3–34.4 kcal mol^{−1} higher than the corresponding energies of heterolytic dissociation) are indicative of the single-electron transfer mechanism and provide evidence that the proton and electron transfer in the final oxidation step is more probable than the hydrogen abstraction.

Analogously, the probability of homolytic and heterolytic cleavage of the neutral and radical cationic forms of NADH in water (Scheme 2) was estimated for the first time:⁵⁶



R is adenosine diphosphoribosyl.

The following dissociation energies (kcal mol^{−1}) were obtained:

	NADH ^{•+}	NADH
ΔH_{het}	5.1	53.6
ΔH_{hom}	36.3	79.3

Therefore, the proton transfer from the NADH^{•+} radical cation in aqueous solutions should occur more readily than the hydrogen abstraction, *i.e.*, the EPE sequence is most probable of all possible mechanisms in living systems.

In a series of studies concerned with the hydride transfer mechanism, the possibility of the formation of a charge transfer complex and its position in the reaction coordinate were examined.^{57,58} The existence of charge transfer complexes was proved by calculations of changes in the activation enthalpy for the reactions of substituted dihydroacridines with *p*-benzoquinone derivatives and tetracyanoethylene.²⁶ The reaction rate was found to depend on the temperature. It was also demonstrated that the nature of the solvent influences the reaction enthalpy change. Calculations of the equilibrium constants of the electron and proton transfer steps demonstrated that deprotonation of radical cations is the rate-determining step.

The stepwise hydride transfer mechanism was suggested based on the results of calculations of the free energy changes of elementary reactions involved in the one-step and multistep mechanisms of reduction of metal cations and quinones by NADH models combined with measurements of the kinetic isotope effects.^{59–61}

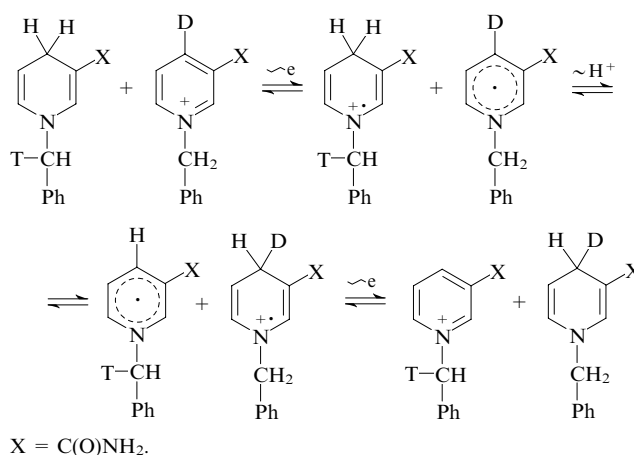
Based on the results of theoretical studies performed for various models of nicotinamide adenine dinucleotides, it is impossible to unambiguously decide whether the hydride-labile hydrogen transfer occurs by the one-step or stepwise mechanism. It should be taken into account that most of calculations were carried out for models in the gas phase without consideration of

the solvent effect. However, these calculations can be used for comparing the reactivities of dihydropyridine derivatives.

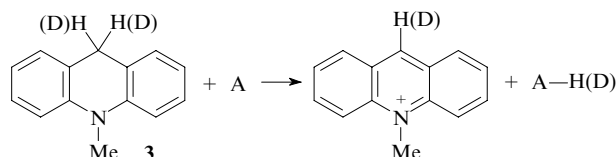
The influence of such factors as the primary and secondary isotope effects, acid–base catalysis, the nature of the solvent, the steric and electronic effects of substituents in the substrate, the presence of metal complexes or ions and photoinitiation on the hydride transfer rate was examined.^{24,62–66} The experimental data can be interpreted in favour of both the one-step hydride transfer and the multistep (single-electron transfer) mechanism.

Measurements of the isotope effects, *viz.*, the kinetic effects (primary and secondary) and the label distribution in the reaction products, provide information on the rate-determining step of the C–H bond cleavage and give evidence for the existence of intermediates. The maximum primary kinetic isotope effect K_H/K_D , which is associated with the concerted hydride transfer and was calculated for the C–H bonds, is ~ 7 . The usual secondary kinetic isotope effects characterising the change in hybridisation of the carbon atom ($sp^3 \rightarrow sp^2$) in the transition state are $K_H/K_D \sim 1$.^{26,43,44,54}

A detailed study of the hydride transfer mechanism was carried out for deuterium- (D) and tritium- (T) labelled *N*-benzyl-dihydronicotinamides and their quaternary salts.⁶⁷ The course of the reactions was monitored based on the changes in radioactivity of the starting reactants and final reaction products. The secondary tritium isotope effects for the hydrogen transfer were anomalous, whereas the primary deuterium isotope effect was identical to the expected value. The typical secondary tritium isotope effects corresponding to the hydride transfer should be equal to ~ 1.2 and ~ 0.83 upon the change in hybridisation from sp^3 to sp^2 and from sp^2 to sp^3 , respectively. Anomalies of the secondary effects of the isotope are attributed to the larger contribution of the inductive isotope effect to stability of the radical cation generated as a result of electron transfer. In this case, the equilibrium constant of the single-electron step increases, which is responsible for the appearance of an anomaly. Due to symmetry of the reactants and the reaction products, the free-energy profile should also be symmetrical. Hence, the only mechanism consistent with the symmetry of the reaction involves the successive electron–proton–electron transfer (EPE). For BNAH, this sequence can be represented as follows:

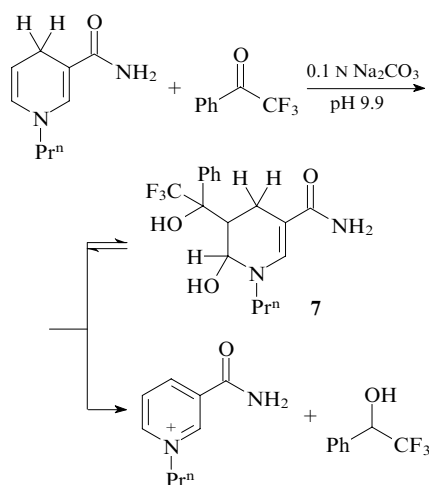


The presence of isotope effects in the hydride transfer does not provide an unambiguous answer to the question as to the form in which hydrogen is abstracted (proton, the hydrogen atom or the hydride ion) in the rate-determining step. Studies of the secondary isotope effects, in particular, the tritium isotope effects, can provide information on the changes in the transition state. However, Colter *et al.*⁶⁸ were doubtful about this expectation. The authors studied *N*-methylacridane (**3**), which gives rather stable radical species due to annulation of the pyridine ring to the benzene rings, as the NADH model. Oxidation of the latter affords the acridinium cation.



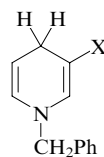
A is benzoquinone, tetracyanoquinodimethane, chloranil or tetracyanoethylene.

The authors⁶⁸ considered two reaction mechanisms: the one-step hydride transfer and the electron and hydrogen transfer. No explanation was provided for the anomalous isotope effects, and it was only hypothesised that tunnelling can occur. Large primary isotope effects and the fact that they are in agreement with the isotope label distribution in the products are most likely indicative of the stepwise rather than the concerted mechanism. It should be emphasised that the measured isotope effects should be interpreted with care considering the results of detailed investigation of the reaction mixtures, the possibility of side reactions and concerted and equilibrium processes. All these data can have a substantial effect on the conclusions. For example, in one of the most-cited studies, Steffens and Chipman⁶⁹ observed the abnormally high primary isotope effects in reactions of different dihydropyridines with trifluoroacetophenone. The label distribution in the products differs from that determined by the reaction kinetics. Based on this fact, the authors suggested the existence of radical ionic intermediates in the hydride transfer. However, more recently Chipman refuted the earlier conclusions by reporting⁷⁰ that the disagreement between the isotope effects is due to the reversible formation of covalent adduct **7**, which does not lie in the redox reaction coordinate.



Unusual condensation of the reaction products of *N*-(α,α -dichlorobenzyl)pyridinium chloride with the chloride ion or pyridines was documented.⁷¹ Presumably, the proton in 4-substituted 1,4-dihydropyridines is transferred from the geminal unit of the dihydropyridine ring to the benzyl dichloromethylene group which is accompanied by the replacement of the chlorine atom to form the corresponding pyridinium cations. Experiments with the use of deuteropyridine confirmed the fact that the redox process involves the transfer of hydrogen (or deuterium) as the cation rather than as the hydride ion or the hydrogen atom.

In the study of oxidation of 3-substituted 1-benzyl-1,4-dihydropyridines **1f** and **8a–c** by copper ions, ferricyanide or *N*-methylacridinium iodide, the influence of substituents at position 3 of the heterocyclic moiety on the reaction rate was estimated.⁷²

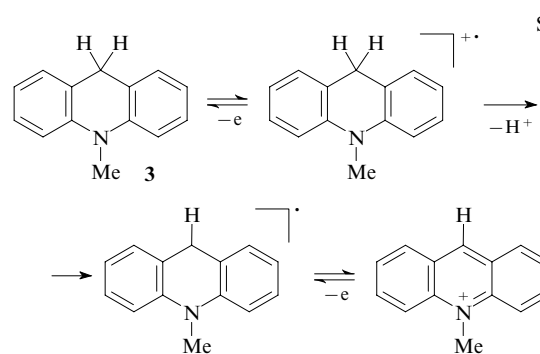


1f, 8a–c

X = C(O)NH₂ (**1f**), C(S)NH₂ (**8a**), CO₂Me (**8b**), Ac (**8c**).

The authors have reached an unexpected (in our opinion) conclusion that oxidation by organic cations is accompanied by the one-step hydride transfer, whereas the reactions with inorganic cations occur by the stepwise single-electron transfer mechanism.

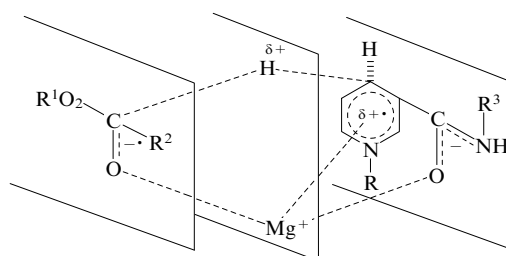
The study of the kinetics and mechanism of oxidation of 10-methyl-9,10-dihydroacridine (**3**) by chromium(VI, V or IV) compounds demonstrated²⁵ that oxidation of AcrH₂ to AcrH⁺ by chromate ions in a water–acetonitrile mixture occurs by the single-electron transfer mechanism and is inhibited by oxygen. The first step involves the formation of the AcrH₂^{•+} radical cation followed by ionisation to the neutral radical and, finally, the electron transfer to form AcrH⁺ (Scheme 3).



Scheme 3

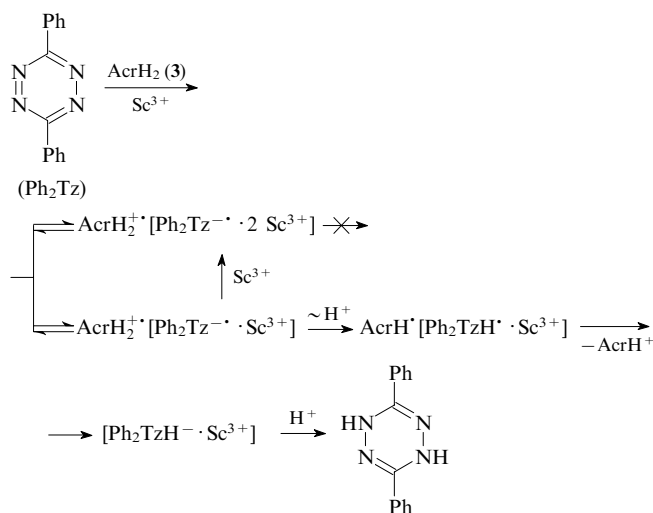
Dihydropyridine–electron acceptor systems, in which the H[−] transfer occurs in the presence of metal ions, were extensively studied. These systems are more complex but they are most similar to biochemical processes catalysed by pyridine-dependent dehydrogenases. It is known⁶⁶ that zinc ions accelerate the hydrogen transfer between the coenzyme and the substrate. Reduction of methyl benzoyl formate with an analogue of 1-benzyl-1,4-dihydronicotinamide in the presence of magnesium ions is accompanied by the anomalous kinetic and product isotope effects due to the ability of the metal ion to stabilise the transition state in which the electron is transferred from the dihydro compound to the acceptor.⁷³ The magnesium ion can either enhance the ability of dihydropyridines to donate an electron to α -keto esters, trifluoroacetophenone, diketones and other electron acceptors^{74,75} or decrease this ability, as was exemplified by the reaction of BNAH with thiopivalophenone.⁷³

An attempt was made to explain the role of the metal ion in the electron transfer.⁷⁶ It was assumed that magnesium in the intermediate complex is coordinated by the dihydropyridine molecule and the acceptor (the parallel planes indicate the spatial orientations of the reagents).



As a result of this coordination, the positive charge is accumulated on the C(4) atom of the pyridine ring [the downfield shift of the signal for the H(4) proton in the ^1H NMR spectrum], which is favourable for the proton rather than hydride abstraction. This assumption was confirmed in the study,⁵⁴ where the authors observed that the single-electron oxidation potentials of dihydropyridines are changed in the presence of Mg^{2+} ions on the average by 0.2 V, whereas the oxidation potential of *N*-methylacridane in the presence of Mg^{2+} remains unchanged because acridane does not form complexes with metal.

A number of studies were concerned with oxidation of dihydroacridines by metal ions or their complexes. High reactivity of phenoxide radical complexes of alkali metals (Na and K) was documented.⁷⁷ The primary kinetic isotope effects provide evidence for the electron and proton transfer mechanism. The cobalt complex of tetraphenylporphyrin and decamethylferrocene catalyse the electron transfer from acridane to *p*-benzoquinones.⁷⁸ It was demonstrated⁷⁹ that the hydride transfer from 10-methyl-9,10-dihydroacridine (**3**) to 3,6-diphenyl-1,2,4,5-tetrazine (Ph_2Tz) occurs only in the presence of scandium(III) ions, which promote the electron transfer due to the formation of the Ph_2Tz –metal complex.



The mechanism of stepwise oxidation accompanied by the hydrogen abstraction or elimination of the substituent in 9-alkyl-10-methyl-9,10-dihydroacridines catalysed by monomeric or dimeric cobalt complexes in the presence of perchloric acid was suggested in the publication.⁸⁰ Acceleration of single-electron oxidation of acridane and 1-benzyl-1,4-dihydronicotinamide (**1f**) in the presence of ruthenium(IV) complexes was documented.⁶¹

Due to the observed differences in the influence of metal ions on the rate of the hydrogen or hydride transfer and the uncertainty of the nature of the bond between the metal and the hydride donor (with both the starting compound and the transition state), no reliable conclusions can be drawn regarding the mechanism of these complex reactions. Apparently, the systems under study should be simplified by separately elucidating the nature of interactions of the metal cation with dihydro compounds, hydride acceptors and radical ionic intermediates and estimating the possibilities of stabilisation of these species, removal from the solvation cage, *etc.*

2. Electrochemical simulation

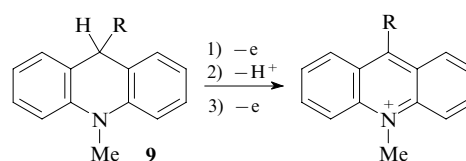
Nicotinamide cofactors are involved in the electron and proton transport, due to which studies of the redox properties of these compounds with the use various model compounds have attracted attention of chemists and biologists.^{21, 22, 24, 27} Measurements of the oxidation potentials of NADH at different electrodes, the determination of the conditions of its electrochemical regeneration, biocatalysis and electrocatalytic oxidation of NADH were described in the studies.^{81–86} It is commonly accepted²³ that due

to the specific features of electrode reactions in solution and the specificity of the electric layer at the electrode–solution interface, the hydride transfer involving dihydropyridines under electrochemical conditions is a very approximate model of real electrochemical reactions in organisms. However, the electrochemical method enables not only the measurements of individual electrochemical characteristics of substances but also the detection of short-lived particles, the electroorganic synthesis, mediated catalysis and transformations of NADH, NAD and their models. In the last decade, the number of publications (see, for example, Refs 85–89) in the field of bioelectrochemistry concerned with regeneration of nicotinamide derivatives, the construction and immobilisation of new electrode systems and the design of electrochemical enzyme reactors has steadily increased, providing evidence that this direction of investigation holds promise.

The electrochemical behaviour of the oxidised and reduced forms of the nicotinamide cofactor was investigated.⁸⁴ Mediated electrocatalysis and electrode modifications were found^{88, 89} to substantially decrease the overvoltage, facilitate oxidation of NADH and enable an increase in the yield of NAD. Organic compounds, which are involved in redox two-electron transfer reactions and simultaneously act as proton donors/acceptors (for example, *ortho*- and *para*-substituted quinones, phenylenediamines, aminophenols), readily oxidise NADPH. NADH-Dependent enzymes existing in contact with an electrode provide high efficiency of bioelectrocatalytic oxidation of NADPH, which was observed, for example, in experiments with the use of diaphorase combined with various quinones, flavins or viologens. The structure–activity relationships of artificial analogues of NADP^+ and the possibility of their immobilisation were investigated.⁹⁰ The possibility of their use instead of natural NADP^+ was examined.⁹¹

The influence of the structure of dihydropyridines (Hantzsch esters) on their reactivity was studied.⁹² The authors mentioned the drawbacks of electrochemical simulation of oxidation of dihydropyridines, which ignores the influence of the nature and structure of the oxidant partner and of the solvent. Based on a comparison of the enzymatic and electrochemical oxidation of dihydropyridines, it is impossible to make an unambiguous choice between the fundamentally different mechanisms of this process involving the hydride and hydrogen transfer.⁹³ It appeared that 3,5-bifunctional 1,4-dihydropyridine derivatives are irreversibly oxidised at a rotating platinum electrode to the corresponding pyridines with consumption of two electrons and two protons, where the proton abstraction is not the rate-determining step.⁹⁴ However, the authors of the publication⁹⁵ observed the potential-determining influence of the deprotonation step of the radical cation generated after the electron transfer from the dihydropyridine molecule.

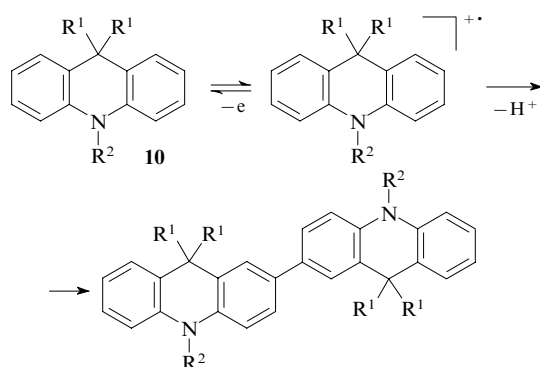
Many studies were concerned with electrochemical oxidation of 9-substituted 9,10-dihydroacridines **9** combined with chemical and spectroscopic methods. Oxidation of these compounds by a divalent copper salt revealed⁹⁶ that 2 mol of Cu^{2+} are consumed per mole of acridane. It was also found that electrochemical oxidation of acridanes, like other dihydroazines,^{97, 98} occurs by the EPE mechanism analogous to that presented in Scheme 3.



R = Me, Ph, NPhMe.

The results of the study⁹⁶ were confirmed by more recent investigations^{99–101} of oxidation of various 9,10-dihydroacridines. The data from cyclic voltammetry, controlled potential electrolysis and chemical syntheses demonstrated that 9,9-disubstituted 9,10-dihydroacridines **10** are oxidised to radical mono-

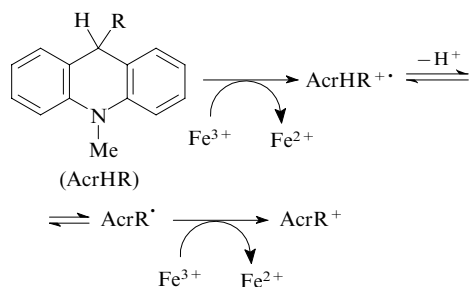
cations (reversible single-electron transfer), and, after the proton abstraction, the resulting radicals undergo dimerisation to readily oxidisable 2,2'-bi(acridane) systems.¹⁰⁰



R¹ = Me; R² = H, Me; R¹ = H, R² = Ph.

By contrast, oxidation of 9*H*-acridanes **9** occurs by the EPE mechanism to give the acridinium cation, a peak assigned to reduction of protons being observed in the cyclic voltammogram, which is an additional argument for the proposed oxidation scheme.

A series of 9-alkylacridanes **9** (AcrHR) were studied by cyclic voltammetry.¹⁰² The reversible formation of radical cations and radicals in the case of oxidation of acridanes and reduction of conjugated cations, respectively, was observed by varying the potential scan rate. The EPE mechanism was confirmed for electrochemical and chemical oxidation (by a trivalent iron salt).

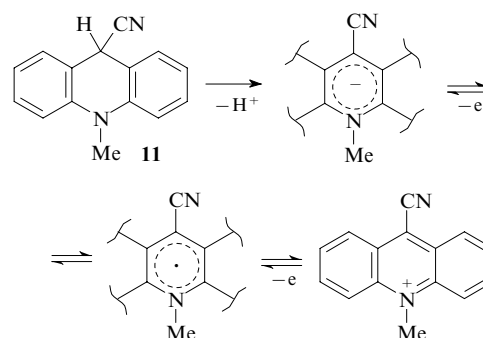


R = Alk.

This example demonstrates that deprotonation of the radical cation is the rate-determining step. A substituent in the geminal unit of acridane favours an increase in the oxidation potential compared to the unsubstituted compound (AcrH₂). This increase is insignificant in the case of alkyl electron-donating substituents and is more substantial in the case of electron-withdrawing substituents.

Earlier, the EPE oxidation mechanism has been observed for 1-benzyl-1,4-dihydronicotinamide derivatives containing different substituents in the benzene ring.⁵⁴ Electron-donating substituents at position 9 of the acridinium cation favour an increase in the negative potentials of single-electron reduction and the formation of neutral radicals in the reaction pathway of electrochemical oxidation of the corresponding acridane.²⁶ Electron-withdrawing substituents in the C(sp³)-H fragment of dihydro compounds substantially decrease their tendency to undergo hydride abstraction and increase the electron affinity of the conjugated azinium cations.¹⁰³ For example, the introduction of the cyano group at position 9 of acridane leads to oxidation of the dihydro compound not only by the EPE mechanism but also by the EEP mechanism. Moreover, under certain conditions, hydrogen can be abstracted from dihydro derivatives as a proton.^{104, 105} For example, oxidation of 9-cyanoacridane **11** in the presence of sodium nitrite used

as a base is accompanied by the proton abstraction followed by the two-electron transfer (the PEE mechanism).¹⁰⁶



Electrochemical oxidation of unsubstituted *N*-methylacridane (**3**) to the *N*-methylacridinium cation in the presence of pyridinium bases also occurs by the single-electron transfer mechanism (EPE).¹⁰¹ The deprotonation rate constants of the AcrH₂^{•+} radical cation were determined depending on the strength of the base with the use of spectrophotometric and electrochemical methods, and the constants p*K*_a were calculated.

Therefore, electrochemical simulation of oxidation of dihydroazines enables the detection of short-lived intermediates in the hydride transfer, *viz.*, radical ions and radicals. The existence of these types of intermediates was confirmed by different physicochemical methods.

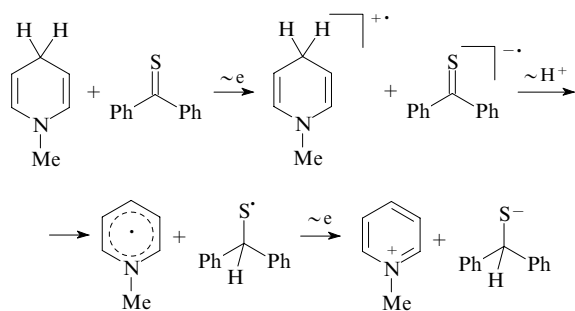
3. Detection of radical products

The radical forms of nicotinamide cofactors (NAD[•]) can be involved in enzyme-catalysed oxidation and reduction reactions. The pyridyl radicals are generated by the addition of one electron to the pyridinium ion or the hydrogen abstraction from dihydropyridine, for example, under irradiation. These radicals are generated also from pyridinium charge-transfer complexes in photochemical reactions, dihydropyridines being able to act as electron donors in charge-transfer complexes. The pyridyl radicals can undergo dimerisation to form unusual π complexes (π -mers).

Single-electron processes in hydride transfer reactions can be directly observed by ESR spectroscopy, which, like electrochemical methods, enables the detection of intermediate radical and radical ionic species.

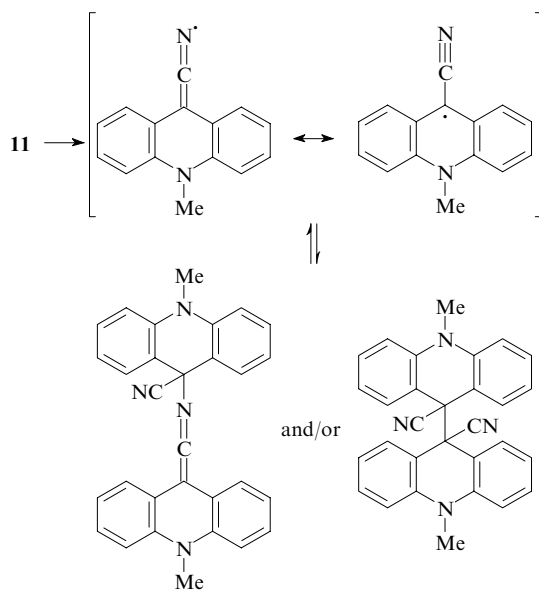
The generation of radicals in chemical oxidation of different dihydro adducts of the pyridine series was confirmed by the formation of dimeric products^{107–109} and with the use of radical traps [diphenylpicrylhydrazyl, 2,4,6-tri(*tert*-butyl)phenol, nitroxides, *etc.*].^{21, 110} Direct reduction of stable radicals and radical cations by 1,4-dihydropyridines made it possible to observe radical derivatives of pyridines by ESR spectroscopy.⁴⁸ The free radical products were detected by UV irradiation of a ternary mixture consisting of bromobenzene, aromatic imine and 1-benzyl-1,4-dihydronicotinamide in acetonitrile.¹¹¹ Radicals and radical cations were found also in the study of photoinduced oxidation of 1,4- and 1,2-dihydropyrimidines with quinones.¹¹²

The direct detection of pyridyl radicals presents difficulties because of their high reactivity toward oxidising agents. Nevertheless, it has been possible to detect radicals generated in oxidation of BNAH with quinones and acids with the use of the ESR method by varying the reaction conditions and the structures of dihydro adducts and using special techniques for observing fast processes.^{113–116} The thiobenzophenone radical anion was detected by freezing a solution of dihydropyridine and thiobenzophenone in THF, the radical anion being then transformed into the free radical and anion, whereas dihydropyridine is oxidised to the pyridinium cation through the successive electron-proton-electron transfer.¹¹⁷



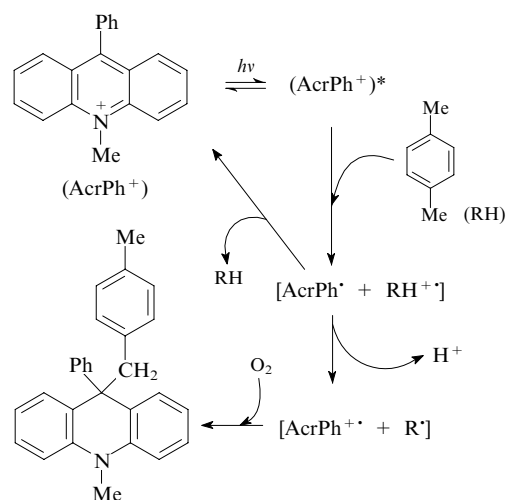
Radicals generated in reduction of the 4-acetyl-1-benzyl-*N,N*-diisopropylnicotinamide (ABNA) and 1-benzyl-4-phenylnicotinamide (PhBNA) cations in the presence of trivalent scandium cations, which form complexes with the corresponding pyridines, were detected by ESR spectroscopy.¹¹⁸

Benzannulation of the pyridine ring and the introduction of an electron-withdrawing substituent into the geminal unit stabilise the radical intermediates generated in oxidation of dihydro compounds. The generation of the stable 9-cyanoacridinyl radical in oxidation of acridane **11** by atmospheric oxygen in the presence of cyanide ions and potassium *tert*-butoxide used as bases was documented.¹⁰⁴ The acridine radical stable for several hours was prepared by oxidation of 9-cyano-10-methyl-9,10-dihydroacridine (**11**) in the presence of nitrite ions under an inert atmosphere in an electrochemical cell, which was placed in a resonator of an ESR spectrometer.¹⁰⁶ This radical can undergo reversible dimerisation in the temperature range from -30 to 20 °C.¹¹⁹

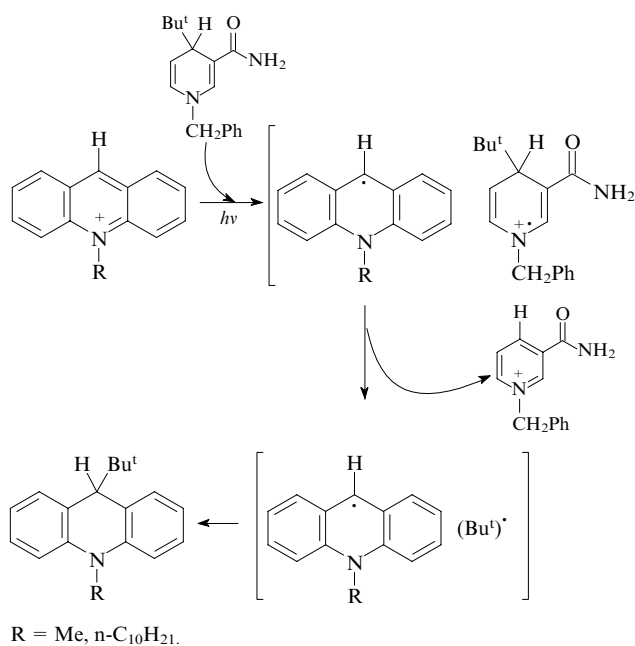


Chemical oxidation of acridane **11** in DMF by *p*-benzoquinone and atmospheric oxygen in the presence of lithium nitrite also enabled the detection of the cyanoacrydinyl radical by ESR. Such spectra were recorded in the case of reduction of the *N*-methylacridinium cation with the cyanide ion and of the 9-cyano-*N*-methylacridinium cation with sodium borohydride,¹²⁰ which confirms the possibility of the single-electron transfer from these compounds.^{121, 122}

The radical ionic and radical products generated in the photo-initiated reaction of 10-methyl-9-phenyl-9,10-dihydroacridine with *p*-xylene were directly detected by Ohkubo and Fukuzumi.¹²³



Photoinduced alkylation of the acridinium cation with 1-benzyl-4-*tert*-butyl-1,4-dihydronicotinamide was investigated.¹²⁴ Not only the detection of radical species, but also elimination of the *tert*-butyl radical from the radical cationic analogue of NADH due to the influence of the steric factors on the properties of dihydro compounds and intermediates of their oxidation are of interest.

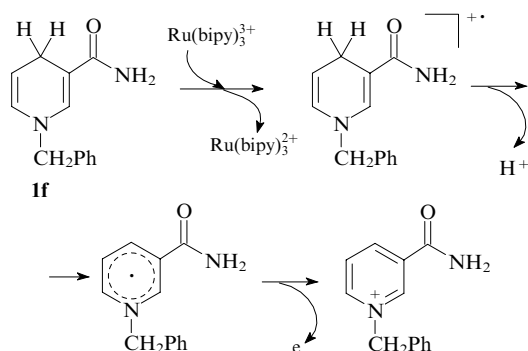


R = Me, *n*-C₁₀H₂₁.

In more recent studies (see, for example, Ref. 125), the acridinium cation was used as a catalyst for photoinduced selective oxidation of aromatic compounds, which occurs through the formation of radical products.

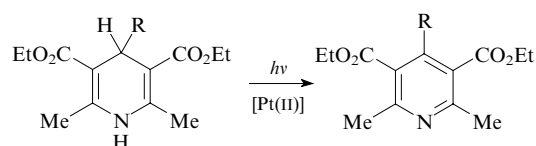
The radical cations of 9-substituted *N*-methylacridanes **9** were observed with the use of the stopped-flow rapid-mixing ESR technique.¹⁰²

Direct evidence for the formation of the 1-benzyl-1,4-dihydronicotinamide radical cation in oxidation of this compound with the iron(III) and rubidium(III) bipyridyl complexes was obtained.^{53, 126, 127}



The results of measurements of the deprotonation rate of the 1-benzyl-1,4-dihydropyridine radical cation and the observed kinetic isotope effect are indicative of the single-electron transfer mechanism.

The predominant reaction pathway through the formation of radical intermediates was described for photocatalytic oxidation of Hantzsch esters in the presence of the platinum terpyridyl complex.¹²⁸



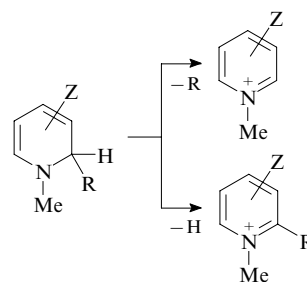
Useful information on the mechanism of processes involving radicals can be obtained by ESR spectroscopy combined with other instrumental methods for monitoring chemical reactions. However, in spite of numerous facts of the detection of radical ionic species in oxidation of dihydroazines and published results of investigation of the properties of pyridinyl radicals, it is still doubtful that ESR spectroscopy provides an unambiguous answer to the question whether the observed radical species lie on the reaction coordinate.

4. Mass spectrometric fragmentation

Ionisation of substrates can be studied by electron-impact mass spectrometry and correlated with the mechanisms of chemical reactions of various nature. In addition, mass spectrometry provides information on the relationship between the molecular structure and the reactivity.^{129, 130}

Stability of tetrahydropyrazines with annulated five- and six-membered heterocycles was studied by mass spectrometry.¹³¹ Criteria were proposed for the mass-spectrometric estimation of stability. The validity of estimates of stability of annulated tetrahydropyrazines based on the proposed mass-spectrometric criterion (the ratio of the peaks of the molecular ion or the radical cation and the 1,4-diazinium ion) was confirmed by chemical experiments. Stability of tetrahydropyrazines was demonstrated to depend on the nature and orientation of the heterocycle as well as on the nature and size of the substituent.

In the study,¹³² the results of measurements of stability to electron impact and the tendency of dihydroazines to undergo aromatisation were correlated for the first time with the experimental data on chemical oxidation of these compounds. Aromatisation of these compounds is characterised by the formation of conjugated cations from dihydroazines due to elimination of both the substituent and hydride-labile hydrogen.

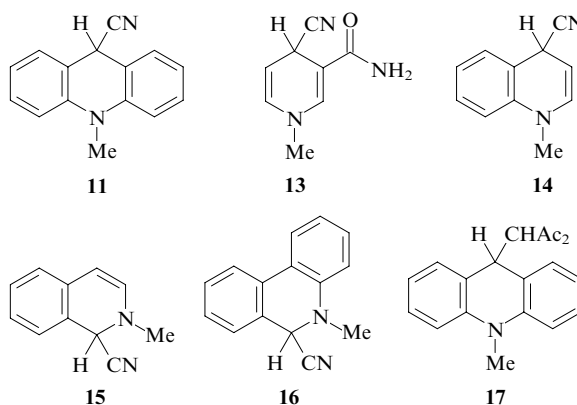


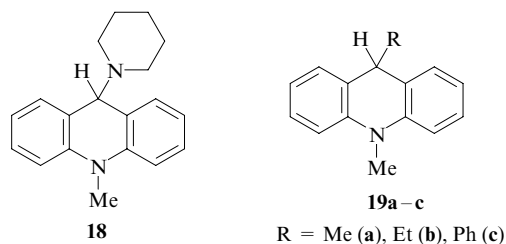
The intensity ratio of the peaks of radical cations generated upon electron impact to the peaks corresponding to the hydrogen abstraction or elimination of a substituent from molecular ions was used as the mass-spectrometric criterion for the pathways of aromatisation of dihydroazines. It should be noted that the single-electron redox mechanism implies the formation of a radical cation identical to the molecular ion (M^+) generated upon electron impact. This indicates that aromatisation of dihydro compounds under electron impact correspond to chemical transformations under the action of dehydrogenating agents. However, it should be remembered that chemical oxidation in solution can differ substantially from the process in the gas phase.

In studies of aromatisation of dihydropyridine derivatives containing electron-donating or electron-withdrawing substituents in the geminal unit (Table 1), a rather good correlation between the products of chemical oxidation and the results of mass-spectrometric experiments was obtained. This can be attributed (with a certain degree of approximation) to the formation of a radical cation as the primary intermediate of the chemical oxidation reaction.^{24–27, 102–104}

Table 1. Data from mass-spectrometric fragmentation of dihydroazines.¹³²

Compound	Characteristic peaks, m/z (intensity, %)			Fragment elimination of which is the most probable in aromatisation
	M^+	$[\text{M}-\text{H}]^+$	$[\text{M}-\text{R}]^+$	
11	220 (49)	219 (77)	194 (31)	$-\text{H}^+$
13	163 (39)	162 (26)	137 (100)	$-\text{CN}^+$
14	170 (41)	169 (69)	144 (36)	$-\text{H}^+$
15	170 (99)	169 (99)	144 (100)	$-\text{H}^+$, $-\text{CN}^+$
16	220 (36)	219 (34)	194 (100)	$-\text{CN}^+$
17	293 (39)	292 (4)	194 (100)	$\text{CH}(\text{COMe})_2^+$
18	278 (12)	—	194 (100)	$-\text{C}_5\text{H}_8\text{N}^+$
19a	209 (43)	208 (6)	194 (100)	$-\text{CH}_3^+$
19b	223 (7)	—	194 (100)	$-\text{C}_2\text{H}_5^+$
19c	271 (100)	270 (39)	194 (14)	$-\text{H}^+$





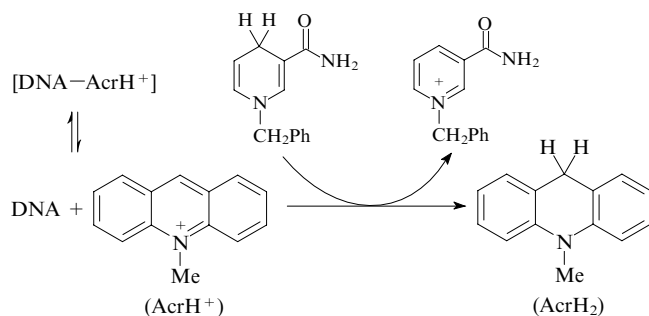
Since the reactions occur in the gas phase at high temperature and radical cations are generated under drastic conditions, the mass spectra give only an approximate model of chemical experiments. Nevertheless, the results of studies demonstrated that mass spectrometry can provide useful information for estimating the influence of the electronic effects of substituents, the steric factors and hetero- and benzannulation on stability of NADH models and the possible pathways of aromatisation.

5. Modelling of biochemical reactions

In recent years, investigations of the hydride transfer mechanism with the use of various models approximating chemical systems to biochemical systems have increased in number. These studies were concerned primarily with catalysis of redox reactions by metal ions and complexes, photoinitiation of processes and the use of mediators and intermediates.^{30–32, 133, 134} Quantum-chemical methods are widely used for calculations of the energies of the hydride transfer processes involving enzymes.^{40, 135–137}

Japanese chemists¹³⁸ studied oxidation of NADH by a system that models the respiratory chain and demonstrated that the ATP synthesis is accompanied by electron transfer. The fact of electron transfer from NADH to the flavin analogue and then to a hemin complex and oxygen was established by spectroscopic studies. Analogous model reactions were performed.^{84, 139, 140}

A study of the structure–activity relationships for artificial analogues of NADP⁺ and examination of the possibility of immobilising these derivatives⁹⁰ revealed the conditions for the use of these compounds instead of natural compounds.⁹¹ The influence of DNA on oxidation of BNAH by photoinduced oxygen¹⁴¹ and acridinium cations and on reduction of the quinolinium cation by a ruthenium bipyridyl complex was investigated.¹⁴² The photoinduced electron transfer from the donor [Ru(bipy)₃²⁺] to the quinolinium cation (QuH⁺) is efficiently accelerated by DNA, as is evidenced by the shift of the single-electron reduction potential of the QuH⁺ cation to positive values due to intercalation of QuH⁺ with DNA molecules. The QuH[•] radical generated upon the electron transfer can be stabilised through π – π intercalation with two bases of the DNA chain. The electronic spectrum of this system was recorded by laser flash photolysis (in the absence of DNA, absorption was not observed). The opposite situation is observed when DNA is involved in the hydride transfer from BNAH to the AcrH⁺ cation. In the presence of DNA, oxidation of dihydro compounds is inhibited, which is attributed to the intercalation of the bulky AcrH⁺ ion with bases from the DNA chain.¹⁴³



The isotope effects and their dependence on the temperature for proton transfer reactions involving transhydrogenases were described.¹⁴⁴ Various compact chemical coenzyme reactors were designed based on nicotinamide compounds.^{145, 146} An enzyme reactor for enantioselective reduction of pyruvate to L-lactate in high yield can be mentioned as an example.¹⁴⁷

Arguments in favour of the EPE mechanism of reduction of lipophilic quinones with NADH models were presented by Zlatovic *et al.*¹⁴⁸ The dynamics of the photoinduced electron transfer during oxidation of 1-benzyl-1,4-dihydropyridine by the DNA-intercalated acridinium, quinolinium and phenanthridinium cations in the presence of a ruthenium bipyridyl complex was investigated.¹⁴⁹ The shift of the reduction potentials of cations intercalated into DNA to more positive values and acceleration of the reaction in the presence of metal complexes additionally support the stepwise hydride transfer mechanism. However, the possibility of the single-electron mechanism of reduction of flavins by NADH was not denied.¹⁵⁰ In the study cited, the formation of a charge-transfer complex was detected by stopped-flow electron spectroscopy.

Presumably,¹⁵¹ insignificant kinetic isotope effects observed in the case of reduction of D-xylose by dihydronicotinamide attest to the one-step hydride transfer mechanism. However, thermodynamic analysis of reduction of quinones by NADPH¹⁵² provided evidence for the stepwise EPE mechanism of hydride-labile hydrogen abstraction.

Photobacterial catalysis of the single-electron transfer from NADPH to ferredoxin or flavodoxin was examined.¹⁵³ Kinetic studies by the stopped-flow technique confirmed the stepwise mechanism of reduction of flavodoxin by enzymes. The equilibrium in the NADPH–flavin system was described in the study,¹⁵⁴ where intermediates of the hydride transfer were observed by spectroscopic and electrochemical methods.

The stereoselectivity of reduction of NO-containing cytochromes by dihydropyridines can be considered as evidence for the direct hydride transfer.¹⁵⁵ However, intermediates of hydride transfer were detected in the analogous NADH–cytochrome system,¹⁵⁶ and the oxidation rate was demonstrated to depend on the substituents.

Based on the characteristic features of the reactions involving dihydropyridines in model or real biological systems and understanding of the mechanism of hydride transfer reactions and ways of controlling these reactions, many of the known compounds were recommended as biomimetics and bioprotectors, inhibitors of bacterial processes, neuroprotectors and neuromodulators, radioprotectors, antidiabetic and anti-dermatitis drugs, *etc.* (Refs 157–163).

Therefore, a combination of chemical, electrochemical and enzyme models holds promise for investigation of the hydride transfer reactions.

III. Three-dimensional structures of dihydropyridines and stereospecificity of hydride transfer

In studies of processes that model NADH–NAD transformations, it is necessary to take into account that the dihydropyridine–pyridinium cation system undergoes a substantial rearrangement because hybridisation of the geminal carbon atom changes from sp³ to sp². In this case, not only the aromaticity, chemical, magnetic, electrochemical, physical and energy characteristics of the molecule but also its spatial structure are changed. It is known that biological activity of compounds is related to their structures. Enzymes, for which a dihydronicotinamide derivative is a cofactor, are sensitive to the stereoconfiguration of the substrates involved in the interaction, *i.e.*, the spatial structure of the latter is responsible for stereospecificity of biochemical processes.^{29–31}

The development of X-ray spectroscopy enabled the direct examination of the structures of dihydropyridines and estimation of the influence of various substituents on the conformation of NADH analogues.

The presence of sp^3 -hybridised carbon atoms in dihydropyridines leads to a distortion of the planarity characteristic of aromatic pyridinium salts. X-Ray diffraction data for 3,5-di(methoxycarbonyl)-1-methyl-4-phenyl-1,4-dihydropyridine demonstrated that the strain causes bending of the plane of the pyridine ring along the N–C(4) axis (Fig. 1)¹⁶⁴ and a certain degree of shielding of hydride-labile hydrogen in the geminal unit.^{165, 166}

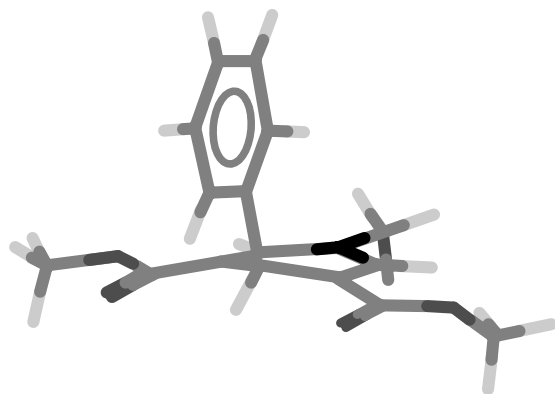
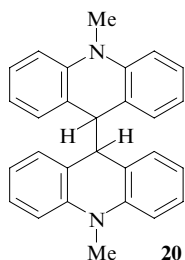


Figure 1. Three-dimensional structure of 3,5-di(methoxycarbonyl)-1-methyl-4-phenyl-1,4-dihydropyridine.¹⁶⁴

Shielding of the geminal hydrogen atom by bulky substituents decreases the ‘hydride activity’ of dihydro derivatives, with the result that steric hindrances prevail over the electronic effects.¹⁶⁷ It would be interesting to estimate the $C(sp^3)–H$ bond length and energy in the geminal unit in a series of related compounds. It is the steric factors that are apparently responsible for elimination of substituents, which is sometimes observed in the case of oxidation of dihydropyridines.^{54, 102, 132}

For 9-substituted 10-methyl-9,10-dihydroacridines, the pyridine ring is also strongly puckered along the N–C(9) axis, which is characterised by the average dihedral angle of 150° .^{168–171} The ease of dissociation of recombination products of acridinyl radicals is attributed to the strained structures of heterocyclic systems,¹⁷² which was exemplified by acridine dimer **20** (Fig. 2).^{119, 169}



The spatial structures of dihydroacridine radical cations generated in oxidation of 9,10-dihydroacridines by an iron(III) salt were discussed.¹⁰² Radical cations of 9-substituted *N*-methylacridanes **9** were detected with the use of the stopped-flow rapid-mixing ESR technique. The hyperfine splitting constants were calculated by comparing the observed ESR spectra with the results of computer simulation using molecular orbital calculations. The calculations demonstrated that the acridane system adopts a boat conformation with the substituent R in an axial position and the hydrogen atom at C(9) in an equatorial position. It was hypoth-

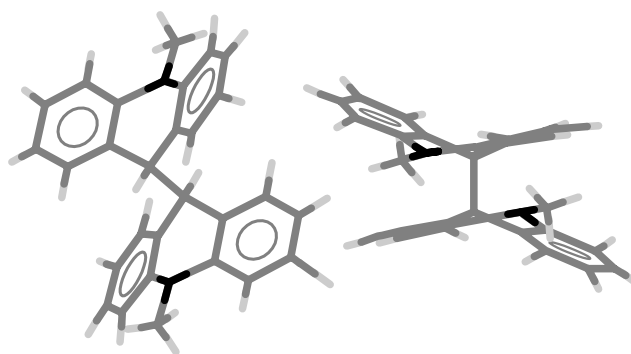
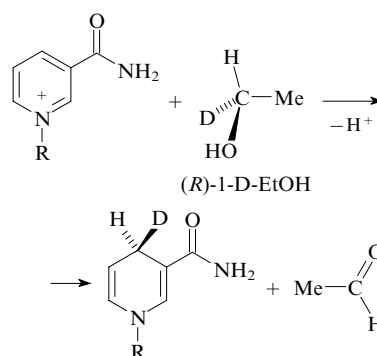


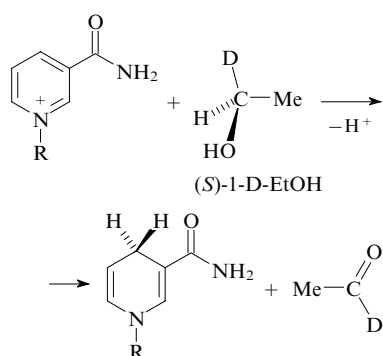
Figure 2. Three-dimensional structure of *N*-methylacridine dimer **20**.

esised that the steric demands are responsible for the reactivity of the radical cations.

In our opinion, the calculations demonstrating the nonequivalence of the axial and equatorial hydrogen atoms in unsubstituted dihydroacridine are of considerable interest. It is quite probable that the steric effects are not the only factors responsible for differentiation of the geminal hydrogen atoms. Thermodynamic instability of systems that lost aromaticity is also increased by the charge effects, which act together with the structural factors. Presumably, this facilitates stereospecificity of reduction of various substrates by unsubstituted dihydropyridines, which exist in the activated transition state initiated by the single-electron transfer. After the proton abstraction, the sterically hindered active pyridinium radical cation is transformed into the neutral radical structurally similar to the cation, and the secondary electron transfer gives rise to the thermodynamically more favourable planar molecule of the aromatic pyridinium cation or its analogue.¹⁷³

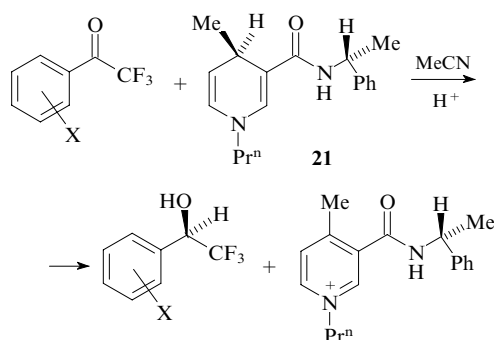
The characteristic feature of the processes in organisms is that only particular stereoisomers are involved in the reactions, resulting in the formation of stereochemically pure products.^{30, 174} The stereospecificity is responsible for the fact that only one of enantiomers exhibits biological properties and this lies at the basis of the active principle of many pharmaceuticals. In enzymatic processes in living organisms, the protein chain acts as the chiral recognising fragment. Reduction processes involving NADH are stereoselective. The formation of one of stereoisomers is associated with the fact that enzymes (dehydrogenases) distinguish the enantiotopic hydrogen atoms at the C(4) atom in the 1,4-dihydropyridine ring. The stereospecificity of the transfer of hydride-labile hydrogen was experimentally proved by studying oxidation of deuterium-labelled ethanol. Actually, after oxidation of (*R*)-1-D-ethanol, deuterium was found in the reduced form of NADD at the C(4) atom having the *R* configuration, whereas deuterium completely goes to acetaldehyde in the case of oxidation of (*S*)-1-D-ethanol.³⁰





To model natural processes, chiral substituents are deliberately introduced into synthetic dihydropyridines. In the case of formation of reactive chiral complexes, the mutual arrangement of the reactants is determined only by the structural factors. The resulting energy difference of diastereomeric transition states provides an enantiomeric excess of one of the adducts. In recent years, the regiospecific NAD–NADH conversion has been extensively studied because NADH is a necessary component of various bioorganic processes accompanied by the formation of chiral organic compounds.

As an example, let us mention stereoselective reduction of ketones, which was performed by Ohno and co-workers¹⁷⁵ with the use of specially prepared model compounds **21**. The process is characterised by high enantioselectivity.



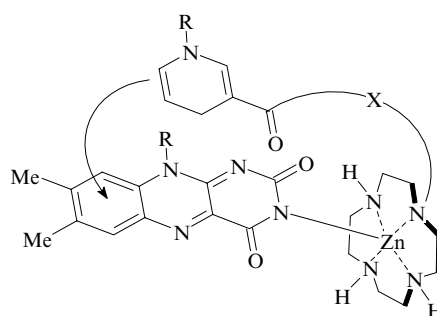
X = H, Me, OMe, Cl, Br.

The chiral recognition is provided by steric interactions along with the electronic effects of the substituents. The stereoselectivity of oxidation of NADH by *p*-quinone derivatives controlled by the electronic effect of the carbonyl group was documented.⁶³ The structural effects of the substituents at position 4 are responsible also for the reactivity of 1,4-dihydropyridines in reactions with stable radicals.⁵⁰

Quantum-chemical calculations of the potential energy surface for isomers of 2-methyl-4(*R* or *S*)-methyl-1,4-dihydropyridines in the gas phase and in solution were performed by the extended Hartree–Fock method with the 6-311 basis set.¹⁷⁶ The stereoselectivity of reduction with NADH analogues was demonstrated to be controlled by the steric and electronic properties of substituents at position 4 as well as by the solvent polarity.

Enantioselective reactions often proceed through the formation of active prochiral radical species. Numerous examples of such reactions were cited in the review.¹⁷⁷ This is indicative of the single-electron nature of reduction processes based on dihydropyridine derivatives.

Chiral NADH models providing stereoselectivity of the hydride transfer were designed based on benzo[*b*]-1,6-naphthyrindines.¹⁷⁸ A system consisting of dihydronicotinamide and a zinc complex was used for reduction of flavin.¹⁷⁹

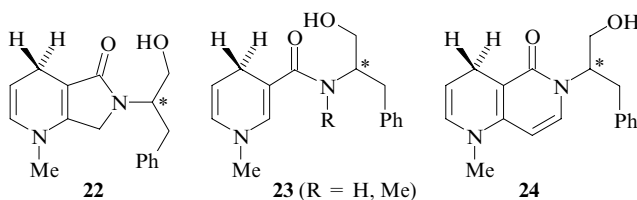


X is a chiral linking group.

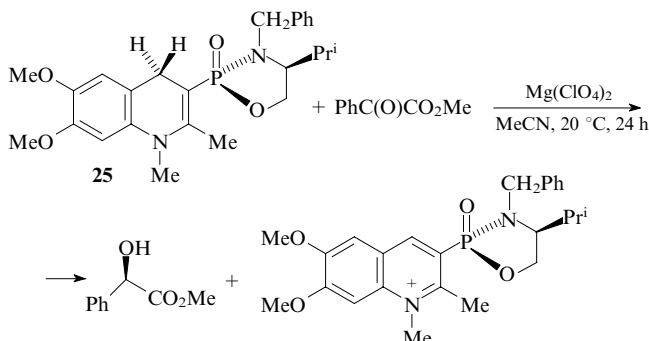
The involvement of bipyridyl complexes of ruthenium and other metals in regioselective reduction of substrates by NADH models was documented.^{180, 181}

Data on stereospecificity of the hydride transfer in NAD-dependent synthases in the antibiotic synthesis were published in the literature.¹⁸² The conformational exchange of the carbothioamide group in the hydride transfer between transhydrogenase and the thionicotinamide analogue of NADH was documented.¹⁸³ The factors influencing the stereoselectivity of the hydride transfer between the NADH model and the NO-bound cytochrome P450,¹⁵⁵ keto esters¹⁸⁴ and dehydrogenases were reported.¹⁸⁵

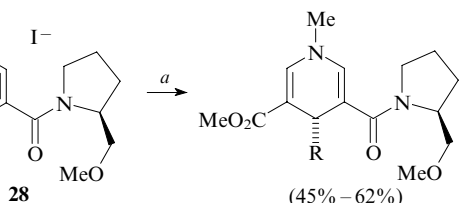
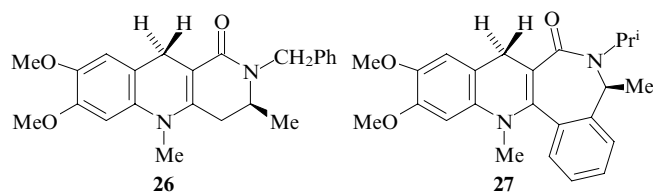
A series of studies on the synthesis and the use of chiral NADH models were performed by French researchers. Detailed NMR studies of asymmetric reduction of methyl benzoylformate by dihydropyridines **22**–**24** were carried out.¹⁸⁶



New chiral NADH models were designed based on hydrogenated quinoline.^{187–189} It appeared that electron-donating groups in the benzene ring of quinoline enhance its ability to eliminate the hydride ion, thus providing a high degree of reduction of methyl benzoylformate with quinoline in the presence of magnesium ions. The enantioselectivity of reduction is determined by the concentration of metal ions. The best results (*ee* 45%) were obtained for dihydroquinoline **25**.¹⁸⁷

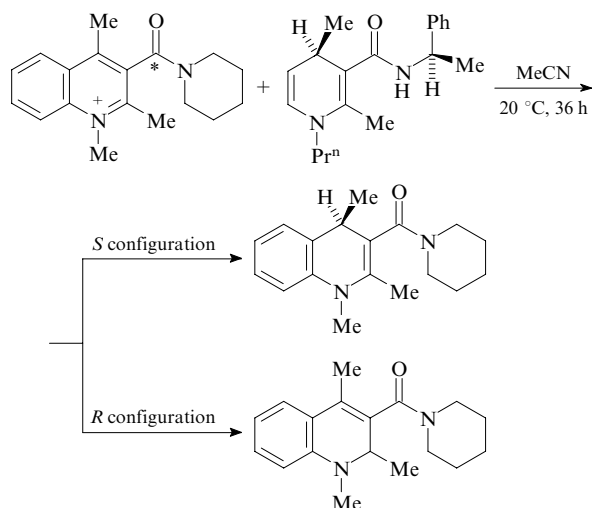


Models favourable for an increase in the stereoselectivity of the hydride transfer were synthesised based on benzo[*b*]-1,6-naphthyrindine **26**, its analogue **27**¹⁷⁸ and pyridinium salts **28**.¹⁹⁰



R = Me, Buⁿ, Ph; (a) (1) R₂CuLi, (2) (Cl₃CCO)₂O, (3) MeONa.

The optically active model NAD compound based on quinoline was reduced by chiral dihydropyridine¹⁹¹ to form a mixture of the corresponding 1,2- and 1,4-dihydroquinolines. The orientation of the carbonyl group in quinoline is responsible for regio- and enantioselectivity of the reaction products. Thus, the *S* isomer forms predominantly the chiral 1,4-adduct with *ee* 96%.



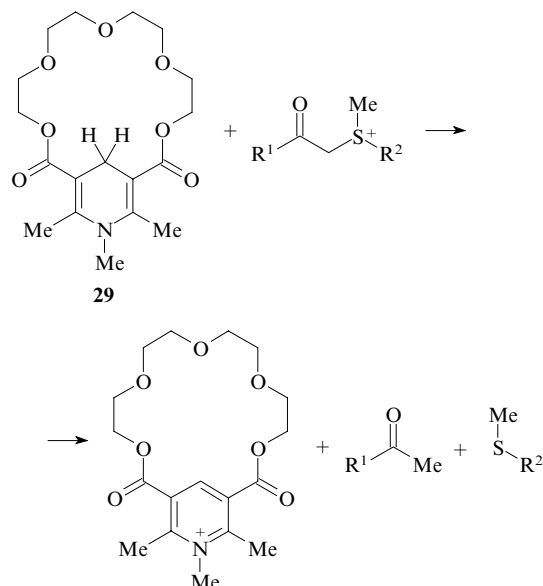
Regioselective reduction of 1-benzylnicotinamide triflate in the presence of a ruthenium bipyridyl complex was documented.¹⁹² Many bridged NADH analogues¹⁴⁷ and 1-benzyl-3-(*p*-toluenesulfonyl)-1,4-dihydropyridine derivatives¹⁹³ have high enantioselective reducing ability.

Due to ability of NADH and their synthetic models to be involved in enantioselective reactions along with their tendency to perform the single-electron transfer, dihydropyridines and their analogues are unique compounds, because the optical activity is not generally retained upon the formation of radicals.

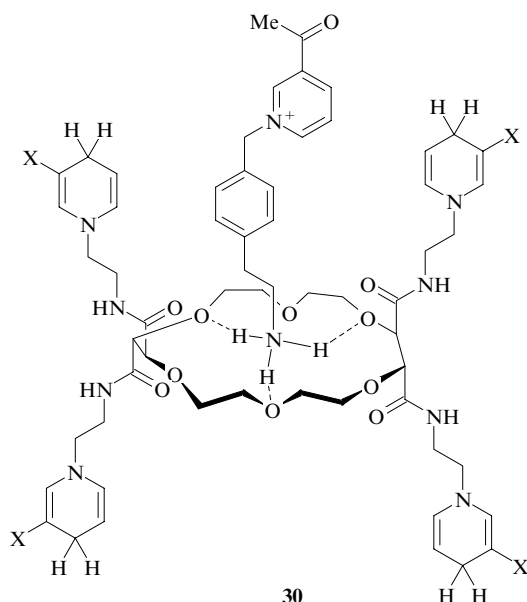
IV. Molecular devices based on dihydropyridines

Supramolecular chemistry deals with structures containing non-bonded interactions, such as hydrogen bonds, electrostatic effects, hydrophobic forces, *etc.* These interactions are responsible for fast and reversible changes of biological molecular structures, such as nucleic acids, proteins and enzymes.¹⁹⁴ In the design of supramolecular devices, studies of hydride transfer processes in chemical models of NADH, investigation of the fine mechanism of these reactions and elucidation of the structure–property relationship are of considerable interest.

For example, it was found that macrocycles containing the 1,4-dihydropyridine fragments substantially accelerate the hydrogen transfer. In the studies,^{195, 196} crown ether of dihydropyridine **29** was used as the hydride ion donor. The rate of the reaction of ether **29** with acceptors is 2700 times higher than that of the reactions of classical Hantzsch esters or 1-methyl-1,4-dihydropyridine.



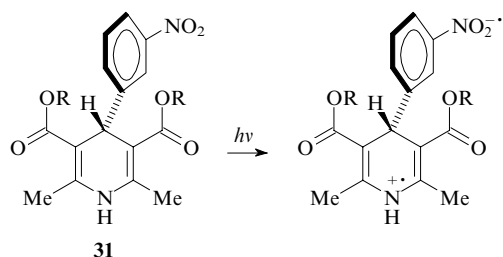
Efficient reduction of the pyridinium fragments within supramolecular compounds of type **30** through the hydrogen transfer from dihydropyridines in the peripheral positions was documented.¹⁹⁷



X = C(O)NHBuⁿ.

Such first-order intracomplex reactions are inhibited by cations capable of complex formation.¹⁹⁴ As mentioned above, the influence of metal ions or complexes on the hydrogen transfer is a characteristic feature of oxidation of dihydropyridines.

It was suggested to use 4-(*m*-nitrophenyl)dihydropyridine **31** for the design of new photoinduced intramolecular electron-transfer systems.¹⁹⁸



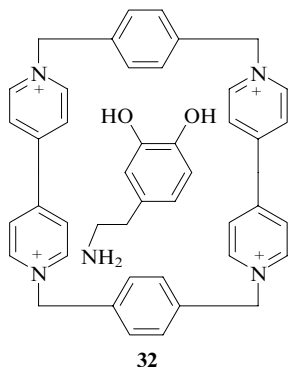
R = Alk.

Molecular magnetism is, in essence, a supramolecular phenomenon, because it is associated with the collective properties of the system components that contain unpaired electrons, and depends on the relative arrangement of these compounds in organised ensembles and crystal structures. A search for high-spin components of the organic (free radicals, carbenes or charge-transfer salts), organometallic (metal complexes) or inorganic (coordination metal centres) nature is presently an important problem.^{199–202} This is why the radical ionic salts based on dihydropyridine derivatives have attracted interest. The synthesis and the mechanism of formation of radical anionic salts in the reactions of unsubstituted acridane, *N*-methylacridane or 1-propyl-1,4-dihydropyridine with π -electron acceptors (tetracyanoquinodimethane, dicyanodichloro-*p*-benzoquinone, tetra-cyanoethylene, *etc.*) were described.²⁰³

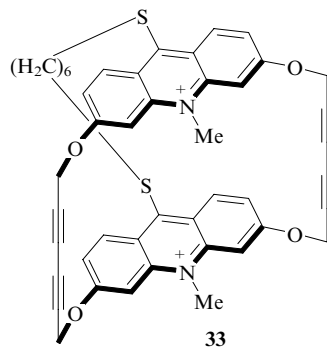
We synthesised analogous compounds by oxidation of 9-cyano-10-methyl-9,10-dihydroacridine (**11**) to the corresponding radical anionic and dianionic salts with the cyanoacridinium cation. These salts have a very narrow electrochemical gap, *i.e.*, a small difference between the reversible oxidation and reduction potentials. These systems hold promise for the design of molecular switches, conductors, semiconductors, visible light converters into the electric energy (solar elements) and, on the contrary, nonlinear optical materials, *etc.*

Hydrogen bonding, π - π -stacking interactions or Coulombic interactions can be employed for recognition of amino acids, nucleotides and heterocycles through complementary binding. It was mentioned¹⁴² that such interactions have an effect on the electron and hydride transfer involving DNA in redox reactions of DNA intercalates with NAD and NADH models.

Coulombic interactions and structural factors can be efficiently used for the recognition of systems containing the charged pyridine rings. Supramolecular charge-transfer complexes formed by cyclobis(paraquat-*p*-phenylene) as a model of a molecular receptor and different neuromediators (for example, by dopamine in compound **32**) were studied.²⁰⁴ Analogous structures were described in the publications.^{205–207}

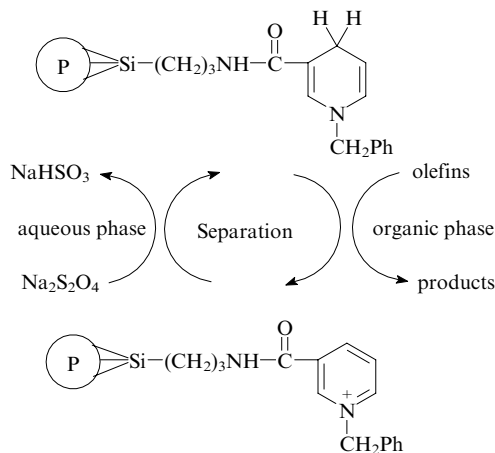


N-Methylacridinium derivatives, which are acceptors of anionic and neutral nucleophiles, can be involved in macrocyclic bis-intercalates (for example, compound **33**) capable of interacting with nucleosides, nucleotides and planar anionic substrates.^{208, 209}

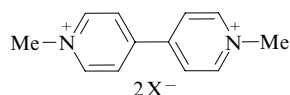


Along with homogeneous processes of molecular recognition in solution, heterogeneous recognition on the surface or in the bulk of organised ordered phases and solid materials is also known. Examples of these reactions are the formation of solid inclusion compounds, *viz.*, clathrates, with the use of zeolites or other natural sorbents, as well as intercalation in the formation of hollow clays and the design of hybrid organic–inorganic structures by sol–gel methods.¹⁹⁴ A polysiloxane-immobilised NADH model compound was prepared.²¹⁰ This compound provides easy reduction of olefins as well as isolation of the reaction products and recycling of the reducing agent. This environmentally safe process for olefin reduction by immobilised dihydropyridine in a two-phase system is an example of green chemistry (Scheme 4). Catalytic transformations of natural compounds under mild conditions, which are accompanied by the conversion of the reagents, are among such processes.²¹¹

Scheme 4

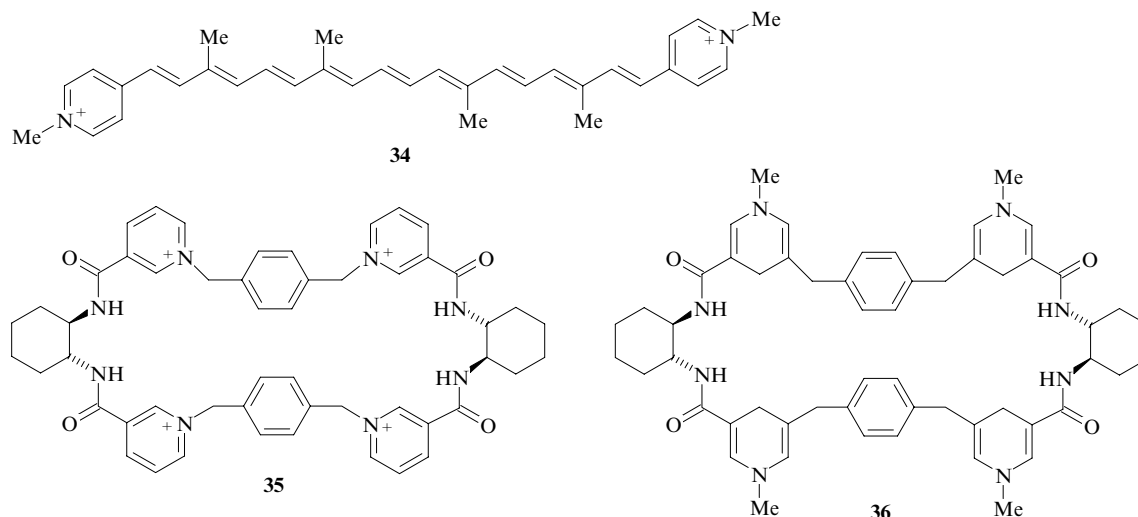


Redox processes involved in NAD–NADH transformations can be performed in molecular devices which convert molecular recognition events into electronic signals. Quinones and the 1,1'-dimethyl-4,4'-bipyridinium dication were examined as such compounds.²⁰⁷



Pyridinium cations **34** linked by a long chain of conjugated C=C bonds are fragments of so-called molecular wires.¹⁹⁴ In such oligomers, pyridinium cations are used as electron acceptors capable of forming stable radicals.

The design of supramolecular ensembles based on the 10-carboxymethyl-9-mesitylacridinium ion and the fullerene cluster with titanium(IV) oxide or tin(IV) oxide for light energy conversion was documented.^{212, 213} Systems consisting of donor–acceptor metal complexes, dihydropyridine-based hydride donors and



acceptors and acridinium cations have been designed and found use as photocatalysts.²¹⁴

Macrocyclic NADH models containing two or four nicotinamide fragments were prepared.²¹⁵ In the presence of magnesium ion as a catalyst, these macrocyclic dihydropyridines selectively reduce ethyl benzoylformate. Macrocyclic NAD (compound **35**) and NADH models (compound **36**), which can form host–guest complexes were synthesised based on the pyridinium cation and dihydropyridine.^{216, 217}

The above data demonstrate that investigations of the hydrogen transfer mechanism $\text{NAD} \rightleftharpoons \text{NADH}$ with the use of model compounds provide a deeper insight into processes in living nature and give possibilities for designing different-purpose devices, receptors and new materials.

* * *

A review of studies on oxidation of dihydropyridines and their analogues leads to the conclusion that, in spite of a continuing discussion regarding the one-step or stepwise mechanism of hydride transfer, evidence in favour of the latter mechanism prevails in the modern literature. It should be noted that the successive electron–proton–electron transfer (EPE mechanism) was accepted by chemists as the most probable pathway of hydride transfer involving coenzymes.

The Nobel laureate Albert Szent-Györgyi stated that electrons drive life. In living systems, electrons move to higher energy levels due to sunlight absorption by the substance and then electrons portionwise release an excess energy. It should be emphasised that electrons perform this cycle one-by-one by being excited and passing through cytochromes, because the central metal atom in cytochrome can undergo only single-electron transformations.²¹⁸

In recent years, studies on the fine mechanism of the $\text{C}(\text{sp}^3)\text{--H}$ bond cleavage in dihydroazines have received new impetus due to the design of new pharmaceuticals and technical materials, enzyme reactors, bioelectrochemical systems and molecular devices (switches, antennas, sensors, etc.) based on these compounds and the use of partially hydrogenated heteroarenes as reagents for stereoselective reduction of various unsaturated systems.

References

- O N Chupakhin, V N Charushin, H C van der Plas *Nucleophilic Aromatic Substitution of Hydrogen* (New York: Academic Press, 1994)
- F Terrier *Nucleophilic Aromatic Displacement. The Influence of the Nitro Group* (New York: VCH, 1991)
- D N Kozhevnikov, V L Rusinov, O N Chupakhin *Adv. Heterocycl. Chem.* **82** 261 (2002)
- S Ostrowski, N Urbńska, A Mikus *Tetrahedron Lett.* **44** 4373 (2003)
- C M A Sanches, M J Iglesias, I J P Alvarez, F L Ortiz *Tetrahedron Lett.* **44** 8441 (2003)
- M Makosza, K Wojciechowski *Chem. Rev.* **104** 2631 (2004)
- J Joule, K Mills *Heterocyclic Chemistry* (Oxford: Blackwell, 2000)
- O A Reutov, A L Kurts, K P Butin *Organicheskaya Khimiya* (Organic Chemistry) (Moscow: Binom, 2005)
- O N Chupakhin, I Ya Postovskii *Usp. Khim.* **45** 908 (1976) [*Russ. Chem. Rev.* **45** 454 (1976)]
- V N Charushin, O N Chupakhin *Usp. Khim.* **53** 1648 (1984) [*Russ. Chem. Rev.* **53** 956 (1984)]
- O N Chupakhin, V N Charushin, H C van der Plas *Tetrahedron* **44** 1 (1988)
- V N Charushin, O N Chupakhin, H C van der Plas *Adv. Heterocycl. Chem.* **43** 301 (1988)
- O N Chupakhin, V N Charushin, A I Chernyshev, in *Progress in NMR Spectroscopy* Vol. 20 (Eds J M Emsley, J Feeney, L H Sutcliffe) (Oxford, New York: Pergamon Press, 1988) p. 95
- V N Charushin, S G Alexeev, O N Chupakhin, H C van der Plas *Adv. Heterocycl. Chem.* **46** 73 (1989)
- O N Chupakhin, S G Alexeev, B V Rudakov, V N Charushin *Heterocycles* **33** 931 (1992)
- D N Kozhevnikov, V L Rusinov, O N Chupakhin *Usp. Khim.* **67** 707 (1998) [*Russ. Chem. Rev.* **67** 633 (1998)]
- O N Chupakhin, D G Beresnev *Usp. Khim.* **71** 803 (2002) [*Russ. Chem. Rev.* **71** 707 (2002)]
- V N Charushin, V L Rusinov, L I Rusinova, O N Chupakhin *Vestn. UGTU-UIPI* **37** 26 (2004)
- V N Charushin, O N Chupakhin *Pure Appl. Chem.* **76** 1621 (2004)
- I N Egorov, G V Zyryanov, V L Rusinov, O N Chupakhin *Usp. Khim.* **74** 1176 (2005) [*Russ. Chem. Rev.* **74** 1073 (2005)]
- E Kosower *Free Radicals in Biology* (Ed. W A Pryor) (New York: Academic Press, 1976)
- I Ya Postovskii, O N Chupakhin, A I Matern *Khim. Geterotsikl. Soedin.* 1299 (1984)^a
- A F Pozharskii *Teoreticheskie Osnovy Khimii Geterotsiklov* (Theoretical Foundations of Heterocyclic Chemistry) (Moscow: Khimiya, 1985)
- A Ohno *J. Phys. Org. Chem.* **8** 567 (1995)
- O Pestovsky, A Bakac, J H Espenson *J. Am. Chem. Soc.* **120** 13422 (1998)
- S Fukuzumi, K Ohkubo, Y Tokuda, T Suenobu *J. Am. Chem. Soc.* **122** 4286 (2000)
- P N Barlett, E Simon *J. Am. Chem. Soc.* **125** 4014 (2003)
- S Fukuzumi *Bull. Chem. Soc. Jpn.* **79** 177 (2006)

29. V I Slesarev *Khimiya. Osnovy Khimii Zhivogo* (Chemistry. Foundations of Chemistry of Live) (St Petersburg: Khimizdat, 2005)
30. N A Tyukavkina, Yu I Baukov *Bioorganicheskaya Khimiya* (Bioorganic Chemistry) (Moscow: Drofa, 2005)
31. S D Varfolomeev *Khimicheskaya Enzimologiya* (Chemical Enzymology) (Moscow: Akademiya, 2005)
32. S Fukuzumi *Org. Biomol. Chem.* **609** (2003)
33. O Yu Okhlobystin *Perenos Elektrona v Organicheskikh Reaktsiyakh* (Electron Transfer in Organic Reactions) (Rostov-on-Don: Rostov State University, 1974)
34. C Costentin, M Robert, J-M Savéant *J. Electroanal. Chem.* **588** 197 (2006)
35. M M Baizer (Ed.) *Organic Electrochemistry* (New York: Marcel Dekker, 1973)
36. D F Shriver, P W Atkins *Inorganic Chemistry* (Oxford: Oxford University Press, 1999)
37. M V Bazilevskii, V I Faustov *Usp. Khim.* **61** 1185 (1992) [*Russ. Chem. Rev.* **61** 651 (1992)]
38. R A Marcus *Angew. Chem., Int. Ed. Engl.* **32** 1111 (1993)
39. I Tinoko, K Sauer, J C Wang, J D Puglisi *Physical Chemistry: Principles and Applications in Biological Sciences* (New Jersey: Prentice Hall, 2002)
40. P Varnai, A Warshel *J. Am. Chem. Soc.* **122** 3849 (2000)
41. H C Lo, R H Fish *Angew. Chem., Int. Ed.* **41** 478 (2002)
42. R Reichenbach-Klinke, M Kruppa, B Konig *J. Am. Chem. Soc.* **124** 12999 (2002)
43. S R Billeter, S P Webb, P K Agarwal, T Iordanov, S Hammes-Schiffer *J. Am. Chem. Soc.* **123** 11262 (2001)
44. I Rostov, S Hammes-Schiffer *J. Chem. Phys.* **115** 285 (2001)
45. S Hammes-Schiffer *Curr. Opin. Struct. Biol.* **14** 192 (2004)
46. S Hammes-Schiffer *Chem. Phys. Chem.* **3** 33 (2002)
47. I-S H Lee, K-H Chow, M M Kreevoy *J. Am. Chem. Soc.* **124** 7755 (2002)
48. X-Q Zhu, Y Liu, B-J Zhao, J-P Cheng *J. Org. Chem.* **66** 370 (2001)
49. X-Q Zhu, H-L Zhou, P-W Yuan, Y Liu, L Cao, J-P Cheng *J. Chem. Soc., Perkin Trans. 2* 1857 (2000)
50. C Yañez, C López-Alarcón, C Camargo, V Valanzuela, J A Squella, L J Nuñez-Vergara *Bioorg. Med. Chem.* **12** 2459 (2004)
51. Y Lu, Y Zhao, K L Handoo, V D Parker *Org. Biomol. Chem.* **1** 173 (2003)
52. D E Berning, B C Noll, D L DuBois *J. Am. Chem. Soc.* **121** 11432 (1999)
53. S Fukuzumi, O Inada, T Suenobu *J. Am. Chem. Soc.* **125** 4808 (2003)
54. S Fukuzumi, S Koumitsu, K Hironaka, T Tanaka *J. Am. Chem. Soc.* **109** 305 (1987)
55. X-Q Zhu, H R Li, Q Li, T Ai, J V Lu, Y Yang, J-P Cheng *Chem. – Eur. J.* **9** 871 (2003)
56. X-Q Zhu, Y Yang, M Zhang, J-P Cheng *J. Am. Chem. Soc.* **125** 15298 (2003)
57. J K Kochi *Adv. Phys. Org. Chem.* **29** 185 (1994)
58. M Chanon, M Rajzmann, F Chanon *Tetrahedron* **46** 6193 (1990)
59. J-P Cheng, Y Lu, X-Q Zhu, L Mu *J. Org. Chem.* **63** 6108 (1998)
60. N Scherbak, A Strid, L A Eriksson *Chem. Phys. Lett.* **414** 243 (2005)
61. T Matsuo, J M Mayer *Inorg. Chem.* **44** 2150 (2005)
62. G-X He, A Blasko, T C Bruce *Bioorg. Chem.* **21** 423 (1993)
63. A Ohno, Y Ishikawa, N Yamazaki, M Okamura, Y Kawai *J. Am. Chem. Soc.* **120** 1186 (1998)
64. H R Memarian, A Mirjafari *Bioorg. Med. Chem. Lett.* **15** 3423 (2005)
65. B Han, Z Liu, Q Liu, L Yang, Z-L Liu, W Yu *Tetrahedron* **62** 2492 (2006)
66. C A Coleman, J G Rose, C J Murray *J. Am. Chem. Soc.* **114** 9755 (1992)
67. P van Eikeren, D Grier *J. Am. Chem. Soc.* **99** 8057 (1977)
68. A K Colter, G Saito, F J Sharom *Can. J. Chem.* **55** 2741 (1977)
69. J J Steffens, D M Chipman *J. Am. Chem. Soc.* **93** 6694 (1971)
70. D M Chipman, R Yaniv, P van Eikeren *J. Am. Chem. Soc.* **102** 3244 (1980)
71. L I Belen'kii, I S Poddubnyi, M M Krayushkin *Khim. Geterotsikl. Soedin.* **830** (1995)^a
72. K K Park, H-G Kim, J W Park *Bull. Korean Chem. Soc.* **10** 448 (1989)
73. A Ohno, S Yasui, H Yamamoto, S Oka, Y Ohnishi *Bull. Chem. Soc. Jpn.* **51** 294 (1978)
74. A Ohno, H Kobayashi, T Goto, S Oka *Bull. Chem. Soc. Jpn.* **57** 1279 (1984)
75. L L Miller, J R Valentine *J. Am. Chem. Soc.* **110** 3982 (1988)
76. A Ohno, T Kimura, H Yamamoto, S G Kim, S Oka, Y Ohnishi *Bull. Chem. Soc. Jpn.* **50** 1535 (1977)
77. S Itoh, H Kumei, S Nagatomo, T Kitagawa, S Fukuzumi *J. Am. Chem. Soc.* **123** 2165 (2001)
78. S Fukuzumi, K Ohkubo, T Okamoto *J. Am. Chem. Soc.* **124** 14147 (2002)
79. S Fukuzumi, J Yuasa, T Suenobu *J. Am. Chem. Soc.* **124** 12566 (2002)
80. S Fukuzumi, T Okamoto, Y Tokuda, C P Gros, R Guillard *J. Am. Chem. Soc.* **126** 17059 (2004)
81. D J Astles, M Girard, D Griller, R J Kolt, D D M Wayner *J. Org. Chem.* **53** 6053 (1988)
82. F Silber, C Bräuchle, N Hampp *J. Electroanal. Chem.* **390** 83 (1995)
83. P Ramesh, S Sampath *Anal. Chem.* **72** 3369 (2000)
84. S H Baik, C Kang, I C Jeon, S E Yun *Biotechnol. Techniq.* **13** 1 (1999)
85. P de los Santos-Álvarez, P G Molina, M J Lobo-Castañón, A J Miranda-Ordieres, P Tuñón-Blanco *Electroanalysis* **14** 1543 (2002)
86. P de los Santos-Álvarez, M J Lobo-Castañón, A J Miranda-Ordieres, P Tuñón-Blanco *Electroanalysis* **16** 881 (2004)
87. S M Golabi, L Irannejad *Electroanalysis* **17** 985 (2005)
88. A S Santos, L Gorton, L T Kubota *Electroanalysis* **14** 805 (2002)
89. F-D Munteanu, D Dicu, I C Popescu, L Gorton *Electroanalysis* **15** 383 (2003)
90. R Katakya, E Morgan *Biosens. Bioelectron.* **18** 1407 (2003)
91. J Hendle, A F Buckmann, W Achle, D Schomburg, R D Schmidt *Eur. J. Biochem.* **213** 947 (1993)
92. Ya R Uldrikis, A O Kumerova, G Ya Dubur *Khim. Geterotsikl. Soedin.* 691 (1973)^a
93. L C Kurz, J L Kurz *Eur. J. Biochem.* **90** 283 (1978)
94. J Klima, L Kurfurst, L Kuthan, J Volke *Tetrahedron Lett.* **18** 2725 (1977)
95. Ya P Stradyn, Yu I Beilis, G Ya Duburs, T Ya Slonskaya *Izv. Akad. Nauk Latv. SSR, Ser. Khim.* 372 (1978)
96. I M Sosonkin, V A Subbotin, V N Charushin, O N Chupakhin *Dokl. Akad. Nauk SSSR* **229** 888 (1976)^b
97. J Moiroux, S Deycard, T Malinski *J. Electroanal. Chem.* **194** 99 (1985)
98. J Ludvic, J Volke, J Klima *Electrochim. Acta* **32** 1063 (1987)
99. V I Shilov, O N Chupakhin, I M Sosonkin, V A Subbotin *Zh. Org. Khim.* **16** 202 (1980)^c
100. T Sturm, H Kiese, E Daltrozzi *Chem. Ber.* **111** 227 (1978)
101. P Hapiot, J Moiroux, I M Saveant *J. Am. Chem. Soc.* **112** 1337 (1990)
102. S Fukuzumi, Y Tokuda, T Kitano, T Okamoto, Y Otera *J. Am. Chem. Soc.* **115** 8960 (1993)
103. I M Sosonkin, O N Chupakhin, A I Matern *Zh. Org. Khim.* **15** 1976 (1979)^c
104. J W Happ, E G Janzen *J. Org. Chem.* **35** 96 (1970)
105. A R Katritzky, A F Pozharski *Handbook of Heterocyclic Chemistry* (New York: Pergamon Press, 2000) p. 216
106. O N Chupakhin, I M Sosonkin, A I Matern, G N Strogov *Dokl. Akad. Nauk SSSR* **250** 875 (1980)^b
107. O N Chupakhin, V N Charushin, I M Sosonkin, E G Kovalev, G L Kalb, I Ya Postovskii *Khim. Geterotsikl. Soedin.* 90 (1977)^a
108. O N Chupakhin, V I Shilov, V F Gryazev *Khim. Geterotsikl. Soedin.* 1136 (1979)^a
109. S Tamagaki, M Ueno, W Tagaki *Bull. Chem. Soc. Jpn.* **65** 55 (1992)
110. O N Chupakhin *Izv. Sib. Otd. Akad. Nauk SSSR, Ser. Khim.* **46** (1980)
111. M Jin, D Zhang, L Yang, Y Liu, Z Liu *Tetrahedron Lett.* **41** 7357 (2000)

112. I M Magin, A I Kruppa, T V Leshina, V Lúsis, D Muceniece *J. Photochem. Photobiol. A* **155** 119 (2003)
113. A Marcinek, J Adamus, K Huben, J Gebicki, T J Bartczak, P Bednarek, T Bally *J. Am. Chem. Soc.* **122** 437 (2000)
114. A Marcinek, J Rogowski, J Adamus, J Gebicki, P Bednarek, T Bally *J. Phys. Chem. A* **104** 718 (2000)
115. J Gebicki, A Marcinek, J Adamus *Wiadomosci Chem.* **56** 397 (2002)
116. I Nakanishi, C Nishizawa, K Ohkubo, K Takeshita, K T Suzuki, T Ozawa, S M Hecht, M Tanno, S Sueyoshi, N Miyata, H Okuda, S Fukuzumi, N Ikota, K Fukuhara *Org. Biomol. Chem.* **3** 3263 (2005)
117. A Ohno, N Kito *Chem. Lett.* 369 (1972)
118. S Fukuzumi, O Inada, N Satoh, T Suenobu, H Imahori *J. Am. Chem. Soc.* **124** 9181 (2002)
119. A I Matern, V V Yanilkin, V N Nastapova, V I Morozov, V N Charushin, O N Chupakhin *Izv. Akad. Nauk, Ser. Khim.* 1444 (2006)^d
120. I M Sosonkin, A I Matern, O N Chupakhin *Khim. Geterotsikl. Soedin.* 1377 (1983)^a
121. E C Ashby, R N De Priest, T N Pham *Tetrahedron Lett.* **24** 2825 (1983)
122. W F Hendrickson Jr, W D McDonald, S T Howard, E J Coligato *Tetrahedron Lett.* **26** 2939 (1985)
123. K Ohkubo, S Fukuzumi *Org. Lett.* **2** 3647 (2000)
124. S Fukuzumi, K Ohkubo, T Suenobu, K Kato, M Fujitsuka, O Ito *J. Am. Chem. Soc.* **123** 8459 (2001)
125. K Ohkubo, K Suga, K Morikawa, S Fukuzumi *J. Am. Chem. Soc.* **125** 12850 (2003)
126. S Fukuzumi, S Fujita, T Suenobu, H Imahori, Y Araki, O Ito *J. Phys. Chem. A* **106** 1465 (2002)
127. S Fukuzumi, O Inada, T Suenobu *J. Am. Chem. Soc.* **124** 14538 (2002)
128. D Zhang, L-Z Wu, L Zhou, X Han, Q-Z Yang, L-P Zhang, C-H Tung *J. Am. Chem. Soc.* **126** 3440 (2004)
129. N A Klyuev, U S Brodskii *Ros. Khim. Zh.* (4) 57 (2002)^e
130. V G Zaikin, A V Varlamov, A I Minaya *Mass-spektrometriya Organicheskikh Soedinenii* (Mass Spectrometry of Organic Compounds) (Moscow: Nauka, 2001)
131. N A Klyuev, V G Baklykov, V N Charushin, O N Chupakhin *Khim. Geterotsikl. Soedin.* 532 (1989)^a
132. O N Chupakhin, V G Baklykov, N A Klyuev, A I Matern *Khim. Geterotsikl. Soedin.* 1083 (1989)^a
133. H Park, G G Girdaukas, D B Northrop *J. Am. Chem. Soc.* **128** 1868 (2006)
134. R A Dick, T W Kensler *J. Biol. Chem.* **279** 17269 (2004)
135. D J Rodrigues, J D Venning, P G Quirk, J B Jackson *Eur. J. Biochem.* **268** 1430 (2001)
136. M Yamaguchi, C D Stout, Y Hatefi *J. Biol. Chem.* **277** 33670 (2002)
137. C Carra, N Iordanova, S Hammes-Schiffer *J. Am. Chem. Soc.* **125** 10429 (2003)
138. A Ohno, T Kimura, S Oka, Y Ohnishi, M Kagami *Tetrahedron Lett.* **16** 2371 (1975)
139. O Almarsson, T C Bruice *J. Am. Chem. Soc.* **115** 2125 (1993)
140. L P Olson, T C Bruice *Biochemistry* **34** 7335 (1995)
141. I Nakanishi, S Fukuzumi, T Konishi, K Ohkubo, M Fujitsuka, O Ito, N Miyata *J. Phys. Chem. B* **106** 2372 (2002)
142. M Nishimine, K Ohkubo, T Komori, S Fukuzumi *Chem. Commun.* 1886 (2003)
143. S Fukuzumi, K Yukimoto, K Ohkubo *J. Am. Chem. Soc.* **126** 12794 (2004)
144. J B Lackson, S J Peake, S A White *FEBS Lett.* **464** 1 (1999)
145. E C Stevenson, P L Spedding *J. Chem. Technol. Biotechnol.* **65** 286 (1999)
146. B R Riebel, P R Gibbs, W B Wellborn, A S Bommarius *Adv. Synth. Catal.* **345** 707 (2003)
147. N Kanomata, T Nakata *J. Am. Chem. Soc.* **122** 4563 (2000)
148. M Zlatovic, D Sladic, M J Gasic *J. Serb. Chem. Soc.* **64** 647 (1996)
149. S Fukuzumi, M Tanaka, M Nishimine, K Ohkubo *J. Photochem. Photobiol., A* **175** 79 (2005)
150. H J Lee, J Basran, N S Scrutton *Biochemistry* **37** 15513 (1998)
151. B Nidetzky, M Klimacek, P Mayr *Biochemistry* **40** 10371 (2001)
152. Z Anusevičius, J Šarlauskas, N Čėnas *Arch. Biochem. Biophys.* **404** 254 (2002)
153. I Nogues, I Perez-Dorado, S Frago, C Bittel, S G Mayhew, C Gomez-Moreno, J A Hermoso, M Medina, N Cortez, N Carrillo *Biochemistry* **44** 11730 (2005)
154. R Neeli, O Roitel, N S Scrutton, A W Munro *J. Biol. Chem.* **280** 17634 (2005)
155. R Oshima, S Fushinobu, F Su, L Zhang, N Takaya, H Shoun *J. Mol. Biol.* **342** 207 (2004)
156. D C Lamb, Y Kim, L V Yermalitskaya, V N Yermalitsky, G L Lepesheva, S L Kelly, M R Waterman, L M Podust *Structure* **14** 51 (2006)
157. G Tirzitis, E Kazush, G Duburs *Khim. Geterotsikl. Soedin.* 355 (1998)^a
158. A Hilgeroth, A Billich, H Lilie *Eur. J. Med. Chem.* **36** 367 (2001)
159. A Hilgeroth *Mini Rev. Med. Chem.* **2** 235 (2002)
160. A Hilgeroth, H Lilie *Eur. J. Med. Chem.* **38** 495 (2003)
161. S Broussy, V Bernardes-Genisson, A Quemard, B Meunier, J Bernadou *J. Org. Chem.* **70** 10502 (2005)
162. T J Sullivan, J J Truglio, M E Boyne, P Novichenok, X Zhang, C F Stratton, H-J Li, T Kaur, A Amin, F Johnson, R A Slayden, C Kisker, P J Tonge *ACS Chem. Biol.* **1** 43 (2006)
163. S Fukuzumi, H Miyao, K Ohkubo, T Suenobu *J. Phys. Chem. A* **109** 3285 (2005)
164. A Hilgeroth, G Hempel, U Baumeister, D Reichert *Magn. Reson. Chem.* **37** 376 (1999)
165. O Ishitani, S Yanagida, S Takamuku, C Pac *J. Org. Chem.* **52** 2790 (1987)
166. S Yamada, C Morita *J. Am. Chem. Soc.* **124** 8184 (2002)
167. J I Bardagi, S E Vaillard, R A Rossi *Tetrahedron Lett.* **47** 3149 (2006)
168. S S C Chu, R D Rosenstein *Acta Crystallogr., Sect. B* **35** 480 (1979)
169. H Jiang, Y-C Liu, J Li, G-W Wang, Y-D Wu, Q-M Wang, T C W Mak *Chem. Commun.* 882 (2002)
170. T Suzuki, A Migita, H Higuchi, H Kawai, K Fujiwara, T Tsuji *Tetrahedron Lett.* **44** 6837 (2003)
171. H Jiang *Chin. Chem. Lett.* **15** 159 (2004)
172. J Preuss, V Zanker, A Gieren *Acta Crystallogr., Sect. B* **33** 2317 (1977)
173. O M Huta, I O Patsaj, A Konitz, J Meszko, J Blazejowski *Acta Crystallogr., Sect. C* **58** o295 (2002)
174. E L Eliel *Elements of Stereochemistry* (New York: Wiley, 1971)
175. S Yasui, K Nakamura, A Ohno, S Oka *Bull. Chem. Soc. Jpn.* **55** 196 (1982)
176. H Zhong, J P Bowen *J. Mol. Graph. Model.* **24** 1 (2005)
177. M P Sibi, S Manyem, J Zimmerman *Chem. Rev.* **103** 3263 (2003)
178. J-L Vasse, V Levacher, J Bourguignon, G Dupas *Tetrahedron: Asymmetry* **13** 227 (2002)
179. S C Ritter, M Eiblmaier, V Michlova, B König *Tetrahedron* **61** 5241 (2005)
180. H Konno, K Sakamoto, O Ishitani *Angew. Chem., Int. Ed.* **39** 4061 (2000)
181. A Kobayashi, R Takatori, I Kikuchi, H Konno, K Sakamoto, O Ishitani *Organometallics* **20** 3361 (2001)
182. Z Huang, K Kakinuma, T Eguchi *Bioorg. Chem.* **33** 82 (2005)
183. A Singh, J D Vennig, P G Quirk, G I van Boxel, D J Rodrigues, S A White, J B Jackson *J. Biol. Chem.* **278** 33208 (2003)
184. U Vitinius, K Schaffner, M Demuth *J. Photochem. Photobiol. A* **169** 197 (2005)
185. B Bhushan, A Halasz, J Hawari *Biochem. Biophys. Res. Commun.* **337** 1080 (2005)
186. C Vitry, J Bédar, Y Prigent, V Levacher, G Dupas, I Salliot, G Quéguiner, J Bourguignon *Tetrahedron* **57** 9101 (2001)
187. J-L Vasse, S Goumain, V Levacher, G Dupas, G Quéguiner, J Bourguignon *Tetrahedron Lett.* **42** 1871 (2001)
188. C Vitry, J-L Vasse, G Dupas, V Levacher, G Quéguiner, J Bourguignon *Tetrahedron* **57** 3087 (2001)
189. S Leleu, C Papamicaäl, F Marsais, G Dupas, V Levacher *Tetrahedron: Asymmetry* **15** 3919 (2004)
190. M-L Bennasar, E Zulaica, Y Alonso, J Bosch *Tetrahedron: Asymmetry* **14** 469 (2003)
191. Y Mikata, S Aida, S Yano *Org. Lett.* **6** 2921 (2004)

192. H C Lo, C Leiva, O Buriez, J B Kerr, M M Olmstead, R H Fish *Inorg. Chem.* **40** 6705 (2001)
193. J Li, Y-C Liu, J-G Deng, X-Z Li, X Cui, Z Li *Tetrahedron: Asymmetry*, **11** 2677 (2000)
194. J-M Lehn *Supramolecular Chemistry. Concepts and Perspectives* (Weinheim: VCH, 1995)
195. T J van Bergen, R M Kellogg *J. Am. Chem. Soc.* **99** 3882 (1977)
196. R M Kellogg *Angew. Chem.* **96** 769 (1984)
197. J-P Behr, J-M Lehn *J. Chem. Soc., Chem. Commun.* 143 (1978)
198. E Fasani, M Fagnjini, D Dondi, A Albini *J. Org. Chem.* **71** 2037 (2006)
199. V I Ovcharenko, R Z Sagdeev *Usp. Khim.* **68** 381 (1999) [*Russ. Chem. Rev.* **68** 345 (1999)]
200. V T Kalinnikov, Yu V Rakitin, V M Novotortsev *Usp. Khim.* **72** 1123 (2003) [*Russ. Chem. Rev.* **72** 995 (2003)]
201. S P Gubin, Yu A Koksharov, G B Khomutov, G Yu Yurkov *Usp. Khim.* **74** 539 (2005) [*Russ. Chem. Rev.* **74** 489 (2005)]
202. E A Karakhanov, A L Maksimov, E A Runova *Usp. Khim.* **74** 104 (2005) [*Russ. Chem. Rev.* **74** 97 (2005)]
203. G Saito, A K Colter *Tetrahedron Lett.* **18** 3325 (1977)
204. A R Bernardo, J F Stoddart, A E Kaifer *J. Am. Chem. Soc.* **114** 10624 (1992)
205. M B Nielsen, J O Jeppesen, J Lau, C Lomholt, D Damgaard, J P Jacobsen, J Becher, J F Stoddart *J. Org. Chem.* **66** 3559 (2001)
206. G Doddi, G Ercolani, P Mencarelli, A Piermattei *J. Org. Chem.* **70** 3761 (2005)
207. P-N Cheng, P-Y Huang, W-S Li, S-H Ueng, W-C Hung, Y-H Liu, C-C Lai, Y Wang, S-M Peng, I Chao, S-H Chiu *J. Org. Chem.* **71** 2373 (2006)
208. S Claude, J-M Lehn, F Schmidt, J-P Vigneron *J. Chem. Soc., Chem. Commun.* 1182 (1991)
209. M Žinić, P Čidić, V Škarić, J-P Vigneron, J-M Lehn *Tetrahedron Lett.* **33** 7417 (1992)
210. B Zhang, X-Q Zhu, J-Y Lu, J He, P G Wang, J-P Cheng *J. Org. Chem.* **68** 3295 (2003)
211. O N Chupakhin, V N Charushin, in *Zelenaya Khimiya v Rossii* (Green Chemistry in Russia) (Eds V V Lunin, P Tundo, E S Lokteva) (Moscow: Moscow State University, 2004) p. 24
212. T Hasobe, S Hattori, H Kotani, K Ohkubo, K Hosomizu, H Imahori, P V Kamat, S Fukuzumi *Org. Lett.* **6** 3103 (2004)
213. T Hasobe, S Hattori, P V Kamat, Y Wada, S Fukuzumi *J. Mater. Chem.* 372 (2005)
214. S Fukuzumi, H Imahori, K Okamoto, H Yamada, M Fujitsuka, O Ito, D M Guldi *J. Phys. Chem. A* **106** 1903 (2002)
215. U Gran, O Wennerström, G Westman *Tetrahedron: Asymmetry* **11** 3027 (2000)
216. U Gran, O Wennerström, G Westman *Tetrahedron* **57** 8897 (2001)
217. U Gran *Tetrahedron* **59** 4303 (2003)
218. A Szent-Györgyi *Submolecular Biology* (New York: Academic Press, 1960)

^a — *Chem. Heterocycl. Compd. (Engl. Transl.)*

^b — *Dokl. Chem. (Engl. Transl.)*

^c — *Russ. J. Org. Chem. (Engl. Transl.)*

^d — *Russ. Chem. Bull., Int. Ed. (Engl. Transl.)*

^e — *Mendeleev Chem. J. (Engl. Transl.)*

Radical chemistry of iron carbonyls

Yu A Belousov

Contents

I. Introduction	41
II. Iron carbonyl radical anions	42
III. Reactions of iron carbonyls with Lewis bases. Activating complex formation	43
IV. Reactions of (hydrido)carbonylferrate anions with Brønsted and Lewis acids	45
V. Reactions of iron carbonyls with carbonylferrate anions	47
VI. Nucleophilic substitution and catalytic conversions of iron carbonyls induced by electron transfer	48
VII. Iron carbonyls as reducing agents	48
VIII. Catalytic processes involving iron carbonyl radical anions	49
IX. Reactions with possible involvement of iron carbonyl complexes	50
X. Redox disproportionation of transition metal carbonyls	51
XI. Conclusion	54

Abstract. It is shown that catalytic carbonylation of various compounds using iron carbonyl complexes is based on two types of reactions [redox disproportionation of iron carbonyl induced by Lewis bases and oxidative addition of Brønsted and Lewis acids to (hydrido)carbonylferrate anions] comprising single-electron initiation steps and subsequent radical chain reactions. The role of iron carbonyl radical anions as catalysts for carbonylation processes with controlled reduction potential of the medium is noted. Characteristic features of the radical chemistry of iron and other transition metal carbonyls is analysed. The bibliography includes 262 references.

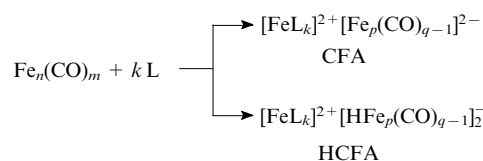
I. Introduction

The chemistry of transition element carbonyls has been developed for more than a century since the initial discovery in 1890 of complexes of transition metals with CO ligands, first, nickel tetracarbonyl¹ and then iron pentacarbonyl.^{2,3} The discovery of the Fischer–Tropsch process for hydrocarbon synthesis from synthesis gas (CO + H₂)^{4–7} and hydroformylation of organic compounds made a major impact on the development of this field of chemistry.⁸ Metal carbonyls are used as catalysts in all these processes. The development of homogeneous catalytic systems for the Reppe synthesis and the replacement of synthesis gas by water gas (CO + H₂O)⁹ may be regarded as the major achievements of these studies. As far as carbon monoxide is a key component of the CO + H₂ and CO + H₂O gas mixtures, the mechanism of catalysis by transition element-based catalysts should be governed by the chemistry of metal carbonyls. Owing to the structural and chemical similarities between a metal surface with adsorbed CO molecules and carbonyl metal complexes, the latter can be

regarded as simple models of catalytic processes, because studies of heterogeneous transformations are often extremely labour-consuming (see for example Refs 5–7, 10 and 11).

It is quite possible that in the nearest future the humankind will solve the energy problem by using renewable sources of energy instead of oil and gas; however there is no substitute for hydrocarbons in the industrial organic synthesis. The problem of alternative sources of raw materials for petrochemical industry will inevitably arise as the world oil supply gradually diminishes.^{5,6,12} Hydrocarbons and other organic products obtained from CO may be such an alternative. In spite of some successful examples of application of CO conversion processes, in most cases they cannot compete with the petrochemical ones for economic reasons. The main problem is lack of inexpensive and selective catalysts for operation under mild conditions. The search for such catalysts requires a detailed investigation of the reactions of various coordination compounds with CO. The iron carbonyl complexes are regarded as the most promising ones, as they are readily available, stable and highly catalytically active in a variety of transformations.

In the early 1930s, Hieber and co-workers started to study the properties of iron carbonyls, particularly their reactions with Lewis bases (cited from^{13,14}). They have shown that the two-electron redox disproportionation is the predominant pathway of these reactions. This process results in the formation of Fe²⁺ salts with carbonyl-ferrate dianions (CFA) and (or) with their protonated analogues, hydridocarbonyl-ferrate monoanions (HCFA).



$n = 1, m = 5; n = 2, m = 9; n = 3, m = 12; p = 1, q = 5; p = 2, q = 9; p = 3, q = 12; p = 4, q = 14; 2 \leq k \leq 6; \text{L}$ is a nucleophilic ligand (a neutral Lewis base).

Yu A Belousov A N Nesmeyanov Institute of Organoelement Compounds, Russian Academy of Sciences, ul. Vavilova 28, 119991 Moscow, Russian Federation. Fax (7-495) 135 50 85, tel. (7-495) 135 92 21, e-mail: belyur@ineos.ac.ru

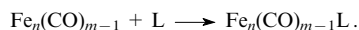
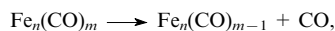
Received 18 July 2006

Uspekhi Khimii 76 (2) 46–65 (2007); translated by D S Yufit

Besides, these reactions may yield the products of substitution of nucleophilic ligands for the CO groups. Rearrangements of the metal core accompanied by the change in the number of metal

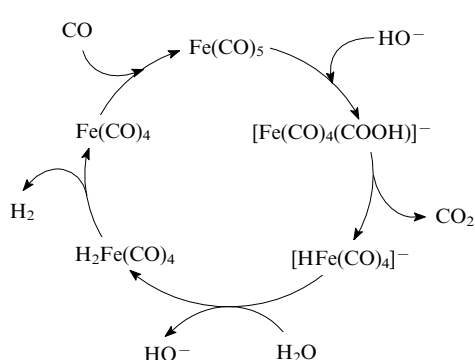
atoms in a cluster also may take place in these reactions. Numerous iron carbonyl complexes containing various functional groups have been obtained nowadays.^{15, 16}

Studies of the mechanisms of transformations of iron carbonyls are crucial for elucidation of their catalytic activity. The mechanisms are usually described by schemes that include 16-electron coordinatively unsaturated species. Thus, the following sequence of reactions was suggested for substitution processes:^{2, 5, 14–16}



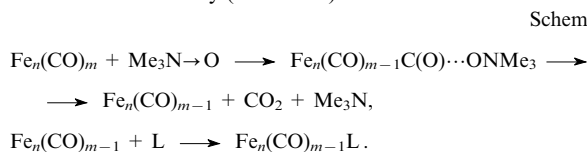
$n = 1, m = 5; n = 2, m = 9; n = 3, m = 12$; L is a nucleophilic ligand.

The catalytic scheme of water–gas shift reaction (Scheme 1) suggested by Pettit and co-workers^{17, 18} is another example of transformations catalysed by iron carbonyl complexes. The same scheme with only minor variations was also used by the same authors for the description of the mechanism of Reppe synthesis. The most general and complete version of this scheme has been published by King *et al.*^{19, 20} The nucleophilic addition of a base to a carbonyl ligand takes place at the first stage of the catalytic cycle, which is followed by decarboxylation and the formation of hydridocarbonylferrate anion. The Scheme contains two redox reactions.



Scheme 1

The substitution of nucleophilic ligands for the CO groups during the activation of iron carbonyls by trimethylamine oxide proceeds in a similar way (Scheme 2).^{21–24}



Scheme 2

The three abovementioned schemes are unified by a common paradigm, which has been formed over more than a century, concerning the major role of 16-electron intermediate species in the transformations of metal carbonyls. The paradigm is formulated as the Tolman rule,²⁵ which states that the predominant pathway of these reactions consists of consecutive formation of 18-, 16- and 18-electron complexes ($18e \rightarrow 16e \rightarrow 18e$).

The formation of 16-electron coordinatively unsaturated species, for example $\text{Fe}(\text{CO})_4$, is postulated on the basis of their detection by IR spectroscopy in the gas phase^{26, 27} and in noble gas matrices at 4–20 K.^{28–31} However, only recently, was the existence of $\text{Fe}(\text{CO})_4$ in a solution registered by femtosecond IR spectroscopy during UV photolysis of iron pentacarbonyl. The lifetime of such species is 660 ps (6.6×10^{-10} s).^{32, 33} Obviously, special experimental conditions of flash photolysis and the so short lifetime of iron tetracarbonyl cast doubt upon its participation in the processes in the liquid phase.

II. Iron carbonyl radical anions

Alongside with neutral and charged iron carbonyl complexes containing an even number of electrons, iron derivatives with an odd number of electrons may also exist. We are talking about iron carbonyl radical anions (ICRA) $[\text{Fe}_n(\text{CO})_m]^{-\cdot}$ ($n = 1, m = 5$; $n = 3, m = 12$) and $[\text{Fe}_n(\text{CO})_{m-1}]^{-\cdot}$ ($n = 1, m = 5$; $n = 2, m = 9$; $n = 3, m = 12$; $n = 4, m = 14$), which may be generated by various methods.

Electrochemical single-electron reduction of iron carbonyls in various solvents leading to the formation of ICRA has been studied by polarography using dropping mercury electrodes^{34–39} and by cyclic voltammetry using platinum,^{37–41} gold^{42, 43} and glassy-carbon electrode.³⁹

Iron carbonyl radical anions were also obtained by chemical methods: either by reactions of iron carbonyls with strong reducing agents such as alkali metals or sodium benzophenone ketyl,^{44–46} or by oxidation of carbonylferrate anions by, for example, ferrocenium or silver salts.^{46, 47} Iron carbonyl radical anions are formed also during UV or ⁶⁰Co γ -irradiation of the corresponding iron carbonyls or CFA.^{43, 45, 48–52}

The formation of $[\text{Fe}(\text{CO})_4]^{-\cdot}$ in noble gas matrices at low temperatures has been observed in the same experiments in which the 16-electron $\text{Fe}(\text{CO})_4$ species have been registered.^{31, 53, 54} In order to suppress the formation of mono- and polynuclear iron carbonyl radical anions, a stabilising agent, namely, 0.02% of CCl_4 , has been added to the system (the mechanism of stabilisation is discussed in Section VII).³¹ The $[\text{Fe}(\text{CO})_4]^{-\cdot}$ radical anion in Ne or Ar matrices has C_{3v} symmetry and its IR spectrum exhibits a CO absorption band at 1859.7 cm^{-1} (in Ne) or at 1853.5 cm^{-1} (in Ar).^{31, 48, 53, 54}

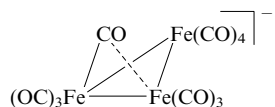
Only the signals of terminal CO groups [$\nu_{\text{CO}} = 2057 \text{ (vw)},^\dagger$ 2017 (w), 1984 (vw), 1966 (m), 1922 cm^{-1} (w, sh)]^{55, 56} are present in the IR spectra of $[\text{Fe}_3(\text{CO})_{11}]^{-\cdot}$ in THF, while in a solution in aqueous THF in the presence of NaOH, the spectrum changes [$\nu_{\text{CO}} = 2057 \text{ (vw)}, 2019 \text{ (vw, sh)}, 1982 \text{ (vw)}, 1969 \text{ (m)}, 1960 \text{ (m, sh)}, 1933 \text{ (w)}, 1916 \text{ cm}^{-1}$ (w, sh)].⁵⁷

The ESR spectra of iron carbonyl radical anions in different solvents at various temperatures were studied in a number of papers.^{38, 44–46, 49, 58, 59} The ESR spectral parameters of ICRA and their hydrido analogues (g -factor and hyperfine splitting constants a on the ¹H, ¹³C and ⁵⁷Fe nuclei) are given in Table 1.

The iron carbonyl radical anions in which one or several CO groups are replaced by phosphine or phosphite ligands are also known.^{37, 44, 45, 60, 61}

Low-temperature ESR-spectroscopic studies of ICRA in crystalline matrices and solid solutions have been performed.^{47, 50–52, 62, 63}

The most stable iron carbonyl radical anion, $[\text{Fe}_3(\text{CO})_{11}]^{-\cdot}$, has been isolated as bis(triphenylphosphine)iminium (PPN^+) and $[\text{PPh}_4]^+$ salts and characterised by elemental and X-ray diffraction analysis. The X-ray study has shown that the anion consists of a triangular core of iron atoms with one semibridging and ten terminal CO ligands.^{55, 56}



The photoelectron spectra of the $[\text{Fe}(\text{CO})_4]^{-\cdot}$ radical anion have been reported,^{64–66} and its reactivity towards various compounds in the gas phase was studied by mass spectroscopy and ion cyclotron resonance.^{67–70} Besides, clusterisation of ICRA in the

[†] The following notation is used for the band intensities in the IR spectra: v. is very, w. is weak, s is strong, m. is medium; sh (shoulder) is a signal superimposed as a shoulder on another signal.

Table 1. ESR data of some ICRA and its hydride analogues.

Species	<i>g</i>	<i>a</i> /mT (the number of nuclei)			Temperature /°C	Solvent	Ref.
		¹ H	¹³ C	⁵⁷ Fe			
[Fe(CO) ₄] ^{−•} (1)	2.0486				−80	THF, MeTHF	43, 49
[Fe ₂ (CO) ₈] ^{−•} (2)	2.0385			3.7 (2)	−80	THF	46
[Fe ₃ (CO) ₁₁] ^{−•} (3)	2.0497			5.2 (1)	−80	THF	46
[Fe ₃ (CO) ₁₂] ^{−•} (4)	2.0016		3.55 (12)	3.1 (3)	−80	THF	46
[Fe ₄ (CO) ₁₃] ^{−•} (5)	2.0134		16.2 (3), 14.2 (3), 2.5 (6), 7.9 (1)	1.27 (3), 5.8 (1)	−80	THF	46
[HFe(CO) ₄] [•] (6)	2.0545	22.60 (1)			−110	n-C ₅ H ₁₂	49
[HFe ₂ (CO) ₈] [•] (7)	2.0122	22.22 (1)	12.37 (2)		−110	n-C ₅ H ₁₂	49
	2.0120	22.2 (1)	12.3 (2)	3.60 (2)	−100	n-C ₅ H ₁₂ , cyclo-C ₃ H ₆	58
						n-C ₅ H ₁₂	49
[HFe ₃ (CO) ₁₁] [•] (8)	2.0641	18.95 (1)	10.0 (3)		−80	THF	58
	2.0635	18.4 (1)			−80	THF	58
[H ₃ Fe(CO) ₃] [•]	2.0459	24.9 (2), 2.9 (1)			−80	n-C ₅ H ₁₂	49
H ₃ Fe ₂ (CO) ₇ [•]	2.0161	16.7 (1), 5.0 (2)			−80	n-C ₅ H ₁₂	49
[H ₂ Fe(CO) ₃] ^{−•} (9)	2.0529	22.2 (2)			−110	MeTHF	59
[H ₂ Fe ₂ (CO) ₇] ^{−•} (10)	2.0435	22.4 (2)			−80	MeTHF	59
[H ₂ Fe ₃ (CO) ₁₀] ^{−•} (11)	2.0489	24.2 (2)			−40	MeTHF	59

Note. MeTHF is 2-methyltetrahydrofuran.

reactions of [Fe(CO)₄]^{−•} with iron pentacarbonyl in the gas phase were studied^{71–73} and IR spectra of the clusters formed were obtained.⁷⁴

Thus, on the one hand, we have got 16-electron intermediate complexes, formed during iron carbonyl transformations, which are short-lived and ghostly ‘as the Cheshire cat smile’ (the comparison was made by Poliakoff, one of the founders of this field of chemistry). On the other hand, the relatively stable ICRA resulting from single-electron reduction of iron carbonyls, are regarded at best as by-products of processes involving iron carbonyls.

III. Reactions of iron carbonyls with Lewis bases. Activating complex formation

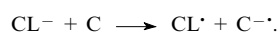
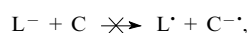
During investigation of the reactions of iron carbonyls with various Lewis bases in anionic or neutral form, it was found that radical anions are easily generated in an ESR spectrometer cavity even at early stages of reactions at low conversions of the initial complexes.^{75–79} Nevertheless, the concentrations of the ICRA were relatively high (10^{−5}–10^{−2} mol litre^{−1}).

Naturally, these data may be interpreted as evidence in favour of single-electron reduction of iron carbonyls similar to the electrochemical reduction or to the action of strong reducing agents such as the sodium mirror and sodium benzophenone ketyl. However, the Lewis bases used (supposed electron donors) may hardly be regarded as reducing agents, because their oxidation potentials are too high (for example, these values for Cl[−] and HO[−] in acetonitrile are equal to +2.24 and +0.92 V, respectively⁸⁰). These processes have to be interpreted as anomalous reactions proceeding ‘against the potential’, which are similar to the reactions between *p*-quinones and bases studied by Pedersen.⁸¹

The concept of the ‘activating complex formation’ was suggested by Abakumov^{82,83} to explain the mechanisms of this type of reactions. As applied to iron carbonyls, this concept may be formulated as follows: if a donor L[−] (a Lewis base in its anionic form) is unable to reduce directly an acceptor C (an iron carbonyl) but forms a complex CL[−], which becomes a reducing agent with respect to the initial iron carbonyl molecule, then a single-electron process becomes possible (Scheme 3).

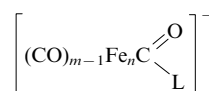
The Lewis bases used are, most often, quite simple molecules (or ions) containing localised σ-bonds without a π-electronic conjugated system. Elimination of an electron from such a compound results in a significant change in the atomic charge of

Scheme 3



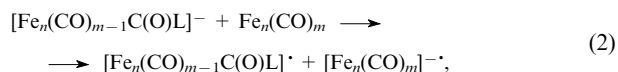
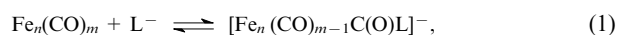
the ‘key’ atom. This process is energetically unfavourable. On the contrary, the CL[−] complex formed acquires donor properties and electron elimination stabilises the complex due to delocalisation.

The activating complex formation for the reactions of iron carbonyls with Lewis bases consists of the addition of the base to the carbonyl group.



The structure of such adducts is well known (see, for example, the review⁸⁴). The kinetics of formation of hydroxycarbonyl (L = OH) and methoxycarbonyl (L = OMe) iron complexes in solution has been studied.^{85–87} The thermodynamic and kinetic aspects of the formation of such derivatives in the gas phase are described in papers.^{67,88–92}

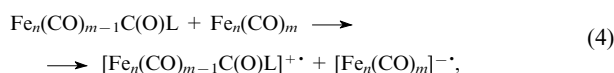
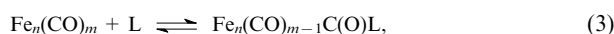
In some cases it is possible to isolate an adduct of an iron carbonyl with Lewis base. This fact was used to confirm the second redox step in Scheme 3. Thus, the salt (PPN)[Fe(CO)₄.C(O)OMe] has been isolated.^{86,93} No ESR signals have been observed for this salt in solution, as for the initial iron pentacarbonyl. The reaction of the salt with iron pentacarbonyl directly in the cavity of an ESR spectrometer reveals that fast reduction of the iron carbonyl yielding ICRA takes place even at temperatures below −80 °C. The type of ESR spectrum and the character of its gradual change are similar to those for the reaction of Fe(CO)₅ with sodium methoxide.⁷⁷ Therefore, the reaction of iron carbonyl with anionic Lewis bases may be represented as follows:



n = 1, *m* = 5; *n* = 2, *m* = 9; *n* = 3, *m* = 12.

This scheme of formation of radical anions is general and does not depend on the type of iron carbonyl or Lewis bases. A great number of anionic Lewis bases in the form of sodium derivatives NaL [$\text{L} = \text{OR}, \text{SR}, \text{NR}_2, \text{CR}_2\text{NO}_2$ ($\text{R} = \text{H}, \text{Alk}, \text{Ph}$)], alkali metal and complex cation salts M^+L^- (M is an alkali metal, PPN, NR_4 ; $\text{L} = \text{H}, \text{F}, \text{Cl}, \text{Br}, \text{I}, \text{CN}, \text{SCN}, \text{N}_3, \text{MeCO}_2, \text{CF}_3\text{CO}_2, \text{MeSO}_3, \text{NO}_2$) as well as sodium salts of dianions $\text{S}^{2-}, \text{CO}_3^{2-}, \text{SO}_4^{2-}$ have been studied in the reactions with $\text{Fe}(\text{CO})_5$, $\text{Fe}_2(\text{CO})_9$ and $\text{Fe}_3(\text{CO})_{12}$.^{76–79} Tetrahydrofuran, 2-methyltetrahydrofuran, diethyl ether, monoglyme, dioxane, methylene chloride, methanol, ethanol and THF–water (10:1 by volume) were used as solvents.⁷⁸

Redox disproportionation of iron carbonyls induced by neutral Lewis bases is much more difficult. Particularly, the interaction of $\text{Fe}(\text{CO})_5$ with neutral bases ($\text{ROH}, \text{RSH}, \text{R}_2\text{NH}$) yields a set of radicals, which is virtually identical to that formed in the reactions of anionic forms; however the process is considerably slower and takes place only at high temperature.⁷⁷ The rate of ICRA generation may be lower due to both a smaller equilibrium constant of the first step of activating complex formation [reaction (3)] and the additional energy expenditure for the generation and separation of charges during the second, redox stage of the process [reaction (4)].



$n = 1, m = 5; n = 2, m = 9; n = 3, m = 12$.

Besides the abovementioned reactions, the reactions of iron carbonyls with standard solvents and reagents, such as pyridine, DMF, DMSO, *o*-phenanthroline⁷⁷ and trimethylamine oxide⁷⁹ were studied by ESR. All these neutral Lewis bases possess electron-donating properties.

A study on the rates of reactions between Lewis bases and $\text{Fe}(\text{CO})_5$, $\text{Fe}_2(\text{CO})_9$ and $\text{Fe}_3(\text{CO})_{12}$ has shown that the rate is the lowest for $\text{Fe}(\text{CO})_5$ and the highest for $\text{Fe}_3(\text{CO})_{12}$. The difference is a result of the higher reduction potential ($E_{1/2\text{red}}$) for $\text{Fe}_3(\text{CO})_{12}$ (which is in the range from -0.32 to -0.44 V)^{38, 39} in comparison with that for $\text{Fe}(\text{CO})_5$ ($E_{1/2\text{red}} = -1.77$ V).³⁹ The electron transfer step [reactions (2) and (4)] proceeds much easier for $\text{Fe}_3(\text{CO})_{12}$ for this reason. Probably, the heterogeneity of the $\text{Fe}_2(\text{CO})_9\text{--L}$ (or L^-) system does not affect the process rate in this particular case. The electron transfer from the activated complex formed to the neighbouring iron carbonyl molecule [reactions (2) and (4)] proceeds on the surface of a crystal and is accompanied by charge delocalisation over the crystal, thus reducing the energy required for the process and compensating the diffusion limitations.

Thus, the scheme comprising a complex formation stage followed by the transfer of one electron from the activated complex to another substrate molecule may be regarded as general for the disproportionation reactions of iron carbonyls with Lewis bases.

However, for a long time there has been no answer to the main question: 'Do the radicals take part in the reaction or are they just by-products?' In order to solve this problem, kinetic studies of the reactions of iron carbonyls with various Lewis bases have been performed. The following conclusions may be drawn from the obtained data:

1. The initial stage of the interaction of iron carbonyls with Lewis bases is a reversible bimolecular reaction having the first order with respect to each of the components,^{84, 86, 87, 94} which consists of activating complex formation [reaction (1)]. The subsequent processes are multistep.^{86, 95}

2. A scheme of transformations including (according to the Tolman rule²⁵) the formation of 16-electron coordinatively unsaturated species of the $\text{Fe}(\text{CO})_4$ type underlay all kinetic calculations.

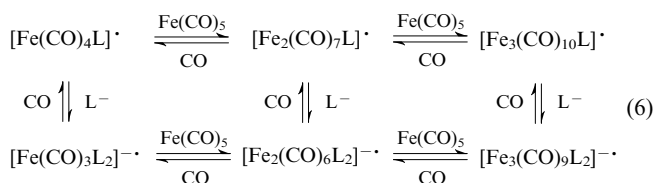
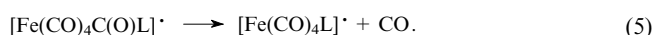
3. Methods that determine only the parameters of the initial reactants and final reaction products were used in kinetic studies of the multistep processes. (The complexes with the bases formed at the first step of the reaction were an exception.) The absence of the kinetic data on the intermediate catalytically active species makes such schemes look like a 'black box' (*i.e.*, the change of the input parameters results in the change in the output parameters, but there is no way to find out what is going on inside the box).

The radical chain mechanism of the process was first proved by studying the kinetics of accumulation and loss of the intermediate radical species, namely, iron carbonyl radical anions.⁹⁶ A well studied reaction of iron dodecacarbonyl with tetraethylammonium ethanethiolate in THF was used as a model. For this reaction, the structures of intermediate radical species^{77, 97} and final products are known.⁹⁸ The reaction was carried out directly in the cavity of an ESR spectrometer in a flow system using the stopped flow method. It was shown⁹⁶ that the experimental results on the kinetics of accumulation and loss of intermediate radical anions **3** and **4** correspond well to the calculated ones. These calculations were based on the suggested mechanism of two-step redox formation of ICRA [reactions (1) and (2)].

The iron in complexes with Lewis bases formed in reactions (2) and (4) are in the formal oxidation states (+1) and (−1), respectively.[‡] These complexes initiate two chains of transformations caused by substitution reactions in the coordination sphere of the radicals. Whereas $\text{Fe}(-1)$ radicals are intrinsically stable and easily detectable, the registration of $\text{Fe}(+1)$ radicals is much more challenging, because such complexes (the iron configuration is d^7) are usually extremely unstable. In the case of hard Lewis bases (L), the coordination sphere of the carbonyl complex is destabilised with elimination of CO ligands and oxidation of the iron atom to Fe^{2+} . This gives inorganic compounds of the FeL_2 type (L is an anion) or salts of the $[\text{FeL}_k]^{2+}$ cation (L is a neutral base).^{13, 14} Stabilisation of the coordination sphere of an iron carbonyl complex becomes possible in the case of soft Lewis base L (or in the case of transition of hard base into a soft one, *e.g.*, NO_2^- into NO^{76}) or when the η -bonding of ligand L with the metal core increases during the reaction. Sometimes such iron(+1) radicals may be detected by ESR either directly or as spin adducts.^{76, 99}

The radical complexes $[\text{Fe}(\text{CO})_{5-n}\text{L}_n]^{+ \cdot}$ ($n = 1, 2$), in which one or two CO groups are replaced by phosphine or phosphite ligands are most stable.^{100–103} The complex $[\text{Fe}(\text{CO})_3(\text{PPh}_3)_2] \cdot [\text{PF}_6] \cdot 0.5 \text{CH}_2\text{Cl}_2$ has been isolated¹⁰⁰ and characterised by X-ray crystallography.¹⁰⁴

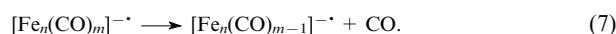
The reactions of iron carbonyls with sodium hydrosulfide and thiolates, which may be regarded as soft Lewis bases, are suitable for the detection of radical complexes of $\text{Fe}(+1)$. These bi- and trinuclear radical anions of the $[\text{Fe}_2(\text{CO})_6(\text{SR})_2]^{- \cdot}$ and $[\text{Fe}_3(\text{CO})_9(\text{SR})_2]^{- \cdot}$ types formed in the reaction with $\text{Fe}(\text{CO})_5$ may be detected.^{77, 97} The number of metal atoms may change as a result of exchange of the CO ligands with the starting iron carbonyl or the L^- ion. These processes take place in the coordination sphere of the initially formed $\text{Fe}(+1)$ complexes [reaction (2)].^{77, 105}



[‡] Strictly speaking, the oxidation stages should be noted as $+(1/n)$ and $-(1/n)$, where n is the number of iron atoms in the corresponding species. One should keep this in mind when regarding the designations used in this review.

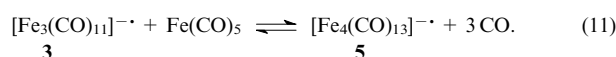
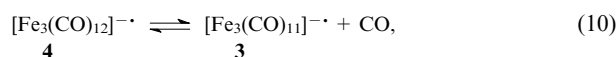
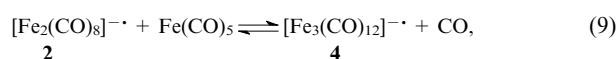
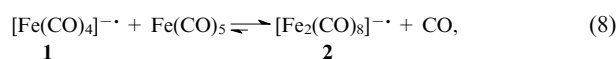
In this situation, $\text{Fe}(\text{CO})_5$ acts as a peculiar spin trap stabilising the radical $\text{Fe}(\text{I})$ complex by delocalisation of the unpaired electron over the iron carbonyl fragment. The subsequent oxidation, which happens during either disproportionation or catalysis, and substitution by electron transfer (ETC mechanism, see Section VI), yields the final diamagnetic products. The sequences of the reactions (6) represent the case where no transitions of the L^- ligand in the metal coordination sphere take place. The delocalisation of the unpaired electron on the ligand makes possible the reorganisation (reduction, oxycarbonyl bond formation, *etc.*) of this ligand followed by coordination of the modified ligands. The formation of bi- and polynuclear iron complexes with unusually coordinated modified ligands is well known.^{106, 107}

As it was mentioned before, the reactions of iron carbonyls with Lewis bases generate unstable (with exception of radical anion **4**, see Table 1) electron-rich ICRA $[\text{Fe}_n(\text{CO})_m]^-$. These ICRA are formed during single-electron redox disproportionation [reactions (2), (4)]. The ICRA are transformed into more stable electron-deficient species $[\text{Fe}_n(\text{CO})_{m-1}]^{2-}$ by decarbonylation. According to the Sedgwick's rule of closed 18-electron configuration, the transition from 19- to 17-electron complexes takes place during this process:⁸

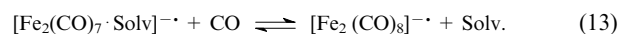
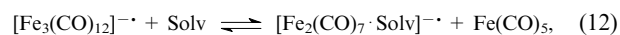


Usually, the formation of ICRA **2–5** is observed in any combination of the starting iron carbonyl and the base.^{76–79} Differences are only in the succession of their generation and consumption at various stages of the process. For example, in the reactions of $\text{Fe}(\text{CO})_5$ with the bases, the radical anions are generated in the sequence **1**, **2**, **4** and **3**, **5**. The mononuclear radical anion **1** was detected at the initial stages of the reaction of $\text{Fe}(\text{CO})_5$ with strong bases, such as NaOMe and NaOEt , in 2-methyltetrahydrofuran at -100°C .⁷⁸ In similar reactions of $\text{Fe}_3(\text{CO})_{12}$ the radical anions **3**, **4** are produced first and the radicals **2**, **5** are formed later. Species **2** is generated initially in the heterogeneous system containing $\text{Fe}_2(\text{CO})_9$; radical anions **3–5** emerge at later stages. Similar succession of ICRA generation was observed during the reduction of iron carbonyls over a sodium mirror.⁴⁶ The equilibrium between ICRA **2–5** with the trinuclear radical anion **3** as the major component was observed at room temperature when the reaction was performed in a closed system, *e.g.*, in a sealed ampoule. Higher temperature shifts the equilibrium towards the species containing more metal atoms. At the same time the ESR signals of species **2–5** appear and become dominant during the generation of penta- and hexanuclear $[\text{Fe}_5\text{C}(\text{CO})_{14}]^{2-}$ and $[\text{Fe}_6\text{C}(\text{CO})_{16}]^{2-}$ radical anions in the temperature range from -30°C to 50°C .⁷⁷

The coordination sphere of iron carbonyl radical anions **1–5** is quite labile and capable of fast ligand and electron exchange. This enables interconversions of radical ion clusters



Donor compounds, particularly the solvent molecules (Solv), may take part in these processes¹⁰⁴



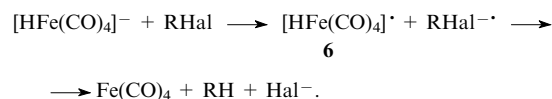
The reactions (8)–(11) represent a sort of radical-ion ‘oligomerisation’ of iron pentacarbonyl in solution. The same reaction may take place in the gas phase.^{72–74} The reverse process, namely, a catalytic conversion of $\text{Fe}_3(\text{CO})_{12}$ into $\text{Fe}(\text{CO})_5$ by electron transfer, has been described.¹⁰⁸

Being labile electron-deficient species, ICRA **1**, **2**, **3** and **5** tend to fill their electronic shells. Therefore, in the reactions of iron carbonyls with Lewis bases they convert into carbonylferrate dianions $[\text{Fe}_n(\text{CO})_{m-1}]^{2-}$, containing 18, 34, 48 and 60 cluster valence electrons for $n = 1, 2, 3$ and 4 respectively. The unstable intermediate complexes of $\text{Fe}(\text{I})$ mentioned above may act as reducing agents for iron carbonyl radical anions.⁷⁷

Thus, in general, the reactions of iron carbonyls with Lewis acids proceed as two-electron disproportionations and afford traditional products of these transformations, the CFA salts.^{13, 14}

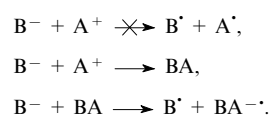
IV. Reactions of (hydrido)carbonylferrate anions with Brønsted and Lewis acids

The (hydrido)carbonylferrate anion–Brønsted (or Lewis) acid system is the antipode of the previously discussed iron carbonyl–Lewis base system. It is very important to note that most of the carbonylation processes are catalysed by one of these systems.^{19, 20, 84, 109, 110} Besides, the interaction of CFA and HCFA with Brønsted and Lewis acids may take place in non-catalytic processes as well, namely, in stoichiometric reactions giving aldehydes, ketones, carboxylic acids, esters and amides,¹¹¹ α -diketones,¹¹² and in the reduction of α, β -unsaturated carbonyl compounds.^{113, 114} The iron carbonyl radical species were detected in early investigations of these reactions, but not identified, and this explains the interest in these processes.^{113, 115} For example, the radicals are formed during the direct reduction of an alkyl halide (Lewis acid) by HCFA.^{116, 117}



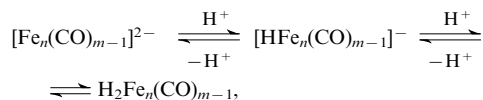
The formation of a 16-electron intermediate species of the $\text{Fe}(\text{CO})_4$ type is traditionally suggested in this reaction, as in Schemes 1 and 2. The existence of this species in solution has been discussed in the Introduction. Besides, the direct reduction of RHal is also thermodynamically unlikely and possible only in the case of aromatic iodides with the smallest negative reduction potentials.^{109, 118} Intensive generation of ICRA **2–5** in the reactions of CFA and HCFA with Lewis and Brønsted acids has been observed by ESR spectroscopy.⁵⁹ These radical anions are identical to those formed in the reactions of iron carbonyls with Lewis bases. The hypothesis of ‘activating complex formation’, used previously to explain the mechanism of the reactions of iron carbonyls with Lewis bases (see Section 3), has been used to explain this fact too. The only difference between these two cases is that CFA or HCFA play a donor role (B^-), while their complexes (BA) with the acid (A^+) are acceptors. If the donor (CFA or HCFA) cannot directly reduce an acceptor (an acid), but the formation of their complex is still possible, then this complex may take part in a single-electron transfer, which thus becomes achievable (Scheme 4).

Scheme 4



[§]In fact, the electron shells of ICRA **1–5** contain 17, 33, 47, 49 and 59 cluster valence electrons respectively. The 18-electron closed shell configuration rule is conventionally accepted for clarity and in order to compare the complexes with different numbers of metal atoms.

According to Scheme 4, the activating complex formation stage corresponds to the well known processes: either the protonation of CFA or HCFA



$n = 1, m = 5; n = 2, m = 9; n = 3, m = 12; n = 4, m = 14;$

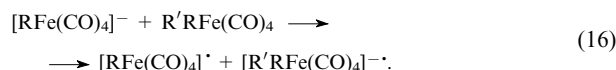
or the oxidative addition of alkyl and acyl halides to them^{15, 93, 109, 111, 113, 119–124}



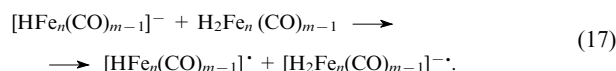
$\text{R} = \text{H}; \text{R}' = \text{Alk}, \text{AlkC}(\text{O}); \text{R} = \text{R}' = \text{Alk}, \text{Ar}, \text{AlkC}(\text{O}), \text{ArC}(\text{O});$
 $\text{X} = \text{Cl}, \text{Br}, 4\text{-MeC}_6\text{H}_4\text{SO}_2 (\text{Ts}).$

The reactions (14) and (15) are given for well studied mononuclear iron complexes, which are most active in the redox transformations affecting the metal coordination centres.[¶]

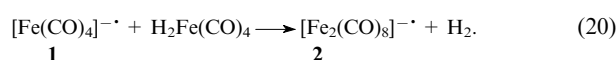
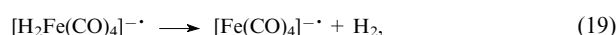
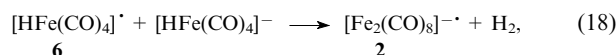
The electron transfer itself happens at the next step during the reduction of the formed neutral complex $\text{R}'\text{RFe}(\text{CO})_4$



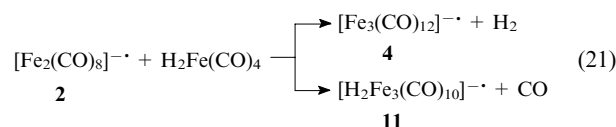
A similar electron transfer stage for protonated complexes CFA looks as follows:



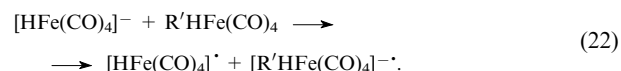
The pure starting compounds without any traces of the oxidation products are required in order to confirm that the electron transfer occurs during this stage of the reaction. This was achieved, for example, by vacuum distillation of complex $\text{H}_2\text{Fe}(\text{CO})_4$ [$\text{R} = \text{R}' = \text{H}$ in reaction (16) or $n = 1, m = 5$ in reaction (17)] directly into an ampoule located in the cavity of an ESR spectrometer.⁵⁹ No ESR signals were observed in a solution of $\text{H}_2\text{Fe}(\text{CO})_4$ in 2-methyltetrahydrofuran at temperatures below -60°C . A similar situation has been found in the case of a solution of $(\text{PPN})[\text{HFe}(\text{CO})_4]$ in MeTHF over a wide range of temperatures up to room temperature. At the same time, the reaction of $\text{H}_2\text{Fe}(\text{CO})_4$ with $(\text{PPN})[\text{HFe}(\text{CO})_4]$ in this solvent results in the appearance of ICRA signals at as low as -100°C . It was shown,⁵⁹ that 17-electron radical $[\text{HFe}(\text{CO})_4]^\cdot$ and 19-electron radical anion $[\text{H}_2\text{Fe}(\text{CO})_4]^{-\cdot}$, formed at the electron-transfer stage of the reaction, are unstable under these conditions and are quickly converted into $[\text{Fe}_2(\text{CO})_8]^{-\cdot}$ by reactions (18) and (19), respectively.



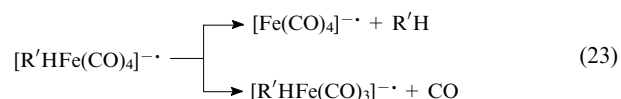
Radical anions **3–5, 11** containing greater numbers of metal atoms arise in reactions (21) and (9)–(11).



The transformations of $\text{RR}'\text{Fe}(\text{CO})_4$ complexes ($\text{R} = \text{H}, \text{R}' = \text{Alk}, \text{Ac}$) should be particularly noted. These are the key compounds in many processes involving $[\text{HFe}(\text{CO})_4]^-$ (Ref. 106). In this case, reaction (16) is as follows:

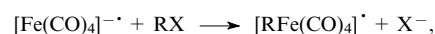


The unstable 19-electron complex $[\text{R}'\text{HFe}(\text{CO})_4]^{-\cdot}$ formed initially is transformed into the more stable 17-electron species by elimination of $\text{R}'\text{H}$ or CO [reaction (23)]. In the latter case, the $[\text{R}'\text{HFe}(\text{CO})_3]^{-\cdot}$ radical anions are formed. They were detected in the reactions of acyl halides $\text{R}'\text{X}$ ($\text{R}' = \text{Ac}, \text{Bz}$) with $[\text{HFe}(\text{CO})_4]^-$ (Ref. 59).

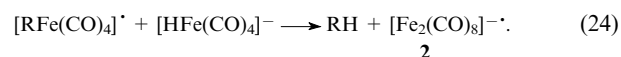


It is remarkable that the $[\text{R}'\text{Fe}(\text{CO})_4]^-$ and $[\text{HFe}(\text{CO})_4]^-$ anions do not react with each other. For instance, propionaldehyde is not formed in the reaction between $[\text{EtC}(\text{O})\text{Fe}(\text{CO})_4]^-$ and $[\text{HFe}(\text{CO})_4]^-$; however it is formed in 57% yield when the acetic acid, which partially protonates the $[\text{HFe}(\text{CO})_4]^-$, is added to the reaction mixture.¹²⁵ This confirms that the process proceeds according to pathway (22). The yield of the target compound, which is approximately half of the theoretical one, points out to the partial protonation of $[\text{HFe}(\text{CO})_4]^-$ and its consumption according to reactions (16) (for $\text{R} = \text{R}' = \text{H}$) and (18)–(20).

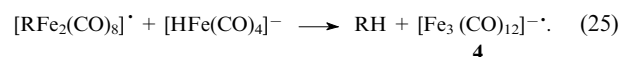
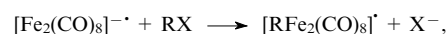
As it was noted before, on the one hand, ICRA are relatively stable species (during the reaction their steady-state concentrations may be fairly high). On the other hand, these ICRA are coordinatively unsaturated electron-deficient systems with labile coordination sphere capable of fast ligand and electron exchange. An important consequence of these two characteristics is the ability of ICRA to add Brønsted or Lewis acids. These reactions are the key stages in a number of reduction and carbonylation processes of various compounds. Initially, the radical anion reacts with an electron acceptor (the corresponding acid):



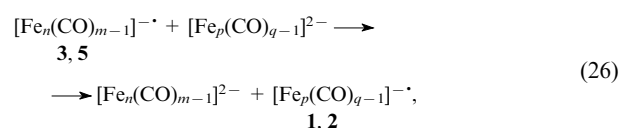
and then, similarly to reaction (18), species **2** are formed.



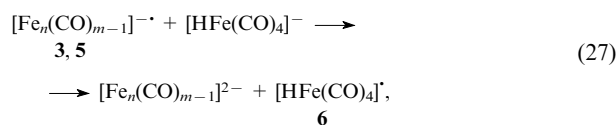
The subsequent transformations of the ICRA are of the radical chain type and are accompanied by the increase in the number of metal atoms in the radical complex:



Radical anions **3** and **5** are reduced to corresponding CFA by reactions (26) and (27) at the final stages of the interaction of (hydrido)carbonylferrate anions with Brønsted and Lewis acids. The reduction potentials of these CFA make the processes thermodynamically favourable.^{42, 126}



¶ Tri- and tetranuclear CFA can be alkylated and acylated at the carbonyl group resulting in the formation of the $[\text{Fe}_n(\text{CO})_{m-2}(\text{COR})]^-$ ($\text{R} = \text{Me}, \text{Ac}; n = 3, m = 12; n = 4, m = 14$) complexes, which mainly tend to undergo transformations of the carbonyl ligand.¹⁵



$n = 3, m = 12$ (3); $n = 4, m = 14$ (5); $p = 1, q = 5$ (1); $p = 2, q = 9$ (2).

The final products of the reaction are diamagnetic compounds, mainly the modified organic ligands and polynuclear CFA and HCFA.

Thus, the reactions of (hydrido)carbonylferrate anions with the Brønsted and Lewis acids, like the reactions of iron carbonyls with Lewis bases, may be described as radical chain processes which include the preliminary activating complex formation and the redox initiation stage.

V. Reactions of iron carbonyls with carbonylferrate anions

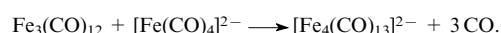
It is believed that the nucleophilic displacement of the CO groups in the reactions of diamagnetic iron carbonyls and carbonylferrate anions results in the formation of CFA with an increased number of metal atoms. Thus, the reaction of $\text{Fe}(\text{CO})_5$ with $[\text{Fe}(\text{CO})_4]^{2-}$ yields $[\text{Fe}_2(\text{CO})_8]^{2-}$ [reaction (28)].^{42, 43, 113, 127–129}



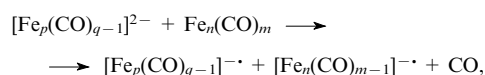
The $[\text{Fe}_3(\text{CO})_{11}]^{2-}$ anion is formed from $\text{Fe}(\text{CO})_5$ and $[\text{Fe}_2(\text{CO})_8]^{2-}$ (Ref. 127)



while the reaction of $[\text{Fe}_3(\text{CO})_{12}]$ with $[\text{Fe}(\text{CO})_4]^{2-}$ results in the formation of $[\text{Fe}_4(\text{CO})_{13}]^{2-}$ (Ref. 130):



It was shown⁷⁷ that the $[\text{Fe}(\text{CO})_4]^{2-}$ and $[\text{Fe}_2(\text{CO})_8]^{2-}$ anions easily react with $\text{Fe}(\text{CO})_5$ and $\text{Fe}_3(\text{CO})_{12}$, ICRA 2–5 being formed at the initial steps of the reaction. At the same time, the reactions of tri- and tetranuclear CFA salts, $[\text{Fe}_3(\text{CO})_{11}]^{2-}$ or $[\text{Fe}_4(\text{CO})_{13}]^{2-}$, with $\text{Fe}_3(\text{CO})_{12}$ give first mainly heavier radical anions 3–5. It should be noted that the reaction of $(\text{PPN})_2[\text{Fe}_3(\text{CO})_{11}]$ with $\text{Fe}_3(\text{CO})_{12}$ is the preparative method for the synthesis of the stable radical anion salt, $(\text{PPN})[\text{Fe}_3(\text{CO})_{11}]^{\cdot-}$ (Ref. 131). These data show that in the reactions of carbonylferrate anions with iron carbonyls, single-electron transfer takes place at low degrees of conversion.



for $p = 1, q = 5$ and $p = 2, q = 9$: $n = 1, m = 5$; $n = 2, m = 9$; $n = 3, m = 12$; for $p = 3, q = 12$ and $p = 4, q = 14$: $n = 3, m = 12$.

Such process may be regarded as direct single-electron reduction of iron carbonyls,[†] which is quite natural, taking into account the high reduction potentials of CFA (Fig. 1).⁴²

The two-electron reduction potential ($E_{\text{red}} = -1.77\text{ V}$)³⁹ for $\text{Fe}(\text{CO})_5$ is shown in Fig. 1. This potential, probably, corresponds to the reduction of iron pentacarbonyl in very fast reactions of types (7) (for $n = 1, m = 5$) and (8) followed by the reduction of $[\text{Fe}_2(\text{CO})_8]^{\cdot-}$ to the corresponding anion. In the electrochemical terms, this corresponds to the two-electron reduction with an intermediate chemical stage (ECE). The value $E_{1/2\text{red}} = -2.67\text{ V}$

[†] This scheme of the direct reduction may be regarded as a variant of the redox disproportionation with the preliminary activating complex formation stage, if the ‘additional’ lone pair of CFA is considered as a donor ligand.

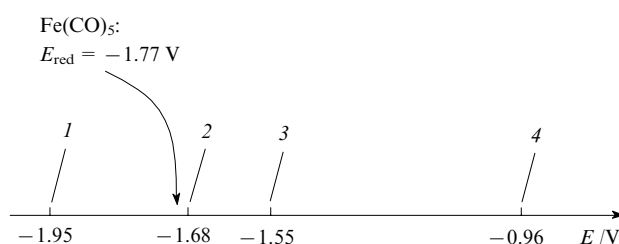
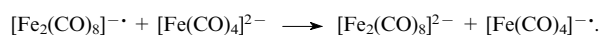
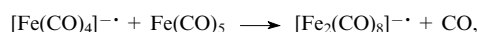


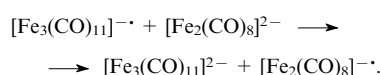
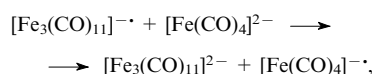
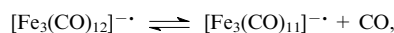
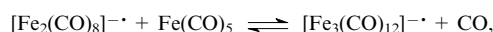
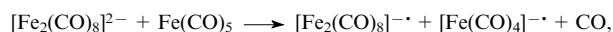
Figure 1. The scale of the redox potentials of the following pairs: $[\text{Fe}(\text{CO})_4]^{2-}/[\text{Fe}(\text{CO})_4]^{\cdot-}$ (1), $[\text{Fe}_2(\text{CO})_8]^{2-}/[\text{Fe}_2(\text{CO})_8]^{\cdot-}$ (2), $[\text{Fe}_3(\text{CO})_{11}]^{2-}/[\text{Fe}_3(\text{CO})_{11}]^{\cdot-}$ (3) and $[\text{Fe}_4(\text{CO})_{13}]^{2-}/[\text{Fe}_4(\text{CO})_{13}]^{\cdot-}$ (4) in THF.⁴²

has been reported⁴³ for the reduction potential of $\text{Fe}(\text{CO})_5$, which is probably related to the supporting electrolyte used, Bu_4NBF_4 ($E_{1/2\text{red}} = -2.75\text{ V}$)¹³².

Whereas the interaction of trinuclear $[\text{Fe}_3(\text{CO})_{11}]^{2-}$ and $\text{Fe}_3(\text{CO})_{12}$ complexes ($E_{1/2\text{red}}$ from -0.32 to -0.44 V ^{38, 39}) in an open system results in the formation of trinuclear ICRA 3 and 4, the reaction of tetracarbonylferrate anion with iron pentacarbonyl proceeds as a radical chain reaction. The reaction gives $[\text{Fe}_2(\text{CO})_8]^{2-}$ when the concentrations of the starting compounds are equimolar [see reaction (28)].

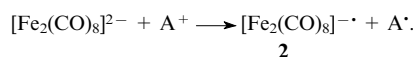


With excess iron pentacarbonyl, the process continues further to give trinuclear CFA incapable any more of reducing the starting iron pentacarbonyl at ambient temperature at the final stage of the reaction.



The radical chain process with single-electron redox steps ends in the formation of diamagnetic complexes. In a closed system, when CO is not removed from the reaction vessel, the iron carbonyl radical anions 2–5 are in equilibrium [reactions (9)–(13)].

A series of papers^{127, 131, 133–137} dealing with the reactions of CFA with other metal carbonyls and the reactions of anionic carbonyl compounds of various metals with iron carbonyls should be noted. The electron transfer between such complexes and the formation of ICRA at the intermediate stages of the process have been discussed.^{127, 134, 135, 137} The charge transfer in the $\text{A}_2[\text{Fe}_2(\text{CO})_8]$ salts, where A are *N*-methylated pyridine derivatives, PPN, Ph_4P or the organometallic cation $[\text{CpFe}(\text{C}_6\text{H}_6)]^+$ (Cp is cyclopentadienyl), has been described.¹³⁸ The electron transfer in this system results in the formation of radical anion 2, which undergoes subsequent conversions.



The structures of $[\text{Li}_2(\text{THF})_6\text{Fe}_2(\text{CO})_8]$ and $[\text{Li}_2(\text{THF})_4\text{Fe}_2(\text{CO})_8]_n$ complexes in which the iron carbonyl fragment contains two bridging CO ligands with coordinated $\text{Li}(\text{THF})_3$ and $\text{Li}(\text{THF})_2$ groups have been determined by X-ray

crystallography.¹³⁹ A similar structure of the $\text{Fe}_2(\text{CO})_8$ fragment was suggested for the $[\text{Fe}_2(\text{CO})_8]^{-\bullet}$ radical anion.^{7,63} On the contrary, the structure of the corresponding carbonylferrate anion $[\text{Fe}_2(\text{CO})_8]^{2-}$ does not contain any bridging groups, two $\text{Fe}(\text{CO})_4$ fragments being linked only by the Fe–Fe bond.^{133, 138, 140, 141} It should be noted that the lithium salt with the $[\text{Fe}(\text{CO})_4]^{2-}$ anion is unknown in a pure state. As the reduction potential of Li^+ ($E_{1/2\text{red}}$ from -1.42 to -1.82 V)^{142, 143} is less negative than the redox potential of the $[\text{Fe}(\text{CO})_4]^{2-}/[\text{Fe}(\text{CO})_4]^{-\bullet}$ pair (see Fig. 1), the reduction of Li^+ occurs. In the case of $[\text{Li}_2(\text{THF})_6\text{Fe}_2(\text{CO})_8]$ and $[\text{Li}_2(\text{THF})_4\text{Fe}_2(\text{CO})_8]_n$ complexes, when the redox potential of the $[\text{Fe}_2(\text{CO})_8]^{2-}/[\text{Fe}_2(\text{CO})_8]^{-\bullet}$ pair (see Fig. 1) falls in the $E_{1/2\text{red}}$ region of lithium, charge transfer from CFA to Li^+ may take place followed by the rigid fixation of the cation in a contact ion pair. The presence of two different types of lithium atoms in the structure of the polymeric complex also supports this suggestion.

Thus the carbonylferrate anions are quite strong reducing agents, able to take part in the direct single-electron reduction of various substrates, including iron carbonyls. The iron carbonyl radical anions are formed in these processes and the radicals undergo further conversions by a radical chain mechanism.

VI. Nucleophilic substitution and catalytic conversions of iron carbonyls induced by electron transfer

A series of papers on the nucleophilic substitution of CO by phosphine, phosphite and isocyanate ligands in iron carbonyl complexes under the conditions of preliminary chemical or electrochemical reduction of the initial complex to the corresponding radical anion was published in the early 1980s. The trinuclear iron carbonyl complex $\text{Fe}_3(\text{CO})_{12}$ (Refs 60, 144–146) and complexes of the $\text{Fe}_3(\mu_3\text{-E})_2\text{L}(\text{CO})_8$ type, where $\text{L} = \text{CO}$; $\text{E} = \text{NAr}$, PPh , S , Se ;^{147–151} E_2 is 2,3-diazanorbornene;¹⁵² $\text{L} = \text{C}_3\text{H}_2\text{S}_2$, $\text{E} = \text{S}$ ^{153, 154} were the main objects of these studies. The replacement of CO in iron pentacarbonyl by phosphine and phosphite ligands, initiated by sodium benzophenone ketyl, has been described.¹⁵⁵ It appeared that these processes correspond to the known substitution reactions or to the catalytic conversions induced by electron transfer:^{156–158}

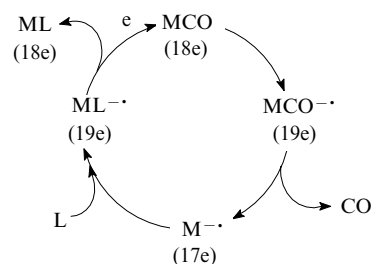


MCO is iron carbonyl complex,

$\text{L} = \text{PR}_3, \text{P}(\text{OR})_3, \text{NCR}$ ($\text{R} = \text{Alk}, \text{Ar}$).

If the standard electrochemical potentials of reactions (29) and (32) obey the inequality $E_2^\circ > E_1^\circ$, then the electron-induced nucleophilic substitution, EINS, takes place.^{140, 155} If $E_1^\circ > E_2^\circ$, then a catalysed reaction called electron-transfer chain catalysis (ETC) takes place.^{146, 157, 158} The catalytic cycle is shown in Scheme 5.

Reactions (29)–(33) and Scheme 5 represent the simplest case of an ETC process without taking into account the interconversions of the intermediate 19-electron ($\text{MCO}^{-\bullet}$ and $\text{ML}^{-\bullet}$) and 17-electron ($\text{M}^{-\bullet}$) radical anions. After the electron addition in reaction (29) the reorganisation of the radical anions accompanied by the change in the number of iron atoms in the metal core and rearrangement of the coordination sphere are possible [see, for

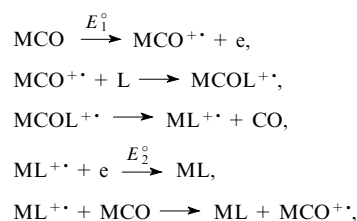


Scheme 5

example, reactions (6), (8)–(10) in Section III and also the papers^{108, 159}].

In spite of the fact that no data on the ETC processes involving intermediate 17-electron radical cations are known for iron carbonyls, similar reactions for the carbonyls of Group VI metals were described in the literature.¹⁶⁰ As applied to the iron carbonyls, these transformations may be described as follows (Scheme 6):

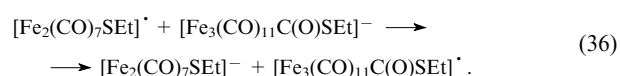
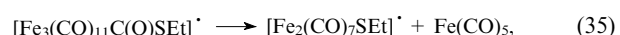
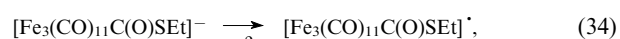
Scheme 6



MCO is iron carbonyl complex,

$\text{L} = \text{PR}_3, \text{P}(\text{OR})_3$ ($\text{R} = \text{Alk}, \text{Ar}$).

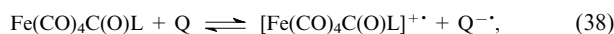
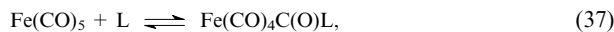
If $E_1^\circ > E_2^\circ$, then electron-induced nucleophilic substitution takes place. For instance, the nucleophilic substitution of the CO group in the $[\text{Fe}(\text{CO})_3(\text{PPh}_3)_2]^{+\bullet}$ radical cation yielding the $[\text{Fe}(\text{CO})_2 \cdot (\text{PPh}_3)_2(\text{L}-\text{L})]^{+\bullet}$ complex, where $\text{L}-\text{L}$ are 1,2-diketones, *o*-chloranil, 1,2-naphthoquinone, belongs to this type of reaction.^{102, 161} If $E_2^\circ > E_1^\circ$, the catalytic ETC process occurs. Only one example of ETC process in which the addition of the nucleophilic anion (EtS^-) is followed by rearrangement of the metal skeleton is known for 17-electron $\text{Fe}(\text{I})$ carbonyl complexes.⁹⁶



Thus, in the ETC processes involving complex iron carbonyl radical ions, ligand exchange takes place in the coordination sphere of a complex with incomplete 17-electron configuration. This is a radical chain process; however its final products are diamagnetic.

VII. Iron carbonyls as reducing agents

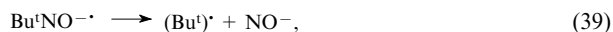
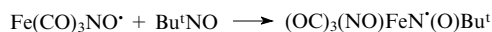
It was shown in Section III that disproportionation reactions of iron carbonyls with Lewis bases include a stage of activating complex formation followed by single-electron transfer from the carbonyl complex activated by the electron donor to another molecule of the starting carbonyl. This gives complexes of iron in the oxidation state (+1) and radical anions containing iron in the oxidation state (−1) [see reactions (1)–(4)]. If the reaction mixture contains a third component (Q), more easily reducible than the starting iron carbonyl, then the reduction of only this component is possible.



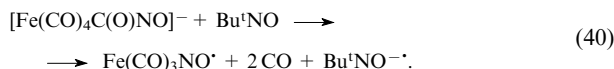
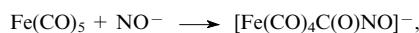
L is a Lewis base.

The situation represented by reactions (37) and (38) occurs when the reduction potentials of the compound Q are higher than those of iron pentacarbonyl [$E_{1/2\text{red}} = -1.77$ V in THF vs. the saturated calomel electrode (SCE)],³⁹ as, for example in the case of the nitroso compound Bu^tNO [$E_{1/2\text{red}} = -1.36$ V (MeCN, SCE)];¹⁶² haloalkanes, viz., CCl₄ [$E_{1/2\text{red}} = -0.78$ V (dioxane, SCE)]¹⁶³ and CHCl₃ [$E_{1/2\text{red}} = -1.68$ V (dioxane, SCE)],¹⁶³ as well as sulfur [$E_{1/2\text{red}} = -1.077$ V in DMF vs. the Fe/Fe⁺ couple (Fe is ferrocene)]¹⁶⁴.

A study of the reaction of Fe(CO)₅ with 2-methyl-2-nitrosopropane (Bu^tNO) in THF or toluene in the absence of electron donors has shown that at 20 °C, the induction period of the reaction is rather long (~20 min).⁷⁶ The fast accumulation of the Fe(CO)₃NO[•] [Fe(1⁺)] and Bu^tNO^{•-}, which are subsequently converted into the stable radicals (OC)₃(NO)FeN[•](O)Bu^t and Bu₂NO[•], takes place after this period.



The intermediate nitrosyl anion NO^{•-} initiates the already discussed scheme of redox disproportionation of Fe(CO)₅ under the action of an anionic nucleophile.



After the end of the induction period, the process proceeds as a chain reaction, which is provided by the formation of Bu^tNO^{•-} in reaction (40) and its decomposition [reaction (39)]. In the case of excess Fe(CO)₅ relative to Bu^tNO, after complete decomposition of nitroso compound, the resulting Bu₂NO[•] [$E_{1/2\text{red}} = -1.63$ V (MeCN, SCE)]¹⁶⁵ is reduced to the hydroxylamine anion according to a scheme similar to reaction (38).

The Fe(CO)₅–Lewis base system (L = DMF, HMPA, tertiary amines, etc.) is widely used as an initiator for radical addition, telomerisation of olefins with haloalkanes and the reduction of polychloro-substituted compounds.^{166–171} Haloalkanes (mainly, polyhaloalkanes) are quite reactive in these processes, because they are reduced more easily than iron pentacarbonyl. The scheme of the process initiation may be represented by reactions (37), (38), where L is DMF or HMPA, and Q is an easily reduced haloalkane RX. The resulting RX^{•-} radical anion decomposes to give the R[•] radical, which subsequently participates in the radical process, and a halide ion X⁻. The latter reacts with Fe(CO)₅, as a Lewis base, as described above, thus enhancing the initiation of subsequent transformations. The intermediate species of the single electron redox process, namely, the Fe⁺ carbonyl complexes, for example Cl(OC)₄FeN[•](O)Bu^t, and alkyl radicals, were identified by spin-trap methods.^{99, 169–171} In the presence of olefins, diamagnetic Fe²⁺ complexes and the products of addition of haloalkanes to the double C=C bond are the final products of telomerisation. Without olefins the reaction of Fe(CO)₅ with polyhalomethanes CCl₃X (X = Cl, Br) in the presence of DMF yields hexachloroethane, which is also evidence for the radical Cl₃C[•] generation.^{172, 173} In the presence of hydrogen donors (alcohols, mercaptans, organosilicon hydrides), the hydrogen atom adds to the RCCl₂[•] radical formed upon decomposition of RCCl₃. Thus, readily available compounds containing a trichloromethyl group are reduced to dichloro derivatives.¹⁶⁹

A study¹⁷⁴ of the reaction of Fe(CO)₅ with sulfur (S₈) in THF at 20 °C has demonstrated that after the induction period (> 10 min), the ESR spectra exhibit a broadened signal for S₃^{•-} with $g = 2.031$ (according to the literature, $g = 2.032$ ¹⁷⁵ and 2.033 ¹⁷⁶). However, no ICRA are detected. The stable radical anion S₃^{•-}, together with S_n²⁻ ($n < 8$), is formed from S₈^{•-} through a relatively complicated disproportionation.^{164, 177, 178} The polysulfide dianions S_n²⁻, being Lewis bases, initiate the redox process according to reactions (38) and (39), where Q = S₈. The identification of the Fe⁺ radical carbonyl complexes in this system is difficult, because their signals overlap with the broad signal of S₃^{•-}. However, the formation of diamagnetic complexes of the S₂Fe₂(CO)₆, S₂Fe₃(CO)₉ and SFe₃(CO)₁₀ type^{179–181} points to the fact that their precursors are the Fe⁺ radical ion complexes, which are involved in the transformations similar to reaction (6).

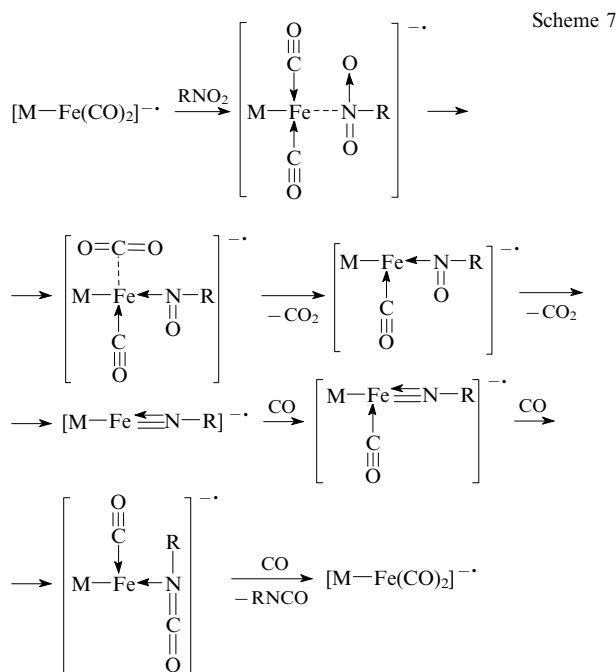
If an unsaturated compound is introduced in the reaction of an iron carbonyl with S₈, the S_n^{•-} radical anions appearing in the system will add to the double bond, forming cyclic polysulfides, various organic sulfur derivatives and their iron carbonyl complexes.^{181, 182} This process may be used for the low-temperature vulcanisation of resins. It was also reported that Fe(CO)₅ in the presence of sulfur is an effective catalyst of lignite and bituminous coal liquefaction under hydrogen^{183, 184} or water gas (CO + H₂O)¹⁸⁵ gasifications.

Thus, in the reactions with Lewis bases in the presence of compounds reduced more easily than iron pentacarbonyl, Fe(CO)₅ forms an activated complex with a Lewis base and acts as a single-electron reducing agent. The resulting Fe⁺ radical carbonyl derivatives are then oxidised either to Fe²⁺, or to diamagnetic carbonyl complexes of the L₂Fe₂(CO)₆, L₂Fe₃(CO)₉ and LFe₃(CO)₁₀ type, where L is a nucleophilic ligand. Another reaction pathway is determined by the Q^{•-} radical anion formed upon the reduction.

VIII. Catalytic processes involving iron carbonyl radical anions

The catalytic transformations of iron carbonyls in the processes of carbonylation of various compounds are usually described by a scheme constructed according to the Tolman rule for determination of the major reaction pathway *via* complexes with even numbers of electrons in the outer shell (18e → 16e → 18e). However, all attempts to prove this mechanism failed. In fact, catalytic processes of carbonylation with iron carbonyl complexes include reactions of two types: the redox disproportionation of iron carbonyls induced by Lewis bases (see Section III) and the oxidative addition of Brønsted and Lewis acids to the (hydrido)-carbonylferrate anions (see Section IV).^{19, 20, 84, 109, 110} In both cases, ICRA 2–5 are formed. These ICRA are fairly stable and their steady-state concentrations during the reaction may be high (10⁻⁵–10⁻² mol litre⁻¹). At the same time, ICRA 2, 3 and 5 are coordinatively unsaturated electron-deficient systems with a labile coordination sphere, capable of fast ligand and electron exchange. Usually reactions involving these ICRA follow a radical chain mechanism (see Sections III and IV); therefore these species are, most likely, catalysts of carbonylation. The catalytic activity of ICRA was demonstrated for the first time in the reductive carbonylation of nitro and nitroso compounds⁷⁶ and was confirmed later^{56, 57} with [Fe₃(CO)₁₁]^{•-} as a model compound.^{56, 57} Radical anion nitrene complexes were found by ESR method in the reactions of Bu^tNO₂ and Bu^tNO with participation of the ICRA (Scheme 7).

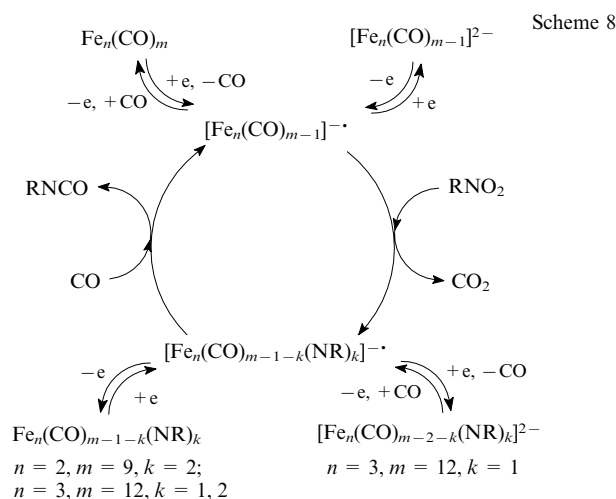
Scheme 7 depicts the case where only one molecule of nitro compound is present in the coordination sphere of an iron carbonyl cluster. This molecule is reduced consecutively to nitroso derivative and then to the nitrene complex. If the process is carried out in the catalytic mode with a controlled negative reduction potential of the medium, the intermediate nitrene complexes are carbonylated to give isocyanates and the starting ICRA. The iron



oxidation state (−1) in the catalytic species remains unchanged in this process. The addition of the second molecule of the nitro compound yields intermediate radical species containing ligands with nitro groups reduced to different extent.⁷⁶

If the reaction is carried out with a stoichiometric component ratio, the reduction of nitrogen-containing ligands may end after the formation of nitrene structures. In the absence of an adequate reduction potential of the medium and with additional supply of carbon monoxide, the nitrogen-containing ligands in intermediate complexes are reduced at the expense of oxidation of Fe(−1) into Fe(+1). Further on, the radical anions lose the unpaired electron to be transformed into well known diamagnetic complexes with d⁷ electron configuration of the iron atom, for example, into Fe₂(CO)₆(NR)₂, Fe₃(CO)₉(NR)₂, Fe₃(CO)₁₀NR, *etc.*^{186, 187} This results in withdrawal of the complex from the catalytic cycle, and the subsequent formation of isocyanates becomes impossible (Scheme 8).

In the presence of proton donors in the reaction mixture, the nitro compounds are reduced to amines.^{56, 188} The intermediate radical anion nitrene complexes may be stabilised by being



reduced to diamagnetic anions, [Fe₃(CO)₉NR]^{2−} and [HFe₃(CO)₉NR][−] (Ref. 56).

It is noteworthy that the catalytically active species are 17-electron radical anions; in the process of catalysis, they add a ligand, *e.g.*, CO, and are transformed into 19-electron species. The latter eliminate the product being thus converted into the original electron-deficient form. There is a possibility of the transformation of an electron-rich system into an electron-deficient one upon cluster core rearrangement due to breaking of the Fe–Fe or Fe–N bonds and upon localisation of the excessive electron on the ligand. In these cases, a new bond is formed between the coordinated ligands, for example, CO–NR, or their reduction, for example into the RNH ligand, takes place in the presence of proton donors. These transformations afford various diamagnetic complexes, which may be isolated upon the reaction of iron carbonyls with nitro compounds.^{186, 189}

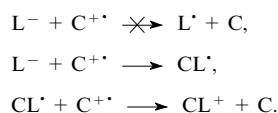
Thus, the catalytic cycle of reductive carbonylation of nitro and nitroso compounds catalysed by ICRA includes transformations *via* complexes 17e → 19e → 17e, and the process itself has a radical chain character.

IX. Reactions with possible involvement of iron carbonyl complexes

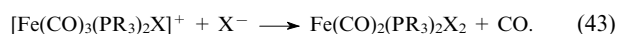
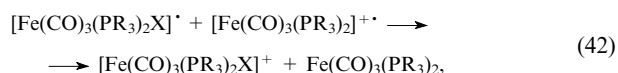
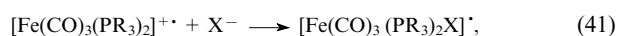
The concept of the ‘activating complex formation’ discussed in Section III describes adequately a wide variety of redox processes in organic and organometallic chemistry,^{82, 83} for example, the reactions of ferrocenium salts with different nucleophilic reagents.¹⁹⁰

If the neutral complex C in Scheme 2 is replaced by the radical cation C^{•+}, we get Scheme 9. This may explain the halide-induced disproportionation of radical cations [Fe(CO)₃(PR₃)₂]^{•+} containing iron atom in the formal oxidation state 1+ into the complexes Fe(CO)₃(PR₃)₂ [Fe(0)] and Fe(CO)₂(PR₃)₂X₂ [Fe(II)], where X = Cl, Br, I.^{100, 101, 103}

Scheme 9



The ‘activating complex formation’ produces at the first stage the known^{100, 101} radical [Fe(CO)₃(PR₃)₂X][•] [reaction (41)]. This is followed by an electron transfer from this compound to the starting radical cation and the formation of the coordination sphere of Fe(+2) carbonyl complex [reactions (42) and (43)].



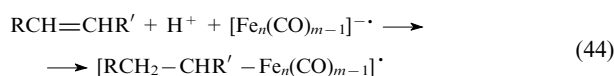
The mechanism of single-electron redox disproportionation of iron carbonyls induced by Lewis bases, resulting in the formation of ICRA, is quite common and may be applied to a wide variety of bases (see Section III). However, this mechanism has to be proved in every particular case. For instance, some authors^{23, 24} regard the N-oxide-induced ligand substitution in iron carbonyls as a special type of transformations caused by ‘oxygen atom transfer reagents’ (see Scheme 2 in Introduction). However, it was shown⁷⁹ that, in reality, such processes start with the formation of ICRA according either to reactions (1) and (2) (L[−] = OH[−]), if commercial Me₃NO · 2 H₂O available as [Me₃NOH]⁺OH[−] · H₂O is applied, or to reactions (3) and (4) (L = Me₃NO), if the preliminarily dehydrated amine oxide is used. This is followed by nucleophilic displacement of CO in the formed ICRA according

to reactions (29)–(33), which is a typical electron transfer induced catalysis (see Section VI).

The activation of nucleophilic substitution and CO exchange in $\text{Fe}(\text{CO})_5$ under the action of salts (such as CoHal_2 and NiHal_2)¹⁹¹ or transition metal complexes^{192,193} occurs in a similar way. These compounds are able to dissociate yielding negatively charged species, for example, halide ions X^- , which act as Lewis bases. They react with $\text{Fe}(\text{CO})_5$ to form complexes $[\text{Fe}(\text{CO})_4\text{C}(\text{O})\text{X}]^-$ [reaction (1)], which subsequently react with the starting $\text{Fe}(\text{CO})_5$ molecule according to equation (2), producing iron carbonyl radical anions.⁷⁸ It is important to note that in these compounds, the transition metal is in a low oxidation state and is unable to oxidise the emerging radical anions. The activation of such processes by potassium hydride¹⁹⁴ and by the complex hydride derivatives, R_3BH^- ($\text{R} = \text{H}, \text{Alk}, \text{AlkO}$) and AlH_4^- (Refs 194 and 195), which produce the $[\text{Fe}(\text{CO})_4\text{C}(\text{O})\text{H}]^-$ formyl iron complex^{196–199} proceeds by a similar way.

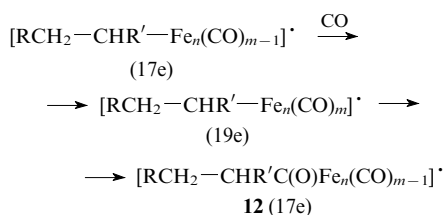
The kinetic data on one of the most important carbonylation processes, Reppe olefin hydroformylation in alkaline solutions containing $\text{Fe}(\text{CO})_5$,⁹ have been interpreted according to the traditional scheme based upon the Tolman rule. Several intermediate 16-electron species, the possible existence of which was not proved, are included in this scheme.

However, the very same data can be consistently interpreted by assuming the formation of ICRA in the iron carbonyl–Lewis base system and their radical chain transformations through complexes $17e \rightarrow 19e \rightarrow 17e$, which do exist in solution and are easily detectable by ESR spectroscopy. The key stage of the process is the addition of an olefin to the coordinatively unsaturated 17-electron radical anion in the presence of a proton donor. As a result, an alkyl-containing iron carbonyl radical is generated [reaction (44)].



$\text{R}, \text{R}' = \text{Alk}; n = 2, m = 9; n = 3, m = 12.$

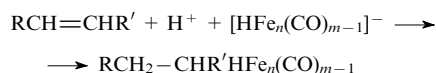
The next stage is the addition of CO producing a 19-electron species and the transformation of the latter into the 17-electron radical upon carbonylation of the $\text{Fe}-\text{Alk}$ bond.



The subsequent reaction of radical **12** with $[\text{HFe}(\text{CO})_4]^-$ produces an aldehyde and radical anion with an increased number of iron atoms, similarly to the reactions of acyl derivative $[\text{RFe}(\text{CO})_4]^{\cdot-}$ [reactions (24) and (25)]. The hydridocarbonylferrate anion $[\text{HFe}(\text{CO})_4]^-$ is formed in this process as a result of redox disproportionation of $\text{Fe}(\text{CO})_5$ in the presence of a proton donor.^{19,20,109} In the presence of carbon monoxide, ICRA **2–5** interconvert^{76–78,96,108} according to reactions (8)–(11). This provides the regeneration of radical anions **2** and **3** and thus determines the catalytic character of the process.

Stoichiometric reduction of various unsaturated compounds (alkenes,²⁰⁰ 1,3-dienes,²⁰¹ α,β -unsaturated carbonyl compounds,^{113,114} enamines,²⁰² a number of nitrogen-containing heterocycles and anthracene²⁰³) by HCFA occurs in the absence of CO in a proton donor medium. During the reduction, ESR signals that may be assigned to ICRA **2–4** were detected. However, the formation of such species was usually attributed to side processes.¹¹³

An alkyl-containing complex is formed at the first step of the reduction.



$\text{R}, \text{R}' = \text{Alk}; n = 1, m = 5; n = 2, m = 9.$

The subsequent process is believed to proceed according to reactions (22) and (23) (see Section IV), *i.e.*, the scheme of single-electron redox disproportionation in the HCFA–Lewis acid system, resulting in the formation of ICRA and reduction products, is implemented. The iron carbonyl radical anions react with the starting compounds [see reactions (44), (24) and (25)]. As a result, the hydrocarbonylferrate anion is completely spent for the reduction of unsaturated compound.

The transformation schemes *via* the $17e \rightarrow 19e \rightarrow 17e$ complexes may be applied also to the explanation of other processes, which involve the iron carbonyl–Lewis base and HCFA–Lewis (or Brønsted) acid systems. However, the validity of using such schemes should be proved in each particular case.

X. Redox disproportionation of transition metal carbonyls

The redox disproportionation induced by Lewis bases is a typical reaction of transition metals carbonyls. As a result of this reaction, the reduction of carbonyls to carbonylmetallate or hydridocarbonylmetallate anions and their oxidation to positively charged complexes take place. The general features of the formation of stable complexes, namely, binary carbonyls containing only the metal atoms and carbonyl ligands, should be considered in the discussion of these processes, because the relationship between the stability and reactivity is important for the choice of potential carbonylation catalysts.

All complexes require the 18-electron configuration of the outer electron shell of a metal atom in order to achieve the thermodynamic stability (the Sidgwick rule). The number of CO ligands coordinated to the metal (not more than 6) is an important factor determining the stability of carbonyl complexes obtained in various processes. The size of the metal atom is another such factor. The larger is the metal atom and the smaller is the number of CO groups required for its coordination, the more pronounced is the tendency of the complex to form cluster structures. This fact is reflected in the concept of close packing of ligands on a metal core surface.²⁰⁴ For instance, the vanadium atom, which possesses a d^5 electron configuration, forms a stable 17-electron radical, $[\text{V}(\text{CO})_6]^{\cdot-}$, unable to dimerise. On treatment with a Lewis base (L), this radical easily disproportionates yielding the salt $[\text{VL}_n][\text{V}(\text{CO})_6]_2$ ($n = 3, 6$), in which the mononuclear anion $[\text{V}(\text{CO})_6]^-$ obtains the closed 18-electron configuration.²⁰⁵

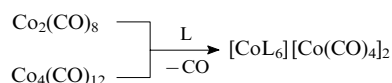
A stable mononuclear carbonyl $\text{Ni}(\text{CO})_4$ with a closed 18-electron shell is known for nickel (electron configuration d^{10}). During the redox disproportionation induced by Lewis bases (L), it transforms into salts of polynuclear carbonyl-containing $\text{Ni}(-2)$ anions, $[\text{NiL}_n][\text{Ni}_p(\text{CO})_q]$ with $p \geq 5$ nickel atoms in the anion cluster, for example $[\text{Ni}_6(\text{CO})_{11}]^{2-}$, $[\text{Ni}_9(\text{CO})_{18}]^{2-}$ or $[\text{Ni}_{12}(\text{CO})_{21}]^{4-}$ (Refs 206–208). Platinum, which is located in the Periodic Table in the same group as nickel, but in Period 6, does not form a stable mononuclear carbonyl $\text{Pt}(\text{CO})_4$, but produces a polymeric cluster $[\text{Pt}(\text{CO})_2]_x$ instead.²⁰⁹ The same is true for carbonylplatinates, for example for $[\text{Pt}_3(\mu-\text{CO})_3(\text{CO})_3]_n^{2-}$ (Ref. 210).

Group VI metals, Cr, Mo and W, form very stable hexacarbonyls $\text{M}(\text{CO})_6$, which disproportionate only under the action of strong bases and under drastic conditions. For instance, the reactions of $\text{M}(\text{CO})_6$ with KOH produces $[\text{HM}_2(\text{CO})_{10}]^-$ binuclear anions,^{211,212} and the reactions of $\text{Cr}(\text{CO})_6$ with KOH in the presence of the cryptand **222** (4,7,13,16,21,24-hexaoxa-1,10-

diazabicyclo[8.8.8]hexacosane) result in the formation of the $[\text{HCr}(\text{CO})_5]^-$ anion.²¹³ Dianionic carbonylmetallates, $[\text{M}_2(\text{CO})_{10}]^{2-}$ ($\text{M} = \text{Cr}, \text{Mo}, \text{W}$), are also known for these metals.^{212, 214–216} When less basic nucleophiles are used, the redox disproportionation does not occur. The reactions stop after the formation of complexes at the CO group, for example $[\text{M}(\text{CO})_5\text{C}(\text{O})\text{L}]^-$ [$\text{M} = \text{Cr}$: $\text{L} = \text{N}_3, \text{H}, \text{NEt}_2$ (Ref. 214); $\text{M} = \text{W}$, $\text{L} = \text{OMe}$ (Ref. 217)]. The subsequent transformations are accompanied by replacement of the carbonyl group and yield either $[\text{M}(\text{CO})_5\text{L}]^-$ anions ($\text{M} = \text{Cr}, \text{Mo}, \text{W}$; $\text{L} = \text{NCS}, \text{H}, \text{CN}, \text{Cl}, \text{Br}, \text{I}$) or neutral compounds $\text{M}(\text{CO})_5\text{L}$ ($\text{M} = \text{W}$: $\text{L} = \text{THF}, \text{NAlk}_3, \text{AlkCN}$).^{216, 218}

Group VII metals, $\text{Mn}, \text{Tc}^\ddagger$ and Re (with the electron configuration d^7), form stable binuclear carbonyls $\text{M}_2(\text{CO})_{10}$ with a closed 18-electron shell. Their redox disproportionation induced by Lewis bases (L) produces the $[\text{ML}_6][\text{M}(\text{CO})_5]_2$ salts ($\text{M} = \text{Mn}, \text{Re}$).^{219–221} The oxidation state of the metal in the pentacarbonylmetallate anions is -1 . In the case of manganese, the formation of complex salts $[\text{Mn}(\text{CO})_{6-n}\text{L}_n]^+[\text{Mn}(\text{CO})_5]^-$ [$n = 3$ or 6 ; L is pyridine (Py), amines, *etc.*] is possible.²²²

Stable binuclear $[\text{Co}_2(\text{CO})_8]$ and tetranuclear $[\text{Co}_4(\text{CO})_{12}]$ carbonyl complexes with 18-electron closed shells are typical of cobalt (the electron configuration d^9).^{223, 224} Their disproportionation induced by Lewis acids (L) generates the mononuclear $[\text{Co}(\text{CO})_4]^-$ anion.



The disproportionation of $\text{Co}_2(\text{CO})_8$ in the presence of pyridine may give also the trinuclear $[\text{Co}_3(\text{CO})_{10}]^-$ anion. Depending on the conditions, the counter-ions are represented by Co^+ and Co^{2+} complexes, such as $[\text{Co}(\text{CO})_4\text{Py}]^+$, $[\text{Co}(\text{CO})_4\text{Py}_3]^+$, $[\text{CoPy}_3]^{2+}$ and $[\text{CoPy}_4]^{2+}$ (Ref. 224).

The cobalt group metals, Rh and Ir , also form dimeric carbonyls $\text{M}_2(\text{CO})_8$; however these carbonyls are unstable and are converted into tetranuclear complexes, $\text{M}_4(\text{CO})_{12}$.^{209, 225} The clusters $\text{M}_6(\text{CO})_{16}$ are also known for rhodium and iridium.^{209, 225} The reduction of the carbonyls of these metals results in the formation of the mononuclear anion $[\text{M}(\text{CO})_4]^-$; however, the anionic Rh and Ir carbonylmetallate complexes usually exist as polynuclear clusters $[\text{M}_p(\text{CO})_q]^{n-}$ with the number of metal atoms $p \geq 5$ and the charge n ranging from -1 to -4 , for example, $[\text{M}_5(\text{CO})_{16}]^-$, $[\text{M}_6(\text{CO})_{16}]^{2-}$, $[\text{Ir}_{12}(\text{CO})_{26}]^{2-}$, $[\text{Rh}_{22}(\text{CO})_{37}]^{4-}$ and $[\text{Rh}_{26}(\text{CO})_{32}]^{2-}$ (Refs 204, 209, 225 and 226).

Iron (the electron configuration d^8) forms stable 18-electron carbonyls, $\text{Fe}(\text{CO})_5$, $\text{Fe}_2(\text{CO})_9$ and $\text{Fe}_3(\text{CO})_{12}$, and also a carbidocarbonyl cluster $\text{Fe}_5\text{C}(\text{CO})_{15}$. The redox disproportionation of iron carbonyls produces the salts of carbonylferrate or hydrocarbonylferrate anions with the number of iron atoms from 1 to 4 (see Introduction). Carbidocarbonyl anionic clusters $[\text{Fe}_5\text{C}(\text{CO})_{14}]^{2-}$ and $[\text{Fe}_6\text{C}(\text{CO})_{16}]^{2-}$ are formed in the reactions of iron carbonyls at temperatures around 150°C .^{204, 227} These clusters contain the largest number of iron atoms. The redox transformations of these compounds produce complexes with fewer number of iron atoms.⁷⁸

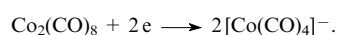
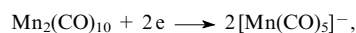
The iron group metals, Ru and Os , have a larger atom size and produce stable trinuclear carbonyls $\text{M}_3(\text{CO})_{12}$, while mononuclear pentacarbonyls of these atoms $\text{M}(\text{CO})_5$ are unstable. The redox disproportionation of $\text{Ru}_3(\text{CO})_{12}$ under the action of KOH produces the $[\text{HRu}_3(\text{CO})_{11}]^-$ and $[\text{Ru}_6(\text{CO})_{18}]^{2-}$ anionic complexes,²²⁸ and its pyrolysis gives the $\text{Ru}_6\text{C}(\text{CO})_{17}$ cluster.²⁰⁹ The thermal destruction of $\text{Os}_3(\text{CO})_{12}$ yields new polynuclear

carbonyls, $\text{Os}_5(\text{CO})_{16}$, $\text{Os}_6(\text{CO})_{18}$, $\text{Os}_7(\text{CO})_{21}$ and $\text{Os}_8(\text{CO})_{23}$.²⁰⁹ The polynuclear anionic clusters of Ru and Os , for instance $[\text{Ru}_{10}\text{C}_2(\text{CO})_{24}]^{2-}$ and $[\text{Os}_{10}\text{C}(\text{CO})_{24}]^{2-}$, are also known (Refs 204, 228 and 229).

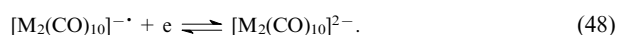
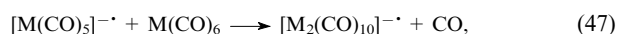
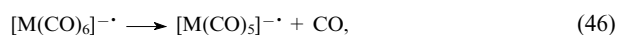
Generally, the anionic carbonyl clusters of platinum group metals are able to combine into polynuclear clusters with larger number of metal atoms, up to several dozens or even hundreds. The resulting clusters have a metal core like a crystal lattice with a 'coat' of CO ligands at the surface. This seriously hinders the determination of their structure, because during the X-ray study of such clusters the localisation of carbonyl ligands and determination of their number is problematic due to high absorption of X-rays and strong scattering by metal atoms.²⁰⁴ Besides, the '18-electron configuration rule', which is valid for mono- and polynuclear complexes of transition metals, does not work for large clusters. The stable forms of these structures are described in terms of the concept of cluster valence electrons (CVE) and cluster core electrons (CCE), which are directly involved in the metal–metal bonding.²⁰⁴

Thus, the disproportionation of Group V–VII metals and Fe or Co , which belong to Group VIII of Period 4 of the Periodic Table, produces either stable mononuclear carbonyl complexes or clusters of few metal atoms. Polynuclear cluster structures are more typical of carbonyls of platinum Group VIII metals of Periods 5 and 6.

The reducing ability of metal carbonyls is an important factor, affecting the rate of the redox disproportionation induced by Lewis bases. This ability is determined by the single-electron reduction potential (E_{red}°). There are some difficulties in measuring E_{red}° , caused by chemical transformations of carbonyl complexes during electrolysis. The initially formed electron-rich radical anion of a metal carbonyl tends to transform into an electron-deficient one (transition $19e \rightarrow 17e$) by elimination of CO or by breaking of the metal–metal bond. More energetically favourable radical anion is formed in the former case. The unpaired electron of this radical anion is located in the highest occupied molecular orbital, which is lower than the lowest unoccupied molecular orbital bearing the unpaired electron of the initial 19-electron radical anion. The breaking of the metal–metal bond may be accompanied either by a decrease in the number of metal atoms in the complex or by rearrangement of the cluster core. For example, the initial 19-electron radical anions $[\text{Mn}_2(\text{CO})_{10}]^{\cdot -}$ and $[\text{Co}_2(\text{CO})_8]^{\cdot -}$ decompose quickly into 18-electron anions $[\text{Mn}(\text{CO})_5]^-$ and $[\text{Co}(\text{CO})_4]^-$ and 17-electron radicals $[\text{Mn}(\text{CO})_5]^\cdot$ and $[\text{Co}(\text{CO})_4]^\cdot$ respectively.^{134, 222, 224, 230, 231} The latter are then easily reduced to the corresponding anions, because their reduction potentials are less negative.²³² As a result, the two-electron reduction of the starting metal carbonyl takes place; in this process, the electrochemical stages are accompanied by a chemical reaction (ECE mechanism).²³³



The two-electron reduction in the ECE-reactions is also typical of $\text{Fe}(\text{CO})_5$ (see Section V, Fig. 1 and its caption) and for Group VI metal carbonyls $\text{M}(\text{CO})_6$ ($\text{M} = \text{Cr}, \text{Mo}, \text{W}$) [reactions (45)–(48)]. In these cases, as in the previous example, the reduction potential of the formation of binuclear complexes at the second electrochemical stage (48) is less negative than the potential of stage (45).^{43, 234}



[†] The chemistry of the carbonyl complexes of radioactive technetium is barely known. Only the reduction of $\text{Tc}_2(\text{CO})_{10}$ to $[\text{Tc}(\text{CO})_5]^-$ is described.²¹⁹

Another interpretation of this process with the same final product, instead of stages (47), (48), includes further reduction of $[\text{M}(\text{CO})_5]^{-\bullet}$ to $[\text{M}(\text{CO})_5]^{2-}$ and either the reaction of the latter with the starting complex $\text{M}(\text{CO})_6$ ($\text{M} = \text{Cr}$)⁴³ or its dimerisation, resulting in the formation of $[\text{M}_2(\text{CO})_{10}]^{2-}$ ($\text{M} = \text{Cr}, \text{Mo}, \text{W}$).⁴⁰ However, irrespective of the possible reaction pathway, the two-electron potential of the ECE process may be regarded, with some restrictions, as the potential of single-electron reduction of the metal carbonyl. The ECE process includes fast chemical transformations and the diffusion-controlled first stage [reaction (45)] with the most negative reduction potential.

In some cases, when relatively stable radical anions, *e.g.* $[\text{Fe}_3(\text{CO})_{12}]^{-\bullet}$, are formed, it is possible to determine two consecutive single-electron reduction potentials (Table 2).^{37–39}

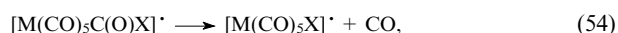
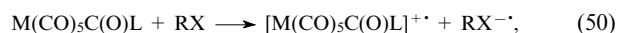
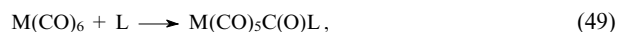
Table 2. Reduction potentials of metal carbonyls.

Starting complex	Product	Potential /V (method) ^a	Number of electrons ^b	Ref.
$\text{V}(\text{CO})_6$	$[\text{V}(\text{CO})_6]^{-}$	−0.21 (C)	1	40
$\text{Cr}(\text{CO})_6$	$[\text{Cr}_2(\text{CO})_{10}]^{2-}$	−2.66 (C) −2.7 (P)	2 1–2 ?	40 34
$\text{Mo}(\text{CO})_6$	$[\text{Mo}_2(\text{CO})_{10}]^{2-}$	−2.59 (C) −2.7 (P)	2 1 ?	40 34
$\text{W}(\text{CO})_6$	$[\text{W}_2(\text{CO})_{10}]^{2-}$	−2.63 (C) −2.9 (P)	2 1 ?	40 34
$\text{Fe}(\text{CO})_5$	$[\text{Fe}_2(\text{CO})_8]^{2-}$	−2.38 (C) −1.67 (C) −1.77 (P) −2.4 (P)	2 2 2 1 ?	40 37 39 34
$\text{Ni}(\text{CO})_4$	—	−2.70 (C) −2.80 (C) −2.9 (P)	2 2 1 ?	40 235 34
$\text{Mn}_2(\text{CO})_{10}$	$[\text{Mn}(\text{CO})_5]^{-}$	−1.65 (C) −1.8 (P)	2 2	40 34
$\text{Re}_2(\text{CO})_{10}$	$[\text{Re}(\text{CO})_5]^{-}$	−2.36 (C) −2.3 (P)	2 2	40 34
$\text{Co}_2(\text{CO})_8$	$[\text{Co}(\text{CO})_4]^{-}$	−0.75 (C)	2	235
$\text{Fe}_3(\text{CO})_{12}$	$[\text{Fe}_3(\text{CO})_{12}]^{-\bullet}$	−0.32 (P) −0.26 (C) −0.44 (C)	1 1 1	39 37 38
$\text{Ru}_3(\text{CO})_{12}$	$[\text{Ru}_3(\text{CO})_{12}]^{2-}$	−0.815 (P) −0.97 (P) −1.00 (C) −1.49 (P)	1 2 2 2	37 236 236 237
$\text{Os}_3(\text{CO})_{12}$	$[\text{Os}_3(\text{CO})_{12}]^{2-}$	−1.16 (P) −1.31 (P) −1.54 (C)	1 2 2	37 236 236

^aThe determination method is either the cyclic voltammetry (C) or polarography (P). ^bThe number of electrons, which determines the character (one- or two-electron) of the reduction potential, is indicated. The question mark means that the authors doubt the reliability of the value.

The reduction potentials listed in Table 2 were measured by different methods and under different conditions. These potentials describe the ECE processes, which are irreversible in some cases, but on the basis of these data, some qualitative conclusions about the ability of a carbonyl complex to undergo Lewis base-induced redox disproportionation may yet be drawn. The complexes $\text{M}(\text{CO})_6$ ($\text{M} = \text{Cr}, \text{Mo}, \text{W}$), possessing the most negative reduction potentials, are difficult to disproportionate. Therefore, the processes in which metal carbonyls reduce, for example, organic compounds are typical of the carbonyls of these metals. These complexes are used as the initiators of radical addition reactions, the olefin telomerisation with haloalkanes and the

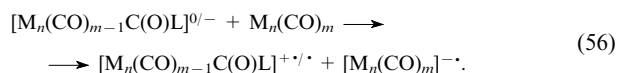
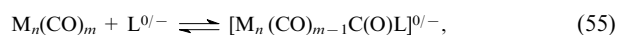
reduction of polychlorinated compounds.^{166–171, 238} Their transformations in the presence of Lewis bases may be described by reactions (49)–(54) similarly to reactions (37), (38) and (1), (2), (5) for $\text{Fe}(\text{CO})_5$.



$\text{M} = \text{Cr}, \text{Mo}, \text{W}$; $\text{X} = \text{Cl}, \text{Br}, \text{I}$; L is a Lewis base.

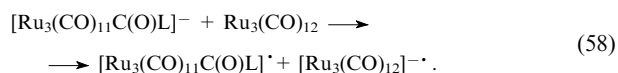
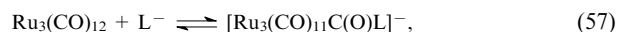
The radicals $\text{M}(\text{CO})_5\text{Cl}^{\bullet}$ ($\text{M} = \text{Cr}, \text{Mo}, \text{W}$), detected by the spin trap method, may be regarded as a proof for the suggested scheme.^{99, 166, 168, 169, 171, 238} Other metal carbonyls possessing low reduction potentials such as $\text{Re}_2(\text{CO})_{10}$, $\text{Mn}_2(\text{CO})_{10}$, $\text{Ni}(\text{CO})_4$, are also used as the initiators of similar reactions.^{166–171, 238, 239} In the case of binuclear complexes $\text{Re}_2(\text{CO})_{10}$, $\text{Mn}_2(\text{CO})_{10}$ and $\text{Co}_2(\text{CO})_8$, the initiation may proceed as a result of photolytic generation of monomeric radicals $[\text{M}(\text{CO})_5]^{\bullet}$ ($\text{M} = \text{Re}, \text{Mn}$) and $[\text{Co}(\text{CO})_4]^{\bullet}$, respectively.

The metal carbonyls possessing high reduction potentials, *e.g.*, $\text{V}(\text{CO})_6$, $\text{Co}_2(\text{CO})_8$ and $\text{Fe}_3(\text{CO})_{12}$, disproportionate easily. It is reasonable to suggest that this process proceeds according to a scheme similar to that proposed for iron carbonyls [see Section III, reactions (1)–(4)]:



The formation of the adducts $[\text{M}_n(\text{CO})_{m-1}\text{C}(\text{O})\text{L}]^{0/-}$ (see §) in the reactions of metal carbonyls with Lewis bases in the neutral (L^0) or anionic (L^{-}) form [reaction (55)] is well known and has been discussed in a review.⁸⁴ The higher is the reduction potential of the complex, the easier is the redox disproportionation according to equation (56). The detection of carbonyl radical anions in these processes is difficult due to their low stability, although they are known for most metal carbonyls. For instance, the $[\text{Ni}(\text{CO})_3]^{-\bullet}$ (Ref. 240), $[\text{Ni}_2(\text{CO})_7]^{-\bullet}$ (Ref. 241) and $[\text{M}(\text{CO})_5]^{-\bullet}$ ($\text{M} = \text{Cr},^{43, 241} \text{Mo}, \text{W}^{242}$) radical anions and the $[\text{M}(\text{CO})_5]^{\bullet}$ ($\text{M} = \text{Mn}, \text{Re}$)^{243–245} and $[\text{Co}(\text{CO})_4]^{\bullet}$ (Ref. 232) radicals formed upon decomposition of the $[\text{M}_2(\text{CO})_{10}]^{2-}$ and $[\text{Co}_2(\text{CO})_8]^{-\bullet}$ radical anions respectively, have been studied.

The $[\text{Ru}_3(\text{CO})_{12}]^{-\bullet}$ radical anion was detected in the reaction of $\text{Ru}_3(\text{CO})_{12}$ with anionic forms of bases: HO^{-} , MeO^{-} , EtO^{-} , EtS^{-} , Et_2N^{-} , H^{-} and Cl^{-} (Ref. 78). Taking into account the fact that the first stage of this reaction yields the $[\text{Ru}_3(\text{CO})_{11}\text{C}(\text{O})\text{L}]^{-}$ anion,⁸⁷ the scheme of single-electron redox disproportionation may be represented by reactions (57) and (58).

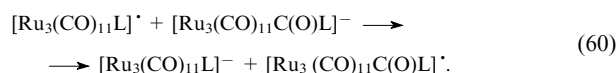


The CO group of the $[\text{Ru}_3(\text{CO})_{12}]^{-\bullet}$ radical anion may be substituted by another ligand (ETC process), similarly to the substitutions in iron carbonyl radical anions [see Scheme 5 and reactions (30), (31) and (33)], as occurs, for example, in the electrochemical generation of this species in the reactions of $\text{Ru}_3(\text{CO})_{12}$ with PPh_3 .²³⁶ The only difference is in the method of generation of the radical anion. This scheme describes well the

§ The superscript after the slash indicates the alternative charge.

nature of the catalytic action of various Lewis bases in the substitution of CO by phosphine ligands, which was studied in a series of papers.^{246–250} The catalytic activity of the $\text{Ru}_3(\text{CO})_{12}-\text{Et}_4\text{NCl}$ system in the reductive carbonylation of nitro compounds²⁵¹ may also be related to the generation of the radical anion $[\text{Ru}_3(\text{CO})_{12}]^{\cdot-}$, which is a total analogue of ICRA, which are the catalysts of these processes (see Section VIII).

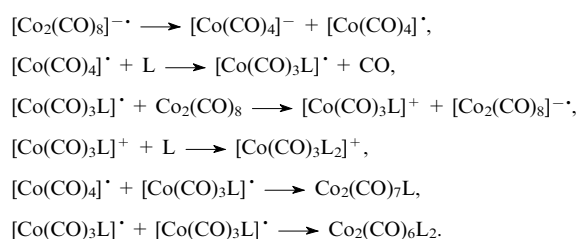
An important feature of the $\text{Ru}_3(\text{CO})_{12}$ complex should be noted: the main products of its reactions with such Lewis bases as halide ions are trinuclear complexes with halide ligands, and the yield of the (hydrido)carbonylruthenate anions is negligible.^{246, 248, 249} Probably, this is caused by the fact that the rearrangement of the radical product $[\text{Ru}_3(\text{CO})_{11}\text{C}(\text{O})\text{L}]^{\cdot}$ is accompanied by ETC process and, similarly to $\text{Fe}_3(\text{CO})_{12}$ [see reactions (34)–(36)], may be represented by the following equations:



Taking into account reaction (57), in the overall process, a significant part of reactants is converted into the final product $[\text{Ru}_3(\text{CO})_{11}\text{L}]^-$. The role of the single-electron transfer (58) in this process is reduced to the initial generation of the $[\text{Ru}_3(\text{CO})_{11}\text{C}(\text{O})\text{L}]^{\cdot}$ radical. Reactions (59) and (60) describe the formation of a possible product, $[\text{Ru}_3(\text{CO})_{11}\text{L}]^-$. Other products, $[\text{Ru}_3(\mu_2\text{-L})(\text{CO})_{10}]^-$ ($\text{L} = \text{Cl}, \text{Br}, \text{I}$) and $[\text{Ru}_3(\mu_3\text{-L})(\text{CO})_9]^-$ ($\text{L} = \text{I}$),²⁴⁸ are produced upon the subsequent transformation of the ligand L in the coordination sphere of the radical $[\text{Ru}_3(\text{CO})_{11}\text{L}]^{\cdot}$ followed by reduction.

The more negative is the reduction potential of a metal carbonyl, the less important are the processes of its redox disproportionation induced by Lewis bases. For instance, for the $\text{M}(\text{CO})_6$ ($\text{M} = \text{Cr}, \text{Mo}, \text{W}$),^{214, 217} the formation of the carbonyl group adducts $[\text{M}(\text{CO})_5\text{C}(\text{O})\text{L}]^-$ and their transformation into $[\text{M}(\text{CO})_5\text{L}]^-$ may be represented by reactions (57)–(60). In these reactions, thermodynamically the most unfavourable redox stage (58) is the first stage of the process initiation.

Whereas for metal carbonyls with the most negative reduction potentials the transformations of M^+ complexes formed at the redox disproportionation step of process (58) are typical, in the case of complexes with higher reduction potentials, the transformations of the $\text{M}(0)$ derivatives become more significant. The reaction of $\text{Co}_2(\text{CO})_8$ with ligands L ($\text{L} = \text{AsPh}_3, \text{PBu}_3, \text{PPh}_3, ^{13}\text{CO}$) is an example of such transformation. The initiation of the reaction of the starting metal carbonyl by a base first produces the $[\text{Co}_2(\text{CO})_8]^{\cdot-}$ radical anion [reactions (55) and (56)]; its further transformations proceed as follows:²³¹



Substituted cobalt carbonyls $\text{Co}_2(\text{CO})_7\text{L}$ ($\text{L} = \text{AsPh}_3$), $\text{Co}_2(\text{CO})_6\text{L}_2$ ($\text{L} = \text{AsPh}_3, \text{PBu}_3$) and the ionic complex $[\text{Co}(\text{CO})_3\text{L}_2][\text{Co}(\text{CO})_4]$ ($\text{L} = \text{PBu}_3, \text{PPh}_3$) are the final products of the radical chain process. Similar radical chain substitution of CO by various basic ligands during photochemical disproportionation of $\text{Mn}_2(\text{CO})_{10}$ has been described.²³⁰

Thus, the reactions of metal carbonyls with Lewis bases may be represented by a single scheme of redox disproportionation. This scheme includes the stage of activating complex formation (55) followed by single-electron transfer from a carbonyl complex

activated by an electron donor to another metal carbonyl molecule. The radical and radical ion complexes formed at stage (56) may undergo two types of transformations: (i) further disproportionation yielding stable cationic metal complexes containing Lewis bases in the coordination sphere and (hydrido)carbonylmethylate anions; (ii) radical chain ETC processes, resulting in the formation of diamagnetic derivatives of metal carbonyl complexes with initial oxidation state of the metal $\text{M}(0)$.

XI. Conclusion

Two types of redox reactions underlie catalytic carbonylation of various compounds by iron carbonyls. The first type is the redox disproportionation of iron carbonyl induced by Lewis bases (see Section III), while the second type is the oxidative addition of the Brønsted or Lewis acids to carbonylferrate and hydridocarbonylferrate anions (see Section IV). The reactions of both types include single-electron stages of redox initiation and subsequent radical chain transformations of iron carbonyl complexes. The resulting iron carbonyl radical anions are coordinatively unsaturated electron-deficient systems with labile coordination sphere, capable of the fast ligand and electron exchange. These particular properties allow one to suggest that ICRA are the catalytically active species in carbonylation processes (see Section VIII). It is very important to note that a catalytic cycle with radical anions as catalysts is based on the transformations which include consecutive formation of the odd-electron complexes ($17e \rightarrow 19e \rightarrow 17e$), the whole process having a radical chain character. This scheme uncontradictorily describes from a unified standpoint the two-electron redox processes of iron carbonyls and explains the formation of all known reaction products. Besides, this scheme is able to interpret the main chemical transformations of other metals carbonyls, to suggest new promising catalytic systems for carbonylation and to propose the optimal conditions for homogeneous catalysis (the heterogeneous catalysis is beyond the scope of the present review).

Mononuclear complexes and small clusters are effective homogeneous catalysts of various processes with CO participation. It is advisable to use either carbonyl complexes of the Period 4 transition metals, which do not form big clusters, or to use complexes with bulky substituents, which prevents the clusterisation of the platinum-group metals, such as, for example, the Wilkinson catalyst $[\text{RhCl}(\text{PPh}_3)_3]$ or the complex $\text{RhH}(\text{CO}).(\text{PPh}_3)_3$. These platinum group metal-based catalysts may be effectively applied in the small-scale organic synthesis of expensive chemicals,²⁵² but they are not cost-effective in the large-scale industrial processes. Moreover, in the course of the process the ligands in the metal coordination sphere may be replaced by molecules of the main process participants (in our case, CO). This results in the change in the catalytic system properties. The metal carbonyl-based complexes are suitable catalysts as they contain the ligands taking part in the catalysis. In this respect, the commercially available carbonyl complexes of Group VIII metals, namely, Fe, Co and Ni, are the most promising as catalysts. The cobalt carbonyl complexes are industrially important and used in hydroformylation.^{6, 12} Numerous studies of Fe and Ni carbonyl complexes have revealed their reduced catalytic activity in comparison with that of the platinum-group metal carbonyls in, for example, hydroformylation and water gas conversion^{6, 17} and in the reductive carbonylation of nitro compounds.²⁵³ A possible reason for such reduced activity may be the traditional approach towards the catalytic processes with participation of metal carbonyls, according to which they are carried out under the conditions similar to those of their synthesis (high pressure and temperature). Assuming that in the case of Fe and Ni, the metal carbonyl radical anions are the catalytically active species in carbonylation, it is possible to suggest that the optimal conditions for their catalytic activity will be controlled reduction potential of the medium and also relatively low temperature and a nearly

atmospheric CO pressure. This results in a new approach to catalytic carbonylation processes, namely, the idea to carry out the process under conditions favourable for chain propagation reactions rather than under the traditional conditions involving high pressures and temperatures. The traditional conditions increase the role of chain termination reactions and decrease the catalytic activity of metal carbonyl radical anions.

The reduction potential of the reaction medium is an important condition for the formation of Fe and Ni carbonyl complexes from their inorganic salts. For instance, the following compounds were obtained at room temperature and atmospheric CO pressure: $\text{Na}_2\text{Fe}(\text{CO})_4$ from FeCl_3 and $[\text{Na}^+(\text{C}_{10}\text{H}_8)^-]^-$;²⁵⁴ $[\text{HFe}(\text{CO})_4]^-$ from FeCl_3 and NaBH_4 upon acetic acid treatment;²⁵⁵ $\text{Ni}(\text{CO})_4$ from $\text{Ni}(\text{acac})_2$ (acac is acetylacetonate) upon reduction with Bu_2AlH , Bu^nLi or Pr^nMgBr ;²⁵⁶ $\text{Ni}(\text{CO})_2(\text{bipy})$ (bipy is bipyridyl) upon electrochemical reduction of $[\text{Ni}(\text{bipy})]^{2+}$ (Ref. 257). It should also be noted that the catalytic synthesis of ammonia from N_2 and H_2 (using the coal-supported $\text{K}_2\text{Fe}(\text{CO})_8$ – metallic sodium system²⁵⁸ as a catalyst), quite similar to carbonylation, also proceeds in reductive media.

It is necessary to note the second important aspect of the catalytic processes, namely, that they follow a radical chain mechanism proceeding through the $17e \rightarrow 19e \rightarrow 17e$ complexes. Similar radical reaction schemes were discussed in the late 1970s,^{259,260} but this idea has not been generalised and was regarded as a specific case. The traditional approach, which describes the process in usual terms of the Tolman rule about 16-electron intermediates, has prevailed. However, the latest studies attest more and more often to the radical chain mechanism as the major one for such catalytic processes. For example, the electrochemical studies of very well known complexes, the Wilkinson catalyst and $\text{RhH}(\text{CO})(\text{PPh}_3)_3$, have revealed that they easily form radical cations ($E_{1/2\text{ox}} = +0.035 \text{ V}$, Ref. 261, and $E_{1/2\text{ox}} = -0.48 \text{ V}$, Ref. 262, respectively). This means that, according to the Nernst equation, the radical cation concentration in a catalytic process may reach tens of percent even when the electrochemical potential of the reaction medium is close to neutral. The role of such active species must be taken into account.

Thus, the features of the radical chemistry of iron carbonyls discussed in the present review provide new opportunities in the search for effective catalysts for metal carbonyl-based carbonylation processes and in carrying out these processes as radical chain ones with odd-electron (17 and 19) intermediates and under the controlled electrochemical potential of the reaction media.

References

1. L Mond, C Langer, F Quincke *J. Chem. Soc.* 749 (1890)
2. M Berthelot *C.R. Seances Acad. Sci.* **112** 1343 (1891)
3. L Mond, F Quincke *J. Chem. Soc.* 604 (1891)
4. H Pichler, H Schulz *Chem. Ing. Techn.* **42** 1162 (1970)
5. G Henrici-Olivé, S Olivé *The Chemistry of the Catalyzed Hydrogenation of Carbon Monoxide* (New York: Springer, 1984)
6. R A Sheldon *Chemicals from Synthesis Gas* (Dordrecht: Reidel, 1983)
7. M Röper, in *Catalysis in C₁ Chemistry* (Ed. W Keim) (Dordrecht: Reidel, 1983) p. 41
8. O Rölen *Angew. Chem.* **60** 62 (1948)
9. W Reppe, H Vetter *Liebigs Ann. Chem.* **582** 133 (1953)
10. W A Herrmann *Angew. Chem., Int. Ed. Engl.* **21** 117 (1982)
11. B N Kuznetsov, V I Koval'chuk *Kinet. Katal.* **36** 353 (1995)^a
12. W Keim (Ed.) *Catalysis in C₁ Chemistry* (Dordrecht: Reidel, 1983)
13. W Hieber *Adv. Organomet. Chem.* **8** 1 (1970)
14. F Calderazzo, R Ercoli, G Natta in *Organic Syntheses via Metal Carbonyls* Vol. 1 (Eds I Wender, P Pino) (New York: Wiley, 1968) p. 1
15. D F Shriver, K H Whitmire, in *Comprehensive Organometallic Chemistry* Vol. 4 (Ed. G Wilkinson) (Oxford: Pergamon Press, 1982) p. 243
16. K H Whitmire, in *Comprehensive Organometallic Chemistry II* Vol. 7 (Eds D F Shriver, M I Bruce) (Oxford: Pergamon Press, 1995) p. 1
17. H C Kang, C H Mauldin, T Cole, W Slegier, K Cann, R Pettit *J. Am. Chem. Soc.* **99** 8323 (1977)
18. R Pettit, C H Mauldin, T Cole, H Kang *Ann. N.Y. Acad. Sci.* **295** 151 (1977)
19. R B King, A D King *Izv. Akad. Nauk, Ser. Khim.* 1533 (1994)^b
20. R B King *J. Organomet. Chem.* **586** 2 (1999)
21. J-K Shen, Y-C Gao, Q-Z Shi, F Basolo *Organometallics* **8** 2144 (1989)
22. F Basolo *J. Organomet. Chem.* **383** 579 (1990)
23. F Basolo *Polyhedron* **9** 1503 (1990)
24. J-K Shen, Y-C Gao, Q-Z Shi, F Basolo *Coord. Chem. Rev.* **128** 69 (1993)
25. C A Tolman *Chem. Soc. Rev.* 337 (1972)
26. A J Ouderkirk, P Werner, N L Schultz, E Weitz *J. Am. Chem. Soc.* **105** 3354 (1983)
27. T A Seder, A J Ouderkirk, E Weitz *J. Chem. Phys.* **85** 1977 (1986)
28. M Poliakoff, J J Turner *J. Chem. Soc., Dalton Trans.* 1351 (1973)
29. M Poliakoff, J J Turner *J. Chem. Soc., Dalton Trans.* 2276 (1974)
30. M Poliakoff, E Weitz *Acc. Chem. Res.* **20** 408 (1987)
31. M Zhou, L Andrews, C W Bauschlicher Jr *Chem. Rev.* **101** 1931 (2001)
32. P T Snee, C K Payne, K T Kotz, H Yang, C B Harris *J. Am. Chem. Soc.* **123** 2255 (2001)
33. M Poliakoff, J J Turner *Angew. Chem., Int. Ed.* **40** 2809 (2001)
34. R E Dessy, F E Stary, R B King, M Waldrop *J. Am. Chem. Soc.* **88** 471 (1966)
35. R E Dessy, R B King, M Waldrop *J. Am. Chem. Soc.* **88** 5112 (1966)
36. R E Dessy, L E Bares *Acc. Chem. Res.* **5** 415 (1972)
37. A M Bond, P A Dawson, B M Peake, B H Robinson, J Simpson *Inorg. Chem.* **16** 2199 (1977)
38. D Miholova, J Klima, A A Vlček *Inorg. Chim. Acta* **27** L67 (1978)
39. N El Murr, A Chaloyard *Inorg. Chem.* **21** 2206 (1982)
40. C J Pickett, D Pletcher *J. Chem. Soc., Dalton Trans.* 879 (1975)
41. G J Bezems, P H Rieger, S Visco *J. Chem. Soc., Chem. Commun.* 265 (1981)
42. C Amatore, J-N Verpeaux, P J Krusic *Organometallics* **7** 2426 (1988)
43. C Amatore, P J Krusic, S U Pedersen, J-N Verpeaux *Organometallics* **14** 640 (1995)
44. B M Peake, B H Robinson, J Simpson, D J Watson *J. Chem. Soc., Chem. Commun.* 945 (1974)
45. P A Dawson, B M Peake, B H Robinson, J Simpson *Inorg. Chem.* **19** 465 (1980)
46. P J Krusic, J S Filippo Jr, B Hutchinson, R L Hance, L M Daniels *J. Am. Chem. Soc.* **103** 2129 (1981)
47. J R Morton, K F Preston, Y Le Page, P J Krusic *J. Chem. Soc., Faraday Trans. 1* **85** 4019 (1989)
48. P A Breeze, J K Burdett, J J Turner *Inorg. Chem.* **20** 3369 (1981)
49. P J Krusic, D J Jones, D C Roe *Organometallics* **5** 456 (1986)
50. B M Peake, M C R Symons, J L Wyatt *J. Chem. Soc., Dalton Trans.* 1171 (1983)
51. S A Fairhurst, J R Morton, K F Preston *J. Chem. Phys.* **77** 5872 (1982)
52. J R Morton, K F Preston, J-P Charland, P J Krusic *J. Mol. Struct.* **223** 115 (1990)
53. M Zhou, V Chertihin, L Andrews *J. Chem. Phys.* **109** 10893 (1998)
54. M Zhou, L Andrews *J. Chem. Phys.* **110** 10370 (1999)
55. F Ragaini, D L Ramage, J-S Song, G L Geoffroy, A L Rheingold *J. Am. Chem. Soc.* **115** 12183 (1993)
56. F Ragaini, J-S Song, D L Ramage, G L Geoffroy, G A P Yap, A L Rheingold *Organometallics* **14** 387 (1995)
57. F Ragaini *Organometallics* **15** 3572 (1996)

58. P J Krusic *J. Am. Chem. Soc.* **103** 2131 (1981)
59. Yu A Belousov *Izv. Akad. Nauk, Ser. Khim.* 1048 (1997)^b
60. F-H Luo, S-R Yang, C-S Li, J-P Duan, C-H Cheng *J. Chem. Soc., Dalton Trans.* 2435 (1991)
61. A S Huffadine, B M Peake, B H Robinson, J Simpson *Aust. J. Chem.* **36** 613 (1983)
62. A Grand, P J Krusic, L Noodleman, R Subra *J. Mol. Struct. (THEOCHEM)* **226** 251 (1991)
63. P J Krusic, J R Morton, K F Preston, A J Williams, F L Lee *Organometallics* **9** 697 (1990)
64. P C Engelking, W C Lineberger *J. Am. Chem. Soc.* **101** 5569 (1979)
65. A E Stevens, C S Feigerle, W C Lineberger *J. Am. Chem. Soc.* **104** 5026 (1982)
66. P W Villalta, D G Leopold *J. Chem Phys.* **98** 7730 (1993)
67. K Lane, L Sallans, R R Squires *J. Am. Chem. Soc.* **106** 2719 (1984)
68. R R Squires *Chem. Rev.* **87** 623 (1987)
69. R N McDonald, A K Chowdhury, P L Schell *J. Am. Chem. Soc.* **106** 6095 (1984)
70. R N McDonald, P L Schell *Organometallics* **7** 1820 (1988)
71. R L Dunbar, J F Ennever, J P Fackler Jr *Inorg. Chem.* **12** 2734 (1973)
72. J Wronka, D P Ridge *Int. J. Mass Spectrom. Ion Phys.* **43** 23 (1982)
73. J Wronka, D P Ridge *J. Am. Chem. Soc.* **106** 67 (1984)
74. D T Moore, J Oomens, J R Eyler, G Meijer, G von Helden, D P Ridge *J. Am. Chem. Soc.* **126** 14726 (2004)
75. V N Babin, Yu A Belousov, V V Gumenyuk, R M Salimov, R B Materikova, N S Kochetkova *J. Organomet. Chem.* **241** C41 (1983)
76. Yu A Belousov, T A Kolosova *Polyhedron* **6** 1959 (1987)
77. Yu A Belousov, T A Kolosova, V N Babin *Polyhedron* **8** 603 (1989)
78. Yu A Belousov, T A Belousova *Izv. Akad. Nauk, Ser. Khim.* 248 (1996)^b
79. Yu A Belousov, T A Belousova *Polyhedron* **18** 2605 (1999)
80. P K S Tsang, P Cofre, D T Sawyer *Inorg. Chem.* **26** 3604 (1987)
81. J A Pedersen *J. Chem. Soc., Perkin Trans. 2* 424 (1973)
82. G A Abakumov, Doctoral Thesis in Chemical Sciences, Gor'kii State University, Gor'kii, 1975
83. G A Abakumov, in *Metalloorganicheskie Soedineniya i Radikaly* (Organometallic Compounds and Radicals) (Ed. M I Kabachnik) (Moscow: Nauka, 1985) p. 85
84. P C Ford, A Rokicki *Adv. Organomet. Chem.* **28** 139 (1988)
85. D C Gross, P C Ford *Inorg. Chem.* **21** 1702 (1982)
86. R J Trautman, D C Gross, P C Ford *J. Am. Chem. Soc.* **107** 2355 (1985)
87. D C Gross, P C Ford *J. Am. Chem. Soc.* **107** 585 (1985)
88. K R Lane, R E Lee, L Sallans, R R Squires *J. Am. Chem. Soc.* **106** 5767 (1984)
89. K R Lane, L Sallans, R R Squires *J. Am. Chem. Soc.* **107** 5369 (1985)
90. K R Lane, L Sallans, R R Squires *J. Am. Chem. Soc.* **108** 4368 (1986)
91. K R Lane, R R Squires *J. Am. Chem. Soc.* **108** 7187 (1986)
92. L S Sunderlin, R R Squires *J. Am. Chem. Soc.* **115** 337 (1993)
93. W O Siegl, J P Collman *J. Am. Chem. Soc.* **94** 2516 (1972)
94. R E Stevens, W L Gladfelter *Inorg. Chem.* **22** 2034 (1983)
95. R Massoudi, J H Kim, R B King, A D King Jr *J. Am. Chem. Soc.* **109** 7428 (1987)
96. Yu A Belousov, E F Brin *Polyhedron* **20** 2765 (2001)
97. Yu A Belousov, T A Kolosova, E A Viktorova, V A Sergeev, V N Babin *Izv. Akad. Nauk SSSR, Ser. Khim.* 1652 (1987)^b
98. D Seyferth, G B Womack, J C Dewan *Organometallics* **4** 398 (1985)
99. R G Gasanov, R Kh Freidlina *Dokl. Akad. Nauk SSSR* **235** 1309 (1977)^c
100. P K Baker, N G Connelly, B M R Jones, J P Maher, K R Somers *J. Chem. Soc., Dalton Trans.* 579 (1980)
101. R N Bagchi, A M Bond, C L Heggie, T L Henderson, E Mocellin, R A Seikel *Inorg. Chem.* **22** 3007 (1983)
102. N G Connelly *Chem. Soc. Rev.* **18** 153 (1989)
103. L Song, W C Trogler *J. Am. Chem. Soc.* **114** 3355 (1992)
104. J H MacNeil, A C Chiverton, S Fortier, M C Baird, R C Hynes, A J Williams, K F Preston, T Ziegler *J. Am. Chem. Soc.* **113** 9834 (1991)
105. Yu A Belousov, in *Proceedings of the Xth FEChem Conference on Organometallic Chemistry, Agia Pelagia, Greece, 1993* p. 108
106. P J Fagan, in *Comprehensive Organometallic Chemistry II* Vol. 7 (Eds D F Shriver, M I Bruce) (Oxford: Pergamon Press, 1995) p. 231
107. M Akita, in *Comprehensive Organometallic Chemistry II* Vol. 7 (Eds D F Shriver, M I Bruce) (Oxford: Pergamon Press, 1995) p. 259
108. S L Yang, C S Li, C H Cheng *J. Chem. Soc., Chem. Commun.* 1872 (1987)
109. J-J Brunet *Chem. Rev.* **90** 1041 (1990)
110. A L Lapidus, E Z Gil'denberg, A R Sharipova, N F Kononov, Ya T Eidus *Kinet. Katal.* **17** 1483 (1976)^a
111. J P Collman *Acc. Chem. Res.* **8** 342 (1975)
112. M Periasamy, A Devasagayaram, U Radhakrishnan *Organometallics* **12** 1424 (1993)
113. J P Collman, R G Finke, P L Matlock, R Wahren, R G Komoto, J I Brauman *J. Am. Chem. Soc.* **100** 1119 (1978)
114. R Noyori, I Umeda, T Ishigami *J. Org. Chem.* **37** 1542 (1972)
115. S Sabo-Etienne, H des Abbayes, L Toupet *Organometallics* **6** 2262 (1987)
116. S C Kao, C T Spillett, C E Ash, R J Lusk, Y K Park, M Y Darensbourg *Organometallics* **4** 83 (1985)
117. K H Whitmire, T R Lee, E S Lewis *Organometallics* **5** 987 (1986)
118. J-J Brunet, D de Montauzon, M Taillefer *Organometallics* **10** 341 (1991)
119. R G Finke, T N Sorrell *Org. Synth.* **59** 102 (1979)
120. J P Collman, R G Finke, J N Cawse, J I Brauman *J. Am. Chem. Soc.* **99** 2515 (1977)
121. H Alper, M Tanaka *J. Am. Chem. Soc.* **101** 4245 (1979)
122. D W Hensley, W L Wurster, R P Stewart Jr *Inorg. Chem.* **20** 645 (1981)
123. P Laurent, S Sabo-Etienne, A-M Laronneur, H des Abbayes *J. Chem. Soc., Chem. Commun.* 929 (1988)
124. P Laurent, J-Y Salaun, G Le Gall, M Sellin, H des Abbayes *J. Organomet. Chem.* **466** 175 (1994)
125. J C Barborak, K Cann *Organometallics* **1** 1726 (1982)
126. M Tilset, V D Parker *J. Am. Chem. Soc.* **111** 6711 (1989)
127. Y Zhen, J D Atwood *Organometallics* **10** 2778 (1991)
128. H Strong, P J Krusic, J S Filippo Jr *Inorg. Synth.* **24** 157 (1988)
129. D J Curran, P B Graham, M D Rausch *Organometallics* **12** 2380 (1993)
130. G L Geoffroy, W L Gladfelter *J. Am. Chem. Soc.* **99** 7565 (1977)
131. F R Furuya, W L Gladfelter *J. Chem. Soc., Chem. Commun.* 129 (1986)
132. H O House, E Feng, N P Peet *J. Org. Chem.* **36** 2371 (1971)
133. N K Bhattachaya, T J Coffy, W Quintana, T A Salupo, J C Bricker, T B Shay, M Payne, S G Shore *Organometallics* **9** 2368 (1990)
134. M S Corrairie, J D Atwood *Organometallics* **10** 2647 (1991)
135. M S Corrairie, J D Atwood *Organometallics* **10** 2985 (1991)
136. W L Gladfelter, G L Geoffroy *Adv. Organomet. Chem.* **18** 207 (1980)
137. M Y Darensbourg, C E Ash, L W Arndt, C P Janzen, K A Youngdahl *J. Organomet. Chem.* **383** 191 (1990)
138. T M Bockman, H-C Cho, J K Kochi *Organometallics* **14** 5221 (1995)
139. B Neumüller, W Petz *Organometallics* **20** 163 (2001)
140. H B Chin, M B Smith, R D Wilson, R Bau *J. Am. Chem. Soc.* **96** 5285 (1974)
141. J M Cassidy, K H Whitmire, G J Long *J. Organomet. Chem.* **427** 355 (1992)
142. S Wawzonek, M E Runner *J. Electrochem. Soc.* **99** 457 (1952)
143. R C Larson, R T Iwamoto *J. Am. Chem. Soc.* **82** 3239 (1960)
144. M I Bruce, D C Kehoe, J G Matison, B K Nicholson, P H Rieger, M L Williams *J. Chem. Soc., Chem. Commun.* 442 (1982)

145. M I Bruce, T W Hambley, B K Nicholson *J. Chem. Soc., Dalton Trans.* 2385 (1983)
146. M Arewgoda, B H Robinson, J Simpson *J. Am. Chem. Soc.* **105** 1893 (1983)
147. H H Ohst, J K Kochi *J. Chem. Soc., Chem. Commun.* 121 (1986)
148. H H Ohst, J K Kochi *Inorg. Chem.* **25** 2066 (1986)
149. H H Ohst, J K Kochi *J. Am. Chem. Soc.* **108** 2897 (1986)
150. T M Bockman, J K Kochi *J. Am. Chem. Soc.* **109** 7725 (1987)
151. T M Bockman, Y Wong, J K Kochi *New J. Chem.* **12** 387 (1988)
152. P Lahuerta, J Latorre, M Sanau *J. Organomet. Chem.* **286** C27 (1985)
153. A Darchen, C Mahe, H Patin *J. Chem. Soc., Chem. Commun.* 243 (1982)
154. A Darchen, C Mahe, H Patin *Nouv. J. Chim.* **6** 539 (1982)
155. S B Butts, D F Shriver *J. Organomet. Chem.* **169** 191 (1979)
156. M O Albers, N J Coville *Coord. Chem. Rev.* **53** 227 (1984)
157. M Chanon *Acc. Chem. Res.* **20** 214 (1987)
158. W Kaim *Coord. Chem. Rev.* **76** 187 (1987)
159. A Darchen, E K Lhadi, H Patin, D Grandjean, A Mousser *J. Organomet. Chem.* **385** C4 (1990)
160. J W Hersherberger, R J Klingler, J K Kochi *J. Am. Chem. Soc.* **104** 3034 (1982)
161. P K Baker, K Broadley, N G Connelly *J. Chem. Soc., Dalton Trans.* 471 (1982)
162. H Sayo, Y Tsukitani, M Masui *Tetrahedron* **24** 1717 (1968)
163. M Stackelberg, W Stracke *Z. Elektrochem.* **53** 118 (1949)
164. E Levillain, F Gaillard, P Leghie, A Demortier, J P Lelieur *J. Electroanal. Chem.* **420** 167 (1997)
165. A K Hoffmann, A T Henderson *J. Am. Chem. Soc.* **83** 4671 (1961)
166. R Kh Freidlina, F K Velichko, S S Zlatskii, D L Rakhmankulov, A B Terent'ev *Radikal'naya Telomerizatsiya* (Radical Telomerisation) (Moscow: Khimiya, 1988)
167. R Kh Freidlina, F K Velichko, A B Terent'ev *Usp. Khim.* **53** 370 (1984) [*Russ. Chem. Rev.* **53** 222 (1984)]
168. E Ts Chukovskaya, R G Gasanov, I I Kandror, R Kh Freidlina *Zh. Vsesous. Khim. O-va im D I Mendeleeva* **24** 161 (1979)^d
169. R Kh Freidlina, R G Gasanov, N D Kuz'mina, E Ts Chukovskaya *Usp. Khim.* **54** 1127 (1985) [*Russ. Chem. Rev.* **54** 662 (1985)]
170. R G Gasanov, R Kh Freidlina *Usp. Khim.* **56** 447 (1987) [*Russ. Chem. Rev.* **56** 264 (1987)]
171. R G Gasanov, R Kh Freidlina *Izv. Akad. Nauk SSSR, Ser. Khim.* 1045 (1983)^b
172. W Hieber, A Wirsching *Z. Anorg. Allg. Chem.* **245** 35 (1940)
173. V I Tararov, A P Pisarevskii, Yu N Belokon' *Izv. Akad. Nauk, Ser. Khim.* 916 (1996)^b
174. T A Kolosova, Candidate Thesis in Chemical Sciences, M V Lomonosov Moscow State University, Moscow, 1988
175. J H Lunsford, D P Johnson *J. Chem. Phys.* **58** 2079 (1973)
176. S-I Tobishima, H Yamamoto, M Matsuda *Electrochim. Acta* **42** 1019 (1997)
177. F Gaillard, E Levillain *J. Electroanal. Chem.* **398** 77 (1995)
178. E Levillain, F Gaillard, P Leghie *J. Electroanal. Chem.* **440** 243 (1997)
179. N S Nametkin, V D Tyurin, M A Kukina *J. Organomet. Chem.* **149** 355 (1978)
180. N S Nametkin, V D Tyurin, M A Kukina *Usp. Khim.* **55** 815 (1986) [*Russ. Chem. Rev.* **55** 439 (1986)]
181. N S Nametkin, V D Tyurin, G G Aleksandrov, I V Petrosyan, B I Kolobkov, A M Krapivin, Yu T Struchkov *Izv. Akad. Nauk SSSR, Ser. Khim.* 2572 (1981)^b
182. A I Nekhaev, S D Alekseeva, B I Kolobkov, G G Aleksandrov, M T Toshev, H B Dustov, N A Parpiev *J. Organomet. Chem.* **401** 65 (1991)
183. Y Watanabe, O Yamada, K Fujita, Y Takegami, T Suzuki *Fuel* **63** 752 (1984)
184. T Suzuki, O Yamada, Y Takahashi, Y Watanabe *Fuel Process. Technol.* **10** 33 (1985)
185. Y Watanabe, H Yamada, N Kawasaki, K Hata, K Wada, T Mitsudo *Fuel* **75** 46 (1996)
186. H Alper *Inorg. Chem.* **11** 976 (1972)
187. G D Williams, R R Whittle, G L Geoffroy, A L Rheingold *J. Am. Chem. Soc.* **109** 3936 (1987)
188. V I Manov-Yuvenskii, B K Nefedov *Usp. Khim.* **50** 889 (1981) [*Russ. Chem. Rev.* **50** 470 (1981)]
189. S Aime, G Gervasio, L Milone, R Rossetti, P L Stanghellini *J. Chem. Soc., Dalton Trans.* 534 (1978)
190. L G Abakumova, Candidate Thesis in Chemical Sciences, Rostov State University, Rostov-on-Don, 1978
191. M O Albers, N J Coville, E Singleton *J. Chem. Soc., Dalton Trans.* 1069 (1982)
192. M O Albers, N J Coville, C P Nicolaides, R A Webber, T V Ashworth, E Singleton *J. Organomet. Chem.* **217** 247 (1981)
193. M O Albers, N J Coville, E Singleton *J. Chem. Soc., Chem. Commun.* 96 (1982)
194. I C Bricker, M W Payne, S G Shore *Organometallics* **6** 2545 (1987)
195. R L Keiter, E A Keiter, K H Hecker, C A Boecker *Organometallics* **7** 2466 (1988)
196. J A Gladysz *Adv. Organomet. Chem.* **20** 1 (1982)
197. S R Winter, G W Cornett, E A Thompson *J. Organomet. Chem.* **133** 339 (1977)
198. S W Lee, W D Tucker, M G Richmond *J. Organomet. Chem.* **398** C6 (1990)
199. W O Siegl *J. Organomet. Chem.* **92** 321 (1975)
200. H Masada, M Mizuno, S Suga, Y Watanabe, Y Takegami *Bull. Chem. Soc. Jpn.* **43** 3824 (1970)
201. Y Takegami, Y Watanabe, I Kanaya, T Mitsudo, T Okajima, Y Morishita, H Masada *Bull. Chem. Soc. Jpn.* **41** 2990 (1968)
202. T Mitsudo, Y Watanabe, M Tanaka, S Atsuta, K Yamamoto, Y Takegami *Bull. Chem. Soc. Jpn.* **48** 1506 (1975)
203. T J Lynch, M Banah, H D Kaesz, C R Porter *J. Org. Chem.* **49** 1266 (1984)
204. S P Gubin *Khimiya Klasterov* (The Chemistry of Clusters) (Moscow: Nauka, 1987)
205. N G Connelly, in *Comprehensive Organometallic Chemistry* Vol. 3 (Ed. G Wilkinson) (Oxford: Pergamon Press, 1982) p. 647
206. W Hiber, J Ellermann, E Zahn *Z. Naturforsch., B* **18** 589 (1963)
207. P W Jolly, in *Comprehensive Organometallic Chemistry* Vol. 6 (Ed. G Wilkinson) (Oxford: Pergamon Press, 1982) p. 3
208. A F Masters, J T Meyer *Polyhedron* **14** 339 (1995)
209. V I Spitsyn, I V Fedoseev *Karbonil'nye Kompleksy Platinovykh Metallov* (Carbonyl Complexes of Platinum Metals) (Moscow: Nauka, 1980)
210. G Longoni, P Chini *J. Am. Chem. Soc.* **98** 7225 (1976)
211. M D Grillone, L Palmisano *Transition Met. Chem.* **14** 81 (1989)
212. J K Burdett *Coord. Chem. Rev.* **27** 1 (1978)
213. D J Darensbourg, A Rokicki, M Y Darensbourg *J. Am. Chem. Soc.* **103** 3223 (1981)
214. S W Kirtley, in *Comprehensive Organometallic Chemistry* Vol. 3 (Ed. G Wilkinson) (Oxford: Pergamon Press, 1982) p. 783
215. S W Kirtley, in *Comprehensive Organometallic Chemistry* Vol. 3 (Ed. G Wilkinson) (Oxford: Pergamon Press, 1982) p. 1079
216. S W Kirtley, in *Comprehensive Organometallic Chemistry* Vol. 3 (Ed. G Wilkinson) (Oxford: Pergamon Press, 1982) p. 1255
217. A Bates, M T Muraoka, R J Trautman *Inorg. Chem.* **32** 2651 (1993)
218. S Woodward, in *Comprehensive Organometallic Chemistry II* Vol. 5 (Eds E W Abel, F G A Stone, G Wilkinson) (Oxford: Pergamon Press, 1995) p. 215
219. A P Sattelberger, J C Bryan, in *Comprehensive Organometallic Chemistry II* Vol. 6 (Eds E W Abel, F G A Stone, G Wilkinson) (Oxford: Pergamon Press, 1995) p. 151
220. N M Boag, H D Kaesz, in *Comprehensive Organometallic Chemistry* Vol. 4 (Ed. G Wilkinson) (Oxford: Pergamon Press, 1982) p. 161
221. P M Treichel, in *Comprehensive Organometallic Chemistry* Vol. 4 (Ed. G Wilkinson) (Oxford: Pergamon Press, 1982) p. 1

222. P M Treichel, in *Comprehensive Organometallic Chemistry II* Vol. 6 (Eds E W Abel, F G A Stone, G Wilkinson) (Oxford: Pergamon Press, 1995) p. 1
223. R D W Kemmitt, D R Russell, in *Comprehensive Organometallic Chemistry* Vol. 5 (Ed. G Wilkinson) (Oxford: Pergamon Press, 1982) p. 1
224. R L Sweany, in *Comprehensive Organometallic Chemistry II* Vol. 8 (Eds E W Abel, F G A Stone, G Wilkinson) (Oxford: Pergamon Press, 1995) p. 1
225. C E Barnes, in *Comprehensive Organometallic Chemistry II* Vol. 8 (Eds E W Abel, F G A Stone, G Wilkinson) (Oxford: Pergamon Press, 1995) p. 419
226. P Chini *J. Organomet. Chem.* **200** 37 (1980)
227. M Tachikawa, R L Geerts, E L Muetterties *J. Organomet. Chem.* **213** 11 (1981)
228. M I Bruce, in *Comprehensive Organometallic Chemistry* Vol. 4 (Ed. G Wilkinson) (Oxford: Pergamon Press, 1982) p. 889
229. R D Adams, J P Selegue, in *Comprehensive Organometallic Chemistry* Vol. 4 (Ed. G Wilkinson) (Oxford: Pergamon Press, 1982) p. 967
230. A E Stiegman, A S Goldman, C E Philbin, D R Tyler *Inorg. Chem.* **25** 2976 (1986)
231. M Absi-Halabi, J D Atwood, N P Forbus, T L Brown *J. Am. Chem. Soc.* **102** 6248 (1980)
232. T M Bockman, J K Kochi *J. Am. Chem. Soc.* **111** 4669 (1989)
233. P Lemoine *Coord. Chem. Rev.* **83** 169 (1988)
234. J R Phillips, W C Trogler *Inorg. Chim. Acta* **198–200** 633 (1992)
235. D de Montauzon, R Poilblanc *J. Organomet. Chem.* **104** 99 (1976)
236. A J Downard, B H Robinson, J Simpson, A M Bond *J. Organomet. Chem.* **320** 363 (1987)
237. J E Cyr, P H Rieger *Organometallics* **10** 2153 (1991)
238. R G Gasanov, Doctoral Thesis in Chemical Sciences Institute of Organoelement Compounds, Academy of Sciences of the USSR, Moscow, 1981
239. T Kunieda, T Tamura, T Takizawa *J. Chem. Soc., Chem. Commun.* 885 (1972)
240. M Zhou, L Andrews *J. Am. Chem. Soc.* **120** 11499 (1998)
241. J R Morton, K F Preston *Inorg. Chem.* **24** 3317 (1985)
242. R C Hynes, K F Preston, J J Springs, A J Williams *Organometallics* **9** 2298 (1990)
243. D R Kidd, T L Brown *J. Am. Chem. Soc.* **100** 4095 (1978)
244. M C R Symons, R L Sweany *Organometallics* **1** 834 (1982)
245. W K Meckstroth, R T Walters, W L Waltz, A Wojcicki, L M Dorfman *J. Am. Chem. Soc.* **104** 1842 (1982)
246. G Lavigne, H D Kaesz *J. Am. Chem. Soc.* **106** 4647 (1984)
247. G Lavigne, N Lugan, J-J Bonnet *Inorg. Chem.* **26** 2345 (1987)
248. S-H Han, G L Geoffroy, B D Dombek, A L Rheingold *Inorg. Chem.* **27** 4355 (1988)
249. T Chin-Choy, W T A Harrison, N Keder, G D Stucky, P C Ford *Inorg. Chem.* **28** 2028 (1989)
250. J-K Shen, F Basolo *Izv. Akad. Nauk, Ser. Khim.* 1540 (1994)^b
251. F Ragaini, A Ghitti, S Cenini *Organometallics* **18** 4925 (1999)
252. S D Ittel *Homogeneous Catalysis: the Applications and Chemistry of Catalysis by Soluble Transition Metal Complexes* (2nd Ed.) (New York: Wiley, 1992)
253. F Paul *Coord. Chem. Rev.* **203** 269 (2000)
254. A Devasagayaraj, M Periasamy *Transition Met. Chem.* **16** 503 (1991)
255. C Rameshkumar, M Periasamy *Organometallics* **19** 2400 (2000)
256. F Boix, F Camps, J Coll, J M Moreto, J Torras *Synth. Commun.* **17** 1149 (1987)
257. M Oçafain, M Devaud, M Troopel, J Perichon *J. Chem. Soc., Chem. Commun.* 2331 (1995)
258. V B Shur, S M Yunusov, Z Rummel', M Varen, M E Vol'pin *Dokl. Akad. Nauk SSSR* **292** 1409 (1987)^c
259. J K Kochi *Organometallic Mechanisms and Catalysis*. Academic Press New York 1978
260. J Halpern, in *Fundamental Research in Homogeneous Catalysis* Vol. 3 (Ed. M Tsutsui) (New York: Plenum, 1979) p. 25
261. F Barriere, W E Geiger *Organometallics* **20** 2133 (2001)
262. D Menglet, A M Bond, K Coutinho, R S Dickson, G G Lazarev, S A Olsen, J R Pilbrow *J. Am. Chem. Soc.* **120** 2086 (1998)
 - ^a — *Kinet. Catal. (Engl. Transl.)*
 - ^b — *Russ. Chem. Bull., Int. Ed. (Engl. Transl.)*
 - ^c — *Dokl. Chem. (Engl. Transl.)*
 - ^d — *Mendeleev Chem. J. (Engl. Transl.)*

Methods for investigation of the free volume in polymers

Yu P Yampolskii

Contents

I. Introduction	59
II. Positron annihilation lifetime spectroscopy	60
III. ^{129}Xe NMR spectroscopy	64
IV. Inverse gas chromatography	65
V. Miscellaneous methods	67
VI. Simulation of the free volume by molecular dynamics	68
VII. Conclusion	72
VIII. Appendix	73

Abstract. Experimental probe methods for investigation of the free volume in polymers (positron annihilation lifetime spectroscopy, ^{129}Xe NMR spectroscopy and inverse gas chromatography) and relevant theoretical approaches (computer simulation) are considered. Various definitions of the free volume and related terms are given. The physical principles that underlie particular probe methods as well as the scope and limitations of each method are discussed. A systematic comparison of the size of free-volume elements in polymers determined by different methods is carried out. The bibliography includes 175 references.

I. Introduction

The notion of the free volume is of paramount importance for physical chemistry of polymers. Being initially formulated for liquid state,¹ it was extended to amorphous polymers that are either above or below the glass transition temperature (T_g).^{2–5} The free volume in polymers determines their viscosity, relaxation and mechanical properties (deformation), thermal expansion, as well as the rates of interdiffusion of polymers and diffusion of low-molecular-mass species (gases and vapours) in polymers. Considering the free volume in polymers, one should keep in mind that this is not only an abstract physical parameter (although it can of course be described quantitatively), but also a real physical object characterised by an average size and shape of the ‘hole’ (a free-volume element, FVE), FVE size distribution, topology and connectivity (closed or open internal porosity). The FVE in glassy polymers are treated as ‘frozen’ in the polymer matrix. For rubbers, where the free volume has a fluctuation nature like in liquids, both the size of randomly formed FVE and the rate of their diffusion in the polymer matrix are essential.

The early phenomenological models treated the free volume as an abstract notion not related to the chemical structure and geometry of constituting polymeric chains. At temperatures

above T_g , one can distinguish, in the free volume, the ‘hole’ component characterised by zero energy expenditure for redistribution (*i.e.*, motion) of FVE and the interstitial component that becomes accessible to transport owing to energy fluctuations greater than kT . At temperatures below T_g , yet another component of the free volume appears corresponding to the nonequilibrium thermodynamic state of glassy polymers.^{4,5}

Elaboration of additive incremental (group contribution) methods for inclusion of the effect of the chemical structure of polymers on their properties became an important step towards establishment of relations between the free volume and physical properties of polymers. These methods were developed to correctly estimate the occupied volume in the polymer, which makes it possible to calculate the macroscopic free volume using the van der Waals atomic radii and particular concepts of chain packing in polymer.^{6–8} Here, the calculated free volume is considered as the property of solely the polymer; however, only a fractional free volume ‘sensed’ by different molecular probes can be estimated.⁹ This group of methods is useful for constructing correlations between the free volume and various characteristics of polymers (*e.g.*, gas diffusion and permeability coefficients), but their analysis is beyond the scope of the present review because our goal is to consider methods for investigation (first of all, experimental) of the free volume on the microscopic (molecular) level.

In connection with the development of methods of computer simulation of polymers, the fractional free volume and related notions had to be redefined more rigorously.^{10,11} These methods treat polymeric chains as consisting of rigid atomic spheres with the corresponding van der Waals radii. The occupied volume (V_{oc}) is the total volume of the polymeric chains in the region under study. The unoccupied volume (voids) is defined as the volume including all points lying outside the van der Waals atomic spheres that form the polymer. Thus, the specific volume (V_{sp}) of the polymer can be represented by the sum of the occupied and void volume. Because free volume calculations are most often carried out in connection with analysis of gas diffusion, a very important notion ‘accessible volume’ (V_{ac}) was introduced. The accessible volume is the volume including the points that can be occupied by the centres of mass of penetrant molecules without overlap between the van der Waals volumes of the penetrant molecules and the atoms of the polymeric chains. Hence, it follows that the accessible volume is the property of the polymer–gas system, *i.e.*, V_{ac} in a given polymer will be considerably different for, *e.g.*, He and Xe atoms. It should be noted that the void volume is the

Yu P Yampolskii A V Topchiev Institute of Petrochemical Synthesis, Russian Academy of Sciences, Leninsky prosp. 29, 119991 Moscow, Russian Federation. Fax (7-495) 230 22 24, tel. (7-495) 955 42 10, e-mail: Yampol@ips.ac.ru

Received 7 February 2006

Uspekhi Khimii 76 (1) 66–87 (2007); translated by A M Raevskiy

property of each polymer. The accessible volume forms clusters in the interior of the polymer, the cluster size and geometry being significantly different for different penetrants.

Experimental investigations of the free volume in polymers are often carried out using probe methods. Common features of these techniques consist of introducing certain molecules (probes) into the polymer and monitoring their behaviour. The results of observations allow conclusions about the structure of the free volume to be drawn. These methods use probes of different nature and size and provide differently detailed information. For instance, in ^{129}Xe NMR spectroscopy the only probe (^{129}Xe atom) 'explores' the free volume in different polymers. In studies of polymers by positron annihilation lifetime spectroscopy (PALS), an electron-positron pair (positronium atom) serves as a probe. In inverse gas chromatography (IGC), the role of probes is played by series of structurally similar compounds.

The present review concerns the principles, fields of possible applications and results obtained by different probe methods of investigation of the free volume. The chemical formulae and names of the polymers mentioned in the text are listed in the Appendix.

II. Positron annihilation lifetime spectroscopy

Positron annihilation lifetime spectroscopy allows one to obtain information on the size, size distribution and concentration of free volume elements as well as on the effect of temperature, pressure, mechanical deformations and phase compositions of polymers on the free volume.^{12–15} This method makes it possible to follow changes in the free volume occurring in the course of physical ageing of polymers, as a result of sorption and swelling and during cross-linking. Parameters of positron annihilation lifetime spectra strongly depend on the polymer structure but only slightly depend on the molecular mass,¹⁶ which facilitates comparison of different polymers. In addition, these parameters are fairly reproducible in studies of different polymer samples and, as showed investigations carried out in different research laboratories, in the experiments with reference samples.¹⁷

The PALS method is based on measuring the positron lifetimes in matter. In polymers, positrons can exist in both free (e^+) and bound states, the latter being represented by H-like positronium atom, *i.e.*, an electron–positron pair (Ps or e^-e^+). The singlet state of this species, *p*-Ps, has antiparallel spins and a short lifetime (0.125 ns in vacuum), whereas the triplet state, *o*-Ps, with parallel spins has a much longer lifetime (142 ns in vacuum). It is believed that long-lived species, *o*-Ps, appear in the regions with reduced electron density (*i.e.*, in the FVE).^{18–20} Due to overlap between the wave functions of *o*-Ps and electrons of atomic groups that form the FVE walls, the *o*-Ps lifetimes become much shorter compared to annihilation in vacuum, lying usually in the range from 1.5 to 4.0 ns. The observed lifetimes depend on the FVE size, namely, the larger the FVE the longer the positron lifetime in the polymer. The lifetime spectrum is a set of experimental characteristic times τ_i (ns) and corresponding statistical weights or intensities I_i (%). It is assumed that the intensity of the positronium component depends on the concentration of FVE, although it can also be affected by other factors.

Usually, ^{22}Na isotope with a half-life time of 2.6 years serves as a source of positrons. Particles formed are characterised by energies distributed between zero and 0.540 MeV with a maximum at ~ 0.2 MeV and a mean free path of ~ 1 mm in conventional polymers. In matter, positrons are rapidly (within ~ 10 ps) thermalised and all subsequent processes involve particles with thermal energies.

An experimental setup for measuring positron annihilation lifetimes (see Fig. 1) consists of a source of positrons placed between two samples of the polymer under study (a plate, a stack of films or a powder). The lifetimes are measured using an electronic system (time–amplitude converter). The circuit measures the time interval between two events, namely, the appearance

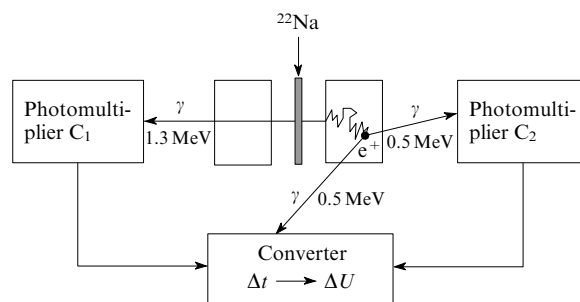


Figure 1. Scheme of a setup for measuring positron annihilation lifetime spectra.

of primary γ -quanta from the source and the appearance of quanta that accompany positron annihilation. Once detected a total of 10^5 – 10^7 events by a photomultiplier, an experimental positron lifetime distribution curve $y(t)$ is plotted, which shows the number of events y as function of the time elapsed t (Fig. 2).

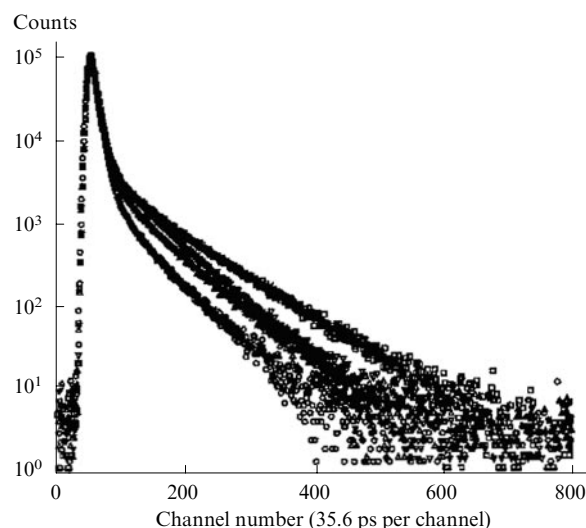


Figure 2. Typical experimental positron annihilation lifetime distributions of various polyimides.²¹

The primary experimental dependences $y(t)$ can be interpreted in the framework of analysis based on a discrete or continuous model. In the former case, the $y(t)$ curve is represented by the sum of several exponents

$$I_i \lambda_i \exp(-\lambda_i t), \quad (1)$$

where I_i is the intensity (in %) and $\lambda_i = 1/\tau_i$ (in ns^{-1}) is the annihilation rate. The number of exponents n is set in such a manner that the deviation from the experimental $y(t)$ curve be minimum. Traditionally, it is assumed that $n = 3$, although for many polymers studied recently one has $n > 3$. The first two spectral components τ_1 and τ_2 (times ~ 0.1 – 0.2 and ~ 0.3 – 0.5 ns, respectively) are due to annihilation of *p*-Ps and the free e^+ , being not related to probing of the free volume in polymers. At the same time, the 'long-lived' components τ_i ($i = 3$ or 4) are due to annihilation of *o*-Ps located within the FVE. It is analysis of these spectral components that forms the basis for the use of PALS as probe method. Discrete analysis of primary data is performed using different programmes, *e.g.*, PATFIT.²² Continuous data analysis using the CONTIN^{23,24} or MELT²⁵ programmes gives the probability density function of positron annihilation characterised by a given lifetime in the polymer.

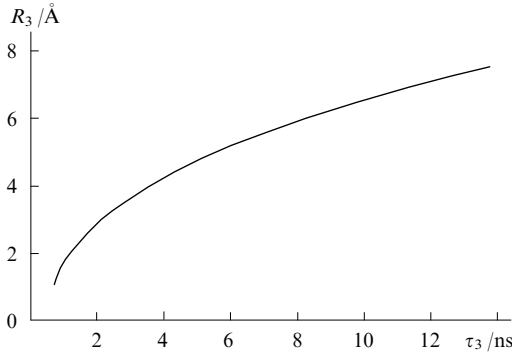


Figure 3. Correlation between positronium lifetime and average FVE radius in polymers according to the Tao–Eldrup relationship.

Here, the number of components in the lifetime spectrum is chosen by the programme automatically.

A semiempirical expression relating the lifetime of *o*-Ps (τ_3) to the average radius (R_3) of a spherical FVE in a polymer (the Tao–Eldrup relationship)^{19,20} has the form

$$\tau_3 = \frac{1}{2} \left[1 - \left(\frac{R_3}{R_0} \right) + \frac{1}{2\pi} \sin \left(\frac{2\pi R_3}{R_0} \right) \right]^{-1}, \quad (2)$$

where $R_0 = R_3 + \Delta R$ (the fitting parameter $\Delta R = 1.66$ Å was determined from analysis of the data for media with the known ‘hole’ size including zeolites). The FVE radii increase almost linearly as τ_3 increases (see Fig. 3).

A similar relationship is used in the case of several lifetimes of *o*-Ps. Assuming spherical geometry and a known radius, the FVE volume (v_f) or the volume distribution are found

$$v_f = \frac{4\pi}{3} R_3^3.$$

The assumption of spherical geometry of FVE in polymers seems to be somewhat incorrect (see Section VI). Cylindrical and ellipsoidal FVE were also considered and the corresponding relations for calculating the FVE volumes from the known *o*-Ps lifetimes are available in the literature.^{26–29} However, most probing studies of free volume in polymers were carried out using the Tao–Eldrup relationship.

Variations of the free volume in polymers can be illustrated by the data listed in Table 1. Here, the polymers are arranged in almost the same order as the gas permeability and radius R_3 increase. The barrier materials (*e.g.*, Vectra copolyester) are characterised by the smallest size of FVE. As the gas permeability increases, the lifetimes of *o*-Ps and the FVE size increase. It was established (see, *e.g.*, Ref. 33) that the conventional glassy polymers have a monomodal size distribution of FVE (*i.e.*, the *o*-Ps lifetime spectrum includes one time τ_3) and the lifetime distribution can be represented by Gaussian peaks when analysing the data using the CONTIN programme. However, statistical processing of spectra reveals bimodal lifetime and FVE size distributions that appear starting with particular free volume and gas permeability values (Fig. 4). For instance, the long-lived components in the lifetime spectra of PVTMS and certain relatively high-permeability polyimides³⁶ have a ‘shoulder’ or superposition of two Gaussian peaks, whereas two *o*-Ps lifetimes appear, namely, τ_3 and τ_4 (see Fig. 4) for polymers with even greater permeabilities. When treated with the CONTIN programme, maxima in the curves coincide with the lifetimes obtained by discrete processing of the primary data. Bimodal (or even polymodal) FVE size distributions were found in numerous studies of highly permeable polymers.^{37–42} Note that the average FVE size and the size distribution determined from PALS data are consistent with the data obtained by other probe methods and with the results of

Table 1. Gas permeability coefficients (P_{O_2}) and FVE size in glassy polymers.

Polymer	P_{O_2} /Barrer ^a	R_3 /Å	v_{f3} /Å ³	R_4 /Å	v_{f4} /Å ³	Ref.
Vectra copolyester	0.0005	2.1	39	—	—	30
PMMA	0.09	2.6	74	—	—	31
PS	2.9	2.9	102	—	—	32
PC	1.6	2.94	106	—	—	33
Polyimides						
6FDA-ODA	2.4	3.19	136	—	—	34
6FDA-BAAF	14.2	3.62	198	—	—	34
PVTMS	44	3.21	138	4.35	345	35
PTMSS	56	2.71	83	3.74	219	35
PPrSiDPA	230	3.83	235	6.38	1088	35
AF2400	1140	2.68	81	5.95	882	35
PTMSP	7700	3.41	166	6.81	1323	35

^a 1 Barrer = 10^{-10} cm³ (normal conditions) cm cm⁻² s⁻¹ (cm Hg)⁻¹; this is the flow of gas taken by a volume of 1 cm³ under normal conditions through a surface area of 1 cm² of a membrane 1 cm thick per s at a pressure drop of 1 cm Hg.

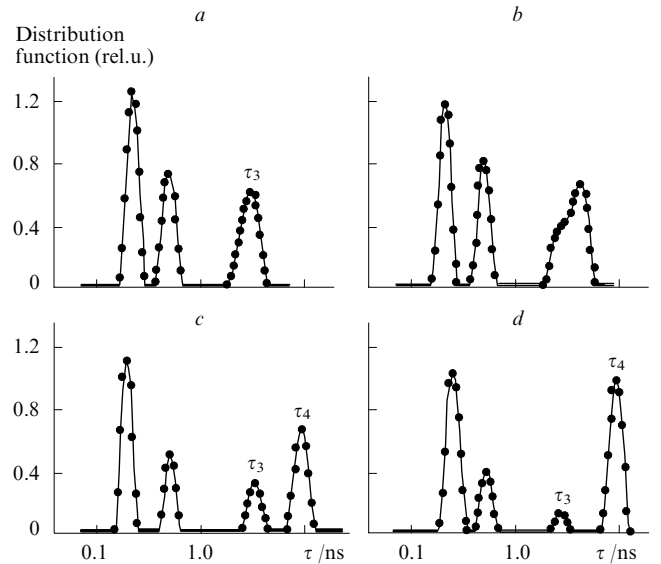


Figure 4. CONTIN positronium lifetime distributions obtained for glassy polymers with the increasing free volume.³⁵ Polymer: PFPDMSS (a), PVTMS (b), PPrSiDPA (c), and PTMSP (d).

molecular dynamics (MD) simulation of the free volume in polymers (see Sections IV and VI).

Free volume elements of even larger sizes were found in polymeric sorbents and organic clusters. In particular, PALS data showed that hypercross-linked polystyrene sorbents contain cavities with a radius of 14 Å and their content is ~20% of the total number of FVE in the material.^{43,44} A cluster prepared by the reaction of terephthalic acid with chromium nitrate, hydrogen fluoride and water has pores ~3 nm in diameter and a specific surface area of 5900 m² g⁻¹ (Ref. 45). This is much larger than the maximum specific surface area in zeolites. Even larger cubic cavities (volume is ~8000 Å³) were identified in the crystal lattice of a phthalocyanine macrocycle.⁴⁶ Similar cavities probably form an open system of pores, which is important, in particular, for separation processes in membranes.

Thus, the PALS technique provides a microscopic description of the free volume in terms of the average FVE radii and corresponding volumes v_f . To relate these parameters to macro-

scopic characteristics of polymers, one should know the average FVE concentrations N (cm^{-3}) and then estimate the fractional free volume (FFV) as the product $v_f N$. This can be done using various approaches.

According to the simplest early models,^{32, 47, 48} the intensity I_3 was assumed to be proportional to N . Then, if we know the coefficient of proportionality, A , from independent data, the concentration N is given by

$$N = AI_3,$$

and therefore one gets

$$\text{FFV} = AI_3 v_f.$$

However, a more correct treatment showed that the intensity I_3 also depends on the probability of o -Ps formation, trapping rate of o -Ps by FVE and on the 'decay' of positronium under the action of polar groups (e.g., C=O groups in imidazole rings of polyimides).³⁵ Because of this, the simple model mentioned above is no longer used. A number of more reliable methods of determination of the parameter N were developed.

1. The temperature dependences of τ_3 and FVE volume are very similar to the classical dilatometric curves for polymers, i.e., the temperature dependences of the specific volume that determine the volumetric expansion coefficients of polymers. However, there is a significant quantitative difference between these dependences. Namely, the thermal expansion coefficients of a polymer (i.e., its specific volume) below and above T_g (α_g , α_r) are of the order of 10^{-4} K^{-1} , whereas the thermal expansion coefficients of the free volume (α_{hg} , α_{hr}) are an order of magnitude larger. A natural explanation for this fact is as follows: the α_g and α_r values characterise the thermal expansion of both the FVE and the more dense matrix (walls surrounding the FVE). By comparing the temperature dependences of the specific volume V_{sp} and τ_3 (or v_f) one can choose N values suitable for both dependences, i.e., one can determine the parameter N .^{49–52} Recently, this approach was systematically used for estimating the concentration N in various amorphous polymers.^{49, 53, 54} It was shown that in most cases the concentrations N depend only slightly on the chemical structure of polymers and their values lie in the range $(2–8) \times 10^{20} \text{ cm}^{-3}$ at $T = T_g$ and show a relatively weak temperature dependence.

2. The N values can also be determined from PALS data obtained in studies of gas sorption by polymers. The time τ_3 is shortened upon gas sorption. This can be interpreted as a result of selective sorption by FVE of different sizes. Because the amount of gas molecules sorbed by polymers in the course of sorption experiments under different conditions is known, Kirrheim and co-workers⁵⁵ postulated different types of FVE size distributions and estimated the N values that are consistent with the dependences $\tau_3(p)$ and $I_3(p)$, where p is the pressure. However, the N values for polycarbonate and tetramethylpolycarbonate lie in the range $(2–4) \times 10^{21} \text{ cm}^{-3}$ and seem to be overestimated. Indeed, they correspond to the situation where the fractional free volume in these polymers is from 30% to 100%. Here, the polymer volume per FVE should be 200 \AA^3 , which corresponds to a cube with a nearly 6 \AA -edge. With allowance for the average FVE diameter this means that the neighbouring FVE should nearly contact one another, thus indicating an open porosity, which does not occur in these polymers. An attempt to estimate the parameter N from the results of sorption experiments gave a more realistic value of $4 \times 10^{20} \text{ cm}^{-3}$ for three polycarbonates.⁵⁶

3. Yet another method of estimation of the N value is based on detailed analysis of the kinetics of formation and annihilation of o -Ps in polymers.^{57, 58} According to this approach, only a fraction of positrons that form o -Ps contributes to the long-lived component of the PAL spectrum. Therefore, the intensities I_3 and I_4 should depend not only on N , but also on the probability of trapping of o -Ps by FVE. The trapping rate is given by equation

$$v_i^t = 4\pi D_{Ps} R_i N_i \quad (i = 3, 4), \quad (3)$$

where D_{Ps} is the diffusion coefficient of non-localised o -Ps and N_i is the concentration of a particular type of traps (FVE) of radius R_i .

To determine N_i , one should know the coefficient D_{Ps} from independent data. The D_{Ps} estimates available in the literature³¹ lie in the range $(0.5–15) \times 10^{-5} \text{ cm}^2 \text{ s}^{-1}$. Probably, the value $D_{Ps} = 1.3 \times 10^{-5} \text{ cm}^2 \text{ s}^{-1}$ obtained for polyimides⁴⁹ is the most reliable, because it is consistent with the N values determined from the temperature dependence of τ_i below and above T_g . Of course, one should also know how the coefficient D_{Ps} varies for different polymers. Analysis of the D -vs.- d^2 dependences (D is the diffusion coefficient of molecules with the gas-kinetic diameter d lying between 2.5 and 4 \AA) for different polymers showed that extrapolation to the o -Ps size ($\sim 1 \text{ \AA}$) gives the diffusion coefficients that fall in a relatively narrow range of one decimal order of magnitude.

The concentration N in partially crystalline polymers can be estimated from the densities of polymers of different crystallinity.⁵⁹ Assuming that the specific volume of the crystalline phase equals the occupied volume, one can determine the fraction of the specific volume of the amorphous phase h . Then N is given by

$$N = \frac{h}{v_h}, \quad (4)$$

where v_h is the average FVE volume found from PALS data.

At last, the N values for polymeric sorbents and some high-permeability open-pore polymers can be estimated from joint analysis of the annihilation parameters and pore size distribution obtained according to Brunauer–Emmet–Teller.⁴³

An indirect estimate of N can be obtained using the average size of FVE in polymers. The average volume of the polymer matrix per FVE in a polymer should be much larger than the FVE volume. Assuming that the specific volume of the polymer is about $1 \text{ cm}^3 \text{ g}^{-1}$ and N is nearly $\sim 10^{20} \text{ g}^{-1}$ (or $\sim 10^{20} \text{ cm}^{-3}$), one gets the volume per FVE $v = 10^4–10^3 \text{ \AA}^3$. This corresponds to a cube with a $20–10 \text{ \AA}$ -edge. The average diameter of FVE in polymers is $\sim 5–13 \text{ \AA}$; therefore, one can conclude that the average distance (k) between neighbouring FVE is 5 to 10 \AA . At much smaller k values, the regularities of gas transport in polymers will be similar to those in porous media, which contradicts the majority of experimental data. At $N > 10^{21} \text{ cm}^{-3}$, the parameter k should take negative values. Note also that the k values determined are in good agreement with the diffusion jump lengths of gas molecules in polymers estimated using the Meares model.⁶⁰ The values of N obtained by different methods for different polymers are listed in Table 2.

Table 2. FVE concentrations in different polymers according to PALS data.

Polymer	$10^{-20} N / \text{cm}^{-3}$	Ref.
PE	6–8	59
Polyolefins	5	61
EVA	6, 7	62
Rubbers	2–6	52
PVC (plasticised)	8	54
PC	40	55
	6–11	50
	4	56
PVTMS, PTMSP, AF2400, AF1600, PTMSS, etc.	6–15	35, 49
Poly(ether imides)	4–8	49

Thus, the PALS technique allowed one to obtain a fundamental result, namely, the FVE concentration in all polymers lies in a narrow range from 10^{20} to 10^{21} cm^{-3} .

1. Free volume in thin films and on the surface of solids

Traditionally, the PALS method is used in studies of the free volume inside a polymer matrix. However, there is a variety of objects [free thin polymer films (membranes), coatings on the surface of various materials, *etc.*] for which the surface rather than bulk properties of polymers are important. Glass transition temperature,^{63,64} density,^{65,66} chain mobility and some other characteristics⁶⁷ of polymers measured for the bulk phase (polymer matrix) and at interfaces can be significantly different.

Positrons used in traditional version of the PALS technique have an average energy of 200 keV and a braking distance of ~ 1 mm. The latter value is several orders of magnitude larger than the characteristic thickness of surface layers; therefore, the positron lifetimes in PALS experiments contain information on the free volume in the matrix. Studies of the free volume in near-surface layers require that the positron beam energy be much lower than 200 keV (positrons should not penetrate into the interior of the sample and annihilate in the near-surface layers). The development of monochromatic low-energy positron beam techniques⁶⁸ with much lower controllable positron energies (0.2–20 keV) made it possible to probe the free volume in thin polymer layers (of the order of a few nanometres) and to plot the corresponding free volume profiles.

The surface layers at polymer–vacuum interfaces have been best studied,^{69,70} whereas investigations at the polymer–polymer interface are less detailed.⁷¹ As the positron energy decreases, the *o*-Ps lifetimes (τ_3) in different glassy polymers [an epoxide copolymer, polystyrene, poly(methyl methacrylate)] increase compared to the lifetimes measured in conventional PALS experiments where the depth of position penetration is larger.^{69,70,72,73} Taking into account the Tao–Eldrup relationship, this suggests an increase in the size of FVE in the near-surface layers. Using the density profile, it was shown⁷¹ that there is a variable-density layer 30–40 Å thick near the interface where the size of FVE does increase. The FVE size distribution is broadened near the polymer–vacuum interface.⁷⁰ An unexpected result was obtained for polystyrene, namely, a bimodal positron lifetime distribution with τ_4 values lying in the interval from 8 to 14 ns was revealed,^{71,72} which corresponds to FVE size from 5.7 to 6.2 Å and exceeds considerably the size of FVE in polystyrene matrix. However, it cannot be ruled out that we deal with an artifact due to superposition with positron annihilation in vacuum characterised by much longer Ps lifetimes.

Yet another observation has no reasonable explanation so far. In addition to a very thin near-surface layer (a few tens of ångström thick) characterised by densification with an increase in the distance from the interface, there is a much thicker (a few micrometres) layer the density of which decreases as the distance from the interface increases. This is indicated by changes in the densities of glassy polymers and in the coefficients of gas diffusion therein.^{65,66} Probably, harmonisation of these data requires further studies.

2. Effect of chemical structure on the free volume in polymers

Analysis of the results of numerous PALS studies showed that the free volume in polymers is highly sensitive to the chemical structure of the monomer unit. That is why the gas permeability and gas diffusion coefficients of polymeric materials depend on their structure (Table 3).

An efficient method of increasing the free volume of a polymer consists of introducing bulky substituents [first of all, Si(CH₃)₃ groups] into the main chain (see the data for two metathesis-derived polynorbornenes in Table 3). The introduction of other substituents (*e.g.*, a methyl group) into aromatic nuclei of the main chain also causes a systematic increase in the positron lifetime and FVE size (in Table 3, this can be followed using the data for polyimides and polycarbonates).

Table 3. Effect of polymer structure on lifetimes τ_3 and FVE radii.

Polymer	τ_3 /ns	R_3 /Å	Ref.
Poly(norbornene)	2.15	2.9	74
(CH ₃) ₃ Si-Substituted poly(norbornene)	2.70	3.4	75
6FDA-Polyimides with different number of methyl groups (<i>n</i>) in phenylenediamine residue			76
<i>n</i> = 0 (6FDA-PDA)	2.57	3.3	76
<i>n</i> = 1 (6FDA-1)	2.80	3.5	76
<i>n</i> = 2 (6FDA-2)	3.15	3.7	76
<i>n</i> = 3 (6FDA-P14)	3.63	4.0	76
<i>n</i> = 4 (6FDA-P13)	3.94	4.2	76
Polycarbonate	2.1	2.9	33
Tetramethylpolycarbonate	2.4	3.2	33

3. Effect of temperature

The temperature dependences of Ps lifetimes were mentioned above in connection with the estimation of FVE concentration in polymers. Numerous studies (see, *e.g.*, Refs 33, 47, 52–54, 77, 78) showed a linear increase in τ_3 in the glassy-state region followed by a kink near T_g and subsequent linear increase in τ_3 (with a greater slope) in a highly elastic state with an increase in temperature. This is illustrated in Fig. 5. Most polymers are characterised by thermal expansion coefficients of FVE of $1 \times 10^{-3} \text{ K}^{-1}$ below the glass transition temperature and $(2-10) \times 10^{-3} \text{ K}^{-1}$ above T_g (see Refs 52, 53 and 77).

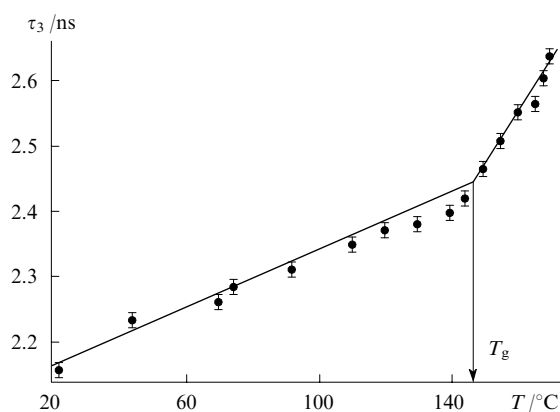


Figure 5. Temperature dependence of positronium lifetime τ_3 in polycarbonate.⁷⁸

Interestingly, some polymers present exceptions. For instance, a study of PTMSP (polymer with the largest FVE and record high gas permeability) showed that the times τ_3 and τ_4 are independent of temperature.³⁹ Probably, for this polymer the effect of temperature on small-scale motions of atomic groups in the FVE walls (these motions should govern the temperature dependences of τ_3 in conventional glassy polymers) is less pronounced due to abnormally large FVE size. Substantiation of this hypothesis requires additional measurements of the $\tau_i(T)$ dependences for other polymers with large free volumes.

4. Effect of pressure

The nanostructure of the free volume (average FVE radius and FVE size distribution) in polymeric materials can be significantly changed by applying high pressure. These changes are well ‘sensed’ by the PALS technique. In particular, the average FVE

radius in polyepoxide decreases from 2.5 to 0.73 Å and the FVE size distribution becomes narrower as the pressure increases from 0 to 14 kbar.⁷⁹ The effect of high pressure on the polymer also manifests itself as an aftereffect, namely, the lifetimes τ_3 and corresponding FVE size decrease after decompression.^{48, 80, 81}

5. Mechanical effects

The PALS method is also suitable for probing changes in the free volume (cavity size and concentration) due to deformation of polymers. However, because orientation of polymeric films can be accompanied by crystallisation and the changes in the supra-molecular structure and in FVE geometry, interpretation of experimental data can be ambiguous. If deformation of amorphous polymers (*e.g.*, polycarbonate⁷⁸) at room temperature causes no crystallisation at small relative elongations (less than 2%, *i.e.*, in the region of quasielastic deformation), the time τ_3 linearly increases with the relative elongation thus indicating an increase in FVE. At the same time biaxial orientation of poly(ethylene terephthalate), poly(ethylene naphthenate) and their copolymers at temperatures above T_g causes only minor changes in τ_3 and I_3 and significant changes in the gas permeability and diffusion coefficients. This points to predominance of sample morphology (lengthening of ‘diffusion paths’).⁸² Much greater changes in the annihilation parameters were observed at larger relative elongations Δl upon deformation of partially crystalline polymers (taking polyethylene as an example).⁸³ As Δl increases, the positron lifetime, τ , corresponding to the fractional free volume in the amorphous phase initially decreases and then (at large Δl) remains unchanged. It was assumed that the changes in τ characterise a change in the shape of FVE from nearly spherical in undeformed sample to ellipsoidal in oriented polymer. Other examples of PAL studies of mechanical effects in polymers can be found in the review.¹⁵

One of the first PAL studies of the phenomena accompanying deformation of polymers was reported by Askadskii *et al.*⁸⁴ Unfortunately, the authors studied a polyimide based on pyromellitic dianhydride and 4,4'-diaminodiphenyl oxide, which is also known as Kapton polyimide. This and numerous subsequent studies (see, *e.g.*, Refs 31, 85 and 86) revealed that the PAL spectrum of this polymer shows only one relatively short-lived component (lifetime 0.3–0.4 ns) instead of three components. It is noteworthy that this feature allows Kapton polyimide to be used as a component of the source of positrons, because Kapton films do not change the positron lifetimes in the sample under study. Apparently, this is due to the fact that at high concentration of dicarboximide rings in this polymer the positronium production is efficiently inhibited through trapping of positrons by the ring carbonyl groups. As a result, annihilation mainly involves free positrons and occurs in relatively close-packed polymer domains rather than FVE. Again, the absence of the long-lived component ($I_3 = 0$) shows that the parameter I_3 cannot serve as a measure of FVE concentration, because it depends on the positronium yield. Otherwise, Kapton should be characterised by zero free volume, whereas the gas diffusion coefficients for the polymer are similar to those found for other polymers (*e.g.*, $D_{O_2} = 0.29 \times 10^{-8} \text{ cm}^2 \text{ s}^{-1}$ according to Ref. 87). Also note that the absence of the τ_3 component can be due to a decrease in the FVE concentration owing to an increase in the concentration of cross-links, as shown for oligo(ester acrylates).⁸⁸

III. ^{129}Xe NMR spectroscopy

Chemical shifts in the ^{129}Xe NMR spectra are highly sensitive to the free volume in the medium where gaseous xenon is sorbed. Qualitatively, the larger the FVE size the smaller the ^{129}Xe chemical shift relative to the chemical shift characteristic of the gas phase. In this respect, polymers differ insignificantly from other condensed media, namely, large chemical shifts are observed in, *e.g.*, the media with high refractive indices. In this connection we can say that the xenon atom placed inside the FVE is in a local

low-refraction medium and characterised by a smaller chemical shift.⁸⁹

Note that the ^{129}Xe chemical shift is sensitive to structural and morphological features of partially crystalline and cross-linked polymers, polymer blends and block copolymers; it also changes near the glass transition temperature.^{90–97}

According to Fraissard and co-workers^{98, 99} who studied the sorption of xenon in various zeolites, the chemical shift in the NMR spectrum of a ^{129}Xe atom sorbed in nanoporous medium in the absence of paramagnetic species or admixtures producing a strong local electric field (*e.g.*, cations) can be written as follows:

$$\delta_{\Sigma} = \delta_0 + \delta + \delta_{\text{Xe/Xe}} \rho, \quad (5)$$

where δ_0 is a constant, δ is the chemical shift due to collisions with the FVE walls, $\delta_{\text{Xe/Xe}}$ is the chemical shift due to collisions with other xenon atoms in the gas phase and ρ is the density of the gas phase. Therefore, after extrapolation to zero pressure of gaseous xenon the difference

$$\delta = \delta_{\Sigma} - \delta_0$$

should characterise only the collisions with the walls within the FVE. Based on analysis of the data for zeolites, an empirical relation for the experimentally measured chemical shift was proposed⁹⁸

$$\delta = \frac{499.1}{2.054 + \lambda}, \quad (6)$$

where λ (in Å) is the mean free path of a xenon atom within the FVE. Note in advance that this method is only applicable to studies of those FVE the size of which exceeds that of the xenon atom. Assuming different FVE geometries, from the λ value one can estimate the diameter of either a spherical cavity (D_{sp}) or a cylindrical FVE (D_c) with a large length-to-diameter ratio,

$$\lambda = \frac{D_{\text{sp}}}{2} - 2.2, \quad (7)$$

$$\lambda = D_c - 4.4. \quad (8)$$

The free terms in relations (7) and (8) are the radius and diameter of the xenon atom, respectively. This approach is based on the possibility of determining the size of the lattice cell from X-ray diffraction data for zeolites¹⁰⁰ and availability of various characteristics of xenon. By extending relationships (6)–(8) to other nanoporous systems (in particular, polymers) it is possible to estimate their FVE sizes. However, it should be noted that there are some difficulties related to, *e.g.*, a large scatter of numerical characteristics of the size of xenon atom determined by different methods (see details below).

The FVE size was determined from the results of ^{129}Xe chemical shift measurements of xenon sorbed in different polymers. NMR measurements were carried out at low pressures or extrapolation to low pressures was used. ^{129}Xe NMR data obtained assuming spherical and cylindrical FVE geometries are listed in Table 4. For comparison, we also present the results obtained by other probe methods for different polymers. Analysis of these data allows one to draw some general conclusions.

First of all, the ^{129}Xe chemical shift can be considered as a characteristic property of the polymer, as indicated by coincidence of the chemical shifts for the polymers studied by different authors (*e.g.*, for PE and PS).

Polymers studied to date can be divided into two groups. Polymers with relatively small free volume and low gas permeability are characterised by the chemical shifts (δ) in the region δ 200–214. This corresponds to the FVE radii lying between 2.5 and 2.9 Å, being in good agreement with the PALS data (see Table 4). Significantly smaller δ values are observed for high-permeability perfluorinated polymers.¹⁰¹ Because small δ values correspond to larger FVE radii, this was interpreted as substantiation of the higher permeability of such polymers. However,

Table 4. Radii of spherical (R_{sp}) and cylindrical (R_c) FVE (Å) determined by different methods.

Polymer	^{129}Xe NMR spectroscopy					PALS			IGC	
	δ	λ /Å	R_{sp}	R_c	Ref.	R_{sp}	R_c	Ref.	R_{sp}	Ref.
AF2400	63.3	5.83	8.04	5.12	101	5.95	6.33	36	6.4	102
AF1600	76.7	4.46	6.66	4.43	101	4.89	5.43	36	5.8	103
AD 80X	83.6	3.92	6.12	4.16	101	—	—			
AD 60X	85.3	3.80	6.00	4.10	101	—	—			
PTFE	90	3.49	5.69	3.94	26	4.2	4.9	26		
PTMSP	148	1.32	3.52	2.9	89	6.8	6.5	36	—	
	178	0.75	3.0	2.6	104					
PPO	180	0.72	2.92	2.56	26	3.4	4.2	26	3.4	105
	185	0.64	2.84	2.52	106					
	188	0.60	2.80	2.50	107					
LDPE	203	0.40	2.60	2.40	26	3.3	4.1	26		
	200	0.44	2.64	2.42	90					
	200	0.44	2.64	2.42	97					
PC	214	0.28	2.48	2.34	26	2.9	3.8	26		
	212	0.30	2.50	2.35	90					
PS	210	0.32	2.52	2.36	108	2.88	3.76	33		
PEMA	203	0.40	2.60	2.40	97	3.0	3.9	109		

other factors affecting the chemical shift can exist. This is indicated by the δ values measured for PTMSP (polymer with the largest free volume and record high gas permeability).^{89,104} Typical of perfluorinated polymers are relatively low refractive indices n_D equal to ~ 1.3 , which corresponds to the molecular refraction

$$R_m = \frac{n_D^2 - 1}{n_D^2 + 2} = 0.187,$$

whereas conventional polymers (*e.g.*, PS, PC, PEMA) are characterised by n_D value lying between 1.5 and 1.7 (molecular refraction is ~ 0.3 – 0.4).¹¹⁰ One can assume that the ^{129}Xe nuclei arrive at regions with lower refraction upon collisions with the FVE walls in perfluorinated polymers, *i.e.*, the lower polarisabilities of chemical bonds in these materials cause less pronounced perturbations of ^{129}Xe nuclei.⁸⁹ The aforesaid suggests that the FVE radii calculated from relations (6)–(8) and listed in Table 4 seem to be somewhat overestimated. This does not contradict the PALS and IGC data that are also shown in Table 4. Only PTMSP presents an exception, namely, the FVE size estimates for this polymer not only do contradict the data for other polymers, but are also inconsistent with the PALS data. Probably, errors in estimation of the FVE size from expressions (7) and (8) are due to the complex geometry of the free volume in PTMSP.¹¹¹

The second problem is related to uncertainty in the size of the xenon atom, which is used for estimation of FVE. Different methods of determination of the atomic diameter (d) of xenon (from viscosity of gas, second virial coefficient, intermolecular interaction potentials, liquid and crystal densities) give the values in the range from 3.2 to 4.6 Å (values obtained before 1990 were summarised in Ref. 112). Traditionally, it is accepted that d equals 4.4 Å (this value was obtained using the van der Waals radii corrected by Pauling and reported by Breck¹⁰⁰). However, Breck also reported a smaller value (3.96 Å) calculated using the Lennard-Jones potential of intermolecular interactions. The data listed in Table 5 illustrate the effect of d value on the theoretical radius of spherical FVE for two polymers with large free volume. Clearly, agreement with the data obtained by other probe methods is more or less depending on the d value chosen. However, a broad FVE size distribution found from MD simulation suggests that the FVE radii mentioned above fall in the range of possible values.

The results of experiments on encapsulation of ^{129}Xe atoms in C_{60} fullerene and measurement of ^{129}Xe NMR spectrum¹¹³ offered some prospects for refinement of the ^{129}Xe NMR data (see above). On the one hand, the synthesis of inclusion compound

Table 5. Atomic diameter of xenon and FVE radii obtained by different methods.

δ	$\lambda / \text{\AA}$	$d / \text{\AA}$	$R_{\text{sp}} / \text{\AA}$			Ref.
			^{129}Xe NMR spectroscopy	PALS	MDS / \AA (see ^a)	
Polymer PTMSP						
148	1.32	3.2	2.9	6.8	2–10	89
		3.96	3.3			
		4.4	3.5			
178	0.75	3.2	2.4	—	—	104
		3.96	2.7			
		4.4	3.0			
Polymer AF2400						
63.3 (powder)	5.83	3.2	7.4	6.0	1.5–12	101
		3.96	7.8			
		4.4	8.0			
64.7 (film)	5.63	3.2	7.2	—	—	101
		3.96	7.6			
		4.4	7.8			

^a MD simulation data were taken from Ref. 111.

^a MD simulation data were taken from Ref. 111.

$\text{Xe}@\text{C}_{60}$ is quite unexpected, because the diameter of xenon atom (4.4 Å) exceeds that of the fullerene cavity. This could be evidence of smaller $d(\text{Xe})$ value. On the other hand, the measured ^{129}Xe chemical shift in this compound is δ 179.24, which gives an estimate of 5 to 6 Å for the inner diameter of the C_{60} cavity. Probably, in this case estimation from expressions (6)–(8) is not substantiated, because we can assume that the xenon atom encapsulated in C_{60} cavity will simultaneously interact with a few (probably, all) fullerene carbon atoms and this will cause large chemical shifts, thus making the Fraissard model inapplicable.¹¹⁴ However, this result indicates the necessity of taking into account the interactions between xenon atom and FVE walls in polymers.

IV. Inverse gas chromatography

Inverse gas chromatography (IGC) is used to study the thermodynamics of sorption of gases and vapours in polymers and to determine their physicochemical parameters.^{115,116} To this end, a polymer is applied on the surface of a solid porous substrate and the sorbate is introduced in the carrier gas flow. Under particular

conditions, by measuring the retention times t_r one can calculate various thermodynamic parameters of the polymer–gas system.

From the known t_r values, it is possible to calculate the net retention volume V_n of a sorbate

$$V_n = (t_r - t_a)J_n^m F_c \frac{273}{T}, \quad (9)$$

where t_a is the retention time of the ‘non-sorbable’ component (e.g., air), which takes into account the dead volume of the chromatograph; J_n^m is the correction for pressure drop in the column; F_c is the rate of the carrier gas; and T is the temperature (in K) at which the experiment is carried out.

A correct application of IGC technique in studies of bulk sorption in polymers implies no diffusion control of the chromatographic experiments; namely, the characteristic times of diffusion into the bulk of the supported polymer should be shorter than the ‘effective’ times of contacts of a sorbate with the polymer phase. Experimentally, this can be achieved using lower rates of the carrier gas, by applying thinner polymer films or by carrying out measurements at higher temperatures.

The main thermodynamic characteristic of bulk sorption (in contrast to adsorption on polymer surface) is the specific retention volume V_g defined as follows:

$$V_g = \frac{V_n}{\omega_L}, \quad (10)$$

where ω_L is the mass of the polymer in the column. With this parameter known, one can calculate¹¹⁷ the solubility factors (S) at infinite dilution

$$S = V_g \frac{\rho}{p_0} \exp \left[(2B_{11} - V_1)J_n^m \frac{p_0}{RT} \right], \quad (11)$$

where ρ is the density of the polymer at temperature T ; p_0 is the standard pressure (1 atm); the exponential term, which includes the second virial coefficient B_{11} and the molar volume of the sorbate V_1 , takes into account the non-ideal state of vapours; R is the universal gas constant.

Yet another important thermodynamic characteristic determined using V_g is the activity coefficient $(a_1/w_1)_\infty$ at infinite dilution

$$\ln \left(\frac{a_1}{w_1} \right)_\infty = \ln \left(\frac{273R}{V_g p_1^0 M_1} \right) - \frac{p_1^0}{RT} (B_{11} - V_1), \quad (12)$$

where M_1 is the molecular mass of the sorbate and p_1^0 is the vapour pressure of the sorbate at temperature T .

The partial molar enthalpy of mixing, ΔH_m , characterises the sorbate–polymer interaction and can be calculated from the temperature dependence of the activity coefficient.

$$\Delta H_m = R \frac{\partial \ln(a_1/w_1)_\infty}{\partial (1/T)}. \quad (13)$$

It can also be estimated from the temperature dependence of the solubility coefficient

$$S = S_0 \exp \left(-\frac{\Delta H_s}{RT} \right), \quad (14)$$

because the enthalpy of sorption can be represented by the sum

$$\Delta H_s = \Delta H_c + \Delta H_m, \quad (15)$$

where ΔH_c is the enthalpy of condensation, which is tabulated for different sorbates.¹¹⁸

Studies of several glassy polymers [polysulfone,¹¹⁹ poly(vinyl-trimethylsilane),¹²⁰ poly(phenylene oxide)¹⁰⁵ and amorphous Teflons AF^{102, 121}] showed that the ΔH_m values strongly depend on the size of the sorbate molecule. The ΔH_m values of n -alkanes

C₃–C₁₂ initially decrease as the molecular masses of these hydrocarbons increase, pass through minima at particular sizes of the sorbate molecules (these sizes are different for different polymers) and then increase again. It was assumed¹²² that the critical size of the sorbate molecule, which corresponds to the minimum and the highest exothermicity of mixing, is also related to the average size of FVE. This hypothesis is substantiated by establishment of correlations between the minimum ΔH_m values and the diffusion coefficients and gas permeabilities of glassy polymers. Probably, this behaviour is due to the ability of FVE to uptake molecules with sizes smaller than the FVE size. Sorption within FVE requires no energy expenditure to overcome the intermolecular interaction forces; therefore, the observed ΔH_m values are negative. The smaller the size difference between the sorbate molecule and FVE size the softer the restrictions imposed on the internal degrees of freedom of the sorbed molecule; as a result, the entropy of mixing ΔS_m , which correlates with ΔH_m , also passes through a minimum.¹²² Thus, the IGC technique permits estimation of the FVE size. The IGC data can be compared with the results obtained using other methods of investigation of the free volume.

The effect of the critical volume V_c used as a measure of the molecular size of sorbates (n -alkanes) on the ΔH_m of particular polymers is illustrated in Fig. 6a. The ΔH_m values pass through minima the coordinates of which ($V_{c, \min}$) are in qualitative correlation with the gas permeability and diffusion coefficient of a given polymer, namely, polymers with larger $V_{c, \min}$ values are characterised by higher diffusion coefficients and gas permeabilities and *vice versa*.

Figure 6b presents the FVE size distributions plotted from PALS data. The ordinate axis denotes the probability density

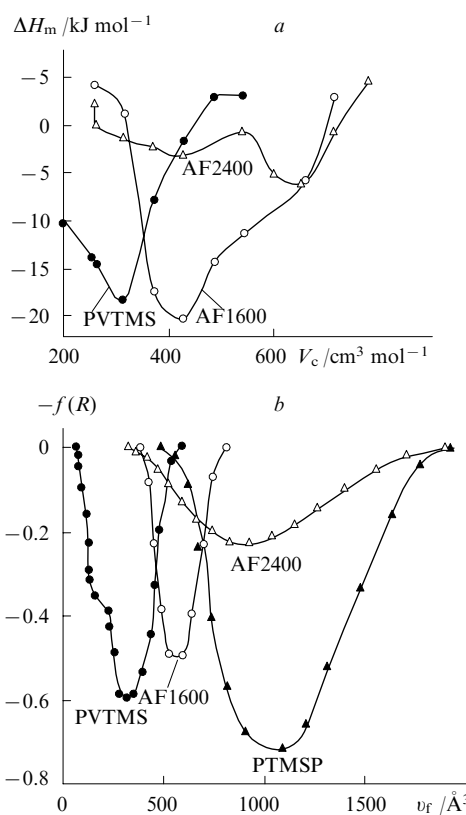


Figure 6. FVE size distribution in glassy polymers.¹²¹

Partial molar enthalpies of mixing plotted vs. critical volumes of sorbates (n -alkanes) according to IGC data (a) and the probability density functions $f(R)$ for polymers with FVE of different size according to PALS data (b).

function $f(R)$ determined using the CONTIN program. The radii of FVE were calculated for spherical geometry using the Tao–Eldrup relationship and then the v_f were found. For clear visual comparison with the dependence on V_c (Fig. 6a), it is appropriate to recalculate the necessary parameters per mole of a particular compound, *i.e.*

$$v_f' = v_f N_A \text{ (cm}^3 \text{ mol}^{-1}\text{)},$$

where N_A is the Avogadro constant. A comparison of the plots shown in Fig. 6a and Fig. 6b shows a clear analogy between the FVE size distributions obtained by two independent methods. Consider this result in more detail.

1. The relative positions of the curves in Fig. 6a and Fig. 6b are very similar. Both methods assign the smallest FVE size to PVTMS and the largest one to AF2400. Minima in the $\Delta H_m(V_c)$ curves for AF1600 and PVTMS correspond to alkanes C_6 and C_7 , respectively, whereas for AF2400 the minima correspond to bulkier sorbates C_{10} and C_{11} (minima at V_c and v_f' equal to $\sim 600 \text{ cm}^3 \text{ mol}^{-1}$).

2. According to PALS data, polymer AF1600 has a much narrower FVE size distribution compared to AF2400. Probably, the narrower this size distribution the stricter the size segregation of the molecules sorbed in FVE. This conclusion is also consistent with the IGC data, namely, the minimum in the ΔH_m curve is much broader for AF2400 than for AF1600.

Quantitative determination of the FVE size from IGC data requires substantiated choice of the probe size (probes are the *n*-alkanes sorbed in polymers). To this end, different parameters can be used, *e.g.*, the van der Waals volume V_w ,¹²³ the molar volume in the liquid phase V_b (at the corresponding boiling temperature T_b)¹²⁴ and the critical volume V_c .¹²⁵ Although these quantities are significantly different from one another (see Table 6), they show the same trend of changes among the polymer–sorbate systems studied. A comparison with other probe methods (PALS, ¹²⁹Xe NMR spectroscopy) and with the results of MD simulation¹¹¹ showed that the best agreement is achieved using V_b or even V_c as a measure of FVE. This is probably due to the fact that linear *n*-alkane molecules should adopt a folded conformation in order to be arranged within (postulated) spherical FVE; because of this, a rather large excluded volume should be added to the intrinsic (van der Waals) volume of the probe.

Some features and limitations of the IGC technique should be pointed. First of all, the FVE size determined using this method is found from the temperature dependence of ΔH_m , *i.e.*, the IGC method provides a temperature-averaged value. Though, with allowance for the thermal expansion coefficient of FVE (about 10^{-3} K^{-1} for glassy polymers according to PALS data) these

differences seem to be insignificant for the temperature intervals (nearly 100 degrees) corresponding to operating conditions. Another problem is related to a limited set of compounds suitable for free volume determination by IGC. The dependences of ΔH_m on the sorbate size in rubbers do not pass through minima due to another mechanism of dissolution and mixing. Additionally, the diffusion coefficients of many glassy polymers are insufficiently high so that the experiments are carried out with diffusion limitations. The results obtained show that the IGC technique is applicable to free-volume studies of polymers characterised by oxygen permeabilities $P_{O_2} > 20$ Barrer at room temperature. However, the number of such polymers is rather large. Polymers with lower permeabilities can be investigated at elevated temperatures.

V. Miscellaneous methods

Many processes involving low-molecular-mass compounds dissolved in polymers are controlled by mobilities of these compounds. The rate of translational (or rotational) mobility strongly depends on the molecule (probe)-to-FVE size ratio in a given polymer. Therefore, by following the mobility of probes of different size in different polymers one can obtain information on the free volume.

1. The photochromic probe technique

The technique is based on a hypothesis,¹²⁷ according to which the implementation of monomolecular chemical reactions (in particular, photoisomerisation) in glassy matrices requires a minimum (critical) FFV in the immediate vicinity of the dissolved probe molecule. This method involves measurements of the degree of *cis*–*trans*-photoisomerisation of a probe in a glassy polymer and in a dilute solution in a model non-viscous solvent where the free volume imposes no restrictions on the isomerisation. Having determined the ratio of these parameters as a function of the probe size (more exactly, as a function of the volume necessary for isomerisation to occur), one can estimate the average size of FVE. Victor and Torkelson¹²⁸ studied the free volume in glassy polystyrene using various stilbene and azobenzene derivatives with the van der Waals volumes in the range of 127–571 Å³ as probes. The implementation of photoisomerisation requires an additional volume for the rearrangement of the molecule that undergoes isomerisation in the excited state. This volume can be estimated from geometric considerations. It was found that more than 90% of the FFV in PS exceeds 120–130 Å³, no FVE with size $> 400 \text{ Å}^3$ are present, and the maximum in the FVE size distribution curve is at $\sim 270 \text{ Å}^3$. Assuming, as in other cases, spherical symmetry of FVE, one gets a FVE radius of $\sim 4 \text{ Å}$, which is somewhat larger than the values obtained using other probe methods (2.4–3.8 Å, see Table 4).

Data on changes in the free volume during physical ageing of glassy polymers obtained by this method worth mentioning. Larger FVE are the first to disappear in the ageing of poly(methyl methacrylate) and PS.¹²⁹ At the same time, an ageing study of polycarbonate characterised by a broader FVE size distribution showed that both large and small free-volume elements disappear simultaneously.¹³⁰

2. The spin probe technique

This was one of the first methods used for estimating the free volume in polymers. It is based on the concept that the mobility (rotational frequency ν_{cor}) of spin probes, namely, stable nitroxyl radicals, first of all 2,2,6,6-tetramethylpiperidine-1-oxyl (TEMPO), is sensitive to the dynamic or structural features of the polymers in which the probes are dissolved.¹³¹ The probe rotational frequency ν_{cor} can be estimated from EPR spectral parameters. Depending on the ν_{cor} values, slow ($0.2 \times 10^9 < \nu_{\text{cor}} < 10^7 \text{ s}^{-1}$) and fast ($\nu_{\text{cor}} > 0.5 \times 10^9 \text{ s}^{-1}$) motions of probes in polymers are distinguished. At room temperature, the rotational frequencies of probes in rubbers decrease as

Table 6. Molecular volumes (Å³ per molecule) and FVE radii (Å) corresponding to minima in ΔH_m -vs.- v_f plots.¹²⁶

Polymer ^a	$\frac{V_w}{R}$	$\frac{V_b}{R}$	$\frac{V_c}{R}$
PVTMS (C_6)	$\frac{113}{3.0}$	$\frac{235}{3.8}$	$\frac{611}{5.3}$
AF1600 (C_7)	$\frac{130}{3.1}$	$\frac{269}{4.0}$	$\frac{708}{5.5}$
PDSNb (C_8)	$\frac{147}{3.3}$	$\frac{316}{4.2}$	$\frac{807}{15.8}$
AF2400 (C_{11})	$\frac{198}{3.6}$	$\frac{436}{4.7}$	$\frac{1096}{6.4}$

Note. The molecular volumes are given in the numerator and the FVE radii are given in the denominator.

^a *n*-Alkane corresponding to minimum ΔH_m value is given in parentheses.

the glass transition temperature increases. Initially, it was accepted that the FVE size in glassy polymers is less than the probe size and therefore only slow motions should occur, as is the case of, *e.g.*, polystyrene. However, it was unexpectedly found that TEMPO radicals execute fast motions while larger spin probes execute slow motions in PVTMS.¹³² Thus, estimation of the FVE size in PVTMS, which possesses rather high permeability, showed that it exceeds the size of the TEMPO molecule (more exactly, it is larger than the volume necessary for rotation of the TEMPO molecule by an angle of 1 radian). Later, similar relations were established by different probe methods for a number of polymers with relatively large FVE sizes.¹³³

However, it was shown^{134, 135} that the model for rotation used in the interpretation of the EPR spectra of the spin probes is simplified and the character of the motion and librations of spin probes in glassy polymers and low-molecular-mass glasses is more complex. Nevertheless, even assuming that the parameter v_{cor} does not reflect the actual dynamics of spin probe motions in FVE, it can be considered as an indicator of the probe-to-FVE size ratio in polymers, which shows the relative differences in the FVE values in different polymers.

3. The electrochromic probe technique

The electrochromic effect, *i.e.*, a change in colour under the action of an electric field, is due to the effect of the electric field on the light-absorption of organic compounds. Orientation of light-absorbing molecules in an electric field changes their extinction coefficients. This can be used for estimating the molecular mobility or the free volume in polymers.¹³⁶ To this end, the light-absorbing molecules acting as probes are dissolved in polymers. Experiments involve detection of changes in the extinction coefficients upon switching the electric field on and then off when random reorientation of the dissolved probe molecules occurs. To make the effect more pronounced, the probe molecules should have large dipole moments, *e.g.*, azo dyes with the van der Waals volumes lying in the range of 770–2900 Å³.¹³⁷ Note that so large probe sizes correspond to hypothetical FVE sizes that are absent in real polymers. In addition, molecules with large dipole moments can strongly interact with polar groups in the polymer structure. Therefore, the electrochromic probe technique is not a ‘non-perturbative’ one, *i.e.*, the FVE size thus determined should sense distortions produced by the introduction of the probe molecules. Nevertheless, the results obtained by this method were useful in the early stages of investigations of the free volume in polymers.

To estimate the average FVE size, one has to analyse the kinetic curves of changes in the optical density upon orientation of dipoles by the electric field and after switching this field off. Experiments are carried out with probes of different sizes. The FVE size is determined using the Cohen–Turnbull model.^{2, 3}

Studies of glassy polymers (PS, PVTMS and PTMSP)^{138, 139} using the electrochromic probe technique gave a ‘correct’ order of changes in the free volume in these polymers, *i.e.*, its increase with an increase in the gas permeabilities and diffusion coefficients. Interestingly, the temperature dependence of the average FVE size in PTMSP was found to be an order of magnitude weaker than in PS; this was confirmed by PALS data.³⁹

The average FVE size in PS was found to be in good agreement with that obtained by the photochromic probe technique.¹²⁸ However, studies by both methods were carried out using very large probes; therefore, it cannot be ruled out that the FVE sizes are overestimated. For instance, the value $v_f = 3290$ Å³ found for PTMSP corresponds to a spherical cavity with the radius of 9 Å. This exceeds considerably the value obtained from PALS data for this polymer (according to results of MD simulation, the presence of so large cavities seems not to be improbable, see Section VI). Based on the aforesaid, data of free-volume studies carried out using large probes should be analysed with special care. Additionally, when comparing different polymers taking into account the

matrix-perturbing effects, it is more correct to consider the probe mobility as a semiquantitative characteristic of the free volume.

4. The conformation probe technique

To probe the free volume in polymers, it was proposed to use organic compounds that can exist as two conformers with different IR spectra.^{140–142} The FVE size can be estimated from the shift of the conformational equilibrium for such probes introduced into glassy polymers. If no conformational transitions occur at a certain temperature (conformational equilibrium is ‘frozen’), the FVE size is less than the critical probe size necessary for its isomerisation. At certain temperature, the ratio of the conformers changes, which means that the FVE size at this temperature is comparable with the probe size. The experimentally used conformation probes were dichloroethane, 1,2-bromofluoroethane, 1,1,2,2-tetrabromoethane and some other compounds. Free-volume studies were carried out for polystyrene, poly(vinyl chloride), poly(methyl methacrylate) and some other glassy polymers. For each probe, the characteristic IR bands corresponding to *trans*- or *gauche*-conformations were chosen. At low temperatures, the optical density ratio $D_{\text{gauche}}/D_{\text{trans}}$ is independent of temperature, then an inflection is observed at certain T_f value after which this ratio (in the $1/T$ coordinates) linearly decreases with temperature. Because the volume necessary for isomerisation of a given probe is known, one can estimate the FVE size at T_f . As the probe size increases, the T_f increases. This makes it possible to estimate the temperature dependence of the limiting FVE size ($V^\#$) necessary for the conformational transition (isomerisation) of the probe in the polymer under study. An example of this dependence for poly(methyl methacrylate) is presented in Table 7. The results obtained are comparable with the PALS data.¹⁴³

Table 7. Temperature dependence of FVE size in PMMA from the conformation probe technique data.¹⁴³

Probe	T_f /K	$V^\#$ /Å ³
1-Bromo-2-fluoroethane	190 ± 20	13.0
1,2-Dichloroethane	195 ± 10	29.5
1,1,2,2-Tetrabromoethane	239 ± 9	56.6
1,2-Di(<i>p</i> -bromophenyl)ethane	326 ± 18	108.2

Experiments with the same probe in different polymers showed that for polymers with high permeabilities the conformational mobility of the probe unfreezes at much lower temperatures than for polymers with low permeabilities. For instance, $T_f = 326$ K for PMMA and 163 K for PTMSP with 1,2-di(*p*-bromophenyl)ethane as probe. Unfreezing of conformation transitions of a smaller probe (1,1,2,2-tetrabromoethane) in PTMSP occurs at even lower temperatures ($T_f < 90$ K).

However, this method is of limited use for studying the free volume in polymers due to the overlap of the spectral bands of the probe and polymer, scarcity of probes and problems associated with the introduction of the probe into the polymer from a common solvent.

On the whole, the methods considered in this Section cannot compete in reliability and informativity with the PALS technique. However, some of them played an important role in the early stage of development of studies on the free volume in polymers and still remain suitable for obtaining additional useful information.

VI. Simulation of the free volume by molecular dynamics

So far, we considered experimental methods of investigation of the free volume. Recently, methods of computer simulation of the nanostructure of polymers aimed at predicting many properties of

polymeric materials [in particular, the diffusion (D) and gas solubility (S) coefficients] have become increasingly important. When solving such problems, the construction of a correct model for the free volume in the polymer under study is prerequisite for obtaining accurate results. The results of computer simulation are analysed using relevant data obtained by probe techniques for substantiation of the reliability of calculations. At the same time, MD simulation provides valuable information that cannot be obtained by the probe methods (see below).

The free volume in polymers can be simulated by, *e.g.*, the Monte Carlo method,^{8, 144–148} molecular mechanics,^{8, 149, 150} theory of transition state and related approaches.^{8, 151, 152} MD simulation appeared to be the most efficient method and a large number of polymers were studied by this method in recent years. In this Section we will consider the results of MD simulation of the free volume in amorphous polymers.

In MD simulation of amorphous polymers, the free volume is described using a cubic box filled with polymer chains. The results of analysis of the free volume and theoretical parameters including D and S can depend on the size of the cubic box, which is undesirable. Calculations with small boxes (cube edge is shorter than 20 Å) take a shorter time. Starting with a certain size (cube edge of about 40–50 Å) this correlation is no longer valid, but the results become more reliable. Usually, the model boxes contain 2000 to 10 000 atoms in the polymer chain.¹⁵³ All atoms in the polymer chains are represented by spheres of preset diameters and masses. The interactions of covalently bonded atoms are described with allowance for the bond lengths, bond angles and torsion angles. Non-covalent intermolecular interactions are described using commonly accepted (most often, the Lennard-Jones and Coulomb) potentials. The chemical structure of the polymer studied is determined in different approximations. The ‘United Atoms’ method ignores all hydrogen atoms and treats all quasi-spherical atomic groups (*e.g.*, CH₂, CH₃) as individual species in order to reduce the computing time. More reliable results can be obtained using the ‘All-Atom Strategy’.¹¹

The sum of all atom–atom interactions expressed as the potential energy model of the packing is called the force field. A correctly determined force field is the key for successful MD simulation of the nanostructure of the system. The force field should reproduce the equilibrium structure, thermodynamic and dynamic properties of the polymer under study and govern the accuracy of prediction of all parameters of the system. One of the most popular force field types is known as the COMPASS (Condensed-phase Optimized Molecular Potentials for Atomistic Simulation Studies)¹⁵⁴ force field (for details, see Ref. 8).

Theodorou and Suter^{155, 156} proposed an efficient box-filling procedure, which allows the length of the polymer chain to be chosen in such a manner that the packing be completely amorphous. The polymer chains are generated using the so-called periodic boundary conditions. Namely, as a propagating virtual chain reaches a cube face and starts to ‘penetrate’ it, a similar propagating chain is automatically introduced on the opposite face. The box is filled until a preset, experimentally determined density of the polymer is reached. Therefore, the polymer density serves as an ‘input parameter’ for calculations. This can cause some difficulties, because the densities of glassy polymers depend on the sample prehistory, amount of residual solvent, *etc.* Since the number of possible types of packing within the cubic box is infinitely large, a packing containing domains with too low or too high local density can be formed in the initial stage. Obtaining a more realistic packing requires an additional stage of the process, namely, the relaxation stage. Various procedures are used to accelerate relaxation. In particular, molecules of ‘plasticiser’ (*e.g.*, methanol) can be introduced into the box and then removed upon relaxation. Detailed consideration of the polymer structure models can be found in, *e.g.*, Refs 8, 111, 153, 157 and 158.

Computer simulation opens new, additional prospects for investigation of the free volume in polymers, most of which are inaccessible in principle to probe methods:

- visualisation of the free volume;
- analysis of connectivity of free-volume elements (cluster size, closed or open porosity);
- construction of FVE size distribution;
- studies of mobility (dynamics) of the free volume elements in polymers.

Consider as an example model nanostructures of the free volume^{111, 157} in a polymer with moderate permeability, poly(*p*-trimethylsilylstyrene) (P_{O_2} = 56 Barrer¹⁵⁹) and in two polymers with high permeabilities and large FVE (according to PALS and IGC data), namely, poly(trimethylsilylpropyne) and amorphous Teflon AF2400 (P_{O_2} = 7700 and 1140 Barrer, respectively^{41, 160}). The force field was calculated using the COMPASS programme,¹⁵⁴ which includes interactions of all atoms in the monomer unit in explicit form and optimizes the bond lengths, bond angles, dihedral angles and the Coulomb and van der Waals potentials. Calculations involve optimisation of the force field in order to correctly reproduce the physical properties of the polymer in the block. The *cis:trans* ratio in PTMSP, which contains double bonds in the main chain, was set to 1 : 1 assuming random distribution of *cis* and *trans* units over the chain. In this approximation all dihedral angles were determined based on the Boltzmann distribution obtained using the torsion potentials included in the COMPASS force field for particular bonds with allowance for local non-bonding interactions.

It is convenient to carry out visualisation by slicing the cubic boxes generated. In boxes with 4–5 nm edges, the neighbouring layers are separated by a distance of about 0.3 nm (Fig. 7). In Fig. 7a, the white background denotes the free volume; the free volume elements in PTMSP represent compact aggregates the size of which is comparable with the slice-to-slice separation. For instance, the visible FVE in slice c_4 is not seen in the neighbouring slices c_3 and d_1 . This means that the FVE size is comparable with the slice-to-slice separation of ~0.3 nm. The visible ‘diameter’ of FVE in this slice is also similar to this value. Thus, our simplest analysis shows that the shape of the free volume elements in PTMSP is nearly spherical or ellipsoidal with similar lengths of semiaxes. PTMSP has another shape of the free volume elements (Fig. 7b). Here, the characteristic size of FVE is much larger and the same FVE can be seen in many slice sequences in the cubic box. This can be considered as a proof of the assumptions of quasi-open porosity in this polymer, which were based on some indirect observations.^{161, 162} A broad FVE size distribution was also obtained in another study¹⁵² where it was found that larger FVE tend to form channels.

According to MD simulation data, the other polymer with high permeability, *viz.*, amorphous Teflon AF2400, has yet another type of the nanostructure of the free volume elements. The results of MD simulation of the packing in this polymer showed¹¹¹ that the FVE size here is also rather large, but the FVE no longer pierce the whole cubic box, as in the case of PTMSP. Elongated FVE rarely extend to more than one or two slices. Thus, the structure of the AF2400 polymer is rather characterised by the closed porosity.

It is interesting to follow how these microscopic properties are reflected in the macroscopic behaviour of membrane materials, in particular their gas permeabilities and diffusion coefficients (Table 8). Since

$$P = DS,$$

the changes in P in series of penetrants are governed by the kinetic (D) or thermodynamic (S) factors. For all polymers their D values decrease, although at different rates, as the size or molecular mass of penetrant increase. On the contrary, the solubility coefficients S , which characterise the ability of transition to condensed state,

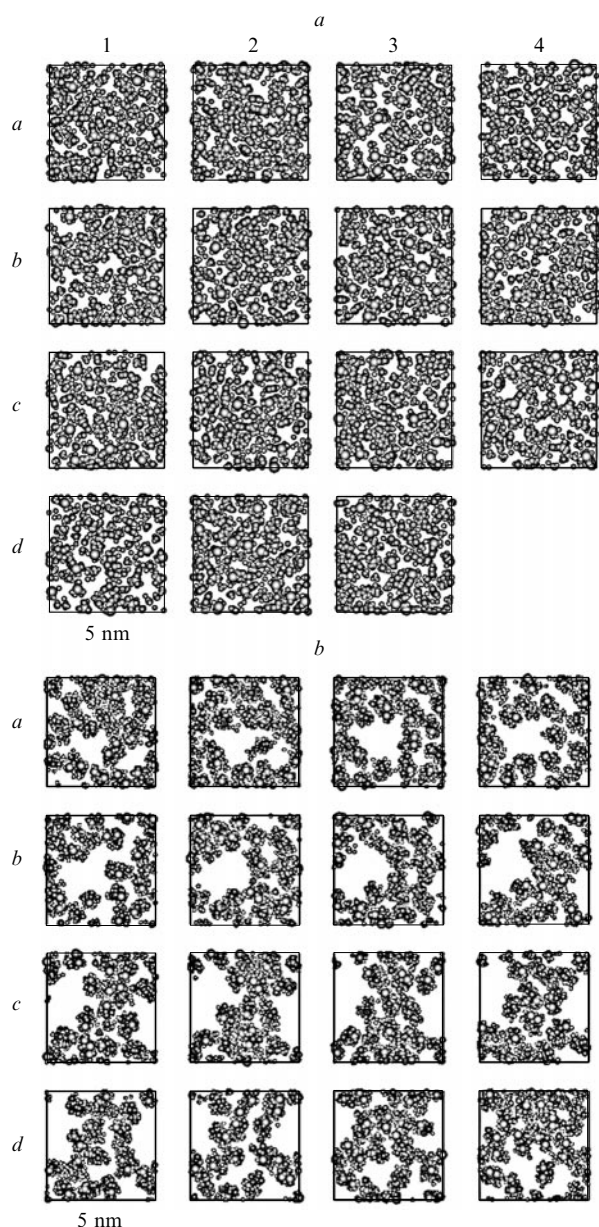


Figure 7. Model representation of the free volume in PTMSS (a) and PTMSP (b).¹⁵⁷

Cube edge is about 5 nm, slice-to-slice separation is nearly 0.3 nm; slices are shown as follows: $a_1 \dots a_4$, $b_1 \dots b_4$, $c_1 \dots c_4$, $d_1 \dots d_3(d_4)$.

Table 8. Permeability and diffusion coefficients of hydrocarbons in AF2400 and PTMSP.

Gas	P /Barrer		$10^7 D$ /cm ² s ⁻¹	
	AF2400 ⁴¹	PTMSP ¹⁶³	AF2400 ⁴¹	PTMSP ¹⁶³
CH ₄	435	15 000	—	240
C ₂ H ₆	252	31 000	3.6	110
C ₃ H ₈	97	38 000	0.42	98
C ₄ H ₁₀	—	78 000 ^a	0.24	—

^a Data taken from Ref. 162.

increase in this case. In polymers the with open porosity characterised by low barriers to diffusion the parameter P is more

strongly affected by the solubility coefficient S . It is this behaviour that is typical of PTMSP, which has a relatively weak dependence of D on the size of the penetrant. Contrary to this, polymer AF2400 behaves as a conventional glassy polymer and demonstrates a rather strong dependence of D on the size of the penetrant; therefore, here the P values decrease on going from CH₄ to C₃H₈. Thus, the connectivity of the free volume elements has a crucial effect on the selectivity of glassy membrane materials.

Using MD simulation, it is possible to determine the FVE size distribution. The corresponding procedure involves filling of the box with probes of different size and calculations of the volume where the rigid spheres of the probes and polymer atoms do not overlap. However, because the free volume in polymers has a complex geometry (irregular shape; for details, see, *e.g.*, Refs 164–167), the results obtained can depend on how the notion ‘FVE’ used in analysis of the computer model is defined. Hofmann *et al.*^{111, 157, 168} put forward two definitions of the FVE in polymers; these are illustrated in Fig. 8. One limiting case (V_{connect} approximation) corresponds to a topological situation where a given FVE contains all points having at least one neighbour with no overlap of the rigid spheres of the probe and atoms of the polymer chain. This approach makes it possible to identify cavities that can be large and have irregular shape. In the other limiting case (R_{max} approximation), the FVE contains only the points located at the shortest distance to the atoms of the polymer chain surrounding the FVE. This approach allows partition of large FVE having irregular or extended shape into smaller ‘local’ regions, as shown in Fig. 8.

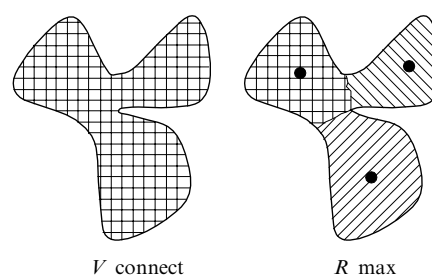


Figure 8. Schematic illustration of two approaches to visualisation of the free volume in glassy polymers.¹⁵⁷

The V_{connect} approximation characterises the ‘global’ FVE, while the R_{max} approximation characterises the ‘fractional’ FVE more similar to spherical.

Now consider how the shape of the FVE size distribution in polymers, obtained using these two approximations, are represented. PTMSP is characterised by a nearly Gaussian distribution with a maximum at $R = 2$ Å (Fig. 9), which is consistent with the results of qualitative analysis of the cubic box (see above and Fig. 7a). For this polymer, both approximations give similar FVE size distributions. Another pattern was obtained for the polymers with high permeabilities and large free volumes. As examples, Fig. 10 presents the FVE size distributions obtained for amorphous Teflon AF2400 in the R_{max} and V_{connect} approximations. In the former case, this is a broadened continuous FVE size distribution with radii of up to 13 Å. In the latter case, we have a clearly seen bimodal distribution consistent with the results of PALS data processing using the CONTIN programme (see Section II). Because the real structure of the free volume in polymers should be considered as superposition of these two limiting models, it seems that we get even better agreement between the predictions of MD simulations and experimental results obtained using probe methods.

Similar characters of the distributions obtained in the V_{connect} and R_{max} approximations were also established for PTMSP

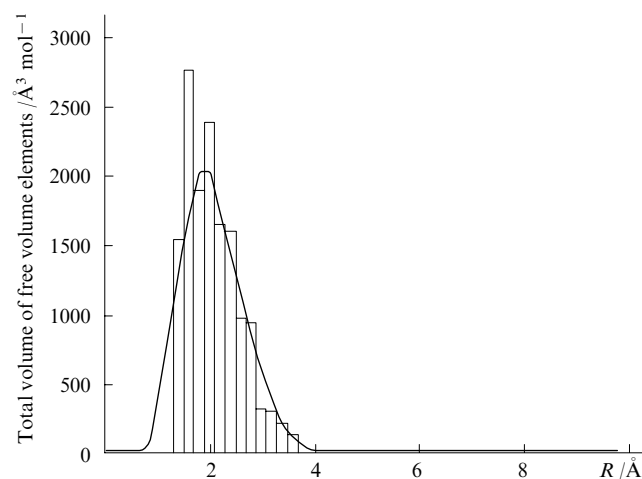


Figure 9. Size distribution of free volume elements in PTMSS.¹⁵⁷ Rectangles denote the results obtained in the R_{\max} approximation. The curve corresponds to averaged data.

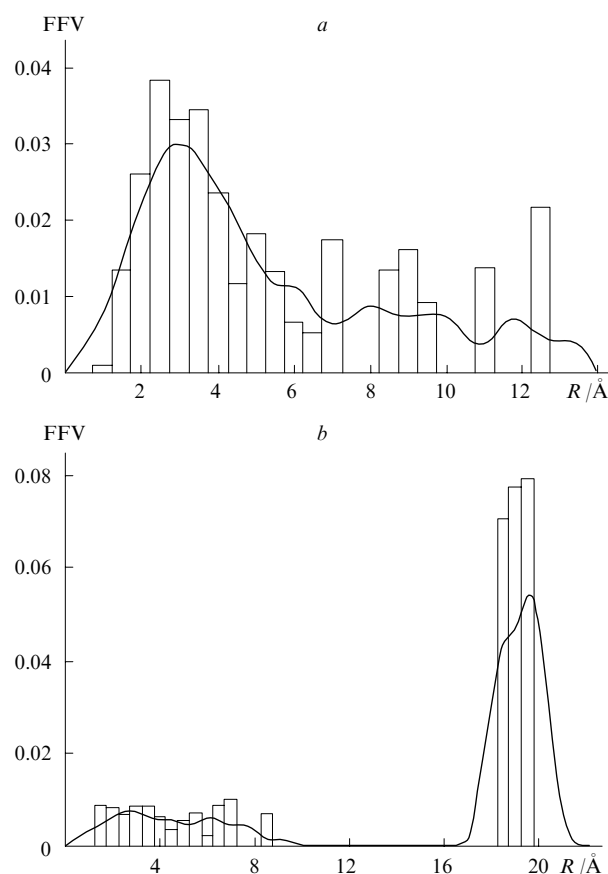


Figure 10. Size distribution of free volume elements in perfluorinated polymer AF2400.¹¹¹ Results obtained in the R_{\max} (a) and V_{connect} (b) approximations. Rectangles denote the corresponding theoretical results and the curves correspond to averaged data.

and other polymers with high permeabilities.¹¹¹ Bimodal distributions in the V_{connect} approximation were also obtained in simulation of polymers with smaller permeabilities (polyimides, see Fig. 11). However, a decrease in gas permeability (and free volume) of polyimides is followed by rapid transformation of the bimodal distribution to monomodal (Gaussian).¹⁶⁸

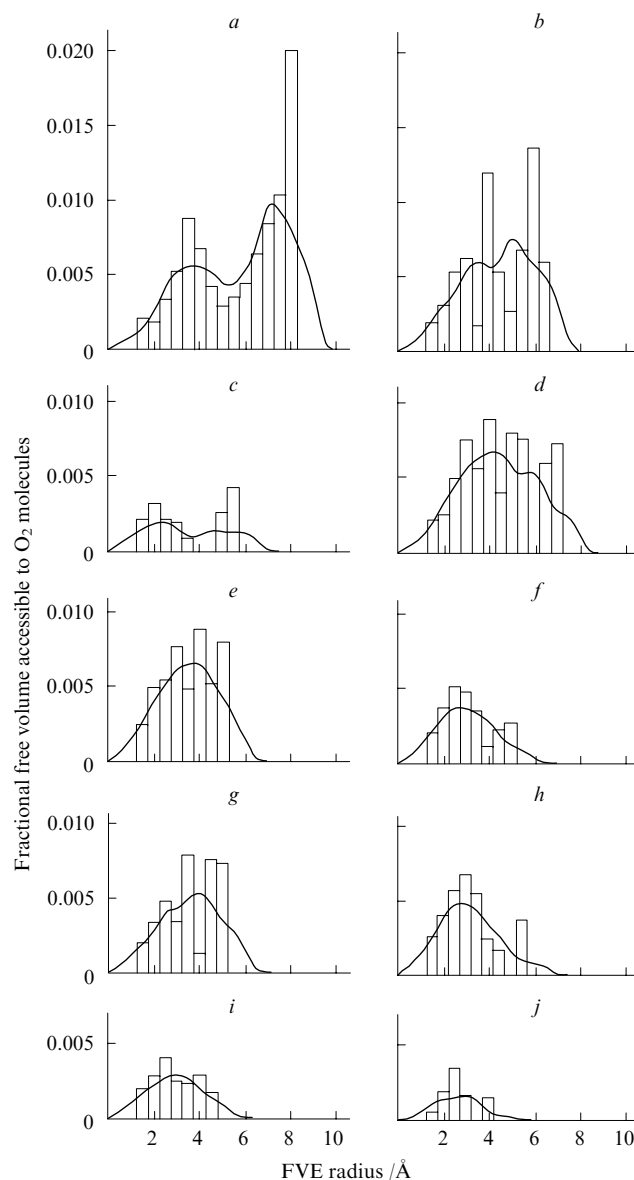


Figure 11. Size distribution of free volume elements in different polyimides.¹⁶⁸

Shown is the evolution of the size distribution upon a change in the polymer permeability P_{O_2} /Barrer: P13, $P_{O_2} = 124$ (a); P14, $P_{O_2} = 137$ (b); T6, $P_{O_2} = 69$ (c); B4, $P_{O_2} = 54$ (d); BAFF, $P_{O_2} = 13$ (e); MDX, $P_{O_2} = 11$ (f); PDA, $P_{O_2} = 5$ (g); ODX, $P_{O_2} = 4$ (h); DDS, $P_{O_2} = 3$ (i); and KAP, $P_{O_2} = 0.5$ (j).

The character of the FVE size distribution depends on the probe size. For instance, the use of oxygen molecules (van der Waals radius 1.73 Å) instead of *o*-Ps (Bohr radius 1.06 Å) as probes causes the distribution to be shifted to the left at larger radii; however, the overall distinctions between the two distributions are insignificant.¹¹¹

By substantially reducing the probe size, one can plot the 'total' FVE size distribution^{157,169} (Table 9), which includes even so small cavities that cannot participate in transport of the smallest molecules. For most glassy polymers extrapolation to zero probe size gives a FFV of about 0.3, but in some cases (e.g., PTMSP) it can be as high as 0.5 (Ref. 157). Taking atactic polypropylene as an example, Greenfield and Theodorou¹⁴⁴ showed that a decrease in the probe size causes a rapid increase in continuous free-volume clusters in the polymer, which overcome the percolation threshold. Indeed, an infinite cluster is

Table 9. FFV estimates obtained from MD simulation with probes of different sizes.¹⁵⁷

Polymer	Probe size /Å	FFV
PTMSS	1.1	0.02
	0.43	0.185
	0.18	0.331
	extrapolation to zero	~0.36
PTMSP	1.1	0.211
	0.43	0.369
	0.18	0.469
	extrapolation to zero	~0.50

formed at a virtual (unnatural) probe radius of 0.9 Å (*cf.* a range from 1.20 to 1.30 Å reported by different authors for the van der Waals radius of the He atom).

Correctness of the results of MD simulation of the free volume in polymers can be assessed not only by comparing them with the results obtained by experimental probe methods, but also by checking for consistence with the FVE size distributions in the same polymers treated using different computational approaches (see, *e.g.*, Refs 157 and 169). To date, MD simulations of the free volume in many glassy polymers (polyimides, polysulfones, polystyrenes, polyacetylenes, *etc.*) have been carried out.^{110, 148, 160, 163, 164} For most polymers, the FVE radii lie in the range 2–4 Å, which is consistent with the data obtained by two probe methods, PALS and ¹²⁹Xe NMR spectroscopy. However, for some polymers with high permeabilities MD simulation gives much larger FVE radii (up to 10–20 Å), which undoubtedly determines unusual transport properties of these compounds. Selected results of MD simulation of the free volume and experimental PALS data are listed in Table 10. Taking into account a large number of admissions made in both MD simulation and experimental free-volume studies, the degree of consistency obtained for most polymers can be considered reasonable.

In the aforesaid we considered the static free volume in polymers. However, MD methods are also suitable for studying the redistribution dynamics of FVE in polymers. For rubbers [*e.g.*, polydimethylsiloxane, poly(methyloctylsiloxane)^{172–174} and poly(dimethylsilamethylene)¹⁵⁸] the average lifetime of FVE in a certain domain within the box is a few picoseconds while the opening of channels connecting the neighbouring FVE seems to take even shorter time. Glassy polymers, *e.g.*, polyimides and poly(ether-ether-ketone)^{172, 175} are characterised by much longer average lifetimes, but reliable data on these times are unavailable as yet, because analysis of the events occurring on a few-nano-second time scale requires unreasonably high computational resources.

The time necessary for visualisation of FVE redistribution in glassy polymers is much longer than several nanoseconds.¹⁵⁸

Consider the dynamics of FVE redistribution in rubbers^{153, 158, 172} in more detail. Simulation of the free volume in poly(methyloctylsiloxane) rubber showed that the opening time of a channel between neighbouring FVE is of the order of nanoseconds, *i.e.*, is two orders of magnitude longer than the ‘settled’ lifetime of the penetrant molecule (H₂O). Channels being opened are rather broad; as a result, two neighbouring FVE coalesce. This provides an explanation for the well-known phenomenon of low-selectivity diffusion in rubbers; indeed, here size selection of the diffusing molecules in the opening channels is impossible. Microscopically, migration of FVE (or, which is the same, opening of channels) is a consequence of both segmental mobility and small-scale mobility of side groups (CH₃ and C₈H₁₇ for poly(dimethylsiloxane) and poly(methyloctylsiloxane),¹⁵³ respectively).

Table 10. FVE radii (Å) in polymers obtained from molecular dynamics simulation and by PALS.

Polymer	MD simulation			PALS			
	R_m	$R_{1/2}$	Ref.	R	R_3	R_4	Ref.
6FDA-polyimides							
P13	3.0	1.3–4.5	168	4.2			76
P14	2.7	1.4–4.4	168	4.0			76
BAAF	2.7	1.3–4.0	168	3.6			76
	2.7	1.3–3.7	170				
PDA	2.6	1.3–4.0	168	3.4			76
ODA	2.6	1.3–3.8	168	3.2			76
PS	3.2	2.9–3.6	167	2.7;			33
				2.9			171
PTMSS	1.9	1.3–2.8	157		2.6	3.8	159
PFPDMSS	1.8	1.3–2.6	157	3.6			157
PSP	1.2	0.8–2.2	170	2.8			34, 172
PVTMS	2.6	1.3–4.4	111	3.4			111
PTMSP	4.5	1.7–8.0	111		3.3	6.3	111, 157
	5.6	4.7–7.4	169				
PPrSiDPA	3.1	1.3–4.9	111		4.4	6.5	111
PPHSiDPA	2.7	1.0–4.7	111		2.6	4.1	111
AF2400	4.7	3.3–5.5	169		2.7	6.0	111
AF1600	3.1	1.6–5.2	111		2.5	4.9	111
						4.8	40

Note. R_m is the FVE radius at the distribution maximum; the width of the FVE size distribution is represented by the range of $R_{1/2}$ (radii at half-height) values; PALS data are represented by either a unique radius of spherical FVE (R) or two values (R_3 and R_4) if the size distribution is bimodal.

Similar conclusions were also drawn in studies of the dynamics of fluctuating FVE in another organosilicon rubber, poly(dimethylsilamethylene).¹⁵⁸ MD simulation of this polymer was carried out for the free volume ‘sensed’ by two penetrant molecules of different sizes, namely, methane and a spherical penetrant with diameter of 2.8 Å (similar to the size of H₂ molecule). The FVE concentrations accessible to methane molecule appeared to be much lower than those accessible to the smaller penetrant. In both cases the larger FVE were characterised by longer ‘settled’ lifetimes compared to the smaller FVE. The spatial FVE distribution significantly changed after a period of 10 ns (time interval between two successive ‘frames’ in MD simulation of the free-volume dynamics); the effective diffusion coefficients of FVE were of the order of 10^{-3} – 10^{-4} cm² s⁻¹. This provides an explanation for fast gas diffusion in rubbers.

VII. Conclusion

At present, the free volume in polymers is studied by experimental methods based on different physicochemical principles and measuring techniques. On the whole these techniques give mutually consistent results. Among them, analysis of positron annihilation lifetimes has been best developed and most often used. Despite some admissions associated with uncertainties in the hypothesis of spherical geometry of the FVE in polymers and some doubt concerned with bimodal FVE size distribution, this method gave a clear description of the free volume in hundreds of polymers. Also, it is at least equally important that the method makes it possible to study changes in the free volume upon chemical modification of polymers, sorption and plastification, upon change in temperature and under the action of pressure and deformations.

The results obtained showed that other probe methods are of much more limited use. However, their role should not be under-

estimated. Indeed, reasonable agreement between the FVE sizes determined by different methods increases the degree of confidence for the principle of probing the free volume in polymers. This made it possible to establish various correlations between the free volume and particular characteristics (*e.g.*, diffusion coefficients and gas permeabilities), which are suitable for quantitative predictions.

Recently, MD methods have become of particular importance for the description and prediction of free-volume parameters. The results obtained by the probe methods are still needed to confirm the results of simulation, but it seems likely that in the future the

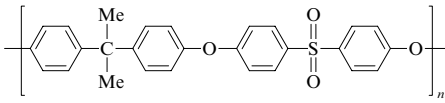
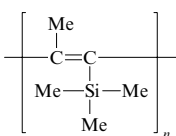
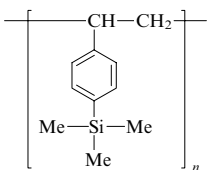
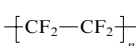
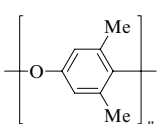
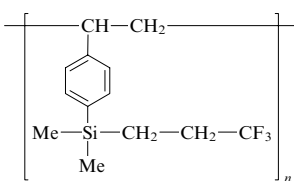
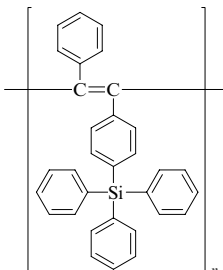
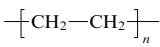
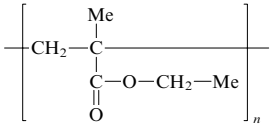
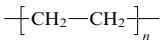
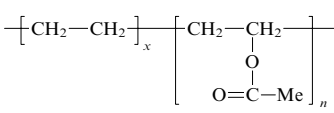
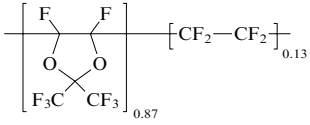
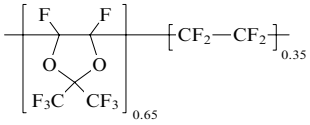
MD methods will become the main tool of studying the free volume in polymers. It is also of crucial importance that MD simulation provides not only local characteristics of the free volume (FVE size and FVE size distribution), but also information on its topology (closed or open porosity, percolation phenomena, *etc.*). This is inaccessible to probe methods. The aforesaid suggests that the results of studies on the properties of polymers (*e.g.*, membrane polymers) should be complemented with the data obtained by probe methods and by the results of MD simulation of the free volume in polymers.

VIII. Appendix

List of polymers.

Notation	Name	Formula
PVA	poly(vinyl acetate)	$\left[\begin{array}{c} \text{CH}_2 - \text{CH} \\ \\ \text{O} \\ \\ \text{C} = \text{O} \\ \\ \text{Me} \end{array} \right]_n$
PVTMS	poly(vinyltrimethylsilane)	$\left[\begin{array}{c} \text{CH}_2 - \text{CH} \\ \\ \text{Me} - \text{Si} - \text{Me} \\ \\ \text{Me} \end{array} \right]_n$
PVC	poly(vinyl chloride)	$\left[\begin{array}{c} \text{CH}_2 - \text{CH} \\ \\ \text{Cl} \end{array} \right]_n$
PDMS	poly(dimethylsiloxane)	$\left[\begin{array}{c} \text{Me} \\ \\ \text{Si} - \text{O} \\ \\ \text{Me} \end{array} \right]_n$
PDSNb	poly(disilylnorbornene)	$\left[\begin{array}{c} \text{Me} \quad \text{Me} \\ \diagdown \quad \diagup \\ \text{Si} \quad \text{Si} \\ \diagup \quad \diagdown \\ \text{Me} \quad \text{Me} \end{array} \right]_n$
PC	bisphenol-A polycarbonate	$\left[\begin{array}{c} \text{Me} \\ \\ \text{C} \\ \\ \text{Me} \end{array} \begin{array}{c} \text{O} \\ \\ \text{C} - \text{O} \end{array} \right]_n$
PMMA	poly(methyl methacrylate)	$\left[\begin{array}{c} \text{Me} \\ \\ \text{CH}_2 - \text{C} \\ \\ \text{C} - \text{O} - \text{Me} \\ \\ \text{O} \end{array} \right]_n$
PPrSiDPA	poly{1-phenyl-2-[<i>p</i> -(triisopropylsilyl)phenyl]acetylene}	$\left[\begin{array}{c} \text{C}_6\text{H}_5 \\ \\ \text{C} = \text{C} \\ \\ \text{C}_6\text{H}_4 \\ \\ \text{CH} - \text{Si} - \text{CH} \\ \quad \quad \\ \text{Me} \quad \text{CH} \quad \text{Me} \\ \quad \\ \text{Me} \quad \text{Me} \end{array} \right]_n$
PS	polystyrene	$\left[\begin{array}{c} \text{CH}_2 - \text{CH} \\ \\ \text{C}_6\text{H}_5 \end{array} \right]_n$

List of polymers (continued).

Notation	Name	Formula
PSP	polysulfone	
PTMSP	poly(trimethylsilylpropyne)	
PTMSS	poly(<i>p</i> -trimethylsilylstyrene)	
PTFE	poly(tetrafluoroethylene)	
PPO	poly(1,3-dimethyl-2,5-phenylene oxide)	
PFPDMSS	poly[<i>p</i> -(3,3,3-trifluoropropyl)dimethylsilyl]styrene	
PPHSiDPA	poly{1-phenyl-2-[<i>p</i> -(triphenylsilyl)phenyl]}acetylene	
PE	polyethylene	
PEMA	poly(ethyl methacrylate)	
LDPE	low-density polyethylene	
EVA	ethylene – vinyl acetate copolymer	
AF-2400	random copolymer of 2,2-bis(trifluoromethyl)-4,5-difluoro-1,3-dioxole (87 mol.%) and tetrafluoroethylene (13 mol.%)	
AF-1600	random copolymer of 2,2-bis(trifluoromethyl)-4,5-difluoro-1,3-dioxole (65 mol.%) and tetrafluoroethylene (35 mol.%)	

List of polymers (continued).

Notation	Name	Formula
6FDA-ODA	polyimide based on 1,1,1,3,3,3-hexafluoro-2,2-bis(3,4-dicarboxyphenyl)propane dianhydride and 4,4'-diaminodiphenyl ether	
6FDA-BAAF	polyimide based on 1,1,1,3,3,3-hexafluoro-2,2-bis(3,4-dicarboxyphenyl)propane dianhydride and 2,2-bis(4-aminophenyl)hexafluoropropane	
6FDA-P13	polyimide based on 1,1,1,3,3,3-hexafluoro-2,2-bis(3,4-dicarboxyphenyl)propane and 2,3,5,6-tetramethyl-p-phenylenediamine	
6FDA-P14	polyimide based on 1,1,1,3,3,3-hexafluoro-2,2-bis(3,4-dicarboxyphenyl)propane dianhydride and 2,4,6-trimethyl-m-phenylenediamine	
6FDA-2	polyimide based on 1,1,1,3,3,3-hexafluoro-2,2-bis(3,4-dicarboxyphenyl)propane dianhydride and 2,5-dimethyl-p-phenylenediamine	
6FDA-1	polyimide based on 1,1,1,3,3,3-hexafluoro-2,2-bis(3,4-dicarboxyphenyl)propane dianhydride and methyl-p-phenylenediamine	
6FDA-PDA	polyimide based on 1,1,1,3,3,3-hexafluoro-2,2-bis(3,4-dicarboxyphenyl)propane dianhydride and p-phenylenediamine	
6FDA-T6	polyimide based on 1,1,1,3,3,3-hexafluoro-2,2-bis(3,4-dicarboxyphenyl)propane dianhydride and 4,4''-diamino-3,5,2',5',3'',5''-hexamethylterphenyl	
6FDA-B4	polyimide based on 1,1,1,3,3,3-hexafluoro-2,2-bis(3,4-dicarboxyphenyl)propane dianhydride and 4,4'-diamino-3,5,3',5'-tetramethylbiphenyl	
6FDA-MDX	polyimide based on 1,1,1,3,3,3-hexafluoro-2,2-bis(3,4-dicarboxyphenyl)propane dianhydride and 4,4'-diamino-3,5,3',5'-tetramethyldiphenylmethane	
DDS	polyimide based on 1,1,1,3,3,3-hexafluoro-2,2-bis(3,4-dicarboxyphenyl)propane dianhydride and 4,4'-diaminodiphenyl sulfone	
KAP	polyimide of pyromellitic dianhydride and 4,4'-diaminodiphenyl oxide	

List of polymers (continued).

Notation	Name	Formula
Hyflon AD80X	random copolymer of 2,2,4-trifluoro-5-trifluoromethoxy-1,3-dioxolane (80 mol.%) and tetrafluoroethylene (20 mol.%)	
Hyflon AD60X	random copolymer of 2,2,4-trifluoro-5-trifluoromethoxy-1,3-dioxolane (60 mol.%) and tetrafluoroethylene (40 mol.%)	
Vectra	copolyester of <i>p</i> -hydroxybenzoic acid and 6-hydroxy-2-naphthoic acid	

References

1. Ya I Frenkel' *Sobranie Izbrannykh Trudov. Kineticheskaya Teoriya Zhidkostei* (Collected Selected Works. Kinetic Theory of Liquids) (Moscow, Leningrad: Academy of Sciences of the USSR, 1959) Vol. 3
2. M H Cohen, D Turnbull *J. Chem. Phys.* **31** 1164 (1959)
3. D Turnbull, M H Cohen *J. Chem. Phys.* **34** 120 (1961)
4. J S Vrentas, J L Duda, in *Encyclopedia of Polymer Science and Engineering* Vol. 5 (New York: Wiley, 1986) p. 36
5. J L Duda, J M Zelinsky *Free-Volume Theory in Diffusion in Polymers* (Ed. P Neogi) (New York: Marcel Dekker, 1996)
6. A A Askadskii, Yu I Matveev *Khimicheskoe Stroenie i Fizicheskie Svoistva Polimerov* (Chemical Structure and Physical Properties of Polymers) (Moscow: Khimiya, 1983)
7. A A Askadskii, V I Kondrashchenko, in *Komp'yuternoe Materialovedenie Polimerov. Atomno-molekulyarnyi Uroven'* (Computer Materials Science of Polymers. Atomic-molecular Level) (Moscow: Nauchnyi Mir, 1999) Vol. 1, p. 54
8. A Bondi *Physical Properties of Molecular Crystals, Liquids and Gases* (New York: Wiley, 1968)
9. J Y Park, D R Paul *J. Membr. Sci.* **125** 23 (1997)
10. D N Theodorou, in *Molecular Simulations of Sorption and Diffusion in Amorphous Polymers in Diffusion in Polymers* (Ed. P Neogi) (New York: Marcel Dekker, 1996) p. 67
11. D N Theodorou, in *Principles of Molecular Simulation of Gas Transport in Polymers. (Materials Science of Membranes for Gas and Vapour Separation)* (Eds Yu Yampolskii, I Pinnau, B D Freeman) (New York: Wiley, 2006) p. 47
12. D M Shrader, Y C Jean (Eds) *Positron and Positronium Chemistry* (Amsterdam: Elsevier, 1988)
13. R A Pethrick *Prog. Polym. Sci.* **22** 1 (1997)
14. A Hill, in *High Temperature Properties and Applications of Polymeric Materials (ACS Symp. Ser.)* (Eds M R Tant, J W Connell, H L N McManus). (Washington, DC: American Chemical Society, 1995) Vol. 603, p. 63
15. J Bartos, in *Encyclopedia of Analytical Chemistry* (Ed. R A Meyers) (New York: Wiley, 2000) p. 7968
16. M Ban, M Kyoto, A Uedono, T Kawano, S Tanigawa *J. Polym. Sci., Part B: Polym. Phys.* **34** 1189 (1996)
17. C Westlund, M Eldrup, F H J Maurer *Nucl. Instrum. Methods Phys. Res., Sect. B* **143** 575 (1998)
18. W Brandt, J Spirn *Phys. Rev.* **142** 231 (1966)
19. J Tao *J. Chem. Phys.* **56** 5499 (1972)
20. M Eldrup, D Lightbody, J N Sherwood *Chem. Phys.* **63** 51 (1981)
21. A Shimazu, T Miyazaki, S Katayama, Y Ito *J. Polym. Sci., Part B: Polym. Phys.* **41** 308 (2003)
22. P Kirkegaard, N J Pederson, M Eldrup *PATFIT-88: A Data Processing System for Positron Annihilation Spectra on Main-frame and Personal Computers*, Roskilde, Denmark, 1989 Risoe-M-2740
23. S W Provencher *Comput. Phys. Commun.* **27** 229 (1982)
24. R B Gregory *J. Appl. Phys.* **70** 4665 (1991)
25. C-L Wang, F H J Maurer *Macromolecules* **29** 8249 (1996)
26. B Nagasaka, T Eguchi, H Nakayama, N Nakamura, Y Ito *Radiat. Phys. Chem.* **58** 581 (2000)
27. B G Olson, T Prodpran, A M Jamieson, S Nazarenko *Polymer* **43** 6775 (2002)
28. Y C Jean, H Shi *J. Non-Cryst. Solids* **172–174** 806 (1994)
29. T Goworek, K Ciesielski, B Jasinska, J Wawrzyszuk *Radiat. Phys. Chem.* **58** 719 (2000)
30. T Hsieh, C Tiu, G P Simon *J. Appl. Polym. Sci.* **82** 2252 (2001)
31. V P Shantarovich, Yu P Yampolskii, Yu M Sivergin, O B Salamatina, V V Gustov, D Khofmann *Khim. Fiz.* **22** 87 (2003)^a
32. J Liu, Q Deng, Y C Jean *Macromolecules* **26** 7149 (1993)
33. Y C Jean, J-P Yuan, J Liu, Q Deng, H Yang *J. Polym. Sci., Part B: Polym. Phys.* **33** 2365 (1995)
34. K Tanaka, K Okamoto, H Kita, Y Ito *Polym. J. (Tokyo)* **25** 577 (1993)
35. V Shantarovich, I Kevdina, Yu Yampolskii, A Alentiev *Macromolecules* **33** 7453 (2000)
36. A Shimazu, T Kanaya, T Miyazaki, S Katayama, Y Ito *Mater. Sci. Forum* **445–446** 249 (2004)
37. K Okamoto, K Tanaka, M Ito, H Kita, Y Ito *Mater. Sci. Forum* **175–178** 743 (1995)
38. V Shantarovich, Z Azamatova, Yu Novikov, Yu Yampolskii *Macromolecules* **31** 3963 (1998)
39. G Consolati, I Genco, M Pegoraro, L Zanderighi *J. Polym. Sci., Part B: Polym. Phys.* **34** 357 (1996)
40. W J Davies, R A Pethrick *Eur. Polym. J.* **30** 1289 (1994)
41. A Yu Alentiev, Yu P Yampolskii, V P Shantarovich, S M Nemser, N A Plate *J. Membr. Sci.* **126** 123 (1997)
42. G Consolati, R Rurali, M Stefanetti *Chem. Phys.* **237** 493 (1998)
43. V P Shantarovich, T Suzuki, C He, V A Davankov, A V Pastukhov, M P Tsyurupa, K Kondo, Y Ito *Macromolecules* **35** 9723 (2002)
44. V P Shantarovich, T Suzuki, C He, I B Kevdina, V A Davankov, A V Pastukhov, M P Tsyurupa *High Energy Chem.* **38** 274 (2004)
45. G Ferey, C Mellot-Draznieks, C Serre, F Millange, J Dutour, S Surble, I Margiolaki *Science* **309** 2040 (2005)
46. N B McKeown, S Makhseed, K J Msayib, L L Ooi, M Helliwell, J E Warren *Angew. Chem., Int. Ed.* **44** 7718 (2005)

47. Y Kobayashi, W Zheng, E F Meyer, J D McGervey, A M Jamieson, R Simha *Macromolecules* **22** 2302 (1989)
48. Y Y Wang, H Nakanishi, Y C Jean, T C Sandreczki *J. Polym. Sci., Part B: Polym. Phys.* **28** 1431 (1990)
49. V Shantarovich, T Suzuki, C He, Y Ito, Yu Yampolskii, A Alentiev *Radiat. Phys. Chem.* **73** 45 (2005)
50. J Kristiak, J Bartos, K Kristiakova, O Sausa, P Bandzuch *Phys. Rev. B* **49** 6601 (1994)
51. H A Christov, B Bolan, A F Yee, L Xie, D W Gidley *Macromolecules* **29** 8507 (1996)
52. R Srithawatpong, Z L Peng, B G Olson, A M Jamieson, R Simha, J D McGervey, T R Meier, A F Halasa, H Ishida *J. Polym. Sci., Part B: Polym. Phys.* **37** 2754 (1999)
53. G Dlubek, K Saarinen, H M Fretwell *J. Polym. Sci., Part B: Polym. Phys.* **36** 1513 (1998)
54. G Dlubek, V Bondarenko, J Pionteck, M Supej, A Wutzler, R Krause-Rehberg *Polymer* **44** 1921 (2003)
55. J Bohlen, J Wolff, R Kirchheim *Macromolecules* **32** 3766 (1999)
56. S S Jordan, W J Koros *Macromolecules* **28** 2228 (1995)
57. V P Shantarovich *J. Radioanal. Nucl. Chem.* **210** 357 (1996)
58. V P Shantarovich, V I Goldanskii *Hyperfine Interact.* **116** 67 (1998)
59. G Dlubek, J Stejny, T Lüpke, D Bamford, K Peters, C Hubner, M A Alam, M J Hill *J. Polym. Sci., Part B: Polym. Phys.* **40** 65 (2002)
60. A Alentiev, Yu Yampolskii *J. Membr. Sci.* **206** 291 (2002)
61. G Dlubek, D Bamford, A Rodriguez-Gonzalez, S Bornemann, J Stejny, B Schade, M A Alam, M Arnold *J. Polym. Sci., Part B: Polym. Phys.* **40** 434 (2002)
62. G Dlubek, T Lüpke, J Stejny, M A Alam, M Arnold *Macromolecules* **33** 990 (2000)
63. J L Keddie, R A L Jones, R A Cory *Europhys. Lett.* **27** 59 (1994)
64. J A Forrest, K Dalnoki-Veress, J R Stevens, J R Dutcher *Phys. Rev. Lett.* **77** 2002 (1996)
65. B A Rozenberg, V I Irzhak, L M Bogdanova *Prog. Colloid Polym. Sci.* **80** 187 (1989)
66. S M Shishatskii, Yu P Yampolskii, K-V Peinemann *J. Membr. Sci.* **112** 275 (1996)
67. A L Volynskii, N F Bakeev *Vysokomol. Soedin., Ser. B* **45** 1209 (2003)^b
68. D Schodbauer, G Kögel, P Sperr, W Triftshauser *Phys. Status Solidi A* **102** 549 (1987)
69. Y C Jean, H Cao, G H Dai, R Suzuki, T Ohdaira, Y Kobayashi, K Hirata *Appl. Surf. Sci.* **116** 251 (1997)
70. H Cao, J-P Yuan, R Zhang, C S Sundar, Y C Jean, R Suzuki, T Ohdaira, B Nielsen *Appl. Surf. Sci.* **149** 116 (1999)
71. J Algers, PhD Thesis, Lund University, Sweden, 2004
72. J Algers, R Suzuki, T Ohdaira, F H J Maurer *Macromolecules* **37** 4201 (2004)
73. J Algers, R Suzuki, T Ohdaira, F H J Maurer *Polymer* **45** 4533 (2004)
74. Yu P Yampolskii, E Sh Finkel'shtein, K L Makovetskii, I Ya Ostrovskaya, E B Portnykh, M L Gringol'ts, Yu G Ishutina, I B Kevdina, V P Shantarovich *Vysokomol. Soedin., Ser. A* **38** 1480 (1996)^b
75. Yu P Yampolskii, E Sh Finkel'shtein, K L Makovetskii, V I Bondar, V P Shantarovich *J. Appl. Polym. Sci.* **62** 349 (1996)
76. K Tanaka, M Katsube, K Okamoto, H Kita, O Sueoka, Y Ito *Bull. Chem. Soc. Jpn.* **65** 1891 (1992)
77. K Hagiwara, T Ougizawa, T Inoue, K Hirata, Y Kobayashi *Radiat. Phys. Chem.* **58** 525 (2000)
78. L Xie, D W Gidley, H A Hristov, A F Yee *J. Polym. Sci., Part B: Polym. Phys.* **33** 77 (1995)
79. Q Deng, Y C Jean *Macromolecules* **26** 30 (1993)
80. H F Szocs, O Sausa, K Kristiakova, J Kristiak, M Klimova *Eur. Polym. J.* **31** 1019 (1995)
81. J M Schmidt, F H J Maurer *Macromolecules* **33** 3879 (2000)
82. E-A McGonigle, J J Liggat, R A Pethrick, S D Jenkins, J H Daly, D Hayward *Polymer* **42** 2413 (2001)
83. G Dlubek, T Lüpke, H M Fretwell, M A Alam, A Wutzler, H-J Radusch *Acta Polym.* **49** 2326 (1998)
84. A A Askadskii, S A Tishin, V V Kazantseva, O V Kovriga *Vysokomol. Soedin., Ser. A* **32** 2437 (1990)^b
85. K Okamoto, K Tanaka, N Katsube, O Sueoka, Y Ito, in *Proceedings of the 9th International Conference on Positron Annihilation. ICPA-9, Hungary, 1991* D-100
86. V P Shantarovich, T Suzuki, C He, V W Gustov *Radiat. Phys. Chem.* **67** 15 (2003)
87. Y Hirayama, T Yoshinaga, Y Kusuki, K Ninomiya, T Sakakibara, T Tamari *J. Membr. Sci.* **111** 169 (1996)
88. I B Kevdina, Yu M Sivergin, V P Shantarovich *Khim. Vys. Energ.* **30** 145 (1996)^c
89. Y Wang, P T Inglefield, A J Jones *Polymer* **43** 1867 (2002)
90. A P M Kentgens, H A van Bortel, R J Verweel, W S Veeman *Macromolecules* **24** 3712 (1991)
91. G J Kennedy *Polym. Bull.* **23** 605 (1990)
92. D R Morgan, E O Stejskal, A L Andrady *Macromolecules* **32** 1897 (1999)
93. M Mansfeld, W S Veeman *Chem. Phys. Lett.* **213** 153 (1993)
94. S K Brownstein, J E L Roovers, D Worsfold *Magn. Reson. Chem.* **26** 392 (1988)
95. T Suzuki, H Yoshimizu, Y Tsujita *Desalination* **148** 359 (2002)
96. T T P Cheung, P J Chu *J. Phys. Chem.* **96** 9551 (1992)
97. T R Stengle, K L Williamson *Macromolecules* **20** 1428 (1987)
98. J Demarquay, J Fraissard *J. Chem. Phys. Lett.* **136** 314 (1987)
99. J Fraissard, T Ito *Zeolites* **8** 350 (1988)
100. D W Breck *Zeolite Molecular Sieves* (New York: Wiley, 1974)
101. G Golemme, J B Nagy, A Fonseca, C Algieri, Yu Yampolskii *Polymer* **44** 5039 (2003)
102. V I Bondar, B D Freeman, Yu P Yampolskii *Macromolecules* **32** 6163 (1999)
103. Yu P Yampolskii, V G Berezkin, T P Popova, A P Korikov, B D Freeman, V I Bondar, T C Merkel *Polym. Sci., Ser. A* **42** 1023 (2000)^b
104. T C Merkel, L G Toy, A L Andrady, H Gracz, E O Stejskal *Macromolecules* **36** 353 (2003)
105. M B Davydova, Yu P Yampolskii *Vysokomol. Soedin., Ser. A* **33** 574 (1991)^b
106. G Golemme, J B Nagy, A Fonseca, C Algieri, in *Euromembrane 2000 (Abstracts of Papers)*, Maale Hachamisha, Israel, 2000 p. 312
107. T Suzuki, M Miyauchi, M Takegawa, H Yoshimizu, Y Tsujita, T Kinoshita *Macromolecules* **34** 3805 (2001)
108. J H Simpson, W Wen, A A Jones, J T Bendler *Macromolecules* **29** 2138 (1996)
109. B D Malhotra, R A Pethrick *Macromolecules* **16** 1175 (1983)
110. *Entsiklopediya Polimerov* (Encyclopaedia of Polymers) (Moscow: Sovetskaya Entsiklopediya, 1972)
111. D Hofmann, M Entrialgo-Castano, A Lerbret, M Heuchel, Yu Yampolskii *Macromolecules* **36** 8528 (2003)
112. V V Teplyakov, Doctoral Thesis in Chemical Sciences, Institute of Petrochemical Synthesis, Russian Academy of Sciences, Moscow, 1991
113. M S Syamala, R J Cross, M Saunders *J. Am. Chem. Soc.* **124** 6216 (2002)
114. M Saunders, H A Jimenez-Vasquez, J Cross, S Mroczkowski, M L Gross, D E Giblin, P J Poreda *J. Am. Chem. Soc.* **116** 2193 (1994)
115. J M Braun, J E Guillet *Adv. Polym. Sci.* **21** 107 (1976)
116. A E Nesterov, Yu S Lipatov *Obrashchennaya Gazovaya Khromatografiya v Termodinamike Polimerov* (Inverse Gas Chromatography in Thermodynamics of Polymers) (Kiev: Naukova Dumka, 1976)
117. M Kawakami, S Kagawa *Bull. Chem. Soc. Jpn.* **51** 75 (1978)
118. D R Stull, E F Westrum, G C Sinke *The Chemical Thermodynamics of Organic Compounds* (New York: Wiley, 1969)
119. K C B Dangayach, D C Bonner *Polym. Eng. Sci.* **20** 59 (1980)
120. Yu P Yampolskii, N E Kaliuzhnyi, S G Durgaryan *Macromolecules* **19** 846 (1986)
121. A Yu Alentiev, V P Shantarovich, T C Merkel, V I Bondar, B D Freeman, Yu P Yampolskii *Macromolecules* **35** 9513 (2002)
122. Yu Yampolskii, S Durgaryan, in *Chromatography and Thermodynamics. Determination of Physicochemical Parameters* (Warsaw: Institute of Physical Chemistry, Polish Academy of Sciences, 1986) p. 185
123. D W Van Krevelen *Properties of Polymers: Their Correlation with Chemical Structure* (3rd Ed.) (Amsterdam: Elsevier, 1990)

124. *Gas Encyclopaedia. L'Air Liquide* (Amsterdam: Elsevier, 1976)
125. R C Reid, T K Sherwood *The Properties of Gases and Liquids* (New York: McGraw-Hill, 1966)
126. Yu P Yampolskii, S A Soloviev, M L Gringolts *Polymer* **45** 6945 (2004)
127. C S Paik, H Morawetz *Macromolecules* **5** 171 (1972)
128. J G Victor, J M Torkelson *Macromolecules* **20** 2241 (1987)
129. J S Royal, J G Victor, J M Torkelson *Macromolecules* **25** 729 (1992)
130. J S Royal, J M Torkelson *Macromolecules* **25** 4792 (1992)
131. A M Vasserman, A L Kovarskii *Spinovye Zondy i Metki v Fizicheskoi Khimii Polimerov* (Spin Probes and Labels in Physical the Chemistry of Polymers) (Moscow: Nauka, 1986)
132. Yu P Yampolskii, A M Vasserman, A L Kovarskii, S G Durgar'yan, N S Nametkin *Dokl. Akad. Nauk SSSR* **249** 150 (1979)^d
133. Yu P Yampolskii, M V Motyakin, A M Wasserman, T Masuda, M Teraguchi, V S Khotimskii, B D Freeman *Polymer* **40** 1745 (1999)
134. A Kh Vorobiev, V S Gurman, T A Klimenko *Phys. Chem. Chem. Phys.* **2** 379 (2000)
135. S V Paschenko, S A Dzuba, A Kh Vorobiev, Yu V Toropov, Yu D Tsvetkov *J. Chem. Phys.* **110** 8150 (1999)
136. F P Chernyakovskii *Usp. Khim.* **48** 563 (1979) [*Russ. Chem. Rev.* **48** 306 (1979)]
137. A I Kornilov, A N Shchapov, E F Oleinik, N L Murav'eva, F P Chernyakovskii *Dokl. Akad. Nauk SSSR* **260** 124 (1981)^d
138. N I Murav'eva, F P Chernyakovskii, Yu P Yampolskii, S G Durgar'yan *Zh. Fiz. Khim.* **61** 1894 (1987)^e
139. Yu P Yampolskii, V P Shantarovich, F P Chernyakovskii, A I Kornilov, N A Plate *J. Appl. Polym. Sci.* **47** 85 (1993)
140. A A Stolov, D I Kamalova, A B Remizov, O E Zgadzai *Polymer* **37** 3049 (1996)
141. A A Stolov, D I Kamalova, A B Remizov *Polymer* **39** 5711 (1998)
142. D I Kamalova, A A Stolov, S A Petrova, A B Remizov *Zh. Fiz. Khim.* **74** 1997 (2000)^e
143. S A Petrova, Candidate Thesis in Chemical Sciences, Kazan State Technological University, Kazan, 2002
144. M L Greenfield, D N Theodorou *Macromolecules* **26** 5461 (1993)
145. V M Shah, S A Stern, P J Ludovice *Macromolecules* **22** 4660 (1989)
146. S Neyertz, D Brown *J. Chem. Phys.* **115** 708 (2001)
147. S Trohalaki, C C De Bolt, J E Mark, H L Frisch *Macromolecules* **23** 813 (1990)
148. I A Ronova, E M Rozhkov, A Yu Alentiev, Yu P Yampolskii *Macromol. Theory Simul.* **12** 425 (2003)
149. S Misra, W L Mattice *Macromolecules* **26** 7274 (1993)
150. S Niemela, J Leppanen, F Sundholm *Polymer* **37** 4155 (1996)
151. R Voorinhtolt, M T Kusters, G Vegter, G Vriend, W G J Hol *J. Mol. Graphics Modell.* **7** 243 (1989)
152. T Zheng, J R Fried *Sep. Sci. Technol.* **36** 959 (2001)
153. D Hofmann, L Fritz, J Ulbrich, C Schepers, M Böhning *Macromol. Theory Simul.* **9** 293 (2000)
154. H Sun *J. Phys. Chem. B* **102** 7338 (1998)
155. D N Theodorou, U W Suter *Macromolecules* **18** 1467 (1985)
156. D N Theodorou, U W Suter *Macromolecules* **19** 139 (1986)
157. D Hofmann, M Heuchel, Yu P Yampolskii, V Khotimskii *Macromolecules* **35** 2129 (2002)
158. V E Raptis, I G Economou, D N Theodorou, J Petrou, J H Petropoulos *Macromolecules* **37** 1102 (2004)
159. V S Khotimskii, V G Filippova, I S Bryantseva, V I Bondar, V P Shantarovich, Yu P Yampolskii *J. Appl. Polym. Sci.* **78** 1612 (2000)
160. Y Ichiraku, S A Stern, T Nakagawa *J. Membr. Sci.* **34** 5 (1987)
161. R Srinivasan, S R Auvil, P M Burban *J. Membr. Sci.* **86** 67 (1994)
162. I Pinnau, L G Toy *J. Membr. Sci.* **116** 199 (1996)
163. T C Merkel, V Bondar, K Nagai, B D Freeman *J. Polym. Sci., Part B: Polym. Phys.* **38** 273 (2000)
164. E Schmidtke, K Günter-Schade, D Hofmann, F Faupel *J. Mol. Graphics Modell.* **22** 309 (2004)
165. C Nagel, E Schmidtke, K Günter-Schade, D Hofmann, D Fritsch, T Strunkus, F Faupel *Macromolecules* **33** 2242 (2000)
166. K Ciesielski, A L Dawidowicz, T Goworek, B Jasinska, B Wawryszczuk *J. Chem. Phys. Lett.* **289** 41 (1998)
167. H Schmitz, F Müller-Plathe *J. Chem. Phys.* **112** 1040 (2000)
168. M Heuchel, D Hofmann, P Pullumbi *Macromolecules* **37** 201 (2004)
169. X Y Wang, K M Lee, Y Lu, M T Stone, I C Sanchez, B D Freeman *Polymer* **45** 3907 (2004)
170. X Y Wang, P J Veld, Y Lu, I C Sanchez, B D Freeman, I C Sanchez *Polymer* **46** 9155 (2005)
171. H F M Mohamed, N S Abd El-Aziz *Polymer* **42** 8013 (2001)
172. D Hofmann, L Fritz, J Ulbricht, D Paul *Comput. Theor. Polym. Sci.* **10** 419 (2000)
173. L Fritz, D Hofmann *Polymer* **38** 1035 (1997)
174. D Hofmann, L Fritz, J Ulbricht, D Paul *Polymer* **38** 6145 (1997)
175. E Tocci, D Hofmann, D Paul, N Russo, E Drioli *Polymer* **42** 521 (2001)

^a — *Chem. Phys. Rep. (Engl. Transl.)*

^b — *Polym. Sci. (Engl. Transl.)*

^c — *High Energy Chem. (Engl. Transl.)*

^d — *Dokl. Phys. Chem. (Engl. Transl.)*

^e — *Russ. J. Phys. Chem. (Engl. Transl.)*

Determination of biologically active phenols and polyphenols in various objects by chromatographic techniques

M V Kochetova, E N Semenistaya, O G Larionov, A A Revina

Contents

I. Introduction	79
II. General characteristics of biologically active phenols and polyphenols	79
III. Sample preparation	81
IV. Chromatographic determination of phenols and polyphenols in various objects	82

Abstract. Chromatographic techniques for determination of biologically active phenols and polyphenols are considered. Various methods for sample preparation and detection are compared. The advantages of high performance liquid chromatography with spectrophotometric detection for determination of antioxidants are demonstrated. Data on determination of biologically active phenols and polyphenols published in the period from 1995 to 2005 are analysed. The bibliography includes 270 references.

I. Introduction

During the last decade, the number of publications devoted to chromatographic studies of natural and synthetic biologically active compounds has sharply increased.^{1–8} The studies of the antioxidant activity of, in particular, phenol and polyphenol derivatives attract special attention of researchers. The environment deterioration and the increase in the number of stress situations decrease the defense forces in humans. This, in turn, increases the risk of pathological states (cardiovascular diseases, inflammatory processes, atherosclerosis, etc.). Studies of the active forms and the mechanisms of action *in vitro* and *in vivo* of natural and synthetic biologically active compounds is a topical problem related to preservation of human health.

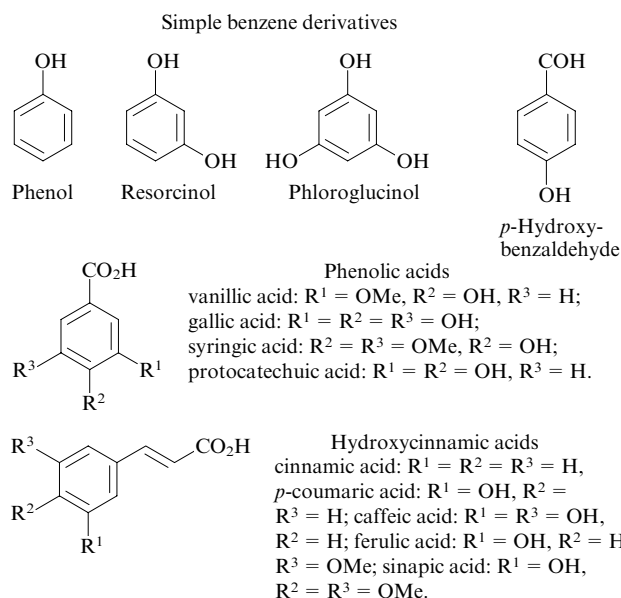
Phenols and polyphenols possess a broad spectrum of biological activities: they exert antioxidant,^{9–11} antiinflammatory,¹² antitumour,¹³ capillary strengthening^{14,15} and hepatoprotector¹⁶ actions. They are able to form chelates with metals. These chelates can exhibit both antioxidant and prooxidant[†] activities.^{17–19} This accounts for the use of biologically active compounds in medicine, pharmacology, biochemistry and food industry. Despite the wide use of polyphenols as antioxidants, the mechanisms of their action *in vitro* and *in vivo* and the cases where these compounds behave as prooxidants²⁰ are still not entirely clear. This is due, on the one hand, to the existence of numerous natural derivatives of these compounds and the diversity of their oxidised forms and, on the

other hand, to the complexity of composition of the extracts from which these compounds are isolated and determined. Therefore, to analyse biologically active compounds, one needs information on their transformations during all stages of sample preparation.

This review considers the studies devoted to chromatographic methods for determination of biologically active phenols and polyphenols published over the last 10 years. The attention is focused on the most widely used procedures.

II. General characteristics of biologically active phenols and polyphenols

Phenol derivatives constitute a widely encountered and abundant class of natural products exhibiting biological activity. They are distinguished by the presence of free or bound OH group as a substituent in the benzene ring.



M V Kochetova, E N Semenistaya, O G Larionov, A A Revina

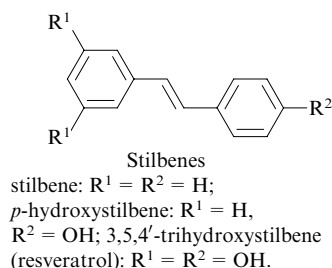
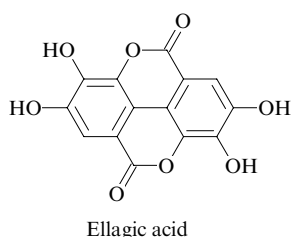
A N Frumkin Institute of Physical Chemistry and Electrochemistry,
Russian Academy of Sciences, Leninsky prosp. 31, 119991 Moscow,
Russian Federation. Fax/tel. (7-495) 952 00 65, e-mail: marie_k@bk.ru
(M V Kochetova), EN_Semenistaya@mail.ru (E N Semenistaya),
kolom@phyche.ac.ru (O G Larionov), tel. (7-495) 955 00 17,
e-mail: revina@mail333.com (A A Revina)

Received 13 February 2006

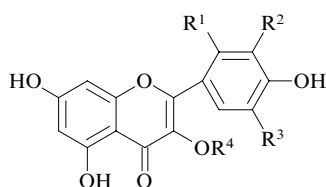
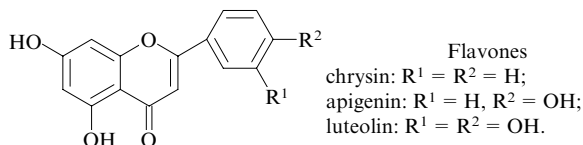
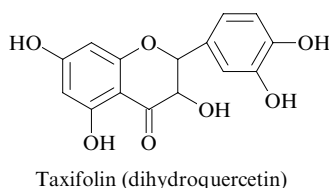
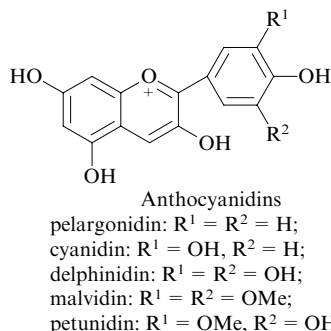
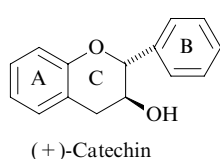
Uspekhi Khimii 76 (1) 88–100 (2007); translated by Z P Bobkova

[†]Prooxidant activity of a compound usually implies an increase in the yield of active oxygen-centred radicals in the presence of this compound.

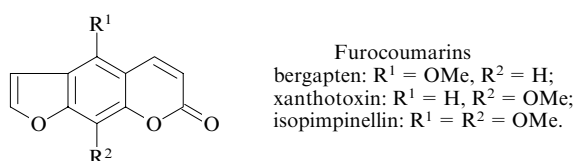
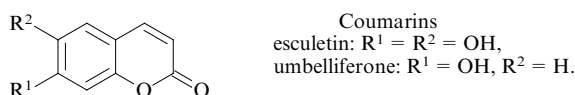
Aromatic compounds containing two or more non-fused aromatic rings



Flavonoids (arylbenzo[*b*]pyrans) and coumarins



kaempferol: $R^1 = R^2 = R^3 = R^4 = H$;
morin: $R^1 = OH$, $R^2 = R^3 = R^4 = H$;
quercetin: $R^1 = R^3 = R^4 = H$, $R^2 = OH$;
myricetin: $R^1 = R^4 = H$, $R^2 = R^3 = OH$;
quercetrin (quercetin rhamnoside): $R^1 = R^3 = H$, $R^2 = OH$,
 $R^4 = \alpha\text{-L-Rhap}$; rutin (quercetin rutinoside):
 $R^1 = R^3 = H$, $R^2 = OH$, $R^4 = \beta\text{-D-Glcp-(6}\leftarrow\text{1)}\text{-}\alpha\text{-L-Rhap}$.



Phenols are present almost in all plants either as glycosides or in the free state in amounts from 0.1% to 7%.²¹

Phenolic alcohols and their glycosides favour the increase in human performance capability and the organism resistance against adverse effects. Hydroxycinnamic acids (*p*-coumaric, caffeic, ferulic and sinapic acids) are present in many plants²² and fruits^{23,24} in various combinations, either in the free state or as glycosides or esters. Caffeic acid and its derivatives (chlorogenic acid and its isomers), which have antiinflammatory and choleric actions, are found in nature most often. Chlorogenic acid occurs in large amounts in coffee beans, bilberry, mountain tobacco, wild chamomile leaves, *etc.* Ferulic acid is a part of plant cell walls.²⁵ Caffeic, chlorogenic, ferulic and coumaric acids together have a hypouricemic effect, enhance the kidney function and stimulate the detoxifying function of the liver. Hydroxycinnamic acids are also present in echinacea, burdock root, hawthorn and rhubarb.

Ellagic acid is abundant in many fruits and vegetables, especially in raspberry, strawberry and pomegranates. Stilbenes are mainly contained in various kinds of wood (pine tree, gum-tree, *etc.*).

Catechins were found in many fruits²⁶ (apples, peaches, apricots, queen-apples and plums) and berries (cherry, strawberry, currant, raspberry, gooseberry and cowberry). Large amounts of catechins are present in tea-plant browses²⁷ (up to 20%–25% of the dry weight) and acacia catechu browses (which gave rise to the name of these compounds), in grapes (mainly in stones and peel),²⁸ and in cocoa beans.²⁹ Catechins show high biological activity; in the human body, they control the capillary permeability and increase the wall elasticity and also increase the bioavailability of ascorbic acid. Therefore, catechins are classified as substances having P-vitamin activity and are used in the therapy of diseases related to capillary dysfunction and edemas.³⁰

The cell vacuoles of many flowers and fruits contain pigments such as anthocyanidins and anthocyanins [as oligomeric and polymeric forms (proanthocyanidins) or complexes with metals, proteins and polysaccharides], which are responsible for their bright colour.^{31,32} Proanthocyanidins were found in most fruits³³ and vegetables³⁴ and in leaves of many plants. The main source of these compounds on an industrial scale are grape stones and peel and the cluster pine cork. In medicine, they are used to prevent the cardiovascular diseases and to reduce the cholesterol level in blood.³⁵ Studies of the antitumour activities of anthocyanidins are in progress.³⁶ The instability and structural diversity of anthocyanidins complicate their qualitative analysis.

Flavonols (dihydroflavonols) are mainly present in coniferous wood (pine tree, larch tree and cedar) and some leaf wood (eucalyptus, beech, cherry). Flavanones are encountered in citrus plants. Hesperetin and its glycoside, hesperidin, are contained in the orange, lemon and citron pulp; the glycoside naringin is responsible for the bitterish taste of grapefruit, and eriodictyol occurs in lemons.^{37,38}

Like flavones, flavonols are yellow pigments,³⁹ which are distributed in plants most widely (almost universally).⁴⁰ Compounds of this group encountered most frequently include kaempferol, quercetin, myricetin and their numerous derivatives. 3,5,4'-Trihydroxystilbene (*trans*-resveratrol) present in red wine is an interesting biologically active polyphenol, which has been the subject of a large number of studies in recent years. It was found⁴¹ that *trans*-resveratrol protects the membrane lipids from peroxidation; it quenches free radicals less effectively than flavonoids but it is more effective in chelating copper ions.

Coumarins are also widely distributed in nature.^{42–44} They are present in umbelliferous, leguminous and rue plants, being mainly concentrated in roots and fruits.⁴⁵ Owing to the availability and the ease of chemical modification, coumarins can be used for the development of medicinal drugs.⁴⁶ A meptazinol derivative based on coumarin is more easily uptaken in the body than the starting drug,⁴⁷ and the coumarin derivative with *trans*-

resveratrol is a more efficient vasodilator than *trans*-resveratrol itself.⁴⁸ Coumarins are used as anticoagulants;⁴⁹ they exhibit bactericidal,⁵⁰ fungicidal⁵¹ and antitumour⁵² activities.

The relationship between the antioxidant activity and the chemical structure of polyphenols has not been ultimately elucidated as yet. Chromatographic methods can be used to study the relationship between the structures and some properties of phenols.⁵³ This is done by modelling the retention in various versions of chromatography^{54–56} and by numerical methods.⁵⁷ It has been established⁵⁸ that the antioxidant activity of polyphenols increases in the following cases:

(i) in the presence of a 2,3-double bond of the heterocyclic ring, as this seems to allow electron delocalisation between rings A and B [see the structure of (+)-catechin] and, hence, stabilisation of the aryloxy radical formed;

(ii) in the presence of hydroxy groups in positions 2 and 4 of ring B, because this apparently also contributes to radical stabilisation;

(iii) on passing from polyphenol glycosides to aglycons, because carbohydrate residues in glycosides markedly decrease the antioxidant activity;

(iv) in the presence of a free phenolic hydroxy group.

It is known^{59–65} that vegetables, fruits, red wine, chocolate, and other foodstuffs rich in polyphenols, when eaten on a regular basis, decrease substantially the risk of cardiovascular diseases.

Depending on the type and concentration of the initiator of free radicals, polyphenols can behave as either antioxidants or prooxidants.^{66–69} The understanding and interpretation of the dual behaviour of polyphenols is complicated by the fact that despite the large body of data on high biological activity accumulated in recent years, the questions concerning the mechanism of their action and existence in the active forms *in vitro* and *in vivo* are still open. Therefore, development of procedures for determination of phenols and polyphenols in various objects by various analytical techniques, including chromatographic ones, is a topical task.

III. Sample preparation

An important problem that researchers are often faced with when investigating complex mixtures is the need to isolate the analytes from natural sources and thoroughly purify the extracts prior to the analysis.

The strategy of determination of biologically active compounds in plants depends on the nature and structure of the compound under study, the object of analysis (sample) and goals of analysis and cannot be completely unified. The following main stages of the investigation can be distinguished: extraction of the compounds from the sample, purification of the extract from accompanying compounds, separation and identification.

1. Extraction of compounds from natural sources

As a rule, biologically active compounds come from plant sources. Therefore, the primary task of a research is to extract the target compounds from the raw material as fully as possible, better in the native form. Usually, this is done by liquid or supercritical fluid extraction, in some cases, by high-pressure steam extraction. The extraction methods that permit preliminary purification of the extract from accompanying compounds are preferred.

The plant material is crushed and defatted by treatment with light petroleum, hexane or chloroform. If it is necessary to isolate a particular compound or a group of compounds from a complex sample, successive extractions with solvents in the order of increasing polarity is carried out (hexane, diethyl ether, ethyl acetate, butanol, water–ethanol mixtures).⁷⁰ In simple cases, one-stage extraction with methanol^{71,72} or dichloromethane is performed.⁷³ Pinelo *et al.*⁷⁴ used ethanol for complete extraction of biologically active phenols from the almond shell and pine sawdust, while polyphenols were selectively extracted with methanol. In another study,⁷⁵ phenols were extracted from lablab

stems, flowers and fruit coat with 90% methanol and from leaves, with 90% ethanol. Preliminary separation of the flavonoids in plant extracts is carried out using preparative thin layer chromatography or preparative reversed phase chromatography.⁷⁶ The isolation of polyphenols from plant material is performed most often using 80% ethanol. The purity of the resulting fractions is checked by thin layer chromatography.^{77–79}

Anthocyanins and anthocyanidins are extracted and separated in an acidic medium in order to avoid the destruction of non-acylated derivatives. In addition, the most stable resonance form of anthocyanins, flavylium cation, is formed at pH < 2. The extraction of anthocyanins from the ghost plant (*Graptopetalum paraguayense*) leaves with water and water–ethanol mixtures at different temperatures has been studied.⁸⁰ The highest antioxidant activity was found for a 50% ethanolic extract (extraction for 3 h at 75 °C). A mixture of water, acetonitrile and formic acid (1:1:0.1)⁸¹ or trifluoroacetic acid (1:1:0.5)⁸² was used to extract anthocyanins from liliaceous plant petals. Extraction with water⁸³ or methanol⁸⁴ with addition of an acid is also possible; however, the extraction time in this case is 12–16 h. Water–methanol–organic acid mixtures are more efficient. These extractants were used to isolate anthocyanidins of ornamental plants.^{85–87} The extraction efficiency increases when an ultrasonic bath or a magnetic stirrer is used.

Sample preparation of procyanidins has some specific features. These compounds readily form complexes with metals, polysaccharides and proteins, which hampers their extraction using solid sorbents. The extraction of procyanidins from the seed coats or fruit pulp is complicated by the fact that procyanidins are oxidised during fruit ripening. This yields procyanidin–polysaccharide complexes and the solubility of procyanidins thus decreases.⁸⁸

Rohr *et al.*⁸⁹ proposed a procedure for quantitative determination of procyanidins (three dimers and a trimer of epicatechin) in hawthorn leaves and flowers by reversed phase high performance liquid chromatography. The most complete extraction of procyanidin oligomers (yield 99%) was achieved using 70% aqueous acetone. However, during acetone evaporation, polymerisation and precipitation of the target compounds may take place. Extraction with 70% aqueous methanol has been reported.^{90,91} Methanol was used to obtain extracts from olive tree, hawthorn and oregano leaves.⁹² The extraction of procyanidins from the cat's claw (*Uncaria tomentosa*) bark by refluxing with water has been reported.⁹³ Flavonoid glycosides and anthocyanidins can be destroyed by acid hydrolysis carried out at ~90 °C for several hours. The effect of the addition of an acid during extraction on the antioxidant activity of plant extracts has been studied.⁹⁴ The activity was found to increase in the vast majority of cases.

The higher the pressure, the higher the efficiency in liquid extraction. Papagiannopoulos *et al.*⁹⁵ identified 41 polyphenols in an aqueous acetone extract of algaroba obtained in this way. By varying temperature and pressure, biologically active phenols have been selectively extracted with water from rosemary⁹⁶ and other plants.⁹⁷ By combined use of solid-phase extraction and high performance liquid chromatography, an automated procedure for determination of procyanidins in malt was developed.⁹⁸

Using supercritical fluid extraction technique, one can substantially increase the yield of labile compounds from biological matrices. As a rule, supercritical carbon dioxide is used. Since the polarity of CO₂ is relatively low, a polar modifying agent is often added. The effects of temperature, pressure and polar additives on the extraction kinetics and antioxidant properties of the ginger oil have been studied.⁹⁹ The efficiency of supercritical fluid extraction of phenols from the olive tree leaves with supercritical CO₂ has increased after the addition of methanol.¹⁰⁰ Thermodynamic modelling of quercetin solubility in supercritical CO₂ in the presence of ethanol has been carried out.¹⁰¹ A scheme for broad-scale supercritical fluid extraction of the rosemary oil followed by liquid chromatography–mass spectrometry analysis of the obtained fractions has been proposed.¹⁰² The use of supercritical

CO₂ for the fractionation of plant extracts has been reported.¹⁰³ New extraction techniques such as supercritical fluid extraction and automated tunnelling solid-phase microextraction has been described.¹⁰⁴ The extent of extraction of polyphenols from grape stones with liquid–liquid, solid-phase and supercritical fluid extraction have been compared.¹⁰⁵ The highest yield was achieved by the last-mentioned technique, possibly, due to the fact that the sample was located in a carbon dioxide atmosphere and was protected from light. This minimised decomposition of unstable compounds such as catechins.

A comparison of the efficiency of extraction from natural sources by liquid–liquid, solid-phase and supercritical fluid extraction techniques and by high-pressure extraction using various solvents has been reported.¹⁰⁶

Usual objects of analysis, *i.e.*, plants, berries, fruits and vegetables, contain diverse phenols and polyphenols. However, substantial portions of these compounds are often lost during extraction, isolation and purification. Therefore, correct choice of the sample preparation method is a key issue in the qualitative and quantitative analysis of complex multicomponent mixtures.^{107, 108}

2. Methods for extract purification and preconcentration

A number of techniques for the extraction and purification of phenols from complex mixtures have been reported,^{109, 110} specifically, supercritical fluid extraction, semipreparative high performance liquid chromatography, high-speed counter-current liquid chromatography and superheated solvent extraction. Liquid–liquid and solid-phase extractions are used most widely for purification and preconcentration of polyphenols.^{111–120}

For correct quantitation of phenol derivatives, it is necessary to take into account their possible transformations. This is especially important for analysis of food and beverages. During their production, phenols present in the raw materials undergo various transformations.

The influence of different wine manufacture processes on the composition of phenols and the antioxidant properties of the red wine Spatburgurder (Pinot Noir) and Cabernet Franc have been studied.¹²¹ The processes included the grape peel fermentation, mash heating and a combination of these processes. The highest concentrations of anthocyanins, flavan-3-ols, flavonols and stilbenes were found in the red wine prepared by process combination. Lower concentrations of biologically active compounds were present in the wine prepared by mash heating; the wine produced by peel fermentation contained the lowest amount of anthocyanins. The process of fermentation during production of wine from blackberry and cherry berries caused ~25% decrease in the content of the total polyphenol fraction.¹²²

Table 1. Eluents used for fractionation and separation of extracts.

Phenols	Thin layer, preparative and column chromatography
Procyanidins	MeOH, acetone–water, ethyl acetate–HOAc–H ₂ O
Anthocyanins	Bu ⁿ OH–HOAc–H ₂ O (4:5:1); Bu ⁿ OH–2 N HCl (1:1), 1% HCl, HOAc–HCl–H ₂ O (15:3:82)
Anthocyanidins	HOAc–HCl–H ₂ O (30:3:10); HCO ₂ H–HCl–H ₂ O (5:2:3)
Phenolic acids	Bu ⁿ OH–HOAc–H ₂ O (4:5:1); EtAc–HOAc–H ₂ O (3:1:1); EtOH–H ₂ O–NH ₄ OH (16:3:1); toluene–HOAc–H ₂ O (40:10:5)

Note. The following mixture are used as eluents in high performance liquid chromatography: organic solvent (methanol, acetonitrile, ethanol)–water–acid (HCl, acetic, trifluoroacetic, formic, phosphoric) or organic solvent–acid.

In the extraction of phenols from grapefruit and orange juices¹²³ and dry leaves of green tea,¹²⁴ high yields were attained by repeated liquid–liquid extraction with aqueous methanol and acidified methanol. However, solid-phase extraction¹²⁵ ensures higher yield of phenols and polyphenols from various samples than liquid–liquid extraction. The main eluents for fractionation and separation of extracts are presented in Table 1.

IV. Chromatographic determination of phenols and polyphenols in various objects

1. Determination in plant materials

Determination of phenols in objects with a large number of components (complex mixtures) is performed most often by chromatography and capillary electrophoresis. Due to the thermal and chemical lability of most compounds to be determined, thin layer chromatography, its high performance version, capillary electrophoresis and high performance liquid chromatography are used. Thin layer and flash chromatography were the first methods used to separate many biologically active compounds of the plant origin. These methods are distinguished by low cost and simplicity. High-performance and two-dimensional thin layer chromatography can be used for analysis of complex natural sources of phenols.

Plant extracts do not require thorough purification by thin layer chromatography. Examples of such analyses are qualitative and quantitative determination of flavonoids in the passion flower (*Passiflora coerulea*)¹²⁶ and beech extracts.¹²⁷ Flavonoids were detected by exposure to UV light,¹²⁸ while procyanidins and anthocyanins were visualised by spraying with a 5% solution of vanillin in an ethanol–HCl (4:1) mixture.¹²⁹ Aglycons and glycosides were detected in the UV light and then visualised by spraying with a solution of H₂SO₄ and heating.¹³⁰ Scanning densitometry was used to analyse plant pigments.¹³¹ Simultaneous separation and detection of compounds with antioxidant properties was carried out on plates with 1,1-diphenylpicrylhydrazide¹³² and silver nanoparticles¹³³ applied thereon as indicators.

Gas chromatography is of limited utility for the analysis of natural biologically active compounds due to the necessity of derivatisation of phenols into methyl or trimethylsilyl derivatives. Nevertheless, such analysis is practised. Gas chromatography with mass spectrometric detection was used to determine phenolic acids in a coriander extract,¹³⁴ the main flavonoids and their glycosides in the willow wood¹³⁵ and phenols in the wormwood oil.¹³⁶ Fiamegos *et al.*¹³⁷ have developed a procedure for simultaneous extraction and derivatisation of flavonoids and phenolic acids for their determination in plant extracts by gas chromatography with mass spectrometric detection.

High performance liquid chromatography is used most often for determination of phenols. This is due to the following advantages of the method: high selectivity of the sorbents, sensitivity and selectivity of the diode array, ultraviolet, fluorescence and mass spectrometric detectors and mild conditions of analysis under which the analytes are not decomposed. High performance liquid chromatography on reversed phase columns with binary solvent systems and diode array detector is used both for routine analyses and to study plant extracts with complex composition. The detection limit of flavonoids can be reduced by using electrochemical or fluorescence¹³⁸ detectors. Examples of solvent systems and columns for this type of chromatography of plant extracts are summarised in Table 2.

Chromatography with amperometric detection is used to estimate the antioxidant activities of foodstuffs, beverages and drugs.^{149, 150} Most natural biologically active phenols can be oxidised on an electrode; therefore, the amperometric detector is convenient for their determination. This allows one to establish the presence of unknown compounds in complex natural sources of phenols, whereas classical chemical methods¹⁵¹ are only

Table 2. Results of analyses of the extracts of some flavonoids in plant samples by high performance liquid chromatography.

Sample	Identified compounds	Extractant	Column	Mobile phase	Detection	Ref.
Red clover	11 flavonoids	ethanol, methanol; acid hydrolysis	HP ODS Hypersil	H ₂ O/AcOH – MeOH	UV-MS	139
Passion flower (<i>Passiflora incarnata</i>)	10 flavonoids	'dry' extract	LiChrospher RP-18	H ₂ O – THF – MeCN – Pr ⁱ OH	UV-MS	140
Cistus (<i>Cistus ladanifer</i>)	8 flavonoids	chloroform, methanol	LiChrosorb RP-18	0.1 M NH ₄ OAc in H ₂ O – THF – MeCN – Pr ⁱ OH	UV-MS	141
Goatweed herb (<i>Hypericum perforatum</i> , St John's wort)	16 phenolic compounds	methanol	TP 544 RP-18	H ₂ O/H ₃ PO ₄ – MeCN – MeOH	UV-MS	142
Oregano, caraway, fennel	flavonoids, methoxyflavonoids	methanol – water (62.5%)	Phenomenex RP C ₁₈	H ₂ O/HCO ₂ H – MeOH	UV, MS-MS	143
Siberian larch and Gmelin larch bark	21 flavonoids	ethyl acetate	TLC: silica gel, HPLC: Separon C ₁₈	H ₂ O/AcOH – MeCN	UV, IR, NMR	144
Gnidia (<i>Gnidia socotrana</i>) herb	flavone and coumarin derivatives	ethanol, heptane, ethyl acetate, n-butanol	RP 18	MeOH; H ₂ O/AcOH – MeCN	UV, UV-MS	145
Cyclopia	8 flavonoids, two isomers separated	methanol	Phenomenex Synergy MAX-RP C ₁₂	H ₂ O/AcOH – MeCN – THF	electrochemical detector	146
Veronica (<i>Veronica thymoides</i>)	acylated flavonoids and glycosides	methanol, light petroleum	polyamide column for flash chromatography, TLC: silica gel	MeOH – CHCl ₃ , MeOH – H ₂ O	fluorescence detector	147
Brazilian pine tree	6 flavonoids	methanol – water, hexane	Phenomenex Synergy C18	MeOH – CHCl ₃ /HCO ₂ H	DAD, MS	148

Notes. The following designations are used: UV-MS a combination of UV and mass spectrometric detectors, MS-MS is tandem mass spectrometry, TLC is thin layer chromatography, DAD is diode array detector.

suitable for estimating the overall antioxidant activity of the sample or the activity of a known compound.

The difficulties arising in the determination of phenols by chromatographic methods are mainly related (apart from the necessity of preliminary purification of the extracts before the introduction into the column) to the lack of standards due to the great diversity of natural forms of these compounds. Therefore, the so-called fingerprint method is used in some cases for analysis of complex plant extracts.^{152, 153} These fingerprints are specific for each plant species and can be used to identify the source of a plant raw material. Secondary metabolites, including phenolic acids and flavonoids, are used as chemical markers in the fingerprints.¹⁵⁴ The plants species are differentiated based on the variation of the composition and content of these compounds.¹⁵⁵ A combination of the fingerprint method and chromatographic analysis of biological fluids is used to identify fake drugs.¹⁵⁶

A number of methods have been described for quantitative and qualitative determination of proanthocyanidins and their derivatives,¹⁵⁷ chromatography and spectrometry being used most often.

The spectrometric methods are based on reactions giving chromophores (the Folin–Ciocalteu reagent, the use of HCl–BuOH, vanillin, and so on). However, these methods do not provide information on the amounts and structures of oligomers with different degrees of polymerisation. Spectrophotometry is used to determine the total amount of procyanidins in complex samples,⁹³ however lately it has been replaced by mass spectrometry. Gel chromatography,¹⁵⁸ thin layer and column chromatography are used to isolate anthocyanin and procyanidin fractions and to separate them according to the degree of polymer-

isation.^{92–94} A mixture of individual procyanidins (from monomers to trimers) can be separated by reversed phase high performance liquid chromatography.^{99, 159} The method proposed by Svedstrom *et al.*⁹¹ made it possible to separate epicatechin oligomers (from monomers to hexamers) present in the extract of hawthorn leaves and to isolate previously unknown trimers and pentamers using a polyamide column and an acetonitrile-based eluent.

Capillary electrophoresis is gaining increasing acceptance for determination of pharmacologically important compounds in plants.^{160–162} *trans*-Resveratrol was determined using a borate buffer (pH 8–11), as borates form complexes with the hydroxy groups of flavonoids, thus facilitating the separation.¹⁶³ The buckthorn flavonoids were separated in the presence of a modifying agent, dimethyl- β -cyclodextrin.¹⁶⁴ Anthocyanins have been separated by capillary electrophoresis in an acidic medium.¹⁶⁵

Neutral molecules can be separated in an electric field by micellar electrokinetic capillary chromatography. By varying the concentration of the micelle-forming agent (most often, sodium dodecyl sulfate), the system selectivity can be changed. Various modifying agents are used: methanol for determination of flavonoids, phenolic acids and aldehydes,¹⁶⁶ butan-1-ol for flavonoids and iridoids¹⁶⁷ and acetonitrile for coumarins.¹⁶⁸ Drawbacks of the method include lower sensitivity and reproducibility compared to high performance liquid chromatography.

2. Determination in foodstuffs and beverages

Most often, phenols are detected by spectrophotometry using a number of wavelengths: 230, 280, 360, 503 nm, *etc.* In some studies dealing with particular groups of flavonoids, only one

wavelength was used, namely 280 nm for catechins^{169–173} and 520 nm for anthocyanins.^{174–178} Other studies made use of wavelengths of 280, 306 and 360 nm for phenol detection.^{179–184} Since many phenols have several absorption maxima, they are often determined using simultaneous scanning at several wavelengths called diode array detection.^{185–190} High performance liquid chromatography with diode array detection is often used to determine phenols present in foodstuffs and beverages. The key advantage of this method is the low detection limits. For example, the detection limit for catechins in the green tea extract was reported to be 0.05 mg ml⁻¹ (with detection at 205 nm).¹⁹¹ Examples of using the diode array detection in the determination of phenols and polyphenols in fruit and vegetable extracts and in

beverages by high performance liquid chromatography are summarised in Table 3.

Determination of phenols in foodstuffs and beverages is often carried out by reversed phase chromatography on modified silica gels, because reversed phase columns ensure high separation selectivity and better reproducibility of the results and have longer service life. Some types of modified silica gels used most often in the analysis of phenols in various objects are summarised in Table 4.

To increase the sensitivity and selectivity of determination of phenolic acids and aldehydes, simultaneous diode array and fluorescence detection is used. In order to ensure the highest sensitivity of the analysis, a fluorescence detector should be time

Table 3. Results of determination of phenol and polyphenol antioxidants in fruits, vegetables and beverages by high performance liquid chromatography.

Object	Identified compounds	Detector	Quantifiable concentrations	Ref.
Apples, grapes, beans	(+)-catechin, (-)-epicatechin, 3 catechin derivatives	DAD	0.1–3.9 mg per kg — —	192
Grapefruit juice	naringin	DAD 280 nm	2.5 mg litre ⁻¹	193
Grape berries	<i>trans</i> -resveratrol, rutin, quercetin, quercitrin	DAD 306 nm	4.5–10.1 mg per 100 g — 0.16–0.45 mg per 100 g —	194
Bulgarian wine, 11 brands	quercetin, myricetin, morin, kaempferol	DAD 360 nm	the highest total content of flavonols in the brand Melnic: 12.2–16.9 mg litre ⁻¹	195
Green and black tea	16 phenols including (-)-epigallocatechin	DAD 205 nm	2.84 mg g ⁻¹ (black tea) (23.46–36.53) mg g ⁻¹ (green tea)	196–199
Juices and beverages	21 phenols including: quercetin (-)-quininic acid	DAD 215 nm	0.03 mg litre ⁻¹ 12.5 mg litre ⁻¹	200

Table 4. Characteristics of some reversed phase columns used in analysis of phenol derivatives in various objects by high performance liquid chromatography.

Object	Column			Elution time and mode	Identified compounds	Ref.
	sorbent type	sorbent grain diameter /μm	column size /mm			
Juices (apple and multifruit)	Shim-Pack VP-ODS	5	250 × 4.6	80 min, gradient	31 phenols	201
Cranberry	XDR C ₁₈	5	150 × 4.6	47 min, gradient	13 phenols	202
Apples, pears	Nucleosil 120 C ₁₈	5	250 × 4.6	25 min, gradient	5 phenols	203
Green and black tea, 8 brands	PartiSphere 5 C ₁₈	3	110 × 4.6	27 min, gradient	15 phenols	191
Chocolate, 11 brands	Hypersil ODS	5	250 × 4.6	30 min, isocratic	9 phenols	173
Grapefruit, orange	μ-Bondapak C ₁₈	5	250 × 4.6	20 min, isocratic	3 phenols	204
White wine, 11 brands	Alltima	3	100 × 4.6	20 min, isocratic	4 phenols	205
Grape berries	Hypersil ODS	5	150 × 4.6	25 min, gradient	4 phenols	206
Red and white wine, 5 brands	Nova-Pak C ₁₈	4	150 × 3.9	34 min, gradient	17 phenols	207
Onion, soy	Hypersil 120	3	125 × 4.6	30 min, gradient	5 phenols	208
Green tea	YMC-Pack ODS-AQ	5	150 × 4.6	50 min, isocratic	6 phenols	209
Orange juice	Luna	3	150 × 2.0	15 min, gradient	10 flavonoids	181
Lemon peel	Nova Pak C ₁₈	5	150 × 4.6	60 min, gradient	7 flavonoids	210
Wine ^a	Spherisorb ODS 2	3	250 × 4.6	55 min, gradient	17 phenols	211
Orange and grapefruit juice concentrates	Alltech C ₁₈	5	250 × 4.6	30 min, isocratic	3 flavonoid glycosides	123
French wine ^b	Nucleosil 100 C ₁₈	5	250 × 4.0	75 min, gradient	1 phenol	212
Linseed	Spherisorb S-ODS	5	250 × 4.0	50 min, isocratic	6 phenols	213
Lentil, beans	Nucleosil 120 C ₁₈	5	250 × 4.6	20 min, gradient	5 phenols	214

^a The wine brand was not specified. ^b Red and white wine, 5 brands each.

programmed for the optimal excitation and fluorescence wavelengths for the group of phenols with similar spectral characteristics. The use of statistic multivariate methods is of interest for composing an optimal program for detection of a complex sample.¹⁸⁸ After optimisation of all individual parameters of the analysis, the detection limit for *trans*-resveratrol using fluorescence detector was 0.003 mg litre⁻¹, and using diode array detector, this value was an order of magnitude higher, 0.02 mg litre⁻¹ (Ref. 187).

The sensitivities of various versions of detection in the determination of flavonoids in orange juice by high performance liquid chromatography have been compared.²¹⁵ The detection limits and the concentrations of some flavonoids found in orange juice are presented in Table 5. It can be seen that all detection methods ensured high reproducibility and allowed quantitative determination of low levels of flavonoids.

Table 5. Detection limits and results of quantitative determination of flavonoids in orange juice by high performance liquid chromatography with different detectors.¹⁸⁶

Compound	Detector		
	UV	mass spectrometer	electro-chemical
Detection limits (μg in 1 ml) for some flavonoids			
Quercetin	0.15	0.2	0.3
Narirutin	0.2	0.1	1.0
Eriocitrin	0.2	0.08	0.5
Hesperidin	0.3	0.1	0.5
Naringin	0.25	0.15	1.0
Content (mg per 100 g) of flavonoids detected in juice			
Quercetin	1.34 ± 0.15	0.90 ± 0.03	1.18 ± 0.11
Narirutin	5.10 ± 0.17	5.4 ± 0.2	5.0 ± 0.6
Eriocitrin	1.0 ± 0.2	0.9 ± 0.3	—
Hesperidin	73 ± 7	78.9 ± 0.4	79.3 ± 0.5
Naringin	2.6 ± 0.3	0.14 ± 0.0	—

The compounds to be determined may have a broad range of polarity; therefore, their analysis requires either a gradient elution mode or several mobile phases with isocratic elution. Thus the isocratic mode was used to determine anthocyanins, flavan-3-ols, flavonols and phenolic acids in three brands of Bulgarian wine and gradient elution was employed to determine stilbenes in the same brands of wine.¹²² In some cases, virtually no sample preparation was required. For analysis of *trans*-resveratrol isomers in red wine, the sample was directly applied (without the sample preparation stage) on a chromatographic column and the fractions containing each of the target stilbenes were isolated by reversed phase high performance liquid chromatography.²¹⁶ Then these fractions were analysed by the gas chromatography–mass spectrometry technique.[‡]

A popular method for detection of phenols is coulometric detection. Unlike amperometric analysis, in this case the analyte is completely oxidised. The coulometric detector has been used for qualitative and quantitative determination of phenols in vegetable oils.¹⁹⁵ The advantages of this detector are the simple design and the possibility of simultaneous determination of eluates with different oxidation potentials. This detector ensures a lower detection limit and a higher selectivity than the UV detector when used for quantitative determination of biologically active

phenols in plant extracts. However, it suffers from a number of drawbacks, namely, contamination of the electrode by oxidation products and, as a consequence, a change in the electrode characteristics, dependence of the signal on the eluent flow rate and limited applicability in the gradient elution mode.²¹⁸ It has been found²¹⁹ that phenolic acids and tocopherol show the maximum coulometric detector response at low potentials (100–450 mV), while flavonoids show the maximum responses in two ranges: 0–300 and 600–900 mV.

In the studies of complex natural objects by any chromatographic method, identification of the components is an important stage. This task is solved by comparing the retention times, spectroscopic data and/or retention indices of the analytes with the same parameters of standard (reference) compounds. In analysis of natural objects, the most informative data can be obtained by combined use of all characteristics.²²⁰ The phenol derivatives determined by high performance liquid chromatography are identified by comparison of spectroscopic characteristics (mass spectra)²²¹ and retention indices^{222, 223} with the respective characteristics of the standard compounds. In the absence of standard compounds,²²⁴ the impurities in dihydroquercetin can be identified by combined consideration of the retention indices and spectral ratios at different wavelengths. It is possible to use retention indices in micellar electrokinetic chromatography.²²⁵

In recent years, high performance liquid chromatography with mass spectrometric detection^{226–230} or combinations of diode array and mass spectrometric detection with various ionisation sources^{231–234} have been used most often to identify phenols present in plant raw materials and foodstuffs. The latter technique is especially valuable in the study of acylated flavonoid glycosides present in plants, vegetables or fruits in small amounts.

Using high performance liquid chromatography with mass spectrometric detection and with chemical ionisation under atmospheric pressure, extracts of about 40 fruit and vegetable species have been characterised qualitatively and quantitatively.²³⁵ Seven flavonoids were isolated and identified. For example, apples contained up to 2 mg of quercetin per 100 g of the sample weight and parsley contained up to 185 mg of apigenin per 100 g of the sample weight.

Studies of flavonoids in many spice plants carried out by high performance liquid chromatography with electrospray ionisation mass spectrometry detection have shown¹⁴³ the possibility of determining molecular masses of aglycons and glycosides.

Capillary electrophoresis starts to be actively used to determine phenols in juices, tea, vegetable oils, wines and berries.^{236–241} Advantages of this method include the possibility of introducing the sample into a capillary in a dilute form under pressure,²⁴² i.e., the sample preparation stage is avoided, and performing the experiments over a broader pH range^{243, 244} than in the case of high performance liquid chromatography.

A review²⁴⁵ cites an interesting example of using capillary electrophoresis for the separation of six diastereomeric flavanone-7-*O*-glycosides. The separation was carried out at pH 10 in a phosphate buffer with addition of chiral compounds, viz., cyclodextrins and their derivatives, to the supporting electrolyte. Under chosen conditions, lemon juice was analysed and the mixture of four flavanone-7-*O*-glycosides present was separated into isomers.

Currently, capillary electrophoresis is used as a technique supplementary to high performance liquid chromatography for the separation and determination of phenols.

3. Determination in biological fluids

Biological fluids (blood, urine) are analysed for the presence of antioxidants and to estimate the bioavailability of these compounds (after consuming various kinds of food), study their metabolism and influence on the human health. In virtually all studies of this type, high performance liquid chromatography and capillary electrophoresis techniques are used. The applications of

‡ The original procedure for the analysis of hydrophobic samples including direct injection of plant or animal fats into a column has been reported.²¹⁷ The procedure is applicable to determination of biologically active compounds in plant oils.

capillary electrophoresis, in particular, that with mass spectrometric detection, for analysis of antioxidants, metabolites and toxins have been surveyed.²⁴⁵ In the present review, we will consider the use of high performance liquid chromatography in more detail.

The extraction of flavonoids from biological fluids is rather simple. A sample is centrifuged to remove proteins and other polymeric components and is subjected to solid-phase extraction with elution by methanol, ethanol and ethyl acetate. If necessary, enzymatic or acid hydrolysis is carried out. Sample preparation methods for blood samples have been compared.²⁴⁶ The addition of anticoagulants does not influence noticeably the accuracy of analysis, 1% ascorbic acid mixed with orthophosphoric acid (10 $\mu\text{l ml}^{-1}$) being the best stabiliser. The samples should be stored at -20°C .

Isoflavones were the first flavonoids to be determined quantitatively in human urine. Routine methods for analysis of human blood and urine for the presence of daidzein and equol (120 ng ml^{-1})²⁴⁷ using reversed phase high performance liquid chromatography with UV detection have been developed. The high performance liquid chromatography technique with electrochemical detector is more sensitive, permitting determination of daidzein, genistein and equol at a level of 1–2 ng ml^{-1} (Ref. 248). By gas chromatography–mass spectrometry, isofla-

vone metabolites were identified in blood serum and rat internal tissues at a minimum content of 10–20 pg mg^{-1} (Ref. 249). A fast method for determination of isoflavone in urine by immunofluorometric assay was proposed by Uehara *et al.*²⁵⁰ The method is sensitive (0.1 ng ml^{-1}) and reproducible (the root-mean-square deviation is 2%–10% between the series of analyses); however, like gas chromatography with the same detection method, this method is expensive and labour-consuming.

The total amount of quercetin and its metabolites in biological samples is determined using liquid chromatography with mass spectrometric detection^{251–254} and some other methods, for example, versions of high performance liquid chromatography with mass spectrometric,²⁵² UV,^{255,256} affinity chromatographic,²⁵⁷ fluorescence and electrochemical^{258,259} detection. Gas chromatography with mass spectrometric detection has been proposed for determining quercetin and its conjugates in human urine and blood plasma in concentrations of down to 10 pg ml^{-1} (Ref. 260). The characteristics of some methods for determination of quercetin and other biologically active phenols are given in Table 6.

Thus, nowadays, reversed phase high performance liquid chromatography combined with various detection techniques (most often, diode array and mass spectrometric detection) is

Table 6. Characteristics of some methods for determination of biologically active phenols in various samples.

Sample	Identified compounds	Extractant	Hydrolysis	Method ^a	Detection limit / ng ml^{-1}	Ref.
Blood, human blood serum and plasma, rat urine	(+)-catechin, quercetin, <i>trans</i> -resveratrol	ethyl acetate	see ^b	GC-MS	0.01	261
Human blood and urine	quercetin and its glycosides	aqueous methanol	HCl–methanol, 5 h (blood), 8 h (urine)	HPLC, fluorescence detector	—	262
Rat blood plasma	quercetin	preliminary purification on a C_{18} column, extraction with a toluene– CH_2Cl_2 mixture	ascorbic acid + β -glucuronidase	HPLC, electrochemical detector	0.63	263
Rat urine and blood	flavonoids, phenylalkanoic acids	water, methanol, fractionation (SPE C_{18})	HCl–methanol, 45 min	RP HPLC-UV (C_8 , C_{18})	—	264
Human blood plasma	naringin, naringenin	ethanol, fractionation (Sep-Pak, C_{18} , 80% methanol)	—	RP HPLC-UV (C_{18})	2	265
Human blood plasma	catechin, epicatechin, 3 derivatives	ethyl acetate	HCl–methanol, 30 min	RP HPLC-UV (C_{18})	—	266
Human urine	apigenin, acacetin	addition of 2 M NaOAc + 10% ascorbic acid	β -glucuronidase + arylsulfatase, 60 min	RP HPLC-UV with column switching (C_8 , C_{18})	10–70	267
Human blood plasma	naringenin, hesperetin	SPE on a C_{18} cartridge	β -glucuronidase + arylsulfatase, 18 h	HPLC-UV, C_8	10	268
Rat blood, urine, tissues	a mixture of 8 catechins	methanol–ethyl acetate–sodium dithionite (2 : 1 : 3)	β -glucuronidase + arylsulfatase, 45 min	RP HPLC (C_{18}), electrochemical detector	5	269
Human blood serum	6 phenolic acids and aldehydes	formic acid–acetone–water (4 : 140 : 56)	—	HPLC-MS (C_{18})	8	270

Notes. The following designations are used: GC-MS is gas chromatography–mass spectrometry, RP HPLC-UV is reversed phase high performance liquid chromatography with UV detection, SPE is solid-phase extraction, HPLC-UV is high performance liquid chromatography with UV detection, HPLC-MS is high performance liquid chromatography with mass spectrometric detection.

^a The hydrocarbon sorbent is indicated in parentheses. ^b Prior to the analysis, the sample was modified with bis(trimethylsilyl)trifluoroacetamide.

one of the most efficient methods for separation and identification of biologically active phenols and polyphenols in various objects.

References

1. J Alanko, A Ruita, P Holm, I Mucha, T Metsa-Ketela *Free Radical Biol. Med.* **26** 193 (1999)
2. W Deng, X Fang, J Wu *Radiat. Phys. Chem.* **50** 271 (1997)
3. A Saija, M Scalese, M Lanza, D Marzullo, F Ronina, F Castelli *Free Radical Biol. Med.* **19** 481 (1995)
4. Q Guo, B Zhao, M Li, S Shen, W Xin *Biochim. Biophys. Acta* **1304** 210 (1996)
5. J Jodoin, M Demeule, R Beliveau *Biochim. Biophys. Acta* **1542** 149 (2002)
6. A A Semenov *Ocherk Khimii Prirodnykh Soedinenii* (Essay on the Chemistry of Natural Compounds) (Novosibirsk: Nauka, 2000)
7. J-M Kong, L-S Chia, N-K Goh, T-F Chia, R Brouillard *Phytochemistry* **64** 923 (2003)
8. C A Williams, R J Gray *Nat. Prod. Rep.* **21** 539 (2004)
9. A A Revina, O G Larionov, M V Kochetova, T K Lutsik, G I El'-Registan *Izv. Akad. Nauk, Ser. Khim.* **11** 2257 (2003)^a
10. A A Revina, Author's Abstract of Doctoral Thesis in Chemical Sciences, Institute of Physical Chemistry, Russian Academy of Sciences, Moscow, 1995
11. A A Revina, in *The IIIrd International Symposium on Colourants, Princeton, USA, 1998* p. 278
12. E Middleton Jr, C Kandaswami, T C Theoharides *Pharmacol. Rev.* **52** 673 (2000)
13. H Nishino, M Murakoshi, X Y Mou, S Wada, M Masuda, Y Ohsaka, Y Satomi, K Jinno *Oncology* **69** 38 (2005)
14. M N Diaz, B Frei, J A Vita, J F Keaney *New Engl. J. Med.* **337** 408 (1997)
15. K J Joshupura, F B Hu, J E Manson, M J Stampfer, E B Rimm, F E Speizer, G Colditz, A Ascherio, B Rosner, D Spiegelman, W C Willett *Ann. Intern. Med.* **134** 1106 (2001)
16. P Vitaglione, F Morisco, N Caporaso, V Fogliano *CRC Crit. Rev. Food Sci. Nutr.* **44** 575 (2004)
17. M M Silva, M R Santos, G Caroco, R Rocha, G Justino, L Mira *Free Radical Res.* **36** 1219 (2002)
18. A A Revina, P M Zaitsev, D M Fedulov, G A Zheltukhina, V E Nebol'sin *Zh. Fiz. Khim.* **77** 364 (2003)^b
19. L Mira, M T Fernandez, M Santos, R Rocha, M H Florêncio, K R Jennings *Free Radical Res.* **36** 1199 (2002)
20. G Galati, P J O'Brien *Free Radical Biol. Med.* **37** 287 (2004)
21. K E Heim, A R Tagliaferro, D J Bobilya *J. Nutr. Biochem.* **13** 572 (2002)
22. Y Cai, Q Luo, M Sun, H Corke *Life Sci.* **74** 2157 (2004)
23. Y-Y Soong, P J Barlow *Food Chem.* **88** 411 (2004)
24. M Nacz, F Shahidi *J. Chromatogr., A* **1054** 95 (2004)
25. S Mathew, T E Abraham *Crit. Rev. Biotechnol.* **4** 59 (2004)
26. J-B Ruidavets, P-L Teissedre, J Ferrieres, S Carando, G Bougard, J-C Cabanis *Atherosclerosis (Shannon, Irel.)* **153** 107 (2000)
27. J Peterson, J Dwyer, S Bhagwat, D Haytowitz, J Holden, A L Eldridge, G Beecher, J Aladesanmi *J. Food Compos. Anal.* **18** 487 (2005)
28. S Tsanova-Savova, F Ribarova, M Gerova *J. Food Compos. Anal.* **18** 691 (2005)
29. M Arlorio, J D Coisson, F Travaglia, F Varsaldi, G Miglio, G Lombardi, A Martelli *Food Res. Int.* **38** 1009 (2005)
30. G Lill, S Voit, K Schror, A-A Weber *FEBS Lett.* **546** 265 (2003)
31. K Takeda, A Osakabe, S Saito, D Furuyama, A Tomita, Y Kojima, M Yamadera, M Sakuta *Phytochemistry* **66** 1607 (2005)
32. A M González-Paramás, F L da Silva, P Martín-López, G Macz-Pop, S González-Manzano, C Alcalde-Eon, J J Pérez-Alonso, M T Escribano-Bailón, J C Rivas-Gonzalo, C Santos-Buelga *Food Chem.* **94** 428 (2006)
33. N P Seeram, R A Momin, M G Nair, L D Bourquin *Phytomedicine* **8** 362 (2001)
34. A F Vinha, F Ferreres, B M Silva, P Valentão, A Gonçalves, J A Pereira, M B Oliveira, R M Seabra, P B Andrade *Food Chem.* **89** 561 (2005)
35. F Galvano, L La Fauci, G Lazzarino, V Fogliano, A Ritieni, S Ciappellano, N C Battistini, B Tavazzi, G Galvano *J. Nutr. Biochem.* **15** 2 (2004)
36. D Cooke, W P Steward, A J Gescher, T Marczylo *Eur. J. Cancer.* **41** 1931 (2005)
37. D Di Majo, M Giammanco, M La Guardia, E Tripoli, S Giammanco, E Finotti *Food Res. Int.* **38** 1161 (2005)
38. M A Anagnostopoulou, P Kefalas, V P Papageorgiou, A N Assimopoulou, D Boskou *Food Chem.* **94** 19 (2006)
39. R E Asenstorfer, Y Wang, D J Mares *J. Cereal Sci.* **43** 108 (2006)
40. S A Aherne, N M O'Brien *Nutrition* **18** 75 (2002)
41. E M Marinova, N V Yanishlieva, I R Totseva *Int. J. Food Sci. Technol.* **37** 145 (2002)
42. S A Matasova, N A Mitina, G L Ryzhova, D O Zhuganov, K A Dychko *Khim. Rastit. Syr'ya* (2) 119 (1999)
43. V Yu Andreeva, G I Kalinkina *Khim. Rastit. Syr'ya* (2) 79 (2000)
44. K-H Lee, H-B Chai, P A Tamez, J M Pezzuto, G A Cordell, K K Win, M Ti-Wa *Phytochemistry* **64** 535 (2004)
45. P Zhou, Y Takaishi, H Duan, B Chen, G Honda, M Itoh, Y Takeda, O K O K Kodzhimatov, K-H Lee *Phytochemistry* **53** 689 (2000)
46. D Voora, H L McLeod, C Eby, B F Gage *Pharmacogenomics* **6** 503 (2005)
47. O Xie, X Wang, X Wang, Z Jiang, Z Qiu *Bioorg. Med. Chem. Lett.* **15** 4953 (2005)
48. S Vilar, E Quezada, L Santana, E Uriarte, M Yanez, N Fraiz, C Alcade, E Cano, F Orallo *Bioorg. Med. Chem. Lett.* **16** 257 (2006)
49. I Manolov, N Danchev *Eur. J. Med. Chem.* **30** 717 (1995)
50. A M El-Sayed, O A Abd-Allah *Phosphorus, Sulfur Silicon Relat. Elem.* **170** 75 (2001)
51. A M El-Agrody, M S Abd El-Latif, N A El-Hady, A H Fakery, A H Bdair *Molecules* **6** 519 (2001)
52. Z M Nofal, M I El-Zahar, S S Abd El-Karim *Molecules* **5** 99 (2000)
53. M H Abraham, J M R Gola, R Kumarsingh, J E Cometto-Muniz, W S Cain *J. Chromatogr., B* **745** 103 (2000)
54. T Hanai *J. Chromatogr., A* **1027** 279 (2004)
55. N Sanli, G Fonrodona, J Barbosa, G A Özkan, J L Beltran *Anal. Chim. Acta* **537** 53 (2005)
56. J K Törnblom, T F W Bureyko, C D MacKinnon *J. Chromatogr., A* **1095** 68 (2005)
57. R M Smith *J. Chromatogr., A* **656** 381 (1993)
58. C A Rice-Evans, N J Miller, G Paganda *Free Radical Biol. Med.* **20** 933 (1996)
59. P A Morrissey, K M O'Brien *Int. Dairy J.* **8** 463 (1998)
60. M Sato, D Bagchi, A Tosaki, D K Das *Free Radical Biol. Med.* **31** 729 (2001)
61. L Fremont, L Belguendouz, M T Gozzelino, A Linard *Atherosclerosis (Shannon, Irel.)* **134** 202 (1997)
62. C Casalini, M Lodovici, C Briani, G Paganelli, S Remy, V Cheynier, P Dolara *Eur. J. Nutr.* **38** 190 (1999)
63. M Bergman, L Varshavsky, H E Gottlieb, S Grossman *Phytochemistry* **58** 143 (2001)
64. S V Nigdikar, A N Howard *Atherosclerosis (Shannon, Irel.)* **134** 203 (1997)
65. K Robards *J. Chromatogr., A* **1000** 657 (2003)
66. E Sergediene, K Jonsson, H Szymusiak, B Tyrakowska, I Rietjens, N Cenas *FEBS Lett.* **462** 392 (1999)
67. D Metodiewa, A K Jaiswal, N Cenas, E Dickanait, J Segura-Aguilar *Free Radical Biol. Med.* **26** 107 (1999)
68. O Dangles, C Dufour, G Fargeix *J. Chem. Soc., Perkin Trans. 2* 1215 (2000)
69. S Auriol, H Ohshima, Y Yoshie, I Gilibert *Free Radical Biol. Med.* **25** 1057 (1998)
70. O M Palomino, P Gomes-Serranillos, E Carretero, A J Villar *J. Chromatogr., A* **731** 103 (1996)
71. R Aqino, S Morelli, M R Lauro, S Abdo, A Satija, A Tomaino *J. Nat. Prod.* **64** 1019 (2001)
72. C Poullain, E Girard-Valenciennes, J Smadja *J. Ethnopharmacol.* **95** 19 (2004)
73. J-H Liu, S Zschocke, R Bauer *Phytochemistry* **49** 211 (1998)

74. M Pinelo, M Rubilar, J Sineiro, M J Nunez *Food Chem.* **85** 267 (2004)
75. P Siddhuraju, P S Mohan, K Becker *Food Chem.* **79** 61 (2002)
76. U Hohl, B Neubert, H Pforte, I Schonhof, H Bohm *Eur. Food Res. Technol.* **213** 205 (2001)
77. J F Stevens, M Ivancic, V L Hsu, M L Deinzer *Phytochemistry* **44** 1575 (1997)
78. R Aquino, A Cáceres, S Morelli, L Rastrelli *J. Nat. Prod.* **65** 1773 (2002)
79. L M Sokmen, M Angelova, E Krumova, S Pashova, S Ivancheva, A Sokmen, J Serkedjieva *Life Sci.* **76** 2981 (2005)
80. E Walther, Y-C Chung, S-J Chen, C-K Hsu, C-T Chang, S-T Chou *Food Chem.* **91** 419 (2005)
81. V I Deineka, A M Grigor'ev *Zh. Anal. Khim.* **59** 305 (2004) ^c
82. R Norbaek, T Kondo *Phytochemistry* **50** 1181 (1999)
83. K Toki, N Saito, T Honda *Phytochemistry* **48** 729 (1998)
84. E Pale, M Nacro, M Vanhaelen, R Vanhaelen-Fastré, R Ottinger *Phytochemistry* **48** 1433 (1998)
85. F Tatsuzawa, N Saito, H Seki, R Hara, M Yokoi, T Honda *Phytochemistry* **45** 173 (1997)
86. N Saito, F Tatsuzawa, A Nishiyama, M Yokoi, A Shigihara, T Honda *Phytochemistry* **38** 1027 (1995)
87. F Tatsuzawa, N Saito, M Yokoi, A Shigihara, T Honda *Phytochemistry* **49** 869 (1998)
88. M A S Marles, H Ray, M Y Gruber *Phytochemistry* **64** 367 (2003)
89. G E Rohr, B Mier, O Sticher *J. Chromatogr., A* **835** 59 (1999)
90. U Svedstrom, H Vuorela, R Konstiainen, I Laasko, R Hiltunen *J. Chromatogr., A* **968** 53 (2002)
91. U Svedstrom, H Vuorela, R Konstiainen, J Tuominen, J Kokkonen, J-P Rauha, I Laasko, R Hiltunen *Phytochemistry* **60** 821 (2002)
92. M Skerget, P Kotnik, M Hadolin, A R Hra, M Simonic, Z Knez *Food Chem.* **89** 191 (2005)
93. C Goncalves, T Dinis, M T Batista *Phytochemistry* **66** 89 (2005)
94. M Kosar, H J D Dorman, R Hiltunen *Food Chem.* **91** (3) 525 (2005)
95. M Papagiannopoulos, H R Wollseifen, A Mellenthin, B Haber, R Galesa *J. Agric. Food Chem.* **52** 3784 (2004)
96. E Ibanez, A Kubatova, F J Senorans, S Caverio, G Reglero, S B Hawthorne *J. Agric. Food Chem.* **51** 375 (2003)
97. E S Ong, S M Len *Anal. Chim. Acta* **482** 81 (2003)
98. M Papagiannopoulos, B Zimmermann, A Mellenthin, M Krappe, G Maio, R Galesa *J. Chromatogr., A* **958** 9 (2002)
99. K C Zancan, M O M Marques, A J Petenate, M A A Meireles *J. Supercrit. Fluids* **24** 57 (2002)
100. F Le Floch, M T Tena, A Rios, M Valcarcel *Talanta* **46** 1123 (1998)
101. A Chafer, T Fornari, A Berna, R P Stateva *J. Supercrit. Fluids* **32** 89 (2004)
102. F J Senorans, E Ibanez, S Caverio, J Tabera, G Reglero *J. Chromatogr., A* **870** 491 (2000)
103. B-J Wang, C-T Liu, C-Y Tseng, Z-R Yu *LWT — Food Sci. Technol.* **38** 281 (2005)
104. J Wu, W Xie, J Pawliszyn *Analyst (Cambridge)* **125** 2216 (2000)
105. L T Taylor, M Palma *J. Chromatogr., A* **849** 117 (1999)
106. M Bonoli, E Marconi, M F Caboni *J. Chromatogr., A* **1057** 1 (2004)
107. D Tura *J. Chromatogr., A* **975** 71 (2002)
108. M Antolovich, P Prenzler, K Robards, D Ryan *Analyst (Cambridge)* **125** 989 (2000)
109. L-J Chen, D E Games, J Jones *J. Chromatogr., A* **988** 95 (2003)
110. Y Shibusawa, A Yanagida, A Ito, Kichihashi, H Shindo, Y Ito *J. Chromatogr., A* **886** 65 (2000)
111. M Palma, Z Pineiro, C G Baroso *J. Chromatogr., A* **921** 69 (2001)
112. P Swatsitang, G Tucker, K Robards, D Jardine *Anal. Chim. Acta* **417** 231 (2000)
113. R Slimestad, A Marston, K Hostettmann *J. Chromatogr., A* **719** 438 (1996)
114. A Degenhardt, P Winterhalter *Eur. Food Res. Technol.* **213** 277 (2001)
115. L S Hutabarat, H Greenfield, M Mulholland *J. Chromatogr., A* **886** 55 (2000)
116. N Nakatani, H Kikuzaki, J Hikida, M Ohba, O Inami, I Tamura *Phytochemistry* **38** 755 (1995)
117. A L Davis, J R Lewis, Y Cai, C Powell, A P Davis, J P G Wilkins, P Pudney, M N Clifford *Phytochemistry* **46** 1397 (1997)
118. A Garsia, M Brenes, P Garsia, C Romero, A Garrido *Eur. Food Res. Technol.* **216** 520 (2003)
119. D Matejcek, B Klejdus, O Mikes, D Sterbova, V Kuban *Anal. Bioanal. Chem.* **377** 340 (2003)
120. D A Guillen, C G Barroso, J A Perez-Bustamante *J. Chromatogr., A* **730** 39 (1996)
121. M Netzel, G Strass, I Bitsch, R Konitz, M Christmann, R Bitsch *J. Food Eng.* **56** 223 (2003)
122. A Czyzowska, E Pogorzelski *Eur. Food Res. Technol.* **214** 148 (2002)
123. W E Bronner, G Rbecher *J. Chromatogr., A* **705** 247 (1995)
124. Y Zuo, H Chen, Y Deng *Talanta* **57** 307 (2002)
125. B Suarez, A Picinelli, J J Mangas *J. Chromatogr., A* **727** 203 (1996)
126. E Pastene, M Montes, M Vega *J. Planar. Chromatogr. — Mod. TLC* **10** 362 (1997)
127. E Wollenweber, J F Stevens, M Dorr, A C Rozefelds *Phytochemistry* **62** 1125 (2003)
128. M Watanabe, Y Ohshita, T Tsushida *J. Agric. Food Chem.* **45** 1039 (1997)
129. C W Beninger, G L Hosfield, M G Nair *J. Agric. Food Chem.* **46** 2906 (1998)
130. Y Ju, J N Sacalis, C C Still *J. Agric. Food Chem.* **46** 3785 (1998)
131. S Cobzas, G Cimpan, N Olah, S Gocan *J. Planar. Chromatogr. — Mod. TLC* **12** 26 (1999)
132. M A Hawryl, E Soczewinsky, T H Dzido *J. Chromatogr., A* **886** 75 (2000)
133. O G Larionov, A A Revina, O G Tataurova, A Yu Budunova *Sorbts. Khromatogr. Protsessy* **3** (1) 19 (2003)
134. E A Melo, J M Filho, N B Guera *Lebensm.-Wiss. Technol.* **38** 15 (2005)
135. S P Pohjamo, J E Hemming, S M Willfor, M H T Reunanen, B R Holmbom *Phytochemistry* **63** 165 (2003)
136. L Khaled, F El-Massry, A H El-Ghorab, A Farouk *Food Chem.* **79** 331 (2002)
137. Y C Fiamegos, C G Nanos, J Vervoort, C D Stalikas *J. Chromatogr., A* **1041** 11 (2004)
138. M Lopez, F Martinez, C Del Valle, M Ferrit, R Luque *Talanta* **60** 609 (2003)
139. X He, L Lin, L Lian *J. Chromatogr., A* **755** 127 (1996)
140. A Raffaelli, G Moneti, V Mercati, E Toja *J. Chromatogr., A* **777** 223 (1997)
141. N Chaves, J J Rios, C Gutierrez, J C Escudero, J M Olias *J. Chromatogr., A* **799** 111 (1998)
142. M Broliis, B Gabetta, N Fuzzati, R Pace, F Panzeri, F Peterlongo *J. Chromatogr., A* **825** 9 (1998)
143. U Justesen *J. Chromatogr., A* **902** 369 (2000)
144. S Z Ivanova, T E Fedorova, N V Ivanova, S V Fedorov, L A Ostroukhova, Yu A Malkov, V A Babkin *Khim. Rastit. Syr'ya* (4) 5 (2002)
145. K Franke, A Porzel, J Schmidt *Phytochemistry* **61** 873 (1996)
146. E Jourbet, F Otto, S Gruner *Eur. Food Res. Technol.* **216** 270 (2003)
147. I Saracoglu, M Varel, U S Harput, A Nagatsu *Phytochemistry* **65** 2379 (2004)
148. L F Yamaguchi, D G Vassao, J Kato, P Di Mascio *Phytochemistry* **66** 2238 (2005)
149. V M Misin, L A Goncharov, E V Maiorov, Ya I Yashin, E I Korotkova, A V Ivanova, R R Farkhutdinov, in *Biotechnologiya-2005: Vos'moi Mezhdunarodnyi Seminar-prezentatsiya Innovatsionnykh Nauchno-tehnicheskikh Proektov, Pushchino, 2005* (Biotechnology-2005: Eighth International Seminar-presentation of Innovation Scientific and Technical Projects, Pushchino, 2005) p. 58
150. A Ya Yashin, Ya I Yashin *Ros. Khim. Zh.* **66** (4) 109 (2002) ^d

151. M Antolovich, P D Prenzler, E McDonald, K Robards *Analyst (Cambridge)* **127** 183 (2002)
152. N G Goryacheva, M V Kochetova, E F Shanenko, A A Revina, O G Larionov *Pivo Zhizn* **37** 27 (2003)
153. V Katalinic *J. Chromatogr.*, **A 775** 359 (1997)
154. P Drasar, J Moravcova *J. Chromatogr.*, **B 812** 3 (2004)
155. R F Viera, R J Grayer, A J Paton *Phytochemistry* **63** 555 (2003)
156. J-lan Zhang, M Cui, Y He, H-Yu, D-Guo *J. Pharm. Biomed. Anal.* **36** 1029 (2005)
157. P Schofield, D M Mbugua, A N Pell *Anim. Feed Sci. Technol.* **91** 21 (2001)
158. A Yanagida, T Shoji, Y Shibusawa *J. Biochem. Bioph. Methods* **56** 311 (2003)
159. T Fuleki, J M Ricardo da Silva *J. Agric. Food Chem.* **45** 1156 (1997)
160. Y Cao, Q Chu, J Ye *J. Chromatogr.*, **B 812** 231 (2004)
161. H-B Li, Y Jiang, F Chen *J. Chromatogr.*, **B 812** 277 (2004)
162. I Molnar-Perl, Z Fuzfai *J. Chromatogr.*, **A 1073** 201 (2005)
163. M Vahner, M Koel *J. Chromatogr.*, **A 990** 225 (2005)
164. M-E Yue, T-F Jiang, Y-P Shi *Talanta* **62** 695 (2004)
165. V Bicaud, A Fougerousse, R Brouillard *J. Liq. Chromatogr. Relat. Technol.* **22** 541 (1999)
166. M A Rodriguez-Delgado, M L Perez, R Corbella, G Gonzalez, F J G Montelongo *J. Chromatogr.*, **A 871** 427 (2000)
167. H Y Cheung, W P Lai, M S Cheung, F M Leung, D J Hood, W F Fong *J. Chromatogr.*, **A 989** 303 (2003)
168. W Ketai, L Huitao, C Xingguo, Z Yunkun, H Zhide *Talanta* **54** 753 (2001)
169. C del Mar Verde Mendez, M P Forster, M A Rodriguez-Delgado, E M Rodriguez-Rodriguez, C D Romero *Eur. Food Res. Technol.* **217** 287 (2003)
170. A Escarpa, M C Gonzalez *J. Chromatogr.*, **A 897** 161 (2000)
171. A Escarpa, M C Gonzalez *Eur. Food Res. Technol.* **212** 439 (2001)
172. G N Magoma, F N Washira, M Obanda, M Imbuga, S G Agong *Genet. Resour. Crop Evol.* **47** 107 (2000)
173. O Tokusoglu, M K Unal *Eur. Food Res. Technol.* **215** 340 (2002)
174. H Morais, C Ramos, E Forgacs, T Cserhati, J Oliveira *J. Chromatogr.*, **B 770** 297 (2002)
175. B Berente, D De la Calle Garcia, M Reichenbacher, K Danzer *J. Chromatogr.*, **A 871** 95 (2000)
176. E Mataix, M D Luque de Castro *J. Chromatogr.*, **A 910** 255 (2001)
177. B Berente, M M Reichenbacher, K Danzer *Fresenius J. Anal. Chem.* **371** 68 (2001)
178. N Terahara, Y Takede, A Nesumi, T Honda *Phytochemistry* **56** 359 (2001)
179. M Lopez, F Marhnez, C Del Valle, C Orte, M Miro *J. Chromatogr.*, **A 922** 359 (2001)
180. R M Alonso-Salces, S Guyot, C Herrero, L A Berrueta, J F Drilleau, B Gallo, F Vicente *Anal. Bioanal. Chem.* **379** 464 (2004)
181. M Materska, S Piacente, A Stochmal, C Pizza, W Oleszek, I Perucka *Phytochemistry* **63** 893 (2003)
182. Y Amakura, M Okada, S Tsuji, Y Tonogai *J. Chromatogr.*, **A 891** 183 (2000)
183. F M Pirisi, A Angioni, P Cabras, V L Garau, M T S di Teulada, M K dos Santos, G Bandino *J. Chromatogr.*, **A 768** 207 (1997)
184. A Schieber, P Keller, R Carle *J. Chromatogr.*, **A 910** 265 (2001)
185. E Revilla, J-M Ryan *J. Chromatogr.*, **A 881** 461 (2000)
186. R Tsao, R Yang *J. Chromatogr.*, **A 1018** 29 (2003)
187. I Arozarena, A Casp, R Marin, M Navarro *Eur. Food Res. Technol.* **212** 108 (2000)
188. A Pena-Neira, T Hernandez, C Garcia-Vallejo, I Estrella, J A Suarez *Eur. Food Res. Technol.* **210** 445 (2000)
189. C Inocencio, D Rivera, F Alcouraz, F A Tomas-Barberau *Eur. Food Res. Technol.* **212** 70 (2000)
190. M C Gonzalez, A Escarpa *J. Chromatogr.*, **A 830** 301 (1999)
191. B-L Lee, C-N Ong *J. Chromatogr.*, **A 881** 439 (2000)
192. Y Amakura, M Okada, S Tsuji, Y Tonogai *J. Chromatogr.*, **A 896** 87 (2000)
193. D A Guillen, C G Barroso, J A Perez-Bustamante *J. Chromatogr.*, **A 724** 117 (1996)
194. M Fiorini *J. Chromatogr.*, **A 692** 213 (1995)
195. A Cert, W Moreda, M C Perez-Camino *J. Chromatogr.*, **A 881** 131 (2000)
196. A M van Nederkassel, M Daszykowski, D L Massart, Y V Heyden *J. Chromatogr.*, **A 1096** 117 (2005)
197. C Chilla, D A Guillen, C G Barroso, J A Perez-Bustamante *J. Chromatogr.*, **A 750** 209 (1996)
198. A Crozier, E Jensen, M E J Lean, M S McDonald *J. Chromatogr.*, **A 761** 315 (1997)
199. A Escarpa, M C Gonzalez *J. Chromatogr.*, **A 823** 331 (1998)
200. M Lores, C M Garcia, R Cela *J. Chromatogr.*, **A 683** 31 (1994)
201. G Shui, L P Leong *J. Chromatogr.*, **A 977** 89 (2002)
202. H Chen, Y Zuo, Y Deng *J. Chromatogr.*, **A 913** 387 (2001)
203. A Escarpa, M C Gonzalez *Anal. Chim. Acta* **427** 119 (2001)
204. A Ortuno, I Reynaldo, M D Fuster, J Botia, D G Puig, I Porras, A G Lidon, F Sabater, J A Del-Rio *Sci. Hortic.* **68** 231 (1997)
205. S Tsanova-Savova, F Ribarova *J. Food Compos. Anal.* **15** 639 (2002)
206. O Palomino, M P Gomez-Serranillos, K Slowing, E Carretero, A Vilar *J. Chromatogr.*, **A 870** 449 (2000)
207. M A Rodriguez-Delgado, S Malovana, J P Perez, T Borges, F J G Motelongo *J. Chromatogr.*, **A 912** 249 (2001)
208. W Andlauer, M J Martena, P Furst *J. Chromatogr.*, **A 849** 341 (1999)
209. A Ogawa, H Arai, H Tanizawa, T Miyahara, T Toyo'oka *Anal. Chim. Acta* **383** 221 (1999)
210. A Baldy, R T Rosen, E K Fukuda C-T Ho *J. Chromatogr.*, **A 718** 89 (1995)
211. S Perez-Magarino, I Revilla, M L Gonzalez-SanJose, S Beltran *J. Chromatogr.*, **A 847** 75 (1999)
212. G Deffieux, J C Cabanis, P Waffo-Teguo, S Carando, P L Teissedre, J M Merillon *J. Chromatogr.*, **A 849** 617 (1999)
213. T Kraushofer, G Sontag *Eur. Food Res. Technol.* **215** 529 (2002)
214. A Escarpa, M D Morales, M C Gonzalez *Anal. Chim. Acta* **460** 61 (2002)
215. M Careri, L Elviri, A Mangia, M Musci *J. Chromatogr.*, **A 881** 449 (2000)
216. D M Goldberg, N E Karumanchiri, Y Yan, E P Diamandis, G J Soleas *J. Chromatogr.*, **A 708** 89 (1995)
217. J F Noguera-Ort, G Ramis-Ramos, R M Villanueva-Camanas *Anal. Chim. Acta* **402** 81 (1999)
218. V V Brazhnikov *Detektory dlya Khromatografii* (Detectors for Chromatography) (Moscow: Mashinostroenie, 1992)
219. M N Peyrat-Maillard, S Bonnelly, C Berset *Talanta* **51** 709 (2000)
220. M V Kochetova, A A Revina, O G Larionov *Sorbts. Khromatograf. Protessy* (3) 12 (2003)
221. X-G He *J. Chromatogr.*, **A 880** 203 (2000)
222. V M Kosman, I G Zenkevich, N F Komissarenko *Rastit. Resursy* **33** (3) 32 (1997)
223. V M Kosman, I G Zenkevich *Rastit. Resursy* **33** (2) 14 (1997)
224. I G Zenkevich, V M Kosman *Zh. Anal. Khim.* **60** 837 (2005)^c
225. P G Muijselaar *J. Chromatogr.*, **A 780** 117 (1997)
226. S Guyot, T Doco, J-M Souquet, M Moutounet, J-F Drilleau *Phytochemistry* **44** 351 (1997)
227. G Shui, L P Leong *J. Chromatogr.*, **A 1022** 67 (2004)
228. M Careri, P Lombardi, A Cappiello, G Famiglini, F Mangani, C Mucchino *J. Chromatogr.*, **A 855** 515 (1999)
229. F Sanchez-Rabaneda, O Jauregui, R M Lamuela-Raventos, J Bastida, F Viladomat, C Codina *J. Chromatogr.*, **A 1008** 57 (2003)
230. G K Poon *J. Chromatogr.*, **A 794** 63 (1998)
231. J Bakker, P Bridle, T Honda, H Kuwano, N Saito, N Terahara, C F Timberlake *Phytochemistry* **44** 1375 (1997)
232. G J Soleas, E P Diamandis, G Tomlinson, D M Goldberg *Atherosclerosis (Shannon, Irel.)* **134** 207 (1997)
233. I Revilla, S Beltran, S Perez-Magarino, M L Gonzalez-SanJose *J. Chromatogr.*, **A 847** 83 (1999)
234. G Stecher, C W Huck, M Popp, G K Bonn *Fresenius' J. Anal. Chem.* **371** 73 (2001)
235. P Knuthsen, U Jistesén, T Leth *J. Chromatogr.*, **A 799** 101 (1998)
236. J Sadecka, J Polonsky *J. Chromatogr.*, **A 880** 243 (2000)

237. G Cartoni, F Coccioli, R Jasionowska *J. Chromatogr., A* **709** 209 (1995)
238. M Bonoli, M Montanucci, T G Toschi, G Lercker *J. Chromatogr., A* **1011** 163 (2003)
239. R Saenz-Lopez, P Fernandez-Zurbano, M T Tena *J. Chromatogr., A* **990** 247 (2003)
240. D B Gomis, N F Palomino, J J M Alonso *Anal. Chim. Acta* **426** 111 (2001)
241. X Gu, Q Chu, M O'Dwyer, M Zeece *J. Chromatogr., A* **881** 471 (2000)
242. M R Bronze, L F V Boas, A P Belchior *J. Chromatogr., A* **768** 143 (1997)
243. C T da Costa, S A Margolis, D Horton, B C Nelson *J. Chromatogr., A* **799** 321 (1998)
244. N Gel-Moreto, R Streich, R Galensa *J. Chromatogr., A* **925** 279 (2001)
245. M T Galceran, L Puignou *TrAC — Trends Anal. Chem.* **24** 743 (2005)
246. M V Martinez-Ortega, M C Garcia-Parrilla, A M Troncoso *Anal. Chim. Acta* **502** 49 (2004)
247. Y Zhang, G Wang, T T Song, P A Murphy, S Hendrich *J. Nutr.* **129** 957 (1999)
248. P H Gamache, I N Acworth *Proc. Soc. Exp. Biol. Med.* **217** 274 (1998)
249. S Heinonen, K Wahala, H Adlercreutz *Anal. Biochem.* **274** 211 (1999)
250. M Uehara, O Lapcik, R Hampl, N Al-Maharik, T Makela, K Wahala, H Mikola, H Adlercreutz *J. Steroid Biochem. Mol. Biol.* **72** 273 (2000)
251. J Wittig, M Herderich, E U Stewart, A Crozier *J. Chromatogr., B* **753** 237 (2001)
252. A J Day, F Mellon, D Barron, G Sarrazin, M R Morgan, G Williamson *Free Radical Res.* **35** 941 (2001)
253. W Mullen, R C Hartley, A Crozier *J. Chromatogr., A* **1007** 21 (2003)
254. L Wang, M E Morris *J. Chromatogr., B* **821** 194 (2005)
255. F M Wang, T W Yao, S Zeng *J. Pharm. Biomed. Anal.* **33** 317 (2003)
256. S E Nielsen, L O Dragsred *J. Chromatogr., B* **707** 81 (1998)
257. D Bongartz, A Hesse *J. Chromatogr., B* **673** 223 (1995)
258. C Manach, C Morand, V Crespy, C Demigne, O Texier, F Regerat, C Remesy *FEBS Lett.* **426** 331 (1998)
259. W Mullen, B A Graf, S T Caldwell, R C Hartley, G G Duthie, C A Edwards, M E Lean, A Crozier *J. Agric. Food Chem.* **50** 6902 (2002)
260. D G Watson, E J Oliveira *J. Chromatogr., B* **723** 203 (1999)
261. G J Soleas, J Yan, D M Goldberg *J. Chromatogr., B* **757** 161 (2001)
262. P C P Hollman, J M P van Trijp, M Buysman, M Gaag, M Mengelers, J de Vries, M Katan *FEBS Lett.* **418** 152 (1997)
263. I Erlund, G Alftan, H Siren, K Ariniemi, A Aro *J. Chromatogr., B* **727** 179 (1999)
264. P G Pietta, C Gardana, P L Mauri, R Maffei-Facino, M Carini *J. Chromatogr., B* **673** 75 (1995)
265. K Ishii, T Furuta, Y Kasuya *J. Chromatogr., B* **683** 225 (1996)
266. G Maiani, M Stefani, M Salucci, E Azzini, A Ferro-Luzzi *J. Chromatogr., B* **692** 211 (1997)
267. S E Nielsen, L O Dragsted *J. Chromatogr., B* **713** 379 (1998)
268. F I Kanaze, E Kokkalou, M Georgarakis, I Niopas *J. Chromatogr., B* **801** 363 (2004)
269. F O Chu, C C Wang, M S Rogers, K W Choy, C P Pang *J. Chromatogr., B* **810** 187 (2004)
270. X L Chen Yu, Y Cai, G Liu, J Jia, Y Wang *J. Chromatogr., B* **820** 41 (2005)

^a — *Russ. Chem. Bull., Int. Ed. (Engl. Transl.)*

^b — *Russ. J. Phys. Chem. (Engl. Transl.)*

^c — *Russ. J. Anal. Chem. (Engl. Transl.)*

^d — *Mendeleev Chem. J. (Engl. Transl.)*

The mechanism of electronic excitation in the bacterial bioluminescent reaction

E V Nemtseva, N S Kudryasheva

Contents

I. Introduction	91
II. General characteristics of the bioluminescent reaction of bacteria	92
III. Formation of the emitter in the bioluminescent reaction	93
IV. Excitation of secondary emitters of bacterial bioluminescence	96
V. Conclusion	99

Abstract. The current state of the problem of formation of the electron-excited product in the chemiluminescent reaction that underlies the bacterial luminescence is analysed. Various schemes of chemical transformations capable of producing a bacterial bioluminescence emitter are presented. The problem of excitation of secondary emitters is considered; two possible mechanisms of their excitation are analysed. The bibliography includes 76 references.

I. Introduction

The bioluminescence, *i.e.* glowing of living organisms, is based on chemiluminescent reactions catalysed by biological catalysts, *i.e.*, enzymes that are called luciferases.^{1,2} Luminescence is inherent in more than 700 animal species, the best studied of which are bacteria, fireflies, marine coelenterates (jelly-fishes, hydranths, *etc.*), fishes, and so on.¹ Among the luminescent organisms, only bacteria emit light continuously. Being developed on organic remainders formed, they make a substantial contribution to the ocean glow. It is believed that by luminous bacteria attract more advanced species (for example, fish or shrimp) and thus they can populate their organs as symbiotes or parasites.¹ However, the signal function of bioluminescence may be secondary. Many researchers suggest an important metabolic role of light-producing systems,³ in particular, the relationship between the bioluminescent reactions and the antioxidant system of the organisms is considered.^{4–6} Presumably, bioluminescence is due to the hereditary change in the mechanisms that protect cells specially releasing reactive oxygen species for particular purposes from self-destruction.⁷ In addition, it has been suggested that luciferases and their substrates perform only metabolic functions in the cells, while emission of a light quantum is a ‘random’ process.^{4–6} According to a hypothesis, the bioluminescent reaction serves for hydrogen peroxide deactivation by the cells under

conditions of intensive energy metabolism.⁸ The excess energy is emitted as a light quantum; otherwise, its dissipation as heat or side chemical reactions would threaten the cell viability.

The substrates of bioluminescent reactions (traditionally called luciferins) present in various organisms differ in chemical structure and belong to different classes of organic compounds.^{1,9} The amino acid composition and structure of luciferases are also different even for related species of luminescent bacteria.¹⁰ Currently, about 30 bioluminescent reactions, *i.e.*, about 30 luciferin – luciferase combinations, are known.

Unlike most chemiluminescent processes in the inanimate nature, the luminescence of living organisms has a high intensity. This is due, first, to high rates of enzymatic chemiluminescent reactions, and second, to high quantum yields of the luminescence of the reaction products, *viz.*, emitters. Despite the fact that emitter molecules of various bioluminescent organisms belong to different classes of chemical compounds, they bear similarity in the electronic structure: they belong to the same spectral luminescent group in the classification of molecules according to spectral luminescence properties.¹¹ The molecules of this group are characterised by high quantum yields of $\pi\pi^*$ fluorescence and high efficiency of intramolecular relaxation of energy from upper excited states.

In addition, certain contribution to the high bioluminescence yields (the number of quanta per reaction event) is made by the protein environment of the bioluminescence emitters, which protects them from energy transfer and transformation processes competing with light emission. In this case, the protein can act as a matrix that ensures rigid fixation of the fluorophore. In some bioluminescent reactions, the yields of bioluminescence are close to unity.^{2,9}

High efficiency of formation of the light quantum distinguishes bioluminescence from another type of biological glow, namely, weak and ultraweak chemiluminescence, which always accompanies the vital activity of an organism. In the case of ultraweak luminescence of animal tissues, photons are usually formed as by-products of free radical autoxidation of unsaturated fatty acids.¹² In addition, bioluminescence usually performs a definite biological function (*e.g.*, attracts a partner or deters beasts from prey) and in this sense, the light quantum is physiologically the main reaction product.

A common feature of all biological light emitting reactions is that molecular oxygen is always a reaction component.

The luminescence of bacteria has been attracting the attention of researchers for four decades; in some aspects, this is one of the best studied bioluminescent processes.^{2,13} This, however, does not refer to the chemical mechanism of formation of the electron-

E V Nemtseva Department of Physics, Krasnoyarsk State University, prosp. Svobodnyi 79, 660041 Krasnoyarsk, Russian Federation.
Fax (7-3912) 44 87 81, tel. (7-3912) 44 08 41,
e-mail: NEV@lan.krasu.ru

N S Kudryasheva Institute of Biophysics, Siberian Branch of the Russian Academy of Sciences, Akademgorodok, 660036 Krasnoyarsk, Russian Federation. Fax (7-3912) 43 34 00, tel. (7-3912) 49 42 42,
e-mail: kudr@ibp.ru

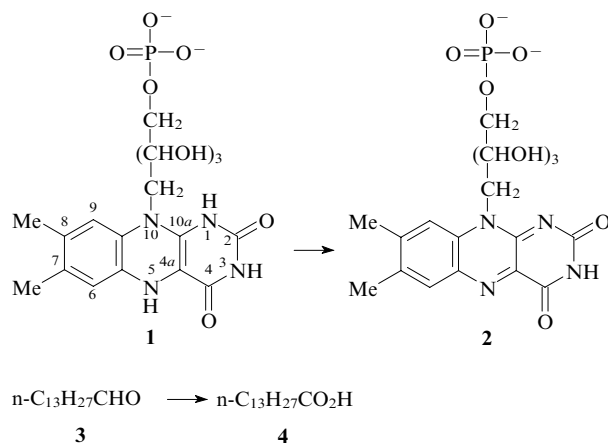
Received 25 May 2006

Uspekhi Khimii 76 (1) 101–112 (2007); translated by Z P Bobkova

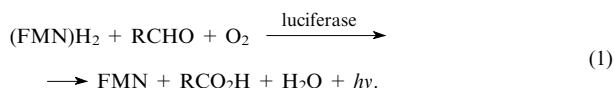
excited product in the bioluminescent reaction; this question still remains open and arouses the interest of chemists and physicists who study chemiluminescence. Throughout the history of investigations of bacterial luminescence, a dozen of possible routes for the excitation of chemiluminescence in the bacterial luciferase-catalysed reaction have been proposed. This review gives comparative analysis of the main excitation mechanisms in the bioluminescent reaction of bacteria.

II. General characteristics of the bioluminescent reaction of bacteria

It has been found long ago¹³ that the chemical grounds of bacterial luminescence include the enzymatic oxidation of the reduced flavin mononucleotide [(FMN)H₂, **1**] to flavin mononucleotide (FMN, **2**) and oxidation of long-chain aldehyde **3** to myristic acid (**4**) with atmospheric oxygen.



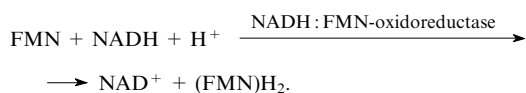
The overall reaction can be written as follows:



The bacterial luciferase is a heterodimer with a molecular mass of ~80 kDa. The components of the bioluminescent reaction can also react without an enzyme but the efficiency of chemiluminescence in this process is 10 orders of magnitude lower.² From this standpoint, bacterial luciferase is considered to be the most catalytically active known enzyme.

The heat of this reaction is 110 kcal mol⁻¹; this comprises the heats of oxidation of (FMN)H₂ (40 kcal mol⁻¹) and the aldehyde (70 kcal mol⁻¹).⁷ The overall heat of the reaction is greater than the energy of the bioluminescence quantum equal to ~60 kcal mol⁻¹. However, it can be seen that the oxidation energy of only (FMN)H₂ does not suffice for the observed light quantum emission.

It is noteworthy that none of the starting reactants of the discussed reaction can exist in a bacterial cell in the free state, in particular, (FMN)H₂ (**1**) is rapidly autoxidised, while aldehyde **3** is a poison and is not produced by organisms. Therefore, bacteria have special enzyme systems that facilitate the reduction of FMN (**2**) and carboxylic acid **4** only for the purpose of bioluminescence. The reduction of FMN in bacteria is believed to be catalysed by NADH:FMN-oxidoreductase (NADH is the reduced form of nicotinamide adenine dinucleotide):

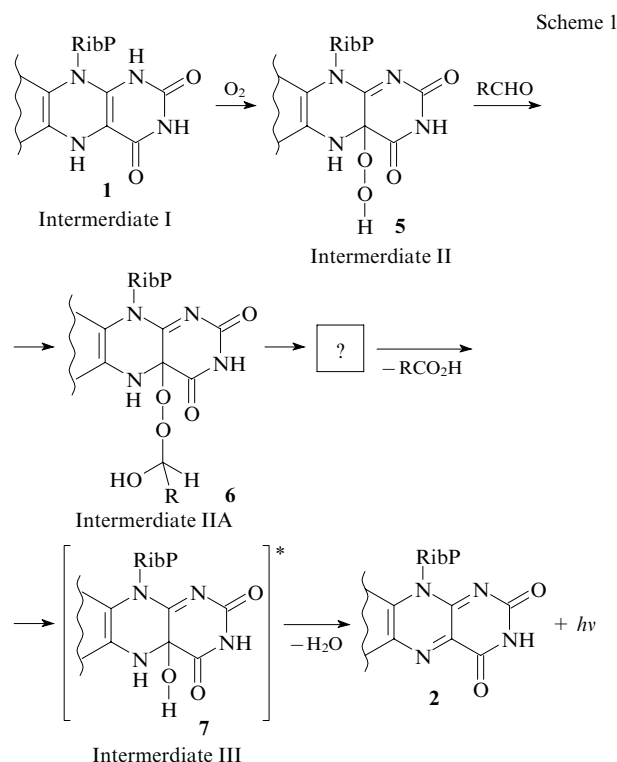


The question of the transfer mechanism of the reduced flavin mononucleotide between the oxidoreductase and bacterial luciferase still remains open.

There is indirect evidence for both the independent operation of these enzymes¹⁴ and the formation of a strong complex between them.^{15,16} This problem has been studied in detail.¹⁶⁻¹⁸

Luciferases from various sources have different specificities with respect to the second substrate (aldehyde). The affinity of the aldehyde for luciferase is due to the hydrophobic interactions between the aliphatic fragment of the aldehyde and the hydrophobic groups of the enzyme. Therefore, as the length of the carbon chain in the aldehyde increases, the aldehyde becomes more strongly bound to luciferase.^{1,13} In addition, the length of the aliphatic chain determines the position of the aldehyde carbonyl group involved in the chemical rearrangements in the luciferase active site. Perhaps, this is why aldehydes with chains shorter than the octanal chain are not involved in the luminescent reaction. Tetradecanal (**3**) is considered to be the natural substrate of bacterial luciferase,¹⁹ because the enzymatic system that reduces a carboxylic acid for the purpose of bioluminescence is specific exactly toward myristic acid (**4**).²⁰

The general scheme of reactant transformation in the reaction catalysed by bacterial luciferase was proposed more than forty years ago²¹ and confirmed by subsequent investigations. According to this scheme, the reaction proceeds *via* three intermediate complexes (intermediates) formed by flavin derivatives with luciferase (Scheme 1). Complex I contains reduced flavin, (FMN)H₂, complex II, flavin hydroperoxide and complex IIA, flavin peroxyhemiacetal (the numbers **1**, **2**, and **5**–**7** refer to the proper substrates rather than to their complexes). The existence of intermediates I and II was proved by NMR spectroscopy.²² The formation of intermediate IIA has not been proven experimentally as yet, but is recognised as a necessary step of the reaction.⁹ It was shown by NMR spectroscopy that the major chemical transformations during the reaction affect the C(4a) atom of the FMN isoalloxazine fragment.²² The results of these studies made it possible to compose the sequence of chemical transformations of the reduced flavin mononucleotide in the active site of bacterial luciferase (see Scheme 1) (this and subsequent schemes show only the part of flavin that is involved in transformations).



Here and below, RibP = CH₂(CHOH)₃CH₂OP(O)(OH)₂.

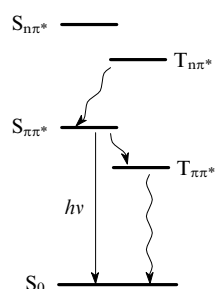
There is still no unified opinion concerning the mechanism of transformation of intermediate IIA [5-hydroxyflavin mononucleotide 4*a*-peroxyhemiacetal (**6**) bonded to luciferase] into the excited emitter. This step, designated by the interrogation mark in Scheme 1, may comprise several steps. The problem of identification of the structure of the emitting chromophore (emitter) has not been completely solved either. It has been accepted by most researchers that luciferase-bound 4*a*-hydroxy-5-hydroxyflavin mononucleotide (**7**) acts as the bacterial bioluminescence emitter. We will call this complex intermediate III. The photoluminescence spectrum of compound **7** (in the bound state) is similar to the emission spectrum recorded during the bioluminescent reaction. The problem of formation of the emitter is considered in more detail in Section III.

The key steps of the bacterial bioluminescent reaction are as follows.^{12, 23}

1. Formation of intermediates I, II and IIA [the energy range of the possible excited states of intermediates is approximately 260–390 kJ mol⁻¹ (21 700–32 700 cm⁻¹)].
2. Elementary excitation event in which the intermediate IIA is converted into emitter P* (intermediate III).
3. Light emission step P* → P + *hν*.

The optical properties of the reactants deserve attention. The spectrum of bacterial bioluminescence is a nearly symmetrical Gaussian distribution over the frequency scale with a peak at a wavelength of ~490 nm. The position of the peak does not depend on the acidity or temperature of the reaction mixture. The bioluminescence yield in this reaction ranged from 0.1 to 0.3 under optimal conditions, depending on the luciferase and aldehyde types.² According to NMR studies,²² the reduced flavin, (FMN)H₂ (**1**), is bound to luciferase as the (FMN)H⁻ anion. The absorption spectra of intermediates I, II, IIA and III differ little from one another and have a peak at 380 nm characteristic of all hydroflavins.^{2, 21} Among these intermediates, noticeable fluorescence (with a peak at ~490 nm) is observed only for luciferase-bound hydroxyflavin **7**.

The emitter of bacterial bioluminescence **7** refers to group V of the classification of molecules in terms of their spectral luminescence properties.¹¹ This group includes all aromatic heterocyclic compounds characterised by high quantum yields of fluorescence. The energy levels of the electron-excited states of the molecules of this group, taking into account the orbital nature and multiplicity, can be represented as follows:



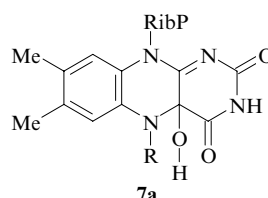
These molecules have upper excited states of the $n\pi^*$ type and undergo effective conversion of the excitation into the fluorescent $S_{\pi\pi^*}$ state from the $T_{\pi\pi^*}$ and $S_{n\pi^*}$ states.²⁴

As noted above, an interesting fact is that the emitters of bioluminescent reactions of other organisms (for example, glow-worms and jelly-fishes) also belong to group V of the spectral-luminescent classification, although the chemical structures of the emitters differ from that of the bacterial emitter.

Thus, the bioluminescent reaction of bacteria is an efficient chemiluminescent process which passes, like most known liquid-phase chemiluminescent reactions, through the formation and decomposition of organic peroxides. However, this reaction is still an exception, because no other efficient chemiluminescent processes involving hydroperoxides (such as derivative **5**) have been found as yet.⁹

III. Formation of the emitter in the bioluminescent reaction

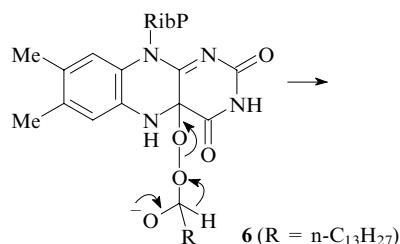
Kurfurst and Hastings²⁵ identified and characterised the emitting intermediate of reaction (1). While monitoring both the variation of the absorption and bioluminescence intensity during the reaction of intermediate II [luciferase complex with 4*a*-hydroperoxy-5-hydroxyflavin mononucleotide (**5**)] with decanal, the researchers detected the formation of two forms of enzyme-bound flavin. The greater part of bound flavin was FMN (**2**) responsible for characteristic absorption peaks at 370 and 440 nm and a fluorescence maximum at 530 nm. The second form of the enzyme complex with flavin exhibited an absorption maximum at 360 nm and a fluorescence maximum at 490 nm and was identified as the intermediate responsible for bioluminescence. Based on the spectral-luminescent characteristics, the researchers postulated that the fluorophore of this intermediate has the structure of 4*a*-hydroxyflavin **7**. It was found that the emitting intermediate has a relatively short lifetime (7 min at 9 °C) and its fluorophore is readily oxidised to FMN (**2**) by dissolved oxygen (the activation energy for this process equals 83 kJ mol⁻¹).²⁶ The ultimate identification of 4*a*-hydroxyflavin **7** as an emitting fluorophore (*i.e.*, emitter) is hampered by the fact that this compound has not yet been synthesised in a stable form, which is required to describe comprehensively its spectral-luminescent properties. The studied stable analogues of this compound, even those having suitable absorption spectra, exhibit very weak luminescence and provide much lower yields in chemiluminescent reactions (10⁻⁴–10⁻⁷).^{27, 28} Only recently was a paper published describing a model derivative of flavin with acceptable luminescent characteristics.²⁹ The authors studied binding to bacterial luciferase and fluorescence quantum yields for 5-decyl-4*a*-hydroxyflavin mononucleotide (**7a**). It was found that this compound having weak fluorescence in the free state provided a fluorescence quantum yield of 0.08 (this makes about 50% of the yield of bacterial bioluminescence) and a maximum intensity at 440 nm when bound to bacterial luciferase. In the opinion of the researchers cited, this fact confirms the identity of 4*a*-hydroxyflavin **7** and the natural bacterial bioluminescence emitter.



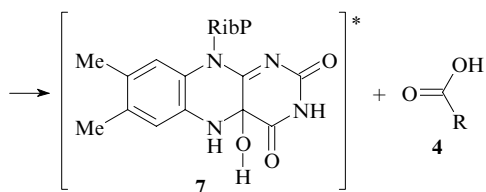
R = n-C₁₀H₂₁.

Of the multitude of mechanisms of excitation of the bacterial bioluminescence emitter proposed to date, six main mechanisms discussed below are most interesting from our standpoint.

The first mechanism was proposed rather long ago by Eberhard and Hastings.³⁰ Having postulated the key steps of reaction (1), they suggested that flavin peroxyhemiacetal **6** incorporated in intermediate IIA undergoes the Baeyer–Villiger rearrangement to give directly carboxylic acid **4** and excited hydroxyflavin **7**.



6 (R = n-C₁₃H₂₇)



An objection to this hypothesis is the fact that in chemical reactions, the Baeyer–Villiger rearrangement does not give electron-excited products.³¹

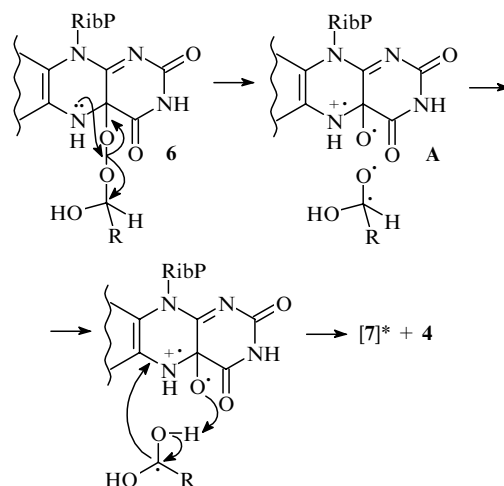
Subsequently, Kosower proposed another route to the bioluminescence emitter.³² It is worth noting that this mechanism is the first attempt to rationalise the excitation process based on analysis of elementary physicochemical processes. According to this hypothesis (Scheme 2), the excited state results from dissociative electron transfer from the flavin semiquinone radical **8a**. The peroxide radical anion $\text{RCH}(\text{O}_2)\text{O}^{\cdot-}$ formed after the superoxide attack abstracts a hydrogen atom from the luciferase SH group; this is followed by cleavage of the C–H bond in aldehyde to give protonated flavin mononucleotide **8b** in the excited state, which acts as the emitter.

Three critical remarks are pertinent as regards the above mechanism. First, this hypothesis is considered doubtful because it implies the occurrence of free radical steps in this reaction, which have not yet been detected by EPR.³³ (However, this may be due to limitations of the method.) Second, this mechanism implies involvement of the enzyme mercapto group in the process. Indeed, it has now been found³⁴ that the active site of the bacterial luciferase contains a cysteine residue Cys106, which could theoretically provide the SH group for the reaction with the peroxy radical anion $\text{RCH}(\text{O}_2)\text{O}^{\cdot-}$. However, the subsequent studies showed that this amino acid residue is not involved in the bioluminescent process, because its replacement by serine, alanine or valine does not result in the loss of bioluminescent activity of the enzyme.³⁵ It was found that the SH group of the Cys106 residue influences the aldehyde binding and the stability of intermediate IIA.³⁶ Third, an analogue of reduced flavin has been synthesised that cannot form the *N*(1)-protonated form [1-deaza-(FMN) H_2] but is nevertheless involved in the bacterial luciferase-catalysed reaction with emission of a light quantum.³⁷

The mechanism proposed by Kosower can be criticised regarding several points; however, its main value is that the

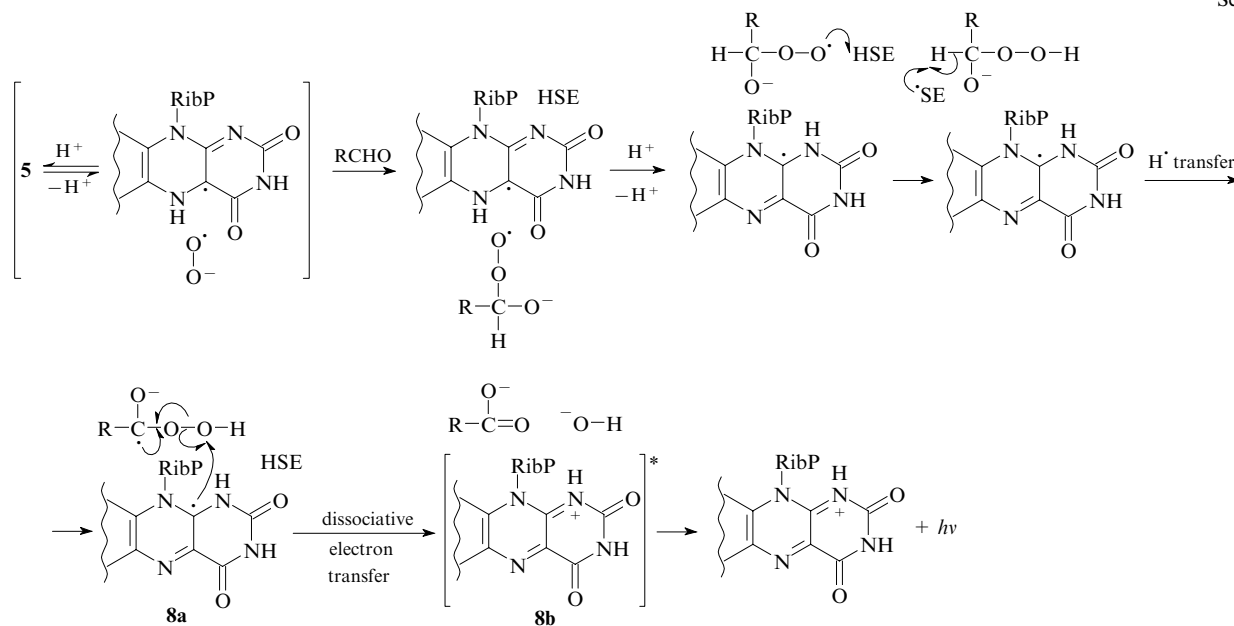
excitation of molecules during bioluminescence was related for the first time to dissociative electron transfer, *viz.*, one of the key probable mechanisms of chemiluminescence.

After the discovery³⁸ of chemically initiated electron exchange luminescence (CIEEL) as a mechanism of chemiluminescent reactions, Mager and Addink attempted³⁹ to adopt this mechanism to bacterial bioluminescence. The CIEEL process typical of the chemiluminescence of some peroxides implies the following steps: (i) the reaction of peroxide with an electron donor and the formation of a radical ion pair, (ii) the transformation of the radical anion into the carboxyl radical and the reverse electron transfer to give the excited fluorophore. According to the Mager and Addink concept,³⁹ the formation of flavin peroxyhemiacetal **6** within intermediate IIA is followed by intramolecular single-electron rearrangement to give hydroxyflavin radical cation **A**. This rearrangement includes the transfer of an electron from the *N*(5) atom of flavin to the antibonding orbital of the peroxide fragment and the subsequent localisation of this electron on an oxygen atom accompanied by simultaneous homolytic cleavage of the peroxide bond.



Presumably, radical cation **A** is a key intermediate in the reverse electron transfer giving rise to either excited hydroxyflavin **7** or excited carboxylic acid **4**. The existence of 4*a*-hydroxyflavin

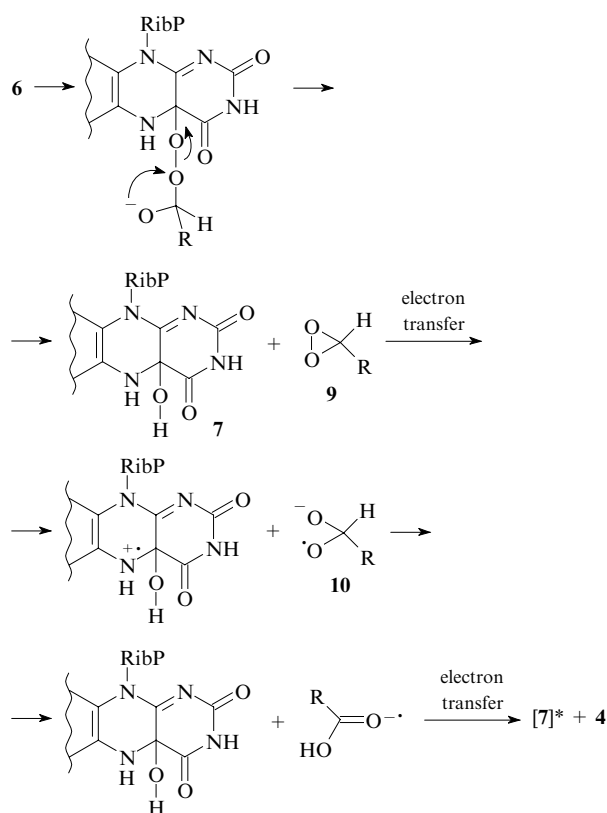
Scheme 2



HSE is luciferase.

radical cations structurally related to radical **A** has been shown using electrochemistry and radiolysis of model systems.⁴⁰ The efficiency of this reaction is controlled, first of all, by the single-electron transfer rate. On this basis, numerous attempts to verify this hypothesis using modified flavins with different redox properties have been undertaken. Eckstein *et al.*⁴¹ generalised the results of these studies. The kinetic parameters of bioluminescence for the reaction with FMN analogues having different substituents at C(8) were measured. An inverse correlation has been found between the rate constant for the first-order reaction and the single-electron redox potential of FMN analogues. In the researchers' opinion, this means that in the rate-limiting step the flavin moiety of the complex loses the negative charge. This result is consistent with the intramolecular CIEEL mechanism for the bacterial luciferase-catalysed reaction. The Baeyer–Villiger type rearrangement of the intermediates implies an inverse dependence of the rate on the redox potential of flavins. Nevertheless, McCapra criticised⁴² the study by Eckstein *et al.*⁴¹ He noted that the obtained dependences were due to the shift of the equilibrium between flavin derivatives **6** and **7**; it was concluded that no evidence for preference of the CIEEL mechanism for the bacterial luciferase reaction is currently available.

Yet another line of research in the studies of the mechanism of bacterial bioluminescence has been pursued by Raushel and Baldwin.⁴³ They were the first to propose⁴³ the 'dioxirane' mechanism of the bioluminescent reaction catalysed by bacterial luciferase. According to their hypothesis, instead of elimination of the α -proton from the carbonyl carbon of the aldehyde (initiating the Baeyer–Villiger rearrangement), the formation of flavin peroxyhemiacetal **6** is followed by an attack by the aldehyde oxygen atom on the peroxide bond, resulting in its cleavage to give 4*a*-hydroxyflavin **7** and dioxirane **9**.



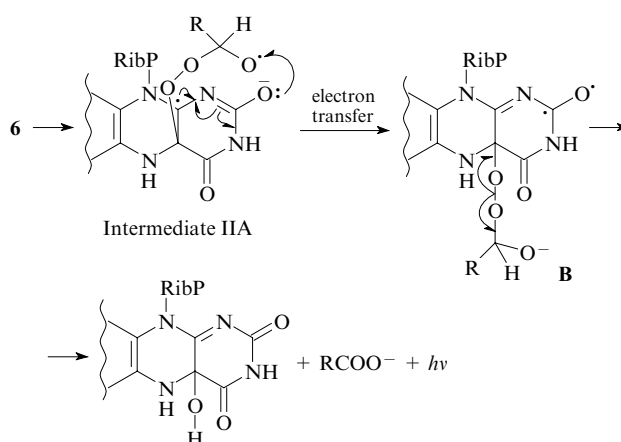
The formation of dioxirane is the key point of this hypothesis. There are two possible ways of dioxirane decomposition. First, dioxiranes can undergo homolytic cleavage of the peroxide bond to give radical anion **10**, which rearranges to give carboxylic acid (in either singlet or triplet excited state). This pathway bears direct analogy with decomposition of dioxetanes. Hydroxyflavin **7** is this type of a fluorophore, which can accept the electron excitation

energy from both triplet and singlet states of the dioxirane decomposition product. Second, the excited fluorophore can be formed *via* CIEEL in which dioxirane accepts an electron from fluorophore thus forming a radical ion pair. The subsequent transformation of the dioxirane radical anion into the carboxyl radical and the reverse electron transfer give the electron-excited fluorophore. Both the first and second route of dioxirane decomposition release sufficient energy for occupation of the excited states capable of emitting a photon upon deactivation, even in the blue region.

The Raushel and Baldwin's research group have studied the isotope effect of deuterated aldehyde on the rate of the bioluminescent reaction under various conditions.⁴⁴ This gave a relatively low but reliable k_H/k_D value in the range of 1.5–1.9, which is consistent with the theoretical calculations of the same researchers carried out with the assumption of intermediate formation of dioxiranes.

However, there are some serious objections to the formation of dioxiranes in the bacterial luciferase reaction, in particular, those stated by McCapra.⁹ First, no cases of dioxirane formation from an aldehyde are known to date.⁴⁵ Usually, the loss of a proton by an aldehyde results directly in carboxylic acid. Second, dioxiranes are highly reactive molecules,⁴⁵ and their formation would result in oxidation (injury) of the enzyme in the active site.

A distinctive feature of the next mechanism proposed by Kudryasheva *et al.*⁴⁶ is the occurrence of only intramolecular rearrangements during the formation of the excited structure of the bioluminescent emitter upon transition from structure **6** to **7**. The possibility of occupation of the upper excited states as the primary states of the bioluminescent emitter through the intramolecular electron transfer from the deprotonated ketoimide group to the peroxyhemiacetal fragment of intermediate **IIA** has been substantiated.⁴⁶



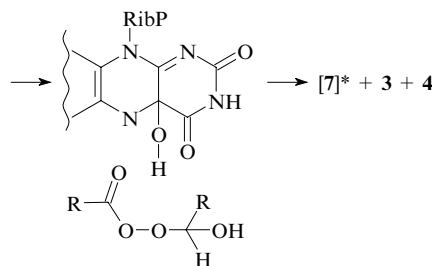
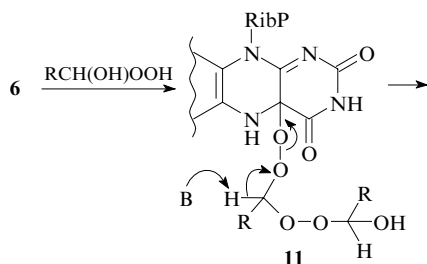
For flavins **5–7**, the $T_{n\pi^*}$ states are not the lowest excited states. The authors suggested that it is in this excited state (structure **B**) that flavin is formed in the bioluminescent reaction. According to this hypothesis, the formation of the excited carbonyl group is followed by intramolecular transfer of energy to the fluorescence state, $T_{n\pi^*} \rightarrow S_{n\pi^*}$, which is allowed as a transition between the levels of different orbital nature and multiplicity (the El-Sayed rule⁴⁷). The prohibition as regards multiplicity is eliminated due to spin–orbit coupling. This fact has been explained previously in a study by Plotnikov,²⁴ who calculated the rate constants for intramolecular transitions in this type of molecules; the resulting values were high, being equal to 10^{10} – 10^{11} s⁻¹. The importance of spin–orbit couplings in the physicochemical processes has been emphasised by Minaev *et al.*^{48–50} The efficiency of intramolecular transitions between the levels of different multiplicity was proved for many complex heteroaromatic compounds. Indeed, for a series of aromatic compounds including flavins, photoexcitation is known to be typically accompanied by reverse intersystem crossing from the

upper excited triplet states to the excited singlet states followed by fluorescence during transition to the ground state.⁵¹

The above-described relaxation process of the excitation in the bioluminescence emitter is associated with rearrangements of the electronic structure of the emitter molecule. The excitation located on the carbonyl group ($n\pi^*$ excitation) is delocalised throughout the molecule ($\pi\pi^*$ excitation). The process ends by the radiative transition $S_{\pi\pi^*} \rightarrow S_0$. It was noted²⁴ that the upper triplet states of these structures have too short lifetimes (10^{-10} – 10^{-11} s) to be detected by EPR. It is noteworthy that this course of bioluminescent reaction also predicts an inverse dependence of the rate constant for the first-order reaction on the single-electron oxidation potential of FMN analogues, which was mentioned above in the discussion of the CIEEL mechanism.³⁹ The data obtained using the FMN derivative in which oxygen at the C(2) atom was replaced by sulfur (2-thio-1,5-dihydroflavin mononucleotide) as the substrate of the bioluminescent reaction are also in line with this hypothesis.⁵² This is accompanied by a shift of the bioluminescence spectrum toward longer wavelengths (to 535 nm).

The fluorescence spectroscopy techniques have been used to carry out a number of studies aimed at detection of upper excited states of the bacterial bioluminescence emitter.^{53–55} In particular, the energy transfer to exogenous molecules introduced in the bioluminescent reaction has been attempted.^{53,54} Fluorescent aromatic molecules with energies of the first singlet excited state in the range of 22 000–32 000 cm^{-1} (i.e., higher than the analogous energy of the emitter molecule) have been used as the exogenous molecules (potential acceptors of excitation energy). Note that the absorption spectra of the chosen molecules did not overlap with the bioluminescence spectrum. During the bioluminescent reaction in the presence of these compounds, their sensitised luminescence was observed as low-intensity bands in the short-wavelength region of the spectrum. This result was attributed to non-radiative energy transfer from the upper electron-excited states of the emitter to the levels of these exogenous molecules, probably, by the exchange-resonance (collision) mechanism. Since the sensitised luminescence was detected only for compounds with an energy of the fluorescent state of not more than 26 000 cm^{-1} , this energy was taken as the characteristics of the upper electron-excited state of the bacterial bioluminescence emitter.⁵⁴ A study of the fluorescence anisotropy decay of the acceptor molecules in the presence of bacterial luciferase proved the possibility of hydrophobic binding of acceptor molecules to luciferase, and, hence, these molecules can approach the emitter to distances appropriate for energy transfer by the exchange mechanism.⁵⁵

The last mechanism of bacterial bioluminescence to be mentioned was proposed by McCapra.⁹ He considered the following advantages of this mechanism over all other mechanisms: (i) this mechanism is consistent with the isotope effect data⁴⁴ and with experimental results obtained by variation of substituents;⁴¹ (ii) this mechanism has a chemiluminescent analogy, namely, the reaction of peroxy esters with fluorescent compounds. McCapra postulated that the formation of intermediate IIA in the bacterial luciferase reaction is followed by the addition of hydrogen peroxide and second aldehyde molecule to the peroxyhemiacetal fragment of the complex.⁹



B is a base.

The resulting adduct **11** decomposes to hydroxyflavin and peroxy ester. The next step involves decomposition of the ester in the presence of fluorescent compound (hydroxyflavin) to give the excited molecules of the latter. This reaction route is confirmed by the detected enhancement of bioluminescence upon the addition of hydrogen peroxide.⁵⁶ The spontaneous formation of H_2O_2 adduct with two aldehyde molecules is also a proven fact.⁵⁶ The McCapra scheme proposed for bacterial bioluminescence is rather original and substantiated; however, as the author himself admits, this does not explain the key step, viz., the formation of the emitter, because the mechanism of chemiluminescence of peroxy esters has not been ultimately established as yet.

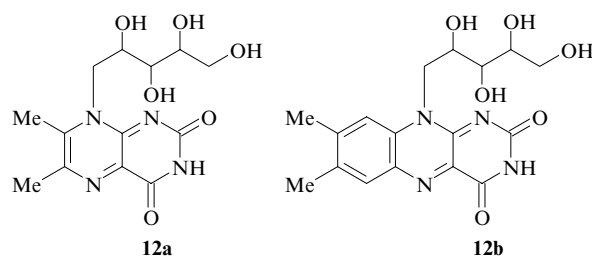
Thus, the question of the excitation mechanism of the molecules in the reaction catalysed by bacterial luciferase is still debated. The proposed schemes are diverse and cover almost all mechanisms currently applied to liquid-phase chemiluminescent reactions. However, as some researchers remark, none of the proposed reaction mechanisms is consistent with the whole set of experimental data accumulated throughout a five-decade history of the studies of bioluminescence.

IV. Excitation of secondary emitters of bacterial bioluminescence

1. Characteristics of the fluorescent proteins, secondary emitters of luminescent bacteria

The fact that bacterial luminescence is based on reaction (1) was established by 1965. However, the difference between the spectral characteristics of bioluminescence of the bacteria themselves (bioluminescence *in vivo*) and luminescence in the reactions of the reagents isolated from them (bioluminescence *in vitro*) has remained uninterpreted for many years. The position of the spectral peaks of bioluminescent reactions depends on the luciferase type but is confined within the range of 487–505 nm. Meanwhile, the bioluminescence maxima of living bacteria differ much more appreciably. Indeed, some bright strains of luminescent bacteria of the *Photobacterium* genus emit light with a maximum at 475 nm,¹³ while the bioluminescence of the Y1-strain of *Vibrio fischeri* discovered in the mid-1970s has a maximum at 545 nm.⁵⁷ It has now been proven that the reason for the change in the spectral composition of the above-mentioned bacterial emission is the presence of specific fluorescent proteins functioning as bioluminescence emitters, i.e., in these cases, indirect or sensitised chemiluminescence takes place.

The fluorescent proteins of luminescent bacteria are protein complexes with low-molecular fluorophores capable of fluorescing in the visible spectral region. A fluorescent protein was isolated from the bacteria *Photobacterium*; this protein was called the lumazine protein (LumP), as its fluorophore is represented by 6,7-dimethyl-8-(1-D-ribityl)lumazine (**12a**).⁵⁸ The yellow green strain of *V. fischeri* was found to contain^{59,60} the so-called yellow fluorescent protein (YFP) with a similar mass and, as has been found later,^{61,62} with a primary structure also similar to that of LumP. The YFP fluorophore is represented by FMN (**2**) or riboflavin (**12b**).⁶³



The key characteristics of these fluorescent proteins are given in Table 1.

To avoid confusion, we will designate the protein parts of LumP and YFP, which remain after removal of the fluorophore (this is called apoprotein), by LumP_A and YFP_A, respectively. The proteins LumP_A and YFP_A are notable by the fact that, unlike most other proteins, they do not quench the fluorescence of flavin bound to them.⁶⁴ On binding to LumP_A and YFP_A, the fluorescence maxima of their natural fluorophores shift to opposite directions (see Table 1): a hypsochromic shift is observed for lumazine **12a** and a bathochromic shift is observed for flavin **2**. However, both these facts indicate a high polarity of the micro-environment of the above fluorophores in the binding site of the protein (since it is known that with a decrease in the solvent polarity, the peak of flavin fluorescence shifts to shorter wavelengths and the peak of lumazine luminescence shifts to longer wavelengths).^{2, 64}

It was found that in the presence of micromolar concentrations of LumP or YFP, the following effects can be observed depending on the type of luciferase, the length of the aldehyde carbon chain and the source of the fluorescent protein: (i) a shift of the emission peak (hypsochromic in the presence of LumP or bathochromic in the presence of YFP); (ii) an increase in the emission intensity (up to a threefold in the presence of LumP and up to tenfold in the presence of YFP).² The mechanisms that underlie these effects are considered in more detail below.

Since the effect of fluorescent proteins on the characteristics of the bacterial bioluminescent reaction starts to be observed at low effective concentrations, they probably (or even obviously) form complexes with the reaction intermediates. It was shown by fluorescent spectroscopy and chromatography that LumP and YFP form 1 : 1 complexes with intermediates II and III (but not with free luciferase).^{65, 66} The lack of interaction with luciferase looks reasonable, because otherwise, the addition of the fluorescent protein would prevent the substrates of the bioluminescent reaction (mainly reduced flavin **1**) from accessing the active site of this enzyme. The binding constant of intermediate III with the YFP determined by fluorescent titration is equal to $7 \times 10^{-7} \text{ mol litre}^{-1}$ (0 °C), which is comparable with the effective concentration at which the effect of this protein on the bioluminescent reaction starts to be observed.⁶⁶

A study of the kinetics of bioluminescent reactions involving LumP and YFP has shown that an important role in the formation of protein complexes is played by aliphatic components (aldehydes, carboxylic acids, alcohols).⁶⁷ In the absence of aliphatic components, no reaction was detected between the proteins.

2. The mechanism of the change in the spectral composition of bioluminescence by fluorescent proteins

Comparison of the changed patterns of the bioluminescence spectra with the fluorescence spectra of LumP and YFP on photoexcitation indicates unambiguously that these proteins are involved in the light emission event resulting from the reaction. The problem of the excitation mechanism of the fluorescent proteins upon their introduction into reaction (1) is still debated. A non-radiative inductive resonance energy transfer (IRET) from the primary emitter due to weak dipole–dipole interaction could be the simplest and most attractive mechanism responsible for the excitation of secondary emitters. The rate constant for this transition k_{ET} is determined by the Förster equation:

$$k_{\text{ET}} = A Q_D k^2 \tau^{-1} R^{-6} J,$$

Table 1. Comparative characteristics of fluorescent proteins of luminescent bacteria.

Characteristics	Values for proteins ^a	
	LumP	YFP ^b
Molecular mass /kDa	21	24
Fluorophore	Lumazine derivative 12a	FMN
Binding constant of the fluorophore with the protein /mol litre ⁻¹	1.6×10^{-8} (20 °C, pH 7)	1×10^{-8} (4 °C, pH 7)
Long-wavelength absorption maximum of the fluorophore in the free/bound state /nm	406/417	445/470
Molar extinction coefficient of the fluorophore in the free/bound state /litre mol ⁻¹ cm ⁻¹	10 300 (406 nm)/10 300 (414 nm)	12 500 (445 nm)/12 500 (460 nm)
Fluorescence spectral maximum of the fluorophore in the free/bound state /nm	490/475 (water)	525/538 (water)
Fluorescence quantum yield of the fluorophore in the free/bound state	0.45 (water, 22 °C)/0.58 (water, 20 °C)	0.26 (water, 22 °C)/—
Lifetime of the fluorescent state of the fluorophore in the free/bound state /ns	8.9 (20 °C)/1.7 (2 °C)	4.7 (20 °C)/5.5 (2 °C)
Rotational correlation time ^c of the fluorophore in the free/bound state /ns	0.15 (2 °C)/20 (0 °C)	0.2 (0 °C)/20 (0 °C)
Overlap integral of the absorption spectrum of the fluorescent protein with the bioluminescence spectrum /cm ³ litre mol ⁻¹	2×10^{-15}	1.54×10^{-14}

^a The conditions of determination of the parameters are given in parentheses. ^b Characteristics are given for the best studied YFP form with FMN (**2**) as the fluorophore. ^c The rotational correlation time is the characteristic time of the exponential decay of the fluorescence anisotropy of the molecule upon pulse excitation.

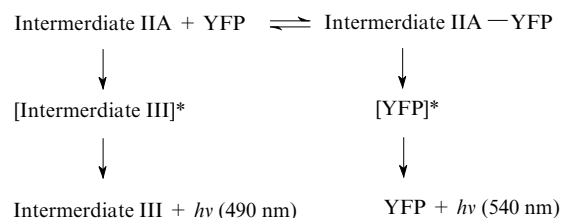
where A is a constant, Q_D is the quantum yield of the donor fluorescence, k^2 is the orientation factor, τ is the lifetime of the fluorescent state of the donor in the absence of the acceptor, R is the distance between the energy donor and acceptor, J is the overlap integral of the absorption spectrum of the acceptor and the emission spectrum of the donor. The acceptor properties are characterised by three quantities in this formula: the distance R , the orientation factor k^2 and overlap integral J . The values of the first two can be such that they would favour a high rate of the IRET from hydroxyflavin **7** to fluorescent proteins: the proven existence of complexes formed by intermediate III with LumP and YFP can ensure a proximate arrangement and a favourable orientation of the fluorophores. The last factor, *viz.*, the overlap integral of the spectra, is high for YFP and low for LumP (see Table 1).

It is the small overlap integral of the absorption spectrum of LumP with the bioluminescence spectrum that draws objections against effective accepting of energy by this protein according to the inductive resonance mechanism. In addition, the fluorescence maximum of hydroxyflavin **7** is at 495 nm, while the maximum of the absorption spectrum of LumP is at ~ 420 nm, and the hypothetical energy transfer should be followed by an increase in the emitted quantum energy, which is not observed in the photoluminescence of dyes in solutions. A great contribution to the investigation of this problem was made by Lee's research group.^{2,67–71} Initially, Lee and co-workers attributed⁶⁹ the effect of the lumazine protein to the existence of a high-energy precursor of the bacterial bioluminescence emitter with an excited state energy of $\sim 25\,000\text{ cm}^{-1}$. They assumed that this precursor transmits the electron excitation energy to either hydroxyflavin or the lumazine protein. However, subsequently, Lee refuted the high-energy precursor concept and attributed^{2,64} the efficiency of IRET to a special orientation of the donor and the acceptor with a small overlap integral of the spectra. Fluorescence spectroscopy studies^{64,68} revealed the existence of a short-time component in the fluorescence anisotropy decay of intermediates II and III complexed with LumP (on excitation to the flavin absorption band at 370 nm). This fast decay of the anisotropy was attributed to the occurrence of the IRET from flavin, incorporated in the intermediates, to lumazine **12a**. The results were adequately described by a model in which the rate constant for the IRET varied from 4×10^8 to 10^9 s^{-1} (depending on the luciferase type and LumP source).^{65,68} Since the rate constant for the radiative transition of the primary emitter containing fluorophore **7** is 10^8 s^{-1} , it was concluded that the change of the spectral characteristics in the bioluminescent reaction in the presence of LumP can occur *via* the IRET. Lee's calculations⁶⁴ showed that a fixed distance of 1.5 nm and a favourable mutual orientation of flavin **7** and the lumazine fluorophore **12a** can make up for the small overlap integral of the spectra and account for the observed high efficiency of the 'anti-Stokes' migration of the excitation energy to LumP. Note that the spectral properties of the intermediate III – LumP donor–acceptor pair, namely, the close arrangement of the emission spectral peaks of the donor and the acceptor (490 and 475 nm, respectively), do not allow one to study the energy transfer by classical fluorescence spectroscopy methods. Usually, the energy transfer rate is determined from the change in the quantum yield of the donor in the presence of the acceptor (upon excitation to the donor absorption band).

Study of the energy transfer processes in the bioluminescent emitter – YFP system is easier than that for the LumP-containing system due to the large bathochromic shift between the emission peaks of the presumptive energy donor and acceptor. Hence, the emission bands of the donor and the acceptor can be effectively separated and the energy transfer rate can be measured more precisely from the change in the lifetime of the fluorescent state of the donor. This study has been carried out.⁶⁷ The rate constant for the IRET to the YFP ($4 \times 10^9\text{ s}^{-1}$) was found from the change in the rate constant for the fluorescence decay of intermediate III. Thus, it was found that the IRET rate for the YFP system is about

ten times as high as that for the LumP system.⁶⁰ The overlap integrals of the absorption spectrum with the bioluminescence spectra of LumP and YFP differ by a factor of 7.7. The authors⁶⁷ consider this to confirm the assumption that the secondary emitters are excited through weak dipole–dipole interaction according to the Förster (inductive resonance) mechanism.

The bioluminescence spectra in the presence of YFP consist of two bands: a strong yellow-green band with a peak at 540 nm and a weak blue band with a peak at 490 nm. For more detailed determination of the mechanism of formation of this spectrum, Eckstein *et al.*⁷² studied the kinetics of reaction (1) in the presence of YFP. They found a complex and, what is more important, different patterns of variation of the time decay rates for the 'blue' and 'yellow-green' bioluminescence components. In the researchers' opinion, this indicates that the classical non-radiative energy transfer alone cannot account for the effect of YFP on the bacterial luciferase-catalysed reaction. A scheme was proposed according to which YFP forms a complex with intermediate IIA, thus decreasing its lifetime. This complex decomposes to give excited YFP, while the 'blue' component of the bioluminescence is emitted only by non-bonded intermediate III.



This mechanism resembles the intermolecular activated chemiluminescence where the fluorophore catalyses decomposition of the peroxide through charge or electron transfer, thus passing to the excited state. The mathematical model constructed according to the proposed scheme described adequately the experimental data obtained for the kinetics of two bioluminescence components (for low YFP concentrations). As has already been noted, subsequent studies showed that, upon photoexcitation, the IRET from intermediate III to YFP in the complex is a very efficient process.⁶⁷ Its rate is more than an order of magnitude greater than the rate of the radiative transition for hydroxyflavin **7** in intermediate III. Therefore, this excitation pattern for the yellow-green bioluminescence in a system involving YFP should not be underestimated.

3. Change in the bioluminescence intensity in the presence of fluorescent proteins

As noted above, both natural bacterial fluorescent proteins (LumP and YFP) increase the bioluminescence intensity of reaction (1). However, these effects were found to be due to different mechanisms.

The addition of LumP to the bioluminescent reaction was found to increase the bioluminescence yield. The reason for this increase (trivial, in the opinion of some researchers^{2,67}) is as follows: the quantum yield of LumP fluorescence (0.58) is almost twice as high as that of luciferase-bound hydroxyflavin **7** (0.28–0.33). Therefore, the emission event is more efficient with LumP. We would like to note that this explanation is reasonable if the rate of energy transfer to LumP actually exceeds the rate of the intrinsic radiative transition in hydroxyflavin **7** by a large factor (4–10), as it was estimated in the works cited.^{65,68} Unfortunately, the spectroscopic properties of the intermediate III – LumP system preclude precise measurement of the energy transfer rate; hence, the explanation for the high efficiency of this transfer casts doubts due to the small overlap integral of the spectra.

The fluorescence quantum yields of YFP and hydroxyflavin **7** differ slightly; therefore, despite the known⁶⁷ high rate constant for the energy transfer in the YFP system, no increase in the total

number of the emitted quanta takes place in the reaction involving this secondary emitter.

The emission intensity of the bioluminescent reaction in the presence of YFP is controlled in a somewhat different way. It was found⁷³ that in the presence of this protein the rate of reaction (1) substantially increases. A unique feature of this system is that this effect is enhanced with a decrease in temperature. The highest efficiency of YFP defined as the ratio of the emission intensity at 540 nm (I_{540}) to the intensity at 490 nm (I_{490}) is observed at 4 °C. Some researchers argue⁷³ that this system is perhaps the only enzyme system having a negative temperature coefficient. The loss of YFP activity with the temperature rise cannot be attributed to dissociation of flavin and YFP_A alone (for example, on heating of the reaction mixture from 4 to 15 °C in the presence of 4×10^{-6} mol litre⁻¹ of YFP, only 15% of YFP molecules dissociate, while the I_{540}/I_{490} value decreases threefold). A change in the conformation of this protein on heating could be an additional factor contributing to YFP inactivation with the temperature rise, but this phenomenon has not found experimental proof or disproof. It is also of interest that not only the optimal reaction temperature but also the optimal length of the aldehyde carbon chain change in the presence of YFP.⁷⁴ The highest efficiency of YFP is attained in the reaction involving octanal, whereas in the absence of YFP, the highest intensity was observed for aliphatic aldehydes containing no less than 12 carbon atoms. This was attributed to the fact that the longest lifetime of intermediate IIA in reaction (1) is observed with octanal (compared with reactions involving other aldehydes). As a consequence, YFP has more opportunities to react with this intermediate and to 'switch' the reaction to the pathway leading to excitation of the 'yellow-green' chromophore.⁷⁴

The biological role of the secondary emitters of luminescent bacteria is not entirely clear. Most assumptions concerning this issue imply that the main function of bioluminescence is signalling. From this standpoint, the involvement of LumP in the light emission provides at least a gain in the luminescence intensity (due to the increase in the bioluminescence yield). And YFP allows bacteria to glow over a broad temperature range (from 5 to 25 °C). It is also assumed that the high luminescence intensity of 'yellow-green' bacteria at 4 °C (*i.e.*, at a temperature where their metabolic processes are retarded) makes them attractive symbionts for fishes or other organisms.⁷³

If the hypothesis of 'non-thermal energy discharge' in a bioluminescent process is taken as the basis,⁸ the possibility of changing the energy of the 'discharged' quantum in the presence of secondary emitters can be considered as an important adaptation feature of bacteria under conditions of variable amounts of energy entering the cell (for example, in the presence of different amounts of hydrogen peroxide).

To conclude this Section, we would like to note that any proposed scheme of the bioluminescent reaction should be consistent with the above-described effects produced by fluorescent proteins. This is especially true for the lumazine protein, as it gives rise to a hypsochromic shift of the bioluminescence spectrum. Of the six schemes presented in the previous Section, the last four schemes imply occupation of the electron-excited states of the secondary emitter, which can be represented by LumP. If the reaction follows the CIEEL mechanism, this may give excited carboxylic acid, which then functions as the energy donor for fluorescent molecules. Similarly, dioxirane decomposition can involve LumP and result in the excitation of the lumazine chromophore. According to the scheme proposed by Kudryashova *et al.*,⁴⁶ LumP is capable of accepting energy from highly excited levels of the hydroxyflavin intermediate. The reaction proposed by McCapra may also involve another fluorophore (apart from hydroxyflavin) in the step of peroxy ester decomposition followed by excitation of this fluorophore.

Thus, although the secondary emitters of bacterial bioluminescence (the lumazine and yellow fluorescent proteins) induce different changes in the spectral characteristics of the biolumines-

cent reaction, they still resemble each other in their properties: their proteins have similar structures and interact efficiently with the bioluminescent reaction intermediates, thus creating conditions for the excitation of the secondary fluorophore. The highly effective change in the spectra and bioluminescence intensity upon the addition of fluorescent proteins is due, first of all, to the formation of protein complexes. Therefore, their fluorophores occur in the vicinity of the luciferase active site, almost at the centre of events, and can be involved in some chemical steps of the process and the physical transfer of the excitation energy. To date, it can be stated that neither 'physical' nor 'chemical' way of excitation of secondary emitters can alone explain the whole set of effects of fluorescent proteins on the bacterial bioluminescence parameters. It is noteworthy that the uncertainty in the mechanism of energy transfer to secondary emitters is partly due to the uncertainty of the mechanism of the proper reaction catalysed by bacterial luciferase. Subsequent studies of the pathways leading to the primary emitter of bacterial bioluminescence would apparently make corrections in the proposed schemes of excitation of fluorescent proteins. Conversely, investigation of the interactions of the secondary bioluminescence emitters with the components of the main chemical process can, in the future, shed light on the mechanism of the bioluminescent reaction.

V. Conclusion

Bioluminescence is a unique natural phenomenon and an exceptionally convenient tool that can be used in various fields of human activities ranging from environmental monitoring and clinical analysis to investigations of gene expression and regulation.^{3,75} The transformation of the chemical reaction energy into light with a high quantum efficiency in bioluminescent reactions has always attracted the interest of scientists. By now, the sequences of formation of chemical intermediates have been established and the spectral and kinetic characteristics of bioluminescent reactions involving enzymes (luciferases) have been described. Genetic engineering works aimed at modification of luciferase are in progress.⁷⁶ However, since bioluminescence is traditionally a subject studied by biologists (physiologists, microbiologists and biochemists), the formation of excitation is the most debated issue. Solving this problem requires the use of results obtained in structural, luminescence and chemiluminescence studies based on analysis of elementary physicochemical processes. Thus classification of molecules in terms of their spectral luminescent properties developed in the 1970–1980s shows that the emitters of all bioluminescent organisms belong to the group of molecules characterised by high $\pi\pi^*$ -fluorescence quantum yields. The belonging of bioluminescence emitters to this group of compounds determines (together with enzymatic catalysis) the high bioluminescence intensity. In our opinion, study of the intramolecular energy transfer, the use of the theory of intermolecular migration of the excitation energy developed for solutions of fluorescent dyes and data for chemiluminescent oxidation reactions would allow researchers to achieve considerable insight in the processes giving electron-excited states of molecules upon bioluminescence.

This review was prepared with financial support of the Ministry of Education and Science of the Russian Federation and the American Civilian Research and Development Foundation (the Programme 'Fundamental Research and Higher Education', Grants RUX0-002-KR-06 and Y1-B-02-13), the Federal Central Science and Engineering Programme 'Studies and Projects along the Priority Lines of Science and Engineering' for the 2002–2006 (the Programme 'Scientific Research Carried out by Young Scientists', Grant 2006-RI-19.0/001/454), the Russian Academy of Sciences (the Programme 'Molecular Cell Biology', Grant 'Molecular Mechanisms of Formation of the Emitter in Bioluminescent Reactions of Various Organisms', 2005–2007) and the Krasnoyarsk Regional Science Foundation (Grant 15G120).

References

1. J W Hastings, in *Cell Physiology* (3rd Ed.) (Ed. N Sperelakis) (New York: Academic Press, 2001) p. 1115
2. J Lee, I B C Matheson, F Muller, D J O'Kane, J Vervoort, A J W G Visser, in *Chemistry and Biochemistry of Flavins and Flavoenzymes* Vol. 2 (Ed. F Muller) (Orlando, FL: CRC Press, 1991) p. 109
3. I I Gitel'zon, V A Kratasyuk, V N Lopatin, A D Aponasenko, V S Filimonov, V V Fishov, Z G Kholostova, N A Gaevskii, Yu S Grigor'ev, A A Tikhomirov *Ekologicheskaya Biofizika. Fotobiofizika Ekosistem* (Ecological Biophysics. Photobiophysics of Biosystems) (Moscow: Logos, 2002) Vol. 1
4. J F Rees, B de Wergifosse, O Noiset, M Dubuisson, B Janssens, E M Thompson *J. Exp. Biol.* **201** 1211 (1998)
5. H Watanabe, T Nagoshi, H Inaba *Biochim. Biophys. Acta* **1141** 297 (1993)
6. M P Barros, E J H Bechara *Free Radical Biol. Med.* **24** 767 (1998)
7. Yu A Labas, A V Gordeeva *Priroda* (2) 25 (2003)
8. V N Karnaukhov *Luminescentnyi Spektrol'nyi Analiz Kletki* (Luminescent Spectral Analysis of Cell) (Moscow: Nauka, 1978)
9. F McCapra *Methods Enzymol.* **305** 3 (2000)
10. B A Illarionov, M V Protopopova, V A Karginov, N P Mertvetsov, I I Gitel'zon *Bioorg. Khim.* **14** 412 (1988)^a
11. D N Shigorin, G A Val'kova, E A Gastilovich, V A Godik, G G Konoplev, M A Pak, A N Rodionova, N S Strokach *Elektronno-vozbuzhdennye Sostoyaniya Mnogoatomnykh Molekul* (Electron-excited States of Polyatomic Molecules) (Moscow: Nauka, 1993)
12. A I Zhuravlev, in *Biokhemiyluminesentsiya* (Biochemiluminescence) (Ed. A I Zhuravlev) (Moscow: Nauka, 1983) p. 3
13. I I Gitel'zon, E K Rodicheva, S E Medvedeva, G A Primakova, S I Bartsev, G A Kratasyuk, V N Petushkov, V V Mezhevikin, E S Vysotskii, V V Zavoruev, V A Kratasyuk *Svetyashchiesya Bakterii* (Luminescent Bacteria) (Novosibirsk: Nauka, 1984)
14. V N Petushkov, G A Kratasyuk, N S Rodionova, A M Fish, P I Belobrov *Biokhimiya* **49** 692 (1984)^b
15. T M Schmidt, K Kopecky, K H Neelson *Appl. Environ. Microbiol.* **55** 2607 (1989)
16. J C Low, S C Tu *Photochem. Photobiol.* **77** 446 (2003)
17. B F Lei, S C Tu *Biochemistry* **37** 14623 (1998)
18. C E Jeffers, S C Tu *Biochemistry* **40** 1749 (2001)
19. S Ulitzur, J W Hastings *Proc. Natl. Acad. Sci. USA*, **76** 265 (1979)
20. E A Meighen *FASEB J.* **7** 1016 (1993)
21. J W Hastings, Q H Gibson *J. Biol. Chem.* **238** 2537 (1963)
22. J Vervoort, F Muller, D J O'Kane, J Lee, A Bacher *Biochemistry* **25** 8067 (1986)
23. R F Vasil'ev *Izv. Akad. Nauk SSSR, Ser. Fiz.* **46** 323 (1982)^c
24. V G Plotnikov *Usp. Khim.* **49** 327 (1980) [*Russ. Chem. Rev.* **49** 172 (1980)]
25. M Kurfurst, S Ghisla, P Macheroux, J W Hastings, in *Flavins and Flavoproteins* (Eds R C Bray, P C Engel, S C Mayhew) (Berlin, New York: Walter de Gruyter, 1984) p. 657
26. I B C Matheson, J Lee *Photochem. Photobiol.* **38** 231 (1983)
27. H I X Mager, D Sazou, Y H Liu, S C Tu, K M Kadish *J. Am. Chem. Soc.* **110** 3759 (1988)
28. T W Kaaret, T C Bruice *Photochem. Photobiol.* **51** 629 (1990)
29. B F Lei, Q Z Ding, S C Tu *Biochemistry* **43** 15975 (2004)
30. A Eberhard, J W Hastings *Biochem. Biophys. Res. Commun.* **47** 348 (1972)
31. K-D Gundermann, F McCapra *Chemiluminescence in Organic Chemistry* (Berlin: Springer, 1987)
32. E M Kosower *Biochem. Biophys. Res. Commun.* **92** 356 (1980)
33. V N Petushkov *Biofizika* **30** 49 (1985)^d
34. A J Fischer, T B Thompson, J B Thoden, T O Baldwin, I Rayment *J. Biol. Chem.* **271** 21956 (1996)
35. H M Abu-Soud, A C Clark, W A Francisco, T O Baldwin, F M Raushel *J. Biol. Chem.* **268** 7699 (1993)
36. O Paquatte, S C Tu *Photochem. Photobiol.* **50** 817 (1989)
37. M Kurfurst, P Macheroux, S Ghisla, J W Hastings *Eur. J. Biochem.* **181** 453 (1989)
38. G B Schuster *Acc. Chem. Res.* **12** 366 (1979)
39. H I X Mager, R Addink, in *Flavins and Flavoproteins* (Eds R C Bray, P C Engel, S C Mayhew) (Berlin, New York: Walter de Gruyter, 1984) p. 37
40. H I X Mager, S C Tu *Photochem. Photobiol.* **62** 607 (1995)
41. J W Eckstein, J W Hastings, S Ghisla *Biochemistry* **32** 404 (1993)
42. F McCapra, in *Proceedings of the 9th International Symposium on Bioluminescence and Chemiluminescence. Bioluminescence and Chemiluminescence: Molecular Reporting with Photons, Woods Hole, MA, 1996* p. 7
43. F M Raushel, T O Baldwin *Biochem. Biophys. Res. Commun.* **164** 1137 (1989)
44. W A Francisco, H M Abu-Soud, A J DelMonte, D A Singleton, T O Baldwin, F M Raushel *Biochemistry* **37** 2596 (1998)
45. V P Kazakov, A I Voloshin, D V Kazakov *Usp. Khim.* **68** 283 (1999) [*Russ. Chem. Rev.* **68** 253 (1999)]
46. N S Kudryasheva, P I Belobrov, V A Kratasyuk, D N Shigorin *Dokl. Akad. Nauk SSSR* **321** 837 (1991)^e
47. M A El-Sayed *J. Chem. Phys.* **38** 2834 (1963)
48. B F Minaev, S Lunell *Z. Phys. Chem.* **182** 263 (1993)
49. B F Minaev, S Knuts, H Agren *Chem. Phys.* **181** 15 (1994)
50. S Knuts, B F Minaev, O Vahtras, H Agren *Int. J. Quantum Chem.* **55** 23 (1995)
51. V L Ermolaev *Usp. Khim.* **70** 539 (2001) [*Russ. Chem. Rev.* **70** 471 (2001)]
52. I B C Matheson, J Lee, F Muller *Proc. Natl. Acad. Sci. USA* **78** 948 (1981)
53. N S Kudryasheva, E V Nemtseva, Yu P Meshalkin, A G Szykh *Luminescence* **16** 243 (2001)
54. N S Kudryasheva, E V Nemtseva, A G Szykh, V A Kratasyuk, A J W G Visser *J. Photochem. Photobiol., B* **68** 88 (2002)
55. N S Kudryasheva, E V Nemtseva, A J W G Visser, A van Hoek *Luminescence* **18** 156 (2003)
56. H Watanabe, J W Hastings *J. Biochem. (Tokyo)* **101** 279 (1987)
57. E G Ruby, K H Neelson *Science* **196** 432 (1977)
58. D J O'Kane, J Lee *Biochemistry* **24** 1467 (1985)
59. P Macheroux, K U Schmidt, P Steinerstauch, S Ghisla, P Colepiccolo, R Buntic, J W Hastings *Biochem. Biophys. Res. Commun.* **146** 101 (1987)
60. K W Cho, P Colepiccolo, J W Hastings *Photochem. Photobiol.* **50** 671 (1989)
61. T O Baldwin, M L Treat, S C Daubner *Biochemistry* **29** 5509 (1990)
62. D J O'Kane, B Woodward, J Lee, D C Prasher *Proc. Natl. Acad. Sci. USA* **88** 1100 (1991)
63. V N Petushkov, B G Gibson, J Lee *Biophys. Biochem. Res. Commun.* **211** 774 (1995)
64. J Lee *Biophys. Chem.* **48** 149 (1993)
65. V N Petushkov, B G Gibson, J Lee *Biochemistry* **34** 3300 (1995)
66. V N Petushkov, B G Gibson, J Lee *Biochemistry* **35** 8413 (1996)
67. V N Petushkov, M Ketelaars, B G Gibson, J Lee *Biochemistry* **35** 12086 (1996)
68. J Lee, Y Wang, B G Gibson *Biochemistry* **30** 6825 (1991)
69. J Lee, Y Wang, B G Gibson *J. Fluorescence* **1** 23 (1991)
70. J Lee *Photochem. Photobiol.* **36** 689 (1982)
71. J Lee, Y Wang, B G Gibson *Anal. Biochem.* **185** 220 (1990)
72. J W Eckstein, K W Cho, P Colepiccolo, S Ghisla, J W Hastings, T Wilson *Proc. Natl. Acad. Sci. USA* **87** 1466 (1990)
73. G Sirokman, T Wilson, J W Hastings *Biochemistry* **34** 13074 (1995)
74. G Sirokman, J W Hastings *Photochem. Photobiol.* **66** 198 (1997)
75. A Roda, P Pasini, M Mirasoli, E Michellini, M Guardigli *Trends Biotechnol.* **22** 295 (2004)
76. A Tsuji, M Matsumoto, M Maeda, L J Kricka, P E Stanley (Eds) *Bioluminescence and Chemiluminescence: Progress and Perspectives. Proceedings of the 13th International Symposium on Bioluminescence and Chemiluminescence* (Singapore: World Sci. Publ., 2005)

^a — *Russ. J. Bioorg. Chem. (Engl. Transl.)*^b — *Biochemistry (Moscow) (Engl. Transl.)*^c — *Bull. Russ. Acad. Sci., Phys. (Engl. Transl.)*^d — *Biophysics (Engl. Transl.)*^e — *Dokl. Biochem. Biophys. (Moscow) (Engl. Transl.)*

Crystal chemistry and features of the structure formation of mercury oxo- and chalcahalides

S A Magarill, N V Pervukhina, S V Borisov, N A Pal'chik

Contents

I. Introduction	101
II. Mercury chalcahalides	102
III. Mercuric oxohalides	113
IV. Stable atomic groups (building blocks) in mercury compounds	116
V. The modular principle in the structure formation of mercury oxo- and chalcahalides	124
VI. Crystal chemical features of the MHgYX compounds (M = Cu or Ag; Y = S or Se; X = Cl, Br or I)	127
VII. Conclusion	129

Abstract. Characteristic features of the crystal structures of mercury oxohalides, chalcahalides and related compounds are surveyed. The structures of these compounds are described using both the traditional way and a modern approach based on the identification of stable building blocks coupled with the analysis of their packing. The crystallographic and crystal chemical data for the title compounds are given. The bibliography includes 123 references.

I. Introduction

Crystal chemistry of mercury compounds is unique being principally different from that of lighter neighbours of mercury in Group 12 of the Periodic system, *viz.*, Zn and Cd. In contrast to zinc and cadmium, the Hg^{2+} ions are capable of forming two linear shortened strong bonds that are prone to further association, in addition to ordinary tetrahedral bonds. The complexity and multiplicity of crystal chemistry of mercury compounds is also manifested in the co-existence of various combinations of ionic and covalent bonds in a mercury compound with various anions Y (N, O, S, Se or Te) and X (F, Cl, Br or I). Yet another characteristic feature consists of the frequently occurring short covalent bonds between mercury atoms giving rise to cluster-like polyatomic fragments, such as $[\text{Hg}_2]^{2+}$ dumbbells or $[\text{Hg}_3]^{4+}$ triangles (with the Hg–Hg bond lengths of 2.5–2.7 Å). There are a number of structures where mercury atoms form covalent bonds with other crystal chemically similar cations (*e.g.*, Ag, Pb and Cu) to generate, for instance, $[\text{Ag}_3\text{Hg}]^{3+}$ or $[\text{Ag}_2\text{Hg}_2]^{4+}$ tetrahedra, *etc.* The mercury atoms in these cluster fragments occur in an oxidation state lower than +2. It is interesting to note that the

$[\text{Hg}_2]^{2+}$ dumbbells tend to linear coordination to Y atoms to yield covalently bound $\text{Y} - [\text{Hg}_2]^{2+} - \text{Y}$ moieties, which can further be involved as building blocks in diverse assemblies (including extended ones), in addition to the $\text{Y} - \text{Hg}^{2+} - \text{Y}$ group. A similar behaviour is also typical of the $[\text{Hg}_3]^{4+}$ triangular clusters.

The results of structural investigations into inorganic compounds containing mercury atoms either in the bivalent (Hg^{2+}) or a 'low-valence' (*i.e.*, $[\text{Hg}_2]^{2+}$, *etc.*) states gathered to date reveal a variety of covalently bound chains, layers and frameworks as building blocks to form the general structural motifs. These compounds also contain additional isolated or extended atomic groups, which compensate for the charges and fill in the voids of the structure presumably favouring the formation of specific motifs in some cases (owing to the so-called 'template' synthesis mechanism).

A special interest in the crystal chemistry of mercury compounds is partially explained by the fact that this environmentally important element is highly mobile in the earth's crust, waters and atmosphere. Presently, about 100 mercury-based and mercury-containing minerals are known. Among them, mercury amalgams, sulfo salts, oxo compounds (predominantly oxohalides) and sulfohalides can be distinguished as the most representative groups. Furthermore, about 30 minerals (mainly halides, oxohalides and oxochromates) contain low-valence mercury as $[\text{Hg}_2]^{2+}$ or $[\text{Hg}_3]^{4+}$ cluster fragments.

Several aspects of the crystal chemistry of mercuric inorganic compounds with Y and X anions have been elucidated for the first time by Karin Aurivillius.¹ The linear $\text{Y} - \text{Hg} - \text{Y}$ fragment [with a YHgY bond angle of $\sim 180^\circ$ and short Hg–Y bond lengths: $(\text{Hg} - \text{O})_{\text{av}}$ of 2.04 Å and $(\text{Hg} - \text{S})_{\text{av}}$ of 2.34 Å] was recognised as the main building block in the crystal structures known at that time. It was also noted that two major types of assemblies based on these fragments are possible: the fragments can occur as isolated ions or molecules (such as linear $\text{X} - \text{Hg} - \text{X}$ molecules in the crystal structures of mercuric halides or complex cation $[\text{OHg}_3\text{Cl}_3]^+$ in the structure of Hg_3OCl_4); or they can join into infinite chains characterised by a certain sequence of the HgYHg angles between the neighbouring $\text{Y} - \text{Hg} - \text{Y}$ fragments. Aurivillius introduced¹ a classification of such chains including three distinct types: helical chains that can be either right-handed (+) or left-handed (–) (in particular, they occur in the hexagonal modification of HgO), zigzag chains '+ –' (occur in the orthorhombic modification of HgO) and crankshaft chains '+ + – –' (occur in $\text{Hg}_5\text{O}_4\text{Br}_2$). The exact geometry of a chain is determined by the HgYHg angle, which in turn depends on the nature of the Y

S A Magarill, N V Pervukhina, S V Borisov A V Nikolaev Institute of Inorganic Chemistry, Siberian Branch of the Russian Academy of Sciences, prosp. Akad. Lavrent'eva 3, 630090 Novosibirsk, Russian Federation. Fax (7-383) 330 94 89, tel. (7-383) 330 94 66, e-mail: svetlana@che.nsk.su (S A Magarill, S V Borisov), pervukh@che.nsk.su (N V Pervukhina)

N A Pal'chik Institute of Geology and Mineralogy, Siberian Branch of the Russian Academy of Sciences, prosp. Akad. Kopt'yuga 3, 630090 Novosibirsk, Russian Federation. Fax (7-383) 333 27 92, tel. (7-383) 333 29 03, e-mail: nadezhda@uiggm.nsk.su

Received 3 July 2006

Uspekhi Khimii 76 (2) 115–146 (2007); translated by Ya V Zubavichus

anion (for instance, different forms of crankshaft chains '+ + - -' are realised in oxo- and sulfoxo compounds, such as $\text{Hg}_5\text{O}_4\text{Br}_2$ and $\text{Hg}_3\text{S}_2\text{Cl}_2$). These chains can assemble into various planar or puckered ribbons, layers or frameworks.

Bivalent, low-valence and mixed-valence mercury compounds (nitrates, molybdates, tungstates, vanadates, arsenates and so on containing the Hg^{2+} , $[\text{Hg}_2]^{2+}$ or $[\text{Hg}_3]^{4+}$ cations) have been the subject of investigations by many research groups, including the ones headed by Brodersen, Jeitschko, Beck, Keller, Mayer, *etc.* The group headed by Voroshilov has contributed a lot into the structural studies of mercuric ternary chalcogenides. Over the recent years, about fifty mercury inorganic compounds in different oxidation states have been synthesised and characterised by Weil and co-workers. Over the recent years in Russia, the crystal chemical analysis of factors affecting the structure formation for these compounds has been in the focus of research interest of a group headed by Borisov.

Various aspects of crystal chemistry of naturally occurring and synthetic compounds containing low-oxidation-state mercury [including mixed-valence compounds, compounds with polyatomic groups $[\text{Hg}_n]^{n+}$ ($n > 2$), low-valence mercury compounds with organic ligands and mercury-containing transition metal clusters] have been surveyed in two reviews^{2,3} and a monograph.⁴

The structures of inorganic mercury compounds are of significant interest from the viewpoint of the crystal formation process encompassing all changes in the interactions between atoms upon their incorporation into a crystalline phase imposed by the regular packing, symmetry and long-range ordering requirements. A number of characteristic representatives of those compounds have been analysed using an original software package KAP-PLATS⁷ within a concept considering the crystalline state to be a result of ordering of atoms or rigid atomic fragments produced by families of parallel equi-distant (crystallographic) planes.^{5,6} Such an approach has been extended to a wider range of mercury compounds in a recent review by Borisov *et al.*⁸

The present review is concerned with specific features of the crystal structure of mercury oxo- and chalcogenides and closely related compounds, which are determined to a large extent by crystal chemical preferences of the mercury atoms, in particular, their tendency to form strong covalent bonds yielding stable atomic fragments, the so-called 'rigid' atomic groups. The structures of compounds are described both in the traditional way and using a modern approach based on the recognition of such stable 'building blocks' coupled with the analysis of their packings.

II. Mercury chalcogenides

1. Preparation, properties and occurrence in nature

Within the Hg-S binary system, there are at least three sulfides corresponding to the composition HgS .⁹ Two stoichiometric modifications, *viz.*, low-temperature α modification, cinnabarite, and high-temperature β modification, metacinnabarite, are widely known. The third phase that becomes stable at even higher temperature mentioned for the first time in the mid 1960s¹⁰ as non-stoichiometric γ - HgS has been later referred to as hypercinnabarite.

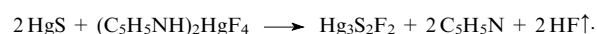
Mercuric sulfide occurs in nature predominantly as crimson cinnabarite (cinnabar, vermilion), whereas velvet black metacinnabarite is very scarce.⁹ There has been some evidence¹⁰ of natural occurrence of non-stoichiometric hypercinnabarite with iron impurities as well. Mercury selenide and telluride occur as rare minerals,¹¹ *viz.*, purple black tiemannite HgSe and dark grey coloradoite HgTe .

Ternary mercury chalcogenides (with a 3:2:2 composition) $\text{Hg}_3\text{Y}_2\text{X}_2$ ($\text{Y} = \text{S, Se, Te; X} = \text{Cl, Br, I}$) have been known for a long time. Recently, they start to attract a great interest from researchers due to their potential application in advanced technologies. These compounds manifest photoconductivity, large refraction indices and large specific angle-of-polarisation rotation in the visible light range. In particular, cubic mercury chalcogenides simultaneously demonstrate the optical activity and linear electrooptic effect, which makes them promising optical and gyrotropic materials in optoelectronics.

Comprehensive investigations into the crystal structures of ternary mercury chalcogenides started in the early 1960s. For instance, the crystal structures of $\text{Hg}_3\text{S}_2\text{Cl}_2$, $\text{Hg}_3\text{Se}_2\text{Cl}_2$, $\text{Hg}_3\text{Te}_2\text{Cl}_2$ and $\text{Hg}_3\text{Te}_2\text{Br}_2$ belonging to one of 9 rare cubic space symmetry groups, $I2_13$, which contain non-intersecting three-fold symmetry axes, were reported.^{12,13} Polymorphism is very typical of these compounds. Puff *et al.*¹⁴ elucidated polymorphism in a number of mercury sulfochlorides and sulfobromides. According to their results, the low-temperature cubic α - $\text{Hg}_3\text{S}_2\text{Cl}_2$ modification can be crystallised from a stoichiometric mixture of HgS and HgCl_2 at 300 °C. The high-temperature cubic β - $\text{Hg}_3\text{S}_2\text{Cl}_2$ modification is formed at 400 °C. The low-temperature α - $\text{Hg}_3\text{S}_2\text{Cl}_2$ modification can reversibly transform into β - $\text{Hg}_3\text{S}_2\text{Cl}_2$ under hydrothermal conditions at 300 ± 0.5 °C. The orthorhombic γ - $\text{Hg}_3\text{S}_2\text{Cl}_2$ phase can be produced at ~ 750 °C and is probably metastable over the entire temperature range studied.

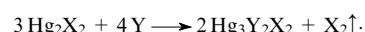
The orthorhombic low-temperature modification of mercury sulfobromide, α - $\text{Hg}_3\text{S}_2\text{Br}_2$, can be synthesised from HgS and HgBr_2 at 200 °C, the high-temperature (also orthorhombic) phase β - $\text{Hg}_3\text{S}_2\text{Br}_2$ is formed from the same reactants at ~ 420 °C. The metastable γ - $\text{Hg}_3\text{S}_2\text{Br}_2$ phase was prepared *via* the interaction of a HgBr_2 solution with an excess of KBr and sodium thiosulfate at 80 °C. No single crystal of this modification has been grown, but the authors claimed that it was isomorphous to the tetragonal phase of mixed mercury sulfobromiodide $\text{Hg}_3\text{S}_2\text{Br}_{0.5}\text{I}_{0.5}$.¹⁴

Single crystals of mercury sulfofluoride $\text{Hg}_3\text{S}_2\text{F}_2$ were grown by heating of a mixture of HgS and dipyrindinium tetrafluoromercurate up to 260 °C in vacuum according to the reaction



This compound was isomorphous to cubic α - $\text{Hg}_3\text{S}_2\text{Cl}_2$; isomorphous mercury selenofluoride $\text{Hg}_3\text{Se}_2\text{F}_2$ can be prepared in a similar way.¹⁵

Earlier, an oxidative method for the synthesis of these compounds has been suggested,¹⁶ which implied heating of the respective reaction mixtures in sealed evacuated ampoules at a temperature of the onset of exothermic effects:



Among all possible combinations, only $\text{Hg}_3\text{Te}_2\text{F}_2$ could not be prepared in pure form by this method, owing to the fact that heating of mixtures of Hg_2F_2 and Te in a temperature range of 180–350 °C always yielded liquid mercury. The oxidative synthesis of mercury seleno- and tellurohalides was successfully realised. The preparation of cubic mercury $\text{Hg}_3\text{S}_2\text{I}_2$ sulfoiodide was also reported.¹⁷

Systematic investigations into the ternary mercury chalcogenides are performed by a group of Ukrainian researchers starting from the early 1980s.^{18–23} The preparation, physical and crystallographic characterisation of cubic α - $\text{Hg}_3\text{S}_2\text{Cl}_2$, $\text{Hg}_3\text{Se}_2\text{Cl}_2$, $\text{Hg}_3\text{Te}_2\text{Cl}_2$, $\text{Hg}_3\text{Te}_2\text{Br}_2$ and $\text{Hg}_3\text{S}_2\text{I}_2$ were reported.¹⁹ The phase equilibria in the HgS-HgTe-HgCl_2 ternary system were elucidated.²² The existence of a single ternary compound, $\text{Hg}_3\text{S}_2\text{Cl}_2$, in the HgS-HgCl_2 system was confirmed, which occurs as three polymorph modifications, *viz.*, low-temperature α modification with a cubic structure, high-temperature cubic β modification with the double lattice parameter and metastable γ modification. It turned out that the structure of the γ phase belonged to the so-called order-disorder type. In addition to the ternary compound $\text{Hg}_3\text{Te}_2\text{Cl}_2$, another compound with a composition Hg_3TeCl_4 was found in the HgTe-HgCl_2 system.

A study of the HgS-HgBr_2 system revealed²³ two modifications of mercury sulfobromide $\text{Hg}_3\text{S}_2\text{Br}_2$, *viz.*, low- (α) and high-temperature (β) ones. According to single-crystal X-ray diffraction data, both compounds belong to the monoclinic system. No confirmation of the existence of a metastable phase γ - $\text{Hg}_3\text{S}_2\text{Br}_2$

was found. Two ternary mercury tellurobromides, *viz.*, cubic $\text{Hg}_3\text{Te}_2\text{Br}_2$ and Hg_3TeBr_4 isomorphous to their chloro analogue, Hg_3TeCl_4 , were found in the $\text{HgTe}-\text{HgBr}_2$ system. Within the $\text{HgTe}-\text{HgI}_2$ system, only one ternary compound Hg_3TeI_2 was identified.

Voroshilov and Slivka¹⁸ have observed for the first time the formation of ternary compounds $\text{Hg}_3\text{S}_2\text{I}_2$ (at 658 K) with an orthorhombic lattice and $\text{Hg}_3\text{Se}_2\text{I}_2$ (at 693 K), in the $\text{HgS}-\text{HgI}_2$ and $\text{HgSe}-\text{HgI}_2$ systems, respectively. Syntheses of $\text{Hg}_3\text{S}_2\text{I}_2$ and $\text{Hg}_3\text{Se}_2\text{I}_2$ by heating stoichiometric mixtures of the respective mercury chalcogenides and iodine in sealed evacuated ampoules at 260 °C for 2–3 days were reported.²⁴

Based on the analysis of equilibrium diagrams for the $\text{HgY}-\text{HgX}_2$ system, Voroshilov and Slivka¹⁸ concluded that the reactivity of mercuric chalcogenides towards mercuric halides increases on going from sulfur to tellurium (an increase in the ionic character of bonding) and from iodine to chlorine (an increase in the covalency of bonding).

In nature, mercuric sulfosalides occur as typical but rare exogenous minerals within the oxidation zone of mercury deposits, which are often characterised by a variable composition, depending on the number and type of halogen atoms incorporated into the crystal structure. These include the following minerals: corderoite $\alpha\text{-Hg}_3\text{S}_2\text{Cl}_2$,²⁵ lavrentievite $\text{Hg}_3\text{S}_2(\text{Cl},\text{Br})_2$ and arzakite $\text{Hg}_3\text{S}_2(\text{Br},\text{Cl})_2$,^{26,27} grechishchevite $\text{Hg}_3\text{S}_2(\text{Br},\text{Cl},\text{I})_2$,²⁸ radtkiteite $\text{Hg}_3\text{S}_2\text{ClI}$ ²⁹ and kenshuaitite $\gamma\text{-Hg}_3\text{S}_2\text{Cl}_2$.³⁰

The data given above indicate that both naturally occurring and synthetic mercury chalcogenides are of interest in terms of their polymorphism and possible isomorphous replacements of the halogen atoms in the crystal structures.

2. The crystal structures of ternary mercury chalcogenides

The rare mineral metacinnabarite ($\beta\text{-HgS}$) crystallises in the sphalerite structural type (the $\text{Hg}-\text{S}$ bond length is 2.54 Å).³¹

The more common trigonal modification, $\alpha\text{-HgS}$ (cinnabar),³¹ possesses a unique structure with no close analogues among monosulfides, since it involves chains combined into helices with the mercury atoms surrounded by two closest S atoms at 2.368 Å, two more S atoms at 3.10 Å and two even more distant S atoms at 3.30 Å. The $\text{S}-\text{Hg}-\text{S}$ and $\text{Hg}-\text{S}-\text{Hg}$ bond angles are 173° and 105°, respectively (Fig. 1). Similar to $\beta\text{-HgS}$, HgSe (tiemannite) and HgTe (coloradoite) crystallise in the sphalerite structural type ($\text{Hg}-\text{Se}$ 2.615, 2.634 Å, $\text{Hg}-\text{Te}$ 2.797 Å, the YHgY angle of 109.47°). Upon compression to 1.5–2 GPa, the crystal structures of HgSe and HgTe are transformed into that of $\alpha\text{-HgS}$.³²

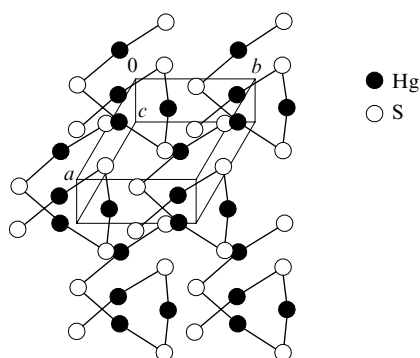


Figure 1. The crystal structure of $\alpha\text{-HgS}$ (cinnabarite).

a. 3:2:2 Mercury chalcogenides

The crystal structure of synthetic $\alpha\text{-Hg}_3\text{S}_2\text{Cl}_2$ (natural mineral corderoite²⁵) was determined by means of single-crystal X-ray diffraction.^{33,34} An analysis of the interatomic distances and angles taking into account the tendency of mercury atoms towards

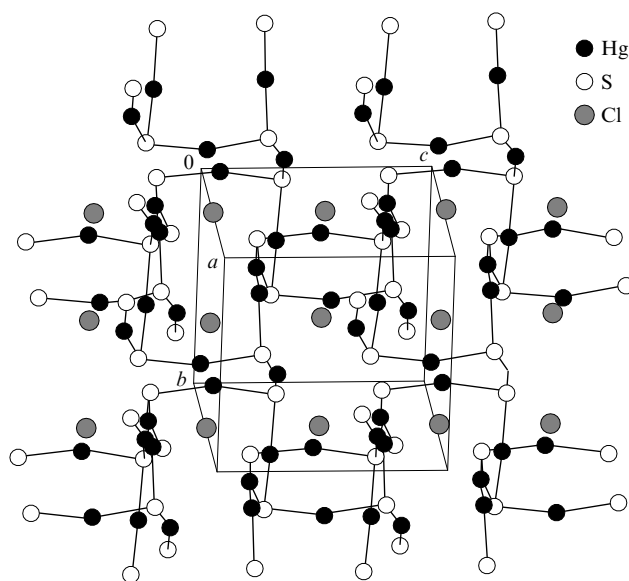


Figure 2. The crystal structure of $\alpha\text{-Hg}_3\text{S}_2\text{Cl}_2$ (corderoite).

the formation of infinite chains¹ $(-\text{S}-\text{Hg}-\text{S}-)_{\infty}$ identified a $[\text{Hg}_3\text{S}_2]_{\infty}^{2n+}$ framework in the structure, which can be described in two ways. From the one side, the infinite nearly planar $(-\text{S}-\text{Hg}-\text{S}-)_{\infty}$ chains of the ‘+ + –’ type (Table 1, Fig. 2) can be considered as major building block of the structure. The chains go through the unit cell near the $z = \pm 1/4$ planes and include 8 out of 12 mercury atoms and all 8 sulfur atoms of a unit cell. The remaining mercury atoms combine the chains *via* the $\text{S}-\text{Hg}-\text{S}$ bridges into a $[\text{Hg}_3\text{Y}_2]_{\infty}^{2n+}$ spatial framework with the halogen atoms localised in its cavities.³³ The cubic symmetry (space group $I2_13$) provides the equivalency of all three chain orientations.

The same authors³³ suggested an alternative method for the description of the $\alpha\text{-Hg}_3\text{S}_2\text{Cl}_2$ structure based on the identification of the trigonal pyramidal SHg_3 groups. The sulfur atoms located on the spatial diagonal of the cubic cell, *i.e.*, on the three-fold axis, coordinate three mercury atoms with $\text{Hg}-\text{S}$ bond lengths of 2.42 Å. These three mercury atoms compose regular triangles with an edge of 3.543 Å. The distance from the centre of such a triangle to the sulfur atoms in the pyramid apex is 1.30 Å. The SHg_3 groups are combined into a common framework by sharing mercury vertices. Large cavities present in the framework are occupied by the chlorine atoms. Very long $\text{Hg}-\text{Cl}$ bond lengths (2.87 Å) are indicative of the ionic character of bonding.

Frueh and Gray³⁴ described this structure in a more traditional way: each Hg atom is octahedrally coordinated by two S and four Cl atoms. Strongly distorted $[\text{HgY}_2\text{X}_4]$ octahedra are interlinked by face sharing.

Structural data on the isostructural compounds of the $\alpha\text{-Hg}_3\text{Y}_2\text{X}_2$ family ($\text{Y} = \text{S}, \text{Se}$ and Te ; $\text{X} = \text{F}, \text{Cl}, \text{Br}$ and I)¹² that crystallise in the enantiomorphous space group $I2_13$ with four formula units per unit cells are given in Table 1.

In order to rationalise the interatomic interactions in $\text{Hg}_3\text{S}_2\text{Cl}_2$, $\text{Hg}_3\text{S}_2\text{F}_2$, $\text{Hg}_3\text{Se}_2\text{Cl}_2$, $\text{Hg}_3\text{Te}_2\text{Cl}_2$ and $\text{Hg}_3\text{Te}_2\text{Br}_2$, a crystal chemical analysis of their structures has been accomplished.¹⁸ The authors note that the interactions between the mercury and chalcogen atoms are predominantly covalent. The $\text{Hg}-\text{Y}-\text{Hg}$ bond angles imply a significant contribution of the chalcogen p electrons to the chemical bond (the coordination is trigonal prismatic). Meanwhile, the $\text{Y}-\text{Hg}-\text{Y}$ angles close to 180° are characteristic of six-coordinated mercury atoms in distorted $[\text{HgY}_2\text{X}_4]$ octahedra. The packing density of the structure calculated based on mean specific volumes of the atoms involved estimated from their effective radii is 65%–71%, which

Table 1. Crystallographic and crystal chemical parameters of ternary mercury chalcogenides.

Compound	Space group (<i>R</i> _f)	Unit cell parameters		<i>Z</i>	<i>d</i> _{exp} , <i>d</i> _{calc} /g cm ^{−3}	Bond lengths ^a /Å		Bond angles ^a /deg.		Ref.
		translations /Å	β angle /deg.			Hg–Y	Hg–X	YHgY	HgYHg	
3 : 2 : 2 Chalcahalides										
α-Hg ₃ S ₂ Cl ₂	<i>I</i> 2 ₁ 3 (0.065)	<i>a</i> = 8.940		4	6.74 6.90	2.42	2.86, 3.39	165.1	94.1	33
	<i>I</i> 2 ₁ 3 (0.08)	<i>a</i> = 8.949		4	6.895 6.827	2.45	2.87, 3.38	166	92	34
β-Hg ₃ S ₂ Cl ₂	<i>Pm</i> $\bar{3}$ <i>n</i> (0.035)	<i>a</i> = 17.925		32	— 6.798	2.36–2.40	2.70–3.64	166.9–176.5	94.8–98.0	22
γ-Hg ₃ S ₂ Cl ₂ (polytype 1)	<i>Pbmn</i> (0.135)	<i>a</i> = 9.328 <i>b</i> = 8.410 <i>c</i> = 4.541		2	6.83 6.814	2.37–2.44	2.67–3.55	157.8–176.0	94.0–96.0	35
γ-Hg ₃ S ₂ Cl ₂ (polytype 2)	<i>A</i> 2 <i>mm</i> (0.213)	<i>a</i> = 4.664 <i>b</i> = 16.820 <i>c</i> = 9.081		4	6.83 6.814	2.37–2.44	2.67–3.55	157.8–176.0	94.0–96.0	35
γ-Hg ₃ S ₂ Cl ₂ (kenshuaitaie)	see ^b —	<i>a</i> = 9.332 <i>b</i> = 16.820 <i>c</i> = 9.108		8	6.83 6.87	—	—	—	—	30
α-Hg ₃ S ₂ Br ₂	<i>C</i> 2/ <i>m</i> (0.0535)	<i>a</i> = 17.996 <i>b</i> = 9.281 <i>c</i> = 10.289	116.4	8	— 7.110	2.384–2.416	2.848–3.706	162.4–176.5	95.8–98.5	23
β-Hg ₃ S ₂ Br ₂	<i>C</i> 2/ <i>m</i> (0.086)	<i>a</i> = 17.273 <i>b</i> = 9.374 <i>c</i> = 9.473	89.78	8	— 7.13	2.24–2.69	2.64–3.39	137.8–180.0	84.4–109.3	23
Hg ₃ S ₂ I ₂	<i>Imma</i> (0.0449)	<i>a</i> = 9.799 <i>b</i> = 18.703 <i>c</i> = 9.462		8	— 7.045	2.399–2.423	—	160.8–169.9	99.11–99.50	24
Hg ₃ Se ₂ Cl ₂	<i>I</i> 2 ₁ 3 —	<i>a</i> = 9.06		4	—	2.51	2.90	167	92	12
Hg ₃ Se ₂ Br ₂	<i>C</i> 2/ <i>m</i> (0.0517)	<i>a</i> = 17.529 <i>b</i> = 9.408 <i>c</i> = 9.775	89.51	8	— 7.577	2.496–2.536	2.815–3.305	159.2–180.0	92.9–94.6	36
Hg ₃ Se ₂ I ₂	<i>C</i> 2/ <i>m</i> (0.0749)	<i>a</i> = 19.392 <i>b</i> = 9.652 <i>c</i> = 10.918	116.54	8	— 7.37	2.36–2.66	2.79–4.09	150.7–166.4	85.7–108.4	36
	<i>Imma</i> (0.0518)	<i>a</i> = 9.766 <i>b</i> = 19.381 <i>c</i> = 9.633		8	— 7.384	2.501–2.522	3.034–3.304	161.58–171.80	96.53–97.39	24
Hg ₃ Te ₂ Cl ₂	<i>I</i> 2 ₁ 3 —	<i>a</i> = 9.336		4	—	2.65	2.99	167	91	12
Hg ₃ Te ₂ Br ₂	<i>I</i> 2 ₁ 3 —	<i>a</i> = 9.54		4	—	2.64	3.08	167	91	12
Hg ₃ Te ₂ I ₂	<i>C</i> 2/ <i>c</i> (0.076)	<i>a</i> = 14.22 <i>b</i> = 9.70 <i>c</i> = 14.34	79.9	8	—	2.648–2.702	2.981–3.499	155.23–180.0	89.75–97.60	37
	<i>Cc</i> (0.0483)	<i>a</i> = 14.276 <i>b</i> = 9.722 <i>c</i> = 14.382	100.11	8	— 7.508	2.57–2.77	2.99–3.97	180.0	88.3–100.0	38
Hg ₃ Te ₂ BrI	<i>C</i> 2 (0.1045)	<i>a</i> = 18.376 <i>b</i> = 9.587 <i>c</i> = 10.575	90.12	8	— 7.585	2.526–2.761	2.850–3.711 (Br) 3.270–3.838 (I)	—	88.7–100.2	39
Hg ₃ S ₂ F ₂	<i>I</i> 2 ₁ 3 —	<i>a</i> = 8.14		4	8.64 8.68	—	—	—	—	15
Hg ₃ Se ₂ F ₂	<i>I</i> 2 ₁ 3 —	<i>a</i> = 8.387		4	—	—	—	—	—	15

Table 1 (continued).

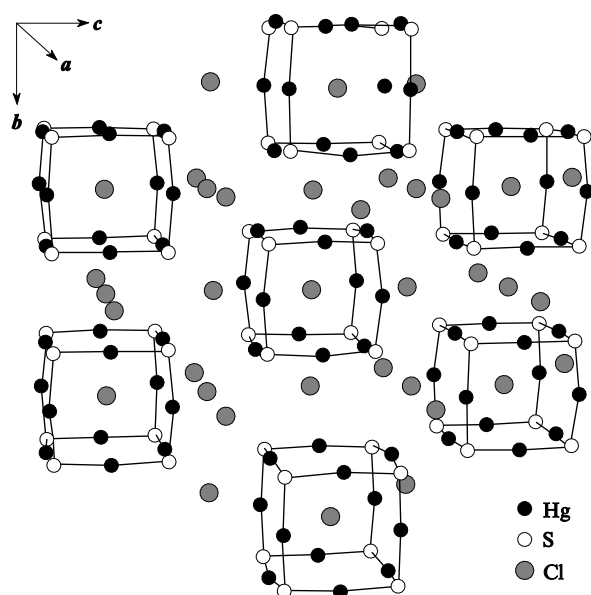
Compound	Space group (<i>R</i> _{<i>t</i>})	Unit cell parameters		<i>Z</i>	<i>d</i> _{exp} , <i>d</i> _{calc} /g cm ^{−3}	Bond lengths ^a /Å		Bond angles ^a /deg.		Ref.
		translations /Å	β angle /deg.			Hg–Y	Hg–X	YHgY	HgYHg	
3 : 2 : 2 Chalcahalides										
Hg ₃ S ₂ Br _{1.0} Cl _{0.5} I _{0.5}	<i>Pbnm</i> (0.0363)	<i>a</i> = 13.249 <i>b</i> = 13.259 <i>c</i> = 8.710		8	— 7.396	2.358–2.459	2.768–2.804 (Cl) 3.040–3.078 (Br) 3.259–3.304 (I)	140.9–172.9	95.95–104.91	40
Hg ₃ S ₂ Cl _{1.0} I _{1.0}	<i>C</i> 2/ <i>m</i> (0.0527)	<i>a</i> = 16.827 <i>b</i> = 9.117 <i>c</i> = 13.165	130.17	8	— 7.130	2.240–2.474	2.783–2.961 (Cl) 3.083–3.216 (I)	146.1–180.0	94.7–102.9	41
Hg ₃ S ₂ Cl _{1.5} Br _{0.5} (I)	<i>C</i> 2/ <i>m</i> (0.0528)	<i>a</i> = 16.841 <i>b</i> = 9.128 <i>c</i> = 9.435	90.08	8	— 6.952	2.372–2.484	2.703–2.801 (Cl) 3.070–3.099 (Cl, Br) ^c	158.42–180.0	93.06–96.21	42
Hg ₃ S ₂ Cl _{1.54} Br _{0.46} (II)	<i>Pm</i> $\bar{3}$ <i>n</i> (0.0282)	<i>a</i> = 18.0409		32	— 6.851	2.387–2.410	2.715–3.294 (Cl) 3.576 (Br) 2.884–3.448 (Cl, Br) ^c	166.0–176.1	95.4–96.6	42
Hg ₃ S ₂ Br _{1.5} Cl _{0.5} (III)	<i>C</i> 2/ <i>m</i> (0.0513)	<i>a</i> = 17.824 <i>b</i> = 9.238 <i>c</i> = 10.269	115.69	8	— 7.005	2.366–2.430	2.826–2.854 (Cl) 2.923–3.697 (Br)	163.0–176.3	96.3–97.6	43
Hg ₃ S ₂ Br _{1.5} Cl _{0.5} (IV)	<i>Pm</i> $\bar{3}$ <i>n</i> (0.0380)	<i>a</i> = 18.248		32	— 7.026	2.385–2.414	2.773–3.537 (Cl, Br) ^c 3.318–3.591 (Br)	165.2–175.0	95.7–96.5	43
3 : 1 : 4 Chalcahalides										
Hg ₃ TeCl ₄	<i>Pbca</i> (0.0388)	<i>a</i> = 11.522 <i>b</i> = 12.140 <i>c</i> = 12.683		8	— 6.523	2.631–2.637	2.357–3.691	—	89.89–97.61	22
Hg ₃ TeBr ₄	<i>Pbca</i> (0.1181)	<i>a</i> = 12.360 <i>b</i> = 12.523 <i>c</i> = 12.868		8	— 7.00	2.62–2.71	2.64–3.49	—	81.85–99.07	23
Hg ₃ TeI ₄	<i>F</i> $\bar{4}$ 3 <i>m</i> (0.1181)	<i>a</i> = 6.244		—	7.03 —	—	2.704	—	—	44

^a Y = S, Se, Te; X = Cl, Br, I; ^b the crystals are orthorhombic, the possible space groups are *Ammm*, *A2mm*, *Am2m*, *Amm2* and *A222*; ^c the position is statistically occupied by Cl and Br.

indicates that the structure is organised similar to a dense packing typical of many chalcogenides and halides.

In the crystal structure of β -Hg₃S₂Cl₂, virtually linear –S–Hg–S– groups forming closed isolated [Hg₁₂S₈] cubes with the S atoms in their vertices (Table 1, Fig. 3) can be identified.²² The Cl atoms are located both in the centres of the cubes and between them. According to an analysis of the interatomic distances and bond angles, the sulfur atoms are coordinated (similar to those in α -Hg₃S₂Cl₂) by three mercury atoms to form strong covalently bound trigonal pyramidal SHg₃ groups, which can be considered as basic building blocks of the structure. Closed isolated [Hg₁₂S₈] cubes are composed of eight SHg₃ groups. It is interesting to note that in both of these cubic structures (*i.e.*, α - and β -Hg₃S₂Cl₂), each sulfur atom is located on the spatial diagonal of the cubic lattice, *i.e.*, on the three-fold axis, in the intersection point of three virtually perpendicular linear –S–Hg–S– groups. Such isolated cubes occur also in other classes of compounds, in particular, they are similar to the [Si₈O₁₂] cubes found⁴⁵ in octasilsesquioxanes (and can be actually regarded as their antitypes).

The crystal structure of the γ modification of Hg₃S₂Cl₂ was solved³⁵ as belonging to the order–disorder type. It is composed of different polytypes with the prevalence of blocks with the *A2/m* or *F2/m* symmetries. The crystal structure includes layers built up of the SHg₃ groups interlinked by sharing mercury vertices to

Figure 3. A fragment of the crystal structure of β -Hg₃S₂Cl₂.

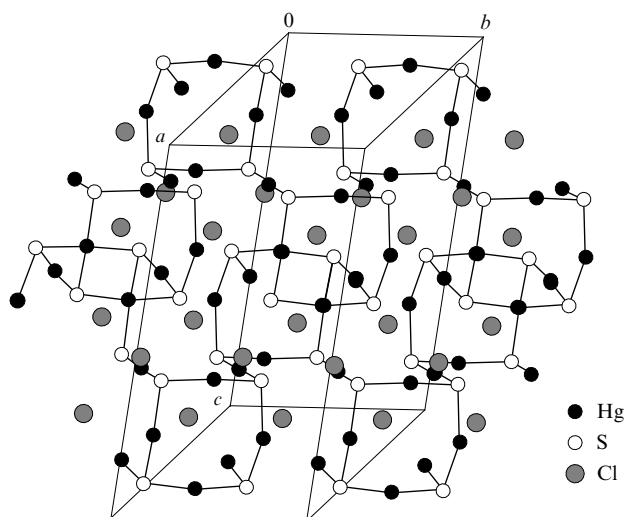


Figure 4. $[\text{Hg}_3\text{S}_2]_{\infty}^{2+}$ pucker layers with closed $[\text{S}_4\text{Hg}_4]$ rings in the crystal structure of $\gamma\text{-Hg}_3\text{S}_2\text{Cl}_2$.

form $[\text{Hg}_3\text{S}_2]_{\infty}^{2+}$ polycations. Within the layers, the Hg–S and Hg–Cl bonds are covalent and ionic, respectively (Table 1, Fig. 4). A comparison of the polycationic motifs in $\alpha\text{-Hg}_3\text{S}_2\text{Cl}_2$ and $\gamma\text{-Hg}_3\text{S}_2\text{Cl}_2$ reveals that in the case of $\alpha\text{-Hg}_3\text{S}_2\text{Cl}_2$, these groups are characterised by the $3m$ symmetry and the covalent Hg–S bonds form a spatial framework. In the γ modification, the SHg_3 groups appear distorted and the network of the covalent Hg–S bonds extends only in two dimensions. Each pair of neighbouring layers is bridged by a system of the Hg–S bonds. However, the whole structure is joined only by significantly weaker Hg...Cl contacts. This explains the perfect cleavage of the $\gamma\text{-Hg}_3\text{S}_2\text{Cl}_2$ crystals parallel to the (100) plane.

Two polymorph modifications of $\text{Hg}_3\text{S}_2\text{Br}_2$, viz., α and β , were prepared and characterised.²³ In the case of the α phase, nearly undistorted SHg_3 groups act as the basic structural unit. Similar to the situation observed in $\beta\text{-Hg}_3\text{S}_2\text{Cl}_2$, eight such groups linked by the mercury atoms compose isolated closed $[\text{Hg}_{12}\text{S}_8]$ cubes with the S atoms in their vertices, which can be regarded as main building blocks of the structure. The Br atoms are located both in the centres of the cubes and between them.

The monoclinic modification $\beta\text{-Hg}_3\text{S}_2\text{Br}_2$ (Ref. 23) is isostructural to $\text{Hg}_3\text{Se}_2\text{Br}_2$.³⁶ X-Ray diffraction patterns of $\text{Hg}_3\text{Se}_2\text{Br}_2$, $\gamma\text{-Hg}_3\text{S}_2\text{Cl}_2$ and $\beta\text{-Hg}_3\text{S}_2\text{Br}_2$ are very similar.²³ The crystal structure of $\gamma\text{-Hg}_3\text{S}_2\text{Br}_2$ remains unknown.

The crystal structures of isomorphous $\text{Hg}_3\text{S}_2\text{I}_2$ and $\text{Hg}_3\text{Se}_2\text{I}_2$ have been reported.²⁴ The mercury atoms therein are covalently bound to two chalcogen atoms with the mean Hg–Y bond lengths of 2.411 Å and 2.512 Å for Y = S and Se, respectively. The Y–Hg–Y bond angles lie in the range of 160.8–163.9° and 161.48–171.78° for $\text{Hg}_3\text{S}_2\text{I}_2$ and $\text{Hg}_3\text{Se}_2\text{I}_2$, respectively. The mercury and chalcogen atoms form Hg–Y chains with the mean Hg–Y–Hg angles of 99.3° and 96.9° for $\text{Hg}_3\text{S}_2\text{I}_2$ and $\text{Hg}_3\text{Se}_2\text{I}_2$, respectively. The Hg–Y chains go along the *a* axis parallel to each other and are interlinked by the mercury atoms to form step-like ribbons (Fig. 5). Since the tricoordinated chalcogen atoms in the YHg_3 groups are characterised by the oxidation state –2, these one-dimensional polycations can be formulated as $[\text{Hg}_3\text{Y}_2]_{\infty}^{2+}$. The Hg–I interatomic distances exceeding 3 Å clearly indicate the ionic character of bonding. The iodide ions are located both inside the covalently bound ribbons and between them. Therefore, the structures of $\text{Hg}_3\text{S}_2\text{I}_2$ and $\text{Hg}_3\text{Se}_2\text{I}_2$ reveal a new type of the mutual disposition of the trigonal YHg_3 groups for compounds of the $\text{Hg}_3\text{Y}_2\text{X}_2$ family (Y = S, Se or Te; X = Cl, Br or I).

Minets *et al.*³⁶ reported on the synthesis and structural studies of selenohalides $\text{Hg}_3\text{Se}_2\text{Br}_2$ and $\text{Hg}_3\text{Se}_2\text{I}_2$. The former compound is isostructural to $\beta\text{-Hg}_3\text{S}_2\text{Br}_2$. Each mercury atom is covalently

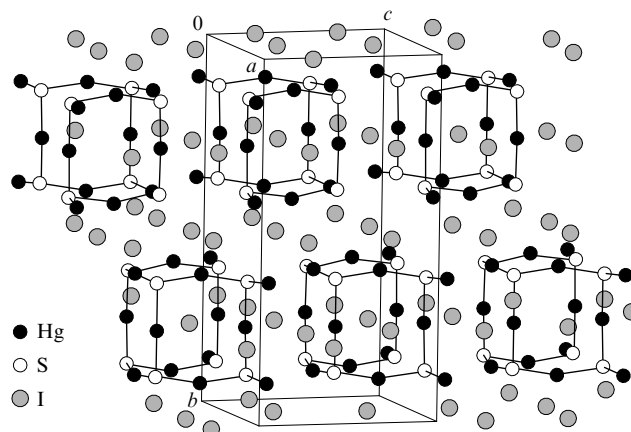


Figure 5. $[\text{Hg}_3\text{Y}_2]_{\infty}^{2+}$ step-like polycationic ribbons composed of the closed $[\text{S}_4\text{Hg}_4]$ rings going along the [100] direction in the crystal structure of $\text{Hg}_3\text{S}_2\text{I}_2$.

bound to two selenium atoms, whereas each selenium atom is connected with three mercury atoms to form the SeHg_3 groups (see Table 1). These groups are linked by sharing Hg vertices into $[\text{Hg}_{12}\text{Se}_8]_{\infty}$ pucker layers. The majority of the Hg–Se bonds (5/6) are involved into closed $[\text{Hg}_4\text{Se}_4]$ rings oriented in two different ways and the remaining bonds combine the rings into layers *via* the Hg–Se–Hg bridges. The Br atoms are localised inside the $[\text{Hg}_{12}\text{Se}_8]_{\infty}$ layers and between them. Similar pucker layers are observed in the crystal structure of $\gamma\text{-Hg}_3\text{S}_2\text{Cl}_2$.³⁵

The authors³⁶ assign the structure of $\text{Hg}_3\text{Se}_2\text{I}_2$ to the same type as $\alpha\text{-Hg}_3\text{S}_2\text{Br}_2$, *i.e.*, the structure containing isolated closed $[\text{Hg}_{12}\text{Se}_8]$ cubes with the Se atoms in their vertices. The I atoms are located both in the centres of the cubes and between them. It is of note that this conclusion contradicts the results reported by Beck and Hedderick.²⁴

The crystal structure of $\text{Hg}_3\text{Te}_2\text{I}_2$ has been studied by several authors.^{36,37} Its unit cell contains three types of Hg atoms in the sites with point symmetries 1, $\bar{1}$ and 2. The coordination polyhedron of the Hg atoms in the inversion centres can be described as a distorted octahedron with four relatively long Hg–I bonds (3.425–3.499 Å) and two short Hg–Te bonds (2.648 Å, the TeHgTe angle is 180°). Meanwhile, the Hg atoms residing on the 2-fold axes are surrounded by two Te atoms with the Hg–Te bond lengths of 2.678 Å and two I atoms at longer distances [$(\text{Hg}–\text{I})_{\text{av}}$ of 3.093 Å, the TeHgTe and IHgI angles are 157.80° and 100.99°, respectively]. Therefore, this type of crystallographically independent mercury atoms is characterised by the tetrahedrally distorted ‘butterfly’ coordination. The shortest Hg...Hg distance is 3.782 Å. According to a crystal chemical analysis, a complex framework of the Hg–Te bonds is realised in the $\text{Hg}_3\text{Te}_2\text{I}_2$ structure. It is built up of the $[\text{Te}_8\text{Hg}_{12}]$ fragments, which are in turn a combination of two $[\text{Te}_4\text{Hg}_4]$ rings related to each other by the two-fold symmetry axis parallel to the ring plane linked by a Te–Hg–Te bond. These fragments are assembled into a crankshaft ribbon, which differs from the $[\text{Y}_4\text{Hg}_6]_{\infty}$ ribbon in that only a half of the rings therein are closed and open rings form bonds with the neighbouring translationally equivalent chains. This gives rise to a framework with non-uniformly distributed bonds: 2/3 of the Hg–Te bonds form identically oriented closed $[\text{Te}_4\text{Hg}_4]$ rings, whereas 1/3 of the bonds link these rings by the Hg–Te–Hg bridges (Fig. 6). The eight-membered $[\text{Te}_4\text{Hg}_4]$ rings in the crystal structure of $\text{Hg}_3\text{Te}_2\text{I}_2$ have no shared edges with neighbouring rings, which is typical of other ribbon and layered Hg–Y motifs; this constitutes the principal distinction of this structural type from the structures of other known chalcogenides. All four Te–Hg–Te bonds formed by a ring are bridging, they link the ring with four neighbouring ones at different levels.

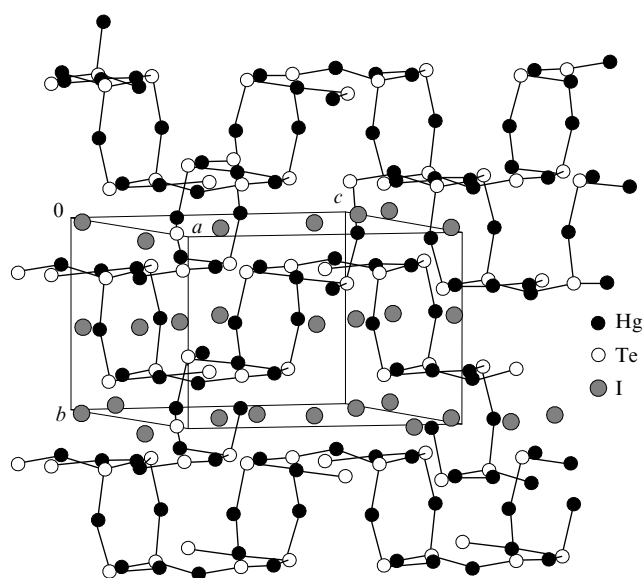


Figure 6. A complicated framework of the Hg–Te bonds in the crystal structure of $\text{Hg}_3\text{Te}_2\text{I}_2$.

Voroshilov and Minets³⁹ described the crystal structure of $\text{Hg}_3\text{Te}_2\text{BrI}$, which belongs to the structural type of $\beta\text{-Hg}_3\text{S}_2\text{Br}_2$ ($\text{Hg}_3\text{Se}_2\text{Br}_2$). Due to the presence of two different halogens, the morphotropic transition $\text{Hg}_3\text{Se}_2\text{Br}_2 \rightarrow \text{Hg}_3\text{Te}_2\text{BrI}$ is accompanied by lowering of the structure symmetry (space group $C2/m \rightarrow C2$) with the approximate retention of the unit cell parameters due to the regular iodide substitution for a half of the bromide ions.

Mercury sulfosalides rarely occur in nature. Only a few minerals within the ternary $\text{Hg}_3\text{S}_2\text{Cl}_2\text{--Hg}_3\text{S}_2\text{Br}_2\text{--Hg}_3\text{S}_2\text{I}_2$ system are known, all of them have structures closely related to each other. One of them (corderoite) has been discussed above in the beginning of Section II.2.a.

Crystals of a synthetic mercury chalcogenide that represents the analogue of naturally occurring mineral grechishchevite²⁸ have been structurally elucidated by means of X-ray diffraction.⁴⁰ In agreement with the refined stoichiometry $\text{Hg}_3\text{S}_2\text{Br}_{1.0}\text{Cl}_{0.5}\text{I}_{0.5}$, each mercury atom is connected with two sulfur atoms. As in other structures of mercury chalcogenides with a common formula $\text{Hg}_3\text{Y}_2\text{X}_2$, covalently bound S--Hg--S and SHg_3 groups assembled into a general motif can be readily identified in the crystal structure. A significant deviation of some of the SHgS angles (141.8° and 140.9°) from the linearity typical of bivalent mercury compounds¹ is of note. The halogen atoms are located between the zigzag chains. The eight-membered $[\text{Hg}_4\text{S}_4]$ rings composed of the SHg_3 groups are assembled into infinite crankshaft ribbons going along the $[001]$ direction. As has been mentioned above, similar polycationic motifs were found²⁴ in $\text{Hg}_3\text{S}_2\text{I}_2$ and $\text{Hg}_3\text{Se}_2\text{I}_2$. In these structures, all ribbons are translationally equivalent, whereas they are related to each other by the inversion centre and 2_1 -axis in $\text{Hg}_3\text{S}_2\text{Br}_{1.0}\text{Cl}_{0.5}\text{I}_{0.5}$. This difference is sufficient to classify the structure of the grechishchevite analogue as a new structural type (Fig. 7).

Naturally occurring mercury sulfosalide $\text{Hg}_3\text{S}_2\text{ClI}$ was characterised as a new mineral radtkite in 1991.²⁹ A few years later, its synthetic analogue $\text{Hg}_3\text{S}_2\text{Cl}_{1.00}\text{I}_{1.00}$ was prepared and its crystal structure was determined.⁴¹ As in the case of $\text{Hg}_3\text{S}_2\text{Br}_{1.0}\text{Cl}_{0.5}\text{I}_{0.5}$,⁴⁰ the SHgS groups deviate significantly from the linearity (see Table 1). The SHg_3 groups form $[\text{Hg}_{12}\text{S}_8]_\infty$ puckered layers similar to those found in the crystal structures of $\gamma\text{-Hg}_3\text{S}_2\text{Cl}_2$,³⁵ $\beta\text{-Hg}_3\text{S}_2\text{Br}_2$ ²³ and $\text{Hg}_3\text{Se}_2\text{Br}_2$.³⁶ The orientation of the layers strictly corresponds to the planes of perfect cleavage of the crystals.

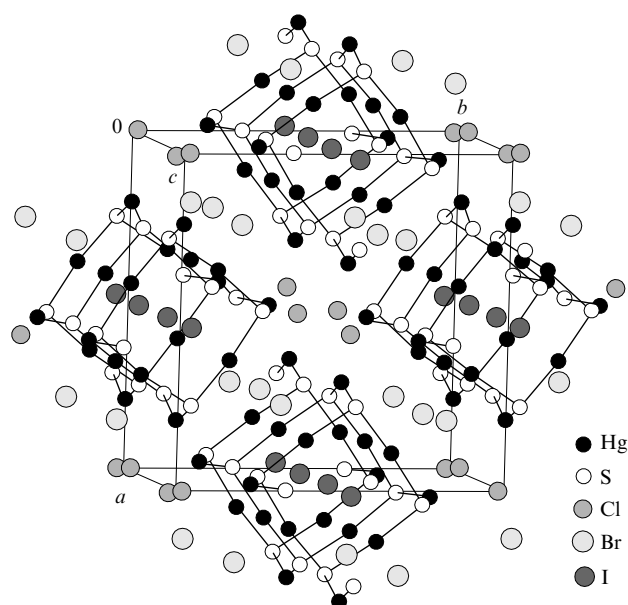


Figure 7. Crankshaft ribbons composed of closed $[\text{S}_4\text{Hg}_4]$ rings going along the $[001]$ direction in the crystal structure of the synthetic analogue of grechishchevite $\text{Hg}_3\text{S}_2\text{Br}_{1.0}\text{Cl}_{0.5}\text{I}_{0.5}$.

A series of isostructural minerals $\text{Hg}_3\text{S}_2\text{Cl}_m\text{Br}_n$ ($m+n=2$; $m>n$, lavrentievite and $m<n$, arzarkite)^{26,27} have not been studied by means of X-ray crystallography due to the lack of suitable single crystals. Attempted syntheses of these minerals afforded new mercury chalcogenides corresponding to compositions $\text{Hg}_3\text{S}_2\text{Cl}_{1.5}\text{Br}_{0.5}$ (I), $\text{Hg}_3\text{S}_2\text{Cl}_{1.54}\text{Br}_{0.46}$ (II)⁴² and $\text{Hg}_3\text{S}_2\text{Br}_{1.5}\text{Cl}_{0.5}$ (III, IV),⁴³ which have been successfully characterised by single-crystal X-ray diffraction (see Table 1).

Compound I is isostructural to synthetic $\gamma\text{-Hg}_3\text{S}_2\text{Cl}_2$, $\beta\text{-Hg}_3\text{S}_2\text{Br}_2$, $\text{Hg}_3\text{Se}_2\text{Br}_2$ and $\text{Hg}_3\text{S}_2\text{ClI}$ (a synthetic analogue of radtkite). A part of the halogen sites in the structure are statistically occupied by Cl and Br.

Compound II is isostructural to $\beta\text{-Hg}_3\text{S}_2\text{Cl}_2$ except for some increase in the lattice parameter a due to the incorporation of larger bromine atoms. The monoclinic modification III is isostructural to the synthetic compound $\alpha\text{-Hg}_3\text{S}_2\text{Br}_2$, and the cubic modification IV is isostructural to $\beta\text{-Hg}_3\text{S}_2\text{Cl}_2$. In the latter structure, 64 Br atoms are located in the nodes of a sublattice with a sublattice constant $a/4$, and eight $[\text{Hg}_{12}\text{S}_8]$ groups are arranged in a way similar to that found in $\beta\text{-W}$: they are located in the nodes and in the centre of the unit cell; additionally, each face of the unit cell accommodates these two groups.

b. 3 : 1 : 4 Mercury chalcogenides

Two isomorphous compounds Hg_3TeCl_4 and Hg_3TeBr_4 were found in the HgTe--HgCl_2 (see Ref. 22) and HgTe--HgBr_2 (Ref. 23) systems (see Table 1). Both Hg_3TeX_4 compounds ($\text{X} = \text{Cl}$ or Br) have layered structures with puckered layers stacked nearly parallel to the crystallographic xz plane, which agrees with the fact that the crystals manifest perfect cleavage along the (010) plane. Double layers oriented perpendicular to the y axis contain the halogen, tellurium and mercury atoms along with the TeHg_3 pseudotrigonal pyramids analogous to the SHg_3 groups observed in the $\text{Hg}_3\text{Y}_2\text{X}_2$ chalcogenides described above. The isolated TeHg_3 groups are arranged in such a way that two mercury atoms are located in the same layer as the tellurium atom, whereas the third Hg atom is located in the neighbouring layer (Fig. 8) thus making a covalent contribution into the predominantly ionic bonding between the atoms within a double layer. Owing to the stoichiometry change, the TeHg_3 groups are slightly more distorted than the YHg_3 groups in $\text{Hg}_3\text{Y}_2\text{X}_2$ ($\text{Y} = \text{S}, \text{Se}$ or

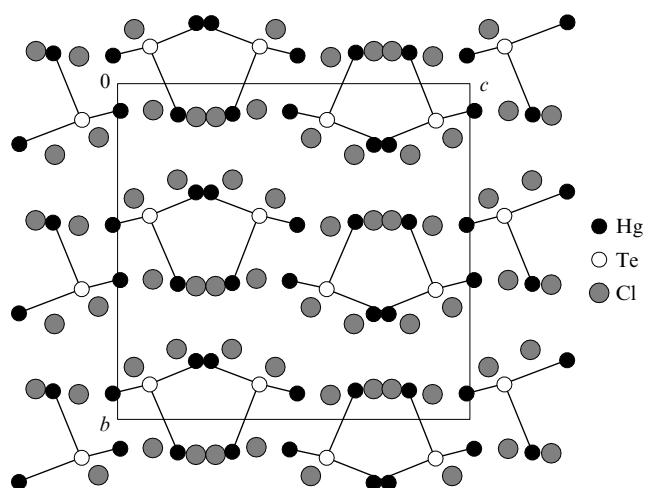


Figure 8. A projection of the crystal structure of Hg_3TeCl_4 onto the (100) plane.

Te; $X = \text{Cl, Br or I}$); the spread in the HgYHg bond angles increases from 3° (in $\text{Hg}_3\text{S}_2\text{Cl}_2$) to 7° (in Hg_3TeCl_4).

In a study of the HgTe-HgI_2 system, a new compound Hg_3TeI_4 has been found and an attempt at determining its structure from powder X-ray diffraction data has been undertaken.⁴⁴ According to the results obtained, the compound possesses a structure similar to that of sphalerite (ZnS) with a statistical distribution of atoms over the available sites, which can be described as a cubic close packing of the anions with the mercury cations statistically occupying its tetrahedral cavities (see Table 1). The authors also suggested that Hg_3TeI_4 in the ordered form can contain fragments of the red modification of HgI_2 bridged by chains composed of the HgX_4 tetrahedra ($X = \text{Te or I}$) in a way similar to that observed in the crystal structure of SiS_2 .

3. Preparation and crystal structures of quaternary mercury chalcogenides

a. Synthesis and crystal structures of MHgYX compounds

($M = \text{Cu or Ag}$; $Y = \text{S or Se}$; $X = \text{Cl, Br or I}$)

Silver and copper halides are well known cationic conductors. With this regard, the crystal structures of compounds of the MHgYX family ($M = \text{Cu or Ag}$; $Y = \text{S or Se}$; $X = \text{Cl, Br or I}$) have been in the focus of intense investigations. Main methods for their preparation can be classified into two types: (a) solid-state reactions of appropriate stoichiometric amounts of the binary precursors MX and HgY in sealed evacuated ampoules upon heating to a specific temperature for a certain time; (b) hydrothermal reactions of the starting binary components MX and HgY in concentrated or dilute solutions with HCl , HBr or HI as solvents in sealed evacuated ampoules at a certain temperature.

The major crystallographic and crystal chemical parameters of the MHgYX compounds are summarised in Table 2.

The quaternary sulfosalides CuHgSCl and CuHgSBr are isostructural. According to the X-ray diffraction study of their orthorhombic single crystals,⁴⁶ both crystal structures include planar crankshaft $-\text{S}-\text{Hg}-\text{S}-$ chains assembled into a spatial framework with pairs of strongly distorted $[\text{CuS}_2\text{X}_2]$ tetrahedra sharing an $X-X$ edge (Fig. 9). The coordination polyhedron of the mercury atoms is supplemented to a distorted octahedron with the halogen atoms. The coordination polyhedron of the copper atoms can be regarded as a strongly distorted $[\text{CuS}_2\text{X}_2]$ tetrahedron, where the copper atom occupies a position shifted from the centre of the tetrahedron (see Table 2). The sulfobromide CuHgSBr undergoes a phase transition at 323 K transforming into another orthorhombic phase with the halved parameter b . The crystal structures of CuHgSBr (at 358 K) and $\beta\text{-AgHgSI}$

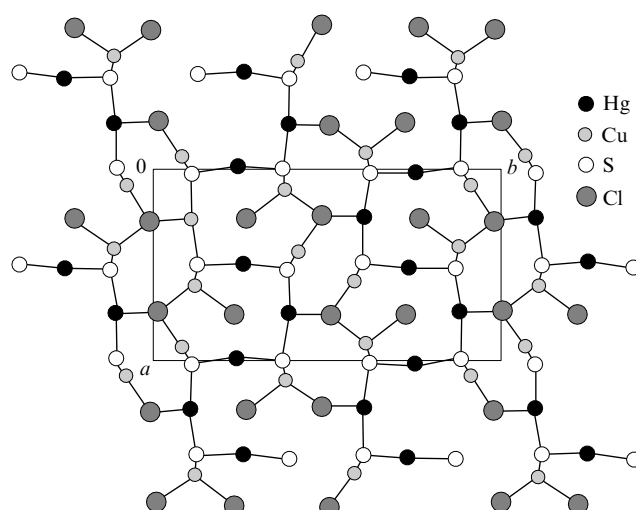


Figure 9. A projection of the crystal structure of CuHgSCl onto the (001) plane.

(Ref. 50) become virtually identical after the y and z axes in the former crystal structure are interchanged.

The crystal structure of CuHgSI has been determined independently by two research groups using the Rietveld refinement of a powder X-ray diffraction pattern⁴⁸ and single-crystal X-ray diffraction.⁴⁷ As major structural units therein, the $-\text{I}-\text{Cu}-\text{I}-$ and $-\text{S}-\text{Hg}-\text{S}-$ zigzag chains going along the c axis can be identified (Fig. 10). The copper atoms are tetrahedrally coordinated by the S and I atoms, whereas the Hg atoms are linearly coordinated (see Table 2). The structure of CuHgSI is similar to those of CuHgSCl and CuHgSBr , except for the fact that the shape of the $-\text{S}-\text{Hg}-\text{S}-$ chains is distorted in the two latter structures.

As a part of an investigation into the CuCl-HgSe system, a new compound CuHgSeCl has been synthesised and character-

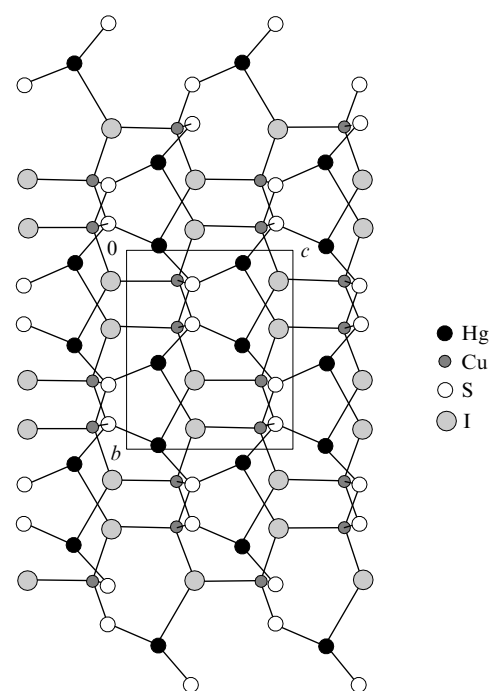


Figure 10. A projection of the crystal structure of CuHgSI onto the (100) plane.

Table 2. Crystallographic and crystal chemical parameters of quaternary mercury chalcogenides.

Compound	Space group (R_f)	Unit cell parameters /Å	Z	$d_{\text{calc}} / \text{g cm}^{-3}$	Bond lengths ^a /Å				Bond angles ^a /deg.						Ref.
					Hg–Y	M–Y	Hg–X	M–X	YHgY	HgYHg	YMY	XHgX	XXM	XYM	
Chalcohalides with a 1 : 1 cation-to-anion ratio															
CuHgS ₂ Cl	<i>Pbam</i> (0.049)	$a = 9.84$ $b = 17.75$ $c = 4.09$	8	6.16	2.362– 2.369	2.258– 2.281	2.955– 3.091	2.273– 2.559	172.4– 172.5	96.0– 96.6	—	87.75	—	101.79– 114.78	46
CuHgSBr (295 K)	<i>Pbam</i> (0.032)	$a = 10.03$ $b = 18.33$ $c = 4.124$	8	6.58	2.369– 2.371	2.266– 2.282	3.051– 3.192	2.412– 2.787	171.6– 175.2	97.4– 97.9	—	85.06	—	98.54– 114.16	46
CuHgSBr (358 K)	<i>Pmam</i> (0.068)	$a = 10.092$ $b = 9.184$ $c = 4.138$	4	6.57	2.361– 2.367	2.284	3.061– 3.265	2.430– 2.931	171.4– 180.0	97.9	—	85.07	97.6	—	46
CuHgSI	<i>Pna</i> 2 ₁ —	$a = 7.183$ $b = 8.343$ $c = 6.989$	4	—	2.359– 2.369	2.311– 2.322	3.212– 3.999	2.633– 2.743	153.8	98.8	—	—	106.5	103.8– 116.0	47
	<i>Pna</i> 2 ₁ (0.0416)	$a = 7.1748$ $b = 8.3356$ $c = 6.9855$	4	—	2.373	2.324	3.213	2.649	153.45	—	114.70	78.78	108.70	—	48
CuHg ₂ S ₂ I	<i>Cmc</i> 2 ₁ —	$a = 12.618$ $b = 7.224$ $c = 6.937$	4	—	2.374	2.368– 2.417 ^b	3.214– 4.034	3.089 ^b	—	—	113.4– 125.8 ^b	—	—	92.8– 106.6 ^b	47
CuHgSeCl (see ^c)	<i>Pbam</i> (0.071)	$a = 6.9444$ $b = 12.7561$ $c = 4.2526$	4	—	2.477– 2.486	2.379	3.105– 3.270	2.268– 2.882	171.31	89.14	126.74	—	—	98.05– 114.82	49
CuHgSeBr	<i>Pmma</i> (0.0591)	$a = 10.201$ $b = 4.312$ $c = 9.256$	4	—	2.462– 2.475	2.392	3.073– 3.358	2.434– 2.787	173.02– 180.0	—	128.7	—	—	109.52	50
AgHgSBr	<i>Pmma</i> (0.0547)	$a = 9.648$ $b = 4.661$ $c = 9.426$	4	—	2.354– 2.363	2.498	3.092– 3.357	2.679– 3.109	171.4– 180.0	—	137.80	—	—	109.23	50
α-AgHgSI	<i>P</i> 2 ₁ 2 ₁ 2 ₁ —	$a = 7.075$ $b = 7.732$ $c = 8.475$	4	—	2.351	2.561– 2.635	3.482– 3.745	2.748– 2.982	172.5	98.1	—	—	115.24	94.7– 130.4	51
β-AgHgSI	<i>Pmma</i> —	$a = 10.159$ $b = 4.648$ $c = 9.849$	4	—	2.376	2.535	3.268– 3.453	2.802– 3.209	171.4– 180.0	—	132.9	—	—	112.4	50
Ag ₂ HgSI ₂	<i>Cmc</i> 2 ₁ (0.0567)	$a = 13.834$ $b = 7.470$ $c = 7.103$	4	6.35	2.38– 2.52	2.52	3.375– 3.590	2.778– 2.950	175.5	93.1	—	—	103.1– 110.5	100.0– 130.7	52

Table 2 (continued).

Compound	Space group (R_f)	Unit cell parameters /Å	Z	d_{calc} /g cm ^{−3}	Bond lengths ^a /Å				Bond angles ^a /deg.						Ref.
					Hg–Y	M–Y	Hg–X	M–X	YHgY	HgYHg	YMY	XHgX	XXM	XYM	
Chalcohalides with a 3 : 4 cation-to-anion ratio															
Hg ₂ SnS ₂ Br ₂ (see ^d)	$P2_1/n$ (0.0543)	$a = 9.356$ $b = 8.028$ $c = 10.630$	4	6.352	2.345– 2.369	2.909– 2.921	—	2.840– 2.966	171.5– 173.5	86.8– 105.0	—	—	—	—	53
Hg ₂ PbS ₂ I ₂	$P4/mbm$ (0.039)	$a = 13.501$ $c = 4.593$	4	7.349	2.382– 2.386	2.989	3.301– 3.441	3.427– 4.385	171.06	98.84	73.71– 100.4	—	—	—	54
Naturally occurring chalcohalides															
Hg _{4.6} Ag _{4.4} S _{4.6} · (Cl ₂ Br _{0.8} I _{1.6}) (perroudite)	$P2_12_12_1$ (0.100)	$a = 17.430$ $b = 12.240$ $c = 4.350$	2	6.60	2.29– 2.43	2.46– 2.78	3.13– 3.47	2.74– 3.03	173.0– 176.0	96.0– 102.0	92.0 140.0	—	—	—	55
HgAgS(Cl,Br,I) (capgaronnite)	$P2_12_12_1$ (0.170)	$a = 6.803$ $b = 12.870$ $c = 4.528$	4	6.43	2.40– 2.49	2.44– 2.61	2.90– 3.34	2.71– 3.05	—	—	—	—	—	—	56
HgAgS(Cl,Br) (iltisite)	$P6_2$ —	$a = 8.234$ $c = 19.381$	12	6.59	—	—	—	—	—	—	—	—	—	—	57

^a M = Cu, Ag, Sn, Pb; Y = S, Se; X = Cl, Br, I; ^b the position is occupied by the Cu and Hg atoms in a 0.53 : 0.47 ratio; ^c the Cl–Cl distance is 3.738 Å; ^d β = 102.68°; the HgSSn angles are 95.7–113.9°.

^a M = Cu, Ag, Sn, Pb; Y = S, Se; X = Cl, Br, I; ^b the position is occupied by the Cu and Hg atoms in a 0.53 : 0.47 ratio; ^c the Cl–Cl distance is 3.738 Å; ^d $\beta = 102.68^\circ$; the HgSn angles are $95.7–113.9^\circ$.

ised.⁴⁹ Its structure represents a framework assembled from the $-\text{Se}-\text{Hg}-\text{Se}-$ chains running along the $[100]$ direction. Two chains related to each other by a translation along c are bridged by distorted $[\text{CuSe}_2\text{Cl}_2]$ tetrahedra involving two Se atoms from different chains and two Cl atoms. The copper atoms in these tetrahedra are strongly shifted from the centres. Pairs of these tetrahedra combined by sharing a $\text{Cl}-\text{Cl}$ edge assemble the $-\text{Se}-\text{Hg}-\text{Se}-$ chains lying in the xy plane into a framework. The geometry of the $-\text{Se}-\text{Hg}-\text{Se}-$ chains in CuHgSeCl differs from that of the $-\text{S}-\text{Hg}-\text{S}-$ chains in MHgSX ($\text{M} = \text{Cu}$ or Ag ; $\text{X} = \text{Cl}, \text{Br}$ or I).⁵⁸ The $-\text{Se}-\text{Hg}-\text{Se}-$ chains are similar to the chains present in the structures of HgO , $\text{Hg}(\text{OHg})_4\text{Br}$ and $\text{Hg}_2\text{O}_2\text{NaI}$ described as zigzag chains (the ‘+ – + –’ type) by Aurivillius,¹ whereas the chains in CuHgSeCl are of the ‘+ + – –’ type (*i.e.*, crankshaft chains) according to the same classification.

The preparation methods and crystal structures of isostructural chalcogenides CuHgSeBr , AgHgSBr and $\beta\text{-AgHgSI}$ have been reported by Beck *et al.*⁵⁰ The structures are built up of puckered layers composed of crankshaft chains with the covalent $\text{Hg}-\text{Y}$ bonds. These chains are assembled into a framework by pairs of strongly distorted $\text{M}[\text{Y}_2\text{X}_2]$ tetrahedra with shared $\text{X}-\text{X}$ edges (Table 2, Fig. 11).

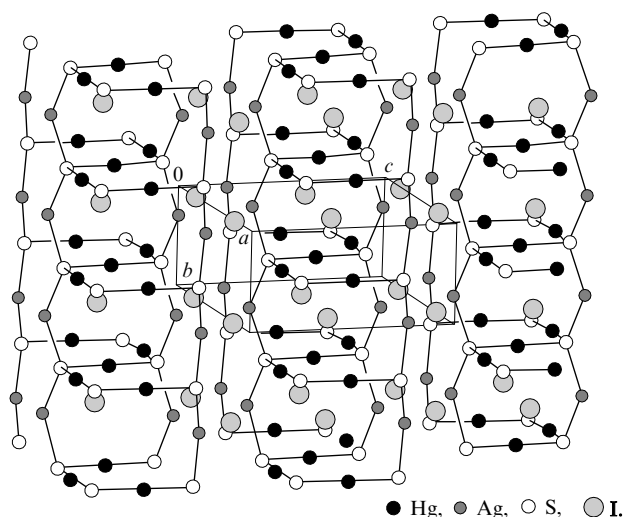


Figure 11. Puckered layers constituted by the $\text{Hg}-\text{S}$ and $\text{Ag}-\text{S}$ bonds in the crystal structure of $\beta\text{-AgHgSI}$.

A new phase, $\alpha\text{-AgHgSI}$, has been synthesised recently.⁵¹ Its structure is based on a distorted hexagonal close packing of the sulfur and iodine atoms. One fourth of the tetrahedral cavities of the packing is occupied by the silver atoms, whereas a half of the octahedral sites is occupied by the mercury atoms. The mercury atoms, like those in other mercuric compounds, are connected to two sulfur atoms. The $-\text{S}-\text{Hg}-\text{S}-$ chains (of the ‘+ – + –’ type) oriented along the $[100]$ direction are assembled into a framework by pairs of distorted $[\text{AgS}_2\text{I}_2]$ tetrahedra with shared $\text{I}-\text{I}$ edges (Fig. 12). Each tetrahedron includes two S atoms from different chains and two I atoms. The low-temperature modification $\beta\text{-AgHgSI}$ is transformed into high-temperature $\alpha\text{-AgHgSI}$ at 273°C .

We conclude this section by considering two compounds that do not formally fall into the MHgYX family, although they also correspond to a 1 : 1 cation-to-anion ratio. The crystal structures of $\text{CuHg}_2\text{S}_2\text{I}$ (Ref. 47) and Ag_2HgSI_2 (Ref. 52) are similar. Each mercury atom is linearly coordinated to two sulfur atoms (see Table 2). In these structures, the planar (in the yz plane) zigzag $-\text{S}-\text{Hg}-\text{S}-$ chains go along the c axis (Fig. 13). The coordination polyhedron of the Hg atoms is supplemented by the I atoms to a distorted octahedron. In the crystal structure of

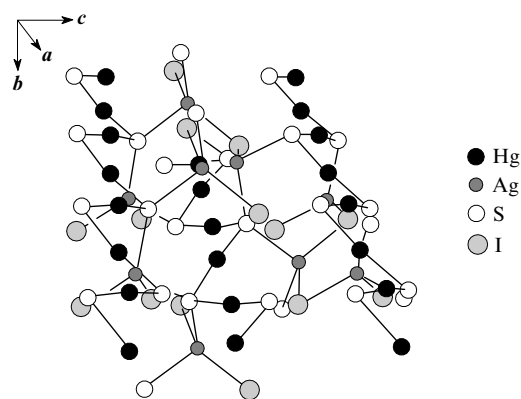


Figure 12. A fragment of the crystal structure of $\alpha\text{-AgHgSI}$.

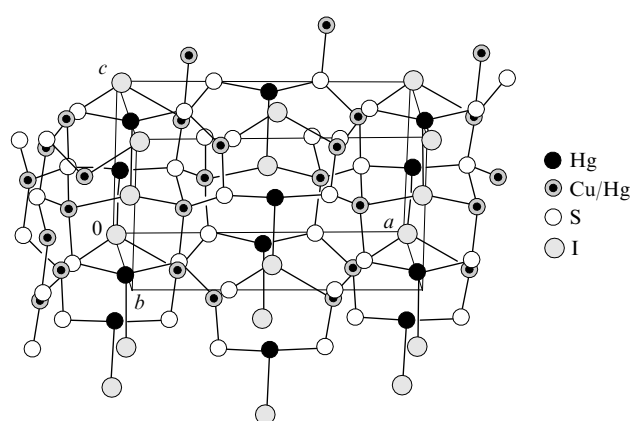


Figure 13. The crystal structure of $\text{CuHg}_2\text{S}_2\text{I}$.

$\text{CuHg}_2\text{S}_2\text{I}$, one of the cationic sites is statistically occupied by mercury and copper in a 0.47 : 0.53 ratio. The Hg/Cu cation is characterised by a distorted tetrahedral coordination environment composed of three S and one I atoms. The $[(\text{Hg},\text{Cu})\text{S}_3\text{I}]$ tetrahedra assemble the $-\text{S}-\text{Hg}-\text{S}-$ chains into a framework by vertex-sharing. In the crystal structure of $\text{AgHg}_2\text{S}_2\text{I}$, the silver atoms are surrounded by three I and one S atoms forming distorted tetrahedra. These tetrahedra assemble the $-\text{S}-\text{Hg}-\text{S}-$ chains into a framework by sharing their S vertices.

b. Quaternary mercury chalcogenides with a cation-to-anion ratio of 3 : 4

Blachnik *et al.*⁵³ reported on the synthesis of $\text{Hg}_2\text{SnS}_2\text{Br}_2$ by a solid-state reaction of HgS and SnBr_2 . In the crystal structure of this compound, helical $-\text{S}-\text{Hg}-\text{S}-$ chains, which are nearly square in the cross-section, oriented parallel to $[010]$ are packed into a tetragonal structure giving rise to voids accommodating the Sn_2Br_4 fragments (Fig. 14). The Hg atoms are characterised by a distorted octahedral coordination (two S plus four Br atoms, see Table 2).

In a study of quaternary compounds within the $\text{HgS}-\text{PbI}_2$ system involving elements of Groups 12, 14, 16 and 17,⁵⁴ a new sulfoiodide $\text{Hg}_2\text{PbS}_2\text{I}_2$ has been synthesised (see Table 2). In its crystal structure, the Hg atoms form two covalent bonds with the S atoms, and four longer $\text{Hg}-\text{I}$ bonds supplement its coordination environment to distorted octahedral one. The coordination polyhedron of the Pb atoms can be described as a monoclapped trigonal prism composed of four S and three I atoms. The sulfur atoms are tetrahedrally coordinated by two Hg and two Pb atoms. The 3D structure is built up of planar $[\text{Hg}_4\text{S}_4]$ rings stacked in columns along the $[001]$ direction. The columns are linked by the

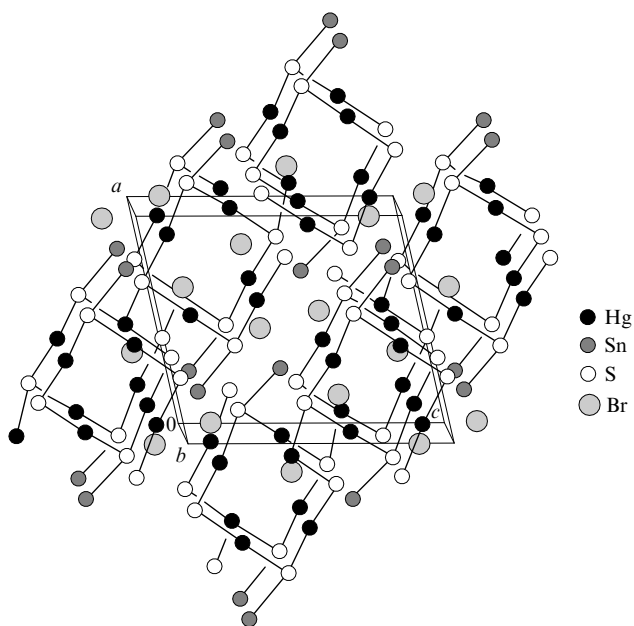


Figure 14. Helical axes $-S-Hg-S-$ going along the $[010]$ direction in the crystal structure of $Hg_2SnS_2Br_2$.

Pb atoms coordinated to four S atoms from four $[Hg_4S_4]$ rings of two neighbouring columns into a spatial framework; the iodine atoms occupy its cavities (Fig. 15).

As has been noted by Blachnik *et al.*,⁵⁴ $Hg_2PbS_2I_2$ can be considered as a cinnabarite (α - HgS) (see Fig. 1) derivative built up of helical $-S-Hg-S-$ chains.¹ The replacement of an S^{2-} ion in cinnabarite with two I^- ions gives rise to the $Hg_3S_2I_2$ structure,²⁴ where the chains are joined by the Hg bridges. The coordination number of the sulfur atoms increases to three. The sulfoiodide $Hg_2PbS_2I_2$ can be regarded as a $Hg_3S_2I_2$ derivative that is obtained by the Pb^{2+} substitution for one third of the Hg^{2+} ions, this modification is accompanied by a change of the sulfur coordination to the tetrahedral one (2 Pb plus 2 Hg).

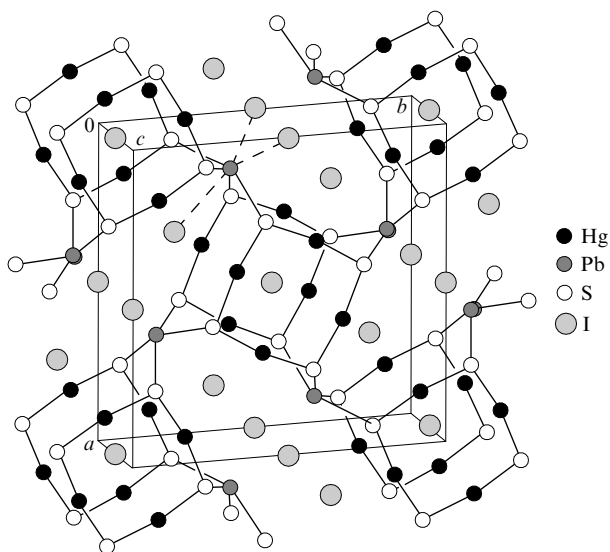


Figure 15. Columns of the $[Hg_4S_4]$ rings linked by the Pb atoms in the crystal structure of $HgPbS_2I_2$. The Pb–I bonds supplementing the coordination environment of the lead atoms to a monocapped trigonal prism are shown as dashed lines.

c. Naturally occurring quaternary mercury chalcogenides

Presently, there are only three known rare minerals falling into the class of quaternary mercury chalcogenides, *viz.*, perroudite, capgaronnite and iltisite. Perroudite and capgaronnite contain three halogens (Cl, Br and I) at once; among naturally occurring ternary mercury sulfosalts, all three halogens are present simultaneously only in grechishchevite.²⁸

In the structure of perroudite $Hg_5Ag_4S_5(Cl,Br,I)_4$, the mercury atoms are covalently bound to two sulfur atoms to form specific crankshaft chains parallel to b .⁵⁵ The coordination environment of the mercury atoms is supplemented by the halogen X atoms to the distorted octahedral one; the halogen sites are occupied by the Cl, Br and I ions statistically. The silver atoms of the first type are tetrahedrally coordinated by three S and one X atoms ($Ag-S$ 2.46–2.78 Å, $Ag-X$ 2.99 Å), whereas those of the second type are tetrahedrally coordinated by three X and one S atoms ($Ag-S$ 2.66 Å, $Ag-X$ 2.59–3.03 Å). The $S-Hg-S$ chains are assembled into a framework by the $[Ag(S,X)_4]$ tetrahedra (Fig. 16). An accurate refinement of the crystal structure indicated the complete mutual isomorphous substitution of the halogen atoms, Cl substitution for a part of the sulfur atoms and Ag substitution for a part of the mercury atoms. The mineral was finally formulated as $Hg_{4.6}Ag_{4.4}S_{4.6}Cl_{2.0}Br_{0.8}I_{1.6}$.

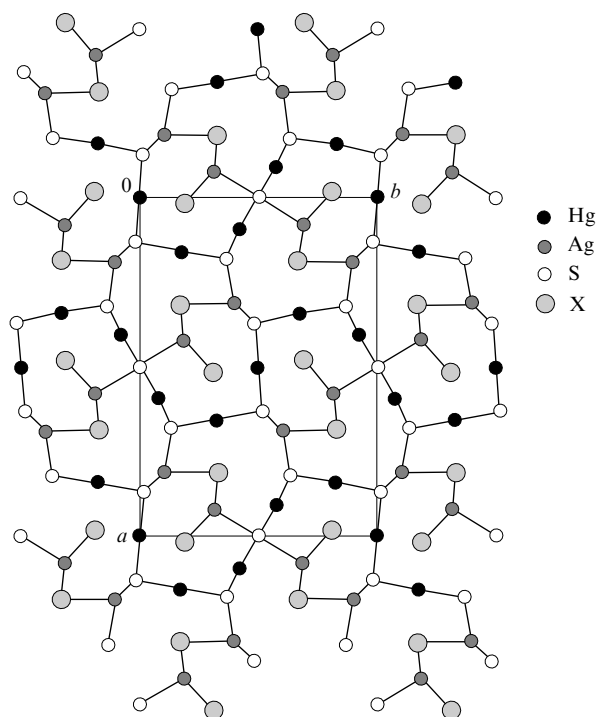


Figure 16. A projection of the crystal structure of perroudite $Hg_5Ag_4S_5X_4$ ($X = Cl, Br$ or I) onto the (001) plane.

The mineral capgaronnite corresponds to the stoichiometry $HgAgS(Cl,Br,I)$. In contrast to the framework structure of perroudite considered above, in the crystal structure of capgaronnite, the zigzag $-S-Hg-S-$ chains (of the ‘+ – + –’ type) are assembled into layers parallel to the (010) plane by pairs of edge-sharing $[AgS_2X_2]$ tetrahedra (Fig. 17).⁵⁶ The mercury atoms inside the chains are linearly coordinated by two S atoms, and four X atoms supplement their coordination to the octahedral one. The Ag atoms are tetrahedrally coordinated by two S and two X atoms.

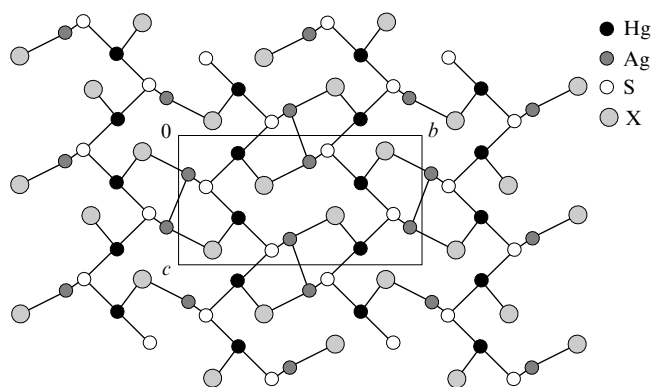


Figure 17. A projection of the crystal structure of capgaronnite HgAgSX ($\text{X} = \text{Cl}, \text{Br}$ or I) onto the (100) plane.

A hexagonal polymorph of the orthorhombic capgaronnite, *viz.*, iltsite $\text{HgAgS}(\text{Cl}, \text{Br})$, has been reported by Sarp *et al.*,⁵⁷ although its crystal structure has not been determined so far.

The major crystallographic and crystal chemical parameters of quaternary mercury chalcogenides are summarised in Table 2.

III. Mercuric oxohalides

Two binary mercury oxides are well known, *viz.*, yellow orthorhombic (natural mineral montroidite) and red hexagonal phases.

According to investigations into the pressure-induced polymorphism in HgO ,⁵⁹ a black polycrystalline powder with the tetragonal symmetry (the Laue class is $4/mmm$) is formed at 35 GPa. The authors assume that the $-\text{Hg}-\text{O}-\text{Hg}-\text{O}-$ chains are preserved in the new structure, *i.e.*, no dramatic structural rearrangement occurs.

A new triclinic phase of mercuric oxide has been reported by Benjamin.⁶⁰ It is spontaneously formed as a thin film on the surface of pure mercury under the action of oxygen under humidity. Meanwhile, stirring of mercury in ozonated oxygen affords a mixture of the orthorhombic and triclinic HgO modifications. According to X-ray diffraction data, the film represents the triclinic HgO modification with the double parameters of the orthorhombic unit cell. The structure contains zigzag $-\text{Hg}-\text{O}-\text{Hg}-\text{O}-$ chains with the bond lengths and angles typical of the HgO structures. Nevertheless, the $\text{Hg}-\text{Hg}$ distance between the neighbouring chains is ~ 2.64 Å, which is rather typical of compounds of monovalent mercury. Therefore, Benjamin suggested this compound to be a mixed-valence one.

Mercury forms various oxo salts. In particular, a series of mercuric oxochlorides $n\text{HgO} \cdot \text{HgCl}_2$ ($n = 0.5, 2, 3, 4$) and an oxobromide $\text{Hg}(\text{OHg})_4\text{Br}_2$ are known.

There are only a few quaternary mercury oxohalides. The heating of a mixture of PbO , PbBr_2 , HgBr_2 and H_2O in a 3 : 1 : 2 : 1 ratio in a sealed evacuated ampoule at 280 °C yields⁶¹ $\text{HgPb}_2\text{O}(\text{OH})\text{Br}_3$. Within the $\text{PbO}-\text{HgCl}_2$ system, single crystal of $\text{HgPb}_2\text{O}_2\text{Cl}_2$ has been synthesised by heating a mixture of PbO and HgCl_2 (in a 2 : 1 ratio) in a sealed evacuated ampoule at 275–300 °C.⁶² As a part of investigations into Hg-containing high-temperature superconductors, the first barium mercury oxochloride $\text{BaHg}_2\text{O}_2\text{Cl}_2$ has been synthesised by heating a mixture of BaO_2 and Hg_2Cl_2 in a sealed ampoule at 360 °C for three days.⁶³ The first strontium mercury oxochloride $\text{SrHg}_2\text{O}_2\text{Cl}_2$ has been prepared as reddish brown powder by the solid-state reaction of strontium peroxide SrO_2 with calomel Hg_2Cl_2 .⁶⁴

The crystal structure of the orthorhombic HgO modification reveals infinite planar zigzag $-\text{O}-\text{Hg}-\text{O}-\text{Hg}-$ chains (of the

$+ - + -$ type)¹ lying in the *ac* plane parallel to *a* ($\text{Hg}-\text{O}$ 2.039–2.067 Å, the OHgO and HgOHg angles are 179.5° and 107.3°, respectively). A comparison of the crystal structures of HgO and the hexagonal modification of mercury sulfide (cinnabarite) reveals similar principles of their structural organisation. The planar zigzag $-\text{O}-\text{Hg}-\text{O}-\text{Hg}-$ chains in oxide correspond to the infinite helical $-\text{S}-\text{Hg}-\text{S}-\text{Hg}-$ chains oriented parallel to *c* in sulfide. In both cases, the $\text{X}-\text{Hg}-\text{X}$ bond angles do not deviate substantially from 180°. A decrease in the $\text{Hg}-\text{X}-\text{Hg}$ bond angle on going from oxygen (109°) to sulfur (105°) fully reproduces the respective trend observed in other structures.

The crystal structure of hexagonal red mercury oxide is built up of infinite helical $(-\text{O}-\text{Hg}-\text{O}-)_\infty$ chains going parallel to the *c* axis. The $\text{Hg}-\text{O}$ bond lengths (2.03 Å) and $\text{Hg}-\text{O}-\text{Hg}$ (108°) and $\text{O}-\text{Hg}-\text{O}$ (176°) bond angles inside the chains are nearly the same as in the planar zigzag chains of the orthorhombic modification.⁵⁹ Four O atoms at 2.79–2.90 Å supplement the coordination polyhedron of the Hg ions to a strongly distorted octahedron. Inside the chains, the $\text{Hg}-\text{O}$ bond in the hexagonal modification is of the same type as in the orthorhombic modification but the interchain bonds are significantly weaker (the $\text{Hg} \cdots \text{O}$ distances are 2.79 and 2.90 Å, the $\text{Hg} \cdots \text{Hg}$ distances are 3.30, 3.58 and 3.72 Å, the $\text{O} \cdots \text{O}$ distances are 3.41–4.06 Å).

1. The crystal structures of ternary mercuric oxohalides

The basic crystallographic and crystal chemical parameters of mercury oxohalides are listed in Table 3.

The structure of Hg_3OCl_4 ($n = 0.5$) includes the Cl^- anions and pyramidal $[\text{OHg}_3\text{Cl}_3]^+$ cations (Ref. 65). The O atoms are located on the body diagonals of the cubic unit cell (that is on the three-fold axes) coordinating three mercury atoms. The oxygen atoms are shifted by 0.30 Å from the centres of regular triangles composed of the mercury atoms. Furthermore, each mercury atom is connected to a chlorine atom (2.302 Å) in a way that three linear $\text{Cl}-\text{Hg}-\text{O}$ groups intersect at the central oxygen atom. Therefore, the triangle composed of mercury atoms is located inside the regular triangle of the chlorine atoms; their edges are virtually parallel. The remaining chlorine atoms are situated at significantly larger distances from the mercury atoms. Each $[\text{OHg}_3\text{Cl}_3]^+$ pyramidal cation is surrounded by three Cl^- anions and *vice versa* each Cl^- anion is surrounded by three $[\text{OHg}_3\text{Cl}_3]^+$ cations. The bonds inside the pyramidal cation are covalent, as evidenced by the respective $\text{Hg}-\text{O}$ and $\text{Hg}-\text{Cl}$ bond lengths (see Table 3). The $\text{Hg}-\text{O}-\text{Hg}$ bond angle (118°) is also indicative of the covalent bonding between the oxygen and mercury atoms.

A similar nearly planar $[\text{O}(\text{HgI})_2(\text{HgOH})]^+$ cation occurs⁷¹ in two isostructural compounds $[\text{O}(\text{HgI})_2(\text{HgOH})]\text{ClO}_4$ and $[\text{O}(\text{HgI})_2(\text{HgOH})]\text{BF}_4$ ($\text{Hg}-\text{O}$ 1.99–2.12 Å, HgOHg 115.4–128.1°; $\text{Hg}-\text{OH}$ 1.98 Å, $\text{Hg}-\text{I}$ 2.57 Å, OHgI 175.0–177.2°, OHgOH 175.9°).

In the structure of $\alpha\text{-Hg}_3\text{O}_2\text{Cl}_2$ ($n = 2$), two crystallographically independent mercury atoms are characterised by different coordination environments: the first type Hg atoms are linearly coordinated by two O atoms ($\text{Hg}-\text{O}$ 2.07 Å), whereas the second type Hg atoms are coordinated by three O atoms ($\text{Hg}-\text{O}$ 2.17, 2.32 and 2.33 Å).⁶⁶ Nearly planar HgO_3 triangles are combined by edge- and vertex-sharing into puckered layers lying in the *ac* plane. The layers are further assembled into a framework by the linearly coordinated Hg atoms. The chlorine atoms occupy cavities of the framework (Fig. 18). Examples of non-linear coordination types involving a third O atom (T-shaped, *etc.*), which are less typical of Hg^{2+} cations, can be found elsewhere.³

There is another modification of this compound, $\beta\text{-Hg}_3\text{O}_2\text{Cl}_2$, which can be alternatively formulated as $\text{Hg}_6\text{O}_4\text{Cl}_4$.⁶⁷ Its structure is more complex than that of the α phase, which is evidenced by a four times larger unit cell volume. A unit cell of the β -phase

Table 3. Crystallographic and crystal chemical parameters of mercury oxohalides.

Compound	Space group (<i>R</i> _f)	Unit cell parameters		<i>Z</i>	<i>d</i> _{exp} , <i>d</i> _{calc} /g cm ^{−3}	Bond lengths ^a /Å				Bond angles ^a /deg.					Ref.
		translations /Å	β angle /deg.			Hg—O	Hg—X	M—O	M—X	OHgO	HgOHg	OHgX	MOM	HgOM	
Ternary oxohalides															
Hg ₃ OCl ₄	<i>P</i> 2 ₁ 3 (0.108)	<i>a</i> = 9.236		4	6.43 6.45	2.062	2.302, 2.987– 3.085			—	118.0	175.7			65
α-Hg ₃ O ₂ Cl ₂	<i>P</i> 2 ₁ / <i>c</i> (0.059)	<i>a</i> = 6.3100 <i>b</i> = 6.8657 <i>c</i> = 6.8579	114.36	2	8.53 8.59	2.07– 2.23	2.706– 3.259			82, 123, 149, 180	98.3– 114.3	—			66
β-Hg ₃ O ₂ Cl ₂ ≡Hg ₆ O ₄ Cl ₄	<i>P</i> 2 ₁ / <i>c</i> (0.059)	<i>a</i> = 10.838 <i>b</i> = 9.317 <i>c</i> = 11.564	108.90	4	8.44 8.47	2.028– 2.184, 2.436– 2.781	2.364, 2.753– 2.934			154.9– 175.1	104.9– 120.7	158.9			67
β-Hg ₃ O ₂ Cl ₂	<i>P</i> 2 ₁ / <i>c</i> (0.04)	<i>a</i> = 10.826 <i>b</i> = 9.310 <i>c</i> = 11.515	71.04	8	8.53 8.53	2.035– 2.778	2.362– 3.368			154.46– 174.04	85.5– 121.9	156.91			68
Hg ₅ O ₄ Br ₂	<i>Ibam</i> (0.105)	<i>a</i> = 11.888 <i>b</i> = 6.185 <i>c</i> = 11.746		4	9.23 9.43	2.05– 2.09	2.958			86–133, 163, 175	113	—			69
Hg ₅ O ₄ Cl ₂ (pinchite)	<i>Ibam</i> (0.030)	<i>a</i> = 11.619 <i>b</i> = 6.105 <i>c</i> = 11.710		4	— 9.29	2.04– 2.71	2.916– 3.142			67.0– 134.2	113.2	—			70
Quaternary oxohalides															
HgPb ₂ O(OH)Br ₃	<i>Aba</i> 2 (0.0653)	<i>a</i> = 14.652 <i>b</i> = 14.6491 <i>c</i> = 7.782		8	—	2.07	2.422– 3.347	2.29– 2.42	—	—	—	—	103.27– 108.32	114.61– 116.48	61
HgPb ₂ O ₂ Cl ₂	<i>C</i> 2/ <i>m</i> (0.047)	<i>a</i> = 11.788 <i>b</i> = 3.910 <i>c</i> = 7.749	122.64	2	—	2.054	2.981	2.340– 2.388	3.291– 3.402	—	—	—	105.99– 109.87	108.26– 113.10	62
BaHg ₂ O ₂ Cl ₂	<i>P</i> 4/ <i>mbm</i> (0.0621)	<i>a</i> = 11.8442 <i>c</i> = 4.2865		4	—	2.03– 2.09, 2.382	3.030– 3.107	2.72	3.119– 3.220	169	101	—	—	—	63
SrHg ₂ O ₂ Cl ₂	<i>P</i> 2 ₁ / <i>n</i> (0.0598)	<i>a</i> = 9.943 <i>b</i> = 7.023 <i>c</i> = 8.288	102.4	4	—	2.046– 2.491	—	2.542– 2.684	—	—	108.42– 108.56	—	107.24– 113.16	103.88– 119.13	64
^a M = Ba, Pb, Sr; X = Cl, Br.															

^a M = Ba, Pb, Sr; X = Cl, Br.

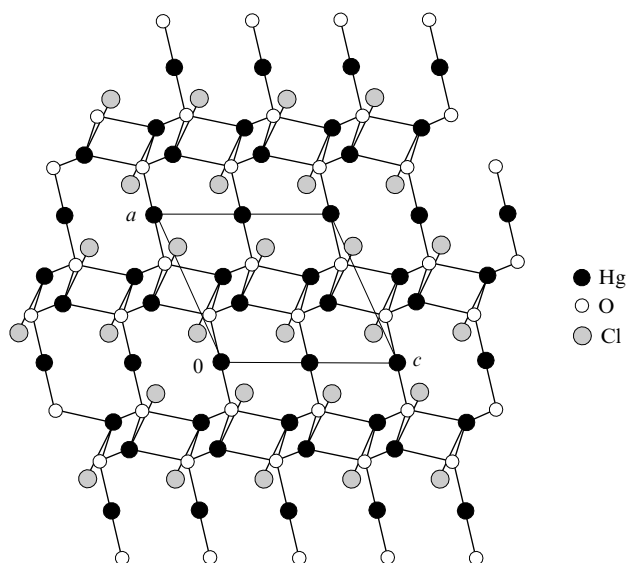


Figure 18. A projection of the crystal structure of α - $\text{Hg}_3\text{O}_2\text{Cl}_2$ onto the (010) plane.

contains six crystallographically independent mercury atoms. One of them is linearly coordinated by two oxygen atoms ($\text{Hg}-\text{O}$ 2.068 and 2.099 Å, the OHgO angle is 175.1°), four types of the Hg atoms are coordinated (similarly to the structure of α - $\text{Hg}_3\text{O}_2\text{Cl}_2$) by three O atoms in the 2+1 manner ($\text{Hg}-\text{O}$ 2.028–2.184 and 2.436–2.781 Å, the OHgO angles are 154.9 – 171.4°). The last type of the Hg atoms forms close contacts with two O atoms ($\text{Hg}-\text{O}$ 2.100 and 2.586 Å) and binds covalently a Cl atom ($\text{Hg}-\text{Cl}$ 2.364 Å, the OHgCl angle is 158.9°). The structure is built up of infinite Hg–O chains (of the ‘+ + – –’ type).¹ Four these symmetry-related chains cross a unit cell nearly parallel to the [001] direction, a repeating unit of a chain forms two O–Hg–O bonds with the nearest chain, *i.e.*, individual chains are assembled into pairs forming 12-membered $(\text{Hg}-\text{O})_6$ rings. Taking into account slightly longer contacts, these double chains are joined by pairs into extended ribbons. The sixth type of the Hg atoms is connected to a chain oxygen atom and a Cl atom to form a finite –Hg–Cl side chain. As a result, extended double ribbons with the general formula $[\text{Hg}_2(\text{OHg})_4\text{Cl}^{3+}]_n$ act as the primary building blocks of the structure. The ribbons are further assembled by the Hg atoms into a complicated framework with the remaining Cl atoms occupying its cavities. The Hg–Cl bonds with these Cl atoms are essentially ionic, according to their lengths. The authors of this study proposed to write the crystal chemical formula of this compound as $[\text{Hg}_2(\text{OHg})_4\text{Cl}]\text{Cl}_3$. It is of note that the structure of this phase was determined independently by another research group⁶⁸ and they described its structure as a motif of condensed cationic oxo-centred tetrahedra (see Section IV.1).

The presence of extended virtually planar –O–Hg–O– chains containing two of three crystallographically independent types of the Hg atoms and all O atoms constitutes the main structural feature of mercury oxobromide $\text{Hg}(\text{OHg})_4\text{Br}_2$ ($n = 4$).⁶⁹ They can be classified as crankshaft chains of the ‘+ + – –’ type ($\text{Hg}-\text{O}$ 2.05 and 2.09 Å, the OHgO angles are 175° and 163° , whereas the HgOHg angles are 113°). The remaining Hg atoms bridging the chains into a framework are located between the planes of the chains; these Hg atoms are tetrahedrally coordinated by the oxygen atoms ($\text{Hg}-\text{O}$ 2.24 Å, the OHgO angles are 86 – 133°). Cavities of the framework accommodate the Br atoms (Fig. 19). The crystal structure of naturally occurring mercury oxochloride $\text{Hg}_5\text{O}_4\text{Cl}_2$, or $\text{Hg}(\text{OHg})_4\text{Cl}_2$ (pinchite), as determined by Hawthorne *et al.*,⁷⁰ appeared fully analogous to that of $\text{Hg}(\text{OHg})_4\text{Br}_2$.

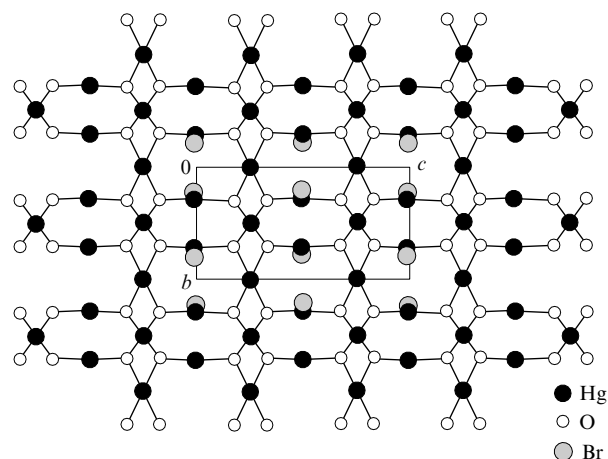
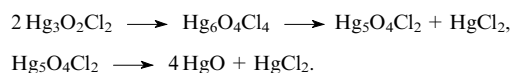


Figure 19. A projection of the crystal structure of $\text{Hg}(\text{OHg})_4\text{Br}_2$ onto the (100) plane.

The Cl atoms play different roles in the structures of the mercury oxochlorides. Above, in α - $\text{Hg}_3\text{O}_2\text{Cl}_2$ and $\text{Hg}_5\text{O}_4\text{Cl}_2$, all bonds between the Cl atoms and the respective frameworks ($[\text{Hg}_3\text{O}_2^{2+}]_n$ and $[\text{Hg}_5\text{O}_4^{2+}]_n$, respectively) are ionic. In β - $\text{Hg}_3\text{O}_2\text{Cl}_2$ and Hg_3OCl_4 , a fraction of the Cl atoms (25% and 75%, respectively) form covalent bonds with the mercury atoms giving rise to the $[\text{Hg}_6\text{O}_4\text{Cl}^{3+}]_n$ ribbons in the former case and isolated $[\text{OHg}_3\text{Cl}_3]^+$ cations in the latter one. The –O–Hg–O– fragments with terminal covalently bound Cl atoms present in the structure of β - $\text{Hg}_3\text{O}_2\text{Cl}_2$ loose them upon heating and the compound converts into $\text{Hg}_5\text{O}_4\text{Cl}_2$ with the liberation of HgCl_2 . The similarity between the crystal structures of β - $\text{Hg}_3\text{O}_2\text{Cl}_2$ and α - $\text{Hg}_3\text{O}_2\text{Cl}_2$ is not obvious. The presence of planar HgO_3 groups is their common structural feature. The β - $\text{Hg}_3\text{O}_2\text{Cl}_2$ phase is more stable at 25°C . Upon heating in air at 200°C for 70 h, both modifications convert into $\text{Hg}_5\text{O}_4\text{Cl}_2$; its structure is similar to that of β - $\text{Hg}_3\text{O}_2\text{Cl}_2$. The α - $\text{Hg}_3\text{O}_2\text{Cl}_2$ phase can be transformed into the β -modification by annealing in vacuum at 200°C for a week. A subsequent heating at 230°C for three days affords a mixture of $\text{Hg}_5\text{O}_4\text{Cl}_2$ and HgCl_2 , as evidenced by powder X-ray diffraction data. Therefore, β - $\text{Hg}_3\text{O}_2\text{Cl}_2$ remains stable at about 200°C , whereas $\text{Hg}_5\text{O}_4\text{Cl}_2$ becomes more stable at 230°C . In overall, solid oxohalides undergo the following reactions upon heating in vacuum in the above temperature range:⁶⁷



2. The crystal structures of quaternary mercuric oxohalides

In the crystal structure of $\text{HgPb}_2\text{O}(\text{OH})\text{Br}_3$, it is a complex fragment $[\text{Hg}_2\text{Pb}_4\text{O}_2(\text{OH})_2]^{6+}$ with the so-called heterocubane skeleton that acts as the principal building block.⁶¹ The central empty tetrahedron therein is constituted by the lead cations; four exterior tetrahedra sharing faces with the central one contain interstitial oxygen atoms in their centres, whereas their exterior vertices are occupied by two mercury and two hydrogen atoms. The mercury atoms in the structure are linearly coordinated by O and Br at 2.07 Å and 2.42 Å, respectively (the OHgBr angle is 166.7°). The coordination polyhedron of the mercury atoms is supplemented to a distorted trigonal bipyramid with three Br atoms at larger distances. The $[\text{Hg}_2\text{Pb}_4\text{O}_2(\text{OH})_2]^{6+}$ moieties are assembled into a framework by sharing Br vertices of the mercury polyhedra (Fig. 20).

Mercury lead oxochloride $\text{HgPb}_2\text{O}_2\text{Cl}_2$ is characterised by a significantly different structure.⁶² In this case, the $[\text{OHgPb}_3]$ tetrahedra and the linear –O–Hg–O– groups can be considered as basic structural units. The $[\text{OHgPb}_3]$ tetrahedra are

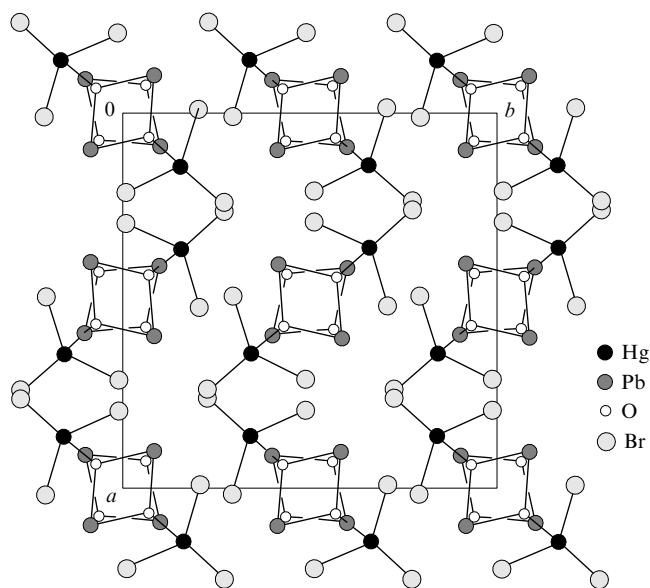


Figure 20. A projection of the crystal structure of $\text{HgPb}_2\text{O}(\text{OH})\text{Br}_3$ onto the (001) plane. The $[\text{Hg}_2\text{Pb}_4\text{O}_2(\text{OH})_2]^{6+}$ groups are localised in the nodes of the unit cell and in the centres of its faces (the H atoms are omitted for clarity).

assembled into puckered $[\text{HgPb}_2\text{O}_2^{2+}]_{\infty}$ layers in the ab plane by sharing vertices and edges. The Cl^- anions are located between the layers (Fig. 21).

The crystal structure of $\text{BaHg}_2\text{O}_2\text{Cl}_2$ has been solved from powder X-ray diffraction data.⁶³ The Hg atoms in the structure form two covalent bonds with the O atoms with bond lengths of 2.03–2.09 and 2.382 Å. The coordination environment of the Hg atoms is supplemented to a distorted octahedron by four Cl atoms (see Table 3). The coordination polyhedron of the Ba atoms can be described as a monocapped trigonal prism composed of four O (Ba–O 2.72 Å) and three Cl atoms. The structure is built up of planar Hg_4O_4 rings stacked into columns along the [001] direction.

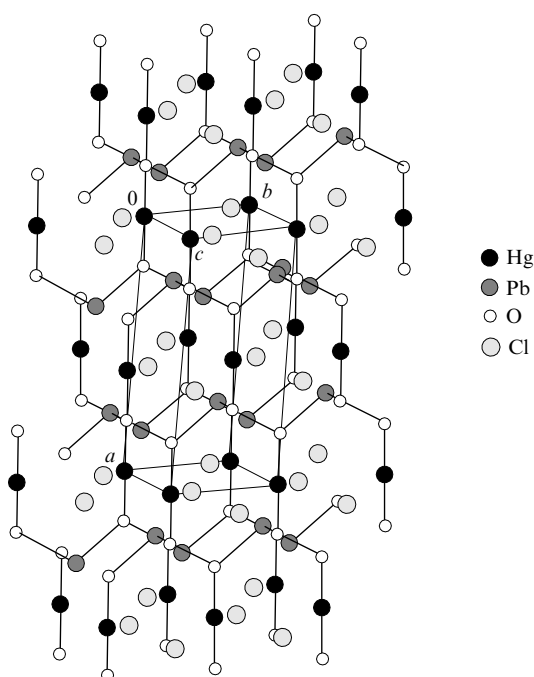


Figure 21. The crystal structure of $\text{HgPb}_2\text{O}_2\text{Cl}_2$.

These columns are assembled into a framework *via* the Ba atoms coordinated by four O atoms from four Hg_4O_4 rings belonging to two neighbouring columns; cavities of the framework accommodate the Cl atoms. Oxochloride $\text{BaHg}_2\text{O}_2\text{Cl}_2$ is isostructural to sulfiodide $\text{Hg}_2\text{PbS}_2\text{I}_2$ (see Fig. 15), its structure contains columns of isolated Hg_4S_4 squares.

The crystal structure of $\text{SrHg}_2\text{O}_2\text{Cl}_2$ has been determined using powder X-ray diffraction owing to the lack of suitable single crystals.⁶⁴ Two crystallographically independent types of mercury atoms present in the structure are characterised by different coordination environments. The first type Hg atoms are linearly coordinated by two O atoms ($\text{Hg}-\text{O}_{\text{av}}$ 2.07 Å), whereas the second type Hg atoms have the so-called T-shaped HgO_3 coordination.^{3,4} Two HgO_3 groups form four-membered rings, which are further assembled into extended $[\text{Hg}_2\text{O}_2]_{\infty}$ puckered layers oriented perpendicular to the [101] direction with the linear $-\text{O}-\text{Hg}-\text{O}-$ bridges. The $[\text{Hg}_2\text{O}_2]_{\infty}$ layers are joined together into a framework (Fig. 22) by the Sr^{2+} cations, which are characterised by irregular coordination polyhedra composed of three oxygen and five chlorine atoms. Thus the structure of $\text{SrHg}_2\text{O}_2\text{Cl}_2$ can be classified as a new structural type. The crystallographic and crystal chemical parameters of quaternary mercuric oxohalides are summarised in Table 3.

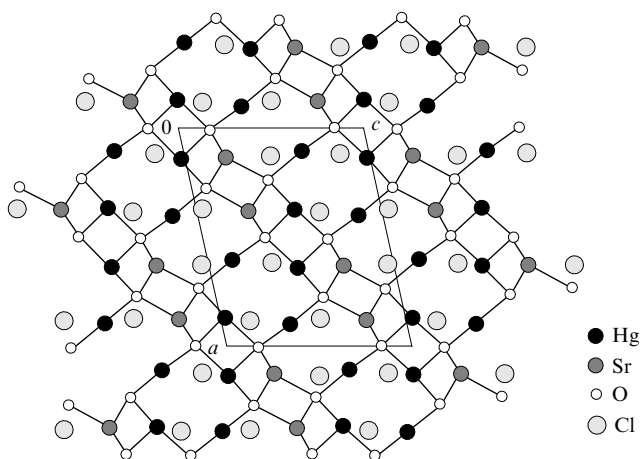


Figure 22. A projection of the crystal structure of $\text{SrHg}_2\text{O}_2\text{Cl}_2$ onto the (010) plane.

IV. Stable atomic groups (building blocks) in mercury compounds

1. Oxo-centred complexes in mercury compounds

In addition to the traditional crystal chemical approach to the structure description based on the coordination polyhedra of cations, an alternative method relying on the identification of anion-centred $[\text{M}_4\text{Y}]$ tetrahedra ($\text{M} = \text{Hg}, \text{Cu}, \text{Pb}$ or Ln ; $\text{Y} = \text{O}$ or N) in the structures came in use starting from 1968.⁷² More details on this concept can be found elsewhere.^{73–77}

The $[\text{Hg}_4\text{O}]$ tetrahedra that are stable in terms of their shape and size are capable of forming finite groups, chains, ribbons, layers and spatial frameworks in the crystal structures of mercury oxo compounds.⁷⁸ The Hg–O bond lengths in the oxo-centred tetrahedra lie in the range of 1.90–2.78 Å. The upper limit significantly exceeds the sum of the ionic radii of Hg and O, which implies that no chemical bonding is realised in such cases. It is worth noting that the spread in the Hg–O bond lengths in mercury oxo compounds is much larger than that in the M–O bond lengths for the $[\text{M}_4\text{O}]$ tetrahedra ($\text{M} = \text{Cu}, \text{Pb}$ or Ln).⁷⁵ This is explained by the ability of Hg atoms to form strong covalent bonds with only one or two oxygen atoms, which gives rise to a

shift of the O^{2-} anion from the centre of the Hg-tetrahedron to one or two of its vertices.

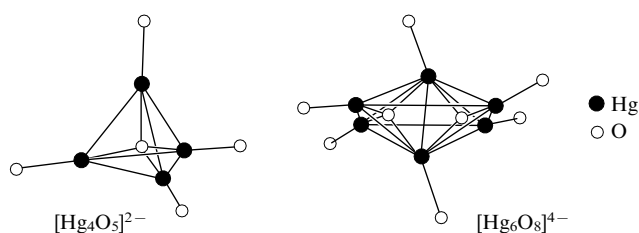
As has been demonstrated by theoretical calculations, not only Hg—O covalent bonds are of importance in the $[Hg_4O]$ tetrahedra, but the interactions between the mercury atoms as well, despite relatively large Hg—Hg interatomic distances (~ 3.5 Å).⁷⁹ This fact additionally justifies the consideration of these groups in crystal structures. The relative spread in the Hg...Hg distances in the oxo-centred tetrahedra is smaller than that in the Hg—O bond lengths. Therefore, the interatomic interactions in the $[Hg_4O]$ groups (or in the $[Hg_4O_5]$ groups formed by the addition of external covalent Hg—O bonds to the oxo-centred tetrahedron) cannot be represented as a mere sum of the pairwise Hg—O contacts. It is a more complex system of many-body interactions also involving the Hg...Hg bonding.⁷⁹

The oxo-centred $[Hg_4O]$ tetrahedra can form topologically complicated assemblies by sharing vertices and edges. Their examples can be found elsewhere.⁷⁸ The Hg:O* ratio (where O* is the so-called free oxygen, *i.e.*, oxygen atoms not involved into stable groups, such as AsO_4 or CrO_4 acid anions, *etc.*) is the main parameter governing the type of the structures. Below, a series of such crystal structures are considered, where all oxygen atoms are 'free' and the remaining anions are represented by halogens.⁸⁰ These compounds contain mercury in different oxidation states. The crystallographic and crystal chemical parameters of some of these compounds are given in Tables 3 and 4.

The structure of the mineral poyarkovite⁸¹ Hg_3OCl , or $[Hg_2]_3O_2Cl_2$, is determined both by the covalent Hg—Hg bonds in the binuclear Hg_2 fragments and the Hg—O bonds giving rise to the bond angles of 87.9 – 121.6° at the central oxygen atom.⁷⁸ Taking into account the geometry of the covalent bonds, a $[Hg_6O_2]$ moiety composed of two edge-sharing oxo-centred mercury tetrahedra can be identified in the structure. The convex polyhedron, which is a joint coordination polyhedron of two

central oxygen atoms of the two tetrahedra, has been considered earlier for the structures of rare-earth metal fluorides and denoted as *r*-octahedron, *i.e.*, rhombically distorted octahedron.⁹⁰ It can be considered as a fragment of a cubic close packing, which means that its long edge and diagonal have lengths of $a_r\sqrt{2}$ and $a_r\sqrt{3}$, respectively (where a_r is the length of its short edge).

In order to confirm the reasonability of the consideration of this moiety, quantum chemical calculations on $[Hg_4O_5]^{2-}$ and $[Hg_6O_8]^{4-}$ have been accomplished using the ZORA method⁹² as implemented in the software code ADF-2002.02.⁹¹ In addition to the internal oxygen atoms in the moiety, the covalent bonds formed by the Hg atoms with the 'external' O atoms were taken into account. According to the results obtained,⁹³ the $[Hg_6O_8]^{4-}$ fragment is substantially more preferable in terms of energy as compared to the isolated oxo-centred tetrahedron $[Hg_4O_5]^{2-}$.



This implies that these energetically favourable fragments would spontaneously form during the crystallisation provided that appropriate conditions are realised (the required Hg/O stoichiometry, the availability of suitable charge-compensating components, *etc.*). The crystal structure formation is completed by the packing of such hinged joint moieties and remaining components in an ordered way. Indeed, many structures of mercury oxohalides support this concept.

Table 4. Crystallographic and crystal chemical parameters of low-valence and mixed-valence mercury oxohalides.

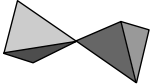
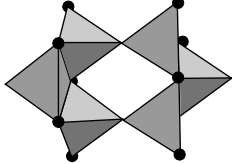
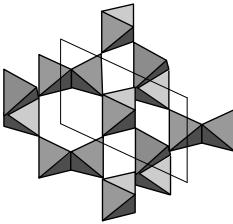
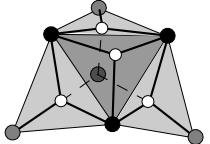
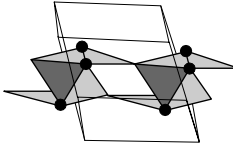
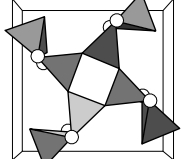
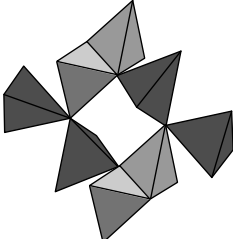
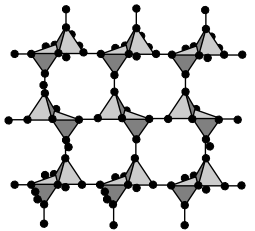
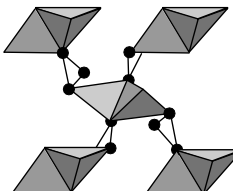
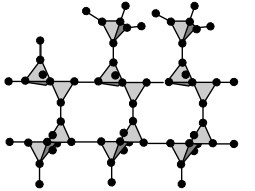
Compound	Space group (<i>R</i> _f)	Unit cell parameters		<i>Z</i>	<i>d</i> _{calc} /g cm ^{−3}	Bond lengths ^a /Å			Bond angles ^a /deg.		Ref.
		translations /Å	β angle /deg.			Hg—Hg	Hg—O	Hg—X	OHgO	OHgHg	
Hg_3OCl (poyarkovite)	<i>C</i> 2/ <i>c</i> (0.0607)	<i>a</i> = 19.009 <i>b</i> = 9.018 <i>c</i> = 16.848	β = 110.84	24	9.643	2.502–2.565	1.95–2.60	2.816–3.043	77.5–82.1	116.9–173.2	81
$Hg_6O_2HCl_3$ (eglestonite)	<i>Ia</i> $\bar{3}d$ (0.044)	<i>a</i> = 16.036		16	—	2.516	2.165	3.010–3.095	114.6	162.6	82
Hg_2OI (aurivilliusite)	<i>C</i> 2/ <i>c</i> (0.036)	<i>a</i> = 17.603 <i>b</i> = 6.981 <i>c</i> = 6.701	β = 101.61	8	8.96	2.534	2.128–2.471	3.466–3.761	—	174.6	83, 84
$Hg_7O_3Cl_2$ (hanawaltite)	<i>Pmba</i> (0.049)	<i>a</i> = 11.796 <i>b</i> = 13.890 <i>c</i> = 6.471		4	9.51	2.536–2.544	2.10–2.65	2.992–3.340	—	175.4–177.0	85
$Hg_8O_4Br_3$	<i>P</i> 2 ₁ / <i>n</i> 0.068	<i>a</i> = 6.8554 <i>b</i> = 6.3033 <i>c</i> = 31.093	β = 96.09	4	9.49	2.517–2.557	2.10–2.57	≥ 3.02	79.6–176.7	102.0–172.4	86
$Hg_4O_2Cl_2$ (terlinguaite) ^b	<i>C</i> 2/ <i>c</i> —	<i>a</i> = 11.953 <i>b</i> = 5.904 <i>c</i> = 9.466	β = 105.5	4	9.35 ^c	2.703	2.234–2.462	2.587	—	—	87
Hg_3AsO_4Cl (kuznetsovite) ^b	<i>P</i> 2 ₁ 3 —	<i>a</i> = 8.3790		4	8.763	2.675	—	2.17–2.28	—	—	88
Vasilyevite ^d	<i>P</i> $\bar{1}$ —	<i>a</i> = 9.344 <i>b</i> = 10.653 <i>c</i> = 18.265	α = 93.262 β = 90.548 γ = 115.422	2	9.57	2.533–2.595	2.00–2.32	—	—	157.1–176.0	89

^a X = Cl, Br, I; ^b the HgHgHg angles are 60° ; ^c *d*_{meas} = 9.40 g cm^{−3}; ^d $Hg_{20}O_6I_3Br_2Cl(CO_3)$, *i.e.*, $[(Hg_2^{2+})_{10}O_6]I_3Br_2Cl(CO_3)$.

Table 5. Building blocks in the structures of mercury oxohalides with tetrahedral anions.^a

Compound, Hg:O* ratio	Geometry parameters of the [OM ₄] tetrahedron (M is a metal)		Structure-forming fragment	Ref.	Compound, Hg:O* ratio	Geometry parameters of the [OM ₄] tetrahedron (M is a metal)		Structure-forming fragment	Ref.
Hg ₅ O ₄ Cl ₂ (pinchite) 5:4	Hg—O	2.045–2.707 Å		70	Hg ₃ OCl (poyarkovite) 3:1	Hg—O	1.949–2.601 Å		81
	Hg...Hg	3.416–3.945 Å				Hg...Hg	3.109–3.943 Å		
	HgOHg	100.4–113.5°				HgOHg	87.9–121.6°		
Hg ₄ O ₂ Cl ₂ (terlinguaite) 4:2	Hg—O	2.016–2.486 Å		87	Hg ₈ O ₄ Br ₃ 2:1	Hg—O	2.041–2.571 Å		86
	Hg...Hg	3.408–3.963 Å				Hg...Hg	3.225–3.948 Å		
	HgOHg	91.6–123.3°				HgOHg	88.1–118.3°		
Hg ₇ O ₃ Cl ₂ (hanawaltite) 7:3	Hg—O	2.095–2.642 Å		85					
	Hg...Hg	3.311–3.937 Å							
	HgOHg	81.52–124.8°							
α-Hg ₃ O ₂ Cl ₂ 3:2	Hg—O	2.063–2.319 Å		66					
	Hg...Hg	3.511–3.766 Å							
	HgOHg	98.3–112.5°							
β-Hg ₃ O ₂ Cl ₂ 3:2	Hg—O	1.891–2.588 Å		67, 68					
	Hg...Hg	3.338–3.989 Å							
	HgOHg	104.9–120.7°							
			layer 1		Hg ₆ O ₂ Cl ₃ H (eglestonite) 3:1	Hg—O ^b	1.23–2.179 Å		82
						Hg...Hg	3.654–3.994 Å		
						HgOHg	105.0–113.6°		
			layer 2						
Hg ₂ OI 2:1	Hg—O	2.128–2.471 Å		83, 84	Hg ₅ O ₂ CrO ₄ (wattersite) 5:2	Hg—O	2.064–2.705 Å		94
	Hg...Hg	3.590–3.775 Å				Hg...Hg	3.217–3.814 Å		
	HgOHg	101.3–111.0°				HgOHg	86.6–121.9°		

Table 5 (continued).

Compound, Hg : O* ratio	Geometry parameters of the [OM ₄] tetrahedron (M is a metal)	Structure-forming fragment	Ref.	Compound, Hg : O* ratio	Geometry parameters of the [OM ₄] tetrahedron (M is a metal)	Structure-forming fragment	Ref.
Hg ₅ OS ₂ CrO ₄ (deanesmithite) 5 : 1	Hg—O 2.014–2.585 Å Hg...Hg 3.404–3.987 Å HgOHg 87.3–125.5°		95	HgPb ₂ O ₂ Cl ₂ 3 : 2	Hg—O 2.048 Å Pb—O 2.341–2.388 Å Pb...Pb 3.777–3.980 Å Hg...Pb 3.560–3.706 Å PbOPb 105.99–109.87° HgOPb 108.26–113.10°		62
Hg ₃ O ₂ CrO ₄ 3 : 2	Hg—O 2.161–2.583 Å Hg...Hg 3.552–3.843 Å HgOHg 100.65–112.69°		96	HgPb ₂ O(OH)Br ₃ 3 : 2	Hg—O 2.117 Å Pb—O 2.240–2.456 Å Pb...Pb 3.699–3.781 Å Hg...Pb 3.611–3.763 Å PbOPb 100.27–107.32° HgOPb 114.61–116.48°		61
HgPb ₂ O ₂ CrO ₄ 3 : 2	Hg—O 2.019 Å Pb—O 2.375–2.395 Å Pb...Pb 3.579–4.044 Å Hg...Pb 3.665–3.940 Å PbOPb 97.25–111.76° HgOPb 110.28–116.20°		97	BaHg ₂ O ₂ Cl ₂ 3 : 2	(see Table 3)		63
SrHg ₂ O ₂ Cl ₂ 3 : 2	Hg—O 2.046–2.491 Å Hg...Hg 3.194–3.689 Å HgOHg 108.42–108.56°		64	Hg ₂₀ O ₆ I ₃ Br ₂ Cl. . (CO ₃) ≡ [(Hg ₂ ²⁺) ₁₀ O ₆]. . I ₃ Br ₂ Cl(CO ₃) (vasilyevite) 5 : 3	Hg—O 2.00–2.735 Å Hg...Hg 3.041–3.497 Å HgOHg 92.9–121.1°		89
[Hg ₃] ₂ HgO ₂ (PO ₄) ₂ 7 : 2	Hg—O 2.031–2.526 Å Hg...Hg 3.563–3.607 Å HgOHg 101.61–119.83°		98				
						layer 1	
						layer 2	

^a Some discrepancies in the listed geometry parameters as compared to those reported in Tables 3, 4 and 6 are due to the use of different software codes for their calculation (based on the same structural data);

^b 1.23 Å is the O—H distance in the [OM₃H] tetrahedron.

Table 5 lists possible types of building blocks based on the $[\text{OHg}_4]$ tetrahedra and $[\text{Hg}_6\text{O}_2]$ *r*-octahedra realised in the crystal structures of some natural and synthetic mercury oxohalides.

The dimensions of the *r*-octahedra determine the unit cell parameters and, to a some extent, its symmetry. Most frequently, they are packed in a herringbone manner. Herringbone layers of the *r*-octahedra represent stable structural units, which occur in various structures.

Two independent *r*-octahedra can be identified in the structure of poyarkovite $[\text{Hg}_3\text{O}_2\text{Cl}_2]$. A crystallographic inversion centre resides in the centre of one of them. The second *r*-octahedron has no symmetry elements, although its geometry is close to that of the first one. All cation vertices of an *r*-octahedron covalently link them with the neighbouring *r*-octahedra *via* the Hg—Hg bonds. If the $[\text{Hg}_2]^{2+}$ dumbbell is taken as the cation, the ideal poyarkovite stoichiometry 3 : 2 : 2 is resulted. It is important to note that the unit cell parameters of the poyarkovite structure are determined by the size and orientation of the cationic *r*-octahedra coupled with the lengths of the Hg—Hg bonds that join the *r*-octahedra together (these are the so-called contact links). The poyarkovite structure is composed of two types of layers made up of the *r*-octahedra oriented parallel to the *yz* plane.

The structure of $\alpha\text{-Hg}_3\text{O}_2\text{Cl}_2$ analysed earlier in Section III.1 can be regarded as a result of the Hg^{2+} 'isomorphous' substitution for the $[\text{Hg}_2]^{2+}$ dumbbells in the poyarkovite structure; this is accompanied by a reduction in the length of the contact link between the *r*-octahedra to zero, *i.e.*, the octahedra are directly linked by sharing Hg vertices. In a unit cell of $\alpha\text{-Hg}_3\text{O}_2\text{Cl}_2$, there are two symmetry-related *r*-octahedra. Furthermore, there are two types of the mutual orientations of the neighbouring *r*-octahedra: the neighbouring *r*-octahedra are translationally equivalent along the *x* axis, which means that the translation *a* is equal to their long diagonal. In other directions, translationally equivalent *r*-octahedra alternate with the *r*-octahedra transformed by a 2_1 screw axis or a *c* gliding reflection plane. As a result, the unit cell parameters *b* and *c* are nearly identical being equal to the vector sum of two short edges of the *r*-octahedra.

The structure of mixed-valence Hg_2OI takes^{83,84} a position intermediate between those of poyarkovite and $\alpha\text{-Hg}_3\text{O}_2\text{Cl}_2$. In these structures, only two Hg-vertices of the *r*-octahedra are replaced with the $[\text{Hg}_2]^{2+}$ dumbbells. The layer of vertex-sharing *r*-octahedra analogous to that in the structure of $\alpha\text{-Hg}_3\text{O}_2\text{Cl}_2$ is located in the *yz* plane, which gives rise to nearly identical *b* and *c* in these two structures. Two vertices of an *r*-octahedron (at the ends of the long diagonal) are occupied by the $[\text{Hg}_2]^{2+}$ dumbbells extended along the *a* axis. The vector sum of the parameter *a* with the long diagonal of the *r*-octahedron is $a/2 = 8.8$ Å, which is close to the parameter *b* of the poyarkovite structure. The residual free volume is filled with bulky I^- anions.

In the structure of $\alpha\text{-Hg}_3\text{O}_2\text{Cl}_2$, the translation parameters of the orthogonal two-dimensional lattice of the herringbone layer are 6.8657 and 6.8759 Å, whereas its thickness is ~ 6 Å. The structure of Hg_2OI can be represented as two herringbone layers parallel to *x*, which are linked by the Hg—Hg dumbbells (~ 2.5 Å) also oriented along the *x* axis, rather than by shared Hg vertices. Thus the *a* parameter of the Hg_2OI structure corresponds to the doubled *a* of the $\alpha\text{-Hg}_3\text{O}_2\text{Cl}_2$ structure (6.310 Å) plus two Hg—Hg bond lengths: 17.603 Å $\approx 2 \times 6.310 + 2 \times 2.50$ Å.

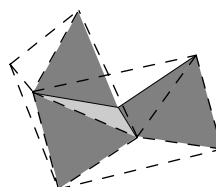
The symmetry centre of an *r*-octahedron often coincides with the crystallographic inversion centre of the structure, which implies that the 'rigid' moiety partially determines the structure symmetry in addition to the unit cell dimensions. In particular, a single $[\text{Hg}_4\text{O}]$ tetrahedron with no inversion centre can possess a dipole moment. Meanwhile, a pair of the inversion-related tetrahedra mutually compensate for their dipole moments in the minimum volume, which gives rise to the stabilisation of such a structural fragment.

In contrast to the $\alpha\text{-Hg}_3\text{O}_2\text{Cl}_2$ structure, a $[\text{Hg}_{10}\text{O}_4]$ moiety with an inversion centre localised in the middle of an edge shared by two *r*-octahedra acts as the basic building block in the

β -modification of $\text{Hg}_3\text{O}_2\text{Cl}_2$ due to the condensation of a part of the *r*-octahedra. Dimensions of this moiety determine the unit cell parameters *b* and *c*: the double *r*-octahedra centred at $1/2, 1/2, 1/2$ form a layer in the *yz* plane, the packing of the moieties in the layer is determined by the symmetry (*a c* plane and a 2_1 axis). This layer is stacked along *a* on another layer constituted by two types of the *r*-octahedra formed around oxygen atoms of two other types with the inversion centres at $00, 1/2$ and $0, 1/2, 1/2$. The condensation of the two *r*-octahedra changes the Hg : O stoichiometry, a ratio of Hg : O = 5 : 4 is expected provided that each vertex of the double *r*-octahedron is shared with the neighbouring ones. In order to compensate for the stoichiometry violation, two Hg atoms from the $[\text{Hg}_{10}\text{O}_4]$ fragment become terminal; this is accompanied by the introduction of a Cl^- anion at a distance of 2.36 Å (the sum of ionic radii of Hg and Cl is 2.50 Å!) into their coordination environments in place of oxygen. Taking into account that all other vertices of the *r*-octahedra in the structure are bridging, this configuration restores the 3 : 2 Hg : O stoichiometry.

The ratio of mercury cations to oxygen anions (taking into account dumbbell groups) in the structure of mixed-valence hanawaltite $[\text{Hg}_2]_3\text{HgO}_3\text{Cl}_2$ is 4 : 3, *i.e.*, it includes a larger amount of cations than $\text{Hg}_3\text{O}_2\text{Cl}_2$. As a result, isolated $[\text{Hg}_4\text{O}]$ tetrahedra are present in the structure in addition to the *r*-octahedra. The *r*-octahedra are grouped nearby the inversion centres $1/2, 1/2, 1/2$ filling the space between the mirror planes that accommodate the isolated $[\text{Hg}_4\text{O}]$ tetrahedra. The unit cell parameter *c* is determined by the length of the long diagonal of the *r*-octahedron. The only Hg^{2+} atom resides in an inversion centre and is characterised by the strictly linear O—Hg—O coordination.

Despite a relatively small number of cations in the structure of pinchite $\text{Hg}_5\text{O}_4\text{Cl}_2$, all oxygen atoms therein are tetrahedrally surrounded by the cations. There are two types of the *r*-octahedra with partially overlapping volumes; their centres are located at an inversion centre $1/4, 1/4, 1/4$ (the packing of this type of polyhedra determines the structure in the *ab* plane) and at a two-fold axis parallel to *x*, respectively.



In overall, the pinchite structure can be represented as an assembly of four symmetry-related columns composed of the *r*-octahedra extended along the *b* axis. The bonding between the columns is realised by sharing Hg vertices. Within the columns, the bonding is stronger: each *r*-octahedron shares a common $[\text{Hg}_4\text{O}]$ tetrahedron with a neighbouring one. Therefore, this represents a new pattern of bonding between structural units, *viz.*, partial volume-sharing in addition to known types, such as vertex-, edge- and face-sharing.

The structure of mixed-valence oxobromide $\text{Hg}_8\text{O}_4\text{Br}_3$ reveals a complex combination of structural elements observed in pinchite and poyarkovite. All four basic oxygen atoms are involved in *r*-octahedra but only one of the *r*-octahedra (composed of the mercury atoms forming dimeric $[\text{Hg}_2]$ groups) is located at an inversion centre ($1/2, 00$). This type of the *r*-octahedra form a layer in the *xy* plane (layer 1), which is similar in terms of its structure to layers present in poyarkovite. Two other types of the *r*-octahedra with partly overlapping volumes (similar to those found in the pinchite structure) occupy larger volume filling the space between the layers composed of the first type *r*-octahedra separated by *c*/2 (layer 2). Pairs of overlapping *r*-octahedra are linked by sharing Hg^{2+} vertices in such a way that one of the typical coordination types is realised for all mercury atoms. The unit cell parameter *b* is equal to the long diagonal of the *r*-octahedron (like *b* parameter of pinchite, *c* parameter of hanawaltite and *b* parameter of $\alpha\text{-Hg}_3\text{O}_2\text{Cl}_2$).

In the mineral terlinguaite $[\text{Hg}_3]\text{HgO}_2\text{Cl}_2$, the $[\text{Hg}_3]^{4+}$ triangular clusters and $[\text{Hg}_6\text{O}_2]$ *r*-octahedra (taking into account the covalent Hg–O interactions) act as basic structure-forming units. The structure is built up by their packing together with the Cl^- anions. A unit cell includes one type of the *r*-octahedra centred at the inversion centre in the origin (000). In agreement with the space group $C2/c$, they are arranged in a way that all equatorial Hg-vertices are bridging and all axial vertices are terminal, which provides the required stoichiometry $\text{Hg} : \text{O} = 4 : 2$. The first type of the mercury atoms are characterised by the linear O–Hg–O coordination; the second type of the Hg atoms reside in the plane composed of two oxygen atoms and two mercury atoms of the third type; the latter are characterised by a non-typical $2\text{O} + 2\text{Hg} + \text{Cl}$ coordination. These structural peculiarities are due to the presence of the $[\text{Hg}_3]^{4+}$ cluster fragment, which includes two mercury atoms of different types.

In Hg-deficient structures, a part of vertices of the *r*-octahedra can be occupied by other cations (Sr, Pb), which results in only insignificant geometry changes ($\text{SrHg}_2\text{O}_2\text{Cl}_2$, $\text{HgPb}_2\text{O}_2\text{Cl}_2$, see Table 5). The approach based on the identification of ‘rigid’ atomic groups in crystal structures becomes increasingly more popular.^{99–102} In particular, very similar atomic arrangements were found in gold $[\text{Au}_6\text{O}_2]$ (Ref. 103) and mixed gold–rhodium $[\text{Rh}_2\text{Au}_4\text{O}_2]$ (Ref. 104) clusters. These fragments manifest a high stability due to the formation of Au–Au (3.008 Å) and Au–Rh (3.00 Å) bonds.

In the structure of $\text{SrHg}_2\text{O}_2\text{Cl}_2$, a cationic *r*-octahedron with an inversion centre and two strontium atoms occupying two its vertices can be identified. The $[\text{Sr}_2\text{Hg}_4\text{O}_2]$ *r*-octahedra are assembled by isolated $[\text{Sr}_2\text{Hg}_2\text{O}]$ tetrahedra into a three-dimensional motif, like that in the hanawaltite structure. The formation of stable atomic groups explains many structural features of these compounds, in particular, irregular coordination polyhedra of some atoms, as noted by Harrison *et al.*⁶⁴

In the above compounds, the charge-compensating halogen atoms play an insignificant structure-forming role, since rigid polyatomic moieties ($[\text{Hg}_4\text{O}]$ tetrahedra and $[\text{Hg}_6\text{O}_2]$ *r*-octahedra) by far exceed them in terms of both mass and size. In this class of compounds, they play a secondary role merely filling available space.

In the majority of structures analysed above, *r*-octahedra possess only inversion centres, their short edges, long edges and long diagonals are 3.40–4.00 Å, 5.30–5.40 Å and 6.10–6.30 Å, respectively. Each Hg vertex of the polyhedra is involved into covalent bonding with external oxygen atoms belonging to neighbouring *r*-octahedra in addition to one or two internal oxygen atoms. Therefore, these groups can be regarded as isolated ones only formally similar to, for instance, SiO_4 tetrahedra in framework silicates. It is the mutual packing of these polyhedra that governs the crystal structure. Although Hg vertices of *r*-octahedra are also involved into external covalent bonding, in particular, with neighbouring *r*-octahedra, the spread in the respective bonding angle is significantly larger than for the internal bonds. It is worth noting that up-to-date methods for the quantitative simulation of chemical bonding fully support the emergence of intuitively apparent cation–cation bonds in these groups.^{79, 105}

2. Stable structural units in mercury compounds with the AO_4 tetrahedral anions (A = Cr, P, As or V)

A number of crystal structures of naturally occurring and synthetic mercury sulfo- and oxochromates reveal even more complex fragmentation patterns. The crystal structures of mercury compounds with the AO_4 tetrahedral anions (A = Cr, P, As or V) include, in addition to the Hg–S and Hg–O covalent bonds formed by the mercury atoms, covalent A–O bonds within the $[\text{AO}_4]$ tetrahedral complexes, which are also incorporated into the structure as ‘rigid’ moieties.¹⁰⁶ The crystallographic and crystal chemical parameters of these compounds are summarised in

Table 6, whereas the types of cationic and anionic ‘rigid’ atomic fragments are listed in Table 7.

With an increase in the effective size of the anionic fragments, their role in the structure formation becomes more important. The $[\text{AO}_4]$ tetrahedra can combine into inversion centre-related pairs in such a way that two triangular faces looking toward each other form an octahedral cavity of oxygen atoms. For example, such pairs are present in the structures of edoylerite and deanesmithite (see Table 7); the distances between the centres of the tetrahedra in these structures are 4.10 and 4.30 Å, respectively. The cationic part of the edoylerite structure is represented by zigzag chains composed of the $[\text{Hg}_4\text{S}_4]$ rings that separate the anionic fragments from each other. The centres of gravity of these rings coincide with the crystallographic inversion centres. In the deanesmithite structure, a three-dimensional framework of Hg–Hg and Hg–S covalent bonds constitutes the cationic part.

The crystal structures of mercury chromates (HgCrO_4 , $\text{Hg}_3\text{O}_2\text{CrO}_4$ and $\text{HgPb}_2\text{O}_2\text{CrO}_4$) contain various configurations of the $[\text{CrO}_4]$ tetrahedra retaining the same type of contacts *via* the octahedral cavity of oxygen atoms. Edge-sharing oxo-centred tetrahedra, which can be identified as $[\text{Hg}_6\text{O}_2]$ and $[\text{Hg}_2\text{Pb}_4\text{O}_2]$ *r*-octahedra and $[\text{HgPb}_2\text{O}]$ triangles (in $\text{HgPb}_2\text{O}_2\text{CrO}_4$), act as the cationic parts of these structures. Similar structural units occur in the crystal structure of $[\text{Hg}_3]\text{HgO}_2(\text{PO}_4)_2$ (see Table 5), where centrosymmetrical $[\text{Hg}_6\text{O}_2]$ *r*-octahedra are assembled into a framework by shared vertices and the $[\text{Hg}_3]^{4+}$ cluster cation; the $[\text{PO}_4]^{3-}$ tetrahedra together with the centrosymmetric empty oxygen octahedra separating them from each other form zigzag columns, which run through the cationic framework parallel to the *z* axis.

In the crystal structure of mineral wattersite $[\text{Hg}_2^{2+}]_2\text{Hg}^{2+}\text{O}_2\text{CrO}_4$, a more complex moiety acts as the basic unit, which in the ideal shape is known as stella quadrangula.¹¹¹ The central core of this unit comprises an empty $[\text{Hg}_4]$ tetrahedron (Hg...Hg 3.30–3.72 Å) capped with two $[\text{Hg}_4\text{O}]$ and two $[\text{CrHg}_3\text{O}]$ tetrahedra at each face; the rotation axis 2 of this group coincides with the crystallographic two-fold axis. Along the *z* axis, the groups are sharing Hg vertices (these Hg atoms reside in the inversion centres so that the Hg–Hg distance is $c/2 = 3.30$ Å); in other directions, these groups are bridged by the $[\text{Hg}_2]^{2+}$ dumbbells. Zigzag columns formed by the $[\text{CrO}_4]$ tetrahedra alternating with the centrosymmetrical empty oxygen octahedra are strongly elongated (the Cr–Cr distance is 5.407 Å), which implies that they play only a secondary role in the structure formation as compared to the cationic moiety. In the wattersite structure, the $[\text{Hg}_6\text{O}_2]$ cationic group can be represented in terms of both composition and geometry as a distorted *r*-octahedron in which one of the long Hg–Hg edges is shortened to ~ 3.5 Å. Taking into account two additional relatively close oxygen atoms of the $[\text{CrO}_4]$ tetrahedra along with the chromium atoms themselves, this group can be considered as an intermediate case between an *r*-octahedron and a more symmetric stella quadrangula.

The crystal structure of $\text{HgPb}_2\text{O}(\text{OH})\text{Br}_3$ reveals a similar fragment referred to as ‘heterocubane skeleton’ (see Table 5), which is similar to the aforementioned group in terms of both symmetry and dimensions.⁶¹ The central empty tetrahedron is formed by four Pb cations, four adjacent (face-sharing) tetrahedra contain interstitial oxygen anions, two mercury and two hydrogen atoms act as external vertices. This example as well as the structure of $\text{HgPb}_2\text{O}_2\text{CrO}_4$ described above demonstrate similar crystal chemistry of Pb^{2+} and Hg^{2+} cations in compounds of the approximate compositions.¹¹² Notwithstanding, there are substantial differences between them: the mercury atoms preferably form linear O–Hg–O fragments and thus tend to occupy equatorial positions of the *r*-octahedra, whereas the lead atoms tend to form three covalent bonds with the oxygen atoms and can occupy both equatorial and apical positions.

Quite different atomic groups occur in the HgCrO_4 structure (see Tables 6, 7): these include two $[\text{CrHg}_2\text{O}]$ triangles sharing a

Table 6. Crystallographic and crystal chemical parameters of mercury compounds with AO₄ tetrahedral anions (A = Cr, P, As or V).

Compound	Space group (<i>R</i> _F)	Unit cell parameters		<i>Z</i>	<i>d</i> _{calc} /g cm ⁻³	Interatomic distances /Å		Bond angles /deg.		Ref.
		translations /Å	angles /deg.							
Hg ₃ S ₂ CrO ₄ (edoylerite)	<i>P</i> 2 ₁ / <i>c</i> (0.079)	<i>a</i> = 7.528 <i>b</i> = 14.832 <i>c</i> = 7.463	β = 118.8	4	7.11	Hg—O 2.441–2.580 Hg—S 2.365–2.415	SHgS HgSHg	163.70–173.93 93.52–125.42		107
Hg ₅ S ₂ OCrO ₄ ≡ [Hg ₂ ²⁺](Hg ²⁺) ₃ S ₂ OCrO ₄ (deanesmithite)	<i>P</i> $\bar{1}$ (0.0292)	<i>a</i> = 8.129 <i>b</i> = 9.492 <i>c</i> = 6.894	α = 100.4 β = 110.2 γ = 83.0	2	8.14	Hg—Hg 2.536 Hg—O 2.11 Hg—S 2.352–2.442	HgHgS	167.6–171.3		95
HgCrO ₄	<i>P</i> 2 ₁ / <i>n</i> (0.049)	<i>a</i> = 7.342 <i>b</i> = 8.522 <i>c</i> = 5.202	β = 94.0	4	6.47	Hg—O 2.000–2.047	—			108
Hg ₃ O ₂ CrO ₄	<i>P</i> 3 ₂ 21 (0.0768)	<i>a</i> = 7.137 <i>c</i> = 10.017		3	8.45	Hg—O 2.161–2.170	OHgO HgOHg	166.27 102.83–122.47		96
HgPb ₂ O ₂ CrO ₄	<i>P</i> $\bar{1}$ (0.049)	<i>a</i> = 6.505 <i>b</i> = 7.201 <i>c</i> = 7.605	α = 91.82 β = 92.17 γ = 111.33	2	7.65	Hg—O 1.993–2.019 Pb—O 2.236–2.448	OHgO HgOHg	174.45 112.65		97
[Hg ₃] ₂ HgO ₂ (PO ₄) ₂	<i>P</i> 2 ₁ / <i>c</i> (0.028)	<i>a</i> = 6.2506 <i>b</i> = 9.9366 <i>c</i> = 9.6663	β = 95.783	2	7.65	Hg—Hg 2.652–2.705 Hg—O 2.031–2.600	OHgO HgHgHg	180 58.927–60.880		98
Hg ₅ O ₂ CrO ₄ ≡ [Hg ₂ ²⁺] ₂ Hg ²⁺ O ₂ CrO ₄ (wattersite)	<i>C</i> 2/ <i>c</i> (0.055)	<i>a</i> = 11.274 <i>b</i> = 11.669 <i>c</i> = 6.603	β = 98.19	4	8.891	Hg—Hg 2.526 Hg—O 2.06–2.16	HgHgO	153.3–169.5		94
AgHg ₂ PO ₄	<i>Pbam</i> —	<i>a</i> = 9.256 <i>b</i> = 8.614 <i>c</i> = 6.152		4	8.18	Hg—Hg 2.608 Ag—Ag 2.824 Hg—Ag 2.840, 2.941 Hg—O 2.224–2.348	HgHgO	101.2		109
[Ag ₃ Hg][(V,As)O ₄] (tillmannsite)	<i>I</i> $\bar{4}$ (0.037)	<i>a</i> = 7.727 <i>c</i> = 4.648		2	7.733	Hg/Ag—Hg/Ag 2.752, 2.738 (see ^a) Hg/Ag—O 2.395–2.449	—			110
[Ag ₃ Hg]VO ₄	<i>I</i> $\bar{4}$ (0.0365)	<i>a</i> = 7.7095 <i>c</i> = 4.6714		2	7.645	Hg/Ag—Hg/Ag 2.723, 2.739 Hg/Ag—O 2.373–2.444	Hg/Ag—Hg/Ag—Hg/Ag 59.60–60.198			100
[Ag ₂ Hg ₂] ₃ (VO ₄) ₄	<i>I</i> $\bar{4}$ 2 <i>d</i> (0.0508)	<i>a</i> = 12.6295 <i>c</i> = 12.566		4	7.657	Hg/Ag—Hg/Ag 2.684– 2.739	Hg/Ag—Hg/Ag—Hg/Ag 59.31–60.77			100
AgHgVO ₄	<i>C</i> 2 (0.0358)	<i>a</i> = 9.9407 <i>b</i> = 5.5730 <i>c</i> = 7.1210	β = 94.56	4	7.151	Hg—O 2.084–2.699 Ag—O 2.282–3.133	—			100
[Ag ₂ Hg ₂] ₂ (HgO ₂)(AsO ₄) ₂	<i>P</i> 3 ₁ <i>c</i> (0.0480)	<i>a</i> = 6.0261 <i>c</i> = 21.577		2	8.537	Hg/Ag—Hg/Ag 2.710– 2.774 Hg/Ag—O 2.214–2.597 Hg—O 2.00–2.24	Hg/Ag—Hg/Ag—Hg/Ag 59.56–62.38			100

^a Hg/Ag means that the respective sites are occupied statistically.

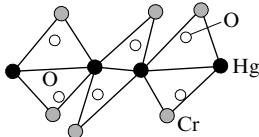
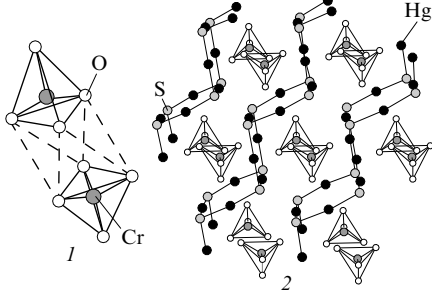
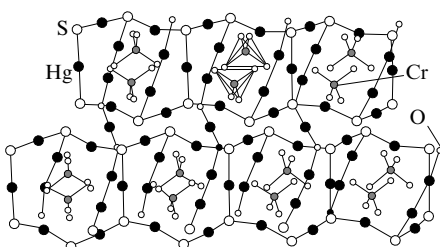
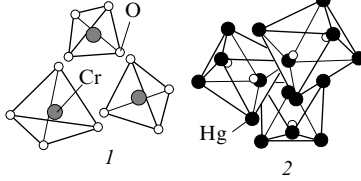
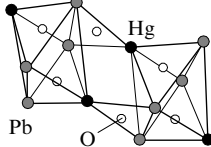
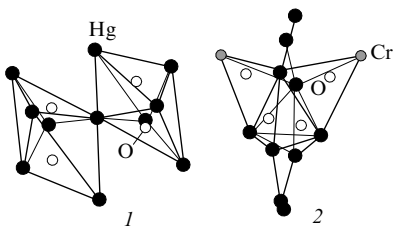
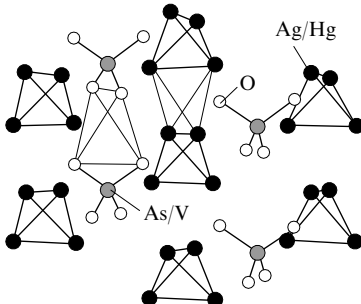
common Hg—Hg edge (~ 3.5 Å) (an inversion centre is located in the middle of this bond) forming a nearly planar rhombus.

A non-typical combination of cationic and anionic fragments occurs in the crystal structure of AgHg₂PO₄ (see Table 6).¹⁰⁹ Its cationic part is represented by an [Ag₂Hg₄] *r*-octahedron composed of two [Ag₂Hg₂] tetrahedra sharing an Ag—Ag edge with the crystallographic inversion centre in the middle. In contrast to the structures described above, the tetrahedra are substantially smaller since they contain no interstitial oxygen atoms. A pair of the [PO₄] tetrahedra separated by an empty oxygen octahedron constitutes the anionic fragment of the structure. The centres of the complex cations and anions are packed into a pseudocubic *I*-centred cell with the following parameters: $\mathbf{a}' = \frac{1}{2}\mathbf{a} + \frac{1}{2}\mathbf{b}$

(6.32 Å); $\mathbf{b}' = -\frac{1}{2}\mathbf{a} + \frac{1}{2}\mathbf{b}$ (6.32 Å); $\mathbf{c}' = \mathbf{c}$ (6.152 Å); $\alpha' = \beta' = \gamma' = 94.12^\circ$.

The recently solved tetragonal crystal structure of tillmannsite [Ag₃Hg][(V,As)O₄] (see Tables 6, 7)¹¹⁰ also includes an 'empty' [Ag₃Hg] cationic tetrahedron with three Ag and one Hg atoms statistically distributed over four vertices. The [(V,As)O₄]³⁻ tetrahedra alternating with empty oxygen tetrahedra and combined with them by shared edges form a ribbon going along the *z* axis, and the centres of both tetrahedra types have the $\bar{4}$ point symmetry. Two other sites with the 4 symmetry are located in the centres of the aforementioned cationic tetrahedron and another adjacent, also 'empty', [Ag₃Hg] tetrahedron sharing cation—cation edges with the former one. The latter tetrahedron is

Table 7. Anionic and cationic ‘rigid’ atomic moieties in mercury compounds with AO_4 tetrahedral anions ($\text{A} = \text{Cr}, \text{P}, \text{As}$ or V).

Compound	Types of anionic and cationic fragments	Anionic and cationic fragments	Ref.
HgCrO_4	isolated chains of the $[\text{Cr}_2\text{Hg}_2\text{O}_2]$ rhombs incorporating the $[\text{CrO}_4]$ tetrahedra		108
$\text{Hg}_3\text{S}_2\text{CrO}_4$ (edoylerite)	(1) isolated pairs of the $[\text{CrO}_4]_2$ tetrahedra; (2) zigzag ribbons of the $[\text{Hg}_4\text{S}_4]$ rings		107
$\text{Hg}_5\text{S}_2\text{OCrO}_4 \equiv [\text{Hg}_2^{2+}](\text{Hg}^{2+})_3\text{S}_2\text{OCrO}_4$ (deanesmithite)	isolated pairs of the $[\text{CrO}_4]_2$ tetrahedra inside a spatial framework of the $\text{S}-\text{Hg}-\text{Hg}-\text{O}$, $\text{S}-\text{Hg}-\text{S}$ and $\text{O}-\text{Hg}-\text{O}$ bonds		95
$\text{Hg}_3\text{O}_2\text{CrO}_4$	(1) isolated helical chains of tetrahedra $[\text{CrO}_4]_\infty$; (2) a spatial framework of the $[\text{Hg}_6\text{O}_2]$ r -octahedra linked by vertex-sharing		96
$\text{HgPb}_2\text{O}_2\text{CrO}_4$	ribbons of the $[\text{Hg}_2\text{Pb}_4\text{O}_2]$ r -octahedra linked by the $[\text{HgPb}_2\text{O}]$ triangles		97
$\text{Hg}_5\text{O}_2\text{CrO}_4 \equiv [\text{Hg}_2]_2^{2+}\text{Hg}^{2+}\text{O}_2\text{CrO}_4$ (wattersite)	(1) a fragment of a chain composed of distorted $[\text{Hg}_6\text{O}_2]$ r -octahedra; (2) $[\text{Cr}_2\text{Hg}_6\text{O}_4]$ stella quadrangula, a fragment of the cationic framework		94
$[\text{Ag}_3\text{Hg}][(\text{V},\text{As})\text{O}_4]$ (tillmannsite)	alternating pairs of r -octahedra composed of $[\text{Ag}_3\text{Hg}]$ ‘empty’ cationic tetrahedra and ribbons of the $[(\text{V},\text{As})\text{O}_4]$ anions sharing edges with empty O-tetrahedra		110

tetragonally distorted along the z axis [the Ag(Hg)–Ag(Hg) side edges are 3.316 Å]. As in the AgHg₂PO₄ structure, the two adjacent edge-sharing cationic tetrahedra can be considered as a deformed ‘empty’ r -octahedron. The overall crystal structure is built up of ribbons of such r -octahedra packed in the xy projection together with the ribbons of anionic tetrahedra in a herringbone manner. The positions of (Ag,Hg) and (V,As) cations themselves form a pseudocubic F -centred sublattice with a volume constituting 2/5 of the unit cell volume with the following parameters: $a' = 3/5a + 1/5b = 4.90$ Å; $b' = -1/5a + 3/5b = 4.90$ Å; $c' = c = 4.648$ Å; $\alpha' = \beta' = \gamma' = 90^\circ$.

A series of compounds with the [Ag,Hg]₄ clusters have been synthesised within the Ag–Hg–E–O system ($E = V^{5+}$, As^{5+}) (see Table 6). In the tetragonal structure of [Ag₃Hg]VO₄, the tetrahedral cluster is formed by the statistical distribution of the Ag and Hg atoms in a 3 : 1 ratio over the available positions. Meanwhile, the tetragonal clusters corresponding to the [Ag₂Hg₂] stoichiometry also with the statistical distribution of Ag and Hg with a mean metal–metal distance of 2.72 Å are present in tetragonal [Ag₂Hg₂]₃(VO₄)₄ and trigonal [Ag₂Hg₂]₂HgO₂·(AsO₄)₂. Assuming the [Ag,Hg]₄ moieties and the VO₄ or AsO₄ tetrahedra to be pseudospherical ‘building blocks’, the structures of [Ag₃Hg]VO₄ and [Ag₂Hg₂]₂HgO₂(AsO₄)₂ can be described as a cubic close packing with the (ABC) stacking sequence and a mixed-layer packing with the ABACACAB stacking sequence, respectively, where A is the layer formed by VO₄ or AsO₄, B and C are the layers formed by the [Ag₂Hg₂] clusters. The crystal structure of [Ag₂Hg₂]₃(VO₄)₄ cannot be described in a similar way. It is interesting that another compound synthesised in this system, AgHgVO₄, which has a monoclinic structure, contains no cluster groups; the cations therein are characterised by usual coordination types: Ag and V are tetrahedrally coordinated by oxygen, the Hg coordination is a distorted octahedron.¹⁰⁰

Therefore, it might be concluded that the crystal structures considered above represent the net result of two major structure-forming factors: the ‘chemical’ one, which induces the formation of stable atomic fragments that can undergo only minor changes after their formation and the crystallographic one, which promotes their dense packing into highly symmetric extended assemblies by fixing centres of these groups or single atoms at specific families of crystallographic planes.

V. The modular principle in the structure formation of mercury oxo- and chalcogenides

The presence of linear Y–Hg–Y groups ($Y = O, S, Se$ or Te) is commonly accepted as a specific structural feature of mercury oxo- and chalcogenides. Additionally, trigonal pyramidal [YHg₃] groups, in which the Y atom is connected to three mercury atoms forming variable Hg–Y–Hg bond angles in a range from 110° to 90° frequently occur in the crystal structures of ternary chalcogenides with the 3 : 2 : 2 stoichiometry, *i.e.*, Hg₃Y₂X₂ ($Y = S$ or Se , Te ; $X = Cl, Br$ or I). These groups can be assembled into various one-, two- or three-dimensional motifs.¹ Typically, large monovalent halogens ($X = Cl, Br$ or I) in these structures merely fill the space between chains, ribbons or frameworks formed by these stereochemically active structural elements and compensate for their positive charge. A more thorough analysis shows¹¹³ that the halogen atoms tend to form a pseudocubic primitive sublattice with a periodicity constant of 4.4–5.4 Å, depending on the nature of X.

The original software package KAP-PLATS⁷ can be efficiently applied to objectively evaluate the role played by all types of atoms in the crystal structure formation and identify common structural features of these compounds. As a starting postulate, this approach assumes that the atoms most important for the structure formation are characterised by most densely occupied atomic planes within the range of interplane distances d_{hkl} of the order of shortest interatomic distances. Furthermore, an analysis of the distribution of special positions, *i.e.*, of the location of

different types of atoms with respect to space group symmetry elements, is of importance. This is due to the fact that any special position represents a locus of intersection of both symmetry elements and closely packed atomic layers and thus they serve as natural boundaries in dividing a structure into fragments.

1. The role of halogen atoms in the structures of ternary mercury chalcogenides Hg₃Y₂X₂ ($Y = S, Se$ or Te ; $X = Cl, Br$ or I)

In the crystal structure of α -Hg₃S₂Cl₂ (corderoite) (see Table 1), a single basis Cl atom occupies a special position 8(a) on a three-fold axis. These atoms form a primitive cubic sublattice with a translation vector $a' = a/2 = 4.47$ Å. Deviations of the Cl atoms from expected ideal positions of the sublattice nodes do not exceed 0.15 Å. The sulfur atoms are located in the centres of cubes of the Cl sublattice, their deviations from the geometric centres being ~ 0.3 Å. The mercury atoms centre three of six faces intersecting in a vertex deviating from the centres by ~ 0.5 Å. Therefore, the chlorine atoms (as well as other atoms) can shift along the three-fold axis and appear most rigidly ordered in the lattice since they are located in the intersection of the (200), (020) and (002) planes and planes derived from them, such as (222).

A similar situation is observed in the structure of β -Hg₃S₂Cl₂ (see Table 1); its unit cell comprises 64 cubic Cl sublattices ($a' = a/4 = 4.48$ Å). The Cl atoms are dominantly localised in special positions and are most rigidly ordered by systems of the {004}, {044} and {444} planes, which intersect in nodes of the sublattice. The sulfur atoms localised in the centres of the Cl sublattices are ordered nearly as rigidly, whereas the mercury atoms deviate substantially from the centres of faces of the Cl sublattice.

In the monoclinic structure of β -Hg₃S₂Br₂ (see Table 1), all Br atoms are located on the mirror reflection planes, which determine one of the lattice parameters of the Br sublattice as $b/2$. Two other lattice parameters are $a/4$ and $c/2$, since the intersection points of the (400), (020) and (002) crystallographic planes most densely occupied by the Br ions form a pseudocubic primitive sublattice with exactly these translation vectors: $a' = 4.42$, $b' = 4.69$ and $c' = 4.72$ Å. The S atoms localised in the centres of cubes of the Br sublattice are ordered by the same systems of crystallographic planes but are phase-shifted by 180°. The ordering of the S atoms is again less rigid than that of the Br atoms due to the fact that the sulfur atoms occupy general positions in the structure. The disposition of the Hg atoms is even less ordered.

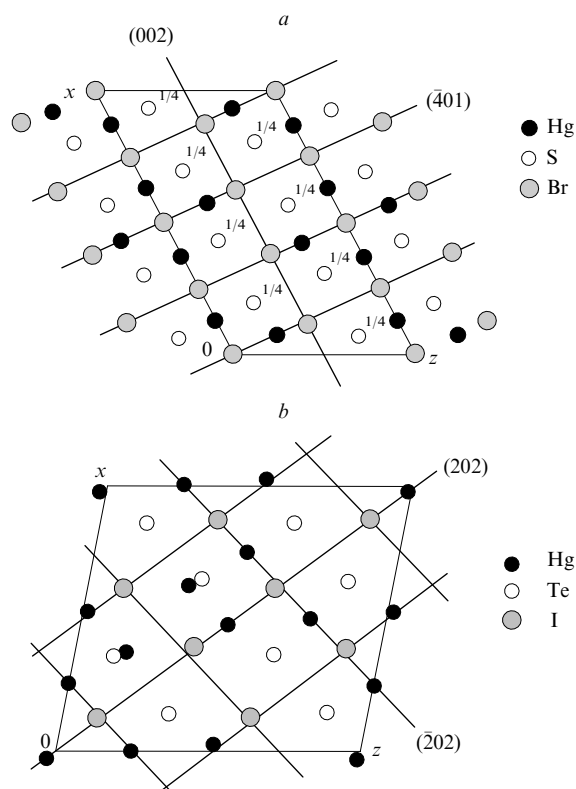
In the crystal structure of the α -modification of this compound (α -Hg₃S₂Br₂) (see Table 1), a unit cell is constructed from the Br sublattices in a different manner as compared to the β -phase, thus the sublattice of nodes occupied by Br is formed by the intersection locus of the (401), (020) and (002) crystallographic planes, which cut a pseudocubic sublattice with $a' = a/4 = d_{401} = 4.50$, $b' = b/2 = 4.64$ and $c' = d_{002} = 4.62$ Å (Fig. 23 a). The sulfur atoms are arranged nearly as regularly as the bromine atoms, whereas the mercury atoms are distinctly shifted from the centres of faces of the Br cubes.

The unit cell of Hg₃Te₂I₂ (see Table 1) is constructed of the iodine sublattices in an even more complicated manner. It is formed by the intersection of families of the (202), (020) and (202) crystallographic planes. They cut a parallelepiped with edges of 5.47, 4.85 and 5.45 Å and angles close to 90° (Fig. 23 b).

Therefore, the structures of Hg₃Y₂X₂ compounds ($Y = S, Se, Te$) despite their formal diversity are constructed, to the first approximation, from ‘cubic’ modules with the halogen atoms in the vertices, chalcogen atoms in the centres and the mercury atoms in the centres of three faces intersecting in a common vertex. Such a cubic module is further attached to a common motif by bonds going out from the centres of three faces towards the centres of neighbouring modules. Each of them can be connected by sharing a face in four possible orientations differing from each other by the rotation around the Y–Hg–Y bond by 90°. Using this algorithm, various puckered ribbon, layered and spatial frameworks can be assembled from them (Table 8). The dimensions of a

Table 8. The Hg–Y motifs in the structures of 3 : 2 : 2 ternary mercury chalcogenides.

Compound	Hg–Y motif type	Examples of isomorphous compounds	Ref.
α -Hg ₃ S ₂ Cl ₂ (corderoite)	a uniform framework of the –Hg–S–Hg– bonds devoid of closed rings (see Fig. 2)	α -Hg ₃ Se ₂ Cl ₂ , Hg ₃ Te ₂ Cl ₂ , Hg ₃ Te ₂ Br ₂ , Hg ₃ S ₂ F ₂ , Hg ₃ Se ₂ F ₂	12, 15, 33, 34
β -Hg ₃ S ₂ Cl ₂	isolated [Hg ₁₂ S ₈] groups (see Fig. 3)	Hg ₃ S ₂ Cl _{1.54} Br _{0.46} , α -Hg ₃ S ₂ Br ₂ , Hg ₃ Se ₂ I ₂ (monoclinic), Hg ₃ S ₂ Br _{1.5} Cl _{0.5} (monoclinic), Hg ₃ S ₂ Br _{1.5} Cl _{0.5} (cubic)	22, 23, 36, 42, 43
β -Hg ₃ S ₂ Br ₂	the [Hg ₃ S ₂] ²⁺ layers incorporating the [Hg ₄ S ₄] rings in two different orientations (see Fig. 4)	γ -Hg ₃ S ₂ Cl ₂ , Hg ₃ Se ₂ Br ₂ , Hg ₃ S ₂ Cl _{1.5} Br _{0.5} (monoclinic), Hg ₃ S ₂ ClI (radtkelte), Hg ₃ Te ₂ BrI	23, 35, 36, 39, 41, 42
Hg ₃ S ₂ I ₂	[Hg ₃ S ₂] ²⁺ double crankshaft ribbons (see Fig. 5)	Hg ₆ S ₄ Br ₂ ClI (grechishchevite), Hg ₃ Se ₂ I ₂ (orthorhombic)	24, 40
Hg ₃ Te ₂ I ₂	a spatial framework with identically oriented closed [Hg ₄ Te ₄] rings (see Fig. 6)	–	37, 38

**Figure 23.** Projections of the crystal structures of Hg₃Y₂X₂.

(a) A partial projection $0 \leq y \leq 1/2$ of the crystal structure of α -Hg₃S₂Br₂ onto the xz plane; the Br sublattice is formed by the (401), (020) and (002) planes;

(b) a projection of the crystal structure of Hg₃Te₂I₂ onto the xz plane; the I sublattice is formed by the (202), (020) and (020) planes.

module determine the unit cell dimensions and partially the general symmetry of the structure, although the prevailing contribution is made by the specific pattern of the covalent bonding distribution.¹¹³

Signatures of the modular structure preserved to a greater or lesser extent can be observed in the crystal structures of a number of mercury oxohalides and more complex compounds.

2. The role of halogen atoms in the structures of mercury oxohalides

In the crystal structure of the orthorhombic mineral pinchite Hg₅O₄Cl₂ (see Table 3), the halogen atoms form a planar network with the translation periods of the Cl sublattices of 4.13 and 4.34 Å. This network is centred by the mercury atoms. In addition to these eight centring mercury atoms, a unit cell contains 12

mercury atoms, which constitute together with the oxygen atoms a second layer, where two distorted tetragonal networks of oxygen atoms sandwich a hexagonal network composed of the mercury atoms. The commensurability of the (Hg₄Cl₄) and (Hg₆O₈) networks is provided by a change in the geometry of the latter, which gives rise to a non-typical flattened tetrahedral oxygen coordination of the mercury atoms within the hexagonal network. Meanwhile, the Hg atoms of the tetragonal network are characterised by the linear O–Hg–O coordination supplemented to an octahedral one by a square of the Cl atoms.

The halogen atoms play a key role in the structure formation of some low-valence mercury halides. In particular, in the crystal structure of the cubic mineral kuznetsovite [Hg₃]AsO₄Cl (see Table 4), the Cl atoms occupy special positions on a three-fold axis (xxx , $x \approx 0.23$). A point on the three-fold axis with a coordinate $x = 0.25$ corresponds to the intersection of families of the (200), (020) and (002) crystallographic planes (with phases of 180° for all planes), which cut a unit cell into eight cubes with an edge $a' = a/2 = 4.19$ Å. A half of nodes of this sublattice are occupied by the Cl atoms according to the chessboard pattern; the centres of the sublattices are alternately filled with the [Hg₃]⁴⁺ triangles and [AsO₄]^{3–} tetrahedra. In the crystal structure of cubic eglestonite [Hg₂]₃O₂HCl₃ (see Table 4), which is characterised by a lattice parameter nearly doubled as compared to that of kuznetsovite, the cubic sublattice ($a' = a/4 = 4.01$ Å) is formed by the intersection of families of the (400), (040) and (004) crystallographic planes, which gives rise to 64 sublattice nodes per unit cell. Among them, 48 nodes are occupied by the Cl atoms and 16 nodes remain vacant. The centres of the sublattices virtually coincide with the centres of the [Hg₂]²⁺ dumbbells (again 48 centres out of 64 sublattices are occupied). Two latter examples demonstrate that in the absence of large S^{2–} anions, space-filling structural units larger than the oxygen atoms, such as [Hg₃]⁴⁺, [AsO₄]^{3–} or [Hg₂]²⁺ moieties are required to preserve the cubic sublattice of halogen atoms. In both cases, the sublattice has vacant nodes, which gives rise to its slight contraction with respect to the sublattice with no vacancies.¹¹³

3. General trends in the structure formation and an analysis of the structure-forming factors in the crystal structures of mercury oxo- and chalcogenides

The crystal structures of mercury oxo- and chalcogenides fully confirm general regulation of the structure formation formulated by Borisov *et al.*^{5,6,114} Rigid multiatomic fragments, *e.g.*, [M₄O], [M₆O₂], [M₁₀O₄], [AO₄], *etc.*, are most probably generated in a reaction medium even prior to the initiation of crystallisation. The forces driving the transition of a substance into the crystalline state are substantially weaker than the interatomic interactions within these fragments, thus they remain nearly unchanged upon the nucleation and crystal growth. The dimensions and shape of the rigid multiatomic fragments determine the unit cell parameters and partially the space symmetry group, since the sym-

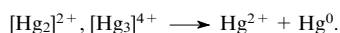
metry element intrinsic to these groups often convert into the symmetry elements of the whole crystal structure.

In some complicated cases, the software package KAPPLATS⁷ helps a lot in the analysis of structure-forming factors. Among the crystallographic planes it separates those are closely populated by atoms or gravity centres of rigid multiatomic moieties.^{115, 116} The crystal structure is then interpreted as a result of the spatial ordering of these atoms and centres of moieties by a set of basis crystallographic planes.⁶ The stability of the crystal structure is increased if these planes are related to each other by symmetry operations (even provided that these operations are slightly violated^{6, 114}).

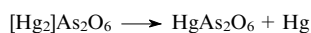
As has been shown by Borisov *et al.*,¹¹⁶ the relative space-filling density for isolated Hg atoms is significantly lower than that for centres of rigid fragments, which implies that the effect of the ordering of isolated mercury atoms is weakly pronounced and the overall structure is predominantly determined by the ordering of centres of rigid atomic fragments.

The spatial segregation of Hg cations with different oxidation states over different layers¹¹⁶ facilitates solid-state mercury disproportionation reactions, since the pre-existing layers with bivalent mercury are retained thus stabilising the structure-forming motif, whereas the low-valence mercury (*i.e.*, Hg in the $[\text{Hg}_3]^{4+}$ and $[\text{Hg}_2]^{2+}$ clusters) partly leave the structure. It has to be noted that naturally occurring compounds with 'cluster' mercury, *e.g.*, $[\text{Hg}_2]^{2+}$ or $[\text{Hg}_3]^{4+}$ moieties, are characterised by a cation-to-anion ratio distinctly different from that of more common rock-forming minerals. In particular, in known mercury minerals, this ratio is close to unity, whereas it is about 1.5 in poyarkovite. The minerals growing in an anion-deficient medium are obliged to saturate the valence bonds by forming Hg...Hg contacts, which gives rise to cluster fragments. Due to the deficit, anions can act as a core for the formation of polyatomic groups, which probably exist in a mother liquor even prior to the initiation of crystallisation.

Since the total sequence of solid-state transformations happening to a mercury mineral upon its transition into an oxygen-rich medium and giving rise to the complete mercury oxidation, which is actually realised in nature, cannot be elucidated, the relevant information can be retrieved from an analysis of methods for the synthesis of compounds containing the $[\text{Hg}_3]^{4+}$ and $[\text{Hg}_2]^{2+}$ clusters and their stepwise oxidation as realised under laboratory conditions. Typically, the synthesis is accomplished starting from Hg^{2+} oxides and other components in sealed evacuated ampoules at a temperature $> 400^\circ\text{C}$ or under hydrothermal conditions at a sufficiently high temperature. It would be reasonable to assume that minerals with the $[\text{Hg}_3]^{4+}$ and $[\text{Hg}_2]^{2+}$ clusters are formed in nature under similar conditions. When the minerals are transferred to the earth's surface, the mercury disproportionation processes are initiated:



In a laboratory, the disproportionation of 'cluster' mercury to Hg^{2+} and Hg^0 is typically carried out in an open system, since mercury vapour is liberated. The process proceeds at a high rate at $200\text{--}450^\circ\text{C}$, however presumably, this process proceeds at a lower temperature and thus at a lower rate under natural conditions. A pair of closely related compounds, $[\text{Hg}_2]\text{As}_2\text{O}_6$ and HgAs_2O_6 , offer a very illustrative example of this process.¹¹⁷ These compounds include identical layers of interlinked AsO_6 octahedra; layers formed by the Hg cations are also similar provided that the centres of the $[\text{Hg}_2]^{2+}$ dumbbells are taken as cations in the former case. Therefore, the reaction



can be interpreted as a progressive withdrawal of a half of the mercury atoms from the cationic layers of the $[\text{Hg}_2]\text{As}_2\text{O}_6$ structure, which gives rise to the replacement of the $[\text{Hg}_2]^{2+}$ dumbbells with single Hg^{2+} cations. This transformation is

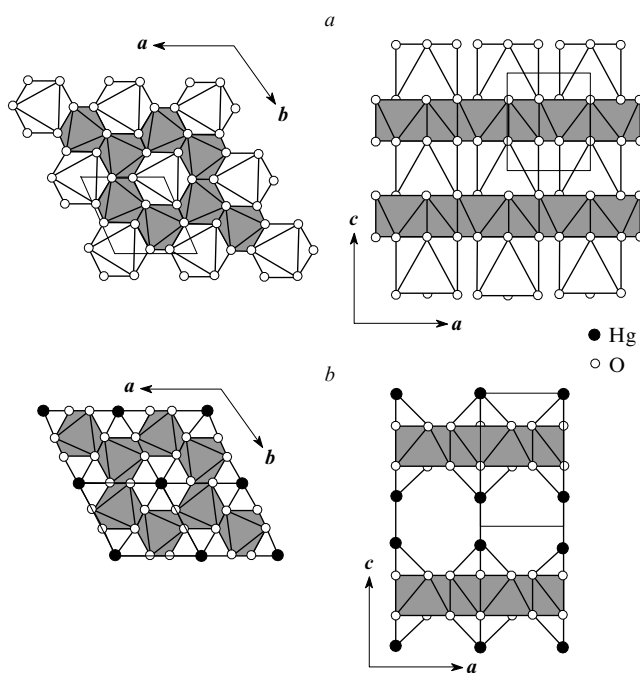


Figure 24. Projections of the crystal structures of HgAs_2O_6 (a) and $[\text{Hg}_2]\text{As}_2\text{O}_6$ (b) drawn to a common scale.

Plain octahedra denote HgO_6 , grey octahedra denote AsO_6 ; the As atoms are not shown for clarity, the Hg atoms are shown only in Fig. b. Although the projections onto the *ab* plane are identical, those onto the *ac* plane differ by a length of the Hg–Hg dumbbell (2.5 \AA) along the *c* axis.

accompanied only by a decrease in the *c* parameter of the hexagonal lattice (Fig. 24).

The conversion of a part of mercury atoms from cluster moieties into the bivalent state with the simultaneous withdrawal of free mercury metal from the structure is well possible, especially in the surface regions of crystals owing to the fact that many crystal structures reveal large voids and channels (in particular, channels with a diameter as large as $\sim 13.6\text{ \AA}$ are present in the structure of the mineral szymanskiite¹¹⁸). This process can serve as a source of mercury in natural waters and atmosphere.¹¹⁹

The segregation of different types of mercury over different layers observed in the structures of some minerals¹¹⁶ can be a consequence of processes directed towards most stable forms, which slowly proceed under natural conditions. Solid-state transformations changing the overall composition but retaining the structure of large fragments occur most easily exactly in layered compounds. The mechanism of the 'layer-by-layer' transformation was suggested by Hawthorne *et al.*⁷⁰ within a discussion of the crystal structures of monoclinic terlinguaite and orthorhombic pinchite, which are tightly associated in nature.

The important role in the crystal structure formation played by large anions (Cl, Br and I) has already been noted above as a part of discussion concerning mercury chalcogenides (see Tables 1 and 8). Mercury and chalcogen atoms are bound by strong covalent bonds and thus are incorporated into the structure as extended atomic groups with constrained variations in the bond lengths and angles. In contrast, quite bulky and large halide anions are not involved into strictly oriented chemical bonding and thus are free to form a more ordered sublattice.¹¹³

The phenomenon of ordering of various atomic groups by independent systems of crystallographic planes has earlier been observed for other classes of compounds, including rare-earth metal sulfides.¹²⁰ Normally, the subdivision into groups is performed according to the spectrum of shortest cation–cation, anion–anion and cation–anion interatomic distances. Within

this approach, the effective size of an atom or atomic group rather than only their chemical nature are of importance.⁶

Therefore, the crystal structure formation in mercury compounds can be formally subdivided into two steps.⁶ As the first step, larger 'building blocks' are ordered by basis families of planes (which are the coordinate planes constituting the translation sublattice of these large blocks). As the second step, which proceeds simultaneously, smaller building blocks and single atoms are ordered by basis planes of independent sublattices within a range of shorter interplane distances d_{hkl} . Some atoms of large building blocks are also involved in the second step. The crystal formation means that an initial set of independent sublattices possible for all combinations of atoms and 'rigid' atomic groups converts into a common lattice (least common multiple) with a unit cell composed of an integer number of sublattices and the ordering families of planes become crystallographic planes, which requires the respective indices to be integers.

VI. Crystal chemical features of the MHgYX compounds (M = Cu or Ag; Y = S or Se; X = Cl, Br or I)

1. An analysis of the anion packing

According to several groups of authors,^{46–52} the two-layer hexagonal close packing is realised in the crystal structures of MHgYX (M = Cu or Ag; Y = S or Se; X = Cl, Br or I). On the other hand, the anion packing therein is rather close to body-centred cubic packing, at least for some representatives of this class of compounds, according to our results.¹¹³

A comprehensive analysis of all closely packed anionic planes for typical structures of MHgYX^{46–52} as well as of Ag₂HgSI₂ (Ref. 52) and CuHg₂S₂I,⁴⁷ which are characterised by similar stoichiometries, was performed using the software package KAP-PLATS⁷ to establish the character of their anionic packings. It was demonstrated that idealised hexagonal close packing (hcp) and body-centred cubic packing (bcc) differ from each other only in the stacking sequence of dense hexagonal layers³⁶ and some distortions of the layers themselves, which complicates the straightforward assignment of real structures to one of the two packing types.⁵⁸

For all the structures, the degree of anion ordering significantly (by 15%–20%) exceeds that of cation ordering for the same range of interplane distances d_{hkl} essential for the crystal packing formation. This is surprising taking into account the respective results for the structures of heavy metal fluorides, oxides and sulfides,^{114,120} where cations are more ordered.

In the series of the compounds considered, the anion packing varies from ideal hcp (*e.g.*, in CuHgSI)^{47,48} to ideal bcc (*e.g.*, in Ag₂HgSI₂).⁵² This result requires additional elucidation for the cases of large differences in the sizes of the Y^{2–} and X[–] anions ($r = 1.84$ Å and 2.20 Å for S^{2–} and I[–], respectively). According to an analysis of the arrangement of all atoms in these structures,⁵⁸ the relatively small radii of an S^{2–} anion is compensated for by the fact that all direct S–S contacts, which could have distorted the packing (due to a large difference as compared to typical lengths of the I–I or I–S contacts) involve cations, which results in either linear S–Hg–S or bent S–M–S fragments, and the S...S contact appears comparable in length with the S–I and I–I distances (in the former case, S...S ~ 4.7 Å). Therefore, the mercury atoms, due to the covalent Hg–S and, to a lesser extent, M–S interactions, actually occupy positions with a coordination number of 2, which are non-typical from the classical viewpoint, thus acting as an auxiliary spacer to the S–S contact, which apparently increases its length to that of the I–I contact of the anion packing. The resultant commensurability of the strongest covalent S–Hg–S bond and the van der Waals contact between the large I[–] anions enables the regularity of a stable collective packing involving anions with different sizes.

Within this concept, the reason for a less ordered arrangement of cations becomes evident: it is controlled by the covalent interactions between cations and anions and between cations, which is a more powerful factor than mere ordering. As has been mentioned in Section IV.4, weak attractive Hg...Hg interactions in the oxo-centred [Hg₄O] tetrahedra exist at a Hg–Hg distance of ~ 3.5 Å.⁷⁹ Thus it would be reasonable to consider the crystal structures in more detail taking into account both well known Hg–Y interactions and possible Hg...Hg and Hg...M interactions.

2. The structure-forming role of the [(Hg,M)₄Y] tetrahedra

According to structural studies on quaternary chalcogenides MHgYX (M = Ag or Cu; Y = S or Se; X = Cl, Br or I) and closely related Ag₂HgSI₂ and CuHg₂S₂I, the S^{2–} anions in these compounds are characterised by the stable tetrahedral surrounding by cations (in contrast to the umbrella-like environment typical of mercury chalcogenides). A similar environment of the sulfur anions is observed in the structures of Hg₂PbS₂I₂ (Ref. 54), perroudite Hg_{4.6}Ag_{4.4}S_{4.6}(Cl,Br,I)_{4.8} (Ref. 55) and capgaronnite HgAgS(Cl,Br,I),⁵⁶ where the [M₂Hg₂S] tetrahedra similar to the oxo-centred [Hg₄O] tetrahedra present in mercury oxosalts can be identified. These tetrahedra can be considered as Y-centred; it would be reasonable to assume that it is the sp³-hybridised orbitals of the chalcogen atoms that are involved into the bonding with the cations, since sulfur and selenium are similar to oxygen in terms of the valence electron structures.⁵⁸

Experimental data summarised in Table 9 indicate that the cationic tetrahedra surrounding the S^{2–} anions (only one example is available for Se^{2–}) are sufficiently stable in terms of the geometry parameters.

Tetrahedron edge	Length / Å
Hg–Hg	3.56–3.60
Cu–Cu	4.08–4.14
Hg–Cu	3.48–3.90
Hg–Ag	3.63–4.08
Ag–Ag	4.56–4.83

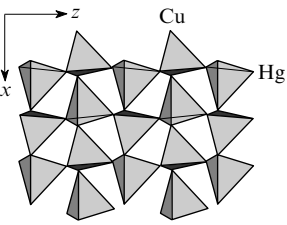
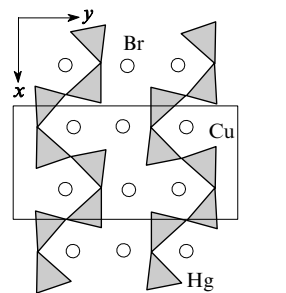
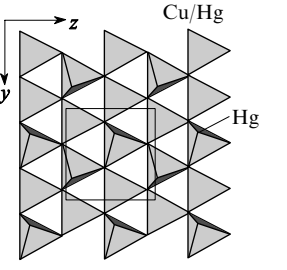
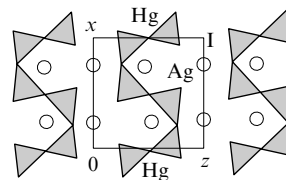
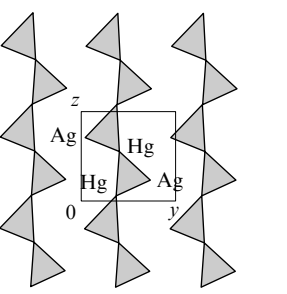
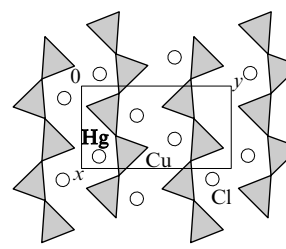
Noting the small variations in the cation–anion distances (see Table 2), the [(M,Hg)₄Y] tetrahedra can be considered as 'rigid' atomic moieties (building blocks), which are incorporated into a crystal structure as a whole. This is due to both well known Hg–S and Hg–Hg covalent interactions and less elucidated M–S, M–Hg and M–M bonding.

In the crystal structure of CuHgSI, a chain of the [Cu₂Hg₂S] tetrahedra going along the 2₁ axis parallel to the *z* axis acts as the 'load-bearing' structural unit, which includes the strongest inter-atomic interactions, *i.e.*, Hg–S and Hg...Hg. A unit cell includes two such chains, *viz.*, in the origin and in the centre of the *xy* projection. The chains are assembled into a common framework by sharing Cu vertices, the I atoms coordinated (like the S atoms) by four cations (2 Hg + 2 Cu) fill the interchain cavities.

In the structure of CuHg₂S₂I, the [(Cu,Hg)₄S] tetrahedra are assembled into a layer in the *yz* plane by sharing (Hg,Cu) vertices. The layers are further assembled into a framework by sharing Hg vertices. As outlined in Table 9, some edges of the [(Cu,Hg)₄S] tetrahedra are shorter than 3.8 Å, which assumes attractive interactions.

In both CuHg₂S₂I and Ag₂HgSI₂, mercury and sulfur are present in a 1 : 1 ratio. Although the anion packings in the two structures are similar (positions of the S and I ions are interchanged), the covalent skeleton in Ag₂HgSI₂ involves only isolated chains composed of the [Ag₂Hg₂S] tetrahedra going along the *z* axis together with a virtually linear rows of the Hg atoms with Hg–Hg ≈ *c*/2 = 3.55 Å. In a projection onto the *xy* plane, the chains of the [Ag₂Hg₂S] tetrahedra go through the origin and the centre of the unit cell composing an approximate hexagonal packing of these isolated one-dimensional fragments in this cross-section.

Table 9. Frameworks of the $[(M,Hg)_4Y]$ tetrahedra in the structures of some quaternary mercury chalcogenides.

Compo- und	Metal–metal distance ^a /Å	Motif of the $[(M,Hg)_4Y]$ tetrahedra	Ref.	Compo- und	Metal–metal distance ^a /Å	Motif of the $[(M,Hg)_4Y]$ tetrahedra	Ref.
CuHgSI	3.589 (Hg–Hg) 3.617–3.970 (Hg–Cu) 4.078 (Cu–Cu)		47	CuHgSBr (295 K) (see ^c)	3.568 (Hg–Hg) 3.530–3.831 (Hg–Cu) 4.124 (Cu–Cu) 3.576 (Hg–Hg) 3.481–3.881 (Hg–Cu) 4.124 (Cu–Cu)		46
CuHg ₂ S ₂ I	3.775–4.152 (Hg–Hg/Cu) ^b 3.696–3.832 (Hg/Cu–Hg/Cu)		47	β -AgHgSI	3.598 (Hg–Hg) 3.999 (Hg–Ag) 3.776 (Hg–Ag) 4.648 (Ag–Ag)		50
Ag ₂ HgSI ₂	3.559 (Hg–Hg) 3.629–4.112 (Hg–Ag) 4.555 (Ag–Ag)		52	CuHgSeCl	3.483 (Hg–Hg) 3.592, 4.121 (Hg–Cu) 4.253 (Cu–Cu)		49

^a For the Hg–Y, Cu–Y and Ag–Y distances, see Table 2; ^b Hg/Cu means that the respective site is statistically occupied by Hg and Cu (see Fig. 13);

^c data for crystallographically independent $[(M,Hg)_4Y]$ tetrahedra are given.

In the crystal structures of CuHgSBr (295 K),⁴⁶ the vertex-sharing $[Cu_2Hg_2S]$ tetrahedra form puckered layers lying in the xz plane. The mercury atoms in these structures are arranged into zigzag rows [in contrast to the linear Hg–Hg columns that determine the respective unit cell parameters in the above structures (the double Hg–Hg distance is ~ 7 Å)]. Two Hg–Hg–Hg fragments intersect at an angle close to 90° and thus $a \approx 7\sqrt{2} = 9.84$ Å. A unit cell accommodates two layers related to each other by a glide-reflection plane associated with a shift by $b/2 = 9.17$ Å. Meanwhile, unit cells of similarly organised β -AgHgSI and CuHgSBr (358 K) accommodate only one such layer. These structures feature a short translation (~ 4 Å) normal to the mirror reflection plane.

In the structure of CuHgSeCl, the Se^{2-} anions are also characterised by the tetrahedral environment (2 Cu and 2 Hg, see Table 9). The structure is based on chains of the $[Cu_2Hg_2Se]$ tetrahedra formed around linear rows of the Hg^{2+} cations with the doubled Hg–Hg distance of $a = 6.94$ Å. The chains are assembled into a layer in the xz plane by sharing Cu vertices. Due to the short translation c (4.25 Å), the Cl atoms lie in the same plane as the Cu atoms, thus the layers formed by the $[Cu_2Hg_2Se]$ tetrahedra are separated from each other by layers of the Cl^- anions. In the structure of α -AgHgSI,⁵¹ symmetry factors do not prevent the formation of a framework of vertex-sharing $[Ag_2Hg_2S]$ tetrahedra; cavities of the framework are occupied by the large iodine atoms.

3. Crystal structure-forming factors for the MHgYX structures

Summarising structural data outlined above, we conclude that it is the Hg–Y covalent interactions and Hg \cdots Hg bonding contacts that act as the prevailing structure-forming factors in the crystals of quaternary mercury chalcogenides.⁵⁸ Linear or zigzag $\cdots Hg\cdots Hg\cdots Hg\cdots$ chains (with Hg–Hg distances of ~ 3.5 Å) determine one of the unit cell dimensions. Other unit cell dimensions are dictated by the necessity to combine the $[(M,Hg)_4Y]$ tetrahedra by vertex-sharing. The commensurability of the Hg \cdots Hg, X \cdots X and X \cdots Y contacts enables the close packing of anions and a rather high symmetry of the resultant crystal structure. The stability of a structure towards isomorphous substitution of components can be regarded as an additional argument in favour of its robustness. In particular, the isomorphous substitution $HgS \rightleftharpoons AgX$ over a wide concentration range with the preservation of the crystal structure type (minerals perroudite⁵⁵ and capgaronnite⁵⁶) has been reported. Structural investigations into the synthetic analogues of minerals greischchevite, lavrentievite, arzakite, radtkite (corresponding to the $Hg_3Y_2X_2$ stoichiometry) confirm the ability of the anion packings to remain unchanged over significant variations in the halogen composition within the $Hg_3S_2Cl_2$ – $Hg_3S_2Br_2$ – $Hg_3S_2I_2$ system.^{40–43} The halogen atoms always occupy positions in the nodes of a primitive cubic sublattice centred by the S^{2-} anions. The introduction of monovalent atoms, *i.e.*, Cu and Ag, relieves this limitation making the X and Y anions more equivalent.

Within the approach adopted (based on the identification of stable 'building blocks') it would be interesting to compare the structures of two natural HgS modifications, *viz.*, trigonal α -HgS (cinnabar or cinnabarite) and cubic β -HgS (metacinnabarite). These structures are traditionally considered as distinctly different. Our approach to the crystal chemical analysis aimed at the identification of densely packed crystallographic planes⁷ (separately for cations and anions) established that the cationic matrices are identical in both phases. It can be represented as the three-layer cubic close packing (with the stacking sequence ABC).¹²¹ In the cubic phase, both anions and cations are packed according to this pattern and thus the overall structure can be considered as a three-dimensional motif of [S₄Hg] or, alternatively, [Hg₄S] tetrahedra. Meanwhile, the anion packing is significantly different in the trigonal phase. The S²⁻ anions are shifted from the initial cationic tetrahedron through a common face to a neighbouring cationic octahedron while the bonds with two Hg atoms are preserved and remain the strongest in the new location. *F*-centred cubic and rhombohedral cells are equivalent provided that $c_R/a_R = 2.45$.¹²² For the cinnabar structure, this ratio is 2.29, which means that the rhombohedron of Hg atoms somewhat deviates from cube: $a'_R = 5.74$ Å; $\alpha'_R = 92.5^\circ$ (Fig. 25).

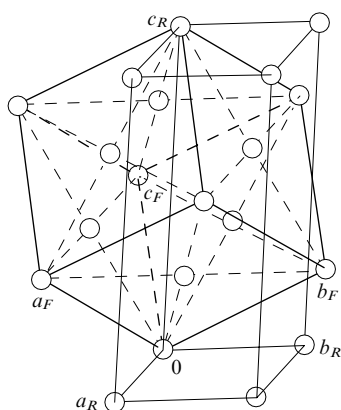


Figure 25. A relation between the rhombohedral and *F*-centred cubic cells in the cinnabarite (α -HgS) structure. Only mercury atoms involved into a lattice close to the *F*-centred cubic one are shown.

The stability of the cationic framework both in α - and β -HgS is confirmed by its preservation upon the Al substitution for 1/4 of the Hg cations, as evidenced by the crystal structure of Hg₃AlF₆O₂H (space group $R\bar{3}m$, $a = 7.262$ Å, $c = 10.441$ Å, $Z = 3$).¹²³ In contrast to the framework realised in α -HgS, the *F*-centred cubic sublattice of cations is deformed in the opposite direction, *i.e.*, the cube is elongated along the three-fold axis: $a'_R = 5.449$ Å, $\alpha'_R = 83.57^\circ$. This pseudocubic cationic sublattice corresponds to a hexagonal one with $a_R = a/2 = 3.631$ and $c_R = c = 10.441$ Å. In this case, the $c_R/a_R = 2.88$, which by far exceeds the ideal value of 2.45 (Fig. 26). We note that the F atoms in this structure occupy cationic tetrahedra, whereas the O atoms composing the linear O—Hg—O fragments are characterised by a less regular coordination environment.

The fact that the coordination of an S atom to only two Hg atoms is preferred can be a reason for the 'dissolution' of cinnabar in specific natural processes, which gives rise to the replacement of two remote Hg atoms in the coordination environment of the sulfur atoms with two Cu, Ag, Pb, *etc.* atoms. The incorporation of these cations is accompanied by the introduction of charge-compensating anions, *viz.*, Cl, Br or I, which results in the formation of structures considered above corresponding to the MHgXY stoichiometry with HgS:MX = 1:1.

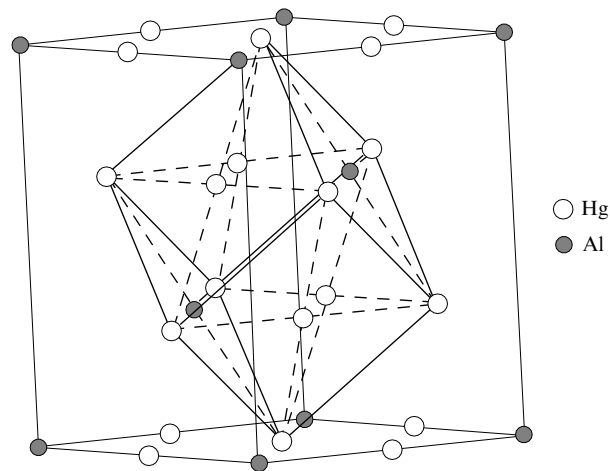


Figure 26. The cationic *F*-centred sublattice in the crystal structure of Hg₃AlF₆O₂H.

In the case of more mercury-excessive compounds (here, we focus on the Hg:Y:X = 3:2:2 stoichiometry, since it is best represented by structurally studied compounds), the crystal structures emerge under the action of two factors: covalent bonding between the Hg and S atoms giving rise to isolated, ribbon, layer or framework assemblies and arrangement of the halogen atoms into a packing close to a primitive cubic one.^{8,113} As has already been stated above, the 'cubic' unit in these structures provides the commensurability of the geometric parameters of this two components resulting in the stability of the packing motifs even against substantial variations in the halogen composition. The freedom in the rotation of the blocks upon their assembling produces [HgS]_n moieties with diverse topologies, which explains rich polymorphism intrinsic to these class of compounds.

VII. Conclusion

The crystal chemical analysis of natural and synthetic inorganic mercury compounds with anions abundant in nature (O, S, Se, Te, F, Cl, Br, I, CrO₄, PO₄ and AsO₄) also containing auxiliary cations similar to mercury in terms of structural preferences (*i.e.*, Cu, Ag and Pb) demonstrate a huge diversity of their crystal structures. As has been established, some atomic groups with strong covalent Hg—O, Hg—Y (Y = S, Se or Te) and A—O (A = Cr, P or As) bonds are not substantially deformed in the course of the crystallisation. These include oxo-centred [Hg₄O] tetrahedra (which also involve weaker attractive Hg...Hg interactions), S- and Se-centred [(M,Hg)₄Y] tetrahedra, [Hg₆O₂] *r*-octahedra, *etc.* The centres of these 'rigid' groups upon their incorporation into a crystal structure undergo ordering by systems of parallel (crystallographic) planes to form sublattices and the true translation lattice.

In the crystal structures of compounds with the 3:2:2 stoichiometry, the monovalent anions are more strictly ordered than the cations. This is explained by the fact that large weakly bound anions adapt much easier to the sublattice requirements than the covalently bound Hg—Y component of the structure.

Specific features of the assembly of these covalently bound groups and their ability to change the configuration without substantial redistribution of the bonding topology facilitate polymorph transitions and other structural transformations therein. This observation can shed light upon complex associations between naturally occurring mercury-containing minerals. A deep understanding of the mechanisms underlying structural transitions in associations of these minerals is of great environmental significance.

This review was written with a partial financial support from the Russian Foundation for Basic Research (Project No. 04-05-64058).

References

1. K. Aurivillius *Ark. Kemi* **24** 151 (1965)
2. N V Pervukhina, G V Romanenko, S V Borisov, S A Magarill, N A Pal'chik *Zh. Strukt. Khim.* **40** 561 (1999)^a
3. N V Pervukhina, S A Magarill, S V Borisov, G V Romanenko, N A Pal'chik *Usp. Khim.* **68** 683 (1999) [*Russ. Chem. Rev.* **68** 615 (1999)]
4. S A Magarill, N V Pervukhina, S V Borisov, N A Pal'chik *Kristalloghimiya Soedinenii Nizkovaletnoi Rtuti* (Crystal Chemistry of Compounds of Low-valence Mercury) (Moscow: Yanus-K, 2001)
5. S V Borisov *Zh. Strukt. Khim.* **33** (6) 123 (1992)^a
6. S V Borisov, R F Klevtsova, S A Magarill, N V Pervukhina, N V Podberezskaya *Zh. Strukt. Khim.* **43** 664 (2002)^a
7. N A Bliznyuk, S V Borisov *Zh. Strukt. Khim.* **33** (2) 145 (1992)^a
8. S V Borisov, S A Magarill, N V Pervukhina, E V Peresypkina *Crystallogr. Rev.* **11** 87 (2005)
9. R W Potter II, H L Barnes *Am. Mineral.* **63** 1143 (1978)
10. A G Mikolaichuk, Ya I Dutchak *Mineral. Sb. L'vovsk. Gos. Univ.* **19** 368 (1965)
11. V I Vasil'ev *Mineralogiya Rtuti* (Mineralogy of Mercury) Pt. 1 (Novosibirsk: Siberian Branch of Russian Academy of Sciences, 2004)
12. H Puff, J Küster *Naturwissenschaften* **49** 464 (1962)
13. H Puff, R Kohlschmidt *Naturwissenschaften* **49** 299 (1962)
14. H Puff, A Harpain, K-P Hoop *Naturwissenschaften* **53** 274 (1966)
15. H Puff, D Heine, G Lieck *Naturwissenschaften* **55** 298 (1968)
16. S S Batsanov, L I Abaulina *Izv. Sib. Otd. Akad. Nauk SSSR* (10) 67 (1961)
17. S S Batsanov, V N Kolomiichuk, S S Derbeneva, R S Erenburg *Izv. Akad. Nauk SSSR, Neorg. Mater.* **9** 1098 (1973)^b
18. Yu V Voroshilov, V Yu Slivka *Anoksidnye Materialy dlya Elektronnoi Tekhniki* (Anoxide Materials for Electronics) (L'vov: Vyscha Shkola, 1989)
19. Yu V Voroshilov, Z P Gad'mashi, V Yu Slivka, V A Khudolii *Izv. Akad. Nauk SSSR, Neorg. Mater.* **17** 2022 (1981)^b
20. V A Khudolii, V V Pan'ko, M S Shelemba, L I Lopit, A S Fedor, Yu V Voroshilov *Zh. Neorg. Khim.* **38** 1584 (1993)^c
21. V V Pan'ko, Yu V Voroshilov, V A Khudolii, M S Shelemba *Zh. Neorg. Khim.* **41** 1731 (1996)^c
22. Yu V Voroshilov, V A Khudolii, V V Pan'ko *Zh. Neorg. Khim.* **41** 287 (1996)^c
23. Yu V Voroshilov, V A Khudolii, V V Pan'ko, Yu V Minets *Neorg. Mater.* **32** 1466 (1996)^b
24. J Beck, S Hedderich *J. Solid State Chem.* **151** 73 (2000)
25. E E Foord, P Berendsen, L O Storey *Am. Mineral.* **59** 652 (1974)
26. V I Vasil'ev, N A Pal'chik, O K Grechishchev *Geol. Geofiz.* (7) 54 (1984)
27. V I Vasil'ev, Yu G Lavrent'ev, N A Pal'chik *Dokl. Akad. Nauk SSSR* **290** 948 (1986)^d
28. V I Vasil'ev, L V Usova, N A Pal'chik *Geol. Geofiz.* (7) 61 (1989)
29. J K McCormack, F W Dickson, M P Leshendok *Am. Mineral.* **76** 1715 (1991)
30. J K McCormack, F W Dickson *Can. Mineral.* **36** 201 (1998)
31. T Schleid, P Lauxmann, C Schneck *Z. Kristallogr.* **16** (Suppl.) 95 (1999)
32. A San-Miguel, N G Wright, M I McMahon, R J Nelves *Phys. Rev. B: Condens. Matter* **51** 8731 (1995)
33. K. Aurivillius *Ark. Kemi* **26** 497 (1967)
34. A J Frueh, N Gray *Acta Crystallogr., Sect. B* **24** 156 (1968)
35. S Đurovič *Acta Crystallogr., Sect. B* **24** 1661 (1968)
36. Yu V Minets, Yu V Voroshilov, V V Pan'ko, V A Khudolii *J. Alloys Compd.* **365** 121 (2004)
37. V A Lyakhovitskaya, N I Sorokina, A A Safonov, I A Verin, V I Andrianov *Kristallografiya* **34** 835 (1989)^e
38. Yu V Minets, Yu V Voroshilov, V V Pan'ko, in *IX Nauchno-tekhnichna Konferentsiya 'Khimiya, Fizika i Tekhnologiya Khal'kogenidiv ta Khal'kogalogenidiv' (Tez. Dok.)*, Uzhgorod, 1998 [The IXth Scientific Engineering Conference 'The Chemistry, Physics and Technology of Chalcogenides and Chalcogenides' (Abstracts of Reports), Uzhgorod, 1998] p. 87
39. Yu V Voroshilov, Yu V Minets *Nauk. Visn. Uzhgorodsk. Univ., Ser. Khim.* (3) 39 (1998)
40. N V Pervukhina, V I Vasil'ev, S V Borisov, S A Magarill, D Yu Naumov *Can. Mineral.* **41** 1445 (2003)
41. N V Pervukhina, V I Vasil'ev, D Yu Naumov, S V Borisov, S A Magarill *Can. Mineral.* **42** 87 (2004)
42. N V Pervukhina, V I Vasil'ev, S A Magarill, S V Borisov, D Yu Naumov *Can. Mineral.* **44** 1239 (2006)
43. N V Pervukhina, V I Vasil'ev, S A Magarill, S V Borisov, D Yu Naumov *Can. Mineral.* **44** 1247 (2006)
44. H Wiedemeier, M A Yutchins, Y Grin, C Feldmann, H G von Schnering *Z. Anorg. Allg. Chem.* **623** 1843 (1997)
45. N V Podberezskaya, S A Magarill, I A Baidina, S V Borisov, L E Gorsh, A N Kanev, T N Martynova *Zh. Strukt. Khim.* **23** (3) 120 (1982)^a
46. J Beck, M Rompel *Z. Anorg. Allg. Chem.* **629** 421 (2003)
47. H-L Keller, L Wimbart *Z. Anorg. Allg. Chem.* **630** 331 (2004)
48. M Moro'oka, H Ohki, K Yamada, T Okuda *J. Solid State Chem.* **177** 1401 (2004)
49. M Guillo, B Mercey, P Labbé, A Deschanvres *Acta Crystallogr., Sect. B* **36** 2520 (1980)
50. J Beck, H-L Keller, M Rompel, L Wimbart *Z. Anorg. Allg. Chem.* **627** 2289 (2001)
51. J Beck, H-L Keller, M Rompel, L Wimbart, B Ewald *Z. Anorg. Allg. Chem.* **630** 1031 (2004)
52. H-L Keller, L Wimbart *Z. Anorg. Allg. Chem.* **629** 2337 (2003)
53. R Blachnik, K Lytze, H Reuter *J. Solid State Chem.* **126** 95 (1996)
54. R Blachnik, W Buchmeier, H A Dreisbach *Acta Crystallogr., Sect. C* **42** 515 (1986)
55. W G Mumme, E H Nickel *Am. Mineral.* **72** 1257 (1987)
56. B Mason, W G Mumme, H Sarp *Am. Mineral.* **77** 197 (1992)
57. H Sarp, J Sanz-Gysler, P Perroud *Arch. Sci. (Geneve)* **50** 1 (1997)
58. S V Borisov, S A Magarill, N V Pervukhina *Z. Kristallogr.* **220** 946 (2005)
59. V A Voronin, V V Shchennikov *Kristallografiya* **34** 491 (1989)^e
60. D J Benjamin *Mater. Res. Bull.* **17** 179 (1982)
61. H-J Riebe, H-L Keller *Z. Anorg. Allg. Chem.* **574** 191 (1989)
62. H-L Keller, R Langer *Z. Anorg. Allg. Chem.* **620** 977 (1994)
63. W T A Harrison, L Liu, A J Jacobson *Angew. Chem., Int. Ed. Engl.* **35** 625 (1996)
64. W T A Harrison, L Liu, A J Jacobson, T Vogt *Inorg. Chem.* **37** 834 (1998)
65. K. Aurivillius *Ark. Kemi* **22** 517 (1964)
66. K. Aurivillius, C Stålhandske *Acta Crystallogr., Sect. B* **30** 1907 (1974)
67. K. Aurivillius, C Stålhandske *Acta Crystallogr., Sect. B* **34** 79 (1978)
68. M A Neuman, D R Petersen, G Y S Lo *J. Cryst. Mol. Struct.* **6** 177 (1976)
69. K. Aurivillius *Ark. Kemi* **28** 279 (1968)
70. F C Hawthorne, M Cooper, P K Sen Gupta *Am. Mineral.* **79** 1199 (1994)
71. K Kohler, G Thiele, D Brettinger *Z. Anorg. Allg. Chem.* **418** 79 (1975)
72. G Bergerhoff, J Paeslack *Z. Kristallogr.* **126** 112 (1968)
73. S V Krivovichev, S K Filatov *Acta Crystallogr., Sect. B* **55** 664 (1999)
74. S V Krivovichev, S K Filatov *Am. Mineral.* **84** 1099 (1999)
75. S V Krivovichev, S K Filatov *Kristalloghimiya Mineralov i Neorganicheskikh Soedinenii s Kompleksami Anionotsentrirovannykh Tetraedrov* (Crystal Chemistry of Minerals and Inorganic Compounds with Complexes of Anion-centred Tetrahedra) (St Petersburg: St Petersburg State University, 2001)

76. S V Krivovichev, S K Filatov, T F Semenova *Z. Kristallogr.* **212** 411 (1997)
77. S V Krivovichev, S K Filatov, T F Semenova *Usp. Khim.* **67** 155 (1998) [*Russ. Chem. Rev.* **67** 137 (1998)]
78. S A Magarill, G V Romanenko, N V Pervukhina, S V Borisov, N A Pal'chik *Zh. Struct. Khim.* **41** 116 (2000)^a
79. E Le Fur, R Gautier, E Furet, J Y Pivan *Inorg. Chem.* **41** 4227 (2002)
80. S V Borisov, S A Magarill, N V Pervukhina *Zh. Struct. Khim.* **44** 1102 (2003)^a
81. V I Vasil'ev, N V Pervukhina, G V Romanenko, S A Magarill, S V Borisov *Can. Mineral.* **37** 119 (1999)
82. K Mereiter, J Zemann, A W Hewat *Am. Mineral.* **77** 839 (1992)
83. C Stålhandske, K Aurivillius, G-I Bertinsson *Acta Crystallogr., Sect. C* **41** 167 (1985)
84. A C Roberts, J A R Stirling, A J Criddle, G E Dunning, J Spratt *Mineral. Mag.* **68** 241 (2004)
85. J D Grice *Can. Mineral.* **37** 775 (1999)
86. C Stålhandske *Acta Chem. Scand., Ser. A* **41** 576 (1987)
87. K Brodersen, G Gobel, G Liehr *Z. Anorg. Allg. Chem.* **575** 145 (1989)
88. G V Romanenko, N V Pervukhina, S V Borisov, S A Magarill, V I Vasil'ev *Zh. Struct. Khim.* **40** 324 (1999)^a
89. M A Cooper, F C Hawthorne *Can. Mineral.* **41** 1173 (2003)
90. S V Borisov, N V Podberezskaya *Zh. Struct. Khim.* **22** (6) 18 (1981)^a
91. Amsterdam Density Functional (ADF) Program, Release 2002 02, Vrije Universiteit, Amsterdam, 2002
92. G Te Velde, F M Bickelhaupt, E J Baerends, C F Guerra, S J A Van Gisbergen, J G Snijders, T Ziegler *J. Comput. Chem.* **22** 931 (2001)
93. S V Borisov, S V Kozlova, S P Gabuda *Zh. Struct. Khim.* **45** 162 (2004)^a
94. L A Groat, A C Roberts, Y Le Page *Can. Mineral.* **33** 41 (1995)
95. J T Szymanski, L A Groat *Can. Mineral.* **35** 765 (1997)
96. T Hansen, H Müller-Buschbaum, L Walz *Z. Naturforsch., B* **50** 47 (1995)
97. W Klein, J Curda, K Friese, M Jansen *Acta Crystallogr., Sect. C* **58** i23 (2002)
98. M Weil, R Glaum *J. Solid State Chem.* **157** 68 (2001)
99. M Weil *Z. Anorg. Allg. Chem.* **631** 1346 (2005)
100. M Weil, E Tillmanns, D Yu Pushcharovsky *Inorg. Chem.* **44** 1443 (2005)
101. G D Ilyushin, V A Blatov, Yu A Zakutkin *Acta Crystallogr., Sect. B* **58** 948 (2002)
102. G D Ilyushin *Kristallografiya* **50** 1123 (2005)^c
103. Y Yang, V Ramamoorthy, P R Sharp *Inorg. Chem.* **32** 1946 (1993)
104. H Shan, P R Sharp *Angew. Chem., Int. Ed. Engl.* **35** 635 (1996)
105. S G Wang, Y X Qiu, E Neumann, H J Deiseroth, W H E Schwarz *Z. Anorg. Allg. Chem.* **629** 1718 (2003)
106. S V Borisov, S A Magarill, N V Pervukhina *Zh. Struct. Khim.* **45** 471 (2004)^a
107. P C Burns *Can. Mineral.* **37** 113 (1999)
108. C Stålhandske *Acta Crystallogr., Sect. B* **34** 1968 (1978)
109. R Masse, J-C Guitel, A Durif *J. Solid State Chem.* **23** 369 (1978)
110. H Sarp, D Yu Pushcharovsky, E J MacLean, S J Teat, N V Zubkova *Eur. J. Mineral.* **15** 177 (2003)
111. H Nyman, S Andersson *Acta Crystallogr., Sect. A* **35** 934 (1979)
112. S V Krivovichev, P C Burns *Eur. J. Mineral.* **13** 801 (2001)
113. S V Borisov, S A Magarill, N V Pervukhina *Zh. Struct. Khim.* **42** 516 (2001)^a
114. S V Borisov *Kristallografiya* **45** 779 (2000)^c
115. S V Borisov, S A Magarill, N V Pervukhina, N A Kryuchkova *Zh. Struct. Khim.* **43** 317 (2002)^a
116. S V Borisov, S A Magarill, N V Pervukhina *Zh. Struct. Khim.* **44** 494 (2003)^a
117. M Weil *Z. Naturforsch., B* **55** 699 (2000)
118. J T Szymanski, A C Roberts *Can. Mineral.* **28** 709 (1990)
119. S V Borisov, S A Magarill, G V Romanenko, N V Pervukhina *Khim. Inter. Ustoich. Razv.* **7** 497 (1999)^f
120. S V Borisov, N V Podberezskaya, N V Pervukhina, S A Magarill *Z. Kristallogr.* **213** 253 (1998)
121. S A Magarill, S V Borisov, N V Pervukhina, V I Vasil'ev *Khim. Inter. Ustoich. Razv.* **15** 71 (2007)^f
122. S A Gromilov, S V Borisov *Zh. Struct. Khim.* **44** 724 (2003)^a
123. M Weil *Acta Crystallogr., Sect. C* **58** i37 (2002)

- ^a — *J. Struct. Chem. (Engl. Transl.)*
^b — *Inorg. Mater. (Engl. Transl.)*
^c — *Russ. J. Inorg. Chem. (Engl. Transl.)*
^d — *Dokl. Chem. (Engl. Transl.)*
^e — *Crystallogr. Rep. (Engl. Transl.)*
^f — *Chem. Sust. Develop. (Engl. Transl.)*

Sonochemical synthesis of inorganic materials

A Ye Baranchikov, V K Ivanov, Yu D Tretyakov

Contents

I. Introduction	133
II. Methods of generation of acoustic vibrations	134
III. Action of ultrasound on liquid-phase systems	134
IV. Cavitation parameters	135
V. Sonochemical reactions in aqueous media	138
VI. Sonochemical processes in non-aqueous media	142
VII. Sonochemical processes under hydrothermal conditions	144
VIII. Solid-phase sonochemical processes	145
IX. Conclusion	148

Abstract. Methods of synthesis of highly dispersed inorganic materials based on the use of ultrasonic treatment are considered. Particular attention is paid to current trends in sonochemistry, namely, ultrasonic hydrothermal treatment and high-temperature ultrasonic processing of liquid- and solid-phase systems. The bibliography includes 218 references.

I. Introduction

The synthesis of modern inorganic materials usually presents significant difficulties. Indeed, such systems are multicomponent and a number of successive stages of formation of intermediates should be carried out in order to obtain target products. The multistage character of the synthesis is responsible for inhomogeneity of chemical and phase compositions (this presents a severe problem in the formation of single phase multicomponent products) and the microstructure of materials. These problems are solved using a variety of chemical homogenisation techniques,^{1,2} which make it possible to obtain reaction mixtures in which the starting reactants are in highly dispersed reactive state. Good mixing of reactants provides the possibility of formation of numerous interfacial contacts and, as a consequence, the emergence of a developed reaction interface. The rate of formation of new phases near the developed reaction interface much exceeds the rate of interaction between reactants in conventional state. However, by no means all interfacial contacts formed in the course of homogenisation become reaction interfaces during the synthesis. This is first of all due to the compaction of reactant

particles, breakdown of the contacts formed in the course of mechanical mixing of reactants and demixing of reaction mixtures owing to different chemical nature of the reactants.

Solving a number of problems in the synthesis of inorganic materials requires the use of novel methods that allow one to change the character of the reaction zone or the reaction mechanism in a targeted manner and to additionally activate the reaction mixtures.³ Recently, synthetic methods based on utilisation of microwave radiation have been progressed rapidly.^{4–6} Microwave irradiation makes it possible to considerably accelerate such important physicochemical processes as dehydration, decomposition of salt and hydroxide precursors, synthesis of multicomponent composites and sintering of ceramics. This approach is promising due to high rate of heating and short delay of the process in contactless regime (no contact between the heater and the heated body) and to the possibility of selective heating of the components of reaction mixtures.⁷ Nevertheless, practice shows that prediction of the behaviour of a system under microwave irradiation is a very complicated task. The reason is that the electrophysical and thermophysical characteristics responsible for the absorbance of compounds strongly depend on temperature. Correct allowance for this factor is a practically insoluble problem. The situation becomes even more complicated for the systems in which chemical processes occur, because changes in the phase composition of such systems cause jumpwise and often uncontrollable changes in their electrophysical and thermophysical characteristics.

Yet another important problem in modern inorganic chemistry and inorganic materials science consists in the need of elaboration of methods for targeted synthesis of nanodisperse materials.⁸ Methods of preparation of nanopowders have been studied for a rather long time and many of them are successfully used not only in laboratory practice, but also in industry. The mechanisms of formation of free nanoparticles have been a subject of intensive research and some of them have found experimental substantiation. This made it possible to choose the strategies of the synthesis of nanopowders with preset physicochemical properties, however some problems are still to be solved.⁹ In particular, highly dispersed powders have an excess surface energy, which causes their aggregation. Additionally, enhanced reactivity of nanopowders compared to bulk crystals predetermines their instability to the action of various media and rapid degradation. These problems can be solved by introducing nanopowders into

A Ye Baranchikov, V K Ivanov N S Kurnakov Institute of General and Inorganic Chemistry, Russian Academy of Sciences, Leninsky prosp. 31, 119991 Moscow, Russian Federation. Fax (7-495) 954 12 79, tel. (7-495) 236 20 44, e-mail: a.baranchikov@gmail.com (A Ye Baranchikov), van@igic.ras.ru (V K Ivanov)

Yu D Tretyakov Department of Chemistry, Department of Materials Science, M V Lomonosov Moscow State University, Leninskie Gory, 119992 Moscow, Russian Federation. Fax (7-495) 939 09 98, tel. (7-495) 939 20 74, e-mail: yudt@inorg.chem.msu.ru

Received 25 May 2006

Uspekhi Khimii 76 (2) 147–168 (2007); translated by A M Raevskiy

inert matrices or by using low- and high-molecular-mass surfactants that form a shell on the surface of nanoparticles in the course of the synthesis and thus protect them from aggregation and degradation.^{10, 11}

A promising method for solving a number of problems mentioned above is sonication. Utilisation of ultrasonic vibrations in chemistry and materials science has long gone beyond research laboratories. Ultrasound is widely used in industry for intensification of many technological processes including degassing of metal melts, dispersion of liquids and solids, extraction, filtration and cleaning of various surfaces.^{12, 13} Considerable attention has been paid to applications of ultrasound in chemical synthesis including the synthesis of advanced inorganic materials. Progress of research in this field led to emergence of a new branch of chemical science, sonochemistry.[†]

A number of reviews and monographs devoted to various aspects of application of sonication in inorganic chemistry and materials science have been reported in the last decade.^{14–20} At present, chemically- and materials-science-attractive features of sonochemical synthesis have been well documented. The advent of promising sonochemical research avenues, *e.g.*, high-temperature synthesis of complex oxides²¹ and synthesis of highly dispersed oxide materials under concurrent hydrothermal and ultrasonic treatment²² should also be pointed out. In the course of preparation of the present review the authors tried to outline general ideas of the synthetic potential of the methods involving ultrasonic treatment, to consider the mechanisms of processes occurring under sonication and to systematise recent advances in sonochemical synthesis.

II. Methods of generation of acoustic vibrations

Acoustic vibrations are elastic (mechanical) longitudinal vibrations that propagate through a medium. The frequency spectrum of acoustic vibrations is usually divided into three regions, namely, infrasound (frequencies lower than 30 Hz), audible sound (frequency range from 30 Hz to 20 kHz) and ultrasound (frequencies higher than 20 kHz). This classification is to a great extent conditional, being based on human perception of acoustic vibrations.

From the standpoint of applications, ultrasonic vibrations are grouped into low-frequency vibrations (frequency range from 20 kHz to 1 MHz) and high-frequency (frequencies higher than 1 MHz) ones.²³ Low-frequency ultrasonic vibrations are mainly utilised in industry, chemistry and materials science (production of metals and alloys with specified microstructure, ultrasonic cutting and welding,²⁴ pressing,²⁵ synthesis of various compounds and materials,¹⁵ sample preparation in analytical chemistry,²⁶ *etc.*). High-frequency (diagnostic) ultrasound is used in non-destructive methods of analysis (ultrasonic defectoscopy and microscopy, studies of biological objects, *etc.*); in particular, it is widely used for contactless precision measurements of fluid parameters in flow systems.²⁶ The speed of propagation of an acoustic wave is determined by the properties of the medium through which the wave propagates; therefore, any changes in the liquid phase caused by, *e.g.*, the occurrence of a chemical reactions will change the speed of propagation of the wave and, as a consequence, change the time interval between the generation of an acoustic pulse and reception of the echo signal. Ultrasound diagnostic methods are used if a large number of contactless measuring devices are available (in, *e.g.*, petrochemical industry).^{27–29}

Generation of ultrasonic vibrations is based on transformation of electromagnetic oscillations to elastic mechanical vibra-

tions using specific devices. Electrical energy is converted to mechanical energy using the magnetostriction or piezoelectric effect.³⁰ These phenomena are due to the ability of certain materials to change their linear dimensions upon the action of alternating electric or magnetic field (piezoelectric effect and magnetostriction, respectively).

Magnetostrictive transducers characterised by ultrasound intensity of up to several tens of Watt per cm² (electroacoustic efficiency in liquid media exceeds 50%) at frequencies below 30 kHz are best for solving various problems in preparative chemistry and metallurgy. The maximum amplitude of acoustic vibrations is ~2 µm for ferrite transducers and more than 10 µm for metallic transducers.

Piezoelectric transducers are mainly used for generation of high-frequency (500 kHz–100 MHz) ultrasonic vibrations in defectoscopes, sonars and acoustoelectronic devices. The radiation intensity can be as high as 60 W cm⁻² and even reach the values 200–500 W cm⁻² at an efficiency of 60%–65% in, *e.g.*, pulsed mode of operation.¹³

In order to increase the acoustic wave intensity in a local spatial domain compared to its intensity at the surface of ultrasonic radiation source, the so-called concentrators are used.³¹ Rod-like concentrators (acoustic waveguides) are most widely used because of simple design and ease of replacement. A rod-like concentrator increases the amplitude of vibrations due to a decrease in its cross-section or density in accordance with the momentum conservation law. The gain coefficient of a waveguide (with respect to acoustic wave intensity) depends on the shape of the waveguide. The stepwise and conical concentrators have the simplest design while the highest gains are provided by exponential and catenoidal concentrators. The best materials for manufacturing of concentrators with maximum amplitude of the vibrational speed are titanium and its alloys. However, the maximum operating temperatures of these materials are at most 500–600 °C and therefore operation at higher temperatures requires the use of various steels with high acoustic characteristics (*e.g.*, steels with high content of silicon, manganese and chrome).

III. Action of ultrasound on liquid-phase systems

The basic phenomena accompanying propagation of an acoustic wave through a liquid are summarised in Fig. 1. Numerical data presented below (including the acoustic wave intensities) refer to the low-frequency ultrasonic region.

At a rather low intensity (usually, less than 0.1 W cm⁻²), the behaviour of the system can be quite correctly described using the classical wave equation. In this case no phenomena that could be

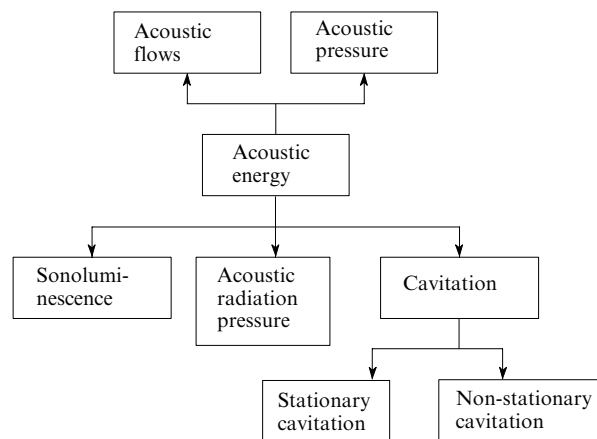


Figure 1. Physical phenomena accompanying the action of high-power acoustic radiation on liquids.

[†] In 1994, Elsevier B V (now a part of Reed – Elsevier Group) established a scientific journal *Ultrasonics Sonochemistry*. This fact substantiates that research in this field is in high demand.

useful for preparative chemistry and materials science are observed. As mentioned above, low-power ultrasound can only be used for solving particular diagnostic problems.

An increase in the acoustic energy flux density to $\sim 1 \text{ W cm}^{-2}$ and more causes the onset of some non-linear phenomena in the liquid. Among them, the most important is cavitation.^{14, 32–34}

The mechanism of the onset of cavitation can be described as follows.^{14, 35} Propagation of acoustic vibrations through a liquid causes the appearance of alternating rarefaction and compression zones in this liquid. A negative pressure is produced in the rarefaction zone. At high acoustic energy densities, it can exceed a critical value corresponding to discontinuity in the liquid and formation of cavitation bubbles in the bulk (Fig. 2, curve *AC* or *ABL*). The critical acoustic pressure for an ideal liquid should be equal to the difference between the atmospheric pressure and the pressure at which boiling of the liquid occurs at a given temperature (P_s). Actually, the critical pressure is much lower than this difference due to the presence of dissolved gases and mechanical impurities in the liquid. In this connection the formation of cavitation bubbles in a real system can be treated as a transition *AF* (see Fig. 2).

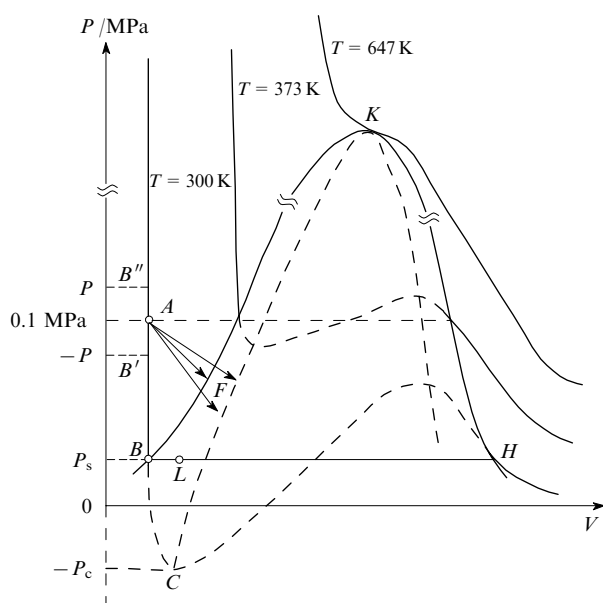


Figure 2. The phase diagram of water.¹⁴

Notations of points: *AF* is cavitation, *K* is critical point, *BKH* is binodal, *BK* is onset of boiling, *KH* is condensation of vapour, *CK* is spinodal, *P* is acoustic pressure, P_s is saturated vapour pressure, P_c is ultimate tensile stress.

At present, there are two main approaches to explanation of the mechanism of initiation of sonochemical reactions. One approach is usually called the 'hot spot' theory. It is widely used by researchers and is based on the following considerations.

During certain time interval the size of an emerged cavitation bubble and the external acoustic field execute almost in-phase oscillations. Then, due to a large difference between the hydrostatic pressure of the liquid and the pressure within the cavity of the cavitation bubble and to an abrupt increase in the acoustic pressure in the liquid in the compression zone of the ultrasonic wave the liquid moves towards the centre of the bubble and the bubble collapses (Fig. 3).³⁶ This is accompanied by concentration of energy similarly to the focussing of a converging shock wave. A high pressure developed in the central region of the collapsing bubble causes generation of a diverging spherical shock wave.³⁷ It is accepted that collapse of a cavitation bubble leads to the formation of a 'hot spot' at the centre, characterised by a local

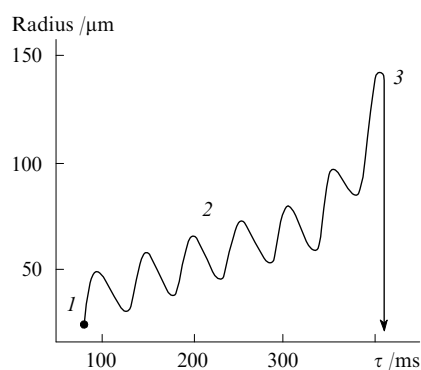


Figure 3. Evolution of a cavitation bubble.³⁴ Generation (1), growth and oscillations (2), collapse (3).

temperature of about $5 \times 10^3 \text{ K}$ [up to $(2-3) \times 10^4 \text{ K}$]³⁸ and a pressure ranging from 500 to 1000 atm.³⁹ The rate of cooling of the 'hot spot' can be as high as 10^{10} K s^{-1} (Ref. 40). Note that these numerical values were obtained ignoring the effects of heat exchange, surface tension and viscosity of the medium on the parameters of collapse and no correction for non-ideal character of the gas was applied.^{41–44}

Thus, the key idea of the 'hot spot' theory is that ultrasonic cavitation causes concentration of acoustic energy within very small spatial domains in the medium. This leads to production of extremely high local energy densities (mainly in the form of heat), which thus initiates the sonochemical reactions.⁴⁵

The second approach to explanation for the mechanism of initiation of sonochemical processes involves analysis of electrical phenomena accompanying the evolution of cavitation bubbles. The approach has been best developed by Margulis,^{42, 46–50} who proposed a theory of local electrification of cavitation bubbles. The key ideas of this theory are as follows. The action of an acoustic energy flux causes partial removal of the electrical double layer near the liquid–cavitation bubble interface. As a result, an uncompensated electric charge appears on the surface of the cavitation bubble. Later on, oscillations of the size of cavitation bubbles under sonication lead to the loss of stable spherical shape and to formation of various microirregularities (branches and jogs) on the surface of cavitation bubbles. In the limiting case, deformation of cavitation bubbles leads to their fission and abstraction of fragment bubbles. Deformation of the bubble surface creates favourable conditions for the appearance of high local densities of uncompensated electric charge, which eventually leads to electrical breakdown. Electrical discharge is accompanied by excitation and splitting of the gas and liquid molecules in the cavitation bubble. Thus, the mechanism of sonochemical reactions is closely related to the processes occurring during electrical discharge in a vapour–gas medium in the cavity of the cavitation bubble.

It should be noted that the local electrification theory reasonably describes some experimental results that cannot be explained in the framework of the 'hot spot' theory,⁴² including the occurrence of sonochemical reactions at very low ultrasound intensities (about $10^{-3} \text{ W cm}^{-2}$) or at high ultrasound frequencies ($> 100 \text{ Hz}$) and an increase in the efficiency of suppression of sonochemical reactions using high-boiling additives, etc.

IV. Cavitation parameters

Cavitation can be characterised by three main parameters, namely, intensity, cavitation threshold and stationarity.⁵¹

The cavitation intensity means the volume-average intensity (power) of spherical shock waves generated in a liquid medium upon collapse of cavitation bubbles. The higher the power of the shock waves the higher the cavitation intensity.

The intensity of vibrations I (energy transferred per unit time through a unit surface area) can be estimated from the relation

$$I = \frac{1}{\tau} \int_0^{\tau} I(\zeta) d\zeta = \frac{P^2}{2\rho c_0} = \frac{\xi^2 \omega^2 \rho c_0}{2},$$

where τ is time, ζ is the integration constant, $P = \xi \omega \rho c_0$ is the amplitude of acoustic pressure, ρ is the density of the medium, c_0 is the velocity of sound, ξ is the amplitude of acoustic vibrations and $\omega = 2\pi f$ is the angular frequency of vibrations.

It should be noted that the specific power (intensity) of acoustic vibrations is usually expressed in W cm^{-2} (power per unit surface area of acoustic radiator) or in W cm^{-3} (power per unit volume of irradiated sample).⁵²

Clearly, the relation presented above is appropriate for determination of the acoustic energy flux density only if the wave propagates through a continuous isotropic medium with no scattering of acoustic power and the propagation of sound through the system treated causes no non-linear physicochemical effects (pre-cavitation regime).

Otherwise, one should use indirect methods of determination of the energy flux density.^{52, 53} The most widely used method is a calorimetric technique⁵⁴ based on the assumption that a large proportion of the acoustic energy absorbed by the system is released in the form of heat. The main advantage of the technique is simplicity of both practical implementation and corresponding calculations. The method involves measurements of the rate of an increase in the temperature of the medium to which the acoustic wave radiation is transferred followed by calculations of the specific acoustic power using the relation

$$I = \frac{C_p \Delta T v}{S \tau},$$

where C_p is the molar (mass) heat capacity of the medium, ΔT is the experimentally determined change in the temperature during the time interval τ , v is the mass of the substance being processed and S is the radiating surface area of the waveguide (or the volume of the system treated).

Using the definition of specific absorbed acoustic power, it is possible to estimate the efficiency (η_{ef}) of a sonochemical process

$$\eta_{\text{ef}} = \frac{m}{S I \tau},$$

where m is the amount of the substance (in moles) involved in the sonochemical reaction. The yield of a sonochemical process (η) can be defined⁵⁵ using the transferred power of the source of vibrations W instead of absorbed acoustic power

$$\eta = \frac{m}{W \tau}.$$

However, the calorimetric technique described above has a number of significant drawbacks.⁵⁶ First, this is an intense heat exchange between the metallic waveguide contacting the cavitating liquid. Second, the heat capacities of cavitating media may differ appreciably from the heat capacity of the liquid (one should also keep in mind that the properties of the cavitating liquid differ from those of the same liquid in its normal state). Third, large local temperature gradients can be produced in the liquid in the course of experiments.

An alternative method is the comparative calorimetric technique.⁵⁷ This approach involves initial irradiation of the liquid with ultrasound over a short period (τ) and measurements of the dependence of the temperature of the liquid on the duration of the treatment stage (curve A). After cooling, the liquid is heated again using a conventional technique (by, *i.e.*, an electrical resistive heater) and the dependence of the temperature of the liquid on time (curve B) is also measured. Then, by varying the

power of the heater the shape of curve B is changed in order to match curve A . Once matched, the output power of the heater is considered equal to the acoustic power absorbed by the liquid. The most favourable conditions for calorimetric measurements are as follows: a slight increase in temperature (0.1–0.4 °C), short-term operation of the source of ultrasound (5–15 s) and efficient mixing of the liquid.

The cavitation threshold is a minimum intensity of ultrasonic waves at which cavitation emerges. Cavitation is quantitatively characterised by the so-called critical cavitation number (χ_c) defined by the relation

$$\chi_c = \frac{P_0 - P_s}{P_c},$$

where P_0 is the external pressure. Interestingly, the χ_c value corresponding to the onset of cavitation usually differs from the value corresponding to its disappearance, *i.e.*, hysteresis occurs. The χ_c value depends on many parameters that characterise both the state of the liquid (content of dissolved gases, temperature, presence of impurities) and the acoustic field (frequency, pulse duration, *etc.*). For instance, the cavitation threshold increases as the concentration of gas dissolved in the liquid decreases, the frequency of acoustic vibrations increases, the pulse duration decreases and the flow turbulence enhances.

Depending on the lifetime of cavitation bubbles, cavitation is classified into two types,²³ stationary and non-stationary cavitation. Non-stationary cavitation bubbles are formed at an acoustic energy density of the order of 10 W cm^{-2} and exist during one or a few acoustic cycles. The bubble radius becomes at least twice as large as the initial radius and then the bubbles are rapidly collapsed in the liquid compression stage. Some bubbles disintegrate into smaller bubbles that in turn form cavitation centres. Non-stationary cavitation is characterised by high intensity because the vapour pressure in the bubble cavities is very low owing to short bubble lifetimes.

Stationary cavitation bubbles are characterised by relatively long lifetimes and high vapour pressure in cavities. They are formed at rather low ultrasound intensities ($1\text{--}3 \text{ W cm}^{-2}$).

It has been accepted for long that only non-stationary cavitation can induce sonochemical processes. However, recent calculations showed that the temperature and pressure produced in the collapsing stationary bubbles are only slightly lower than in the collapsing non-stationary bubbles. Additionally, the stable cavitation bubbles have much longer lifetimes and therefore a stronger effect on the course of the sonochemical reaction.¹⁴

The key parameters of acoustic cavitation (cavitation intensity and threshold) depend on various factors. The most important factors are listed below.

Ultrasound power and frequency. The ultrasound power necessary for carrying out a sonochemical reaction should be chosen taking into account the need of overcoming the power threshold associated with the onset of cavitation ($1\text{--}5 \text{ W cm}^{-2}$ for aqueous solutions) and the optimum power ($10\text{--}50 \text{ W cm}^{-2}$ for aqueous solutions), because further increase in acoustic power makes the process less efficient.²³ The limitation imposed on the second parameter is due to the formation of a cavitation cloud near the radiating surface at high ultrasound power, which precludes the development of cavitation in the bulk of the liquid.¹⁴

Sonochemical processes are usually carried out with 20–500 kHz ultrasound, because at lower frequencies the role of vapour cavitation increases appreciably, which reduces the overall cavitation intensity. At the same time at acoustic frequencies of 2–3 MHz the cavitation threshold substantially increases¹⁴ and the efficiency of the sonochemical processes decreases.

Physical properties of solvent. It is accepted⁴⁰ that an increase in the viscosity of the medium causes a substantial increase in the cavitation threshold and a decrease in cavitation intensity.

According to calculations⁵⁸ for acoustic vibrations at 23 kHz, an increase in the viscosity of the medium from 0.001 to 0.1 Pa s leads to more than twofold decrease in cavitation intensity. As the viscosity of the liquid phase increases to 1.0 Pa s, cavitation almost disappears.

Based on analysis of experimental data, the following relation between the viscosity of the liquid medium η and cohesion pressure p_{co} (characterises the hydraulic resistance of the liquid to the formation of cavitation bubbles) was proposed⁵⁹

$$\log\left(\frac{\eta}{\eta_0}\right) = -3.05p_{co},$$

where $\eta_0 = 0.13$ MPa s and the empirical constant -3.05 is expressed in atm^{-1} .

The cohesion pressure cannot be measured directly, but it can be expressed through the experimentally measured parameters, namely, the amplitude of acoustic pressure (p_{min}) and the intensity of ultrasonic waves corresponding to the onset of acoustic cavitation (I_{min}), i.e., the cavitation threshold⁶⁰

$$p_{co} = p_0 - p_{min} = p_0 - \sqrt{2I_{min}\rho v_{us}},$$

where p_0 is the hydrostatic pressure and v_{us} is the speed of ultrasonic waves in the liquid medium.

Not only the viscosity, but also the surface tension of the liquid phase has a strong effect on the cavitation intensity and threshold. Experiments⁶¹ showed that a decrease in the surface tension of the liquid from 0.072 to 0.040 N m⁻¹ causes a more than threefold acceleration of sonochemical reactions. The main reason for this effect is the decrease in the cavitation threshold.⁶¹

According to calculations,⁵⁸ the surface tension of the liquid sonicated at 23 kHz has no pronounced effect on the cavitation intensity. At the same time an increase in the surface tension of the liquid medium from 0.020 to 0.1 N m⁻¹ reduces the cavitation intensity by a factor of nearly 2.5 for sonication at high frequencies (2–3 MHz).

Thus, a correct choice of the medium is of crucial importance for carrying out sonochemical reactions, namely, the liquid media of low viscosity (weak intermolecular interaction) and surface tension are more appropriate for the onset of intense low-threshold acoustic cavitation.

Presence of dissolved gases and purity of reaction system. An abrupt drop of external pressure in a liquid causes liberation of gas dissolved in it. If an acoustic wave is in the rarefaction phase, the dissolved gases liberate in the form of small bubbles, which can act as nuclei of cavitation centres, and the cavitation threshold decreases appreciably.⁶² Additional cavitation nuclei are usually produced by bubbling an inert gas (nitrogen or argon) through the liquid.

Any microinhomogeneities or free surfaces present in the liquid medium also act as nuclei of cavitation bubbles; this considerably decreases the cavitation threshold.⁶³

Temperature. Experiments⁶² showed that raising the temperature favours a decrease in the cavitation threshold on the one hand and an increase in the rate of solvent evaporation and in the partial pressure of the solvent inside the bubble on the other hand. Because of this, a transition is possible from gas cavitation to vapour cavitation⁶⁴ characterised by an abrupt decrease in the efficiency of collapse of cavitation bubbles and in the intensity of acoustic cavitation. For instance, the oxidation of aqueous FeSO₄ solution under sonication is suppressed at 50 °C and sonolysis of water resulting in the formation of H₂O₂ is suppressed at 67 °C.⁶² Thus, the operating temperature for sonochemical processes in open systems should be much lower than the boiling point of the solvent.

External pressure. The cavitation threshold depends on the pressure developing in the rarefaction phase. This pressure exceeds the hydrostatic pressure of the liquid medium in absolute

value. An increase in external pressure reduces the difference between the acoustic pressure in the rarefaction phase and the hydrostatic pressure. At high external pressure, this difference can appear to be insignificant for formation of cavitation bubbles in the liquid medium. In this case the onset of cavitation requires a substantial decrease in the acoustic pressure in the rarefaction phase (increase in the amplitude of acoustic vibrations). Experimental studies¹⁴ showed that the optimum external pressure for sonochemical processes in open systems ranges from 0.1 to 0.5 MPa.

Thus, cavitation emerged upon sonication of liquid-containing systems enhances the efficiency of ultrasonic treatment due to concentration of acoustic energy in small spatial domains. Using this effect, one can solve a number of chemical, materials science and technological problems, e.g., fabrication of metal slabs with homogeneous microstructure,^{65–68} finely dispersed powders,⁶⁹ emulsions^{60,70} and aerosols.^{71–73} Additionally, sonication is successfully utilised for etching of surfaces,²³ regeneration of catalysts,⁷⁴ monitoring of precipitation,²³ etc.

Ultrasonic dispersion procedure is based on violation of symmetry of collapse of a cavitation bubble near the interface (e.g., liquid–solid interface, Fig. 4).¹⁵ As a result, intense local fluid microflows towards the phase boundary are produced; the speed of propagation of such flows reaches several tens of metres per second. Physicochemical consequences of this phenomenon can be followed taking ultrasonic treatment of various suspensions as examples.

It was experimentally established⁷⁵ that sonication of suspensions of inorganic oxide and sulfide materials in organic solvents causes a considerable increase in the surface area of target powders (20–30-fold increase after ~45 min at an initial specific surface area of 0.3–0.5 m² g⁻¹) due to collisional disintegration of particles. Chemical processes in the liquid–solid systems can also occur at higher rates under these conditions;⁷⁶ this particularly concerns molecular intercalation into layered inorganic materials. For instance, the intercalation rate of amines, metal-locenes, metallic sulfide clusters and some other compounds into ZrS₂, V₂O₅, TaS₂, MoS₂ and MoO₃ under sonication increases by more than two orders of magnitude compared to conventional intercalation rates. Ultrasonic treatment of suspensions under normal conditions can initiate reactions giving binary compounds from elements (Fig. 5).⁷⁷

A common feature of the fields of application of high-power ultrasound mentioned above is utilisation of mainly mechanical effects of sonication of liquids. At the same time there is a broad spectrum of pure chemical problems that can also be solved using acoustic treatment of the liquid phase.

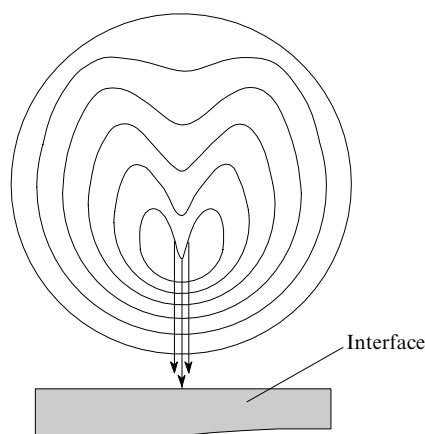


Figure 4. Collapse of a cavitation bubble near interface.¹⁵ The direction of the liquid flow after collapse of the bubble is shown by arrows.

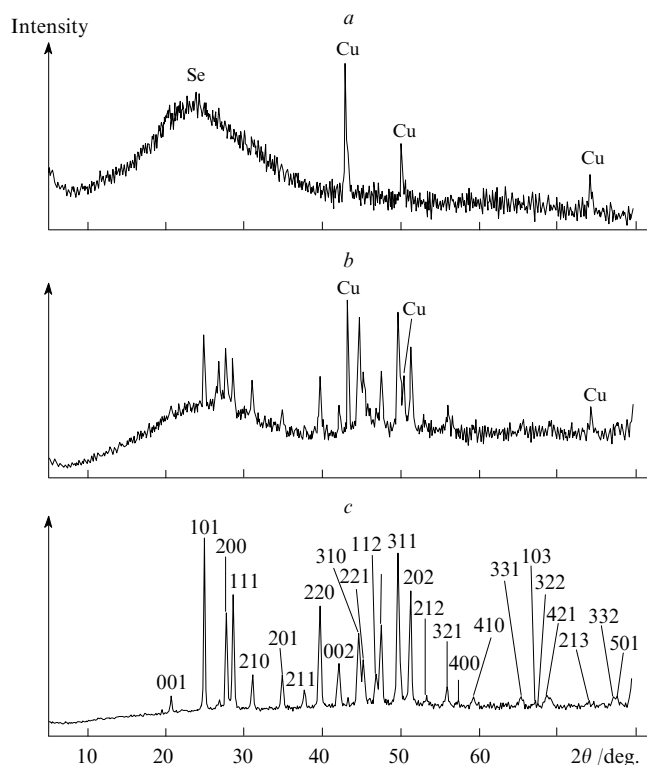
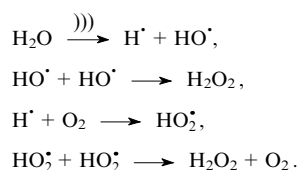


Figure 5. Powder X-ray diffraction data of the samples obtained upon irradiation of a suspension of Cu/Se mixture in methanol with ultrasound for 30 (a), 120 (b), and 480 min (c).⁷⁷ The X-ray diffraction pattern in Fig. c corresponds to single Cu₃Se₂ phase; the reflections were indexed according to [PDF 47-1745].

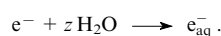
V. Sonochemical reactions in aqueous media

The chemistry of aqueous solutions under sonication has been studied in considerable detail.^{8, 14, 33, 78} In most cases sonochemical reactions in aqueous solutions are due to the fact that water vapour present in the cavity of a cavitation bubble at the instant of bubble collapse experiences the action of high temperature and high pressure; as a consequence, water molecules undergo the so-called sonolysis^{79, 80}

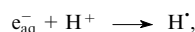


The rate of formation of HO[•] radicals in solutions in the absence of oxygen dissolved in water is ~25 μmol litre⁻¹ min⁻¹ and the rate of formation of hydrogen peroxide in air-saturated solutions is 0.6 mmol litre⁻¹ min⁻¹ (Ref. 81).

Sonication of water causes ionisation of water molecules at the instant of collapse of the cavitation bubble and emergence of hydrated electrons⁸²



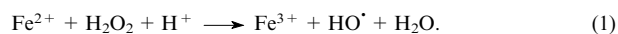
The presence of solvated electrons in an aqueous solution strongly depends on the acidity of the medium.⁸³ For instance, in an acidic medium the solvated electrons participate in the formation of hydrogen atoms following the reaction



whereas another process occurs in a basic medium



Thus, sonication of aqueous solutions should initiate redox and radical reactions in them. For instance, sonication of an acidified aqueous solution of Mohr's salt in air causes oxidation of Fe(II) to Fe(III) as follows⁸⁴



The oxidation of iodide ions in aqueous KI solution occurs under similar conditions



Reactions (1)–(3) are considered as reference reactions in sonochemistry. They are used, in particular, for dosimetric purposes in the determination of specific acoustic power from the data of kinetic experiments, because it is clear that the rates of these redox reactions are related to the acoustic power absorbed by the solution.⁵³ In addition to the oxidation reactions of divalent iron and iodide anion, the decomposition reactions of various porphyrin derivatives, *e.g.*, 5,10,15,20-tetrakis(4-sulfophenyl)porphyrin (TPPS)⁸⁵ (Fig. 6), are also used as reference reactions.

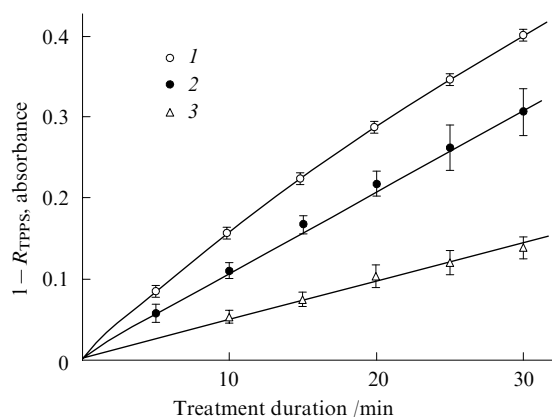
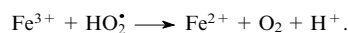


Figure 6. Extent of decomposition of TPPS (1) and absorbances of Fe³⁺ (2) and I⁻ (3) solutions plotted vs. duration of ultrasonic treatment.⁸⁵ $R_{\text{TPPS}} = c_{\text{TPPS}}/c_{\text{TPPS}}^0$ is the ratio of the TPPS concentration after ultrasonic treatment to the initial TPPS concentration.

Reduction reactions, *e.g.*, reduction of Fe(III) upon sonication of weak acid or neutral aqueous solution of complex K₃[Fe(C₂O₄)₃] in air⁸⁶ can also proceed in aqueous solutions



Reduction of Ce(IV) to Ce(III) under ultrasonic treatment of acidified aqueous cerium(IV) sulfate solution proceeds analogously.⁸⁷

Particular attention should be paid to a series of studies of oscillation processes in ultrasonic field taking the Belousov–Zhabotinsky reaction as an example; the results obtained are summarised in a monograph.¹⁴ It was shown that the parameters of the self-oscillatory chemical process (frequency, intensity, duration of vibrations) strongly depend on the instant (within the period of oscillations of the concentration of reaction mixture components) at which the acoustic energy is transferred to the irradiated medium.

Radical processes occurring under high-power ultrasound in aqueous solutions saturated with an oxygen–nitrogen mixture have also been studied.^{88–90} It was established that molecular nitrogen undergoes a series of chemical transformations involving the formation of nitrate and nitrite ions at nearly the same rates (about 0.03 μmol litre⁻¹ W⁻¹).⁹⁰

As mentioned above, sonolysis of water in the course of ultrasonic treatment of aqueous and aqueous alcoholic solutions creates favourable conditions for redox reactions, which can be used for the synthesis of various compounds in highly dispersed state. In this connection it is convenient to consider direct and indirect sonochemical redox reactions. In the former case the chemical reaction is solely driven by hydrogen peroxide formed in the course of sonolysis while in the latter case the oxidising (or reducing) agent is added to the reaction mixture during the synthesis.

It should be noted that often the role of sonication during the synthesis of disperse powders from aqueous solutions is reduced to intensification of the mixing of the reaction medium, disaggregation of particles, renewal of their surfaces, fabrication of uniform heterogeneous mixtures of solids, *etc.* Thus, sonolysis of water has almost no effect on the physicochemical features of synthesis.

1. Reduction of metals from aqueous solutions

Metals characterised by large positive redox potentials corresponding to semireactions (gold, platinum, palladium) can be reduced by direct sonochemical reduction (no additional reducing agents) to give disperse elements. For instance, ultrasonic treatment of aqueous tetrachloroaurate solutions in argon atmosphere makes it possible to prepare colloidal solutions of 10-nm gold particles⁹¹ with very narrow size distribution. The addition of aliphatic alcohols to the reaction mixture significantly accelerates the formation of colloidal solution, the effect being even more pronounced with enhancement of the hydrophobic properties of the alcohol. Similar results were obtained⁹² in a study of the influence of aliphatic alcohols on the rate of reduction of platinum from H_2PtCl_6 . The effect seems to be due to the fact that the interaction of alcohols with primary radicals H^\bullet and HO^\bullet formed in the sonolysis of water results in more stable and long-lived secondary radicals, which then act as reducing agents. As the hydrophobic fragments of molecules increase, the concentration of alcohol at the cavitation bubble–solution interface increases. As a consequence, most primary radicals interact with the alcohol molecules, thus favouring an increase in the yield of the secondary radicals. Therefore, the highest rate of sonochemical reactions in aqueous solutions is expected in the presence of surfactants.

Indeed, the rate of sonochemical reduction of some metals in the absence of surfactants is very low. For instance, the reduction of hexachloroplatinum acid and formation of nanodisperse platinum particles with the size of 3 nm occurs only in the presence of anionic surfactants (sodium dodecyl sulfate, sodium dodecylbenzene sulfonate or polyethylene glycol sodium monostearate); moreover, the reaction rate remains almost unchanged if the surfactant concentration becomes higher than the critical micelle concentration ($0.1\text{--}5\text{ mmol litre}^{-1}$).⁹³

The effect of the surfactant concentration on the micro morphology of nanodisperse powders formed under sonochemical reduction conditions was studied.⁹⁴ With no surfactant, ultrasonic treatment of aqueous hydrogen tetrachloroaurate solution in the presence of poly-*N*-vinyl-2-pyrrolidone resulted in the formation of highly dispersed almost spherical gold particles (average size $\sim 7\text{ nm}$). The particles formed in the presence of $\text{NaO}_3\text{SC}_{12}\text{H}_{23}$ have different morphologies including spherical, needle-shaped, disk-like and triangular crystals (Fig. 7). As the $[\text{HAuCl}_4]:[\text{NaO}_3\text{SC}_{12}\text{H}_{23}]$ ratio decreased from 1 to 0.05 with an increase in the surfactant concentration, the average particle size reduced from 18 to 10 nm and almost all triangular particles disappeared (only disk-like or spherical gold particles formed at high surfactant concentrations).

A negative consequence of the presence of surfactants in solution consists in reduction of cavitation efficiency due to the decrease in the surface tension of the solution. Because of this, the efficiency of formation of primary radicals decreases.

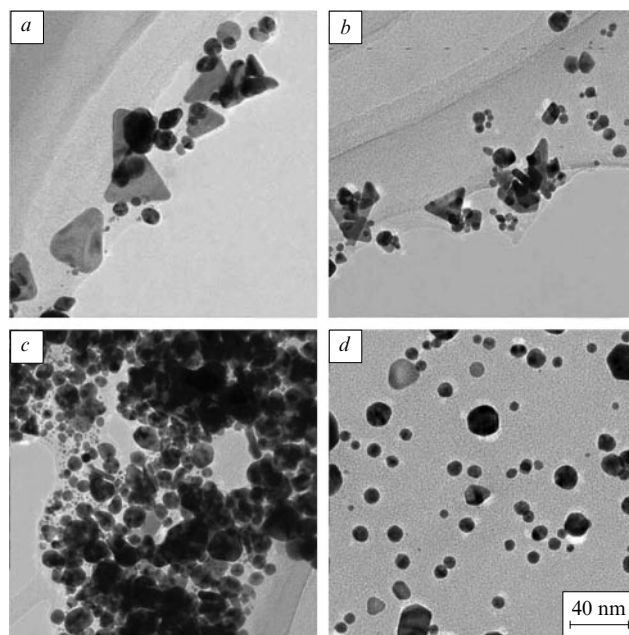


Figure 7. Micrographs of nanodisperse gold particles prepared by ultrasonic treatment for 1 h at a $[\text{HAuCl}_4]:[\text{NaO}_3\text{SC}_{12}\text{H}_{23}]$ ratio of 1 (a), 0.2 (b), 0.1 (c), 0.05 (d).⁹⁴

A study⁹⁴ of the effect of the acoustic power on the micro-morphology and average size of gold particles showed that an increase in the acoustic power from 30 to 90 W causes the average particle size to decrease from 20 to 10 nm. Additionally, nearly perfect spherical particles formed under high-power treatment, whereas low-power sonication resulted in the formation of disk-like, prismatic and needle-shaped particles. The authors believe that an increase in the ultrasound power increases the reduction rate of gold ions and the nucleation rate of the new phase and, correspondingly, the average particle growth rate decreases. Hydrogen peroxide that is formed during sonolysis of water is not a unique reducing agent; other compounds can also play this role. The mechanism of sonication is most likely associated with initiation of redox reactions due to the appearance of reactive radicals in the aqueous solution. The synthesis⁹⁵ of nanodisperse copper particles of size 50–70 nm from copper(II) hydrazine carboxylate can also be treated as indirect sonochemical reduction.

The results obtained in a study⁹⁶ of sonochemical reduction of potassium dicyanoaurate(I) in the presence of ascorbic acid deserve particular attention. It was shown that strongly aggregated gold particles of irregular shape are formed in aqueous solution. At the same time, gold nanoparticles formed in polyethylene glycol (PEG-400) have a needle-shaped morphology (diameter $\sim 40\text{ nm}$ at an anisotropy coefficient of about 15). It was assumed that the mechanism of formation of needle-shaped particles is due to the fact that individual 3-nm gold particles formed in the redox reaction form chains owing to coordination by OH and C–O–C groups of the polymer solvent molecules. Then, these chains aggregate to form needle-shaped particles. This mechanism was confirmed by the results of a study of the effect of potassium dicyanoaurate(I) concentration on the micromorphology of particles formed. The size and anisotropy coefficients of aggregates formed upon sonochemical reduction of gold from solutions with higher salt concentrations considerably increased and the content of particles with dendritic morphology also increased.

At present, studies on the synthesis of inorganic composite materials based on simple metals using sonochemical reduction techniques are scarce. In particular, direct sonochemical reduction of HAuCl_4 , AgNO_3 and PdCl_2 was successfully used^{97–101} for preparation of nanocomposites based on SiO_2 xerogels and containing 4–7-nm nanoparticles of corresponding metals. The matrix (SiO_2) plays an important role in the formation of nanodisperse metal particles. First, the xerogel pore diameter determines the size of the metal particles and, second, the matrix precludes aggregation of individual particles. Nanodisperse ruthenium particles were synthesised in a similar fashion by sonochemical reduction of ruthenium trichloride in the presence of mesoporous silica SBA-15.¹⁰²

Sonochemical reduction of HAuCl_4 and H_2PtCl_6 was also employed to prepare conducting composite materials based on polypyrrole¹⁰³ and polyaniline.¹⁰⁴ It was shown that acoustic treatment makes it possible to significantly accelerate (by ~ 50 times) the formation of the composite and to increase the yield of the reaction product.

2. Sonochemically induced reduction of metal oxides and hydroxides from aqueous media

Iron, chromium and manganese cannot be obtained from aqueous solutions by sonochemical reduction (standard electrode potential of semireactions is negative or has a small positive value). However, sonication can be utilised for preparation of corresponding highly dispersed oxides. In particular, nanocrystalline Fe_3O_4 powder comprising needle-shaped particles (average size 14×48 nm) was obtained by ultrasonic treatment of $\text{Fe}(\text{OAc})_2$ solution under argon bubbling.¹⁰⁵ Good examples of typical publications in this field are provided in Refs 83, 106 and 107. In particular, highly dispersed (50–200 nm) powders of X-ray amorphous manganese and chromium oxides Mn_2O_3 and Cr_2O_3 were synthesised from potassium permanganate and ammonium bichromate, respectively.¹⁰⁷ The addition of ethanol to the reaction mixture considerably increased the rate of sonochemical synthesis due to the formation of secondary radicals (α -hydroxyethyl radical). A study of the effect of temperature of the solution treated on the sonochemical reaction showed that the yield of the reaction product increases (but not decreases) with the increase in temperature due to a decrease in the cavitation intensity. Probably, in this case the thermodynamic and kinetic factors predominate. Recently, various modifications of the sonochemical synthesis of manganese oxides from aqueous solutions have attracted considerable attention because these compounds are promising in the design of materials for d.c. sources.^{108–110}

As mentioned above, in some cases the mechanism of sonochemical synthesis does not involve the redox processes and the role of cavitation is reduced to various mechanical effects. The reaction products obtained under sonication can differ in phase composition and micromorphology from those synthesised under similar conditions without sonication. In particular, this was observed¹¹¹ in the course of preparation of nanodisperse α - $\text{Ni}(\text{OH})_2$ powder (particle size 20 nm) by precipitation from aqueous solutions of nickel salts under ultrasonic treatment. The reaction carried out under similar conditions with no sonication resulted in the β -modification of nickel hydroxide characterised by somewhat larger particle size (70 nm).

A number of highly dispersed simple metal oxides were prepared in a similar fashion by sonohydrolysis.⁸ In particular, nanodisperse ceria was synthesised^{112,113} from cerium ammonium nitrate, hexamethylenetetramine, and polyethylene glycol. The procedure resulted in relatively small particles (size 2–4 nm) with narrow size distribution. Additionally, it was shown that the micromorphology of powder obtained by precipitation from a solution containing cerium nitrate and azoformamide noticeably

changes upon addition of some bases. In particular, the addition of quaternary ammonium bases gave monodisperse CeO_2 powder with a particle size of 3.3 nm.

Recently, extensive literature on the synthesis of titania powders under sonication has been published.^{114–122} Interest in preparation of highly dispersed titania is first of all due to the fact that this compound is a promising photocatalyst, which finds application in cleaning of waste water from organic waste. Most often, the sonochemical synthesis of TiO_2 is carried out by hydrolysis of titanium tetraisopropoxide in ethanol–water mixture followed by thermal annealing of the product at relatively low temperatures (400–500 °C). In this case spherical dense or mesoporous monophase anatase particles (average size 100–500 nm) or a mixture of anatase with brookite are formed depending on the reaction conditions.^{117,119} In some cases preparation of spherical particles during the synthesis requires the addition of high-molecular-mass compounds, *e.g.*, polyethylene glycol¹¹⁵ or octadecylamine.¹¹⁸ It should be noted that synthesis of titania from titanium tetrachloride results in monophase rutile^{119,121} with needle-shaped or dendritic morphologies.

Acoustic treatment of rutile suspensions in sodium hydroxide solution¹²² leads to formation of nanotubes and needle-shaped particles of approximate composition $\text{H}_2\text{Ti}_3\text{O}_7 \cdot 0.5 \text{H}_2\text{O}$. No such structures are formed without sonication. The authors assumed that this is due to partial dissolution of TiO_2 upon sonication.

The photocatalytic activity of titania can be considerably enhanced by carrying out the photodegradation reaction under sonication (Fig. 8).¹²³ This effect is due to continuous renewal and activation of the surface of titania particles.

A study¹¹⁴ of the photocatalytic activity of titania powders synthesised by sonohydrolysis of titanium tetraisopropoxide in aqueous and aqueous-alcohol media showed that this procedure makes it possible to prepare photocatalysts whose catalytic activities are at least comparable with those of the samples of commercially available materials (comparison with the Degussa-P25 sample was made, see Fig. 9).

More complex compounds, in particular aluminates,¹²⁴ nickelates and manganites⁸ were synthesised using similar sonochemical procedures (addition of precipitating agent to aqueous metal salt solutions).

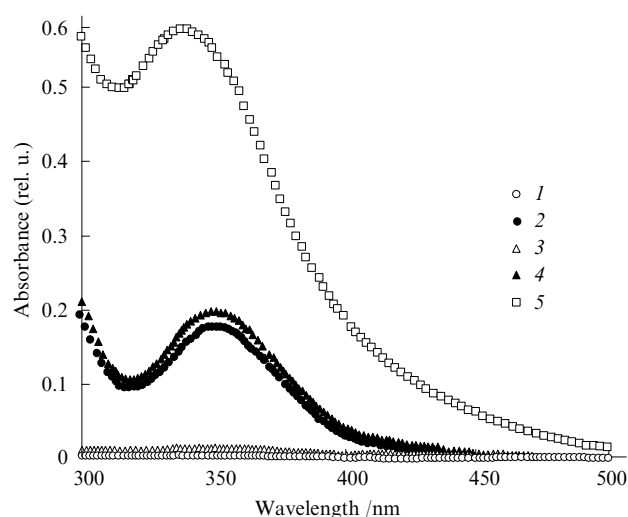


Figure 8. Absorption spectra of: aqueous KI solution irradiated with UV light (1) and ultrasound (2), aqueous KI solution with TiO_2 additive (3), pure aqueous KI solution (4) and aqueous KI solution with TiO_2 additive simultaneously irradiated with UV light and ultrasound (5).¹²³

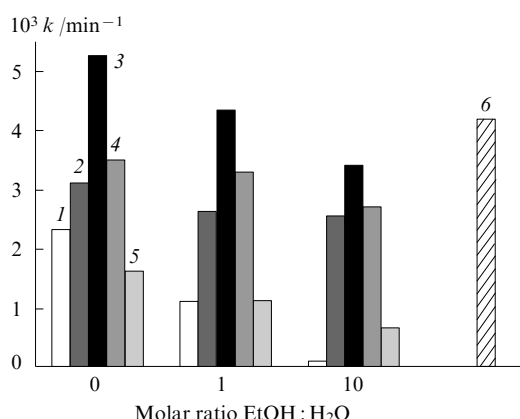


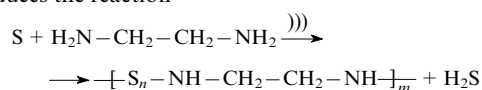
Figure 9. Apparent rate constants (k) for photocatalytic degradation of acetone plotted vs. solvent composition and calcination temperature of titania samples prepared by ultrasonic irradiation.¹¹⁴ $T/^{\circ}\text{C}$: 100 (1), 400 (2), 500 (3), 600 (4) and 700 (5); Degussa-P25 sample (6).

3. Sonochemical synthesis of metal chalcogenides

Recently, extensive literature has been devoted to sonochemical synthesis of transition metal chalcogenides. This method was used for preparation of nanodisperse ZnS ,^{125–127} Sb_2S_3 ,^{128, 129} HgSe ,¹³⁰ HgS ,¹³¹ SnS_2 ,¹³² CdS ,^{133–137} CdSe ,^{133, 138} PbX ($\text{X} = \text{S}, \text{Se}, \text{Te}$),^{139–141} CuS ,^{96, 142} Cu_{2-x}Se , Cu_3Se_2 , CuSe ,^{143–145} $\text{Bi}_2\text{Se}_x\text{Te}_{3-x}$, Ag_2Se , Ag_2Te , Cu_5Se_4 , PbSe , Ni_3Se_4 ,¹⁴⁶ Ag_2Se , $\text{NiS}_{1-x}\text{Se}_x$,^{142, 147} MoS_2 ,¹⁴⁸ Ag_2S ,¹⁴⁹ $\text{RuS}_{1.7}$,¹⁵⁰ Bi_2S_3 ,¹⁵¹ HgTe ,¹⁵² MoTe_2 ,¹⁵³ and Bi_2Te_3 powders.¹⁵⁴

Here, salts are most widely used as the source of metal. First of all, these are acetates,^{125, 130, 139} nitrates and chlorides.¹³² The source of sulfur is provided by thioacetamide, thiourea, elemental sulfur or sodium thiosulfate. Selenides and tellurides are mainly synthesised from elemental selenium and tellurium as the sources of the non-metals; at the same time, the syntheses of selenides and tellurides using sodium selenite or tellurite were reported.^{138, 146}

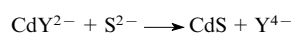
The most often used solvents are water or aqueous-alcohol solutions;^{125, 134, 136} however, in some cases ethylenediamine^{145, 147, 149, 152, 155} or polyethylene glycol^{130, 140} is more appropriate. This concerns the reactions involving elemental sulfur (or selenium) as the source of the non-metal, because sonication of a suspension of a chalcogen in ethylenediamine induces the reaction



resulting in liberation of hydrogen sulfide.¹⁴⁹ Nanodisperse sulfides are formed as a result of the interaction of hydrogen sulfide with a metal salt or a metal complex.¹⁵⁶ By carrying out reactions in polyethylene glycol it is possible to substantially reduce the minimum acoustic power necessary for the sonochemical synthesis of chalcogenides.¹³⁰ In some cases polyethylene glycol also acts as a reducing agent.¹³⁰ Additionally, the synthesis of metal chalcogenides in the presence of polyethylene glycol or other polymers capable of playing the role of complex-forming agents (e.g., hydroxyethylcellulose¹³⁶) permits fabrication of submicron disperse particles with strip and dendritic morphologies. A similar procedure [sonochemical oxidation of iron(II) acetate in aqueous solution in β -cyclodextrin matrix] was used for preparation¹⁰⁵ of needle-shaped magnetite (Fe_3O_4) nanoparticles.

It should be noted that low-molecular-mass complex-forming agents affect the micromorphologies of the powders formed in the course of sonochemical synthesis. This concerns, in particular, sodium tartrate and sodium citrate.^{143, 151} However, the most interesting results were obtained using ethylenediaminetetraacetic acid (EDTA) as complex-forming agent. Namely, the reactions of formation of needle-shaped or strip-like nanodisperse Bi_2S_3 ,¹⁵¹

PbS ,¹⁴¹ and CdS ¹³⁶ particles in the presence of EDTA were substantially accelerated. The formation of highly anisotropic particles in the presence of EDTA was explained using a mechanism involving the formation of a very stable pentadentate complex between EDTA (Y^{4-}) and Cd^{2+} ion. Steric hindrances allow the interaction between Cd^{2+} and S^{2-} ions



to follow only one direction.¹⁶ Correspondingly, the chalcogenide particles grow in this direction (Fig. 10).

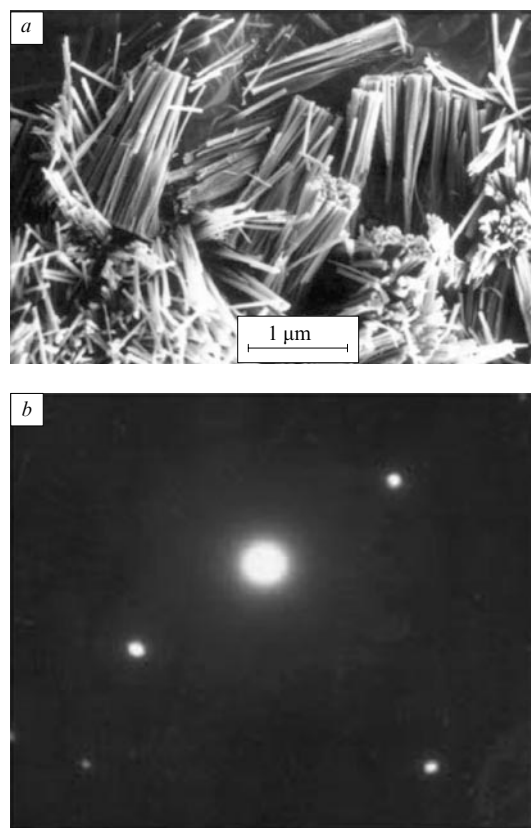


Figure 10. Micrograph of rod-like CdS crystals (~ 80 nm in diameter, ~ 1.3 μm long) formed under ultrasonic treatment in the presence of EDTA (a) and an electron diffraction pattern of an individual rod (b).¹⁶

When chalcogenides are synthesised in aqueous media, the compositions and structures of reaction products are strongly influenced by the pH value of the solution. Taking mercury sulfides as examples, it was shown that nanodisperse α -HgS powders can only be synthesised from solutions with pH 9–11.¹³¹ In more acidic media, coarse-grained precipitate is formed rapidly. If the medium pH is controlled by adding ammonia (triethanolamine), the powder formed is characterised by an average particle size of ~ 35 nm (10–15 nm, spherical particles). The smaller particle size in the case of triethanolamine was explained¹³¹ by the fact that this compound is an effective ligand that forms stable complexes with Hg^{2+} . The synthesis of nanodisperse β -HgS powder only proceeds at pH values from 3 to 5. Reactions in media of lower acidity result in coarse-grained β -HgS precipitate. Additionally, it was shown that the β -HgS particle size also depends on the treatment duration, namely, the average particle size changes from 13 to 20 nm as the duration of sonochemical synthesis increases from 0.5 to 1 h. This effect can be due to recrystallisation and growth of nanodisperse particles.

By and large, the micromorphologies of products of sonochemical synthesis are to a great extent determined by the reaction conditions. For instance, the synthesis of Sb_2S_3 gave both amor-

phous nanospheres and needle-shaped nanoparticles.¹²⁸ Star-like Sb_2S_3 particles were synthesised under somewhat different conditions.¹²⁹

The mechanism¹³⁹ of sonochemical formation of nanodisperse lead sulfide powders can probably be extended to other metal sulfides and selenides provided that the source of the non-metal is elemental sulfur or selenium. Sonication of such systems increases the rate of dissolution of the non-metal (conventionally, this is the limiting stage of the chalcogenide formation reactions) and, hence, the formation of E^{2-} ($\text{E} = \text{S}, \text{Se}, \text{Te}$) ions. Additionally, ultrasonic treatment precludes aggregation of chalcogenide particles.

VI. Sonochemical processes in non-aqueous media

As shown above, in the course of sonochemical reactions in aqueous media the cavity of a cavitation bubble is only filled with water vapours and dissolved gases, because usually the volatilities of other components of the aqueous solution are negligible. The mechanism of sonochemical processes in aqueous solutions involves the formation of mainly H^\bullet , HO^\bullet , and HO_2^\bullet radicals upon collapse of cavitation bubbles and subsequent interaction of these species with compounds in solution.

In the case of non-aqueous solutions the number of compounds capable of competing with the solvent in volatility considerably increases and includes, *e.g.*, various metal complexes. Large amounts of such compounds can be present in the gaseous phase within the cavitation bubble along with the solvent molecules. Collapse of the cavitation bubble causes their decomposition and formation of solid-phase products of sonolysis. Since each collapsing cavitation bubble can be treated as a specific microreactor, sonochemical decomposition products are characterised by very high degree of dispersion.

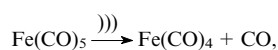
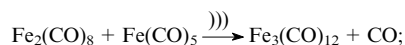
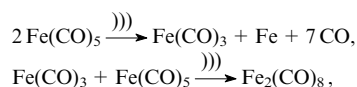
Sonolysis of non-aqueous solutions makes it possible to obtain simple (metals) and complex substances (*e.g.*, binary compounds including nitrides, carbides, oxides, sulfides, silicides, borides) and composites based on them.¹⁵ The compositions and structures of nanomaterials strongly depend on the characteristics of the reaction medium, namely, the type of solvent, chemical inertness of the solvent or its ability to interact with the substance treated; the presence of surfactants and/or high-molecular-mass compounds; the oxidative, reductive or inert character of the atmosphere in which ultrasonic treatment is carried out.

1. Synthesis of nanodisperse metals and alloys

Sonolysis of solutions of transition metal carbonyls [$\text{Fe}(\text{CO})_5$, $\text{Ni}(\text{CO})_4$, $\text{Co}(\text{CO})_3\text{NO}$, $\text{Mn}_2(\text{CO})_{10}$, $\text{Re}_2(\text{CO})_{10}$, $\text{Cr}(\text{CO})_6$, $\text{Mo}(\text{CO})_6$] in high-boiling alkanes leads to formation of nanosized clusters of amorphous metal particles.^{39, 157–161} In particular, high-power ultrasonic treatment of a solution of iron pentacarbonyl in decane under argon bubbling at 0 °C led to weak aggregation of amorphous particles of elemental iron of size at most 5–6 nm.³⁹ Subsequent heat treatment of the powder thus obtained in inert atmosphere at 350 °C resulted in partial crystallisation of iron.

Starting from a mixture of metal carbonyls, one can prepare nanodisperse alloys. For instance, sonication of a solution of iron and cobalt carbonyls in decane gave a highly dispersed Fe–Co alloy (particle size 6–10 nm).¹⁶² By varying the concentrations of the starting compounds it is possible to obtain a continuous series of iron–cobalt alloys from pure iron to pure cobalt.^{162, 163} Similar results were obtained in the synthesis of Co–Ni and Fe–Ni alloys.^{164, 165}

Not only elemental iron, but also carbonyl complexes of more complex structures are formed³⁹



It is impossible to obtain $\text{Fe}_3(\text{CO})_{12}$ by thermolysis of photolysis of $\text{Fe}(\text{CO})_5$ as well as by other methods. Therefore, the synthesis of compound $\text{Fe}_3(\text{CO})_{12}$ can be considered as specific sonochemical reaction.

Small metal and alloy particles formed in the sonochemical reaction undergo strong aggregation. The degree of dispersion of powders obtained can be considerably increased using surfactants and some other compounds. A method of synthesis of stable colloidal solutions of elemental iron and cobalt using high-power sonication was proposed.^{166–168} The technique is based on sonochemical decomposition of iron pentacarbonyl or cobalt carbonyl-nitrosyl in decane in the presence of stabilisers (poly-*N*-vinyl-2-pyrrolidone, oleic acid^{8, 15} or higher aliphatic alcohols).^{167, 168} As a result, a stable colloidal solution of nanosized paramagnetic iron particles (size range 8–10 nm) is formed (Fig. 11). A modified procedure was used for the synthesis of colloidal Fe_2O_3 solution stabilised with oleic acid.⁸

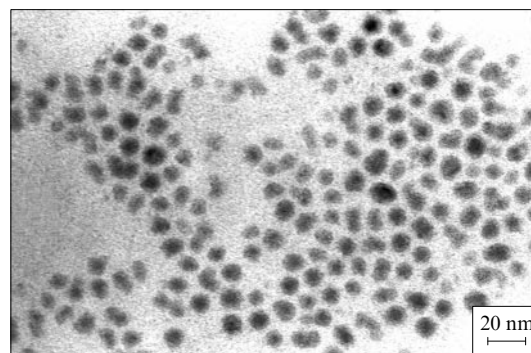


Figure 11. Micrograph of colloidal iron sample obtained under sonochemical irradiation and stabilised by oleic acid.¹⁵

It should be noted that nanodisperse metals can be sonochemically synthesised in non-aqueous media not only from carbonyls, but also from other volatile metal compounds. For instance, a colloidal solution of nickel particles (size 3.9–4.3 nm) in diethyl ether was prepared from nickel acetylacetonate in the presence of triphenylphosphine with diethyl aluminium hydride as reducing agent at –40 °C.¹⁶⁹ Colloidal particles can be separated and redispersed in another polar solvent, *e.g.*, pyridine. Colloidal particles are stabilised by the triphenylphosphine shell on the surface.

The use of transition metal β -diketonates instead of carbonyl and carbonyl-nitrosyl complexes is not very promising because of rather high metal–oxygen and oxygen–carbon bond energies. Therefore, sonolysis of solutions of transition metal β -diketonates (even carried out in high-boiling alkanes C_{12} – C_{17}) only results in partial decomposition of these compounds and formation of products with high content of organic residues.^{170, 171}

Catalysis is one of the largest fields of application of nanodisperse metals.¹⁷² The vast majority of metals used as heterogeneous catalysts represent supported catalysts. Here, compounds characterised by large specific surface area (usually, alumina or silica) act as substrates. A conventional method of synthesis of heterogeneous catalysts involves the soaking of a porous substrate with a corresponding metal salt solution followed by heat treatment in reductive atmosphere. Clearly, in this case metal particles

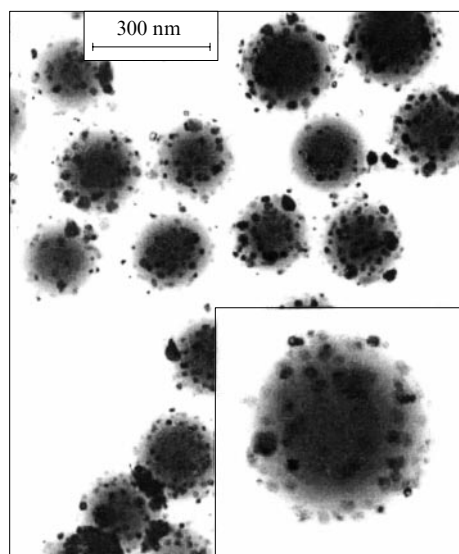


Figure 12. Micrograph of a sample prepared by sonolysis of iron pentacarbonyl in decalin in the presence of silica microspheres followed by hydrogen reduction.¹⁷⁴

are adsorbed not only on the surface, but also within the pores of the substrate, which significantly reduces the specific activity of the catalyst. In this connection the development of sonochemical methods for the synthesis of catalysts with uniformly distributed nanodisperse metal particles with narrow size distribution (Fig. 12) on the substrate surface seems to be quite promising.^{173, 174}

Sonolysis of iron pentacarbonyl in decane in the presence of silica gel results in nanodisperse powders of amorphous metallic iron (3–8 nm); the powder particles are uniformly distributed over the surface of silica particles.¹⁷⁵ The catalytic activity of the material thus obtained was studied taking the Fischer–Tropsch reaction as an example. A comparison of its catalytic activity with that of a catalyst prepared by the soaking technique showed that at the same loading the activity of the sonochemically prepared catalyst was nearly tenfold higher than the activity of the ‘soaked’ catalyst. The former catalyst exhibited a high activity at relatively low temperatures (< 250 °C), whereas the activity of the latter catalyst in this temperature range was very low (Fig. 13).

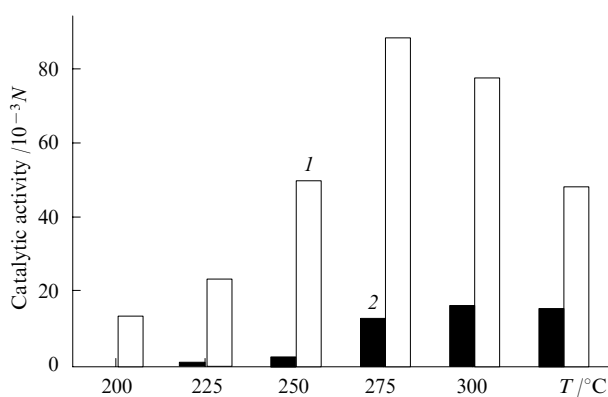


Figure 13. Catalytic activity of Fe/SiO₂ plotted vs. hydrogenation temperature of carbon monoxide.¹⁷⁵

N is the number of hydrogenated CO molecules per active site per second; catalysts were prepared by ultrasonic treatment (1) and by soaking (2).

2. Synthesis of binary compounds

Metal carbonyls can serve as precursors in the synthesis of binary metal compounds, *e.g.*, carbides and chalcogenides. Depending on the synthesis conditions and the character of subsequent treatment, a variety of products can be obtained.¹⁷⁶ Often, preparation of the end product involves high-temperature heat treatment of an intermediate. For instance, the sonochemical decomposition of molybdenum hexacarbonyl in hexadecane followed by heating of the product in CH₄–H₂ atmosphere resulted in a nanosized Mo₂C_{1.02} powder with particle size of 3–5 nm.¹⁶²

In order to synthesise metal chalcogenides, the corresponding carbonyl and elemental chalcogen are sonicated in a high-boiling non-polar solvent. In particular, ultrasonic treatment of a solution of molybdenum hexacarbonyl and sulfur in tetramethylbenzene under argon bubbling results in the formation of nanocrystalline MoS₂ (particle size ~15 nm) with unusual morphology (aggregates of porous spherical particles).¹⁴⁸ Molybdenum telluride MoTe₂ was synthesised¹⁵³ by sonicating tellurium and Mo(CO)₆ in decalin under argon bubbling for 4 h. The product obtained immediately after sonication was X-ray amorphous powder characterised by high degree of aggregation of particles of size 50–150 nm. The powder obtained at shorter duration of the synthesis had a different micromorphology and comprised plate-like particles of nearly the same size (50–150 nm). Subsequent thermal annealing of the products of sonochemical synthesis at 650 °C for 10 h gave a molybdenum telluride powder the particles of which were nanotubes of length 100–500 nm and 20–50 nm in diameter.

Nanosized amorphous cobalt ferrite (CoFe₂O₄) powder was obtained by sonochemical decomposition of iron carbonyl Fe(CO)₅ and cobalt carbonyl-nitrosyl Co(CO)₃NO in decalin at 0 °C under oxygen flow.¹⁷⁷ Nanosized amorphous nickel ferrite NiFe₂O₄ was prepared under similar conditions.¹⁷⁸ Subsequent annealing of the amorphous products at 450 °C led to partial crystallisation with retention of the nanosized state.

Composite materials can also be synthesised using the procedure described above. Considerable advances in this field were made by a research group headed by Prof. Gedanken. Most studies of researchers from this group were devoted to preparation of reactive catalytic materials.^{8, 15} In particular, a novel method of fabrication of molybdenum oxide–silica and molybdenum carbide–silica composites was reported.¹⁷⁹ These materials were synthesised by ultrasonic treatment of a suspension of silica microspheres and molybdenum hexacarbonyl in decane. Treatment in air gave amorphous powder of Mo₂O₅–SiO₂ composite, whereas ultrasonic treatment in argon atmosphere resulted in amorphous Mo₂C–SiO₂ composite.

Preparation of nanodisperse amorphous oxides, in particular, nickel and cobalt oxides can also be treated as specific methods of sonochemical synthesis. It is believed¹⁸⁰ that similar compounds can be synthesised only under sonochemical treatment, because one should attain unusually high cooling rates (up to 10¹⁰–10¹¹ K s⁻¹).

It should be noted that sonochemical reactions in non-aqueous media are far from being reduced to the transformations of metal carbonyls. Extensive literature is devoted to sonochemical transformations of organic (alkanes, halogenated hydrocarbons) and organometallic compounds; Diels–Alder synthesis, Friedel–Crafts reaction, *etc.* under sonication. It was shown that concurrent microwave and ultrasonic treatment is promising for acceleration of hydrazinolysis of esters.¹⁸¹ A scheme of a setup for combined microwave–ultrasonic treatment is shown in Fig. 14. A number of reviews concerned with various aspects of liquid-phase and heterophase sonochemistry of non-aqueous media are available.^{14, 23, 33, 182}

Thus, at present the most often used starting compounds for sonochemical synthesis of nanodisperse inorganic materials in non-aqueous media are transition metal carbonyl and carbonyl-

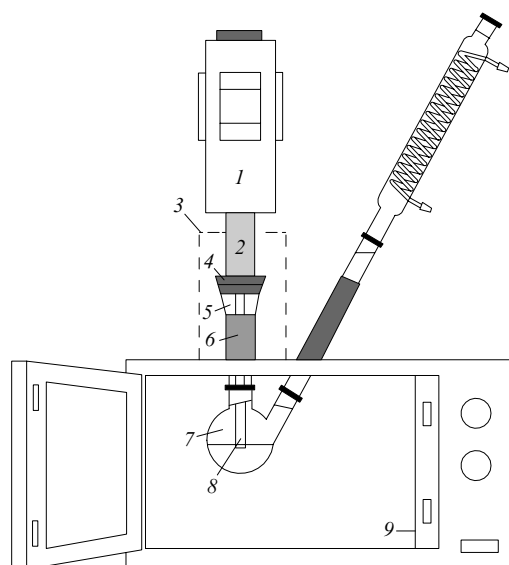


Figure 14. Scheme of an apparatus for combined microwave–ultrasonic treatment of solutions.¹⁸¹

Transducer housing (1), upper part of the waveguide (2), copper mesh screen (3), rubber stopper (4), adapter (5), port (6), flask (7), detachable horn (8), microwave oven (9).

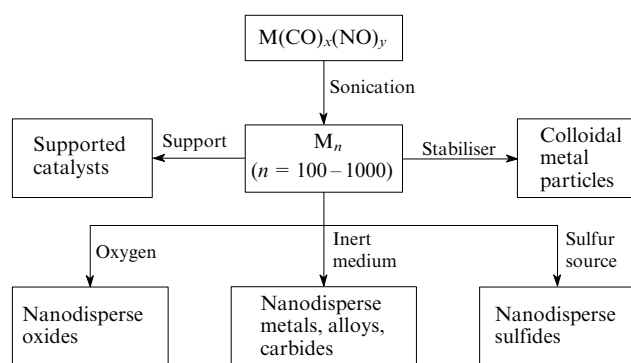


Figure 15. Sonochemical methods of synthesis of various nanodisperse inorganic materials in non-aqueous media.¹⁵

nitrosyl complexes. Possible methods of synthesis of such materials are shown in Fig. 15.

VII. Sonochemical processes under hydrothermal conditions

Initially, hydrothermal synthesis was used as efficient method of growth of single crystals of various inorganic compounds and for production of high-purity inorganic materials.^{183, 184} Later on, the method was shown to be promising for the synthesis of highly dispersed (including nanodisperse) inorganic materials. At present, hydrothermal method is widely used for preparation of both single crystals and highly dispersed powders of simple and complex oxides, chalcogenides, hydroxides, phosphates, zeolites, supramolecular and many other classes of compounds.¹⁸⁵

The promise for using concurrent hydrothermal and ultrasonic treatment for the synthesis of disperse powders has been documented.^{22, 186–188} The authors assumed that the main effects accompanying sonication of liquid-phase and heterogeneous liquid–solid systems under conventional conditions (cavitation, sonolysis and sonochemical redox reactions, intense local microflows of liquids and shock waves) should also be observed under hydrothermal conditions. At the same time the possibility of onset

of cavitation in aqueous solutions at temperatures above 100 °C required experimental substantiation. This was done in analysis of the level of acoustic noise in an aqueous medium measured by a broadband hydrophone.¹⁸⁶ It was established that the cavitation intensity at 250 °C is 70%–80% of the cavitation intensity at room temperature. Unfortunately, the temperature dependence of the cavitation intensity in the temperature range from 100 to 250 °C was not measured. Additionally, the influence of the physicochemical properties of liquid media at temperatures above 100 °C (viscosity, surface tension, saturated vapour pressure, etc.) on the cavitation parameters was also not studied.

It was also shown¹⁸⁶ that sonication of hydrothermal solutions initiates redox processes in them. The authors assumed that the oxidation of divalent cobalt salts and hydroxide to Co₃O₄ involves HO• radicals generated in aqueous solutions during sonolysis of water. It should be noted that nanodisperse Co₃O₄ particles formed under concurrent hydrothermal and ultrasonic treatment of a cobalt nitrate solution have a well-developed mesoporous structure (Fig. 16). Under conventional hydrothermal treatment of solutions, mesoporous metal oxide powders are formed at such concentrations at which the rates of nucleation processes (they dominate at low concentrations) and growth of crystallites (they dominate at high concentrations) are commensurable.¹⁸⁹ It was shown experimentally that the growth of crystallites predominates under hydrothermal treatment of solutions of cobalt(II) salts. At the same time sonication probably increases the rate of nucleation of the new phase, which leads to a shift of the hydrothermal synthesis towards the transient ‘nucleation–crystallite growth’ region characterised by the best conditions for the formation of mesoporous oxide powders.

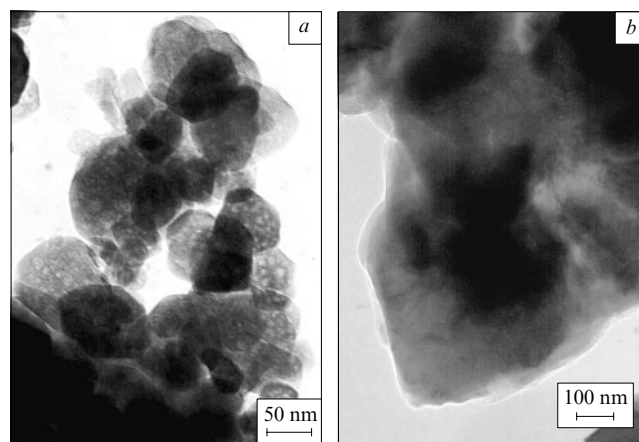


Figure 16. Micrographs of Co₃O₄ samples synthesised by concurrent hydrothermal and ultrasonic treatment (a) and by conventional hydrothermal treatment (b).¹⁸⁶

A study¹⁹⁰ of the synthesis of mixed nickel–zinc ferrites showed that ultrasonic treatment under hydrothermal conditions causes a slight increase (by 10%–20%) in the size of nanodisperse product crystallites and the formation of powders with a narrower crystallite size distribution compared to the particle size distribution typical of conventional hydrothermal synthesis.

Sonication under hydrothermal synthesis also has a moderate effect on the micromorphology of titania and zirconia powders prepared by crystallisation of X-ray amorphous zirconyl and titanyl hydroxide gels.¹⁹⁰ At the same time the TiO₂ and ZrO₂ powders synthesised under concurrent hydrothermal and ultrasonic treatment are characterised by significantly different phase compositions compared to powders prepared under conventional hydrothermal conditions. For instance, hydrothermal treatment of amorphous zirconyl hydroxide gel for 3 h at 250 °C results in the formation of a mixture of two crystalline polymorphs of

zirconia, namely, a thermodynamically stable monoclinic modification ($\sim 12\%$) and a metastable tetragonal modification ($\sim 88\%$). Hydrothermal treatment of amorphous gel $\text{ZrO}_2 \cdot n\text{H}_2\text{O}$ under similar conditions with concurrent sonication leads to appreciable acceleration of crystallisation of the amorphous phase and to an increase in the content of thermodynamically stable monoclinic modification of zirconia (to $\sim 30\%$) in the reaction product.

Similar results were obtained in the synthesis of nanodisperse titania by high-temperature hydrolysis of aqueous $\text{H}_2\text{TiO}(\text{C}_2\text{O}_4)_2$ solution.¹⁹⁰ A conventional hydrothermal treatment of the solution gave a mixture of thermodynamically stable (rutile) and metastable (anatase) TiO_2 polymorphs, the content of rutile being at most 10%. Concurrent hydrothermal and ultrasonic treatment led to an increase in the content of rutile to 20%.

At the same time sonication in the course of hydrothermal synthesis of ZrO_2 and TiO_2 from zirconyl nitrate and X-ray amorphous $\text{TiO}_2 \cdot n\text{H}_2\text{O}$ gel, respectively, had almost no effect on the phase composition of reaction products.

Thus, sonication during the hydrothermal synthesis of oxide powders can be accompanied by (i) substantial acceleration of crystallisation of X-ray amorphous gels and formation of highly dispersed and nanodisperse powders, (ii) an increase in the content of thermodynamically stable phases in the products of synthesis provided that the oxide being synthesised exists as a number of polymorphs and (iii) initiation of redox reactions in aqueous solutions resulting in highly dispersed (including mesoporous) particles.

VIII. Solid-phase sonochemical processes

The mechanisms of liquid-phase sonochemical reactions are closely related to a number of non-linear effects emerging upon sonication of solutions and suspensions (first of all, cavitation). Clearly, cavitation cannot be the driving force of the processes occurring in the solids irradiated with high-power ultrasound. Therefore, the mechanism of the action of ultrasound on solids should be fundamentally different.

Consider the effect of acoustic vibrations on the real structure of solids. At present, such studies are only carried out for polycrystalline metals and alloys¹⁹¹ as well as for single crystals of ionic compounds (alkali metal halides) and $\text{A}^{\text{II}}\text{B}^{\text{VI}}$ and $\text{A}^{\text{III}}\text{B}^{\text{V}}$ semiconductor crystals.¹⁹² Main trends in the behaviour of these systems under alternating stresses are similar.

Sonication causes the following processes in solids to occur.

1. Dislocation motion and redistribution over the volume of the crystal, which is only possible upon attainment of a threshold amplitude of ultrasonic vibrations ($\xi_{\text{threshold}}$).^{193, 194} Translational motion of dislocations mainly follows one direction in spite of periodic changes in the sign of the stress, because the chain of point defects, small dislocation loops and dislocation dipoles formed behind the moving dislocation precludes the change in the direction of the dislocation motion. The speed of translational motion of dislocations in various crystals varies from 0.2 to $2.4 \mu\text{m min}^{-1}$ (Ref. 192). The action of ultrasound on crystals induces the appearance of stable dislocation patterns, thus having much in common with thermal annealing.^{195, 196}

2. Dislocation multiplication and an increase in the concentration of dislocations to a certain limiting value (saturation) occur at stresses corresponding to the dynamic yield stress σ_f^0 . Sonication causes an increase in the concentration of dislocations by several orders of magnitude to $10^8 - 10^{10} \text{ cm}^{-2}$ (Ref. 194). The dislocation distribution over the volume is highly non-uniform; dislocations are mainly concentrated near sources (at grain boundaries, cracks and other macroscopic structural defects).

3. Formation of point defects, which can occur at dislocation jogs or follow the mechanism of annihilation of dislocations of opposite sign.^{197, 198}

It should be noted that the concentration of structural defects in ultrasonically treated material is a non-linear function of both

the acoustic power and the treatment temperature. Here, a considerable (by more than an order of magnitude) increase in defectiveness of the crystal is observed in particular temperature and ultrasound power ranges,¹⁹¹ *i.e.*, there is well-defined synergism between acoustic and heat treatment. Clearly, such a change in the real structure of a solid should lead to considerable enhancement of the diffusion mobility of ions in the crystal structure and, correspondingly, to acceleration of certain solid-phase reactions.

The simplest types of solid-phase reactions are polymorphic transformations and phase decomposition. In the text below we summarise the results of studies on the effect of sonication on solid-phase austenite transformations in steels.

The effect of ultrasonic radiation on the kinetics of intermediate (beinite) transformation of 30XГCH2A steel was studied.¹⁹⁹ The ultrasonically treated samples showed a considerable increase in the content of beinite, *i.e.*, acoustic treatment favoured acceleration of the austenite transformation. Electron microscopy studies revealed that the dislocation density in the untreated samples was an order of magnitude lower (10^8 cm^{-2}) than in the samples exposed to ultrasonic irradiation (at least 10^9 cm^{-2}). The ultrasonically treated steel samples showed that dislocations are present both in the interior of grains and at grain boundaries. Additionally, the dislocation structure of austenite developed under sonication rapidly disappears upon short-term heat treatment of the steel samples. The authors¹⁹⁹ suggested the following mechanism of austenite transformations. The interaction of point defects that are formed abundantly under sonication with dislocations during high-temperature annealing is due to diffusion and subsequent annihilation of the defects. Acceleration of the beinite transformation under ultrasonic treatment results from enhancement of the mobility of carbon atoms, which in turn is a consequence of an increase in the density of lattice defects (dislocations and vacancies).

The effect of sonication on the reverse martensite transformation in iron/nickel (29% Ni) alloy pre-annealed from 950 °C was a subject of yet another study.²⁰⁰ It was established that the process slows down upon ultrasonic treatment. The authors²⁰⁰ pointed out that austenisation on heating causes the formation of concentration inhomogeneities, namely, regions with higher and lower concentration of nickel atoms. According to the phase diagram of the Fe–C system, the nickel-enriched martensite phase should transform into austenite at lower temperatures compared to the Ni-depleted phase. Continuous ultrasonic irradiation results in a high concentration of vacancies and, as a consequence, enhanced mobility of nickel atoms. Here, the formation of the nickel-enriched zones becomes less probable. As a result, the reverse martensite transformation is shifted towards the higher-temperature region.

Studies of the effect of acoustic activation on polymorphic transformations were carried out for a few oxides, in particular, PbO ²⁰¹ and zirconia.²⁰² For instance, it was shown²⁰¹ that ultrasonic treatment of $\beta\text{-PbO}$ initiates the $\beta\text{-PbO} \rightarrow \alpha\text{-PbO}$ phase transition even in the absence of additional heat treatment; the degree of transformation was about 5%. The efficiency of sonication in the course of phase transition appreciably increases as the temperature increases. At 400–475 °C, the $\alpha\text{-PbO}$ phase formed under sonication is partially oxidised to Pb_3O_4 . A kinetic study of the $\beta\text{-PbO} \rightarrow \alpha\text{-PbO}$ phase transition and oxidation of $\alpha\text{-PbO}$ to Pb_3O_4 at 425 °C showed that an increase in the duration of ultrasonic treatment of $\beta\text{-PbO}$ causes the overall extent of the transformation $\beta\text{-PbO} \rightarrow \alpha\text{-PbO} + \text{Pb}_3\text{O}_4$ to increase. Then, the rate of the phase transition decreases and the curve of the $\beta\text{-PbO}$ content reaches saturation stage. The maximum extent of transformation of $\beta\text{-PbO}$ under concurrent sonication and heat treatment is 0.85, which is in good agreement with the results obtained in studies of mechanochemical activation of the $\beta\text{-PbO} \rightarrow \alpha\text{-PbO}$ transition.²⁰³

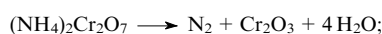
Sonochemical initiation of the phase transformation ‘metastable polymorph \rightarrow stable polymorph’ of zirconia proceeds in a

similar fashion.²⁰² Under conventional heat treatment the tetragonal polymorph of zirconia remains stable on heating up to 600 °C, whereas under concurrent high-temperature and ultrasonic treatment the monoclinic modification is formed at 500 °C (the content of the latter is 18%).

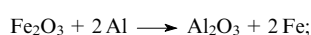
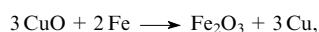
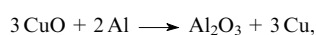
More complex types of solid-phase reactions undoubtedly include processes in binary and multicomponent systems, because reactions in such systems occur at grain boundaries.

Enikolopov *et al.*²⁰⁴ were the first who studied the possibility for solid-phase chemical processes to occur under ultrasonic treatment in mixed (not pure metallic) systems. The following reactions were carried out under sonication:

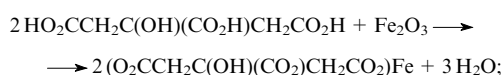
(1) decomposition



(2) substitutions in metal–oxide systems (metallothermy)



(3) exchange in the citric acid–iron oxide system



(4) azo couplings in solid-phase synthesis of some azo dyes (Bismarck brown, pigment Red G) from stoichiometric mixtures including an aromatic amine and sodium nitrite.

It was shown that in all these systems ultrasonic treatment favours initiation of solid-phase reactions. For instance, irradiation of metal–metal oxide systems with ultrasound (vibrational amplitude 5 μm) initiated reactions that completed in 15–25 s depending on the system. An increase in the amplitude had no effect on the reaction rate. Sonication had similar action on the reactions of ammonium bichromate decomposition and interaction of iron(III) oxide with citric acid. In the latter case the maximum extent of transformation was only 50% and did not increase with an increase in the duration of ultrasonic treatment and in the acoustic power delivered, apparently, due to the formation of a dense layer of reaction product on the Fe_2O_3 surface. On the contrary, the synthesis of azo dyes appeared to be sensitive to the ultrasonic power, namely, the rate of the reaction increased on the average by 30%–40% upon an increase in the vibrational amplitude from 10 to 15 μm .

It was established that each system studied is characterised by a particular threshold amplitude of ultrasonic vibrations (no reaction initiation occurs at smaller amplitudes). Solid-phase sonochemical reactions require a rather high density of compaction of the starting powder.²⁰⁴ For instance, initiation of the decomposition of ammonium bichromate under sonication occurred only if the density of the starting pellet was at least 80% of the theoretical value. This is probably due to the need of creation of good acoustic interparticle contacts in powder (if no contacts are available, acoustic power substantially dissipates at interfaces and the efficiency of sonication considerably decreases).

It was assumed²⁰⁴ that the initiating action of ultrasound causes an appreciable reduction of diffusion limitations, which allows solid-phase reactions to proceed at rather high rates under relatively mild conditions. However, in this case the role of acoustic activation is likely reduced to initiation of the solid-phase reactions mentioned above. In particular, it is known that metallothermic processes and decomposition of ammonium bichromate release much heat. Ultrasonic deformations can cause local heating in powder systems; for instance, heat release occurs at interparticle contacts at the instant of reaction initiation. At high density of compacted samples, the energy released is almost not dissipated, being completely spent for heating of the surrounding particles and thus initiating further interaction. Then the reaction proceeds by a mechanism similar to high-temperature

self-propagating synthesis (in this case ultrasound acts as initiator of the reaction). This assumption is consistent with the fact that an increase in the amplitude of ultrasonic vibrations upon attainment of a threshold value does not accelerate the reaction, because after initiation the effect of sonication on the process becomes negligible compared to the effect of heating of the reaction mixture due to heat released.

Obviously, the data on the formation of complex organic compounds²⁰⁴ could not be interpreted in the framework of the diffusion formalism. In this case the reaction mixtures are multicomponent systems including not only ionic, but also molecular compounds, and the chemical reaction involves formation of numerous intermediate products.

The effect of sonication on high-temperature self-propagating synthesis of Ti_5Si_3 and TiSi_2 in the titanium–silicon system was studied.²⁰⁵ This is a multiphase system and therefore the reaction product can contain a variety of intermediates depending on the blend composition and synthesis conditions. Sonication causes changes in both the temperature profile of the combustion wave (heating zone is extended) and the rate of combustion. Ultrasonic treatment reduces the reaction rate and the maximum temperature of the synthesis. It was assumed that alternating stresses produced at contacts between the reactant particles induce local heating of the starting mixture. This can cause the formation of intermediate reaction products in the heating zone and thus change the reaction conditions; as a consequence, the amount of heat released will be smaller compared to the combustion of mixtures without sonication.

A study by Khanukaev and Khanukaeva²⁰⁶ was a logical continuation of an earlier investigation.²⁰⁴ The authors²⁰⁶ also studied a number of solid-phase processes occurring under ultrasonic treatment:

(1) decomposition of ammonium bichromate, chromate and sulfate;

(2) dehydration of copper(II) and magnesium sulfate crystal hydrates;

(3) decomposition of $\text{Mg}(\text{OH})_2$ and $\text{Fe}(\text{OH})_2$;

(4) synthesis of copper(I) phthalocyanine from *o*-phthalonitrile



The results obtained in both studies appeared to have much in common. The vast majority of the reactions studied were characterised by a threshold amplitude of ultrasonic vibrations ($\sim 5 \mu\text{m}$) and by a threshold density of compact samples (no reaction at lower densities). Acceleration of the reactions under ultrasonic treatment was associated with the overcoming of diffusion limitations.

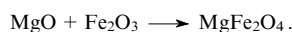
New information was as follows. First, it was found that the amplitude of ultrasonic vibrations has a strong effect on the reaction kinetics in these systems. In particular, the mass loss rates during the decomposition of hydroxides, $\text{Mg}(\text{OH})_2$ and $\text{Fe}(\text{OH})_2$, appeared to be proportional to the squared amplitude of vibrations at the end face of the waveguide at the same treatment durations (*i.e.*, the reaction rates are proportional to the transferred acoustic power). Additionally, almost all reactions were characterised by rather long induction periods (3–8 min), which was associated with the need of accumulation of the energy necessary for initiation and keeping up the reactions in the reaction volume. The distribution of the reaction product over the sample volume has a cylindrical symmetry.

The threshold pattern of ultrasonically treated solid-phase reactions was explained as follows. First, effective mixing of reactants occurs under such conditions where the stress due to ultrasonic vibrations exceeds the corresponding yield points. The threshold amplitude was estimated at $\sim 5 \mu\text{m}$, which coincides with experimental data. Second, it is well known that initiation of any chemical reaction requires the overcoming of an energy barrier (threshold amplitude of ≥ 10 – $11 \mu\text{m}$).

According to a model proposed,²⁰⁶ the key factors responsible for acceleration of ultrasonically treated solid-phase reactions are renewal of the reactant surfaces and removal of the reaction product layer between the interacting particles rather than the overcoming of diffusion limitations by generation of structural defects.

We believe that both mechanisms of acoustic activation of solid-phase processes take place in real systems.

The fact that sonication of a solid-phase reaction mixture can accelerate the interaction between the mixture components due to elimination of diffusion limitations was first experimentally proved in studies^{207–209} on the kinetics and mechanism of ultrasonically treated high-temperature reaction



At 800 °C, the rate of magnesium ferrite formation under ultrasonic activation was noticeably higher (by 15%–20%) than the rates of the blank reactions (no activation). On the contrary, the rate of the solid-phase reaction carried out at 700 °C under ultrasonic activation decreased to some extent. At 900 °C, ultrasonic treatment of the samples had almost no effect on the rate of ferrite formation. The results obtained correlate with the characteristics of the defectiveness of the iron(III) oxide samples, which is formed upon ultrasonic treatment in the temperature range 700–900 °C.^{209,210} The character of changes in the defectiveness of $\alpha\text{-Fe}_2\text{O}_3$ directly affects the formation kinetics of MgFe_2O_4 , namely, if the sonicated Fe_2O_3 samples have less defect structures compared to the products of the blank reactions (700 °C), the formation of MgFe_2O_4 and the yield of the reaction product in the former case is lower than in the latter case. However, if the reaction is carried out at 800 °C, both the defectiveness of the Fe_2O_3 samples and the rate of MgFe_2O_4 formation from the ultrasonically treated samples are higher than those for the blank reactions. At 900 °C, the ultrasonically processed samples and the untreated ones are characterised by the same defectiveness and the formation of MgFe_2O_4 occurs at nearly the same rates.

Additionally, alternating stresses at 700–900 °C should obviously cause the same mechanical effect of renewal of the reactant surfaces. Thus, it is the diffusion mobility of ions that governs all changes in the reaction rates under ultrasonic treatment compared to the rates of the blank reactions.

These non-linear changes in the defectiveness of $\alpha\text{-Fe}_2\text{O}_3$ crystallites and in the rate of solid-phase reactions of $\alpha\text{-Fe}_2\text{O}_3$ were explained^{207–209} by the occurrence of the following concurrent processes in the system: generation of structural defects under sonication; thermal annealing of defects, which dominates at 900 °C; and annihilation of extensive defects in the acoustic field upon ultrasonic annealing.

The effective activation energies of the solid-phase reactions carried out under ultrasonic treatment and without it were determined from formal kinetic analysis of experimental data. It was found that in both cases the formation of MgFe_2O_4 is a diffusion-limited process. Analysis of the Arrhenius relation $\ln k = f(T^{-1})$ (k is the rate constant for the reaction in the framework of the kinetic model chosen) gave an apparent activation energy of 180 kJ mol⁻¹ for the samples formed in the blank reactions. The relationship between $\ln k$ and T^{-1} for the reaction conducted under combined heat and ultrasonic treatment is non-linear. The temperature range studied can be divided into two intervals, 700–800 °C and 800–900 °C, which are characterised by the apparent activation energies of 320 and 100 kJ mol⁻¹, respectively.

The efficiency of sonication performed to accelerate diffusion was also demonstrated taking the solid-phase reaction of iron(III) oxide with lithium carbonate as an example.²¹¹

An additional substantiation of interrelation between the mechanism of ultrasonic activation of solid-phase reactions and elimination of diffusion limitations is provided by the results of a study²¹² of ion exchange in acid tantalum and zirconium phos-

phates in the presence of caesium chloride under ultrasonic treatment.

It was shown that dehydration of mixtures of acid tantalum phosphate with caesium chloride upon sonication occurs at a higher temperature, being characterised by smaller mass loss. This effect is most pronounced for the decrease in the mass loss in the low-temperature region corresponding to the loss of weakly bound water. This is due to partial substitution of caesium ions for $(\text{H}_3\text{O}_2)^+$ ions in acid tantalum phosphate. The ultrasonically treated samples also show a smaller mass loss corresponding to solid-phase ion exchange accompanied by liberation of HCl. The major effect of sonication is achieved in the initial stages of treatment; additional processing of the samples in the reactor has a much weaker effect. Probably, this is due to the fact that solid-phase ion exchange between $(\text{H}_3\text{O}_2)^+$ and caesium ions is controlled by cation diffusion through the layer of reaction product. Therefore, initially (at zero degree of conversion and diffusion layer thickness) the reaction rate is rather high, being exponentially decreased with the development of the reaction.²¹³ The overall extent of ion exchange and dehydration reduces on the average by 15%–20% due to ultrasonic treatment.

Sonication has a similar effect on ion exchange between acid zirconium phosphate $\text{Zr}(\text{HPO}_4)_2 \cdot \text{H}_2\text{O}$ and alkali metal chlorides. The ultrasonically treated samples were also characterised by the mass loss at higher temperatures compared to the untreated samples. This effect was observed for both dehydration (80–350 °C) and ion exchange ($T > 450$ °C). As in the preceding case, this is an indication of solid-phase ion exchange induced by ultrasonic vibrations.

A series of recent studies^{21,214–218} was devoted to detailed investigations of the effect of ultrasonic activation on high-temperature solid-phase synthesis of various ferrites including LiFe_5O_8 , ZnFe_2O_4 and NiFe_2O_4 (Fig. 17). Kinetic studies of the solid-phase reactions of iron(III) oxide with zinc oxide, nickel oxide and lithium α -orthoferrite and investigations of the evolution of the structure of the reactants during the synthesis of the final phases revealed similarity of the mechanisms of ultrasonic

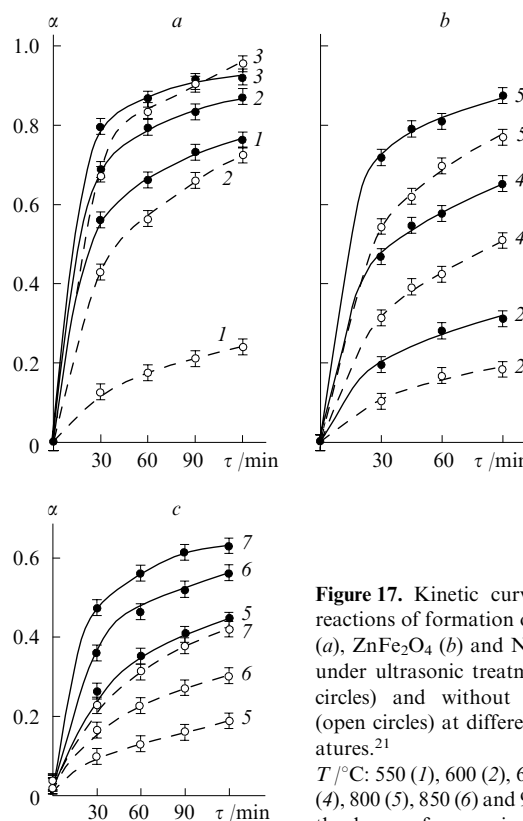


Figure 17. Kinetic curves of the reactions of formation of LiFe_5O_8 (a), ZnFe_2O_4 (b) and NiFe_2O_4 (c) under ultrasonic treatment (filled circles) and without sonication (open circles) at different temperatures.²¹ T / °C: 550 (1), 600 (2), 650 (3), 700 (4), 800 (5), 850 (6) and 900 (7); α is the degree of conversion.

activation of these reactions. With no sonication, the reaction products (LiFe_5O_8 , ZnFe_2O_4 , NiFe_2O_4) are formed only on the outer surface of iron(III) oxide particles representing dense aggregates of primary Fe_2O_3 crystallites. The microstructure of the starting Fe_2O_3 shows no significant changes [the size of the coherent scattering domains (CSD) in iron(III) oxide remains almost unchanged in the corresponding temperature ranges for all reaction mixtures] and small particles of reaction products rapidly aggregate into relatively large crystallites, as indicated by rapid increase in the CSD size in the initial stages of the reactions.

At the same time the reactions of ferrite formation under ultrasonic treatment are characterised by a decrease in the size of the primary iron(III) oxide crystallites and by prolonged retention of small size of the CSDs in lithium, zinc and nickel ferrites that are formed. This indicates non-uniformity of the reaction front, which penetrates into the bulk of Fe_2O_3 aggregates with the development of the reaction due to intensification of ion transfer through diffusion along Fe_2O_3 grain boundaries (Fig. 18).

IX. Conclusion

An undoubted advantage of ultrasonic treatment consists in the possibility of concurrent use of the technique and other methods of activation of reaction mixtures including conventional thermal activation procedures. Such 'combined' methods are characterised by manifestation (to some extent) of characteristic physical effects of sonication. Targeted use of ultrasonic treatment makes it possible to considerably enhance the possibilities of the available synthetic approaches and to synthesise novel inorganic materials in a targeted manner. The main effects accompanying the action of high-power ultrasound on liquid- and solid-phase systems are listed below.

Liquid-phase systems	Solid-phase systems
Processes accompanying sonication	
1. Cavitation. Local heating to ~ 5000 K, local increase in pressure to ~ 1000 atm, microflows of liquids with velocities of up to 100 m s^{-1} , intense local electric discharge.	1. Motions, generation and multiplication of dislocations (nearly 1 000-fold increase in concentration).
2. Considerable intensification of mass transfer.	2. Nearly tenfold increase in effective diffusion coefficients.
	3. Formation of interparticle contacts through mutual motions of particles.
Main physicochemical consequences of ultrasonic treatment	
1. Decomposition of volatile components of solutions.	1. Acceleration of solid-phase reactions.
2. Initiation and acceleration of redox reactions.	2. Reduction of reaction temperature
3. Disaggregation of particles.	
4. Formation of stable suspensions and emulsions.	
5. Degassing of solution.	
Main fields of application of high-power ultrasonic waves	
1. Organic and inorganic syntheses.	1. Activation of solid-phase reactions; synthesis at lower temperatures.
2. Preparation of nanodisperse materials based on amorphous and crystalline metals, simple and complex oxides, etc.	2. Targeted formation of the structure of solids.
3. Design of materials with preset morphologies of aggregates.	

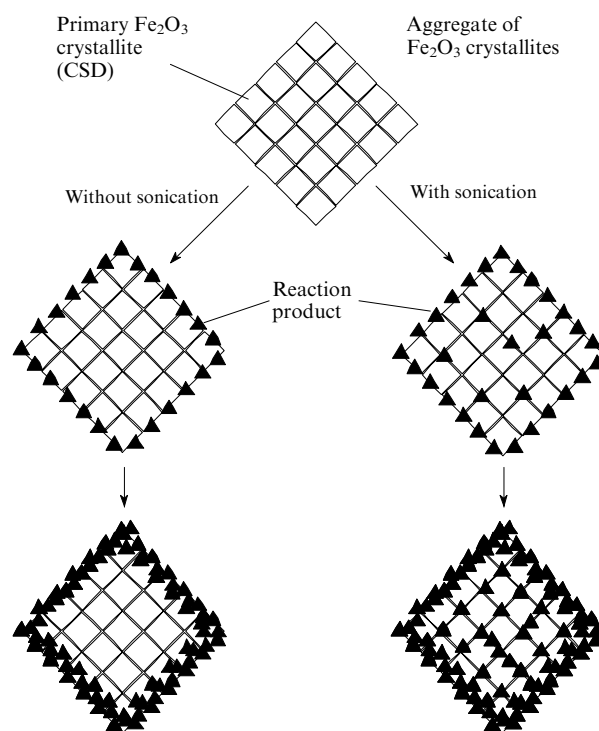


Figure 18. Mechanisms of reactions of ferrite formation under ultrasonic treatment and without it.²¹

Summing up, it should be emphasised that sonication techniques open new prospects for targeted synthesis of various inorganic materials. Sonochemical treatment allows one not only to considerably accelerate chemical transformations (first of all, in heterogeneous systems), but also often to prepare highly dispersed phases with controllable micromorphology.

This review has been written with the financial support from the Russian Foundation for Basic Research (Project Nos 06-03-33042 and 05-03-33036), the Foundation for Support of Domestic Science, the Chemistry and Materials Science Division of the Russian Academy of Sciences (in the framework of the Programme 'Development of Scientific Foundations of Advanced Chemical Technologies and Synthesis of Pilot Batches of Compounds and Materials') and the Presidium of the Russian Academy of Sciences (in the framework of the Programme 'Elaboration of Methods of Synthesis of Chemical Compounds and Design of Advanced Materials').

References

1. Yu D Tretyakov, V I Putlyaev *Vvedenie v Khimiyu Tverdogaznykh Materialov* (Introduction in the Chemistry of Solid-phase Materials) (Moscow: Nauka, 2006)
2. Yu D Tretyakov, N N Oleinikov, O A Shlyakhtin *Cryochemical Technology of Advanced Materials* (London: Chapman and Hall, 1997)
3. A V Knot'ko, I A Presnyakov, Yu D Tretyakov *Khimiya Tverdogo Tela* (The Chemistry of Solid) (Moscow: Akademiya, 2006)
4. E T Thostenson, T W Chou *Composites, Part A* **30** 1055 (1999)
5. R E Newnham, S J Jang, M Xu *Ceram. Trans.* **21** 23 (1991)
6. A S Vanetsev, Candidate Thesis in Chemical Sciences, Moscow State University, Moscow, 2004
7. D E Stein (Ed.) *Microwave Processing of Materials* (Washington, DC: Academic Press, 1994)
8. C N R Rao, A Müller, A K Cheetham (Eds) *The Chemistry of Nanomaterials: Synthesis, Properties and Applications* Vol. 2 (Weinheim: Wiley-VCH, 2004)

9. G M Chow, K E Gonsalves (Eds) *Nanotechnology: Molecularly Designed Materials* (Washington, DC: American Chemical Society, 1996)
10. A S Edelstein, R C Cammarata (Eds) *Nanomaterials: Synthesis, Properties and Applications* (Bristol, Philadelphia: Institute of Physics, 1997)
11. G V Lisichkin (Ed.) *Khimiya Privykh Poverkhnostnykh Soedinenii* (The Chemistry of Graft Surface Compounds) (Moscow: Fizmatlit, 2003)
12. O V Abramov *Kristallizatsiya Metallov v Ul'trazvukovom Pole* (Crystallisation of Metals in Ultrasonic Field) (Moscow: Metallurgiya, 1972)
13. B G Novitskii *Primenenie Akusticheskikh Kolebaniy v Khimiko-tekhnologicheskikh Protseessakh* (Application of Acoustic Oscillations in Chemical and Technological Processes) (Moscow: Khimiya, 1983)
14. M A Margulis *Sonochemistry and Cavitation* (Luxembourg: Gordon and Breach, 1995)
15. K S Suslick *Annu. Rev. Mater. Sci.* **29** 295 (1999)
16. A Gedanken *Ultrason. Sonochem.* **11** 47 (2004)
17. Y Mastai, A Gedanken, in *The Chemistry of Nanomaterials: Synthesis, Properties and Applications* Vol. 1 (Eds C N R Rao, A Müller, A K Cheetham) (Weinheim: Wiley-VCH, 2004) p. 113
18. Y Zhao, R Feng, Y Shi, M Hu *Ultrason. Sonochem.* **12** 173 (2005)
19. T J Mason *Ultrason. Sonochem.* **10** 175 (2003)
20. K E Gonsalves, H Li, R Perez, P Santiago, M Jose-Yacamán *Coord. Chem. Rev.* **206–207** 607 (2000)
21. A Ye Barantchikov, V K Ivanov, N N Oleynikov, Yu D Tretyakov *Mendeleev Commun.* 143 (2004)
22. P E Meskin, Yu V Kolenko, A Ye Barantchikov, V K Ivanov, B R Churagulov, N N Oleynikov *Mater. Res. Soc. Symp. Proc.* **788** L8.12.1 (2004)
23. T Mason, J Lindley, R Davidson *Chemistry with Ultrasound* (New York: Elsevier, 1990)
24. O V Abramov *Vozdeistvie Moshchnogo Ul'trazvuka na Zhidkie i Tverdye Metally* (Effect of High-power Ultrasound on Liquid and Solid Metals) (Moscow: Nauka, 2000)
25. T M Soboleva, I F Lunin, V A Mashtakova, V N Monakhov, O A Troitskii, V M Avdyukhina *Sverkhprovodimos': Fiz. Khim. Tekhnol.* **4** 199 (1991)
26. R C Asher *Ultrasonics* **25** 17 (1987)
27. M J Millen, B D Sowerby, P J Coghill, J R Tickner, R Kingsley, C Grima *Flow. Meas. Instrum.* **11** (3) 153 (2000)
28. A R Guilbert, M Law, M L Sanderson *Ultrasonics* **34** 435 (1996)
29. M S Greenwood, J R Skorpiak, J A Bamberger, R V Harris *Ultrasonics* **37** 159 (1999)
30. G I Eskin *Ul'trazvuk v Metallurgii* (Ultrasound in Metallurgy) (Moscow: Metallurgizdat, 1961)
31. *Ul'trazvuk. Malen'kaya Entsiklopediya* (Ultrasound. Small Encyclopaedia) (Moscow: Sovetskaya Entsiklopediya, 1979)
32. *Moshchnye Ul'trazvukovye Polya* (High-power Ultrasonic Fields) (Moscow: Nauka, 1960)
33. M A Margulis *Osnovy Zvukokhimii* (Foundations of Sonochemistry) (Moscow: Khimiya, 1984)
34. *Ultrasound, its Chemical, Physical and Biological Effects* (New York: Wiley-VCH, 1988)
35. J P Lorimer, in *Sonochemistry. The Uses of Ultrasound in Chemistry* (Cambridge: Royal Society of Chemistry, 1990) p. 9
36. K S Suslick, in *Kirk-Othmer Encyclopedia of Chemical Technology* Vol. 26 (4th Ed.) (New York: Wiley, 1998) p. 517
37. T J Mason (Ed.) *Advances in Sonochemistry* Vols 1–3 (London: JAI Press, 1990–1993)
38. L A Crum, R A Roy *Science* **266** 233 (1994)
39. K S Suslick, S B Choe, A A Cichowas *Nature (London)* **353** 414 (1991)
40. E B Flint, K S Suslick *Science* **253** 1397 (1991)
41. E A Neppiras *Phys. Rep.* **61** 159 (1980)
42. M A Margulis, A F Dmitrieva *Zh. Fiz. Khim.* **55** 23 (1981)^a
43. M A Margulis, A F Dmitrieva *Zh. Fiz. Khim.* **56** 170 (1982)^a
44. M A Margulis *Usp. Fiz. Nauk* **170** 263 (2000) [*Physics-Uspekhi* **43** 259 (2000)]
45. M Gutierrez, A Henglein, F Ibanez *J. Phys. Chem.* **95** 6044 (1995)
46. M A Margulis, I M Margulis *Zh. Fiz. Khim.* **71** 1890 (1997)^a
47. M A Margulis, I M Margulis *Ultrason. Sonochem.* **9** 1 (2002)
48. M A Margulis, I M Margulis *Ultrason. Sonochem.* **6** 15 (1999)
49. M A Margulis, I M Margulis *Khim. Vys. Energ.* **38** 323 (2004)^b
50. M A Margulis, I M Margulis *Zh. Fiz. Khim.* **71** 1885 (1997)^a
51. E A Neppiras *Ultrasonics* **18** 201 (1980)
52. T J Mason, J Berlan, in *Advances in Sonochemistry* Vol. 4 (Greenwich, UK: JAI Press, 1996) p. 1
53. S Koda, T Kimura, T Kondo, H Mitome *Ultrason. Sonochem.* **10** 149 (2003)
54. J Raso, P Manas, R Pagan, F J Sala *Ultrason. Sonochem.* **5** 157 (1999)
55. J Berlan, T J Mason *Ultrasonics* **30** 203 (1992)
56. I M Margulis, M A Margulis *Akustich. Zh.* **51** 802 (2005)^c
57. I M Margulis, M A Margulis *Zh. Fiz. Khim.* **77** 1318 (2003)^a
58. S Sochard, A M Wilhelm, H Delmas *Chem. Eng. Sci.* **53** 239 (1998)
59. H Briggs, J Johnson, W Mason *J. Acoust. Soc. Am.* **19** 664 (1947)
60. O Behrend, K Ax, H Shubert *Ultrason. Sonochem.* **7** 77 (2000)
61. S Majumdar, P Senthil Kumar, A B Pandit *Ultrason. Sonochem.* **5** 113 (1998)
62. I E El'piner *Ul'trazvuk. Fiziko-khimicheskoe i Biologicheskoe Deistvie* (Ultrasound. Physicochemical and Biological Effects) (Moscow: Fizmatgiz, 1963)
63. W Mason (Ed.) *Physical Acoustics. Principles and Methods* Vol. 1 (New York: Academic Press, 1964)
64. M Degrois, P Baldo *Ultrasonics* **12** 25 (1974)
65. M Abdel-Reihim, I W Reif *Metal* **12** 1156 (1984)
66. O V Abramov *Ultrasonics* **25** 73 (1987)
67. J Seifert, F Fischer *Ultrasonics* **15** 154 (1977)
68. V S Arakelyan *Acta Phys. Hung.* (2) 185 (1987)
69. R Pohlman, K Heisler, H Chicos *Ultrasonics* **12** 11 (1974)
70. T J Mason *Ultrasonics* **30** 192 (1992)
71. A Agranat *Ul'trazvukovaya Tekhnologiya* (Ultrasonic Technology) (Moscow: Metallurgiya, 1974)
72. M Blesik, Z Saponjic, J M Nedeljkovic *Mater. Lett.* **54** 298 (2002)
73. I Taniguchi, C Lim, D Song *Solid State Ionics* **146** 239 (2002)
74. T Inui, J L Li *Appl. Catal. A* **139** 87 (1996)
75. K Chatakondur, M Green, M Thompson, K Suslick *J. Chem. Soc., Chem. Commun.* 900 (1987)
76. K S Suslick, D J Casadonte, M Green, M E Thompson *Ultrasonics* **25** 56 (1987)
77. T Ohtani, M Araki, M Shohno *Solid State Ionics* **172** 197 (2004)
78. R Roy *J. Solid State Chem.* **111** 11 (1994)
79. M A Margulis, V A Gavrilov *Zh. Fiz. Khim.* **66** 771 (1992)^a
80. P Birkin, J Power, T Leighton *Chem. Commun.* 2230 (2001)
81. M Mizukoshi, R Oshima, Y Maeda, Y Nagata *Langmuir* **15** 2733 (1999)
82. M Gutierrez, A Hehglein, J Dohrmann *J. Phys. Chem.* **91** 6687 (1987)
83. A K Pikaev *Impul'snyi Radioliz Vody i Vodnykh Rastvorov* (Pulse Radiolysis of Water and Aqueous Solutions) (Moscow: Nauka, 1965)
84. M A Margulis *Zh. Fiz. Khim.* **50** 2267 (1976)^a
85. H Nomura, S Koda, K Yasuda, Y Kojima *Ultrason. Sonochem.* **3** 153 (1996)
86. M A Margulis, A N Mal'tsev *Vestn. Mosk. Univ., Ser. 2: Khim.* (3) 34 (1969)^d
87. M A Margulis *Zh. Fiz. Khim.* **50** 2271 (1976)^a
88. A Virtanen, N Ellfolk *J. Am. Chem. Soc.* **72** 1046 (1950)
89. M A Margulis, Yu T Didenko *Zh. Fiz. Khim.* **58** 1402 (1984)^a
90. Supeno, P Kruus *Ultrason. Sonochem.* **7** 109 (2000)
91. Y Nagata, Y Mizukoshi, K Okitsu, Y Maeda *Radiat. Res.* **146** 333 (1996)
92. R A Caruso, M Ashokkumar, F Griezner *Colloids Surf., A* **169** 219 (2000)
93. Y Mizukoshi, E Takagi, H Okuno, R Oshima, Y Maeda, Y Nagata *Ultrason. Sonochem.* **8** 1 (2001)
94. J E Park, M Atobe, T Fuchigami *Ultrason. Sonochem.* **13** 237 (2006)
95. N A Dhas, C P Raj, A Gedanken *Chem. Mater.* **10** 1446 (1998)
96. X F Qui, J J Zhu, H Y Chen *J. Cryst. Growth* **257** 378 (2003)
97. W Chen, W P Cai, C H Liang, L D Zhang *Mater. Res. Bull.* **36** 335 (2001)
98. W Chen, J Zhang, W Cai *Scr. Mater.* **48** 1061 (2003)

99. W Chen, W Cai, G Wang, L Zhang *Appl. Surf. Sci.* **174** 51 (2001)
100. W Chen, J Zhang, Y Di, Z Wang, Q Fang, W Cai *Appl. Surf. Sci.* **211** 280 (2003)
101. W Chen, W Cai, Y Lei, L Zhang *Mater. Lett.* **50** 53 (2001)
102. S M Zhu, H S Zhou, M Hibino, I Honma *J. Mater. Chem.* **13** 1115 (2003)
103. J E Park, M Atobe, T Fuchigami *Electrochim. Acta* **51** 849 (2005)
104. M Sivakumar, A Gedanken *Synth. Met.* **148** 301 (2005)
105. R Vijayakumar, Yu Koltypin, X N Xu, Y Yeshurun, A Gedanken, I Felner *J. Appl. Phys.* **89** 6324 (2001)
106. F Grier *Stud. Surf. Sci. Catal.* **130** 57 (1997)
107. N A Dhas, Yu Koltypin, A Gedanken *Chem. Mater.* **9** 3159 (1997)
108. H Kawaoka, M Hibino, H Zhou, I Honma *Solid State Ionics* **176** 621 (2005)
109. H Kawaoka, M Hibino, H Zhou, I Honma *J. Power Sources* **125** 85 (2004)
110. A Odani, A Nimberger, B Markovsky, E Sominsky, E Levi, V G Kumar, M Motiei, A Gedanken, P Dan, D Aurbach *J. Power Sources* **119–121** 517 (2003)
111. P Jeevanadam, Yu Koltypin, A Gedanken *Nano Lett.* **1** 263 (2001)
112. H Wang, J J Zhu, J M Zhu, X H Liao, S Xu, T Ding, H Y Shen *Phys. Chem. Chem. Phys.* **4** 3794 (2002)
113. L Yin, Y Wang, G Pang, Yu Koltypin, A Gedanken *J. Colloid Interface Sci.* **246** 78 (2002)
114. J C Yu, J Yu, L Zhiang, W Ho *J. Photochem. Photobiol., A* **148** 263 (2002)
115. L Zhang, J C Yu *Chem. Commun.* 2078 (2003)
116. W Guo, Z Lin, X Wang, G Song *Microelectron. Eng.* **66** 95 (2003)
117. J C Yu, J Yu, W Ho, L Zhiang *Chem. Commun.* 1942 (2001)
118. Y Q Wang, S G Chen, X H Tang, O Palchik, A Zaban, Yu Koltypin, A Gedanken *J. Mater. Chem.* **11** 521 (2001)
119. W Huang, X Tang, Y Wang, Y Koltypin, A Gedanken *Chem. Commun.* 1415 (2000)
120. G Wei-Lin, W Xi-Kui *J. Mater. Sci.* **39** 3265 (2004)
121. K Yang, J Zhu, J Zhu, S Huang, X Zhu, G Ma *Mater. Lett.* **57** 4639 (2003)
122. Y Zhu, H Li, Yu Koltypin, Y R Hacohen, A Gedanken *Chem. Commun.* 2616 (2001)
123. T Tuziuti, K Yasui, Y Iida, H Taoda, S Koda *Ultrasonics* **42** 597 (2004)
124. P Jeevanadam, Yu Koltypin, A Gedanken *Mater. Sci. Eng., B* **90** 125 (2002)
125. G Z Wang, B Y Geng, X M Huang, Y W Wang, G H Li, L D Zhang *Appl. Phys. A* **77** 922 (2003)
126. J L Yin, X F Qian, J Yin, M Shi, G Zhou *Mater. Lett.* **57** 3859 (2003)
127. J F Xu, W Ji, J Y Lin, S H Tang, Y W Du *Appl. Phys. A* **66** 639 (1998)
128. H Wang, Y N Lu, J J Zhu, H Y Chen *Inorg. Chem.* **42** 6404 (2003)
129. J H Zhang, Z Chen, Z L Wang, N B Ming *J. Mater. Res.* **18** 1804 (2003)
130. T Ding, J J Zhu, J M Hong *Mater. Lett.* **57** 4445 (2003)
131. H Wang, J J Zhu *Ultrason. Sonochem.* **11** 293 (2004)
132. H Mukaibo, A Yoshizawa, T Momma, T Osaka *J. Power Sources* **119** 60 (2003)
133. H L Li, Y C Zhu, S G Chen, O Palchik, J P Xiong, Yu Koltypin, Y Gofer, A Gedanken *J. Solid State Chem.* **172** 102 (2003)
134. G Z Wang, Y W Wang, W Chen, C H Liang, G H Li, L D Zhang *Mater. Lett.* **48** 269 (2001)
135. S M Zhou, Y S Feng, L D Zhang *Mater. Lett.* **57** 2936 (2003)
136. G S Wu, X Y Yuan, T Xie, G C Xu, L D Zhang, Y L Zhuang *Mater. Lett.* **58** 794 (2004)
137. M Shao, Z Wu, F Gao, Y Ye, X Wei *J. Cryst. Growth* **260** 63 (2004)
138. J P Ge, Y D Li, G Q Yang *Chem. Commun.* 1826 (2002)
139. Q Li, Y Ding, M W Shao, J Wu, G H Yu, Y T Qian *Mater. Res. Bull.* **38** 539 (2003)
140. T Ding, H Wang, S Xu, J J Zhu *J. Cryst. Growth* **235** 517 (2002)
141. S M Zhou, X H Zhang, X M Meng, X Fan, S T Lee, S K Wu *J. Solid State Chem.* **178** 399 (2005)
142. H Wang, J R Zhang, X N Zhao, S Xu, J J Zhu *Mater. Lett.* **55** 253 (2002)
143. S Xu, H Wang, J J Zhu, H Y Chen *J. Cryst. Growth* **234** 263 (2002)
144. H L Li, Y C Zhu, S Avivi, O Palchik, J P Xiong, Yu Koltypin, V Palchik, A Gedanken *J. Mater. Chem.* **12** 3723 (2002)
145. B Li, Y Xie, J Huang, Y Qian *Ultrason. Sonochem.* **6** 217 (1999)
146. J P Ge, Y D Li *J. Mater. Chem.* **13** 911 (2003)
147. N Chen, J Zeng, F Li, W Zhang, Y Qian *J. Cryst. Growth* **235** 505 (2002)
148. M M Mdeleni, T Hyeon, K S Suslick *J. Am. Chem. Soc.* **120** 6189 (1998)
149. R V Kumar, O Palchik, Yu Koltypin, Y Diamant, A Gedanken *Ultrason. Sonochem.* **9** 65 (2002)
150. P Jeevanadam, Yu Koltypin, Y Gofer, Y Diamant, A Gedanken *J. Mater. Chem.* **10** 2769 (2000)
151. J M Zhu, K Yang, J J Zhu, G B Ma, X H Zhu, S H Zhou, Z G Liu *Opt. Mater. (Amsterdam)* **23** 89 (2003)
152. H Song, K Cho, H Kim, J S Lee, B Min, H S Kim, S W Kim, T Noh, S Kim *J. Cryst. Growth* **269** 317 (2004)
153. L Qiu, V G Pol, Y Wei, A Gedanken *J. Mater. Chem.* **13** 2985 (2003)
154. Y Y Zheng, T J Zhu, X B Zhao, J P Tu, G S Cao *Mater. Lett.* **59** 2886 (2005)
155. J H Zhan, X G Yang, S D Li, D W Wang, Y Xie, Y T Qian *Int. J. Inorg. Mater.* **3** 47 (2001)
156. M Behboudnia, M H Majlesara, B Khanbabaee *Mater. Sci. Eng., B* **122** 160 (2005)
157. M W Grinstaff, A A Cichowlas, S B Choe, K S Suslick *Ultrasonics* **30** 168 (1992)
158. M W Grinstaff, M B Salamon, K S Suslick *Phys. Rev. B* **48** 269 (1993)
159. R Bellissent, G Galli, M W Grinstaff, P Migliardo, K S Suslick *Phys. Rev. B* **48** 15797 (1993)
160. K S Suslick, J W Goodale, H H Wang, P F Schubert *J. Am. Chem. Soc.* **105** 5781 (1983)
161. K S Suslick, P Schubert *J. Am. Chem. Soc.* **105** 6042 (1983)
162. T Hyeon, M Fang, A Cichowlas, K Suslick *Mater. Sci. Eng., A* **204** 186 (1995)
163. R Bellissent, G Galli, T Hyeon, S Magazu, D Majolino, P Migliardo, K S Suslick *Phys. Scr.* **T57** 79 (1995)
164. K V P M Shafi, A Gedanken, R Prozorov *J. Mater. Chem.* **83** 769 (1998)
165. K V P M Shafi, A Gedanken, R B Goldfarb, I Felner *J. Appl. Phys.* **81** 6901 (1997)
166. K S Suslick, M Fang, T Hyeon *J. Am. Chem. Soc.* **118** 11960 (1996)
167. G Kataby, A Ulman, R Prozorov, A Gedanken *Langmuir* **14** 1512 (1998)
168. K V P M Shafi, S Wize, T Prozorov, A Gedanken *Thin Solid Films* **318** 38 (1998)
169. A Duteil, G Schmid, W Meyer-Zaika *J. Chem. Soc., Chem. Commun.* 31 (1995)
170. S I Nikitenko, P Moisy, I A Tcharushnikova, P Blanc, C Madic *Ultrason. Sonochem.* **7** 177 (2000)
171. S I Nikitenko, P Moisy, A F Seliverstov, P Blanc, C Madic *Ultrason. Sonochem.* **10** 95 (2003)
172. I Chorkendorff, J W Niemantsverdriet *Concepts of Modern Catalysis and Kinetics* (New York: Wiley, 2003)
173. K J Klabunde, Y X Li, in *Selectivity in Catalysis* (Washington, DC: American Chemical Society, 1993)
174. S Ramesh, R Prozorov, A Gedanken *Chem. Mater.* **9** 2996 (1997)
175. K S Suslick, T Hyeon, M Fang, A A Cichowlas, in *Advanced Catalysts and Nanostructured Materials* (New York: Academic Press, 1996) p. 197
176. K S Suslick, T Hyeon, M Fang *Chem. Mater.* **8** 2172 (1996)
177. V Kirikka, P Shafi, A Gedanken, R Prozorov, J Balogh *Chem. Mater.* **10** 3445 (1998)
178. V Kirikka, P Shafi, Yu Koltypin, A Gedanken, R Prozorov, J Balogh *J. Phys. Chem. B* **101** 6409 (1997)
179. A N Dhas, A Gedanken *Chem. Mater.* **9** 3144 (1997)

180. G Katabi, X Cao, A Gedanken, R Prozorov, Yu Koltypin *J. Non-Cryst. Solids* **201** 159 (1996)
181. Y Peng, G Song *Green Chem.* **3** 302 (2001)
182. K S Suslick *Adv. Organomet. Chem.* **25** 73 (1986)
183. B N Litvin, V I Popolitov *Gidrottermal'nyi Sintez Neorganicheskikh Soedinenii* (Hydrothermal Synthesis of Inorganic Compounds) (Moscow: Nauka, 1984)
184. A N Lobachev (Ed.) *Gidrottermal'nyi Sintez i Vyrashchivanie Monokristallov* (Hydrothermal Synthesis and Growing of Single Crystals) (Moscow: Nauka, 1982)
185. K Byrappa, M Yoshimura *Handbook of Hydrothermal Technology. A Technology for Crystal Growth and Materials Processing* (Norwich, New York: William Andrew Publishing, 2000)
186. P E Meskin, A E Baranchikov, V K Ivanov, E V Kisterev, A A Burukhin, B R Churagulov, N N Oleinikov, Sh Komarneni, Yu D Tretyakov *Dokl. Akad. Nauk* **389** 207 (2003)^e
187. P E Meskin, V K Ivanov, A E Baranchikov, B R Churagulov, Yu D Tretyakov *Ultrason. Sonochem.* **13** 47 (2006)
188. C Aymonier, M Bottreau, B Berdeu, F Cansell *Ind. Eng. Chem. Res.* **39** 4734 (2000)
189. A A Burukhin, B R Churagulov, N N Oleynikov *High Pressure Res.* **20** 255 (2001)
190. P E Meskin, A E Baranchikov, V K Ivanov, D R Afanas'ev, A I Gavrilov, B R Churagulov, N N Oleinikov *Neorg. Mater.* **40** 1208 (2004)^f
191. A V Kulemin *Ul'trazvuk i Diffuziya v Metallakh* (Ultrasound and Diffusion in Metals) (Moscow: Metallurgiya, 1978)
192. N A Tyapunina, E K Naimi, G M Zinenkova *Deistvie Ul'trazvuka na Kristally s Defektami* (Effect of Ultrasound on Crystals with Defects) (Moscow: Moscow State University, 1999)
193. N A Tyapunina, E V Shtrom, G M Zinenkova *Vestn. Mosk. Univ., Ser. 2, Fiz. Astronom.* **19** 33 (1978)
194. A Mateo, L Llanes, L Iturgoyen, M Anglada *Acta Mater.* **44** 1143 (1996)
195. M V Klassen-Neklyudova, A P Kapustin *Dokl. Akad. Nauk SSSR* **77** 1019 (1951)^e
196. A V Kulemin, O M Smirnov *Problemy Metallovedeniya i Fiziki Metallov. Sbornik 1* (Problems of Metal Research and Physics of Metals. Collection 1) (Moscow: Metallurgiya, 1972)
197. S Ostapenko *Appl. Phys. A* **69** 225 (1999)
198. L V Borkovska, M P Baran, N O Korsunskaya, I V Markevich, O F Singaevsky, M K Sheinkman, T V Torchynska *Physica B: Condens. Matter* **340–342** 258 (2003)
199. A V Kulemin, S Z Nekrasova, A G Kozlova, R I Entin *Fiz. Khim. Obrab. Mater.* **5** 111 (1981)
200. G Ya Bazelyuk, Yu P Barabanov, V G Gorbach *Metallofizika* **8** 53 (1986)
201. A E Baranchikov, V K Ivanov, A N Baranov, N N Oleinikov, Yu D Tretyakov *Zh. Neorg. Khim.* **46** 2067 (2001)^g
202. A E Baranchikov, V K Ivanov, V A Ketsko, D E Sklovskii *Kondens. Sredy, Mezhfaz. Granitsy* **8** 278 (2005)
203. G Heinicke *Tribochemistry* (Berlin: Akademie-Verlag, 1984)
204. N S Enikolopov, O V Abramov, B B Khanukaev *Vysokomol. Soedin., Ser. A* **36** 588 (1994)^h
205. V V Klubovich, M M Kulak, V M Mal'tsev *Inzh.-Fiz. Zh.* **65** 471 (1993)ⁱ
206. B B Khanukaev, N S Khanukaeva *Zh. Fiz. Khim.* **72** 1607 (1998)^a
207. V M Kuznetsov, A N Baranov, N N Oleinikov, E V Kisterev, O V Abramov, Yu D Tretyakov *Dokl. Akad. Nauk* **352** 355 (1997)^e
208. A N Baranov, N N Oleinikov, V M Kuznetsov, E V Kisterev, O V Abramov, Yu D Tretyakov *Zh. Neorg. Khim.* **43** 567 (1998)^g
209. A E Baranchikov, N N Oleinikov, A N Baranov, V M Kuznetsov, E V Kisterev *Neorg. Mater.* **34** 352 (1999)^f
210. A E Baranchikov, A N Baranov, V K Ivanov, N N Oleynikov, Yu D Tretyakov *Solid State Ionics* **141–142** 689 (2001)
211. A E Baranchikov, V K Ivanov, N N Oleinikov, Yu D Tretyakov *Zh. Neorg. Khim.* **48** 42 (2003)^g
212. M N Kisilitsyn, A E Baranchikov, V K Ivanov, Yu D Tretyakov, A B Yaroslavl'tsev *Neorg. Mater.* **38** 858 (2002)^f
213. A B Yaroslavl'tsev *Solid State Ionics* **97** 281 (1997)
214. A E Baranchikov, V K Ivanov, N N Oleinikov, Yu D Tretyakov *Zh. Neorg. Khim.* **48** 1828 (2003)^g
215. A E Baranchikov, V K Ivanov, G P Murav'eva, N N Oleinikov, Yu D Tretyakov *Dokl. Akad. Nauk* **397** 201 (2004)^e
216. A E Baranchikov, V K Ivanov, N N Oleinikov, Yu D Tretyakov *Neorg. Mater.* **40** 1243 (2004)^f
217. A E Baranchikov, V K Ivanov, N N Oleinikov, V A Ketsko, Yu D Tretyakov *Zh. Neorg. Khim.* **49** 1776 (2004)^g
218. A Ye Baranchikov, V K Ivanov, Yu D Tretyakov *Ultrason. Sonochem.* **14** 131 (2007)

^a — *Russ. J. Phys. Chem. (Engl. Transl.)*

^b — *High Energ. Chem. (Engl. Transl.)*

^c — *Acoust. Phys. (Engl. Transl.)*

^d — *Moscow Univ. Bull., Chem. (Engl. Transl.)*

^e — *Dokl. Chem. (Engl. Transl.)*

^f — *Inorg. Mater. (Engl. Transl.)*

^g — *Russ. J. Inorg. Chem. (Engl. Transl.)*

^h — *Polym. Sci. (Engl. Transl.)*

ⁱ — *J. Eng. Phys. Thermophys. (Engl. Transl.)*

Oxidative catalysis on high-temperature ionic melts

Yu S Chekryshkin, T A Rozdyalovskaya, A A Fyodorov, G V Lisichkin

Contents

I. Introduction	153
II. Experimental techniques for the work with molten catalysts	154
III. Characteristic features of reactions proceeding on melts	154
IV. Relationship between the catalytic reactions proceeding on solid and molten catalysts	155
V. Electrochemical control of the activity and selectivity of molten catalysts	157
VI. Oxidation of organic compounds	158
VII. Conclusion	164

Abstract. The results of studies of the catalytic oxidation of organic compounds in the presence of molten transition metal salts and oxides are surveyed. The attention is focused on extensive oxidation of halogen-containing compounds. The bibliography includes 197 references.

I. Introduction

Molten salts, in particular, alkali, alkaline earth and rare earth metal halides, carbonates, sulfates, molybdates, tungstates and vanadates, are distinguished by thermal and radiation stability, low volatility, low viscosity, and high electrical and thermal conductivities over a broad temperature range. Owing to these properties, ionic melts are of interest as high-temperature electrolytes,^{1,2} energy storage devices and heat carriers,^{1–5} and as gas- and dust-trapping liquids.^{6–8} Molten electrolytes (metal oxides and salts) are used in coating of metal surfaces^{9,10} and in thermal and electrochemical storage cells and fuel cells.^{1,2,9,11–13} The present review considers the use of metal oxide and salt melts as catalysts of oxidation of some organic and inorganic compounds and as the media for these reactions.

In recent years, considerable attention has been devoted to the so-called ionic liquids, *i.e.*, salts formed by quaternised nitrogenous heterocycles (or amines) and Lewis acids, which are liquid under normal conditions. The application of these compounds as catalysts for skeletal isomerisation of alkanes and for metathesis, alkylation, disproportionation and oligomerisation of alkenes has been described.^{14–25} High catalytic activity of ionic liquids, which is attributable to their high polarity and high acidity, was noted. Thus they induce isomerisation of alkanes at 30–70 °C.

Yu S Chekryshkin, T A Rozdyalovskaya, A A Fyodorov Institute of Technical Chemistry, Urals Branch of the Russian Academy of Sciences, ul. Lenina 13a, 614990 Perm, Russian Federation. Fax (7-3422) 37 82 62, tel. (7-3422) 37 82 88 (Yu S Chekryshkin), (7-3422) 37 82 53 (T A Rozdyalovskaya), (7-3422) 37 82 91 (A A Fyodorov), e-mail: cheminst@mpm.ru

G V Lisichkin Department of Chemistry, M V Lomonosov Moscow State University, Leninskie Gory, 119992 Moscow, Russian Federation. Fax (7-495) 236 05 33, tel. (7-495) 939 46 38, e-mail: lisich@petrol.chem.msu.ru

The salt melts considered in this review are also ionic liquids.[†] These high-temperature melts are used to carry out reactions that are thermodynamically allowed only at elevated temperatures (cracking, dehydrogenation). In addition, due to the high thermal conductivity, it is expedient to use molten salts in the processes accompanied by pronounced heat evolution or absorption, for example, pyrolysis, partial and extensive (complete) oxidation of organic compounds, coal gasification, and so on.

Molten catalysts (MC) have the following specific features which make them unique.

1. Unlike the conventional heterogeneous catalysts, MC exhibit high performance stability, because the ‘liquid–vapour (or gas) phase’ interface is constantly renovated during the catalysis.^{28–30}

2. High thermal conductivity of ionic melts provides easy solution to the heat supply or withdrawal problem in highly endo(or exo)thermic reactions. The risk of local overheating resulting in the destruction of active sites, which is typical of traditional catalysts, markedly decreases.

3. An important advantage of MC is the simplicity of their preparation. They are usually prepared by simultaneous or consecutive fusion of the components. There is no need to be concerned about optimisation of the surface texture and the surface area, the mechanical strength or the grain-size distribution of the catalyst, *etc.*

4. High electrical conductivity of ionic melts allows one to use electrochemical methods for the monitoring and control of MC composition during the process.

5. The reactions on MC proceed in the absence of water or aqueous solutions; this is very important as regards environment protection (no wash water).

However, molten catalysts are not free from drawbacks, first of all, this is their relatively high corrosion activity and the need to use special reactors.

Despite the fact that the first studies dealt with reactions of organic compounds catalysed by melts were published more than a hundred years ago,³¹ these catalysts have not yet found wide use in industry. Apart from the high corrosion activity of the melts, this is due to poor knowledge of their catalytic properties. Currently, melts are used on an industrial scale only for the synthesis of isoalkanes^{26,27,32–34} and for chlorination of hydro-

Received 19 June 2006

Uspekhi Khimii 76 (2) 169–186 (2007); translated by Z P Bobkova

[†]In particular, isomerisation of alkanes on a molten salt mixture $\text{AlCl}_3\text{–SbCl}_3\text{–KCl}$ also proceeds at 30–70 °C.^{26,27}

carbons^{3, 12, 35–41} and on a pilot scale for coal gasification.^{11, 12, 42–44}

The purpose of this review is to summarise the published data on the characteristic features of processes catalysed by melts.

II. Experimental techniques for the work with molten catalysts

The catalytic processes on molten metal salts and oxides are carried out using special equipment and procedures. Several versions of process implementation involving molten catalysts have been proposed. Most often, MC-catalysed reactions are carried out by bubbling vapour of the feedstock with or without a carrier gas through a melt bed.^{35, 43, 44} Bubble-type reactors are used for this purpose,^{45–47} and the contact time of the reaction mixture with the catalyst is controlled by changing the height of the melt bed.^{47, 48}

In the bubbling of a gas–vapour mixture through a melt, the contact area of the gas–liquid phases and, hence, the degree of feedstock conversion depends on the degree of dispersion of the gas flow. In an ideal case, a gas bubble has a diameter of less than 1 mm, *i.e.*, it is a microreactor with a great surface-to-volume ratio. Therefore, in these systems, the processes that tend to acquire an explosive character when carried out in usual reactors become easily controllable.⁴⁹

A study of thermal properties of a $\text{KPO}_3\text{--V}_2\text{O}_5$ melt has shown^{50, 51} that oxygen is evolved from the melt in discrete portions. This was attributed to the formation of oxygen microbubbles, which have no time to unite into large particles. The minimum volume of an evolved bubble was calculated to be $5 \times 10^{-5} \text{ cm}^3$. Each bubble acts as a microreactor on the walls of which free radicals are ‘quenched’ and, hence, chain reactions cannot switch to the explosive mode. Probably, this accounts for the possibility of safe extensive oxidation of phthalic anhydride and nitrobenzene production wastes on the $\text{K}_2\text{O--V}_2\text{O}_5$ melt,^{52, 53} whereas their combustion in an open flame is accompanied by explosion.

Gas-phase oxidation of *o*-xylene with oxygen bubbled through an eutectic (eut) melt $\text{K}_2\text{SO}_4\text{--V}_2\text{O}_5$ (39 mass %) and a melt $\text{K}_2\text{S}_2\text{O}_7\text{--V}_2\text{O}_5$ (14 mass %) has been reported.^{54, 55} The experimental data were processed, to determine the bubbling velocity (U), using the equation

$$U = \frac{H}{(H-h)(\pi R^2/Q)} = -\frac{1}{h\pi R^2} \frac{dQ}{d(1/H)},$$

where H is the effective height of the melt; h is height of the melt at a zero gas velocity; Q is the gas volume flow rate at the melt temperature; R is the radius of the reactor. The resulting velocity was used to determine the residence time of the mixture in the reaction zone.

In the 509–570 °C temperature range for $Q = 40 \text{ cm}^3 \text{ s}^{-1}$, the U value varied from 9 to 18 cm s^{-1} . At 500 °C, the conversion of *o*-xylene in a mixture with oxygen reached 35–42%. (Note that oxidation of *o*-xylene mixed with nitrogen under the same conditions results in a low conversion of the hydrocarbon, *viz.*, 2.5%–4.5%.) The residence time of the gas–vapour bubbles in the melt zone was $\sim 2 \text{ s}$. It is believed^{54, 55} that the higher reaction selectivity observed in the melt compared with a solid catalyst having the same composition is due to the isothermal mode of the process, resulting in a decrease in the yields of extensive oxidation products.

The kinetics of reactions on MC is usually studied using a tubular reactor with a melt layer applied onto its internal surface.⁵⁶ The residence time is controlled by varying the feed rate of the reaction mixture or the reactor length. The reactor can operate in either continuous or pulse mode.^{56, 57} Processing of the experimental results obtained with a pulse-type reactor has been described in detail.⁵⁸ For reactors operating in the displacement

mode, a dependence of the substrate conversion on time was derived using different forms of kinetic equations.

If it is necessary to increase the specific surface area of a molten catalyst, this is applied on a sorbent surface.^{59, 60} In this case, reactors traditional for heterogeneous catalysis are utilised. The use of supported MC often results in higher yields of the target products with respect to those obtained in the bubbling mode.

The combined reactor and regenerator in which the catalyst reduction and reoxidation stages occur separately appears to be the best version. The ammoxidation process of *m*-xylene using this reactor design has been reported.⁶¹ The reaction mixture enters the reactor at a high rate through a specially designed nozzle and sprays the melt. The reaction proceeds in a vessel filled with finely dispersed drops of the melt. The partially reduced melt flows into a tank from which it moves again into the reactor by means of a gas lift[‡] with simultaneous oxidation. The non-consumed hydrocarbons and ammonia are separated from the reaction products and recycled.

The necessity to separate the reactor zones in which the reaction occurs and the catalyst is regenerated is quite common. Thus the oxidative dehydrogenation of ethylbenzene and aliphatic alcohols on the $\text{K}_2\text{O--V}_2\text{O}_5$ melt proceeds more easily than the reaction of vanadium(IV) with oxygen (catalyst regeneration);^{46, 62} therefore, it is expedient to carry out the oxidation of vanadium(IV) with oxygen at higher temperatures ($> 640 \text{ °C}$) and to carry out the oxidation of organic compounds at 500 °C in another reactor zone.

The catalyst regeneration (saturation with oxygen in the case of oxidation) can be performed during gas lift transportation of the melt.⁶³ The melt is first saturated with oxygen and then excess oxygen is removed in the separation zone until a specified partial pressure is attained. To increase the selectivity of oxidation of organic compounds⁶⁴ and prevent the formation of explosive mixtures, it is necessary to eliminate the contact of the hydrocarbon feedstock and reaction products with oxygen. This allows one to carry out simultaneously two processes with opposite signs of thermal effect (an endothermic process in one zone and an exothermic process in the other zone) and thus to balance the heat flows. For example, such reactor has been used for the production of synthesis gas by oxidation of lower alkanes ($\text{C}_1\text{--C}_4$) in a flow of molten metal oxides.⁶⁵ The proper oxidation was carried out in one reactor zone, while in the other zone, the oxidation products were reformed. This endothermic process yielded synthesis gas virtually free from nitrogen. The partially reduced melt was routed into the regeneration zone for oxidation with atmospheric oxygen.

A special reactor has been developed for the processing of solid urban waste by fusion in a slag melt under conditions of air bubbling. In this reactor, solid waste particles of different sizes are captured by melt drops, get into the high-temperature region (1250 °C) and burn. This process for urban waste destruction has already been tested on an industrial scale.^{66–68}

Non-friable bulk materials are processed using tanks filled with a molten catalyst.^{69, 70} The possibility of using molten catalysts for extensive oxidation of organic polymers containing a metal cord with subsequent recovery of the metal from wastes formed in the manufacture and applications of various reinforced polymeric and rubber articles has been demonstrated.⁷¹

III. Characteristic features of reactions proceeding on melts

Owing to the high thermal conductivity of inorganic melts, the heat supply to the reactor in the case of endothermic reactions (hydrocarbon pyrolysis and cracking) and the heat withdrawal from the reaction zone in the case of oxidation (especially,

[‡] Gas lift is a device for lifting a liquid by the energy contained in the compressed gas that is mixed with this liquid.

extensive oxidation) of organic compounds are easier for the reactions with MC. This allows one to intensify the processes.

The by-products (tars and coke) formed during high-temperature reactions are either collected on the melt surface (and, hence, they can easily be removed mechanically from the reaction zone) or distributed throughout the bulk of the melt without the formation of a continuous crust^{30, 72} (this facilitates their removal by oxygen bubbling, *i.e.*, burning out³⁰). The addition of glass-forming metal oxides (boron oxide²⁹ or metal oxides that increase coke wettability⁷³) favours the uniform distribution of coke throughout the melt. High rate of oxidation of soot was attributed⁷⁴ to good wettability of soot in the presence of the V₂O₅ melt.

Since metal oxides and inorganic salts exist as melts over a broad temperature range and have a high thermal conductivity, the temperature in the reactor can be quickly changed and finely controlled, which is important for catalytic reactions carried out under non-steady-state conditions.⁷⁵ The perturbations introduced into a heterogeneous catalytic system (the changes in the reactant concentration, temperature and electrode potential) are controlled more easily when the reaction is carried out on the melts rather than on solid catalysts for which the surface structure is poorly reproducible.

High diffusion coefficients of oxygen in melts, in particular, 10^{-7} – 10^{-5} cm² s⁻¹ (Refs 75 and 76), determine high rate of structure relaxations and allow one to study fast steps of a heterogeneous catalytic process. Structural changes in a molten catalyst can be induced and detected by various methods, including electrochemical ones. In this case, the reaction products are simultaneously detected, which is important to gain information on the process mechanism.^{77, 78} This possibility was demonstrated for the first time in a study of SO₂ oxidation mechanism under non-steady-state conditions on a K₂S₂O₇–V₂O₅ melt.^{75, 76}

The relatively high oxidation temperatures of organic compounds on MC do not prevent investigation of the kinetic effects, namely, the isotope (KIE) and compensation effects. For example, for the oxidative dehydrogenation of *para*-substituted and deuterated ethylbenzene on the KVO₃–V₂O₅ eutectic melt, primary KIE and inverse secondary KIE were observed and the log *k* vs. σ_R^0 dependence was established.^{56, 79} It was concluded that oxidative dehydrogenation of ethylbenzene derivatives is a multi-step process. At a temperature of up to 550 °C, the oxidation involves sorbed oxygen and follows an associative (concerted) mechanism, which switches to the stepwise oxidation–reduction mechanism at higher temperatures. The first step is the reaction of V₂O₅ as the MC component with the aromatic system of the benzene ring. Presumably, the reaction is facilitated by the replacement of hydrogen atoms in the benzene ring by deuterium. This leads to an increase in the equilibrium concentration of the initially formed π -complex, which is then converted into styrene, and to an increase in the dehydrogenation rate (inverse secondary KIE). The replacement of hydrogen atoms at α -carbon in ethylbenzene by deuterium results in a twofold decrease in the rate constant for ethylbenzene dehydrogenation (or a 25% decrease per deuterium atom). This relatively high (in view of the fact that the rate constants were determined at 540–600 °C) primary KIE value indicates that the hydrogen atom is rather remote from the carbon atom in the transition state.

This assumption is supported by the dependence of the rate constants for oxidative dehydrogenation of *para*-substituted ethylbenzenes on the σ_R^0 Hammett constants of the substituents R.⁵⁶ The equation for this dependence at 600 °C has the form

$$\log k = -0.187 \pm 0.016 + (1.345 \pm 0.120) \sigma_R^0$$

($r = 0.9907$, $s = 0.0173$),

where r and s are correlation parameters.

The dependence of log *k* on σ_R^0 shows that in the transition state the substituent is involved in resonance interaction with the aromatic system. The polarity of the transition state is also

confirmed by high reaction constant ($\rho = 1.345$ at 600 °C), which suggests a radical mechanism of the process. On the basis of elemental and powder X-ray diffraction analyses of solidified catalyst samples taken before and after the reaction, it was concluded that the reaction follows a stepwise mechanism, which switches to a concerted mechanism at temperatures below 550 °C.⁸⁰

A study of the oxidation kinetics of ethanol on K–V–M oxide catalysts containing various metal oxides (about 300 compositions) over a broad temperature range (573–873 K, below and above the melting points of the systems) has revealed^{81, 82} a kinetic compensation effect, *i.e.*, parallel variation of the activation energies (E_a) and pre-exponential factors (A) in the Arrhenius equation. This effect is expressed by the relation

$$\log A = cE_a + d = E_a/2.3RT_s + \log k_s,$$

where c and d are constants, T_s and k_s are isokinetic parameters.

Different dependences of log A on E_a for oxidative dehydrogenation of ethanol to acetaldehyde, extensive oxidation of ethanol to CO₂ and dehydration of ethanol to ethylene indicate that these processes occur on different active sites of the catalyst.^{82, 83} The aggregation state of the oxide composition does not influence the pattern of isokinetic dependence.

IV. Relationship between the catalytic reactions proceeding on solid and molten catalysts

Molten catalysts can be used as models to search for new catalytic systems, to establish correlations between the catalyst composition and activity and to study the catalysed reaction mechanisms. The surface of melts has a more uniform composition than that of solid-phase catalysts, which have surface defects and structural and chemical inhomogeneities.^{51, 84, 85}

The features elucidated in the studies of properties and action of MC can be used when preparing solid catalysts. However, one should take into account the correspondence of the conditions of application of molten and solid catalysts, for example, coincidence of the temperature range. A large number of salt and oxide systems with melting points ranging from room temperature to 900 °C are available.⁸⁶ This makes it possible to select melt compositions with melting points below the temperatures used to carry out most of petroleum refining and petrochemistry processes such as pyrolysis and cracking of petroleum hydrocarbons, oxidation of alcohols and alkylaromatic hydrocarbons and production of monomers.

Analysis of the published data shows that the principles of selection of the chemical composition of molten and solid catalysts do not differ much. For example, the chemical composition (in particular, the content of vanadium with the oxidation state +4 in the KVO₃–V₂O₅ melt) was found to correlate with specific oxygen desorption from the melt and its catalytic activity with respect to ethanol oxidation.^{85, 87} It is noteworthy that the relationship between the nature of the transition metal oxide added to the K₃V₅O₁₄ melt and the catalyst activity in the oxidation of ethanol (Fig. 1) is similar to the relationship established⁸⁸ for solid catalysts.

In the oxide catalysts with a more complex chemical composition, the dependence of the catalytic activity on the composition is more complicated. Thus for the oxidation of ethanol, the curve for the activity of the K₃V₅O₁₄–MoO₃ melt vs. the content of MoO₃ has three maxima for MoO₃ concentrations of 13.3 mol %, 20.5 mol % and 34 mol % (*i.e.*, for molar ratios K₃V₅O₁₄:MoO₃ = 2:1, 1:1 and 1:2, respectively).^{85, 87} However, the curve for solid catalysts having a simpler composition, V₂O₅–MoO₃, has only one maximum at a MoO₃ content of about 30 mol %. The lack of other maxima on the catalytic activity curve can be attributed to the formation, on the surface of catalyst grains, of a compound with the same composition (irrespective of

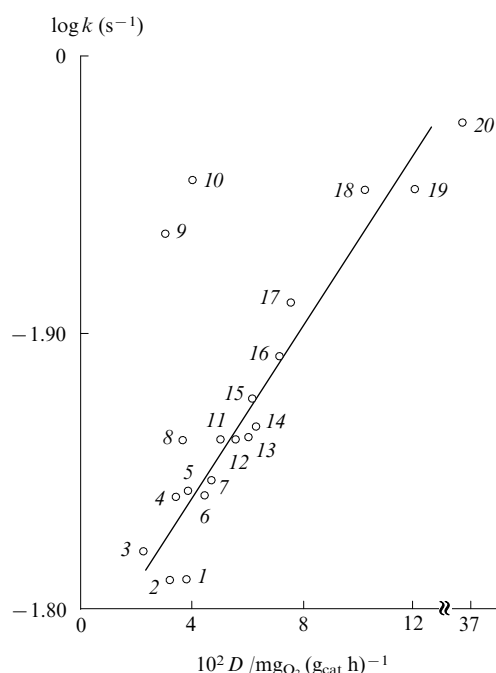


Figure 1. Correlation between the catalytic activity of the $K_3V_5M_{0.33}O_{14}$ melts in the oxidation of ethanol at 500 °C and specific desorption of oxygen from these melts at 600 °C.

M: (1) Ni, (2) Ba, (3) Cr, (4) Co, (5) Al, (6) none, (7) Ti, (8) Zn, (9) Fe, (10) Fe (V : Fe = 7), (11) Pb, (12) Sn, (13) Sb, (14) Bi, (15) Ag, (16) W, (17) B, (18) Mo, (19) Mn, (20) Cu.

the amount of MoO_3), which is thermodynamically more stable under these conditions.

A clear correlation between the catalytic activity of melts based on vanadium oxides in oxidative dehydrogenation of ethylbenzene and the content of vanadium +4 in the melts has been noted.⁸⁰ The rate of transformation of ethylbenzene into styrene on $K_2O-V_2O_5-V_2O_4$ melts was found to decrease with a decrease in the V_2O_5 concentration. The extrapolation to a zero rate shows the lack of activity for a catalyst with the composition 6 mass % V_2O_4 , 69 mass % V_2O_5 and 25 mass % K_2O . In the phase diagram of the $K_2O-V_2O_5-V_2O_4$ system, this composition corresponds to the bronze $K_{(2+2x)}V_2O_{16}$ ($x = 0.35-0.45$)⁸⁹ the presence of which in solidified samples taken from the melt was proved by powder X-ray diffraction.⁸⁰ For solid-phase catalysts it was found⁹⁰ that the phase Ψ of the $K_2O-V_2O_5-V_2O_4$ system containing 3 mol % – 8 mol % V_2O_4 exhibits the lowest activity in the oxidation of *o*-xylene as compared with other formulations of the same system. In the oxidation of alcohols, the activity of the molten $K_2O-V_2O_5$ catalyst is governed by the $KV_4O_{(10.5-x)}$ concentration.^{81,85} The activity of the solid catalyst with the same composition in the oxidation of naphthalene was also higher than the activity of other potassium vanadates.⁹¹

The similarity of action of a catalytic system in the solid or molten states can be revealed by comparing the reaction rates at temperatures above and below the catalyst melting point. The results obtained are useful for solving the problem concerning the role of the chemical composition and the solid surface in the catalysis.

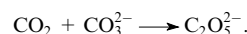
The kinetic parameters for catalytic reactions proceeding on melts and on the solid phase have been compared by many researchers (see, for example, Refs 75, 85, 92–94). In particular, the activation energies of some oxidation reactions at temperatures below and above the catalyst melting points were determined.^{75,85,92} Presumably, the invariable activation energy of the process on going through the melting point can serve as evidence for the predominant influence of the chemical composition of the

catalyst rather than the pattern of its surface on the reaction rate. However, the decrease in the activation energy upon melting observed in some cases is attributable to the fact that the process occurs not only on the surface but also in the bulk of the molten catalyst. For example, oxidation of SO_2 to SO_3 on the $K_2S_2O_7-V_2O_5$ melt proceeds both on the melt surface and in the bulk, depending on the conditions, which was established in a study of the thickness of an ‘operating’ catalyst film.^{76,92,95} This results in a more than twofold decrease in E_a for the reaction on melts compared with the reaction on the solid catalyst surface.⁶² The activation energy also increases upon partial crystallisation of the melt.⁷⁶ High solubility of sulfur dioxide in the $K_2S_2O_7-V_2O_5$ melt was also proved.^{75,76}

The decrease in the activation energy upon passing the catalyst melting point is not common to all the studied reactions. Thus the activation energy for elimination of HCl from alkyl chlorides is the same for catalysis by $ZnCl_2$ solid phase and melt,⁹³ which is explained by the fact that the process occurs only on the melt surface. Analogous data were obtained for oxidative dehydrogenation of ethylbenzene on the $KVO_3-V_2O_5$ catalyst applied onto alumina grains,⁹⁶ and also for benzene oxidation on vanadium oxide catalysts.⁹⁴

A similar dependence of the activation energy on the catalyst aggregation state was found in the oxidation of hydrogen chloride on $CuCl_2$ melt.^{38,97} On solidification of the molten catalyst, the activation energy of this reaction sharply increases.

Oxidation of naphthalene on the $K_2SO_4-V_2O_5$ melt has been investigated.⁹⁷ The activation energy for the reaction on the melt was found to be lower by 36 kJ mol^{−1} than that on the solid catalyst with the same composition. No data on the solubility of naphthalene in the melt of the given composition are available from the literature; however, according to calculations, molecules with sizes greater than the size of the benzene molecule (about 0.6 nm) are poorly soluble in such systems. For example, the solubility of naphthalene in potassium chloride melt was calculated to be 10^{-12} g·mol (cm³ Pa)^{−1} at 400 °C.⁹⁸ The solubility of CO_2 (the size of the molecule is ~0.3 nm) in the $Li_2CO_3-Na_2CO_3-K_2CO_3$ eutectic melt at 700 °C found experimentally equals 9.5×10^{-7} g·mol (cm³ Pa)^{−1} (Ref. 99). The enhanced solubility of CO_2 in alkali metal carbonate melts was attributed⁹⁹ to the formation of the dicarbonate ion:



In the oxidation of naphthalene on the potassium–vanadium–sulfate melt, the rates of naphthalene consumption and oxygen adsorption are proportional to the surface area of the melt and do not depend on its volume.⁹⁷ Therefore, the decrease in the E_a for naphthalene oxidation upon passing of the catalyst from the solid to the molten state can hardly be attributed to occurrence of the reaction in the melt bulk.

The few kinetic data presented above were obtained for processes differing in the nature of the substrate, the composition of the catalyst and reaction conditions. The E_a values for the formation of acetaldehyde from ethanol on a number of molten

Table 1. Activation energy for the formation of acetaldehyde from ethanol on molten and solid catalysts.⁸⁵

Catalyst composition (mol %)			T_m /K	E_a /kJ mol ^{−1}	
K_2O	V_2O_5	M_xO_y		$T < T_m$	$T > T_m$
30.7	48.8	20.5 (MoO_3)	698	76	76
37.0	59.1	3.9 (NiO)	673	113	58
37.0	59.1	3.9 (Ag_2O)	673	91	94
35.6	56.8	7.6 (SnO_2)	683	118	85
37.0	59.1	3.9 (Sb_2O_5)	673	140	79
37.0	59.1	3.9 (Mn_2O_3)	668	80	80

and solid catalysts containing V_2O_5 and other transition metal oxide additives were determined⁸⁵ (Table 1). These data were obtained under identical conditions for catalysts with similar compositions; therefore, their comparison is more vivid than a comparison of the results reported by different authors. The activation energy of the reaction remains unchanged or increases on going from the melt to the solid phase. The different influence of transition of the catalyst through the melting point on E_a can hardly be attributed to the catalytic action of the bulk of the melt. It is unlikely that the addition of 4 mass %–7 mass % of NiO , SnO_2 and Sb_2O_5 would sharply increase the solubility of ethanol in the $K_2O-V_2O_5$ melt, while the same amounts of molybdenum, silver and manganese oxides would not affect the solubility. The assumption that the mechanism of ethanol oxidation changes on passing from high to low temperatures (from 650 to 570 K) on some systems also appears doubtful in view of the fact that on other systems this mechanism is retained.

It is worth noting that the pattern of dependence of the activity of $K_3V_5O_{14}-MoO_3$ catalyst on the MoO_3 content (from 0 mol % to 60 mol %) in the ethanol oxidation is the same at 823 K (melt) and at 673 K (solid phase). Presumably, the structure of the catalyst active sites does not change significantly upon the melt solidification.

The results presented in Table 1 were obtained for catalysts in the solid and molten states. In this case, the possibility of melt solidification to give glasses cannot be ruled out. The structures of the molten and glassy catalysts are similar; therefore, their catalytic activity is the same. Raman and IR spectroscopic data show¹⁰⁰ that the local ordering is the same in both glassy and molten $ZnCl_2$, but differs from that in crystalline zinc chloride. The similarity of structures of glasses and melts for the $K_2SiO_3-KAlSi_3O_8$ systems was established¹⁰¹ on the basis of Raman spectra. The conclusion concerning the identity of the structural units of the melts and 'quenched' glasses was also derived from the IR spectra of sodium metaphosphate.¹⁰²

The results of X-ray diffraction studies of high-temperature melts led researchers¹⁰³ to conclusion that an increase in the temperature to a value 400–700 °C above the T_m changes only slightly the short-order parameters of the mutual arrangements of atoms.

In the case where cooling is accompanied by crystallisation of the system, the environment of the active sites and the distances between them can sharply change with respect to those in the liquid state. This might account for the difference in the activities of catalysts having the same composition in the solid and molten states. For example, in crystalline vanadium(V) oxide, according to the FT EXAFS X-ray absorption data, the V–O bond lengths are 0.16 and 0.19 nm, while after melting the bond lengths become equal to 0.18 nm.¹⁰⁴ Other researchers¹⁰⁵ have shown by X-ray scattering that amorphous V_2O_5 obtained by superfast cooling of the vanadium(V) oxide melt has a tetrahedral coordination with a V–O distance of 0.18 nm. The formation of either amorphous or crystalline product depends on the cooling rate of the melt. The cooling rate that is critical for the amorphisation of melts and the duration and temperature of incubation are determined by the difference between the ionic radii and the thermal conductivity of components.¹⁰⁶

This phenomenon is responsible for the increase in the activity of crystalline silicate catalysts after the 'heat shock'. For increasing the activity, the catalyst is first heated at a rate of 0.5–560 K s^{−1} to 1200 °C, kept for 0.1 to 1200 s and rapidly cooled to 500 °C.^{107, 108} A short heating of superconductor oxide compositions to a temperature of 1000 °C (above T_m) at a rate of ~2000 K min^{−1} followed by cooling at a rate of 100 K min^{−1} is also proposed in another study.¹⁰⁹

The validity of assumptions that the structure of active sites and the distances between them are crucial for the catalyst activity could be verified by investigating the transition of the catalyst from the solid to the molten state: for all catalysts of the same type,

the activation energy of the same reaction should decrease upon this transition. In addition, the dependence of E_a on the aggregation state of the system presented in Table 1 might change for the oxidation of other organic compounds on these catalysts. Unfortunately, no facts either supporting or disproving these assumptions are now available.

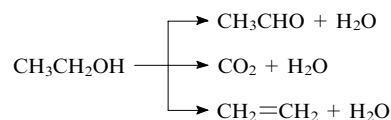
Thus, when working with molten catalysts, one can determine quickly and reliably the correlations between the structures of compounds present as catalyst components and the catalyst activity and to reproduce more precisely the definite ratios of the catalyst components, which is important for the search for conditions for selective formation of the target products.

V. Electrochemical control of the activity and selectivity of molten catalysts

Due to high electrical conductivity of molten metal oxides and salts, catalytic processes can be carried out under conditions of electrolysis.^{110–113} The electrochemical treatment is especially topical for catalytic oxidation of organic compounds accompanied by a change in the oxidation state of transition metals in the catalyst. For example, V_2O_5 widely used as a component of oxidation catalysts is reduced to vanadium(IV) under the reaction conditions.^{85, 110, 114–118} Vanadium(V) is regenerated ($V^{4+} \rightarrow V^{5+}$) under the action of oxygen present in the reaction mixture; as a rule, this is the rate-limiting step for the whole catalytic oxidation of organic compounds.^{80, 92, 110, 119} It has been shown⁸⁰ that in the oxidation of ethylbenzene, the vanadium(IV) concentration in the molten $KVO_3-V_2O_5$ catalyst depends on the ratio of the partial pressures of oxygen and the hydrocarbon. The redox reactions in the melts containing vanadium oxides can also occur during electrolysis; by varying electrolysis parameters, one can obtain specified phases of vanadium oxide bronzes.¹²⁰ The catalytic activity of the vanadium oxide-based melts in the oxidation of organic compounds can be controlled by varying the redox potential of the medium.¹²¹

The changes in the equilibrium potential of the $K_2O-V_2O_5-M_xO_y$ melts depend on the amount of oxygen evolved from the melt,^{83, 122, 123} which, in turn, depends on the rate constant for ethanol oxidation on these catalysts (Fig. 2). The electrochemical control of the catalyst activity includes the change in the redox potential of the medium and the shift of the equilibria in the system. The results of electrochemical studies provide grounds for predicting the catalytic activity of molten oxide–salt systems in the oxidation.

The effect of the redox potential of the $KVO_3-V_2O_5$ melt on the course of ethanol oxidation has been studied.^{111–113} The changes in the redox (for acetaldehyde and CO_2) or acid–base (for ethylene) properties of the melt can be derived from the ratio of the products.



In reality, all three reactions occur simultaneously giving rise also to by-products: C_2H_6 , CO , CH_4 , CH_3COOH .

The conversion and the ratio of the products of ethanol oxidation on melts containing 100 mass %, 90 mass % and 72 mass % of KVO_3 (823 K, molar ratio oxygen : ethanol = 1.5, contact time 0.5 s) depend on the electrode potential.

The dependence of the composition of ethanol oxidation products on the magnitude and sign of the working electrode potential indicates that the oxidation of ethanol under the conditions studied proceeds in the catalyst melt, and regeneration of the catalyst occurs upon electrochemical reactions on the electrodes. Thus, electrochemical processes yield mediators (electron carrier catalysts), which change the catalytic characteristics

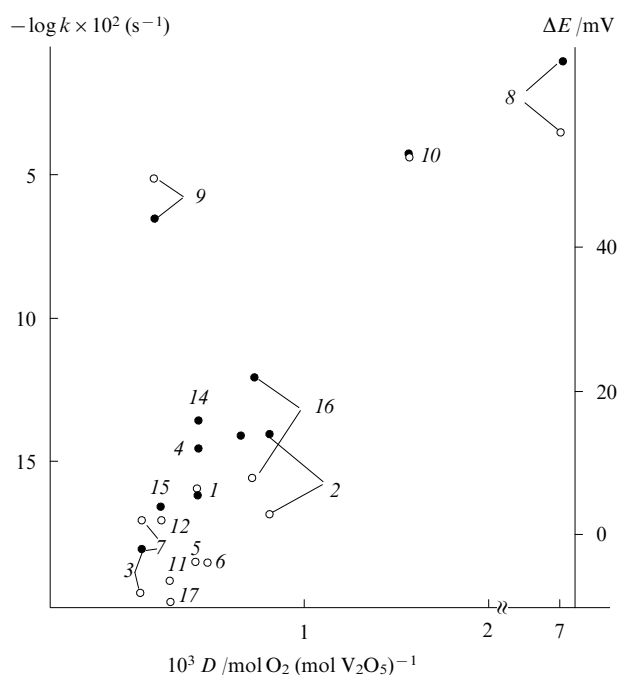


Figure 2. Dependences of the emf (ΔE) of the galvanic cell $\text{Pt}, \text{O}_2 | \text{K}_3\text{V}_5\text{O}_{14} || \text{K}_3\text{V}_5\text{O}_{14} + \text{M}_x\text{O}_y | \text{Pt}, \text{O}_2$ (open circles) and rate constant (at 500 °C) for ethanol oxidation (closed circles) vs. specific desorption (D) of oxygen from the melt for $\text{K}_3\text{V}_5\text{O}_{14} + \text{M}_x\text{O}_y$ systems with different chemical composition for $\text{M} : \text{V} = 1 : 15$.

Additive (M): (1) Al, (2) B, (3) Ba, (4) Bi, (5) Ca, (6) Co, (7) Cr, (8) Cu, (9) Fe, (10) Mn, (11) Ni, (12) Pb, (13) Sb, (14) Sn, (15) Ti, (16) W, (17) Zn.

of the melt, in particular, the reaction rate, selectivity and direction.¹²⁴

The features of transformation of ethanol on the $\text{K}_3\text{V}_5\text{O}_{14}$ or NaOH melts and their solutions in the LiCl–KCl melt are determined by the nature, redox properties and the redox potential of the melt components.^{112, 113, 115} Over the whole range of potentials studied (from +1 to –1 V), the conversion of ethanol and the yield of acetaldehyde upon electrolysis proved to be higher than in the case where the melt was not subjected to electrolysis.

VI. Oxidation of organic compounds

1. Partial oxidation

a. Alkanes and alkenes

The catalytic oxidation of methane yields ethylene (oxidative dimerisation of methane) and liquid hydrocarbons (ethylene oligomerisation). This process is important for practical purposes,^{125–127} because its use on a commercial scale would provide conversion of natural gas into monomers and liquid motor fuel. However, despite the extensive research dealing with optimisation of this process, the conversion of methane in this reaction is only 3%–20%, the selectivity with respect to liquid hydrocarbons varies from 40% to 70%, and the yield of C_2 hydrocarbons does not exceed 25%.¹²⁵

A number of patents^{125, 128, 129} propose the use of melts as catalysts for the oxidative dimerisation of methane. The molten catalysts are composed of mixtures of metal oxides, alkali metal carbonates or sulfates and a reducible transition metal oxide (Mn, Sn, Sb, Pb, Bi, etc.). Transition metal oxides insoluble in the melt and not melting at the reaction temperature should better be fixed on a support that forms a suspension in the salt melt. For better dispersion of the initial gas mixture, particles inert with respect to the melt (the so-called immersed packing) can be added. When the melts are used, the methane conversion is carried out at a temperature of 500–1000 °C and at a pressure of 0.01–3 MPa. The

methane to oxygen volume ratio in the initial mixture varies from 1 to 50. The methane conversion reaches 24%, while the selectivity with respect to higher hydrocarbons, equal to 57%, increases upon a decrease in the methane conversion, as the process follows a parallel-consecutive mechanism.¹²⁵

Lithium carbonate melt was used as the catalyst of oxidative coupling of methane.¹³⁰ The experiments were carried out in a bubble column reactor. In order to keep lithium in the form of carbonate, CO_2 was added to the reaction mixture. It was found that on a Li_2CO_3 –MgO melt (powdered magnesium oxide), the selectivity with respect to hydrocarbons markedly increased with temperature, while the yield of CO decreased with the amount of CO_2 remaining the same. The researchers note that no catalyst deactivation usual for fixed-bed reactors takes place in the bubble reactor.

The oxidative dimerisation of methane on a $\text{Ba}(\text{OH})_2$ melt at a temperature of 800 °C and the ratio $\text{CH}_4 : \text{O}_2 = 3 : 1$ has been studied.¹³¹ The conversion of methane reaches 20%, while the selectivity of formation of C_2 products equals 33%–38%. The authors assumed¹³¹ that the process involves peroxide structures such as the superoxide ion $\text{O}_2^{\cdot -}$, which are stabilised upon enhanced basicity of the medium due to dehydration of $\text{Ba}(\text{OH})_2$. An increase in the basicity increases also the conversion of methane and the yield of C_2 hydrocarbons.

The oxidation of methane to give formaldehyde on a potassium nitrate melt has been studied.^{132, 133} The process is catalysed most likely by NO species formed upon decomposition of potassium nitrate.

The oxidation of methane on sodium metaphosphate-based melts containing transition metal compounds was accompanied by reduction of Cr(VI), V(V) and Co(III) to lower oxidation states.¹³³ The concentration ratio of ^{18}O and ^{16}O isotopes in the melt on bubbling of air or a methane–air mixture was studied by mass spectrometry. The results led the authors to a conclusion that the oxidation of methane on a Na_3PO_3 melt containing d-metal ions involves both reversibly dissolved molecular oxygen (extensive oxidation of methane) and oxygen incorporated into an oxygenated metal complex (partial oxidation of methane).

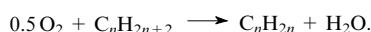
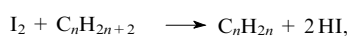
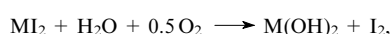
Oxidation of methane with oxygen on a Na_2MoO_4 melt containing V_2O_5 and $\text{K}_4\text{B}_2\text{O}_7$ has been reported.¹³⁴ Despite the changes in the temperature, catalyst composition, the volume feed rate of the reaction mixture and the methane : oxygen ratio, high yield of formaldehyde could not be attained. Similar results have been obtained on an HPO_3 melt with iron oxide additives.³² It is noteworthy that methane conversion and the selectivity of formation of partial oxidation products on solid catalysts are also low.¹³⁵

The oxidation of alkanes and alkenes in molten media are widely studied in order to develop methods of preparation of commercially important monomers, buta-1,3-diene (divinyl) and 2-methylbuta-1,3-diene (isoprene). In the oxidative dehydrogenation, oxygen and its mixtures with hydrogen sulfide, ammonia and sulfur dioxide are used as hydrogen atom acceptors. Eutectic mixtures of metal chlorides, viz., lithium and potassium, sodium and potassium, and magnesium and calcium chlorides serve as molten catalysts, which also contain up to 20 mass % of Group II, IV and VII metal chlorides as promoters.¹³⁶ Presumably,¹³³ the use of melts provides easy solution of the problem of heat withdrawal from the reaction zone owing to high thermal conductivity and melt circulation. The isothermal character of the process results in a higher selectivity with respect to the oxidative dehydrogenation products. For example, bubbling of a butane, hydrogen sulfide, air and ammonia mixture in a 1 : 4 : 2 : 8 molar ratio through molten lithium, potassium and manganese chlorides at 650 °C affords divinyl in a 52% yield, the total yield of divinyl and butenes being 70%.

The dependences of the degree of conversion of n-butane and selectivity of formation of C_4 alkenes on the nature of the melt have been studied.²⁸ The relatively high yields of alkenes are also

observed for molten sodium, potassium and cadmium chlorides (39.9 mass % Cd) or molten lithium and potassium chlorides (37.2 mass % K). The effect of addition of some other metal chlorides on the oxidative dehydrogenation of butane was studied. It was found that barium and manganese chloride additives decrease the conversion of n-butane but increase the yield of alkenes. The conversion of butane increases with an increase in the hydrogen sulfide concentration in the mixture. The selectivity with respect to C₄ alkenes is maximum at a hydrogen sulfide to butane molar ratio of four and decreases upon further increase in the amount of H₂S due to extensive oxidation of hydrocarbons and the formation of sulfur-containing compounds (mainly, thiophene) and elemental sulfur.

It has been proposed¹³⁷ to carry out the oxidative dehydrogenation of alkanes and alkylbenzenes on molten lithium and lead iodides at 500–650 °C in the presence of iodine for hydrocarbon oxidation in a two-chamber reactor. The process is described by the following reactions (for a divalent metal):



Molecular iodine is generated *in situ* upon the oxidation of metal iodides. Saturated hydrocarbons react with iodine to give the target products and HI, which is absorbed by the melt. The metal iodides present in the melt are reoxidised by oxygen in another compartment. This allows one to eliminate direct contact of the hydrocarbon with oxygen, which is a stronger oxidant than I₂ and thus to decrease the formation of complete oxidation products. The results of a study of hydrocarbon reactivity suggest a free radical mechanism of oxidative dehydrogenation of alkanes in the presence of iodine.¹³⁷ Despite the high conversions of hydrocarbons and the selectivity of alkene formation (for ethane, these values are ~80% and >90%, respectively), industrial implementation of this method is precluded by high cost, volatility and high corrosion activity of iodine.

The CuCl–KCl melt pre-saturated with air was used¹³⁸ to convert ethane into acetaldehyde in ~75% yield. On air bubbling, CuCl in the melt is oxidised to CuO·CuCl₂. Apart from acetaldehyde, this reaction affords vinyl chloride.

The results of kinetic and mechanistic studies of the oxidative dehydrogenation of propane on a LiOH–LiI melt have been reported.¹³⁹ At 600 °C and a propane:air ratio of 1:2, the selectivity with respect to propylene is equal to ~75% and that with respect to benzene is 7%–14%. The reaction proceeds by a radical mechanism, the yield of propylene being mainly governed by the concentration ratio of the (Prⁿ)[•] and (Prⁱ)[•] radicals.

A patent¹⁴⁰ describes a process of preparation of acetaldehyde from C₂ hydrocarbons (ethane with ethylene impurity) on transition metal (Mn, Ni, Fe, Cu, Co, Cr) chloride melts in an air flow in the temperature range of 370–540 °C at a pressure of 0.1–1.5 MPa and a contact time from 1 to 60 s. At a <12% conversion of ethane, the selectivity with respect to acetaldehyde reaches 50%–80%.

The oxidation of propylene with oxygen on bubbling the reaction mixture through a KVO₃ melt in the temperature range of 500–650 °C has been studied.¹⁴¹ Since the optimum temperature was lower than the melting point of the catalyst, the yield of aldehydes decreased with increasing temperature.

The partial oxidation of propane on melts representing complex mixtures of potassium, sodium, tungsten, molybdenum and vanadium oxides as well as B₂O₃, K₂Cr₂O₇ and NaOH has been studied.¹⁴² It was found that, for some melts, the conversion of propane in a flow-type bubble reactor at 580–600 °C reaches 70%–90% at rather high yields of carbonyl compounds. K₂Cr₂O₇, NaOH and B₂O₃ melts proved inapplicable for this

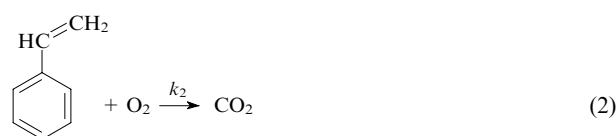
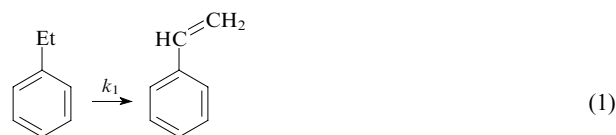
reaction due to irreversible changes in the catalyst, including reduction, transformation into carbonate and sublimation, respectively.

b. Aromatic hydrocarbons

Oxidative dehydrogenation. Alkylbenzenes, for example, ethyl- and isopropylbenzenes are readily converted into the corresponding alkenylarenes on LiI and PbI₂ melts in the presence of iodine. At a high conversion of the starting hydrocarbon (up to 99%), the reaction selectivity reaches 95%.¹³⁷ Propylbenzene is converted into a mixture of allyl- and *cis*- and *trans*-propenylbenzenes. As the side chain of the hydrocarbon becomes longer, the fraction of the cracking products increases. Indeed, ethane and styrene are produced in almost equal amounts upon dehydrogenation of n-butylbenzene, while the major reaction product is naphthalene resulting from dehydrocyclisation (yield 72%).¹³⁷

The oxidative dehydrogenation of ethylbenzene by oxygen on a molten KVO₃–V₂O₅ catalyst has been studied in most detail.^{46, 56, 79, 80, 96} In particular, the activities of the catalyst in the molten and the solid states were compared and the mechanism of the process and its separate steps was studied.^{56, 80, 96}

The kinetics of the oxidative dehydrogenation of ethylbenzene on an alumina-supported melt KVO₃–V₂O₅ (22 mol %) has been studied in a flow-type setup with a rotating catalyst, which ruled out the influence of mass transfer on the process rate.⁹⁶ This reaction gave styrene (St) and CO₂.



At temperatures of 450–550 °C and ethylbenzene and oxygen partial pressures of 3.7×10^{-3} – 6.7×10^{-3} MPa and 3.3×10^{-3} – 6.25×10^{-3} MPa, respectively, this process is described by the following kinetic equations:

$$V_{\text{EtPh}} = k_1[\text{EtPh}]^{1.12}[\text{O}_2]^{0.68},$$

$$V_{\text{St}} = k_1[\text{EtPh}]^{1.12}[\text{O}_2]^{0.68} - k_2[\text{St}]^{0.53}[\text{O}_2]^{0.53},$$

$$V_{\text{CO}_2} = k_2[\text{St}]^{0.53}[\text{O}_2]^{0.53},$$

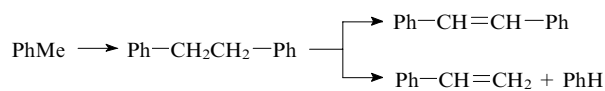
where V_{EtPh} , V_{St} , V_{CO_2} are the consumption rate of ethylbenzene and the formation rates of styrene and carbon dioxide, respectively, k_1 and k_2 are the rate constants for reactions (1) and (2).

It was found⁸⁰ that the accumulation of V₂O₄ in the melt is accompanied by the formation of a complex, inactive in oxidative dehydrogenation of ethylbenzene, with a composition corresponding to the bronze χ . From the temperature dependence of the rate constants for oxygen sorption in the KVO₃–V₂O₅ melt, it was found that oxygen is sorbed by the melt in two forms differing in the activation energies: 170.8 kJ mol^{−1} at 500–550 °C and 327.3 kJ mol^{−1} at 550–600 °C. In the temperature range of 500–550 °C, the removal of oxygen from the melt results in an increase in the catalyst activity in oxidative dehydrogenation of ethylbenzene.

Molten catalysts are suitable not only for the oxidation of organic compounds, but also for the synthesis of complex molecules containing more carbon atoms than the starting compound. Alkyl-substituted aromatic hydrocarbons (for example, toluene and xylenes) and heteroaromatic compounds [for example, picolines (methylpyridines)] form dimerisation products on alkali metal hydroxide melts.^{143–145} These oxidative dehydrodimerisation reactions are currently the subject of extensive research,

because their mechanism resembles that of methane conversion into liquid hydrocarbons.

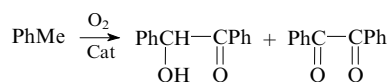
It was found¹⁴⁴ that the transformation of toluene on alkali metal hydroxide melts proceeds as follows:



The bibenzyl formation step is highly sensitive to the nature of the melt. The melts with high basicity catalyse efficiently dimerisation of toluene. The conversion of toluene on the NaOH and KOH melts and their mixtures is much higher than on the melt composed of a sodium and potassium chloride mixture. The conversion of toluene increases if up to 10 mass % of vanadium(V) or phosphorus(V) oxide is added to the alkali metal hydroxide melt.¹⁴⁴

A study of the transformations of *o*-, *m*- and *p*-xylenes on a sodium hydroxide melt has shown that, apart from the dimerisation products, the reaction mixture contains the corresponding methylstyrenes.¹²² The reactivities of the *meta*- and *para*-isomers were almost the same; the selectivity of formation of *m*- and *p*-methylstyrenes, respectively, from these isomers was also the same. The selectivity of formation of *o*-methylstyrene was almost four times lower due to steric effect on the dimerisation. This is consistent with the assumption that transformations of methylbenzenes (in particular, toluene and xylenes) involve the intermediate formation of benzyl radicals. Thus the enthalpies of formation of *meta*- and *para*-methyl-substituted benzyl radicals are 124 kJ mol⁻¹ (Ref. 146) and the enthalpy of formation of unsubstituted benzyl radical is 188 kJ mol⁻¹. This is why the observed conversion of toluene is much lower than that of xylenes.

An increase in the catalyst acidity decreases the yield of dimers, while the yield of products of more extensive oxidation of hydrocarbons increases. An acidic catalyst, namely, V₂O₅-K₂SO₄ melt supported on SiO₂ converts toluene into oxygen-containing products, benzoin (2-hydroxy-1,2-diphenylethanone) and benzil (diphenylethanedione), in the presence of atmospheric oxygen at 400–450 °C.¹⁴⁴ No stilbene or bibenzyl were detected among the reaction products.

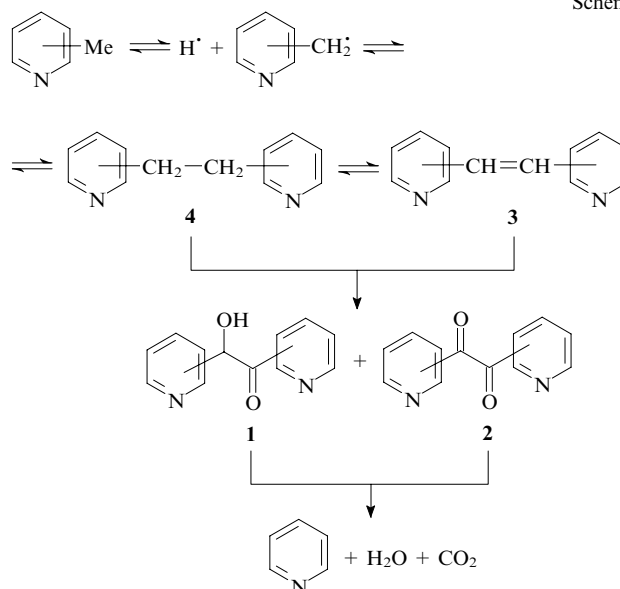


In a similar experiment, 2-methylpyridine was converted into 2-pyridoin (1) and 2,2'-pyridil (2). The proposed reaction mechanism involves the formation of a benzyl-type heterocyclic radical (Scheme 1).

On an eutectic melt KVO₃-V₂O₅ containing 12 mass % of MoO₃, toluene is converted into benzaldehyde and benzoic acid, and methylpyridines are converted into pyridine. In the presence of γ-Al₂O₃-supported K₂CO₃, KOH, KCl and KNO₃ catalysts, methylpyridines are converted into pyridine, CO₂ and water. No methylpyridine dimerisation products were detected. An increase in the temperature, content of air in the reaction mixture or the contact time results in higher yields of 1,2-dipyridylethylenes 3. Note that the conversion of 3-methylpyridine is lower than that of 4-methylpyridine.¹⁴⁵

As noted above, the mechanisms of dehydrodimerisation of methylbenzenes and methylpyridines on basic catalysts are similar to the mechanism of oxidative dimerisation of methane. In the latter reaction, the formation and dimerisation of radicals occur on the catalyst surface and subsequently the dimerisation products pass to the gas phase. Presumably, oxygen-containing products are formed from ethane 4 and ethylene 3 derivatives (see Scheme 1), which were found among the reaction products.

Scheme 1

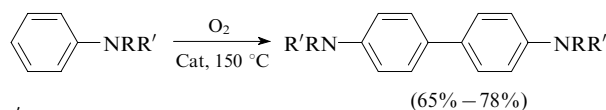


However, upon the toluene oxidation catalysed by V₂O₅-K₂SO₄/SiO₂, no toluene dimerisation products (bibenzyl or stilbene) were detected.

The difference between the composition of products formed on basic and acidic catalysts is due to the difference between the heats of adsorption of organic molecules on different surfaces. Higher heats of adsorption of aromatic and heteroaromatic molecules on acidic catalysts and, as a consequence, an increase in the contact time of the molecule with the catalyst account for more extensive oxidation of the dimerisation products of methylpyridines on the V₂O₅-K₂SO₄/SiO₂ catalyst.

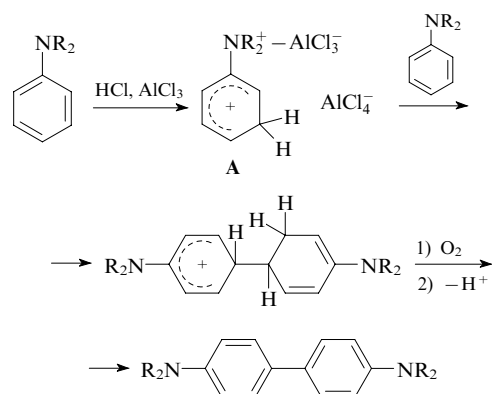
Apparently, the reaction of toluene or picolines with a basic catalyst involves the methyl groups (as in the case of oxidative dimerisation of methane), while in the case of acidic catalysts the substrate is adsorbed upon interaction of the catalyst with the aromatic π-system.

Dimerisation of aromatic amines PhNRR' (R, R' = H, Me) in a NaCl-KCl mixture of molten salts containing Lewis acids (AlCl₃ or ZnCl₂) to give benzidines has been studied with varied temperature, reaction time, reactant ratio and salt and gas phase compositions.¹⁴⁷



R, R' = H, Me.

The highest yield of benzidines was obtained at 150–200 °C in the presence of oxygen. If amine is used as a base, small amount of chlorobenzidines is formed, whereas the use of aniline hydrochlorides results in chlorinated derivatives as the major products (> 50%). The molecular chlorine formed *in situ* upon the oxidation of HCl serves as the chlorinating agent. The dimerisation of amines is markedly influenced by the nature of the Lewis acid, weaker acids such as ZnCl₂ or SnCl₄ being inefficient in this reaction. When two different amines are introduced in the reaction, a mixture of two symmetrical and one asymmetrical benzidines is formed. High regiospecificity of aniline dimerisation was noted: the reaction involves exclusively the *para*-position with respect to the amino group of the most stable σ-complex A formed upon the reaction of aniline with the Lewis acid.



Ammoxidation process. A number of US patents describe one-step synthesis of nitriles, amides, amines and other nitrogen-containing compounds by conjugated oxidation of organic compounds and ammonia on treatment with molecular oxygen in the gas phase on transition metal oxide melts.^{61, 148–152}

For example, ammoxidation of propane on Mn, Co, Cr, Cu chloride and oxychloride melts yields acrylonitrile.¹⁴⁹ In the ammoxidation of the reaction mixture composed of propane, ammonia, air and oxygen on molten copper and potassium chlorides at a contact time of 4.8 s, the conversion of propane was 21%, while the acrylonitrile content in the products was 52.8%.

An eutectic $K_2O-V_2O_5$ mixture was proposed as the MC for ammoxidation.^{61, 150–152} In this case, the process can be carried out in the absence of oxygen in the reaction mixture.¹⁵⁰ For example, a mixture of *m*-xylene and ammonia (molar ratio ~ 0.3) was converted into a mixture (mol %) of benzonitrile (9.49), toluenitrile (58.05) and isophthalonitrile (4.02). The conversion of *m*-xylene was 15.23%.¹⁵⁰ For implementing a continuous process, simultaneous melt regeneration under the action of atmospheric oxygen has been proposed.⁶¹

Benzaldehyde and phthalic anhydride. The oxidation of alkylaromatic hydrocarbons or naphthalene to give benzaldehyde or phthalic anhydride is accompanied by evolution of a large amount of heat, resulting in a sharp increase in the temperature in the reaction zone, which may induce thermal decomposition of the target products. In order to withdraw heat evolved upon toluene oxidation, Volynkin¹⁵³ proposed placing the suspended or floating catalyst, molybdenum oxide supported on ferrochrome grains or crushed MoO_3 , into molten metals or alloys. The yield of benzaldehyde increased in this case to 20%–30% (based on the converted toluene). The product composition depended on the nature of the molten metal. In particular, the yield of benzaldehyde was higher when MoO_3 was suspended in an aluminium alloy. Meanwhile, molten lead was converted into lead oxide under the reaction conditions, and lead oxide catalysed further oxidation of benzaldehyde.

The oxidation of toluene to benzaldehyde on a series of molten catalysts consisting of vanadium or molybdenum oxide or their mixtures doped with sodium, potassium, copper, silver and tin oxides has been studied.¹⁵⁴ As the temperature of the liquid catalyst decreased from 670 to 550 °C, the yield of benzaldehyde sharply decreased, as on solid catalysts. Volynkin studied the oxidation of benzene and phenol into maleic anhydride using the same catalytic systems. The highest activity was found for the catalysts the electrical conductivity of which does not change much upon melt solidification.

The oxidation of *o*-xylene on the $K_2S_2O_7-K_2SO_4-V_2O_5$ melt using electrochemical methods has shown that potassium sulfate not only serves as the solvent for V_2O_5 but also as a reactant involved in the oxidation.¹¹⁰ Regeneration is carried out using the V^{5+}/V^{4+} redox system, which serves as a ‘relay switch’ between the S^{6+}/S^{4+} and O^0/O^{2-} electrochemical pairs. The reduction of the sulfate by the hydrocarbon and the oxidation of vanadium(IV)

by molecular oxygen may be the rate-limiting steps. The reaction orders for the overall oxidation process with respect to *o*-xylene and oxygen are 0.5 and 1.2, respectively. The activation energy is 79 kJ mol⁻¹, which almost coincides with the activation energy for the oxidation of *o*-xylene on solid vanadium catalysts reported in a review.¹⁵⁵

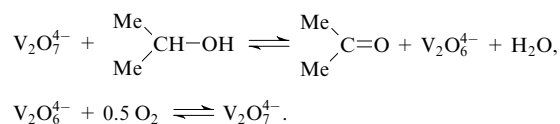
The major naphthalene oxidation products in a molten eutectic mixture of K_2SO_4 and $K_2S_2O_7$ in the presence of V_2O_5 include phthalic and maleic anhydrides and naphthoquinone, the last-mentioned compound being an intermediate in the anhydride synthesis.^{156, 157} For a constant air to naphthalene volume ratio, the yields of the products depend most appreciably on the V_2O_5 concentration.

c. Oxygen-containing organic compounds

The vapour-phase oxidation of C_1-C_4 aliphatic alcohols on heterogeneous catalysts is an industrial method for the production of carbonyl compounds. The oxidation of ethyl and propyl alcohols on $K_2O-V_2O_5$ (5 mass %–24 mass %) melts by a flow-type bubble method has been studied.^{45, 158–162} As the catalyst operates and vanadium(IV) is being accumulated in the melt, the yield of aldehydes somewhat increases. After the equilibrium between the oxidation and vanadium reduction has been attained, the degree of conversion of the alcohol becomes constant.

Studies of the transformation of alcohols in an oxygen and nitrogen atmosphere have shown¹⁵⁹ that the qualitative composition of the products in these reactions is the same. It was thus concluded that the process follows a redox mechanism at the expense of oxygen atoms contained in the melt components. The presence of molecular oxygen in the reaction mixture promotes oxidative dehydrogenation, while the lack of oxygen is favourable for dehydration of the alcohol.

The oxidation of isopropyl alcohol on the $KVO_3-V_2O_5$ eutectic melt in a flow mode has been studied.^{132, 163} On the basis of IR, ¹H NMR and EPR spectroscopic data, it was assumed that the alcohol is first oxidised by vanadium compounds and then the reduced forms of vanadium are reoxidised by molecular oxygen.¹⁶³



The kinetics of the oxidation of n-butanol, n-butanal and n-butyl n-butyrate ($Pr^nCO_2Bu^n$) by chemically bound (lattice) oxygen of the melt with the empirical formula $K_{21}V_{35}O_{107}$ has been studied by pulse chromatography.⁴⁷ The studies were carried out in the temperature range of 430–550 °C in a bubble-type reactor with the bubbling height of the melt varying from 2 to 16 cm. The qualitative composition of the oxidation products proved to be the same for all three compounds; however, their ratios were substantially different.⁴⁷ Under the experimental conditions, the degree of conversion (x) of the initial compounds reached 80%–90% and the reaction slowed down with time. From the decrease in the process rate with an increase in x , it follows that the kinetic dependences are described by the Frost equation

$$k = \frac{1}{\tau} \log \frac{1}{1-x} - \frac{\beta x}{\tau}, \quad (3)$$

where the parameter β (inhibition coefficient) is the slope of the straight line $(1/\tau) \log [1/(1-x)]$ vs. x/τ (τ is time).¹⁶⁴ A comparison of the k values calculated from Eqn (3) and the E_a values demonstrated that in terms of stability against oxidation, these compounds can be arranged in the sequence: butyl butyrate > butanal > butanol.

The oxidation of dimethyl ether to formaldehyde has been studied.^{165–168} The reaction was carried out with oxygen by the flow method in the bubbling mode under atmospheric pressure in the temperature range of 400–500 °C. Melts consisting of Li, K, Na, Mo, V, P oxides (>60 formulations) were used as the catalysts. In the case of melts consisting of vanadium and molybdenum oxides promoted by alkali metal oxides and small amounts of other oxides at an optimum temperature of 420–440 °C, the conversion of dimethyl ether was 45%–54% and the selectivity with respect to the target product (formaldehyde) was 90%–99%. The latter value is much higher than the selectivity (70%–80%) obtained with solid oxide catalysts. A mechanism of the process has been proposed¹⁶⁵ according to which the ether reacts with molybdenum(VI), which results from oxidation of Mo(V) with vanadium pentoxide, with transfer of electrons to the molecular oxygen. The degree of conversion of dimethyl ether increases with an increase in the number of reduced Mo and V ions.

2. Extensive oxidation of organic compounds

The extensive catalytic oxidation and destruction of organic compounds on molten catalysts are of interest, first of all, as environmentally safe methods for waste utilisation. Other applications of these reactions are to produce heat¹⁶⁹ and generate synthesis gas by the reforming of carbon black residues (tar, coke) with steam.⁶⁵

The oxidation of formaldehyde by atmospheric oxygen in molten $\text{KVO}_3\text{--KBr}$ (20 mol %) ($T_m = 491$ °C) and LiCl--KCl (47 mol %) ($T_m = 352$ °C) eutectic mixtures in a flow-type bubble reactor has been studied in the 550–800 °C and 400–800 °C temperature ranges, respectively.¹⁷⁰ At 500 °C, the conversion of formaldehyde in the lithium and potassium chloride melt exceeds 32%, whereas in the gas phase (upon thermal decomposition), it reaches 98%. The oxidation in the salt melts is more mild, as follows from the high content of CO in the products; in the gas phase, the aldehyde is oxidised to CO_2 .

Complete and fast oxidation of organic wastes to carbon dioxide and water is often carried out on MC containing vanadium pentoxide.⁵² Unlike the known methods of incineration of organic compounds in the media of molten metals, glasses and slags,¹⁷¹ the oxidation in the presence of V_2O_5 -based melts can involve not only atmospheric oxygen, but also the oxygen from vanadium(V) oxide. Hence, it is possible to supply the organic feedstock and oxygen to the reactor separately or to carry out oxidation of organic compounds with vanadium pentoxide in one reactor zone and oxidation of the formed vanadium(IV) in another zone and thus to avoid the formation of explosive mixtures.⁶³

The incineration of organic wastes on molten catalysts occurs at the interface. Chain oxidation cannot immediately propagate to the bulk of compounds fed to the reactor; therefore, the process occurs smoothly, under isothermal conditions, and the heat evolved during incineration is absorbed by the molten catalyst, which has a high heat capacity and high thermal conductivity. For example, the $\text{K}_2\text{O}_5\text{--V}_2\text{O}_5$ melt (with a V_2O_5 content of 40 mass % to 83 mass %) was used to oxidise wastes from the production of phthalic anhydride (tar)⁵² and nitrobenzene,^{52,53} while their incineration in usual furnaces is accompanied by explosion. For this reason, these wastes are usually diluted with water prior to combustion, which reduces the efficiency of using the supplied heat and requires combined fuel combustion.

Molten mixtures of inorganic salts, alkali metal oxides and transition metal oxides are also used as catalysts for the oxidation of carbon monoxide.¹⁷²

The possibility of detoxification of mixed organic wastes containing radionuclides using catalytically active melts has been studied.^{172–174} Depending on the nature and concentration, the radioactive metal ions can either be retained in the melt or precipitate, which leads to the necessity of melt regeneration.¹⁷³ The oxidation of model extractants containing uranium and

plutonium in melts based on alkali metal carbonate has been carried out. Analysis of the effluent gases and the melt composition after completion of the experiments showed high efficiency of oxidation of organic components from radioactive wastes and complete absorption of phosphorus and radionuclides by the melt.¹⁷³

A method for processing of solid urban wastes by fusion in a bubbled slag melt has been proposed.^{66–68,175,176} Owing to the manufacture of special design reactors in which unique aerohydrodynamic conditions are produced, solid urban waste particles of various sizes are captured by melt drops, get into the high-temperature region and pass to the liquid (molten) state. Fast heating to a temperature above 1250 °C in ambient atmosphere promotes complete oxidation of organic compounds, and fast cooling of the gaseous products contemplated by the process flow diagram prevents the transformation of the feedstock components into dioxins.¹⁷⁷ This process flow diagram has passed pilot tests.⁶⁸

a. Oxidation of organohalogen compounds

Let us consider extensive oxidation processes of organohalogen compounds and disposal of polymeric materials in more detail.

Molten catalysts are suitable for extensive oxidation of halogen-containing organic compounds,^{122,178–180} while their oxidation on solid catalysts is complicated by the reactions of Cl_2 and HCl formed with components of the catalyst. The demand for an effective catalyst for the oxidation of halogen derivatives is due to the fact that the amount of such wastes reaches 1.5×10^6 tpy in Russia alone.¹⁸¹ In addition, neutralisation of fluorine-containing compounds, which are components of chemical weapons now becomes a highly topical problem. Extensive oxidation on molten electrolytes is also used for this purpose. Thus exhaustive oxidation of sarin and soman in molten alkali metal salts was recommended in the USA for large-scale destruction of chemical agent stockpiles.^{182,183} As a method for extermination of chemical weapon components, their catalytic destruction by metal melts at high temperature has been considered.¹⁸⁴

An attempt to carry out extensive oxidation of polychlorobiphenyls on the molten $\text{KVO}_3\text{--V}_2\text{O}_5$ (60 mass %) catalyst supported on alumina in a flow-type tubular reactor at 600–750 °C has been undertaken.¹⁸⁵ The kinetic and energetic parameters of the process were determined. Carbon oxides and HCl were found to be the major products under these conditions.

Chlorodioxins present in wastes are neutralised by the reaction with molten salts¹⁷³ or by incineration after pre-treatment with molten metallic sodium.¹⁸⁶ Pilot plant tests carried out for a long period of time demonstrated the efficiency of oxidation of toxic organic compounds such as polychlorobiphenyls and tetrachloroethylene on melts.¹⁷³

The company ATG Inc. (USA) developed an industrial process ensuring the destruction of halogen-containing wastes based on injection of the material to be treated into a sodium carbonate melt or melts of other similar salts.¹⁸⁷ At 650–700 °C, organohalogen components are destroyed to give non-toxic salts (e.g., sodium chloride). It was noted¹⁸⁷ that this process is 30%–40% less expensive than the traditional method of waste disposal by incineration followed by gas scrubbing.

The company Molten Metal Technology Inc. (USA) proposed¹⁸⁸ performing neutralisation of toxic chlorine-containing wastes using a reactor containing a molten metal acting as the catalyst. The wastes are thus converted into utilisable products such as CO , HCl , ceramics, metallic alloys, and the exhaust gases of the reactor do not contain dioxins or chlorodibenzofurans.

Organohalogen compounds are also oxidised by treatment in a tank with a melt through which an oxygen-containing gas mixture is passed.¹⁸⁹ The melt contains an alkaline earth metal and an alkaline earth metal halide. The halogen formed upon extensive oxidation of wastes reacts with the metal; as a result, the alkaline earth metal halide is accumulated in the melt. This

method is rather expensive due to the high cost of the alkaline earth metal; however, its use for treatment of highly toxic substances seems to be cost-effective.

A method for treatment of exhaust gases from waste incinerators used for hazardous wastes (chlorinated organic compounds) has been proposed¹⁹⁰ and prepared for commercial use. The oxidation occurring on a molten eutectic mixture of Na, Li and K carbonates at 700–800 °C does not require any expensive construction materials. The effluent gases of the reactor contain less than 0.01 % of the initial organic compounds.

The results of a study on extensive oxidation of halogen-containing compounds, *viz.*, CHCl₃, CCl₄, and fluorocarbon fluid M-1, on molten catalysts I–X (Table 2) depending on the temperature, air feed rate and the nature of the substrate have been reported.^{122, 179} It was shown that the extensive oxidation of CCl₄ and CHCl₃ on catalyst I yields CO₂, Cl₂ or HCl. However, these compounds are absent in the effluent gases, as they are absorbed by the melt. In the oxidation of CCl₄ and CHCl₃ on catalyst II, carbon dioxide appears in the effluent gases in the very beginning of the experiment, and its concentration gradually increases. The degrees of conversion of CCl₄ and CHCl₃ increase from ~99.0% at 350 °C (the ratio air : substrate = 1.8) to 100% at 400 °C. The conversion of chlorohydrocarbons reaches a maximum with a decrease in the load on the catalyst. The reactor effluent gases first contain no chlorine (it reacts with sodium and potassium hydroxides) but after long-term experiment, chlorine appears. Chloride anions were found in the spent catalysts. The presence of sodium and potassium chlorides in the catalysts was confirmed by powder X-ray diffraction data. In the case of catalyst IV (*T*_m = 710 °C), no complete oxidation of halohydrocarbons is observed even at 720 °C and the reaction products contain CO.

Table 2. Composition of the molten catalysts for extensive oxidation of halogen-containing compounds.^{124, 174}

Catalyst	Primary melt	Additives (mass %)
I	NaOH–KOH (eut.)	–
II	NaOH–KOH (eut.)	V ₂ O ₅ (10)
III	NaOH–KOH (eut.)	CuO (10)
IV	Na ₂ CO ₃ –K ₂ CO ₃ (eut.)	–
V	Na ₂ CO ₃ –K ₂ CO ₃ (eut.)	V ₂ O ₅ (10)
VI	Na ₂ CO ₃ –K ₂ CO ₃ (eut.)	V ₂ O ₅ (15)
VII	LiCl–KCl (eut.)	–
VIII	LiCl–NaCl–KCl (eut.)	–
IX	LiCl–NaCl–KCl (eut.)	V ₂ O ₅ (10)
X	LiCl–NaCl–KCl (eut.)	V ₂ O ₅ (15)

When air is bubbled through melt IV containing V₂O₅ (10 mass %), the reactor effluent gases contain CO₂, resulting from thermocatalytic decomposition of carbonates. Thus, during catalyst preparation, CO₂ is removed due to the reaction of sodium and potassium carbonates with V₂O₅ and oxygen. However, CO₂ formed upon passing of CCl₄ and CHCl₃ vapours through the melt and their oxidation is absorbed by the melt. Hence, in the early period of catalyst operation, the CO₂ concentration in the reaction products is lower than that calculated theoretically, while at 650 °C, it approaches the calculated value.

The results of investigation of the oxidation of fluorohydrocarbon fluid M-1 on melts I, IV, VI–X have been reported.^{122, 179} Upon saturation of these melts with atmospheric oxygen (without supply of the fluorohydrocarbon), evolution of chlorine from catalysts IX and X was noted. The oxidation of chloride ions to molecular chlorine by V₂O₅ and atmospheric oxygen attests to the possibility of melt regeneration.

It was shown that fluorine and hydrogen fluoride formed upon decomposition of fluid M-1 are absorbed by the melt. The

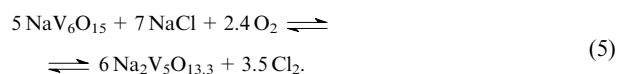
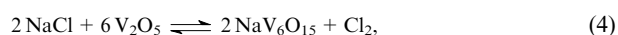
best properties as regards extensive oxidation were found for the melt of sodium and potassium carbonates having the eutectic composition with the addition of 15 mass % of vanadium pentoxide. However, the chloride melt X containing 15 mass % of V₂O₅ showed better stability against fluoride ions and molecular fluorine. The transformation pathway of fluorinated fluid M-1 depends appreciably on the nature of the melt. In the case of melts IV and VIII, thermal decomposition of fluid M-1 and oxidation of the pyrolysis products by atmospheric oxygen take place. In the case of doping of alkali metal chloride or carbonate melts with vanadium pentoxide, which reacts with alkali metal ions and catalyses the formation of CO₂ from carbonates and the formation of molecular chlorine from chloride ions, fluorinated fluid M-1 undergoes catalytic oxidation.

It was shown by differential thermal, elemental and powder X-ray diffraction analyses¹⁷⁹ that the oxidation of halohydrocarbons on molten catalysts NaOH–KOH (eut.), Na₂CO₃–K₂CO₃ (eut.) or LiCl–NaCl–KCl (eut.) containing V₂O₅ affords an equilibrium mixture containing alkali metal hydroxides, carbonates, halides and vanadates and vanadium oxide bronzes, their ratio in the mixture depending on the partial pressures of the halogen, CO₂, water vapour and oxygen. Based on these studies, a catalyst for extensive oxidation of halogenated compounds stable against halogens was proposed, in particular a LiCl–NaCl–KCl (eut.) mixture containing 15 mass % of V₂O₅.

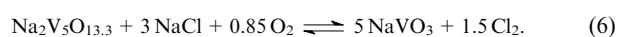
The process of gaseous chlorine evolution from melts has been described.^{122, 191} The NaCl–V₂O₅ (5 mass %, 10 mass %, 20 mass %) and NaCl–NaVO₃ (13.4 mass %) systems were studied in an inert atmosphere and in the presence of atmospheric oxygen at 820 and 880 °C as molten catalysts for extensive oxidation of organohalogen compounds. The derivatograms of the samples obtained by fusing NaCl with 10 mass % of V₂O₅ in air or with continuous air supply to the melt at a rate of 2.5 litre h^{–1} exhibit endothermic effects corresponding to the melting points of NaCl (780 °C), the NaVO₃–Na₂V₅O_{13.3} eutectics (525 °C) and sodium metavanadate (630 °C). The derivatogram of the NaCl–V₂O₅ (10 mass %) sample molten in air shows an endothermic effect indicating the presence of the NaV₆O₁₅ bronze (670 °C). The derivatogram of a sample of the NaVO₃ melt recorded after bubbling CCl₄ (fed as a liquid at a rate of 2 ml h^{–1}) for 3 h and air (2.5 litre h^{–1}) through the melt contains minima corresponding to the melting points of NaVO₃ (630 °C) and NaCl (800 °C). The endothermic effect at 525 °C is due to melting of the NaVO₃–Na₂V₅O_{13.3} eutectics. The Na₂V₅O_{13.3} bronze results from the reaction of sodium metavanadate with chlorine formed upon oxidation of CCl₄. The mass of the catalyst samples does not change over the temperature range studied.

When air is bubbled through a NaCl melt at 820 °C, no molecular chlorine is evolved. Chloride ions might be oxidised with oxygen to give oxides, peroxides and superoxides, but the equilibrium constants of these reactions are low.¹⁹² If V₂O₅ has been added to the NaCl melt, molecular chlorine does form, its amount increasing with an increase in the V₂O₅ concentration and with increasing temperature.

The initial reaction products formed in the NaCl–V₂O₅ system are oxide bronzes, β-type NaV₆O₁₅ and κ-type Na₂V₅O_{13.3}.^{193, 194}



Then the Na₂V₅O_{13.3} bronze is converted into NaVO₃:



The oxidation of chloride ions in an inert atmosphere is due to the redox reaction accompanied by partial reduction of vanadium(V) to vanadium(IV) to give the β-type NaV₆O₁₅ bronze [reaction (4)].

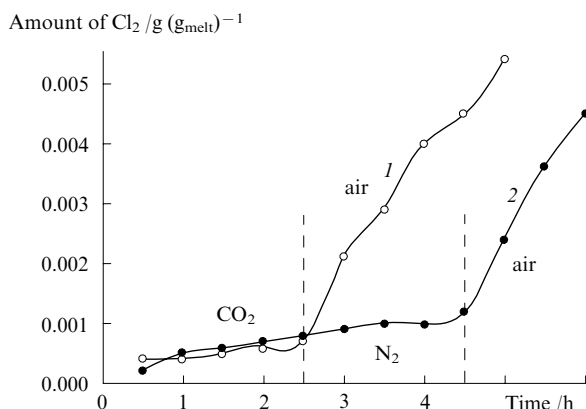


Figure 3. Kinetics of chlorine evolution from the NaCl + 10 mass % V_2O_5 melt depending on the nature of bubbled gas at 820 °C: (1) CO_2 then air, (2) N_2 then air. The gas feed rate is 2.5 litre h^{-1} (Ref. 117).

It has been found¹⁹¹ that the amount of chlorine evolved upon bubbling of nitrogen or carbon dioxide through the NaCl– V_2O_5 (10 mass %) melt is the same and is much lower than that in the case of passing of atmospheric oxygen through this melt (the initial sections of the curves in Fig. 3). If the gas bubbled through the melt is replaced by air, the amount of the evolved chlorine sharply increases (see Fig. 3).

The dynamics of chlorine formation in the NaCl– $NaVO_3$ (13.4 mass %) melt upon bubbling of air (volume flow rate 2.5 litre h^{-1}) has been studied.¹²² The concentrations of sodium metavanadate formed in this mixture and in the NaCl– V_2O_5 (10 mass %) system in the presence of air are the same in the case of complete transformation of V_2O_5 (Table 3). The reaction affords sodium divanadate. The amount of chlorine evolved in this case is minor and the rate constant for the reaction of $NaVO_3$ with NaCl is about two orders of magnitude lower than that for the formation of chlorine in the NaCl– V_2O_5 system. In an inert atmosphere (bubbling of pure CO_2), almost no chlorine is evolved.

Table 3. Rate constants for the oxidation of chloride ions according to reaction (4) for the NaCl– V_2O_5 systems.¹²²

Air passing mode	Content of V_2O_5 (mass %)	$T/^\circ C$	$10^4 k_1/s^{-1}$
Bubbling	5	820	0.59 ± 0.03
Bubbling	10	820	0.79 ± 0.02
	10	880	1.31 ± 0.13
Surface	10	820	0.69 ± 0.03

Presumably, under these conditions, V_2O_5 is first converted into non-stoichiometric compounds corresponding in composition to vanadium oxide bronzes and then into more stable $NaVO_3$. Thus, equal rate constants for the oxidation of Cl^- with air bubbling through the NaCl– V_2O_5 systems suggest simultaneous existence and fast interconversion of vanadium-containing compounds.

The reactivity of vanadium compounds in the oxidation of Cl^- decreases in the sequence $V_2O_5 \gg NaV_6O_{15} \gg Na_2V_5O_{13.3} \gg NaVO_3$. Upon an increase in the temperature and partial pressures of oxygen and chlorine, the rate of transition of one species into another becomes higher than the oxidation rate of the chloride ion. Therefore, when using the NaCl– V_2O_5 system as the catalyst for extensive oxidation of chlorinated organic compounds, the catalyst activity can be controlled by varying the conditions of the process and the composition of the initial mixture.

The apparent activation energy for the oxidation of Cl^- in the NaCl– NaV_6O_{15} – O_2 system was determined. The relatively high value (109 kJ mol^{-1}) indicates that diffusion has a slight influence on the chlorine evolution.

The interactions in the NaCl– M_xO_y (where $M = Cu, Co, Cr, Mo, Sb$) and NaCl–CuCl systems in air or nitrogen atmosphere were studied by differential thermal, powder X-ray diffraction and elemental analyses. The activity of these catalysts in the oxidation of chloride ions was found to depend on the nature of the metal oxide and to decrease in the sequence:¹⁹⁵ $CrO_3 > V_2O_5 > V_2O_5 + Sb_2O_5 > MoO_3 > Sb_2O_5 > Cr_2O_3 > Co_3O_4 > CuCl$.

In the absence of oxygen, the oxidation of chloride ions takes place in the reaction of sodium chloride with vanadium, chromium(VI) and molybdenum oxides. When the reaction mixture contains oxygen, metal oxides act as catalysts of the oxidation of chloride ions by oxygen; as a result, regular evolution of chlorine is observed.

The results of studies of chloride ion oxidation to chlorine indicate that one can select NaCl– M_xO_y systems containing mixtures of transition metal oxides that would ensure that a rate of chlorine formation and evolution from the melt would be commensurable with the rate of chlorine supply from extensive oxidation of halohydrocarbons. Thus, these catalysts would also be suitable for the latter process.

b. Disposal of polymers

It has been proposed⁷¹ to clean metal cord and fixtures from polymeric materials by extensive oxidation of the polymers (burning at 350–600 °C) in a molten catalyst with air bubbling through the melt. The NaOH–KOH melt with 5 mass %–10 mass % of transition metal oxide added is used as the catalyst. The relatively low temperature of the process rules out the formation of nitrogen oxides and the catalytic oxidation of compounded rubber is not accompanied by evolution of gaseous organic compounds or soot. The metal wire is recovered from the processed wastes from reinforced hoses, where the polymers contain mixed rubbers, low density polyethylene, plasticisers (dibutyl phthalate, paraffin, rosin, etc.), or from cord debris obtained from waste automobile tyres by pressing,¹⁹⁶ where different amounts of compounded rubber could be present.

The rate of extensive oxidation of compounded rubber and polymeric materials depends on the amount and the nature of transition metal oxides added. The carbon dioxide formed upon the oxidation of polymers is partly absorbed by the melt, together with the sulfur (IV and VI) oxides formed upon oxidation of compounded rubber. This yields a mixture of salts. In the presence of atmospheric oxygen and water vapour, alkali metal carbonates present as components of the melt can partially decompose to give carbon dioxide; therefore, the spent catalyst represents a mixture of carbonates, sulfites and sulfates as well as transition metal salts; as a result, the melting point of the mixture increases.

VII. Conclusion

Analysis of the properties and possible applications of MC demonstrates that molten metals, metal oxides and salts can be successfully used as the media and the catalysts for various processes. Depending on the melt composition and the nature of the organic compound that reacts with the melt, this can function as a solvent, a chemical reagent or heterogeneous or homogeneous catalyst. The high rate of heterogeneous exchange of the components of a melt containing transition metal oxides with the gas-phase oxygen, the high thermal and electrical conductivities of these systems and the simplicity and reproducibility of the catalyst preparation stage and the activity parameters allow researchers to use molten oxides and salts for mechanistic studies of catalytic reactions and for establishing the composition–catalytic activity relationships. The physicochemical properties attest to advantages of molten catalysts over other types of catalysts, especially as

regards oxidation of organic compounds accompanied by substantial heat evolution, coking or formation of explosive mixtures.

The electrical conductivity of molten oxides and salts allows one to use electrochemical methods for increasing the catalytic activity; this enhances the reliability of operation of reactors in the case of violation of the organic compound to oxygen ratio.

Promising applications of molten electrolytes are those for treatment of exhaust gases and destruction of chemical production wastes. By varying the physicochemical properties of these systems over wide limits, it is possible to use diverse techniques and equipment for the treatment processes and separate and utilise compounds with complex chemical compositions and aggregation states present in the wastes.

Molten salts and oxides demonstrate high stability and capacity (the bulk of the melt rather than only the surface, as in the solid catalysts, is involved in operation) with respect to impurities, which are often poisonous for solid catalysts even when present in minor concentrations. Therefore, the starting compounds can be used without pretreatment and complex mixtures can also be processed using melts.

The use of melts based on alkali metal chlorides containing transition metal oxides, most often V_2O_5 , appears to be promising for the oxidation of chlorine-containing organic compounds. Vanadium(V) oxide increases the catalytic activity and durability of melt performance and improves the heterogeneous exchange between the catalyst and oxygen; thus, it becomes possible to separate the zone for melt saturation with oxygen (catalyst regeneration) and the zone for oxidation of organic compounds. Besides, the addition of V_2O_5 increases the catalyst service life, as it favours the evolution of CO_2 and Cl_2 from the melt giving rise to an equilibrium mixture of K, Na, OH, CO_3 , Cl and V ions in the reactor. The presence of V_2O_5 in the molten catalyst favours oxidation of aromatic hydrocarbons.

Molten catalysts can act as reagents with respect to the halogen evolved upon extensive oxidation of organic compounds; hence, trapping of toxic products by adsorbents is not required. According to published data,¹⁷³ burial of organohalogen compounds formed in the deactivation is more cost-effective than absorption of effluent gases in absorbing towers followed by neutralisation.

Due to the specific character of the catalysts and high cost of reactors used for the melt-catalysed oxidation, it is expedient to use this technique for combusting highly toxic wastes or wastes containing metals and halogens. Thus, it is better to design small-capacity units which can be combined into blocks if necessary. For destruction of highly toxic wastes, the incineration units can be placed into boxes and an additional treatment of the gaseous products formed can be provided.

Molten catalysts are promising systems for effective disposal of solid polymeric and metal polymeric wastes.

Thus, the prospects of development of this field are related to practical implementation of extensive oxidation and destruction of diverse wastes.

In conclusion, we would like to mention one more application of molten catalytic systems, which has not yet been practically implemented, namely, their use as solvents for metal complex catalysts of high-temperature processes such as dehydrogenation.¹⁹⁷

References

1. Yu K Delimarskii, in *Ionnye Rasplavy* (Ionic Melts) (Kiev: Naukova Dumka, 1975) No. 3, p. 3
2. S V Volkov *Teor. Eksp. Khim.* **18** 3 (1982)^a
3. C N Kenney *Catal. Rev. Sci. Eng.* **11** 197 (1975)
4. J F Knifton, in *Aspects of Homogeneous Catalysis* Vol. 6 (Ed. R Ugo) (Dordrecht: Reidel, 1988) p. 1
5. D H Kerridge *Pure Appl. Chem.* **41** 355 (1975)
6. M V Smirnov, V A Khokhlov, V P Stepanov, V P Rychkov, G N Gornova *Rasplavy* (3) 84 (1989)^b
7. G N Gornova, V A Khokhlov, V P Stepanov, M V Smirnov, V P Rychkov, V A Samarina *Rasplavy* (3) 87 (1989)^b
8. V P Stepanov, M V Smirnov, V A Khokhlov, V P Rychkov, V P Obrosof, G N Gornova *Rasplavy* (3) 89 (1989)^b
9. Yu K Delimarskii, L P Barchuk *Prikladnaya Khimiya Ionnykh Rasplavov* (Applied Chemistry of Ionic Melts) (Kiev: Naukova Dumka, 1988)
10. Ya B Chernov, A I Anfinogenov, N I Shurov *Borirovanie Stalei v Ionnykh Rasplavakh* (Boronising of Steels in Ionic Melts) (Ekaterinburg: Urals Branch of Russian Academy of Sciences, 2001)
11. E A Feigin, E A Raud *Primenenie Rasplavlennykh Sred v Protessakh Neftepererabotki i Neftekhimii* (Applications of Molten Media in Petroleum Refining and Petrochemistry) (Moscow: TsNIITENEFTEKhim, 1983)
12. B W Hatt, D H Kerridge *Chem. Br.* **15** (2) 78 (1979)
13. E Arato, B Bosio, P Costa, F Parodi *J. Power Sources* **102** 74 (2001)
14. G P Smith, R M Pagni, in *Molten Salt Chemistry: Introduction and Selected Applications* (Proceedings of NATO Advanced Study Institute on Molten Salt Chemistry, Camerino, Italy, 1986) (Eds G Mamantov, R Marassi) (Dordrecht: Reidel, 1987) p. 383
15. G Mamantov, C B Mamantov, J Braunstein (Eds) *Advances in Molten Salt Chemistry* Vol. 6 (Amsterdam: Elsevier, 1987)
16. K R Seddon *J. Chem. Technol. Biotechnol.* **68** 351 (1997)
17. K R Seddon, in *Molten Salt Chemistry and Technology 5* (Proceedings of the 5th International Symposium on Molten Salt Chemistry and Technology) (Uetikon, Zürich: Trans. Tech. Publ., 1998) Vol. 5–6, p. 53
18. V A Ksenofontov, A N Pryakhin, L M Kustov, V V Lunin *Katal. Prom-sti* (5) 29 (2003)^c
19. V A Ksenofontov, A N Pryakhin, L M Kustov, V V Lunin *Katal. Prom-sti* (6) 23 (2003)^c
20. Ya S Vygodskii, E I Lozinskaya, A S Shaplov *Dokl. Akad. Nauk* **381** 634 (2001)^d
21. R C Buijsman, E van Vuuren, J G Sterreburg *Org. Lett.* **3** 3785 (2001)
22. D Semeril, H Olivier-Bourbigou, C Runeau, P H Dixneuf *Chem. Commun.* 146 (2002)
23. N Audic, H Clavier, M Mauduit, J C Guillemin *J. Am. Chem. Soc.* **125** 9248 (2003)
24. Q Yao, Y Zhang *Angew. Chem., Int. Ed.* **42** 3395 (2003)
25. A V Vasnev, A A Greish, N B Bespalova, L M Kustov, O V Shuvalova *Neftekhimiya* **45** 25 (2005)^e
26. USSR P. 1162480; *Ref. Zh. Khim.* 1L204P (1986)
27. V G Ryabov, A B Solomonov, A N Ketov, A M Bugaichuk *Khim. Tekhnol. Topl. Masel* 6 (1979)^f
28. N J Gaspar, J S Pasternak, M Vadekar *Can. J. Chem. Eng.* **52** 793 (1974)
29. US P. 3876527; *Ref. Zh. Khim.* 5P137 (1976)
30. M P Fazleev, O S Chekhov, E A Ermakov *Zh. Prikl. Khim.* **57** 1872 (1984)^g
31. A F Dobryanskii *Kreking s Khloristym Alyuminiem* (Cracking with Aluminium Chloride) (Leningrad: Khimteoret, 1938)
32. I M Kolesov, V Ya Pavlov, L Ya Perevozchikov, G P Davydov, in *Geterogennye Khimicheskie Reaktsii* (Tr. Permsk. Gos. Farm. In-ta) [Heterogeneous Chemical Reactions (Proceedings of Perm State Pharmaceutical Institute)] (Perm: Perm State Pharmaceutical Institute, 1974) No. 3, p. 131
33. W M J Ruedisulj, H D Evans, E B Fountain *Hydrocarbon Process. Petrol. Refin.* **42** (7) 125 (1963)
34. USSR P. 488800; *Ref. Zh. Khim.* 22R521 (1976)
35. S Kikkawa, T Hayashi, M Nomura, N Otsu *Bull. Chem. Soc. Jpn.* **48** 90 (1975)
36. V A Mireev, V V Safonov *Rasplavy* (5) 67 (1992)^b
37. S Kikkawa, M Nomura *J. Synth. Org. Chem. Jpn.* **33** 593 (1975)
38. F P B Holroyd, C N Kenney *Chem. Eng. Sci.* **26** 1971 (1971)
39. W Verbeek, W Sundermeyer *Angew. Chem.* **78** 307 (1966)
40. Y Tamai, Y Ohtsuka *Bull. Chem. Soc. Jpn.* **46** 1996 (1973)
41. USSR P. 423493; *Byull. Izobret.* (14) (1974)
42. R T Struck, C W Zielke *Fuel* **60** 795 (1981)
43. Y Ogino *Catal. Rev. Sci. Eng.* **23** 505 (1981)

44. N S Pechuro, O Yu Pesin, V N Konokhov, in *Tekhnologiya Organicheskikh Veshchestv (Itogi Nauki i Tekhniki)* [Technology of Organic Substances (Advances in Science and Engineering Series)] (Moscow: Izd. VINITI, 1984) Vol. 9, p. 3
45. O K Koz'minykh, N A Makarevich, A N Ketov *Izv. Vyssh. Uchebn. Zaved., Khim. Khim. Tekhnol.* 723 (1973)
46. E V Pantelev, Yu S Chekryshkin, A N Ketov, M N Stepanova, A I Sterlyagov *Neftekhimiya* 21 361 (1981)^c
47. I V Shakirov, A N Ketov, Yu S Chekryshkin *Zh. Prikl. Khim.* 57 369 (1984)^g
48. N S Pechuro, O Yu Pesin, I A Dorofeev, in *Khimiya i Khimicheskaya Tekhnologiya (Tr. MITKhT im. M V Lomonosova)* [The Chemistry and Chemical Technology (Proceedings of M V Lomonosov Moscow Institute of Fine Chemical Technology)] (Moscow: Lomonosov Moscow Institute of Fine Chemical Technology, 1976) p. 157
49. N P Belyaeva *Kat. Prom-sti* (2) 16 (2004)^c
50. I V Shakirov, Yu S Chekryshkin *Rasplavy* (2) 94 (1987)^b
51. I V Shakirov, V I Abanin, in *Okislitel'nyi Kataliz v Khimicheskoi Tekhnologii i Promyshlennoi Ekologii* (Oxidative Catalysis in Chemical Technology and Industrial Ecology) (Ed. Yu S Klyachkin) (Sverdlovsk: Urals Branch of the USSR Academy of Sciences, 1990) p. 19
52. USSR P. 911091; *Ref. Zh. Khim.* 3T825P (1983)
53. V A Sekirin, A N Ketov, Yu S Chekryshkin *Zh. Prikl. Khim.* 58 2389 (1985)^g
54. C N Satterfield, J Loftus *AIChE J.* 11 1103 (1965)
55. C N Satterfield, J Loftus *Ind. Eng. Chem. Proc.* 4 102 (1965)
56. E V Pantelev, A N Ketov, Yu S Chekryshkin, M N Stepanova *Kinet. Katal.* 28 736 (1987)^h
57. E V Pantelev, A N Ketov, Yu S Chekryshkin, A I Sterlyagov, M N Stepanova *Kinet. Katal.* 22 1082 (1981)^h
58. A Miyamoto, Y Ogino *J. Catal.* 37 133 (1975)
59. S V Adel'son, O V Lysykh, Ya M Paushkin *Neftekhimiya* 15 836 (1975)^c
60. US P. 6565820; *Ref. Zh. Khim.* 03-19L142 (2004)
61. US P. 3945804; *Ref. Zh. Khim.* 1N226 (1977)
62. L A Perevozchikov, L P Kostin, A N Ketov *Izv. Vyssh. Uchebn. Zaved., Khim. Khim. Tekhnol.* 24 308 (1982)
63. USSR P. 980806; *Ref. Zh. Khim.* 18I136P (1983)
64. I V Shakirov, A N Ketov, Yu S Chekryshkin *Zh. Prikl. Khim.* 55 2498 (1982)^g
65. US P. 5478370; *Ref. Zh. Khim.* 5P196P (1998)
66. V V Mechev, A V Grechko, V F Denisov, E I Kalnin, L D Shishkina, M I Gertseva *Izv. Vyssh. Uchebn. Zaved., Tsvet. Metallurg.* 26 (1993)ⁱ
67. Russ. P. 2062949; *Byull. Izobret.* (18) 235 (1996)
68. A V Grechko, V F Denisov *Khim. Prom-st.* (1) 115 (1998)^j
69. US P. 5191154; *Ref. Zh. Khim.* 19I515P (1994)
70. BRD Appl. 4217854; *Ref. Zh. Khim.* 1I465P (1995)
71. Russ. P. 2151696; *Byull. Izobret.* (18) 324 (2000)
72. F P B Holroyd, C N Kenney *Chem. Eng. Sci.* 26 1963 (1971)
73. K J Hüttenger, R Minges *Fuel* 64 491 (1985)
74. B A A L Setten, R van Dijk, S J Jelles, M Makkee, J A Moulijn *Appl. Catal., B* 21 51 (1999)
75. B S Bal'zhinimaev, V E Ponomarev, G K Borekov, A A Ivanov, V S Sheplev, V M Sadovskaya *React. Kinet. Catal. Lett.* 28 81 (1985)
76. B S Bal'zhinimaev, A A Ivanov *Relaksatsionnye Metody v Geterogenom Katalize. Eksperimental'nye Rezul'taty* (Relaxation Methods in Heterogeneous Catalysis. Experimental Results) (Novosibirsk: Institute of Catalysis, Siberian Branch of the Academy of Sciences of the USSR, 1985) Ch. II
77. B S Bal'zhinimaev, A A Ivanov *Relaksatsionnye Metody v Geterogenom Katalize. Eksperimental'naya Tekhnika* (Relaxation Methods in Heterogeneous Catalysis. Experimental Technique) (Novosibirsk: Institute of Catalysis, Siberian Branch of the Academy of Sciences of the USSR, 1985) Ch. I
78. A A Ivanov, B S Bal'zhinimaev, Yu S Chekryshkin, in *Nestatsionarnye Protssy v Katalize (Tez. Dokl. Mezhdunar. Konf.)*, Novosibirsk, 1990 [Non-steady-state Processes in Catalysis (Abstracts of Reports of the International Conference), Novosibirsk, 1990] p. 39
79. E V Pantelev, Yu S Chekryshkin, in *Heterogeneous Catalysis. (Proceedings of the VIth International Symposium)*, Sofia, 1987 p. 448
80. E V Pantelev, A N Ketov, Yu S Chekryshkin *Kinet. Katal.* 24 376 (1983)^h
81. I V Shakirov, Yu S Chekryshkin, in *Okislitel'nyi Kataliz v Khimicheskoi Tekhnologii i Promyshlennoi Ekologii* (Oxidising Catalysis in Chemical Technology and Industrial Ecology) (Ed. Yu S Klyachkin) (Sverdlovsk: Urals Branch of Academy of Sciences of the USSR, 1990) p. 25
82. Yu S Chekryshkin, I V Shakirov, P S Dukhanin *Rasplavy* (6) 65 (1991)^b
83. Yu S Chekryshkin, A A Fedorov, O A Tetenova *Rasplavy* (2) 47 (2000)^b
84. Yu S Chekryshkin, E V Pantelev, I V Shakirov, A P Khaimenov *Neorganicheskie Rasplavy — Katalizatory Prevrashcheniya Organicheskikh Veshchestv* (Inorganic Melts as Catalysts of Conversion of Organic Substances) (Moscow: Nauka, 1989)
85. I V Shakirov, Yu S Chekryshkin, V I Abanin *Kinet. Katal.* 26 356 (1985)^h
86. A Gordon, R Ford *A Chemist's Companion* (New York: Wiley-Interscience, 1973)
87. Yu S Chekryshkin, I V Shakirov, in *Ionnye Rasplavy i Tverdye Elektrolity* (Ionic Melts and Solid Electrolytes) (Kiev: Naukova Dumka, 1987) No. 2, p. 36
88. L N Kurina, L M Potalitsyna *Zh. Fiz. Khim.* 53 728 (1979)^k
89. A A Fotiev, V L Volkov, V K Kapustkin *Oksidnye Vanadievye Bronzy* (Oxide Vanadium Bronzes) (Moscow: Nauka, 1978)
90. M Gasior, B Grzybowska, S Haber, T Machej, J Ziolkowski *J. Catal.* 58 15 (1979)
91. A Kato, S Kawadze, C Isida, T Ino, T Seyama *J. Chem. Soc. Jpn.: Pure Chem. Sec. (Nippon Kagaku Zasshi)* 91 843 (1970)
92. G M Polyakova, G K Borekov, A A Ivanov, L P Davydova, G A Marochkina *Kinet. Katal.* 12 666 (1971)^h
93. C N Kenney, in *Tr. IV Mezhdunar. Kongressa po Katalizu* (Proceedings of the IVth International Congress on Catalysis) (Nauka: Moscow, 1970) Vol. 2, p. 425
94. K Mori, M Inomata, A Miyamoto, Y Murakami *J. Chem. Soc., Faraday Trans. 1* 2655 (1984)
95. G K Borekov, V A Dzis'ko, D V Tarasova, G P Balaganskaya *Kinet. Katal.* 11 181 (1970)^h
96. E V Pantelev, Candidate Thesis in Chemical Sciences, Lomonosov Moscow Institute of Fine Chemical Technology, Moscow, 1973
97. P V Butt, C N Kenney, in *Proceedings of the 6th International Congress on Catalysis* (London: Imperial College, 1976) p. B.17
98. A K K Lee, E F Johnson *Ind. Eng. Chem. Fundam.* 8 726 (1969)
99. P Claes, D Moyaux, D Peeters *Eur. J. Inorg. Chem.* 583 (1999)
100. M L Cacciola, S Magazú, P Migliardo, F Aliotta, C Vasi *Solid State Commun.* 57 513 (1986)
101. V E Eremyashev, A A Osipov, V N Bykov *Rasplavy* (4) 9 (2005)^b
102. L R Bazarashvili, N I Buryak, V A Bandur, S V Volkov *Ukr. Khim. Zh.* 56 115 (1990)
103. E A Pastukhov, N A Vatolin *Difraktsionnye Issledovaniya Stroeniya Vysokotemperaturnykh Rasplavov* (Diffraction Investigations of the Structures of High-Temperature Melts) (Ekaterinburg: Urals Branch of the Russian Academy of Sciences, 2003)
104. M Miyake, M Okuno, T Suzuki, F Marumo *J. Chem. Soc. Jpn.: Chem. Ind. Chem.* 905 (1982)
105. A Mosset, P Lecante, J Galy, J Livage *Philos. Mag.* B 46 137 (1982)
106. K V Gamayunov, T V Maslova, V V Osiko, V M Tatarintsev *Izv. Akad. Nauk SSSR, Neorg. Mater.* 23 264 (1987)^l
107. US P. 4582694; *Ref. Zh. Khim.* 22L190 (1986)
108. US P. 4623636; *Ref. Zh. Khim.* 6N204 (1988)
109. Jpn. Appl. 323271; *Ref. Zh. Khim.* 18L79P (1993)
110. M Kerkeni, PhD Thesis, Toulouse, 1980; *Ref. Zh. Khim.* 3B1334D (1983)
111. P S Dukhanin, Yu S Chekryshkin, A P Khaimenov *Rasplavy* (4) 49 (1990)^b

112. P S Dukhanin, Yu S Chekryshkin *Rasplavy* (2) 50 (1995)^b
113. Yu S Chekryshkin, P S Dukhanin, A P Khaimenov, A A Fyodorov, in *Molten Salt Chemistry and Technology 5 (Proceedings of the 5th International Symposium on Molten Salt Chemistry and Technology)* Vol. 5–6 (Uetikon, Zürich: Trans. Tech. Publ., 1998) p. 497
114. Yu S Chekryshkin, E V Panteleev, I V Shakirov, in *Issledovaniya v Oblasti Khimii Ionnykh Rasplavov i Tverdykh Elektrolitov* (Investigations in the Field of Ionic Melts and Solid Electrolytes) (Kiev: Naukova Dumka, 1985) p. 30
115. Zh G Bazarova *Kinet. Katal.* **12** 948 (1971)^h
116. V E Ponomarev, B S Bal'zhinimaev, A A Ivanov, in *Nestatsionarnye Protsessy v Katalize. Ch. 1. (Tez. Dokl. III Vsesoyuzn. Konf.)*, Novosibirsk, 1986 [Non-steady-state Processes in Catalysis (Abstracts of Reports of the IIIrd All-Union Conference), Novosibirsk, 1986] Pt. 1, p. 49
117. V M Mastikhin, G M Polyakova, Ya Zyulkovski, G K Borekov *Kinet. Katal.* **11** 1463 (1970)^h
118. V E Ponomarev, A N Ketov, B S Balzhinimaev, A A Ivanov, S V Kozyrev *React. Catal. Lett.* **18** 421 (1981)
119. P Mars, J G H Maessen *J. Catal.* **10** 1 (1968)
120. USSR P. 1366554; *Ref. Zh. Khim.* 13L216P (1988)
121. A P Tomilov, S G Mairanovskii, M Ya Fioshin, V A Smirnov *Elektrokhimiya Organicheskikh Soedinenii* (Electrochemistry of Organic Compounds) (Leningrad: Khimiya, 1968) p. 559
122. Yu S Chekryshkin, T A Rozdyalovskaya, A A Fedorov *Geterogenno-kataliticheskoe Glubokoe Okislenie Galogensoderzhashchikh Organicheskikh Veshchestv na Rasplavakh Elektrolitov* (Heterogeneous Catalytic Extensive Oxidation of Halogen-containing Organic Substances on Electrolyte Melts) (Ekaterinburg: Urals Branch of the Russian Academy of Sciences, 2005)
123. Yu S Chekryshkin, I V Shakirov, P S Dukhanin, in *Rasplavlennyye Elektrolity (Tez. Dokl. V Ural'skoi Konf. po Vysokotemperaturnoi Fizicheskoi Khimii i Elektrokhimii)* [Molten Electrolytes (Abstracts of Reports of the Vth Urals Conference on High-temperature Physical Chemistry and Electrochemistry)] (Sverdlovsk: Urals Branch Academy Sciences of the USSR, 1989) Vol. 1, p. 256
124. O A Petrii, B I Podlovchenko, in *Kataliz (Fundamental'nye i Prikladnye Issledovaniya)* [Catalysis (Fundamental and Applied Investigations)] (Eds O A Petrii, V V Lunin) (Moscow: Moscow State University, 1987) p. 39
125. US P. 4678862; *Ref. Zh. Khim.* 9N4 (1988)
126. V S Arutyunov, O V Krylov *Usp. Khim.* **74** 1216 (2005) [*Russ. Chem. Rev.* **74** 1111 (2005)]
127. V S Arutyunov, A L Lapidus *Vestn. Ros. Acad. Nauk* (8) 683 (2005)^m
128. US P. 4665261; *Ref. Zh. Khim.* 6N6 (1988)
129. Fr. Appl. 2603573; *Ref. Zh. Khim.* 3N1P (1989)
130. J W M H Geerts, H M N van Kasteren, K van der Wiele *J. Chem. Soc., Chem. Commun.* 802 (1990)
131. C Moneuse, M Cassir, C Piolet, J Devynck *Appl. Catal.* **63** 67 (1990)
132. V A Bandur, N I Buryak, S V Volkov, in *Ionnyye Rasplavy i Tverdye Elektrolity* (Ionic Melts and Solid Electrolytes) (Kiev: Naukova Dumka, 1986) No. 1, p. 41
133. S V Volkov, V A Bandur, N I Buryak *Rasplavy* (6) 72 (1991)^b
134. I M Kolesov, S V Zekhov, in *Razvitie Khimicheskoi i Neftekhimicheskoi Promyshlennosti Zapadnogo Urala i Zadachi po Povysheniyu Kachestva i Effektivnosti Proizvodstva (Tez. Dokl. VII Oblastnoi Nauchno-tehnicheskoi Konferentsii po Khimii i Khimicheskoi Tekhnologii)* [Development of Chemical and Petrochemical Industry of West Ural and Tasks on Increasing the Production Efficiency (Abstracts of Reports of the VIIth Regional Scientific and Technical Conference on Chemistry and Chemical Technology)] (Perm: Perm Polytechnic Institute, 1979) p. 68
135. O V Krylov, M D Shibanova (Eds) *Glubokoe Kataliticheskoe Okislenie Uglevodorodov* (Extensive Catalytic Oxidation of Hydrocarbons) (Moscow: Nauka, 1981) Vol. 18
136. USSR P. 345117; *Ref. Zh. Khim.* 9N6 (1973)
137. C T Adams, S G Brandenbergen, J B DuBois, G S Mill, M Nager, D B Richardson *J. Org. Chem.* **42** 1 (1977)
138. BRD P. 2247343; *Auszuge aus der Auslege Schriften* [Patent Schriften 05.04.1973]
139. I M Dahl, K Grande, K-J Jens, E Rytter, Å Slagtern *Appl. Catal.* **77** 163 (1991)
140. US P. 3869518; *Ref. Zh. Khim.* 1N51 (1976)
141. O K Koz'minykh, V A Skvortsov, in *Geterogennye Khimicheskie Reaktsii (Tr. Permsk. Gos. Farm. In-ta)* [Heterogeneous Chemical Reactions (Proceedings of Perm State Pharmaceutical Institute)] (Perm: Perm State Pharmaceutical Institute, 1974) No. 6, p. 125
142. A G Vilenskii, A Ya Averbukh, A S Turbin, N G Gerleman, in *Kataliticheskie Protsessy i Katalizatory* (Catalytic Processes and Catalysts) (Ed. I P Mukhlenov) (Leningrad: Leningrad Technological Institute, 1982) p. 29
143. USSR P. 1353769; *Ref. Zh. Khim.* 11N91P (1988)
144. Yu S Chekryshkin, O A Tetenova, A A Fedorov *Neftekhimiya* **41** 298 (2001)^e
145. Yu S Chekryshkin, O A Tetenova, A A Fedorov *Neftekhimiya* **42** 41 (2002)^e
146. V N Kondrat'ev (Ed.) *Energii Razryva Khimicheskikh Svyazei. Potentsialy Ionizatsii i Srodstvo k Elektronu* (Rupture Energy of Chemical Bonds. Ionisation Potentials and Electron Affinity) (Moscow: Nauka, 1974)
147. H Imaizumi, S Sekuguchi, K Matsui *Bull. Chem. Soc. Jpn.* **50** 948 (1977)
148. US P. 3444234; Patent Official Gazette USA, **862** (19), 2 (1969)
149. US P. 3652638; *Ref. Zh. Khim.* 2N83 (1973)
150. US P. 3812171; *Ref. Zh. Khim.* 7N161 (1975)
151. US P. 3803205; *Ref. Zh. Khim.* 6N170 (1975)
152. US P. 3846473; *Ref. Zh. Khim.* 22N258 (1975)
153. N I Volynkin *Zh. Prikl. Khim.* **41** 1376 (1968)^g
154. N I Volynkin *Zh. Prikl. Khim.* **44** 1853 (1971)^g
155. S L Kiperman *Kineticheskie Problemy v Geterogennom Okislitel'nom Katalize. Kinetika i Kataliz (Itogi Nauki i Tekhniki)* [Kinetic Problems in Heterogeneous Oxidative Catalysis. Kinetics and Catalysis (Advances in Science and Engineering Series)] (Moscow: Izd. VINITI, 1979) Vol. 6
156. M S Medimagh, E Ben Mamou, M L Bouguerra *J. Ir. Chem. Soc.* **5** (Spec. Issue) 73 (1980); *Ref. Zh. Khim.* 17N111 (1984)
157. M S Medimagh, M L Bouguerra *J. Chim. Phys. Phys.-Chim. Biol.* **88** 451 (1991)
158. USSR P. 352874; *Ref. Zh. Khim.* 15N41 (1973)
159. N A Makarevich, O K Koz'minykh, A N Ketov, in *Geterogennye Khimicheskie Reaktsii (Tr. Permsk. Gos. Farm. In-ta)* [Heterogeneous Chemical Reactions (Proceedings of Perm State Pharmaceutical Institute)] (Perm: Perm State Pharmaceutical Institute, 1974) No. 6, p. 118
160. N A Makarevich, O K Koz'minykh, M V Kosheleva, in *Geterogennye Khimicheskie Reaktsii (Tr. Permsk. Gos. Farm. In-ta)* [Heterogeneous Chemical Reactions (Proceedings of Perm State Pharmaceutical Institute)] (Perm: Perm State Pharmaceutical Institute, 1974) No. 6, p. 114
161. O K Koz'minykh, N A Makarevich, A N Ketov, in *Sbornik Nauchnykh Trudov Permskogo Politehnicheskogo Instituta* (Collected Scientific Works of Perm Polytechnic Institute) (Perm: Perm Polytechnic Institute, 1973) Vol. 135, p. 23
162. O K Koz'minykh, N A Makarevich, A N Ketov, in *Khimiya i Tekhnologiya Vanadievnykh Soedinenii* (Chemistry and Technology of Vanadium Compounds) (Perm: Perm Book Publishing, 1974) p. 236
163. S V Volkov, V A Bandur, N I Buryak *Ukr. Khim. Zh.* **46** 906 (1980)
164. A I Dinkes, A V Frost *Dokl. Akad. Nauk SSSR* **3** 510 (1934)^d
165. E V Dolbilkina, M V Kosheleva, O K Koz'minykh, A N Ketov *Okislenie Dimetilovogo Efera v Rasplave KVO₃–MoO₃* (Oxidation of Dimethyl Ether in a KVO₃–MoO₃ Melt); articles deposited in VINITI, Moscow, 1981, No 1441
166. USSR P. 593727; *Ref. Zh. Khim.* 8L185 (1979)
167. USSR P. 413139; *Ref. Zh. Khim.* 6N29 (1975)

168. E V Dolbilina, in *Geterogenyye Khimicheskie Reaktsii* (Tr. Permsk. Gos. Farm. In-ta) [Heterogeneous Chemical Reactions (Proceedings of Perm State Pharmaceutical Institute)] (Perm: Perm State Pharmaceutical Institute, 1974) No. 6, p. 110
169. G K Borekov, E A Levitskii, Z R Ismagilov *Zh. Vses. Khim. O-va im D I Mendeleeva* **29** 19 (1984)ⁿ
170. I M Kolesov, Z V Zekhov, in *Khimiya i Tekhnologiya Protssesov, Protekayushchikh v Srede Rasplavlennykh Solei* (Mezhvuz. Sb. Nauch. Trudov No. 210) [Chemistry and Technology of Processes in Molten Salts (International Collection of Scientific Works No. 210)] (Perm: Perm State University, 1977) p. 26
171. BRD Appl. 2612560; *Izobret. za Rubezhom* (19) (1976)
172. M A Kerzhentsev, M G Adamson, Z R Ismagilov, Yu S Chekryshkin, in *Advances in Molten Salts. From Structural Aspects to Waste Processing* (Proceedings of the European Research Conference on Molten Salts. Porquerolles Island, France, 1998) (Ed. M Gaune-Escard) (New York: Begel House Inc., 1999) p. 279
173. M G Adamson, P C Hsu, D L Hipple, K G Foster, R W Hopper, T D Ford, in *Advances in Molten Salts. From Structural Aspects to Waste Processing* (Proceedings of the European Research Conference on Molten Salts. Porquerolles Island, France, 1998) (Ed. M Gaune-Escard) (New York: Begel House Inc., 1999) p. 1
174. Z R Ismagilov, M A Kerzhentsev, V A Rogov, V G Balakhonov, G V Beklemyshev, V S Zagumennov, in *Vseros. Molodezhnaya Nauchnaya Konf. po Fundamental'nym Problemam Radiokhimii i Atomnoi Energetiki* (Tez. Dokl.), Nizhnii Novgorod, 2001 [The First All-Russian Youth Scientific Conference on Fundamental Problems of Radiochemistry and Nuclear-power Engineering (Abstracts of Reports), Nizhnii Novgorod, 2001] p. 17
175. A V Grechko, V F Denisov *Khim. Prom-st.* **61** (1998)^j
176. V V Mechev, in *Ekologicheskii Chistaya Tekhnologiya Pere-rabotki Bytovykh Otkhodov* (Tez. Dokl. 2-go Mezhdunarodnogo Kongressa po Upravleniyu Otkhodami VeistTek-2001), Moskva, 2001 [Environmentally Clean Process of Domestic Waste Treatment (Abstracts of Reports of Second International Congress on Control of Waste, Wastetech-2001)] p. 115
177. L A Fedorov *Dioksiny kak Ekologicheskaya Opasnost': Retrospektiva i Perspektivy* (Dioxins as Ecological Danger: Retrospective and Perspectives) (Moscow: Nauka, 1993)
178. Yu S Chekryshkin, T A Rozdvalovskaya, A A Fedorov, L A Chekryshkina *Inzhen. Ekolog.* (3) **36** (2005)
179. Yu S Chekryshkin, T A Rozdvalovskaya, Z R Ismagilov, M A Kerzhentsev, O A Tetenova, A A Fedorov *Eurasian Chem. Technol. J.* **5** 201 (2003)
180. L E Johnston *Environ. Health Perspect.* **60** 339 (1985)
181. L N Zhanavskii, O A Konorev, V A Aver'yanov *Khim. Prom-st.* (2) **3** (2002)^j
182. V L Zhdanov, V M Koshelev, V K Novikov, A A Shuvalov *Ros. Khim. Zh.* **37** (3) 22 (1993)ⁿ
183. M S Haralampiev *Univ. Chem. Technol. Met.* **37** 29 (2002)
184. G Yu Udal'tsova, N A Tankovich, L P Lyangasov *Ros. Khim. Zh.* **37** 17 (1993)ⁿ
185. N M Kazakova, S B Kholostov, M N Stepanova, A A Fedorov, N V Cheremukhina, in *Vysokotemperaturnaya Fizicheskaya Khimiya i Elektrokhimiya* (Tez. Dokl. IV Ural'skoi Konf.), Sverdlovsk, 1985 [High-temperature Physical Chemistry and Electrochemistry (Abstracts of Reports of the IVth Urals Conference), Sverdlovsk, 1985] Pt. 2, p. 3
186. *New Sci.* **130** (1774) 28 (1991)
187. *Chem. Eng. (USA)* **107** 23 (2000); *Ref. Zh. Khim.* 0109-191529 (2001)
188. D L Hoey, B Cox, K Lesker, C Lütge *Chem. Ing. Techn.* **68** 1159 (1996)
189. BRD P. 38136139; *Ref. Zh. Khim.* 19N16 P (1990)
190. *Chem. Eng. (USA)* **100** (10) 23 (1993); *Ref. Zh. Khim.* 9N453 (1995)
191. T A Rozdvalovskaya, Yu S Chekryshkin, Zh A Vnutskikh, V N Nekrasov, O V Limanovskaya *Rasplavy* (4) **75** (2004)^b
192. V N Nekrasov *Rasplavy* (2) **58** (1993)^b
193. A A Fotiev, B V Slobodin, M Ya Khodos *Vanadaty: Sostav, Sintez, Struktura, Svoistva* (Vanadates: Composition, Synthesis, Structure, Properties) (Moscow: Nauka, 1988)
194. A A Fotiev, M Ya Khodos, E D Pletneva, in *Oksidnye Bronzy* (Oxide Bronzes) (Ed. V I Spitsyn) (Moscow: Nauka, 1982) p. 17
195. T A Rozdvalovskaya, A N Chudinov, Yu S Chekryshkin, A A Fedorov, in *Problemy i Perspektivy Razvitiya Khimicheskoi Promyshlennosti na Zapadnom Urale* (Problems and Perspectives of Development of Chemical Industry on West Ural) (Perm: Perm State Technology University, 2005) p. 33
196. USSR P. 1497021; *Byull. Izobret.* (28) (1989)
197. G V Lisichkin, A Yu Fadeev, A A Serdan, P N Nesterenko, P G Mingalev, D B Furman *Khimiya Privitykh Poverkhnostnykh Soedinenii* (Chemistry of Grafted Surface Compounds) (Moscow: Fizmatlit, 2003)

^a — *Theor. Exp. Chem. (Engl. Transl.)*

^b — *Melts (Engl. Transl.)*

^c — *Catal. Indust. (Engl. Transl.)*

^d — *Dokl. Chem. (Engl. Transl.)*

^e — *Petrol. Chem. (Engl. Transl.)*

^f — *Chem. Technol. Fuels Oils (Engl. Transl.)*

^g — *Russ. J. Appl. Chem. (Engl. Transl.)*

^h — *Kinet. Catal. (Engl. Transl.)*

ⁱ — *Nonferr. Metall. Trans. (Engl. Transl.)*

^j — *Ind. Chem. (Engl. Transl.)*

^k — *Russ. J. Phys. Chem. (Engl. Transl.)*

^l — *Inorg. Mater. (Engl. Transl.)*

^m — *Herald Russ. Acad. Sci. (Engl. Transl.)*

ⁿ — *Mendeleev Chem. J. (Engl. Transl.)*

The use of tetrazolium salts in inorganic analysis

K B Gavazov, A N Dimitrov, V D Lekova

Contents

I. Introduction	169
II. Preparation and properties of tetrazolium ion-associated complexes	169
III. Analytical applications of tetrazolium ion-associated complexes	173
IV. Miscellaneous applications of tetrazolium salts in inorganic analysis	177
V. Conclusion	177

Abstract. The use of tetrazolium salts for extraction, spectrophotometric and potentiometric determination of various elements and ions is described. The optimum conditions for extraction of tetrazolium ion-associated complexes are analysed. Chromogenic and other systems derived from tetrazolium salts and their applications in the analysis of industrial and natural samples are discussed. The bibliography includes 118 references.

I. Introduction

Tetrazolium salts (TS) are heterocyclic compounds the five-membered rings in which contain four nitrogen atoms; one of these atoms bears a positive charge. The methods for synthesis, properties and applications of TS have been described.¹ Substituted TS usually contain up to three substituents, *viz.*, at the carbon atom in position 5 and at two nitrogen atoms. The following combinations of positions of substitution in the tetrazolium ring are possible: 1, 2, 5; 1, 3, 5; 1, 4, 5 and 2, 3, 5. The most extensively studied 2,3,5-trisubstituted TS (Table 1) are the topic of the present review.

The first tetrazolium salt, *viz.*, 2,3,5-triphenyltetrazolium chloride, was synthesised in the late 19th century independently by H von Pechman and E Bamberger. Tetrazolium salts attracted the attention of investigators by virtue of their ability to be converted into coloured formazans under the action of chemical and biological reducing agents. Commercial production of TS began half a century later. Tetrazolium salts came into wide use as redox indicators for determination of enzymes and other systems.^{1,2} At present, tetrazolium salts are among the most efficient reagents in cell biology designed for determination of metabolic activities of various cells (from mammalian to bacterial).² In addition, TS have found application as catalysts and photo-sensitive materials.¹

In the 1960–1970s, a new trend in the chemistry of TS emerged, namely, the chemistry of ion-associated complexes (IAC) of tetrazolium cations with simple and complex anions.^{3,4}

Unlike the original salts, these complexes are poorly soluble in water and can selectively be extracted with appropriate organic solvents. Due to the ability to form IAC, tetrazolium salts served as the basis for the development of analytical (*e.g.*, extraction–photometric, *etc.*) techniques for the determination of metal ions and non-metal derivatives incorporated in such complexes.

The first surveys^{3,4} of the extraction and analytical applications of tetrazolium ion-associated complexes (TIAC) published before 1983 appeared in 1984. Since then, numerous data have been reported on ion-associated complexes with different tetrazolium cations and their applications for the extraction of various ions and elements. Competitive extraction–photometric and potentiometric methods making use of TIAC and photometric and catalytic photometric methods based on TS reduction were also developed.

The aim of the present review is to generalise and to systematise the data on the applications of TS in inorganic analysis published between 1984 and 2006.

II. Preparation and properties of tetrazolium ion-associated complexes

Tetrazolium ion-associated complexes are crystalline compounds that are stable under ordinary conditions, poorly soluble in water and easily soluble in diverse organic solvents. They are decomposed upon heating to 180–220 °C (Refs 5 and 6) or under direct sunlight.^{3,4,7,8} In weakly basic solutions, *e.g.*, at pH ~10, the N(2)–N(3) bond of the tetrazolium ring is cleaved to yield coloured formazans.^{1,3,4,7}

The chromophore properties of TIAC usually represent a combination of chromophore properties of the constituent ions, *viz.*, tetrazolium cations and complex anions. This suggests the predominantly ionic nature of the chemical bond in TIAC. The tetrazolium salts absorb light in the visible and UV spectral regions, their absorption maxima usually lie at 200–260 nm with exception of MTT, which has an absorption maximum in the visible region (~380 nm).

TIAC are widely employed in analytical chemistry as components of extraction systems. They are used for both isolation of ions from complex mixtures and quantitative determination of metal cations and other inorganic ions in various natural and industrial samples by extraction–spectrophotometric methods. The properties of TIAC allow their extraction from aqueous solutions and govern the extraction characteristics of systems employed in the analysis (Tables 2 and 3). In addition to the general characteristics of the method (*e.g.*, solvents, extraction time, pH, *etc.*), these tables list the extraction constants (which

K B Gavazov, A N Dimitrov, V D Lekova Department of Chemistry, Plovdiv University 'Paisii Hilendarski', Tsar Assen st. 24, 4000 Plovdiv, Bulgaria. Fax (359-32) 62 83 90, tel. (359-32) 26 14 20, e-mail: kgavazov@abv.bg (K B Gavazov), vanlek@pu.acad.bg (V D Lekova), tel. (359-32) 26 13 24, e-mail: andim@pu.acad.bg (A N Dimitrov)

Received 4 July 2006

Uspekhi Khimii 76 (2) 187–198 (2007); translated by R L Birnova

Table 1. Tetrazolium salts used for the preparation of ion-associated complexes.

Formula	Name	Abbreviation	Mol. mass	Formula	Name	Abbreviation	Mol. mass
	2,3,5-triphenyl-2 <i>H</i> -tetrazolium chloride	TT	334.41		3,3'-(4,4'-biphenylene)-bis(2,5-diphenyl-2 <i>H</i> -tetrazolium) chloride (Neotetrazolium chloride)	NT	667.60
	2-(4-nitrophenyl)-3,5-diphenyl-2 <i>H</i> -tetrazolium chloride	p-NT	379.82		3,3'-(3,3'-dimethoxy-4,4'-biphenylene)bis(2,5-diphenyl-2 <i>H</i> -tetrazolium) chloride (Tetrazolium Blue chloride)	BT	727.66
	3-(1-naphthyl)-2,5-diphenyl-2 <i>H</i> -tetrazolium chloride (Tetrazolium Violet)	TV	384.86		3,3'-(3,3'-dimethoxy-4,4'-biphenylene)bis[2-(4-nitrophenyl)-5-phenyl-2 <i>H</i> -tetrazolium] chloride (Nitro Blue Tetrazolium chloride)	NBT	817.65
	3-(4,5-dimethylthiazol-2-yl)-2,5-diphenyl-2 <i>H</i> -tetrazolium bromide (Thiazolyl Blue Tetrazolium Bromide)	MTT	414.31		3,3'-(3,3'-dimethoxy-4,4'-biphenylene)bis[2,5-di(4-nitrophenyl)-2 <i>H</i> -tetrazolium] chloride (Tetranitro-tetrazolium Blue chloride)	TNBT	907.6
	3-(4-iodophenyl)-2-(4-nitrophenyl)-5-phenyl-2 <i>H</i> -tetrazolium chloride	INT	505.70				

Table 2. Extraction characteristics of tetrazolium ion-associated complexes with inorganic anions.

Extraction system		pH	Time of extraction /min	log K_{ex}	log K_{D}	log β	R (%)	Ref.
TIAC	solvent							
(INT ⁺)BrO ₃ [−]	CHCl ₃	broad range	3	1.9	1.19	0.7	93.9	9
(MTT ⁺)BrO ₃ [−]	CHCl ₃	the same	3	1.9	1.29	0.6	95.1	9
(TT ⁺)BrO ₃ [−]	CHCl ₃	"	3	0.8	0.35	0.4	69.1	9
(TNBT ²⁺)[Cd(SCN) ₄] ^{2−}	C ₂ H ₄ Cl ₂ + + (CH ₃) ₂ O	2–6	2	2.8	0.85	2.0	87.6	10
(TT ⁺) ₂ [Cd(SCN) ₄] ^{2−}	C ₂ H ₄ Cl ₂	broad range	3	5.6	1.52	4.1	97.1	11, 12
(INT ⁺) ₂ [Cd(SCN) ₄] ^{2−}	C ₂ H ₄ Cl ₂	the same	3	5.9	1.35	4.5	95.7	11, 12
(MTT ⁺) ₂ [Cd(SCN) ₄] ^{2−}	C ₂ H ₄ Cl ₂	"	3	5.9	1.13	4.7	93.1	13
(NBT ²⁺)[Cd(SCN) ₄] ^{2−}	C ₂ H ₄ Cl ₂	"	4	2.9	0.60	2.3	80.2	11, 14
(NT ²⁺)[Cd(SCN) ₄] ^{2−}	C ₂ H ₄ Cl ₂	"	4	2.8	0.64	2.2	81.3	11, 14
(INT ⁺)ClO ₃ [−]	CHCl ₃	"	3	3.2	0.88	2.4	88.6	15
(MTT ⁺)ClO ₃ [−]	CHCl ₃	"	3	3.3	1.04	2.3	91.7	15
(TT ⁺)ClO ₃ [−]	CHCl ₃	"	3	2.3	0.14	2.2	58.4	15
(INT ⁺)ClO ₄ [−]	CHCl ₃	"	3	4.0	1.42	2.6	96.3	9
(MTT ⁺)ClO ₄ [−]	CHCl ₃	"	3	4.0	1.57	2.4	97.4	9
(TT ⁺)ClO ₄ [−]	CHCl ₃	"	3	3.6	1.27	2.3	94.9	9
(TT ⁺) ₂ [Co(SCN) ₄] ^{2−}	C ₂ H ₄ Cl ₂	"	3	6.5	2.07	4.5	99.2	16
(NBT ²⁺)[Co(SCN) ₄] ^{2−}	C ₂ H ₄ Cl ₂	1–8 (0.01– 0.66 M H ₂ SO ₄)	3	4.1	2.07	2.0	99.2	16, 17
(TV ⁺) ₂ [Co(SCN) ₄] ^{2−}	C ₂ H ₄ Cl ₂	2.7–7.6	3	6.4	1.86	4.6	98.6	8
(MTT ⁺) ₂ [Co(SCN) ₄] ^{2−}	C ₂ H ₄ Cl ₂	2.7–7.6	3	6.6	1.81	4.8	98.5	13
(TNBT ²⁺)[Co(SCN) ₄] ^{2−}	C ₂ H ₄ Cl ₂ + + (CH ₃) ₂ O	2–6	2	4.3	2.08	2.3	99.2	10
(MTT ⁺) ₃ [Cr(SCN) ₆] ^{3−}	C ₂ H ₄ Cl ₂	1.8–7.2 M HCl	0.5	—	—	—	—	18

Table 2 (continued).

Extraction system		pH	Time of extraction /min	log K_{ex}	log K_D	log β	R (%)	Ref.
TIAC	solvent							
(MTT ⁺) ₃ [Cr(ClO ₄) ₆] ³⁻	CHCl ₃	2.4–5.5 M HCl	—	—	—	—	—	18
(NT ²⁺)[CrO ₃ Cl] ₂ ⁻	C ₂ H ₄ Cl ₂	0.36–1.08 M HCl	0.17	—	—	—	—	19
(NBT ²⁺)[CrO ₃ Cl] ₂ ⁻	C ₂ H ₄ Cl ₂	0.25–0.6 M HCl	0.25	—	—	—	—	20
(TT ⁺)[CrO ₃ Cl] ⁻	C ₂ H ₄ Cl ₂	0.3–1.5 M HCl	1	2.9	0.76	2.1	85.2	21
(INT ⁺)[CrO ₃ Cl] ⁻	C ₂ H ₄ Cl ₂	0.1–1.1 M HCl	0.5	4.2	1.36	2.8	95.6	8, 22
(TV ⁺)[CrO ₃ Cl] ⁻	C ₂ H ₄ Cl ₂	0.07–0.36 M HCl	0.5	4.5	1.42	3.1	96.4	8, 22
(MTT ⁺)[CrO ₃ Cl] ⁻	C ₂ H ₄ Cl ₂	0.15–0.42 M HCl	1	4.0	1.38	2.6	96.0	23
(MTT ⁺)[GaCl ₄] ⁻	CHCl ₃	6.1–6.6 M HCl	15	4.7	0.67	4.0	82.4	24
(TV ⁺)[HgBr ₃] ⁻	C ₂ H ₄ Cl ₂	broad range	1	4.5	1.60	2.9	97.6	25
(TV ⁺)[HgI ₃] ⁻	CHCl ₃	1–9	1	4.1	1.03	3.1	91.5	25
(INT ⁺)[HgI ₃] ⁻	C ₂ H ₄ Cl ₂	0.2–5.5 M H ₂ SO ₄	0.25	4.2	1.18	3.0	93.8	8, 26
(TT ⁺)[HgI ₃] ⁻	CHCl ₃	1–9 (0.1–4.5 M H ₂ SO ₄)	0.5	4.5	1.32	3.2	95.4	27
(MTT ⁺)[HgI ₃] ⁻	CHCl ₃	1–8	0.5	4.5	1.22	3.3	94.3	28
(TV ⁺)I ⁻	C ₂ H ₄ Cl ₂	1–6 (0.25–1.8 M HCl)	0.25	—	—	—	—	29
(TV ⁺)IO ₄ ⁻	CHCl ₃	broad range	3	4.3	0.97	3.3	90.3	30
(INT ⁺)[La(S ₂ O ₃) ₂] ⁻	CHCl ₃	5–7.4	1	—	—	—	—	31
(MTT ⁺)MnO ₄ ⁻	C ₂ H ₄ Cl ₂	5–8 (0.01–0.16 M H ₂ SO ₄)	0.08	4.5	1.34	3.2	95.6	32
(TT ⁺)MnO ₄ ⁻	C ₂ H ₄ Cl ₂	6–7 (0.01–0.3 M H ₃ PO ₄)	0.033	3.3	1.25	2.1	94.7	8, 33
(INT ⁺)MnO ₄ ⁻	C ₂ H ₄ Cl ₂	0.01–0.125 M HCl	0.05	3.2	1.38	1.8	96.0	34
(TV ⁺)MnO ₄ ⁻	C ₂ H ₄ Cl ₂	0.01–0.03 M H ₃ PO ₄	0.17	4.5	1.75	2.8	98.2	35
(NBT ²⁺)[MnO ₄] ₂	C ₂ H ₄ Cl ₂	1–9 (0.01–0.2 M H ₂ SO ₄)	0.5	11.0	1.55	9.5	97.2	8
(MTT ⁺) ₃ [MoO(SCN) ₆] ³⁻	C ₂ H ₄ Cl ₂	0.9 M H ₂ SO ₄	0.5	—	—	—	—	36
(p-NT ⁺)ReO ₄ ⁻	CHCl ₃	1–10	3	3.0	0.97	2.1	90.3	37
(TV ⁺)ReO ₄ ⁻	CHCl ₃	3–10	3	4.2	1.86	2.1	98.6	38
(MTT ⁺)ReO ₄ ⁻	CHCl ₃	2–10	3	4.0	1.59	2.4	97.5	39, 40, 41
(INT ⁺)ReO ₄ ⁻	CHCl ₃	3–10	3	4.6	1.80	2.8	98.4	39, 40, 41
(NT ²⁺)(ReO ₄) ₂ ⁻	CHCl ₃	4–10	3	8.0	1.18	6.8	93.8	39, 40, 41
(NBT ²⁺)(ReO ₄) ₂ ⁻	CHCl ₃	broad range	3	9.0	1.22	7.8	94.3	40, 41
(INT ⁺) ₂ [ReCl ₆] ²⁻	C ₂ H ₄ Cl ₂	2–7	60	—	1.38	—	96.0	42
(NT ²⁺)[ReCl ₆] ²⁻	C ₂ H ₄ Cl ₂	3–7	60	4.5	0.46	4.0	74.0	43
(MTT ⁺)[Sb(OH) ₂ Cl ₄] ⁻	C ₆ H ₆ + diethyl ether (3:1)	> 1.65 M HCl	1	—	—	—	—	44
(TV ⁺)[Sb(OH) ₂ Cl ₄] ⁻	CHCl ₃	6 M HCl	60	—	—	—	—	5
(TV ⁺)[Sb(OH) ₂ Cl ₄] ⁻	C ₆ H ₆	> 6 M HCl	10	—	—	—	—	45
(MTT ⁺)[TiCl ₄] ⁻	C ₆ H ₆ + diethyl ether (3:1)	0.01–1.0 M HCl	1	5.3	1.72	3.6	98.1	41, 44
(TV ⁺)[TiCl ₄] ⁻	C ₆ H ₆	0.05–6.0 M HCl;	1	—	—	—	—	45
(TT ⁺) ₂ [Zn(SCN) ₄] ²⁻	C ₂ H ₄ Cl ₂	broad range	3	8.3	1.05	7.3	91.8	46
(INT ⁺) ₂ [Zn(SCN) ₄] ²⁻	C ₂ H ₄ Cl ₂	the same	3	8.3	1.02	7.2	91.2	46
(NBT ²⁺)[Zn(SCN) ₄] ²⁻	C ₂ H ₄ Cl ₂	"	3	5.1	1.68	3.4	98.0	46
(NT ²⁺)[Zn(SCN) ₄] ²⁻	C ₂ H ₄ Cl ₂	"	3	5.1	1.57	3.5	97.4	46
(TNBT ²⁺)[Zn(SCN) ₄] ²⁻	C ₂ H ₄ Cl ₂ + (CH ₃) ₂ O	2–6	0.5	5.1	1.68	3.4	98.0	10
(TV ⁺) ₂ [Zn(SCN) ₄] ²⁻	C ₂ H ₄ Cl ₂	2–8	0.02	8.5	1.03	7.5	91.4	8, 47
(MTT ⁺) ₂ [Zn(SCN) ₄] ²⁻	C ₂ H ₄ Cl ₂	broad range	3	8.0	1.16	6.8	93.5	13

Note. Here and in Table 3, K_{ex} is the extraction constant ($K_{ex} = K_D \times \beta$); K_D is the distribution constant of the ionic associate between the phases; β is the stability constant of the associate (association constant) and R is the degree of extraction.

characterise the extraction in the system under consideration on the whole), distribution constants of the ionic associate between phases (*i.e.*, the concentration ratios in organic and aqueous phases), stability constants of ionic associates (which describe the associate formation in the aqueous phase) and the degree of extraction, *i.e.*, the percentage of the substance extracted into the organic phase.

Chloroform or dichloroethane are commonly used as an organic phase for extraction; benzene and n-butanol are used less often. Sometimes, the use of mixtures of these solvents^{67, 68} or their mixtures with ethers and acetone is more preferable.^{10, 44}

The extraction time varies from several seconds to several minutes. The relatively slow extraction processes of [Sb(OH)₂Cl₄]⁻ and [ReCl₆]²⁻ represent an exception, shaking for ~1 h is required.^{5, 42, 43} The difference between extraction

Table 3. Extraction characteristics of tetrazolium ion-associated complexes with chelate anions.

Extraction system		pH	Time of extraction /min	log K_{ex}	log K_D	log β	$R(\%)$	Ref.
TIAC ^a	solvent							
(MTT ⁺) ₂ [Ge(NPC) ₃] ²⁻	CHCl ₃	2.9–3.5	2	11.2	1.11	9.1	92.8	48
(TT ⁺) ₂ [Ge(NPC) ₃] ²⁻	CHCl ₃	4.0–4.5	2	11.2	1.52	9.7	97.1	49
(TV ⁺) ₂ [MoO ₂ (NPC) ₂] ²⁻	C ₂ H ₄ Cl ₂	1.2–2.6	2	8.5	1.75	6.7	98.2	50
(BT ²⁺) ₂ [MoO ₂ (NPC) ₂] ²⁻	C ₂ H ₄ Cl ₂	1.8–4.0	2	5.4	—	—	—	51
(TT ⁺)[MoO ₂ (OH)·(H ₂ O)(NPC)] ⁻	CHCl ₃	1.8–2.5	1	5.2	0.88	4.3	88.4	52
(MTT ⁺) ₂ [MoO ₂ (NPC) ₂] ²⁻	CHCl ₃	2.1–3.4	2	9.6	1.12	8.5	93.0	6
(INT ⁺) ₂ [MoO ₂ (NPC) ₂] ²⁻	C ₂ H ₄ Cl ₂	1.5–3.0	10	10.0	0.47	9.5	74.0	53
(MTT ⁺)[MoO ₂ (OH)·(H ₂ O)(DHN)] ⁻	CHCl ₃	1.6–3.8	2	5.3	1.17	4.2	93.7	6
(INT ⁺)[MoO(OH)(DHN) ₂] ⁻	CHCl ₃	0.7–1.9	10	5.3	1.13	4.2	93.2	53
(TV ⁺)[MoO(OH)(PC) ₂] ⁻	C ₂ H ₄ Cl ₂	0.3–1.4	1	5.0	0.76	4.3	85.2	52
(MTT ⁺) ₂ [MoO ₂ (THBA) ₂] ²⁻	C ₂ H ₄ Cl ₂	2.6–3.2	0.25	9.1	0.85	8.2	87.6	54
(NBT ²⁺) ₂ [MoO ₂ (THBA) ₂] ²⁻	CHCl ₃	0.03–0.08 M HCl	0.5	5.1	1.54	3.6	97.2	55
(INT ⁺)[NbO(PC) ₂] ⁻	CHCl ₃	0.09–1.4 M H ₂ SO ₄	15	5.2	1.74	3.4	98.0	56
(INT ⁺)[NbO(DHN) ₂] ⁻	CHCl ₃	0.09–1.2 M H ₂ SO ₄	15	5.3	1.86	3.5	98.9	56
(TV ⁺)[NbO(PG) ₂] ⁻	C ₂ H ₄ Cl ₂	0.25–1.25 M H ₂ SO ₄	15	4.6	1.49	3.1	96.9	57, 58
(TV ⁺)[NbO(NPC) ₂] ⁻	C ₂ H ₄ Cl ₂	0.25–1.25 M H ₂ SO ₄	15	4.5	1.61	3.0	97.6	57, 58
(TV ⁺)[NbO(PC) ₂] ⁻	CHCl ₃	1 M H ₂ SO ₄	15	5.5	1.54	3.9	97.2	58, 59
(TV ⁺)[NbO(DHN) ₂] ⁻	CHCl ₃	0.5–1 M H ₂ SO ₄	15	5.5	1.51	4.0	97.0	58, 59
(TT ⁺)[NbO(PC) ₂] ⁻	CHCl ₃	0.4–1 M H ₂ SO ₄	15	5.1	1.84	3.2	98.8	60
(INT ⁺)[Ti(OH)·(H ₂ O)(DHN) ₂] ⁻	CHCl ₃ (C ₂ H ₄ Cl ₂)	1.2–2.8	15	—	—	—	—	61
(TT ⁺) ₂ [TiO(DHN) ₂] ²⁻	CHCl ₃	1.7	10–15	—	—	—	—	62
(TT ⁺) ₂ [TiO(PC) ₂] ²⁻	C ₂ H ₄ Cl ₂	2.2	10–15	—	—	—	—	63
(INT ⁺) ₂ [TiO(NPC) ₂] ²⁻	CHCl ₃	1.0	15	7.4	0.74	6.6	84.0	63
(TV ⁺) ₂ [TiO(NPC) ₂] ²⁻	CHCl ₃	1.4–1.8	15	12.1	1.90	10.0	98.7	63
(INT ⁺) ₂ [VO(NPC) ₂] ²⁻	CHCl ₃	3.9–4.5	5	10.6	1.4	9.2	96.0	64
(INT ⁺) ₃ [VO ₂ (NPC) ₂] ³⁻	CHCl ₃	4.7–5.1	5	—	0.39	—	71.1	65, 66
(NT ²⁺) ₃ [VO ₂ (NPC) ₂] ³⁻	CHCl ₃ –BuOH	4.9	20	—	—	8.9	96.1	67
(NT ²⁺) ₃ [VO(NPC) ₂] ²⁻	CHCl ₃ –BuOH	3.9–4.7 (4.5–5.5)	15	—	—	—	—	68
(INT ⁺) ₃ [VO(DHN) ₂] ³⁻	CHCl ₃	4.6–5.2	3	4.8	1.03	3.7	92.0	69
(NT ²⁺) ₃ [VO ₂ (TAR) ₂] ³⁻	CHCl ₃	4.5–5.0	2	8.2	1.21	7.0	93.8	70
(TT ⁺) ₃ [VO ₂ (TAR) ₂] ³⁻	CHCl ₃	4.3–5.3	2	15.1	1.13	14.0	93.0	71
(MTT ⁺) ₃ [VO ₂ (TAR) ₂] ³⁻	CHCl ₃	4.3–5.3	2	17.9	1.16	16.7	93.5	72
(TV ⁺) ₃ [VO ₂ (TAR) ₂] ³⁻	CHCl ₃	4.3–5.3	2	18.7	1.07	17.6	92.0	72
(INT ⁺) ₃ [VO ₂ (TAR) ₂] ³⁻	CHCl ₃	4.3–5.3	2	16.3	0.92	15.4	88.9	72
(BT ²⁺) ₃ [VO ₂ (TAR) ₂] ³⁻	CHCl ₃	4.7–5.7	2	9.7	1.12	8.6	92.9	72
(NBT ²⁺) ₃ [VO ₂ (TAR) ₂] ³⁻	CHCl ₃	5.2–5.7	2	8.4	0.69	7.7	83.1	72
(TV ⁺) ₃ [VO ₂ (PAR) ₂] ³⁻	C ₂ H ₄ Cl ₂	5.2–6.3	2	17.9	1.48	16.4	96.8	73
(INT ⁺) ₃ [VO ₂ (PAR) ₂] ³⁻	CHCl ₃	5.5–7.5	2	16.4	1.59	14.8	97.5	74, 75
(MTT ⁺) ₃ [VO ₂ (PAR) ₂] ³⁻	CHCl ₃	5.1–6.5	2	17.5	1.61	15.9	97.5	76
(TT ⁺) ₃ [VO ₂ (PAR) ₂] ³⁻	CHCl ₃	5.2–6.3	2	—	—	14.7	—	see ^b
(NBT ²⁺) ₃ [VO ₂ (PAR) ₂] ³⁻	CHCl ₃	4.7–5.7	2	—	—	7.6	—	see ^b
(TNBT ²⁺) ₃ [VO ₂ (PAR) ₂] ³⁻	CHCl ₃	5.7–6.0	2	—	—	6.7	—	see ^b
(NT ²⁺) ₃ [VO ₂ (PAR) ₂] ³⁻	CHCl ₃	4.8–6.7	2	8.5	1.26	7.2	94.8	77
(NT ²⁺) ₃ [VO ₂ (PG) ₂] ³⁻	BuOH	4.8–5.1	0.5	—	—	—	—	78
(INT ⁺) ₃ [VO ₂ (PG) ₂] ³⁻	BuOH	2.6–3.3	0.5	—	—	—	—	79
(INT ⁺) ₂ [VO(PG) ₂] ²⁻	BuOH	2.9–3.5	0.5	—	1.21	8.1	94.2	80
(NT ²⁺) ₃ [VO(PG) ₂] ³⁻	BuOH	3.8–4.3	0.5	—	1.37	3.8	95.8	80
(TT ⁺)[WO(OH)(DHN) ₂] ⁻	CHCl ₃	0.04–0.09 M H ₂ SO ₄	10	5.2	1.28	3.9	95.0	81
(INT ⁺)[WO(OH)(DHN) ₂] ⁻	CHCl ₃	0.10–1.10 M H ₂ SO ₄	1	5.0	0.81	4.2	86.5	82
(TV ⁺)[WO(OH)(DHN) ₂] ⁻	CHCl ₃	0.08–0.35 M H ₂ SO ₄	10	5.0	1.93	3.1	98.8	83
(TV ⁺) ₂ [WO ₂ (NPC) ₂] ²⁻	CHCl ₃	4.2–5.7	3	10.4	1.56	8.9	97.3	82
(TT ⁺) ₂ [WO ₂ (NPC) ₂] ²⁻	CHCl ₃	3.5–5.0	1	10.3	1.05	9.2	91.9	82
(MTT ⁺) ₂ [WO ₂ (NPC) ₂] ²⁻	CHCl ₃	1.2–3.6	2	10.3	1.03	9.3	91.5	84

Table 3 (continued).

Extraction system		pH	Time of extraction /min	log K_{ex}	log K_D	log β	$R(\%)$	Ref.
TIAC ^a	solvent							
(TT ⁺)[WO(OH)(DNC) ₂] [−]	CHCl ₃	0.25–0.40 M H ₂ SO ₄	2	10.6	1.06	9.6	91.8	82
(TT ⁺)[WO(OH)(PC) ₂] [−]	CHCl ₃ (C ₆ H ₆)	0.005–4.0 M H ₂ SO ₄	20	—	—	—	—	85

^a Abbreviations: NPC is 4-nitropyrocatechol; DHN is 2,3-dihydroxynaphthalene; PC is pyrocatechol; THBA is 3,4,5-trihydroxybenzoic acid; PG is pyrogallol; TAR, 4-(2-thiazolylazo)resorcinol; PAR is 4-(2-pyridylazo)resorcinol; DNC is 3,5-dinitropyrocatechol. ^b K Gavazov, unpublished data.

times of different TIAC can be used for ion separation and identification (qualitative analysis).

The composition of the extract can differ from the composition of the aqueous phase, this depends on a number of factors, *e.g.*, the nature of the central atom of the complex, its oxidation state, concentration of the starting reagents and pH.

Contrary to amines, tetrazolium cations can be used as IAC components without preliminary protonation. Therefore, the changes in the acidity of the aqueous phase do not prevent quantitative extraction of many inorganic anions, *e.g.*, ReO₄[−], [Zn(SCN)₄]^{2−}, [HgI₃][−], *etc.* in the form of the respective TIAC. At the same time, the control over pH is important for the extraction of complexes with metal-containing anions prone to hydrolysis (as a rule, the hydrolysed forms are not extracted) as well as complexes with organic ligands. For TIAC containing organic ligands with higher molecular masses, the pH optimum range tends to be broader (see Table 3).

The optimisation of reagent concentrations plays the key role in extraction and spectrophotometric measurements.

As TS are usually taken in a large excess, their concentrations (or changes in concentrations) have little effect on the results of analysis.⁴¹ Moreover, in many cases TS have beneficial effects. Thus it inhibits the reduction of V(V) to V(IV) by polyphenolic compounds such that vanadium(V) is stable in ternary complexes with chelating polyphenolic ligands.^{67,79} In contrast to other

cationic dyes, only in rare cases the excess of TS interfere with spectrophotometric measurements.⁶⁷ The concentration of a ligand involved in the formation of a complex anion was found to depend on its stability constant, it varies in a broad range.⁴¹

The results of several studies suggest^{41,75,86,87} that the association constant of TIAC is proportional to the molecular mass of the tetrazolium cation: the higher the molecular mass the higher the association constant. This ratio can be used for the prediction of the possibility of formation of associates^{41,86} and of the association constants of newly formed complexes in a given class of compounds.^{41,86,87} However, this ratio is violated if the tetrazolium cation of TS-based extraction systems contains a nitrophenyl substituent (Refs 72 and 75 and Fig. 1).

III. Analytical applications of tetrazolium ion-associated complexes

1. 1. Extraction – photometric analysis

Some characteristics of extraction – photometric methods for determination of certain elements as TIAC are presented in Table 4. Spectrophotometric determinations with such complexes (or their decomposition products) are usually carried out by measuring absorption in the UV or visible spectral regions.

All tetrazolium complexes strongly absorb light in the UV region. However, analytical applications of UV spectra are complicated due to high absorption of the reference sample (blank experiment) and specific requirements for equipment and solvents. Therefore, very often preference is given to methods that employ compounds specially designed for spectrophotometric measurements in the visible spectral region. These include, for example, MTT complexes, TIAC containing a coloured complex anion, conversion products of TIAC (formazans formed upon reduction of tetrazolium cations in basic media),^{31,45} complexes obtained by replacement of tetrazolium cations by coloured cations (*e.g.*, rhodamine B)⁴ and complexes produced in competitive reactions or their decomposition products.^{10,47,109,110}

The following approaches are used to increase the sensitivity of determination.

(1) Selection of an appropriate extraction system containing intensely coloured TIAC and solvents ensuring recovery close to 100%. In the context of this approach, MTT complexes containing yellow-coloured anions, *e.g.*, [Ge(NPC)₃]^{2−} (Ref. 48), are especially promising, since they contain two chromophore ions absorbing in the same spectral region.

(2) Extraction of large amounts of coloured complexes by small volumes of an organic phase.

To attain the required selectivity, special attention is paid to the selection of adequate extraction-photometric conditions, *i.e.*, wavelength,^{59,62,81,103,104} pH,^{77,82} reagent concentrations,⁶⁹ the order of their addition¹⁰⁷ and extraction time.^{82,84} Masking is also popular.

Some TIAC-based procedures are sufficiently selective to allow direct determinations without additional steps.

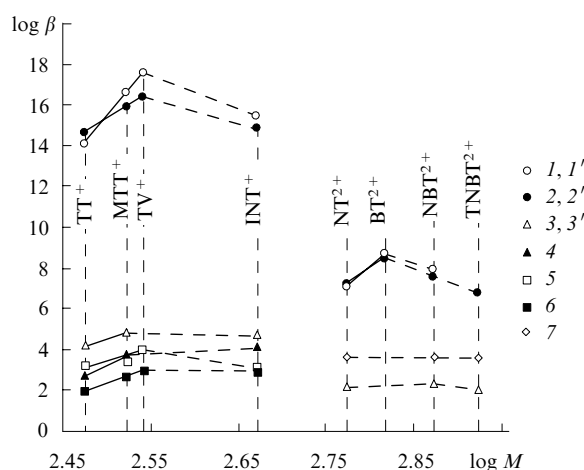


Figure 1. Dependence of the logarithm of the association constant of TIAC (β) on the logarithm of the molecular mass of the tetrazolium cation (M).

Anions: (1, 1') [VO₂(TAR)₂]^{3−}, (2, 2') [VO₂(PAR)₂]^{3−}, (3, 3') [Cd(SCN)₄]^{2−}, (4) [TiCl₄][−], (5) [HgI₃][−], (6) [CrO₃Cl][−], (7) [Zn(SCN)₄]^{2−}.

The values of β for tetrazolium ion-associated complexes containing nitro groups (INT⁺, NBT²⁺, TNBT²⁺) are lower than expected on the assumption that the association constant increases linearly with the molecular mass (solid lines).

Table 4. Extraction-spectrophotometric methods based on TIAC.

Analyte	Reagents	Solvent	pH	Linearity range ^a /mg ml ⁻¹	λ /nm (see ^b)	$10^{-4}\epsilon$ (see ^c)	Samples	Ref.
Co(II)	NBT + SCN ⁻	C ₂ H ₄ Cl ₂	1–8	0.5–9	625	0.76	soils	17
	TV + SCN ⁻	C ₂ H ₄ Cl ₂	2.7–7.6	0.5–9	630	4.0	soils, plants	88
	MTT + SCN ⁻	C ₂ H ₄ Cl ₂	2.7–7.6	0.5–10	625	0.67	soils	89
Cr(III)	MTT + SCN ⁻	C ₂ H ₄ Cl ₂	1.8–7.2 M HCl	0.01–0.06	235	0.465	"	18
Cr(VI)	NBT	C ₂ H ₄ Cl ₂	0.25–0.6 M HCl	0.01–0.4	260	8.2	soils, steels	20
	NT	C ₂ H ₄ Cl ₂	0.36–1.08 M HCl	0.05–1.5	255	3.12	steels, soils, plants	19
	TT	C ₂ H ₄ Cl ₂	0.1–1.2 M HCl	0.04–0.3	250	3.03	soils, plants	90, 91
	TT	C ₂ H ₄ Cl ₂	0.3–1.5 M HCl	4.2–39.5	450	0.25	steels, plants	21, 92
	INT	C ₂ H ₄ Cl ₂	0.1–1.1 M HCl	0.02–0.3	250	3.70, 8.8	steels, soils, vegetables	93, 94, 95, 96
	TV	C ₂ H ₄ Cl ₂	0.07–1.1 M HCl	0.02–0.3	230	12.2	the same	94, 96
	MTT	C ₂ H ₄ Cl ₂	0.15–0.42 M HCl	0.04–1	245	2.96	soils, steels, plants	23, 91
	NPC + MTT	CHCl ₃	2.5–3.9	0.15–1.88	410	5.11	model mixture	48
	NPC + TT	CHCl ₃	4.0–4.5	0.2–3.0	420	2.88	the same	49
	Hg(II)	TV + I ⁻	0.1–4.5 M H ₂ SO ₄	0.1–1.4	250	10.2	soils	97
	INT + I ⁻	C ₂ H ₄ Cl ₂	0.2–5.5 M H ₂ SO ₄	0.1–1.2	260	10.0	"	26
	TT + I ⁻	CHCl ₃	0.2 M H ₂ SO ₄	0.1–0.8	255	6.45	"	27
I ⁻	MTT + I ⁻	CHCl ₃	2	0.1–1	255	6.55	"	28
	TV	C ₂ H ₄ Cl ₂	1–6 (0.25–1.8 M HCl)	0.4–5	230	11.5	"	29
IO ₃ ⁻	TT + I ⁻	C ₂ H ₄ Cl ₂		0.04–0.7		7.48	drinking water	98
	INT + I ⁻	C ₂ H ₄ Cl ₂	0.1–2.4 M HCl	0.02–0.5	295	16.4	"	99
IO ₄ ⁻	TT + I ⁻	C ₂ H ₄ Cl ₂		0.02–0.35		9.09	"	98
	INT + I ⁻	C ₂ H ₄ Cl ₂	0.1–3.0 M HCl	0.02–0.5	295	16.7	"	99
Mn(VII)	MTT	C ₂ H ₄ Cl ₂	0.01–0.16 M H ₂ SO ₄	0.1–1.75	250	1.0	soils, plants	32
	TT	C ₂ H ₄ Cl ₂	0.01–0.7 M H ₂ SO ₄	0.5–12	530	0.556	soils, steels	33
	INT	C ₂ H ₄ Cl ₂	0.01–0.125 M HCl	0.5–12	530	0.694	soils	34
	TV	C ₂ H ₄ Cl ₂	0.01–0.03 M H ₃ PO ₄	0.05–0.6	235	6.67	"	35
	NBT	C ₂ H ₄ Cl ₂	0.01–0.2 M H ₂ SO ₄		260	10	plants, soils	8, 100
Mo(VI)	NPC + TV	C ₂ H ₄ Cl ₂	1.2–2.6	0.31–3.1	440	2.06	steels	50
	NPC + BT	C ₂ H ₄ Cl ₂	1.8–4.0	0.2–6.7	445	2.38	steels, ferromolybdenum	51
	NPC + TT	CHCl ₃	1.8–2.5	0.5–10.0	445	2.28	model mixture	52
	NPC + MTT	CHCl ₃	2.1–3.4	0.2–7.0	440	2.41	steels, ferromolybdenum	6
	NPC + INT	C ₂ H ₄ Cl ₂	1.5–3.0	0.24–6.9	430	1.94	the same	53
	PG + TV	C ₂ H ₄ Cl ₂	0.3–1.4	0.5–6.0	432	0.72	the same	52
	THBA + NBT	CHCl ₃	0.03–0.08 M HCl	0.5–5	260	15.0	soils	101
	THBA + MTT	C ₂ H ₄ Cl ₂	2.6–3.2	0.15–3	245	1.67	soils, vegetables	54, 102
	MTT + SCN ⁻	C ₂ H ₄ Cl ₂	0.9 M H ₂ SO ₄	0.1–1.5	470	5.7	plants (lettuce)	36
	DHN + TT	CHCl ₃	0.07 M H ₂ SO ₄		360, 500, 625	0.81 (Mo at 360 nm)	steels	103
Nb(V)	NPC + TV	C ₂ H ₄ Cl ₂	0.7 M H ₂ SO ₄	0.41–4.54	440	1.59	"	57
	PC + TT	CHCl ₃	0.4–1 M H ₂ SO ₄	1.25–11.78	390	1.60	"	60
	DHN + TV	CHCl ₃	0.5–1 M H ₂ SO ₄	0.20–3.29	400	1.18	"	59
Re(VII)	p-NT	CHCl ₃	1–10	0.2–16	255	2.1	copper concentrate	37
	TV	CHCl ₃	3–10	0.2–17	280	1.32	copper ore	38
	MTT	CHCl ₃	2–10	0.2–18	280	0.82	molybdenum concentrates	39
	INT	CHCl ₃	3–10	0.5–24	280	1.45	the same	39
	NT	CHCl ₃	4–10	0.5–26	280	0.73	"	39

Table 4 (continued).

Analyte	Reagents	Solvent	pH	Linearity range ^a /mg ml ⁻¹	λ /nm (see ^b)	$10^{-4}\epsilon$ (see ^c)	Samples	Ref.
Ti(IV)	DHN + INT	C ₂ H ₄ Cl ₂	1.2–2.8	0.24–5.2	370	2.57	aluminium alloys	61
Ti(IV), W(VI)	DHN + TT	CHCl ₃	1.7	0.12–1.66 (Ti)	380, 470	2.74 (Ti)	steels	62
Ti(IV)	PC + TT	C ₂ H ₄ Cl ₂	2.2	0.24–2.6	390	1.15	aluminium alloys	62
	NPC + TV	CHCl ₃	1.4–1.8	0.20–2.00	440	4.4	the same	63
Tl(III), Sb(V)	MTT	C ₆ H ₆ + diethyl ether (3:1)	0.2 M HCl (Ti); 1.8 M HCl (Ti + Sb)	1.0–15.0 (Ti); 1.0–16.0 (Sb)	400.5		cadmium	44
	TV	C ₆ H ₆	0.05–6.0 M HCl (Ti); > 6 M HCl (Sb)	1.0–20.0 (Ti); 0.5–9.5 (Sb)	520		"	45
V(V)	NPC + INT	CHCl ₃	5.0	0.2–2.6	400	1.7	steels	65
V(IV)	NPC + NT	CHCl ₃ + BuOH (7:3)	4.75	0.5–3.0	605	1.15	"	104
V(V)	TAR + TT	CHCl ₃	4.75	0.1–2.5	550	2.37	catalysts	105
	TAR + MTT	CHCl ₃	4.75	0.1–2.5	550	2.60	"	72
	PAR + TV	C ₂ H ₄ Cl ₂	5.2–6.3	0.05–2.5	555	4.0	"	105
V(V), V(IV)	PAR + TV	C ₂ H ₄ Cl ₂	5.8	0.003–1.45	555	3.05	"	106
	PAR + MTT	CHCl ₃	5.8	0.21–1.5	560	3.30	"	76
	PAR + INT	CHCl ₃	5.5–7.5	up to 1.5	560	2.4	natural waters	107
V(V)	PAR + INT	CHCl ₃	5.5–7.5	up to 1.5	560	2.4	aluminium alloys	107
	PAR + NT	CHCl ₃	4.8–6.7	0.15–3.5	560	2.95	steels	77
	PAR + TT	CHCl ₃ + PrOH	5.8	–	560	4.7	soils	108
	DHN + INT	CHCl ₃	4.6–5.2	0.1–0.9	340	2.5	steels	69
W(VI)	DHN + TT	CHCl ₃	0.04–0.09 M H ₂ SO ₄	0.5–6.0	440	1.16	"	81
	DHN + INT	CHCl ₃	0.10–1.10 M H ₂ SO ₄	0.7–7.4	420	0.938	"	82
	DHN + TV	CHCl ₃	0.08–0.35 M H ₂ SO ₄	0.9–12.9	440	0.766	"	83
	NPC + TV	CHCl ₃	5.4	0.7–10.3	425–430	2.69	steels, ferrotungsten	82
	DNC + TT	CHCl ₃	0.25–0.40 M H ₂ SO ₄	0.5–7.4	400	2.12	steels	82
	NPC + MTT	CHCl ₃	1.2–3.6	0.9–8.8	415	2.8	steels, ferrotungsten	84
Zn(II)	p-NT + SCN ⁻ + Co(II)	C ₂ H ₄ Cl ₂	1–7	1.7–13.3	630		cadmium	109
	MTT + SCN ⁻ + Co(II)	C ₂ H ₄ Cl ₂	2–6	3.3–18.3	630		"	110
	TNBT + SCN ⁻ + Co(II)	C ₂ H ₄ Cl ₂ + Me ₂ O (1:1)	2–6	0.75–8.75	630		"	10
	TV + SCN ⁻ + Co(II)	C ₂ H ₄ Cl ₂	2–6	0.5–8	630		"	47

^a The concentration range in which the signal is proportional to the analyte concentration enables quantitative determination. ^b Wavelength. ^c ϵ is the molar extinction coefficient (litre mol⁻¹ cm⁻¹) (the values were taken from the cited papers). However, they were not always calculated using standard methods and different volumes of the aqueous and organic phases were employed.

a. Determination of cobalt

The extraction-photometric procedure for determination of cobalt in soils^{17,88,89} and plants⁸⁸ is based on the formation of ion-associated complexes (NBT)[Co(SCN)₄]¹⁷ (TV)₂[Co(SCN)₄] (Ref. 88) and (MTT)₂[Co(SCN)₄] (Ref. 89) and their subsequent extraction with 1,2-dichloroethane in a broad pH range. The relative standard deviation (RSD), detection limit (DL) and molar extinction coefficient (ϵ) for the most sensitive procedure based on the use of TV are equal to 1.15%, 1.5×10^{-3} μ g ml⁻¹ and 4×10^4 litre mol⁻¹ cm⁻¹, respectively.⁸⁸

b. Determination of chromium

The interactions of solutions of Cr(VI) in hydrochloric acid with NT,¹⁹ NBT,²⁰ MTT,²³ TT,⁹⁰ INT⁹³ and TV⁹⁴ were studied by Kamburova *et al.* The complexes were efficiently extracted with 1,2-dichloroethane. Apparently, the Cr(VI)–TV complex is the most suitable for the determination of Cr(VI) in the presence of ascorbic acid and NH₄F as masking reagents in soils,⁹⁴ steels⁹⁴ and vegetables⁹⁶ [$\epsilon_{230} = 1.22 \times 10^5$ litre mol⁻¹ cm⁻¹, RSD = (0.4%–0.7%)].

The use of a ternary chromium(III) complex with thiocyanate and MTT for the determination of chromium in soils has been described;⁹ however, the sensitivity of this method is low ($\epsilon_{235} = 4.65 \times 10^3$ litre mol⁻¹ cm⁻¹).

c. Determination of germanium

Two procedures for the determination of Ge(IV) based on formation of ternary complexes with 4-nitropyrocatechol and extraction with chloroform have been described.^{48,49} The best of them⁴⁸ employs MTT ($\epsilon_{410} \approx 5.1 \times 10^4$ litre mol⁻¹ cm⁻¹). The interfering effects of Al³⁺, Fe³⁺ and Cr³⁺ are eliminated with Na-EDTA. The presence of Mo(VI), V(IV), W(VI), I⁻ and Cl⁻ interferes with the assay.

d. Determination of mercury

Determination of mercury in soils included extraction of mercury(II) halide complexes with chloroform.^{8,26–28,97} The complexes (TV)[HgI₃] and (TV)[HgBr₃] manifested the highest molar extinction coefficients (1.02×10^5 litre mol⁻¹ cm⁻¹ and 1×10^6 litre mol⁻¹ cm⁻¹, respectively).⁹⁷ Other fast and sensitive

methods for the determination of mercury(II) are based on the use of the complexes (INT)[HgI₃],²⁶ (TT)[HgI₃]²⁷ and (MTT)[HgI₃].²⁸ Ascorbic acid and fluoride ions were used as masking reagents.

e. Determination of iodide, iodate and periodate

A sensitive method for the determination of iodide ions in soils was developed by Kamburova.²⁹ It is based on extraction, with 1,2-dichloroethane, of ion-associated TV complexes with iodide oxidation products. Hydrogen peroxide was found to be the oxidant of choice. The majority of ions, except for Hg²⁺, BrO₃⁻ and S₂O₃²⁻, do not interfere.

The optimum complexation conditions in TS–iodate–iodide–dichloroethane and TS–periodate–iodide–dichloroethane systems have been studied. Two procedures for the determination of iodates and periodates in drinking water using (TT⁺)I₃⁻ and (INT⁺)I₃⁻ have been described.^{98,99} The procedure based on TT is more sensitive:⁹⁸ $\epsilon_{295} = (1.64 \pm 0.02) \times 10^5$ litre mol⁻¹ cm⁻¹ (for IO₃⁻), $\epsilon_{295} = (1.67 \pm 0.05) \times 10^5$ litre mol⁻¹ cm⁻¹ (for IO₄⁻). The presence of other ions has no interfering effect on the assay. The RSD value lies in the range from 0.8% to 1.3%.

f. Determination of manganese

Several methods were developed for the determination of manganese(VII) in natural and industrial samples.^{8,32–35,100} All of them included extraction, with 1,2-dichloroethane, of tetrazolium ion-associated complexes with the permanganate anion. Complexes with TT³³ and INT³⁴ were used for the determination of manganese in soils^{33,34} and steels³³ at $\lambda = 530$ nm; however, the sensitivity of these methods was rather low. Higher sensitivity was achieved through the use of MTT ($\epsilon_{250} = 1.0 \times 10^4$ litre mol⁻¹ cm⁻¹),³² TV ($\epsilon_{235} = 6.67 \times 10^4$ litre mol⁻¹ cm⁻¹)³⁵ and NBT ($\epsilon_{260} = 1.0 \times 10^5$ litre mol⁻¹ cm⁻¹)^{8,100} in the UV region. The NBT complex was used for the determination of manganese in diverse vegetable samples. Interfering ions were masked using saturated solutions of ascorbic acid. The RSD value did not exceed 1.8%.

g. Determination of molybdenum

A series of sensitive spectrophotometric procedures for the determination of molybdenum [$\epsilon_{430-445} = (1.94-2.41) \times 10^4$ litre mol⁻¹ cm⁻¹] using 4-nitropyrrocatechol and various tetrazolium cations were developed by Dimitrov *et al.*^{6,50–53} In particular, this method was used for the determination of molybdenum in ferrous metallurgy products. Other TIAC-forming reagents, *e.g.*, pyrogallol,⁵² 2,3-dihydroxynaphthalene¹⁰³ and 3,4,5-trihydroxybenzoic acid, are also employed.^{54,101,102} The use of 3,4,5-trihydroxybenzoic acid and MTT for the determination of molybdenum in soils⁵⁴ and vegetables¹⁰² (RSD = 1.1% and 1.9%, respectively) has been described. A highly sensitive procedure for the analysis of soils¹⁰¹ is based on the use of 3,4,5-trihydroxybenzoic acid and NBT ($\epsilon_{260} = 1.5 \times 10^5$ litre mol⁻¹ cm⁻¹) and does not require preliminary isolation of molybdenum.

A method based on the use of thiocyanate and MTT for the determination of molybdenum in lettuce has been described.³⁶ Fe(III) and V(V) ions were masked with oxalic and ascorbic acids; the RSD value did not exceed 1.2%.

A procedure for simultaneous determination of molybdenum, tungsten and niobium in steels with the use of their ternary complexes with 2,3-dihydroxynaphthalene and TT has been developed.¹⁰³ The determination of molybdenum was carried out at 625 nm; the total content of W + Mo and W + Mo + Nb was determined at 500 and 360 nm, respectively. Interfering ions were masked with EDTA. The RSD values for molybdenum,

tungsten and niobium were equal to (0.5–1.07)%, (4.0–6.9)% and (5.2–8.0)%, respectively.

h. Determination of niobium

Several methods based on the use of Nb(V) complexes with TS and polyphenols (4-nitropyrrocatechol,⁵⁷ 2,3-dihydroxynaphthalene^{59,103} and pyrocatechol⁶⁰) for the determination of niobium in steels have been developed. 4-Nitropyrrocatechol–TV⁵⁷ and pyrocatechol–TT systems⁶⁰ are more suitable for the analysis of steels containing no molybdenum or tungsten. Other interfering ions are masked with EDTA or ascorbic acid. If a steel contains 0.021% Nb, its RSD value is equal to 4.7%.⁵⁷

If a steel contains Mo(VI) or W(VI), the 2,3-dihydroxynaphthalene–TV system is used.⁵⁹ In the presence of W(VI), absorption was measured at 400 and 490 nm; in the presence of Mo(VI), at 400 and 582 nm. This approach can also be used,¹⁰³ if a steel contains simultaneously Mo and W (see Section III.1.g).

i. Determination of rhenium

ReO₄⁻ ions form ion-associated complexes with tetrazolium cations,^{37–39} which enables reliable determination of rhenium in industrial samples, *e.g.*, copper concentrates,³⁷ copper ores³⁸ and molybdenum concentrates.³⁹ Extraction with chloroform is carried out in a broad pH range. The method based on *p*-NT is the most sensitive ($\epsilon_{255} = 2.1 \times 10^4$ litre mol⁻¹ cm⁻¹) and selective.³⁷ The assay procedure is not interfered with by Mo(VI), Ni(II), Co(II), Cu(II), Fe(II), Mg(II), Mn(II), Cd(II), V(V) or W(VI). The RSD value is 2.1% at the rhenium content of $(1.58-1.75) \times 10^{-3}\%$.

j. Determination of titanium

Determination of titanium in aluminium alloys^{61–63} and steels⁶² is based on the use of its yellow-coloured TIAC involving 2,3-dihydroxynaphthalene,^{61,62} pyrocatechol⁶² and 4-nitropyrrocatechol.⁶³ The 4-nitropyrrocatechol–TV system⁶³ is the best for extraction in respect of sensitivity ($\epsilon_{440} = 4.4 \times 10^4$ litre mol⁻¹ cm⁻¹) and reproducibility (the RSD value does not exceed 1.05%). This system was used for the determination of titanium in aluminium alloys with ascorbic acid as a masking reagent.

The 2,3-dihydroxynaphthalene–TT system was used⁶² for simultaneous determination of titanium and tungsten in steels. The values of molar extinction coefficients were as follows: $\epsilon_{380} = 2.74 \times 10^4$ litre mol⁻¹ cm⁻¹ and $\epsilon_{470} = 0$ litre mol⁻¹ cm⁻¹ for titanium and $\epsilon_{380} = 6.33 \times 10^3$ litre mol⁻¹ cm⁻¹ and $\epsilon_{470} = 4.3 \times 10^3$ litre mol⁻¹ cm⁻¹ for tungsten. Interfering ions were masked with ascorbic acid. The RSD values for titanium and tungsten were equal to 3.5% and 2.0%, respectively.

k. Determination of thallium and antimony

Two methods for the simultaneous determination of antimony and thallium in cadmium were developed by Kostova *et al.*^{44,45} They are based on extraction, with an organic solvent, *e.g.*, benzene⁴⁵ or a benzene–ether system (3:1),⁴⁴ of thallium(III) and antimony(V) TIAC. Both procedures imply preliminary addition of an oxidising reagent to the tested solution containing Tl(I) or Sb(III).

Only Tl(I) undergoes oxidation to Tl(III) in dilute solutions of hydrochloric acid. However, in hydrochloric acid solutions of moderate concentration both Tl(I) and Sb(III) are oxidised to Tl(III) and Sb(V). Thus, variation in solution acidity enables stepwise determination of Tl(III) and Sb(V) in the same sample.

The first procedure is more simple.⁴⁴ The use of ternary complexes with MTT allows direct determination of Tl(III) and Sb(V) in the visible spectral region (at 400.5 nm). The RSD values for Tl and Sb are equal to 1.01% and 1.45%.

The second, more sensitive procedure⁴⁵ includes reduction of TV with $\text{NH}_2\text{OH} \cdot \text{HCl}$ to formazan which absorbs at 520 nm. The detection limit is $1 \mu\text{g ml}^{-1}$ for Tl and $0.5 \mu\text{g ml}^{-1}$ for Sb.

I. Determination of vanadium

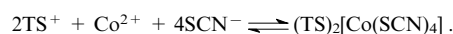
It was recommended to use ternary TIAC with 4-nitropyrocatechol,^{65, 104} 2,3-dihydroxynaphthalene,⁶⁹ 4-(2-pyridylazo)resorcinol^{76, 77, 105–108} and 4-(2-thiazolylazo)resorcinol^{72, 105} for the determination of V(V) in the environment and in industrial samples. It was found that 4-(2-pyridylazo)resorcinol is the most sensitive and convenient reagent for the determination and identification of vanadium. If selective determination of V(V) is required, diaminocyclohexanetetraacetic acid (DCTA)⁷⁷ or DCTA + NH_4F are added to the solution as masking reagents^{106, 107} as a result of which V(IV) is masked. This method is employed in indirect determination of the V(IV) content from the difference in the absorption measured in the presence and in the absence of the reagent used for the oxidation of V(IV) to V(V).^{106, 107} The use of NH_4F as a secondary masking reagent results in instantaneous colouration and provides better selectivity with respect to definite ions including V(IV).^{106, 107} Determination of vanadium in various natural water samples,¹⁰⁷ aluminium alloys,¹⁰⁷ catalysts,^{86, 105, 106} steels⁷⁷ and soils¹⁰⁸ was carried out by varying detection parameters, such as the nature of TS, order of addition of the reactants, *etc.*

m. Determination of tungsten

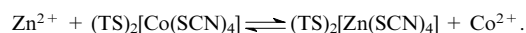
A series of procedures for the determination of tungsten in steels and ferrotungsten have been developed. These methods are based on the formation of tungsten(VI) TIAC with 2,3-dihydroxynaphthalene,^{81–83} 3,5-dinitropyrocatechol⁸² and 4-nitropyrocatechol.^{82, 84} The highest sensitivity ($\epsilon_{415} = 2.80 \times 10^4$ litre $\text{mol}^{-1} \text{cm}^{-1}$) was achieved with 4-nitropyrocatechol and MTT.⁸⁴ The interfering effects of Fe(III), Al(III), Cr(III) and V(V) were eliminated by precipitation/coprecipitation at pH 11 in the course of sample preparation. The RSD value did not exceed 0.53%.

n. Determination of zinc

A series of spectrophotometric procedures for the determination of zinc in cadmium have been developed^{10, 47, 109, 110} based on predominant formation of thiocyanate cobalt complexes with TS cations in the presence of cadmium and their selective extraction. Blue-coloured cobalt complexes are formed upon addition of a cobalt salt, an excess of thiocyanate and a small amount of a tetrazolium salt to the tested sample:



The presence of Zn^{2+} ions in the system makes the blue colouration of the solution less intensive due to a shift of the reaction equilibrium towards less soluble weakly coloured zinc complexes:



It was found that the decrease in absorption at 630 nm is proportional to Zn^{2+} concentration in the tested solution in a rather broad range: $0.5\text{--}8 \mu\text{g ml}^{-1}$ (for a TV^+ complex),⁴⁷ $3.3\text{--}18.3 \mu\text{g ml}^{-1}$ (for a MTT^+ complex),¹¹⁰ $1.7\text{--}13.3 \mu\text{g ml}^{-1}$ (for a $p\text{-NT}^+$ complex)¹⁰⁹ and $0.75\text{--}8.75 \mu\text{g ml}^{-1}$ (for a TNBT^{2+} complex).¹⁰ The detection limit for zinc in cadmium can be decreased to $6.9 \times 10^{-3}\%$ in the presence of TV.⁴⁷

2. Application in potentiometric analysis

Two sensitive and selective potentiometric methods for the determination of Hg(II)¹¹¹ and Tl(III)¹¹² based on the ability of these ions to form ion-associated complexes with TT^+ have been described.

The use of the complex $\text{TT}[\text{HgI}_3]$ in the construction of a modified mercury-selective carbon paste electrode has been

described.¹¹¹ The electrode shows a stable, near-Nernstian response for $1 \times 10^{-3}\text{--}6 \times 10^{-6}$ mol litre⁻¹ $[\text{HgI}_3]^-$ (the anionic slope in the pH range 4.0–9.0 is 55.5 ± 0.4 mV). The lower detection limit is 4×10^{-6} mol litre⁻¹; the response time is 30–50 s. The interfering effects of the majority of tested ions were negligibly small. The electrode was used for direct determination of mercury in waste waters, metal amalgams and dental alloys.

The application of a membrane sensor based on $\text{TT}[\text{Ti}^{\text{III}}\text{Cl}_4]$ dispersed in a PVC matrix plasticised with dioctyl phthalate has been described.¹¹² The electrode shows a stable, near-Nernstian response at $1 \times 10^{-3}\text{--}4 \times 10^{-6}$ mol litre⁻¹ Tl(III) (the anionic slope is 56.5 ± 0.5 mV in the pH range 3–6). The lower detection limit is 2×10^{-6} mol litre⁻¹; the response time is 30–60 s. The electrode was successfully employed for the determination of thallium in spiked waste waters and zinc concentrates. The RSD value at $10 \mu\text{g ml}^{-1}$ was 1.6%.

IV. Miscellaneous applications of tetrazolium salts in inorganic analysis

A method for the determination of trace amounts of selenium based on its catalytic effect on the reduction of TNBT with dithiothreitol has been described.¹¹³ The method proved to be a simple, fast and efficient procedure for the determination of several forms of selenium. A similar procedure using the MTT–dithiothreitol system was used in the analysis of lobsters.¹¹⁴

A procedure for photometric determination of selenium in aqueous media (at the level of $10\text{--}120 \mu\text{g litre}^{-1}$) with 2-(*p*-nitrophenyl)-3,5-diphenyltetrazolium chloride was developed by Moskvina *et al.*¹¹⁵ The sample preparation step includes gas extraction of selenium (in the form of hydrogen selenide) followed by its liquid-adsorption extraction from the gaseous phase to an aqueous solution of reagents to yield water-insoluble formazan. A similar procedure¹¹⁶ based on 5-(benzo-1,3-dioxol-5-yl)-2-(4-iodophenyl)-3-phenyl-2*H*-tetrazolium chloride was used to determine arsenic at the level of $1\text{--}120 \mu\text{g litre}^{-1}$.

A method for determination of sulfur in steels, nickel alloys, chromium, tin, sodium dihydrophosphate, galena and $\text{RbAg}_4\text{I}_{5-x}\text{S}_x$ was developed by Kolesnikova *et al.*¹¹⁷ Here, the determination makes use of formazans formed upon reduction of TT, INT and NBT.

Nagaraja *et al.*¹¹⁸ developed a highly sensitive spectrophotometric method for the determination of silver ($\epsilon_{510} = 4.51 \times 10^5$ litre $\text{mol}^{-1} \text{cm}^{-1}$) that involves silver-enhanced reduction of TT with semicarbazide hydrochloride. This procedure was used for the determination of Ag(I) in photographic process waste water.

V. Conclusion

Tetrazolium salts are popular and readily available multifunctional reagents for liquid–liquid extraction, spectrophotometric and potentiometric determination of different ions and elements in environmental objects and industrial samples. Each tetrazolium-containing extraction system has its own advantages and disadvantages in terms of sensitivity, selectivity, accuracy, reliability and rapidity. On the whole, these systems are efficient and enable solution of complex analytical problems. The characteristics of some of these methods are comparable with those of atomic absorption spectrometry (AAS) and inductively coupled plasma–atomic emission spectroscopy (ICP–AES). However, in contrast with the latter, these methods are inexpensive and do not require costly equipment.

Altogether, these data suggest that complexes of the mono-tetrazolium salts MTT, TV and INT and of the ditetrazolium salt BT hold considerable promise for further investigations. Thus MTT is a convenient reagent for extraction and spectrophoto-

metric determination of colourless anions, while TV and INT having higher molecular masses form more stable and readily extractable complexes. The properties of INT complexes are less predictable, but their application offers a significant gain in sensitivity and/or selectivity. BT complexes are the least studied; however, there are strong grounds to believe that they are more efficient in comparison with other tetrazolium salts.

The authors thank Professor A V Alexandrov, former Head of the Department of General and Inorganic Chemistry of the Plovdiv University and recognised leader in the field, for helpful discussions and inestimable experience shared to the authors of this review.

References

1. A B Zhivich, G I Koldobskii, V A Ostrovskii *Khim. Geterotsikl. Soedin.* **12** 1587 (1990)^a
2. M V Berridge, P M Herst, A S Tan *Biotechnol. Annu. Rev.* **11** (Suppl.) 127 (2005)
3. A Alexandrov *Tertazolium Salts for Solvent Extraction of Elements as Ion Association Complexes. Review* (Saarbrücken: Universität des Saarlandes, 1984)
4. A Alexandrov *The Application of Tetrazolium Salts in Analytical Chemistry. Review* (Saarbrücken: Universität des Saarlandes, 1984)
5. S Kostova, B Boyanov *J. Radioanal. Nucl. Chem., Lett.* **200** 427 (1995)
6. A N Dimitrov, V D Lekova, K B Gavazov, B S Boyanov *Cent. Eur. J. Chem.* **3** 747 (2005)
7. W D Hooper *Pure Appl. Chem.* **19** 221 (1969)
8. M Kamburova, Doctoral Thesis in Chemical Sciences, BAS, Sofia, Bulgaria, 1999
9. Zh Simeonova, A Aleksandrov, K Bukovinov *Nauch. Tr. Plovdiv Univ., Khim.* **27** 27 (1989)
10. M Kamburova *Zh. Anal. Khim.* **48** 1161 (1993)^b
11. M Kamburova, PhD Thesis, BAS, Sofia, Bulgaria, 1986
12. A Aleksandrov, M Kamburova *Nauch. Tr. Plovdiv Univ., Khim.* **22** 25 (1984)
13. A Aleksandrov, M Kamburova *Higher School Agricult. Plovdiv, Sci. Works* **32** 155 (1987)
14. A Aleksandrov, M Kamburova *Nauch. Tr. Plovdiv Univ., Khim.* **22** 35 (1984)
15. Zh Simeonova, A Aleksandrov *Nauch. Tr. Plovdiv Univ., Khim.* **27** 17 (1989)
16. A Alexandrov, M Kamburova *J. Radioanal. Nucl. Chem.* **97** 271 (1986)
17. M Kamburova, A Aleksandrov *Zh. Anal. Khim.* **54** 277 (1999)^b
18. M Kamburova, A Aleksandrov *Zh. Anal. Khim.* **50** 1292 (1995)^b
19. M Kamburova *Anal. Lett.* **30** 305 (1997)
20. M Kamburova *Mikrochim. Acta* **128** 177 (1998)
21. M Kamburova *Zh. Anal. Khim.* **45** 678 (1990)^b
22. M Kamburova, T Popov, A Aleksandrov *Higher School Agricult. Plovdiv, Sci. Works* **35** 41 (1990)
23. M Kamburova *Zh. Anal. Khim.* **46** 1538 (1991)^b
24. Z Pancheva, A Dimitrov, S Kostova, A Alexandrov *Bulg. Chem. Ind.* **73** 17 (2002)
25. M Kamburova *Higher School Agricult. Plovdiv, Sci. Works* **35** 61 (1990)
26. M Kamburova, N Nikolov, A Nikolov *Chem. Anal. (Warsaw)* **38** 161 (1993)
27. M Kamburova *Talanta* **40** 719 (1993)
28. M Kamburova, T Popov, D Nikitova *Zh. Anal. Khim.* **47** 799 (1992)^b
29. M Kamburova *Zh. Anal. Khim.* **46** 1534 (1991)^b
30. Zh J Simeonova, A V Alexandrov, M B Stoyanova *Bulg. Chem. Commun.* **35** 5 (2003)
31. S Kostova, A Aleksandrov, in *The 3rd National Conference on Chemistry (Abstracts of Reports)*, Plovdiv, Bulgaria, 1998 p. 241
32. M Kamburova *Mikrochim. Acta* **124** 129 (1996)
33. M Kamburova *Chem. Anal. (Warsaw)* **40** 93 (1995)
34. M Kamburova *Zh. Anal. Khim.* **50** 614 (1995)^b
35. M Kamburova *Anal. Lett.* **27** 1999 (1994)
36. M Kamburova, A Aleksandrov *Zh. Anal. Khim.* **53** 589 (1998)^b
37. A Aleksandrov, Z Simeonova, M Vasileva *Nauch. Tr. Plovdiv Univ., Khim.* **25** 47 (1987)
38. Z Simeonova, A Aleksandrov, N Stoimenov *Nauch. Tr. Plovdiv Univ., Khim.* **27** 39 (1989)
39. A Aleksandrov, Z Simeonova *Mikrochim. Acta* **1** 447 (1985)
40. A Alexandrov, Zh Simeonova *Thermochim. Acta* **107** 123 (1986)
41. A Aleksandrov, Doctoral Thesis in Chemical Sciences, BAS, Sofia, Bulgaria, 1987
42. Z Simeonova, A Alexandrov, M Dzharkova *Fresenius' J. Anal. Chem.* **348** 329 (1994)
43. Z Simeonova, A Alexandrov, S Dicheva *Talanta* **42** 867 (1995)
44. A Aleksandrov, A Dimitrov, S Kostova *Nauch. Tr. Plovdiv Univ., Khim.* **24** 41 (1986)
45. S Kostova, A Dimitrov, A Aleksandrov *Nauch. Tr. Plovdiv Univ., Khim.* **29** 3 (2000)
46. A Alexandrov, M Kamburova *Mikrochim. Acta* **3** 159 (1985)
47. M Kamburova *Chem. Anal. (Warsaw)* **38** 371 (1993)
48. A Dimitrov, S Kostova *Bulg. Chem. Ind.* **70** 88 (1999)
49. A Dimitrov, S Kostova, A Alexandrov *Anal. Lab.* **7** (1) 20 (1998)
50. A Dimitrov, S Kostova, Z Pancheva, V Lekova *Bulg. Chem. Ind.* **73** 20 (2002)
51. A Dimitrov, V Lekova, K Gavazov, B Boyanov *Zh. Anal. Khim.* **62** 138 (2007)^b
52. S Kostova, A Dimitrov *Bulg. Chem. Ind.* **71** 44 (2000)
53. V Lekova, A Dimitrov, M Slavova *J. Univ. Chem. Tech. Met.* **38** 901 (2003)
54. M Kamburova *Anal. Lett.* **31** 2255 (1998)
55. M Kamburova *Higher School Agricult. Plovdiv, Sci. Works* **43** 17 (1998)
56. A Aleksandrov, S Kostova, O Navratil *Collection Czech. Chem. Comm.* **50** 2369 (1985)
57. S Kostova, A Aleksandrov, I Ilieva *Nauch. Tr. Plovdiv Univ., Khim.* **27** 67 (1989)
58. A Aleksandrov, S Kostova *Nauch. Tr. Plovdiv Univ., Khim.* **24** 53 (1986)
59. S Kostova, A Aleksandrov, S Statkova *Nauch. Tr. Plovdiv Univ., Khim.* **27** 53 (1989)
60. A Alexandrov, S Kostova *J. Radioanal. Nucl. Chem.* **83** 247 (1984)
61. S Kostova, V Stajkovska, A Aleksandrov *Nauch. Tr. Plovdiv Univ., Khim.* **29** 9 (2000)
62. S Kostova, A Alexandrov, A Dimitrov *Anal. Lab.* **7** (1) 13 (1998)
63. S Kostova, A Dimitrov, A Alexandrov *Chem. Pap.* **54** 66 (2000)
64. Z Simeonova, K Gavazov, A Alexandrov *Nauch. Tr. Plovdiv Univ., Khim.* **33** 5 (2005)
65. Z Simeonova, K Gavazov, A Alexandrov *Anal. Lab.* **7** (4) 184 (1998)
66. K Gavazov, PhD Thesis, BAS, Sofia, Bulgaria, 2000
67. K Gavazov, Z Simeonova, A Alexandrov *Nauch. Tr. Plovdiv Univ., Khim.* **31** 5 (2002)
68. K Gavazov, V Lekova, A Dimitrov, in *National Scientific Conference with International Participation, Union of Scientists of Bulgaria — Branch Smolyan, Smolyan, Bulgaria (CD Proceedings)*, 2006
69. Z Simeonova, K Gavazov, A Alexandrov *Cent. Eur. J. Chem.* **4** 258 (2006)
70. K Gavazov, V Lekova, A Dimitrov *J. Univ. Chem. Tech. Met.* **41** 217 (2006)
71. K Gavazov, Z Simeonova *Nauch. Tr. Plovdiv Univ., Khim.* **32** 15 (2004)
72. K Gavazov, V Lekova, A Dimitrov, G Patronov *Cent. Eur. J. Chem.* 2006; published online DOI: 10.2478/s11532-006-0053-x
73. K Gavazov, Z Simeonova, A Alexandrov *J. Univ. Chem. Tech. Met.* **38** 909 (2003)
74. Z Simeonova, K Gavazov, A Alexandrov *Zh. Neorg. Khim.* **44** 676 (1999)^c
75. K Gavazov, A Dimitrov, V Lekova, E Karaasheva *Nauch. Tr. Plovdiv Univ., Khim.* **34** 17 (2006)
76. K Gavazov, V Lekova, G Patronov *Acta Chim. Slovenica* **53** 506 (2006)
77. K Gavazov, Z Simeonova, A Alexandrov *Anal. Lab.* **7** (3) 127 (1998)

78. K Gavazov, Z Simeonova, A Aleksandrov, in *Scientists Union of Bulgaria — Jubilee Scientific Session (Abstracts and Papers)*, Plovdiv, 1998 Vol. 3, p. 189
79. K Gavazov, Z Simeonova, A Alexandrov *Zh. Neorg. Khim.* **46** 494 (2001)^c
80. K Gavazov, Z Simeonova, A Alexandrov *Zh. Neorg. Khim.* **45** 142 (2000)^c
81. A Alexandrov, A Dimitrov, A Patcheva, M Vrchlabsky *Scr. Fac. Sci. Natl. Univ. Purkynianae Brun.* **15** 497 (1985)
82. A Dimitrov, A Alexandrov *Anal. Lab.* **4** (3) 172 (1995)
83. A Aleksandrov, A Dimitrov *Nauch. Tr. Plovdiv Univ., Khim.* **24** 17 (1986)
84. V D Lekova, K B Gavazov, A N Dimitrov *Chem. Pap.* **60** 283 (2006)
85. A Dimitrov, A Alexandrov, A Hrdlička, M Vrchlabsky *Scr. Fac. Sci. Nat. Univ. Purkynianae Brun.* **14** 91 (1984)
86. A Alexandrov, Z Simeonova, M Kamburova *Commun. Dept. Chem. Bulg. Acad. Sci. (Bulg. Chem. Commun.)* **23** 542 (1990)
87. M Kamburova *Higher School Agricult. Plovdiv, Sci. Works* **43** 31 (1998)
88. M Kamburova, A Alexandrov, K Trifonov *Chem. Anal. (Warsaw)* **39** 639 (1994)
89. M Kamburova, A Alexandrov *Chem. Anal. (Warsaw)* **43** 1021 (1998)
90. M Kamburova, *Chem. Anal. (Warsaw)* **38** 189 (1993)
91. M Kamburova, T Mokreva *Higher School Agricult. Plovdiv, Sci. Works* **43** 27 (1998)
92. M Kamburova, V Rankov *Higher School Agricult. Plovdiv, Sci. Works* **35** 49 (1990)
93. M Kamburova *Talanta* **40** 725 (1993)
94. M Kamburova *Talanta* **40** 707 (1993)
95. M Kamburova, V Rankov *Higher School Agricult. Plovdiv, Sci. Works* **36** 163 (1991)
96. M Kamburova, T Mokreva *Higher School Agricult. Plovdiv, Sci. Works* **43** 21 (1998)
97. M Kamburova *Chem. Anal. (Warsaw)* **40** 791 (1995)
98. M Kamburova *Talanta* **39** 997 (1992)
99. M Kamburova *Zh. Anal. Khim.* **53** 140 (1998)^b
100. M Kamburova, D Nikitova *Higher School Agricult. Plovdiv, Sci. Works* **42** 113 (1997)
101. M Kamburova, A Alexandrov *Chem. Anal. (Warsaw)* **44** 745 (1999)
102. M Kamburova, D Nikitova *Higher School Agricult. Plovdiv, Sci. Works* **41** 59 (1996)
103. A Aleksandrov, A Dimitrov, S Kostova *Nauch. Tr. Plovdiv Univ., Khim.* **24** 67 (1986)
104. K Gavazov, Z Simeonova, A Aleksandrov *Nauch. Tr. Plovdiv Univ., Khim.* **31** 13 (2002)
105. K Gavazov, G Patronov, in *Balkan Conference of Young Scientists, (Scientific Researches of the Union of Scientists. Series C. Technics and Technologies)*, Plovdiv, 2005 Vol. 5, p. 290
106. K Gavazov, V Lekova, G Patronov, M Turkyilmaz *Chem. Anal. (Warsaw)* **51** 221 (2006)
107. K Gavazov, Z Simeonova, A Alexandrov *Talanta* **52** 539 (2000)
108. E A Morgen, L M Dimova *Industr. Lab.* **50** 947 (1984)
109. A Aleksandrov, M Kamburova, A Karanova *Nauch. Tr. Plovdiv Univ., Khim.* **25** 59 (1987)
110. A Aleksandrov, M Kamburova, S Dimitrov *Nauch. Tr. Plovdiv Univ., Khim.* **25** 73 (1987)
111. M N Abbas, G A E Mostafa *Anal. Chim. Acta* **478** 329 (2003)
112. M M Hassanien, Kh S Abou-El-Sherbini, G A E Mostafa *Talanta* **59** 383 (2003)
113. W C Hawkes *Anal. Chim. Acta* **183** 197 (1986)
114. E Aoyama, N Kobayashi, M Shibata, T Nakagawa, H Tanaka *Anal. Sci.* **7** 103 (1991)
115. L N Moskvina, A V Bulatov, E A Rudenko, D V Navolotskii, G I Koldobskii *Zh. Anal. Khim.* **61** 29 (2006)^b
116. L N Moskvina, A V Bulatov, G L Grigor'ev, G I Koldobskii *Zh. Anal. Khim.* **58** 955 (2003)^b
117. A M Kolesnikova, A I Lazarev, V I Lazareva *Zav. Lab.* **51** (11) 1 (1985)
118. P Nagaraja, M C Hemantha Kumar, H S Yathirajan *Anal. Sci.* **18** 815 (2002)
- ^a — *Chem. Heterocycl. Compd. (Engl. Transl.)*
- ^b — *Russ. J. Anal. Chem. (Engl. Transl.)*
- ^c — *Russ. J. Inorg. Chem. (Engl. Transl.)*

Gold nanoparticles: preparation, functionalisation and applications in biochemistry and immunochemistry

L A Dykman, V A Bogatyrev

Contents

I. Introduction	181
II. Methods of preparation of colloidal gold	183
III. Functionalisation of gold nanoparticles	184
IV. Colloidal gold in solid-phase assays	185
V. Application of colloidal gold for the quantitative protein determination	186
VI. Application of gold nanoparticles in studies of biologically active compounds by vibrational spectroscopy	186
VII. Gold nanoparticles as antigen carriers	187

Abstract. The review summarises data on the synthesis and functionalisation of gold nanoparticles and their applications in biological investigations. Particular attention is given to applications of colloidal gold in solid-phase assays, immunoassay and studies of biologically active compounds by vibrational spectroscopy. A special section deals with the use of gold nanoparticles as antigen carriers in immunisation. The bibliography includes 406 references.

I. Introduction

Gold was one of the first metals discovered by humans, and the history of its study counts several thousands of years. First data on colloidal gold (CG) can be found in treatises by Chinese, Arabic and Indian scientists, who prepared CG and used it, in particular, for medical purposes as early as 5–4th centuries B.C. In the Middle Ages, alchemists in Europe actively studied and used CG. Probably, wonderful colour changes that accompany condensation of gold atoms prepared by reduction of salt solutions led alchemists to believe in transformations of elements, CG being considered as a panacea.¹ For example, Paracelsus wrote about the therapeutic properties of '*quinta essentia auri*,' which was prepared by reduction of gold chloride by ethanolic extracts of plants. In 1583, the doctor of the French king Louis XIII, the alchemist David de Planis-Campy, recommended the use of a colloidal solution of gold in water as an elixir of longevity. The first book on colloidal gold preserved to our days was published by the philosopher and doctor of medicine Francisco Antonii in 1618.² This book contains information on the formation of CG and its medical uses, including practical advices. From the mid-17th century, CG was used for the production of red (ruby) glasses, decoration on porcelain (purple of Cassius) and silk colouration.

The beginning of scientific research on CG dates back to the mid-19th century, when Michael Faraday published an article³ devoted to methods of synthesis and properties of CG. In this article, Faraday described, for the first time, aggregation of CG in the presence of electrolytes, the protective effect of gelatin and other high-molecular-mass compounds and the properties of thin films of CG. Colloidal gold solutions prepared by Faraday are still stored in the Royal Institution of Great Britain in London.

In the late 19th century—early 20th century, Richard Zsigmondy^{4,5} published a series of fundamental papers on the properties of CG. He was the first to describe methods of synthesis of CG with different particle sizes with the use of hydrogen peroxide, formaldehyde and white phosphorus as reducing agents and report on important physicochemical (including optical) properties of gold sols. Zsigmondy used colloidal gold as the main experimental object when inventing (in collaboration with Siedentopf) an ultramicroscope. In 1925, Zsigmondy was awarded the Nobel Prize in Chemistry 'for his demonstration of the heterogeneous nature of colloid solutions and for the methods he used, which have since become fundamental in modern colloid chemistry'.

Studies by the Nobel Prize laureate Theodor Svedberg on the preparation, analysis of mechanisms of colloidal gold formation and sedimentation properties of CG (with the use of the ultracentrifuge he had invented)⁶ are also among classical studies. Svedberg investigated the kinetics of reduction of gold halides and formulated the main concepts about the mechanism of formation (chemical condensation) of colloidal gold particles.

Later studies were concerned with various procedures for the synthesis of gold sols based on both disintegration of metallic gold by electric arc and (primarily) synthesis of colloidal particles from gold halides with the use of chemical reducing agents or irradiation.^{7–11}

Nowadays, colloidal gold is used by scientists as a perfect subject for studies of the optical properties of metal particles^{12–15} and fractal clusters¹⁶ and the mechanisms of aggregation and stabilisation of colloids.^{17–21} Colloidal gold is also applied in analytical chemistry,^{22,23} geomicrobiology, geobiochemistry²⁴ and photography.²⁵ Colloidal gold, unlike crystalline gold, shows a pronounced catalytic activity.²⁶ Colloidal gold immobilised on an electrode surface is used in investigations of catalytic processes and electron transport in biomacromolecules.²⁷

Examples of the application of CG in medicine, in particular, in colour reactions for proteins which are present in the cerebrospinal fluid and blood serum are documented.^{28,29} Methods

L A Dykman, V A Bogatyrev Institute of Biochemistry and Physiology of Plants and Microorganisms, Russian Academy of Sciences, prosp. Entuziastov 13, 410049 Saratov, Russian Federation. Fax (7-8452) 97 03 83, tel. (7-8452) 97 04 03, e-mail: dykman@ibppm.sgu.ru (L A Dykman), bog@ibppm.sgu.ru (V A Bogatyrev)

Received 17 October 2006

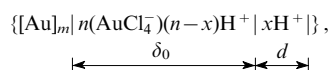
Uspekhi Khimii 76 (2) 199–213 (2007); translated by T N Safonova

developed for these purposes are based on the properties of proteins to serve (depending on their physicochemical properties) as either flocculants or stabilisers of colloidal gold particles. Methods for the treatment of rheumatoid arthritis with CG solutions were developed.³⁰ Colloidal solutions of the ¹⁹⁸Au isotope (the half-life is 65 h) are successfully used for therapeutic purposes in oncology.³¹ Non-radioactive CG has found wide application in the diagnosis and treatment of cancer diseases.^{32–35}

Gold particles are used for studying the transport of substances into cells by endocytosis,³⁶ the delivery of genetic material to cell nucleus by biolistic transfection³⁷ and targeted drug delivery.³⁸

However, colloidal gold is most widely applied in medicine as an immunochemical marker. An ideal marker should be readily distinguishable with an electron microscope, have a specified size, shape and structure, be stable against aggregation, be strongly bound to biomolecules and not decrease their activity. Colloidal gold meets all these requirements. For the first time, colloidal gold conjugates with immunoglobulins were used as immunochemical markers in 1971.³⁹ After the publication in 1973 of the study by Frens⁴⁰ concerned with methods of synthesis of CG with a desired particle size, CG-based biospecific markers have found wide application in different fields of biology. Abundant information on the most important aspects of the preparation and application of CG-based immunochemical markers in biology and medicine was summarised in monographs^{41–43} and reviews.^{44–47}

A colloidal gold particle consists of the crystalline nucleus $[\text{Au}]_m$ and AuCl_4^- ions adsorbed on the surface of the nucleus. These ions determine the negative charge of colloidal gold particles, compose the inner layer of the ionic (electric) double layer and determine the adsorption potential. The H^+ ions are present in an intermicellar solution (some of them are located in the adsorption region; other, in the diffuse region of the electric double layer). The gold micelle can be represented as follows:



where $[\text{Au}]_m$ is the micelle nucleus (m is the number of gold atoms, which can vary from several hundreds to millions), n is the number of adsorbed AuCl_4^- ions ($n \ll m$), δ_0 is the adsorption layer thickness and d is the thickness of the diffuse region of the electric double layer.⁴⁸

A high electron density, the ability to scatter and emit secondary electrons, the characteristic absorption and scattering in the visible region of the electromagnetic spectrum and the intense red colour of gold-containing markers enable easy detection of gold particles by different physicochemical methods (microscopy,[†] photometry, flow cytometry, *etc.*). The possibility of preparing gold sols with different particle sizes and a narrow particle size distribution provides a high resolution of these methods and, in addition, enables simultaneous labelling of two or more antigens (or other ligands). After the corresponding immunochemical reaction, the size of CG particles can be increased by silver⁴⁹ or gold⁵⁰ enhancement (autometallography), which substantially extends the scope of these methods.

In the last 10–15 years, metal nanoparticles (particularly, gold nanoparticles) have found increasing application as efficient optical transducers of the results of biospecific interactions (for example, of an antibody with an antigen adsorbed on CG particles) into the detected optical signal in devices called biochips and biosensors.⁵¹ These devices are based on the unique optical properties of CG, in particular, the surface plasmon resonance (SPR, see below).⁵² The changes in physicochemical parameters of biochips and biosensors that occur in the course of biospecific

reactions are detected with the use of visual observations, light-scattering methods, vibrational spectroscopy, *etc.*

Biospecific interactions of biomolecules adsorbed on gold nanoparticles in systems, where nanoparticles exist as ordered self-assembled structures (thin films)⁵³ or are encapsulated in polymeric matrices,⁵⁴ have been extensively studied. Such structures are popular for the detection of biomolecules and microorganisms, for the design of DNA chips, *etc.* In these systems, the optical signal from the marker is sharply enhanced due to a strengthening of the local excitation field in an aggregate formed from gold nanoparticles.

Of nanosize structures, which are the subject of numerous fundamental studies, clusters are of particular interest. They occupy an intermediate position between individual atoms and solids and exhibit properties different from those of both atoms and solids. In particular, their physical characteristics substantially depend on the type and number of atoms involved in these structures, and this dependence becomes weaker as the number of atoms increases, which is indicative of the transformation of the material from the cluster to bulk state (quantum-size effects). Among clusters of simple substances, metal clusters (gold nanoparticles is a typical example) are of particular interest. These compounds attract considerable attention due to the characteristic features of their electronic structures and the relative simplicity of their preparation.

The present stage of development of physics of metal clusters dates back to 1993, when the electron shell structure of these clusters was discovered.^{55,56} This structure resembles in many aspects the shell structure of atoms. The experimental discovery of electron shells in polyatomic clusters was almost simultaneously confirmed by theoretical methods.

The theoretical approach was based on the property of metal valence electrons to leave the atoms (to be delocalised) and form a conduction band. It appeared that it is these shared electrons that determine the energy structure of the cluster and its unusual collective properties.⁵⁷ In particular, delocalised electrons in metal clusters have an effect on the behaviour of clusters in interactions with external fields. Recent extensive studies of interactions of metal clusters with electromagnetic fields revealed giant maxima (resonances) in electromagnetic absorption spectra. These resonances are associated with excitation of collective vibrations of the electronic system analogous to plasma vibrations of the electronic gas in the plasma and macroscopic metal bodies. These vibrations are called plasmon vibrations; the resonance, the surface plasmon resonance. The amplitude and the frequency range of plasmon resonance in clusters differ from those in macroscopic crystals.

If particles form aggregates, the corresponding plasmon peak is shifted to longer wavelengths or is broadened due to dipole–dipole interactions of light-induced dipole moments of particles in aggregates.⁵⁸ Therefore, optical excitations in aggregates composed of metal nanoparticles have a collective nature. As a result, local optical fields acting on metal particles in a fractal aggregate can be substantially higher than the mean field, which leads to giant non-linear effects.⁵⁹

It is of principal importance that the optical response of nanoparticles or their aggregates (particularly, ordered) substantially depends on the particle size and shape, the interparticle distance and the local dielectric environment of the particles.⁶⁰ This enables the tuning of the optical parameters of sensors.

The design and practical applications of biosensors based on metal nanoparticles were considered in reviews.^{51,61–68} New unique technologies, in particular, the monolayer self-assembly of metal particles,⁶⁹ nanolithography,⁷⁰ vacuum evaporation,⁷¹ *etc.*, are employed in the design of biosensor devices. Biosensors based on gold nanoparticles are used in immunoassay⁷² and for the nucleotide sequence determination.^{73,74} Recently, record sensitivities (in a zeptomole range) of such sensors have been achieved,^{75,76} and it has been demonstrated that resonance scattering spectra of individual particles can be recorded. This

[†] In addition to conventional transmission electron microscopy, scanning electron microscopy, light microscopy and different modifications of atomic force microscopy are also widely used.

opens up the possibility of observing intermolecular interactions at the single-molecule level.⁷⁷

The unique optical properties of silver and gold nanoparticles, which are determined by the localised surface plasmon resonance, are nowadays widely applied in single-electron transistors,⁷⁸ near-field optical microscopy,⁷⁹ surface-enhanced Raman scattering⁸⁰ (including at the single-molecule level⁸¹), SPR microscopy, SPR spectroscopy,⁸² *etc.* The optical properties of metal nanoparticles and their conjugates with biomacromolecules have been reviewed.^{83–88}

The present review summarises data on different methods of synthesis and functionalisation of gold nanoparticles and their applications in biological studies. Particular attention is given to applications of colloidal gold particles in solid-phase assays, immunoassays and studies of biomolecules by vibrational spectroscopy (the use of gold nanoparticles in electron microscopic methods is only briefly mentioned). A special section is devoted to applications of gold nanoparticles as antigen carriers in immunisation.

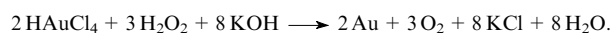
II. Methods of preparation of colloidal gold

Methods of synthesis of CG (and other metal colloids) can be arbitrarily divided into the following two large groups: dispersion methods (metal dispersion) and condensation methods (reduction of the corresponding metal salts).

Dispersion methods for the preparation of CG are based on destruction of the crystal lattice of metallic gold in high-voltage electric field. If an electric arc is created in a liquid between two gold electrodes under electric field, its blazing leads to the mass transfer between electrodes accompanied by the colloidal gold formation. The yield and shape of gold particles formed under electric current depend not only on the voltage between electrodes and the current strength, but also on the presence of electrolytes in solution. The use of direct current leads to the formation of non-uniform gold particles. The addition of even very small amounts of alkalis or chlorides and the use of high-frequency alternating current for dispersion substantially improve the quality of gold hydrosols.

Condensation methods are more commonly employed than dispersion methods. Colloidal gold is most often prepared by reduction of gold halides (for example, of HAuCl₄) with the use of chemical reducing agents and/or irradiation (ultrasonic and UV irradiation, pulse or laser radiolysis).^{47,89} Various organic and inorganic compounds serve as chemical reducing agents.²³ In the pioneering studies by Faraday and Zsigmondy,^{3,4} formaldehyde, ethanol and white phosphorus were used, *inter alia*, as reducing agents. These compounds are still successfully used for the preparation of sols with an average particle diameter of 5–12 nm.^{90,91} In addition, sodium citrate⁹² (for the preparation of CG with an average particle diameter of 20 nm), ascorbic acid⁹³ (12 nm), ethylenediaminetetraacetic acid (EDTA)⁸ (20 nm), sodium citrate in the presence of tannin (~5 nm),^{94,95} sodium borohydride,⁹⁶ borohydride in a mixture with sodium citrate⁹⁷ or EDTA⁹⁸ and cyanoborohydride⁹⁹ (for the preparation of CG with an average particle diameter of ~5 nm) have found application in the synthesis of gold sols. Ultradispersed sols (the particle diameter of 2–3 nm) can be prepared with the use of sodium or potassium thiocyanate.¹⁰⁰ Other reducing agents, such as oxalic and tartaric acids, carbon monoxide, tin chloride, hydrazine, hydrogen peroxide, carbohydrates, phenols, aromatic aldehydes, essential oils and many other compounds (up to an aqueous extract of Dutch cigars),⁹⁰ which were extensively applied in the synthesis of CG early in the 20th century, are not presently used.

Zsigmondy and Svedberg^{5,6} studied the kinetics of reduction of gold halide solutions and formulated the principal notions of the mechanism of formation of gold particles using reduction of HAuCl₄ with hydrogen peroxide as an example



This reaction produces only one electrolyte and, consequently, it can be monitored by conductometry.

According to Zsigmondy and Svedberg, ~30% of HAuCl₄ is initially reduced (to form a highly supersaturated gold solution in which the concentration of atomic metal is 6 orders of magnitude higher than that in a saturated solution), after which the reaction rate sharply decreases. The slow step involves condensation of gold to form very small particles (new phase nuclei). The latter form large but unstable aggregates (coagulation followed by peptisation), the sol solution turning blue. Particles involved in aggregates gradually enlarge and become centres of further rapid reduction of HAuCl₄. Once nuclei reach a particular critical size, a stable red sol is formed.

Taking into account the condensation mechanism of formation of a colloidal phase, several parameters determining the degree of dispersity of a gold suspension can be mentioned. Evidently, the rate of new phase nucleation depends on the concentrations of the reactants and the chemical nature of the reducing agent. At a low rate of nucleation and a rather high rate of particle condensation (the low degree of supersaturation of an HAuCl₄ solution), rather bulky particles are formed in small amount. At a high rate of nucleation and a rather low rate of particle condensation (the high degree of supersaturation of an HAuCl₄ solution), the probability of the formation of small particles increases. The increase in the concentration of the reducing agent is limited by aggregation stability of colloidal gold (rather high stability is achievable only in low-ionic-strength media).

In the case of self-nucleation, the larger the number of nucleation centres the higher the degree of dispersity of sols. In most cases, the nucleation and nucleus growth occur simultaneously (*i.e.*, reduced metal is consumed simultaneously in both processes). A decrease in the nucleation rate also leads to the formation of more coarse-dispersed hydrosols; a decrease in the nucleus growth rate, to the formation of finely dispersed hydrosols. Studies of numerous gold sols prepared by chemical reduction demonstrated that most of them were characterised by low stability and a broad particle size distribution.¹⁰¹ Relatively monodispersed particles with a diameter of 10–60 nm can be prepared only by the Frens method⁴⁰ using sodium citrate for reduction of HAuCl₄.

According to Zsigmondy, a sol with a narrow Au particle size distribution can be prepared by adding presynthesised Au seeds, on which condensation will occur, to an HAuCl₄ solution. In this method, sodium citrate or hydroxylamine can serve as reducing agents.^{102–104} Isodisperse and isomorphous sols can be prepared only if the formation of new nuclei is prevented. As a rule, it is achieved by performing the process in two steps. Initially, a new phase nucleates, and then weak supersaturation is created in the sol, due to which new nuclei are not produced any more and only the already formed nuclei grow.¹⁰⁵

Another procedure for the preparation of monodispersed gold sols was developed.¹⁰⁶ This method is based on reduction of a concentrated HAuCl₄ solution (0.5 mol litre⁻¹) by isoascorbic acid in the presence of gum arabic as the protective colloid. Under these conditions, condensation is accompanied by aggregation to form virtually monodispersed spherical gold particles with a diameter from 80 nm to 5 μm (depending on the acidity of the medium and the concentration of the reducing agent).

Gold nanoparticles can also be prepared by the two-phase microemulsion method. In the first step, metal-containing reagents are transferred from an aqueous to an organic phase. After the addition of a surfactant solution to this system, a microemulsion, *i.e.*, a dispersion of two immiscible liquids, is formed. The reduction reaction proceeds in a dispersed phase in which the drop size is at most 100 nm. As a result, virtually monodispersed sols are formed.¹⁰⁷ Later, a single-phase method without the use of aqueous solutions was developed.¹⁰⁸

In microemulsion methods of synthesis of CG, alkanethiols are often added to the reaction solution, and these additives form dense self-assembled monolayers on the gold surface. This method was employed for the preparation of self-assembled two- and three-dimensional ensembles of gold nanoparticles.^{109–111} Some ligands, such as alkanethiols, amines, silanes, phosphines and chitosan, can be involved in digestive ripening, *i.e.*, in a process in which a polydispersed colloidal suspension is transformed into monodispersed state upon refluxing in a solvent containing surfactant ligands.¹¹²

In recent years, synthetic polymers, such as polyethylene glycol (PEG), polyethyleneimine, polyvinylpyrrolidone, poly(vinyl acetate), polyamidoamine (dendrimer), polydithiafulvene, chitosan, *etc.*, have found application in the synthesis of monodispersed CG.^{113–117} Particles formed in the presence of these polymers are characterised by a higher size and shape uniformity.^{118, 119} Sodium borohydride,^{120, 121} alcohols and ethers,¹²² hydrazine¹²³ and sodium diphenylaminosulfonate,¹²⁴ as well as ultrasonic radiation,¹²⁵ can be used for reduction. A tyrosine residue of a polyfunctional peptide served as a reducing agent.¹²⁶ Colloidal gold with the required particle size can be prepared by choosing a particular reducing agent and taking into account the characteristic features of the kinetics of formation of a colloidal phase.^{127–130} A procedure for the synthesis of a marker for lectins with the use of PEG modified by carbohydrates and thiol groups was described.¹³¹

Physical (based on ultrasonic, UV, IR or ionising radiation or laser photolysis)^{8, 9, 132–138} and electrochemical¹³⁹ methods of reduction are much less commonly employed than chemical methods. The advantages of the former methods are that impurities of chemical compounds are absent in the resulting sols (on the metal particle surface).¹⁴⁰

In electron microscopic biological studies, gold clusters consisting of 11–67 atoms (undecagold, Nanogold[®]) with a diameter of 0.82–1.4 nm are used as markers. These clusters are prepared by reduction of a gold triarylphosphine complex with sodium borohydride^{11, 141, 142} or by reduction of HAuCl₄ in methanol with glutathione.^{143, 144}

The application of microorganisms and plant and animal cells for the CG synthesis is a new line of investigations in nanobiotechnology.^{145–148}

In recent years, CG particles uniformly distributed in polymeric matrices and particles consisting of the metal core and a dielectric shell,^{149–151} as well as non-spherical particles (spheroids, rods, chains)[‡] and shell and planar structures,^{152–162} have been much in demand due to the use of CG in biosensors. The latter structures can be prepared by reduction of gold salts in reverse micelles,¹⁶³ by the photochemical method¹⁶⁴ and with the use of porous aluminium or quartz templates and carbon nanotubes.^{165, 166} These methods were also employed for the synthesis of composite materials, for example, of gold–iron (possessing magnetic properties),¹⁶⁷ gold–silver^{168, 169} and other bimetallic nanoparticles.⁴⁷

III. Functionalisation of gold nanoparticles

A gold hydrosol is a typical lyophobic colloid the particles of which bear a large negative surface charge (the surface potential is ~50 mV)¹⁷⁰ and, hence, it is stable only in very low-ionic-strength solutions. In lyophobic systems, the dispersion medium and the dispersed phase are substantially different in the chemical composition and the interface structure, as a result of which the surface forces at the interface are uncompensated. These systems are thermodynamically unstable and require special stabilisation.^{17, 170, 171}

The stability of a sol can be increased by coating particles with a polymeric layer (conjugation with a polymer).^{18–21, 172} This method of stabilisation was proposed by Faraday, who studied the protective properties of gelatin.³ The addition of even a small amount of a polymer (particularly, of polyelectrolytes) to lyophobic colloids can substantially increase their aggregation stability.

The formation of an adsorbed polymeric layer on the particle surface leads to a decrease in the interphase tension due to a strengthening of interactions between the dispersed phase and the dispersion medium, resulting in a substantial increase in the entropy component of the system (due to the involvement of molecules and ions of the surface layer in thermal motion together with particles of the dispersed phase). As a result, the aggregation stability of the system increases. The adsorption layer favours the formation of a solvate layer with the result that the particle surface becomes lyophilic and the lyophobic sol becomes much less sensitive to coagulation by electrolytes (due to electrostatic and hydrophobic interactions and structural mechanical stability).

The efficiency of stabilisation depends on solubility of the protective polymer in a dispersion medium, the ability of lyophobic particles to adsorb the polymer on their surface and the degree of the surface coverage by the polymer.

Not only the molecular mass of a polymer, but also the charge of its functional groups are of importance for the protective action. Polymers containing simultaneously acidic and basic groups (for example, protein analogues) or weakly basic polycationic macromolecules having the pH-dependent protective action are the most efficient stabilisers of gold hydrosols.^{19, 20, 173}

The ability of polymers (including biospecific macromolecules) to stabilise lyophobic colloids underlies the preparation of stable bioconjugates, *e.g.*, complexes of CG with immunoglobulins, lectins, enzymes, hormones, lipoproteins, *etc.*¹⁷⁴

The attachment of biospecific probes to CG can be performed by adsorption and chemisorption methods. Each method has characteristic features of its own. It is commonly accepted that stabilisation of CG by recognising biomolecules (functionalisation) occurs through passive adsorption of a polymer on the particle surface by electrostatic and hydrophobic interactions.^{43, 90} A strong negative charge of the gold particle surface provides their strong adsorption interactions with high-molecular-mass compounds. The presence of Coulomb interactions between the NH₂ groups of lysine residues of a protein adsorbed on the gold nanoparticle surface with the citrate ions was reported.¹⁷⁵

In recent years, an important role of cysteine SH groups in binding of proteins to the surface of gold particles has been documented.¹⁷⁶

The advantage of physical adsorption is that gold particles have a minimum effect on the structure of a macromolecule (a probe). Electrostatic (rather than covalent) interaction of a label with a probe ensures to the greatest extent the conservation of the native character of the probe and, consequently, the activity and specificity of its interactions with the target molecule. However, when using this procedure for the preparation of bioconjugates, the possibility of desorption of recognising molecules from the gold nanoparticle surface and their binding to the target molecules must be taken into account. The main distinguishing feature of polymer adsorption is that polymers are usually adsorbed in amounts substantially larger than those required for the formation of a monomolecular layer. Adsorption isotherms of polymer adsorption from dilute solutions show no inflection points, which could be indicative of the formation of a discrete monolayer, as is observed for low-molecular-mass surfactants. This is due to formation of a relatively large number of contacts between macromolecules and the surface. The simultaneous cleavage of these contacts is statistically improbable,²⁰ and consequently, in most cases, adsorption of individual macromolecules is irreversible.

‡ It is known that the particle shape has a profound effect on their optical properties.

Sulfur and gold atoms are known to form dative bonds.^{22, 177} Hence, it was proposed that alkanethiol linkers $\text{HS}(\text{CH}_2)_n\text{R}$ ($\text{R} = \text{COOH}$, OH or SO_3H ; $n = 11-22$) were used to achieve stronger attachment of biomolecules to gold particles (the chemisorption method).¹⁷⁸ Interactions of these linkers with gold afford thiolates $[\text{Au}^0]_m \cdot \text{Au}^+ \text{S}^-(\text{CH}_2)_n\text{R}$,⁶⁹ which form a monolayer on the particle surface.

In 1996, Mirkin *et al.*⁷³ performed thiolation of oligonucleotides at the 5'-end before their attachment to gold particles with a size of 15 nm. As a result, very stable conjugates (resistant to high and low temperatures) were prepared, which were employed for colourimetric determination of DNA in solution. Cyclic disulfides¹⁷⁹ and tris(ω -mercaptohexyl) derivatives¹⁸⁰ were used as linkers for the preparation of bioconjugates with gold particles with sizes of 30 and 100 nm, respectively. Conjugates with gold nanoparticles (nanospheres and nanorods) were prepared from thiolated proteins, immunoglobulins and avidin.^{168, 181} In addition to alkanethiols, ligands containing phosphino, amino or carboxy groups served as linkers.⁴⁷ The advantages of chemisorption are most pronounced in the case of linear molecules (for example, DNA). Adsorption of these molecules leads to the formation of structures characterised by close spatial orientation of the attached molecules.

However, non-covalent (adsorption) conjugation is still most commonly employed for the preparation of gold markers for immunochemical studies. In this approach, the native structure of biomacromolecules and, as a consequence, their functional properties are retained to the greatest extent.

IV. Colloidal gold in solid-phase assays

In early steps of development of immunoassay methods, preference was given to liquid-phase procedures. However, in recent years, solid-phase methods have found increasing use because they enable substantial simplification of experiments and a decrease in the background signal. For the first time, the solid-phase procedure was applied in radioimmunoassays of proteins.¹⁸²

The problem is that the liquid-phase assays require the use of an antigen in solution; however, not all antigens are water-soluble.⁸ There is a large number of antigens, which can be transformed into the soluble state only in the presence of dissociating additives, such as sodium dodecyl sulfate, urea, guanidinium chloride, *etc.* These dissociating additives prevent the formation of immune complexes.¹⁸³ These difficulties can be avoided by immobilising antigens on solid supports. Microtitration plates and nitrocellulose (NC) filters have gained wide acceptance in solid-phase assays.¹⁸⁴

Radioactive isotopes (^{125}I , ^{14}C and ^3H), enzymes (peroxidase, alkaline phosphatase, *etc.*)¹⁸⁵⁻¹⁸⁷ and, in recent years, CG have found wide application as labels in membrane tests. In 1984, the use of CG as labels for solid-phase immunoassays was documented in several publications.¹⁸⁸⁻¹⁹¹ Colloidal gold conjugates have found application in solid-phase assays due to the intense red colour of gold-containing markers. The appearance of the colour in the course of the reaction enables visualisation of the process.¹⁹²⁻¹⁹⁴

Non-specific staining of proteins on NC filters was carried out using the gold stain AuroDye^{195, 196} (see[¶]). This method was further improved and modified.¹⁹⁷⁻¹⁹⁹ Non-specific staining of proteins by gold stains is rather simple, convenient and highly sensitive.²⁰⁰ The staining intensity is proportional to the logarithm of the protein concentration and its molecular mass.²⁰¹ Elution of CG-immobilised proteins and the photometric determination of

the protein concentration from the light absorption of the resulting complex at 540 nm were described.²⁰² The gold stain was used also for direct protein staining in gels,²⁰³ for detection of nucleic acids immobilised on blots,²⁰⁴ for protein determination by electron microscopy^{205, 206} and for the colourimetric determination of proteins in solution.²⁰⁷

In assays, an antigen immobilised on a membrane is incubated with a solution of the corresponding CG-labelled antibodies (or other biospecific probes). Immunoglobulins,^{189, 191, 208, 209} Fab and scFv fragments of antibodies,^{123, 210} protein A,^{188, 190} lectins,^{211, 212} enzymes,²⁰⁴ streptavidin or antibiotin antibodies (in studies of biotinylated specimens),^{213, 214} *etc.*, were applied as probes in 'gold' dot-blot assays. To visualise different antigens on a membrane, several labels can simultaneously be used (for example, CG and peroxidase^{215, 216} or alkaline phosphatase²¹⁷). Colloidal gold conjugates also have found application in tissue blots,²¹⁸ in which tissue prints are blotted onto nitrocellulose filters and the sought-for components are visualised with labelled probes, as well as in linear blots.²¹⁹

In membrane tests, CG was used for diagnosis of parasitic,²²⁰⁻²²³ viral²²⁴⁻²²⁷ and fungal^{228, 229} diseases, tuberculosis,²³⁰ melioidosis,²³¹ syphilis,²³² brucellosis²³³ and shigellosis,²³⁴ for the determination of early pregnancy²³⁵ and blood groups,²³⁶ for the identification of plant antigens^{237, 238} and for dot-blot hybridisation.²³⁹

Attempts were made (in our opinion, not quite convincing) to stain samples with CG in wells of microtitration plates²⁴⁰⁻²⁴⁴ or on the cover glass surface²⁴⁵ and to use colloidal silver²⁴⁶ or coal particles²⁴⁷ instead of CG in solid-phase immunoassays. The application of CG in assays of large series of antigens in micro-matrices (immuno-chips) holds more promise.²⁴⁸ The latter method enables the determination of analytes at a concentration of 60-70 ng litre⁻¹. In this case, up to 384 samples can simultaneously be analysed using microlitre amounts of an analyte and an immunogold marker as the detecting agent.

Depending on the form in which an antigen is immobilised on a membrane, immunodot and immunoblot assays are distinguished. The former is employed in assays of non-fractionated specimens; the latter, in assays of pre-fractionated specimens. The immunodot assay is one of the simplest methods of analysis of antigens immobilised on membranes and, in some cases, enables their quantitative estimation. The immunodot assay is most often used for soluble antigens.²⁴⁹ Studies of whole bacterial cells by dot assay with an enzymatic label or by colony blot assay were also documented.²⁵⁰⁻²⁵³ The dot assay of whole bacterial cells using visualisation of the reaction products with biospecific markers, *viz.*, CG conjugates, (cell-gold immunoblotting) was used^{254, 255} for serotyping of nitrogen-fixing soil microorganisms. More recently, this method was applied to the diagnosis of intestinal infections.²⁵⁶

The sensitivity of a label depends on the gold particle size [the light attenuation coefficient increases with increasing particle diameter (> 40 nm)].²⁵⁷ This is the reason why most of companies producing gold markers recommend to use conjugates of a probe with CG particles with a diameter of 20-30 nm in blot assays. The sensitivity in dot assays was increased by using conjugates of recognising molecules with gold nanoparticles as nanorods and nanoshells.^{258, 259}

In the 1990s, some companies began to produce immunochemical diagnostic test kits. Due to high specificity and sensitivity of the immunoassay technique, these tests have found wide application in the determination of narcotic drugs and toxins, the early pregnancy diagnosis and screening of especially dangerous infections and urogenital diseases.²⁶⁰⁻²⁶⁷ In recent years, procedures have been developed for DNA hybridisation²⁶⁸ and tuberculosis diagnosis.²⁶⁹ Immunochromatography is a technique for rapid immune tests, which is most actively developed and widely used in practice.

Immunochromatographic assays are based on the motion of an eluent along a membrane (lateral diffusion), which is accom-

§ For example, a wide class of corpuscular antigens, such as whole bacterial cells, are among water-insoluble antigens.

¶ The gold stain is a gold sol partially stabilised by polymers, such as PEG 20M, Tween-20, *etc.*

panied by the formation of specific immune complexes in different membrane regions visualised as coloured bands.²⁷⁰ Enzymes, coloured latexes and, most often, CG are used as labels in these systems.^{271, 272}

Examinations of these test systems demonstrated their high stability, reproducibility of the results and correlation with alternative methods. The degree of inhomogeneity of the detected bands estimated by densitometry is in the range of 5%–8%, which enables reliable visualisation of the results of assays. These tests are very simple and convenient in use. However, the technology of production of components of such test kits (unlike dot-blot tests) is rather complicated and is the property of manufacturers, which limits the use of these methods in routine laboratory practice.

V. Application of colloidal gold for the quantitative protein determination

Dot-blot assays with the use of CG conjugates have found increasing use and gained wide acceptance due to high sensitivity and simplicity. However, this method has some limitations, among which are difficulties of rigorous quantitative interpretation of the results and operations with low-molecular-mass ligands and considerable problems associated with the detection of components of complex biological systems (homogenates, exudates, etc.).

In 1980, Leuvers *et al.*²⁷³ developed a new immunoassay method called the sol particle immunoassay (SPIA). This method employs two important properties of gold sols: (1) the typical bright red colour of sols, which remains virtually unchanged upon adsorption of high-molecular-mass compounds on gold particles, and (2) changes in the colour of sols upon aggregation of gold particles, which is detected from changes in absorption in the visible spectral region. These changes in absorption are clearly detected both spectrophotometrically and visually.

The SPIA method is rather simple in use. Solutions of a gold-containing marker and the sample under study are mixed in a reaction vessel, and either the spectrophotometric characteristics of the suspension are monitored or the colour of the suspension is visually estimated during the incubation period (0.5–2 h). If the biospecific reaction proceeding on the CG surface is accompanied by destabilisation of the sol resulting in aggregation of gold particles (in the case of polyclonal antibodies, this process is called agglutination), the absorption spectrum of the suspension shows substantial changes associated with a noticeable change in its colour (from red to blue or gray). Antigens can be quantitatively determined with spectrophotometers and colourimeters.

Later,^{274–277} this method was modified and optimised to detect human chorionic gonadotropin in the urine in pregnancy (larger gold particles and monoclonal antibodies to different antigen regions were used). Based on the results of these investigations, home-use test kit Discretest[®] for early pregnancy is produced (Chefaro company, the Netherlands). The immunocolorimetric test kits for the rheumatoid factor and streptolysin is produced by PLIVA Lachema company (Czech Republic).

More recently, this method was applied to immunoassays of *Schistosoma*²⁷⁸ and *Rubella*²⁷⁹ antigens, the determination of affinity constants for different isotypes of mouse monoclonal IgG²⁸⁰ and quantitative determination of immunoglobulins^{281, 282} and cystatin C (an endogenous marker for the filtration ability of kidney glomeruli).²⁸³

In 2002, Thanh and Rosenzweig²⁸⁴ rediscovered this method and applied it to the quantitative determination of antibodies to protein A with the use of the conjugate of protein A with CG. In recent years, new methods for the detection of a response of a system (for example, antigen–antibody labelled by CG) to interactions, such as photothermal spectroscopy,²⁸⁵ double-beam laser absorption spectroscopy²⁸⁶ and hyper-Rayleigh scattering,²⁸⁷ have enabled an increase in the assay sensitivity. The

combined use of agglutination of latex and gold particles (heterogeneous SPIA) was proposed.²⁸⁸

All versions of the SPIA method are very simple in use and are characterised by high sensitivity and specificity. However, researchers faced with the fact that antigen–antibody interactions on sol particles not always lead to destabilisation of the system (particle aggregation). In some cases, in spite of the obvious pair complementarity, the colour of the solution and, consequently, the absorption spectra change only slightly, if at all.

After a series of preliminary experiments, it was hypothesised²⁸⁹ that in these cases a second protein layer is formed on gold particles without loss of aggregation stability of the sol. In this case, changes in the spectra due to adsorption of the second biopolymer and, correspondingly, changes in the structure of the biopolymer layer on the metal particle surface are relatively small. However, even such small changes in the absorption spectra can be recorded and used for quantitative assays in biological applications.^{290, 291}

Another version of the above-described method was proposed by Mirkin and co-workers.⁷³ This version is based on the colourimetric determination of polynucleotides interacting with complementary oligonucleotides immobilised on gold nanoparticles. This process is accompanied by the formation of an ordered three-dimensional structure of gold nanoparticles, which leads to changes in the absorption spectrum of the solution and is detected visually⁷³ or photometrically.²⁹²

The formation of ordered three-dimensional structures in the reactions of IgG-functionalised gold nanoparticles with antigens^{176, 293} or with aptamers was documented.²⁹⁴ It was demonstrated that biologically programmed ensembles of gold nanoparticles can be prepared with the use of an avidin–biotin system.^{295, 296} An analogous approach was applied for the detection of lectins.¹⁴⁶ Ca²⁺-dependent aggregation of gold nanoparticles coated with carbohydrates was described.²⁹⁷

In spite of the fact that the SPIA method is very simple in use, the real practical applications of this method during 20 years have been described in rather modest number of papers. Only in the very recent past, this method has been demonstrated to be promising as a high-performance clinical test. In our opinion, the SPIA method has little use because the physicochemical and optical mechanisms of the conversion of signals, which are generated upon the biospecific binding of target molecules to CG conjugates, into characteristics of light attenuation or scattering by suspensions are poorly understood.

A new version of the SPIA method with the use of microtitration plates and microplate reader and a trypsin (proteolytic enzyme) conjugate with CG as a specific visualising agent for proteins was proposed.²⁹⁸ This assay holds considerable promise for the rapid, sensitive and quantitative protein determination.

VI. Application of gold nanoparticles in studies of biologically active compounds by vibrational spectroscopy

Raman spectroscopy is an efficient tool to investigate molecular structures because the set of intramolecular vibrational frequencies is uniquely related to the molecular structure as well as to intermolecular and intramolecular interactions.^{299, 300} However, since the intensity of the Raman signal is relatively low, the detection of this signal is a rather complex problem and requires the use of modern laser sources and photon counting systems. In 1974, Fleischman *et al.*³⁰¹ suggested that the effective number of molecules involved in scattering from the adsorbed monolayer could be increased by increasing the real surface area with retention of the ‘visible’ surface area illuminated with pumping radiation. For this purpose, the silver surface was made coarse by anodic etching and the spectra of compounds adsorbed on this surface were recorded. The intensity of Raman scattering increased by a factor of 10⁶–10⁷, while the surface area after

etching of the silver electrode surface increased by only an order of magnitude.³⁰¹ More recently, it was demonstrated that the observed enhancement of Raman scattering is associated with a new non-linear effect called the surface-enhanced Raman scattering (SERS) effect.[†]

Surface-enhanced Raman scattering has some features distinguishing it from conventional Raman scattering. First, SERS cross-sections for vibrational modes of adsorbed molecules can be increased by a factor of 10^{10} or more compared to the analogous parameters for unadsorbed molecules. Second, the enhancement of scattering varies depending of the excitation frequency and the degree of roughness of the support according to a law specific for SERS. Third, the SERS spectra of many adsorbed molecules are substantially different from the corresponding Raman spectra of molecules in the free state. This is manifested in the selective enhancement of particular vibrations and the appearance of new bands in the SERS spectrum.

Abundant information on applications of surface-enhanced Fourier-transform IR and SERS spectroscopy in biological studies is summarised in the reviews.^{303–306} Vibrational spectroscopic methods are used for studying individual biomolecules, as well as cells and tissues.^{307–311}

In most of the cited studies, vibrations of biomolecules were enhanced due to their adsorption on metal electrodes or thin films. However, in recent years the methods in which signals are enhanced with the use of colloidal metals (primarily, gold and silver), have gained wide acceptance.^{312–316} In these methods, the signal is enhanced by giant non-linear local fields that are produced in metal clusters.^{317,318} Different versions of immunoassay with the use of antibodies or antigens adsorbed on gold nanoparticles and vibrational spectroscopic methods were developed.^{319–323}

It was demonstrated for the first time³²⁴ that Fourier-transform IR spectroscopy can be employed for the sensitive determination of interactions of protein molecules with the gold particle surface and for the reliable and simple monitoring of biospecific reactions. This method (that is called spectroimmunochemical) can serve as a basis for the development of test systems detecting biospecific antigen–antibody, enzyme–substrate, lectin–polysaccharide, *etc.* interactions. The observed changes in the spectra of biomolecules immobilised on gold particles are evidence that these biomolecules are indeed adsorbed. The proposed method along with other methods (for example, SERS) can be used for controlling the quality of gold conjugates.

VII. Gold nanoparticles as antigen carriers

Let us briefly consider two interrelated problems of modern immunology that attract the attention of many researchers. These are the preparation of antibodies against non-immunogenic low-molecular-mass compounds (haptens) and the design of new generation vaccines based on natural (microbial) or synthetic peptides.^{325–328}

The biosynthesis of antibodies in organisms is known to be induced by compounds possessing a rather developed structure (immunogenicity). These compounds include proteins and polysaccharides.³²⁹ However, many biologically active compounds (neuromediators, hormones, vitamins, antibiotics, *etc.*) have rather low molecular masses. Low-molecular-mass antigens belong to the so-called weak antigens, *i.e.*, a pronounced immune response against these antigens (biosynthesis of the corresponding antibodies) is not developed.

The preparation of antibodies against haptens has attracted interest for several reasons. First, antibodies to particular fragments of biomacromolecules can serve as a highly efficient tool for

investigating their topography and structures. Second, the preparation of antibodies to such low-molecular-mass compounds, as antibiotics, hormones and some pharmaceuticals, would enable the control of their amount in the blood of patients, in meat and dairy products and in cultural media. The drug monitoring is widely used in all developed countries. This method enables substantial enhancement of the efficiency of curing and prevention of complications. Among various procedures for the detection of such compounds, immunochemical assay is most convenient and highly sensitive, which implies the preparation of antibodies to these low-molecular-mass compounds. Antibodies to low-molecular-mass compounds hold considerable promise in immunotherapeutic practice.^{325,330} Third, attempts are made to use synthetic peptides for the design of artificial (acellular) vaccines containing only protective antigens and inert carriers.

Since haptens exhibit weak immunogenicity, the choice of an optimal carrier (a delivery system) providing a high immune response and the preparation of sufficiently pure antibodies are important problems to be solved in the preparation of antibodies to haptens. These problems are traditionally solved by covalent coupling of a hapten to a protein matrix, the so-called *schlepper* (which comes from the German word 'schleppen', which means 'to drag, lug') with the use of adjuvants and intensive schemes of animal immunisation by the resulting conjugate.^{325,331} Bovine serum albumin, ovalbumin, thyroglobulin, hemocyanin, diphtheria or tetanus anatoxins (for synthetic peptides), *etc.* are usually used as *schleppers*. However, these processes give antibodies against both a hapten and immunodeterminant sites of a carrier. The use of such carriers not necessarily gives rise to a pronounced immune response to weak antigens. In addition, the subsequent purification and screening of the resulting antibodies are time-consuming and expensive, and their titer and affinity are often low.

Most of the presently used adjuvants based on oil emulsions and suspensions of inorganic compounds are, as a rule, prone to phase separation, their immunogenic properties change with time, and many of such adjuvants cause local and systemic toxic effects.^{332,333} The application of antibody phage display is seemingly the most promising solution of the problem of the preparation of antibodies against haptens.³³⁴ However, this technique is virtually inapplicable in vaccinology.

In recent years, studies have been carried out on the design of the so-called complex antigens, *i.e.*, artificial macromolecular complexes containing both the desired antigenic determinants and carriers and/or adjuvants. In particular, synthetic polyelectrolytes [poly-L-lysine, polyacrylic acid, polyvinylpyridine, poly(styrenesulfonate), Ficoll, *etc.*] were proposed as carriers.³³⁵ For example, the influenza vaccine Grippol was designed based on the cation exchange resin 'Polyoxonium'. These polymeric compounds are synthesised by radical polymerisation of the corresponding monomers.³³⁶ The simplicity of the chemical synthesis of polyelectrolytes and the possibility of preparation of polymer chains in a broad molecular mass range (*i.e.*, of different length), solubility in water and other properties (the ability to undergo conformational transformations, complex formation with proteins, *etc.*) opened up possibilities for their application in immunological studies.³³⁷ These carrier-adjuvants can form a depot of antigens at the site of injection, enhance the presentation of antigens to immunocompetent cells and induce the production of required cytokines. However, low immunogenicity of such complexes associated with a low epitopic density stimulated a search for new non-toxic and efficient carriers having, in addition, adjuvant properties.

In our opinion, nanosized corpuscular carriers, such as polymeric nanoparticles [for example, poly(methyl methacrylate)],³³⁸ liposomes, proteosomes and microcapsules,^{339–341} fullerenes,^{342,343} carbon nanotubes,³⁴⁴ *etc.*, hold considerable promise in this respect. The use of such carriers leads to a change in the form of manifestation of immunogenicity of the required compound in the immune system of host organisms. An antigen

[†] Adsorption of molecules of the compound under study on the metal surface is accompanied also by changes in luminescence, absorption and non-linear effects and the appearance of induced optical activity.³⁰²

adsorbed to, or encapsulated in, nanoparticles can be used as an adjuvant for optimisation of the immune response of the organism upon vaccination. For example, an analysis of the dynamics of an immune response demonstrated that the titer of antibody in response to an antigen introduced together with fullerenes was equal to the titer of antibody in response to the antigen introduced together with the Freund's complete adjuvant (FCA) and was approximately an order of magnitude larger than the titer of antibody in response to the antigen introduced without an adjuvant.

In 1986, the successful preparation of antibody to glutamic acid with the use of CG particles as a carrier was reported in the pioneering study by Japanese researchers.³⁴⁵ (It should be noted that colloidal metals were used for stimulation of an immune response to haptens and complete antigens as early as 1920th by Zil'ber and co-workers.^{346–348}) More recently, this method has been applied and improved for the preparation of antibodies to the following haptens and complete antigens: amino acids,^{349,350} platelet activating factor,^{351,352} quinolinic acid,³⁵³ biotin,³⁵⁴ immunophilin,³⁵⁵ lysophosphatidic acid,³⁵⁶ endostatin,³⁵⁷ peptides of hepatitis C virus capsid,³⁵⁸ surface antigens of *Yersinia*³⁵⁹ and brucellas.³⁶⁰ In all the above-mentioned studies, haptens were directly conjugated with CG particles, mixed with FCA and used for immunisation of animals. As a result, high-titer antisera, which did not require further purification from ballast antibodies, were obtained.

In 1993, Australian scientists³⁶¹ suggested that haptens should be added to a carrier protein before conjugation with CG. More recently, this approach was applied for the preparation of antibodies against a number of synthetic^{362–365} and natural³⁶⁶ peptides, amino acids,^{367,368} citrulline³⁶⁹ and phenyl β -D-thiogluconide.³⁷⁰ In these studies, FCA or *N*-acetylmuramyl-L-alanyl-D-isoglutamine were used as adjuvants.³⁶³ Antibodies prepared according to this procedure have high specificity for antigens under examination and a higher titer (the authors of the publication³⁶¹ referred to this titer as extremely high), from 1:250 000 to 1:1 000 000, compared to antibodies prepared according to a conventional procedure (by conjugation with a schlepper).

In 1996, researchers from the Khabarovsk Research Institute of Epidemiology and Microbiology demonstrated³⁷¹ for the first time that CG particles in a viral vaccine can be used as carriers of tick-borne encephalitis virus capsid protein antigen. According to the results of this study, in spite of the fact that no adjuvants are present in the vaccine, the latter has higher protective properties compared to commercial analogues. In 2003, a new procedure for the preparation of antibodies against A β peptides, which is a molecular marker of Alzheimer's disease, was described.³⁷² The authors designed a molecular mimic of the fibrillar form of A β peptides by covalently binding prethiolated oligomers to the gold particle surface. Antibodies to antigens that were synthesised according to this procedure, have very high specificity and affinity for both soluble and fibrillar forms of A β peptides.

Numerous studies were devoted to applications of CG particles in the design of DNA vaccines. In DNA immunisation, gene constructions coding proteins to which it is necessary to prepare antibodies, are introduced into organisms. In the case of efficient gene expression, these proteins serve as antigens for the development of an immune response.^{373,374} In early studies, immunisation was performed with subcutaneous or intramuscular injections of 'naked' DNA. However, the biolistic transfection with nanoparticles began to be applied for this purpose almost at the same time. This procedure proved to be very efficient due apparently to multiple sites of interactions between a transgene and tissues. The injection material began to be administered subcutaneously, epicutaneously or intranasally.^{375,376}

Among nanoparticles, colloidal gold particles are most widely applied as DNA carriers.^{377–383} Initially, gold has been used only as a carrier, but more recently gold was demonstrated to enhance

an immune response *in vivo*.³⁸⁴ However, to our knowledge, data on the mechanisms of this action of gold particles are lacking.

Gene immunisation (it is often called DNA immunisation), which has been developed in tests on animals, is highly efficient, particularly, against viral infections, such as tick-borne encephalitis, HIV infection, hepatitis B and some other. The DNA immunisation has some advantages over conventional vaccination. One recombinant vector can simultaneously direct the synthesis of several antigens, which decreases the number of immunisations. This eliminates problems associated with the difficulties of penetration of proteins into organisms and, in addition, substantially decreases the risk of side effects, which depend on toxicity of inactive proteins introduced in the case of conventional vaccination or virulence in bacteria and viruses. In the coming years, DNA immunisation would be expected to be among the most efficient methods of gene therapy.^{37,385,386}

The preparation of antibodies to complete antigens and haptens of different nature using CG particles as carriers was documented.^{387,388} It was demonstrated that CG as an antigen carrier activates phagocytic activity of macrophages and influences the functioning of lymphocytes, which is apparently responsible for its immunomodulation effect. The most interesting aspect of manifestation of the immunogenic properties by haptens upon their immobilisation on colloidal gold is that CG particles act simultaneously as adjuvants and carriers, *i.e.*, present haptens to T-cells. Gold nanoparticles conjugated with antigens were found to influence activation of T-cells (an increase in proliferation by a factor of 10 compared to that upon the addition of the native antigen). This fact shows that the targeted activation of T-cells (for example, by antigens of *Mycobacterium tuberculosis*, HIV, *etc.*) followed by activation of macrophages and pathogen killing is possible, in principle, which holds considerable promise for the design of new generation vaccines.

The question is what is responsible for the adjuvant properties of CG. Nowadays, there is no answer to this question. However, let us give some comments.

In our opinion, conclusions about the preferable macrophage response to corpuscular antigens, unlike soluble antigens, is undoubtedly valid.³⁶¹ This fact was confirmed in the studies^{379,381,384} where the mechanism of action of DNA vaccines was elucidated and gold particles were used for delivery of genetic material into cells. In these studies, the role of the Kupffer cells and the Langerhans islets in the immune response was revealed. Moreover, CG particles were used in the studies^{389,390} of endocytosis by macrophages. (Gold particles included in phagocyte lysosomes even received their own name 'aurosomes'.) The influence of dendrite cells on the immune response to antigens conjugated with gold nanoparticles was discussed.³⁹¹ In addition, the authors mentioned that, when using nanoparticles in medical practice, it is necessary that lipopolysaccharides be absent on their surface.

However, these data do not reveal further mechanisms of presentation of antigens to T helpers. According to modern views,^{329,392} the presentation of antigens to T-cells is preceded by processing (protein cleavage into peptide fragments) followed by the formation of compounds with molecules of the major histocompatibility complex, which performs the delivery of an antigen fragment to the surface of antigen-presenting cells. Hence, it remains unclear how this process can occur with haptens. The assumption about the existence of a multivalent antigen, *i.e.*, the antigen that is formed due to a high local concentration of monovalent antigens on the gold particle surface, also does not answer this question.

At the same time, the influence of gold salts on the immune system has long been known.^{393–397} Treatment of a number of autoimmune diseases, in particular, of rheumatoid arthritis, is based on the ability of gold to change non-specific immune reactions of an organism. For example, the successful therapy of rheumatoid arthritis by a colloidal gold solution was documented.^{30,398} According to the results of another study,³⁹⁹ in this

case the function of CG is to inhibit monocyte-induced proliferation of lymphocytes. The transformation of Au(0) into Au(I) in immune system cells under the action of certain amino acids was discussed.⁴⁰⁰

Contradictory results were obtained in the studies^{401–403} aimed at examining the sensitivity of mammalian organisms to the introduction of metallic gold. In particular, it was noted^{401,402} that the injection of CG into laboratory animals can lead to inflammatory reactions, accumulation of gold in reticular cells of lymphoid tissues and activation of cellular and humoral immunity. However, in the study⁴⁰³ dealt with the influence of gold nanoparticles on the immune system cells, it was concluded that CG particles is a non-cytotoxic, non-immunogenic and biocompatible material for the potential application in different fields of nanoimmunology, nanomedicine and nanobiotechnology.

In recent years, the use of gold nanoparticles for targeted drug delivery has been considered in a number of publications (see, for example, Refs 32 and 404–406). In this connection, it should be noted that, in our opinion, this problem must be considered with caution taking into account that antibodies against the administered drug adsorbed on CG particles can be formed in animal and human organisms.

In conclusion, it should be noted that it is apparently the time to consider not only biochemistry, but also biophysics of the immune response, because it is the unique biophysical properties of metal particles, in particular, the surface charge and the electrostatic field of the particles (which influence the charge, orientation and polarisation of antigenic molecules adsorbed on the particles) that have a substantial effect on the immune response.

This review has been written with the financial support of the Russian Foundation for Basic Research (Project Nos 04-04-48224 and 05-02-16776).

References

1. J Sadoul *Alchemists and Gold* (New York: Putnam Publ. Group, 1972)
2. F Antonii *Panacea Aurea-Auro Potabile* (Hamburg: Bibliopolio Frobeniano, 1618)
3. M Faraday *Philos. Trans. R. Soc. London* **147** 145 (1857)
4. R Zsigmondy *Ann. Chim.* **301** 29 (1898)
5. R Zsigmondy *Das Kolloide Gold* (Leipzig: Akademische Verlagsgesellschaft, 1925)
6. T Svedberg *Colloid Chemistry (ACS Monography 16)* (New York: Chem. Catalog. Co, 1924)
7. L De Brouckere, J Casimir *Bull. Soc. Chim. Belg.* **57** 517 (1948)
8. A Fabrikanos, S Athanassiou, K H Lieser *Z. Naturforsch., B* **18** 612 (1963)
9. C L Beigent, G Müller *Experimentia* **36** 472 (1980)
10. J Turkevich *Gold Bull.* **18** 86 (1985)
11. J F Hainfeld *Science* **236** 450 (1987)
12. G Mie *Ann. Phys.* **25** 377 (1908)
13. J Turkevich, G Garton, P C Stevenson *J. Colloid Sci., Suppl. 1* **9** 26 (1954)
14. C F Bohren, D R Huffman *Absorption of Light by Small Particles* (New York: Wiley, 1983)
15. U Kreibitz, M Vollmer *Optical Properties of Metal Clusters (Springer Series in Materials Science)* (Heidelberg: Springer, 1995)
16. M Y Lin, H M Lindsay, D A Weitz, R C Ball, R Klein, P Meakin *Phys. Rev. A* **41** 2005 (1990)
17. H R Kruyt *Colloid Science* (Amsterdam: Elsevier, 1952)
18. W Heller, T L Pugh *J. Polym. Sci.* **47** 203 (1960)
19. H Thiele, K Hoppe, G Moll *Kolloid-Z. Z. Polym.* **185** 45 (1962)
20. A A Baran *Polimersoderzhashchie Dispersnye Sistemy* (Polymer-containing Disperse Systems) (Kiev: Naukova Dumka, 1986)
21. M K Chow, C F Zukoski *J. Colloid Interface Sci.* **165** 97 (1994)
22. R J Paddephatt *The Chemistry of Gold* (Amsterdam: Elsevier, 1978)
23. A I Busev, V M Ivanov *Analiticheskaya Khimiya Zolota* (Analytical Chemistry of Gold) (Moscow: Nauka, 1973)
24. S A Marakushev *Geomikrobiologiya i Biokhimiya Zolota* (Geomicrobiology and Biochemistry of Gold) (Moscow: Nauka, 1991)
25. M J Ware *J. Photogr. Sci.* **42** 157 (1994)
26. G C Bond, C Louis, D T Thompson *Catalysis by Gold* (London: Imperial College Press, 2006)
27. S Q Liu, D Leech, H X Ju *Anal. Lett.* **36** 1 (2003)
28. F Green *The Colloidal Gold Reaction of the Cerebrospinal Fluid* (Berlin: Medizin Fritz-Dieter Söhn, 1925)
29. N F MacLagan *Br. J. Exp. Pathol.* **25** 15 (1944)
30. G E Abraham, P B Himmel *J. Nutr. Med.* **7** 295 (1997)
31. E E Rogoff, R Romano, E W Hahn *Radiology* **114** 225 (1975)
32. G F Paciotti, L Myer, D Weinreich, D Goia, N Pavel, R E McLaughlin, L Tamarkin *Drug Deliv.* **11** 169 (2004)
33. C M Pitsillides, E K Joe, X Wei, R R Anderson, C P Lin *Biophys. J.* **84** 4023 (2003)
34. I H El-Sayed, X H Huang, M A El-Sayed *Nano Lett.* **5** 829 (2005)
35. C Loo, A Lin, L Hirsch, M-H Lee, J Barton, N Halas, J West, R Drezek *Technol. Cancer Res. Treat.* **3** 33 (2004)
36. E J Andreu, J J M de Llano, I Moreno, E Knecht *J. Histochem. Cytochem.* **46** 1199 (1998)
37. A V Zelenin *Vestn. Ros. Akad. Nauk* **71** 387 (2001)^a
38. G A Hughes *Nanomedicine* **1** 22 (2005)
39. W Faulk, G Taylor *Immunochemistry* **8** 1081 (1971)
40. G Frens *Nature Phys. Sci.* **241** 20 (1973)
41. M A Hayat (Ed.) *Colloidal Gold: Principles, Methods, and Applications* (San Diego, CA: Academic Press, 1989)
42. G R Bullock, P Petrusz (Eds) *Techniques in Immunocytochemistry* (London: Academic Press, 1982)
43. J De Mey, M Moeremans, in *Advanced Techniques in Biological Electron Microscopy* (Ed. J K Koehler) (Berlin: Springer, 1986) p. 229
44. M D Rekhter, A A Mironov *Usp. Sovrem. Biol.* **109** 467 (1990)
45. L A Dykman, V A Bogatyrev *Biokhimiya* **62** 411 (1997)^b
46. W R Glomm *J. Dispers. Sci. Technol.* **26** 389 (2005)
47. M C Daniel, D Astruc *Chem. Rev.* **104** 293 (2004)
48. H B Weiser *Inorganic Colloid Chemistry* (New York: Wiley, 1933)
49. G Danscher *Histochemistry* **71** 81 (1981)
50. Z F Ma, S-F Sui *Angew. Chem., Int. Ed.* **41** 2176 (2002)
51. Th Schalkhammer *Monatsh. Chem. (Chem. Monthly)* **129** 1067 (1998)
52. M Malmqvist *Nature (London)* **361** 186 (1993)
53. M D Musick, C D Keating, L A Lyon, S L Botsko, D J Peña, W D Holliway, T M McEvoy, J N Richardson, M J Natan *Chem. Mater.* **12** 2869 (2000)
54. A N Shipway, E Katz, I Willner *ChemPhysChem* **1** 18 (2000)
55. W A De Heer *Rev. Mod. Phys.* **65** 611 (1993)
56. M Brack *Rev. Mod. Phys.* **65** 677 (1993)
57. G Schmid, L F Chi *Adv. Mater.* **10** 515 (1998)
58. V M Shalaev, M I Shtokman *Zh. Eksp. Teor. Fiz.* **92** 509 (1987)^c
59. A V Butenko, P A Chubakov, Yu E Danilova, S V Karpov, A K Popov, S G Rautian, V P Safonov, V V Slabko, V M Shalaev, M I Stockman *Z. Phys. D* **17** 283 (1990)
60. A C Templeton, J J Pietron, R W Murray, P Mulvaney *J. Phys. Chem. B* **104** 564 (2000)
61. S G Penn, L He, M J Natan *Curr. Opin. Chem. Biol.* **7** 609 (2003)
62. P Schuk *Annu. Rev. Biophys. Biomol. Struct.* **26** 541 (1997)
63. W M Mullett, E P C Lai, J M Yeung *Methods* **22** 77 (2000)
64. C M Niemeyer *Angew. Chem., Int. Ed.* **40** 4128 (2001)
65. D A Schultz *Curr. Opin. Biotechnol.* **14** 13 (2003)
66. W J Parak, D Gerion, T Pellegrino, D Zanchet, C Micheel, S C Williams, R Boudreau, M A Le Gros, C A Larabell, A P Alivisatos *Nanotechnology* **14** R15 (2003)
67. J C Riboh, A J Haes, A D McFarland, C R Yonzon, R P Van Duyne *J. Phys. Chem. B* **107** 1772 (2003)
68. A Moores, F Goettmann *New J. Chem.* **30** 1121 (2006)
69. A Ulman *Chem. Rev.* **96** 1533 (1996)
70. C L Haynes, R P Van Duyne *J. Phys. Chem. B* **105** 5599 (2001)
71. L A Lyon, M D Musick, M J Natan *Anal. Chem.* **70** 5177 (1998)
72. M Adamczyk, J A Moore, Z Yu *Methods* **20** 319 (2000)
73. C A Mirkin, R L Letsinger, R C Mucic, J J Storhoff *Nature (London)* **382** 607 (1996)

74. P Bao, A G Frutos, Ch Greef, J Lahiri, U Muller, T C Peterson, L Warden, X Y Xie *Anal. Chem.* **74** 1792 (2002)
75. G Raschke, S Kowarik, T Franzl, C Sönnichsen, T A Klar, J Feldmann, A Nichtl, K Kürzinger *Nano Lett.* **3** 935 (2003)
76. A D McFarland, R P Van Duyne *Nano Lett.* **3** 1057 (2003)
77. A Csáki, G Maubach, D Born, J Reichert, W Fritzsche *Single Mol.* **3** 275 (2002)
78. D L Feldheim, C D Keating *Chem. Soc. Rev.* **27** 1 (1998)
79. S I Bozhevolnyi, in *Optics of Nanostructured Materials (Wiley Series in Lasers and Applications)* (Eds V A Markel, Th F George) (New York: Wiley-Interscience, 2000) p. 73
80. K Kneipp, H Kneipp, I Itzkan, R R Dasari, M S Feld *J. Phys.: Condens. Matter* **14** R597 (2002)
81. W E Doering, S M Nie *J. Phys. Chem. B* **106** 311 (2002)
82. B Rothenhäusler, W Knoll *Nature (London)* **332** 615 (1988)
83. J Belloni *Curr. Opin. Colloid Interface Sci.* **1** 184 (1996)
84. J Yguerabide, E E Yguerabide *Anal. Biochem.* **262** 137 (1998)
85. V I Roldugin *Usp. Khim.* **69** 899 (2000) [*Russ. Chem. Rev.* **69** 821 (2000)]
86. G C Schatz *J. Mol. Struct. (THEOCHEM)* **573** 73 (2001)
87. N G Khlebtsov, A G Melnikov, L A Dykman, V A Bogatyrev, in *Photopolarimetry in Remote Sensing* (Eds G Videen, Y Yatskiv, M Mishchenko) (Dordrecht: Kluwer Academic, 2004) p. 265
88. E Katz, I Willner *Angew. Chem., Int. Ed.* **43** 6042 (2004)
89. T Teranishi, in *Encyclopedia of Surface and Colloid Science* (Ed. A Hubbard) (New York: Marcel Dekker, 2002) p. 3314
90. J Roth, in *Techniques in Immunocytochemistry* (Eds G R Bullock, P Petrusz) (London: Academic Press, 1983) p. 217
91. D A Handley, in *Colloidal Gold: Principles, Methods and Applications* (Ed. M A Hayat) (San Diego, CA: Academic Press, 1989) p. 13
92. J Turkevich, P C Stevenson, J Hillier *Discuss. Faraday Soc.* **11** 55 (1951)
93. E C Stathis, A Fabricanos *Chem. Ind. (London)* **27** 860 (1958)
94. H Mühlfordt *Experientia* **38** 1127 (1982)
95. J W Slot, H J Geuze *Eur. J. Cell Biol.* **38** 87 (1985)
96. J Tschopp, E R Podack, H J Muller-Eberhard *Proc. Natl. Acad. Sci. USA* **79** 7474 (1982)
97. G B Birrel, K K Hedberg *J. Electron Microsc. Tech.* **5** 219 (1987)
98. N G Khlebtsov, V A Bogatyrev, L A Dykman, A G Melnikov *J. Colloid Interface Sci.* **180** 436 (1996)
99. R G DiScipio *Anal. Biochem.* **236** 168 (1996)
100. W Baschong, J M Lucocq, J Roth *Histochemistry* **83** 409 (1985)
101. J M Thomas *Pure Appl. Chem.* **60** 1517 (1988)
102. K R Brown, M J Natan *Langmuir* **14** 726 (1998)
103. K R Brown, D G Walter, M J Natan *Chem. Mater.* **12** 306 (2000)
104. N R Jana, L Gearheart, C J Murphy *Langmuir* **17** 6782 (2001)
105. J P Wilcoxon, P P Provencio *J. Am. Chem. Soc.* **126** 6402 (2004)
106. D V Goia, E Matijević *Colloids Surf., A* **146** 139 (1999)
107. H Hirai, H Aizawa *J. Colloid Interface Sci.* **161** 471 (1993)
108. M Green, P O'Brien *Chem. Commun.* 183 (2000)
109. M Giersig, P Mulvaney *Langmuir* **9** 3408 (1993)
110. M Brust, D Walker, D Bethell, D J Schiffrin, R Whyman *J. Chem. Soc., Chem. Commun.* 801 (1994)
111. M Brust, C J Kiely *Colloids Surf., A* **202** 175 (2002)
112. S Stoeva, K J Klabunde, C M Sorensen, I Dragieva *J. Am. Chem. Soc.* **124** 2305 (2002)
113. Y Zhou, H Itoh, T Uemura, K Naka, Y Chujo *Chem. Commun.* 613 (2001)
114. S Sato, K Toda, S Oniki *J. Colloid Interface Sci.* **218** 504 (1999)
115. Y Tan, X Dai, Y Li, D Zhu *J. Mater. Chem.* **13** 1069 (2003)
116. K Esumi, N Takei, T Yoshimura *Colloids Surf., B* **32** 117 (2003)
117. A Pal *J. Nanoparticle Res.* **6** 27 (2004)
118. T Sugimoto *Adv. Colloid Interface Sci.* **28** 65 (1987)
119. L Longenberger, G Mills *J. Phys. Chem.* **99** 475 (1995)
120. T Teranishi, M Miyake *Hyomen (Japan)* **35** 439 (1997)
121. S Nuss, H Böttcher, H Wurm, M L Hallensleben *Angew. Chem., Int. Ed.* **40** 4016 (2001)
122. H Hirai, Y Nakao, N Toshima *J. Macromol. Sci. Chem., A* **13** 727 (1979)
123. J P Spatz, S Mössmer, M Möller *Chem. – Eur. J.* **12** 1552 (1996)
124. Q Liu, H Liu, Q Zhou, Y Liang, G Yin, Z Xu *J. Mater. Sci.* **41** 3657 (2006)
125. K Esumi, A Susuki, N Aihara, K Usui, K Torigoe *Langmuir* **14** 3157 (1998)
126. J M Slocik, M O Stone, R R Naik *Small* **1** 1048 (2005)
127. L A Dykman, A A Lyakhov, V A Bogatyrev, S Yu Shchegolev *Kolloid. Zh.* **60** 757 (1998)^d
128. S T Wang, J C Yan, L Chen *Mater. Lett.* **59** 1383 (2005)
129. A V Singh, B M Bandgar, M Kasture, B L V Prasad, M Sastry *J. Mater. Chem.* **15** 5115 (2005)
130. C E Hoppe, M Lazzari, I Pardiñas-Blanco, M A López-Quintela *Langmuir* **22** 7027 (2006)
131. H Otsuka, Y Akiyama, Y Nagasaki, K Kataoka *J. Am. Chem. Soc.* **123** 8226 (2001)
132. S A Yeung, R Hobson, S Biggs, F Grieser *J. Chem. Soc., Chem. Commun.* 378 (1993)
133. W Chen, W Cai, L Zhang, G Wang, L Zhang *J. Colloid Interface Sci.* **238** 291 (2001)
134. M Mandal, S Kundu, S K Ghosh, T Pal *Bull. Mater. Sci.* **25** 509 (2002)
135. Y Niidome, A Hori, T Sato, S Yamada *Chem. Lett.* 310 (2000)
136. E Gachard, H Remita, J Khatouri, B Keita, L Nadjio, J Belloni *New J. Chem.* **22** 1257 (1998)
137. F Mafuné, J-Y Kohno, Y Takeda, T Kondow, H Sawabe *J. Phys. Chem. B* **105** 5114 (2001)
138. K Mallick, M J Witcomb, M S Scurrall *Appl. Phys. A* **80** 395 (2005)
139. H Ma, B Yin, S Wang, Y Jiao, W Pan, S Huang, S Chen, F Meng *ChemPhysChem* **5** 68 (2004)
140. B G Ershov *Ros. Khim. Zh.* **45** (3) 20 (2001)^e
141. P A Bartlett, B Bauer, S J Singer *J. Am. Chem. Soc.* **100** 5085 (1978)
142. J F Hainfeld, R D Powell *J. Histochem. Cytochem.* **48** 471 (2000)
143. T G Schaaff, R L Whetten *J. Phys. Chem. B* **104** 2630 (2000)
144. C J Ackerson, P D Jadzinsky, G J Jensen, R D Kornberg *J. Am. Chem. Soc.* **128** 2635 (2006)
145. J L Gardea-Torresdey, J G Parsons, E Gomez, J Peralta-Videa *Nano Lett.* **2** 397 (2002)
146. C S Shankar, A Ahmad, R Pasricha, M Sastry *J. Mater. Chem.* **13** 1822 (2003)
147. M Gericke, A Pinches *Gold Bull.* **39** 22 (2006)
148. A Anshup, J S Venkataraman, C Subramaniam, R R Kumar, S Priya, T R S Kumar, R V Omkumar, A John, T Pradeep *Langmuir* **21** 11562 (2005)
149. M S Kunz, K R Shull, A J Kellok *J. Colloid Interface Sci.* **156** 240 (1993)
150. M K Corbierre, N S Cameron, M Sutton, S G J Mochrie, L B Lurio, A Rühm, R B Lennox *J. Am. Chem. Soc.* **123** 10411 (2001)
151. S T Selvan, J P Spatz, H-A Klock, M Möller *Adv. Mater.* **10** 132 (1998)
152. N R Jana, L Gearheart, S O Obare, C J Murphy *Langmuir* **18** 922 (2002)
153. N R Jana, L Gearheart, C J Murphy *J. Phys. Chem. B* **105** 4065 (2001)
154. B Nikoobakht, M A El-Sayed *J. Phys. Chem. A* **107** 3372 (2003)
155. J J Mock, S J Oldenburg, D R Smith, D A Schultz, S Schultz *Nano Lett.* **2** 465 (2002)
156. T Pham, J B Jackson, N J Halas, T R Lee *Langmuir* **18** 4915 (2002)
157. T Ung, L M Liz-Marzán, P Mulvaney *Colloids Surf., A* **202** 119 (2002)
158. Y Sun, Y Xia *Science* **298** 2176 (2002)
159. H Liao, C L Nehl, J H Hafner *Nanomedicine* **1** 201 (2006)
160. N G Khlebtsov, A G Melnikov, V A Bogatyrev, L A Dykman, A V Alekseeva, L A Trachuk, B N Khlebtsov *J. Phys. Chem. B* **109** 13578 (2005)
161. A V Alekseeva, V A Bogatyrev, B N Khlebtsov, A G Mel'nikov, L A Dykman, N G Khlebtsov *Kolloid. Zh.* **68** 725 (2006)^d
162. N G Khlebtsov, V A Bogatyrev, L A Dykman, B N Khlebtsov *Nanotekhnika* **4** 1 (2006)
163. F Chen, G-Q Xu, T S A Hor *Mater. Lett.* **4325** 1 (2003)

164. F Kim, J H Song, P Yang *J. Am. Chem. Soc.* **124** 14316 (2002)
165. B M I van der Zande, M R Böhmer, L G J Fokink, C Schönenberger *Langmuir* **16** 451 (2000)
166. S L Pan, M Chen, H L Li *Colloids Surf., A* **180** 55 (2001)
167. T Kinoshita, S Seino, K Okitsu, T Nakayama, T Nakagawa, T A Yamamoto *J. Alloys Compd.* **359** 46 (2003)
168. I D Walton, S M Norton, A Balasingham, L He, D F Oviso, D Gupta, P A Raju, M J Natan, R G Freeman *Anal. Chem.* **74** 2240 (2002)
169. M P Mallin, C J Murphy *Nano Lett.* **2** 1235 (2002)
170. Yu G Frolov *Kurs Kolloidnoi Khimii. Poverkhnostnye Yavleniya i Dispersionnye Sistemy* (Course of Colloid Chemistry. Surface Effects and Dispersion Systems) (Moscow: Khimiya, 1989)
171. E D Shchukin, A V Pertsov, E A Amelina *Kolloidnaya Khimiya* (Colloid Chemistry) (Moscow: Moscow State University, 1982)
172. E D Goddard, B Vincent *Polymer Adsorption and Dispersion Stability (ACS Symp. Ser.)* (Washington, DC: American Chemical Society, 1984)
173. A B R Mayer, J E Mark *Pure Appl. Chem.* **11** 2151 (1997)
174. G T Hermanson *Bioconjugate Techniques* (San Diego, CA: Academic Press, 1996)
175. M Donbrow (Ed.) *Microcapsules and Nanoparticles in Medicine and Pharmacy* (Boca Raton, FL: CRC Press, 1992)
176. W Shenton, S A Davis, S Mann *Adv. Mater.* **11** 449 (1999)
177. L H Dubois, R G Nuzzo *Annu. Rev. Phys. Chem.* **43** 437 (1992)
178. C R Lowe *Curr. Opin. Struct. Biol.* **10** 428 (2000)
179. R L Letsinger, R Elghanian, G Viswanadham, C A Mirkin *Bioconjugate Chem.* **11** 289 (2000)
180. Z Li, R S Jin, C A Mirkin, R L Letsinger *Nucleic Acids Res.* **30** 1558 (2002)
181. S S Ghosh, P M Kao, A W McCue, H L Chappelle *Bioconjugate Chem.* **1** 71 (1990)
182. K J Catt, G W Tregear *Science* **158** 1570 (1967)
183. A T Mikhailov, V N Simirskii *Metody Immunokhimicheskogo Analiza v Biologii Razvitiya* (The Methods of Immunochemical Assay in Developmental Biology) (Moscow: Nauka, 1991)
184. R Hawkes, E Niday, J Gordon *Anal. Biochem.* **119** 142 (1982)
185. W F Glass, R C Briggs, L S Hnilica *Science* **211** 70 (1981)
186. M L Bell, E Engvall *Anal. Biochem.* **123** 329 (1982)
187. R Jahn, W Schiebeler, P Greengard *Proc. Natl. Acad. Sci. USA* **81** 1684 (1984)
188. D Brada, J Roth *Anal. Biochem.* **142** 79 (1984)
189. M Moeremans, G Daneels, A van Dijk, G Langanger, J De Mey *J. Immunol. Methods* **74** 353 (1984)
190. B Surek, E Latzko *Biochem. Biophys. Res. Commun.* **121** 284 (1984)
191. Y-H Hsu *Anal. Biochem.* **142** 221 (1984)
192. M Moeremans, G Daneels, M De Raeymaeker, J De Mey, in *Handbook of Immunoblotting of Proteins* (Eds O J Bjerrum, N H H Heegaard) (Orlando: CRC Press, 1988) p. 137
193. R Rohringer, in *Colloidal Gold: Principles, Methods and Applications* (Ed. M A Hayat) (San Diego, CA: Academic Press, 1989) p. 396
194. S J Fowler *Methods Mol. Biol.* **32** 239 (1994)
195. M Moeremans, G Daneels, J De Mey *Anal. Biochem.* **145** 315 (1985)
196. G Daneels, M Moeremans, M De Raeymaeker, J De Mey *J. Immunol. Methods* **89** 89 (1986)
197. D Egger, K Bienz *Anal. Biochem.* **166** 413 (1987)
198. A H V Schapira, G Keir *Anal. Biochem.* **169** 167 (1988)
199. K Jamaguchi, H Asakawa *Anal. Biochem.* **172** 104 (1988)
200. D Egger, K Bienz *Mol. Biotechnol.* **1** 289 (1994)
201. K W Li, W P Geraerts, R van Elk, J Joosse *Anal. Biochem.* **182** 44 (1989)
202. S Cheley, H Bayley *BioTechniques* **10** 730 (1991)
203. P Casero, G B Del Campo, P G Righetti *Electrophoresis* **6** 367 (1985)
204. E Saman *Gene Anal. Tech.* **3** 1 (1986)
205. G L Jones, J A Bailey, R J O'Connell *Mycol. Res.* **99** 567 (1995)
206. B H Juurlink, R M Devon *Experientia* **47** 75 (1991)
207. C M Stoschek *Anal. Biochem.* **160** 301 (1987)
208. D Poulain, A Ayadi, J Fruit *Ann. Biol. Clin.* **45** 565 (1987)
209. S R Kimball, S L Rannels, M B Elenski, L S Jefferson *J. Immunol. Methods* **106** 217 (1988)
210. V A Velikov, O S Ermoshina, I V Volokhina, M I Chumakov *Mol. Gen., Mikrobiol. Virusol.* (1) 21 (2006)
211. J Seitz *Biol. Chem. Hoppe-Seyler* **368** 442 (1987)
212. W P Li, C Zuber, J Roth *Histochemistry* **100** 347 (1993)
213. A Nespolo, G Bianchi, A Salmaggi, M Lazzaroni, D Cerrato, L M Tajoli *Electrophoresis* **10** 34 (1989)
214. S Tomlinson, A Luga, E Huguenel, N Dattagupta *Anal. Biochem.* **171** 217 (1988)
215. P G Righetti, P Casero, G B Del Campo *Clin. Chim. Acta* **157** 167 (1986)
216. M L Poor, P F Santa, G S Sittampalam *Anal. Biochem.* **175** 191 (1988)
217. W Steffen, R W Linck *Electrophoresis* **10** 714 (1989)
218. K M Makkouk, A Comeau *Eur. J. Plant Pathol.* **100** 71 (1994)
219. D Raoult, G A Dasch *J. Immunol. Methods* **125** 57 (1989)
220. B Petchclai, S Hiranras, U Potha *Am. J. Trop. Med. Hyg.* **45** 672 (1991)
221. J M Scott, W G Shreffler, H W Ghalib, A el Asad, M Siddig, R Badaro, S G Reed *Am. J. Trop. Med. Hyg.* **44** 272 (1991)
222. Y S Liu, W P Du, Z X Wu *Int. J. Parasitol.* **26** 127 (1996)
223. Y S Liu, W P Du, Y M Wu, Y G Chen, K Y Zheng, J M Shi, X Z Hu, G Y Li, C F You, Z X Wu *J. Trop. Med. Hyg.* **98** 151 (1995)
224. F Chu, Q Ji, R-M Yan *Chin. J. Integr. Trad. Western Med.* **21** 504 (2001)
225. V S Dar, S Ghosh, S Broor *J. Virol. Methods* **47** 51 (1994)
226. D Fernandez, I Valle, R Llamas, M Guerra, L Sorell, J Gavilondo *J. Virol. Methods* **48** 315 (1994)
227. J L Yee, M B Jennings, J R Carlson, N W Lerche *Lab. Anim. Sci.* **41** 119 (1991)
228. A C Reboli *J. Clin. Microbiol.* **31** 518 (1993)
229. D Poulain, D W R Mackenzie, J van Cutsem *Mycoses* **34** 221 (1991)
230. L Vera-Cabrera, A Rendon, M Diaz-Rodriguez, V Handzel, A Laszlo *Clin. Diagn. Lab. Immunol.* **6** 686 (1999)
231. M Kunakorn, B Petchclai, K Khupulsup, P Naigowit *J. Clin. Microbiol.* **29** 2065 (1991)
232. Q Huang, X Lan, T Tong, X Wu, M Chen, X Feng, R Liu, Y Tang, Z Zhu *J. Clin. Microbiol.* **34** 2011 (1996)
233. T Yu Zagorskina, E Yu Markov, A I Kalinovskii, E P Golubinskii *Zh. Mikrobiol. Epidemiol. Immunol.* (6) 64 (1998)
234. V A Lazarchik, L P Titov, T N Vorob'eva, T S Ermakova, O N Vrublevskaya, N V Vlasik *Izv. NAN Belarus., Ser. Med. Nauk* (3) 44 (2005)
235. Z Xu *Chung Hua I Hsueh Tsa Chih (Taipei)* **72** 216 (1992)
236. S Matsuzawa, H Kimura, Y Itoh, H Wang, T Nakagawa *J. Forensic Sci.* **38** 448 (1993)
237. M V Sumaroka, L A Dykman, V A Bogatyrev, N V Evseeva, I S Zaitseva, S Yu Shchyogolev, A D Volodarsky *J. Immunoassay* **21** 401 (2000)
238. L A Dykman, V A Bogatyrev, I S Zaitseva, M K Sokolova, V V Ivanov, O I Sokolov *Biofizika* **47** 632 (2002)^f
239. A F Cremers, N Jansen in de Wal, J Wiegant, R W Dirks, P Weisbeek, M van der Ploeg, J E Landegent *Histochemistry* **86** 609 (1987)
240. A G Walker, K I Dawe *J. Immunol. Methods* **104** 281 (1987)
241. E B Smithwick, L G Young *J. Androl.* **11** 246 (1990)
242. T Hatakeyama, K Murakami, Y Miyamoto, N Yamasaki *Anal. Biochem.* **237** 188 (1996)
243. S Vazquez, G Lemos, M Pupo, O Ganzon, D Palenzuela, A Indart, M G Guzman *Clin. Diagn. Lab. Immunol.* **10** 1074 (2003)
244. R Kaur, M Raje *J. Immunol. Methods* **279** 33 (2003)
245. L Duan, Y Wang, S S Li, Z Wan, J Zhai *BMC Infect. Dis.* **5** 53 (2005)
246. A G Poltavchenko, D A Poltavchenko, T Yu Zagorskina *Sibir' – Vostok* (3) 10 (2002)
247. T Yu Zagorskina, A G Poltavchenko, A A Dokorina *Sibir' – Vostok* (8) 8 (2002)

248. A Han, M Dufva, E Belleville, C B V Christensen *Lab Chip* **3** 329 (2003)
249. N F Starodub, V P Artyukh, V I Nazarenko, L I Kolomiets *Ukr. Biokhim. Zh.* **59** 108 (1987)
250. J McCarvil, A J McKenna, C Grief, C S Hoy, D Sesardic, M C J Maiden, I M Feavers *Mol. Microbiol.* **10** 203 (1993)
251. R Liang, D W Emerich *Anal. Biochem.* **164** 488 (1987)
252. M Achacha, K R Mittal *Vet. Rec.* **139** 539 (1996)
253. A Fenoll, I Jado, D Vicioso, J Casal *J. Clin. Microbiol.* **35** 764 (1997)
254. V A Bogatyrev, L A Dykman, L Yu Matora, B I Shvartsburd *Mikrobiologiya* **60** 524 (1991) ^g
255. V A Bogatyrev, L A Dykman, L Yu Matora, B I Shvartsburd *FEMS Microbiol. Lett.* **96** 115 (1992)
256. L A Dykman, V A Bogatyrev *FEMS Immunol. Med. Microbiol.* **27** 135 (2000)
257. M A Jeppesen, R B Barlow *J. Opt. Soc. Am.* **52** 99 (1962)
258. A V Alekseeva, V A Bogatyrev, L A Dykman, B N Khlebtsov, L A Trachuk, A G Melnikov, N G Khlebtsov *Appl. Opt.* **44** 6285 (2005)
259. B N Khlebtsov, L A Dykman, V A Bogatyrev, V Zharov, N G Khlebtsov *Nanoscale Res. Lett.* **2** 6 (2007)
260. A H Peruski, L F Peruski *Clin. Diagn. Lab. Immunol.* **10** 506 (2003)
261. G W Long, T O'Brien *J. Appl. Microbiol.* **87** 214 (1999)
262. C B Bird, R L Miller, B M Miller *J. AOAC Int.* **82** 625 (1999)
263. S J Wu, H Paxton, B Hanson, C G Kung, T B Chen, C Rossi, D W Vaughn, G S Murphy, C G Hayes *Clin. Diagn. Lab. Immunol.* **7** 106 (2000)
264. H A Escalante, O C Huamanchay, K A Davelois *Rev. Peru. Med. Exp.* **18** 57 (2001)
265. K H Engler, A Efstratiou, D Norn, R S Kozlov, I Selga, T G Glushkevich, M Tam, V G Melnikov, I K Mazurova, V E Kim, G Y Tseneva, L P Titov, R C George *J. Clin. Microbiol.* **40** 80 (2002)
266. R H Shyu, H F Shyu, H W Liu, S S Tang *Toxicon* **40** 255 (2002)
267. S Chanteau, L Rahalison, L Ralafiarisoa, J Foulon, M Ratsitorahina, L Ratsifasoamanana, E Carniel, F Nato *Lancet* **361** 211 (2003)
268. K Glynou, P C Ioannou, T K Christopoulos, V Syriopoulou *Anal. Chem.* **75** 4155 (2003)
269. M P Grobusch, D Schormann, S Schwenke, D Teichmann, E Klein *J. Clin. Microbiol.* **36** 3443 (1998)
270. B B Dzantiev, A V Zherdev, V O Popov, Yu Yu Vengerov, T A Starovoitova, R T Toguzov *Klin. Lab. Diagn.* (8) 25 (2002)
271. J-H Cho, S-H Paek *Biotechnol. Bioeng.* **75** 725 (2001)
272. S Wang, C Zhang, J Wang, Y Zhang *Anal. Chim. Acta* **546** 161 (2005)
273. J H W Leuvers, P J H M Thal, M van der Waart, A H W M Schuurs *J. Immunoassay* **1** 77 (1980)
274. J H W Leuvers, P J H M Thal, M van der Waart, A H W M Schuurs *J. Immunol. Methods* **45** 183 (1981)
275. J H W Leuvers, B C Coverde, P J H M Thal, A H W M Schuurs *J. Immunol. Methods* **60** 9 (1983)
276. J H W Leuvers, P J H M Thal, A H W M Schuurs *J. Immunol. Methods* **62** 175 (1983)
277. T J C Gribnau, J H W Leuvers, H van Hell *J. Chromatogr.* **176** 175 (1986)
278. A M Deelder, M H Dozy *Acta Leiden.* **48** 17 (1982)
279. F Wielaard, A Denissen, L van der Veen, I Rutjes *J. Virol. Methods* **17** 149 (1987)
280. R Van Erp, T J C Gribnau, A P van Sommeren, H P Bloemers *J. Immunoassay* **12** 425 (1991)
281. R Zeisler, S F Stone, R P Viscidi, E H Cerny *J. Radioanal. Nucl. Chem.* **167** 445 (1993)
282. V K Gasparyan *J. Clin. Lab. Anal.* **19** 124 (2005)
283. M Tanaka, K Matsuo, M Enomoto, K Mizuno *Clin. Biochem.* **37** 27 (2004)
284. N T K Thanh, Z Rosenzweig *Anal. Chem.* **74** 1624 (2002)
285. H Sakashita, A Tomita, Y Umeda, H Narukawa, H Kishioka, T Kitamori, T Sawada *Anal. Chem.* **67** 1278 (1995)
286. N T K Thanh, J H Rees, Z Rosenzweig *Anal. Bioanal. Chem.* **374** 1174 (2002)
287. C X Zhang, Y Zhang, X Wang, Z M Tang, Z H Lu *Anal. Biochem.* **320** 136 (2003)
288. M J Benecky, D R Post, S M Schmitt, M S Kocher *Clin. Chem.* **43** 1764 (1997)
289. L A Dykman, Ya M Krasnov, V A Bogatyrev, N G Khlebtsov *Proc. SPIE* **4241** 37 (2001)
290. P Englebienne *Analyst* **123** 1599 (1998)
291. P Englebienne, A van Hoonacker, M Verhas, N G Khlebtsov *Comb. Chem. High Throughput Screen.* **6** 777 (2003)
292. J J Storhoff, R Elghanian, R C Mucic, C A Mirkin, R L Letsinger *J. Am. Chem. Soc.* **120** 1959 (1998)
293. S Mann, S A Davis, S R Hall, M Li, K H Rhodes, W Shenton, S Vaucher, B Zhang *J. Chem. Soc., Dalton Trans.* 3753 (2000)
294. J Liu, Y Lu *Angew. Chem., Int. Ed.* **45** 90 (2006)
295. S Connolly, D Fitzmaurice *Adv. Mater.* **11** 1202 (1999)
296. S Mann, W Shenton, M Li, S Connolly, D Fitzmaurice *Adv. Mater.* **12** 147 (2000)
297. A J Reynolds, A H Haines, D A Russell *Langmuir* **22** 1156 (2006)
298. L A Dykman, V A Bogatyrev, B N Khlebtsov, N G Khlebtsov *Anal. Biochem.* **341** 16 (2005)
299. G S Landsberg *Optika* (Optics) (Moscow: Nauka, 1976)
300. S E M Colaiani, J Aubard, S H Hansen, O F Nielsen *Vib. Spectrosc.* **9** 111 (1995)
301. M Fleischman, P J Hendra, A J McQuillan *Chem. Phys. Lett.* **26** 163 (1974)
302. O A Aktsipetrov *Soros. Obraz. Zh.* **7** 109 (2001)
303. A Campion, P Kambhampati *Chem. Soc. Rev.* **27** 241 (1998)
304. K Kneipp, H Kneipp, I Itzkan, R R Dasari, M S Feld *Chem. Phys.* **247** 155 (1999)
305. D I Kreimer, T H Nufert *J. Mol. Biol. Biotechnol.* **1** 4 (1999)
306. F Maroun, F Ozanam, J-N Chazalviel, W Thei *Vib. Spectrosc.* **19** 193 (1999)
307. D Naumann, D Helm, H Labischinski *Nature (London)* **351** 81 (1991)
308. D Naumann, S Keller, D Helm, Ch Schultz, B Schrader *J. Mol. Struct.* **347** 399 (1995)
309. H H Mantsch, D Chapman *Infrared Spectroscopy of Biomolecules* (New York: Wiley, 1996)
310. K Brandenburg, U Seydel *Chem. Phys. Lipids* **96** 23 (1998)
311. M Osawa *Top. Appl. Phys.* **81** 163 (2001)
312. K Kneipp, Y Wang, R R Dasari, M S Feld, B D Gilbert, J Janni, J I Steinfield *Spectrochim. Acta, Part A* **51** 2171 (1995)
313. S R Emory, S Nie *Anal. Chem.* **69** 2631 (1997)
314. T Vo-Dinh *TrAC — Trends Anal. Chem.* **17** 557 (1998)
315. X Dou, Y M Jung, H Yamamoto, S Doi, Y Ozaki *Appl. Spectrosc.* **53** 133 (1999)
316. J A Seelenbinder, C W Brown, P Pivarnik, A G Rand *Anal. Chem.* **71** 1963 (1999)
317. K Kneipp, H Kneipp, R Manoharan, E B Hanlon, I Itzkan, R R Dasari, M S Feld *Appl. Spectrosc.* **52** 1493 (1998)
318. R F Aroca, D J Ross, C Domingo *Appl. Spectrosc.* **58** 324A (2004)
319. C W Brown, Y Li, J A Seelenbinder, P Pivarnik, A G Rand, S V Letcher, O J Gregory, M J Platek *Anal. Chem.* **70** 2991 (1998)
320. D S Grubisha, R J Lipert, H Y Park, J Driskell, M D Porter *Anal. Chem.* **75** 5936 (2003)
321. X Dou, Y Yamaguchi, H Yamamoto, S Doi, Y Ozaki *J. Raman Spectrosc.* **29** 739 (1998)
322. J Ni, R J Lipert, G B Dawson, M D Porter *Anal. Chem.* **71** 4903 (1999)
323. S Xu, X Ji, W Xu, X Li, L Wang, Y Bai, B Zhao, Y Ozaki *Analyst* **129** 63 (2004)
324. A A Kamnev, L A Dykman, P A Tarantilis, M G Polissiou *Biosci. Rep.* **22** 541 (2002)
325. I E Kovalev, O Yu Polevaya *Biokhimicheskie Osnovy Immuniteta k Nizkomolekulyarnym Khimicheskim Soedineniyam* (Biochemical Foundations of Immunity to Low-molecular Chemical Compounds) (Moscow: Nauka, 1985)

326. V T Ivanov, O M Vol'pina, T M Andronova *Zh. Vses. Khim. O-va im D I Mendeleeva* **33** 523 (1988)^c
327. R Arnon, R J Horwitz *Curr. Opin. Immunol.* **4** 449 (1992)
328. T Ben-Yedidia, R Arnon *Curr. Opin. Biotechnol.* **8** 442 (1997)
329. J Roitt, J Brostoff, D Male *Immunology* (London: Mosby, 1998)
330. W J Harris, C Cunningham *Antibody Therapeutics* (Berlin: Springer, 1995)
331. M-P Marco, S Gee, B D Hammock *TrAC — Trends Anal. Chem.* **14** 415 (1995)
332. V A Sergeev *Virusnye Vaktsiny* (Viral Vaccines) (Kiev: Urozhai, 1993)
333. J F Stills *ILAR J.* **46** 280 (2005)
334. J McCafferty, A D Griffiths, G Winter, D J Chiswell *Nature (London)* **348** 552 (1990)
335. R V Petrov, R M Khaitov *Immunologiya* (1) 4 (1998)
336. R V Petrov, V A Kabanov, R M Khaitov *Zh. Vses. Khim. O-va im. D I Mendeleeva* **33** 502 (1988)^c
337. V A D'yakonova, S V Dambaeva, N M Golubeva, V V Burakov, G V Sharonov, E E Komogorova, B V Pinegin *Fiziol. Patolog. Immunoi Sist.* **8** 100 (2004)
338. J Kreuter *Pharm. Biotechnol.* **6** 463 (1995)
339. G Gregoriadis *Immunol. Today* **11** 89 (1990)
340. M Fukasawa *FEBS Lett.* **441** 353 (1998)
341. W Morris *Vaccine* **12** 5 (1994)
342. O V Masalova, A V Shepelev, S N Atanadze, Z N Parnes, V S Romanova, O M Vol'pina, Yu A Semiletov, A A Kushch *Dokl. Akad. Nauk* **369** 411 (1999)^h
343. S M Andreev, A A Babakhin, A O Petrukhina, V S Romanova, Z N Parnes, R V Petrov *Dokl. Akad. Nauk* **370** 261 (2000)^h
344. D Pantarotto, C D Partidos, J Hoebeke, F Brown, E Kramer, J-P Briand, S Muller, M Prato, A Bianco *Chem. Biol.* **10** 961 (2003)
345. S Shiosaka, H Kiyama, A Wanaka, M Tohyama *Brain Res.* **382** 399 (1986)
346. L A Zil'ber, V V Frize *Zh. Eksp. Biol.* **11** 128 (1929)
347. J Zozaya, J Clark *J. Exp. Med.* **57** 21 (1933)
348. L A Zil'ber *Osnovy Immunologii* (Foundations of Immunology) (Moscow: Medgiz, 1958)
349. O P Ottersen, J Storm-Mathisen *Trends Neurosci.* **10** 250 (1987)
350. A Wanaka, Y Shiotani, H Kiyama, T Matsuyama, T Kamada, S Shiosaka, M Tohyama *Exp. Brain Res.* **65** 691 (1987)
351. A Tomii, F Masugi *Jpn. J. Med. Sci. Biol.* **44** 75 (1991)
352. N Tatsumi, Y Terano, K Hashimoto, M Hiyoshi, S Matsuura *Osaka City Med. J.* **39** 167 (1993)
353. J R Moffett, M G Espey, M A A Namboodiri *Cell Tissue Res.* **278** 461 (1994)
354. L A Dykman, L Yu Matora, V A Bogatyrev *J. Microbiol. Methods* **24** 247 (1996)
355. L D Walensky, P Gascard, M E Fields, S Blackshaw, J G Conboy, N Mohandas, S H Snyder *J. Cell Biol.* **141** 143 (1998)
356. J Chen, F Zou, N Wang, S Xie, X Zhang *Bioorg. Med. Chem. Lett.* **10** 1691 (2000)
357. A L Feldman, L Tamarkin, G F Paciotti, B W Simpson, W M Linehan, J C Yang, W E Fogler, E M Turner, H R Alexander, S K Libutti *Clin. Cancer Res.* **6** 4628 (2000)
358. L V Olenina, E F Kolesanova, Yu V Gervaziev, I S Zaitseva, T E Kuraeva, B N Sobolev, A I Archakov *Med. Immunol.* **3** 231 (2001)
359. S A Staroverov, D N Ermilov, A A Shcherbakov, S V Semenov, C Yu Shchegolev, L A Dykman *Zh. Mikrobiol. Epidemiol. Immunol.* (3) 54 (2003)
360. T Yu Zagorskina, Doctoral Thesis in Medical Sciences, Pacific Institute of Bioorganic Chemistry, Far East Branch of the Russian Academy of Sciences, Vladivostok, 2003
361. D V Pow, D K Crook *J. Neurosci. Methods* **48** 51 (1993)
362. A Baude, Z Nusser, E Molnár, R A J McIlhinney, P Somogyi *Neuroscience* **69** 1031 (1995)
363. L Pickard, J Noël, J M Henley, G L Collingridge, E Molnar *J. Neurosci.* **20** 7922 (2000)
364. S Holmseth, Y Dehnes, L P Bjornsen, J-L Boulland, D N Furness, D Bergles, N C Danbolt *Neuroscience* **136** 649 (2005)
365. D P Harris, H-M Vordermeier, A Arya, K Bogdan, C Moreno, J Ivanyi *Immunology* **88** 348 (1996)
366. M K-H Schäfer, H Varoqui, N Defamie, E Weihe, J D Erickson *J. Biol. Chem.* **277** 50734 (2002)
367. M J Schell, M E Molliver, S H Snyder *Proc. Natl. Acad. Sci. USA* **92** 3948 (1995)
368. M J Schell, O B Cooper, S H Snyder *Proc. Natl. Acad. Sci. USA* **94** 2013 (1997)
369. M J L Eliasson, S Blackshaw, M J Schell, S H Snyder *Proc. Natl. Acad. Sci. USA* **94** 3396 (1997)
370. N Staimer, S J Gee, B D Hammock *Fresenius' J. Anal. Chem.* **369** 273 (2001)
371. V A Demenev, M A Shchinova, L I Ivanov, R N Vorob'eva, N I Zdanovskaya, N V Nebaikina *Vopr. Virusol.* **41** 107 (1996)
372. R Kayed, E Head, J L Thompson, T M McIntire, S C Milton, C W Cotman, C G Glabe *Science* **300** 486 (2003)
373. D W Kowalczyk, H C J Ertl *Cell. Mol. Life Sci.* **55** 751 (1999)
374. U A Hasan, A M Abai, D R Harper, B W Wren, W J W Morrow *J. Immunol. Methods* **229** 1 (1999)
375. Z Cui, R J Mumper *Eur. J. Pharm. Biopharm.* **5** 11 (2003)
376. L Zhang, G Wiedera, D Rabussay *Bioelectrochemistry* **63** 369 (2004)
377. M J Roy, M S Wu, L J Barr, J T Fuller, L G Tussey, S Speller, J Culp, J K Burkholder, W F Swain, R M Dixon, G Wiedera, R Vessey, A King, G Ogg, A Gallimore, J R Haynes, D Heydenburg, D H Fuller *Vaccine* **19** 764 (2000)
378. C M Leutenegger, F S Boretti, C N Mislin, J N Flynn, M Schroff, A Habel, C Junghans, S A Koenig-Merediz, B Sigrist, A Aubert, N C Pedersen, B Wittig, H Lutz *J. Virol.* **74** 10447 (2000)
379. D Chen, L G Payne *Cell Res.* **12** 97 (2002)
380. D Chen, C Zuleger, Q Chu, Y F Maa, J Osorio, L G Payne *AIDS Res. Hum. Retroviruses* **18** 715 (2002)
381. H J Dean, D Fuller, J E Osorio *Comp. Immunol. Microbiol. Infect. Dis.* **26** 373 (2003)
382. M Thomas, A M Klivanov *Proc. Natl. Acad. Sci. USA* **100** 9138 (2003)
383. A K Salem, C F Hung, T W Kim, T C Wu, P C Searson, K W Leong *Nanotechnology* **16** 484 (2005)
384. Z Zhao, T Wakita, K Yasui *J. Virol.* **77** 4248 (2003)
385. M A Liu, M R Hillerman, R Kurth *Ann. N. Y. Acad. Sci.* **772** 1 (1995)
386. S Gurunathan, D M Klinman, R A Seder *Annu. Rev. Immunol.* **18** 927 (2000)
387. L A Dykman, M V Sumaroka, S A Staroverov, I S Zaitseva, V A Bogatyrev *Izv. Akad. Nauk, Ser. Biol.* **31** 86 (2004)ⁱ
388. L A Dykman, V A Bogatyrev, S A Staroverov, D V Pristensky, S Yu Shchyogolev, N G Khlebtsov *Proc. SPIE* **6164** 38 (2006)
389. S M Moghimi, I S Muir, L Illum, S S Davis, V Kolbbafofen *Biochim. Biophys. Acta* **1179** 157 (1993)
390. H S Kruth, J Chang, I Ifrim, W Y Zhang *Eur. J. Cell Biol.* **78** 91 (1999)
391. H Vallhov, J Qin, S M Johansson, N Ahlberg, M A Muhammed, A Scheynius, S Gabrielson *Nano Lett.* **6** 1682 (2006)
392. V T Ivanov (Ed.) *Belki Immunoi Sistemy* (Proteins of Immune System) (Moscow: Institute of Bioorganic Chemistry, Russian Academy of Sciences, 1997)
393. R H Persellin, E V Hess, M Ziff *Arthritis Rheum.* **10** 99 (1967)
394. J W Measel *Infect. Immun.* **11** 350 (1975)
395. M Harth *J. Rheumatol. Suppl.* **5** 7 (1979)
396. A J Lewis, J Cottney, D D White, P K Fox, A McNeillie, J Dunlop, W E Smith, D H Brown *Agents Actions* **10** 63 (1980)
397. S Bajaj, I Ahmad, M Fatima, S Raisuddin, S B Vohora *Immunopharmacol. Immunotoxicol.* **21** 151 (1999)
398. J Stejskal, V D M Stejskal *Neuroendocrinol. Lett.* **20** 351 (1999)
399. G Graham *Agents Actions Suppl.* **44** 209 (1993)
400. B Merchant *Biologicals* **26** 49 (1998)
401. R Eisler *Biol. Trace Elem. Res.* **100** 1 (2004)
402. R Eisler *Biogeochemical, Health, and Ecotoxicological Perspectives on Gold and Gold Mining* (Boca Raton, FL: CRC Press, 2004)
403. R Shukla, V Bansal, M Chaudhary, A Basu, R R Bhonde, M Sastry *Langmuir* **21** 10644 (2005)

404. Z P Xu, Q H Zeng, G Q Lu, A B Yu *Chem. Eng. Sci.* **61** 1027 (2006)
405. H Gu, P L Ho, E Tong, L Wang, B Xu *Nano Lett.* **3** 1261 (2003)
406. H M Joshi, D R Bhumkar, K Joshi, V Pokharkar, M Sastry *Langmuir* **22** 300 (2006)

^a — *Herald Russ. Acad. Sci. (Engl. Transl.)*

^b — *Biochemistry (Moscow) (Engl. Transl.)*

^c — *J. Exp. Theor. Phys. (Engl. Transl.)*

^d — *Colloid J. (Engl. Transl.)*

^e — *Mendeleev Chem. J. (Engl. Transl.)*

^f — *Biophysics (Engl. Transl.)*

^g — *Microbiology (Engl. Transl.)*

^h — *Dokl. Biochem. Biophys. (Engl. Transl.)*

ⁱ — *Biol. Bull. (Engl. Transl.)*

1,2,3,4,5-Pentathiepines and 1,2,3,4,5-pentathiepanes

L S Konstantinova, S A Amelichev, O A Rakitin

Contents

I. Introduction	195
II. Methods of synthesis	195
III. Chemical properties	201
IV. Spectroscopic studies	208
V. Stereochemical aspects: conformation and chirality	208
VI. Quantum-chemical calculations of pentathiepine molecules	209
VII. Biological activity and practical applications of pentathiepines	209

Abstract. Data on the synthesis and properties of seven-membered heterocyclic compounds containing five successive sulfur atoms and a carbon–carbon bond, 1,2,3,4,5-pentathiepines and -pentathiepanes, are generalised and described systematically. The bibliography includes 104 references.

I. Introduction

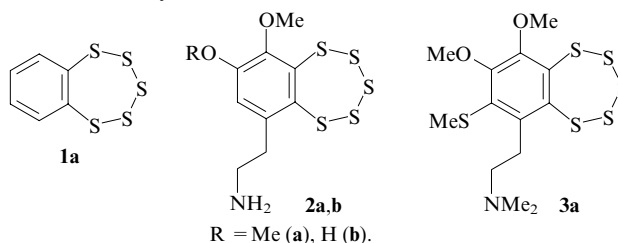
Among seven-membered polysulfur-containing heterocycles containing five sulfur atoms and two carbon atoms, there are 1,2,3,4,5-pentathiepines and -pentathiepanes and 1,2,3,4,6- and 1,2,3,5,6-pentathiepanes. Data on the two last-mentioned classes of compounds, whose properties are substantially different from those of 1,2,3,4,5-isomers, are beyond the scope of the present review. We review data on methods for the synthesis and reactions of seven-membered rings, which contain a carbon–carbon double or single bond and a chain of five sulfur atoms, *viz.*, 1,2,3,4,5-pentathiepines and their hydrogenated analogues, 1,2,3,4,5-pentathiepanes.



Fehér was the first to synthesise such derivatives: pentathiepanes in 1967 (Ref. 1) and pentathiepines in 1971.² Twenty years later, a seven-membered polysulfur-containing ring was found in natural antibiotics isolated from marine organisms (cited in Ref. 3). In recent years, pentathiepines have attracted considerable interest as antitumour, antifungal and antiseptic drugs. Apparently, it is the heterocycle that is responsible for their biological activity. In addition, 1,2,3,4,5-pentathiepines have found application in industry, for example, as cathodic materials. These compounds are also valuable starting com-

pounds in synthetic organic chemistry, because they can be used for the preparation of various sulfur-containing derivatives, both cyclic (1,4-dithiines, 1,2,4,5-tetrathiocines and 1,3-dithioles) and acyclic (vicinal 1,2-dithiols and many other compounds).

Among natural and synthetic pentathiepines, benzopentathiepine (**1a**) and its analogues containing a substituted benzene ring are best studied. Natural compounds, such as varacin (**2a**), lissoclinotoxin A (**2b**) and *N,N*-dimethyl-5-(methylthio)-varacin (**3a**), have antiseptic and antifungal activities and inhibit protein kinase C. In addition, varacin exhibits antitumour activity.



In 2004, we published a review³ on the chemistry of pentathiepines. Data on reviews on pentathiepanes are lacking in abstract journals, although data on both classes of compounds were included in chapters of the monograph *Comprehensive Heterocyclic Chemistry*.⁴ In the present review, the results of research into the chemistry of 1,2,3,4,5-pentathiepanes are analysed for the first time. Since the synthesis methods, chemical properties and spectroscopic characteristics of 1,2,3,4,5-pentathiepines and their hydrogenated analogues are rather similar, it is worthwhile to consider and compare data on these heterocycles in one paper, with a supplement of studies on pentathiepines published in the last three years.

II. Methods of synthesis

1. Sulfurisation of sulfur-containing compounds by elemental sulfur

a. Synthesis of pentathiepines from aromatic vicinal dithiols

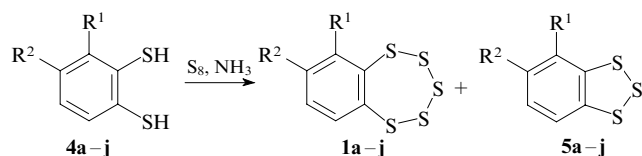
Benzopentathiepine (**1a**) and its 7-chloro-substituted analogue (**1b**) were synthesised by Sato *et al.*⁵ by the reaction of the corresponding arene-1,2-dithiols (**4a,b**) with elemental sulfur in liquid ammonia. The reactions were performed in a titanium

L S Konstantinova, S A Amelichev, O A Rakitin N D Zelinsky Institute of Organic Chemistry, Russian Academy of Sciences, Leninsky prosp. 47, 119991 Moscow, Russian Federation. Fax (7-495) 135 53 28, tel. (7-495) 135 53 27, e-mail: dlt@ioc.ac.ru (L S Konstantinova), stas_a@mail.ru (S A Amelichev), orakitin@ioc.ac.ru (O A Rakitin)

Received 9 November 2006

Uspekhi Khimii 76 (3) 219–236 (2007); translated by T N Safonova

autoclave at 20 °C. More recently, this method was improved (for example, dichloromethane was used as the solvent), and a wide range of monosubstituted benzopentathiepienes **1c–j** were synthesised.^{6–8} In addition to thermodynamically stable pentathiepienes **1a–j**, sulfurisation of arene-1,2-thiols with elemental sulfur affords less stable benzo-1,2,3-trithioles **5a–j** as by-products. Unfortunately, the yields of the reaction products were not reported in the cited studies.

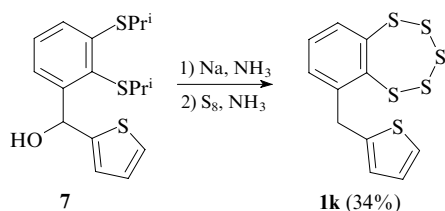


R¹ = H; R² = H (**a**), Cl (**b**); R² = H; R¹ = SiMe₃ (**c**), SiMe₂Bu^t (**d**), SiEt₃ (**e**), SiPh₃ (**f**), CH₂CH₂NH₂ (**g**), CH₂CH₂NHBoc (**h**), CH₂Py (**i**), CH₂Pyrm (**j**)

Boc is *tert*-butoxycarbonyl, Py is 2-pyridyl, Pyrm is 2-pyrimidyl.

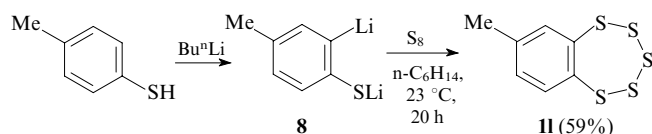
This method was used for the synthesis of 6-(2-aminoethyl)benzopentathiepine (**1g**) and 6,7-dimethoxybenzopentathiepine (**6a**) as structural analogues of the natural antibiotic varicin (**2a**).⁷

The reaction can be performed with *S,S*-dialkyl-substituted arene-1,2-dithiols instead of thioles. In this case, the pentathiepine ring is synthesised in two steps. Compound **7** is dealkylated by sodium in liquid ammonia, which is accompanied by reduction of the hydroxy group, and the subsequent reaction with sulfur produces pentathiepine **1k**.⁸



Recently, the synthesis of phthalocyanines fused with the pentathiepine ring by the reaction of the corresponding 4,5-(*o*-xylylenedithio)phthalonitrile derivatives with lithium amide and elemental sulfur has been documented.⁹

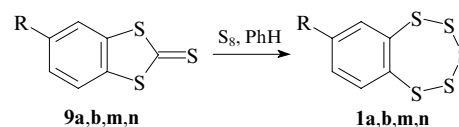
As an exception, let us mention the reaction ideologically similar to the above-considered method. In this reaction, aromatic monothiol was used as the starting compound. The treatment of dilithium intermediate **8**, which is generated *in situ* by the reaction of *p*-toluenethiol with butyllithium, with sulfur affords pentathiepine **1l**.¹⁰



b. Synthesis from fused 1,3-dithiole-2-thiones

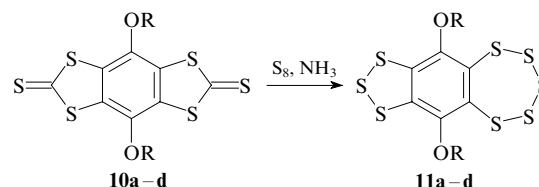
R Sato *et al.*⁵ synthesised benzopentathiepine (**1a**) and its 7-monosubstituted analogues **1b,m,n** from fused 1,3-dithiole-2-thiones **9a,b,m,n** by the reaction with sulfur in liquid ammonia. The use of benzene as the solvent led to an increase in the yield of the reaction products. However, attempts to synthesise 7-nitrobenzopentathiepine according to this method failed. Interestingly, pentathiepine **1a** is derived from compound **9a** in higher yield compared to the reaction with benzene-1,2-dithiol (**4a**), although the latter is produced by hydrolysis of

benzodithiole **9a** and is, presumably, an intermediate in the synthesis of pentathiepine **1a**.



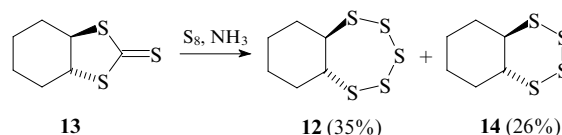
R = H (**a**, 82%), Cl (**b**, 59%), MeO (**m**, 99%), NH₂ (**n**, 91%).

The reaction of benzobis(dithiolethiones) **10a–d** with sulfur in liquid ammonia gives trithiolobenzopentathiepienes **11a–d** in high yields rather than the corresponding benzobis(pentathiepienes).¹¹ Under these conditions, the reaction of benzobis(1,3-dithiole-2-thione) containing no alkoxy groups yields only polymers of unknown structure.



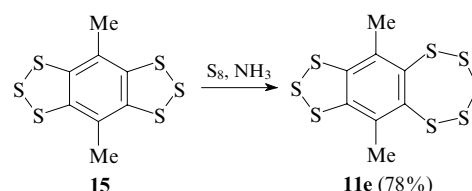
R = Me (**a**, 82%), Et (**b**, 99%), Prⁱ (**c**, 99%), PhCH₂ (**d**, 62%).

Pentathiepane **12** fused with the cyclohexane ring was synthesised from 1,3-dithiole-2-thione **13** in low yield (35%) due to formation of tetrathiine **14** as a by-product.¹²



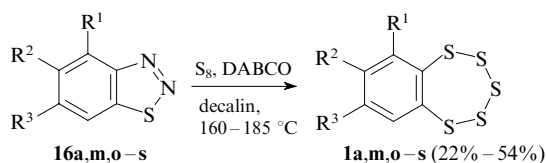
c. Synthesis from benzo-1,2,3-trithioles

Pentathiepienes can be synthesised starting from benzo-1,2,3-trithioles. For example, the treatment of benzobis(trithiole) **15** with sulfur in liquid ammonia affords pentathiepine **11e** in good yield.¹³



d. Synthesis from annulated 1,2,3-thia(selena)diazoles

A procedure for the synthesis of benzopentathiepienes from the corresponding 1,2,3-thiadiazoles was proposed and developed by Chenard *et al.*^{14,15} The reaction proceeds upon heating (160–185 °C) of benzothiadiazoles **16a,m,o–s** with elemental sulfur in decalin. In the presence of diazabicyclo[2.2.2]octane (DABCO), final products **1a,m,o–s** were obtained in higher yields. The authors attributed this fact to high nucleophilicity of the organic base necessary for the S₈ ring opening. Benzothiadiazoles react as latent *o*-mercaptodiazonium salts. Apparently, the reaction initially leads to cleavage of the heterocycle in compound **16** accompanied by elimination of the nitrogen molecule and the resulting intermediate reacts with the activated [S₈–DABCO] species.

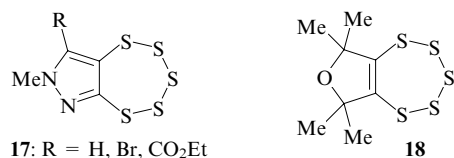


$\text{R}^1 = \text{R}^2 = \text{R}^3 = \text{H}$ (**a**); $\text{R}^2 = \text{R}^3 = \text{H}$; $\text{R}^1 = \text{Br}$ (**o**), CF_3 (**p**);

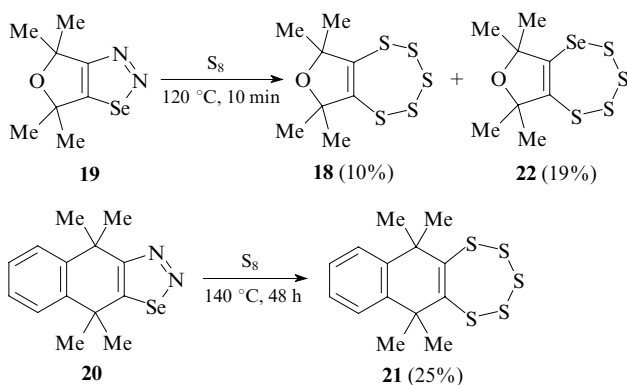
$\text{R}^1 = \text{R}^3 = \text{H}$; $\text{R}^2 = \text{OMe}$ (**m**), NMe_2 (**q**); $\text{R}^1 = \text{R}^2 = \text{H}$;

$\text{R}^3 = \text{Cl}$ (**r**), CF_3 (**s**).

This method allowed the synthesis of a series of pentathiepinanes annulated with heterocyclic rings, such as the pyrazole ring (**17**, 36%–44% yields)¹⁵ or the dihydrofuran ring (**18**, 22%).¹⁶

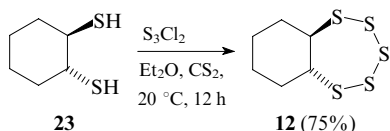


Analogously, 1,2,3-selenadiazoles **19** and **20** are transformed into pentathiepinanes **18** and **21**, respectively. The reaction with compound **19** proceeds very rapidly to give predominantly 1-selena-2,3,4,5-tetrathiepine **22**.¹⁷

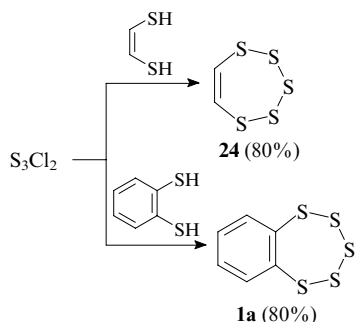


2. Sulfurisation of vicinal dithiols with other reagents

The first compound belonging to pentathiepanes, *viz.*, perhydrobenzopentathiepane (**12**), was synthesised by Fehér and Degen¹ from *trans*-cyclohexane-1,2-dithiol (**23**) with the use of the rare reagent dichlorotrithiane (S_3Cl_2). The reaction was carried out in a mixture of diethyl ether and carbon disulfide at room temperature.

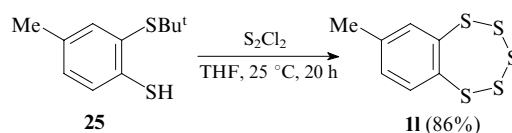


The parent compound of pentathiepinanes, *viz.*, unsubstituted pentathiepine (**24**), and benzopentathiepine (**1a**) were

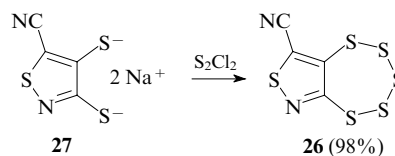


synthesised for the first time by the reaction of ethylene- and benzene-1,2-dithiols, respectively, with S_3Cl_2 .²

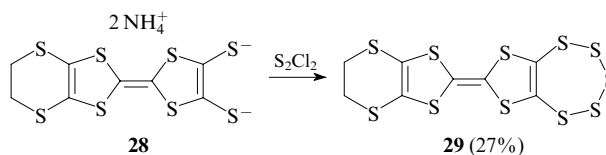
More recently, this reaction was extended to other vicinal 1,2-dithiols. In these reactions, cheaper sulfur monochloride (S_2Cl_2) was used instead of S_3Cl_2 . The limitations of this method are associated exclusively with stability and accessibility of the starting compounds. The reaction with sulfur monochloride can be performed also with mono-*S*-alkylated derivatives, for example, with compound **25**.¹⁰ In this case, dealkylation occurs under mild conditions in the presence of a sulfur-containing reagent; the resulting benzothiepine **11** was isolated by silica gel column chromatography.



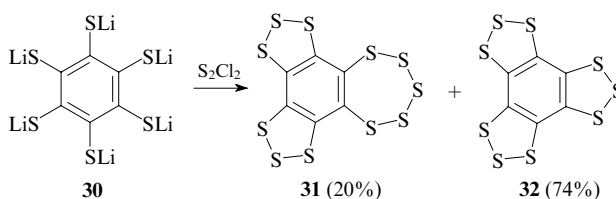
The synthesis of annulated pentathiepinanes from salts, 1,2-dithiolates, was documented.^{18–20} In particular, cyano-substituted pentathiepinisothiazole **26** was synthesised from the corresponding disodium salt **27** in almost quantitative yield.¹⁸



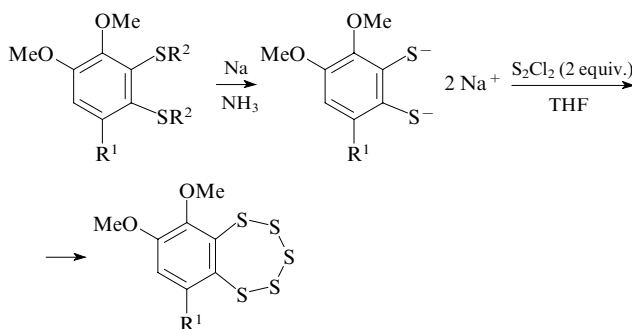
However, the analogous reaction with diammonium salt **28** produced pentathiepine **29** in substantially lower yield.²⁰



The reaction with the hexalithium salt of hexamercapto-benzene **30** afforded products in rather high total yield; however, pentathiepine **31** was obtained as a minor component of the mixture, and the reaction produced predominantly benzotris(trithiole) **32**.¹⁹

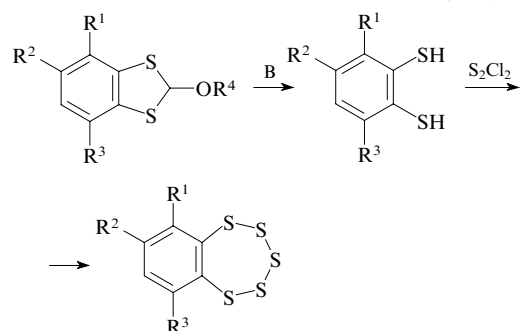
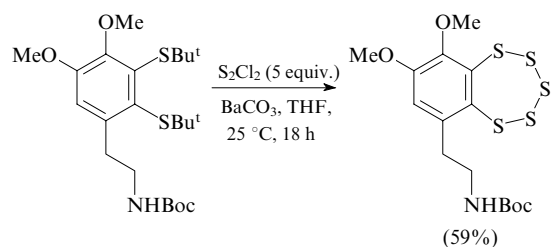


It should be noted that vicinal dithiols can be generated *in situ* from various 1,2-bifunctional compounds.^{10, 15, 21–26} Examples of reactions, in which intermediate dithiolate anions form the 1,2,3,4,5-pentathiepine ring, are given below. It

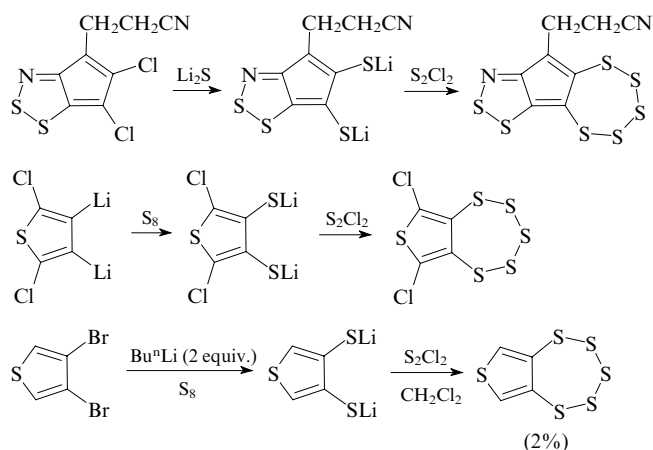


$\text{R}^1 = (\text{CH}_2)_2\text{NHCO}_2(\text{CH}_2)_2\text{SiMe}_3$; $\text{R}^2 = \text{Pr}^n$ (28%), Bu^n (47%).

should be noted that this reaction was described^{10, 21–23} as one of steps in the total synthesis of natural pentathiepine analogues.



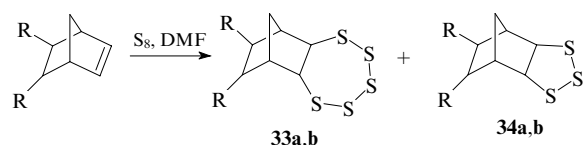
B is a base [Na, NH₃ (liq), *etc.*]; R¹ = H, Me; R² = R³ = H, R⁴ = Buⁿ; R¹ = R² = OMe, R³ = (CH₂)₂NHBoc, R⁴ = iso-C₅H₁₁.



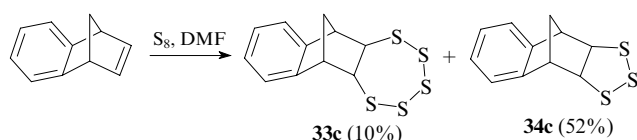
3. Cyclosulfurisation at a carbon–carbon multiple bond

a. Reactions with elemental sulfur

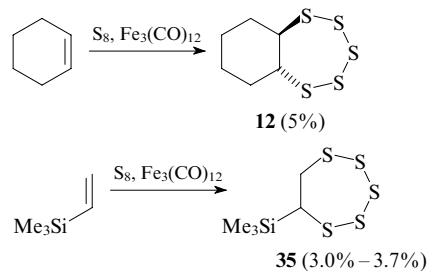
One of the commonly used procedures for the synthesis of pentathiepanes is based on the reactions of cyclic and linear alkenes with elemental sulfur. However, this reaction generally gives products in low yields. For example, the reactions of norbornene derivatives with sulfur in DMF afford pentathiepanes **33a–c** in low yields, whereas the corresponding trithiolanes **34a–c** are obtained as the major products.²⁷



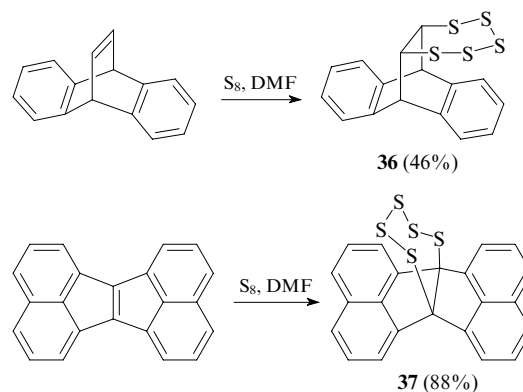
Compound	R–R	Yield (%)	
		33	34
a	2 H	6.5	30
b	CH ₂ CH=CH	5	40



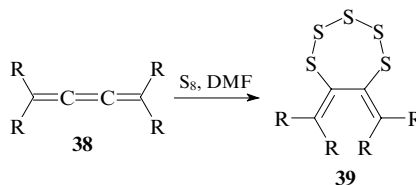
To stabilise intermediates, Fe₃(CO)₁₂ was added to the reaction mixture.^{28, 29} However, the use of this carbonyl as the catalyst for the reactions of cyclohexene²⁸ and vinyltrimethylsilane²⁹ with sulfur did not lead to an increase in the yield of pentathiepanes **12** and **35**.



The reactions with polycyclic aromatic alkenes produce fused pentathiepanes in considerably higher yields. For example, pentathiepanes **36** and **37** were synthesised by the reaction of barrelene³⁰ or acenaphtho[1,2-*a*]acenaphthylene³¹ with elemental sulfur in DMF in 46% and 88% yields, respectively.

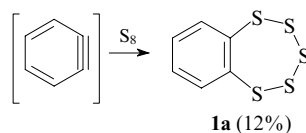


Due to steric hindrance, the analogous reaction of 1,1,4,4-tetrasubstituted buta-1,2,3-trienes **38** with sulfur proceeds regioselectively at the central C=C double bond to give compounds **39**, as a rule, in good yields.^{17, 32}

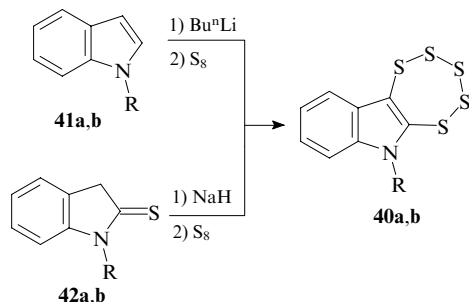


R = Ph (87%), 4-MeC₆H₄ (65%), 4-ClC₆H₄ (56%), 1-adamantyl (19%).

It should also be noted that benzopentathiepine (**1a**) was obtained as one of products in the reaction of dehydrobenzene with sulfur at low temperature.³³ Unlike the above-considered reactions, this reaction results in the addition of elemental sulfur to the carbon–carbon triple bond.

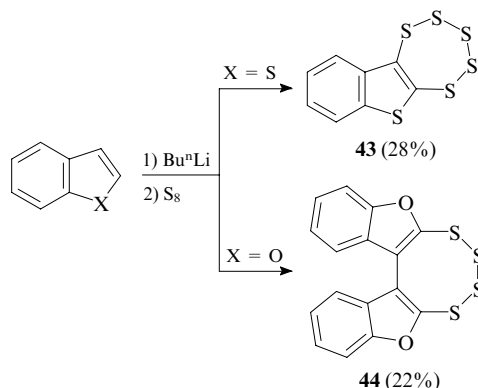


2,3-Benzannulated five-membered heterocycles containing one heteroatom readily react with electrophilic sulfur in the presence of strong bases. In these reactions, the double bond of the starting molecule, which is involved in the heteroaromatic system, remains intact, and the process can be considered as the formal replacement of hydrogen atoms. Pentathiepinino[6,7-*c*]indoles **40a,b** were synthesised by Bergman and co-workers³⁴ from indole derivatives **41a,b** and thioxindole **42a,b**. The reaction with sulfur is preceded by the treatment of the heterocycles by butyllithium or sodium hydride.

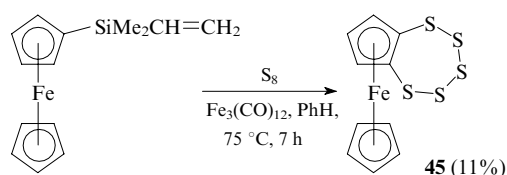


Starting compound	R	Yield of 40 (%)
41a	H	29
41b	Me	22
42a	H	42
42b	Me	13

The reaction of benzo[*b*]thiophene with butyllithium and S₈ produces benzothienopentathiepine **43**, whereas the reaction of benzo[*b*]furan performed under analogous conditions gives only bis(benzofuro)tetrathiocine **44**.³⁵



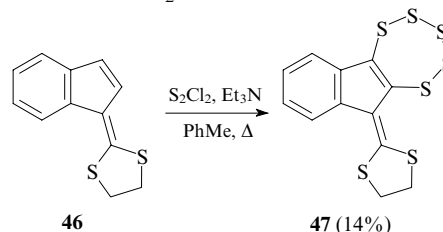
In the presence of a mixture of elemental sulfur and iron carbonyl Fe₃(CO)₁₂, (vinyltrimethyl)silylferrocene is transformed into the corresponding pentathiepine fused with ferrocene (**45**).³⁶ In this reaction, not only the hydrogen atom, but also the silicon-containing group are replaced.



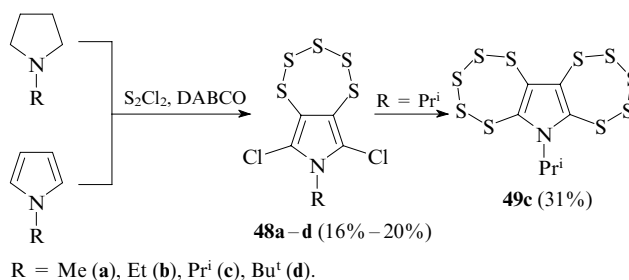
b. Reactions with sulfur monochloride

Commercially available sulfur monochloride is used as a reagent for cyclosulfurisation of various compounds to form

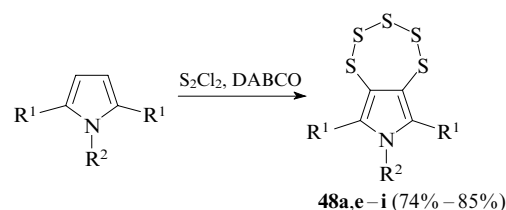
pentathiepinines. For example, refluxing of indene derivative **46** in toluene with S₂Cl₂ in the presence of triethylamine afforded pentathiepine **47**.³⁷ Apparently, the initial electrophilic replacement of two hydrogen atoms gives rise to a 2,3-bis(chlorodithio) derivative, which reacts with the third sulfur monochloride molecule to form the pentathiepine ring after elimination of SCl₂.



Recently, we have demonstrated^{38,39} that the reactions of five-membered electron-donating heterocycles, such as pyrrole, thiophene and their derivatives, with S₂Cl₂ in the presence of a base can be used as a one-pot method for the synthesis of annulated pentathiepinines. Pentathiepinines **48a–d** fused at positions 3 and 4 of the pyrrole ring were synthesised from *N*-substituted pyrroles and pyrrolidines. These reactions are also accompanied by the replacement of the hydrogen atoms in the β position. It should be noted that the reaction of *N*-isopropylpyrrolidine with S₂Cl₂ and DABCO produced pyrrolo-bis(pentathiepine) **49c**, which is the first representative of compounds containing two pentathiepine rings in one molecule.

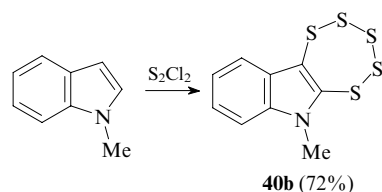


In the reactions with 1,2,5-trisubstituted pyrroles, cyclo-sulfurisation products **48a,e–i** are formed in good yields.



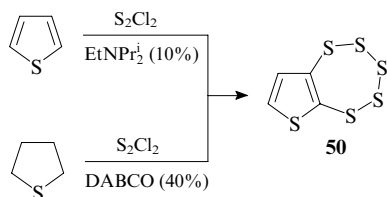
R¹ = Cl, R² = Me (**a**); R¹ = Me: R² = Me (**e**), Et (**f**), Prⁿ (**g**), Prⁱ (**h**), CH₂Ph (**i**).

Under analogous conditions, the reaction of *N*-methylindole produced pentathiepinino[6,7-*c*]indole **40b**.

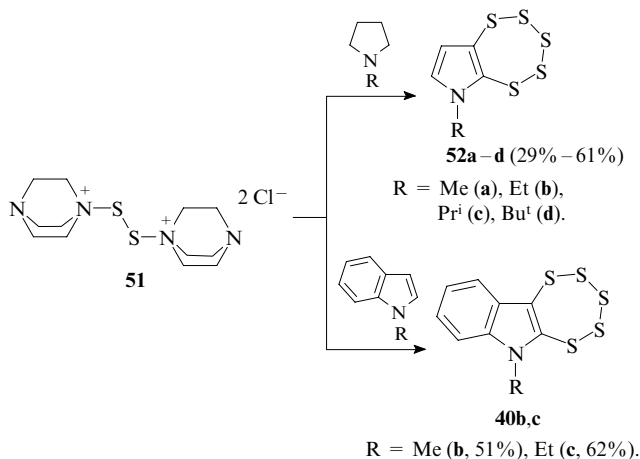


The reaction of thiophene with S₂Cl₂ in the presence of diisopropylethylamine gives pentathiepine **50** in substantially

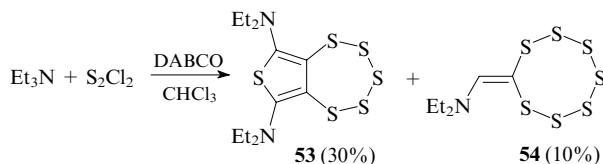
lower yield than that obtained in the reaction of tetrahydrothiophene with S_2Cl_2 in the presence of DABCO.



Pentathiepinines fused with the pyrrole, thiophene or indole rings can also be prepared by the reactions of the corresponding heterocycles with a prestored mixture of sulfur monochloride and DABCO.⁴⁰ The authors hypothesised that 1-(4-aza-1-azoniabicyclo[2.2.2]oct-1-ylidithio)-4-aza-1-azoniabicyclo[2.2.2]octane dichloride (**51**) is the main reacting species in these transformations. The formation of the latter was established by IR spectroscopy based on the disappearance of the S–Cl absorption band. It should be noted that in these reactions, annulation products **52a–d** at positions 2 and 3 of the pyrrole ring are generated from *N*-substituted pyrrolidines.



High reactivity of salt **51** was confirmed by its unexpected transformations. For example, the addition of triethylamine to a solution of this salt in chloroform followed by heating of the reaction mixture afforded thienopentathiepine **53** and heptathiocane **54**.⁴¹ X-Ray diffraction study demonstrated that the polysulfur rings of these compounds exist as chair and crown conformations, respectively.



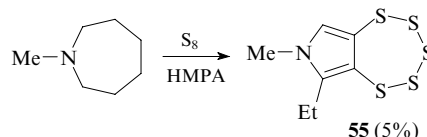
The reactions of other tertiary ethylamines with S_2Cl_2 proceed analogously, although these reactions afford products in lower yields. The thiophene ring in compound **53** is constructed from the ethyl groups of two amine molecules (the new C–C bond is formed between two non-activated methyl groups); the pentathiepine ring, as a result of the reaction of intermediate thiophene with salt **51** (by analogy with the above-considered examples). The probable reaction mechanisms were proposed in the cited studies.

In spite of low yields of the products, the advantage of this method is that these products are generally formed in one step from cheap starting reagents.

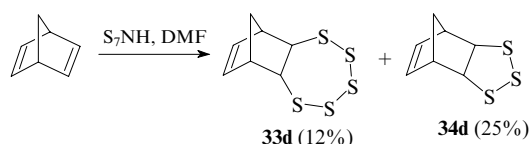
4. Other methods

In conclusion, let us consider several original approaches to the synthesis of pentathiepinines.

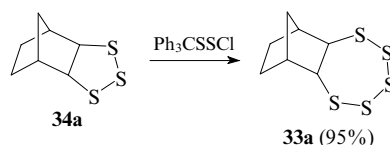
Cyclosulfurisation with elemental sulfur accompanied by the intramolecular rearrangement of the starting compound was documented. The reaction of *N*-methylazepane with sulfur in the presence of hexamethylphosphoramide (HMPA) produced pentathiepinopyrrole **55** in low yield.⁴² Unfortunately, no suggestions about the reaction mechanism were made.



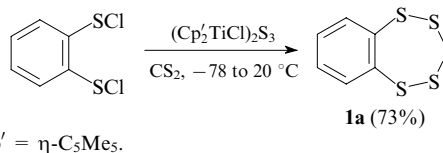
In some cases, pentathiepanes and pentathiepinines were synthesised with the use of non-traditional reagents. For example, pentathiepane **33d** was synthesised from norbornadiene with the use of the sulfurising reagent S_7NH , which is more reactive than elemental sulfur (see Section II.3.a). Although the reaction was performed under mild conditions (at room temperature), pentathiepane **33d** was produced in low yield (12%), and trithiole **34d** was obtained as the major product.²⁷



Structurally similar trithiole **34a** was transformed into the corresponding pentathiepane **33a** in high yield in the reaction with triphenylmethylthiosulfenyl chloride (Ph_3CSSCl).⁴³



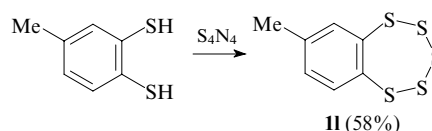
One of the most rational methods for the synthesis of pentathiepinines is based on the introduction of three sulfur atoms into 1,2-bis(chlorosulfonyl)benzene under the action of bis(pentamethylcyclopentadienyl)titanium dichloride trisulfide. This reaction gives benzopentathiepine (**1a**) in good yield.⁴⁴

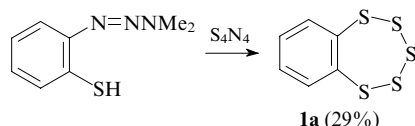


$Cp^* = \eta-C_5Me_5$.

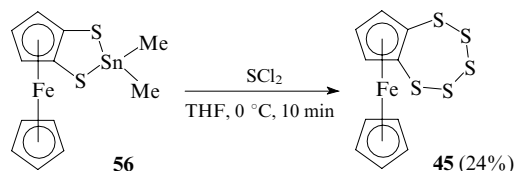
This method was also used for the synthesis of pentathiepane **33b** from the corresponding bis(sulfonyl chloride). This reaction produced compound **33b** in 9% yield.⁴⁵

Tetrasulfur tetranitride (S_4N_4) can also be used as the sulfurising reagent in the synthesis of benzopentathiepinines. For example, refluxing of S_4N_4 in xylene with 4-methylbenzene-1,2-dithiol and (*ortho*-mercaptophenyl)triazene⁴⁶ afforded compounds **1l** and **1a**, respectively.

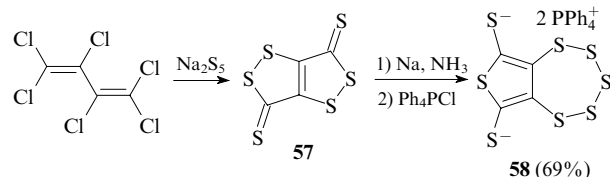




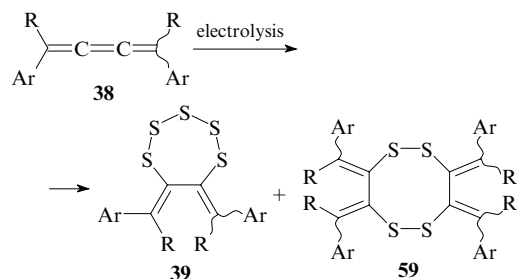
Pentathiepine fused with ferrocene (**45**) was synthesised by the reaction of dithiastannole **56** with a large excess of sulfur dichloride.⁴⁷



Perchlorobuta-1,3-diene reacts with Na_2S_5 to form bis(dithiolethione) **57**. The reaction of the latter with sodium in liquid ammonia followed by the treatment with $Ph_4P^+Cl^-$ affords thienopentathiepine salt **58**.⁴⁸

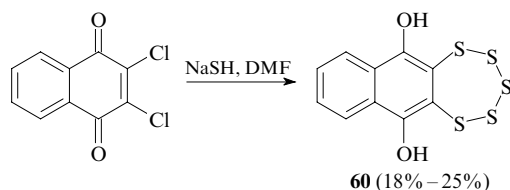


Sulfurisation of 1,1,4,4-tetrasubstituted buta-1,2,3-trienes **38** to form pentathiepanes can be performed by electrolysis on a sulfur graphite electrode in DMF in the presence of Et_4NOTs .^{49, 50} The reactions with tetraaryl derivatives **38** ($R = Ar$) afforded pentathiepanes **39** ($R = Ar$) as the major products (61%–86% yields). By contrast, 1,4-bis(trifluoromethyl)-1,4-diarylbuta-1,2,3-trienes gave predominantly 1,2,5,6-tetrathiocines **59**, whereas pentathiepanes **39** ($R = CF_3$) were isolated in yields from 1% to 25%.



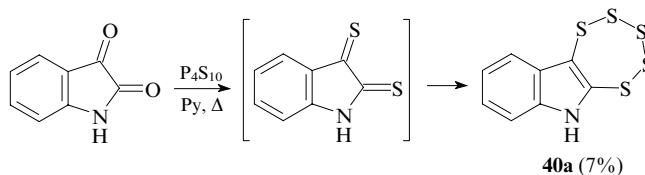
$R = CF_3$ or Ar ; $Ar = 4-XC_6H_4$ ($X = H, Me, Cl, MeO$).

Some approaches to the synthesis of pentathiepienes were discovered accidentally. For example, the reaction of 2,3-dichloro-1,4-naphthoquinone with sodium hydrosulfide in DMF unexpectedly produced naphthopentathiepine **60**.⁵¹

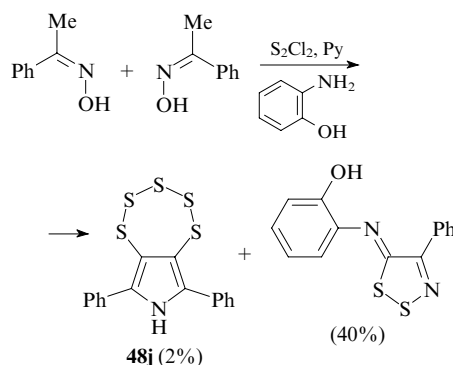


It appeared that the reaction of isatin with P_4S_{10} under reflux in pyridine does not stop at the formation of dithioisatin; instead, it produces pentathiepinino[6,7-*c*]indole **40a**. This fact is

indicative of thermodynamic stability of the final products, fused pentathiepienes.⁵²



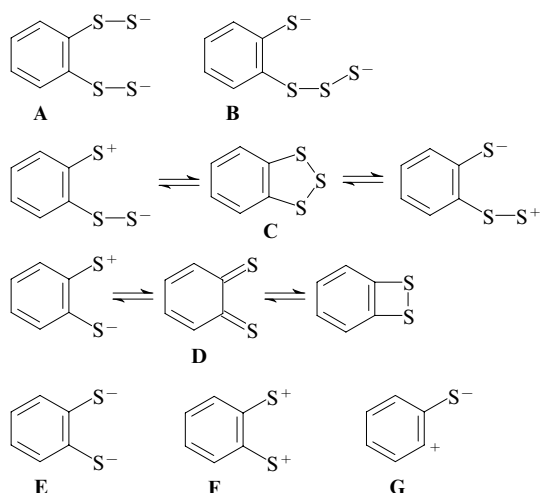
Pentathiepinino[6,7-*c*]pyrrole **48j** was isolated as a by-product in the reaction of acetophenone oxime with sulfur monochloride in the presence of pyridine and *o*-aminophenol.⁵³ This reaction gives substituted dithiazole as the major product.



To summarise, there are several approaches to the construction of the pentathiepine ring based on different starting compounds and sulfur-containing reagents.

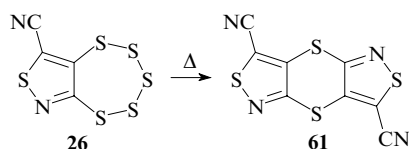
III. Chemical properties

Most reactions of pentathiepienes and pentathiepanes considered in this Section involve the nucleophilic or electrophilic attack on the S atom, resulting in the pentathiepine ring opening and elimination of one to five sulfur atoms.⁵⁴ These reactions proceed through the formation of various charged and neutral intermediates **A–G**.⁵⁵

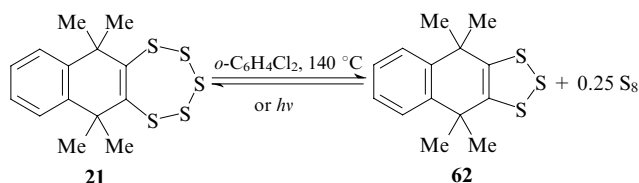


1. Thermolysis and photolysis

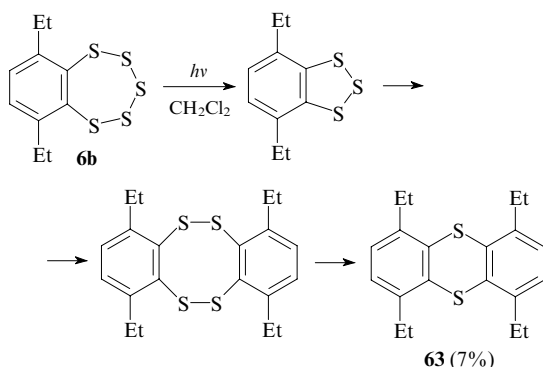
Thermal and photochemical transformations of pentathiepienes generally lead to a loss of two, three or four sulfur atoms. These reactions produce 1,2,3-trithioles, dimeric tetrathiocines and 1,4-dithiines. For example, pyrolysis of pentathiepinisothiazole **26** affords 1,4-dithiine **61**.¹⁷



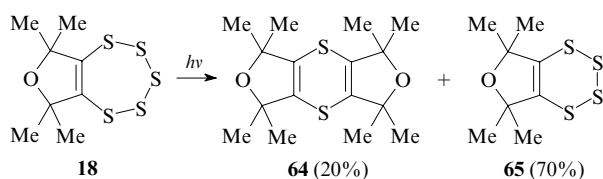
Heating of dihydronaphthopentathiepine **21** in 1,2-dichlorobenzene to 140 °C or its irradiation with a high-pressure mercury lamp (100 W) affords an equilibrium mixture of the starting pentathiepine, 1,2,3-trithiole **62** and elemental sulfur.⁵⁶



Irradiation of a solution of 6,9-diethylbenzopentathiepine (**6b**) in dichloromethane leads to successive desulfurisation, dimerisation and ring contraction. The corresponding trithiole and tetrathiocin were detected as intermediates, and 1,4-dithiine **63** was obtained as the final transformation product.⁵⁷

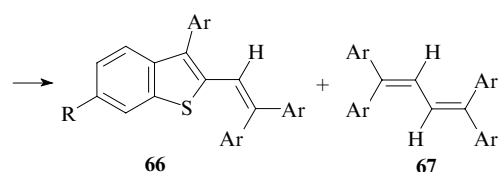
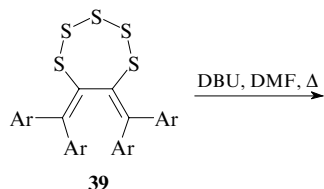


Under analogous conditions, dihydropentathiepin[6,7-c]-furan **18** also gave 1,4-dithiine **64**; however, compound **65** belonging to the poorly known class of 1,2,3,4-tetrathiines was isolated as the major photolysis product.¹⁶



2. Desulfurisation with bases

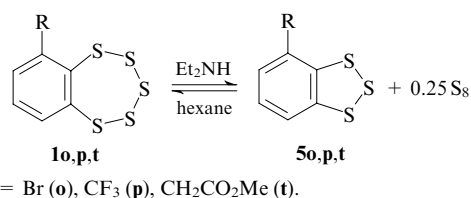
The reactions of pentathiepinines and pentathiepanes with bases {for example, with 1,8-diazabicyclo[5.4.0]undec-7-ene (DBU) and other tertiary or secondary amines} involve desulfurisation of the substrate accompanied by a loss of two to five sulfur atoms. For example, refluxing of pentathiepanes **39** in the presence of DBU in DMF affords the corresponding benzothiophenes **66** and buta-1,3-dienes **67**.³² In the authors' opinion, the mechanism of formation of these products and their



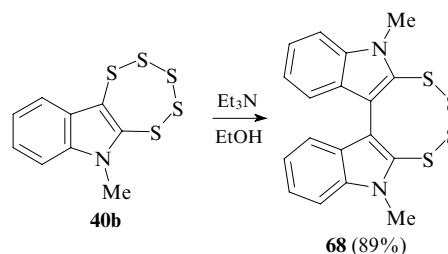
Ar	Yield (%)	
	66	67
Ph	12	52
4-MeC ₆ H ₄	33	40
4-ClC ₆ H ₄	2	32

ratio depend on the relative stability and reactivity of radical intermediates.

The reactions of benzopentathiepinines **10,p,t** substituted at position 6 with diethylamine in hexane yield the corresponding trithioles **50,p,t**.¹⁵ In the reaction with trifluoromethyl derivative **1p**, an equilibrium is established (**1p**:**5p** = 46:54).



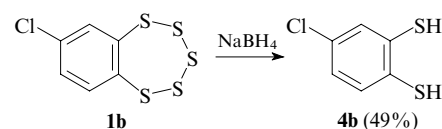
Heating of pentathiepin[6,7-c]indole **40b** with triethylamine in ethanol affords bis(indolo)-fused 1,2,3,4-tetrathiocine **68** in high yield.³⁴ The reaction mechanism involves elimination of three sulfur atoms to form dithioindole, which undergoes dimerisation to give product **68**.



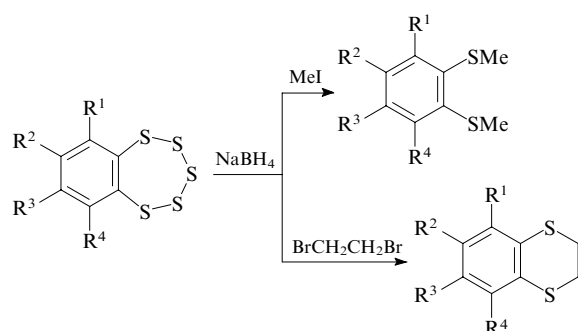
Evidently, the role of the base in these transformations is to cleave the polysulfide chain.

3. Reduction

Benzopentathiepinines are reduced most often with sodium borohydride.¹⁵ These reactions generally produce arene-1,2-dithiols. For example, 7-chlorobenzopentathiepine (**1b**) was reduced with NaBH₄ to dithiol **4b**.¹⁵

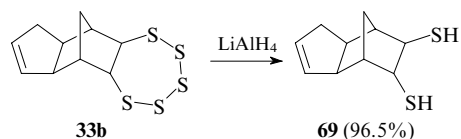


In the presence of an electrophilic reagent (for example, alkyl halide) in the reaction mixture, intermediate dithiol is readily alkylated to form stable 1,2-di(alkylthio) derivatives. *S,S*-Dialkyl-substituted arene-1,2-dithiols were synthesised from various benzopentathiepinines according to this method.^{11, 13, 15}

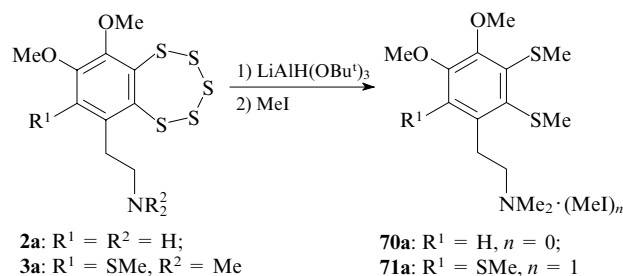


$R^1 = R^3 = R^4 = \text{H}; R^2 = \text{Cl}, \text{NMe}_2$;
 $R^1 = R^4 = \text{Me}; R^2-R^3 = -\text{SSS}-, -\text{SCH}_2\text{CH}_2\text{S}-$;
 $R^1 = R^4 = \text{OMe}, R^2-R^3 = -\text{SSS}-$.

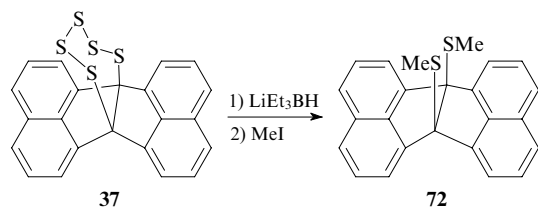
1,2-Dithiol **69** was prepared from pentathiepane **33b** with the use of lithium aluminium hydride. Compound **69** is rather stable; it was isolated in almost quantitative yield and characterised by different physicochemical methods.²⁷



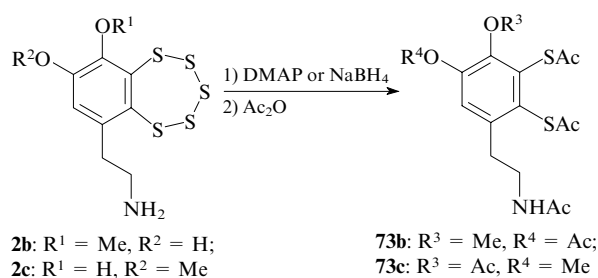
Varacin (**2a**) and its derivative **3a** were reduced with lithium tris(*tert*-butoxy)aluminium hydride.^{58,59} Subsequent alkylation of the intermediate with iodomethane afforded amine **70a** and quaternary ammonium salt **71a**, respectively.



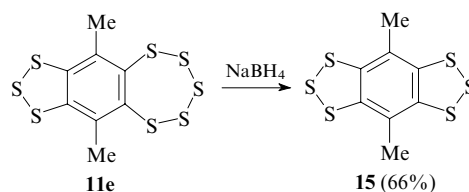
Polycyclic pentathiepane **37** was reduced with lithium triethyl borohydride. The treatment of the reaction mixture with iodomethane gave the bis(methylthio) derivative of acenaphtho[1,2-*a*]-acenaphthene **72**.³¹



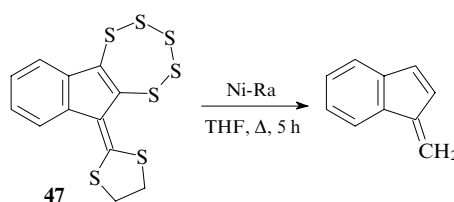
The reactions can be performed with acylating reagents instead of alkylating reagents. For example, the reaction of lissoclinotoxin A (**2b**) with acetic anhydride in the presence of 4-dimethylaminopyridine (DMAP) in DMF at room temperature produces compound **73b**.⁶⁰ Apparently, three sulfur atoms are eliminated through the nucleophilic attack of DMAP. In the analogous reaction (with NaBH_4 and acetic anhydride), isolissoclinotoxin A (**2c**) gives isomer **73c**.²²



It should be noted that the pentathiepine ring can be reduced in such a way that the trithiole ring remains intact. For example, mild reduction of trithiolobenzopentathiepine **11e** with sodium borohydride afforded benzobis(trithiole) **15** in good yield.¹³

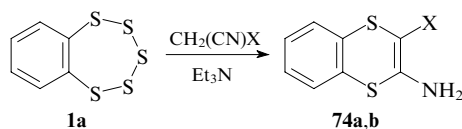


Pentathiepine **47** is reduced under reflux with Raney nickel in THF with a loss of all five sulfur atoms and cleavage of the dithiole ring to form benzofulvene.³⁷



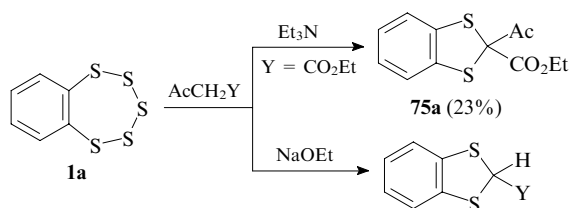
4. Reactions with compounds containing the activated methylene group

In the presence of bases (triethylamine or sodium ethoxide), compounds containing the CH -acidic methylene group (malononitrile, ethyl cyanoacetate, ethyl acetoacetate, ethyl 2-chloropropionate and acetylacetone) react with benzopentathiepine (**1a**) to form 1,4-dithiines, 1,3-dithiols and 1,2,4-trithiines.⁶¹ Under these conditions, malononitrile and ethyl cyanoacetate give dithiines **74** in high yields.



$\text{X} = \text{CN}$ (**a**, 87%), CO_2Et (**b**, 76%).

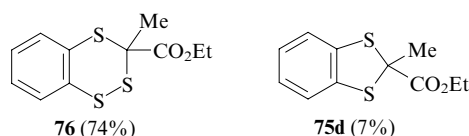
The reaction of benzopentathiepine (**1a**) with ethyl acetoacetate in the presence of triethylamine produces benzo-1,3-dithiole **75a**; the reaction with ethyl acetoacetate and acetyl-



75b: $\text{Y} = \text{CO}_2\text{Et}$ (57%);
75c: $\text{Y} = \text{Ac}$ (42%)

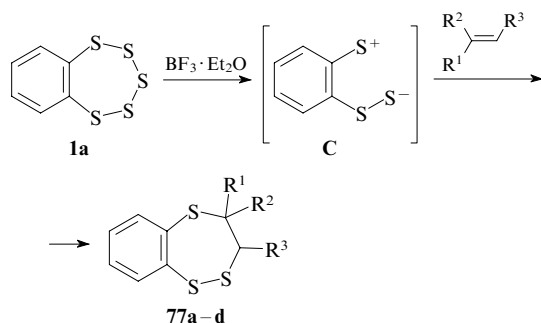
acetone in the presence of sodium ethoxide gives benzodithioles **75b,c**.

Dithioles **75a** (40% yield) and **75b** (42%) are formed also from benzopentathiepine (**1a**) and ethyl 2-chloroacetoacetate. However, the reaction of compound **1a** with ethyl 2-chloropropionate and sodium ethoxide gives trithiine **76** rather than dithiole **75d** as the major product. Presumably, the latter reaction proceeds through the above-considered intermediates **C**, **D** or **F** (see the beginning of Section III).



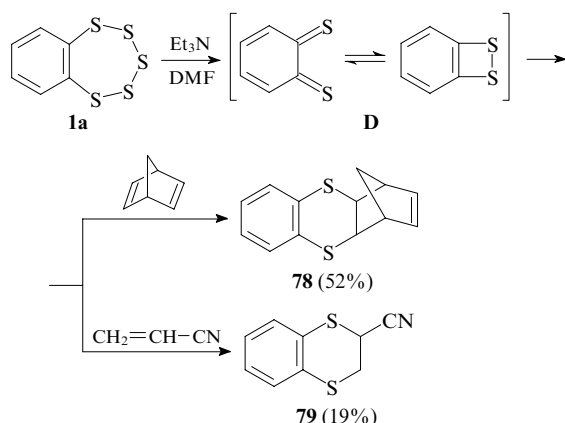
5. Reactions with unsaturated compounds

The reactions of benzopentathiepienes with unsaturated compounds (alkenes, alkynes and arenes) give rise to new S—C bonds. Benzopentathiepine (**1a**) reacts with alkenes in the presence of a Lewis acid or triethylamine. The reaction catalysed by $\text{BF}_3 \cdot \text{Et}_2\text{O}$ produces unsymmetrical benzo-1,2,5-trithiepienes **77a–d**. In this case, pentathiepine is involved in the reaction as a 1,5-dipole (**C**).⁶² Other Lewis acids are less efficient catalysts for the pentathiepine ring opening than $\text{BF}_3 \cdot \text{Et}_2\text{O}$.



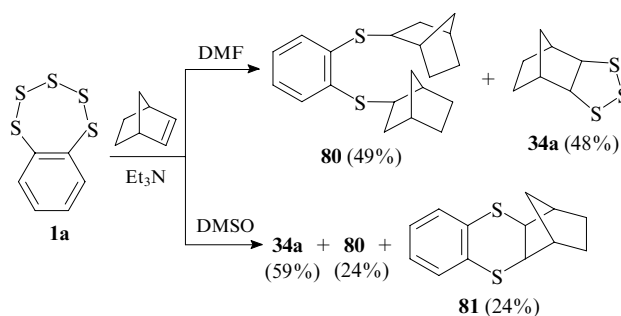
Compound 77	R ¹	R ²	R ³	Yield (%)
a	H	(CH ₂) ₄		81
b	H	(CH ₂) ₃		68
c	Me	H	Me	58
d	Et	H	Et	39

In the presence of triethylamine in DMF, the reaction of compound **1a** with norbornadiene and acrylonitrile is accompanied by a loss of three sulfur atoms; 1,4-dithianes **78** and **79** are apparently formed through intermediate **D**.⁵⁵

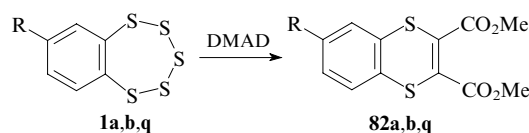


The direction of the reaction of benzopentathiepine (**1a**) with norbornene in the presence of triethylamine depends on

the nature of the solvent. The reaction in DMF produces an equimolar mixture of 1,2,3-trithiolane **34a** and adduct **80** generated as a result of addition of two norbornene molecules at the sulfur atoms. The analogous reaction in DMSO gives not only compounds **34a** and **80**, but also dithiane **81**.

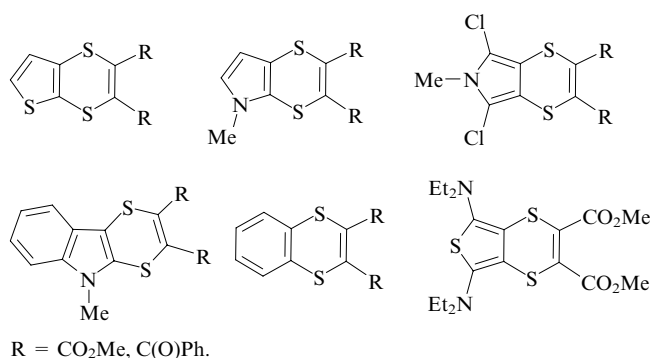


Benzopentathiepienes **1a,b,q** slowly react with dimethyl acetylenedicarboxylate (DMAD) to form benzo-1,4-dithiines **82a,b,q**, the reaction being substantially accelerated in the presence of triphenylphosphine or triethylamine in DMF.^{15, 55}

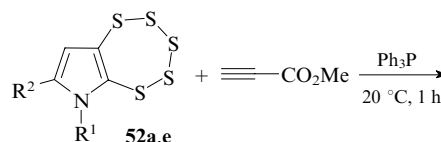


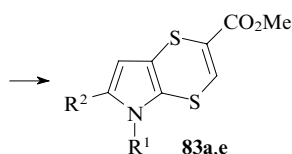
Product 82	R	Reaction conditions	Yield (%)
a	H	Et_3N , DMF	84
b	Cl	xylene	15
q	NMe ₂	Ph_3P , CH_2Cl_2	51

The reaction of electron-withdrawing alkynes with pentathiepienes fused with aromatic and heterocyclic rings in the presence of triphenylphosphine is characteristic of this class of compounds; the corresponding 1,4-dithiines are formed in high yields (64%–93%).^{41, 63} Examples of compounds prepared according to this procedure are given below.



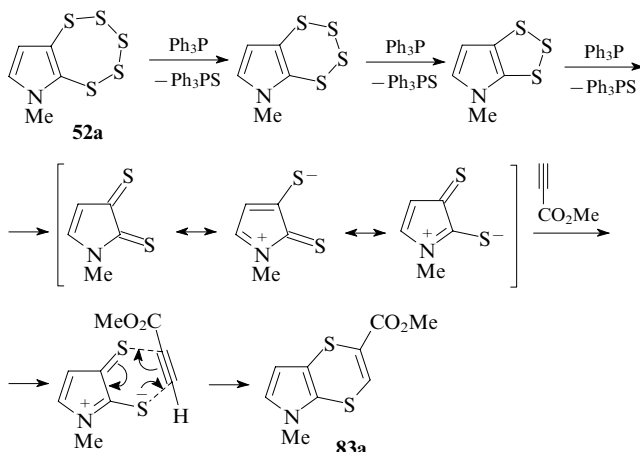
In the presence of triphenylphosphine, pentathiepieno-[6,7-*b*]pyrroles **52a,e** regioselectively add to an unsymmetrical alkyne molecule.⁶³ For example, in compliance with the electron density distribution in the intermediates, which are generated according to the proposed reaction mechanism, the addition products of methyl propiolate, viz., fused 1,4-dithiines **83a,e**, were obtained.



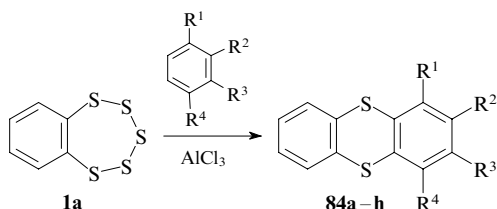


$R^1 = \text{Me}, R^2 = \text{H}$ (**a**); $R^1 = \text{Et}, R^2 = \text{Cl}$ (**e**).

Apparently, triphenylphosphine, acting as a nucleophile, attacks molecule **52a**, which is accompanied by the pentathiepine ring opening and successive elimination of three sulfur atoms to give intermediate of type **D**,⁵⁵ and the latter adds to alkyne (see also Section III.6, the reaction with the Grignard reagent).

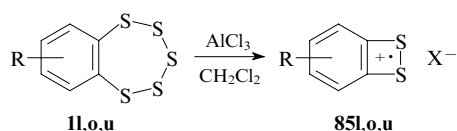


Benzopentathiepine (**1a**) reacts with benzene and some of its derivatives in the presence of a Lewis acid (for example, AlCl_3) as the catalyst. The corresponding 1,4-dithiines **84a–h** are generally formed in good yields.⁶⁴



Compound 84	R^1	R^2	R^3	R^4	Yield (%)
a	H	H	H	H	44
b	Me	H	H	Me	75
c	Pr^i	H	H	Pr^i	62
d	Me	Me	Me	Me	83
e	1,2- C_6H_4		H	H	93
f	Me	1,2- $\text{SC}_6\text{H}_4\text{S}$		Me	20
g	H	H	1,2- $\text{C}_6\text{H}_4\text{S}$		43
h	H	H	1,2- $\text{C}_6\text{H}_4\text{S}$		43

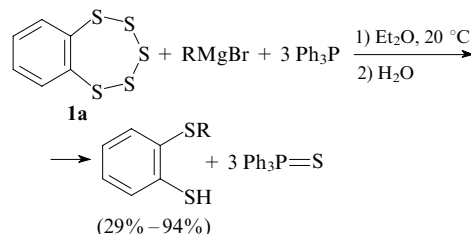
Under the action of AlCl_3 in dichloromethane, pentathiepienes **11,o,u** are transformed into radical cations **851,o,u**, which are apparently intermediates in Friedel–Crafts reactions.⁶⁵ The formation of radical cations **85** was detected by EPR spectroscopy.



$R = 7\text{-Me}$ (**l**), 6-Br (**o**), 7-CF_3 (**u**); $X = \text{Cl}$ or AlCl_4 .

6. Reactions with Grignard reagents

R Sato *et al.*⁶⁶ developed convenient procedures for the synthesis of 2-alkyl(aryl)sulfenylthiophenols. These authors demonstrated that benzopentathiepine (**1a**) reacts with alkyl- and arylmagnesium bromides under mild conditions in the presence of triphenylphosphine.

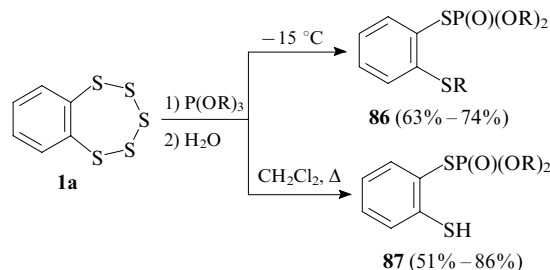


$R = \text{Alk}, \text{Ar}$.

In the absence of triphenylphosphine, the reactions give products in low yields. The presumable mechanism of these reactions involves elimination of three sulfur atoms from benzopentathiepine (**1a**) under the action of triphenylphosphine to form intermediate of type **D**, which adds a Grignard reagent. Hydrolysis of the reaction mixture leads to organyl-sulfenylthiophenols.

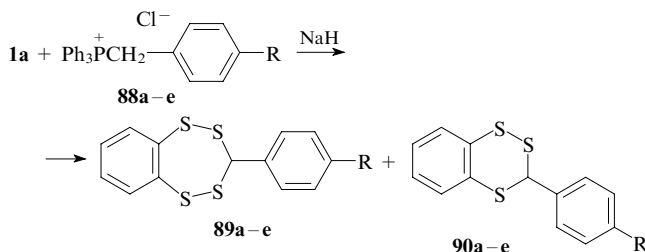
7. Reactions with phosphorus-containing compounds

The reactions of benzopentathiepine (**1a**) with neutral and cationic organophosphorus compounds were documented. The reactions with trialkyl phosphites regioselectively produce thiophosphonates **86** or **87** depending on the reaction conditions.⁶⁷ The former products are generated at -15°C ; the latter products, under reflux of the reagents in dichloromethane. Apparently, the reaction is accompanied by elimination of three sulfur atoms under the action of $\text{P}(\text{OR})_3$, and the resulting intermediate **D** adds the phosphite molecule.



$R = \text{Me}, \text{Et}, \text{Pr}^i, \text{Bu}^n, \text{Ph}$.

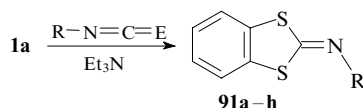
The nucleophilic attack on benzylphosphonium salts **88** in the presence of sodium hydride in pentathiepine **1a** results in a mild ring opening.⁶⁸ These reactions produce mixtures of tetrathiepienes **89** and trithiines **90** in moderate yields.



Compound	R	Yields (%)	
		89	90
a	H	15	52
b	NO_2	0	55
c	Me	19	51
d	OMe	45	25
e	Cl	7	53

8. Reactions with isothiocyanates

2-Iminobenzo-1,3-dithioles **91a–h** were synthesised in good yields from benzopentathiepine (**1a**) and isothiocyanates in the presence of triethylamine.⁶⁹ Aryl isothiocyanates react more readily than alkyl derivatives, and their reactions are accelerated in the presence of electron-donating groups in the molecule. However, unsubstituted phenyl isothiocyanate does not react with pentathiepine **1a**, and compound **91h** was synthesised with the use of phenyl isoselenocyanate.

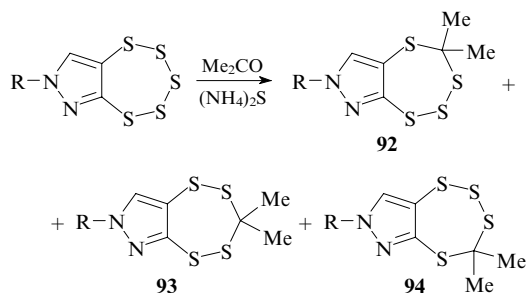


E = S: R = Me (**a**, 81%), Et (**b**, 59%), Prⁿ (**c**, 47%), 4-MeC₆H₄ (**d**, 77%), 4-ClC₆H₄ (**e**, 84%), 4-MeOC₆H₄ (**f**, 74%), 2-MeOC₆H₄ (**g**, 86%);

E = Se, R = Ph (**h**, 78%).

9. Reactions with acetone

Condensation of pentathiepine[6,7-*c*]pyrazoles with acetone in the presence of ammonium sulfide at room temperature gives a mixture of tetrathiepines **92–94** in low yields.⁷⁰

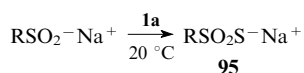


R	Yield (%)		
	92	93	94
Me	10	15	0
Ph	22	21	14

The structures, the energies of transformation and conformational dynamics of isomeric tetrathiepines were studied. However, the mechanism of formation of these compounds remains unclear. Presumably, the pentathiepine ring is cleaved as a result of the nucleophilic attack of the sulfide ion. This reaction is accompanied by extrusion of S₂ to form bis-nucleophilic intermediates analogous to intermediates **A** and **B**, which are fused with acetone.

10. Unusual transformations of pentathiepines

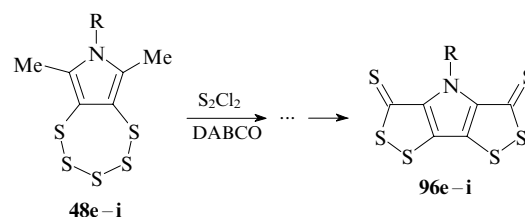
Pentathiepines can serve as sources of sulfur atoms. For example, in the reactions with benzopentathiepine (**1a**), sodium alkyl- and arylsulfonates are transformed into thiosulfonates **95** in high yields.⁷¹



R = Me (78%), Ph (99%), PhCH₂ (81%), PhCH₂CH₂ (86%), Cl(CH₂)₄ (78%), 4-MeC₆H₄ (100%), 4-ClC₆H₄ (82%), 4-MeOC₆H₄ (96%), 4-BrC₆H₄ (85%), EtO₂CCH₂CH₂ (69%).

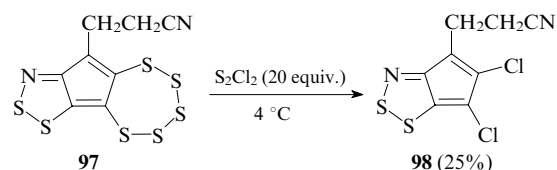
The treatment of *N*-substituted pentathiepine[6,7-*c*]pyrroles **48e–i** with a prestored mixture of sulfur monochloride and DABCO at room temperature leads to an unusual cascade transformation giving rise to bis(dithiolo)pyrroles **96e–i** in high yields.³⁹ The authors described the presumable reaction

mechanism involving oxidation of an enamine tautomer with a disulfide reagent as the key step.



R = Me (**e**, 85%), Et (**f**, 80%), Prⁿ (**g**, 74%), Prⁱ (**h**, 79%), CH₂Ph (**i**, 84%).

The treatment of pentathiepine **97** with a large excess of S₂Cl₂ unexpectedly leads to elimination of all sulfur atoms to form vicinal dichloride **98**.²⁴ At 4 °C, the reaction is completed in a few days.

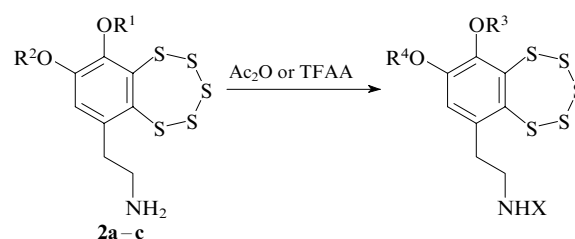


Analogous transformations of other pentathiepines are unknown.

11. Reactions of substituents in aromatic rings of benzopentathiepines

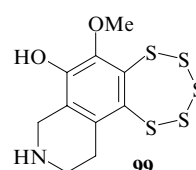
a. Reactions of amino and hydroxy groups

Reactions of the phenol hydroxy group and an aminoalkyl-aromatic fragment of benzopentathiepine derivatives are of interest primarily as procedures for modifying natural pentathiepines and their analogues. It should be noted that the pentathiepine ring is very sensitive to the nucleophilic attack, for example, by the nitrogen atom of the unsubstituted amino group of a peripheral substituent.⁸ For this reason, the protection of the amino group by acylation leads to substantial stabilisation of pentathiepines. *N*-Acetylation and trifluoroacetylation of amines are generally performed with acetic^{60, 72} or trifluoroacetic (TFAA) anhydrides,^{22, 73} Ac₂O reacting also with free phenol groups.



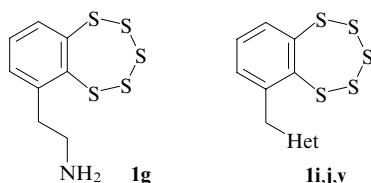
R¹ = Me: R² = Me (**2a**), H (**2b**); R¹ = H, R² = Me (**2c**); R³ = Me, R⁴ = X = Ac; R³ = X = Ac, R⁴ = Me; R³ = R⁴ = Me, X = COCF₃; R³ = Me, R⁴ = H, X = COCF₃; R³ = H, R⁴ = Me, X = COCF₃.

Lissoclinotoxin B (**99**) is easily acylated with acetic anhydride in pyridine at room temperature. The reaction proceeds both at the nitrogen atom of the amino group and the oxygen atom of the phenol hydroxy group.²²



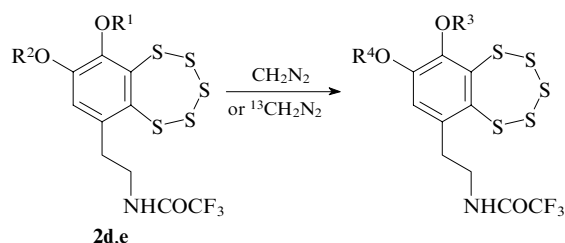
It should be noted that the pentathiepine ring remains intact in the transformation of the amino group of the side chain in varacin (**2a**) into the urea fragment in the course of the reaction with (*S*)-(+)-1-(1-naphthyl)ethyl isocyanate.⁷⁴

Since benzopentathiepine **1g** containing the free aminoethyl group is unstable, it is generally used as hydrochloride. By contrast, compounds **1i,j,v** containing less nucleophilic heterocyclic fragments (pyridine or pyrimidine) and thiophene are rather stable.⁸



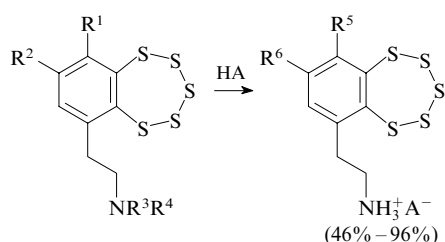
Het = 2-Py (**i**), 2-Pyrm (**j**), 2-thienyl (**v**).

Methylation of the phenol group in compounds **2d,e** with diazomethane and ¹³C-labelled diazomethane made it possible to establish the structure of lissoclinotoxin A.⁷³ In this reaction, the pentathiepine ring also remains intact.



2d,e
 $R^1 = \text{H}, R^2 = \text{Me}$ (**d**); $R^1 = \text{Me}, R^2 = \text{H}$ (**e**);
 $R^3 = R^4 = \text{Me}$; $R^3 = \text{Me}, R^4 = {}^{13}\text{CH}_3$; $R^3 = {}^{13}\text{CH}_3, R^4 = \text{Me}$.

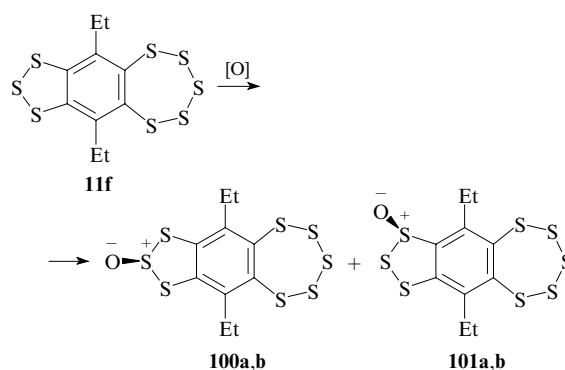
Derivatives of varacin and lissoclinotoxin A containing primary or secondary amino groups can be transformed into stable hydrochlorides and trifluoroacetates.^{8, 10, 22, 23}



$A = \text{CF}_3\text{CO}_2$; $R^1 = R^2 = R^5 = R^6 = \text{OMe}, R^3 = \text{H},$
 $R^4 = \text{CO}_2(\text{CH}_2)_2\text{SiMe}_3, \text{Boc}$; $R^1 = \text{OCH}_2\text{OMe}, R^2 = R^6 = \text{OMe},$
 $R^3 = \text{H}, R^4 = \text{CO}_2(\text{CH}_2)_2\text{SiMe}_3, R^5 = \text{OH};$
 $A = \text{Cl}$; $R^1 = R^2 = R^3 = R^5 = R^6 = \text{H}, R^4 = \text{Boc};$
 $R^1 = R^2 = R^5 = R^6 = \text{OMe}, R^3 = \text{CHO}, R^4 = \text{Boc}.$

b. Oxidation and reduction of the trithiole ring

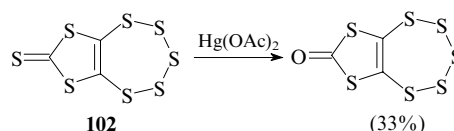
Tricyclic compounds **11** containing the trithiole ring along with the pentathiepine ring were oxidised with various reagents. It appeared that the reactions with *m*-chloroperoxybenzoic acid (MCPBA)⁷⁵ or the $\text{Ti}(\text{OPri})_4$ –DET– Bu^tOOH [DET is (*R,R*)-diethyl tartrate] system⁷⁶ occur only at the trithiole ring.



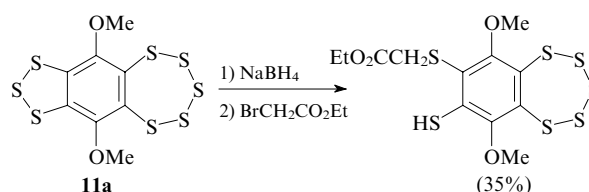
Oxidant	Yield (%)			
	100a	100b	101a	101b
MCPBA	16	13	26	32
Bu^tOOH		29	18	23

Sulfoxides **100a,b** and **101a,b** were isolated from the reaction mixture. Compounds **100a,b** were demonstrated to exist as achiral centrosymmetric conformers, whereas compounds **101a,b** are unsymmetrical diastereomers containing the sulfoxide group in different conformations with respect to the pentathiepine ring (the stereochemistry is considered in more detail in Section V).

Upon oxidation with mercury acetate, the pentathiepine ring also remains intact. For example, the reaction between this reagent and 1,3-dithiole-2-thione fused with pentathiepine **102** produces the corresponding keto derivative.⁷⁷

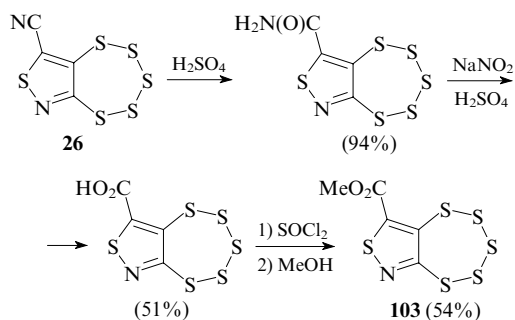


It is known that sodium borohydride NaBH_4 can reduce the pentathiepine ring.¹⁵ However, the treatment of trithiolo-benzopentathiepine **11a** with two equivalents of NaBH_4 followed by alkylation with ethyl β -bromoacetate afforded tetrasubstituted benzopentathiepine.¹¹ This is evidence that the trithiole ring is more sensitive to reducing reagents than the pentathiepine ring.



Reactions of carboxylic acid derivatives

High stability of the pentathiepine ring to acids and nitrosating reagents was exemplified by cyanoisothiazole derivative **26**.¹⁵ For example, the cyano group was hydrolysed in concentrated sulfuric acid to give the amide group in high yield. Then the amide was transformed under the action of sodium nitrite and concentrated sulfuric acid into the acid; its treatment with thionyl chloride and methanol afforded methyl ester **103**. In all these transformations, the pentathiepine ring remains intact.



IV. Spectroscopic studies

1. UV and IR spectroscopy

The character and positions of absorption bands in UV spectra depend on the structure of pentathiepine. The spectrum of unsubstituted pentathiepine (**24**) shows weak and diffuse signals at 206 [the extinction coefficient (ϵ) is 9730], 253 ($\epsilon = 3440$) and 315 nm ($\epsilon = 1510$).¹ Most pentathiepinines are characterised by only one intense band at ~ 210 nm ($\epsilon = 25\,000\text{--}32\,000$).^{1, 15, 60, 73} The spectra of benzopentathiepinines **11e,f** annulated with the trithiole ring show absorption bands at 292–294 nm ($\epsilon = 15\,100\text{--}15\,500$).⁷⁸ For pentathiepinines fused with pyrrole, pyrazole or thiophene, the absorption maxima are observed at 230–240 nm.^{15, 42} The UV spectra of pentathiepanes fused with carbocycles (for example, compounds **12**, **33a,d** and **35**) show two characteristic bands at 231–233 ($\epsilon = 3750\text{--}5500$) and 278–281 nm ($\epsilon = 3090\text{--}3480$).^{1, 2, 29}

The IR spectra contain absorption bands of the S–S bond in pentathiepinines at $460\text{--}485\text{ cm}^{-1}$ (Ref. 29).

2. Raman spectroscopy

All pentathiepinines fused with aromatic or heterocyclic rings are characterised by strong absorption at 485 cm^{-1} in Raman spectra.¹⁵ Most often, Raman spectra of pentathiepinines show two absorption bands, the most intense band being observed at $490 \pm 5\text{ cm}^{-1}$. The Raman spectra of benzopentathiepinines have two additional characteristic absorption bands at $425 \pm 5\text{ cm}^{-1}$ (of weak to medium intensity) and $180 \pm 5\text{ cm}^{-1}$ (strong), which can be used for the identification of these compounds.

3. NMR spectroscopy

The ring protons in the ^1H NMR spectrum of unsubstituted pentathiepine (**24**) have a chemical shift (δ) of 7.42 ppm. The spectrum of benzopentathiepine (**1a**) is characterised by an AA'BB' system centred at $\delta = 7.52$.¹ The signals for the carbon atoms of the pentathiepine ring are observed in the ^{13}C NMR spectrum at low field ($\delta = 135\text{--}145$).^{18, 22, 32, 56, 59, 77}

The corresponding NMR spectra of pentathiepanes **33a,c,d** show signals for the ring hydrogen atoms at $\delta 3.93\text{--}4.06$ and signals for the carbon atoms of the pentathiepane ring at $\delta 69.8\text{--}72.7$.²⁷

4. Mass spectrometry

Mass spectrometry is one of the main methods for establishing the structures of pentathiepinines and pentathiepanes. Generally, samples are transformed into the ionised state under electron impact. Almost in all cases, the intensity of the molecular ion peak is low (from 0.6% to 25%), and the $[\text{M} - \text{S}_2]^+$ ion peak corresponding to a loss of two sulfur atoms is the most characteristic peak (the intensity is 40%–100%) upon fragmentation.^{34, 35, 42, 46, 49, 56, 60, 77–79} Pentathiepinines can also be identified by FAB (Fast Atom

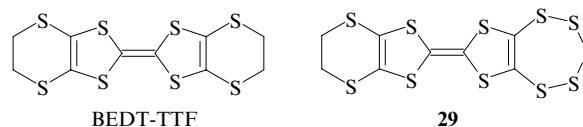
Bombardment) mass spectrometry,^{72, 73} however this method has not gain wide acceptance.

5. X-Ray diffraction

The molecular structures of more than 30 compounds containing the pentathiepine or pentathiepane rings were established by X-ray diffraction. In most compounds, polysulfur-containing rings adopt a chair conformation. The S–S bond length varies from 2.039 (in benzopentathiepine **1a**)⁸⁰ to 2.063 Å (in dithiolopentathiepine **102**),⁸¹ which is similar to the bond length in the S_8 molecule (2.051 Å). The S–S–S and S–S–S–S angles are also comparable with those in S_6 and S_8 . The S–C bond lengths in pentathiepinines and pentathiepanes (1.744–1.795 Å) are comparable with the S–C(sp²) single bond length (1.78 Å).^{15, 81, 82}

6. Electrochemical methods

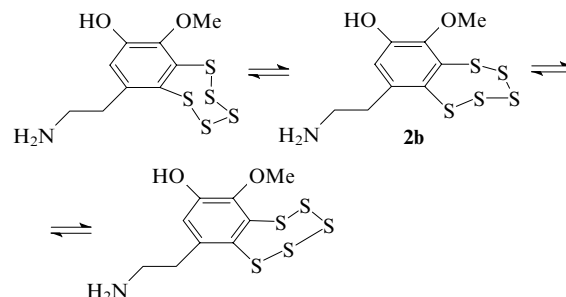
The electrochemical properties of pentathiepine **29** were studied by cyclic voltammetry. This compound is characterised by two pairs of reversible redox potentials with the following values: +0.69 and +1.06 V. These potentials are higher than those for the structurally similar BEDT-TTF compound (+0.53 and +0.89 V).²⁰ This indicates that the electron-donor properties of pentathiepine **29** are weaker than those of BEDT-TTF. Apparently, this fact can be attributed to the induction effect due to the larger number of sulfur atoms in the pentathiepine ring.



A comparison of the electrochemical behaviour of pentathiepineindole **40b** and 1-methylindole demonstrated that the introduction of a polysulfur-containing ring into an inactive molecule gives rise to electrochemical activity.⁸³

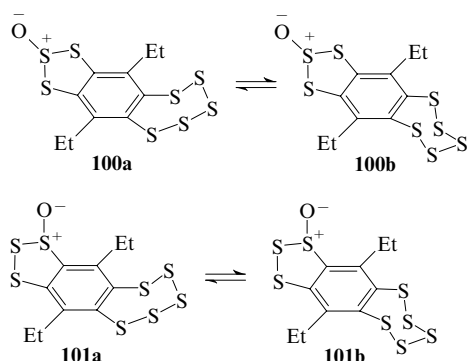
V. Stereochemical aspects: conformation and chirality

The ^1H NMR spectra of varacin (**2a**) and lissoclinotoxin A (**2b**) show complex signals for the protons of the benzyl group.^{73, 74} A complication of the signals is a consequence of a high energy barrier (30 kcal mol^{−1}) for inversion of the pentathiepine ring, resulting in asymmetry of the molecule and diastereotopicity of the benzyl protons. An increase in temperature from 25 to 100 °C leads to narrowing of the signals and the signals for all protons are clearly observed. The high energy barrier is apparently attributed to unfavourable overlap of the isolated orbitals of the sp³-hybridised sulfur atom during ring inversion through the half-chair transition state.⁷³

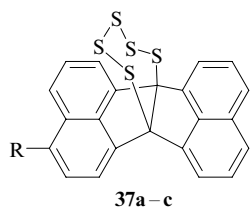


The structures of four sulfoxides (**100a,b** and **101a,b**), which were synthesised by oxidation of trithiolobenzopentathiepine **11f** with *m*-chloroperoxybenzoic acid, were estab-

lished by X-ray diffraction.⁷⁵ For pairs of 2- and 1-oxides, the activation parameters of the pentathiepine ring inversion in chloroform at room temperature were determined. It appeared that the free energy change ($^{298}\Delta G^\ddagger$) after complete inversion is from 105.0 to 113.4 kJ mol⁻¹ in each case.⁷⁶



Analogous investigations were performed for pairs of isomers of monosubstituted pentathiepanoacenaphtho[1,2-*a*]acenaphthylenes **37a–c**; for the complete inversion, $^{298}\Delta G^\ddagger$ was 103.8–108.5 kJ mol⁻¹.³¹



R = Et (**a**), Ph (**b**), (**c**).

VI. Quantum-chemical calculations of pentathiepine molecules

The conformations of pentathiepine (**24**), benzopentathiepine (**1a**) and thieno[3,4-*f*]pentathiepine (**1v**) were studied by the semiempirical AM1 method.⁸⁴ It was found that the rigid chair-like conformation of the heterocycle is the most stable one. The results of calculations by the CNDO method correlate well with the observed positions of absorption bands in UV spectra.

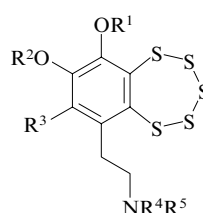
Ab initio molecular orbital calculations (SCF and MP-2) of the conformational behaviour of benzopentathiepine (**1a**) are in good agreement with the experimental data. According to the results of calculations, the chair conformation is more stable than the boat and twist conformations.⁷⁰ Calculations of the highest occupied molecular orbital and the lowest unoccupied molecular orbital for compound **1a** by the PM3 method demonstrated that the nucleophilic attack of trialkyl phosphites occurs predominantly on the sulfur atom at position 2 to give products **86** and **87**, as was described above (see Section III.7).⁶⁷

The structures of pentathiepinanes and their reactions were studied in detail by Greer⁸⁵ by density functional theory (DFT). The calculations demonstrated that decomposition of unsubstituted pentathiepine (**24**) upon the nucleophilic attack on the hydrosulfide anion unexpectedly starts with the attack on the S(1) atom rather than with the more expected attack on the S(2) atom. This gives rise to the delocalised enethiolate anion, which initiates the subsequent liberation of the S₃

species.[†] The S₃ molecule was detected by the reactions with norbornene and 2,3-dimethylbuta-1,3-diene; these adducts are analogous to the reaction products with S₂.⁸⁶

VII. Biological activity and practical applications of pentathiepinanes

Varacin (**2a**) isolated from the marine organisms *Lissoclinum vareau* in 1991 was the first known natural pentathiepine.⁵⁸ More recently, several structurally analogous compounds were isolated: lissoclinotoxin A (**2b**) from the ascidians *Lissoclinum* sp.,⁷³ lissoclinotoxin B (**99**) from the tunicate *Lissoclinum perforatum* found near the Palau Islands,⁶⁰ *N,N*-dimethyl-5-(methylthio)varacin (**3a**) from the ascidians *Lissoclinum japonicum*, 5-(methylthio)varacin (**3b**) in a mixture with the corresponding trithiole (in a 2:3 ratio) and demethylated varacin (**2f**) from various species of the marine organisms *Lissoclinum* and *Eudistoma* found near the Pohnpei Island, respectively.⁵⁹



R¹ = R² = Me, R³ = R⁴ = R⁵ = H (**2a**);

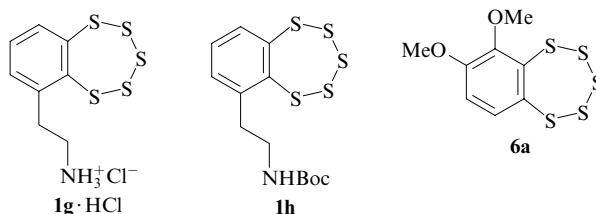
R¹ = R² = Me, R³ = SMe, R⁴ = R⁵ = H (**3b**);

R² = R³ = R⁴ = R⁵ = H: R¹ = H (**2f**), Me (**2b**);

R¹ = Me, R² = R⁵ = H, R³–R⁴ = CH₂ (**99**).

Synthetic and natural pentathiepinanes have various biological activities. The antitumour properties of these compounds were tested. High cytotoxicity of varacin was demonstrated with several types of cancer cells (*IC*₅₀ varies from 1 to 50 nmol litre⁻¹).⁸⁷ The cytotoxicity against HCT 116 human colon cancer cells is characterised by *IC*₅₀ = 0.05 mg ml⁻¹. Varacin is 100 times more active and 1.5 times less toxic to CHO EM9 tumour cells compared to 5-fluorouracil (the antitumour drug belonging to antimetabolites).⁵⁸

N,N-Dimethyl-5-(methylthio)varacin (**3a**) and synthetic benzopentathiepinanes **1g** (as hydrochloride), **1h** and **6a** have the cytotoxicity *IC*₅₀ = 0.26, 3.2 and 6.1 mg ml⁻¹, respectively, against HeLa53 cells. Pentathiepine hydrochloride **1g** is 10 times more active in these experiments than the corresponding starting arene-1,2-dithiol.⁷



[†] The appearance of the previously unknown S₃ species is considered as an important factor in chemical and, which is particularly important, biochemical transformations of pentathiepinanes, for example, in the explanation of the mechanism of antitumour action of varacin (**2a**). Elimination of S₃ is attributed also to the presence of the side aminoalkyl group, which was found in all natural pentathiepinanes. The intramolecular attack of the primary or secondary (but not tertiary!) amino group on the S(1) atom of fused pentathiepine is the key step of elimination of the S₃ species.

7-Methylbenzopentathiepine (**11**) has a thiol-dependent DNA-binding ability. This is the first direct evidence that pentathiepinanes can act on DNA in physiological conditions.⁸⁸ Recently, it has been demonstrated⁸⁹ that the nucleophilic attack of thiols leads to a more rapid opening of the pentathiepine ring in 7-methylbenzopentathiepine (**11**) compared to the analogous reactions with di- and trisulfides. Apparently, this is responsible for the cytotoxic role of natural pentathiepinanes interacting with endogenous cellular trisulfides. Varacin has an efficient DNA-binding ability both in the presence and in the absence of 2-mercaptoethanol, and this activity increases with increasing concentration of thiol.⁸⁷

Since all natural pentathiepinanes contain the aminoethyl fragment, the positively charged amino group of pentathiepine antibiotics is presumably favourable for their interactions with DNA.^{88,89} Demethylated varacin (**2f**) and *N,N*-dimethyl-5-(methylthio)varacin (**3a**) inhibit protein kinase C with $IC_{50} = 0.5$ and 3.0 mg ml^{-1} , respectively.⁵⁹

Lissoclinotoxin A (**2b**) and lissoclinotoxin B (**99**) are strong antimicrobial drugs, the former compound showing activity toward a number of microorganisms similar to that of cefotaxim.⁶⁰ Compounds **2b** and **99** were found to have activity against a fish pathogenic strain similar to that of ampicillin.

Varacin (**2a**), lissoclinotoxin A (**2b**) and benzopentathiepine (**1a**) exhibit high *in vitro* activity against the microorganisms *Candida albicans* and *Bacillus subtilis*.^{58,72,73} This activity of the benzopentathiepine system is independent of the presence of an amino group in the side chain. The fungicidal activity of pentathiepinoinisothiazole **26** was tested and covered by patents^{90–93} for the tomato fungus *Phytophthora infestans*⁹⁴ and the fungus *Venturia inaequalis* in infected apple trees.⁹⁵ 7-Trifluoromethylbenzopentathiepine (**1u**) at a concentration of 100 ppm provides 100% protection against the apple scab; its 7-dimethylamino analogue **1q**, 100% protection against the cucumber mosaic virus.⁹⁶

Pentathiepinanes derived from norbornene and its derivatives were proposed as catalysts for vulcanisation of diene rubbers.⁹⁷ Benzo- and perhydrobenzopentathiepinanes were used in photography as additives to emulsion layers or adjacent hydrophilic colloidal layers as antifogging agents;⁹⁸ other pentathiepinanes have found application for the improvement of properties of photographic materials.^{99–104} In 2005, Japanese researchers proposed that pentathiepinoinidole **40a** be used as a cathodic material for storage batteries.⁸³

* * *

In conclusion, it should be noted that 1,2,3,4,5-pentathiepinanes and 1,2,3,4,5-pentathiepanes are the most stable C_2S_n heterocycles because they are thermodynamically controlled products of numerous sulfurisation reactions. Although only a rather small amount of time has passed since the first synthesis of pentathiepanes (in 1967) and pentathiepinanes (in 1971) and isolation of natural antibiotics containing the pentathiepine ring from marine organisms (in 1991), a large number of studies on these compounds have been published. These compounds have attracted considerable interest because of their surprising stability, high inversion barriers of the chair-like pentathiepine ring and various biological activities.

The pentathiepine ring can easily be formed with the use of known synthetic methods; however, these heterocycles are often formed accidentally as a result of quite unexpected transformations of sulfur-containing substrates. Since there are numerous possibilities for both the nucleophilic and electrophilic attack on all five sulfur atoms, the pentathiepine ring can be involved in various chemical reactions. Unfortunately, scarce examples were documented for such transformations, the mechanisms of these transformations often

remaining unknown. Hence, further investigations in this interesting field of heterocyclic chemistry are required.

This review has been written with the financial support of the Russian Foundation for Basic Research (Project No. 05-03-32032).

References

1. F Fehér, B Degen *Angew. Chem., Int. Ed. Engl.* **6** 703 (1967)
2. F Fehér, M Langer *Tetrahedron Lett.* **12** 2125 (1971)
3. L S Konstantinova, O A Rakitin, C W Rees *Chem. Rev.* **104** 2617 (2004)
4. G N Nikonov, A S Balueva, in *Comprehensive Heterocyclic Chemistry II* Vol. 9 (Ed. G R Newkome) (Oxford: Elsevier, 1996) p. 371
5. R Sato, S Saito, H Chiba, T Goto, M Saito *Chem. Lett.* 349 (1986)
6. S Ogawa, N Yomoji, S Chida, R Sato *Chem. Lett.* 507 (1994)
7. R Sato, T Ohyama, S Ogawa *Heterocycles* **41** 893 (1995)
8. R Sato, T Ohyama, T Kawagoe, M Baba, S Nakajo, T Kimura, S Ogawa *Heterocycles* **55** 145 (2001)
9. T Kimura, T Suzuki, Y Takaguchi, A Yomogita, T Wakahara, T Akasaka *Eur. J. Org. Chem.* 1262 (2006)
10. F D Toste, I W J Still *J. Am. Chem. Soc.* **117** 7261 (1995)
11. R Sato, T Kimura, T Goto, M Saito *Tetrahedron Lett.* **29** 6291 (1988)
12. R Sato, S Saito, H Chiba, T Goto, M Saito *Bull. Chem. Soc. Jpn.* **61** 1647 (1988)
13. R Sato, T Kimura, T Goto, M Saito, C Kabuto *Tetrahedron Lett.* **30** 3453 (1989)
14. B L Chenard, T J Miller *J. Org. Chem.* **49** 1221 (1984)
15. B L Chenard, R L Harlow, A L Johnson, S A Vladuchick *J. Am. Chem. Soc.* **107** 3871 (1985)
16. W Ando, Y Kumamoto, N Tokitoh *Tetrahedron Lett.* **28** 4833 (1987)
17. W Ando, N Tokitoh, Y Kabe *Phosphorus, Sulfur Silicon Relat. Elem.* **58** 179 (1991)
18. S A Vladuchick, T Fukunaga, H E Simmons, O W Webster *J. Org. Chem.* **45** 5122 (1980)
19. E Fanghänel, R Herrmann, H Naarmann *Tetrahedron* **51** 2533 (1995)
20. E Ojima, H Fujiwara, H Kobayashi *Adv. Mater.* **11** 758 (1999)
21. P W Ford, B S Davidson *J. Org. Chem.* **58** 4522 (1993)
22. P W Ford, M R Narbut, J Belli, B S Davidson *J. Org. Chem.* **59** 5955 (1994)
23. V Behar, S J Danishefsky *J. Am. Chem. Soc.* **115** 7017 (1993)
24. S Macho, C W Rees, T Rodriguez, T Torroba *Chem. Commun.* 403 (2001)
25. M J Earle, A G Massey, A R Al-Soudani, T Zaidi *Polyhedron* **8** 2817 (1989)
26. F Trigalo, M Guyot, F Frappier *Nat. Prod. Lett.* **4** 101 (1994)
27. P D Bartlett, T Ghosh *J. Org. Chem.* **52** 4937 (1987)
28. N S Nametkin, V D Tyurin, I V Petrosyan, A V Popov, B I Kolobkov, A M Krapivin *Izv. Akad. Nauk SSSR, Ser. Khim.* 2841 (1980)^a
29. E A Chernyshev, O V Kuz'min, A V Lebedev, A I Gusev, N I Kirillova, N S Nametkin, V D Tyurin, A M Krapivin, N A Kubasova *J. Organomet. Chem.* **252** 133 (1983)
30. J Nakayama, Y Ito, A Mizumura *Sulfur Lett.* **14** 247 (1992)
31. Y Sugihara, H Takeda, J Nakayama *Eur. J. Org. Chem.* 597 (1999)
32. N Tokitoh, H Hayakawa, M Goto, W Ando *Tetrahedron Lett.* **29** 1935 (1988)
33. E M Brzostowska, A Greer *J. Org. Chem.* **69** 5483 (2004)
34. G W Rewcastle, T Janosik, J Bergman *Tetrahedron* **57** 7185 (2001)
35. T Janosik, B Stesland, J Bergman *J. Org. Chem.* **67** 6220 (2002)
36. A V Lebedev *Zh. Obshch. Khim.* **63** 1780 (1993)^b
37. Z S Ariyan, C I Courduvelis, J T O'Brien, W D Spall *J. Chem. Soc., Perkin Trans. 1* 447 (1974)
38. S A Amelichev, L S Konstantinova, K A Lyssenko, O A Rakitin, C W Rees *Org. Biomol. Chem.* 3496 (2005)

39. S A Amelichev, R R Aysin, L S Konstantinova, N V Obruchnikova, O A Rakitin, C W Rees *Org. Lett.* **7** 5725 (2005)
40. L S Konstantinova, O A Rakitin, C W Rees, S A Amelichev *Mendeleev Commun.* 91 (2004)
41. L S Konstantinova, O A Rakitin, C W Rees, L I Souvorova, D G Golovanov, K A Lyssenko *Org. Lett.* **5** 1939 (2003)
42. J Perregaard, S Scheibye, H J Meyer, I Thomsen, S O Lawesson *Bull. Soc. Chim. Belg.* **86** 679 (1977)
43. A Z Rys, D N Harpp *Tetrahedron Lett.* **41** 7169 (2000)
44. R Steudel, K Hassenberg, V Muenchow, O Schumann *Eur. J. Inorg. Chem.* 921 (2000)
45. M Kustos, R Steudel *J. Org. Chem.* **60** 8056 (1995)
46. J L Morris, C W Rees *J. Chem. Soc., Perkin Trans. 1* 211 (1987)
47. H Muraoka, S Ogawa, N Nagahora, Y Kawai, R Sato *Bull. Chem. Soc. Jpn.* **78** 2026 (2005)
48. J-H Chou, T B Rauchfuss *Z. Naturforsch., B* **52** 1549 (1997)
49. A Kunugi, K Kuwamura, H Uno *Electrochim. Acta* **42** 2399 (1997)
50. A Kunugi, K Hayashi, H Yumoto, H Uno *Electrochim. Acta* **44** 2899 (1999)
51. S G Polonik, P S Dmitrenok, V V Makhan'kov, V F Anufriev, *Zh. Org. Khim.* **42** 316 (2006)^c
52. J Bergman, C Stålhandske *Tetrahedron Lett.* **35** 5279 (1994)
53. K Emayan, C W Rees *Bull. Soc. Chim. Belg.* **106** 605 (1997)
54. R Sato *Heteroatom. Chem.* **13** 419 (2002)
55. R Sato, K Chino, M Saito *Sulfur Lett.* **10** 233 (1990)
56. N Tokitoh, H Ishizuka, W Ando *Chem. Lett.* 657 (1988)
57. T Kimura, K Tsujimura, S Mizusawa, S Ito, Y Kawai, S Ogawa, R Sato *Tetrahedron Lett.* **41** 1801 (2000)
58. B S Davidson, T F Molinski, L R Barrows, C M Ireland *J. Am. Chem. Soc.* **113** 4709 (1991)
59. R S Compagnone, D J Faulkner, B K Carté, G Chan, A Freyer, M E Hemling, G A Hofmann, M R Mattern *Tetrahedron* **50** 12785 (1994)
60. M Litaudon, F Trigalo, M-T Martin, F Frappier, M Guyot *Tetrahedron* **50** 5323 (1994)
61. R Sato, Y Kanazawa, Y Akutsu, M Saito *Heterocycles* **29** 2097 (1989)
62. R Sato, A Onodera, T Goto, M Saito *Chem. Lett.* 2111 (1989)
63. S A Amelichev, L S Konstantinova, N V Obruchnikova, O A Rakitin, C W Rees *Org. Lett.* **8** 4529 (2006)
64. R Sato, A Onodera, T Goto, M Saito *Heterocycles* **27** 2563 (1988)
65. H Bock, B L Chenard, P Rittmeyer, U Stein *Z. Naturforsch., B* **43** 117 (1988)
66. R Sato, K Ishigami, M Saito *Sulfur Lett.* **12** 61 (1990)
67. R Sato, T Murata, S-I Chida, S Ogawa *Chem. Lett.* 1325 (1993)
68. S Ogawa, M Wagatsuma, R Sato *Heterocycles* **44** 187 (1997)
69. R Sato, S Yamaichi *Chem. Lett.* 355 (1991)
70. B L Chenard, D A Dixon, R L Harlow, D C Roe, T Fukunaga *J. Org. Chem.* **52** 2411 (1987)
71. R Sato, Y Akutsu, T Goto, M Saito *Chem. Lett.* 2161 (1987)
72. T N Makarieva, V A Stonik, A S Dmitrenok, B B Grebnev, V V Isakov, N M Rebachyk *J. Nat. Prod.* **58** 254 (1995)
73. P A Searle, T F Molinski *J. Org. Chem.* **59** 6600 (1994)
74. B S Davidson, P W Ford, M Wahlman *Tetrahedron Lett.* **35** 7185 (1994)
75. T Kimura, M Hanzawa, E Horn, Y Kawai, S Ogawa, R Sato *Tetrahedron Lett.* **38** 1607 (1997)
76. T Kimura, M Hanzawa, K Tsujimura, T Takahashi, Y Kawai, E Horn, T Fujii, S Ogawa, R Sato *Bull. Chem. Soc. Jpn.* **75** 817 (2002)
77. C P Galloway, D D Doxsee, D Fenske, T B Rauchfuss, S R Wilson, X Yang *Inorg. Chem.* **33** 4537 (1994)
78. N Yomoji, S Takahashi, S-I Chida, S Ogawa, R Sato *J. Chem. Soc., Perkin Trans. 1* 1995 (1993)
79. A I Mikaya, E A Trusova, V G Zaikin, V D Tyurin, O V Kuz'min, A V Lebedev *J. Organomet. Chem.* **256** 97 (1983)
80. F Fehér, B Z Engelen *Z. Anorg. Allg. Chem.* **452** 37 (1979)
81. V N Baumer, V A Starodub, V P Batulin, E E Lakin, V P Kuznetsov, O A Dyachenko *Acta Crystallogr., Sect. C* **49** 2051 (1993)
82. J D Korp, I Bernal, S F Watkins, F R Fronczek *J. Heterocycl. Chem.* **19** 459 (1982)
83. H Tsutsumi, H Higashiyama, K Onimura, T Oishi *J. Power Sources* **146** 345 (2005)
84. G Buemi, F Zuccarello, A Raudino *J. Mol. Struct. (THEOCHEM)* **167** 245 (1988)
85. A Greer *J. Am. Chem. Soc.* **123** 10379 (2001)
86. E M Brzostowska, A Greer *J. Am. Chem. Soc.* **125** 396 (2003)
87. A H F Lee, A S C Chan, T Li *Chem. Commun.* 2112 (2002)
88. T Chatterji, K S Gates *Bioorg. Med. Chem. Lett.* **8** 535 (1998)
89. T Chatterji, K S Gates *Bioorg. Med. Chem. Lett.* **13** 1349 (2003)
90. Belg. P. 853648; *Chem. Abstr.* **89** 18357 (1978)
91. US P. 4094985; *Chem. Abstr.* **89** 215448 (1978)
92. US P. 2387236; *Chem. Abstr.* **91** 193346 (1979)
93. US P. 4275073; *Chem. Abstr.* **95** 150654 (1981)
94. Neth. P. 7704108; *Chem. Abstr.* **90** 137878 (1979)
95. Jpn. P. 78127489; *Chem. Abstr.* **90** 82132 (1979)
96. WO PCT 8404921; *Chem. Abstr.* **102** 185115 (1985)
97. BRD P. 10114025; *Chem. Abstr.* **135** 332437 (2001)
98. Jpn. P. 02157745; *Chem. Abstr.* **114** 52848 (1991)
99. Jpn. P. 02256046; *Chem. Abstr.* **114** 196310 (1991)
100. Jpn. P. 04115249; *Chem. Abstr.* **118** 29180 (1993)
101. Jpn. P. 06194775; *Chem. Abstr.* **122** 20369 (1995)
102. Jpn. P. 09061956; *Chem. Abstr.* **126** 299653 (1997)
103. Jpn. P. 11119368; *Chem. Abstr.* **130** 344985 (1999)
104. Jpn. P. 2000047344; *Chem. Abstr.* **132** 173319 (2000)
- ^a — *Russ. Chem. Bull., Int. Ed. (Engl. Transl.)*
- ^b — *Russ. J. Gen. Chem. (Engl. Transl.)*
- ^c — *Russ. J. Org. Chem. (Engl. Transl.)*

Thermodynamics and mechanisms of the formation of supramolecules and supramolecular assemblies of s, p, d and f elements: problems and prospects

A Yu Tsivadze, G V Ionova, V K Mikhalko, Yu N Kostrubov

Contents

I. Introduction	213
II. Molecular recognition in biology and coordination chemistry	214
III. Transition d and f elements as structural components of polymers	215
IV. Complexes of d and f elements as the building blocks in macrocycles	217
V. Thermodynamic properties of macrocyclic complexes in solution	227
VI. Conclusion	231

Abstract. The experimental results concerning the mechanism and thermodynamics of formation of three classes of supramolecular systems, namely, polymers, discrete ring nanostructures and macrocyclic complexes (with crown ethers, cryptands, *etc.*) are surveyed. The thermodynamic factors, in particular, the bond energy between the ‘building blocks’, determining the stability of supramolecular assemblies are analysed. The energy contributions of the metal–ligand and metal–metal interactions and hydrogen bonds to the thermodynamics and mechanism of self-assembly are compared. The principles of design of new polynuclear assemblies of s, p, d and f elements are considered. The bibliography includes 165 references.

I. Introduction

The subject of supramolecular chemistry (SMCh) is the formation of new chemical structures upon self-assembly of molecules and molecular aggregates into supramolecular assemblies (SMA). A founder of this new scientific trend, J-M Lehn proposed^{1,2} the following definition: ‘Beyond molecular chemistry based on the covalent bond, there lies the field of supramolecular chemistry, whose goal it is to gain control over the intermolecular bond’.

Initially, the task of SMCh was formulated (according to Lehn’s views) as the study of ‘non-covalent interaction of two or more subunits’³ or ‘spontaneous interaction of molecules to give structured, stable, non-covalently bound aggregates’.⁴ However, as experimental data on the synthesis of SMA such as supramacrocycles (SMC), macrocyclic complexes (MC) and supramolecular polymers (SMP) have been accumulated, the definition of SMCh was modified. For example, it was stated⁵ that, whereas non-covalent interactions play a key role in the formation of secondary and tertiary structures in natural

macromolecules, in the case of linear supramolecular polymers, strong, highly directed interactions are more desirable in order to create materials with bonds able to make an alternative to covalent bonds. Currently, there is no consensus of opinions about this issue. It has been even doubted⁶ whether it is possible to distinguish between the chemistry of polynuclear metal complexes and SMCh. Generalisation of the proposed mechanisms of SMA formation^{1–8} shows that they include all types of interactions between structural units ranging from weak intermolecular^{1–4} to strong coordination bonds.^{5,7,8} No new, previously unknown types of interaction have been found in the SMCh.

The concepts and notions borrowed from biology have played a significant role in the formation of supramolecular chemistry as a separate field of science. The most important of such concepts are the molecular recognition and cooperativity. The formation of SMA is considered^{1–20} to be a cooperative process based on the molecular recognition of the interacting ‘building blocks’ related to the complementarity principle.

The structural blocks in SMCh include nitrogen- and sulfur-containing heteroaromatic compounds, polypyridine ligands, cyano-substituted aromatic ligands, hydroxamates, *o*-catecholamides, calixarenes, *etc.*^{6–25} Recent reviews are devoted to the synthesis and properties of crown-substituted porphyrinates and phthalocyaninates;⁷ stereochemical aspects of chiral self-assembly;⁶ development of the assembly principle of SMC;^{8,9} dendrimers;^{10,11} tetrathiafulvalenes;¹² rotaxanes;¹³ molecular ‘containers’;¹⁴ crown ethers;¹⁵ the photochromism of SMA;¹⁶ molecular wires;^{17,18} helical polycyanides and SMP¹⁹ and supramolecular fullerene aggregates.²⁰ Some studies discuss the synthesis of new SMA (including SMC) and their practical application as sensors;²¹ nanopores and mesopores; the properties of individual nanoparticles and metallic nanoclusters;²³ and plastic cylinders.²⁴ Although s-, p- and d-metal complexes are used as building blocks,²⁵ preference is given to soft (according to Pearson’s classification²⁶) metal cations: Cu⁺, Ag⁺, Au⁺, Pd²⁺, Pt²⁺, Cd²⁺, Pd⁴⁺, Pt⁴⁺, and cations having intermediate properties: Fe²⁺, Co²⁺, Ni²⁺, Ru²⁺, Os²⁺, Rh³⁺ and Ir³⁺. A number of publications deal with the SMCh of lanthanides^{7,27} and actinides.²⁸ The preparation of polymetallic SMA for Ln³⁺ and An³⁺ may provide a new solution to an important processing problem, namely, the separation of these elements by extraction.

According to Pearson,²⁶ all Ln and An cations are classified as hard acids, irrespective of the oxidation state. The

A Yu Tsivadze, G V Ionova, V K Mikhalko, Yu N Kostrubov A N Frumkin Institute of Physical Chemistry and Electrochemistry, Russian Academy of Sciences, Leninsky prosp. 31, 119991 Moscow, Russian Federation. Fax (7-495) 952 53 08, tel. (7-495) 952 04 62, e-mail: tsiv@phyche.ac.ru (A Yu Tsivadze), tel. (7-495) 429 94 66, e-mail: ionova@ipc.rssi.ru (G V Ionova), mikhalko@ipc.rssi.ru (V K Mikhalko), kostrubov@ipc.rssi.ru (Yu N Kostrubov)

Received 2 February 2006

Uspekhi Khimii 76 (3) 237–259 (2007); translated by Z P Bobkova

hardness of Ln and An was characterised quantitatively depending on the oxidation state.^{29,30} It was shown^{31,32} that An³⁺ ions are softer acids than Ln³⁺ and they should be better coordinated to soft bases.

Supramolecular assemblies can contain three and more metal ions. For example, a metallodendrimer containing 64 ferrocenyl ions and a polycobaltocene dendrimer with 32 cobalt ions have been obtained in solutions.¹⁰ The strategy of self-assembly allows one to prepare SMA with pre-specified properties.⁹ In these SMA, metal ions can exhibit new and unexpected redox and magnetic properties. The unique features of SMA include the selective inclusion of guest ions and molecules into the cavities to give new SMA of the guest–host type.^{1,2,8,9}

This review is concerned with SMA constructed from s-, p-, d- and f-metal ion complexes. In these SMA, discrete structures formed through coordination bonding and incorporating metal ions are combined into large stable assemblies. As the experimental data have been accumulated, it became necessary to perform quantitative analysis of the interaction energies between the building blocks, which contribute to the formation enthalpy of SMA. In this review, we attempted to compare quantitatively different mechanisms for SMA formation, in particular, the formation through weak intermolecular interactions,^{1–4,18} strong coordination and ionic interactions^{5–17,19} and mixed type interactions.^{1,2,6,18,22}

Comparison of the energetic characteristics of metal-containing building blocks and the structural fragments linking them to form SMA is an important stage in the study of the thermodynamics of SMA formation. In SMC, the metal–metal interaction even at large distances, as well as interaction through bridging ligands may play a significant role in the formation of stable SMA. All available estimates of the $D_0(\text{AB})$ bond energy are based on the structural thermodynamic model (STM).^{32–34} The basis equations include the following parameters: the radius of the maximum electron density R_0 , which can be found by solving the Schrödinger equation with allowance for relativistic corrections for free atoms in the ground state; the experimental $R_e(\text{AB})$ value, *i.e.*, the equilibrium internuclear distance for the A–B bond in the given compound; R_e^{di} is the experimental internuclear distance in the diatomic AB(g) molecule; $\chi(\text{A})$ and $\chi(\text{B})$ are the chemical potentials of atoms A and B, respectively; $\chi(\text{AB})$ is the relative chemical potential, which is close to the Pauling electronegativity; $\chi^{\text{di}}(\text{AB})$ corresponds to a diatomic AB(g) molecule.

$$\ln[D_0(\text{AB})] = \chi(\text{AB}) + \gamma(\text{AB}) = \lambda(\text{AB});$$

$$D_0(\text{AB}) = ke^{\lambda(\text{AB})}, k \approx 1 \text{ eV};$$

$$\chi(\text{AB}) = \chi(\text{A}) + \chi(\text{B}) = \chi^{\text{di}}(\text{AB})e^y;$$

$$y = (R_e - R_e^{\text{di}})(R_e + R_e^{\text{di}})^{-1};$$

$$\gamma(\text{AB}) = \gamma(\text{A}) + \gamma(\text{B});$$

$$\gamma(\text{A}) = [R_0(\text{A})][R_e(\text{AB})]^{-1} - [R_e(\text{AB})][R_0(\text{A})]^{-1}.$$

In a number of studies,^{30,32,33,35–38} the STM has been used to calculate the thermodynamic properties of d- and f-element complexes with various ligands (H_2O , NO_3 , O-, S- and N-donor ligands, F, Cl, Br). The $D_0(\text{AB})$ bond energies determine the thermodynamic properties of compounds, in particular, the standard enthalpies of their formation in solution $\Delta H_f^\circ(\text{aq})$, in the crystalline state $\Delta H_f^\circ(\text{s})$ and in the gaseous state $\Delta H_f^\circ(\text{g})$. If ΔH_f° have not been measured, they can be calculated from known $D_0(\text{AB})$ values; conversely, if ΔH_f° have been measured, they can be used to evaluate the accuracy of $D_0(\text{AB})$ by solving the inverse problem.

The following properties were calculated^{35,36} for compounds of d elements: $\Delta H_f^\circ(\text{ML}_4, \text{g})$ and $\Delta H_f^\circ(\text{ML}_4, \text{s})$, L = Cl, Br; $\Delta H_f^\circ(\text{MCl}_6^{2-}, \text{g})$, $\Delta H_f^\circ(\text{MCl}_6^{2-}, \text{aq})$ and

$\Delta H_f^\circ(\text{A}_2\text{MCl}_6, \text{s})$, where M are 4d, 5d, 6d and 5f elements (Zr, Hf, Th, Rf; Nb, Ta, Pa, Db; Mo, W, U, Sg; Tc, Re, Np, Bh; Ru, Os, Pu, Hs; Rh, Ir, Am, Mt; Pd, Pt, Cm, ¹¹⁰TAn; TAn are transactinides). The ΔH_f° values for many compounds of 3d, 4d, 5d and 5f elements have been measured. The calculations^{30,32,33,35–38} of ΔH_f° and $D_0(\text{AB})$ reproduce the experimental values to within $\pm 15 \text{ kJ mol}^{-1}$; this has stimulated the use of the STM for predicting the properties of transactinides [$D_0(\text{TAn} - \text{Hal})$ and $\Delta H_f^\circ(\text{TAnHal}_4)$]^{35,36} and the properties of SMA. The structural thermodynamic model has also been used to estimate the thermodynamic parameters for the extraction of Ln³⁺ and An³⁺ ions with amides,³² acids R₂PSSH and O-containing co-extractants such as phosphates, amides and phosphine oxides.^{30,37}

In supramolecular chemistry, polypyridine ligands, for example, 2,2':6',2''-terpyridine, are widely used as building blocks. Data on the thermodynamic properties of the complexes of f elements with this class of ligands are scarce.²⁷ The stability constants $K(\text{LnL}^{3+})$ for 70 complexes with these ligands were calculated, while for 15 complexes they were measured.³⁸ The accuracy of calculation was $\pm 10\%$ of the experimental $\log K(\text{LnL}^{3+})$ values.

II. Molecular recognition in biology and coordination chemistry

The progress in the development of nanochemistry and nanotechnology is largely due to the use of biological concepts.^{8,39–42} The idea of designing machines at the molecular level has also come to chemistry from biology: numerous biological ‘machines’, for example, cell proton pumps, transmembrane ion channels, *etc.*, are known.⁴² A classical example of molecular recognition in biology is the complementary binding of nucleotides into the DNA double helix.^{1,43} A classification of different types of molecular recognition has been proposed.^{2,44} Weak specific interactions between the receptor and the substrate play an important role in the formation of complex biological structures at the cellular level, hydrogen bonds being especially significant.^{43,45}

The supramolecular chemistry usually considers two limiting mechanisms for SMA formation: non-covalent^{1,2,45} and covalent interactions.⁴² However, this differentiation is rather conventional.^{5,6} The formation of SMA through hydrogen bonds has been discussed in the literature.^{18,41,43,45} Coordination bonds can also act as strong interactions.

The coordination mechanism of SMA formation, which is also called metal-directed self-assembly,^{8,9,42} is an alternative to the mechanism based on weak intermolecular interactions (this is called in some cases the biological mechanism). The key features of the coordination mechanism include^{8,39,42} the directional character of the metal–ligand bonds; the diversity of SMA caused by the diversity of building blocks (polydentate ligands and metals), a combination of strong and weak bonds,²² the possibility of a control over the reaction mechanism, *i.e.*, of carrying out the reaction under thermodynamic or kinetic control.^{8,9,39}

The molecular recognition principle in the coordination mechanism is based on the stereochemical model developed in a number of papers.^{8,9,39} It is noteworthy that the decrease in the free energy upon the formation of SMA according to this mechanism is due to the appearance of weak coordination bonds between the metal atoms either directly ($\text{M} \cdots \text{M}$) or through bridging ligands ($\text{M} \cdots \text{L} \cdots \text{M}$).¹⁵ The properties of cations (the electronic configuration and the size determining the geometry of the polyhedra in the local environment), the softness or hardness of cations and ligands and the chelation effects are to be taken into account in the coordination mechanism of SMA formation. Chelating polypyridine ligands have found extensive use in SMCh.^{1,2,6,8,9,14,18,39,42} It was

shown⁴⁶ that in the formation of the ML_n^{3+} complexes, where $M = Ln^{3+}$ ($Ln = La, Ce, \dots, Lu$) and An^{3+} ($An = Pu, Am, Cm$), with such ligands, the chelation effect can stabilise complexes both by increasing the entropy and by decreasing the enthalpy, depending on the cation and the number of ligands n ($n = 1-3$). The effect of chelation on the thermodynamics of self-assembly of molecules to SMA has not yet been considered.

III. Transition d and f elements as structural components of polymers

The self-assembly giving rise to supramolecular systems is a new line of research in the polymer science.⁵ This research is at the boundary of organic, bioorganic and inorganic chemistry. Polymers of new generation are synthesised based on a preset (*i.e.*, inherent in the synthetic strategy)⁴⁷ combination of intramolecular and/or intermolecular interactions.⁶ A prominent achievement in this field is the synthesis of polymers with one-dimensional structure. The search for and the targeted synthesis of quasi-one-dimensional systems is an important problem in the solid-state physics and chemistry. This Section deals with the properties of the new-generation polymers.

1. Self-assembly in the formation of inorganic polymers: the effect of the electronic structures of metals and ligands

In recent years, dinuclear metal complexes have been actively used to design molecular assemblies. The synthesis of one-dimensional tetracarboxylate SMP where the blocks containing Rh_2^{4+} or Re_2^{6+} are combined by hydrogen bonds has been reported.⁴⁷ Many polymers of this type in which dinuclear blocks are connected by bridging ligands have been studied previously. The structure of the first inorganic formate-containing polymer $Rh_2(HCOO)_4 \cdot H_2O$ (**1**) with the Rh^{2+} ions linked by bridging oxygen atoms $Rh^{2+} \dots O \dots Rh^{2+}$ has been reported in a review;⁴⁸ the references cited therein have initiated the study of SMP based on dinuclear d-element cations. Although dimeric Cr, Rh, Cu and Mo carboxylates were the first to be prepared, their structural studies were performed somewhat later. Using the results of early synthetic and structural works^{48,49} and later publications,^{47,50-52} we compared the bond energies in the polymers constructed from the same dinuclear blocks connected by either bridging ligands^{48,49} or hydrogen bonds.^{5,47,50-52}

Inorganic metal-containing SMP can exist in different conformations: helical, zigzag and so on. A theoretical model interpreting the reasons and the mechanism for the formation of a particular conformation in inorganic SMP should take into account the electronic structure of the metal cation.

As an example, consider compounds of monovalent elements of the copper group: Cu^+ , Ag^+ and Au^+ . In the crystals of $KCu(CN)_2$ (**2**), the Cu atoms have a coordination number (C.N.) of 3. The C and N atoms and the Cu atoms to which they are bonded are nearly coplanar.⁵³ One CN group is terminal and the other two groups are bridging. This gives rise to helical polymeric chains $\dots CN \dots Cu \dots CN \dots$. In the $KCu_2(CN)_3 \cdot H_2O$ crystal, the polymeric layers $[Cu_2(CN)_3]_n^-$ are composed of helical $(CuCN)_n$ chains (as in compound **2**) and zigzag $(CuCN)_n$ chains; the Cu atoms in the polymeric chains with different conformations are linked through the third cyano group. It should be emphasised that the anions in $KAg(CN)_2$ (**3**) and $KAu(CN)_2$ (**4**) are discrete and form no polymeric structures.⁵³ A linear coordination and C.N. equal to 2 have also been found for the Ag atom in $AgSCN$ and $AgCN$, which are zigzag polymers in the solid state.

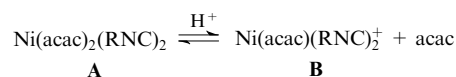
A triangular coordination of the metal atom like that in compound **2** may arise in the case of ds^2 , dp^2 or sp^2 hybridisation. The Cu, Ag and Au atoms have the same electronic configuration $nd^{10}(n+1)s^1$, $n = 3-5$; however, the formation

of the $nd^9(n+1)s^2$ electronic configuration corresponding to these types of hybridisation requires different energy expenditures $\Delta E(ds)$. The $\Delta E(ds)$ value is abnormally high for Ag and is the lowest for Cu:⁵⁴

Element	Cu	Ag	Au
$\Delta E(ds) / kJ mol^{-1}$	34.4	91.8	40.2

As a result, among the three compounds with the same composition $KM(CN)_2$, compound **2** has a polymer structure (the C.N. of Cu is 3) and compounds **3** and **4** have a discrete structure (the C.Ns of Ag and Au are 2). Thus, the electronic structure determines the C.N. Note that the mechanism of formation of these inorganic polymers is determined by strong (ionic and covalent) rather than weak interactions. Thus the thermal stability and low solubility of the acetylenide polymer $Cu_2C_2 \cdot H_2O$ are due to the formation of strong π -bonds.⁵³ Transitions between conformations of inorganic polymers require, most often, large energy expenditure.

Concluding this Section, consider an interesting example in which the metal complex serves as the polymerisation catalyst of aliphatic and aromatic isocyanides.¹⁹



Complex **A** has a *trans*-configuration; however, for polymerisation to start, the complex must have two vacant *cis*-sites. Complex **B** formed under the action of an acid serves as an efficient polymerisation catalyst. The driving force of this reaction is the transformation of formally divalent carbon in the monomer into the tetravalent carbon in the polymer. The reaction readily proceeds at room temperature, the reaction heat being $81.4 kJ mol^{-1}$. It cannot be ruled out that the heat of polymerisation is related to the electron excitation energy accompanying the transition of carbon into the tetravalent state.

The considered examples demonstrate the importance of electronic effects in the thermodynamics of the formation of polymers involving metals and non-metals.

2. Coordination mechanism of the formation of inorganic carboxylate polymers containing M_2^{4+} dimers of d elements

Quasi-one-dimensional systems have long been of only theoretical interest as hypothetical models in the solid-state physics and chemistry; they were used to start the solution of many problems. However, more recently, synthetic chemists have manufactured species that can be regarded, to a first approximation, as one-dimensional solids.⁵⁵ Among these, an important place is occupied by divalent 3d-element carboxylates. For example, the compound $Cu(PhCOO)_2 \cdot 3 H_2O$ is a one-dimensional ferromagnet and is described by the Heisenberg model.⁵⁵ On the basis of M_2^{4+} carboxylate complexes ($M = Cr, Mo, Cu, Rh$), polymers with a quasi-one-dimensional chain structure have been prepared. The simplest compound, dirhodium tetraformate monohydrate $Rh_2(HCOO)_4 \cdot H_2O$ (**1**) consists of two types of complexes:⁴⁸ $Rh_2(HCOO)_4 \cdot (H_2O)_2$ (**1a**) and $Rh_2(HCOO)_4$ (**1b**). Complexes **1a** have a distorted octahedral geometry and consist of $Rh^{2+}-Rh^{2+}$ dimers connected by four bridging $HCOO^-$ groups, and two H_2O molecules occupy the *trans*-positions with respect to the $Rh^{2+}-Rh^{2+}$ bond. Complex **1b** contains no coordinated H_2O molecules; they are replaced by the O atoms of the $HCOO^-$ groups of the neighbouring complexes **1a**. The $Rh^{2+}-Rh^{2+}$ bonds are oriented either along the polymer axis or at an angle, which is favourable for binding Rh_2^{4+} dimers through the bridging O atoms: $Rh_2^{4+} \dots O \dots Rh_2^{4+}$. Compound **1** has one coordination vacancy. In the polymer, weak cooperative charge ordering is formed along the $(Rh_2^{4+\delta} \dots Rh_2^{4-\delta})_x$ axis, resulting in polymer stabilisation. The coordinatively saturated compound

$\text{Rh}_2(\text{OAc})_4(\text{H}_2\text{O})_2$ (**5**) does not form a polymer, as the 'excess' water molecule (missing from compound **1**) saturates the coordination. Numerous non-polymeric compounds $\text{M}_2(\text{RCOO})_4\text{L}_2$ ($\text{M} = \text{Cr}, \text{Mo}, \text{Cu}, \text{Rh}$, etc., L is a neutral ligand) have been prepared; they do not undergo disproportionation to give two complementary complexes.⁴⁹

The interatomic distances $R(\text{Rh}-\text{Rh}) = 2.38 \pm 0.02 \text{ \AA}$, $R[\text{Rh}-\text{O}(\text{water})] = 2.20 \pm 0.06 \text{ \AA}$, average $R(\text{Rh}-\text{O}) = 2.03 \pm 0.05 \text{ \AA}$ in polymer **1**⁴⁸ are much shorter than the $R(\text{Rh}-\text{O}) = 2.45 \pm 0.03 \text{ \AA}$ distance to the inter-moiety bridging oxygen atom. Here and below, the bond energies in the structural blocks were calculated²² based on the STM^{32,33} with experimental $R(\text{A}-\text{B})$ distances reported in the studies cited and with handbook⁵⁶ data for R_{e}^{di} : $D_0(\text{Rh}^{2+}-\text{Rh}^{2+}) = 233.5$, $D_0(\text{Rh}^{2+}-\text{O}) = 246.9$ and $D_0(\text{Rh}^{2+}-\text{OH}_2) = 178.8 \text{ kJ mol}^{-1}$, while the energy of the bridging $\text{Rh}^{2+}-\text{O}$ bonds combining these blocks into a polymer, $D_0(\text{Rh}^{2+}-\text{O})$ is equal to $111.2 \text{ kJ mol}^{-1}$.

The driving force of polymerisation is disproportionation $2\text{I} \rightarrow \text{1a} + \text{1b}$, resulting in alternation of the complementary complexes **1a** and **1b**. It follows from the bond energies that complexes **1a** and **1b** are constructed through strong coordination bonds and are connected to each other by weaker bridging bonds.

3. Mechanism of formation of supramolecular polymers containing M_2^{4+} dimers of d elements with participation of hydrogen bonds

In recent years, the trend of using combinations of strong valence bonds with weak intermolecular contacts ($\pi-\pi$ -interactions, hydrogen bonds and so on) has started to develop in the SMP synthesis. In order to connect metal-containing blocks into the SMP through hydrogen bonds, pyridinecarboxylic acids and their amides are used most often.^{57,58} Another synthetic strategy for the preparation of one-dimensional SMP using dinuclear M_2 fragments was developed in parallel.^{51,52} The two possible limiting M_2 orientations with respect to the polymeric chain dictate the range of bridging ligands: parallel (axial bridges) and perpendicular (equatorial bridges) orientations. The complexes containing Rh_2^{4+} or Re_2^{6+} dimers were used to prepare one-dimensional SMP:⁴⁷ $\text{Rh}_2(\text{OAc})_4(\text{INA})_2 \cdot 2 \text{Me}_2\text{CO}$ (**6**); $\text{Rh}_2(\text{OAc})_4(\text{NIA})_2 \cdot 2 \text{Me}_2\text{CO}$ (**7**); *cis*- $\text{Re}_2(\text{OAc})_2\text{Cl}_4(\text{INA})_2$; *cis*- $\text{Re}_2(\text{OAc})_2\text{Cl}_4 \cdot (\text{NIA})_2 \cdot 2(\text{NIA})$, where INA is isonicotinamide and NIA is nicotinamide. The idea was to replace two water molecules in complex **5**, which cannot be self-assembled due to the coordination saturation, by the ligands NIA or INA, which form hydrogen bonds like other amides. Pyridinecarboxamides are used as donors in the axial positions, while hydrogen bonds are formed due to complementarity of the amide groups. The conformation of SMP depends on the geometry of the linkers (NIA and INA). As a result, compound **6** contains linear polymer chains and complex **7** contains zigzag chains.

Presumably, the stability of the dirhodium SMP is due to the presence of a stable diamagnetic structural block, $\text{Rh}^{2+}-\text{Rh}^{2+}$. Then one can expect that $R(\text{Rh}-\text{Rh})$ in SMP **6**, **7** and in compound **5** would be different. Although these differences are slight: $R(\text{Rh}-\text{Rh}) = 2.4034(16)$ (for **6**), $2.3972(12)$ (for **7**), $2.3855(5)$ (for **5**), $2.38(2) \text{ \AA}$ (for **1**),⁴⁷⁻⁴⁹ the secondary effect is still observed, namely, the $\text{Rh}^{2+}-\text{Rh}^{2+}$ bonds in complexes **6** and **7** are slightly weaker than those in non-polymeric compound **5**, and these bonds in complex **1** are slightly stronger than those in **5**. The $D_0(\text{Rh}-\text{Rh})$ values were calculated in terms of the STM (to the accuracy of $\pm 2 \text{ kJ mol}^{-1}$): $D_0(\text{Rh}-\text{Rh}) = 224$ (for **6**) ≤ 226 (for **7**) < 231 (for **5**) $\leq 234 \text{ kJ mol}^{-1}$ (for **1**).

The average $R(\text{Rh}-\text{O})$ distances to the carboxylate oxygen atoms in the three SMP are similar:^{47,48} $R(\text{Rh}-\text{O}) = 2.03(5)$ (**1**); $2.036(6)$ (**6**) and $2.037(4) \text{ \AA}$ (**7**). The key difference between

the SMP **1** and **6**, **7** is related to the energetic properties of linkers, i.e., the $\text{Rh}_2^{4+} \cdots \text{O} \cdots \text{Rh}_2^{4+}$ bridging bonds in complex **1** and hydrogen bonds in complexes **6** and **7**. The interaction energy between the blocks upon the formation of hydrogen bonds is much lower than the bridging bond energies, which accounts for the higher stability of polymers of type **1**.

The difference between the energetic properties of linear and zigzag polymers **6** and **7** is due to the difference between the $R(\text{Rh}-\text{N})$ distances to the pyridine N atoms: $R(\text{Rh}-\text{N}) = 2.205(7)$ (INA) and $2.224(5) \text{ \AA}$ (NIA). The calculated values, $D_0[\text{Rh}-\text{N}(\text{INA})] = 240$ and $D_0[\text{Rh}-\text{N}(\text{NIA})] = 232 \text{ kJ mol}^{-1}$, differ by 8 kJ mol^{-1} . The stronger $\text{Rh}-\text{N}$ bond in SMP **6** results in weakening of hydrogen bonds: $R(\text{N}-\text{H} \cdots \text{O}) = 2.922 \text{ \AA}$ with respect to $R(\text{N}-\text{H} \cdots \text{O}) = 2.865 \text{ \AA}$ in SMP **7**.

The thermodynamic and structural properties of compounds with hydrogen bonds have been studied in numerous works.^{5,18,41,43,59-64} The first estimates of the energies of such bonds concern the peptide structure.⁶¹ Then the energies of the $\text{O}-\text{H} \cdots \text{O}$, $\text{O}-\text{H} \cdots \text{N}$, $\text{N}-\text{H} \cdots \text{O}$, $\text{N}-\text{H} \cdots \text{N}$, $\text{O}-\text{H} \cdots \text{Cl}$, $\text{N}-\text{H} \cdots \text{F}$, $\text{N}-\text{H} \cdots \text{Cl}$, $\text{F}-\text{H} \cdots \text{F}$ and other hydrogen bonds were determined from thermodynamic properties of the corresponding compounds or from spectroscopic data⁶³⁻⁶⁵ or calculated in terms of the STM.⁶⁶ In a review,⁴¹ the reference values for hydrogen bond energies have been compared with the energies of conventional single bonds. The $\text{S}-\text{S}$, $\text{C}-\text{P}$, $\text{C}-\text{N}$, $\text{C}-\text{Cl}$, $\text{C}-\text{C}$, $\text{N}-\text{H}$, $\text{C}-\text{H}$, $\text{H}-\text{H}$ and $\text{O}-\text{H}$ bond energies vary in the range of $260-460 \text{ kJ mol}^{-1}$, while hydrogen bond energies lie in the $10-65 \text{ kJ mol}^{-1}$ range; however, if the hydrogen bond is formed with an ion (for example, $\text{HCOOH} \cdots \text{F}^-$), the range is broadened to $40-190 \text{ kJ mol}^{-1}$.

It follows from the reported data^{18,41,60,63,64,66} that the dependence of the hydrogen bond energy $D(\text{AH} \cdots \text{B})$ ($\text{A} = \text{N}$; $\text{B} = \text{O}, \text{Cl}$; $\text{A} = \text{B} = \text{O}$, and so on) on the $R(\text{A} \cdots \text{B})$ distance is described by the equation

$$D(\text{AH} \cdots \text{B}) = \alpha \exp[-\beta R(\text{A} \cdots \text{B})],$$

where α and β are empirical constants.

Using this equation, $D(\text{AH} \cdots \text{B})$ can be estimated from the measured $R(\text{A} \cdots \text{B})$ values to the accuracy of $\pm 3\%$ relative to the values determined from spectroscopic and thermodynamic characteristics of the corresponding compounds.⁶³⁻⁶⁵ The hydrogen bond energies were calculated in terms of the STM.⁶⁶

The hydrogen bond energies for SMP **6** and **7** were found to be 6.5 and 7.6 kJ mol^{-1} , respectively. Since each complex is linked to two neighbouring complexes by four hydrogen bonds, the total energy difference for two conformations is equal to $\sim 5 \text{ kJ mol}^{-1}$. Hydrogen bonds formed at so long distances ($2.8-2.9 \text{ \AA}$) cannot be strong. The energies of the bridging coordination bonds [$D_0(\text{Rh}^{2+}-\text{O}) = 111.2 \text{ kJ mol}^{-1}$] in inorganic polymer **1** are much higher than the hydrogen bond energies in SMP **6** and **7** [$4 D_0(\text{N}-\text{H} \cdots \text{O}) \approx 30 \text{ kJ mol}^{-1}$]. Apart from hydrogen bonds, other non-valent contacts should also be taken into account in the structures of complexes **6** and **7**; however, they are also present in SMP **1**.

The $\text{N}-\text{H} \cdots \text{O}$ distances and the hydrogen bond energies in polymers **6** and **7** fall in the range typical of biological systems. Indeed, in the case of peptides,⁶³ the $R(\text{NH} \cdots \text{O})$ distance ranges from 2.80 to 3.16 \AA . However, a value of 2.90 \AA equal to the sum of the van der Waals radii of the oxygen and nitrogen atoms $R^{\text{VW}}(\text{NO})$ is encountered most often. Meanwhile, in the linear SMP **6**, $R(\text{N} \cdots \text{O}) = 2.922 \text{ \AA} > R^{\text{VW}}(\text{NO})$, and in the zigzag SMP **7**, $R(\text{N} \cdots \text{O}) = 2.865 \text{ \AA} < R^{\text{VW}}(\text{NO})$.

It has been noted above that the presence of axial ligands relative to the $\text{Rh}-\text{Rh}$ bonds prevents the formation of SMP, because these complexes are coordinatively saturated. This is also valid for other metal compounds. Thus all non-solvated compounds $\text{Cr}_2(\text{O}_2\text{CR})_4$ form polymeric chains in the crystalline state where $R(\text{Cr}-\text{Cr})$ varies from 2.2 to 2.5 \AA ,⁴⁹ and the

bond energy $D_0(\text{Cr}^{2+} - \text{Cr}^{2+})$ that we calculated falls in the range of 154–232 kJ mol⁻¹. However, the lack of axial ligands is a necessary but not a sufficient condition for self-assembly to give SMP. If very short bonds, $R(\text{Cr} - \text{Cr}) < 1.9 \text{ \AA}$, are formed in the complexes, their energy sharply increases and the complexes lose flexibility. These complexes contain no axial ligands but still they do not tend to self-assemble.

Thus, a comparison of the two mechanisms of SMP formation from identical dinuclear blocks (through bridging oxygen ligands or hydrogen bonds) indicates that the bridging coordination bond energy for inorganic polymer **1** is higher than the total energy of all hydrogen bonds in SMP **6** and **7** and that the stronger the coordination bonds in the initial building block, the weaker the hydrogen bonds between the blocks.

4. Self-assembly of trivalent lanthanide and actinide complexes

As mentioned above, the lanthanide ions Ln^{3+} are classified as hard acids; they form strong bonds with hard bases.^{26,67} However, in recent years, interest has arisen in Ln^{3+} compounds in which the coordination sphere contains both hard and soft donor atoms: (F, S, O),⁶⁸ (O, S, N).^{30,36–38,69,70} These compounds were found to exhibit unusual properties not inherent in Ln^{3+} compounds containing either only hard or only soft ligands. These properties have already found application in the separation of Ln^{3+} and An^{3+} ions by extraction.^{30,36–38} In sulfur-containing crystalline compounds, Sm and Eu are known to exhibit mixed valence.⁶⁷ The reactions of metallic Sm and Eu with mercury perfluorobenzenethiolate $\text{Hg}(\text{SC}_6\text{F}_5)_2$ in THF give dimer $[(\text{THF})_2\text{Sm}(\text{SC}_6\text{F}_5)_2 \cdot (\mu\text{-SC}_6\text{F}_5)]_2$ (**8**) and one-dimensional polymer $[(\text{THF})_2\text{Eu} \cdot (\text{SC}_6\text{F}_5)_2(\mu\text{-SC}_6\text{F}_5)]_n$ (**9**), respectively.⁶⁸ In dimer **8**, two thiolate ligands form rings through the Sm–S and Sm–F bonds, while the bridging thiolate ligands are not coordinated by F atoms. The coordination sphere is completed by two THF ligands. In compound **9** (unlike dimer **8**), the bridging thiolates interact with Eu atoms through F atoms, thus forming an SMP. This is a rare example where a ‘hard’ F atom is coordinated as a neutral donor and, in combination with a ‘soft’ S atom, gives rise to an eight-coordinate Eu^{2+} (4S + 2F + 2O).

The charge transfer energies from the higher occupied non-bonding molecular orbitals (MO) $\Delta E(\text{L} \rightarrow \text{M}^{3+})$ (L = S, F) in S- and F-containing lanthanide and actinide compounds (M = La, Ce, Pr, ..., Lu; Ac, Th, Pa, ..., Lr) have been discussed.^{30,37} On the basis of the $\Delta E(\text{L} \rightarrow \text{M}^{3+})$ values, one can find out what lanthanides (apart from Eu) and light actinides (from Ac to Am) could form SMP similar to polymer **9** according to the same mechanism. The $\Delta E(\text{L} \rightarrow \text{M}^{3+})$ values are known to correlate with the reduction potentials $E^\circ(3+/2+)$. It was found experimentally^{30,37} that the lowest $\Delta E(\text{S} \rightarrow \text{Ln}^{3+})$ values in the lanthanide series (in eV) are found for Eu (2.79), Yb (3.26) and Sm (3.77), while among light actinides, this is observed for Am (4.22). The corresponding $E^\circ(3+/2+)$ values are 0.35 (Eu), 1.05 (Yb), 1.55 (Sm) and 2.3 V (Am).³⁷ The measured distances, $R(\text{Sm} - \text{S}) = 2.822$ (**8**) and $R(\text{Eu} - \text{S}) = 3.034 \text{ \AA}$ (**9**),⁶⁸ correspond to the ionic radii $R_{\text{ion}}(\text{Sm}^{3+})$ and $R_{\text{ion}}(\text{Eu}^{2+})$. Using the correlation between $E^\circ(3+/2+)$ for Eu, Yb, Sm, Am and the measured $R(\text{Sm} - \text{S})$ and $R(\text{Eu} - \text{S})$ values, one gets $R(\text{Yb} - \text{S}) = 2.954$ and $R(\text{Am} - \text{S}) = 2.850 \text{ \AA}$. These distances correspond to ionic radii $R_{\text{ion}}(\text{Am}^{3+}) = 1.106$ and $R_{\text{ion}}(\text{Yb}^{2+}) = 1.186 \text{ \AA}$. The qualitative estimates lead to the conclusion that Am, like Sm, would not be reduced within the thiolates under discussion, while Yb is expected to be reduced like Eu. In the former case, the reaction gives a dimer and in the latter case, an SMP is formed. It can be seen that the polymer is formed if the $E^\circ(3+/2+)$ and $\Delta E(\text{L} \rightarrow \text{M}^{3+})$ values obey the following

conditions: $0.35 \leq E^\circ(3+/2+) < 1.55 \text{ V}$ and $2.79 \leq \Delta E(\text{L} \rightarrow \text{M}^{3+}) < 3.26 \text{ eV}$.

An exceptionally high level of cooperative $\pi - \pi$ -interaction of the thiolate rings has been noted⁶⁸ for the SMP.

IV. Complexes of d and f elements as the building blocks in macrocycles

The square planar (M = Pd^{2+} , Pt^{2+}), tetrahedral (M = Cu^+) and octahedral (M = Fe^{2+} , Co^{2+} , Ni^{2+}) complexes are used most often in self-assembly reactions. To date, supramacrocycles containing from 2 to 12 metal atoms have been prepared in the solid state and in solution. These can be classified into three types: (1) SMC in which the metal atoms are separated by bridging ligands; however, a weak $\text{M} \cdots \text{M}$ interaction exists and contributes to the thermodynamics of SMC formation; (2) SMC in which the metal atoms are shielded by bulky ligands, the distances $\text{M} \cdots \text{M} > 5 \text{ \AA}$ and $\text{M} \cdots \text{M}$ interaction is lacking; (3) SMC with short and strong $\text{M} \cdots \text{M}$ bonds making an appreciable contribution to the thermodynamics of SMC formation.

In the SMC chemistry, the principle of SMA formation is formulated^{8,9,14,39} as metal-directed self-assembly. The most typical features of the self-assembly of discrete metal-containing blocks into large cyclic aggregates have been summarised in a review:⁸ (1) upon self-assembly, the blocks are selectively bound by coordination bonds based on the molecular recognition principle; (2) self-assembly is a cooperative process; (3) the SMA formed are discrete. The above-listed publications mention all types of interactions ranging from weak intermolecular to ionic and covalent ones. Therefore, we consider it important to compare the energetic properties of the strong coordination bonds $\text{M} \cdots \text{M}$, $\text{M} \leftarrow \text{L}$ and hydrogen bonds ($\text{OH} \cdots \text{O}$, $\text{NH} \cdots \text{O}$, $\text{NH} \cdots \text{Cl}$), which contribute to the formation energy of SMC.

Note that the properties of SMC are determined by not only the nature of intermolecular interactions but also the electronic structure of the metal ions, their Lewis acid properties (soft or hard),^{26,69} their redox potentials and their dependence on the number (q) of p^q , d^q and f^q electrons.^{29,70}

It is necessary to emphasise that the macrocyclic systems we discuss differ fundamentally from the previously studied polynuclear metal complexes by the fact that the large ring system exists not only in the solid state but is also formed and retained in solutions. This feature opens up broad prospects for the use of these systems in nanotechnology and molecular-level technology.

The experimental thermodynamic data concerning the free energy or enthalpy of formation of SMC are few. As a rule, they are used to draw qualitative conclusions concerning the driving force of the formation of various SMC: some studies assume the entropy mechanism and other studies, the enthalpy or mixed (enthalpy and entropy) mechanisms. We attempted to estimate quantitatively the contribution of weak and strong interactions to the formation of SMC.

1. Mechanism of self-assembly of macrocycles

A number of mechanisms for the self-assembly of macrocycles have been considered in biology and coordination chemistry.^{8,39} A fast kinetic process and thermodynamic equilibrium between the reactants and products in every reaction stage are the key features of the self-assembly mechanism typical of coordination chemistry. This mechanism has been called³⁹ thermodynamic or strict. The ratio of the products in the final stage of self-assembly is determined by their thermodynamic stability. The thermodynamic self-assembly should result in one, most stable product to be of practical value.² Other self-assembly mechanisms characteristic of both biology and coordination chemistry also exist. They have been classi-

fied and analysed.⁷¹ (1) An irreversible or kinetically controlled mechanism of self-assembly induces a cascade of irreversible reactions and the equilibrium is not reached. (2) An assisted mechanism involving an auxiliary reagent that does not participate in either self-assembly or the formation of the final product but prevents the formation of intermediate products. (3) The directed mechanism requires the presence of a recognition pattern reagent, which directs the self-assembly without being involved in the formation of the final product. Other mechanisms assuming various ways of modification of either reactants prior to self-assembly or final products after the self-assembly (post-modification) have also been considered.⁷¹ Although many SMA have been prepared according to the thermodynamic mechanism of self-assembly, other self-assembly mechanisms (irreversible, directed, and self-assembly with post-modification) are also widely used, for example, in Sauvage's studies.^{72–74} Molecular knots, most of catenanes and some kinetically stable helical SMA have been prepared by self-assembly with post-modification.^{75, 76}

The present review considers the SMA prepared according to the thermodynamic self-assembly mechanism. Note once again that the so-called biological (*i.e.*, caused by intermolecular interactions) and coordination self-assembly mechanisms are not always easily differentiated. For example, complexes of the type MA_2X_2 , where $M = Pd^{2+}, Pt^{2+}$, A is a neutral ligand, X is an anion, are widely used in the SMC synthesis.^{1, 2, 9, 10, 39} In the solid state, these compounds form islet structures MA_2X_2 in which the complexes are linked by weak intermolecular interactions. For example, in the *cis*-isomer of dichlorodiammineplatinum, a 'column motif' is repeated.⁷⁷ In the neighbouring columns, two Cl atoms of the same complex are linked to two NH_3 groups of another complex by hydrogen bonds with the distances $R[Cl(1) \cdots N(2)] = 3.34$ and $R[Cl(2) \cdots N(1)] = 3.30$ Å.⁷⁷ The $R(Pt-Pt)$ distances are 3.372 and 3.409 Å. Each pair of complexes in the columns is linked by two hydrogen bonds the energies of which (our calculations) are as follows (in $kJ\ mol^{-1}$): $D_0[NH_3 \cdots Cl(1)] = 49.7$; $D_0[NH_3 \cdots Cl(2)] = 45.6$. The $Pt-Pt$ bonds also contribute to stabilisation of the *cis*-isomer: $D_0(Pt-Pt) = 28.7\ kJ\ mol^{-1}$ for $R(Pt-Pt) = 3.409$ Å; $D_0(Pt-Pt) = 29.9\ kJ\ mol^{-1}$ for $R(Pt-Pt) = 3.372$ Å. For each pair of complexes in neighbouring columns, the intermolecular interaction energy is relatively high: $\Sigma D_0 \approx 125\ kJ\ mol^{-1}$. This example demonstrates that weak intermolecular $M-M$ contacts may be important both for the coordination chemistry and in SMC by determining the self-assembly process.

It is emphasised in a review⁸ that self-assembly is a cooperative process. A monograph⁵⁵ devoted to the theory of cooperative processes and order-disorder type models presents the result of a quasichemical approximation in the solution of the Ising problem for the Bethe lattice, which represents a tree within the framework of the graph theory. Numerous dendrimers with this type of structural motif have been described in reviews.^{10, 11} Theoretical physicists have anticipated, to some extent, the existence of some structural motifs, which have been later considered in the SMCh. Similarly, theoretical physicists have predicted⁵⁵ some structural motifs and called them 'ladder cluster', 'ladder pseudo-assembly' and so on; more recently, the SMA called the 'ladder', 'rack' and 'grid' have been synthesised in solution and in the solid state.^{1, 39}

2. Structural factors in the formation of supramacrocycles

The structural principles of the design of SMC were developed at a qualitative level in the studies by Lehn,^{78, 79} Raymond,⁸⁰ Verkade,⁸¹ Fujita^{9, 82} and Stang.⁸ Lehn introduced into practice^{78, 79, 83} the method of SMA formation with the use of branched chelating ligands, which are highly pre-organised and have a large binding energy to metals. As compared with

monodendate ligands, the benefit in the free energy is due to the chelation effect. At an early stage of the development of SMCh, various SMA have been synthesised by mere screening diverse ligands and metals. Subsequently, rational approaches to the synthesis of these assemblies have been developed; these can be described systematically as two models.⁸

The first approach was called the symmetry interaction model.^{8, 79–83} This model considers free metal ions and ligands, most often, rather rigid bi- and tridentate chelating ligands as the starting fragments. The preferential coordination number and the preferential polyhedron for a given metal are taken into account. On the basis of analysis of the point group of symmetry of the target assembly with allowance for the mutual arrangement of the symmetry axes of various types, the synthesis is planned with particular metal ions and particular ligands. For more precise description of the geometric relations between the ligands and the metal ion, a number of special terms were defined (chelation vector, chelate plane, approach angle).^{8, 80}

The other ideology can be called a molecular library model.^{1, 2, 8, 9, 39} In this case, coordinatively unsaturated metal-containing fragments with vacant sites oriented at a definite angle rather than free metal ions are considered as the starting blocks. These are supplemented by linking fragments with different numbers of donor atoms (di-, tri- and tetrapotic) and different geometry (linear, angular, *etc.*). By combining a moderate number of such elementary blocks, one can construct a variety of cyclic and polyhedral SMA. It is assumed that the geometric parameters (first of all, the angles) of the free blocks do not change much upon association.

Thus, the use of only ditopic ligands resulted in diverse SMA (ranging from a triangle to a dodecahedron) with many d and f elements.^{83–99}

3. Macrocycles based on d and f elements and their thermodynamic properties

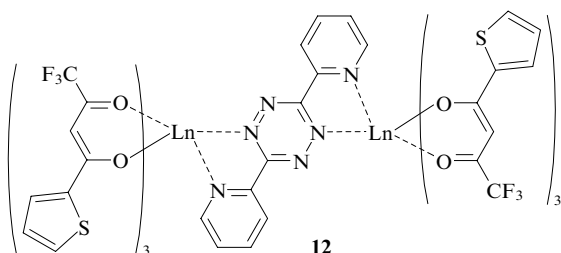
a. Dinuclear structures

Numerous dimers have been prepared in coordination chemistry and their physicochemical properties (spectral, thermodynamic, magnetic, and so on) were studied. The dimers $Cu_2(OAc)_4 \cdot 2H_2O$, which interact through hydrogen bonds in the solid state, have been reported;⁵³ the distance $R(Cu-Cu) = 2.64$ Å is somewhat larger than in the metal, while the exchange interaction between the Cu atoms is $\sim 300\ cm^{-1}$. The water molecules can be replaced by dioxane, pyridine or aniline.

Many dinuclear assemblies with different metals have been obtained; these metals include Cu,^{84, 98} Ag,⁸⁵ Mo,⁸⁶ Cd,⁸⁷ Zn,⁸⁸ Fe, Ga,⁸⁹ Os,⁹⁰ and, most often, Pd and Pt,^{91–97} which is not surprising, because Pd^{2+} and Pt^{2+} dimers have been studied for a very long period.^{48, 77} Let us compare the previously studied⁷⁷ dimer $[PdL_2Cl_2]_2$ (**10**) ($L = NH_2CHMeCHMeNH_2$) with the recently synthesised⁹⁶ SMC $[PdL_2Cl_2]_2$ (**11**) [L is 3,5-bis(dimethylaminomethyl)pyridine]. In SMC **11**, the Pd atoms are coordinated by two N atoms (the pyridine atom of one L and the aminomethyl N atom of the other L molecule) and two Cl atoms. The distance $R(Pd-Pd) = 4.6$ Å is rather long; therefore, the interaction between the metal ions does not contribute to dimer stabilisation. In dimer **10**, the Pd atoms also form two $Pd-Cl$ bonds and two $Pd-N$ bonds. Dimerisation is due to weak $Pd-Pd$ intermolecular interactions and hydrogen bonds,⁹⁷ which, according to a definition,^{1–4} are rather characteristic of SMCh: $R(NH \cdots Cl) = 3.29$ and 3.35 Å, and the distance $R(Pd-Pd) = 3.34$ Å is shorter than that in SMC **11**. The following energy values correspond to these distances (in $kJ\ mol^{-1}$): $D_0(Pd \cdots Pd) = 12.8$; $D_0(NH \cdots Cl) = 50.6$ and 44.7 . The overall contribution to dimerisation enthalpy is rather high: $\Sigma D_0 = 12.8 + 2(50.6 + 44.7) = 203.4\ kJ\ mol^{-1}$.

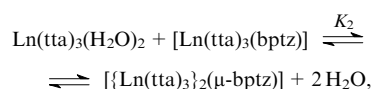
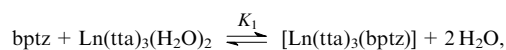
Both SMC **11** and dimer **10** contain usual Pd–N and Pd–Cl coordination bonds present in compounds of the ML_2Cl_2 type ($\text{M} = \text{Pd}, \text{Pt}$). However, the structural difference is obvious: in the case of SMC **11**, the self-assembly stops after formation of the dimer (*i.e.*, a discrete ring) both in the solid state and in solution, while in compound **10**, dimers form an infinite structure in the solid state due to weak intermolecular contacts.

The experimental thermodynamic data on the formation of dinuclear SMC in solutions are still scarce. It has been shown¹⁰⁰ that the complexes $\text{Ln}(\text{tta})_3(\text{H}_2\text{O})_2$ [tta is 2-thenoyl-(trifluoro)acetone] react with bis-bidentate bridging ligand bptz [3,6-bis(2-pyridyl)tetrazine] in aqueous ethanol to form mononuclear complexes $[\text{Ln}(\text{tta})_3(\text{bptz})]$ ($\text{Ln} = \text{La}, \text{Nd}$) for the first half of the lanthanide series and dinuclear complexes $[\{\text{Ln}(\text{tta})_3\}_2(\mu\text{-bptz})]$ (**12**) ($\text{Ln} = \text{Gd}, \text{Er}, \text{Yb}$) for the second half of the lanthanide series.



$\text{Ln} = \text{Gd}, \text{Er}, \text{Yb}$.

The stability constants (K_1 and K_2) of the complexes formed in the following reactions, respectively, were measured:

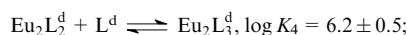
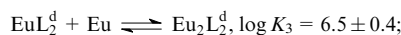
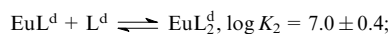
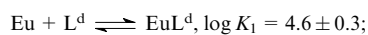


Ln	$\log K_1$	$\log K_2$
La	6.32	5.42
Yb	6.0	4.8

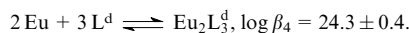
However, dinuclear complex **12** was isolated only with Yb but not with La. In dimer **12**, the C.N. of the Ln^{3+} ion is equal to 8 ($2\text{N} + 6\text{O}$), the coordination polyhedron has an approximate square antiprism geometry. This geometry is also characteristic of solvated cations of heavy lanthanides ($\text{Ln} = \text{Dy}, \text{Ho}, \dots, \text{Lu}$),¹⁰¹ whereas solvated cations of light lanthanides have a tricapped trigonal prismatic coordination and C.N. 9. Thus, light lanthanides do not form dimers, because the coordination geometry required for dimer formation is associated with considerable steric hindrance.

The change in the thermodynamic parameters (ΔH° , $T\Delta S^\circ$ and ΔG°) upon the formation of Ln^{3+} complexes with chelating ligands has been considered along the lanthanide series.^{27, 102} It was shown that $\gamma = |\Delta H^\circ / T\Delta S^\circ| \approx 0.25 \pm 0.1$. With this γ for dimer **12** with the measured¹⁰⁰ value of $\Delta G^\circ = -62.1 \text{ kJ mol}^{-1}$, one gets the approximate values $\Delta S^\circ \approx 165 \pm 20 \text{ J mol}^{-1} \text{ K}^{-1}$; $\Delta H^\circ \approx -13 \pm 6 \text{ kJ mol}^{-1}$. The formation of dimer **12** is mainly an entropy-driven process, like all other processes of formation of Ln^{3+} complexes in aqueous solutions.²⁷

The thermodynamics of the Eu^{3+} self-assembly in MeCN with the bis[1-methyl-2-(6-[1-(3,5-dimethoxybenzyl)benzimidazol-2-yl])pyridin-2-yl]benzimidazol-5-yl]methane ligand (L^d), composed of two tridentate bis(benzimidazolyl)pyridine fragments, has been studied.¹⁰³ The stepwise and overall stability constants were measured for the reactions:



overall reaction

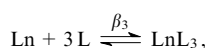
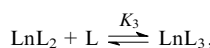
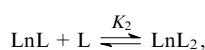
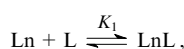


From these data, it follows that

$$\log \beta_4 \approx \log K_1 + 3 \log K_3 = 4.6 + 3 \times 6.5 = 24.1,$$

which is similar to the experimental value equal to 24.3. The first step of the reaction depends on the energy expenditure for the change in the ligand conformation, while the subsequent steps, on the properties of ligands and their interactions with cations.

The relations between the stability constants of the Ln complexes with monotopic chelating ligands have been derived for the reactions below^{31, 46}



$$\log K_1 > \log K_2 > \log K_3,$$

$$\log K_1 - \log K_2 \approx \log K_2 - \log K_3,$$

$$\log \beta_3 \approx 3 \log K_2.$$

These relations hold with high accuracy for approximately 200 Ln complexes with monotopic ligands and for a Eu^{3+} complex with the ditopic ligand L^d . No other data on Ln complexes with ditopic ligands are available. The enthalpy changes upon the formation of dinuclear Eu^{3+} complexes have not been measured. Presumably, $\Delta S_f^\circ < 0$, because it is known that in MeCN, lanthanide complexes are formed by an enthalpy mechanism rather than by an entropy mechanism²⁷ as in aqueous solutions.

The thermodynamics of formation of the dinuclear Eu^{3+} complex with the ditopic ligand L^d implies an important role of ligand pre-organisation at the first stage of the reaction.¹⁰³ For the subsequent stages, the derived relations between $\log K_i$ ($i = 2, 3, 4$) and $\log \beta_3$ allow one to calculate the stability constants. Using lanthanide complexes ($\text{Ln} = \text{La}, \text{Nd}, \text{Gd}, \text{Er}, \text{Yb}$) with tta and $\mu\text{-bptz}$ as examples, the role of the cation size in the formation of dinuclear SMC in aqueous solutions has been demonstrated.¹⁰⁰

b. Trinuclear structures

Triangular structures with weak M–M bonds. According to the molecular library model, the triangular SMC may be formed based on three building blocks arranged at 60° angles and linked by three linear fragments. The M_3 building blocks are widely known in the cluster chemistry. They can be combined to form tetrahedra, octahedra and other polyhedra.^{104–110} The M_3 metal rings with the M–M or M–L–M bonds can behave as both Lewis acids and bases;¹⁰⁴ hence, they can be used for the synthesis of SMC with diverse ligands in solution and in the solid state. A number of reviews^{105–110} have discussed the concept of the ‘magic’ number of valence electrons $m = 48$ for the M_3 clusters composed of d elements. Deviations from $m = 48$ exist, *i.e.*, this number is not universal^{105–110} even for elements of the same group, for example, $\text{M} = \text{Cu}, \text{Ag}, \text{Au}$ or $\text{M} = \text{Ni}, \text{Pd}, \text{Pt}$. Indeed, inclusion of

relativistic effects for Pt or Au metal rings would change the sequence and structure of the MO.

Two factors, *viz.*, the electronic structure of the metal and the effect of bridging groups, determine the M–M interaction.^{111–115} As was discussed in Section IV.3.a, many metals form dimeric complexes $M_2(OAc)_4L_2$ (M = Cu, Rh, Ru, Re, Cr, Mn, but not Pd or Pt). In the crystalline state, Pd^{2+} diacetate $Pd_3(OAc)_6 \cdot H_2O$ (**13**) contains trimeric ring complexes. The Pd atoms form a nearly regular triangle with the distances $R(Pd-Pd) = 3.105-3.203$ Å (on average, 3.154 Å) and $R(Pd-O) = 1.973-2.014$ Å (on average, 1.99 Å).¹¹² Although, according to STM calculations,^{32,33} the Pd–Pd bond energy is markedly lower than the energy of one Pd–O coordination bond: $D_0(Pd-Pd) = 19.5$ kJ mol^{−1}, $D_0(Pd-O) = 191.6$ kJ mol^{−1}, the contribution of three Pd–Pd bonds equal to ~ 60 kJ mol^{−1} stabilises trimer **13**. The palladium acetatoacetoneoximate $Pd_3(OAc)_3 \cdot (ONCMe_2)_3 \cdot 0.5 C_6H_6$ (**14**) has a similar structure;⁷⁷ however, the $R(Pd-Pd)$ distances (3.009 Å) are shorter and the energy of three Pd–Pd bonds [$3 D_0(Pd-Pd) = 3 \times 27.3 = 81.9$ kJ mol^{−1}] is greater than those in the acetate.

A number of SMC have been prepared on the basis of palladium acetate. The reaction of $Pd(OAc)_2$ with 1,3-bis(1-R-benzimidazol-2-yl)benzene (RbzimPh) gives the compound $[Pd(RbzimPh)(OAc)]_3 \cdot 9 MeCN$ (**15**), where R = Me, Et, CH_2D .^{39,114,115} Supramacrocycles **15** are based on the structural motifs of compounds **13** and **14**. In the solid state, the cavity is occupied by the MeCN molecules. The triangular shape of these rings is due to the acetate structure in which the carboxy groups combine three Pd^{2+} cations (rather than two, as in Cr, Mn, Cu, Ru, Rh and Re dimers).

It is noteworthy that in SMC **15**, as in trimers **13** and **14**, the Pd atoms are separated by bridging ligands but the shortest Pd–Pd distances allow the metal–metal interaction, which is weak but still stabilises the triangular shape. The $R(Pd-Pd)$ distances vary from 3.0 to 3.5 Å and the energy of one bond, $D_0(Pd-Pd)$, ranges from 28 to 10 kJ mol^{−1}.

The bis(2-mercaptoethyl) sulfide anion is a promising ligand for the synthesis of triangular SMC. The crystal structure of $Pd_3(SCH_2CH_2SCH_2CH_2S)_3$ resembles that of palladium acetate trimers.⁷⁷ Each Pd atom is coordinated by four sulfur atoms (approximately square planar geometry); the Pd atoms form a triangle with $R(Pd-Pd) = 3.41$, 3.49 and 3.66 Å, the corresponding bond energies being $3 D_0(Pd-Pd) = 11.0 + 9.3 + 6.6 = 26.9$ kJ mol^{−1}.

Platinum complexes of this type have been prepared. The acetate groups and the bis(2-mercaptoethyl)sulfide anion draw the metal atoms towards one another, shorten the M–M bonds and thus strengthen the M_3 core.

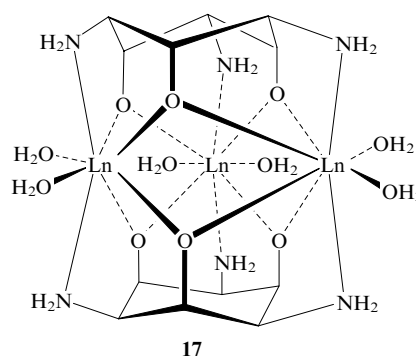
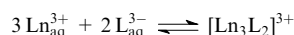
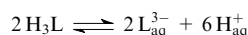
Triangular structures without stabilising M–M bonds. Bulky nitrogen-containing hetaryl ditopic bridging ligands shield the M–M interaction. Many SMC have been prepared with these ligands, in particular, $[Pd(dmpze)Cl_2]_3$ [dmpze is 1,2-bis(3,5-dimethylpyrazol-1-yl)ethane];¹¹⁶ $[Cu(tacn)(imd)]_3^{3+}$ (tacn is 1,4,7-triazacyclononane, imd is imidazolate);¹¹⁷ $[Fe(ttpO)]_3$ (ttpOH is 2-hydroxytetrakis-4'-tolylporphyrin).¹¹⁸

The triangular SMC $[(en)M(pyrXpyr)_2]_3(NO_3)_6$ (**16**) (M = Pd, Pt; en = $H_2NCH_2CH_2NH_2$, pyr is 4-pyridyl; X = *p*- C_6H_4 , $C \equiv C$, $C \equiv C-C \equiv C$) have been prepared in an aqueous solution using bis-hetaryl ligands and $Pd(en)(NO_3)_2$.¹¹⁹ In solution, these complexes occur in equilibrium with square SMC. In our opinion, the presence of flexible linking pyrXpyr ligands and the absence of M–M contacts in SMC **16** reduce the stability of these supramacrocycles. The reaction of $Pt(en)(NO_3)_2$ in H_2O with 2,2'-bipyrazine (2,2'-bpz) yields only the triangular SMC $[Pt(2,2'-bpz)]_3(NO_3)_6$, while in the case of Pd, only the mononuclear chelate complex is formed.¹²⁰

The above information leads to conclusions concerning the similarity of, and the differences between, the palladium and platinum SMA. Although Pd and Pt compounds, most often, have similar structures, thermodynamic characteristics of their SMC may be different. The difference between the cohesion energies¹²¹ of metallic palladium and platinum is ~ 200 kJ mol^{−1}; the Pt–Pt bonds are stronger than the Pd–Pd bonds. In the absence of M–M bonds in SMC and in the formation of π -bonds with polydentate ligands, it is important that the 5d atomic orbitals of platinum are more diffuse than the 4d atomic orbitals of palladium and form stronger π -bonds with ligands. In addition, platinum atom has a higher electron affinity than palladium (2.1251 and 0.5621 eV, respectively). The electron affinity of platinum is nearly equal to that of sulfur and higher than that of oxygen (1.465 eV). Thus, the effective charges on the platinum atoms are much lower than those on palladium atoms and the bonds with ligands are stronger and more covalent.

Macrocycles with strong M–M bonds. Quite a few examples of triangular macrocycles formed by d elements and stabilised through the formation of M–M bonds can be cited. Thus the $Pt_3[\mu-C(OMe)C_6H_4Me-4]_3(CO)_3$ trimers have¹²² short Pt–Pt distances (2.62 Å), the corresponding energy $D_0(Pt-Pt)$ is equal to 73 kJ mol^{−1} (*i.e.*, 219 kJ mol^{−1} for three bonds).

The first lanthanide-containing SMC were prepared not long ago.^{123,124} The hexadentate 1,3,5-triamino-1,3,5-trideoxy-*cis*-inositol ligand (H_3L) and Ln^{3+} form the $[Ln_3L_2]^{3+}$ complex (**17**) in an aqueous solution according to the reactions



$Ln = Gd, Lu.$

Structural similarity of complexes **17** for $Ln = Gd$ and Lu has been established: the Ln^{3+} cations are bound to two ligands through two N atoms and four O atoms; two water molecules complete the C.N. of the metal ion to 8. Three Ln^{3+} ions form a nearly regular triangle similarly to many other metal rings formed by d elements,¹⁰⁴ for example, $[M_3(\mu-H)_3(CO)_{12}]$ (M = Mn, Tc, Re); $[M_3(\mu-CO)_3(PR_3)_n]$ ($n = 3, 4$; M = Pd, Pt). Despite numerous studies of the triangular clusters and SMC of this type, the thermodynamics of self-assembly in solution has been reported only in two studies.^{123,124} It was found that (a) the self-assembly is a purely entropic process: $\Delta S^\circ > 0$, $\Delta H^\circ > 0$; (b) the stability of SMC **17** increases from La to Lu in parallel with a decrease in the ionic radius R_{ion} ; (c) $\Delta G^\circ [La_3L_2]^{3+}$ and $\Delta G^\circ [Lu_3L_2]^{3+}$ differ almost threefold. Such a pronounced change in the thermodynamic characteristics is unusual for the chemistry of Ln^{3+} complexes. This unexpected fact of the thermodynamics of SMC is attributable to the difference between the thermodynamic parameters of desolvation of the $[Ln_{aq}]^{3+}$ cations. The change in ΔG° during the reaction can be represented as follows:

Table 1. Change in the thermodynamic parameters of the formation of complexes **17** in the lanthanide series (at 298 K).

Parameter /kJ mol ⁻¹	Pr	Sm	Gd	Dy	Er	Lu
$\delta\Delta G^\circ$	-48	-83	-95	-104	-111	-122
$\delta\Delta G_f^\circ[\text{Ln}_3\text{L}_2]^{3+}$	-27	-50	-11	-32	-66	-89
$-3\delta\Delta G_f^\circ(\text{Ln}_{\text{aq}}^{3+})$	-21	-33	-84	-72	-45	-33
$\delta\Delta H^\circ$	-24	-58	-72	-80	-76	-88
$\delta\Delta H_f^\circ[\text{Ln}_3\text{L}_2]^{3+}$	-14.4	-3.1	-4.8	-38.6	-72.1	-67.6
$-3\delta\Delta H_f^\circ(\text{Ln}_{\text{aq}}^{3+})$	-9.6	-54.9	-67.2	-41.4	-3.9	-20.4
$-\delta T\Delta S^\circ$	-24	-25	-22.6	-24.4	-34.6	-33.6
$-\delta T\Delta S_f^\circ[\text{Ln}_3\text{L}_2]^{3+}$	-12.6	-46.9	-6.2	6.6	6.1	-21.4
$3\delta T\Delta S_f^\circ(\text{Ln}_{\text{aq}}^{3+})$	-11.4	21.9	-16.8	-30.6	-41.1	-12.6

$$\Delta G^\circ = \Delta G_f^\circ[\text{Ln}_3\text{L}_2]^{3+} - 3\Delta G_f^\circ(\text{Ln}_{\text{aq}}^{3+}) - 2\Delta G_f^\circ(\text{L}_{\text{aq}}^{3-}) + 6\Delta G_f^\circ(\text{H}_{\text{aq}}^+),$$

where $\Delta G_f^\circ[\text{Ln}_3\text{L}_2]^{3+}$, $\Delta G_f^\circ(\text{Ln}_{\text{aq}}^{3+})$, $\Delta G_f^\circ(\text{L}_{\text{aq}}^{3-})$ and $\Delta G_f^\circ(\text{H}_{\text{aq}}^+)$ are the standard free energies for the formation of the complex, the Ln^{3+} aqua ions, hydrated ligands and protons, respectively.

Then the difference between the ΔG° values of the reaction ($\delta\Delta G^\circ$) for different Ln^{3+} ions (with respect to $\text{Ln} = \text{La}$) is given by

$$\delta\Delta G^\circ = \delta\Delta G_f^\circ[\text{Ln}_3\text{L}_2]^{3+} - 3\delta\Delta G_f^\circ(\text{Ln}_{\text{aq}}^{3+}),$$

where

$$\delta\Delta G_f^\circ[\text{Ln}_3\text{L}_2]^{3+} = \Delta G_f^\circ[\text{Ln}_3\text{L}_2]^{3+} - \Delta G_f^\circ[\text{La}_3\text{L}_2]^{3+},$$

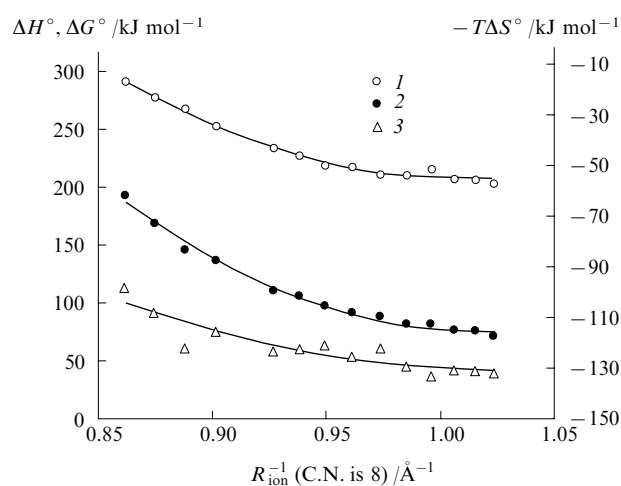
$$\delta\Delta G_{\text{of}}^\circ(\text{Ln}_{\text{aq}}^{3+}) = \Delta G_f^\circ(\text{Ln}_{\text{aq}}^{3+}) - \Delta G_f^\circ(\text{La}_{\text{aq}}^{3+}).$$

The corresponding values are presented in Table 1; the $\Delta G_f^\circ[\text{Ln}_3\text{L}_2]^{3+}$ values were taken from the work by Chapon *et al.*,¹²⁴ and the $\Delta G_f^\circ(\text{Ln}_{\text{aq}}^{3+})$ values were reported by Morss.¹²⁵

The reaction thermodynamics is determined by the contributions of two opposite effects: the energy gain due to the formation of two $\text{Ln}^{3+}-\text{N}$ bonds and four $\text{Ln}^{3+}-\text{O}(\text{L})$ bonds and energy loss for the cleavage of six $\text{Ln}^{3+}-\text{O}(\text{OH}_2)$ bonds. The $\Delta G_f^\circ(\text{Ln}_{\text{aq}}^{3+})$ values (in kJ mol⁻¹) increase on passing from La to Gd and decrease from Gd to Lu:¹²⁵ $\Delta G_f^\circ(\text{Ln}_{\text{aq}}^{3+}) = -688$ (La), -660 (Gd); -677 (Lu). The contribution of the desolvation effect $3\delta\Delta G_f^\circ(\text{Ln}_{\text{aq}}^{3+})$ to $\delta\Delta G^\circ$ is from 30% to 70%. Two effects, *i.e.*, the decrease in the energy consumption for desolvation for heavy elements and the increase in the $\text{Ln}^{3+}-\text{N}$ and $\text{Ln}^{3+}-\text{O}(\text{L})$ bond energies in the SMC of these elements, caused by the lanthanide contraction partially counterbalance each other. The enthalpy contribution of desolvation, $3\delta\Delta H_f^\circ(\text{Ln}_{\text{aq}}^{3+})$ (see Table 1), determines almost completely the $\delta\Delta H^\circ$ values for Sm and Gd, whereas the gain in energy caused by the formation of two $\text{Ln}^{3+}-\text{N}$ bonds and four $\text{Ln}^{3+}-\text{O}(\text{L})$ bonds ($\text{Ln} = \text{Er}$, Lu) makes the major contribution to $\delta\Delta H^\circ$ of these elements. The balance of the two contributions to the reaction enthalpy results in a monotonic variation of $\delta\Delta H^\circ$ versus the ionic radius R_{ion} of the cations (C.N. 8) and allows one to estimate the ΔH° values for the SMC of Ce, Nd, Eu, Tb, Ho, Tm, Yb, which have not been measured. The entropy contribution $T\Delta S^\circ$ to the self-assembly reaction is documented¹²⁴ with the accuracy of ± 7.5 kJ mol⁻¹. The $\delta T\Delta S^\circ$ values for Gd, Dy and Er are determined almost completely by the difference in the desolvation entropies $\delta T\Delta S_f^\circ(\text{Ln}_{\text{aq}}^{3+})$ (see Table 1, Fig. 1). The qualitative aspects of the variation of thermodynamic parameters upon the formation of SMC have been considered.^{50, 126–128}

c. Supramacrocycles with square or rectangular geometry

Many metal complexes with square planar, trigonal bipyramidal, tetrahedral and octahedral coordination can be used as

**Figure 1.** Variation of the thermodynamic parameters of the formation of Ln^{3+} complexes with 1,3,5-triamino-1,3,5-trideoxy-*cis*-inositol depending on the Ln nature.

(1) ΔH , (2) ΔG , (3) $T\Delta S$.

angular structural fragments in the construction of homonuclear square assemblies. The tetragonal SMC were prepared for the following metals: Ti;^{8, 129} V, Cr;^{14, 81} Mn;^{14, 130, 131} Fe;^{8, 14, 39, 130, 132} Co;^{8, 14, 39, 130, 131, 133, 134} Ni;^{130, 131} Cu;^{8, 14, 39, 130, 135} Zn;^{8, 14, 39, 130} Zr, Nb, Mo;^{8, 14, 81, 136, 137} Tc, Ru;^{39, 138, 139} Rh;^{8, 140} Pd, Pt;^{8, 9, 14, 39} Ag;^{8, 39, 141} Cd;^{39, 130, 131} Hf, Ta, W;^{14, 81} Re;^{8, 142, 143} Os, Ir, Au, Hg;³⁹ Na, Cs;⁸ Ga;¹³⁷ and Mg;¹³¹ heteronuclear SMC have also been prepared: Pt–Pd, Ti–Pt, Re–Pd.⁸ The supramacrocycles with a square geometry refer to the simplest representatives of the family of nanoassemblies. The steric strain in a square SMC depends on the ligands that form the square sides; therefore, their self-assembly is not always thermodynamically favourable; in these cases, kinetically labile oligomers are formed. In the self-assembly of square SMC, flexible or semiflexible linkers are used, for example, 4,4'-bipy; 1-(2-thiouracil-4-methylene)-3,6-diazahexane; bis(4-pyridyl)methane and -ethane; bis[4-(2-diphenylphosphinoethyl)phenyl] ether; 1,4-bis(4-pyridylmethyl)-2,3,5,6-tetrafluorobenzene, amines and substituted bis-phosphonates; tetrakis(2-pyridyl)thiocarbazine and so on.

In the future, square supramacrocycles could find extensive practical use:^{1, 2, 8, 9, 14, 18, 39} they participate in the hydrophobic/hydrophilic molecular recognition; form host–guest complexes by inclusion of various molecules into the cavity where they demonstrate high selectivity; they are used to transport salts into the organic phase and as artificial receptors. A promising trend in electrochemistry is the use of square SMC which change the oxidation state depending on the M–M interaction, *e.g.*, the metallacyclophane ‘host’ with four

reduced metal centres can transfer four electrons to a guest molecule. The redox reactions in a 'host-guest' system result in the change in properties (reactivity, magnetism, optical properties). Square SMC based on imine or azine Re complexes possess luminescent properties and are of interest as new promising sensors. The influence of the guest molecules on the excited states of the host molecule is considered as a new line of research in optics. The use of paramagnetic metal ions in square SMC allows one to study intermolecular interactions inside molecular layers; porphyrin-containing SMC are used to study the photochemical properties of the bound porphyrin layers, in particular, the processes occurring in the active sites of photosynthesis and in light-accumulating bacteria are modelled in this way; finally, square assemblies are used in catalysis.

In square rings, the M–M interactions are shielded by bulky ligands, however the design of SMC as a rectangle from two dimers with relatively short M–M bonds connected by substituted aryl ligands gives SMC of a new type. This approach makes use of rhenium complexes with alkoxy¹⁴² or thiolate¹⁴³ ligands. The reaction of the dimer $[(OC)_4Re(\mu-SPr)_2]$ with 4,4'-bipyridyl (L) in chloroform gives SMC having a rectangular structure with two shorter sides $(OC)_3Re(\mu-SPr)_2Re(CO)_3$ and two longer sides, Re–L–Re [$R(Re-Re) = 3.81$ and 11.57 Å].¹⁴³ The shorter side of the rectangle, *i.e.*, the dimeric fragment, is stabilised by the Re–Re interaction, while the longer side, by Re–N coordination bonds [$D_0(Re-Re) = 2 \times 18.3 = 36.6$ kJ mol^{−1}].

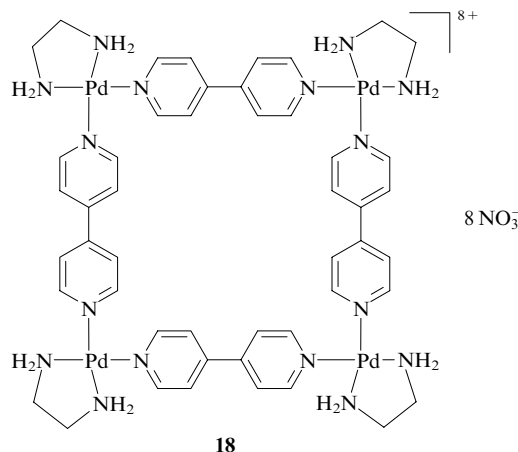
The longer side of this SMC can be shortened by replacing bipyridyl by pyrazine; the Re–Re contact would also contribute to stabilisation of the ring. Generally, the development of this strategy appears to hold promise. When designing rectangular SMC, one can choose various dimers of transition d elements with strong or weak M–M bonds.⁴⁹ The length of the other two bonds in the rectangular SMC can be varied by 'elongating' the 4,4'-bipy ligand, *i.e.*, by using pyrXpyr ligands of different length, for example, X = *p*-C₆H₄, C≡C, C≡C–C≡C. Rectangular supramacrocycles are able to accommodate neutral aromatic guest molecules.

Among the factors that stabilise SMC, a new type of ligand–ligand interaction, the so-called π – π -stacking interaction, is often mentioned. However, it is difficult to confirm this effect experimentally. It was hypothesised⁸ that the ring structure of the tetranuclear assembly $[Cu_4(dppn)_4](OTf)_4$ [dppn is 3,6-bis(2-pyridyl)pyradazine, OTf = CF₃SO₃] with a distorted tetrahedral coordination of Cu(I) is stabilised by the π – π -stacking interaction of two pairs of ligands. This could be accepted if Cu⁺ compounds with C.N. 4 devoid of the stabilising π – π -stacking interactions were unstable. However, in all compounds (both with σ and with π Cu⁺–L interactions, in polymers, and in isolated molecules, and now in SMC), Cu⁺ has a tetrahedral coordination and all these compounds are stable. Now the role of π – π -stacking interactions between the aryl ligands in the SMC remains an interesting hypothesis. The variation of the stability of $[LnL_3]^{3-}$ complexes (L is pyridine-2,6-dicarboxylate) along the lanthanide series was attributed¹²⁸ to the π – π -stacking interaction between the ligands. It turned out, however, that in the complexes of heavy Ln, the conformation of the ligands changes. Probably, the π – π -stacking interaction is important for biological systems, but in the case of SMC containing metals that form strong $d\pi(M) - p\pi(L)$ bonds, multicentre $L(\pi-\pi) - M - (\pi-\pi)L$ interactions arise. The problem of π – π -stacking interactions is related to the important theoretical problem of the degree of electron delocalisation in SMC.

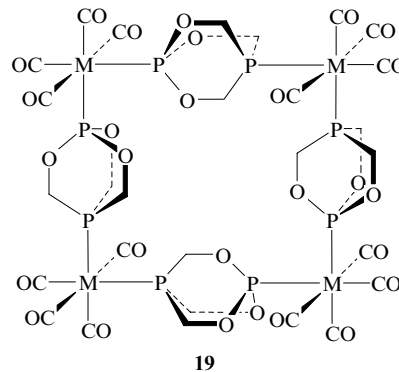
Although many metals form square assemblies, Pd²⁺ and Pt²⁺ complexes possess a number of specific properties. A square coordination geometry is typical of the electronic configuration d⁸. Square Pd²⁺ and Pt²⁺ complexes are self-

assembled to form a square SMC in the case where the *cis*-positions of the complex are 'protected', *i.e.*, they do not interact with other ligands.

A square supramacrocycle, $[Pd(en)(4,4'-bipy)]_4^{8+}$ (**18**), has been synthesised⁸² by the reaction between a ditopic non-chelating ligand, 4,4'-bipyridyl, and the kinetically labile Pd(en)(NO₃)₂ complex. The 4,4'-bipy ligand replaces the nitrate anions in the *trans*-positions with respect to N atoms of ethylenediamine and forms bonds with two cations.

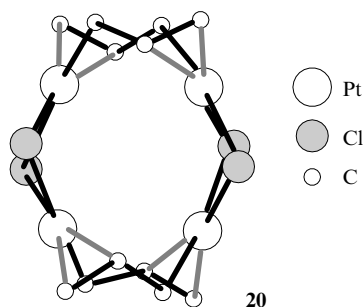


This method of synthesis, *i.e.*, self-assembly of *cis*-protected Pd²⁺, Pt²⁺ and other metal complexes has been analysed in many publications,^{6, 8, 12, 14, 18, 39} as it allows one to prepare SMC with different types of bonds, ranging from strong coordination M–N, M–O, M–C, M–P and M–Cl bonds to weak intermolecular M···M and hydrogen bonds. However, in the Jones opinion,¹⁴ the studies^{9, 82} are not pioneering, because the first square-shaped SMC **19** were prepared, based on the same idea (the use of *cis*-protecting ligands), ten years earlier, in particular, by reactions of $M(CO)_6$ (M = Cr, Mo, W) with ditopic donor $P(OCH_2)_3P$ ligands.⁸¹



M = Cr, Mo, W.

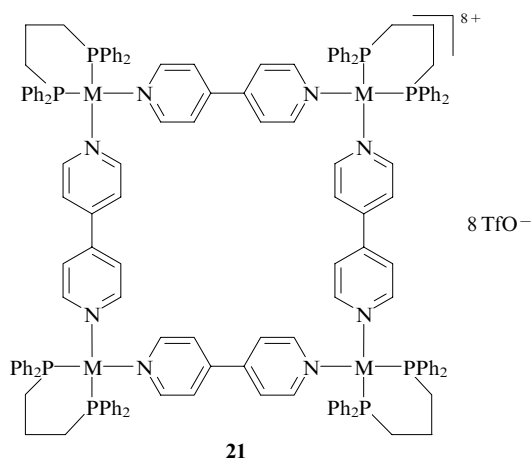
Even earlier, an extensive class of Pd and Pt metallacycles, for example, allylplatinum chloride $[(\pi-C_3H_5)PtCl]_4$ (**20**), have been studied in the solid state.¹⁴⁴ In the solid tetramer **20**, each



Pt atom is coordinated in the π -mode by the C=C bond of the allyl group, in the σ -mode by the CH₂ fragment of another allyl group and also by chlorine atoms. The bridging allyl ligands in complex **20** protect the *cis*-positions, similarly to the en and CO ligands in compounds **18** and **19**, respectively. It seems likely that the proper idea of *cis*-protection has long been used for the synthesis of tetramers with a rectangular or square coordination.⁷⁷ The Pt atoms in tetramer **20** are arranged at the corners of a square, the Pt–Pt distances being 3.270 and 3.235 Å, and the contribution of Pt–Pt bonds into the tetramer formation is essential [$D_0(\text{Pt}–\text{Pt}) = 2 \times 33.3 + 2 \times 34.6 = 135.8 \text{ kJ mol}^{-1}$].

One can compare the properties of tetramers **18** and **20**. According to NMR spectroscopy and mass spectrometry, the structure of the ring in **18** is the same in solution as in the crystalline state (determined by X-ray diffraction). No experimental data on the structure of tetramer **20** in solution are available. The sides of rings **18** and **20** are ~ 8 and < 3 Å long, respectively; note that the size of the former can be varied. The supramacrocycle **18** is capable of molecular recognition, as it can host some guest molecules such as benzene, naphthalene, and so on; the ring size in tetramer **20** is too small for the insertion of guest molecules. The difference between Pt and Pd is noteworthy.⁸ Thus Pt(en)(NO₃)₂ and 4,4'-bipy react to give a mixture of oligomers from which a thermodynamically stable square-shaped SMC can be isolated on heating. This effect was attributed to the fact that the Pd–N(bipy) bond is weaker than Pt–N. For the statistically average distances, $R(\text{Pd}–\text{N}) = 2.04$ and $R(\text{Pt}–\text{N}) = 2.06$ Å,⁷⁷ the bond energies we calculated are as follows: $D_0(\text{Pt}–\text{N}) = 274$, $D_0(\text{Pd}–\text{N}) = 238 \text{ kJ mol}^{-1}$.

Square-shaped SMC have also been synthesised from bis-phosphine derivatives [M(dppp)(OTf)₂] [M = Pt, Pd; dppp = Ph₂P(CH₂)₃PPh₂] and 4,4'-bipy in a non-aqueous solvent (CH₂Cl₂).^{145,146} The existence of the square SMC [M(dppp)(4,4'-bipy)]₄(OTf)₈ (**21**) was proved by NMR spectroscopy. The researchers cited noted a remarkable fact: even with a 100-fold excess of the 4,4'-bipy ligand, only square SMC **21** are formed in solution, *i.e.*, a fragment corresponding to a side or a corner of the SMC cannot be isolated.



M = Pd, Pt.

For solid compound **21** with M = Pt, it was shown that a square side is equal to 11.2 and the diagonal is 14.3 Å. The Pt²⁺ ions have C.N. 4: each Pt²⁺ ion is connected to two P atoms of the dppp ligand and two N atoms of the two 4,4'-bipy ligands. The N–Pt–N bond angles are equal to 84° and the P–Pt–P angles are about 90°, so that the whole ring is essentially non-planar. It was assumed¹⁴⁵ that the stability of this SMC is related to the strong π – π -stacking interaction between the ligands, in particular, between the π -electrons of

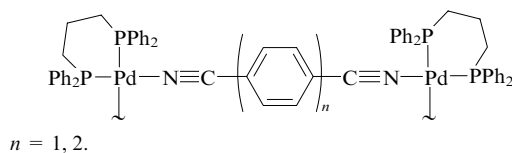
the benzene rings of the chelating bis-phosphine ligands and π -electrons of one of bipyridyl rings. If this interaction was responsible for the stability of SMC **21**, the effect would be manifested in the interatomic distances in square SMC compared to those in the Pt²⁺ and Pd²⁺ complexes studied previously.⁷⁷ Our analysis of the reported structural data^{8,9,14,77,145} has shown that the M²⁺–N and M²⁺–P distances (M = Pt, Pd) in the phosphine and pyridine complexes and in square SMC **21** are equal to within the accuracy of measurements. Indeed, in Pd[Ph₂P(CH₂)₂PPh₂](SCN)₂, the measured⁷⁷ distances are $R(\text{Pd}–\text{P}) = 2.245–2.260$ Å, while in SMC **21**, $R(\text{Pt}–\text{P}) = 2.23–2.25$ Å.¹⁴⁵ An early publication⁷⁷ reports the average $R(\text{Pt}–\text{N})$ and $R(\text{Pd}–\text{N})$ values in the Pt²⁺ and Pd²⁺ pyridine compounds to be 2.02–2.06 Å, and the $R(\text{Pt}–\text{N})$ distances in SMC are 2.03–2.07 Å.^{8,9,14,145} Thus, the assumption of stabilisation of the SMC by π – π -stacking interactions between the ligands is not confirmed.

Analogous square SMC based on *cis*-phosphine derivatives have been obtained:¹⁴⁵ [M(PEt₃)₂X]₄(OTf)₈ (M = Pd²⁺, Pt²⁺; X is 4,4'-bipy, 2,7-diazapyrene, and so on). For all square SMC considered above, the *cis*-positions in the starting complexes (*i.e.*, the square corners) are protected by bidentate (en, dppp) or monodentate (PEt₃) ligands, which form strong M–P bonds. Neutral phosphines are strong electron donors, therefore, their interaction with metals is accompanied by a substantial charge transfer.³⁷ In the initial MA₂X₂ complexes (M = Pd, Pt; A = PEt₃; X is anion), the $R(\text{Pt}–\text{P})$ and $R(\text{Pd}–\text{P})$ distances vary in the 2.22–2.34 Å range.⁷⁷ According to our estimates, the M–P bond energy is fairly high [$D(\text{M}–\text{P}) = 415–358 \text{ kJ mol}^{-1}$]; phosphine ligands protect the *cis*-positions of the structural blocks by a thermodynamic mechanism, *i.e.*, they stabilise the SMC by a great contribution of the M–PEt₃ and M–PPh₂ interaction energy. In addition, the PPh₂ ligands provide a steric protection of the *cis*-positions, which opens up broad opportunities for the synthesis of SMC using these ligands.^{8,14,39}

In the absence of groups shielding the *cis*-positions, square-coordinated SMP may form. For example, this is the case in the reaction of Co(NCS)₂ with 4,4'-bipy.¹⁴⁷

Although the properties of many palladium and platinum SMC are largely similar, note once again the difference in the self-assembly mechanisms: under the same conditions, square SMC are formed for palladium but oligomer mixtures are formed for platinum, because the Pd–N bonds are weaker than Pt–N bonds and more labile in the self-assembly processes giving SMC.⁸

The reaction of [Pd(dppp)(OTf)₂] with *p*-NC(C₆H₄)_nCN-*p* (*n* = 1, dcp; *n* = 2, dcdp) in CH₂Cl₂ produces square SMC [Pd(dppp)(dcp)]₄(OTf)₈ (**21a**) and [Pd(dppp)(dcdp)]₄(OTf)₈ (**21b**), the sides of which can be represented as follows:

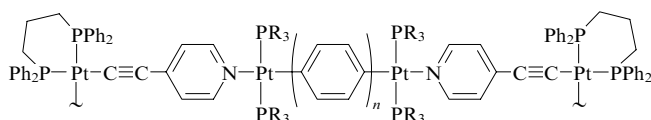


Thus, although a large number of homonuclear and heteronuclear SMC based on complexes of almost all of d elements have been prepared in recent years, nitrogen-containing SMC with Pt²⁺ and Pd²⁺ are most numerous. This can be attributed to several reasons. The Pt²⁺ and Pd²⁺ ions are soft acids and the nitrogen atom, being a softer ligand than oxygen, forms numerous complexes with these ions, which is not so typical of other d elements. The Pd–N and Pt–N bond energies are higher than the Pd–O and Pt–O bond energies. This is an important thermodynamic factor affecting the self-assembly. As an illustration, one can compare the energies of

the Pd–N and Pd–O bonds having standard interatomic distances, $R(\text{Pd–O}) = 2.0$ and $R(\text{Pd–N}) = 2.05$ Å.⁷⁷ The calculated energies are as follows: $D_0(\text{Pd–N}) = 243.4$, $D_0(\text{Pd–O}) = 191.6$ kJ mol^{–1}, so that the energy gain due to the formation of two Pd–N bonds instead of two Pd–O bonds is significant: $\delta D_0 = 2[D_0(\text{Pd–N}) - D_0(\text{Pd–O})] = 2 \times (243.4 - 191.6) = 85.6$ kJ mol^{–1}.

The thermodynamics of the self-assembly process is substantially affected by the solvent. The formation of complexes of d elements and lanthanides in aqueous solutions is entropy controlled, while in non-aqueous solutions, it is enthalpy controlled.^{26, 121} Without experimental data, it is unknown whether this would be valid for the self-assembly of SMC from complexes. Various hypotheses on the thermodynamics of the self-assembly of SMC have been put forward; it was noted³⁹ that the formation of ring structures is preferred over the formation of linear structures from the enthalpy standpoint, while the formation of small rings is preferred over the formation of large rings (at low concentrations) from the entropy standpoint.^{126, 127}

Nanosized square SMC have now been prepared.^{8, 111} For example, the addition of a solution of *cis*-[(dppp)Pt{C≡C(C₅H₄N-4)}₂] in CD₂Cl₂ to the solid bis-triflates TfOPt(PR₃)₂(*p*-C₆H₄)_nPt(PR₃)₂OTf gave square SMC of different size the side of which can be represented as



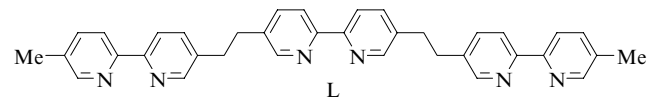
R = Et: $n = 1, 2$; R = Ph: $n = 2, 3$.

This nanosquare contains 12 platinum ions; each side has four ions, two of these being common to two sides. Generally, the synthetic strategy is the same as for the smaller SMC described previously (**18**, **21** and so on), namely, *cis*-protection of the metal ion. The calculated square diagonal is ~ 36 Å long.⁸

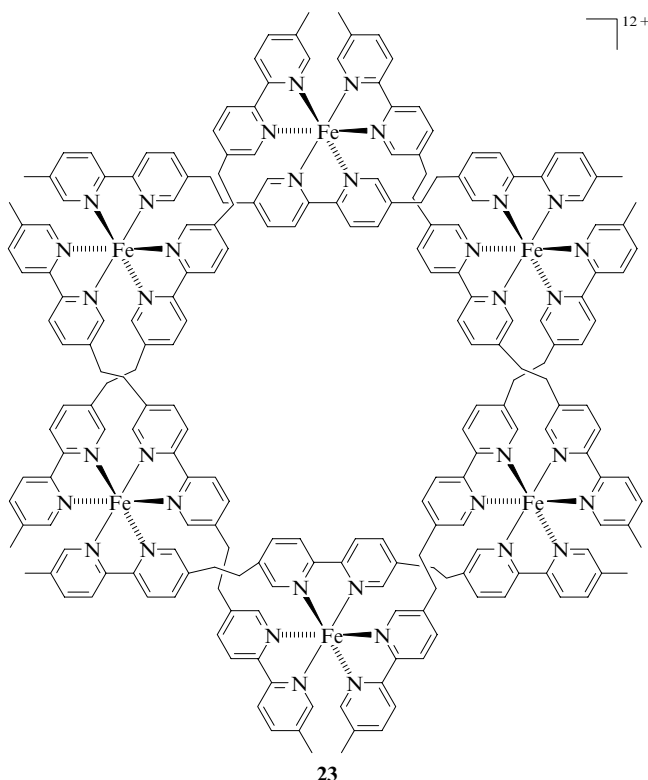
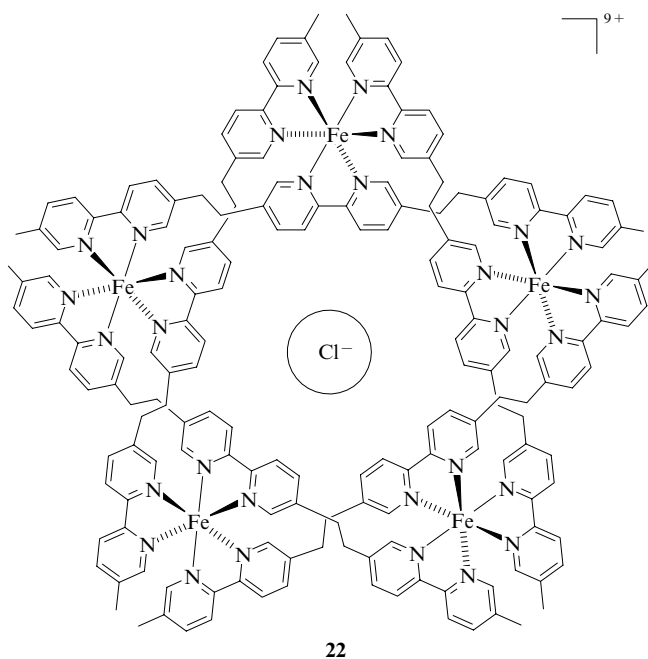
Nanosquares of this type are promising for the design of molecular switches and molecular machines. Another possibility is to use the magnetic properties of these SMC. These macrocycles are classified as ultrathin particles with a diagonal dimension of 3.4–4.8 nm. Nanoparticles applied onto a substrate are known to form ordered one-, two- and three-dimensional structures,²³ which find application due to the possibility of magnetic transitions (paramagnet – ferromagnet – antiferromagnet) or metal – dielectric phase transition.⁷⁶

d. Polygonal supramacrocycles and three-dimensional structural motifs

Pentagonal and hexagonal supramacrocycles. The first SMC with pentagonal or hexagonal geometry were obtained by Lehn^{148, 149} in ethylene glycol using FeCl₂ or FeSO₄, respectively, in the presence of NH₄PF₆ and ligand L.



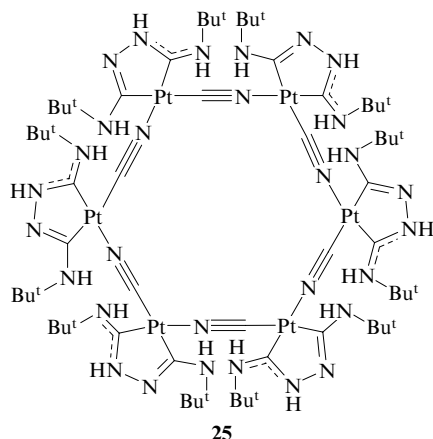
These are helical SMC $\{[\text{FeL}]_5\text{Cl}\}(\text{PF}_6)_9$ (**22**) and $[\text{FeL}]_6(\text{PF}_6)_{12}$ (**23**). In compound **22**, the Cl[–] ion resides in the SMC cavity. By analogy with SMC **22**, the compound $\{[\text{NiL}]_5\text{Cl}\}(\text{PF}_6)_9$ (**24**) was prepared.³⁹



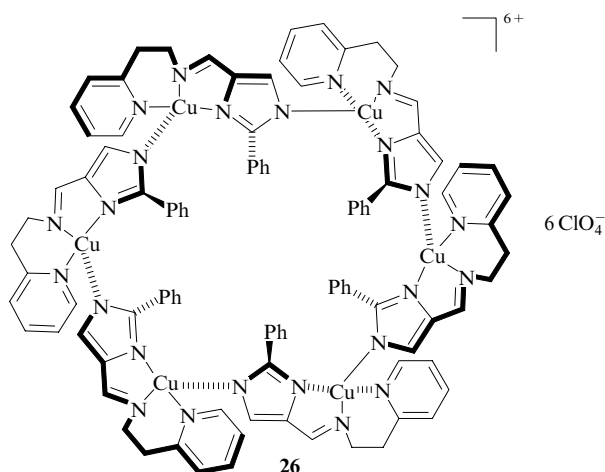
The authors¹⁴⁸ noted that the inner cavity of SMA **22** has a radius of 1.75 Å. The size of the Cl[–] ion (the ionic radius is 1.7 Å) fits the cavity and strong binding is due to the high positive charge of the SMA. However, when FeSO₄ is used, a large six-membered SMA containing no anion is formed. Analogous SMA were synthesised with Fe(BF₄)₂ and FeSiF₆. The use of FeBr₂ resulted in an approximately equimolar mixture of five- and six-membered SMA. Thus, it was concluded that the structure of SMA is influenced by the size rather than the charge of the counter-ion. However, the mechanism of this influence remains an open question, *i.e.*, whether the anion serves as the template in the SMA formation

or the assemblies capable of strong binding of the anion (substrate) as receptors are formed owing to the reversibility of self-assembly.

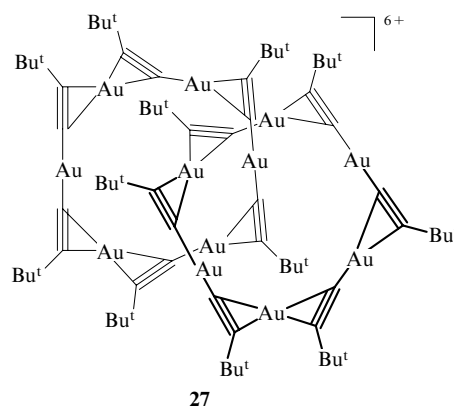
Using K_2PtCl_4 , H_2NNH_2 and Bu^tNC , SMC **25** has been synthesised in an aqueous solution.¹¹² This compound possesses luminescent properties being responsible for a strong band in the visible region at 356 nm. This band was assigned to a $\text{Pt} \rightarrow \pi(\text{carbene})$ charge transfer transition. An X-ray diffraction study showed that the SMC is non-planar, its conformation resembling the 'chair' conformation. The $\text{CN}-\text{Pt}-\text{CN}$ angles are equal to 92.4° and the $\text{Pt}-\text{N}\equiv\text{C}$ and $\text{Pt}-\text{C}\equiv\text{N}$ fragments are nearly linear (angle 174°).



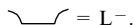
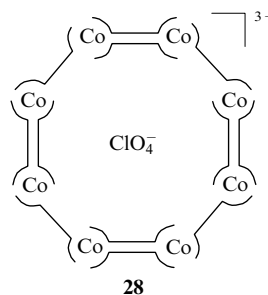
Six-membered SMC have also been prepared for other metals. The compound $[\text{CuL}]_6(\text{ClO}_4)_6$ (**26**) was synthesised¹³⁵ by triethylamine-induced deprotonation of the complex $\text{Cu}(\text{HL})(\text{ClO}_4)_2$, where HL is *N*-(2-phenylimidazol-4-ylmethylidene)-2-aminoethylpyridine.



The complex $[\{\text{Au}(\text{C}\equiv\text{CBu}^t)\}_6]_2$ (**27**) was isolated upon the reaction of $[\text{Au}(\text{NH}_3)_2]\text{BF}_4$ with $\text{Bu}^t\text{C}\equiv\text{CH}$ in acetonitrile.¹⁵⁰ It was found that this compound is a catenane consisting of two interlinked six-membered SMC; each SMC contains six Au^+ ions and six acetylene groups. Within each ring, metal ions form a planar hexagon in which the $R(\text{Au}-\text{Au})$ distances are 3.30–3.36 Å. Although these distances are longer than those in metallic gold (2.88 Å), the $\text{Au}-\text{Au}$ contacts determine the stability of this SMC. The energy of six $\text{Au}-\text{Au}$ bonds $D_0(\text{Au}-\text{Au})$ [for average $R(\text{Au}-\text{Au}) = 3.33$ Å] equals $6 \times 26 = 156 \text{ kJ mol}^{-1}$.



Octagonal supramacrocycles. The reaction of $[\text{Co}(\text{OAc})_2(\text{H}_2\text{O})_4]$ with the salt KL {L is bis[3-(2-pyridyl)pyrazol-1-yl]dihydroboronate} in MeOH with the addition of KPF_6 or NaClO_4 for precipitation gave¹⁵¹ SMC containing eight Co^{2+} cations, twelve L^- bridging ligands and the PF_6^- or ClO_4^- anion: $[\text{M}_8\text{L}_{12}\text{A}]^{3+}(\text{A}^-)_3$, $\text{M} = \text{Co}, \text{Ni}$; $\text{A} = \text{ClO}_4, \text{PF}_6$. The ligand $\text{L} = \text{C}_5\text{H}_4\text{N}-\text{C}_3\text{H}_2\text{N}_2-\text{BH}_2-\text{N}_2\text{C}_3\text{H}_2-\text{C}_5\text{H}_4\text{N}$ forms a bridge between the neighbouring Co^{2+} ions.

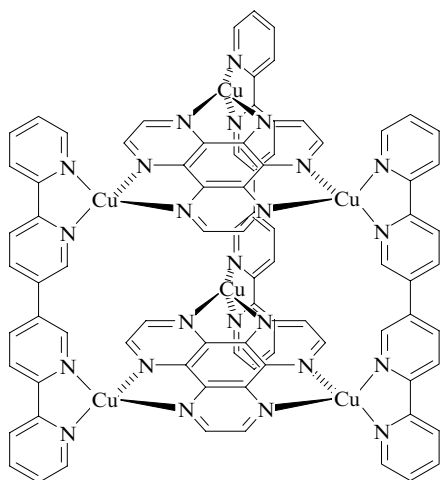


According to electrospray mass spectrometry and X-ray diffraction analysis, one anion resides in the SMC cavity of $[\text{Co}_8\text{L}_{12}(\text{ClO}_4)]^{3+}(\text{ClO}_4^-)_3$ (**28**). No $[\text{M}_8\text{L}_{12}]^{4+}$ cation without an anion in the cavity was detected; thus, the anion stabilises the eight-membered ring and, apparently, controls its size. We present our interpretation of this effect based on the thermodynamics of anion formation in solution. Note first of all that in the hexagonal SMC **26** of a smaller size, the ClO_4^- anion is not inserted in the cavity, *i.e.*, the size effect is significant for SMC **26** and **28**.

It is known that thermodynamics of formation of anions affects their outer- or inner-sphere coordination. Thus the standard free energies of formation¹²¹ $\Delta G_f^\circ(\text{ClO}_4^-)_{\text{aq}} = 7163.5$ and $\Delta G_f^\circ(\text{Cl}^-)_{\text{aq}} = -164.5 \text{ kJ mol}^{-1}$ are similar but the coordination of the ClO_4^- anion is usually outer-sphere, while the Cl^- ion can be coordinated as both an outer- and an inner-sphere ligand. The standard entropy of formation of the ClO_4^- anion in an aqueous or ethanolic solution is positive and high, while that of the Cl^- ion is negative [$\Delta S_f^\circ(\text{ClO}_4^-)_{\text{aq}} = +118.7$, $\Delta S_f^\circ(\text{Cl}^-)_{\text{aq}} = -8.7 \text{ J mol}^{-1} \text{ K}^{-1}$]. Thus, the entropy factor mainly determines the outer-sphere coordination of the ClO_4^- anion, because the inner-sphere coordination is entropically unfavourable. For insertion into an SMC, the ClO_4^- anion should be stabilised by a gain in enthalpy, *i.e.*, by the formation of strong bonds with the atoms of SMC, in order to counterbalance both the entropy and enthalpy loss. Apparently, this is the case for SMC **28** in which the ClO_4^- anion is strongly bound to atoms of the eight-membered ring⁸ and the size effect allows the anion to be inserted into the cavity. The possibility of insertion of the SO_4^{2-} , Cl^- and ClO_4^- anions has been studied from the standpoint of the size effect.^{148, 151}

However, it should be borne in mind that thermodynamics of their insertion into SMC are fundamentally different due to different thermodynamics of their formation in solutions. Thus the values $\Delta S_f^\circ(\text{SO}_4^{2-})_{\text{aq}} = -112.2$ and $\Delta S_f^\circ(\text{ClO}_4^-)_{\text{aq}} = +118.7 \text{ J mol}^{-1} \text{ K}^{-1}$ are close in magnitude but have opposite signs. The insertion of $(\text{SO}_4^{2-})_{\text{aq}}$ into SMC is entropically favourable but the enthalpy loss is high because $\Delta H_f^\circ(\text{SO}_4^{2-})_{\text{aq}} = -875.9 \text{ kJ mol}^{-1}$. The $(\text{ClO}_4^-)_{\text{aq}}$ anion has the maximum entropy of formation and the $(\text{SO}_4^{2-})_{\text{aq}}$ ion has the minimum enthalpy of formation. Hence, in order to surpass the enthalpy loss upon the insertion of SO_4^{2-} , it is necessary to select an appropriate SMC with very strong bonds between its atoms and the inserted SO_4^{2-} anion.

Apart from two-dimensional SMC, three-dimensional SMA with a tetrahedral,¹⁵² prismatic⁹¹ or cylindrical^{28,98} geometry have also been prepared. For example, SMA **29** was synthesised by the reaction of $[\text{Cu}(\text{MeCN})_4]\text{BF}_4$ with hexaphenylhexaazatriphenylene and quaterpyridine in chloroform.⁹⁸ The structure of this SMA was determined by X-ray diffraction analysis. By introduction of various fragments (acetylene, benzene and so on) into quaterpyridine, the height of SMA **29** can be increased to 33 Å.⁷⁸



29 (the phenyl groups are omitted for clarity)

As the conclusion of this Section, we would like to note that Pt^{4+} and Pd^{4+} compounds could also be used in the SMCh. However, this would require an absolutely different strategy of the preparation of SMA. The stereochemistry of these compounds, for example, R_3PtX ($\text{R} = \text{Me, Et; X} = \text{OH, Cl, I}$), shows¹⁴⁴ that the PtR_3^+ groups tend to acquire a pyramidal structure and Pt^{4+} tends to an octahedral geometry. This gives compounds with a cubane structure, which is based on a cube with vertices occupied by alternating Pt^{4+} and X^- ions. In these systems, the $R(\text{Pt}-\text{Pt})$ distances vary from 3.41 (Me_3PtOH) to 3.90 Å (Me_3PtI , Et_3PtCl), so that the contribution to the enthalpy stabilisation ranges from $D_0(\text{Pt}-\text{Pt}) = 4 \times 28.7 = 114.8$ to $D_0(\text{Pt}-\text{Pt}) = 4 \times 17.8 = 71.2 \text{ kJ mol}^{-1}$. As a result of competition between the tendency of PtR_3^+ to form a pyramidal coordination and the tendency of Pt^{4+} to an octahedral coordination, depending on the number and the coordination capacity of the anions and polar molecules, either oligomers or SMC are formed.

4. Thermodynamic factors in the formation of supramacrocycles

The role of thermodynamic factors in the formation of SMC has been considered in a number of studies.^{8,39,50,71,126,128} As noted above, several mechanisms have been proposed^{8,39,71} for the formation of supramolecular systems, which reflect to one or another extent the thermodynamics of self-assembly,

namely, these are thermodynamic, kinetically controlled and irreversible, assisted, directed mechanism, *etc.* According to the thermodynamic mechanism of the self-assembly in solution, a thermodynamic equilibrium between the starting reactants and one, thermodynamically the most stable product is attained. Thermodynamically unstable products either dissociate or are formed in minor amounts with respect to the major product. The self-assembly of the structural blocks to give SMC or a linear oligomer decreases the disorder in the system and, hence, results in a negative change in entropy, which can be counterbalanced by the enthalpy effect. In a review,⁸ it has been suggested that both the enthalpy and entropy changes are favourable for the self-assembly of SMC. It has been shown above, using numerous examples, that the metal-metal bonds present in SMC contribute considerably to the enthalpy of formation of SMC.

The thermodynamic parameters of the self-assembly process largely depend on the properties of the solvent.¹²⁴ It was found experimentally that the formation of Ln^{3+} and An^{3+} complexes in acetonitrile is characterised by the following relationship between the enthalpy and entropy contributions to the free energy:^{153–155}

$$\Delta S^\circ < 0, \Delta H^\circ < 0, |T\Delta S^\circ| < |\Delta H^\circ|.$$

However, in water, the formation of Ln^{3+} and An^{3+} complexes with various N- and O-donor ligands obeys other relations:^{125,156}

$$\Delta S^\circ > 0, \Delta H^\circ < 0, T\Delta S^\circ > |\Delta H^\circ|.$$

In water, the $3 \text{ Ln}^{3+} + 2 \text{ L}$ self-assembly to give triangular SMC **17** is entropy-driven, *i.e.*, similar to the formation of Ln^{3+} and An^{3+} complexes.¹⁵⁶ However, it is not clear whether this conclusion can be extended to the formation of SMC with other metals, a different geometry (for example, squares), and in other solvents.

The self-assembly processes often use chelating n -dentate ligands. In SMC **17**, the ligand is hexadentate ($n = 6$); two ligands form a common electronic system; therefore, for two chelating ligands, we get $n = 12$. Let us assume that the change in entropy upon self-assembly is due to the chelation effect. The entropy change caused by the chelation effect is determined¹⁵⁶ by the equation

$$\Delta S^\circ = R(n-1) \ln M = 367 \text{ J mol}^{-1} \text{ K}^{-1},$$

where R is the universal gas constant, M is the molality of water. The change ΔS° upon the formation of SMC **17** ranges¹²⁴ from 329 (La) to $442 \text{ J mol}^{-1} \text{ K}^{-1}$ (Lu). With allowance for the inaccuracy of ΔS° equal to $\pm 25 \text{ J mol}^{-1} \text{ K}^{-1}$, the average entropy of self-assembly for SMC **17** is $\Delta S^\circ = 408 \text{ J mol}^{-1} \text{ K}^{-1}$ (Ref. 124); this value is consistent with the estimate $\Delta S^\circ = 367 \pm 50 \text{ J mol}^{-1} \text{ K}^{-1}$ made using the chelation model.

The role of the solvent is highly important in both complexation and the self-assembly: the free energy of formation of SMC **17** ΔG_f° correlates with the free energy of formation of the aqua ions $3 \Delta G_f^\circ(\text{Ln}_{\text{aq}}^{3+})$; therefore, from the known $\Delta G_f^\circ(\text{Ln}_{\text{aq}}^{3+})$ and $\Delta G_f^\circ(\text{An}_{\text{aq}}^{3+})$ values and the measured $\Delta G_f^\circ(\text{17})$ values, one can estimate the standard free energy of formation of similar SMC with other metals and, hence, the changes in the free energy ΔG° for the corresponding self-assembly reactions:

Ln	Eu	Pu	Am	Cm
$\Delta G^\circ / \text{kJ mol}^{-1}$	104	83.6	93.3	90.0

An important problem in the processing of radioactive elements is the separation of Eu^{3+} , Am^{3+} and Cm^{3+} . The obtained values $\delta \Delta G^\circ(\text{Eu}-\text{Am}) = 10.7$ and $\delta \Delta G^\circ(\text{Eu}-\text{Cm}) = 14.0 \text{ kJ mol}^{-1}$ show that using SMC, one

can achieve high selectivity in the separation of Ln^{3+} and An^{3+} ions.

The properties of solvents (dielectric constant, polarisability, the ability to form hydrogen bonds, viscosity) determine the soft or hard behaviour of the solvent.^{44, 156} Using the set of these properties, it is possible to predict that the self-assembly involving hard Ln^{3+} cations in water is an entropy-driven process, that in acetonitrile or pyridine is enthalpy-driven, the process in octanol is rather enthalpy-driven, *etc.* In addition, it was shown¹²⁴ that ΔG° and the $\Delta S^\circ/\Delta H^\circ$ ratio for the self-assembly depend on the properties of cations. It is beyond doubt that the effects of solvents on the self-assembly thermodynamics should be different for compounds of soft M^+ ($\text{M} = \text{Cu}, \text{Ag}, \text{Au}, \text{Tl}, \text{Hg}$), M^{2+} ($\text{M} = \text{Pd}, \text{Pt}, \text{Cd}, \text{Hg}$) and hard (Ln^{3+} , An^{3+}) cations. Even among the same family (soft or hard cations), the $\Delta S^\circ/\Delta H^\circ$ ratio would substantially depend on the desolvation of this cation. Ten years ago the ΔG° values for self-assembly were still calculated using two-parameter models,¹⁵⁷ which define the electron-donor (C_D) and -acceptor (C_A) properties of the interacting Lewis acids and bases

$$\Delta G^\circ = \text{const } C_D C_A.$$

As new data have been accumulated, it became clear that these simplified models do not reflect either quantitative or qualitative features of thermodynamics of the SMA formation.

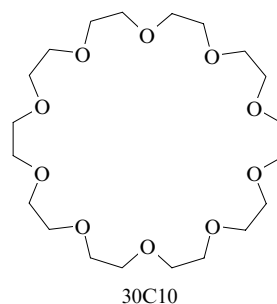
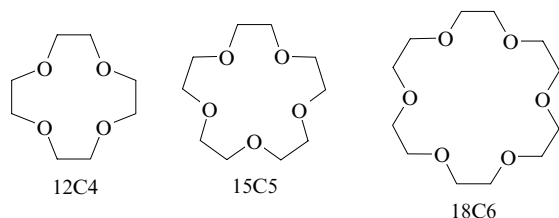
V. Thermodynamic properties of macrocyclic complexes in solution

Among the macrocyclic ligands, crown ethers, cryptands, spherands, calixarenes and their derivatives have been most studied.^{1, 2, 7, 128, 158–161} The advances in the synthesis of the alkali and alkaline earth metal complexes^{1, 2, 7, 159–162} have stimulated the development of analogous studies dealing with lanthanides.^{27, 128, 161, 162} The particular interest in this field is related to the extensive use of lanthanides in catalysis, in the manufacture of glass, ceramics, optical and electronic devices, in nuclear power engineering (separation processes), in biology and medicine.

As regards the stability of Ln complexes with crown ethers containing 4, 5, 6 and 10 oxygen atoms, it has been noted¹⁶² that the plots $\log \beta$ vs. $R_{\text{ion}}^{-1}(\text{Ln})$ do not show any general trend, some passing through an extremum and some other monotonically descending or ascending. This reflects the relationship between parameters such as the ion diameter and the size of the ligand cavity. Although the idea of size fitting has not lost its importance in analysis of the selectivity of complexation of macrocyclic ligands with alkali and alkaline earth metals, the experimental data indicate that other properties of cations such as desolvation parameters and the ability to accept electron density have a substantial influence on the thermodynamic properties of MC.

1. Size selectivity of macrocyclic ligands with respect to cations

It was found that the ratio of the cation to cavity dimensions ($R_{\text{ion}}/R_c = r$) is an important factor determining the selectivity of complexation with the crown ethers, 12-crown-4 (12C4), 15-crown-5 (15C5), 18-crown-6 (18C6), 21-crown-7 (21C7) and 30-crown-10 (30C10) in solution.



The stability constants $\log \beta_1$ of lanthanide(III) complexes with a number of crown ethers in propylene carbonate (PC) were measured and the $\log \beta_1$ values were statistically processed depending on r :¹⁶²

Crown ether	21C7	18C6	15C5	12C4
$\log \beta_1(\text{La} - \text{Lu})$	5.0–7.5	7.0–9.0	6.0–7.5	5.0–5.5
r	0.6–0.75	0.75–0.95	1.20–1.40	1.70–2.0

The $\log \beta_1$ values are maximum for the complexes with 18C6. For $r \ll 1$ or $r \gg 1$, the stability of the complexes decreases. For the complexes of light lanthanides with 18C6, $r \approx 1$, which accounted for their higher stability compared to heavy lanthanide complexes. The decrease in $\log \beta_1$ of the complexes with this crown ether in methanol¹⁶⁰ following an increase in $Z(\text{Ln})$ from La to Eu could also be attributed to the better fit between R_{ion} and R_c . It may seem that the trends in variation of $\log \beta_1$ upon complexation of alkali metals with crown ethers can also be interpreted in this way; however, on going from Na^+ to Cs^+ the ionic radius increases 1.6-fold and on going from La^{3+} to Lu^{3+} , only 1.2-fold. This implies the need for essential preorganisation of macrocyclic ligands for the reaction with M^+ : in the complexes with 18C6, the K^+ cation fits in the plane of the ligand molecule with D_{3d} symmetry, while the large Cs^+ ion deviates from this plane. However, the Na^+ ion is too small for the large ring; therefore, its symmetry is highly distorted compared to D_{3d} .

The enthalpy of desolvation (ΔH_h) and electronegativity of cations play an important role in the complexation. Compare two ion pairs, $\text{Sr}^{2+}/\text{Pb}^{2+}$ and Rb^+/Tl^+ , having similar ΔH_h , R_{ion} and similar enthalpies of complexation with 18C6 [$\Delta H(18\text{C6})$]:

Sr^{2+} and Pb^{2+} :

$$\Delta H_h = -1521 \text{ and } -1556 \text{ kJ mol}^{-1};$$

$$R_{\text{ion}} = 1.18 \text{ and } 1.19 \text{ \AA},$$

$$\Delta H(18\text{C6}) = -15.1 \text{ and } -21.8 \text{ kJ mol}^{-1};$$

Rb^+ and Tl^+ :

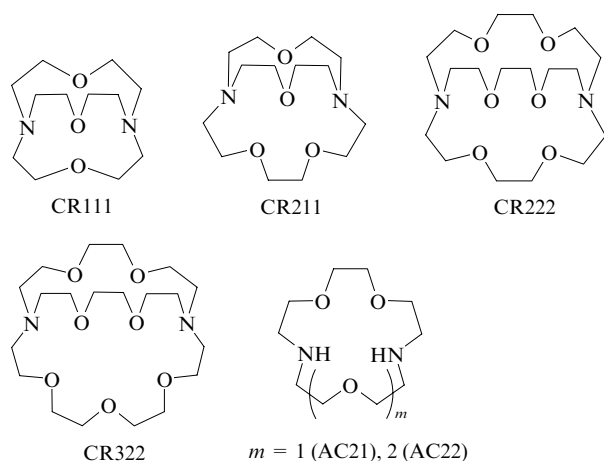
$$\Delta H_h = -339 \text{ and } -364 \text{ kJ mol}^{-1};$$

$$R_{\text{ion}} = 1.52 \text{ and } 1.50 \text{ \AA},$$

$$\Delta H(18\text{C6}) = -15.9 \text{ and } -18.4 \text{ kJ mol}^{-1}.$$

The negative $\Delta H(18\text{C6})$ values larger in magnitude found for Pb^{2+} and Tl^+ were attributed¹⁵⁶ to higher electronegativity of Pb (1.8) and Tl (1.8) compared to Sr (1.0) and Rb (0.8); apparently, the 5d-AO of lead and thallium participate in the formation of bonds with macrocyclic ligand atoms, resulting in more exothermic complexation.

In the case of cryptands, the size fitting principle is believed¹⁵⁶ to be more significant than for crown ethers or tetraazamacrocycles, which is reflected in the stability constants $\log K_{211}$, $\log K_{222}$, $\log K_{322}$.



The highest stability is attained for smaller cations, which fit in small cavities:

$$\text{Li}^+: R_{\text{ion}} = 0.675 \text{ \AA},$$

$$\log K_{211} > \log K_{221};$$

$$\text{Na}^+: R_{\text{ion}} = 1.0 \text{ \AA},$$

$$\log K_{211} < \log K_{221} > \log K_{222} < \log K_{322};$$

$$\text{K}^+: R_{\text{ion}} = 1.376 \text{ \AA},$$

$$\log K_{221} < \log K_{222} > \log K_{322};$$

$$\text{Ca}^{2+}: R_{\text{ion}} = 0.72 \text{ \AA},$$

$$\log K_{211} < \log K_{221} > \log K_{222} < \log K_{322};$$

$$\text{Ba}^{2+}: R_{\text{ion}} = 1.389 \text{ \AA},$$

$$\log K_{221} < \log K_{222} > \log K_{322} < \log K_{332}.$$

The reason is in the greater hardness of cryptands CR111–CR322 and higher preorganisation compared to crown ethers.

2. Effect of the charge transfer energy from the ligand to the cation on the stability of macrocyclic complexes

Presumably, the interaction of macrocyclic ligands (cryptands and azacrown ethers, AC) with Ln^{3+} ions occurs through electron density transfer from the O and N atoms of the ligand to the cations. The higher the electron-acceptor capacity of the cation and the lower the electron transfer energy from the occupied MO of the ligands to vacant or partially occupied 4f-AO of the cation, the more stable the complex. If this hypothesis is valid, the charge transfer energy $\Delta E[2p(\text{O}) \rightarrow 4f(\text{Ln}^{3+})]$ and $\Delta E[2p(\text{N}) \rightarrow 4f(\text{Ln}^{3+})]$ should correlate with $\log \beta[\text{Ln}(\text{CR221})]^{3+}$ and $\log \beta[\text{Ln}(\text{AC21})]^{3+}$. The $\Delta E[2p(\text{O}) \rightarrow 4f(\text{Ln}^{3+})]$ have been measured for many complexes and systematised,^{29,35} whereas no data on $\Delta E[2p(\text{N}) \rightarrow 4f(\text{Ln}^{3+})]$ are available. Figure 2 compares the trends of variation of $\Delta E[2p(\text{O}) \rightarrow 4f(\text{Ln}^{3+})]$ (Ref. 35) and $\log \beta[\text{Ln}(\text{CR221})]^{3+}$ or $\log \beta[\text{Ln}(\text{AC21})]^{3+}$ (Ref. 161). It can be seen that in the first half of the series, on going from Pr to Eu, the stability of complexes $[\text{Ln}(\text{CR221})]^{3+}$ increases in line with a decrease in $\Delta E[2p(\text{O}) \rightarrow 4f(\text{Ln}^{3+})]$, i.e., with an increase in the electron-acceptor ability of the cation. The extreme points of $\log \beta[\text{Eu}(\text{CR221})]^{3+}$ and $\log \beta[\text{Eu}(\text{AC21})]^{3+}$ correspond to the minimum of $\Delta E[2p(\text{O}) \rightarrow 4f(\text{Eu}^{3+})]$. The antiparallel variation of $\log \beta[\text{Ln}(\text{CR221})]^{3+}$ and $\Delta E[2p(\text{O}) \rightarrow 4f(\text{Eu}^{3+})]$ in the second half of the lanthanide series from Gd to Yb is beyond doubt. The $\log \beta[\text{Lu}(\text{CR221})]^{3+}$ has not been measured: in the model considered, one can expect that $\log \beta[\text{Lu}(\text{CR221})]^{3+} < \log \beta[\text{Yb}(\text{CR221})]^{3+}$. As a conclusion of this Section, note

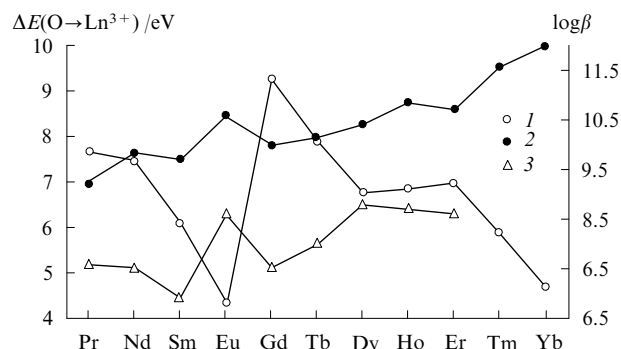


Figure 2. Energies of charge transfer from the oxygen atoms to the Ln^{3+} 4f-AO in the Ln^{3+} complexes (1), stability constants of the complexes with cryptand CR221 (2) and azacrown ether AC21 (3) in MeOH.

that the charge transfer energy in the MC of transition d elements has not been studied experimentally, although this could provide direct information on the electron density transfer from the ligands to the cations inserted in the cavity.

3. Effect of desolvation of cations on the stability of macrocyclic complexes

The stability of lanthanide cryptates depends on the solvent and increases in the sequence¹⁶¹ $\text{DMF} < \text{DMSO} < \text{H}_2\text{O} < \text{MeOH} < \text{MeCN} \ll \text{PC}$. In highly solvating solvents (DMF, DMSO, H_2O , MeOH), the lower the expenditure for desolvation, the higher the stability of complexes ($\log \beta$) (or the greater the magnitude of the negative ΔG° upon complexation). The free desolvation energy is determined by the free energy of formation of solvated ions; in the aqueous solution, the $-\Delta G_f^\circ(\text{Ln}_{\text{aq}}^{3+})$ values vary in the range from 576 (Eu) to 688 kJ mol^{-1} (La).^{125, 153–155}

Ln	$-\Delta G_f^\circ(\text{Ln}_{\text{aq}}^{3+}) / \text{kJ mol}^{-1}$	Ln	$-\Delta G_f^\circ(\text{Ln}_{\text{aq}}^{3+}) / \text{kJ mol}^{-1}$
La	688	Tb	668
Ce	676	Dy	664
Pr	681	Ho	675
Nd	672	Er	673
Sm	677	Tm	671
Eu	576	Yb	639
Gd	660	Lu	677

It was noted¹⁶¹ that the dependences of $\log \beta[\text{Ln}(\text{CR221})]^{3+}$ and $\log \beta[\text{Ln}(\text{AC21})]^{3+}$ on $Z(\text{Ln})$ are essentially non-monotonic. It should be emphasised that in the first half of the series, the extremal point is found for Eu in both cases. Evidently, neither the size of the cavity nor the ionic radius, which is a monotonic function $Z(\text{Ln})$, can be responsible for the non-monotonic variation of the stability of the complexes and the presence of extremal points for Eu. Probably, the variation of $\log \beta[\text{Ln}(\text{CR221})]^{3+}$ and $\log \beta[\text{Ln}(\text{AC21})]^{3+}$ is determined by the desolvation parameters of the cations. Since there are no experimental data on the free energy of formation of Ln^{3+} in MeOH, we use the reported¹²⁵ experimental values of $\Delta G_f^\circ(\text{Ln}_{\text{aq}}^{3+})$. A comparison of $|\Delta G_f^\circ(\text{Ln}_{\text{aq}}^{3+})|$ for Sm, Eu and Gd shows that the extremal points in the $\log \beta[\text{Ln}(\text{CR221})]^{3+}$ and $\log \beta[\text{Ln}(\text{AC21})]^{3+}$ plots corresponding to an increase in the stability of Eu complexes with respect to Sm and Gd complexes are related to the desolvation of cations. The antiparallel variations of $|\Delta G_f^\circ(\text{Ln}_{\text{aq}}^{3+})|$ and $\log \beta[\text{Ln}(\text{CR221})]^{3+}$ or $\log \beta[\text{Ln}(\text{AC21})]^{3+}$ can be clearly seen (see Fig. 2).

If the correlation between $\log \beta[\text{Ln}(\text{CR221})]^{3+}$ and $|\Delta G_f^\circ(\text{Ln}_{\text{aq}}^{3+})|$ is applied only to two elements, La and Yb, one

can determine $\log \beta[\text{Ln}(\text{CR221})]^{3+}$ for $\text{Ln} = \text{Ce}, \text{Pr}, \text{Nd}, \text{Sm}, \text{Gd}, \text{Tb}, \text{Dy}$. The difference between these estimates and the experimental values equal to ± 0.4 for $\log \beta$ (or $\sim 2.4 \text{ kJ mol}^{-1}$ for ΔG°) signifies not only a qualitative but also a quantitative relationship between the MC stability and the desolvation energy of the cations inserted in the cavity. However, the $|\Delta G_f^\circ(\text{Ln}_{\text{aq}}^{3+})|$ values for $\text{Ln} = \text{Ho}$ (675), Er (673) and Tm (671) differ by only 2 kJ mol^{-1} (Ref. 125). This is apparently lower than the experimental error in the determination of $\log \beta$; for these three elements, the variations of $\log \beta$ can be determined by other factors.

4. Effect of the solvent on the stabilisation of the unusual oxidation states of lanthanides and actinides

The charge transfer energies $\Delta E[2p(\text{O}) \rightarrow 4f(\text{Ln}^{3+})]$ can serve as a quantitative characteristics of the redox potentials $E^\circ(3+/2+)$.^{153–155} The lowest $\Delta E[2p(\text{O}) \rightarrow 4f(\text{Ln}^{3+})]$ values for europium, samarium and ytterbium correspond to their most stable, divalent states in the series of lanthanides. The divalent state of europium, samarium and ytterbium can be stabilised upon complexation with cryptands or even coronands¹⁶¹ in H_2O , MeOH and DMF . In these solvents, the cryptates and coronates of trivalent lanthanides are reduced at higher potentials than free (solvated) cations, which attests to stabilisation of the lanthanide(II) complexes. In MeCN or PC , no systematic stabilisation of the divalent state is observed.

Therefore, it may be promising to use cryptands and coronands for the separation of $\text{Ln}^{2+}/\text{Ln}^{3+}$ and $\text{An}^{2+}/\text{An}^{3+}$ pairs by extraction based on the difference between the redox potentials $E^\circ(3+/2+)$. It has been noted above that the separation of Eu^{3+} , Am^{3+} and Cm^{3+} , which are deservedly called the ‘Bermuda Triangle’ in the extraction chemistry is a challenge. The problem is that complexes of these cations in solutions have very similar thermodynamic characteristics due to the small difference between the free energies of formation of solvated cations ΔG_f° , in particular, in aqueous solutions, $\Delta G_f^\circ = -576$ (Eu^{3+}), -603 (Am^{3+}) and -594 kJ mol^{-1} (Cm^{3+}).¹²⁵ Upon complex formation with cryptands and coronands in aqueous solutions, Am^{3+} and Cm^{3+} are not reduced, unlike Eu^{3+} . However, the heavy actinide ions (Cf^{3+} , Es^{3+} , Fm^{3+} like Sm^{3+} , and Md^{3+} like Eu^{3+}) should be reduced to the divalent state. The good prospects of using cryptands and coronands for the separation of these elements are due to the use of readily available solvents and environmentally safe extractants, which do not give rise to the third phase, unlike the classical phosphorus-containing extractants.

5. Complexation with preorganised ligands

The thermodynamic characteristics, *i.e.*, the free energy and enthalpy changes upon the formation of $[\text{Ln}(\text{CR221})]^{3+}$ complexes in MeCN and PC , were measured¹⁶¹ for $\text{Ln} = \text{La}, \text{Pr}, \text{Nd}, \text{Er}$ and for $\text{Ln} = \text{La}, \text{Pr}, \text{Nd}$, respectively. The ligand is hard and highly preorganised and both solvents are non-solvating. Presumably, the $\Delta G^\circ[\text{Ln}(\text{CR221})]^{3+}$, $\Delta H^\circ[\text{Ln}(\text{CR221})]^{3+}$ and $\Delta S^\circ[\text{Ln}(\text{CR221})]^{3+}$ values are controlled by the size effect. The experimental values of ΔG° and ΔH° for seven lanthanides depend linearly on the ionic radii of the cations (C.N. 9) with a correlation factor of 0.99. This allows one to estimate $\Delta G^\circ[\text{Ln}(\text{CR221})]^{3+}$, $\Delta H^\circ[\text{Ln}(\text{CR221})]^{3+}$ and $T\Delta S^\circ[\text{Ln}(\text{CR221})]^{3+}$ for $\text{Ce}, \text{Sm}, \text{Eu}, \text{Gd}, \text{Tb}, \text{Tm}, \text{Yb}, \text{Lu}$ in MeCN and PC . Thus, in the case of MC $[\text{Ln}(\text{CR221})]^{3+}$ we have at hand the $\Delta G^\circ[\text{Ln}(\text{CR221})]^{3+}$ values for all lanthanides in MeOH , MeCN and PC and the $\Delta H^\circ[\text{Ln}(\text{CR221})]^{3+}$ and $T\Delta S^\circ[\text{Ln}(\text{CR221})]^{3+}$ values in MeCN and PC .

In the complexation of Ln^{3+} with O- and N-donor ligands in MeCN , both the entropy and enthalpy changes are negative;^{128, 156} therefore, it is not unexpected that $\Delta S^\circ[\text{Ln}(\text{CR221})]^{3+} < 0$ and $\Delta H^\circ[\text{Ln}(\text{CR221})]^{3+} < 0$ in the

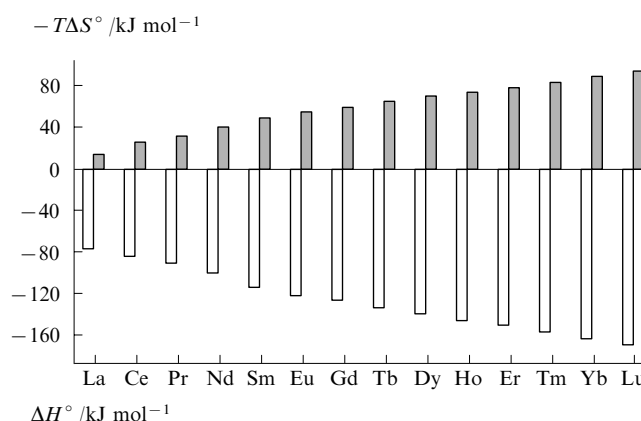


Figure 3. Enthalpy and entropy changes upon the formation of cryptates $[\text{Ln}(\text{CR221})]^{3+}$ in MeCN .

case of formation of $[\text{Ln}(\text{CR221})]^{3+}$ in MeCN (Fig. 3). However, it is difficult to explain why ΔS° for complexation in PC changes the sign: for light lanthanides, $\Delta S^\circ > 0$ ($\text{La} - \text{Nd}$), in the middle of the series, $\Delta S^\circ \approx 0$ (Eu, Gd) and in the second half of the series, $\Delta S^\circ < 0$ ($\text{Tb} - \text{Lu}$). The change in the entropy sign is rarely encountered in the chemistry of complex compounds; it is attributed to a change in the composition of complexes or the conformation of the ligands.¹⁵⁶ As regards the complexation of Ln^{3+} with CR221 in other solvents (H_2O or MeOH), the $\Delta S^\circ[\text{Ln}(\text{CR221})]^{3+}$ values may be expected to be positive and the entropy contribution to the change in the free energy of complexation would predominate over the enthalpy contribution.

6. Macrocyclic effect

When studying MC, it is general practice to estimate the macrocyclic effect by comparing the thermodynamic properties of the MC and its acyclic analogue; however, such an analogue cannot be easily selected.¹⁵⁶ We chose the lanthanide complexes with highly preorganised macrocyclic ligand CR221 synthesised in MeCN and MeOH and with a non-preorganised edta ligand in H_2O . Each ligand has six coordinating atoms ($2\text{N} + 4\text{O}$). The presence of the same donor atoms results in some linear relationships for the free energy of complexation $\Delta G_{\text{CR221}}^\circ(\text{MeCN})$, $\Delta G_{\text{CR221}}^\circ(\text{MeOH})$ ¹⁰¹ and $\Delta G_{\text{edta}}^\circ(\text{H}_2\text{O})$ ¹⁵⁶ (all values are expressed in kJ mol^{-1}):

$$\Delta G_{\text{edta}}^\circ(\text{H}_2\text{O}) = \Delta G_{\text{CR221}}^\circ(\text{MeCN}) - 23.5, \quad (1)$$

$$\Delta G_{\text{edta}}^\circ(\text{H}_2\text{O}) = 0.985 \Delta G_{\text{CR221}}^\circ(\text{MeOH}) - 36.5. \quad (2)$$

However, the trends in the variation of $\Delta H_{\text{CR221}}^\circ(\text{MeCN})$ and $\Delta H_{\text{edta}}^\circ(\text{H}_2\text{O})$ as well as $T\Delta S_{\text{CR221}}^\circ(\text{MeCN})$ and $T\Delta S_{\text{edta}}^\circ(\text{H}_2\text{O})$ are different. The change in the C.N. in lanthanide complexes with edta (C.N. is 10 for $\text{La} - \text{Nd}$, 9.5 for Sm and Gd , 9 for $\text{Tb} - \text{Lu}$)¹⁰² is responsible for the non-monotonic variation of the entropy along the series and, as a consequence, a non-monotonic variation of the enthalpy (Fig. 4). Both $\Delta H_{\text{CR221}}^\circ(\text{MeCN})$ and $T\Delta S_{\text{CR221}}^\circ(\text{MeCN})$ vary monotonically along the lanthanide series. This is a consequence of high preorganisation of the ligand and the effect of the non-solvating solvent. As long as experimental $\Delta H_{\text{CR221}}^\circ(\text{MeOH})$ and $\Delta H_{\text{CR221}}^\circ(\text{H}_2\text{O})$ values are missing, it is difficult to draw conclusions about the nature (either enthalpy or entropy) of the macrocyclic effect. It is clear that the degree of ligand preorganisation depends on the solvent. At a qualitative level, it can be noted that if a thermodynamic effect of ligand preorganisation in solvating solvents is pronounced, this can

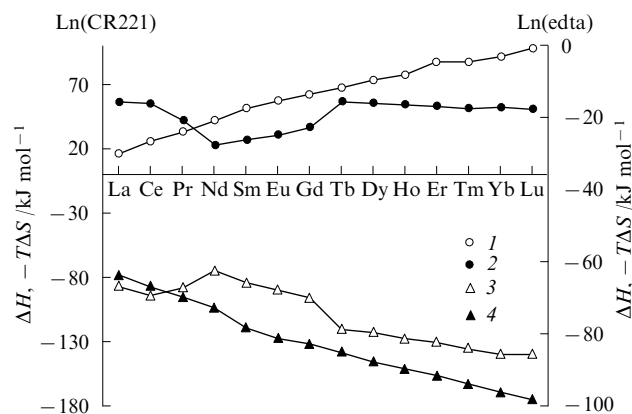


Figure 4. Changes in entropy (1, 3) and enthalpy (2, 4) upon the formation of complexes Ln(edta) in H₂O (2, 3) and Ln(CR221) in MeCN (1, 4).

mask the non-monotonic entropy and enthalpy changes along the lanthanide series.

For predicting the macrocyclic effect, it is important that in Eqns (1) and (2), the coefficient at $\Delta G_{\text{CR221}}^\circ$ is ~ 1 . Hence, the macrocyclic effect along the lanthanide series can be estimated using known ΔG° for the appropriate ligands with the same number and nature of the donor atoms as in the macrocycle, for example, nitrilotriacetate (1 N + 3 O), ethylenediaminetetraacetate (2 N + 4 O), ethylenetriaminepentaacetate (3 N + 5 O), etc.

7. Calixarenes and crown ethers

a. Interaction of calixarenes with lanthanide aqua ions

Water-soluble calixarenes are considered as promising ligands for the synthesis of MC.¹⁶³ *p*-Sulfocalix[4]arenes (*p*-SC[4]A) form SMA with a variety of guest molecules in both solution and the solid state. Two-dimensional hydrogen-bonded SMP with $\text{Ln}_{\text{aq}}^{3+} \cdot [\text{Ln}(\text{H}_2\text{O})_8]^{3+}[\text{p-SC[4]A}]$ (Ln = Gd, Tb, Tm) have been synthesised. In the two-dimensional SMP, each aqua ion is connected by hydrogen bonds to four neighbouring sulfonate groups of *p*-SC[4]A, thus forming an infinite structure. For example, in the Tb complex, each $[\text{Tb}(\text{H}_2\text{O})_8]^{3+}$ ion forms eight hydrogen bonds with the distances $R(\text{O} \cdots \text{H} \cdots \text{O}) = 2.741 \text{ \AA}$ and the energy $\Sigma D_0(\text{O} \cdots \text{H} \cdots \text{O}) = 8 \times 12.98 = 103.8 \text{ kJ mol}^{-1}$.

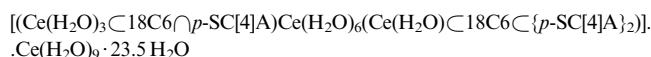
The enthalpy and entropy changes upon the formation of $\text{O} \cdots \text{H} \cdots \text{O}$ bonds have been reported^{43,60} to be approximately equal, i.e., $\Delta H^\circ/T\Delta S^\circ \approx 1.0$. In view of the reported $\Sigma D_0(\text{O} \cdots \text{H} \cdots \text{O})$, the change ΔS° upon the formation of hydrogen bonds of each aqua ion with four sulfonate groups equals $\Delta S^\circ(\text{O} \cdots \text{H} \cdots \text{O}) = 174 \pm 40 \text{ J mol}^{-1} \text{ K}^{-1}$. The standard entropy of formation of the aqua ions is negative:¹¹¹ $\Delta S_f^\circ(\text{Ln}_{\text{aq}}^{3+}) = -219, -224$ and $-236 \text{ J mol}^{-1} \text{ K}^{-1}$ for Ln = Gd, Tb and Tm, respectively;¹²⁵ hence, upon binding of $\text{Ln}_{\text{aq}}^{3+}$ with *p*-SC[4]A, $\Delta S_f^\circ(\text{Ln}_{\text{aq}}^{3+})$ is largely counterbalanced by $\Delta S^\circ(\text{O} \cdots \text{H} \cdots \text{O})$.

A fundamental issue is the relationship between the coordination and hydrogen bond energies in the $[\text{Ln}_{\text{aq}}^{3+} \cdots \text{calixarene}]$ SMA and their variation along the lanthanide series. Structural data for solving this problem appeared only recently:¹⁶⁴ for the $[\text{LnL}(\text{NO}_3)_2(\text{H}_2\text{O})_2]\text{NO}_3$ complexes [Ln = Eu, Gd, Tb, Dy, Ho, Er, Tm, Yb, Lu; L is 2,6-bis(2-pyridyl)-4-amino-1,3,5-triazine], the lengths of the coordination bonds $R(\text{Ln} \cdots \text{O})$ and the hydrogen bonds $R(\text{O} \cdots \text{H} \cdots \text{O})$ were measured. Using about 200 measured¹⁶⁴ $R(\text{Ln} \cdots \text{O})$ and $R(\text{O} \cdots \text{H} \cdots \text{O})$ values, it was established^{30,31} that the greater $R(\text{Ln} \cdots \text{O})$, the smaller $R(\text{O} \cdots \text{H} \cdots \text{O})$. Thus, the interaction of $\text{Ln}_{\text{aq}}^{3+}$ with *p*-SC[4]A is

accompanied by a decrease in $R(\text{Ln} \cdots \text{O})$ and an increase in $R(\text{O} \cdots \text{H} \cdots \text{O})$ on passing from light lanthanides to heavy ones. The energy of intermolecular hydrogen bonds $\text{Ln}_{\text{aq}}^{3+} \cdots \text{calixarene}$ decreases to the end of the series, whereas the energy of the coordination bonds increases.

b. Crown ethers and cryptands as guest molecules in calixarenes: encapsulation according to the 'matreshka doll' pattern

On the basis of a structural conformation analysis, structural reorganisation of crown ethers taking place upon the reaction of 18C6 with *p*-SC[4]A and $\text{Ln}_{\text{aq}}^{3+}$ was studied. The SMA of a complicated structure formed in the case of Ce can be represented¹⁶³ by the following formula (the sign \subset designates inclusion and the sign \cap attests to the arrangement of the crown ether molecule above the calixarene bowl):



The partially hydrated Ce(1) ion is incorporated in the 18C6 ring forming six $\text{Ce} \cdots \text{O}(18\text{C}6)$ bonds, three $\text{Ce} \cdots \text{O}(\text{H}_2\text{O})$ bonds and one $\text{Ce} \cdots \text{O}(\text{p-SC[4]A})$ bond. The Ce(2) ion is also incorporated into the 18C6 ring; remarkably, $[\text{Ce}(2) + 18\text{C}6]$ are encapsulated by two *p*-SC[4]A ligands. Atwood¹⁶³ has called such encapsulation the 'matreshka doll'. One 18C6 molecule serves as the host for the Ce(1) guest ion but $[\text{Ce}(2) + \text{other } 18\text{C}6]$ serve themselves as a guest for two *p*-SC[4]A molecules. The Ce(3) ion is bound to two sulfonate groups from two *p*-SC[4]A ligands, whereas the Ce(4) ion is completely hydrated, forms no coordination bonds with macrocyclic ligands and is involved only in the formation of hydrogen bonds. The energy spectrum of this SMA is fairly complicated (Fig. 5): the $\text{Ce}(1) \cdots \text{O}(18\text{C}6)$ bonds are weaker than $\text{Ce}(1) \cdots \text{O}(\text{H}_2\text{O})$; the encapsulation of $[\text{Ce}(2) + 18\text{C}6]$ in two *p*-SC[4]A strengthens all bonds in the inner 'doll', which is compressed by the outer one. The modification of all bonds is rather significant; for example, the hydrated $\text{Ce}(4)(\text{H}_2\text{O})_9^{3+}$ ion in SMA is distorted due to the formation of hydrogen bonds to such an extent that $R(\text{Ce} \cdots \text{OH}_2)$ varies from 2.352 to 2.674 Å. This cation does not resemble the hydrated cation with a nearly regular tricapped trigonal prismatic coordination considered in the traditional lanthanide chemistry.

As a conclusion of this Section, note that the chemistry of host–guest systems based on calixarenes, crown ethers and

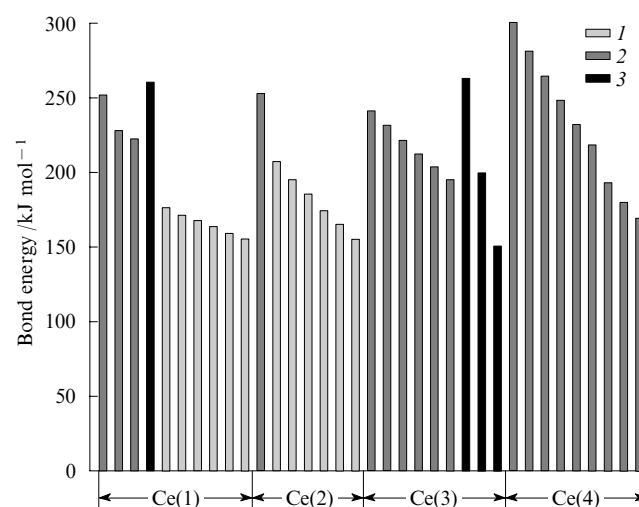


Figure 5. Energies of the $\text{Ce}^{3+} \cdots \text{O}$ bonds with crown ether (1), water (2) and *p*-sulfonatocalix[4]arene (3).

cryptands represents a new field of SMC; which is most amazing, this is a new type of 'matreshka doll' encapsulation.

VI. Conclusion

The synthesis and structure of supramolecular assemblies containing ions of d and f transition elements is a relatively new and rapidly developing field of SMC. These SMA attract particular attention of researchers owing to a set of unique properties, which may enable their extensive practical use in the future.

The synthesis of quasi-one-dimensional polymeric structures, which had been previously considered to be only theoretical models, was an achievement in the supramolecular chemistry. A number of such SMP in which separate dinuclear metal-containing blocks are linked by coordination or hydrogen bonds have now been prepared. A necessary (but not sufficient) condition for the formation of SMP is the absence of axial ligands in the initial complex. The formation of SMP or discrete aggregates (for example, dimers) is determined by the electronic structure of the metal and the ligands. Depending on the geometry of the binding ligands, one can obtain SMP in various conformations (linear, zigzag and so on).

Supramolecular rings are apparently the most numerous class of SMA. The variation of metal-containing fragments and ditopic ligands connecting them gives SMC of various sizes and geometries. Currently, systematic approaches to their synthesis have been developed, which allows targeted design of the structure with a definite parameters.

Several mechanisms of the self-assembly of the structural blocks in SMC are known. Of these, thermodynamic mechanism is studied in most detail and used most often; according to this mechanism, equilibrium between the reactants and products is established in each step and, finally, the thermodynamically most stable product is formed. In the SMC synthesis, Pd^{2+} and Pt^{2+} complexes are used most widely; however, many SMC with other metals are also known (Cr, Mo, Cu, Au, etc.).

The stability of SMC depends on a number of factors among which the metal-metal interaction is the most important. In some cases, a contribution of π - π -stacking is probable. The self-assembly process depends considerably on the solvent properties.

A distinctive feature of SMC is that their structure is retained in solutions. As a result, the ring may function as the host molecule for small ions or molecules exhibiting high selectivity. This feature is of particular interest for researchers, the more so, because the SMC can be varied by selecting appropriate ligands.

Three- and four-membered SMC are best studied; however, examples of five-, six- and eight-membered and even larger rings are also known.

The advances in the synthesis and practical use of alkali and alkaline earth metal macrocyclic complexes stimulated the development of analogous research for lanthanides and actinides. Crown and azacrown ethers, cryptands, calixarenes and so on are used as macrocyclic ligands. Of particular interest is the study of the variation of MC stability along the lanthanide and actinide series. The elucidation of these trends with allowance for the electronic characteristics of metal ions and the solvent effect would open up the way to the development of an efficient method for the separation of poorly separable Ln^{3+} and An^{3+} ions. The differences between the reduction potentials $E^\circ(3+/2+)$, which correlate with the charge transfer energy $\Delta E[2p(\text{O}) \rightarrow 4f(\text{Ln}^{3+})]$ can be used for the same purpose.

Thus, a large body of experimental data on the synthesis of diverse SMA has now been accumulated. In the next stage, it is necessary to carry out in-depth studies of the mechanisms of

their formation based on the methods and concepts of chemical thermodynamics, kinetics, and theoretical and quantum chemistry.^{22, 165}

References

1. J-M Lehn, A Rigault, J Siegel, J Harrowfield, B Chevrier, D Moras *Proc. Natl. Acad. Sci. USA* **84** 2565 (1987)
2. J-M Lehn *Supramolecular Chemistry: Concepts and Perspective* (New York: VCH, 1995)
3. P Tecilla, R P Dixon, G Slobodkin, D S Alavi, D H Waldeck, A D Hamilton *J. Am. Chem. Soc.* **112** 9408 (1990)
4. G M Whitesides, J P Mathias, C T Seto *Science* **254** 1312 (1991)
5. D C Sherrington, K A Taskinen *Chem. Soc. Rev.* **30** 83 (2001)
6. O Mamula, A von Zelewsky *Coord. Chem. Rev.* **242** 87 (2003)
7. A Yu Tsivadze *Usp. Khim.* **73** 6 (2004) [*Russ. Chem. Rev.* **73** 5 (2004)]
8. S Leininger, B Olenyuk, P J Stang *Chem. Rev.* **100** 853 (2000)
9. M Fujita *Chem. Soc. Rev.* **27** 417 (1998)
10. G R Newkome, E He, C N Moorefield *Chem. Rev.* **99** 1689 (1999)
11. A W Bosman, H M Janssen, E W Meijer *Chem. Rev.* **99** 1665 (1999)
12. T Jørgensen, T K Hansen, J Becher *Chem. Soc. Rev.* **23** 41 (1994)
13. M-J Blanco, M C Jiménez, J-C Chambron, V Heitz, M Linke, J-P Sauvage *Chem. Soc. Rev.* **28** 293 (1999)
14. C J Jones *Chem. Soc. Rev.* **27** 289 (1998)
15. A Yu Tsivadze *Zh. Neorg. Khim.* **48** 81 (2003)^a
16. M Irie *Chem. Rev.* **100** 1685 (2000)
17. F Barigelletti, L Flamigni *Chem. Soc. Rev.* **29** 1 (2000)
18. J Rebek Jr *Chem. Soc. Rev.* **25** 255 (1996)
19. R J M Nolte *Chem. Soc. Rev.* **23** 11 (1994)
20. F Diederich, M Gómez-López *Chem. Soc. Rev.* **28** 263 (1999)
21. C A Bigozzi, R Argazzi, C J Kleverlaan *Chem. Soc. Rev.* **29** 87 (2000)
22. A Yu Tsivadze, G V Ionova, V K Mikhalko, Yu N Kostrubov, in *Tezisy Mezhdunarodnoi Konferentsii 'Fiziko-khimicheskie Osnovy Noveishikh Tekhnologii XXI Veka'*, Moskva, 2005 (Proceedings of International Conference 'Physicochemical Foundations of Newest Technologies of the XXIst Century, Moscow, 2005) p. 23
23. C N Ramachandra, G U Kulkarni, P J Thomas, P P Edwards *Chem. Soc. Rev.* **29** 27 (2000)
24. S Matile *Chem. Soc. Rev.* **30** 158 (2001)
25. J-P Sauvage (Ed.) *Comprehensive Supramolecular Chemistry* Vol. 9 (Oxford: Pergamon Press, 1996)
26. R G Pearson (Ed.) *Hard and Soft Acids and Bases* (Stroudsburg, PA: Dowden Hutchinson and Ross, 1973)
27. J-C G Bünzli, C Piquet *Chem. Rev.* **102** 1897 (2002)
28. J L Sessler, A E Vivian, D Seidel *Coord. Chem. Rev.* **216**–**217** 411 (2001)
29. G Ionova, J C Krupa, I Gerard, R Guillaumont *New J. Chem.* **19** 677 (1995)
30. G Ionova, S Ionov, C Rabbe, C Hill, C Madic, R Guillaumont, G Modolo, J C Krupa *New J. Chem.* **25** 491 (2001)
31. G Ionova, D Guillaumont, R Guillaumont, S Ionov, C Madic, in *International Conference 'Sciences for the Future Nuclear Fuel Cycles'*, Atlanta, 2004 p. 87
32. G Ionova, R Guillaumont, S Ionov, C Madic, M J Hudson *J. Alloys Compd.* **275**–**277** 785 (1998)
33. S P Ionov, N T Kuznetsov *Zh. Neorg. Khim.* **48** 97 (2003)^a
34. S P Ionov, N T Kuznetsov *Ros. Khim. Zh.* **44** (4) 5 (2000)^b
35. G V Ionova *Usp. Khim.* **71** 461 (2002) [*Russ. Chem. Rev.* **71** 401 (2002)]
36. G V Ionova, V K Mikhalko, G A Gerasimova, Yu N Kostrubov, N I Suraeva *Koord. Khim.* **30** 377 (2004)^c
37. G Ionova, S Ionov, C Rabbe, C Hill, C Madic, R Guillaumont, J-C Krupa *Solv. Extraction Ion Exchange* **19** 391 (2001)
38. G Ionova, C Rabbe, R Guillaumont, S Ionov, C Madic, J-C Krupa, D Guillauneux *New J. Chem.* **26** 234 (2002)
39. G F Swiegers, T J Malefeste *Chem. Rev.* **100** 3483 (2000)
40. P F H Schwab, M D Levin, J Michl *Chem. Rev.* **99** 1863 (1999)

41. C B Aakeröy, K R Seddon *Chem. Soc. Rev.* **22** 397 (1993)
42. L M Greig, D Philp *Chem. Soc. Rev.* **30** 287 (2001)
43. P Schuster, G Zundel, C Sandorfy (Eds) *The Hydrogen Bond. Recent Developments in Theory and Experiments Vols I–III* (Amsterdam: North-Holland, 1976)
44. F Vogtle, E Weber (Eds) *Host Guest Complex Chemistry. Macrocycles, Synthesis, Structures, Applications* (Berlin, New York: Springer, 1985)
45. S C Zimmermann, F Zeng, D E C Reichert, S V Kolotuchin *Science* **271** 1095 (1996)
46. G Ionova, R Guillaumont, C Hill, C Rabbe, S Ionov, M-C Charbonnel, D Guillaumont, C Madic, in *Proceedings of the International Conference 'Modelling Chemical Reactions', Nancy, France, 2003* p. 14
47. J K Bera, T-T Vo, R A Walton, K R Dunbar *Polyhedron* **22** 3009 (2003)
48. M A Porai-Koshits, T S Khodasheva, A S Antsishkina, in *Kristalloghimiya (Itogi Nauki i Tekhniki)* [Crystal Chemistry (Advances in Science and Engineering Series)] (Moscow: Izd. VINITI, 1971) Vol. 7, p. 1
49. F A Cotton, R A Walton *Multiple Bonds between Metal Atoms* (New York: Wiley, 1982)
50. D S Lawrence, T Jiang, M Levett *Chem. Rev.* **95** 2229 (1995)
51. F A Cotton, C Lin, C A Murillo *Acc. Chem. Res.* **34** 759 (2001)
52. J K Bera, B W Smucker, R A Walton, K R Dunbar *Chem. Commun.* 2562 (2000)
53. F A Cotton, G Wilkinson *Advanced Inorganic Chemistry* (New York: Interscience, 1962)
54. C Moore *Atomic Energy Levels Vols 1–3* (Washington, DC: National Bureau of Standards, 1952–1955)
55. J M Ziman *Models of Disorder. The Theoretical Physics of Homogeneously Disordered Systems* (London: Cambridge University Press, 1979)
56. K S Krasnov, N V Filipenko, V A Bobkova *Molekulyarnye Postoyannye Neorganicheskikh Soedinenii* (Molecular Constants of Inorganic Compounds) (Ed. K S Krasnov) (Leningrad: Khimiya, 1979)
57. D Braga, L Maini, F Grepioni, C Elschenbroich, F Paganelli, O Shiemann *Organometallics* **20** 1875 (2001)
58. C B Aakeröy, A M Beatty, D S Leinen, K R Lorimer *Chem. Commun.* 935 (2000)
59. G E Shulz, R H Shirmer *Principles of Protein Structures* (Ed. C Cantor) (New York, Berlin: Springer, 1979)
60. M V Vol'kenshtein *Molekulyarnaya Biofizika* (Molecular Biophysics) (Moscow: Nauka, 1975)
61. L Pauling, R B Corey, H R Branson *Proc. Natl. Acad. Sci. USA* **37** 205 (1951)
62. G I Tishchenko, in *Kristalloghimiya (Itogi Nauki i Tekhniki)* [Crystal Chemistry (Advances in Science and Engineering Series)] (Moscow: Izd. VINITI, 1979) Vol. 13, p. 189
63. G C Pimentel, A L McClellan *The Hydrogen Bond* (San Francisco, London: Freeman, 1960)
64. P L Huyskens, W A Luck, T Zeegers-Huyskens (Eds) *Intermolecular Forces. Introduction to Modern Methods and Results* (Berlin: Springer, 1991)
65. N D Sokolov, V M Chulanovskii (Eds) *Vodorodnaya Svyaz'* (The Hydrogen Bond) (Moscow: Nauka, 1964)
66. S P Ionov, N T Kuznetsov *Koord. Khim.* **26** 563 (2000)^c
67. G V Ionova *Usp. Khim.* **59** 66 (1990) [*Russ. Chem. Rev.* **59** 39 (1990)]
68. J Melman, T J Emge, J G Brennan *Inorg. Chem.* **40** 1078 (2001)
69. G V Ionova *Zh. Neorg. Khim.* **47** 601 (2002)^a
70. G V Ionova *Koord. Khim.* **28** 254 (2002)^c
71. J S Lindsey *New J. Chem.* **15** 153 (1991)
72. J C Chambron, C O Dietrich-Buchecker, J-P Sauvage, in *Comprehensive Supramolecular Chemistry* Vol. 9, Ch. 2 (London: Elsevier, 1996)
73. C O Dietrich-Buchecker, J-P Sauvage *Chem. Rev.* **87** 795 (1987)
74. J-P Sauvage *Acc. Chem. Res.* **23** 319 (1990)
75. L J Charbonnière, M-F Gilet, K Bernauer, A F Williams *Chem. Commun.* 39 (1996)
76. Ch P Pole Jr, F J Owens *Introduction to Nanotechnology* (New Jersey: Wiley-Interscience, 2003)
77. M A Porai-Koshits, G A Kukina, in *Kristalloghimiya (Itogi Nauki i Tekhniki)* [Crystal Chemistry (Advances in Science and Engineering Series)] (Moscow: Izd. VINITI, 1974) Vol. 9, p. 1
78. P N W Baxter, J-M Lehn, D Fenske *Chem. – Eur. J.* **5** 102 (1999)
79. P N W Baxter, J-M Lehn, B O Kneisel, G Baum, D Fenske *Chem. – Eur. J.* **5** 1132 (1999)
80. D L Caulder, K N Raymond *J. Chem. Soc., Dalton Trans.* 1185 (1999)
81. M Stricklen, J Verkade *J. Am. Chem. Soc.* **105** 2494 (1983)
82. M Fujita, K Ogura *Bull. Chem. Soc. Jpn.* **69** 1471 (1996)
83. C M Drain, J-M Lehn *J. Chem. Soc., Chem. Commun.* 2313 (1994)
84. A W Maverick, F E Klavetter *Inorg. Chem.* **23** 4129 (1984)
85. C M Hartshorn, P J Steel *Inorg. Chem.* **35** 6902 (1996)
86. S C Davies, A-K Duhme, D L Hughes *Inorg. Chem.* **37** 5380 (1998)
87. M J Hannon, C L Painting, W Errington *Chem. Commun.* 307 (1997)
88. M A Houghton, A Bilyk, M M Harding, P Turner, T W Hambley *J. Chem. Soc., Dalton Trans.* 2725 (1997)
89. D L Caulder, K N Raymond *Angew. Chem., Int. Ed. Engl.* **36** 1440 (1997)
90. K-S Jeong, Y L Cho, J U Song, H-Y Chang, M-G Choi *J. Am. Chem. Soc.* **120** 10982 (1998)
91. M Fujita, S Nagao, K Ogura *J. Am. Chem. Soc.* **117** 1649 (1995)
92. M Fujita *Acc. Chem. Res.* **32** 53 (1999)
93. M Fujita, F Ibukuro, H Seki, O Kamo, M Imanari, K Ogura *J. Am. Chem. Soc.* **118** 899 (1996)
94. M Fujita, M Aoyagi, F Ibukuro, K Ogura, K Yamaguchi *J. Am. Chem. Soc.* **120** 611 (1998)
95. R Schneider, M W Hosseini, J-M Planeix, A de Cian, J Fischer *Chem. Commun.* 1625 (1998)
96. M C Lagunas, R A Gossage, W J J Smeets, A L Spek, G van Koten *Eur. J. Inorg. Chem.* **163** (1998)
97. E J Enemark, T D P Stack *Angew. Chem., Int. Ed.* **37** 932 (1998)
98. P N Baxter, J-M Lehn, A De Cian, J Fischer *Angew. Chem., Int. Ed. Engl.* **32** 69 (1993)
99. T Beissel, R E Powers, K N Raymond *Angew. Chem., Int. Ed. Engl.* **35** 1084 (1996)
100. N M Shavaleev, S J A Pope, Z R Bell, S Faulkner, M D Ward *Dalton Trans.* 808 (2003)
101. F David, V Vokhmin, G Ionova *J. Mol. Liq.* **90** 45 (2001)
102. G V Ionova, C Madic, R Guillaumont *Koord. Khim.* **27** 471 (2001)^c
103. J Hamacek, S Blanc, M Elhabiri, E Leize, A Van Dorsselaer, C Piquet, A-M Albrecht-Gary *J. Am. Chem. Soc.* **125** 1541 (2003)
104. D Imhof, L M Venanzi *Chem. Soc. Rev.* **23** 185 (1994)
105. S P Gubin *Usp. Khim.* **54** 529 (1985) [*Russ. Chem. Rev.* **54** 305 (1985)]
106. Yu L Slovokhotov, Yu T Struchkov *Usp. Khim.* **54** 556 (1985) [*Russ. Chem. Rev.* **54** 323 (1985)]
107. G P Kostikova, D V Korol'kov *Usp. Khim.* **54** 591 (1985) [*Russ. Chem. Rev.* **54** 344 (1985)]
108. V I Spitsyn, A F Kuzina, A A Oblova, S V Kryuchkov *Usp. Khim.* **54** 619 (1985) [*Russ. Chem. Rev.* **54** 373 (1985)]
109. N K Eremenko, E G Mednikov, S S Kurasov *Usp. Khim.* **54** 637 (1985) [*Russ. Chem. Rev.* **54** 394 (1985)]
110. V E Fedorov, V E Mishchenko, V P Fedin *Usp. Khim.* **54** 671 (1985) [*Russ. Chem. Rev.* **54** 408 (1985)]
111. J Manna, C J Kuehl, J A Whiteford, P J Stang, D C Muddiman, S A Hofstadler *J. Am. Chem. Soc.* **119** 11611 (1997)
112. S-W Lai, K-K Cheung, M C W Chan, C M Che *Angew. Chem., Int. Ed.* **37** 182 (1998)
113. O Mamula, A von Zelewsky, G Bernardinelli *Angew. Chem., Int. Ed.* **37** 290 (1998)
114. S Rüttimann, G Bernardinelli, A F Williams *Angew. Chem., Int. Ed. Engl.* **32** 392 (1993)
115. R F Carina, A F Williams, G Bernardinelli *J. Organomet. Chem.* **548** 45 (1997)
116. A T Baker, J K Crass, M Maniska, D C Craig *Inorg. Chim. Acta* **225** 225 (1995)

117. J Padilla, D Gatteschi, P Chaudhuri *Inorg. Chim. Acta* **260** 217 (1997)
118. J Wojaczynski, L Latos-Grazynski, M M Olmstead, A L Balch *Inorg. Chem.* **36** 4548 (1997)
119. M Fujita, O Sasaki, T Mitsuhashi, T Fujita, J Yazaki, K Yamaguchi, K Ogura *Chem. Commun.* 1535 (1996)
120. R-D Schnebeck, L Randaccio, E Zangrando, B Lippert *Angew. Chem., Int. Ed.* **37** 119 (1998)
121. J C Bailar (Ed.) *Comprehensive Inorganic Chemistry* Vols 2, 3 (New York: Pergamon Press, 1973)
122. J C Jeffrey, I Moore, M Murray, F G A Stone *J. Chem. Soc., Dalton Trans.* 1741 (1982)
123. R Hedinger, M Ghisletta, K Hegetschweiler, E Toth, A E Merbach, R Sessoli, D Gatteschi, V Gramlich *Inorg. Chem.* **37** 6698 (1998)
124. D Chapon, J-P Morel, P Delangle, C Gateau, J Pécaut *Dalton Trans.* 2745 (2003)
125. L Morss, in *Handbook on the Physics and Chemistry of Rare Earths* Vol. 18 (Eds K A Gschneidner Jr, L Eyring) (Amsterdam: North Holland, 1991) p. 239
126. X Chi, A J Guerin, R A Haycock, C A Hunter, L D Sarson *J. Chem. Soc., Chem. Commun.* 2563 (1995)
127. X Chi, A J Guerin, R A Haycock, C A Hunter, L D Sarson *J. Chem. Soc., Chem. Commun.* 2567 (1995)
128. C Piquet, J-C G Bünzli *Chem. Soc. Rev.* **28** 347 (1999)
129. S C Dixit, R Sharan, R N Kappoor. *Inorg. Chim. Acta* **158** 109 (1989)
130. A W Schwabacher, J Lee, H Lei *J. Am. Chem. Soc.* **114** 7597 (1992)
131. R W Saalfrank, A Stark, K Peters, H G von Schnering *Angew. Chem., Int. Ed. Engl.* **27** 851 (1988)
132. E C Constable *Chem. Commun.* 403 (1998)
133. C-y Duan, Z-h Liu, X-z You, F Xue, T C W Mak *Chem. Commun.* 381 (1997)
134. T Kajiware, T Ito *J. Chem. Soc., Chem. Commun.* 1773 (1994)
135. N Matsumoto, Y Motoda, T Matsuo, T Nakashima, N Re, F Dahan, J-P Tuchagues *Inorg. Chem.* **38** 1165 (1999)
136. F A Cotton, L M Daniels, C Lin, C A Murillo *J. Am. Chem. Soc.* **121** 4538 (1999)
137. T Beissel, R E Powers, T N Parac, K N Raymond *J. Am. Chem. Soc.* **121** 4200 (1999)
138. K Funatsu, A Kimura, T Imamura, Y Sasaki *Chem. Lett.* 765 (1995)
139. R Ziessel, D Matt, L Toupet *J. Chem. Soc., Chem. Commun.* 2033 (1995)
140. R P Bonar-Law, T D McGrath, N Singh, J F Bickley, A Steiner *Chem. Commun.* 2457 (1999)
141. M J Hannon, C L Painting, W Errington *Chem. Commun.* 1805 (1997)
142. S M Woessner, J B Helms, Y Shen, B P Sullivan *Inorg. Chem.* **37** 5406 (1998)
143. K D Benkstein, J T Hupp, C L Stern *Inorg. Chem.* **37** 5404 (1998)
144. M A Porai-Koshits, G A Kukina, in *Kristalloghimiya (Itogi Nauki i Tekhniki)* [Crystal Chemistry (Advances in Science and Engineering Series)] (Moscow: Izd. VINITI, 1974) Vol. 10
145. P J Stang, B Olenyuk *Acc. Chem. Res.* **30** 502 (1997)
146. P J Stang, D H Cao, S Saito, A M Arif *J. Am. Chem. Soc.* **117** 6273 (1995)
147. J Lu, T Paliwala, S C Lim, C Yu, T Niu, A J Jacobson *Inorg. Chem.* **36** 923 (1997)
148. B Hasenknopf, J-M Lehn, B O Kneisel, G Baum, D Fenske *Angew. Chem., Int. Ed. Engl.* **35** 1838 (1996)
149. B Hasenknopf, J-M Lehn, N Boumidjene, A Dupont-Gervais, A van Dorsselaer, B Kneisel, D Fenske *J. Am. Chem. Soc.* **119** 10956 (1997)
150. D M P Mingos, J Yau, S Menzer, D J Williams *Angew. Chem., Int. Ed. Engl.* **34** 1894 (1995)
151. P L Jones, K J Byrom, J C Jeffery, J A McCleverty, M D Ward *Chem. Commun.* 1361 (1997)
152. R W Saalfrank, A Stark, M Bremer, H-U Hummel *Angew. Chem., Int. Ed. Engl.* **29** 311 (1990)
153. G V Ionova, V I Spitsyn *Elektronnoe Stroenie Aktinidov* (Electronic Structure of Actinides) (Moscow: Nauka, 1986)
154. G V Ionova, V I Spitsyn *Effektivnye Zaryady v Soedineniyakh Aktinidov* (Effective Charges in Actinide Compounds) (Moscow: Nauka, 1989)
155. G V Ionova, V I Spitsyn, V G Vokhmin *Zakonomernosti Izmeneniya Svoistv Lantanidov i Aktinidov* (Regularities in the Variation of Properties of Lanthanides and Actinides) (Moscow: Nauka, 1990)
156. A E Martell, R D Hancock *Metal Complexes in Metal Solution* (New York: Plenum, 1996)
157. H-J Schneider *Chem. Soc. Rev.* **23** 227 (1994)
158. D J Cram, T Kaneda, R C Helgeson, S B Brown, C B Knobler, E Maverick, K N Trueblood *J. Am. Chem. Soc.* **107** 3645 (1985)
159. A Yu Tsivadze *Ros. Khim. Zh.* **40** (4–5) 43 (1996)^b
160. A Yu Tsivadze, V I Zhilov, S V Demin *Koord. Khim.* **22** 143 (1996)^c
161. F Arnaud-Neu *Chem. Soc. Rev.* **23** 235 (1994)
162. J-C G Bunzli, F Pilloud *Inorg. Chem.* **28** 2638 (1989)
163. J L Atwood, L J Barbour, S Dalgarno, C L Raston, H R Webb *J. Chem. Soc., Dalton Trans.* 4351 (2002)
164. M G B Drew, M J Hudson, P B Iveson, C Madic, M L Russel *J. Chem. Soc., Dalton Trans.* 2711 (2000)
165. A Yu Tsivadze, G V Ionova, V K Mikhalko, Yu N Kostrubov, in *Proceedings of International Summer School 'Supramolecular Systems in Chemistry and Biology', Tuapse, 2006* p. 42

^a — *Russ. J. Inorg. Chem. (Engl. Transl.)*

^b — *Mendelev Chem. J. (Engl. Transl.)*

^c — *Russ. J. Coord. Chem. (Engl. Transl.)*

Physicochemical properties of plasma – solution systems and prospects for their use in technology

A G Zakharov, A I Maksimov, Yu V Titova

Contents

I. Introduction	235
II. Plasma – solution systems	235
III. The effect of gas discharges on physicochemical properties of solutions	237
IV. Plasma-initiated chemical processes in solution	238
V. Potentials and prospects of plasma initiation of industrial processes in aqueous solutions	246
VI. Conclusion	250

Abstract. Gas discharge initiation of chemical processes in electrolyte solutions is considered. Data on the types of chemical transformations in plasma – solution systems are presented. The processes of generation of primary reactive species in solutions under gas discharge and the key routes for their further reactions are analysed. The prospects for practical application of plasma – solution systems in solving technological and environmental problems are considered. The bibliography includes 109 references.

I. Introduction

Nonequilibrium gas-discharge plasma finds practical application in implementation of numerous physicochemical processes¹ due to its extremely high chemical activity at relatively low temperatures of treated materials. As a penalty, the high reactivity entails low selectivity of chemical reactions initiated by plasma. This necessitates a search for such conditions that would combine the high reactivity of plasma with the selectivity of its effect. The fundamental way for solving this problem is presented by the plasma activation of chemical reactions in electrolyte solutions. Successful realisation of these processes requires the knowledge of physics of gas discharges (in our case, discharge that interacts with the solution), and the mechanism and kinetics of generation of active species (in liquid and gas phases) and their chemical reactions in solution. All these questions are as yet little understood, although the studies of chemical effects initiated by the simplest plasma – solution system, namely, a glow discharge with the electrolyte that plays the role of the electrode, date back to nearly 100 years ago. Güntherschulze (*e.g.*, see Ref. 2) studied the electroforming of aluminium and tantalum electrodes in electrolytic cells with dilute electrolyte solutions ($\text{Na}_2\text{B}_4\text{O}_7$ – HBO_3 and $\text{Na}_2\text{B}_4\text{O}_7$) and observed that the anodic sparkling was accom-

panied by the gas evolution on the anode at a rate higher than the value calculated based on the Faraday law and also the appearance of hydrogen peroxide in the solution. A hypothesis was advanced according to which gases were formed in a region immediately adjacent to the discharge zone as a result of the four-body recombination of oxygen and hydrogen atoms delivered from the discharge zone. Fundamental cycles of studies were accomplished by schools of Klemenc^{3–7} in Germany and Hickling^{8–16} in England. Although the interpretation of their results has now substantially changed, these studies are still of interest, the more so that no such comprehensive systematic studies were carried out since that time and no exhaustive reviews on this subject are known.

II. Plasma – solution systems

1. Specific features and types of plasma – solution systems

The interaction of a gas discharge with solutions can be realised in the following two ways:

- (1) with a discharge that contacts the liquid and is generated between two electrodes located in the gas phase;
- (2) with a discharge in which the electrolyte solution plays the role of one or both electrodes.

In both cases, the properties of the system and the achieved results substantially depend on whether we deal with a (quasi)stationary discharge or a high-voltage pulsed discharge. The present review is chiefly devoted to plasma – solution systems (PSS) with stationary discharges; however, the studies of pulsed PSS are also discussed.

The first-type processes resemble conventional heterogeneous plasma-chemical processes in which active species generated in plasma diffuse to the interface to initiate chemical reactions in the solution. In the second-type systems, the discharge current passes through the electrolyte, which substantially changes the properties of the plasma – liquid interface. In this case, plasma can be generated either in the original plasma-forming gas that contains solvent vapours or within a vapour blanket formed in the liquid phase due to the superheat instability. Figure 1 shows possible configurations of systems differing in the roles of the metal and electrolyte electrodes. The Figure also shows different orders of alternation of interfaces formed by metals, plasma and solutions in PSS of different types. A plasma – solution system can be distinguished from a classical electrochemical system by the presence of one or two plasma – solution interfaces. Note that the

A G Zakharov, A I Maksimov, Yu V Titova Institute of Solution Chemistry, Russian Academy of Sciences, ul. Akademicheskaya 1, 153045 Ivanovo, Russian Federation. Fax (7-4932) 33 62 37, tel. (7-4932) 33 62 59, e-mail: agz@isc-ras.ru (A G Zakharov), tel. (7-4932) 33 62 64, e-mail: aim@isc-ras.ru (A I Maksimov), jvt@isc-ras.ru (Yu V Titova)

Received 26 October 2006

Uspekhi Khimii 76 (3) 260–278 (2007); translated by T Ya Safonova

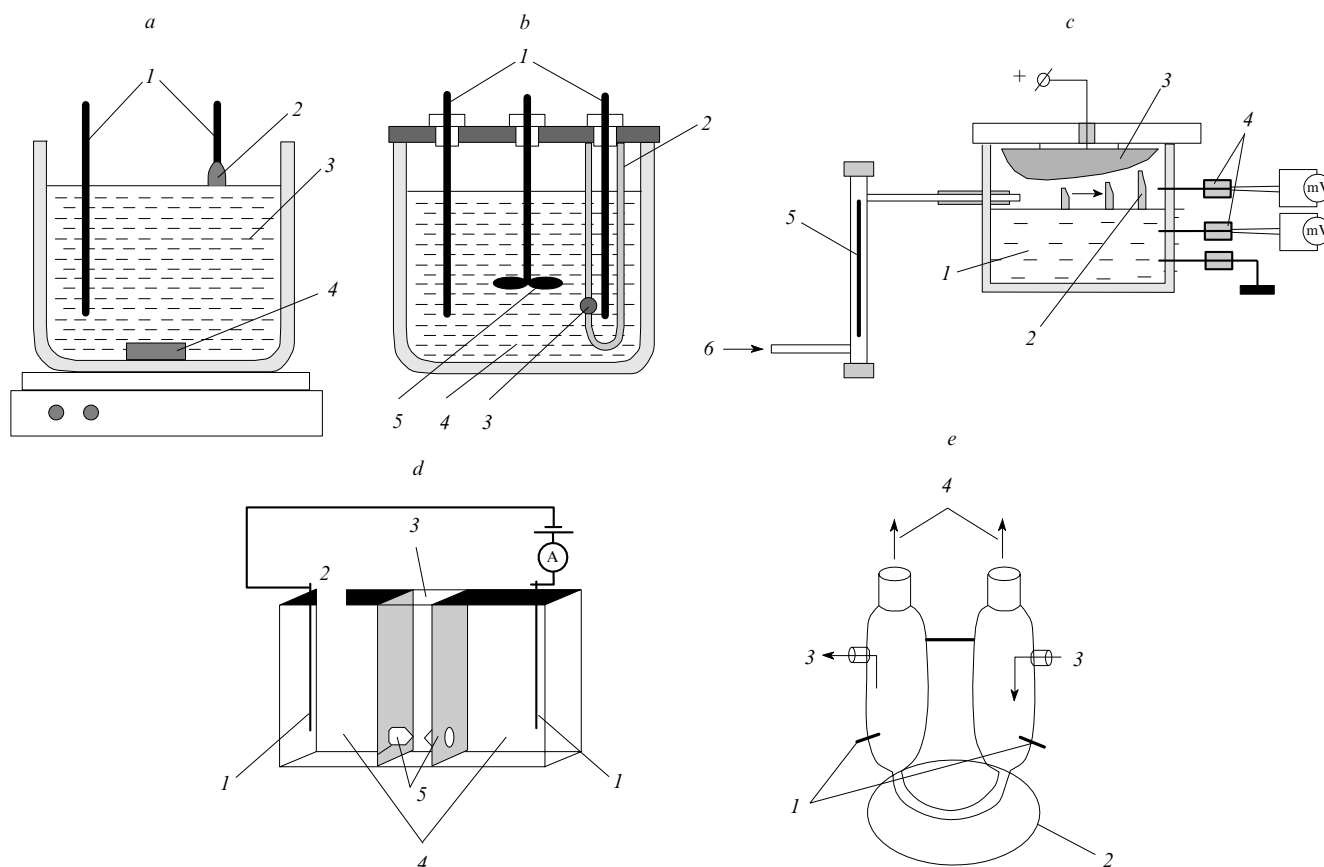


Figure 1. Configurations of discharge cells. In parentheses, the order of alternation of interfaces formed between metal (M), plasma (P) and electrolyte solution (E) is shown.

(a) Glow-discharge cell (M–E–P–M): (1) electrodes, (2) plasma zone, (3) electrolyte, (4) magnetic stirrer.

(b) Diaphragm discharge cell (M–E–P–E–M): (1) electrodes, (2) quartz ampoule, (3) diaphragm (plasma zone), (4) electrolyte, (5) stirrer.

(c) Gliding arc discharge cell (M–E–P–M): (1) solution, (2) gliding arc discharge, (3) special-shape electrode (anode), (4) thermocouple entry, (5) flow meter, (6) gas inlet.

(d) Diaphragm discharge cell with buffer compartments (M–E–P–E–M): (1) electrodes, (2) plasma zone, (3) active zone, (4) buffer compartments, (5) quartz ampoules with diaphragms.

(e) Cell for initiation of volume discharges in a tube filled with a solution (M–E–P–E–P–E–M): (1) electrodes, (2) discharge zone, (3) circulation of electrolyte solution, (4) to a reflux condenser.

plasma structures in these systems may be in direct contact with neither metal electrodes nor the external atmosphere.

The glow discharge in which the electrolyte solution serves as one of the electrodes (most often, the cathode) was studied most thoroughly (see Fig. 1a).^{3–16} Apparently, anodic microdischarges that arise as a result of the breakdown of the oxide film on the surface of such metals as Al, Ta, Nb, which are immersed into the solution, can also be assigned to the same type.^{17–22} Special mention should be made of PSS in which the plasma formed in the solution has a sufficiently large volume, which allows one to treat materials by combining the impacts of plasma and the plasma-activated solution (see Fig. 1e).²³

From our viewpoint, any strict classification of plasma–solution systems is hardly possible to date. A classification based on the analysis of the number of metal–solution and plasma–solution interfaces and the order of their alternation was proposed.²⁴ It is the dynamic plasma–solution interface that is the key feature of any PSS. Few available experimental data characterising this interface were obtained only for a glow discharge with electrolyte electrodes and exclusively for the case where the electrolyte serves as the cathode. For non-stationary continuous discharges, e.g., diaphragm discharge, such studies are more cumbersome and are virtually unknown to date. According to our viewpoint, the most important

properties of the dynamic plasma–solution interface are similar for the mentioned discharge types. This is why below we consider only the glow discharge with the electrolyte as the cathode.

Drawing the analogy between a glow discharge with the electrolyte cathode and a classical low-pressure glow discharge, it should be noted that the cathodic potential drop at the electrolyte surface is determined by two characteristics, namely, the coefficient of electron emission from the solution (γ) and the Townsend coefficient of volume ionisation (α).²⁴ Measurements gave the cathodic potential drop at the electrolyte surface in the range from 300 to 800 V.²⁵ These values substantially exceed the usual cathodic potential drops obtained for glow discharges with metal electrodes, which apparently can be associated with the low coefficient γ . Estimates, which were based on an assumption that at low discharge currents (not exceeding tens of mA), the glow discharge with an electrolyte cathode can be considered as a conventional glow discharge, gave the values $\gamma = 10^{-4}–10^{-3}$ (Ref. 26).

The high potential drop at the surface of electrolyte cathodes determines the sufficiently high yields of primary active species in the thin surface layer of the solution. To our knowledge, the energy distribution of ions bombarding the

solution surface is yet unknown. However, it is evident that the maximum possible energy should correspond to the potential drop at the cathode surface.

Ionic bombardment of the solution surface not only leads to its effective chemical activation but also gives rise to an effect similar to the classical cathode sputtering, *i.e.*, the transfer of solution components into the plasma zone. According to the results of measurements,^{27,28} the transfer coefficient of solvent (water) molecules, which is determined as the number of water molecules knocked out from the solution per incident ion exceeds 10^2 ; the transfer coefficient of the solute is approximately proportional to its mole fraction in the solution. The vapour jet that arises as a result of cathodic sputtering has a linear velocity of $50\text{--}100\text{ cm s}^{-1}$. The energy consumed in its formation reaches 50% of the total discharge energy.²⁹ Estimates of average energy consumed in the transfer of a single water molecule to the plasma zone correspond to $\sim 50\text{ kJ mol}^{-1}$, which does not differ much from the thermodynamically equilibrium consumption (43.3 kJ mol^{-1} at $40\text{ }^{\circ}\text{C}$ ³⁰).

The presence of non-equilibrium vapour jet leads to the fact that regardless of the nature of the main plasma-forming gas, the ionisation of water molecules plays the key role in the formation of plasma; moreover, according to certain estimates,²⁵ the main ions in the plasma zone are $\text{H}_3\text{O}^+ \cdot \text{H}_2\text{O}$. The role played by this jet in the discharge-initiated processes in solution is of no less importance. The analysis of the mechanism of these processes requires taking into account the ion-bombardment-induced transfer of reagents and products into the gas zone.³¹ The fact that recombination processes that involve primary active species (HO^\bullet , H^\bullet , e_{soln}^-) almost exclusively occur in the cathodic spot zone necessitates the separate consideration of the rates of processes initiated by primary species in the cathodic spot and those initiated by secondary species (*e.g.*, hydrogen peroxide) in the rest solution volume.³¹

2. The mechanism of chemical activation of solutions in plasma–solution systems

Despite the substantial difference in the PSS mentioned above, the main reason for the plasma activation of solutions is their bombardment with ions accelerated near the solution surface in the vicinity of the near-electrode (mainly cathodic) potential drop. This causes non-equilibrium dissociation and ionisation of, first of all, solvent molecules. As a result, H^\bullet , HO^\bullet radicals and solvated electrons appear in the solution. This mechanism of activation followed by chemical reactions is close to that comprehensively studied in radiation chemistry.³² The yields of primary active species depend on the cathodic potential drop formed. Another important effect of ionic bombardment is the transfer of solution components into the plasma zone. The data on its kinetics under the conditions of an atmospheric-pressure glow discharge are available.^{26–28} Undoubtedly, the transfer processes initiated by ionic bombardment substantially affect the properties of other non-stationary PSS, including the migration of plasma wisps in solution. In the case of non-stationary discharges (diaphragm and volume discharges), a shock wave is initiated in the electrolyte bulk, the propagation of which can also affect the chemical processes in the solution.^{33,34}

The contact of the plasma zone with the solution surface apparently activates the solution *via* the ‘dissolution’ of active species formed in the plasma by fairly well known mechanisms. However, the quantitative contribution of this activation mechanism to the observed yields of chemical reaction products in solutions still remains unclear. Obviously, this

contribution can be higher when the plasma zone is located within the solution as in the case of anodic microdischarges or a diaphragm discharge.

3. Yields of primary active species in plasma–solution systems

Within the framework of the simplified scheme described above in the absence of discharge-initiated chain reactions in solutions, the yields of final products of redox reactions cannot exceed the yields of primary active species. Experimental results that allow one to directly check this assumption are scarce. Thus it was found^{8,9,13,14} that with an increase in the salt concentration, the yields of oxidation products of Fe^{2+} and Ce^{3+} approach the yields of HO^\bullet radicals found in the same studies. As a whole, these results do not contradict the above assumption. The only exclusion was the far too high yield observed³⁵ in the oxidation of Fe^{2+} to Fe^{3+} with a very low discharge current (0.1 mA). Table 1 shows the discussed results.

III. The effect of gas discharges on physicochemical properties of solutions

Initiation of redox reactions in solutions should be accompanied by the changes in their acidity. At the same time, the observed pH changes sometimes cannot be explained by this effect. As demonstrated for a corona discharge⁴³ and, later, for a gliding arc discharge burning between two metal electrodes in the immediate vicinity of the solution surface,⁴⁴ the pH of aqueous solutions in contact with a gas discharge decreased. In both studies, the discharge-activated gas was in contact with the aqueous solution surface but no discharge current passed through the solution. Moreover, according to the authors of these studies, the effect of a powerful gliding arc discharge on the solution pH completely resembled the titration of a strong alkali with a strong acid (*i.e.*, the pH changes were sharp and great). The simplest explanation of this effect assumes the formation of nitrogen oxides in the plasma zone followed by their dissolution.

In the studies of the effect of a glow discharge on the acidity of solutions of alkali metal chlorides,²⁶ no oxidation processes initiated in the liquid phase were found; however, in dilute solutions, a strong and steady decrease in the pH was observed, where the changes in the proton concentration in solution corresponded to the quantity of electricity passed. It was assumed⁴⁵ that the observed effect can be attributed to a redox process initiated by ion bombardment and localised in the gas phase. This process gave alkali metal atoms and chlorine molecules observed experimentally in the gas phase. Under the experimental conditions used, virtually no sodium returned to the liquid phase, in contrast to chloride. Thus, in this case, the changes in the solution acidity were determined by the transfer rate of the solute to the gas phase under the action of ion bombardment.

The changes in the acidity of solutions subjected to a gas discharge were accompanied by the changes in the solution conductivity.⁴⁶ The conductivity of concentrated acids and alkalis subjected to a diaphragm discharge decreased, whereas the conductivity of salt solutions remained unchanged.⁴⁷ Taking into account the mechanisms of conduction in these solutions, this effect was explained by the changes in the structural characteristics of acid and alkali solutions, which affected the effectiveness of the relay mechanism of charge transfer in them.

Table 1. Yields of the primary active species or the products of redox processes initiated by these species.

Species or process	Yield /mol F ⁻¹ (see ^a)	Conditions	Ref.
HO·, H·	7.3	glow discharge (25–125 Torr), FeSO ₄ solution	9
	7.6	glow discharge (25–125 Torr), Ce ₂ (SO ₄) ₃ solution	10
	8.3	glow discharge (25–125 Torr), NaN ₃ solution	10
	3.16–3.58	microdischarges in aqueous solution of NH ₃ + H ₃ BO ₃	18
e _{solv} ⁻	3.3	glow discharge, sulfuric acid solution	3
	6.0 ± 0.6	solutions of salts of chloroacetic acid	17
H ₂ O ₂	0.532	low-pressure glow discharge, current 60 mA, 1 M H ₂ SO ₄	4
	1.1–1.9	glow discharge (75–100 Torr), current 50–100 mA, pH 1–8	8
	0.66–1.1	contact discharge (1 atm), sulfate buffer	36
	0.42	glow discharge (750 Torr), current 25 mA, 0.49 M NH ₃ (aq.)	37
	3.39	glow discharge (100 Torr), phosphate buffer with addition of 0.9 mol litre ⁻¹ ethanol, bubbling of O ₂ through the solution (900 cm ³ s ⁻¹), current 30 mA	38
	0.64–9.75	glow discharge (1 atm), 0.01–0.5 M Na ₂ SO ₄ , KCl, KOH, current 8–30 mA	39
I ⁻ → I ₂	0.18–2.88	glow discharge (1 atm), current 6 mA, 0.15–0.25 M KI	29
	3.2	glow discharge, 0.02 M KI, neutral phosphate buffer (the maximum yield is shown)	40
Fe ²⁺ → Fe ³⁺	7.3	glow discharge (50, 75, 100 Torr), current 25–100 mA, 0.005–0.075 M FeSO ₄ (the limiting yield reached at the maximum salt concentration is shown)	9, 10
	11; 25	glow discharge in air (25 Torr), current 4.2 or 0.1 mA, 0.01 M iron ammonium sulfate solution in 0.5 M H ₂ SO ₄	35
Ce ³⁺ → Ce ⁴⁺	7.6	glow discharge (50, 75, 100 Torr), currents 25–100 mA, 0.005–0.075 M Ce ₂ (SO ₄) ₃ (the limiting yield reached at the maximum salt concentration is shown)	9, 10
K ₄ [Fe(CN) ₆] → → K ₃ [Fe(CN) ₆]	7.3	glow discharge in air, nitrogen, oxygen (50 Torr), currents 75 mA (limiting yields reached at the increase in the salt concentration to 0.45 mol litre ⁻¹ are shown)	41
	5.7	glow discharge in hydrogen (50 Torr), current 75 mA (limiting yields reached at the increase in the salt concentration to 0.45 mol litre ⁻¹ are shown)	41
	0.5–0.9	atmospheric-pressure glow discharge, current 5 or 10 mA, K ₄ [Fe(CN) ₆] concentrations 1 × 10 ⁻³ –5 × 10 ⁻² mol litre ⁻¹	42
KMnO ₄ → MnO ₂	1.25	atmospheric-pressure glow discharge in air, current 20 mA	29
	0.66	atmospheric-pressure gliding arc discharge in air, current 20 mA	29

^a From hereon, F corresponds to Faraday, *i.e.*, an off-system unit widely used in electrochemistry, namely, 1 F ≈ 9.65 × 10⁴ C.

IV. Plasma-initiated chemical processes in solution

Table 2 shows examples of redox processes that occur in solution under the action of gas discharges.

Table 2. Examples of redox processes initiated by gas discharge in aqueous electrolyte solutions.

Reaction	Medium
Oxidation reactions	
I ⁻ → I ₂ → IO ₄ ⁻	neutral, acidic
Br ⁻ → Br ₂ → BrO ₄ ⁻	the same
S ²⁻ → S → SO ₃ ²⁻ → SO ₄ ²⁻	"
Cl ⁻ → Cl ₂ → ClO ₂ ⁻	"
Mn ²⁺ → MnO ₂	"
Cr ³⁺ → Cr ₂ O ₇ ²⁻	"
Fe ²⁺ → Fe ³⁺	"
[Fe(CN) ₆] ⁴⁻ → [Fe(CN) ₆] ³⁻	neutral
Ce ³⁺ → Ce ⁴⁺	acidic
Tl ⁺ → Tl ³⁺	the same
Reduction reactions	
MnO ₄ ⁻ → MnO ₂	neutral
Cr ₂ O ₇ ²⁻ → Cr ₂ O ₃	the same
VO ₃ ⁻ → VO ²⁺	"

The number of studies devoted to chemical reactions in solutions initiated by different types of gas discharge is sufficiently large. However, the comprehensive analysis of all these data is complicated because the experimental conditions used were substantially different and often described in insufficient detail.

1. Hydrogen peroxide generation in electrolyte solutions subjected to the gas-discharge plasma

Klemenc *et al.*^{3–6} pioneered the quantitative studies of the formation of hydrogen peroxide in PSS. Hickling *et al.*^{8, 15} carried out further comprehensive investigations of the hydrogen peroxide formation in aqueous solutions subjected to a low-pressure discharge (50–75 Torr) with the anode located in the gas phase. According to their results, hydrogen peroxide was formed in an amount proportional to the quantity of electricity passed, the accumulation of hydrogen peroxide was accompanied by its decomposition, which ultimately led to its steady-state concentration. The amount of H₂O₂ formed in the solution upon the passage of a given charge through it was independent of both the current and the factors that determine the discharge nature and can be described by the following expression:

$$C_{eq} = \frac{F}{k} \left[1 - \exp\left(-\frac{akq}{V}\right) \right],$$

where C_{eq} is the steady-state concentration of H_2O_2 , F is the Faraday constant, k is the rate constant for the hydrogen peroxide decomposition, a is a numerical coefficient equal to 1.1–1.9 which corresponds to the number of hydrogen peroxide equivalents primarily formed per Faraday of electricity (the initial yield is G_0), q is the quantity of electricity in Faradays, V is the solution volume.

The process followed the same mechanism in the pH range from 1 to 9. However, beyond this range, the H_2O_2 yield decreased. In strongly alkaline solutions, no hydrogen peroxide was detected. Presumably, this can be associated with its anodic decomposition at the discharge of hydroxyl ions. The primary formation of hydroxyl radicals dimerisation of which yields peroxide was assumed to occur in the solution. At high concentrations, hydrogen peroxide decomposed in the reaction with the mentioned HO^\bullet radical. The hydrogen peroxide yield was observed to depend relatively weakly on the electrolyte concentration (including aqueous ammonia and sulfuric acid solutions) and also on the nature of the primary plasma-forming gas and its pressure.^{11–16}

Considering the formation of hydrogen peroxide as a result of dimerisation of HO^\bullet radicals, one can expect the appearance of H_2O_2 in alcohol solutions. However, in the glow-discharge-treated solution of 0.3 M $LiClO_4$ in methanol, formaldehyde was the main product and no hydrogen peroxide was detected.³³ A totally different situation was observed upon plasma treatment of aqueous ethanol in the presence of oxygen.³⁸ The action of an anodic glow discharge on ethanol in its neutral aqueous solution (a phosphate buffer) afforded acetaldehyde, butane-2,3-diol and hydrogen peroxide. The yields of these products strongly depended on both the oxygen flow and stirring. With the increase in the discharge current, the maintenance of the hydrogen peroxide yield at a constant level requires the increase of the oxygen consumption. Under experimental conditions, the amount of formed H_2O_2 linearly increased with the increase in the quantity of electricity passed, *i.e.*, no discharge-induced decomposition of hydrogen peroxide took place.

Kinetic curves of hydrogen peroxide accumulation measured^{8, 15, 40, 48} under different conditions were processed in our studies with the use of an exponential relationship similar to that proposed by Hickling^{8, 15}

$$C = C_{lim} [1 - \exp(-BQ)],$$

where C is the current concentration of hydrogen peroxide, C_{lim} is the maximum concentration of hydrogen peroxide obtained by using this processing procedure, B is the empirical coefficient, Q is the quantity of electricity passed through the system. Table 3 shows the obtained results.

Table 3. Kinetic characteristics of the hydrogen peroxide accumulation under different conditions.^a

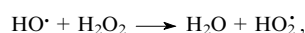
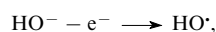
Experimental conditions	$10^3 C_{lim}$ /mol litre ⁻¹	$10^3 B$ /F ⁻¹	v (see ^b) /mol F ⁻¹	Ref.
Contact discharge (1 atm), 0.05 M K_2SO_4	0.2	1.88	0.376	8
Glow discharge (50 Torr), current 75 mA, 0.4 M H_2SO_4	1.7	0.405	0.688	15
Glow discharge (50 Torr), current 110 mA, 0.05 M $NaHSO_4$	2	0.403	0.806	40
Contact discharge (1 atm), current 110 mA, 0.02 M H_2SO_4	10	0.189	1.89	48

^a Initial current yield of H_2O_2 were practically the same (~ 1.5 mol F⁻¹);

^b v is the formation rate of H_2O_2 .

For similar discharge currents, the initial current yields of hydrogen peroxide were virtually the same, whereas its limiting concentrations differed by more than an order of magnitude. Moreover, the maximum difference was observed for only one type of discharge, namely, the contact discharge, *i.e.*, the explanation should be sought in the discharge as such. This means that even for the same discharge type, the rates of discharge-induced hydrogen peroxide decomposition can differ by two orders of magnitude.

In the aforementioned studies, Hickling also examined the decomposition of hydrogen peroxide for the cases where 0.05 M solutions of H_2SO_4 , Na_2HPO_4 and $NaOH$ with different starting H_2O_2 concentrations were subjected to the discharge. It was found that in discharge-treated sulfuric acid and sodium phosphate solutions, the amount of hydrogen peroxide changed until its steady-state concentrations corresponding to those found in experiments on the peroxide synthesis were reached. In the alkaline solution, decomposition of hydrogen peroxide with the current efficiency equal to 1 persisted, which was explained by the following anodic processes:



2. Oxidation processes initiated by a gas discharge in aqueous solutions of inorganic substances

A gas discharge initiates both oxidation and reduction reactions in solution (see Table 2). According to available data, the discharge initiates all thermodynamically permissible redox reactions that involve primary active HO^\bullet species. At the same time, the rate of the process strongly depends on the ratio of redox potentials of the corresponding half-reactions.

The oxidation of $FeSO_4$, NaN_3 and $Ce_2(SO_4)_3$ initiated by a glow discharge at reduced pressure (125–250 Torr) in the argon atmosphere was studied.^{9, 10, 13, 14, 35, 44}

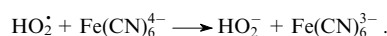
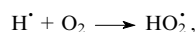
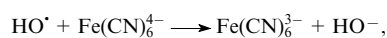
It was found⁹ that the yield of oxidation products of $FeSO_4$ (G /equiv F⁻¹) can be described by the relationship

$$G = 1 + n \frac{[Fe^{2+}] + A}{[Fe^{2+}] + A + B},$$

where n is the number of equivalents of the oxidant, which were formed per Faraday of electricity, A and B are empirical constants.

Presumably, the majority of obtained experimental results can be explained based on the assumption that the HO^\bullet radical is the primary oxidation agent. The kinetic model, which was developed based on the experimental data, has led to a relationship similar to that shown above and allowed the empirical kinetic characteristics for the oxidation of three substrates mentioned above to be found. The initial yield of HO^\bullet (mol F⁻¹) was determined to be 7.3 for iron sulfate, 7.6 for cerium sulfate and 8.3 for sodium azide (the limiting yields obtained at the maximum salt concentration are shown).^{9, 10}

Glow-discharge-induced oxidation of $K_4[Fe(CN)_6]$ was studied.⁴¹ With the increase in the concentration of oxidised ions, the yield of oxidation products tended to a limit of 7 mol F⁻¹ (at the salt concentration of 0.45 mol litre⁻¹). Presumably, the main oxidation reactions were as follows:



The reduction of $K_3[Fe(CN)_6]$ under the action of hydrogen atoms was neglected.

The oxidation of $K_4[Fe(CN)_6]$ to $K_3[Fe(CN)_6]$ initiated by a 'positive' atmospheric-pressure glow discharge between an electrode-tip in the gas phase and the surface of an aqueous electrolyte solution was studied⁴² as a function of the gas discharge current and the concentration of the starting compound. The currents of 5 and 10 mA were used, the voltage at electrodes did not exceed 5 kV. Table 4 shows the results obtained.

Table 4. Initial oxidation rates (v_0) of potassium hexacyanoferrate(II) and current yields (G) for different discharge conditions.⁴²

Discharge current /mA	$10^3 C_0$ /mol litre ⁻¹ (see ^a)	$10^7 v_0$ /mol litre ⁻¹ s ⁻¹	G^b
10	5	2.27	0.88
	2	1.91	0.74
	1	1.99	0.77
	0.5	2.34	0.90
	0.25	2.45	0.94
5	0.5	0.904	0.70
	0.25	0.728	0.56
	1	0.683	0.53

^a C_0 is initial concentration of $K_4[Fe(CN)_6]$.

^b Average current yield is expressed as the number of $K_3[Fe(CN)_6]$ molecules formed per incident ion.

The oxidation of ammonium ions under the discharge conditions was studied.³⁷ Air-saturated stirred aqueous ammonia (50 ml) served as the working solution. In the 'positive' discharge, the main products were hydrogen peroxide, hydrazine, hydroxylamine and nitrite ions. In the 'negative' discharge, neither hydrogen peroxide nor hydrazine were detected. In both cases, no formation of nitrate ions was observed. Both anodic and cathodic discharges afforded nitrogen and hydrogen as the gaseous products. In a cooled trap behind the discharge cell, only NH_3 and H_2O were detected.

Sulfuric acid oxidation was studied back in the work by Klemenc and Eder.⁴ They have found that the oxidation products of sulfuric acid under the action of a glow discharge were (in addition to hydrogen peroxide) peroxydisulfuric ($H_2S_2O_8$) and peroxymonosulfuric (H_2SO_5) acids. The effect of minor additives on this process was studied⁵ (see below). Denaro and Hough⁴⁸ studied the oxidation of sulfuric acid under a glow discharge in 0.4 M H_2SO_4 under a nitrogen atmosphere, at a pressure of 50 Torr and a discharge current of 57 mA. The authors observed the formation of the same products; however, according to their data, hydrogen peroxide was produced in the highest yield, whereas the yield of peroxydisulfuric acid was very low. The total yield of oxidation products, which was assumed equal to the sum of yields of hydrogen peroxide and peroxydisulfuric acid was found as well as individual yields of each product mentioned. Figure 2 shows the dependence of the overall concentration of oxidation products on the quantity of electricity passed.

The following reactions that lead to the formation of oxidation products were considered:⁴⁸

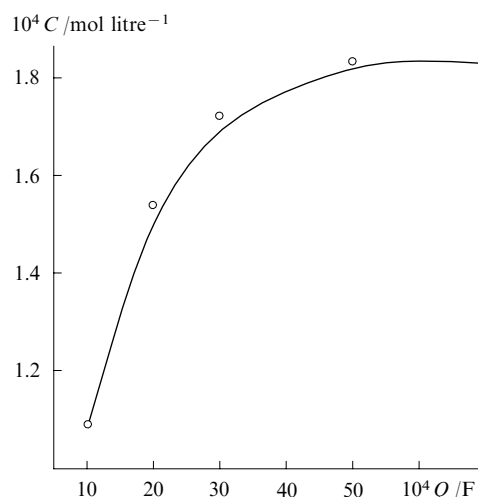
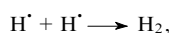
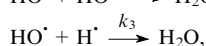
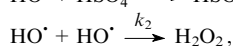
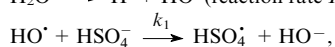
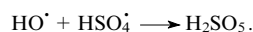
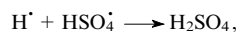


Figure 2. Dependence of the overall concentration (C) of sulfuric acid oxidation products ($H_2SO_5 + H_2O_2$) under a glow discharge on the quantity of electricity (Q) passed.



Using the values of rate constants $k_1 \approx 8 \times 10^5$, $k_2 = 1 \times 10^{10}$, $k_3 = 3.2 \times 10^{10}$ litre mol⁻¹ s⁻¹ and assuming that the thickness of the active layer at the cathodic spot was ~ 1 nm, the authors assessed the rate (R_i) of generation of radicals and their concentrations to be $R_i = 261$ mol litre⁻¹ s⁻¹, $[HO^\bullet] = 8.17 \times 10^{-5}$, $[H^\bullet] = 6 \times 10^{-5}$ mol litre⁻¹ (the latter quantity pertains to the primary reaction zone with a thickness of ~ 400 nm).

Oxidation of potassium iodide solutions was also studied.⁴⁰ The effect of a glow discharge on acidic and neutral KI solutions in hydrogen atmosphere was explored. Solutions were prepared from 0.4 M H_2SO_4 and a neutral phosphate buffer (0.1 M $Na_2HPO_4 + 0.1$ M KH_2PO_4). The formation of molecular iodine and hydrogen peroxide was expected. Hydrogen peroxide complicated the analysis because it could react both during the discharge and after its quenching. To solve this problem, 1 ml of 20% ammonium molybdate solution was added to the cell as the catalyst of the hydrogen peroxide reaction with iodide ions. Under these conditions, I_2 was expected to become the only product of this process. Figure 3 shows the measured total yields of oxidation products. In contrast to other cases [oxidation of bivalent iron, potassium hexacyanoferrate(II), *etc.*], the dependences of the yield of oxidation products passed through the maximum rather than tended to a limit.

Oxidation of potassium iodide subjected to a gliding arc discharge was studied.⁴⁴ For a discharge power of 1 kW dissipated in 50 ml of solution, the steady-state concentration of oxidation products was attained in ~ 1 h.

Spectrophotometric studies^{29, 49–51} were devoted to the oxidation of iodide ions under a glow discharge. The changes in the absorption of a neutral potassium iodide solution subjected to a stationary discharge were studied at a wavelength of 460 nm for different starting concentrations. During the plasma treatment, the optical density of the solution passed through a maximum the height and position of which strongly depended on the starting concentration of iodide ions. The initial segments of optical density curves were almost linear. The curves' segments at greater times described the optical density to descend by approximately the exponential law.

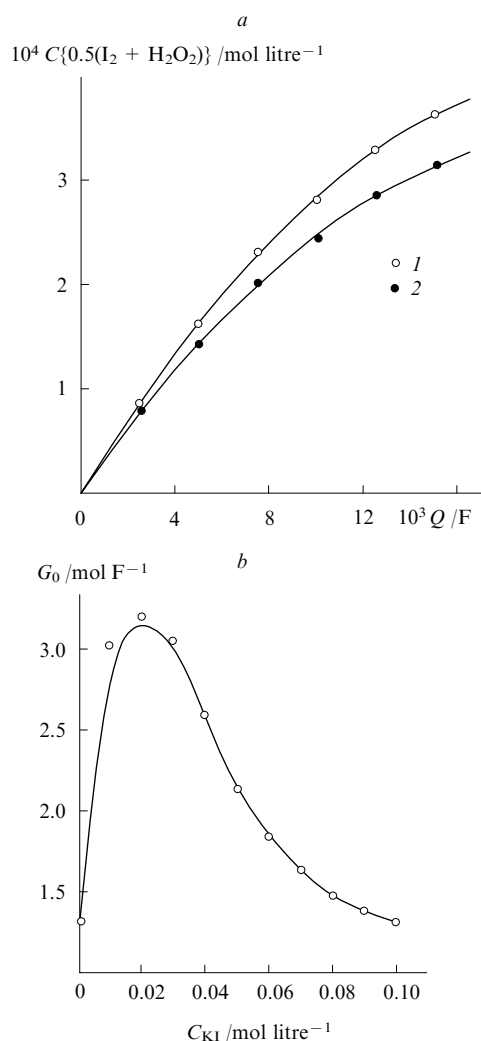


Figure 3. Dependences (a) of the overall concentration of KI oxidation products under the action of a glow discharge on the quantity of electricity passed through the solution and (b) of the initial current efficiency on the KI concentration in solution. Hydrogen atmosphere (50 Torr), current 75 mA.
(1) Acidic medium, (2) alkaline medium.

Table 5 shows the characteristics of gas-discharge-initiated oxidation of iodide ions calculated from experimental results.

Due to a high rate of the transformation of molecular iodine to triiodide ions,⁵² the initial segments of absorption curves measured at moderate starting concentrations of iodide ions directly illustrated the accumulation of triiodide ions. This conclusion was confirmed by the absorption spectra of KI

Table 5. Oxidation rates (v) of iodide ions and current yields (G_0) of the oxidation product (stationary glow discharge, discharge current 6 mA).²⁹

$10^3 C_0(KI) / \text{mol litre}^{-1}$	$10^7 v / \text{mol litre}^{-1} \text{ s}^{-1}$	$G_0 / \text{mol F}^{-1}$
0.9	1.57	0.45
1.8	0.63	0.18
3.6	1.38	0.4
7.23	9.8	2.88
15	3.4	0.96

solutions treated in plasma. At short treatment times, merely the absorption of triiodide ions was observed, which monotonically increased with an increase in the exposure time. Experiments at low starting concentrations of iodide ions showed that the optical density of solutions descended for the greater doses of treatment, *i.e.*, the formation of polyiodide ions was merely the first stage of oxidation. Qualitative chemical analysis of solutions thus treated indicated the formation of iodates.

Studies of the effect of plasma formed in a stationary glow discharge and a gliding arc discharge on aqueous solutions of sodium sulfide have shown²⁹ that plasma-initiated oxidation of sulfide ions proceeds *via* sulfur and polysulfide ions to ultimately afford sulfites and sulfates. These conclusions were drawn based on spectral measurements and the qualitative chemical analysis of treated solutions.

3. Reduction of inorganic compounds

Plasma-initiated reduction reactions in solutions were far less studied as compared with oxidation reactions. Early studies by Klemenc^{3,4} provided the most systematic data. The precipitation of metal or metal oxide from salt solutions and the reduction of certain acids (HClO_3 , HBrO_3 , HClO_4 , HNO_3 , *etc.*) were investigated.³

The reduction of potassium chlorate in a neutral solution yielded chloride ions. The reduction of KBrO_3 proceeded quite efficiently even in neutral solutions (like the reduction of chlorates in acidic solutions). Chromic acid was reduced almost completely to a chromium(III) salt. Perchloric acid failed to be reduced in the conventional electrolysis. A glow discharge initiated its reduction with the conversion degree dependent on the concentration. Table 6 compares the reduction processes that occur in the classical electrolysis and with the plasma activation.

The studies⁴ of the reduction of perchloric and chloric acids and their salts have revealed the following specific features.

1. The discharge-induced reduction of perchloric and chloric acids and their salts can occur with either anode or cathode located in the gas phase.

2. The reduction of perchloric acid in the region of the cathodic potential drop (when the anode is located in the gas

Table 6. Features of reduction under conditions of classical electrolysis and glow discharge.³

Electrolyte	Classical electrolysis	Glow discharge ^a	Notes
KNO_3	the products are NH_3 and NH_2OH	the products are HNO_2 , NO and N_2O	alkaline solution
$\text{Fe}_2(\text{SO}_4)_3$	easily reduced	reduced insignificantly	sulfuric acid solution
KClO_3	no or insignificant reduction on a Cu–Pt electrode, substantial reduction on a Fe electrode	reduction (12%)	neutral solution
KBrO_3	readily reduced on a Pt electrode	reduction (90%)	acidic solution
H_2CrO_4	reduction to $\text{Cr}_2(\text{CrO}_4)_3$	reduction (90%)	neutral or acidic solution
HClO_4	no reduction	reduction (88%)	—
		stepwise reduction (up to 40%)	Cu or Pt electrode

^a In parentheses, the yield of reduction products is shown.

Table 7. Reduction of perchloric and chloric acids and their salts under conditions of classical electrolysis in a glow discharge.⁴

Electrolyte	Classical electrolysis	Reduction in a glow discharge (%)	
		cathode in the gas phase	anode in the gas phase
HClO ₃ , 1 M	insignificant reduction on a Pt electrode	500	2600
HClO ₄ , 1 M	is not reduced on a Cu–Pt electrode	20	200
KClO ₃ , 0.26 M	insignificant reduction on conventional electrodes	90	500
NaClO ₄ , 0.5 M	is not reduced on a Pt electrode	insignificant reduction	60
	insignificant reduction on a Ni–Fe electrode	the same	no noticeable reduction

phase) demonstrates the strongest (40-fold in 2.5 M solution) increase in the yield of products over the faradaic yields.

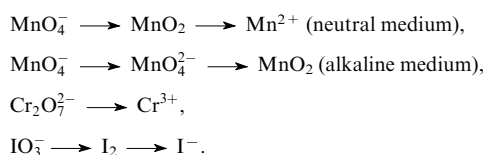
3. The reduction of perchloric acid corresponds to its decomposition to HCl and O₂.

4. Side reactions that produce detonating gas occur at a rate, which is the higher the slower the corresponding reduction reaction in the electrolyte.

5. The ratio of current efficiencies observed in the anodic and cathodic compartments is the same for the oxidation of sulfuric acid solutions and the reduction of perchloric acid.

Table 7 compares the reduction processes that occur in the classical electrolysis with the corresponding plasma-electrolytic reactions.

The reduction of inorganic ions under the action of a stationary glow discharge at atmospheric pressure was studied^{53,54} (the discharge current was 10 mA, the solution volume was 400 ml). The following processes were observed:



4. Gas evolution processes

In 'classical' electrolysis of aqueous electrolyte solutions, the evolution of main gaseous products (oxygen and hydrogen) is associated with the electrode processes of the discharge of hydroxyl and hydronium ions. The situation changes crucially when the electrode represents the plasma in contact with a solution. Ions accelerated in the region of the potential drop at the solution surface initiate dissociation of solvent molecules. This gives rise to many effects including the evolution of gaseous products, which does not obey the Faraday law. At the same time, ions that came to solution from the plasma zone and underwent thermalisation can either be solvated or recombine with solution counter-ions, which ultimately affords gaseous products in yields corresponding to the Faraday law. Hence, the analysis of the gas evolution in the course of the plasma treatment of solutions might shed light on the behaviour of ions injected into the solution from the plasma zone and answer the question on the role of their solvation.

It was noted⁵ that, if exclude the secondary effects, the gas evolution was never observed in the cathodic spot region on the solution surface. This makes the bulk recombination of ions injected into the plasma zone quite unlikely.

It was shown⁷ that in addition to the faradaic ('polar', according to the authors of Ref. 7) gas evolution, the electrolysis in a glow discharge always produces the detonating gas. The cathodic spot is the source of active species that lead to the formation of the latter gas. The amount of evolved detonating gas can be many times increased if one surrounds the cathodic spot with a narrow glass cylinder. The effect manifests itself to the full extent only if the cylinder is completely immersed into the electrolyte. Based on these experiments, it was concluded⁵ that the 'non-polar' formation of detonating gas occurs only as a result of a heterogeneous process.

The formation of oxygen and hydrogen in the anodic and cathodic discharges was studied.¹² A solution of 0.05 M K₂SO₄ served as the electrolyte. Figure 4 shows the dependences of the oxygen and hydrogen yields on the quantity of electricity passed through the solution and the potential drop in the discharge gap for a 'positive' contact discharge. As seen from the Figure, the processes that do not obey the Faraday law make the main contribution to the formation of gaseous products. In a 'negative' contact discharge, the yields of oxygen (1.84 mol F⁻¹) and hydrogen (2.73 mol F⁻¹) also substantially exceeded their faradaic yields.

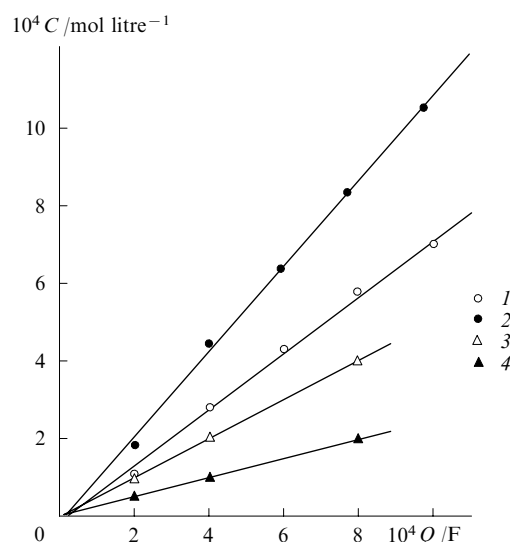


Figure 4. Dependences of (1) oxygen and (2) hydrogen yields on the quantity of electricity passed under the action of a glow discharge on a K₂SO₄ solution; (3) and (4) corresponding 'faradaic' yields.

5. Oxidation processes initiated by a glow discharge in solutions of organic compounds

a. Oxidation of alcohols

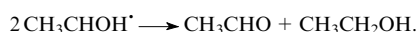
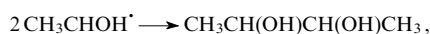
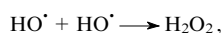
The effect of a glow discharge on a methanol solution was studied.³⁸ In the cathodic glow discharge, the main products were formaldehyde and formic acid. The anodic discharge produced fomadehyde and insignificant amounts (~1% of the HCOH yield) of formic acid, ethylene glycol and dimethoxy-methane. No hydrogen peroxide formation was observed. In both cathodic and anodic discharges, hydrogen, methane and carbon monoxide were the main gaseous products. Trace amounts of ethane, ethylene and acetylene were detected.

The medium becomes acidic under the action of a 'positive' discharge and alkaline when subjected to a 'negative' discharge.

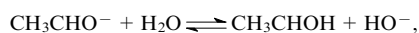
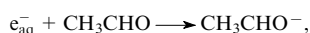
The effect of a glow discharge on the ethanol solution was considered in the same publication. Oxygen and argon at a pressure of 100 Torr served as the working gas. The main

reaction products included acetaldehyde, hydrogen peroxide and butane-2,3-diol. Their yields strongly depended on the presence of oxygen in this system and the intensity of its flow. The other key factors were the gas pressure, the intensity of stirring, the discharge current and the quantity of electricity passed. The hydrogen peroxide yield increased with an increase in the oxygen flow rate. The following mechanism of the processes was put forward. In the absence of oxygen and at a sufficient concentration of ethanol, the main initial reaction was the capture of hydroxyl radicals by ethanol molecules. The reactions of hydrogen atoms and solvated electrons proceeded more slowly. The reaction of H^\bullet and HO^\bullet radicals with ethanol is sufficiently well studied. A HO^\bullet radical abstracts a hydrogen atom from an ethanol molecule to form the following products: $\text{CH}_3\text{CH}_2\text{O}^\bullet$ (2.5%), $\text{CH}_3\text{CHOH}^\bullet$ (84.3%), $\text{CH}_2\text{CH}_2\text{OH}^\bullet$ (13.2%). The rate of the reaction of hydrogen atoms with ethanol molecules was lower by approximately two orders of magnitude. The main process was the elimination of a hydrogen atom from the CH_2 group to afford molecular hydrogen and a $\text{CH}_3\text{CHOH}^\bullet$ radical. In turn, radicals $\text{CH}_3\text{CH}_2\text{O}^\bullet$ and $\text{CH}_2\text{CH}_2\text{OH}^\bullet$ abstracted a hydrogen atom from an ethanol molecule. In the second case, this led to the conversion of the HO^\bullet radical into the 1-hydroxyethyl radical.

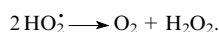
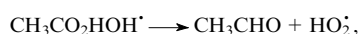
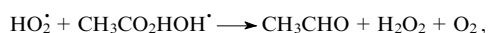
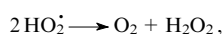
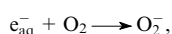
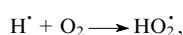
The action of a glow discharge on a water–ethanol solution of a neutral phosphate buffer under the argon atmosphere produced hydrogen peroxide, butanediol and acetaldehyde.³⁸



The following solvated electron reactions were considered:



The hydroperoxyl radical HO_2^\bullet played an important role in the discussed processes.



Thus, the presence of oxygen in the system gives rise to two additional channels for the formation of hydrogen peroxide. One channel is associated with the intermediate formation of organic peroxy radicals and the second corresponds to the formation of hydroperoxyl radicals.

Bugaenko *et al.*^{21,55} studied the conversion of 0.1–3 M solutions of methanol and ethanol in a carbonate electrolyte under the action of microdischarges on an aluminium anode. Table 8 shows the main reaction products and their energy yields. The products of ethanol conversion were formed both within gas-vapour bubbles and in the near-surface liquid layer (the yield of the latter amounted to no more than 20% of the total yield).

The results shown above allow one to qualitatively compare the effects of a glow discharge (at reduced pressure) and anodic microdischarges on methanol and ethanol solutions. The reaction products for both PSS types by and large coincided. However, it should be mentioned that the reaction

Table 8. Energy yields of reaction products of 2 M ethanol and 2 M methanol in a 0.03 M solution of sodium carbonate under the action of microdischarges on an aluminium anode (voltage 500 V, current 90 mA, error of yield determination < 10%).^{21,55}

Product	Yield /number of molecules per 100 eV	
	ethanol solution	methanol solution
H_2	1.90	2.60
CO	0.72	1.30
CH_4	0.29	0.27
C_2H_6	0.17	—
C_2H_4	0.40	—
$\text{C}_2\text{H}_6 + \text{C}_2\text{H}_4$	—	0.11
C_3H_8	0.056	0.0086
$\text{C}_2\text{H}_2 + \text{C}_3\text{H}_6$	0.19	0.010
C_4H_{10}	0.13	—
CH_3OH	0.030	—
$\text{CH}_3\text{CH}(\text{OH})\text{CH}_2\text{OH}$	0.015	—
$\text{CH}_3\text{CH}(\text{OH})\text{CH}(\text{OH})\text{CH}_3$	0.015	—
CH_2O	0.041	0.28
$(\text{CH}_2\text{O})_2$	—	0.098
HCOOH	—	0.058
CH_3CHO	0.260	—
CH_3COOH	0.050	—
H_2O_2	0	0

Note. The consumption of ethanol and methanol (calculated from the yields of products) was 1.83 and 2.38 molecules per 100 eV of energy, respectively.

products formed under the action of a glow discharge on a methanolic solution of LiClO_4 included dimethoxymethane, which was absent when methanol in aqueous sodium carbonate solutions was subjected to anodic microdischarges. The quantitative comparison of yields of products in these PSS is complicated by the fact that the yields are expressed in different units, namely, per 100 eV of consumed energy (anodic microdischarges) and in mol F^{-1} (glow discharge). However, bearing in mind that the authors of these studies^{21,55} assessed the average energy of ions that have passed to the solution from the anodic microdischarge zone as 100 eV, it can be assumed that the yield per 100 eV coincides with the yields expressed as the number of moles per Faraday of electricity. This allows one to compare certain values found for the glow discharge and anodic microdischarges (Table 9).

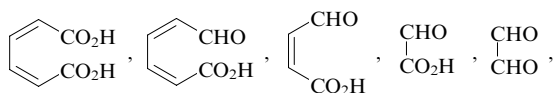
Table 9. Yields of products (mol F^{-1}) under the action of a glow discharge³⁸ and anodic microdischarges^{21,55} on an aqueous ethanolic solution.

[$\text{C}_2\text{H}_5\text{OH}$] /mol litre ⁻¹	CH_3CHO			Butane-2,3-diol	
	glow dis- charge in O_2	glow dis- charge in Ar	anodic micro- discharge	glow dis- charge in Ar	anodic microdis- charges
0.01	0.18	0.25	—	0.05	—
0.1	2.39	1.83	0.024	0.90	0.0007
0.3	6.47	4.67	0.043	1.14	0.0015
0.9	6.44	4.56	—	1.20	—
1.0	—	—	0.14	—	0.078

The difference between the yields obviously exceeds the possible errors and may point to a difference in the mechanisms of processes in these PSS.

b. Oxidation of aromatic compounds under pulsed discharges

Since the early 1990s, in line with the solution of environmental problems, keen attention has been paid to the oxidation of aromatic compounds in aqueous solutions under the action of either pulsed discharges in liquids or pulsed discharges between a metal electrode located in the gas phase and the solution surface.^{55–69} These studies preferentially dealt with phenol and its derivatives. In the phenol oxidation generated by pulsed discharges, pyrocatechol, hydroquinone, *p*-benzoquinone and (in small amounts) resorcinol were detected as the primary products.^{60, 68} Figure 5 shows the kinetics of decomposition of phenol and accumulation of its primary destruction products. Presumably, the first stage of this process is the hydroxyl radical reaction with a phenol molecule, which results in either the addition of HO• to the benzene ring to afford a dihydroxycyclohexadienyl radical or the elimination of a hydrogen atom from the OH group to form a phenoxyl radical. The radical reactions produced the intermediates listed above. Subsequent stages involved the benzene ring opening to form acyclic products



and also oxalic and formic acids, acetaldehyde and formaldehyde. Figure 6 illustrates the kinetics of accumulation of formic acid in aqueous phenol subjected to a corona discharge.⁶⁰

The oxidation of phenol in aqueous solutions under anodic microdischarges was described.^{22, 70} For relatively low initial phenol concentrations ($\sim 10^{-5}$ – 10^{-2} mol litre⁻¹), its concentration was found to decrease in time according to the exponential law; however, for high initial concentrations, two characteristic kinetic regions were observed, namely, the initial fast and the subsequent slow regions. Presumably, the deceleration of the oxidative destruction of phenol observed in its concentrated solutions was associated with the accumulation of stable intermediates and their competition with phenol molecules for HO• radicals.

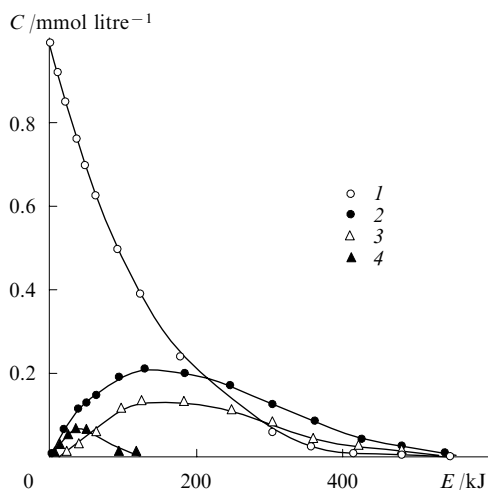


Figure 5. Kinetics of oxidation of phenol and accumulation of its primary destruction products: (1) phenol, (2) pyrocatechol, (3) hydroquinone, (4) *p*-benzoquinone.

c. Oxidation of organic dyes in aqueous solutions

The corona-discharge generated oxidation of Methylene Blue and Malachite Green dyes in aqueous solutions was studied⁷¹

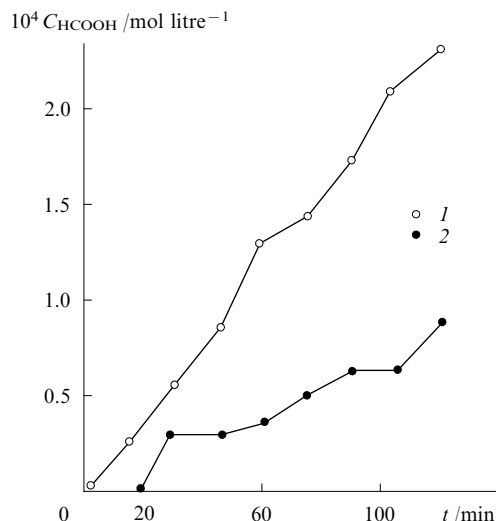


Figure 6. Kinetics of formic acid accumulation under the action of a pulsed corona discharge on an aqueous phenol solution: (1) in argon, (2) in air.⁶⁰

(the solution volume was 100 ml, the starting concentrations of dyes was 6 mg litre⁻¹, the discharge current was varied from 40 to 150 μ A). The kinetics of this process was monitored by following variation of the light absorption by the dissolved dye. The results strongly depended on stirring and the distance between the electrode and the solution surface. Chloride ions inhibited this process. Presumably, ozone, oxygen atoms, HO• radicals and hydroxyl ions were the active species that initiated the dye oxidation. After the treatment, the solution ceased to absorb light at 200–900 nm.

The oxidation of an aqueous solution of Monochlorotriazine Blue (or Bright Blue) dye (MCTB) under glow or gliding arc discharges was considered.^{72, 73} In all experiments, the dye was decolourised (Fig. 7). However, the initial period of this process could be different for different discharge currents and types. Thus when the times of MCTB exposure did not exceed 2–3 min, the absorption could uniformly decrease over the whole visible spectrum range; however, the process could lead to a decrease in the absorption in the vicinity of the maximum (~ 600 nm) and its simultaneous increase in the vicinity of the

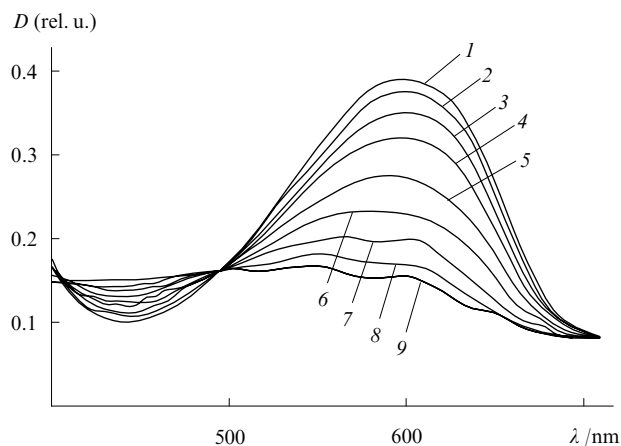


Figure 7. Changes in the absorption spectrum of a solution of Chlorotriazine Blue under a gliding arc discharge. Exposure time (min): (1) 0, (2) 2, (3) 4, (4) 6, (5) 8, (6) 10, (7) 12.5, (8) 15, (9) 17.5.

absorption minimum (~ 450 nm). For long-term exposure, the absorption at 450 nm passed through a maximum and the absorption in the near UV range increased. The changes in the absorption spectrum of the dye could be observed for several hours after the cessation of the plasma treatment.

Based on the results of spectrophotometric measurements, kinetic curves that reflect the changes in the dye concentration were plotted. In doing so, it was assumed that oxidative destruction products of a dye do not absorb in the long-wave region. Figure 8 shows the examples of kinetic curves.

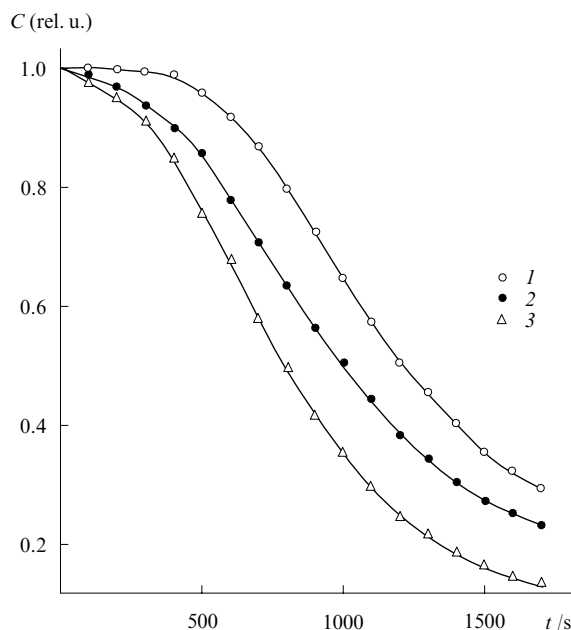


Figure 8. Kinetics of destruction of Monochlorotriazine Blue under a glow discharge with the plasma zone of different length (mm): (1) 1.34, (2) 2.3, (3) 3.8.

Experimental kinetic curves were interpreted within the framework of a simple model that assumes the plasma-initiated formation of an oxidant and its one-stage reaction with the dye, which is of the first order with respect to the oxidant. The rate of oxidant formation (ω_o) is constant within the framework of this model. The accumulation of oxidant after switching on the discharge is determined by ω_o and the oxidant lifetime (τ_o). The model gives the following expression for the time dependence of the relative dye concentration (C/C_0):

$$\ln \frac{C}{C_0} = -\left(\frac{k\omega_o\tau_o}{2}\right)t^2 - (k\omega_o\tau_o^2)(e^{-t/\tau_o} - 1),$$

where k is the effective rate constant for oxidation.

Figure 8 shows the dependence of the dye oxidation rate on the distance between the anode and the solution surface. An increase in the discharge current results in the substantial acceleration of the dye destruction (Fig. 9). Extrapolation to the zero inter-electrode distance gives the reaction rate for the solution activation by exclusively the ions accelerated in the region of the near-surface potential drop and injected into the liquid phase. The increase in the reaction rate with the increase in the plasma column height points to the possibility of initiation of the reaction by neutral active species generated in the gas phase.

The effect of the pre-treatment of a MCTB solution with a corona discharge on the rate of the MCTB oxidation under a stationary glow discharge was studied.²⁹ For the treatment

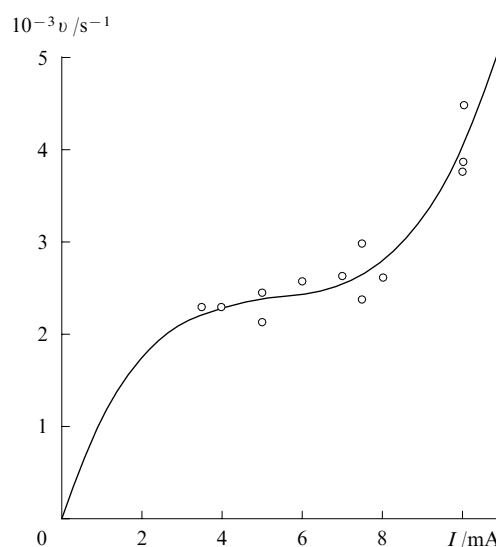


Figure 9. Initial destruction rate of Monochlorotriazine Blue during the plasma treatment vs. discharge current (the rate was assessed from the changes in the optical density of solution).

time of no longer than 30 min, the decolouration of the solution under the direct action of a corona discharge with a current of 50–100 μ A was hardly visible. At the same time, the subsequent oxidation of the dye under the action of a glow discharge sharply accelerated.

The oxidation of Methylene Blue in aqueous solutions under the action of glow and diaphragm discharges was considered^{74,75} (the current was varied in a range of 20–50 mA). The kinetics of dye destruction was studied using a spectrophotometric technique in wavelength ranges of 220–350 and 450–750 nm ($\lambda_{\max} = 667$ nm) with periodic sampling of the solution.

Discharges of both types favoured a decrease in the optical density of solutions in the visible spectrum of the dye. In an acidic medium ($\text{pH} < 4$), the increase in the discharge current led to the acceleration of dye destruction. It should be noted that for all other factors equal, the decolouration was faster at the diaphragm discharge. The absorption spectra in the region of 450–750 nm remained virtually unchanged, being identical for both discharge types. At the same time, the changes in the UV spectrum substantially depended on the discharge type. The increase in the optical density of solutions with the increase in the time of their exposure to plasma was one order of magnitude greater for the glow discharge (for equal exposure times and similar discharge currents and pH values). This fact can be interpreted as a result of the deeper oxidative destruction of the dye under the action of a diaphragm discharge. Presumably, these results point to the difference in the mechanisms of processes initiated by glow and diaphragm discharges. This was assumed to be due to the effect of a shock wave that appears during the burning of a diaphragm discharge.

In the same publications, the post-effect, which was observed in solutions treated with a discharge was discussed. The studies were carried out by several methods.

1. Dye solutions ($\text{pH } 3$) were exposed to the plasma of the glow and diaphragm discharges at a current of 50 mA for 2, 5 and 10 min, then samples were taken and the time variations of the absorption spectra in the absence of plasma treatment were studied.

2. Electrolyte solutions ($\text{H}_2\text{O} + \text{H}_2\text{SO}_4 + \text{Na}_2\text{SO}_4$) with $\text{pH } 3$ were exposed to discharges of both types for 2, 5 and 10 min; immediately a dye was added up to a concentration of

0.01 g litre⁻¹. Then, solution samples were taken and their absorption spectra were analysed in certain time intervals.

3. Experiments were carried out as described above (point 2), but the dye was added in 20 min rather than immediately.

The deviations in the effects of glow and diaphragm discharges also showed up in the post-effect characteristics. Under the same conditions, the diaphragm discharge produced a stronger effect (Fig. 10). Upon the cessation of the discharge, the dye concentration decreased to the same level for both the direct plasma treatment of dye solutions and when the dye was added to the electrolyte pre-activated by a discharge. At the same time, the kinetics of the post-effect strongly depended on the experimental conditions, *e.g.*, on the illumination (Fig. 11).

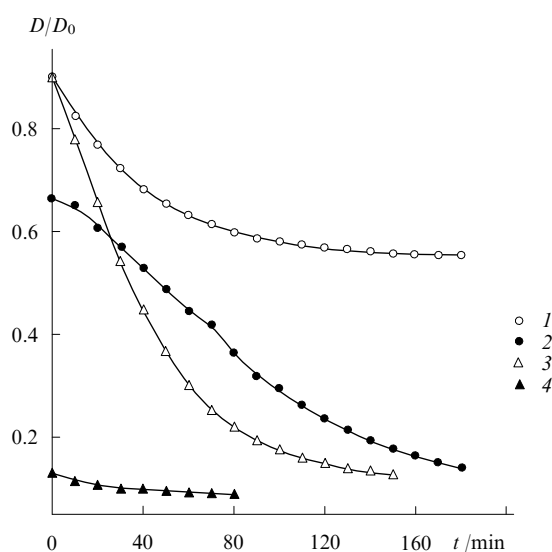


Figure 10. Changes in the optical density of a Methylene Blue solution upon its exposure to plasma (discharge current 50 mA, pH ~ 3, $\lambda_{\text{max}} = 667$ nm): (1) glow discharge, exposure time 5 min; (2, 3, 4) diaphragm discharge (exposure times 2, 5 and 10 min, respectively).

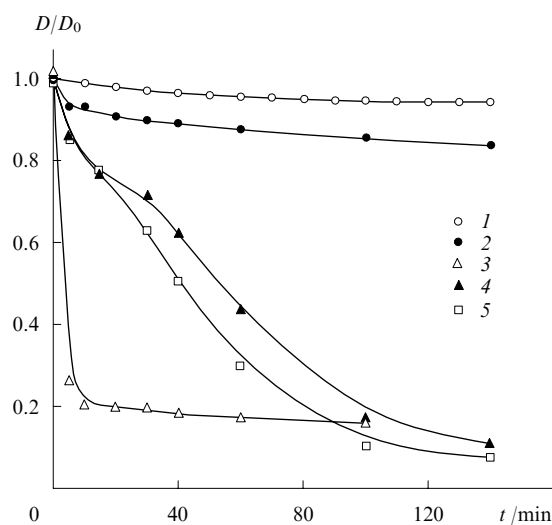


Figure 11. Changes in the optical density of a plasma-pre-activated Methylene Blue solution.

(1) Glow discharge: exposure time 10 min, the solution was kept in the dark; (2–5) diaphragm discharge: exposure time 10 min (2) in the dark and (3) in the light; exposure time 5 min (4) in the dark and (5) in the light.

To explain the results obtained, it was assumed that, in principle, the exposure of solutions to gas discharges can give rise to three different effects, namely, solution activation, solute activation and changes in the solution structure. Among these effects, only the solution activation is sufficiently well studied. Insofar as the differences between the glow and diaphragm discharges were observed both at their direct action on dye solutions and as the post-effect in preliminary treated dye solutions and also as the changes in the destruction rate of a dye added to electrolyte solutions (pre-treated with a discharge in the absence of the dye), the role of direct activation of the solute can hardly be great. At the same time, the post-effect could not be caused by short-lived primary active species; and, moreover, the addition of hydrogen peroxide to a dye solution, which was not pre-treated with a discharge, did not lead to results resembling the post effect. Thus, the reason for the long-term and strong post-effect should be sought in the effect of the discharge on the solution structure, which can cause changes in both thermodynamic and kinetic characteristics of processes that occur in solutions. This effect can be stronger in the presence of a shock wave at the diaphragm discharge.

d. Syntheses of organic compounds initiated by a gas discharge in electrolyte solutions

Harada and co-workers^{76, 77} studied the asparagine formation under the action of a glow discharge on a solution containing a mixture of amino acids (glycine, alanine and β -alanine) with amides of simple carboxylic acids.

Denaro and Hough⁷⁸ studied the acrylamide polymerisation initiated by a glow discharge between the air-located metal anode and an aqueous solution of the monomer. They have found the dependences of the polymer yield and its average molecular mass on the quantity of electricity passed, the acrylamide concentration and the air pressure. The results obtained were explained within the framework of a simple kinetic model. Two reaction zones were singled out. The first zone represented a thin near-surface solution layer in the vicinity of the cathodic spot. No polymerisation was observed in this zone. The concentration of radicals in this zone was very high; hence, their recombination prevailed. Only ~0.2% of radicals reached the second zone with a volume of ~0.4 cm³. Here, the radicals initiated the chain polymerisation reaction. The polymer yield increased virtually linearly with the increase in both the quantity of passed electricity and the acrylamide concentration. The average molecular mass also increased linearly with the increase in the monomer concentration. Under the conditions of the experiment described, the polymer yield reached 15 mol F⁻¹. With the increase in the air pressure, these characteristics decreased. Moreover, the efficiency of this process also decreased in the alkaline medium.

V. Potentials and prospects of plasma initiation of industrial processes in aqueous solutions

The surface modification of polymeric materials including fabrics with natural and synthetic fibres (pre-treatment of fabrics before printing, dyeing, *etc.*), bleaching (especially of linen), delignification of wood, *etc.* may be assigned to the heterogeneous processes presumably initiated by the plasma – solution treatment. At present, this field remains virtually unexplored.

1. Plasma modification of starch glue. Treatment of microcrystalline cellulose

The modification of starch by different reagents is one of the methods used in practice for the preparation of starch and its products with desired properties. The treatment of starch with oxidants, for example, sodium or potassium hypochlorites, is most popular. Hydrogen peroxide, potassium permanganate

in alkaline media, chloramine T, *etc.* are also used. The diverse goals of starch modification, the long time required when traditional methods are used and the environmental problems associated with the use of such reagents as hypochlorites send the scientists in search for alternative methods of modification. The effect of the glow-discharge plasma treatment on the properties of starch glue was studied.^{79,80} The glue viscosity was considered as the criterion of its modification degree. The viscosity was observed to increase in the initial period of treatment. The decrease in the viscosity at long-term treatment pointed to the predomination of destruction processes. Note that it takes a short time to reach the maximum viscosity even for discharges with quite moderate power densities.

The use of atmospheric-pressure plasma in processing of cellulose-containing materials attracts attention because cellulose is one of the basic raw materials used in the pharmaceutical, textile and food industries. The surface modification of cellulose by the gas-discharge activation can change its reactivity.

The effect of gas-discharge activation on the electrokinetic properties of aqueous suspensions of cellulose powder (electrophoresis mobility of cellulose particles) was considered.⁸¹ Glow and diaphragm discharges served as the sources of activation. A 0.04% solution of cellulose powder with colloid particles <63 µm in diameter was studied. The required solution conductivity was achieved by adding sodium chloride (10^{-3} mol litre⁻¹). The acidity of the dispersed medium was controlled by the addition of sodium hydroxide or hydrochloric acid. The studies of the electrophoretic mobility of processed cellulose have shown that the isoelectric point is at pH 2.5 and the maximum electrophoretic mobility is reached at pH 6.5. The exposure (20 min) of the dispersed system studied to the discharge led to the increase in the electrophoretic mobility of cellulose particles as compared with the reference untreated solution; moreover, the greatest effect was observed for the glow discharge. The latter effect can be associated with the fact that a diaphragm discharge not only generates reactive species but also gives rise to a shock wave in the solution.

2. Destruction of aqueous emulsions of hydrocarbons in anodic microdischarges

Under the action of an anodic microdischarge (aluminium cathode) on a pentadecane emulsion in a carbonate electrolyte, the alkane is destroyed to form hydrogen, carbon monoxide, gaseous hydrocarbons and an insoluble product, namely, a polycondensate that gives rise to the formation of spherical hollows filled with gas.^{82–85}

It was assumed that the primary process is the reaction between pentadecane and a hydroxyl radical, which consists of the elimination of a hydrogen atom from the alkane. A secondary aliphatic radical formed can either dimerise to afford a branched product or add an oxygen molecule. In turn, the peroxide radical gives rise to various secondary products, namely, alcohols, ketones, acids, hydroperoxides. The appearance of spherical particles points to the formation of a three-dimensional network; hence, dimeric products are subjected to the secondary attack of HO• radicals and decomposition products of hydroperoxides or react with fragment radicals formed in gas – vapour bubbles (GVB).

The energy yields of gaseous hydrocarbons C₁–C₅ and CO were independent of the emulsion concentration in the liquid phase. The overall curves of accumulation of gaseous products were linear for degrees of pentadecane conversion not exceeding 50% (at higher degrees of conversion, the curves tended to a certain limit). The partial curves of accumulation of individual gases with the exception of hydrogen were linear. The sum of energy yields of gaseous products increased non-linearly with the increase in the pentadecane concentration. The destruction of pentadecane to form light hydrocarbons almost

totally proceeded within gas – vapour bubbles. Hydrogen molecules were largely formed in the pentadecane layer on the GVB surface upon the reaction of the hydrogen atoms formed in GVB with pentadecane molecules. Carbon monoxide was also formed in GVB but upon the oxidation processes.

The microdischarge treatment of an emulsion containing 0.0012 mol litre⁻¹ of pentadecane and 0.005 mol litre⁻¹ of styrene resulted in the destruction of both pentadecane and styrene in energy yields of 0.16 and 0.50 molecules, respectively, per 100 eV of consumed energy, which was close to their yields in emulsions containing only individual components.⁸⁶

3. Plasma treatment of cellulose-containing and other phytogetic materials in aqueous media. Refining of textile materials

In addition to the search for new kinds and sources of raw materials, the development of fundamentally new methods for processing of traditional raw materials is of great importance. The processing of wood and resulting cellulose (including microcrystalline cellulose) forms the basis of many industrial processes (in pulp and paper industry, manufacturing of synthetic fibres, *etc.*).

Traditional processing of wood into cellulose, which involves mechanical grinding of wood, removal of lignine, (*e.g.*, by sulfite-alkaline digestion), bleaching, washing and drying, is an energy-consuming process accompanied by the formation of vast amounts of toxic sewage.

Thus, the plasma – solution activation of the listed processes in the stationary (or quasi-stationary) plasma or pulsed-discharge plasma in the liquid phase attracts attention. In these two cases, the chemical activation conditions are different; moreover, pulsed discharges give rise to a shock wave, *i.e.*, lead to the mechanochemical activation.

The studies of the effect of pulsed discharges in aqueous media on raw plant materials date back to the 1970s. Thus it was shown⁸⁶ that the processing of winter wheat straw in water and weak alkaline solutions leads to the partial destruction of the lignocarbon complex in straw and can form the basis of an industrial process of straw treatment for feeding livestock. It was proposed⁸⁷ to use high-voltage pulsed discharges in aqueous media for washing and degreasing wool. It was shown⁸⁸ that the electrohydraulic treatment of chlorella improves the digestibility of nitrogen-containing substances, while the similar processing of pine needles⁸⁹ makes it possible to produce a vitamin – protein concentrate. The action of pulsed discharges in water on kitchen herbs (parsley, dill) leads to the formation of a protein – lipid complex, a precursor of the vitamin – protein paste.⁹⁰ It was found⁹¹ that the electrohydraulic treatment of aqueous solutions of saccharose and glucose results in their hydrolysis, where a part of molecules decompose to afford formaldehyde. The possibility of using pulsed discharges at different stages of the wet treatment processes in industry, including textile production, was studied.⁹² A method for production of fibres from stems of fibre crops in which the wetting procedure was combined with high-voltage discharges at a voltage of 30–50 kV has been developed.⁹³

Detailed studies of the pulsed-discharge treatment of plant raw materials in aqueous media were carried out later.^{94,95} Wheat straw (coarse chopped, 3–10 mm) was subjected to pulsed discharges in water and the aqueous solutions of NH₄OH (0.5%–5%) and hydrogen peroxide (1%–5%). A stainless-steel reactor served as the cathode, a cylindrical anode was placed at the reactor axis above the solution surface. A power source allowed application of voltage pulses of 20–35 kV at a frequency of 0.1–0.5 Hz, period of 4–5 µs and energy of 120–2500 J. The treatment involved series of 100–1000 pulses. Both liquid and solid phases of the system formed upon the action of pulses were analysed. Table 10

Table 10. Liquid phase characteristics (in % of the original straw mass) after 100 discharge pulses as a function of single-discharge energy.⁹⁴

Determined characteristics	Discharge energy /J				
	120	240	540	960	2500
Extractive substances	0.04	0.09	0.55	0.13	0.58
Lignine	0.32	0.27	0.25	0.42	0.6
Polysaccharides	0.05	0.06	0.07	0.08	0.04
Colloidal suspension	1.1	1.2	1.0	1.5	1.5
Ash content	0.33	0.51	0.56	0.69	1.0

shows the results of the analysis of the liquid phase after 100 pulses with different energies.

Under the electrohydraulic impact, wheat straw is effectively chopped and its lignine–carbon complex is destroyed. The solid residue is freed from nitrogen-containing (proteins and their products) and silicon-containing compounds that enter into the ash composition. The short-term destruction of the lignine–carbon complex is the characteristic feature of the electrohydraulic treatment of plant biomass. The deeper destruction of the lignine–carbon complex was observed in the processing of wheat straw in NH_4OH and H_2O_2 solutions; although, due to the high conductivity of these solutions, a part of energy was consumed in the pre-breakdown stage, which affected the effectiveness of the electrohydraulic impact.

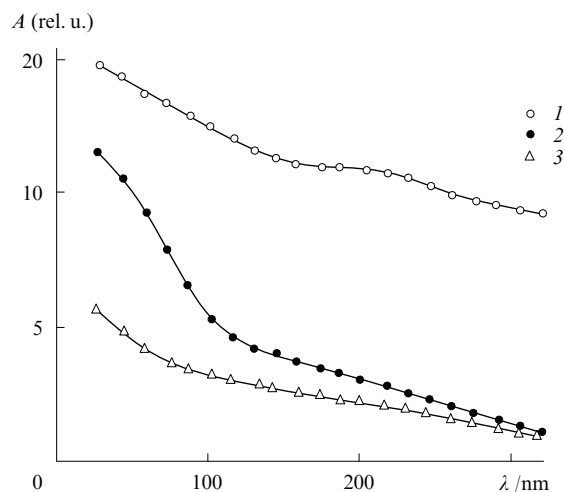
Similar processes occurred in alkaline aqueous suspensions of hydrolytic lignine, which were subjected to high-voltage pulsed discharges.⁹⁵ Lignine was dispersed and freed from mineral and organic low-molecule substances. However, gummy and lignohumic compounds were not removed. The gummy substances were washed out in alkalis, which was considerably accelerated under the simultaneous treatment with electric pulses.

All aforementioned studies devoted to the use of pulsed discharges failed to separate the contributions of chemical process and mechanochemical activation.

The effect of the solution activation in a glow discharge on the surface properties of cellulose-containing materials placed in solutions and also on the extraction of lignine was studied.^{29,96} Linen and roving fabrics were studied as well as wood in the form of sawdust. The process was carried out in aqueous NaOH at constant stirring, either without the gas flow or with oxygen bubbling through the solution. A 'positive' stationary glow discharge was used. It was found that the plasma–solution treatment allows one to increase the capilarity of fabrics; moreover, the effect strongly depended on the solution pH and might not correlate with the lignine destruction.

To check the selectivity of the effect of an activated solution on the cellulose-containing materials, the products obtained in the treatment of delignified cellulose and wood-extracted lignine, which have passed to solution, were analysed separately. The effect was followed by the analysis of absorption spectra of treated solution samples. Figure 12 shows the results obtained in an alkaline solution after the treatment of cellulose (with and without plasma activation) and lignine. According to these data, a plasma-activated aqueous solution that contains no specially added oxidants exerts a selective effect on the cellulose-containing materials.

The presence of such selectivity allows one to assume the possibility of using the mentioned method in the bleaching of fabrics. The samples of linen fabric were treated in the plasma-activated solution in the absence of specially added oxidants. The absorption spectra of the solution and the scattering spectra of the fabrics were studied simultaneously. The results obtained confirmed that the effect of fabric bleaching is present

**Figure 12.** Absorption spectra of solutions of (1) lignine and (2) cellulose upon treatment in a glow discharge (NaOH solution with concentration 1 g litre⁻¹, discharge current 20 mA, exposure time 20 min) and (3) spectrum of a solution of cellulose unexposed to plasma.

and the products accumulated in solution substantially affect this process.

The use of a volume discharge described quite recently in the treatment of cellulose-containing materials in the plasma–solution system was discussed.⁹⁷ Presumably, to achieve the greatest effect in the modification of polymeric materials, it is necessary to develop a PSS in which the reactions in the activated solution would occur simultaneously with the direct effect of plasma on the material modified. The discharge was ignited in a tube of silicon rubber that connected two stainless-steel vessels, which served as the electrodes; the circulation of solution was performed using a peristaltic pump. Linen roving of four-fold milling and purified cellulose were studied. The average degree of polymerisation, the lignine content and the moisture absorption were measured for the case of linen roving. In the case of cellulose, the measured characteristics included the degree of polymerisation and the contents of α -cellulose and the aldehyde and carboxyl groups. The treatment time was 10 min.

The treatment of linen roving in a PSS with a discharge in the electrolyte volume (NaOH) resulted in a greater decrease in the lignine content as compared with the conventional thermal

Table 11. Properties of linen roving treated in a plasma–solution system (volume discharge).⁹⁷

Sample	C_{NaOH} /g litre ⁻¹	Lignine content ^a (%)		Degree of poly- merisation	Moisture absorp- tion (%)
		ASL	AIL		
Original roving (4-fold milling)		1.5	10.5	4750	1010
Samples after treatment					
boiling ^b	50	0.4	9.3	3200	980
discharge ^c	50	0.21	5.2	2986	1030
boiling ^b	100	0.5	8.8	5500	1250
discharge ^c	100	0.2	4.6	1450	1142
boiling ^b	150	0.42	9.2	4500	1210
discharge ^c	150	0.19	4.6	2785	1205

^a ASL and AIL are acid-soluble and acid-insoluble lignine, respectively;

^b at 98 °C for 1 h; ^c in solution for 10 min.

Table 12. The effect of cellulose treatment in a volume discharge on its physicochemical properties.⁹⁷

Treatment conditions			Degree of polymerisation	Content of α -cellulose (%)	10 ⁵ δ (see ^a) (%)
C_{NaOH} /g litre ⁻¹	time /min	tube diameter /mm			
Original sample			1400	91.4	5.3
50	20	10	825	93.24	3.39
50	20	8	905	91.3	3.51
50	15	8	900	90.7	3.76
10	30	10	940	89.4	2.9
10	15	10	960	88.1	3.3
10	15	8	892	91.84	2.98
5	20	8	959	88.67	3.47
See ^b	20	8	981	88.77	2.98

^a δ is the content of aldehyde groups; ^b in this case, the electrolyte was 0.1 M Na₂SO₄.

treatment in alkali with a longer exposure time. The plasma–solution treatment in the volume discharge sharply reduced the degree of polymerisation; however, the moisture absorption changed insignificantly (Table 11). Table 12 shows the data obtained in the studies of cellulose.

4. The use of plasma–solution systems in cleaning and sterilisation of water, aqueous solutions and articles

The use of plasma discharges in aqueous media for their sterilisation and also for the sterilisation of articles was extensively studied since the beginning of the 1970s.^{98–106}

High-voltage electropulsed discharges can be considered as an environmentally clean source of UV radiation the short-wave spectrum of which is not ‘cut off’ by glass walls as in the case of UV lamps. Under the action of reactive species formed in water, decomposition of amino acids and proteins, depolymerisation of nucleic acids and destruction of other biologically active substances take place. Moreover, a pulsed discharge generates intense acoustic waves capable of tearing apart bacterial cells thus destroying them. The disinfecting effect persists for a long time after the cessation of the discharge treatment (days, weeks and longer) due to the effect of the microorganism decomposition products obtained in the active phase of the process. According to the data of Ref. 106, the pronounced antibacterial effect was observed at a discharge energy of $(0.6–0.8) \times 10^2$ J. In the same study, quantitative estimates of energy consumed in the water disinfection were obtained. The calculated relationships were derived under the assumption that the main effect is associated with the shock wave impact and that the destruction of simplest unicellular microorganisms requires an acceleration of 100–1000 *g*. The pressure in the compression wave front was assessed by the semi-empiric relationship

$$P = 0.6 \times 10^{-5} E_0^{0.6} \tau^{-0.8} r^{-1},$$

where P is the pressure (mPa), E_0 is the discharge energy (J), τ is the time of energy generation (s), r is the distance from the discharge centre to the measurement point (m).

If ρ_0 and a_0 are the density of the liquid and the sound velocity in it, then the liquid acceleration in the wave is

$$W = \frac{2P}{\rho_0 a_0 \tau}.$$

Hence, for the relative acceleration K_p , we obtain the following expression:

$$K_p = \frac{2P}{g \rho_0 a_0 \tau} = 0.8 \times 10^{-5} \frac{2E_0^{0.6}}{g r \rho_0 a_0 \tau^{1.8}}.$$

The volume of water cleaned is assessed from the distance at which the acceleration of the liquid in a wave is not lower than a given critical value.

The disinfecting efficiency of an atmospheric-pressure glow discharge that burned over the water surface in a flow-through system was assessed.¹⁰⁷ The concentration of hydrogen peroxide formed under the discharge (the discharge current was 200 mA, the output voltage reached 5 kV) was taken as the criterion of water decontamination efficiency. For a discharge gap of 10 mm and the power of ~ 90 W, the maximum accumulation of hydrogen peroxide was observed, namely, 3.6 g m⁻³ (1×10^{-4} mol litre⁻¹) at the minimum energy consumed in its formation (~ 250 kW h kg⁻¹). The fact that the maximum H₂O₂ concentration was achieved under these conditions was attributed to the maximum area of the cathodic spot. The hydrogen peroxide concentration decreased with an increase in the water consumption, whereas the efficiency with respect to H₂O₂ increased. This was explained by the fact that a part of hydrogen peroxide synthesised in the discharge was destroyed by the discharge itself. As a result, at the higher water consumption, the larger amount of H₂O₂ was brought out from the discharge zone without destruction. The overall content of hydrogen peroxide also depended on the electrode erosion products, which often catalyse H₂O₂ decomposition.

Sterilisation of conducting solutions and objects immersed in them under a glow discharge or a low-voltage diaphragm discharge (alternating current) was studied.^{33, 108, 109} The inhibiting effect of the atmospheric-pressure glow and diaphragm discharges on asporogenic microorganisms *Escherichia coli* M-17 was discussed. Microbiological studies of strains of the culture tested revealed that totally sterile solutions were obtained in 1–20 min depending on the exposure time, the type and intensity of discharge, the nature of the object sterilised and the nature and concentration of the bacterial culture. (Table 13).

Table 13. Results of gas-discharge sterilisation of solutions containing microorganisms *Escherichia coli* M-17 (see ^a).¹⁰⁹

Composition of the medium ^b		Treatment time ^d /min		
		DDC	RIF	ECS
Glow discharge				
I	10 ⁴	6	11	16
II	10 ⁴	5	10	15
	10 ⁷	10	16	20
Diaphragm discharge				
II	10 ⁴	1	2.5	3
	10 ⁷	5	10	12

^a Discharge parameters. Glow discharge: current 50 mA, voltage 1500 V; diaphragm discharge: current 50 mA, voltage 500 V; ^b Composition of the medium: (I) aqueous NaOH solution (1.5 g litre⁻¹) and nitrilotrimethylphosphonic acid; (II) physiological solution of NaCl (2 g litre⁻¹); ^c C is relative concentration of microorganisms (number of colonies in 1 ml of solution); ^d treatment time necessary for a decrease in the density of colonies (DDC), for observation of rare individual formations (RIF), for reaching the effect of complete sterility (ECS).

VI. Conclusion

Plasma–solution systems in which an electrolyte solution plays the role of one or both gas-discharge electrodes represent non-equilibrium systems where the chemical activation predominantly proceeds in a thin near-surface solution layer and is substantially determined by the parameters of the gas discharge and related processes on the plasma–solution interface. The combination of the chemical activity of plasma with the possibility of carrying out selective processes in solutions allows one to use plasma–solution systems in cleaning of water and aqueous solutions from organic and inorganic impurities, sterilisation of solutions and objects immersed in them and also in the modification of surface properties of natural and synthetic polymeric materials.

The physical chemistry and physics of PSS were studied far less comprehensively than the corresponding properties of the classical reduced and atmospheric pressure plasma in contact with solid objects. The most important trends in the physico-chemical studies of PSS are associated with the kinetics of generation of reactive species in both the solution surface layer and the adjacent plasma layer and also with the reactions of these species depending on the type of initiating gas discharge and the properties of the solution. It is the processes at the plasma–solution interface that are the governing factor.

References

1. M N Vasil'ev, in *Entsiklopediya Nizkotemperaturnoi Plazmy. Vvodnyi Tom IV* (Encyclopaedia of Low-temperature Plasma. Entrance Volume IV) (Ed. V E Fortov) (Moscow: Nauka, 2000) p. 331
2. A Güntherschulze *Z. Electrochem.* **31** 187 (1925)
3. A Klemenc, H F Hohn *Z. Phys. Chem., Abt. A* **154** 385 (1931)
4. A Klemenc, R Eder *Z. Phys. Chem., Abt. A* **179** 1 (1937)
5. A Klemenc, H Kalisch *Z. Phys. Chem., Abt. A* **182** 1 (1938)
6. A Klemenc, G Heinrich *Z. Phys. Chem., Abt. A* **183** 217 (1938)
7. A Klemenc *Z. Phys. Chem., Abt. A* **183** 297 (1938)
8. R A Davies, A Hickling *J. Chem. Soc.* 3595 (1952)
9. A Hickling, J K Linacre *J. Chem. Soc.* 711 (1954)
10. A R Denaro, A Hickling *Electrochem. Soc.* **105** 265 (1958)
11. A Hickling, G R News *J. Chem. Soc.* 5177 (1961)
12. A Hickling, G R News *J. Chem. Soc.* 5186 (1961)
13. A Hickling, M D Ingram *Trans. Faraday Soc.* 783 (1964)
14. A Hickling, in *Modern Aspects of Electrochemistry* Vol. 6 (Eds J O M Bockris, B E Conway) (London: Butterworth, 1971) p. 329
15. A Hickling, M D Ingram *J. Electroanal. Chem.* **8** 65 (1964)
16. A R Denaro, A Hickling *J. Electrochem. Soc.* **105** 265 (1958)
17. V V Bakovets, O V Polyakov, I P Dolgovesova, in *Plazmennoelektroliticheskaya Anodnaya Obrabotka Metallov* (Plasma-electrolytic Anodic Metal Working) (Novosibirsk: Nauka, 1991) p. 168
18. O V Polyakov, V V Bakovets *Khim. Vys. Energ.* **17** 291 (1983)^a
19. E G Vol'f, L T Bugaenko, G V Kovalev, A M Sizikov, E P Kalyazin *Khim. Vys. Energ.* **22** 377 (1988)^a
20. L T Bugaenko, E G Vol'f, E P Kalyazin, G V Kovalev, A M Sizikov, in *Plazmokhimiya-90* (Plasma Chemistry-90) Pt. 1 (Moscow: Department of Scientific and Technical Information of Institute of Petrochemical Synthesis, Academy of Sciences of the USSR, 1990) p. 8
21. L T Bugaenko, E G Vol'f, E P Kalyazin, G V Kovalev, A M Sizikov *Khim. Vys. Energ.* **29** 456 (1995)^a
22. O V Polyakov, A M Badalyan, L F Bakhturova *Khim. Interes. Ustoich. Razv.* **8** 855 (2000)^b
23. A I Maksimov, L A Kuz'micheva, A Y Nikiforov, J V Titova *Plasma Chem. Plasma Proc.* **26** 205 (2006)
24. S Braun *Elementarnye Protssy v Plazme Gazovogo Razryada* (Elementary Processes in Plasma of Gas Discharge) (Moscow: Gosatomizdat, 1961)
25. A M Kutepov, A G Zakharov, A I Maksimov *Dokl. Akad. Nauk* **357** 782 (1997)^c
26. A V Khlyustova, A I Maksimov *Elektron. Obrab. Mater.* **217** 35 (2002)
27. A V Khlyustova, A I Maksimov *Elektron. Obrab. Mater.* **227** 79 (2004)
28. A V Khlyustova, A I Maksimov, V A Titov *Khim. Vys. Energ.* **38** 227 (2004)^a
29. Yu V Titova, Candidate Thesis in Chemical Sciences, Institute of Solution Chemistry, Russian Academy of Sciences, Ivanovo, 1999
30. *Tablitsy Fizicheskikh Velichin* (The Tables of Physical Values) (Ed. I K Kikoin) (Moscow: Atomizdat, 1976)
31. A I Maksimov, Yu V Titova, L A Kuz'micheva, in *Gorenie i Plazmokhimiya (Sb. tr. III Mezhdunarodnogo Simpoziuma), Almaty, 2005* [Combustion and Plasma Chemistry (Proceedings of the IIIrd International Symposium), Almaty, 2005] p. 347
32. A K Pikaev, S A Kabakchi, I E Makarov *Vysokotemperaturnyye Radioliz Vody i Vodnykh Rastvorov* (High-temperature Radiolysis of Water and Aqueous Solutions) (Moscow: Energoatomizdat, 1988)
33. I K Stroikova, Candidate Thesis in Chemical Sciences, Institute of Solution Chemistry, Russian Academy of Sciences, Ivanovo, 2001
34. I K Stroikova, A I Maksimov *Elektron. Obrab. Mater.* **219** 52 (2003)
35. H A Dewhurst, J F Flagg, P K Watson *J. Electrochem. Soc.* **106** 366 (1959)
36. S K Sengupta, O P Singh *J. Electroanal. Chem.* **369** 113 (1994)
37. G A Mazzocchi, G Bontempelli, F Magno *J. Electroanal. Chem.* **42** 3698 (1973)
38. M A Almubarak, A Wood *J. Electrochem. Soc.* **124** 1356 (1977)
39. L A Kuz'micheva, Yu V Titova, A I Maksimov *Elektron. Obrab. Mater.* **228** 57 (2004)
40. A R Denaro, A Mitchell, M R Richardson *Electrochim. Acta* **16** 755 (1971)
41. A R Denaro, P A Owens *Electrochim. Acta* **13** 157 (1968)
42. L A Kuz'micheva, A I Maksimov, Yu V Titova *Elektron. Obrab. Mater.* **233** 41 (2005)
43. J L Brisset, J Lelievre, A Doubla, J Amouroux *Rev. Phys. Appl.* **25** 535 (1990)
44. M Chabchoub, J-L Brisset, A Czernichowski, in *Proceedings of 12th International Symposium on Plasma Chemistry, Minneapolis, 1995* Vol. 2, p. 801
45. A V Khlyustova, Candidate Thesis in Chemical Sciences, Institute of Solution Chemistry, Russian Academy of Sciences, Ivanovo, 2004
46. A I Maksimov, A V Khlyustova, S V Troshenkova *Elektron. Obrab. Mater.* **230** 31 (2004)
47. I K Stroikova, A I Maksimov, A V Grechin, in *Sb. Materialov 3 Mezhdunarodnogo Simpoziuma po Teoreticheskoi i Prikladnoi Plazmokhimii, Ples, 2002* (Proceedings of the 3rd International Symposium on Theoretical and Applied Plasma Chemistry, Ples, 2002) Vol. 2, p. 345
48. A R Denaro, K O Hough *Electrochim. Acta* **17** 549 (1972)
49. A G Zakharov, J V Titova, A I Maksimov, in *Problems of Solvation and Complex Formation in Solutions. (Proceedings of the 7th International Conference)*. Ivanovo 1998. P. 420
50. A M Kutepov, A G Zakharov, A I Maksimov, in *Vestn. Khar'kovsk. Un-ta* **27** 1 (1999)
51. Yu V Titova, A I Maksimov *Elektron. Obrab. Mater.* **192** 87 (1998)
52. V I Ksenzenko, D S Stasinevich *Khimiya i Tekhnologiya Broma, Ioda i ikh Soedinenii* (The Chemistry and Technology of Bromine, Iodine and their Compounds) (Moscow: Khimiya, 1979)
53. L A Kuz'micheva, Yu V Titova, A I Maksimov, in *Sb. Materialov 4 Mezhdunarodnogo Simpoziuma po Teoreticheskoi i Prikladnoi Plazmokhimii, Ivanovo, 2005* (Proceedings of the 4th International Symposium on the Theoretical and Applied Plasma Chemistry, Ivanovo, 2005) Vol. 2, p. 121

54. L A Kuz'micheva, Yu V Titova, A I Maksimov, in *Sb. Materialov 4 Mezhdunarodnogo Simpoziuma po Teoreticheskoi i Prikladnoi Plazmokhimii, Ivanovo, 2005* (Proceedings of the 4th International Symposium on the Theoretical and Applied Plasma Chemistry, Ivanovo, 2005) Vol. 2, p. 125
55. L T Bugaenko, E G Vol'f, G V Kovalev, A M Sizikov *Khim. Vys. Energ.* **36** 453 (2002)^a
56. A K Sharma, B R Locke, P Arce, W C Finney *Hazard. Waste Hazard. Mater.* **10** 209 (1993)
57. A A Joshi, B R Locke, P Arce, W C Finney *J. Hazard. Mater.* **41** 3 (1995)
58. P Sunka, V Babicky, M Člupek, P Lukes, M Simek, J Schmidt, M Černák *Plasma Sourc. Sci. Technol.* **8** 258 (1999)
59. Yu B Bark, E M Barkhudarov, Yu N Kozlov, I A Kossyl, V P Silakov, M I Taktakishvili, S M Temchin *J. Phys. D: Appl. Phys.* **33** 859 (2000)
60. W F L M Hoeben, E M van Veldhuizen, W R Rutgers, C A M G Cramers, G M W Kroesen *Plasma Sourc. Sci. Technol.* **9** 361 (2000)
61. A M Anpilov, E M Barkhudarov, Yu B Bark *J. Phys. D: Appl. Phys.* **33** 993 (2000)
62. W F L M Hoeben, E M van Veldhuizen, W R Rutgers, C A M G Cramers, G M W Kroesen *J. Phys. D: Appl. Phys.* **32** 133 (1999)
63. B Sun, M Sato, J S Clements *J. Electrostat.* **39** 189 (1997)
64. D Hayashi, W F L M Hoeben, G Dooms, E M van Veldhuizen, W R Rutgers, G M W Kroesen *J. Phys. D: Appl. Phys.* **33** 2769 (2000)
65. A T Sugiarto, M Sato *Thin Solid Films* **386** 295 (2001)
66. D Hayashi, W F L M Hoeben, G Dooms, E M van Veldhuizen, W R Rutgers, G M W Kroesen *J. Phys. D: Appl. Phys.* **33** 1484 (2000)
67. P Sunka *Phys. Plasmas* **8** 2587 (2001)
68. P Luceš, Ph.D. Thesis, Institute of Plasma Physics, Academy of Sciences of Czech Republic, Prague, 2001
69. J Goodman, A Hickling, B Schofield *J. Electroanal. Chem.* **48** 319 (1973)
70. A M Badalyan, O V Polyakov, L F Bakhturova *Goren. Plazmokhim.* **1** 187 (2003)
71. S C Goheen, D E Durham, M McCulloch, O William, in *Chemical Oxidation Technology for the Nineties (Proceedings of the Second International Symposium)*, Nashville, TN, 1992 p. 356
72. A G Zakharov, A I Maksimov, Yu V Titova *Tekstil. Khim.* **13** 20 (1998)
73. J Janca, S Kuzmin, A Maximov, J Titova, A Czernichovski *Plasma Chem. Plasma Proc.* **19** 53 (1999)
74. I N Sergeeva, Yu V Titova, A I Maksimov *Elektron. Obrab. Mater.* **216** 34 (2002)
75. Yu V Titova, I N Sergeeva, A I Maksimov, in *Sb. Materialov 3 Mezhdunarodnogo Simpoziuma po Teoreticheskoi i Prikladnoi Plazmokhimii, Ples, 2002* (Proceedings of the 3rd International Symposium on the Theoretical and Applied Plasma Chemistry, Ples, 2002) Vol. 2, p. 99
76. T Munegumi, A Shimoyama, K Harada *Chem. Lett.* 393 (1997)
77. K Harada, M Takasaki, H Naraoka, S Nomoto *Origin Life* **14** 107 (1984)
78. A R Denaro, K O Hough *Electrochim. Acta* **18** 863 (1973)
79. I N Sergeeva, Yu V Titova, A I Maksimov, in *Aktual'nye Problemy Khimii i Khimicheskoi Tekhnologii (Tez. Dokl. II Mezhdunarodnoi Nauchno-tehnicheskoi Konferentsii)*, Ivanovo, 1999 [Topical Problems of the Chemistry and Chemical Technology (Abstracts of Reports of the Second International Scientific and Technical Conference), Ivanovo, 1999] p. 211
80. I N Sergeeva, Yu V Titova, A I Maksimov, in *Tekstil'naya Khimiya-2000 (Tez. Dokl. II Mezhdunarodnoi Konferentsii)*, Ivanovo, 2000 [Textile Chemistry-2000 (Abstracts of Reports of the Second International Conference), Ivanovo, 2000] p. 114
81. K N Zheleznov, A I Maximov *Mendeleev Commun.* 214 (2005)
82. A M Sizikov, T A Kalinina, I A Glizdinskii, L T Bugaenko *Khim. Vys. Energ.* **35** 219 (2001)^a
83. T A Kalinina, A M Sizikov, L T Bugaenko *Khim. Vys. Energ.* **35** 393 (2001)^a
84. T A Kalinina, A M Sizikov, L T Bugaenko, G V Kovalev *Khim. Vys. Energ.* **36** 156 (2002)^a
85. T A Kalinina, A M Sizikov, L T Bugaenko, G V Kovalev *Khim. Vys. Energ.* **37** 38 (2003)^a
86. V I Naumenko, N A Zhuravleva, S A Tarchenko, V A Apostoli *Elektron. Obrab. Mater.* **55** 89 (1974)
87. V N Pisarevskii, V V Kovriga, N A Zhuravleva, A P Yarosh *Elektron. Obrab. Mater.* **56** 81 (1974)
88. L D Pidorenko, M A Yatsko, L L Korinetskaya, V V Petrichenko, in *Mekhanizatsiya i Elektrifikatsiya Sel'skogo Khozyaistva, Kiev, 1975* (Mechanisation and Electrification of Agriculture, Kiev, 1975) No. 32, p. 115
89. M A Yatsko, G M Balan *Zhivotnovodstvo* (12) 38 (1973)
90. M A Yatsko, G M Balan, L L Korinetskaya *Elektron. Obrab. Mater.* **64** 62 (1975)
91. M A Yatsko, L L Khonina, L D Pidorenko *Elektron. Obrab. Mater.* **63** 59 (1975)
92. N E Gevorkyan, S A Khachatryan, N G Grigoryan, in *Elektroavtomatika Tekhnologicheskogo Oborudovaniya Tekstil'noi i Legkoi Promyshlennosti (Tr. I Vsesoyuzn. Nauchno-tehnicheskoi Konferentsii)*, Erevan, 1973 [Electroautomation of the Equipment in Textile and Light Industry (Proceedings of the First All-Union Scientific and Technical Conference), Erevan, 1973] S. 178
93. USSR P. 362080; *Byull. Izobret.* (2) 64 (1973)
94. V G Gorokhova, L N Petrushenko, A A Shishko, V G Chernova, N V Ivanova, O A Kolomakina, N A Koshilev, V A Babkin, M G Voronkov *Dokl. Akad. Nauk* **343** 62 (1995)^c
95. N V Ivanova, A A Shishko, V G Gorokhova, N A Koshilev, N V Lebedev, V A Babkin, M G Voronkov *Dokl. Akad. Nauk* **343** 486 (1995)^c
96. I N Sergeeva, Yu V Titova, A I Maksimov, in *Aktual'nye Problemy Khimii i Khimicheskoi Tekhnologii (Tez. Dokl. II Mezhdunarodnoi Nauchno-tehnicheskoi Konferentsii)*, Ivanovo, 1999 [Topical Problems of the Chemistry and Chemical Technology (Abstracts of Reports of the Second International Scientific and Technical Conference), Ivanovo, 1999] p. 210
97. Yu V Titova, M I Voronova, A I Maksimov, in *Sb. Materialov 4 Mezhdunarodnogo Simpoziuma po Teoreticheskoi i Prikladnoi Plazmokhimii, Ivanovo, 2005* (Proceedings of the 4th International Symposium on the Theoretical and Applied Plasma Chemistry, Ivanovo, 2005) Vol. 2, p. 414
98. R A Bretosh, L A Rudenko, A F Urusov *Elektron. Obrab. Mater.* **45** 79 (1971)
99. A E Zhuk, E G Zhuk *Elektron. Obrab. Mater.* **64** 60 (1975)
100. L N Zykina, V S Goldaev *Elektron. Obrab. Mater.* **62** 68 (1974)
101. L A Yutkina, O N Mel'nikova, A K Postoev, A Yu Zemlyanoi *Elektron. Obrab. Mater.* **77** 67 (1978)
102. E G Zhuk *Elektron. Obrab. Mater.* **80** 80 (1978)
103. V N Bubentsov, E G Zhuk, Yu V Yakunin *Elektron. Obrab. Mater.* **85** 42 (1983)
104. N D Ryazanov, E N Perevyazkina *Elektron. Obrab. Mater.* **122** 43 (1984)
105. A P Shvedchikov, E V Belousova, A V Polyakova, A Z Ponizovskii, V L Goncharov *Khim. Vys. Energ.* **27** 63 (1993)^a
106. A G Ryabinin *Elektron. Obrab. Mater.* **176** 77 (1994)
107. A A Ivannikov, V M Lelevkin, A V Tokarev, V A Yudanov *Khim. Vys. Energ.* **37** 148 (2003)^a
108. Russ. P. 2195961; *Byull. Izobret.* (1) (2003)
109. I K Stroikova, A I Maksimov *Elektron. Obrab. Mater.* **218** 43 (2002)

^a — *High Energy Chem. (Engl. Transl.)*^b — *Chem. Sust. Develop. (Engl. Transl.)*^c — *Dokl. Chem. (Engl. Transl.)*

Post-metallocene catalysts for olefin polymerisation

K P Bryliakov

Contents

I. Introduction	253
II. Monocyclopentadienyl complexes	254
III. Complexes of late transition metals	256
IV. Complexes with bis(imino)pyridyl and similar ligands	260
V. Complexes with phenoxyimine, pyrrolylimine and similar ligands	265
VI. Miscellaneous complexes	270
VII. Conclusion	271

Abstract. The main types of post-metallocene catalysts for olefin polymerisation based on bis(imino), bis(imino)pyridyl, bis(phenoxyimino), bis(pyrrolylimino) and other complexes of transition metals developed in the last 10–15 years and having prospects for practical use are considered. Modern views on the mechanism of action of these catalysts are discussed. The bibliography includes 375 references.

I. Introduction

During the last 30 years the main attention of scientists studying catalytic olefin polymerisation has been attracted to the catalysts based on metallocene complexes of Group 4 elements in combination with activators, namely, Lewis acids [methylaluminoxane (MAO), fluoroarylboron derivatives and some others],^{1–11} which have replaced the Ziegler–Natta catalysts. The cationic nature of the active sites (an activator should form a non-coordinating anion) and the correlation between the ligand structure and the structure of polymer are typical of metallocene-based catalytic systems. Such properties of metallocene systems as high catalytic activity, narrow range of molecular masses of the obtained polyolefins, the ability of catalysing co-polymerisation of ethylene with higher α -olefins, the possibility of controlling the catalytic properties by variation of ligand structure, have stimulated their broad industrial production in the 1990s,^{12, 13} which was even called a ‘metallocene revolution’.^{11, 14} However, at present the scope of industrial applications of metallocene systems is smaller than it was predicted. This is a result of some disadvantages of such systems, namely, significant consumption of expensive activators increasing the cost of products and the oxophilicity of Group 4 metals, which makes them unsuitable for the synthesis of co-polymers with functionalised olefins. Obviously, catalysts of other classes are required in order to increase the

variety of polyolefins. This has inspired the search for more effective and inexpensive catalysts. Moreover, in view of the higher resistance of complexes of the so-called ‘late’ transition metals (Ni, Pd, Co) to heteroatomic fragments compared to that of complexes of ‘early’ transition metals (Ti, Zr, V), one could hope for the development of catalysts that would be active in co-polymerisation of ethylene and olefins with polar functional groups.^{14, 15}

Thus as early as the first half of the 1990s the interest in the synthesis of a new type of homogeneous one-centred catalysts of polymerisation, *viz.* of a non-metallocene (or, according to the chronology, post-metallocene), catalysts increased. During this period, a significant attention was paid to complexes of Group 4 metals with one cyclopentadienyl ligand and other ligands containing donor heteroatoms. An important event in the development of post-metallocene systems was the synthesis of nickel(II) bis(imine) complexes capable of catalysing ethylene polymerisation.¹⁶ Later, systems based on nickel complexes and not requiring an activator have been found.¹⁷ At the end of the 1990s, iron bis(imino)pyridyl complexes highly active in ethylene polymerisation were discovered.^{18, 19} In addition, it was found that not only MAO but also trialkylaluminium derivatives may be used as activators.^{20–22} This substantially simplified and decreased the cost of a catalytic system.

In recent years, significant interest has arisen in titanium and zirconium bis(phenoxyimine) complexes²³ and titanium bis(pyrrolylimino) complexes.²⁴ These compounds are able to catalyse the so-called ‘living’ polymerisation of olefins²⁵ and produce polymers with narrow molecular mass distribution (the ratio M_w/M_n is around 1.1) and high molecular masses.

In order to convert post-metallocene catalysts to an active form (as for metallocene catalysts), co-catalysts are required. These co-catalysts are Lewis acids, which produce cationic active centres with a high olefin affinity. Immobilisation of active catalytic systems on a solid support is of a great practical importance, as it facilitates the system handling, simplifies the catalyst composition (as the support itself may work as an activator; both a catalyst and an activator may be deposited on the same support), increases the resistance of the system against adverse external effects (*e.g.*, heating and oxidation) and also improves the morphology of the product.

To date, a series of reviews,^{14, 15, 26} books^{27, 28} and generalising reports^{23, 24} on the non-metallocene olefin polymerisa-

K P Bryliakov G K Boreskov Institute of Catalysis, Siberian Branch of the Russian Academy of Sciences, prosp. Acad. Lavrentieva 5, 630090 Novosibirsk, Russian Federation. Fax (7-383) 330 80 56, tel. (7-383) 330 68 77, e-mail: bryliako@catalysis.ru

Received 30 May 2006

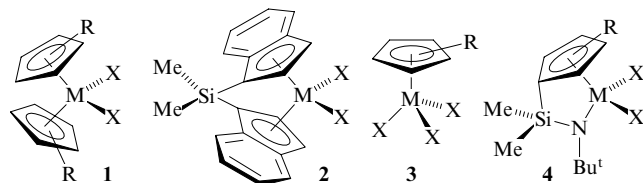
Uspekhi Khimii 76 (3) 279–304 (2007); translated by D S Yufit

tion catalysts have been published. However, these papers were written before 2003 and usually discuss only one particular type of catalytic systems and reflect the contribution of only one research group. The author of the present review has aimed at following the development of studies of post-metallocene catalytic systems of olefin polymerisation during the recent years. The attention is focused on the most scientifically and industrially important systems. To this end, it appeared expedient to abandon the traditional systematisation of the post-metallocene complexes according to the metal position in the Periodic Table^{15,26} and classify them according to the type of ligand, because catalysts based on different metals with several main types of ligands are known. The order of discussion of the ligands in the present review mainly corresponds to the chronology of their appearance in the literature.

It should be noted that some caution is needed when comparing the properties of catalysts reported by different authors, because no universal procedure of catalyst testing exists and the experimental data are affected by particular reaction conditions, such as the reactor configuration, stirring speed, the method of activation, *etc.* Quite often the authors do not report the kinetics of polymerisation (or even the lifetime of a catalyst), but provide, for example, the data about the activity of a catalyst during the first 1–5 min of the reaction, which may create an inadequate idea of the catalytic properties of a complex in the case of its rapid deactivation. A slightly modified scale suggested by Gibson and co-workers²⁶ is used here for the activity classification: very low, low, medium (moderate) and high, which correspond to the following values < 1, 1–10, 10–100, 100–1000 and higher in terms of (kg of polymer) (1 mol of catalyst)^{–1} h^{–1} bar^{–1} units (or in the abbreviated form, kg mol^{–1} h^{–1} bar^{–1}), respectively.

II. Monocyclopentadienyl complexes

Up to the mid-1990s, most papers on the catalytic olefin polymerisation dealt with metallocene (**1**), including *ansa*-metallocene (**2**), and monocyclopentadienyl catalysts, particularly with ‘half-titanocenes’ (**3**) and the so-called ‘constrained geometry’ complexes (**4**).^{1–11}



M = Ti, Zr, Hf; X = Cl, Alk; R = Alk.

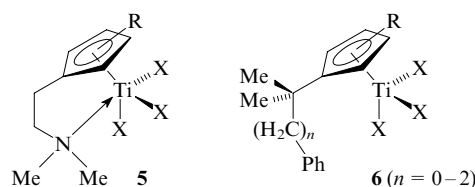
To date, the processes that take place upon the activation of metallocene complexes with alkylaluminium chlorides,^{29–31} methylaluminoxane^{32–41} and the trialkylaluminum–tetrakis(pentafluorophenyl)borate system,^{42–45} have been studied in detail. The cationic complexes that are the precursors of active intermediates have been detected and identified by NMR spectroscopy. The genuine intermediates, *i.e.*, the complexes in which the central atom is coordinated by the growing polymeric chain, were also detected.^{33,36,46}

Naturally, the initial attempts of the search for new catalysts were aimed at the synthesis of non-metallocene complexes of Group 4 metals. Monocyclopentadienyl complexes of titanium and zirconium and of some other metals with additional donor atoms are discussed in this Section. Generally, the monocyclopentadienyl complexes are less active in olefin polymerisation than their bis(cyclopentadienyl) ana-

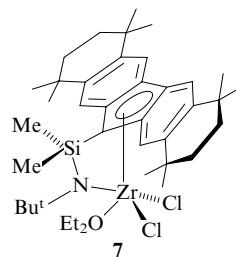
logues, but more active in ethylene co-polymerisation with α -olefins. The incorporation of additional donor atoms into catalysts often adds new important properties, for example, high thermal stability (as in the case of complexes **4** with constrained geometry) and high polymerisation activity.

1. Complexes of Group 4 metals with one cyclopentadienyl ligand and an additional ligand containing a donor atom

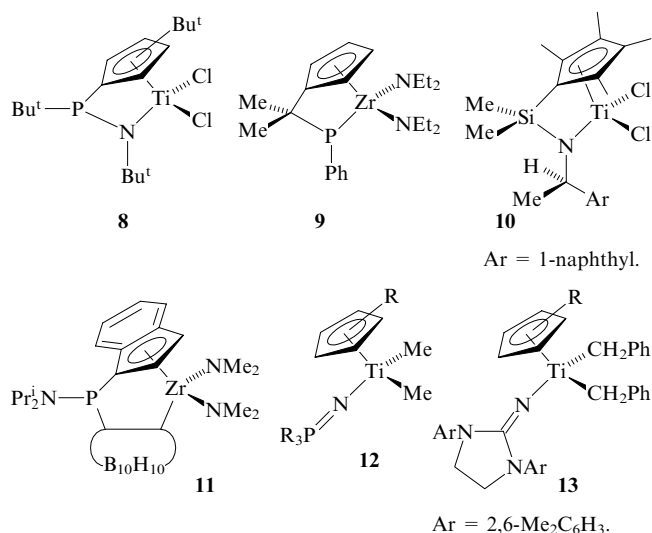
As noted above, titanium(IV) and zirconium(IV) monocyclopentadienyl complexes **3** are less active in olefin polymerisation than their bis(cyclopentadienyl) analogues.^{47–49} Complexes **4** and **5** (R = H, X = Cl) with the activity of about 2500 kg mol^{–1} h^{–1} bar^{–1} (Ref. 50) were obtained by introduction of an additional ligand containing a donor atom (for example, N). However, such complexes are highly sensitive to traces of oxygen which deteriorates the process.⁵¹ Another possible modification is introduction of a non-coordinating substituent into the cyclopentadienyl ring (complex **6**).⁵² Interestingly, complex **6** (X = Cl, *n* = 0) is able to catalyse highly selective ethylene trimerisation when activated by MAO.⁵³ The role of pendant phenyl ring in this process is discussed comprehensively in a review.⁵⁴



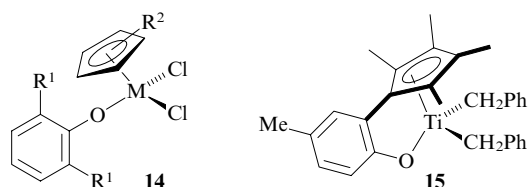
The monocyclopentadienyl systems in which an additional ligand containing a donor atom is covalently bonded to the metal have also become popular. Such catalysts (*e.g.*, complex **4**) are applied in industry due to their high thermal stability and ability to initiate co-polymerisation.^{55,56} The catalytic properties of the complexes may be controlled by introducing substituents (including heteroatoms) into the cyclopentadienyl ring. Thus the application of fluorenyl complex **7** in the co-polymerisation of ethylene with higher α -olefins yields ethylene co-polymers with cycloolefins^{57–65} and also with oct-1-ene (the octene content > 70 mol %, Ref. 61).



Several attempts at changing the nature of the bridging and the donor atom were described. For instance, linear high-molecular-mass polyethylene (PE) was obtained by using complex **8**,⁶⁵ while complex **9** and its titanium analogue catalyse the co-polymerisation of ethylene with octene.⁶⁶ The presence of a bulky aromatic substituent in complex **10** facilitates the polymerisation of propylene with a relatively high degree of isotacticity (*[mmmm]* = 56%).⁶⁷ Complex **11** containing the C-donor bridge C₂B₁₀H₁₀ is able to initiate the ϵ -caprolactone polymerisation besides being a catalyst of ethylene polymerisation.⁶⁸ The activity of complexes with ligands similar to phosphinimide (**12**)⁶⁹ and guanidinate (**13**)⁷⁰ is > 1000 (kg PE) mol^{–1} h^{–1} bar^{–1}.



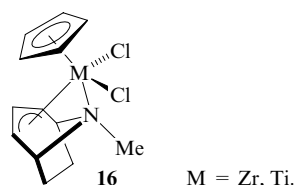
The aryloxy complexes **14**^{71,72} and **15**⁷³ should be mentioned; in the latter complex, the aryloxy group is linked to the cyclopentadienyl ligand. The complexes of type **14** are highly active in ethylene polymerisation [>2000 (kg PE) mol⁻¹ h⁻¹ bar⁻¹ for M = Ti and >4000 (kg PE) mol⁻¹ h⁻¹ bar⁻¹ for M = Zr], while the activity of complex **15** is somewhat lower. Complexes **14** and **15** are also able to catalyse propylene and styrene polymerisation.



M = Ti, Zr; R¹ = Alk; R² = H, Alk.

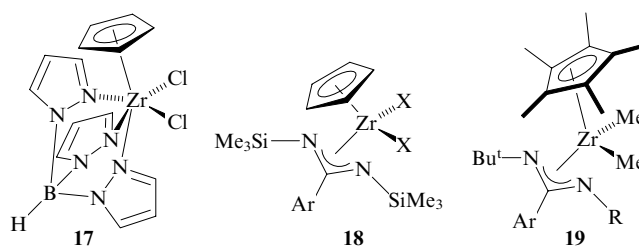
2. Complexes of Group 4 metals with one cyclopentadienyl ligand and an additional ligand containing several donor atoms

Among derivatives of Group 4 metals with one cyclopentadienyl ligand, complexes **16** proposed by Bergman and co-workers⁴⁹ should be noted. The zirconium complex with a tropidinyl fragment, isoelectronic to cyclopentadienyl, is highly active in ethylene polymerisation in the presence of MAO (comparable with the activity of Cp₂ZrCl₂, Cp = η⁵-C₅H₅); the corresponding titanium complex is less active.⁴⁹

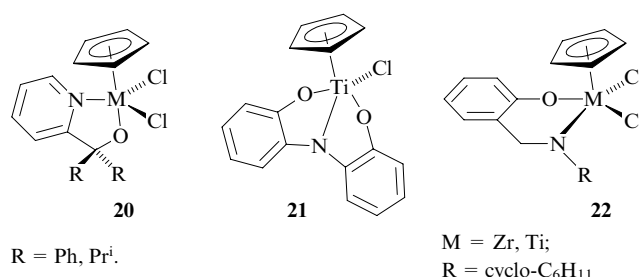


Nakazawa *et al.*⁷⁴ have described complex **17** with a tris(pyrazolyl)borate ligand, which is active in ethylene polymerisation. The complexes LZrCl₃ and LTiCl₃ with additional bulkier mesityl-substituted tris(pyrazolyl)borate ligands L are slightly more active in ethylene polymerisation; they are able to catalyse the co-polymerisation of ethylene with hex-1-ene.^{75,76} In the presence of an activator B(C₆F₅)₃, complex **17** yields high-molecular-mass polyethylene [$M_w = (4-6) \times 10^5$]. Moderately active catalysts **18** can be activated by both MAO (X is a halogen)⁷⁷ and perfluoroarylborate compounds

(X = Me).⁷⁸ Structurally similar complexes **19** (R = Alk, Ar) are able to catalyse living polymerisation of hex-1-ene with [PhMe₂NH][B(C₆F₅)₄] as an activator.⁷⁹

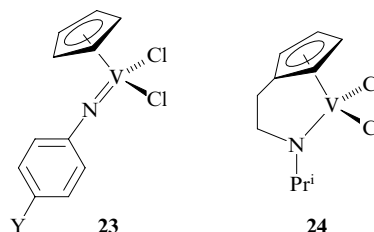


Among other monocyclopentadienyl complexes of Group 4 metals, compounds **20–22**^{80–82} with alkoxy and aryloxy ligands deserve attention. They exhibit moderate activity in ethylene polymerisation.

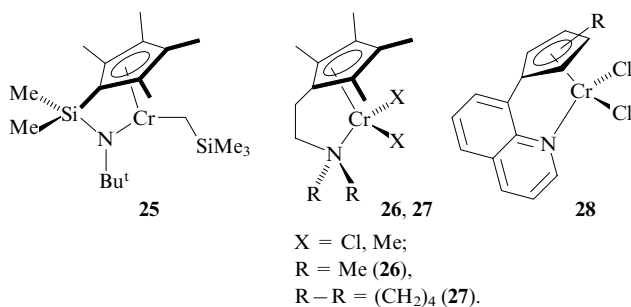


3. Monocyclopentadienyl complexes of other metals with additional ligands containing donor atoms

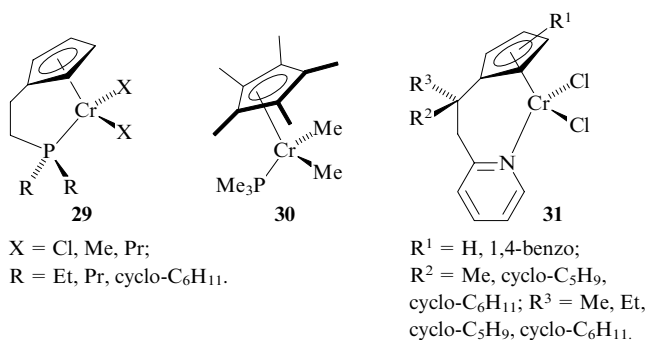
Group 5 metals in the formal oxidation state +4 and +5 form monocyclopentadienyl complexes that are active in ethylene polymerisation (it should be noted that the metal oxidation state may change during activation of the catalyst¹⁵). Thus complex **23** (Y = Me)⁸³ is slightly active [27 (kg PE) mol⁻¹ h⁻¹ bar⁻¹] when activated by MAO; the fast deactivation of the catalyst is caused by the formation of inactive dinuclear vanadium complexes.⁸⁴ Immobilisation of the active centres of complex **23** on polystyrene (Y is polystyrene) increases the lifetime of the active species which results in the production of high-molecular-mass polyethylene ($M_w = 1.9 \times 10^6$) when activated by diethylaluminium chloride.⁸⁵ Among vanadium(IV) derivatives, complex **24**, isostructural to the 'constrained geometry' catalysts based on Group 4 metals should be noted. This complex is less active in ethylene polymerisation than its titanium analogue.⁸⁶



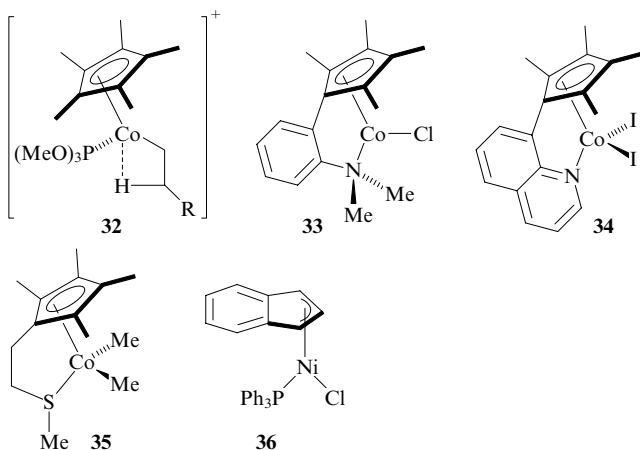
Chromium(III) complex **25** is almost catalytically inactive in ethylene polymerisation⁸⁷ and is able to catalyse only oligomerisation or isomerisation of higher α-olefins, while complex **26** is relatively active [8300 (kg PE) mol⁻¹ h⁻¹ bar⁻¹] when activated by MAO.⁸⁸ Structurally similar complex **27** is even more active in these reactions.⁸⁹ Compounds **28** are able to catalyse the polymerisation of ethylene⁹⁰ and propylene⁹¹ (to give atactic polypropylene).



Complexes with phosphine ligands **29**,^{92,93} which provide ethylene conversion into oligomers and low-molecular-mass polyethylene upon activation by methylaluminoxane, and complex **30**,⁹⁴ which ensures the formation of linear saturated hydrocarbons due to the chain transfer from MAO to aluminium are also known. Complex **31** with an additional pyridyl ligand is active in ethylene polymerisation [up to 1000 (kg PE) mol⁻¹ h⁻¹ bar⁻¹, Ref. 95]. In general, chromium cyclopentadienyl complexes containing an additional ligand with a donor atom exhibit significant polymerisation activity.^{96,97}

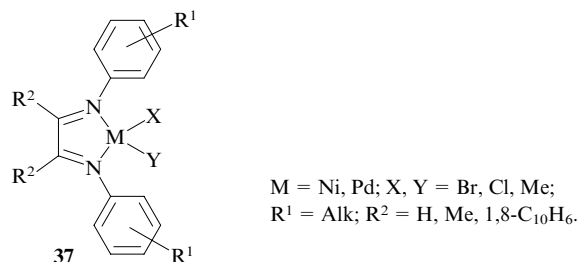


The monocyclopentadienyl complexes of late transition metals should also be noted. Thus complexes **32** show low activity in living ethylene polymerisation ($M_w/M_n = 1.1-1.2$).⁹⁸ The polymerisation activity of complexes **33** and **34**⁹⁹ is several orders of magnitude lower than the activity of their chromium analogues.⁹⁹ Branched polyethylene (up to 10 branches per 1000 carbon atoms) was obtained when complex **35** with a sulfide donor fragment was used,¹⁰⁰ and the application of nickel complex **36** with monoindenyl and phosphine ligands yielded high-molecular-mass polyethylene [the activity of the complex was up to 130 (kg PE) mol⁻¹ h⁻¹ bar⁻¹].¹⁰¹



III. Complexes of late transition metals

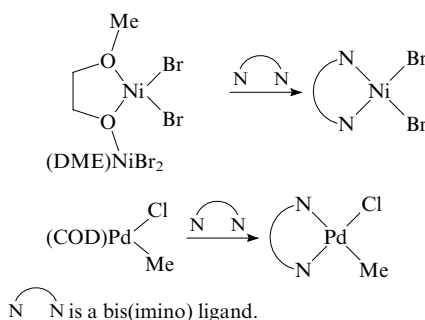
The catalysts briefly discussed in Section II are generally not used in industry (except for the constrained geometry catalysts of type **4**). The discovery of nickel and palladium bis(imino) complexes **37** and their analogues by Brookhart and co-workers¹⁶ has become an important event in the search for new catalysts of polymerisation. The complexes with bis(imino) ligands are widely used due to the specific properties of ligands, namely, their ability to effectively stabilise organometallic compounds, relatively high steric hindrance and the possibility of fine tuning of their electronic and steric properties by introduction of substituents into the aryl rings. A number of such complexes were found to be active in polymerisation of ethylene, linear α -olefins, styrene, norbornene, and in co-polymerisation of ethylene with higher olefins and polar co-monomers.



The complexes that do not require activation (the transformation into cationic form) were developed. The main types of nickel and palladium bis(imino) and other complexes are discussed below as well as the development of the views on the mechanism of polymer chain growth and the effect of ligand structure on the catalytic properties.

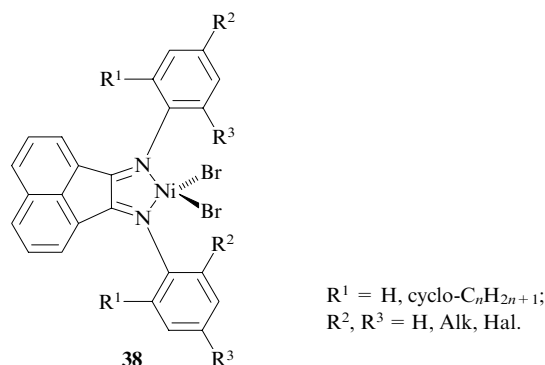
1. Nickel and palladium bis(imino) complexes

The first studies of nickel and palladium bis(imino) complexes were published by Brookhart.^{16, 102-105} The simplest way of their synthesis is the reaction of a ligand with a metal derivative, for example, (DME)NiBr₂, (COD)PdMeCl (DME is 1,2-dimethoxyethane, COD is cycloocta-1,5-diene) and others.¹⁴

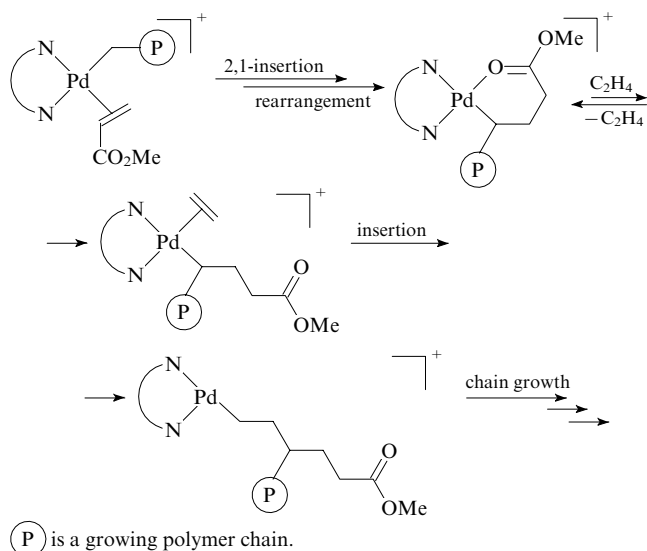


Active centres in these complexes are formed upon alkylation and then activation by transformation into a cationic form. Both boron derivatives {NaBAF, H(Et₂O)₂BAF, BAF = [B(3,5-(CF₃)₂C₆H₃)₄]⁻} and MAO may be used as activators. Nickel(II) complexes **37** are highly active [up to 11 000 (kg PE) mol⁻¹ h⁻¹ bar⁻¹] in ethylene polymerisation.¹⁶ β -Elimination of a hydrogen atom with subsequent secondary 2,1-addition (see below) results in the formation of branched polymers with up to 70 and more branches per 1000 carbon atoms. Polyethylene with molecular mass of up to 10⁶ may be obtained by varying the temperature and pressure as well as the structure of the ligand. The polymerisation of α -olefins at low temperatures (-10°C) follows a living mechanism (the polypropylene obtained had $M_n = 1.6 \times 10^5$ and

$M_w/M_n = 1.13$), which allows one to produce di- and tri-block co-polymers.^{104, 106} The living polymerisation of a series of α -olefins (from but-1-ene to oct-1-ene) with catalysts **38** ($R^1 = \text{H}$, $R^2 = \text{C}^*\text{HMePh}$, $R^3 = \text{Me}$) was observed in the temperature range from -30 to -40 °C by Coates and co-workers.¹⁰⁶ Besides, the syndiotactic polypropylene may be obtained at low temperature.¹⁰⁷



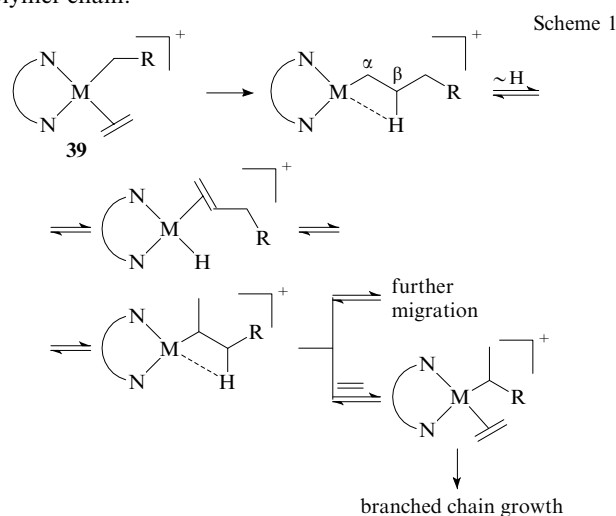
Palladium(II) complexes **37** are usually less active and produce highly branched amorphous polyethylene with up to 100 branches per 1000 carbon atoms.^{16, 108, 109} Palladium complexes are able to catalyse co-polymerisation of ethylene with α -olefins and with functionalised co-monomers (methyl acrylate, methyl vinyl ketone).^{102, 103} Thus the incorporation of up to 25% of co-monomer was achieved in co-polymerisation of ethylene with methyl acrylate. The activity of such catalysts in co-polymerisation of ethylene with α -olefins is substantially lower than that in homopolymerisation; the introduction of a co-monomer sharply reduces the polymer molecular mass and narrows its molecular mass distribution. The suggested mechanism of co-polymerisation of ethylene with methyl acrylate includes 2,1-insertion of co-monomer with the formation of an intermediate cyclic adduct followed by the insertion of ethylene molecule.¹⁰³



Note that palladium bis(imino) complexes are also active in the living polymerisation. For example, polyethylene with polydispersity of 1.05 was obtained by Gottfried and Brookhart in polymerisation of ethylene at 5 °C in the presence of palladium(II) bis(imino) complex **37** ($R^1 = 2,6\text{-Pr}_2$; $R^2 = \text{X} = \text{Me}$; $\text{Y} = \text{Cl}$) activated by NaBAF.¹¹⁰

The ability of nickel(II) and palladium(II) bis(imino) complexes to catalyse the formation of branched polymers is unique: the topology of the resulting polymers varies from

linear with a small number of branches up to the hyper-branched one (in the latter case, oils are formed). A migratory insertion mechanism of the ethylene polymerisation into branched polyethylene (Scheme 1) was suggested on the basis of low-temperature ^1H NMR studies.^{16, 111} A key feature of the mechanism is that the main form of the catalyst is alkyl-ethylene complex **39**. Note that for early transition metals such intermediates have never been observed. The limiting step of the reaction is the addition of ethylene to complex **39**; therefore, the rate of the chain growth is of zero order with respect to ethylene. The energy barrier to ethylene insertion is 17–18 kcal mol⁻¹ for $\text{M} = \text{Pd}$ ^{16, 112} and 13.5–14 kcal mol⁻¹ for $\text{M} = \text{Ni}$.¹¹² This explains the difference between the observed activities of the polymerisation catalysts. The β -elimination of a hydrogen atom leading to the formation of alkenyl hydride complex may follow the ethylene insertion. The repeated 2,1-addition of coordinated olefin may take place in the coordination sphere of this complex resulting in branching of the polymer chain.

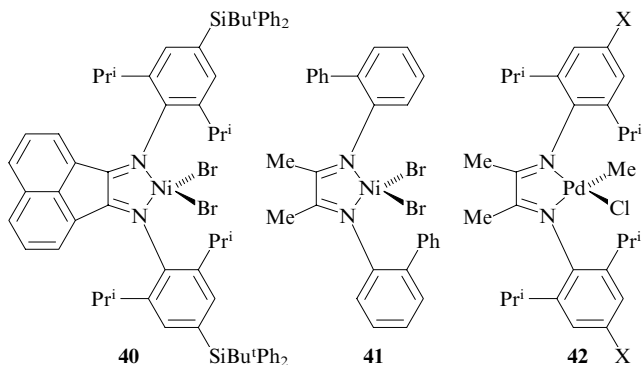


The effect of conditions of the process on the activity of the catalyst and the properties of the polymers formed was studied.^{113–121} Various aspects of the mechanism of polymerisation were discussed in a number of theoretical studies (see for example, Refs 122–129).

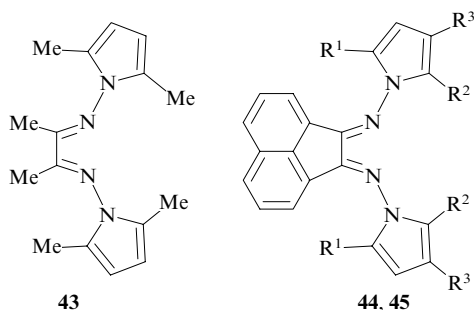
In all of the previously discussed schemes, MAO, ionic tetrakis(aryl)borate derivatives or alkylaluminium chlorides were used as activators. If $\text{B}(\text{C}_6\text{F}_5)_3$ is used, the activity of the ethylene polymerisation catalyst is significantly lower.¹³⁰ Nevertheless, $\text{B}(\text{C}_6\text{F}_5)_3$ was used in co-polymerisation of ethylene with acrylates in the presence of nickel bis(imino) complexes,^{131, 132} and the achieved degrees of co-monomer incorporation were higher than those in the presence of palladium complexes.

The substituents in the aromatic rings greatly affect the catalytic properties of bis(imino) complexes: the shielding of a vacant coordination position of the central atom due to an increase in the bulk of the *ortho*-substituents decreases the catalytic activity; at the same time, the chain propagation rate decreases and, as a consequence, the molecular mass of the polymer increases. The size of the *ortho*-substituent does not affect the number of short-chain branches very much; however, this number rapidly increases with temperature. Oligomeric products are obtained in the presence of complexes with one *ortho*-substituent.^{14–16, 26, 133} Complexes **37** containing aliphatic substituents in the aromatic rings are able to function at temperatures up to 50 °C, but at higher temperatures, their activities significantly decrease. Ivanchev and co-workers have shown^{133–136} that the incorporation of bulky *o*-cycloalkyl substituents into 1,2-bis(arylimino)acenaphthyl complexes **38**

slightly increases the thermal stability of the catalysts. Other nickel and palladium complexes (such as **40–42**)^{137–139} and different bis(imino) ligands (for example **43–45**)^{16,28} are also in use.



X are electron-withdrawing substituents



44: $R^1 = R^2 = \text{Alk}$, $R^3 = \text{H}$;
45: $R^1 = \text{Alk}$, $R^2 - R^3 = 1,4\text{-benzo}$.

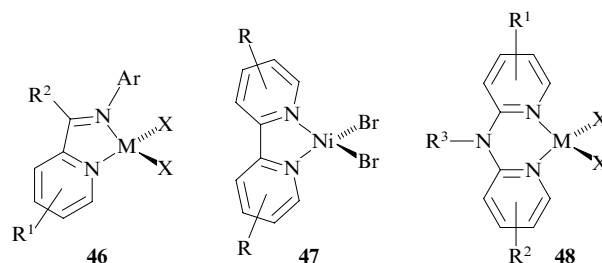
The nickel and palladium bis(imino) complexes are applied in the production of polymers by the so-called in-reactor blending methods. In essence, most of these methods consist of the introduction of a composite catalyst containing a metallocene complex of earlier transition metal in combination with a complex of later transition metal, into the reactor.^{135, 140–143} The resulting polymeric product possesses an extended molecular mass distribution, which facilitates its processing.

The bis(imino) complexes are catalytically active in polymerisation of cycloolefins and in co-polymerisation of linear olefins with cycloolefins. Thus complexes **38** catalyse polymerisation of cyclopentene in the presence of ethylaluminium chloride.¹⁴⁴ In co-polymerisation of ethylene with norbornene, nickel bis(imino) complexes are inactive. At the same time, palladium complexes **37** are able to catalyse this process. Depending on the structure of the ligand, the molecular mass of the resulting co-polymers of ethylene with norbornene was up to 8×10^5 (and higher) and the degree of incorporation of norbornene was as high as 90%.¹⁴⁵

2. Miscellaneous nickel and palladium N,X-donor chelate complexes

A series of complexes with other *N,N*-chelate ligands (**46–51**) deserve attention. It should be noted that efficient olefin polymerisation requires sterically hindered ligands; otherwise, β -elimination with subsequent dissociation of the coordinated olefin will result in the predominant formation of higher α -olefins.¹⁴⁶ Complexes **46** with various (alkyl, aryl and other, including polar) substituents in the pyridine and benzene rings of the ligand are less active in ethylene polymerisation than bis(imino) complexes and produce polymers with lower molecular masses.^{147–153} Complexes **47–49** in the presence of

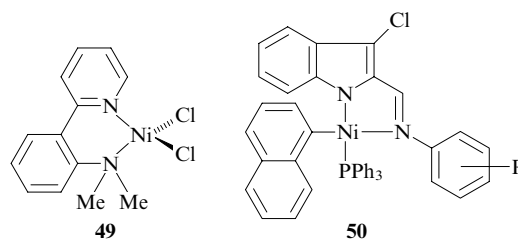
various co-catalysts [MAO, modified methylaluminoxane (MMAO), $\text{Al}_2\text{Et}_3\text{Cl}_3$] produce mainly α -alkenes.^{144, 146, 154, 155} Ethylene oligomerisation proceeds slowly in the presence of complex **50** without a neutral co-catalyst.¹⁵⁶ Complex **51** is active in the polymerisation and oligomerisation of hex-1-ene.¹⁵⁷ The catalysts with this type of ligand are described in patents; the corresponding references can be found in a review.¹⁴ Various types of post-metallocene catalysts immobilised on polymeric supports have been discussed.¹⁵⁸



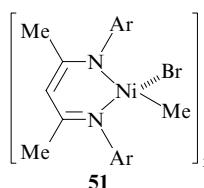
$R^1 = \text{Alk}$, Ar etc.;
 $R^2 = \text{Alk}$, Ar .

$R = \text{Alk}$.

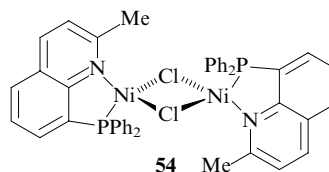
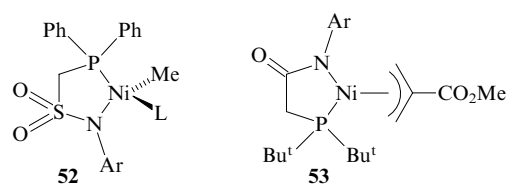
$R^1 = R^2 = R^3 = \text{H}$,
 Alk ; $X = \text{Cl}$, Br



$R = \text{H}$, Alk .



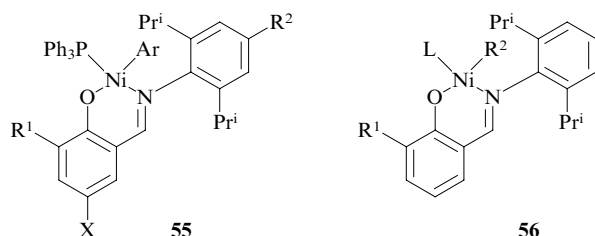
Complexes with *N,P*-chelating ligands **52–54** have been reported.^{159–161} Among the variety of catalysts, compounds with bis(imino), *N,N*-chelate (see above) and *N,O*-chelate ligands, which will be discussed later, turned out to be most active.



3. Nickel salicylaldimine and other N,O-chelate complexes

In 1998, Grubbs and co-workers¹⁶² have prepared catalysts based on nickel salicylaldimine complexes **55** with bulky substituents. Ethylene polymerisation has been performed in the presence of two equivalents of a co-catalyst [$\text{Ni}(\text{COD})_2$ or $\text{B}(\text{C}_6\text{F}_5)_3$]. The productivity of the catalyst (13.3–253 kg PE per 1 mol of catalyst in 40 min under ethylene pressure from 7 to 14 atm) and the molecular mass of the polymer ($M_w = 4 \times 10^3 - 3.6 \times 10^4$) strongly depended on the substitu-

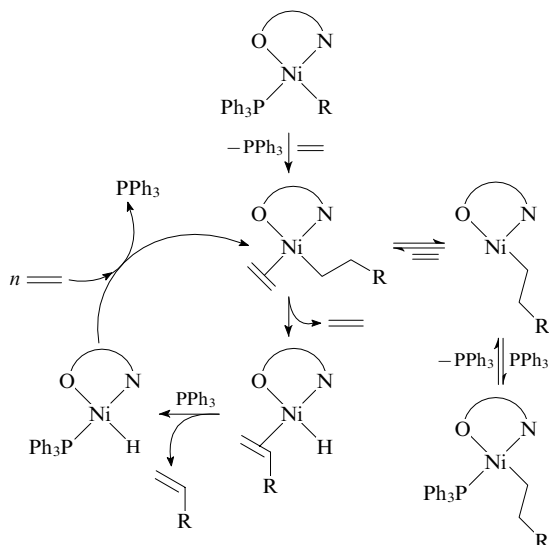
ent. The number of branches in the obtained polyethylene samples varied from 5 (for $R^1 = \text{Ph}$, $X = \text{H}$) to 55 per 1000 carbon atoms (for $R^1 = \text{Bu}^t$, $X = \text{H}$). The molecular mass distribution fluctuated from 1.4 to 12.4. Theoretical studies have shown that elimination of the donor group PPh_3 from complex **55** takes place in the initial step of the process.¹⁶³ Catalysts **56** (R^1 is anthracenyl, $R^2 = \text{Ph}$) turned out to be more active: their productivity was up to 6400 (kg PE) $\text{mol}^{-1} \text{h}^{-1}$ under the pressure of 17 atm.¹⁷ Triphenylphosphine as well as acetonitrile may be used as the ligand L.



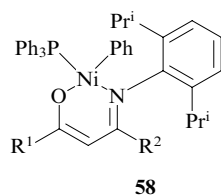
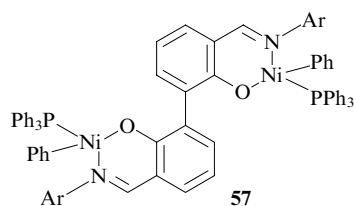
$R^1 = \text{H, Alk, Ar, CHO, NO}_2$;
 $R^2 = \text{H, Pr}^i$;
 $X = \text{H, OMe, NO}_2, \text{Cl}$;

$R^1 = 9\text{-anthracenyl}$;
 $R^2 = \text{Ph, Me}$;
 $L = \text{PPh}_3, \text{MeCN}$.

Some of the discussed catalysts are able to function without a co-catalyst (the testing was continued for 1–2 h).^{17, 164} The following catalytic cycle of polymerisation with nickel salicylaldimine complexes has been suggested on the basis of ^{31}P NMR studies.

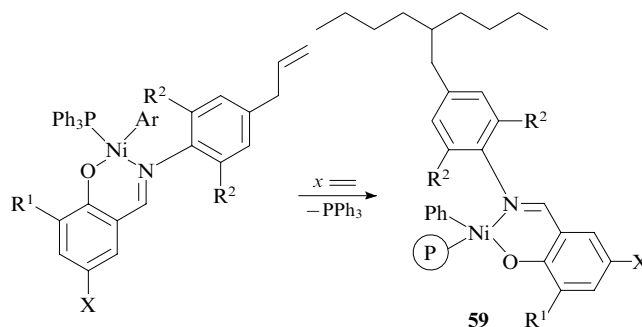


Data on dinuclear complex **57** which exhibits similar catalytic properties, have been published recently.¹⁶⁵ Catalysts of this type are quite resistant to the effect of polar functional groups; this makes it possible to obtain co-polymers of ethylene with substituted norbornenes and α,ω -functionalised olefins^{17, 166, 167} and also to perform polymerisation in polar and protic solvents.^{168, 169} However, the co-polymerisation of olefins with vinyl-functionalised co-monomers turned out to be impossible due to the catalyst deactivation.¹⁷⁰ Nevertheless, Li



$R^1 = \text{Ph, CF}_3$;
 $R^2 = \text{Me, CF}_3$.

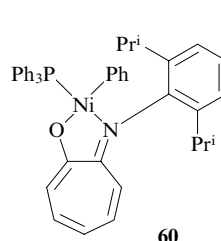
*et al.*¹⁷¹ have managed to perform homo- and co-polymerisation of ethylene with methyl metacrylate (the incorporation of co-monomer was up to 16.7%) on catalyst **58** and MMAO as a co-catalyst. The co-polymerisation of ethylene with methyl metacrylate on nickel catalysts activated by $\text{Ni}(\text{COD})_2$ and then by methylaluminoxane has been discussed.¹⁷² It was shown¹⁷³ that complexes containing a vinyl substituent in the aromatic ring are transformed into 'self-immobilised' catalysts **59** during ethylene polymerisation.



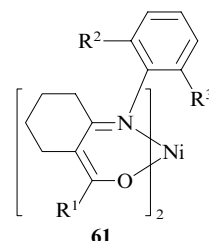
$X = \text{H, NO}_2, \text{Me}$; $R^1 = \text{H, Bu}^t, \text{Ph, NO}_2$; $R^2 = \text{Me, Pr}^i$.

Hicks and Brookhart¹⁷⁴ have reported nickel anilinetropolone complex **60**, which does not require a co-catalyst in olefin polymerisation. This complex produces polyethylene with molecular mass $M_n = 1 \times 10^5 - 3 \times 10^5$, a rather narrow molecular mass distribution ($M_w/M_n = 1.7 - 2.0$) and the number of branches ranging from 8 to 100 per 1000 carbon atoms. Later, it was shown that the polymerisation has a migratory mechanism (see Scheme 1), the predominant state of the catalyst being the complex $\text{LNiR}(\text{C}_2\text{H}_4)$ (L is the anilinetropolone ligand, R is the polymeric chain); the activation parameters of separate stages of the process were also evaluated.¹⁷⁵

The effect of reaction conditions on ethylene polymerisation in the presence of dinitro-substituted nickel catalysts **55** ($R^1 = X = \text{NO}_2$, $R^2 = \text{H, Pr}^i$) and methylaluminoxane has been studied.¹⁷⁶ A linear polyethylene of high molecular mass has been obtained and the activity of the catalyst was as high as 200 (kg PE) $\text{mol}^{-1} \text{h}^{-1} \text{bar}^{-1}$. A tenfold increase in the activity of the catalytic system was achieved by varying the content of trimethylaluminium in MAO.¹⁷⁷ It was shown¹⁷⁸ that complex **55** ($R^1 = \text{cyclo-C}_6\text{H}_{11}$, $R^2 = \text{H}$, $X = \text{Me}$) is able to catalyse ethylene polymerisation and its co-polymerisation with functionalised substrates (*tert*-butyl undec-10-enoates, methyl undec-10-enoates, pent-4-en-1-ol) when activated by $\text{Ni}(\text{COD})_2$. A similar catalyst ($R^1 = \text{cyclo-C}_6\text{H}_{11}$, $R^2 = \text{H}$, $X = \text{Cl}$) is active in the homo- and co-polymerisation of ethylene with esters of undecenoic acid when $\text{Ni}(\text{COD})_2$ or AlBu_3 are used as co-catalysts.¹⁷⁹ Nickel *N,O*-chelates are very convenient as they are applicable to various substrates. For instance, β -ketoiminate complexes **61** are inactive in olefin polymerisation; however they catalyse the norbornene polymerisation when activated by MAO. The activity of such system may reach 1600 (kg polynorbornene) $\text{mol}^{-1} \text{h}^{-1} \text{bar}^{-1}$ with $M_w/M_n = 1.3 - 2.0$.¹⁸⁰



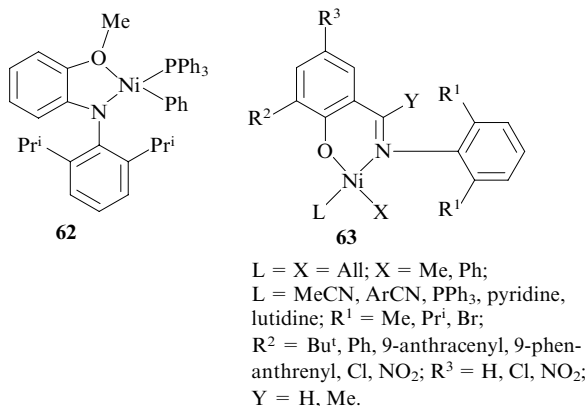
60



61

$R^1 = \text{Me, Ph}$; $R^2, R^3 = \text{Me, Pr}^i$.

Among other nickel *N,O*-chelates, worthy of note are complexes **62**¹⁶⁰ and **55** ($X = \text{Cl}$, $R^1 = \text{CHO}$, Ar is 1-naphthyl),¹⁸¹ which are active in ethylene oligomerisation with $\text{B}(\text{C}_6\text{F}_5)_3$ and MAO co-catalysts, respectively. The results of a systematic study of the effect of substituents in various positions of salicylaldimine ligands (complexes **63**) on the structure of the polymers obtained were reported.^{17, 162, 182–184}

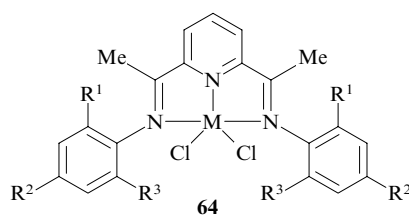


Thus the introduction of bulky substituents in the *ortho*-position of aryl ligand at the nitrogen atom results in the increase in linearity and molecular mass of polyethylene. A linear polyethylene with the highest molecular mass was obtained using catalysts with bulky substituents in the *ortho*-position relative to the phenoxy group. These catalysts also possess the longest lifetimes. More branched polyethylene was obtained when a halogen atom was placed in the *ortho*-position of the aryl substituent or when primary imino group was replaced by a secondary one. The activity of these catalysts remained almost the same; however, the molecular mass of the polymer decreased. Besides, the catalytic activity of nickel salicylaldimine complexes increased when substituents such as Cl and NO_2 , were placed in the *ortho*- and *para*-positions of the phenoxy ring.

Thus, unlike polymerisation catalysts based on Group 4 metals, complexes of the late transition metals are able to catalyse not only homopolymerisation of linear olefins, but also other processes such as oligomerisation, co-polymerisation of olefins with polar co-monomers, living polymerisation, polymerisation in polar media and may produce branched polymers if the mechanism of β -elimination followed by repeated 2,1-insertion takes place. However, unlike Group 4 metal complexes, no obvious correlation between the ligand structure and the microstructure of the obtained polymers has yet been established for the late transition metal complexes.

IV. Complexes with bis(imino)pyridyl and similar ligands

In 1998 the groups of Brookhart¹⁸ and Gibson¹⁹ published independently the first studies dealing with olefin polymerisation catalysts based on iron(II) and cobalt(II) complexes **64** with bis(imino)pyridyl ligands and MAO as a co-catalyst.

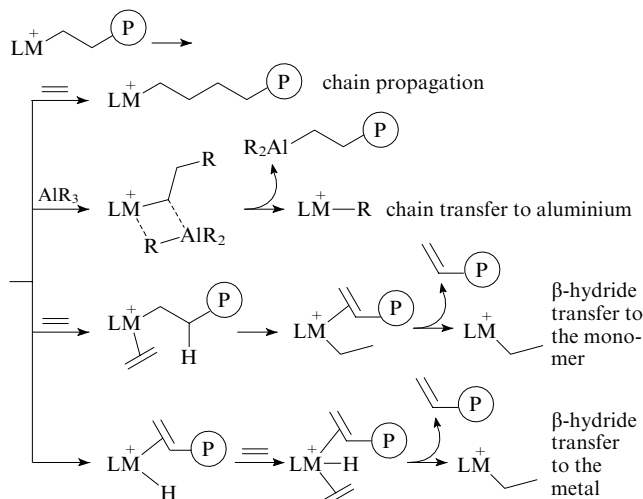


$M = \text{Fe}, \text{Co}$; $R^1, R^2, R^3 = \text{H}, \text{Alk}$.

The extremely high activity of such systems [up to $11\,000\text{ (kg PE mol}^{-1}\text{ h}^{-1}\text{ bar}^{-1})$, which is higher than the activity of Group 4 metal complexes] has attracted attention of scientists and chemical industry professionals. This type of catalysts produce linear polyethylene with wide molecular mass distribution ranging from oligomers to a high-molecular-mass polyethylene. The presence and the bulk of substituents in the phenyl rings at the imine nitrogen atoms strongly affect the activity of the catalyst and the molecular mass of the polymer. Later, it was shown that simpler and cheaper activators, particularly trialkylaluminium, may be used for these catalysts;^{20–22, 185, 186} supported catalysts were developed as well as the catalysts based on complexes of other metals (V, Cr) with bis(imino)pyridyl ligands.

1. Iron(II) bis(imino)pyridyl complexes and their analogues

Iron(II) complexes **64** catalyse ethylene polymerisation producing linear polyethylene with M_w up to 6×10^5 (Ref. 187), which usually has a broad molecular mass distribution ($M_w/M_n = 2.3–144$), including a bimodal distribution.^{26, 187} This can be explained by the suggestion that besides β -elimination,¹⁸⁸ chain transfer to aluminium may take place in this type of systems.¹⁸⁷ The following processes are possible in catalytic systems based on iron bis(imino)pyridyl complexes:

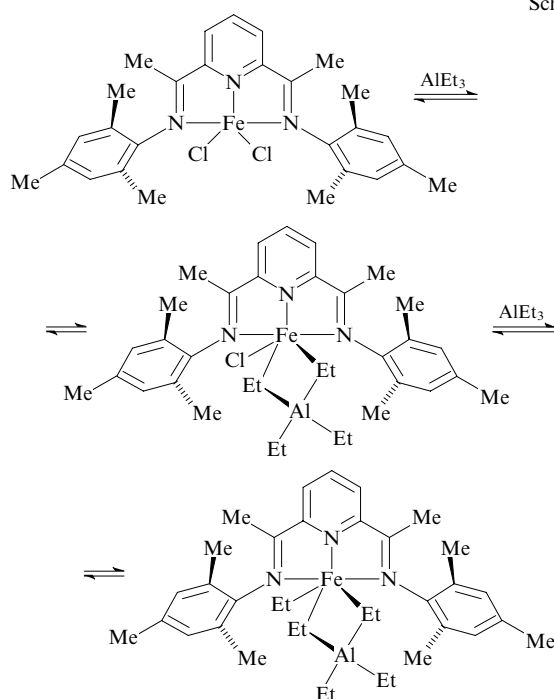


$R = \text{Me}, \text{Bu}^i$; LM^+ is the active catalyst.

The complexes containing two substituents in the *ortho*-positions of aryl rings at the nitrogen atom ($R^1 = R^3 = \text{Alk}$, $R^2 = \text{H}$) are more active than complexes with one *ortho*-substituent ($R^1 = \text{Alk}$, $R^2 = R^3 = \text{H}$), and the introduction of a *para*-substituent increased the catalyst activity and the molecular mass of the polymer to even a greater extent.^{18, 19} Meanwhile, iron bis(imino)pyridyl complexes are able to catalyse the oligomerisation of ethylene to give α -olefins with high selectivity if the aryl rings contain one small substituent in the *ortho*-position ($R^1 = \text{Me}$, $R^2 = R^3 = \text{H}$) or if the ligand is non-symmetric (*i.e.*, two different amines are used in the synthesis of the ligand).^{189–191}

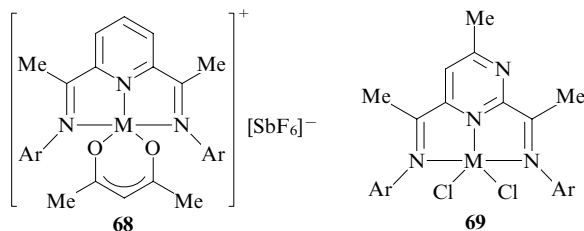
Predominant formation of oligomeric products was also observed when only 3- and 4-substituents are present in the aryl fragments at the nitrogen atoms in complexes **64**.¹⁹² It was established¹⁹² that in the presence of acetylaminopyridine complexes **65**, ethylene oligomerisation proceeds with high selectivity (the content of α -alkenes is up to 82%).

The mechanism of activation of iron(II) bis(imino)pyridyl complexes is shown in Scheme 2. In order to explain the observed bimodal molecular mass distribution of the polymerisation products, Wang and co-workers²¹⁴ have suggested, on the basis of electron microscopy data, the formation of two types of catalytically active species (Scheme 3) in the activation of iron(II) bis(imino)pyridyl chloride complexes by triethylaluminium. Barabanov *et al.*^{215, 216} have made an attempt to establish the nature of active centres in such systems. They estimated the concentration of these centres and the rate constant for chain propagation with inhibition of polymerisation by the addition of ¹⁴CO. Two types of active centres were found in the system with AlEt₃. Presumably, the most active (less stable) centres are responsible for the formation of the low-molecular-mass polyethylene fraction. Similar measurements were performed for supported systems and the relative amount of active centres in the supported systems turned out to be significantly lower than that in homogeneous systems.^{199, 217}

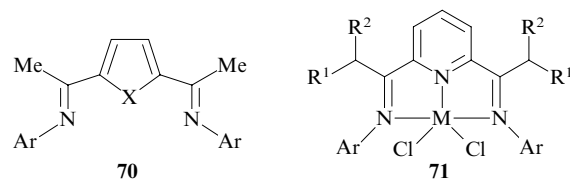


Scheme 3

The diversity of bis(imino)pyridyl complexes is based on the variety of ligand structures. Thus the cationic complex **68** is highly active in ethylene polymerisation when activated by MAO or by the AlMe₃–B(C₆F₅)₃ system.²¹⁸ The replacement of the pyridine ring by a pyrimidine ring (complex **69**) somewhat decreases the catalyst activity.²¹⁹



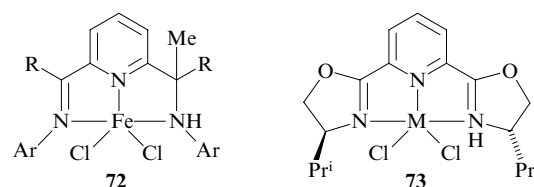
The attempts to isolate complexes with ligands containing a five-membered heterocycle (compounds **70**) instead of the pyridine ring were unsuccessful.²¹⁹ The replacement of methyl groups in the ketimine fragments by bulkier substituents resulted in the formation of highly active catalysts of ethylene polymerisation **71**.²²⁰



X = N, H, O, S.

R¹, R² = H, Me, CH₂Ph.

However, *N,N'*-bis(diphenylmethyl)-2,6-bis(imino)pyridyl complexes do not react with ethylene, while *N,N'*-difluorophenyl-2,6-bis(imino)pyridyl complexes are highly active in its oligomerisation.^{193, 221} Non-symmetric iron bis(imino)pyridyl complexes exhibit high activity in ethylene polymerisation.^{193, 222} If one (or both) imine fragments are replaced by neutral amino groups (complex **72**), the observed decrease in activity is 1–2 orders of magnitude.²²³ Series of studies were performed to elucidate the influence of various substituents at the imine nitrogen atoms in iron and ruthenium bis(oxazoline)pyridine (**73**)^{224, 225} and bis(hydrazono)pyridine^{226, 227} complexes on their activities. Several attempts were made to explain the effect of substituents in aromatic rings^{228–230} and activators^{231, 232} on the behaviour of the polymerisation catalysts and also on the structure and molecular mass of the polymers.



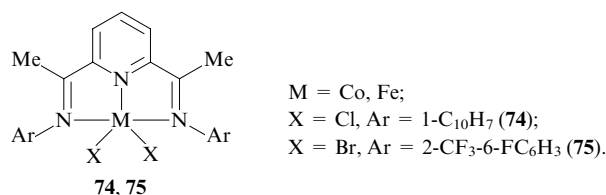
R = H, Me.

M = Fe, Ru.

Iron bis(imino)pyridyl complexes are fairly active in propylene polymerisation.^{233, 234} Small and Brookhart²³³ have reported the activity of up to 950 (kg propylene) mol^{−1} h^{−1} bar^{−1}, the polymerisation proceeding with a high proportion of 2,1-insertion; the content of the *[mm]* diads in the resulting low-molecular-mass propylene (*M*_n ≈ 6500) was as high as 67%. These catalysts show low degree of α -olefin insertion, therefore, they are unsuitable for co-polymerisation.¹⁵

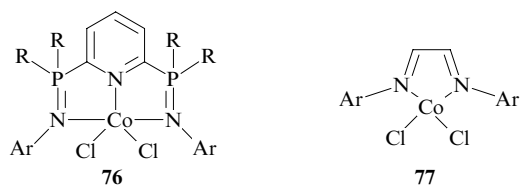
2. Cobalt(II) bis(imino)pyridyl complexes

The catalysts of olefin polymerisation based on cobalt(II) bis(imino)pyridyl complexes **64** (M = Co) were discovered simultaneously with similar iron(II) complexes.^{18, 19} Very often, the new iron and cobalt bis(imino)pyridyl ligands were studied in parallel.^{18, 19, 187, 218, 219, 226, 228–230, 235–239} Some papers describe supported iron and cobalt catalysts.^{205, 239} Interestingly, cobalt complexes with ligands containing bulky polynuclear aromatic substituents at the nitrogen atoms are relatively active in ethylene polymerisation; indeed, the activity of cobalt complex **74** was up to 673 against 950 (kg PE) mol^{−1} h^{−1} bar^{−1} for the similar iron complex when activated by MAO.²⁴⁰ The activity decreases and the polymer molecular mass increases with an increase in the bulk of the *ortho*-substituents in the phenyl rings at the nitrogen atom. The presence of both *ortho*-substituents is required in order to obtain polyethylene, while in the case of only one substituent, lower oligomers predominate among the products. Generally, the cobalt complexes are an order of magnitude less active than similar iron complexes and produce linear polymers with somewhat narrower molecular mass distribution (*M*_w/*M*_n for cobalt complexes rarely exceeds 10, while it is as high as several tens for iron complexes).



Cobalt bis(imino)pyridyl complexes are rather active in the polymerisation of vinyl ethers in the presence of MAO (iron complexes are significantly less active)²⁴¹ and in the copolymerisation of ethylene with methylcyclopropanes.²⁴² The cobalt catalysts containing electron-withdrawing substituents are extremely active in selective dimerisation and oligomerisation of α -olefins. Particularly, the selectivity of propylene dimerisation to give hex-1-ene catalysed by complex **75** is 72% and the activity of the catalyst is 19.3 (kg products) (g Co)⁻¹ h⁻¹ bar⁻¹; this catalyst is also active in ethylene polymerisation, its activity being up to 129 000 (kg PE) mol⁻¹ h⁻¹ bar⁻¹ (however, only for polymerisation time of 2 min).²⁴³ This is a record value for Group 9 metals, complex **75** being the first example of a system where a cobalt complex is more active than its iron analogue. Catalysts **64** (M = Co; R¹ = Me; R² = Me, OMe) are highly active in α -olefins formation. Such complexes in combination with [*rac*-ethylene-bis(indenyl)]zirconium(IV) dichloride²⁴⁴ or with a constrained geometry complex²⁴⁵ (the reactor blending) are used in ethylene polymerisation to produce linear low-density polyethylene with ethyl, butyl and other long alkyl branches in the side chain.

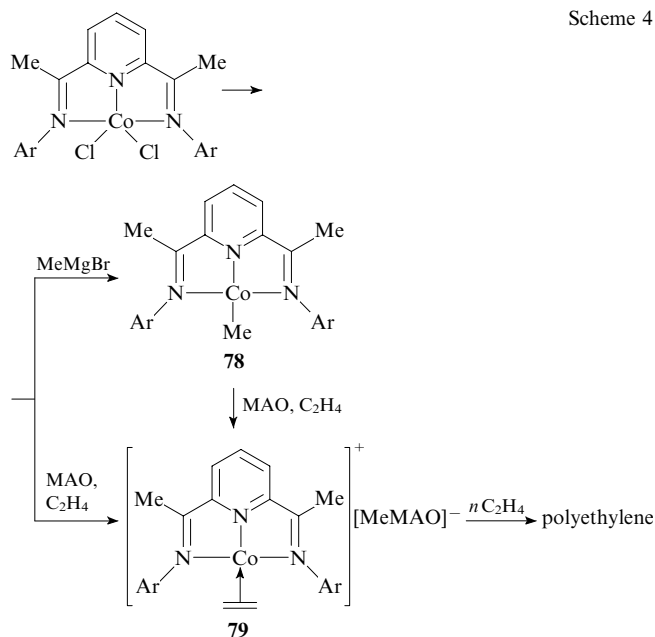
Of the analogues of cobalt(II) bis(imino)pyridyl complexes, compounds **76** deserve attention: the introduction of phosphinimide fragments results in the formation of moderately active catalysts.^{246, 247} In contrast to similar nickel compounds, branched oligomeric products are formed when cobalt bis(imino) complexes **77** are used in ethylene polymerisation in the presence of MAO.²⁴⁸



R = Ph, cyclo-C₆H₁₁;
Ar = 2,6-Pr₂C₆H₃, 2,4,6-Me₃C₆H₂.

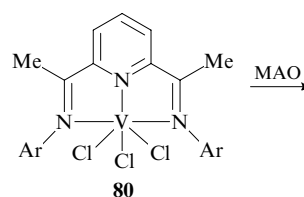
The structure of the active intermediates in cobalt-based systems has not been determined so definitely as in the case of similar iron(II) complexes. Some authors claim that cobalt(I) derivatives may be the active species.^{249, 250} The activation process suggested for systems based on cobalt bis(imino)pyridyl complexes is shown in Scheme 4. Gibson *et al.*²⁴⁹ have synthesised cobalt(I) complex **78**, a supposed precursor of the active intermediate, and have shown that after MAO activation, the same polymer is formed at the same rate as in the case of the starting cobalt(II) complex. Complex **78** itself is unable to add ethylene, it must be transformed into an active cationic form **79**.^{249, 251} According to NMR data, the observed intermediates represent ionic pairs of the types LMeCo(II)Cl-MAO or LMeCo(II)Me-MAO.²² The activation of cobalt bis(imino)pyridyl complexes by methylaluminumoxanes was also studied by electronic spectroscopy.²⁵²

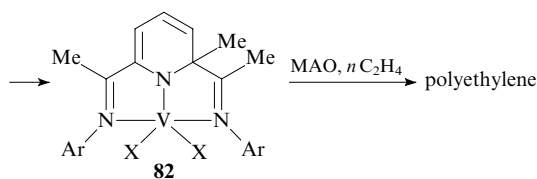
Scheme 4



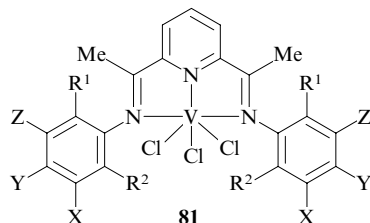
3. Vanadium(III) and chromium(III) complexes with bis(imino)pyridyl and other nitrogen-containing chelating ligands

Soon after the discovery of iron(II) and cobalt(II) bis(imino)pyridyl complexes, similar catalysts based on other metals were developed. Thus Gambarotta and co-workers²⁵³ have observed high activity of vanadium complex **80** in ethylene polymerisation [up to 3300 (kg PE) mol⁻¹ h⁻¹] in the presence of MAO. The resulting polymers possessed a bimodal molecular mass distribution and the value of M_w/M_n was as high as 50. Several years later, Schmidt *et al.*^{254, 255} have studied systematically the effect of substituents in aromatic rings on the activity of catalysts **81** and the properties of the products. It was found that in contrast to similar iron(II) complexes, oligomeric products are formed predominantly when vanadium complexes are used.²⁵⁵ Low-molecular-mass polyethylene was formed only if the aromatic rings contained two or more relatively bulky substituents (Et, Prⁱ). The introduction of electron-withdrawing substituents into the *ortho*- and *para*-positions of the phenyl ring sometimes increased the activity.²⁵⁵ Grassi and co-workers²⁵⁶ have reported low activity of similar complexes in the presence of MAO or Al₂Et₃Cl₃ in the processes of homo- and co-polymerisation of butadiene with ethylene. The mechanism of activation of vanadium catalysts is not yet clear. It was found²⁵³ that alkylation of the ligand takes place when the excess of MAO is added to catalyst **80**. It was suggested that it is complex **82** formed (X = Cl) that catalyses ethylene polymerisation. The activation processes of vanadium catalysts were studied by electronic spectroscopy.²⁵⁷ The results were interpreted by assuming the formation of complex **82** (X = Me) as the precursor of the active intermediate.



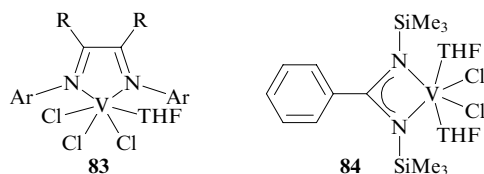


Ar = 2,6-Pr₂C₆H₃; X = Cl, Me.

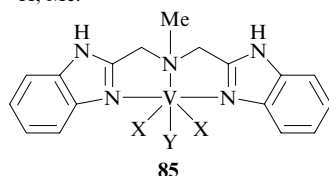


R¹, R² = H, Alk; X, Y, Z = H, Alk, Cl, Br.

Vanadium(III) bis(imino) complexes **83** have shown low activity in ethylene polymerisation in the presence of MAO and AlEt₂Cl.²⁵⁸ On the contrary, catalyst **84** supported on modified MgCl₂ was rather active [up to 3100 (kg PE) mol⁻¹ h⁻¹ bar⁻¹]; polyethylene formed had high molecular mass and a narrow molecular mass distribution (M_w up to 7×10^5 , $M_w/M_n = 2.0-2.3$).²⁵⁹ Vanadium(III) bis(benzimidazole) complexes **85** are highly active in ethylene polymerisation in the presence of AlMe₂Cl and produce polyethylene with M_w up to 10^6 and $M_w/M_n = 2.4-3.3$.²⁶⁰

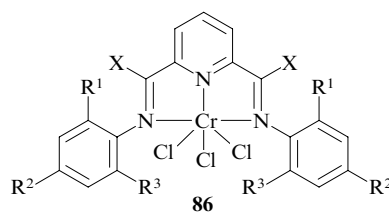


R = H, Me.



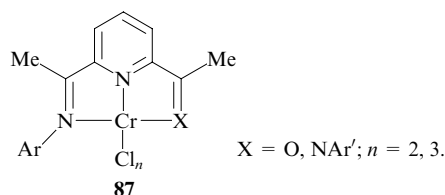
X = Y = Cl; X = OPrⁱ, Y = O.

There are very few studies on chromium(III) bis(imino)pyridyl complexes. The first publications on the synthesis of chromium(III) bis(imino)pyridyl complexes **86**²⁶¹ and on the study of their catalytic activity in ethylene polymerisation in the presence of MAO, AlBu₃ and triisobutylaluminum²⁶² appeared in 2002–2004. The resulting polymers usually possess low molecular masses (M_w up to several tens of thousands) and narrow molecular mass distribution [the ratio $M_w/M_n = 1.3-1.9$ is the lowest among bis(imino)pyridyl complexes of various metals] and the activity of the catalysts is very high [for R¹ = R² = R³ = Me, the activity was up to 25 000 (kg PE) mol⁻¹ h⁻¹ bar⁻¹ in the presence of MAO and 15 000 (kg PE) mol⁻¹ h⁻¹ bar⁻¹ in the presence of AlBu₃, polymerisation time 30 min]. A systematic study of the effect of substituents revealed general trends for all bis(imino)pyridyl complexes: the presence of *ortho*-substituents in the aromatic rings is required to achieve high activity and an increase in the bulk of these substituents results in a decrease in the activity and an increase in the molecular masses of the polymers.



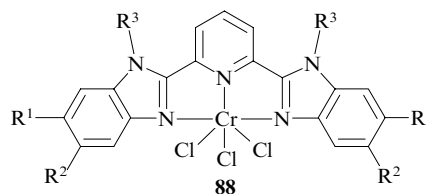
X = Me, Ph; R¹, R², R³ = H, Alk, AlkO, CF₃.

Small *et al.*²⁶³ have studied the catalytic properties of a series of other complexes of the type **87**, including non-asymmetrical ones, mainly in the reaction of ethylene oligomerisation. It was found that at room temperature the monoimine complexes **87** (X = O) are moderately active in ethylene polymerisation ($M_w = 34 \times 10^3-103 \times 10^3$) and at higher temperatures (80–100 °C) they behave similarly to the bis(imine) complexes [produce low-molecular-mass PE, the catalyst activity being up to 14 000 (kg PE) mol⁻¹ h⁻¹ bar⁻¹].

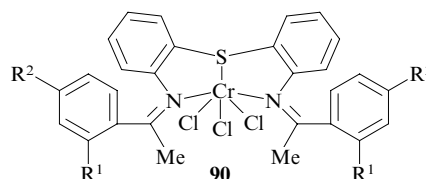
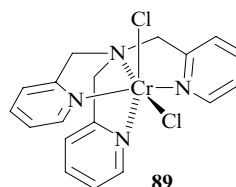


X = O, NAr'; n = 2, 3.

Nakayama *et al.*²⁶⁴ have studied a number of chromium(III) complexes with halo-substituted bis(imino)pyridyl ligands. The activity of such complexes in the presence of MMAO ranged from moderate to high. Among the analogues of bis(imino)pyridyl complexes, compound **88** has to be noted. This complex produces a mixture of oligomeric products alongside with low-molecular-mass polyethylene.²⁶⁵ The chromium(II) and chromium(III) complexes with tris(pyridylmethyl)amine (TPA) **89** show low activity in ethylene polymerisation.^{266, 267} Complexes **90** containing a donor sulfur atom are moderately active in the presence of MMAO [72–188 (kg PE) mol⁻¹ h⁻¹ bar⁻¹] and yield relatively high-molecular-mass linear product (M_w up to 3.94×10^5).²⁶⁸



R¹, R², R³ = H, Alk.



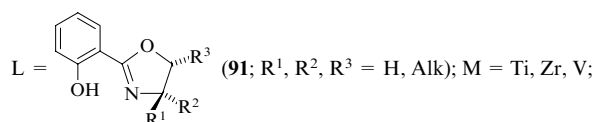
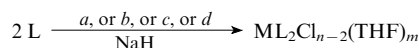
R¹, R² = H, Me.

It should be noted that chromium and vanadium bis(imino)pyridyl complexes are not currently used for ethylene polymerisation as extensively as the iron complexes. This is attributable, first, to the fact that they were discovered later than iron and cobalt complexes and, second, to the fact that they are less active and the molecular masses of the obtained polymers are lower. The zirconium(IV), titanium(III), titanium(IV) and manganese(II) bis(imino)pyridyl complexes have also been reported;^{269, 270} however, due to their low activity, they would hardly find any industrial application.

Taking into account the above-mentioned features of bis(imino)pyridyl complexes, one may conclude that the iron(II) and chromium(III) complexes are the most active in ethylene polymerisation; the iron-based catalysts produce polyethylene with a broad molecular mass distribution ($M_w/M_n > 10$), while the chromium derivatives produce polyethylene with a narrow molecular mass distribution ($M_w/M_n < 10$, sometimes even 1.3–1.9). The cobalt(II) and vanadium(III) complexes are less active and the polymers formed usually have $M_w/M_n < 10$ and a lower molecular mass than those obtained with iron- and chromium-based catalysts. The vanadium-based catalysts mainly produce oligomeric products. The product characteristics strongly depend in all cases on the substituents in the aromatic rings at the imino-group nitrogen atoms.

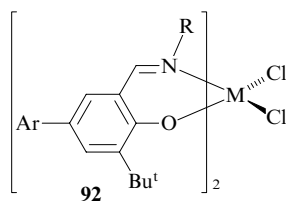
V. Complexes with phenoxyimine, pyrrolylimine and similar ligands

The first catalysts of ethylene polymerisation based upon titanium(III), titanium(IV) and zirconium(IV) complexes with N,O-donor bis(hydroxyphenyloxazoline) ligands **91** were synthesised by Floriani's research group in 1995; however the activities of these catalysts were very low.^{271, 272}

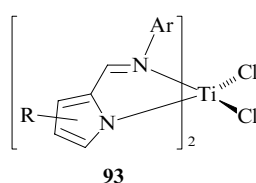


(a) $\text{TiCl}_3(\text{THF})_3$, (b) $\text{TiCl}_4(\text{THF})_2$, (c) $\text{ZrCl}_4(\text{THF})_2$, (d) $\text{VCl}_3(\text{THF})_3$.

Later, at the end of the 1990s, the synthesis of new highly active catalysts of olefin polymerisation based on complexes of Group 4 metals with bis(phenoxyimine) ligands **92** was reported.^{273, 274} The activity of these catalysts was equal to or even higher (depending on the substituents) than the activity of metallocene-based systems. Some complexes were able to catalyse living polymerisation of ethylene, stereospecific polymerisation of propylene and even co-polymerisation of ethylene and α -olefins with polar co-monomers.^{23, 275} Later, highly effective bis(pyrrolylimine) catalysts **93** have been synthesised.²⁴



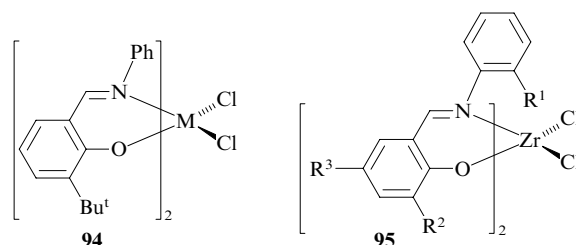
$\text{R} = \text{Ph}, \text{polyfluorophenyl}, 2\text{-MeC}_6\text{H}_4, 2\text{-Pr}^i\text{C}_6\text{H}_4$; $\text{M} = \text{Zr}, \text{Ti}$.



$\text{R} = \text{Alk}$.

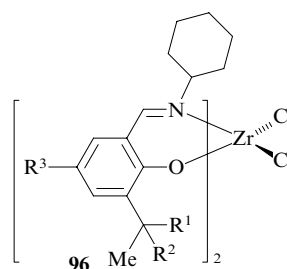
1. Zirconium complexes with phenoxyimine ligands

The optimal structure of the ligand for complexes **94** which makes them active catalysts in ethylene polymerisation upon activation with MAO was found even in the first studies of Fujita and co-workers.^{276–278} Whereas the titanium and hafnium complexes were highly active [3300 and 6500 (kg PE) $\text{mol}^{-1} \text{h}^{-1} \text{bar}^{-1}$ respectively], the zirconium complex has shown a unique activity of 519 000 (kg PE) $\text{mol}^{-1} \text{h}^{-1} \text{bar}^{-1}$ at 25 °C and polymerisation time of 5 min. Zirconium catalyst **94** effectively maintained the activity for at least 30 min at room temperature. In the presence of MAO, the maximum activity was observed at 40 °C [587 000 (kg PE) $\text{mol}^{-1} \text{h}^{-1} \text{bar}^{-1}$]; the polyethylene obtained had $M_w = 10^4$. However, if the $\text{Ph}_3\text{CB}(\text{C}_6\text{F}_5)_4\text{-AlBu}_3$ combination was used as an activator, the activity drastically decreased [down to 11 000 (kg PE) $\text{mol}^{-1} \text{h}^{-1} \text{bar}^{-1}$ at 50 °C] and ultrahigh-molecular-mass polyethylene was obtained.²⁷⁹ The catalytic properties were strongly affected by the presence of substituents in the aromatic ring and the aniline fragment. Thus, the introduction of alkyl substituents ($\text{R}^1 = \text{Alk}$) in the *ortho*-position of the aniline ring (complex **95**) resulted in a decrease in the catalyst activity and in an increase in the polymer molecular mass in the presence of MAO.²⁸⁰

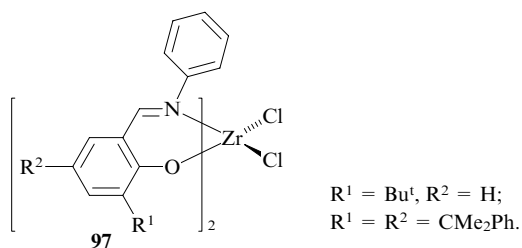


$\text{M} = \text{Ti}, \text{Zr}, \text{Hf}$.

Further development of this catalytic system involved mainly the modification of ligands. The activity was increased by selecting bulky R^2 substituents and the activity of complex **95** ($\text{R}^1 = \text{H}$, $\text{R}^2 = \text{CMe}_2\text{Ph}$, $\text{R}^3 = \text{Me}$) reached 2.1×10^6 (kg PE) $\text{mol}^{-1} \text{h}^{-1} \text{bar}^{-1}$ (Ref. 279). The replacement of aniline by cyclohexylamine increased the activity of these catalysts even more. In the presence of MAO, complex **96** ($\text{R}^1 = \text{R}^2 = \text{Ph}$, $\text{R}^3 = \text{OMe}$) has shown the activity of 9 350 000 (kg PE) $\text{mol}^{-1} \text{h}^{-1}$ under a pressure of 9 bar at 75 °C during 15 min of polymerisation.^{23, 280, 281} Matsui and Fujita²⁷⁹ have called these highly active catalysts 'FI Catalysts'.



Polyethylene with a relatively narrow molecular mass distribution ($M_w/M_n = 1.1\text{--}2.5$) is obtained in the presence of most zirconium bis(phenoxyimine) complexes. However, polyethylene obtained in the presence of complexes **97** possesses a trimodal distribution (each maximum has $M_w/M_n \approx 2$) and the content of the high-molecular-mass fractions may be controlled by temperature variation.²⁸² It was suggested that this effect is caused by existence of equilibrium of several coordination isomers of the catalyst.

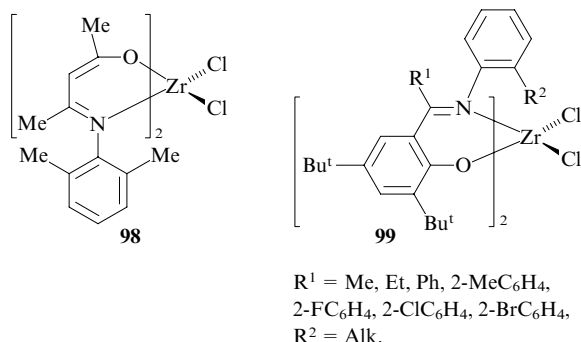


In the presence of MAO and $\text{Ph}_3\text{C}[\text{B}(\text{C}_6\text{F}_5)_4] - \text{AlBu}_3^i$, zirconium systems are able to catalyse propylene polymerisation²⁷⁷ and also co-polymerisation of ethylene with propylene^{279, 280} (with 20%–30% of propylene content) including co-polymerisation which produces an ultrahigh-molecular-mass co-polymer ($M_w = 10.2 \times 10^6$).²⁸³ The catalytic properties of phenoxyimine catalysts and the structures of the resulting polymers have been surveyed.^{284, 285}

It was found that these catalysts may also be activated by activators other than MAO and $\text{Ph}_3\text{C}[\text{B}(\text{C}_6\text{F}_5)_4]$, for example, by AlEt_3 and a phosphomolybdenum heteropoly compound²⁸⁶ or even by trialkylaluminium derivative alone.²⁸⁷ In the latter case, the molecular masses of the products are higher and their molecular mass distribution is broader than those in the case of MAO activation, while the activity of catalysts remains approximately the same. The $\text{MgCl}_2 - \text{R}_m\text{Al}(\text{OR})_n$ system was used as an activator and a support for zirconium, titanium and vanadium bis(phenoxyimine) complexes.^{288, 289} Also, highly active ‘self-immobilised’ zirconium and titanium systems containing an allyl substituent in the aniline ring were proposed, the molecular mass distribution ($M_w/M_n = 3.5 - 19.2$) attained with the ‘self-immobilised’ catalysts being wider than that for similar homogeneous systems ($M_w/M_n < 3$).²⁹⁰

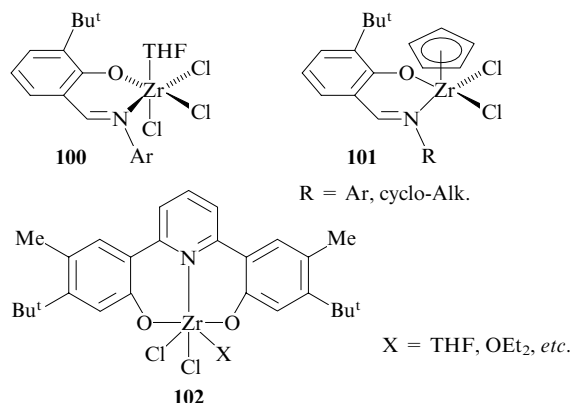
The mechanism of polymerisation with zirconium bis(phenoxyimine) complexes is little studied. Makio and Fujita²⁹¹ have attempted to detect active intermediates by ^1H NMR spectroscopy, but the results were not highly informative.

Bis(ketimine) complexes **98**, which are moderately active in ethylene polymerisation, should be noted among the analogues of zirconium bis(phenoxyimine) complexes.²⁹² Highly active bis(phenoxyketimine) complexes **99** were synthesised; the introduction of the R^1 substituents into the imine group results in an increase in the catalyst activity and the molecular mass of polyethylene.²⁹³



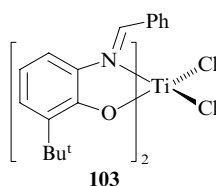
It is remarkable that removal of one phenoxyimine ligand or its replacement by cyclopentadienyl results in a significant decrease in the activity of complexes **100** and **101**.^{82, 294} Complexes **102** with tridentate N,O,O-donor ligands are highly active in ethylene polymerisation and co-polymerisation of ethylene with propylene in the presence of MAO [up to 5700 (kg PE) $\text{mol}^{-1} \text{h}^{-1} \text{bar}^{-1}$ at 25 °C for polymerisation time of 5 min] and $\text{Ph}_3\text{CB}(\text{C}_6\text{F}_5)_4 - \text{AlBu}_3^i$ [up to 36 590 (kg PE) $\text{mol}^{-1} \text{h}^{-1} \text{bar}^{-1}$ under similar conditions].

The increase in temperature has resulted in a decrease in the polymer molecular mass and in the narrowing of the molecular mass distribution due to acceleration of chain transfer processes.²⁹⁵ The catalysts containing phenoxyimine ligands linked by a polymethylene bridge were also highly active.²⁹⁶ The zirconium complexes containing bis(phenoxyimine) ligands linked by different types of bridges were moderately active in the polymerisation^{297–299} and oligomerisation of ethylene.^{300, 301}



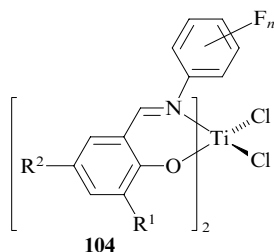
2. Titanim complexes with phenoxyimine ligands

In contrast to zirconium complexes, titanium complexes with bis(phenoxyimine) ligands are not highly active in polymerisation but produce polymers with higher molecular masses. Thus the activity of titanium complexes **94**^{276–280, 302} in ethylene polymerisation in the presence of MAO was equal to 2280–4150 (kg PE) $\text{mol}^{-1} \text{h}^{-1} \text{bar}^{-1}$; a high-molecular-mass polyethylene ($M_w = 2.9 \times 10^5 - 8.8 \times 10^5$) was obtained at 25–75 °C. This complex is less active in the presence of $\text{Ph}_3\text{CB}(\text{C}_6\text{F}_5)_4 - \text{AlBu}_3^i$; however, the resulting polyethylene had an ultrahigh molecular mass ($M_w = 3.9 \times 10^6 - 5.9 \times 10^6$). Note that titanium complex **94** may be reduced by triisobutylaluminium to a phenoxyamine derivative, which is active in polymerisation of higher olefins, particularly, hex-1-ene.³⁰³ Structurally related *N*-benzylidene complex **103** is also highly active in ethylene polymerisation in the presence of MAO or $\text{Ph}_3\text{CB}(\text{C}_6\text{F}_5)_4 - \text{AlBu}_3^i$ yielding high-molecular-mass polyethylene.³⁰⁴

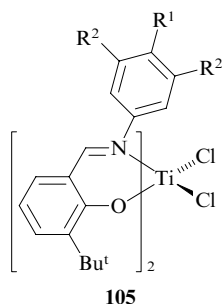


The most interesting properties were found for catalysts with electron-withdrawing substituents in the aniline ring. Thus it was established that complexes **104** ($R^1 = \text{Bu}^t$, $R^2 = \text{H}$) are able to catalyse living polymerisation of ethylene³⁰⁵ and propylene with high syndiospecificity ($[rr]$ of up to 87%–93%, $M_w/M_n \sim 1.1$) in the presence of MAO.^{306, 307} The presence of even one fluorine atom in the *ortho*-position of the aniline fragment is sufficient to trigger the living polymerisation mechanism; the highest activity [up to 36 000 (kg PE) $\text{mol}^{-1} \text{h}^{-1} \text{bar}^{-1}$ at 50 °C] was achieved with a catalyst containing a pentafluorinated phenyl ring, and the polymer molecular mass was also the highest in this case ($M_n = 4.24 \times 10^5$).^{23, 308} Complexes containing fluorine atoms only in the *meta*- and/or *para*-positions of the aniline ring are also highly active but do not catalyse living polymerisation ($M_w/M_n = 1.78 - 2.18$).^{23, 305–308} It is characteristic that upon introduction of electron-withdrawing substituents into the

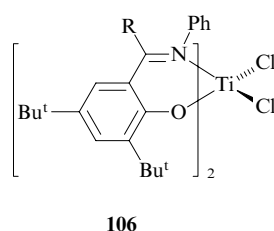
salicylaldimine ring, polymerisation in the presence of titanium bis(phenoxyimine) complexes **104** ($R^1 = R^2 = \text{I}$; $F_n = 2,6\text{-F}_2$) is no more living and the activity of the catalyst decreases. Complexes **104** are able to catalyse the production of block co-polymers with styrene.^{309–311} It should be noted that in all cases, the polymerisation time was very short (from 1 to 5 min).



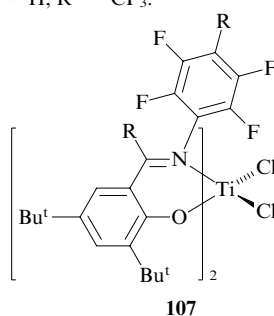
Titanium fluorinated phenoxyimine complexes were used for the production of ethylene-propylene block co-polymers.³¹² Trifluoromethyl groups (complex **105**) can also be used as substituents that increase the activity; the higher the number of electron-withdrawing groups the higher the catalyst activity and the polymer molecular mass.³¹³ Coates and co-workers³¹⁴ have found that titanium complexes **106** with phenoxyketimine ligands without electron-withdrawing substituents in the aniline ring may be used as catalysts of living polymerisation of ethylene. Complexes **107** produce polyethylene with a relatively broad molecular mass distribution ($M_w/M_n = 4-5$).³¹⁵



$R^1 = \text{CF}_3$, $R^2 = \text{H}$;
 $R^1 = \text{H}$, $R^2 = \text{CF}_3$.



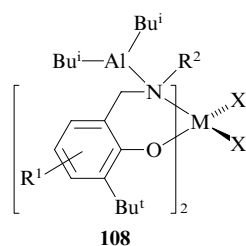
$R = \text{H, Me, Et, Ph}$.



$R = \text{H, CF}_3$.

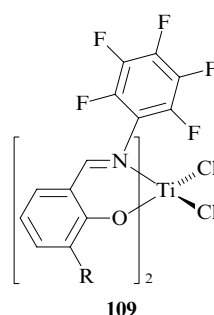
A number of interesting properties were found for fluorinated phenoxyimine catalysts **104** in living polymerisation of propylene.^{306, 307} Particularly, the syndiotactic polypropylene with a high melting point (up to 149–156 °C) was obtained in the presence of MAO.³¹⁶ It is quite remarkable that chain propagation occurs according to the 2,1-insertion mechanism.^{317, 318} If the $\text{Ph}_3\text{CB}(\text{C}_6\text{F}_5)_4\text{-AlBu}_3$ system is used as a co-catalyst, a high-molecular-mass atactic polypropylene is produced; the zirconium and hafnium analogues of complex **104** in combination with this co-catalyst form isotactic polypropylene.³¹⁹ This was attributed to the reduction of the imine bond leading to compounds **108**, which possess different catalytic properties.³²⁰ Particularly, these compounds are less active than phenoxyimines and their activity in the polymer-

isation of higher olefins increases in the series hex-1-ene < oct-1-ene < dec-1-ene < 4-methylpent-1-ene.



$R^1 = \text{Alk}$; $R^2 = \text{X} = \text{Bu}^i$.

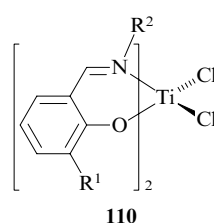
Bis(phenoxyimine) complexes may be used as catalysts of ethylene co-polymerisation with higher olefins. Co-polymerisation of ethylene with propylene, hex-1-ene and norbornene catalysed by titanium bis(phenoxyimine) complexes **94** has been studied.³²¹ Complexes **109** may catalyse the production of block co-polymers with hex-1-ene, oct-1-ene, dec-1-ene with narrow molecular mass distributions ($M_w/M_n = 1.1-1.3$) and co-monomer contents of up to 30%.³²² The homopolymerisation of higher α -olefins ($\text{C}_6\text{-C}_{10}$) in the presence of titanium bis(phenoxyimine) complexes and $\text{Ph}_3\text{CB}(\text{C}_6\text{F}_5)_4\text{-AlBu}_3$ have been discussed by Fujita and co-workers;³²³ atactic polyolefins with high molecular mass were obtained ($M_w = 8.5 \times 10^5 - 1.5 \times 10^6$).



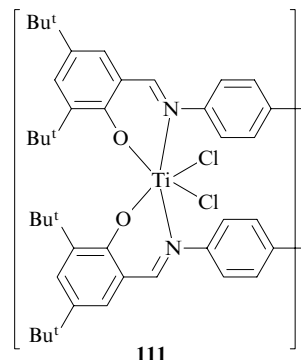
$R = \text{H, Me, Bu}^i, \text{Pr}^i, \text{cyclo-C}_6\text{H}_{11}$.

The search for other co-catalysts has brought some results. Particularly, polyethylene³²⁴ and syndiotactic polypropylene³²⁵ were obtained with fluorinated catalysts activated by isobutylaluminium 2-ethylhexyloxide [$\text{Bu}_m^i\text{Al}(\text{OR})_n$] with MgCl_2 . Similar co-catalyst systems were used for activation of titanium, zirconium and vanadium phenoxyimine complexes.²⁸⁸ The first papers on the solid-phase phenoxyimine systems have appeared. For example, Klapper and co-workers³²⁶ supported titanium bis(phenoxyimine) complex on latex particles and obtained ultrahigh-molecular-mass ($M_w > 6 \times 10^6$) polyethylene with $M_w/M_n = 3$.

The structure of phenoxyimine ligands was varied in a number of studies. Complexes **110** with bulky substituents in the aniline ring had a low activity.³²⁷ Bravaya and co-workers³²⁸ synthesised dinuclear titanium complex **111**, which was highly active in ethylene polymerisation in the

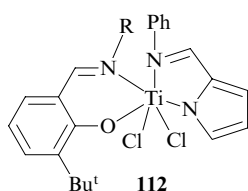


$R^1 = \text{H}$, $R^2 = \text{Ph}$,
2,6- $\text{Me}_2\text{C}_6\text{H}_3$, 2,6- $\text{Pr}_2\text{C}_6\text{H}_3$,
2,6- $\text{F}_2\text{C}_6\text{H}_3$, 1- C_{10}H_7 ;
 $R^1 = \text{F}$, $R^2 = 2,6\text{-F}_2\text{C}_6\text{H}_3$.

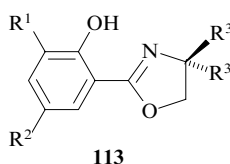


presence of MAO and produced high-molecular-mass polyethylene ($M_n = 2.5 \times 10^6$).

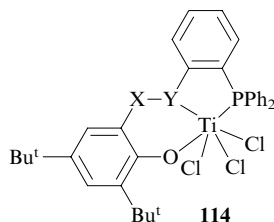
Bochmann and co-workers⁸² have synthesised titanium monocyclopentadienyl monophenoxyimine and phenoxyamine complexes similar to zirconium complexes **101**; these compounds were active in the polymerisation of 1-alkenes in the presence of MAO. The monosalicylaldimine compounds, for example, the titanium analogues of complexes **100**, exhibit relatively low activities [up to 440 (kg PE) mol⁻¹ h⁻¹ bar⁻¹].^{294, 329} The hybrid salicylaldiminato pyrrolyliminate catalysts **112** are highly active [up to 85 000 (kg PE) mol⁻¹ h⁻¹ bar⁻¹, polymerisation time 2 min, 20 °C]; however, they are unable to activate living polymerisation.³³⁰ Recently, it has been found that the titanium and zirconium complexes L₂MCl₂ with salicyloxazoline ligands **113** bearing substituents R¹, R², R³ = H, Me, Prⁱ, Bu^t are highly active catalysts of ethylene polymerisation [up to 280 000 (kg PE) mol⁻¹ h⁻¹ bar⁻¹, polymerisation time 1 min, 22 °C].³³¹



R = Ph, C₆F₅.



Tang and co-workers³³² have shown that titanium complexes **114** with tridentate N,O,P-donor ligands are active in ethylene polymerisation in the presence of MMAO and are also able to catalyse co-polymerisation of ethylene with propylene, hexene and norbornene.



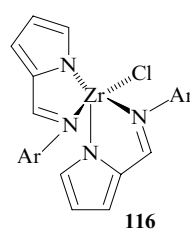
X–Y = CH=N, CH₂–NH.

It should be noted that zirconium phenoxyimine and other related complexes particularly, titanium complexes are usually rapidly deactivated; therefore, most of the authors use only the initial parts of polymerisation curves (1–5 min) in the calculation of catalytic activities.

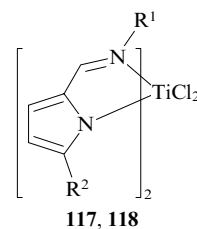
In the case of titanium phenoxyimine catalysts, active intermediates have been studied in more detail than their zirconium analogues. Thus Fujita and co-workers²⁸⁹ have identified a series of titanium(IV) complexes in the catalytic system **109** (R = Bu^t) with MAO by ¹H NMR spectroscopy. Later, Talsi and co-workers³³³ have used ¹H, ¹³C and ¹⁹F NMR to detect and identify a series of cationic intermediates, including species **115**, in the catalytic systems comprising compound **109** (R = Bu^t) and MAO (Scheme 5) and also with AlMe₃–Ph₃CB(C₆F₅)₄. It was established that reduction of the metal to titanium(III) and the transfer of the phenoxyimine ligand to aluminium, resulting in the formation of LAlMe₂, are the main routes of deactivation of the active species.

3. Group 4 metal complexes with pyrrolylimine ligands

The first complexes of Group 4 metals with pyrrolylimine ligands were synthesised and tested in polymerisation by Fujita and co-workers^{24, 334, 335} and Bochmann and co-workers.³³⁶ Zirconium complex **116** was moderately active in ethylene polymerisation in the presence of MAO [63.8 (kg PE) mol⁻¹ h⁻¹ bar⁻¹], while titanium complexes **117** proved to be much more active [up to 33 200 (kg PE) mol⁻¹ h⁻¹ bar⁻¹ in the presence of MAO, R¹ = cyclo-C₈H₁₅] to produce linear high-molecular-mass polyethylene ($M_w = 3.1 \times 10^6$). When Ph₃CB(C₆F₅)₄–Bu₃Al was used as a co-catalyst, the activity decreased severalfold and M_w increased (up to 4.9×10^6), as in the case of phenoxyimine catalysts (see above). Later, it was shown³³⁷ that complex **117** (R¹ = cyclo-C₆H₁₁) is able to catalyse living polymerisation of ethylene with norbornene, the co-monomer content being up to 44%–48%, and the product formed has M_n up to 8×10^5 and $M_w/M_n = 1.1$ –1.2. Fujita and co-workers²⁴ have generally termed the bis(pyrrolylimine) catalysts as ‘PI Catalysts’.



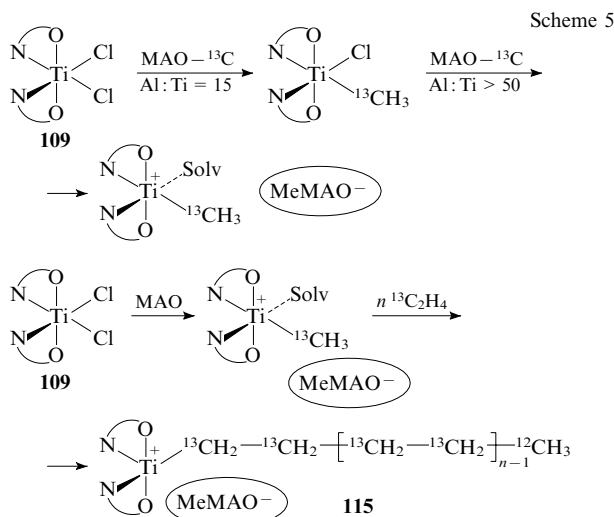
Ar = 2,6-Pr₂C₆H₃.



117: R² = H; R¹ = Et, Ph, n-C₆H₁₃, cyclo-C₆H₁₁, cyclo-C₈H₁₅;

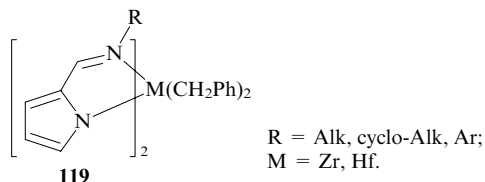
118: R¹ = Ph; R² = H, Me, Bu^t, SiMe₃.

Titanium bis(pyrrolylimine) complexes are more active than their zirconium analogues and, hence, it is studies of titanium complexes that are the most advanced. Attaining high activity of such complexes does not require necessarily the presence of a bulky substituent in the vicinity of the active centre. Indeed, the complex with R² = H is the most active in the series of catalysts **118**.²⁴ Probably, the higher content of propylene (up to 20%–30% against 4.5% for phenoxyimine systems) and hex-1-ene (up to 1.9% against 0.4% for phenoxyimine systems) obtained upon co-polymerisation of ethylene with these co-monomers may be explained by greater steric accessibility of the central atom in pyrrolylimine complexes.^{24, 321} A similar picture was also observed in co-polymerisation of ethylene with norbornene.²⁴ Details of studies on living co-polymerisation of ethylene with norbornene have been reported.^{24, 337} Analysis of the co-polymer structure has revealed that alternating norbornene–ethylene units predominate. Interestingly, the homopolymerisation of ethylene is not living polymerisation (the obtained polymer has $M_w/M_n = 2.1$) and norbornene is not polymerised at all.³³⁸ For the first time, the authors have managed to obtain block co-polymers of ethylene with norbornene that contained polyethylene and alternating ethylene–norbornene segments.^{338, 339} The cal-

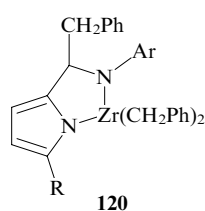


culations for ethylene insertion into the metal–carbon bond, which take place in the polymerisation on bis(pyrrolylimine) catalysts, were performed in a theoretical study.³⁴⁰

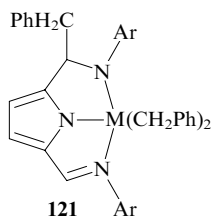
Apart from the titanium bis(pyrrolylimine) complexes, similar hafnium and zirconium complexes have been studied. In contrast to complexes **117**,³³⁶ compounds **119** are extremely active in ethylene polymerisation when activated by MAO or $\text{B}(\text{C}_6\text{F}_5)_3\text{-AlBu}_3^i$ [up to 22 900 (kg PE) $\text{mol}^{-1} \text{h}^{-1} \text{bar}^{-1}$] and zirconium complexes are approximately an order of magnitude more active than the hafnium ones.^{341, 342}



A study of titanium complexes **112** with one pyrrolylimine and one phenoxyimine ligands has shown that they are able to catalyse co-polymerisation of ethylene not only with norbornene, but also with hex-1-ene or cyclopentene (in the latter case, the co-monomer content reached 37 mol %).^{329, 343} Mashima and co-workers^{344–346} have synthesised and studied a series of complexes **120** and **121**, which are active in polymerisation of ethylene in the presence of MAO or MMAO. However, their activity is lower than those of titanium bis(pyrrolylimine) complexes.



Ar = 4-MeC₆H₄, 4-MeOC₆H₄.

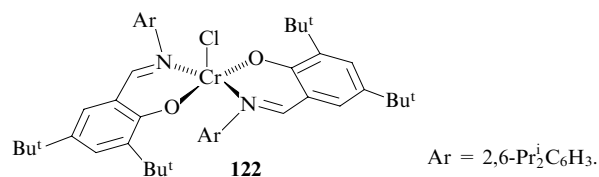


M = Zr, Hf; Ar = 2-MeC₆H₄,
4-MeC₆H₄, 4-MeOC₆H₄,
2,6-Me₂C₆H₃, 2,6-Pr₂C₆H₃.

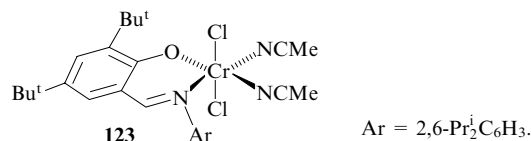
Thus, the titanium bis(pyrrolylimine) complexes are quite attractive as catalysts: they are more active in ethylene polymerisation than the metallocene systems, they are able to catalyse living co-polymerisation of ethylene with norbornene yielding the products with high norbornene content, and are suitable for production of block co-polymers of ethylene and norbornene.

4. Phenoxyimine and pyrrolylimine complexes of other metals and their analogues

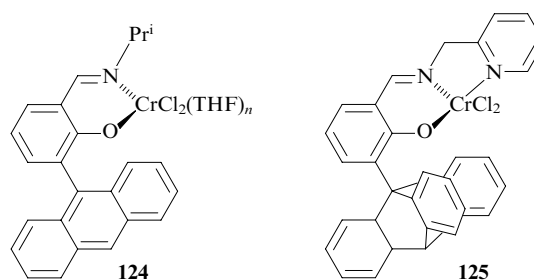
Titanium and zirconium compounds are catalytically the most active in ethylene polymerisation among metal phenoxyimine and pyrrolylimine complexes known so far. Similar complexes of other metals are also able to catalyse this process. Thus the activity of chromium bischelat complex **122** was up to 96 (kg PE) $\text{mol}^{-1} \text{h}^{-1} \text{bar}^{-1}$ with AlEt_2Cl as an activator.³⁴⁷



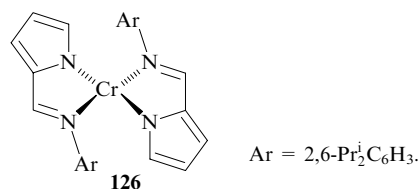
Monochelate phenoxyimine complex **123** is more active [130 (kg PE) $\text{mol}^{-1} \text{h}^{-1} \text{bar}^{-1}$],³⁴⁸ and AlEt_2Cl is also more efficient as an activator than MAO.



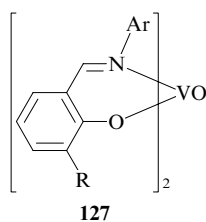
Monochelate complex **124** containing a bulky anthracenyl substituent is better activated by methylaluminoxane yielding ultrahigh-molecular-mass polyethylene.³⁴⁹ Complex **125** (and a number of similar complexes) with the tridentate O,N,N-donor ligand was found during screening of a wide variety of ligands. Such complexes are highly active in ethylene polymerisation [6970 (kg PE) $\text{mol}^{-1} \text{h}^{-1} \text{bar}^{-1}$] producing linear low-molecular-mass polyethylene.^{349, 350}



Chromium pyrrolylimine complexes are less active than similar titanium complexes. The activity of catalyst **126** combined with AlEt_2Cl is up to 70 (kg PE) $\text{mol}^{-1} \text{h}^{-1} \text{bar}^{-1}$ (Ref. 351). Subsequently, it was shown³⁵² that AlMe_2Cl may be used for activation of complex **126**; this results in an increase in the polymer molecular mass and in narrowing of the molecular mass distribution. Complex **126** shows no noticeable activity in the presence of MAO.³⁵²



Among other catalysts, vanadium bis(phenoxyimine) complexes should be noted; in particular, compounds **127** (R = H, Ar = Ph) in combination with a heterogeneous activator, $\text{MgCl}_2\text{-Et}_m\text{Al}(\text{OEH})_{3-m}$ (OEH is 2-ethylhexyloxy), is highly active in ethylene polymerisation at high temperature [65 000 (kg PE) $\text{mol}^{-1} \text{h}^{-1} \text{bar}^{-1}$ at 75 °C] and also in the co-polymerisation of ethylene with propylene ($M_w = 697\,000$, propylene content 21.3 mol %). It should be noted that compounds **127** are the first vanadium-based highly active ther-

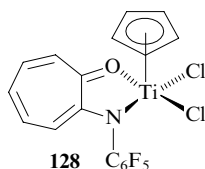


mally stable single-centred catalysts of polymerisation.^{285, 353} Redshaw *et al.*³⁵⁴ have used AlMe_2Cl for activation of complexes **127** [$\text{R} = \text{CH}(\text{OHC}_6\text{H}_4)_2$, $\text{Ar} = 2,6\text{-Pr}_2\text{C}_6\text{H}_3$]. The activities were somewhat lower [up to $24\,900\text{ (kg PE) mol}^{-1}\text{ h}^{-1}\text{ bar}^{-1}$ at $75\text{ }^\circ\text{C}$]; ethyl trichloroacetate, which increases the catalyst thermal stability and service life, was added as a re-activator.

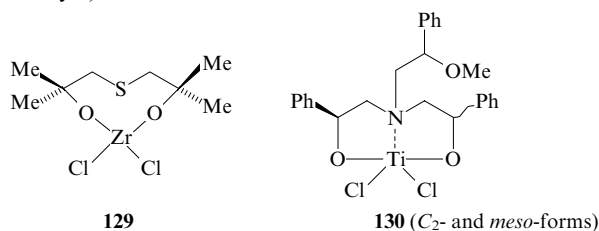
Aluminium(III) mono(phenoxyimine) complexes, which showed low activity in the polymerisation of ethylene and propylene in the presence of AlEt_3 or AlMe_3 and $\text{B}(\text{C}_6\text{F}_5)_3$, should also be noted.^{355–357}

VI. Miscellaneous complexes

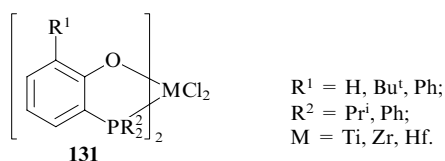
We discussed the key complexes used as catalysts of olefin polymerisation and synthesised in the late 1990s and in the early 2000s. However, a number of other complexes, which have been synthesised recently and may turn out to be perspective in the future, should be noted. Thus titanium(IV) complexes **128** containing aminotropolone ligands were synthesised. These complexes combined with MAO are able to to catalyse polymerisation of ethylene and propylene and their activities are comparable with those of metallocene catalysts.^{174, 358, 359}



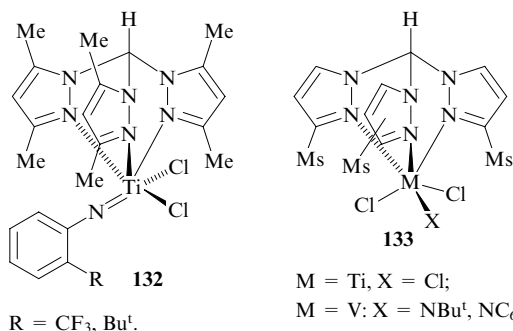
Carpentier and co-workers³⁶⁰ have synthesised and characterised a series of titanium and zirconium complexes with dialkoxy ligands containing a sulfur bridge. In the presence of MAO, some of these complexes were highly active in ethylene polymerisation [for example, the activity of complex **129** was $7190\text{ (kg PE) mol}^{-1}\text{ h}^{-1}\text{ bar}^{-1}$]. Titanium complex **130** effectively catalyses polymerisation of hex-1-ene in the presence of MAO, the resulting polymer having a narrow molecular mass distribution ($M_w/M_n = 1.07\text{--}1.11$). This implies that polymerisation follows a living mechanism; the isotacticity of the *mmmm*-pentad was 80%–85% (for the C_2 -form of the catalyst).³⁶¹



Gibson and co-workers³⁶² have described Group 4 metal complexes **131** with P,O-donor ligands that are active in olefin polymerisation. The activity of the catalyst with $\text{M} = \text{Zr}$, $\text{R}^1 = \text{Bu}^t$, $\text{R}^2 = \text{Ph}$ in ethylene polymerisation during 1 h at $20\text{ }^\circ\text{C}$ was equal to $26\,700\text{ (kg PE) mol}^{-1}\text{ h}^{-1}\text{ bar}^{-1}$. This is a very high value for non-metallocene systems.

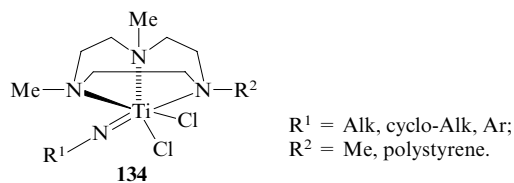


Titanium complexes **132** with the tris(pyrazolyl)methane ligand show varying activities depending on the substituent at the nitrogen atom. The complexes with $\text{R} = \text{CF}_3$, Bu^t were

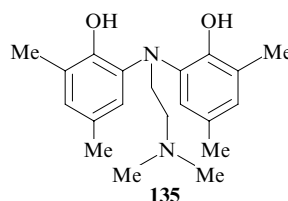


extremely active under nearly industrial conditions ($100\text{ }^\circ\text{C}$, 7 bar, 10 min), their activities being $133\,700$ and $152\,500\text{ (kg PE) mol}^{-1}\text{ h}^{-1}\text{ bar}^{-1}$ (Ref. 363). Titanium and vanadium complexes **133** catalyse ethylene polymerisation in the presence of MAO or the $\text{AlBu}_3\text{--MAO}$ system, their activity exceeding $10^4\text{ (kg PE) mol}^{-1}\text{ h}^{-1}\text{ bar}^{-1}$. High-molecular-mass polyethylene ($M_w = 1.2\text{--}1.6 \times 10^6$) may be obtained with the vanadium complex ($\text{X} = \text{NBu}^t$).³⁶⁴

The synthesis and the catalytic activity in ethylene polymerisation for several tens of imidotitanium complexes **134** containing triazacyclic ligands have been reported³⁶⁵ (only triazacyclononane complexes are shown but triazacyclohexane complexes were also studied). The activities of some complexes reached $4000\text{--}10\,000\text{ (kg PE) mol}^{-1}\text{ h}^{-1}\text{ bar}^{-1}$ at $100\text{ }^\circ\text{C}$ for a polymerisation time of 10 min.



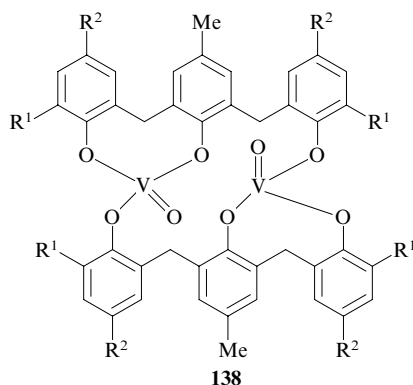
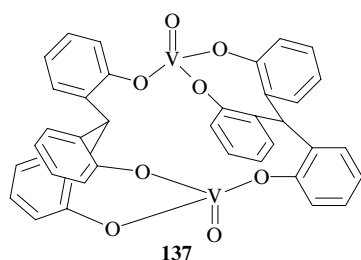
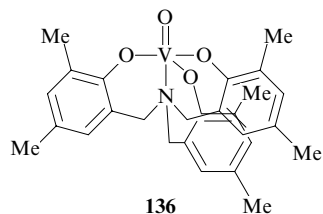
A series of complexes containing vanadium in various oxidation states ranging from +2 to +5 with O,N,N,O-donor ligands **135** have recently been reported. In the presence of AlEtCl_2 , these complexes are moderately active in ethylene polymerisation and in co-polymerisation of ethylene with hex-1-ene and norbornene (the content of norbornene is up to 29 mol%).³⁶⁶



Catalysts **136–138** based on mono- and dinuclear vanadium complexes synthesised and studied by Redshaw and co-workers^{355, 367} may be of considerable interest. Complex **136** is highly active in ethylene polymerisation in the presence of AlMe_2Cl and ethyltrichloroacetate as the reactivator [up to $96\,500\text{ (kg PE) mol}^{-1}\text{ h}^{-1}\text{ bar}^{-1}$ at $80\text{ }^\circ\text{C}$, polymerisation time 15 min, $\text{Al}:\text{V} = 2500$]; a decrease in the temperature to $25\text{ }^\circ\text{C}$ results in a 3.5-fold decrease in activity; however, the molecular mass increases by more than an order of magnitude ($M_w = 5.18 \times 10^6$).³⁵⁴

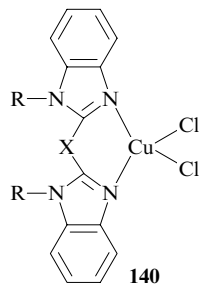
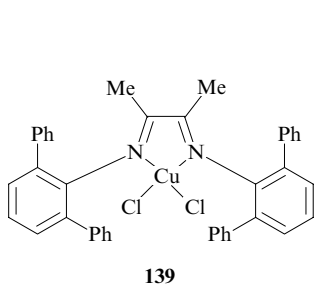
The activity of dinuclear complex **137** was similar under similar conditions.³⁵⁴ The activity of complex **138** ($\text{R}^1 = \text{Bu}^t$, $\text{R}^2 = \text{Me}$) was formally a record [up to $640\,000\text{ (kg PE) mol}^{-1}\text{ h}^{-1}\text{ bar}^{-1}$ at $80\text{ }^\circ\text{C}$], but only in the presence of a huge excess of AlMe_2Cl ($\text{Al}:\text{V} = 150\,000$) and polymerisation

time of 1 min. The melting point of the product obtained under these conditions was 135 °C, which is typical of linear ultra-high-molecular-mass polyethylene.³⁶⁷ Among other new complexes, vanadium complexes with tris(pyrazolyl)borate ligands supported on SiO₂ should be noted. These systems are highly active [up to 1900 (kg PE) mol⁻¹ h⁻¹ bar⁻¹] in the presence of MAO, AlMe₃, AlPr₃ (Ref. 368).



R¹ = Bu^t, R² = Me; R¹ = R² = Bu^t.

No copper complex-based catalysts of olefin polymerisation are discussed in this review because the activity of even the most active ones (complexes **139**³⁶⁹ and **140**³⁷⁰) does not exceed 300 (kg PE) mol⁻¹ h⁻¹ bar⁻¹. However, copper bis-(benzimidazole) complexes **140** are able to catalyse co-polymerisation of ethylene with acrylic acid esters in the presence of MAO.^{370, 371} Recently, studies of copper complexes with other *N,O*-³⁷² and *N,N*-chelating³⁷³ ligands were reported. The state-of-the-art of the studies into olefin polymerisation catalysts based on rare earth metal complexes, including non-metallocene ones, has been reviewed.³⁷⁴



R = Alk; X = CH₂,
CHOH, 2,2'-biphenyl.

VII. Conclusion

At the boundary of the century, a great number of new non-metallocene catalytic systems for olefin polymerisation have emerged. Among these systems, the transition metal bis(imine) and bis(imino)pyridyl, bis(phenoxyimine) and bis(pyrrolylimine) complexes stand out. These systems have overcome their metallocenic predecessors in the activity and variety of the obtained polymer products. New classes of ligands have appeared that allow one to control the catalytic properties of the active centres over a broad range by variation and modification of the ligands' structure. In contrast to metallocene systems, which use expensive Lewis acids (methylaluminoxane, perfluoroarylboron derivatives) as activators, much cheaper activators such as trialkylaluminium, alkoxylaluminium derivatives on MgCl₂, etc., may be used for activation of post-metallocene systems. At present, the main target of the studies of these systems is maximum control over the parameters (molecular mass, composition, structure) of the resulting products. Undoubtedly, very soon we can expect new achievements in this field, as big research groups have started a systematic search for new catalytic systems by employing the 'high-throughput screening' methodology.^{15, 350} The experimental and theoretical studies of the structures of active intermediates and the mechanisms of catalytic polymerisation are also in progress.

In an early review on the new catalytic systems, Gibson has mentioned that overcoming of the stereotype that the search for new catalysts should be limited by a narrow class of metals, which have already proved themselves in the formation of active polymerisation centres, and that the development of new systems will be restricted only by imagination of a scientist, would form the distinctive features of the 'post-metallocene age' of olefin polymerisation catalysts.²⁶ Some research groups proceeded, from the very beginning, from the assumption that the ligand structure is the most important factor because the olefin affinity is pronounced for all transition metals.²⁴ According to this ligand-oriented approach, high polymerisation activity requires a suitable ligand with balanced electron-releasing and -withdrawing properties. Indeed, up to now, among all complexes of the first row transition metals, the highly active catalytic systems for olefin polymerisation are practically unknown only for manganese complexes. However, this situation is already changing: manganese(I) hydrotris(pyrazolyl)borate complexes are reported.³⁷⁵

At the same time, it should be noted that the development of studies of post-metallocene systems has not resulted so far in a broad commercial application of these systems. On the one hand, some time is required for bringing new processes to large-scale industrial production. On the other hand, the industry demands, first of all, active systems stable at higher temperatures (preferably supported). At present, most of the post-metallocene catalytic systems do not meet these criteria. Therefore, it is obvious that the traditional processes based upon Ziegler–Natta and metallocene catalysts will not be quickly replaced and mainly those post-metallocene systems that produce valuable polyolefin-based materials with new properties will be used by industry in the future.

The author is grateful to professors V A Zakharov and E P Talsi for important comments during the preparation of the present review.

References

1. R Mulhaupt *Nachr. Chem. Technol. Lab.* **41** 1341 (1993)
2. M Bochmann *Top. Catal.* **7** 9 (1999)
3. H H Brintzinger, D Fischer, R Mulhaupt, B Rieger, R M Waymouth *Angew. Chem., Int. Ed. Engl.* **34** 1143 (1995)

4. A Thayer *Chem. Eng. News* **72** 4 (1994)
5. T J Marks J C Stevens (Eds) *Top. Catal.* **7** (Special Issue on Advances in Polymerization Catalysis. Catalysts and Processes) (1999)
6. W Kaminsky (Ed.) *Metalorganic Catalysts for Synthesis and Polymerization: Recent Results by Ziegler-Natta and Metallocene Investigations* (Berlin: Springer, 1999)
7. R F Jordan (Ed.) *J. Mol. Catal.* **128** (Special Issue on Metallocene and Single-Site Olefin Catalysts) (1998)
8. W Kaminsky, M Arndt *Adv. Polym. Sci.* **127** 143 (1997)
9. M Bochmann *J. Chem. Soc., Dalton Trans.* 255 (1996)
10. R F Jordan *Adv. Organomet. Chem.* **32** 325 (1991)
11. E Y X Chen, T J Marks *Chem. Rev.* **100** 1391 (2000)
12. K B Sinclair, R B Wilson *Chem. Ind.* (21) 857 (1994)
13. S S Ivanchev *Katal. Prom-sti* (6) 15 (2002)
14. S D Ittel, L K Johnson, M Brookhart *Chem. Rev.* **100** 1169 (2000)
15. V C Gibson, S K Spitzmesser *Chem. Rev.* **103** 283 (2003)
16. L K Johnson, C M Killian, M Brookhart *J. Am. Chem. Soc.* **117** 6414 (1995)
17. T R Younkin, E F Conner, J I Henderson, S K Friedrich, R H Grubbs, D A Bansleben *Science* **287** 460 (2000)
18. B L Small, M Brookhart, A M A Bennet *J. Am. Chem. Soc.* **120** 4049 (1998)
19. G J P Britovsek, V C Gibson, B S Kimberley, P J Maddox, S J McTavish, G A Solan, A J P White, D J Williams *Chem. Commun.* 849 (1998)
20. K R Kumar, S Sivaram *Macromol. Chem. Phys.* **201** 1513 (2000)
21. E P Talsi, D E Babushkin, N V Semikolenova, V N Zudin, V N Panchenko, V A Zakharov *Macromol. Chem. Phys.* **202** 1816 (2001)
22. N V Semikolenova, V A Zakharov, E P Talsi, D E Babushkin, A P Sobolev, L G Echevskaya, M M Khusniyarov *J. Mol. Catal. A* **182–183** 283 (2002)
23. H Makio, N Kashiwa, T Fujita *Adv. Synth. Catal.* **344** 477 (2002)
24. Y Yoshida, S Matsui, T Fujita *J. Organomet. Chem.* **690** 4382 (2005)
25. G W Coates, P D Hustad, S Reinartz *Angew. Chem., Int. Ed.* **41** 2237 (2002)
26. G J P Britovsek, V C Gibson, D F Wass *Angew. Chem., Int. Ed.* **38** 428 (1999)
27. A O Patil, G G Hlatky (Eds) *Beyond Metallocenes: Next-Generation Polymerization Catalysts* (Oxford: Oxford University Press, 2003)
28. B Rieger, L S Baugh, S Kacker, S Striegler (Eds) *Late Transition Metal Polymerization Catalysis* (Weinheim: Wiley-VCH, 2003)
29. R Minott, G Fink, W Fenzl *Angew. Makromol. Chem.* **154** 1 (1987)
30. G Fink, W Fenzl, R Minott *Z. Naturforsch., B* **40** 158 (1985)
31. G Fink, R Rottler *Angew. Makromol. Chem.* **94** 25 (1981)
32. I Tritto, S X Li, M C Sacchi, P Locatelli, G Zannoni *Macromolecules* **28** 5358 (1995)
33. I Tritto, R Donetti, M C Sacchi, P Locatelli, G Zannoni *Macromolecules* **32** 264 (1999)
34. I Tritto, R Donetti, M C Sacchi, P Locatelli, G Zannoni *Macromolecules* **30** 247 (1997)
35. I Tritto, M Sacchi, S Li *Macromol. Rapid Commun.* **15** 217 (1994)
36. I Tritto, M Sacchi, P Locatelli, S Li *Macromol. Symp.* **89** 289 (1995)
37. D E Babushkin, N V Semikolenova, V A Zakharov, E P Talsi *Macromol. Chem. Phys.* **201** 558 (2000)
38. K P Bryliakov, D E Babushkin, E P Talsi, A Z Voskoboynikov, H Gritz, L Shröder, H R Damrau, U Wieser, F Schaper, H H Brintzinger *Organometallics* **24** 894 (2005)
39. D E Babushkin, H H Brintzinger *J. Am. Chem. Soc.* **124** 12869 (2002)
40. K P Bryliakov, M Bochmann, E P Talsi *Organometallics* **23** 149 (2004)
41. K P Bryliakov, N V Semikolenova, D V Yudaev, V A Zakharov, H H Brintzinger, M Ystenes, E Rytter, E P Talsi *J. Organomet. Chem.* **683** 92 (2003)
42. M Bochmann, S J Lancaster *Angew. Chem., Int. Ed. Engl.* **33** 1634 (1994)
43. C Götz, A Rau, G Luft *J. Mol. Catal. A* **184** 95 (2002)
44. X Yang, C L Stern, T J Marks *J. Am. Chem. Soc.* **116** 10015 (1994)
45. L Jia, X Yang, A Ishihara, T J Marks *Organometallics* **14** 3135 (1995)
46. C R Landis, K A Rosaaen, D R Sillars *J. Am. Chem. Soc.* **125** 1710 (2003)
47. M Bochmann, S J Lancaster *Organometallics* **12** 633 (1993)
48. J C Flores, J C W Chien, M D Rausch *Organometallics* **13** 4140 (1994)
49. S J Skoog, C Mateo, G G Lavoie, F J Hollander, R G Bergman *Organometallics* **19** 1406 (2000)
50. J C W Chien, Z T Yu, M M Marques, J C Flores, M D Rausch *J. Polym. Sci., Part A* **36** 319 (1998)
51. M S Blais, J C W Chien, M D Rausch *Organometallics* **17** 3775 (1998)
52. J Sassmannshausen, A K Powell, C E Anson, S Wocadlo, M Bochmann *J. Organomet. Chem.* **592** 84 (1999)
53. P J W Deckers, B Hessen, J H Teuben *Angew. Chem., Int. Ed.* **40** 2516 (2001)
54. B Hessen *J. Mol. Catal. A* **213** 129 (2004)
55. A L McKnight, R M Waymouth *Chem. Rev.* **98** 2587 (1998)
56. US P. 6265338; *Chem. Abstr.* **135** 107722 (2001)
57. N Naga *J. Polym. Sci., Part A* **43** 1285 (2005)
58. G Lanza, I L Fragalà, T J Marks *Organometallics* **21** 5594 (2002)
59. G Xu, D Cheng *Macromolecules* **34** 2040 (2001)
60. W Kaminsky, P D Tran, R Werner *Macromol. Symp.* **213** 101 (2004)
61. L J Irwin, J H Reibenspies, S A Miller *J. Am. Chem. Soc.* **126** 16716 (2004)
62. I Tritto, L Boggioni, D R Ferro *Coord. Chem. Rev.* **250** 212 (2006)
63. S Martinez, J Ramos, V L Cruz, J Martinez-Salazar *Polymer* **47** 883 (2006)
64. S Martinez, M T Exposito, J Ramos, V Cruz, M C Martinez, M Lopez, A Munoz-Escalona, J Martinez-Salazar *J. Polym. Sci., Part A* **43** 711 (2005)
65. V V Kotov, E V Avtonomov, J Sundermeyer, K Harms, D A Lemenovskii *Eur. J. Inorg. Chem.* 687 (2002)
66. K Kunz, G Ecker, S Döring, R Fröhlich, G Kehr *J. Am. Chem. Soc.* **123** 6187 (2001)
67. R Kleinschmidt, Y Griebenow, G Fink *J. Mol. Catal. A* **157** 83 (2000)
68. H Wang, H S Chan, J Okuda, Z Xie *Organometallics* **24** 3118 (2005)
69. D W Stephan, J C Stewart, F Guerin, R Spence, W Xu, D G Harrison *Organometallics* **18** 1116 (1999)
70. W P Kretschmer, C Dijkhuis, A Meetsma, B Hessen, J H Teuben *Chem. Commun.* 608 (2002)
71. K Nomura, M Naga, M Miki, K Yanagi, A Imai *Organometallics* **17** 2152 (1998)
72. A Antinolo, F Carrillo-Hermosilla, A Corrochano, J Fernandez-Baeza, A Lara-Sanchez, M R Ribeiro, M Lanfranchi, A Otero, M A Pellinghelli, M F Portela, J V Santos *Organometallics* **19** 2837 (2000)
73. Y X Chen, P F Fu, C L Stern, T J Marks *Organometallics* **16** 5958 (1997)
74. H Nakazawa, S Ikai, K Imaoka, Y Kai, T Yano *J. Mol. Catal. A* **132** 33 (1998)
75. S Murtuza, O L Casagrande, R F Jordan *Organometallics* **21** 1882 (2002)
76. M P Gil, J H dos Santos, O L Casagrande *Macromol. Chem. Phys.* **202** 319 (2001)
77. R Gómez, R Ducheteau, A N Chernega, J H Teuben, F T Edelman, M L H Green *J. Organomet. Chem.* **491** 153 (1995)
78. R Gómez, M L H Green, J Haggit *J. Chem. Soc., Chem. Commun.* 2607 (1994)
79. D Kissouko, J C Fetting, L R Sita *Inorg. Chim. Acta* **345** 121 (2003)
80. S Doherty, R J Errington, A P Jarvis, S Collins, W Clegg, M R J Elsegood *Organometallics* **17** 3408 (1998)

81. J Huang, B Lian, Y Qian, W Zhou, W Chen, G Zheng *Macromolecules* **35** 4871 (2002)
82. R K J Bott, D L Hughes, M Schormann, M Bochmann, S J Lancaster *J. Organomet. Chem.* **665** 135 (2003)
83. M P Coles, V C Gibson *Polym. Bull. (Berlin)* **33** 529 (1994)
84. M C W Chan, J M Cole, V C Gibson *Chem. Commun.* 2345 (1997)
85. M C W Chan, K C Chew, C I Dalby, V C Gibson, A Kohlmann, I R Little, W Reed *Chem. Commun.* 1673 (1998)
86. P T Witte, A Meetsma, B Hessen *Organometallics* **18** 2944 (1999)
87. Y Liang, G P A Yap, A L Rheingold, K H Theopold *Organometallics* **15** 5284 (1996)
88. R Emrich, O Heinemann, P W Jolly, C Krüger, G P J Verhovnik *Organometallics* **16** 1511 (1997)
89. A Dohring, J Gohre, P W Jolly, B Kryger, J Rust, G P J Verhovnik *Organometallics* **19** 388 (2000)
90. M Enders, G Kohl, H Pritzkow *Organometallics* **23** 3832 (2004)
91. M Enders, P Fernandez, G Ludwig, H Pritzkow *Organometallics* **20** 5005 (2001)
92. A Dohring, V R Jensen, P W Jolly, W Thiel, J C Weber *Macromol. Symp.* **173** 117 (2001)
93. A Dohring, V R Jensen, P W Jolly, W Thiel, J C Weber *Organometallics* **20** 2234 (2001)
94. J S Rogers, G C Bazan *Chem. Commun.* 1209 (2000)
95. H Zhang, J Ma, Y Qian, J Huang *Organometallics* **23** 5681 (2004)
96. U Peucker, W Heitz *Macromol. Rapid Commun.* **19** 159 (1998)
97. U Peucker, W Heitz *Macromol. Chem. Phys.* **202** 1289 (2001)
98. M J Tanner, M Brookhart, J M DeSimone *J. Am. Chem. Soc.* **119** 7617 (1997)
99. M Enders, G Ludwig, H Pritzkow *Organometallics* **20** 827 (2001)
100. O Daugulis, M Brookhart, P S White *Organometallics* **22** 4699 (2003)
101. P Longo, F Grisi, A Proto, A Zambelli *Macromol. Rapid Commun.* **19** 31 (1998)
102. L K Johnson, S Mecking, M Brookhart *J. Am. Chem. Soc.* **118** 267 (1996)
103. S Mecking, L K Johnson, L Wang, M Brookhart *J. Am. Chem. Soc.* **120** 888 (1998)
104. C M Killian, D J Tempel, L K Johnson, M Brookhart *J. Am. Chem. Soc.* **118** 11664 (1996)
105. J Feldman, S J McLain, A Parthasarathy, W J Marshall, J C Calabrese, S D Arthur *Organometallics* **16** 1514 (1997)
106. J M Rose, A E Cherian, G W Coates *J. Am. Chem. Soc.* **128** 4186 (2006)
107. C Pelleccia, A Zambelli *Macromol. Rapid Commun.* **17** 333 (1996)
108. D Mader, P Walter, J Heinemann, R Mülhaupt *Polym. Prepr. (Am. Chem. Soc., Div. Polym. Chem.)* **40** 719 (1999)
109. J Heinemann, R Mülhaupt, P Brinkmann, G Luinstra *Macromol. Chem. Phys.* **200** 384 (1999)
110. A C Gottfried, M Brookhart *Macromolecules* **34** 1140 (2001)
111. S A Svejda, L K Johnson, M Brookhart *J. Am. Chem. Soc.* **121** 10634 (1999)
112. D J Tempel, M Brookhart *Organometallics* **17** 2290 (1998)
113. D P Gates, S K Svejda, E Onate, C M Killian, L K Johnson, P S White, M Brookhart *Macromolecules* **33** 2320 (2000)
114. O I R Neto, R S Mauler, R F de Souza *Macromol. Chem. Phys.* **202** 3432 (2001)
115. L C Simon, R F de Souza, J B P Soares, R S Mauler *Polymer* **42** 4885 (2001)
116. F F N Escher, R S Mauler, R F de Souza *J. Braz. Chem. Soc.* **12** 47 (2001)
117. L C Simon, R S Mauler, R F de Souza *J. Polym. Sci., Part A* **37** 4656 (1999)
118. R S Mauler, R F de Souza, D V V Vesccia, L C Simon *Macromol. Rapid Commun.* **21** 458 (2000)
119. R J Maldanis, J S Wood, A Chandrasekaran, M D Rausch, J C W Chien *J. Organomet. Chem.* **645** 158 (2002)
120. S P Meneghetti, J Kress, P J Lutz *Macromol. Chem. Phys.* **201** 1823 (2000)
121. Z Guan *Chem. – Eur. J.* **8** 3086 (2002)
122. T K Woo, P M Margl, L Deng, T Ziegler *ACS Symp. Ser.* **712** 128 (1998)
123. L Deng, P Margl, T Ziegler *J. Am. Chem. Soc.* **119** 1094 (1997)
124. L Deng, T K Woo, L Cavallo, P M Margl, T Ziegler *J. Am. Chem. Soc.* **119** 6177 (1997)
125. A Michalak, T Ziegler *Organometallics* **18** 3998 (1999)
126. T K Woo, P M Margl, P E Bloechl, T Ziegler *J. Phys. Chem. B* **101** 7877 (1997)
127. D G Musaev, R D Froese, K Morokuma *Organometallics* **17** 1850 (1998)
128. T K Woo, T Ziegler *J. Organomet. Chem.* **591** 204 (1999)
129. T K Woo, P E Bloechl, T Ziegler *J. Phys. Chem. A* **104** 121 (2000)
130. J W Strauch, G Erker, G Kehr, R Frohlich *Angew. Chem., Int. Ed.* **41** 2543 (2002)
131. L Johnson, A Bennett, K Dobbs, E Hauptman, A Ionkin, S Ittel, E McCord, S McLain, C Radzewich, Z Yin, L Wang, Y Wang, M Brookhart, in *PMSE-Preprints of the 223rd ACS National Meeting, Orlando, FL* (Washington, DC: American Chemical Society, 2002) Vol. 86, p. 319
132. S J McLain, K J Sweetman, L K Johnson, E McCord, in *PMSE-Preprints of the 223rd ACS National Meeting, Orlando, FL* (Washington, DC: American Chemical Society, 2002) Vol. 86, p. 320
133. S S Ivanchev, G A Tolstikov, V K Badaev, N I Ivancheva, I I Oleinik, S Ya Khaikin, I V Oleinik *Vysokomol. Soedin., Ser. A* **44** 1478 (2002)^a
134. I I Oleinik, I V Oleinik, I B Abdrakhmanov, S S Ivanchev, G A Tolstikov *Zh. Obshch. Khim.* **74** 1534 (2004)^b
135. S S Ivanchev, V K Badaev, N I Ivancheva, E V Sviridova, D G Rogozin, S Ya Khaikin *Vysokomol. Soedin., Ser. B* **46** 1959 (2004)^a
136. I I Oleinik, I V Oleinik, S S Ivanchev, G A Tolstikov *Zh. Org. Khim.* **41** 1354 (2005)^c
137. H R Liu, P T Gomes, S I Costa, M T Duarte, R Branquinho, A C Fernandes, J C W Chien, R P Singh, M M Marques *J. Organomet. Chem.* **690** 1314 (2005)
138. H Zou, F M Zhu, Q Wu, J Y Ai, S A Lin *J. Polym. Sci., Part A* **43** 1325 (2005)
139. C Popeney, Z Guan *Organometallics* **24** 1145 (2005)
140. S Mecking *Macromol. Rapid Commun.* **20** 139 (1999)
141. R F de Souza, O L Casagrande *Macromol. Rapid Commun.* **22** 1293 (2001)
142. F F Mota, R S Mauler, R F de Souza, O L Casagrande *Macromol. Chem. Phys.* **22** 1 (2001)
143. F A Kunrath, R F de Souza, O L Casagrande *Macromol. Rapid Commun.* **21** 277 (2000)
144. S J McLain, J Feldman, E F McCord, K H Gardner, M F Teasley, E B Coughlin, K J Sweetman, L K Johnson, M Brookhart *Macromolecules* **31** 6705 (1998)
145. US P. 6265506; *Chem. Abstr.* **135** 122919 (2001)
146. C M Killian, L K Johnson, M Brookhart *Organometallics* **16** 2005 (1997)
147. T V Laine, M Klinga, M Leskela *Eur. J. Inorg. Chem.* 959 (1999)
148. T V Laine, K Lappalainen, J Liimatta, E Aitola, B Lofgren, M Leskela *Macromol. Rapid Commun.* **20** 487 (1999)
149. T V Laine, U Piironen, K Lappalainen, M Klinga, E Aitola, M Leskela *J. Organomet. Chem.* **606** 112 (2000)
150. S P Meneghetti, P J Lutz, J Kress *Organometallics* **18** 2734 (1999)
151. A Koppl, H G Alt *J. Mol. Catal. A* **154** 45 (2000)
152. WO PCT 9849208; *Chem. Abstr.* **130** 4185 (1999)
153. X Tang, W H Sun, T Gao, J Hou, J Chen, W Chen *J. Organomet. Chem.* **690** 1570 (2005)
154. T Schareina, G Hillebrand, H Fuhrmann, R Kempe *Eur. J. Inorg. Chem.* 2421 (2001)
155. Z L Li, W H Sun, Z Ma, Y L Hu, C X Shao *Chin. Chem. Lett.* **12** 691 (2001)
156. J Li, T Gao, W Zhang, W H Sun *Inorg. Chem. Commun.* **6** 1372 (2003)
157. J Zhang, H Gao, Z Ke, F Bao, F Zhu, Q Wu *J. Mol. Catal. A* **231** 27 (2005)
158. J Zhang, X Wang, G X Jin *Coord. Chem. Rev.* **250** 95 (2006)

159. M J Rachita, R L Huff, J L Bennett, M Brookhart *J. Polym. Sci., Part A* **38** 4627 (2000)
160. WO PCT 0020377; *Chem. Abstr.* **132** 278733 (2000)
161. W H Sun, Z L Li, H Hu, B Wu, H Yang, N Zhu, X Leng, H Wang *New J. Chem.* **26** 1474 (2002)
162. C Wang, S Friedrich, T R Younkin, R T Li, R H Grubbs, D A Bansleben, M W Day *Organometallics* **17** 3149 (1998)
163. M S W Chan, L Q Deng, T Ziegler *Organometallics* **19** 2741 (2000)
164. B M Novak, G Tian, M Nodono, P Boyle, in *PMSE-Preprints of the 223rd ACS National Meeting, Orlando, FL* (Washington, DC: American Chemical Society, 2002) Vol. 86, p. 326
165. T Hu, L M Tang, X F Li, Y S Li, N H Hu *Organometallics* **24** 2628 (2005)
166. E N Jacobsen, R Breinbauer *Science* **287** 437 (2000)
167. E F Connor, T R Younkin, J I Henderson, S Hwang, R H Grubbs, W P Roberts, J J Litau *J. Polym. Sci., Part A* **40** 2842 (2002)
168. F M Bauers, S Mecking *Angew. Chem., Int. Ed.* **40** 3020 (2001)
169. F M Bauers, S Mecking *Macromolecules* **34** 1165 (2001)
170. A W Waltman, T R Younkin, R H Grubbs *Organometallics* **23** 5121 (2004)
171. X F Li, Y G Li, Y S Li, Y X Chen, N H Hu *Organometallics* **24** 2502 (2005)
172. C Carlini, V De Luise, M Martinelli, A M R Galletti, G Sbrana *J. Polym. Sci., Part A* **44** 620 (2006)
173. D Zhang, G X Jin, N Hu *Chem. Commun.* 574 (2002)
174. F A Hicks, M Brookhart *Organometallics* **20** 3217 (2001)
175. J C Jenkins, M Brookhart *J. Am. Chem. Soc.* **126** 5827 (2004)
176. C Carlini, A Macinai, F Masi, A M R Galletti, R Santi, G Sbrana, A Sommazz *J. Polym. Sci., Part A* **42** 2534 (2004)
177. C Carlini, V E G Fernandes, M Martinelli, A M R Galletti, G Sbrana *Macromol. Rapid Commun.* **26** 808 (2005)
178. J Q Sun, Y H Shan, Y J Xu, Y G Cui, H Schumann, M Hummert *J. Polym. Sci., Part A* **42** 6071 (2004)
179. Y H Shan, J Q Sun, Y J Xu, Y G Cui, F Lin *Chin. J. Polym. Sci.* **23** 301 (2005)
180. G Gui, F Bao, H Gao, F Zhu, Q Wu *J. Coord. Chem.* **59** 107 (2006)
181. Y M Zhang, Q Lin, T B Wei, D H Zhang, S Y Jie *Inorg. Chim. Acta* **358** 4423 (2005)
182. WO PCT 9830609; *Chem. Abstr.* **129** 149362 (1997)
183. WO PCT 9842664; *Chem. Abstr.* **129** 276509 (1998)
184. WO PCT 9842665; *Chem. Abstr.* **129** 276510 (1998)
185. S T Babik, G Fink *J. Mol. Catal.* **188** 245 (2002)
186. Q Wang, H Yang, Z Fan *Macromol. Rapid Commun.* **23** 639 (2002)
187. G J P Britovsek, M Bruce, V C Gibson, B S Kimberley, P J Maddox, S Mastroianni, S J McTavish, C Redshaw, G A Solan, S Stromberg, A J P White, D J Williams *J. Am. Chem. Soc.* **121** 8728 (1999)
188. G J P Britovsek, S P D Baugh, O Hoarau, V C Gibson, D F Wass, A J P White, D J Williams *Inorg. Chim. Acta* **345** 279 (2003)
189. D L Small, M Brookhart *J. Am. Chem. Soc.* **120** 7143 (1998)
190. G J P Britovsek, S Mastroianni, G A Solan, S P D Baugh, C Redshaw, V C Gibson, A J P White, D J Williams, M R J Elsegood *Chem. – Eur. J.* **6** 2221 (2000)
191. WO PCT 0158874; *Chem. Abstr.* **135** 181084 (2001)
192. M E Bluhm, C Folli, M Döring *J. Mol. Catal. A* **212** 13 (2004)
193. Z Ma, W H Sun, Z L Li, C X Shao, Y L Hu, X H Li *Polym. Int.* **51** 994 (2002)
194. M W Bouwkamp, E Lobkovsky, P J Chirik *J. Am. Chem. Soc.* **127** 9660 (2005)
195. Russ. P. 2194056; *Byull. Izobret.* **34** (2) 240 (2002)
196. S S Ivanchev, A V Yakimanskii, D G Rogozin *Dokl. Akad. Nauk* **393** 504 (2003)^d
197. I I Oleinik, I V Oleinik, I B Abdrakhmanov, S S Ivanchev, G A Tolstikov *Zh. Obshch. Khim.* **74** 1698 (2004)^b
198. S S Ivanchev, G A Tolstikov, V K Badaev, I I Oleinik, N I Ivancheva, D G Rogozin, I V Oleinik, S V Myakin *Kinet. Katal.* **45** 192 (2004)^e
199. V A Zakharov, N V Semikolenova, T B Mikenas, A A Barabanov, G D Bukatov, L G Echevskaya, M A Mats'ko *Kinet. Katal.* **47** 305 (2006)^e
200. F A R Kaul, G T Puchta, H Schneider, F Bieleert, D Mihalios, W A Herrmann *Organometallics* **21** 74 (2002)
201. Z Ma, W H Sun, N Zhu, Z Li, C Shao, Y Hu *Polym. Int.* **51** 349 (2002)
202. N V Semikolenova, V A Zakharov, E A Paukshtis, I G Danilova *Top. Catal.* **32** 77 (2005)
203. S S Ivanchev, V K Badaev, N I Ivancheva, E V Sviridova, S Ya Khaikin, D G Rogozin, A S Abakunchik *Vysokomol. Soedin., Ser. A* **47** 934 (2005)^a
204. S Ray, S Sivararn *Polym. Int.* **55** 854 (2006)
205. I Kim, B Han, J Kim, C S Ha *Catal. Lett.* **101** 249 (2005)
206. Jpn. P. 200/1213913; *Chem. Abstr.* **135** 137853 (2001)
207. D Armspach, D Matt, F Peruch, P Lutz *Eur. J. Inorg. Chem.* **5** 805 (2003)
208. M Ohnishi, T Konakazawa, J Amano, T Fujimura *Polym. Bull. (Berlin)* **56** 1 (2006)
209. Russ. P. 2248374; *Chem. Abstr.* **142** 317239 (2005)
210. E P Talsi, D E Babushkin, N V Semikolenova, V N Zudin, V A Zakharov *Kinet. Katal.* **42** 165 (2001)^e
211. K P Bryliakov, N V Semikolenova, V N Zudin, V A Zakharov, E P Talsi *Catal. Commun.* **5** 45 (2004)
212. K P Bryliakov, N V Semikolenova, V A Zakharov, E P Talsi *Organometallics* **23** 5375 (2004)
213. G J P Britovsek, G K B Clentsmith, V C Gibson, D M L Goodgame, S J McTavish, Q A Pankhurst *Catal. Commun.* **3** 207 (2002)
214. S Wang, D Liu, R Huang, Y Zhang, B Mao *J. Mol. Catal. A* **245** 122 (2006)
215. A A Barabanov, G D Bukatov, V A Zakharov, N V Semikolenova, L G Echevskaya, M A Matsko *Vysokomol. Soedin., Ser. B* **47** 2203 (2005)^a
216. A A Barabanov, G D Bukatov, V A Zakharov, N V Semikolenova, L G Echevskaja, M A Matsko *Macromol. Chem. Phys.* **206** 2292 (2005)
217. A A Barabanov, G D Bukatov, V A Zakharov, N V Semikolenova, T B Mikenas, L G Echevskaja, M A Matsko *Macromol. Chem. Phys.* **207** 1368 (2006)
218. G J P Britovsek, V C Gibson, S K Spitzmesser, K P Tellmann, A J P White, D J Williams *J. Chem. Soc., Dalton Trans.* 1159 (2002)
219. G J P Britovsek, V C Gibson, O D Hoarau, S K Spitzmesser, A J P White, D J Williams *Inorg. Chem.* **42** 3454 (2003)
220. WO PCT 0123396; *Chem. Abstr.* **134** 281263 (2001)
221. Z Ma, W H Sun, H Vang, W D Yang, Y L Hu *Acta Polym. Sin.* 703 (2002)
222. Z Ma, W H Sun, Z L Li, C X Shao, Y L Hu *Chin. J. Polym. Sci.* **20** 205 (2002)
223. G J P Britovsek, V C Gibson, S Mastroianni, D C Oakes, C Redshaw, G A Solan, A J P White, D J Williams *Eur. J. Inorg. Chem.* 431 (2001)
224. K Nomura, W Sidokmai, Y Imanishi *Bull. Chem. Soc. Jpn.* **73** 599 (2000)
225. K Nomura, S Warit, Y Imanishi *Macromolecules* **32** 4732 (1999)
226. G J P Britovsek, V C Gibson, B S Kimberley, S Mastroianni, C Redshaw, G A Solan, A J P White, D J Williams *J. Chem. Soc., Dalton Trans.* 1639 (2001)
227. WO PCT 0050470; *Chem. Abstr.* **133** 208316 (2000)
228. I Kim, B H Han, Y S Ha, C S Ha, D W Park *Catal. Today* **93** 281 (2004)
229. I Kim, B H Han, J S Kim, C S Ha *Macromol. Res.* **13** 2 (2005)
230. J Y Liu, Y Zheng, Y G Li, L Pan, Y S Li, N H Hu *J. Organomet. Chem.* **690** 1233 (2005)
231. Q Wang, L D Li *Polym. Int.* **53** 1473 (2004)
232. Q Wang, L D Li, Z Q Fan *Eur. Polym. J.* **41** 1170 (2005)
233. B L Small, M Brookhart *Macromolecules* **32** 2120 (1999)
234. C Pellecchia, M Mazzeo, D Pappalardo *Macromol. Rapid Commun.* **19** 651 (1998)
235. A M A Bennett *Chemtech* **29** 24 (1999)
236. Y F Chen, R F Chen, C T Qian, X C Dong, J Sun *Organometallics* **22** 4312 (2003)

237. K Lappalainen, K Yliheikkilä, A S Abu-Surrah, M Polamo, M Leskeli, T Repo *Z. Anorg. Allg. Chem.* **631** 763 (2005)
238. F Pelascini, F Peruch, P J Lutz, M Wesolek, J Kress *Eur. Polym. J.* **41** 1288 (2005)
239. I Kim, B H Han, C S Ha, J K Kim, H Suh *Macromolecules* **36** 6689 (2003)
240. A S Abu-Surrah, K Lappalainen, U Piironen, P Lehmus, T Repo, M Leskeli *J. Organomet. Chem.* **648** 55 (2002)
241. I Kim, Y S Ha, C S Ha *Macromol. Rapid Commun.* **25** 1069 (2004)
242. D Takeuchi, K Anada, K Osakada *Bull. Chem. Soc. Jpn.* **78** 1868 (2005)
243. K P Tellmann, V C Gibson, A J P White, D J Williams *Organometallics* **24** 280 (2005)
244. H Wang, Z Ma, Y C Ke, Y L Hu *Polym. Int.* **52** 1546 (2003)
245. M Frediani, C Bianchini, W Kaminsky *Kinet. Katal.* **47** 210 (2006)^c
246. S Al-Benna, M J Sarsfield, M Thornton-Pett, D L Ormsby, P J Maddox, P Bres, M Bochmann *J. Chem. Soc., Dalton Trans.* 4247 (2000)
247. K Kreischer, J Kipke, M Bauerfeind, J Sundermeyer *Z. Anorg. Allg. Chem.* **627** 1023 (2001)
248. T V Laine, M Klinga, A Maaninen, E Aitola, M Leskela *Acta Chem. Scand.* **53** 968 (1999)
249. V C Gibson, M J Humphries, K P Tellmann, D F Wass, A J P White, D J Williams *Chem. Commun.* 2252 (2001)
250. T M Kooistra, Q Knijnenburg, J M M Smits, A D Horton, P H M Budzelaar, A W Gal *Angew. Chem., Int. Ed.* **40** 4719 (2001)
251. M J Humphries, K P Tellmann, V C Gibson, A J P White, D J Williams *Organometallics* **24** 2039 (2005)
252. H K Luo, Z H Yang, B Q Mao, R G Tang, D S Yu, W Xie *Acta Polym. Sin.* 720 (2001)
253. D Reardon, F Conan, S Gambarotta, G Yap, Q Y Wang *J. Am. Chem. Soc.* **121** 9318 (1999)
254. R Schmidt, M B Welch, R D Knudsen, S Gottfried, H G Alt *J. Mol. Catal. A* **222** 9 (2004)
255. R Schmidt, M B Welch, R D Knudsen, S Gottfried, H G Alt *J. Mol. Catal. A* **222** 17 (2004)
256. E Colamarco, S Milione, C Cuomo, A Grassi *Macromol. Rapid Commun.* **25** 450 (2004)
257. R Schmidt, P K Das, M B Welch, R D Knudsen *J. Mol. Catal. A* **222** 27 (2004)
258. S Milione, G Cavallo, C Tedesco, A Grassi *J. Chem. Soc., Dalton Trans.* 1839 (2002)
259. J R Severn, R Duchateau, J C Chadwick *Polym. Int.* **54** 837 (2005)
260. A K Tomov, V C Gibson, D Zaher, M R J Elsegood, S H Dale *Chem. Commun.* 1956 (2004)
261. H Sugiyama, G Aharonian, S Gambarotta, G P A Yap, P H M Budzelaar *J. Am. Chem. Soc.* **124** 12268 (2002)
262. M A Esteruelas, A M Lopez, L Mendez, M Olivan, E Onate *Organometallics* **22** 395 (2003)
263. B L Small, M J Carney, D M Holman, C E O'Rourke, J A Halfen *Macromolecules* **37** 4375 (2004)
264. Y Nakayama, K Sogo, H Yasuda, T Shiono *J. Polym. Sci., Part A* **43** 3368 (2005)
265. W Zhang, W H Sun, S Zhang, J Hou, K Wedeking, S Scholtz, R Fröhlich, H Song *Organometallics* **25** 1961 (2006)
266. N J Robertson, M J Carney, J A Halfen *Inorg. Chem.* **42** 6876 (2003)
267. M J Carney, N J Robertson, J A Halfen, L N Zakharov, A L Rheingold *Organometallics* **23** 6184 (2004)
268. J Y Liu, Y S Li, J Y Liu, Z S Li *J. Mol. Catal. A* **244** 99 (2006)
269. WO PCT 0069923; *Chem. Abstr.* **134** 5263 (2001)
270. F Calderazzo, U Englert, G Pampaloni, R Santi, A Sommazzi, M Zinna *Dalton Trans.* 914 (2005)
271. P G Cozzi, C Floriani, A Chiesi-Villa, C Rizzoli *Inorg. Chem.* **34** 29 (1995)
272. P G Cozzi, E Gallo, C Floriani, A Chiesivilla, C Rizzoli *Organometallics* **14** 4994 (1995)
273. Eur. P. 0874005; *Chem. Abstr.* **129** 331166 (1998)
274. WO PCT 01/55231; *Chem. Abstr.* **135** 137852 (2001)
275. R Furuyama, J Saito, S Ishii, H Makio, M Mitani, H Tanaka, T Fujita *J. Organomet. Chem.* **690** 4398 (2005)
276. S Matsui, Y Tohi, M Mitani, J Saito, H Makio, H Tanaka, M Nitabaru, T Nakano, T Fujita *Chem. Lett.* 1065 (1999)
277. S Matsui, M Mitani, J Saito, Y Tohi, H Makio, H Tanaka, T Fujita *Chem. Lett.* 1163 (1999)
278. S Matsui, M Mitani, J Saito, N Matsukawa, H Tanaka, T Nakano, T Fujita *Chem. Lett.* 554 (2000)
279. S Matsui, T Fujita *Catal. Today* **66** 63 (2001)
280. S Matsui, M Mitani, J Saito, Y Tohi, H Makio, N Matsukawa, Y Takagi, K Tsuru, M Nitabaru, T Nakano, H Tanaka, N Kashiwa, T Fujita *J. Am. Chem. Soc.* **123** 6847 (2001)
281. N Matsukawa, S Matsui, M Mitani, J Saito, K Tsuru, N Kashiwa, T Fujita *J. Mol. Catal. A* **169** 99 (2001)
282. Y Tohi, H Makio, S Matsui, M Onda, T Fujita *Macromolecules* **36** 523 (2003)
283. S Ishii, J Saito, S Matsuura, Y Suzuki, R Furuyama, M Mitani, T Nakano, N Kashiwa, T Fujita *Macromol. Rapid Commun.* **23** 693 (2002)
284. Y Nakayama, M Mitani, H Bando, T Fujita *J. Synth. Org. Chem. Jpn.* **61** 1124 (2003)
285. M Mitani, J Saito, S I Ishii, Y Nakayama, H Makio, N Matsukawa, S Matsui, J I Mohri, R Furuyama, H Terao, H Bando, H Tanaka, T Fujita *Chem. Rec.* **4** 137 (2004)
286. H Bando, Y Nakayama, Y Sonobe, T Fujita *Macromol. Rapid Commun.* **24** 732 (2003)
287. D B Liu, S B Wang, H T Wang, W Chen *J. Mol. Catal. A* **246** 53 (2006)
288. Y Nakayama, H Bando, Y Sonobe, T Fujita *J. Mol. Catal. A* **213** 141 (2004)
289. Y Nakayama, H Bando, Y Sonobe, T Fujita *Bull. Chem. Soc. Jpn.* **77** 617 (2004)
290. D Zhang, G X Jin *Appl. Catal. A* **262** 85 (2004)
291. H Makio, T Fujita *Macromol. Symp.* **213** 221 (2004)
292. J Kim, J W Hwang, Y Kim, M H Lee, Y Han, Y Do *J. Organomet. Chem.* **620** 1 (2001)
293. S T Chen, X F Zhang, H W Ma, Y Y Lu, Z C Zhang, H Y Li, Z X Lu, N N Cui, Y L Hu *J. Organomet. Chem.* **690** 4184 (2005)
294. D A Pennington, W Clegg, S J Coles, R W Harrington, M B Hursthouse, D L Hughes, M E Light, M Schormann, M Bochmann, S J Lancaster *Dalton Trans.* 561 (2005)
295. M C W Chan, K H Tam, N Y Zhu, P Chiu, S Matsui *Organometallics* **25** 785 (2006)
296. S Ishii, M Mitani, J Saito, S Matsuura, R Furuyama, T Fujita *Stud. Surf. Sci. Catal.* **145** 49 (2003)
297. J P Corden, W Errington, P Moore, M G H Wallbridge *Chem. Commun.* 323 (1999)
298. P D Knight, A J Clarke, B S Kimberley, R A Jackson, P Scott *Chem. Commun.* 352 (2002)
299. T Repo, M Klinga, P Pietikainen, M Leskelä, A M Uusitalo, T Pakkanen, K Hakala, P Aaltonen, B Lofgren *Macromolecules* **30** 171 (1997)
300. M Wang, H Zhu, K Jin, D Dai, L Sun *J. Catal.* **220** 392 (2003)
301. H Zhu, M Wang, C Ma, B Li, C Chen, L Sun *J. Organomet. Chem.* **690** 3929 (2005)
302. J Saito, M Mitani, S Matsui, Y Tohi, H Makio, T Nakano, H Tanaka, N Kashiwa, T Fujita *Macromol. Chem. Phys.* **203** 59 (2002)
303. J Saito, M Mitani, S Matsui, N Kashiwa, T Fujita *Macromol. Rapid Commun.* **21** 1333 (2000)
304. Y Suzuki, N Kashiwa, T Fujita *Chem. Lett.* 358 (2002)
305. J Saito, M Mitani, J Mohri, Y Yoshida, S Matsui, S Ishii, S Kojoh, N Kashiwa, T Fujita *Angew. Chem., Int. Ed.* **40** 2918 (2001)
306. J Saito, M Mitani, J Mohri, S Ishii, Y Yoshida, T Matsugi, S Kojoh, N Kashiwa, T Fujita *Chem. Lett.* 576 (2001)
307. M Mitani, R Furuyama, J Mohri, J Saito, S Ishii, H Terao, N Kashiwa, T Fujita *J. Am. Chem. Soc.* **124** 7888 (2002)
308. M Mitani, J Mohri, Y Yoshida, J Saito, S Ishii, K Tsuru, S Matsui, R Furuyama, T Nakano, H Tanaka, S Kojoh, T Matsugi, N Kashiwa, T Fujita *J. Am. Chem. Soc.* **124** 3327 (2002)

309. M S Weiser, M Wesolek, R Mülhaupt *J. Organomet. Chem.* **691** 2945 (2006)
310. M S Weiser, R Mülhaupt *Macromol. Rapid Commun.* **27** 1009 (2006)
311. M S Weiser, R Mülhaupt *Macromol. Symp.* **236** 111 (2006)
312. S Kojoh, T Matsugi, J Saito, M Mitani, T Fujita, N Kashiwa *Chem. Lett.* 822 (2001)
313. S Ishii, J Saito, M Mitani, J Mohri, N Matsukawa, Y Tohi, S Matsui, N Kashiwa, T Fujita *J. Mol. Catal. A* **179** 11 (2002)
314. S Reinartz, A F Mason, E B Lobkovsky, G W Coates *Organometallics* **22** 2542 (2003)
315. S C Gagieva, T A Sukhova, D V Savinov, V A Optov, N M Bravaya, Y M Belokon, B M Bulychev *J. Appl. Polym. Sci.* **95** 1040 (2005)
316. M Mitani, R Furuyama, J Mohri, J Saito, S Ishii, H Terao, T Nakano, H Tanaka, T Fujita *J. Am. Chem. Soc.* **125** 4293 (2003)
317. J Saito, M Mitani, M Onda, J Mohri, S Ishii, Y Yoshida, T Nakano, H Tanaka, T Matsugi, S Kojoh, N Kashiwa, T Fujita *Macromol. Rapid Commun.* **22** 1072 (2001)
318. R Furuyama, J Saito, S Ishii, M Mitani, S Matsui, Y Tohi, H Makio, N Matsukawa, H Tanaka, T Fujita *J. Mol. Catal. A* **200** 31 (2003)
319. J Saito, M Onda, S Matsui, M Mitani, R Furuyama, H Tanaka, T Fujita *Macromol. Rapid Commun.* **23** 1118 (2002)
320. J Saito, Y Suzuki, T Fujita *Chem. Lett.* **32** 236 (2003)
321. Y Yoshida, T Nakano, H Tanaka, T Fujita *Isr. J. Chem.* **42** 353 (2002)
322. R Furuyama, M Mitani, J Mohri, R Mori, H Tanaka, T Fujita *Macromolecules* **38** 1546 (2005)
323. J Saito, Y Suzuki, T Fujita, H Makio, H Tanaka, M Onda, T Fujita *Macromolecules* **39** 4023 (2006)
324. Y Nakayama, H Bando, Y Sonobe, H Kaneko, N Kashiwa, T Fujita *J. Catal.* **215** 171 (2003)
325. Y Nakayama, J Saito, H Bando, T Fujita *Macromol. Chem. Phys.* **206** 1847 (2005)
326. C Naundorf, S Matsui, J Saito, T Fujita, M Klapper, K Mullen *J. Polym. Sci., Part A* **44** 3103 (2006)
327. A Parssinen, T Luhtanen, M Klinga, T Pakkanen, M Leskela, T Repo *Eur. J. Inorg. Chem.* 2100 (2005)
328. S Ts Gagieva, T A Sukhova, D B Savinov, N M Bravaya, Yu N Belokon', B M Bulychev *Izv. Akad. Nauk, Ser. Khim.* 2652 (2004)^f
329. D A Pennington, D L Hughes, M Bochmann, S J Lancaster *Dalton Trans.* 3480 (2003)
330. D A Pennington, S J Coles, M B Hursthouse, M Bochmann, S J Lancaster *Chem. Commun.* 3150 (2005)
331. R K J Bott, M Hammond, P N Horton, S J Lancaster, M Bochmann, P Scott *Dalton Trans.* 3611 (2005)
332. W Q Hu, X L Sun, C Wang, Y Gao, Y Tang, L P Shi, W Xia, J Sun, H L Dai, X Q Li, X L Yao, X R Wang *Organometallics* **23** 1684 (2004)
333. K P Bryliakov, E A Kravtsov, D A Pennington, S J Lancaster, M Bochmann, H H Brintzinger, E P Talsi *Organometallics* **24** 5660 (2005)
334. Y Yoshida, S Matsui, Y Takagi, M Mitani, M Nitabaru, T Nakano, H Tanaka, T Fujita *Chem. Lett.* 1270 (2000)
335. Y Yoshida, S Matsui, Y Takagi, M Mitani, T Nakano, H Tanaka, N Kashiwa, T Fujita *Organometallics* **20** 4793 (2001)
336. D M Dawson, D A Walker, M Thornton-Pett, M Bochmann *J. Chem. Soc., Dalton Trans.* 459 (2000)
337. Y Yoshida, J Saito, M Mitani, Y Takagi, S Matsui, S Ishii, T Nakano, N Kashiwa, T Fujita *Chem. Commun.* 1298 (2002)
338. Y Yoshida, J Mohri, S Ishii, M Mitani, J Saito, S Matsui, H Makio, T Nakano, H Tanaka, M Onda, Y Yamamoto, A Mizuno, T Fujita *J. Am. Chem. Soc.* **126** 12023 (2004)
339. Jpn. P. 2004/155989; *Chem. Abstr.* **141** 8033 (2004)
340. K Vanka, Z T Xu, T Ziegler *Organometallics* **23** 2900 (2004)
341. S Matsui, T P Spaniol, Y Takagi, Y Yoshida, J Okuda *J. Chem. Soc., Dalton Trans.* 4529 (2002)
342. S Matsui, T P Spaniol, Y Yoshida, Y Takagi, J Okuda *J. Organomet. Chem.* **689** 1155 (2004)
343. D A Pennington, S J Coles, M B Hursthouse, M Bochmann, S J Lancaster *Macromol. Rapid Commun.* **27** 599 (2006)
344. Y Matsuo, K Mashima, K Tani *Chem. Lett.* 1114 (2000)
345. H Tsurugi, T Yamagata, K Tani, K Mashima *Chem. Lett.* 756 (2003)
346. H Tsurugi, Y Matsuo, T Yamagata, K Mashima *Organometallics* **23** 2797 (2004)
347. V C Gibson, S Mastroianni, C Newton, C Redshaw, G A Solan, A J P White, D J Williams *J. Chem. Soc., Dalton Trans.* 1969 (2000)
348. V C Gibson, C Newton, C Redshaw, G A Solan, A J P White, D J Williams *J. Chem. Soc., Dalton Trans.* 827 (1999)
349. D J Jones, V C Gibson, S Green, P J Maddox *Chem. Commun.* 1038 (2002)
350. D J Jones, V C Gibson, S M Green, P J Maddox, A J P White, D J Williams *J. Am. Chem. Soc.* **127** 11037 (2005)
351. V C Gibson, P J Maddox, C Newton, C Redshaw, G A Solan, A J P White, D J Williams *Chem. Commun.* 1651 (1998)
352. V C Gibson, C Newton, C Redshaw, G A Solan, A J P White, D J Williams *J. Chem. Soc., Dalton Trans.* 4017 (2002)
353. Y Nakayama, H Bando, Y Sonobe, Y Suzuki, T Fujita *Chem. Lett.* 766 (2003)
354. C Redshaw, M A Rowan, D M Homden, S H Dale, M R J Elsegood, S Matsui, S Matsuura *Chem. Commun.* 3329 (2006)
355. P A Cameron, V C Gibson, C Redshaw, J A Segal, G A Solan, A J P White, D J Williams *J. Chem. Soc., Dalton Trans.* 1472 (2001)
356. P A Cameron, V C Gibson, C Redshaw, J A Segal, M D Bruce, A J P White, D J Williams *Chem. Commun.* 1883 (1999)
357. D Pappalardo, C Tedesco, C Pellecchia *Eur. J. Inorg. Chem.* 621 (2002)
358. F A Hicks, J C Jenkins, M Brookhart *Organometallics* **22** 3533 (2003)
359. M Mazzeo, M Lamberti, A Tuzi, R Centore, C Pellecchia *Dalton Trans.* 3025 (2005)
360. L Lavanant, L Toupet, C W Lehmann, J F Carpentier *Organometallics* **24** 5620 (2005)
361. P Sudhakar, G Sundararajan *Macromol. Rapid Commun.* **26** 1854 (2005)
362. R J Long, V C Gibson, A J P White, D J Williams *Inorg. Chem.* **45** 511 (2006)
363. H R Bigmore, S R Dubberley, M Kranenburg, S C Lawrence, A J Sealey, J D Selby, M A Zuideveld, A R Cowley, P Mountford *Chem. Commun.* 436 (2006)
364. A C A Casagrande, M P Gil, O L Casagrande *J. Braz. Chem. Soc.* **16** 1283 (2005)
365. N Adams, H J Arts, P D Bolton, D Cowell, S R Dubberley, N Friederichs, C M Grant, M Kranenburg, A J Sealey, B Wang, P J Wilson, M Zuideveld, A J Blake, M Schroder, P Mountford *Organometallics* **25** 3888 (2006)
366. C Lorber, F Wolff, R Choukroun, L Vendier *Eur. J. Inorg. Chem.* 2850 (2005)
367. C Redshaw, L Warford, S H Dale, M R J Elsegood *Chem. Commun.* 1954 (2004)
368. A C A Casagrande, P S dos Anjos, D Gamba, O L Casagrande, J H Z dos Santos *J. Mol. Catal. A* **255** 19 (2006)
369. V C Gibson, A Tomov, D F Wass, A J P White, D J Williams *J. Chem. Soc., Dalton Trans.* 2261 (2002)
370. R T Stibrany, D N Schulz, S Kacker, A O Patil, L S Baugh, S P Rucker, S Zushma, E Berluche, J A Sissano *Macromolecules* **36** 8584 (2003)
371. L S Baugh, J A Sissano, S Kacker, E Berluche, R T Stibrany, D N Schulz, S P Rucker *J. Polym. Sci., Part A* **44** 1817 (2006)
372. X Q Lu, F Bao, D S Kang, Q Wu, H Q Liu, F M Zhu *J. Organomet. Chem.* **691** 821 (2006)

373. B Bushuev, V P Krivopalov, N V Semikolenova,
E V Peresypkina, A V Virovets, L A Sheludyakova,
L G Lavrenova, V A Zakharov, S V Larionov *Koord. Khim.* **32**
208 (2006) ^g
374. Y Nakayama, H Yasuda *J. Organomet. Chem.* **689** 4489 (2004)
375. M Nabika, Y Seki, T Miyatake, Y Ishikawa, K Okamoto,
K Fujisawa *Organometallics* **23** 4335 (2004)

^a — *Polym. Sci. (Engl. Transl.)*

^b — *Russ. J. Gen. Chem. (Engl. Transl.)*

^c — *Russ. J. Org. Chem. (Engl. Transl.)*

^d — *Dokl. Phys. Chem. (Engl. Transl.)*

^e — *Kinet. Catal. (Engl. Transl.)*

^f — *Russ. Chem. Bull., Int. Ed. (Engl. Transl.)*

^g — *Russ. J. Coord. Chem. (Engl. Transl.)*

RNA bulges as targets for selective cleavage by metal ions and organic compounds

I L Kuznetsova, M A Zenkova, V V Vlassov

Contents

I. Introduction	279
II. Structure of RNA bulge loops	279
III. Phosphodiester bond cleavage in RNA bulges	282
IV. Conclusion	287

Abstract. The results of studies of RNA bulge structures are reviewed. Cleavage of the phosphodiester bonds within RNA bulges is considered. Attention is focused on the factors influencing the cleavage efficiency. The state-of-the-art of the problem of targeted RNA cleavage induced by various reagents is discussed. The bibliography includes 101 references.

I. Introduction

Most RNA molecules are single-stranded polynucleotide chains with a complex three-dimensional structure (tertiary structure) stabilised through hydrogen bonds between complementary or partially complementary sequences (Watson–Crick complementary base pairing), stacking interactions between loops and binding of loops to metal ions.^{1–3} A combination of various interactions gives rise to a unique RNA packaging, which can be compared with a complex protein packaging.

Short double-stranded regions (or stems) and four types of single-stranded regions, *viz.*, single-stranded fragments, hairpin loops, internal loops (symmetric or asymmetric) and junctions, are typical elements of the RNA secondary structure.¹

Bulges are a special case of asymmetric internal loops, *i.e.*, RNA regions where the adjacent stems are stacked. Bulges are frequently occurring secondary structure elements. They provide flexibility for the ribose phosphate backbone necessary for RNA folding. RNA bulge loops containing nucleotides that lack complementary bases in the opposite RNA strand play an important biological role. They determine the RNA tertiary structure,⁴ represent specific RNA–protein binding sites^{5,6} and form active sites of ribozymes.^{7,8}

Single-base bulges were studied and characterised in most detail. Single-adenosine bulges most frequently occur in natural RNAs. Bulged adenosine residues (bulge A) serve as specific protein-binding sites, for example, in *E. coli* ribosomal

RNAs (5S rRNA–protein L18 and 16S rRNA–protein S8)^{9,10} and in the operator region of mRNAs encoding the capsid proteins of bacteriophage MS2.⁵ Single-uridine bulges were found in many RNAs. For example, this bulge is present in the catalytic site of RNase P,^{11,12} in the high-affinity binding sites for the Rev protein to HIV-1 RNA^{13,14} and for the Tar protein to HIV-2 RNA.¹⁵ Single-cytosine or -guanine bulges are much more rare; however, such bulges play an important role in organisation of the tertiary structure of natural RNAs.^{16,17}

Numerous low-molecular-weight compounds capable of RNA cleavage under physiological conditions (pH 7.0, 37 °C) have been synthesised in recent years.^{18–25} RNA cleavage induced by these compounds occurs predominantly at regions that are not involved in secondary structure formation. RNA cleavage within apical hairpin loops has been most extensively studied. RNA cleavage at linkages in bulge loops has been studied to a lesser degree, although bulges have advantages when used as targets for selective RNA cleavage. Both bulges in natural RNAs and tailor-made bulges in RNAs by hybridisation with partially complementary DNA or RNA oligonucleotides can serve as such targets.

II. Structure of RNA bulge loops

1. Methods of investigation of the bulge structure in DNA and RNA duplexes

X-Ray diffraction analysis is most commonly used in studies of DNA and RNA duplex structures.^{26–28} In spite of high accuracy of this method, X-ray crystallography of nucleic acids offers only an approximate estimate of general structural parameters of duplexes. It is impossible to construct a satisfactory structural model based on these parameters without invoking data from other methods. Potential energy calculations provide a general insight into internal mobility of RNA molecules. Among spectroscopic methods, NMR is used most often.^{29–31} Analysis of nucleic acid structures by NMR spectroscopy provides insight into the molecular dynamic structure in solution and complements X-ray diffraction data, which are somewhat limited due to the static state of the subjects under study. The influence of bulges on the RNA tertiary structure is analysed by gel retardation assay,³² fluorescence resonance energy transfer (FRET)³³ and transient electric birefringence (TEB).³⁴ The classification of structural elements of RNAs and their abundance in natural and synthetic RNAs studied by X-ray diffraction and NMR spectroscopy is available through

I L Kuznetsova, M A Zenkova, V V Vlassov Institute of Chemical Biology and Fundamental Medicine, Siberian Branch of the Russian Academy of Sciences, prosp. Akad. Lavrentieva 8, 630090 Novosibirsk, Russian Federation. Fax (7-383) 333 36 77, tel. (7-383) 333 37 61, e-mail: irakuzn@yahoo.com (I L Kuznetsova), marzen@niboch.nsc.ru (M A Zenkova), tel. (7-383) 333 33 28, e-mail: valentin.vlassov@niboch.nsc.ru (V V Vlassov)

Received 6 October 2006

Uspekhi Khimii 76 (3) 305–316 (2007); translated by T N Safonova

the Internet (SCOR: Structural Classification of RNA, <http://scor.lbl.gov/index.html>).

2. Structures of single-nucleotide bulges

Single-nucleotide bulges appear in RNAs if one nucleotide in the polynucleotide chain lacks a complementary base and is located between two classical Watson–Crick or non-canonical base pairs.³⁵ This unpaired nucleotide can adopt two main conformations, *e.g.*, can be either looped out of the helix (Fig. 1 *b*) or be stacked into the helix with adjacent bases (Fig. 1 *a*).³⁶ The conformation of the bulged nucleotide depends on both the nature of the nitrogen base and the adjacent bases. There are examples when the same bulge adopts different conformations, which change depending on intermolecular interactions.

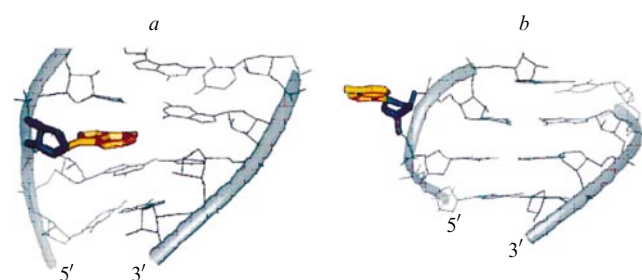


Figure 1. Three-dimensional structure of the RNA double strand containing a single-nucleotide bulge, which is stacked in the helix (*a*) or is looped out from the helix (*b*).³⁶

About 30 single-adenine bulges that are present in RNA structures studied by NMR spectroscopy and X-ray diffraction were derived from the SCOR database. In 11 structures, adenosine is located within the helix; in the other structures it is looped out. Generally, the X-ray diffraction method^{13,28,37–41} shows that in crystals, a bulged adenosine residue is looped out from the RNA helix (Fig. 2), whereas the NMR method^{42–45} indicates that this adenosine is located within the helix and is involved in stacking interactions with

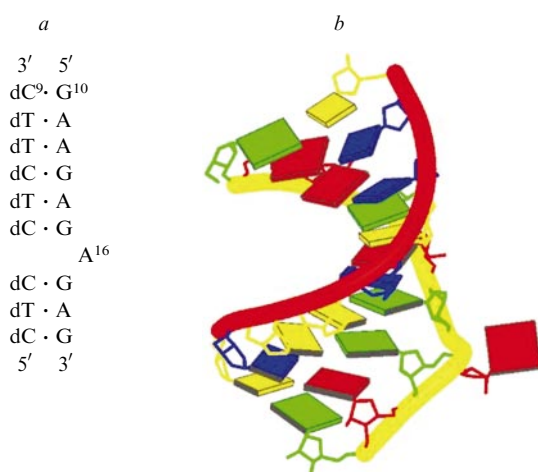


Figure 2. Sequence (*a*) and the three-dimensional structure (*b*) of the RNA–DNA duplex containing a single-nucleotide A bulge.²⁸

Hereinafter, G bases are green, A bases, red; C bases, yellow; U bases, dark blue (or pale blue).

The PDB code for the bulge A structure is 1EFO (<http://www.rcsb.org/pdb/explore.do?structureId=1EFO>).

adjacent bases. Apparently, a bulged adenosine residue is highly mobile, and its position at each instant of time is determined by intra- and intermolecular interactions. Therefore, the discrepancy between the data can be attributed to different conditions in which RNAs exist during experiments: in solution (NMR experiments) or in the solid phase (X-ray diffraction analysis).

In crystals, the duplex structure is stabilised by intermolecular bonds. In addition, intermolecular stacking interactions between flipped-out nucleoside bases located in different duplexes can exist. The looped-out conformation of a bulged adenosine residue in crystals can also be due to the fact that crystallisation is performed in the presence of divalent metal cations, for example, of Mg^{2+} , which can stabilise this structure.³⁸ NMR spectroscopic studies of duplex structures are performed in solution, where RNA molecules adopt the energetically most favourable conformation. In this conformation, a duplex contains a bulged adenosine oriented inside the helix. As a result of high mobility of a bulged adenosine, different conformations of a bulged adenosine were established in the same RNA duplexes.^{27,46,47}

To understand which conformation is adopted by a bulged adenosine depending on its environment, an attempt was made to determine the energetically most favourable conformation by computer simulation methods.^{48,49} An hierarchical approach was used⁴⁹ to investigate various sterically possible low-energy conformations of single-base bulge loops. The method is based on the assumption that a bulge and adjacent base pairs are responsible for the conformational deformation of the double helix. Computer simulations and calculations of all possible conformations were performed for 6-mer RNA duplexes containing one bulged adenosine. The duplex in which the bulged adenosine lies inside the helix and is involved in stacking interactions with adjacent nucleotides has the lowest energy. Higher Gibbs energies were obtained for RNA duplexes in which the bulged adenosine is located inside the helix and forms a triplex with a base pair at the 5' end (in the minor groove). According to the calculations, duplexes containing a bulged-out adenosine are characterised by the highest energies. It should be noted that a somewhat different situation was observed for analogous DNA duplexes containing a bulged adenosine. The stacked conformation of a bulged adenosine was also energetically most favourable. However, next in the Gibbs energy was the conformer with a bulged-out adenosine, whereas the conformer in which the bulged adenosine forms a triplex was energetically least favourable.

Single-guanosine bulges (bulge G) have been much less studied. In the structures of all known duplexes containing a bulged guanosine, this nucleoside is looped out from the helix.^{16,50,51} In natural RNAs, a bulged guanosine was found in the α -sarcin loop region 23–28 S of rRNA, where it forms the so-called G-bulged motif.¹⁶ This motif is located in an imperfect stem of a 29-mer hairpin in the 5'GGAACC·3'CAUGACU sequence, where the bulged guanosine (printed in boldface type) is flanked by non-canonical A–A, C–C and U–C base pairs (Fig. 3).

G-Bulged motifs have an important biological function (interactions with α -sarcin and elongation factor G). These motifs were found in the rRNA large subunits of rat and *E. coli* ribosomal RNAs and in the E loop of 5 S rRNA from the frog *Xenopus laevis*.^{9,16,52–54} The specific structural feature of the G-bulged motif is that the bulged guanosine is flanked by the non-canonical purine-purine base pair A–A on the 5' side and forms the G·U·A triplex with the adjacent base pair on the 3' side (see Fig. 3). This leads to a widening of the major groove of RNA by 5 Å, the groove depth remaining typical of the A-form RNA structure.¹⁶ An analysis of mutant 28 S rRNAs demonstrated that a conserved bulged guanosine, which allows RNAs to fold into a unique tertiary structure, is absolutely

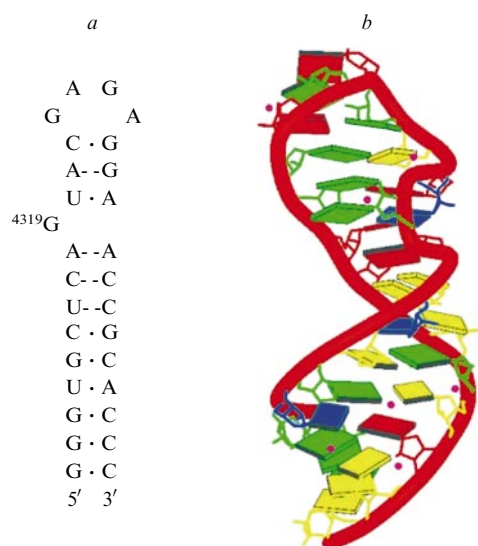


Figure 3. Sequence (*a*) and the three-dimensional structure (*b*) of the α -sarcin loop of the rat 28S rRNA containing a single-nucleotide G bulge.¹⁶

The PDB code for the bulge G structure is 430D (<http://www.rcsb.org/pdb/explore.do?structureId=430D>).

necessary in the α -sarcin hairpin for rRNAs to exhibit biological activity (binding with the elongation factor).¹⁶

According to X-ray diffraction data, an uridine residue in single-nucleotide bulges (bulge U) is generally looped out, and it is not only looped out from the helix, but also forms a complex intramolecular structure (for example, it can be directed inward the minor groove).^{13,55} The main distinguishing feature of this conformation of the bulged uridine is that it is stabilised by intramolecular (rather than intermolecular) interactions, to be more precise, by hydrogen bonds between adjacent nucleotides either directly or through aqua bridges. The bulged uridine directed inward the minor groove changes the conformations of adjacent nucleotides. The twist angle of the helix near this bulge increases to 50° (over-twist).⁵⁵ The only bulged uridine adopting a stacked conformation inside the helix was found in a ribozyme (Fig. 4).⁵⁶ Interestingly, the

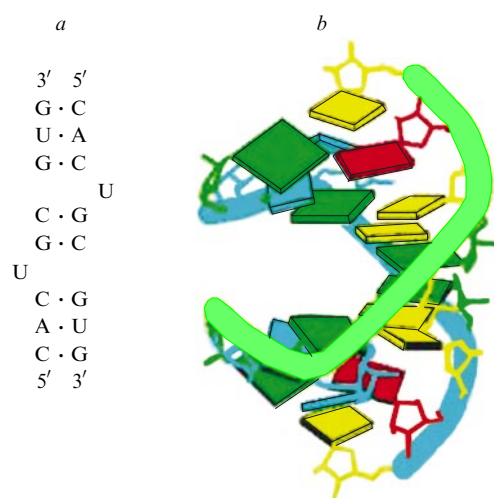


Figure 4. Sequence (*a*) and the three-dimensional structure (*b*) of the duplex containing a bulged uridine.⁵⁶

The PDB code for the bulge U structure is 1J9H (<http://www.rcsb.org/pdb/explore/images.do?structureId=1J9H>).

replacement of this uridine by any other nucleoside does not change the activity of the ribozyme, which is not typical of single-stranded regions of catalytic RNAs.⁵³

A conserved single-cytidine bulge (bulge C) was found in 5S rRNA.^{17,57} The structure of this bulge was studied in detail in an 8-mer RNA duplex (Fig. 5) corresponding to the helix II region of 5S rRNA from the frog *Xenopus laevis*.⁵¹ Crystals of the duplex were studied at 2.2 and 1.7 Å resolution. In both crystal structures, the bulged cytidine is looped out, and the helix axis deviates from the straight line by an angle smaller than 10°. In the crystals studied at 2.2 Å resolution, the bulged base is directed toward the 3' end of the duplex; in the crystals studied at 1.7 Å resolution, to the 5' end. The existence of two conformations of the bulged cytidine was attributed to its mobility. In crystal, the bulged cytidine, like the bulged uridine, is involved in several intermolecular hydrogen bonds with nucleotides of the adjacent duplexes as well as in stacking interactions with purine bases.

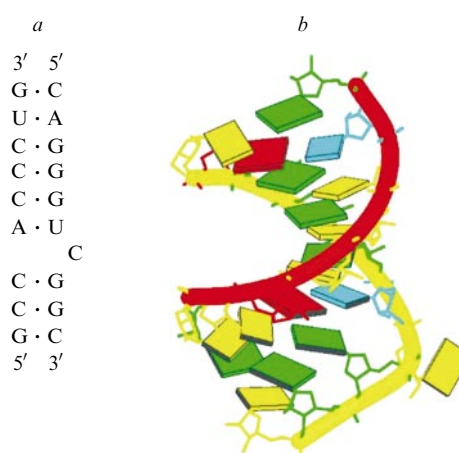


Figure 5. Sequence (*a*) and the three-dimensional structure (*b*) of the duplex containing a bulged cytosine.¹⁷

The PDB code for the bulge C structure is DQH1 (<http://www.rcsb.org/pdb/explore.do?structureId=DQH1>).

The structure of single-nucleotide bulges in RNA·DNA duplexes was established by X-ray diffraction study of the homopyrimidine·homopurine heteroduplex d(C¹TCCTC·TTC⁹)·r(G¹⁰AAGAGA¹⁶GAG¹⁹) containing a bulged adenosine (printed in boldface type) (see Fig. 2).²⁸ It was demonstrated that the bulged adenosine adopts a looped-out conformation, the ribose ring of the adenosine being almost perpendicular to the helix axis. A comparison of the structure of this duplex with the structure of the RNA·DNA duplex with the same sequence but lacking a bulged adenosine demonstrated that the presence of a bulge has only a slight effect on the bend angle of the helix axis of the RNA·DNA duplex (6°). This behaviour of a bulged adenosine in the RNA·DNA duplex substantially differs from that in RNA·RNA and DNA·DNA duplexes. In crystals, the bulged adenosine (A¹⁶) forms the (C⁹·G¹⁰)·A¹⁶ triplex with the terminal C⁹·G¹⁰ base pair of the symmetrically arranged molecule of the heteroduplex through intermolecular hydrogen bonds.

3. Structures of bulges containing two or more nucleotides

As mentioned above, one of the functions of bulges in nature is to organise the RNA tertiary structure, to be more precise, to provide orientation of two adjacent double-stranded RNA regions relative to one another.^{1,58} The influence of the length and the nucleotide composition of a bulge on the RNA

structure was characterised in the studies^{32–34,59} dealing with electrophoretic mobility of bulge-containing RNA·RNA duplexes. An analysis of homo-A and homo-U bulges containing from 1 to 7 nucleotides demonstrated that an increase in the length of the bulge leads to a decrease in electrophoretic mobilities of duplexes,³² duplexes with U_n bulges always having a higher electrophoretic mobility than duplexes with A_n bulges.⁵⁹

The X-ray data on changes in the bend angle of the axis of a bulge-containing helix were confirmed by the data obtained by the FRET³³ and TEB³⁴ methods. It appeared that the bend angle depends on two parameters, *viz.*, the length of the bulge (an increase in the number of nucleotides in the bulge leads to an increase in the bend angle) and its nucleotide composition (bulges containing primarily purine bases bend the helix axis to a lesser extent than bulges containing pyrimidine bases).³⁴

X-Ray diffraction and NMR spectroscopic data demonstrated that bulges consisting of several nucleotides are generally stabilised by a complex system of intermolecular hydrogen bonds, intra- and intermolecular stacking interactions and interactions with metal ions.^{38,51,60–62} The diversity of nucleotide sequences and the environments of bulges consisting of several nucleotides is responsible for the infinite diversity of their structural forms. The structures of two motifs with particular sequences and structures are known: the above-described G bulges in the α -sarcin hairpin of rRNA and the 'kink-turn' or 'K-turn' structure. The K-turn structure was found for a three-base bulge flanked by two G·C base pairs at the 5' end and by two or three non-canonical G·-A base pairs at the 3' end.⁵¹ As a result, the helix axis is bent by 120° at the bulge (Fig. 6). The K-turn motifs play an important biological role. For example, five K-turn motifs were found in 23S rRNA, and all these motifs serve as binding sites for ribosomal proteins.

Therefore, an analysis of X-ray diffraction and NMR spectroscopic data shows that the looped-out conformation rather than stacked into a helix is more typical of single-nucleotide uridine, guanosine and cytidine bulges. Single-adenosine bulges have higher mobility and can adopt different conformations. Double-stranded RNA regions containing bulges are highly mobile. The major groove of the A helix in the bulge region is widened (predominantly, on the 5' end of the bulge) due to which it is accessible for interactions with other molecules. In addition, the helix axis is bent at bulges. Numerous multi-membered bulges are known; however, except for the K-turn motif, there are no clear criteria for

predicting the three-dimensional structure of bulges with an arbitrary nucleotide sequence.

III. Phosphodiester bond cleavage in RNA bulges

1. Geometric parameters of internucleotide bonds and RNA stability

RNA cleavage occurs predominantly in single-stranded regions (hairpin loops, mismatches, internal loops, bulges, junctions and single-stranded fragments). However, it is difficult to determine which bonds and in which sequences are cleaved more rapidly because of complexity of the secondary and tertiary structure of natural RNAs. Many ribozymes and natural and artificial ribonucleases cleave RNA by phosphodiester bond transesterification.⁶³ It is hypothesised that RNA transesterification can occur only when the attacking oxygen atom of the 2'-hydroxy group of the nucleophile is in-line with the 5'-oxy anion of the leaving group, *i.e.*, the arrangement of the leaving group (the oxygen atom of the 5'-hydroxy group), the phosphorus atom and the nucleophile (the oxygen atom of the 2'-hydroxy group) is strictly linear.⁶⁴

Double-stranded RNAs and RNAs involved in RNA·DNA duplexes generally assume an A-form helix, in which the 2'-oxy anion and the 5'-oxy anion of the leaving group are arranged so that the formation of a linear conformation is hindered, resulting in higher stability of double-stranded regions of RNAs and RNA·DNA duplexes compared to single-stranded RNA regions, in which the phosphodiester bonds are labile and can spontaneously adopt an in-line configuration. Therefore, the rate of phosphodiester bond cleavage in RNA bulges would be determined by their ability to adopt an in-line configuration. A phosphodiester bond can spontaneously assume an in-line configuration in the case of sufficient mobility of the corresponding region of the RNA structure. The mobility of a bulge is determined by its size, the nucleotide sequence and the efficiency of intra- and intermolecular stacking interactions between bases.⁶⁴

Nowadays, it is impossible to predict theoretically the sensitivity of the bonds in each particular RNA bulge to cleavage and, much less, to suggest the geometric parameters for the design of a catalytic group capable of performing selective cleavage. In spite of the fact that the specificity toward the RNA structure is always determined for all new compounds exhibiting ribonuclease activity, the dependence of the site and efficiency of cleavage on the RNA primary and secondary structure was studied systematically mainly for divalent metal ions.^{65–70}

2. RNA cleavage at bulge sites by metal ions

RNA cleavage by metal ions or metal ion complexes can occur either by the transesterification mechanism^{71,72} or by metal-dependent redox reactions.^{73,74} Many metals catalyse cleavage of internucleotide phosphodiester bonds in RNAs.^{75,76} Initially, oligomers containing a 2',3'-cyclophosphate at the 3' end are formed and these oligomers are then hydrolysed to give a mixture of 2'- and 3'-phosphates (Zn^{2+} ions)⁷⁷ or only 3'-phosphate (for example, in the presence of Pb^{2+} ions).⁷⁸

Among divalent metal ions, lead ions most efficiently cleave RNA under physiological conditions.⁷⁹ Cleavage of various oligoribonucleotides containing bulges of different length by lead ions (Fig. 7a) was analysed.⁶⁷ The oligoribonucleotides differed not only in the length, nature and nucleotide sequence of bulges, but also in flanking bases. Adenine bulges flanked by G·C base pairs on both sides are not cleaved by Pb^{2+} ions. The replacement of the G·C base pair on the 5' side by the U·A or U·G base pair facilitates phosphodiester bond cleavage in bulges. This fact was attributed to the difference in staking interactions between a bulged base and flanking bases. The efficiency of stacking interactions decreases in the series

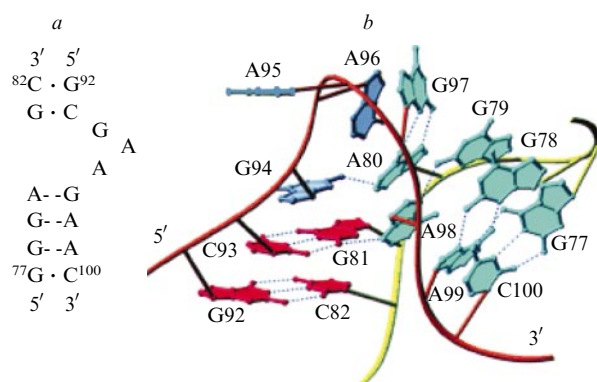


Figure 6. Sequence (a) and the three-dimensional structure (b) of the K-turn motif of the protein-binding site of 23S rRNA *Haloarcula marismortui*.⁵¹ The G·C base pairs at the 5' end are red, the G·A base pairs at the 3' end are green and nucleotides in the bulge are blue.

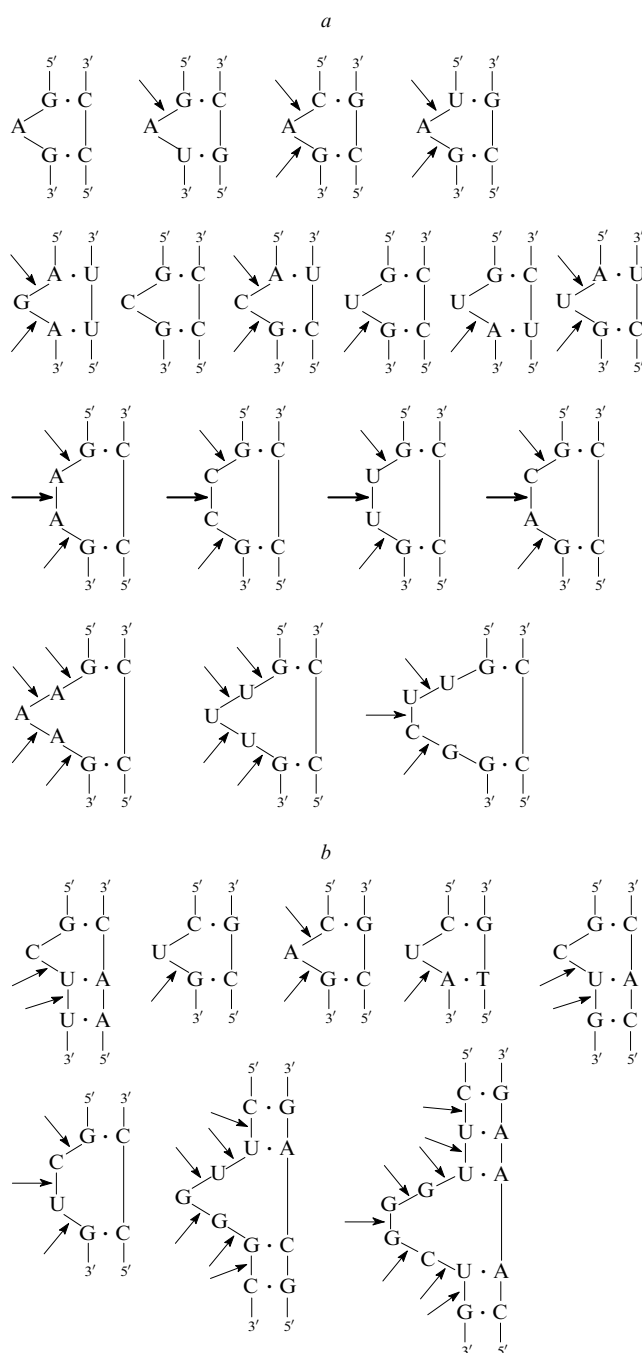


Figure 7. Sensitivity of the phosphodiester bonds in RNA bulges to cleavage by lead ions (a)⁶⁷ and magnesium ions (b).⁶⁸ The arrow thickness corresponds to the cleavage efficiency of a particular phosphodiester bond.

$\text{Pu} \cdot \text{Pu} > \text{Py} \cdot \text{Pu} > \text{Py} \cdot \text{Py}$,⁸⁰ the base on the 5' side of the bulge making the largest contribution. If a base in a bulge takes part in stacking interactions with adjacent bases, the phosphodiester bonds of the nucleotide in the bulge adopt a configuration similar to that in double-stranded RNA and become slightly sensitive to cleavage.

All known oligoribonucleotides with two-membered bulges (AA, CC, UU and CA) located between two G·C base pairs were cleaved by Pb^{2+} ions, all three phosphodiester bonds in the bulge being cleaved. The bond in the middle of the bulge was cleaved most efficiently. The same situation was observed for three-membered bulges. Phosphodiester bonds in

bulges and hairpin loops containing the same nucleotide sequences substantially differ in sensitivity to cleavage by metal ions. For example, the UUCG sequence in an apical hairpin loop is stable and does not undergo cleavage, whereas this sequence in a bulge is readily cleaved by lead ions.⁶⁷

The sensitivity of the phosphodiester bonds in RNA bulges to cleavage by magnesium ions was studied.⁶⁸ The formation of bulges composed of 1–4 nucleotides in the 5'-end region of a 132-mer RNA was induced by hybridisation with oligodeoxyribonucleotides. Magnesium ions at a concentration of 2.5 mmol litre⁻¹ in weak alkaline solutions (pH 8.0) at 60 °C can cleave RNAs at single-stranded regions,⁶⁸ all bulges in RNA·oligonucleotide complexes being cleaved (Fig. 7b).

In single-nucleotide bulges, cleavage occurs predominantly at the phosphodiester bonds on the 3' side for bulged nucleotides, whereas cleavage of these bonds on the 5' side for bulged nucleotides is less efficient. The appearance of secondary cleavage sites on the 5' side for bulges was attributed to the increased flexibility of the bulged nucleotide after cleavage of the most sensitive bond (primary cleavage). When a bulge is flanked on the 3' side by A·U(T) base pairs, secondary cleavage sites are observed also at sites involved in binding of oligodeoxyribonucleotides, which is attributed to stability of heteroduplexes with a single cleavage site.

Unlike lead ions, magnesium ions cleave all single-nucleotide bulges with the same efficiency independently of the type of the bulged base and the flanking base pairs. When the length of an artificial bulge is increased up to 2–4 nucleotides, primary RNA cleavage at the phosphodiester bond on the 3' side of the bulge occurs simultaneously with extensive cleavage of the analogous bond in the double-stranded region adjacent to the bulge on the 5' side. It should be noted that phosphodiester bond cleavage in artificial bulges is accompanied by cleavage of these bonds in all other single-stranded regions in a 132-mer RNA. A comparison of phosphodiester bond cleavage in RNA bulges with cleavage in artificial mismatches demonstrated that, as opposed to bulges, cleavage of sequences flanking mismatches is induced.⁶⁸

The study⁸¹ dealt with phosphodiester bond cleavage by zinc ions in 1–5-nucleotide bulges of a 2'-O-methyl oligoribonucleotide, in which only one nucleotide was not modified at 2' position. Since cleavage of 2'-O-methyl oligoribonucleotides occurs not by the transesterification mechanism, the use of such model RNAs allowed the authors to analyse the sensitivity of each particular phosphodiester bond in bulges. The most efficient cleavage was observed for the phosphodiester bond formed by an unmodified uridine residue (rU), which was located in the middle of a five-base bulge. This bond is cleaved two times more rapidly than the analogous bond in a single-stranded oligoribonucleotide. Four- and three-nucleotide bulges containing riboadenosine or ribouridine in the apical position are cleaved by zinc ions at approximately the same rate. In the case of single- and two-nucleotide bulges, the cleavage rate sharply decreases.

The computer analysis⁸¹ of the structures of bulge-containing oligoribonucleotides demonstrated that five-base bulges with a ribose unit, which is either in the apical position or located closer to the 5' side of a bulge, adopt the same conformation in which all nucleotides are located inside the helix. Two-nucleotide bulges have a similar structure. The cleavage rates of two- and five-nucleotide bulges in which a ribonucleotide is located closer to the 5' end are, respectively, 3 and 6 times lower than the cleavage rate of a five-nucleotide bulge with ribose in the apical position. The geometric parameters of phosphodiester bonds determined by molecular dynamics methods for all types of bulges are substantially different from the parameters typical of the in-line configuration of these bonds.⁸¹ Presumably, the lability of phospho-

diester bonds in bulges is an important feature responsible for sensitivity of these bonds to cleavage.

The above-considered data show that most bulges in RNAs and RNA·DNA complexes can be cleaved by divalent metal ions, cleavage of bulges being different from that of mismatches and apical hairpin loops. Cleavage of bulges has a random character. Thus, phosphodiester bonds located on the 3' side (in some cases, on the 5' side) from bulges are cleaved. In addition, some phosphodiester bonds in an RNA·DNA duplex located near a bulge loop can undergo cleavage. In most cases, RNA cleavage at the bonds in bulges has no effect on the pattern (level) of phosphodiester bond cleavage in other RNA regions.

3. RNA cleavage within artificial bulge loops by metal complex – oligonucleotide conjugates

One of promising approaches to selective RNA injury is based on RNA cleavage by antisense oligonucleotide conjugates containing RNA-cleaving groups. First conjugates containing an RNA-cleaving group covalently bound to the 5' end of oligonucleotides were constructed in the mid-1990s.^{82,83} These conjugates cleaved RNA targets at bonds located in a single-stranded region on the 3' side from heteroduplexes. However, the conjugates described^{82,83} cannot cleave RNAs in a catalytic manner because of slow dissociation of complexes of the conjugate with the cleavage product. To cleave RNAs in a catalytic manner, it is necessary that an RNA·conjugate complex be more stable than the cleavage product·conjugate complex. In other words, RNA cleavage should occur within RNA·oligonucleotide duplexes. However, such duplexes are poor substrates for cleavage because the catalytic (imidazole- or metal-containing) group in such substrates occurs in the double-stranded RNA region.^{84–86}

This problem can be solved by creating artificial bulges in RNAs using hybridisation with partially complementary oligonucleotides containing RNA-cleaving groups. Haner and co-workers were the first to apply this approach.⁸⁶ They used oligodeoxyribonucleotides that contained thymidine

modified by a La^{3+} or Eu^{3+} macrocomplex in the middle of the sequence (Fig. 8a). Upon binding to RNA, these conjugates induced the formation of two-nucleotide AA or GA bulges. In this case, a modified thymidine bearing a metal complex was located not exactly opposite to the artificial bulge in the RNA target but was shifted to the 3' or 5' end of RNA by 4 nucleotides, due to which the RNA-cleaving group can approach the bulged bonds from the side of either the minor or major groove of the duplex.

Conjugates of oligonucleotides entirely complementary to a 32-mer RNA target (except for two nucleotides that form a bulge in the RNA) efficiently cleave the phosphodiester bonds in this bulge and near the bulge (the extent of cleavage is 92%, 16 h), the conjugates containing the Eu^{3+} complex (see Fig. 8a) performing more efficient RNA cleavage compared to conjugates containing the La^{3+} complex.

The experiments demonstrated that the most favourable position of a modified base bearing an RNA-cleaving group is such that provides cleavage through the minor groove of a heteroduplex.⁸⁶ Interestingly, the conjugate, in which the Eu^{3+} complex was covalently attached to the 5' end of a bulge forming oligonucleotide, also efficiently cleaved RNA at the phosphodiester bonds in the bulge. It should be noted that binding of RNA to the conjugate gave rise to a free 10-mer single-stranded fragment at the 5'-end region of the conjugate, which was subjected to cleavage to an insignificant extent. The cleavage occurred primarily at the bonds in the region of the artificial bulge. The above data demonstrate that the phosphodiester bonds in bulges are more sensitive to cleavage than those in other single-stranded RNA regions. This is apparently attributed to the fact that the phosphodiester bonds in bulges assume a configuration more favourable for transesterification compared to their configuration in single-stranded RNA regions.

RNA cleavage by Eu^{3+} complex – oligodeoxyribonucleotide conjugates occurred efficiently; however, the reaction proceeded in a non-catalytic manner. The replacement of an oligodeoxyribonucleotide by 2'-methoxyethoxy derivatives

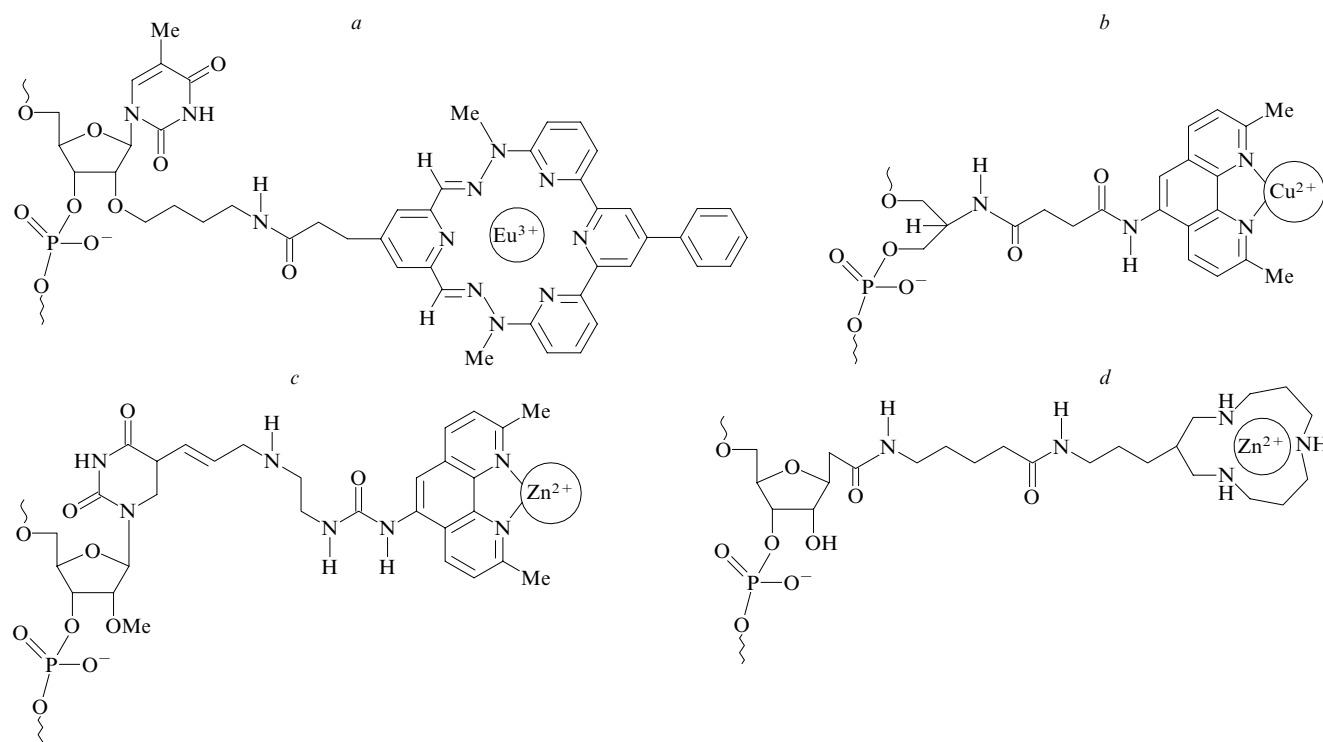


Figure 8. Structure of modified nucleotide units containing an RNA-cleaving group.^{86, 89, 91, 92}

having a higher affinity for RNA enabled a decrease in the length of an antisense oligonucleotide by a factor of two.⁸⁷ The conjugate of this 10-mer oligonucleotide with the Eu^{3+} complex cleaved a 23-mer RNA target in a catalytic manner; one molecule of the conjugate was able to cleave 39 RNA molecules under physiological conditions in 64 h.⁸⁸

Another type of RNA-cleaving conjugates includes oligonucleotides in which one nucleotide is modified by phenanthroline (Fig. 8b) or terpyridine complexes of Cu^{2+} or Zn^{2+} . It was demonstrated⁸⁹ that site-directed RNA cleavage at the phosphodiester bond in an artificial single-base bulge can be performed with the use of oligonucleotide conjugates containing serinol modified by phenanthroline or terpyridine Cu^{2+} complexes instead of one of nucleotides. As opposed to conjugates described earlier,⁸⁶ metal complexes in the conjugates under consideration were attached not to ribose but to its analogue (serinol) incorporated into the ribose-phosphate backbone of an antisense oligodeoxyribonucleotide.⁸⁹ This non-nucleotide insertion was located directly opposite to artificial RNA bulge. Depending on the nature of the copper complex, the efficiency of cleavage decreased in the series: 2,9-dimethyl-*o*-phenanthroline complex \gg terpyridine complex $>$ *o*-phenanthroline complex. The extent of site-directed 159-mer RNA cleavage by the 2,9-dimethyl-*o*-phenanthroline complex was as high as 80%. Unfortunately, the authors failed to perform this reaction in a catalytic fashion. Efficient RNA cleavage was observed only in the presence of a 500-fold excess of the conjugate with respect to the RNA substrate.

Stromberg and co-workers^{90,91} synthesised 2'-*O*-methyl-oligoribonucleotides containing a modified uridine (Fig. 8c) or cytidine residue bearing the 2,9-dimethylphenanthroline zinc complex in the middle of the nucleotide sequence. The oligoribonucleotides used were completely complementary to the RNA under study, except for nucleotides involved in homo-A bulges containing from 1 to 5 nucleotides. These conjugates cleave RNAs at the phosphodiester bonds in bulges containing from 2 to 5 nucleotides in a catalytic fashion, single-base bulges remaining uncleaved.

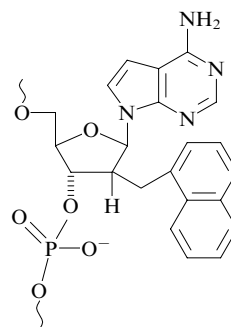
Unlike macrocyclic Ln^{3+} complex-oligonucleotide conjugates, which cleave RNAs at the phosphodiester bonds in bulges or near the bulges, conjugates with zinc complexes cleave RNAs only at the bonds in bulges.⁹⁰ The cleavage rate depended on the length of an artificial bulge and the mode of attachment of the 2,9-dimethylphenanthroline Zn^{2+} complex to the antisense oligonucleotide. Four-nucleotide AAAA bulges were cleaved most efficiently, the phosphodiester bonds between the first three adenosine residues were cleaved much more rapidly than the last bond in the bulge.

A comparison of different modes of covalent binding of the 2,9-dimethylphenanthroline zinc complex to heterocyclic bases demonstrated that the attachment at the C(5) atom of uracil is most favourable (see Fig. 8c). Apparently, this arrangement of the complex allows the Zn^{2+} ion to approach the internucleotide bonds in bulges at the shortest distance. A conjugate containing two nucleotides modified by the 2,9-dimethylphenanthroline Zn^{2+} complex (in the middle and at the 5' end of the oligonucleotide chain) was synthesised to increase the efficiency of RNA cleavage. Surprisingly, the presence of the second RNA-cleaving group led to a sharp decrease in the extent of RNA cleavage, which was attributed to steric factors.⁹⁰

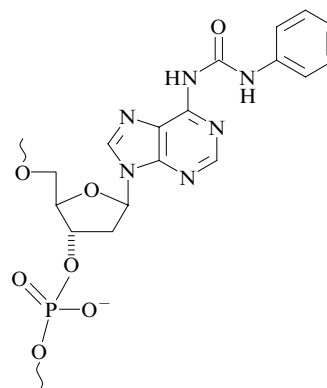
Phenanthroline zinc complex-oligonucleotide conjugates efficiently cleaved RNAs in the presence of a 4-fold excess of an RNA with respect to the conjugate. However, due to weak complexation of Zn^{2+} ions with phenanthroline, the presence of a 25-fold excess of Zn^{2+} ions in the reaction mixture is necessary for the reaction to proceed efficiently. To decrease the concentration of Zn^{2+} ions in the reaction mixture, complexes of macrocyclic polyamines, in particular, 1,5,9-

triazacyclododecan-3-yl (aza crown) zinc complexes (Fig. 8d),⁹² were used instead of phenanthroline zinc complexes. In solution, these complexes are four times more stable than phenanthroline complexes. These conjugates also cleaved oligoribonucleotides at the phosphodiester bonds in artificial bulges, but the reaction rate was an order of magnitude lower than that achieved with conjugates containing phenanthroline complexes.

Stromberg and co-workers⁹³ suggested that antisense oligonucleotides, which bear not only an RNA-cleaving group, but also a group that decreases mobility of an RNA bulge, be used for RNA cleavage. It was found that oligonucleotides containing 2'-(1-naphthylmethyl)-2'-deoxytubercidin can specifically stabilise artificial bulges.



Other authors used an adenosine derivative containing a phenylurea substituent at position 6 of the heterocyclic base.⁹⁴



This modified adenosine has a high ability of stacking interactions with adjacent bases and corresponds in size to the complementary A · T base pair. When this nucleoside is present in a duplex, it pushes the opposite nucleotide out of the helix. The phosphodiester bonds on the 3' and 5' sides with respect to these bulged-out nucleotides are cleaved by magnesium ions at a higher rate than the phosphodiester bonds in a single-base bulge or a mismatch. The construction of conjugates, which contain simultaneously nucleosides (adenosine) bearing groups that stabilise bulges and nucleosides bearing an RNA-cleaving group, is presently underway.

4. RNase A- and artificial RNase-induced cleavage at bulge sites

Earlier, it has been demonstrated that RNA cleavage under physiological conditions proceeds efficiently in the presence of small synthetic molecules bearing RNA-cleaving groups. These molecules mimic active sites of natural RNases.^{21, 22, 25} Imidazole is the simplest RNA-cleaving agent. In concentrated solutions of this compound (1 or 2 M), RNA undergo random cleavage at the phosphodiester bonds located in single-stranded regions.⁶⁹ More complex RNA-cleaving compounds (artificial RNases, artificial ribonucleases; hereinafter referred to as aRNases) generally contain an RNA-binding fragment

(for example, an intercalator, a cationic structure or an oligonucleotide).^{21, 22, 24, 95}

The sensitivity of RNA bulges to imidazole, RNase A and various aRNases was examined.^{96, 97} A 96-mer RNA fragment of influenza virus M2 protein mRNA was used as an RNA target. In this fragment, bulges of different length (from 1 to 7 nucleotides) and sequences were formed by hybridisation with partially complementary oligodeoxyribonucleotides (Fig. 9) analogously to a procedure used earlier.⁶⁸

It was demonstrated that the character of RNA cleavage within the bulges induced by imidazole is similar to the cleavage by metal ions, *i.e.*, all phosphodiester bonds in bulges and all bonds in a single-stranded RNA regions are cleaved. However, unlike RNA cleavage by magnesium ions, imidazole does not induce cleavage of the bonds adjacent to the bulges (< 5 nucleotides). Cleavage of RNA containing longer bulges (from 5 to 7 nucleotides) by imidazole occurs at the phosphodiester bonds both in the bulges and adjacent regions. Presumably, this is associated with the fact that RNA oligonucleotide complexes containing short bulges are more stable than complexes containing longer bulges. In the latter complexes, RNA remaining in the dissociated state over a long period of time ('breathing' complexes).⁹⁶

Natural RNase A cleaves RNAs at the phosphodiester bonds in all bulges except for single-base bulges. In addition to the phosphodiester bonds in bulges, RNase A cleaves phosphodiester bonds in other single-stranded RNA regions. Similar pattern of RNA cleavage was observed for aRNases. The extent of phosphodiester bond cleavage in bulges depends on the length and the nucleotide sequence of the bulges.

The concept 'selectivity' was introduced to estimate the difference in sensitivity of the phosphodiester bonds in artificial bulges and other phosphodiester bonds. The selectivity means the ratio of the extent of RNA cleavage at the bonds in a bulge to the total extent of RNA cleavage including all other

phosphodiester bonds. It appeared that the selectivity of cleavage depends on the type of aRNase. RNase A cleaves the bonds within bulges with a low selectivity (no higher than 0.1). In other words, cleavage at the bonds in bulges occurs at a rate lower than or similar to that at the other cleaved phosphodiester bonds in RNAs.

The selectivity of RNA cleavage by artificial RNases, which are short cationic peptides, was also low.⁹⁷ The highest selectivity of cleavage was observed for aRNases containing the 1,4-diazabicyclo[2.2.2]octane residue.^{98, 99} The CA phosphodiester bond in a four-membered bulge was cleaved with the highest selectivity (0.4). The cleaved phosphodiester bond was in the apical position. The presence of the second CA motif in a bulge increases the selectivity of phosphodiester bond cleavage up to 0.5.

Interestingly, the selectivity of cleavage in RNA · oligonucleotide complexes, in which the oligonucleotide contains a non-complementary adenosine residue opposite to the bulge, was always higher than that in complexes in which this non-complementary base was absent. It should be noted that, according to the data from gel shift analysis, binding of oligonucleotides containing an additional adenosine residue to RNAs does not differ from binding of oligonucleotides in which a non-complementary adenosine residue is absent.⁹⁶ Consequently, in this case high selectivity of cleavage can be attributed to a more flexible structure of the bulge, which provides for efficiency of transesterification. Therefore, artificial ribonucleases containing the 1,4-diazabicyclo[2.2.2]octane residue, unlike short cationic peptides, predominantly cleave bonds in bulges.

5. RNA cleavage at bulge sites by artificial RNases in the presence of magnesium ions

It is known that Mg^{2+} ions stabilise the RNA structure by decreasing its mobility,¹⁰⁰ resulting in a decrease in efficiency

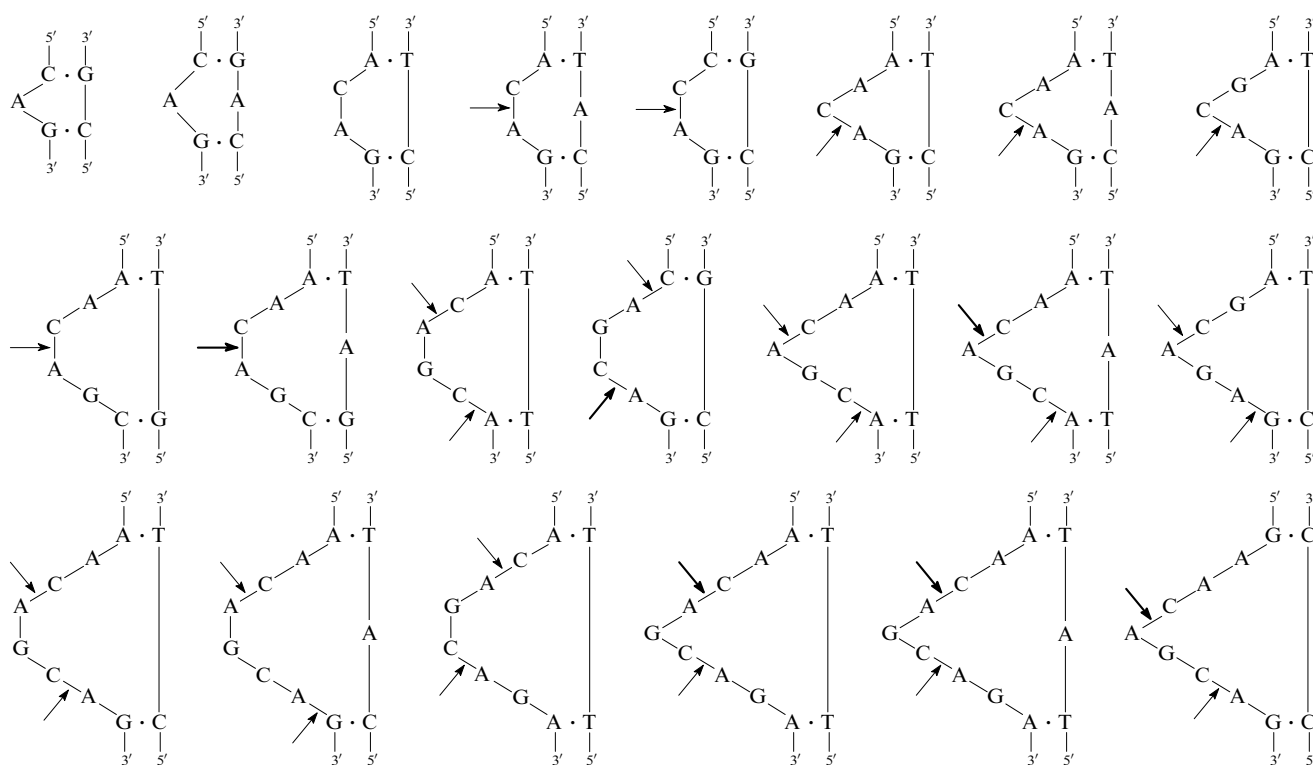


Figure 9. Sensitivity of the phosphodiester bonds in RNA bulges to cleavage by artificial RNases (the arrow thickness corresponds to the cleavage efficiency of a particular phosphodiester bond).^{96, 97}

of RNA cleavage by different agents. At the same time, magnesium ions stabilise such RNA structural elements as bulges. In the presence of magnesium ions, the total extent of M2-96 RNA cleavage by artificial RNases decreases. However, in the presence of MgCl_2 at a concentration of 10 mmol litre^{-1} , RNA·oligonucleotide complexes are cleaved by aRNases containing 1,4-diazabicyclo[2.2.2]octane predominantly at the bonds in bulges, whereas cleavage at other regions is suppressed to a substantial degree.^{96,97} In the presence of magnesium ions, the selectivity of cleavage of four- and seven-membered bulges increases to 0.68 and 0.75, respectively, *i.e.*, the formation of bulges in RNAs entirely changes the cleavage pattern by aRNases containing 1,4-diazabicyclo[2.2.2]octane. An increase in selectivity of cleavage in the presence of magnesium ions was observed for neither RNase A nor short cationic peptides.⁹⁷

These data correlate with the X-ray diffraction data for the single-nucleotide A bulge in the $[\text{r}(\text{GCG})\text{d}(\text{ATATA})\text{r}(\text{CGC})]_2$ duplex. In the presence of Mg^{2+} ions, the phosphodiester bond in the bulge adopts a nearly in-line configuration, unlike the configuration observed in the crystals grown in the presence of spermine.⁴¹ Apparently, Mg^{2+} ions can stabilise the in-line configuration of the phosphodiester bonds in bulges, which is favourable for transesterification.

IV. Conclusion

The idea for construction of specific catalysts for RNA cleavage has attracted attention for many years. Theoretical studies demonstrated that oligonucleotides that contain RNA-cleaving groups and form artificial bulges in a complementary RNA sequence can selectively inactivate RNAs in a catalytic manner and do not require additional enzymes or cofactors. However, there are problems with implementation of this approach in practice. The sensitivity of the phosphodiester bonds in bulges depends not only on the length and the nucleotide sequence of the bulge, but also on the nature of the RNA-cleaving group. An RNA-cleaving group should not only be an efficient catalyst for cleavage, but also be in an optimal orientation with respect to the cleaved bond. One of requirements imposed on the oligonucleotide moiety of the conjugate is that the DNA·RNA complex should be sufficiently stable before cleavage and readily dissociate after cleavage. In the case of long RNAs, this problem is complicated by a search for RNA regions accessible for binding with oligonucleotides. Therefore, the construction of efficient artificial RNases performing site-directed RNA cleavage requires a complex approach.

Two main approaches are available for site-directed RNA cleavage by artificial RNases. One approach is based on the synthesis of antisense oligonucleotides containing RNA-cleaving groups (see Section III.3). Another approach consists in constructing binary systems composed of a low-molecular-weight RNA-cleaving unit and a complementary oligonucleotide. The latter contains a group enhancing the sensitivity of a particular region or particular bonds in RNAs to cleavage.^{96,97,101} Site-directed RNA cleavage with the use of this system was first exemplified by cleavage of a short model 36-mer RNA in which all bonds, except for the bond subjected to cleavage, were protected by complexation with complementary oligonucleotides.⁹³

The approach proposed by Vlassov *et al.*⁹⁶ is based on an increase of sensitivity of phosphodiester bonds in RNAs to cleavage due to their bulging. It was demonstrated that in the presence of magnesium ions, the phosphodiester bonds in (4–7)-member bulges, which are formed in RNAs by hybridisation with a partially complementary oligonucleotide, are selectively cleaved by aRNases at a rate several times higher than the rate of cleavage of other phosphodiester bonds in

RNA molecules. Selective RNA cleavage within a bulge occurs apparently due to the appearance of constraints, which is necessary for efficient transesterification, and stabilisation of the other parts of the RNA molecule in the presence of magnesium ions. As a result, the RNA molecule becomes poorly sensitive to cleavage at all bonds except those in bulges.^{96,97} To summarise, selective RNA cleavage at phosphodiester bonds in bulges can be performed with the use of a binary system consisting of aRNase and an oligonucleotide partially complementary to RNA.

This review has been written with the financial support of the Russian Foundation for Basic Research (Project No. 05-04-49109), Programs of Basic Research of the Russian Academy of Sciences ('Molecular and Cellular Biology' and 'Fundamental Sciences for Medicine'), the Federal Centre of Scientific and Technological Programs (Grants RI-012/001/254 and RI-19.0/001/826), the Siberian Branch of the Russian Academy of Sciences (Grant for State Support of Young Scientists) and the Russian Science Support Foundation (Grant 'Doctors of Science of the Russian Academy of Sciences').

References

1. R T Batey, R P Rambo, J A Doudna *Angew. Chem., Int. Ed.* **38** 2326 (1999)
2. J D Robertus, J E Ladner, J T Finch, D Rhodes, R S Brown, B F Clark, A Klug *Nature (London)* **250** 546 (1974)
3. A M Pyle *J. Biol. Inorg. Chem.* **7** 679 (2002)
4. C R Woese, R R Gutell *Proc. Natl. Acad. Sci. USA* **86** 3119 (1989)
5. K Valegard, J B Murray, N J Stonehouse, S van den Worm, P G Stockley, L Liljas *J. Mol. Biol.* **270** 724 (1997)
6. G L Olsen, T E Edwards, P Deka, G Varani, S T Sigurdsson, G P Drobny *Nucleic Acids Res.* **33** 3447 (2005)
7. S Schmidt, L Beigelman, A Karpeisky, N Usman, U S Sorensen, M J Gait *Nucleic Acids Res.* **24** 573 (1996)
8. T Tanaka, T Ando, S Haga, Y Kikuchi *Biosci., Biotechnol., Biochem.* **68** 1388 (2004)
9. B Wimberly, G Varani, I Tinoco Jr *Biochemistry* **32** 1078 (1993)
10. H Moine, C Cachia, E Westhof, B Ehresmann, C Ehresmann *RNA* **3** 255 (1997)
11. M Schmitz, I Tinoco Jr *RNA* **6** 1212 (2000)
12. D N Frank, A E Ellington, N R Pace *RNA* **2** 1179 (1996)
13. J A Ippolito, T A Steitz *J. Mol. Biol.* **295** 711 (2000)
14. S Iwai, C Pritchard, D A Mann, J Karn, M J Gait *Nucleic Acids Res.* **20** 6465 (1992)
15. J D Puglisi, R Tan, B J Calnan, A D Frankel, J R Williamson *Science* **257** 76 (1992)
16. C C Correll, A Munishkin, Y L Chan, Z Ren, I G Wool, T A Steitz *Proc. Natl. Acad. Sci. USA* **95** 13436 (1998)
17. Y Xiong, M Sundaralingam *RNA* **6** 1316 (2000)
18. B N Trawick, A T Daniher, J K Bashkin *Chem. Rev.* **98** 939 (1998)
19. J R Morrow *Adv. Inorg. Biochem.* **9** 41 (1994)
20. K Shinozuka, Y Nakashima, K Shimizu, H Sawai *Nucleosides, Nucleotides, Nucleic Acids* **20** 117 (2001)
21. M A Podyminogin, V V Vlassov, R Giege *Nucleic Acids Res.* **21** 5950 (1993)
22. M Zenkova, N Beloglazova, V Sil'nikov, V Vlassov, R Giege *Methods Enzymol.* **341** 468 (2001)
23. M Perello, B Barbier, A Brack *Int. J. Pept. Protein Res.* **38** 154 (1991)
24. C H Tung, Z Wei, M J Leibowitz, S Stein *Proc. Natl. Acad. Sci. USA* **89** 7114 (1992)
25. N L Mironova, D V Pyshnyi, E M Ivanova, M A Zenkova, H J Gross, V V Vlassov *Nucleic Acids Res.* **32** 1928 (2004)
26. W Saenger *Printsipy Strukturnoi Organizatsii Nukleinovyykh Kislot (Principles of Nucleic Acid Structure)* (Moscow: Mir, 1987; translated into Russian)

27. L Joshua-Tor, F Frolow, E Appella, H Hope, D Rabinovich, J L Sussman *J. Mol. Biol.* **225** 397 (1992)
28. C Sudarsanakumar, Y Xiong, M Sundaralingam *J. Mol. Biol.* **299** 103 (2000)
29. M W Kalnik, D G Norman, M G Zagorski, P F Swann, D J Patel *Biochemistry* **28** 294 (1989)
30. M A Rosen, D Live, D J Patel *Biochemistry* **31** 4004 (1992)
31. U Dornberger, A Hillisch, F A Gollmick, H Fritzsche, S Diekmann *Biochemistry* **38** 12860 (1999)
32. A Bhattacharyya, D M Lilley *Nucleic Acids Res.* **17** 6821 (1989)
33. D M Lilley *Proc. Natl. Acad. Sci. USA* **92** 7140 (1995)
34. M Zacharias, P J Hagerman *J. Mol. Biol.* **247** 486 (1995)
35. T Hermann, D J Patel *Structure* **8** R47 (2000)
36. T Hermann, D J Patel *J. Mol. Biol.* **294** 829 (1999)
37. Y T van den Hoogen, A A van Beuzekom, E de Vroom, G A van der Marel, J H van Boom, C Altona *Nucleic Acids Res.* **16** 5013 (1988)
38. J H Cate, A R Gooding, E Podell, K Zhou, B L Golden, C E Kundrot, T R Cech, J A Doudna *Science* **273** 1678 (1996)
39. B L Golden, A R Gooding, E R Podell, T R Cech *Science* **282** 259 (1998)
40. S H van den Worm, N J Stonehouse, K Valegard, J B Murray, C Walton, K Fridborg, P G Stockley, L Liljas *Nucleic Acids Res.* **26** 1345 (1998)
41. S Portmann, S Grimm, C Workman, N Usman, M Egli *Chem. Biol.* **3** 173 (1996)
42. J S Smith, E P Nikonowicz *Biochemistry* **37** 13486 (1998)
43. P N Borer, Y Lin, S Wang, M W Roggenbuck, J M Gott, O C Uhlenbeck, I Pelczar *Biochemistry* **34** 6488 (1995)
44. L Jiang, A K Suri, R Fiala, D J Patel *Chem. Biol.* **4** 35 (1997)
45. L Varani, M Hasegawa, M G Spillanti, M J Smith, J R Murrell, B Ghetti, A Klug, M Goedert, G Varani *Proc. Natl. Acad. Sci. USA* **96** 8229 (1999)
46. L Joshua-Tor, D Rabinovich, H Hope, F Frolow, E Appella, J L Sussman *Nature (London)* **334** 82 (1988)
47. V Tereshko, S T Wallace, N Usman, F E Wincott, M Egli *RNA* **7** 405 (2001)
48. W D Cornell, P Cieplak, C I Bayley, I R Gould, K M Merz, D M Ferguson, D C Spellmeyer, T Fox, J W Caldwell, P A Kollman *J. Am. Chem. Soc.* **117** 5179 (1995)
49. M Zacharias, H Sklenar *J. Mol. Biol.* **289** 261 (1999)
50. B T Wimberly, D E Brodersen, W M Clemons Jr, R J Morgan-Warren, A P Carter, C Vornrhein, T Hartsch, V Ramakrishnan *Nature (London)* **407** 327 (2000)
51. D J Klein, T M Schmeing, P B Moore, T A Steitz *EMBO J.* **20** 4214 (2001)
52. K Seggerson, P B Moore *RNA* **4** 1203 (1998)
53. A A Szewczak, P B Moore *J. Mol. Biol.* **247** 81 (1995)
54. A A Szewczak, P B Moore, Y L Chang, I G Wool *Proc. Natl. Acad. Sci. USA* **90** 9581 (1993)
55. Y Xiong, Y Deng, C Sudarsanakumar, M Sundaralingam *J. Mol. Biol.* **313** 573 (2001)
56. S E Butcher, F H Allain, J Feigon *Nat. Struct. Biol.* **6** 212 (1999)
57. O Theunissen, F Rudt, U Guddat, H Mentzel, T Pieler *Cell (Cambridge)* **71** 679 (1992)
58. J R Wyatt, I Tinoco Jr, in *RNA Structural Elements and RNA Function. The RNA World* (Eds R F Gesteland, J F Atkins) (Cold Spring Harbor: Cold Spring Harbor Laboratory Press, 1993) p. 465
59. K J Luecke, I Tinoco Jr *Biochemistry* **35** 11677 (1996)
60. J A Ippolito, T A Steitz *Proc. Natl. Acad. Sci. USA* **95** 9819 (1998)
61. J H Cate, R L Hanna, J A Doudna *Nat. Struct. Biol.* **4** 553 (1997)
62. J M Ogle, D E Brodersen, W M Clemons Jr, M J Tarry, A P Carter, V Ramakrishnan *Science* **292** 897 (2001)
63. R T Raines *Chem. Rev.* **98** 1045 (1998)
64. G A Soukup, R R Breaker *Proc. Natl. Acad. Sci. USA* **96** 3584 (1999)
65. I Zagorowska, S Kuusela, H Lonnberg *Nucleic Acids Res.* **26** 3392 (1998)
66. H Hosaka, I Sakabe, K Sakamoto, S Yokoyama, H Takaku *J. Biol. Chem.* **269** 20090 (1994)
67. J Ciesiolka, D Michalowski, J Wrzesinski, J Krajewski, W J Krzyzosiak *J. Mol. Biol.* **275** 211 (1998)
68. D Husken, G Goodall, M J Blommers, W Jahnke, J Hall, R Haner, H E Moser *Biochemistry* **35** 16591 (1996)
69. K Breslow, M Labelle *J. Am. Chem. Soc.* **108** 2655 (1986)
70. A Bibillo, M Figlerowicz, K Ziomek, R Kierzek *Nucleosides, Nucleotides, Nucleic Acids* **19** 977 (2000)
71. G L Eichhorn, in *Inorganic Biochemistry* Vol. 2 (Ed. G L Eichhorn) (Amsterdam: Elsevier, 1973) p. 1210
72. N K Kochetkov, E L Budovskii (Eds) *Organicheskaya Khimiya Nukleinovykh Kislot* (Organic Chemistry of Nucleic Acids) (Moscow: Khimiya, 1970)
73. D W Celander, T R Cech *Biochemistry* **29** 1355 (1990)
74. C E Holmes, B J Carter, S M Hecht *Biochemistry* **32** 4293 (1993)
75. J Sumaoka, M Yashiro, K Komiyama *J. Chem. Soc., Chem. Commun.* 1707 (1992)
76. S A Kazakov, in *Bioorganic Chemistry. Nucleic Acids* Pt. 1 (Ed. S M Hecht) (New York: Oxford University Press, 1995) p. 244
77. R Breslow, D-L Huang *Proc. Natl. Acad. Sci. USA* **88** 4080 (1991)
78. W R Farkas *Biochim. Biophys. Acta* **155** 401 (1968)
79. R S Brown, B E Hingerty, J C Dewan, A Klug *Nature (London)* **303** 543 (1983)
80. W Saenger *Principles of Nucleic Acid Structure* (New York: Springer, 1984)
81. U Kaukinen, L Bieleki, S Mikola, R W Adamiak, H T Lonnberg *J. Chem. Soc., Perkin Trans. 2* 1024 (2001)
82. V Vlassov, T Abramova, T Godovikova, R Giege, V Silnikov *Antisense Nucleic Acid Drug Dev.* **7** 39 (1997)
83. J Hall, D Husken, U Piesles, H E Moser, R Haner *Chem. Biol.* **1** 185 (1994)
84. M A Reynolds, T A Beck, P B Say, D A Schwartz, B P Dwyer, W J Daily, M M Vaghefi, M D Metzler, R E Klem, L J Arnold *Nucleic Acids Res.* **24** 760 (1996)
85. K Kolasa, J Morrow, A Sharma *Inorg. Chem.* **32** 3983 (1993)
86. J Hall, D Husken, R Haner *Nucleic Acids Res.* **24** 3522 (1996)
87. A De Mesmaeker, R Haner, P Martin, H E Moser *Acc. Chem. Res.* **28** 366 (1995)
88. R Haner, J Hall, A Pfutzer, D Husken *Pure Appl. Chem.* **70** 111 (1998)
89. W C Putnam, A T Daniher, B N Trawick, J K Bashkin *Nucleic Acids Res.* **29** 2199 (2001)
90. H Astrom, R Stromberg *Org. Biomol. Chem.* **2** 1901 (2004)
91. H Astrom, N H Williams, R Stromberg *Org. Biomol. Chem.* **1** 1461 (2003)
92. T Niittymaki, H Lonnberg *Bioconjugate Chem.* **15** 1275 (2004)
93. A Maddar, R Ehrl, R Stromberg *Nucleosides, Nucleotides, Nucleic Acids* **22** 1289 (2003)
94. S Nakano, Y Uotani, K Uenishi, M Fujii, N Sugimoto *J. Am. Chem. Soc.* 127 518 (2005)
95. N G Beloglazova, M M Fabani, M A Zenkova, E V Bichenkova, N N Polushin, V V Sil'nikov, K T Douglas, V V Vlassov *Nucleic Acids Res.* **32** 3887 (2004)
96. I L Kuznetsova, M A Zenkova, H J Gross, V V Vlassov *Nucleic Acids Res.* **33** 1201 (2005)
97. I L Kuznetsova, M A Zenkova, V V Vlassov *Izv. Akad. Nauk, Ser. Khim.* 1236 (2006)^a
98. N Koval'ov, I Kuznetsova, E Burakova, V Sil'nikov, M Zenkova, V Vlassov *Nucleosides, Nucleotides, Nucleic Acids* **23** 977 (2004)
99. D Konevets, I Beck, N Beloglazova, I Sulimenkov, V Sil'nikov, M Zenkova, G Shishkin, V Vlassov *Tetrahedron* **55** 503 (1999)
100. V K Misra, D E Draper *Biopolymers* **48** 113 (1998)
101. A Kuzuya, R Mizoguchi, T Sasayama, J M Zhou, M Komiyama *J. Am. Chem. Soc.* **126** 1430 (2004)

^a — *Russ. Chem. Bull., Int. Ed. (Engl. Transl.)*

Synthesis, structures and reactivity of polyhalo[60]fullerenes[†]

A A Goryunkov, N S Ovchinnikova, I V Trushkov, M A Yurovskaya

Contents

I. Introduction	289
II. Synthesis, structures and physical properties of polyhalo[60]fullerenes	289
III. Reactions of C ₆₀ F ₁₈ and other polyfluoro[60]fullerenes	294
IV. Reactions of polychloro[60]fullerenes	306
V. Reactions of polybromo[60]fullerenes	309

Abstract. Methods for the synthesis of polyfluoro(chloro, bromo) derivatives of C₆₀ fullerene and their structures are described. The reactivity of these compounds is demonstrated considering redox reactions, nucleophilic substitution, radical addition, cycloaddition and electrophilic arylation. The bibliography includes 185 references.

I. Introduction

Polyhalofullerenes are the best studied fullerene polyadducts, and halogenation reactions were among the first reactions of fullerenes performed in the early 1990s.^{1–8} These compounds have attracted interest primarily because they hold promise for the design of new materials, which would be expected to exhibit unique properties. In particular, an idea of the synthesis of chemically inert perfluorinated fullerene C₆₀F₆₀ similar in properties to Teflon (the so-called ‘Teflon Buckyballs’) was very popular at one time.^{1,9} However, later it has been found^{10,11} that polyfluorofullerenes are not as chemically stable as polyfluoroalkanes, and it is impossible to prepare exohedral C₆₀F₆₀. Nevertheless, polyhalofullerenes have continued to attract attention, and investigations into halogenation of fullerenes for more than one decade led to the development of efficient methods for the synthesis of polyfluoro-, polychloro- and polybromofullerenes. The structures of individual polyhalofullerenes were established.

Compounds containing an aromatic annulene fragment bearing conjugated C=C bonds only in *trans* configuration (all-*trans* annulenes or trannulenes) were first synthesised based on polyfluorofullerenes.¹² It has been repeatedly suggested^{12–15} that polyhalofullerenes hold promise for the synthesis of donor–acceptor dyads with improved electron-

withdrawing properties and for the design of molecular devices. This has stimulated studies of the redox,^{16,17} electrochemical^{18–21} and photophysical^{22–24} behaviour of polyhalofullerenes and their derivatives. The design of new polyhalofullerene-based materials requires that both physical and chemical properties of these compounds were known. The aim of the present review is to systematise and analyse methods for the synthesis, structural features, chemical properties and characteristics of chemical transformations of polyhalo derivatives of the C₆₀ ([60]fullerene) molecule.

II. Synthesis, structures and physical properties of polyhalo[60]fullerenes

Being polyunsaturated compounds, fullerenes are prone to be involved in radical and nucleophilic addition and cycloaddition reactions, but they very rarely react with strong electrophilic reagents.^{25,26} Polyhalofullerenes are usually synthesised by the reactions of fullerene with a wide range of halogenating agents. Preparative procedures for the synthesis of various polyfluoro-, polychloro- and polybromofullerenes are available. Polyiodofullerenes are presently unknown, although the existence of molecular crystals with the composition C₆₀·2 I₂ was proved.^{27,28} In spite of the fact that the number of possible geometric isomers of polyhalofullerenes is very large, in practice only a few of them were prepared by halogenation of fullerene. The formation of particular isomers is generally controlled by thermodynamic factors and only in rare cases by kinetic factors.

The present review deals only with polyhalo derivatives of C₆₀ fullerene. Polyhalogenated C₇₀ fullerenes and polyhalogenated higher fullerenes have been studied in much less detail. However, the available data suggest that their chemical properties are analogous to those of polyhalo[60]fullerenes.

1. Synthesis and structures of polyfluoro[60]fullerenes

Polyfluorofullerenes are most numerous of all isolated and characterised polyhalofullerenes (Fig. 1).^{29–36} For example, the structures of C₆₀F₁₈ with the symmetry group C_{3v},^{37–39} three isomers of C₆₀F₃₆ (with *T*, *C*₃ and *C*₁ symmetry)^{40–42} and *D*₃ and *S*₆ isomers of C₆₀F₄₈ (Refs 43 and 44) were studied. Polyfluorofullerenes C₆₀F_{2n} (*n* = 1–4),^{45,46} C_s-C₆₀F₁₆

A A Goryunkov, N S Ovchinnikova, I V Trushkov, M A Yurovskaya,
Department of Chemistry, M V Lomonosov Moscow State University,
Leninskie Gory, 119992 Moscow, Russian Federation.
Fax (7-495) 939 12 40, tel. (7-495) 939 53 73,
e-mail: aag@thermo.chem.msu.ru (A A Goryunkov),
natasha@thermo.chem.msu.ru (N S Ovchinnikova),
tel. (7-495) 939 48 95, e-mail: trush@org.chem.msu.ru (I V Trushkov),
tel. (7-495) 939 53 76, e-mail: yumar@org.chem.msu.ru
(M A Yurovskaya)

Received 3 October 2006

Uspekhi Khimii 76 (4) 323–347 (2007); translated by T N Safonova

[†] Dedicated to the memory of Roger Taylor.

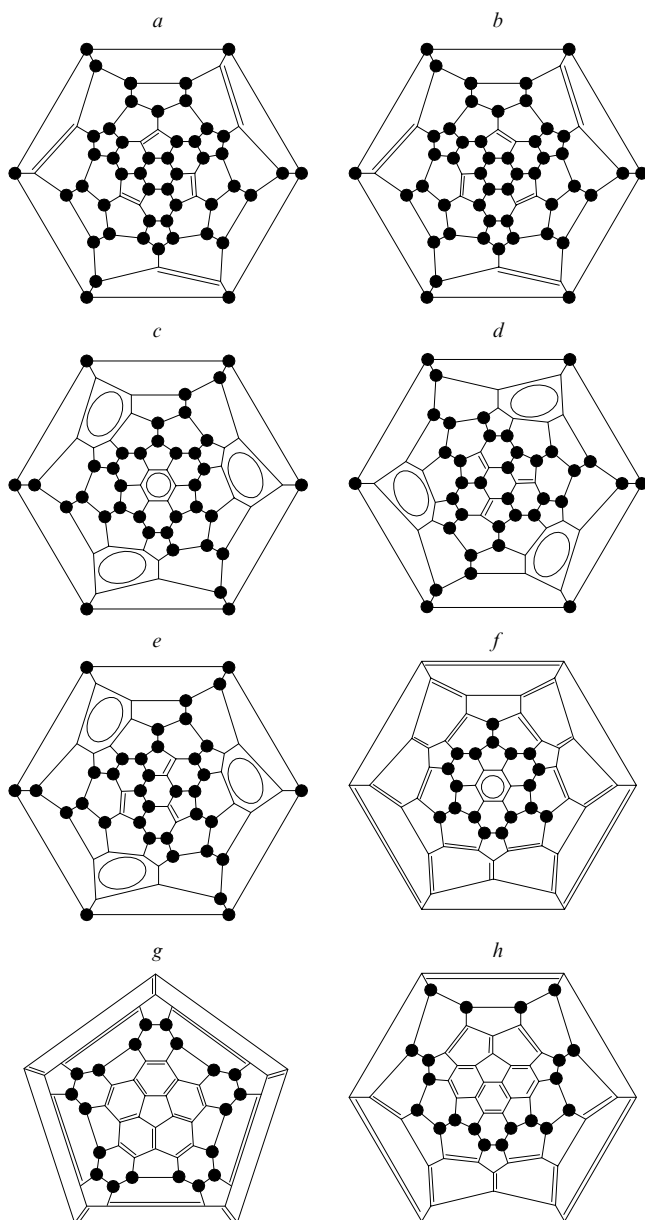


Figure 1. Schlegel diagrams of polyfluorofullerenes $C_{60}F_{48}$ [D_3 (a) and S_6 isomers (b)], $C_{60}F_{36}$ [C_{3v} (c), C_3 (d) and C_1 isomers (e)], C_{3v} - $C_{60}F_{18}$ (f) and two projections of D_{5d} - $C_{60}F_{20}$ (g, h). Hereinafter, the solid circles indicate the binding sites of halogen atoms.

(see ‡),⁴⁷ D_{5d} - $C_{60}F_{20}$,^{48,49} T_h - $C_{60}F_{24}$ (Ref. 50) and $C_{60}F_{38}$ (Ref. 51) were isolated and partially characterised.

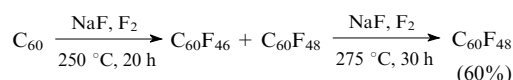
The methods for the synthesis of polyfluoro derivatives of fullerenes can be divided into three groups: (1) fluorination of fullerene by molecular fluorine either directly or in metal fluoride matrices, (2) fluorination of fullerene by fluorides of transition metals in high oxidation states and (3) fluorination of polychloro- and polybromofullerenes.

Higher polyfluorofullerenes, in particular, $C_{60}F_{48}$, can easily be synthesised by the reaction of fullerene with molecular fluorine (see Section II.1.a).⁴³ However, attempts to use this procedure for the synthesis of less fluorinated fullerenes led to the formation of complex mixtures of products. This is due to

the fact that direct fluorination occurs by a radical mechanism. The range of synthetically accessible polyfluorofullerenes was substantially extended due to the use of high-oxidation-state metal fluorides as fluorinating agents. In this case, the reaction apparently proceeds by a mechanism of single-electron oxidation of fullerene (and its partial fluorination products) by metal cations followed by the addition of the fluoride ion to the intermediate radical cation. This assumption is consistent with the observed dependence of the degree of fluorination of fullerene on the metal oxidation potential.^{35,52} The selective formation of polyfluorofullerenes $C_{60}F_{18}$, $C_{60}F_{36}$ and $C_{60}F_{48}$ was also observed in the reactions of fullerene with molecular fluorine in MnF_2 , CoF_2 or NiF_2 matrices.^{53–55} The advantage of this approach is the possibility to synthesise polyfluorofullerenes in a flow reactor, which is of importance for the development of industrial apparatus. Fluorination of polyhalofullerenes under mild conditions affords thermodynamically unstable but kinetically stable T_h - $C_{60}F_{24}$ (see Sections II.1.d and V).⁵⁰

a. Polyfluorofullerene $C_{60}F_{48}$

Fluorination of [60]fullerene with molecular fluorine was historically one of the first studied functionalisation reactions of C_{60} . Early experiments on fluorination of this fullerene often gave complex mixtures of fluoro derivatives of [60]fullerene, the composition of the products varied depending on the reaction temperature and time.^{1,11,56,57} In 1994, Tuinman and Gakh⁴³ developed a preparative procedure for the selective synthesis of $C_{60}F_{48}$ involving two fluorination steps.



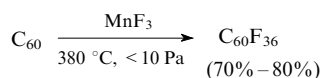
The reaction was performed in the presence of NaF to decrease the exothermicity of fluorination, which made it possible to decrease the degree of ‘combustion’ of fullerene in fluorine atmosphere and increase the yield of the target product. Initially, C_{60} and NaF were heated in a stream of fluorine at 250 °C for 20 h. The resulting mixture of isomers of higher polyfluorofullerenes $C_{60}F_{46}$ and $C_{60}F_{48}$ was extracted with $CFCl_3$ and subjected again to fluorination but at higher temperature (275 °C, 30 h). Polyfluorofullerene $C_{60}F_{48}$ was obtained in yields up to 60%. All attempts to perform further fluorination of $C_{60}F_{48}$ at high temperatures failed. Decomposition of the carbon skeleton of the molecule giving rise to a complex mixture of polyfluorocarbons C_nF_m ($n = 16–30$, $m = 30–50$) occurred instead of the addition of the fluorine atom.⁵⁸ Based on this fact, it was concluded that the maximum possible degree of fullerene fluorination is achieved in polyfluorofullerene $C_{60}F_{48}$. Improved procedures for the synthesis of $C_{60}F_{48}$ were described.^{55,59}

One- and two-dimensional ^{19}F NMR correlation spectroscopy demonstrated that polyfluorofullerene $C_{60}F_{48}$ thus synthesised is a mixture of isomers with the point groups D_3 and S_6 (see Fig. 1 a, b).⁴³ The structures of the D_3 and S_6 isomers were conclusively established by X-ray diffraction.⁴⁴ These molecules are characterised by the presence of six shortened double bonds (1.301 Å), which are located in six five-membered rings of the fullerene cage and are completely shielded by the surrounding fluorine atoms. The F...F distance between the opposite fluorine atoms at the double bond is 4.2 Å. Since the van der Waals diameter of the fluorine atom is 2.7 Å, the open space around the C=C bond is at most 1.5 Å. Such a substantial steric shielding of the double bond is one of the factors that preclude further fluorination of $C_{60}F_{48}$ without destruction of the fullerene cage.¹¹

‡ The point symmetry group of the compound is given in italics as a prefix to the formula.

b. Polyfluorofullerene C₆₀F₃₆

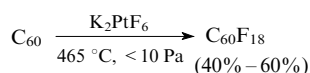
Heating of C₆₀ with MnF₃,⁶⁰ CeF₄³⁵ or MPbF₆ (M = Mg, Ca, Sr or Ba)⁶¹ at 380 °C under dynamic vacuum affords a mixture of *T*, C₃ and C₁ isomers of C₆₀F₃₆ in a yield of > 70% (see Fig. 1 *c–e*).



The structures of the isomers have been initially suggested based on ¹⁹F NMR spectroscopic data.^{40, 62} More recently, the structures of *T*- and C₃-C₆₀F₃₆ were established by X-ray diffraction.^{41, 42} Each isomer contains isolated cyclohexatriene fragments. An analysis of the C–C bond lengths in these rings demonstrates that all these distances are averaged and are similar to the typical bond lengths in aromatic compounds (for example, 1.373 Å for *T*-C₆₀F₃₆ and 1.368 Å for C₆F₆). Taking into account efficient π -electron density delocalisation and small deviations from planarity (about 0.01 Å) of the cyclohexatriene fragments, these rings can be considered as benzenoid. In the most symmetrical isomer *T*-C₆₀F₃₆, the fluorine atoms are arranged so that four isolated benzenoid fragments are retained. The molecules of the less symmetrical isomers (C₃-C₆₀F₃₆ and C₁-C₆₀F₃₆) contain three such fragments, whereas the remaining three double bonds are localised in the five-membered rings. It should be noted that all three isomers of C₆₀F₃₆ are structurally related to each other and can easily be derived from each other as a result of the 1,3-shift of one fluorine atom (interconversions of the C₃ and C₁ isomers)⁶³ or three fluorine atoms (interconversions of the *T* and C₃ isomers) within one or three five-membered rings, respectively. These rearrangements are also confirmed by the fact that fluorination of isomers of C₆₀F₃₆ by molecular fluorine affords higher polyfluorofullerenes D₃- and S₆-C₆₀F₄₈, which cannot occur without migration of the fluorine atom over the surface of the fullerene sphere.⁶⁴ It should be noted that analogous mechanisms were proposed for the explanation of interconversions of polyhydrofullerenes C₆₀H₃₆ isostructural to isomers of C₆₀F₃₆.⁶⁵

c. Polyfluorofullerenes C₆₀F₁₈ and C₆₀F₂₀

Polyfluorofullerene C₆₀F₁₈ can be prepared in yields of up to 60% by heating (465 °C) a mixture of C₆₀ and K₂PtF₆ under dynamic vacuum.^{37, 39} The compounds Cs₃PbF₇,⁶¹ Rb₂PtF₆ and Cs₂PtF₆ (Ref. 66) can be recommended as alternative fluorinating agents for the synthesis of C₆₀F₁₈. The use of KMnF₄,⁴⁶ K₃CoF₆,⁶⁷ Li₄CeF₈ or the KF–MnF₃ system^{49, 67} leads to an increase in the percentage of low-fluorinated by-products or a decrease in the degree of conversion of C₆₀. Hence, these reactions are less attractive for the synthesis of C₆₀F₁₈.



The only isomer of polyfluorofullerene C₆₀F₁₈ with symmetry C_{3v} (see Fig. 1 *f* and 2) was isolated. An important difference between this compound and the above-considered polyfluorofullerenes is that all fluorine atoms in this compound are located in one half of the fullerene cage, whereas another hemisphere remains unfunctionalised. As a result, the molecule assumes a large dipole moment estimated to be 8–15 D.^{38, 68} According to the X-ray diffraction data,^{38, 39} the fullerene hemisphere containing fluorine atoms is substantially flattened (see Fig. 2 *b*). This hemisphere includes the cyclohexatriene pole, in which the bond lengths are equalised and are typical of aromatic systems (1.372 Å). Therefore, like isomers of C₆₀F₃₆, polyfluorofullerene C₆₀F₁₈ contains a

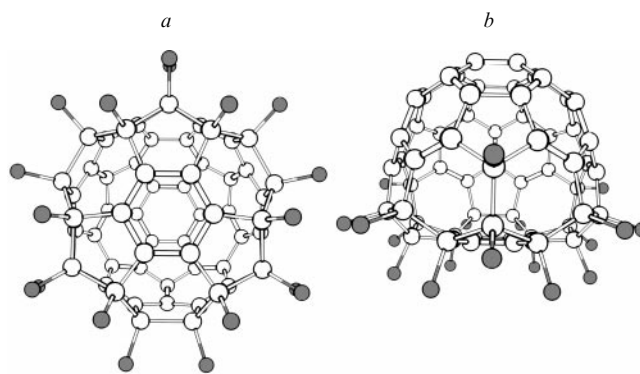


Figure 2. Three-dimensional structure of C_{3v}-C₆₀F₁₈: top view (*a*) and side view (*b*).

benzenoid fragment. The bond lengths and the shape of the pole of the fullerene hemisphere free of fluorine atoms are very similar to the corresponding parameters of non-modified fullerene. The C₆₀F₁₈ molecule contains four types of fluorine atoms, one of which is sterically most accessible, and the distance from such fluorine atoms to the carbon atoms bearing them (1.396 Å) is larger than the lengths of the other fluorine–carbon bonds (1.361–1.385 Å). Evidently, this longest bond is the weakest one, *i.e.*, this type of fluorine atoms is most reactive in the C₆₀F₁₈ molecule. The higher reactivity of this type of atoms compared to other fluorine atoms is also attributed to the fact that the involvement of the latter in chemical transformations results in a deviation from planarity and destabilisation of the aromatic π system of the benzene-like fragment.

Polyfluorofullerene C₆₀F₂₀ was isolated from fluorination products of C₆₀ with complex manganese and cerium fluorides in 5%–8% yields.^{48, 49, 66, 69} (It should be noted that this compound was found in trace amounts, if at all, among the reactions products of fullerene with K₂PtF₆ and Cs₂PtF₆, but it was detected in the analogous reaction with Rb₂PtF₆). A ¹⁹F NMR spectroscopic study demonstrated that all 20 fluorine atoms in the C₆₀F₂₀ molecule are equivalent. This is consistent with the structure shown in Figs 1 *g, h* and 3.⁴⁸ Fullerene D_{5d}-C₆₀F₂₀ contains the equatorial belt of sp³-hybridised carbon atoms (CF)₂₀, which divides the fullerene cage into two equivalent dehydrocorannulene fragments. Although the alternative structure of C₆₀F₂₀ described in Ref. 48 formally satisfies the condition of equivalence of 20 fluorine atoms, conclusive evidence in favour of the initially proposed structure containing the equatorial (CF)₂₀ belt was

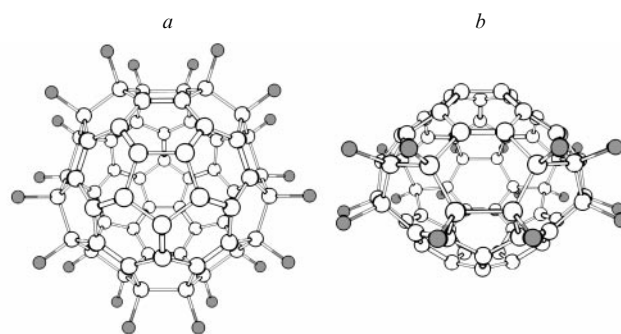


Figure 3. Three-dimensional structure of D_{5d}-C₆₀F₂₀: top view (*a*) and side view (*b*).

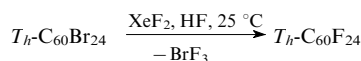
given in a more recent study.⁴⁹ Evidently, polyfluorofullerene D_{5d} - $C_{60}F_{20}$ cannot be generated from C_{3v} - $C_{60}F_{18}$ without substantial rearrangements of the fluorine atoms. This suggests that the pathways giving rise to these two compounds include different intermediate fluorination products.⁴⁸

Due to the presence of two dehydrocorannulene fragments, which are located at the poles of the $C_{60}F_{20}$ molecule and can independently bind donor or acceptor groups, these derivatives are promising starting compounds for the formation of donor–acceptor complexes and polymers.⁷⁰

d. Polyfluorofullerene T_h - $C_{60}F_{24}$

A possible method for the synthesis of polyhalofullerenes is based on the replacement of one halogen atom by another halogen. In early studies,^{71, 72} it has been demonstrated that chlorine (bromine) atoms in polychloro(bromo)fullerenes can be replaced by fluorine atoms in reactions with molecular fluorine or XeF_2 . However, the authors failed to isolate individual compounds. By contrast, bromination of lower polychloro derivatives $C_{60}Cl_n$ ($n = 6, 8, 12$ or 14) by liquid bromine affords T_h - $C_{60}Br_{24}$,⁷³ the chlorination of which by antimony pentachloride at high temperature gives rise to T_h - $C_{60}Cl_{24}$.⁷⁴

Fluorination of T_h - $C_{60}Br_{24}$ with xenon difluoride in anhydrous HF at room temperature is the only known example of the successful selective formation of polyfluorofullerene by the substitution reaction.⁵⁰



Under the above-mentioned conditions, bromine atoms in polyhalofullerene are replaced by fluorine atoms. According to the ^{19}F NMR spectroscopic data, this reaction produces the highly symmetrical T_h - $C_{60}F_{24}$ compound isostructural to the starting $C_{60}Br_{24}$ compound (Fig. 4). According to quantum chemical calculations,⁵⁰ this polyfluorofullerene is metastable and, consequently, can undergo isomerisation or disproportionation to form more stable structures. However, this process is kinetically hindered; at least, it was not detected at room temperature.

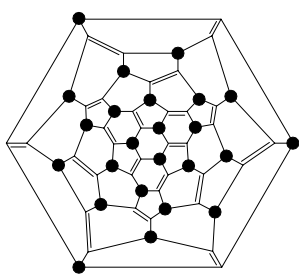


Figure 4. The Schlegel diagram of T_h - $C_{60}F_{24}$.

e. Other polyfluoro derivatives of [60]fullerene

In addition to $C_{60}F_{18}$ and $C_{60}F_{20}$, fluorination of C_{60} fullerene by complex metal fluorides (K_2PtF_6 , $KMnF_4$, Cs_2PbF_6 , Li_4CeF_8 , etc.) gives other lower polyfluorofullerenes [$C_{60}F_{2n}$ ($n = 1-3$),^{45, 46} two isomers of $C_{60}F_8$,^{45, 46, 75} $C_{60}F_{12}$, $C_{60}F_{14}$,⁴⁹ $C_{60}F_{16}$ (Ref. 47)], oxopolyfluorofullerenes [$C_{60}F_2O$,⁴⁵ $C_{60}F_{2n}O$ ($n = 2-4$),⁷⁶ $C_{60}F_{16}O$,⁷⁷ $C_{60}F_{18}O$,⁷⁸⁻⁸⁰ $C_{60}F_{18}O_2$ (Ref. 81)] and mixed perfluoroalkylfluoro derivatives [$C_{60}F_7CF_3$,^{45, 46} $C_{60}F_{17}CF_3$, $C_{60}F_{17}C_2F_5$ (Ref. 82)]. Impurities

of oxopolyfluorofullerenes and perfluoroalkylpolyfluorofullerenes are always present in certain amounts among fluorination products of fullerenes. These compounds are formed because of imperfections in vacuum apparatus used for their preparation, due to the presence of traces of oxygen in crystalline fullerene, reagents or on the surface of the reactor and as a result of thermal destruction of polyfluorofullerenes (for more details, see Section III.4.b). Although the percentage of these compounds is low (the yields are usually lower than 5%), they were isolated by chromatography and partially characterised. The structures of most of these compounds were proposed based on ^{19}F NMR spectroscopic data. The structures of some derivatives were confirmed by the results of other spectroscopic methods (for example, by IR and Raman spectroscopy) interpreted with the use of quantum chemical calculations. The structures of some compounds were established by X-ray diffraction. For example, it was demonstrated that the C_s and C_1 isomers of fullerene $C_{60}F_{17}CF_3$ are isostructural to $C_{60}F_{18}$. These molecules contain the CF_3 group instead of one of three sterically most accessible fluorine atoms.⁸² An X-ray diffraction study showed that oxohomofullerene C_s - $C_{60}F_{18}O$ dominates among oxygen-containing products.⁸⁰ In this compound, the oxygen atom is introduced into the longest [5,6] C(F)–C(F) bond[§] of the $C_{60}F_{18}$ molecule, which is accompanied by cleavage of this bond.

2. Solubility of polyfluoro[60]fullerenes

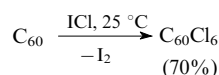
Only a few studies were concerned with the determination of solubility of polyfluorofullerenes and investigation of their stability in solution.⁸³⁻⁸⁵ It should be noted that the lack of information on stability of polyfluorofullerenes in different solvents led to erroneous interpretation of the experimental data in some early studies in favour of the formation of $C_{60}F_{60}$.^{1, 86, 87}

Stability of polyfluorofullerenes in solution depends on the chemical properties of these compounds. As will be demonstrated below, polyfluorofullerenes are prone to nucleophilic substitution reactions, in particular, to hydrolysis and can act as oxidising agents. Hence, to prevent non-destructive dissolution of polyfluorofullerenes, it is necessary to avoid the use of nucleophilic or protic solvents (for example, alcohols, amines, pyridine, etc.), solvents that are difficult to purify from traces of water or alcohols (for example, acetone and chloroform) and solvents that are readily involved in redox reactions (ethers, particularly, for higher polyfluorofullerenes).

Among the solvents recommended for use in experiments with polyfluorofullerenes, hydrocarbons (alkanes and arenes) and their halogeno derivatives should be mentioned. The solubilities of C_{60} and polyfluorofullerenes $C_{60}F_{18}$, $C_{60}F_{36}$ and $C_{60}F_{48}$ in some organic solvents are given in Table 1.

3. Synthesis and structures of polychloro[60]fullerenes

Unlike polyfluoro[60]fullerenes, polychloro derivatives of fullerene C_{60} have been less studied. For example, only $C_{60}Cl_6$ has been synthesised (by the reaction of fullerene with iodine monochloride) so far and reliably characterised.⁸⁹⁻⁹¹



Fullerene C_{60} is known to react only with highly reactive electrophiles; however, this compound is readily involved in radical addition reactions. Hence, it is reasonable to suggest

§ The carbon–carbon bond between the five- and six-membered rings is enclosed in brackets [5,6].

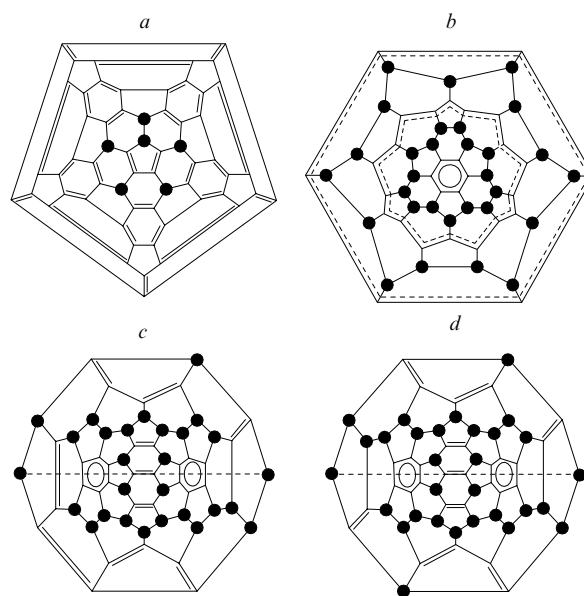
Table 1. Solubility of C₆₀ and polyfluoro[60]fullerenes in organic solvents at 25 °C (in mg ml⁻¹).

Solvent	C ₆₀	C ₆₀ F ₁₈	C ₆₀ F ₃₆	C ₆₀ F ₄₈
Aromatic hydrocarbons				
Benzene	1.5 ^a	0.48 ^b	—	1.5
Toluene	2.9 ^a	0.52 ^b	—	1.4
<i>o</i> -Xylene	8.7 ^a	0.75 ^b	—	4.8
<i>m</i> -Xylene	1.4 ^a	1.23 ^b	—	11.1
<i>p</i> -Xylene	5.9 ^a	0.96 ^b	—	9.1
Mesitylene	2.4 ^a	—	—	0.31
n-Alkanes				
n-Pentane	—	—	0.36	19.4 ^c
n-Hexane	—	—	0.50	11.6 ^c
n-Heptane	—	—	0.60	10.8 ^c
n-Octane	—	—	0.44	11.6 ^c
n-Nonane	—	—	0.89	9.9 ^c
n-Decane	—	—	0.61	9.0 ^c
n-Undecane	—	—	—	6.5 ^c
Tolyl halides				
<i>o</i> -MeC ₆ H ₄ Cl	—	5.6	2.1	14.8
<i>m</i> -MeC ₆ H ₄ Cl	—	6.4	3.3	18.2
<i>p</i> -MeC ₆ H ₄ Cl	—	8.2	2.1	8.2
<i>o</i> -MeC ₆ H ₄ Br	—	5.6	1.6	8.2
<i>m</i> -MeC ₆ H ₄ Br	—	6.4	2.2	6.4
<i>p</i> -MeC ₆ H ₄ Br	—	4.2	1.8	6.4
<i>p</i> -MeC ₆ H ₄ F	—	4.2	3.4	11.4

^a Ref. 88, ^b Ref. 83, ^c Ref. 85. Other values were taken from Ref. 84.

that chlorination of C₆₀ proceeds by a radical mechanism.⁸⁹ This assumption is consistent with the influence of solvents on the reaction rate. It was found that the reaction proceeds more rapidly in benzene or chlorobenzene than in toluene. Evidently, toluene captures part of the radicals, resulting in a decrease in the rate of chlorination of fullerene. Since ICl is a weak Lewis acid, chlorination of C₆₀ in benzene or toluene gives aryl-containing fullerenes as by-products.^{91,92} Apparently, this reaction proceeds analogously to arylation of fullerenes and polychlorofullerenes in the presence of aluminium chloride⁹³ (see Section IV.2). The yields of aryl-containing fullerenes that are formed as by-products can be substantially decreased using monochloro- and dichlorobenzenes, which are less reactive in Friedel–Crafts reactions, and by removing unconsumed ICl from the reaction mixture as quickly as possible.^{91,94}

The structure of polychlorofullerene C₆₀Cl₆ (Fig. 5a) was established by ¹³C NMR spectroscopy⁸⁹ and was then confirmed by X-ray diffraction.⁹⁵ In the molecule, five chlorine atoms surround one of the pentagonal faces of the fullerene, whereas the sixth chlorine atom is directly attached to this five-membered ring to form a 1,2 contact with the adjacent chlorine atom (this structure is generally described as a truncated pentagonal pyramid). This addition pattern of addends to the fullerene cage was demonstrated⁹⁶ to be energetically most favourable in the presence of bulky substituents, including chlorine atoms. To the contrary, the formation of *trans*-chains of 1,2 contacts (the so-called *S* addition pattern) is favourable for small substituents, such as H and F atoms. This difference is evidently associated with steric strain due to interactions between the adjacent bulky groups. The presence of one 1,2 contact between chlorine atoms in the C₆₀Cl₆ molecule leads to

**Figure 5.** The Schlegel diagrams of C₅-C₆₀Cl₆ (a), D_{3d}-C₆₀Cl₃₀ (b), C₁-C₆₀Cl₂₈ (c) and C₂-C₆₀Cl₃₀ (d).

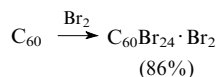
a slight elongation of the corresponding C–Cl bond and, as a consequence, to its weakening. At the same time, most reactions with C₆₀Cl₆ consist of the replacement of all five chlorine atoms surrounding the five-membered ring with retention of the chlorine atom in the ring. This is due to the fact that elimination of this atom as the chloride anion should give rise to a fragment of the cyclopentadienyl cation with pronounced antiaromatic properties. By contrast, elimination of other chlorine atoms affords stable allyl-type cations.

Syntheses of a series of polychloro derivatives of fullerene C₆₀ with a larger number of chlorine atoms [for example, C₆₀Cl₈, C₆₀Cl₁₀,⁹⁴ C₆₀Cl₁₂,^{4,94,97} C₆₀Cl₁₄,^{94,97} C₆₀Cl₂₄,² C₆₀Cl₂₆ (Ref. 94)] were documented. However, only indirect evidence for the formation of these molecules was presented, and these data can be interpreted ambiguously. Higher polychlorofullerenes, *viz.*, T_h-C₆₀Cl₂₄, C₁-C₆₀Cl₂₈, C₂-C₆₀Cl₃₀ and D_{3d}-C₆₀Cl₃₀ (see Fig. 5), have been synthesised and structurally characterised only very recently.⁷⁴ These compounds can be prepared by heating fullerene with such chlorinating agents as ICl, PCl₅, SbCl₅, VCl₄, KICl₄, MoCl₅ or VOCl₃.^{74,98} Polychlorofullerene T_h-C₆₀Cl₂₄ is isostructural to the halogeno derivatives T_h-C₆₀Br₂₄ and T_h-C₆₀F₂₄. The structure of the compound D_{3d}-C₆₀Cl₃₀ (see Fig. 5b) contains two benzenoid poles and the [18]trannulene ‘equator’ (see Section III.2.c) with a high degree of delocalisation. The aromatic character of these fragments is confirmed by the C–C bond lengths (1.368 and 1.375 Å in the six-membered rings and 1.386 and 1.392 Å in the trannulene ring).⁹⁹ In the D_{3d}-C₆₀Cl₃₀ molecule, the C=C double bonds are involved only in aromatic rings, due to which this polychlorofullerene is thermally more stable (*T*_{decomp} = 450–500 °C) than other polychlorofullerenes (*T*_{decomp} = 280–350 °C).^{74,99,100} Although the reactivity of these compounds remains unstudied, their unusual structures will undoubtedly attract attention of researchers in the nearest future.

4. Synthesis and structures of polybromo[60]fullerenes

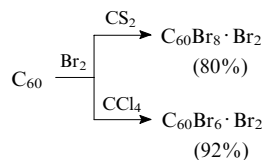
Polybromo[60]fullerenes can be synthesised by the reaction of C₆₀ with liquid bromine or its solution in an appropriate

solvent. For example, dissolution of C_{60} in liquid Br_2 affords orange crystals of $C_{60}Br_{24} \cdot n Br_2$.⁷



The structure of $C_{60}Br_{24}$ was established by X-ray diffraction.^{7, 101} All the attached bromine atoms are located in the fullerene cage so that 1,2 contacts between these atoms are absent (Fig. 6a). There is the only possible arrangement for 24 attached bromine atoms without 1,2 contacts. It corresponds to the structure with high symmetry T_h . The average C—Br, C—C and C=C bond lengths are normal for these types of bonds (1.994, 1.510 and 1.344 Å, respectively). Further addition of the bromine atoms leads to appearance of 1,2 contacts between these atoms, and, as a result, to destabilisation of the molecule due to strong steric strains caused by repulsions between the bulky substituents. Therefore, the highest degree of bromination of C_{60} is apparently achieved in polybromofullerene $C_{60}Br_{24}$.

Bromination of [60]fullerene by molecular bromine in some organic solvents affords polybromofullerenes $C_{60}Br_6$ and (or) $C_{60}Br_8$, the selectivity being dependent on the nature of the solvent.⁵ In CS_2 or $CHCl_3$, dark-brown crystals of $C_{60}Br_8$ containing solvated bromine molecules precipitate from the reaction mixture (in 80% and 50% yields, respectively).⁵



Bromination of C_{60} in benzene or CCl_4 gives rise to $C_{60}Br_6$ (in ~50% and 92% yields, respectively) as dark-claret plates.⁵

In the study cited,⁵ the observed selectivity of the formation of polybromofullerenes in various solvents was attributed to selective precipitation of insoluble polybromofullerene, due to which it does not undergo further transformations. However, more recent investigations demonstrated¹⁰² that the reagent ratio also has a principal effect on the selectivity of formation of polybromofullerenes. In particular, both $C_{60}Br_6$ and $C_{60}Br_8$ were synthesised in nearly quantitative yields with the use of 1,2-dichlorobenzene as the solvent in the reactions with a 40- and 400-fold excess of Br_2 , respectively.¹⁰²

The structures of polybromofullerenes $C_{60}Br_6$ and $C_{60}Br_8$ (see Fig. 6b,c) were unambiguously established by X-ray diffraction.^{5, 101, 103} The molecules have C_s and C_{2v} symmetry, respectively. The C—Br bond lengths vary in a narrow range (1.986–1.998 Å). The changes in the C—C bond lengths in the molecule C_s - $C_{60}Br_6$ compared to those in C_{60} fullerene are substantial only for the brominated hemisphere, the largest elongation being observed for the bonds involving sp^3 -hybridised carbon atoms. Five bromine atoms surround the five-membered ring containing the butadiene fragment with two double $C(sp^2)=C(sp^2)$ bonds (1.350 Å) and one elongated $C(sp^2)-C(sp^2)$ single bond (1.462 Å). The characteristic features of the addition pattern of the bromine atoms in the molecule C_{2v} - $C_{60}Br_8$ are responsible for the presence of the isolated $C=C$ double bonds with typical lengths of 1.333 and 1.339 Å in the brominated fragment of the fullerene cage. The $C(sp^2)-C(sp^3)$ bonds of predominantly ordinary character have an average length of 1.510 Å. The remote region of the fullerene sphere is characterised by the C—C bond lengths typical of [60]fullerene.

Polybromofullerenes are the thermally least stable polyhalo derivatives of fullerenes and decompose to give C_{60} and molecular bromine upon heating to 100–200 °C, the thermal stability being increased in the series $C_{60}Br_6 < C_{60}Br_8 < C_{60}Br_{24}$.^{7, 102} Polybromofullerenes are characterised by low solubility and low stability in solution, which limits their use in organic synthesis.⁸⁹⁻

III. Reactions of $C_{60}F_{18}$ and other polyfluoro[60]fullerenes

In the previous sections, it was noted that $C_{60}F_{18}$ is a synthetically accessible, rather stable and reactive polyfluorofullerene. Its structure is characterised by the presence of a flattened fluorine-substituted fragment and the unfluorinated fullerene hemisphere. These structural features are responsible for the diversity of chemical transformations of this compound, such as redox, nucleophilic substitution, arylation and cycloaddition reactions. Hence, it is not surprising that the chemical properties of this compound have been studied in most detail. In addition to $C_{60}F_{18}$, scarce published data on the chemical properties of other polyfluoro[60]fullerenes are considered below.

1. Redox reactions

It is known that C_{60} fullerene exhibits oxidation properties and forms the $C_{60}^{\cdot -}$ radical anion at a relatively positive potential [the first half-wave potential $E_{1/2}^I = -0.59$ V in CH_2Cl_2 vs. the saturated calomel electrode (SCE)].^{18, 19, 21} The addition of electronegative groups to the fullerene cage should, on the

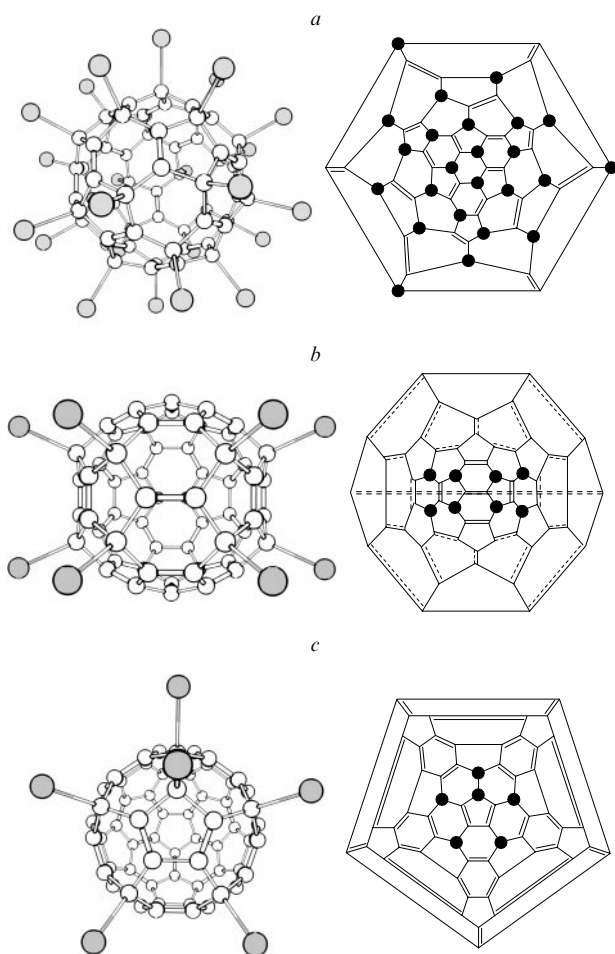
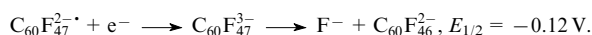
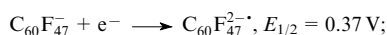
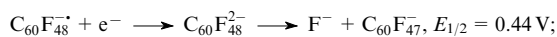


Figure 6. Three-dimensional structures and the Schlegel diagrams of polybromofullerenes T_h - $C_{60}Br_{24}$ (a), C_{2v} - $C_{60}Br_8$ (b) and C_s - $C_{60}Br_6$ (c).

whole, lead to an increase in electron-withdrawing properties. As a result, the reduction potentials of polyfluorofullerenes are more positive. This shift achieves 1.38 V for C₆₀F₄₈ against C₆₀.²¹ The high electron affinity of polyfluorofullerenes is also confirmed by the fact that long-lived polyfluorofullerene dianions^{20, 21, 104–106} and even the C₆₀F₄₈^{3–} trianion¹⁷ were detected in the gas phase by mass spectrometry.

The processes that occur during electrochemical reduction of polyfluorofullerene C₆₀F₄₈ were studied in detail.²¹ One-electron reversible reduction of C₆₀F₄₈ giving rise to the C₆₀F₄₈^{•–} radical anion occurs at the potential $E_{1/2}^I = 0.79$ V (CH₂Cl₂, SCE). Since the reduction potential of C₆₀F₄₈ is more positive than the oxidation potentials of the I[–]/I₃[–] (0.26 V, SCE) and I₃[–]/I₂ pairs (0.65 V, SCE), the reaction of C₆₀F₄₈ with the iodide anion occurs with elimination of molecular iodine.^{21, 107} This process is accompanied by the formation of the long-lived (> 20 s) C₆₀F₄₈^{•–} radical anion.

Further reduction of C₆₀F₄₈ at potentials $E_{1/2}^{II} = 0.44$, $E_{1/2}^{III} = 0.37$ and $E_{1/2}^{IV} = -0.12$ V (CH₂Cl₂, SCE) leads to irreversible processes accompanied by defluorination of polyfluorofullerenes.²¹ To elucidate the mechanism of these processes, the reaction products of C₆₀F₄₈ with various reducing agents were studied by electrospray ionisation mass spectrometry. The reducing agents were chosen in such a way that their oxidation potentials were as close to the potential of the corresponding process as possible. For example, reduction of C₆₀F₄₈ with ferrocene (Fc) with the oxidation potential [$E(\text{Fc}/\text{Fc}^+) = 0.31$ V vs. SCE] close to the second reduction potential of polyfluorofullerene affords the C₆₀F₄₇[–] anion. It was hypothesised that the reaction initially produces the unstable C₆₀F₄₈^{2–} dianion, which decomposes to form the F[–] and C₆₀F₄₇[–] anions. The latter yields C₆₀F₄₇^{2–}. The reaction of C₆₀F₄₈ with the stronger reducing agent, viz., decamethylferrocene [$E(\text{DmFc}/\text{DmFc}^+) = -0.11$ V vs. SCE], produces C₆₀F₄₆^{2–}. In the authors' opinion, the latter is formed as a result of elimination of F[–] from the initially formed C₆₀F₄₇^{3–} trianion. The schemes of the reactions involved in the successive reduction of C₆₀F₄₈ and their reduction potentials in CH₂Cl₂ vs. SCE are given below.



It should be noted that the process is not stopped at this moment, and the percentage of polyfluorofullerenes containing a smaller number of fluorine atoms increases with time.

Electrochemical transformations of polyfluorofullerenes containing smaller amounts of halogen have been investigated.^{16, 18, 19, 108} Reduction of these compounds was demonstrated to be accompanied by a loss of fluorine atoms. For example, the reaction of C₆₀F₁₈ with chloroanil produces the C₆₀F₁₇[–] ion,¹⁰⁸ and reduction of C₆₀F₂ and C₆₀F₄ affords the C₆₀^{•–} anion.¹⁸

The reduction potential of polyfluorofullerenes monotonically increases with increasing number of the attached fluorine atoms or upon introduction of other electron-withdrawing fragments into the molecule (Table 2). The arrangement of the fluorine atoms at the fullerene cage also has an effect on the potential. For example, of the three studied isomers of C₆₀F₃₆, it is most difficult to reduce the *T* isomer; the *C*₁ and *C*₃ isomers are reduced at 30 and 80 mV higher potentials, respectively.¹⁰⁸ This fact correlates with higher chemical stability of the *T*-C₆₀F₃₆ isomer compared to the *C*₁ and *C*₃ isomers (see Section III.2.a).^{109, 110}

Interesting results were obtained in the study of the trannulene dyads C₆₀F₁₅[C(CO₂Et)₂CO₂R]₃ (R = Et, pyrene-,

Table 2. Reduction potentials of polyfluorofullerenes and some their derivatives in CH₂Cl₂.

Compound	$E_{1/2}^I/\text{V}$		Ref.
	vs. SCE	vs. C ₆₀ /C ₆₀ [–]	
C ₆₀	–0.59	0.00	18, 19, 21
C ₆₀ F ₂	–0.55	0.04	18
C ₆₀ F ₄	–0.51	0.08	18
C ₆₀ F ₁₈	–0.33	0.26	108
C ₆₀ F ₁₈ O	–0.28	0.31	108
C ₆₀ F ₁₅ [C(CO ₂ Et) ₂ CO ₂ R] ₃ ^a	–0.10 to –0.005	0.49–0.51	14, 22, 111
<i>T</i> -C ₆₀ F ₃₆	0.04	0.63	108
<i>C</i> ₁ -C ₆₀ F ₃₆	0.07	0.66	108
<i>C</i> ₃ -C ₆₀ F ₃₆	0.12	0.71	108
C ₆₀ F ₃₆ ^b	0.24	0.82	19
C ₆₀ F ₄₈	0.78	1.38	21, 108

^a R = Et, pyrene-, perylene-, ferrocene- or tetrathiafulvalene-containing fragments; ^b a mixture of the *T*-C₆₀F₃₆ and *C*₃-C₆₀F₃₆ isomers (1 : 10).

perylene-, ferrocene- or tetrathiafulvalene-containing fragments).^{14, 22, 111} The first reduction potential of these compounds corresponding to the single-electron reversible transfer varies from –0.005 to –0.10 V (CH₂Cl₂, SCE), which is substantially higher than the reduction potential of C₆₀F₁₈ (–0.33 V, CH₂Cl₂, SCE).¹⁰⁸ The observed process is attributed to reduction of the [18]trannulene fragment in the compounds under study.

Polyfluorofullerenes are stronger oxidising agents than fullerene, which was demonstrated back in early studies. A mixture of higher polyfluorofullerenes C₆₀F₄₄ and C₆₀F₄₆ was found to oxidise the iodide anion to I₂.¹⁰⁷ Reduction of polyfluorofullerenes is accompanied by a loss of fluorine atoms to form a complex mixture of compounds, from C₆₀F₃₆ to C₆₀F₄₀. The reactions of higher polyfluorofullerenes with Br[–] proceed with difficulty and are accompanied by elimination of only a small amount of Br₂.

Organic compounds can also be oxidised and even fluorinated by higher polyfluorofullerenes. For example, heating of a mixture of C₆₀F₄₄ and C₆₀F₄₆ in PrOH affords acetone,¹⁰⁷ whereas heating of solutions of polyfluorofullerenes in aromatic solvents in the presence of Lewis acids leads to defluorination of fullerenes^{112–114} accompanied by partial fluorination of solvent molecules. Under these conditions, even pyridine, which exhibits low reactivity in electrophilic substitution reactions, gives 2-fluoropyridine in a yield of up to 10%.¹⁰⁷ In the presence of higher polyfluorofullerenes, polymerisation of THF occurs;^{87, 110, 115} an analogous process is also observed upon dissolution of these compounds in acetone (in the latter case, a polymer is formed as a result of aldol condensation induced by HF).¹

Therefore, polyfluorofullerenes are very strong oxidants, the redox reactions involving these reagents being accompanied by defluorination of the starting polyfluorofullerenes. The degree of defluorination is generally determined by the strength of the reducing agent and the possibility of competitive substitution and addition reactions. Some other examples of reduction of polyfluorofullerenes observed in the course of nucleophilic substitution and cycloaddition reactions are given in Sections III.2 and III.4.a.

2. Nucleophilic substitution reactions

The mechanisms of nucleophilic substitution in polyhalofullerenes are virtually unknown. The ideas about the processes involved in these reactions changed with time. However, numerous uncertainties and ambiguities concerning these

mechanisms still persist. The problem is that the substitution of different nucleophiles and polyhalofullerenes occurs apparently by different pathways. Hence, there is good reason to discuss the most probable mechanisms of these reactions in the present review. We expect that further experimental studies will provide conclusive information on these mechanisms.

a. Reactions with O-nucleophiles

Even in early studies, it was found that polyfluorofullerenes, which have initially been believed to be chemically inert, are involved in nucleophilic substitution reactions.^{56, 86, 115, 116} These reactions have been discovered accidentally. The mass spectrometric analysis of fluorination products of C₆₀ fullerene revealed the presence of oxopolyfluoro derivatives containing from 1 to 18 oxygen atoms.^{8, 57, 117}

It is unlikely that oxygen atoms are inserted into polyfluorofullerene molecules upon oxidation by atmospheric oxygen because solid samples of polyfluorofullerenes were found^{29, 59, 86} to be unchanged in air for an indefinitely long period of time. However, dissolution of highly fluorinated fullerenes in polar solvents (for example, THF) containing traces of water is accompanied by an exothermic reaction resulting in a loss of fluorine atoms.^{110, 115} Hence, it was hypothesised that oxo derivatives of polyfluorofullerenes are formed through the nucleophilic displacement of F by OH followed by elimination of HF from the adjacent F and OH substituents.^{57, 115, 116} This transformation occurs so easily that oxopolyfluorofullerenes have long been considered as primary reaction products.^{57, 117} However, hydroxypolyfluorofullerenes are precursors of these compounds, as has been recently exemplified by the individual isomers C₃- and C₁-C₆₀F₃₆.¹⁰⁹

The discovery of 'accidental'³⁴ epoxidation of polyfluorofullerenes has inflated studies of targeted nucleophilic displacement of fluorine atoms by oxygen-containing nucleophiles. It was found that C₆₀F₃₆ (Ref. 40) and higher polyfluorofullerenes^{115, 116} are easily hydrolysed in the presence of organic co-solvents (the presence of the latter is necessary because polyfluorofullerenes are insoluble in water). For example, dissolution of C₆₀F₃₆ in wet toluene or chloroform affords the compounds C₆₀F₃₅OH, C₆₀F₃₃(O)OH and C₆₀F₃₂(O)₂.¹¹⁸ The treatment of polyfluorofullerenes with methanolic NaOMe leads to methoxydefluorination. The nucleophilic displacement of fluorine atoms with sodium acetate in acetic acid was also documented.¹¹⁵ Therefore, unlike polyfluoroalkanes and most of their derivatives, polyfluorofullerenes are rather good substrates for nucleophilic substitution reactions. The mechanism of this reaction deserves a detailed discussion.

The nucleophilic substitution involves the carbon–leaving group bond cleavage and the carbon–nucleophile bond formation. These processes can be either concerted (the so-called S_N2 mechanism) or sequential. The concerted mechanism is impossible for polyhalofullerenes because it involves the backside attack of a nucleophile with respect to the leaving group, *i.e.*, from the inside of the fullerene sphere. In early studies on nucleophilic substitution in polyhalofullerenes, the direct nucleophilic displacement of halogen has been believed to be a result of the frontal attack of a nucleophile. However, this mechanism was rejected in more recent studies. Actually, the frontal attack of a nucleophile is a forbidden process according to the orbital symmetry rules. *Ab initio* quantum chemical studies with an extended basis set taking into account diffuse and polarisation functions demonstrated that the energy barrier to the frontal attack is 165–190 kJ mol^{−1} higher than that to the backside attack even in simplest halomethanes.¹¹⁹

Nucleophilic substitution reactions at a carbonyl carbon atom or at a silicon atom proceed by an addition–elimination mechanism (the leaving group is eliminated only after the

formation of a bond with a nucleophile). However, it is evident that this mechanism is impossible for polyfluorofullerenes. The S_N1 mechanism can also be rejected. First, the formation of carbocations from electron-deficient polyfluorofullerenes in the absence of Lewis acids is hardly probable. Second, the substitution reaction rate was found to depend on the strength of a nucleophile. For example, up to 65% of fluorine atoms are replaced in the reaction with sodium methoxide in methanol for 12 h, whereas only 15% of fluorine atoms are replaced in the reaction with the weaker nucleophilic agent, *viz.*, sodium acetate, in acetic acid (which is often used as the solvent in S_N1 reactions) even after 550 h.¹¹⁵

The nucleophilic substitution reaction can be considered as a single-electron transfer from a nucleophile to the leaving group. Before the reaction, the nucleophile bears a lone electron pair, whereas the leaving group contains one electron of the R–X bond. After completion of the reaction, the nucleophile bears one electron of the R–Y bond, whereas the leaving group contains a lone electron pair. This electron density shift can occur either simultaneously with the bond cleavage–formation steps or independently of these processes (or one of these processes).

All possible nucleophilic substitution mechanisms can be represented by a three-dimensional reaction diagram (Fig. 7).^{120–122} The degree of the R–Y bond formation is on the *x* axis; the degree of the R–X bond cleavage, on the *y* axis; the degree of electron density transfer from one fragment to another, on the *z* axis. The S_N1 mechanism is described by the movement of the system from the point *A* to the point *C* through the point *B*. The movement along the *ADC* path corresponds to the addition–elimination mechanism. The transformation of the system from the state *A* to the state *C* without intersections of other nodes in the diagram corresponds to the concerted S_N2 reaction.

If the electron shift from the nucleophile (Y:) to the substrate (RX) is not accompanied by the Y–R bond formation and the R–X bond cleavage, the mechanism involves the single-electron transfer (path *A–F*). If the electron shift is not accompanied by the formation of the Y–R bond but is accompanied by the cleavage of the R–X bond, the mechanism involves the dissociative electron transfer (path *A–G*). The strong electron-withdrawing properties of fullerene and, particularly, of polyfluorofullerenes suggest the possibility of the single-electron transfer mechanism.

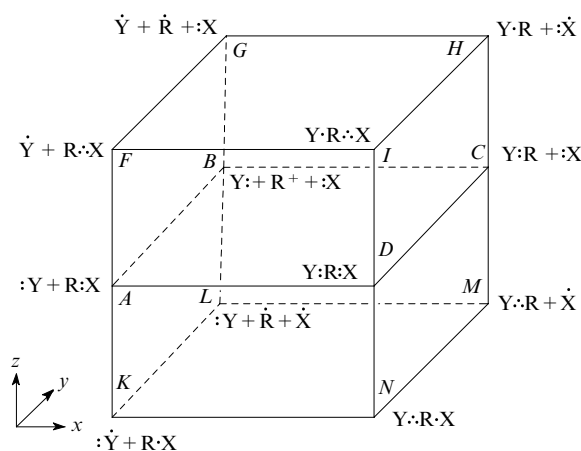
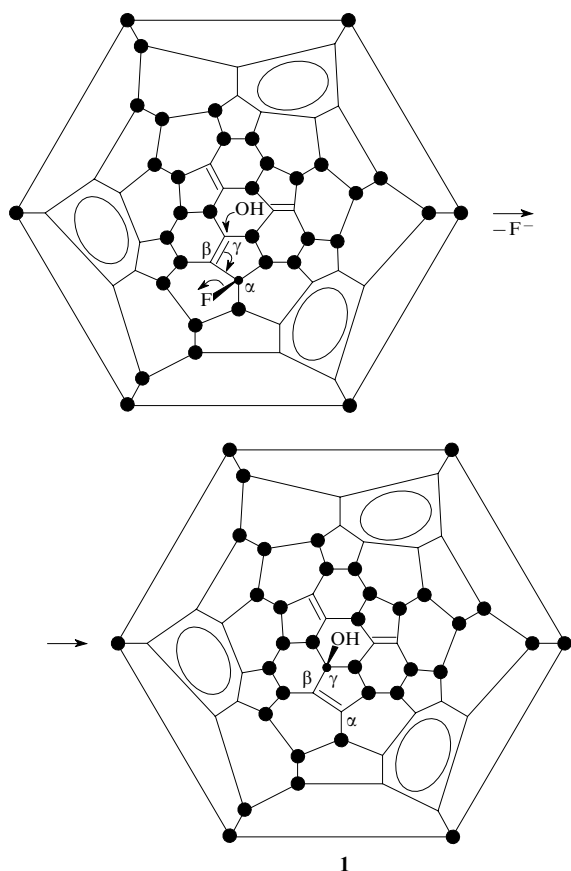


Figure 7. Three-dimensional reaction diagram for nucleophilic substitution reactions. See comments in the text.

The single-electron transfer from various donors to polyfluorofullerenes is rather well known (see Section III.1).^{16, 18, 19, 21} These reactions are usually accompanied by complete or partial defluorination. Actually, it was found that hydrolysis of S_6 - and D_3 - $C_{60}F_{48}$ in aqueous acetone affords a complex mixture of products, including $C_{60}F_{42}O$, $C_{60}F_{40}O$, $C_{60}F_{38}O$, *etc.*¹¹⁰ These data can be considered as evidence for the single-electron transfer mechanism in the case of hydrolysis of the strongest electron-withdrawing polyfluorofullerene, $C_{60}F_{48}$.

The C_{3v} - $C_{60}F_{18}$ and T - $C_{60}F_{36}$ compounds are stable with respect to hydrolysis. Hydrolysis of the C_3 and C_1 isomers of $C_{60}F_{36}$ proceeds without a loss of additional fluorine atoms.^{109, 110} This would be impossible in the case of the single-electron transfer mechanism. Consequently, the nucleophilic substitution reactions of these substrates proceed by another pathway. A comparison of the structures of the T - $C_{60}F_{36}$ isomer, which withstands hydrolysis, and the hydrolysable isomers C_3 - $C_{60}F_{36}$ and C_1 - $C_{60}F_{36}$ (see Fig. 1 *c-e*) gives the answer to this question. In the T - $C_{60}F_{36}$ molecule, all double bonds adjacent to the fluorine atoms are involved in the aromatic benzenoid six-membered rings. This isomer contains only $Ph-C(F)RR'$ -type fragments. In two other isomers, there are three isolated double bonds containing the $C(F)RR'$ fragment in the allylic position. It is known that nucleophiles can attack allyl halides both at the α - and γ -carbon atoms. The latter attack leads to the shift of the $C=C$ double bond (the so-called S_N2' mechanism). The nucleophilic substitution in polyhalofullerenes should proceed by this mechanism.

Actually, dissolution of C_3 - $C_{60}F_{36}$ in wet toluene affords C_1 - $C_{60}F_{35}OH$ (**1**), which is consistent with the S_N2' mechanism.¹⁰⁹



The isomers of hydroxypolyfluorofullerene C_1 - $C_{60}F_{35}OH$, *viz.*, compounds **1** and **2** (Fig. 8), obtained upon hydrolysis of C_3 - and C_1 - $C_{60}F_{36}$, respectively, were isolated and characterised.¹⁰⁹ It was found that only the allylic fluorine atoms are

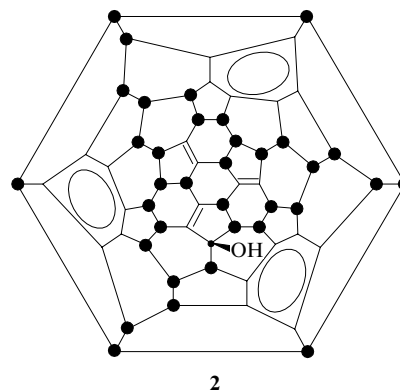
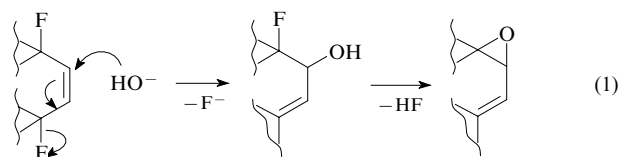


Figure 8. The Schlegel diagram of C_1 - $C_{60}F_{35}OH$ (**2**).

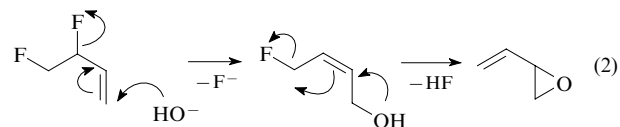
replaced. On the contrary, the fluorine atoms that are surrounded only by other fluorine atoms or benzenoid rings remain intact.

Compounds **1** and **2** easily undergo dehydrofluorination to give $C_{60}F_{34}O$. In this case, the oxygen atom is, apparently, involved in the epoxide ring. However, it should be borne in mind that some oxopolyfluorofullerenes generated as by-products in fluorination reactions of [60]fullerene, *viz.*, $C_{60}F_{2n}O$ ($n = 1-4$),⁴⁵ $C_{60}F_{18}O$ ⁸⁰ and $C_{60}F_{36}O$,¹⁰⁹ contain an oxygen atom as an intramolecular ether group.

It was hypothesised^{36, 57} that epoxide is formed by elimination of HF from the adjacent OH and F groups. Therefore, the overall process of epoxide formation is described by reaction (1).



However, we are doubtful about this mechanism because the formation of the epoxide ring from halohydrins generally occurs by the S_N2 mechanism, which, as demonstrated above, is impossible in the case under consideration. Hence, the S_N2' mechanism described by reaction (2) seems to be more probable. Unfortunately, it is impossible to draw an unambiguous conclusion about the mechanism of this step because it is necessary to establish the structures of the resulting epoxides.



The further substitution of fluorine atoms can also occur. The $C_{60}F_{33}(O)OH$ and $C_{60}F_{32}O_2$ compounds were also detected among the hydrolysis products of the polyfluorofullerene $C_{60}F_{36}$.¹¹⁸ The formation of these compounds is accompanied by migration of double bonds, which destabilises the molecule as a whole. Hence, the percentage of the latter compounds is low.

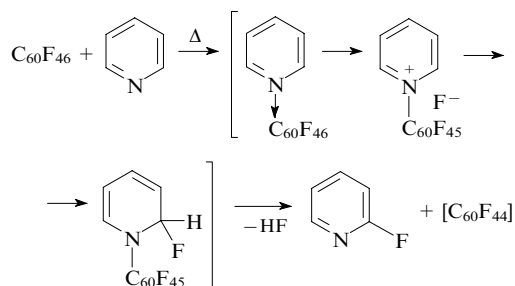
The analogous S_N2' mechanism of the substitution of fluorine atoms is observed for dissolution of D_3 - and S_6 - $C_{60}F_{48}$ in THF or acetone in the presence of water.¹¹⁰ This treatment leads to the replacement of up to 12 halogen atoms. This is consistent with the presence of six double bonds, for which the S_N2' mechanism is possible. Subsequent elimination of HF gives fragments containing up to six epoxide rings.

Calculations of the formation energies of possible intermediates containing a hydroxy group demonstrated that the energy difference between these intermediates is small. Consequently, hydrolysis of $C_{60}F_{48}$ can afford complex mixtures of isomers.¹¹⁰

Thus, the nucleophilic substitution in polyfluorofullerenes occurs by the S_N2' mechanism or *via* the electron transfer and is possible only in the presence of the activated carbon–carbon double bond that is not involved in the aromatic ring and occupies the β position with respect to the leaving atom. Hence, the C_3 - and C_1 - $C_{60}F_{36}$ isomers containing three allylic fragments are much more reactive in nucleophilic substitution reactions than T - $C_{60}F_{36}$ in which the π -electron density is completely delocalised over the aromatic rings. It should also be noted that the double bonds containing several fluorine atoms in the nearest environment are more reactive. As a result, O-nucleophiles react more readily with higher polyfluorofullerenes than with lower polyfluorofullerenes, in particular, with $C_{60}F_{18}$, which are less reactive in these reactions.^{109, 110}

b. Reactions with N-nucleophiles

The reactions of polyfluorofullerenes with N-nucleophiles are less studied than the reactions with O-nucleophiles. It is known that higher polyfluorofullerenes react readily with primary and secondary amines. For example, up to 55% of fluorine atoms are substituted in reactions of higher polyfluorofullerenes with Et_2NH during 1 h (^{19}F NMR spectroscopic data), and the percentage of the replaced fluorine atoms increases to 65% when the reaction time is increased to 12 h.¹¹⁵ Pyridine also reacts slowly with higher polyfluorofullerenes $C_{60}F_{44}$ – $C_{60}F_{46}$ with selective formation of 2-fluoropyridine.¹⁰⁷ To explain this fact, the authors suggested the mechanism involving the N addition followed by the migration of the fluorine atom.



This unexpected result may be of importance in the preparative chemistry of pyridine, because it is virtually impossible to synthesise 2-fluoropyridine by other methods. Besides, this is the first example of the use of higher polyfluorofullerenes as fluorinating agents for heterocyclic compounds.

c. Reactions with C-nucleophiles

Reactions with organometallic compounds. The formation of a new carbon–carbon bond is the most important reaction in synthetic chemistry of fullerenes. Hence, the reactions with C-nucleophiles attract the largest interest among nucleophilic substitution reactions of polyfluorofullerenes. Alkyl- and aryllithium compounds are known to be very reactive nucleophiles. In an early study on the chemical properties of polyfluorofullerenes,¹¹⁵ it was demonstrated that these compounds react readily with typical C-nucleophiles, such as Grignard reagents and organolithium compounds. However, the products have not been isolated and analysed. Further detailed studies on the reaction of polyfluorofullerenes $C_{60}F_{44}$ – $C_{60}F_{46}$ with alkyllithium reagents showed that this is one of the most efficient routes to polymethylated and polyphenylated [60]fullerenes with high degree of addition.¹²³

Products with the compositions $C_{60}Me_n$ ($n = 2$ –28) and $C_{60}Ph_n$ ($n = 2$ –20) were synthesised by the reactions of a mixture of polyfluorofullerenes $C_{60}F_{44}$ – $C_{60}F_{46}$ with an excess of MeLi and PhLi, respectively.¹²³ The formation of compounds with the number of methyl (phenyl) groups smaller than the number of fluorine atoms in the starting polyfluorofullerene is evidence for partial defluorination of the substrate in the course of the reaction. This suggests that the reactions of polyfluorofullerenes with organolithium compounds proceed by the single-electron transfer mechanism. This reaction pathway is also supported by the fact that a considerable amount of biphenyl was detected in the reaction with phenyllithium.¹⁰⁷ Fullerene methylation (or phenylation) products are orange (or brown), very readily soluble in non-polar organic solvents, thermally stable at least up to 300 °C and storage-stable in air over a long period of time. It is of note that refluxing of polyfluorofullerenes in diethyl ether for 3 h is required to achieve the complete substitution of methyl groups for all fluorine atoms. At room temperature, mixed derivatives $C_{60}F_xMe_y$ are formed. The necessity of prolonged heating of the reaction mixture for the complete substitution of fluorine atoms is attributed to the fact that the electron-withdrawing properties of fullerene are decreased as the degree of substitution of methyl groups for the fluorine atoms increases and, as a consequence, to the incomplete reaction under milder conditions (*cf.* Ref. 115).

Arylation of $C_{60}F_{18}$. An alternative procedure for the introduction of aryl substituents into the fullerene cage is the Friedel–Crafts reaction. In this reaction, polyfluorofullerenes and aromatic compounds act as electrophiles and nucleophiles, respectively. In other words, the arylation reactions of polyfluorofullerenes belong to nucleophilic substitution reactions. Many arylated fullerenes, which are of practical interest, were synthesised by the reactions of fullerenes or polyhalofullerenes with aromatic compounds in the presence of Lewis acids. Arylfullerenes are soluble in organic solvents and storage-stable.

The Friedel–Crafts reaction with polyhalofullerenes was first described for polychlorofullerenes² (arylation of polychlorofullerenes is considered in detail in Section IV.1). Since alkyl fluorides are more reactive in the Friedel–Crafts reaction than analogous chlorides,¹²⁴ it can be expected that polyfluorofullerenes would also be involved in this reaction. Actually, it was found that the electrophilicity of polyhalofullerenes increases in the series $Br < Cl < F$.¹²⁵

It can also be expected that of all polyfluorofullerenes the lower polyfluorofullerenes would be most reactive in the Friedel–Crafts reaction because fluorine atoms in these compounds are sterically more accessible. For example, $C_{60}F_{18}$ reacts with benzene in the presence of $FeCl_3$ at room temperature. On the contrary, attempts to replace fluorine atoms in higher polyfluorofullerenes $C_{60}F_{36}$ and $C_{60}F_{48}$ by phenyl groups using the Friedel–Crafts reaction failed.¹¹²

The trefoil-shaped triphenyl derivative $C_{60}F_{15}Ph_3$ (**3**), which was called triumphene (Fig. 9), was isolated from arylation products of polyfluorofullerene C_{3v} - $C_{60}F_{18}$ and completely characterised.¹¹²

Based on the ^{19}F NMR spectroscopic data, which are indicative of the C_{3v} symmetry of this molecule, evidence for the direct nucleophilic substitution of fluorine atoms according to the S_N1 mechanism was reported.¹¹² This mechanism is facilitated by the Friedel–Crafts catalyst. An increase in the reaction temperature results in the formation of $C_{60}Ph_{18}$, in which all fluorine atoms are replaced by phenyl groups. It was hypothesised^{36, 112} that, in spite of presumable steric hindrance, the phenyl groups occupy the positions of fluorine atoms in the precursor. However, this is doubtful. The mass spectra of the reaction products show a low-intensity peak of

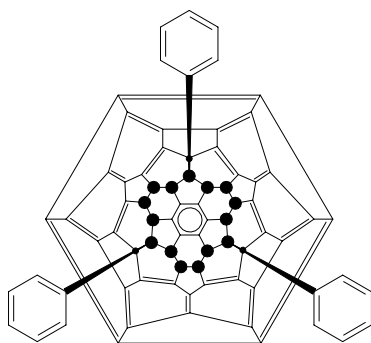


Figure 9. The Schlegel diagram of $C_{3v}\text{-C}_{60}\text{F}_{15}\text{Ph}_3$ (**3**).

the $\text{C}_{60}\text{Ph}_{19}^+$ ion. Apparently, this compound is formed as a result of further phenylation of the fullerene cage. This reaction is analogous to the well-known reaction of fullerene with benzene in the presence of AlCl_3 .⁹³ In addition, $\text{C}_{60}\text{F}_{15}\text{Ph}_7$ and other phenylation products of polyfluorofullerene were detected in the reaction mixture.¹¹²

In studies of the reaction of polyfluorofullerene $\text{C}_{60}\text{F}_{18}$ with a wide range of aromatic compounds catalysed by FeCl_3 , mono-, bis- and tris(aryl) derivatives **4**–**6** (Fig. 10) were detected.^{112, 113} The results of these experiments are summarised in Table 3.

The degree of substitution of F atoms depends on the nature of the aromatic reagent. For example, the reactions of $\text{C}_{60}\text{F}_{18}$ with bulky arenes, such as naphthalene, biphenylene, pyrene or fluoranthene, yield monosubstituted compounds **4** as the major products. On the contrary, bis- (5) and/or trisubstituted (**6**) products dominate in the reactions of $\text{C}_{60}\text{F}_{18}$ with smaller arenes, such as benzene, chloro- and 1,2-dichlorobenzenes, toluene, biphenyl, fluorene, *etc.* Some aromatic compounds do not give arylation products because of steric hindrance (for example, mesitylene), self-condensation side reactions¹¹³ or low reactivity of the substrate (for example, trifluoromethylbenzene). Serious steric hindrance or self-con-

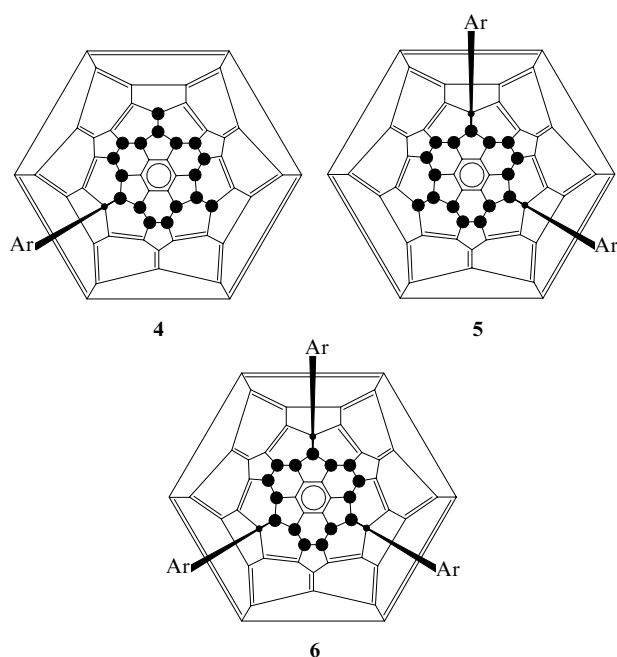


Figure 10. The Schlegel diagrams of electrophilic mono- (**4**), di- (**5**) and tri-substitution products (**6**) in $\text{C}_{60}\text{F}_{18}$ by different arenes (see Table 3).

Table 3. Results of the replacement of fluorine atoms in $\text{C}_{60}\text{F}_{18}$ by different agents.

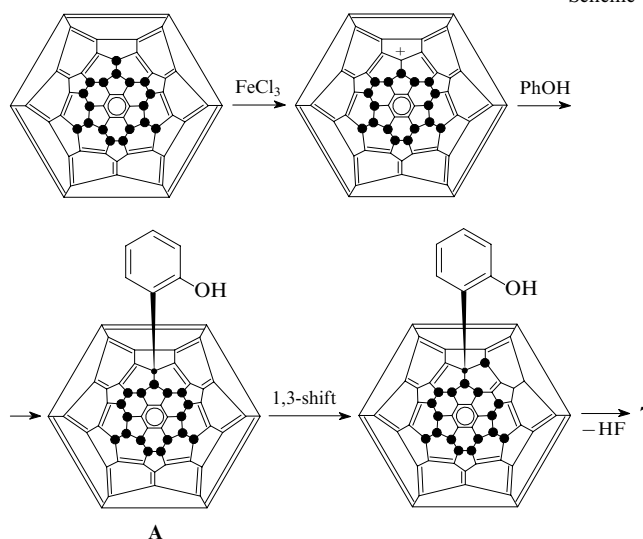
Arene	Product		
	4	5	6
Benzene	—	—	+
Chlorobenzene	—	—	+
1,2-Dichlorobenzene	—	—	+
Toluene ^a	+	+	+
Anisole	+	+	+
Diphenyl ether	+	+	+
Biphenylene	+	+	+
Naphthalene	+	+	+
Biphenyl	+	—	+
Fluorene ^b	+	—	+
Pyrene	+	—	—
Fluoranthene	+	+	—
Mesitylene	—	—	—
Perylene ^b	—	—	—
Coronene	—	—	—
Thiophene ^c	—	—	—
Azulene ^b	—	—	—
Trifluoromethylbenzene ^c	—	—	—

^a The *para* isomer is generated as the major product, although fractions containing *ortho*- and *meta*-substitution products were isolated; ^b chlorination and/or self-condensation of arene are side processes; ^c the reaction does not proceed.

densation and chlorination of arenes in the presence of FeCl_3 as side reactions precluded synthesis of the substitution products of $\text{C}_{60}\text{F}_{18}$ with thiophene, perylene and azulene.

The reactions of $\text{C}_{60}\text{F}_{18}$ with hydroxyl-containing aromatic compounds (phenol, hydroquinone and 2-naphthol) are not stopped after electrophilic defluoroarylation, but are accompanied by elimination of HF to give benzofuran derivatives of fullerene **7**, **8** and **9**, respectively (Fig. 11).^{113, 125} The elimination of HF was described as a result of the direct attack of the OH group on the F atom, which becomes adjacent to the 2-hydroxyphenyl substituent after the 1,3-shift (Scheme 1). The possibility of the 1,3-migration of the fluorine atom was exemplified⁶³ by the transformations of isomers of $\text{C}_{60}\text{F}_{36}$.

Scheme 1



An alternative step of dehydrofluorination of the intermediate **A** involves the attack of the OH group on the adjacent

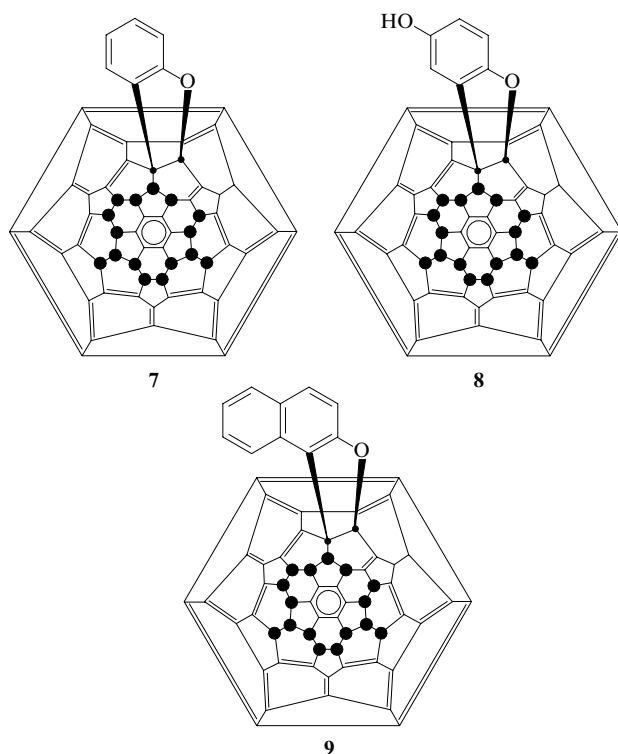
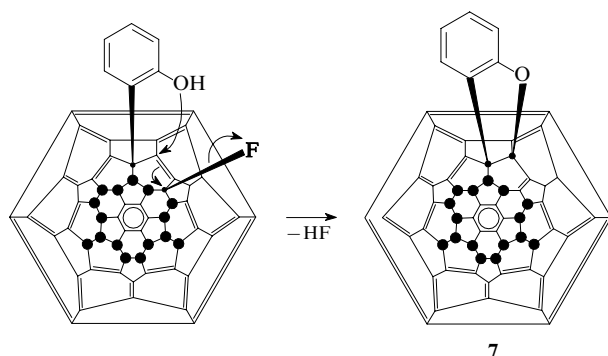


Figure 11. The Schlegel diagrams of compounds 7–9 prepared by the reactions of $C_{60}F_{18}$ with phenol, hydroquinone and 2-naphthol, respectively.

double bond accompanied by the migration of the electron pair and elimination of the fluorine atom (S_N2' reaction). Taking into account the discussion in Section III.2.a, the second pathway seems to be more probable.



The reaction of $C_{60}F_{18}$ with 2-naphthol affords naphtho[2,1-*b*]furano[*d*-1,2][60]fullerene as a by-product, which is formed as a result of complete defluorination of polyfluorofullerene.¹²⁵ The formation of this compound can be considered as evidence for the competitive single-electron transfer from naphthol to polyfluorofullerene. This process is not observed in the reaction of $C_{60}F_{18}$ with water, because water molecules are hard acids and non-polarisable nucleophiles and are rarely involved in electron transfer reactions. To the contrary, readily oxidisable 2-naphthol is much more prone to donate electrons to an appropriate acceptor.

The reaction of $C_{60}F_{18}$ with benzene in the presence of $SbCl_5$ afforded the expected $C_{60}F_{15}Ph_3$ product (3) along with two oxygen-containing derivatives.¹¹⁴ One of these products is fluoroxyfullerene $C_{60}F_{14}OFPh_3$ (10) (Fig. 12); the second, a mixture of oxahomo derivatives (intramolecular ethers) $C_{60}F_{14}O_2Ph_3$.

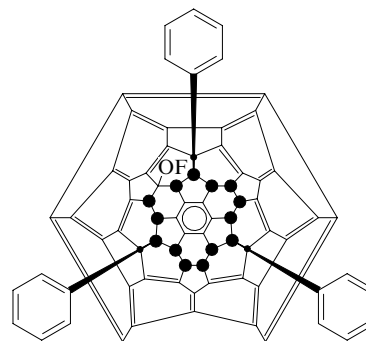


Figure 12. The Schlegel diagram of $C_{60}F_{14}OFPh_3$ (10).

Anomalous Bingel reaction. Since $C_{60}F_{18}$ can serve as a precursor for the formation of donor–acceptor dyads having stronger electron-withdrawing properties, attempts were made to involve this compound in reactions, which are generally used for the synthesis of analogous structures from C_{60} . The Bingel reaction is most often used for this purpose. This reaction involves the nucleophilic addition of the stabilised α -halocarbocation to the fullerene cage followed by the intramolecular substitution of the halogen atom to give methanofullerenes.^{126, 127}

However, it appeared that the reaction of diethyl bromomalonate with $C_{60}F_{18}$ in the presence of 1,8-diazabicyclo[5.4.0]undec-7-ene (DBU) proceeds by a mechanism different from the [2 + 1]-cycloaddition.¹² The reaction was found to give mono-, di- and trisubstitution products of diethyl bromomalonate groups for the fluorine atoms, *viz.*, the compounds $C_{60}F_{18-n}[CBr(CO_2Et)_2]_n$ ($n = 1–3$) (Fig. 13). The degree of substitution can be regulated by the rate of addition of the base.^{12, 128} Due to the presence of a leaving group (even a

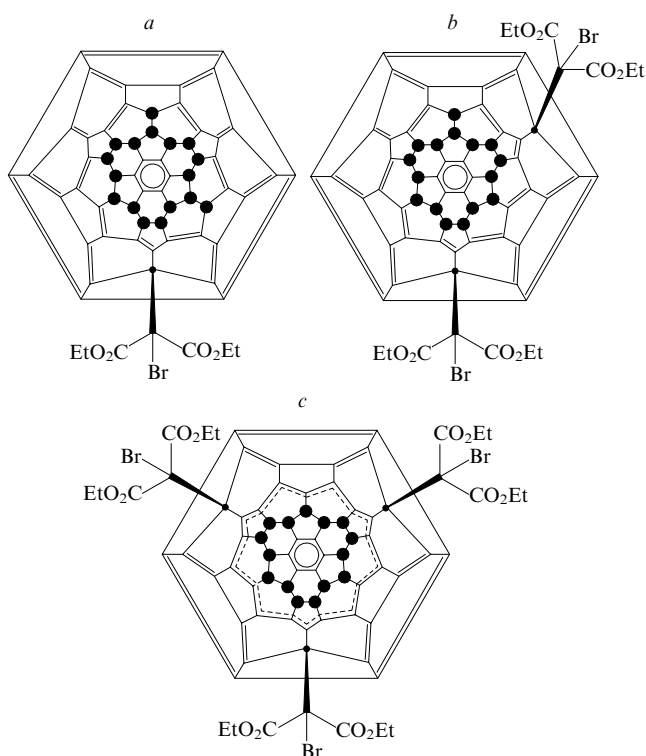
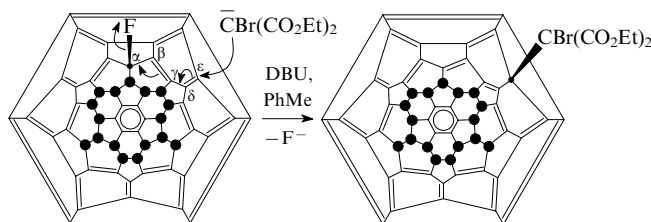


Figure 13. The Schlegel diagrams of $C_{60}F_{17}[CBr(CO_2Et)_2]$ (a), $C_{60}F_{16}[CBr(CO_2Et)_2]_2$ (b) and $C_{60}F_{15}[CBr(CO_2Et)_2]_3$ (11) (c).

poor leaving group, such as the fluoride anion) in fullerene, after the addition of the diethyl bromomalonate carbanion to the polyfluorofullerene cage the reaction proceeds not as cyclopropanation. This follows a pathway analogous to the S_N2' reaction considered above in the discussion of the formation of epoxides from polyfluorofullerenes in the presence of atmospheric moisture (see Section III.2.a).^{109, 110} The only difference is that the fluoride ion is eliminated as a result of the nucleophilic attack not on the γ -carbon atom, but on the more distant ε -carbon atom (to emphasise this fact, some authors used the notation S_N2'' mechanism, Scheme 2).^{12, 14, 129}

Scheme 2



Apparently, the attack of the bulky nucleophiles $-CBr(CO_2Et)_2$ on the γ -carbon atom (the S_N2' mechanism) is hindered due to steric effects caused by adjacent fluorine atoms. On the contrary, the attack on the ε -carbon atom (the S_N2'' mechanism) remote from fluorine atoms occurs without noticeable steric repulsions. As a result, one to three most sterically accessible fluorine atoms, which are adjacent to the double bond and are bound to carbon atoms bearing the largest positive charge are subjected to nucleophilic substitution in the $C_{60}F_{18}$ molecule. Semiempirical quantum chemical calculations by the AM1 and PM3 methods demonstrated¹²⁸ that among the carbon atoms of the $C_{60}F_{18}$ cage, the carbon atoms that lose fluorine atoms bear the largest positive charge. Of the fluorine atoms in the $C_{60}F_{18}$ molecule, the largest negative charges are accumulated on the leaving atoms.¹²⁸ Therefore, the reaction involves the successive replacement of three fluorine atoms and finally gives the trisubstituted product, which is not prone to further reactions.

The structure of the C_{3v} -symmetrical trisubstituted derivative $C_{60}F_{15}[CBr(CO_2Et)_2]_3$ (**11**) established by X-ray diffraction deserves special attention.¹² This compound is characterised by the presence of the equatorial [18]annulene belt (see Fig. 13 c). Since all double bonds involved in the belt are in *trans* configurations, this fragment is called [18]trannulene according to the term proposed in the early theoretical study.¹³⁰ An analysis of the C—C bond lengths in the [18]trannulene fragment in $C_{60}F_{15}[CBr(CO_2Et)_2]_3$ shows that these bonds are substantially equalised (the maximum difference is 0.018 Å) and vary from 1.392 to 1.410 Å. By contrast, these bonds in the starting $C_{60}F_{18}$ vary in a wider range (from 1.368 to 1.528 Å, *i.e.*, the difference is as large as 0.160 Å).³⁹

It should be noted that π -electron delocalisation in the [18]trannulene fragment resulting in the equalisation of the bond lengths can be explained as a result of the formation of a single aromatic π -system. However, commonly known aromatic systems are annulenes, in which C=C bonds are either in *cis* (for example, benzene), or *cis,trans* configurations (for example, [18]annulene). These conformations are more favourable because the π orbitals involved in aromatic conjugation are perpendicular to the plane of the annulene ring. Nevertheless, the possibility of the existence of aromatic systems, which are additionally stabilised due to overlap of the π orbitals lying in the $[n]$ annulene plane, has theoretically been predicted earlier.^{131, 132} In particular, it was theoretically demonstrated¹³⁰ that aromatic stabilisation can be achieved

by fixing the *trans* configuration of the $[n]$ annulene ring (*i.e.*, the formation of $[n]$ trannulene) upon its involvement in the molecular cage. The calculated geometry, energy and magnetic properties indicate that $[n]$ trannulenes obey the Hückel rule, *e.g.*, $(4n+2)$ π -electron systems are aromatic, whereas $4n$ π -electron systems are antiaromatic. Therefore, due to the rigid fullerene cage and the arrangement of the addends in the $C_{60}F_{15}[CBr(CO_2Et)_2]_3$ molecule, [18]annulene adopts the *trans* configuration, which satisfies the Hückel rule, resulting in aromatic conjugation. The aromaticity of the [18]trannulene fragment in the $C_{60}F_{15}[CBr(CO_2Et)_2]_3$ molecule leads to a slight bond-length alternation in this ring,^{12, 23} gives rise to the diamagnetic ring current induced by the external magnetic field¹³³ and leads to an increase in chemical stability of the $C_{60}F_{15}[CBr(CO_2Et)_2]_3$ molecule compared to the starting polyfluorofullerene $C_{60}F_{18}$.^{23, 110} Analogous [18]trannulene structural fragments were found in the fullerene derivatives $D_{3d}-C_{60}Cl_{30}$,⁹⁹ $S_6-C_{60}[CMe(CO_2Et)_6]$ and $S_6-C_{60}[CMe.(CO_2Bu^t)_6]$ synthesised more recently.¹³⁴ The mono- and disubstituted products $C_{60}F_{18-n}[CBr(CO_2Et)_2]_n$ ($n = 1$ or 2), unlike trisubstituted compound **11**, do not contain the [18]trannulene belt because of the presence of $C(sp^3)$ atoms disrupting the equatorial π -conjugation system (see Fig. 13 a,b).

Turning back to the discussion of the Bingel reaction mechanism, it should be noted that the formation of the [18]trannulene fragment is one of the factors responsible for the regiochemistry of nucleophilic substitution in $C_{60}F_{18}$. Actually, one of the three most activated fluorine atoms can be subjected to the nucleophilic displacement through the attack of a nucleophilic species both on the ε - and γ -carbon atoms (see Scheme 2). However, the formation of the aromatic [18]trannulene fragment is possible only upon the addition of a nucleophile at the ε -carbon atom, resulting in additional thermodynamic and kinetic stabilisation of the fullerene. After the formation of $C_{60}F_{15}[CBr(CO_2Et)_2]_3$, the fluorine atoms that remain in the molecule are separated from double bonds by aromatic π -systems of the benzenoid and [18]trannulene rings, which prevents further nucleophilic substitution.

The nucleophilic displacement of three fluorine atoms in the C_{1v} - and C_s - $C_{60}F_{18}O$ isomers by $-CBr(CO_2Et)_2$ anions afforded the corresponding [18]trannulenes, *viz.*, C_{1v} - and C_s - $C_{60}F_{15}O[CBr(CO_2Et)_2]_3$, and these products were characterised.¹²⁹ These results demonstrate that the presence of the oxygen atom in the molecule results in neither steric nor electronic effects hindering the formation of trannulenes.

The reactions of $C_{60}F_{18}$ with a large number of malonates $HCX(CO_2R)_2$, with different ester $[R = Me, Et, PhCH_2$ or $3,5-(MeO)_2C_6H_3CH_2]$ and acceptor groups $[X = F, Cl, Br, CN, CO_2Et, NO_2, P(O)(OMe)_2, SO_2CH_2Ph$ or $C(O)CH_2.(CH_2Ph)]$, were studied to elucidate the influence of the nature of substituents and the size of the $-CX(CO_2R)_2$ carbanion on the possibility of the synthesis of trannulenes.^{14, 23, 129}

Almost all known malonates [except for oxomalonate $HC(C(O)CH_2CH_2Ph)(CO_2Et)_2]$ were found to be involved in nucleophilic substitution reactions with $C_{60}F_{18}$. The inactivity of the oxomalonate under these conditions was attributed to the keto–enol tautomerism of the reagent.¹⁴ The anions derived from fluoro- and cyanomalonates do not form trannulenes; instead, they give mono- or disubstituted products, *viz.*, $C_{60}F_{17}[CF(CO_2Et)_2]$, $C_{60}F_{17}[C(CN)(CO_2Et)_2]$ and $C_{60}F_{16}.[C(CN)(CO_2Et)_2]_2$, in low yields. Based on the differences in the ^{19}F NMR spectra of the fullerene derivatives $C_{60}F_{17}[C(CN)(CO_2Et)_2]$ and $C_{60}F_{17}[CBr(CO_2Et)_2]$, it was concluded¹²⁸ that cyanomalonate reacts at the γ position, *i.e.*, by the S_N2' mechanism.¹⁴ However, it should be noted that the determination of the structure of $C_{60}F_{17}[C(CN)(CO_2Et)_2]$ only from ^{19}F NMR spectroscopic data is insufficiently reliable.

The reactions of $C_{60}F_{18}$ with $HC(SO_2CH_2Ph)(CO_2Et)_2$ and $HC[PO(OMe)_2](CO_2Et)_2$ afford trannulene-containing products in low yields.¹⁴ The reaction of phosphorus-containing malonate is accompanied by dephosphonylation giving rise to $C_{60}F_{15}[CH(CO_2Et)_2]_3$. This is confirmed by the absence of signals in the ^{31}P NMR spectrum and resonances of the methoxy groups in the 1H NMR spectra of the isolated product. Since potassium fluoride is known to induce dephosphonylation of tertiary phosphonates,¹³⁵ dephosphonylation of the trannulene belt is apparently initiated by fluoride anions generated in the reaction.¹⁴

Good yields of the corresponding trannulenes ($\sim 30\%$) were achieved in the reactions of $C_{60}F_{18}$ with $HCBBr(CO_2R)_2$, where $R = CH_2Ph$ ¹²⁹ or $CH_2C_6H_3(OMe)_2$,²³ or with $HCHX(CO_2Et)_2$, where $X = Cl$,¹²⁹ Br ,^{12, 128} CO_2Et or NO_2 .¹⁴ It should be noted that an increase in the bulk of the ester group leads to a decrease in the degree of substitution in $C_{60}F_{18}$. This can be overcome by increasing the malonate-to-fullerene ratio or introducing a bridge into malonate, resulting in an increase in the distance between the bulky substituent and the carbanionic centre.²³

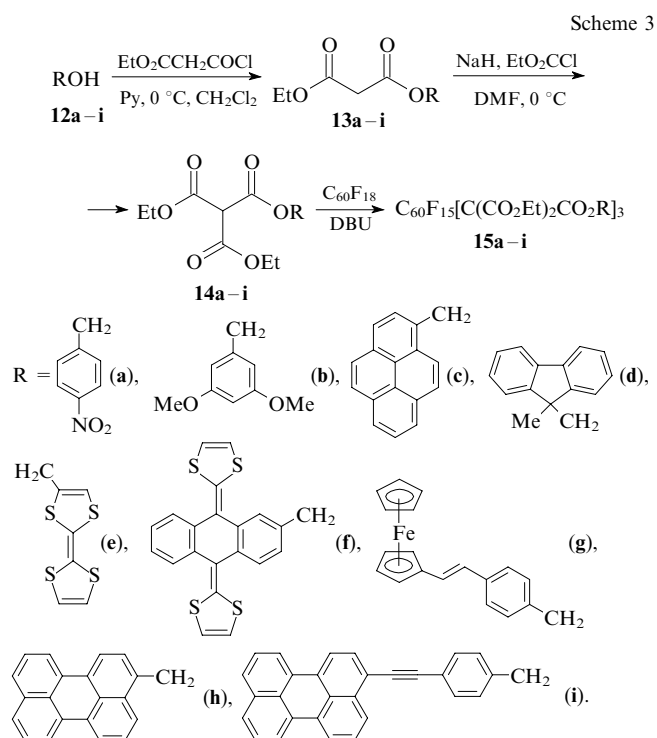
A series of trannulenes were synthesised by the reactions of $C_{60}F_{18}$ with methanetricarboxylates containing various photoactive functional groups.^{22, 23} Methanetricarboxylates serve as an attractive alternative to halo- and nitromalonates. The advantages of the latter compounds are low pK_a , high nucleophilicity of anions, the absence of the keto–enol tautomerism, a rather large steric demands and stability. To achieve the efficient formation of trannulenes from $C_{60}F_{18}$, CH-acids should meet these requirements.

The starting methanetricarboxylates can easily be synthesised from the corresponding alcohols (Scheme 3). Commercially available alcohols **12a–i** containing photoactive fragments were used. Treatment of these alcohols with ethyl malonyl chloride afforded the corresponding malonates **13a–i**, which were deprotonated and coupled with ethyl chloroformate to form methanetricarboxylates **14a–i**. Trannulenes **15a–i** were synthesised from methanetricarboxylates **14a–i** and $C_{60}F_{18}$.

The results of the above studies demonstrate that the larger the bulk of the substituent shielding the nucleophilic carbanionic centre, the larger the amount of methanetricarboxylate **14** required for the synthesis of trannulene. Attempts to use perylene ester **14h** for the synthesis of trannulene **15h** failed in spite of a variation of the reaction conditions over a wide range. In all cases, bis-adduct **16** was obtained as the major product due to the size of the perylene fragment (Scheme 4).

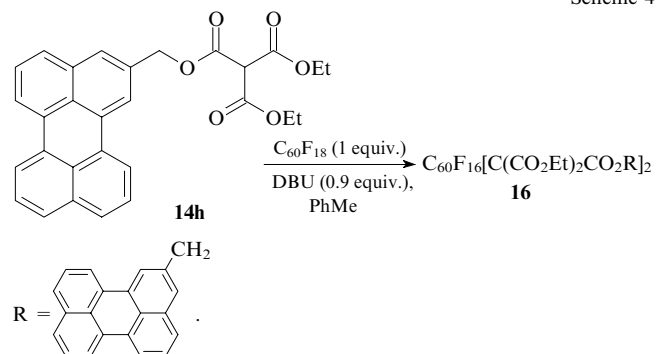
The steric barrier was overcome by removing the bulky fragment from the reaction centre after the introduction of the phenylacetylene bridge between the perylene moiety and the methanetricarboxylate group. For example, the reaction of ester **14i** with $C_{60}F_{18}$ in the presence of a base produces trannulene **15i** in 31% yield.

All compounds **15** are emerald-green, which is typical of fullerene trannulenes^{12, 23, 129, 134} due to intense absorption of the [18]trannulene fragment at 610–670 nm. In addition, the presence of this fragment leads to an increase in electron-withdrawing properties of the molecule, which is manifested in a substantial increase in the first potential of single-electron reversible reduction (from -0.005 to -0.10 V, CH_2Cl_2 , SCE)^{14, 22, 111} compared to that for $C_{60}F_{18}$ (-0.33 V, CH_2Cl_2 , SCE).¹⁰⁸ To summarise, fullerene trannulenes have better chromophoric properties, more efficiently stabilise the negative charge compared to traditional fullerene derivatives prepared by the Bingel reaction and retain low reorganisation energy for transition into the charge-separated state due to the rigid fullerene cage. Based on this fact, it was suggested that



Compound	14 : $C_{60}F_{18}$: DBU ratio	Yield of 15 (%)
a	1.0:1.0:1.0	41
b	1.6:1.0:1.3	34
c	1.6:1.0:1.3	28
d	1.6:1.0:1.3	33
e	1.5:1.0:1.0	28
f	1.8:1.0:1.7	26
g	1.6:1.0:1.3	28
h	2.0:1.0:1.7	traces
i	1.6:1.0:1.3	31

trannulene derivatives of $C_{60}F_{18}$ are promising molecular 'building blocks' for the design of components of single-electron devices, molecular switches and sensors.^{14, 22, 23, 136} In particular, studies of single-electron transfer in the tetrathiafulvalene–trannulene dyad demonstrated that these molecules can accumulate energy of photoexcitation in the long-lived (870 ns) charge-separated state.²² However, it should be borne in mind that the use of fullerene trannulenes as electron-withdrawing building blocks is sometimes complicated by considerable activation barriers to the transition into the charge-separated state.¹¹¹



In conclusion of this section, it should be noted that the anomalous Bingel reaction (synthesis of trannulenes) can be accompanied by the formation of classical cyclopropanation products. For example, the reaction of $C_{60}F_{18}$ with diethyl bromomalonate generated *in situ* (from diethyl malonate and CBr_4) in the presence of DBU affords the usual cyclopropanation product $C_1-C_{60}F_{18}C(CO_2Et)_2$ in low yield.¹²⁸ It was hypothesised that the classical Bingel reaction proceeds as a result of the attack of the carbanion on the fluorine-free fullerene hemisphere. In addition, the $C_{60}F_{16}C(CO_2Et)_2$ adduct, which was generated as a result of a loss of two fluorine atoms upon cyclopropanation, was detected. The formation of this compound was attributed to defluorination of $C_{60}F_{18}$ with a base.

3. Cycloaddition to lower polyfluoro[60]fullerenes

The development of efficient methods for the synthesis and isolation of lower polyfluorofullerenes in the individual state allowed investigation of a number of cycloaddition reactions, which are widely used for functionalisation of C_{60} .¹³⁷ On the one hand, the presence of a large number of the attached fluorine atoms in polyfluorofullerene molecules leads to a strong increase in the electron affinity of these compounds compared to C_{60} and, consequently, to an increase in their electron-withdrawing properties. On the other hand, the presence of large fluorine-free fragments of the fullerene cage in lower polyfluorofullerenes allows the cycloaddition reactions to proceed without substantial steric hindrance, which is unlikely in the case of higher polyfluorofullerenes. Therefore, lower polyfluorofullerenes would be expected to be involved in cycloaddition reactions analogously to C_{60} . Due to lower symmetry of polyfluorofullerenes, a larger number of isomeric products can be formed. In addition, the reactions with electron-donating reagents can be accompanied by competitive complete or partial defluorination of substrates.

a. [2 + 3]-Cycloaddition (the Prato reaction)

One of the most widely used methods for the fullerene cage functionalisation is based on the Prato reaction (annulation of the pyrrolidine ring by the reaction of fullerene with azomethine ylides derived from α -amino acid esters and carbonyl compounds).¹³⁸

The reaction of $C_{60}F_{18}$ with *N*-methylaminoacetic acid (sarcosine) and formaldehyde or benzaldehyde produced the corresponding fulleropyrrolidines, which were isolated and partially characterised by 1H and ^{19}F NMR spectroscopy.¹³⁹ It should be noted that, unlike the anomalous Bingel reaction,¹²⁸ the Prato reaction with $C_{60}F_{18}$ proceeds by a traditional pathway, no products of substitution or elimination of fluorine atoms being detected. Cycloaddition to the $C_{60}F_{18}$ molecule at the fluorine-free fullerene hemisphere affords mono- and bis-adducts.

To interpret the structures of the resulting cycloadducts, it is necessary to consider possible cycloaddition patterns of azomethine ylide at $C=C$ double bonds to form the pyrrolidine fragment. It is reasonable to exclude the double bonds involved in the benzenoid ring and the [5,6] bonds from consideration because the cycloaddition at these types of bonds reduces stabilisation due to aromatic conjugation and leads to an increase in strains in the fullerene cage. Consequently, the formation of a monoadduct can occur at one of four non-equivalent bonds, *a*, *b*, *c* or *d* (Fig. 14).

Two products prepared by annulation of the pyrrolidine ring to the $C_{60}F_{18}$ molecule (at the *a* and *c* bonds) should have C_s symmetry, whereas two other annulation products (the addition at the *b* and *d* bonds) are non-symmetrical. It is reasonable to suggest that steric hindrance does not allow the reaction to proceed at the *d* bond. Hence, the formation of three isomeric monoadducts would be expected; the bis-addi-

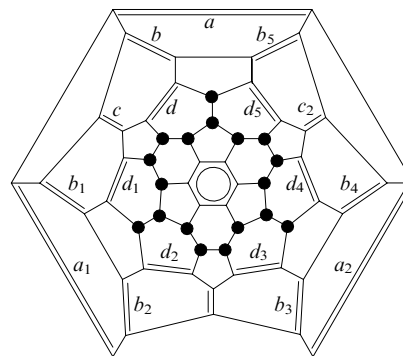


Figure 14. Possible cycloaddition sites in the $C_{60}F_{18}$ molecule.

tion would be expected to give five symmetrical and eight non-symmetrical bis-adducts.

Two monoadducts of three possible adducts were found experimentally (Fig. 15).¹³⁹ This reaction affords C_s -symmetrical monoadduct **17** as the major product as a result of the cycloaddition at the *a* bond most remote from the fluorine atoms. Non-symmetrical cycloadduct **18**, which is formed with the involvement of the *b* bond, is the minor product. The C_s -symmetrical cycloaddition product at the *c* bond was not detected in the reaction mixture. Apparently, the addition to this bond close to the flattened fragment of $C_{60}F_{18}$ leads to an increase in steric hindrance in the fullerene cage.

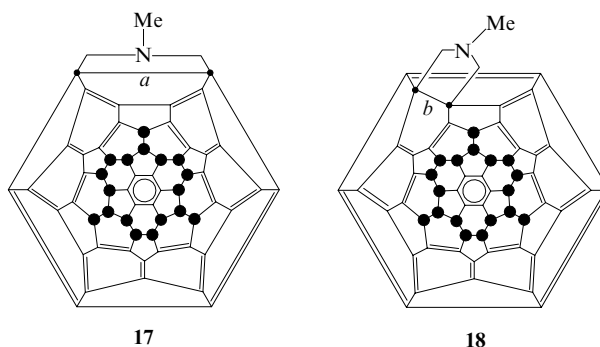


Figure 15. The Schlegel diagrams of the $C_{60}F_{18}(C_3H_7N)$ monoadducts.

Polycycloaddition products were also found, three C_s -symmetrical and four non-symmetrical bis-adducts being isolated. As in the case of monoadducts, the addition of azomethine ylide occurs predominantly at the *a* bond, whereas the addition products at the *c* and *d* bonds are absent. In other words, all bis-adducts are formed as a result of different cycloaddition patterns at the *a* and *b* bonds. For example, annulation of the pyrrolidine fragment at two *a* bonds (Fig. 16a) was proposed¹³⁹ for one of the C_s -symmetrical isomers, *viz.*, compound **19**. However, it should be noted that in this case the pyrrolidine rings are bound to one six-membered ring resulting in destabilisation of this isomer due to repulsion between these rings. Hence, it cannot be ruled out that C_s -symmetrical bis-adduct **19** is formed as a result of cycloaddition at the *b*₁, *b*₄ or *b*, *b*₁ bonds (see Fig. 16b). Unfortunately, no ^{13}C NMR spectroscopic data were reported.¹³⁹

The Prato reaction of $C_{60}F_{18}$ with sarcosine and benzaldehyde proceeds analogously to give a complex mixture of isomeric adducts.¹³⁹ Six major products and four minor

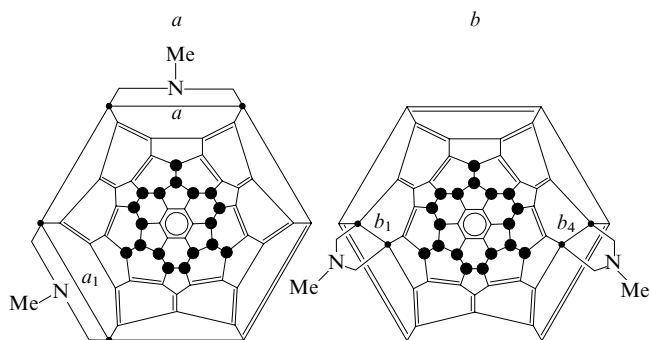


Figure 16. The Schlegel diagrams of two possible C_s -bis-adducts $C_{60}F_{18}(C_3H_7N)_2$ (**19**) (see the discussion in the text).

products were identified. These products were isolated in amounts insufficient for the structure elucidation.

Monoadduct **17** produced by the reaction of $C_{60}F_{18}$ with sarcosine and formaldehyde was unexpectedly detected in the reactions with other aldehydes.¹³⁹ This can be attributed to either the presence of an impurity of formaldehyde in sarcosine or the *in situ* formation of formaldehyde as a result of oxidation of sarcosine catalysed by fluorofullerene. The latter is evidenced by the fact that the major product (monoadduct) of the reaction of $C_{60}F_{18}$ with sarcosine and benzaldehyde is formed by refluxing a toluene solution of $C_{60}F_{18}$ with sarcosine in the absence of benzaldehyde in the reaction mixture! This result is attributed to the presence of traces of benzaldehyde in toluene (0.05%, HPLC data), the amount of which increases due to oxidation of toluene under the reaction conditions.

To summarize, the Prato reaction of lower polyfluorofullerenes is not accompanied by defluorination and produces complex isomeric mixtures of mono- and bis-adducts. The cycloaddition occurs predominantly at the sterically most accessible and fluorine-free fragment of the fullerene cage.

b. [2 + 4]-Cycloaddition reactions

Electron-deficient fullerene and its derivatives can be involved in the Diels–Alder reaction.^{140–142} Polyfluorofullerenes are no exception.^{13, 70} For example, refluxing of a toluene solution of $C_{60}F_{18}$ with anthracene under argon produced monocycloadducts **20** and **21**, which were isolated and partially characterised (in a ratio of 3:2, the total yield was 40%, Fig. 17).¹³ Anthraquinone was found among by-products. The latter compound was also detected in the reactions of anthracene with C_{60} and $C_{60}Cl_6$. Apparently, fullerene or its halogen derivatives either act as oxidants in these reactions or catalyse oxidation of anthracene.

In the electron ionisation mass spectra of **20** and **21**, the molecular ion peak is absent, but the spectra show ions corresponding to $C_{60}F_{18}$ and anthracene, which is evidence that thermodesorption is accompanied by the retro reaction. This process is also typical of cycloadducts of non-halogenated C_{60} .¹⁴²

The structures of monocycloadducts **20** and **21** were proposed based on the analysis of ¹H and ¹⁹F NMR spectroscopic data. In this case, as in the Prato reaction, defluorination products are not observed. The major C_s -symmetrical (**20**) and minor non-symmetrical (**21**) isomers are produced by cycloaddition at the *a* and *b* bonds, respectively (see Fig. 17). Quantum chemical calculations (by the semiempirical AM1 method) of the thermal effects of the Diels–Alder reactions of $C_{60}F_{18}$ with anthracene, butadiene or benzene confirmed that the cycloaddition at the *a* bond is more favourable and this adduct is more stable.¹⁴³ Cycloadducts **20** and **21** partially

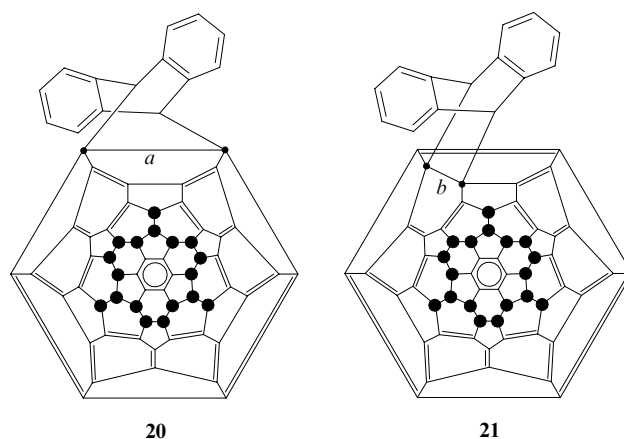


Figure 17. The Schlegel diagrams of monocycloadducts formed in the the Diels–Alder reaction of $C_{60}F_{18}$ with anthracene.

decompose on storage. For example, the degree of decomposition of major compound **20** after two weeks of storage at room temperature is 5.5%. Minor product **21** is much less stable. Virtually immediately after isolation of compound **21** from the reaction mixture, a considerable amount of anthracene was detected by ¹H NMR spectroscopy. Moreover, spontaneous isomerisation of minor product **21** was observed. As a result, compound **20** and a new cycloadduct were obtained. The ¹⁹F NMR spectroscopic study demonstrated that the latter compound has C_s symmetry although it differs from major product **20**. Apparently, this product is generated by the retro Diels–Alder reaction followed by cycloaddition at the *c* bond.

Fullerene $C_{60}F_{20}$ is another promising substrate for cycloaddition reactions. Due to high D_{5d} symmetry of the $C_{60}F_{20}$ molecule, the monoadduct can be formed as a result of cycloaddition to one of two non-equivalent [6,6] bonds (see Fig. 1 g). Since the approach of the reagent to one of these bonds is sterically hindered, the only cycloadduct would be formed.

The [2 + 4]-cycloaddition reaction of anthracene with polyfluorofullerene $C_{60}F_{20}$ was demonstrated⁷⁰ to proceed only under illumination and in the presence of dissolved oxygen. Oxidised non-symmetrical cycloadduct **22** was obtained in a yield of <40%. The structure of this product was proposed based on ¹H and ¹⁹F NMR spectra (Fig. 18). The 'normal' C_s -symmetrical cycloadduct of anthracene and $C_{60}F_{20}$ was detected as an impurity.

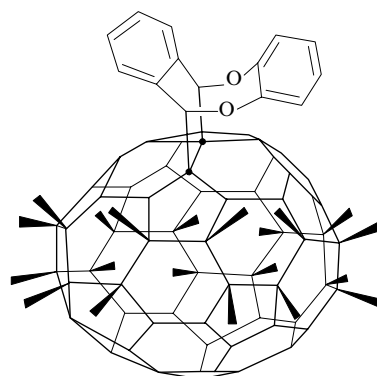
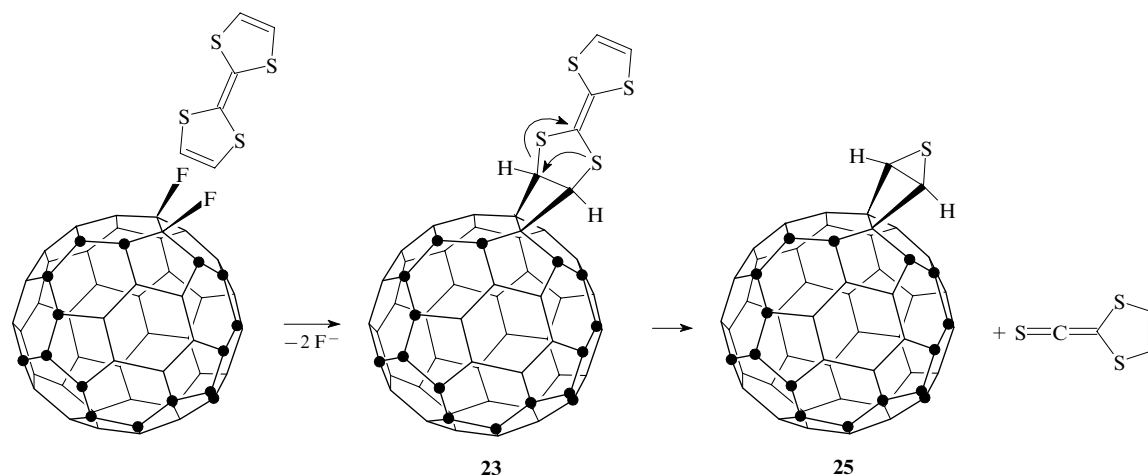


Figure 18. Structure of cycloadduct **22** (for clarity, the C–F bonds are represented as stereobonds).

Scheme 5



4. Miscellaneous reactions

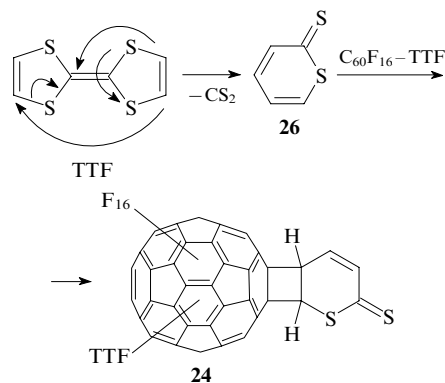
a. Unusual cycloaddition reactions

The use of tetrathiafulvalene (TTF) as an electron donor plays an important role in studies on the photoinduced electron transfer involving fullerene. Attempts to perform the reaction of $C_{60}F_{18}$ with tetrathiafulvalene led to the discovery of the previously unknown cycloaddition reaction.¹⁵ Concentration of a solution of $C_{60}F_{18}$ and tetrathiafulvalene in toluene afforded products **23** and **24**. The non-symmetrical [$C_{60}F_{16}$ -tetrathiafulvalene] adduct (**23**) was obtained as the major product (Scheme 5).

Apparently, this reaction involves at least two steps. Initially, $C_{60}F_{18}$ undergoes partial defluorination due to the redox reaction of $C_{60}F_{18}$ with tetrathiafulvalene. Indeed, dehalogenation of $C_{60}Cl_6$, $C_{60}Br_6$ or $C_{60}Br_8$ with tetrathiafulvalene has been documented earlier,¹⁴⁴ although the reaction products were not isolated and characterised. Intermediate polyfluorofullerene $C_{60}F_{16}$ exhibits high reactivity with respect to tetrathiafulvalene and gives the [2 + 2]-cycloaddition product.

Storage of product **23** leads to its rearrangement to form two compounds with identical molecular masses. The unstable minor adduct was not studied in detail. Major adduct **25**, which is formed upon elimination of the thioketene fragment from derivative **23**, is a new type of fullerene derivatives, *viz.*, thiirano[2,3-*a*]cyclobuta[*c*-1,2]fullerene.

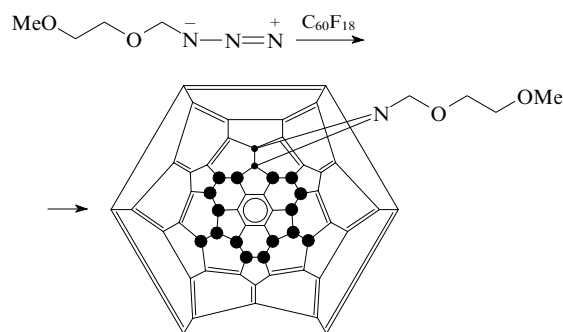
The structure of compound **24** was determined by ¹H NMR spectroscopy and electron ionisation mass spectrometry. In this bis-adduct, unsaturated dithiolactone **26** generated from tetrathiafulvalene by elimination of CS_2 serves as the second addend (Scheme 6).



TTF is tetrathiafulvalene.

An analogous replacement of two fluorine atoms is also observed in the reaction of $C_{60}F_{18}$ with 2-methoxyethoxy-

methyl azide.¹⁴⁵ The reactions of non-modified C_{60} with azides (in particular, with 2-methoxyethoxymethyl azide) generally produce open-cage fulleroid adducts, *viz.*, azahomofullerenes, upon the [2 + 3]-cycloaddition of the azide followed by extrusion of N_2 (see, for example, Ref. 146). As in many above-considered examples, the use of polyfluorofullerenes as the substrate substantially changes the reaction pathway because of the ease of a loss of fluorine atoms giving rise to aziridino-polyfluorofullerene $C_{60}F_{16}N(CH_2OCH_2CH_2OMe)$.



b. Radical reactions

Fullerenes are readily involved in radical addition reactions.²⁵ In particular, the reactions of C_{60} with molecular fluorine^{1, 11, 43} and with radical species generated *in situ* by decomposition of peroxides,¹⁴⁷ alkyl and perfluoroalkyl iodides,^{6, 148} metal trifluoroacetates,¹⁴⁹ *etc.* were documented.

Polyfluorofullerenes are also involved in radical addition reactions but they are less reactive than fullerene. As mentioned above, fluorination of C_{60} with molecular fluorine proceeds by a radical mechanism. Evidently, fluorination of lower polyfluorofullerenes by fluorine also proceeds by a radical mechanism. The transformation of $C_{60}F_{36}$ into $C_{60}F_{48}$ is an example of such reactions.⁶⁴ As was discussed in Section II.1.a, further fluorination occurs under more drastic conditions due to steric strains and is accompanied by decomposition of the fullerene cage.^{11, 58}

The formation of the mixed compounds $C_{60}F_x(R^F)_y$ ($R^F = CF_3$ or C_2F_5), which were detected in the reaction of C_{60} with high oxidation state metal fluorides, is yet another interesting example.^{45, 82, 150} The 1,9- and 1,7- $C_{60}FCF_3$, C_1 - $C_{60}F_5CF_3$,^{150, 151} C_1 - $C_{60}F_7CF_3$ (see Refs 45, 46 and 150) and C_s - $C_{60}F_{17}C_2F_5$ isomers and three isomers of $C_{60}F_{17}CF_3$, *viz.*, one C_s -symmetrical isomer (65% of the total amount) and a pair of C_1 enantiomers (35%),^{82, 152} were isolated from these reaction mixtures by HPLC. The structures of the compounds

Scheme 6

were proposed based on ^{19}F NMR spectroscopic data and results of quantum chemical calculations. It should be noted that $\text{C}_{60}\text{F}_{17}\text{CF}_3$ has initially been considered¹⁵² as the difluoromethanofullerene derivative $\text{C}_{60}\text{F}_{18}\text{CF}_2$. However, more recent X-ray diffraction study demonstrated⁸² that this compound is an analogue of $\text{C}_{60}\text{F}_{18}$, with the only difference that one of the sterically most accessible fluorine atoms is replaced by the CF_3 group.

In a number of studies,^{36, 82, 152} it was hypothesised that mixed fluoro- and perfluoroalkyl derivatives are generated through the insertion of the difluorocarbene $:\text{CF}_2$ into polyfluorofullerene at C–F bonds. The origin of difluorocarbene is attributed to thermal destruction of polyfluorofullerenes. This reaction can proceed analogously to the insertion of methylene into the C_{60} molecule upon hydrogenation¹⁵³ with the only difference that the methylene group is inserted at the double bond of fullerene, whereas difluoromethylene is inserted at the C–F bond. However, it should be noted that the more probable pathway of the formation of perfluoroalkylated fullerene derivatives involves the addition of the $\cdot\text{CF}_3$ or $\cdot\text{C}_2\text{F}_5$ radicals that are generated upon thermal destruction of polyfluorofullerenes to fullerene or its fluorination products. Actually, these radicals were detected upon decomposition of polyfluorofullerenes.^{8, 58, 154, 155} Convincing evidence for the formation of mixed derivatives in the reaction of [60]fullerene with $\cdot\text{CF}_3$ was reported.⁶⁷ It was demonstrated that the independent generation of the $\cdot\text{CF}_3$ radicals at the moment of fluorination of fullerene with K_2PtF_6 gives rise predominantly to mixed fluoro and CF_3 derivatives of fullerene with the compositions $\text{C}_{60}\text{F}_{18-n}(\text{CF}_3)_n$ and $\text{C}_{60}\text{F}_{20-m}(\text{CF}_3)_m$ ($n = 1-5$, $m = 1-6$).

IV. Reactions of polychloro[60]fullerenes

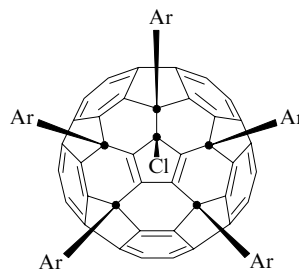
Until recently, C_{60}Cl_6 has been the only polychlorofullerene that was available in preparative amounts in high purity form.⁸⁹ Because of this, the reactions of polychlorofullerenes were studied in most detail for this compound. Higher chlorides, for example, $\text{C}_{60}\text{Cl}_{24}$,¹⁰⁰ $\text{C}_{60}\text{Cl}_{28}$ (Ref. 74) and two isomers of $\text{C}_{60}\text{Cl}_{30}$, were synthesised and isolated in the individual state.⁹⁹ This will help in studying their reactivity in detail and synthesising new derivatives of the fullerene series.

1. Arylation of polychlorofullerenes

Polychlorofullerenes readily enter the Friedel–Crafts reaction.² For example, ^1H and ^{13}C NMR spectroscopic studies demonstrated that stirring of a benzene solution of C_{60}Cl_n with catalytic amounts of AlCl_3 at room temperature for 2 h leads to the formation of polyphenylfullerenes (according to mass-spectrometric data, up to 22 phenyl groups are attached).

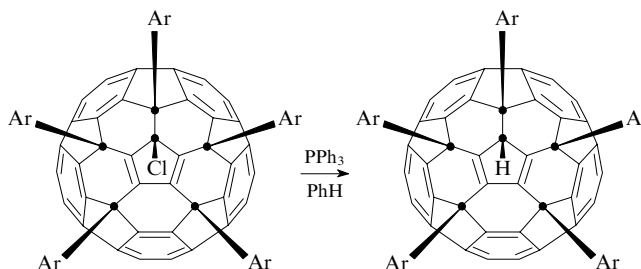


The Friedel–Crafts reaction of fullerene C_{60}Cl_6 with various aromatic substrates was studied in detail.^{156–158} The reactions of C_{60}Cl_6 with arenes in the presence of FeCl_3 were demonstrated to give the corresponding C_s -symmetrical aryl derivatives $\text{C}_{60}\text{Ar}_5\text{Cl}$ in yields ranging from 48% (Ar is thienyl) to 63% (Ar = 4- FC_6H_4). The reaction with toluene proceeds both at the *para* and *ortho* positions. The reactions with anisole and fluorobenzene gave exclusively *para*-substituted products, which were isolated and completely characterised.¹⁵⁷ The replacement of chlorine atoms by aryl groups at the same positions as those occupied by chlorine atoms in C_{60}Cl_6 , indicates that the reaction proceeds through the cationic fullerene intermediate.



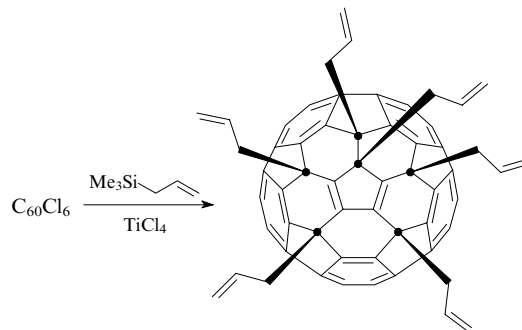
Ar = XC_6H_4 (X = H, Me, MeO, Bu^t, F, Me₃Si), thienyl.

In a more recent detailed study¹⁵⁸ of the reaction of C_{60}Cl_6 with fluorobenzene in the presence of FeCl_3 , the major product [$\text{C}_{60}(4\text{-FC}_6\text{H}_4)_5\text{Cl}$] was detected along with two C_s -symmetrical isomers of 1,4-(4- FC_6H_4)₂ C_{60} , one non-symmetrical isomer of $\text{C}_{60}(4\text{-FC}_6\text{H}_4)_4$ and a small amount of $\text{C}_{60}(4\text{-FC}_6\text{H}_4)_4\text{H}_2$. The following scheme was proposed for the explanation of the formation of the latter compound. Initially, two chlorine atoms are replaced by a hydrogen atom, which is most likely generated from the solvent. The resulting intermediate enters the Friedel–Crafts reaction with fluorobenzene.¹⁵⁹ The substitution of hydrogen for chlorine atoms was also observed in the reaction of $\text{C}_{60}\text{Ar}_5\text{Cl}$ with triphenylphosphine.¹⁵⁷



Ar = 4- FC_6H_4 .

The steric hindrance in C_{60}Cl_6 , which is the presently known bulkiest electrophile, plays an important role. For example, no reaction occurs with sterically hindered mesitylene.¹⁵⁸ At the same time, reagents with lower steric demands can replace all six chlorine atoms. For example, the reaction of C_{60}Cl_6 with an excess of allyltrimethylsilane in the presence of TiCl_4 produces hexaallylfullerene $\text{C}_{60}(\text{CH}_2\text{CH}=\text{CH}_2)_6$ in good yield.¹⁶⁰



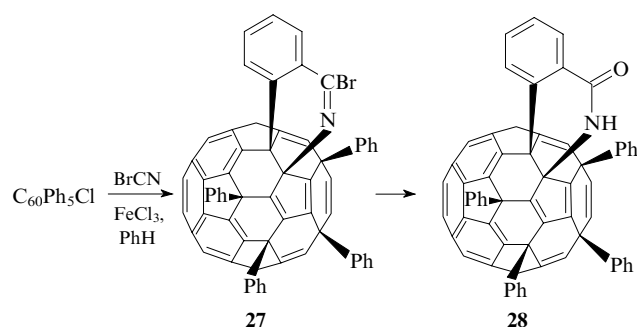
In this case, the steric factors are less significant, which facilitates the complete replacement of chlorine atoms. The pentasubstituted compound $\text{C}_{60}(\text{CH}_2\text{CH}=\text{CH}_2)_5\text{Cl}$ was isolated as a minor reaction product.

A comparative study of the geometry and electronic structures of the compounds $C_{60}Cl_6$, $C_{60}Ph_5Cl$ and $C_{60}Ph_5H$ by quantum chemical calculations (the AM1 method) demonstrated that the nature of functional groups has no noticeable effect on the bond lengths in the fullerene cage (the difference in the lengths of the analogous C—C bonds is at most 0.01 Å).¹⁶¹ For these derivatives, the addition of functional groups leads to a loss of the icosahedral (I_h) symmetry, cleavage of five carbon–carbon double bonds and the appearance of the isolated cyclopentadienyl fragment. The C—C bonds involving sp^3 -hybridised carbon atoms (1.50–1.55 Å) are longer than those in C_{60} . The 1H NMR spectroscopic study revealed free rotation of the phenyl groups at room temperature. This is consistent with the results of calculations by the AM1 method, according to which there is a large number of conformations in a narrow energy range. Therefore, the molecules $C_{60}Ph_5Cl$ and $C_{60}Ph_5H$ are ‘pseudo- C_s -symmetrical’.¹⁵⁶

Calculations of the Mulliken charges illustrated the almost neutral character of chlorine atoms relative to the fullerene cage in $C_{60}Cl_6$ and a weak donor character of the phenyl groups in $C_{60}Ph_5Cl$ and $C_{60}Ph_5H$. Each phenyl group in these compounds donates, on the average, 0.038 (in $C_{60}Ph_5Cl$) and 0.02 electrons (in $C_{60}Ph_5H$) to the carbon cage. The hydrogen atom bound directly to the fullerene cage acts as a strong donor (+0.217 e) and the chlorine atom, as a weak acceptor (−0.044 e). Unlike $C_{60}Ph_5H$, in which the negative charge is almost uniformly distributed over the functionalised fragment, the total charge in $C_{60}Ph_5Cl$ (0.150 e) donated by the addends is mainly redistributed to the intact part of the cage (−0.143 e).

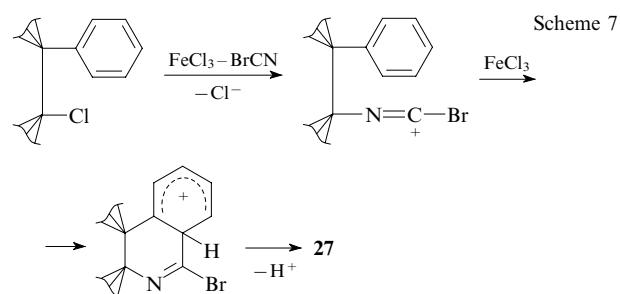
Due to a combination of the aryl substituents and the reactive chlorine atom in the molecules $C_{60}Ar_5Cl$, the latter can be used as the starting compounds for further functionalisation.^{162, 163} For example, a new pathway of spontaneous oxidation of $C_{60}Ph_5X$ ($X = H$ or Cl) to the benzofuran derivative of C_{60} , in which the oxygen atom forms a bridge between the carbon cage and one of the benzene rings, was found (see Section IV.2).¹⁶³

The treatment of $C_{60}Ph_5Cl$ with cyanogen bromide allows the annulation of the quinoline fragment onto the fullerene cage.¹⁶² The reaction is accompanied by a loss of the chlorine atom and the formation of the bromine-substituted CN bridge between the carbon cage and the *ortho* position of the adjacent benzene ring to form 1-bromoisoquinoline derivative **27**.



The structure of this derivative was confirmed by the synthesis of amide **28** by the nucleophilic substitution of a hydroxy group for the bromine atom.¹⁶² Like the other amides, compound **28** is poorly soluble and crystallises from benzene as orange-red plates.

The proposed¹⁶² mechanism of the formation of compound **27** (Scheme 7) is based on the experimental facts that the reaction does not proceed in the absence of $FeCl_3$ and that $C_{60}(4-FC_6H_4)_5Cl$ does not undergo this transformation. The dependence of the process on the presence of a strong Lewis acid is indicative of the involvement of a carbocationic intermediate in this reaction. In this case, the intermediate



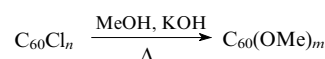
can be generated in the reaction of $FeCl_3$ with either $C_{60}Ph_5Cl$ or $BrCN$.

It should be noted that if the complex of $BrCN$ with iron(III) chloride were an intermediate of this reaction, an electrophile would be formed and the latter would attack the phenyl group in $C_{60}Ph_5Cl$ predominantly at the most accessible *para* or (taking into account the electron-withdrawing character of the fullerene substituent) *meta* position. However, the absence of these products in the reaction mixture suggests that the transformation of $C_{60}Ph_5Cl$ into product **27** proceeds by a different mechanism involving the formation of the $C_{60}Ph_5^+$ cation.

Due to considerable steric hindrance, the $C_{60}Ph_5^+$ cation cannot react with the phenyl group of another $C_{60}Ph_5Cl$ molecule, but can react with the small $BrCN$ molecule at the nitrogen atom. Then the electrophilic attack of the resulting iminium cation on the adjacent phenyl group occurs. The strong electron-withdrawing properties of fullerene hinder the electrophilic substitution in the aryl moiety bound to the fullerene cage. Nevertheless, high electrophilicity of the bromoiminium cation and the intramolecular character of the reaction (the entropy factor) do make this cyclisation possible.¹⁶⁴ In $C_{60}(4-FC_6H_4)_5Cl$, the electronegative fluorine atom is in the *meta* position to the site of attack and has a negative inductive effect, which makes the electrophilic attack even more difficult. In combination with the electron-withdrawing effect of the fullerene cage, this is sufficient for deactivation of the benzene ring even toward the intramolecular attack by the iminium electrophile.

2. Nucleophilic substitution reactions

Polychlorofullerenes are sensitive to hydrolysis and readily react with nucleophiles.² For example, the reaction of a mixture of polychlorofullerenes with excess KOH under reflux in methanol produced polymethoxyfullerenes, the most substituted product containing 26 methoxy groups (mass spectrometric data).²



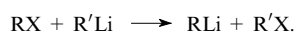
This reaction proceeds simultaneously with partial hydroxylation of the substrate.

The reaction of a benzene solution of $C_{60}Cl_6$ with sodium alkoxide in the corresponding alcohol ROH ($R = Me, Et$) produces $C_{60}(OR)_5Cl$ in moderate yields (15%–20%).¹⁶⁵ The reaction proceeds rather rapidly under reflux, but several days are required for its completion at room temperature. The reaction of $C_{60}Cl_6$ with EtO^- yields $1,4-(EtO)_2C_{60}$ as a by-product. Therefore, the substitution reaction is competitive with elimination of chlorine atoms. When $C_{60}Cl_6$ is heated with an alcohol in the absence of alkoxide ions, which are stronger nucleophiles, dechlorination becomes the main reaction. For example, the reaction of a benzene solution of $C_{60}Cl_6$ with methanol or isopropyl alcohol under reflux for 140 h produces $1,4-(MeO)_2C_{60}$ or $1,4-(Pr^iO)_2C_{60}$ in 11%–30% yields.¹⁶⁵ The

reaction of $C_{60}Cl_6$ with secondary aliphatic amines gives 1,4-diaminofullerenes (in 5%–20% yields) and an inseparable mixture of tetra- and hexaaminofullerenes.¹⁶⁶

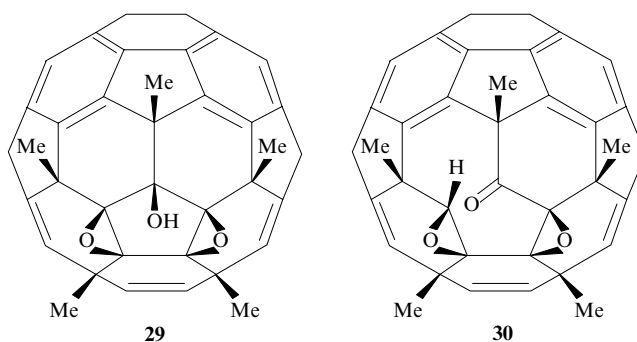
The reaction of $C_{60}Cl_6$ with an excess of methylolithium in a THF–cumene mixture at room temperature affords a complex mixture of products.¹⁶⁷ The completely alkylated derivative $C_{60}Me_6$ and chloropentamethylfullerene $C_{60}Me_5Cl$ are among the major reaction products. Since the arrangement of the addends typical of $C_{60}Cl_6$ is retained in these compounds, it was hypothesised that the reaction involves the frontal replacement of chlorine atoms by nucleophilic species. However, as mentioned above, we are doubtful about this mechanism.

As discussed above, the reactions of higher polyfluorofullerenes with nucleophiles proceed by the S_N2' mechanism. This mechanism is also possible for the transformation of $C_{60}Me_5Cl$ into $C_{60}Me_6$. However, it is inconsistent with the retention of the arrangement of the addends upon the transformation of $C_{60}Cl_6$ into $C_{60}Me_5Cl$, since it is known that alkylolithium compounds are involved in exchange reactions with alkyl halides rather than give coupling products. Presumably, the transformation of $C_{60}Cl_6$ into $C_{60}Me_5Cl$ involves the halogen–metal exchange step:



This process was found to partly proceed in the reaction of phenyllithium with polyfluorofullerenes,¹⁰⁷ as evidenced by the presence of a certain amount of fluorobenzene as one of by-products. It is also known^{168–173} that alkali metal fullerenes smoothly react with alkyl halides to form the corresponding alkylfullerenes.

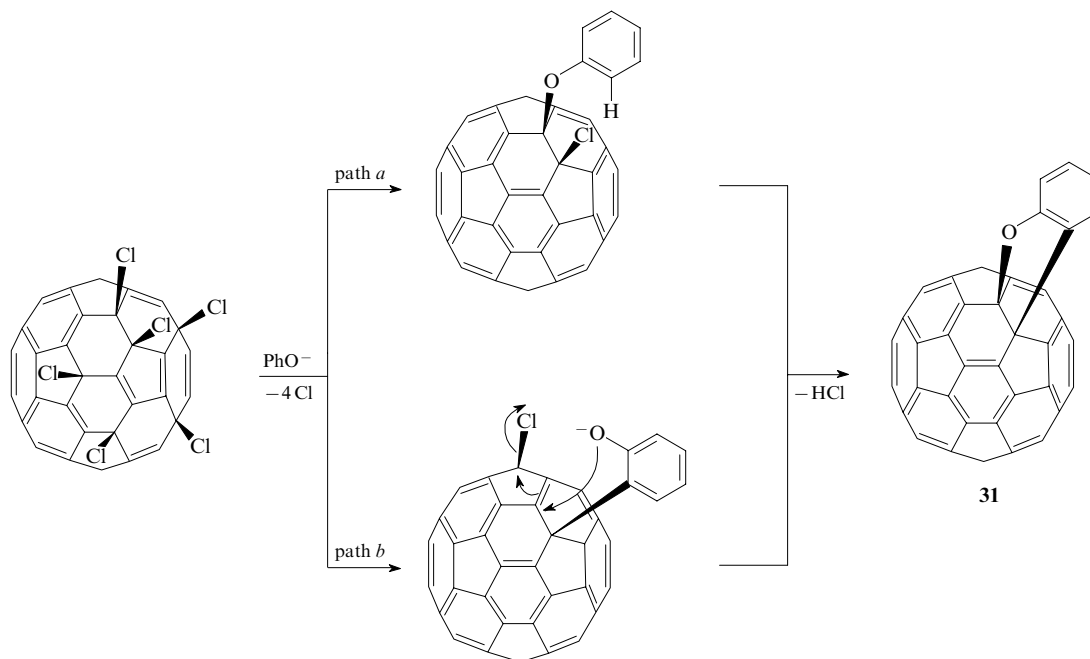
The compound $C_{60}Me_5Cl$ readily undergoes hydrolysis and oxidation.^{165, 167, 174, 175} In the presence of atmospheric oxygen, epoxides with the compositions $C_{60}Me_5(O)OH$, $C_{60}Me_5O_2OH$ and $C_{60}Me_5O_3H$ were obtained. The X-ray diffraction study showed that the hydroxy group in the molecule $C_{60}Me_5O_2OH$ (**29**) occupies the position of the chlorine atom in the molecule $C_{60}Me_5Cl$, and two oxygen atoms form epoxide functions attached at the double bonds of the butadiene fragment in the five-membered ring.¹⁷⁴



The compound $C_{60}Me_5O_3H$ (**30**) isomeric to bis(epoxy)fullerenol **29** is bis-epoxy ketone containing the open-cage fullerene, and compounds **29** and **30** undergo interconversions through the 1,3-tautomeric shift of the hydrogen atom of the hydroxy group.¹⁷⁵ It should be noted that the compounds $C_{60}Ph_5Cl$ and $C_{60}Ph_3H$ containing a truncated pentagonal pyramidal fragment undergo oxidation too. The high reactivity of this fragment is apparently attributed to a high π -electron density on the double bonds.¹⁷⁶ The tendency of these oxygen-containing compounds to undergo decarbonylation during thermolysis, which can lead to an opening of the fullerene cage, is an important but, unfortunately, poorly studied characteristic feature of such compounds.^{158, 167, 174}

The reactions of $C_{60}Cl_6$ with phenols (PhOH, 4-FC₆H₄OH or 4-MeOC₆H₄OH) and aniline in the presence of water and KOH represent an unusual example of the nucleophilic displacement of chlorine atoms followed by cyclisation.¹⁷⁷ The reactions with phenol or its substituted analogues produce benzofuran derivatives **31** (Scheme 8), while aniline gives indolofullerene. It should be noted that, although the reaction can lead to the nucleophilic displacement of several chlorine atoms by phenoxy or anilino groups, only one of these groups undergoes cyclisation to give a heterocyclic (benzofuran or indole) functional group. Other chlorine atoms are either eliminated or are subjected to the nucleophilic substitution without the ring formation. It was demonstrated that thiophene, being a weak nucleophile, does not react, and the

Scheme 8



reaction rate increases in the series $\text{PhOH} < 4\text{-FC}_6\text{H}_4\text{OH} < 4\text{-MeOC}_6\text{H}_4\text{OH} < \text{PhNH}_2$ in accordance with an increase in the nucleophilicity of the reagent.

It was hypothesised¹⁷⁷ that a derivative with a chlorine atom bound to the fullerene cage in the *ortho* position with respect to the arene group, is formed as an intermediate in this reaction, and cyclisation occurs as a result of a loss of the *ortho*-hydrogen atom of the aromatic ring and the chlorine atom (see Scheme 8, path *a*).¹⁷⁷ In our opinion, it is more probable that this reaction involves the initial nucleophilic attack on the polychlorofullerene cage by the *ortho*-carbon atom of the phenoxide ion followed by the substitution of the phenoxide for the chlorine atom (see Scheme 8, path *b*) according to one of the above-considered nucleophilic substitution mechanisms.

V. Reactions of polybromo[60]fullerenes

Unlike reactions of polyfluoro and polychloro derivatives of fullerenes, chemical transformations of polybromofullerenes have not been adequately studied because the use of the latter as synthons is limited by their poor solubility and instability in most of organic solvents.⁸⁹ For example, dissolution of C_{60}Br_6 in chloroform, dichloromethane, 1,2-dichlorobenzene, carbon disulfide or cyclohexane is accompanied by its complete decomposition into C_{60} and Br_2 .^{103, 144} Disproportionation of C_{60}Br_6 giving rise to C_{60} and C_{60}Br_8 upon dissolution in organic solvents was also documented.^{5, 103} Decomposition of C_{60}Br_8 to the starting fullerene and molecular bromine occurs upon heating in organic solvents to 70–80 °C, whereas $\text{C}_{60}\text{Br}_{24}$ does not decompose even upon prolonged refluxing in 1,2-dichlorobenzene (180 °C).¹⁰³ Therefore, thermal stability of polybromofullerenes in organic solvents increases in the series $\text{C}_{60}\text{Br}_6 < \text{C}_{60}\text{Br}_8 < \text{C}_{60}\text{Br}_{24}$, which is consistent with the thermogravimetric data for crystalline polybromofullerenes.¹⁰² Thermal decomposition of polybromofullerenes under an inert atmosphere or under vacuum leads to molecular bromine and C_{60} fullerene. In the presence of oxygen, this process is accompanied by the formation of fullerene oxides, which, under these conditions, are readily involved in the cycloaddition reaction to form difullerenofuran derivatives.¹⁷⁸ It should be noted that thermolysis of polybromofullerenes in the presence of oxygen affords rather easily fullerene oxides. On the contrary, C_{60} fullerene is involved in these reactions only in the presence of strong oxidising agents, *e.g.*, ozone or peroxides, or as a result of photochemical or electrochemical reactions.^{179, 180}

Like other halogen derivatives of fullerenes, polybromofullerenes enter the Friedel–Crafts reaction with arenes catalysed by AlBr_3 or similar Lewis acids.^{2, 181} The reactions of $\text{C}_{60}\text{Br}_{24}$ with benzene, toluene or fluorobenzene in the presence of AlBr_3 produce polyarene derivatives C_{60}Ar_n ($n = 2–16$; $\text{Ar} = \text{Ph}$, MeC_6H_4 or FC_6H_4).¹⁸¹ In the presence of organic electron donors of the tetrathiafulvalene series, C_{60}Br_6 and C_{60}Br_8 undergo debromination accompanied by the formation of C_{60} and the donor radical cation.¹⁴⁴

The reaction of polybromofullerene $\text{C}_{60}\text{Br}_{24}$ with methanolic KOH produces a complex mixture of polymethoxyfullerenes $\text{C}_{60}(\text{OMe})_n$ ($n = 2–26$).¹⁸¹ The treatment of polybromofullerenes with aqueous alkalis or aqueous dioxane leads to their complete hydrolysis to form fullerlenols with complex composition.¹⁸² In the case of aqueous dioxane, the substitution of bromine atoms in fullerenes C_{60}Br_8 and $\text{C}_{60}\text{Br}_{24}$ is the main reaction giving rise to compounds of compositions similar to $\text{C}_{60}(\text{OH})_{10}$ and $\text{C}_{60}(\text{OH})_{26}$, respectively. In reactions with aqueous alkalis, the nucleophilic substitution of bromine atoms is accompanied by the additional attachment of hydroxy groups to the fullerene cage to give fullerlenols containing a large number of hydroxy groups, whatever the composition of the starting polybromofullerene. An elemental analysis

demonstrated that alkali metal fullerlenolates are present among the products obtained by alkaline hydrolysis of polybromofullerenes. This fact accounts for higher solubility of these fullerlenols in water compared to fullerlenols prepared according to other procedures. It should be noted that pH of aqueous solutions of alkali metal fullerlenolates is close to neutral, which is typical of salts of strong acids. This is apparently due to the strong electronegative nature of the fullerene cage functionalised by a large number of electron-withdrawing hydroxy groups.

It was demonstrated that polybromofullerenes react with silver trifluoroacetate upon heating in aromatic hydrocarbons.¹⁸² In the case of C_{60}Br_8 and $\text{C}_{60}\text{Br}_{24}$, the compounds with the compositions $\text{C}_{60}(\text{CF}_3\text{COO})_{2–3}(\text{OH})_{6–5}$ and $\text{C}_{60}(\text{CF}_3\text{COO})_{2–4}(\text{OH})_{6–7}$ were obtained as the major products. It can be seen that the compositions of the resulting compounds do not correlate with the number of the replaced bromine atoms. The formation of hydroxy derivatives was attributed to high sensitivity of the intermediates to atmospheric moisture. However, the products do not undergo further hydrolysis in the presence of HCl . Analogously, phosphorylation of $\text{C}_{60}\text{Br}_{24}$ and C_{60}Br_6 in THF by $(\text{EtO})_2\text{P}(\text{OLi})$ leads to the addition of up to six diethoxyphosphoryl groups $\text{PO}(\text{OEt})_2$ to the fullerene cage.¹⁸¹

The selective substitution of bromine atoms in polybromofullerenes is exemplified by the reactions of $\text{C}_{60}\text{Br}_{24}$ with SbCl_5 (or with KICl_4) at 140–150 °C^{74, 100} and with XeF_2 in liquid anhydrous HF at room temperature.⁵⁰ In both cases, the $T_h\text{-C}_{60}\text{Cl}_{24}$ and $T_h\text{-C}_{60}\text{F}_{24}$ compounds isostructural to the starting polybromofullerene were obtained as the major products. Polychlorofullerenes, in turn, can be transformed into $T_h\text{-C}_{60}\text{Br}_{24}$ by the reactions with liquid bromine.⁷³ In earlier studies,^{71, 183} attempts have also been made to replace bromine and chlorine atoms by fluorine; however, individual compounds have not been obtained.

It should be noted that, according to quantum chemical calculations, fullerene $T_h\text{-C}_{60}\text{F}_{24}$ is thermodynamically unstable and can undergo disproportionation to $\text{C}_{60}\text{F}_{18}$ and $\text{C}_{60}\text{F}_{36}$. Apparently, that is why this compound was not isolated from products of high-temperature syntheses of polyfluorofullerenes under thermodynamic control.^{34, 183} However, $T_h\text{-C}_{60}\text{F}_{24}$ can be synthesised by the reaction of $\text{C}_{60}\text{Br}_{24}$ with XeF_2 under mild conditions, which is evidence for its kinetic stability to further rearrangements. Unfortunately, the mechanism of this reaction remains unknown and it can only be hypothesised that the reaction involves the concerted $\text{Br}–\text{F}$ exchange at the sp^3 -carbon atom or(and) a sequence of addition and elimination reactions.⁵⁰ It cannot be ruled out that the reaction of $\text{C}_{60}\text{Br}_{24}$ with XeF_2 is of the radical cation nature, analogously to that assumed for fluorination of bromopentafluorobenzene $\text{C}_6\text{F}_5\text{Br}$ or bromotetrafluorobenzenes $\text{C}_6\text{F}_4\text{HBr}$ with xenon difluoride in liquid HF.^{184, 185} The reaction of benzene derivatives with XeF_2 is not accompanied by debromination, which is apparently associated with a higher $\text{C}–\text{Br}$ bond energy in these compounds. In the case of polybromofullerenes, in which the bromine atoms are bound to tertiary carbon atoms and cause steric strain in the cage, the $\text{C}–\text{Br}$ bond energy is substantially lower, resulting in elimination of bromine atoms. Nevertheless, mixed compounds with the composition $\text{C}_{60}\text{F}_{25}\text{Br}$ were detected among the reaction products of $\text{C}_{60}\text{Br}_{24}$ with XeF_2 . Therefore, under these conditions, not only the substitution of fluorine for bromine atoms, but also the addition of fluorine atoms to the fullerene cage is observed.

* * *

We thank Professor L N Sidorov for helpful discussion and valuable advice, which have stimulated the writing of this review.

This review has been written with the financial support of the Federal Agency for Science and Innovations of the Russian Federation (Contract No. 02.120.11.80.2) and the Russian Foundation for Basic Research (Project No. 06-03-32942).

References

1. J H Holloway, E G Hope, R Taylor, G J Langley, A G Avent, T J Dennis, J P Hare, H W Kroto, D R M Walton *J. Chem. Soc., Chem. Commun.* 966 (1991)
2. G A Olah, I Bucsi, C Lambert, R Aniszfeld, N J Trivedi, D K Sensharma, G K S Prakash *J. Am. Chem. Soc.* **113** 9385 (1991)
3. H Selig, C Lifshitz, T Peres, J E Fischer, A R McGhie, W J Romanow, J P McCauley Jr, A B Smith III *J. Am. Chem. Soc.* **113** 5475 (1991)
4. F N Tebbe, J Y Becker, D B Chase, L E Firment, E R Holler, B S Malone, P J Krusic, E Wasserman *J. Am. Chem. Soc.* **113** 9900 (1991)
5. P R Birkett, P B Hitchcock, H W Kroto, R Taylor, D R M Walton *Nature (London)* **357** 479 (1992)
6. P J Fagan, B Chase, J C Calabrese, D A Dixon, R Harlow, P J Krusic, N Matsuzawa, F N Tebbe, D L Thorn, E Wasserman *Carbon* **30** 1213 (1992)
7. F N Tebbe, R L Harlow, D B Chase, D L Thorn, G C Campbell Jr, J C Calabrese, N Herron, R J Young Jr, E Wasserman *Science* **256** 822 (1992)
8. A A Tuinman, P Mukherjee, J L Adcock, R L Hettich, R N Compton *J. Phys. Chem.* **96** 7584 (1992)
9. G E Scuseria *Chem. Phys. Lett.* **176** 423 (1991)
10. J Cioslowski *Chem. Phys. Lett.* **181** 68 (1991)
11. A A Tuinman, A A Gakh, J L Adcock, R N Compton *J. Am. Chem. Soc.* **115** 5885 (1993)
12. X-W Wei, A D Darwish, O V Boltalina, P B Hitchcock, J M Street, R Taylor *Angew. Chem., Int. Ed.* **40** 2989 (2001)
13. A G Avent, O V Boltalina, J M Street, R Taylor, X-W Wei *J. Chem. Soc., Perkin Trans. 2* 994 (2001)
14. G A Burley, A G Avent, O V Boltalina, T Drewello, I V Gol'dt, M Marcaccio, D Paolucci, F Paolucci, J M Street, R Taylor *Org. Biomol. Chem.* 2015 (2003)
15. A D Darwish, A G Avent, O V Boltalina, I Gol'dt, I V Kuvychko, T Da Ros, J M Street, R Taylor *Chem. – Eur. J.* **9** 2008 (2003)
16. K Ohkubo, R Taylor, O V Boltalina, S Ogo, S Fukuzumi *Chem. Commun.* 1952 (2002)
17. O V Boltalina, A V Streletsii, I N Ioffe, P Hvelplund, B Liu, S B Nielsen, S Tomita *J. Chem. Phys.* **122** 021102 (2005)
18. A A Popov, J Tarábek, I E Kareev, S F Lebedkin, S H Strauss, O V Boltalina, L Dunsch *J. Phys. Chem. A* **109** 9709 (2005)
19. N Liu, Y Morio, F Okino, H Touda, O V Boltalina, V K Pavlovich *Synth. Met.* **86** 2289 (1997)
20. C Jin, R L Hettich, R N Compton, A Tuinman, A Derecskei-Kovacs, D Marynick, B I Dunlap *Phys. Rev. Lett.* **73** 2821 (1994)
21. F Zhou, G J Van Berkel, B T Donovan *J. Am. Chem. Soc.* **116** 5485 (1994)
22. G A Burley, A G Avent, O V Boltalina, I V Gol'dt, D M Guldi, M Marcaccio, F Paolucci, D Paolucci, R Taylor *Chem. Commun.* 148 (2003)
23. G A Burley, A G Avent, I V Gol'dt, P B Hitchcock, H Al-Matar, D Paolucci, F Paolucci, P W Fowler, A Soncini, J M Street, R Taylor *Org. Biomol. Chem.* 319 (2004)
24. A M Lebedev, K A Menshikov, V G Stankevich, N Yu Svechnikov, A V Ryzkov, O V Boltalina, I V Gol'dt, I A Kamenskikh, L N Sidorov *Nucl. Instrum. Methods Phys. Res., Sect. A* **543** 221 (2005)
25. L N Sidorov, M A Yurovskaya, A Ya Borshchevskii, I V Trushkov, I N Ioffe *Fullereny (Fullerenes) (Moscow: Ekzamen, 2004)*
26. A Hirsch, M Brettreich *Fullerenes* (Weinheim: Wiley-VCH, 2005)
27. Q Zhu, D E Cox, J E Fischer, K Kniaz, A R McGhie, O Zhou *Nature (London)* **355** 712 (1992)
28. M Kobayashi, Y Akahama, H Kawamura, H Shinohara, H Sato, Y Saito *Solid State Commun.* **81** 93 (1992)
29. R Taylor *Izv. Akad. Nauk, Ser. Khim.* 852 (1998)^a
30. R Taylor *Chem. – Eur. J.* **7** 4074 (2001)
31. O V Boltalina, N A Galeva *Usp. Khim.* **69** 661 (2000) [Russ. Chem. Rev. **69** 609 (2000)]
32. L N Sidorov, O V Boltalina *Usp. Khim.* **71** 611 (2002) [Russ. Chem. Rev. **71** 535 (2002)]
33. O V Boltalina *J. Fluorine Chem.* **101** 273 (2000)
34. R Taylor *J. Fluorine Chem.* **125** 359 (2004)
35. A Yu Lukonin, V Yu Markov, O V Boltalina *Vestn. Mosk. Univ., Ser. 2, Khim.* **42** 3 (2001)^b
36. R Taylor *C.R. Chim.* **9** 982 (2006)
37. O V Boltalina, V Yu Markov, R Taylor, M P Waugh *Chem. Commun.* 2549 (1996)
38. I S Neretin, K A Lyssenko, M Yu Antipin, Yu L Slovokhotov, O V Boltalina, P A Troshin, A Yu Lukonin, L N Sidorov, R Taylor *Angew. Chem., Int. Ed.* **39** 3273 (2000)
39. I V Gol'dt, O V Boltalina, L N Sidorov, E Kemnitz, S I Troyanov *Solid State Sci.* **4** 1395 (2002)
40. O V Boltalina, J M Street, R Taylor *J. Chem. Soc., Perkin Trans. 2* 649 (1998)
41. P B Hitchcock, R Taylor *Chem. Commun.* 2078 (2002)
42. A G Avent, B W Clare, P B Hitchcock, D L Kepert, R Taylor *Chem. Commun.* 2370 (2002)
43. A A Gakh, A A Tuinman, J L Adcock, R A Sachleben, R N Compton *J. Am. Chem. Soc.* **116** 819 (1994)
44. S I Troyanov, P A Troshin, O V Boltalina, I N Ioffe, L N Sidorov, E Kemnitz *Angew. Chem., Int. Ed.* **40** 2285 (2001)
45. O V Boltalina, A D Darwish, J M Street, R Taylor, X-W Wei *J. Chem. Soc., Perkin Trans. 2* 251 (2002)
46. A A Goryunkov, I E Kareev, I N Ioffe, A A Popov, I V Kuvychko, V Yu Markov, I V Gol'dt, A S Pimenova, M G Serov, S M Avdoshenko, P A Khavrel, L N Sidorov, S F Lebedkin, Z Mazej, B Žemva, S H Strauss, O V Boltalina *J. Fluorine Chem.* **127** 1423 (2006)
47. A G Avent, O V Boltalina, A Yu Lukonin, J M Street, R Taylor *J. Chem. Soc., Perkin Trans. 2* 1359 (2000)
48. O V Boltalina, V Yu Markov, P A Troshin, A D Darwish, J M Street, R Taylor *Angew. Chem., Int. Ed.* **40** 787 (2001)
49. A A Popov, A A Goryunkov, I V Gol'dt, I V Kuvychko, W-D Hunnius, K Seppelt, S H Strauss, O V Boltalina *J. Phys. Chem. A* **108** 11449 (2004)
50. N I Denisenko, S I Troyanov, A A Popov, I V Kuvychko, B Žemva, E Kemnitz, S H Strauss, O V Boltalina *J. Am. Chem. Soc.* **126** 1618 (2004)
51. J M Street, B W Clare, D L Kepert, R Taylor *J. Phys. Chem. B* **108** 19228 (2004)
52. A A Goryunkov, V Yu Markov, O V Boltalina, B Žemva, A K Abdul-Sada, R Taylor *J. Fluorine Chem.* **112** 191 (2001)
53. N S Chilingarov, A V Nikitin, J V Rau, I V Golyshevsky, A V Kepman, F M Spiridonov, L N Sidorov *J. Fluorine Chem.* **113** 219 (2002)
54. I V Golyshevsky, A Ya Borschevsky, N S Chilingarov, J V Rau, A V Kepman, L N Sidorov *J. Fluorine Chem.* **126** 785 (2005)
55. A V Kepman, V F Sukhoverkhov, A Tressaud, C Labrugere, E Durand, N S Chilingarov, L N Sidorov *J. Fluorine Chem.* **127** 832 (2006)
56. J H Holloway, E G Hope, G J Langley, R Taylor, A G Avent, T J Dennis, J P Hare, H W Kroto, D R M Walton *J. Fluorine Chem.* **58** 257 (1992)
57. R Taylor, G J Langley, J H Holloway, E G Hope, A K Brisdon, H W Kroto, D R M Walton *J. Chem. Soc., Perkin Trans. 2* 181 (1995)
58. A A Gakh, A A Tuinman *J. Phys. Chem. A* **104** 5888 (2000)
59. V F Bagryantsev, A S Zapol'skii, O V Boltalina, N A Galeva, L N Sidorov *Zh. Neorg. Khim.* **45** 1121 (2000)^c
60. O V Boltalina, A Ya Borschevskii, L N Sidorov, J M Street, R Taylor *Chem. Commun.* 529 (1996)
61. P A Troshin, O V Boltalina, N V Polyakova, Z E Klinkina *J. Fluorine Chem.* **110** 157 (2001)
62. A A Gakh, A A Tuinman *Tetrahedron Lett.* **42** 7133 (2001)

63. A G Avent, R Taylor *Chem. Commun.* 2726 (2002)
64. A A Gakh, A A Tuinman *Tetrahedron Lett.* **42** 7137 (2001)
65. A A Gakh, A Y Romanovich, A Bax *J. Am. Chem. Soc.* **125** 7902 (2003)
66. A B Kornev, P A Troshin, A S Peregudov, Z E Klinkina, N V Polyakova, R N Lyubovskaya *Mendeleev Commun.* **16** 157 (2006)
67. O V Boltalina, A A Goryunkov, V Yu Markov, I N Ioffe, L N Sidorov *Int. J. Mass Spectrom.* **228** 807 (2003)
68. G Gigli, G Balducci, V Yu Markov, O V Boltalina, A A Goryunkov, L N Sidorov, R Taylor *J. Chem. Thermodyn.* **34** 57 (2002)
69. P A Troshin, A B Kornev, A S Peregudov, S A Baskakov, R N Lyubovskaya *J. Fluorine Chem.* **126** 1559 (2005)
70. A G Avent, O V Boltalina, J M Street, R Taylor, P A Troshin, X-W Wei *Fullerenes, Nanotubes, Carbon Nanostruct.* **10** 227 (2002)
71. A J Adamson, J H Holloway, E G Hope, R Taylor *Fullerene Sci. Technol.* **5** 629 (1997)
72. N F Yudanov, A V Okotrub, L G Bulusheva, I P Asanov, V I Lisoivan, Yu V Shevtsov *Mol. Mater.* **7** 127 (1998)
73. P A Troshin, S A Baskakov, Yu M Shulga, R N Lyubovskaya *Fullerenes, Nanotubes, Carbon Nanostruct.* **12** 159 (2004)
74. S I Troyanov, N B Shustova, A A Popov, L N Sidorov *Izv. Akad. Nauk, Ser. Khim.* 1608 (2005)^a
75. J P B Sandall, P W Fowler *Org. Biomol. Chem.* 1061 (2003)
76. O V Boltalina, A Yu Lukonin, A G Avent, J M Street, R Taylor *J. Chem. Soc., Perkin Trans. 2* 683 (2000)
77. J M Street, T Drewello, Yu V Vasil'ev, O V Boltalina, R Taylor *Fullerenes, Nanotubes, Carbon Nanostruct.* **12** 753 (2004)
78. A G Avent, O V Boltalina, P W Fowler, A Yu Lukonin, V K Pavlovich, J P B Sandall, J M Street, R Taylor *J. Chem. Soc., Perkin Trans. 2* 1319 (1998)
79. O V Boltalina, B de La Vaissière, P W Fowler, A Yu Lukonin, A K Abdul-Sada, J M Street, R Taylor *J. Chem. Soc., Perkin Trans. 2* 2212 (2000)
80. O V Boltalina, B de La Vaissière, P W Fowler, P B Hitchcock, J P B Sandall, P A Troshin, R Taylor *Chem. Commun.* 1325 (2000)
81. O V Boltalina, B de La Vaissière, A Yu Lukonin, P W Fowler, A K Abdul-Sada, J M Street, R Taylor *J. Chem. Soc., Perkin Trans. 2* 550 (2001)
82. O V Boltalina, P B Hitchcock, P A Troshin, J M Street, R Taylor *J. Chem. Soc., Perkin Trans. 2* 2410 (2000)
83. S I Troyanov, O V Boltalina, I V Kuvytko, P A Troshin, E Kemnitz, P B Hitchcock, R Taylor *Fullerenes, Nanotubes, Carbon Nanostruct.* **10** 243 (2002)
84. Yu A Makeev, Candidate Thesis in Chemical Sciences, M V Lomonosov Moscow State University, Moscow, 2002
85. P A Troshin, Yu A Mackeyev, N V Chelovskaya, Yu L Slovokhotov, O V Boltalina, L N Sidorov *Fullerene Sci. Technol.* **8** 501 (2000)
86. K Kniaz, J E Fischer, H Selig, G B M Vaughan, W J Romanow, D M Cox, S K Chowdhury, J P McCauley, R A Strongin, A B Smith III *J. Am. Chem. Soc.* **115** 6060 (1993)
87. O V Boltalina, A K Abdul-Sada, R Taylor *J. Chem. Soc., Perkin Trans. 2* 981 (1995)
88. W A Scrivens, J M Tour *J. Chem. Soc., Chem. Commun.* 1207 (1993)
89. P R Birkett, A G Avent, A D Darwish, H W Kroto, R Taylor, D R M Walton *J. Chem. Soc., Chem. Commun.* 1230 (1993)
90. P R Birkett, A G Avent, A D Darwish, H W Kroto, R Taylor, D R M Walton *J. Chem. Soc., Chem. Commun.* 683 (1995)
91. I V Kuvytko, A V Streletskii, A A Popov, S G Kotsiris, T Drewello, S H Strauss, O V Boltalina *Chem. – Eur. J.* **11** 5426 (2005)
92. Yu V Vasil'ev, A V Streletskii, I V Kuvytko, O V Boltalina, P R Birkett, E E B Campbell, M V Korobov, T Drewello *Int. J. Mass Spectrom.* **228** 979 (2003)
93. G A Olah, I Bucsi, C Lambert, R Aniszfeld, N J Trivedi, D K Sengharia, G K S Prakash *J. Am. Chem. Soc.* **113** 9387 (1991)
94. P A Troshin, O Popkov, R N Lyubovskaya *Fullerenes, Nanotubes, Carbon Nanostruct.* **11** 165 (2003)
95. N B Shustova, D Yu Chernyshev, S I Troyanov *Mendeleev Commun.* **16** 209 (2006)
96. B W Clare, D L Kepert *J. Mol. Struct. (THEOCHEM)* **621** 211 (2003)
97. K Priyadarsini, H Mohan, P R Birkett, J P Mittal *J. Phys. Chem.* **100** 501 (1996)
98. P A Troshin, A Lapin'ski, A Bogucki, M Polomska, R N Lyubovskaya *Carbon* **44** 2770 (2006)
99. P A Troshin, R N Lyubovskaya, I N Ioffe, N B Shustova, E Kemnitz, S I Troyanov *Angew. Chem., Int. Ed.* **44** 234 (2005)
100. N B Shustova, A A Popov, L N Sidorov, A Turnbull, E Kemnitz, S I Troyanov *Chem. Commun.* 1411 (2005)
101. S I Troyanov, P A Troshin, O V Boltalina, E Kemnitz *Fullerenes, Nanotubes, Carbon Nanostruct.* **11** 61 (2003)
102. P A Troshin, D Kolesnikov, A V Burtsev, R N Lyubovskaya, N I Denisenko, A A Popov, S I Troyanov, O V Boltalina *Fullerenes, Nanotubes, Carbon Nanostruct.* **11** 47 (2003)
103. P A Troshin, E Kemnitz, S I Troyanov *Izv. Akad. Nauk, Ser. Khim.* 2675 (2004)^a
104. A V Streletskii, I N Ioffe, S G Kotsiris, M P Barrow, T Drewello, S H Strauss, O V Boltalina *J. Phys. Chem. A* **109** 714 (2005)
105. A V Streletskiy, P Hvelplund, S B Nielsen, B Liu, S Tomita, A A Goryunkov, O V Boltalina *J. Chem. Phys.* **124** 144306 (2006)
106. T Drewello, H Frauendorf, R Herzschuh, A A Goryunkov, S H Strauss, O V Boltalina *Chem. Phys. Lett.* **405** 93 (2005)
107. A A Gakh, A A Tuinman, J L Adcock, R N Compton *Tetrahedron Lett.* **34** 7167 (1993)
108. D Paolucci, F Paolucci, M Marcaccio, M Carano, R Taylor *Chem. Phys. Lett.* **400** 389 (2004)
109. A G Avent, A K Abdul-Sada, B W Clare, D L Kepert, J M Street, R Taylor *Org. Biomol. Chem.* 1026 (2003)
110. B W Clare, D L Kepert, R Taylor *Org. Biomol. Chem.* 3618 (2003)
111. D M Guldi, M Marcaccio, F Paolucci, D Paolucci, J Ramey, R Taylor, G A Burley *J. Phys. Chem. A* **109** 9723 (2005)
112. O V Boltalina, R Taylor, J M Street *Chem. Commun.* 1827 (1998)
113. A D Darwish, A G Avent, A K Abdul-Sada, I V Gol'dt, P B Hitchcock, I V Kuvytko, R Taylor *Chem. – Eur. J.* **10** 4523 (2004)
114. A D Darwish, A G Avent, I V Gol'dt, J M Street, R Taylor *J. Fluorine Chem.* **125** 1131 (2004)
115. R Taylor, J H Holloway, E G Hope, A G Avent, G J Langley, T J Dennis, J P Hare, H W Kroto, D R M Walton *J. Chem. Soc., Chem. Commun.* 665 (1992)
116. R Taylor, A G Avent, T J Dennis, J P Hare, H W Kroto, D R M Walton, J H Holloway, E G Hope, G J Langley *Nature (London)* **355** 27 (1992)
117. R Taylor, G J Langley, A K Brisdon, J H Holloway, E G Hope, H W Kroto, D R M Walton *J. Chem. Soc., Chem. Commun.* 875 (1993)
118. O V Boltalina, J H Holloway, E G Hope, J M Street, R Taylor *J. Chem. Soc., Perkin Trans. 2* 1845 (1998)
119. M N Glukhovtsev, A Pross, H B Schlegel, R D Bach, L Radom *J. Am. Chem. Soc.* **118** 11258 (1996)
120. I V Trushkov *Ros. Khim. Zh.* **38** (6) 45 (1994)^d
121. I V Trushkov, V V Zhdankin, A S Koz'min, N S Zefirov *Tetrahedron Lett.* **21** 3199 (1990)
122. I V Trushkov, N D Chuvylkin, A S Koz'min, N S Zefirov *New J. Chem.* **17** 161 (1993)
123. E T Mickelson, R H Hauge, J L Margrave *J. Fluorine Chem.* **92** 59 (1998)
124. G A Olah *Friedel-Crafts and Related Reactions* (New York: Wiley-Interscience, 1963)
125. A D Darwish, A G Avent, J M Street, R Taylor *Org. Biomol. Chem.* 1764 (2003)
126. C Bingel *Chem. Ber.* **126** 1957 (1993)
127. C Bingel, H Schiffer *Liebigs Ann.* 1551 (1995)
128. X-W Wei, A G Avent, O V Boltalina, A D Darwish, P W Fowler, J P B Sandall, J M Street, R Taylor *J. Chem. Soc., Perkin Trans. 2* 41 (2002)

129. A D Darwish, I V Kuvychko, X-W Wei, O V Boltalina, I V Gol'dt, J M Street, R Taylor *J. Chem. Soc., Perkin Trans. 2* 1118 (2002)
130. A A Fokin, H Jiao, P v R Schleyer *J. Am. Chem. Soc.* **120** 9364 (1998)
131. J Chandrasekhar, E D Jemmis, P G R Schleyer *Tetrahedron Lett.* **20** 3707 (1979)
132. P v R Schleyer, H Jiao, M N Glukhovtsev, J Chandrasekhar, E Kraka *J. Am. Chem. Soc.* **116** 10129 (1994)
133. G A Burley, P W Fowler, A Soncini, J P B Sandall, R Taylor *Chem. Commun.* 3042 (2003)
134. T Canteenwala, P A Padmawar, L Y Chiang *J. Am. Chem. Soc.* **127** 26 (2005)
135. A Thenappan, D J Burton *J. Org. Chem.* **56** 273 (1991)
136. G A Burley *Angew. Chem., Int. Ed.* **44** 3176 (2005)
137. M A Yurovskaya, I V Trushkov *Izv. Akad. Nauk, Ser. Khim.* 343 (2002)^a
138. M Prato, M Maggini, C Giacometti, G Scorrano, G Sandona, G Farnia *Tetrahedron* **52** 5221 (1996)
139. X-W Wei, A G Avent, O V Boltalina, J M Street, R Taylor *J. Chem. Soc., Perkin Trans. 2* 47 (2002)
140. K Komatsu, Y Murata, N Sugita, K Takeuchi, T S M Wan *Tetrahedron Lett.* **34** 8473 (1993)
141. J A Schlueter, J M Seaman, S Taha, H Cohen, K R Lykke, H H Wang, J M Williams *J. Chem. Soc., Chem. Commun.* 972 (1993)
142. M Tsuda, T Ishida, T Nogami, S Kuroono, M Ohashi *J. Chem. Soc., Chem. Commun.* 1296 (1993)
143. J P B Sandall, P W Fowler, R Taylor *J. Chem. Soc., Perkin Trans. 2* 1718 (2002)
144. Y Yoshida, A Otsuka, O O Drozdova, G Saito *J. Am. Chem. Soc.* **122** 7244 (2000)
145. G A Burley, A D Darwish, J M Street, R Taylor *Tetrahedron Lett.* **45** 3617 (2004)
146. J Zhou, A Rieker, T Grösser, A Skieba, A Hirsch *J. Chem. Soc., Perkin Trans. 2* 1 (1997)
147. L Gan, S Huang, X Zhang, A Zhang, B Cheng, H Cheng, X Li, G Shang *J. Am. Chem. Soc.* **124** 13384 (2002)
148. P J Fagan, P J Krusic, C N McEwen, J Lazar, D H Parkert, N Herron, E Wasserman *Science* **262** 404 (1993)
149. I S Uzikh, E I Dorozhkin, O V Boltalina, A I Boltalin *Dokl. Akad. Nauk* **379** 344 (2001)^e
150. I E Kareev, G S Quinões, I V Kuvychko, P A Khavrel, I N Ioffe, I V Gol'dt, S F Lebedkin, K Seppelt, S H Strauss, O V Boltalina *J. Am. Chem. Soc.* **127** 11497 (2005)
151. A G Avent, O V Boltalina, A A Goryunkov, A D Darwish, V Yu Markov, R Taylor *Fullerenes, Nanotubes, Carbon Nanostruct.* **10** 235 (2002)
152. A G Avent, O V Boltalina, A Yu Lukonin, J M Street, R Taylor *J. Chem. Soc., Perkin Trans. 2* 1 (2000)
153. A D Darwish, A K Abdul-Sada, G J Langley, H W Kroto, R Taylor, D R M Walton *J. Chem. Soc., Perkin Trans. 2* 2359 (1995)
154. Y Matsuo, T Nakajima, S Kasamatsu *J. Fluorine Chem.* **78** 7 (1996)
155. H Steger, U Mische, W Kamke, A Ding, M Fieber-Erdmann, T Drewello *Chem. Phys. Lett.* **276** 39 (1997)
156. A G Avent, P R Birkett, J D Crane, A D Darwish, G J Langley, H W Kroto, R Taylor, D R M Walton *J. Chem. Soc., Chem. Commun.* 1463 (1994)
157. P R Birkett, A G Avent, A D Darwish, I Hahn, H W Kroto, G J Langley, J O'Loughlin, R Taylor, D R M Walton *J. Chem. Soc., Perkin Trans. 2* 1121 (1997)
158. A D Darwish, A G Avent, P R Birkett, H W Kroto, R Taylor, D R M Walton *J. Chem. Soc., Perkin Trans. 2* 1038 (2001)
159. A D Darwish, P R Birkett, G J Langley, H W Kroto, R Taylor, D R M Walton *Fullerene Sci. Technol.* **5** 705 (1997)
160. A K Abdul-Sada, A G Avent, P R Birkett, H W Kroto, R Taylor, D R M Walton *J. Chem. Soc., Perkin Trans. 1* 393 (1998)
161. P-F Coheur, J Cornil, D A dos Santos, P R Birkett, J Ligvin, J L Brgdas, J-M Janot, P Seta, S Leach, D R M Walton, R Taylor, H W Kroto, R Colin *Synth. Met.* **103** 2407 (1999)
162. A K Abdul-Sada, A G Avent, D R M Walton, O B Woodhouse *Chem. Commun.* 307 (1998)
163. A G Avent, P R Birkett, A D Darwish, H W Kroto, R Taylor, D R M Walton *Chem. Commun.* 1579 (1997)
164. K S Currie, G Tennant *J. Chem. Soc., Chem. Commun.* 2295 (1995)
165. A G Avent, P R Birkett, A D Darwish, S Houlton, R Taylor, K S T Thomson, X-W Wei *J. Chem. Soc., Perkin Trans. 2* 782 (2001)
166. O A Troshina, P A Troshin, A S Peregodov, E M Balabaeva, V I Kozlovski, R N Lyubovskaya *Tetrahedron* **62** 10147 (2006)
167. H Al-Matar, A K Abdul-Sada, A G Avent, P W Fowler, P B Hitchcock, K M Rogers, R Taylor *J. Chem. Soc., Perkin Trans. 2* 53 (2002)
168. C Caron, R Subramanian, F D'Souza, J Kim, W Kutner, M T Jones, K M Kadish *J. Am. Chem. Soc.* **115** 8505 (1993)
169. E Allard, L Rivière, J Delaunay, D Dubois, J Cousseau *Tetrahedron Lett.* **40** 7223 (1999)
170. F Cheng, Y Murata, K Komatsu *Org. Lett.* **4** 2541 (2002)
171. N Chronakis, G C Vougioukalakis, M Orfanopoulos *Org. Lett.* **4** 945 (2002)
172. M S Meier, R G Bergosh, M E Gallagher, H P Spielmann, Z Wang *J. Org. Chem.* **67** 5946 (2002)
173. E Allard, J Delaunay, F Cheng, J Cousseau, J Orduna, J Garin *Org. Lett.* **3** 3503 (2001)
174. H Al-Matar, P B Hitchcock, A G Avent, R Taylor *Chem. Commun.* 1071 (2000)
175. H Al-Matar, A K Abdul-Sada, A G Avent, R Taylor *Org. Lett.* **3** 1669 (2001)
176. K M Rogers, P W Fowler *Chem. Commun.* 2357 (1999)
177. A D Darwish, A G Avent, H W Kroto, R Taylor, D R M Walton *J. Chem. Soc., Perkin Trans. 2* 1983 (1999)
178. M R Resmi, S Ma, R Caprioli, T Pradeep *Chem. Phys. Lett.* **333** 515 (2001)
179. S Lebedkin, S Ballenweg, J Gross, R Taylor, W Kratschmer *Tetrahedron Lett.* **36** 4971 (1995)
180. R W Murray, K Iyanar *Tetrahedron Lett.* **38** 335 (1997)
181. C S Lee *J. Korean Chem. Soc.* **40** 515 (1996)
182. P A Troshin, A S Astakhova, R N Lyubovskaya *Fullerenes, Nanotubes, Carbon Nanostruct.* **13** 331 (2005)
183. N I Denisenko, A V Streletskii, O V Boltalina *Phys. Solid State* **44** 539 (2002)
184. G M Brooke *J. Fluorine Chem.* **86** 1 (1997)
185. V V Bardin, L N Shchegoleva, H J Frohn *J. Fluorine Chem.* **77** 153 (1996)

^a — *Russ. Chem. Bull., Int. Ed. (Engl. Transl.)*

^b — *Moscow Univ. Bull., Ser. 2, Chem. (Engl. Transl.)*

^c — *Russ. J. Inorg. Chem. (Engl. Transl.)*

^d — *Mendeleev. Chem. J. (Engl. Transl.)*

^e — *Dokl. Chem. (Engl. Transl.)*

The chemistry of indoloindoles[†]

Sh A Samsoniya, M V Trapaidze

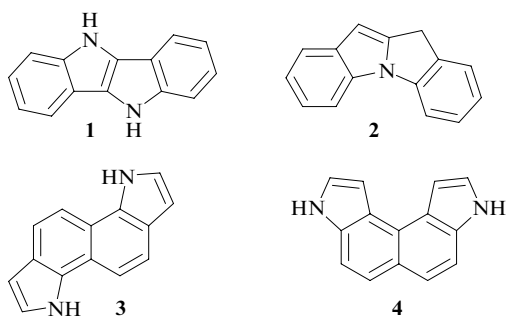
Contents

I. Introduction	313
II. Synthesis and use of indoloindoles with carbon atoms of the pyrrole rings in common	313
III. Indoloindoles with carbon and nitrogen atoms of the pyrrole rings in common	316
IV. Indoloindoles with carbon atoms of the benzene and pyrrole rings in common	316
V. Indoloindoles with carbon atoms of the benzene rings in common	317

Abstract. Methods for the synthesis of substituted and unsubstituted indoloindoles are considered. Characteristic features of electrophilic substitution in the indoloindole system and some transformations in the side chains are discussed. The bibliography includes 86 references.

I. Introduction

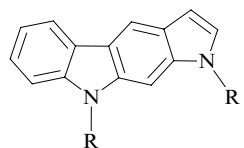
In recent years, considerable attention has been paid to the study of diverse synthetic analogues of indole, which was stimulated by their potential biological activities.^{1,2} Of particular interest among these compounds are indoloindoles in which indole fragments are fused so as to have in common either carbon atoms of the pyrrole rings {e.g., 5*H*,10*H*-indolo[3,2-*b*]indole (**1**)} or carbon and nitrogen atoms of the pyrrole rings {e.g., 10*H*-indolo[1,2-*a*]indole (**2**)}, or carbon atoms of the benzene rings {e.g., 1*H*,6*H*-indolo[7,6-*g*]indole (**3**), 3*H*,8*H*-indolo[4,5-*e*]indole (**4**), etc.}. The last-mentioned compounds are of interest because the reactive pyrrole rings in their molecules remain unsubstituted and capable of various transformations.



Natural compounds containing an indoloindole fragment in which the fused indole rings have the carbon atoms of the benzene rings in common have not yet been found.

Sh A Samsoniya, M V Trapaidze I Javakishvili Tbilisi State University, I Chavchavadze ave. 3, 0128 Tbilisi, Georgia. Fax/tel. (995-32) 22 68 10, e-mail: shotasamsonia@yahoo.de (Sh A Samsoniya), tel. (995-32) 27 87 18 (M V Trapaidze)

The present review generalises data on the synthesis and properties of the above-mentioned indoloindoles and related compounds in which two indole fragments are fused so that three or four carbon atoms of the benzene and pyrrole rings are in common simultaneously. Compounds of the type

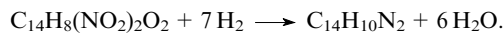


in which the pyrrole ring of one indole molecule is fused to the benzene ring of the other molecule are beyond the scope of this review, because in conformity with the IUPAC rules, they are called pyrrolocarbazoles.

Since no reviews on indoloindoles have been published as yet, we did not restrict ourselves to consideration of only recent studies but also included the results of earlier studies.

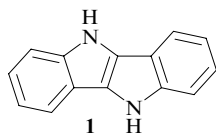
II. Synthesis and use of indoloindoles with carbon atoms of the pyrrole rings in common

The first reported synthesis of indoloindoles dates back to 1884 when P Golubeva³ obtained a neutral compound with the molecular formula $C_{14}H_{10}N_2$ by the reduction of *o,o'*-dinitrobenzil (formed upon oxidation of dinitrodeoxybenzoin) with tin and hydrochloric acid in ethanol

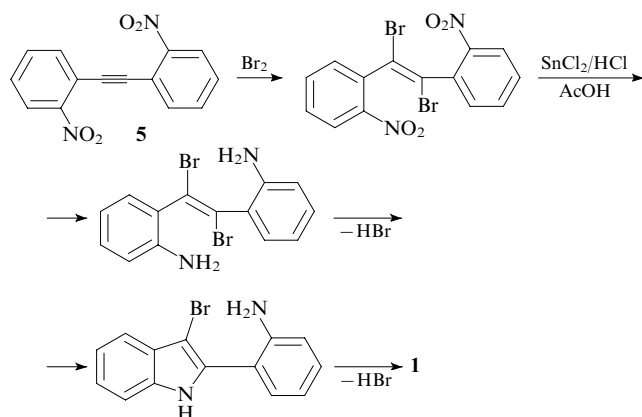


Golubeva³ suggested that this compound is a tolan derivative and called it 'diiminotolan'.

Later, Kliegl and Haas⁴ prepared a compound identified as dinitrobenzil, according to elemental composition, by oxidation of *o,o'*-dinitrotolan with a mixture of chromic and glacial acetic acids. The reduction of this product with tin gave a compound identical to Golubeva's 'diiminotolan'. They suggested that reduction of dinitrobenzil does not give 'diiminotolan', as Golubeva believed, but is accompanied by ring closure to give compound **1**, which they called 'doubly fused indole'.

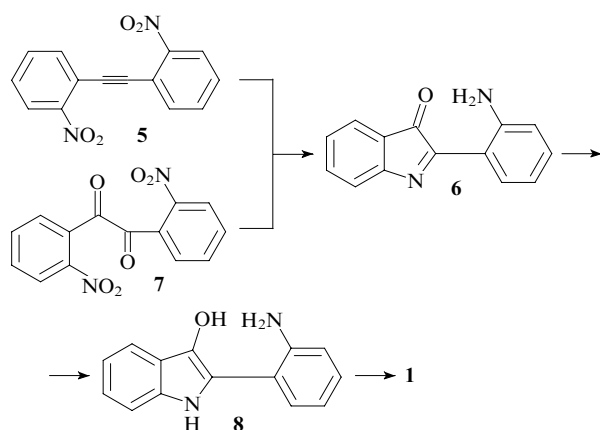


The targeted synthesis of 5H,10H-indolo[3,2-b]indole (**1**) was first performed by Ruggli.⁵ He used *o,o'*-dinitrotolan (**5**), as the starting compound, which was oxidised with bromine to give 1,2-dibromo-1,2-di(*o*-nitrophenyl)ethylene. The reduction of this product with tin(II) chloride[‡] in hydrochloric acid afforded product **1**,



which was almost identical to the 'diiminotolan' obtained by Golubeva in the physicochemical properties.

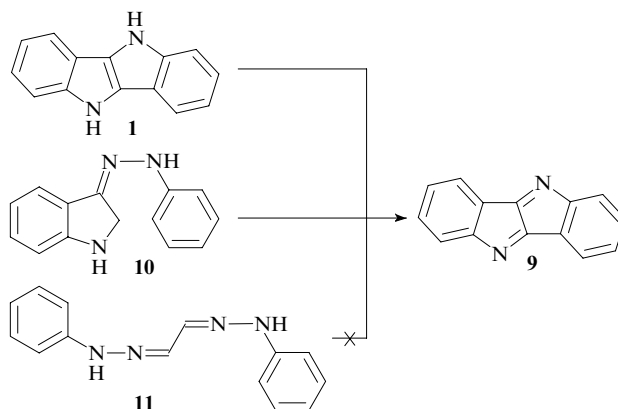
Later, Ruggli and Zaeslin⁷ reported an improvement of the method for the synthesis of indoloindole **1** from *o,o'*-dinitrotolan (**5**). They first prepared 2-(*o*-aminophenyl)indolenin-3-one (**6**) by refluxing compound **5** in an aqueous solution of sodium sulfide followed by reduction with tin(II) chloride in a mixture of hydrochloric and glacial acetic acids at 70 °C to give 5H,10H-indolo[3,2-b]indole (**1**) (yield 78%). Compound **1** was formed as colourless crystals poorly soluble in conventional organic solvents. According to Ruggli and Zaeslin,⁷ it was not 2-(*o*-aminophenyl)indolenin-3-one (**6**) that cyclised in this reaction but its reduced form, compound **8** formed after acidification.



Compound **6** can also be obtained by the reduction of *o,o'*-dinitrobenzil **7** in a neutral solution in the presence of Ni.

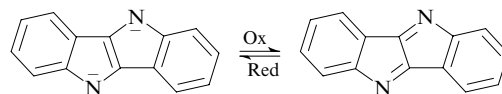
Dehydrogenation of indoloindole **1** on treatment with chloranil⁶ results in a product for which a quinonoid structure

and the name dehydroindoloindole were proposed. The structure of 5,10-didehydroindolo[3,2-*b*]indole (**9**) was confirmed by IR and UV spectroscopic data. Oxidative dehydrogenation of indoloindole **1** (in boiling acid) was also carried out by Treibs.^{8,9} Subsequently, he attempted to develop a more convenient method for the synthesis of 5,10-didehydroindolo[3,2-*b*]indole (**9**). To this end, he investigated the following reactions:⁹

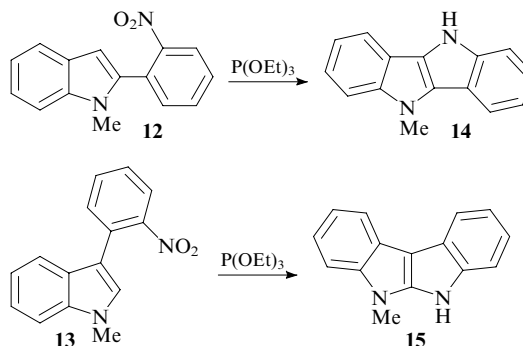


However, it turned out that compound **9** is formed in low yield from indolin-3-one phenylhydrazone (**10**) and is not formed at all from glyoxal diphenylhydrazone (**11**).

Compound **9** and some derivatives of indoloindole **1** were synthesized by Hünig and Steinmetzer^{10–13} in a study of various redox systems, in particular, the system

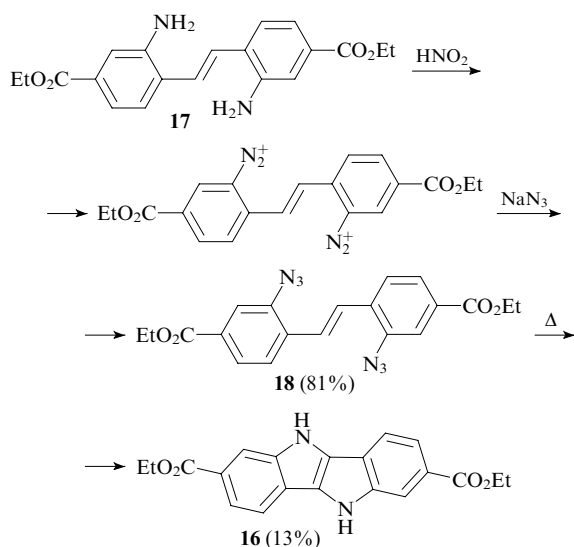


Cadogan *et al.*¹⁴ proposed a new method for the synthesis of carbazoles, indoles, indazoles and related compounds, which involved the reduction of appropriate nitro compounds with triethyl phosphite. It was found that reduction of mono-nitro derivatives gives products in high yields, while in the case of dinitro compounds, the yields are moderate. Thus *o,o'*-dinitrostilbene was converted into indoloindole **1** in a very low yield (2%), whereas treatment of 1-methyl-2-(*o*-nitrophenyl)indole (**12**) and its 3-isomer **13** with triethyl phosphite in cumene at 160 °C resulted in the formation of 10-methyl-5H-indolo[3,2-*b*]indole (**14**) and 6-methyl-5H-indolo[2,3-*b*]indole (**15**), respectively, in good yields.¹⁵

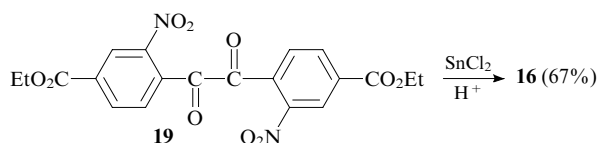


Kaszynski and Dougherty¹⁶ prepared diethyl 5H,10H-indolo[3,2-*b*]indole-2,7-dicarboxylate (**16**) from diethyl 2,2'-diaminostilbene-4,4'-dicarboxylate (**17**) according to the following scheme:

[‡] Heller⁶ proposed the use of zinc dust in acetic acid for the reduction of *o,o'*-dinitrobenzil.

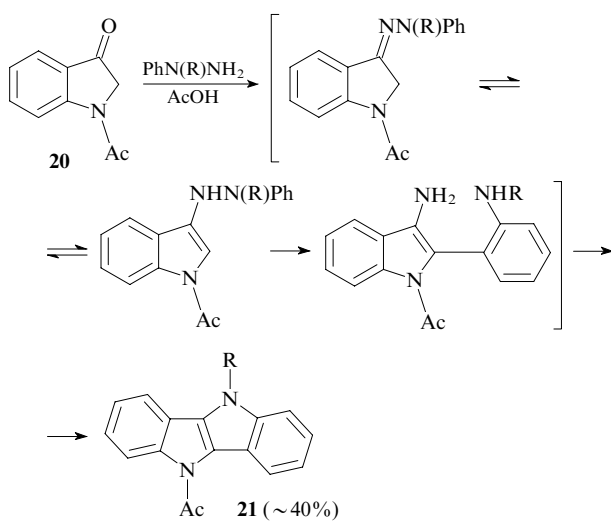


The cyclisation of diazide **18** took place in *o,o'*-dichlorobenzil at 155 °C. In this reaction, indolo[1,2-*b*]indazole derivatives were obtained as by-products. Diester **16** can also be obtained by simultaneous reduction (SnCl_2) and cyclisation of compound **19** in a mixture of hydrochloric and acetic acids.



Kaszynski and Dougherty¹⁶ also synthesised the *N,N'*-dimethyl derivative of compound **16** and studied its electrochemical oxidation in CH_2Cl_2 in the presence of $\text{Bu}_4\text{N}^+\text{ClO}_4^-$ to give stable radical cation **16**^{•+}. It was assumed that the indoloindole obtained could find use in the synthesis of polaronic ferromagnets.

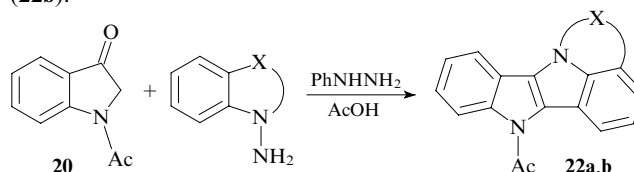
A new synthetic route to indolo[3,2-*b*]indole derivatives based on *N*-substituted indoxyls and phenylhydrazines has been proposed.¹⁷ Refluxing of 1-acetylindolin-3-one (**20**) with substituted phenylhydrazines in acetic acid for 10 min gave the corresponding indolo[3,2-*b*]indoles (**21**).



R = Me, PhCH_2 .

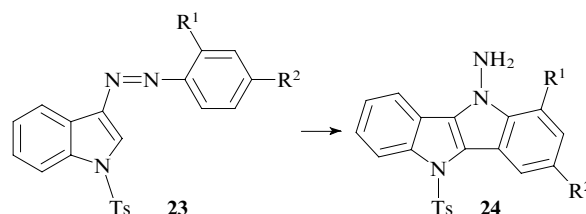
The process involves the formation of hydrazones, which then undergo the Fischer reaction to be converted into the corresponding indoloindoles. The acetyl derivative **20** may be replaced by the tosyl derivative;¹⁸ in this case, the yield of indolo[3,2-*b*]indole is 50%.

The Fischer method has found use in the synthesis of diverse fused heterocycles. In particular, this approach was employed to prepare indolo[3,2-*b*]indolo[1,7*a*,7-*ab*]tetrahydropyridine (**22a**) and indolo[3,2-*b*]indolo[1,7*a*,7-*ab*]diazepinone (**22b**).¹⁹



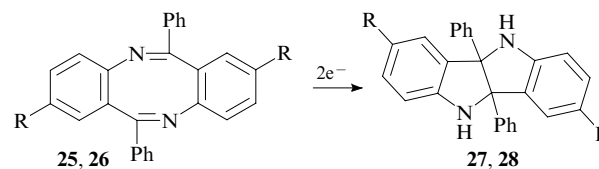
X = $(\text{CH}_2)_3$ (**22a**), $\text{NHC(O)(CH}_2)_2$ (**22b**).

Cyclisation of phenylazindoles **23** in acetic acid at 60–70 °C in the presence of $\text{Na}_2\text{S}_2\text{O}_4$ gave 10-amino-5-tosylindolo[3,2-*b*]indoles **24**.²⁰



$\text{R}^1, \text{R}^2 = \text{H, Hal, Alk.}$

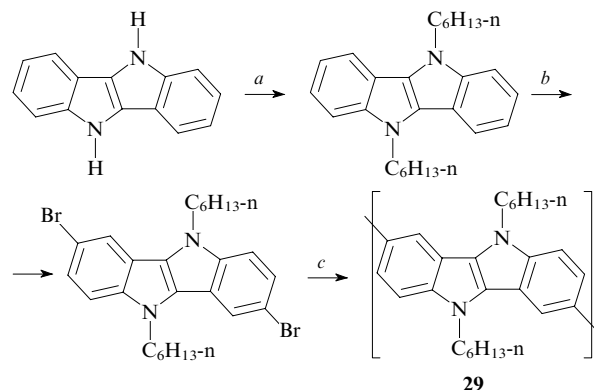
Yet another route to indolo[3,2-*b*]indole derivatives is electrochemical reduction of bis-Schiff bases.²¹ The reduction of 6,12-diphenyldibenzo[*b,f*][1,5]diazocine (**25**) and its 2,8-dichloro derivative **26** gives 4*b*,9*b*-diphenyl-4*b*,5,9*b*,10-tetrahydroindolo[3,2-*b*]indole (**27**) and its 3,8-dichloro derivative (**28**) in 94% and 69% yields, respectively.²²



R = H (**25, 27**), Cl (**26, 28**).

Previously, compounds **27** and **28** were obtained in relatively low yields^{23–25} by the reduction of compounds **25** and **26** with zinc in acetic acid or by platinum oxide-catalysed reduction.

Recent publications describe the use of indolo[3,2-*b*]indoles in the synthesis of high-spin polymeric materials for light emitting diodes. Thus the synthesis and electroluminescent properties of a high-spin polymer, poly(5,10-dihexylindolo[3,2-*b*]indole-2,7-diyl) (**29**), have been reported.²⁶ This



(a) $n\text{-C}_6\text{H}_{13}\text{Br}$, NaH, THF; (b) Br_2 , pyridine, CCl_4 ; (c) Ni(COD)_2 , COD, 2,2'-bipyridine.

polymer possessed good optical and electroluminescent properties, but unfortunately had a low molecular mass and formed poor-quality polymeric films.

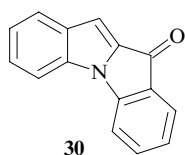
Earlier, high-spin polymers with a similar structure containing an indolo[3,2-*b*]indole fragment in the monomer unit were prepared by Murray *et al.*,²⁷ who have called them the prototypes of polaronic ferromagnets.

A study of the hole conduction of various heterocyclic systems related to the class of 5,10-dihetera-5,10-dihydroindeno[3,2-*b*]indenes²⁸ has shown that 5,10-dihydroindeno[3,2-*b*]indole possesses the best characteristics (luminescent properties and the lifetime).

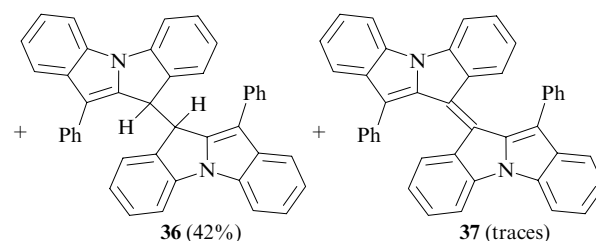
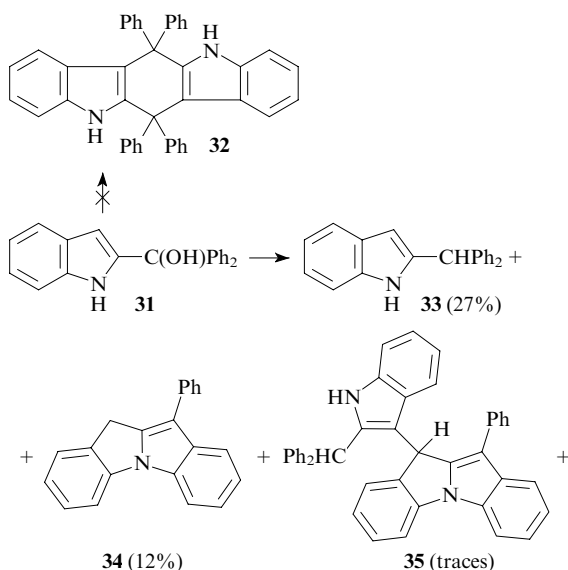
Dobrin and co-workers^{29–32} studied the photophysical properties of 5*H*,10*H*-indolo[3,2-*b*]indole (**1**) and its derivatives (in particular, 5,10-dimethylindolo[3,2-*b*]indole and its 2,7-diethoxycarbonyl derivative) using the spectral and quantum-chemical methods. These compounds can be considered to be stilbene analogues, as they contain a stilbene chromophore as a part of a tetracyclic system.

III. Indoloindoles with carbon and nitrogen atoms of the pyrrole rings in common

The interest in indoloindoles with carbon and nitrogen atoms of the pyrrole rings in common is due to their biological activities. The first derivative with this type of fusion, namely, 10*H*-indolo[1,2-*a*]indol-10-one (**30**), was prepared in 40% yield back in 1953 by Shirley and Roussel³³ upon treatment of *N*-phenylindole with excess *n*-butyllithium and saturation with carbon dioxide. The oxime of compound **30** was also prepared. It was suggested that indoloindole **30** is formed upon the reaction of 2,2'-dilithiated *N*-phenylindole with CO₂.

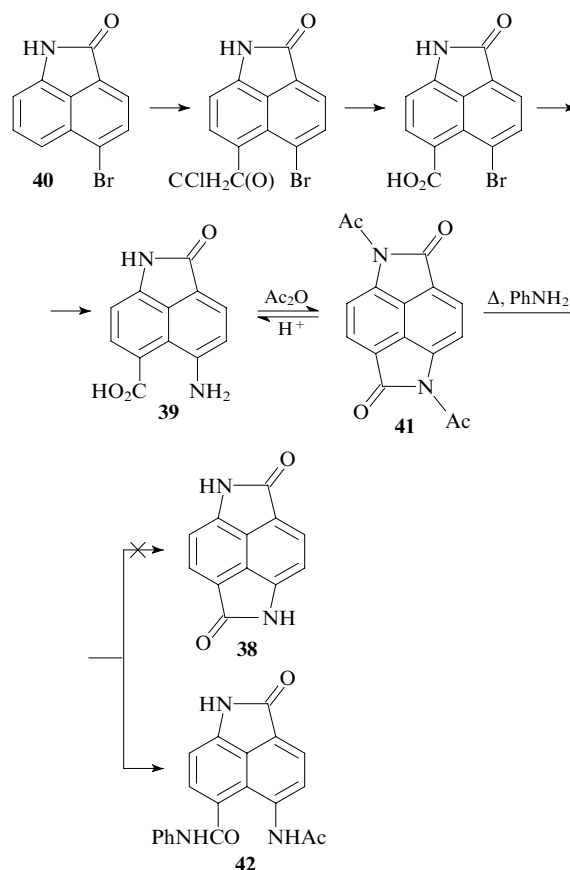


Thermolysis of dilute solutions of 2-(hydroxydiphenylmethyl)indole (**31**) in boiling bromobenzene did not give the expected dimer **32**, but afforded instead a mixture of products **33–37** comprising 11-phenyl-10*H*-indolo-[1,2-*a*]indole (**34**) and its derivatives **35–37**.³⁴ The structures of compounds **34–37** were proposed based on the data from IR and UV spectroscopy.



IV. Indoloindoles with carbon atoms of the benzene and pyrrole rings in common

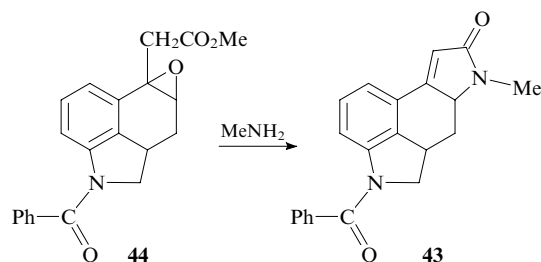
In order to study the possibility of preparing fused heterocyclic compounds with two pyrrole rings upon cyclisation of substituents located in the *peri*-position of the naphthalene nucleus, an attempt was made to synthesise indolo[5,4,3*a*,3-*cde*]indole-2,6-dione (**38**).³⁵ 5-Amino-2-oxobenzo[*c,d*]indoline-6-carboxylic acid (**39**), which was obtained from 5-bromobenzo[*c,d*]indolin-2-one (**40**), was subjected to the cyclisation.



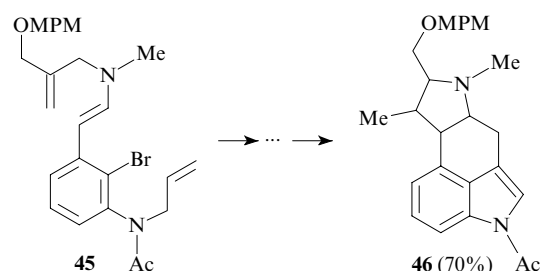
Lactam ring closure in the *peri*-positions of the naphthalene nucleus was attained only by refluxing compound **39** in acetic anhydride. This gave 1,5-diacetyl-1,5-dihydroindolo[5,4,3*a*,3-*cde*]indole-2,6-dione (**41**) in 59% yield. This amide proved unstable; in an acidic medium it was converted into the starting compound **39**. Heating of compound **41** in aniline did not give unsubstituted indolo[5,4,3*a*,3-*cde*]indole-2,6-dione (**38**); instead, opening of one lactam ring took place to give compound **42**.

Yet another indoloindole fused so as to have the carbon atoms of the benzene and pyrrole rings in common, namely, 4-benzoyl-7-methyl-5,5*a*,6,6*a*-tetrahydroindolo[6,5,4-*cd*]indol-8-one (**43**), was isolated at a stage of synthesis of lysergic acid³⁶ by the reaction of 1-benzoyl-5-methoxycarbonylmethyl-

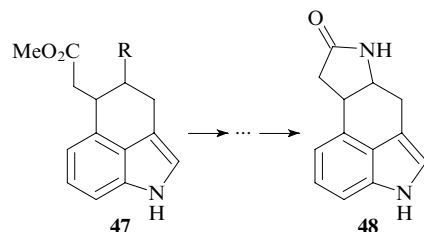
4,5-epoxy-1,2,2a,3,4,5-hexahydrobenz[*c,d*]indole (**44**) with a large excess of methylamine in an autoclave (100 °C, 6 h).



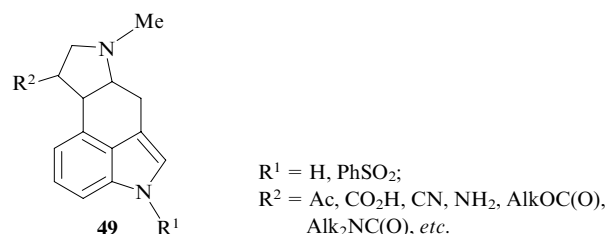
An attempted synthesis of lysergic acid from enamine **45** resulted in indolo[6,5,4-*cd*]indole **46** as one of the products.³⁷



Japanese researchers^{38–40} prepared indolo[6,5,4-*cd*]indole derivatives and used them as prolactin secretion inhibitors and intermediate compounds in the synthesis of drugs. In one study,⁴⁰ they used tetrahydrobenzo[*c,d*]indole **47** (R = NO₂) as the starting compound; refluxing of compound **47** with zinc amalgam in 2 M HCl gave the corresponding amine (R = NH₂). Cyclisation of this product in aqueous methanol containing NaHCO₃ resulted in indolo[6,5,4-*cd*]indole **48** in high yield (87%).



A patent⁴¹ describes the preparation of a large group of substituted hexahydro-4*H*-indolo[6,5,4-*cd*]indoles **49** from agroclavine and ergoline derivatives.



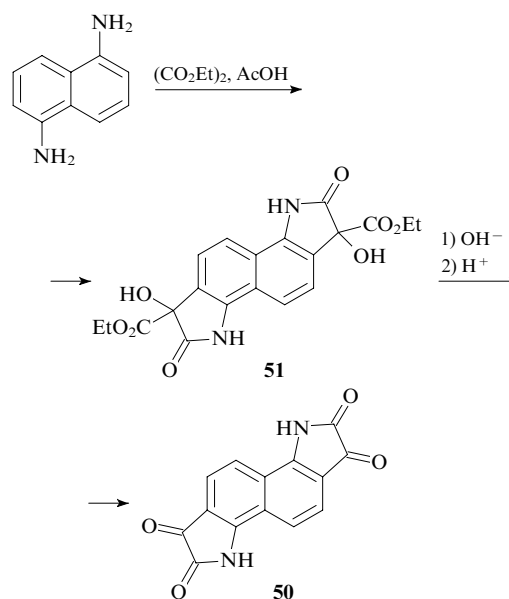
The synthesis of a series of tetracyclic indole derivatives, in particular indolo[3,2,1-*hi*]indoles, using the Fischer reaction has been described; their anticonvulsant activities have been studied.⁴²

V. Indoloindoles with carbon atoms of the benzene rings in common

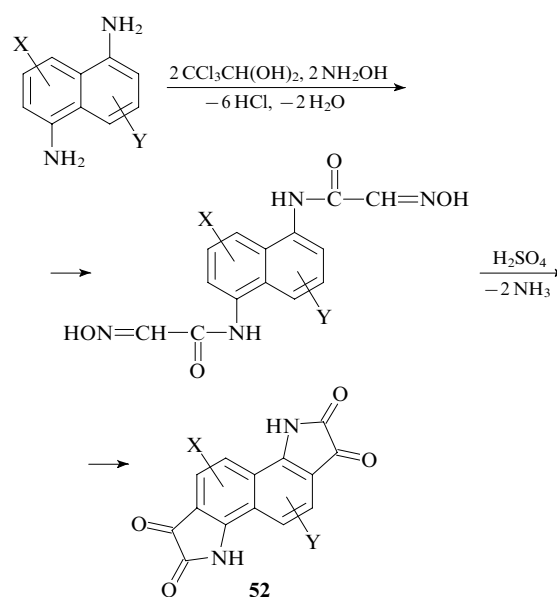
1. Synthesis of substituted indoloindoles

The first indolo[7,6-*g*]indole derivatives, namely, 1*H*,6*H*,2,3,7,8-tetrahydroindolo[7,6-*g*]indole-2,3,7,8-tetraone

(**50**) and its monophenyl- and diphenylhydrazones, were prepared in 1922.⁴³ Compound **50** is formed on heating 1,5-naphthylenediamine with diethyl oxalate in acetic acid followed by hydrolysis of diester **51** with potassium hydroxide and neutralisation with HCl.



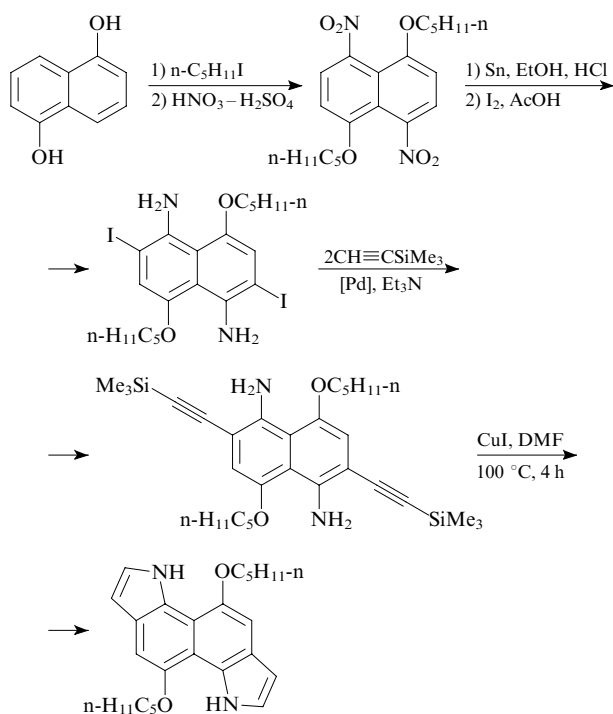
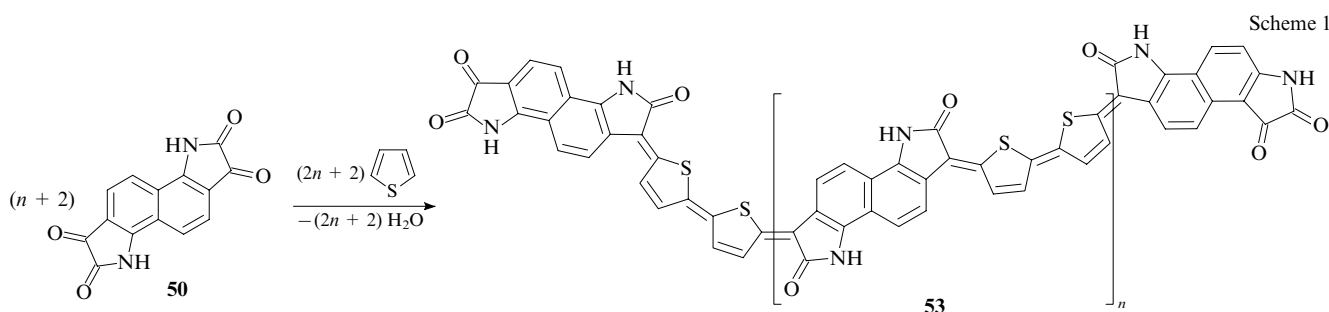
Subsequently, indolo[7,6-*g*]indole tetraoxo derivatives **52** substituted in the benzene ring were prepared⁴⁴ using the classical Sandmeyer synthesis of isatins from diamionaphthalene as shown below.



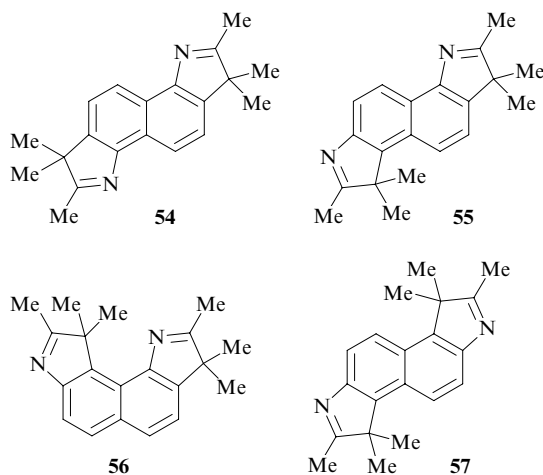
X, Y = H, Hal, Alk, AlkO, NO₂, CN.

Kossmehl and Manecke⁴⁵ prepared indolo[7,6-*g*]indole-tetraone **50** in the same way and then converted this product into polymer **53** containing fragments of this indoloindole. Compound **50** was coupled with thiophene in a mixture of glacial acetic and concentrated sulfuric acids. Polymer **53** was obtained in 84% yield as a dark purple powder, which did not melt up to 600 °C and was insoluble in conventional organic solvents (Scheme 1).

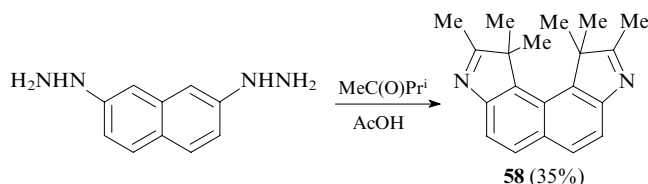
A new approach to the synthesis of substituted indolo[7,6-*g*]indoles using readily available 1,5-dihydroxynaphthalenes as the starting compounds has been proposed.⁴⁶



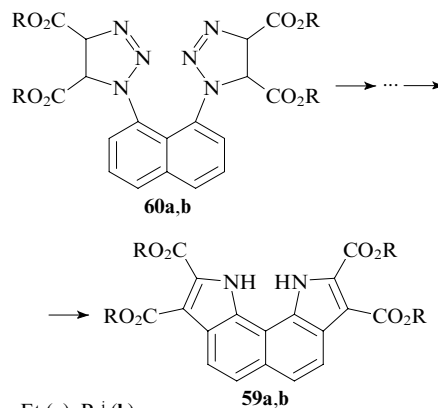
The Fischer cyclisation of isopropyl methyl ketone 1,5-, 1,6-, 1,7- and 2,6-naphthylenedihydrazones gave isomeric hexamethylindoloindoles: 2,3,3,7,8,8-hexamethyl-3*H*,8*H*-indolo[7,6-*g*]indole (**54**), 2,3,3,6,6,7-hexamethyl-3*H*,6*H*-indolo[6,7-*e*]indole (**55**), 2,3,3,9,10,10-hexamethyl-3*H*,10*H*-indolo[7,6-*e*]indole (**56**) and 1,1,2,6,6,7-hexamethyl-1*H*,6*H*-indolo[5,4-*e*]indole (**57**), which were used as hetero residues in the synthesis of carbocyanine dyes.⁴⁷



The researchers cited⁴⁷ were unable to prepare hexamethylindoloindoles from isopropyl methyl ketone 2,7-naphthylenedihydrazone, because only one pyrrole ring was closed in this case due to steric hindrance. Only recently,⁴⁸ was 1,1,2,9,10,10-hexamethyl-1,10-dihydroindolo[4,5-*e*]indole (**58**) synthesised in 35% yield by the Fischer reaction of 2,7-naphthylenedihydrazine and isopropyl methyl ketone in acetic acid without isolation of the dihydrazone.



Substituted indolo[6,7-*g*]indoles **59a,b** were prepared using photolysis of 1,1'-(1,8-naphthylene)bis(1*H*-1,2,3-triazoles) (**60a,b**) (450 W, high-pressure Hg lamp, quartz, 20 °C).⁴⁹ The reaction occurs in two steps, one pyrrole ring being closed first followed by closure of the other ring.



R = Et (**a**), Prⁱ (**b**).

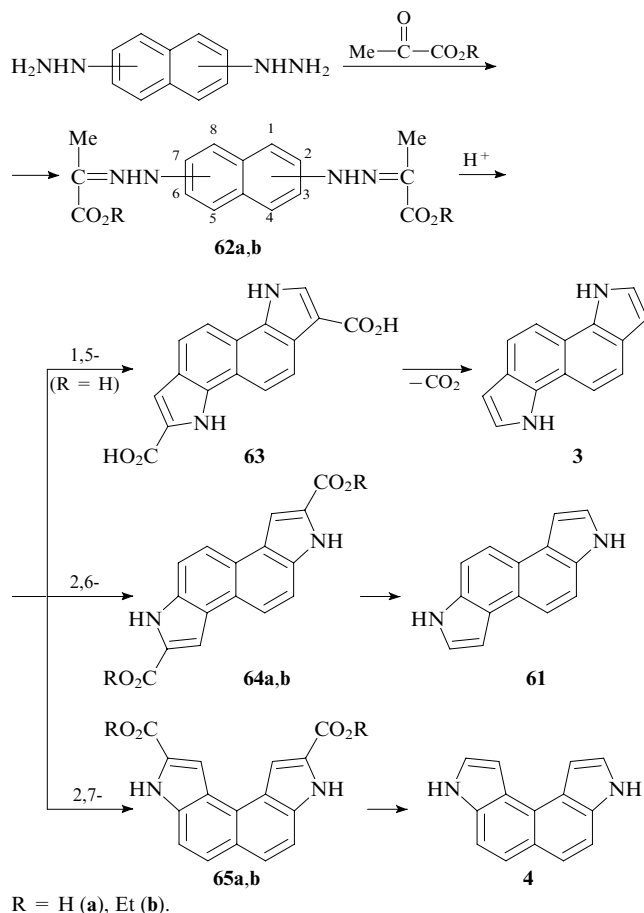
The structure of compound **59a** was confirmed by X-ray diffraction analysis.⁵⁰

2. Synthesis of unsubstituted indoloindoles

The systematic investigation into the synthesis of unsubstituted indoloindoles in which the indole fragments have the carbon atoms of the benzene rings in common was started in 1977 simultaneously at the Chairs of Organic Chemistry of the D I Mendelev Russian University of Chemical Technology and the I Javakhishvili Tbilisi State University.

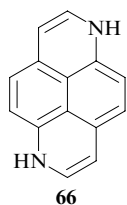
Isomeric unsubstituted indoloindoles **3**, **4** and **61** were obtained by cyclisation of pyruvic acid or ethyl pyruvate 1,5-, 2,6- and 2,7-naphthylenedihydrazones (**62a,b**), which were prepared from the corresponding naphthylenedihydrazines under conditions of the Fischer reaction (Scheme 2).^{51–53}

Scheme 2



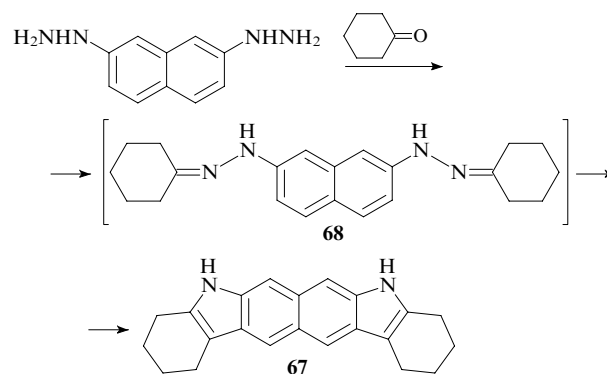
The cyclisation of pyruvic acid naphthylenedihydrazones **62a** was carried out in a mixture of concentrated sulfuric and glacial acetic acids, while the cyclisation of ethyl pyruvate dihydrazones **62b** was performed in a mixture of esters of polyphosphoric acid. The subsequent thermal decarboxylation of diacids **63**, **64a** and **65a** yielded unsubstituted 1H,6H-indolo[7,6-g]indole (**3**), 3H,8H-indolo[5,4-e]indole (**61**) and 3H,8H-indolo[4,5-e]indole (**4**).

Theoretically, one could suggest that cyclisation of pyruvic acid 1,5-naphthylenedihydrazones followed by decarboxylation would give compound **66** with four six-membered rings; however, ¹H NMR spectroscopic data attest to a structure in which protons occur in six- and five-membered rings, which is consistent with structure **3**.⁵⁴

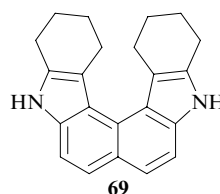


The cyclisation of 2,6- and 2,7-naphthylenedihydrazones may give six isomeric indoloindoles, four symmetrical (two linear and two angular) and two asymmetric ones. Chromatographic monitoring of the cyclisation of dihydrazones showed the presence of several products; however, only one isomer was isolated in each case (namely, compounds **64** and **65**), i.e., in both cases, cyclisation involved more reactive α-positions of the naphthalene nucleus.⁵²

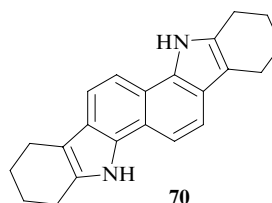
As an attempt to obtain linear indoloindoles, cyclisation of cyclohexanone 2,7-naphthylenedihydrazones was carried out.^{55, 56} In this case, due to the steric influence of the cyclohexane ring, cyclisation of the dihydrazones to give linear structure **67** seemed more likely. Indeed, one-pot reaction carried out in a mixture of concentrated acetic and sulfuric acids gave this compound without isolation of the extremely unstable dihydrazones **68**.



Angular isomer **69** was formed in this reaction as an admixture, which was proved by ¹H NMR spectroscopy.



Similarly, compound **70** was prepared from 1,5-naphthylenedihydrazine and cyclohexanone.⁵⁷



3. Quantum-chemical calculations for unsubstituted indoloindoles

The molecules of indoloindoles **3**, **4** and **61** are tetracyclic fused conjugated hetero systems. According to Albert's classification,⁵⁸ indoloindoles are π-excessive heterocycles, as the number of π-electrons in their aromatic system exceeds the number of atoms in the rings. In this respect, they resemble indoles and benzindoles, but differ from them by the presence of the second heteroatom. Pozharskii⁵⁹ classified these fused π-excessive heterocycles as a separate group, as in these cases, the benzene rings also become π-excessive due to the shift of the π-electron density in the heterocycle. In the molecules of indoloindoles **3**, **4** and **61**, the π-excessive character extends to the naphthalene nucleus.

Quantum-chemical calculations for the molecules of 1H,6H-indolo[7,6-g]indole (**3**),⁶⁰ 3H,8H-indolo[4,5-e]indole (**4**)⁶¹ and 3H,8H-indolo[5,4-e]indole (**61**)⁶² were carried out. The electronic structure of the indoloindole molecule **3** was calculated by the CNDO MO and those of molecules **4** and **61** were determined using the SCF MO method in the CNDO/2 approximation.⁶³ The calculations for molecules **3** and **4** were carried out using the Maslov programme,⁶⁴ those for molecule

61, using software developed at the Department of Chemistry of the Moscow State University (Ref. 65).[§]

It can be seen from the molecular diagrams of indoloindoles **3**, **4** and **61** (Figs 1–3) that the introduction of an additional pyrrole ring into the [4,5]- and [6,7]-benzindole molecules results in a more pronounced electron delocalisation. The charge density and the overall ($\sigma + \pi$) charges are maximum for the atoms located at the β -positions of the pyrrole rings; the electron density is also increased at positions 5,10 (compound **3**), 4,9 (compound **61**) and 4,7 (compound **4**) of the naphthalene nucleus.

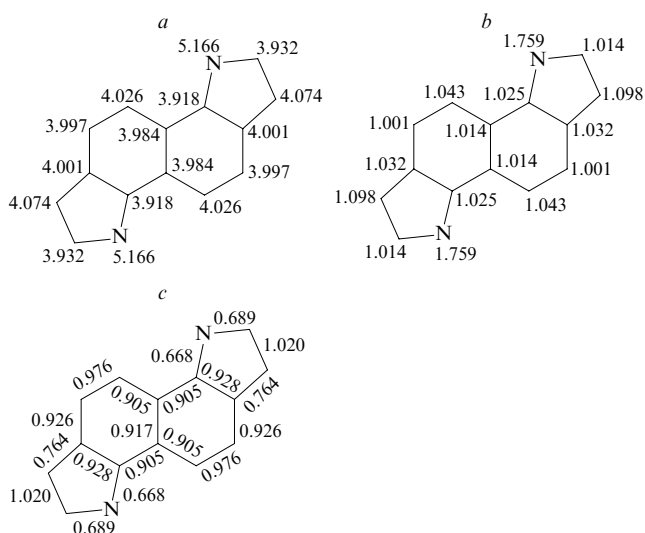


Figure 1. Molecular diagram of indoloindole **3**. (a) Overall ($\sigma + \pi$) charges, (b) π -electron densities, (c) bond orders.

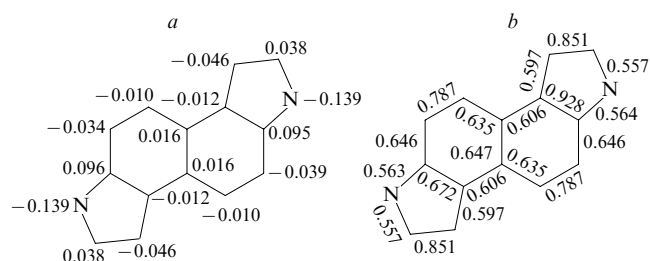


Figure 2. Molecular diagram of indoloindole **61**. (a) Charge density on the atoms, (b) Wiberg indices.

Unlike indole, pyrroloindole⁶⁶ or other indoloindole isomers, in the molecule of indoloindole **4**, the highest π -electron densities occur on the α -carbon atoms of the pyrrole rings,⁶⁷ which is abnormal for the indole ring.

4. Reactions of indoloindoles with the carbon atoms of the benzene rings in common

a. Cycloaddition and cyclocondensation

The reactions of indoloindoles **58** and **54** with 2',3'-dimethoxycarbonylspirofluorene cyclopropene yielded dispiropoly-

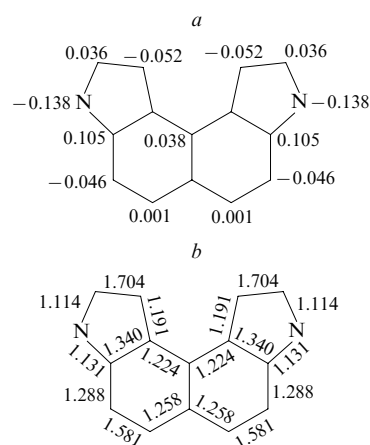
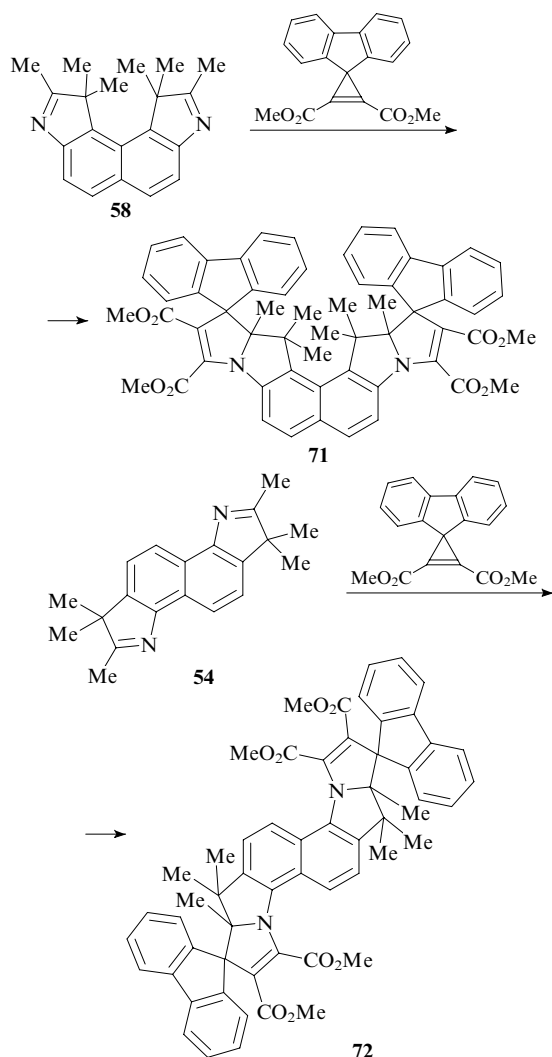


Figure 3. Molecular diagram of indoloindole **4**. (a) Charge density on the atoms, (b) Wiberg indices.

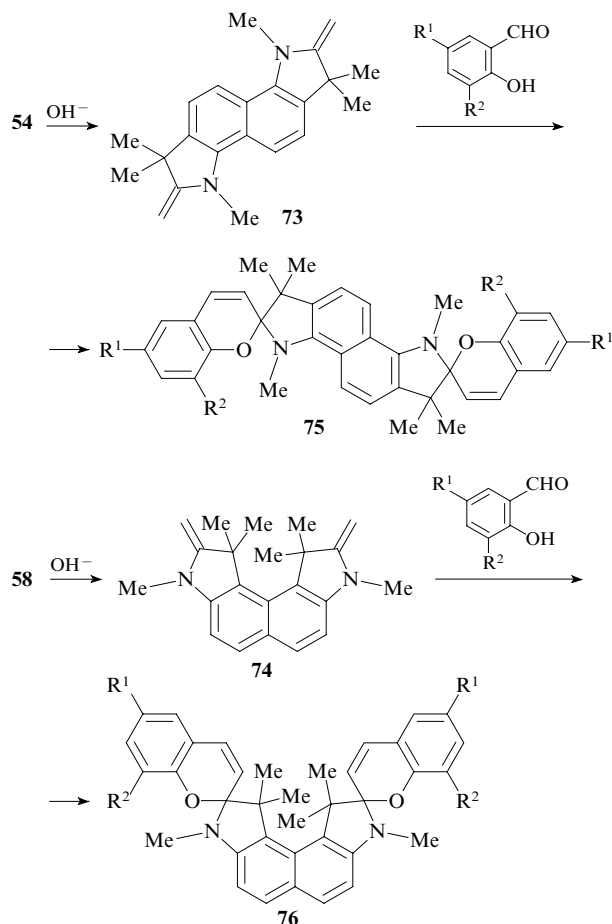
cyclic photochromic systems, namely, compounds **71** and **72**.^{48, 68, 69}



[§] A programme package Viking was designed at the NMR laboratory of the Department of Chemistry of the Moscow State University for the calculation of physicochemical properties of molecules by semiempirical quantum-chemical methods including CNDO/2.

Yet another method for the preparation of spirocyclic compounds based on indolo[7,6-*g*]- and indolo[4,5-*e*]indoles is the condensation of indoloindoles with substituted salicylaldehydes.^{70, 71} To this end, isomeric hexamethyldihydroindolo-

loindoles **54**, **58** were first converted into bis-quaternary salts, which were then treated with a warm solution of alkali to obtain the Fischer bases, viz., 1,3,3,6,8,8-hexamethyl-2,7-dimethylideneindolino[7,6-*g*]indoline (**73**) and 1,1,3,8,10,10-hexamethyl-2,9-dimethylideneindolino[4,5-*e*]indoline (**74**). The latter compound was condensed with 5-nitro-, 3,5-dinitro- or 3,5-dibromosalicylaldehyde to be converted into spiro compounds **75** and **76** substituted at the pyran fragment.



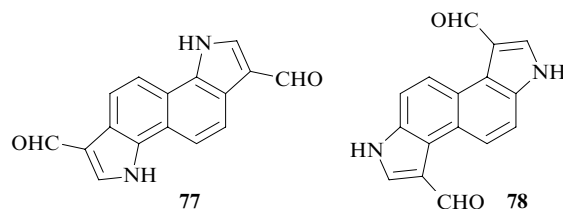
$R^1 = \text{NO}_2, \text{Br}; R^2 = \text{H}, \text{NO}_2, \text{Br}.$

b. Electrophilic substitution in the pyrrole ring

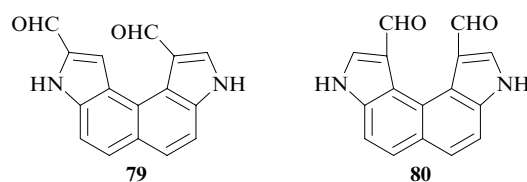
In a study of the chemical properties of indoloindoles with the carbon atoms of the benzene rings in common, it was of interest to elucidate the influence of the mode of fusion of the indole rings on the specific features of various reactions, in particular, electrophilic substitution. It follows from the molecular diagrams of indoloindoles **3**, **4** and **61** that the molecules of these compounds contain two reactive sites most favourable for the electrophilic attack, namely, the β -positions of the pyrrole rings. Since the molecules are symmetrical, these positions are equivalent from both the electronic and steric standpoints. Therefore, it is of interest to find the conditions for selective formation of mono- or disubstituted derivatives and determine the ratios of the yields of mono- and disubstituted products when they are formed simultaneously. One should also take into account the possibility of competitive substitution in the α -positions of the pyrrole rings or in the naphthalene nucleus.

The Vilsmeier reaction. Among numerous methods of formylation of organic compounds, the Vilsmeier–Haack reaction is one of the most synthetically important methods. Indoloindoles **3**, **4** and **61** were formylated using different molar ratios of these compounds to formamide complexes

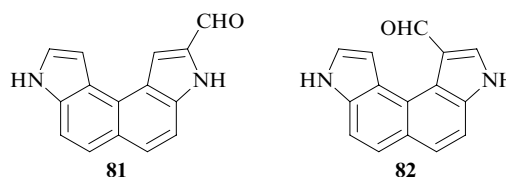
with POCl_3 (Vilsmeier complexes, VC). On treatment of indoloindoles **3** and **61** with a threefold excess of VC, symmetrical dialdehydes, viz., 3,8-diformyl-1*H*,6*H*-indolo[7,6-*g*]indole (**77**) and 1,6-diformyl-3*H*,8*H*-indolo[5,4-*e*]indole (**78**), respectively, were formed in high yields.^{61,72} Note that dialdehyde **77** was obtained in highly pure state under these conditions and did not require additional treatment for the use in subsequent transformations.⁵⁴



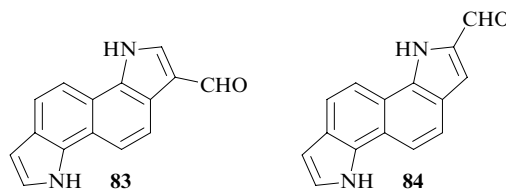
At the same time, indoloindole **4** was converted into a mixture of 1,9- (**79**) and 1,10-diformyl-3*H*,8*H*-indolo[4,5-*e*]indoles (**80**).⁷²



With equimolar amount of VC, indoloindole **4** is converted into α - (**81**) and β -monoaldehydes (**82**). Chromatographic monitoring of the formylation showed also the presence of diformyl derivatives **79** and **80** among the reaction products.^{61,72}



Indoloindole **3** is converted under the same conditions into a 1:1 mixture of 3-formyl- (**83**) and 3,8-diformyl-1*H*,6*H*-indolo[7,6-*g*]indoles (**77**). An attempt has been made⁶⁰ to obtain monoformyl derivative **83**. To this end, the formylation temperature was reduced to 55–60 °C and the reactants were taken in a 1:1 ratio. Under these conditions, the yield of aldehyde **83** was 43%, 2-formyl-1*H*,6*H*-indolo[7,6-*g*]indole (**84**) being formed as a by-product.

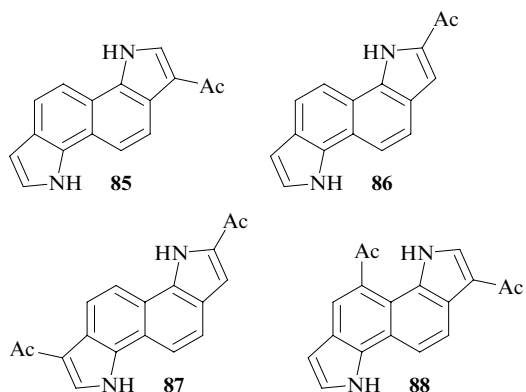


Indolo[7,6-*g*]indole (**3**) does not react with *N,N*-dimethylacetamide at 70–100 °C. An increase in temperature results in the resinification of the starting compound, no acetylation products being detected in the reaction mixture.⁷²

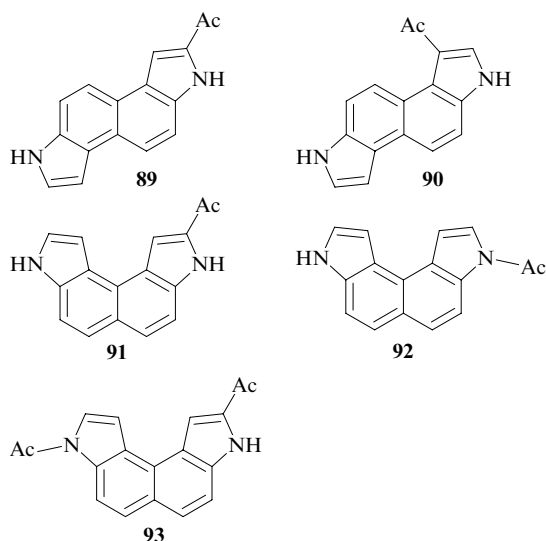
The presented data show that indoloindoles undergo the Vilsmeier–Haack reaction more readily than indole, as indicated by the formation of α -substituted aldehydes in addition to β -substituted products. This is due to the rather high π -electron density on the carbon atoms of the pyrrole ring.

Acetylation. Acetylation of indoloindoles **3**, **4** and **61**^{61,72} with acetic anhydride in the presence of acetic acid affords mixtures of acetyl derivatives in low yield. In the case of

acetylation of indolo[7,6-*g*]indole (**3**), both mono- (**85** and **86**) and disubstituted (**87** and **88**) derivatives were isolated from the reaction mixture by column chromatography.



The acetylation of indolo[5,4-*e*]indole (**61**) with acetyl chloride in the presence of AlCl_3 yields only monosubstituted α - and β -acetyl derivatives **89** and **90**, while acetylation of indolo[4,5-*e*]indole (**4**) under the same conditions affords only α -acetyl derivatives **91**. In the latter case, minor amounts of *N*-acetyl derivatives **92** and **93** are also formed.

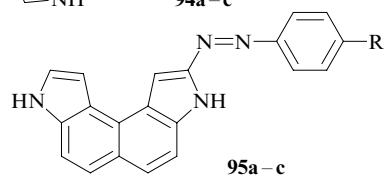
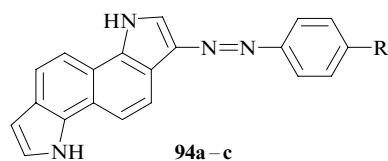


The acetylation of compound **4** at the β -position of the pyrrole ring does not take place, unlike acetylation of indoloindoles **3** and **61**. This is apparently due to steric hindrance created by the closely arranged pyrrole rings in compound **4**. In all cases, the yield of monoacetylated derivatives was substantially higher than the yield of diacetylated products.

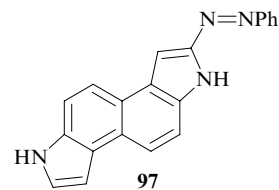
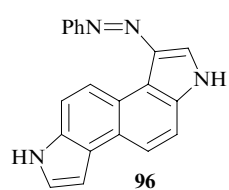
The formation of product substituted in the naphthalene nucleus (compound **88**) upon the acetylation of compound **3** is attributable to an increase in the π -electron density and an additional activation of the naphthalene α -position due to the electronic influence of the pyrrole ring.

Azo coupling. Azo coupling tends to be highly selective. Studies of azo coupling of indoloindoles **3**, **4** and **61** with different diazo components in a neutral medium at a 1 : 3 molar ratio of the substrate to the diazonium salt have been reported.^{61, 72} Under these conditions, indoloindole **3** is converted into the expected monosubstituted β -phenylazo derivatives **94a–c**, while azo coupling of indoloindole **4** follows an abnormal route with a predominant formation of monosubstituted α -phenylazo derivatives **95a–c**. The reaction of indoloindole **61** with phenyldiazonium chloride furnishes 1-phenylazo- (**96**) and 2-phenylazo-3*H*,8*H*-indolo[5,4-*e*]indoles (**97**)

in a 1 : 4.5 ratio; the reaction with *p*-nitrophenyldiazonium chloride results in polymeric products.

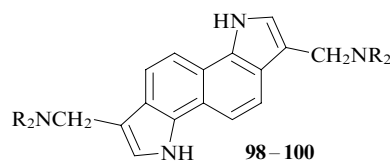


R = H (**a**), Cl (**b**), NO_2 (**c**).



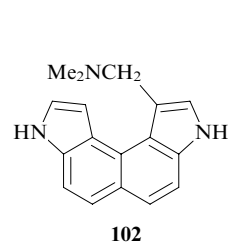
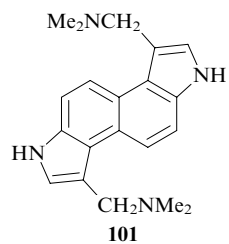
The predominant formation of monosubstituted derivatives in azo coupling may be caused by low electrophilicity of the ArN_2^+ ion, which is insufficient for the subsequent interaction with the monosubstituted phenylazo derivatives formed, in which the electron density of the aromatic system has been reduced by the introduction of the first phenylazo group. The formation of 2-substituted derivatives from compounds **61** and **4** may be due to the steric influence of the pyrrole ring and naphthalene nucleus.

The Mannich reaction. Indoloindole **3** undergoes the Mannich reaction with formaldehyde and amines (dimethylamine, piperidine and morpholine) to give the corresponding disubstituted derivatives **98–100** in high yields.^{73, 74} The reaction is carried out in acetic acid at 60 °C.



$\text{NR}_2 = \text{NMe}_2$ (**98**), N-piperidine (**99**), N-morpholine (**100**).

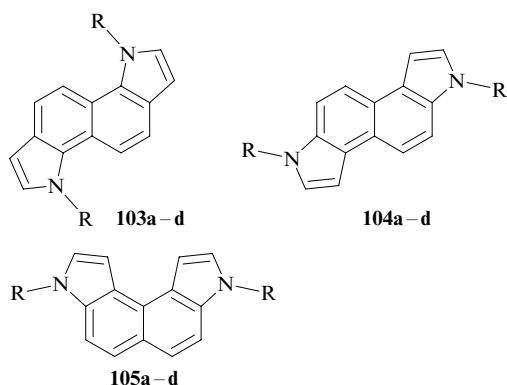
Indoloindoles **61** and **4** are converted into 1,6-bis-(dimethylaminomethyl)-3*H*,8*H*-indolo[5,4-*e*]indole (**101**) and 1-dimethylaminomethyl-3*H*,8*H*-indolo[4,5-*e*]indole (**102**), respectively, with the same ease and in high yields.⁶¹



In order to study the probable biological activities, salts of gramine analogues were prepared, namely, 3,8-bis(dimethylaminomethyl)-1*H*,6*H*-indolo[7,6-*g*]indole dihydrochloride, dimethosulfate, dimethiodide and diethiodide,^{73, 74} 1-dimethylaminomethyl-3*H*,8*H*-indolo[4,5-*e*]indole methiodide and

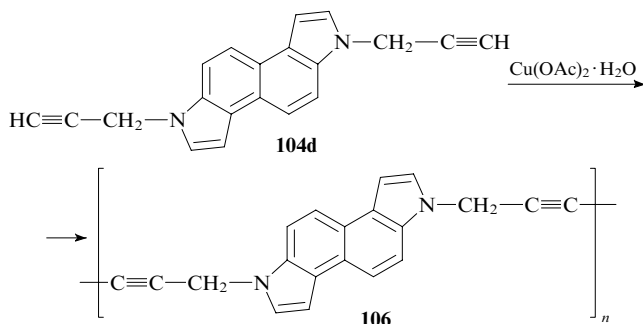
1,6-bis(dimethylaminomethyl)-3*H*,8*H*-indolo[5,4-*e*]indole dimethiodide.

Alkylation. The alkylation of indoloindoles **3**, **4** and **61** was carried out using alkyl halides.⁷⁵ In non-polar solvents (for example, under conditions of phase transfer catalysis in a 50% aqueous solution of NaOH), the reactions proceed slowly (~12 h) despite vigorous stirring at a temperature of 60–65 °C. Probably, this is caused by poor solubility of indoloindoles in non-polar solvents. The alkylation of compounds **3**, **4** and **61** in 1,2-dichloroethane at a catalyst (tetrabutylammonium bromide): substrate molar ratio of 1:5 at 40–45 °C yields mainly *N,N'*-dialkylindoloindoles.⁷⁵ Indolo[4,5-*e*]indole **4** undergoes *N,N'*-dialkylation more easily than compounds **3** and **61**, which is due to its better solubility in 1,2-dichloroethane. Compounds **103–105** were synthesised by alkylation.^{75–77}

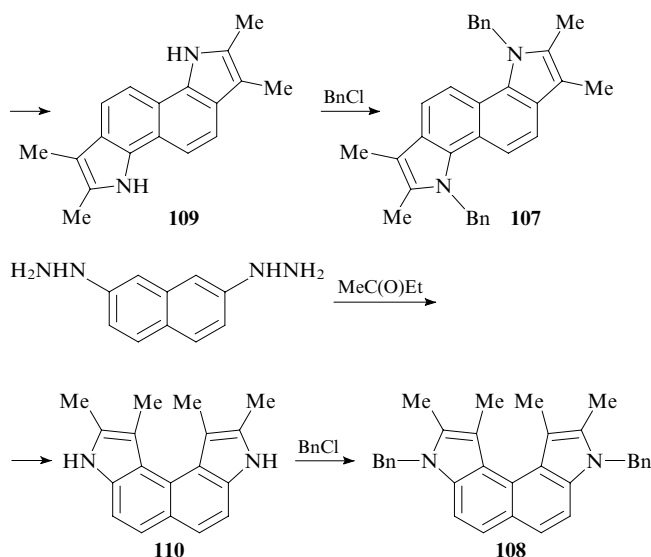
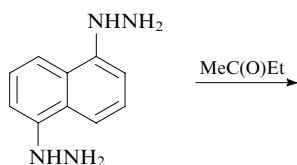


R = Et (**a**), Bn (**b**), CH₂=CHCH₂ (**c**), CH≡CCH₂ (**d**).

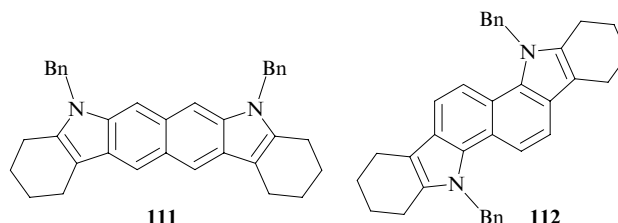
Apart from the purely theoretical interest, compounds **103–105** are of considerable practical value because of their probable biological activities and the use for preparation of polymers. For example, 3,8-dipropargylindolo[5,4-*e*]indole (**104d**) was used as an example in the Glaser–Eglinton reaction to give polyacetylenes **106** containing fused indoloindole fragments in the monomeric unit,⁷⁸ whereas in the case of 3-propargylindole, symmetrical diacetylene was isolated.⁷⁹



N,N'-Dibenzyl-substituted indoloindoles **107** and **108** were obtained by direct Fischer cyclisation of the corresponding naphthylenedihydrazines and alkyl ketones followed by benzylation of the cyclisation products **109** and **110**.^{57, 68, 80}

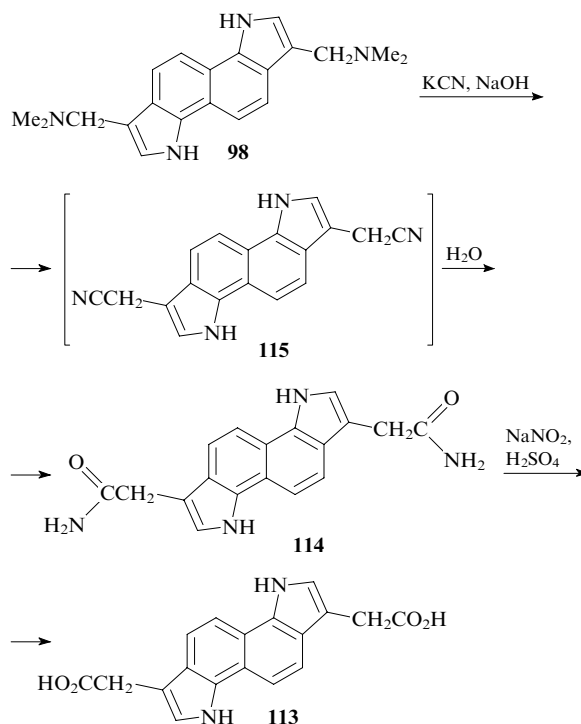


The same publications describe the synthesis of *N,N'*-dibenzyl derivatives **111** and **112** from compounds **67** and **70**.



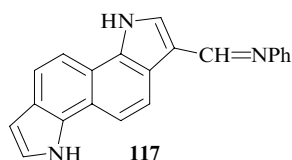
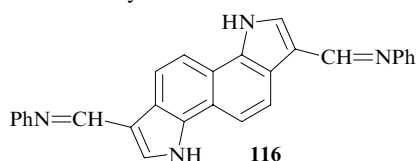
c. Transformations in side chains

Synthesis of heteroauxin analogue. The synthesis of a heteroauxin analogue, *viz.*, 3,8-bis(carboxymethyl)-1*H*,6*H*-indolo[7,6-*g*]indole (**113**), has been reported.⁷³ 3,8-Bis(dimethylaminomethyl)-1*H*,6*H*-indolo[7,6-*g*]indole (**98**) was used as the starting compound.

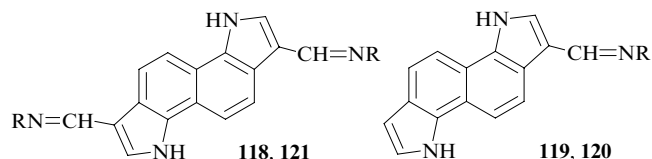


After refluxing of an ethanolic solution of compound **98** in the presence of KCN for 17 h, 3,8-bis(carbamoylmethyl)-1*H*,6*H*-indolo[7,6-*g*]indole (**114**) resulting from partial hydrolysis of the intermediate dinitrile **115** precipitates from the reaction mixture. Due to the poor solubility in an alkaline medium, compound **114** does not undergo further hydrolysis; however, in an acidic medium, the Bouveault reaction of amide **114** yields an oily product in which diacid **113** was detected by chromatography.

Condensation involving indolo[7,6-*g*]indole aldehydes. Aldehydes **77** and **83** are readily coupled with primary amines to give Schiff bases. The reactions of compounds **77** and **83** with aniline resulted in 3,8-diformyl-1*H*,6*H*-indolo[7,6-*g*]indole dianil (**116**) and 3-formyl-1*H*,6*H*-indolo[7,6-*g*]indole anil (**117**), respectively, in high yields.⁶⁰ The reaction proceeds without a catalyst.



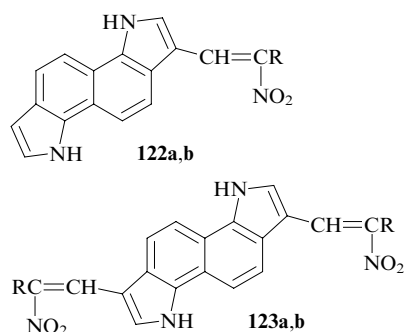
The condensation of compounds **77** and **83** with thiosemicarbazide in the presence of a catalytic amount of an ethanolic solution of HCl (pH 4–5) occurs equally smoothly giving rise to thiosemicarbazones **118** and **119**.



R = NHC(S)NH₂ (**118**, **119**), OH (**120**, **121**).

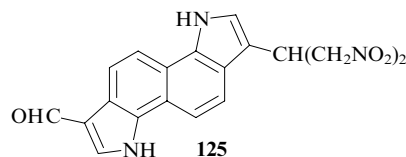
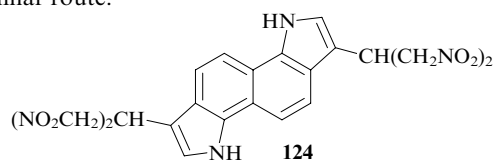
The reaction of monoaldehyde **83** with hydroxylamine proceeds smoothly to yield a mixture of 3-formyl-1*H*,6*H*-indolo[7,6-*g*]indole oxime (**120**) isomers, which could not be separated.⁶⁰ The reaction is carried out in ethanol in the presence of sodium hydrogencarbonate. The condensation of dialdehyde **77** takes place only with a strong oximating reagent, *viz.*, a mixture of hydroxylamine hydrochloride with pyridine. The reaction yields geometric isomers of 3,8-diformyl-1*H*,6*H*-indolo[7,6-*g*]indole dioxime (**121**); both isomers were isolated by chromatography. According to NMR spectroscopy, these isomers had *syn,syn*- and *anti,anti*-configurations and existed in the cisoid conformation,⁶⁰ which is sterically more favourable than the transoid conformation of the aldoxime groups.

The condensation of monoaldehyde **83** with excess nitromethane (or nitroethane) proceeds in the presence of a catalytic amount of ammonium acetate yielding 3-(2-nitrovinyl)- (**122a**) or 3-(2-nitroprop-1-enyl)indolo[7,6-*g*]indole (**122b**) (the nitroalkane serves as the solvent).^{81,82} The reactions of dialdehyde **77** with these nitroalkanes follow different routes depending on the amount of the nitroalkane. When a stoichiometric amount of nitroalkane is used and the reaction is carried out in DMF in the presence of ammonium acetate, disubstituted derivatives **123a,b** are formed.

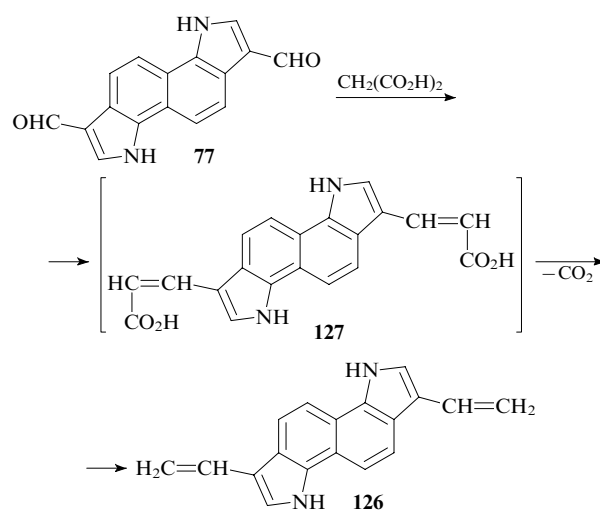


R = H (**a**), Me (**b**).

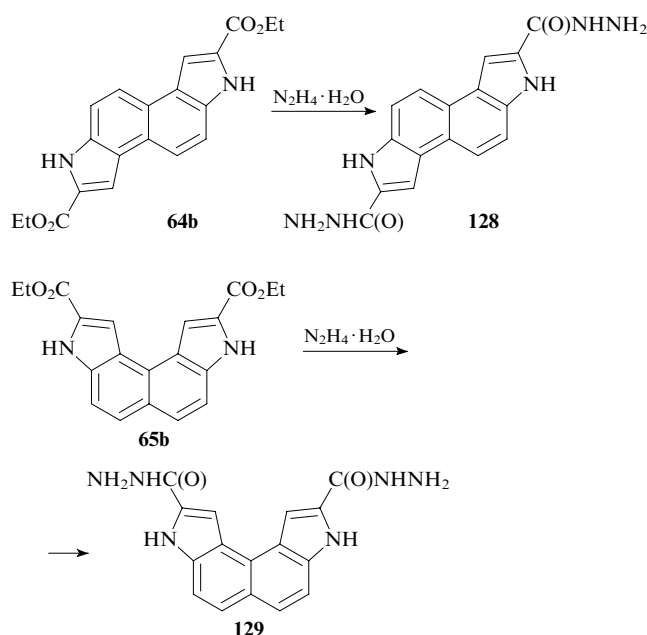
With a large excess of nitromethane and a 50% solution of NaOH as the catalyst, the reaction of dialdehyde **77** with nitromethane does not stop after the formation of compound **123a**, but proceeds further to give small amounts (isolated yields 5%–8%) of the addition products of nitromethane to compound **123a**, namely, 3,8-bis(1,3-dinitroisopropyl)-1*H*,6*H*-indolo[7,6-*g*]indole (**124**) and 3-(1,3-dinitroisopropyl)-8-formyl-1*H*,6*H*-indolo[7,6-*g*]indole (**125**), as followed from their elemental composition and spectroscopic data. The addition of nitromethane to 3-(2-nitrovinyl)indole follows a similar route.⁸³



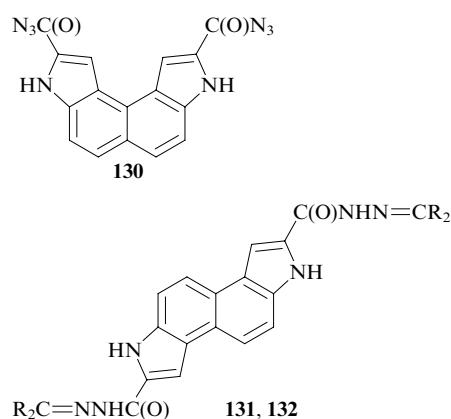
The condensation of dialdehyde **77** with malonic acid in pyridine in the presence of piperidine affords 3,8-divinyl-1*H*,6*H*-indolo[7,6-*g*]indole (**126**), which is the key compound in the synthesis of various monomeric and polymeric products.⁸⁴ Presumably, the condensation gives diacid **127**, which is decarboxylated under the reaction conditions to give compound **126**.



Synthesis and transformations of indoloindole dihydrazides. Refluxing of diesters **64b** and **65b** with hydrazine hydrate in propan-2-ol yielded 2,7-di(hydrazinocarbonyl)-3*H*,8*H*-indolo[5,4-*e*]indole (**128**) and 2,9-di(hydrazinocarbonyl)-3*H*,8*H*-indolo[4,5-*e*]indole (**129**).^{85, 86}



Nitrosation of dihydrazide **129** using sodium nitrite and concentrated HCl gives 2,9-di(azidocarbonyl)-3*H*,8*H*-indolo[4,5-*e*]indole (**130**).⁸⁵ Treatment of dihydrazide **128** with ethyl methyl ketone or hexanone resulted in dihydrazones **131** and **132**, respectively.



$\text{R}_2\text{C=NNHC(O)}$ **131, 132**
 $\text{N=CR}_2 = \text{N=CMeEt}$ (**131**), N= (cyclohexyl) (**132**).

References

1. *The Chemistry of Synthetic Indole Systems. Selected Methods for Synthesis and Modification of Heterocycles (InterBioScreen Monograph Series)* Vol. 3 (Ed. V G Kartsev) (Moscow: IBS Press, 2004)
2. J Bergman, T Janosik, N Wahlstrom *Adv. Heterocycl. Chem.* **80** 1 (2001)
3. P Golubeva *Zh. Rus. Fiz.-Khim. O-va* **16** 577 (1884) [P Golubew *Berichte* **17c** 581 (1884)]
4. A Kliegl, K Haas *Berichte* **44** 1209 (1911)
5. P Ruggli *Berichte* **50** 883 (1917)
6. G Heller *Berichte* **50** 1202 (1917)
7. P Ruggli, H Zaeslin *Helv. Chim. Acta* **18** 845 (1935)
8. W Treibs *Naturwissenschaften* **48** 130 (1961)
9. W Treibs *Chimia* **22** 467 (1968)
10. S Hünig, H-C Steinmetzer *Tetrahedron Lett.* **13** 643 (1972)
11. S Hünig, H-C Steinmetzer *Justus Liebigs Ann. Chem.* **6** 1090 (1976)
12. S Hünig, H-C Steinmetzer *Justus Liebigs Ann. Chem.* **6** 1039 (1976)
13. H Quast, S Hünig *Chem. Ber.* **99** 2017 (1966)
14. J I G Cadogan, M Cameron-Wood, R K Mackie, R J G Searle *J. Chem. Soc.* 4831 (1965)
15. A H Jackson, D N Johnston, P V R Shannon *J. Chem. Soc., Chem. Commun.* 911 (1975)
16. P Kaszynski, D A Dougherty *J. Org. Chem.* **58** 5209 (1993)
17. A N Grinev, S Yu Ryabova *Khim. Geterotsikl. Soedin.* 199 (1982)^a
18. J Y Merour, L Savelon *Heterocycles* **32** 849 (1991)
19. A N Grinev, E V Lomanova, Yu I Trofimkin *Khim. Geterotsikl. Soedin.* 1201 (1983)^a
20. USSR P. 764321; *Byull. Izobret.* (32) 271 (1989)
21. R W Koch, R E Dessy *J. Org. Chem.* **47** 4452 (1982)
22. W Metlesics, T Resnick, G Silverman, R Tavares, L H Sternbach *J. Med. Chem.* **9** 633 (1966)
23. W Metlesics, L H Sternbach *J. Am. Chem. Soc.* **88** 1077 (1966)
24. W Metlesics, R Tavares, L H Sternbach *J. Org. Chem.* **31** 3356 (1966)
25. US P. 3282958 (1966)
26. Y Jin, K Kim S Song, Ji Kim, Ja Kim, S H Park, K Lee, H Suh *Bull. Korean Chem. Soc.* **27** 1043 (2006)
27. M M Murray, P Kaszynski, D A Kaisaki, W Chang, D A Dougherty *J. Am. Chem. Soc.* **116** 8152 (1994)
28. S J Jacobs, T P Pollagi, M B Sinclair, R D Scurlock, P R Ogilby *Fall Meeting of Materials Research Society, Boston, MA, 1995*
29. M Gil, J Marczyk, S Dobrin, P Kaszynski, J Waluk *J. Mol. Struct.* **475** 141 (1999)
30. S Dobrin, A Starukhin, P Kaszynski, Ya Valuk *Opt. Spektrosk.* **83** 669 (1997)^b
31. S Dobrin, P Kaszynski, S Ikeda, J Waluk *Chem. Phys.* **216** 179 (1997)
32. S Dobrin, P Kaszynski, J Waluk *J. Photochem. Photobiol., A* **105** 149 (1997)
33. D A Shirley, P A Roussel *J. Am. Chem. Soc.* **75** 375 (1953)
34. L J Dolby, P D Lord *J. Org. Chem.* **34** 2988 (1969)
35. G I Bystritskii, G N Vorozhtsov, N S Dokunikhin, S V Ovsyannikova *Zh. Org. Khim.* **11** 1731 (1975)^c
36. E C Kornfeld, E J Fornefeld, G B Kline, M J Mann, D E Morrison, R G Jones, R B Woodward *J. Am. Chem. Soc.* **78** 3087 (1956)
37. Y Özlü, D E Cladingboel, P J Parsons *Tetrahedron* **50** 2183 (1994)
38. Jpn. P. 55/034985 (1989)
39. M Somei, Y Karasawa, C Kaneko *Chem. Lett.* 813 (1980)
40. M Somei, F Yamada, H Ohnishi, Y Makita, M Kuriki *Heterocycles* **26** 2823 (1987)
41. US P. 4742075 (1989)
42. J L Stanton, M A Ackerman *J. Med. Chem.* **26** 986 (1983)
43. J Martinet, F Vacher *Bull. Soc. Chim. Fr.* **31** 435 (1922)
44. GB P. 1251082; *Chem. Abstr.* **77** 151907 (1972)
45. G Kossmehl, G Manecke *Makromol. Chem.* **176** 333 (1975)
46. J Soloducho *Tetrahedron Lett.* **40** 2429 (1999)
47. A M Kolesnikov, F A Mikhailenko *Zh. Org. Khim.* **18** 441 (1982)^c
48. Sh A Samsoniya, G Dürr, M V Trapaidze, E R Chkhaidze, E O Gogrichiani *Khim. Geterotsikl. Soedin.* 1423 (2001)^a
49. Y Nagawa, K Honda, H Nakanishi *J. Chem. Soc., Chem. Commun.* 989 (1988)
50. Y Nagawa, M Goto, K Honda, H Nakanishi *Bull. Chem. Soc. Jpn.* **62** 3109 (1989)
51. Sh A Samsoniya, M V Trapaidze, I M Gverdtsiteli, N N Suvorov *Khim. Geterotsikl. Soedin.* 1279 (1977)^a
52. Sh A Samsoniya, M V Trapaidze, N N Suvorov, I M Gverdtsiteli *Soobshch. Akad. Nauk Gruz. SSR* **91** 361 (1978)

53. Sh A Samsoniya, M V Trapaidze, S V Dolidze, N A Esakiya, N N Suvorov, A M Kolesnikov, F A Mikhailenko *Khim. Geterotsikl. Soedin.* 352 (1984)^a
54. M V Trapaidze, Candidate Thesis in Chemical Sciences, I Javakhishvili Tbilisi State University, Tbilisi, 1980
55. M V Trapaidze, S V Dolidze, Sh A Samsoniya *Tezisy Dokladov I Vsesoyuznoi Nauchnoi Konferentsii 'Khimiya, Biokhimiya i Farmakologiya Proizvodnykh Indola'*, Tbilisi, 1986 (Abstracts of Reports of the First All-Union Scientific Conference 'The Chemistry, Biochemistry and Pharmacology of Indole Derivatives', Tbilisi, 1986) p. 155
56. D O Kadzhirishvili, S V Dolidze, Sh A Samsoniya, N N Suvorov *Khim. Geterotsikl. Soedin.* 346 (1990)^a
57. M Trapaidze, N Machaidze, Sh Samsoniya *Bull. Georgian Acad. Sci.* 161 246 (2000)
58. A Albert *Heterocyclic Chemistry. An Introduction* (London: The Athlone Press, 1958)
59. A F Pozharskii *Khim. Geterotsikl. Soedin.* 723 (1977)^a
60. Sh A Samsoniya, M V Trapaidze, L N Kurkovskaya, D A Kereselidze, N N Suvorov *Khim. Geterotsikl. Soedin.* 1501 (1980)^a
61. Sh A Samsoniya, M V Trapaidze, S V Dolidze, N A Esakiya, L N Kurkovskaya, N N Suvorov *Khim. Geterotsikl. Soedin.* 1205 (1988)^a
62. N A Esakiya, Candidate Thesis in Chemical Sciences, I Javakhishvili Tbilisi State University, Tbilisi, 1986
63. J A Pople, D L Beveridge *Approximate Molecular Orbital Theory* (New York: McGraw Hill, 1970) p. 214
64. V G Maslov *Zh. Strukt. Khim.* 18 414 (1977)^d
65. *Kvantovokhimicheskie Metody Rascheta Molekul* (Quantum-Chemical Analysis of Molecules) (Ed. Yu A Ustynyuk) (Moscow: Khimiya, 1985)
66. Sh A Samsoniya, N L Targamadze, N N Suvorov *Usp. Khim.* 63 866 (1994) [*Russ. Chem. Rev.* 63 815 (1994)]
67. S V Dolidze, Candidate Thesis in Chemical Sciences, I Javakhishvili Tbilisi State University, Tbilisi, 1985
68. Sh A Samsoniya, M V Trapaidze, N N Machaidze, G Dürr *Khim. Geterotsikl. Soedin.* 461 (2002)^a
69. Sh A Samsoniya, M V Trapaidze, E R Chkhaidze, N N Machaidze *The Chemistry of Synthetic Indole Systems. Selected Methods for Synthesis and Modification of Heterocycles (InterBioScreen Monograph Series)* Vol. 3 (Ed. V G Kartsev) (Moscow: IBS Press, 2004) p. 544
70. Sh A Samsoniya, M V Trapaidze, E O Gogrichiani, E A Katsadze, J P Maisuradze, K G Japaridze *Azotsoderzhashchie Geterotsikly (Trudy III Mezhdunarodnoi Konferentsii 'Khimiya i Biologicheskaya Aktivnost' Azotsoderzhashchikh Geterotsiklov')*, Chernogolovka, 2006 [Nitrogen-containing Heterocycles (Proceedings of the Third International Conference 'The Chemistry and Biological Activity of Nitrogen-containing Heterocycles')] Vol. 1, p. 445
71. Sh A Samsoniya, M V Trapaidze, J P Maisuradze, N G Makharashvili, K G Japaridze *The Chemistry of Synthetic Indole Systems. Selected Methods for Synthesis and Modification of Heterocycles (InterBioScreen Monograph Series)* Vol. 3 (Ed. V G Kartsev) (Moscow: IBS Press, 2004) p. 546
72. Sh A Samsoniya, M V Trapaidze, L N Kurkovskaya, L G Tretyakova, T K Efimova, N N Suvorov *Khim. Geterotsikl. Soedin.* 1221 (1979)^a
73. Sh A Samsoniya, M V Trapaidze, N N Suvorov *Soobshch. Akad. Nauk Gruz. SSR* 93 613 (1979)
74. Sh A Samsoniya, M V Trapaidze, N L Targamadze, I Sh Chikvaidze, N N Suvorov, Yu A Ershova, V A Chernov *Soobshch. Akad. Nauk Gruz. SSR* 100 337 (1980)
75. Sh A Samsoniya, N A Esakiya, N N Suvorov *Khim. Geterotsikl. Soedin.* 464 (1991)^a
76. N A Esakiya, S V Dolidze, M V Trapaidze, Z Sh Lomtadze, Sh A Samsoniya *Tezisy Dokladov II Vsesoyuznoi Nauchnoi Konferentsii 'Khimiya, Biokhimiya i Farmakologiya Proizvodnykh Indola'*, Tbilisi, 1991 (Abstracts of Reports of the Second All-Union Scientific Conference 'The Chemistry, Biochemistry and Pharmacology of Indole Derivatives', Tbilisi, 1991) p. 95
77. Sh A Samsoniya, N A Esakiya, S V Dolidze, M V Trapaidze, Z Sh Lomtadze, N N Suvorov *Khim.-Farm. Zh.* (9) 40 (1991)^c
78. N A Esakiya, Sh A Samsoniya *Tezisy Dokladov II Vsesoyuznoi Nauchnoi Konferentsii 'Khimiya, Biokhimiya i Farmakologiya Proizvodnykh Indola'*, Tbilisi, 1991 (Abstracts of Reports of the Second All-Union Scientific Conference 'The Chemistry, Biochemistry and Pharmacology of Indole Derivatives', Tbilisi, 1991) p. 147
79. Sh A Samsoniya, N A Esakiya, M S Melua, N N Suvorov *Zh. Org. Khim.* 21 275 (1985)^c
80. M Trapaidze, E Chkhaidze, Sh Samsoniya *Bull. Georgian Acad. Sci.* 160 275 (1999)
81. G I Zhungietu, V A Budylin, A N Kost *Preparativnaya Khimiya Indola* (Preparative Chemistry of Indole) (Kishinev: Shtiintsa, 1975)
82. E H P Joung *J. Chem. Soc.* 3493 (1958)
83. N N Bulatova, Candidate Thesis in Chemical Sciences, Moscow D I Mendeleev Chemical Technological Institute, Moscow, 1969
84. M V Trapaidze, Sh A Samsoniya, N N Suvorov *Zh. Org. Khim.* 16 1779 (1980)^c
85. Sh A Samsoniya, M V Trapaidze, N A Kuprashvili, N Sh Samsoniya, N N Suvorov *Khim. Geterotsikl. Soedin.* 1048 (1994)^a
86. N Nikoleishvili, E Onashvili, N Esakia, M Trapaidze, Sh Samsoniya *International Conference 'Advanced Materials and Technologies'*, Tbilisi, 2006 p. 60

^a — *Chem. Heterocycl. Compd. (Engl. Transl.)*

^b — *Opt. Spectroscop. (Engl. Transl.)*

^c — *Russ. J. Org. Chem. (Engl. Transl.)*

^d — *Russ. J. Struct. Chem. (Engl. Transl.)*

^e — *Pharm. Chem. J. (Engl. Transl.)*

Synthesis of arylenephosphamacrocycles using tri- and pentavalent phosphorus compounds

E E Nifantsev, P V Slitkov, E N Rasadkina

Contents

I. Introduction	327
II. Syntheses using trivalent phosphorus compounds	327
III. Syntheses using pentavalent phosphorus compounds	337
IV. Conclusion	337

Abstract. Key results of research into the reactions of cyclophosphorylation of dibasic phenols and related compounds with tri- and pentavalent phosphorus compounds are analysed. Structural features and chemical modification of macrocyclic systems obtained are considered. The bibliography includes 63 references.

I. Introduction

Research into macrocyclic phosphorus-containing systems began after the discovery of plasmids that are giant DNA molecules containing cyclic structures.¹ Probably, this fact and considerable advances in the synthesis and investigations of crown ethers and other macroheterocycles gave an impetus to intensive studies dealing with the design and chemical properties of cyclic systems containing tri- and pentavalent phosphorus acid residues.^{2–5} It should be noted that the attention of researchers was focussed on the products of cyclophosphorylation of dibasic phenols. The results obtained in this field allow one to relate the reactivities of the cyclic compounds to their sizes, mutual position of phosphorus-containing groups and other factors. Now one can expect the design of original supramolecular assemblies based on novel phosphorus-containing macrocycles, observation of molecular recognition effects,^{6,7} discovery of novel catalytic systems, *etc.*

At present, cyclic compounds of different nature are available. Their molecules comprise two to six phosphorus-containing fragments and the same number of arylene substituents. In this review we will dwell on the studies devoted to the synthesis and investigations of the properties of such systems that mainly include the phosphite and phosphonite moieties.

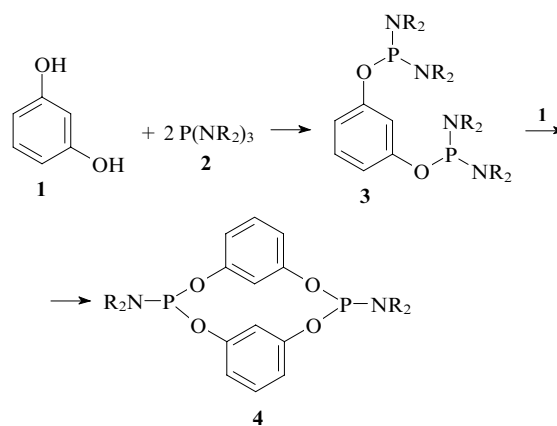
II. Syntheses using trivalent phosphorus compounds

1. Syntheses of diphosphamacrocycles

This problem attracted the attention of scientists from several research centres. They studied the reactions of dibasic phenols with equivalent and inequivalent amounts of phosphorylating agents (direct cyclophosphorylation and molecular assembly techniques, respectively).

a. Cyclophosphorylation of dihydroxybenzenes and 4,4'-dihydroxybiphenyl

The first phosphacyclophanes comprising two resorcinol (**1**) residues linked by two phosphoramidite bridges were synthesised in 1997 by the reactions of **1** with hexaalkylphosphorous triamides **2** taken in a 1 : 2 molar ratio.^{8–10} Then, 1,3-bis(phosphordiamidite)benzene **3** formed in the first stage was introduced into the reaction with an equimolar amount of **1**:



R = Me, Et.

In addition to this process (we will call it ‘molecular assembly’), a direct reaction between equimolar amounts of resorcinol and phosphorous triamide is also possible. This reaction, which can be called ‘direct cyclophosphorylation’ or ‘direct synthesis’, is more convenient and often gives better results. Both reactions proceed in acetonitrile or 1,4-dioxane at room temperature.

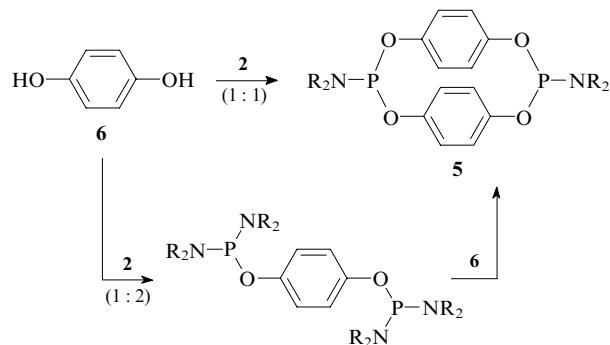
E E Nifantsev, P V Slitkov, E N Rasadkina Department of Chemistry, Moscow State Pedagogical University, Nesvizhskii per. 3, 119021 Moscow, Russian Federation. Fax (7-495) 246 77 66, tel. (7-495) 246 57 90, (E E Nifantsev, E N Rasadkina), (7-495) 246 54 53 (P V Slitkov), e-mail: chemdept@mtu-net.ru

Received 25 September 2006

Uspekhi Khimii 76 (4) 362–374 (2007); translated by A M Raevskiy

Cyclic bis(phosphoramidites) **4** are oily substances characterised by good solubility in conventional organic solvents and high oxidisability.

Cyclic phosphoramidites **5** based on hydroquinone **6** were also synthesised by the molecular assembly and direct phosphorylation techniques (from this point on, figures in parentheses above or below the arrow denote the reactant ratio).¹¹



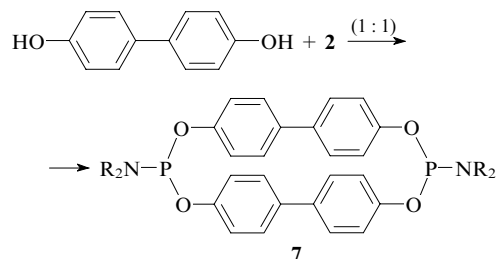
R = Me, Et.

The direct phosphorylation method resulted in higher yields of compounds **5** compared to the molecular assembly technique.

The structures and individuality of the reaction products as well as cyclic phosphoramidites and their derivatives (see below) were proved by physicochemical methods (¹H and ³¹P NMR spectroscopy, IR spectroscopy and mass spectrometry) and confirmed by the results of elemental analysis. Cyclic phosphoramidites **5** synthesised in different ways exhibited identical physicochemical characteristics. These are solid, low-melting and poorly soluble substances that are unstable upon storage even in inert atmosphere. Probably, the labile behaviour of these compounds is due to strain in the macrocycle caused by the proximate arrangement of two aromatic rings. This assumption was confirmed by the results of calculations of the most stable conformations, according to which the molecules of cyclic bis(phosphoramidites) **5** have an eclipsed cyclophane structure.¹²

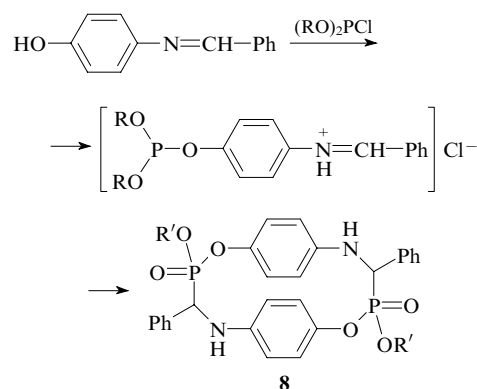
Compounds **5** readily add oxygen and sulfur to give corresponding cyclic bis(phosphoramidates) and bis(phosphoramidothioates).

Similar heterophanes (hereafter, phosphacyclophanes) **7** are formed in the reactions of 4,4'-dihydroxybiphenyl with phosphorous triamides **2**.¹¹



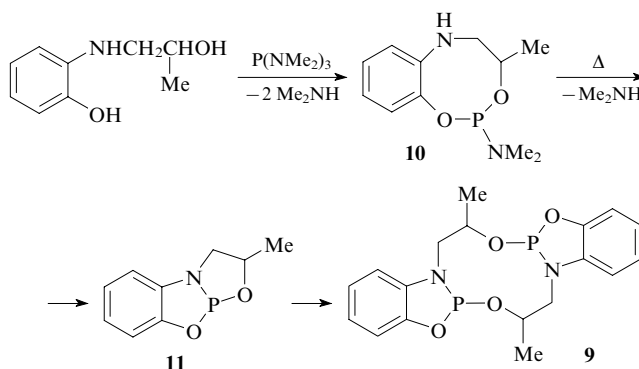
Compounds **5** and **7** were introduced into the oxidation reactions and into complexation with Mo(CO)₆ and Rh(CO)₂(acac) (acac stands for acetylacetonate). The oxidation and complexation with Rh(CO)₂(acac) occurred in dichloromethane at room temperature. Complexes with Mo(CO)₆ formed only on heating in dioxane (95 °C) in the presence of excess carbonyl. All derivatives were isolated and studied by physicochemical methods (¹H and ³¹P NMR spectroscopy and IR spectroscopy).

Nitrogen-containing phosphacyclophanes **8** were obtained from (*N*-benzylidene)-*p*-aminophenol and dialkylphosphorochloridites (RO)₂P(O)Cl.¹³ The reactions proceeded in chloroform at room temperature and completed in 5 days.



R = R' = Et; (RO)₂ = OCH₂CH₂O, R' = CH₂CH₂Cl.

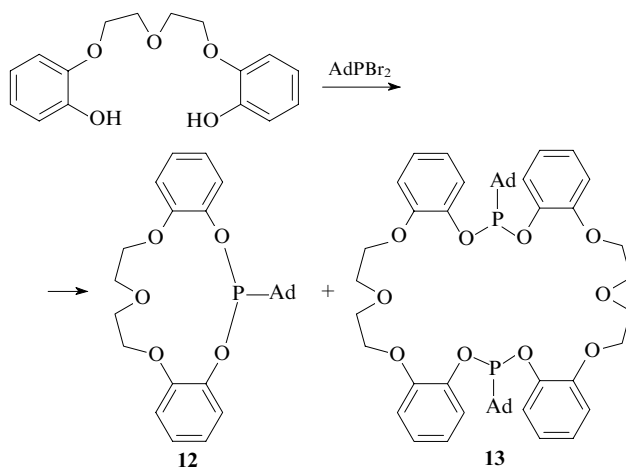
Phosphacyclophane **9** was synthesised by phosphorylation of *N*-(β-hydroxypropyl)-*o*-aminophenol with hexamethylphosphorous triamide.¹⁴ Monitoring by ³¹P NMR spectroscopy revealed the formation of cyclic compound **10** with one phosphorus-containing fragment. When heated, compound **10** transformed into heterobicyclic **11** which in turn experienced spontaneous dimerisation into phosphoramidite **9**. The structure of compound **9** was proved by X-ray analysis.



At 20 °C, the transformation **11** → **9** takes a very long time to complete (about a year).

b. Cyclophosphorylation of organylenebisphenols

Among the first examples of this type of chemical transformation is the reaction of 1,7-bis(2-hydroxyphenyl)-1,4,7-trioxaheptane with 1-adamantyldibromophosphine (AdPBr₂).¹⁵

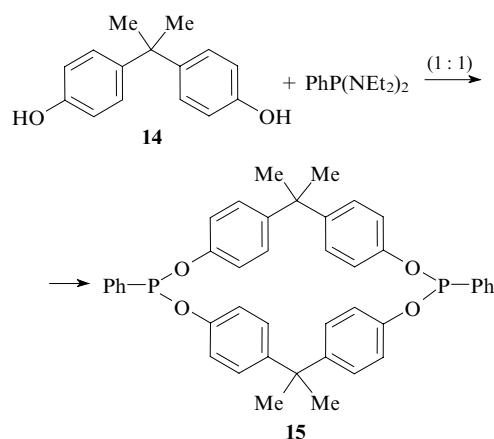


Ad is 1-adamantyl.

This cyclophosphorylation results in the fourteen-membered adamantylphosphonous acid diester **12** (yield 10%) and

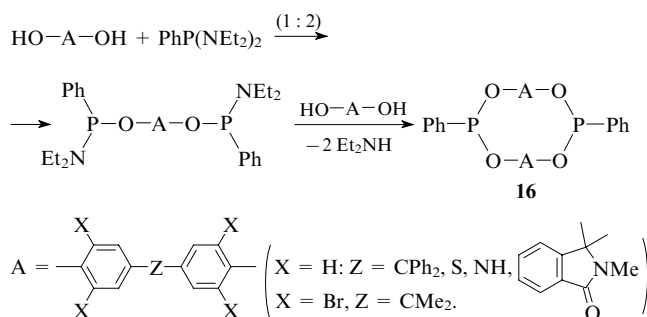
diphosphorus cyclic compound **13** (yield 11%–44%). The structures of the products were confirmed by NMR spectroscopy and by measuring the molecular mass (ebullioscopy). Substance **13** appeared to be a stable and convenient reactant, which can be oxidised, alkylated, *etc.*

The cyclophosphorylation of an available commercial product, namely, 2,2-bis(*p*-hydroxyphenyl)propane (DIAN) (**14**) with phenylphosphonous acid tetraethyldiamide was studied in the 1990s.¹⁶



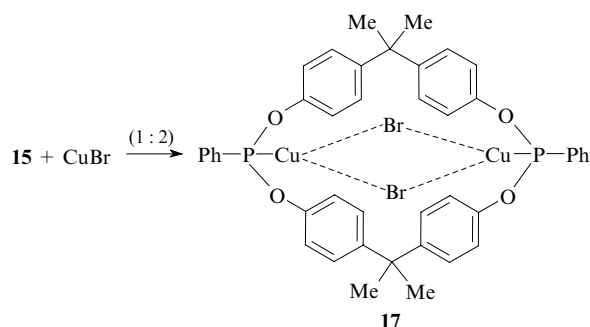
The reaction was carried out in toluene under (relatively) severe conditions (115–120 °C). The structure of cyclophenylphosphonite **15** was studied by X-ray analysis.¹⁷ The phosphorus atoms and the quaternary carbon atoms approximately occupy the corners of a square. The angle between the DIAN aromatic rings is 35° so the whole system has a cavity. The diphosphonite macrocycle **15** was found to be a stable compound.

This allowed one to extend the range of dinuclear bisphenols used in cyclocondensation and synthesise new macrocycles **16** containing not only isopropylidene, but also sulfide, imide and other bridges.¹⁸



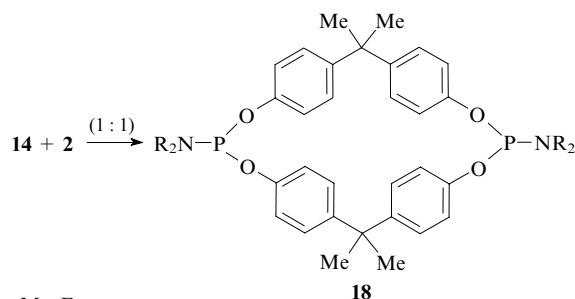
Cyclic bis(phenylphosphonites) **16** were introduced into the complexation, oxidation and sulfurisation reactions, easily

resulting in cyclophosphonates and their thio analogues. An X-ray diffraction study revealed considerable changes in the cavity volume and configuration for cyclic bis(phosphonates) compared to the starting cyclic bis(phenylphosphonites).¹⁸ Some cyclic bis(phenylphosphonites), *e.g.*, compounds **15** and **16**, can form complexes with CuBr.^{19,20} The assumption of metal coordination to two phosphorus atoms was confirmed by ³¹P NMR data.



Complexes **17** exhibit high catalytic activity in the reactions accompanied by transfer of hydrogen atoms in homogeneous media.

Phosphorylation of bisphenol **14** with equimolar amount of phosphorous triamides **2** under mild conditions results in reactive cyclic phosphoramidites **18**.²¹

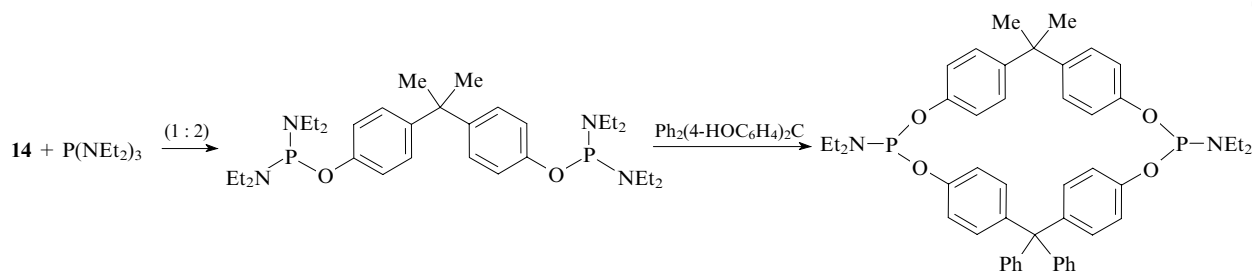


This approach can be extended to molecular assembly of unsymmetrical bis(phosphoramidite) macrocycles (Scheme 1).

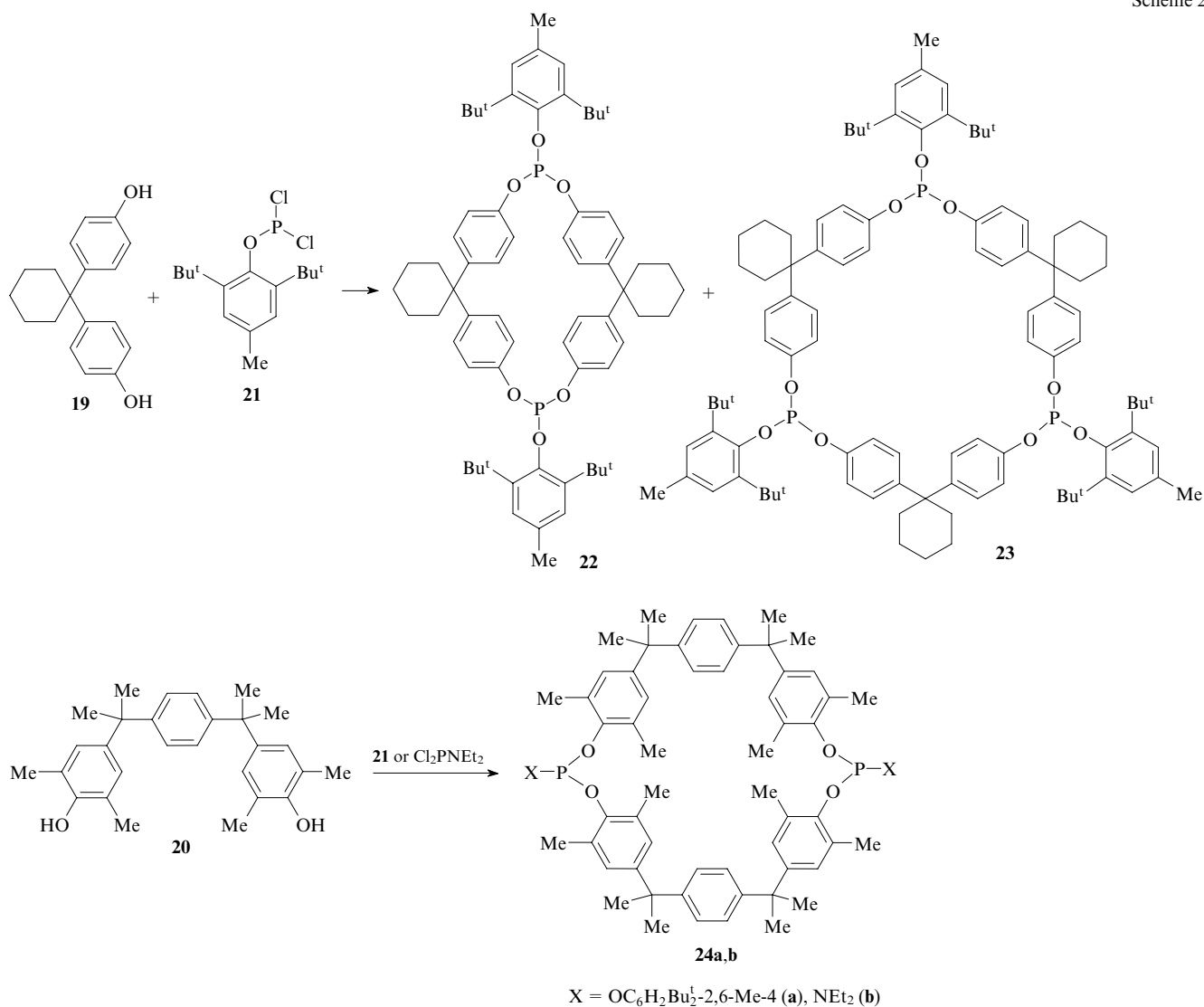
Using bisphenols **19** and **20** as matrices and 2,6-di-*tert*-butyl-4-methylphenylphosphonous dichloride (**21**) and diethylamidophosphonous dichloride as phosphorylating reagents, in the last decade Habicher and Bauer^{22–25} synthesised a series of even more complex macrocycles **22–24**. The syntheses were carried out at room temperature in toluene in the presence of triethylamine upon high dilution (Scheme 2).

Habicher and Bauer also established that many unsymmetrical macrocycles undergo spontaneous symmetrisation. For instance, the interaction of bisphenol **14** with bis(phosphorodiamidite) based on bisphenol **20** results in cyclic phos-

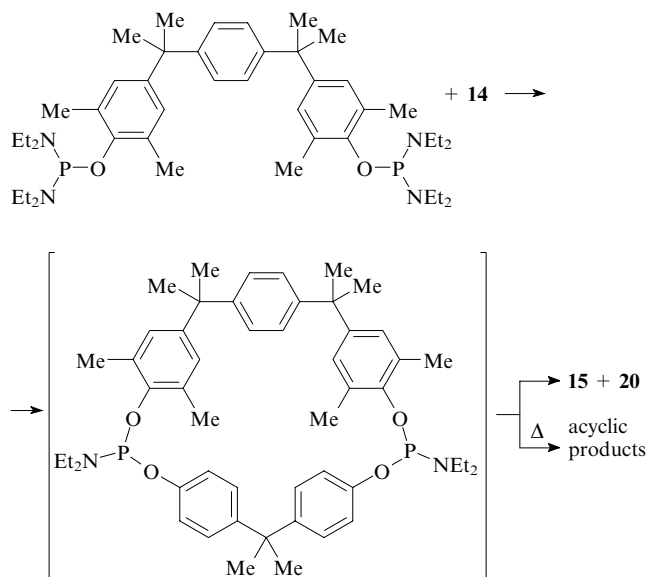
Scheme 1



Scheme 2

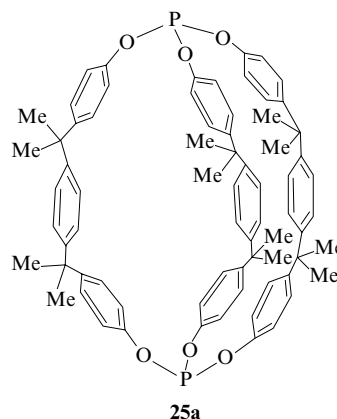


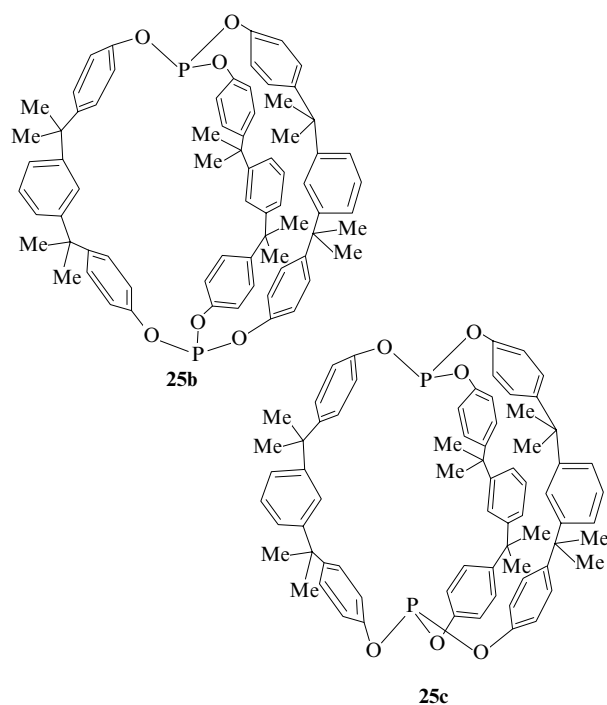
phoramidite **15** and free bisphenol **20**. When carried out on heating, this reaction affords acyclic oligomeric products.



The above series of reactions is completed by the synthesis of phosphorus-containing cryptands **25a–c** by the reaction of bisphenol **20** with phosphorus trichloride.²⁶

Analysis of the structures of cryptands **25** revealed the ‘in–out’ isomerism. All three stereoisomers were chromatographically separated. The structures of isomers **25a–c** were proved by NMR spectroscopy and X-ray diffraction analysis. In addition, all three cryptands were introduced into the

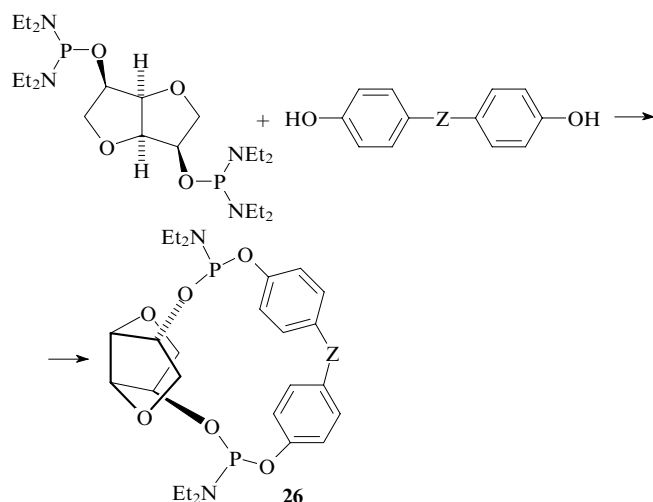




reactions characteristic of simple phosphites.²⁷ The synthesis and investigations of the chemical features of cyclic phosphites and phosphorus-containing cryptands have been well documented in a review.²⁸

At present, cyclophosphorylation reactions are carried out using phosphorochloridites and phosphoramidites, the latter often being more convenient because they react with phenols at room temperature in various solvents and do not require removal of amines released. Additionally, the amide groups show different reactivities, namely, the first amide group is replaced rapidly while the third amide group remains almost unsubstituted. At the same time the use of reaction mixtures based on phosphorochloridites requires introduction of acceptors in order to bind hydrogen chloride evolved, all chlorine atoms being almost equally reactive. Probably, the next stage of research and development in this field of synthetic chemistry will require optimisation of reaction conditions, *e.g.*, the search for appropriate catalysts.

Progress in the synthesis of complex macrocyclic diphosphorus systems using phosphorous triamides **2** led to the preparation of multinuclear chiral structures **26** based on the

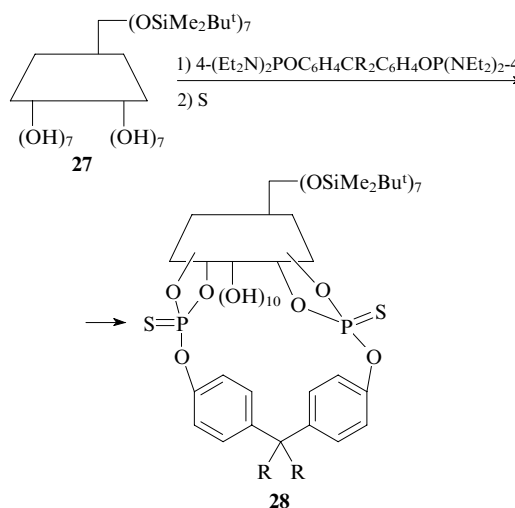


Z = O, S, CMe₂, CPh₂.

available bisphosphorylated 1,4;3,6-dianhydro-D-mannitol derivative.^{29–31} The reaction was carried out in benzene with distillation of diethylamine (75 °C) in inert atmosphere.

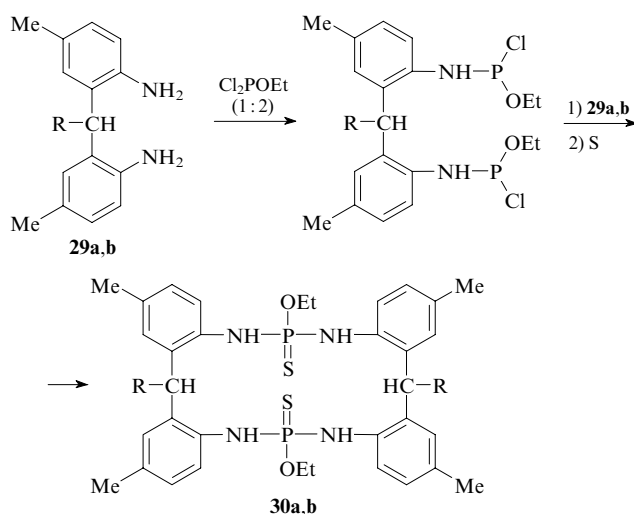
Products **26** were converted *in situ* into corresponding bis(thiophosphates), which were isolated from the reaction medium in 60%–88% yields by column chromatography.

Structures with large cavities were also synthesised starting from silylated β -cyclodextrin derivative **27** and various dinuclear phosphorylated bisphenols.³² The reactions in benzene at 75 °C completed in 6 h and resulted in the so-called ‘capped’ cyclodextrins **28** isolated in 62%–75% yields by column chromatography. ‘Capping’ of the cyclodextrin molecule enhances its ability to form inclusion complexes with various ‘guest’ molecules.



R = Me, Ph.

In addition to bisphenols, aromatic diamines were also employed to design related macrocyclic systems. For instance, bis(2-amino-5-methylphenyl)methane (**29a**) and its phenyl analogue **29b** served as building blocks for the synthesis of 16-membered nitrogen-containing macrocycles **30a,b**.³³ The reaction was carried out using the molecular assembly technique in dioxane in the presence of triethylamine at 5 °C with ethyl phosphorodichloridite as phosphorylating agent.



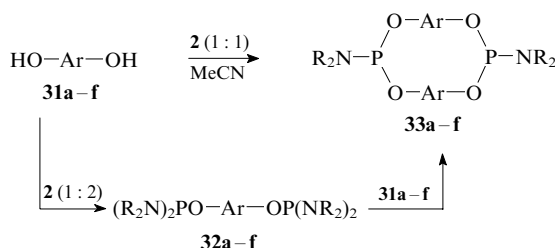
R = H (a), Ph (b).

The best results were obtained in the phosphorylation of primary amines with alkyl phosphorodichloridites. ³¹P and ¹H NMR studies showed that the macrocycles synthesised exist as mixtures of two conformers.

c. Cyclophosphorylation of dihydroxynaphthalenes and dihydroxyanthracenes

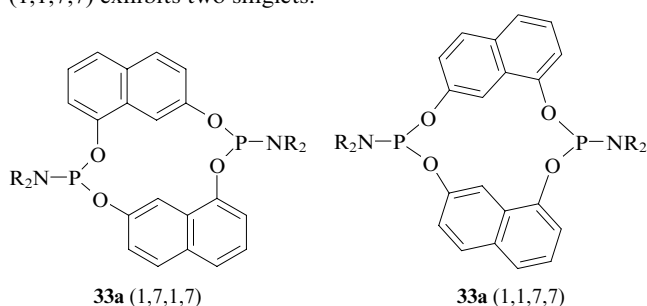
The cyclophosphorylation of dihydroxynaphthalenes is a promising method for the synthesis of previously unknown phosphacyclophanes. At present, it has been shown that both symmetrical (1,5-; 2,6-; 2,7-) and unsymmetrical (1,3-; 1,6- and 1,7-) dihydroxynaphthalenes **31** efficiently react with phosphorous triamides **2** following the single-step or two-step (involving intermediate amido esters **32**) schemes.^{17, 34–39}

All reactions were carried out in acetonitrile at room temperature and completed in 3 to 40 h depending on the substituent in the phosphorylating agent. The cyclic products **33a–f** were obtained in 70%–80% yields.

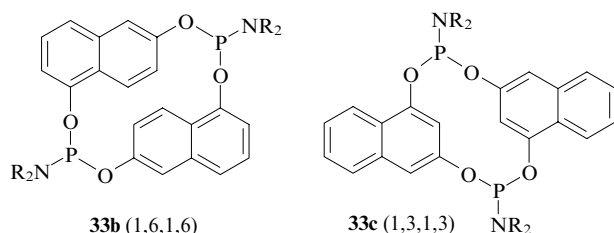


R = Me, Et, Prⁱ; R–R = (CH₂)₅; Ar = *i,j*-naphthylene;
i = 1; *j* = 7 (**a**), 6 (**b**), 3 (**c**), 5 (**d**); *i* = 2; *j* = 7 (**e**), 6 (**f**).

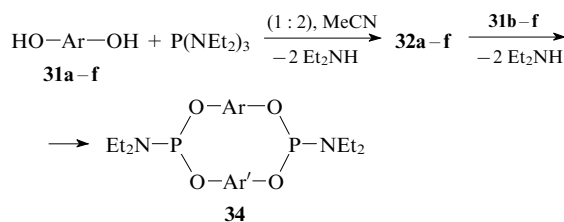
Cyclophosphorylation of 1,7-dihydroxynaphthalene (**31a**) results in two structural isomers with differently arranged naphthylenedioxy groups, namely, a series arrangement in compound **33a** (1,7,1,7) and a pairwise arrangement in compound **33a** (1,1,7,7). The former isomer was isolated and studied by NMR spectroscopy and X-ray diffraction analysis.^{36, 37} Its ³¹P NMR spectrum exhibits a singlet. The second isomer was characterised by ¹H NMR spectroscopy in the form of thio derivative. The ³¹P NMR spectrum of **33a** (1,1,7,7) exhibits two singlets.



Products of cyclophosphorylation of 1,6- or 1,3-dihydroxynaphthalene exist as single structural isomers [compounds **33b** (1,6,1,6) or **33c** (1,3,1,3), respectively] with a series arrangement of naphthylenedioxy groups in the ring.^{38, 39}

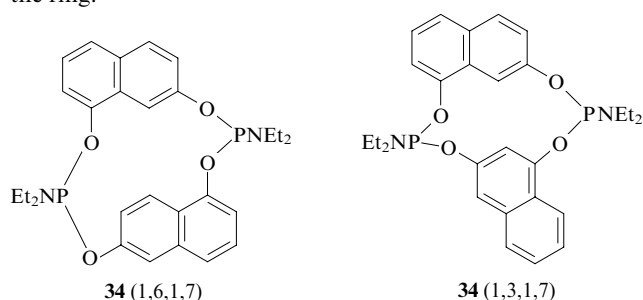


The molecular assembly technique was also used for the synthesis of phosphacyclophanes **34** the molecules of which comprise different arylene moieties. A number of 'non-uniform' naphthophosphacyclophanes containing two different naphthylenedioxy units were obtained.⁴⁰



Ar = *i,j*-naphthylene, Ar' = *i',j'*-naphthylene; {*ij*} ≠ {*i'j'*}.

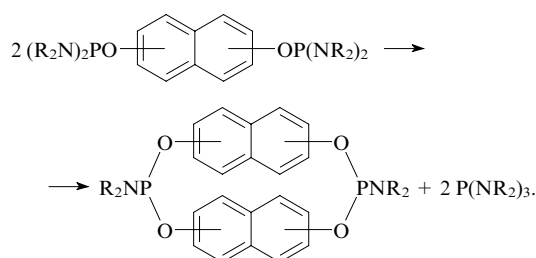
Similarly to the case of 'uniform' naphthophosphacyclophanes based on 1,6- and 1,3-dihydroxynaphthalenes, cyclophosphorylation of unsymmetrical 1,7-, 1,6- and 1,3-dihydroxynaphthalenes only resulted in structural isomers with a series arrangement of the naphthylenedioxy groups in the ring.



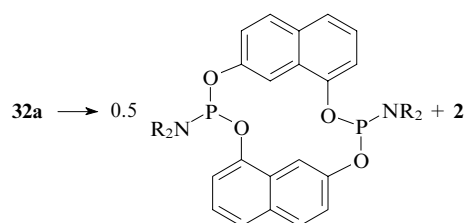
The reaction is regioselective; therefore, the products were isolated in a pure state. The naphthophosphacyclophanes **33** and **34** were oxidised and sulfurised. The reactions in dichloromethane at room temperature took a short time (20 h) to complete. Thiophosphoramidates were isolated by column chromatography (yields ~55%) and cyclophosphoramidates were isolated by reprecipitation (yields ~90%). The structures and individual character of all macrocycles **33**, **34** and their thio and oxo derivatives were confirmed by ¹H, ¹³C and ³¹P NMR spectroscopy and by MALDI mass spectrometry. MM2 calculations of the steric energies of the 'uniform' and 'non-uniform' naphthophosphacyclophanes made it possible to predict the stabilities of corresponding phosphites, thiophosphates and phosphates.

Cyclic phosphoramidites **33** and **34** readily form complexes with Mo(0) and Rh(I). The complexation of 'uniform' naphthophosphacyclophanes occurs more easily than that of 'non-uniform' compounds.

Recently, the syntheses of naphthalene-based phosphacyclophanes using dismutation of bis(phosphoramidites) were reported.^{41, 42} The process can be described as follows:



The rate of this reaction depends on position of substitution in naphthylenedioxy groups and on the nature of the substituent at the phosphorus atom. In particular, the reaction of unsymmetrical 1,7-dihydroxynaphthalene results in one structural isomer with a series arrangement of naphthylenedioxy groups in the ring.³⁷

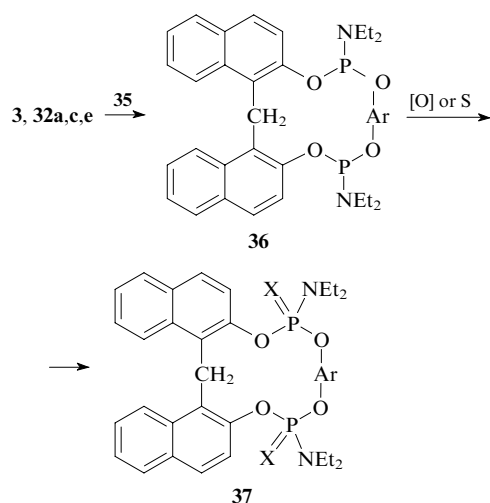


As mentioned above, the direct synthesis and molecular assembly techniques afford a mixture of two structural isomers, one with a series (1,7,1,7) and the other with a pairwise (1,1,7,7) arrangement of naphthylendioxy groups in the ring. Therefore, the dismutation is a regioselective reaction.

The dismutation of bis(phosphoramidites) based on dibasic phenols and naphthols has been studied in considerable detail.^{41, 42} The process is governed by many factors including the nature of the aromatic fragment, the substituent at the phosphorus atom, the solvent and especially the existence of conjugation in the starting reactant molecule. The derivatives of condensed aromatic systems undergo dismutation faster than their mononuclear analogues. Dismutation of the amide derivatives with aliphatic substituents at nitrogen also proceeds more readily than that of their heterocyclic analogues. The reaction in dichloromethane proceeds at the highest rate irrespective of the aromatic component and substituents at phosphorus. Non-polar solvents (benzene, diethyl ether) do not favour dismutation. Temperature does not affect the duration of the dismutation reaction. In the presence of a catalyst (amine hydrochloride) the process time is shortened by a factor of 1.5–2.

In addition, MM2 calculations of the steric energies were carried out for all the compounds synthesised. Generally, the steric energies of phosphorous diamido esters **32** are higher than those of phosphorous amido diesters **33**, **34**.

Cyclic phosphoramidites **36** were synthesised from bisphosphorylated aromatic diols **3**, **32a,c,e** and 2,2'-dihydroxy-1,1'-dinaphthylmethane (**35**) by the molecular assembly technique at room temperature in dioxane.⁴³

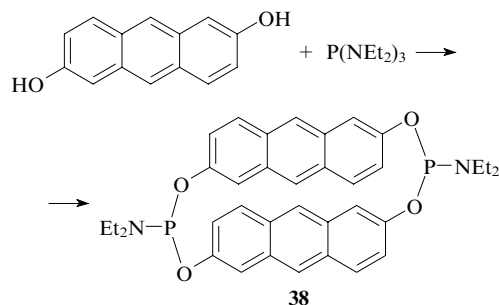


Ar = 1,3-phenylene, 1,7-, 1,3- or 2,7-naphthylene; X = S, O.

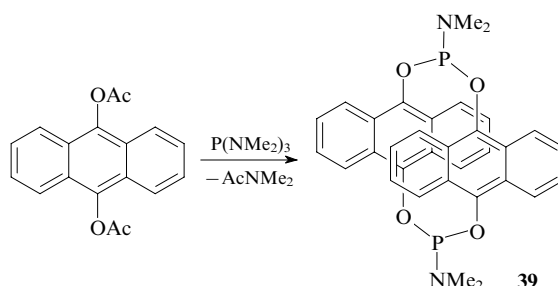
The oxidation occurred in dioxane or dichloromethane at room temperature and completed in 24 h. The structures of the resulting macrocycles **37** were confirmed by ¹H, ¹³C and ³¹P NMR spectroscopy and by MALDI mass spectrometry.

Phosphacyclophanes were also synthesised from dihydroxyanthracenes. For instance, the reaction of 2,6-dihydroxyanthracene with hexaethylphosphorous triamide results in a symmetrical ring system **38**.⁴⁴ This compound is similar in

chemical properties to the naphthalene analogues studied earlier.



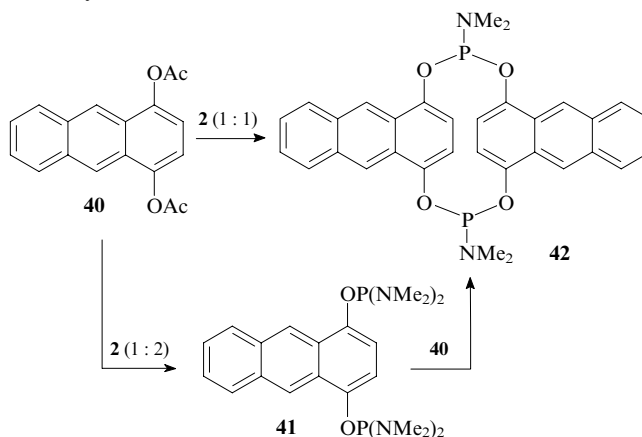
A cage product **39** comprised of two anthracene residues linked by two phosphoramidite bridges at positions 9,10 was prepared from 9,10-diacetoxyanthracene, which was used instead of very unstable 9,10-dihydroxyanthracene, and hexamethylphosphorous triamide.^{45, 46}



The reaction proceeded at 20 °C and completed after 96 h. Phosphacyclophane **39** was isolated in a 42% yield using two methods, at equimolar reactant ratio and by dismutation.

Product **39** appeared to be unstable in solution and decomposed with release of anthraquinone. This is consistent with the results of MM2 calculations.

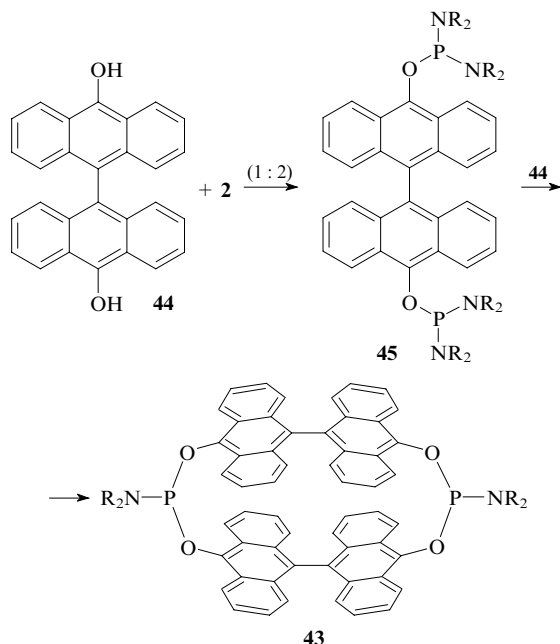
A dimer based on 1,4-dihydroxyanthracene was also synthesised from its diacetate derivative **40** using the molecular assembly technique involving bis(phosphoramidite) **41** and the direct synthesis.^{46, 47}



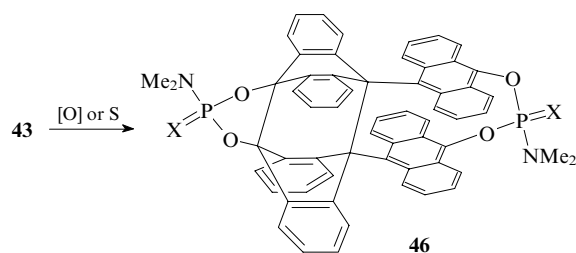
The reaction was carried out at room temperature. Phosphacyclophane **42** was isolated in 37% (molecular assembly technique) and 58% (direct synthesis) yields. A MALDI mass spectrometric study showed that the cyclic product contains two anthracene moieties and two phosphorus-containing groups. Compound **42** is much more stable than compound **39**, because the aromatic fragments in the former can be more distant from each other.

Macrocycle **43** is based on dianthrone **44**, a bisphenol containing two mutually perpendicular 9-anthrone residues

linked by a C—C bond at positions 10.⁴⁸ It was phosphorylated with phosphorous amides **2** in pyridine only on heating in the temperature range of 50–120 °C depending on the substituent in the phosphorylating agent. Cyclic systems **43** were only synthesised by the molecular assembly technique using corresponding bisphosphorylated derivatives **45**.

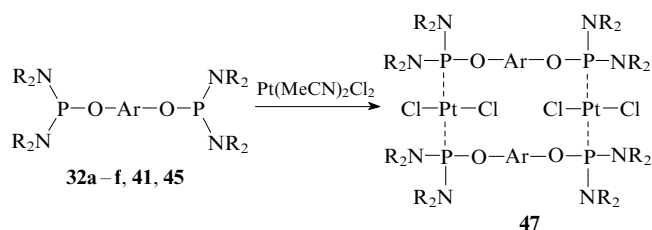


The direct synthesis affords a mixture of cyclic systems containing two to four dianthracene residues. It was established that oxidation of cyclic compound **43** ($R = \text{Me}$) results in a 'cross-linked' structure **46** containing a five-membered ring with two quaternary carbon atoms. It was assumed that in this case one deals with isomerisation, which obeys the pattern of intramolecular Diels–Alder reaction and is similar to intramolecular cycloaddition of some compounds with two anthracene residues.



$X = \text{S}, \text{O}$.

Metallaphane complexes **47** containing bridging $\text{Pt}(\text{II})$ atoms are based on dihydroxynaphthalene derivatives **32a–f** and bisphosphorylated dihydroxyanthracenes **41** and **45**. The synthesis was carried out in dichloromethane or pyridine at room temperature with diacetonitriledichloroplatinum(II) as the starting complex.^{35, 49–51}

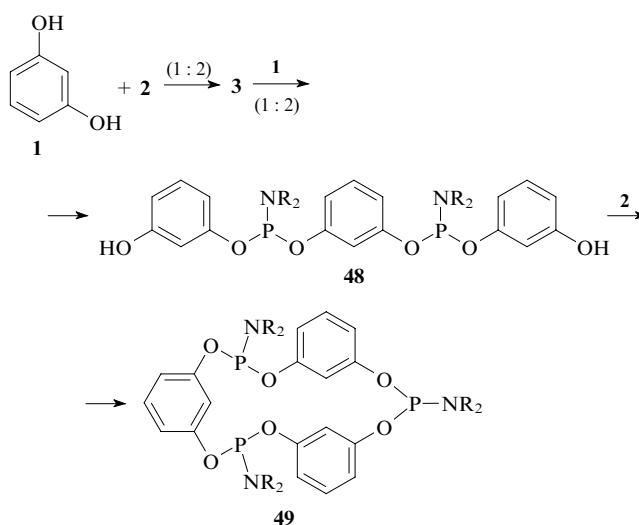


Complexes **47** are powder-like compounds which decompose upon melting. They were isolated in 60%–80% yields. The structures and compositions of the complexes were confirmed by ^1H and ^{31}P NMR spectroscopy and by cryoscopy. The spin–spin coupling constants $^1J_{\text{PPt}}$ equal to 3441 and 3347 Hz indicate that the complexes are *trans*-isomers.

2. Synthesis of triphosphamacrocycles

Recently, macrocyclic compounds larger than molecule **4** containing regularly arranged phosphoramidite groups and resorcinol fragments have been synthesised. The resulting compounds resemble Pedersen's crown ethers.⁶ Therefore, they or corresponding pentavalent phosphorus derivatives can find practical applications in supramolecular chemistry.

The simplest representatives of these macrocyclic compounds were synthesised following the scheme:

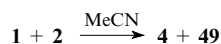


$R = \text{Me}, \text{Et}$.

The reactions of resorcinol and phosphorous amides **2** were carried out at 1:2 molar ratio of the reactants at room temperature. Then, phosphorodiamidite **3** was introduced into the reaction with resorcinol. Linear reaction product **48** undergoes cyclisation in the reaction with phosphoramidite **2**.^{52–54}

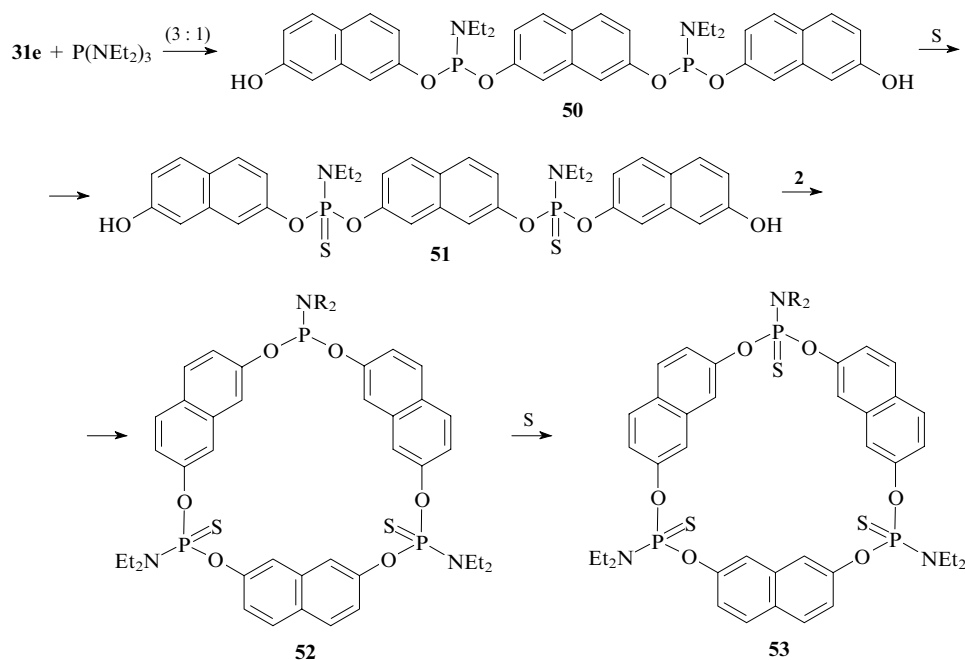
Sulfurisation of macrocyclic tris(phosphoramidite) **49** results in a crystalline *cis,cis,trans*-product (one P atom is above and the other two P atoms are below the macrocycle plane); its structure was established by X-ray diffraction analysis.⁵³ Later on, dismutation of macrocyclic pentakis(phosphoramidite) (see Section II.3) afforded the *cis,cis,cis*-isomer of heterocycle **49** (all P atoms are on one side of the macrocycle), which significantly differs from the *cis,cis,trans*-isomer in properties.^{54, 55}

Mention should be made of the possibility of bis(phosphoramidite) **4** formation in the first stage of this reaction. Unfortunately, other procedures for the synthesis of cyclic phosphoramidites are also non-selective. For instance, the reactions of resorcinol with phosphorous triamides **2** in acetonitrile result in cyclic bis(phosphoramidite) **4** and cyclic tris(phosphoramidites) **49** as the major products.^{8, 9}



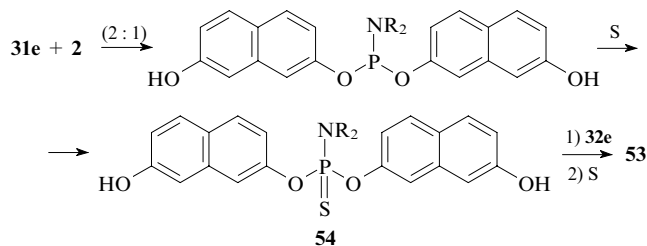
Cyclic tris(naphthylenephosphoramidites) have also been synthesised (Scheme 3).^{51, 56} One route to these compounds begins with the synthesis of linear bis(phosphoramidite) **50** containing three naphthylene fragments, two of which bear hydroxyl groups, at a 1:3 ratio of the starting reactants (this is

Scheme 3



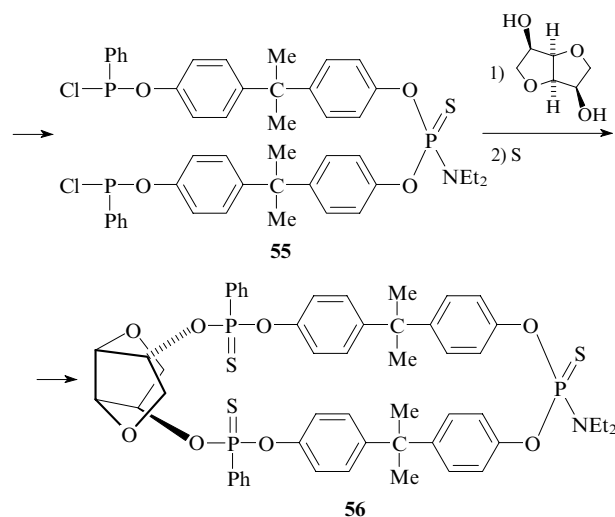
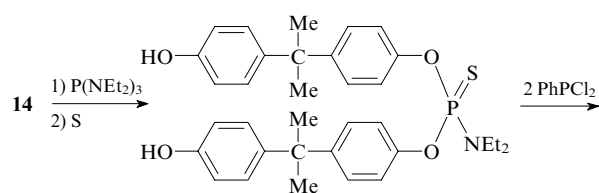
a necessary condition). Otherwise, the reaction results in cyclic bis(phosphoramidite) **33e**. Bisphenol **50** was sulfured and product **51** was isolated by column chromatography. Phosphocyclisation of **51** with phosphorous triamides **2** resulted in compound **52** which was again sulfured. Tris(thiophosphate) **53** was isolated by column chromatography in ~60% yield.

The second method involves the synthesis of stable acyclic *O,O*-bis(7-hydroxy-2-naphthyl) *N,N*-dialkyl thiophosphoramidates **54**. Cyclisation of **54** with bisphosphorylated 2,7-dihydroxynaphthalene **32e** followed by sulfuration affords the desired cyclic tris(thiophosphate) **53**.



Cyclic thiophosphates **53** synthesised using both methods exhibited fully identical physicochemical characteristics.^{51, 56} These tris(thiophosphates) can be used as, *e.g.*, ligands for binding 'soft' metals or as starting compounds in syntheses of cyclic tris(phosphites).

Bisphenol **14**, $P(NEt_2)_3$ and phenylphosphonous dichloride were used for the synthesis of a phosphorylating agent **55**, which was then employed in the phosphorylation of 1,4;3,6-dianhydro-D-mannitol³¹ in order to obtain a chiral large-cavity system **56**.

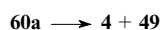


The reaction was carried out in benzene, the second and third stages being conducted in the presence of triethylamine. Macrocycle **56** was isolated in 40% yield and characterised by ³¹P and ¹H NMR spectroscopy.

3. Synthesis of higher phosphorus-containing macrocycles

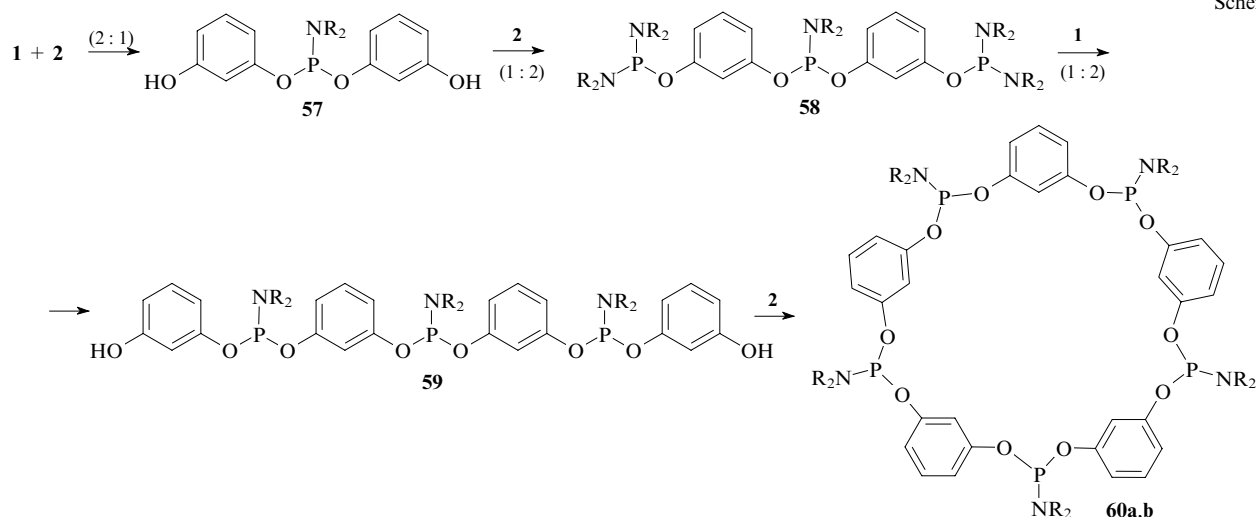
Higher macrocyclic systems were designed using the molecular assembly technique starting from resorcinol and phosphorous triamides **2** (see above). The oligomer chain terminated with hydroxyl groups at both ends was extended in a sequential manner. Then, the diols thus obtained were cyclophosphorylated with phosphorous triamides **2**. One-pot synthesis under control of the composition of intermediates **57–59** resulted in cyclic pentakis(phosphoramidites) **60** (Scheme 4).^{53, 54}

The reaction was carried out in acetonitrile or benzene at room temperature. Cyclic compound **60a** is unstable and undergoes a rearrangement resulting in cyclic bis- and tris(phosphoramidites) when stored in benzene solution.



In contrast to this, cyclic pentakis(phosphoramidite) **60b** does not undergo rearrangement.^{54, 55}

Scheme 4

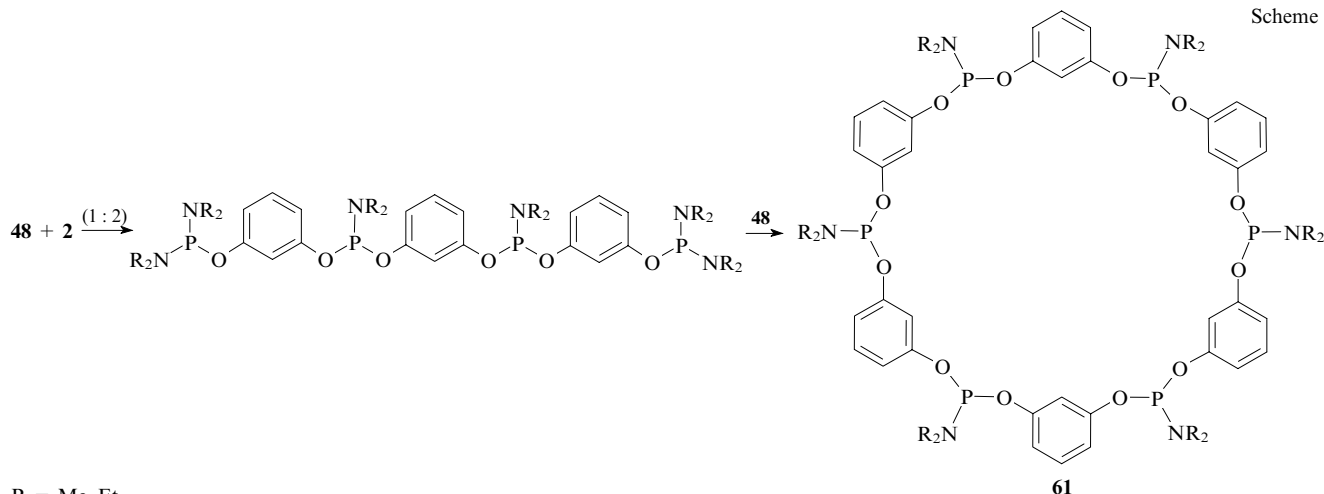


R = Me (a), Et (b).

Regarding even more complex macrocycles, it is appropriate to synthesise them from two fragments of a target system with similar compositions. An example is provided by the synthesis of cyclic hexakis(phosphoramidites) **61** (Scheme 5).

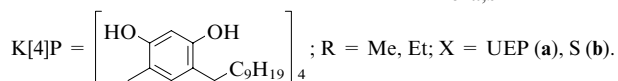
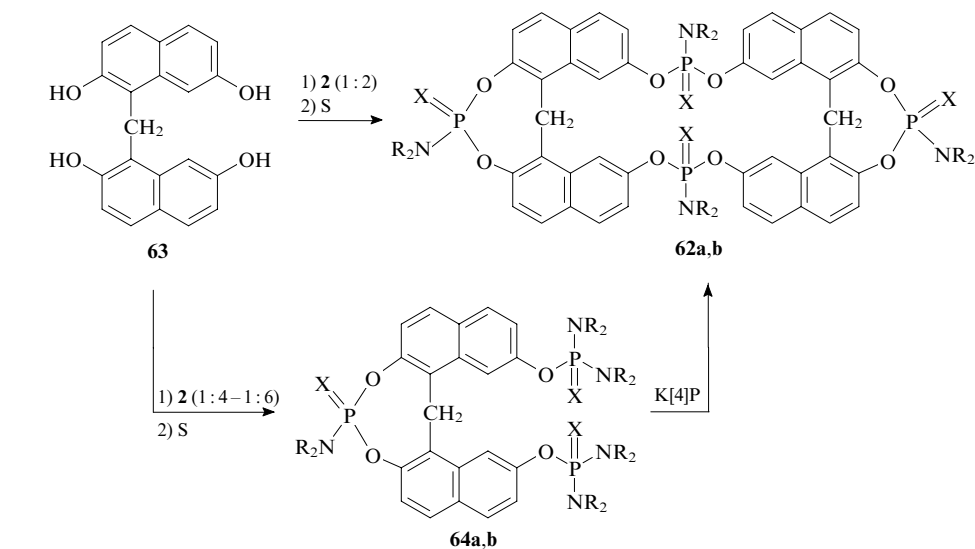
Cyclic oligomeric phosphoramidites considered above were introduced into the sulfurisation and oxidation reactions. Some of them were introduced into the complexation reactions with $\text{Rh}(\text{CO})_2(\text{acac})$. The results of cryoscopic determination

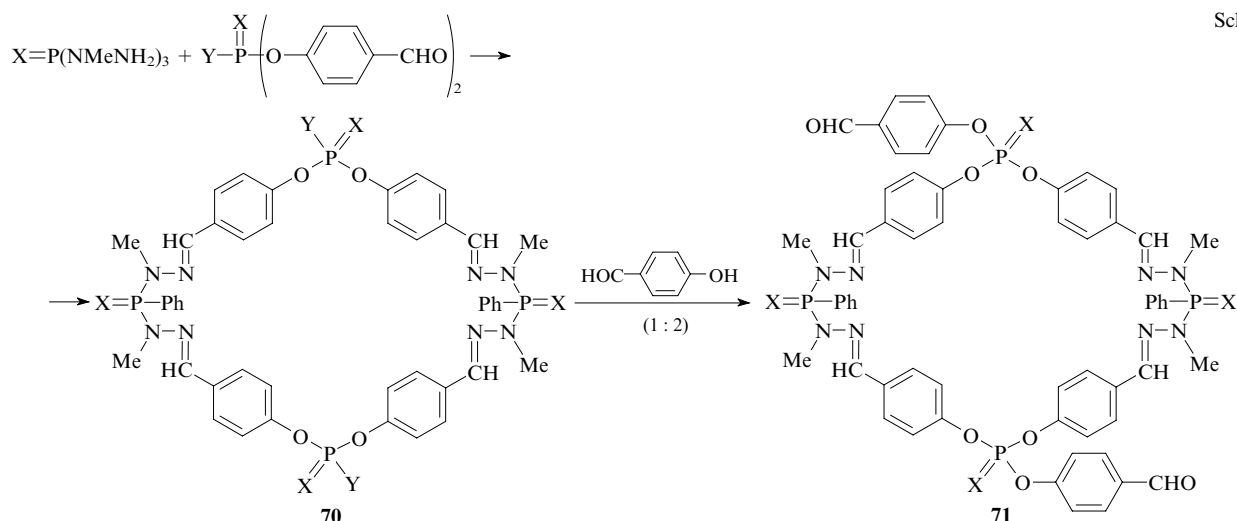
Scheme 5



R = Me, Et.

Scheme 6



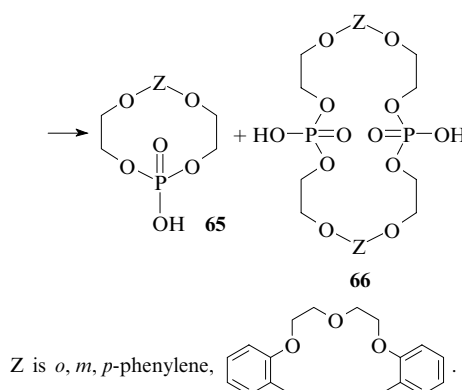
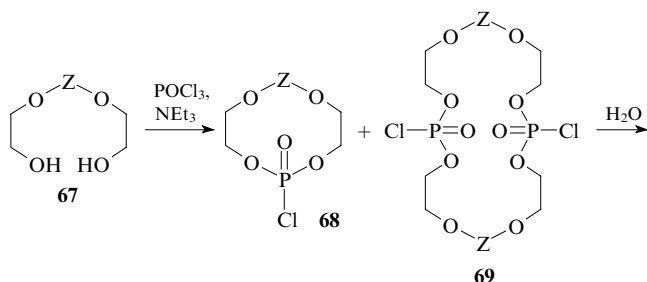


of the molecular masses and the NMR spectra confirm the structures of these compounds.

Macrocycles **62** were synthesised based on 2,2',7,7'-tetrahydroxy-1,1'-dinaphthylmethane **63**. Macrocycles **62** contain four phosphorus atoms, two of them form phosphocine fragments. Phosphorous triamides **2** served as phosphorylating agents. Macrocycles **62** can be synthesised using two procedures, by direct phosphorylation at 1 : 2 reactant ratio and in a stepwise reaction using the action of calix[4]resorcinarene (K[4P] with bulky hydrophobic substituents in the lower rim on the phosphate derivative **64** in the second stage.⁵⁷ All reactions were carried out in dioxane under argon at room temperature (Scheme 6). The yields of the target products **62** were 55%–63%.

III. Syntheses using pentavalent phosphorus compounds

Compared to trivalent phosphorus compounds, pentavalent phosphorus derivatives are usually poor phosphorylating agents. Nevertheless, in some cases it is more appropriate to synthesise complex phosphorus-containing macrocyclic systems using phosphochloridates, phosphoramidates and other pentavalent phosphorus derivatives. This is confirmed by the stereochemical features of the pentavalent phosphorus derivatives and by their stabilities against oxidation and disproportionation and, therefore, by the stability upon storage. Recently, novel polyfunctional crown ethers representing macrocyclic phosphates and phosphonates have been synthesised. For instance, arylenephosphate **65** and bis(arylenediphosphate) **66** were synthesised in two stages by the reactions of various arylenediols **67** with phosphorus oxochloride in the presence of triethylamine followed by hydrolysis of intermediate phosphochloridates **68**, **69** (compounds **69** were not isolated).⁵⁸



Pentavalent phosphorus derivatives were also employed to design polyfunctional phosphate-phosphonate macrocyclic systems **70** and **71** reported by Caminade *et al.*^{59–61} Of particular interest are those systems that can be readily modified due to the presence of aldehyde groups (*e.g.*, compound **71**), which favour chain extension and formation of bulky cryptands, crown ethers and dendrimers (Scheme 7).^{62, 63}

IV. Conclusion

Summing up, an original field of chemistry of phosphorus-containing macroheterocycles has emerged in the last decade. Progress in this research avenue is due to the availability of reactants and efficiency of synthetic methods. The strategies of synthesis have been well developed, the molecular assembly technique being used more often. In turn, the alternative route, the direct synthesis of bismacrocyclic systems, is sometimes more preferable because it ensures higher yields of end products. Carrying out reactions at high temperatures and under solvent-free conditions can result in macrocycles containing more than two phosphorus-containing groups. Usually, the best results are obtained in phosphorylation and cyclophosphorylation with amides, which results in a smaller content of side products. Research on the synthesis of novel phosphorus-containing heterocycles revealed a number of interesting chemical facts including the 'in-out' structural isomerism of cage structures and dismutation of unsymmetrical aromatic mono- and bisphosphorus systems.

References

1. *Plasmids. A Practical Approach* (Ed. K G Hardy) (Oxford: Oxford University Press, 1989)
2. L N Markovskii, V I Kal'chenko *Zh. Vses. Khim. O-va im. D I Mendeleeva* **30** 528 (1985)^a
3. A-M Caminade, J-P Majoral *Chem. Rev.* **94** 1183 (1994)
4. M V Alfimov *Izv. Akad. Nauk, Ser. Khim.* 1303 (2004)^b
5. P Finocchiaro, S Failla, G Consiglio *Izv. Akad. Nauk, Ser. Khim.* 1313 (2005)^b
6. J-M Lehn *Supramolecular Chemistry. Concepts and Perspectives* (Weinheim: VCH, 1995)
7. J H Hartley, T D James, C J Ward *J. Chem. Soc., Perkin Trans. I* 3155 (2000)
8. E E Nifantsev, E N Rasadkina, I V Yankovich *Zh. Obshch. Khim.* **67** 1812 (1997)^c
9. E E Nifantsev, E N Rasadkina, I V Yankovich, L K Vasyanina, V K Belsky, A I Stash *Zh. Obshch. Khim.* **69** 36 (1999)^c
10. E E Nifantsev, S V Suvorkin, E N Rasadkina, O V Selyutina, A V Shishin *Zh. Obshch. Khim.* **72** 1263 (2002)^c
11. E E Nifantsev, E N Rasadkina, Yu B Evdokimenkova *Zh. Obshch. Khim.* **71** 401 (2001)^c
12. Yu B Evdokimenkova, Candidate Thesis in Chemical Sciences, Moscow State Pedagogical University, Moscow, 2002
13. M N Dimukhametov, V F Mironov, R Z Musin *Mendeleev Commun.* 48 (2006)
14. S A Terent'eva, M A Pudovik, O N Kataeva, I A Litvinov, A N Pudovik *Zh. Obshch. Khim.* **70** 556 (2000)^c
15. R I Yurchenko, E E Lavrova, A G Yurchenko *Zh. Obshch. Khim.* **65** 1445 (1995)^c
16. E E Nifantsev, Yu I Blokhin, M Ya Ergashev *Dokl. Akad. Nauk* **325** 73 (1992)^d
17. Yu I Blokhin, D V Gusev, V K Belsky, A I Stash, E E Nifantsev *Phosphorus, Sulfur, Silicon Relat. Elem.* **102** 143 (1995)
18. Yu I Blokhin, F M Galiaskarova, D V Gusev, M Ya Ergashov, V K Belsky, E E Nifantsev *Phosphorus, Sulfur, Silicon Relat. Elem.* **111** 170 (1996)
19. D V Gusev, Candidate Thesis in Chemical Sciences, Moscow State Pedagogical University, Moscow, 2000
20. Yu I Blokhin, D V Gusev, K N Kornilov *International Symposium on Advanced Science in Organic Chemistry, Sudak, 2006* S-075
21. E E Nifantsev, E N Rasadkina, S V Suvorkin, D V Gusev *Zh. Obshch. Khim.* **71** 1403 (2001)^c
22. I Bauer, W D Habicher *Phosphorus, Sulfur, Silicon Relat. Elem.* **128** 79 (1997)
23. I Bauer, W D Habicher, P G Jones, H Thonnessen, R Schmutzler *Phosphorus, Sulfur, Silicon Relat. Elem.* **143** 19 (1998)
24. I Bauer, W D Habicher *Phosphorus, Sulfur, Silicon Relat. Elem.* **147** 23 (1999)
25. I Bauer, W D Habicher *Tetrahedron Lett.* **43** 5245 (2002)
26. I Bauer, O Rademacher, M Gruner, W D Habicher *Chem. – Eur. J.* **6** 3043 (2000)
27. I Bauer, M Gruner, S Goutal, W D Habicher *Chem. – Eur. J.* **10** 4011 (2004)
28. I Bauer, W D Habicher, I S Antipin, O G Sinyashin *Izv. Akad. Nauk, Ser. Khim.* 1348 (2004)^b
29. G I Kurochkina, M K Grachev, L K Vasyanina, A E Piskaev, E E Nifantsev *Dokl. Akad. Nauk* **371** 189 (2000)^d
30. G I Kurochkina, N O Soboleva, M K Grachev, E E Nifantsev *Phosphorus, Sulfur, Silicon Relat. Elem.* **177** 2059 (2002)
31. M K Grachev, G I Kurochkina, N O Soboleva, L K Vasyanina, E E Nifantsev *Zh. Obshch. Khim.* **72** 1918 (2002)^c
32. G I Kurochkina, M K Grachev, A A Sutyagin, E E Nifantsev *Zh. Obshch. Khim.* **73** 2056 (2003)^c
33. N M Selezneva, Candidate Thesis in Chemical Sciences, Moscow State Pedagogical University, Moscow, 2000
34. E N Rasadkina, E E Nifantsev *Zh. Obshch. Khim.* **69** 510 (1999)^c
35. E E Nifantsev, E N Rasadkina, Yu B Evdokimenkova, L K Vasyanina, A I Stash, V K Bel'skii *Zh. Obshch. Khim.* **71** 203 (2001)^c
36. E E Nifantsev, E N Rasadkina, Yu B Evdokimenkova *Izv. Akad. Nauk, Ser. Khim.* 883 (2001)^b
37. E E Nifantsev, E N Rasadkina, Yu B Evdokimenkova, A I Stash, V K Belsky, L K Vasyanina *Heteroat. Chem.* **14** 404 (2003)
38. E N Rasadkina, P V Slitkov, M S Mel'nik, A I Stash, V K Bel'skii, E E Nifantsev *Zh. Obshch. Khim.* **74** 1170 (2004)^c
39. E N Rasadkina, P V Slitkov, M P Pechkina, L K Vasyanina, A I Stash, E E Nifantsev *Zh. Obshch. Khim.* **75** 2000 (2005)^c
40. E N Rasadkina, P V Slitkov, M S Mel'nik, E E Nifantsev *Izv. Akad. Nauk, Ser. Khim.* 362 (2004)^b
41. E E Nifantsev, E N Rasadkina, P V Slitkov, L K Vasyanina *Phosphorus, Sulfur, Silicon Relat. Elem.* **180** 513 (2005)
42. E N Rasadkina, P V Slitkov, E E Nifantsev *Zh. Obshch. Khim.* **76** 196 (2006)^c
43. E E Nifantsev, E N Rasadkina, P V Slitkov, V A Bogoyavlenskii *International Symposium on Advanced Science in Organic Chemistry, Sudak, 2006* S-154
44. E E Nifantsev, E N Rasadkina, A V Petrov *Zh. Obshch. Khim.* **75** 698 (2005)^c
45. A V Petrov, E N Rasadkina, E E Nifantsev *VIII Nauchnaya Shkola-konferentsiya po Organicheskoi Khimii, Kazan', 2005* (The VIIIth Scientific School Conference on Organic Chemistry, Kazan, 2005) p. 70
46. E N Rasadkina, A V Petrov, E E Nifantsev *Phosphorus, Sulfur, Silicon Relat. Elem.* (2007) (in the press)
47. A V Petrov, E N Rasadkina, E E Nifantsev *Mezhdunarodnaya Konferentsiya po Organicheskoi Khimii 'Organicheskaya Khimiya ot Butlerova i Beil'shteina do Sovremennosti' (Tezisy Dokladov), Sankt-Peterburg, 2006* [International Conference on Organic Chemistry 'Organic Chemistry from Butlerov and Belstein to the Present (Abstracts of Reports), St Petersburg, 2006] p. 396
48. E N Rasadkina, A V Petrov, E E Nifantsev *Zh. Obshch. Khim.* **77** 268 (2007)^c
49. P V Slitkov, A V Petrov, E N Rasadkina, E E Nifantsev *Mezhdunarodnaya Konferentsiya po Organicheskoi Khimii 'Organicheskaya Khimiya ot Butlerova i Beil'shteina do Sovremennosti' (Tezisy Dokladov), Sankt-Peterburg, 2006* [International Conference on Organic Chemistry 'Organic Chemistry from Butlerov and Belstein to the Present (Abstracts of Reports), St Petersburg, 2006] p. 543
50. P V Slitkov, A V Petrov, E N Rasadkina, E E Nifantsev *Koord. Khim.* **33** 296 (2007)^c
51. P V Slitkov, Candidate Thesis in Chemical Sciences, Moscow State Pedagogical University, Moscow, 2004
52. I V Yankovich, Candidate Thesis in Chemical Sciences, Moscow State Pedagogical University, Moscow, 1999
53. E E Nifantsev, E N Rasadkina, I V Yankovich, L K Vasyanina, V K Belsky, A I Stash *Heteroat. Chem.* **9** 643 (1998)
54. E E Nifantsev, V I Maslennikova, E N Rasadkina *Zh. Obshch. Khim.* **69** 1813 (1999)^c
55. E E Nifantsev, E N Rasadkina, I V Yankovich, V K Belsky, A I Stash *Heteroat. Chem.* **11** 129 (2000)
56. E N Rasadkina, P V Slitkov, Yu B Evdokimenkova, E E Nifantsev *Zh. Obshch. Khim.* **73** 1279 (2003)^c
57. V I Maslennikova, T Yu Sotova, L K Vasyanina, I Bauer, W D Habicher, E E Nifantsev *Tetrahedron Lett.* **46** 4891 (2005)
58. A A Chaikovskaya, T N Kudrya, A V Podgornyi, A M Pinchuk *Zh. Obshch. Khim.* **64** 765 (1994)^c
59. A-M Caminade, J-P Majoral *Synlett* 1019 (1996)
60. A-M Caminade, R Kraemer, J-P Majoral *New J. Chem.* **21** 627 (1997)
61. G Margo, A-M Caminade, J-P Majoral *Tetrahedron Lett.* **44** 7007 (2003)
62. J-P Majoral, A-M Caminade *Chem. Rev.* **99** 845 (1999)
63. A Balueva, S Merino, A-M Caminade, J-P Majoral *J. Organomet. Chem.* **643–644** 112 (2002)

^a — *Mendeleev Chem. J. (Engl. Transl.)*

^b — *Russ. Chem. Bull., Int. Ed. (Engl. Transl.)*

^c — *Russ. J. Gen. Chem. (Engl. Transl.)*

^d — *Dokl. Chem. (Engl. Transl.)*

^e — *Russ. J. Coord. Chem. (Engl. Transl.)*

Detonation-synthesis nanodiamonds: synthesis, structure, properties and applications

V Yu Dolmatov

Contents

I. Introduction	339
II. Detonation synthesis of nanodiamonds: mechanisms	339
III. Detonation synthesis of nanodiamonds: key features and regularities	341
IV. Novel method of synthesis and revised elemental compositions of nanodiamonds and diamond blend	343
V. Chemical purification of nanodiamonds: theory vs. practice	345
VI. Industrial synthesis of nanodiamonds	346
VII. Properties of nanodiamonds	346
VIII. Fields of application of nanodiamonds	350

Abstract. The review outlines the theoretical foundations and industrial implementations of modern detonation synthesis of nanodiamonds and chemical purification of the nanodiamonds thus obtained. The structure, key properties and promising fields of application of detonation-synthesis nanodiamonds are considered. The bibliography includes 135 references.

I. Introduction

Detonation-synthesis nanodiamonds (ND) were first synthesised by researchers from the USSR in 1963 by explosive decomposition of high-explosive mixtures with negative oxygen balance in a non-oxidising medium.^{1,2} Nanodiamonds are characterised by nanoscale particle sizes and have chemically inert cores and reactive peripheral regions called shells. A micrograph of a typical ND particle is shown in Fig. 1.

The detonation synthesis offers the following advantages over the static synthesis of ND: (1) high performance due to the lack of limitations associated with the size and the weight of charges; (2) no need for expensive and scarce expendable materials (hard alloys, alloy steels) and metal catalysts (nickel, manganese); and (3) possibility of preparation of unique polycrystalline ND powders under strongly non-equilibrium conditions.

A drawback of the technique consists in potential explosion risk when carrying out blasting operations, fabrication and transportation of charges.

II. Detonation synthesis of nanodiamonds: mechanisms

No commonly accepted theory of the detonation synthesis of ND is available at the moment. Different authors propose

different (sometimes, significantly different) ND formation mechanisms. In this Section we will consider a number of theoretical models for ND formation.

A mechanism of ND formation from TNT–hexogen (RDX) mixtures is as follows.^{3,4} In the zone of the detonation wave the explosive molecules disintegrate into atoms. Carbon atoms thus released are condensed into an amorphous carbon phase by means of diffusion and liquid droplet coalescence. Subsequently, amorphous carbon particles undergo a phase transition to diamond. It is believed that the degree of conversion increases from 0% to 100% in the pressure range 17–23 MPa. The formation of the diamond phase in this pressure range (it corresponds to the region of chemical peak of the detonation wave) was confirmed in other studies.^{5–7} According to the data mentioned above, the formation of ND takes a time of 0.2 to 0.5 μ s.

The diamond phase repeatedly experiences the action of reflected shock waves, and the ND temperature increases. As a

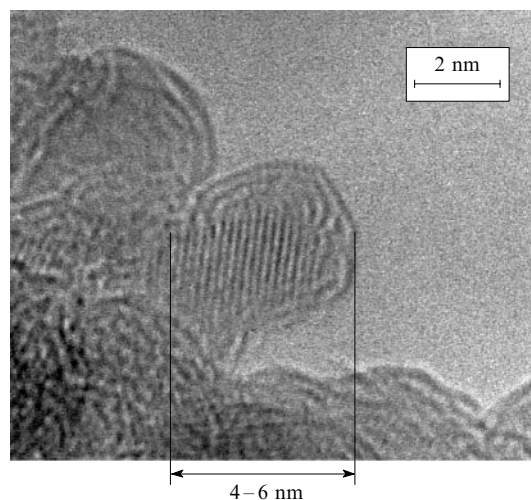


Figure 1. Micrograph of a single nanodiamond particle. Courtesy of Professor A Ya Vul' (Ioffe Physico-Technical Institute, Russian Academy of Sciences, St Petersburg).

V Yu Dolmatov Federal State Unitary Enterprise Special Design-Technology Bureau (FSUE SDTB) 'Tekhnolog' at the St Petersburg State Institute of Technology (Technical University), Sovetskii prosp. 33A, 192076 St Petersburg, Russian Federation. Fax (7-812) 700 38 98, tel. (7-812) 700 38 98, e-mail: alcen@peterstar.ru

Received 18 January 2007

Uspekhi Khimii 76 (4) 375–397 (2007); translated by A M Raevskiy

consequence, the thermodynamic state of detonation products corresponds to the graphite stability region and partial graphitisation of ND occurs.

A study of the isotopic composition of the condensed products formed upon detonation of a TNT/octogen (HMX) mixture (TNT was labelled with ^{13}C at methyl group) showed that detonation-synthesis ND are mainly formed from the carbon atoms of TNT.⁸ Similar conclusions were made in the studies of ND synthesis from a mixture of RDX with TNT labelled with ^{14}C at position 1 of the benzene ring.^{9,10} It was also established that the yield of condensed carbon linearly decreases as the TNT content in the mixtures decreases, while the ND content in the diamond blend (DB), an intermediate product of ND synthesis, monotonically increases and reaches a constant value (for mixtures with RDX and HMX denoted TNT/RDX and TNT/HMX, respectively).¹¹

The addition of heterocyclic and aliphatic nitramines has a little effect on the formation of ND. The role of the additives is to produce the necessary pressure and temperature for the phase transition to occur.¹²

The dispersion of ND depends on the nature of the carbon source.¹³ For instance, the average particle size of the diamond phase formed upon detonation of mixtures of HMX with liquid organic additives varied from 1.8 (for glycerol) to 4.1 nm (for ethanol).

The maximum yield of ND was obtained using TNT/HMX or TNT/RDX mixtures containing 60 mass % to 70 mass % of TNT (density 1630 kg m^{-3}).¹¹

According to Lin,¹⁴ the key step in ND formation is the appearance of cyclohexane molecules (nuclei of the diamond structure). Collisions between the nuclei cause their aggregation into small clusters followed by growth of mesoscopic structures with long-range crystal order. Subsequent interaction of the mesoscopic structures with one another and with nuclei causes the formation of ND.

Anisichkin¹⁵ put forward an original hypothesis, according to which the initial decomposition stages of explosive materials occur with the release of hydrogen as methane and carbon in the diamond phase. Then, these products are oxidised. The extent of carbon conversion to the diamond phase is determined by the detonation parameters.

It was shown that the chemical reaction zone extends as the dimensions of the explosive charge increase and that energy release also continues behind the Chapman–Jouguet plane.¹⁶ Carbon coagulation and crystallisation can occur upon adiabatic expansion of detonation products. This was established in the studies^{2,17} of the effect of the mass of the charge and the heavy shell surrounding it on the ND particle size. For instance, an increase in the charge mass from 0.6 to 10 kg using a water shell causes the particle size to increase from 4 to 6 nm (specific surface area is reduced from 330 to $200\text{ m}^2\text{ g}^{-1}$, see Ref. 2). The detonation of a 140-kg charge in water shell afforded ND particles with an average size of about 8 nm and individual polycrystals of size up to 85 μm .¹⁷

According to Danilenko,¹⁸ the formation of ND can proceed by the known mechanism of homogeneous condensation of ultradisperse phases in highly supersaturated vapour (vapour–liquid–crystal mechanism) and result in spherical particles. Because of rapid exhaustion of the gas–vapour medium the average particle size does not increase with increasing duration of existence of the particle-growth conditions.

Crystallisation from vapour usually gives spherical nanoparticles of size $\leq 20\text{ nm}$, which also holds for ND.¹⁹

Additionally, Danilenko reported¹⁸ that the assumption of ND crystallisation from the liquid phase was substantiated by

the fact that the shape of the ND particle size distribution is typical of liquid droplet coalescence.²⁰

The most probable values of the detonation pressure and temperature in the Chapman–Jouguet plane are listed in Table 1. The Chapman–Jouguet parameters of TNT/RDX alloys correspond to liquid nanocarbon.¹⁸ At higher densities of explosive materials (ρ), carbon condensed in the reaction zone consists of nanodroplets only.

Table 1. Parameters of the ideal detonation in the Chapman–Jouguet plane.¹⁸

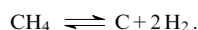
Explosive	$\rho/\text{kg m}^{-3}$	P/GPa		T/K	
		experi- ment	calcula- tions	experi- ment	calcula- tions
TNT	1600–1640	18–19	18.3–20.1	3700 ^a	3500–3618
RDX	1780–1800	34.5–35.4	34.7–35.0	4500 ^b	4200
TNT/RDX					
36:64	1713–1730	27–29.2	27.4–29.3	—	3931–4063
50:50	1670–1680	24.6	24.4–25.5	—	3225–3900
Tetryl	1700	—	23.9–25.4	3700, 4300 ^c	3991–4063

$\rho = 1510,^a 1660^b$ and 1610^c kg m^{-3} .

The formation of ND in the detonation wave involves the following processes:¹⁸

- condensation of carbon in the reaction zone with the formation of primary clusters ($d < 1\text{ nm}$);
- cluster–cluster interaction (liquid droplet coalescence) with the formation of nanodroplets;
- crystallisation of nanodroplets with formation of ND provided a sufficiently long period of cooling by turbulent detonation products or amorphisation of nanodroplets and clusters resulting in free and bound soot.

Possible reasons for soot release in DB are (i) imperfect detonation in certain regions of the charge volume (initiation zone, boundary regions) characterised by low P and T values and leading to carbon condensation by the vapour–amorphous carbon mechanism and (ii) formation of methane,¹⁵ which decomposes to soot upon detonation according to the reaction



Detonation in real systems occurs in non-ideal and non-steady-state regimes. Here, carbon is oxidised to CO rather than CO_2 . The process is characterised by lower pressures and temperatures and, correspondingly, by lower content of free carbon in detonation products and a decrease in the yield of ND. For instance, calculations²¹ showed that the $P_{50}:P_{100}$ and $T_{50}:T_{100}$ ratios are respectively equal to 0.337 and 0.546 at 50% conversion, *i.e.*, the pressure decreases about twice faster than the temperature.

As the mass of the water shell surrounding the charge increases, the ND yield increases and reaches a maximum value at the shell mass equal to ten charge masses.^{22,23} Optimum conditions for the synthesis of ND require the use of explosive charges with minimum porosity (highest density) and the blast conditions that provide the minimum possible imperfection of detonation.

The general conditions for optimum synthesis resulting in the maximum ND yield and the corresponding experimental methods are listed below.

Synthesis conditions	Implementation methods
Condensation of maximum possible, for a given explosive, amount of free carbon. Carbon condensation in the liquid nanocarbon region.	Detonation of explosive charges with the minimum porosity and imperfection. Use of TNT/RDX or TNT/HMX alloys with pressures higher than 22 GPa in the Chapman–Jouguet plane.
Maximum possible times of existence of liquid nanocarbon conditions in the detonation products and crystallisation of nanocarbon at pressures higher than 10 GPa in detonation products.	Detonation of explosive charges heavier than 5 kg in a water shell weighing more than ten charges.
Blasting under conditions that ensure the absence of amorphisation, oxidation and graphitisation.	Blasting charges in a massive water shell.

Thus, the chemical reaction zone of the detonation wave involves formation of carbon nanodroplets, which then crystallise into ND upon adiabatic expansion of detonation products in the pressure range from 16.5 to 10.0 GPa and in the temperature range from 3400 to 2900 K (ND stability region).¹⁸ When the charge is surrounded by a water shell, the unloading (pressure drop) in this pressure interval slows down and the temperature of detonation products is halved. As a consequence, the degree of oxidation of ND decreases and the effect of chamber walls on the yield of ND becomes less pronounced. Soot in the resultant mixture is treated as the product of amorphisation of carbon nanodroplets rather than graphitisation of ND. In the case of adiabatic expansion of detonation products, crystallisation of nanodroplets with $d < 1$ nm is impossible at all, amorphisation of nanodroplets with $d < 2$ nm occurs under conditions corresponding to the diamond region in the phase diagram of carbon, while amorphisation of nanodroplets with $d > 2$ nm, under conditions corresponding to the graphite region.

Another model for ND formation was proposed by Breusov.²⁴ A comparison of the energy released upon detonation of explosives with the energies of chemical bonds in the starting (explosive) molecules revealed impossibility of release of free carbon. Indeed, the energy released upon detonation is at most 809 kJ mol⁻¹ for TNT and 1240 kJ mol⁻¹ for RDX.²⁵

The energies of some chemical bonds (in kJ mol⁻¹)²⁶ are listed below.

C–H	CC	C–N	C=N	N=O	N–N
413.6 (in alkanes)	346.1 (in alkanes)	305.0	615.9	188.6 (in nitro com- pounds)	163.4
421.9 (in benzene)	487.7 (in benzene)				

Cleavage of all C–H and C–N bonds in the molecule requires a total of 3000 kJ mol⁻¹ for TNT and 3071 kJ mol⁻¹ for RDX; *i.e.*, the energy released upon detonation of each explosive or their mixture is several times lower than that needed for intermediate formation of elemental carbon. Therefore, a fraction of volatile chemically bonded components should not be consumed in the initial stages of the process.

In the shock-wave front zone certain bonds in the starting molecules can break down. According to Breusov,²⁴ radicals thus produced favour the formation of the carbon cage to which many molecules of volatile products are chemically bonded in the initial stages. Depending on the P – T detonation conditions and corresponding electronic hybridisation of carbon atoms, one can deal with either a graphite-like or a diamond-like frame.

Nucleation and growth of diamond particles are accompanied by accumulation of volatile low-molecular-mass detonation products (nitrogen, hydrogen, CO, CO₂, N_xO_y, H₂O, *etc.*) in the interparticle space, which precludes the delivery of carbon-containing ‘building’ material to the growing particles and finally the growth ceases.

It is believed²⁴ that methane and methyl radical are most suitable for growth of diamond particles and ‘healing’ their structural defects.

III. Detonation synthesis of nanodiamonds: key features and regularities

The design of the blast chamber is of great importance for the synthesis of nanodiamonds. Roughly, 1 to 4 m³ of the chamber volume are required per kg of explosive.²

In design of large blast chambers (> 50 m³) one should allow for the fact that the larger the chamber volume the lower the mechanical strength of the chamber.² The effect of the scale factor can be explained by brittle fracture of large items made of plasticised steel in the elastic deformation region. The thicker the chamber walls the more probable the appearance of structural defects that reduce the fracture stress.

The effect of the scale factor can be significantly reduced using blast chambers with multilayer walls made of, *e.g.*, steel strips or glass fibre. This significantly increases the crack resistance of the material.

Industrial blast chambers are usually relatively small and have a volume of 2 m³ [FSUE ‘Federal Research and Production Centre (FRPC) Altai’, FSUE ‘Elektrokhimpribor’ Integrated Plant, FSUE SDTB ‘Tekhnolog’, facilities in China]. They have long operating life (failure-free operation since mid-1980s). The mass of the explosive charges varies from 0.5 to 1.0 kg; this allows up to 2.5 kg of nanodiamonds to be synthesised over a period of 8 h. These chambers are reliable and simple in operation.

Larger blast chambers, *e.g.*, 11 m³ in volume, are also used [RPA ‘Sinta’, Belarus; Russian Federation Nuclear Centre – All-Russian Research Institute of Technical Physics (RFNC – ARITP), Snezhinsk, Russia]. Here, the explosive charges have a mass of 2 kg and therefore such blast chambers are characterised by higher performance. However, they are unreliable in service.

The Closed Joint-Stock Company (CJSC) ‘Alit’ (Kiev, Ukraine) successfully employs for more than a decade a 100 m³ blast chamber (mass of explosive charge is 10 kg), which provides a high performance with respect to ND. However, the blast chamber has a complex hand-driven charging system; sometimes, ice armour weighing at least 60 kg is used. The blast chamber looks like a railway tank and is rail tracked. The charge is blasted at the centre of the ‘tank’. The action of the shock waves on the blast chamber walls is non-uniform and the undesired effects are quenched by spraying water in the chamber upon explosion. As a result, the content of incom-bustible impurities (products of chamber wall corrosion) in the condensed carbon is rather high (16 mass % to 26 mass %).²

Thus, in choosing the volume and design of industrial blast chambers one should allow for not only the performance, but also simplicity and safety of operations with explosives and the content of impurities in the condensed carbon.

Nanodiamonds can be synthesised using various individual explosives and high-explosive mixtures. The type of the explosive governs the detonation characteristics and the composition of detonation products. In the case of adiabatic (isentropic) expansion of detonation products the temperature drop rate also depends on the type of the explosive, the state of the charge surface and the charge shape and on the atmosphere in the blast chamber. The key parameters affecting the final temperature and the corresponding rate constant (and, hence,

Table 2. Yields of diamond blend (M_{DB}) and ND (M_{ND}) as functions of the type of explosive.²⁷

Explosive	$M_{\text{Expl.}} / \text{g (see } ^a)$	$\rho / \text{kg m}^{-3}$	$M_{DB}/M_{\text{Expl.}} (\%)$	$M_{ND}/M_{DB} (\%)$	$M_{ND}/M_{\text{Expl.}} (\%)$
<i>z</i> -Takot	153.2	1603	18.4	19.2	3.34
<i>z</i> -Takot : HMX (80 : 20)	250.7	1580	14.3	30	4.3
<i>z</i> -Takot : HMX (70 : 30)	294.5	1740	12.3	69	8.6
HNAB	263.5	1630	9.47	71	6.63
TATB : HMX (70 : 30)	324.6	1850	9.9	54	5.3
TNT ^b	280	1605	18.1	15.7	2.8
TNT/HMX (70 : 30)	310	1700	12.5	65.7	8.2

^a $M_{\text{Expl.}}$ is the charge mass. ^b Data taken from Refs 10 and 28.

the yield of ND) include the heat capacity, the content and the reactivity of the medium. An increase in the volume of the gas, its initial pressure and heat capacity in the blast chamber favour efficient reduction of the residual temperature and improves the yield of ND. The most pronounced effect is attained using CO_2 .

A general rule is as follows: the larger the ratio of the mass of the medium surrounding the blasting charge to the mass of the explosive charge, the higher the yield of ND.

The possibility of synthesis of ND upon detonation of the following aromatic nitro compounds: 1,3,5-triamino-2,4,6-trinitrobenzene (TATB), bis(2,4,6-trinitrophenyl)diazine (HNAB) and 2,4,8,10-tetranitro-5*H*-benzotriazolo[2,1-*a*]benzotriazolium (*z*-Takot) was studied.²⁷ To improve the detonation parameters, in some cases the explosives were mixed with HMX and then used in the experiments.

Analysis of experimental data (Table 2) showed that the syntheses of ND upon detonation of the explosives under study and TNT obey the same pattern. Indeed, if the detonation parameters of an explosive and TNT are similar, the ND yields are also similar. The data for *z*-Takot show that, similarly to the TNT/RDX and TNT/HMX compositions, the content of the diamond phase in the DB released increases as the HMX proportion in the charge increases.

In the case of HNAB the thermodynamic parameters produced are sufficiently high to efficiently form ND without HMX additives. However, in this case the overall yield of DB is nearly halved compared to that obtained using TNT and *z*-Takot; therefore, the yield of ND is somewhat lower than the yields reached using optimum TNT/RDX compositions.

The results obtained using TATB deserve particular attention. Despite the higher detonation pressure (compared to *z*-Takot and TNT), the content of the diamond phase in DB was lower. This is probably due to the lower detonation temperature, which hampers efficient growth of the diamond particles.

Nanodiamonds are also formed upon detonation of hexanitrostilbene,²⁹ picric acid,³⁰ tetryl³¹ and TNT/nitroguanidine, RDX/polybutadiene and RDX/aluminum mixtures.³²

Long experience in industrial synthesis of ND has shown that TNT/RDX mixtures remain the most appropriate explosives. Indeed, these substances have well-known characteristics and are produced on a large scale. Processing of these explosives faces no problems, charges are castable and mouldable and can be shaped in any desired fashion. The yield of industrially synthesised ND can be as high as about 14%.

The synthesis of ND in the presence of organic admixtures to high explosives (RDX or HMX) is of considerable interest. The yield of ND produced in the presence of benzene, benzyl alcohol, allyl alcohol, allylamine, acetonitrile, nitrobenzene, propargyl alcohol and aniline admixed to HMX (~25 vol.%) is 6%–10% per unit mass of the mixture. Lower yields (~3%) were obtained with paraffin admixtures (hexane, decane),

alcohols (pentyl and octyl alcohols) and the lowest yield (~2%) was obtained using tetradecane.

The temperature and pressure developed upon detonation of explosives reach up to 4000 K and 30 GPa, respectively.

Table 3 lists the yields of diamond blend and ND obtained under different detonation synthesis conditions, namely, in the atmosphere of gaseous detonation products or an inert gas; in a water shell surrounding the explosive charge; and in an ice armour.^{33, 34} High yield of ND in the presence of a water shell or ice armour is due to prolonged action of pressure in the diamond stability region.

As shown above, the process affords the raw carbonaceous material (DB) consisting of ND, graphite-like particles and contaminants (metals and metal compounds).

The yields of ND and DB also depend on the charge mass-to-chamber volume ratio and on the site where the explosion is initiated. The ND content in diamond blend is plotted vs. water shell thickness at different charge geometries (TNT : RDX = 40 : 60) in Fig. 2. In the case of long cylindrical charge ($l/d > 2$) the amount of ND is much higher compared to those obtained

Table 3. Yields of DB and ND under different detonation synthesis conditions.^{33, 34}

Quality parameters of final product	Synthesis conditions		
	inert gas medium	aqueous medium	ice armour
DB yield (mass %)	3–8	6–12	8–14
ND content in DB (mass %)	20–40	40–63	55–75
ND yield calculated with respect to explosive	0.6–3.2	2.4–7.6	4.4–10.5

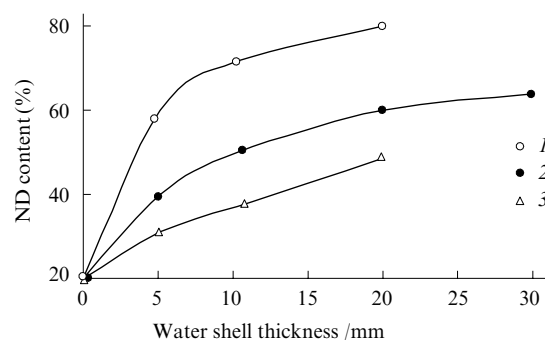


Figure 2. ND content in diamond blend plotted vs. water shell thickness at different charge geometries (TNT : RDX = 40 : 60 charge, mass 100 g).³⁵ Charge shape: cylinder (1), disc (2) and sphere (3).

with disc-like of spherical charges under identical explosion conditions.³⁵

To obtain the maximum possible yield of ND and DB, one should use long cylindrical charges of the highest possible density, a water shell or an ice armour surrounding the charge and a hardest booster pulse.

The yield of ND and DB also depends on the procedure used for cooling of detonation products in the blast chamber. If the charge is surrounded by a water shell or ice armour (so-called 'wet' synthesis), intense cooling of detonation products is due to transformation of their energy to heat (heating and vapour formation) and the kinetic energy of water and turbulent mixing with water. Additionally, water and ice are convenient substances, because they do not damage the walls of the blast chamber and ice does not require a container.

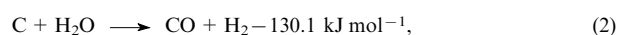
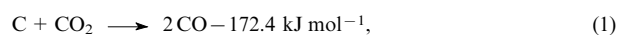
'Wet' synthesis (in water) can be carried out in optimum manner using a TNT/RDX charge with a TNT content of 40%. The composition produces a high synthesis temperature, while rapid cooling with water provides a higher degree of conservation of ND.

The so-called 'dry' synthesis involves blasting of a charge in gaseous medium. Here, carbon dioxide is the most efficient coolant of ND. Detonation products of a preceding blast can be used as coolant gas. A TNT/RDX charge containing 60% of TNT is optimum for the 'dry' method. Since for this alloy the detonation pressure and detonation temperature are lower than those reported for the composition with 40% of TNT, the yield of ND is nearly halved.

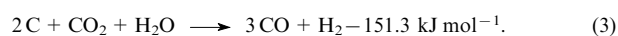
As the number of blasts in unventilated chamber increases, the composition of the gaseous atmosphere significantly changes. Namely, the concentrations of carbon dioxide, nitrogen and oxygen decrease, while the concentration of carbon monoxide increases, which makes the cooling of detonation products less efficient.³⁵ Therefore, it is desired to introduce carbon dioxide into the chamber after each series of four or five blasts.

The synthesis takes at most 0.5 μ s, which approximately corresponds to the time of chemical reaction (or chemical peak) in the detonation (explosive) decomposition of TNT.⁶

The elemental composition of DB is governed by hetero-phase endothermic processes of gasification of the blend with carbon dioxide and water vapour



which can be described by the overall reaction



At high temperature, two competing processes proceed in the chamber, namely, gasification of DB (first of all, gasification of the non-diamond carbon as the more reactive DB component) and graphitisation of ND.

In the course of chemical purification (on going from DB to ND) the texture of the material changes non-monotonically (in stepwise fashion), which distinguishes the DB from other carbonaceous materials.³⁶ This is due to the fact that DB is an organised three-dimensional structure formed as a result of multistage aggregation of primary particles rather than a mixture of ND and non-diamond carbon.

IV. Novel method of synthesis and revised elemental compositions of nanodiamonds and diamond blend

A novel method of synthesis of ND^{37,38} permits significant improvement of the qualitative and quantitative characteristics of ND and DB. Namely, it allows one to change the elemental

composition towards higher content of carbon as the major element, to considerably increase the yield of ND and DB and to reduce the content of incombustible impurities.

A charge made of TNT – RDX alloy containing 40 mass % of TNT (TNT/RDX 40) was blasted in a blast chamber surrounded by a water shell (chamber volume 1 m³, charge mass 0.6 kg, blast atmosphere: products of previous detonations). The explosive : water mass ratio was maintained at 1 : 6. A number of readily oxidisable reducing agents (hydrazine hydrate, urotropin, urea, ammonia) were added to water, the explosive : reducing agent ratios being 1 : (0.1 – 10.0). The DB was purified to ND by dilute nitric acid at 513 K and a pressure of ~ 80 atm.³⁹

Additionally, a new procedure for elemental analysis of DB and ND was elaborated. It differs from conventional procedure by more severe conditions.^{37,38} Namely, a weighed sample is kept *in vacuo* (0.01 – 10.0 Pa) at 120 – 140 °C (DB) or 423 – 453 K (ND) for 3 – 5 h and then treated with oxygen passing at a flow rate that ensures complete combustion of the sample at 1323 – 1473 K over a period of 40 – 50 s. Subsequent determination of the elemental composition is carried out by conventional analytical techniques.

According to published data,^{36,40} the detonation synthesis of ND involves four stages. In the first stage, the detonation transformation of the explosive mainly occurs within the volume occupied by the charge. When using a condensed shell (water or ice), the detonation products are for some time confined within this volume, which favours a more complete transformation of carbon into the diamond prastructure.

Completion of the detonation process requires rapid gas-dynamic cooling of products to protect ND formed in the chemical reaction zone (or behind this zone¹⁸). The second stage consists in adiabatic expansion of gaseous detonation products.

The third stage of the detonation synthesis of ND involves circulation of the shock wave reflected from the chamber walls and turbulent mixing of detonation products with the medium in the chamber.

The fourth stage of the process involves intense cooling of the blast-heated medium surrounded (and thus confined) by the cold shell. In addition to various gaseous products (CO₂, CO, O₂, H₂, N₂, CH₄, NO, NO₂, NH₃, H₂O), the blast chamber contains highly disperse suspension of carbon particles possessing high radiating capacity. Therefore, cooling of this medium occurs through simultaneous heat transfer by convection and radiation.

The retention of condensed carbon is governed by hetero-phase gasification reactions with carbon dioxide and water vapour. Two competing processes proceed in the blast chamber in the third and fourth stages at the high residual temperature. These are gasification of condensed carbon (first of all, non-diamond carbon as the most reactive component) and graphitisation (or amorphisation¹⁸) of ND.

At a constant composition and density of the explosive, it is impossible to influence the first stage of the synthesis (*i.e.*, the formation of ND) by adding various admixtures to the condensed phase (water, ice) surrounding the charge. The processes occurring in the second stage can also hardly be affected by the substances in the condensed phase even with allowance for non-ideal character of gas-dynamic cooling of detonation products upon expansion. On the contrary, the addition of more readily oxidisable compounds (reducing agents) in the third stage (turbulisation of products), where condensed carbon reacts with CO₂, H₂O and other corrosive (under these conditions) compounds, will strongly affect the results of the synthesis. Of course, the oxidising agents (CO₂, H₂O, O₂, NO₂, N₂O₃) first of all react with more readily oxidisable reducing agents (in our case, hydrazine hydrate, urotropin, urea, ammonia) rather than with hardly oxidisable

Table 4. Elemental compositions and the DB and ND yields upon blasting of TNT/RDX 40 charges surrounded by water shell with different reducing agents.³⁸

Reducing agent	Explosive : reducing agent ratio (mass to mass)	Elemental composition of DB (mass %)				Content of incombustible impurities in DB (mass %)	Content of ND in DB (mass %)	DB yield calculated with respect to explosive (mass %)	ND yield calculated with respect to explosive (mass %)
		C	H	N	O				
Hydrazine hydrate	1:0.1	90.2	3.3	3.0	0.4	3.1	51.1	14.4	7.36
	1:0.5	90.5	3.0	2.9	0.8	2.8	54.7	15.8	8.64
	1:2.0	90.1	3.7	3.2	0.4	2.6	53.8	16.0	8.61
Urotropin	1:0.25	94.1	1.6	2.2	0.5	1.6	51.6	12.4	6.4
	1:0.5	91.2	3.0	2.6	0.9	2.3	51.7	12.2	6.3
	1:1	92.7	2.8	2.8	0.3	1.4	51.9	16.3	8.46
Urea	1:0.5	90.1	3.6	3.1	0.5	2.7	51.2	14.1	7.22
Ammonia	1:0.5	91.1	3.0	2.8	0.9	2.2	51.0	13.4	6.83
No additive	—	84.2	0.9	8.3	3.1	3.5	45.0	7.2	3.24

carbon, especially ND. Therefore, one should expect an increase in the yield of DB and, hence, ND and quantitative changes in the elemental composition.

Additionally, the presence of readily oxidisable reducing agents among the detonation products also affects the fourth stage of the process, namely, the temperature of the products decreases due to decomposition of a fraction of the reducing agent, which favours protection of ND and a decrease in the extent of its graphitisation.

The elemental compositions of DB and the content of the major impurity (incombustible metal oxides and carbides) are listed in Table 4. As can be seen, introduction of organic or inorganic reducing agents (at least 10 mass %, calculated with respect to the initial explosive) causes a significant increase (by ~4 mass %–7 mass %) in the content of carbon in DB. The content of hydrogen remains almost unchanged, but those of nitrogen and oxygen decrease dramatically (3- to 10-fold). The amount of incombustible impurities also decreases 1.5–2-fold, which makes the DB thus produced suitable for immediate use in plating, finish polishing, polymer chemistry, oil composites, etc. Additionally, this DB can be much more readily purified, which leads to high-quality ND.

The content of ND in the DB synthesised in the presence of reducing agents increases by about 5 mass %–7 mass %, whereas the overall mass of the DB is doubled and therefore the yield of ND calculated with respect to the starting explosive increases 2.5-fold.

The elemental compositions and amount of impurities in the ND isolated by chemical purification of the DB produced by the novel method are listed in Table 5. The content of the

major component (carbon) in the detonation-synthesis ND prepared by the new technique is considerably larger (by 4 mass %–6 mass %) and amounts to 96.0 mass %. Irrespective of the synthesis conditions, the content of nitrogen varies in a narrow region, from 2.2 to 2.9 mass %, which indicates a quite uniform distribution of this element within all ND layers. Contrary to this, the amounts of hydrogen and oxygen change considerably (from 0.4 mass % to 2.4 mass % and from 0.7 mass % to 2.3 mass %, respectively). This points to accumulation of H and O in the outer layers of ND particles and to strong dependence of the contents of these elements on the synthesis conditions.

The lowest amount of incombustible impurities was found in the ND produced in the presence of urotropin. This is due to the fact that urotropin is a strong complex-forming agent, which reacts with metal impurities (Fe, Ni, Cr, Cu, etc.) to form soluble complexes which can be easily removed during chemical purification (upon treatment with nitric acid).

Because of the low content (0.1 mass %–0.3 mass %) of incombustible impurities (metal oxides and carbides) ND thus produced can be used in all technologies. At the same time the content of the non-diamond carbon in ND is almost constant (0.8 mass %–1.4 mass %) and has no effect on the technologies that use ND. The content of the diamond phase in the purified ND can be as high as 99.1 mass %.

The elemental compositions of a large number of ND samples produced at different facilities in Russia, China, Ukraine and Belarus were determined using the recently proposed procedure.^{37,38} The contents of the constituent elements in ND vary within the following limits (in mass %):

Table 5. Elemental composition and purity of ND isolated by nitric-acid purification from DB prepared using different types of reducing agents.³⁷

Reducing agent	Explosive : reducing agent (mass to mass ratio)	Elemental composition of ND (mass %)				Content of incombustible impurities in ND (mass %)	Content of oxidisable carbon in ND (mass %)	ND purity (ND content in the solid phase) (mass %)
		C	H	N	O			
Hydrazine hydrate	1:0.1	93.6	1.2	2.3	1.7	1.2	1.0	97.8
	1:0.5	94.4	0.4	2.5	2.3	0.4	1.1	98.5
	1:2.0	95.2	0.7	2.3	1.6	0.2	1.0	98.8
Urotropin	1:0.25	94.9	1.1	2.5	1.4	0.1	0.8	99.1
	1:0.5	95.2	1.0	2.2	1.5	0.1	1.0	98.9
	1:1	96.0	0.4	2.6	0.7	0.3	0.9	98.8
Urea	1:0.5	94.3	1.6	2.7	0.8	0.6	1.4	98.0
Ammonia	1:0.5	92.7	2.4	2.9	1.3	0.7	0.9	98.4
No additive ⁴¹	—	88.5	1.1	2.2	8.2	—	—	—

90.3–93.8 for C, 0.4–4.8 for H, 1.5–2.3 for N and 2.3–4.5 for O.

The actual elemental composition of ND is as follows:

Element	C	H	N	O
Content (mass %)	93–95	1–2	~2.5	2–3.5

V. Chemical purification of nanodiamonds: theory vs. practice

The specific features of DB include high dispersion, defectness of the carbon structures, developed active surface and, as a consequence, enhanced reactivity.

Besides, the detonation blend contains metal particles resulting from wear of the operating surfaces of the blast chambers and foreign impurity particles.

All the known ND purification techniques are based on the use of different stability of the diamond and non-diamond forms of carbon to oxidants.⁴² Liquid-phase oxidants offer an undoubted advantage over gas–solid systems, because they allow one to obtain higher reactant concentrations in the reaction zone and, therefore, provide high reaction rates.

Nevertheless, a method of oxidation of the non-diamond carbon by ozone was reported.⁴³ The ozone–air mixture is passed through DB at 120–400 °C. Despite quite a high degree of purification of DB from the non-diamond carbon, it still contains unburnt impurities (mainly iron oxides and carbides, up to 25 mass %; CJSC ‘Alit’, Ukraine). These impurities can be dissolved using liquid oxidants (strong acids).

The liquid-phase oxidation proceeds at sufficiently high rates at high temperature. Therefore, the oxidising mixtures are prepared using high-boiling acids (HClO₄, H₃PO₄, H₂SO₄) and oxidising agents (HNO₃, nitrogen oxides, H₂O₂, NaClO₄, CrO₃, K₂Cr₂O₇, etc.). Initially, perchloric acid was widely used as the high-temperature single-component oxidising agent. However, this is a hazardous substance (operation with and storage of this acid are expensive) and therefore it is no longer used for isolation of ND despite the unique properties.

There are three conventional ND purification techniques used in industry:

(1) action of chromium anhydride (CrO₃) solution on DB in concentrated sulfuric acid (RFNC–ARITP; FSUE ‘Elektrokhimpribor’ Integrated Plant, Lesnoy, Russia; CJSC ‘Alit’, Ukraine; facilities in China);

(2) use of nitric acid/oleum mixtures (‘FRPC Altai’, Biysk, Russia); and

(3) use of dilute nitric acid (FSUE SDTB ‘Tekhnolog’, St Petersburg, Russia; CJSC ‘Sinta’, Minsk, Belarus; Beijing Technological Institute, China).

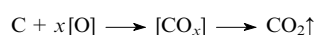
In particular, DB was mechanically filtered, treated with concentrated sulfuric acid, then heated and the non-diamond carbon was removed by adding oxidising agent (aqueous chromium anhydride solution) to the mixture of DB with concentrated sulfuric acid.⁴⁴ After the oxidation, ND were washed with water. The primary treatment of DB with sulfuric acid was carried out at 105–110 °C for 1.0–1.5 h. Nanodiamonds were first washed from acid treatment products with water to pH 5–6 at 60–70 °C and then with hot distilled water until negative reaction for chromium ions in rinse water. As a result, the amount of metal impurities in ND reduced to 0.9 mass % and the content of the major component increased to 98.5 mass %. This multistage chemical purification technique⁴⁴ is complex and expensive and produces very toxic waste.

The main advantages of the nitric acid/oleum oxidising systems consist in the availability and cheapness of the components. They are also simple in design and technological operation.⁴⁵ The drawbacks of the technique include low quality of purified ND (ND content is ~90 mass %), large

consumption of the acids (up to 57 kg per kg of DB), complexity of the regeneration and utilisation of the multicomponent mixture and contamination of the diamond surface with sulfur and nitrogen compounds.

Yet another group of methods of liquid-phase purification of ND is based on the principle of free dispersion of carbonaceous material in all stages of treatment.⁴⁶ The reaction suspensions of DB in liquid oxidising mixtures are homogeneous, colloidally stable (no ND precipitate), highly disperse and characterised by low viscosity. During the reaction, the oxidising agent has unrestricted access to the solid particles, which practically removes the diffusion limitations on the reaction rate.

High reactivity of DB allows the following oxidising systems to be used for purification:



Oxidation system	Reaction products
HNO ₃ –H ₂ SO ₄ –SO ₃ HNO ₃ –H ₂ SO ₄ HNO ₃ –H ₂ SO ₄ –H ₂ O	CO ₂ + H ₂ O + NO _x + SO _y
HNO ₃ –H ₂ O HNO ₃ –H ₂ O–H ₂ O ₂	CO ₂ + H ₂ O + NO _x
H ₂ O ₂ –H ₂ O–catalyst O ₂ –H ₂ O–catalyst	CO ₂ + H ₂ O

The total concentration of acids, specific consumption of reactants, amount and toxicity of gaseous reaction products and corrosion activity of the reaction medium decrease while the economic and environmental characteristics of technological processes are improved along the arrow.

Hydrogen peroxide is an attractive oxidising agent. Indeed, its reaction with carbon results in only two products, carbon dioxide and water.⁴⁷ The reaction also causes the development of a specific surface of the diamond material, which is free from sulfo and nitro derivatives. The use of hydrogen peroxide based oxidising systems for purification of ND significantly simplifies the process infrastructure, first of all the environmental protection system and waste reclamation. The main drawbacks of the technique include the impossibility of removal of unburnt impurities, the need of using equipment for high-pressure operation and incomplete removal of the non-diamond carbon.

These problems can be solved on going to aqueous nitric acid solutions. This fundamentally improves the quality of ND purification, because sulfur-containing derivatives cannot be formed on the diamond surface.³⁹ The process is carried out at elevated pressure. The equipment operating at high temperature is made of corrosion resistant materials.

High-purity ND (carbon content ≥ 98.5 mass %) can be obtained from DB upon 30–40 min of its residence in hot zone under high pressure. This process has been implemented in Russia, China and Belarus.

The use of complicated but efficient method of high-temperature oxidation with nitric acid under pressure makes it possible to implement a high-performance process characterised by low content of hazardous waste. The dissolution of metal-containing impurities and their transformation into water-soluble products are combined with oxidation within this method.

The simplest and the most readily available oxidising agent is atmospheric oxygen. Using specific features of the detonation blend, the non-diamond carbon was selectively oxidised by blowing air through an aqueous DB suspension in the presence of catalysts.⁴⁶ The procedure offers all advantages of the liquid-phase ND purification techniques and has the same

drawbacks as the method based on purification with hydrogen peroxide.

Analysis of the simplest, convenient and environmentally safe purification methods unambiguously shows that only dilute nitric acid should be used in large-scale production.

At present, the two-step ND purification technique based on treatment of DB with aqueous nitric acid solutions is practically implemented at some facilities. The first stage involves treatment of DB with concentrated (50–99)% nitric acid at 80–180 °C. In the second stage the material is treated with (10–40)% nitric acid at 220–280 °C.³⁹

A novel promising method of chemical purification of ND by combined treatment of DB with (2–40)% nitric acid and atmospheric oxygen at 200–280 °C under pressure (5–15 MPa) was developed.³⁷ The treatment involves renewal of the outer boundary layer of ND particles and has almost no effect on the structure of the diamond core. Therefore, purification is the key stage in the formation of the application characteristic of ND, because it is this stage that determines the possibility of preparation of various modifications of the product.

VI. Industrial synthesis of nanodiamonds

Technologically, production of ND involves the detonation synthesis, chemical purification and washing of ND from acids and conditioning of the product,^{34,36} recovery and utilisation of acid vapours and gases, pretreatment and recycling of nitric acid and water treatment.

Usually, industrial detonation synthesis (Fig. 3) is a periodic process. Every time an explosive charge equipped with electric detonator is manually loaded through a top hatch (not shown) of a hermetically closed blast chamber. Depending on the process used at the plant, a cylindrical charge (either non-armoured or surrounded by a water shell or ice armour) is suspended on strips to a hook welded at the top of the blast chamber. The charge is blasted from a distant explosion-proof room by applying an electric pulse to the detonator. The blast chambers of volume ~2 m³ are used most often.

In addition to DB, 60% nitric acid, air and desalinated water are used. The process results in ND as the end product in the form of either thickened stabilised suspension in distilled water or dry powder.

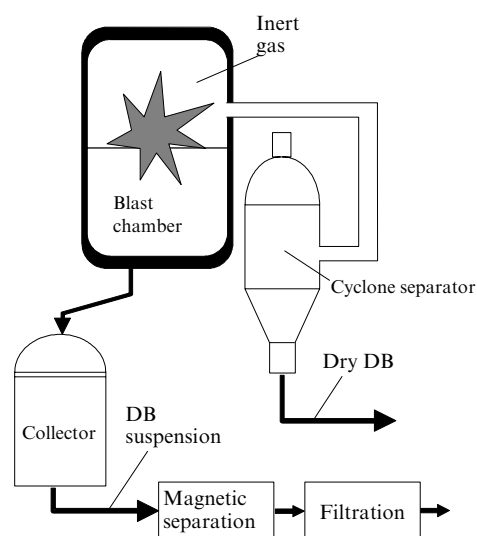


Figure 3. Detonation synthesis of nanodiamonds: flow chart of the process.³

A simplified scheme illustrating the key stages of purification process is shown in Fig. 4. Generally, the ND purification procedure involves the following steps.³⁶

1. Preparation of DB.
2. Preparation of aqueous nitric acid solutions.
3. Preparation of thin homogenated suspensions of DB in aqueous nitric acid solutions.
4. Continuous thermal-oxidation treatment of DB suspensions under pressure (~500 K, 8–10 MPa). This is the key stage, which requires the use of tailor-made equipment. The process is carried out in a flow reactor cascade with a particular temperature profile (smooth variation of the temperature along the reactor cascade) under equilibrium pressure.
5. Separation of thermal-oxidation treatment products.
6. Recycling of nitric acid.
7. Washing of ND from acids.
8. Waste processing.
9. Preparation of stabilised ND suspensions in distilled water.
10. Preparation of ND in the form of dry uniform powder.

Modern technology of ND purification by thermal oxidation using liquid-phase high-temperature oxidation of nitric acid provides high and stable characteristics of purification and is readily scalable and best practically implemented.

VII. Properties of nanodiamonds

Nanodiamonds are complex objects usually having a three-layer structure^{48,49} comprised of

- a diamond core 4–6 nm in size, containing from 70% to 90% of the total number of carbon atoms;
- a transient carbon shell (intermediate layer) surrounding the core and consisting of X-ray amorphous carbonaceous structures 0.4–1.0 nm thick, containing from 10% to 30% of the total number of carbon atoms; and
- a surface layer comprised of carbon atoms and other heteroatoms (N, O, H) that form various functional groups; the nitrogen atoms are quite uniformly distributed among all layers.

Detonation-synthesis ND are chemically inert and hardly oxidisable.⁴⁹ The diamond core can be partially decomposed by prolonged etching under severe conditions (in strong acids or acid mixtures, *e.g.*, conc. HNO₃, HNO₃ + HCl, HNO₃ + H₂SO₄ + SO₃, *etc.* at corresponding boiling temperatures for 50–100 h). Oxidation (etching) of ND has a complex character because the process does not involve a conventional layer-by-layer removal of the non-diamond and diamond phases (*i.e.*, their oxidation to gaseous products). Etching of the carbon matrix (up to the diamond phase) proceeds at structural defects within the intermediate layer. When the process involves the diamond core (mass loss of 30 mass % and more with respect to starting ND), not only the chemical composition of the surface functional groups, but also the structure of the intermediate layer is reproduced. It was shown that highly etched ND particles (mass loss of 40 mass %–60 mass %) possess nearly the same properties as the starting detonation-synthesis ND. The formation of almost the same intermediate shell was proved in many studies by various analytical methods. The oxidation processes first of all affect unstable (excited) atoms in the material. The most excited carbon atoms are on the surface of particles near structural defects. Thus, here we deal with selective etching of the most defect fragments of the near-surface structures near the most excited carbon atoms, resulting in the formation of nearly identical intermediate layer.

It should be noted that the greatest difficulties during chemical purification of detonation-synthesis ND by oxidation of DB are encountered in the oxidation of the ‘last’

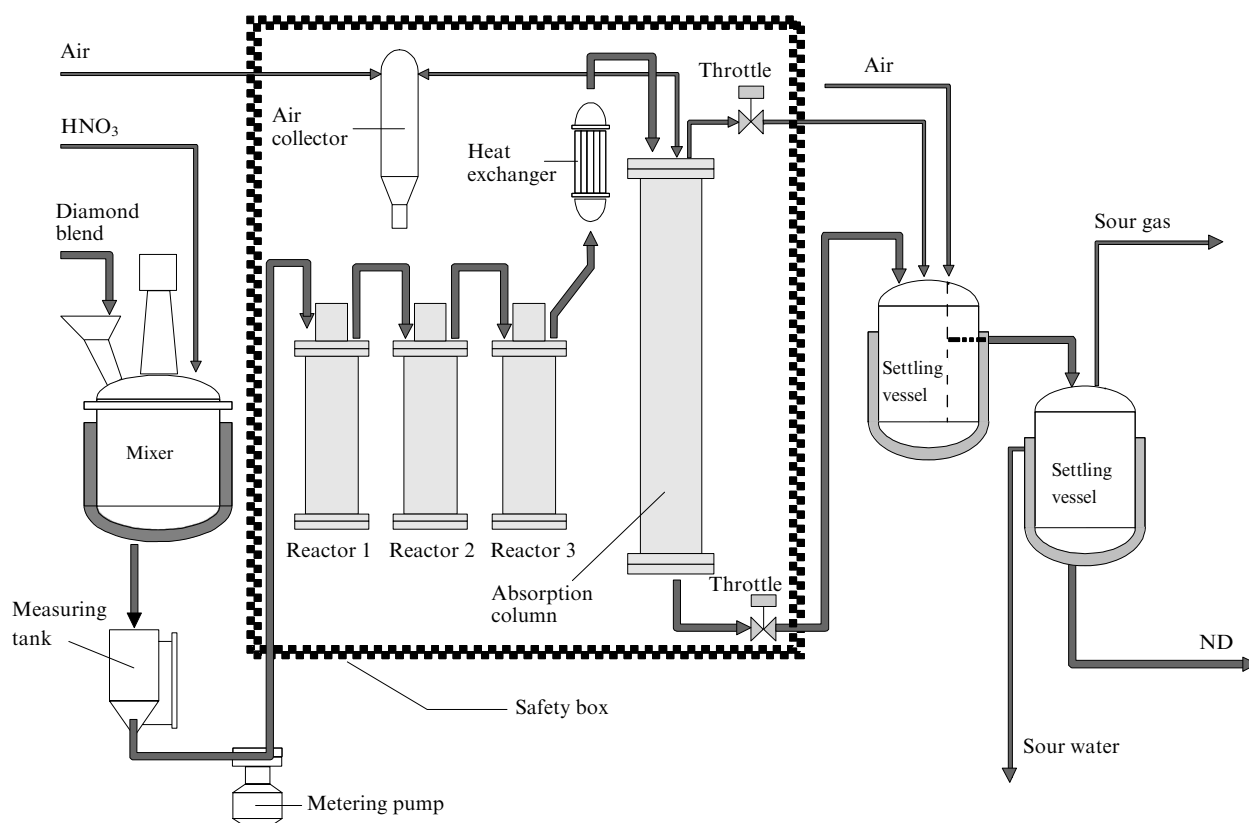


Figure 4. Simplified nanodiamond purification flow chart.³⁶

The mixer is filled with DB and HNO_3 . A suspension thus formed is fed to the measuring tank and then to Reactor 1. The ND suspension in spent HNO_3 passes through the heat exchanger and then is delivered to the adsorption column where gas separation occurs. Gases are absorbed by water and by alkali solution and the sour suspension is fed to the system of settling vessels and subsequent washing. The air collector is used to smooth pressure surges and to produce prepressure at the start-up in the operating mode, thus acting as a high-pressure throttle.

18 mass %–20 mass % of the non-diamond carbon, *i.e.*, in this case the residual carbon also shows a diamond-like behaviour.

The intermediate layer of purified ND has inhomogeneous structure. The inner sphere of the intermediate shell, which is adjacent to the diamond core, is comprised of continuous onion-like carbon (OLC) layers formed by hexagons.⁴⁸ The intermediate layer also contains graphite-like monolayers localised in peripheral regions. However, the overall structure of the intermediate layer is still to be clarified.

The complex structure of the intermediate layer is due to incomplete transformation of the carbon component of the ND particle to the diamond under the synthesis conditions. During the action of the detonation wave and in the course of the unloading step, when detonation products expand and reflected shock waves pass through them at rapidly dropping pressure but still at a very high temperature, structural fragments of the molecules of initial explosives chaotically combine with one another in the chemical reaction zone.^{1, 2, 10, 28, 36} Secondary processes, namely, graphitisation of detonation-synthesis ND and amorphisation of the crystalline phase are also highly probable under these conditions.

It is likely that the structure of the intermediate layer is comprised of a randomly combined praunits of those chemical compounds that release from ND upon extraction and thermal desorption. However, it is still unclear what these units and compounds made of them look like and how they are bonded

to one another, embedded into the intermediate-layer cage and stabilised.

Undoubtedly, it is vast variety and high reactivity of chemically bonded prastructures (in addition to the reactivity of functional groups on the surface of ND particles) that are responsible for the high reactivity of detonation-synthesis ND. Amazingly, the bulk mass concentrated in the diamond core remains chemically inert. Therefore, the behaviour of detonation-synthesis ND in various systems is hard to predict.

The average ND particle size is 4.2 nm. A simplified model for the surface of an ND particle with different functional groups is shown in Fig. 5. The number of atoms in such a particle is quite difficult to estimate owing to imperfection of the crystal, complication in the determination of the actual number and types of functional groups and uncertainty associated with characteristics of the intermediate carbon shell of the nanocrystal.

The number of carbon atoms in 4.2-nm ND particles reported by different authors varies from 300 to 20 000.^{36, 50} (Usually, the elemental composition was calculated for a perfect crystal.) The average number of atoms (including heteroatoms) in octahedral ND crystal (edge length 4.4 nm) is $\sim 20\,000$.⁵¹

A spherical ND particle of 4.2 nm size comprises nearly 7000 carbon atoms. The results of some calculations of the elemental composition of ND are listed in Table 6. According to Shenderova, the number of surface carbon atoms is ~ 1000 or $\sim 15\%$ of the total number of atoms.

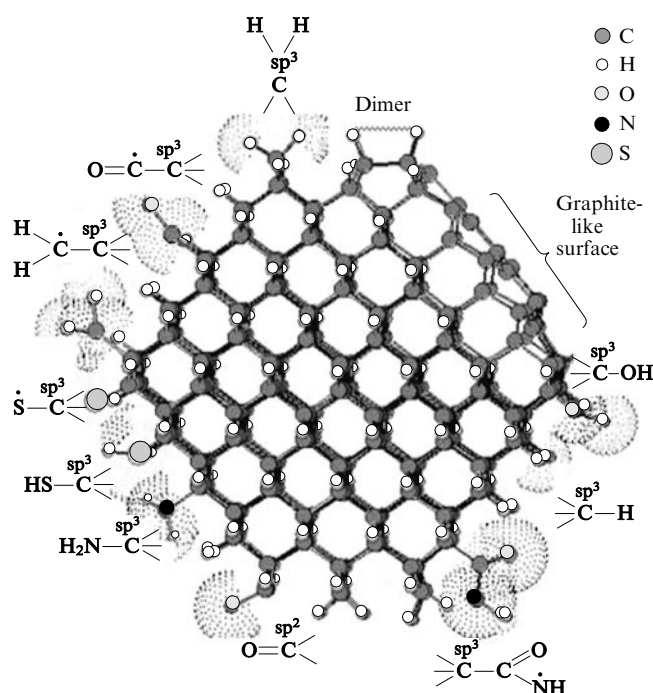


Figure 5. Nanodiamond particle with different surface functional groups (according to Shenderova, International Technology Center, USA). The structure was optimised by the semiempirical quantum-chemical method PM3.

Most often, functional groups appear on the surface of ND particles during purification of DB with strong oxidising agents. All oxygen and hydrogen atoms belong to the surface groups of ND.^{36, 50, 52–55} Nitrogen atoms are incorporated not only into the diamond lattice, but also the surface groups (amide groups⁵³ and nitro groups^{54, 56}).

The surface functional groups were analysed by IR spectroscopy,^{53–59} temperature-programmed desorption,⁵³ chem-

ical titration,^{59, 60} polarography^{36, 60} and X-ray photoelectron spectroscopy.⁵⁸

The surface groups were identified as hydroxyl groups (OH) in the form of sorbed water, carboxyl group and tertiary alcohol;^{53–57, 61} amide groups [NC(O)–H];⁵³ hydrocarbon groups (C–H) in the form of CH, CH₂ and CH₃;^{53, 56, 58, 62, 63} carbonyl groups (C=O) in the form of ketone, carboxyl group, acid anhydride, ester and lactone;^{53, 55–58, 63} C–O–C groups in the form of ether, acid anhydride, lactone and epoxy group.^{54–57, 62}

A study of fluorinated ND revealed the presence of surface CF, CF₂ and CF₃ groups.⁵⁸

The electrokinetic potential (ξ -potential) is one of the key characteristics of the ND surface, which strongly depends on the surface state. Different fractions of the same ND sample and, moreover, of ND samples purified and surface-modified in different manner are usually characterised by different ξ -potentials.

The ξ -potentials of three fractions (precipitate, intermediate and aqueous suspension) of the ND produced at the RFNC–ARITP were +16, +32 and +39 mV, respectively.⁶⁴ The ξ -potential of non-fractionated ND (UDD-TAH brand) produced at the FSUE SDBT ‘Tekhnolog’ is +33 mV (aqueous medium).

Three types of modified ND (UD-HP, UD-SO and UD-M brands) are produced at the RPA ‘Sinta’.⁶⁵ The ξ -potentials of their aqueous suspensions equal –16 (UD-HP), –87 (UD-SO) and +24.9 (UD-M) mV.

Dry ND is a light-grey polydisperse powder with a bulk density of about 0.5 g cm^{–3}. It is comprised of agglomerates of size from a few to hundreds of micrometres. Two main types of impurities in ND are incombustible and oxidisable carbon (the latter remains on the surface of ND particles after chemical purification). The admissible content of each of the two impurities is at most 1.0 mass %. Well-purified ND contains at most 0.5 mass % of each type of impurity. Practical applications of ND are mainly interfered with the presence of incombustible impurities; their compositions for three commercially available ND brands is presented in Table 7.^{50, 66}

An aqueous suspension of pure ND in water cannot be neutral (Fig. 6); the ND particles should behave in water like

Table 6. Contents of chemical elements (%) with allowance for various functional groups on the surface of spherical diamond particle 4.2 nm in diameter.

Surface composition		C _{diamond}	H	O	N	C–X (hetero- atom)	C _{tot}
atom or group	content (%)						
H	100	98.7	1.3				
OH	100	81.9	1.0	17.1			
OH	50	89.5	1.2	9.3			
H	50						
COOH	50	77.0	1.0	16.0		6.0	83.0
H	50						
H	63.8	88.7	1.17	5.68	2.34	2.09	90.79
OH	10						
COOH	5						
CO	10						
NH ₂	11						
NO ₂	0.1						
NO ₃	0.1						

Note. All surface groups provide a 100% ‘coverage’ of unsaturated bonds. (Calculated by Shenderova, International Technology Center, USA).

Table 7. Contents of incombustible impurities (mass %) in ND samples according to atomic emission spectroscopy data (analysed by Chukhaeva, RFNC–ARITP).^{50, 66}

Impurity	Aqueous ND suspension ^a		Typical ND ^b
	UDD-SWS powder	UDD-TAH powder	
Fe	0.15	0.1	0.1
Cr	0.07	0.05	0.5
Xi	0.3	0.1	0.15
Al	0.005	0.001	0.01
Na	0.03	0.003	0.05
K	0.002	0.002	0.002
Cu	0.005	0.002	0.003
Ca	0.002	0.002	0.01
Mg	0.005	0.003	0.005
Mn	0.001	see ^c	0.001
Ti	0.01	0.005	0.002
Pb	0.001	0.001	0.001
Total	0.58	0.27	0.84
Incombustible residue (%)	0.95	0.4	1.4

^a Produced at FSUE SDBT ‘Tekhnolog’. ^b Produced at RFNC–ARITP.

^c Undetected at a sensitivity of 5×10^{-4} mass %.

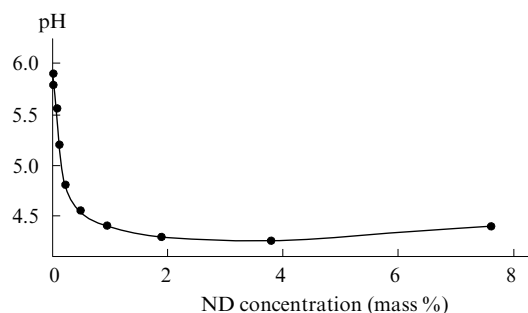


Figure 6. The pH values of a washed aqueous ND suspension plotted vs. ND content.⁶⁷

an acid due to the presence of surface carboxyl groups.⁶⁷ Indeed, they do behave as poorly soluble weak organic acids. The rapid coagulation threshold of ND particles, *i.e.*, the loss of sedimentation stability, corresponds to a pH value of 5.5.

Earlier (see, *e.g.*, Ref. 68), it was shown that the phase transition occurs on heating of ND from 720 to 1400 K in inert atmosphere.

The lines in the Raman spectra of ND coincide with maxima of the phonon state density functions of diamond and graphite. This indicates the presence of small amounts of amorphous diamond and graphite in the ND material. Nanodiamond clusters exist only in the form of aggregates;⁶⁹ the amorphous phase is likely to occur in the interior. The presence of the amorphous phase is also confirmed by X-ray diffractometry data; the characteristic size of this phase was estimated at about 1.5 nm.

According to X-ray diffractometry data, nucleation of the graphite phase occurs only at $T > 1200$ K. The diamond–graphite structural phase transition occurs on annealing in inert atmosphere and begins at the surface of ND clusters; the graphite phase nucleates in the form of equidistant nanoplates.

The phase transition onset temperature correlates with the electron microscopy data,⁷⁰ according to which the decrease in the size of the ND core begins only at $T > 1300$ K. The process is accompanied by transition of the outer carbon atoms to the OLC phase.

Later on, it was found that graphitisation of diamond can be induced by heat treatment and by the action of reactive gases and maintained using metal catalysts and also by emission from various sources.⁷¹ On the one hand, graphitisation sets limitations on the temperature range and conditions for efficient use of diamond. On the other hand, it provides the possibility of design of novel nanoscale carbonaceous materials. It was shown⁷¹ that annealing of 2–5-nm ND particles gives rise to the OLC phase,[†] whereas the annealing of micrometre-size diamond particles leads to formation of closed bent graphite-like structures, such as nanotubes, nanohelices, *etc.* Based on the results of molecular modeling by the molecular mechanics, molecular dynamics and Hartree–Fock methods, it was assumed that the formation of the OLC and closed bent graphite-like structures on the surface of diamond particles exhibits specific features of self-assembly processes.

Nanodiamond particles have a large specific surface area and therefore their physical and chemical properties are strongly affected by the surface groups. Controlled functionalisation provides a powerful tool of specific modification of ND particles. Using this approach, one can involve ND in various chemical reactions, enhance their interaction with solvents, components of composite materials, polymers and catalysts. The surface groups stabilise the surface of ND

particles and preclude their graphitisation. Decomposition of the surface groups causes graphitisation of ND and formation of bucky-diamonds (intermediates of the transformation of ND to OLC) and, finally, to OLC. With allowance for high stability of the hydrocarbon groups the most thermally stable ND can be prepared by surface hydrogenation.

Various graphitisation mechanisms were reported for the ‘low’- and ‘high’-temperature regions.⁷¹ In the high-temperature region, the rate of graphitisation is controlled by the detachment of a single atom from the diamond surface. In the low-temperature region, the mechanism of graphitisation involves incomplete detachment of carbon atoms from the surface of diamond particles and the external planes (faces) of diamond crystal are gradually transformed into the graphite planes. These temperature regions are separated by the Debye temperature of diamond (1910 K).

By varying the ND graphitisation rate it is possible to prepare diamond/nanographite composites with different ratios between the diamond core and bent graphite shells (so-called sp^2/sp^3 -nanocomposites). The presence of interfaces between the nanoscale diamond cores and graphite shells and, probably, high concentrations of the open graphite edges can predetermine unusual electronic properties of these composites.

Selected characteristics of the static-synthesis diamonds and detonation-synthesis ND are listed in Table 8. The differences between the particle size, specific surface area and content of volatile impurities are most pronounced.

Table 9 lists selected properties of ND and technological parameters of large-scale production of ND for three leading manufacturers of detonation-synthesis ND in the CIS.⁷² The maximum yield of ND is obtained using the novel method of synthesis at the FSUE SDTB ‘Tekhnolog’. Additionally, the content of incombustible impurities even in DB is minimum and their content in pure ND is very low.

Table 8. Characteristics of detonation-synthesis nanodiamonds and static-synthesis diamonds.⁷²

Parameter	Nanodiamonds	Diamonds
Phase composition	cubic diamond, $a = 0.3565$	cubic diamond, $a = 0.3567$
Picnometric density /g cm ⁻³	3.30	3.51
Particle size /nm	4–15	30–2000
Specific surface area /m ² g ⁻¹	200–450	13.5
Content of incombustible impurities (mass %)	< 1.5	< 0.2
Content of volatile impurities (mass %)	10–12	1–2
Temperature corresponding to the onset of intense oxidation in air /K	800	780
Maximum exothermic effect in air /K	960–1000	900
Temperature corresponding to the onset of graphitisation <i>in vacuo</i> /K	1373	1373
Electrical resistivity /Ω m	7.7×10^9	1×10^{10}
Specific magnetic susceptibility, $10^8 \chi /m^3 \text{ kg}^{-1}$	< 1.0	0.5
Surface functional groups	OH, C=O, CO ₂ H, NH ₂	HO, C=O, CO ₂ H

[†] Complete annealing results in OLC particles while partial annealing affords diamond/OLC core–shell particles.

Table 9. Technological parameters and properties of samples produced by the leading manufacturers of detonation-synthesis ND in the CIS area.⁷²

Parameter	FSUE SDTB 'Tekhnolog', St Petersburg, Russia	CJSC 'Alit', Kiev, Ukraine	'FRPC Altai', Biysk, Russia
Blast conditions in chamber	water shell (3 kg) of complex composition	water shower/water shower + ice armour (100 kg)	gaseous atmosphere
Mass of explosive charge /kg	0.6	10.0	0.6
Explosive charge composition (TNT/RDX mixture) (mass % of TNT)	40%	40%	60%
ND yield relative to the mass of explosive (%)	10–14	5–7/8–12	4–5
ND content in diamond blend (mass %)	55–75	50–60/~70	30–40
Content of incombustible impurities in DB (mass %)	1.5–3.0	16–26	5–12
Chemical purification procedure and its parameters	55%–60% HNO ₃ , 513 K, ~8 MPa	1) HCl (boiling) 2) H ₂ SO ₄ + H ₂ Cr ₂ O ₇ (boiling) 3) HCl + HNO ₃ (boiling)	H ₂ SO ₄ + SO ₃ + HNO ₃ , 523 K
ND size (coherent scattering range) /nm	4–5	6–8	4–6
ND specific surface area /m ² g ⁻¹	330	200	250–350
Content of incombustible residue in ND (mass %)	0.1–0.6	2.5–3.0	4–5
Content of oxidisable carbon in ND (mass %)	0.5–0.8	0.8–1.5	4–5

VIII. Fields of application of nanodiamonds

Nanodiamonds incorporated into materials act as powerful structure-forming agents that ensure dispersion strengthening of composites.

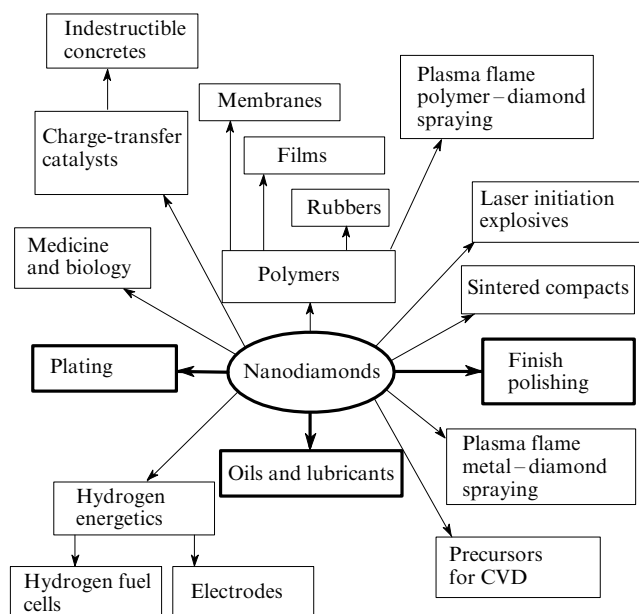
In search for optimum cost–quality relation for ND-containing products one should allow for the following:

— simple ND synthesis technology makes it possible to establish large-scale production of cheap ND the cost of which is mainly determined by the cost of explosives;

— in many fields of application ND can be replaced by crude DB, which is much cheaper than purified ND;

— positive effect is attained upon introduction of (0.1 mass %–1.0 mass %) of ND additive into the material.

Nanodiamonds have a broad spectrum of applications (Fig. 7), three of them being the major ones. These are finish polishing (~70% of the total amount of ND), metal plating (~25%) and oil composites (~5%). In the nearest future, production of polymer–diamond composites, charge-transfer catalysts and modified biologically stable concretes can develop into large-scale industries.

**Figure 7.** Fields of application of nanodiamonds.

Thick and thin arrows denote the current and future fields of application, respectively.

1. Metal plating

Nanodiamonds present in the electrolyte of a galvanic bath should be in the suspended state. To this end, an aqueous ND suspension is added to the electrolyte. In the preparation of metal–diamond composite electrochemical coatings, the suspended state of ND is maintained by gas evolution and thermal convection.

The introduction of ND into electrochemical coatings significantly improves their microhardness, wear resistance, corrosion resistance, throwing power, makes the visual appearance of goods more attractive and reduces porosity. The main reason for these changes consists in reduction of the size of metal domains in the coatings. Nanodiamond particles are small and therefore sufficiently dense and uniform distribution over the coating can be attained even at very low content of these species (few tenth of a per cent).

A number of ND-containing composite electrochemical coatings based on chromium, nickel, tin, zinc, copper, gold, silver, aluminium, iron and various alloys were developed. Selected physicomachanical characteristics of such coatings are listed in Table 10.

a. Chromium plating

Investigations on metal–diamond coatings began with the studies of electrochemical deposition of chromium and ND.^{73–75} Later on, they attracted the greatest interest because chromium coatings are most often used to provide for high wear resistance of tools and workpieces.

Table 10. Physicomechanical characteristics of metal–diamond coatings.

Coating	Wear resistance increases by a factor of n , where n is	H_V /kg mm ⁻² (see ^a)	Porosity decreases by a factor of m , where m is	Corrosion resistance increases by a factor of p , where p is
Cr + ND	2–12	up to 2300	2–3	3–6
Ni + ND	5–6	up to 600	no pores	2–5
Cu + ND	9–10	160	the same	no corrosion
Au + ND	2–5	200	6	the same
Ag + ND	10–15	180	8	"
Zn + ND	—	—	6–8	2–4
Sn + ND	4–5	150	7	1.5
Al + ND	10–13	600–700	3	no corrosion
Fe + ND	6–8	800	8–10	3–4
Ni + B + ND	6	8000	—	no corrosion
Sn + Pb + ND	—	31	no pores	5–7
Sn + Sb + ND	2.5	25	5–6	2–3
Ag + Sb + ND	1.5–1.7	150	—	—

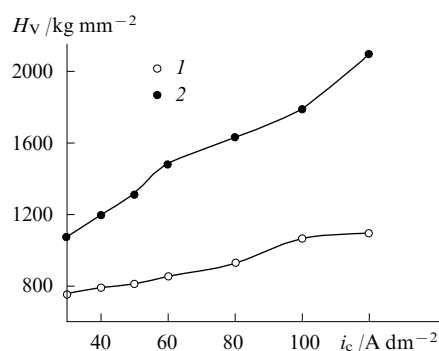
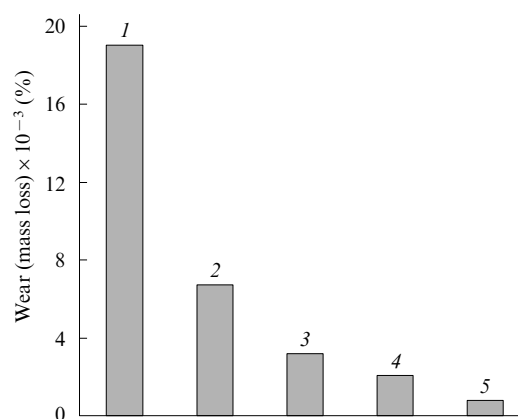
^a Microhardness.

Either solid chromium plating electrolytes or buffer electrolytes are used as chromium/ND plating electrolytes. The content of ND in the coating is 0.3 mass %–1.0 mass %.

The content of ND in the chromium coating is analysed as follows. A chromium–diamond coating (CDC) 55–60 μm thick is deposited on a stainless steel plate. Then, the CDC is electrolytically dissolved in 10% aqueous NaOH solution at a cathode current density (i_c) of 10 A dm⁻² and a temperature of 303 K. A sodium chromate solution containing the ND suspension is passed through a preliminarily weighed Schott filter. The ND precipitate on the filter is successively washed with hot water, 10% H₂SO₄, water, 20% HCl and again water. The filter with the precipitate is dried at 423–473 K, the absolute amount of ND is determined from the mass difference and then the ND concentration in CDC is calculated (knowing the mass of the dissolved coating).

The microhardness of chromium coating depends on the ND concentration in the electrolyte, namely, the microhardness increases as the ND concentration increases.⁷⁶ As i_c increases, the microhardness also increases. The most impressive results were obtained using a composite diamond additive comprised of detonation-synthesis ND and static-synthesis diamonds (Fig. 8).⁷⁷

In Fig. 9 the wear of various chromium coatings is compared with that of titanium nitride coatings.⁷⁷

**Figure 8.** Microhardness of solid Cr-ND-ASM-coating plotted vs. cathodic current density (standard electrolyte).⁷⁷ No ND additives (1) and in the presence of ND (ND : ASM = 5 : 5) (2); ASM brand is synthetic diamond nanopowder.**Figure 9.** Wear of titanium nitride (TiN) and chromium coatings.⁷⁷ TiN (1), hard Cr (2), wear-resistant Cr (3), Cr + ND (4) and Cr + ND + ASM (5).

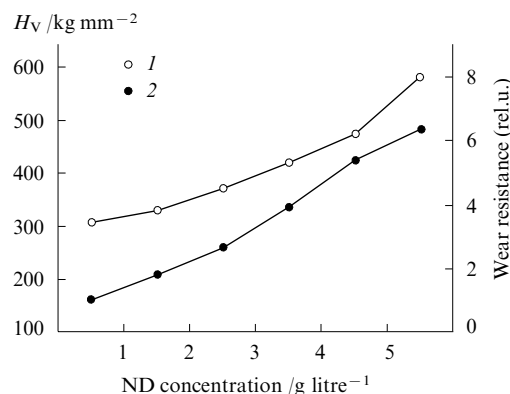
Chromium plating using ND is widely used in Russia, USA and South Korea.

b. Nickel plating

Analysis of the data listed in Table 11 and the plots shown in Fig. 10 reveals a positive effect of ND on the quality of nickel–diamond coatings.^{76, 78, 79}

Table 11. Effect of ND content on microhardness, wear resistance and porosity of nickel coatings at different cathodic current densities.^{76, 78}

ND content /g litre ⁻¹	H_V /kg mm ⁻²			Porosity /number of pores per cm ²		Wear resistance (rel.u.)
	1.0 ^a	1.5 ^a	5.0 ^a	1.0 ^a	1.5 ^a	5.0 ^a
No additives	251	286	308	20	15	1.0
0.5	301	312	330	15	10	1.8
1	320	331	354	15	5	2.3
2	359	380	378	15	5	3.8
5	370	408	472	10	5	5.7
10	395	467	583	6	4	6.4

^a The i_c values (in A dm⁻²).**Figure 10.** Microhardness (1) and wear resistance (2) of nickel coating plotted vs. ND concentration in sulfuric acid electrolyte.³⁶ $i_c = 5$ A dm⁻².

The content of ND in the coating increases from 0.1 mass % to 0.7 mass % as the ND concentration in the electrolyte increases from 0.5 to 10.0 g litre⁻¹. At a 5 g litre⁻¹ ND concentration in the electrolyte, the microhardness of the coating becomes nearly doubled (see Fig. 10) and the wear resistance shows a nearly sixfold increase. The coating thus prepared is fine-grained, dense and has a low porosity.

c. Gold plating

If the ND concentration in the electrolyte varies from 0.1 to 10.0 g litre⁻¹, the ND content in the gold coating changes from 0.2 mass % to 0.8 mass %. The microhardness of the coating reaches a value of 200 kg mm⁻² and the wear resistance increases two- to five-fold.^{36, 80–82}

The structure and properties of the coating vary non-monotonically. Figures 11 and 12 show bimodal plots.⁶⁵ The first peak appears at low ND concentrations and its intensity depends on both the electrolyte composition and the type of the co-deposited diamond-containing additive. The second peak appears at higher ND concentrations. Nanodiamonds can be incorporated into the coating in the form of individual particles or as large aggregates depending on their colloidal state in the electrolyte. The second peak appears in the concentration range corresponding to co-deposition of gold with ND aggregates. In this region some technological characteristics (*e.g.*,

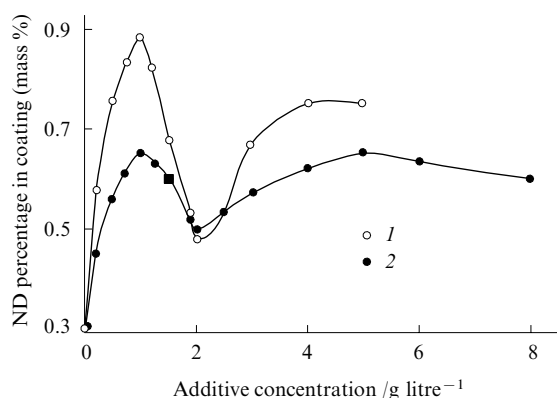


Figure 11. Mass percentage of co-deposited ND particles in gold coating plotted vs. concentration of the diamond-containing additive in the electrolyte for two types of additives: DB (1) and ND (2).⁶⁵

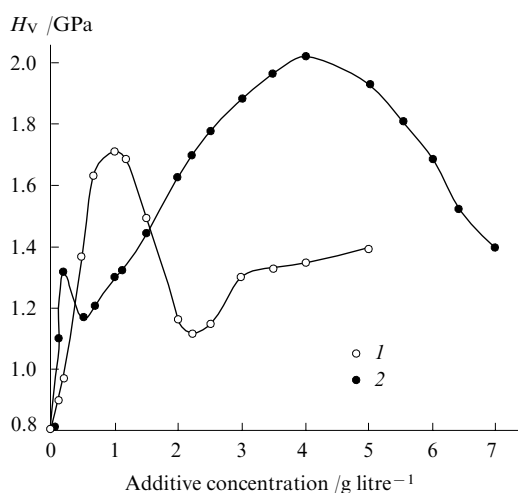


Figure 12. Microhardness of gold coating plotted vs. concentration of the diamond-containing additive in the electrolyte for two types of additives: DB (1) and ND (2).⁶⁵

sedimentation rate and the yield of gold calculated with respect to electric current) are deteriorated.

The gold plating process has been implemented on a large scale.

g. Silver plating

Using ND, it is possible to prepare dense, fine-grained semi-bright silver coatings containing up to 1.0 mass % of ND.^{36, 80, 83}

Depending on the electrolysis conditions, composition and type of electrolyte, the microhardness of the silver–diamond coating increases by 200–700 MPa compared to that of microhardness of pure silver. The wear resistance of the coatings shows a ten- to fifteen-fold increase (Fig. 13), the solderability of this coating is identical to that of pure silver. The silver plating process has been implemented on a large scale.³⁶

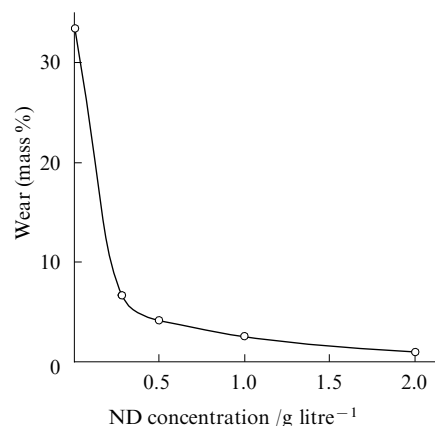


Figure 13. Wear resistance (mass loss) of silver–diamond coating plotted vs. ND concentration in electrolyte.^{36, 80}

d. Zinc plating

The optimum concentration of ND in the zinc plating electrolyte is 10 g litre⁻¹, which corresponds to the ND content in the coating of 0.7 mass %.^{36, 76, 84} As the amount of ND in the electrolyte increases, the precipitates become more finely grained.

Passivation of zinc/ND coatings thus obtained by conventional chromium plating or phosphating significantly increases

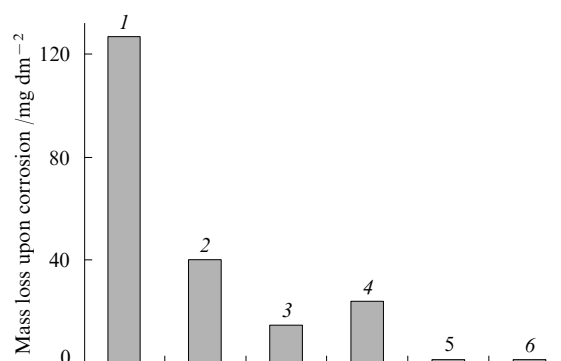


Figure 14. Corrosion resistance (mass loss) of zinc coatings compared to that of unprotected steel and cadmium coating (NaCl fog, 60 h).^{36, 76, 84} Unprotected steel (1), Zn-coating (2), Cd-coating (3), Zn + ND (4), Zn + ND + chromating (5) and Zn + ND + phosphating (6).

their corrosion resistance (Fig. 14). Phosphating was found to be much more efficient and environmentally safe.

e. Anodic oxidation of aluminium

Anodic oxidation is the main method of corrosion protection, and increasing the strength and wear resistance of aluminium and aluminium alloys.

During oxidation, the ND particles fill pores and remain in them due to mechanical and van der Waals forces. The mass of the filled oxide film increases two- to four-fold.^{36, 76, 85} The wear resistance of such a film increases to a much greater extent (by 10 to 13 times; see Fig. 15) and so do its corrosion resistance and dielectric properties. The film turns grey.

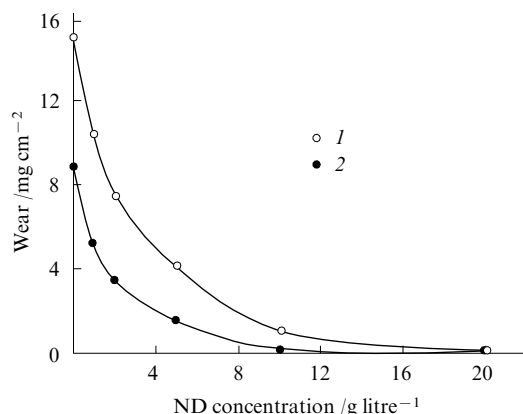


Figure 15. Wear of anodically oxidised aluminium film based on D-16 alloy (Germany) plotted vs. ND concentration in anodic oxidation electrolyte ($i_a = 1.5 \text{ A dm}^{-2}$).^{36, 76, 85} At 10 °C (1) and at 20 °C (2).

g. Iron plating

The hardness of electrochemical iron coating approaches that of steel. Such coatings become even harder when using ND.⁸⁶ For iron plating, it is more appropriate to use DB rather than purified ND. The best results were obtained using partially oxidised DB prepared following a known procedure.⁸⁷

The effect of ND and partially oxidised DB on the microhardness and wear of iron coatings is illustrated in Figs 16 and 17. The advantage of using the cheaper product (DB) is clearly seen.

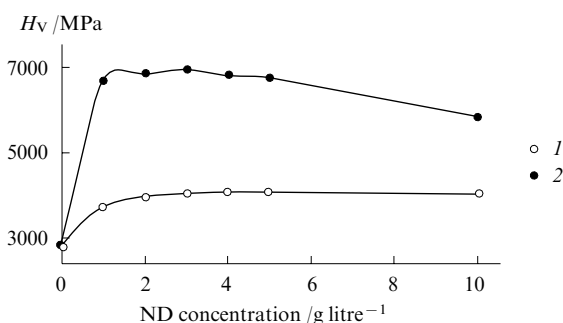


Figure 16. Effect of ND (1) and DB (2) concentration on microhardness of iron coating ($i_c = 4 \text{ A dm}^{-2}$).⁸⁶

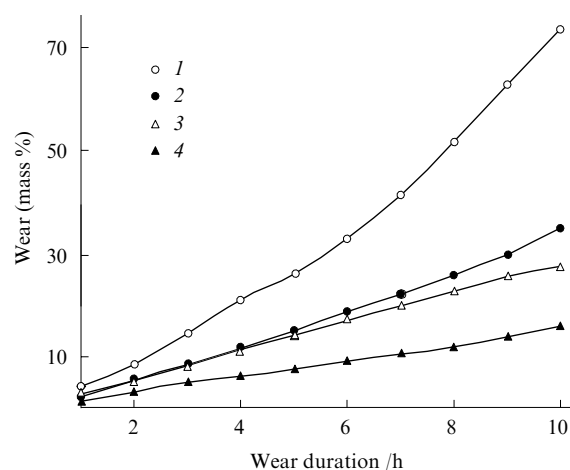


Figure 17. Effect of various diamond-containing additives on wear of an iron coating (concentrations of all additives were 5 g litre^{-1} , $i_c = 4 \text{ A dm}^{-2}$).⁸⁶ No additives (1), ND (2), conventional DB (3) and oxidised DB (4).

2. Polishing

Introduction of ND into polishing composites improves the characteristics of chemico-mechanical polishing and the efficiency of the overall surface treatment.^{36, 50, 88–93}

The colloidal, sedimentation and mechanical properties of ND clusters aggregated into complex fractal structures depend on the procedure for preparation and on the composition of the liquid dispersion medium. Nanodiamonds introduced into the liquid (ND content of 0.1 mass %–0.3 mass %) act as powerful structure-forming agent. Using low-filled aqueous, organic and aqueous-organic ND dispersions, one can obtain ideally smooth surfaces of materials processed, in which the micro-roughness is comparable in size with interatomic distances.

The fractal structure of ND favours efficient relief of local stress produced as the working surfaces approach each other. Large loose ND aggregates easily break down upon slightest action on the suspension and appear again also easily.

The fractal ND aggregates act as a kind of damper, which makes rigid point-to-point interactions between the working surfaces less probable. This prevents the material being processed from deformations and stress in the near-surface layer.

When the polishing pads and treatment regimes on most buffing machines were chosen appropriately, all materials showed smoothing of relief and formation of flat mirror surfaces without macroscopic defects.

Preparation of polycrystalline micropowders with different nanostructures of porous particles seems to be promising for polishing. Powders are prepared by milling large aggregates formed upon compaction of ND powder.

Polishing using ND is employed to improve the operating characteristics of almost all materials, namely, composites, semiconductors, dielectrics and conductors having a crystal, polycrystal, glassy or some other structure.⁹²

The key parameters of polishing are the rate of removal of material, surface roughness, flatness and plane-parallel arrangement of surfaces of working pieces. They are determined by the properties of ND and to a great extent by the design of buffing machines, types of polishing pads, their pre-treatment and other factors. Therefore, a particular ND powder (or polishing composite) should be 'tuned' to a technology of treatment of a material in hand or working pieces made of it.

Table 12. ND-containing polishing compositions.⁹⁴

State	Medium	ND content (mass %)
Suspension	water, ethylene glycol, aqueous KOH or FeSO ₄ solution, petroleum oil	3–5
Polishing compound	lipids, polymers	3–5
Solids of specified shape	cured silicone, nitrile, <i>etc.</i> rubbers	2–3
	cured formaldehyde and epoxy resins	2–5
	metal (aluminum, nickel)	< 50

Nanodiamond-containing polishing compositions can provide a high flatness (to 1 μm) and reproducible surface roughness from a few fractions of a nanometre to a few nanometres for more than thirty crystalline substances. The number of such materials increases and the polishing quality is improved, which indicates a versatile character of this technology.

Table 12 lists the components of some polishing compositions.⁹⁴ The results of treatment of materials characterised by different hardness and plasticity are listed below.⁹⁴

Material	Surface roughness /nm
Hard alloy	1–5
Steel	5–6
Sapphire	5–6
Quartz	0.5–1.5
Molten silica	0.5–1.0
Silicon	0.5–1.5
NaCl crystal	2–3
KBr crystal	2–3

A decrease in the diamond particle size from 1 μm to 3–5 nm is accompanied by a decrease in the relief roughness and by the change in the mechanism of mass transfer on the surfaces of alloys and composite materials from anisotropic (plastic deformation) to isotropic (nanoscratching) removal of material.

3. Oils and lubricants

Nanodiamonds, as modifiers of the friction surfaces, offer the following advantages over other types of surface modifiers:^{36, 50, 95–97}

- efficiency at very low concentrations in the base oil;
- compatibility with various types of synthetic and mineral oils; and
- environmental safety of the carbon additive to oils compared to metal particles or fluorocarbons.

The addition of diamond blend containing a large number of ultrasmall graphite-like particles and ND causes the properties of lubricants and the character of the interaction between the friction surfaces to change. Namely, the viscosity of the liquid, the strength of the lubricating film and, as a consequence, the loading capacity of tribomating increase. Selected characteristics of diamond-containing lubricant compositions and their efficiency are listed below.

Parameter	Numerical value
ND content (mass %)	0.01–0.3
Particle concentration / cm^{-3}	$\sim 10^{14}$
Reduction of temperature in the contact zone (%)	16–20
Reduction of the friction coefficient (%)	20–30
Increase in limiting load of a friction pair (steel–bronze) /MPa	from 16 to 72 (approximately fourfold)
Reduction of wear of mating components by a factor of n	$n = 1.5–3.0$
Combustion engines	
Engine run-in time reduction by a factor of m	$m = 10–12$
Fuel economy (%)	3–6
Power increase (%)	4–8
Cylinder compression increase (%)	10–17
Cooling-lubricating liquids (CLL)	
Cutting torque reduction (%)	20–30
Increase in operating life of tools by a factor of p	$p = 1.5–4.0$

The most interesting parameters are the very low content of ND, considerable increase in the limiting load, reduction of wear of mating components, engine run-in time reduction and an increase in the operating life of tools. ND-containing lubricant compositions can be based on mineral or synthetic oils and CLL.

The DB in a lubricant composition produces a complex effect consisting in:

- filling of dips on the friction surfaces with carbon clusters and subsequent reduction of boundary friction and wear;

- an increase in viscosity of the lubricant composition in thin films due to dispersion structuring of carbon clusters;

- a decrease in viscosity of the lubricant composition at low temperatures due to reduction of glass transition threshold of the dispersion-filled medium;

- after-effect (duration over 60 h) upon replacement of the lubricant composition by the base oil; the effect is due to strong mechanical, adsorption and diffusion immobilisation of carbon clusters on the friction surfaces;

- operation of ND clusters as microscopic antifriction bearings under high load at maximum displacement of the liquid phase between friction surfaces, which permits an increase in the limiting load of the friction pair.

The content of DB in the lubricant composition depends on the character and operation mode of a particular device.

Diamond blend has a strong effect on most structural-mechanical and operating characteristics of almost all types of lubricants. The use of preservation greases reduces the chemical and electrochemical metal corrosion because many additives (usually, corrosive substances) are no longer used. The use of sealing greases and thread lubricants improves the tightness of joints, reduces corrosion of the contact surfaces and stabilises and reduces the shear stress and torque.

Cooling-lubricating liquids are most efficient in screw cutting and holmaking in hard-to-machine materials.^{98–100} Introduction of DB (1 mass %–5 mass %) into lubricants used in plastic metal working significantly reduces the friction coefficient and improves the quality of the surface of goods.¹⁰¹

Diamond blend-containing oil compositions are used in Russia, Germany, Italy, Turkey and China.

4. Polymer – diamond composites

Numerous studies showed efficiency of the introduction of ND and DB into polymeric composites and films based on poly(fluoroelastomers), perfluorocarbons, polysiloxanes, poly(isoprenes), butadiene–styrene rubbers, polyurethanes, polyimides, *etc.*^{36, 50, 91, 102–107}

The introduction of ND improves the overall elasticity and strength characteristics and in some cases provides polymers with unique tribotechnical properties.

The introduction of DB significantly reduces the permeability of fluoroelastomer films.^{103–105} Based on some optimisation parameters, poly(vinylidene fluoride-*co*-perfluoropropyl ether) (CVPE) filled with DB to different extent (from 2 to 50 parts by mass) was chosen as the elastomeric component. A comparative analysis of mass thermograms of the elastomer and nanocomposites based on it showed an increase in the thermal degradation onset temperature, on average, by 40 °.

At a DB content of 5 mass %, the tear resistance of the fluoroelastomer is doubled (Fig. 18). The physicochemical characteristics of the fluoroelastomers based on this DB measured in the course of thermal ageing at 522 K are identical to or better than those of non-aged conventional vulcanisates.

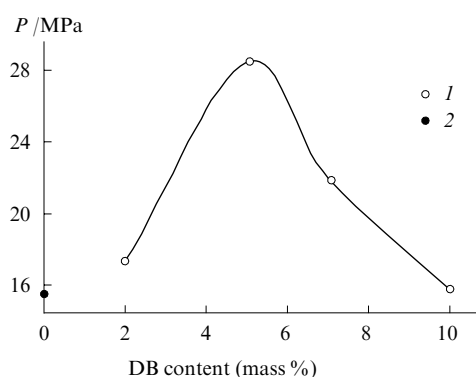


Figure 18. Tensile strength of perfluorinated polymer (film) CVPE plotted vs. additive concentration. Additives: diamond blend (1) and carbon black (2).¹⁰⁵

A fluoropolymer filled with DB (2 parts by mass) demonstrated a decrease in the coefficient of sliding friction at the metal–rubber interface to 7.0×10^{-3} . Rubber mixtures based on DB-modified fluoroelastomers showed an increase in the abrasive wear resistance by a factor of 1.5–2.0.

Thus, DB is the most reactive filler of fluoroelastomers and provides a highly cross-linked vulcanisation network, minimum thermal ageing, low friction coefficient of film coatings and extends their operating life by 25%–40% in the friction units.

a. Polyisoprene and butadiene–styrene copolymer

The modifying action of DB was demonstrated in relation to conventional filled polymer blends based on polyisoprene and butadiene–styrene rubbers, which are widely used in Russia.¹⁰⁸

Diamond blend-modified rubbers are characterised by higher degree of vulcanisation, a 35% higher conditional tensile strength at 300% elongation and a 30% lower degree of swelling in toluene. Such rubbers have better strength characteristics (about 30% higher than those of conventional

rubbers) under normal test conditions and better wear endurance. The addition of DB to rubber in a (2–4) : 100 ratio (by mass) is optimum from the standpoint of the overall effect on the physicochemical characteristics of rubbers.

As the DB content increases, the cohesion strength of rubbers increases by a factor of 1.3–2.0. The maximum cohesion strength is attained at the DB content of 7.5 parts (by mass). The introduction of DB into polyisoprenes causes the tear strength to increase by a factor of about 1.5.

To determine the effect of the rubber matrix on the modifying activity of DB, the latter was introduced in excess (2, 3 and 4 parts by mass) into a conventional rubber blend based on butadiene–styrene copolymer containing 30% of styrene units. The rubber blends containing 3 and 4 parts (by mass) of DB showed an increase in the cohesion strength by a factor of 1.5 to 2.0 compared to the reference samples. The tear resistance of DB-containing vulcanisates is doubled compared to that of the reference samples (Fig. 19). Thus the modifying action of DB introduced into rubber matrices of different nature manifests itself in different manner.

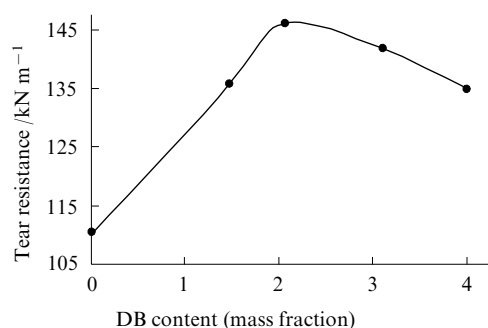
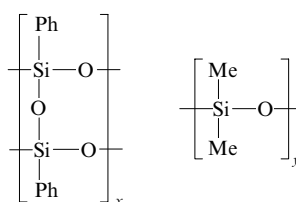


Figure 19. Tear resistance of butadiene–styrene rubber CKCM-30 APK (Russia) at different diamond blend content.¹⁰⁸

b. Polysiloxanes

Polysiloxanes were studied using a polyblock copolymer of ladder phenylsesquioxane and poly(dimethylsiloxane) (LPS-PDMS) as the polymer matrix.¹⁰⁶



This copolymer is cold-resistant to 200 K and thermally stable to 673 K. It can be used as the basic component of film-forming materials having a broad spectrum of applications from protective coatings to selectively permeable membranes.

Nanodiamond powders were pre-calcined and the ND particle surfaces were modified using the silylation reaction (Fig. 20).

When the modified fillers were used in their individual state, the strength parameters of the modified films increase by 20%–30% in the practically valuable interval of deformations and their elastic properties remain reasonably good. The effect is attained at filling degrees of less than 5 mass %.

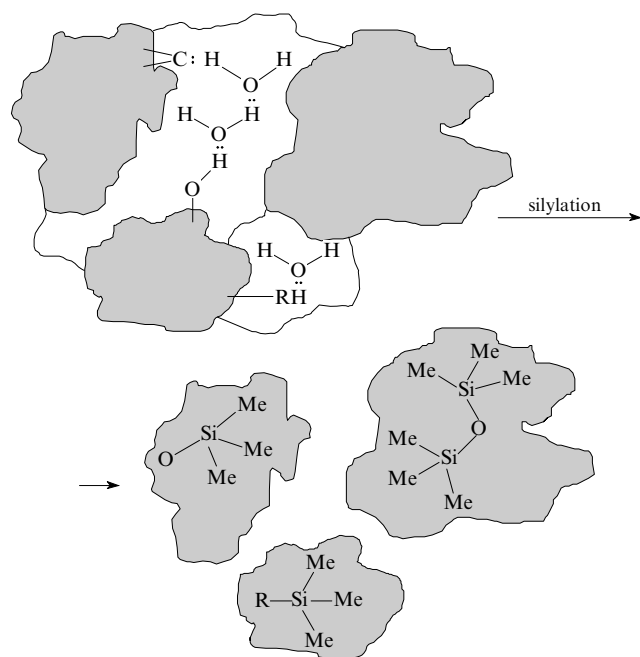


Figure 20. Modification of ND surface with silylating agents.¹⁰⁶

The following silylating composites were used: Me_3SiCl : $(\text{Me}_3\text{Si})_2\text{NH}$ = 1 : 1, $(\text{CH}_2=\text{CH})_2\text{SiCl}_2$: Me_3SiNH_2 = 1 : 1; R is the functional group containing 'reactive' proton (OH, NH_2 , COOH, etc.).

c. Polyurethanes

The introduction of DB (0.2 mass %) into polyurethanes causes the conditional strength to increase by a factor of 3 upon an increase in the polymer elasticity by a factor of 1.5.

The introduction of DB (0.3 mass %) into polyurethane foams leads to an increase in the compression strength by a factor of 1.5 and improvement of process performance in the preparation of this polymer.

d. Cold-resistant butadiene–nitrile rubber

Introduction of DB (to 1 mass %) into cold-resistant butadiene–nitrile rubber causes a significant (up to 70%) increase in the relative ultimate elongation of the rubber. Additionally, the wear resistance increases and the friction coefficient is halved compared to that of gum rubber.^{109, 110} At 223 K, the cold resistance increases by 50%.

The resistance of rubbers in hydrocarbon media increases by 20% upon introduction of DB. The addition of DB (0.1%–0.5%) improves the key operating characteristics, namely, the friction coefficient decreases and the wear resistance, elasticity and cold resistance of the materials increase. Additionally, the rubbers studied had lower hysteresis losses under dynamic loading; this is responsible for longer operating life.

e. Explosive decompression-resistant rubbers

The introduction of DB (0.1 mass % to ~2 mass %) into commercially available, explosive decompression-resistant rubbers based on various polymers having an elastic modulus of up to 8 MPa causes the tear resistance and wear resistance to increase by 60% and 40%, respectively.¹¹¹

f. Plasma-flame-spraying polymeric coating

A process was developed for plasma flame spraying of single- and multilayer polymeric coatings containing disperse ND.¹¹²

Bilayer metal–polymer coatings containing 0.5 mass % of ND prepared by plasma flame spraying technique provide reliable protection of immersion pump bearings and rotors and other parts from combined action of corrosion and wear, which allows them to retain high operating characteristics over a long period of time.

5. Diamond sintered samples and compacts

Experience in sintering of diamond micropowders has shown that a decrease in the grain size causes deterioration of the physicomechanical properties of sintered polycrystals. The reason lies in high back pressure of desorbed gases at $T > 1773$ K and at pressures > 5 GPa.^{113–115}

Desorption of gases physisorbed on the surface of ND particles was achieved by heat treatment of compacts *in vacuo* for 2 h at 773 K and a residual gas pressure of 10^{-3} Pa.¹¹⁶

As the sintering temperature increases, the degree of graphitisation increases. Removal of carbonyl and hydroxyl groups from the surface of diamond particles as a result of its chemical modification decreases the degree of graphitisation of ND on sintering. Here, raising the temperature is accompanied by densification of the sintered polycrystals; as a consequence, their strength and hardness increase (maximum hardness is 28 GPa).¹¹⁶

By cold pressing of ND one can prepare compacts with a density of 1830 (at 4.5 GPa) and 1950 kg m^{-3} (at 8 GPa). At the pressing temperature of 1773 K, the density slowly increases and at 2273 and 2573 K it decreases.¹¹⁷ The samples prepared at 1273 K and higher temperatures showed graphitisation of ND, which develops at the grain boundaries. The optimum sintering duration is 36 s. The sintering of ND is governed by two parameters, the initial density of ND and the quality of purification of the particle surfaces.

The data on the ND sintering conditions and the characteristics of their structural state are listed in Table 13.¹¹⁵ Two processes occur during the sintering of ND, that is, transformation of the structural state of ND and the diamond → graphite phase transition.

A possible method of counteracting the effect of desorbed gases on the sintering of ND involves the introduction of getters (elements or compounds that form chemical bonds with gas molecules) into the reaction volume.¹¹⁸ For instance, by modifying the surface of ND particles with cobalt and nickel, a fraction of volatile oxides was replaced by non-volatile ones; as a consequence, gas evolution in the course of hot compaction reduced and the density and hardness of the compacts increased.¹¹⁹

The approach involving the introduction of compounds favouring glass formation into the ND powder proved to be fruitful.¹²⁰ In particular, the addition of B_2O_3 , SiO_2 , CaO or B (1 mass % to 3 mass %) made it possible to reduce the sintering pressure from 7 to 5 GPa and to increase the temperature and duration of sintering; graphitisation and recrystallisation of diamond slowed down.

The density and hardness of sintered ND samples can also be increased by sintering mixtures of ND with static-synthesis diamond micropowders produced on a large scale. The drawing dies for metal cord fabrication showed a halved wear compared to the dies sintered from static-synthesis diamond micropowders only.

By introducing DB into copper–graphite collectors one can eliminate the wear problems of both the collector and the copper wire (minimum wear).

Rolled tungsten + aluminium + ND composite (thickness 4 mm) is used for production of body armour.²

Table 13. Characteristics of starting ND and ND-based compacts prepared under different conditions of heat treatment under pressure.¹¹⁵

Treatment conditions			Phase composition	Composition of the diamond component					
P /GPa	T /°C	τ /s		polycrystalline particles		aggregates		single-crystal grains	
				size	content (%)	size /Å	content (%)	size /Å	content (%)
1	—	—	starting diamond	I	90				
				II	10				
4.5	1000	36	diamond + graphite	I + II	100	—		—	
4.5	1500	36	the same	I + II	80	100–150	20		
8	750	36	diamond	I + II	100	—		—	
8	1000	36	diamond + graphite	I + II	100	—		—	
8	1500	36	the same	I + II	80	100–150	20	—	
8	2000	12	"	I + II	20	100–200	70	100–300	10
8	2000	36	"	—		100–500	70	100–500	30
8	2300	12	"	—		100–500	20	500–1500	80

Note. Notations used in this Table are as follows: 'I' for particle size from 3 to 50 Å and 'II' for particle size from 100 to 150 Å.

6. Biological activity of nanodiamonds

Modern antioxidants used for chemotherapy of cancer patients are very toxic compounds. This makes the search for novel antioxidants of low toxicity topical.

Diamonds are non-toxic and non-tumourigenic species, possess no mutagenic properties and are insoluble in biological liquids. The biological activity of ND has not been studied as yet.

An ND crystal has a chemically inert classical diamond core (almost round or oval in shape) and a quite reactive surface 'fringe' comprised of functional groups that are safe for living organism and impart the surface with hydrophilic properties.^{121,122} Additionally, each ND crystal has a large number of unpaired electrons, being in essence a multiradical.¹²³

Nanodiamonds belong to fundamentally novel antitumour agents.^{124,125} They can be treated as polyfunctional supra-molecular structures bearing polar groups [OH, NH₂, C(O)NH₂] that govern the antioxidant activity and the ability to participate in free-radical processes in living cells.

A large number of functional groups on the surface of ND particles can provide both additional generation and quenching of excess radicals in metabolic processes. It is the ability to control free-radical processes under the action of ND that can appear to be a basis for their antitumour action.

In all studies, ND showed a marked beneficial effect, which manifests itself in the extension of life of cancer patients compared to predictions. Figure 21 shows the initial and final stages of the attack of ND on malignant cells in human body.

Generally, the results obtained using aqueous ND suspensions are as follows: significant or even complete relief of severe pain; normalisation of intestinal peristalsis, including recovery of gut permeability; improvement of blood characteristics; significant activation of the immune system and the mental status of patients (incredible eagerness for life was observed).

It is possible to design ND-based pharmaceuticals for activation of the enzymatic subsystem of the antioxidative cell protection system.^{126,127}

Thus, the results of a few available studies of biological activity of ND are as follows.

1. At present, ND have no analogues, with allowance for their physical state (insoluble solid powder), from the standpoint of complex action on human organism.

2. The use of ND along with chemotherapy and radiotherapy can appear to be promising in treatment of malignant neoplasms.

3. ND are highly efficient for normalisation of gastro-intestinal function.

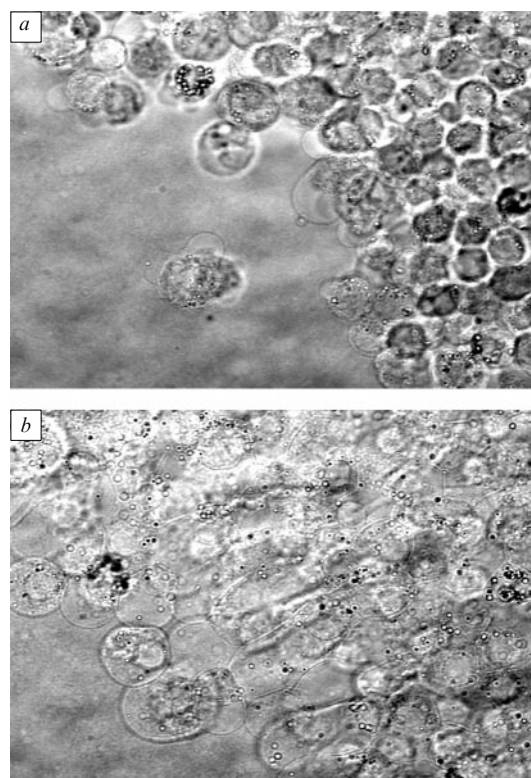


Figure 21. Initial (a) and final (b) stage of ND attack on malignant cells in human organism.¹²⁶

Nanodiamonds are also of great interest for biochemistry as a novel kind of sorbents suitable for separation and purification of proteins.^{128–131} Nanodiamonds can selectively adsorb recombinant apoobelin from the protein extract of the cells of *Escherichia Coli*. It was found that ND particles also can adsorb phytoprotein on their surface.¹²⁹ An ND–obelin composition was grafted onto the surface of aluminium substrate and a prototype of planar luminescent sensors (biochips) was created.¹²⁸

Recently, a highly sensitive test method for determination of the presence and type of antibodies and antigen markers of different nosology using ND has been developed. The technique does not require any equipment and solutions other than analysed one.

7. Other fields of application of nanodiamonds

A novel initiation composition VS-2 based on 5-hydrazino-tetrazolylmercury(II) and poly(methylvinyltetrazole) containing ND (Table 14) was developed.^{132, 133} The substance is sensitive to low-temperature laser radiation.

Table 14. Parameters of VS-2 explosive initiation with a laser pulse.

VS-2 charge + additive		Initiation energy /μJ
additive	additive content (%)	
No additive	—	310
Soot	0.5	2450
	1	2550
	2	3050
	3	3250
Nanodiamonds	0.5	260
	1	200
	3	180
	5	340
Fullerenes	1	630
	3	830
	5	730
Nanotubes	0.5	640
	1	590
	2	640
	3	850

Laser initiation is a relatively new safe procedure for blasting explosives. It provides a high degree of isolation of the light-initiated detonator from a false pulse because of the lack of powerful random light sources suitable for blasting the detonator in the optical region. The additives to the VS-2 composition, namely, finely disperse soot, fullerenes or nanotubes (1%–3%) increase the threshold of initiation by a single pulse of a neodymium laser. On the contrary, the introduction of detonation-synthesis ND (0.5%–3%) reduces this threshold.

The composition provides simultaneous enhancement of sensitivity to the laser pulse by a factor of 1.5–1.7 and high adhesion to the contact surface due to improvement of the adhesive properties of poly(methylvinyltetrazole) caused by the presence of ND. The minimum initiation energy drops from 310 to 180 μJ for the ND-containing material.

To protect architectural monuments made of white Carrara marble, ND-containing organic–silicate coatings were developed and evaluated.^{134, 135} Nanodiamonds present in such coatings inhibit the growth of the most abundant, in urban environment, fungi and bacteria that destroy the structure of stone materials. The coatings are prepared from tetraethoxysilane-based sols containing ND. They can be used to modify the surface of particles of the powder components of cements and concretes. This permits a significant extension of the operating life of buildings, motorways, hydroelectric power plants and other facilities made of concrete.

References

1. K V Volkov, V V Danilenko, V I Elin *Fiz. Gorennya Vzryva* **26** (3) 123 (1990)^a
2. V V Danilenko *Sintez i Spekanie Almaza Vzryvom* (Synthesis and Caking of Diamond by Explosion) (Moscow: Energoatomizdat, 2003)
3. Yu A Babushkin, A I Lyamkin, G A Chiganova *Ul'tradispersnye Poroshki, Nanostruktury, Materialy* (Ultradispersed Powders, Nanostructures and Materials) (Krasnoyarsk: Krasnoyarsk State Technological University, 1996) p. 10
4. A Yu Babushkin, A I Lyamkin *Fizikokhimiya Ul'tradispersnykh Sistem* (*Sb. Nauch. Tr. IV Vseros. Konf.*) [Physicochemistry of Ultradispersed Systems (Proceedings of the IVth All-Russian Conference)] (Moscow: Moscow Engineering Physics Institute, 1999) p. 125
5. S V Pershin, D N Tsaplin *V Vsesoyuznoe Soveshchanie po Detonatsii* (The Vth All-Union Meeting on Detonation) (Chernogolovka: Small-scale Enterprise Imtek, 1991) Vol. 2, p. 237
6. A M Staver, A P Ershov, A I Lyamkin *Fiz. Gorennya Vzryva* **20** (3) 79 (1984)^a
7. E E Lin *Fizikokhimiya Ul'tradispersnykh Sistem* (*Sb. Nauch. Tr. IV Vseros. Konf.*) [Physicochemistry of Ultradispersed Systems (Proceedings of the IVth All-Russian Conference)] (Moscow: Moscow Engineering Physics Institute, 1999) p. 40
8. V F Anisichkin, B G Derendyaev, V A Koptug, Yu I Mal'kov, N F Salakhutdinov, V M Titov *Fiz. Gorennya Vzryva* **24** (3) 121 (1988)^a
9. N V Kozyrev, G V Sakovich, S Ch Su, M S Shtein *V Vsesoyuznoe Soveshchanie po Detonatsii* (The Vth All-Union Meeting on Detonation) (Chernogolovka: Small-scale Enterprise Imtek, 1991) Vol. 1, p. 176
10. N V Kozyrev, P M Brylyakov, S Ch Su, M S Shtein *Dokl. Akad. Nauk SSSR* **314** 889 (1990)^b
11. N V Kozyrev, E S Golubeva *Fiz. Gorennya Vzryva* **28** (5) 119 (1992)^a
12. A L Vereshchagin *Detonatsionnye Nanoal'mazy* (Detonation-synthesis Nanodiamonds) (Barnaul: Altai State Technological University, 2001)
13. Yu I Mal'kov *Fiz. Gorennya Vzryva* **27** (5) 136 (1991)^a
14. E E Lin *Fizikokhimiya Ul'tradispersnykh Sistem* (*Sb. Nauch. Tr. V Vseros. Konf.*) [Physicochemistry of Ultradispersed Systems (Proceedings of the Vth All-Russian Conference)] (Moscow: Moscow Engineering Physics Institute, 2000) p. 40
15. V F Anisichkin *Fiz. Gorennya Vzryva* **30** (5) 100 (1994)^a
16. B G Loboiko *Fiz. Gorennya Vzryva* **36** (6) 45 (2000)^a
17. B A Vyskubenko, V V Danilenko, E E Lin, V A Mazanov, T V Serova, V I Sukharev, A P Tolochko *Fiz. Gorennya Vzryva* **28** (2) 108 (1992)^a
18. V V Danilenko *Fiz. Gorennya Vzryva* **41** (5) 104 (2005)^a
19. V V Danilenko *Fiz. Gorennya Vzryva* **41** (4) 110 (2005)^a
20. V M Titov, V F Anisichkin, I Yu Mal'kov *Fiz. Gorennya Vzryva* **25** (3) 117 (1989)^a
21. C L Mader *Numerical Modeling of Explosives and Propellants* (New York: CRC Press, 1998)
22. A L Vereshchagin, G V Sakovich, L A Petrova, V V Novoselov, P M Brylyakov *Dokl. Akad. Nauk SSSR* **315** 104 (1990)^b
23. RF P. 2230702; *Byull. Izobret.* (17) (2004)
24. O N Breusov *Khim. Fiz.* **21** (11) 110 (2002)^c
25. L V Dubnov, N S Bakharevich, A N Romanov *Promyshlennyye Vzryvchatyye Veshchestva* (Industrial Explosives) (Moscow: Nedra, 1973)
26. A N Nesmeyanov, N A Nesmeyanov *Nachala Organicheskoi Khimii* (Principles of Organic Chemistry) (Moscow: Khimiya, 1969) Vol. 1, p. 344
27. V F Anisichkin, I Yu Mal'kov, F A Sagdiev *V Vsesoyuznoe Soveshchanie po Detonatsii* (The Vth All-Union Meeting on Detonation) (Chernogolovka: Small-scale Enterprise Imtek, 1991) Vol. 1, p. 27
28. A M Staver, N V Gubareva, A I Lyamkin, E A Petrov *Fiz. Gorennya Vzryva* **20** (5) 100 (1984)^a
29. V V Odintsov, S A Gubin, V I Pepekin, L N Akimova *Khim. Fiz.* **10** 687 (1991)^c
30. S V Pershin, V N Tsaplin, A N Dremine, A G Antipenko *Fiz. Gorennya Vzryva* **27** (4) 117 (1991)^a

31. S V Pershin, V N Tsaplin, A G Antipenko *V Vsesoyuznoe Soveshchanie po Detonatsii* (The Vth All-Union Meeting on Detonation) (Chernogolovka: Small-scale Enterprise Imtek, 1991) Vol. 2, p. 233
32. F Volk *Philos. Trans. R. Soc. London, Ser. A* **339** 335 (1992)
33. V Yu Dolmatov *Sverkhtv. Mater.* (4) 38 (2003)^d
34. V Yu Dolmatov, M V Veretennikova, V A Marchukov, V G Sushchev *Fiz. Tv. Tela* **46** 596 (2004)^e
35. A M Staver, A I Lyamkin *Ul'tradispersnye Materialy. Poluchenie i Svoistva (Mezhvuzovskii Sbornik)* [Ultradispersed Materials. Production and Properties (Intercollegiate Collection)] (Krasnoyarsk: Krasnoyarsk Polytechnic Institute, 1990) p. 3
36. V Yu Dolmatov *Ul'tradispersnye Almazy Detonatsionnogo Sintez* (Ultradispersed Detonation-synthesis Diamonds) (St Petersburg: St Petersburg State Pedagogical University, 2003)
37. Appl. PCT WO 000686 (2005)
38. Appl. PCT WO 000685 (2005)
39. RF P. 2109683; *Byull. Izobret.* (12) 215 (1998)
40. V A Mazanov *Fiz. Tv. Tela* **46** 614 (2004)^e
41. US P. 5916955; *Chem. Abstr.* **121** 208474 (1994)
42. A A Putyatin, A V Nikol'skaya, Ya A Kalashnikov *Sverkhtv. Mater.* (2) 2 (1982)^d
43. RF P. 2019502; *Byull. Izobret.* (17) 79 (1997)
44. RF P. 2077476; *Byull. Izobret.* (11) (1997)
45. RF P. 1770271; *Byull. Izobret.* (39) (1992)
46. T M Gubarevich, R R Sataev, V Yu Dolmatov *V Vsesoyuznoe Soveshchanie po Detonatsii* (The Vth All-Union Meeting on Detonation) (Chernogolovka: Small-scale Enterprise Imtek, 1991) Vol. 2, p. 272
47. T M Gubarevich, V Yu Dolmatov, V F Pyaterikov, I S Larionova *Zh. Prikl. Khim.* **65** 2512 (1992)^f
48. A E Aleksenskii, M V Baidakova, A Ya Vul', V I Siklitskii *Fiz. Tv. Tela* **41** 740 (1999)^e
49. V Yu Dolmatov *Sverkhtv. Mater.* (1) 28 (2005)^d
50. V Yu Dolmatov *Usp. Khim.* **70** 687 (2001) [*Russ. Chem. Rev.* **70** 607 (2001)]
51. E Osawa *Proceedings of the NATO ARW 'Synthesis, Properties and Applications of Ultrananocrystalline Diamond'* (Dordrecht: Springer, 2004) p. 231
52. V F Loktev, V I Makal'skii, I V Stoyanova, A V Kalinkin, V A Likhonov, V N Mitkin *Carbon* **29** 817 (1991)
53. T Jiang, K Xu *Carbon* **33** 1663 (1995)
54. V L Kuznetsov, M N Aleksandrov, I V Zagoruiko, A L Chuvilin, E M Moroz, V N Kolomichuk, V A Likhonov, P M Brylyakov, G V Sakovich *Carbon* **29** 665 (1991)
55. F Cataldo, A P Koscheev *Fullerenes, Nanotubes, Carbon Nanostruct.* **11** 201 (2003)
56. E Mironov, A Koretz, E Petrov *Diamond Relat. Mater.* **11** 872 (2002)
57. L-C L Huang, H-C Chang *Langmuir* **20** 5879 (2004)
58. Y Liu, X Gu, J L Margrave, V N Khabashesku *Chem. Mater.* **16** 3924 (2004)
59. I I Kulakova *Phys. Solid State* **46** 636 (2004)
60. G Post, V Yu Dolmatov, V A Marchukov, M V Veretennikova, A E Sal'ko *Zh. Prikl. Khim.* **75** 773 (2002)^f
61. S Ji, T Jiang, K Xu, S Li *Appl. Surf. Sci.* **133** 231 (1998)
62. A Dandekar, R T K Baker, M A Vannice *Carbon* **36** 1821 (1998)
63. X Xua, Z Yua, Y Zhuh, B Wang *Diamond Relat. Mater.* **14** 206 (2005)
64. S I Chukhaeva, P Ya Detkov, A P Tkachenko, A D Toropov *Sverkhtv. Mater.* (4) 29 (1998)^d
65. T M Gubarevich, L E Chernukho *Proceedings of the NATO ARW 'Synthesis, Properties and Applications of Ultrananocrystalline Diamond'* (Dordrecht: Springer, 2004) p. 345
66. V Yu Dolmatov, V G Sushchev, V A Marchukov, M V Veretennikova *Porodorazrushayushchii i Metallo-obrabatyvayushchii Instrument — Tekhnika i Tekhnologiya ego Izgotovleniya i Primeneniya (Nauchnye Trudy ISM im. V N Bakulya NAN Ukrainy, Kiev, 2004)* [Rock-destroying and Metal-working Instrument: Technique and Technology of Its Production and Application (Proceedings of V N Bakul Institute for Superhard Materials of National Academy of Sciences of Ukraine, Kiev 2004)] No. 7, p. 176
67. V Yu Dolmatov, T Fujimura *Proceedings of the NATO ARW 'Synthesis, Properties and Applications of Ultrananocrystalline Diamond'* (Dordrecht: Springer, 2004) p. 217
68. A E Aleksenskii, M V Baidakova, A Ya Vul' *Fiz. Tv. Tela* **39** 1125 (1997)^e
69. G V Sakovich, V D Gubarevich, F Z Badaev *Dokl. Akad. Nauk SSSR* **310** 402 (1990)^b
70. V L Kuznetsov, A L Chuvilin, Yu V Butenko *Proceedings of Symposium 'Science and Technology of Fullerene Materials'* Vol. 359 (Pittsburg: Materials Research Society, 1995) p. 105
71. O A Shenderova, D M Gruen *Ultrananocrystalline Diamond: Synthesis, Properties and Applications* (New York: William Andrew Publishing, 2006)
72. V Yu Dolmatov *Proceedings of the 4th International Conference on Materials Processing for Properties and Performance (MP³-IV), Tsukuba Science City, Ibraki, Japan, 2005* p. 284
73. Appl. PCT WO 89/07668; *Chem. Abstr.* **111** 242622 (1989)
74. USSR P. 1694710; *Byull. Izobret.* (44) 91 (1991)
75. Jpn P. 05106195; *Chem. Abstr.* **116** 141825 (1992)
76. G K Burkat, V Yu Dolmatov *Fiz. Tv. Tela* **46** 685 (2004)^e
77. Korean P. 10-0634125 (2006)
78. V Yu Dolmatov, G K Burkat *Sverkhtv. Mater.* (1) 84 (2000)^d
79. Yu V Timoshkov, T M Gubarevich, T I Orekhovskaya, I S Molchan, V I Kurmashov *Gal'vanotekh. Obrab. Poverkh. 7* (2) 20 (1999)
80. V Yu Dolmatov, G K Burkat, V Yu Saburbaev, A E Sal'ko, M V Veretennikova *Sverkhtv. Mater.* (2) 52 (2001)^d
81. RF P. 2191227; *Byull. Izobret.* (29) 345 (2002)
82. E N Loubnin, S M Pimenov, A Blatter, F Schwager, P Ya Detkov *New Diamond Front. Carbon Technol.* **9** (4) 273 (1999)
83. USSR P. 1668490; *Byull. Izobret.* (29) 123 (1991)
84. RF P. 2169798; *Byull. Izobret.* (18) 279 (2001)
85. RF P. 2169800; *Byull. Izobret.* (18) 279 (2001)
86. Appl. RF 2005 131916 (2005)
87. RF P. 2046094; *Byull. Izobret.* (29) 189 (1995)
88. T M Gubarevich, V Yu Dolmatov *Zh. Prikl. Khim.* **66** 1878 (1993)^f
89. RF P. 2082738; *Byull. Izobret.* (18) 141 (1997)
90. A A Zakharov, V A Yuzova, N V Eristova *Ul'tradispersnye Materialy. Poluchenie i Svoistva (Mezhvuzovskii Sbornik)* [Ultradispersed Materials. Production and Properties (Intercollegiate Collection)] (Krasnoyarsk: Krasnoyarsk Polytechnic Institute, 1990) p. 170
91. G V Sakovich, V F Komarov, E A Petrov *V Vsesoyuznoe Soveshchanie po Detonatsii* (The Vth All-Union Meeting on Detonation) (Chernogolovka: Small-scale Enterprise Imtek, 1991) Vol. 2, p. 273
92. A S Artemov *Fiz. Tv. Tela* **46** 670 (2004)^e
93. T Kurobe, T Fujimura, H Ikeda *Fiz. Tv. Tela* **46** 730 (2004)^e
94. V F Komarov *Tekhn. Mashinostr.* **4** (14) 106 (1997)
95. A I Lyamkin, V E Red'kin *Nauka — Proizvodst.* **3** (28) 59 (2000)
96. Appl. RF 87/00249 (1987)
97. Appl. RF 4923749 (1992)
98. V M Sannikov, Yu M Koreibo *Ul'tradispersnye Materialy. Poluchenie i Svoistva (Mezhvuzovskii Sbornik)* [Ultradispersed Materials. Production and Properties (Intercollegiate Collection)] (Krasnoyarsk: Krasnoyarsk Polytechnic Institute, 1990) p. 155

99. A P Shangin, V E Red'kin, E D Rakshin, S V Seligeev *Ul'tradispersnye Materialy. Poluchenie i Svoistva (Mezhvuzovskii Sbornik)* [Ultradispersed Materials. Production and Properties (Intercollegiate Collection)] (Krasnoyarsk: Krasnoyarsk Polytechnic Institute, 1990) p. 165
100. RF P. 2009186; *Byull. Izobret.* (5) 124 (1994)
101. V N Istomin, E D Rakshin, Yu D Akimov *Ul'tradispersnye Materialy. Poluchenie i Svoistva (Mezhvuzovskii Sbornik)* [Ultradispersed Materials. Production and Properties (Intercollegiate Collection)] (Krasnoyarsk: Krasnoyarsk Polytechnic Institute, 1990) p. 161
102. A P Voznyakovskii, L F Shelokhneva, V Yu Dolmatov, V S Bodrova *Kauchuk Rezina* **6** 27 (1996)
103. RF P. 2100389; *Byull. Izobret.* (36) 295 (1997)
104. V Yu Dolmatov, A P Voznyakovskii, M V Veretennikova *Sverkhtv. Mater.* (6) 81 (2001)^d
105. A P Voznyakovskii, V Yu Dolmatov, E A Levintova, T M Gubarevich *Doklady Mezhdunarodnoi Konferentsii po Kauchuku i Rezine* (Reports of International Conference on Rubber) (Moscow: Moscow State University, 1994) Vol. 2, p. 80
106. A P Voznyakovskii, V Yu Dolmatov, M V Veretennikova *Sverkhtv. Mater.* (4) 27 (2003)^d
107. N V Sirotinkin, A P Voznyakovskii, A N Ershova *Fiz. Tv. Tela* **46** 725 (2004)^e
108. V Yu Dolmatov, A P Voznyakovskii, K A Shevtsova, V S Kutyanina, M V Veretennikova *Porodorazrushayushchii i Metalloobrabatyvayushchii Instrument — Tekhnika i Tekhnologiya ego Izgotovleniya i Primeneniya (Nauchnye Trudy ISM im. V N Bakulya NAN Ukrainy, Kiev, 2005)* [Rock-destroying and Metal-working Instrument: Technique and Technology of Its Production and Application (Proceedings of V N Bakul Institute for Superhard Materials of National Academy of Sciences of Ukraine, Kiev 2005) No. 7, p. 160]
109. O A Adrianova, M D Sokolova, S N Popov *Kauchuk Rezina* **6** 11 (1999)
110. RF P. 2129132; *Byull. Izobret.* (11) 375 (1999)
111. L A Akopyan, M N Zlotnikov, B V Romyantsev, N L Abramova, M V Zobina, T L Mordvintseva *Fiz. Tv. Tela* **46** 722 (2004)^e
112. P A Vityaz' *Fiz. Tv. Tela* **46** 591 (2004)^e
113. A A Shul'zhenko, V G Gargin, V A Shishkin, A A Bochechka *Polikristallicheskie Materialy na Osnove Almaza* (Polycrystalline Materials Based on Diamond) (Kiev: Naukova Dumka, 1989)
114. A A Bochechka *Fiz. Tv. Tela* **46** 652 (2004)^e
115. A A Bochechka *Sverkhtv. Mater.* (4) 10 (1998)^d
116. A A Shul'zhenko, A A Bochechka, L A Romanko, A M Kutsai, V G Kargin *Sverkhtv. Mater.* (6) 50 (2000)^d
117. V V Danilenko, I A Petrusha, G S Oleinik, N V Danilenko *Sverkhtv. Mater.* (4) 53 (1998)^d
118. A A Shul'zhenko, A A Bochechka, V G Gargin, A G Gontar', L A Romanko, V N Tkach *Sverkhtv. Mater.* (4) 46 (1998)^d
119. V B Shipilo, I M Starchenko, T M Gubarevich *Poroshk. Metall.* **18** 126 (1995)^g
120. V B Shipilo, I M Starchenko, E V Zvonarev, V T Senyut' *Materialy, Tekhnologii, Instrumenty* **2** (4) 61 (1997)
121. I I Kulakova, V Yu Dolmatov, T M Gubarevich, A P Rudenko *Sverkhtv. Mater.* (1) 46 (2000)^d
122. A L Vereshchagin, L A Petrova, V V Brylyakov *Sverkhtv. Mater.* (1) 14 (1992)^d
123. T A Nachal'naya, V G Malogolovets, G A Podzerei, Yu I Nikitin, N V Novikov, Yu A Polkanov *Sverkhtv. Mater.* (1) 36 (2000)^d
124. V Yu Dolmatov, L N Kostrova *Sverkhtv. Mater.* **3** 82 (2000)^d
125. RF P. 2203068; *Byull. Izobret.* (12) 72 (2003)
126. A P Puzyr, D A Neshumayev, S V Tarskikh, G V Makarskaya, V Yu Dolmatov, V S Bondar *Diamond Relat. Mater.* **13** 2020 (2004)
127. A P Puzyr, V Yu Dolmatov, I V Shigalei, S V Tarskikh, G V Makarskaya, V S Bondar *Proceedings of NATO ARW 'Innovative Superhard Materials and Sustainable Coating'* (Dordrecht: Springer, 2004) p. 155
128. K V Purtov, V S Bondar', A P Puzyr' *Dokl. Akad. Nauk* **380** 411 (2001)^b
129. V S Bondar', A P Puzyr' *Dokl. Akad. Nauk* **373** 251 (2000)^b
130. V S Bondar', I O Pozdnyakova, A P Puzyr' *Fiz. Tv. Tela* **46** 737 (2004)^e
131. A P Puzyr', I O Pozdnyakova, V S Bondar' *Fiz. Tv. Tela* **46** 740 (2004)^e
132. Appl. RF 2004134657 (2004)
133. M A Ilyushin, I V Tselinsky, I A Ugryumov, V Yu Dolmatov, I V Shugalei *Cent. Eur. J. Energ. Mater.* **2** (1) 21 (2005)
134. O V Frank-Kamenetskaya, T Fujimura, O A Shilova, V Yu Dolmatov, D Yu Vlasov *Proceedings of the 10th International Conference on New Diamond Science and Technology (ICNDST-10), Comenius University, Bratislava, 2005* p. 170
135. A M Marugin, M A Arkhipova, O V Frank-Kamenetskaya, D Yu Vlasov, V Yu Dolmatov, O A Shilova, V P Chelibanov, T Fujimura *Proceedings of International Conference SREN 2005, Florence, Italy, 2005* p. 130

^a — *Comb. Explos. Shock Waves (Engl. Transl.)*

^b — *Dokl. Phys. (Engl. Transl.)*

^c — *Chem. Phys. Rep. (Engl. Transl.)*

^d — *J. Superhard Mater. (Engl. Transl.)*

^e — *Phys. Solid State (Engl. Transl.)*

^f — *Russ. J. Appl. Chem. (Engl. Transl.)*

^g — *Power Metall. Met. Ceram. (Engl. Transl.)*

Ion-selective electrodes in medicinal drug determination

S V Kharitonov

Contents

I. Introduction	361
II. Principles of operation of membrane ion-selective electrodes	362
III. Mechanism of electrode selectivity of ionophore-based membranes	365
IV. Components of ion-selective electrode membranes and methods of potentiometric determination of medicinal drugs	370

Abstract. Data published in the past 10 years on the use of ion-selective electrodes in direct potentiometry and potentiometric titration for the determination of organic medicinal drugs are analysed. In the vast majority of cases, ion-sensitive membranes contain associates of drug cations or anions with appropriate counter-ions. The theoretical approaches to optimisation of the characteristics of ion-selective electrodes are discussed. The mechanism of electrode response generation for neutral and charged carriers of organic ions is considered. The bibliography includes 314 references.

I. Introduction

The advance of the pharmaceutical science is marked by the appearance of 30–40 new medicinal drugs annually. At present, there are more than 10 000 medicinal drugs (MD) and over 100 000 drug preparations registered all over the world.^{1,2}

According to the data issued by the Ministry of Health and Social Development, since 1997, the number of MD registered in the Russian Federation has increased almost 1.5-fold (Fig. 1), of which ~80% pertains to reproduced preparations.² Figure 2 illustrates the dynamics in the development of original Russian MD in the period from 1997 to 2003. The average number of new MD introduced into the national health protection practice amounted to 40–60 items per year.

In line with the progressively increasing number of new MD, the problem of their identification and determination in both individual samples (*in vitro*) and living organisms (*in vivo*) becomes urgent. The demand for the accumulation, generalisation and systematisation of data on the MD monitoring and analysis resulted in the appearance of specialised scientific periodicals. Since 1983, the international *Journal of Pharmaceutical and Biomedical Analysis* (*J. Pharm. Biomed. Anal.*), which deals with the studies in the field of the MD analysis, analytical biochemistry, pharmacokinetics, forensic toxicology and other related fields, has been published. *Fresenius' Journal of Analytical Chemistry* has been published under a new title,

viz., *Analytical and Bioanalytical Chemistry* since 2002. Among the other international issues that publish the results of studies in the field of MD analysis, mention should be made of journals *American Journal of Pharmaceutical Education*, *Archiv der Pharmazie*, *Drug Information Journal*, *European Journal of Pharmaceutical Sciences*, *Il Farmaco*, *International Journal of Pharmaceutics*, *Journal of Chromatography B: Biomedical Sciences and Applications*, etc. The main Russian journal devoted to this field is the *Khimiko-farmatsevticheskii Zhurnal* [*Pharm. Chem. J. (Engl. Transl.)*], which has been published since 1967.

Considering the data published in original papers in *J. Pharm. Biomed. Anal.*, it can be stated with confidence that the chromatographic methods of analysis still occupy the leading position (more than 1500 publications in 10 years). They amount more than 50% of all methods of MD determination (Fig. 3), of which 45% fall on HPLC, 23% correspond to liquid chromatography, 14% are devoted to liquid chroma-

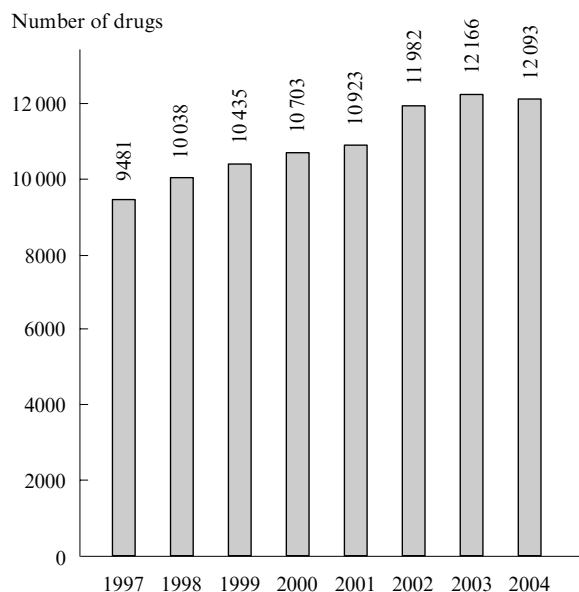


Figure 1. Increase in the number of registered medicinal drugs in Russia in 1997–2004 (according to the Ministry of Health and Social Development of the Russian Federation).

S V Kharitonov St Petersburg State Institute of Technology (Technical University), Moskovsky prosp. 26, 190013 St. Petersburg, Russian Federation. Fax (7-812) 712 77 91, tel. (7-812) 316 29 91, e-mail: kharitonov@hotmail.ru

Received 10 October 2006

Uspekhi Khimii 76 (4) 398–432 (2007); translated by T Ya Safonova

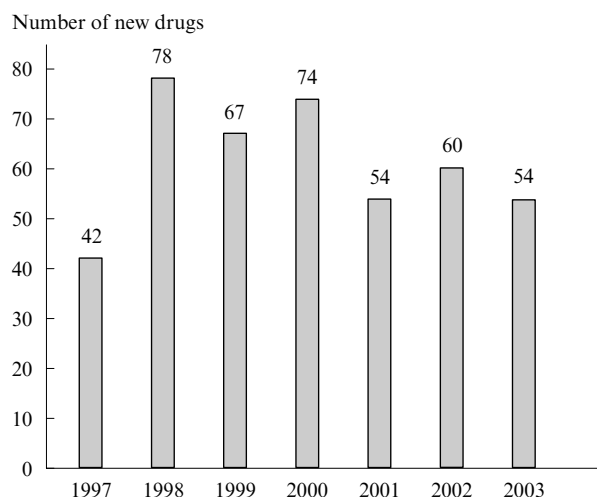


Figure 2. Dynamics in the development of new medicinal drugs in Russia in 1997–2003 (according to the data issued by the Ministry of Health and Social Development of the Russian Federation).

tography with mass spectrometric detection, 7% deal with gas chromatography and 11% fall on the rest chromatographic techniques.

According to the number of publications in *J. Pharm. Biomed. Anal.*, the electrochemical methods of the MD analysis occupy the third place after photometry and spectrophotometry, ~20% of publications being devoted to the potentiometric determination of MD.

Equilibrium electrochemical methods of the MD analysis, which include direct potentiometry (ionometry) and potentiometric titration, are extremely convenient, simple and make it

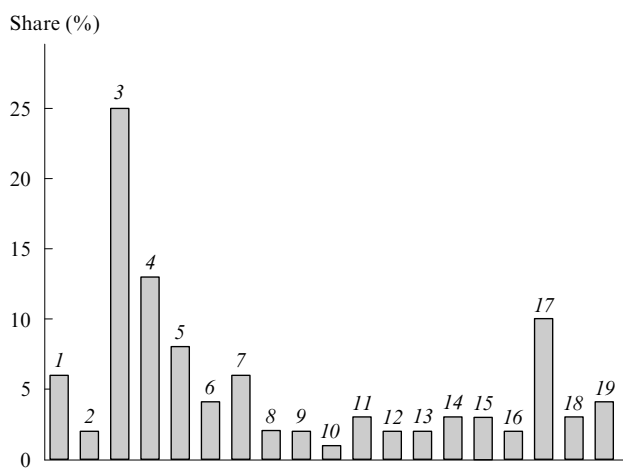


Figure 3. Distribution (%) of different instrumental methods for quantitative determination of MD (according to publications in *J. Pharm. Biomed. Anal.* in 1995–2005).

(1) Capillary (including zone) electrophoresis (6%); (2) bioanalysis and biosensors (2%); (3) HPLC (25%); (4) liquid chromatography (13%); (5) liquid chromatography with mass spectrometric detection (8%); (6) gas chromatography (4%); (7) other chromatographic methods (6%); (8) mass spectrometry (2%); (9) immunoassay and radioimmunoassay (2%); (10) IR spectroscopy and Raman spectroscopy (1%); (11) voltammetry (3%); (12) inversion voltammetry (2%); (13) ionometry (2%); (14) miscellaneous electrochemical methods (3%); (15) fluorimetry (3%); (16) NMR (2%); (17) spectrophotometry and photocolourimetry (10%); (18) flow-injection analysis (3%); (19) miscellaneous analytical methods (4%).

possible to determine those MD that can be converted into the corresponding ionic forms. As a rule, they combine sufficient selectivity with the precision of determination, which can substantially be enhanced even in the direct determination by operating the sensors *via* the mechanism of super-Nernstian response. Moreover, potentiometric detectors are capable of operation under the conditions of on-line analysis and can sufficiently easily be miniaturised to serve as micro- and ultra-microelectrodes.

In 1980–1990, many reviews were devoted to the use of ion-selective electrodes (ISE) in the pharmacological, clinical and biomedical assay. The biomedical aspects of the use of ISE and microelectrodes,^{3,4} the application of ISE in the medicinal practice and the potentiometric determinations *in vivo*^{5,6} were considered. The peculiarities of the use of ISE, including the application of potentiometric measurements with ISE and transducers in the clinical chemistry, were discussed.^{7–14} The data on the use of various ISE (with liquid and film membranes, ‘coated wire’ ISE, heterogeneous ISE with matrix-incorporated ion exchangers, pseudoliquid ISE, *etc.*) in pharmacy and pharmacological analysis were systematised.^{15–25}

However, in the past decade, a vast number of new MD appeared and different ISE types were elaborated for their determination, which necessitates the systematisation of the corresponding literature data.

II. Principles of operation of membrane ion-selective electrodes

An ion-selective electrode can be defined as an electrochemical sensor with a membrane the potential of which serves as the measure of the activity of a certain ion.²⁶ An ISE membrane may represent a crystalline or non-crystalline, homogeneous or heterogeneous phase, which, as a rule, exhibits high ionic conductivity. Crystalline membranes are based on single crystals (*e.g.*, LaF_3 for F^- -ISE), polycrystalline compounds (*e.g.*, Ag_2S for Ag^+ - and S^{2-} -ISE), heterogeneous mixtures pressed into pellets or incorporated into an inert binding material (matrix) (the Pungor electrodes). Glass, liquid and plasticised membranes are classified with non-crystalline membranes. The latter are used most extensively. The main requirement to a membrane is the ability to exchange ions of only one type. For an ISE to be selective with respect to a single type of ions, its membrane should contain a substance that can reversibly bind the ion under determination and at the same time exhibit the minimum solubility in aqueous solutions. Substances with such properties are called electroactive compounds (EAC). According to the mechanism of EAC reactions with the determined ion, the EAC are divided into charge carriers or ion-exchangers (the ion is transferred by an active ion-exchange site due to electrostatic interactions), neutral carriers or ionophores (the ion transfer follows the mechanism of selective complexation) and chelate-forming carriers (the ion transfer proceeds due to both electrostatic interactions and the complexation).²⁶

Ion-selective electrodes are classified according to the type of membranes used. Solid-phase, liquid-phase and film ISE are distinguished, which can be divided further to various groups depending on the nature of EAC used and the design of the ISE itself. Thus gas electrodes, enzyme electrodes, solid-contact electrodes and microelectrodes are often singled out into individual groups. Figure 4 shows the designs of most popular ISE types.

In addition to EAC, other components are often introduced into membranes to improve the functional properties of ISE. These can be additives that affect the electrophysical characteristics of membranes or substances capable of additional specific or non-specific interactions with the membrane or solution components.

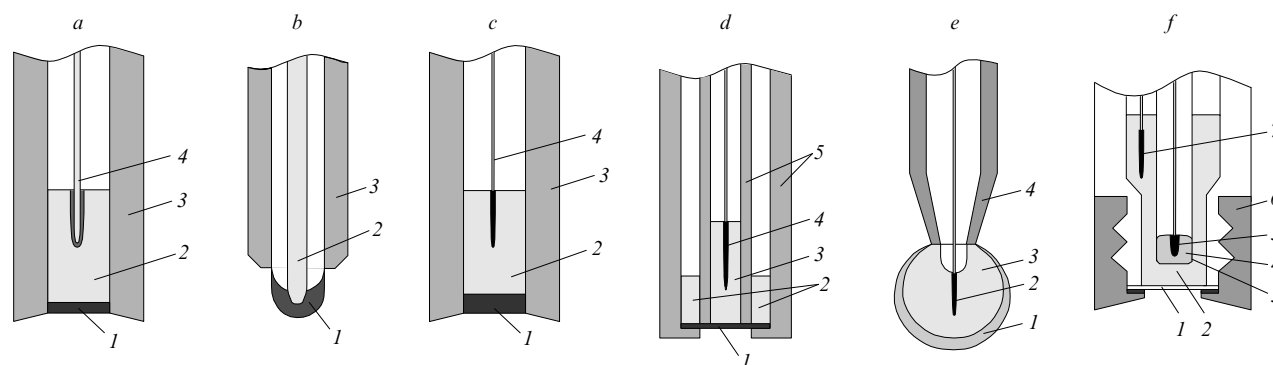


Figure 4. Designs of main types of ion-selective electrodes.

- (a) Solid-phase ISE with crystalline or heterogeneous membranes: (1) ion-selective membrane, (2) hydrophobic graphite layer, (3) case (a PVC or PTFE tube), (4) electron conductor (steel wire).
 (b) Solid-contact electrodes of the 'coated wire' type: (1) ion-selective membrane, (2) electron conductor (Au, Pt or Cu wire), (3) case (usually glass).
 (c) ISE with a polymeric membrane and an internal liquid contact: (1) ion-selective membrane, (2) internal standard solution, (3) case, (4) internal reference electrode (Ag/AgCl).
 (d) ISE with a liquid membrane: (1) porous plate impregnated with EAC solution, (2) EAC solution in an organic solvent, (3) internal standard solution, (4) internal reference electrode (Ag/AgCl), (5) case.
 (e) Glass ISE: (1) ion-selective glass membrane, (2) internal reference electrode (Ag/AgCl), (3) internal standard solution, (4) case.
 (f) Gas-sensitive ISE: (1) gas-permeable membrane, (2) internal solution, (3) ISE with (4) standard solution and (5) reference electrode, (6) case, (7) internal reference electrode

Ion-selective electrodes can be used in the determination of both organic and inorganic ions and certain neutral molecules. As will be shown below, the vast majority of studies dealing with the ISE for medicinal drugs were associated with the development of procedures for the quantitative determination of MD in model solutions, drug preparations, more rarely, in biological fluids and raw materials used in chemical and pharmaceutical industries. Much fewer studies were aimed at relating the physicochemical, electrochemical and transport properties of selective membranes to the potentiometric characteristics of the relevant ISE.^{27–38}

In the majority of cases, the charged carriers, *i.e.*, ion associates (IA) formed by MD cations or anions with the corresponding counter-ions, are introduced into selective membranes as the EAC. In addition to ion-exchange properties and the minimum solubility in water, an EAC should be compatible with the other components of the ion-sensitive membrane. The mechanism of operation of such ISE is described by a model of charged carriers.³⁹

Pungor^{40,41} has considered the processes that occur on the membrane surface and in its bulk and assessed the contributions of individual components to the membrane potential. In discussing the anomalies that arise in the interpretation of the mechanism of ISE operation, he took into account⁴⁰ the Donnan effect, the response time, the surface morphology, *etc.* The modified electrodes the chemical reaction on which involves the potential-determining ion were found to demonstrate a surface response. For IA-based ISE, the lyotropic series rule is valid; the surface reactions are also possible; however, such electrodes not always demonstrate the Nernstian response. Such aspects as the energy of the transfer of charged species across the electrode–solution interface were also considered.

For polymeric membranes that contain charged ion-exchangers and neutral carriers as the ionophores, it was proposed^{42–45} to quantitatively describe the ISE response based on the consideration of the ion-exchange equilibrium at the membrane–solution interface. The validity range of the Nikolskii–Eisenman equation used in the calculation of the selectivity coefficient of ISE was discussed. It was shown that the derived mathematical relationships allow more accurate calculations of ISE selectivity coefficients in the presence of

interfering ions with different charges. It was concluded that this approach can be applied in assessing the selectivity of most ISE with polymeric membranes.

The studies aimed at the optimisation of electroanalytical properties of membrane ISE were largely developed in two directions, namely, the optimisation of the internal near-membrane solution and the introduction of different ions and molecules into the membrane.

The first direction was developed in the studies by Pretsch and Bakker. In 1997, Pretsch and co-workers⁴⁶ demonstrated that the introduction of hydrophilic (thus, incapable of penetrating into the membrane) complexing agents that can form stable complexes with the determined ion, into the intramembrane solution intensifies the ion fluxes from the external solution to the membrane phase and dramatically lowers the detection limit. The development of these ideas made it possible to create a new model describing the detection limit of ISE and to elaborate new sensors with superhigh sensitivity.

The processes that lead to lowering of the detection limits of ionophore-based ISE are described by a steady-state model of ion fluxes.^{47,48} It was found that the ion-exchange and extraction equilibria at both sides of a membrane stimulate the appearance of concentration gradients in the membrane phase and can affect the detection limit through the ion fluxes. The concentration variations in the near-membrane internal solution can change the ISE detection limits by more than five orders of magnitude. However, it is necessary to produce high gradients of concentration to achieve adequate ISE characteristics. It was shown that the appearance of a superlow detection limit of ISE (10^{-9} – 10^{-12} mol litre⁻¹) cannot be defined according to the IUPAC rules. The impurities present in minor concentrations in the membrane phase can have a strong effect on the ISE characteristics when the electrodes operate at the concentrations of determined substances below 1 μ mol litre⁻¹.

Mention should be made of studies^{42,49–53} on the effect of different parameters on the ISE characteristics, which were based on the steady-state model.^{47,48} The effect of interfering ions, the composition of near-membrane and intramembrane solutions, the selectivity coefficients, the analyte lipophilicity, the concentrations of ionophore and lipophilic additives in the membrane, the thicknesses of the Nernstian diffusion layer and

the membrane and the diffusion coefficients of ions in both phases were studied. Based on the results obtained, it was concluded that all these factors might contribute to the lowering of the detection limit of potentiometric sensors.⁵³

The most general theoretical description of the stationary potentiometric response of ISE membranes was presented.^{54–56} Membrane systems that contain any number of ionophores with ion-exchange centres fixed on a polymeric matrix were considered. The thermodynamic model explains the characteristics of ISE selectivity based on different diffusion-induced effects associated with trans-membrane ion fluxes at zero emf. The appearance of super- and sub-Nernstian responses and the upper and lower limits of the determined concentrations were discussed; the temporal characteristics of ISE were considered. The approach developed allows one to considerably improve the selectivity coefficients and detection limits of ionophore-containing ISE. These studies open up new possibilities and prospects for the wide application of ISE techniques, which can compete with the most sensitive analytical methods.

A non-classical interpretation of the electrode response of sensors based on ionophores was discussed.⁵⁷ Several new concepts on the development of ionophore-based ISE were considered. Various long-known ISE for simple cations and anions are widely used in the industry and clinical chemistry. However, further studies that would allow the optimisation of ISE properties for analytical purposes are necessary. These studies should be carried out in the following directions:

- reduction of the lower limit of determined concentrations by governing the analyte ion fluxes through the membrane;
- development of methods for the determination of ion concentrations using sensors that exhibit the effect of the intensification of ion fluxes to the internal near-membrane solution;
- targeted search for ionophores that can provide the super-Nernstian response to the ions determined;
- development of ion-exchange membranes sensitive to polyions according to a non-equilibrium mechanism of electrode response;
- development of membranes selective to molecules of non-ionogenic surfactants;
- development of ISE with the electrode response formed due to redox reactions between the ionophore and the detected ion.

Insofar as the current practice consists of the incorporation of membrane-active complexones (ionophores) synthesised for this purpose^{58–106} into the ISE, the results of studies mentioned above^{42–57} are of fundamental importance for the development of ionometry of MD.

The second direction in the optimisation of ISE properties dates back to the pioneering studies of 1970s in which polymeric matrices with fixed charges were used for the improvement of electrode characteristics of membranes.³⁹ Later, this idea gave impetus to the development of mobile anionic sites in the membrane by the introduction of highly lipophilic ions such as tetraphenylborate anions.^{39, 107–109} It is believed that due to the poor solubility in water, these species indeed reside in the organic phase of a membrane. Lipophilic ions should remove the analyte anions to one extent or another from the membrane rather than compete with the ionophore for the formation of complexes with cations. As a result, the effect of the anion permeability that deforms the cationic response of the ISE is diminished or totally eliminated. Such compounds proved to be promising for ISE based on dissociating ion exchangers.¹¹⁰ This made it possible not only to extend the interval of the ISE electrode response, but also to considerably enhance the electrode selectivity.

The mechanism of operation of ISE based on liquid ion-exchangers, which are incorporated in the membrane in a mixed form, *viz.*, preferentially as a salt with an ion modifier and partially as a salt with the determined ions, was considered.¹¹¹ The ion modifier should be much more lipophilic than the determined ion to ensure the virtually constant concentrations of both salts in the membrane surface layer in the course of an ion exchange reaction that occurs once the membrane is brought into contact with the aqueous solution containing ions to be determined. The boundary conditions for the linearity of the electrode function for ISE of such a kind in solutions of determined ions were formulated. It was proved theoretically and demonstrated experimentally that for electrodes under consideration, the extraction selectivity of the ion-exchanger with respect to the determined ion can be adequately converted into the potentiometric form.

At present, almost all electrodes (including ISE based on ion associates) for the determination of both cations and anions employ membranes modified with lipophilic additives, which considerably improve their characteristics. The incorporation of ionic components into ISE membranes based on neutral carriers also proved to be advantageous due to the substantial reduction of the Ohmic resistance in the membrane.

The operation limits of ISE are the important characteristics. The dynamic range of the ISE operation can be substantially extended by either modifying the membrane or introducing a special buffer into the internal solution of the ISE. In the first case,¹¹⁰ the ISE membrane will operate by the mixed mechanism, namely, the addition of a lipophilic salt will increase the ISE selectivity (due to the stabilisation of counterions in the membrane) and also decrease the negative effect of co-ions that cause degeneration of the ISE electrode function.

The studies on the effect of the intramembrane buffer on the detection limit have shown^{42, 46, 49, 50, 112–114} that the buffer can affect the ion fluxes and thus change the detection limit of conventional ISE. Such parameters as the composition of the internal electrolyte, the membrane thickness, the nature and concentration of the ion exchanger were studied with the aim of achieving the lower detection limits of ISE. The experimental data were explained based on the fundamental concepts of theoretical models of the diffusion transfer.

Reliable information on the effect of the membrane composition and the ion-exchanger properties on the electrochemical and analytical characteristics of ISE retrieved by studying the transfer of potential-determining species across interfaces under both equilibrium and non-equilibrium conditions. The state of EAC based on MD ion associates in the membrane phase,^{27–36} the nature and physicochemical properties of ion exchangers in the membrane solvent^{27–29, 33} and the processes associated with the effect of water on the properties of interfaces³⁷ were considered.

Studies on the kinetics of the ion-exchange sorption of MD cations on the surface of ion-selective membranes have shown that the degree of ion exchange is determined by the lipophilicity of the eluting ion, while the time of the establishment of the equilibrium state is controlled by the diffusion. A mechanism of the exchange of hydrophobic organic ions on the surface of liquid membranes with strongly associating active sites was proposed.³⁸

The effect of the nature of the polymeric matrix on the electroanalytical properties of ISE was discussed.¹¹⁵ The studies on the transport of organic cations through membranes involved the determination of their transport numbers. The dependences of the selectivity coefficients on the transport properties of polymeric matrices and on the coefficients of MD distribution between aqueous and membrane phases were obtained.

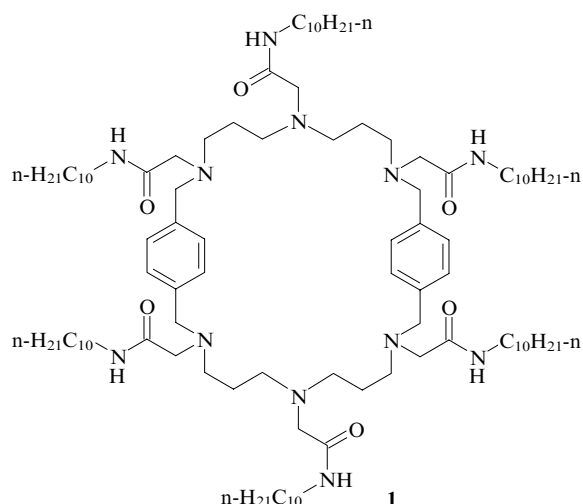
III. Mechanism of electrode selectivity of ionophore-based membranes

Neutral carriers (ionophores) were used as EAC in the ISE for different MD, namely, protonated amines, quaternary ammonium compounds, amino acids, peptides, nucleotides.^{58–106} The use of neutral carriers as the receptors for organic ions is based on their specific reactions and the formation of ‘host–guest’ complexes. In the formation of such complexes, the hydrophobic effects, van der Waals forces, hydrogen bonds and π -cationic interactions play the great role.¹¹⁶ The stability of complexes formed is determined by the following factors:¹¹⁷

- the correspondence between the geometrical sizes of the molecule-guest and the cavity of the molecule-host,
- the conformational flexibility of the ligand,
- the presence of functional groups in ionophore molecules,
- the nature of the solvent.

The membrane potential in a cell with an ISE based on a neutral carrier is formed as a result of processes of selective molecular recognition between the ionophore and the potential-determining ion, which occur at the interface.

To find the principles of potentiometric selectivity of ionophores with respect to organic ions and molecules, it is expedient to consider the effect of the polarity of structural fragments in organic compounds.¹¹⁸ For polar organic ions, the appearance of a specific membrane potential was associated with the electrostatic interaction and/or the formation of hydrogen bonds between the functional groups of the ionophore and the polar fragments of the organic molecule (ion). Such a mechanism of selective recognition is typical of macrocyclic polyamines with long-chain hydrocarbon substituents, which can form multicharged cations upon protonation. These ionophores are selective with respect to multicharged organic anions such as adenine nucleotides and anions of certain dicarboxylic acids.^{119–121} Moreover, the potentiometric selectivity of ionophores depends on the charge of organic ions (the potentiometric response decreases in the sequence $\text{ATP}^{4-} \gg \text{ADP}^{3-} \gg \text{AMP}^{2-}$)^{119, 121} or on the localisation of the negative charge on the organic anion [the potentiometric response decreases in the sequences *cis*- $-\text{OOC}-\text{CH}=\text{CH}-\text{COO}^- > \text{trans}-\text{OOC}-\text{CH}=\text{CH}-\text{COO}^-$; *o*- $\text{C}_6\text{H}_4(\text{COO}^-)_2 > m\text{-C}_6\text{H}_4(\text{COO}^-)_2 > p\text{-C}_6\text{H}_4.(\text{COO}^-)_2$] (Refs 120, 121). Thus macrocyclic hexamine **1** was used as the neutral carrier in the benzoate-ISE.⁵⁸ The selectivity of an electrode based on amine **1** with respect to anions decreased in the sequence $\text{PhCOO}^- \approx \text{Cl}^- \approx \text{SO}_4^{2-} \approx \text{PO}_4^{3-} > \text{AcO}^- > \text{NO}_3^- > \text{citrate}$.



Macrocyclic hexamine **1** exhibits a pronounced anionic receptor function at the pH from 4 to 6 due to the presence of amide groups in the β -positions relative to the nitrogen atoms of the polyamine ring, which enhance the affinity of the ionophore for hydrogen ions and improve its receptor function with respect to anions.¹²² The same ionophore was used as the EAC in an ion-selective electrode sensitive with respect to anions of adenosine diphosphate and adenosine monophosphate; moreover, the electrode function slope proved to be close to the theoretical slope.⁵⁹

The effect of positively charged nitrogen atoms formed upon protonation of ionophores on their complexation properties was demonstrated by the example of cyclic and acyclic polyamines.¹²¹

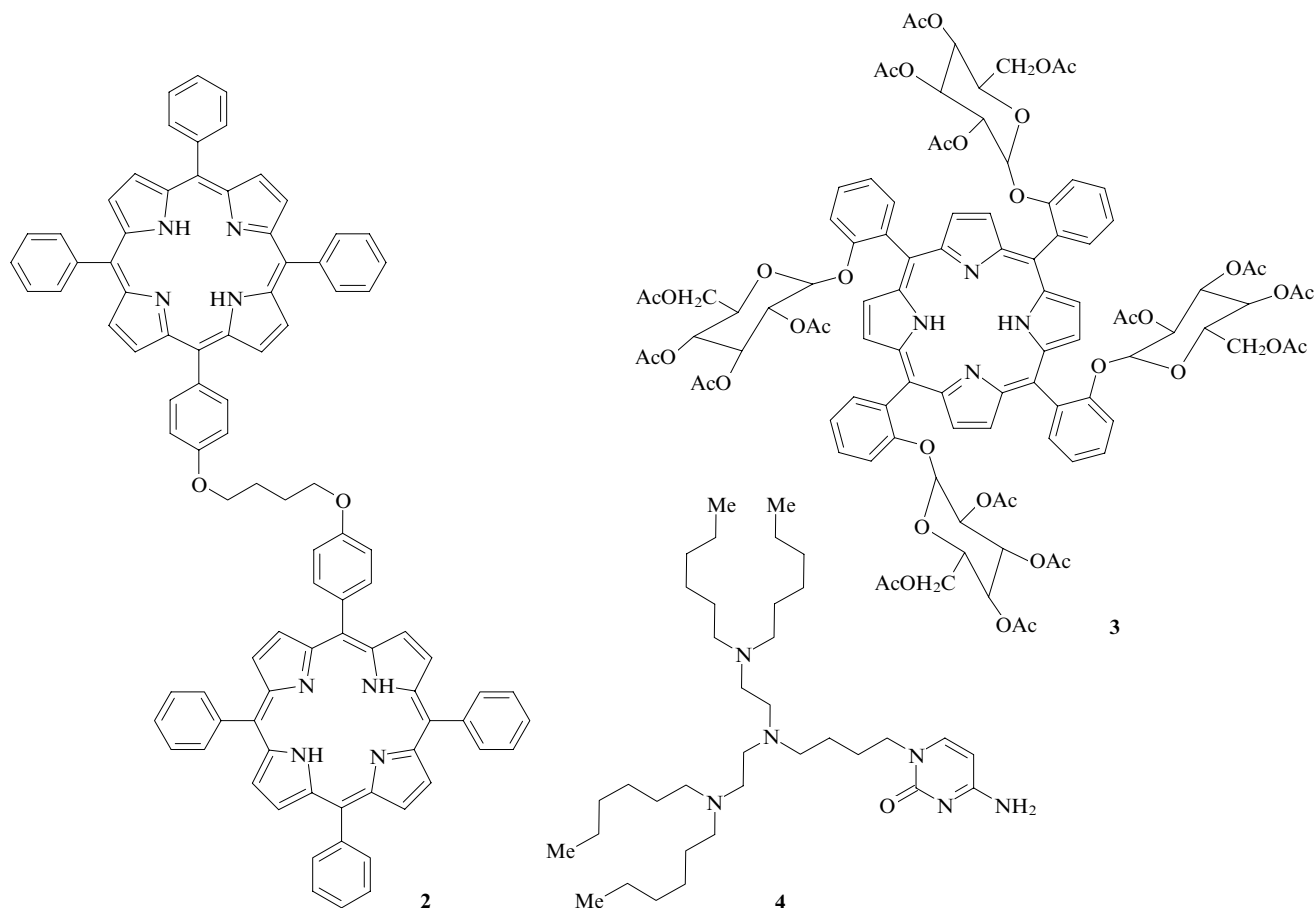
Porphyrine and its derivatives represent typical cyclic polyamines (azacrown compounds) with donating nitrogen atoms, which are softer bases as compared with oxygen atoms. They were used in ISE sensitive with respect to salicylate and valproate anions.^{60, 63–65} 5-*n*-{[4-(10,15,20-Triphenyl-5-porphynato)phenoxy]-1-butoxy}phenyl-10,15,20-triphenylporphyrine (**2**) and 5,10,15,20-tetrakis[2-(2,3,4,6-tetraacetyl- β -D-glucopyranosyloxyphenyl)]porphyrine (**3**) served as specific ionophores in ISE for alkaloid berberine.^{61, 62}

The studies on the reaction of ionophores **2** and **3** with berberine cations involved the analysis of electron absorption spectra of their solutions in chloroform and nitromethane, which were measured before and after these solutions were brought into contact with an aqueous solution of berberine cations.⁶² The absorption peaks of porphyrin **3** at 418, 516, 588 and 654 nm observed upon the contact with the solution of a berberine salt shifted to the long-wave region on average by 4 nm and the peak at 544.5 nm disappeared. This was also observed for ionophore **2**. At the same time, the absorption spectra of a manganese(II) complex with porphyrin **3** remained unchanged both before and after its contact with the berberine salt.

A comparison of IR spectra of PVC membranes based on ionophore **3** before and after their contact with a berberine salt revealed the shifts of absorption bands at 1643.9, 1218.7 and 707.9 cm^{-1} to 1647.1, 1221.9 and 720.0 cm^{-1} , respectively, and the appearance of a new characteristics peak at 1046.5 cm^{-1} associated with the valence vibrations of the amino group in the berberine molecule. This made it possible to assume⁶² the reversible complexation of ionophores with the berberine cation.

A more complicated process that accompanies the complexation is the formation of hydrogen bonds between the ‘guest’ and ‘host’ molecules. In this case, the potentiometric selectivity was demonstrated for liquid membranes that contained ionophore **4** with a dual receptor function and were capable of recognising guanine- and adenine-containing nucleotides with high selectivity with respect to the former.¹²³

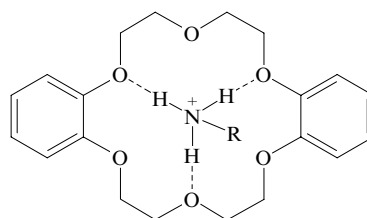
The selectivity of ionophores with respect to organic compounds depends on the presence of non-polar fragments of different nature and structure and, in the general case, is determined by the hydrophilic–lipophilic balance in the organic molecule as a whole. Although the ability for the incorporation of organic molecules into the hydrophobic cavities of the matrices of molecules-hosts is one of the key factors in the molecular recognition, for example, for cyclodextrins and cyclophans in aqueous solutions, the membrane systems pose certain difficulties in the realisation of this selectivity mechanism due to the presence of competitive interactions between ionophores, organic molecules and membrane components. This is why the potentiometric selectivity of ionophores is associated with such properties of organic molecules as lipophilicity and chirality.^{118, 124–126}



The enantiomeric potentiometric selectivity of ionophores with respect to protonated amines and esters of amino acids was demonstrated for PVC membranes based on crown ethers,^{127, 128} natural ionophores¹²⁹ and cyclodextrins.¹³⁰ Due to the peculiarities of their three-dimensional structure, calix[n]arene derivatives exhibited selectivity with respect to primary amines and catecholamines.¹³¹

Cyclic coronands (crown ethers) such as 18-crown-6, dibenzo-15-crown-5, dibenzo-18-crown-6, dibenzo-21-crown-7, dibenzo-24-crown-8, dibenzo-30-crown-10, dicyclohexano-18-crown-6, 4',4''(5'')-di-*tert*-butylcyclohexano-18-crown-6 and dicyclohexano-24-crown-8 were used in the ISE sensitive with respect to chlorphenoxamine,⁶⁶ mexitol⁶⁷ and amphetamine stimulators.^{68, 69}

Potentiometric selectivity of crown ethers is associated with the lipophilicity of organic ions. The formation of complexes between 'guest' and 'host' molecules is accompanied by the formation of hydrogen bonds, which is typical of, *e.g.*, any protonated primary amines. Thus the selectivity of dibenzo-18-crown-6 with respect to primary ammonium cations correlates with the $\log P$ and decreases in the following sequence: octylammonium (3.06 ± 0.18) \approx adamantylammonium (2.22 ± 0.24) > phenethylammonium (1.46 ± 0.19) > benzylammonium (1.09 ± 0.21) \approx *tert*-butylammonium (0.56 ± 0.21). Its selectivity with respect to catecholamines decreases in the sequence dopamine (0.12 ± 0.22) > adrenaline (-0.63 ± 0.28) > noradrenaline (-0.88 ± 0.27) (Ref. 70).[†] The structure of resulting complexes is as follows.



In certain cases, the lipophilicity of an organic cation is not the key factor for the potentiometric selectivity of crowns. It was assumed that an ISE based on dibenzo-18-crown-6 should be more selective with respect to the hydrophobic cations of phentermine ($\log P = 2.16 \pm 0.21$) as compared with less hydrophobic cations of amphetamine ($\log P = 1.81 \pm 0.20$) and phenethylamine ($\log P = 1.46 \pm 0.19$). However, its selectivity turned out to be approximately the same with respect to all mentioned cations.⁶⁸ Here, the key role is played by the steric factor that directly affects the stability of complexes formed. In the phentermine molecule, steric accessibility of the positively charged nitrogen atom for complexation is restricted by two α -methyl groups. The use of an acyclic ionophore with carboxamide fragments made it possible to develop an ISE with the higher selectivity with respect to phentermine. The ISE selectivity decreased with the decrease in the lipophilicity of the organic cation in the series phentermine > amphetamine > phenethylamine. This suggests that the stability of complexes of a series of (phenylalkyl)amines with an acyclic ionophore is independent of the steric accessibility of the NH_3^+ group. The peculiarities of the complexation of crown ethers with nitrogen-containing organic compounds were discussed.¹¹⁷

Acyclic oxygen-, nitrogen- and phosphorus-containing podands, namely, *N,N*-bisoctadecyl-*N',N'*-dipropyl-3,6-

[†] Logarithms of coefficients of distribution in the water – n-octanol system were calculated using the ACD Labs software with a $C \log P$ predictor for the deprotonated amine form.

dioxaocanediamide (Pb^{2+} -ionophore I, ETH 322); bisdodecyl ether of triethylene glycol; N,N,N',N' -tetrakis(cyclohexyl)-oxybis(*o*-phenyleneoxy)diacetamide (Ba^{2+} -ionophore I); N,N,N',N' -tetrakis(cyclohexyl)diglycolamide (Ca^{2+} -ionophore II, ETH 129); N,N,N',N' -tetrakis(cyclohexyl)-1,2-phenylenedioxydiacetamide (Na^+ -ionophore III, ETH 2120) and tris[(2-(2-diphenylphosphinylmethyl)phenoxy)ethyl]amine, which are traditionally used in the ISE reversible with respect to metal ions, turned out to be selective ionophores with respect to amphetamine preparations,^{68,69} β -lactam antibiotics,⁷¹ anions of hydroxy-, mono- and dicarboxylic acids and surfactants.⁷²

Calix[*n*]arenes can form π -complexes due to the presence of aromatic rings. Such complexes are formed with organylammonium, -iminium and tropylium cations; their stability depends first of all on the conformational peculiarities of the calix[*n*]arene molecule.¹³² Thus complexes of amino acids, aliphatic amines, guanidine, creatinine with methyl, ethyl and propyl ethers of calix[6]arene proved to be more stable than the complexes of amino acids with cyclodextrins and crown ethers.¹³³

Theoretical calculations and the results of computer simulations have confirmed that the complexing ability of a calix[*n*]arene directly depends on the size and conformational peculiarities of its macrocycle and the presence of functional groups.^{134–137}

It was assumed that the reaction of calix[*n*]arenes with amines in solutions can be described¹³⁸ by the following sequence of reactions:



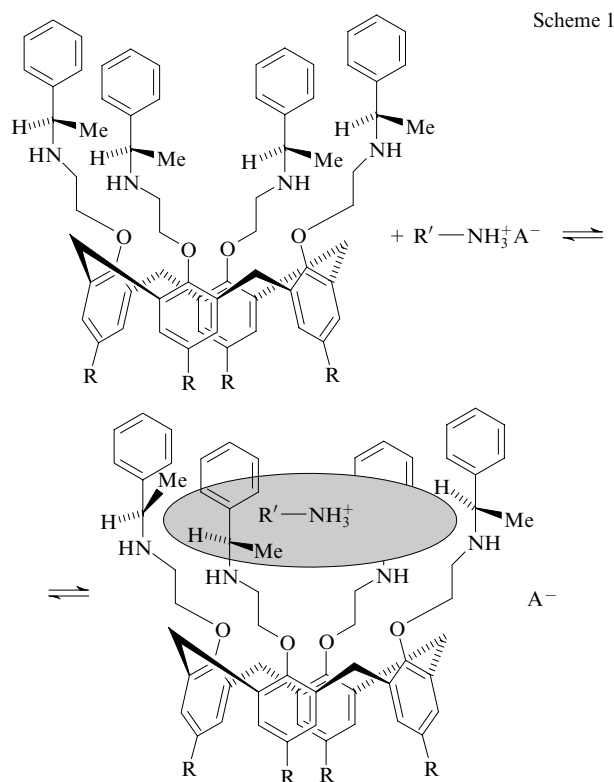
In the first stage, a mobile proton is transferred from the calix[*n*]arene molecule to the amine molecule. In the second stage, complexation with association of ions occurs, where the ammonium cation can be incorporated into the conical hollow in the ionophore matrix due to the π -cationic interaction.^{139–141}

For example, Scheme 1 illustrates the reaction of 25,26,27,28-tetrakis[*(S)*-(–)-(1)-phenylethylaminoethoxy]calix[4]arene with anions of amino acids or aliphatic amines in water–organic media.¹⁴²

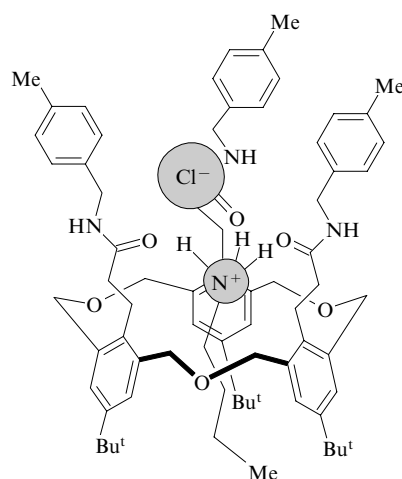
Complexes with the different composition (other than 1 : 1) are formed if the reaction proceeds by the following mechanism: encapsulation of the amine molecule by a macrocycle, formation of a coordination bond between the ‘host’ molecule and another amine molecule.

As a rule, the arrangement of amine molecules is such that hydrocarbon radicals are located in the intramolecular cavities of the calixarene matrix.¹⁴³

Chemical modification of calix[*n*]arenes is a sufficiently simple, effective and versatile approach to the synthesis of receptors highly selective with respect to both cations and anions.¹⁴⁴ The introduction of different functional groups into calix[*n*]arene molecules makes it possible to change the selectivity of ionophores with respect to organic ions. Thus N,N -diethylamide of hexahomotrioxacalix[3]arene extracts 97.8% of Bu^nNH_3^+ , 48.1% of Bu^iNH_3^+ and 35.4% of Bu^tNH_3^+ from the salt mixture. The introduction of a (4-methylbenzyl)aminocarbonyl group into the same calix[3]arene results in the total loss of its specificity with respect to metal ions, whereas the selectivity with respect to nitrogen-containing organic cations such as tetrabutylammonium and trimethylphenylammonium appears as a result of higher electron density on the oxygen atom of the carbonyl group due to the conjugation in the $\text{N}=\text{C}=\text{O} \leftrightarrow \text{N}^+=\text{C}=\text{O}^-$ fragment.^{145–149} As the result of the formation of hydrogen bonds between the neighbouring NH and CO groups, the calixarene molecule loses its affinity for ‘soft’ and ‘hard’ metal cations.¹⁵⁰ In the formation of a complex with the Bu^nNH_3^+ cation, the alkyl substituent travels

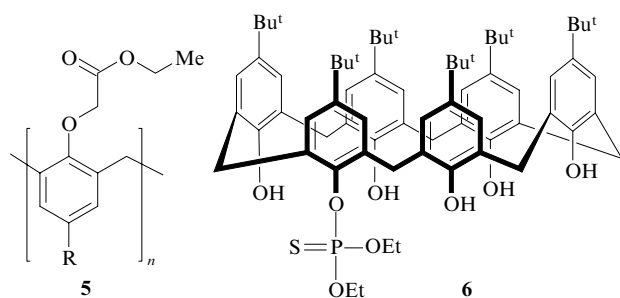


through the ligand π -cavity thus causing changes in the calixarene conformation; moreover, no intramolecular hydrogen bonds are formed in this conformation. The anion (Cl^-) is located within the complex and does not leave it due to the formation of an intramolecular hydrogen bond with the NH group.



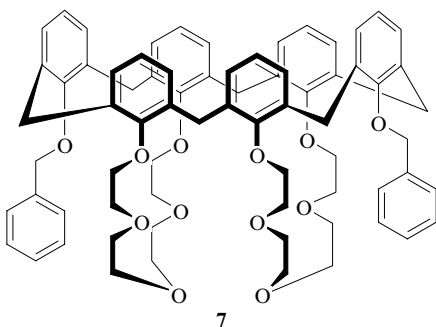
The peculiarities of complexation of calix[*n*]arenes with nitrogen-containing organic compounds (amines, quaternary ammonium cations, iminium ions, amino acids, peptides) were discussed in several reviews.^{116, 151}

Derivatives of calix[6]- and calix[8]arenes (**5** and **6**, respectively) with specific complexing properties with respect to histamine, dopamine, norephedrine, serotonin⁷³ and chlorphenoxamine⁶⁶ were synthesised and used as the specific receptors in ISE membranes.

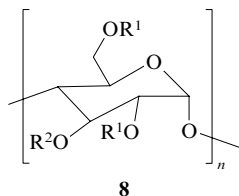


R = H, Bu^t; $n = 6, 8$.

Calix[6]crown ethers were tested as the ISE ionophores in the determination of catecholamines (epinephrine, norepinephrine, dopamine).⁷⁴ ISE based on compound **7** exhibited the best potentiometric characteristics. The selectivity of such an electrode doped with a lipophilic compound decreased in the sequence epinephrine > K⁺ ≈ dopamine > NH₄⁺ > norepinephrine > Na⁺. The detection limit for epinephrine was 1.86×10^{-5} mol litre⁻¹. The calculated values of log P were -0.17, -0.39, -0.97 for dopamine, epinephrine and norepinephrine, respectively. The inversed order of the extraction selectivity for catecholamines suggests that the complexation of ionophores with the epinephrine cation makes the main contribution in the formation of the potentiometric response of an ISE.

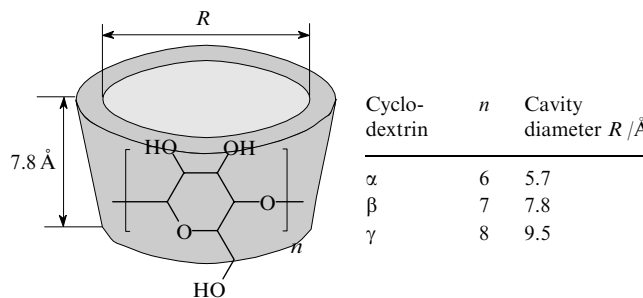


Cyclodextrins (CD) are cyclic oligosaccharides that consist of D-glucopyranose residues linked with one another with α -1,4-glycosidic bonds. Their lipophilic derivatives **8** were incorporated into selective membranes for the determination of diclofenac sodium,⁷⁵ protonated physiologically active amines, namely, dopamine,⁷⁶ (S)-enalapril,⁷⁷ tricyclic antidepressants (desipramine, imipramine, trimipramine),⁷⁸ local anaesthetics (bupivacaine, lidocaine, procaine, prilocaine),⁷⁹ propranolol, acetylcholine, methacholine, metformin, norephedrine, phenformin, choline, ephedrine.⁸⁰⁻⁸³



$n = 6$: R¹ = n-C₈H₁₇, R² = H (50% or 57%) + n-C₈H₁₇ (50% or 43%);
 $n = 7$: R¹ = n-C₁₂H₂₅, R² = H;
 R¹ = n-C₈H₁₇, R² = H (48%) + n-C₈H₁₇ (52%).

α -, β -, γ -Cyclodextrins differ from one another in the number of glucopyranose residues in the molecule and, correspondingly, in the diameter of the inner cavity.¹⁵²



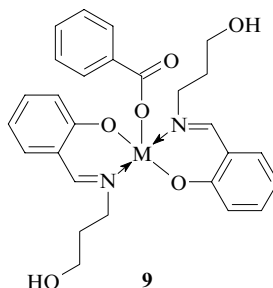
The presence of an inner cavity makes it possible for cyclodextrin molecules to form inclusion compounds with both inorganic and organic molecules and ions.

Cyclodextrin derivatives that exhibit enantiomeric selectivity can be used in ISE for the determination of organic compounds.⁸¹ Thus ISE based on lipophilic 2,6-diethyl- α -cyclodextrin and 2,6-bisdodecyl- α -cyclodextrin allow the selective determination of the (-)-(1*R*,2*S*)-ephedrine cation in the presence of its three stereoisomers, even though the free energies of the formation of isomer complexes differed by merely 2.5 kJ mol⁻¹. The method of proton magnetic relaxation, which was used in the studies of diastereomeric complexes of ephedrine and its analogues with lipophilic cyclodextrins, has demonstrated the difference in the degree of hydrogen bond formation between the structural fragments NH⁺...O in the complex compounds.⁸⁴ As a result of stereo-differentiation in the formation of cyclodextrin complexes with ephedrine cations, a more stable complex of the corresponding stereoisomer was formed.⁸¹

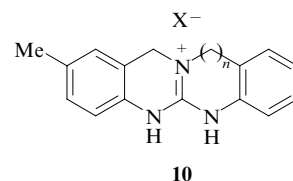
A guanidinium ion and 2,6-bisdodecyl- β -cyclodextrin form a 1:1 complex, and the ISE on its basis exhibited approximately equal sensitivity with respect to organic cations with the structures close to that of guanidine.⁸¹ The occasional independence of the ISE electrode response on the cyclodextrin structure (α -, β -, OH- and alkylcyclodextrins) was associated with the formation of a primary hydrogen bond between the positively charged nitrogen atom and the oxygen atom of the cyclodextrin molecule.⁸⁰

Certain cyclodextrin derivatives can form supramolecular polymers, intramolecular inclusion complexes and more intricate supramolecular systems, which extends the possibilities of their practical application as specific receptors.¹⁵³

Complexes of aluminium, tin(IV) and copper(II) with tetra(*tert*-butyl)phthalocyanine and oxo(phthalocyaninato)-vanadium(IV) and -molybdenum(IV) were used as ionophores in liquid⁸⁵⁻⁸⁹ and solid-contact⁹⁰ membranes of salicylate-selective electrodes. Metallocenes [bis(cyclopentadienyl) Co(II), Fe(II), Ni(II), Hf(IV), Nb(V), Ti(IV) and Zr(IV)], tribenzyltin(IV), phenolates and carboxylates, phenylboronic acid derivatives, heptyl 4-(trifluoroacetyl)benzoate, complexes of Al(III) and Sn(IV) with *N,N'*-bis(salicylidene)-*o*-phenylenediamine, complexes of Schiff base **9**, guanidine derivatives **10** and tetra-azo[14]annulene copper(II) also proved to be suitable



M = Co(III), Mn(III)



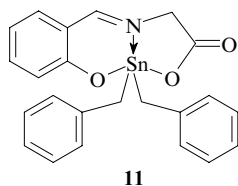
$n = 2$, X = ClO₄; $n = 3$, X = BF₄

ionophores for the ISE selective with respect to salicylate anions (Sal^-).^{91–95}

Spectrophotometry,^{63, 88, 89, 96} IR spectroscopy⁶³ and the electrochemical impedance method⁹⁷ were used for the elucidation of the mechanism of the potentiometric response of ISE to salicylate anions. Spectral methods provided information on the mechanism of complex formation, while the electrochemical impedance method afforded data on the kinetic characteristics and limiting stages of the transfer processes.

Based on experimental data, it was shown that the reaction of tetra(*tert*-butyl)phthalocyaninato(iodo)cobalt(III) with salicylate anions proceeds *via* the substitution of a salicylate ion for the axial iodide ion. This was not the case for tetra(*tert*-butyl)phthalocyaninato(chloro)rhodium(III) due to the very strong Rh–Cl bond and the hindered coordination through the free sixth axial position on the metal, because the radius of the Rh(III) ion substantially exceeds the size of the phthalocyanine cavity so that the metal ion ‘leaves’ the plane in the direction of the axial chloride ion. An ion-selective electrode based on tetra(*tert*-butyl)phthalocyaninato(chloro)rhodium(III) does not respond to salicylate anions, whereas an ISE based on tetra(*tert*-butyl)phthalocyaninato(iodo)cobalt(III) demonstrates an electrode function with a slope S of $50 \pm 2 \text{ mV (pC)}^{-1}$ and a detection limit of $6.3 \times 10^{-5} \text{ mol litre}^{-1}$ of Sal^- (Ref. 88).

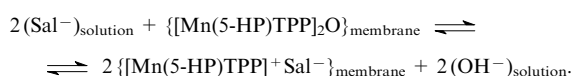
An ion-selective electrode based on complex **11** formed by dibenzyltin with a Schiff base produced a super-Nernstian response [$S = 65.5 \pm 1.8 \text{ mV (pC)}^{-1}$] to salicylate anions in the range of $1.0 \times 10^{-1} - 4.0 \times 10^{-6} \text{ mol litre}^{-1}$ of Sal^- (Ref. 97).



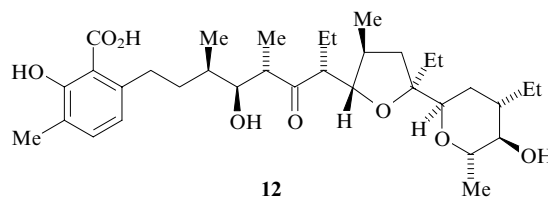
11

The appearance of the super-Nernstian response was associated with the ability of the ionophore to form dimers and more complex aggregates in the organic phase of the membrane, while the increase in the electrode function slope is the consequence of the changes in the stoichiometry of the ionophore reaction with the salicylate anion (2 : 1 in place of 1 : 1). Based on the analysis of electron absorption spectra of ionophore solutions in chloroform measured before and after their contact with the NaSal solution, the potentiometric selectivity of a membrane with respect to Sal^- was associated with the thermodynamically preferential coordination of the Sal^- anion at the central metal atom of the ionophore. The results of impedance measurements made it possible to assume the diffusion-controlled transfer of salicylate anions.⁹⁷

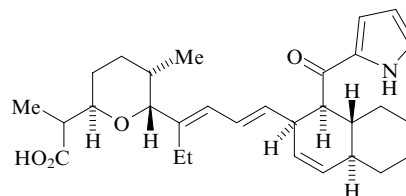
The mechanism of the potentiometric response of an ISE with a membrane based on μ -oxobis[5-(*p*-hydroxyphenyl)-10,15,20-triphenylporphyrinato]manganese(III) $\{[\text{Mn(5-HP).TPP}]_2\text{O}\}$ was studied by IR and UV spectroscopic techniques.⁶³ The selectivity of the ISE electrode with respect to Sal^- was associated with the formation of charged carriers in the membrane as a result of the following reaction:



Acyclic polyether antibiotics lasalocid (**12**) and omomycin (**13**) were shown to exhibit enantiometric selectivity with respect to optical isomers of methyl esters of amino acids.⁹⁸



12



13

The electrode function of ISE in solutions of L-isomers had a slope close to theoretical. The coefficient of enantiometric selectivity for L- and D-isomers of methyl phenylalaninate was 2.38 for lasalocid-based membranes and 1.85 for membranes containing omomycin. According to the transport tests, it was shown that lasalocid can transfer protonated cations of methyl phenylalaninate across the liquid membrane–solution interface according to the antiport principle at a rate close to that of the transfer of cations by other ionophore antibiotics.

Phenylboronic acid derivatives and complexes of hydroxamic acids with boric acid were used as ionophores for ISE membranes sensitive to protonated forms of catecholamines (adrenaline, dobutamine, dopamine, noradrenaline),^{95, 99} phenolic acids (gallic, homoprotocatechuic, caffeic and salicylic acids).^{94, 99} The electrode response of ISE membranes was associated with the trend of polyhydroxycompounds for the fast and reversible formation of covalent ester bonds with boric acid derivatives.^{94, 95, 99}

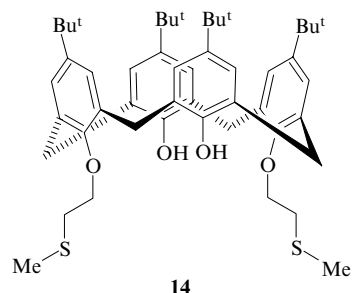
Of other ionophores, 2,3,5-triphenyl-2H-tetrazolium tungstophosphate was used in the ISE for ascorbic acid,¹⁰⁰ a complex of iron(II) with 2,4,6-tri(piperidino)-1,3,5-triazine was used in ISE for diclofenac sodium,¹⁰¹ O-(2,4-dichlorophenyl) O-ethyl S-propyl dithiophosphate was employed in ISE for histamine,¹⁰² heptyl 4-(trifluoroacetyl)benzoate was used as the ionophore in salicylate-ISE.¹⁰³

Studies were carried out devoted to the development and optimisation of characteristics of ISE for polyions (heparin and protamine).^{154–164} The equilibrium response of sensors to polyions of different structure was compared for ISE based on tri(dodecyl)methylammonium chloride and tetra(dodecyl)ammonium chloride. The deviations in the emf changes were used as the basis for stating a correlation between the energy of interaction of ionic pairs and the polyion charge. A threshold mass of polyion molecules was required for reaching the maximum emf value. The effect of lipophilic additions on the ISE response was studied. It was shown that the ISE may be used in the monitoring of the enzymatic hydrolysis of protazoline with tripsin.

A modernised ISE for protamine, which was based on its associate with dinonylnaphthalenesulfonate, was developed for the whole blood analysis.¹⁶³ The electrode operates by the mechanism of non-equilibrium response in the concentration range of $0.5 - 20 \text{ mg litre}^{-1}$ and can be used in both direct potentiometry and potentiometric titration of heparin with protamine. The results of ISE determinations agreed with the data of other (independent) analytical techniques. It was shown that the procedure of potentiometric titration of heparin using this ISE allows complete automation.

The development and optimisation of solid-contact ISE for heparin was discussed.¹⁶⁴ The temporal instability of the potential is the main drawback of solid-contact ISE. To

remove this drawback, silver(I) complexes with a lipophilic derivative of *tert*-butylcalix[4]arene **14** were incorporated into the membrane in addition to EAC [tri(dodecyl)methylammonium chloride].



This complex serves as the reversible electron carrier between the polymeric membrane and the current lead and favours the stabilisation of the potential of the solid-contact sensor.

IV. Components of ion-selective electrode membranes and methods of potentiometric determination of medicinal drugs

As was mentioned above, IA formed by MD cations and anions with the corresponding counter-ions are used most often as the EAC in selective membranes. Table 1 presents different EAC types, which are incorporated into the composition of ISE membranes both directly and in the form of ion associates with MD. Tetraphenylborate and its derivatives are used most extensively in EAC for cation-selective electrodes, while the cations of quaternary ammonium bases (QAB) are employed in EAC for anion-selective electrodes.

Nitrobenzene derivatives (in ISE with liquid membranes), nitrophenol ethers, esters of *o*-phthalic, adipic, sebacic, phosphonic and phosphoric acids are used most often as the solvents-plasticisers. Table 2 shows membrane solvents used in ion-selective membranes. *o*-Nitrophenyl octyl ether, dibutyl phthalate and dioctyl phthalate are the most common plasticisers of the polymeric binder, *i.e.*, polyvinyl chloride (PVC). Depending on the particular case, one or another membrane

Table 1. Electroactive compounds incorporated into the selective membrane either directly or as ion associates with medicinal drugs.

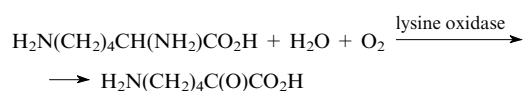
Class of compounds	Compound	Ref.
Tetraphenylborate derivatives	sodium tetraphenylborate	86, 87, 106, 165–219
	sodium tetrakis(4-methylphenyl)borate	37, 170
	potassium tetrakis(4-chlorophenyl)borate	37, 66, 68, 73, 74, 76, 80, 83, 86, 170, 171, 191, 192, 211, 220–226
	potassium tetrakis[3,5-bis(trifluoromethyl)phenyl]borate	37, 67, 78–82, 192, 227, 228
	sodium tetrakis[3,5-bis(1,1,1,3,3,3-hexafluoro-2-methoxyisopropyl)phenyl]borate Na[B(C ₁₄ H ₉ O ₂ F ₁₂) ₄]	64, 67, 102, 229
Heteropoly compounds	molybdophosphoric acid H ₃ [PMo ₁₂ O ₄₀]	32, 34, 36, 165, 170, 172, 175, 184, 189, 198, 230–246
	molybdosilicic acid H ₄ [SiMo ₁₂ O ₄₀]	32, 34, 36, 170, 172, 231, 239, 240, 246
	tungstophosphoric acid H ₃ [PW ₁₂ O ₄₀]	32, 34, 36, 100, 170–172, 177, 184, 195, 196, 208, 212, 233–235, 238–241, 243–261
	tungstosilicic acid H ₄ [SiW ₁₂ O ₄₀]	32, 34, 36, 170, 172, 195, 202, 232, 240, 262–266
1,10-Phenanthroline and its derivatives	1,10-phenanthroline	267, 268
	4,7-diphenyl-1,10-phenanthroline (batophenanthroline)	267, 269–271
Quaternary ammonium and phosphonium cations	<i>N,N,N,N</i> -tetraoctylammonium	272–274
	<i>N,N,N,N</i> -tetraakis(decyl)ammonium	31, 170, 275, 276
	<i>N</i> -methyl- <i>N,N,N</i> -triethylammonium	71, 87, 220, 277–280
	<i>N,N,N,N</i> -tetradodecylammonium	75
	<i>N</i> -hexadecylpyridinium	281
	<i>N,N,N</i> -tridodecyl- <i>N</i> -methylammonium	58, 103
	<i>N,N,N</i> -tributyl- <i>N</i> -hexadecylphosphonium	71
	bis(triphenylphosphoranilidene)ammonium [Ph ₃ P=N ⁺ =PPh ₃]	64, 273, 282, 283
Nitroaromatic compounds	2,2',4,4',6,6'-hexanitrodiphenylamine (dipicrylamine)	271, 284–286
	2,4,6-trinitrophenol (picric acid)	34, 100, 204
	3-methyl-4-nitro-1- <i>p</i> -nitrophenylpyrazol-5-one (picrolonic acid)	100, 287, 288
Miscellaneous salts (anions) and acids	sodium dodecyl sulfate	285, 288, 289
	Reinecke salt anion [Cr(NH ₃) ₂ (NCS) ₄] [–]	32, 34, 197–199, 201, 210, 214–216, 225, 242, 253, 255, 261
	tetraiodobismuthate	32, 34, 183, 204
	tetraiodomercurate	32, 34, 197, 204, 290, 291
	tetraiodocadmate	292
	trioctyloxybenzenesulfonic acid	293
	hexathiocyanoferrate(III) anion	294
	tetrathiocyanocobaltate(II) anion	242
	5-nitropyrimidine-2,3,6-trione (5-nitrobarbituric acid)	295

Table 2. Solvents-plasticisers used in membranes of liquid and polymeric ion-selective electrodes.

Plasticiser type	Name of compound	Ref.
Plasticisers with high permittivity		
Nitro compounds	nitrobenzene	284
	2-nitrotoluene	100
	1-isopropyl-4-nitrobenzene	222, 274
	2-nitrophenyl octyl ether (NPOE)	35, 61–63, 67, 71, 73–75, 78–83, 85, 91–96, 103, 104, 171, 174, 180, 182, 189, 192, 197, 207, 208, 221–225, 227, 233, 234, 243, 261, 263, 266, 269–273, 279, 281–283, 296
	2-nitrophenyl dodecyl ether	227
	2-nitrophenyl phenyl ether	213, 222, 233
	2-nitrophenyl 2-fluorophenyl ether	67, 76, 192, 229
Plasticisers with low permittivity		
Esters of <i>o</i> -phthalic acid	dibutyl phthalate (DBP)	31, 32, 34, 36, 37, 61, 105, 169, 170, 177, 179, 182, 184–186, 188, 195–197, 204, 206, 228, 239, 240, 244, 254, 262, 275–277, 281, 293
	bis(2-ethylhexyl) phthalate	65, 90
	dioctyl phthalate (DOP)	32, 34, 36, 61, 62, 66, 67, 85, 172–174, 177, 186, 187, 190, 191, 193, 195–199, 201, 202, 204, 212, 214–216, 218, 230–232, 235, 238, 239, 243, 245, 246, 256–260, 266–268, 275, 276, 279, 281, 284, 290, 291, 294, 297
	diisooctyl phthalate	62
	bis(2-ethyloctyl) phthalate	96
	dinonyl phthalate (DNP)	58, 192, 278
	diisononyl phthalate (DiNP)	36, 202, 262
Esters of adipic acid	bis(2-ethylhexyl) adipate	91, 226
	bis(1-butylpentyl) adipate	80, 83, 86, 91
Esters of sebacic acid	diethyl sebacate (DES)	85, 94, 95
	dibutyl sebacate (DBS)	197, 214, 225, 266, 281
	bis(2-ethylhexyl) sebacate (EHS)	32, 61, 66, 68, 104, 182, 192, 205, 222, 225, 227, 273, 275, 276
	dioctyl sebacate (DOS)	36, 62, 74, 202, 224
	dinonyl sebacate	86
Esters of phosphoric and phosphonic acids	tributyl phosphate	85
	dioctyl phenyl phosphonate (DOPP)	51, 277
	tritoyl phosphate (mixture of isomers) (TTP)	36, 67, 202, 230, 239
	bis(2-ethylhexyl) phosphate	225
	tris(2-ethylhexyl) phosphate	67, 69, 192, 225
	trioctyl phosphate	226
Esters of miscellaneous acids and non-ester plasticisers	chlorobenzene	181
	n-octanol	292
	heptyl benzoate	32, 34, 275
	bis(1-butylpentyl)decan-1,10-diyl diglutarate	64
	tetrakis(2-ethylhexyl) pyromellitate	192

solvent may prove to be more suitable for the achievement of optimum electroanalytical characteristics of ISE for MD.

In the organic analysis, arrays of sensors (multisensor systems of the 'electronic tongue' type) are used. A multisensor system has been developed for the determination of lysine in foodstuffs.²⁹⁸ The array of sensors comprised an enzyme electrode based on lysine oxidase with NH_4^+ -ISE and a set of solid-contact ISE for H^+ , NH_4^+ , K^+ , Na^+ , Ca^{2+} , Mg^{2+} and Li^+ cations. The response of the enzyme electrode was associated with the enzymatic reaction



Insofar as the selectivity of the enzyme electrode with respect to other cations is low, the cross-selectivity-based potentiometric response of a multisensor system can be deter-

mined using the multiversion regression analysis. Among the methods for mathematical processing of potentiometric data, the least-squares technique with partial regression, which provides the smallest prediction errors, has shown the best results.²⁹⁸

An ISE-based method of precipitation potentiometric titration was also used for the determination of MD and drug preparations. Sodium tetraphenylborate commonly used as the titrant in the cationic MD determination proved to be suitable for determination of both individual MD^{266, 268, 291} and multicomponent MD mixtures.²⁹⁹

The method of precipitation potentiometric titration was also used in the flow analysis. In the determination of ephedrine by potentiometric titration, a flow-injection cell with a tubular indicator electrode containing tetrapentylammonium tetraphenylborate dissolved in *o*-nitrophenyl pentyl ether has been developed.²¹³ An ISE-containing individual channel in the cell was provided for the ephedrine determination. The

Table 3. Composition of membranes and characteristics and electroanalytical properties of ion-selective electrodes for determination of medicinal drugs.

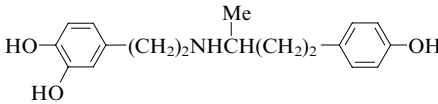
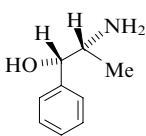
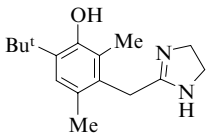
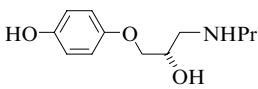
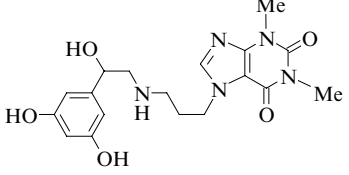
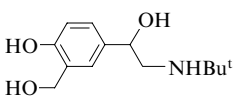
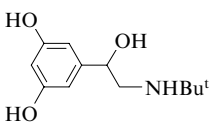
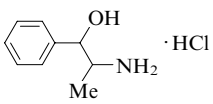
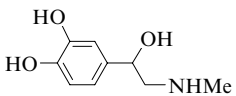
Medicinal drug	Formula	Membrane composition and electrode type ^a	Major electrode characteristics ^b	Ref.
Adrenomimetics and sympathomimetics				
Dobutamine		PPVCM (NPOE or DES) with phenylboronic acid derivatives	LR $1.0 \times 10^{-2} - 5.0 \times 10^{-4}$, DL = 1.7×10^{-5} , S = 58, pH 6.3–8.0	95
Norephedrine		PPVCM [bis(1-butylpentyl) adipate] with a lipophilic derivative of β -CD and addition of $K[B(C_6H_4Cl-4)_4]$ PPVCM (NPOE) with derivatives of calix[n]arenes ($n = 6, 8$) and addition of $K[B(C_6H_4Cl-4)_4]$	DL = 7.9×10^{-6} , S = 58 LR $1.0 \times 10^{-2} - n \times 10^{-6}$, S = 50–57	82 73
Oxymetazoline		PPVCM (DOP) based on IA of MD cations with $[PW_{12}O_{40}]^{3-}$	LR $1.0 \times 10^{-2} - 2.0 \times 10^{-5}$, S = 57.2, pH 1.0–9.4	260
Prenalterol		PPVCM (DOP) based on IA of MD cations with BPh_4^-	LR $3.2 \times 10^{-2} - 1.2 \times 10^{-5}$, S = 56.3, pH 2.2–7.5	187
Reproterol		PPVCM with individual IA of MD cations with $[PW_{12}O_{40}]^{3-}$ and $[PMO_{12}O_{40}]^{3-}$ or their mixture	LR $1.0 \times 10^{-1} - 6.3 \times 10^{-6}$, pH 2.0–9.0	241
Salbutamol		ISE for FIA with PPVCM (DOP) based on IA of MD cations with $[PW_{12}O_{40}]^{3-}$ and $[PMO_{12}O_{40}]^{3-}$ SC-ISE (glassy carbon substrate) with an ion-electron transducer (polyaniline), PPVCM based on IA of MD cations with BPh_4^-	LR $1.0 \times 10^{-1} - 6.3 \times 10^{-6}$, S = 57–67, pH 2.0–11.0 LR $1.0 \times 10^{-1} - 4.0 \times 10^{-5}$, DL = 1.2×10^{-5} , S = 60.4, pH 3.9–7.8	235, 238 194
Terbutaline		PPVCM based on IA of MD cations with $[PW_{12}O_{40}]^{3-}$	—	250
Phenylpropanolamine hydrochloride		PPVCM (DBP or DOP) based on IA of MD cations with BPh_4^- and $[PW_{12}O_{40}]^{3-}$	LR $8.9 \times 10^{-3} - 1.0 \times 10^{-5}$	177
Epinephrine		PPVCM (DOS) with calix[6]crowns and addition of lipophilic $K[B(C_6H_4Cl-4)_4]$	LR $1.0 \times 10^{-2} - 1.0 \times 10^{-4}$, DL = 1.9×10^{-5} , S = 45, pH 7.2	74

Table 3 (continued).

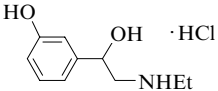
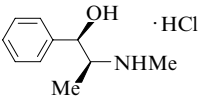
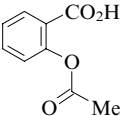
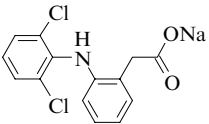
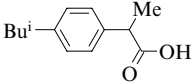
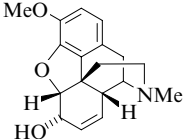
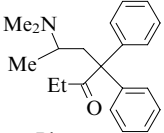
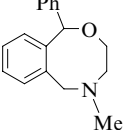
Medicinal drug	Formula	Membrane composition and electrode type ^a	Major electrode characteristics ^b	Ref.
Adrenomimetics and sympathomimetics				
Etilefrine		PPVCM (DOP) based on IA of MD cation with BPh ₄ [−] and [PW ₁₂ O ₄₀] ^{3−}	LR $1.0 \times 10^{-1} - 6.3 \times 10^{-5}$,	212
Ephedrine		microsensor based on a field transistor and a sensitive membrane modified with β-cyclodextrin PPVCM [bis(1-butylpentyl) adipate] with a lipophilic derivative of β-CD and addition of K[B(C ₆ H ₄ Cl-4) ₄] tubular ISE for FIA with PPVCM based on IA [(n-C ₅ H ₁₁) ₄ N] ⁺ [BPh ₄] [−] PPVCM with a mixture of IA formed by ephedrine cations with BPh ₄ [−] , [Cr(NH ₃) ₂ (NCS) ₄] [−] and by phenylephedrine cations with [Cr(NH ₃) ₂ (NCS) ₄] [−]	LR $1.0 \times 10^{-1} - 3.0 \times 10^{-6}$, <i>S</i> = 58, pH 3.0–8.0 DL = 2.5×10^{-7} , <i>S</i> = 60 LR $1.0 \times 10^{-1} - 3.8 \times 10^{-6}$, <i>S</i> = 56.4, pH 2.5–11.5 LR $1.0 \times 10^{-1} - 1.0 \times 10^{-5}$, DL = 4.0×10^{-6} , <i>S</i> = 50–55, pH 2.0–9.0	303 80, 83 213 215
Analgesic drugs (narcotic and non-narcotic analgesics)				
Acetylsalicylic acid (AcSA)		tubular flow ISE for salicylate anions formed upon alkaline hydrolysis of AcSA flow ISE, PPVCM (NPOE) with addition of tetraoctylammonium salicylate and <i>p</i> -(<i>tert</i> -octyl)phenol for the determination of AcSA after its preliminary hydrolysis tubular flow SC-ISE based on ethylene–vinyl acetate co-polymer, trioctylmethylammonium salicylate and addition of K[B(C ₆ H ₄ Cl-4) ₄], sensitive to salicylate anions formed upon hydrolysis of AcSA	LR $4.0 \times 10^{-2} - 4.0 \times 10^{-3}$, pH 8 LR $1.0 \times 10^{-2} - 5.0 \times 10^{-5}$, DL = 5.0×10^{-5} , <i>S</i> = 56 LR $5.0 \times 10^{-1} - 5.0 \times 10^{-3}$, DL = 2.5×10^{-3} , <i>S</i> = 58.3, pH 6–10	304 272 220
Diclofenac sodium		PPVCM (NPOE) with addition of α-CD and [(n-C ₁₂ H ₂₅) ₄ N]Br PPVCM based of IA of diclofenac with a Fe(II) complex with 2,4,6-tris(2-pyridyl)-1,3,5-triazine	LR $1.0 \times 10^{-2} - 5.0 \times 10^{-6}$, DL = 1.0×10^{-6} , <i>S</i> = 57.5, pH 8.2–12.7 LR $n \times 10^{-2} - n \times 10^{-6}$, pH 5.5–9.5	75 101
Ibuprofen		PPVCM based on IA of MD anions with cations of different QAB PPVCM (DOP) with IA formed by MD anions with a Fe(II) complex with phenanthroline	— LR $1.0 \times 10^{-2} - 2.0 \times 10^{-5}$, DL = $0.8 - 1.3 \mu\text{g ml}^{-1}$, <i>S</i> = 59–60	305 268
Codeine		PPVCM (DOP) with IA of MD cations with BPh ₄ [−] and [Cr(NH ₃) ₂ (NCS) ₄] [−]	LR $1.0 \times 10^{-2} - n \times 10^{-5}$, DL = 3.5×10^{-5} , <i>S</i> = 50–60, pH 2.5–8.0	199, 214
Methadone		PPVCM (NPOE) with IA of MD cations with [B(C ₆ H ₄ Cl-4) ₄] [−]	LR $1.0 \times 10^{-1} - 2.5 \times 10^{-5}$, <i>S</i> = 59.5, pH 2.0–9.0	221
Nefopam		PPVCM with a nefopam–picrolonate complex	LR $5.0 \times 10^{-2} - 5.0 \times 10^{-4}$, DL = 7.9×10^{-5} , <i>S</i> = 56	287

Table 3 (continued).

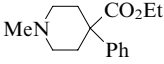
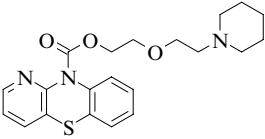
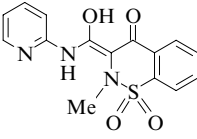
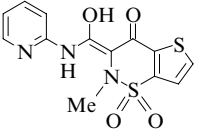
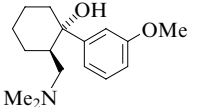
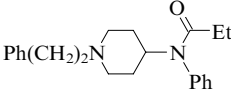
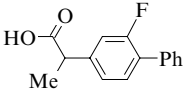
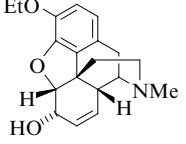
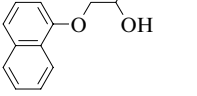
Medicinal drug	Formula	Membrane composition and electrode type ^a	Major electrode characteristics ^b	Ref.
Analgesic drugs (narcotic and non-narcotic analgesics)				
Pethidine		PPVCM (DBP) with IA of MD cations with BPh ₄ [−] and [SiW ₁₂ O ₄₀] ^{4−}	LR $1.0 \times 10^{-2} - 1.0 \times 10^{-5}$, DL = 2.2×10^{-6} , $S = 51.8$, pH 2.0–8.0	206, 265
Pipazetate		PPVCM (DOP) with IA of MD cations with [PMo ₁₂ O ₄₀] ^{3−} and [PW ₁₂ O ₄₀] ^{3−}	LR $1.0 \times 10^{-1} - 6.3 \times 10^{-5}$, $S = 45 - 50$, pH 2.0–9.0	245
Piroxicam		PPVCM (DNP) with IA of MD anions with trioctylmethyl ammonium cations (Aliquat 336S)	LR $1.0 \times 10^{-2} - n \times 10^{-5}$, DL = $(2.4 - 6.0) \times 10^{-6}$, $S = 54 - 56$, pH 4.0–7.5	278
Tenoxicam		the same	the same	278
Tramadol		SC-ISE with PM (DOP or DBPhos) and IA of MD cations with [PW ₁₂ O ₄₀] ^{3−}	LR $1.0 \times 10^{-2} - n \times 10^{-5}$, DL = 2.3×10^{-6} , $S = 55.9 \pm 0.4$, pH 1.0–7.0	249, 257
Fentanyl		PPVCM with IA of MD cations with [B{(C ₆ H ₃ (CF ₃) ₂ -3,5) ₄ }] [−]	LR $1.0 \times 10^{-2} - 1.0 \times 10^{-5}$, DL = 6.29×10^{-6} , $S = 57.9$	228
Flurbiprofen		PPVCM with IA of MD anions with Aliquat 336S	LR $1.0 \times 10^{-2} - 7.0 \times 10^{-5}$	280
Ethylmorphine		SC-Sensor (Si/Si ₃ N ₄ substrate) with PPVCM based on IA of MD cations with BPh ₄ [−] and addition of K[B(C ₆ H ₄ Cl-4) ₄]	LR $1.0 \times 10^{-2} - 2.5 \times 10^{-5}$, DL = $1.0 \mu\text{g ml}^{-1}$, pH 2.5–6.5	211
Antiadrenergics and dopamine mimetics				
Propranolol		PPVCM (DiNP or DOP) with IA of MD cations with [SiW ₁₂ O ₄₀] ^{4−} , [PMo ₁₂ O ₄₀] ^{3−} or [SiMo ₁₂ O ₄₀] ^{4−} PPVCM (NPOE) with a lipophilic derivative of β-CD and addition of K[B(C ₆ H ₄ Cl-4) ₄]	LR $2 \times 10^{-2} - n \times 10^{-6}$, DL = $(1.0 - 10.0) \times 10^{-7}$, $S = 30.0 - 54.7$, pH 4.0–8.0 DL = 1.0×10^{-5} , $S = 60$	231, 262 83

Table 3 (continued).

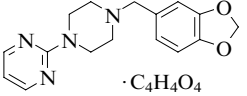
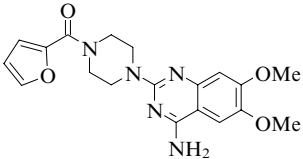
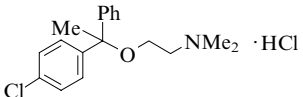
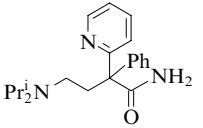
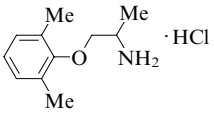
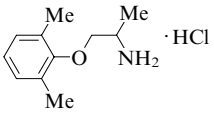
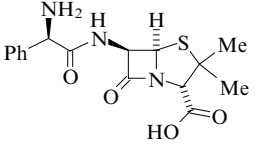
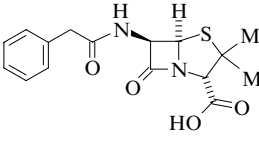
Medicinal drug	Formula	Membrane composition and electrode type ^a	Major electrode characteristics ^b	Ref.
Antiadrenergics and dopamine mimetics				
Piribedil		PPVCM (DBP and DOP) based on IA of MD cations with BPh_4^- , BiI_4^- or HgI_4^{2-}	LR $n \times 10^{-2} - n \times 10^{-6}$, $S = 30 - 57$, pH 3.0–6.4	186, 204
Prazosin		PPVCM based on IA of MD cations with $[\text{PW}_{12}\text{O}_{40}]^{3-}$	LR $1.0 \times 10^{-2} - 2.7 \times 10^{-6}$, pH 1.5–6.4	248
Chlorphenoxamine		PPVCM containing a mixture of ionophores (18-crown-6, dibenzo-18-crown-6 or 37,38,39,40,41-pentakis[(diethoxythiophosphoryl)oxy]-5,11,17,23,29,35-hexakis(1,1-dimethylethyl)calix[6]arene-42-ol) with $\text{K}[\text{B}(\text{C}_6\text{H}_4\text{Cl}-4)_4]$	LR $5.0 \times 10^{-2} - 6.3 \times 10^{-6}$, DL = 5.9×10^{-6} , $S = 35 - 55$, pH 3–8	66
Antiarrhythmic drugs				
Disopyramide		PPVCM (2-nitro-2'-fluorodiphenyl ether) with $\text{Na}[\text{B}(\text{C}_{14}\text{H}_9\text{O}_2\text{F}_{12})_4]$	LR $1.0 \times 10^{-4} - 6.0 \times 10^{-6}$, DL = 8.0×10^{-7} , $S = 55 - 63$, pH 7.4 (buffer)	229
Mexitil		PPVCM with IA of MD cations with dodecyl sulfate	LR $n \times 10^{-2} - n \times 10^{-5}$, DL = 7.1×10^{-8} , pH 2.0–6.5	289
Mexitil		PPVCM based on 4',4''(5'')-di(<i>tert</i> -butyl)cyclohexano-18-crown-6 and $\text{Na}[\text{B}(\text{C}_{14}\text{H}_9\text{O}_2\text{F}_{12})_4]$	LR $1.0 \times 10^{-2} - 1.0 \times 10^{-5}$, DL = 3.0×10^{-6} , $S = 54 - 59$, pH 7.4 (buffer)	67
Antibiotics				
Ampicillin		PPVCM (NPOE) containing tris{[2-(2-diphenylphosphonylmethyl)phenoxy]ethyl}amine PPVCM (DMP) based on IA of MD anions with $[(n\text{-C}_{10}\text{H}_{21})_4\text{N}]^+$	LR $10^{-3} - 10^{-4}$, DL = 3.1×10^{-5} , $S = 58 \pm 1$ LR $n \times 10^{-1} - n \times 10^{-6}$, DL up to 6.3×10^{-6} , $S = 58 - 62$, pH 5.0–9.2	71 31
Penicillin G		the same PPVCM (NPOE) containing $[\text{Bu}_3(n\text{-C}_{16}\text{H}_{33})\text{P}]\text{Br}$ or $[(n\text{-C}_8\text{H}_{17})_3\text{MeN}]\text{Cl}$ ISFT (Ta_2O_5 substrate) with immobilised enzyme penicillinase (β -lactamase) microsensor for FIA based on $\text{Si}-\text{SiO}_2-\text{Ta}_2\text{O}_5$ PM (NPOE) based on PVC and ethyl vinyl ether and containing manganese(III) 5,10,15,20-tetraphenylporphyrinate and lipophilic additives	the same LR $1.0 \times 10^{-1} - 2.5 \times 10^{-5}$, DL = 1.0×10^{-5} , $S = 49 - 57$, pH 4.5–8.0 LR $1.0 \times 10^{-3} - 5 \times 10^{-5}$, DL = 5.0×10^{-6} , $S = 120 \pm 10$ LR $5.0 \times 10^{-3} - 1 \times 10^{-4}$, $S = 135$ LR $1.0 \times 10^{-1} - 2.0 \times 10^{-5}$, $S = 59 - 61$	31 71 306 307 296

Table 3 (continued).

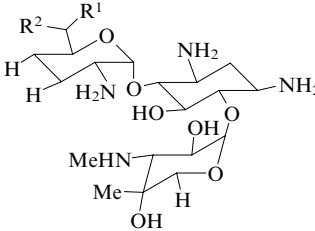
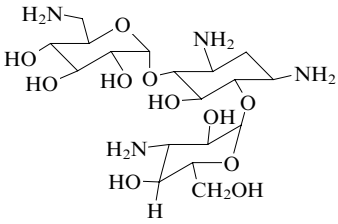
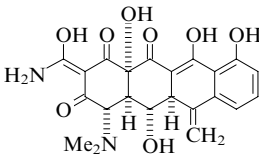
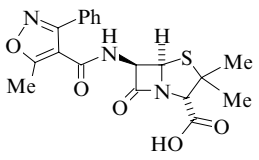
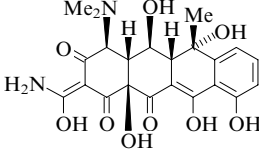
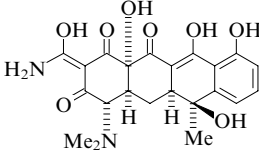
Medicinal drug	Formula	Membrane composition and electrode type ^a	Major electrode characteristics ^b	Ref.
Antibiotics				
Gentamycin	 <p> $R^1 = H, R^2 = NH_2$; $R^1 = Me; R^2 = NH_2, NHMe$ </p>	PPVCM (DBP) with IA of MD cations with BPh_4^-	LR $1.0 \times 10^{-1} - 1.0 \times 10^{-6}$, DL = 1.0×10^{-6} , $S = 26 \pm 2$, pH 5.5–6.0	169, 188
Kanamycin		the same	the same	169, 188
Metacycline		PPVCM (DOP) with IA of MD cations and BPh_4^-	LR $3.0 \times 10^{-2} - 6.0 \times 10^{-6}$, DL = 3.4×10^{-6} , $S = 52.9$, pH 2.6	195
Oxacillin		PPVCM (NPOE) containing copper tetra(<i>tert</i> -butyl)phthalocyaninate or $[Bu_3^0(n-C_{16}H_{33})P]Br$ PPVCM(DBP) with IA of MD anions with $[(n-C_{10}H_{21})N]^+$	LR $1.0 \times 10^{-1} - 2.0 \times 10^{-5}$, DL = 8.0×10^{-6} , $S = 57 \pm 2$, pH 4.5–8.0 LR $1.0 \times 10^{-2} - 3.2 \times 10^{-6}$, DL = 3.1×10^{-6} , $S = 65 \pm 3$, pH 5.0–6.0	71 31
Oxytetracycline		SC-ISE with PPVCM (DBP) with IA of the cationic form of MD with BPh_4^- , $[PMo_{12}O_{40}]^{3-}$ or $[PW_{12}O_{40}]^{3-}$	LR $n \times 10^{-2} - n \times 10^{-7}$, $S = 59 - 62$, DL up to 1.0×10^{-7} , pH 4.0–11.0	184, 185
Tetracycline		PM (NPOE or EHS) based on a mixture of PVC and ethylene–vinyl acetate co-polymer with addition of $K[B(C_6H_4Cl-4)_4]$	LR $1.0 \times 10^{-2} - 1.2 \times 10^{-4}$, $S = 57.4$, pH 2.0–3.8	223

Table 3 (continued).

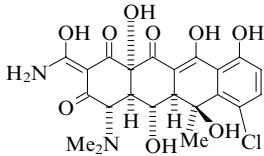
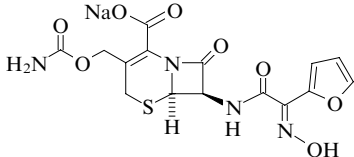
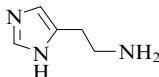
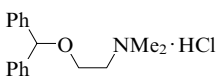
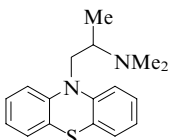
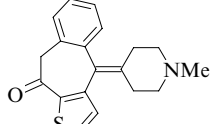
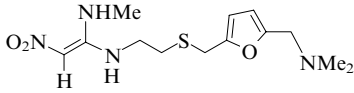
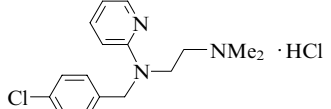
Medicinal drug	Formula	Membrane composition and electrode type ^a	Major electrode characteristics ^b	Ref.
Antibiotics				
Chlortetracycline		PPVCM based on IA of MD cations with $[\text{PMo}_{12}\text{O}_{40}]^{3-}$ and $[\text{PW}_{12}\text{O}_{40}]^{3-}$	LR $1.0 \times 10^{-2} - 1.0 \times 10^{-6}$, $S = 60 - 67$, pH 5.5–11.5	252
Cefuroxime		PPVCM (NPOE or EHS) (including those for FIA) with IA of MD anions with $[(n\text{-C}_8\text{H}_{17})_4\text{N}]^+$ and bis(triphenylphosphoranylidene)ammonium cations and addition of <i>p</i> -(<i>tert</i> -octyl)phenol	DL = 1.3×10^{-4} , $S = 50 - 55$, pH 3.5 ($\text{H}_3\text{PO}_4 - \text{NaH}_2\text{PO}_4$ buffer)	273
Antihistamine drugs				
Histamine		PPVCM with <i>O</i> -(2,4-dichlorophenyl) <i>O</i> -ethyl <i>S</i> -propyl dithiophosphate and $\text{Na}[\text{B}(\text{C}_{14}\text{H}_9\text{O}_2\text{F}_{12})_4]$ PPVCM (NPOE) with derivatives of calix[<i>n</i>]arenes ($n = 6, 8$) and $\text{K}[\text{B}(\text{C}_6\text{H}_4\text{Cl}_4)_4]$	LR $1.0 \times 10^{-2} - 5.0 \times 10^{-5}$, DL = 2.0×10^{-5} , $S = 56$ —	102 73
Diphenhydramine hydrochloride		PPVCM based on IA of MD cations with $[\text{PW}_{12}\text{O}_{40}]^{3-}$, BPh_4^- and $[\text{Cr}(\text{NH}_3)_2(\text{NCS})_4]^-$ SC-ISE with PPVCM (DOP) based on IA of MD with $\text{H}_3[\text{PMo}_{12}\text{O}_{40}]$ and $\text{H}_4[\text{SiW}_{12}\text{O}_{40}]$ and poly(α -naphthylamine) as the transducer	LR $n \times 10^{-2} - 3.5 \times 10^{-5}$, $S = 57.5$, pH 2.0–7.5 LR $1.0 \times 10^{-2} - 1.0 \times 10^{-5}$, DL = 3.0×10^{-6} , $S = 57.5$, pH 2–6	253 232
Promethazine		PPVCM (DOP) based on IA of MD cations with organic and inorganic anions PPVCM (NPOE or EHS) (including those for FIA) with IA of MD cations with BPh_4^-	LR $3.2 \times 10^{-2} - 1.0 \times 10^{-5}$, DL = 3.5×10^{-6} , $S = 41 - 55$, pH 2.5–6.0 LR $1.0 \times 10^{-2} - 5.0 \times 10^{-5}$, DL = 2.0×10^{-5} , pH 6.0 (phosphate buffer)	172 207
Ketotifen		PPVCM based of IA of MD cations with $[\text{B}\{\text{C}_6\text{H}_3(\text{CF}_3)_2-3,5\}_4]^-$	—	227
Ranitidine		Ag/AgCl SC-ISE with PPVCM (DNP) and IA of MD cations and BPh_4^-	LR $1.0 \times 10^{-1} - 5.0 \times 10^{-4}$, DL = 2.8×10^{-4} , $S = 59.7$, pH 8.2 (phosphate buffer)	192
Chloropyramine		PPVCM based on IA of MD cations with anions $[\text{B}(\text{C}_6\text{H}_4\text{Cl}_4)_4]^-$, $[\text{Cr}(\text{NH}_3)_2(\text{NCS})_4]^-$, $[\text{PW}_{12}\text{O}_{40}]^{3-}$, $[\text{PMo}_{12}\text{O}_{40}]^{3-}$ and $[\text{SiMo}_{12}\text{O}_{40}]^{4-}$	LR $1.0 \times 10^{-2} - 2.3 \times 10^{-5}$, DL = 1.1×10^{-5} , $S = 48 - 55$, pH 2.6–5.5	225, 246

Table 3 (continued).

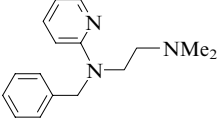
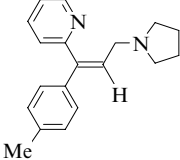
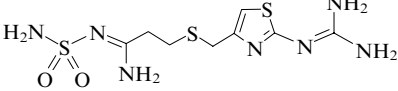
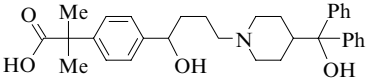
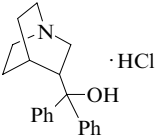
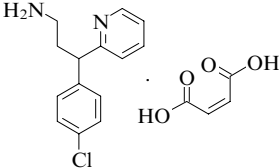
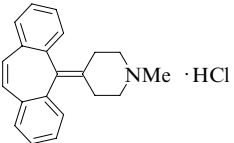
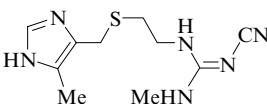
Medicinal drug	Formula	Membrane composition and electrode type ^a	Major electrode characteristics ^b	Ref.
Antihistamine drugs				
Tripelenamine		tubular and conventional ISE with PPVCM and IA of MD cations with BPh ₄ ⁻	LR $1.0 \times 10^{-1} - 4.0 \times 10^{-5}$	182
Triprolidine		membrane ISE, carbon-paste and graphite-supported electrodes; PPVCM (DBP) and IA of MD cations with BPh ₄ ⁻	LR $1.0 \times 10^{-2} - 2.0 \times 10^{-5}$, $S = 54 - 56$, pH 4.7–8.8	196
Famotidine		PPVCM based on IA of MD cations with BPh ₄ ⁻	LR $1.0 \times 10^{-3} - 1.0 \times 10^{-5}$, pH 1.0–5.0	178
Fexofenadine		PPVCM, IA of MD cations with BPh ₄ ⁻ , HgI ₄ ²⁻ and [Cr(NH ₃) ₂ (NCS) ₄] ⁻	LR $1.0 \times 10^{-2} - 2.5 \times 10^{-6}$, DL = 1.3×10^{-6} , $S = 62$, pH 2.0–4.5	197
Quifenadine		PPVCM based on IA of MD cations with [PW ₁₂ O ₄₀] ³⁻ , [PMO ₁₂ O ₄₀] ³⁻ and [SiMO ₁₂ O ₄₀] ⁴⁻	LR $1.0 \times 10^{-2} - 5.4 \times 10^{-5}$, DL = 3.6×10^{-5} , $S = 43 - 50$, pH 2.8–5.0	219
Chlorpheniramine maleate		ion-selective piezoelectric sensors with PVC membranes based on IA of MD cations with dipicrylamine, BiI ₄ ⁻ and BPh ₄ ⁻ AgCl/Ag SC-ISE with membranes based on carbamide-formaldehyde resin with dispersed KCl and IA of MD cations with BPh ₄ ⁻	LR $1.0 \times 10^{-3} - 1.0 \times 10^{-8}$, DL = 6.0×10^{-9} —	183 209
Cyproheptadine		PPVCM and IA of MD cations with [B(C ₆ H ₄ Cl-4) ₄] ⁻ and dipicrylamine anions	LR $n \times 10^{-2} - n \times 10^{-7}$, pH 2.5–7.0	222
Cimetidine		PPVCM based on IA of MD cations with [PW ₁₂ O ₄₀] ³⁻	LR $1.0 \times 10^{-2} - 1.0 \times 10^{-5}$, DL = 5.0×10^{-6} , $S = 58$, pH 3.0–5.5	247

Table 3 (continued).

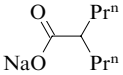
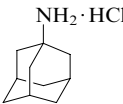
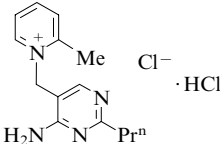
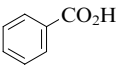
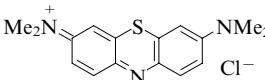
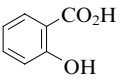
Medicinal drug	Formula	Membrane composition and electrode type ^a	Major electrode characteristics ^b	Ref.
Anticonvulsants				
Sodium valproate		PPVCM based on a Ga(III) complex with tetraphenylporphyrine and bis(1-butylpentyl)decane-1,10-diyl diglutarate (ETH 469)	LR $1.0 \times 10^{-2} - 5.0 \times 10^{-5}$, DL = 2.0×10^{-5} , $S = 55$, pH 5.5 (buffer)	64
Antiseptics and viricides				
Amantadine		PPVCM (DOP) based on IA of MD cations with BPh ₄ ⁻ and [Cr(NH ₃) ₂ (NCS) ₄] ⁻	—	173
Amprolium		PPVCM (DOP) based on IA of MD cations with BPh ₄ ⁻ and [Cr(NH ₃) ₂ (NCS) ₄] ⁻	LR $1.0 \times 10^{-1} - 1.0 \times 10^{-5}$, pH 7.0–11.0	216
Benzoic acid		PPVCM with a macrocyclic polyamine and a lipophilic additive PPVCM based on heptyl 4-(trifluoroacetyl)benzoate	LR $1.0 \times 10^{-2} - 1.0 \times 10^{-4}$, DL = 1.0×10^{-4} , pH 5.0 LR $5.0 \times 10^{-2} - 2.0 \times 10^{-4}$, DL = 1.0×10^{-4}	58 308
Methylene Blue		PM (DBP) with trioctyloxybenzenesulfonic acid as an ion exchanger	LR $1 \times 10^{-4} - 1.0 \times 10^{-6}$, DL = 6.2×10^{-7} , $S = 53.3 \pm 0.5$, pH 4.0–11.0	293
Salicylic acid		ISE based on complexes of Co(II) with bis(salicylaldehyde)diaminodipropylamine or Co(III) with Schiff bases as the carriers PPVCM based on IA of 3-(4-tolylazo)phenylboronic acid with tetrahexylethylenediamine PM based on Sn(IV) complexes with 8-hydroxyquinoline and tetra(<i>tert</i> -butyl)phthalocyanine PPVCM with μ -oxobis[5-(4-hydroxyphenyl)-10,15,20-triphenylporphyrinato]-manganese(III)] as the ionophore PPVCM with tribenzyltin phenolates or carboxylates as ionophores PPVCM (NPOE) with a guanidinium ionophore PPVCM with different metallocenes as ionophores PPVCM (dinonyl sebacate) with [2,9,16,23-tetra(<i>tert</i> -butyl)phthalocyaninato]tin(IV) and addition of KBPh ₄ PPVCM with heptyl 4-(trifluoroacetyl)benzoate as the ionophore and addition of tri(dodecyl)methylammonium chloride PPVCM (DBP) with a neutral carrier SCE (graphite substrate), PPVCM containing Al(III) and Sn(IV) complexes with Salophen as ionophores with addition of NaBPh ₄	LR $1.0 \times 10^{-1} - n \times 10^{-6}$, DL up to 8.0×10^{-7} , $S = 66.8$, pH 4.0 or 5.5 LR $1.0 \times 10^{-1} - 5.0 \times 10^{-5}$, DL = 1.5×10^{-5} , $S = 54 \pm 1$ — LR $1.0 \times 10^{-1} - 6.3 \times 10^{-7}$, $S = 57 \pm 3.5$, pH 6.0 (phosphate buffer) LR $1.0 \times 10^{-1} - n \times 10^{-6}$, DL up to 1.0×10^{-6} , $S = 57$, pH = 5.5 (phosphate buffer) LR $1.0 \times 10^{-1} - 1.0 \times 10^{-3}$, DL = 1.3×10^{-4} , pH 6.0 LR $1.0 \times 10^{-1} - 1.0 \times 10^{-3}$, $S = 58$, pH 5.5; 7.4 LR $1.0 \times 10^{-1} - 1.0 \times 10^{-5}$, DL = 6.3×10^{-6} , pH 5.5 LR $1.0 \times 10^{-2} - 2.0 \times 10^{-4}$, DL = 4.0×10^{-5} , $S = 55$, pH 7.4 LR $1.0 \times 10^{-1} - 2.5 \times 10^{-6}$, DL = 1.0×10^{-6} , $S = 57 \pm 2$, pH 5.0 LR $1.0 \times 10^{-1} - 1.0 \times 10^{-6}$, DL $\sim 1.0 \times 10^{-6}$, $S = 57 - 59$, pH 3.0–8.0	96, 309 94 85 63 92, 93 104 91 86 103 105 106

Table 3 (continued).

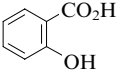
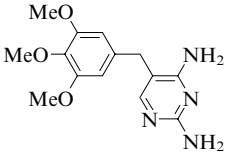
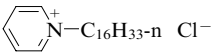
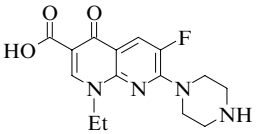
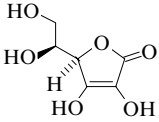
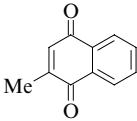
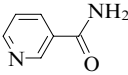
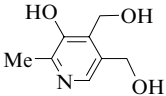
Medicinal drug	Formula	Membrane composition and electrode type ^a	Major electrode characteristics ^b	Ref.
Antiseptics and viricides				
Salicylic acid		PPVCM with chloro(tetraphenylporphyrinato)chromium(III) PPVCM with oxo(phthalocyaninato)vanadium(IV) and -molybdenum(IV) as ionophores SCE (graphite substrate), PPVCM with aluminium phthalocyaninate	LR $n \times 10^{-1} - n \times 10^{-6}$, pH 3.0–9.0 LR $n \times 10^{-1} - n \times 10^{-7}$, pH 6.0–9.0 LR $1.0 \times 10^{-1} - 5.0 \times 10^{-6}$, $S = 59 \pm 1$	65 87 90
Trimethoprim		PPVCM with IA of MD cations with $[\text{PMo}_{12}\text{O}_{40}]^{3-}$ ion-selective piezoelectric sensor with PPVCM (DBP) based on IA of MD cations with $[\text{PW}_{12}\text{O}_{40}]^{3-}$ PPVCM (DOP) with IA of MD cations with BPh_4^- , $[\text{Cr}(\text{NH}_3)_2(\text{NCS})_4]^-$ or $[\text{PW}_{12}\text{O}_{40}]^{3-}$	LR $1.0 \times 10^{-2} - 2.3 \times 10^{-6}$, $S = 56.5$, pH 1.6–6.2 LR $2.0 \times 10^{-3} - 2.0 \times 10^{-8}$, DL = 2.0×10^{-8} , pH 4.0 LR $1.0 \times 10^{-2} - n \times 10^{-6}$, DL = $n \times 10^{-6}$, $S = 57 - 59$, pH 1.8–6.3	237 254 201, 256
Cetylpyridinium chloride		PPVCM (DOP) with IA of cetylpyridinium with iron(III) thiocyanate PPVCM (DOP) with IA of MD cations with HgI_4^{2-}	LR $1.0 \times 10^{-3} - 1.0 \times 10^{-6}$, DL = 8.0×10^{-7} , $S = 57.5 \pm 0.4$, pH 1.0–6.0 LR $1.0 \times 10^{-3} - 2.0 \times 10^{-6}$, DL = 4.0×10^{-7} , $S = 29.0 \pm 0.4$, pH 3.0–6.0	294 291
Enoxacin		PPVCM with IA of MD cations with BPh_4^- and an internal pin Ag/AgCl reference electrode	LR $1.0 \times 10^{-2} - 7.9 \times 10^{-5}$, DL = 2.0×10^{-5} , $S = 30.4$	176
Vitamins and their analogues				
Ascorbic acid		SC-ISE based on a PVC matrix modified with ionophores. A polymeric ISFT film based on MnO_2 nanoparticles immobilised on the transducer surface is fixed between the electrode and the PVC membrane ISE with liquid membrane based on 2-nitrotoluene with dissolved IA of triphenyltetrazolium with $[\text{PW}_{12}\text{O}_{40}]^{3-}$	LR $5.0 \times 10^{-3} - 5.0 \times 10^{-6}$, DL = 2.0×10^{-6} LR $1.3 \times 10^{-3} - 2.0 \times 10^{-5}$, DL = 1.0×10^{-5} LR $1.0 \times 10^{-2} - 2.0 \times 10^{-4}$, $S = 56 - 58$, pH 3.0–12.0	310 167 100
Menadione		PPVCM (NPOE) with IA of MD anions with complex cations of nickel(II) or iron(II) with batophenanthroline	LR $1.0 \times 10^{-1} - n \times 10^{-5}$, DL = 2.0×10^{-5} , $S = 51 - 58$, pH 1.0–5.0	270
Nicotinamide		ion-selective piezoelectric sensor with PVC membrane based on IA of MD cations with $[\text{SiW}_{12}\text{O}_{40}]^{4-}$	LR $1.0 \times 10^{-3} - 1.0 \times 10^{-9}$, pH 7.0	264
Pyridoxine		PPVCM (NPOE) with IA of MD cations with $[\text{PMo}_{12}\text{O}_{40}]^{3-}$ or $[\text{PW}_{12}\text{O}_{40}]^{3-}$	LR $1.0 \times 10^{-2} - 6.0 \times 10^{-5}$, DL = 4.0×10^{-5} , $S = 54$, pH 2–4	233, 234

Table 3 (continued).

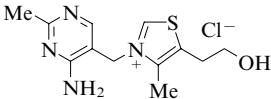
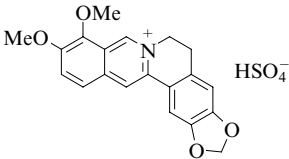
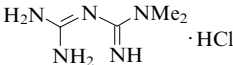
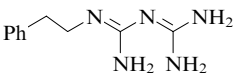
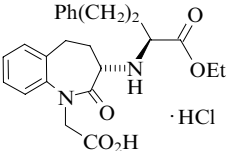
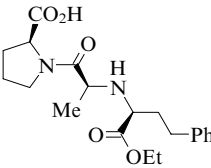
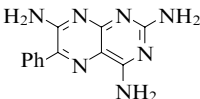
Medicinal drug	Formula	Membrane composition and electrode type ^a	Major electrode characteristics ^b	Ref.
Vitamins and their analogues				
Thiamine chloride		electrode represents a graphite disk covered with successive layers of conductive epoxy resin and ionophore-containing PVC membrane	LR $1.0 \times 10^{-1} - 1.0 \times 10^{-6}$	311
Choline chloride	$\text{Me}_3\text{N}^+\text{CH}_2\text{CH}_2\text{OH} \text{ Cl}^-$	PPVCM (NPOE) with lipophilic β -CD derivatives and addition of $\text{Na}[\text{B}\{\text{C}_6\text{H}_3(\text{CF}_3)_2\text{-3,5}\}_4]$	DL up to 4.0×10^{-7} , $S = 61$, pH 7.0	80–82
Hepatotropic drugs				
Berberine bisulfate		PPVCM (different esters) based on porphyrins	LR $5.0 \times 10^{-3} - n \times 10^{-7}$, $S = 60 - 66$, pH 3.7–11.2	61, 62
Hypoglycemic drugs				
Metformin		PPVCM with IA of MD cations with $[\text{PMo}_{12}\text{O}_{40}]^{3-}$ or $[\text{PW}_{12}\text{O}_{40}]^{3-}$ PPVCM (DOP, NPOE or DBS) with IA of MD cations with $[\text{Cr}(\text{NH}_3)_2(\text{NCS})_4]^-$ and $[\text{SiW}_{12}\text{O}_{40}]^{4-}$ PPVCM (NPOE) with lipophilic β -CD derivative and addition of $\text{Na}[\text{B}\{\text{C}_6\text{H}_3(\text{CF}_3)_2\text{-3,5}\}_4]$	LR $1.0 \times 10^{-2} - n \times 10^{-5}$, $S = 58$, pH 3.0–11.0 LR $n \times 10^{-1} - n \times 10^{-5}$, pH 5.0–11.0 DL = $n \times 10^{-6}$, $S = 56 - 61$	236, 251 266 80, 81
Phenformin		the same	the same	80, 81
Hypotensive drugs				
Benazepril hydrochloride (Amlodipine)		'coated wire' electrode with PVC membrane based on benazepril– BPh_4^- associate	LR $5.8 \times 10^{-3} - 1.3 \times 10^{-5}$, pH 2.5–9.2	217
Sodium nitroprusside	$\text{Na}_2[\text{Fe}(\text{CN})_5\text{NO}]$	PPVCM with IA of MD anions with cetylpyridinium	LR $1.0 \times 10^{-2} - 3.0 \times 10^{-5}$, DL = 2.0×10^{-5} , $S = 27 \pm 1$, pH 2.0–10.0	281
Enalapril		ISE based on graphite paste (a mixture of graphite powder with kerosene) impregnated with a solution of 2-hydroxy-3-trimethylammonioethyl- β -CD chloride	LR $6.4 \times 10^{-2} - 3.6 \times 10^{-5}$, DL = 1.0×10^{-5} , $S = 55 \pm 0.3$, pH 3.0–6.0	77
Diuretics				
Triamterene		'coated wire' electrode with PVC membrane and IA of MD cations with BPh_4^-	LR $3.5 \times 10^{-2} - 1.0 \times 10^{-6}$, pH 4.5–7.5	179

Table 3 (continued).

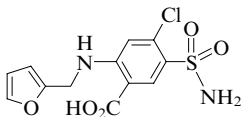
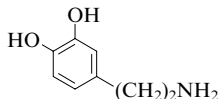
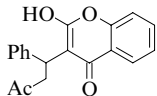
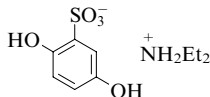
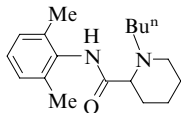
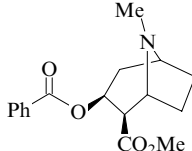
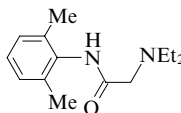
Medicinal drug	Formula	Membrane composition and electrode type ^a	Major electrode characteristics ^b	Ref.
Diuretics				
Furosemide		PPVCM (DBP or DOPP) with IA of MD anions with trioctylmethylammonium	LR $1.0 \times 10^{-2} - 1.6 \times 10^{-4}$, DL = 1.2×10^{-4} , $S = 58.9$, pH 7–10	277
Dopaminergic drugs				
Dopamine		Graphite-based SC-sensor with a membrane of carboxylated PVC with addition of β -CD, $K[B(C_6H_4Cl-4)_4]$ and 2-nitro-2'-fluorodiphenyl ether electrode for FIA, PPVCM (NPOE) with bis(triphenylphosphoranylidene)-ammonium periodate	LR $1.0 \times 10^{-1} - 5.0 \times 10^{-5}$, DL = 3.0×10^{-6} , $S = 59$, pH 2.0–7.5	76
		PPVCM (NPOE) with devivatives of calix[n]arenes ($n = 6, 8$) and addition of $K[B(C_6H_4Cl-4)_4]$	LR $2.7 \times 10^{-1} - 8.0 \times 10^{-3}$ g litre ⁻¹ , $S = 310.1 \pm 7.4$	283
			—	73
Coagulants and anticoagulants				
Warfarin		PPVCM with IA of MD anions and complex cations of Ni(II) and Fe(II) with phenanthroline	LR $n \times 10^{-1} - n \times 10^{-5}$, DL = 0.8–5.3 $\mu\text{g ml}^{-1}$, $S = 51 - 60$	268, 271
Etamsylate (Dicinone)		the same	the same	268, 271
Local anesthetics				
Bupivacaine		PVC or polyurethane membranes (NPOE) with lipophilic derivatives of β -CD and addition of $Na[B\{C_6H_3(CF_3)_2-3,5\}_4]$	LR $1.0 \times 10^{-2} - 1.0 \times 10^{-4}$, DL = 1.3×10^{-5} , $S = 54 - 62$, pH 6.84	79
Cocaine		PPVCM [tetrakis(2-ethylhexyl) pyromellitate] with IA of MD cations with $[B\{C_6H_3(CF_3)_2-3,5\}_4]^-$	LR $1.0 \times 10^{-2} - 1.0 \times 10^{-6}$, DL = 4.0×10^{-7} , $S = 56$, pH 1.0–8.0	192
Lidocaine		PPVCM (NPOE or DOS) modified with 2,6-disdodecyl- β -CD and $K[B(C_6H_4Cl-4)_4]$ (for FIA)	LR $1.0 \times 10^{-1} - n \times 10^{-5}$, DL = 1.6×10^{-5} , $S = 55$	224
		PVC or polyurethane membranes (NPOE) with lipophilic derivatives of β -CD and addition of $Na[B\{C_6H_3(CF_3)_2-3,5\}_4]$	LR $1.0 \times 10^{-1} - 1.0 \times 10^{-3}$, DL up to 1.5×10^{-4} , $S = 61 - 67$, pH 6.84	79
		PPVCM based in IA of MD cations with $[Co(SCN)_4]^{2-}$, $[PMo_{12}O_{40}]^{3-}$ and $[Cr(NH_3)_2(NCS)_4]^-$	LR $1.0 \times 10^{-1} - 1.0 \times 10^{-5}$, pH 3.0–7.0	242

Table 3 (continued).

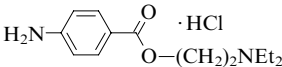
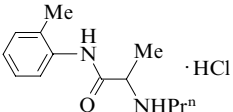
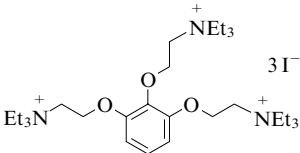
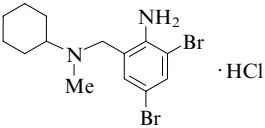
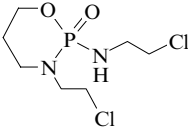
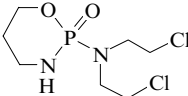
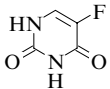
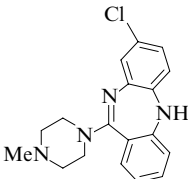
Medicinal drug	Formula	Membrane composition and electrode type ^a	Major electrode characteristics ^b	Ref.
Local anesthetics				
Procaine		piezoelectric sensor with selective PVC membrane based on IA of MD cations with BPh ₄ ⁻ PPVCM (NPOE) with lipophilic derivatives of β-CD and addition of Na[B{C ₆ H ₃ (CF ₃) ₂ -3,5 ₂ }] ₄	LR 5.0×10^{-3} – 8.3×10^{-8} , DL = 8.3×10^{-8} , pH 5.0 DL up to 1.0×10^{-5} , <i>S</i> = 61, pH 6.84	203 79
Prilocaine		the same	the same	79
Muscle relaxants				
Gallamine		carbon-paste electrode impregnated with IA gallamine–BPh ₄ ⁻	LR 1.0×10^{-3} – 2.0×10^{-6} , DL = 1.0×10^{-6} , <i>S</i> = 17.0 ± 0.7 , pH 5.0–8.0	219
Mucolytic drugs				
Bromhexine		PPVCM (DOP) with IA of MD cations with BPh ₄ ⁻	LR 1.0×10^{-1} – 4.0×10^{-4} , <i>S</i> = 57.5	218
Antitumour drugs				
Iphosphamide		PPVCM (DOP) or a membrane based on carboxylated PVC (NPOE) with IA of MD cations with BPh ₄ ⁻	LR $n \times 10^{-2}$ – $n \times 10^{-5}$, <i>S</i> = 50–55, pH 4–7	174
Cyclophosphan		the same	the same	174
Fluorouracil		PPVCM (DOP) based on IA of 5-fluorouracil with Ni(II) and Fe(II) complexes with batophenanthroline and Fe(II) complexes with phenanthroline	LR 1.0×10^{-3} – 1.0×10^{-5} , DL = 1.0×10^{-5} , <i>S</i> = 28–34, pH 5–9	267
Psychotropic drugs				
Azaleptine		PPVCM (DOP or TTP) with IA of azaleptine cations with BPh ₄ ⁻ or [PMO ₁₂ O ₄₀] ³⁻	LR 1.0×10^{-2} – 1.0×10^{-5} , DL = 2.8×10^{-6} , <i>S</i> = 45–54, pH 4.0–7.0	230

Table 3 (continued).

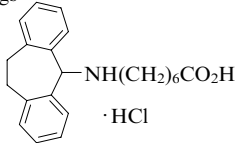
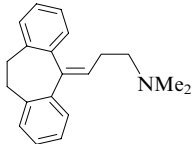
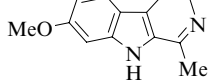
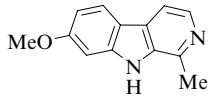
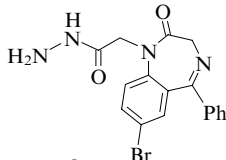
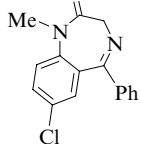
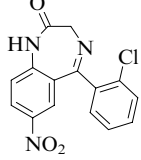
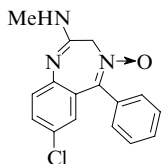
Medicinal drug	Formula	Membrane composition and electrode type ^a	Major electrode characteristics ^b	Ref.
Psychotropic drugs				
Amineptine		PPVCM (DOP or TTP) with IA of azaleptine cations with BPh ₄ [−] or [PMo ₁₂ O ₄₀] ^{3−}	LR $1.0 \times 10^{-2} - 3.2 \times 10^{-6}$, $S = 54 - 58$, pH 2.0–3.9	165
Amitriptyline		PPVCM with IA clonidine–BPh ₄ [−] against 10 ^{−3} M solution of NaCl and 10 ^{−3} M solution of clonidine	LR $1.0 \times 10^{-3} - 1.0 \times 10^{-8}$, DL = 5×10^{-9} , $S = 58.4$	166
Garmaline		sensors for FIA with PPVCM based on IA of MD cations with BPh ₄ [−] and [Cr(NH ₃) ₂ (NCS) ₄] [−]	LR 10 ^{−2} –10 ^{−6} , DL up to 2 μg ml ^{−1} , pH 3.0–8.0	210
Garmin		the same	the same	210
Hydazepam		PPVCM (DBP) with IA of MD cations with heteropolyanions and [C ₆ H ₄ Cl-4) ₄] [−] and addition of a lipophilic compound	LR $n \times 10^{-3} - n \times 10^{-5}$, DL up to 4.8×10^{-6} , $S = 50 - 57$, pH 2.5–5.3	170
Diazepam (Relanium)		the same PPVCM (NPOE) based on IA of MD cations with BPh ₄ [−] and [PW ₁₂ O ₄₀] ^{3−}	the same LR 31.57–0.29 mg ml ^{−1} , DL up to 0.7 mg ml ^{−1} , $S = 50 - 65$, pH 4.0–7.0	170 171, 208
Clonazepam		the same PPVCM (DBP) with IA of MD cations with hereropolyanions and [C ₆ H ₄ Cl-4) ₄] [−] and addition of a lipophilic compound	the same LR $n \times 10^{-3} - n \times 10^{-6}$, DL up to 6.6×10^{-7} , $S = 48 - 60$, pH 2.5–5.3	171, 208 170
Chlordiazepoxide (Elenium)		the same SC-ISE (DOP) with ion-selective transducer [poly(<i>o</i> -aminophenol)] and IA of MD cations with [PW ₁₂ O ₄₀] ^{3−} SC-ISE (DBP) with IA of MD cations with [PMo ₁₂ O ₄₀] ^{3−} and [PW ₁₂ O ₄₀] ^{3−}	the same DL = 6.7×10^{-6} , $S = 55.6$, pH 2.4–6.3 LR $1.0 \times 10^{-2} - 3.2 \times 10^{-6}$, $S = 59 - 61$, pH 2.0–4.5	170 259 244

Table 3 (continued).

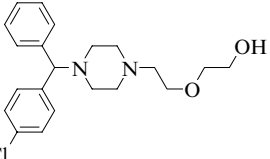
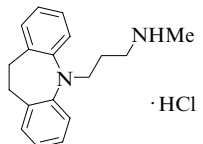
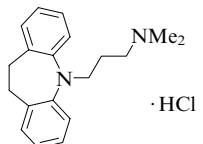
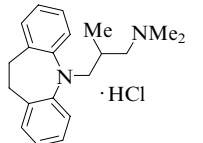
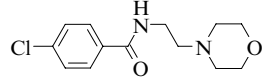
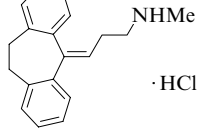
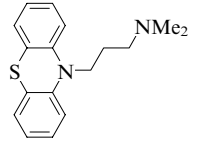
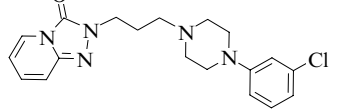
Medicinal drug	Formula	Membrane composition and electrode type ^a	Major electrode characteristics ^b	Ref.
Psychotropic drugs				
Hydroxyzine		PPVCM (NPOE) with IA of MD cations with $[\text{SiW}_{12}\text{O}_{40}]^{4-}$	LR $1.0 \times 10^{-2} - 6.0 \times 10^{-7}$, DL = 2.5×10^{-7} , $S = 57$, pH 2.8–6.9	263
Desipramine	 ·HCl	PPVCM (NPOE) with alkylated CD and addition of $\text{Na}[\text{B}\{\text{C}_6\text{H}_3(\text{CF}_3)_2-3,5\}_4]$	DL up to 2.5×10^{-6} , $S = 56 - 62$, pH 7.0	78
Imipramine	 ·HCl	the same	the same	78
Trimipramine	 ·HCl	the same	the same	78
Moclobemide		PPVCM with IA of MD cations with dodecyl sulfate	LR $10^{-2} - 10^{-5}$, DL = 1.1×10^{-10} , pH 2.0–6.5	289
Nortriptyline	 ·HCl	PPVCM (DOP) with IA of MD cations with BPh_4^- and $[\text{B}(\text{C}_6\text{H}_4\text{Cl}-4)_4]^-$	LR $n \times 10^{-2} - n \times 10^{-5}$, DL = $(8.0 - 9.0) \times 10^{-5}$, $S = 52 - 54$, pH 6.0–7.0	191
Promazine		ISE with liquid membrane based on IA of MD cations with CdI_4^{2-} in n-octanol PPVCM (EHS) with IA of MD cations with BPh_4^-	LR $1.0 \times 10^{-3} - 5.0 \times 10^{-6}$, $S = 61$, pH 4.0–7.0 LR $1.0 \times 10^{-2} - 1.0 \times 10^{-5}$, DL = 1.0×10^{-5} , $S = 58.0 \pm 1.5$, pH 2.0–6.0	292 205
Trazodone		'coated wire' electrode (Cu) based on PPVCM (DOP) with IA trazodone– BPh_4^-	LR $8.9 \times 10^{-3} - 1.4 \times 10^{-5}$, DL = 1.0×10^{-5} , $S = 59$, pH 2.4–9.0	193

Table 3 (continued).

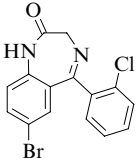
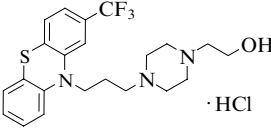
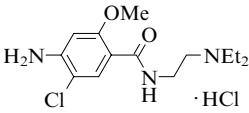
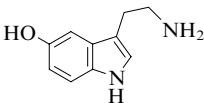
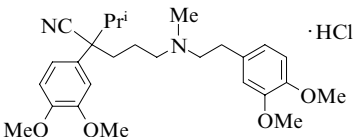
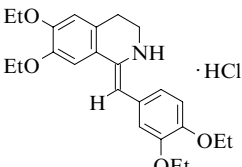
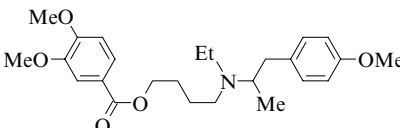
Medicinal drug	Formula	Membrane composition and electrode type ^a	Major electrode characteristics ^b	Ref.
Psychotropic drugs				
Phenazepam		PPVCM (DBP or DOP) with IA of MD cations with $[\text{PMo}_{12}\text{O}_{40}]^{3-}$, $[\text{PW}_{12}\text{O}_{40}]^{3-}$ and $[\text{SiMo}_{12}\text{O}_{40}]^{4-}$	LR $1.0 \times 10^{-2} - 1.0 \times 10^{-5}$, $S = 43 - 54$, pH 1.0–3.0	239
Fluphenazine		PPVCM (DOP) with IA of MD cations with BPh_4^- and addition of $\text{K}[\text{B}(\text{C}_6\text{H}_4\text{Cl}-4)_4]$	LR $n \times 10^{-3} - n \times 10^{-5}$, $\text{DL} = (4.5 - 5.5) \times 10^{-5}$, $S = 59$, pH 6–7	191
Antiemetic drugs				
Metoclopramide		PPVCM (DOP) based on IA of MD cations with HgI_4^{2-} or $[\text{PW}_{12}\text{O}_{40}]^{3-}$	LR $1 \times 10^{-2} - 6.0 \times 10^{-5}$, $\text{DL} = 4.0 \times 10^{-5}$, $S = 53 \pm 0.5$, pH 3.0–7.0	258, 290
Serotonergic drugs				
Serotonin		PPVCM (NPOE) with derivatives of calix[n]arenes ($n = 6, 8$) and addition of $\text{K}[\text{B}(\text{C}_6\text{H}_4\text{Cl}-4)_4]$	—	73
Spasmolytics				
Verapamil		microsensor based carboxylated PVC and Nafion on a graphite substrate	LR $1.0 \times 10^{-2} - 1.0 \times 10^{-5}$, $\text{DL} = 4.1 \times 10^{-6}$, $S = 56 - 57$, pH 2.0–8.0	297
Drotaverine (No Spa)				
Drotaverine (No Spa)		PPVCM based on IA of MD cations with derivatives of tetraphenylborate and organic and inorganic anions	LR $5.0 \times 10^{-2} - n \times 10^{-7}$, DL up to 1×10^{-7} , $S = 51 - 61$, pH 1.8–7.0	32, 37
		carbon-paste electrode for FIA with PPVCM (esters of phthalic acid and TTP) containing IA of MD cations with $[\text{SiW}_{12}\text{O}_{40}]^{4-}$ and BPh_4^-	LR $1.0 \times 10^{-2} - 5.0 \times 10^{-7}$, $\text{DL} = 5.0 \times 10^{-7}$, $S = 59 \pm 2$, pH 2.5–7.0	202
Mebeverine		SC-ISE (for FIA) and ISE with PM (DBP) based on IA of MD cations with heteropolyanions	LR $1.0 \times 10^{-2} - 4.0 \times 10^{-6}$, $\text{DL} = 3.1 \times 10^{-6}$, $S = 55 - 59$, pH 1.0–7.2	36

Table 3 (continued).

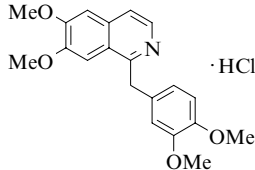
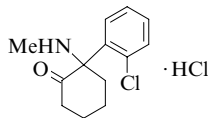
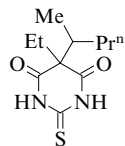
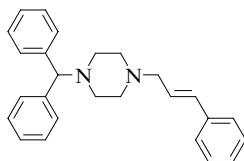
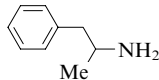
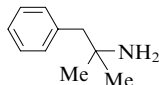
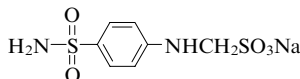
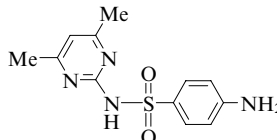
Medicinal drug	Formula	Membrane composition and electrode type ^a	Major electrode characteristics ^b	Ref.
Spasmolytics				
Papaverine		ISE with liquid membrane (chlorobenzene) based on IA of MD cations with BPh ₄ [−] PPVCM based on IA of MD cations with organic and inorganic anions	LR $5.0 \times 10^{-2} - 1.0 \times 10^{-5}$, $S = 62.6$, pH 3.5–5.5 LR $5.0 \times 10^{-2} - 1.0 \times 10^{-5}$, DL = 3.7×10^{-6} , $S = 42 - 56$, pH 2.0–6.0	181 34
Anaesthetics				
Ketamine hydrochloride		membrane with active ion-exchange sites synthesised by polymerisation directly in the plasticiser medium (NPOE)	LR $1.0 \times 10^{-2} - 1.0 \times 10^{-5}$, DL = 1.0×10^{-6} , $S = 59$, pH 4.0–8.5	35
Thiopental		graphite SC sensor with polyurethane membrane based on IA of thiopental with complexes of Co(II) and Cu(II) with batophenanthroline	LR $1.0 \times 10^{-1} - 5.0 \times 10^{-5}$, DL = 5.0×10^{-6} , $S = 28$, pH 6–11	269
Drugs for improving blood circulation of internal organs and tissues				
Cinnarizine		PPVCM (DOP) with IA of MD cations with BPh ₄ [−] , flavianate, [Cr(NH ₃) ₂ (NCS) ₄] [−] and [PMo ₁₂ O ₄₀] ^{3−}	LR $n \times 10^{-2} - n \times 10^{-6}$, DL = $(1.1 - 8.1) \times 10^{-6}$, $S = 27.1 - 38.2$, pH 2.0–3.3	198
Stimulators of central nervous system				
Amphetamine		PPVCM (EHS) based on neutral carriers	LR $1.0 \times 10^{-2} - 2.0 \times 10^{-6}$, DL = 7.0×10^{-7} , $S = 53 - 55$, pH 5.0	68
		PPVCM with an <i>N,N</i> -dioctadecyl- <i>N',N'</i> -dipropyl-3,6-dioxaoctanediamide ionophore and addition of Na[B(C ₁₄ H ₉ O ₂ F ₁₂) ₄]	LR $1.0 \times 10^{-2} - 2.0 \times 10^{-6}$, DL = 1.0×10^{-6} , $S = 59$, pH 5.0	69
Phentermine		PPVCM (EHS) based on dibenzo-18-crown-6 and other ionophores with addition of K[B(C ₆ H ₄ Cl-4) ₄]	LR $1.0 \times 10^{-2} - 2.0 \times 10^{-6}$, DL = 7.0×10^{-7} , $S = 53 - 55$, pH 5.0 (acetic acid – magnesium acetate buffer)	68
Sulfonamides				
Streptocidum soluble		PPVCM with IA of MD anions with different QAB cations	LR $1.0 \times 10^{-1} - 1.0 \times 10^{-5}$, DL up to 7.4×10^{-6} , $S = 42 - 57$, pH 7.0–11.0	29, 275, 276
Sulfamethazine		the same	the same	29, 275, 276

Table 3 (continued).

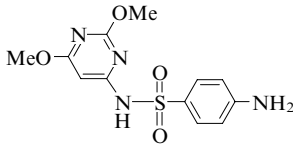
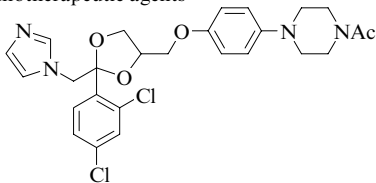
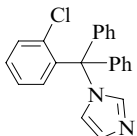
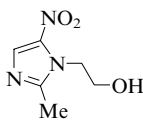
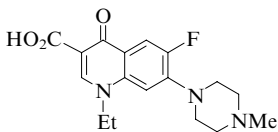
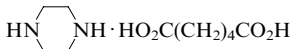
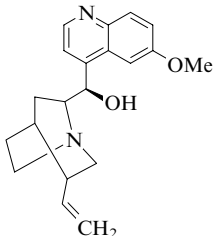
Medicinal drug	Formula	Membrane composition and electrode type ^a	Major electrode characteristics ^b	Ref.
Sulfonamides				
Sulfadimethoxine		PPVCM with IA of MD cations with different QAB cations	LR $1.0 \times 10^{-1} - 1.0 \times 10^{-5}$, DL up to 7.4×10^{-6} , $S = 42 - 57$, pH 7.0–11.0	29, 275, 276
Miscellaneous chemotherapeutic agents				
Ketoconazole		PPVCM (NPOE) based on IA of MD cations with BPh_4^- or $[\text{PMo}_{12}\text{O}_{40}]^{3-}$	LR $6.3 \times 10^{-3} - 7.1 \times 10^{-6}$, DL = 5.0×10^{-6} , $S = 72 \pm 2$, pH 3.0–5.0	180
Clotrimazole		the same	LR $1.0 \times 10^{-3} - 1.4 \times 10^{-5}$, DL = 1.0×10^{-5} , $S = 59 \pm 2$, pH 1.5–2.5	189
Metronidazole		PVC membrane with Mn(III) complex with 5,10,15,20-tetrakis[2-(2,3,4,6-tetra- <i>O</i> -acetyl-β-D-glucopyranosyloxy)phenyl]porphyrin and with addition of graphite powder and epoxy resin	LR $2.9 \times 10^{-3} - 5.8 \times 10^{-8}$, DL = 5.8×10^{-8} , $S = 25 - 28$, pH 4.3	312
Perfloxacin		PPVCM with IA of MD cations with BPh_4^-	LR $1.0 \times 10^{-2} - 5.0 \times 10^{-5}$, $S = 23$	200
Piperazine adipate		PPVCM (DOP) based on IA of MD cations with heteropolyanions	LR $1.0 \times 10^{-1} - 1.0 \times 10^{-4}$, DL = 3.2×10^{-5} , $S = 35$, pH 3–8	240
Quinine		PPVCM based on lipophilic derivatives of tetraphenylborate	LR $1.0 \times 10^{-2} - 6.3 \times 10^{-6}$, DL = 2.5×10^{-6} , $S = 52 - 59$, pH 4.4–8.0	312

Table 3 (continued).

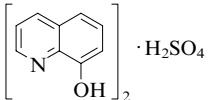
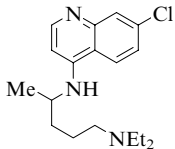
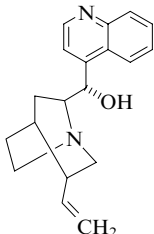
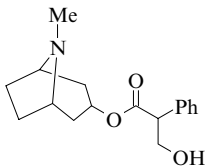
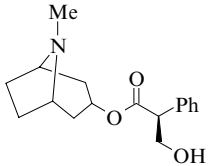
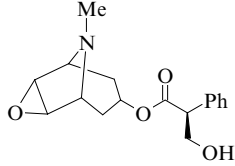
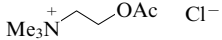
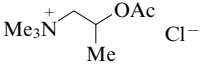
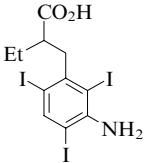
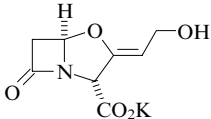
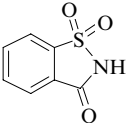
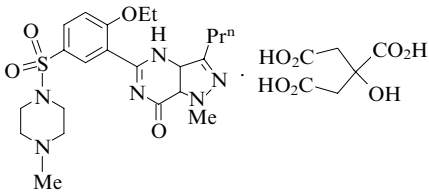
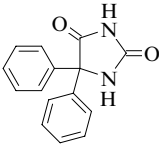
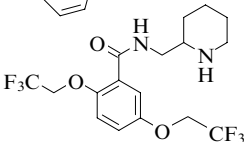
Medicinal drug	Formula	Membrane composition and electrode type ^a	Major electrode characteristics ^b	Ref.
Miscellaneous chemotherapeutic agents				
Oxine		SC-ISE (graphite substrate) with PPVCM (DOP) and IA of MD cations with BPh ₄ [−]	LR $1.0 \times 10^{-1} - 1.0 \times 10^{-6}$, DL = 4.0×10^{-7} , $S = 59.0 \pm 0.5$, pH 1.8–4.7	190
Chloroquine (Lariam)		PPVCM with IA of MD cations with [B(C ₆ H ₄ Cl-4) ₄] [−] (ISE for FIA)	DL up to 5.0×10^{-7} , $S = 28 - 32$	226
Cinchonine		IA cinchonine–picrolonate in an electropolymerised <i>o</i> -phenylenediamine film on the gold electrode surface	LR $1.3 \times 10^{-5} - 2.5 \times 10^{-7}$, DL = 1.0×10^{-7} , pH 7.0	288
Anticholinergic drugs				
Atropine		ion-selective piezoelectric microquartz sensor based on PVC membrane with IA atropine–BPh ₄ [−] and atropine–dipicrylamine anion	LR $1.0 \times 10^{-3} - 1.0 \times 10^{-8}$, DL = 5.0×10^{-9} , pH 3.0–8.0	168
Hyoscyamine		ISE and FIA sensors with PPVCM based on IA of MD cations with BPh ₄ [−] and [PW ₁₂ O ₄₀] ^{3−}	LR $1.3 \times 10^{-2} - 1.0 \times 10^{-5}$, DL = 3.9×10^{-6} , $S = 56.5 - 57.8$, pH 3.0–10.0	255
Scopolamine		PPVCM with IA of MD cations with 5-nitrobarbiturate PPVCM with IA of MD cation with [PMo ₁₂ O ₄₀] ^{3−}	LR $1.0 \times 10^{-2} - 1.0 \times 10^{-4}$ LR $1.0 \times 10^{-2} - 1.0 \times 10^{-6}$, DL = 8.0×10^{-7} , $S = 54.5 \pm 0.5$, pH 3.0–7.0	295 243
Acetylcholine chloride		PPVCM (NPOE) with lipophilic derivatives of β-CD and addition of Na[B{C ₆ H ₃ (CF ₃) ₂ -3,5}4]	DL up to 2.0×10^{-7} , $S = 60 - 62$, pH 7.0	80–82

Table 3 (continued).

Medicinal drug	Formula	Membrane composition and electrode type ^a	Major electrode characteristics ^b	Ref.
Choline mimetic				
Methacholine		PPVCM (NPOE) with lipophilic derivatives of β -CD and addition of $\text{Na}[\text{B}\{\text{C}_6\text{H}_3(\text{CF}_3)_2\text{-3,5}\}_4]$	DL up to 2.0×10^{-7} , $S = 60\text{--}62$, pH 7.0	80–82
Miscellaneous drugs				
Iopanoic acid		IA of the acid anion with $[(n\text{-C}_8\text{H}_{17})\text{N}]^+$ in <i>p</i> -isopropylnitrobenzene	LR $5.0 \times 10^{-3}\text{--}5.0 \times 10^{-5}$, pH 12	274
Potassium clavulanate		PPVCM (NPOE) based on IA clavulanate–bis(triphenylphosphoranylidene)ammonium with addition of <i>p</i> -(<i>tert</i> -octyl)phenol	LR $1.0 \times 10^{-1}\text{--}2.4 \times 10^{-3}$, DL = 8.0×10^{-4} , $S = 59.4 \pm 0.9$, pH 4.8–7.1	282
Saccharin		tubular ISE for FIA, PVC membrane with IA of MD anions with organic dye cations PPVCM (NPOE or DOP) with IA of Aliquat 336S cations with MD anions	LR $2.0 \times 10^{-2}\text{--}1.0 \times 10^{-4}$, DL = 8.0×10^{-5} , $S = 53.1 \pm 0.4$, pH 2.5 LR $1.0 \times 10^{-1}\text{--}5.0 \times 10^{-5}$, DL = 3.0×10^{-5} , $S = 59\text{--}60$, pH 4.5–11.0	313 279
Sildenafil citrate (Viagra)		PM containing IA of MD cations with BPh_4^- and $[\text{PMo}_{12}\text{O}_{40}]^{3-}$	LR $n \times 10^{-2}\text{--}n \times 10^{-5}$, $S = 54\text{--}56$, pH 3.0–6.0	175
Phenytoin		surface acoustic wave selective PVC sensor	LR $8.0 \times 10^{-4}\text{--}6.7 \times 10^{-8}$, DL = 1.0×10^{-8} , pH 10.0	314
Flecainide		PPVCM based on IA of MD cations with dipicrylamine anions and dodecyl sulfate	LR $n \times 10^{-2}\text{--}n \times 10^{-5}$, DL = $(1\text{--}830) \times 10^{-9}$, $S = 51\text{--}54$	285, 286

^a PM and PPVCM stand for the plasticised membrane and the plasticised PVC membrane (plasticiser is shown in parentheses, see Table 2; DBPhos is dibutyl phosphate), FIA is flow-injection analysis, SC-ISE is solid-contact ISE, ISFT is ion-selective field transistor.

^b LR is the linearity range of the electrode function (mol litre^{-1}); DL is the detection limit (mol litre^{-1}), S is the slope of the electrode function [mV (pC)^{-1}].

accuracy of MD determination in the flow mode was $98.6 \pm 2.5\%$. The electrode was also used in the determination of tetraphenylborate anions at pH from 2.5 to 11.5; the electrode function slope was $56.4 \text{ mV (pC)}^{-1}$, the detection limit was $3.8 \times 10^{-6} \text{ mol litre}^{-1}$.

In the mercurimetric titration of barbiturates, a $\text{Hg}(\text{ClO}_4)_2$ solution was used as the titrant and an I^- -ISE served as the indicator electrode.³⁰⁰ The titration curve demonstrated two jumps, the first corresponding to the stoichiometric reaction of mercury(II) with the titrated MD and the second, to the titrant reaction with the borate buffer solution.

Redox titration was used in the flow-injection determination of ascorbic acid, where the latter was consumed in the reduction of IO_3^- ions to I^- (Ref. 301). An I^- -ISE monitored the concentration of iodide ions. A specially developed computer-governed system of automatic control over the ascorbic acid content provided the automation of this procedure and the reduction of experimental errors. This method can be used in the acid concentration range from 7.5 to 15.0 mmol litre⁻¹ ($S_r \sim 0.01$).

The method of artificial neural networks was used in the processing of results of potentiometric titration of mixtures of derivatives of hydroxycinnamic acid (*p*-coumaric and sinapic acids) and hydroxybenzoic acid (vanillic and isovanillic acids) with a solution of tetrabutylammonium hydroxide in propan-2-ol.³⁰² A four-layer recurrent neural network with back propagation of errors was used in the modelling of the non-linear dependence between the analytical signal and the hydroxy acid concentration. To test the chosen model and train the neural network, the results of potentiometric titration of a series of standard solutions with different concentrations of the determined component were processed. The obtained results served as the basis for the formation of a random data sample, which was used in the training of the neural network. The changes in the signal elements were normalised in a range of 0.1–0.9 according to the equation

$$X_N = 0.1 + \frac{0.8(X - X_{\min})}{(X_{\max} - X_{\min})},$$

where X_N is the normalised signal (at the input and output of the network), X is the initial signal, X_{\min} and X_{\max} are the minimum and maximum signal values.

The optimisation of the network architecture involved choosing the number of layers (the input layer, one or two inner layers and the output layer) and the number of neurons in each layer. Two neurons were used in the input layer (the analytical signal and the titrant volume) as the variables independent from one another. Neurons in the inner layer were optimised for each concrete solution and their mixture, and the number of neurons was determined by the choice of the neural network (this is very important, because the correctness of the results of determination depends on the choice). The chosen network employed the algorithm of back propagation of errors, which allowed minimisation of the least-squares deviation of the current output of a multilayer perceptron from the desired output.

The developed procedure makes it possible to analyse four-component mixtures of *p*-coumaric, sinapic, vanillic and isovanillic acids with the total concentration of $n \times 10^{-3} \text{ mol litre}^{-1}$ by the acid–base potentiometric titration with 0.02 M solution of tetrabutylammonium hydroxide in propan-2-ol with the relative error of less than 5%.³⁰²

Ion associates of MD with the corresponding counter-ions were used as the EAC in membrane ISE with liquid filling and solid-contact ISE. Table 3 shows the data on the composition of selective membranes and the basic electroanalytical characteristics of ISE for the MD determination.

* * *

In the past 10 years, different versions of ISE (membrane ISE with liquid filling, solid-contact and flow ISE), which can operate under conditions of flow-injection analysis, were developed for the determination of MD in patented medicinal drugs and biological fluids. The composition of selective membranes may include both the IA of MD cations and anions with lipophilic counter-ions and the neutral carriers. The latter allows one to enhance the ISE selectivity in the presence of lipophilic ions. The linearity range of the electrode function of ISE is usually in a range of $10^{-1} - 10^{-5} \text{ mol litre}^{-1}$.

References

1. *Lekarstvennye Preparaty v Rossii. Spravochnik Vidal'* (Medicines in Russia. Handbook Vidal) (Moscow: AstraFarmServis, 2005)
2. *Farmatsevt. Vestn.* (22) (2004)
3. R L Solsky *CRC Crit. Rev. Anal. Chem.* **14** 1 (1983)
4. Y Ma *Shengwu Huaxue Yu Shengwu Wuli Jinzhan* **18** 260 (1991)
5. V A Popkov, V Yu Reshetnyak *Farmatsiya* **32** 79 (1983)
6. M J Martin, P Rolfe *Anal. Proc.* **23** 303 (1986)
7. J H Ladenson *Anal. Proc.* **20** 554 (1983)
8. U Oesch, D Ammann, W Simon *Clin. Chem.* **32** 1448 (1986)
9. M E Meyerhoff, W N Opdycke *Adv. Clin. Chem.* **25** 1 (1986)
10. P Nabet *Analysis* **15** 379 (1987)
11. T P Byrne *Sel. Electrode Rev.* **10** 107 (1988)
12. M Maj-Zurawska, A Hulanicki *Chem. Anal.* **34** 197 (1989)
13. P Vadgama, M Desai, P Crump *Electroanalysis* **3** 597 (1991)
14. A Lewenstam, M Maj-Zurawska, A Hulanicki *Electroanalysis* **3** 727 (1991)
15. L G Chatten *J. Pharm. Biomed. Anal.* **1** 491 (1983)
16. C Wang *Yaowu Fenxi Zazhi* **5** 252 (1985)
17. G J Patriarche *J. Pharm. Biomed. Anal.* **4** 789 (1986)
18. M A Zarechenskii, A N Gaidukevich, E G Kizim *Farmatsiya* **37** 88 (1988)
19. K Vytras *J. Pharm. Biomed. Anal.* **7** 789 (1989)
20. V A Cosofret, R P Buck *Crit. Rev. Anal. Chem.* **24** 1 (1993)
21. M A Zarechenskii, I Yu Petukhova, O M Gaidukevich *Farm. Zh.* (3) 40 (1993)
22. A V Granzhan, A K Charykov *Khim.-Farm. Zh.* (7) 51 (1993)^a
23. T Katsu, K Watanabe *Jpn. J. Toxicol. Environ. Health.* **42** 453 (1996)
24. S K Menon, A Sathyapalan, Y K Agrawal *Rev. Anal. Chem.* **16** 333 (1997)
25. E G Kulapina, O V Barinova *Khim.-Farm. Zh.* (12) 40 (1997)^a
26. E Bakker, Y Oin *Anal. Chem.* **78** 3965 (2006)
27. E G Kulapina, O V Barinova *Zh. Anal. Khim.* **56** 518 (2001)^b
28. E G Kulapina, O V Barinova *Elektrokhimiya* **37** 935 (2001)^c
29. S V Kharitonov *Elektrokhimiya* **37** 1490 (2001)^c
30. S V Kharitonov *Zh. Anal. Khim.* **58** 199 (2003)^b
31. E G Kulapina, V V Baraguzina, O I Kulapina *Zh. Anal. Khim.* **59** 971 (2004)^b
32. S V Kharitonov *Anal. Bioanal. Chem.* **382** 1642 (2005)
33. E G Kulapina, V V Baraguzina, O I Kulapina, D V Chernov *Elektrokhimiya* **41** 981 (2005)^c
34. S V Kharitonov *Anal. Lett.* **39** 259 (2006)
35. N Alizadeh, R Mehdipour *J. Pharm. Biomed. Anal.* **30** 725 (2002)
36. H Ibrahim, Y M Issa, H M Abu-Shawish *J. Pharm. Biomed. Anal.* **36** 1053 (2005)
37. S V Kharitonov *Zh. Anal. Khim.* **61** 975 (2006)^b
38. S V Kharitonov *Kolloid. Zh.* **65** 672 (2003)^d
39. W Morf *The Principles of Ion-Selective Electrodes and of Membrane Transport* (Amsterdam: Elsevier, 1981)
40. E Pungor *Anal. Sci.* **14** 249 (1998)
41. E Pungor *Talanta* **44** 1505 (1997)
42. E Bakker, P Bühlmann, E Pretsch *Electroanalysis* **11** 915 (1999)
43. E Bakker, D Diamond, A Lewenstam, E Pretsch *Anal. Chim. Acta* **393** 11 (1999)
44. E Bakker, E Pretsch, P Bühlmann *Anal. Chem.* **72** 1127 (2000)
45. E Bakker *Electroanalysis* **9** 7 (1997)

46. T Sokalski, A Ceresa, T Zwickl, E Pretsch *J. Am. Chem. Soc.* **119** 11347 (1997)
47. T Sokalski, T Zwickl, E Bakker, E Pretsch *Anal. Chem.* **71** 1204 (1999)
48. T Sokalski, A Ceresa, M Fibbioli, T Zwickl, E Bakker, E Pretsch *Anal. Chem.* **71** 1210 (1999)
49. A Ceresa, T Sokalski, E Pretsch *J. Electroanal. Chem.* **501** 70 (2001)
50. A Ceresa, E Bakker, B Hattendorf, D Gunther, E Pretsch *Anal. Chem.* **73** 343 (2001)
51. T Zwickl, T Sokalski, E Pretsch *Electroanalysis* **11** 673 (1999)
52. W Qin, T Zwickl, E Pretsch *Anal. Chem.* **72** 3236 (2000)
53. E Bakker, E Pretsch *TRAC-Trends Anal. Chem.* **20** 11 (2001)
54. W E Morf, M Badertscher, T Zwickl, P Reichmuth, N F de Rooij, E Pretsch *J. Phys. Chem., B* **104** 8201 (2000)
55. W E Morf, M Badertscher, T Zwickl, N F de Rooij, E Pretsch *J. Phys. Chem., B* **103** 11346 (1999)
56. T Vigassy, W E Morf, M Badertscher, A Ceresa, N F de Rooij, E Pretsch *Sens. Actuators, B* **76** 477 (2001)
57. E Bakker, M E Meyerhoff *Anal. Chim. Acta* **416** 121 (2000)
58. L Bulgariu, H Radecka, M Pietraszkiewicz, O Pietraszkiewicz *Anal. Lett.* **36** 1325 (2003)
59. I Szymanska, H Radecka, J Radecki, M Pietraszkiewicz, O Pietraszkiewicz *Combinator. Chem. High Through. Scr.* **3** 509 (2000)
60. X M Lin, K Umezawa, K Tohda, H Furuta, J L Sessler, Y Umezawa *Anal. Sci.* **14** 99 (1998)
61. Z-Z Li, X-B Zhang, C-C Guo, G-L Shen, R-Q Yu *Anal. Lett.* **34** 2035 (2001)
62. X-B Zhang, C-C Guo, S-H Chen, G-L Shen, R Q Yu *Fresenius' J. Anal. Chem.* **369** 422 (2001)
63. X-B Zhang, C-C Guo, L-X Jian, G-L Shen, R-Q Yu *Anal. Sci.* **16** 1285 (2000)
64. T Katsu, K Ido, A Moriya, Y Nakae, I Sakata *Electroanalysis* **12** 1282 (2000)
65. S Shahrokhian, A Hamzehloei, M Bagherzadeh *Anal. Chem.* **74** 3312 (2002)
66. M M Zareh, S M Teleb, E S Ahmed *Anal. Lett.* **35** 17 (2002)
67. T Katsu, Y Mori, K Furuno, Y Gomita *J. Pharm. Biomed. Anal.* **19** 585 (1999)
68. T Katsu, K Ido, K Kataoka *Anal. Sci.* **17** 745 (2001)
69. T Katsu, K Ido, K Kataoka *Sens. Actuators, B* **81** 267 (2002)
70. K Odashima *J. Inclusion Phenom. Mol. Recognit.* **32** 165 (1998)
71. N V Shvedene, S V Borovskaya *Zh. Anal. Khim.* **58** 1208 (2003) ^b
72. N V Shvedene, N N Bel'chenko, N V Starushko, V E Baulin, I V Pletnev *Vestn. Mosk. Univ. Ser. 2, Khim.* **39** 383 (1998) ^c
73. T Katsu, N Okaki, K Watanabe, K Takaishi, H Yokosu *Anal. Sci.* **19** 771 (2003)
74. H Yeo, H K Lee, K C Nam, S Jeon *Bull. Korean Chem. Soc.* **25** 361 (2004)
75. A M Pimenta, A N Araujo, M C B S M Montenegro *Anal. Chim. Acta* **470** 185 (2002)
76. J L F C Lima, M C B S M Montenegro *Mikrochim. Acta* **131** 187 (1999)
77. H Y Aboul-Enein, R I Stefan, J F van Staden *Anal. Sci.* **27** 53 (1999)
78. R Katakay, S Palmer, D Parker, D Spurling *Electroanalysis* **9** 1267 (1997)
79. R Katakay, S Palmer *Electroanalysis* **8** 585 (1996)
80. P M Kelly, R Katakay, D Parker, A F Patti *J. Chem. Soc., Perkin Trans. 2* 1955 (1995)
81. D Parker, R Katakay, P M Kelly, S Palmer *Pure Appl. Chem.* **68** 1219 (1996)
82. R Katakay, D Parker *Analyst* **121** 1829 (1996)
83. R Katakay, D Parker, P M Kelly *Scand. J. Clin. Lab. Invest.* **55** 409 (1995)
84. G C Best, P B Dervan *J. Am. Chem. Soc.* **117** 1187 (1995)
85. Yu N Blikova, N N Leizerovich, N A Pasekova, N V Shvedene *Vestn. Mosk. Univ. Ser. 2, Khim.* **41** 259 (2000) ^c
86. J-Z Li, X-Y Pang, D Gao, R-Q Yu *Talanta* **42** 1775 (1995)
87. A R Firooz, M K Amini, S Tangestaninejad, S Shahrokhian *Anal. Lett.* **34** 661 (2001)
88. N V Shvedene, N N Bel'chenko, N V Starushko, M M Shcherbakova, L G Tomilova, I V Pletnev *Vestn. Mosk. Univ. Ser. 2, Khim.* **40** 160 (1999) ^c
89. N V Shvedene, N N Leizerovich, E V Kostalyndina, Ya N Koval', I V Pletnev *Vestn. Mosk. Univ. Ser. 2, Khim.* **41** 34 (2000) ^c
90. S Shahrokhian, M K Amini, S Kolagar, S Tangestaninejad *Microchem. J.* **63** 302 (1999)
91. H Hisamoto, D Siswanta, H Nishihara, K Suzuki *Anal. Chim. Acta* **304** 127 (1995)
92. D Liu, W-C Chen, G-L Shen, R-Q Yu *Analyst* **121** 1495 (1996)
93. Z-Q Li, X-P Song, G-L Shen, R-Q Yu *Anal. Lett.* **31** 1473 (1998)
94. O A Mukhina, I A Nazarova, N V Shvedene *Vestn. Mosk. Univ., Ser. 2, Khim.* **44** 131 (2003) ^c
95. I V Pletnev, N V Shvedene, I V Lyutikova, I A Nazarova, I M Litvak, I V Mikhura, Yu A Zolotov *Fresenius' J. Anal. Chem.* **364** 682 (1999)
96. Y Chai, F Jiang, R Yuan, L Xu, W Xu *Anal. Lett.* **36** 2379 (2003)
97. L Xu, R Yuan, Y-Q Chai, X-L Wang *Anal. Bioanal. Chem.* **381** 781 (2005)
98. N V Shvedene, M Yu Nemilova, E V Ekimova, M F Timchenko, M M Shcherbakova, I V Pletnev *Vestn. Mosk. Univ., Ser. 2, Khim.* **39** 317 (1998) ^c
99. I A Nazarova, N V Starushko, K N Otkidach, N V Shvedene, A A Formanovskii, I V Pletnev *Vestn. Mosk. Univ., Ser. 2, Khim.* **42** 33 (2001) ^c
100. P G Veltsistas, T I Sikalos, M I Prodromidis, C D Papadimitriou, M I Karayannis *Mikrochim. Acta* **135** 113 (2000)
101. S S M Hassan, W H Mahmoud, M A F Elmosallamy, M H Almarzooqi *Pharmazie* **58** 29 (2003)
102. T Katsu, H Hirodo *Anal. Chim. Acta* **396** 189 (1999)
103. T Katsu, Y Mori *Talanta* **43** 755 (1996)
104. R S Hutchins, P Bansal, P Molina, M Alajarin, A Vidal, L G Bachas *Anal. Chem.* **69** 1273 (1997)
105. M Ying, R Yuan, Z-Q Li, Y-Q Song, G-L Shen, R-Q Yu *Anal. Lett.* **31** 1965 (1998)
106. S Shahrokhian, M K Amini, R Kia, S Tangestaninejad *Anal. Chem.* **72** 956 (2000)
107. E Bakker, E Pretsch *Anal. Chim. Acta* **309** 7 (1995)
108. K Tohda, T Higuchi, D Drago, Y Umezawa *Anal. Sci.* **17** 833 (2001)
109. T Vigassy, R E Gyurcsányi, E Pretsch *Electroanalysis* **15** 375 (2003)
110. U Schaller, E Bakker, U E Spichiger, E Pretsch *Anal. Chem.* **66** 391 (1994)
111. V V Egorov, N D Borisenko, E M Rakhman'ko, A P Podterob, A L Gulevich, V A Repin *Elektrokhimiya* **34** 150 (1998) ^c
112. W E Morf, N F de Rooij, E Pretsch *J. Electroanal. Chem.* **581** 265 (2005)
113. S Plaza, Z Szigeti, M Geisler, E Martinoia, E Pretsch *Anal. Biochem.* **347** 10 (2005)
114. K Tompa, K Birbaum, A Malon, T Vigassy, E Bakker, E Pretsch *Anal. Chem.* **77** 7801 (2005)
115. N I Karandeeva, V I Tkach, O I Glukhova, L P Tsyganok, O V Mushik *Zh. Anal. Khim.* **53** 619 (1998) ^b
116. L Mutihac, H-J R Buschmann, R-C Mutihac, E Schollmeyer *J. Inclusion Phenom. Macrocycl. Chem.* **51** 1 (2005)
117. H-J Buschmann, L Mutihac, K Jansen *J. Inclusion Phenom. Macrocycl. Chem.* **39** 1 (2001)
118. K Odashima, K Koga *Comprehensive Supramolecular Chemistry* Vol. 2, Ch. 5 (Ed. F Vogtle) (Oxford: Elsevier, 1996)
119. Y Umezawa, M Kataoka, W Takami, E Kimura, T Koike, H Nada *Anal. Chem.* **60** 2392 (1988)
120. M Kataoka, R Naganawa, K Odashima, Y Umezawa, E Kimura, T Koike *Anal. Lett.* **22** 1089 (1989)
121. R Naganawa, M Kataoka, K Odashima, Y Umezawa, E Kimura, T Koike *Bunseki Kagaku* **39** 671 (1990); *Chem. Abstr.* **114** 139159 (1991)
122. I Szymanska, H Radecka, J Radecki, M Pietraszkiewicz, O Pietraszkiewicz *Electroanalysis* **15** 294 (2003)
123. K Tohda, M Tange, K Odashima, Y Umezawa, H Furuta, J L Sessler *Anal. Chem.* **64** 960 (1992)

124. D Ammann, W E Morf, P Anker, P C Meier, E Pretsch, W Simon *Ion-Select. Electrode Rev.* **5** 3 (1983)
125. K Kimura, T Shono *Studies in Organic Chemistry* Vol. 45, Ch. 4 (Ed. M Hiraoka) (Amsterdam: Elsevier, 1992)
126. J C Lockhart *Comprehensive Supramolecular Chemistry* Vol. 1, Ch. 16 (Ed. G W Gokel) (Oxford: Elsevier, 1996)
127. W Bussmann, W Simon, U Oesch, J-M Lehn, P Plumeré *Helv. Chim. Acta* **64** 657 (1981)
128. T Shinbo, T Yamaguchi, K Nishimura, M Kikkawa, M Sugiura *Anal. Chim. Acta* **193** 367 (1987)
129. K Maruyama, H Sohmiya, H Tsukube *Tetrahedron* **48** 805 (1992)
130. R Katakya, P S Bates, D Parker *Analyst* **117** 1313 (1992)
131. K Odashima, K Yagi, K Tohda, Y Umezawa *Anal. Chem.* **65** 1074 (1993)
132. L F Lindoy, I M Atkinson *Self-Assembly in Supramolecular Systems* (Cambridge: Royal Society of Chemistry, 2000)
133. M M Stone, A H Franz, C B Lebrilla *J. Am. Soc. Mass Spectrom.* **13** 964 (2002)
134. F Fraternali, G Wipff *An. Quim.* **93** 376 (1997)
135. M L Lamb, W L Jorgensen *Curr. Opin. Chem. Biol.* **1** 449 (1997)
136. T Harada, J M Rudzinski, S Shinkai *J. Chem. Soc., Perkin Trans. 2* 2109 (1992)
137. A Casnati, A Pochini, R Ungaro, F Ugozzoli, F Arnaud, S Fanni, M-J Schwing, R J M Egberink, F de Jong, D N Reinhoudt *J. Am. Chem. Soc.* **117** 2767 (1995)
138. C D Gutsche, M Iqbal, I Alam *J. Am. Chem. Soc.* **109** 4314 (1987)
139. A Ikeda, S Shinkai *Chem. Rev.* **97** 1713 (1997)
140. K Araki, H Shimizu, S Shinkai *Chem. Lett.* 205 (1993)
141. S Shinkai *Tetrahedron* **49** 8933 (1993)
142. M Tabakci, B Tabakci, M Yilmaz *J. Inclusion Phenom. Macrocycl. Chem.* **53** 51 (2005)
143. C Bavoux, M Perrin *J. Inclusion Phenom. Macrocycl. Chem.* **14** 247 (1992)
144. V Böhmer *Angew. Chem., Int. Ed. Engl.* **34** 713 (1995)
145. H Matsumoto, S Nishio, M Takeshita, S Shinkai *Tetrahedron* **51** 4647 (1995)
146. T Yamato, F L Zhang *J. Inclusion Phenom. Macrocycl. Chem.* **39** 55 (2001)
147. T Yamato, F L Zhang, H Tsuzuki, Y Miura *Eur. J. Org. Chem.* 1069 (2001)
148. T Yamato, M Haraguchi, J Nishikawa, S Jde *J. Chem. Soc., Perkin Trans. 1* 609 (1998)
149. T Yamato, M Haraguchi, J Nishikawa, S Jde, H Tsuzuki *Can. J. Chem.* **76** 989 (1998)
150. T Yamato, F Kitajima, J T Gil *J. Inclusion Phenom. Macrocycl. Chem.* **53** 257 (2005)
151. W Abraham *J. Inclusion Phenom. Macrocycl. Chem.* **43** 159 (2002)
152. T Hayashita, A Yamauchi, A-J Tong, J C Lee, B D Smith, N Teramae *J. Inclusion Phenom. Macrocycl. Chem.* **50** 87 (2004)
153. M Miyauchi, Y Kawaguchi, A Harada *J. Inclusion Phenom. Macrocycl. Chem.* **50** 57 (2004)
154. M E Meyerhoff, B Fu, S-C Ma, E Bakker, J-H Yun, V C Yang, J A Wahr *Divis. Blood Gas Electrolyte Am. Ass. Clin. Chem. Newslett.* **10** 4 (1995)
155. B Fu, E Bakker, V C Yang, M E Meyerhoff *Macromolecules* **28** 5834 (1995)
156. E Bakker, B Fu, J H Yun, V C Yang, M E Meyerhoff *Pittsburgh Conference on Analytical Chemistry and Applied Spectroscopy, New Orleans, LA, 1995* p. 1082
157. B Fu, E Bakker, J H Yun, E Wang, V C Yang, M E Meyerhoff *Electroanalysis* **7** 823 (1995)
158. D Liu, R K Meruva, R B Brown, M E Meyerhoff *Anal. Chim. Acta* **321** 173 (1996)
159. S Mathison, E Bakker *J. Pharm. Biomed. Anal.* **19** 163 (1999)
160. S Dai, J M Esson, O Lutze, N Ramamurthy, V C Yang, M E Meyerhoff *J. Pharm. Biomed. Anal.* **19** 1 (1999)
161. J H Yun, M E Meyerhoff, V C Yang *Anal. Biochem.* **224** 212 (1995)
162. I H Badr, N Ramamurthy, V C Yang, M E Meyerhoff *Anal. Biochem.* **250** 74 (1997)
163. N Ramamurthy, N Baliga, J A Wahr, U Schaller, V C Yang, M E Meyerhoff *Clin. Chem.* **44** 606 (1998)
164. O Lutze, R K Meruva, A Frielich, N Ramamurthy, R B Brown, R Hower, M E Meyerhoff *Fresenius' J. Anal. Chem.* **364** 41 (1999)
165. Y M Issa, N T Abdel-Ghani, A F Shoukry, H M Ahmed *Mikrochim. Acta* **132** 83 (1999)
166. C-Y Wang, X-Y Hu, Z-Z Leng, G-D Jin *Electroanalysis* **15** 709 (2003)
167. X-L Luo, J-J Xu, W Zhao, H-Y Chen *Anal. Chim. Acta* **512** 57 (2004)
168. Y Long, W Li, D He, L Nie, S Yao, L Lei *Analyst* **124** 1629 (1999)
169. E G Kulapina, V V Baraguzina, O I Kulapina *Khim.-Farm. Zh.* (9) 48 (2004)^a
170. S V Kharitonov, V I Zarembo *Sensor* **1** 13 (2005)
171. A A Salem, B N Barsoum, E L Izake *Anal. Chim. Acta* **498** 79 (2003)
172. S V Kharitonov, I P Gorelov *Khim.-Farm. Zh.* (11) 54 (2000)^a
173. N T Abdel-Ghani, A F Shoukry, S H Hussein *J. Pharm. Biomed. Anal.* **30** 601 (2002)
174. S S Hassan, M M Amer, S A Abd El-Fatah, A M El-Kosasy *Talanta* **46** 1395 (1998)
175. A M Othman, N M H Rizk, M S El-Shahawi *Anal. Chim. Acta* **515** 303 (2004)
176. C-I Huang, R-f Li, R Xiu *Chem. Res. Chin. Univ.* **19** 409 (2003)
177. S S Badawy, A F Youssef, A A Mutair *Anal. Chim. Acta* **511** 207 (2004)
178. M M Ayad, A Shalaby, H E Abdellatif, H M Elsaid *J. Pharm. Biomed. Anal.* **29** 247 (2002)
179. M Arvand, M F Mousavi, M A Zanjanchi, M Shamsipur *J. Pharm. Biomed. Anal.* **33** 975 (2003)
180. M Shamsipur, F Jalali *Anal. Sci.* **16** 549 (2000)
181. B Magnuszewska, J Ostrowska, Z Figaszewski *Chem. Anal.* **45** 105 (2000)
182. J L F C Lima, M C B S M Montenegro, M G F Sales *J. Pharm. Biomed. Anal.* **14** 931 (1996)
183. Y Long, W Li, L Nie, S Yao *Anal. Chim. Acta* **395** 33 (1999)
184. Y M Issa, A L El-Ansary, A S Tag-Eldin *Mikrochim. Acta* **135** 97 (2000)
185. X X Sun, X Zhang, H Y Aboul-Enein *IL Farmaco* **59** 307 (2004)
186. Y M Issa, M M Hassouna, F M Abdel-Gawad, E M Hussien *J. Pharm. Biomed. Anal.* **23** 493 (2000)
187. S Khalil, M A El-Ries *Talanta* **59** 1259 (2003)
188. E G Kulapina, V V Baraguzina, O I Kulapina *Zh. Anal. Khim.* **60** 592 (2005)^b
189. M Shamsipur, F Jalali *Anal. Lett.* **35** 53 (2002)
190. H A M Arida *Anal. Lett.* **35** 2421 (2002)
191. N A El-Ragehy, A M El-Kosasy, S S Abbas, S Z El-Khateeb *Anal. Chim. Acta* **418** 93 (2000)
192. K Watanabe, K Okada, H Oda, K Furuno, Y Gomita, T Katsu *Anal. Chim. Acta* **316** 371 (1995)
193. S Khalil *Analyst* **124** 139 (1999)
194. X X Sun, L Z Sun, H Y Aboul-Enein *Electroanalysis* **12** 853 (2000)
195. H Y Aboul-Enein, X X Sun, C J Sun *Sensors* **2** 424 (2002)
196. S I M Zayed *Anal. Sci.* **20** 1043 (2004)
197. M N Abbas, A A Abdel-Fattah, E A Zahran *Anal. Sci.* **20** 1137 (2004)
198. S S M Hassan, R M Abdel-Aziz, A B Abbas *Anal. Chim. Acta* **321** 47 (1996)
199. A S Amin, M M Zareh *Monatsh. Chem.* **127** 1123 (1996)
200. G Zhou, H Fan, T Han, J Pan *J. Shanxy Univ. Natur. Sci. Ed.* **18** 300 (1995)
201. M A Ahmed, M M Elbeshlawy *Anal. Lett.* **28** 2123 (1995)
202. Y M Issa, H Ibrahim, H M Abu-Shawish *Mikrochim. Acta* **150** 47 (2005)
203. L Lei, X Su, Q Xie, J He, S Yao *Mikrochim. Acta* **134** 63 (2000)
204. F M Abdel-Gawad, Y M Issa, M E M Hassouna, E M Hussien *Mikrochim. Acta* **141** 7 (2003)
205. M M Ayad, A Shalaby, H E Abdellatif, H M Elsaid *Mikrochim. Acta* **140** 93 (2002)

206. Z-H Liu, M-L Wen, Y Yao, J Xiong *Fresenius' J. Anal. Chem.* **368** 335 (2000)
207. J L F C Lima, M C B S M Montenegro, M G F Sales *J. Pharm. Sci.* **86** 1234 (1997)
208. A E A Salem, B N Barsoum, G R Saad, E L Izake *J. Electroanal. Chem.* **536** 1 (2002)
209. C-L Huang, J-J Ren, D-F Hu *Talanta* **43** 2061 (1996)
210. S S M Hassan, E M Elnemma, M A Hamada *Electroanalysis* **7** 656 (1995)
211. S S M Hassan, E M Elnemma, E M El-Naby *Anal. Lett.* **32** 271 (1999)
212. A F Shoukry, Y M Issa, M S Rizk, R M El-Nashar *Anal. Lett.* **29** 1463 (1996)
213. M N M P Alcáda, J L F C Lima, M C B S M Montenegro *J. Pharm. Biomed. Anal.* **13** 459 (1995)
214. E M Elnemma, M A Hamada *Mikrochim. Acta* **126** 147 (1997)
215. M M Zareh *Mikrochim. Acta* **126** 271 (1997)
216. Y M Issa, M S Rizk, A F Shoukry, E M Atia *Mikrochim. Acta* **129** 195 (1998)
217. S Khalil, A S El-Aliem *J. Pharm. Biomed. Anal.* **27** 25 (2002)
218. S Khalil, M M Elrabiehi *Microchem. J.* **62** 237 (1999)
219. M N Abbas, G A E Mostafa *J. Pharm. Biomed. Anal.* **31** 819 (2003)
220. L Rover Jr, C A B Garcia, G de Oliveira Neto, L T Kubota, F Galembeck *Anal. Chim. Acta* **366** 103 (1998)
221. S Khalil, A Kelzieh *J. Pharm. Biomed. Anal.* **31** 601 (2003)
222. J Drozd, H Hopkala *Desalination* **163** 119 (2004)
223. M G F Sales, M C B S M Montenegro *J. Pharm. Sci.* **90** 1125 (2001)
224. R Katakya, K Toth, S Palmer, Z Feher *Talanta* **50** 939 (1999)
225. H Hopkala, J Drozd, A Gumieniczek *Chem. Anal.* **47** 75 (2002)
226. B Saad, Z M Zin, M S Jab, I A Rahman, M I Saleh, S Mahsufi *Anal. Sci.* **21** 521 (2005)
227. H Hopkala, J Drozd *Chem. Anal.* **44** 603 (1999)
228. L J Peng, M L Wen, Y Yao *Anal. Sci.* **17** 815 (2001)
229. T Katsu, Y Mori *Anal. Chim. Acta* **343** 79 (1997)
230. T A Ivon, L P Tsyganok, V I Tkach *Zh. Anal. Khim* **56** 56 (2001)^b
231. S V Kartamyshev, S S Ryasenskii, I P Gorelov *Khim.-Farm. Zh.* (5) 50 (2002)^a
232. M V Kuznetsova, S S Ryasenskii, I P Gorelov *Khim.-Farm. Zh.* (11) 34 (2003)^a
233. G A E Mostafa *Zh. Anal. Khim* **58** 1196 (2003)^b
234. G A H Mostafa, S E S Ghazy *Ann. Chim.* **93** 691 (2003)
235. N T Abdel-Ghani, M S Rizk, R M El-Nashar *Anal. Lett.* **35** 39 (2002)
236. M S Rizk *J. Chem. Technol. Biotechnol.* **61** 67 (1994)
237. M Aboudan, Y M Issa, A F Shoukry *J. Chem. Technol. Biotechnol.* **61** 31 (1994)
238. N T Abdel-Ghani, M S Rizk, R M El-Nashar *Analyst* **125** 1129 (2000)
239. T A Bubel', N A Lyakhovaya, R B Gladyshev, V I Tkach, L P Tsyganok *Zh. Anal. Khim.* **56** 1185 (2001)^b
240. S V Kharitonov, I P Gorelov, I G Davydova *Khim.-Farm. Zh.* (4) 49 (2001)^a
241. A F Shoukry, Y M Issa, R M El-Nashar *Microchem. J.* **69** 189 (2001)
242. Y M Issa, A F Shoukry, M S Rizk, E M Atia *J. Chem. Technol. Biotechnol.* **64** 379 (1995)
243. G A E-H Mostafa *Anal. Sci.* **18** 1335 (2002)
244. Y M Issa, N T Abdel-Ghani, A F Shoukry, H M Ahmed *Anal. Sci.* **21** 1037 (2005)
245. N T Abdel-Ghani, A F Shoukry, R M El-Nashar *Analyst* **126** 79 (2001)
246. S V Kharitonov, V I Zarembo *Izv. Vyssh. Uchebn. Zaved., Khim. Khim. Tekhnol.* **49** 28 (2006)
247. M Shamsipur, F Jalali, S Haghgoo *J. Pharm. Biomed. Anal.* **27** 867 (2002)
248. S Khalil, A Kelzieh, S A Ibrahim *J. Pharm. Biomed. Anal.* **33** 825 (2003)
249. L J Peng, M L Wen, Y Yao *J. Pharm. Biomed. Anal.* **30** 667 (2002)
250. M S Rizk, N T Abdel-Ghani, R M El-Nashar *Microchem. J.* **70** 93 (2001)
251. A F Shoukry, M S Rizk, H M Abdel-Fattah, Y M Issa, E M Atia *J. Chem. Technol. Biotechnol.* **60** 217 (1994)
252. A L El-Ansary, Y M Issa, A S Tag-Eldin *Electroanalysis* **13** 1203 (2001)
253. A Erdem, M Ozsoz, L Kirilmaz, E Kilinc, T Dalbasti *Electroanalysis* **9** 932 (1997)
254. W Li, X Su, H Guo, W Wei, S Yao *Analyst* **124** 91 (1999)
255. S S Badawy, Y M Issa, A A Mutair *J. Pharm. Biomed. Anal.* **39** 117 (2005)
256. M Aboudan, A F Shoukry, Y M Issa *Anal. Lett.* **29** 19 (1996)
257. Ukrain. P. 48652; *Ref. Zh. Khim.* 19O284P (2005)
258. V V Bolotov, M A Zarechenskii, V P Moroz *Farm. Zh.* (6) 86 (2004)
259. I P Gorelov, S S Ryasenskii, S V Kartamyshev, M V Fedorova *Zh. Anal. Khim.* **60** 74 (2005)^b
260. Y M Issa, S I M Zayed *Anal. Sci.* **20** 297 (2004)
261. S S M Hassan, E M Elnemma, W H Mahmoud, A H K Mohammed *J. Appl. Electrochem.* **36** 139 (2006)
262. H Y Aboul-Enein, X X Sun *Analyst* **28** 855 (2000)
263. A Bouklouze, M Elbouzekraoui, Y Cherrah, M Hassar, J-M Kauffmann *Electroanalysis* **14** 1369 (2002)
264. Y Long, W Li, L Nie, S Yao *J. Pharm. Biomed. Anal.* **24** 361 (2001)
265. Z-H Liu, M-L Wen, J Xiong *Anal. Sci.* **16** 885 (2000)
266. S S M Hassan, W H Mahmoud, M A F Elmosallamy, A H M Othman *Anal. Chim. Acta* **378** 299 (1999)
267. S S M Hassan, M Amer, S A A El-Fatah, A M El-Kosasy *Anal. Chim. Acta* **363** 81 (1998)
268. S S M Hassan, W H Mahmoud, M S Abdel-Samad *Mikrochim. Acta* **129** 251 (1998)
269. N M H Rizk, A-H Othman *Anal. Sci.* **21** 107 (2005)
270. N M H Rizk *Mikrochim. Acta* **138** 53 (2002)
271. S S M Hassan, R M El-Bahnasawy, N M Rizk *Mikrochim. Acta* **126** 217 (1997)
272. H Paseková, M G Sales, M C Montenegro, A N Araújo, M Polásek *J. Pharm. Biomed. Anal.* **24** 1027 (2001)
273. J L F C Lima, M C B S M Montenegro, M G F Sales *J. Pharm. Biomed. Anal.* **18** 93 (1998)
274. D S Panagos, M A Koupparis *Analyst* **120** 1643 (1995)
275. S V Kharitonov, I P Gorelov *Khim.-Farm. Zh.* (12) 45 (2000)^a
276. S V Kharitonov *Zh. Anal. Khim.* **56** 754 (2001)^b
277. D I L Tescarollo, N G de Oliveira, D C Vendramini, C Sommer, J L S Martins, L T Kubota *Anal. Lett.* **37** 35 (2004)
278. S Khalil, N Borham, M A El-Ries *Anal. Chim. Acta* **414** 215 (2000)
279. M A F Elmosallamy, M M Ghoneim, H M A Killa, A L Saber *Mikrochim. Acta* **151** 109 (2005)
280. A A Bunaciu, A Grasu, H Y Aboul-Enein *Anal. Chim. Acta* **311** 193 (1995)
281. M N Abbas *Anal. Lett.* **35** 813 (2002)
282. A M Pimenta, C M C M Couto, A N Araujo, M C B S M Montenegro *Fresenius' J. Anal. Chem.* **371** 400 (2001)
283. M C B S M Montenegro, M Goreti, F Sales *J. Pharm. Sci.* **89** 876 (2000)
284. R-I Stefan, H Y Aboul-Enein, G-E Baiulescu *Sens. Actuators, B* **37** 141 (1996)
285. R-I Stefan, G-E Baiulescu, H Y Aboul-Enein *Analyst* **25** 39 (1997)
286. R-I Stefan, G-E Baiulescu *Pittsburgh Conference on Analytical Chemistry and Applied Spectroscopy, Atlanta, 1997* p. 44P
287. Z-L Wang *Liaoning Shifan Daxue Xuebao. Ziran Kexue Ban* **25** 294 (2002)
288. F Yin, X Xu *Anal. Lett.* **37** 3129 (2004)
289. R-I Stefan *Anal. Chim. Acta* **350** 105 (1997)
290. G A E Mostafa *J. Pharm. Biomed. Anal.* **31** 515 (2003)
291. M N Abbas, G A E Mostafa, A M A Homoda *Talanta* **53** 425 (2000)
292. B Magnuszewska, Z Figaszewski *Chem. Anal.* **43** 265 (1998)
293. E V Nizhnikova, A P Podterob *Zh. Anal. Khim.* **60** 69 (2005)^b
294. G A E Mostafa *Anal. Sci.* **17** 1043 (2001)

295. A Shalaby, M El-Maamly, H Abdellatef *Sci. Pharm.* **68** 247 (2000)
296. E M G Santos, A N Araújo, C M C M Couto, M C B S M Montenegro, A Kejzlarová, P Solich *J. Pharm. Biomed. Anal.* **36** 701 (2004)
297. S S M Hassan, W H Mahmoud, M A F Elmosallamy, M S Abdel-Samad *Mikrochim. Acta* **131** 199 (1999)
298. N Garcia-Villar, J Saurina, S Hernandez-Cassou *Fresenius' J. Anal. Chem.* **371** 1001 (2001)
299. V V Egorov, V A Repin *Zh. Anal. Khim.* **50** 463 (1995)^b
300. S S M Hassan, E H El-Naby, E M Elnemma *Anal. Lett.* **30** 1081 (1997)
301. A P S Paim, C M N V Almeida, B F Reis, R A S Lapa, E A G Zagatto, J L F C Lima *J. Pharm. Biomed. Anal.* **28** 1221 (2002)
302. A H Aktas, S Yasar *Acta Chim. Slov.* **51** 273 (2004)
303. X-W Li, B-L Yang *J. Baoji Coll. Arts Sci. Natur. Sci. Ed.* **23** 195 (2003)
304. L T Kubota, J C B Fernandes, L Rover, G de Oliveira Neto *Talanta* **50** 661 (1999)
305. J Lenik, B Marczevska, C Wardak *Desalination* **163** 77 (2004)
306. A Poghosian, M J Schoning, P Schroth, A Simonis, H Luth *Sens. Actuators, B* **76** 519 (2001)
307. D Rolka, A Poghosian, M J Schoning *Sensors* **4** 84 (2004)
308. T Katsu, N Hanada *Anal. Chim. Acta* **321** 21 (1996)
309. Y-Q Chai, Y Liu, R Yuan, W-J Xu, L Xu *Chem. J. Chin. Univ.* **24** 814 (2003)
310. P G Veltsistas, M I Prodromidis, C E Efstathiou *Anal. Chim. Acta* **502** 15 (2004)
311. E Doniga *Rev. Roum. Chim.* **43** 687 (1998)
312. F-C Gong, X-B Zhang, C-C Guo, G-L Shen, R-Q Yu *Sensors* **3** 91 (2003)
313. O Fatibello-Filho, C Aniceto *Lab. Robot. Autom.* **11** 234 (1999)
314. Y Long, L Lei, L Nie, S Yao, Y Liu *Analyst* **126** 1090 (2001)

^a — *Pharm. Chem. J. (Engl. Transl.)*

^b — *J. Anal. Chem. (Engl. Transl.)*

^c — *Russ. J. Electrochem. (Engl. Transl.)*

^d — *Colloid. J. (Engl. Transl.)*

^e — *Bull. Moscow Univ., Ser. 2, Chem. (Engl. Transl.)*

Microwave-assisted synthesis of individual and multicomponent oxides

A S Vanetsev, Yu D Tretyakov

Contents

I. Introduction	397
II. Foundations of the theory of interaction of microwave radiation with the matter	397
III. Design and key principles of operation of microwave heating systems	401
IV. Use of microwave heating for the synthesis of individual and complex oxides	403
V. Conclusion	411

Abstract. Data on the synthesis of individual and multicomponent oxides from salts with microwave initiation published over the last 15 years are analysed. The advantages and drawbacks of using microwave heating in the synthesis of oxide materials are noted. Criteria for the selection of chemical systems for microwave heating are proposed. The bibliography includes 162 references.

I. Introduction

The development of new synthetic methods that would allow decreasing the energy expenditure and increasing the rate of formation of the final multicomponent products is an important problem of modern inorganic chemistry and materials science. The rate of solid-phase reactions can be often increased by using the starting compounds in the active state (salt or hydroxide co-precipitation, cryochemical crystallisation, spray drying, hydrothermal treatment, *etc.*).¹ Another way for accelerating the reaction is additional treatment (apart from heating, *e.g.*, mechanochemical or ultrasonic treatment) of reaction mixtures, which intensifies diffusion processes *in situ*.^{2,3} It is noteworthy that the physicochemical characteristics of the compounds synthesised using these approaches are not inferior to the characteristics of substances prepared by conventional procedures and, moreover, often surpass them.

Microwave heating of reaction mixtures is a promising method of increasing the rate of solid-phase reactions.^{4–6} Microwave radiation is a non-ionising electromagnetic radiation with a frequency of 300 MHz to 30 GHz. Microwave heating is used to carry out important physicochemical processes such as dehydration, decomposition of salts and hydroxides, synthesis of multicomponent compounds and ceramics sintering. The time and energy expenditures in such processes

are much lower than those in conventional processes. Moreover, in some cases, microwave treatment provides results that cannot be achieved by other methods.^{7,8}

Microwave treatment has a number of advantages over the usual methods of heating of condensed media (solids and liquids), in particular, high speed and low inertia of heating, the absence of contact between the heated body and the heater, the uniformity of heating throughout the whole material bulk, the possibility of selective heating of mixture components and high oven efficiency (50% for the ovens with radiation frequency of 2.45 GHz and 85% for the ovens with radiation frequency of 915 MHz).^{4–7}

The first studies dealing with microwave heating of materials were performed in 1967. Ford⁹ carried out systematic research of the behaviour of oxides and sulfides under microwave heating at a 2.45 GHz frequency. Subsequently, the effect of microwave heating on many oxides¹⁰ and natural minerals¹¹ has been studied.

During the last 10–15 years, the number of publications devoted to the use of microwave heating in various fields of chemistry has increased severalfold. In particular, the synthesis of individual and multicomponent oxides using microwave radiation were documented. Nevertheless, despite the considerable interest in this method, no attempts to generalise the accumulated experience in using microwave heating for the synthesis of oxide materials or to formulate the criteria for evaluating the efficiency of microwave heating for inducing various chemical processes have been undertaken as yet. This review is aimed to fill this gap at least partially.

II. Foundations of the theory of interaction of microwave radiation with the matter

In the electromagnetic radiation scale, the microwave radiation is situated between the IR radiation and radiowaves and corresponds to the wavelengths (λ) from ~ 1 m to 1 cm.¹² The waves with frequencies of 1 to 30 GHz are actively used in radars and the rest frequency range is employed in telecommunication. On the basis of international agreement, frequencies of 2.45 GHz ($\lambda \approx 12.2$ cm) and 915 MHz ($\lambda \approx 32.7$ cm) were allocated for laboratory and domestic microwave ovens (Fig. 1).

Currently, the microwave heating theory has been fairly well developed.^{6–9,12} In this review, we will restrict ourselves to a brief description of the principal mechanisms of absorption of microwave radiation by condensed matter, related to heat

A S Vanetsev N S Kurnakov Institute of General and Inorganic Chemistry, Russian Academy of Sciences, Leninsky prosp. 31, 119991 Moscow, Russian Federation. Fax (7-495) 954 12 79, tel. (7-495) 236 20 44, e-mail: vanetsev@gmail.com

Yu D Tretyakov Department of Chemistry and Department of Materials Science, M V Lomonosov Moscow State University, Leninskie Gory, 119992 Moscow, Russian Federation. Fax (7-495) 939 09 98, tel. (7-495) 939 20 74, e-mail: yudt@inorg.chem.msu.ru

Received 1 June 2006

Uspekhi Khimii 76 (5) 435–453 (2007); translated by Z P Bobkova

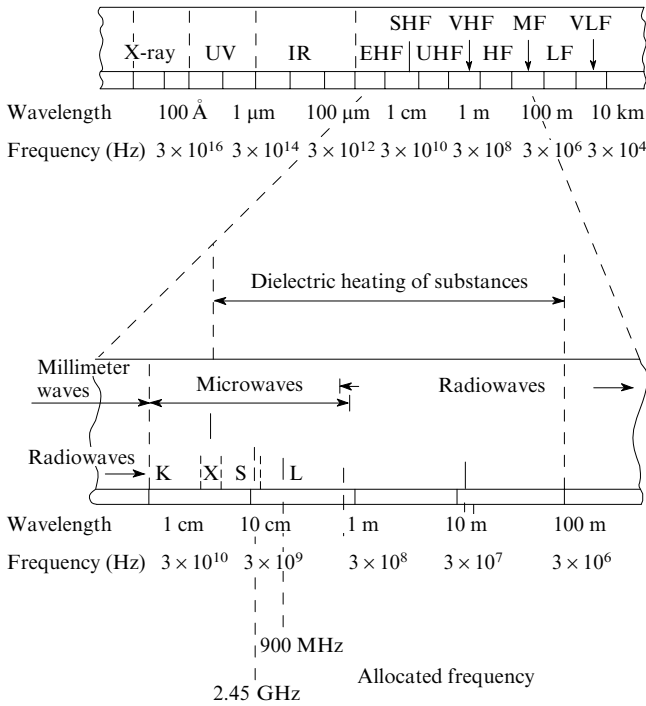


Figure 1. Electromagnetic scale.¹²

EHF are extremely high frequencies, SHF are super high frequencies, UHF are ultra high frequencies, VHF are very high frequencies, HF are high frequencies, MF are medium frequencies, LF are low frequencies, VLF are very low frequencies.

evolution due to dielectric loss on polarisation and to induced currents flowing in the material.

A set of microscopic processes of interaction of electromagnetic waves with charged particles of the matter can correctly be described only by means of quantum mechanical models. Nevertheless, for description of microwave heating, it is often sufficient to take into account the macroscopic properties of the absorbing matter, which are described in terms of classical physics.^{11, 13–17}

Electromagnetic field affects the electric charges in the matter, which are usually classified into free and bound. Free charges can be carried by electrons, vacancies or ions able to move by macroscopic distances. Under the action of an external electric field, conduction currents appear in the matter due to free charge migration

$$\vec{J}_c = \sigma_c \vec{E}, \quad (1)$$

where \vec{J}_c is the conduction current density vector, σ_c is the electrical conductivity of the matter, and \vec{E} is the electrical field vector.

The migration of bound charges is confined to the microscopic size of an atom, a molecule or a crystal cell. Under the action of an external field, the bound charges are merely displaced from their equilibrium states giving rise to macroscopic polarisation. If no free charge carriers are present, the substance is a dielectric and its capacity for polarisation is determined by the relative dielectric permittivity (ϵ_b)

$$\vec{P}_b = (\epsilon_b - 1)\epsilon_0 \vec{E}, \quad (2)$$

where \vec{P}_b is the polarisation vector resulting from bound charges (electrical dipole moment of the unit volume of the substance), $\epsilon_0 = 10^{-9}/36\pi$ (F m⁻¹) is the dielectric permittivity of vacuum.

In the case of an alternating field, the displacement of the bound charges from the equilibrium states is time-dependent; this implies effective movement of charges and, hence, an alternating electric current

$$\vec{J}_b = \frac{\partial \vec{P}_b}{\partial t}, \quad (3)$$

where \vec{J}_b is the polarisation current density.

Thus, in an alternating field, the separation of effects related to the migration of free and bound charges is rather arbitrary.

Currents of any nature in the matter give rise to heat evolution. In the case of high-frequency fields, it is convenient to use field period-averaged characteristics. Therefore, the expression for the power of heat source per unit volume (q) can be written as follows:

$$q = \langle \vec{J} \vec{E} \rangle, \quad (4)$$

where $\vec{J} = \vec{J}_c + \vec{J}_b$ is the total electric field density vector in the matter.

In general due to the inertia of free and bound charge carriers the conduction current and the polarisation vector lag behind the electric field in phase. These effects are often formally described using the so-called complex amplitude method in which all oscillating values are given by

$$\vec{E} = \text{Re}[\vec{E}_\omega \exp(i\omega t)], \quad (5)$$

$$\vec{J} = \text{Re}[\vec{J}_\omega \exp(i\omega t)],$$

etc., where ω is the field circular frequency, t is time, i is the imaginary unit, the values with the subscript ω designate the corresponding complex amplitudes. In the complex form, Eqns (1) and (2) are represented as follows:

$$\vec{J}_{c\omega} = \sigma_c(\omega)\vec{E}_\omega, \quad (6)$$

$$\vec{P}_{b\omega} = [\epsilon_b(\omega) - 1]\epsilon_0 \vec{E}_\omega,$$

where $\sigma_c(\omega) = \sigma'_c(\omega) - i\sigma''_c(\omega)$ and $\epsilon_b(\omega) = \epsilon'_b(\omega) - i\epsilon''_b(\omega)$ are the complex values describing the above-mentioned phase lag of the conduction current and the polarisation vector behind the electric field strength. In the microwave range, the dependence $\sigma_c(\omega)$ and its imaginary part can be neglected for the vast majority of materials, taking that $\sigma_c(\omega) \cong \sigma_c$. The dependence $\epsilon_b(\omega)$ and its imaginary part are determined by the type and properties of the bound charges in the dielectric and can be substantially different for different substances.

Within the complex amplitude formalism, Eqn (4) can be written in the form

$$q = \frac{1}{2}\omega\epsilon_0\epsilon''|\vec{E}_\omega|^2 = \frac{1}{2}\omega\epsilon_0\epsilon'_b\tan\delta|\vec{E}_\omega|^2, \quad (7)$$

where $\epsilon'' = \epsilon''_b + \sigma_c/\omega\epsilon_0$ is the imaginary part of the equivalent dielectric permittivity of a substance, ϵ' is its real part, $\tan\delta \equiv \epsilon''/\epsilon'_b$ is the dielectric loss tangent.

If the substance has pronounced magnetic properties, a term corresponding to the specific power of heat evolution caused by dissipative processes upon magnetisation should be introduced into Eqn (7)

$$q = \frac{1}{2}\omega\epsilon_0\epsilon'_b\tan\delta|\vec{E}_\omega|^2 + \frac{1}{2}\omega\mu_0\mu''|\vec{H}_\omega|^2, \quad (8)$$

where μ_0 is the magnetic permittivity of vacuum, μ'' is the imaginary part of the magnetic permittivity of the substance, \vec{H}_ω is the magnetic field strength complex amplitude.

It can be seen from Eqn (8) that the intensity of heat evolution in a sample being treated depends on many factors, in particular, on electrophysical properties of the material, the frequency and the intensity of the applied field. Note that this equation implies circumstantially the dependence of the heating efficiency on various parameters including the geometric size of the treated sample and the resonator cavity. As characteristics of the microwave treatment system largely depend the field amplitude in the sample, they also affect the heat evolution in its body. For irradiation of a sample with a flat electromagnetic wave with all parameters except ϵ'' being fixed, the highest heating power is observed at some ϵ'' value specific for the given substance. Below this value, the wave would pass through the sample without being significantly absorbed, while above this value, the wave would be largely reflected from the sample.

When selecting the conditions for microwave heating, it is important to take into account the depth of penetration of the electromagnetic wave into the substance under treatment. This factor greatly affects the distribution of the field amplitude in the sample and, hence, uniformity of heat distribution.^{18–21}

If the depth of field penetration into the matter (δ_E) is defined as the distance at which the field strength decreases e -fold (e is the Napierian base), then

$$\delta_E = \frac{\lambda}{\pi \sqrt{2\epsilon'(\sqrt{1 + \tan^2 \delta} - 1)}} \quad (9)$$

If $\tan \delta \ll 1$, then

$$\delta_E = \frac{\lambda}{\pi \sqrt{\epsilon' \tan \delta}} \quad (10)$$

Thus, an increase in frequency entails an increase in not only the heating power but, unfortunately, also in the heating non-uniformity; this may imply overheating of the outer layers of the sample. The penetration depth of the microwave field into material can vary over broad ranges, from several microns to several metres. For example, at 25 °C, the penetration depths of the radiation with 2.45 GHz frequency into copper and graphite are 2.6 and 38 μm , while those into epoxide resin and alumina are 0.73 and 187 m, respectively. If the geometric size of the sample is much larger than the penetration depth of the microwave radiation, heating of the sample will be non-uniform.

It is noteworthy that the δ_E value characterises the heat treatment depth only to a first approximation, because the field penetrates to a greater depth, and its energy may be sufficient for the required heating effect. The dielectric parameters of the matter, and, hence, the penetration depth depends on temperature and can change during heating. Thus, the depth of heat treatment during given technological process can be determined exactly by solving the problem of temperature field in the volume of sample. It is important not only to choose the optimal frequency and amplitude of the electromagnetic field, but also to select the resonator geometry.

In standard domestic microwave ovens with a rectangular resonator (these ovens are still used in most experiments), materials with medium conductivities, *i.e.*, semiconductors, oxides with mixed metal oxidation states, and some powdered metals, are heated more efficiently than good conductors (some metals) or dielectrics (oxides and halides) (Table 1).

This effect may be due to the fact that dielectric losses at room temperature are low for insulators; therefore, no effective heating takes place, although the microwave field penetrates to a high depth. In the case of metals, the microwave radiation is considerably reflected.⁹ Thus, effective heating of substances with low or, conversely, high ϵ'' values requires selection of

Table 1. Efficiency of microwave heating of substances with different types of conduction (radiation frequency 2.45 GHz, power 800 W).^{9,10}

Substance	Resistivity / Ω m	$T/^\circ\text{C}$	Heating duration /min
Metal powders			
Al	$10^{-8} - 10^{-6}$	577	6
Co	$10^{-8} - 10^{-6}$	697	3
Cu	$10^{-8} - 10^{-6}$	228	7
Fe	$10^{-8} - 10^{-6}$	768	7
Mg	$10^{-8} - 10^{-6}$	120	7
Mo	$10^{-8} - 10^{-6}$	660	4
Semiconductors			
FeS ₂	$10^{-5} - 10^{-3}$	1019	7
PbS	$10^{-5} - 10^{-3}$	956	7
CuFeS ₂	$10^{-5} - 10^{-3}$	920	1
Oxides with mixed oxidation states			
Fe ₃ O ₄	$10^{-4} - 10^{-2}$	1258	3
Co ₃ O ₄	$10^{-4} - 10^{-2}$	1290	4
NiO _x	$10^{-4} - 10^{-2}$	1305	6
Graphite	~ 10	1300	4
Alkali metal halides			
KCl	$10^4 - 10^5$	31	3
KBr	$10^4 - 10^5$	46	1
NaCl	$10^4 - 10^5$	83	7
NaBr	$10^4 - 10^5$	40	4
LiCl	$10^4 - 10^5$	35	1
Oxides			
SiO ₂	$10^4 - 10^{14}$	79	7
Al ₂ O ₃	$10^4 - 10^{14}$	78	4
Salts			
KAlSi ₃ O ₈	$10^4 - 10^{14}$	67	7
CaCO ₃	$10^4 - 10^{14}$	74	4

optimal geometric parameters of the resonator. It is often a complicated engineering problem.

In heterogeneous systems containing phases with different dielectric properties, an external electromagnetic field may produce charges at interfaces (the Maxwell–Wagner effect). It has been shown²² that the simplest and most correct description for this type of polarisation is provided by the model of spherical particles of a highly conducting phase distributed uniformly in a dielectric. The reactive component of the dielectric permittivity of such a system can be described by the equation

$$\epsilon_i'' = \frac{(9V\epsilon\omega_{\max})\omega\tau}{1.8 \times 10^{10}\sigma(1 + \omega^2\tau^2)}, \quad (11)$$

where V is the volume fraction of the dispersed phase; ω_{\max} is the circular frequency of the electromagnetic field corresponding to the maximum loss for the dielectric phase; τ is the relaxation time of the dielectric (the time span during which the system returns to the equilibrium state after removal of the electromagnetic field); σ is the conductivity of the dispersed phase. This model was verified experimentally using paraffin with dispersed isotropic particles of copper phthalocyanine as a semiconductor.²³ A good correspondence between the theoretical and experimental results was noted (Fig. 2).

Unfortunately, the contribution of the Maxwell–Wagner effect to the solid- and liquid-phase transformations occurring under microwave irradiation has not been quantitatively

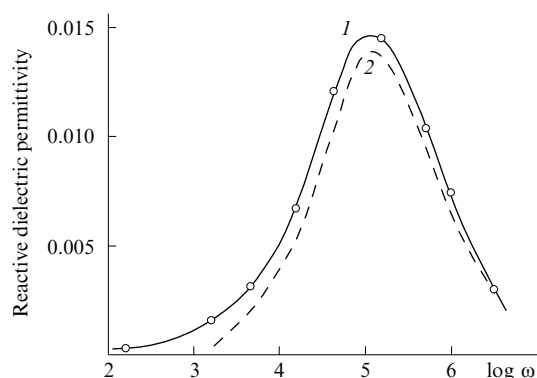


Figure 2. Frequency dependences of the reactive component of the dielectric permittivity of the copper phthalocyanine-paraffin system.²³ (1) Experimental data, (2) calculation by the Maxwell-Wagner model.

estimated as yet. Nevertheless, in some studies (see, for example, Ref. 12), it was suggested that surface polarisation is responsible for the so-called 'non-thermal' effects of microwave treatment resulting in acceleration of processes in a microwave field.

Apart from the above-described features of the propagation of microwave radiation and its interaction with the matter, an important role in microwave heating is played by thermophysical properties of the sample, because the efficiency and uniformity of microwave heating depend on not only the dielectric properties of the material, but also its ability to dissipate the evolved heat throughout the bulk. Thus a main cause of non-uniform heating is the sharp increase in the dielectric loss factor with temperature. The rate of heat dissipation in the sample bulk is insufficient, and areas with higher temperature characterised by more intense absorption of microwave radiation appear in the sample (the so-called 'hot spots'). Thus, despite the widely accepted view that microwave heating produces uniform dissipation of heat throughout the sample bulk (see above), one should thoroughly select the experimental conditions to avoid sharp temperature differences within the sample.²⁴⁻²⁶

When performing any experiments on microwave heating, it is necessary to take into account the following properties of the sample material.

1. Electronic and ionic conduction. There exists an optimal range of electronic conduction that ensures the most efficient interaction of the matter with the microwave field: good insulators are transparent for the microwave field, while substances with high electronic conductivity (metals) reflect microwave radiation. Analysis of published data on microwave heating of substances with high ionic conductivity demonstrated that these substances possess rather high absorption capacity. The absence of substances reflecting microwave field due to high ionic conductivity is attributable to the too low concentration of free ionic charge carriers and their relatively low mobility even in the best ionic conductors.

2. Dielectric permittivity and dielectric loss factor. There exists an optimal range for the dielectric loss factor, which determines the absorption capacity of a substance; an increase in this factor entails a decrease in the depth of penetration of the microwave field into the sample. Thus, the more efficiently the substance absorbs, the smaller is the sample that can be heated in a microwave field without formation of temperature gradients within the sample bulk. It should be borne in mind that at low temperatures the contribution of dielectric losses to microwave heating is quite insignificant for most of substances.

3. Heat conductivity. Heating of substances with low heat conductivity usually produces local overheating giving rise to

above-mentioned 'hot spots', because the evolved heat has no time to dissipate uniformly throughout the bulk. Uniform microwave heating requires a relatively high heat conductivity of the sample. The more efficiently the substance absorbs and the more pronounced is the temperature dependence of the absorption capacity, the higher heat conductivity is expected for this substance.

Thus, one can define the main criteria for the selection of chemical systems for microwave heating and the range of problems that can be solved using this way of heat supply to condensed matter.

1. Non-uniform temperature distribution within the sample bulk can be avoided if the microwave-treated substance has rather high heat conductivity. In each particular case, it is necessary to determine experimentally the maximum dimensions of the sample of a given substance (or a mixture of substances) that can be heated uniformly throughout the whole bulk without formation of pronounced temperature gradients.

2. The substances that can be heated by microwave radiation should possess either a high dielectric loss factor (*i.e.*, they should contain mobile dipoles with a relatively high dipole moment) or a high electronic, hole or ionic conductivity at the experimental temperature. It is noteworthy that for specific conductivity of less than $\sim 10^{-5} \Omega \text{ m}$, the sample starts to reflect the microwave radiation. The dielectric properties depend on temperature and, hence, the absorption mechanism can change during heating not only upon chemical transformations in the sample, but also due to a change in the parameters of microwave radiation absorption by the sample.

It is evident that dipole fragments with zero effective charge have the highest mobility in the crystal structure. Among inorganic compounds, water meets best of all the above requirements (high mobility of molecules and high dipole moment). The Reh binder classification, which is based on the work of isothermally reversible detachment of one mole of water from the material framework, distinguishes three main types of binding of water in solid systems: physicochemical (for example, capillary water), physicochemical (for example, adsorption water) and chemical binding (water of crystallisation, hydroxy groups). Chemically bound water is most interesting for solving synthetic problems, because this is characterised by the highest energy of detachment from the crystal lattice (from 20 to 80 kJ per mole of H_2O approximately depending on the number of water molecules removed from the crystal structure), and the supply of this amount of energy often results in decomposition of the dehydrated substance. Thus, salt crystal hydrates and hydroxides appear promising precursors for the microwave synthesis of oxide compounds.

Analysis of published data on the use of microwave heating for the synthesis of inorganic compounds has shown that, despite the large number of publications, no information that allows predicting the efficiency of the use of microwave radiation for heat treatment of chemical systems is available. Most papers discuss experimental data; the choice of starting reactants for the synthesis is not substantiated, and the discussion of the results concerns the microstructure and the structure-sensitive properties of the products but does not include any fundamental conclusions about their dependence on the physicochemical properties of the starting compounds, the way of organisation of the reaction area, or on the mechanism of interaction of microwave radiation with the sample.

Therefore, of particular interest are papers dealing with the theoretical substantiation of the microwave action on a substance. In most studies of this type, augmentation of mass transfer upon microwave treatment is attributed both to uniform heating of the whole sample bulk and creation of the reversed temperature gradient and to specific 'non-thermal' mechanisms of microwave field action on diffusion processes.

A theoretical substantiation^{27–29} of the ‘non-thermal’ activation of mass transfer under the microwave treatment has been proposed.[†] Consider one-dimensional diffusion of a substance in an alternating electromagnetic field. In this case, mass transfer equation has the form

$$\frac{\partial c}{\partial t} = D \frac{\partial}{\partial x} \left[\frac{\partial c}{\partial x} - U(t) \frac{\partial c}{\partial x} \right]. \quad (12)$$

The additional term $U(t)$ depends on external field parameters $U(t) = qE \cos(\omega t/kT)$, where q is the ion or vacancy charge, ω is the circular field frequency, k is the Boltzmann constant, T is temperature.

No analytical equation relating the rate of mass transfer to the electromagnetic field strength and frequency can be derived for the case of three-dimensional diffusion. However, approximate solution provides the conclusion that the most pronounced influence of the microwave field should be expected at an early stage of the solid-phase process and at short diffusion distances. As the time of action of microwave radiation increases, the process gradually becomes steady-state, and according to Bokhan,²⁷ the contribution of the electromagnetic field to the driving force of diffusion rapidly decreases. In conformity with this model, the diffusion fluxes in the matter are directed from regions with high electric field strength to regions with low electric field strength. The diffusion processes are fairly intense, resulting in redistribution of the electromagnetic field strength and, hence, in a change in the direction of diffusion fluxes. As a consequence, the rate of solid-phase processes increases and the temperature of the process onset decreases.

Unfortunately, this approach is too simplified for the mathematical modelling of processes taking place under microwave heating of solid systems, and the experimental verification of the assumptions made by Bokhan²⁷ is today impossible.

Another approach to the theoretical substantiation of the ‘non-thermal’ effects of microwave heating has been reported.^{30–32} It was assumed that a high-frequency electromagnetic field should create fluxes of charged species (ions or vacancies) in the matter, their intensity being changed in parallel with the strength of the external electromagnetic field. Within the sample bulk, these fluxes counterbalance one another and the overall concentration of charged species remains spatially uniform; however, near the surfaces, discontinuity of the medium gives rise to harmonic oscillations of the charged species concentrations the frequency of which coincides with (or is close to) the electromagnetic field frequency (Fig. 3).

It has been asserted³⁰ that oscillations of this type produce uncompensated fluxes of charged species along any extended crystallite imperfections (free surfaces, phase interfaces or grain boundaries). In the opinion of the researchers cited, this is responsible for the fact that microwave treatment does not increase the rate of charged species migration, but creates an additional driving force for diffusion (F), which is defined by the following expression:

$$F = \frac{c_i}{c_i^0} q_i E, \quad (13)$$

where c_i is the concentration of the i th sort of charged species at the crystallite boundary under the action of an external electromagnetic field, c_i^0 is the concentration of the i th sort of charged species at the crystallite boundary in the absence of an

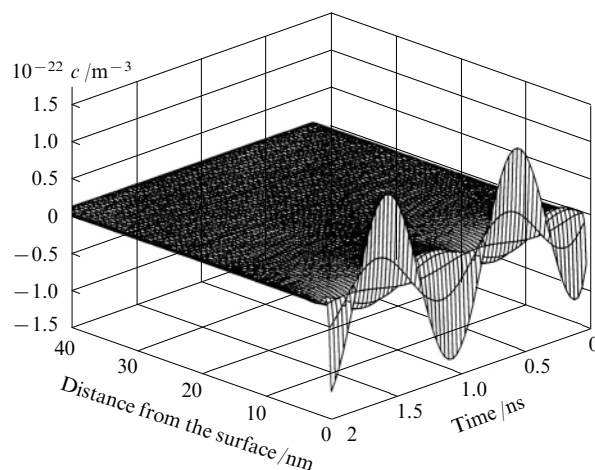


Figure 3. Time dependence of the variation of the concentration of charged species (c) near the surface and in the sample bulk upon the action of high-frequency electromagnetic field (calculated).³²

external electromagnetic field, q_i is the charge of the i th sort of charged species.

According to this theory, the more dispersed the system under treatment, the stronger the ‘non-thermal’ microwave effects. The effect of an external electromagnetic field on the ionic current in the NaCl crystal was studied in order to confirm this hypothesis (Fig. 4).³² It was stated that the experimentally detected change in the ionic current density in the NaCl crystal located in an external electromagnetic field is equal to the calculated gain in the ionic current induced by the microwave field.

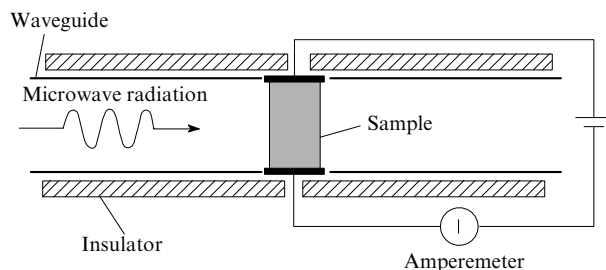


Figure 4. Setup for measurement of the ionic current in a NaCl crystal.³²

It is clear that the proposed model of the ‘non-thermal’ microwave effects on the diffusion processes can hardly be practically verified. Indeed, it is not clear whether the experimentally mentioned above (see Fig. 4) allows one to draw unambiguous conclusions about the change in the mass transfer mechanism during the solid-phase reaction under microwave heating. In any case, verification of this model requires additional experiments.

III. Design and key principles of operation of microwave heating systems

Almost all microwave heating facilities are designed according to a chart shown in Fig. 5. The microwave energy comes out of the source through transmission line and is directed to the working chamber into which the sample is supplied through a loading system. The fraction of energy absorbed by the sample depends on the sample size and electrophysical characteristics briefly considered above. The microwave treatment parame-

[†] The information was partially gained from a Yu I Bokhan’s private communication.

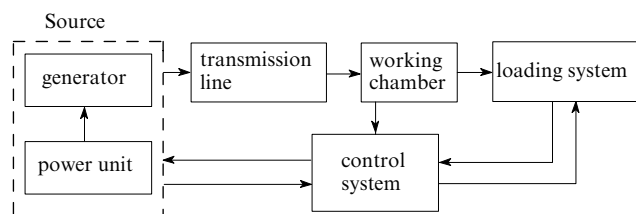


Figure 5. Microwave heating unit.¹¹

ters are controlled by the control system. Some devices envisage a 'feedback', which allows the change in the supplied power during heating following a change in the sample temperature (or pressure in the case of treatment in an autoclave).[‡]

Currently there is no generally accepted classification of microwave heating facilities. Arkhangelskii¹¹ proposed a classification (Fig. 6) in which the power, the design, the mode of operation and the technological purpose of the setup were taken as the determining features. Detailed consideration of the operation principles and the possible designs of microwave heating devices is beyond the scope of this review; therefore, we will present only a brief analysis. More detailed information on this topic can be found elsewhere.^{7, 11, 12, 19, 20} The designs and the main operation principles of magnetron systems will be considered in somewhat more detail, because most studies have been performed using domestic microwave ovens or devices based on them. An important part of the microwave heating device is the working chamber in which the sample is treated. When designing or choosing the working chamber, it is reasonable to consider its dimensions, the pattern of field distribution and type of transmission line as the principal parameters (Fig. 7).

Magnetron is used most often as the microwave radiation source for the synthesis and sintering of oxide materials. Among other sources, mention should be made of gyrotron

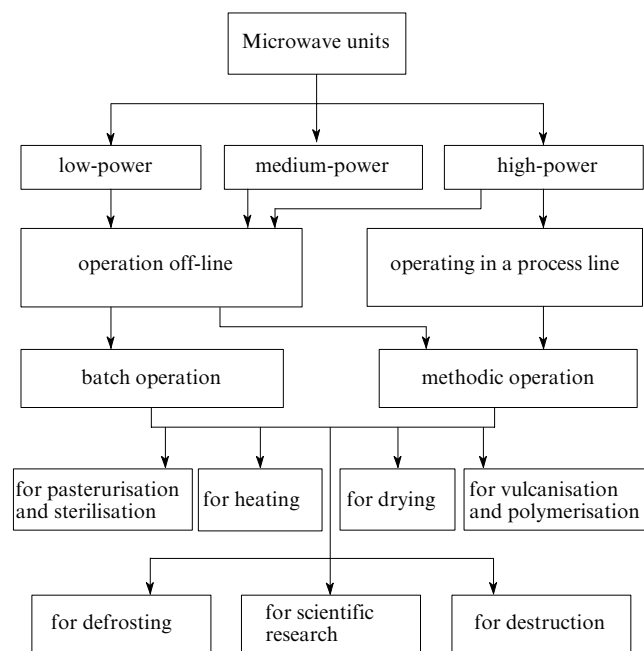


Figure 6. Classification of microwave heating units.¹¹

[‡] Unfortunately, commonly used domestic microwave ovens lack this feedback.

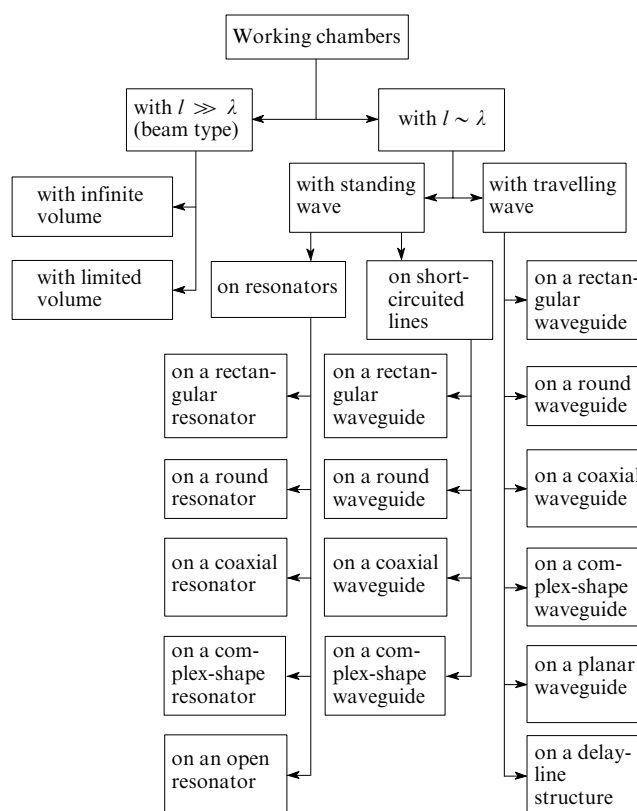


Figure 7. Classification of the working chambers of microwave heating units.¹¹

systems with a radiation frequency of ~ 30 GHz designed at the Institute of Applied Physics of the RAS, klystron tubes and microwave triodes.²⁰ Due to the high radiation frequency, treatment in gyrotron systems is more efficient and less sensitive to the electrophysical characteristics of the material. The gyrotron microwave heating systems are fairly promising for syntheses and especially for sintering. Unfortunately, the complexity of the design and high cost of gyrotron systems hamper their extensive use in scientific practice.

On the one hand, devices based on domestic microwave ovens are used most widely, but on the other hand, they are least adapted for experiments under definitely specified and reproducible conditions. Therefore, it is expedient to consider the operation principle of domestic microwave ovens and the key parameters affecting the operation, in order to find whether it is possible to carry out experiments under controlled conditions in these ovens and what should be done to achieve this goal.

The magnetron used in domestic microwave ovens is a cylindrical diode onto which a magnetic field directed along the cathode is applied. The potential between the cathode and the anode representing a ring of linked cavity resonators reaches several thousand volt. In the non-adjustable magnetron, the oscillators are designed in such a way that they emit energy with a particular frequency. Most domestic microwave devices make use of non-adjustable magnetrons with an output frequency of 2450 ± 13 MHz. This magnetron consumes ~ 1200 W from the supply line; this is converted into a 600 W electromagnetic power output. The rest is converted into heat, which is dissipated by air cooling. The designs of magnetrons and other microwave emitters are described in detail in specialised literature (see, for example, Refs 7, 19 and 20).

In estimation of the power of domestic microwave systems, the averaged rather than the full output power of magnetron is

used. The magnetron duty factor, *i.e.*, the ratio of the time the magnetron is switched on (t_1) to the sweep time (t_s), is used for this purpose. Thus if $t_1 = 5$ s and $t_s = 10$ s, the duty factor is 0.5. Hence, in order to obtain the average radiation power of 300 W (half of the output power), the magnetron of domestic microwave oven should be switched on during some time t_1 and switched off during time t_2 . Domestic microwave ovens usually have the sweep time equal to

$$t_s = t_1 + t_2 = 10 \text{ s.}$$

This long sweep time is undesirable for microwave heating of substances and materials, because with magnetron being switched off for a long period (5 s for a duty factor of 0.5), the loss of heat can be rather high. Most of laboratory microwave heating equipment have shorter sweep times, which is much more convenient for experiments, especially for heating of solids. Many modern facilities provide for the fine power adjustment without switching-off the magnetron.

The full output power of the magnetrons of domestic microwave ovens is usually about 600–700 W. A simple method for its determination is to measure the temperature of a fixed mass of water able to absorb almost all energy supplied to the resonator. Usually, the apparent output power is determined by measuring the temperature of 1 litre of water heated during 2 min at the full magnetron power.

Equation for the calculation of the apparent output power (P/W) has the form⁴

$$P = Kc_p \frac{\Delta Tm}{t}, \quad (14)$$

where K is the conversion factor of the thermodynamic units cal min^{-1} into Watts; c_p is the specific heat capacity/ cal deg^{-1} ; $\Delta T = T_{\text{f}} - T_{\text{u}}$ (the difference between the final and initial temperatures/ $^{\circ}\text{C}$); m is the sample mass/g; t is time/s. If the heated substance is water, Eqn (14) can be simplified

$$P = 35 \frac{\Delta Tm}{t}, \quad (15)$$

where the numerical multiplier includes the conversion factor and water heat capacity. The correctness of power determination depends on the arrangement of sample inside the resonator and on the identity of the containers used. Since energy scattering by a dielectric and energy loss as radiation depend on temperature, the same initial temperature and approximately equal differences ΔT should be used. Power determination is most accurate if the initial temperature of water is equal to 20 ± 2 $^{\circ}\text{C}$.

The output power of the magnetron is markedly affected by the overheating due to reflection of a part of radiation back to the magnetron. The modes that ensure energy transfer from one medium to another without reflection are called wave coupling match. A mismatch may result in magnetron overheating, loss of output power or even failure of the magnetron.⁴ For magnetron protection in case of wave coupling mismatch and for reaching the required output power, devices that eliminate reflection of microwave radiation have been designed. Domestic microwave ovens are usually devoid of such devices, but they are stipulated in industrial microwave systems. The device used most often is the output circulator (ferrite valve or the Faraday isolator), which allows microwave radiation to propagate in the forward direction but directs the reflected radiation to an absorber located outside the resonator, which is a heavy ferrite rod where energy dissipates as heat without damaging the microwave device.⁷ The magnetron-generated microwave radiation is transmitted to the working chamber (resonator) by means of a waveguide made of a reflecting material, for example, a metal sheet.

Considering the working chamber classification shown in Fig. 7, one can see that the working chamber of a domestic microwave oven is a rectangular resonator with stationary waves. In such devices, it is often rather difficult to achieve uniform heating of a sample. In most domestic devices, this problem is solved using a rotating sample holder (usually, as a dish). There exist rotating holders that continuously rotate by 360° and cyclic holders rotating in both directions by 180° . Alternating rotation is used when the sample has various detectors attached. Unfortunately, all these methods for equalisation of the field energy density throughout the resonator volume do not ensure uniform heat treatment of the sample.¹¹

In conclusion of this Section, we will consider a highly important problem of temperature measurement during microwave heating of the sample. Correct measurement of the process temperature is a very complicated problem. A faulty way of introducing a temperature indicator and perturbations induced by the microwave field on the measuring instrument may give rise to substantial errors in the temperature measurement and, hence, in the evaluation of the efficiency of microwave heating.

The use of conventional bimetallic thermocouples is precluded under microwave heating conditions, because a high-frequency electromagnetic field generates additional currents in the thermocouple and induces disturbance on measuring devices. In addition, the introduction of a metallic item into the resonator changes the distribution of the microwave field power, which may result in local overheating.⁴ The only solution to this problem is the use of a screened thermocouple grounded to the resonator wall. It is necessary to determine beforehand the position at which the thermocouple would not disturb the uniform distribution of microwave energy over the resonator volume. Currently, the patterns of electromagnetic field distribution over resonators with different geometries have been determined both experimentally and by calculations.

If the sample is relatively large, the gradients formed upon microwave heating preclude the possibility of accurate characterisation of the sample temperature using only one detector. Accurate temperature measurement requires a good contact between the sample and the measuring detector, which may pose problems if the sample changes its volume or moves during the experiment. The use of other contact methods of temperature measurement is markedly complicated by such effects as indicator heating, screening and local overheating at the site of detector contact with the heated body.^{5,9} When optical devices are used for temperature measurement, it is necessary to establish an accurate correlation between the radiating power of the sample in the given wavelength range and the sample temperature. Apart from temperature, the radiation intensity depends on the state of the sample surface and on the sample homogeneity. If the optical device for temperature measurement and the heated item are separated by a barrier (for example, in domestic microwave ovens, the working chamber door is usually made of metallic grid), it is necessary to take into account attenuation of the radiation from the heated item, as part of radiation is absorbed by the barrier. It should be borne in mind that the attenuation factor depends appreciably on the radiation wavelength. These difficulties can be overcome by using a pyrometer, which measures the temperature based on the ratio of radiation intensities of the sample at two different wavelengths.

IV. Use of microwave heating for the synthesis of individual and complex oxides

It was noted above that microwave radiation is a promising alternative to usual heating for performing various processes including sintering, dehydration, decomposition of salts and hydroxides for the synthesis of individual and multicomponent

compounds, solid-phase and liquid-phase syntheses.⁷ A rather well-developed theory allows one to predict how efficiently a particular substance will absorb microwave radiation. Nevertheless, in practice, it is very difficult to predict the system behaviour in a microwave field. This is mainly due to the fact that electrophysical characteristics that determine the absorption capacity of substances are highly temperature-dependent: as the substance is being heated in a microwave field, its absorption capacity continuously changes. Exact account of this phenomenon is complicated, and data on the temperature dependence of the absorption capacity have been fully accumulated to date only for a limited range of compounds. Apart from the electrophysical characteristics, the heat conductivity and heat capacity of substances and, in many cases, also their micromorphology also change during heating. The change in these parameters affects the absorption of the microwave energy by the substance. Elucidation of the influence of each of the listed parameters on the system behaviour in a microwave field is hardly possible; however, since these characteristics change rather smoothly and monotonically, the heating dynamics can be roughly estimated.

This task becomes much more difficult if chemical processes take place in the system during heating. Upon changes in the chemical and phase composition, electrophysical characteristics of the system change jumpwise and often uncontrollably. As the temperature rises, the sample properties also change. Therefore, it is almost impossible to predict the absorption capacity of the system in which a chemical reaction occurs. This accounts for the lack, in the vast majority of publications, of data on the system behaviour under microwave treatment or attempts at its targeted use for performing processes with allowance for this information.

From the chemical standpoint, sintering is the simplest process; it is not by chance that this application of microwave heating is best studied. Most often, sintering does not change the chemical or phase composition of the sample; the change in the absorption capacity is mainly due to a change in density and grain composition during heating. These characteristics change rather monotonically; therefore, in most cases, one can control sintering to achieve specified results.

Starting with the 1970s, a large number of publications have been devoted to the use of microwave heating for sintering of various materials ranging from weakly absorbing compounds (Al_2O_3 , TiO_2) to compounds that actively interact with the microwave field even at room temperature (SiC , TiB_2 , B_4C).^{33–66} The main advantages of microwave-assisted sintering include high rate and uniformity of heating. This gives rise to ceramics with a more homogeneous microstructure compared to ceramics produced by traditional methods.^{67,68}

Thirty years ago the first experiments on sintering of alumina and zirconia in a microwave unit with a radiation frequency of 2.45 GHz were carried out.³³ This demonstrated both the advantages (high rate of sintering, uniform heating of the whole sample bulk) and specific drawbacks (complexity of temperature measurement and risk of local overheating) of microwave heating. Subsequently, microwave sintering of β -alumina has been studied.^{34,35} It was found that microwave treatment leads to substantial (severalfold) decrease in the sintering time required to reach a nearly theoretical density of the material. Nevertheless, no fine-grain ceramics with a narrow grain size distribution have been obtained in these studies.

The temperature and time dependences of the density of yttrium and cerium oxide-doped zirconia samples during sintering in a microwave oven and in an electric resistance furnace have been considered.³⁶ In the case of low-temperature exposure, samples sintered in a microwave oven had higher density. Nevertheless, nearly theoretical densities are attained in both cases only at temperatures of about 1500 °C. Gener-

ally, the change in the time dependences of sample densities indicates that microwave-induced sintering proceeds at an appreciably higher rate. In addition, samples with equal densities are characterised by much smaller crystallites when sintered in a microwave field. Experiments on microwave field-induced sintering of alumina powders have been described.^{37,41,42} It was shown that densities and microstructures of samples sintered in a microwave oven and in an electric resistance furnace are actually equal. Upon comparison of the results of these studies, one can suggest that the influence of microwave heating on the grain shrinkage and growth during sintering is manifested to a higher extent in substances with ionic conduction than in dielectrics. This probably can be attributed to intensification of diffusion processes caused by microwave field excitation of ionic currents in samples possessing ionic conduction.

Apart from papers devoted to microwave heating of alumina, titania and zirconia, a large number of publications dealing with sintering of oxide powders with complex compositions have appeared in recent years. Microwave radiation has been successfully used^{44,45} for sintering of lead zirconate titanate- and mixed niobium and magnesium zirconate-based powders (PZT and PMNT, respectively) used as piezoelectrics. Note that the use of a microwave system with a magnetron operating at 2.45 GHz⁴⁴ did not result in better ceramic properties compared to those obtained by conventional sintering techniques. Meanwhile, ceramics with much more uniform size distribution of crystallites was produced using a gyrotron system with radiation frequencies of 30 and 83 GHz. Microwave heating was also successfully used for sintering of nanocrystalline hydroxylapatite powders.⁴⁶ The compacted samples reached a density of 95% of the theoretical after a 5-min treatment and 98% after a 15-min treatment, and the microhardness of the ceramic samples was as high as 5.9 ± 0.8 GPa.⁴⁶

Manganese nickel, nickel zinc and nickel copper zinc ferrite powders were sintered using a high-power (3 kW) microwave radiation with a 2.45 GHz frequency.^{47,48} The microstructure and the magnetic properties of the ceramic samples thus obtained were not inferior to the properties of samples annealed in a conventional furnace. The degradation during annealing is much slower for ceramics with a 'microwave' prehistory. The ceramics thus formed was used for the design of multilayer chips the magnetic properties of which were not inferior to the properties of chips manufactured using standard industrial processes, while the manufacture time was significantly reduced.

It is noteworthy that owing to the relative ease of changing the electrophysical characteristics of a sample during sintering, it is often possible to distinguish and describe the specific effects of microwave treatment. Many researchers noted a considerable decrease in temperature during microwave sintering with respect to control experiments carried out using an electric resistance furnace. The most significant result was attained by Janney and Kimrey,^{52,53} who managed to reduce the sintering temperature of an Al_2O_3 powder by 400 °C using radiation at 28 GHz. The decrease in the sintering temperature of ZrO_2 ,^{54,55} $\text{ZrO}_2 - \text{Al}_2\text{O}_3$ composite ceramics⁵⁶ and LaCrO_3 (Ref. 57) was also reported. Similar results were obtained for sintering of ceramics based on oxygen-free compounds, for example, B_4N (Ref. 58) and Si_3N_4 .^{59,60} Analysis of published data showed that the decrease in the sintering temperature is more pronounced at higher frequencies of electromagnetic radiation.^{61,62} A considerable decrease in the sintering temperature can be achieved for microwave heating of dielectrics or ionic conductors but not for electronic conductors, which suggests the influence of the microwave field on the diffusion processes taking place during sintering of powders.^{5,63,64} Unfortunately, the validity of such assumptions largely

depends on the correctness of temperature measurement in the microwave field. In most cases, even using screened thermocouples and fibre optic systems for temperature measurement, one cannot state unambiguously that a significant lowering of the sintering temperature was attained during microwave heating. Indeed, a very thorough investigation of the sintering of stabilised ZrO_2 was carried out.⁶⁹ The sample shrinkage was monitored by dilatometric measurements *in situ*. It was shown that the microwave effect that cannot be reduced to the thermal component does actually exist; however, its contribution is moderate: under identical conditions, shrinkage in a microwave field to the same density as in the case of heat treatment takes place at a 50–80 °C lower temperature. In addition, the contribution of the ‘non-thermal’ factor decreases with an increase in the temperature. This was attributed⁶⁹ to the decrease in the field strength within the sample with an increase in the temperature. Thus, the results of studies published in Refs 52–57 appear to be not quite reliable, as the temperature measurement during sintering was, most likely, improper.

Many researchers totally deny the fact of lowering of the sintering temperature in a microwave field. For example, Levinson *et al.*,⁶⁵ who studied sintering of zinc oxide powders, did not notice any substantial difference between the sintering time in a microwave field and in an electric resistance furnace. In a study³⁹ devoted to the microstructure and the ionic conduction of yttrium oxide-doped ZrO_2 ceramics sintered in a microwave field, no significant differences were noted between the microstructures and properties of samples obtained by microwave treatment and in an electric resistance furnace, except for some decrease in the sintering time. In another publication,⁴⁰ it was concluded that the difference between the properties of ceramics obtained by microwave and conventional sintering is insignificant.

In view of these different opinions, one can suggest that the effect of microwave treatment on the sintering processes depends appreciably on the chemical nature of the sample, in particular, the type of conduction. On the one hand, microwave and thermal sintering of dielectrics and substances with considerable electronic conduction almost do not differ, but on the other hand, the rate of compaction of clear-cut ionic or hole conductors is much higher in a microwave field.

On passing to more complex processes, namely, to the synthesis of individual oxides by decomposition of salts or hydroxides, it is much more difficult to control the absorption properties of the sample and to identify the effect of microwave radiation on the processes. During the synthesis of individual oxides, microwave radiation is mainly used in order to obtain more uniform grain-size composition of the resulting powders and a smaller average particle size. A few papers are devoted to the synthesis of oxide particles with a controlled habit. For example, star-like Cu_2O particles were prepared by microwave-assisted treatment of a copper sulfate solution with sodium hydroxide in the presence of a complex composition containing a surfactant and ascorbic acid as the reducing agent.⁷⁰ Well crystallised copper oxide was prepared by hydrolysis at 95 °C. On the basis of these results, it was concluded that the particle size distribution and habit depend appreciably on the method of heating and on the concentration of a copper sulfate solution. Conventional heating gives rise to cubic copper(I) oxide crystallites with a rather broad size distribution. The use of microwave heating results in practically monosized star-like crystallites. An increase in the concentration of the starting solution of copper sulfate in both cases resulted in particles with a nearly spherical habit. This was attributed to enhancement of the homogeneous nucleation in the case of microwave heating, which suppresses secondary nucleation and promotes fast uniform growth of the nuclei.

The synthesis of zirconia powders by hydrolysis of aqueous ethanolic solutions of zirconyl chloride under microwave treat-

ment has been described.^{71, 72} The uniform heating of the whole bulk of the solution in the microwave field afforded ZrO_2 powders with spherical particles having a monomodal size distribution. It is of interest that, as in the study of Fetter *et al.*,⁷³ microwave heating resulted only in the tetragonal ZrO_2 modification. However, in another study,⁷⁴ the monoclinic modification formed under similar conditions.

Nanocrystalline tin(IV) oxide⁷⁵ and SnCl_2 –graphite composites⁷⁶ were synthesised by hydrolysis of a saturated solution of tin(IV) chloride. The authors emphasised that tin oxide prepared by these procedures is formed in the nanocrystalline state only when microwave heating is used. In their opinion, this is due to acceleration of the olation–oxolation processes in amorphous precipitates under microwave treatment and also to the fact that owing to the uniform heat supply, nucleation predominates over the growth of nuclei.

The synthesis of NiO , ZrO_2 and CeO_2 powders by microwave-assisted hydrolysis of aqueous solutions of the corresponding metal salts in the presence of urea has been described.⁷⁷ It was shown that uniform heat supply to the heated solution produces oxide powders with spherical particles with a narrower size distribution compared to powders obtained by hydrolysis with conventional heating (Fig. 8).

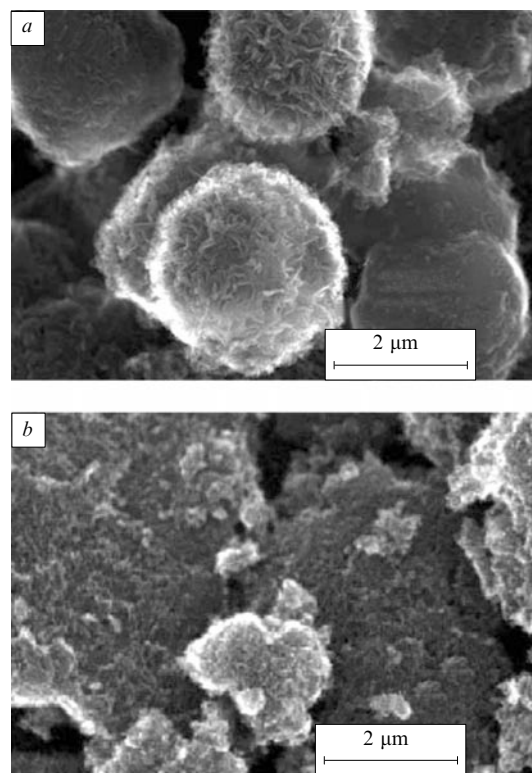


Figure 8. Microphotographs of ZrO_2 powders synthesised by hydrolysis of an aqueous ethanolic solution of zirconyl chloride in a microwave oven (a) and in a conventional furnace (b).⁷⁷

Spatz *et al.*⁷⁸ prepared titanium dioxide nanoparticles from solutions of various titanium alkoxides in reverse micelles of polymeric molecules (Fig. 9 a). It was shown that the sharp decrease in the duration of the synthesis and selective heating of a microquantity of a titanium alkoxide solution inside the micelle allows one to avoid evaporation of HCl , which stabilises micelles, and thus prevent aggregation of TiO_2 nanoparticles in a polymeric matrix (Fig. 9 b).

In recent years, publications dealing with the synthesis of various nanodispersed materials by ‘soft chemistry’ techniques

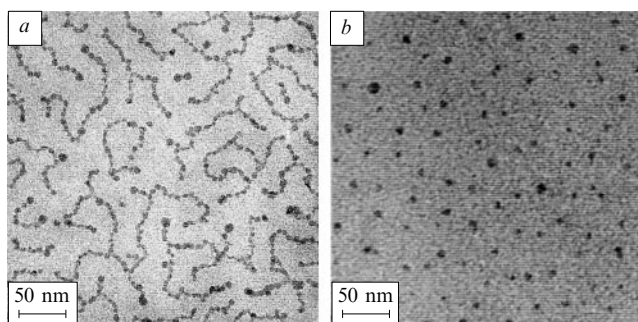
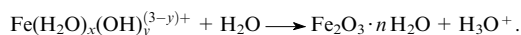


Figure 9. Microphotograph of titanium nanoparticle images in a polymer matrix synthesised in a conventional furnace (a) and a microwave oven (b).⁷⁸

using microwave treatment have appeared more and more often. Many of these publications are devoted to the synthesis of various sulfides and nitrides,^{79–85} but some works deal with the synthesis of nanosized oxides. For example, copper(II)-oxide-based nanostructures have been synthesised.^{86,87} The micromorphology of the obtained powders was shown to be substantially affected by the chemical nature of the initial compounds and the surfactant concentration. For example, hydrolysis of copper acetate in the presence of poly(ethylene glycol) affords virtually isotropic highly aggregated CuO particles, while hydrolysis of an aqueous solution of CuCl₂ in the presence of 1-*n*-butyl-3-methylimidazole tetrafluoroborate yields slightly aggregated nanowhiskers and nanoplates with a narrow size distribution. Note that by using microwave radiation, it is possible to increase substantially the rate of synthesis and increase the degree of crystallinity of the products.

High-temperature hydrolysis of an aqueous iron chloride solution in the presence of poly(ethylene glycol) and urea as the precipitating agent gave an Fe₂O₃ powder with a particle size of 3–5 nm.⁸⁸ However, despite the presence of a surfactant in the solution, powder particles were highly aggregated as shown by transmission electron microscopy. The results of magnetic measurements showed that, as expected, iron oxide nanoparticles occurred in the superparamagnetic state. During annealing at 400 °C, the oxide was crystallised to give α-Fe₂O₃; this was accompanied by an increase in the particle size to 30–40 nm. The researchers discussed the possible mechanism of formation of iron oxide upon high-temperature hydrolysis. According to calorimetric data, the following reaction takes place as an intermediate stage of the process



More uniform heating of the solution exposed to microwave radiation favours the formation of a large number of hydrated oxide nuclei.

The synthesis of nanocrystalline SnO has been reported.⁸⁹ Hydrolysis of an aqueous solution of tin(II) chloride in the presence of ammonia as a precipitating agent afforded tin oxide powders with an average particle size of 30 nm and a specific surface area of ~40 m² g⁻¹. It is of interest that unlike usual heating, microwave heating almost does not induce the oxidation of Sn²⁺ ions to Sn⁴⁺. This was attributed to the fact that, as shown by additional experiments, tin(II) oxide absorbs microwave radiation much more intensively than tin(IV) oxide. The researchers also noted that it was impossible to establish the exact mechanism of the specific ‘non-thermal’ microwave radiation effect in this experiment. The study cited⁸⁹ is a rare example of successful use of the above-discussed change in the absorption capacity of the system upon the change in its phase or component composition.

The synthesis of nanocrystalline SnO₂ by hydrolysis of an aqueous solution of tin(IV) chloride in the presence of urea has been described.⁹⁰ Highly aggregated powders with a crystallite size of ~3 nm were obtained. During the subsequent annealing of these powders, regular particle coarsening and coalescence take place up to micron-size aggregates. The advantage of using microwave radiation is reduced in this case to an increase in the hydrolysis rate.

The synthesis of Mg(OH)₂ nanofibres by hydrolysis of a solution of magnesium hydroxide with a highly dilute aqueous solution of sodium hydroxide supplied through a semipermeable membrane has been reported.⁹¹ Microwave radiation with a relatively low power (20 W) was used and hydrolysis took place at room temperature over a period of 5 days. Owing to these mild conditions, well crystallised magnesium hydroxide powder with 100–150 nm-long and 20–40 nm-thick nanofibre-shaped particles was obtained. The control experiments carried out under similar conditions without microwave heating gave virtually isotropic crystallites with a broad size distribution. Unfortunately, the authors⁹¹ did not discuss the possible mechanism of action of microwave radiation on the crystallisation and the growth of crystallites in this system.

Analysis of the effect of the crystal structure of reactants and the phase composition of the reaction mixture on the intensity of absorption of microwave radiation has been reported.⁹² The author was able to establish the relationship between the crystal structure and absorption capacity of various modifications of Al₂O₃. In particular, it was shown that, owing to the presence of structure-bound water molecules in the mullite-like modification of alumina formed upon hydrolysis of aluminium salts in the presence of alkali metal ions, this compound absorbs microwave radiation much better than α-Al₂O₃ (this oxide is almost transparent for microwave radiation; therefore, it is used for heat insulation of samples during microwave heating). Using this effect, it was possible to perform one-stage synthesis and sintering of β-Al₂O₃-based ceramics without additives that absorb microwave radiation, which are usually added for microwave sintering of alumina-based ceramics.

Microwave heating is also successfully used for sol–gel processes. Thus microwave-induced crystallisation of the SiO₂–TiO₂ xerogel gave⁹³ the phase TS-1 used as a molecular sieve. Crystallisation was shown to proceed at a much higher rate than crystallisation induced by conventional heating (Fig. 10) and the microstructure and the catalytic properties of the product were not inferior to the properties of samples synthesised with conventional heating.

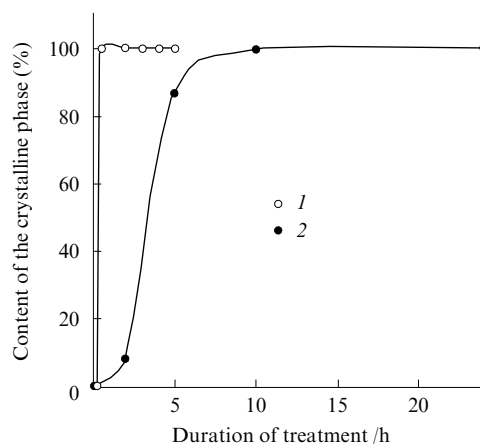


Figure 10. Crystallinity of the TS-1 sample vs. residence time in a microwave oven (1) and a conventional furnace (2).⁹³

The sol–gel synthesis of zirconia-based catalyst powders with copper oxide dispersed over the surface has been reported.⁷³ The effect of pH and the duration of microwave heating on the micromorphology and the catalytic activity of the synthesised powders was established. Upon conventional heating during the sol–gel process, particles of tetragonal ZrO_2 are formed only in the pH range from 3–4 to 13–14, while in the case of microwave heating, these particles are formed irrespective of the pH of hydrolysis of the zirconium *n*-butoxide solution. Unfortunately, the authors offered no interpretation for this finding. Note that the above result⁷³ is at variance with the generally accepted view stating that diffusion processes are intensified in the microwave field, because this field eliminates the kinetic and diffusion hindrance to the metastable modification–stable modification transition. It was also shown that the use of microwave heating results in a more even distribution of copper oxide over the ZrO_2 surface, which in turn results in an increase in the catalyst acidity.

Several papers^{94–96} devoted to the synthesis of highly dispersed cerium dioxide-based catalyst powders using microwave heating have been published. The first of the cited publications represents an attempt to use microwave and ultrasonic treatment for the targeted formation of the micromorphology of cerium dioxide powders prepared by hydrolysis of aqueous solutions of $(\text{NH}_4)_2\text{Ce}(\text{NO}_3)_6$ in the presence of surfactants. As in the studies cited above,^{89–91} microwave-induced high-temperature hydrolysis yielded spherical oxide particles with a rather narrow size distribution. The average particle size was 2–3 nm. Analysis of electron diffraction data showed that the powders were composed of well-crystallised cubic CeO_2 phase. The specific surface area measured by the low-temperature nitrogen adsorption technique was equal to 200–250 $\text{m}^2 \text{g}^{-1}$. Powders with approximately the same micromorphology were synthesised using ultrasonic treatment with conventional heating. The width of the band gap in the resulting nanopowders was 5.5 and 4.1 eV for samples synthesised with ultrasonic and microwave radiation, respectively; that of coarsely crystalline cerium dioxide is 3.19 eV. It is worth noting that the widths of the band gap in the samples with approximately equal average particle sizes obtained by different methods are essentially different. This was attributed⁹⁴ to activation of the surface of particles formed under the action of ultrasound caused by the collapse of cavitation bubbles and formation of microstreams during the sonochemical treatment. The key drawback of this procedure is inevitable contamination of the surface of oxide particles by the surfactant, which would obviously have an adverse influence on the catalytic activity of cerium dioxide.

Solid solutions based on cerium dioxide with partial substitution of zirconium and samarium atoms for cerium were synthesised by thermal and microwave-assisted decomposition of the corresponding nitrates mixed with urea,⁹⁵ glycine, alanine and citric acid.⁹⁶ Presumably, the mechanism of this process is similar to the mechanism of SHS synthesis where metal nitrates act as internal oxidants and urea is the reducing agent. As expected, the oxide particles formed had an order of magnitude greater average size than the particles obtained by Wang *et al.*⁹⁴ (according to X-ray diffraction data, the average particle size was 10–20 nm and the specific surface area was 40–60 $\text{m}^2 \text{g}^{-1}$). An increase in the rate of formation of the oxide phase under microwave radiation was noted.^{95,96} In addition, the effect of the chemical nature of the internal reducing agent on the micromorphology of the oxide powders formed was analysed.⁹⁶ It was noted that the use of citric acid markedly decreases the average particle size (to 6–8 nm); unfortunately, this result was not interpreted.

Hydrothermal synthesis deserves particular attention as an application of microwave radiation in inorganic chemistry. Microwave heating was used for the hydrothermal process to

prepare nanocrystalline strontium, barium and lead titanate, zirconate and niobate powders possessing piezoelectric properties,^{97–99} zinc, nickel and manganese ferrites,¹⁰⁰ various ferrates and bismuthates,^{101,102} layered double hydroxides,¹⁰³ zeolites and molecular sieves^{104–106} and metal powders.¹⁰⁷

As advantages of the microwave-assisted hydrothermal synthesis, most of the cited authors list high rates of phase formation and processes in a microwave field caused by both heat supply features and the possible acceleration of nucleation due to ‘non-thermal’ effects. Thus an order of magnitude higher rate of formation of LiMnO_2 under microwave heating of hydrothermal solutions of lithium hydroxide and $\text{Mn}(\text{O})\text{OH}$ with respect to conventional hydrothermal synthesis has been noted.¹⁰⁸ It was shown¹⁰⁹ that by varying the duration of microwave action, one can control the morphology of the resulting powders. In addition, some hydrothermal processes carried out with microwave heating gave new phases that could not be obtained by conventional methods. For example, titanium and tin phosphates were first synthesised in this way.¹⁰⁶

A promising trend in the use of microwave action is the combination with the sol–gel process. The uniformity and high rate of microwave heating favour fast decomposition of the gel with the formation of powders with narrow particle size distributions. For example, barium molybdate was prepared by precipitation of citrate gels followed by thermal and microwave-induced decomposition.¹¹⁰

The effect of parameters of microwave radiation on the synthesis of layered double hydroxides with hydrotalcite structure by co-precipitation from aqueous solutions of nitrates followed by microwave treatment of the resulting gels has been studied.¹¹¹ The authors were able to prepare layered magnesium aluminium double hydroxides with different cation ratios. For this purpose, they varied the duration and power of microwave action. It was found that the use of microwave heating increases the gel crystallisation rate, which is in line with the assumption of intensification of diffusion processes in a microwave field. Interestingly, the variation of the microwave power is accompanied by parallel variation of the cationic composition. As the power of microwave radiation (W) increases, the Mg : Al ratio in the final product approaches the rated one.[§]

W/W	200	400	600
Mg : Al	5.53	4.54	3.62

This fact was attributed to different diffusion mobility of ions. The researchers also noted¹¹¹ that an increase in the power and duration of microwave heating induces the formation of powders with smaller uniform particles.

The synthesis of LiCoO_2 and $\text{Li}_2\text{Mn}_2\text{O}_{4+\delta}$ powders (used for the preparation of cathode materials) from mixtures of lithium hydroxide hydrate with cobalt (Co_3O_4) and manganese (MnO_2) oxides has been described.^{112,113} It was noted that as regards the particle size and shape, the products of microwave synthesis do not differ much from the powder particles prepared by conventional heating at the same temperature. In both cases, the powder morphology is determined by the morphology of the starting oxides (Fig. 11).

The microwave heating of co-precipitated nickel and aluminium hydroxides was used to prepare nickel aluminate.¹¹⁴ The microwave-induced decomposition of hydroxides yields a single-phase porous nickel aluminate consisting of finely dispersed particles. The attempt to prepare nickel aluminate from gels obtained by hydrolysis of aluminium alkoxide in the presence of nickel nitrate failed: according to

§ The rated ratio of magnesium to aluminium cations is 3.

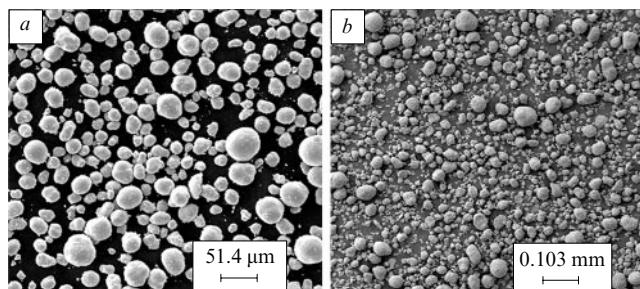


Figure 11. Photomicrographs of initial MnO_2 powder (a) and $\text{Li}_2\text{Mn}_2\text{O}_{4+\delta}$ powder synthesised in a microwave oven (b).¹¹³

IR spectroscopic data, the amorphous intermediate formed upon microwave heating of the gel contained a lot of nitrate ions. Unfortunately, no explanation for the difference between the mechanisms of interaction of various initial mixtures with the microwave field is given in the paper.

Nickel aluminate was synthesised by microwave-assisted decomposition of co-precipitated hydroxides.¹¹⁵ Despite the fairly long microwave treatment of the mixture, the final product was rather poorly crystallised, which is unusual for microwave heating.

The solid-phase reactions between substances that poorly absorb microwave radiation at room temperature are often carried out, like sintering, using the so-called 'hybrid' microwave heating, which implies addition, to the reaction mixture, of a compound that actively absorbs microwave radiation and provides the primary heating of samples. Amorphous carbon or graphite, silicon carbide, copper(I) and copper(II) oxides, MnO_2 , MoSi_2 , etc. are normally used as such additives. Two methods are used most often to introduce the additive, namely, mixing of reactant powders with the powdered absorbing substance and placing the sample into a container made of the absorbing material. Both methods have advantages and drawbacks. Mixing of the reactants with the absorbing additive ensures faster and more uniform heating of the sample; however, there is a risk of contamination of the final product. Placing of the sample into an absorbing container, although decreases the probability of formation of by-products, actually levels-off all the advantages of microwave heating, because in this case, as during of conventional heating, heat is mainly supplied to the sample from the container walls.

Despite these drawbacks, the 'hybrid' microwave heating procedure has found wide use and was employed to synthesise numerous oxide compounds. For example, magnesium aluminate with the spinel structure was prepared by solid-phase reaction of aluminium hydroxide and magnesium oxide in the presence of carbon.¹¹⁶ The optimal amount of the absorbing additive (50 mass %) was found and the micromorphologies and sintering characteristics of powders obtained by microwave and conventional heating were compared. It was shown that the use of microwave heating not only markedly reduces the duration of synthesis but also results in the formation of powders with higher sintering ability. The same method was used to prepare Sr_2CeO_4 ,¹¹⁷ $\text{La}_{0.8}\text{Sr}_{0.2}\text{Ga}_{0.83}\text{Mg}_{0.17}\text{O}_{3-x}$ (Ref. 118) and $\text{Li}_{0.35}\text{La}_{0.55}\text{TiO}_3$.¹¹⁹ In all studies, appreciable acceleration of the solid-phase synthesis upon the use of microwave treatment was noted.

Solid-phase synthesis of a number of niobates and titanates from oxides and salts in the presence of graphite to absorb microwave radiation was carried out.¹²⁰ It was noted that the use of microwave heating reduces the duration of synthesis of these compounds by 1–2 orders of magnitude. This pronounced acceleration of a solid-phase reaction can hardly be attributed to high uniformity and rate of microwave heating

alone; however, researchers¹²⁰ did not make any assumptions on this issue.

If a component of the reaction mixture actively absorbs microwave radiation at room temperature, the reaction can be carried out without an absorbing additive. However, it should be noted that the reactants and products have different absorption capacities, which gives rise to local temperature differentials in the system. This effect was studied in detail¹²¹ in relation to the solid-phase synthesis of barium and yttrium ferrites and nickel aluminate from the corresponding oxides. Each reaction mixture consisted of an oxide efficiently absorbing microwave radiation and a weakly absorbing material (Fe_3O_4 and BaCO_3 , Fe_3O_4 and Y_2O_3 , NiO and Al_2O_3 , respectively). In the researchers' opinion,¹²¹ the particles of highly absorbing oxides functioned as heat sources in the microwave field, while weakly absorbing particles were heat receivers. A permanent temperature gradient was established in the reaction area, which, in turn, resulted in redirection of diffusion fluxes during the solid-phase interaction. Control experiments with the Y_2O_3 and Fe_3O_4 diffusion pair have shown, first, that the difference between the reactant temperatures reaches, in the limiting case, 400 °C, and, second, the diffusion flux is inverted with respect to that observed with conventional heating, in particular, iron ions diffuse in yttrium oxide. It is not quite clear what makes the authors confident that in the case of conventional heating, yttrium ions diffuse into the Fe_3O_4 structure. (In a study¹²² dealing with the mechanism of ferrite formation under conventional heating, diffusion of iron ions into yttrium oxide is considered to be the predominant process.) Nevertheless, this study is of interest for elucidation of specific effects of microwave heating during solid-phase reactions. The diffusion flux is directed from the higher-temperature region to the 'cold' region. If the reaction product actively absorbs microwave radiation, this additionally intensifies the subsequent interaction. The substantial acceleration of solid-phase reactions under microwave treatment observed by many researchers was attributed to this fact.

It is quite probable that the temperature gradient formed during microwave heating of the reaction mixture between reactants with different absorption capacity has actually a considerable effect on the course of reactions, because most data on the acceleration of solid-phase processes concern systems containing both highly and poorly absorbing components. These processes include the preparation of alkali and alkaline-earth metal and lanthanide ferrites, manganites, cobaltites, vanadates, molybdates and cuprates. Uematsu *et al.*¹²³ synthesised Eu^{3+} -doped yttrium vanadate from the corresponding oxides. They also studied the dynamics of absorption of microwave radiation by the reaction mixture depending on the dielectric properties and conductivity of the reactants and the products. It was found that yttrium and europium oxides, like yttrium vanadate, poorly absorb microwave radiation, whereas vanadium oxide intensively absorbs microwave radiation even at low temperatures. After completion of the synthesis, temperature sharply drops, apparently, due to the disappearance of highly absorbing vanadium oxide from the reaction mixture. The authors recommended the use of microwave heating for performing solid-phase processes in which the reactants efficiently absorb microwave radiation, while the products, conversely, are transparent for microwaves.

Yet another approach to the investigation of the mechanisms of solid-phase interactions during microwave heating has been developed¹²⁴ in relation to the kinetics of the reaction between barium carbonate and titanium dioxide under quasi-polythermal conditions (samples were heated as fast as possible to different temperatures and quenched and then the reaction mixtures were analysed quantitatively by powder X-ray diffraction). Using kinetic data, the activation energy of the solid-

phase interaction was calculated in terms of the diffusion model proposed in another publication.¹²⁵ The activation energy of the solid-phase reaction was found to be almost 4 times lower in a microwave field than with conventional heating. The authors noted that this result attests in favour of the intensification of the surface diffusion by the electromagnetic field rather than in favour of the vacancy jump mechanism considered by Katz *et al.*,⁶⁶ as in this case, one would rather expect a change in the pre-exponential factor in the Arrhenius equation but not the activation energy for diffusion.

Solid-phase synthesis of lanthanide chromite and sodium cobaltite with partial replacement of cobalt ions by manganese ions from the corresponding oxides was carried out.^{126, 127} The researchers used a microwave system operating at 28 GHz, which, as they believed, ensured more uniform distribution of the electromagnetic field strength within the sample bulk. It was found that the synthesis of lanthanum chromite with microwave heating can be carried out at 450 °C, which is much lower than that required with conventional heating (about 1200 °C). Measurement of the sample temperature during the process showed that the temperature increases in the first stage (less than 4 min) and then remains constant throughout the whole synthesis. Note that the change in the microwave power from 0.3 to 1 kW does not affect significantly the 'saturation' temperature. Apparently, this temperature is determined by the absorption capacity of components of the reaction mixture and the intensity of heat removal from the sample surface. The latter conclusion contradicts other data,¹²¹ because the sample composition changes appreciably during microwave heating. It cannot be ruled out that these discrepancies are caused by the higher absorption capacity of lanthanum chromite compared with yttrium vanadate.

It is of interest to compare these data with the results of another work¹²⁸ in which lanthanum chromite, cobaltite and nickelate were also synthesised from oxides but in the presence of an absorbing additive (graphite). The temperature substantially increased during the synthesis (to 1100–1200 °C) and the duration of synthesis of the single-phase product was markedly reduced (to 5 min). Thus, the introduction of the absorbing additive was justified in this case.

The $\text{SrFeCo}_{0.5}\text{O}_y$ phase with a mixed conduction type used for the design of solid-state fuel cells was prepared by 'hybrid' microwave heating with SiC as the absorbing additive.¹²⁹ A powder with a narrow particle size distribution and high sintering ability was produced using this procedure.

In the synthesis of complex oxide compounds from salts, it is even more difficult to identify the specific microwave effect, as the number of processes influencing the absorption of microwave radiation by the reaction mixture increases. No studies devoted to the effect of the phase composition of such systems on the absorption of microwave radiation have been published. Most of researchers only state the fact of considerable increase in the reaction rates in the microwave field and make no attempts to determine the reaction mechanisms.

A procedure for the synthesis of a broad range of oxide compounds including individual manganese, iron, cobalt and copper oxides, multicomponent ferrites, manganites and cobaltites based on microwave heating of the corresponding nitrates has been developed.^{130–137} It was shown, that using microwave heating, it is possible not only to shorten the time of synthesis of multicomponent oxide products with various crystal structures, but also, in most cases, to substantially decrease the temperature of synthesis. The latter apparently indicates that microwave heating intensifies the diffusion owing to the appearance of circulating ionic currents on the crystallite surface ('non-thermal' action). The oxide phases synthesised with microwave heating were not inferior in

performance properties to the control samples produced by conventional thermal treatment.

The synthesis of phases based on lanthanum chromite from the corresponding nitrates has been described.^{138, 139} A considerable decrease in the time of synthesis and more uniform micromorphology of the resulting powders upon the use of microwave treatment were noted; in the authors' opinion, this was a consequence of a high uniformity of heat supply favourable for fast formation and even distribution of the oxide phase nuclei.

A method for the synthesis of a powdered MnCo_2O_4 -based catalyst by microwave decomposition of the corresponding nitrates has been developed.^{140, 141} The introduction of some amorphous carbon to the reaction mixture (5 mass % – 30 mass %) with a high specific surface area resulted in a higher rate of formation of the final product and a higher catalytic activity, probably, due to greater surface area. Analysis of the dependence of the specific surface area of the oxide powder on the carbon content demonstrated that after some limiting value has been reached, further increase in the carbon content in the initial mixture does not affect the specific surface area of the oxide powder. Unfortunately, the authors did not analyse the mechanism of microwave action on the reactions and the micromorphology of the final product.

Quite a few papers are devoted to the synthesis of various lithium-containing oxide compounds used as cathodes in lithium rechargeable batteries. The vast majority of these publications deal with the synthesis of materials based on the LiMn_2O_4 phase, which is considered to be most promising for lithium batteries. Nakayama *et al.*¹⁴² compared two procedures of microwave-assisted synthesis of the LiMn_2O_4 phase, *viz.*, decomposition of a mixture of the corresponding nitrates and a mixture of Mn_2O_3 , $\text{LiOH} \cdot \text{H}_2\text{O}$ and copper oxide as the absorbing additive. The former method was preferred, because a single-phase product was formed over a shorter period of time and no LiMnO_2 impurity phase was present. This was attributed to faster attainment of thermal equilibrium in the case of liquid-phase synthesis and to 'non-thermal' effects of microwave heating, which are more pronounced in the absence of an absorbing additive.

Detailed analysis of the effect of the chemical nature of the starting compounds on the course of the reactions in a microwave field has been carried out¹⁴³ using the synthesis of lithium nickelate as an example. Lithium carbonate and hydroxide and nickel hydrocarbonate, hydroxide and oxide in various combinations served as the reactants. Note that the use of microwave treatment markedly reduced the temperature of formation of lithium nickelate. However, in all cases, microwave heating was followed by additional annealing of the sample in a conventional furnace in an oxygen stream in order to obtain a single-phase product. In the authors' opinion, a mixture of hydroxides is the best choice for the synthesis of LiNiO_2 , as in this case slightly aggregated powders with a narrow particle size distribution were produced.

A series of publications^{144–148} report the efficiency of the synthesis of complex ferrites and manganites by microwave-assisted decomposition of nitrate mixtures in the presence of urea. The large volume of gases evolved upon decomposition of nitrates and urea favours deaggregation of the oxide powders. Despite the abundant factual data, the authors unfortunately did not consider the relationship between the microwave treatment conditions and the composition, on the one hand, and the morphology of final products, on the other hand.

A rational approach to the choice of the starting compounds for the microwave-assisted synthesis has been reported.¹⁴⁹ The $\text{La}_{0.7}\text{Ba}_{0.3}\text{MnO}_3$ phase possessing giant magnetoresistance (Fig. 12) was prepared by microwave-induced decomposition of a mixture of metal nitrates. The authors

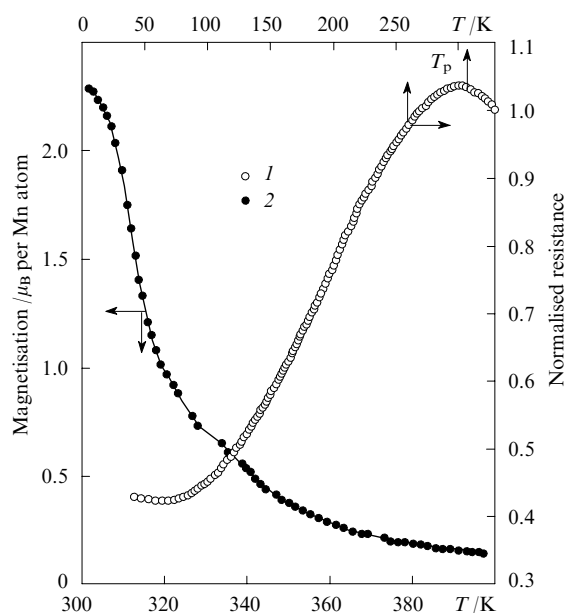


Figure 12. Temperature dependences of the magnetic properties of the ceramics based on the $\text{La}_{0.7}\text{Ba}_{0.3}\text{MnO}_3$ phase synthesised in a microwave field.¹⁴⁹

(1) $T_p = 307\text{ K}$; (2) $H = 0.5\text{ T}$, $T_c = 318\text{ K}$.

substantiated the choice of nitrates as precursors by a large dipole moment of the nitrate ion, which should actively interact with the microwave field. In addition, nitrates readily melt in their water of crystallisation, and aqueous solutions always absorb efficiently microwave radiation. Additional heat is evolved, in the authors' opinion, upon the oxidation of manganese(II), which takes place during decomposition of manganese nitrate. Heat evolution upon oxidation is the main reason why heating does not stop after removal of water from the solution but continues up to decomposition of the precursors to give the oxide phase. It was also found¹⁴⁹ that apart from the substantial decrease in the time of synthesis, the powders obtained by microwave-assisted decomposition of a nitrate mixture have a better microstructure than the powders synthesised by the ceramic technique. It was shown that the properties of ceramics produced using the obtained powders are not inferior to the properties of samples synthesised by the traditional techniques.

In the publications^{147,150} devoted to the synthesis of ferrites $\text{Ni}_{0.25}\text{Cu}_{0.25}\text{Zn}_{0.5}\text{Fe}_2\text{O}_4$ and $\text{SrFe}_{12}\text{O}_{24}$ by pyrolysis of a metal nitrate mixture in the presence of urea, a modification of the procedure considered above was proposed. The reaction of metal nitrates and urea at elevated temperatures is accompanied by evolution of a gas mixture (NH_3 , HNCO , O_2 and NO), which spontaneously ignites after a particular critical temperature has been reached and heats the mixture of solid reaction products to 1000°C or higher. This process lasts for 10–15 min and is accompanied by the formation of single-phase powders of the corresponding ferrites. The microstructure of the synthesised powders is characterised by a loose framework composed of 3- to 6- μm aggregates. The formation of such structures is typical of pyrolysis of salts. Despite the high reaction temperature, the primary crystallites are rather small (50–75 nm) (Fig. 13), which is probably due to high rate of the process. The subsequent annealing of the synthesised samples results in a regular enlargement of particles upon recrystallisation. By correct adjustment of the temperature of the subsequent annealing of the powders, it is possible to reach saturation magnetisations and coercive forces that are rather

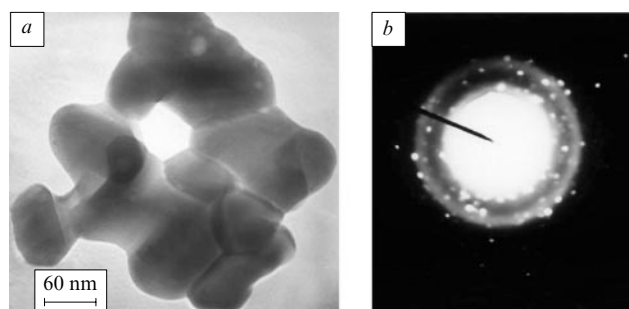


Figure 13. Transmission electron microscopy image (a) and electron diffraction pattern (b) for the particles of the $\text{Ni}_{0.25}\text{Cu}_{0.25}\text{Zn}_{0.5}\text{Fe}_2\text{O}_4$ sample prepared in a microwave field.¹⁵⁰

high for this type of ferrite systems (Fig. 14). Unfortunately, the authors did not compare the properties of samples prepared by microwave-assisted decomposition of a salt mixture with those treated in a conventional furnace; therefore, it is difficult to make conclusions about the advantages of microwave heating. In addition, analysis of the publication¹⁴⁹ casts doubt on the necessity of addition of urea for decomposition of a nitrate mixture in a microwave field.

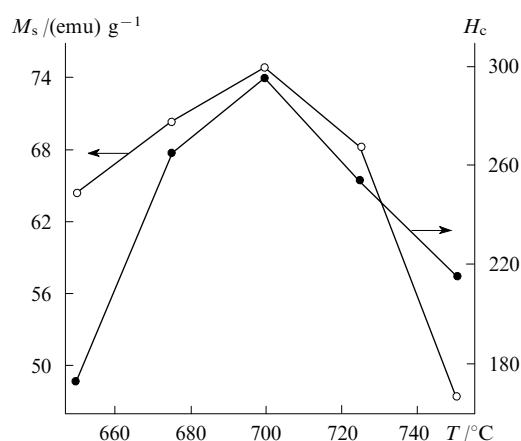


Figure 14. Saturation magnetisation (M_s) and coercive force (H_c) for $\text{Ni}_{0.25}\text{Cu}_{0.25}\text{Zn}_{0.5}\text{Fe}_2\text{O}_4$ samples synthesised in a microwave field vs. temperature of their subsequent heat treatment.¹⁵⁰

The synthesis of layered aluminium and zinc double hydroxides with intercalated sodium dodecyl sulfate molecules has been reported.¹⁵¹ Crystallisation in the microwave field proceeded much faster than that with the use of conventional heating (1–2 h instead of 2–3 days). In addition, crystallisation induced by microwave heating enhances the intercalation of the organic anion into the hydroxide matrix, and thus the starting concentration of sodium dodecyl sulfate can be reduced. The product consists of smaller crystallites with a narrower size distribution than the sample prepared by the conventional heating.

The results of synthesis of the ferrite $\text{Co}_{1-x}\text{Zn}_x\text{Fe}_2\text{O}_4$ ($0 \leq x \leq 0.8$) by precipitation of hydroxides from solutions of the corresponding salts by a solution of KOH in ethylene glycol under microwave treatment followed by separation of the precipitate and annealing at a temperature above 500°C have been reported.¹⁵² The influence of the solution pH and the duration of boiling on the micromorphology of the resulting powders has been studied. It was shown that with an increase in

the pH, the particle size of the powder increases and the degree of agglomeration simultaneously decreases. The addition of ethylene glycol to the solution led to a decrease in agglomeration of the powders.

High-temperature solvolysis of solutions of barium, lead, titanium and zirconium salts in ethylene glycol gave the double oxides BaTiO_3 , BaZrO_3 , PbTiO_3 and $\text{Ba}_6\text{Ti}_{17}\text{O}_{40}$ in the nanocrystalline state.¹⁵³ A specific feature of the synthesis is that the use of ethylene glycol, which functions simultaneously as a solvent, a complexing agent and a surfactant, allows one to vary the powder composition and morphology over a broad range. Note that with the use of microwave heating, it is possible to eliminate a key drawback of the synthesis of oxide phases from solutions in ethylene glycol, *i.e.*, the low reaction rate.

V. Conclusion

The range of physicochemical problems solved successfully by means of microwave radiation is exceptionally broad. This review covers only a small portion mainly related to the synthesis of oxide materials. Not only studies dealing with the synthesis of sulfides,^{80–84} nitrides,^{50, 154} selenides¹⁵⁵ or silicides,¹⁵⁶ but also the applications of microwave treatment such as organic synthesis,^{4, 7, 157–159} analytical chemistry^{4, 160–162} and so on remained beyond the scope of the review. Each of these fields deserves separate consideration and comprises an extended subject matter.

Nevertheless, a general problem should be considered, namely, the possibility to control the processes taking place during microwave treatment of chemical systems, and a closely related problem of evaluating the efficiency of microwave treatment.

Evidently, a satisfactory solution to this problem can now be obtained only for the microwave heating of very simple, more precisely, single-phase systems the physicochemical state of which is not changed much during heating. A good example of such process is the preparation of dense ceramics by sintering of compacted powders, because only the sample morphology is changed most often during compaction, which undoubtedly affects the absorption capacity but this effect is slight and can be taken into account. Similar conditions exist during solution treatment, because these processes usually take place in a rather narrow temperature range and the physicochemical properties of the system do not change much. This range can be supplemented by reactions in inert matrices the specific features of which caused by microwave heating have been poorly studied. In the case of multicomponent systems, it is rather difficult to control the results of microwave treatment due to the large number of processes taking place simultaneously, each affecting significantly the absorption capacity of the whole system. The only practicable way is to accumulate the empirical information on the behaviour of various systems under microwave heating. This would provide an at least qualitative estimate for the efficiency of using such heating. Therefore, systematisation of the accumulated experimental data appears a topical task, which was fulfilled, to some extent, by this review.

Thus, to be able to control the microwave heating in the synthesis or sintering, one should choose systems with the smallest number of components or attain artificially a greater system uniformity by diluting it with an inert matrix or a 'buffer' component the absorption capacity of which depends slightly on the processes that take place. This type of microwave treatment has much in common with the above-mentioned 'hybrid' microwave heating; however, in this case, the added inert component not only enhances the absorption of radiation, but also allows one to control the microwave heating. Thus, the buffer medium should satisfy the same requirements,

namely, it should be chemically inert, absorb efficiently the microwave radiation and be easily separable from the synthesis products after heating has been completed. This route seems especially attractive, as in the future, it may be extended to a rather broad range of physicochemical processes.

This review was written with the financial support of the Russian Foundation for Basic Research (Project No. 06-03-33042), the programme 'Development of the Scientific Potential of Higher School' (government contract No. RNP 2.1.1.1205), the Complex Scientific Research Program of the RAS and the Foundation for the Support of Russian Science. The authors are grateful to Doctor of Science (Physics and Mathematics) V E Semenov for the assistance and valuable remarks made during preparation of the review and to the staff of the Laboratory of Chemical Synergetics of the Institute of General and Inorganic Chemistry of the RAS and the Laboratory of Inorganic Materials Science of the Department of Chemistry, Moscow State University, for fruitful discussion on the issue.

References

1. Yu D Tretyakov *Tverdofaznye Reaktsii* (Solid-phase Reactions) (Moscow: Khimiya, 1978)
2. G Heinicke *Role of Temperature in Tribochemical Reactions* (Sitzungsber: Akad. Wissenschaften, 1981)
3. A E Baranchikov, Candidate Thesis in Chemical Sciences, Institute of Organic and Inorganic Chemistry, Russian Academy of Sciences, Moscow, 2005
4. H M Kingston, L B Jassie *Introduction to Microwave Sample Preparation — Theory and Practice* (Washington, DC: American Chemical Society, 1988)
5. D R Baghurst, A M Chippindale, D M P Mingos *Nature (London)* **332** 311 (1988)
6. D E Clark, D C Folz, S J Oda, R Silbergliet *Ceram. Trans.* **59** 24 (1995)
7. *Microwave Processing of Materials* (Ed. D E Stein) (Washington, DC: National Academy Press, 1994)
8. E T Thostenson, T-W Chou *Composites, Part A* **30** 1055 (1999)
9. J D Ford, D C T Pei *J. Microwave Power Electromagn. Energy* **2** (2) 61 (1967)
10. D Wong, M.Sc. Thesis, University of Alberta, Canada, 1975
11. Yu S Arkhangelskii *SVCh-Elektrotermiya* (Microwave Electrothermy) (Saratov: Saratov State Technical University, 1998)
12. *Microwave-Enhanced Chemistry* (Eds H M Kingston, S J Haswell) (Washington, DC: American Chemical Society, 1997)
13. R E Newnham, S J Jang, M Xu, F Jones *Ceram. Trans.* **21** 23 (1991)
14. L A Vainshtein *Elektromagnitnye Volny* (Electromagnetic Waves) (Moscow: Sovetskoe Radio, 1957)
15. Yu V Novozhilov, Yu A Yappa *Elektrodinamika* (Electrodynamics) (Moscow: Nauka, 1978)
16. B Debye *Polar Molecules* (New York: Chemical Catalog, 1929)
17. I E Tamm *Osnovy Teorii Elektrichestva* (Foundations of Electricity Theory) (Moscow: Gosizdat Tekhniko-teoreticheskoi Literatury, 1954)
18. L Khardman *Elektronika* **20** 30 (1972)
19. I A Rogov, S V Nekrutman *Sverkhvysokochastotnyi i Infrazasnyi Nagrev Pishchevykh Produktov* (Microwave and IR Heating of Foodstuffs) (Moscow: Pishchevaya Prom-st', 1976)
20. *Microwave Power Engineering* (Ed. E Okress) (New York: Academic Press, 1968)
21. *Primenenie SVCh-nagreva v Obshchestvennom Pitanii* (Application of Microwave Heating for Catering) (Eds A N Vysheslavskii, E N Koz'mina) (Moscow: Ekonomika, 1964)
22. K W Wagner *Arch. Elektrotech.* **2** 371 (1914)
23. B V Hamon *Aust. J. Phys.* **6** 304 (1953)

24. M F Iskander *Electromagnetic Fields and Waves* (New Jersey: Prentice Hall, 1992)
25. J W Walkiewicz, G Kazonich, S L McGill *Mineral Metal. Process* **5** (1) 39 (1988)
26. C Kittel *Solid State Physics* (New York: Wiley, 1959)
27. Yu I Bokhan *Dokl. Akad. Nauk Belarusi* **36** 422 (1992)
28. Yu I Bokhan *Pis'ma Zh. Ekp. Teor. Fiz.* **18** (11) 6 (1992)^a
29. Yu I Bokhan, I A Shkrob *Pis'ma Zh. Ekp. Teor. Fiz.* **20** (11) 24 (1994)^a
30. K I Rybakov, V E Semenov *Phys. Rev. B* **49** 64 (1994)
31. Yu V Bykov, K I Rybakov, V E Semenov *J. Phys. D* **34** R55 (2001)
32. J H Booske, R F Cooper, S A Freeman *Mater. Res. Innovations* **1** 77 (1997)
33. A J Berteaud, J C Badot *J. Microw. Power Electromagn. Energy* **11** (4) 315 (1976)
34. P Colomban, J C Badot *Mater. Res. Bull.* **13** 135 (1978)
35. P Colomban, J C Badot *Ind. Ceram. Verr.* **725** 101 (1978)
36. Z Xie, C Wang, X Fan, Y Huang *Mater. Lett.* **38** 190 (1999)
37. Z Xie, J Yang, Y Huang *Mater. Lett.* **37** 215 (1998)
38. D D Upadhyaya, A Ghosh, G K Dey, R Prasad, A K Suri *J. Mater. Sci.* **36** 4707 (2001)
39. F T Ciacchi, S A Nightingale, S P S Badwal *Solid State Ionics* **86–88** 1167 (1996)
40. K-Y Lee, E D Case *J. Mater. Sci. Lett.* **18** 201 (1999)
41. S A Suvorov, I A Turkin, L N Printsev, A V Smirnov *Ogneupory Tekhn. Keram.* **9** 9 (2000)
42. S A Suvorov, I A Turkin, L N Printsev, A V Smirnov *Refract. Ind. Ceram.* **41** (9–10) 295 (2000)
43. A Goldstein, N Travitzky, A Singurindy, M Kravchik *J. Eur. Ceram. Soc.* **19** 2067 (1999)
44. A Goldstein, M Kravchik *J. Eur. Ceram. Soc.* **19** 989 (1999)
45. Yu V Bykov, A G Ereemeev, V V Holoptsev *Proceedings of the 1st World Congress on Microwave Processing of Materials* (Walt Disney Village: American Ceramic Society Press, 1997) p. 25
46. S Vijayan, H Varma *Mater. Lett.* **56** 827 (2002)
47. C Y Tsay, K S Liu, T F Lin *J. Magn. Magn. Mater.* **209** 182 (2000)
48. C Y Tsay, K S Liu, I N Lin *J. Eur. Ceram. Soc.* **21** 1937 (2001)
49. C Siligardi, C Lionelli, F Bondoli, A Corradi, G C Pellacani *J. Eur. Ceram. Soc.* **20** 177 (2000)
50. Y Ch Kim, Ch H Kim, D K Kim *J. Eur. Ceram. Soc.* **17** 1625 (1997)
51. S-T Oh, K Tajima, M Ando, T Ohji *Mater. Lett.* **48** 215 (2001)
52. M A Janney, H D Kimrey *Ceramic Powder Science II* (Ed. G L Messing) (Westerville, OH: American Ceramic Society, 1988) p. 919
53. M A Janney, H D Kimrey *Ceram. Trans.* **7** 382 (1990)
54. M A Janney, C L Calhoun, H D Kimrey *Ceram. Trans.* **21** 311 (1991)
55. M A Janney, H D Kimrey, J O Kiggans *MRS Symp. Proc.* **269** 173 (1992)
56. H D Kimrey, J O Kiggans, M A Janney, R L Beatty *MRS Symp. Proc.* **189** 243 (1991)
57. M A Janney, C L Calhoun, H D Kimrey *J. Am. Ceram. Soc.* **75** 341 (1992)
58. C E Holcombe, N L Dykes *Ceram. Trans.* **21** 375 (1991)
59. T N Tiegs, J O Kiggans, H D Kimrey Jr *MRS Symp. Proc.* **189** 267 (1991)
60. J O Kiggans, T N Tiegs *MRS Symp. Proc.* **269** 285 (1992)
61. A Birnboim, D Gershon, J Calame *J. Am. Ceram. Soc.* **81** 1493 (1998)
62. I-N Lin, W-Ch Lee, K-S Liu, H-F Cheng, M-W Wu *J. Eur. Ceram. Soc.* **21** 2085 (2001)
63. D L Patil, B C Mutsuddy, J Gavulic, M Dahimene *Ceram. Trans.* **21** 301 (1991)
64. J Cheng, J Qui, J Zhou, N Ye *MRS Symp. Proc.* **269** 323 (1992)
65. L M Levinson, H A Comanzo, W N Schultz *MRS Symp. Proc.* **269** 311 (1992)
66. J D Katz, R D Blake, V M Kenkre *Ceram. Trans.* **21** 95 (1991)
67. W H Sutton *Am. Ceram. Soc. Bull.* **68** 376 (1989)
68. W H Sutton *Ceram. Trans.* **36** 3 (1993)
69. R Wroe, A T Rowley *J. Mater. Sci.* **31** 2019 (1996)
70. Z Wu, M Shao, W Zhang, Y Ni *J. Cryst. Growth* **260** 490 (2004)
71. Y T Moon, D K Kim, C H Kim *J. Am. Ceram. Soc.* **78** 1103 (1995)
72. Y T Moon, H K Park, D K Kim, C H Kim, I-S Seog *J. Am. Ceram. Soc.* **78** 2690 (1995)
73. G Fetter, P Bosch, T Lopez *J. Sol-Gel Sci. Technol.* **23** 199 (2002)
74. N T Kalyana Sundaram, T Vasudevan, A Subramania *J. Phys. Chem. Solids* **68** 264 (2007)
75. A Srivastava, K Jiau, Rashui, A K Srivastava, S T Lakshmikummar *Mat. Chem. Phys.* **97** 85 (2006)
76. Y Wang, J Y Lee *J. Power Sources* **144** 220 (2005)
77. A S Vanetsev, V K Ivanov, Yu V Kolen'ko, N N Oleinikov, Yu D Tretyakov *Dokl. Akad. Nauk* **385** 67 (2002)^b
78. J Spatz, S Mößmer, M Möller, M Kocher, D Neher, G Wegner *Adv. Mater.* **10** 473 (1998)
79. D Chen, G Shen, K Tang, S J Lei, H G Zheng, Y T Qian *J. Cryst. Growth* **260** 469 (2004)
80. Y Ni, X Ma, J Hong, Z Xu *Mater. Lett.* **58** 2754 (2004)
81. Y Zhao, J-M Hong, J-J Zhu *J. Cryst. Growth* **270** 438 (2004)
82. A G Saskia *Chem. Soc. Rev.* **26** 233 (1997)
83. Y Ni, F Wang, H Liu, G Yin, J Hong, X Ma, Z Xu *J. Cryst. Growth* **262** 399 (2004)
84. J He, X-N Zhao, J-J Zhu, J Wang *J. Cryst. Growth* **240** 389 (2002)
85. X-H Liao, N-Y Chen, S Xu, S B Yang, J J Zhu *J. Cryst. Growth* **252** 593 (2003)
86. W-W Wang, J-Z Xu, Y-J Zhu, H-Y Chen *J. Cryst. Growth* **244** 88 (2002)
87. W-W Wang, Y-J Zhu, G-F Cheng, Y-H Huang *Mater. Lett.* **60** 609 (2006)
88. X Liao, J Zhu, W Zhong, H-Y Chen *Mater. Lett.* **50** 341 (2001)
89. D-S Wu, C-Y Han, S-Y Wang, N-L Wu, I A Rusakova *Mater. Lett.* **53** 155 (2002)
90. J-J Zhu, J-M Zhu, X-H Liao, J L Fong, M G Zhou, H Y Chen *Mater. Lett.* **53** 12 (2002)
91. H Wu, M Shao, J Gu, X Wei *Mater. Lett.* **53** 121 (2002)
92. R Subasri *Mater. Sci. Eng., B* **112** 73 (2004)
93. W S Ahn, K K Kang, K Y Kim *Catal. Lett.* **72** (3–4) 229 (2001)
94. W Wang, J-J Zhu, J-M Zhu, X-H Liao, S Xu, T Ding, H Y Chen *Phys. Chem. Chem. Phys.* **4** 3794 (2002)
95. Y-P Fu, C-H Lin *J. Alloys Compd.* **354** 232 (2003)
96. D Y Chung, E H Lee *J. Alloys Compd.* **374** 69 (2004)
97. S Komarneni, Q Li, R Roy *Mater. Res. Bull.* **27** 1393 (1992)
98. S Komarneni, Q Li, K M Steffansson, R Roy *J. Mater. Res.* **8** (12) 3176 (1993)
99. F Liu, I R Abothu, S Komarneni *Mater. Lett.* **38** 344 (1999)
100. S Komarneni, M C D'Arrigo, C Leonelli *J. Am. Ceram. Soc.* **81** 3041 (1998)
101. N Kumada, N Kinomura, S Komarneni *Mater. Res. Bull.* **9** 1411 (1998)
102. S Komarneni, V C Menon, Q H Li, R Roy, F W Ainger *J. Am. Ceram. Soc.* **79** 1409 (1996)
103. S Komarneni, Q H Li, R Roy *J. Mater. Res.* **11** 1866 (1996)
104. J Olanrewaju, B L Newlaker, C Mancino, S Komarneni *Mater. Lett.* **45** 307 (2000)
105. M Park, S Komarneni *Microporous Mesoporous Mater.* **20** 39 (1998)
106. S Komarneni, Q H Li, R Roy *J. Mater. Chem.* **4** 1903 (1994)
107. S-E Park, D S Kim, J-S Chang, W Y Kim *Catal. Today* **44** 301 (1998)
108. S Komarneni, Q H Li, R Roy *J. Mater. Res.* **10** 1687 (1995)
109. R Chitrakar, H Kanoh, Y Miyai, K Ooi *J. Solid State Chem.* **163** 1 (2002)
110. J H Ryu, J-W Yoon, C S Lim, K B Shim *Mater. Res. Bull.* **40** 1468 (2005)
111. J A Rivera, G Fetter, P Bosch *Microporous Mesoporous Mater.* **52** 306 (2006)
112. H Yan, X Huang, L Zhonghua, H Huang, R Xue, L Chen *J. Power Sources* **68** 530 (1997)
113. H Yan, X Huang, L Chen *J. Power Sources* **81–82** 647 (1999)
114. M Mohammadpour Amini, L Torkain *Mater. Lett.* **57** 639 (2002)

115. V Fathollahi, M Mohammadpour Amini *Mater. Lett.* **50** 235 (2001)
116. I Ganesh, B Srinivas, R Johnson *J. Eur. Ceram. Soc.* **24** 201 (2004)
117. Y Tang, H Guo, Q Qin *Solid State Commun.* **121** 351 (2002)
118. R Subastri, T Mathews, O M Sreedharan *Mater. Lett.* **57** 1792 (2003)
119. M H Bhat, A Miura, P Vinatier, A Levasseur, K J Rao *Solid State Commun.* **125** 557 (2003)
120. B Vaidhynathan, P Raizada, K J Rao *J. Mater. Sci. Lett.* **16** 2022 (1997)
121. R D Peelmedu, R Roy, D Agrawal *Mater. Res. Bull.* **36** 2723 (2001)
122. L A Bashkurov, V V Pan'kov *Kinetika i Mekhanizm Obrazovaniya Ferritov* (Kinetics and Mechanism of Ferrite Formation) (Minsk: Nauka i Tekhnika, 1988)
123. K Uematsu, K Toda, M Sato *J. Alloys Compd.* **389** 209 (2005)
124. H Liu, L Guo, L Zou, M Cao, J Zhou, S Ouyang *Mater. Sci. Eng., B* **113** 161 (2004)
125. S Freeman, J Booske, R Cooper *MRS Symp. Proc.* **347** 479 (1994)
126. M Iwasaki, H Takizawa, K Uheda, T Endo, M Shimado *J. Mater. Chem.* **8** 2765 (1998)
127. M Iwasaki, H Takizawa, K Uheda, T Endo *J. Mater. Sci. Lett.* **19** 2033 (2000)
128. M Panneerselvam, K J Rao *J. Mater. Chem.* **13** 596 (2003)
129. D Huo, J Zhang, Z Xu *J. Am. Ceram. Soc.* **85** 510 (2002)
130. A S Vanetsev, V K Ivanov, Yu D Tretyakov *Dokl. Akad. Nauk* **387** 640 (2002)^b
131. A S Vanetsev, V K Ivanov, N N Oleinikov, Yu D Tretyakov *Khim. Tekhnol.* **6** 8 (2003)
132. A S Vanetsev, V K Ivanov, N N Oleinikov, Yu D Tretyakov *Mendeleev Commun.* **14** (4) 145 (2004)
133. A S Vanetsev, V K Ivanov, N N Oleinikov, Yu D Tretyakov *Vestn. VGTU* **1** (12) 22 (2002)
134. F A Kulikov, A S Vanetsev, G P Murav'eva, A L Il'inskii, N N Oleinikov, Yu D Tretyakov *Neorg. Mater.* **39** 1244 (2003)^c
135. A E Chekanova, E A Eremina, A S Vanetsev, Yu D Tretyakov *Neorg. Mater.* **40** 420 (2004)^c
136. A S Vanetsev, E V Makshina, N N Oleinikov, Yu D Tretyakov, B V Romanovskii *Dokl. Akad. Nauk* **405** 204 (2005)^b
137. A A Fedorova, A S Vanetsev, I V Morozov, A S Shaporev, Yu D Tretyakov *Khim. Tekhnol.* **12** 18 (2005)
138. H K Park, Y S Han, D K Kim, C H Kim *J. Mater. Sci. Lett.* **17** 785 (1998)
139. R Subastri, T Mathews, K Swaminathan, O M Sreedharan *J. Alloys Compd.* **354** 193 (2003)
140. T Nissinen, T Valo, M Gasik, J Rantanen, M Lampinen *J. Power Sources* **106** 109 (2002)
141. T Nissinen, Y Kiros, M Gasik, M Lampinen *Mater. Res. Bull.* **39** 1195 (2004)
142. M Nakayama, K Watanabe, H Ikute, Y Uchimoto, M Wakihara *Solid State Ionics* **164** 35 (2003)
143. P Kalyani, N Kalaiselvi, N G Renganathan *J. Power Sources* **123** 53 (2003)
144. Y-P Fu, C-H Lin, K-Y Pan *J. Alloys Compd.* **349** 228 (2003)
145. Y-P Fu, C-H Lin, K-Y Pan *J. Alloys Compd.* **364** 221 (2004)
146. Y-P Fu, Y-H Su, C-H Lin *Solid State Ionics* **166** 137 (2004)
147. Y-P Fu, C-S Hsu *J. Alloys Compd.* **391** 185 (2005)
148. Y-P Fu, C-S Hsu *Solid State Commun.* **134** 201 (2005)
149. R K Sahu, M J Rao, S S Manoharan *J. Mater. Sci.* **36** 4099 (2001)
150. Y-P Fu, K-Y Pan, C-H Lin *Mater. Lett.* **57** 291 (2002)
151. M Z B Hussein, Z Zainal, C Y Ming *J. Mater. Sci. Lett.* **19** 879 (2000)
152. J Giri, T Srihasha, D Bahadur *J. Mater. Chem.* **14** 875 (2004)
153. O Palchik, J Zhu, A Gedanken *J. Mater. Chem.* **10** 1251 (2000)
154. J Peng, J Binner *J. Mater. Sci. Lett.* **21** 247 (2002)
155. R Harpeness, A Gedanken *New J. Chem.* **27** 1191 (2003)
156. J R Jokisaari, S Bhaduri, S B Bhaduri *Mater. Sci. Eng., A* **323** 478 (2002)
157. K T J Loones, B U W Maes, G Rombouts, S Hostyna, G Diels *Tetrahedron* **61** 10338 (2005)
158. A M L Hoel, J Nielsen *Tetrahedron Lett.* **40** 3941 (1999)
159. H Glas, W R Thiel *Tetrahedron Lett.* **39** 5509 (1998)
160. A Zlotorzynski *Crit. Rev. Anal. Chem.* **25** 43 (1995)
161. G M B Parkes, P A Barnes, G Bond, E L Charsley *Thermochim. Acta* **356** 85 (2000)
162. J Szpunar, V O Schmitt, O F X Donard, R Lobin'ski *TrAC — Trends Anal. Chem.* **15** (4) 181 (1996)
- ^a — *J. Exp. Theor. Phys. Lett. (Engl. Transl.)*
- ^b — *Dokl. Chem. (Engl. Transl.)*
- ^c — *Inorg. Mater. (Engl. Transl.)*

Ionics of nanoheterogeneous materials

N F Uvarov

Contents

I. Introduction	415
II. General criteria for the choice of composite electrolytes with high ionic conductivity	416
III. Surface disordering of ionic crystals	417
IV. Disorder of ionic crystals at interfaces. Conductivity of microcomposites	420
V. Calculations of physicochemical properties of composites	421
VI. Thermodynamic description of composites. The effect of self-dispersion of ionic salts. Synthesis of nanocomposites	423
VII. Size effects in composites	424
VIII. Conclusion	430

Abstract. The results of studies of composite ionic conductors are considered. The relationship between their properties and the ionic salt disordering and the interfacial interaction between the components of the material is analysed. Special attention is paid to models that describe the surface disordering and the mechanism of defect formation. The methods of calculation of physicochemical characteristics of composites, the thermodynamic stability and peculiarities of the genesis of the nanocomposite morphology are discussed. The bibliography includes 188 references.

I. Introduction

Ionics, *i.e.*, a science that studies ionic processes in systems and materials, is a comparatively new and rapidly progressing field of knowledge.^{1–3} Although it ranks much below electronics in the practical application, its role tends to increase. This is caused first of all by the demands for new and more efficient electrochemical systems for the accumulation and conversion of energy at a constant threat of the shortage of natural energy resources. This problem can be solved given a wide spectrum of electrolytes with different functional characteristics that can be adapted to the specific conditions of operation of various electrochemical systems. Solid electrolytes that exhibit high mechanical strength, thermal stability, unipolar ionic conductivity and can be used in chemical power sources, gas sensors and other electrochemical devices occupy a special place among these electrolytes.

Heterogeneous doping of ionic compounds with dispersed dielectrics that are chemically inert with respect to the ionic salt is known to enhance the conductivity in most cases. Composite solid electrolytes of the ionic salt–oxide (MX–A) type can be considered as a new class of ionic conductors with high ionic conductivity. The combination of high conductivity with the

enhanced mechanical strength together with the wide prospects for the targeted modification of the electrolyte properties by varying the type and concentration of the dopant makes these composites promising materials for real electrochemical systems. The composites LiI–Al₂O₃ synthesised by Liang in 1973 proved to be convenient solid electrolytes for chemical power sources.^{4,5} This achievement has triggered a scientific boom, and a large number of composite ionic conductors were studied in the subsequent years. Actually, doping with dispersed oxides was shown to enhance the conductivity of virtually all composites based on classical (non-superionic) ionic salts, *i.e.*, it is a general effect, which requires scientific explanation and theoretical substantiation.

There are several reviews devoted to the description and the analysis of the ion transport in polycrystalline and composite solid electrolytes.^{6–22} The increase in the ionic conductivity upon heterogeneous doping can be explained within the framework of the space charge model proposed by Wagner and Maier,^{6,7,9,10,12,13,15} which represents a version of the classical Frenkel's model.²³ This model allows the interpretation of many phenomena observed in composites and is the best suited for the explanation of experimental data for composites containing oxides with relatively coarse grains. However, the space charge model in its classical version is correct only for ideal crystals in contact with vacuum or a structure-free medium and obviously ignores the real features of the interphase contact, namely, changes in the structures of ionic crystals (*e.g.*, for epitaxial contacts), the effect of elastic strains, the formation of dislocations, *etc.* Moreover, if the surface concentration of defects is sufficiently high, it is impossible to ignore the interaction between the defects, which results in their ordering and the formation of superstructures and even metastable surface phases.

It is known that the conductivity of composites increases as the size of dopant particles increases. Hence, composites with nanosized grains (about 10 nm) are of particular interest for practice. Obviously, uniform mixing of such an oxide with an ionic component should produce a nanocomposite the properties of which strongly depend on the energy of surface interaction and the peculiarities of the interface between the phases. For composites with coarse-grained dopants, the presence of surfaces or interphase contacts has virtually no effect on the bulk properties of the ionic salt; hence, the

N F Uvarov Institute of Solid State Chemistry and Mechanochemistry, Siberian Branch of the Russian Academy of Sciences, ul. Kutateladze 18, 630090 Novosibirsk, Russian Federation. Fax (7-383) 332 28 47, tel. (7-383) 332 56 45, e-mail: uvarov@solid.nsk.su

Received 11 December 2006

Uspekhi Khimii 76 (5) 454–473 (2007); translated by T Ya Safonova

increase in the conductivity is of the purely surface nature. However, in many cases, it still remains unclear whether the enhanced conductivity is primarily caused by the specific interactions at the interface or by the trivial increase in the surface conductivity as such. To answer this question, information on the conductivity of polycrystals is necessary. In nanocomposites, an ionic salt is virtually totally located at the interface. This is why its structure and thermodynamic characteristics can substantially change. Particularly, for ionic compounds containing high-temperature disordered phases, the latter may prove to be stable at low temperatures in nanocomposites. Therefore, it is important to understand the thermodynamic reasons for the appearance of a disordered phase. To this end, it is necessary to elucidate how the thermodynamic parameters of crystals, particularly, the enthalpy and entropy of phase transitions are related to the lattice disorder.

In this review, the problems of thermodynamic stability of nanocomposites and the genesis of the composite morphology during its sintering are discussed; possible mechanisms of the interfacial interaction and the general trends for the changes in the ionic salt properties are analysed for a wide series of ionic salt – oxide systems; size effects and methods for the quantitative estimation of conductivity and other physicochemical characteristics of composites are considered.

II. General criteria for the choice of composite electrolytes with high ionic conductivity

Even in their first stage, the studies have revealed the following relationships typical of the composite solid electrolytes $\text{MX} - \text{A}$:^{6–8, 10–15}

- due to heterogeneous doping, a region of low-temperature conductivity with a lower activation energy (E_a) appears in the Arrhenius plots of conductivity in addition to the region of intrinsic conductivity (at high temperatures);

- in the low-temperature region, the concentration dependence of the conductivity has a maximum at a dopant concentration of 10 vol.% – 40 vol.%; in certain systems, the maximum is observed at lower dopant concentrations (1 vol.% – 10 vol.%);

- in the high-temperature region, the conductivity monotonously decreases with the increase in the dopant concentration; an analogous effect is observed in superionic phases;

- the conductivity of composites usually increases with the decrease in the size (L_A) of particles of the heterogeneous dopant or with the increase in its specific surface (S_A).

All composite solid electrolytes known can arbitrarily be divided into two groups:²⁴

(1) Composites $\text{MX} - \text{A}$ with the properties similar to those of polycrystals MX (e.g., $\text{LiI} - \text{Al}_2\text{O}_3$, $\text{AgCl} - \text{Al}_2\text{O}_3$, $\text{AgBr} - \text{Al}_2\text{O}_3$ and $\text{TlCl} - \text{Al}_2\text{O}_3$). In this case, the activation energy of the composite $\text{MX} - \text{A}$ is close to E_a of polycrystalline MX and virtually coincides with the enthalpy of migration of a cationic vacancy (E_{cv}) in the single crystal MX . This is an argument for the applicability of the space charge model for the explanation of the conductivity mechanism in composites.^{6–8, 10, 12–15}

(2) Composites with unusual properties. In certain composites, the physicochemical properties of ionic salts substantially differ from those of single-crystal and polycrystalline samples. The activation energy often substantially depends on the type and concentration of a fine-grain dopant and may far deviate from both E_{cv} and E_a . In certain cases, the observed deviations were apparently due to the insufficiently wide temperature ranges in which the conductivity was measured. However, the specific interaction between the composite components can also be a reason for the dramatic changes in the E_a values. For example, in composites $\text{AgI} - \text{Al}_2\text{O}_3$, the temperature of the

β - AgI phase transition into the superionic state was observed to decrease, which was accompanied by a decrease in the enthalpy of the phase transition.^{25, 26} For composites $\text{AgI} - \text{Fe}_2\text{O}_3$ both the changes in the parameters of the AgI phase transition and the increase in the Néel temperature for Fe_2O_3 were observed.²⁷ This suggests that the thermodynamic parameters of both bulk phases are different in composites. In certain composites, in addition to the conventional phases, new phases non-typical of pure ionic crystals were revealed.

These facts suggest that the interfacial interaction in composites may substantially affect the bulk physicochemical properties of the ionic component in a composite. However, so far, no systematic studies were carried out aimed at the synthesis of composites and the investigation of anomalous properties of the constituent ionic salts. The majority of studies were focused on the increase in the ionic conductivity. The theoretical models that describe the increase in the ionic conductivity are usually tested on quite different objects that usually exhibit no high conductivity.

Insofar as the thermodynamic parameters of ionic salts in composites can substantially change, it is important to study their relationship with the surface disordering. The deeper insight into the mechanism and thermodynamic peculiarities of the formation of defects in the crystal bulk, on its surface or on intergrain boundaries requires the knowledge of how the point defects affect the thermodynamic properties of crystals. One may consider the inverse problem, namely, judge on the degree of disordering of a solid based on the analysis of the thermodynamic data. The most distinct changes in vibrational spectra and the degree of disordering occur during the phase transitions and give rise to easily measurable changes in the entropy and enthalpy of a crystal. The presence of grain and phase boundaries affects the concentration of defects in a crystal and can lead to changes in the thermodynamic parameters of phase transitions. Thus, it is expected that the thermodynamic studies of phase transitions would provide information on the disordering of the ionic component in a composite.

In contrast to crystals in which the self-diffusion coefficients may differ by several orders of magnitude, the transport properties of melts are approximately the same for all substances. In this respect, the molten state is universal, most disordered, and the thermodynamic parameters of melting (or crystallisation) contain information on the degree of disordering of a crystal at the melting temperature. Hence, it is the correlations between the parameters of melting and the transport properties of solids that attract the prime interest. Elucidation of the factors responsible for melting allows one to get a clearer insight into the processes that occur in the transition of a substance into the superionic or orientationally disordered state in both pure crystals and ionic salts brought in contact with the surface of another phase.

It was shown^{28–33} that for a wide range of substances a linear correlation is observed between the enthalpy of melting (H_{melt}) and the enthalpy of formation of Schottky defects (h_0) (Fig. 1)

$$h_0 = \beta H_{\text{melt}}. \quad (1)$$

The ratio $h_0/H_{\text{melt}} = \beta = 8.6 \pm 0.6$ is independent of the type of the substance and remains unchanged in binary ionic substances, metals and molecular crystals. In contrast to the correlations such as $h_0 = aT_{\text{mp}}$, which are cited most often but are fulfilled for a limited range of substances, correlation (1) is more general. Within the framework of the phenomenological quasicrystalline model, the melting process can be presented as an abrupt increase in the mole fraction of point defects in a crystal (c) up to a certain critical value c_L followed by the relaxation of the structure around defects. In this approximation, the parameter β has a simple physical meaning and is defined as $\beta = 1/c_L$. The constancy of $c_L = 0.12 \pm 0.02$ for

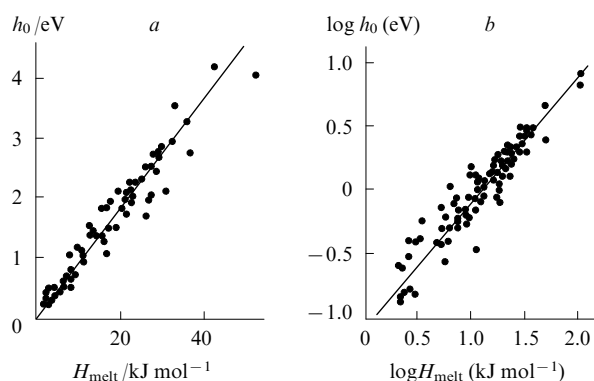


Figure 1. Correlation between the enthalpy of melting (H_{melt}) and the enthalpy of formation (h_0) of the Schottky defects in crystals presented in (a) linear and (b) logarithmic scales.

substances with different types of interatomic interactions may be assumed as a characteristic feature of the liquid state. The relative changes in the volume upon melting ($\Delta V/V$) are associated with the volume of the defect formation v_0 (Ω is the molecular volume)

$$\frac{\Delta V}{V} = c_L \frac{v_0}{\Omega}.$$

This relationship was confirmed experimentally for metals and crystalline alkali metal halides (in this case, v_0 is the volume of formation of the Schottky defect).³³ Melting with the formation of the Schottky defects or the vacancy melting is always accompanied by an increase in the volume. Some substances (H_2O , Bi, Sb, Si, Ge, RbNO_3) melt with a decrease in their volumes. In this case, the melting apparently follows the interstitial mechanism, *i.e.*, involves the formation of Frenkel defects, the volume of formation of which (in contrast to the Schottky defects) can be negative.

If we assume that the vibrational frequencies of atoms or ions in a liquid are equal to those of atoms around a defect in a crystal, it is possible to assess the entropy of the defect formation (s_0) and the concentration of defects in crystals at the melting temperature (c_{mp}). The calculated s_0 and c_{mp} values agree sufficiently well with experimental data for metals and ionic crystals.^{34,35} Insofar as for metals and alkali metal halides, a linear correlation is observed between the enthalpy of defect formation and the enthalpy of migration, one can estimate the absolute magnitudes of the coefficients of self-diffusion or ionic conduction based on H_{melt} .^{28–30,36} The correlations mentioned can be found in the well-known reference book.³⁷

Superionic conductors form an unusual class of ionic conductors characterised by the high conductivity comparable with that of ionic melts and aqueous solutions. The equilibrium concentration of current carriers in superionic conductors is high and comparable with the total amount of mobile ions in the lattice, *i.e.*, h_0 is close to zero. Superionic conductors and ionic melts are known to exhibit common features, for example,

- a diffuse distribution of the ion density along the conduction channels, which is analogous to the broad radial distribution function of the same ions in melts;
- close values of ionic conductivity and, hence, only minor changes in the conductivity in the melting;
- substantial changes in the thermodynamic parameters of substances upon their transition into the superionic state, which are comparable in the magnitude with the corresponding effects in the melting.

High-temperature phases of AgI and Li_2SO_4 are typical examples of superionic conductors. On the qualitative level, a superionic conductor may be represented as a partly ordered system built of two sublattices, one of which is entirely ordered and forms a rigid frame and the other is strongly disordered and resembles a liquid phase that fills the frame. The expressions for the melting temperature, which were derived within the framework of the quasicrystalline model of melting are similar to those obtained by Gurevich for a ‘strong’ superionic transition.^{38–40} This similarity forms the basis for the prediction (if only on the qualitative level) of certain properties of superionic conductors. Apparently, the assumption that $c \approx 1$ is not true for superionic conductors. By analogy with melts, it can be expected that $c \approx c_L = 0.12$. Because no reliable methods were developed so far for the estimation of the defect concentration in superionic conductors, it remains unclear what is the concentration of defects in superionic phases.

An interesting class of ionic conductors is formed by the phases that contain orientationally disordered anions. Obviously, the orientational disordering should entail an increase in the free volume in crystals, which will favour the increase in the diffusion coefficients and in the ionic conductivity. Moreover, the of anion reorientation event may additionally facilitate the transfer of the neighbouring cation by the ‘paddle-wheel’ mechanism proposed by Lunden.⁴¹ The thermodynamic parameters of phase transitions are related to the extent of the crystal disorder at a temperature below the phase transition. This relationship manifests itself most clearly in a series of alkali metal nitrates for which a decrease in the enthalpy and entropy of melting is accompanied by an increase in the conductivity of high-temperature phases.^{24,42} Alkali metal nitrates form an unusual class of inorganic salts, being characterised by phase transitions with orientational disordering in the anionic sublattice.⁴³ Among the nitrates, rubidium nitrate has the lowest H_{melt} and demonstrates three phase transitions associated with the orientational disordering of NO_3^- ions.⁴² The thermodynamic data correlate well with the ionic conductivity, *i.e.*, rubidium nitrate exhibits the highest ionic conductivity in the series of nitrates⁴² and is promising for the development of ionic conductors with the high rubidium conductivity.⁴⁴ This is why, in this review, attention is focused on rubidium nitrate and composites on its basis.

In composites and, particularly, nanocomposites, the interfacial interaction affects the energy of an ionic crystal thus favouring the stabilisation of high-temperature disordered phases. The phase-transition temperature and enthalpy may serve as the convenient parameters that characterise the degree of disordering and the changes in the energy characteristics of a crystal in a composite. For this reason, compounds containing high-temperature superionic or orientationally disordered phases were chosen as the best candidates for the ionic salt component in the ionic salt – oxide composites.

III. Surface disordering of ionic crystals

Embarking on the discussion of the effect of heterophase additives, it is necessary to consider the possible mechanisms of disordering, *i.e.*, the formation of point defects on the free surface of an ionic crystal. It is known that in many cases the conductivity of polycrystalline samples exceeds that of single crystals. Hence, simple dispersion of an ionic crystal MX may be one of the reasons for the increase in its conductivity in composites. This is accompanied by the formation of a large number of free surfaces or grain boundaries MX–MX, which are characterised by the enhanced surface or intergrain conductivity. As a rule, the increase in the concentration of surface defects is associated with the formation of an electrical double layer in the near-surface region of a crystal.

Currently, the interpretation of surface phenomena in ionic crystals widely employs the Frenkel–Kliwer model.^{23, 45–48} This model was first proposed by Frenkel²³ and is based on the assumption that different types of defects can form separately and independently in the crystal bulk due to the difference in their chemical potentials. Frenkel assumed this to be associated with the appearance of an electrical potential in the crystal bulk, which may be considered as a contact potential drop in the crystal surface layer, caused by the difference in the energies of formation of positive and negative defects that appear on the surface.²³ Figure 2a illustrates the changes (in terms of the Frenkel model) in the energy parameters, the defect concentration and the electrical potential on going from the ionic crystal surface to its bulk. This model was analysed most comprehensively in the studies by Kliwer.^{47, 48}

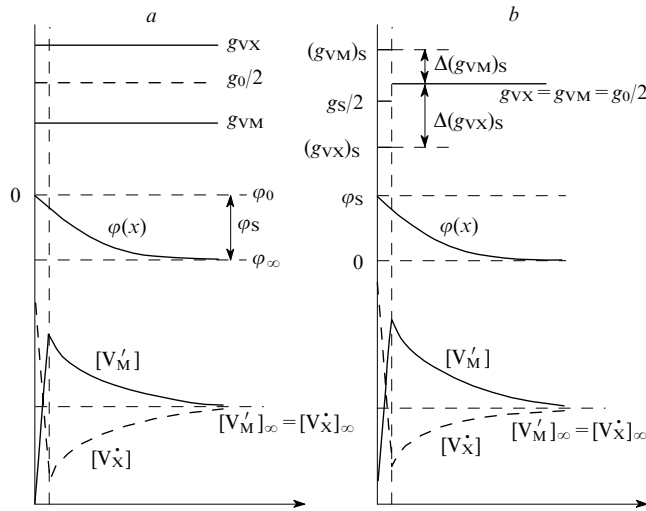


Figure 2. Changes in the energy parameters (g), potential (ϕ) and defect concentration ($[V]$) on going from the surface to the bulk of an ionic crystal.

(a) The Frenkel model; the surface potential ϕ_s is equal to the potential difference between the surface (ϕ_0) and the bulk (ϕ_∞) of a crystal; (b) the Stern model; a case of a diffuse layer enriched with cationic vacancies is considered.

According to this model, the surface potential ϕ_s , *i.e.*, the potential difference between the surface and the bulk of an ionic crystal MX containing intrinsic Schottky defects is

$$e\phi_s = \frac{g_{vX} - g_{vM}}{2}, \quad (2)$$

where e is the electron charge, g_{vX} and g_{vM} are the partial energies of the formation of anionic and cationic vacancies in the crystal bulk the sum of which is equal to the energy of formation (g_0) of the Schottky defect. This expression is remarkable because it contains no characteristics directly related to the surface properties, namely, the quantities g_{vM} and g_{vX} (as well as g_0) are the bulk parameters of the substance; hence, the quantity ϕ_s should be a universal constant of a given substance. However, it is well known that the real surface properties are determined by several specific factors such as the crystal plane type, defects, adsorbed impurities, *etc.*, which casts doubt on the validity of the Frenkel–Kliwer model.

The surface potential can be calculated using a more realistic Stern model,⁴⁹ which implies that the physical properties of a crystal and all its components (native and foreign ions, point defects) on the surface differ from those in the bulk. Particularly, the energies of formation of individual defects on

the surface ($g_{vX})_s$, ($g_{vM})_s$ and the energy of the proper surface disordering $g_s = (g_{vX})_s + (g_{vM})_s$ will differ from the corresponding parameters in the crystal bulk. This difference is the reason for the adsorption (positive or negative) of defects on the crystal surface. If the adsorption energies of oppositely charged defects differ, the excessive defects with the most negative adsorption energies are concentrated on the surface, while the opposite-sign defects form a diffuse layer under the surface. Figure 2b shows the corresponding energy diagram and the distribution of defects in a crystal. According to the Stern model, the surface charge (Q_s) is defined as a sum of contributions of different defects each calculated based on the Langmuir isotherm

$$Q_s = N_s \sum_i q_i \left[1 + \frac{1}{x_i} \exp\left(\frac{\Delta g_i - q_i \phi_s}{kT}\right) \right]^{-1},$$

where N_s is the concentration of accessible surface sites (adsorption centres), q_i is the effective charge of defects, x_i is the mole fraction of defects in the crystal bulk, Δg_i is the adsorption energy of the i th defects (*i.e.*, the excess Gibbs energy of a crystal due to the transition of a defect of the i th kind from the crystal bulk to the surface), k is the Boltzmann constant, T is the absolute temperature; summation is carried out over all possible charged defects. The surface charge is compensated by the charge (Q_d) of a diffuse layer, which is formed under the crystal surface and described by the Gouy–Chapman equation for the diffuse layer charge

$$Q_d = A \left\{ \sum_i N_{0i} x_i \left[\exp\left(-\frac{q_i \phi_{s-1}}{kT}\right) - 1 \right] \right\}^{1/2},$$

where $A = (2\epsilon\epsilon_0 kT)^{1/2}$, ϵ is the dielectric permittivity, ϵ_0 is the dielectric constant; N_{0i} is the bulk concentration of the i th ions in the crystal; ϕ_{s-1} is the potential of the outer Helmholtz plane. The assumption that the surface charges are equal to the diffuse layer charge allows one to obtain a transcendental equation the solution of which gives the surface potential.

The analysis of solutions of this equation⁵⁰ showed that the form of the dependence $\phi_s(T)$ is entirely determined by the values of Δg_i , g_0 and N_s . For positive adsorption energies ($\Delta g^- > 0$, $\Delta g^+ > 0$, negative adsorption), the defect concentration on the crystal surface is lower than in its bulk. In this case, the surface charge and potential are close to zero. For negative adsorption energies of defects ($\Delta g^- < 0$, $\Delta g^+ < 0$, positive adsorption), the cationic and anionic vacancies are concentrated on the surface to form a negative (at $|\Delta g^-| > |\Delta g^+|$) or positive (at $|\Delta g^-| < |\Delta g^+|$) surface charge. Figure 3 shows the dependences of the surface potential on the temperature for a crystal of the NaCl type with the Schottky defects, which were calculated for fixed parameters $g_0 = 1.0$ eV, $\Delta g^- = -0.1$ eV and different values of Δg^+ ($\Delta g^+ < 0$). The analysis has shown that the form of $\phi_s(T)$ curves changes as follows depending on the ratio between g_0 and Δg^+ :

1. For small energies of defect adsorption ($|\Delta g^+| < g_0/4$; $\Delta g^+ < 0$), the quantity $\phi_s(T)$ increases monotonically with the temperature; at $T \rightarrow 0$, $\phi_s \rightarrow 0$ (Fig. 3a). Such a behaviour of the surface potential cannot be explained within the framework of the Frenkel–Kliwer model^{48, 49} and is described by the following approximate formula obtained⁵⁰ for the case of the low potentials $e\phi_s/kT \ll 1$:

$$\phi_s \approx \frac{2kT}{AN_0} N_s \left[\exp\left(-\frac{\Delta g^+}{kT}\right) - \exp\left(-\frac{\Delta g^-}{kT}\right) \right] \times \sqrt{N_0} \exp\left(-\frac{g_0}{4kT}\right). \quad (3)$$

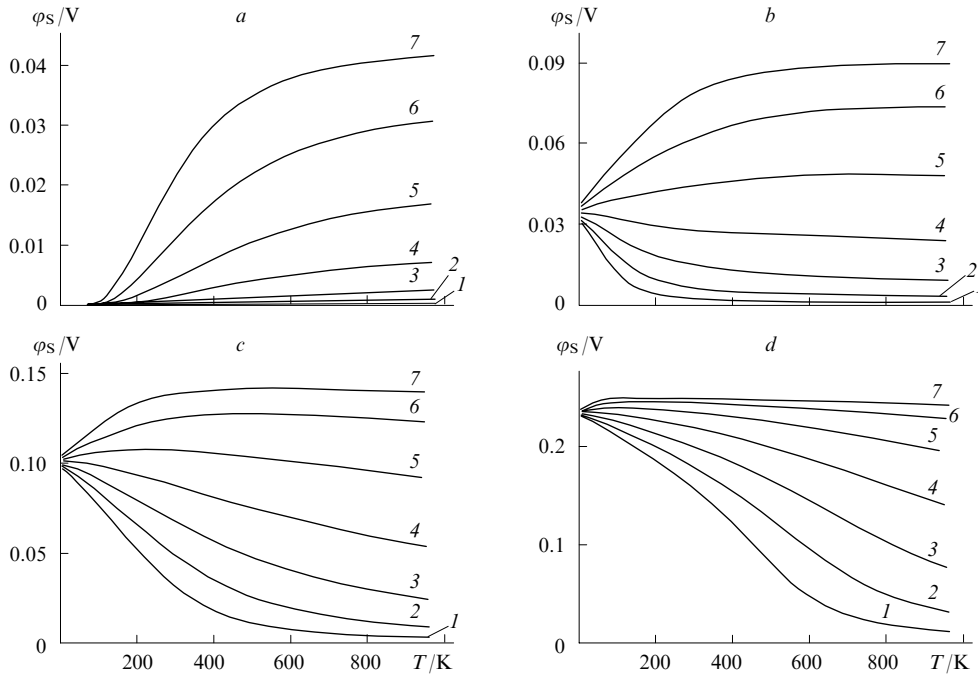


Figure 3. Temperature dependences of the surface potential calculated in terms of the Stern model for $g_0 = 1.0$ eV, $\Delta g^- = -0.1$ eV and $\Delta g^+ = -0.2$ (a), -0.3 (b), -0.4 (c) and -0.6 eV (d). Concentration of surface sites (N_S) is (cm^{-2}): (1) 1×10^{12} , (2) 3×10^{12} , (3) 1×10^{13} , (4) 3×10^{13} , (5) 1×10^{14} (6) 3×10^{14} and (7) 1×10^{15} .

This equation is identical to the expression derived by Lifshits and Geguzin.⁵¹ According to Eqn (3), the surface potential is determined not only by the difference between Δg^+ and Δg^- but also by the energy of defect formation. The quantity ϕ_s increases with the increase in the concentration of surface sites in proportion to the square root of the Schottky defect concentration in a crystal. Thus, for a low adsorption energy, the formation of a double layer is limited not only by the number of surface sites but also by the capacity of the crystal to form a diffuse layer, *i.e.*, by the density of bulk defects.

2. For high adsorption energies ($|\Delta g^+| > g_0/4$; $\Delta g^+ < 0$), the shape of $\phi_s(T)$ curves substantially changes (Fig. 3 b–d). In the limit at $T \rightarrow 0$, the dependence $\phi_s(T)$ tends not to zero but to a certain value ϕ_s^* determined by the relationship

$$e\phi_s^* = \frac{2}{3} \left(-\Delta g^+ - \frac{g_0}{4} \right).$$

In the general case, the surface potential can either increase or decrease depending on the quantities Δg^+ and N_S . For very high adsorption energies $|\Delta g^+|$, the temperature dependences $\phi_s(T)$ differ insignificantly from the curves obtained within the framework of the Poeppele–Blakely model,⁵² which makes an attempt to take into account the effect of the limited number of accessible surface sites on the surface potential. This case is shown in Fig. 3 d, namely, at small N_S , the number of surface sites becomes the limiting factor and the surface potential falls to zero with the increase in the temperature, whereas at large $N_S \sim 10^{15} \text{ cm}^{-2}$, the function $\phi_s(T)$ tends to the high-temperature limit determined by the equation

$$\phi_s = \frac{\Delta g^- - \Delta g^+}{2e}. \quad (4)$$

A comparison of expressions (4) and (2) shows that they are identical under the assumption that

$$\Delta g^- - \Delta g^+ = (\Delta g_{VM})_S - (\Delta g_{VX})_S = g_{VX} - g_{VM}.$$

Thus, for sufficiently high $|\Delta g^+|$ and N_S values and after the renormalisation of the energy values, the Stern model leads to the same result as the Frenkel–Kliwer and Poeppele–Blakely models.

The Stern model allows one to calculate the surface potential in different types of ionic crystals. In the general case, the calculated parameters of this model include the energy of defect formation, the energy of adsorption of defects and impurity ions, the concentration of surface sites, the concentration of impurities and the temperature. This model allows one to calculate ϕ_s in NaCl crystals containing admixed bivalent metals and to assess the isoelectric temperature. The Stern model can be used for the interpretation of experimental ϕ_s values for AgCl and AgBr and also for the calculation of the surface defect concentration in a model superionic oxygen conductor $M_{1-c}^{4+}M_c^{3+}O_{2-0.5c}$. The main advantages of the Stern model are that all its parameters have clear physical meaning, its solution can be found relatively simply and it can be applied to a wide range of problems that include the investigation of segregation effects and the interaction of defects on interfaces.

In the first approximation, the conductivity of a real polycrystalline specimen can be described in terms of a model of cubic blocks by the following expression:^{9, 53}

$$\sigma \approx 2\sigma_{\perp}(4\sigma_{\parallel} + \sigma_b)(2\sigma_{\perp} + \sigma_b)^{-1},$$

where σ_{\perp} and σ_{\parallel} are the contributions of double layers oriented normally and in parallel to the electric field, respectively, to the conductivity; σ_b is the conductivity in the crystal bulk. Usually, for crystals $\sigma_{\perp} \gg \sigma_{\parallel}$, and the conductivity of a specimen is determined by the sum of bulk and surface conductivities. If the same carriers are responsible for the conductivity in the crystal bulk and in the diffuse layer, the conductivity of a polycrystal is expressed by the equation

$$\sigma = \sigma_b \left[1 + \frac{8\lambda_D}{L} \exp\left(\pm \frac{e\varphi_S}{2kT}\right) \right] \quad (5)$$

and is determined by the effective layer thickness equal to the double Debye length of screening ($2\lambda_D$), the block size (L) and the surface potential. The Debye length depends on the concentration of carriers in the crystal bulk and, in the general case, on the temperature. It was shown that the activation energy of conduction of an impurity-free MX crystal is

$$E_a = \frac{h_0}{4} - \frac{e\varphi_S}{2} + E_m, \quad (6)$$

i.e., it is determined by the bulk characteristics of the solid, namely, the enthalpies of formation (h_0) and migration (E_m) of a defect and the surface potential (φ_S).

Studies of polycrystalline AgCl have shown²⁴ that the conductivity of specimens non-subjected to long-term annealing is determined by the conductivity of intergrain boundaries. The estimates of the surface potential based on relationship (6) produce quite reasonable values $\varphi_S = 0.1-0.2$ V, provided the conductivity is assigned to interstitial cations that form the diffuse layer. Polycrystalline specimens demonstrated the dielectric relaxation with a small increment $\Delta\varepsilon/\varepsilon_0 \approx 3$. On annealing, the activation energy of conduction was observed to increase monotonically and the quantity $\Delta\varepsilon/\varepsilon_0$ vanished.

Studies of polycrystalline AgI have shown⁵⁴⁻⁵⁶ that the conductivity of mechanically dispersed samples far exceeds the conductivities of β - and γ -phases of AgI cited in the literature. Upon heating or storage at room temperature, the conductivity decreased, which was accompanied by a gradual increase in the activation energy of conduction from 0.23 to 0.31 eV. For specially purified specimens, the Arrhenius plots demonstrated a bend at a temperature T_b in the range from 0 to 40 °C. After sintering at $T > 150$ °C, the absolute magnitudes of conductivity virtually coincided with that of a β -AgI single crystal. The static permittivity (ε_s), which does not depend on the electrode polarisation, substantially increased to $\varepsilon_s/\varepsilon_0 \sim 50-200$ after the specimens were pressed or mechanically treated, whereas the high-frequency permittivity (ε_∞) ($\varepsilon_\infty/\varepsilon_0 = 8 \pm 2$) was close to the permittivity of pure β -AgI. The observed changes can be explained by the formation of β - γ -polytypes containing randomly alternating closely packed layers (in contrast to the regular packing ABABAB or ABCABCABC in the β - and γ -phases, respectively). Insofar as the unit cells in both phases (in both γ -AgI and β -AgI) possess no inversion centres, the mechanical activation of polytypes can shift the closely packed layers. This is accompanied by changes in the polar axis direction and may result in the formation of a contact between two layers $I^- - Ag^+$. The cations on two sides of the contact plane are in different tetrahedral positions. This contact represents an antiphase boundary, *i.e.*, a boundary between antiphase domains. In this case, the strong Coulomb interaction between the $Ag^+(T_+)$ and $Ag^+(T_-)$ layers is compensated by the partial transition of Ag^+ ions from their regular positions to the vacant tetrahedral and octahedral positions, *i.e.*, to form the Frenkel defects at the antiphase boundary. The accumulation of the space charge at antiphase boundaries is the reason for the high dielectric permittivity of this material.

The presence of a small concentration of a heterogenic admixture (*e.g.*, metallic silver) stabilises the antiphase domains. A qualitatively similar effect was observed in the AgI-poly(tetrafluoroethylene) system.^{57, 58} The mechanism of stabilisation of antiphase boundaries resembles that of dispersion strengthening in metals where fine heterogeneous inclusions prevent the annealing of grain boundaries.

IV. Disorder of ionic crystals at interfaces. Conductivity of microcomposites

The physical reason for the surface interaction in a composite of the ionic salt-oxide type lies in the trend of both substances to decrease their surface energy due to the interaction of surface ions with the ions of the neighbouring phase. The surface energy of the interface between an ionic salt MX and alumina is determined in the first approximation as a sum of the cation-cation ($M^+ - Al^{3+}$), cation-anion ($Al^{3+} - X^-$ and $M^+ - O^{2-}$) and anion-anion ($X^- - O^{2-}$) interactions (E_{M-Al} , E_{X-Al} , E_{M-O} and E_{X-O} , respectively)

$$G_{MX-A}^s = \gamma_{MX-A} S_{MX-A} \approx E_{M-Al} + E_{Al-X} + E_{M-O} + E_{X-O},$$

where γ is the specific surface energy and S is the surface area.

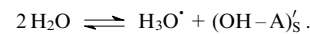
For the sake of simplicity, we assume that, as a result of their interaction, the lattices of MX and A phases are fitted to one another at the interface. Because the energies E_{M-Al} , E_{X-Al} , E_{M-O} and E_{X-O} are different in the magnitude (due to the different energies of interaction in the ion pairs $M^+ - Al^{3+}$, $Al^{3+} - X^-$, $M^+ - O^{2-}$ and $X^- - O^{2-}$), in the interface layers, the ideal structure inherent in individual phases will be distorted in such a way as to provide a gain in the surface energy due to the mutual approach or removal of surface atoms. The relative displacement of ions from their ideal positions is determined by the balance of energies E_i . Insofar as in alumina and in majority of salts MX under discussion, anions exceed cations in size, it can be expected that for close packing, the interface cations will have the larger free volumes and be displaced by longer distances than anions. As a result, in the space between the surface layers, an intermediate positively charged layer enriched with cations is formed, the charge of this layer being compensated by the cationic vacancies (V_M')s that constitute the diffuse layer. The process of structural relaxation can be presented as the following quasichemical reaction:



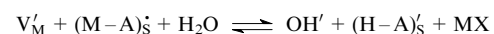
which describes the stage of the surface disordering of MX at the MX-A interface (the superscripts ' and ' correspond to the positive and negative charges of a species, respectively, as compared with the stoichiometric charge of a given lattice site). If an anion is adsorbed on the surface, another reaction proceeds



The isoelectric point of an oxide pE was proposed⁵⁹ as a measure of its surface activity. Indeed, equations similar to Eqns (7) and (8) may be written for the surface interaction of an oxide with water



The first reaction predominates for oxides with $pE > 7$, for instance Al_2O_3 , CeO_2 ; the second prevails for oxides with $pE < 7$ (ZrO_2 , SiO_2). By analogy with aqueous solutions, one can expect that the surface reaction (7) will occur in composites containing basic oxides ($pE > 7$), whereas for acidic oxides ($pE < 7$) the interface interaction will follow the mechanism (8). Unfortunately, to date, due to the insufficient amount of experimental data, it is difficult to check the correctness of the direct transfer of the model of acid-base equilibria in aqueous solutions to the case of composites. Nonetheless, the competition between processes (7) and (9)



can be responsible for the deterioration of the ionic conductivity of composites $\text{AgCl}-\text{Al}_2\text{O}_3$ (Ref. 60) and $\text{AgI}-\text{Al}_2\text{O}_3$ (Ref. 61) and the appearance of the protonic conductivity in composites $\text{Li}_2\text{SO}_4-\text{Al}_2\text{O}_3$ (Ref. 62) and $\text{M}(\text{NO}_3)_n-\text{Al}_2\text{O}_3$ (M is an alkali metal)⁶³ in humid atmosphere.

In essence, reactions (7) and (8) describe the formation of the electrical double layer on the surface of MX in contact with Al_2O_3 . The changes in the energy (Δg_A) upon the displacement of an ion from its normal position into the interfacial space can be considered as the energy of cation adsorption in terms of the Stern model; hence, the quantity Δg_A is related to the surface potential (φ_{SA}) at the interface of a crystal MX

$$\varphi_{SA} \sim -\frac{\Delta g_A}{q_i}, \quad (10)$$

where q_i is the charge of the displaced ion. Insofar as the exact φ_{SA} value is determined not only by the quantity Δg_A but also by the contribution of the relaxation of oxide ions, expression (10) can be considered as merely a correlation between the values Δg_A and φ_{SA} , *viz.*, the surface potential increases with the increase in Δg_A . For $T = 0$ K, on the surface of a salt MX in contact with an oxide, a dense layer similar to the Helmholtz layer exists. With the increase in the temperature, the cationic vacancies form a diffuse layer, which provides the enhanced conductivity of the composite.

Insofar as ions in the dense layer are bound to the surface of oxide A and have limited mobility, the conductivity of MX in composites is determined by the defects that dominate in the diffuse layer. The mobility of defects in the diffuse layer is assumed equal to their mobility in the crystal bulk.^{6, 7, 10, 12, 13, 15} This statement is based on the assumption that the defect concentration in the surface layer remains low; hence, the crystal structure does not change (the absence of deformations, surface phase transitions, *etc.*). Within the framework of these assumptions, the conductivity across the diffuse layer in the composite is described by expression (5), where φ_{SA} should be substituted for φ_S and the migration energy E_m pertains to the defects that form the diffuse layer. For low φ_{SA} , *i.e.*, for a relatively weak surface interaction, the absolute magnitudes of conductivity are low and the activation energy of conduction is

$$E_a = \frac{h_0}{4} - \frac{e\varphi_{SA}}{2} + E_m.$$

The quantity E_a can vary within the limits $(h_0/4 + E_m) > E_a > (h_0/4 + E_m - e\varphi_{SA}/2)$ and is sensitive to the surface state of the $\text{MX}-A$ contact, *i.e.*, to the presence of structural defects, adsorbed admixtures, *etc.*; the measured parameters of conductivity are often characterised by poor reproducibility. Such effects are observed in insufficiently sintered composites.

If as a result of surface interaction, the surface potential increases to its limiting value $e\varphi_S = h_0/2$, the activation energy of conduction decreases to $E_a = E_m$ [see Eqn (6)]. As was shown by Maier,^{10, 13, 15} the activation energy of conduction in composites $\text{MX}-A$ is close to the energy of migration of a cationic vacancy, which indirectly confirms the fact that the surface potential is sufficiently high and reaction (7) proceeds on the interface to afford a diffuse layer built of cationic vacancies.

Most composites considered in the early studies can be classified with microcomposites, because they were prepared from oxides with the average particle size of 0.06–10 μm . The properties of microcomposites are similar to those of polycrystalline specimens, and all physicochemical properties of ionic salts (except for the ionic conductivity) in these systems are analogous to the properties of pure starting compounds. A

typical example of such systems is the composites $\text{AgCl}-\text{Al}_2\text{O}_3$. The dependence of the conductivity (σ) on the mole fraction (x) of the oxide has a maximum at $x = 0.30$, the activation energy of conduction is close to the energy of migration of cationic vacancies.^{6, 60} The estimates of the energy of formation of silver chloride in a composite, which were obtained using an electrochemical cell $\text{Pb}/\text{PbCl}_2/(1-x)\text{AgCl}-x\text{Al}_2\text{O}_3/\text{Ag}$, showed that the thermodynamic properties of AgCl in composites remain virtually unchanged.⁶⁴ The exposure of composites to a humid medium lead to the reduction of their conductivity, particularly, at $x > 0.5-0.6$.⁶⁰

Based on correlations obtained earlier^{65, 66} and an assumption that $E_a = E_m$, it is possible to assess the concentration of current carriers in composites. The following relationship between the conductivity at 25 °C ($\sigma_{25}/\text{S cm}^{-1}$), the defect concentration (n/cm^{-3}) and the activation energy (E_a/eV) was proposed:⁵³

$$\log \sigma_{25} = \log n - 14.5 E_a - 20.55.$$

In composites with the highest conductivity, the concentration of defects proved to be high and comparable with their concentration in superionics. This suggests that additional channels for the defect formation exist in composites so that the correct interpretation of experimental data requires that the specifics of interphase interactions and the real structure of the interface were taken into account. It cannot be ruled out that the disordered surface phases formed at the interface will manifest most strongly their specific properties on going from micro- to nanocomposites. These effects are discussed below.

V. Calculations of physicochemical properties of composites

The model of cubic blocks,^{53, 67} which is similar to that used earlier to describe the conductivity of polycrystalline specimens, may be applied for the quantitative calculation of the physical characteristics of composites $\text{MX}-A$. If a layer with a thickness λ and properties differing from those of the MX phase in the substance bulk exists near the interface, this layer can be conditionally assumed to be the surface phase. The model of cubic blocks allows one to estimate the volume and mole fractions of the surface phase (f_S and x_S , respectively) for the uniform random distribution of equal-size particles MX and A in a composite

$$f_S = \frac{2\beta\lambda f(1-f)}{L_A},$$

$$x_S = \frac{2\beta\lambda\delta x(1-x)}{L_A[1+x(\delta-1)]},$$

where β is the constant determined by the particle geometry, for cubic or spherical particles, $\beta \approx 3$; λ is the surface phase thickness; f and L_A are the volume fraction and the size of particles of the component A in the composite; the coefficient δ is determined by the ratio of densities (d) and molecular masses (μ) of components, namely, $\delta = (\mu_A d_{MX})/(\mu_{MX} d_A)$; x is the mole fraction of the component A . The volume fraction of an ionic salt $(f_{MX})_{\text{bulk}}$ beyond the surface layer can be determined using the expression

$$(f_{MX})_{\text{bulk}} = 1 - f - f_S = \left[1 - \frac{2\beta f \lambda}{L_A}\right](1-f), (f_{MX})_{\text{bulk}} \geq 0, \quad (11)$$

which is very convenient for the estimation of the surface layer thickness provided the size of particles A is known. In real systems, L_A corresponds to the size of an aggregate of particles A and d_A corresponds to the average density of aggregates.

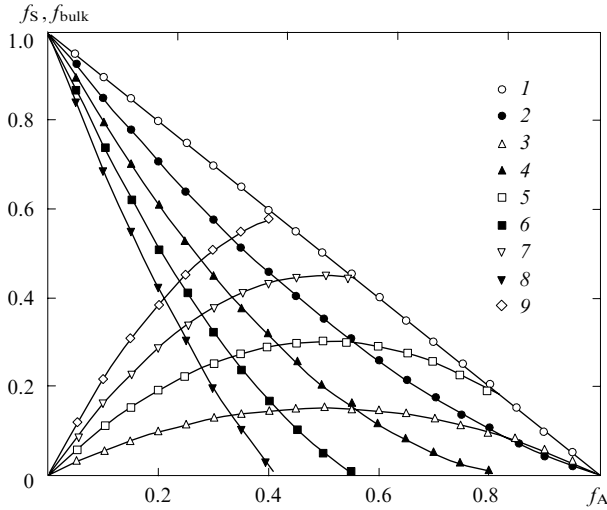


Figure 4. Concentration dependences of (1, 2, 4, 6, 8) bulk (f_{bulk}) and (3, 5, 7, 9) surface (f_s) phases in composites calculated based on the model of cubic blocks for different ratios λ/L_A . $\lambda/L_A = 0$ (1), 0.1 (2, 3), 0.2 (4, 5), 0.3 (6, 7), 0.4 (8, 9).

Expression (11) allows one to determine the ratio λ/L_A based on the concentration dependence of any extensive characteristic of the MX phase; moreover, provided the average size of A particles is known, the absolute magnitude of the surface phase thickness λ can be found (Fig. 4).

To assess the conductivity of composites, the models of effective medium or the theories of percolation, which were adapted to the specific features of the morphology of composites, are used. The most precise calculations of the conductivity of conventional composites of the conductor–dielectric type $(1-f)\text{M}-f\text{A}$ can be performed for the limiting cases ($f \rightarrow 0$ and $f \rightarrow 1$), where the particles of phases A or M pertain to the second-phase matrix and are isolated from one another. As the volume fraction of the second phase increases, its particles are no longer isolated and the calculations of the conductivity of composites require the use of more intricate models. A simpler method for the calculation of the composite conductivity based on the well-known mixing equation was proposed^{68, 69}

$$\sigma^\alpha = (1-f)\sigma_M^\alpha + f\sigma_A^\alpha, \quad (12)$$

where the parameter α is determined by the empirical fitting of dependence (12) to experimental values. The comparison of Eqn (12) with the exact solutions obtained for the limiting cases showed that the parameter α depends on the composite morphology. The morphology of real composites changes as the content of the second component increases, which makes extremely difficult the theoretical calculations of the conductivity within the framework of models mentioned above. The use of rules of mixing allows one to solve this problem by introducing the linear dependence of the power index α in Eqn (12)

$$\alpha \equiv \alpha(f) = \alpha_1(1-f) + \alpha_2 f, \quad (13)$$

where α_1 and α_2 are the constants corresponding to the morphology of composites in the regions of limiting dilution (for $f \rightarrow 0$ and $f \rightarrow 1$, respectively). Taking into account expression (13), it is possible to represent expression (12) in the general form

$$\sigma^{\alpha_1(1-f)+\alpha_2 f} = (1-f)\sigma_M^{\alpha_1(1-f)+\alpha_2 f} + f\sigma_A^{\alpha_1(1-f)+\alpha_2 f}. \quad (14)$$

In the limiting cases, Eqn (14) is reduced to expressions obtained within the framework of the effective medium model. The form of dependences $\log(\sigma/f)$ and $\sigma(f)$ shown in Figs 5a,b is entirely determined by α_1 and α_2 . These dependences allow one to describe the conductivity of composites the morphology of which is determined by quite different factors including the percolation effect. The theoretical curves are close to those obtained using the McLachlan equation,⁷⁰ which is widely employed for the description of the percolation behaviour of composites. Figure 5c shows the experimental conductivity of different composites⁷¹ in comparison with calculated curves.

As in the case of conductor–dielectric composites, the most accurate calculations of the conductivity of solid electrolytes $(1-f)\text{MX}-f\text{A}$ can be performed for the limiting cases ($f \rightarrow 0$ and $f \rightarrow 1$), where isolated particles of phases A or MX are located in the second phase matrix. In the general case, the conductivity of model systems is described in terms of a percolation model¹¹ with two percolation thresholds, namely, p_1 (dielectric MX–ionic conductor) and p_2 (ionic conductor–dielectric A). The most serious difficulties in calculations

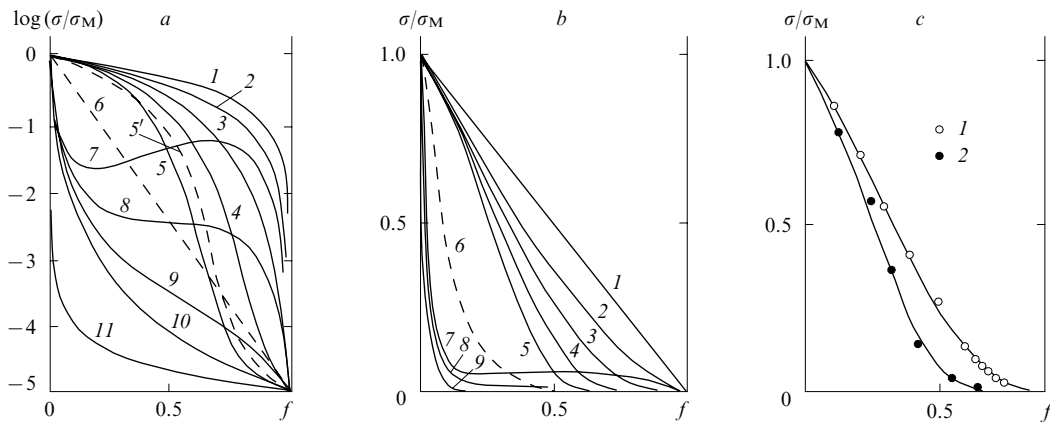


Figure 5. Calculated dependences of the relative conductivity (σ/σ_M) of composites MX–A on the bulk concentration of dielectric (f), shown in (a) logarithmic and (b) linear scales and (c) their comparison with experimental conductivity of composites AgI–Al₂O₃ (1)⁶¹ and AgI–poly(tetrafluoroethylene) (2).^{57, 58}

The curves were obtained for different (α_1, α_2) : (1) (1, 1), (2) (2/3, 2/3), (3) (2/3, 1/3), (4) (2/3, 0), (5) (2/3, −1/3), (6) (0, 0), (7) (−1/3, 2/3), (8) (−1/3, 1/3), (9) (−1/3, 0), (10) (−1/3, −1/3), (11) (−1, −1); curve (5') was calculated using the McLachlan equation.⁷⁰

emerge in the vicinity of percolation thresholds at $f \approx p_1$ or p_2 . In these regions, intricate models^{72–81} are used. Moreover, even for composites with simple morphologies, rather cumbersome analytical expressions with a large number of fitting parameters should be used, which complicates the testing and practical application of these models. The mixing equation can be applied for the description of composite ionic conductors. The additional contribution of the surface conductivity can be taken into account in terms of the model of cubic blocks, which allows one to assess the concentration of the surface conducting phase. The mixing equation should take into account the contribution of this phase and can be presented as follows:

$$\sigma^\alpha = \left[1 - f - 6f(1-f) \frac{\lambda}{L_A} \right] \sigma_M^\alpha + 6f(1-f) \sigma_S^\alpha \left(\frac{\lambda}{L_A} \right) + f \sigma_A^\alpha. \quad (15)$$

For $6(\lambda/L_A)\sigma_S \gg \sigma_{MX}$, the expression takes a simpler form

$$\sigma = \left[6f(1-f) \frac{\lambda}{L_A} \right]^{1/\alpha} \sigma_S. \quad (16)$$

For $\alpha > 0$, dependence (16) has a symmetrical form with the maximum at $f = 0.5$. The introduction of the linear dependence $\alpha = \alpha(f)$ [expression (15)], which takes into account the changes in the morphology, allows one to obtain a modified mixing equation suitable for the description of conductivity of composite solid electrolytes. Analysis showed that the form of curves substantially depends on the parameters α_1, α_2 and that theoretical curves allow one to describe the conductivity as a function of the composition for specimens with totally different morphologies (Figs 6a,b). It is interesting that the conductivity of a composite should increase with the increase in the size of particles of the oxide additive according to the exponential law $\sigma \sim (1/L_A)^\beta$, where $\beta = \alpha^{-1} \geq 1$, and only in the limiting case $\alpha(f) = 1$, it is expressed by the relationship $\sigma \sim (1/L_A)$ conventionally used in the literature.^{15, 22, 25, 26}

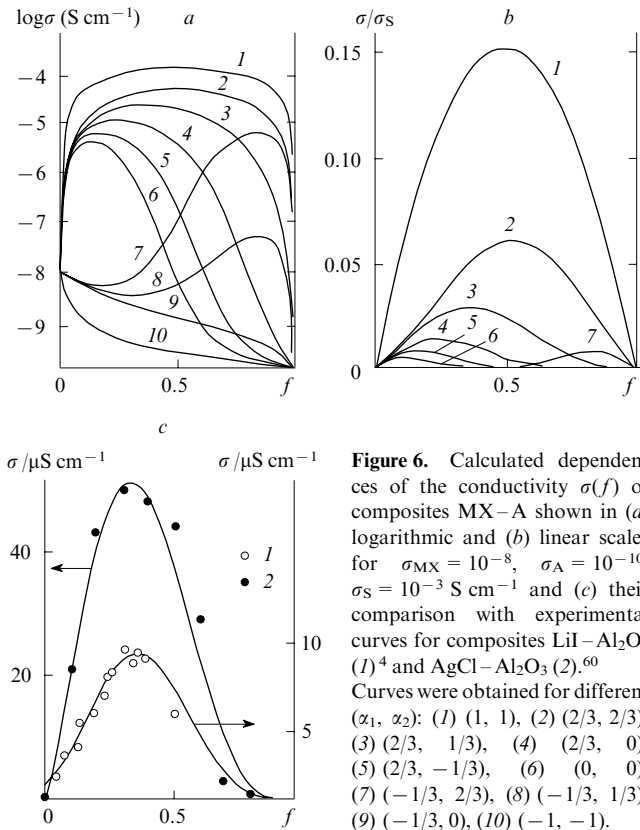


Figure 6. Calculated dependences of the conductivity $\sigma(f)$ of composites MX–A shown in (a) logarithmic and (b) linear scales for $\sigma_{MX} = 10^{-8}$, $\sigma_A = 10^{-10}$, $\sigma_S = 10^{-3}$ S cm⁻¹ and (c) their comparison with experimental curves for composites LiI–Al₂O₃ (1)⁴ and AgCl–Al₂O₃ (2).⁶⁰ Curves were obtained for different (α_1, α_2) : (1) (1, 1), (2) (2/3, 2/3), (3) (2/3, 1/3), (4) (2/3, 0), (5) (2/3, -1/3), (6) (0, 0), (7) (-1/3, 2/3), (8) (-1/3, 1/3), (9) (-1/3, 0), (10) (-1, -1).

Equation (15) type describe well the experimental data for composites LiI–Al₂O₃ (Ref. 4) and AgCl–Al₂O₃ (Ref. 60) (Fig. 6c). The mixing equation in the form (15) is qualitatively consistent with the basic expressions obtained within the framework of the effective medium model and the percolation theory and also with the results of computer calculations.

VI. Thermodynamic description of composites. The effect of self-dispersion of ionic salts. Synthesis of nanocomposites

In the general case, a solid-phase composite represents a complex multicomponent system that comprises several real solid phases. By a real solid phase is meant a combination of single crystals of different sizes, which contain admixtures, lattice defects (point defects and pores), free surfaces, cracks and grain boundaries. Many properties of composites depend on their morphology, viz., the size distributions of particles of each phase and the mutual spatial arrangement of monophase domains. In the presence of the surface interaction between the phases MX and A, the expression for the excess Gibbs energy of the composite can be presented as follows:^{24, 82–84}

$$G = (G_{MX}^\circ + \gamma_{MX} S_{MX} + \Delta G_{MX}^{\text{elas}}) + (G_A^\circ + \gamma_A S_A + \Delta G_A^{\text{elas}}) + \gamma_{MX-A} S_{MX-A}. \quad (17)$$

Here, G_{MX}° and G_A° are the standard changes in the Gibbs energies of the formation of individual components MX and A; $\gamma_{MX} S_{MX}$ and $\gamma_A S_A$ are their excess surface energy determined by the specific surface energy (γ) multiplied by the free surface area; $\Delta G_{MX}^{\text{elas}}$ and ΔG_A^{elas} are the elastic strain contributions; $\gamma_{MX-A} S_{MX-A}$ is the energy of the interface, where γ_{MX-A} is the specific surface energy at the interface; S_{MX-A} is the area of the contact between components MX and A; the contribution of the elastic energy is taken into account by terms $\Delta G_{MX}^{\text{elas}}$ and ΔG_A^{elas} . The expression for the Gibbs energy of the component MX can be obtained from Eqn (17), if we assume that the interface energy is evenly distributed between the components

$$G_{MX} = G_{MX}^\circ + \gamma_{MX} S_{MX} + \frac{\gamma_{MX-A} S_{MX-A}}{2} + \Delta G_{MX}^{\text{elas}}. \quad (18)$$

The contribution of elastic strains ($\Delta G_{MX}^{\text{elas}}$) to the total energy of the MX phase is largely determined by the elastic energy of the misfit in lattice parameters at the interface and the energy of dislocations that arise in the interface regions. The calculations of G^{elas} even for thin films with simple morphologies are very tedious; hence, it is difficult to assess this contribution in composites. Nonetheless, in all the cases irrespective of the nature of elastic strains (dilatational or compression strains), the quantity $\Delta G_{MX}^{\text{elas}}$ is positive and should increase with an increase in S_{MX-A} . Hence, the last two terms in expression (18), which determine the energy of the MX phase depend on the area of the interphase contact in the composite.

Sintering of a mixture of a low-melting component MX (with the higher self-diffusion coefficients) with the nanoparticles of a high-melting component A can be accompanied by both a decrease and an increase in the interface area. In the former case, the sintering is reduced to simple recrystallisation of phases. The latter case is more interesting for solid-state chemistry. The process of the formation of an interphase contact (Fig. 7) is thermodynamically favourable if $dG/dS_{MX-A} < 0$. In this case, the sintering is accompanied by an increase in the interface area S_{MX-A} . If we ignore the dependences of the specific surface energies and the elastic energy on the surface area (or the particle size) [γ_{MX} , γ_A ,

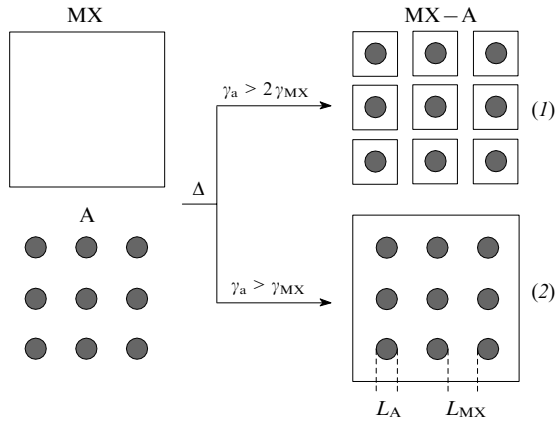


Figure 7. Illustration of self-dispersion of an ionic salt MX at its contact with a nanocrystalline oxide A (see the text).

γ_{MX-A} , G_{MX}^{elas} , $G_A^{elas} \neq f(S_{MX-A})$ and express γ_{MX-A} through the free energy of adhesion (γ_a)

$$\gamma_a = \gamma_{MX} + \gamma_A - \gamma_{MX-A},$$

we can find the change in the Gibbs energy of a composite with the increase in the interface area by dS_{MX-A}

$$\frac{dG}{dS_{MX-A}} = \gamma_{MX} \frac{dS_{MX}}{dS_{MX-A}} + \gamma_A \frac{dS_A}{dS_{MX-A}} + \gamma_{MX} + \gamma_A - \gamma_a. \quad (19)$$

Pines⁸⁵ and Geguzin⁸⁶ considered in detail the mechanism of sintering, *i.e.*, the formation and the growth of the interface. The mechanism and kinetics of sintering differ for two cases determined by the conditions $\gamma_a < 2\gamma_{MX}$ and $\gamma_a > 2\gamma_{MX}$. In the former case, a neck is formed between two grains the shape and size of which are determined by the shape and size of particles and the absolute magnitudes of γ_{MX} , γ_A and γ_a .

The expression

$$\gamma_a > 2\gamma_{MX} \quad (20)$$

is known as the Gibbs–Smith condition for complete spreading. It can be derived from Eqn (19), provided that $dG/dS_{MX-A} < 0$, $dS_A/dS_{MX-A} = -1$, $dS_{MX}/dS_{MX-A} \approx 1$, *i.e.*, if the decrease in the free energy of a component A (substrate) is accompanied by the formation of the equivalent free surface of a component MX (film). The same condition is prerequisite for the stable layer-by-layer growth of films according to the Frank–van der Merve mechanism. Figure 7(1) shows the corresponding changes in the morphology. However, upon sintering of mixtures with an arbitrary microstructure, the newly formed free surfaces of the component MX can overlap if the distances between the surfaces of phase A are sufficiently small [Fig. 7(2)]. At the complete overlap of free surfaces, the derivative dS_{MX}/dS_{MX-A} approaches zero, and the following expression can be derived from Eqn (19):

$$\gamma_a > \gamma_{MX}, \quad (21)$$

which represents a condition of the feasibility in principle of spreading of the component MX over the surfaces of the phase A in a composite. A comparison of condition (21) with the condition (20) for the complete spreading (or epitaxy) in films shows that the interfacial interaction in composites should proceed more actively and at lower energies of adhesion in contrast to ordinary film structures. The surface roughness is known to improve wettability. The roughness coefficient is equal to the ratio of the true contact area to its apparent area and can take values in the range from zero to unity. Equa-

tion (21) corresponds to the limiting roughness coefficient of the phase A equal to unity.

If conditions (20) or (21) are met, the interface area in the system spontaneously increases or the sufficiently well developed surface of nanocrystals A is ‘wetted’ with the substance MX. A comparison of values $\gamma \approx 100–300 \text{ erg cm}^{-2}$ for alkali metal halides⁸⁷ with the specific surface energies of oxides Al_2O_3 , FeO, MgO and SiO_2 ($\gamma \approx 600–1200 \text{ erg cm}^{-2}$) (Refs 88 and 89) suggests that the wetting condition (20) should be fulfilled for composites that consist of ionic halides and high-melting oxides including alumina.

If substance A is in the nanocrystalline state, the effective size of particles of the phase MX should decrease to very small values, *i.e.*, an unusual effect, the self-dispersion of component MX to form a two-phase nanocomposite is observed.²⁴ Indeed, the self-dispersion effect was observed during the solid-phase sintering of composites $\text{AgCl–Al}_2\text{O}_3$,⁶⁰ $\text{AgI–Al}_2\text{O}_3$ (Refs 61, 71 and 90–92) and $\text{Li}_2\text{SO}_4\text{–Al}_2\text{O}_3$,^{82,83,93,94} A similar effect was observed in heterogeneous systems based on alkali metal nitrates [$\text{LiNO}_3\text{–Al}_2\text{O}_3$, $\text{NaNO}_3\text{–Al}_2\text{O}_3$,⁹⁵ $\text{RbNO}_3\text{–Al}_2\text{O}_3$,^{67,96,97} $\text{CsNO}_3\text{–Al}_2\text{O}_3$ (Ref. 96)] and halides [$\text{NaCl–Al}_2\text{O}_3$, $\text{KCl–Al}_2\text{O}_3$ and $\text{RbCl–Al}_2\text{O}_3$ (Ref. 24)], which points to the good adhesion of ionic salts to the alumina surface. Self-dispersion serves as the indicator of strong interfacial interaction in the system and occurs at long-term sintering until the whole surface of the component A is covered with substance MX. In this limiting case, the quantity S_{MX-A} approaches S_A , and the system spontaneously reaches firm metastable equilibrium where

$$G = (G_{MX}^o + G_A^o) + \gamma_{MX-A}S_A + (\Delta G_{MX}^{elas} + \Delta G_A^{elas}),$$

$$G_{MX} = G_{MX}^o + \frac{\gamma_{MX-A}S_A}{2} + \Delta G_{MX}^{elas}. \quad (22)$$

According to the latter expression, the properties of an ionic salt are determined not only by the standard thermodynamic parameters of the substance, but also by the contribution of the energy of interfacial interaction, which increases in proportion to the surface area of the oxide A (or in the inverse proportion to the size of its particles). If the components taken in a volume ratio of 1 : 1 are uniformly mixed so that the total surface of a component A is completely wetted with a component MX, the effective size of MX grains is approximately equal to $L_A/2$. In composites with oxide nanoparticles ($L_A/2 \approx 10 \text{ nm}$), the size of MX particles becomes sufficiently small for the manifestation of pronounced size effects.

VII. Size effects in composites

Size effects in heterogeneous systems⁸⁴ are determined by many factors, namely, the chemical nature of components in the heterogeneous mixture, the morphology of the system and the interfacial interaction between the components. Since it is difficult to take into account these factors, no adequate theoretical description of the size effect in composites has been developed so far. As in the case of pure substances, the most pronounced changes in the properties are observed in nanocomposites, *i.e.*, heterogeneous systems with the average size of particles of both phases below 100 nm. In recent years, the interest in the unusual effects observed in nanosize systems has arisen.^{17–22, 24, 84, 85, 88, 98–128} This is not surprising, since the processes that involve nanosystems form the basis for future solid-state nanotechnologies.

Size effects can conditionally be divided into two types.

1. Weak effects, where the physicochemical properties of a substance change insignificantly with an increase in the specific surface area (or a decrease in the particle size) and all the changes observed can be explained by the additive effect of the

surface on the basic properties of a crystal. According to the classification proposed by Shcherbakov,^{129, 130} these effects may be assigned to capillary effect of the first kind. As a rule, these effects are observed in crystals with the size above 10 nm.

2. Strong phase size effects or, according to the Shcherbakov classification, capillary effects of the second kind responsible for the qualitative changes in the substance properties, which are impossible to explain in terms of ordinary surface phenomena. As a rule, these effects are observed in very small particles the size of which does not exceed 10 nm. It is these systems that should be considered as truly nanosize systems. The concept of Shcherbakov was qualitatively confirmed by the subsequent experimental and theoretical studies^{84, 100–104, 116, 117, 124, 126}.

As a result of spreading or self-dispersion, the Gibbs energy of an ionic salt increases to a value described by expression (22). The excess energy is determined by two main factors, namely, the interface energy, which depends on the nature and the energy of interactions between the surface atoms of phases in contact, and the elastic strains that arise in the bulk of contacting phases.

The mechanism of interactions in composites MX–A is determined by the contribution of non-dispersion interactions, namely, ion–ion, donor–acceptor, dipole–dipole, *etc.* The correct estimation of the interface energy requires consideration of the structure of the contact plane and the real potentials of ion–ion interactions in the contact region, which is an extremely complicated and still unsolved problem. It was shown²⁴ that lithium salts in systems with alumina exhibit a stronger trend for the formation of nanocomposites as compared with rubidium and caesium salts, while iodides more readily form nanocomposites as compared with chlorides and fluorides. This suggests that the polarising power of the cation and the polarisability of the anion in the ionic component play an important role in the surface interaction mechanism.

Studies of thin films have demonstrated that the structure of a solid in the near-interface region depends substantially on the features of the crystallography and energy of planes in contact. As a rule, in very thin films, the epitaxial contact between phases is energetically favourable and the film structure is determined by the effect of the support and can differ from the structure of the same substance in the individual state. With the increase in the film thickness, elastic strains are accumulated in its bulk, which results in the film restructuring upon reaching a certain critical thickness h_{cr} . For a minor misfit in the structural parameters, the film acquires a structure corresponding to the pure component and a network of misfit dislocations is formed on the interface. For a 1%–0.1% misfit in the lattice parameters, the thickness of the epitaxial layer was calculated to be $h_{cr} \approx 5–25$ nm.^{131–133} If the structural parameters of the substrate and the film differ substantially, h_{cr} becomes very small, and the relaxation of the elastic energy of the growing epitaxial layer necessitates the formation of a very large number of dislocations, which becomes energetically unfavourable. In this case, the relaxation of elastic strain energy can proceed through different channels, namely, the film can be divided into separate blocks the size of which increases with the increase in the film thickness or an amorphous surface phase is formed.^{100, 133}

In the above-mentioned cases, the formation of thin epitaxial, nanocrystalline or amorphous films may be considered as the manifestation of the phase size effect in heterogeneous systems, *viz.*, with the increase in the characteristic size (film thickness), new surface phases are formed.

In the composites MX–A the distance between the grains of the oxide component A plays the role of the MX layer thickness. If the size of particles A far exceeds h_{cr} , the properties of the ionic component are similar to those of thick MX

films. If the oxide grains are sufficiently small and comparable with h_{cr} , then at sufficiently high oxide concentrations, the MX phase is localised in nanopores between oxide particles, *i.e.*, under the conditions similar to those of the existence of a thin MX layer on the surface of A. In a real composite, two states always coexist (a ‘normal’ state of coarse MX grains and an ‘interfacial’ state with anomalous properties) in a quantitative ratio determined by the composition and morphology of the composite.

The thermodynamic properties of substances deposited on a solid support to form adsorbed layers or thin films differ from those in the bulk.^{85, 98–100, 131} The characteristic grain size at which noticeable deviations in the thermodynamic properties are observed is ~ 10 nm.^{84, 100–102, 105, 107–111, 113, 116, 117, 124} The temperature of a phase transition (T_t) that occurs in the bulk of an ionic salt MX can be estimated^{24, 100, 115} using the following approximate relationship:

$$\frac{T_t}{T_t^0} = 1 - \left[(\gamma_{MX}^\beta S_{MX}^\beta - \gamma_{MX}^\alpha S_{MX}^\alpha) + \frac{1}{2} (\gamma_{MX-A}^\beta S_{MX-A}^\beta - \gamma_{MX-A}^\alpha S_{MX-A}^\alpha) + \Delta G^{\text{elas}} \right] \frac{1}{H_t},$$

where T_t^0 is the standard temperature of the transition, superscripts α and β correspond to high-temperature and low-temperature phases, respectively, ΔG^{elas} is the difference between the excess elastic energies of phases β and α , H_t is the enthalpy of the phase transition. The interface energies γ_{MX} and γ_{MX-A} decrease with the increase in the temperature; this is why if the phase transition is accompanied by only small changes in the bulk and ΔG^{elas} ($S_{MX}^\alpha \approx S_{MX}^\beta \sim L_{MX}^{-1}$; $S_{MX-A}^\alpha \approx S_{MX-A}^\beta \sim L_A^{-1}$; $\Delta G^{\text{elas}} \approx 0$), the temperature of transformation to the high-temperature α -phase will decrease, which indeed was usually observed for thin films where the layer thickness plays the role of the particle size. The literature offers two types of phase diagrams plotted in coordinates $T_t(T, L^{-1})$ for supported films of different metals;^{85, 98–100} the phase transition temperatures can decrease by hundreds of degrees as L decreases to 10 nm. In the general case, the phase transition temperatures in a composite can either decrease or increase depending on the concrete form of functions $G^0 = f(T)$; $\sigma = f(T)$; $\Delta G^{\text{elas}} = f(T)$ in different phases of a given composite.

The above-described self-dispersion effect caused by the surface interaction of ionic salts with nanodispersed oxides (the particle size not exceeding 10 nm) allowed a wide range of nanocomposites of the MX–A type to be synthesised and studied.^{24, 84, 134–148} Ionic salts in the nanoheterogeneous systems mentioned exhibited several specific features.

1. Crystal structure and morphology. In sintered composites AgI–Al₂O₃,^{61, 71, 90–92} either various polytypes or an amorphous phase were formed depending of the oxide particle size and the conditions of the composite synthesis. Nanocomposites synthesised at 600 °C comprised globular AgI particles measuring 2–5 nm and uniformly distributed over the composite volume (Fig. 8). According to the results of structural studies of composites LiX–Al₂O₃ ($X^- = F^-, Cl^-, Br^-, I^-, 1/3 PO_4^{3-}, 1/2 SO_4^{2-}$) synthesised by decomposition of a precursor, the size of particles in both phases of the composite did not exceed 10 nm, *i.e.*, solid-phase nanocomposites were formed.⁵³ The most thoroughly studied nanocomposites Li₂SO₄–Al₂O₃ exhibited the highest conductivity among these nanocomposites.^{53, 82, 83, 93, 94} On the interfaces of these composites, regardless of the method of their synthesis [by decomposition of the precursor Li₂SO₄·2n Al(OH)₃·m H₂O or by simple mixing of components followed by sintering], an intermediate aluminate layer with a thickness of about 1–2 monolayers was formed to provide a good epitaxial contact

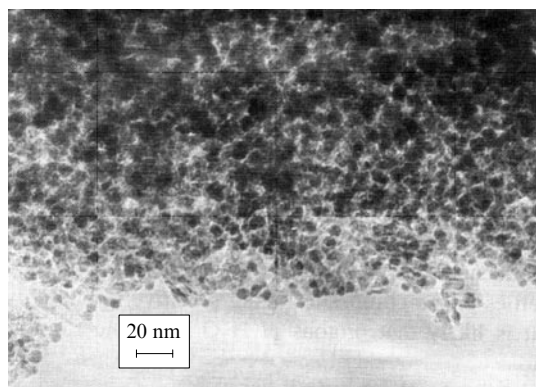


Figure 8. Morphology of the nanocomposite 0.2 AgI–0.8 Al₂O₃ synthesised at 600 °C.

between Li₂SO₄ and Al₂O₃. The average particle size varied in the range of 3–10 nm (Fig. 9). In composites CsCl–Al₂O₃, according to the X-ray diffraction data, a high-temperature face-centred CsCl phase with the particle size in the range of 20–80 nm was stabilised.¹⁴⁴ In nanocomposites based on alkali metal nitrates, amorphous phases of ionic salts were formed.^{67,95–97}

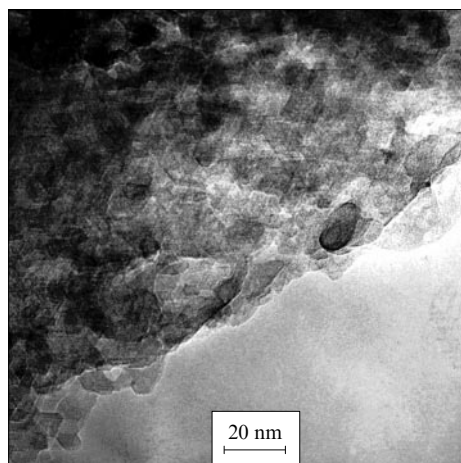


Figure 9. Microstructure of the composite Li₂SO₄–Al₂O₃.

2. Thermodynamic properties. Rubidium nitrate attracts attention because in the temperature range of 25–330 °C it undergoes three polymorphous transitions (at 164, 219 and 286 °C) before melting at 315 °C. The results of differential scanning calorimetry (DSC) studies of composites RbNO₃–Al₂O₃ showed⁶⁷ that sintering did not virtually affect the temperatures of all phase transitions of rubidium nitrate including the melting temperature, while the corresponding enthalpies dramatically decreased (Fig. 10 *a*). At a relatively low mole fraction of the oxide ($x \geq 0.7$), the curves demonstrated no heat effects that would point to the presence of crystalline rubidium nitrate in the composite. In line with the decrease in the enthalpy of crystalline RbNO₃, the DSC curves acquire a new strongly broadened peak at 250 °C. The mentioned effects were not observed in composites containing coarse-grained alumina (with the grain size of several micrometres); hence, the effects were intrinsic in the oxide surface (Fig. 10 *b*). In composites RbNO₃–Al₂O₃, an amorphous phase was formed and the heat effect at 250 °C was caused by the phase transition, namely, its vitrification. The formation of an amorphous phase in nanocomposites was also confirmed by

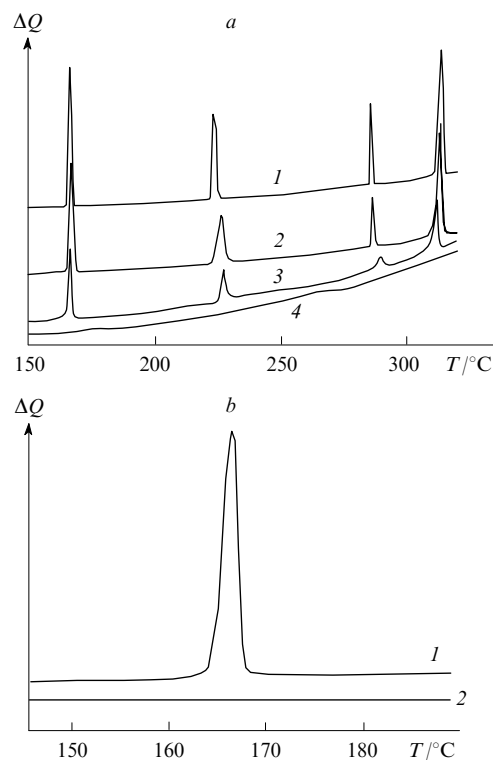


Figure 10. (*a*) DSC curves of composites $(1-x)\text{RbNO}_3-x\text{Al}_2\text{O}_3$ [$x = 0.1$ (1), 0.3 (2), 0.5 (3), 0.7 (4)] containing nanocrystalline alumina ($S_{\text{sp}} = 270 \text{ m}^2 \text{ g}^{-1}$), which were heated at 350 °C and (*b*) segments of DSC curves in the region of phase transition $\text{RbNO}_3\text{-IV} \rightleftharpoons \text{RbNO}_3\text{-III}$ for the composites 0.3 RbNO₃–0.7 Al₂O₃ containing (1) coarse-grain and (2) nanocrystalline alumina.

the disappearance of the heat effect associated with salt melting. The amorphisation of an ionic salt also occurred in composites RbNO₃–SiO₂,¹⁴⁵ CsHSO₄–SiO₂ (Refs 146 and 147) and LiClO₄–Al₂O₃ (Ref. 148). In composites CsCl–Al₂O₃, with the increase in the oxide concentration, the enthalpy of the transition to the high-temperature phase gradually decreased, which was accompanied by the broadening of the hysteresis loop of the phase transition temperature.¹⁴⁴

Expression (11) allows one to assess the ratio λ/L_A and, for a given particle size (L_A), the thickness of the surface phase (λ), based on the concentration dependence of the enthalpy of phase transitions in composites. The λ estimates were 3 and 4 nm in composites AgI–Al₂O₃ (Ref. 92) and RbNO₃–Al₂O₃ (Ref. 97), respectively. For a sufficiently high concentration of the oxide ($x > 0.6–0.7$, which corresponds to the volume ratio $f > 0.5–0.6$), the effective size of MX particles was comparable with λ and virtually the whole volume of the ionic salt was in the amorphous state (Fig. 11).

Self-dispersion of rubidium nitrate in contact with nanocrystalline alumina (the specific surface of $200 \text{ m}^2 \text{ g}^{-1}$) was studied^{97,149} *in situ* by the DSC method; the results are shown in Fig. 12. For non-mixed starting components, the surface interaction began at the rubidium nitrate melting temperature, as indicated by the appearance of the exothermic effect. In the melting, the liquid-phase spreading occurred being accompanied by liberation of the heat of wetting. The DSC curves obtained in the repeated heating of the same specimen corresponded to a mixture of the residual crystalline and amorphous phases. When the starting components were mixed more thoroughly, the surface dispersion and self-dispersion proceeded at noticeable rates even at temperatures substantially

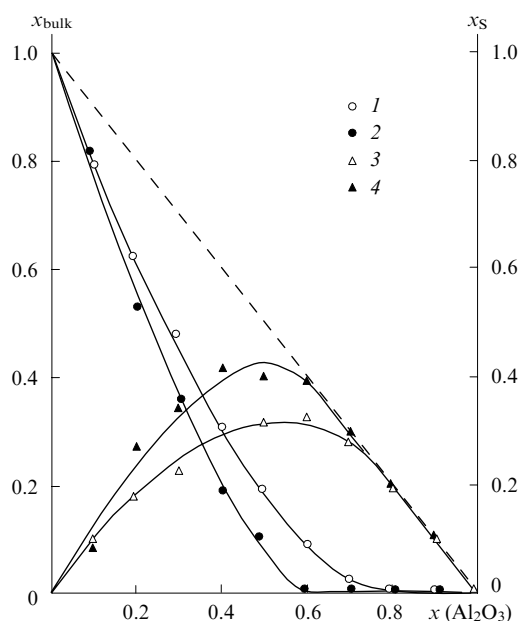


Figure 11. Mole fractions of (1, 2) bulk (x_{bulk}) and (3, 4) surface (x_s) phases in composites (1, 3) $(1-x)\text{AgI}-x\text{Al}_2\text{O}_3$ (Ref. 92) and (2, 4) $(1-x)\text{RbNO}_3-x\text{Al}_2\text{O}_3$ (Ref. 67) as a function of the additive content. Experimental values were calculated from the enthalpy of phase transitions. Theoretical curves were obtained based on Eqn (11). The dashed curve corresponds to the case of $\lambda/L_A = 0$ where the composite altogether lacks the surface phase.

below T_{mp} , *i.e.*, where rubidium nitrate was in the crystalline state. Due to the solid-phase spreading, the amorphous phase was formed, *i.e.*, the crystalline phase spontaneously passed to the amorphous state. The solid-phase spreading to form the amorphous phase was also observed upon sintering of composites $\text{AgI}-\text{Al}_2\text{O}_3$.⁹²

The possible reason for the spontaneous amorphisation of an ionic salt MX in the composites MX-A due to the liquid-phase or solid-phase spreading could be the relaxation of elastic strains that arise in the MX volume formed as a result of the salt spreading over the surface and in the pores of the oxide matrix. If the lattices of the contacting phases do not match one another, the contribution of the elastic energy becomes substantial. Moreover, in contrast to thin films, the MX particles in nanopores are adhesively bound with the randomly oriented oxide surfaces surrounding a pore, which should lead to rather active formation of microdomains of particles and provide the excess surface energy. Apparently, the structural relaxation can occur by spontaneous amorphisation of an ionic salt. This process may be illustrated by a phase diagram shown in Fig. 13.^{97, 139, 140} The amorphisation is possible if with the decrease in the effective particle size, the free energy of the crystalline MX phase becomes higher than the energy of the amorphous phase. A concept of the spontaneous transition from the crystalline to the amorphous state was discussed earlier in the literature in context of the reasons for the mechanical alloying of ionic salts.^{150–158} The data on the amorphisation of alkali metal halides^{159, 160} and certain other inorganic crystalline hydrates^{161–167} in nanopores are available. Amorphous hydrates incorporated into nanoporous matrices turned out to exhibit unusual thermodynamic properties, which are responsible for the changes in the parameters of chemical processes of hydration and dehydration.

3. Ionic conductivity and dielectric properties. In the low-temperature range, all the nanocomposites $(1-x)\text{AgI}-x\text{Al}_2\text{O}_3$ studied exhibited enhanced ionic conduc-

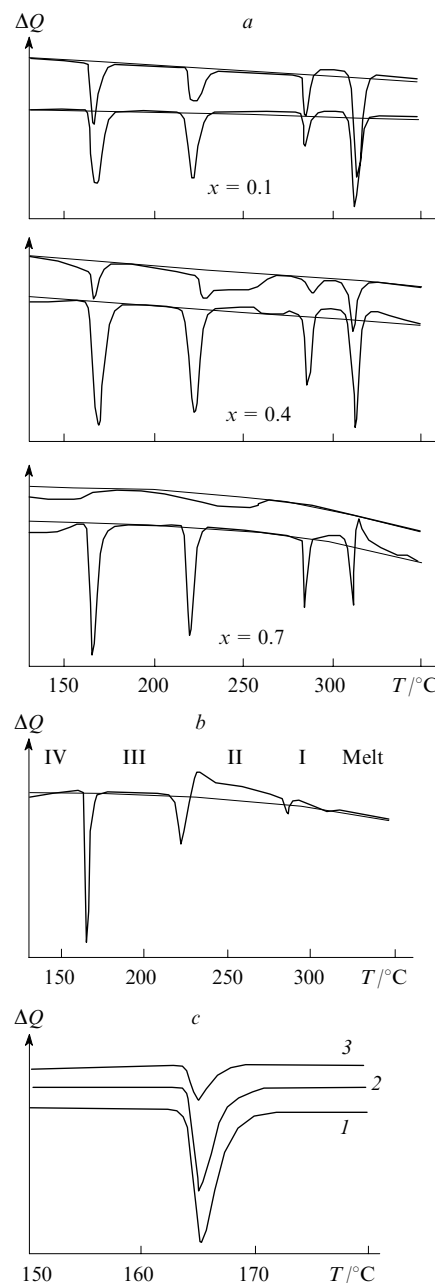


Figure 12. (a) DSC curves of original $\text{RbNO}_3-\text{Al}_2\text{O}_3$ mixtures (lower curves) and the same mixtures in repeated heating (upper curves) for different component ratios; (b) a DSC curve of a thoroughly ground mixture $0.6\text{RbNO}_3-0.4\text{Al}_2\text{O}_3$ obtained in the first heating and (c) a comparison of a segment of this curve (I) with the corresponding segments of DSC curves measured after 1-h exposure of this mixture to temperatures (2) 200 and (3) and 250 °C.

tivity.^{61, 71, 90–92} A comprehensive analysis of the temperature dependence of conductivity and the results of calorimetric studies of composites revealed the presence of two phase transitions. The temperature dependences of conductivity had a non-trivial shape, namely, with the increase in x , the phase-transition hysteresis gradually widened and the conductivities of the high-temperature (superionic) and low-temperature phases gradually became equal, *i.e.*, the phase transition of a salt to the superionic state gradually disappeared^{61, 71, 91} (Fig. 14a). The conductivity maximum ($\sim 10^{-3} \text{ S cm}^{-1}$ at 25 °C) was situated not at $x = 0.20-0.30$ as was observed earlier but at a higher mole fraction of the oxide, $x = 0.5-0.6$

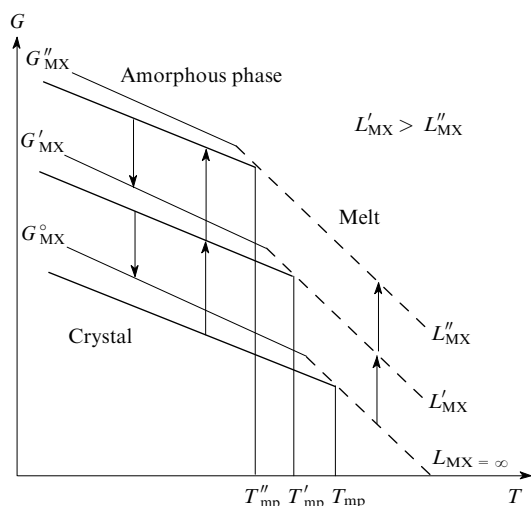


Figure 13. State diagram of an ionic salt in a composite; the changes in the energy of the system in the amorphisation of ionic compounds are indicated.

(Fig. 14b). The activation energy of conduction in both superionic and low-temperature phases increased monotonically with the increase in x . The concentration dependence of

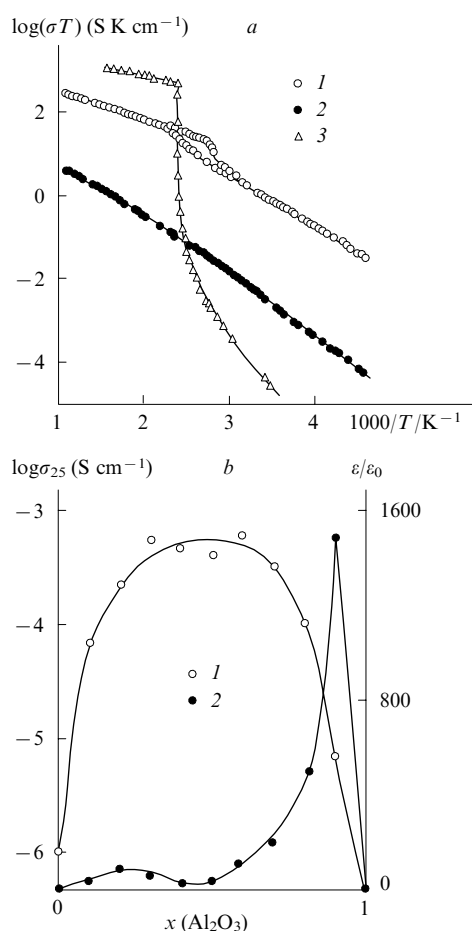


Figure 14. (a) Temperature dependences of conductivity (σT) of composites $(1-x)\text{AgI}-x\text{Al}_2\text{O}_3$ [$x = 0.60$ (1), 0.80 (2), 0 (3)] and (b) isotherms of their (1) conductivity and (2) permittivity at room temperature.⁹²

the dielectric permittivity $\varepsilon(x)$ had two maxima, namely, the first weak maximum at $x = 0.2$ and the second more pronounced maximum at $x = 0.9$ (see Fig. 14b).⁹² These results are consistent with the percolation model¹¹ according to which the permittivity maxima corresponding to two percolation thresholds should be observed at the oxide volume fractions $p_1 = 0.1$ and $p_2 = 0.9$ (i.e., at $x = 0.12$ and 0.94).

The temperature dependence of conductivity of the nanocomposite $\text{Li}_2\text{SO}_4-\text{Al}_2\text{O}_3$ lacked the conductivity jump at 575°C associated with the transition of lithium sulfate to the superionic state (Fig. 15).^{82, 83, 93, 94} The $\sigma(T)$ dependence had a shape typical of solid electrolytes with the fluorite structure in the vicinity of the 'diffuse' phase transition.

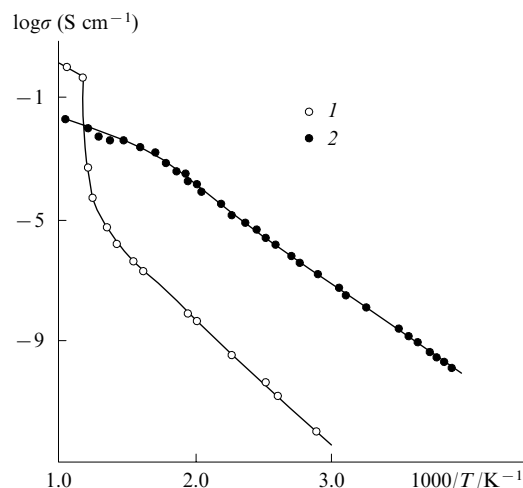


Figure 15. Temperature dependences of conductivity of (1) pure lithium sulfate and (2) a nanocomposite $\text{Li}_2\text{SO}_4-\text{Al}_2\text{O}_3$.⁸²

Studies of the conductivity of composites based on alkali metal nitrates $\text{MNO}_3-\text{Al}_2\text{O}_3$ ($\text{M} = \text{Li}, \text{Na}, \text{K}, \text{Rb}, \text{Cs}$) have shown^{95, 96} that doping of nitrates with alumina with a specific surface area of $270 \text{ m}^2 \text{ g}^{-1}$ is accompanied by a sharp increase in the conductivity (Fig. 16). The dependences of the conductivity on the dopant concentration had a maximum at $x = 0.5-0.7$, and the relative increase in the conductivity

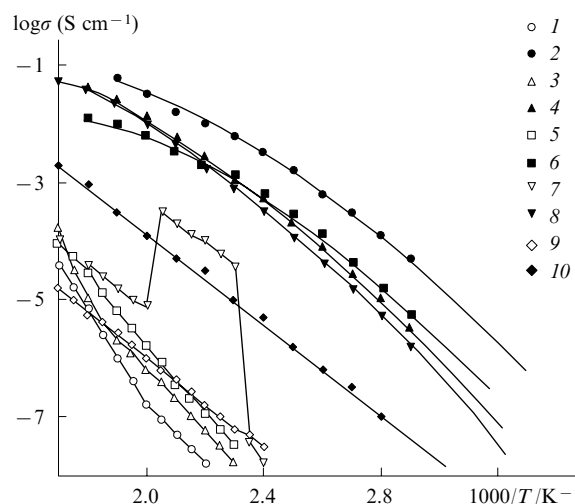


Figure 16. Arrhenius plots of conductivity for (1, 3, 5, 7, 9) pure alkali metal nitrates and (2, 4, 6, 8, 10) a 1:1 composite $\text{MNO}_3-\text{Al}_2\text{O}_3$.^{95, 96} $\text{M} = \text{Li}$ (1, 2), Na (3, 4), K (5, 6), Rb (7, 8), Cs (9, 10).

(σ/σ_0) at 343 K depended on the cation type and varied in the range from 10^2 (in composites $\text{CsNO}_3\text{--Al}_2\text{O}_3$) to 10^8 (in composites $\text{LiNO}_3\text{--Al}_2\text{O}_3$). For $x > 0.5\text{--}0.6$, the Arrhenius plots $\sigma(T)$ of all composites studied were not linear and lacked conductivity jumps at phase transition temperatures. The physicochemical properties of composites based on rubidium nitrate were studied in more detail. The decomposition voltage $U_d = 4$ V assessed from voltammetric curves was close to the corresponding values in fused alkali metal nitrates and halides which allows one to assume that rubidium cations are the main current carriers in the composites $\text{RbNO}_3\text{--Al}_2\text{O}_3$.

In the composites $\text{CsCl--Al}_2\text{O}_3$, with the increase in the oxide concentration, the conductivity jump associated with the transition to the high-temperature phase gradually disappeared, which was associated with the stabilisation of the latter phase (Fig. 17).¹⁴⁴

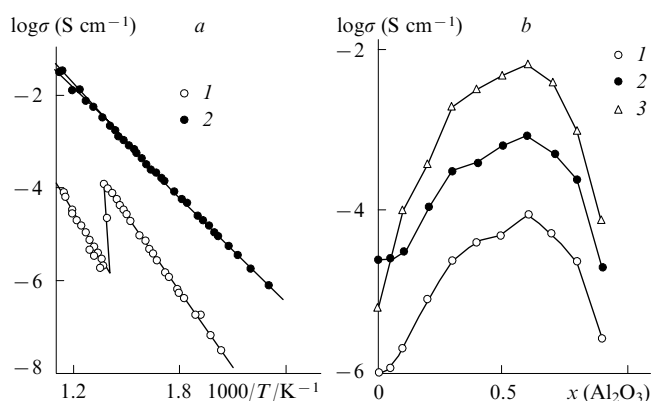


Figure 17. Dependences of conductivity of composites $(1-x)\text{CsCl--}x\text{Al}_2\text{O}_3$ (a) on the temperature and (b) and the oxide concentration. (a) $x = 0$ (1), 0.60 (2); (b) $T = 573$ (1), 673 (2) and 773 K (3).

Thus, in all systems under study, the nature of conduction was observed to change at sufficiently high concentrations of the fine-grain additive. These changes can be associated with either the appearance of new highly conductive amorphous phases atypical of pure ionic compounds (composites based on nitrates, $\text{AgI--Al}_2\text{O}_3$) or with the stabilisation of high-temperature phases (the phase-transition hysteresis in $\text{Li}_2\text{SO}_4\text{--Al}_2\text{O}_3$ and $\text{AgI--Al}_2\text{O}_3$, the formation of a face-centred cubic phase in $\text{CsCl--Al}_2\text{O}_3$) in composites. Moreover, the properties of high-temperature phases stabilised in nanocomposites differed from those of the same phases in pure salts, namely, the former had higher activation energies and modified lattice parameters. A clear trend for the levelling of the characteristics of high-temperature and low-temperature phases was observed, the phase transition region widened and the transition itself became diffuse approaching the second-order phase transitions. Nanocomposites differ basically from polycrystals and microcomposites in their properties; this is explained by the increasing effect of surface interactions on the bulk properties of ionic salts. Under certain conditions, this leads to the appearance of phase size effects or capillary effects of the second kind. Figure 18 illustrates the changes in the ionic salt structure in the vicinity of the MX–A interface, which were observed as the surface interaction increased, *i.e.*, on going from micro- to nanocomposites.

Computer simulation methods can be used for the elucidation of the nanocomposite structure and the conduction mechanism. Nanocomposites $\text{LiI--Al}_2\text{O}_3$ were studied¹⁶⁸ by the molecular dynamics techniques. It was shown that the phase contact was epitaxial, the electrical double layer was

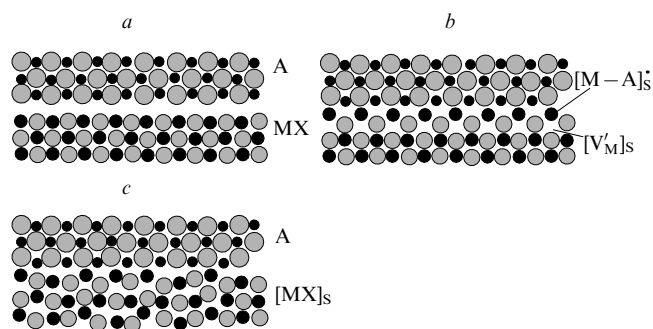


Figure 18. Changes in the ionic salt structure in the vicinity of the MX–A interface with the increase in the effect of surface on the bulk properties of MX, *i.e.*, on going from micro- to nanocomposites.

(a) Original surfaces; (b) weak interfacial interaction, insignificant structural changes, the capillary effect of the first kind; (c) interfacial interaction generates dramatic changes in the ionic salt structure (*e.g.*, amorphisation), phase size effect, the capillary effect of the second kind.

formed at the interface and the activation energy of diffusion of lithium cations was close to the experimental value.

The molecular dynamics methods were also applied¹⁶⁹ for the simulation of the $\text{CsCl--}\alpha\text{-Al}_2\text{O}_3$ interface. The calculation model represented a two-layer heterostructure that comprised 22 080 ions (3840 ions of Cs^+ and Cl^- each and the balance number of Al^{3+} and O^{2-} ions). The calculations were performed for cyclic boundary conditions and involved the use of the Born–Mayer potential. The parameters of the potential were taken from the literature and refined in the preliminary simulation of individual starting components Al_2O_3 and CsCl . The heterostructure was obtained as a result of spontaneous crystallisation of a model CsCl melt, which was followed by the long-term isothermal exposure at $T = 0.8T_{\text{mp}}$ up to the establishment of the steady state (Fig. 19). Caesium chloride crystallised to form a high-temperature phase structure of the NaCl type and did not pass to the low-temperature state as the temperature decreased. The $\text{CsCl--}\alpha\text{-Al}_2\text{O}_3$ interface was realised along the $(110)\text{CsCl} \parallel (10\bar{1}0)\text{Al}_2\text{O}_3$ planes which were off-oriented by a small angle of $\sim 10\text{--}13^\circ$ and contained boundary dislocations at a distance of ~ 5 nm from one another. The boundary dislocations corresponded to the sites of the surface exposure of low-angle boundaries localised in the caesium chloride bulk. Although the bulk of caesium chloride as a whole represented a monolithic crystal, the low-angle boundaries divided it into two microdomains disoriented by $3\text{--}3.5^\circ$.

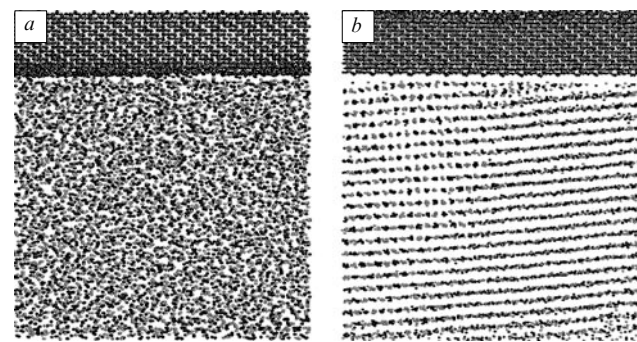


Figure 19. Heterostructure $\text{CsCl--Al}_2\text{O}_3$ calculated by the molecular dynamics method.¹⁶⁹

(a) For temperatures above the melting point of caesium chloride; (b) immediately after its hardening and isothermal exposure at $T = 0.8T_{\text{mp}}$.

In contrast to the system $\text{LiI}-\text{Al}_2\text{O}_3$, no double layer was formed on the interface. Nonetheless, the ions located in the vicinity of the interface and on low-angle boundaries exhibited enhanced mobility. The self-diffusion coefficients of caesium and chloride ions were approximately the same, *i.e.*, equal to $\sim 10^{-6} \text{ cm}^2 \text{ s}^{-1}$ at 700 K, which is smaller than the corresponding values in molten CsCl by merely an order of magnitude. Apparently, the main difference of the system $\text{CsCl}-\text{Al}_2\text{O}_3$ from the system $\text{LiI}-\text{Al}_2\text{O}_3$ is the weak interface interaction. In this case, it is the energy of elastic strains the relaxation of which favours the appearance of intergrain dislocations and small-angle boundaries that makes the main contribution to the changes in the ionic salt properties. Hence, the real composite structure and the mechanism of ionic conduction in nanosized systems depend not only on the energy of interactions, but also on the energy of elastic strains that arise in the interface zone.

The spectrum of phenomena observed in nanocomposites is very wide. Particularly, nanocomposites with protonic conductivity, which are based on acid salts, were shown to exhibit interesting properties.^{146, 170–176} In our studies, we have shown that the physicochemical characteristics of ionic salts depend on the pore size in the silica gel used as the dispersed additive, *viz.*, there is an optimum pore size ($\sim 2 \text{ nm}$) corresponding to the maximum changes in the thermodynamic, structural and transport properties of CsHSO_4 .¹⁷⁰ In our studies, we deliberately ignored the systems with chemical interactions between the components. The chemical reactions make possible the formation of three or four-layer components that include the starting reagents and interfacial phases.¹⁷⁷ Recent years were marked by the discovery of metacomposites, *i.e.*, heterogeneous systems the interfacial interaction in which brings substantial changes into the physicochemical properties of both components.^{149, 178} Moreover, such a heterosystem as a whole exhibits the properties typical of none of its individual components. Such materials form a new interesting class of metamaterials. The transport properties of metamaterials synthesised by the layer-by-layer deposition of nanolayers $\text{CaF}_2/\text{BaF}_2$ were studied.^{179, 180} Nanostructured solid solutions^{181–183} the lattices of which contain separate nanodomains coherently attached to one another and divided by interdomain boundaries are of special interest for solid-state ionics. Highly doped superionic fluorides that comprise extended clusters in their structure are another example of nanoheterogeneous systems.¹⁸⁴ It is not improbable that nanostructuring is the general property of highly doped solid solutions.

Nanoheterogeneous solid-phase systems are of great interest for practice. Like all composite solid materials, they are characterised by the enhanced mechanical strength and thermal stability and can be used in chemical power sources, gas sensors and other electrochemical devices. The high ionic conductivity is among the most important characteristics of nanocomposite solid electrolytes. Nanocomposites based on conventional ionic salts far surpass the corresponding polycrystalline materials and microcomposites in the conductivity. Another valuable characteristics of these materials is that the phase transitions in them are absent or levelled off, which prevents the loss of their mechanical strength at thermal cycling. In model medium-temperature fuel cells with a nanocomposite solid electrolyte $\text{CsHSO}_4-\text{SiO}_2$, sufficiently high current densities were reached.^{185, 186} The performance of a fuel cell with a composite electrolyte compares well with the performance of a cell that employs pure salt as the electrolyte.¹⁸⁷ Nanocomposites $\text{LiClO}_4-\text{Al}_2\text{O}_3$ exhibit high lithium conductivity at 150–200 °C.¹⁴⁸ Studies of medium-temperature lithium cells with solid electrolytes and oxide electrodes

were initiated.¹⁸⁸ Further miniaturisation of these devices, the decrease in the electrolyte thickness and the optimisation of characteristics of electrode materials may provide high power of batteries.

VIII. Conclusion

Summarising the results of studies of composite ionic conductors, it may be concluded that the properties of composite solid electrolytes are determined by both the intrinsic disordering of an ionic salt and the interfacial interaction between the composite components. The intrinsic disordering of a conventional ionic crystal involves the stages of the defect formation in the bulk and on the surface of the crystal. The surface disordering is well described by the Stern model, which allows the surface potential to be easily calculated. The same model can be employed for the description of the mechanism of defect formation as the main stage of the interfacial interaction. Methods for the estimation of the conductivity and other physicochemical characteristics of composites were proposed. The problems of the thermodynamic stability of nanocomposites and the genesis of their morphology during the sintering were considered. The general peculiarities of the variation of ionic salt properties in a wide series of the ionic salt–oxide systems were analysed as well as the size effects.

In heterogeneous systems with sufficiently strong interfacial interaction, the effect of self-dispersion of an ionic salt was observed, which allowed the nanocomposites to be synthesised by the method of liquid-phase or solid-phase spreading. The nanosize state of a salt in systems thus obtained is thermodynamically stable if the size of oxide particles remains constant. Based on the combined studies of a wide series of composites $\text{MX}-\text{A}$ with different ionic compounds, it was shown that nanocomposites are characterised by considerable changes in the thermodynamic and structural properties of ionic salts. These changes manifest themselves most clearly in compounds that contain high-temperature disordered phases, namely, AgI , Li_2SO_4 and alkali metal nitrates. Disordered crystalline surface phases are stabilised in silver iodide and lithium sulfate, whereas the amorphous state is stabilised in nitrates. Rapid quenching of nanocomposites $\text{AgI}-\text{Al}_2\text{O}_3$ allowed amorphous silver iodide to be obtained for the first time. This convincingly proves that the pronounced size effects can be observed on going from microsystems to nanoscale systems, which opens up the possibility for the synthesis of new materials with unusual properties.

I am grateful to my teachers, academician V V Boldyrev and Dr. E F Hairtdinov for their help and constant supervision and also to the scientists of the Institute of Solid State Chemistry and Mechanochemistry of the Siberian Branch of the Russian Academy of Sciences (Novosibirsk) V G Ponomareva, G V Lavrova, L I Brezhneva, V P Isupov, A A Politov, B B Bokhonov, A P Nemudry, V V Zyryanov, I I Gainutdinov, Yu T Pavlyukhin, Yu G Mateishina, A S Ulihin and others who took active part in carrying out experiments and their discussion. I would like to express my sincere gratitude to academician V M Bouznik, corresponding member of RAS Yu A Kotov and professors A Ya Neiman, Yu I Aristov, A K Ivanov-Shits, I V Murin and Yu M Baikov for fruitful discussions of different aspects of these studies; to foreign scientists W Bollmann (Germany), A K Shukla and K J Rao (India), J Maier (Germany), P Vaněk, J Petzelt (Czech Republic) and G Meng (China) for the possibility of carrying out joint studies within the frames of various International programmes and also to academician Yu D Tretyakov for the proposal to publish this review in the special issue of this journal.

References

1. V N Chebotin, M V Perfil'ev *Elektrokhimiya Tverdykh Elektrolitov* (Electrochemistry of Solid Electrolytes) (Moscow: Khimiya, 1978)
2. E A Ukshe, N G Bukun *Tverdye Elektrolity* (Solid Electrolytes) (Moscow: Nauka, 1977)
3. A K Ivanov-Shits, I V Murin *Ionika Tverdogo Tela* (Solid State Ionics) Vol. 1 (St Petersburg: St Petersburg State University, 2000)
4. C C Liang *J. Electrochem. Soc.* **120** 1289 (1973)
5. C C Liang, A V Joshi, N E Hamilton *J. Appl. Electrochem.* **8** 445 (1978)
6. J Maier *J. Phys. Chem. Solids* **46** 309 (1985)
7. J B Wagner *NATO ASI Ser., Ser. E* **101** 77 (1985)
8. A K Shukla, N Vaidehi, K T Jacob *Proc. Indian Acad. Sci., Chem. Sci.* **96** 533 (1986)
9. J Maier *Ber. Bunsen-Ges. Phys. Chem.* **90** 26 (1986)
10. J Maier *J. Electrochem. Soc.* **134** 1524 (1987)
11. R Blender, W Dieterich *J. Phys. C* **20** 6113 (1987)
12. J B Wagner *High Conductivity Conductors: Solid Ionic Conductors* (Ed. T Takahashi) (Singapore: World Sci. Publ., 1989) p. 102
13. J Maier *Superionic Solids and Solid Electrolytes: Recent Trends* (Eds S Chandra, A Laskar) (New York: Academic Press, 1989) p. 137
14. N J Dudney *Annu. Rev. Mater. Sci.* **19** 103 (1989)
15. J Maier *Prog. Solid State Chem.* **23** 171 (1995)
16. R C Agrawal, R K Gupta *J. Mater. Sci.* **34** 1131 (1999)
17. I Kosacki, T Suzuki, V Petrovsky, H U Anderson *Solid State Ionics* **136–137** 1225 (2000)
18. A Yaroslavl'tsev *Russ. J. Inorg. Chem. (Suppl. 3)* **45** 249 (2000)
19. P Heitjans, S Indris *J. Phys.: Condens. Matter* **15** 1257 (2003)
20. J Schoonman *Solid State Ionics* **157** 319 (2003)
21. A B Yaroslavl'tsev, V V Nikonenko, V I Zabolotsky *Usp. Khim.* **72** 438 (2003) [*Russ. Chem. Rev.* **72** 393 (2003)]
22. B S Bokshstein, A B Yaroslavl'tsev *Diffuziya Atomov i Ionov v Tverdykh Telakh* (Diffusion of Atoms and Ions in Solids) (Moscow: Moscow Institute of Steel and Melts, 2005)
23. Ya I Frenkel *Kineticheskaya Teoriya Zhidkosti* (Kinetic Theory of Liquids) (Moscow: Academy of Sciences of the USSR, 1945)
24. N F Uvarov, Doctoral Thesis in Chemical Sciences, Institute of Solid State Chemistry and Mechanochemistry, Siberian Branch of the Russian Academy of Sciences, Novosibirsk, 1998
25. P Chowdhary, V B Tare, J B Wagner *J. Electrochem. Soc.* **132** 123 (1985)
26. A C Khandkar, J B Wagner *Solid State Ionics* **18–19** 1100 (1986)
27. L Chen *Materials for Solid State Batteries* (Eds B V R Chowdari, S Radhakrishna) (Singapore: World Sci. Publ., 1986) p. 69
28. N F Uvarov, E F Hairtdinov, V V Boldyrev *J. Solid State Chem.* **51** 59 (1984)
29. N F Uvarov, E F Hairtdinov, V V Boldyrev *Izv. Sib. Otd. Akad. Nauk, Ser. Khim. Nauk* **1** (3) 3 (1984)
30. N F Uvarov, E F Hairtdinov, V V Boldyrev *Dokl. Akad. Nauk SSSR* **274** 661 (1984)^a
31. N F Uvarov, E F Hairtdinov *J. Therm. Anal.* **33** 279 (1988)
32. N F Uvarov, W Bollmann, E F Hairtdinov *Cryst. Res. Technol.* **24** 413 (1989)
33. W Bollmann, N F Uvarov, E F Hairtdinov *Cryst. Res. Technol.* **24** 421 (1989)
34. N F Uvarov, E F Hairtdinov *Izv. Sib. Otd. Akad. Nauk, Ser. Khim. Nauk* **6** (17) 89 (1986)
35. N F Uvarov, W Bollmann, E F Hairtdinov *Cryst. Res. Technol.* **24** 543 (1989)
36. N F Uvarov, E F Hairtdinov *Izv. Sib. Otd. Akad. Nauk, Ser. Khim. Nauk* **3** (8) 6 (1984)
37. D J Fisher *Rules of Thumb for Physical Scientists* (Aedermannsdorf: Trans Tech Publ., 1988)
38. Yu Ya Gurevich *Dokl. Akad. Nauk SSSR* **222** 143 (1975)^a
39. Yu Ya Gurevich, Yu I Kharkats *Zh. Eksp. Teor. Fiz.* **72** 1845 (1977)^b
40. Yu Ya Gurevich, Yu I Kharkats *Khimiya Tverdogo Tela (Itogi Nauki i Tekhniki)* [Solid State Chemistry (Advances in Science and Engineering Series)] (Moscow: Izd. VINITI, 1987) Vol. 4, p. 3
41. A Lunden *Solid State Commun.* **65** 1237 (1988)
42. N F Uvarov, E F Hairtdinov, V V Boldyrev *Izv. Sib. Otd. Akad. Nauk, Ser. Khim. Nauk* **6** (14) 27 (1981)
43. N Parsonage, L Staveley *Disorder in Crystals* (Oxford: Oxford University Press, 1978)
44. N F Uvarov, I A Gonysheva *Tezisy Dokladov IV Ural'skoi Konferentsii po Vysokotemperaturnoi Fizicheskoi Khimii i Elektrokhimii, Perm', 1985* (Abstracts of Reports of the IVth Urals Conference on High-Temperature Physical Chemistry and Electrochemistry, Perm, 1985) p. 126
45. K Lehovec *J. Chem. Phys.* **21** 1123 (1953)
46. F Kröger *The Chemistry of Imperfect Crystals* (Amsterdam: North-Holland, 1964)
47. K L Kliewer, K S Koehler *Phys. Rev., Sect. A* **140** 1226 (1965)
48. K L Kliewer *J. Phys. Chem. Solids* **27** 705 (1966)
49. O Stern *Z. Electrochem.* **30** 508 (1924)
50. N F Uvarov *Elektrokhimiya* (2007) (in the press)^c
51. I M Lifshits, Ya E Geguzin *Fiz. Tv. Tela* **7** (1) 62 (1965)^d
52. R B Poeppel, J M Blakely *Surf. Sci.* **15** 507 (1969)
53. N F Uvarov, V P Isupov, V Sharma, A K Shukla *Solid State Ionics* **51** 41 (1992)
54. N F Uvarov, E F Hairtdinov *Solid State Ionics* **96** 219 (1997)
55. N F Uvarov, E F Hairtdinov *Solid State Ionics* **96** 227 (1997)
56. N F Uvarov, E F Hairtdinov, A I Rykov, Yu T Pavlyukhin *Solid State Ionics* **96** 233 (1997)
57. N F Uvarov, A K Tsvetnikov, V M Bouznik *Tezisy Dokladov XII Rossiiskoi Konferentsii po Fizicheskoi Khimii i Elektrokhimii Rasplavlennykh i Tverdykh Elektrolitov, Nal'chik, 2001* [Abstracts of Reports of the XIIth Russian Conference on Physical Chemistry and Electrochemistry of Molten and Solid Electrolytes, Nal'chik, 2001] Vol. 2, p. 111
58. *Metallopolimernye Nanokompozity (Poluchenie, Svoistva, Primenenie) (Integratsionnye Proekty SO RAN)* [Metal-polymeric Nanocomposites (Production, Properties and Applications) (Integration Projects of Siberian Branch of the Russian Academy of Sciences)] (Novosibirsk: Siberian Branch of the Russian Academy of Sciences, 2005) No. 2
59. A K Shukla, R Manoharan, J B Goodenough *Solid State Ionics* **26** 5 (1988)
60. N F Uvarov, V G Ponomareva *Dokl. Akad. Nauk* **351** 358 (1996)^a
61. N F Uvarov, E F Hairtdinov, B B Bokhonov, N B Bratel *Solid State Ionics* **86–88** 573 (1996)
62. B Zhu, B-E Mellander *Solid State Ionics* **77** 244 (1995)
63. B Zhu, B-E Mellander *Solid State Ionics* **70–71** 285 (1994)
64. N F Uvarov, J Maier *Solid State Ionics* **62** 251 (1993)
65. N F Uvarov, E F Hairtdinov *J. Solid State Chem.* **62** 1 (1986)
66. N F Uvarov, E F Hairtdinov *Izv. Sib. Otd. Akad. Nauk, Ser. Khim. Nauk* **2** (5) 43 (1985)
67. N F Uvarov, P Vaněk, Yu I Yuzyuk, V ŽeleznyZh, V Studnička, B B Bokhonov, V E Dulepov, J Petzelt *Solid State Ionics* **90** 201 (1996)
68. N F Uvarov *Dokl. Akad. Nauk* **353** 213 (1997)^a
69. N F Uvarov *Solid State Ionics* **136–137** 1267 (2000)
70. D S McLachlan, M Blaszkiewicz, R E Newnham *J. Am. Ceram. Soc.* **73** 2187 (1990)
71. N F Uvarov, E F Hairtdinov, N B Bratel *Elektrokhimiya* **29** 1406 (1993)^c
72. A M Stoneham, E Wade, J A Kilner *Mater. Res. Bull.* **14** 661 (1979)
73. N J Dudney *J. Am. Ceram. Soc.* **68** 538 (1985)
74. J C Wang, N J Dudney *Solid State Ionics* **18–19** 112 (1986)
75. H E Roman, A Bunde, W Dieterich *Phys. Rev. B* **34** 3439 (1986)
76. H E Roman, M Yusouff *Phys. Rev. B* **36** 7285 (1987)
77. H E Roman *J. Phys.: Condens. Matter* **2** 3909 (1990)
78. C W Nan, D M Smith *Mater. Sci. Eng., B* **10** 99 (1991)
79. M Siekierski, J Przyłuski *Proceedings of the 4th Asian Conference on Solid State Ionics* (Singapore: World Sci. Publ., 1994) p. 121

80. S Jiang, J B Wagner Jr *J. Phys. Chem. Solids* **56** 1113 (1995)
81. Mikrajuddin, F G Shi, K Okuyama *J. Electrochem. Soc.* **147** 3157 (2000)
82. N F Uvarov, B B Bokhonov, V P Isupov, E F Hairtdinov *Solid State Ionics* **74** 15 (1994)
83. N F Uvarov, B B Bokhonov, V P Isupov, E F Hairtdinov *Yavleniya Elektroprenosa v Oksidnykh Sistemakh* (Effects of Electricity Transfer in Oxide Systems) (Ekaterinburg: Institute of High-temperature Electrochemistry, Urals Branch of the Russian Academy of Sciences, 1994) p. 45
84. N F Uvarov, V V Boldyrev *Usp. Khim.* **70** 307 (2001) [*Russ. Chem. Rev.* **70** 265 (2001)]
85. B Ya Pines *Ocherki o Metallofizike* (Essays on Physics of Metals) (Kharkov: Kharkov University, 1961)
86. Ya E Geguzin *Fizika Spekaniya* (The Physics of Agglomeration) (Moscow: Nauka, 1984)
87. P W Tasker *Philos. Mag. A* **39** 119 (1979)
88. V L Tauson, M G Abramovich *Fiziko-khimicheskie Prevrashcheniya Real'nykh Kristallov v Mineral'nykh Sistemakh* (Physicochemical Transformations of Real Crystals in Mineral Systems) (Novosibirsk: Nauka, 1988)
89. A Adamson *The Physical Chemistry of Surfaces* (New York: Wiley, 1976)
90. N F Uvarov, M C R Shastri, K J Rao *Rev. Solid State Sci.* **4** 61 (1990)
91. N F Uvarov, B B Bokhonov, A A Politov, P Vaněk, J Petzelt *J. Mater. Synth. Process.* **8** 327 (2000)
92. N F Uvarov, P Vaněk, M Savinov, V ŽeleznyZh, J Studnička, J Petzelt *Solid State Ionics* **127** 253 (2000)
93. N F Uvarov, O P Shrivastava, E F Hairtdinov *Solid State Ionics* **36** 39 (1989)
94. N F Uvarov, O P Srivastava, E F Hairtdinov *Proc. Indian Natl. Sci. Acad., Part A* **55** 703 (1989)
95. N F Uvarov, E F Hairtdinov, I V Skobelev *Solid State Ionics* **86–88** 577 (1996)
96. N F Uvarov, I V Skobelev, B B Bokhonov, E F Hairtdinov *J. Mater. Synth. Process.* **4** 391 (1996)
97. N F Uvarov *The International Symposium on Metastable, Mechanically Alloyed and Nanocrystalline Materials (Abstracts of Papers)*, *Ann Arbor, MI*, 2001 p. 27
98. L S Palatnik, I I Papirov *Epitaksial'nye Plenki* (Epitaxial Films) (Moscow: Nauka, 1971)
99. I D Morokhov, L I Trusov, S P Chizhik *Ul'tradispersnye Metallicheskie Sredy* (Ultradispersed Metallic Media) (Moscow: Atomizdat, 1977)
100. Yu F Komnik *Fizika Metallicheskich Plenok. Razmernye i Strukturnye Effekty* (The Physics of Metallic Films. Size and Structure Effects) (Moscow: Atomizdat, 1979)
101. S A Nepiiko *Fizicheskie Svoistva Malykh Metallicheskich Chastits* (Physical Properties of Small Metallic Particles) (Kiev: Naukova Dumka, 1985)
102. Yu I Petrov *Klastery i Malye Chastitsy* (Clusters and Small Particles) (Moscow: Nauka, 1986)
103. H Gleiter *Prog. Mater. Sci.* **33** 223 (1989)
104. H Gleiter *J. Appl. Crystallogr.* **24** 79 (1991)
105. V G Gryaznov, L I Trusov *Prog. Mater. Sci.* **37** 289 (1993)
106. Yu I Vesnin *Vtorichnaya Struktura i Svoistva Kristallov* (Secondary Structure and Properties of Crystals) (Novosibirsk: Institute of Inorganic Chemistry of Siberian Branch of the Russian Academy of Sciences, 1997)
107. R F Khairutdinov *Usp. Khim.* **67** 125 (1998) [*Russ. Chem. Rev.* **67** 109 (1998)]
108. A I Gusev *Nanokristallicheskie Materialy: Metody Polucheniya i Svoistva* (Nanocrystalline Materials: Methods of Production and Properties) (Ekaterinburg: Urals Branch of Russian Academy of Sciences, 1998)
109. D G Morris *Mechanical Behaviour of Nanostructured Materials (Materials Science Foundations)* (Zuerich: Trans Tech Publ., 1998) Vol. 2
110. R A Andrievskii, A M Glezer *Fiz. Met. Metalloved.* **88** 50 (1999)^e
111. A I Gusev, A A Rempel *Nanokristallicheskie Materialy* (Nanocrystalline Materials) (Moscow: Fizmatlit, 2000)
112. R Z Valiev, I V Aleksandrov *Nanostrukturnye Materialy, Poluchennye Intensivnoi Plasticheskoi Deformatsiei* (Nanostructural Materials, Production by Intensive Plastic Deformation) (Moscow: Logos, 2000)
113. H Gleiter *Acta Mater.* **48** 1 (2000)
114. *Zernogranichnaya Diffuziya i Svoistva Nanostrukturnykh Materialov* (Grain-boundary Diffusion and Properties of Nanostructural Materials) (Eds Yu R Kolobov, R Z Valiev) (Novosibirsk: Nauka, 2001)
115. R A Andrievskii *Usp. Khim.* **71** 967 (2002) [*Russ. Chem. Rev.* **71** 853 (2002)]
116. V Ya Shevchenko, A E Madison *Fiz. Khim. Stekla* **28** 60 (2002)^f
117. V Ya Shevchenko, A E Madison *Fiz. Khim. Stekla* **28** 65 (2002)^f
118. J Maier *Solid State Ionics* **148** 367 (2002)
119. J Maier *Solid State Ionics* **154–155** 291 (2002)
120. G B Sergeev *Nanokhimiya* (Nanotechnology) (Moscow: Moscow State University, 2003)
121. Yu D Tretyakov *Usp. Khim.* **72** 731 (2003) [*Russ. Chem. Rev.* **72** 651 (2003)]
122. V I Roldugin *Usp. Khim.* **73** 123 (2004) [*Russ. Chem. Rev.* **73** 115 (2004)]
123. L I Grechikhin *Fizika Nanochastits i Nanotekhnologii. Obshchie Osnovy, Mekhanicheskie, Teplovy i Emissionnye Svoistva* (The Physics of Nanoparticles and Nanotechnologies. General Foundations, Mechanical, Thermal and Emission Properties) (Minsk: Tekhnoprint, 2004)
124. P Buler *Nanotermodynamika* (Nanothermodynamics) (St Petersburg: Yanus, 2004)
125. F Kh Urakaev, V V Boldyrev *Zh. Fiz. Khim.* **79** 662 (2005)^g
126. I P Suzdalev *Nanotekhnologiya: Fiziko-khimiya Nanoklasteroev, Nanostruktur i Nanomaterialov* (Nanotechnology: Physicochemistry of Nanoclusters, Nanostructures and Nanomaterials) (Moscow: KomKniga, 2005)
127. A I Gusev *Nanomaterialy, Nanostrukturny, Nanotekhnologii* (Nanomaterials, Nanostructures and Nanotechnologies) (Moscow: Fizmatlit, 2005)
128. A L Despotuli, A V Andreeva, B Rambabu *Nano Mikrosistem. Tekh.* (2) 5 (2005)
129. L M Shcherbakov *Issledovaniya v Oblasti Poverkhnostnykh Sil* (Investigation in the Field of Surface Forces) (Moscow: Academy of Sciences of the USSR, 1961) p. 28
130. L M Shcherbakov *Poverkhnostnye Yavleniya v Rasplavakh i Voznikayushchikh iz Nihk Tverdykh Fazakh* (Surface Effects in Melts and Solid Phases Formed in Them) (Kishinev: Shtiintsa, 1974) p. 76
131. L S Palatnik, M Ya Fuks, V M Kosevich *Mekhanizm Obrazovaniya i Substruktura Kondensirovannykh Plenok* (The Mechanism of Formation and Substructure of Condensed Films) (Moscow: Nauka, 1972)
132. W A Jesser, D Kulmann-Wilsdorf *Phys. Status Solidi* **19** 95 (1967)
133. Yu G Sidorov, E M Trukhanov *Poverkhnost'* **6** 106 (1992)
134. N F Uvarov *Izv. Bolg. Akad. Nauk, Khim.* **23** 619 (1990)
135. E F Hairtdinov, N F Uvarov *Mater. Sci. Forum* **88–90** 723 (1992)
136. N F Uvarov, E F Hairtdinov *Solid State Phenomena* **39–40** 27 (1994)
137. N F Uvarov, V G Ponomareva, G V Lavrova, N B Bratel', I V Skobelev, E F Hairtdinov *Fundamental'nye Issledovaniya Novykh Materialov i Protseessov v Veshchestve* (Fundamental Investigations of New Materials and Processes in Substance) (Eds A N Tikhonov, V A Sadovnichii) (Moscow: Moscow State University, 1994) Vol. 1, p. 70
138. N F Uvarov *Solid State Ionics: New Developments.* (Eds B V R Chowdary, M A K L Dissanayake, M A Careem) (Singapore: World Sci. Publ., 1996) p. 311
139. N F Uvarov *Zh. Prikl. Khim.* **73** 970 (2000)^h
140. N F Uvarov, A A Politov, B B Bokhonov *Solid State Ionics: Materials and Devices* (Eds B V R Chowdary, W Wang) (Singapore: World Sci. Publ., 2000) p. 113
141. N F Uvarov, P Vaněk *J. Mater. Synth. Process.* **8** 319 (2000)
142. N F Uvarov, V G Ponomareva, G V Lavrova, L I Brezhneva *Mater. Sci. Forum* **386–387** 639 (2002)

143. N F Uvarov, V G Ponomareva *Nanotechnologies in the Area of Physics, Chemistry and Biotechnology. Fifth ISTC SAC Seminar, St Petersburg, 2002* p. 53
144. N F Uvarov, L I Brezhneva, E F Hairtdinov *Solid State Ionics* **136**–**137** 1273 (2000)
145. G V Lavrova, V G Ponomareva, N F Uvarov *Solid State Ionics* **136**–**137** 1285 (2000)
146. V G Ponomareva, G V Lavrova, N F Uvarov, E F Hairtdinov *Solid State Ionics* **90** 161 (1996)
147. V G Ponomareva, G V Lavrova, N F Uvarov *Solid State Ionics: New Developments* (Eds B V R Chowdary, M A K L Dissanayake, M A Careem) (Singapore: World Sci. Publ., 1996) p. 317
148. A S Ulihin, N F Uvarov, Yu G Mateyshina, L I Brezhneva, A A Matvienko *Solid State Ionics* **177** 2787 (2006)
149. A Ya Neiman, N F Uvarov, N N Pestereva *Solid State Ionics* **177** 3361 (2007)
150. V V Boldyrev *Eksperimental'nye Metody v Mekhanokhimi Tverdykh Neorganicheskikh Veshchestv* (Experimental Methods in Mechanochemistry of Inorganic Solids) (Novosibirsk: Nauka, 1983)
151. V A Pavlov *Fiz. Met. Metalloved.* **59** 629 (1985)^c
152. W L Johnson *Prog. Mater. Sci.* **30** 81 (1986)
153. E G Avvakumov *Mekhanicheskie Metody Aktivatsii Khimicheskikh Protessov* (Mechanical Methods of Activation of Chemical Processes) (Novosibirsk: Nauka, 1986)
154. C C Koch *Annu. Rev. Mater. Sci.* **19** 123 (1989)
155. A V Serebryakov *Metallofizika* **13** (5) 115 (1991)
156. *Mekhanokhimicheskii Sintez v Neorganicheskoi Khimii* (Mechanochemical Synthesis in Inorganic Chemistry) (Ed. E G Avvakumov) (Novosibirsk: Nauka, 1991)
157. *Mechanical Alloying (Mater. Sci. Forum.)* Vols 88–90 (Ed. P H Shingu) (Zuerich: Trans Tech Publ., 1992)
158. P Yu Butyagin *Usp. Khim.* **63** 1031 (1994) [*Russ. Chem. Rev.* **63** 965 (1994)]
159. V A Gusev, V A Gagarina, E M Moroz, E A Levitskii *Kristallografiya* **19** 1289 (1974)ⁱ
160. V A Gusev, V A Gagarina, E M Moroz, E A Levitskii *Kinet. Katal.* **17** 500 (1976)^j
161. Yu I Aristov, M M Tokarev, G Cacciola, G Restuccia *React. Kinet. Catal. Lett.* **59** 325 (1996)
162. Yu I Aristov, M M Tokarev, G Di Marko, G Kachchiola, D Restuchcha, V N Parmon *Zh. Fiz. Khim.* **71** 253 (1997)^g
163. L G Gordeeva, D Restuchcha, G Kachchiola, Yu I Aristov *Zh. Fiz. Khim.* **72** 1236 (1998)^g
164. L G Gordeeva, Candidate Thesis in Chemical Sciences, Institute of Catalysis, Siberian Branch of Russian Academy of Sciences, Novosibirsk, 1998
165. L G Gordeeva, G Restuccia, A Freni, Yu I Aristov *Fuel Process. Technol.* **79** 225 (2002)
166. L G Gordeeva, I S Glaznev, Yu I Aristov *Zh. Fiz. Khim.* **77** 1906 (2003)^g
167. L G Gordeeva, I S Glaznev, V V Malakhov, Yu I Aristov *Zh. Fiz. Khim.* **77** 2048 (2003)^g
168. R W J M Huang Foen Chung, S W de Leeuw *Solid State Ionics* **175** 851 (2004)
169. I I Gainutdinov, N F Uvarov *Solid State Ionics* **177** 1631 (2006)
170. V G Ponomareva, G V Lavrova, L G Simonova *Solid State Ionics* **118** 317 (1999)
171. V G Ponomareva, G V Lavrova *Solid State Ionics* **145** 197 (2001)
172. G V Lavrova, V G Ponomareva *Neorg. Mater.* **38** 1386 (2002)^k
173. V G Ponomareva, G V Lavrova, E B Burgina *Solid State Ionics* **176** 767 (2005)
174. V G Ponomareva, B V Merinov, G V Lavrova *Solid State Ionics* **145** 205 (2001)
175. V G Ponomareva, E S Shutova, A A Matvienko *Neorg. Mater.* **40** 721 (2004)^k
176. V G Ponomareva, E S Shutova *Solid State Ionics* **176** 2905 (2005)
177. E Konisheva, A Neiman, E Gorbunova *Solid State Ionics* **157** 45 (2003)
178. A Ya Neiman, N N Pestereva, A R Sharafutdinov, Yu P Kostikov *Elektrokhimiya* **41** 680 (2005)^c
179. N Sata, K Ebermann, K Eberl, J Maier *Nature (London)* **408** 946 (2000)
180. N Y Jin-Phillipp, N Sata, J Maier, C Scheu, K Hahn, M Kelsch, M Ruhle *J. Chem. Phys.* **120** 2375 (2004)
181. A Nemudry, P Rudolf, R Schöllhorn *Chem. Mater.* **8** 2232 (1996)
182. A Nemudry, E L Goldberg, M Aguirre, M Á Alario-Franco *Solid State Sci.* **4** 677 (2002)
183. N F Uvarov, A P Nemudry *Proceedings of the Xth APAM Topical Seminar 'Nanoscience and Technology', Novosibirsk, 2003* p. 56
184. J M Reau, P Hagenmuller *Appl. Phys. A* **49** 3 (1989)
185. G V Lavrova, M V Russkikh, V G Ponomareva, N F Uvarov *Elektrokhimiya* **41** 556 (2005)^c
186. G V Lavrova, M V Russkikh, V G Ponomareva, N F Uvarov *Solid State Ionics* **177** 2129 (2006)
187. S M Haile, D A Boysen, C R I Chisholm, R B Merle *Nature (London)* **410** 910 (2001)
188. Yu G Mateyshina, N F Uvarov, A S Ulihin, Yu T Pavlyuhin *Solid State Ionics* **177** 2769 (2006)

^a — *Dokl. Chem. (Engl. Transl.)*

^b — *J. Exp. Theor. Phys. (Engl. Transl.)*

^c — *Russ. J. Electrochem. (Engl. Transl.)*

^d — *Phys. Solid State (Engl. Transl.)*

^e — *Phys. Met. Metallogr. (Engl. Transl.)*

^f — *Glass Phys. Chem. (Engl. Transl.)*

^g — *Russ. J. Phys. Chem. (Engl. Transl.)*

^h — *Russ. J. Appl. Chem. (Engl. Transl.)*

ⁱ — *Crystallogr. Rep. (Engl. Transl.)*

^j — *Kinet. Catal. (Engl. Transl.)*

^k — *Inorg. Mater. (Engl. Transl.)*

Nanotechnologies. Properties and applications of nanostructured materials

A A Rempel

Contents

I. Introduction	435
II. Vapour condensation and gas-phase synthesis	436
III. Plasmochemical synthesis	437
IV. Deposition from colloidal solutions	439
V. Pyrolysis	443
VI. Mechanochemical synthesis	443
VII. Detonation-induced synthesis	446
VIII. Self-propagating high-temperature synthesis	446
IX. Compaction of nanopowders	446
X. Crystallisation of amorphous alloys	448
XI. Severe plastic deformation	448
XII. Electric explosion	450
XIII. Ordering of non-stoichiometric compounds as a method for the construction of nanostructures	450
XIV. Properties and application of nanomaterials	453
XV. Conclusion	456

Abstract. The review summarises the main methods for the preparation of nanostructured metals, alloys, semiconductors and ceramics. The formation mechanisms of nanostructures based on two different principles, viz. the assembly principle (bottom-up) and the disintegration principle (top-down), are analysed. Isolated nanoparticles, nanopowders and compact nanomaterials produced by these methods possess different properties. The scope of application of various classes of nanostructured materials is considered and the topicality of the development of nanoindustry is emphasised. The bibliography includes 271 references.

I. Introduction

A large body of the available experimental data on nanomaterials and nanotechnologies provided the basis for the generalisation of fundamental and applied results in reviews and monographs.^{1–20}

Due to the development of the nanoscience in recent years, the data on nanotechnologies and nanomaterials become more abundant and new, sometimes unexpected, properties are revealed. Hence, the present review begins with the author's point of view on the nomenclature and comparative characterisation of the concept of nanomaterials and other similar (often related) notions.

A A Rempel Institute of Solid State Chemistry, Urals Branch of the Russian Academy of Sciences, ul. Pervomaiskaya 91, 620041 Ekaterinburg, Russian Federation. Fax (7-343) 374 44 95, tel. (7-343) 374 73 06, e-mail: rempel@ihim.uran.ru

Received 25 October 2006

Uspekhi Khimii 76 (5) 474–500 (2007); translated by T N Safonova

The term nanotechnology refers to the methods used for the construction of nanomaterials and nanodevices and methods of handling of nanoobjects. Nanotechnologies produce nanometre-size particles. These technologies are based on methods allowing the construction of objects with sizes that are thousand or even million times smaller than those visible to the human eye. The systematic and purposeful development of the fundamentals of nanotechnologies started several decades ago. Nowadays, the results of investigations in this field are introduced in industry. In the present review, emphasis is given to procedures for the preparation of nanostructured materials, their properties and promising fields of application.

Nanotechnologies aimed at preparing nanostructured materials can arbitrarily be divided into the following two groups: bottom-up and top-down. This classification takes into account the key step (or the process) of nanotechnology where a nanostructure is formed. The former group includes methods, in which nanoparticles are formed from atoms and molecules, i.e., the starting species are enlarged to nanometre sizes; the latter group, methods in which nanometre sizes are achieved by disintegration of larger particles, powders or grains. The former group of methods of nanotechnology are based primarily on the chemical approach, while the latter group of methods, on the physical approach. In many cases, nanomaterials with the same chemical composition but with different properties can be prepared using these two different in principle groups of technologies.

A decrease in the particle size of a solid below a certain threshold leads to a considerable change in its properties. For most known materials, the threshold at which a jumpwise change in the properties occurs (the so-called size effect) varies from 1 to 100 nm.

Of course, all materials composed of nanometre-size building blocks can be referred to as nanomaterials. Large molecules, clusters, material particles or polycrystalline grains can

serve as building blocks. However, in this case, the term 'nanomaterial' would be narrowed to the simple statement of the block size, and it would be unclear why the development of nanotechnologies is considered as a new technology revolution. Hence, it is necessary that the concept of a nanomaterial include not only the size of building blocks, but also a jumpwise change in properties of materials that occurs as the nanometre size is achieved.

In some publications, the term nanomaterials refers to highly dispersed, ultrafine-grain, superfine-grain or ultrathin materials. This is unjustified because the concept of nanomaterials includes a quantitative parameter, *viz.*, the size of a particle, grain or building block, reflected in the prefix 'nano'. In the other above-mentioned systems, the building block size is reflected only qualitatively (a small or supersmall size without mentioning its particular value), *i.e.*, the sizes are uncertain and relative. Consequently, the use of the term nanomaterials in relation to these systems should be avoided wherever possible.

The concept of nanomaterials should not be also confused with another commonly accepted concept of submicrocrystalline materials. The properties of submicrocrystalline materials, like those of nanomaterials, differ from the properties of coarsely crystalline, coarse-grain and single-crystalline materials. However, the difference in the properties is associated primarily with increased specific surface area which results in acceleration of various processes, *e.g.*, chemical reactions, but does not lead to a decrease in the activation energy (*i.e.*, to a decrease in the temperature of the beginning of the reaction). In submicrocrystalline materials, the particle, grain or building block size is assumed to be smaller than a micrometre. A micrometre, like a nanometre, is a quantitative characteristic. However, there is a difference in principle between nanomaterials and submicrocrystalline materials. It is the nanostate rather than the submicrocrystalline state that is intermediate between the molecular and solid states. The properties of solids are manifested at nanometre distances. This is also the physical reason of substantial changes in the properties observed on the nanometre-size scale. The fact is that the lengths at which the main physical forces act in materials vary from 1 to 100 nm. It should be noted that different types of interactions, *viz.*, electron–electron, electron–phonon, phonon–phonon, magnon–magnon, *etc.*, are extended to different distances in the same material. Hence these interactions can be observed for different nanoparticle sizes. It is evident that the nanoparticle size is of no fundamental importance for the same or different materials.

Nanomaterials are often called nanocrystalline materials. This is also not always justified. Crystalline particles or grains serve as building blocks in nanocrystalline materials. However, nanomaterials are, as a rule, thermodynamically non-equilibrium systems and, consequently, their building blocks do not necessarily have perfect crystal structures.²¹ It is more likely that the situation is opposite. Building blocks in nanomaterials often have highly defective structures. Sometimes, their state is close to amorphous. In other words, the long-range order in building blocks of nanomaterials can be violated, and multi-particle correlations in the atom arrangement are determined by the short-range order. Hence, the more correct and complete name for nanomaterials should be 'nanostructured materials'.

Different classifications of nanomaterials are associated with their diversity. The most appropriate classification is based on the size of building blocks or their constituent structural elements. The main types of nanomaterials are zero- (0D), one- (1D), two- (2D) and three-dimensional (3D). Nanocluster materials and nanodispersions composed of isolated nanoparticles belong to a zero-dimensional type; nano-

fibre (nanorod) and nanotubular materials, to a one-dimensional type, the fibre (rod) or tube length varying from 100 nm to tens of micrometres. Nanometre-thick films belong to two-dimensional nanomaterials. Nanoparticles in 0D, 1D and 2D nanomaterials are often embedded in a liquid or solid matrix or are deposited onto a support. Powders, fibre, multi-layer and polycrystalline materials, in which 0D, 1D and 2D particles are closely packed together to form interfaces, belong to three-dimensional nanomaterials. A polycrystal containing nanometre-size grains is an example of three-dimensional nanomaterials. In such polycrystals, the total bulk is occupied by nanograins, the free surface of grains is virtually absent, and only grain interfaces are present. The formation of interfaces and the 'disappearance' of the nanoparticle surface in three-dimensional nanomaterials is of fundamental importance for the understanding of the nature of their properties. Actually, the properties of a strongly agglomerated nanopowder can be substantially different from those of a compact nanomaterial consisting of particles of the same size as the powder. In the last two decades, considerable attention was given to the preparation of 3D nanomaterials. It is three-dimensional nanomaterials that will be used in the hard-alloy production, the aircraft construction and hydrogen power engineering in the nearest future.

Nowadays, a rather wide range of nanomaterials is available.^{11–20} In the present review, methods for the preparation of dense three-dimensional and two-dimensional nanostructured materials are considered.

II. Vapour condensation and gas-phase synthesis

One of the simplest procedures for the preparation of nanoparticles is based on vapour condensation in an inert atmosphere under reduced pressure. This method can be applied to the preparation of nanoparticles of both simple and complex compounds. Synthesis of nanoparticles of metal compounds, for example, of oxides, nitrides, carbides, *etc.*, requires that the corresponding reaction gas (oxygen, nitrogen, carbon dioxide, methane, *etc.*) be added. The simplest way to a material vapour is evaporation. The atoms of vaporised substances rapidly lose the kinetic energy and form nanoparticles. In the case of metal compounds, the metal atoms react with the reaction gas. Particles of the desired size can be formed by adjusting the inert gas pressure. The formation of nanoparticles according to this method was systematically studied for Zn, Cd, Se, As and Au. Particles with sizes from 2 to 100 nm were prepared,^{22–24} the optimum inert gas pressure being in the range from 40 to 400 Pa.

It is difficult to collect nanoparticles formed upon condensation because nanoparticles are not deposited under the force of gravity but exist in the suspended state in the Brownian motion. Nanoparticles are usually collected on a cold surface or on filters.

Nanoparticles can also be prepared by dispersing a metal in a liquid with the use of an electric arc followed by condensation of a metal vapour in a liquid vapour.²⁵ The features of condensation in a supersaturated vapour, which proceeds through the nucleation and nucleus growth, were considered in the reviews.^{26–28}

The shapes of nanoparticles prepared by the gas-phase method depend on their size. Nanoparticles with size < 20 nm are spherical in shape due to a change in the relative contribution of the surface energy to the total energy of nanoparticles as their sizes decrease. Larger particles are faceted. Yet another interesting fact associated with the small size of isolated nanocrystals and related to the energy is the absence of dislocations, which are energetically less favourable than disclinations.²⁹

In the gas-phase synthesis, nanoparticles are formed upon cooling of a vapour–gas mixture containing one, two or more chemical elements along with an inert gas. Cooling occurs in the condensation zone the size of which in a particular reaction vessel can be controlled by varying the inert gas pressure. The condensation zone increases with a decrease in pressure and *vice versa*. The influence of the change in the inert gas pressure on the resulting nanoparticle size is manifested both directly and through the condensation zone size. An increase in the gas pressure leads to an increase in density, acceleration of heat removal, a decrease in the formation rate of crystallisation centres in the gas phase, but an increase in the growth rate of crystals and, consequently, the resulting particle size. In the gas-phase synthesis of rather small particles (20–30 nm), the inert gas (usually, helium) pressure is maintained at 40–60 Pa.

Preparation of nanoparticles of metal compounds requires that a reaction gas be added to the inert gas medium. Single-crystalline nanoparticles of metal compounds with different morphologies are formed in these reactions. The particle shape can be controlled by varying the composition of the gas phase. For example, CdS can be prepared as prismatic plates, ribbons, needles, whiskers, threads or tubes upon variation of the temperature and deviation of the Cd:S ratio in the gas phase from the stoichiometric ratio (1:1) toward an increase in the cadmium content.^{30,31} The intermediate clusters $[\text{CdS}]_n$, $[\text{Cd}_2\text{S}]_n$ and $[\text{Cd}_3\text{S}]_n$ serve as the structural basis of the growth of crystals of different shapes. Thus, the ratio of the starting components of the gas phase and the temperature are the main factors determining the particle shape, whereas their size more strongly depends on the inert gas pressure.

Monodisperse nanoparticles with size <2 nm can be prepared by mass separation of clusters in a mass spectrometer. For example, metal vapour is passed through a cell filled with helium under a pressure of ~1000–1500 Pa and then introduced into a vacuum chamber (~10⁻⁵ Pa). The mass of clusters is determined from the flight time by a particular distance in the mass spectrometer. This method was used for the preparation of antimony, bismuth and lead clusters containing 650, 270 and 400 atoms, respectively. The helium gas temperature in the case of Sb and Bi vapour was 80 K; in the case of a Pb vapour, 280 K.³²

Diamond nanoparticles can be synthesised from a gas phase supersaturated with respect to carbon (CO₂, methane, acetylene, propane and other hydrocarbons) under a sub-atmospheric pressure.^{33,34} Condensation of carbon from the gas phase and diamond nucleation are favoured by an excess surface energy at the solid–gas interface. Deposition of diamond nanoparticles is widely used for the construction of diamond and diamond-containing films and coatings.³⁵

Nanocrystalline powders of oxides Al₂O₃, ZrO₂ and Y₂O₃ were prepared by evaporation of oxide targets in a atmosphere helium,³⁶ magnetron sputtering of zirconium in a mixture of argon and oxygen³⁷ and controlled oxidation of yttrium nanocrystals.³⁸ Highly dispersed powders of transition metal nitrides can be synthesised by electron-beam heating of the corresponding metal targets, evaporation being performed in an atmosphere of nitrogen or ammonia at a pressure of 130 Pa.³⁹

Metal carbide, oxide and nitride nanoparticles can be synthesised by pulsed laser heating of metals in an atmosphere of methane (for carbides), oxygen (for oxides), nitrogen or ammonia (for nitrides) under reduced pressure.⁴⁰ Pulsed laser evaporation of metals in an atmosphere of an inert gas (He or Ar) and reaction gases (O₂, N₂, NH₃ and CH₄) affords mixtures of nanocrystalline metal oxides and oxide–nitride and carbide–nitride mixtures. The composition and size of nanoparticles in these mixtures can be controlled by varying the pressure, the composition of the atmosphere, the laser pulse

power and the temperature gradient between the evaporated target and the surface onto which condensation occurs.

Nanoparticles of Fe–Ni, Fe–Mn, Fe–Cr, Fe–Pt and Fe–Co iron-rich alloys are prepared under argon at a pressure of 400 Pa.⁴¹ Deposited particles are spherical in shape. Their average size is 25 ± 5 nm. As a rule, nanoparticles are two-phase (with bcc or hcc lattices), which corresponds to the thermodynamic equilibrium between the components in these alloys.

An yttrium oxide-doped zirconium oxide film with an average crystallite size of 10–30 nm was prepared by pulsed laser evaporation of metals in an oxygen ion beam followed by deposition of oxides onto a support at 350–700 K.⁴²

Nanopowders of ceramic materials can be prepared from organometallic and organoelement compounds. For example, nanocrystalline SiC_xN_y powders were prepared as follows. The starting compound (hexamethyldisilazane) was mixed with an inert carrier gas in a heated tubular reactor serving as an evaporator. Its thermal decomposition affords a continuous cluster or nanoparticle flow, which escapes from the reactor into a working chamber and is condensed in a refrigerator constructed as a rotating cylinder. Nanopowders of SiO₂, SiC and Si₃N₄ can be synthesised by adding water, hydrogen or ammonia, respectively, along with the same precursor to the carrier gas. The success of the reaction is provided by a low concentration of the organoelement compound in the inert gas, fast expansion and cooling of the gas flow at the exit from the reactor into the working chamber and a low pressure in the working chamber.⁴³

III. Plasmochemical synthesis

The plasmochemical synthesis is most commonly used for the synthesis of highly dispersed boride, carbide, nitride and oxide powders. This method makes use of low-temperature (4000–10 000 K) nitrogen, ammonia, hydrogen, hydrocarbon or argon plasmas produced by arc, glow, high-frequency and superhigh-frequency discharges. The characteristics of the resulting powders depend on the nature of the starting material, the technology and the reactor type. Particles of such powders are most often prepared as single crystals with sizes from 10 to 100–200 nm and larger. For nanoparticles to be synthesised by this method, the reaction should be far from equilibrium and the rate of solid-phase nucleation should be high, whereas the rate of nucleus growth should be low. The plasmochemical synthesis provides high formation and condensation rates of compounds and sufficiently high output. Broad particle size distribution (*i.e.*, low selectivity of the process) and heavy contamination of the powder are the main drawbacks of this method. Highly dispersed powders of titanium, zirconium, hafnium, vanadium, niobium, tantalum, boron, aluminium and silicon nitrides, titanium, niobium, tantalum, tungsten, boron and silicon carbides and magnesium, yttrium and aluminium oxides were prepared by the plasmochemical method.^{32,36–51}

At high plasma temperature, all starting compounds pass into the ionised gas state due to which the reaction rates are high and the reaction times are short (10⁻³–10⁻⁶ s). Active particles are formed in arc, high-frequency and superhigh-frequency plasma reactors. Arc plasma reactors are characterised by the highest power and efficiency; however, materials prepared in such reactors are contaminated by electrode erosion products. Electrodeless high-frequency and plasma ultrasonic reactors are free from this drawback. In the next step, quenching results in the isolation of the reaction products. Powders with the desired composition and with a particular particle shape and size can be prepared by varying the quenching region and rate.

Since nanoparticles synthesised by the plasmachemical method have a large excess energy, their chemical and phase compositions can be inconsistent with the equilibrium phase diagram. Additional short-term annealing of the product in a controlled atmosphere helps in preparing nanoparticles of the required stoichiometry. For example, a tungsten carbide powder was synthesised by the plasmachemical method from tungsten oxide (WO_3) and methane in a low-temperature ($\sim 4000\text{--}5000\text{ K}$) hydrogen plasma flow.⁵² A nanocrystalline powder with an average particle size of 20–40 nm was obtained. An X-ray powder diffraction study (Fig. 1 *a*) showed that the powder contained two carbide phases, *viz.*, W_2C ($> 75\text{ mass \%}$) and WC ($\sim 5\text{ mass \%}$), and tungsten ($\sim 18\text{ mass \%}$). Chemical analysis revealed the presence of free carbon in the powder. To achieve the single-phase state, the synthesised powder was additionally annealed under argon at 800–1000 K. The annealed powder contained only hexagonal (space group $P6m2$) tungsten carbide (Fig. 1 *b*). The size of coherent scattering regions in the annealed powder remained virtually unchanged compared to that in the starting powder, but the particle size determined by scanning electron microscopy⁵³ increased to 60–120 nm. This suggests agglomeration of nanoparticles in the annealed powder. The retention of the nanoparticle size of WC in the powder after annealing at 800–1000 K is associated with high thermal stability of this compound, as was demonstrated by magnetic susceptibility measurements.⁵³

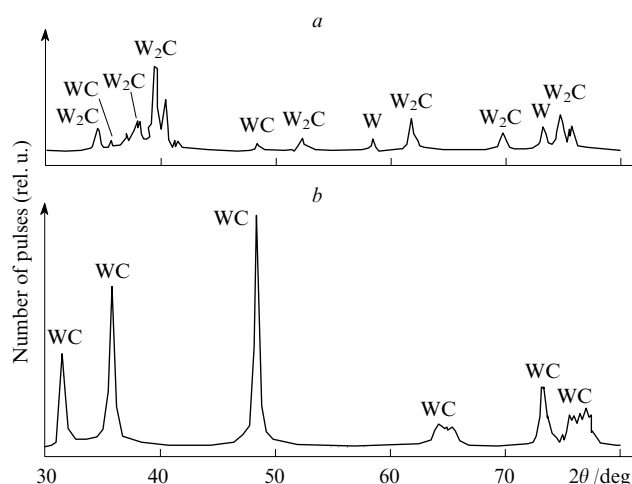


Figure 1. X-Ray powder diffraction patterns of tungsten carbide powders prepared directly by the plasmachemical synthesis (*a*) and after additional homogenising annealing (*b*).⁵² The resulting powder is multiphase; after additional annealing under argon, a single-phase powder was obtained; the average nanoparticle size of the powder was 20–40 nm.

The gas-phase synthesis involving laser heating of a reaction mixture is a version of the plasmachemical synthesis.^{54, 55} This method is highly competitive with other methods due to its reliability and high efficiency. Laser heating excludes contamination of the reaction mixture and allows the control over homogeneous nucleation. Other advantages of laser heating are that surfaces inducing heterogeneous nucleation are absent and the process can be controlled. A laser is a source of high-intensity monochromatic radiation due to which a high degree of its conversion to heat is achieved. The laser-induced synthesis of nanocrystalline Si, Si_3N_4 and SiC powders was described in detail.⁵⁴ Silicon powders were prepared by pyrolysis of gaseous silane (SiH_4) using a CO_2 laser. Silicon grains

were spherical in shape with a diameter of $50 \pm 20\text{ nm}$ and consisted of several crystallites with the size of $\sim 15\text{ nm}$. Silicon nitride powders were synthesised from a gas mixture of silane and ammonia. The resulting powder was amorphous, and the grains were spherical with a diameter of $17 \pm 4\text{ nm}$, the size distribution of grains being narrower than that in a silicon powder (for Si_3N_4 , the size distribution of grains varied from 10 to 25 nm). Unlike silicon nanoparticles, Si_3N_4 grains had no internal structure. Silicon carbide was synthesised from gas mixtures of silane with methane or ethylene. The grain size in the resulting crystalline SiC powder varied from 18 to 26 nm; the average size was 21 nm. The nanoparticle size was demonstrated⁵⁴ to decrease as the intensity of the laser radiation increased due to an increase in the temperature and the heating rate of the reagent gases. Grains of nanopowders synthesised by laser heating are characterised by a narrow size distribution and a spherical shape.

The plasmachemical gas-phase synthesis with the use of laser radiation for the plasma production and maintenance proved to be efficient for the preparation of molecular clusters. The latter have polymorphic cage atomic structures and occupy special place among nanoparticles. Fullerenes, which are allotropes of nanocarbon and differ from the known carbon modifications (graphite and diamond), have received most attention.^{56–58}

Fullerenes can be synthesised by sputtering of graphite in an electric arc under helium at a pressure of $1.33 \times 10^4\text{ Pa}$. Arc burning affords soot that is condensed on a cold surface. The soot is collected and treated with refluxing toluene or benzene. The extract is concentrated to give a black residue containing a mixture of fullerenes C_{60} and C_{70} ($\sim 10\text{--}15\%$). Electron-beam evaporation and laser ablation can be used instead of electric arc sputtering. The diameter of the C_{60} fullerene molecule is 0.72–0.75 nm. Crystallisation of C_{60} affords molecular crystals with a fcc lattice; the unit cell parameter is 1.417 nm. Among carbon nanoparticles fullerene C_{60} is characterised by higher stability, which has been predicted theoretically.^{59, 60}

The plasmachemical synthesis was also used for the preparation of other important molecular nanoclusters, such as fullerene-like $\text{C}_{48}\text{N}_{12}$,⁶¹ the endohedral complex $\text{Ti}@\text{C}_{28}$ (Ref. 62) and the stable charged cluster $\text{Ti}_8\text{C}_{12}^+$ with the linear size of $\sim 0.5\text{ nm}$.^{63, 64}

The clusters M_8C_{12} , where $\text{M} = \text{Zr}, \text{Hf}, \text{V},^{65, 66} \text{Cr}, \text{Mo}$ or $\text{Fe},^{67}$ are called metallocarbohedrenes (Met–Car). In these compounds, transition metal and carbon atoms form a cage-like structure. Metallocarbohedrenes were characterised and the methods for their synthesis were summarised in reviews.^{68, 69}

Interestingly, the plasmachemical gas-phase synthesis^{63, 65, 66} produced predominantly the clusters M_8C_{12} and M_mC_n ($\text{M} = \text{Ti}, \text{Zr}, \text{Hf}$ or V) with a ratio $\text{M}:\text{C} \approx 1.5\text{--}2.0$ rather than nanoparticles of carbides TiC , ZrC , HfC or VC with the structure *B1*. Analogous synthesis in $\text{Ta}\text{--}\text{C}$ and $\text{Nb}\text{--}\text{C}$ systems affords the clusters Ta_mC_n and Nb_mC_n , respectively the composition of which is similar to that of M_8C_{12} along with small amounts of nanoparticles M_mC_n ($m \approx n$) with a cubic structure. Conventional plasmachemical synthesis (without laser heating of a plasma) yields only carbide nanoparticles. Thus, the gas-phase synthesis in transition metal–carbon systems can afford both cubic structures and metallocarbohedrene-like structures.

Metallocarbohedrenes are formed at a high hydrocarbon concentration and a high laser power.⁷⁰ These conditions favour an increase in the carbon content in the plasma. A decrease in the hydrocarbon concentration or a decrease in the laser power leads to a decrease in the carbon content in the plasma. If carbon is present in a deficient amount, carbide

nanoparticles MC with the cubic structure $B1$ are formed. The carbon content in these particles is lower than that in the molecular clusters M_mC_n . This suggests that the formation of cubic or dodecahedral structures in systems $M-C$ under conditions of the gas-phase synthesis is determined primarily by the kinetic rather than thermodynamic factors. The correct answer to the question about the factors responsible for the predominant formation of a particular structure is of practical importance because it allows the targeted synthesis of the desired modification of nanostructured materials.

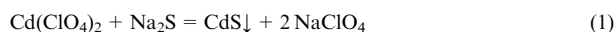
A version of deposition from a plasma is based on magnetron sputtering, which allows the use of not only metal or alloy cathodes, but also of cathodes made of different compounds, thus decreasing the substrate temperature by 100–200 K. This allows the synthesis of a wider range of nanostructured films. However, the degree of ionisation, the kinetic energy of ions and the deposition rate of the product in the case of magnetron sputtering are lower than those obtained with the use of an arc discharge plasma. Intermetallic Ni_3Al films with an average crystallite size of ~ 20 nm were synthesised by magnetron sputtering of the $Ni_{0.75}Al_{0.25}$ target and deposition of a metal vapour on an amorphous substrate.⁷¹

Conventional methods for deposition of films are based on chemical vapour deposition (CVD) and physical vapour deposition (PVD). These methods have long been used for the preparation of films and coatings for different purposes. Generally, crystallites in these materials are rather large in size, but nanostructures can be prepared in multilayer or multiphase CVD films.^{8,72} Vapour deposition is generally associated with high-temperature reactions of metal chlorides in an atmosphere of hydrogen and nitrogen or hydrogen and hydrocarbons. The temperature range of deposition of CVD films is 1200–1400 K, and the deposition rate is $0.03\text{--}0.2\ \mu\text{m min}^{-1}$. The use of laser radiation leads to a decrease in the deposition temperature to 600–900 K, which is favourable for the formation of nanocrystalline films.

IV. Deposition from colloidal solutions

Chemical deposition from colloidal solutions is widely used for the preparation of highly dispersed powders as well as of discrete and continuous films. To prepare nanoparticles from colloidal solutions, the chemical reaction between the solution components is interrupted at a particular instant of time,⁷³ after which the system is converted from the liquid (colloidal) state to the solid (dispersed) state. The method for the preparation of stable colloidal gold solutions and their optical properties were described for the first time by Faraday.⁷⁴

Deposition from aqueous colloidal solutions is used for the synthesis of various metal chalcogenides (sulfides, selenides and tellurides) having semiconducting properties. For example, the synthesis of nanocrystalline sulfide powders involves the reaction of water-soluble metal salts with a sulfidising reagent (a sulfur atom donor). Hydrogen sulfide and sodium sulfide are the simplest sulfidising agents. For example, deposition from a mixture of solutions of cadmium perchlorate and sodium sulfide by the reaction



affords nanostructured cadmium sulfide. The growth of CdS nanoparticles can be interrupted by a jumpwise increase in pH of the solution.

In the synthesis of sulfide nanoparticles of a specified size, thiocarbamide (thiourea) and its derivatives (for example, thiosemicarbazide, thiocarbazine, thioacetamide, allylthiourea, acetylthiourea and sodium thiosulfate) are used as sulfidising reagents. Each of them is characterised by particular formation rates and properties of the resulting films (precip-

itates). In addition, each sulfidising reagent is characterised by particular optimal deposition conditions of metal sulfide. Metal sulfides are deposited as a result of the irreversible reaction; the positive chemical affinity serves as the criterion of the spontaneous formation of sulfide.⁷⁵ [The chemical affinity is equal to the product of the gas constant and the absolute temperature (RT) and the natural logarithm of the ratio of the equilibrium constant of the process under consideration to the product of the concentrations and activities of all components.]

The sizes of PbS particles can be controlled using thiourea and varying the chemical affinity for deposition of the sulfide (Fig. 2). The sulfide particle size, which is equal to the size of coherent X-ray scattering regions at a wavelength λ , was determined^{76–78} by the Williamson–Hall method (Fig. 3) from the dependence of the reduced broadening

$$\beta^*(2\theta) = \frac{\beta(2\theta) \cos \theta}{\lambda}$$

on the scattering vector

$$s = \frac{2 \sin \theta}{\lambda};$$

for the quantitative analysis, the X-ray diffraction line profile was described by the pseudo-Voigt function.^{77,79}

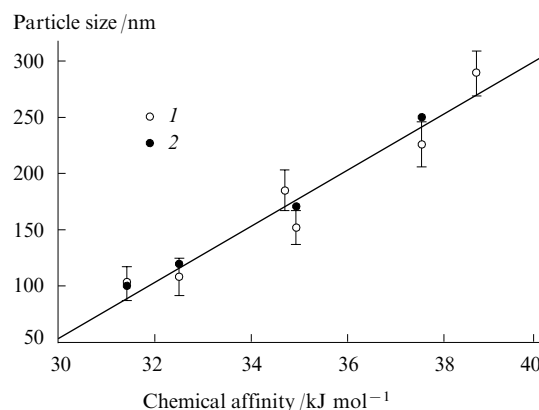


Figure 2. Linear approximation (solid line) of the dependence of the particle size (coherent scattering region) on the chemical affinity for deposition of lead sulfide powders.⁷⁵ (1) X-Ray diffraction, (2) scanning electron microscopy.

The size of cadmium sulfide nanoparticles synthesised by chemical deposition from colloidal solutions with thiourea varied from 2 to 10 nm.^{77,80–83} The structures of nanofilms were studied by a new X-ray diffraction method, the so-called X-ray grazing incidence diffraction, which is also called X-ray scattering under total external reflection conditions. This method was used for studying deposition on a substrate and the atomic structures of films several nanometres thick (Fig. 4)^{21,78,82} and for confirming the hydroxide mechanism of the formation of cadmium sulfide films.⁸²

After deposition of a cadmium sulfide film, the precipitates contained hexagonal prismatic particles several micrometres in size (Figs 5 and 6)⁸⁰ where self-organisation of nanoparticles differed substantially from that observed in analogous compounds prepared by chemical deposition^{84–87} and from that found in SiO_2 (Ref. 88) and TiO_2 (Ref. 89). This is because CdS nanoparticles of several nanometres in size, which form a colloidal crystal several micrometres in size, are arbitrarily

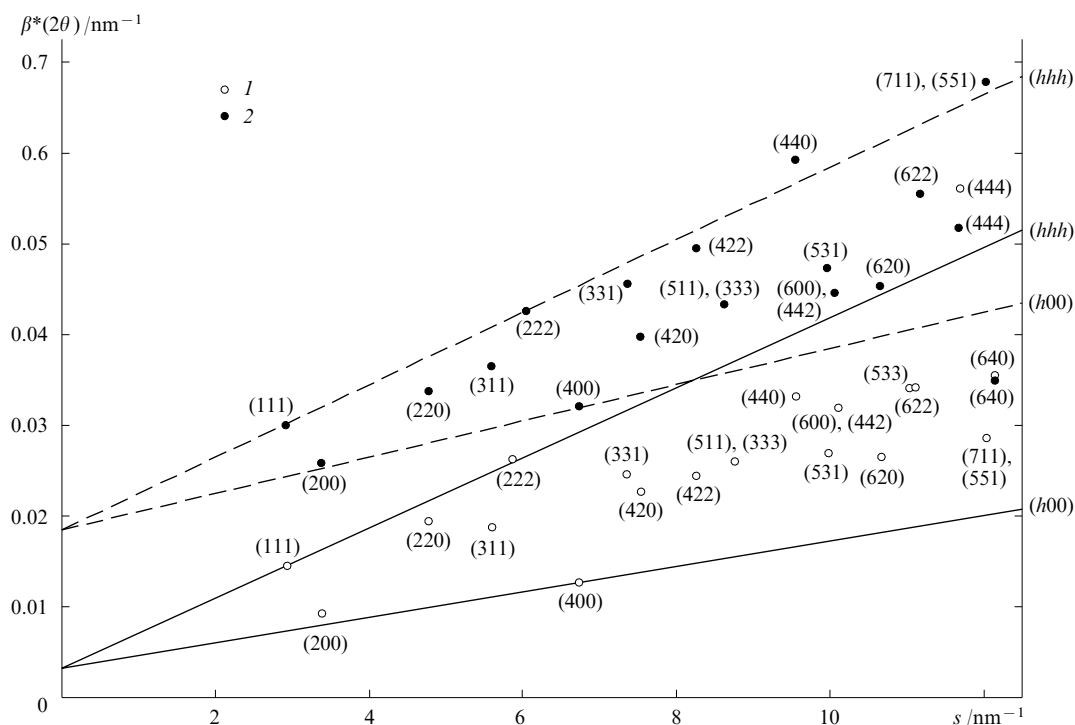


Figure 3. Dependence of broadening of reflections $\beta^*(2\theta)$ on the scattering vector (s) for submicrocrystalline PbS with a particle size of 300 ± 50 nm (1) and nanocrystalline PbS with a particle size of 60 ± 25 nm (2).⁷⁵ The Miller indices for the structure B1 are given.

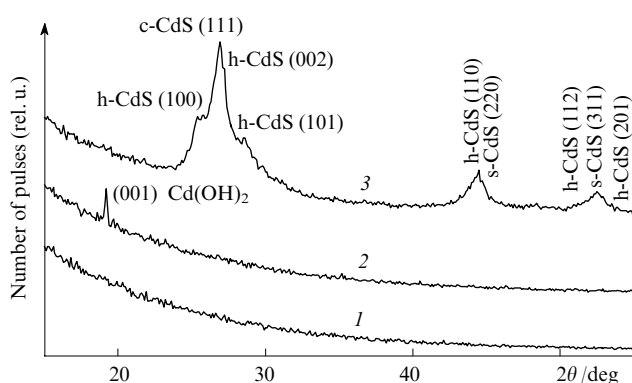


Figure 4. X-Ray diffraction spectra of cadmium sulfide films prepared at 325 K by deposition from the reaction mixture during different periods of time.⁸² The concentrations of the components of the reaction mixture /mol litre⁻¹: $[\text{CdCl}_2]$ is 0.005, $[(\text{NH}_2)_2\text{CS}]$ is 0.025, $[\text{NH}_3]$ is 1.50, $[\text{NaOH}]$ is 0.074; the deposition time /min: (1) 2, (2) 3, (3) 3.

oriented with respect to each other, are irregular in shape and are different in size. Cadmium sulfide nanoparticles are packed closely together in coagulates with the size of ~ 150 nm (Fig. 7).⁸⁰

Self-organisation is a common natural phenomenon.^{90, 91} In recent years, the self-organisation processes in chemistry^{17, 18} have attracted considerable attention because these processes are intended for the use in nanotechnologies for self-assembly of highly efficient schemes for nanoelectronics. The self-assembly mechanism of nanoparticles remains unclear. Emphasis is given to the elucidation of the nature of forces of interparticle interactions, which result in self-organisation and ordering of nanoparticles to form one-, two- and

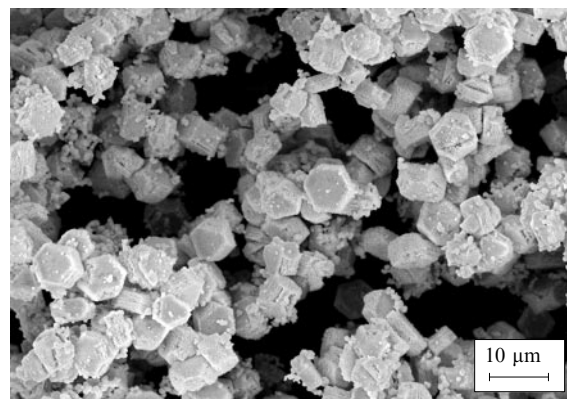
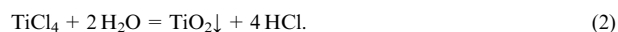


Figure 5. A photomicrograph of a precipitate of cadmium sulfide CdS.⁸⁰ Most of particles are well-faceted hexagonal prisms with approximately the same size of ~ 2.5 μm .

three-dimensional assemblies.⁸⁷ Van der Waals, capillary, electrostatic, steric, *etc.* forces are considered as such forces.

Colloidal metal oxide particles are formed by hydrolysis of salts.^{92–95} For example,



Nanocrystalline titanium, zirconium, aluminium and yttrium oxides can be prepared by hydrolysis of the corresponding chlorides or hypochlorites. Titanium oxide nanoparticles can also be prepared by hydrolysis of titanyl sulfate followed by calcination of the amorphous precipitate at 1000–1300 K. Coagulation of nanoparticles can be prevented by addition of polyphosphates, amines and hydroxide ions to colloidal solutions.

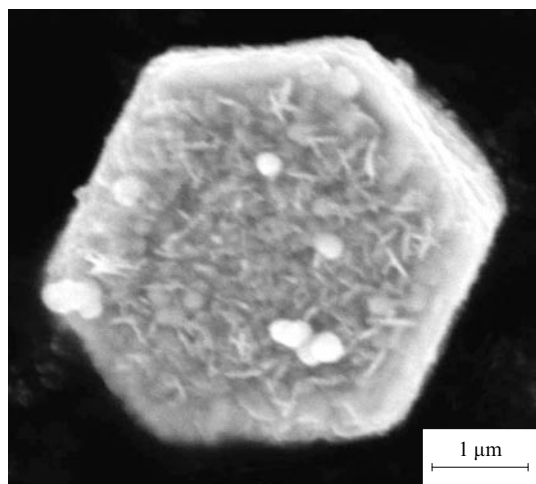


Figure 6. A photomicrograph of a typical colloidal crystal prepared by chemical deposition of CdS.⁸⁰ The crystal side length is $\sim 2.5 \mu\text{m}$.

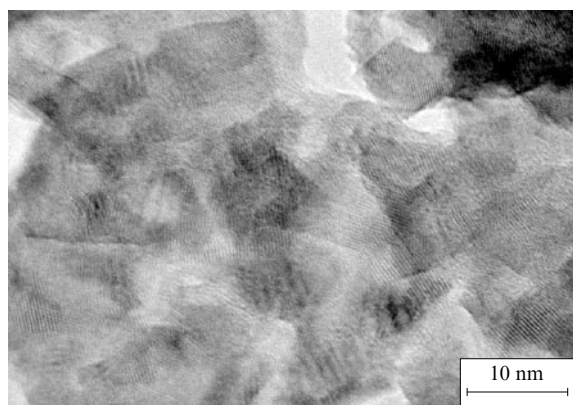


Figure 7. A photomicrograph of coagulates in a chemically deposited CdS powder.⁸⁰ Nanoparticles with the size of 7 nm densely fill the volume inside the coagulates.

Deposition from colloidal solutions is highly efficient for the synthesis of isolated nanoparticles and allows the preparation of nanoparticles characterised by a very narrow size distribution.

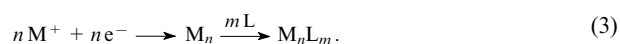
Metal and semiconductor clusters with a narrow size distribution can be prepared inside pores of molecular sieves (zeolites), isolation of clusters inside the pores being retained upon heating to very high temperatures. This method was used for the synthesis of, for example, the semiconductor clusters $(\text{CdS})_4$.⁹⁶ The properties of clusters prepared in zeolite pores were considered in a review.⁹⁷ Larger semiconductor nanoparticles can be synthesised upon attachment of additional molecules to the starting clusters pre-stabilised by organic ligands. This synthesis of large nanoparticles can be considered as polymerisation of inorganic compounds.

Isolated nanoparticles can also be obtained by ultrasonic treatment of colloidal solutions containing large particles.

Deposition from colloidal solutions can be used for the synthesis of nanocrystalline heterostructures, *viz.*, nanoparticles with mixed composition where the core and the shell are formed by semiconductors with different structures of the electron levels (for example, CdSe/ZnS or ZnS/CdSe , HgS/CdS , ZnS/ZnO and $\text{TiO}_2/\text{SnO}_2$). For this purpose, con-

trolled deposition of a semiconductor onto pre-synthesised nanoparticles of a semiconductor of another type should be performed.^{98–101}

An important problem encountered in the deposition from colloidal solutions is prevention of coalescence of the resulting particles and clusters. The chemical synthesis of large stabilised metal clusters with the use of colloidal solutions was described in detail in a review.¹⁰² Generally, colloidal particles and clusters are stabilised by ligands L represented usually by polymers. The reaction scheme for the synthesis of ligand-stabilised metal clusters M_n is as follows:



Metallic gold, platinum and palladium clusters synthesised by this method contain from 300 to 2000 atoms and have cubic or hexagonal close-packed structures. Ligand-stabilised clusters contain the metal core and the external shell formed by the metal atoms that are partially coordinated by ligand molecules. For example, reduction of palladium acetate in acetic acid with hydrogen in the presence of phenanthroline affords stabilised palladium nanoclusters.¹⁰³ The phenanthroline molecules form a shell around the core consisting of the palladium atoms (Fig. 8).

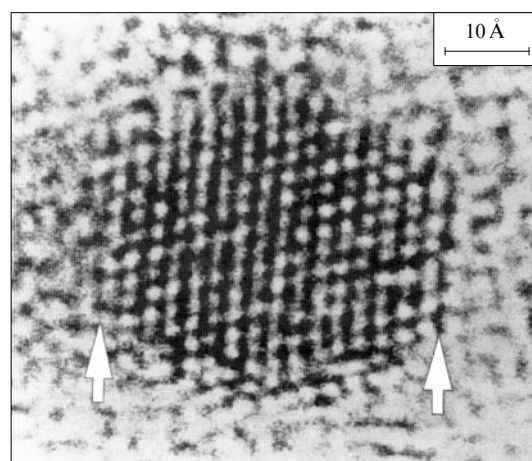


Figure 8. A photomicrograph of a stabilised palladium nanocluster formed by seventeen closely packed atom rows and coated by an eight-layer shell composed of phenanthroline molecules.¹⁰³ The cluster boundaries are indicated by arrows.

Highly dispersed powders can be prepared by calcination of precipitates from colloidal solutions consisting of agglomerated nanoparticles at 1200–1500 K. For example, a nanocrystalline silicon carbide powder ($D \sim 40 \text{ nm}$) was obtained upon hydrolysis of organosilicon compounds followed by calcination in argon at 1800 K.¹⁰⁴ Highly dispersed titanium and zirconium oxide powders are often synthesised by deposition with oxalates.

Nanopowders can also be prepared by cryogenic drying of colloidal solutions.^{9, 11} In this case, a solution is sprayed into a chamber containing a cryogenic medium where the solution is frozen as small particles. Then the gas pressure is reduced to a value lower than the equilibrium pressure above the frozen solvent. Then the material is heated (with continuous evacuation of gases) to remove the solvent. As a result, thinnest porous granules possessing the same composition are formed. Calcination of the latter affords powders.

Various nanostructured mixtures can be synthesised by deposition. An efficient procedure was developed^{105, 106} for the

synthesis of nanocrystalline composites of tungsten carbide and cobalt, which are intended for the preparation of nanostructured solid alloys. Since the synthesis begins in solution, mixing of the components (WC and Co) occurs at the molecular level. Colloidal solutions of tungsten and cobalt salts [for example, $(\text{NH}_4)_6(\text{H}_2\text{W}_{12}\text{O}_{40}) \cdot 4\text{H}_2\text{O}$, CoCl_2 , $\text{Co}(\text{NO}_3)_2$ and $\text{Co}(\text{AcO})_2$] are dried by spraying. Then the resulting powder is subjected to low-temperature carbothermal reduction in a suspended state due to which high dispersity is retained. This technology is covered by a patent¹⁰⁷ under the name the spray conversion process (SCP). A carbidised powder is amorphous. To retard the grain growth and decrease solubility of WC in cobalt, up to 1 mass % of non-stoichiometric vanadium carbide was added to the mixture. The solid alloy prepared from this nanocrystalline composite is characterised by an optimum combination of high hardness and stability. The hardness (H_V) of this alloy is as high as 21.5 GPa, whereas the maximum hardness of the alloy with the same composition prepared from a WC powder is at most 19.5 GPa.^{105–108} An increase in the percentage of vanadium carbide in the alloy leads to an increase in the hardness and a decrease in the grain size of WC. The size distributions of grains in samples of WC alloys containing 6 mass % Co, which were sintered from a nanostructured mixture with 0.83 mass % VC, and in samples of a WC alloy with 6 wt% Co and an additive of 0.32 mass % VC are shown in Fig. 9.¹⁰⁹ As can be seen from Fig. 9, the average grain size of WC in the alloy prepared from an amorphous nanopowder is 250 nm; in the usual alloy, the grain size is almost twice as large (450 nm).

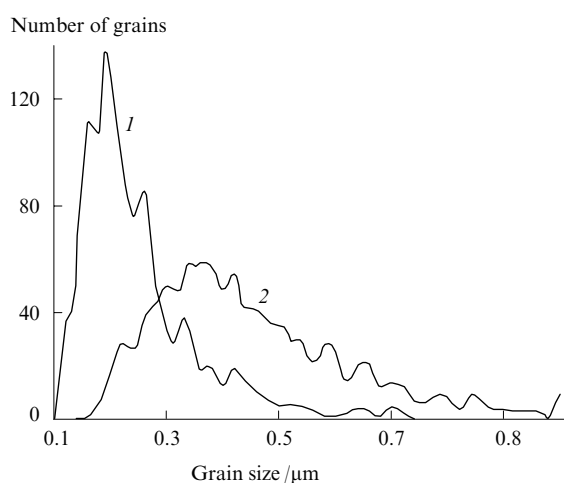


Figure 9. The size distribution of grains in samples of a tungsten carbide alloy; 6 mass % Co.¹⁰⁹

(1) An alloy sintered from a nanostructured mixture of WC and Co with 0.83 mass % VC, which was prepared by co-deposition from a colloidal solution followed by drying and carbothermal reduction (the sample contained 1000 grains); (2) a usual fine-grain WC alloy with 6 mass % Co and 0.32 mass % VC, the sample contained 948 grains.

Each WC–Co nanoparticle with the size of $\sim 75 \mu\text{m}$ was demonstrated^{109,110} to consist of several millions of nanocrystalline WC grains with the size $< 50 \text{ nm}$ distributed in a cobalt matrix (Fig. 10). This nanocrystalline WC–Co powder with a carbide grain size of 20–40 nm is produced in the USA on a commercial scale under the trademark NANOCARB™.

Sintering of a nanostructured mixture of tungsten carbide with 6.8 mass % Co and 1 mass % VC afforded alloys in which 60% of WC grains had sizes of $< 250 \text{ nm}$ and 20% of WC grains, sizes of $< 170 \text{ nm}$. An alloy containing, in addition to tungsten carbide, 9.4 mass % Co, 0.8 mass % Cr_3C_2 and

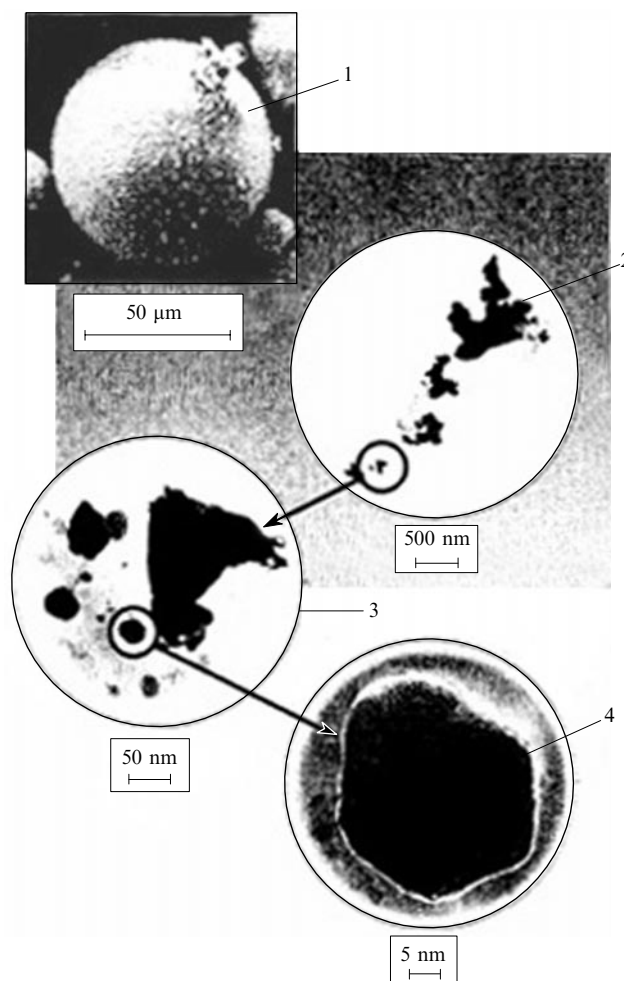


Figure 10. Distribution of nanometre-sized tungsten carbide grains in large particles of an amorphous mixture of WC with 6 mass % Co and 0.83 mass % VC, which was prepared by deposition from a colloidal solution followed by drying and carbothermal reduction.^{109,110}

(1) A particle of a WC–Co composite powder with the size of $75 \mu\text{m}$, (2) fragments of the particle after powder milling, (3) a polycrystalline cluster composed of WC grains in a cobalt matrix, (4) a grain of carbide WC with the size of 30 nm .

0.4 mass % VC had an even finer grain structure. After sintering at 1670 K, 60% of tungsten carbide grains in the alloy had sizes of $< 140 \text{ nm}$ and 20% of grains, sizes of $< 80 \text{ nm}$. Thus, the use of nanostructured WC–Co mixtures synthesised by chemical deposition from colloidal solutions proved to be very efficient for the preparation of nanostructured solid alloys.

Oxide semiconductor films are formed upon deposition onto a support from colloidal solutions. The method involves the preparation of the solution, deposition, drying and annealing. Deposition of oxide nanoparticles afforded ZnO , SnO_2 , TiO_2 and WO_3 semiconductor films.^{111–115} Nanostructured films containing different semiconductor nanoparticles can be synthesised by co-deposition of the latter. The procedure for the preparation of nanocrystalline ZrO_2 films was documented.¹¹⁶

Pulsed electrodeposition is an efficient procedure for the application of coatings and films. This method is also widely used for the preparation of nanostructured metals. A support is soaked in a solution containing ions of an element to be precipitated, and the time-variable (pulsed) potential difference is created between the support and the electrode placed in the solution. The pulsed voltage favours the formation of a

homogeneous coating. A study of the influence of the deposition parameters on the structure and properties of a nickel coating¹¹⁷ demonstrated that the size distribution of grains is narrow, the nickel grain size varying from 13 to 93 nm. Heating of the resulting coating to 380 K did not result in grain growth. The cited study showed also that the grain size and the chemical composition of the nanocrystalline alloy $\text{Ni}_{1-x}\text{Cu}_x$ deposited at room temperature can be controlled by varying the parameters of the pulsed mode and adding organic compounds to the reaction solution.

V. Pyrolysis

In the preparation of nanocrystalline metal powders and their compounds by pyrolysis (thermal decomposition), complex organoelement and organometallic compounds, polymers and metal hydroxides, carbonyls, formates, nitrates, oxalates, amides, imides and azides are generally used as the starting compounds. These compounds contain all or almost all chemical elements, which should be present in the target product. Heating of the starting compounds to a particular temperature results in their decomposition to form the target product and evolution of gaseous compounds.

Highly dispersed metal powders are synthesised by thermal decomposition of various salts.¹¹⁸ For example, metal powders with an average particle size of 100–300 nm were prepared by pyrolysis of iron, cobalt, nickel and copper formates under vacuum or in an inert gas at 470–530 K. Other combinations of pyrolysis and condensation are also used for this purpose. Decomposition of organometallic compounds occurs in a percussion fuse, after which free metal atoms are condensed from a supersaturated vapour, or during supersonic gas flow from a chamber through a nozzle into vacuum.¹¹⁹ The preparation of nanocrystalline metal powders by reduction of metal hydroxides, chlorides, nitrates and carbonates in a hydrogen flow at < 500 K can be considered as a modification of pyrolysis. Low impurity content and a narrow size distribution of particles are advantages of this method.

Thermal decomposition combined with reduction is used for the preparation of supported metal catalysts. This technology is widely employed in industry. In this case, a porous material (silica gel, zeolite, *etc.*) is impregnated with a solution of hydroxide or another compound of the required metal. The impregnated porous support is dried and then calcined in a hydrogen flow to reduce the metal. As a result, catalytically active metal nanoparticles are formed in pores of the support.

However, pyrolysis is most often used for the preparation of nanocrystalline powders of ceramic materials, such as various oxides, carbides, nitrides, borides, carbonitrides, borocarbides, borocarbonitrides, *etc.*

The synthesis of oxide nanomaterials starting from metal carboxylates and their chemical modification products by ethylene glycol was documented.¹²⁰ The compound $\text{Ti}(\text{OCH}_2\text{CH}_2\text{O})_2$ proved to be an efficient precursor for the synthesis of titanium dioxide nanofibres with a diameter from 20 to 100 nm.¹²¹ Titanium glycolate nanofibres were synthesised by heating hydrated titanium dioxide $\text{Ti}(\text{OH})_4$ with ethylene glycol in air. Then titanium glycolate nanofibres were subjected to thermal decomposition in air at a temperature from 400 to 900 °C to prepare TiO_2 nanofibres. Depending on the thermal decomposition temperature, titanium dioxide had a crystal structure of either anatase or rutile, the morphology of the precursor being retained.

A nanocrystalline powder of titanium carbide TiC can be synthesised by pyrolysis of the coordination organometallic compound $(\eta\text{-C}_5\text{H}_5)_2\text{TiMe}_2$ under argon or by pyrolysis of the polymer $[(\text{C}_6\text{H}_4\text{O}_2)_2\text{Ti}]_n$ under argon with the use of hydrogen as the reducing agent.¹²²

Nanocrystalline SiC powders can be prepared by thermal decomposition of polycarbosilanes and polycarbosiloxanes; nanocrystalline silicon nitride Si_3N_4 is produced by pyrolysis of polysilazanes.^{123–125} Since polycarbosiloxanes contain oxygen atoms, their pyrolysis is performed under hydrogen according to the scheme



Initial heating is carried out using a high-temperature plasma or laser radiation followed by additional annealing of pyrolysis products at ~ 1600 K.

Nanocrystalline boron carbide B_4C is obtained upon decomposition of poly(vinylpentaborane) $[\text{C}_2\text{H}_3(\text{B}_5\text{H}_8)]_n$. Polyborazine-, polyborazole- and polyvinylborazine-type boron-containing polymers were suggested¹²⁵ for the use in the synthesis of highly dispersed boron nitride powders and as additives to a titanium powder for the synthesis of nanocrystalline composites $\text{TiN} + \text{TiB}_2$. A nanocrystalline aluminium nitride powder with an average particle size of 8 nm was synthesised by decomposition of $[\text{Al}(\text{NH}_2)_3\text{NH}]_n$ in ammonia at 900 K.¹²⁶

To stabilise the composition and structure of the powders prepared by pyrolysis of monomeric and polymeric compounds, it is necessary to perform their additional annealing; the annealing temperature of nitrides and borides varies from 900 to 1300 K and that of oxides and carbides, from 1200 to 1800 K. The main drawback of thermal decomposition is that the selectivity of the reaction is rather low so that the reaction product represents a mixture of the final product and intermediates.

Nowadays, thermal decomposition is applied to the synthesis of multicomponent amorphous and nanocrystalline ceramic materials. For example, the complex ceramic material $\text{Si}_3\text{B}_1\text{C}_{4.3}\text{N}_2$ was synthesised by decomposition of polyvinylsilazane $[\text{B}(\text{C}_2\text{H}_4\text{SiMeNH})_3]_n$ at 523 K for 1 h and at 623 K for 3 h followed by milling of the product and its dehydrogenation at 1673 K for 2 h.¹²⁷ The influence of annealing on nanocrystallisation and the free volume change in ceramics were examined in detail for the Si–C–B–N system by X-ray diffraction methods and positron annihilation.¹²⁸

A nanostructured mixture of WC and Co can be prepared by pyrolysis of various precursors.¹²² In particular, heating can simultaneously afford WC and Co



where En is ethylenediamine.

VI. Mechanochemistry

Mechanochemistry is one of the most efficient ‘dry’ chemical technologies requiring no or a minimum amount of solvents for chemical reactions. The mechanical treatment of solid mixtures is accompanied by dispersion of substances, acceleration of the mass transfer, mixing of the components at an atomic level and, as a consequence, activation of their chemical reaction.^{129,130} The mechanisms of mechanochemical reactions are characterised by the involvement of many steps. The most important steps are as follows: initial deformation of the crystal structures of the reactants, the formation, accumulation and interactions of point and linear defects, disintegration of substances, the formation of metastable states in the contact zone of different phases, chemical homogenisation and relaxation of the reaction products to the equilibrium state.¹³¹ The reactivity of solids in the course of their deformation and decomposition is the subject of mechanochemistry.

Mechanical milling can result in a decrease in the size of microcrystalline blocks to 10 nm (and smaller), which is equivalent to a decrease in the diffusion length necessary for the reaction.¹²⁹ Simultaneous mechanical treatment of several components of the mixture causes deformation mixing and mechanochemical reactions. The characteristic features of low-temperature mixing of solid reactants associated with the formation of intermediate metastable states and the possibilities of the mechanochemical synthesis of various compounds were covered in detail in the reviews.^{129, 130}

The mechanical milling is an efficient procedure for the preparation of large amounts of nanopowders of various materials, such as metals, alloys, intermetallics, ceramics and composites. Complete solid-state solubility of elements mutual solubility of which under equilibrium conditions is negligibly small can be achieved by mechanical milling and mechanical fusion.^{132, 133} Various mills (reactors) in which the specific mechanical energy imparted to a powder can be as high as 10^2 – 10^3 kJ g⁻¹ are most popular for mechanical activation of powders and mechanochemical processes.

During mechanical milling of powders, the plastic deformation is developed by the dislocation mechanism and it is initially localised in slip bands containing multiple dislocations. As a particular stress level is achieved, these dislocations annihilate, are combined and recombine as small-angle grain boundaries, which separate individual grains, entrapping impurity atoms. In this step of milling, particles with a diameter of 20–30 nm are formed, and their number increases as the particles are ground. In plastic metals, intergrain boundaries are formed by the polygonisation mechanism.¹³⁴ In the next step of milling, the orientation of individual crystallites with respect to each other becomes random due to a slip along the grain boundaries. This behaviour in the course of milling is typical of metals and intermetallics with a bcc lattice.¹³³

The mechanical action during milling of materials is pulsed in character. Hence, the stress field does not act during the entire residence time of particles in the reactor but only at the instant of their collision. During a short period after the collision, partial relaxation occurs. Hence, the character of formation of the stress field in time and the kinetics of subsequent relaxation processes should be taken into account in the mechanochemical synthesis. The mechanical action is not only pulsed, but also local, because it occurs not in the total bulk of the solid, but only where the stress field appears and then relaxes.

Let us consider some results of milling and mechanochemical synthesis with the use of high-energy planetary and vibration mills. A nanocrystalline powder of barium titanate (BaTiO₃) with an average particle size of 25 nm was prepared by the mechanical treatment in a planetary ball mill.¹³⁵ According to the results of electron microscopy, BaTiO₃ nanoparticles contain almost no dislocations. Nanoparticles were combined to form dense aggregates up to 1 µm in size, which in turn form large agglomerates >2 µm in size. The agglomeration is a characteristic property of nanocrystalline powders prepared by mechanical milling.

Mechanochemical synthesis of transition metal boride, carbide, silicide and sulfide powders from powdered mixtures of metals with boron, carbon, silicon and sulfur, respectively, was performed by the so-called explosion method in vibration mills.¹³⁶ In essence, the explosion mechanosynthesis is analogous to the self-propagating high-temperature synthesis; however, unlike the latter method, the fast reaction in the explosion mechanosynthesis is initiated by mechanical activation of powders of the starting components (metal and carbon, boron, silicon or sulfur) for a few minutes rather than by a short-term powerful thermal pulse. X-Ray diffraction and electron microscopic studies of boron, titanium, zirconium,

hafnium, vanadium, tantalum and tungsten carbide powders prepared by the mechanochemical synthesis in eccentric and planetary ball mills demonstrated that the average particle size in these powders varied from 6 to 20 nm.¹³⁷ Metal powders were mechanically milled in planetary and vibration mills under oxygen and nitrogen, respectively to prepare nanocrystalline oxides and nitrides with a particle size of several nanometres.¹³⁸

The mechanochemical synthesis of nanocrystalline carbides TiC, ZrC, VC and NbC with an average particle size of 7 ± 1 nm was carried out by 48-h milling in a planetary ball mill of a mixture of metal and carbon powders.¹³⁹ The formation of carbides starts 4–12 h after the beginning of milling. The study of thermal stability of dispersed nanocrystalline carbides demonstrated¹³⁹ that niobium carbide is the most heat-resistant of all the synthesised carbide nanopowders. The grain size of NbC increases from 7–10 to 30 nm as the temperature increases from 300 to 1300 K. Vanadium carbide is the least thermally stable. Extensive recrystallisation at 1000–1200 K resulted in the VC grain growth to 90 nm.

Vibration ball milling of mixtures of metal powders for 300 h afforded nanocrystalline (the grain size was 5–15 nm) Fe–Ni and Fe–Al alloys with bcc lattices.¹⁴⁰

The synthesis of amorphous nanocrystalline Ni₃Al powders by mechanical milling of an ordered intermetallic alloy Ni₃Al was documented.¹⁴¹ The coarse-grained (with a particle size of ≤ 45 µm) powder had an ordered Cu₃Au-type cubic structure (*L*₁₂) with a long-range parameter of 0.96. After its ball milling for 5 h, superstructure reflections in the X-ray diffraction pattern disappeared (complete ordering of the powder) and the structure reflections corresponding to the fcc lattice broadened. The average crystallite size and the lattice strains were estimated¹⁴¹ from the broadening of the structure reflections of a Ni₃Al powder by the Williamson–Hall method.^{142–144} After 5-h milling, the average crystallite size was 19 nm, and the microstrain was 2×10^{-4} (0.02%). An increase in the milling time to 50 h led to a further broadening of the most intense structure reflections (111) and (200) and the disappearance of other structure reflections. The size of the coherent scattering regions decreased to 8–10 nm. A study of the milled powder by scanning and transmission electron microscopy demonstrated that the nanoparticle size was 2–3 nm, and the electron diffraction pattern for nanoparticles is typical of an amorphous state. Thus, mechanical milling of a coarse-grained powder of the ordered intermetallic Ni₃Al initially resulted in its disorder (the formation of a disordered fcc alloy with an *A*1-type structure) followed by the formation of a nanocrystalline fcc alloy and, in the final step of milling, an amorphous Ni₃Al powder with an average nanoparticle size of ~ 2 nm.

The mechanochemical synthesis can be combined with the synthesis of a nanostructured mixture.¹⁴⁵ In an argon-filled ball mill, a nanostructured mixture of cobalt and tungsten carbide grains with an average size of 11–12 nm is formed after milling of a mixture of coarse-grained (~ 75 µm) tungsten, graphite and cobalt powders for 100 h. In the solid alloy prepared by cold pressing followed by sintering of this mixture at 1310 K, most of WC grains had a size of < 200 nm, *i.e.*, they were several times smaller than those in usual alloys of the same composition. The sintered samples of the alloy had a hardness of ~ 18 GPa and a relative density of 80% of the theoretical value. It was hypothesised¹⁴⁵ that the lower sintering temperature of a nanostructured powdered WC–Co mixture compared to that of a coarse-grained mixture is a consequence of the lower melting point of nanocrystalline cobalt compared to that of the coarse-grained metal.

A complex methodologically correct study of the mechanosynthesis of a nanocrystalline cubic titanium carbide powder was documented.¹⁴⁶ The results of this study deserve a more

detailed discussion. Metallic titanium and graphite powders in a ratio of 44:56 were milled in a sapphire ball mill at room temperature under argon.

After milling for 2×10^3 s, the X-ray diffraction pattern of the reaction mixture (Fig. 11) showed only broad reflections corresponding to elemental Ti and C. After milling for 11×10^3 s, the reflections corresponding to graphite almost disappeared; after milling for 15×10^3 s, reflections of a new cubic phase with the structure B1 (titanium carbide) appeared. This is consistent with the results of investigation¹³⁹ in which the formation of carbide phases was observed after milling of powdered mixtures of transition metal and carbon for four–six hours. An increase in the milling time to 4×10^4 s led to the complete disappearance of X-ray reflections of titanium metal and an increase in the intensities of reflections of titanium carbide. Further increase in the milling time was accompanied by an increase in mechanical deformation of powder particles and a sharp decrease in the grain size, as evidenced by a noticeable broadening of X-ray reflections. Milling for 72×10^4 s afforded nanocrystalline titanium carbide and subsequent increase in the milling time to 10^6 s did not lead to changes in the resulting carbide.

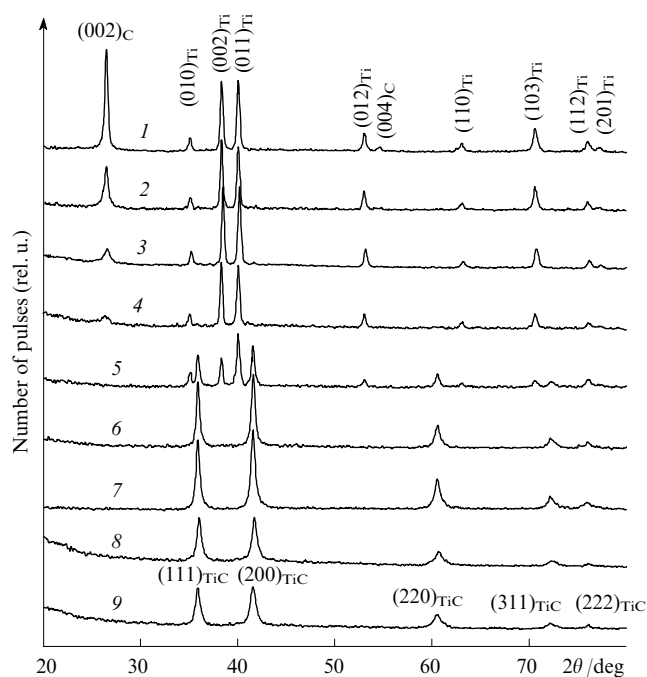


Figure 11. Changes in the X-ray diffraction pattern of powdered 44 Ti + 56 C mixtures prepared at different milling times.¹⁴⁶ The changes in the X-ray diffraction patterns are associated with changes in the phase composition resulting from the formation of titanium carbide and with disintegration of carbide particles to nanometre sizes. The milling time/s: (1) 2×10^3 , (2) 6×10^3 , (3) 8×10^3 , (4) 11×10^3 , (5) 15×10^3 , (6) 22×10^3 , (7) 4×10^4 , (8) 8×10^4 , (9) 72×10^4 .

The changes in the grain size of powders during milling are illustrated in Fig. 12. The formation of nanocrystalline titanium carbide involves four steps presented in Fig. 13. The starting powder (Fig. 13 a) consists of randomly distributed particles of different size and shape. In the first step (the milling time up to 11×10^3 s), very large (with the size of ~ 1 mm) composite Ti/C particles are formed (Fig. 13 b). A metallographic study demonstrated that these particles consist of numerous titanium and carbon layers. The second step (the milling time from 11×10^3 to 2×10^4 s) involves a solid-phase

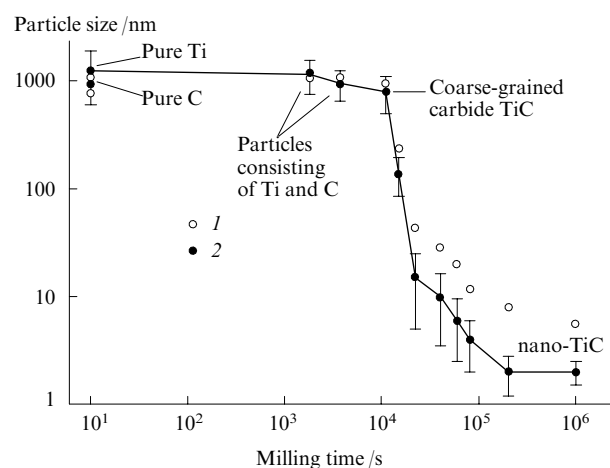


Figure 12. The plot of the particle size of a milled powder containing titanium and carbon particles (44:56) vs. the milling time in the mechano-synthesis of titanium carbide.¹⁴⁶

(1) The particle size determined from the broadening of X-ray reflections; (2) the particle size determined by electron microscopy.

reaction during which titanium and carbon react almost completely with each other to form large titanium carbide grains from 800 to 1000 nm in size. In the third step (the milling time from 2×10^4 to 8×10^4 s), extensive dispersion of large titanium carbide grains affords a finely dispersed powder with a rather broad size distribution of grains (from 5 to 100 nm); the carbide grains form particles with the size of 5–10 μm (Fig. 13 c). In the last step (the milling time from 8×10^4 to 1×10^6 s), the nanocrystalline powder is homogenised with respect to the grain size resulting in the average grain size of $\sim 2 \pm 1$ nm; the grains agglomerate to form spherical particles with the size no larger than 300 nm (Fig. 13 d).

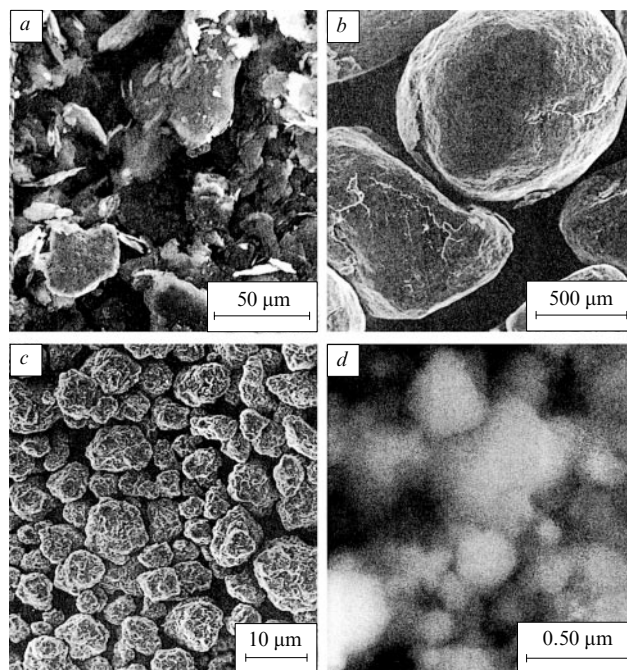


Figure 13. Photomicrographs of particles of the starting powdered mixture of titanium and carbon (44:56) (a) and a powder after ball milling during different periods of time (b–d) see the text.¹⁴⁶

The titanium carbide powder thus prepared was sintered in an activated plasma. The sintering afforded compact titanium carbide samples with high densities (up to 5.2 g cm^{-3}) and hardnesses (up to 3.2 GPa), the average grain size of $< 70 \text{ nm}$ being retained.

The results of the study¹⁴⁶ demonstrated high efficiency of the mechanosynthesis of nanocrystalline titanium carbide. However, it should be noted that the authors' hypothesis that the composition of the starting mixture is identical with that of the synthesised titanium carbide casts doubt, because if this were the case, the superstoichiometric carbide $\text{TiC}_{1.27}$ or the carbide $\text{Ti}_{0.79}\text{C}_{1.00}$ with a defect metal sublattice would be synthesised. The lattice period of the synthesised titanium carbide (0.4326 nm) is somewhat smaller, whereas the measured density (5.2 g cm^{-3}) is higher than the corresponding parameters (0.4328 nm and 4.91 g cm^{-3} , respectively) of the conventional stoichiometric carbide $\text{TiC}_{1.0}$. An excess of carbon atoms in the carbide and its high density can be attributed to the presence of interstitial carbon atoms in the structure B1.

VII. Detonation-induced synthesis

Shock waves is yet another type of mechanical action that creates the conditions for both disintegration of the starting compounds and the synthesis of the final product. Detonation of explosives (the explosion energy) is widely used for performing phase transitions and the synthesis of new compounds. The detonation-induced synthesis of nanopowders proceeds under dynamic conditions where kinetic processes play an important role.

The detonation-induced synthesis of diamond from rhombohedral graphite using a shock wave (the pressure of up to 30 GPa was achieved) was documented.¹⁴⁷ The shock-wave treatment of mixtures of graphite and metals (the duration of a shock wave was 10–20 μs and the produced pressure was 20–40 GPa) afforded¹⁴⁸ diamond powders. These powders were shown to contain single crystals with the size no larger than 50 nm along with assemblies and tightly bound agglomerates with the size of up to 5 μm consisting of individual crystals with sizes of 1–4 and 10–160 nm, respectively.

The 'dry synthesis' based on detonation of condensed carbon-containing explosives with a negative oxygen balance followed by cooling of the detonation products under an inert atmosphere was documented.^{149, 150} Presently, this process is used for industrial production of diamond nanopowders for different technical purposes. The synthesis is performed in explosion chambers with a volume of no smaller than 2–3 m^3 . In the so-called 'aqueous synthesis', which is another version of the detonation-induced synthesis of diamond powders, the diamond particles are cooled with water.

Diamond powders are formed in the zone of chemical decomposition of the starting compounds within $< 0.4 \mu\text{s}$. These powders consist of compact cubic particles with an average size of $\sim 4 \text{ nm}$. Large (up to 1 μm) diamond particles can be prepared with the use of powerful explosives.¹⁵¹

The detonation-induced synthesis of various morphological forms of carbon as well as of aluminium, magnesium, titanium, zirconium and zinc oxide nanopowders was described.^{152, 153} A shock wave passing through a layer of the starting compound (highly porous metal, a chemical compound or a metal hydroxide sol or gel) causes compression and heating of highly porous metals or decomposition of the starting compound to form oxide followed by stabilisation of oxide phases. After the escape of the shock wave on the free surface of the starting compound, materials disperse in the gas atmosphere of the explosion chamber. In a CO_2 atmosphere, carbon nanotubes, spherical carbon particles and thread-like MgO crystals were obtained. The average diameter of thread-

like MgO crystals was 60 nm, and the length to diameter ratio reached 100.

Reactions with chemical compounds as the starting reactants are performed with the use of gaseous and liquid media neutral with respect to the final products, due to which the compounds are rapidly cooled and high-temperature and metastable crystal modifications are stabilised. For example, an yttrium oxide-stabilised cubic ZrO_2 nanopowder was synthesised^{152, 153} by the detonation method. The average particle size was 30 nm.

VIII. Self-propagating high-temperature synthesis

Self-propagating high-temperature synthesis (SHS) is rapidly propagating combustion of solids (of a metal and carbon in the synthesis of carbides or of a metal under nitrogen in the synthesis of nitrides) at a temperature from 2500 to 3000 K.^{154, 155} Since the particle size in the self-propagating high-temperature synthesis products is usually 1–5 μm , it was believed that this method is inapplicable to the preparation of compounds in the nanocrystalline state.

It was suggested¹⁵⁶ that titanium carbide nanopowders would be synthesised by the SHS method in the presence of an inert diluent preventing the particle growth, *e.g.*, using a $\text{Ti} + \text{C} + m\text{NaCl}$ mixture, where $m = 0.2\text{--}0.7$. The particle sizes of the starting Ti, C and NaCl powders were at most 50, 0.1 and 150 μm , respectively. Pellets with a diameter of 30 mm and a height of 40 mm were pressed from the powder mixture. The synthesis was carried out in a standard reactor under argon at a pressure of 0.5 MPa. Combustion was initiated by a current pulse (the voltage was 15–20 V and the pulse duration was 1.0–1.5 s), which was supplied to the sample with a tungsten wire. The combustion temperature decreased from 2500 to 1950 K as the amount of sodium chloride increased (as m changes from 0.2 to 0.7).

The combustion was accompanied by spontaneous homogenisation of the starting mixture due to melting of Ti and NaCl. A microscopic study demonstrated that the resulting titanium carbide particles are distributed in a NaCl melt and are isolated from each other by a thin layer of this melt, which prevented their further growth. No intermediate phases were found. The titanium carbide particle size decreased with the increase in the amount of NaCl in the starting mixture. After washing off NaCl, the titanium carbide powder was studied by X-ray diffraction and electron microscopy. The resulting titanium carbide had the cubic structure B1 with a lattice parameter of 0.433 nm. The powder consisted of particles of irregular shape with a size from 20 to 300 nm; the average particle size was $\sim 100 \text{ nm}$. The optimum amount of NaCl for the synthesis of titanium carbide nanoparticles (m) was found¹⁵⁴ to be 0.4 (or $\sim 30 \text{ mass}\%$). The chemical composition of titanium carbide synthesised in the study¹⁵⁶ was not determined.

IX. Compaction of nanopowders

A method for the preparation of compact dense three-dimensional (3D) nanocrystalline materials named after Gleiter, who was the first to suggest this method,¹⁵⁷ involves the following steps: condensation of nanoparticles under a low-pressure inert gas atmosphere, deposition of particles onto a cold surface of a rotating cylinder and scraping of nanoparticles from the cylinder surface to a collector.¹⁵⁸ After evacuation of the inert gas from the chamber, a nanocrystalline powder was pre-pressed (under a pressure of $\sim 1 \text{ GPa}$) and finally pressed under a pressure of up to 10 GPa. This method can be used for the preparation of cylinders with a diameter from 5 to 15 mm, a thickness of 0.2–3.0 mm and a density of 70%–90% of the theoretical density of the corresponding material. In partic-

ular, the density of nanocrystalline metal powders reaches 97%; the density of nanoceramics, 85%.³ Depending on the evaporation and condensation conditions, compact nanomaterials consist of particles with an average size from 1–2 nm to 80–100 nm. This method was applied to the preparation of compact nanocrystalline nickel with an average particle size of 60 nm.¹⁵⁹

The contact of substances with the environment in the synthesis of nanopowders and their pressing is excluded due to which compact nanocrystalline samples remain uncontaminated. The apparatus described in the papers cited^{157, 158} can be used for the preparation of compact nanocrystalline oxides and nitrides.

The porosity of nanoceramics prepared by pressing of powders is determined primarily by the pores located at triple joints of crystallites and the grain boundaries.² Powders of lower dispersity are less compressible.¹⁶⁰ A uniform porosity distribution is achieved by pressing ceramics at high temperature at which no extensive recrystallisation occurs. For example, conventional sintering of a highly dispersed zirconium oxide powder with a particle size of 40–60 nm at 1370 K for 10 s afforded a material with a relative density of 72% and an average grain size of 120 nm. Hot pressing at the same temperature under a pressure of 1.6 GPa afforded a material with a relative density of 87% and an average grain size of 130 nm.¹⁶¹ Compact oxide ZrO_2 with a relative density of >99% and an average grain size of 85 nm was obtained when the temperature was lowered to 1320 K and the sintering time was increased to 5 h.¹⁶² The most dense (with a relative density of 98%) samples of titanium nitride could be obtained by sintering samples pressed from finely dispersed nanopowders with a grain size of ~8–25 nm and a minimum deviation of the grain size from these values.¹⁶³

Sintering of powders at a high (up to 10 GPa and higher) pressure holds promise for the preparation of dense compact finely grained materials.^{164, 165} For example, a TiN powder with an average particle size of 40 nm was sintered at 3 and 4 GPa at a temperature from 1000 to 1800 K. The maximum density of sintered samples was achieved at 1670 K. An increase in the pressure was accompanied by an increase in the density to 94% of the theoretical value, the crystallite size was 200–300 nm. It should be noted that the crystallite size in samples sintered at 1400–1500 K was at most 60 nm, and the relative density of samples was as high as 92%–93%.

Pressing followed by high-temperature sintering holds promise for the synthesis of compact nanomaterials, particularly, of ceramic materials. To prevent grain enlargement during sintering of pressed samples, it is necessary to use high-density pressing and low sintering temperature $T \leq 0.3T_m$ (T_m is the melting point). The preparation of high-density compact materials presents a serious problem because it is difficult to press nanopowders by conventional static pressing methods. Poor compressibility of nanopowders is associated with adhesion forces the contribution of which to interparticle interactions sharply increases with a decrease in the particle size.

The magnetic pulse method is rather efficient for compaction of nanopowders.^{166–168} This method consists of concentrating the force action of magnetic field of powerful pulse currents, resulting in the appearance of compression waves with an amplitude of up to 5 GPa and a duration of a few microseconds. The parameters of compression waves can rather easily be controlled in this method. The magnetic pulse pressing is environmentally safe, it is much safer than dynamic methods.

Unlike stationary pressing methods, the magnetic pulse method results in extensive heating of powders due to rapid energy release caused by particle friction during packing under the action of a compression wave. If particles are sufficiently

small (≤ 300 nm), the time of their heating is substantially shorter than the characteristic duration of pulse compression waves. Under the same pressure, the magnetic pulse method sometimes allows the preparation of denser compact samples than those prepared by stationary pressing. Aluminium nitride powders prepared by electric explosion (see below) are pressed by the magnetic pulse method under a pressure of 2 GPa to the density of 95% of the theoretical value; Al_2O_3 powders, to the relative density of 86%. This method is applied to the preparation of articles of different shape, which, as a rule, require no additional mechanical treatment. In particular, articles of a complex shape with a density of >95% of the theoretical value were formed from powders of superconducting oxide ceramics.¹⁶⁷ In the general case, interparticle forces are efficiently overcome in the case of rapid motion of a powder medium under the action of pressure pulses due to which the resulting samples have higher density than samples prepared by static pressing. Heating of nanopowders lasts for a short while, which favours a decrease in its recrystallisation at high temperature and the retention of a small particle size.

The magnetic pulse method was used for pressing nanocrystalline Al_2O_3 (see Refs 169 and 170) and TiN powders.¹⁷¹ An increase in the pressing temperature to ~900 K was demonstrated¹⁷¹ to be more efficient than an increase in the pressure in cold pressing. Compact samples of nanocrystalline titanium nitride with a grain size of ~80 nm and a density of ~83% of the theoretical value were prepared under a pulsed pressure of 4.1 GPa at 870 K. A decrease in the pressing temperature to 720 K was accompanied by a decrease in the density to 81%.

A comparative study of compaction of ultradispersed TiN powders by magnetic pulse pressing, high-pressure pressing and conventional pressing was reported.¹⁷² The average particle sizes of the starting powders were 70 and 80 nm. A decrease in the particle size led to a decrease in the degree of compression of samples. An increase in the pressing pressure was accompanied by an increase in the relative density. An increase in the density becomes slower at a pressure of >4 GPa, the density being no higher than 85% even at 7 GPa. It was noted that cold pressing according to different procedures gives very similar results at a pressure of >1 GPa. At 1 GPa, the density of samples prepared by the magnetic pulse method appeared to be somewhat lower than that of samples prepared by static pressing.

Gas-tight ceramic tubes with an external diameter of up to 15 mm and a length of up to 100 mm were produced from nanopowders by radial magnetic pulse pressing.¹⁷³ Powders were placed in a cylindrical gap between a rigid metallic rod and an external cylindrical copper shell. The pressing was performed by radial compression of the external shell under current pulses, the developed pulse pressure being 2 GPa. Aluminium oxide nanopowders and an Y_2O_3 – ZrO_2 mixture with an average particle size of 10–30 nm were used as the starting materials. Radial magnetic pulse pressing of these nanopowders afforded tubes with a relative density of ceramics of >95%.

Ceramic nanopowders can be compacted by dry cold ultrasonic pressing.^{174, 175} Under the action of an ultrasonic field with a power of several kilowatts, interparticle frictions and frictions between particles and walls of the press form decrease, agglomerates and large particles are disintegrated, the surface activity of the powder particles increases and the volume distribution of particles becomes more uniform. This results in an increase in the density of pressed articles, acceleration of diffusion processes, limitation of the grain growth in subsequent sintering and retention of the nanostructure. For example, ultrasonic pressing of an Y_2O_3 -stabilised ZrO_2 nanopowder followed by sintering of samples in air at 1923 K afforded a ceramic material with a relative density of ~90%.

The average particle size in the initial nanopowder was ~ 50 nm.

An interesting procedure for sintering of ceramic compact nanomaterials based on heating of sintered samples with the use of microwave radiation was documented.^{176, 177} Heating is performed by millimetre-range radiation with frequencies from 24 to 84 GHz in a technological gyrotronic device with a power of several kilowatts. The volume energy absorption of microwave radiation provides simultaneous uniform heating of samples because the heating rate is not limited by heat conductivity, as opposed to conventional sintering methods. This allows the preparation of sintered ceramics with a homogeneous microstructure.

Compact samples of Al_2O_3 were prepared by cold isostatic and magnetic-pulse pressing of a nanopowder with an average particle size of 26 nm.¹⁷⁷ The relative densities of the pressed samples were 52% and 70%, respectively. Microwave sintering at maximum temperatures of 1570 and 1770 K afforded samples of Al_2O_3 with a density of 99% of the theoretical value and an average crystallite size of ~ 80 nm.

Conventional sintering methods do not always allow strong connection of different ceramic materials. For example, it is impossible to prepare a mechanically stable composite of ZrO_2 and Al_2O_3 , which is required for the design of devices such as thermal barriers, by conventional methods. This problem can be solved with the use of nanocrystalline materials and microwave sintering.¹⁷⁷ Oxides ZrO_2 and Al_2O_3 are bound to each other with the use of a sintered interlayer made from the nanosized composite ceramic material 60 vol.% ZrO_2 + 40 vol.% Al_2O_3 with an average grain size of 100 nm. The relative density of the interlayer was 96%–98% of the theoretical value. Microwave heating of the ZrO_2 /interlayer/ Al_2O_3 structure over a short period of time to 1700 K afforded a stable composite consisting of oxides ZrO_2 and Al_2O_3 .

X. Crystallisation of amorphous alloys

The above-described methods are based on the assembly principle, *i.e.*, belong to 'bottom-up' nanotechnologies. Methods of 'top-down' technologies are described below.

Nanostructures can be formed in amorphous alloys by crystallisation.¹⁷⁸ Amorphous metal alloys can be prepared by rapid (at a rate of $\geq 10^6$ K s⁻¹) cooling of alloys on the surface of a rotating disc or drum. This method is called spinning. Nanostructures are created by annealing in such a way as to form a large number of crystallisation centres and the crystal growth rate is low.

The amorphous magnetically hard alloy $\text{Fe}_{90}\text{Zr}_7\text{B}_3$ can be referred to as an example.¹⁷⁸ The amorphous alloy was prepared by spinning and then subjected to relaxation annealing at 673 K for 2 h. A nanocrystalline structure formed when the alloy was additionally annealed at 873 K under vacuum (10^{-5} Pa) for 1 h. The transformation of the $\text{Fe}_{90}\text{Zr}_7\text{B}_3$ alloy from the amorphous to the nanocrystalline state results in a change in the X-ray diffraction pattern (Fig. 14): very broad diffuse X-ray reflections become sharp and narrow.¹⁷⁸ The grain size of the crystalline bcc phase α -Fe(Zr) that is formed in the amorphous matrix was ~ 10 nm (results of high-resolution electron microscopy). Considerable attention was given to investigation of the structure of an amorphous matrix containing α -iron nanoparticles.¹⁷⁸ In particular, a study of the atomic structure of the matrix by modern electron–positron annihilation methods revealed a high content of zirconium concentrated at the nucleation sites of the bcc phase α -Fe(Zr).

Crystallisation of amorphous alloys is extensively studied in view of the possibility of constructing nanocrystalline ferromagnetic Fe–Cu–M–Si–B alloys (M = Nb, Ta, W, Mo or Zr) with a very low coercive force and high magnetic permeability, *i.e.*, of magnetically soft materials. The magnetic

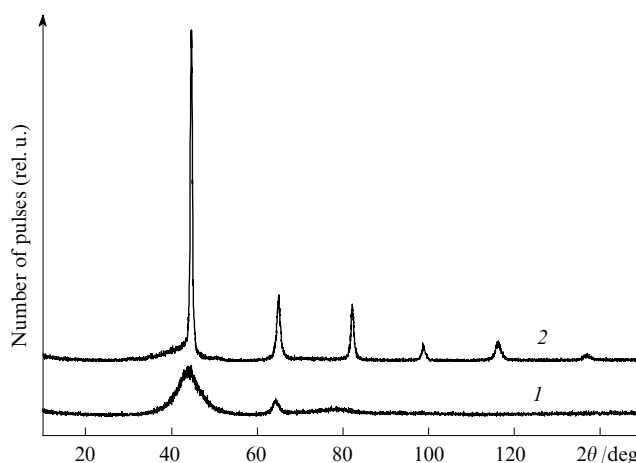


Figure 14. Changes in the X-ray diffraction pattern upon the transformation of the alloy $\text{Fe}_{90}\text{Zr}_7\text{B}_3$ from the amorphous (1) to the nanocrystalline (2) state.¹⁷⁸

The grain size of the bcc phase α -Fe(Zr) is ~ 10 nm.

properties of thin films of the Ni–Fe alloy were demonstrated¹⁷⁹ to be improved as the effective magnetocrystalline anisotropy decreases. This can be achieved by increasing the number of grains involved in exchange interactions in thin magnetic films. In other words, a decrease in the grain size results in an increase in exchange interactions, a decrease in magnetocrystalline anisotropy and, consequently, an improvement of the properties of magnetically soft materials. More recently, this idea has been implemented in targeted crystallisation of multicomponent amorphous alloys.

Silicon-containing steels are magnetically soft materials. Initial attempts to improve the properties of these materials by crystallisation of amorphous alloys were undertaken for alloys of the Fe–Si–B system with addition of copper. However, no alloys with nanocrystalline structures could be obtained in this system. It is only after the introduction of Group IV–VII transition metals along with Cu that a nanostructure was prepared by crystallisation of this system.¹⁸⁰ Crystallisation of amorphous Fe–Cu–Nb–Si–B alloys at 700–900 K afforded an alloy with a homogeneous nanocrystalline structure. In this alloy, grains of the bcc α -Fe(Si) phase with the size of ~ 10 nm and copper clusters with the size of < 1 nm are uniformly distributed in an amorphous matrix.

Positron annihilation studies demonstrated⁷⁹ that $(\text{Fe}_3\text{Si})_{95}\text{Nb}_5$ alloys are thermally stable due to segregation of Nb atoms at the interfaces. Due to the high melting point, niobium hinders complete recrystallisation of the alloy.

The preliminary (before crystallisation annealing) rolling deformation of amorphous Fe–Cu–Nb–Si–B alloys (or their low-temperature annealing) allows a decrease in the grain size to ~ 5 nm.¹⁸¹

Crystallisation of rapidly solidifying aluminium alloys Al–Cr–Ce–M (M = Fe, Co, Ni or Cu) containing 92 at.% Al gave a structure containing an amorphous phase and icosahedral aluminium-rich nanoparticles with the size of ~ 5 –12 nm.¹⁸²

XI. Severe plastic deformation

Severe plastic deformation is a very attractive procedure for the preparation of compact nano- and submicrocrystalline materials.^{19, 183–186} This method is based on the formation of strongly fragmented and disoriented structures with signs of a recrystallised amorphous state. Large deformations of materials can be achieved with the use of the following methods:

twisting under quasi-hydrostatic pressure, equal-channel angular pressing, rolling and three-dimensional forging. These methods consist of performing multiple intense plastic shear deformation of materials, the true logarithmic deformation (e) being 4–7. The use of severe plastic deformation allows not only a decrease in the average grain size but also the production of massive samples with a virtually pore-free structure, which cannot be achieved by compaction of nanopowders.

Twisting under high pressure of disc-shaped samples with the radius R and the thickness l creates shear deformations. The geometric shape of samples is such that the main bulk of materials is deformed under quasi-hydrostatic compression and, hence, the samples are not destroyed in spite of a high degree of deformation. The true logarithmic deformation achieved upon twisting under high pressure is calculated by the equation¹⁸³

$$e = \ln \frac{\theta R}{l}, \quad (7)$$

where θ is the twist angle in radians. The results of numerous investigations demonstrated that after several turns, the structure of samples is disintegrated both at the periphery and in the central part so that it becomes homogeneous throughout the bulk.¹⁹

The most homogeneous structure is formed upon steady-state simple shear deformation. In this method, a material is pressed through two channels of equal cross-section intersecting at an angle of $2\Phi = 90^\circ - 150^\circ$. The intersection plane of the channels contains a homogeneous localised simple shear deformation with an intensity of

$$\Delta\Gamma = 2\cot\Phi. \quad (8)$$

Multiple cycling treatment of a material according to this scheme provides superhigh intense deformations

$$\Gamma = N\Delta\Gamma = 2N\cot\Phi,$$

where N is the number of cycles. The resulting sample exists in a homogeneous stressed deformed state, but its cross-section sizes remain unchanged. The true logarithmic deformation is calculated by the equation

$$e = \operatorname{arsh} \frac{\Gamma}{2} = \ln \left\{ \frac{\Gamma}{2} + \left[\left(\frac{\Gamma}{2} \right)^2 + 1 \right]^{1/2} \right\}. \quad (9)$$

It is most reasonable to use angles 2Φ close to 90° , at which the maximum intensity of deformations is achieved, an increase in the contact pressure being insignificant. A grease is used to minimise contact frictions. This deformation scheme is called equal-channel angular pressing. This method was described for the first time by Segal¹⁸⁷ and was developed further.^{188, 189}

The results of investigations of the structures and properties of submicrocrystalline materials were analysed in reviews.^{19, 185, 190} Annealing of nanocrystalline materials leads to evolution of their microstructures, which can arbitrarily be divided into two steps. In the first step, annealing at a temperature equal to approximately one third of the melting point leads to stress relaxation, the transformation of the grain boundaries from the nonequilibrium to a more equilibrium state and a slight grain growth. In the second step, further increase in the annealing temperature or an increase in the annealing time cause collective recrystallisation (grain enlargement). The first annealing step can readily be observed from the results of microhardness measurements of plastically deformed materials, for example, of Cu, Pd and Ti (Fig. 15).

The severe plastic deformation was applied to obtain nano- and submicrocrystalline structures of metallic Cu,^{191–193}

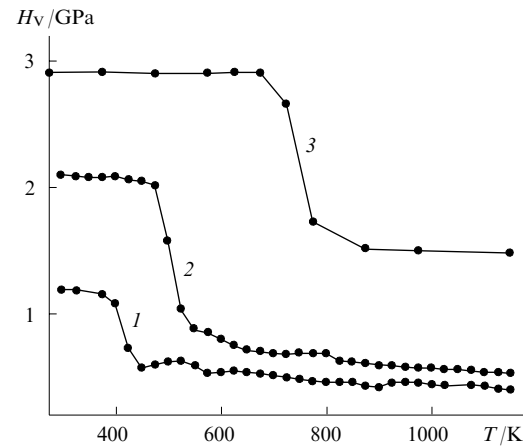


Figure 15. Plots of the microhardness of plastically deformed metals Cu (1), Pd (2) and Ti (3) vs. the annealing temperature.

Pd,^{194–197} Fe,¹⁹⁸ Ni^{191, 193, 199} and Co,²⁰⁰ aluminium-,¹⁸⁴ magnesium-,²⁰¹ and titanium-based^{202, 203} alloys and a number of brittle compounds. Interestingly, after plastic deformation of similar strength, the grain size in brittle compounds was smaller than in metals. For example, a compact nanocrystalline sample with a grain size of $\sim 30 - 40$ nm was prepared for the first time^{204, 205} from a coarsely dispersed nonstoichiometric powder of carbide $\text{TiC}_{0.62}$ (with a particle size of $\sim 2 - 5$ μm) by twisting under quasi-hydrostatic pressure.

The synthesis of nanocrystalline titanium monoxide by twisting under quasi-hydrostatic pressure of 8 GPa was documented.²⁰⁶ The size of coherent scattering regions estimated from the Williamson–Hall plot was ~ 40 nm. In addition, it was found that the cubic lattice parameter of titanium monoxide was increased by 0.0004 nm after mechanical treatment (Fig. 16), which is indicative of a substantial change in the concentration of titanium vacancies.²⁰⁶ Particular attention is given to structural vacancies in this compound, because they are responsible for the properties of the monoxide.

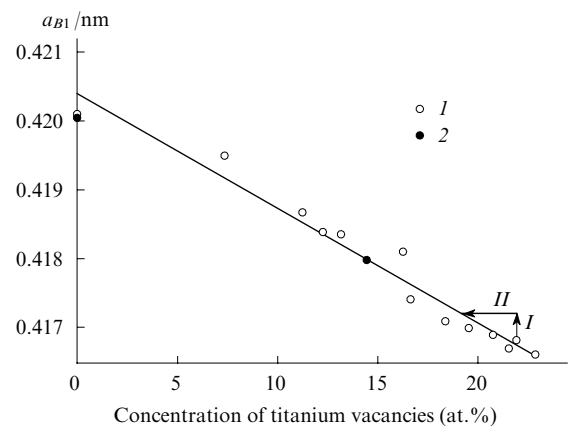


Figure 16. Plot of the lattice parameter of titanium monoxide a_{B1} vs. the concentration of structural vacancies in the metal sublattice for the equilibrium state (I) and the stoichiometric monoxide subjected to a pressure of 8 GPa at high temperature (2).²⁰⁶

The increase in the lattice parameter of titanium monoxide $\text{TiO}_{1.23}$ (I) and the decrease in the concentration of titanium vacancies (II) after severe shear deformation under a pressure of 8 GPa at room temperature are indicated by arrows.

XII. Electric explosion

Nanopowders can be prepared by electric explosion of conductors caused by passing a powerful current pulse with density of 10^4 – 10^6 A mm $^{-2}$ and duration of 10^{-5} – 10^{-7} s.^{207–209} For this purpose, a wire with a diameter of 0.1–1.0 mm is used. An electric explosion of a conductor is accompanied by a sharp change in the aggregation state of metal as a result of intense energy release and by the shock wave generation, enabling rapid (at a rate of higher than 1×10^7 K s $^{-1}$) heating of metals to high temperatures ($T > 10^4$ K). In the initial step of electric explosion, heating of conductors is accompanied by their linear expansion at a rather low rate (1–3 m s $^{-1}$). In the explosion step, the metal is overheated to a temperature higher than the melting point, expansion of the compound occurs at a rate of up to 5×10^3 m s $^{-1}$ and the overheated metal is explosively dispersed.²¹⁰ The pressure and temperature at the shock wave front achieve several hundreds of megapascals (thousands of atmospheres) and $\sim 10^4$ K, respectively. Condensation in a flow of rapidly expanding vapour affords very small particles. Powders with a particle size from 100 μ m to 50 nm can be prepared by controlling the explosion conditions. The average particle size monotonically decreases with an increase in the current density and decrease in the pulse duration. Metal and alloy powders can be prepared by electric explosion in an inert atmosphere. Finely dispersed powders of metal oxides, nitrides and carbides or their mixtures can be prepared by introducing additional reagents (air, a mixture of oxygen and an inert gas, nitrogen, distilled water, decane, paraffin or a technical oil) into a reactor. Copper powders with the maximum of the size distribution corresponding to ~ 20 nm and aluminium powders with an average particle size of ~ 50 nm were prepared by electric explosion at a pressure of 200 Pa.²⁰⁸

According to experimental data,²¹¹ submicrocrystalline powders prepared by electric explosion of a wire have a very high excess energy. For example, the excess energy of aluminium powders with an average particle size of 500–800 nm is 100–200 kJ mol $^{-1}$ and of silver powders with an average particle size of ~ 120 nm is 40–80 kJ mol $^{-1}$, which is several times higher than the heat of melting of a massive substance. This excess cannot be attributed to a contribution of only the surface energy. The observed accumulation of a large excess energy by finely dispersed powders prepared by electric explosion²¹¹ remained unexplained. It was hypothesised²¹² that the excess energy is accumulated as the surface energy, internal defects and charge states. The size distribution of powders is logarithmically normal, and the maximum of distribution is in the range of 10–500 nm. Particles of metal and alloy powders prepared by electric explosion are spherical, whereas particles of nitride powders are faceted.

In recent years, the electroerosion method was developed for the preparation of nano- and submicrocrystalline metal and alloy powders.

XIII. Ordering of non-stoichiometric compounds as a method for the construction of nanostructures

Group IV, V and VI transition metal carbides hold promise for the construction of nanocrystalline ceramic materials having rather high hardness, low fragility and stability against cracking. These ceramics belong to highest-melting compounds and they are inferior only to diamond and cubic boron nitride in hardness.

Group IV and V transition metal monocarbides MC $_x$ are strongly non-stoichiometric compounds.^{213–215} In the disordered state, these compounds have the cubic structure *B1* and contain up to 50% structural vacancies in the non-metal sublattice.^{51, 213–220} At temperatures below 1300 K, the struc-

ture *B1* becomes unstable, and non-stoichiometric carbides undergo first-order disorder–order phase transitions accompanied by a jumpwise change in the volume and the formation of ordered phases with complex superstructures.^{213–221} Since the ordering is a diffusion process, the transformation occurs during a particular temperature-dependent period of time. Carbides are synthesised at 1400–1800 K, which is above the disorder–order phase transition temperatures (T_{trans}). Cooling of carbides to room temperature is accompanied by ordering. In the rapid cooling, ordering is not completed and non-stoichiometric carbide persists in a metastable disordered state. A difference in the lattice parameters of disordered and ordered phases gives rise to stresses, which can lead to cracking of crystallites at interfaces. Nanostructured powders of non-stoichiometric carbides can be prepared by decreasing the domain size of the ordered phase.

An idea of the nanostructure formation by atom-vacancy ordering of non-stoichiometric compounds was applied for the first time to non-stoichiometric vanadium carbide.²²² The latter was chosen for investigation because ordering in this compound is the most pronounced.^{221, 223, 224} In nanocrystalline solids and nanopowders, not only bulk effects (associated with the particle size), but also surface effects (associated with the state and structure of interfaces)^{9–12} play an important role. This is why particular attention was given to the surface state of compounds in the studies on physicochemical properties of vanadium carbide.^{222, 225}

Particles of nanostructured powdered vanadium carbide VC $_{0.875}$ were obtained by carbothermal reduction of oxide V $_2$ O $_5$ followed by cooling to room temperature. Vanadium carbide is nanostructured, and its nanoparticles are curved and petal-shaped. The petals are joined to each other to form a coral-like structure (Fig. 17). An electron microscopic study revealed small deviation of the nanoparticle size. Nanostructured vanadium carbide is unique because this structure has not been found earlier.

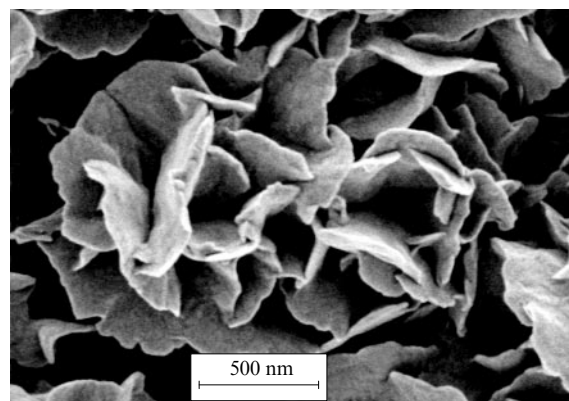


Figure 17. Morphology of particles of the vanadium carbide powder VC $_{0.875}$.²²²

Particles with the size of ~ 1 μ m are two-dimensional nanocrystallites having a shape of curved petal discs with a diameter from 400 to 600 nm and thickness of ~ 15 –20 nm.

The crystal structure of vanadium carbide was studied by X-ray diffraction using CuK $\alpha_{1,2}$ radiation.^{225, 226} The X-ray diffraction spectra of disordered, coarse-grained ordered and nanostructured carbide VC $_{0.875}$ are presented in Fig. 18. The X-ray diffraction pattern of a VC $_{0.875}$ nanopowder (Fig. 18c) shows, along with structure reflections of the basic phase *B1*, only superstructure reflections corresponding to the cubic ordered phase V $_8$ C $_7$ with the space group $P4_332$. The lattice parameter of the disordered phase is

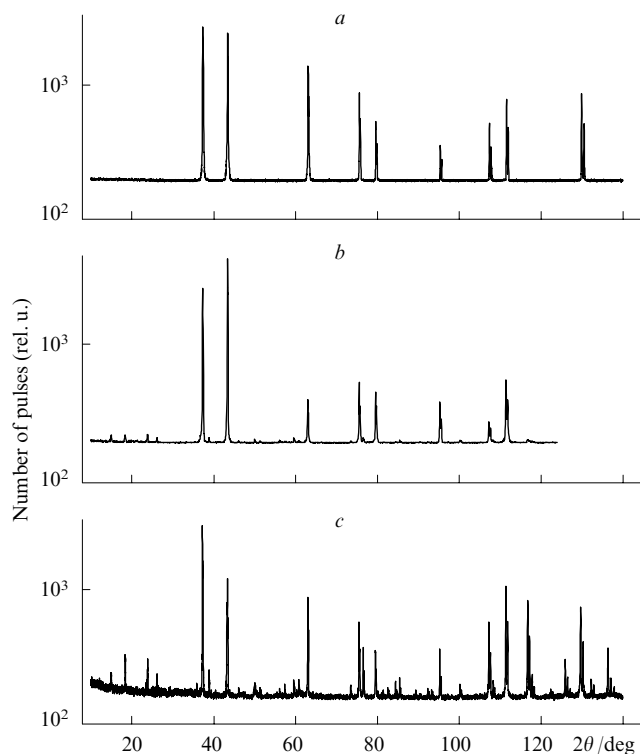


Figure 18. X-Ray powder diffraction patterns of disordered (a), ordered coarse-grained (b) and nanostructured carbide $\text{VC}_{0.875}$ (c) ($\text{CuK}\alpha_{1,2}$ radiation, the intensity is shown on the logarithmic scale; the structure reflections of the phase B1 are indicated).²²⁶ The superstructure reflections in the X-ray diffraction patterns (b) and (c) correspond to the cubic ordered phase V_8C_7 : a_{B1}/nm : (a) 0.41638, (b) 0.41682, (c) 0.41685.

0.8337 ± 0.0001 nm. The ideal M_8C_7 -type cubic superstructure with the space group $P4_332$ has the doubled (compared to the disordered basic phase B1) lattice parameter.^{219, 220, 224} Hence, the lattice parameter of the basic phase a_{B1} of the vanadium carbide under study is 0.41685 nm. This parameter is substantially (by 0.00047 nm) larger than the lattice parameter of disordered carbide $\text{VC}_{0.875}$. Such a large difference can be observed only in the case of the maximum (or nearly maximum) degree of ordering.^{217, 219, 220}

The intensity of superstructure reflections of coarsely crystalline ordered carbide $\text{VC}_{0.875}$ decreases with the increase in the diffraction angle 2θ (Fig. 18 b), whereas the intensity of superstructure reflections of the nanopowder in the angle range $2\theta > 100^\circ$ even increases rather than decreases (Fig. 18 c). This fact remains unexplained.

In spite of the nanometre thickness of nanocrystallites, an analysis of X-ray reflections did not reveal their broadening. Since all atoms in the crystallite scatter coherently, the absence of broadening of X-ray lines is consistent with the presence of a rather large number of atoms in nanocrystallites, as evidenced by a large size of the latter in two other dimensions.

Electron–positron annihilation is the most efficient and sensitive method for studying defects at interfaces and on the surfaces of nanoparticles. The positron trapping by such defects as vacancies or nanopores results in an increase in the positron lifetime compared to that in defect-free materials²²⁷ and in changes in the Doppler broadening spectra of annihilation γ quanta.²²⁸ The defect type can be judged from the lifetime.

The positron lifetime was measured with the use of a $\text{VC}_{0.875}$ carbide powder pre-calcined at 400 K to remove

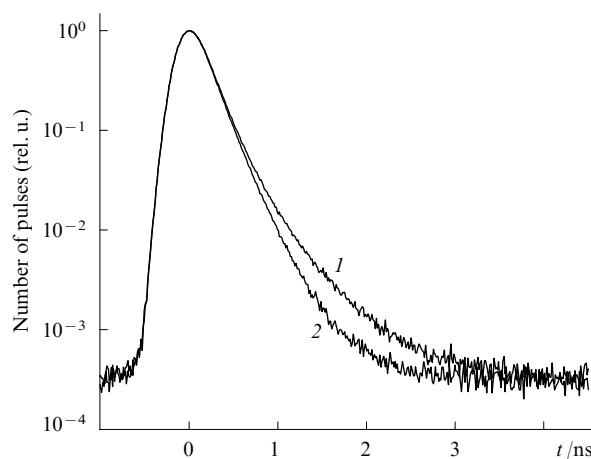


Figure 19. Positron lifetime spectra of nanostructured (1) and coarse-crystalline (2) powders of ordered carbide V_8C_7 .²²² t is the current time.

water.^{222, 225} For comparison, the positron lifetimes were measured in a coarse-grained sintered sample of $\text{VC}_{0.875}$. The positron lifetime spectra are shown in Fig. 19. The average positron lifetime in the nanopowder is substantially longer than that in the polycrystal. The spectrum of the coarse-grained sample of vanadium carbide shows only a short-lifetime component with 157 ± 2 ps, which corresponds to positron annihilation of a structural vacancy in the carbon sublattice.^{229, 230} The spectrum of the nanocrystalline sample contains a short-lifetime component along with a long-lifetime component with 500 ps and a relative intensity of 7%. The long-lifetime component is attributed²²⁷ to positron annihilation in defects on the particle surface. The positron trapping by a structural vacancy is evidence of the absence of long-distance diffusion of positrons. In this case, the intensities of the components are proportional to the volume fractions of phases containing different types of defects. Thus, the relative intensity of the long-lifetime component is consistent with the volume fraction of the surface

$$\Delta V_{\text{surf}} = \delta \frac{S}{V}$$

in the nanopowder. The surface layer was estimated to have thickness $\delta = 0.5\text{--}0.7$ nm or 3–4 atomic monolayers. The results of determination of the positron lifetime show that the inner part of vanadium carbide nanocrystallites contains only non-metal structural vacancies and the surface layer involves vacancy agglomerates as defects.

The observed morphology of the nanocrystalline powder of non-stoichiometric vanadium carbide may be a consequence of grain cracking at the interfaces between the disordered and ordered phases. Actually, high-temperature X-ray diffraction measurements demonstrated²²¹ that a jumpwise increase in the lattice parameter of the fcc sublattice by 0.0004 nm occurs at 1413 ± 20 K as a result of the disorder–order phase transition. The domain size of the ordered phase is ~ 20 nm. It was shown²²³ that ordering occurs according to the mechanism of the first-order phase transition at 1368 ± 12 K. At 300 K, the parameter a_{B1} of the basic crystal lattice of quenched disordered carbide $\text{VC}_{0.875}$ is 0.0002 nm smaller than that of ordered carbide with the same carbon content. The difference between the volumes of the disordered and ordered phases is responsible for the appearance of stresses and subsequent cracking at the interfaces.

The nanostructure formation can proceed according to another mechanism. Unlike the above-considered mechanism associated with the presence of domains of disordered and ordered phases, the mechanism under discussion involves the formation of antiphase domains of the ordered phase. The first-order disorder–order phase transition affords domains of the ordered phase between which stresses occur due to a mismatch of the atomic structures of antiphase domains. In due course, stresses lead to cracking of grains of the initial disordered phase at the antiphase domain boundaries of the ordered phase.

According to this mechanism, the nanostructure formation of a non-stoichiometric $\text{VC}_{0.875}$ powder (see Fig. 17) can be attributed to the $\text{VC}_{0.875} \rightarrow \text{V}_8\text{C}_7$ phase transition. Nanocrystallites of ordered non-stoichiometric vanadium carbide are formed as curved discs with a diameter of < 600 nm and thickness of 15–20 nm through cracking of particles with the size of up to 1 μm . The inner part of nanocrystallites consists of ordered carbide V_8C_7 with a high degree of long-range order and a negligibly small amount of dissolved oxygen. The surface layer of nanocrystallites with a thickness of 0.5–0.7 nm contains chemisorbed oxygen and a large amount of vacancy agglomerates, *i.e.*, has a loose structure.

The ordering allows the nanostructure formation in compact samples of non-stoichiometric compounds.

The structures of annealed and quenched compact samples of $\text{VC}_{0.875}$ were studied by X-ray diffraction. After both annealing and quenching, the X-ray diffraction spectra contain, along with the structure reflections, weak additional reflections (Fig. 20). The positions of additional reflections correspond to superstructure reflections and are assigned to the ordered cubic phase V_8C_7 with the space group $P4_332$. The superstructure reflections for annealed and quenched samples are similar in the integral intensity but strongly differ in the width.

According to the equilibrium phase diagram of the V–C system,²³¹ the ordered V_8C_7 phase is formed after the disorder–order phase transition at 1380 K; the experimental phase transition temperature is 1413 ± 20 K.²²¹ Rapid cooling from 1420 and 1500 to 300 K could result in quenching of non-stoichiometric vanadium carbide $\text{VC}_{0.875}$ and its retention in a metastable state. However, even quenching from 1500 K gives rise to the ordered V_8C_7 phase, the relative intensities of superstructure reflections being approximately equal to those for samples obtained after quenching from 1420 K or annealing at 1370 K (see Fig. 20).

As a consequence of ordering, each grain of the basic disordered phase is divided into domains of an ordered phase. The degree of ordering in domains is high, whereas the mutual spatial arrangement of domains is random to a degree allowed by the ratio between the structures of the ordered phase and the disordered matrix. X-Ray diffraction studies showed that the width of structure reflections is independent of the conditions of thermal treatment of compact $\text{VC}_{0.875}$ samples. Hence, the grain size of the basic phase presumably remains unchanged upon ordering. However, the superstructure lines are substantially broadened, which can be attributed to a small domain size of the ordered phase formed under different conditions of thermal treatment. Since the width of reflections depends on the domain size and the resolution of the instrument used for measurements, the domain size can be determined by measuring the broadening. Let us assume that the deformation broadening is absent in the first approximation and the observed broadening β is associated only with a small domain size, *i.e.*, $\beta = \beta_s$. In this case, the broadening

$$\beta_s(2\theta) \equiv 2\beta_s(\theta),$$

measured in radians is related to the average domain size $\langle D \rangle$ by the Scherrer equation.

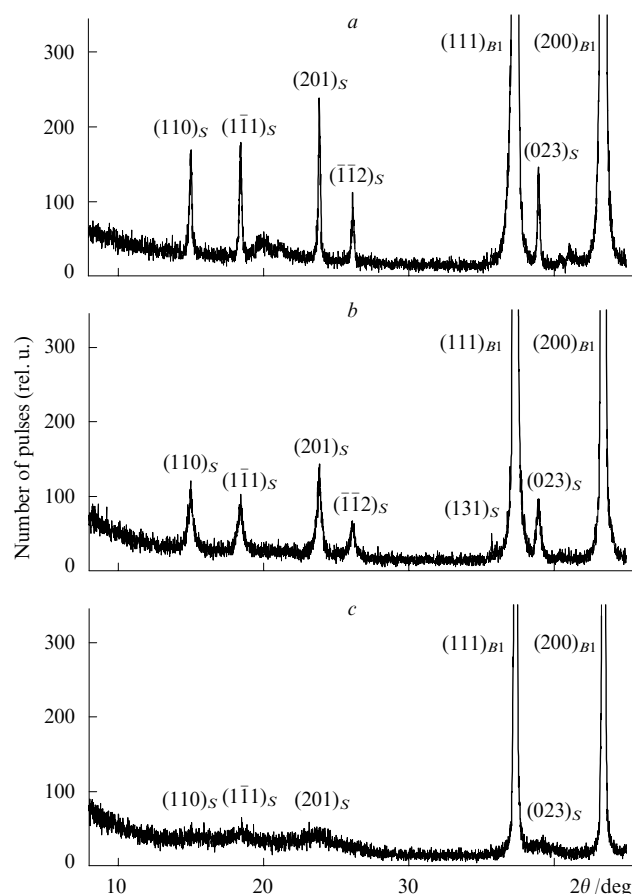


Figure 20. X-Ray diffraction patterns of compact samples of $\text{VC}_{0.875}$ prepared by hot pressing and subjected to additional thermal treatment ($\text{CuK}\alpha_{1,2}$ radiation, the structure reflections of the phase B1 and the superstructure reflections of the phase V_8C_7 are indicated).²²⁶

(a) Annealing at 1370 K for 2 h followed by slow cooling to 300 K; (b) quenching from 1420 to 300 K at a cooling rate of 100 K s^{-1} ; (c) quenching from 1500 to 300 K at a cooling rate of 100 K s^{-1} ; all X-ray diffraction patterns show superstructure reflections of the ordered cubic phase of V_8C_7 ; the most broadened superstructure reflections are seen in the X-ray diffraction pattern of a sample of $\text{VC}_{0.875}$ quenched from 1500 K.

The largest broadening of superstructure reflections is observed for a sample quenched from 1500 K; the least broadening, for a sample annealed at 1370 K. This suggests that the ordered phase in the former sample has the minimum domain size. Annealed vanadium carbide is characterised by the maximum domain size because annealing followed by slow cooling provide more favourable conditions for the domain growth. The determination of the broadening β_s and an estimation of the average domain size of the ordered phase gave the following results: the domain size in annealed samples (see Fig. 20 a) is 127 ± 10 nm with 95% confidence probability; in samples prepared by quenching from 1420 K (see Fig. 20 b) and 1500 K (see Fig. 20 c), the domain sizes are 60 ± 9 and 18 ± 12 nm, respectively, with the same confidence probability.

Thus, annealing and quenching of compact samples of non-stoichiometric carbide $\text{VC}_{0.875}$ from $T_{\text{trans}} \pm 100$ K are accompanied by the nanostructure formation, the nanostructure being composed of domains of the ordered phase. The higher the annealing (quenching) temperature or the higher the cooling rate, the smaller the domain size. The nanostructure

formation in compact non-stoichiometric $\text{VC}_{0.875}$ is associated with the $\text{VC}_{0.875} \rightarrow \text{V}_8\text{C}_7$ phase transition.

The disorder–order transitions accompanied by a change in the volume can be used for the formation of the nanostructured state not only in strongly non-stoichiometric compounds, but also in substitution solid solutions. It was suggested²³² that polymorphic phase transitions would be used for the nanostructure formation in compact compounds.

XIV. Properties and application of nanomaterials

The properties of nanomaterials are substantially different from those of other materials because the properties of nanoparticles differ from those of large particles. In addition, nanoparticles interact with each other in a fashion different from that of large particles because the distances at which interactions occur in electron, phonon and magnon subsystems are comparable with the sizes of nanoparticles. The properties of the latter differ from those of atoms or associations of atoms but are still different from the properties of compounds consisting of a large number of atoms (solid materials). In addition, nanoparticles have no thermodynamically equilibrium atomic-molecular structure due to which their properties can assume a number of values for the same particle size depending on the conditions of synthesis and the temperature prehistory.

Due to high energy of nanoparticles, their structures are not necessarily equilibrium. Accumulation of experimental data on this problem is presently underway. For example, it was demonstrated²¹ that the structure of cadmium sulfide nanoparticles differs from those of this compound in the wurtzite (equilibrium under normal conditions) and sphalerite phases. The atomic structure of nanoparticles is actually disordered to a large degree although the short-range order is almost completely retained. The atomic structure of cadmium sulfide nanoparticles can be represented as disordered superimposed close-packed planes consisting of cadmium and sulfur atoms. The three-dimensional model of CdS nanoparticles containing 3038 cadmium atoms with a disordered structure of the metal sublattice (*ACABCBC*) was described.²¹ The particle height (h) is 2.3 nm, the distance (d) between the lateral faces is 5.7 nm, and the aspect ratio of the particle sizes $d/h \sim 2.5$. Calculations by the Debye equation demonstrated a good agreement between X-ray diffraction spectra and experimental data. A lattice with the space group $P6/mmm$ can be considered as an average crystal lattice of the cadmium sulfide nanophase (Fig. 21).

The properties of isolated nanoparticles along with a disorder are also determined to a large extent by the contribution of the surface layer. For a spherical particle with a diameter D and surface layer thickness δ , the surface layer fraction (ΔV) in the total particle bulk (V) is

$$\frac{\Delta V}{V} = \left[\frac{\pi}{6} D^3 - \frac{\pi}{6} (D - 2\delta)^3 \right] \left(\frac{\pi}{6} D^3 \right)^{-1} \approx \frac{6\delta}{D}.$$

If the surface layer thickness is equal to 3–4 atomic monolayers (0.5–1.5 nm) and the average nanocrystallite size is 10–20 nm, up to 50% atoms of a substance are located in the surface layer.²²² Hence, the properties of nanoparticles are determined by their large specific surface area and the strong effect of the near-surface atoms. The coordination of these atoms and their interatomic distances differ from those of atoms located far from the surface. In many cases, the near-surface atoms have high energy, resulting in a decrease in the temperature of chemical reactions between nanoparticles, and the reaction intensity increases as a consequence of a large specific surface area of nanoparticles.

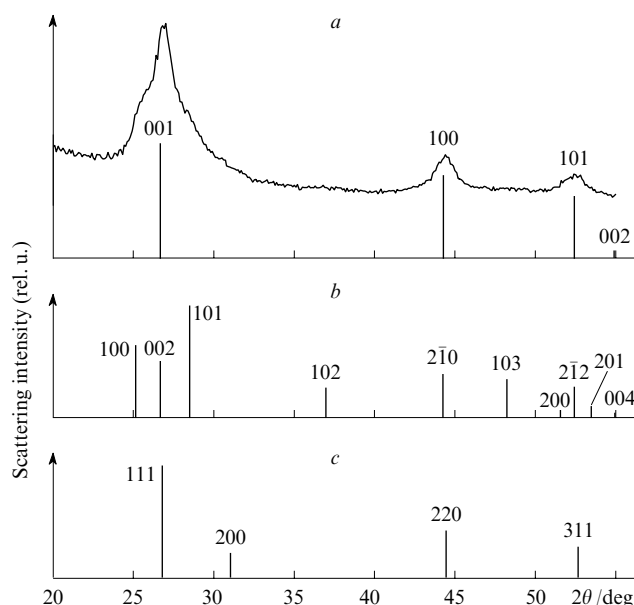


Figure 21. The experimental X-ray diffraction spectrum of a CdS powder (a) and linear spectra of different structures.²¹

(a) The linear spectrum of a disordered structure, the space group of the average lattice is $P6/mmm$; (b) the linear spectrum of the wurtzite structure B4, the space group $P6_3mc$; (c) the linear spectrum of the sphalerite structure B3, the space group $F\bar{4}3m$.

Interactions between nanoparticles differ from those between microparticles. The interfaces between nanoparticles make a large contribution to the properties of assemblies of nanoparticles. For example, the structure of high-angle interfaces between nanoparticles often determines the mechanical properties of nanomaterials. The electric and magnetic properties depend to a large degree on the ratio between the coherence lengths of electron, phonon and magnon interactions and the distances between the centres of nanoparticles. In many cases, the microstructures of nanomaterials are determined by interactions between nanoparticles. For example, the van der Waals forces are responsible for the mutual arrangement of nanoparticles. The interactions result in self-organisation of nanoparticles in nanomaterials.^{17, 18, 80, 87}

In studies of compact nanomaterials, solid materials are considered as assemblies of interacting grain-boundary defects. For example, the symmetry properties of polycrystals in relation to changes in the characteristic scale of structural heterogeneity, *i.e.*, the grain size, are analysed²³³ using the calibration field theory,^{234, 235} which was developed for the description of the structural and physical properties of materials with defects. An increase in the grain size to several nanometres was demonstrated²³³ to lead to the topological transition from isolated waves of orientation shear instability, which are characteristic of the usual polycrystalline state, to spatially periodic defect structures. This topological transition in an assembly of grain-boundary defects is accompanied by a sharp change in the connectivity characteristics and scaling parameters. The validity of this approach is associated with the fact that the concentration of defects in nanomaterials is so high that interactions occur between the defects. For a few nanomaterials in which the concentration of defects is low the application of the calibration field theory is unjustified.

The use of the size effects is convenient for analysing changes in different properties of solids. Actually, there is abundant evidence of the influence of the nanostate on the magnetic properties of ferromagnets, the Curie temperature, coercive forces, the saturation magnetisation and the magnetic

susceptibility of weak para- and diamagnets, the memory effects on the elastic properties of metals, substantial changes in the heat capacity and hardness, changes in the optical and luminescence characteristics of semiconductors and the plasticity of boride, carbide, nitride and oxide materials, which are rather brittle in the usual coarse-grained state.

It has long been known that the properties of small particles differ from those of massive substances. This fact is used in industry. Aerosols, colouring pigments and colouration of glass melts by colloidal metal particles for the preparation of colour glasses can be referred to as examples. Suspensions of metal nanoparticles (generally iron or its alloys) with the size of 30 nm and larger are used as engine oil additives for restoring worn-out details of internal combustion engines directly during operation. Small particles and nanometre-sized elements are used in the production of different aircraft materials, for example, of radio-absorbing ceramics the matrices of which contain randomly distributed metal nanoparticles.

Polymerised rhombohedral fullerene $\text{Rh}-\text{C}_{60}$ has the Curie temperature of 500 K and the hysteresis curve typical of ferromagnets.²³⁶ A light magnet operating at room temperature can be constructed from this nanomaterial. In fullerene crystals, C_{60} molecules are linked to each other by weak van der Waals forces, whereas the presence of nitrogen atoms in the fullerene-like nanomaterial $\text{C}_{48}\text{N}_{12}$ is responsible for the appearance of strong covalent bonds. Hence, the latter material can be employed when a combination of strength and elasticity is required.

Carbon nanotubes show high mechanical stability. Hence, they can be used for the construction of high-strength composites. It is expected that nanotubes will find application in the construction of various mechanical nanodevices.²³⁷ Carbon nanotubes are already used as nanoindenters in microhardness measurements and as probes in atomic-force microscopes.²³⁸ Carbon nanotubes exhibit semiconductivity or metal conductivity depending on the arrangement of carbon atoms in their walls. Due to this fact, these nanotubes are used as conducting elements in nanoelectronics.

Various structures having different properties can be prepared by connecting carbon nanotubes. The synthesis of such structures is of importance for application in electronic technique. Carbon nanotube T-junctions²³⁹ can operate as contact devices. Due to a defect structure, Y-nanotubes²⁴⁰ allow current to pass in one direction at the junction of teeth and operate as diodes.²⁴¹ The stem of Y-nanotubes has a diameter of ~ 60 nm. The diameter of branches is ~ 40 nm. If a controlling voltage is applied to one tooth of an Y-nanotube, the latter will operate as a current stabiliser. The possibility of controlling the current holds promise for the use of Y-nanotubes in nanoelectronics.

Bundles of multilayer carbon nanotubes with a diameter of 20–30 nm that were grown on a substrate coated with a SiO_2 layer, can find application in next generation integrated microcircuits and in microelectromechanical devices.²⁴² Nanotubes can be used as atomic-molecular pumps for depositing individual molecules, atoms or ions onto the surface.²⁴³ The results of investigations and applications of various carbon and non-carbon nanotubes were summarised in reviews.^{244–246}

Catalysis of chemical reactions is an important field of application of metal, alloy and semiconductor nanoparticles.

High catalytic activity of small particles is attributed to the electronic effect. Actually, the number of atoms in an isolated metal particle is small and, consequently, the distance between the energy levels $\delta \approx E_F/N$ (E_F is the Fermi energy and N is the number of atoms in the particle) is comparable with the energy kT . In the limit, when $\delta > kT$, the energy levels are discrete and the particle loses metallic properties. Nanoparticles begin to exhibit catalytic activity at $\delta \approx kT$. For metals, the Fermi

energy is 10 eV. At ~ 300 K, δ is 0.025 eV and, hence, $N \approx 400$. The particle consisting of 400 atoms has a diameter of ~ 2 nm.

As a rule, nanoparticles exhibit catalytic activity in a very narrow size range. For example, rhodium catalysts, which are synthesised by decomposition of the $\text{Rh}_6(\text{CO})_{16}$ clusters deposited on the surface of dispersed silica, catalyse benzene hydrogenation only if the particle size is 1.5–1.8 nm, *i.e.*, only Rh_{12} particles are actually catalytically active in this reaction. High selectivity of the catalytic action is typical also of nanoparticles of such popular catalysts as palladium and platinum. For example, a study of ethylene hydrogenation at 520 K under a hydrogen pressure of 1 atm catalysed by platinum deposited on SiO_2 or Al_2O_3 revealed a pronounced maximum of the reaction rate corresponding to the platinum nanoparticle size of ~ 0.6 nm. Such a high sensitivity of the catalytic action to the size of small particles demonstrates the importance of the development of selective procedures for the preparation of nanoparticles with an accuracy to one atom. Materials characterised by a very narrow size distribution of nanoparticles are required not only for catalysis, but also for nanoelectronics.

A detailed analysis of the size effect of small metal and alloy particles deposited on a support was performed;²⁴⁷ the reviews^{248–250} deal with catalysis involving metal alloys and palladium.

A new field of catalysis on nanoparticles, *viz.*, photocatalysis with the use of semiconductor particles and nanostructured films, holds promise for purification of water from organic contaminants by photocatalytic oxidation and mineralisation. For example, colloidal solutions of semiconducting oxide and sulfide nanoparticles (without deposition on a substrate) and the nanocrystalline heterostructures ZnS/CdSe , HgS/CdS , ZnS/ZnO and $\text{TiO}_2/\text{SnO}_2$ are used in the photocatalytic synthesis and destruction of organic compounds as well as in decomposition of water.^{98–101}

Polymeric composites containing metal nanoparticles are used as conducting film composite materials, the possible amount of the filling agent in the matrix being as high as 90 vol.%. Hybrid metal–polymer composites can be synthesised by the nanoparticle formation in a polymeric matrix.^{251,252} Coloured light guides for computer techniques are produced by introducing metal ions into polymeric fibres. The optical properties of polymers filled with metal, alloy or semiconductor (CdS , CdSe , InP or InAs) nanoparticles are of interest. Such polymers are easily subjected to mechanical treatment and can be used for the preparation of films. Hence, such polymers hold promise as optical elements and light filters.

Multilayer nanostructures are widely applied in the microelectronic device manufacturing. Layered inhomogeneous nanostructures, *viz.*, superlattices consisting of alternating solid superthin layers (with a thickness from several to one hundred crystal lattice parameters or $\sim 1–50$ nm) of two different compounds, can be referred to as an example. This crystal structure contains, along with a usual lattice of periodically arranged atoms, a superlattice consisting of repeated layers with different compositions. Since the nanolayer thickness is comparable with the de Broglie wavelength of the electron, the quantum size effect is manifested in the electronic properties of superlattices. The use of this effect in multilayer nanostructures allows the design of fast-operating electronic devices with a high information capacity. The double-barrier diode $\text{AlAs}/\text{GaAs}/\text{AlAs}$ consisting of a gallium arsenide layer with a thickness of 4–6 nm, which is located between two aluminium arsenide layers with a thickness of 1.5–2.5 nm, is an example of the simplest electronic devices.

Magnetic nanostructures showing giant magnetoresistance are of interest. These nanostructures are multilayer films

composed of alternating layers of ferromagnetic and non-magnetic metals. For example, ferromagnetic Co–Ni–Cu layers and non-magnetic Cu layers alternate in the Co–Ni–Cu/Cu nanostructure. The layer thickness is approximately equal to the electron free path, *i.e.*, to several tens of nanometres. The magnetic configuration of multilayer nanostructures can be changed by varying the external magnetic field intensity from 0 to a particular value H so that the conductivity varies in a very broad range. These films can be used as magnetic field detectors. In the nanostructure under consideration, the largest giant magnetoresistance was achieved for very thin (~ 0.7 nm) copper layers.

In modern microcircuits produced on a large scale, ~ 1000 electrons are required for transistor switching on/off. Due to miniaturisation of microcircuits, the number of required electrons would be decreased to ten in the nearest future.²⁵³ Besides, studies aimed at constructing single-electron transistors are presently underway.²⁵⁴

A device consisting of two condenser plates and a metalised ball hanged between these plates was developed. Under the action of direct-current voltage applied to the plates, the ball swings and transfers the charge. In the nanoversion, such nanopendula (or electronic shuttles) can operate at a frequency of ~ 100 MHz and transfer individual electrons.^{16,255} Such devices would be expected to serve as elements of quantum computers or current interrupters.

Semiconducting heterostructures consisting of two or more different materials are of particular interest. In these heterostructures, a transition layer, *viz.*, the interface between two materials, plays an important role. Moreover, the interface in semiconducting heterostructures can be used as a technical device.²⁵⁶

Molecular-beam and liquid-phase epitaxies allow the growth of heterostructures with a sharp interface. Two interfaces can be located so close to each other that the quantum size effects become to play the key role. Such structures are called quantum wells. In quantum wells, the thickness of the medium layer is several tens of nanometres, resulting in electron level splitting due to the size quantisation effect. This effect, which is manifested as a characteristic stepwise structure of optical absorption spectra of the semiconducting heterostructure GaAs–AlGaAs with a hyperfine GaAs layer (a quantum well), was observed for the first time in 1974.²⁵⁷ In this study, it was also found that characteristic energies are shifted as the thickness of the quantum well (a GaAs layer) decreases. In quantum wells, superlattices and other structures with very thin layers, large deformations are not necessarily accompanied by the appearance of dislocations and, hence, correspondence of the lattice parameters is not required.²⁵⁸ The fundamental characteristics of semiconducting crystals, such as the gap width, the effective masses and the charge carrier mobility, can be controlled with the use of heterostructures, particularly double structures, including quantum wells, quantum wires and quantum dots.

In three-dimensional semiconductors, the density of states $N(E)$ is a continuous function. A decrease in the dimensionality of a semiconductor results in a change in the energy spectrum from continuous to discrete due to its splitting (Fig. 22). The quantum well is a two-dimensional structure in which the charge carrier motion is restricted in the direction perpendicular to the layers, but the charge carriers can freely move in the plane of the layers. In quantum wires, the charge carrier motion is limited in two directions and the charge carriers freely move only along the wire axis. Quantum dots are quasi-zero-dimensional ('0D') structures. In such structures, the charge carrier motion is limited in all three directions and these structures are characterised by completely discrete energy spectra.

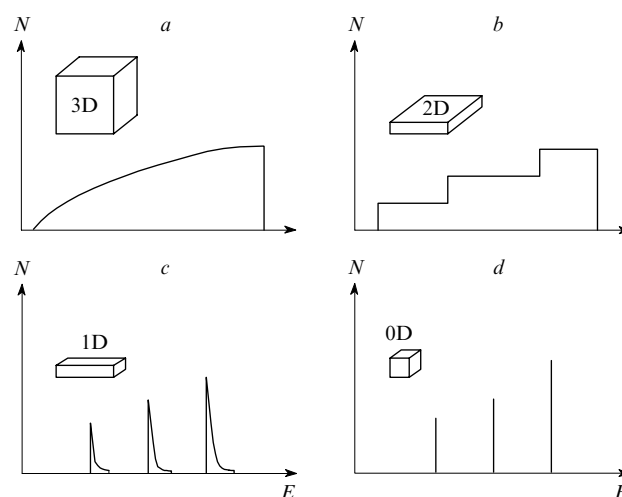


Figure 22. The density of states of N charge carriers as a function of the dimensionality of the semiconductor.¹²

(a) A three-dimensional semiconductor, $dN/dE \sim E^{-1/2}$; (b) a quantum well, $dN/dE \sim \text{const}$; (c) a quantum wire, $dN/dE \sim E^{1/2}$; (d) a quantum dot, $dN/dE \sim \delta(E)$.

The sizes of quantum dots obtained by molecular-beam epitaxy and lithography vary from 100 to 10 nm; smaller quantum dots (1–10 nm) the surface of which is protected by organic molecules preventing particle aggregation can be prepared by methods of colloid chemistry.²⁵⁹

Only nanotechnologies allow a decrease in the size of elements of electronic devices to several nanometres with the use of quantum dots. Time instability of nanostructures at high temperatures is a practical problem to be solved in the construction of quantum dots. Stability of quantum dots is determined by quantum jumps or diffusion of small amounts of atoms, which occur very rapidly on the surface and at interfaces of quantum electronic elements. As a result, destruction of elements or even their migration on a substrate is observed at room temperature.²⁶⁰ The problem of stability of nanoelectronic circuits can be solved with the use of multi-component materials including metal oxides, carbides and nitrides. These compounds have high melting points and low diffusion mobility of atoms and, consequently, show high thermal and time stability.

Special lenses and mirrors with multilayer coatings of alternating thin layers of elements with higher and lower densities (for example, of tungsten and carbon, molybdenum and carbon or nickel and carbon) are used in X-ray and UV optics. Two layers have thicknesses of ~ 1 nm; the layers should be smooth at the atomic level. Multilayer X-ray lenses and mirrors are required in X-ray lithography, which is one of the fields of nanotechnology, and in astrophysical studies. The formation of X-ray mirrors was described in sufficient detail;²⁶¹ this study dealt with multilayer Ni/C nanostructures with a period of ~ 4 nm. The Fresnel zone plates with a minimum zone width of ~ 100 nm and diffraction lattices with a period of < 100 nm are yet other optical devices with nanometre-sized elements intended for use in X-ray diffraction microscopy.

Heterostructures F/S are formed by alternating nanolayers of a ferromagnet (F) and a superconductor (S). Ferromagnetic interlayers of F are generally constructed of Fe, Co, Gd or Ni the Curie temperatures of which are higher than the superconducting transition temperature of metals (Nb, Pb or V) that form an S layer. Experimental studies of such heterostructures were initiated by Hauser *et al.*²⁶² The construction of F/S-type

superlattices can be performed with the use of molecular-beam epitaxy, electron-beam coating or magnetron spraying at direct current.²⁶³ It should be noted that F/S-type heterostructures with layers of atomic thickness can be applied in next generation electronics as logical elements and superconducting current switches.^{264,265} In this case, the superconductivity can be controlled with a weak external magnetic field.²⁶⁶ The properties of multilayer F/S systems including the superconducting transition temperature depend on the thicknesses of the ferromagnetic and superconducting layers. The thickness of a ferromagnetic layer is generally < 1 nm, and the thickness of a superconducting layer varies from 10 to 40–50 nm.²⁶⁶ In F/S heterostructures, the superconducting transition temperature (T_c) not only monotonically decreases but also oscillates as the thickness of the F layer increases. For example, an increase in the thickness of the iron layer in the three-layer system Fe/Nb/Fe from 0.1 to 0.8 nm initially leads to a lowering of T_c from 7 to 4.5 K. Then the temperature rises to 5 K as the layer thickness increases to 1.0–1.2 nm followed by a decrease in the temperature to 3.2–3.4 K as the thickness further increases to 3 nm. In F/S heterostructures, metal and alloy ($\text{Nb}_x\text{Ti}_{1-x}/\text{Co}$ or $\text{V}/\text{Fe}_x\text{V}_{1-x}$) layers can alternate with each other. Superconductor/ferromagnetic semiconductor (for example, NbN/EuO/Pb or NbN/EuS/Pb) heterostructures with the Josephson tunnel transition²⁶⁷ are also of interest. The layer thickness of the ferromagnetic superconductor (EuO, EuS) in these heterostructures is 10–50 nm and the thickness of superconducting layers is > 200 nm.

Ceramic nanomaterials are widely used for the production of components operating at high temperatures, under non-uniform thermal stresses and in corrosive media. Due to superplasticity, these nanomaterials can be used for the preparation of complex-configuration products with highly precise dimensions, in particular, for aerospace technique. Due to biocompatibility and high stability, hydroxylapatite-based nanoceramics are applied in orthopedy for the production of artificial joints and in dental surgery for the production of dental prostheses. Nanocrystalline ferromagnetic alloys Fe–Cu–M–Si–B (M is a Group IV–VI transition metal) have found use as soft magnetic materials for transformers with a very low coercive force and high magnetic permeability.

A method for the manufacture of a detonation diamond nanopowder is implemented in Russian industry. As a result of high pressure and temperature developed during explosion in special chambers, nanodiamond is synthesised from carbon-containing explosives catalysed by particles and metal vapour from ammunition shells.

Ultrasonic pressing of nanopowders is particularly efficient in the construction of complex-shaped articles such as sockets, conical gears, helices, etc.²⁶⁸ The resulting ceramic articles have homogeneous microstructure and density.

The hydrothermal synthesis belonging to 'mild chemistry' methods holds promise for the preparation of nanoceramics. The synthesis proceeds at high temperature and pressure. Oxide nanoceramic materials, for example, TiO_2 , ZrO_2 and HfO_2 ,²⁶⁹ including nanorods can be obtained by this method.²⁷⁰ Nanocrystalline titanium, zirconium and hafnium dioxide powders and composites on their basis have found use as catalysts, gas sensors, dielectric ceramics, dyes, solid electrolytes, diffusion barriers and optical coatings. The development of the hydrothermal synthesis would be expected to expand the field of application of oxide nanoceramics.

To summarise, the analysis of the scope of modern nanotechnologies and prospects of application of different classes of nanostructured materials shows the topicality of the development of nanoindustry.

XV. Conclusion

Studies performed in the last decades provided a deeper insight into the mechanisms of size effects. Emphasis has long been placed on nanoparticles the properties of which are intermediate between those of isolated atoms and polycrystalline solids. The development of methods for the production of compact nanomaterials composed of nanometre-sized building blocks enabled researchers to investigate the properties of solids in the nanostructured state. Nowadays, the following methods are mainly used for the preparation of compact nanomaterials: compaction of isolated nanoclusters, which are obtained by evaporation and condensation, precipitation from solutions or decomposition of precursors, crystallisation of amorphous alloys, severe plastic deformation and ordering of strongly non-stoichiometric compounds and solid solutions. Each method has advantages and drawbacks, and neither is universal.

For a theoretical interpretation of experimental results obtained in studies of isolated nanoparticles and compact nanomaterials, the separation of the surface (associated with interfaces) and bulk (associated with particles sizes) effects is of considerable importance. Nowadays, this problem is far from being solved.

Nanomaterials are characterised by exceptionally high diffusion mobility of atoms along the grain boundaries. This mobility is 5–6 orders of magnitude higher than that in usual polycrystals. However, the mechanisms of diffusion processes in nanomaterials are far from being completely understood, and different explanations of these processes were provided in the literature. The microstructure of nanocrystals, *i.e.*, the structure of interfaces and the atomic density, and the influence of nanopores and the free volume on the properties of nanocrystals are still debated.

The above-considered data suggest that new nanomaterials stable at high temperature will be constructed based on multi-component systems with the use of refractory metals and compounds. Metal oxides, nitrides and carbides with high melting points and thermal stability will be of particular importance in future nanotechnologies. These compounds will find application as components of nanocrystalline materials. The construction of stable-operating systems, which retain their properties throughout the service life, becomes possible with the use of the above-mentioned compounds.

Studies in the field of nanotechnologies and investigations of the nanostate of substances should provide the basis for a new interdisciplinary area of knowledge based on fundamental laws of physics, chemistry and biology.²⁷¹

I thank A I Gusev, N S Kozhevnikova, A A Valeeva, A S Kurllov, A S Vorokh, S Z Nazarova, O V Makarova, V A Moldaver, R R Mulyukov, S I Sadovnikov (Russia), H-E Schaefer, A Magerl, F Hergert (Germany), R Würschum, W Sprengel (Austria), S Van den Berghe, A Leenaers, W van Renterghem (Belgium) and K Reimann (the Netherlands) for collaboration in the synthesis and investigation of nanomaterials.

References

1. H Gleiter *Nanostruct. Mater.* **1** 1 (1992)
2. H-E Schaefer *Mechanical Properties and Deformation Behaviour of Materials Having Ultrafine Microstructure* (Eds M A Nastasi, D M Parkin, H Gleiter) (Dordrecht: Kluwer Academic, 1993) p. 81
3. R W Siegel *J. Phys. Chem. Solids* **55** 1097 (1994)

4. I D Morokhov, L I Trusov, S P Chizhik *Ul'tradispersnye Metallicheskie Sredy* (Ultradispersed Metallic Media) (Moscow: Atomizdat, 1977)
5. A I Gusev *Usp. Fiz. Nauk* **168** 55 (1998) [*Physics-Uspekhi* **41** 49 (1998)]
6. Yu I Petrov *Fizika Malykh Chastits* (The Physics of Small Particles) (Moscow: Nauka, 1982)
7. L N Larikov *Metallofizika* **14** (1) 3 (1992)
8. R A Andrievskii *Usp. Khim.* **63** 431 (1994) [*Russ. Chem. Rev.* **63** 411 (1994)]
9. A I Gusev *Nanokristallicheskie Materialy: Metody Polucheniya i Svoistva* (Nanocrystalline Materials: Methods of Production and Properties) (Ekaterinburg: Urals Branch of Russian Academy of Sciences, 1998)
10. *Nanomaterials: Synthesis, Properties and Applications* (Eds A S Edelstein, R C Cammarata) (Baltimore: Johns Hopkins University, 1998)
11. A I Gusev, A A Rempel *Nanokristallicheskie Materialy* (Nanocrystalline Materials) (Moscow: Fizmatlit, 2000)
12. A I Gusev, A A Rempel *Nanocrystalline Materials* (Cambridge: Cambridge International Science Publ., 2004)
13. K E Drexler *Nanosystems: Molecular Machinery, Manufacturing and Computation* (New York: Wiley, 1992)
14. A ten Wolde *Nanotechnology: Towards a Molecular Construction Kit* (Boston: New World Ventures, 1998)
15. *Nanostructured Materials* (Ed. J Yi-Ru Ying) (New York: Academic Press, 2001)
16. A L Buchachenko *Usp. Khim.* **72** 419 (2003) [*Russ. Chem. Rev.* **72** 375 (2003)]
17. Yu D Tretyakov *Usp. Khim.* **72** 731 (2003) [*Russ. Chem. Rev.* **72** 651 (2003)]
18. V I Roldugin *Usp. Khim.* **73** 123 (2004) [*Russ. Chem. Rev.* **73** 115 (2004)]
19. R Z Valiev, I V Aleksandrov *Nanostrukturnye Materialy, Poluchennye Intensivnoi Plasticheskoi Deformatsiei* (Nanostructured Materials, Production by Intensive Plastic Deformation) (Moscow: Logos, 2000)
20. A I Gusev *Nanomaterialy, Nanostrukturnye, Nanotekhnologii* (Nanomaterials, Nanostructures and Nanotechnologies) (Moscow: Fizmatlit, 2005)
21. A S Vorokh, A A Rempel *Fiz. Tv. Tela* **49** 143 (2007)^a
22. V Kohlschütter, C Ehlers *Z. Elektrochem.* **18** 373 (1912)
23. L Harris, D Jeffries, B M Siegel *J. Appl. Phys.* **19** 791 (1948)
24. M Ya Gen, M S Ziskin, Yu I Petrov *Dokl. Akad. Nauk SSSR* **127** 366 (1959)^b
25. V Tikhomirov, A Lidov *Zh. Russ. Fiz.-khim. O-va* **15** 421 (1883)
26. M Ya Gen, Yu I Petrov *Usp. Khim.* **38** 2249 (1969) [*Russ. Chem. Rev.* **38** 1007 (1969)]
27. B M Smirnov *Usp. Fiz. Nauk* **162** 119 (1992) [*Physics Uspekhi* **35** 37 (1992)]
28. Yu I Petrov, E A Shafranovskii *Izv. Akad. Nauk, Ser. Fiz.* **64** 1548 (2000)^c
29. V I Vladimirov, A E Romanov *Disklinatsii v Kristallakh* (Disclinations in Crystals) (Leningrad: Nauka, 1986)
30. B M Bulakh *Rost Kristallov* (Crystal Growth) (Moscow: Nauka, 1974) Vol. 10, p. 98
31. B M Bulakh, N N Sheftal' *Rost Kristallov* (Crystals Growth) (Moscow: Nauka, 1974) Vol. 10, p. 115
32. J Muhlbusch, E Recknagel, K Sattler *Surf. Sci.* **106** 188 (1981)
33. B V Deryagin, D V Fedoseev *Rost Almaza i Grafita iz Gazovoi Fazy* (Diamond and Graphite Growth from the Gas Phase) (Moscow: Nauka, 1977)
34. A R Badzian, R C de Vries *Mater. Res. Bull.* **23** 385 (1988)
35. D V Fedoseev, Yu N Tolmachev, I G Varshavskaya *Dokl. Akad. Nauk* **349** 212 (1996)^d
36. B Gunther, A Kampmann *Nanostruct. Mater.* **1** 27 (1992)
37. H Hahn, R S Averback *J. Appl. Phys.* **67** 1113 (1990)
38. G Skandan, H Hahn, J C Parker *Scr. Metall. Mater.* **25** 2389 (1991)
39. S Iwama, K Hayakawa, T Arizumi *J. Cryst. Growth* **56** 265 (1982)
40. M S El-Shall, W Slack, W Vann, D Kane, D Hanley *J. Phys. Chem.* **98** 3067 (1994)
41. Yu I Petrov, E A Shafranovskii, Yu F Krupianskii, S V Essine *J. Appl. Phys.* **91** 352 (2002)
42. Yu A Bykovskii, V P Kozlenkov, Yu B Krasil'nikov, I N Nikolaev *Poverkhnost* (12) 69 (1992)
43. B H Kear, P R Strutt *Nanostruct. Mater.* **6** 227 (1995)
44. V N Troitskii, S V Gurov, V I Berestenko *Khim. Vys. Energ.* **13** 267 (1979)^e
45. T N Miller *Izv. Akad. Nauk SSSR, Neorg. Mater.* **15** 557 (1979)^f
46. T Ya Kosolapova, G N Makarenko, D P Zyatkevich *Zh. Vses. Khim. O-va im D I Mendeleeva* **24** 228 (1979)^g
47. V F Petrunin, Yu G Andreev, T N Miller, Ya P Grabis *Poroshk. Metallurg.* (9) 90 (1987)^h
48. I V Blinkov, A V Ivanov, I E Orekhov *Fiz. Khim. Obrab. Mater.* (2) 73 (1992)
49. K Kijima, H Nogushi, M Konishi *J. Mater. Sci.* **24** 2929 (1989)
50. F Thevenot *The Physics and Chemistry of Carbides, Nitrides and Borides* (Ed. R Freer) (Dordrecht: Kluwer Academic, 1990) p. 87
51. A I Gusev *Fizicheskaya Khimiya Nestekhiometricheskikh Tugoplavkikh Soedinenii* (Physical Chemistry of Non-stoichiometric Refractory Compounds) (Moscow: Nauka, 1991)
52. A V Lebedev, V A Moldaver, A S Kurlov, A A Rempel *Khimiya Tverdogo Tela i Funktsional'nye Materialy (Tezisy Dokladov Vserossiiskoi Konferentsii)* [Solid State Chemistry and Functional Materials (Abstracts of Reports of All-Russian Conference)] (Ekaterinburg: Urals Branch of the Russian Academy of Sciences, 2004) p. 237
53. A S Kurlov, S Z Nazarova, A A Rempel *Nanotekhnologiya i Fizika Funktsional'nykh Nanokristallicheskh Materialov* (Nanotechnology and Physics of Functional Nanocrystalline Materials) (Eds V V Ustinov, N I Noskova) (Ekaterinburg: Urals Branch of the Russian Academy of Sciences, 2005) Vol. 1, p. 59
54. J S Haggerty, W R Cannon *Laser-Induced Chemical Processes* (Ed. J I Steinfeld) (New York: Plenum, 1981)
55. N V Karlov, M A Kirichenko, B S Luk'yanchuk *Usp. Khim.* **62** 223 (1993) [*Russ. Chem. Rev.* **62** 203 (1993)]
56. E A Rohlfing, D M Cox, A Kaldor *J. Chem. Phys.* **81** 3322 (1984)
57. H W Kroto, J R Heath, S C O'Brien, R F Curl, R E Smalley *Nature (London)* **318** 162 (1985)
58. R F Curl, R E Smalley *Science* **241** 1017 (1988)
59. E Osawa *Kagaku (Kyoto)* **25** 854 (1970)
60. D A Bochvar, E G Gal'pern *Dokl. Akad. Nauk SSSR* **209** 610 (1973)^d
61. L Hultman, S Stafstrom, Z Czigany, J Neidhardt, N Hellgren, I F Brunell, K Suenaga, C Colliex *Phys. Rev. Lett.* **87** 225503-1 (2001)
62. T Guo, M D Diener, Y Chai, M J Alford, R E Haufler, S M Mclure, T Ohno, J H Weaver, G E Scuseria, R E Smalley *Science* **257** 1661 (1992)
63. T Guo, R E Smalley, G E Scuseria *J. Chem. Phys.* **99** 352 (1993)
64. Z Lin, M B Hall *J. Am. Chem. Soc.* **115** 11165 (1993)
65. B C Guo, S Wei, J Purnell, S Buzza, A W Castleman *Science* **256** 515 (1992)
66. S Wei, B C Guo, J Purnell, S Buzza, A W Castleman *J. Phys. Chem.* **96** 4166 (1992)
67. J S Pilgrim, M A Duncan *J. Am. Chem. Soc.* **115** 4395 (1993)
68. B C Guo, A W Castleman *Advances in Metal and Semiconductor Clusters* (Ed. M Duncan) (Greenwich: JAI Press, 1994) Vol. 2, p. 137
69. A W Castleman *Annu. Rev. Phys. Chem.* **45** 685 (1994)
70. S Wei, B C Guo, H T Deng, K Kerns, J Purnell, S Buzza, A W Castleman *J. Am. Chem. Soc.* **116** 4475 (1994)
71. H van Swygenhoven, P Boni, F Paschoud, M Victoria, M Knauss *Nanostruct. Mater.* **6** 739 (1995)
72. R A Andrievskii *Usp. Khim.* **66** 57 (1997) [*Russ. Chem. Rev.* **66** 53 (1997)]
73. N Herron, Y Wang, M M Eddy, G D Stucky, D E Cox, K Moller, T Bein *J. Am. Chem. Soc.* **111** 530 (1989)
74. M Faraday *Philos. Trans. R. Soc. London* **147** 145 (1857)

75. N S Kozhevnikova, A A Rempel *Fizicheskaya Khimiya Vodnykh Rastvorov: Teoreticheskie Osnovy i Sintez Perspektivnykh Opticheskikh Materialov* (Physical Chemistry of Aqueous Solutions: Theoretical Foundations and Synthesis of Promising Optical Materials) (Ekaterinburg: Ural State Technical University-Ural Polytechnical University, 2006)
76. N S Belova, A A Rempel *Neorg. Mater.* **40** 7 (2004)^f
77. N S Belova, A S Kurlov, A A Uritskaya, A A Rempel *Zh. Strukt. Khim. (Prilozhenie)* **45** 156 (2004)ⁱ
78. A A Rempel, N S Kozhevnikova, A J G Leenaers, S Van den Berghe *J. Cryst. Growth* **280** 300 (2006)
79. L Pasquini, A A Rempel, R Wurschum, K Reimann, M A Muller, B Fultz, H-E Schaefer *Phys. Rev. B* **63** 134114 (2001)
80. A A Rempel, N S Kozhevnikova, S Van den Berghe, W Van Renterghem *Phys. Status Solidi B* **242** (7) R61 (2005)
81. A A Rempel, N S Belova, A S Kurlov, A A Valeeva *The 7th International Conference on Nanostructured Materials 'NANO 2004', Wiesbaden, 2004* p. 307
82. N S Kozhevnikova, A A Rempel, F Hergert, S Jost, A Magerl *The 8th International Conference on Nanostructured Materials 'NANO 2006', Bangalore, 2006* p. 108
83. N S Kozhevnikova, A S Vorokh, A A Rempel *Biosovmestimye Nanostrukturnye Materialy i Pokrytiya Meditsinskogo Naznacheniya (Sbornik Nauchnykh Trudov Rossiiskoi Shkoly-konferentsii Molodykh Uchenykh i Prepodavatelei)* [Biocompatible Nanostructured Materials and Coatings for Medical Purposes (Proceedings of Russian School-conference of Young Scientists and Teachers)] (Belgorod: Institute of Solution Chemistry, Russian Academy of Sciences, 2006) p. 95
84. C B Murray, C R Kagan, M G Bawendi *Science* **270** 1335 (1995)
85. Q Lu, F Gao, D Zhao *Nanotechnology* **13** 741 (2002)
86. D V Talapin, E V Shevchenko, A Kornowski, N Gaponik, M Haase, A L Rogach, H Weller *Adv. Mater.* **13** 1868 (2001)
87. J H Warner, S Djouahra, R D Tilley *Nanotechnology* **17** 3035 (2006)
88. S Wong, V Kitaev, G A Ozin *J. Am. Chem. Soc.* **125** 15589 (2003)
89. A Chemseddine, T Moritz *Eur. J. Inorg. Chem.* 235 (1999)
90. I F Efremov *Periodicheskie Kolloidnye Struktury* (Periodical Colloid Structures) (Leningrad: Khimiya, 1971)
91. G Nikolis, I Prigogine *Self-organization in Nonequilibrium Systems* (New York: Wiley, 1977)
92. A Bleier, R Cannon *Better Ceramics Through Chemistry (MRS Symp. Proc.)* (Eds C J Brinker, D E Clark, D R Ulrich) (Pittsburg: Materials Research Society, 1986) p. 71
93. G Franz, G Schwier *Raw Materials for New Technologies* (Ed. M Kursten) (Stuttgart: Nagele and Obermuller, 1990) p. 139
94. V M Chernov, V I Litvin, I F Mironyuk, V V Tsyryna *Neorg. Mater.* **29** 1019 (1993)^f
95. Y Wang, N Herron *J. Phys. Chem.* **91** 257 (1987)
96. Y Wang, N Herron *J. Phys. Chem.* **92** 4988 (1988)
97. V N Bogomolov *Usp. Fiz. Nauk* **124** 171 (1978) [*Physics-Uspekhi* **21** 77 (1978)]
98. A R Kortan, R Hull, R L Opila, M G Bawendi, M L Steigerwald, P J Carrol, L E Brus *J. Am. Chem. Soc.* **112** 1327 (1990)
99. A Haesselbarth, A Eychmuller, R Eichberger, M Giersig, A Mews, H Weller *J. Phys. Chem.* **97** 5333 (1993)
100. P V Kamat, B Patrick *J. Phys. Chem.* **96** 6829 (1992)
101. I Bedja, P V Kamat *J. Phys. Chem.* **99** 9182 (1995)
102. G Schmid *Nanostruct. Mater.* **6** 15 (1995)
103. G Schmid, M Harms, J-O Malm, J-O Bovin, J van Ruitenbeck, H W Zandbergen, W T Fu *J. Am. Chem. Soc.* **115** 2046 (1993)
104. F Hatakeyama, Sh Kanzaki *J. Am. Ceram. Soc.* **73** 2107 (1990)
105. L E McCandlish, B H Kear, B K Kim *Nanostruct. Mater.* **1** 119 (1992)
106. L Wu, J Lin, B K Kim, B H Kear, L E McCandlish *Proceedings of the 13th International Plansee Seminar Vol. 3* (Eds H Bildstein, R Eck) (Reutte: Metallwerk Plansee, 1993) p. 667
107. US P. 5352269; *Chem. Abstr.* **121** 306171a (1994)
108. Z Fang, J W Eason *Proceedings of the 13th International Plansee Seminar Vol. 3* (Eds H Bildstein, R Eck) (Reutte: Metallwerk Plansee, 1993) p. 625
109. P Seegopaul, L E McCandlish *Adv. Powder Metall. Part. Mater.* **3** 13-3 (1995)
110. P Seegopaul, L E McCandlish, F M Shinneman *Int. J. Refract. Met. Hard Mater.* **15** 133 (1997)
111. S Hotchandani, P V Kamat *J. Phys. Chem.* **96** 6834 (1992)
112. I Bedja, S Hotchandani, P V Kamat *J. Phys. Chem.* **97** 11064 (1993)
113. B O'Regan, M Gratzel, D Fitzmaurice *Chem. Phys. Lett.* **183** 89 (1991)
114. H Yoshiki, K Hashimoto, A Fujishima *J. Electrochem. Soc.* **142** 428 (1995)
115. L Kavan, T Stoto, M Gratzel, D Fitzmaurice, V Shklover *J. Phys. Chem.* **93** 9493 (1993)
116. K Yamada, T Y Chow, T Horihata, M Nagata *J. Non-Cryst. Solids* **100** 316 (1988)
117. H Natter, M Schmelzer, R Hempelmann *J. Mater. Res.* **13** 1186 (1998)
118. I D Morokhov, L I Trusov, V N Lapovok *Fizicheskie Yavleniya v Ul'tradispersnykh Sredakh* (Physical Effects in Ultradispersed Media) (Moscow: Energoatomizdat, 1984)
119. Yu I Petrov *Klasteri i Malye Chastitsy* (Clusters and Small Particles) (Moscow: Nauka, 1986)
120. V N Krasil'nikov, O I Gyrdasova, G V Bazuev *Izv. Akad. Nauk, Ser. Fiz.* **70** 988 (2006)^c
121. V N Krasil'nikov, A P Shtin, O I Gyrdasova, G P Shveikin *VI Nauchnaya Konferentsiya 'Khimiya Tverdogo Tela i Sovremennye Mikro- i Nanotekhnologii' (Teziy Dokladov)* [The VIth Scientific Conference 'Solid State Chemistry and Modern Micro- and Nanotechnologies' (Abstracts of Reports)] (Kislovodsk, Stavropol': North Caucasus State Technological University, 2006) p. 70
122. N T Kuznetsov *Materials Science of Carbides, Nitrides and Borides* (Eds Y G Gogotsi, R A Andrievski) (Dordrecht: Kluwer Academic, 1999) p. 223
123. K E Gonsalves, K T Kembaiyan *Solid State Ionics* **32-33** 661 (1989)
124. M Peuckert, T Vaahs, M Bruck *Adv. Mater.* **2** 398 (1990)
125. M G Mirabelli, A T Lynch, L G Sheddin *Solid State Ionics* **32-33** 655 (1989)
126. T Wade, J Park, E G Garza, C B Ross, D M Smith, R M Crooks *J. Am. Chem. Soc.* **114** 9457 (1992)
127. R Riedel, A Kienzle, W Dreßler, L M Ruwisch, J Bill, F Aldinger *Nature (London)* **382** 796 (1996)
128. K J Reichle, K Reimann, W Sprengel, A A Rempel, A Muller, H-E Schaefer *Int. J. Mater. Res.* **97** 621 (2006)
129. P Yu Butyagin *Usp. Khim.* **63** 1031 (1994) [*Russ. Chem. Rev.* **63** 965 (1994)]
130. V V Boldyrev *Usp. Khim.* **75** 201 (2006) [*Russ. Chem. Rev.* **75** 177 (2006)]
131. N F Uvarov, V V Boldyrev *Usp. Khim.* **70** 307 (2001) [*Russ. Chem. Rev.* **70** 265 (2001)]
132. A Yavari, P J Desre, T Benameur *Phys. Rev. Lett.* **68** 2235 (1992)
133. H-J Fecht *Nanostruct. Mater.* **6** 33 (1995)
134. P Yu Butyagin, A N Streletskii *Fiz. Tv. Tela* **47** 830 (2005)^a
135. V V Zyryanov *Mekhanokhimicheskii Sintez v Neorganicheskoi Khimii* (Mechanochemical Synthesis in Inorganic Chemistry) (Ed. E G Avvakumov) (Novosibirsk: Nauka, 1991) p. 102
136. A A Popovich, V P Reva, V N Vasilenko, V A Popovich, O A Belous *Poroshk. Metallurg.* (2) 37 (1993)^h
137. V Yu Davydkin, L I Trusov, P Yu Butyagin, V V Moskvina, I V Kolbanev, V I Novikov, S S Plotkin *Mekhanokhimicheskii Sintez v Neorganicheskoi Khimii* (Mechanochemical Synthesis in Inorganic Chemistry) (Ed. E G Avvakumov) (Novosibirsk: Nauka, 1991) p. 183
138. N Atsumi, K Yoshioka, T Yamasaki, Y Ogino *Funtai Oyobi Funnatsu Yakin* **40** 261 (1993)
139. A Teresiak, H Kubsch *Nanostruct. Mater.* **6** 671 (1995)

140. D Oleszak, H Matyja *Nanostruct. Mater.* **6** 425 (1995)
141. J S C Jang, C C Koch *J. Mater. Res.* **5** 498 (1990)
142. W H Hall *Proc. Phys. Soc., Sect. A, Pt. 11* **62** 741 (1949)
143. W H Hall, G K Williamson *Proc. Phys. Soc., Sect. B, Pt. 11* **64** 937 (1951)
144. G K Williamson, W H Hall *Acta Metall.* **1** 22 (1953)
145. M A Xueming, J I Gang *J. Alloys Compd.* **245** L30 (1996)
146. M S El-Eskandarany, M Omori, T Kamiyama, T J Konno, K Sumiyama, T Hirai, K Suzuki *Sci. Rep. Res. Inst. Tohoku Univ., Ser. A* **43** 181 (1997)
147. P S de Carli, J C Jamieson *Science* **133** 1821 (1961)
148. L F Trueb *J. Appl. Phys.* **42** 503 (1971)
149. A M Staver, N V Gubareva, A I Lyamkin, E A Petrov *Fiz. Goren. Vzryva* **20** 100 (1984)^j
150. A I Lyamkin, E A Petrov, A P Ershov, G V Sakovich, A M Staver, V M Titov *Dokl. Akad. Nauk SSSR* **302** 611 (1988)^b
151. I Yu Mal'kov, L I Filatov, V M Titov, B V Litvinov, A L Chuvilin, T S Teslenko *Fiz. Goren. Vzryva* **29** 131 (1993)ⁱ
152. A G Beloshapko, A A Bukaemskii, A M Staver *Fiz. Goren. Vzryva* **26** 93 (1990)^j
153. A G Beloshapko, A A Bukaemskii, I G Kuz'min, A M Staver *Fiz. Goren. Vzryva* **29** 111 (1993)^j
154. A G Merzhanov, S Yu Sharivker *Materials Science of Carbides, Nitrides and Borides* (Eds Y G Gogotsi, R A Andrievskii) (Dordrecht: Kluwer Academic, 1999) p. 205
155. A G Merzhanov *Usp. Khim.* **72** 323 (2003) [*Russ. Chem. Rev.* **72** 289 (2003)]
156. H H Nersisyan, J H Lee, C W Won *J. Mater. Res.* **17** 2859 (2002)
157. H Gleiter *Deformation of Polycrystals: Mechanisms and Microstructures* (Eds N Hansen, A Horsewell, T Leffers, H Lilholt) (Roskilde, Denmark: Risø Natl. Laboratory, 1981) p. 15
158. R W Siegel, H Hahn *Current Trends in Physics of Materials* (Ed. M Yussouff) (Singapore: World Sci. Publ., 1987) p. 403
159. E N Yakovlev, G M Gryaznov, V I Serbin, V N Lapovok, L I Trusov, V Ya Ganelin, E V Kapitanov, N B Kukhar', V B Begoulev *Poverkhnost* (4) 138 (1983)
160. R A Andrievskii *Poroshkovoe Materialovedenie* (Powder Materials Science) (Moscow: Metallurgiya, 1991)
161. M D Matthews, A Pechenik *J. Am. Ceram. Soc.* **74** 1547 (1991)
162. D-J Chen, M J Mayo *Nanostruct. Mater.* **2** 469 (1992)
163. T Rabe, R Wasche *Nanostruct. Mater.* **6** 357 (1995)
164. V S Urbanovich *Nanostructured Materials. Science and Technology, Ser. 3 (NATO ASI Ser.)* Vol. 50 (Eds G M Chow, N I Noskova) (Dordrecht: Kluwer Academic, 1998) p. 405
165. R A Andrievskii, V S Urbanovich *Fizikokhimiya Ul'tradispersnykh Sistem (Sbornik Nauchnykh Trudov V Sserossiiskoi Konferentsii)* [Physical Chemistry of Ultradispersed Systems (Proceedings of Vth All-Russian Conference)] (Ekaterinburg: Urals Branch of the Russian Academy of Sciences, 2001) Vol. 2, p. 118
166. G V Ivanov, N A Yavorovskii, Yu A Kotov, V I Davydovich, G A Mel'nikova *Dokl. Akad. Nauk SSSR* **275** 873 (1984)^b
167. V V Ivanov, S N Pararin, E A Gavrilin, A V Petrichenko, Yu A Kotov, S A Lebedev, S M Cheshnitskii *Sverkhprovodimost': Fiz., Khim., Tekh.* 1112 (1992)
168. V V Ivanov, S N Pararin, A N Vikhrev, A A Nozdrin *Materialovedenie* (5) 49 (1997)
169. V V Ivanov, Yu A Kotov, O M Samatov, R Bohme, H U Karow, G Schumacher *Nanostruct. Mater.* **6** 287 (1995)
170. V V Ivanov, A N Vikhrev, A A Nozdrin *Fiz. Khim. Obrab. Mater.* (3) 67 (1997)
171. R A Andrievskii, A N Vikhrev, V V Ivanov, R I Kuznetsov, N I Noskova, V A Sazonova *Fiz. Met. Metalloved.* **81** (1) 137 (1996)^k
172. R A Andrievskii, O M Grebtsova, E P Domashneva, I A Kiyanskii, E N Kurkin, V E Perel'man, V I Sinitsyn, O D Torbova, V I Torbov *Dokl. Akad. Nauk* **331** 306 (1993)^b
173. V V Ivanov, S N Pararin, A V Nikonov, V R Khrustov, S V Dobrov *Fiziko-khimiya Ul'tradispersnykh (Nano-) Sistem (Sbornik Nauchnykh Trudov VI Vserossiiskoi Konferentsii)* [Physical Chemistry of Ultradispersed (Nano-) Systems (Proceedings of the VIth All-Russian Conference)] (Moscow: Moscow Engineering Physics Institute, 2003) p. 194
174. O L Khasanov, E S Dvilis, Yu P Pokholkov, V M Sokolov *Perspektiv. Mater.* (3) 88 (1999)
175. O L Khasanov, V M Sokolov, E S Dvilis, Yu P Pokholkov *Perspektiv. Mater.* (1) 76 (2002)
176. Yu Bykov, A Ereemeev, V Flyagin, V Kaurov, A Kuftin, A Luchinin, O Malygin, I Plotnikov, V Zapevalov *Br. Ceram. Trans.* **59** 133 (1995)
177. S Egorov, A Ereemeev, A Sorokin, Yu Bykov, A Rachkovskii, A Poduretz *Nanoscience and Technology (Proceedings of the Xth APAM Topical Seminar)*, Novosibirsk, 2003 p. 162
178. S Herth, H Rosner, A Rempel, H-E Schaefer, R Wurschum *Z. Metallkd.* **94** 1073 (2003)
179. H Hoffmann *Thin Solid Films* **58** 223 (1979)
180. Y Yoshizawa, S Oguma, K Yamauchi *J. Appl. Phys.* **64** 6044 (1988)
181. N I Noskova, N F Vil'danova, A P Potapov, A A Glazer *Fiz. Met. Metalloved.* **73** (2) 102 (1992)^j
182. A Inoue, H M Kimura, K Sasamori, T Masumoto *Mater. Trans., JIM* **35** 85 (1994)
183. N A Smirnova, V I Levit, V P Pilyugin, R I Kuznetsov, M V Degtyarev *Fiz. Met. Metalloved.* **62** 566 (1986)^k
184. R Z Valiev, N A Krasilnikov, N K Tsenev *Mater. Sci. Eng., A* **137** 35 (1991)
185. R Z Valiev, A V Korznikov, R R Mulyukov *Fiz. Met. Metalloved.* **73** (4) 70 (1992)^k
186. V M Segal *Mater. Sci. Eng., A* **197** 157 (1995)
187. V M Segal, Author's abstract of Doctoral Thesis in Technical Sciences, Physical Technical Institute, Academy of Sciences of the Bel.SSR, Minsk, 1974
188. V M Segal, V I Reznikov, F E Drobyshevskii, V I Kopylov *Izv. Akad. Nauk SSSR, Ser. Metall.* (1) 115 (1981)
189. V M Segal, V I Reznikov, V I Kopylov, D A Pavlik, V F Malyshev *Protsessy Plasticheskogo Strukturoobrazovaniya Metallov* (Processes of Plastic Structurisation of Metals) (Minsk: Nauka i Tekhnika, 1994)
190. R Z Valiev, A V Korznikov, R R Mulyukov *Mater. Sci. Eng., A* **168** 141 (1993)
191. N A Akhmadeev, R Z Valiev, V I Kopylov, R R Mulyukov *Metally* (5) 96 (1992)
192. A A Rempel, A I Gusev, S Z Nazarova, R R Mulyukov *Dokl. Akad. Nauk* **347** 750 (1996)^b
193. A Cziraki, I Geracs, E Toth-Kadar, I Bakonyi *Nanostruct. Mater.* **6** 547 (1995)
194. A A Rempel, A I Gusev, R R Mulyukov, N M Amirkhanov *Metallofiz. Noveish. Tekhnol.* (7) 14 (1996)
195. A A Rempel, A I Gusev *Phys. Status Solidi B* **196** 251 (1996)
196. A A Rempel, A I Gusev, R R Mulyukov, N M Amirkhanov *Nanostruct. Mater.* **7** 667 (1996)
197. A A Rempel, A I Gusev, S Z Nazarova, R R Mulyukov *Dokl. Akad. Nauk* **345** 330 (1995)^b
198. R Z Valiev, R R Mulyukov, V V Ovchinnikov, V A Shabashov *Scr. Metall. Mater.* **25** 2717 (1991)
199. R Z Valiev, Ya D Vishnyakov, R R Mulyukov, G S Fainstein *Phys. Status Solidi A* **117** 549 (1990)
200. Kh Ya Mulyukov, G F Korznikova, R Z Valiev *Phys. Status Solidi A* **125** 609 (1991)
201. R Z Abdulov, R Z Valiev, N A Krasilnikov *J. Mater. Sci. Lett.* **9** 1445 (1990)
202. R M Galeev, O R Valiakhmetov, G A Salishchev *Izv. Akad. Nauk SSSR, Ser. Metall.* (4) 97 (1990)
203. O R Valiakhmetov, R M Galeev, G A Salishchev *Fiz. Met. Metalloved.* **70** (10) 204 (1990)^k

204. A A Rempel, A I Gusev, R R Mulyukov *Khimiya Tverdogo Tela i Noveye Materialy* (Solid State Chemistry and New Materials) (Ekaterinburg: Institute of Solid State Chemistry Urals Branch of the Russian Academy of Sciences, 1996) Vol. 1, p. 244
205. A A Rempel, A I Gusev, R R Mulyukov *Ul'tradispersnye Poroshki, Materialy i Nanostruktury* (Ultradispersed Powders, Materials and Nanostructures) (Ed. V E Red'kin) (Krasnoyarsk: Krasnoyarsk State Technical University, 1996) p. 131
206. A A Valeeva, B A Gizhevskii, V P Pilyugin, A A Rempel *Fiz. Met. Metalloved.* **99** (1) 62 (2005)^k
207. M M Martynyuk *Zh. Tekhn. Fiz.* **44** 1262 (1974)^l
208. Yu A Kotov, N A Yavorskii *Fiz. Khim. Obrab. Mater.* (4) 24 (1978)
209. V A Burtsev, N V Kalinin, A V Luchinskii *Elektricheskii Vzryv Provodnikov i ego Primenenie v Elektrofizicheskikh Ustanovkakh* (Electrical Explosion of Conductors and Its Application in Electrophysical Facilities) (Moscow: Energoatomizdat, 1990)
210. A P Il'in, O B Nazarenko, D V Tikhonov *Ul'tradispersnye Poroshki, Nanostruktury, Materialy (Trudy Vtoroi Mezhrainal'noi Konferentsii)* [Ultradispersed Powders, Nanostructures and Materials (Proceedings of the Second International Conference)] (Krasnoyarsk: Krasnoyarsk State Technical University, 1999) p. 31
211. A P Il'in *Fiz. Khim. Obrab. Mater.* (3) 94 (1994)
212. A P Il'in *Fiz. Khim. Obrab. Mater.* (4) 93 (1997)
213. A I Gusev, A A Rempel *Nestekhiometriya, Beporyadok i Poryadok v Tverdom Tele* (Non-stoichiometry, Disorder and Order in Solids) (Ekaterinburg: Ural Branch of the Russian Academy of Science, 2001)
214. A I Gusev, A A Rempel, A J Magerl *Disorder and Order in Strongly Nonstoichiometric Compounds: Transition Metal Carbides, Nitrides and Oxides* (Berlin, Heidelberg, New York: Springer, 2001)
215. A I Gusev, A A Rempel *Phys. Status Solidi A* **163** 273 (1997)
216. A I Gusev *Usp. Fiz. Nauk* **170** 3 (2000) [*Physics-Uspekhi* **43** 1 (2000)]
217. A I Gusev, A A Rempel *Strukturnye Fazovye Perekhody v Nestekhiometricheskikh Soedineniyakh* (Structural Phase Transitions in Non-stoichiometric Compounds) (Moscow: Nauka, 1988)
218. A A Rempel *Effekty Uporyadocheniya v Nestekhiometricheskikh Soedineniyakh Vnedreniya* (Ordering Effects in Non-stoichiometric Interstitial Compounds) (Ekaterinburg: Nauka, 1992)
219. A A Rempel *Usp. Fiz. Nauk* **166** 33 (1996) [*Physics-Uspekhi* **39** 31 (1996)]
220. A I Gusev, A A Rempel *Phys. Status Solidi A* **135** 15 (1993)
221. T Athanassiadis, N Lorenzelli, C H de Novion *Ann. Chim. (Paris)* **12** 129 (1987)
222. A A Rempel, A I Gusev *Pis'ma Zh. Eksp. Teor. Fiz.* **69** 436 (1999)^m
223. V N Lipatnikov, W Lengauer, P Ettmayer, E Keil, G Grobtho, E Kny *J. Alloys Compd.* **261** 192 (1997)
224. D Rafaja, W Lengauer, P Ettmayer, V N Lipatnikov *J. Alloys Compd.* **269** 60 (1998)
225. A A Rempel, A I Gusev, O V Makarova, S Z Nazarova *Perspekt. Mater.* (6) 9 (1999)
226. A I Gusev, A A Tulin, V N Lipatnikov, A A Rempel *Zh. Obshch. Khim.* **72** 1067 (2002)ⁿ
227. R Würschum, H-E Schaefer *Nanomaterials: Synthesis, Properties and Applications* (Eds A S. Edelstein, R C Cammarata) (Bristol: Institute of Physics Publ., 1996) p. 277
228. A A Rempel, W Sprengel, K Blaurock, K J Reichle, J Major, H-E Schaefer *Phys. Rev. Lett.* **89** 185501 (2002)
229. A A Rempel, M Foster, G-E Shefer *Dokl. Akad. Nauk* **326** 91 (1992)^b
230. A A Rempel, L V Zueva, V N Lipatnikov, H-E Schaefer *Phys. Status Solidi A* **169** R9 (1998)
231. A I Gusev *Zh. Fiz. Khim.* **74** 600 (2000)^o
232. V N Belomestnykh, E P Tesleva *Fiziko-khimiya Ul'tradispersnykh (Nano-) Sistem (Sbornik Nauchnykh Trudov VI Vserossiiskoi Konferentsii)* [Physical Chemistry of Ultradispersed (Nano-) Systems (Proceedings of the VIth All-Russian Conference)] (Moscow: Moscow Engineering Physics Institute, 2003) p. 200
233. O B Naimark *Fiz. Met. Metalloved.* **84** (4) 5 (1997)^k
234. E Kroner *Lecture Notes in Physics* (Eds E Kroner, K Kinchassner) (Heidelberg: Springer, 1986) p. 281
235. A Kadiā, D G B Edelen *A Gauge Theory of Dislocations and Disclinations* (Berlin: Springer, 1983)
236. T L Makarova, B Sundqvist, R Höhne, P Esquinazi, Ya Kopelevich, P Schraff, V A Davydov, L S Kashevarova, A V Rakhmanina *Nature (London)* **413** 716 (2001)
237. K Sohlberg, R E Tuzun, B Sumpter, D W Noid *Nanotechnology* **8** 103 (1997)
238. L Delzeit, C V Nguyen, R M Stevens, J Han, M Meyyappan *Nanotechnology* **13** 280 (2002)
239. M Menon, D Srivastava *Phys. Rev. Lett.* **79** 4453 (1997)
240. J Li, C Papadopoulos, J Xu *Nature (London)* **402** 253 (1999)
241. C Papadopoulos, A Rakitin, J Li, A S Vedenev, J M Xu *Phys. Rev. Lett.* **85** 3476 (2000)
242. B Q Wei, R Vajtai, Y Jung, J Ward, Y Zhang, G Ramanath, P M Ajayan *Nature (London)* **416** 495 (2002)
243. P Kral, D Tomanek *Phys. Rev. Lett.* **82** 5373 (1999)
244. E G Rakov *Usp. Khim.* **70** 934 (2001) [*Russ. Chem. Rev.* **70** 827 (2001)]
245. A L Ivanovskii *Usp. Khim.* **71** 203 (2002) [*Russ. Chem. Rev.* **71** 175 (2002)]
246. V V Pokropivnyi *Poroshk. Metall.* (3–4) 13 (2002)^h
247. M Che, C O Bennet *Adv. Catal.* **36** 55 (1989)
248. V I Bukhtiyarov, M G Slin'ko *Usp. Khim.* **70** 167 (2001) [*Russ. Chem. Rev.* **70** 147 (2001)]
249. V Ponec *Adv. Catal.* **32** 149 (1983)
250. Z Karpinski *Adv. Catal.* **37** 45 (1990)
251. A D Pomogailo *Usp. Khim.* **69** 60 (2000) [*Russ. Chem. Rev.* **69** 53 (2000)]
252. A D Pomogailo, A S Rozenberg, I E Uflyand *Nanochastitsy Metallov v Polimerakh* (Nanoparticles of Metals in Polymers) (Moscow: Khimiya, 2000)
253. J S Kilby *Usp. Fiz. Nauk* **172** 1102 (2002) [Nobel Lectures, Physics 1996–2000 (Ed. G. Eksping) (Singapore: World Sci. Publ., 2002)]
254. D L Klein, R Roth, A K L Lim, A P Alivisatos, P L McEuen *Nature (London)* **389** 699 (1997)
255. A Erbe, C Weiss, W Zwerger, R H Blick *Phys. Rev. Lett.* **87** 096106 (2001)
256. H Kroemer *Usp. Fiz. Nauk* **172** 1091 (2002) [Nobel Lectures, Physics 1996–2000 (Ed. G. Eksping) (Singapore: World Sci. Publ., 2002)]
257. R Dingle, W Wiegmann, C H Henry *Phys. Rev. Lett.* **33** 827 (1974)
258. Zh I Alferov *Usp. Fiz. Nauk* **172** 1072 (2002) [Nobel Lectures, Physics 1996–2000 (Ed. G. Eksping) (Singapore: World Sci. Publ., 2002)]
259. A P Alivisatos *Science* **271** 933 (1996)
260. K Morgenstern *Phys. J.* **1** 95 (2002)
261. Yu P Pershin, E N Zubarev, V V Kondratenko, O V Pol'tseva, A G Ponomarenko, V A Sevryukova, Ya Verkhoeven *Metallofiz. Noveish. Tekhnol.* **24** 795 (2002)
262. J S Hauser, H C Theuerer, N R Werthamer *Phys. Rev.* **142** 118 (1966)
263. B Y Jin, J B Ketterson *Adv. Phys.* **38** 189 (1989)
264. A I Buzdin, A V Vedyayev, N V Ryshanova *Europhys. Lett.* **48** 686 (1999)
265. L R Tagirov *Phys. Rev. Lett.* **83** 2058 (1999)
266. Yu A Izyumov, Yu N Proshin, M G Khushainov *Usp. Fiz. Nauk* **172** 113 (2002) [*Physics-Uspekhi* **45** 109 (2002)]
267. A S Borukhovich *Usp. Fiz. Nauk* **169** 737 (1999) [*Physics-Uspekhi* **42** 653 (1999)]

268. O L Khasanov, E S Dvilis, V M Sokolov, Yu P Pokholkov
Fiziko-khimiya Ul'tradispersnykh (Nano-) Sistem (Sbornik Nauchnykh Trudov VI Vserossiiskoi Konferentsii) [Physical Chemistry of Ultradispersed (Nano-) Systems (Proceedings of the VIth All-Russian Conference)] (Moscow: Moscow Engineering Physics Institute, 2003) p. 180
269. Yu V Kolen'ko, P E Meskin, V A Mukhanov,
B R Churagulov, S V Balakhonov *Zh. Neorg. Khim* **50** 1941 (2005)^p
270. Y V Kolen'ko, K A Kovnir, A I Gavrilov, A V Garshev,
J Frantti, O I Lebedev, B R Churagulov, G Van Tendeloo,
M Yoshimura *J. Phys. Chem. B* **110** 4030 (2006)
271. J H Fendler *Membrane-mimetic Approach to Advance Materials*.
(Berlin, Heidelberg, New York: Springer, 1994)

^a — *Phys. Solid State (Engl. Transl.)*

^b — *Dokl. Phys. (Engl. Transl.)*

^c — *Bull. Russ. Acad. Sci., Phys. (Engl. Transl.)*

^d — *Dokl. Chem. (Engl. Transl.)*

^e — *High Energ. Chem. (Engl. Transl.)*

^f — *Inorg. Mater. (Engl. Transl.)*

^g — *Mendeleev Chem. J. (Engl. Transl.)*

^h — *Powder Metall. Met. Ceram. (Engl. Transl.)*

ⁱ — *J. Struct. Chem. (Engl. Transl.)*

^j — *Comp. Explos. Shock Waves (Engl. Transl.)*

^k — *Phys. Met. Metallogr. (Engl. Transl.)*

^l — *Techn. Phys. (Engl. Transl.)*

^m — *J. Exp. Theor. Phys. Lett. (Engl. Transl.)*

ⁿ — *Russ. J. Gen. Chem. (Engl. Transl.)*

^o — *Russ. J. Phys. Chem. (Engl. Transl.)*

^p — *Russ. J. Inorg. Chem. (Engl. Transl.)*

Multifunctional nanostructured films

E A Levashov, D V Shtansky

Contents

I. Introduction	463
II. Multicomponent nanostructured films for mechanical engineering	464
III. Multifunctional nanostructured films for medicine	467

Abstract. The state-of-the-art of investigation into multifunctional (multicomponent) nanostructured films used in mechanical engineering and medicine is considered. The bibliography includes 113 references.

I. Introduction

New materials form the basis for the technology of the 21st century, and the industry of nanomaterials is a priority field of development of science and engineering. An important vigorously developing trend in the nanomaterial and nanotechnology sciences is the surface engineering, in particular, the design of multicomponent (multifunctional) nanostructured films (MNF) with a characteristic crystallite size of 1 to 100 nm (Fig. 1).¹

What makes nanostructured films unique is the high volume fraction and strength of interfaces, the absence of dislocations inside the crystallites, the possibility of changing the ratio of the volume fractions of the crystalline and amorphous phases and the mutual solubility of metal and non-metal components. The presence of a large interfacial area (the volume fraction may reach 50%) in nanostructured films allows one to change their properties either by material and electronic structure modification[†] or by doping. The strength of the interfaces favours the stability of nanostructured films against deformation. The lack of dislocations inside the crystallites increases the elasticity of these films. These factors altogether allow the production of nanomaterials with improved physicochemical and physicomechanical characteristics, namely, with high hardness ($H > 30$ GPa), elastic recovery ($W_e > 70\%$), strength, thermal stability, and heat and corrosion resistance.

An important feature of the ultrahard nanomaterials based on MNF is that materials with the same hardness may differ in the elastic modulus (E), resistance against elastic strain to failure (H/E) and resistance against plastic deformation (H^3/E^2).²

E A Levashov, D V Shtansky Moscow State Institute of Steel and Alloys (Technology University), Leninsky prosp. 4, 119991 Moscow, Russian Federation. Fax (7-495) 952 53 08, tel. (7-495) 230 45 00, (7-495) 955 00 59, e-mail: levashov@shs.misis.ru (E A Levashov), tel. (7-495) 230 45 35, e-mail: shtansky@shs.misis.ru (D V Shtansky)

Received 10 November 2006

Uspekhi Khimii 76 (5) 501–509 (2007); translated by Z P Bobkova

Multifunctional nanostructured films are used to protect surfaces of articles and tools exposed simultaneously to elevated temperatures, corrosive media and various types of wear. This refers, first of all, to the cutting and press forming tools, mill rolls, parts of aircraft engines, gas turbines and compressors, friction bearings, glass and mineral fibre extrusion nozzles, *etc.* These films are also indispensable in the development of new-generation biocompatible materials, namely, orthopedic and dental implants, craniofacial and maxillofacial surgery implants, fixation of cervical and lumbar spines and so on.

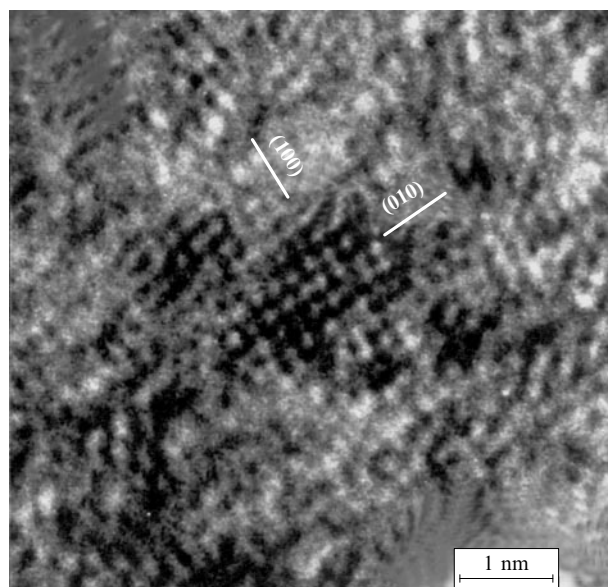


Figure 1. Crystallite with a 1.5 nm size in the Ti–Al–B–N film.¹

Methods for the production of nanostructured materials and films and methods for the investigation of their structures, compositions, and properties have been widely addressed in Russian and foreign publications (see, for example, Refs 3–9).

[†] By changing the charge of the interfaces (by application of an electric field), one can affect the electronic structure of the films and, hence, their magnetic, optical and electric properties and also the mutual solubility of separate components and the formation of new phases.

This review presents a critical account of the promising trends in the application of MNF (based on refractory compounds) in mechanical engineering and medicine, *i.e.*, in those fields where the multifunctional properties of thin-film materials are manifested in full measure. Note that some MNF are used in other fields of technology, for example, in magnetooptics and electronics.

II. Multicomponent nanostructured films for mechanical engineering

Currently, titanium nitride-based films are widely used in industry. The introduction of a third component (for example, Si or B) into the films may markedly improve their physico-mechanical properties and thus extend the scope of application. The interest in the Ti–Si–N films is mainly caused by their high hardness,^{10–12} thermal stability,^{13–15} resistance against high-temperature oxidation^{14, 15} and substantial abrasive wear resistance.¹⁶ Nanostructured Ti–B–N films possess a series of important performance characteristics including high hardness,^{17–19} thermal stability up to 1000 °C (*in vacuo*),^{20–22} heat,¹⁵ wear^{23–26} and corrosion resistance,²⁷ impact resistance²⁸ and high electrical resistance.²⁹ Chromium is known to have a beneficial effect on the stability of titanium carbides, borides and nitrides against oxidation³⁰ and on the wear resistance of articles made of them at elevated temperatures.³¹

Thus, the introduction of doping elements (Al, Si, B and Cr) into protective TiN films provides a combination of high hardness and wear resistance with relatively low friction coefficient (K_f).^{32, 33} In terms of their physico-mechanical and tribological properties, MNF substantially surpass the conventional titanium nitride and carbonitride films. Thus the Ti–B–N and Ti–Cr–B–N films obtained under optimal conditions have hardnesses of 31–34 and 40–47 GPa, elastic moduli of 378 and 506 GPa, friction coefficients of 0.49–0.60 and 0.45–0.52, dry wear rates of $(3.4–4.6) \times 10^{-7}$ and $(6.0–6.8) \times 10^{-7}$ mm³ N^{−1} min^{−1} and substrate adhesion (maximum critical load) of 50 and 42 N, respectively.³²

The nanostructured films are prepared using both physical and chemical methods, among which physical vapour deposition methods (reactive and non-reactive magnetron deposition, cathode sputtering, laser ablation, *etc.*) are used most often. Ion plasma sputtering is an effective method for the synthesis of MNF. The use of multicomponent composite

targets in the magnetron sputtering (MS) process and high-power metal ion beam-assisted MS gives nanostructured Ti–(Si, Cr, Al)–(B, N, C) coatings with controlled composition and high mechanical and tribological parameters.^{33–36}

Coatings of the tribological use must possess high hardness, high fatigue strength and deformation and fracture resistance. All these requirements are satisfied for the tribological ultrahard ($H_v \geq 40$ GPa) nanostructured films composed of immiscible phases (or phases with limited mutual solubility), namely, nanocrystalline (*nc*) and amorphous (*a*) phases. The preparation of these films depends on the possibility of simultaneous deposition of nanocrystalline and amorphous phases. Transition metal nitrides (TiN, CrN, AlN, ZrN, TaN, *etc.*), carbides (TiC, VC, WC, ZrC, *etc.*), borides (TiB₂, CrB₂, WB, ZrB₂, *etc.*), oxides (Al₂O₃, TiO₂, SiO₂, MgO, Y₂O₃, ZrO₂, *etc.*) and silicides (TiSi₂, CrSi₂, ZrSi₂, *etc.*) are used as nanocrystalline phases, and Si₃N₄, BN, C and other substances can act as the amorphous matrices (Table 1).

Veprek *et al.*¹⁴ proposed a theoretical concept for the design of ultrahard nanomaterials according to which these materials should be composed of dislocation-free nanocrystallites (solid phases) of 3–10 nm size separated by a thin (1–2 nm) amorphous phase layer. An idealised model of the ultrahard nanostructured film is shown in Fig. 2. It is noteworthy that complete phase segregation is usually observed when the films are deposited at high temperatures (500–600 °C), while upon deposition at lower temperatures, the interfaces may include both ordered and disordered sections, the amorphous phase being mainly formed as localised areas rather than as thin amorphous interlayers along the crystallite boundaries.⁴²

It has been noted above that the hardness and the elasticity of nanostructured materials depend on the nanocrystallite size. The existence of the characteristic size of nanocrystallites (d_c) ensuring the highest hardness of nanostructured coatings is due to the continuous transition, at distances close to d_c , from the macroscopic dislocation nucleation and motion processes (for $d > d_c$) described by the known Hall–Petch law ($H \approx d^{-1/2}$) for conventional polycrystalline materials to intercrystallite local sliding processes along grain boundaries and interfaces (for $d < d_c$).

Nanocrystallites with a size less than 10 nm are considered to contain no sources of generation of dislocations.⁴⁰ Note that the characteristic size of nanocrystallites as applied to nanocrystalline metallic materials can vary within 2–24 nm.⁴⁸ The

Table 1. Examples of tribological ultrahard nanostructured films consisting of immiscible phases.

Coating	Composition of the sputtered targets	Phase composition of films	Ref.
Ti–B–C–N	TiB + Ti or TiB ₂ + TiC	<i>nc</i> -TiC + <i>nc</i> -TiB ₂ + <i>a</i> -BN	37
Ti–B–N	TiB ₂ + TiN or TiB ₂ + Ti	<i>nc</i> -TiN + <i>nc</i> -TiB ₂ (or <i>a</i> -TiB ₂) + <i>a</i> -BN	33, 36, 38
Ti–Si–N	Ti ₅ Si ₃ + Ti	<i>nc</i> -TiN + <i>nc</i> -TiSi ₂ + <i>a</i> -Si ₃ N ₄	39
	see ^a	<i>nc</i> -TiN + <i>a</i> -Si ₃ N ₄	40
Ti–Cr–B–N	TiB + Ti ₉ Cr ₄ B + Cr ₂ Ti	<i>nc</i> -TiN + <i>nc</i> -CrB ₂ + <i>a</i> -BN + <i>a</i> -TiB ₂	33
Ti–C–B	TiC + TiB ₂	<i>nc</i> -TiB ₂ + <i>nc</i> -TiC + <i>a</i> -B ₄ C	41
Ti–Si–B–N	TiB ₂ + Ti ₅ Si ₃ + Si or TiB ₂ + Si	<i>nc</i> -TiB ₂ + <i>nc</i> -TiN + <i>nc</i> -TiSi ₂ + <i>a</i> -Si ₃ N ₄	35, 36
Ti–Si–C–N	TiC + Ti ₅ Si ₃ or TiC + Ti ₅ Si ₃ C ₂ + TiSi ₂ + SiC	<i>nc</i> -TiC + <i>nc</i> -Ti ₂ SiC ₂ + <i>nc</i> -TiSi ₂ + <i>nc</i> -SiC + <i>a</i> -Si ₃ N ₄	36, 42
Ti–Al–B–N	TiAlBN	<i>nc</i> -TiB ₂ + <i>nc</i> -(Ti _x Al _{1-x})N + <i>a</i> -BN + <i>a</i> -AlN	1
Ti–Al–C–N	TiAl + TiC	<i>nc</i> -TiC + <i>nc</i> -(Ti _x Al _{1-x})N + <i>a</i> -AlN	36
W–C	W + laser ablation of C	<i>nc</i> -WC + <i>a</i> -C	43
W–Si–N	see ^b	<i>nc</i> -W ₂ N + <i>a</i> -Si ₃ N ₄	44
Ti–C	TiC _{0.5}	<i>nc</i> -TiC + <i>a</i> -C	45
Ti–Al–Si–N	TiN + TiAl	<i>nc</i> -(Ti _x Al _{1-x})N + <i>a</i> -Si ₃ N ₄	46
Cr–Si–N	Cr + Si	<i>nc</i> -CrN + <i>a</i> -Si ₃ N ₄	47
Cr–B–N	CrB ₂	<i>nc</i> -CrB ₂ + <i>a</i> -BN	33

Note. In most cases, films were prepared by magnetron sputtering from the targets in an Ar or N₂/Ar atmosphere. ^a The films were obtained by chemical vapour deposition (CVD). ^b The films were obtained by thermal annealing of the amorphous W–Si–N films.

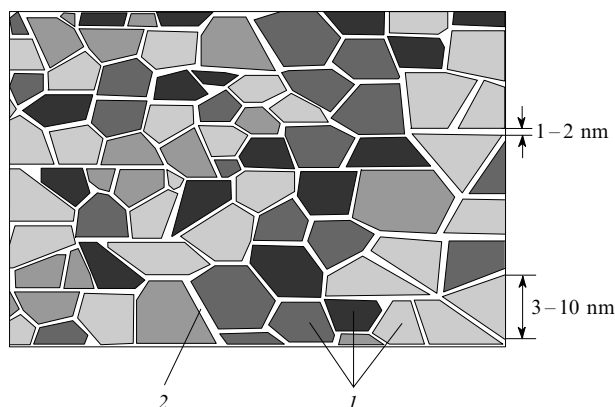


Figure 2. Idealised model of ultrahard nanostructured films. (1) Nanocrystalline phases, (2) amorphous phase.

experimental data on this issue available from the literature are rather scarce and contradictory. Thus a study of the structure of Ti–B–N films by high-resolution transmission electron microscopy⁴⁹ demonstrated the existence of a large number of internal edge dislocations in 5–15-nm crystallites. Figure 3 clearly shows the edge dislocation with the Burgers vector [100] within a 5-nm crystallite. Note also that the interfaces of nanostructured films often accommodate misfit dislocations (see Fig. 3), giving rise to long-range elastic stress fields.

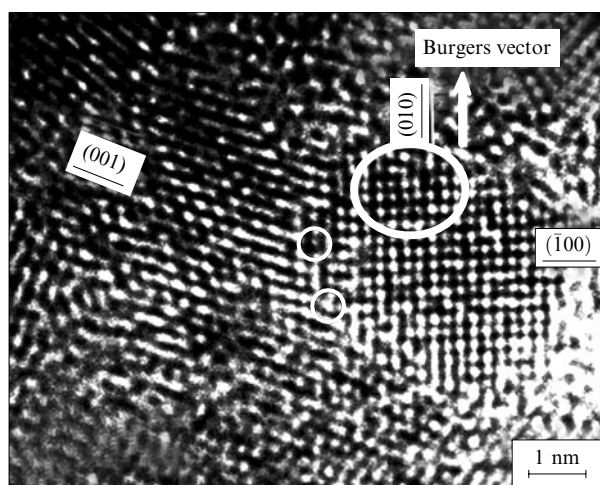


Figure 3. Edge dislocation inside the crystallite (large circle) and misfit dislocation at the crystallite boundary (small circles) in the Ti–Si–B–N film.⁴⁹

The appearance of the amorphous phase in a nanostructured film is usually accompanied by a change in the film structure, namely, transition from the columnar structure,[‡] representing a set of interconnected columns, to a composite structure in which nanocrystallites of one or several phases are separated by thin amorphous interlayers. Controlled introduction of ‘amorphisers’, for example, boron or silicon, allows targeted variation of the structure and properties of nanostructured films. Thus the highest hardness of M–Si–N films (M is a transition metal) was attained in composite nanostructured nc-MN + α -Si₃N₄ films with the characteristic crystallite size

‡ It is believed that undesirable stresses parallel to the substrate surface arise in the films with columnar structure.

$d_c \approx 10$ nm at a silicon content within the 7 at.%–10 at.% range.⁵⁰

Although the reasons for ultrahigh hardness of some composites are not fully understood, the key factors favourable for the increase in hardness can be listed. These include high compression stresses arising due to the difference between the thermal expansion coefficients of the substrate and the coating; distortion of the crystal phase lattice caused by the change in the mutual solubility of elements; high internal stress (or growth stress) and chemical bonds between some phase components.

In addition to high hardness, tribological nanostructured films are expected to have low elastic moduli and high elastic recovery values (W_e), reaching 90%. The numerical values of these characteristics can be measured using a nanohardness tester. Using known parameters E and W_e , one can calculate H/E and H^3/E^2 . The dependences $H = f(E^*)$ [$E^* = E(1 - \nu^2)$ is the effective elastic modulus, where ν is the Poisson coefficient], $H^3/E^2 = f(H)$ and $W_e = f(H)$ are the principal relations describing the mechanical properties of the films.⁵¹

For a series of oxide, carbide, nitride and composite nanostructured films obtained by magnetron sputtering, the dependence $H = f(E^*)$ can be approximated by a straight line, while the dependence $H^3/E^2 = f(H)$, by a parabola.^{44, 45}

$$H = 0.15 E^* - 12,$$

$$\frac{H^3}{E^2} = 4.3 \times 10^{-4} H^2.$$

These equations are useful for predicting the mechanical behaviour of films.

Plastic deformation (W_p) is yet another important characteristics of nanostructured films. No quantitative relationship (as approximating equations) exists between the W_p , H and H^3/E^2 values,⁵² but only a qualitative relationship. As H and H^3/E^2 increase, the W_p value decreases; films with $H > 25$ GPa have relatively low plastic deformation values ($\sim 30\%$).

The local deformation mechanisms in nanostructured thin films have been investigated.^{19, 53} The existence of two local deformation mechanisms for such films was established, namely, homogeneous (with weak chemical bonds between structural elements) and non-homogeneous (with strong bonds between the crystallites). Both deformation mechanisms are implemented by sliding of the structure elements, *i.e.*, separate grains (homogeneous mechanism) or multigrain domains (columnar elements) (non-homogeneous mechanism), parallel to the applied load. In the case of weak chemical bonds between the neighbouring grains, some structure elements can be expelled to the outside as a result of elastic stress relaxation upon load release. In the case of strong chemical bonds between neighbouring grains, the deformation occurs through sliding of the columnar elements, resulting in the formation of shear steps.

The tribological properties of films largely depend on the phase composition of the nanocomposite. Thus for the Ti–B–N and Ti–Cr–B–N films, the friction coefficient decreases to 0.40 with a decrease in the boron content and an increase in the nitrogen content. This low K_f value is due to the presence of the hexagonal α -BN phase.³³ The presence of silicon also enhances the tribological properties of nanostructured films. For example, the friction coefficient of the Ti–Si–B–C–N films in the friction couple with a WC–Co carbide ball decreases to 0.15 as the silicon concentration grows to 12 at.%. Silicon promotes the formation of intermediate solid lubricant layers resulting from tribochemical reactions during friction. Silicon compounds such as TiSi₂, SiC and SiB₄ as the film constituents are known to react with water

and oxygen to give self-lubricated tribolayers of the SiO_2 or $\text{Si}(\text{OH})_4$ type.

An enhanced wear resistance of a material can also be indicated by high values of H/E . This correlation has been confirmed both theoretically and experimentally for a large number of materials.⁵⁴

A number of publications^{43,55,56} describe the first synthesis of 'chameleon' type nanostructured films. These tribological nanocomposite films with low K_{fr} values represent mixtures of hard and soft self-lubricated phases. The hard phases (nitrides, carbides or boride) are responsible for high wear resistance under high load, while soft phases ($a\text{-C}$, $a\text{-WSi}_2$, $a\text{-Si}_3\text{N}_4$, $a\text{-BN}$) significantly decrease K_{fr} of the contact friction couple.

Sputtering of multilayer or functionally gradient nanostructured films with alternating ultrahard and self-lubricated layers is a promising trend in the design of tribological coatings with ultimately low K_{fr} values (<0.05). As an example, consider bilayer WSe_x/TiC , WSe_x/TiCN and $\text{WSe}_x/\text{TiSiN}$ films in which the WSe_x layer consists of WSe_2 and W_3O nanocrystalline phases incorporated in the amorphous $a\text{-WSe}_x$ matrix.⁵⁷ These bilayer compositions had a low friction coefficient both in air ($K_{\text{fr}} = 0.015\text{--}0.05$) and in water ($K_{\text{fr}} = 0.06\text{--}0.07$) throughout the whole series of tribological investigations. A distinctive feature of these films is the absence of starting (break-in) friction coefficient in the beginning of testing, which is usually the highest.

An important factor for increasing the service life of articles at high temperatures is to ensure their thermal stability and high-temperature oxidation resistance (heat resistance). These parameters depend on the elemental and phase composition of the films and on the thermal stability of the constituent individual phases. The thermal stability of nanostructured films has been considered in detail in a review by Andrievskii.⁵⁸

As an example, Fig. 4 shows the dependence of the average crystallite size in nanostructured Ti–B–N and Ti–Cr–B–N films on the annealing temperature. It can be seen that the average size of crystallites does not exceed 5 nm even after annealing of the films *in vacuo* at 1000 °C for 1 h. The same figure shows the dependence of film hardness on the annealing temperature. Both films showed an increase in hardness with an increase in the annealing temperature to 800 °C; for the Ti–Cr–B–N films, this high hardness was retained up to 1000 °C, the hardness of the Ti–B–N films at 1000 °C was

somewhat lower than at 800 °C but nevertheless it was rather high.³³ This extremal pattern of hardness variation with temperature is in good agreement with previous results, indicating the presence of a hardness peak for the Ti–Al–Si–N⁵⁹ and W–Si–N films⁶⁰ at 800 and 900–950 °C, respectively.

The microcrystalline TiN, TiC, TiCN and TiAlN films obtained by physical deposition are known to demonstrate a monotonic decrease in hardness with an increase in temperature.^{61,62} The increase in the hardness of nanostructured films with the increase in temperature may be due to the change in the thickness of intergrain amorphous interlayers and the concentration-induced separation of metastable phases.⁷ In addition, hardness can be affected by stoichiometry of the crystalline phase. Thus the maximum hardness of the Ti–Si–B–N films was achieved at the strictly stoichiometric composition of the $\text{Ti}(\text{B,N})_2$ phase.⁶³

In some publications (see, for example, Ref. 12), it was suggested that the high hardness of the nanostructured films obtained by low-temperature magnetron sputtering is related to the presence of high compression stresses. As the temperature is increased (to 450 °C), elastic stress relaxation takes place and, as a consequence, the hardness of films decreases down to values typical of polycrystalline materials. However, this assumption is at variance with the data obtained for nanostructured Ti–B–N and Ti–Cr–B–N films; these films retain high hardness up to 1000 °C.

The heat resistance of the films has a critical temperature above which the film is completely oxidised and destroyed. The heat resistance varies over a broad range from 400 to 950 °C (Table 2). A common feature of nanostructured films is the polycrystalline structure, which provides direct oxygen access to the substrate along the grain boundaries (by the surface reactive diffusion mechanism). This accounts for the relatively low heat resistance of polycrystalline films.

An efficient way for increasing the heat resistance of solid films is suppression of the recrystallisation of nanocrystallites by creating a dense composite structure in which the crystallites occur in the amorphous matrix containing elements (Si, Al, Cr, B) with high oxygen affinity. It has been shown^{67–70} that the $nc\text{-MN}_x + a\text{-Si}_3\text{N}_4$ ($M = \text{Ta, Zr, Mo}$) compositions with high (>50 at.%) contents of the amorphous phase meet these requirements. These films have a high heat resistance (~ 1000 °C), while retaining high hardness within the 20–40 GPa range.

The positive influence of amorphising elements (Si, Al and B) on the heat resistance of nanostructured Ti–B–N, Ti–Si–B–N, Ti–Si–C–N, Ti–Al–C–N and Ti–C–B films is manifested as an increase in the content of amorphous phases ($a\text{-Si}_3\text{N}_4$, $a\text{-AlN}$, $a\text{-BN}$, $a\text{-B}_4\text{C}$); an increase in the thermal stability of the nanocrystalline state; the formation of a protective oxide layer on the film surface preventing the oxygen access to the substrate.^{36,41,71–74} For example, in the $(\text{Ti,Al})_{1-x}(\text{C,N})_x$ nanostructured films, oxygen is dissolved in

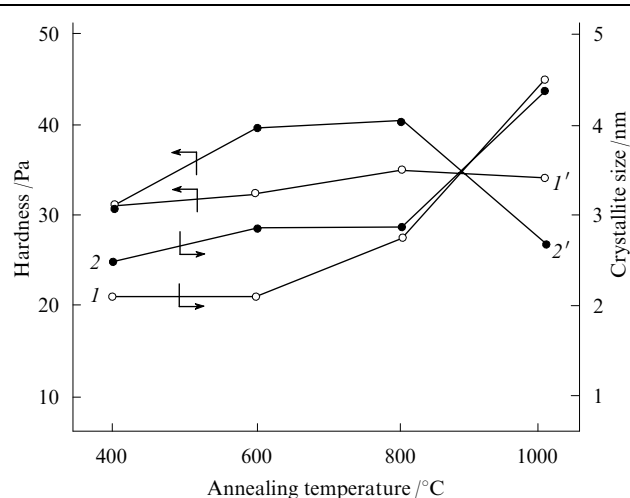


Figure 4. Average size of crystallites (curves 1, 2) and hardness (curve 1', 2') of the Ti–Cr–B–N (1, 1') and Ti–B–N (2, 2') films vs. annealing temperature.

Table 2. Heat resistance of some nanostructured films.

Film	Heat resistance / °C	Ref.
TiC	400	64
TiN	650	30
TiAlN	850	30
(Ti,Al,Y)N	950	65
MSiN ^a	950	66

(M = Ti, Zr, Cr, W, Ta, Mo, Nb)

^a The silicon content does not exceed 10 at.%.

the fcc lattice at 800 °C,[§] while at 1000 °C, aluminium diffuses toward the film surface to form a protective Al₂O₃ layer, which prevents further oxidation.

The results of measurements of the oxidation depth of nanostructured Ti–B–N and Ti–Si–B–N films at various temperatures are presented in Fig. 5. It can be seen that the oxidation resistance of Ti–B–N and Ti–Si–B–N films is higher than that of TiN films, which are oxidised to depth of 800 nm at 550 °C. The Ti–Cr–B–N and Ti–Al–Si–B–N films are even more resistant against high-temperature oxidation: the depth of oxygen penetration into these films did not exceed 800 nm even after annealing at 800 °C. The high heat resistance of the Ti–Cr–B–N and Ti–Al–Si–B–N films is due to the formation of (Ti,Cr)BO₃ and Ti_xAl_ySiO_z oxide-based protective layers on their surfaces. In terms of the high-temperature oxidation resistance, these films can be arranged in the order TiN > Ti–B–N > Ti–Si–B–N > Ti–Cr–B–N > Ti–Al–Si–B–N (the authors' data).

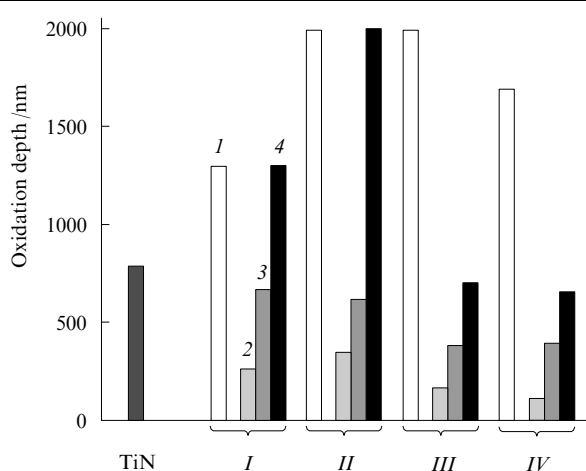


Figure 5. Oxidised layer thickness in the Ti–B–N (I), Ti–Si–B–N (II), Ti–Cr–B–N (III) and Ti–Al–Si–B–N (IV) films vs. annealing temperature. For comparison, the oxidation depth for the TiN coating after annealing at 550 °C is given.

(1) Film thickness, (2) thickness of the oxidised layer after film annealing at a temperature of 600 °C, (3) the same at 700 °C, (4) at 800 °C.

For a number of practical applications, for example, for high-speed cutting or for mechanical tooling in a fluid lubricant, it is important that the films combine high heat resistance with corrosion resistance. The electrochemical testing of the Ti–B–N films carried out in 1 N H₂SO₄ at room temperature demonstrated advantages of chromium-doped films over non-doped or silicon- and aluminium-doped films.³⁶ The Ti–Cr–B–N films have greater positive free corrosion potentials and fourfold lower current density (corrosion rate at the passivation potential) compared to those of the Ti–B–N films, whereas the Ti–Si–B–N and Ti–Al–Si–B–N films have low corrosion and passivation resistances. The corrosion rates of the Ti–Si–B–N and Ti–Al–Si–B–N films under passivation conditions were 6.6 and 14 times higher, respectively, and the free corrosion potentials were more negative than those of the Ti–B–N film. This experiment shows that introduction of chromium in the Ti–B–N films results in stabilisation of the protective oxide layer on the film surface under anodic polarisation conditions.

The above data indicate that the progress in the design of solid wear-resistant nanostructured coatings implies imparting qualitatively new properties and multifunctional character to these coatings. In addition to high hardness and wear resistance, these coatings have low friction coefficients, and high thermal stability and heat and corrosion resistances.

III. Multifunctional nanostructured films for medicine

A topical scientific and technological task of modern biology and materials science is the design of new biomaterials able to accelerate the adaptation of artificial implants to living tissues and markedly increase their service life. The complexity of the problem is due to the fact that none of the materials currently used to produce implants possesses all properties of the bone tissue. New biomaterials for implants should combine the advantages of various materials, in particular, biocompatibility, bioactivity, corrosion stability in physiological media, high fatigue strength and rupture strength, low elastic modulus and friction coefficient, high wear resistance.

Metals and alloys are used most often to produce implants. The use of titanium, stainless steel 316-L and the Cr–Co–Mo alloy (vitallium) in medical practice for the manufacture of implants started back in 1937. However, pure titanium has a relatively low wear resistance; therefore, in medicine it has been replaced by the Ti–Al–V alloys, which are not only biocompatible but also show high mechanical strength, corrosion resistance, fatigue strength and wear resistance. However, the toxicity of vanadium and the side effects caused by the presence of aluminium ions (high risks of thrombus formation and neural disorder) restrict the use of Ti–Al–V alloys in medicine.^{75, 76} In order to eliminate the adverse effect of Al and V ions, new titanium alloys were developed, e.g., Ti–Nb–Zr⁷⁵ and Ti–In–Nb–Ta.⁷⁷

The Ni–Ti, Ni–Cr–Mo and Au–Pt alloys and BT1-0, BT5 and BT14 titanium alloys are often used in medicine. Note that the metal or alloy surface is bioinert and cannot adsorb biological molecules or form chemical bonds with living tissues; therefore, in order to increase the bioactivity of metals and alloys, a hydroxyapatite layer [Ca₁₀(PO₄)₆(OH)₂, HAP], is often applied on their surface.[¶] Unfortunately, HAP cannot be applied on the surfaces of implants operating under load, as it has low strength and crack resistance compared to those of bone tissue.^{78, 79}

Yet another class of materials widely used in medicine includes ceramic materials TiN, TiO₂, SiO₂, Al₂O₃, ZrO₂ and SiC. Thus owing to its excellent mechanical properties, zirconia-based ceramics has been used in endoprosthesis replacement (as parts of artificial joints and couplings) since the late 1960s.^{80, 81} In 2003, the United States Food and Drug Administration (FDA) approved the use of Al₂O₃ in medicine. However, neither ZrO₂ nor Al₂O₃ can form chemical bonds with the bone tissue. Ceramics based on TiN is better suited for medical purposes. Titanium nitride (as a thin coating) is widely used to protect the surface of dentures, artificial hip joints and cardiac valves.^{82–85} This is due to the combination of several useful properties in TiN films, e.g., high hardness, relatively high corrosion stability and biocompatibility. In addition, TiN (Refs 86, 87) and TiO₂ (Ref. 88) films possess high hemocompatibility. However, TiN has a too high friction coefficient and too low wear resistance to ensure a long service life. It is significant to note that SiO₂ and TiO₂ coatings have a negatively charged surface within the human body (environ-

[§] A 800-nm thick titanium oxide layer is formed on the surface of the standard titanium nitride film under the same conditions.

[¶] A layer of HAP and calcium phosphate is often used as a bioactive boundary between the implant and the surrounding tissue due to the close similarity of their chemical and mineral components.

ment acidity pH 7), resulting in the formation of a hydroxyapatite layer.⁸⁹ Amorphous silicon carbide-based alloys are used to improve the biocompatibility of artificial cardiac valves.⁹⁰ The drawbacks of the ceramics include enhanced brittleness, high elastic modulus and low bioactivity if any.

Carbon-based coatings deserve special note. Diamond-like carbon, a metastable form of amorphous carbon containing a considerable number of $C(sp^3)-C(sp^3)$ bonds, is a solid wear- and corrosion-resistant material with a low friction coefficient, chemical inertness and biocompatibility.^{91,92}

Bioactive ceramics initiates the formation of a bone-like apatite layer on its surface, and through this layer the material is bound to the bone tissue. The formation of an apatite layer on the ceramic surface is possible if the ceramics contains some Ca, Si, P, C and O atoms.^{93,94} The formation of an apatite layer is related to the formation of OH groups on the charged surface of bioactive ceramics in the living organism.^{95–97} The silicate ceramics $CaO-SiO_2$ (Refs 95 and 96) and $CaO-MgO-2SiO_2$ (Ref. 98) show good bioactivity and biocompatibility. The introduction of bioinert additives such as ZrO_2 into the bioactive matrix may improve mechanical properties.⁹⁹ A drawback of this ceramics is enhanced brittleness, high elastic modulus, limited plasticity and low cracking resistance.

A possible way of improving the properties of metallic implants operating under load is their coating with protective films with multifunctional properties. Recently a fundamentally new approach to the design of biocompatible thin-film materials has been developed; according to this approach, additional elements (Ca, Zr, Mn, O, P) are introduced into titanium carbide-, carbonitride- or silicide-based films to improve the mechanical and tribological properties of the material and ensure the bioactive properties and biocompatibility of the surface.^{100–104} Inorganic additives, CaO , ZrO_2 , TiO_2 , $KMnO_4$ and HAP, are introduced during the self-propagating high-temperature synthesis (SHS) of composite targets, which are subsequently used for the ion plasma film deposition. The use of high-power metal ion beam-assisted magnetron sputtering of such composite targets allows one to modify the surface of the metallic implants. This process gives dense films with high adhesion strength and controlled elemental composition. The nanocomposite $TiC-CaO$ films can also be manufactured by a mixed PVD/PACVD process, which represents a combination of the magnetron sputtering from a composite target $Ti_{0.5} + CaO$ and plasma assisted chemical vapour deposition (PACVD). The activated plasma is used to increase the ionisation degree of the sputtered particles.^{105–108}

Since the bulk ceramic materials have high Young modulus and rather low plasticity, their deformation is accompanied by the formation and propagation of cracks resulting in fast destruction of the material. An important advantage of MNF is that they possess high hardness and rather low elastic modulus, which is much lower than that of Al_2O_3 , TiN , SiC or ZrO_2 ceramic materials. The low Young modulus of the MNF, similar to that of bone tissue (30 GPa), results in a better bearing of functional loads by a bone tissue and stimulates growth of the bone tissue. Thus, MNF represent a new unique type of material for medical applications combining high hardness with elastic recovery. Whereas the H^3/E^2 parameter of bulk ceramics (TiN , TiO_2 , SiO_2 , ZrO_2 and SiC) does not exceed 0.2 GPa, in the case of MNF, it varies from 0.1 to 0.9 GPa. Multifunctional nanostructured films exhibit high resistance against elastic strain to failure as compared with bulk ceramics.⁵⁴ The H/E parameter is also a measure of the wear resistance of a material.¹⁰⁹

The biocompatibility of new materials is now estimated by two types of testing, first, studies of the *in vitro* cytocompatibility (cytotoxicity) and of the *in vivo* biocompatibility. The adhesion of cells followed by spreading on the implant surface is the first stage of interaction between the organism cells and

the implant. This stage is crucial, as this determines the material biocompatibility. The shape and degree of cell spreading on the substrate depends on the actinic cytoskeleton. Since artificial implants are used most often to replace the bone tissue, of particular interest is their interaction with fibroblasts (connective tissue cells) and osteoblasts (bone tissue cells). The effective spreading of cells is necessary for proliferation and, in the case of osteoblasts, for the subsequent differentiation resulting in the formation of bone tissue from hydroxyapatite.¹¹⁰

Effective implantation requires integration of the implants into the tissue medium and their firm connection to the bone without interlayers, *i.e.*, osteointegration. The effect of the implant material on the capability of bone cells (osteoblasts) for differentiation is estimated in *in vitro* experiments using various cell systems, for example, MC3T3-E1 mice osteoblasts or primary cultures of rat osteoblasts isolated from newborn animals.

The biocompatibility is usually estimated in *in vivo* studies by hypodermic implantation of the materials tested in animals.^{100,101} These studies are necessary, first of all, because the implantation of artificial materials in a living organism usually induces acute and chronic inflammatory processes, the degree of which depends directly on the biocompatibility of the implants. The inflammatory responses are due to polymorphonuclear leucocytes (neutrophils) and lymphocytes, which are accumulated in the inflamed area. Macrophages are also accumulated on the surface of the foreign object; they can be combined to form multinucleate giant cells. It is considered that these giant cells of foreign objects are most active and play the crucial role in the implant destruction.¹¹¹ The activated macrophages produce cytokines ($TNF\alpha$), which accumulate neutrophils and lymphocytes, promoting the inflammation.¹¹² Macrophages can release osteoinductive signals, in particular, bone morphogenetic proteins.^{111,112} Bone osteoinductive proteins are known to stimulate the differentiation of osteoblasts and the formation of bone tissue.¹¹³ The amount of macrophages, neutrophils, lymphocytes and multinucleate giant cells on the implant surface is an important characteristics for the estimation of biocompatibility of the studied materials.

The osteointegration process is evaluated by implanting the tested materials into the bone tissue of laboratory animals. The degree of osteointegration is judged by the degree of resorption of the bone material around the implant, the structure and the maturity of the connective tissue and the newly formed cell structures. Figure 6 shows the interface between the bone and

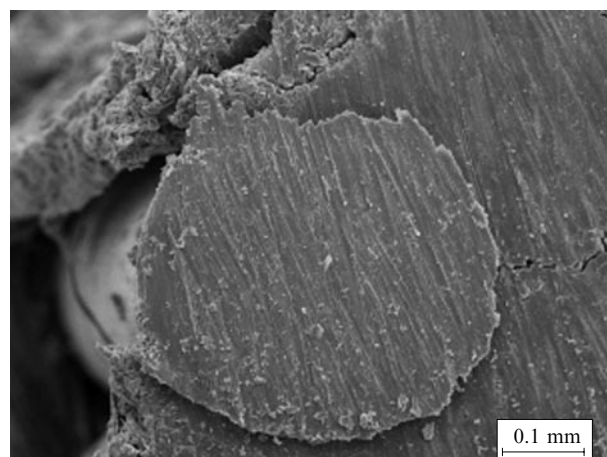


Figure 6. Interface between the bone and the titanium implant surface with the nanostructured $Ti-Ca-P-C-O-N$ coating.

the titanium implant surface with the nanostructured Ti–Ca–P–C–O–N coating 30 days after the implantation. One can see areas of tight contact between the implant and the bone without the formation of coarse-fibred structures, gaps or voids.

The biocompatible MNF obtained to date have high hardnesses (25–40 GPa) and adhesion strengths (critical load > 30 GPa), low elastic moduli (150–250 GPa), low friction coefficients (0.1–0.25) and wear rates ($< 10^{-5}$ mm³ N⁻¹ min⁻¹) in physiological media, high resistances against elastic strain to failure (> 0.1) and plastic deformation (> 0.2 GPa). They are characterised by negative charge on the surface at the acidity of the medium of pH 6–8, surface hydrophilicity and bioactivity, biocompatibility and accelerated osteointegration.^{100, 101}

Thus, MNF have a number of advantages over known bulk and thin-film analogues, which makes them promising materials for implants operating under load.

References

1. D V Shtansky, K Kaneko, Y Ikuhara, E A Levashov *Surf. Coat. Technol.* **148** 206 (2001)
2. D V Shtansky, S A Kulinich, E A Levashov, J J Moore *Fiz. Tv. Tela* **45** 1122 (2003)^a
3. *Nanostructured Coatings* (Eds A Cavaleiro, J T De Hosson) (Berlin: Springer, 2006)
4. P H Mayrhofer, C Mitterer, L Hultman, H Clemens *Prog. Mater. Sci.* **51** 1032 (2006)
5. R A Andrievskii *Usp. Khim.* **74** 1163 (2005) [*Russ. Chem. Rev.* **74** 1061 (2005)]
6. S Veprek, M G J Veprek-Heijman, P Karvankova, J Prochazka *Thin Solid Films* **476** 1 (2005)
7. *Nanostructured Thin Films and Nanodispersion Strengthened Coatings* (Eds A A Voevodin, D V Shtansky, E A Levashov, J J Moore) (Dordrecht: Kluwer Academic, 2004)
8. R A Andrievskii *Ros. Khim. Zh.* **46** (5) 50 (2002)^b
9. D V Shtansky *Ros. Khim. Zh.* **46** (5) 81 (2002)^b
10. P Jedrzejowski, J E Klemberg-Sapieha, L Martinu *Thin Solid Films* **426** 150 (2003)
11. P J Martin, A Bendavid *Surf. Coat. Technol.* **163–164** 245 (2003)
12. S Veprek, A S Argon *J. Vac. Sci. Technol., B* **20** 650 (2002)
13. H-D Männling, D S Patil, K Moto, M Jilek, S Veprek *Surf. Coat. Technol.* **146–147** 263 (2001)
14. S Veprek, M Haussmann, S Reiprich, L Shizhi, J Dian *Surf. Coat. Technol.* **86–87** 394 (1996)
15. S Veprek *J. Vac. Sci. Technol., A* **17** 2401 (1999)
16. M Diserens, J Patscheider, F Lévy *Surf. Coat. Technol.* **108–109** 241 (1998)
17. P Losbichler, C Mitterer, P N Gibson, W Gissler, F Hofer, P Warbichler *Surf. Coat. Technol.* **94–95** 297 (1997)
18. S Veprek, P Nesladek, A Niederhofer, F Glatz, M Jilek, M Sima *Surf. Coat. Technol.* **108–109** 138 (1998)
19. R A Andrievskii, G V Kalinnikov *Surf. Coat. Technol.* **142–144** 573 (2001)
20. R A Andrievskii, G V Kalinnikov, A E Oblezov, D V Shtansky *Dokl. Akad. Nauk* **384** 36 (2002)^c
21. P Karvankova, M G J Veprek-Heijman, O Zindulka, A Bergmaier, S Veprek *Surf. Coat. Technol.* **163–164** 149 (2003)
22. C Mitterer, P H Mayrhofer, J Musil *Vacuum* **71** 279 (2003)
23. D V Shtansky, E A Levashov, N N Khavskii, J J Moore *Izv. Vyssh. Uchebn. Zaved., Tsv. Metallurg.* (1) 59 (1996)
24. J L He, S Miyake, Y Setsuhara, I Shimizu, M Suzuki, K Numata, H Saito *Wear* **249** 498 (2001)
25. C Héau, J P Terrat *Surf. Coat. Technol.* **108–109** 332 (1998)
26. M Stoiber, C Mitterer, T Schoeberl, E Badisch, G Fontalvo, R Kullmer *J. Vac. Sci. Technol., B* **21** 1084 (2003)
27. M Tamura, H Kubo *Surf. Coat. Technol.* **54–55** 255 (1992)
28. C Rebholz, H Ziegele, A Leyland, A Matthews *J. Vac. Sci. Technol., A* **16** 2851 (1998)
29. R A Andrievskii, G V Kalinnikov, N P Kobelev, Ya M Soifer, D V Shtansky *Fiz. Tv. Tela* **39** 1859 (1997)^a
30. L A Donohue, I J Smith, W-D Münz, I Petrov, J E Greene *Surf. Coat. Technol.* **94–95** 226 (1997)
31. E Pflüger, A Schröer, P Voumard, L Donohue, W-D Münz *Surf. Coat. Technol.* **115** 17 (1999)
32. D V Shtansky, A N Sheveiko, M I Petrzhik, F V Kiryukhantsev-Korneev, E A Levashov, A Leyland, A L Yerokhin, A Matthews *Surf. Coat. Technol.* **200** 208 (2005)
33. D V Shtansky, F V Kiryukhantsev-Korneev, A N Sheveiko, I A Bashkova, O V Malochkin, E A Levashov, N B D'yakonova, I V Lyasotskii *Fiz. Tv. Tela* **47** 242 (2005)^a
34. F V Kiryukhantsev-Korneev, D V Shtansky, A N Sheveiko, E A Levashov, I V Lyasotskii, N B D'yakonova *Fiz. Met. Metalloved.* **97** 96 (2004)^d
35. D V Shtansky, E A Levashov, A N Sheveiko, J J Moore *J. Mater. Synth. Process.* **7** 187 (1999)
36. D V Shtansky, E A Levashov, A N Sheveiko, J J Moore *J. Mater. Synth. Process.* **6** 61 (1998)
37. O Knotek, R Breidenbach, F Jungblut, F Löffler *Surf. Coat. Technol.* **43–44** 107 (1990)
38. C Mitterer, M Rauter, P Röthhammer *Surf. Coat. Technol.* **41** 351 (1990)
39. D V Shtansky, I V Lyasotsky, N B Dyakonova, F V Kiryukhantsev-Korneev, S A Kulinich, E A Levashov, J J Moore *Surf. Coat. Technol.* **182** 204 (2004)
40. S Veprek, S Reiprich *Thin Solid Films* **268** 64 (1995)
41. E A Levashov, V I Kosayanin, L M Krukova, J J Moore, D L Olson *Surf. Coat. Technol.* **92** 34 (1997)
42. D V Shtansky, E A Levashov, A N Sheveiko, J J Moore *Metall. Mater. Trans., A* **30** 2439 (1999)
43. A A Voevodin, J P O'Neill, S V Prasad, J S Zabinski *J. Vac. Sci. Technol., A* **17** 986 (1999)
44. C Louro, A Cavaleiro, S Dub, P Smid, J Musil, J Vleck *Surf. Coat. Technol.* **161** 111 (2002)
45. M Stüber, H Leiste, S Ulrich, H Holleck, D Schild *Surf. Coat. Technol.* **150** 218 (2002)
46. S Carvalho, L Rebouta, E Ribeiro, F Vaz, M F Denannot, J Pacaud, J P Rivière, F Paumier, R J Gaboriaud, E Alves *Surf. Coat. Technol.* **177–178** 369 (2004)
47. E Martinez, R Sanjinés, A Karimi, J Esteve, F Lévy *Surf. Coat. Technol.* **180–181** 570 (2004)
48. V G Gryaznov, I A Polonsky, A E Romanov, L I Trusov *Phys. Rev., B* **44** 42 (1991)
49. R A Andrievskii, G V Kalinnikov, D V Shtansky *Fiz. Tv. Tela* **42** 741 (2000)^a
50. J Musil, S Miyake *Novel Materials Processing by Advanced Electromagnetic Energy Sources (MAPEES'04)* (Amsterdam: Elsevier, 2005) p. 345
51. J Musil *Surf. Coat. Technol.* **125** 322 (2000)
52. J Musil, F Kunc, H Zeman, H Poláková *Surf. Coat. Technol.* **154** 304 (2002)
53. D V Shtansky, S A Kulinich, E A Levashov, A N Sheveiko, F V Kiryukhantsev, J J Moore *Thin Solid Films, C* **420–421** 330 (2002)
54. A Leyland, A Matthews *Wear* **246** 1 (2000)
55. A A Voevodin, J J Hu, T A Fitz, J S Zabinski *J. Vac. Sci. Technol., A* **20** 1434 (2002)
56. A A Voevodin, J S Zabinski *Thin Solid Films* **370** 223 (2000)
57. D V Shtansky, T A Lobova, V Yu Fominski, S A Kulinich, I V Lyasotsky, M I Petrzhik, E A Levashov, J J Moore *Surf. Coat. Technol.* **183** 328 (2004)
58. R A Andrievskii *Usp. Khim.* **71** 967 (2002) [*Russ. Chem. Rev.* **71** 853 (2002)]
59. S Veprek, H-D Mannling, M Jilek, P Holubar *Mater. Sci. Eng., A* **366** 202 (2004)
60. A P Marques, A Cavaleiro *Thin Solid Films* **441** 150 (2003)
61. L Karlsson, A Horling, M P Johansson, L Hultman, G Ramanath *Acta Mater.* **50** 5103 (2002)
62. S PalDey, S C Deevi *Mater. Sci. Eng., A* **342** 58 (2003)
63. D V Shtansky, E A Levashov, A N Sheveiko, J J Moore *Izv. Vyssh. Uchebn. Zaved., Tsv. Metallurg.* (1) 67 (1999)
64. W D Münz *J. Vac. Sci. Technol., A* **4** 2717 (1986)

65. I Wadsworth, I J Smith, L A Donohue, W-D Münz *Surf. Coat. Technol.* **94–95** 315 (1997)
66. S Veprek, M Hausmann, S Reiprich *Mater. Res. Soc. Symp. Proc.* **400** 261 (1996)
67. H Zeman, J Musil, P Zeman *J. Vac. Sci. Technol., A* **22** 646 (2004)
68. J Musil, R Daniel, P Zeman, O Takai *Thin Solid Films* **478** 238 (2005)
69. J Musil, P Dohnal, P Zeman *J. Vac. Sci. Technol., B* **23** 1568 (2005)
70. P Zeman, J Musil, R Daniel *Surf. Coat. Technol.* **200** 4091 (2006)
71. D Zhong, J J Moore, B M Mishra, T Ohno, E A Levashov, J Disam *Surf. Coat. Technol.* **163–164** 50 (2003)
72. D V Shtansky, E A Levashov, A N Sheveiko *Galvanotechnik* **88** 3368 (1997)
73. D V Shtansky, E A Levashov, A N Sheveiko, J J Moore *Int. J. Self-Propag. High-Temp. Synth.* **7** 249 (1998)
74. Y Tanaka, T M Gur, M Kelly *J. Vac. Sci. Technol., A* **10** 1749 (1992)
75. J A Davidson, A K Mishra, P Kovacs, R A Poggie *Biomed. Mater. Eng.* **4** 231 (1994)
76. S J Lugowski, D C Smith, A D McHugh, J C Van Loon *J. Biomed. Mater. Res.* **25** 1443 (1991)
77. B-H Lee, Y D Kim, K H Lee *Biomaterials* **24** 2257 (2003)
78. S F Hulbert, F A Young, R S Mathews, J J Klawitter, C D Talbert, F H Stelling *J. Biomed. Mater. Res.* **4** 433 (1970)
79. L L Hench *J. Am. Ceram. Soc.* **74** 1487 (1991)
80. C Piconi, G Maccauro *Biomaterials* **20** 1 (1999)
81. E Adolfsson, L Hermanson *Biomaterials* **20** 1263 (1999)
82. P V Kola, S Daniels, D C Cameron, M S J Hashmi *J. Mater. Process. Technol.* **56** 422 (1996)
83. S Mändl, B Rauschenbach *Surf. Coat. Technol.* **156** 276 (2002)
84. P A Dearnley *Proceedings of the Institution of Mechanical Engineers, Part H (J. Eng. Med.)* Vol. 213 (London: Professional Eng. Publ., 1999) p. 107
85. S Piscanec, L C Ciacchi, E Vesselli, G Comelli, O Sbaizero, S Meriani, A de Vita *Acta Mater.* **52** 1237 (2004)
86. I Dion, X Roques, N More *Biomaterials* **14** 712 (1993)
87. J J A M Van Raay, P M Rozing, C A Van Blitterswijk, R M Van Haastert, H K Koerten *J. Mater. Sci.: Mater. Med.* **6** 80 (1995)
88. N Huang, P Yang, Y X Leng, J Y Chen, H Sun, J Wang, G J Wang, P D Ding, T F Xi, Y Leng *Biomaterials* **24** 2177 (2003)
89. P J Li, C Ohtsuki, T Kokubo, K Nakanishi, N Soga, K de Groot *J. Biomed. Mater. Res.* **28** 7 (1994)
90. A Bolz, M Schaldach *Artif. Organ.* **14** 260 (1990)
91. R Hauert *Diamond Relat. Mater.* **12** 583 (2003)
92. A Grill *Diamond Relat. Mater.* **12** 166 (2003)
93. S H Maxian, J P Zawadsky, M G Dunn *J. Biomed. Mater. Res.* **28** 1311 (1994)
94. X Y Liu, P K Chu, C X Ding *Mater. Sci. Eng., R* **47** 49 (2004)
95. P N De Aza, Z B Luklinska, M R Anseau, M Hector, F Guitivn, S De Aza *Biomaterials* **21** 1735 (2000)
96. T Kokubo, H-M Kim, M Kawashita *Biomaterials* **24** 2161 (2003)
97. P Li, I Kangasniemi, K De Groot *Bioceramics* **6** 41 (1993)
98. T Nonami, S Tsutsumi *J. Mater. Sci.: Mater. Med.* **10** 475 (1999)
99. H Ji, P M Marquis *Biomaterials* **13** 744 (1992)
100. D V Shtansky, N A Glushankova, I A Bashkova, M A Kharitonova, T G Moizhess, A N Sheveiko, F V Kiryukhantsev-Korneev, M I Petrzhik, E A Levashov *Biomaterials* **27** 3519 (2006)
101. D V Shtansky, N A Glushankova, A N Sheveiko, M A Kharitonova, T G Moizhess, E A Levashov, F Rossi *Biomaterials* **26** 2909 (2005)
102. D V Shtansky, E A Levashov, N A Glushankova, N B D'yakonova, S A Kulinich, M I Petrzhik, F V Kiryukhantsev-Korneev, F Rossi *Surf. Coat. Technol.* **182** 101 (2004)
103. D V Shtansky, E A Levashov, N A Glushankova, I V Lyasotskii, F Rossi *Fiz. Met. Metalloved.* **97** 34 (2004)^d
104. D V Shtansky, I A Bashkova, E A Levashov, T A Chipysheva, Yu M Vasil'ev, N A Glushankova *Dokl. Akad. Nauk* **404** 267 (2005)^e
105. W Kulisch, P Colpo, P N Gibson, G Ceccone, D V Shtansky, E A Levashov, F Rossi *Surf. Coat. Technol.* **188–189** 735 (2004)
106. W Kulisch, P Colpo, F Rossi, D V Shtansky, E A Levashov *Surf. Coat. Technol.* **188–189** 714 (2004)
107. W Kulisch, P Colpo, P N Gibson, G Ceccone, D V Shtansky, E A Levashov, M Jelinek, P J M Philip, F Rossi *Appl. Phys. A: Mater. Sci. Process.* **82** 503 (2006)
108. J C Imbert, L de Pouques, C Boisse-Laporte, J Bretagne, M C Hugon, L Teulè-Gay, M Touzeau, D Shtansky, O Voldoire *Surf. Coat. Technol.* **200** 717 (2005)
109. A Leyland, A Matthews *Surf. Coat. Technol.* **177–178** 317 (2004)
110. K Anselme *Biomaterials* **21** 667 (2000)
111. C M Champagne, J Takebe, S Offenbacher, L F Cooper *Bone* **30** 26 (2002)
112. P L E M Van Lent, A B Blom, P Van der Kraan, A E M Holthuysen, E Vitters, N Van Rooijen, R L Smeets, K C A M Nabbe, W B Van den Berg *Arthritis Rheum.* **50** 103 (2004)
113. J M Wozney *Spine* **27** (16S) S2 (2002)

^a — *Phys. Solid. State (Engl. Transl.)*

^b — *Mendeleev Chem. J. (Engl. Transl.)*

^c — *Dokl. Phys. (Engl. Transl.)*

^d — *Phys. Met. Metallogr. (Engl. Transl.)*

^e — *Dokl. Biochem. Biophys. (Engl. Transl.)*

Long-range surface forces and their role in the progress of nanotechnology

L B Boinovich

Contents

I. Introduction	471
II. The surface forces and stability of disperse systems	472
III. Dispersion (van der Waals) forces	472
IV. Ionic electrostatic interactions	475
V. Progress in the theory of dispersion forces	476
VI. Progress in the theory of ionic electrostatic interactions	477
VII. Electrostatic interactions in non-polar media	478
VIII. Interaction forces caused by modified structure of liquid interlayer	479
IX. Conclusion	486

Abstract. Different theories of stability of liquid nanolayers, disperse and colloidal systems are considered. Limitations intrinsic in the classical Derjaguin–Landau–Verwey–Overbeek (DLVO) theory (in particular, calculations of the van der Waals forces acting between macroscopic bodies separated by a thin liquid interlayer) are briefly outlined. Studies devoted to the analysis and calculations of non-DLVO interactions of different nature are reviewed. Particular attention is paid to the forces caused by the inhomogeneity of liquid interlayers. The applicability of the known approaches for solving the nanotechnology challenges (namely, calculations of interaction forces acting through nanolayers and between nanoparticles) is discussed. The bibliography includes 174 references.

I. Introduction

Nanoscience and nanotechnology are two relatively young fields of science and technology. They are based on a theoretical assumption that reduction of the particle size to nanoscale leads to significant changes in the known properties of the corresponding materials and to the appearance of new properties that are not inherent in the bulk state. Later, this assumption was confirmed experimentally. Progress in these new fields of natural science concerns almost all avenues of human activity from biology and medicine to production of polymeric materials, metallurgy, microelectronics, space research, *etc.* Although formally nanoscience and nanotechnology emerged only 20–25 years ago, studies concerned with the dependence of the properties of nanosystems on their size date back to the 1940s. For instance, at that time Derjaguin repeatedly pointed to the dependence of the structure of water in thin liquid interlayers on the interlayer thickness. Manufacture of ultra-disperse powders, a new production area established in the

USSR in the 1950s, was based on the observed dependence of the properties of nanoparticles on the particle size.

A specific feature of small objects is that the smaller the particles the greater the percentage of the molecules (atoms) in the near-interface layer that strongly interact with the phases that bound the object under study. Therefore, reduction of the size of such an object leads to an increase in the surface-to-volume ratio and to a more pronounced effect of the surface phenomena on the properties of the object. Yet another feature of such systems is a stronger effect of the size of small particles on the character of collective phenomena and on the density of states of elementary excitations in the systems.

These features point to the key role of two-phase and three-phase surface phenomena in nanotechnological processes. A considerable proportion of physicochemical studies on these phenomena are carried out using the methods of physics of fluids and colloid chemistry. This is due to the fact that fluids are active participants of liquid-phase chemical synthesis of nanoparticles. The properties of fluids affect the size and stability of particles produced, the course of chemical reactions on the surface of such particles and the strength and character of adsorption at interfaces. In addition, solid nanoparticles prepared using all the known methods¹ were designed for operation under atmospheric conditions or in industry rather than laboratories with controllable gaseous medium. When nanomaterials are exposed to atmosphere, the small size of the objects made of them becomes of crucial importance, because it causes the formation of either capillary condensate in nanoporous media or wetting films on the surfaces of certain particles. As a result, a nanomaterial with well-studied (under laboratory conditions) properties is replaced by a composite nanosystem comprising the solid nanomaterial and a liquid interlayer or capillary bridges. The properties of the system as a whole are determined by the properties of not only the solid phase, but also the liquid interlayer, the character of the interaction between the liquid and the solid nanoparticles and, finally, the character of the interaction between nanoparticles separated by the liquid interlayer. The presence of liquid interlayers can play a decisive role in, *e.g.*, self-organization of nanoparticles, their flowability, *etc.*

Even the examples given above point to particular importance of the studies on the properties of liquids in the nano state

L B Boinovich A N Frumkin Institute of Physical Chemistry and Electrochemistry, Russian Academy of Sciences, Leninsky prosp. 31, 119991 Moscow, Russian Federation. Fax (7-495) 952 53 08, tel. (7-495) 955 46 25, e-mail: boinovich@mail.ru

Received 20 December 2006

Uspekhi Khimii 76 (5) 510–528 (2007); translated by A M Raevskiy

for further progress in nanotechnology. In spite of a variety of challenges in this field, here we will dwell on one problem, namely, stability of liquid nanofilms and disperse and colloidal systems. We believe that this problem is of paramount importance for the development of scientific foundations of nanotechnology; in addition, the author of this review was directly involved in research in this field.

II. The surface forces and stability of disperse systems

A modern physical theory that describes the state and stability of liquid films and the disperse and colloid systems is based on the analysis of the surface forces acting across thin liquid interlayers separating particles or macroscopic surfaces. Here, the surface forces play the same role as the intermolecular interaction forces in condensed systems. In the 1940s, Derjaguin showed² that consideration of the interactions between two surfaces approaching each other is equivalent to consideration of the dependence of the disjoining pressure on the interlayer thickness. The dependence of the disjoining pressure on the thickness of the liquid interlayer is the key thermodynamic characteristic of the thin interlayer that distinguishes it from the bulk liquid. In particular, if the interlayer thickness is such that its medium fragment retains the properties of the bulk phase and, therefore, there is no overlap of the boundary layers adjacent to the interfaces, the disjoining pressure in the interlayer is zero. On the contrary, overlap of the boundary layers leads to anisotropy of the pressure tensor in the interlayer and to appearance of the disjoining pressure $[\Pi(h)]$ dependent on the thickness of the liquid interlayer,

$$\Pi(h) = P_N(h) - P_0, \quad (1)$$

where $P_N(h)$ is the normal component of the pressure tensor in the thin interlayer with thickness h and P_0 is the pressure in the bulk isotropic fluid that is in equilibrium with the interlayer. The character of the dependence of the disjoining pressure on the liquid film thickness characterises the physical nature of the forces that govern the interaction between two surfaces separated by the liquid interlayer. The nature of the interaction forces is naturally determined by three factors, namely, characteristics of the interacting bodies, properties of the fluid, constituting the interlayer and the character of the interaction between the fluid and the boundary phases and, as a consequence, by the dependence of the properties of fluid in the interlayer on the interlayer thickness.

Quantitative analysis of the surface forces is based on the Gouy–Chapman^{3–5} theory of diffuse ionic atmospheres and the theory of molecular forces by London.⁶ These two approaches underlie the Derjaguin–Landau–Verwey–Overbeek (DLVO) theory of stability of lyophobic colloids.^{7,8} In the framework of the DLVO theory, the total interaction energy is determined by the dispersion (van der Waals) and electrostatic mechanisms. Now we will consider them in more detail.

III. Dispersion (van der Waals) forces

The dispersion forces are universal in character and act in all systems. In 1930, London reported a general quantitative theory of the van der Waals forces.⁶ Since then the theory of dispersion interactions between macroscopic bodies separated by an interlayer was developed using two different approaches, a microscopic and a macroscopic one.

The former approach is associated with de Boer⁹ and Hamaker.¹⁰ Here, the force of molecular attraction between identical macroscopic bodies is treated as the resultant of the London attraction forces acting between all pairs of molecules in the body. Details of calculations are available from original

studies and monographs.^{2,8,11} This approach allowed one to derive analytical expressions for calculation of the force of the interaction between two spheres, a sphere and a plane and two planes separated by a vacuum interlayer for both thin and thick interlayers (in the non-retarded limit and with allowance for electromagnetic retardation).[†] Hamaker's interaction constant addition rule¹⁰ makes it possible to extend the microscopic approach to the interactions of condensed bodies separated by a condensed-phase interlayer. However, the state-of-the-art in physics of condensed media is such that the additivity of the London forces in the calculation of the interactions between macroscopic bodies separated by dense-phase interlayers is quite a rough approximation. Thus, the simplicity of the microscopic method of calculations does not compensate for quantitative (in the case of absorbing interlayers, also qualitative) errors in the results of interaction force calculations.

A rigorous macroscopic approach to calculations of dispersion interactions between two bodies separated by a vacuum interlayer or an absorbing condensed phase was reported by Lifshitz *et al.*^{12,13} [Dzyaloshinskii–Lifshitz–Pitaevskii (DLP) theory]. The formalism treats the bodies separated by a thin interlayer as continuous media interacting through fluctuating electromagnetic field. The interlayer thickness is assumed to be much greater than the size of the molecules constituting the bodies. Dzyaloshinskii, Lifshitz and Pitaevskii¹² took into account that the force of the interaction between bodies in vacuum coincides with the zz -component of the averaged Maxwell stress tensor, which was calculated by solving the Maxwell equations with inclusion of fluctuation field sources. To perform the field averaging procedure, the fluctuation-dissipation theorem was applied to the field sources. Later,¹⁴ it was shown that the problem of determination of the stress tensor in the case of two macroscopic bodies separated by vacuum and by an interlayer is reduced to calculations of corresponding Green functions. Since the DLP theory is based on exact Maxwell equations, the retardation effects are included by default. The expression for calculating the disjoining pressure $\Pi(h)$ equal to the specific force of the interaction between macroscopic bodies separated by a homogeneous plane-parallel liquid interlayer of thickness h has the form¹³

$$\begin{aligned} \Pi(h) = & -\frac{kT}{\pi c^3} \sum_{N=0}^{\infty} \xi_N^3 \varepsilon_3^{3/2} \int_1^{\infty} p^2 \left\{ \left[\frac{(s_1+p)(s_2+p)}{(s_1-p)(s_2-p)} \times \right. \right. \\ & \times \exp\left(\frac{2p\xi_N h \varepsilon_3^{1/2}}{c}\right) - 1 \left. \right]^{-1} + \left[\frac{(s_1+ap)(s_2+bp)}{(s_1-ap)(s_2-bp)} \times \right. \\ & \times \exp\left(\frac{2p\xi_N h \varepsilon_3^{1/2}}{c}\right) - 1 \left. \right]^{-1} \left. \right\} dp. \end{aligned} \quad (2)$$

Here k is the Boltzmann constant; T is temperature; c is the speed of light; p is the integration variable, $\xi_N = 2\pi k T N / \hbar$ (N is a natural number, \hbar is the Planck constant); ε_1 , ε_2 and ε_3 are the dielectric permittivities of the macroscopic bodies 1 and 2 and of the liquid interlayer 3 considered as functions of the imaginary field frequency ($\omega = i\xi$), *i.e.*, $\varepsilon = \varepsilon_f(i\xi_N)$; $s_1 = (a - 1 + p^2)^{1/2}$, $s_2 = (b - 1 + p^2)^{1/2}$, where $a = \varepsilon_1/\varepsilon_3$, $b = \varepsilon_2/\varepsilon_3$. The prime at the sum points that the first term in the sum corresponding to $N = 0$ is to be taken with a factor of 0.5. Note that direct substitution of $N = 0$ into Eqn (2) leads to uncertainty because ξ_N equals zero, whereas the integral with

[†] In principle, methods of numerical calculations in the framework of the microscopic approach allow one to calculate the interaction between bodies of arbitrary geometry.

respect to dp diverges. Once the uncertainty is disclosed,¹³ the term with $N = 0$ takes a finite value.

From relation (2) it follows that calculations of the dispersion forces only require knowledge of the frequency dependence of the dielectric permittivities of the contacting media $\varepsilon_j(i\xi_N)$. These can be determined using the Kramers–Kronig relationships[‡] and the values of the imaginary part of dielectric permittivity measured for a broad spectral range.

Analysis of relation (2) shows that the dispersion interaction between identical bodies ($\varepsilon_1 = \varepsilon_2$) is always attractive. However, in the case of different bodies (e.g., wetting films) both attractive and repulsive forces are possible depending on the behaviour of the functions $\varepsilon_j(i\xi_N)$. Moreover, since the behaviour of the functions $\varepsilon_1(i\xi_N)$, $\varepsilon_2(i\xi_N)$ and $\varepsilon_3(i\xi_N)$ in the frequency range important for these bodies is not related to the static dielectric permittivities of the contacting bodies, for certain systems the sign of the interaction force changes with variation of the liquid interlayer thickness (Fig. 1).

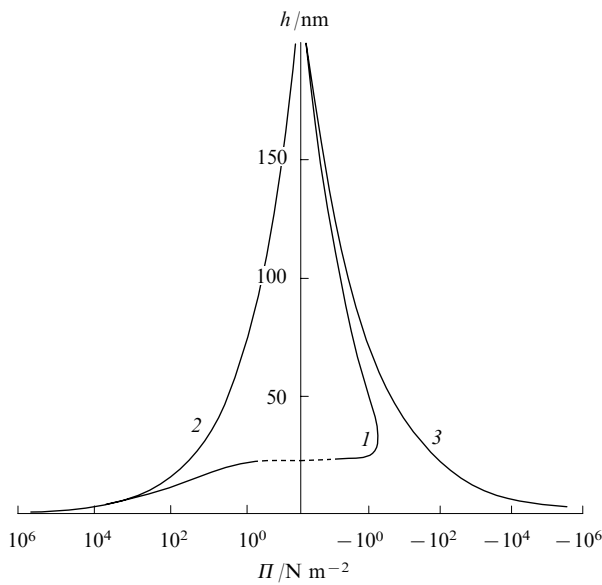


Figure 1. Change in sign of the molecular component of the disjoining pressure (dispersion forces) plotted vs. film thickness (curve 1). Shown are the results of $\Pi(h)$ calculations using Eqn (2) for the air–water–fluorite system. Curves 2 and 3 are calculated using Eqns (3a) and (3b), respectively.

Expression (2) can be simplified using integration over $d\xi = (2\pi kT/\hbar)dN$ instead of summation. However, the force calculation error due to neglect of the contribution of the term with $N = 0$ to the net integral can be significant for the polar fluid interlayers that exhibit strong absorption in the low-frequency range of electromagnetic vibrations. If we compare the interlayer thickness to the main wavelength (λ_0) in the absorption spectra of the contacting media and consider two limiting cases, namely, the thin and thick interlayer limits

‡ These are the integral relationships relating the real and imaginary parts of the complex dielectric permittivity $\varepsilon = \varepsilon'(\omega) + i\varepsilon''(\omega)$. A particular case of the Kramers–Kronig relations is the expression

$$\varepsilon(i\xi_N) = 1 + \frac{2}{\pi} \int_0^\infty \frac{\omega \varepsilon''(\omega)}{\omega^2 + \xi_N^2} d\omega,$$

which determines the values of the ε function of the imaginary argument $\omega = i\xi$. It is these $\varepsilon(i\xi_N)$ values that appear in relation (2).

($h \ll \lambda_0/2\pi$ and $h \gg \lambda_0/2\pi$, respectively), expression (2) is reduced to asymptotic relationships (3a) and (3b) for the delayed and non-delayed dispersion forces, respectively.

$$\Pi(h) = -\frac{\hbar}{8\pi h^3} \int_0^\infty \frac{(\varepsilon_1 - \varepsilon_3)(\varepsilon_2 - \varepsilon_3)}{(\varepsilon_1 + \varepsilon_3)(\varepsilon_2 + \varepsilon_3)} d\xi = -\frac{A_{132}}{6\pi h^3} \text{ at } h \ll \frac{\lambda_0}{2\pi}, \quad (3a)$$

$$\Pi(h) = -\frac{B(\varepsilon_{10}, \varepsilon_{20}, \varepsilon_{30})}{h^4} \text{ at } h \gg \frac{\lambda_0}{2\pi}. \quad (3b)$$

Here ε_{10} , ε_{20} and ε_{30} are the electrostatic dielectric permittivities of the contacting media, A_{132} and $B(\varepsilon_{10}, \varepsilon_{20}, \varepsilon_{30})$ are the dispersion force constants in the non-retarded and retarded limits, respectively. The constant B is determined by the electrostatic dielectric permittivities of the contacting media in the low-frequency range. Analysis of the disjoining pressure values calculated using exact relation (2) shows that marked deviations of the $\Pi(h)$ dependence from the h^{-3} law [expression (3a)] begin at distances of 2–3 nm. As to the h^{-4} law [relationship (3b)], the correctness of the application of this expression to a wide variety of systems is doubtful.¹⁵ In particular, if the systems are characterised by the same sign of the van der Waals forces and the contacting bodies show weak absorption in the radiofrequency and IR region, this law is reasonably obeyed at film thicknesses of 30–40 nm.² At the same time if the van der Waals forces change the sign as h increases, the h^{-4} law can be used as an asymptotic relation only at interlayer thicknesses of the order of hundreds of nanometres (see Fig. 1). From expression (3a) it follows that the dispersion force increases as the dielectric contrast (differences $\varepsilon_1 - \varepsilon_3$ and $\varepsilon_2 - \varepsilon_3$) between the contacting phases increases. As an example, Table 1 lists the Hamaker constants A_{132} of certain systems calculated using relations (2) and (3a).

An alternative approach to calculations of dispersion interactions was proposed by Van Kampen *et al.*¹⁹ The method is based on calculations (in the harmonic approximation) of the excess energy of the normal modes of surface oscillators as function of the interlayer thickness. The approach is somewhat more simple and clear compared to that used in the DLP theory,¹³ however, it proved itself as ‘heuristic and intuitive’.²⁰

Table 1. Hamaker constants of various systems.

System	Hamaker constant (A_{132})/J	Ref.
Gold–water–gold	2.5×10^{-19}	16
Gold–KCl solution–gold	4.0×10^{-19}	17
Platinum–KCl solution–platinum	1.4×10^{-19}	17
Platinum–MgSO ₄ solution–platinum	8.5×10^{-20}	17
Silicon–water–silicon	1.2×10^{-19}	17
Quartz–water–quartz	7.5×10^{-21}	16
Quartz–water–quartz	8.5×10^{-21}	18
Sapphire–water–sapphire	5.3×10^{-20}	18
Poly(vinyl chloride)–water–poly(vinyl chloride)	1.2×10^{-20}	16
Polystyrene–water–polystyrene	1.3×10^{-20}	16
Polyisoprene–water–polyisoprene	7.4×10^{-21}	18
Fluorite–water–fluorite	1.0×10^{-20}	18
Polytetrafluoroethylene–water–polytetrafluoroethylene	3.3×10^{-21}	18
Ice–water–gold	1.6×10^{-21}	16
Ice–water–silicon	-1.7×10^{-21}	16
Ice–water–quartz	3.0×10^{-23}	16
Ice–water–polystyrene	1.2×10^{-22}	16
Quartz–water–air	-1.0×10^{-20}	18
Fluorite–water–air	-1.2×10^{-20}	18

Later, Barash and Ginzburg²¹ reported a substantiation of the Van Kampen approach and analysed its applicability to the solution of new problems with arbitrary media.

Experimental studies of dispersion interactions between bodies were carried out using various model systems containing both symmetrical liquid and gaseous interlayers and wetting films. Comprehensive analysis of these studies was done in a monograph.² Without dwelling on details, note that by and large the interactions between macroscopic bodies separated by vacuum or air and the dispersion interactions of neat non-polar fluids in wetting films can well be described using the macroscopic theory of the van der Waals forces with an error of 15%–30%. Deviations in the behaviour of macroscopic bodies separated by vacuum or air interlayer from the theoretically predicted in the thin interlayer limit are associated^{22–24} with both the effect of the roughness and heterogeneity of the surface of solids and with the formation of the adsorption or oxide layers on the surface (Fig. 2). Although in each case shown in Fig. 2 the experimental data are reasonably described by the inverse cube law, the calculated Hamaker constants differ appreciably and only for curve 3 the value of this constant ($A_{132} = -0.88 \times 10^{-20}$ J) is in good agreement with the theoretical estimates for a hexane wetting film immobilised on fused quartz. At the same time, in some cases the behaviour of solids separated by liquid interlayers strongly differs from that predicted by the theory of the van der Waals forces (Figs 3 and 4). The reasons for the deviation seem to be due to the assumptions underlying the theory in the case of liquid interlayers.

Detailed analysis of the key assumptions in the DLP theory was reported by Barash and Ginzburg.²¹ They used the Green functions for the Maxwell equations to determine the contribution of the long-wavelength equilibrium electromagnetic fluctuations in matter to the free energy of a system comprising macroscopic bodies separated by a thin liquid interlayer. The solutions of the Maxwell equations were expanded over the eigenfunctions of an auxiliary system.²¹ This made it possible to reduce an infinite series for free energy calculations to a rather simple expression suitable for further analysis and reveal limitations on the use of the equations¹³ for calculating the interaction forces acting between two macroscopic bodies.

First, the DLP theory ignores the contribution of the interaction between the long-wavelength fluctuation field and matter to the dielectric permittivity (in essence, the spatial dispersion for an arbitrary system is ignored). Second, the expressions for the energy of the system and the interaction

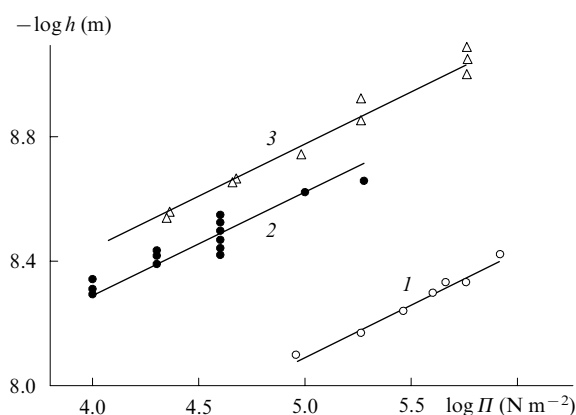


Figure 2. Disjoining pressure isotherms of hexane films on a polished substrate (roughness of about 5 nm) (1) and on molecularly smooth films-substrates (roughness at most 0.5 nm) in the presence of water vapour (2) and in anhydrous nitrogen atmosphere (3).

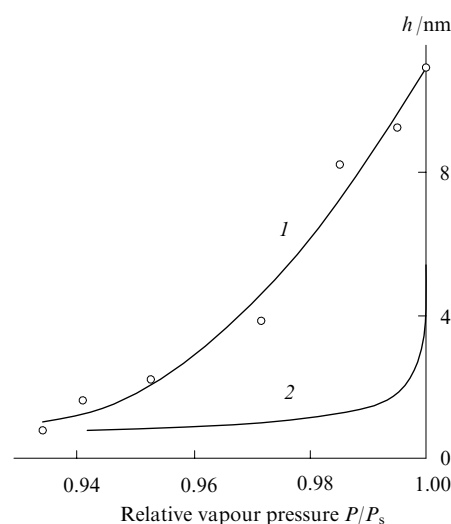


Figure 3. Adsorption isotherm of n-heptan-1-ol on an optical glass K-8. Experimental data by Derjaguin and Zorin²⁵ (1) and theoretical curve for the dispersion component of the disjoining pressure (2).

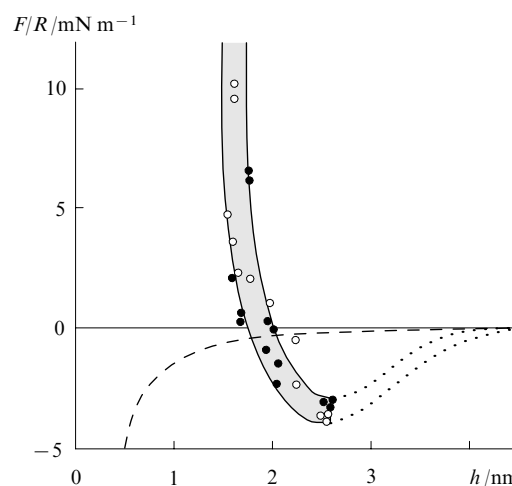


Figure 4. Reduced force (F/R) plotted vs. distance between two mica surfaces in white oil (mixture of branched alkanes) at 22 °C under different experimental conditions.²⁶

Solid circles correspond to completely anhydrous liquid existing in equilibrium with air dried over P_2O_5 , open circles correspond to completely anhydrous liquid in anhydrous nitrogen atmosphere, and the dashed line corresponds to the van der Waals forces.

Here and in Figs 5 and 9, the reduced force is the ratio of the measured force (F) of the interaction between cylindrical surfaces to the surface radius R . The shaded region between the solid lines denotes the limits of scatter of the measured values. The dotted lines denote the expected behaviour of the forces in the case of thick films.

forces derived by Dzyaloshinskii, Lifshitz and Pitaevskii assume that the volumes and dielectric permittivities of the bodies in the system do not change upon the change in the distances between the bodies. This limitation is valid for interacting macroscopic bodies, but in the case of a thin interlayer it is non-rigorous and leads to significant underestimation of the forces produced in the system. Thus, if the dielectric permittivity of the interlayer depends on the interlayer thickness and/or if the interlayer shows a spatial dispersion, the approach developed by Dzyaloshinskii, Lifshitz and Pitaevskii appears to be somewhat incorrect for the description of the interaction forces in a real system.

Both these factors act, as a rule, in complex molecular liquids, especially in the case of thin interlayers. This causes deviations of the experimental interaction curves from the dependences predicted by the DLP theory. In addition, interlayers a few Ångström thick violate one of the DLP theory conditions, according to which the film thickness much exceeds the size of the molecules. In this case, treatment of the liquid as a continuous medium is somewhat incorrect. Finally, calculations of dispersion interactions in the framework of the DLP theory ignore the existence of surface layers of the interacting bodies (dielectric permittivities of these layers can differ appreciably from the corresponding bulk characteristics used in calculations). Thus, theoretical calculations of dispersion interactions between bodies separated by a liquid or gaseous interlayer^{13,19} are reliable only for the interlayers tens of nanometres thick. In the case of thinner interlayers, such calculations are of limited use.

IV. Ionic electrostatic interactions

In the case of ionic fluids and particles having charged surfaces the stability of a liquid film is to a great extent governed by the electrostatic forces due to the overlap of the electric double layers in the liquid interlayer. The main difficulty in calculating these forces consists of the need of determining the spatial arrangement and concentration of ions in the interlayer with allowance for deformation of ionic atmospheres as the surfaces approach each other.

Rigorous calculations of the ionic electrostatic component of the disjoining pressure Π_e based on the solution of the Debye–Hückel equation for strong electrolytes were first reported by Derjaguin.²⁷ He derived equations for calculating the interactions between two identical spheres or two plates separated by a liquid interlayer. Derjaguin used the linearised Debye–Hückel equation, therefore the equations derived by him are only applicable to calculations of electrostatic forces in weakly charged sols.

The interaction of strongly charged particles in electrolyte solutions was studied by Derjaguin and Landau.^{7,28} Using the constant potential approximation for the surfaces brought closer together, they derived relationships for calculating the repulsive forces and the energy of the interaction between flat plates and convex macroscopic surfaces, formulated the coagulation criterion and substantiated the Schulze–Hardy rule according to which the coagulating concentration of electrolyte rapidly decreases as the valence of the counterion increases. Verwey and Overbeek reported an independent study⁸ of the interaction between identical plates in potentials with arbitrary magnitudes, which was also carried out in the constant potential approximation. Additionally, they introduced the Stern correction, which allows for the dense component of the electric double layer.

It should be noted that in solving the problem of electrostatic interaction of charged surfaces separated by an ionic interlayer the boundary conditions are first of all determined by the charging mechanism. In particular, if the surface charging occurs by adsorption of ions from solution and the entropy contribution to the free energy of the system is independent of the amount of adsorbed ions, the charged surfaces will approach each other under the constant-potential boundary condition. If the charging occurs by complete dissociation of surface groups, the constant-charge boundary conditions are applied. In the case of incomplete dissociation of ionised groups or if the entropy depends on the concentration of adsorbed ions, the charge-regulation boundary condition is used.^{29,30} Yet another type of boundary conditions corresponds to the interaction of ‘soft’ ion-permeable particles or polyelectrolyte particles.³¹ If the particle size much exceeds the Debye wavelength, the potential in the bulk of the particle is always equal to the Donnan potential.

The classical theory of ionic electrostatic interactions is restricted to consideration of the first two types of boundary conditions. Both analytical and numerical solutions to the problem of electrostatic interaction between charged identical surfaces (in symmetrical and non-symmetrical electrolytes, see Refs 2 and 31) were derived in the framework of this theory. There is a feature that permits essential simplification of the procedure for evaluation of the ionic electrostatic component of the disjoining pressure Π_e in the systems with unknown or interlayer-thickness-dependent surface charging mechanism. For instance, all possible dependences of Π_e on the interlayer thickness obtained under different boundary conditions lie between the curves corresponding to the constant potential of the diffuse layer boundaries and to the constant density of the surface charge and the charge of the dense Stern monolayer. The former and latter cases correspond to minimum and maximum repulsive forces, respectively.

Later, calculations of the ionic electrostatic component were generalised to electrostatic interactions between different-type particles, which are of particular value in the case of particle–electrode interaction and in electrofiltering and electrophoretic sedimentation. Derjaguin² proposed a graphical method of isodynamic curves, which allows one to estimate the magnitude and character of hetero-interactions at constant potentials of diffuse ionic layers. A feature of the case in point is that the ionic electrostatic forces acting between two likely charged particles bearing non-equal charges are repulsive in character at long distances. The repulsive forces increase as the interlayer thickness decreases, pass through a maximum and then change their character to attractive. The attractive forces increase without limit as the interlayer thickness tends to zero. Analysis showed that the maximum repulsion is determined by the surface potential of the particle bearing the smaller charge.

Considering weakly charged surfaces, an analytical solution to the problem was obtained using the linearised Poisson–Boltzmann equation for both flat interlayers (under constant potential³² and constant charge³³ boundary conditions) and spherical particles of different radii. A simple equation for calculating the energy of the interaction between spherical particles at constant potentials on both surfaces was obtained by Hogg *et al.*³² The problem with the constant charge boundary conditions was first solved by Usui.³⁴ Kar *et al.*³⁵ considered a complex case corresponding to a constant potential on one surface and a constant charge on the other surface for the case of thin (compared to the particle radii) double layers. It should be noted that the solutions were obtained for the problem of the interaction between spherical particles the radii of which much exceed the thicknesses of the liquid interlayers between them.

A general numerical method of solving the non-linear Poisson–Boltzmann equation developed by McCormack *et al.*³⁶ makes it possible to calculate electrostatic interactions between different-type surfaces in flat interlayers of symmetrical electrolytes at large surface charges not only for the abovementioned cases of constant potential and charge at both interfaces simultaneously, but also in the case where the surface of one particle has a constant charge while the other particle has a constant potential. However, it should be emphasised that a wide variety of the laws of variation of the ionic electrostatic component of the disjoining pressure with the interlayer thickness and the dependence of these changes on the boundary conditions^{2,31} can only be observed if the film thickness is smaller than or comparable to the Debye screening length.[§] At long distances, the interaction between both flat and spherical particles exponentially decreases as the interlayer thickness increases irrespective of the surface charging mech-

§ The Debye screening length is the action range of the electric field of a single charge in electrolyte.

anism; this was confirmed by numerous experiments (see, *e.g.*, Ref. 37).

The mechanisms of the van der Waals forces and electrostatic interactions considered above underlie the theory of stability of lyophobic colloids. It is lyophobic surfaces and colloids (their particles are treated as weakly interacting with the dispersion medium) that usually permit a correct description of the stability of interlayers (Fig. 5), kinetics of coagulation and the destabilising effect of electrolyte additives using the two approaches to calculations of surface forces (see above). We believe that the last stage of the evolution of the DLVO theory in its classical form should be dated to the early 1960s; at that time, the macroscopic theory of the van der Waals forces was already elaborated and various theories of calculations of electrostatic interactions between same-type and different-type particles separated by uniform liquid or solvent interlayers were developed. However, the development of the DLVO theory was accompanied by accumulation of experimental data that not only showed poor quantitative agreement, but in some cases qualitatively contradicted the predictions of the classical DLVO theory. Examples are provided by recent studies on the stability of foam films,^{38, 39} wetting films and interlayers between solid surfaces.^{40–44}

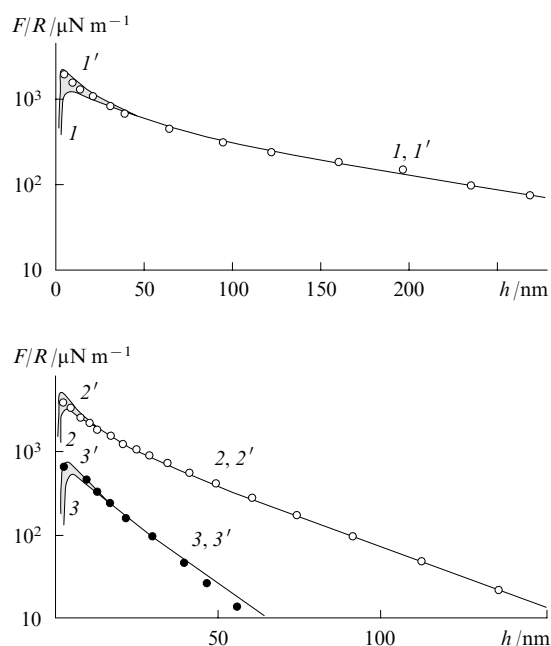


Figure 5. Reduced forces of interaction (F/R) between two crossed cylindrical mica surfaces of radius 1 cm in water (curves 1, 1') and in dilute potassium nitrate solution (10^{-4} M KNO_3 , curves 2, 2') and calcium nitrate solution [10^{-4} M $\text{Ca}(\text{NO}_3)_2$, curves 3 and 3', respectively].¹¹ The open and solid circles denote the experimental data, the solid lines correspond to the results of force calculations using the DLVO theory (the Hamaker constant $A_{132} = 2.2 \times 10^{-20}$ J) in the constant potential (Ψ_0 , curves 1–3) and constant surface charge (curves 1'–3') approximations. For thick interlayers, both approximations give the same results. $\Psi_0 \approx -150$ mV (1, 1'), $\Psi_0 \approx -120$ mV (2, 2') and $\Psi_0 \approx -50$ mV (3, 3').

Attempts to attain agreement between the theory and experiments led, on the one hand, to allowance for specific features of real experimental systems in the framework of the evolution of the classical approaches and, on the other hand, to development of some new mechanisms of long-range surface forces that have a common name 'non-DLVO'-forces.

V. Progress in the theory of dispersion forces

Non-uniformity of a real liquid interlayer due to the change in the film density across the interlayer thickness and to monomolecular or diffuse adsorption of a solution component near the boundary media was included in calculations of the van der Waals interactions in the framework of the model layered systems. Calculations were carried out either assuming identical dielectric properties within each layer^{20, 45–48} or using different laws of the changes in the dielectric properties along the normal to the layers.^{49, 50} In all cases, the results obtained with allowance for non-uniformity were appreciably different from those obtained in the homogeneous interlayer approximation. For instance, the interaction energies calculated using these models for films a few nanometres thick differed by almost an order of magnitude from the values calculated using the DLP theory¹³ with the bulk dielectric permittivities.

An alternative microscopic approach to evaluation of the non-uniformity of the liquid interlayer is based on the molecular statistics methods.^{51, 52} Here, the non-uniformity of the film can be taken into account by augmentation of the equations for interaction energy calculations with an additional term proportional to the inverse cube of the interlayer thickness. This term becomes of particular importance as the interlayer thickness decreases.

Eventually, Derjaguin and Churaev^{2, 53} developed a method of inclusion of the non-uniformity of the interlayer, which involves thermodynamic treatment of adsorption and evaluation of the interaction between components of non-polar solutions and the boundary phases in the framework of the macroscopic approach. Later, the method was extended to solutions of polar substances dissolved in a non-polar solvent.^{54–58} Additional interactions due to non-uniform distribution of the solution components across the interlayer thickness were named 'adsorption component of the disjoining pressure'. Depending on the ratio of the dielectric permittivities of the solvent and solute and on the ratio of the dielectric permittivities of the solvent and boundary phases, these interactions can either stabilise or destabilise the liquid interlayer. It should be noted that the effect of these additional forces is significant only in the case of interlayers a few nanometres thick.

Calculations of dispersion interactions with allowance for the spatial dispersion of dielectric permittivity appeared in the electrolyte solution films were carried out by Gorelkin and Smilga^{59, 60} using either the Dzyaloshinskii–Lifshitz–Pitaevskii method (based on calculations of the temperature Green functions) or the Bogolyubov functions. An analytical solution was obtained for electrolytes modelled by the Debye plasma and collisionless plasma with mirror reflection from the boundaries assuming neutral film boundaries and diagonal dielectric permittivity tensor within the electrolyte interlayer.

A comparison of the equations derived in Refs 59 and 60 with Eqn (2) derived using the DLP theory revealed significant difference only for the term with zero frequency. Therefore, the inclusion of spatial dispersion is of particular importance in studies of the systems where this term plays a significant role. In addition, the spatial dispersion also manifests itself in the appearance of specific effect of interfaces on the character of the frequency dependence of the dielectric permittivity of the interlayer. The effect is expected only for films a few nanometres thick in specific systems, such as metal solutions in ammonia. According to calculations, the presence of dilute electrolyte solution in the system leads to screening of the van der Waals forces at long distances (10^{-7} – 10^{-6} m). At these distances, the molecular forces decrease exponentially rather than in proportion to $\Pi(h) \sim h^{-4}$, as follows from relationship (3b).

VI. Progress in the theory of ionic electrostatic interactions

The evolution of the classical theory of electrostatic interactions between surfaces immersed in electrolyte solutions has been accompanied by revision of its foundations, such as the continuity of charge distribution along the particle surfaces, constant surface potential or constant charge of the approaching surfaces, treatment of ions in solution as point charges and consideration of other (non-Poisson) potentials determining the ion distribution in solution, *etc.*

In particular, Muller showed (see Ref. 2) that drawing colloidal particles closer together is accompanied by rearrangement of not only the diffuse charge, but also the surface charge of the electric double layer except for the chemisorbed part of this layer. He derived an exact parametric equation relating the repulsive energy to the distance between flat plates assuming that the changes in the adsorption of ions as the plates approach each other are described by the Stern isotherm.

Healy and co-workers⁶¹ reported the need of using a charge regulation model instead of the constant potential approximation in calculations of ionic electrostatic interactions at short distances between the charged surfaces.^{29–31} Based on this model, a correction to the DLVO forces of the interaction between hydrophilic surfaces in water was calculated in the framework of constant dielectric permittivity of the solvent with inclusion of the Nernst layer of hydroxyl groups near the interface (this makes the position of the charge plane more distant from the surface).⁶² This approach made it possible to explain the appearance of an additional minimum on the energy curve, which is located between the primary and secondary minima predicted by the DLVO theory.

A general thermodynamic consideration of changes in the charge of the interlayer in the course of approach of differently charged flat surfaces was reported by Lyklema and Duval²⁹ who assumed charge regulation in the Gouy–Stern layer. The approach was used for calculating the potential and charge distributions in plane-parallel interlayers and the forces and energy of the interaction between different-type surfaces in various model systems that simulate the behaviour of complex real systems, *e.g.*, the interaction of clay and metal oxide particles. The constant charge or constant potential approximations of the diffuse double layer were shown to be correct only in the case of thick interlayers. Systems with thin interlayers exhibit deviations from both boundary conditions. To characterise the charge regulation processes occurring within the interlayer as the surfaces approach each other, it is appropriate to introduce the notion of the regulation capacity characterising the possibility of establishment of a new charge distribution in the interlayer without significant change in the potential. The higher the regulation capacity of the interlayer the more correct the description of the behaviour of the system in the constant potential approximation.

The next step in considering ionic electrostatic interactions between surfaces immersed in electrolyte solution is the inclusion of various factors determining the ion distribution in the liquid interlayer. For instance, the theory of the interaction of electric double layers, which is based on the classical Poisson–Boltzmann equation, assumes that ions obey the Boltzmann distribution with the interaction potential obeying the Poisson equation. This theory ignores the effects due to specific nature of the ions in solution. At the same time, experimental data on the stability of disperse systems in electrolyte solutions and on the forces of the interaction between such systems separated by electrolyte interlayers indicate that electrostatic forces depend not only on the valence of ions and the ionic force of the solution, but also on the type of the cations and anions present in the solution.^{63–65}

To describe the specific order of ions with respect to the character of their effect on the interaction between the double layers, it was suggested to augment the Poisson–Boltzmann equation with additional potentials that include, in one way or another, the nature of the ion.^{66–72} For instance, Ninham and Yaminsky⁶⁶ proposed to include the potential of the van der Waals forces acting between the ion and the remaining part of the system in the description of the ion distribution in the solution. In addition to the potential of ion-dispersion interaction including the potential of the van der Waals forces and the Poisson potential, Karraker and Radke⁷² also proposed to take into account the potential of the interaction between ions and their ‘images’ in air, which causes additional repulsion of ions from the water/air interface. Manciu and Ruckenstein^{70,71} considered not only the long-range ion-dispersion potential (see above), but also the short-range ion hydration potential, which describes the ion hydration free energy difference between the solution bulk and the near-interface region.

Thus, the ion redistribution in the solution interlayer in the potentials of ion-dispersion and ion hydration interactions depends on the type of ions. Such a redistribution causes changes in the surface charges and surface potentials and, therefore, affects the interaction between the double layers. Interestingly, the authors of all the approaches mentioned above get satisfactory descriptions for the experimentally observed dependence of the surface tension of electrolyte solutions on the ionic strength of the solutions in spite of different choice of the additional potentials.^{68,70,72}

Correlations in mutual arrangement of ions in the electric double layers and the related additional forces were studied.^{73–75} Additional contributions to the energy of ion–ion interactions in the liquid interlayer are due to correlations of charge density fluctuations in the double layers formed on the opposite surfaces of the liquid interlayer. Taking into account the ion size (passage from point ions presentation to the ions with finite sizes) also causes the energy to change due to additional repulsion between ion shells near the mid-plane of the film. The ‘image’ forces cause deformation of diffuse ionic atmospheres with the corresponding energy contribution. Finally, the ion concentration difference between the actual film and the value predicted using the conventional Poisson–Boltzmann approach leads to a change in the Debye screening length. Analysis showed^{73–75} that the effect of ion–ion correlations mainly involves the appearance of additional attraction between the charged surfaces. This effect is most pronounced in di- and multivalent electrolyte solutions and leads to significant decrease in repulsion between the double layers or to the change in the sign of the interaction. The effect of ion size on the interaction force manifests itself to the greatest extent in the case of thin interlayers, large ionic radii and/or large surface charges. The influence of ion–ion correlations on stability of colloidal solutions with multivalent counterions was experimentally established⁷⁶ by direct measurements of interaction forces between mica surfaces in 0.15 M CaCl₂ solution.

Rejection of the uniformly ‘smeared’ surface charge model led to the development of a family of models^{77–81} that allow for discrete structure of the dense part of the electric double layer at the interface.

For instance, Zhiguleva and Smilga⁷⁹ used the modified Evald method for two-dimensional geometry and analysed the electrostatic field and potential distributions in the electric double layer for various regular flat charge distribution lattices. According to calculations,⁷⁹ the inclusion of discrete structure of the double layer in many systems is necessary because the actual interaction force can be two orders of magnitude higher than the values obtained using the smeared charge model. Similar results were also reported by Kostoglou

and Karabelas⁸⁰ who considered the interaction of surfaces characterised by discrete distribution of round or square-planar potential-determining ions occupying regular lattice sites. They found that the interaction energy differences between the surfaces with discretely distributed and smeared charge are more pronounced (over a wider range of film thicknesses) at a constant potential of the approaching surfaces rather than in the constant charge approximation.

Derjaguin and Muller² established that in the case of delocalised adsorption of ions the discreteness of the surface charge distribution causes correlations in the arrangements of the ions on the opposite film surfaces. According to calculations, these correlations are responsible for the appearance of additional attraction forces that decrease as $\Pi(h) \sim h^{-4}$. In the case of thin interlayer, these correlation forces not only reduce the electrostatic repulsion, but in some cases cause a change in the sign of the interaction.

Analysis of the effect of discreteness of the surface charge distribution on the electrolyte/insulator interface showed⁸¹ that the structure of the diffuse layer in counterions is determined by not only the exponential decay of the field due to the Debye screening, but also additional asymptotics with amplitudes depending on the dielectric permittivity of the insulator.

According to the results of theoretical studies,^{82–84} the electric double layer near the surface bearing a non-uniformly distributed charge has a modified structure compared to the double layer near a uniformly charged surface. The deviation of the structure of the diffuse part of the counterion layer is particularly pronounced in the presence of multiply charged ions and at large average surface charges.

Basu and Sharma⁸⁵ found that repulsive forces additional to those given by the DLVO theory, acting between surfaces can also be due to changes in the static dielectric permittivity of the solvent near the charged interface. Henderson and Lozada-Cassou⁸⁶ attempted to take into account the structure of the thin solvent interlayer by analysing the preferred orientation of the dipole moments of the solvent molecules near the interface, which is interpreted in the framework of the continuum models as dielectric saturation. It was shown that this phenomenon, which manifests itself in a decrease in the static dielectric permittivity, causes an extra repulsion between surfaces (in addition to the DLVO forces) and can be used for explanation of the appearance of hydration forces in electrolyte solutions.

Paunov *et al.*^{87–89} analysed the role of the size of hydrated ions in solution near the interface and showed that the ion size affects the ion distribution not only near the charged interface, but also outside the electric double layer. Redistribution of ions across the film thickness due to the ion size effect and to the changes in the static dielectric permittivity of the solvent near the charged interface requires introduction of a correction to the electrostatic component of the disjoining pressure. The correction describes the additional repulsive in thick and additional attraction in thin interlayers provided that the overlap of the double layers is small.⁸⁹

Discrete dipole distributions along interfaces were studied by different authors.^{54–58, 77, 90–93} For instance, Jönsson and Wennerström⁹⁰ analysed the contribution of image forces to the interaction between surfaces covered with surfactants having bipolar terminal groups using the continuum electrostatic model and pointed that these forces lead to appearance of repulsive forces that can be responsible for the swelling of phospholipid bilayers in aqueous solutions. Kjellander and Marcelja⁹¹ restricted themselves to consideration of dipoles oriented normal to the surface in the hyperchain approximation and showed that the correlation attraction of dipoles located on different surfaces predominates over repulsion between the dipoles and their images. Similar results were obtained by Attard and Mitchell⁹² and by Jönsson *et al.*⁹³ using methods of the perturbation theory and by Martynov and Smilga⁷⁷ who

used the electrostatic approach. As was reasonably argued by Martynov and Smilga,⁷⁷ attraction between dipoles in a symmetrical system is a general result. Since the strength of the field created by the layer adsorbed on one dipole surface alternates in the plane of the second adsorption layer (this is a consequence of the Gauss theorem), at a constant interlayer thickness the dipole lattices on the opposite surfaces are displaced relative to each other in such a manner that the potential electric energy of their interaction be minimum. This in turn causes the appearance of attractive forces acting between the dipole lattices, *i.e.*, a negative disjoining pressure. Jönsson *et al.*⁹³ showed that the inclusion of orientation rotation of dipoles in the framework of perturbation theory (long-wavelength approximation) can cause either attraction or repulsion between the dipole layers. However, in a symmetrical system the repulsion forces are much weaker than the van der Waals attraction.⁹³ It should be noted that the authors of studies^{77, 90–93} considered only symmetrical systems assuming that adsorption is independent of the interlayer thickness and ignoring specific features of the structure of dipole molecules.

VII. Electrostatic interactions in non-polar media

Specific features of ionic electrostatic interactions in non-polar media consist in that usually the bulk ion concentrations in such systems are low and, correspondingly, the Debye screening lengths are of the order of a few thousand nanometres,⁹⁴ which much exceeds the thickness of the interlayers under study. In this case, the interaction between charged surfaces can be treated as the Coulomb interaction ignoring screening. Analysis of the interaction between small charged particles, a polarisable particle and a charged electrode and between polarisable particles in a nonuniform electric field using this approach in the smeared surface charge approximation was reported in a recent review by Adamczyk.⁹⁵ Another approach is based on consideration of the interaction between electric double layers having diffuse parts comprising counterions only.^{94, 96} If the source of counterions is the surface and no ion exchange with the bulk reservoir occurs, the energy of the interaction between two flat charged surfaces can be calculated using the total entropy maximisation approach⁹⁷ with the assumption of charge regulation or constant charge condition.⁹⁶ According to calculations, the long-range repulsion between surfaces separated by non-polar liquid interlayer is more than an order of magnitude weaker compared to ionic electrostatic interaction through a water interlayer. The repulsive forces asymptotically decrease with the interlayer thickness following a power law rather than exponential law predicted by the classical DLVO theory.

The mechanisms of appearance of additional forces of the interaction between surfaces separated by a non-polar liquid interlayer in the presence of polar molecules were considered.^{54–58} This case is of particular importance in the analysis of stability of suspensions in dispersion media represented by solutions of polar components in non-polar solvents. Discrete distributions of the dipoles simulating polar molecules across the interfaces and interlayer thickness cause the appearance of various types of image forces and to dipole–dipole interactions within the interlayer. Both symmetrical and asymmetrical systems characterised by different magnitude and, in some cases, type of adsorption at different interfaces were considered.^{54–58} Equilibrium adsorption calculations were carried out with allowance for not only the specific potential of the interaction between polar adsorbable molecules and active sites at the interface, but also the potentials of the image forces and dispersion interaction of these molecules with the boundary phases. The last two potentials cause a significant dependence of the equilibrium adsorption on the thickness of the liquid interlayer.

The contribution of electrostatic interaction between layers of adsorbed dipole molecules and their images in the confining phases to the disjoining pressure can be rather large even in highly dilute solutions of polar substances in non-polar solvents. Generally, this contribution is a non-monotonic function of the concentration of polar molecules (Fig. 6) and decreases in a $\Pi(h) \sim h^{-4}$ mode as the film thickness decreases. It can cause either attraction or repulsion between film boundaries depending on the character of the changes in the adsorption of the solute across the interlayer thickness, on the ratio of the static dielectric permittivities of the contacting media and on the magnitude of dispersion interaction between the dipole molecules and the confining phases.

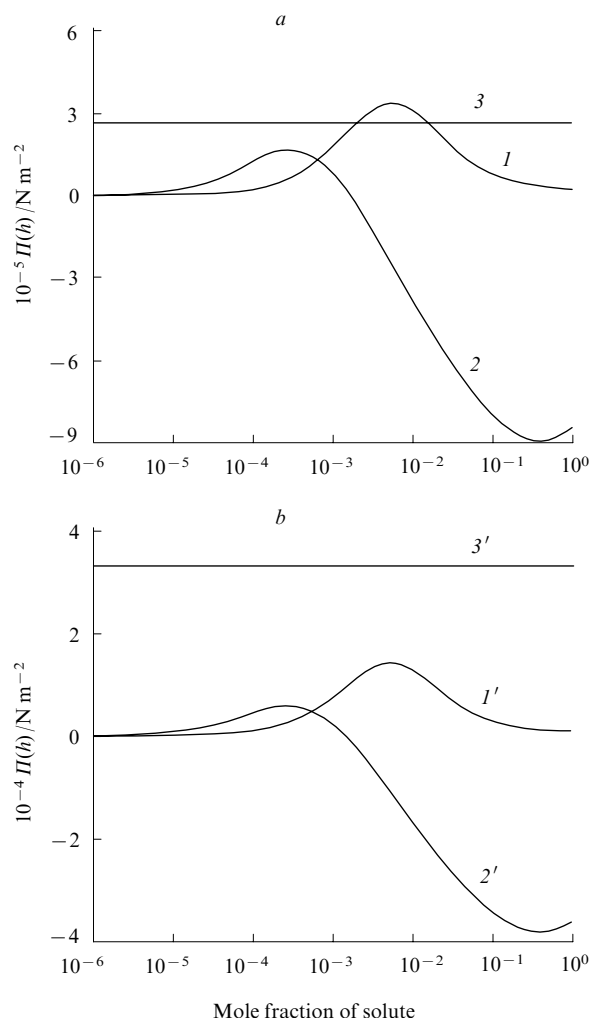


Figure 6. Contribution to the disjoining pressure related to the interaction between the adsorbed monolayer and its images plotted vs. mole fraction of polar solute for films 1 (a) and 2 nm (b) thick. Curves (1, 1') correspond to in-plane and curves (2, 2') correspond to normal orientation of dipoles in the monolayer. Curves (3, 3') correspond to dispersion interaction of bodies (the Hamaker constant $A_{132} = 5 \times 10^{-21}$ J) taken with the opposite sign. Disjoining pressure calculations were carried out for wetting films of solutions of alcohols in oil on the water surface.^{57,58}

Analysis of the expressions derived and numerical calculations carried out for monolayers of adsorbed molecules using different magnitudes and orientations of the dipole moments relative to the interfaces showed^{54–58} that in non-symmetrical thin interlayers (e.g., wetting films) at both in-plane and normal orientations of the dipoles in the monolayer the forces of the interaction between the monolayer and its images can

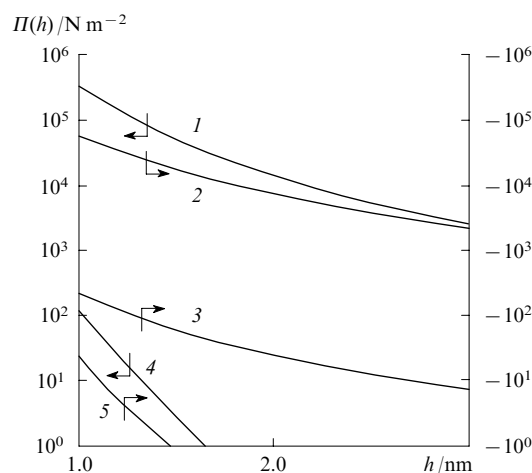


Figure 7. Various components of the disjoining pressure acting in the wetting films of pentanol solution in pentane on water surface plotted vs. film thickness.

Contribution related to the interaction between the adsorbed monolayer of dipole molecules and its images (1); molecular component calculated using published data⁴⁵ (2); adsorption component calculated using the constants of the interaction between pentanol molecules and the boundary phases (taken from Ref. 55) (3); contribution related to excess electrostatic energy of diffusely distributed alcohol molecules (4); and contribution of the correlation attraction of adsorption monolayers (5).

much exceed other types of interaction forces including the forces of the interaction between the diffuse adsorption layers, correlation attraction forces acting between the monolayers adsorbed on the opposite sides of the interlayer and the dispersion forces (Fig. 7). However, the force of dispersion interaction dominates over the image forces in 2–3 nm and thicker films because it decreases in proportion to $\Pi(h) \sim h^{-3}$ as the film thickness decreases.

VIII. Interaction forces caused by modified structure of liquid interlayer

1. Treatment of liquid in a continuum approximation

The assumptions of structural differences between the liquid in the thin interlayer and in the bulk phase and of the existence of long-range surface forces due to this difference were first made by Derjaguin.² Later, these assumptions were repeatedly (and fruitfully) used in discussing the nature of hydration, solvation and structural repulsive forces and hydrophobic attractive forces due to deviations of various structural parameters from the corresponding values in the bulk. One of the first theoretical studies of the processes occurring in a polar solvent as a result of decrease in the thickness of the liquid interlayer was reported by Marcelja and Radic.⁹⁸ They calculated the free energy density using the Landau expansion in the order parameter and showed that the inclusion of only quadratic expansion terms (with respect to the order parameter and its gradient) permits a correct description of the exponentially decreasing repulsive forces acting between the surfaces confining the liquid interlayer provided that variations of the order parameter are small. Later, other authors interpreted the order parameter as a characteristic of the local polarisation of water.^{99–102}

The idea of surface-induced polarisation of water molecules as the source of hydration forces was used by different authors.^{103–106} For instance, Kornyshev and Leikin^{105,106} proposed two different mechanisms of polarisation of water molecules near the interface. One mechanism is based on consideration of the contribution of the interaction between

oppositely charged groups of one electrically neutral surface of a lipid membrane and their images in a non-polar medium separated from the membrane surface by a water interlayer.¹⁰⁵ Spatial correlations of water polarisation fluctuations were included using the methods of non-local electrostatics. It was shown that lateral ordering of polar groups on the membrane surfaces plays the key role in determining the character of the interaction forces between them (Fig. 8). The other, 'chemical', mechanism of ordering of water molecules is based on the use of the Landau free energy functional and introduction of a phenomenological order parameter and inhomogeneous boundary conditions. This approach allowed differences between the states of water near the polar surface and in the bulk phase to be analysed.¹⁰⁶ Both mechanisms predict an exponential decrease in repulsive forces with an increase in the thickness of the water interlayer. These forces are related to the character of ordering of the polar groups on the surface of lipid membranes. Both pre-exponents and correlation lengths depend on the nature and structure of the surfaces confining the interlayer.

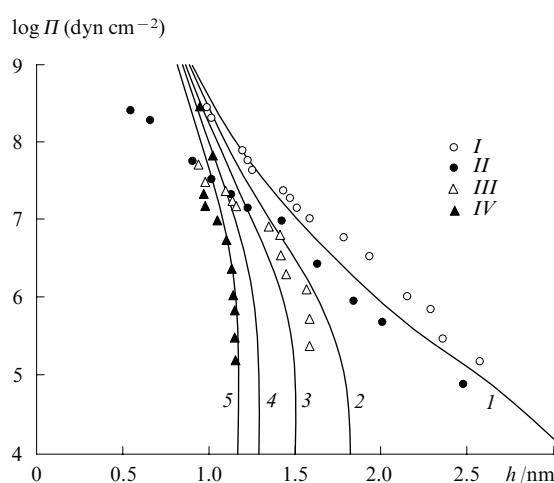


Figure 8. Comparison of theoretically predicted disjoining pressure (solid lines) calculated taking into account the forces of dispersion attraction between membranes¹⁰⁵ with experimental data for various lipids: POPE (I), egg PEt (II), egg PEt – Me (III) and SOPC (IV). Calculated using the following parameters: 8×10^{-21} J for Hamaker constant; 0.5 nm correlation length of water polarisation fluctuations; 0.4 nm for the distance between positively and negatively charged centres in the polar group; 0.5 nm for the distance between the dipole plane and interface; and 0.65 nm^2 for the average surface area per polar group. Theoretical curves were calculated at the following lateral correlation lengths of the polar groups: 0 (I), 0.2 (2), 0.3 (3), 0.5 (4), and 2 nm (5).

Mitlin and Sharma¹⁰⁷ studied the interaction between flat plates separated by a liquid interlayer. They combined, in the framework of the gradient theory, the Cahn approach proposed for analysing wetting transitions at an interface between two media¹⁰⁸ and the approach used by Marcelja and Radic.⁹⁸ The new analytical method¹⁰⁷ made it possible to derive asymptotically exact dependences of the disjoining pressure, free energy and order parameter profile on the interlayer thickness for an arbitrary dependence of the free energy density on the order parameter. It was found that in the general case the disjoining pressure can be described by a sum of exponents with the characteristic lengths proportional to the correlation radius in bulk liquid, the pre-exponent being dependent on both the deviation of the free energy density from the quadratic form in the expansion and on the parameters of the interaction between the liquid in the interlayer and both surfaces confining

the interlayer. The interaction forces between the plates can be either attractive or repulsive. In addition, the sign of the forces changes as the interlayer becomes thinner.

A new approach to account for the interaction between the liquid and the confining surfaces in calculations of forces additional to DLVO was made by Kuklin.¹⁰⁹ The free energy of the system was modelled by the harmonic approximation of the Landau – Ginzburg functional, which depends on the order parameter. In addition to the free energy density expansion terms considered by Marcelja and Radic⁹⁸ and by Kornyshev and Leikin,¹⁰⁶ Kuklin proposed to augment the functional with functions characterising the contribution of direct short-range interaction between the near-surface layers of the liquid and the surface of the solid phase. It was shown¹⁰⁹ that the forces acting between surfaces of different nature can be either attractive or repulsive depending on the interlayer thickness. These forces depend on four scaling parameters, namely, two extrapolation lengths characterising the depth to which the field produced by each surface penetrates into the liquid phase and two field parameters that describe the effect of the solid surface on the properties of the nearest molecular layer in the liquid. When these parameters and the interlayer thickness are chosen appropriately, the forces show a nearly exponential dependence on the thickness of the liquid interlayer.

The approach proposed by Eriksson *et al.*¹¹⁰ is conceptually similar to that developed by Marcelja and Radic. Here, the order parameter characterises the relative local increase in the number of hydrogen bonds per water molecule in the thin interlayer compared to the corresponding characteristic of the bulk phase. Eriksson *et al.*¹¹⁰ considered a system comprising the water interlayer and hydrophobic surfaces confining it and expanded the free energy of the system in terms of the order parameter, minimised it and concluded that an increase in the order parameter near the hydrophobic wall causes the appearance of long-range attractive forces. The action range of such forces is much shorter than that of hydrophobic attraction reported in the literature.

Yushchenko *et al.*¹¹¹ suggested another mechanism of the appearance of hydrophobic attraction forces acting at longer distances. This involves the formation of a cavity filled with vapour of the liquid under study (or with gas) between the interacting lyophobic particles. The hydrophobic attraction forces appeared in this case are in essence capillary forces. This mechanism is possible if the wetting angle exceeds 90° and the cavity is formed only after the interacting bodies are brought into contact. According to calculations,¹¹¹ the cavity is also thermodynamically stable even in the initial appearance of a gap between the plates; however, the energy barrier to cavity formation is as high as tens of kT before the bodies are brought into contact. We believe that this is responsible for the fact that the cavity formed only after the hydrophobic surfaces have preliminarily been brought into contact in water.¹¹²

It should be noted that hydrophobic attraction in the case of thick interlayers was also observed without explicit cavity formation.¹¹³ The cavity formation mechanism proposed to explain the experimental data was based on the hypothesis that the formation of a vapour-filled cavity is preceded by nucleation in the liquid interlayer. Forsman *et al.*¹¹⁴ also reported a decrease in the density of the liquid near the lyophobic wall, which was associated with the presence of gaseous nuclei. Analysis of the density functional of the liquid in the thin interlayer showed that non-uniform decrease in the density across film thickness causes the appearance of attractive forces which can be much stronger than the van der Waals forces for thin films. It is noteworthy that these forces increase rather than decrease (as is traditionally accepted in the literature) in absolute value as the temperature increases.

Other mechanisms leading to appearance of long-range hydrophobic forces related to formation of cavities and micro-bubbles between the interacting surfaces were also proposed.^{115–118}

2. The accounting for discrete structure of liquid

The studies analysed in the preceding Section treated the solvent or the liquid (*i.e.*, the liquid interlayer) in the continuum approximation. However, extensive literature is also available (see, *e.g.*, Refs 119–129) in which the discrete structure of the liquid in the interlayer is included in the framework of the model of the Lennard-Jones fluid or the model of hard spheres. Here, irrespective of the model employed, both analytical methods and computer-aided calculations allow one to reproduce the oscillating character of the interaction forces (Fig. 9) observed in experiments with the liquid interlayers of different nature (see, *e.g.*, Refs 11 and 130).

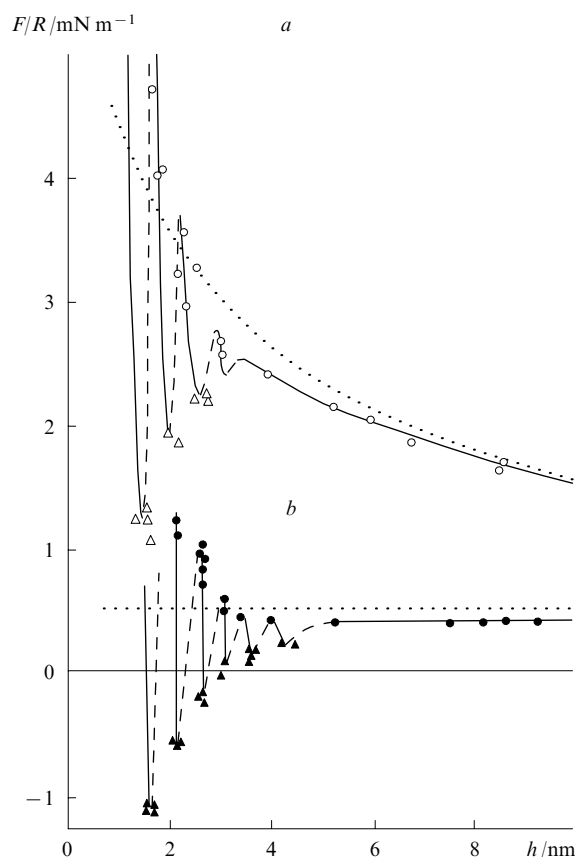


Figure 9. Oscillating forces of the interaction between mica surfaces separated by a propylene carbonate interlayer without electrolyte (a) and upon adding 10^{-4} mol of tetraethylammonium bromide (b).¹³⁰

The circles and triangles denote the results of measurements obtained as the surfaces move away from or approach each other, respectively. The solid and dashed lines connect the experimental points. The dotted lines correspond to theoretically predicted DLVO forces with the Hamaker constant $A_{132} = 10^{-20}$ J.

The main problem in theoretical calculations of the interaction between two solid walls separated by a liquid interlayer consists of maintaining a constant chemical potential of the liquid as the interlayer thickness varies. If for Monte Carlo simulations this condition is explicitly met in the framework of the grand canonical ensemble,¹¹⁹ it is hardly possible in the case of calculations based on analytical theories. There are also some exceptions, namely, approximate theories (*e.g.*, various versions of the mean field theory¹²⁰ and simple theories of

integral equations for inhomogeneous systems¹²¹) in which the closure of the unary distribution functions is attained using the pair distribution functions of the bulk phase. However, the pair distribution functions characteristic of liquid interlayers are anisotropic in nature and therefore the results of corresponding calculations can be incorrect.¹²² In this connection, a number of approaches were proposed, which permit a more correct inclusion of the anisotropy of the liquid in the thin layer.

Kjellander and Sarman¹²³ did their research in the framework of the theory of integral equations based on the solution of the exact Ornstein–Zernicke equation for anisotropic pair correlation function and proposed to use the Percus–Yewick anisotropic closure. Attard¹²⁴ showed that the use of a hyper-chain approximation and its versions in solving the Ornstein–Zernicke equation permits a correct reproduction of the oscillating character of the forces using the model of hard spheres and the Lennard-Jones model of fluid. It should be noted that some authors (see, *e.g.*, Ref. 122) cast doubt on the correctness of the use of the hyperchain approximation for calculations of interaction forces in dense fluids with short-range potentials.

To study molecular liquids having non-spherical molecules, Chandler and Andersen¹²⁵ developed the reference interaction site model (RISM), which is a molecular analogue of the Percus–Yewick approximation of hard spheres for a simple fluid. According to the RISM model, the equilibrium correlations between molecules in the dense fluid are determined by the short-range repulsive component of the intermolecular potential. This model was used for calculating the solvation forces for liquid interlayers comprised of diatomic molecules based on the theory of integral equations.¹²⁶ The results of calculations revealed a high damping of oscillations on going from the model of hard spheres to the RISM model (Fig. 10), which allows for asymmetry of molecules of the liquid.

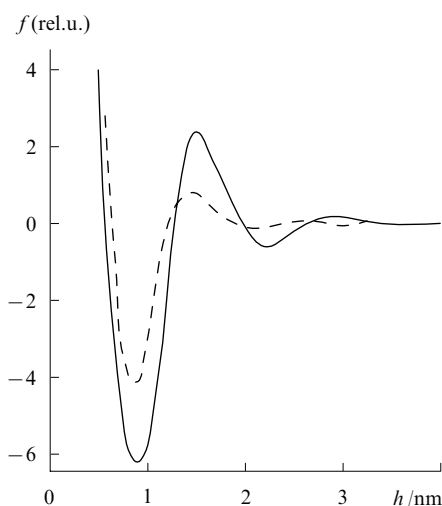


Figure 10. Reduced force of the interaction between two interfaces plotted vs. reduced distance between them for fluids with a reduced density of 0.3584:¹²⁶ the dashed line corresponds to a diatomic fluid with an interatomic distance of 0.6σ (σ is the atom diameter) and the solid line corresponds to the fluid of hard spheres (sphere diameter 1.2146σ).

3. Phonon mechanism of surface forces

As mentioned above, Derjaguin, Churaev and their scientific school (see, *e.g.*, a monograph² and articles^{131, 132} and references cited therein) repeatedly used the idea of the structural

difference between the liquid in the thin interlayer and in the bulk phase in discussing the stability of certain colloidal systems. However, in these studies the structural differences meant static deviations of the local polarisation, intermolecular distances and orientations of molecules relative to interfaces in the interlayer from the corresponding bulk characteristics. Thus, additional surface forces appeared in the system were associated with the overlap of the structure-modified boundary layers in the film.

Another approach to the problem of structuring of the liquid in a system of restricted dimension is based on consideration of the dynamic structure of the liquid.^{133–138} Here, the dynamic structure of the liquid is treated as the set of vibrational and rotational motions of all atoms and molecules in the liquid confined within a thin interlayer. The dynamic structure of liquid strongly depends on both the interlayer thickness and the surface-induced changes in the intermolecular interactions. The dynamic structure differences between bulk liquid and the liquid in the state of restricted dimension manifest themselves in, *e.g.*, the absorption spectra of the liquid in the corresponding state (Fig. 11).

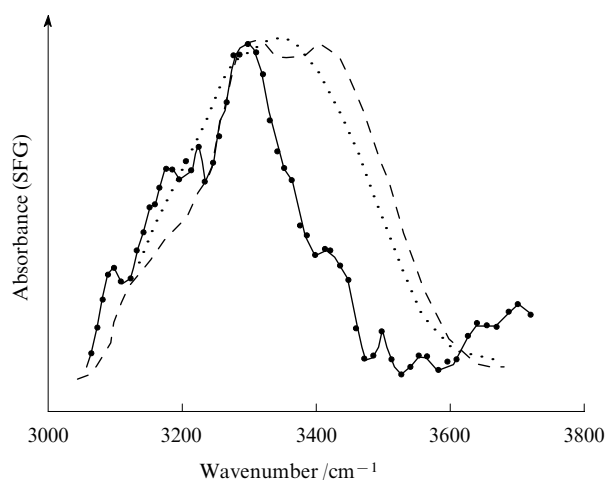


Figure 11. IR spectra of ethanol in the region of OH stretching vibrations.¹³⁶ The dotted curve is the spectrum of the bulk liquid and the dashed line is the spectrum of ethanol interlayer (25 nm thick) separating two fluorite plates. The points connected by the solid line are the sum-frequency generation (SFG) spectrum of ethanol–air interface.

Clearly, these two types of structuring in the thin liquid interlayer complement rather than exclude each other. Therefore, understanding of the character of molecular motions in thin layers of molecular liquids is important for the description of various properties of liquid films and the development of detailed mechanism of structure-induced surface forces.

Generally, molecular motions in bulk liquid are anharmonic. However, if the observation time is short compared to the characteristic relaxation times of the corresponding type of motion^{139, 140} or the region under consideration is small,¹⁴¹ the complex picture of intra- and intermolecular motions in the liquid can quite correctly be represented by a set of collective vibrational states, or normal modes, associated with acoustic waves in the liquid medium. The fruitfulness of this approach to the description of many phenomena in liquids has been well documented. The most important studies are based on the normal-mode approach, *e.g.*, the description of solvation dynamics,¹⁴² calculations of diffusion constants¹⁴³ and

absorption spectra¹⁴⁴ and the description of the nature of the glassy state.¹⁴⁵

The approach developed in our studies^{133–138} also treats the intra- and intermolecular motions in liquids as harmonic processes characterised by corresponding characteristic times and normal-mode spectra. Each normal mode is determined by the parameters of an oscillator involved in a vibrational (rotational) motion and by its interaction with neighbouring oscillators. The probability of realisation of a normal mode of an arbitrary oscillator depends on the ratio of the liquid interlayer thickness (h) to the free path length (L) of phonon corresponding to the normal mode in question, being equal to $\exp(-h/L)$. Because of the normalisation condition for the total number of degrees of freedom at each time instant any oscillator in the film is either involved in collective vibration of the entire ensemble of oscillators propagating normal to the interface or oscillates at a frequency characteristic of the bulk liquid and determined by both the internal force field of the whole molecule and the effective average field produced by the surrounding molecules.

The dynamic structure differences between bulk liquid and the liquid in the thin film are due to the fact that the free path lengths of phonons, orientations of molecules relative to one another and to interfaces and intermolecular distances in the thin interlayer are changed due to the interaction between the molecules and the surface. In addition, the surfaces that bound the thin liquid interlayer induce changes in the conformational states of molecules. All these factors affect the normal-mode spectrum and give rise to an additional contribution to the film free energy, which depends on the interlayer thickness and is given by

$$F^E = \sum_j \int_0^\infty kT \ln \frac{\text{sh}(\hbar\omega/2kT)}{\text{sh}(\hbar\omega_{j0}/2kT)} Z_j(\omega) \exp\left(-\frac{h}{L_j(\omega)}\right) d\omega, \quad (4)$$

where ω_{j0} are the eigenfrequencies of corresponding molecular vibrations in the bulk liquid, $Z_j(\omega)$ is the thermodynamically averaged density of vibrational states determined from the dynamic matrices of instantaneous film states and L_j is the free path length of photons for the j th type of oscillators. Summation is carried out over all types of oscillators (j) associated with branches of the dispersion curve for the liquid interlayer. The product $Z_j(\omega) \exp(-h/L_j(\omega)) d\omega$ is the number of vibrational modes of the j th type per unit surface area of the liquid interlayer with allowance for finite relaxation time of the vibrational mode. For linear waves the free path lengths of phonons are given by the following transcendent relationship

$$L_j(\omega) = v_j(\omega)\tau_0 \left[\int_{L_j(\omega)} \rho(z) \exp\left(\frac{U(z)}{kT}\right) dz \right]^{-1}, \quad (5)$$

where $v_j(\omega)$ is the absolute value of the group velocity of collective vibration at the frequency ω , τ_0 is the average lifetime of oscillators between thermal jumps in the bulk liquid, $\rho(z)$ is the linear density of oscillators along the normal to the film boundaries and $U(z)$ is the excess (compared to bulk liquid) potential barrier to thermal jumps due to the interaction between the oscillators and the boundary phases. Integration is carried out along the chain of oscillators. In the harmonic approximation we neglected the phonon–phonon interaction. In this case the contribution of collective vibrational excitations to the disjoining pressure in the film is given by^{133, 135}

$$\Pi(h) = \sum_j \int_0^\infty \left(-\frac{dK_j}{dh} - \frac{K_j h}{L_j^2(\omega)} \frac{dL_j(\omega)}{dh} + \frac{K_j}{L_j(\omega)} \right) \times \exp\left(-\frac{h}{L_j(\omega)}\right) d\omega, \quad (6)$$

where

$$K_j = Z_j(\omega) kT \ln \frac{\text{sh}(\hbar\omega/2kT)}{\text{sh}(\hbar\omega_{j0}/2kT)}.$$

The contribution to the disjoining pressure described by expression (6) is due to collective vibrational excitations (phonons) in the film; therefore, it was called the phonon component of the disjoining pressure.

From relations (4) and (6) it follows that the excess free energy and the disjoining pressure are calculated as the sums of the contributions of different types of phonons. The signs of the summands are determined by the ratio of the mode frequencies in the film to the corresponding frequencies in the bulk liquid. The magnitudes of the summands are determined by not only the frequency difference, but also the density of phonon states in the nanofilm, the latter contribution being decisive.

Numerical analysis revealed great differences (several orders of magnitude) between the contributions of different types of oscillators. Usually, only a few less localised optical modes essentially contribute to the total disjoining pressure. According to relation (5), the contribution of a certain type of oscillators will first of all be determined by the coupling between these oscillators (both within the same molecule and within neighbouring molecules), which affect the group velocity of phonons. Calculations using the model of coupled oscillators^{135–137} and the force constants of intermolecular interaction characteristic of associated liquids showed that in some cases the contribution of the phonon component of the disjoining pressure to stability of the liquid interlayer can be much larger than that of molecular forces.

From expressions (4) and (6) it follows that the contributions of different oscillators to the disjoining pressure and to the free energy of the film depend exponentially on the film thickness and also implicitly depend on the thickness (this is expressed through the dependence on the free path length of phonons and on the density of vibrational states).

Three terms in square brackets in Eqn (6) describe three different types of the disjoining pressure – film thickness interrelations. The third term dominates in the case of thick films.[¶] Here, the phonon mechanism provides an exponential decrease in the disjoining pressure as the film thickness increases. In a broad range of thicknesses the phonon component of the disjoining pressure is usually described by the sum of several exponentially decreasing terms. This theoretically predicted type of dependence is in good agreement with numerous experimental data (see, e.g., a monograph² and references cited therein).

The first term plays the decisive role for thin films where the discrete structure of the liquid should be taken into account. This discreteness leads to inhomogeneous distribution of molecules across the interlayer due to both the interaction of the liquid with the confining phases and the excluded-volume effect. The last-mentioned factor causes oscillations of the local density across the film thickness. This leads to oscillations of the force constants in the dynamic matrix, which in turn initiates oscillations of the density of vibrational states and,

as a result, oscillations of the excess free energy and disjoining pressure. The use of the phonon mechanism for analysis and description of solvation forces in thin films¹³⁸ made it possible to explain many details of experimental observations, such as anharmonicity of oscillations, changes in the oscillation period with variation of the film thickness and similar oscillations periods for different liquids. Calculations¹³⁸ also clarified the mechanism of disappearance of such oscillations near rough surfaces and in wetting films.

However, it should be emphasised again that the approach under consideration predicts oscillations of forces in thin films with respect to some exponentially decaying function of the film thickness rather than zero. The role of the decaying function is played by the third term in square brackets in Eqn (6).

Eventually, at intermediate thickness of the liquid interlayer the contribution of the oscillations of the density of collective vibrational states can be neglected, but the changes in the mean free path of phonons with variation of the film thickness cannot be ignored. Here, a significant role is played by the second term in square brackets in Eqn (6). The magnitude and sign of this term are determined by the derivative, dL/dh , which mainly depends on the character of the interaction between the oscillators and the phases confining the film.

The effect of the character of the interaction between the liquid and the confining phases on the magnitude and sign of the phonon component of the disjoining pressure deserves particular attention. This effect is first of all due to significant changes in localisation of normal modes near interfaces owing to the interaction between the oscillators and the confining phases. For instance, the free path of phonons increases near the lyophilic surface due to an increase in the energy barrier to thermal jumps and, hence, a significant increase in the relaxation time of the entire ensemble of the oscillators involved in collective vibrations. On the contrary, the energy barrier to thermal jumps decreases near the lyophobic surface, which leads to higher mobility of the molecules near corresponding interface.

Figure 12 shows the normalised relaxation times of a linear ensemble of oscillators in a liquid film plotted vs. film thickness for different constants of the van der Waals interaction between the molecules and the phases confining the film. As can be seen, the effect of the lyophobic substrate manifests itself at much longer distances provided equal, in absolute value, interaction constants. However, the effect of the hydrophobic substrate is not restricted to shortening of the relaxation time of the ensemble of oscillators, but also manifests itself in significant strengthening of intermolecular interactions (e.g., marked strengthening of hydrogen bonds in aqueous media near the hydrophobic surface¹⁴⁶). In turn, the latter factor causes an increase in the group velocity of phonons associated with the O–H vibrations in water molecules. Therefore, for not too thick films the $L_j(\omega)$ parameter, which is sensitive to the interaction of oscillators with the film-confining phases, can vary over a rather wide range as the properties of the confining phases vary only slightly. This was found experimentally for water interlayers separating various lipid membranes.^{147, 148} In the case of inhomogeneous boundary conditions, the free path lengths should fluctuate along the interface; however, these variations of $L_j(\omega)$ can hardly be measured experimentally because in actual experiments we usually measure the integrated characteristics.

Yet another factor affecting the magnitude and sign of the phonon component of the disjoining pressure is the orientation effect of substrate on the molecules in the near-wall layers of the liquid. As a result, the frequency distribution of the density of vibrational states changes significantly. Apparently, this distribution is a consequence of configuration averaging over

¶ Thick films are the films for which the dependence of L and K on the film thickness can be ignored.

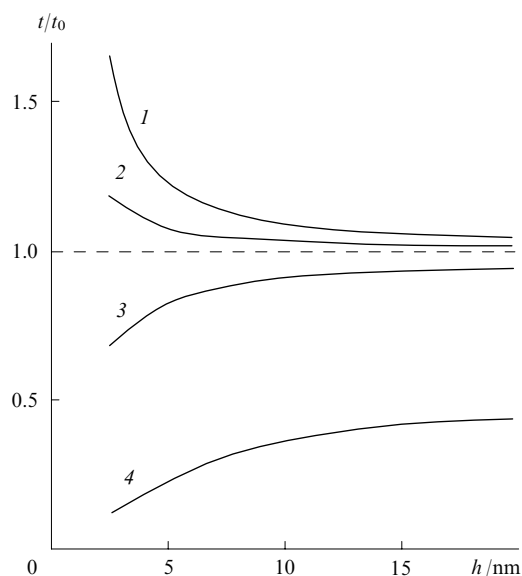


Figure 12. Relaxation time ratio of a linear molecular chain in symmetrical liquid film (t) and in bulk liquid (t_0) plotted vs. film thickness at different constants of dispersion interaction between the liquid molecules and the boundary phases: 1×10^{-49} (1), 2×10^{-50} (2), -2×10^{-50} (3) and $-5 \times 10^{-50} \text{ J m}^{-3}$ (4).

all possible orientations of the molecules in chains (corresponding to instantaneous static structure) with allowance for the statistical weight of each state. For instance, the orientations of molecules and their fragments (oscillators) relative to one another in bulk liquid are only determined by intermolecular interactions. In a liquid film, the field of surface forces of the substrate superimposes the field of intermolecular forces and thus causes redistribution of the statistical weights of different orientations.

We have shown that static structuring even in the first layer of a liquid film strongly affects the dynamic structuring of liquid in the whole film. Therefore, changes in the wettability of the interface resulting in redistribution of the density of vibrational states over frequencies can induce changes in not only the magnitude, but also the sign of the phonon component of the disjoining pressure. In the framework of the phonon mechanism we explained the experimentally observed effect of temperature on the oscillating and exponentially decreasing forces (to a first glance the effect is somewhat contradictory). For instance, theoretical analysis showed¹³⁴ that if the parameters of the dynamic matrix are independent of temperature (neglect of thermal expansion and changes in the state of the surface), the increase in the temperature causes damping of oscillations (Fig. 13) and a decrease in the magnitude and correlation lengths for the exponentially decreasing forces (Fig. 14).

The results of molecular dynamics calculations¹⁴⁹ and measurements of oscillating forces reported by Christenson and Israelachvili¹⁵⁰ (they studied the interaction between mica cylinders separated by an octamethylcyclotetrasiloxane interlayer in the temperature interval 14–40 °C) and by Nakada *et al.*¹⁵¹ (for the interaction between the Si_3N_4 and highly oriented pyrolytic graphite surfaces separated by interlayers of normal alcohols in the temperature range 25–60 °C) are in agreement with the results of theoretical studies indicating a slight damping of oscillations with an increase in temperature.

It is important that the decrease in the disjoining pressure with an increase in temperature, which is theoretically predicted for thick films in the framework of the approach we have developed (see Fig. 14), was repeatedly observed in experi-

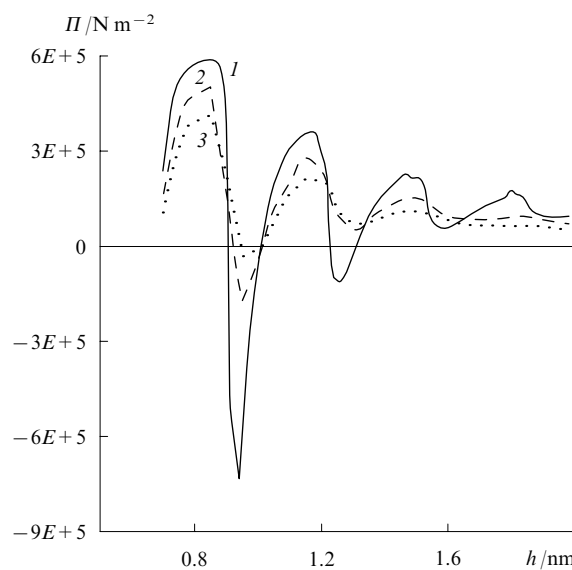


Figure 13. Damping of oscillations of the disjoining pressure with an increase in temperature: $T = 20$ (1), 50 (2), 70 °C (3). Calculated using the coupled oscillator model.¹³⁷

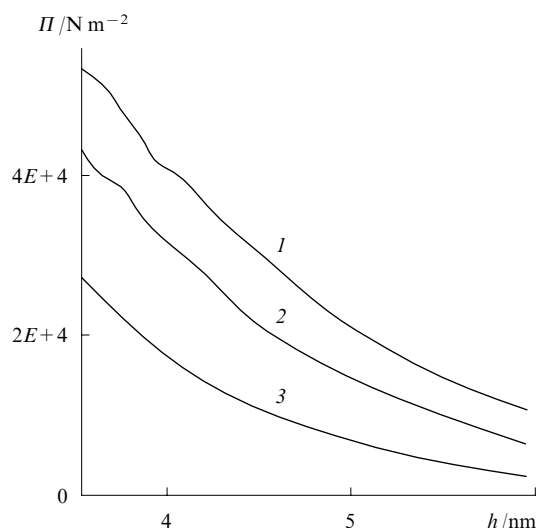


Figure 14. Changes in the non-oscillating portion of the disjoining pressure isotherm with temperature: $T = 20$ (1), 30 (2), 50 °C (3). Calculated using the coupled oscillator model.¹³⁷

ments. Moreover, weakening of the surface forces in water interlayers with an increase in temperature was for long treated as a characteristic property of structural forces and interpreted as a result of partial breakdown of the structure (*e.g.*, disruption of the network of hydrogen bonds).²

The mechanism we have proposed does not contradict this interpretation and provides a better insight into the physical sense of the structural changes occurring in the liquid with an increase in temperature. In particular, an increase in temperature is accompanied by a decrease in the ratio of the energy of hydrogen bonds to kT ; therefore, an increase in the frequency of thermal jumps is accompanied by redistribution of the density of vibrational states over frequencies.

However, the approximation of constant boundary conditions under temperature variation is not always valid. For instance, changes in the boundary conditions with an increase

in temperature can cause significant changes in the density of vibrational states for the interlayers bounded by bilayers, surfactant-coated surfaces, *etc.* This effect is most pronounced near the phase transition temperature in the surface layers. Calculations and theoretical analysis revealed¹³⁴ the possibility of strengthening rather than weakening of exponentially damping forces. Apparently, it is changes in the density of vibrational states that are responsible for the experimentally observed swelling of dipalmitoylphosphatidylcholine¹⁴⁷ and egg phosphatidylcholine¹⁵² bilayers on heating above the melting point.

Thus, the phonon mechanism of surface forces is based on consideration of changes in the frequency spectrum of the liquid upon restriction of its dimension, which was repeatedly observed in the model and real experiments (see, *e.g.*, Refs 146 and 153–155). This mechanism provides better insight into the dynamic processes occurring under limitation of the characteristic sizes of the liquid medium and makes it possible to assess the role of the interaction between the liquid interlayer and the confining phases in the formation of the dynamic structure of the liquid. It should be noted that this mechanism allows one to describe the oscillating (solvation) forces and various manifestations of the exponentially decreasing forces, such as the hydration-induced repulsion between hydrophilic surfaces and hydrophobic attraction.

4. Forces associated with the presence of long-chain surfactants and high-molecular-mass polymers in a liquid interlayer

There is yet another type of forces, which is ignored by the DLVO theory but has a great practical value for colloidal and disperse systems. These are forces associated with the presence of high-molecular-mass polymers and long-chain surfactants in a thin liquid interlayer. In this case the non-DLVO forces are mainly determined by the character of the interaction between polymers (long-chain surfactants) and the surfaces of particles separated by the liquid interlayers. Theoretical analysis of the forces arising in such systems involves consideration of three different cases, namely, reversible and irreversible adsorption of polymers on particles and the 'no adsorption' case.

Determination of the magnitude, sign and action range of forces requires the inclusion of (i) character of the polymer–solvent interaction, which is determined by the Flory–Huggins interaction parameter; (ii) degree of surface coverage with the polymer, (iii) evaluation of the proportion of polymer segments contacting the surface and the adsorption energy per segment and (iv) estimation of the thickness of the adsorption layer and the concentration of the polymer in solution. Finally, the size ratio of colloidal particles to polymer molecules should also be taken into account.

De Gennes¹⁵⁶ and Fleer *et al.*¹⁵⁷ proposed models that describe the interaction between large particles coated with a polymer irreversibly adsorbed from solution. The approach by de Gennes is based on scaling theory methods, being restricted to the case where the polymer occupies a fraction of the available adsorption sites on the surface of a particle and the adsorption energy of each polymer chain is high. The second approach uses the self-consistent field theory and is not restricted to low adsorptions. Both methods are applicable to the case where the phases confining the interlayer approach each other rapidly compared to the rate of establishment of the adsorption equilibrium on the surface but slowly compared to the rate of establishment of the conformational equilibrium in the adlayer. Various types of forces can appear in this case. At low polymer concentrations in a good solvent, bringing the surfaces closer together at constant surface coverages with the polymer causes the appearance of repulsive forces that decrease in proportion to the inverse cube of the separation between the surfaces (the interlayer thickness should be com-

parable with the doubled thickness of the adsorption layer).¹⁵⁸ At high polymer concentrations or under chemisorption conditions, the interaction between surfaces will have another character. An increase in the polymer concentration in solution leads to an increase in the interface coverage and to formation of brush structures (polymer molecules are arranged normal to the interface) under chemisorption conditions. In the latter case the elastic energy of the initially stretched chains in the brush structures decreases as the interlayer thickness decreases. This provides a negative contribution to the disjoining pressure in the film (attraction), which decreases in proportion to $h^{3/4}$. In addition, the osmosis contribution, which includes the change in the entropy of mixing and solvation energy of the polymer segments, and steric effects due to limitation of the number of possible conformations of the polymer molecules confined within the thin interlayer cause the appearance of repulsive forces that increase in proportion to $h^{-9/4}$ as the interlayer thickness decreases. Thus, the sign of the resultant force is determined by competition of the factors mentioned above and the interlayer thickness normalised to the thickness of the adlayer.¹⁵⁸ Numerous experimental data (see, *e.g.*, Refs 159–161) revealed the key role of the steric factor.

It should be noted that the idea of elastic repulsion between the surfactant and polymer adsorption layers was proposed by Reh binder¹⁶² in discussion of the effect of surfactants and polymers on the stability of colloids long before elaboration of theories of steric stabilisation. Recently, Huang and Ruckenstein¹⁶³ showed that changes in the polymer concentration over a wide range can induce a sequence of (re)stabilisation–destabilisation processes. For instance, on the one hand, a considerable increase in the polymer concentration causes an increase in adsorption of the polymer on the surface of particles and thus increases steric repulsion between them. On the other hand, it induces aggregation of the polymer in solution resulting in the appearance of attractive forces due to depletion forces (see below).

As to reversibly adsorbable polymers (usually, homopolymers), both theories, by Fleer¹⁵⁷ and by de Gennes,¹⁵⁶ predict attraction of the surfaces owing to bridging bonding through polymer molecules under equilibrium approach and free desorption of the polymer from the interface.

The effect of non-adsorbable polymers on the interaction between flat plates and spherical particles has been a subject of extensive research (see, *e.g.*, Refs 164–174). In this case, the sign and magnitude of the interaction depend on the thickness of the liquid interlayer, the shape of particles, the charge state of polymer molecules and the ratio of the gyration radius of the polymer to the radius of the colloidal particle. For instance, if macroscopic surfaces immersed in a liquid approach each other and the interlayer thickness is smaller than the length of a free polymer molecule, the concentration of the polymer in the interlayer decreases compared to its concentration in the bulk phase.^{165–168} The osmotic pressure produced in this case causes the appearance of attractive forces (the so-called 'depletion forces'). These forces considerably increase (i) as the polymer concentration increases,^{165, 167–168} (ii) on going from spherical polymer molecules to polymer chains or asymmetrical molecules,^{165, 166} (iii) in the case of charged polymer molecules^{166, 168} and (iv) if the particle–solution interface is covered with an adlayer of a polymer having a higher molecular mass compared to that of the free polymer.¹⁶⁷ Contrary to this, for thick interlayers bringing the surfaces closer together leads to an increase in the concentration of free polymer in the interlayer due to displacement of the solvent, which in turn causes the appearance of repulsive forces.^{167, 168} It should be noted that the repulsive forces at thick interlayers are always weaker than attractive forces at thin interlayers. Nevertheless, an increase in long-range repulsion with an increase in the concentration of a charged polymer at polymer

concentrations > 1 vol.% favours stabilisation of suspensions.¹⁶⁸

The methods and approaches mentioned above are applicable to macroscopic colloidal particles. The interaction of small (compared to the gyration radius of the polymer) particles was also studied.^{169–171} The polymer was treated as an ensemble of monomer units involved in manybody interactions. If the particle size is comparable with the gyration radius of the polymer, the theoretical analysis of the interactions in question is much more complicated.^{172–174} For instance, Tuinier and Fleer¹⁷³ used the notion ‘depletion thickness’ in the framework of the mean-field theory and derived an analytical expression for calculating the potential of depletion forces acting between two disperse particles. This method was also used¹⁷⁴ in a study of the effect of the polymer chain length, bulk concentration and solubility on the polymer segment distribution density across the liquid interlayer and on the magnitude of the depletion forces. It was pointed out that if the disperse particles, polymer molecules and the correlation length in the polymer solution are comparable, the actual magnitudes of depletion forces much exceed those reported in the literature.^{165–168} Thus, for nanodispersions the destabilising role of depletion forces is much more significant than for microdisperse systems.

Summing up, it should be noted that poor understanding of all specific features of the interactions between disperse particles in solutions of polymers or long-chain molecules is to a great extent due to a non-equilibrium character of the approach of the surfaces of particles in polymer solutions.

IX. Conclusion

Usually, the classical DLVO theory permits reliable calculations of the destabilising effects of electrolytes in classical colloidal and disperse systems characterised by a particle size of 100 nm and more and weak particle–dispersion medium interaction.

However, modern nanotechnology deals with much more complex objects. The use of nanocolloidal and nanodisperse systems comprising solid (or liquid) particles comparable in size with not only the Debye screening length, but also the thickness of the liquid interlayer between them requires the introduction of significant corrections for the curvature of the particle surfaces in calculations of the van der Waals and ionic electrostatic interactions and simultaneous inclusion of the specific features of the charge distributions along the surface of particles and across the interlayer separating them.

One of the key problems in nanotechnology is reliable manipulation of the size and properties of the surface of nanoparticles. This involves the use of multicomponent dispersion media characterised by strong interaction between particles and the medium (when it possesses lyophilic or lyophobic properties). This significantly reduces the efficiency of the classical theory in prediction and control of the stability of complex nanocolloidal and nanodisperse systems.

The author hopes that this review of modern theoretical approaches to calculations of surface forces of different nature acting in nanoscale liquid interlayers will help researchers and nanotechnologists to reasonably choose procedures for, and regimes of, treatment of systems containing nanoobjects in order to attain the desired results.

References

1. *Nanoscale Science and Technology* (Eds R W Kelsall, I W Hamley, M Geoghegan) (New York: Wiley, 2005)
2. B V Derjaguin, N V Churaev, V M Muller *Surface Forces* (New York: Consultant Bureau, 1987)
3. G Gouy *J. Phys.* **9** 457 (1910)
4. G Gouy *Ann. Phys.* **7** 129 (1917)
5. D L Chapman *Philos. Mag.* **25** 475 (1913)
6. F London *Trans. Farad. Soc.* **33** 8 (1937)
7. B V Derjaguin, L D Landau *Acta Physicochim. URSS* **14** 633 (1941)
8. E J W Verwey, J T G Overbeek *Theory of the Stability of Lyophobic Colloids* (Amsterdam: Elsevier, 1948)
9. I H de Boer *Trans. Faraday Soc.* **32** 10 (1936)
10. H C Hamaker *Physica* **4** 1058 (1937)
11. J N Israelachvili *Intermolecular and Surface Forces* (London: Academic Press, 1992)
12. E M Lifshitz *Zh. Eksp. Teor. Fiz.* **29** 94 (1955)^a
13. I E Dzyaloshinskii, E M Lifshitz, L P Pitaevskii *Usp. Fiz. Nauk* **73** 381 (1961) [*Physics-Uspekhi* **4** 153 (1961)]
14. M L Levin, S M Rytov *Teoriya Ravnovesnykh Teplovykh Fluktuatsii v Elektrodinamike* (The Theory of Equilibrium Thermal Fluctuations in Electrodynamics) (Moscow: Nauka, 1967)
15. Ya I Rabinovich, N V Churaev *Kolloid. Zh.* **49** 1117 (1987)^b
16. L A Wilen, J S Wettlaufer, M Elbaum, M Schick *Phys. Rev. B* **52** 12426 (1995)
17. B V Derjaguin, V M Muller, Ya I Rabinovich *Kolloid. Zh.* **31** 304 (1969)^b
18. D B Hough, L R White *Adv. Colloid Interface Sci.* **14** 3 (1980)
19. N G Van Kampen, B R A Nijboer, K Schram *Phys. Lett. A* **26** 307 (1968)
20. B W Ninham, V A Parsegian, G H Weiss *J. Stat. Phys.* **2** 323 (1970)
21. Yu S Barash, V L Ginzburg *Usp. Fiz. Nauk* **116** 5 (1975) [*Physics-Uspekhi* **18** 305 (1975)]
22. M Kostoglou, A J Karabelas *J. Colloid Interface Sci.* **171** 187 (1995)
23. J Walz *Adv. Colloid Interface Sci.* **74** 119 (1998)
24. L B Boinovich *Adv. Colloid Interface Sci.* **37** 177 (1992)
25. B V Derjaguin, Z M Zorin *Zh. Fiz. Khim.* **29** 1755 (1955)^c
26. J N Israelachvili, S J Kott, M L Gee, T A Witten *Macromolecules* **22** 4247 (1989)
27. B V Derjaguin *Izv. Akad. Nauk SSSR, Ser. Khim.* 1153 (1937)^d
28. B V Derjaguin, L D Landau *Zh. Eksp. Teoret. Fiz.* **15** 663 (1945)^a
29. J Lyklema, J F L Duval *Adv. Colloid Interface Sci.* **114–115** 27 (2005)
30. H Ohshima, Y Inoko, T Mitsui *J. Colloid Interface Sci.* **86** 57 (1982)
31. H Ohshima *Colloid Stability — The Role of Surface Forces* Pt. I, Vol. 1 (Ed. T F Tadros) (Weinheim: Wiley-VCH, 2007) p. 49
32. R Hogg, T W Healy, D W Fuerstenau *Trans. Faraday Soc.* **62** 1638 (1966)
33. G R Wiese, T W Healy *Trans. Faraday Soc.* **66** 490 (1970)
34. S Usui *J. Colloid Interface Sci.* **44** 107 (1973)
35. G Kar, S Chander, T S Mika *J. Colloid Interface Sci.* **44** 347 (1973)
36. D McCormack, S L Carnie, D Y C Chan *J. Colloid Interface Sci.* **169** 177 (1995)
37. S G Flicker, J L Tipa, S G Bie *J. Colloid Interface Sci.* **158** 317 (1993)
38. R Cohen, G Ozdemir, D Exerowa *Colloids Surf. B* **29** 197 (2003)
39. C Stubenrauch, R Strey *J. Phys. Chem. B* **109** 19798 (2005)
40. B Diakova, C Filiatre, D Platikanov, A Foissy, M Kaisheva *Adv. Colloid Interface Sci.* **96** 193 (2002)
41. M Giesbers, J M Kleijn, M A Cohen Stuart *J. Colloid Interface Sci.* **252** 138 (2002)
42. M M Kohonen, H K Christenson *Eur. Phys. J. E* **6** 315 (2001)
43. A Mukhopadhyay, B M Law *Phys. Rev. Lett.* **83** 772 (1999)
44. P M Claesson, M Kjellin, O J Rojas, C Stubenrauch *Phys. Chem. Chem. Phys.* **8** 5501 (2006)
45. D Langbein *J. Adhes.* **6** 1 (1974)
46. N V Churaev *Colloid Polym. Sci.* **253** 120 (1975)
47. R Podgornik, P L Hansen, V A Parsegian *J. Chem. Phys.* **119** 1070 (2003)
48. R Podgornik, V A Parsegian *J. Chem. Phys.* **120** 3401 (2004)
49. V A Parsegian, G H Weiss *J. Colloid Interface Sci.* **40** 35 (1972)

50. Yu S Barash *Sily Van-der-Vaal'sa* (Van der Waals Forces) (Moscow: Nauka, 1988)
51. E N Trofimova, F M Kuni, A I Rusanov *Kolloid. Zh.* **31** 578 (1969)^b
52. D Y C Chan, D J Mitchell, B W Ninham, B A Pailthorpe *J. Colloid Interface Sci.* **68** 462 (1979)
53. N V Churaev *Adv. Colloid Interface Sci.* **103** 197 (2003)
54. L B Boinovich, A M Emelyanenko *Adv. Colloid Interface Sci.* **104** 93 (2003)
55. L B Boinovich, A M Emelyanenko *Kolloid. Zh.* **65** 735 (2003)^b
56. L B Boinovich, A M Emelyanenko *Kolloid. Zh.* **65** 741 (2003)^b
57. L B Boinovich, A M Emelyanenko *Kolloid. Zh.* **66** 16 (2004)^b
58. L B Boinovich, A M Emelyanenko *Kolloid. Zh.* **66** 23 (2004)^b
59. V N Gorelkin, V P Smilga *Dokl. Akad. Nauk SSSR* **208** 635 (1973)^c
60. V N Gorelkin, V P Smilga *Poverkhnostnye Sily v Tonkikh Plenkakh i Ustoichivost' Kolloidov* (Surface Forces in Thin Films and Stability of Colloids) (Moscow: Nauka, 1974) p. 206
61. R Buscall, R Ettelaie, T W Healy *J. Chem. Soc., Faraday Trans.* **93** 4009 (1997)
62. P M Biesheuvel *Langmuir* **17** 3553 (2001)
63. M G Cacace, E M Landau, J J Ramsden *Q. Rev. Biophys.* **30** 241 (1997)
64. R M Pashley *J. Colloid Interface Sci.* **83** 531 (1981)
65. T W Healy, A Homola, R O James, R G Hunter *Faraday Discuss. Chem. Soc.* **65** 156 (1978)
66. B W Ninham, V V Yaminsky *Langmuir* **13** 2097 (1997)
67. B W Ninham *Prog. Colloid Polym. Sci.* **12** 1 (2002)
68. M Bostrom, D R M Williams, B W Ninham *Langmuir* **18** 6010 (2002)
69. W Kunz, P Lo Nostro, B W Ninham *Curr. Opin. Colloid Interface Sci.* **9** 1 (2004)
70. M Manciu, E Ruckenstein *Adv. Colloid Interface Sci.* **105** 63 (2003)
71. E Ruckenstein, M Manciu *Adv. Colloid Interface Sci.* **105** 177 (2003)
72. K A Karraker, C J Radke *Adv. Colloid Interface Sci.* **96** 231 (2002)
73. P Attard, D J Mitchell, B W Ninham *J. Chem. Phys.* **89** 4358 (1988)
74. R Kjellander *Colloid J.* **69** 20 (2007)
75. V N Paunov, P A Kralchevsky *Colloids Surf.* **64** 265 (1992)
76. R Kjellander, S Marcelja, R M Pashley, J P Quirk *J. Phys. Chem.* **92** 6489 (1988)
77. G A Martynov, V P Smilga *Kolloid. Zh.* **27** 250 (1965)^b
78. R Guidelli *J. Chem. Phys.* **92** 6152 (1990)
79. I S Zhiguleva, V P Smilga *Poverkhnostnye Sily v Tonkikh Plenkakh i Ustoichivost' Kolloidov* (Surface Forces in Thin Films and Stability of Colloids) (Moscow: Nauka, 1974) p. 220
80. M Kostoglou, A J Karabelas *J. Colloid Interface Sci.* **151** 534 (1992)
81. L Foret, A Wurger *J. Phys. Chem. B* **108** 5791 (2004)
82. A G Moreira, R R Netz *Europhys. Lett.* **57** 911 (2002)
83. D B Lukatsky, S A Safran *Europhys. Lett.* **60** 629 (2002)
84. D B Lukatsky, S A Safran, A W C Lau, P Pincus *Europhys. Lett.* **58** 785 (2002)
85. S Basu, M M Sharma *J. Colloid Interface Sci.* **165** 355 (1994)
86. D Henderson, M Lozada-Cassou *J. Colloid Interface Sci.* **162** 508 (1994)
87. V N Paunov, R I Dimova, P A Kralchevsky, G Broze, A Mehreteab *J. Colloid Interface Sci.* **182** 239 (1996)
88. V N Paunov, B P Binks *Langmuir* **15** 2015 (1999)
89. V N Paunov, E W Kaler, S I Sandler, D N Petsev *J. Colloid Interface Sci.* **240** 640 (2001)
90. B Jönsson, H Wennerström *J. Chem. Soc., Faraday Trans.* **2** **79** 19 (1983)
91. R Kjellander, S Marcelja *Chem. Scr.* **25** 112 (1985)
92. P Attard, D J Mitchell *J. Chem. Phys.* **88** 4391 (1988)
93. B Jönsson, P Attard, D J Mitchell *J. Phys. Chem.* **92** 5001 (1988)
94. W H Briscoe, R G Horn *Langmuir* **18** 3945 (2002)
95. Z Adamczyk *Adv. Colloid Interface Sci.* **100** (Spec. Issue) 267 (2003)
96. W H Briscoe, P Attard *J. Chem. Phys.* **117** 5452 (2002)
97. P Attard *Thermodynamics and Statistical Mechanics: Equilibrium by Entropy Maximisation* (London: Academic Press, 2002)
98. S Marcelja, N Radic *Chem. Phys. Lett.* **42** 129 (1976)
99. D W R Gruen, S Marcelja, V A Parsegian *Cell Surface Dynamics* (Eds A S Perelson, C Delisi, F W Wiegand) (New York: Marcel Dekker, 1984)
100. H Huang, M Manciu, E Ruckenstein *J. Colloid Interface Sci.* **263** 156 (2003)
101. E Ruckenstein, M Manciu *Langmuir* **18** 7584 (2002)
102. B W Ninham *J. Phys. Chem.* **84** 1423 (1980)
103. G Cevc, R Podgornik, B Zeks *Chem. Phys. Lett.* **91** 193 (1982)
104. N Ostrovsky, D Sornette *Chem. Scr.* **25** 108 (1985)
105. S Leikin, A A Kornyshev *J. Chem. Phys.* **92** 6890 (1990)
106. A A Kornyshev, S Leikin *Phys. Rev. A* **40** 6431 (1989)
107. V S Mitlin, M M Sharma *J. Colloid Interface Sci.* **157** 447 (1993)
108. J W Cahn *J. Chem. Phys.* **66** 3667 (1977)
109. R N Kuklin *Kolloid. Zh.* **59** 330 (1997)^b
110. J C Eriksson, S Ljunggren, P M Claesson *J. Chem. Soc., Faraday Trans.* **2** **85** 163 (1989)
111. V S Yushchenko, V V Yaminsky, E D Shchukin *J. Colloid Interface Sci.* **96** 307 (1983)
112. H K Christenson, P M Claesson *Science* **239** 390 (1988)
113. P M Claesson, H K Christenson *J. Phys. Chem.* **92** 1650 (1988)
114. J Forsman, B Jönsson, C E Woodward, H Wennerström *J. Phys. Chem. B* **101** 4253 (1997)
115. J L Parker, P M Claesson, P Attard *J. Phys. Chem.* **98** 8468 (1994)
116. A Carambassis, L C Jonker, P Attard, M W Rutland *Phys. Rev. Lett.* **80** 5357 (1998)
117. V V Yaminsky, B W Ninham *Langmuir* **9** 3618 (1993)
118. D R Bérard, P Attard, G N Patey *J. Chem. Phys.* **98** 7236 (1993)
119. M Schoen, T Gruhn, D J Diestler *J. Chem. Phys.* **109** 301 (1998)
120. P Tarazona *Phys. Rev. A* **31** 2672 (1985)
121. D Henderson, F F Abraham, J A Barker *Mol. Phys.* **31** 1291 (1976)
122. M Plischke, D Henderson *J. Chem. Phys.* **84** 2846 (1986)
123. R Kjellander, S Sarman *Chem. Phys. Lett.* **149** 102 (1988)
124. P Attard, J L Parker *J. Phys. Chem.* **96** 5086 (1992)
125. D Chandler, H C Andersen *J. Chem. Phys.* **57** 1930 (1972)
126. M J Grimson, P Richmond *J. Chem. Soc., Faraday Trans.* **2** **76** 1478 (1980)
127. J Gao, W D Luedtke, U Landman *J. Phys. Chem. B* **101** 4013 (1997)
128. G A Martynov *Kolloid. Zh.* **62** 393 (2000)^b
129. E N Brodskaya, V V Zakharov, A Laaksonen *Kolloid. Zh.* **64** 596 (2002)^b
130. H K Christenson *J. Disp. Sci. Techn.* **9** 171 (1988)
131. N V Churaev *Kolloid. Zh.* **58** 725 (1996)^b
132. N V Churaev *J. Colloid Interface Sci.* **172** 479 (1995)
133. L B Boinovich, A M Emelyanenko *Z. Phys. Chem.* **178** 229 (1992)
134. L B Boinovich, A M Emelyanenko *Kolloid. Zh.* **55** (5) 27 (1993)^b
135. L B Boinovich, A M Emelyanenko *Adv. Colloid Interface Sci.* **96** 37 (2002)
136. L B Boinovich *Prog. Colloid Polym. Sci.* **128** 164 (2004)
137. A M Emelyanenko, L B Boinovich *Kolloid. Zh.* **56** 362 (1994)^b
138. L B Boinovich, A M Emelyanenko *Prog. Colloid Polym. Sci.* **112** 64 (1999)
139. B J Berne, R Pecora *Dynamic Light Scattering* (New York: Wiley-Interscience, 1976)
140. R Zwanzig *J. Stat. Phys.* **9** 215 (1973)
141. I Ohmine *J. Phys. Chem.* **99** 6767 (1995)
142. B M Ladanyi, R M Stratt *J. Phys. Chem. A* **102** 1068 (1998)
143. G Seeley, T Keyes, B Madan *J. Phys. Chem.* **96** 4074 (1992)
144. J T Kindt, C A Schmittenmaier *J. Chem. Phys.* **106** 4389 (1997)
145. S D Bembek, B B Laird *Phys. Rev. Lett.* **74** 936 (1995)
146. Q Du, E Freysz, Y R Shen *Science* **264** 826 (1994)
147. L J Lis, M McAlister, N Fuller, R P Rand, V A Parsegian *Biophys. J.* **37** 657 (1982)
148. R P Rand, N Fuller, V A Parsegian, D C Rau *Biochemistry* **27** 7711 (1988)
149. L D Gelb, R M Lynden-Bell *Phys. Rev. B* **49** 2058 (1994)
150. H K Christenson, J N Israelachvili *J. Chem. Phys.* **80** 4566 (1984)

151. T Nakada, S Miyashita, G Sazaki, H Komatsu, A A Chernov
Jpn. J. Appl. Phys. **35** 52 (1996)
152. S A Simon, S Advani, T J McIntosh *Biophys. J.* **69** 1473 (1995)
153. S-B Zhu, G W Robinson *J. Chem. Phys.* **94** 1403 (1991)
154. P B Miranda, Y R Shen *J. Phys. Chem. B* **103** 3292 (1999)
155. L F Scatena, M G Brown, G L Richmond *Science* **292** 908 (2001)
156. P G De Gennes *Macromolecules* **15** 492 (1982)
157. G J Fleer, M A Cohen Stuart, J M H M Scheutjens,
T Cosgrove, B Vincent *Polymers at Interfaces* (London:
Chapman and Hall, 1993)
158. P G De Gennes *Adv. Colloid Interface Sci.* **27** 189 (1987)
159. P M Claesson, A Dedinaite, O J Rojas *Adv. Colloid Interface
Sci.* **104** 53 (2003)
160. R Sedev, D Exerowa *Adv. Colloid Interface Sci.* **83** 111 (1999)
161. C Stubenrauch, R Blomqvist *Colloid Stability — The Role of
Surface Forces* Pt. I, Vol. 1 (Ed. T F Tadros) (Weinheim:
Wiley-VCH, 2007) p. 263
162. P A Rehbinder *Izv. Akad. Nauk SSSR, Ser. Khim.* 639 (1936)^d
163. H H Huang, E Ruckenstein *Langmuir* **22** 4541 (2006)
164. B Vincent *Colloids Surf.* **50** 241 (1990)
165. S Asakura, F Oosawa *J. Chem. Phys.* **22** 1255 (1954)
166. S Asakura, F Oosawa *J. Polym. Sci.* **33** 183 (1958)
167. R I Feigin, D H Napper *J. Colloid Interface Sci.* **75** 525 (1980)
168. J Y Walz, A Sharma *J. Colloid Interface Sci.* **168** 485 (1994)
169. M Schmidt *J. Phys.: Condens. Matter* **11** 10163 (1999)
170. E Eisenriegler *J. Chem. Phys.* **113** 5091 (2000)
171. M Fuchs, K S Schweizer *Phys. Rev. E* **64** 021514 (2001)
172. A A Louis, P G Bolhuis, E J Meijer, J P Hansen *J. Chem. Phys.*
117 1893 (2002)
173. R Tuinier, G J Fleer *Macromolecules* **37** 8764 (2004)
174. S Yang, D Yan, H Tan, A-C Shi *Phys. Rev. E* **74** 041808 (2006)

^a — *J. Exp. Theor. Phys. (Engl. Transl.)*

^b — *Colloid J. (Engl. Transl.)*

^c — *Russ. J. Phys. Chem. (Engl. Transl.)*

^d — *Russ. Chem. Bull., Int. Ed. (Engl. Transl.)*

^e — *Dokl. Phys. Chem. (Engl. Transl.)*

Chemical research at the Siberian Branch of the Russian Academy of Sciences

This issue is devoted to the 50th anniversary of the Siberian Branch of the Russian Academy of Sciences the foundation of which was an outstanding event in the history of Russian science. The intensive exploration of Siberia including mineral resources and development of industry and agriculture, which started in the 1950s and was preceded by evacuation of many factories and scientific institutions from the USSR central regions to Siberia during the World War II, brought about numerous problems to be solved by Russian science. This required creation of an adequate scientific potential of Siberia. Outstanding scientists, Academicians M A Lavrentiev and S A Khristianovich proposed the foundation of a new scientific centre in Siberia. The government supported this proposal and on May 18, 1957, the USSR Council of Ministers established the Siberian Branch of the USSR Academy of Sciences, which was the first regional Branch of the Academy. The Siberian Branch comprised the already existing West-Siberian, East-Siberian, Yakutia and Far Eastern (remained a part of the Siberian Branch of the USSR Academy of Sciences up to 1970) subsidiaries of the USSR Academy of Sciences.

From the very beginning, the activity of the Siberian Branch (SB) was based on advanced principles, which have not still lost their value. These include interdisciplinary fundamental research, integration of science and education and development of the required infrastructure for the practical implementation of scientific achievements, the famous ‘Lavrentiev triangle’.

As soon as the first year of existence of the SB of the USSR Academy of Sciences, it was decided to establish a number of chemistry-oriented institutes in Siberia, namely, the Institute of Chemical Kinetics and Combustion, the Institute of Inorganic Chemistry and the Institute of Organic Chemistry in Irkutsk. However, the first chemistry-oriented Institute of the Academy appeared in Siberia back during World War II (in 1943). This was the Chemicometallurgical Institute founded in Novosibirsk, together with four other Institutes of the Academy within the bounds of the West-Siberian subsidiary of the USSR Academy of Sciences. Today, this institute is called the Institute of Solid State Chemistry and Mechanochemistry of the SB RAS and is among the eleven actively functioning chemical institutes of the Siberian Branch of the RAS, six of which are located in the Novosibirsk Akademgorodok and refer to the Novosibirsk Scientific Centre of the SB RAS. These are the Joint Institute of Catalysis comprising the G K Boreskov Institute of Catalysis, St Petersburg and Volgograd Branches of the Institute, and the Institute of Problems of Hydrocarbon Processing; the A V Nikolaev Institute of Inorganic Chemistry, the N N Vorozhtsov Novosibirsk Institute of Organic Chemistry, the Institute of Chemical Kinetics and Combustion, the International Tomography Centre, and the above-mentioned Institute of Solid State Chemistry and Mechanochemistry. The rest are parts of other scientific centres of the SB RAS, namely, the Irkutsk (A E Favorsky Irkutsk Institute of Chemistry), Krasnoyarsk (Institute of Chemistry and Chemical Technology), Tomsk (Institute of

Oil Chemistry) and Omsk centres (Institute of Problems of Hydrocarbon Processing); the most recently founded Institute for Problems of Chemical and Energetic Technologies is situated in Biysk.

The largest one is the Institute of Catalysis whose staff counts almost 1000. The Institute is a leader in the research of catalytic processes. The works of its founder and the first Director, Academician G K Boreskov, and his school are known all over the world. Boreskov's rule of approximate invariability of the specific catalytic activity of chemicals with invariable chemical and phase composition has underlain the modern theory of heterogeneous catalysis. The Institute's works on mathematical modelling of catalytic processes and development of the strategy for switching from laboratory studies to industrial scale production changed fundamentally the approach to the design of catalytic reactors and prompted the ways for increasing the efficiency of existing industrial processes. A large contribution to the development of physical methods for investigation of catalysts and elaboration of non-traditional ways for performing catalytic reactions was made by Academicians K I Zamaraev and V N Parmon and their co-workers. In particular, they determined the structure of numerous active catalytic sites, developed the methods for stimulation of catalytic processes with light or ionising radiation. Among recent, practically valuable achievements of the Institute of Catalysis, mention should be made of the development of highly efficient titanium–magnesium catalysts for the preparation of a superstrength polymer: ultrahigh-molecular-mass polyethylene. A priority trend in the Institute's activity is the development of environment-oriented processes, in particular, numerous catalytic processes for detoxification of wastes from industry, power engineering and transport.

The history of foundation and development of the Institute of Chemical Kinetics and Combustion (ICKC) is tightly connected with the names of Academician V V Voevodsky, a founder of chemical radiospectroscopy in the USSR, and first Director of the Institute, Corresponding Member of the USSR Academy of Sciences A A Koval'sky. Chemical radiospectroscopy and related studies of the magnetic interactions of molecules, the effect of magnetic field on chemical reactions and the synthesis of stable radicals and molecular magnets are essential priority lines in the research of this Institute. Under direction of Academician Yu D Tsvetkov, the first USSR and European electron spin echo spectrometer specially adapted for investigation of paramagnetic crystals at cryogenic temperatures was devised at the ICKC in 1965. New modifications of the electron spin echo spectroscopy designed and developed at the Institute allow one to study the motion of spin-labelled lipid molecules in biological membranes, the permeability of these membranes, to determine protein conformations and to study electron transfer at the photosynthesis centres. Quantum beats spectroscopy in recombination fluorescence was also developed at the ICKC. This method allows one to study superfast processes in radical ion pairs taking place in solutions over billionth of a second. The works dealing with spin

chemistry carried out at the Institute under the supervision of Academicians Yu N Molin and R Z Sagdeev have gained broad recognition. Studies of the combustion processes in gases and combustion of energetic materials is yet another important scientific trend in the activity of the ICKC. Of special note are works dealing with filtration combustion of gases. In addition, the mechanisms of photochemical reactions and the reactivity of active intermediate species are studied at the Institute. Using a laser on free electrons designed at the G I Budker Institute of Nuclear Physics of the SB RAS, an original method for the investigation of biological macromolecules using terahertz radiation, which does not destroy large molecules, has been developed.

A number of international scientific centres were organised at the base of the Siberian Branch institutes that occupy leading positions in their field of science. One of these centres, the International Tomography Centre (ITC), was founded in 1996 under initiative of Academician R Z Sagdeev in cooperation with the Bruker group of companies. The key lines of research of the ITC include the theory of chemical bond, the reactivity of chemical compounds, the mechanisms of chemical reactions; magnetic phenomena in chemistry and medicine, spin and exchange phenomena, in particular, those in multi-spin coordination compounds; diagnostic NMR imaging and NMR microtomography for physicochemical applications. The unique 3D MYUR procedure developed at the ITC allows visualisation of the peristaltic motion dynamics of free fluid along the hollow biostructures and direct estimation of the physiological rhythm parameters. The development of new contrasting means based on stable aminoxyl radicals for magnetic resonance imaging (MRI) of living organisms is in progress. Magnetic resonance imaging is widely used for chemical investigations, as it makes it possible to study the internal structure and behaviour of samples without their destruction. The method has been successfully used for *in situ* studies of mass transfer within porous materials and also for studies of gas and liquid structure. Using aminoxyl radicals and paramagnetic metal ions, the researchers of the ITC were able to prepare heterospin coordination compounds, which represent a new type of molecular magnets. Pioneering studies on the design of layered polymeric and framework structures were carried out at the ITC. A new in principle class of objects was discovered, the so-called breathing crystals, which tend to change their volume unusually strongly around magnetic transitions upon temperature variation.

A key trend in the activity of the A V Nikolaev Institute of Inorganic Chemistry (NIIC) is the physicochemical research of materials for electronics. A research group of the Institute headed by Academician F A Kuznetsov carried out a large series of works in this field, in particular, they developed the strategy of chemical vapour deposition, which is among the techniques most widely used in industry for the manufacture of microelectronic devices. Yet another important project of the Institute is the development of a crystal growth process for laser technology by the Chokhralsky low-gradient method. A new trend in the NIIC activity is supramolecular chemistry concerned with large molecular arrays self-assembled from geometrically and chemically complementary fragments. Typical examples of supramolecular compounds are 'host-guest' complexes. These complexes are studied at the Institute, in particular, transition metal complexes incorporated into a hydrophobic cavity of large molecular containers, cucurbiturils. It was shown experimentally that the molecules that get in the cavity of such a molecular container can change essentially their physicochemical properties. This method can be used to prepare complexes containing metals in unusual oxidation states with unique reactivity. At the Institute, a method has been developed and a table-top spectrometer NMR-micro has been designed for nanosystem porometry and for studying the

dynamics of nanoliquids under quantum constraint conditions and the properties of the mobile subsystem in ultrathin channels of nanoporous items and heterostructures. Using this method and quantum chemistry methods, the trigger properties of metal nanoclusters, proton and superionic conductors, superconducting systems, nanoporous crystals of the natural zeolite family were studied.

All research trends at the Novosibirsk Institute of Organic Chemistry (NIOC) are associated with the name of its founder, Academician N N Vorozhtsov, a prominent scientist in the chemistry and technology of aromatic compounds, organic intermediates and dyes. He and his followers developed the synthetic chemistry of aromatic compounds, a general approach to the preparation of polyfluorinated aromatic compounds starting from available polychlorinated analogues. One more line of research initiated by N N Vorozhtsov was concerned with the mechanisms of most important reactions of aromatic compounds and the structures and properties of carbocations. This subject was further developed in Academician V A Koptug's studies. The series of studies dealing with carbocations carried out under his supervision was awarded in 1990 the Lenin prize, the most prestigious prize in the USSR. Since Siberian flora is a source of an enormous number of biologically active compounds, N N Vorozhtsov established the Laboratory of Natural Physiologically Active Compounds at the Institute. This research started by Professors V A Pentegova and V A Barkhash was successfully continued by Academician G A Tolstikov. Currently, target-directed synthesis of drugs and modification of plant metabolites form an important field of investigations carried out at the NIOC. In particular, Academician G A Tolstikov supervised the synthesis of new derivatives of betulonic acid, which was synthesised from betulin extracted from the birch bark. Many amides and peptides of betulonic acid are active inhibitors of tumour cell growth. Studies on transformation of readily available plant di- and triterpenoids and diterpene isoquinoline alkaloids aimed at the elaboration of promising antiviral, anaesthetic, cardiostimulating and antitumour drugs are carried out at the Institute.

The main field of research carried out at the Institute of Solid State Chemistry and Mechanochemistry (ISSCM) is related to solid-phase transformations. Academician V V Boldyrev and co-workers elucidated the influence of defects in a solid on the mechanism and the rate of solid-phase transformations. By selecting the methods for the production and pretreatment of solids, they succeeded in carrying out many solid-phase processes not only absolutely without wastes, but also with a considerable decrease in the number of stages and the time of the processing cycle. Among the most recent ISSCM studies, one can mention those of nanoparticle formation upon explosion carried out in cooperation with the G I Budker Institute of Nuclear Physics and the M A Lavrentiev Institute of Hydrodynamics of the SB RAS in the real-time mode using synchrotron radiation. These studies provided a deeper insight into the nature of fast processes and ensured the development of a number of explosion-based industrial processes, in particular, controlled synthesis of nanodiamonds.

The A E Favorsky Irkutsk Institute of Chemistry of the SB RAS (IriC) is among the most prominent Russian centres for fundamental research in organic and organoelement chemistry. A leading Russian scientific school, which continues the tradition of the great Russian organic chemist A E Favorsky, has formed at the Institute. The research carried out at the Institute from the day it was founded has been mainly concerned with acetylene and complex organic and organoelement molecules synthesised based on acetylene. The chemistry of organic compounds of silicon with unusual valence represents yet another leading research trend of the Institute. Under the supervision of Academician

M G Voronkov, compounds with pentacoordinated silicon, the so-called silatranes, were prepared at the IrIC. Many new chemical reactions were discovered, the best known being the reaction of ketoximes with acetylene discovered by Academician B A Trofimov. This reaction gives rise to pyrroles, key fragments of important life-supporting metal complex systems (chlorophyll and haemoglobin) and has been included into monographs and handbooks as the Trofimov reaction. Numerous drugs, environmentally safe pesticides, plant growth regulators, polymers, fragrances, sorbents, complexones and metal and pollutant extractants, corrosion inhibitors, fuel and oil additives, new-generation materials for microelectronics and lithium batteries and energetic compounds for rocket propellants were developed at the Institute. Among new pharmacological agents prepared by Irkutsk chemists, mention should be made of Acyzole, which possesses antidote properties with respect to carbon monoxide, Cobazole, which actively stimulates haemogenesis, and Anavidin, a new-generation antiseptic and disinfectant. A new highly efficient antituberculosis agent Perchlozon active with respect to mycobacteria that are stable against standard antituberculous drugs is under clinical trials.

The setting of research of Siberian chemical institutes have always included a regional component. First of all, this implies systematic studies into the composition of diversified fossil and renewable raw materials and development of the methods for reasonable use of these resources, in particular, development of environmentally safe methods for their processing. The Institute of Chemistry and Chemical Technology of the SB RAS (ICCT) has accumulated highly valuable experience in the processing of plant biomass to produce various target products; in particular, methods for the production of microcrystalline cellulose from wood wastes were developed. The Institute contributed significantly to the development of the theory of structure of the surface and near-surface layers of minerals, in particular, those formed on sulfides in chemical and electrochemical reactions. On the basis of microscopic cenospheres present in the ash from carbon-based heat electric generation plants, microspherical zeolite sorbents, encapsulated inorganic ion-exchange materials and organic extractants for purification of liquid radioactive wastes of nuclear plants and waste waters of hydrometallurgical plants from radionuclides and nonferrous and noble metal ions were developed.

The Institute of Problems of Hydrocarbon Processing (recently, this was the Omsk Branch of the Institute of Catalysis of the SB RAS), together with the Institute of Catalysis were engaged in a highly important State innovation project in 2003–2006 and thus developed (and prepared for commercialisation) new catalysts for two important oil refining processes, namely, cracking and reforming; engine fuel production at Russian plants was successfully upgraded.

The Institute of Petroleum Chemistry of the SB RAS carries out extensive fundamental and applied studies directed at the creation of new science-intensive, environmentally safe, energy-saving processes for enhanced oil refining. Large-scale industrial use of these processes would extend the period of commercial production from fields at later stages of development and start the development of fields with oil reserves which are difficult to refine, in particular, with high-viscosity oils. The development and perfection of physicochemical, hydrodynamic, steam and microbiological methods for reservoir development and integrated processes that combine these ways of stimulation are in progress.

An essential contribution to the production of new highly energetic substances was made by one of the youngest Institutes of the SB RAS, the Institute for Problems of Chemical and Energetic Technologies, founded in 2001 by the Siberian Branch in close cooperation with the Federal State Unitary Enterprise 'Altay' in order to pursue the fundamental and

applied studies in the development and use of energetic compounds, development of the methods of fine organic synthesis, and manufacture of new materials. An achievement of the Institute is the design of new high-enthalpy polymers and other components of rocket propellants with the record-breaking characteristics accomplished by Academician G V Sakovich.

When considering the chemistry-related studies carried out at the Siberian Branch of the RAS, it should be noted that they are far from being limited to the above-listed chemical institutes. For example, extensive advanced studies in bioorganic chemistry and physicochemical biology are carried out at the Institute of Chemical Biology and Fundamental Medicine (formerly, this was the Institute of Bioorganic Chemistry formed from a department of the Novosibirsk Institute of Organic Chemistry) and also in a number of other biological institutes.

The works on the design of new materials including nanomaterials and nanotechnologies are carried out at physical institutes. At some institutes of the SB RAS, research into the chemical essence of natural phenomena and objects is actively carried out (chemistry of atmosphere, geochemistry, *etc.*). Noteworthy are very promising studies of gas hydrates in permafrost zones and aquatic areas representing inexhaustible reserves of methane and physicochemical and analytical studies dealing with Baikal.

Finally, institutes of different disciplines make a great contribution to the development of new instruments and procedures and their adapting to the investigation of chemical processes and materials, as was mentioned above.

The principles of work of the Siberian Branch established by its founders allowed the Branch to survive during the hard years of perestroika and to adapt to work under market. The high level and the integrated character of fundamental research allow the Institutes to compete for, and win grants from, Russian and foreign funds and to award contracts with leading foreign companies. The system of training of scientific staff in the SB RAS ensures preservation of the scientific potential of the Branch at a high level, and the engineering design and pilot departments established at the institutes allow one to bring the scientific results to the level required for commercialisation, thus opening the way for new science-intensive industrial processes and attraction of investments. An important achievement of the SB RAS is the active functioning of world-level scientific schools. The works of scientists of the Branch have been repeatedly rewarded with prestigious prizes, prizes of the RF government and the Russian Academy of Sciences. Many scientists of the SB RAS are international prize winners, members of foreign Academies and international scientific associations.

This issue of the journal composed with significant participation of Professor V P Fedin includes reviews prepared by senior researchers of the chemical institutes of the SB RAS. Of course, this covers only a minor portion of results of studies carried out at these institutes. The subsequent issues of the journal would continue to acquaint the readers with the scientific results obtained by chemists of the Siberian Branch of the RAS.

Academician V N Parmon
Chairman of the Joint Academic Council
on Chemical Sciences of the SB RAS

Quantum beats in radical pairs

V A Bagryansky, V I Borovkov, Yu N Molin

Contents

I. Introduction	493
II. The nature and detection of quantum beats in radical pairs	493
III. Theory of quantum beats in recombination luminescence of spin-correlated radical ion pairs	496
IV. Spectroscopy of quantum beats in radical pairs	499
V. Conclusion	505

Abstract. Possible fields of application of the phenomenon of quantum beats in spin-correlated radical pairs in studies of the properties of short-lived radicals (lifetimes of up to a few nanoseconds) in liquid solutions are considered. The theoretical approaches to the description of this phenomenon and modern experimental data are analysed. The bibliography includes 82 references.

I. Introduction

Shortly after the discovery of chemically induced dynamic nuclear polarisation (CIDNP) in the late 1960s it was established that the course of radical reactions in solutions may be affected by external magnetic fields, resonance microwave radiation and hyperfine interactions (magnetic isotope effect). The new field of research on the effects of electron and nuclear spin dynamics on elementary chemical reactions is for brevity called ‘spin chemistry’ or ‘dynamic spin chemistry’. Recent advantages, research potential and specific features of this field of chemical science have been well documented (see monographs^{1–4} and reviews^{5–21}).

Most phenomena studied by spin chemistry are due to dynamic (not associated with paramagnetic relaxation) transitions between different states of electron spins in a radical pair (RP) emerged in a coherent (singlet or triplet) spin state. Corresponding methods of investigation also employ this feature. These dynamic transitions, or quantum beats, are similar to quantum beats in other systems, which allows spin chemistry to be considered as a ‘companion’ to yet another new avenue of research, namely, femtochemistry, and to some spectroscopic methods of investigations that also utilise quantum interference. In both spin chemistry and femtochemistry the quantum beats in the populations of reactant states modulate the yield of reaction products. To describe these

phenomena, one should allow for the oscillation phase of the wave function. This unusual, for chemistry, feature offers basically new opportunities for control of chemical reactions through variation of the phase relations in the wave packet by varying external factors. In addition, frequency analysis of quantum beats provides information on the properties of reacting species and offers new horizons for experimentalists.

Most experimental approaches used in spin chemistry involve analysis of time-average manifestations of the spin evolution in RPs. A typical example is provided by measurements of the magnetic field effect (dependence of the yield of final products of radical reactions on the magnetic field strength). The magnetic field affects positions of electron-spin energy levels and, as a consequence, the evolution of the spin state of the RP. Since the reaction is spin selective, the yield of reaction products changes with the magnetic field strength. The change in the product yield is thus an integrated ‘fingerprint’ of the temporal evolution of the spin state in the RP.

Development of pulsed methods of generation of radical pairs and relevant detection instruments with nanosecond temporal resolution permitted real-time monitoring of manifestations of quantum oscillations of the spin state in RP. In this review we will consider methods of detection of quantum beats based on recombination luminescence of RPs and the results of recent studies obtained by these techniques.

II. The nature and detection of quantum beats in radical pairs

1. A qualitative model

Dynamic singlet–triplet transitions in spin-correlated RPs are related to the quantum nature of electron spins. Spin-correlated pairs are produced upon rupture of chemical bonds or after ionisation of molecules. The total spin of the unpaired electrons remains unchanged, which means that the state (singlet or triplet) of a radical pair is the same as that of its precursor.

Quantum beats are due to the fact that the singlet and triplet states of RP are superpositions of several stationary states. In turn, this is due to the spin–orbit and hyperfine couplings in radicals. Quantum beats occur in any system whose states are coherent superpositions of stationary states.^{22,23} In the simplest case the initial state of a quantum system

$$|\Psi(0)\rangle = c_a|a\rangle + c_b|b\rangle,$$

V A Bagryansky, V I Borovkov, Yu N Molin Institute of Chemical Kinetics and Combustion, Siberian Branch of the Russian Academy of Sciences, ul. Institutskaya 3, 630090 Novosibirsk, Russian Federation. Fax (7-383) 330 73 50, tel. (7-383) 333 23 81, e-mail: vbag@kinetics.nsc.ru (V A Bagryansky), tel. (7-383) 330 97 92, e-mail: borovkov@kinetics.nsc.ru (V I Borovkov), tel. (7-383) 333 16 07, e-mail: molin@kinetics.nsc.ru (Yu N Molin)

Received 9 April 2007

Uspekhi Khimii 76 (6) 535–549 (2007); translated by A M Raevskiy

is a superposition of two vectors of the stationary states $|a\rangle$ and $|b\rangle$ of the system with the energies E_a and E_b , respectively (c_a and c_b are constants). At arbitrary instant $t > 0$, the state of the system is described by the vector

$$|\Psi(t)\rangle = c_a|a\rangle e^{-iat} + c_b|b\rangle e^{-ibt}, \quad (1)$$

where $a = E_a/\hbar$, $b = E_b/\hbar$. Let x be the operator of an observable quantity and let x have no explicit dependence on time. The average value of x in the state (1) is given by

$$\begin{aligned} \langle x(t) \rangle &= \langle \Psi(t) | x | \Psi(t) \rangle = \\ &= |c_a|^2 x_{aa} + |c_b|^2 x_{bb} + 2|c_a^* c_b x_{ab}| \cos[(a-b)t + \varphi]. \end{aligned} \quad (2)$$

The first two terms in the right side of Eqn (2) are the weight-average of x and the last term is the cross-term modulated by the frequency of the transition between the states a and b (here φ is the relative phase of the complex coefficients c_a and c_b). If the initial state is composed of more than two vectors of stationary states, the average value of the physical quantity is modulated by several frequencies.

The simplest example of quantum beats in a radical pair is provided by two noninteracting radicals differing in their isotropic g -factors. The energies of the stationary states of the pair in a strong magnetic field are shown in Fig. 1. Two states of the pair, with the energies E_1 and E_4 , are the triplet states T_+ and T_- , whereas the other two states with the energies E_2 and E_3 are mixed states composed of the spin states S and T_0 taken with equal weights. This means that emergence of a radical pair in, e.g., the singlet state will cause coherent population of two energy levels, E_2 and E_3 . This will be accompanied by the onset of singlet–triplet oscillations at the frequency

$$\omega = \frac{\beta B}{\hbar} (g_1 - g_2),$$

corresponding to the difference E_2 and E_3 . If isotropic hyperfine couplings (HFC) occur in the radicals, the oscillation frequencies are given by

$$\omega = \frac{\beta B}{\hbar} (g_1 - g_2) + \sum_{i1} a_{i1} m_{i1} - \sum_{i2} a_{i2} m_{i2},$$

where β is the Bohr magneton, B is the induction of external magnetic field, g is the g -factor, a_i is the constant of HFC with the i th nucleus, and m_i is the projection of the spin of the i th nucleus on the direction of the magnetic field; the subscripts '1' and '2' enumerate different radicals in the pair.

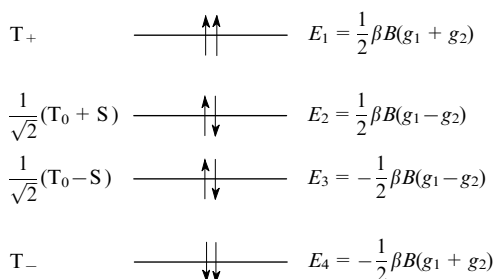


Figure 1. Energy levels of a radical pair comprising radicals with different g -factors in strong magnetic field.

The visual pattern of beats in an RP in a constant magnetic field (magnetic field strength much exceeds the constants of HFC in the radicals in the pair) is illustrated by the vector

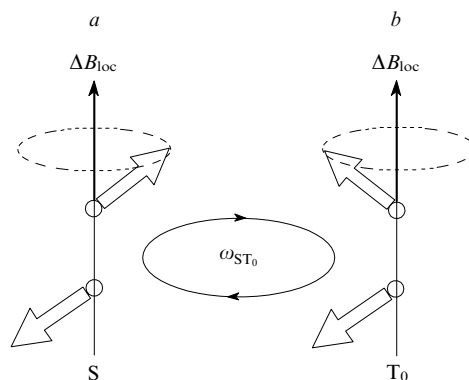


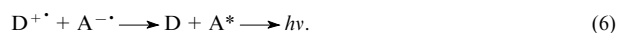
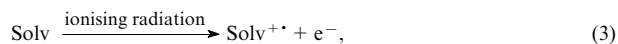
Figure 2. Vector diagram illustrating the onset of $S-T_0$ oscillations of the spin state of a radical pair in strong magnetic field. Oscillations are due to the Larmor frequency difference between electron spins in different local magnetic fields.

diagram shown in Fig. 2. The pair emerged in the singlet (S) spin state corresponds to the antiparallel orientation of the radical spins in the vector diagram (Fig. 2a). Then, in a strong magnetic field the spins undergo precession about the magnetic field direction. However, the spin precession frequencies differ due to differences between the 'internal magnetic fields' owing to different spin–orbit and hyperfine interactions in radicals. As a result, the pair periodically goes to the T_0 state in which the vector sum of the spins differs from zero and is oriented normal to the magnetic field direction (Fig. 2b).

2. Quantum beats in recombination luminescence

The possibility of experimental observation of quantum oscillations in RP is due to the fact that the yield of the products of recombination of the radicals in the pair depends on the total spin of the radicals at the instant of recombination. This means that oscillations of the singlet state population of the RP can be monitored by observing the kinetics of formation of the product of singlet recombination.

Experiments involving detection of recombination luminescence of radical ion pairs formed upon the action of a pulse of ionising radiation on non-polar solutions of electron donors and acceptors appeared to be the most fruitful for observation of quantum beats in the spin state of RP. The formation and recombination of radical ion pairs can be described by the following scheme:



In the first stage (3), irradiation of dilute solutions of electron donors (D) and acceptors (A) causes ionisation of solvent molecules (Solv) and formation of a primary RP comprised of an electron and the solvent hole ($\text{Solv}^{+\bullet}/e^-$). Since the solvent molecule was in the singlet spin state before irradiation, the primary RP emerged upon ionisation is also in the singlet state.

This correlation also holds for the secondary pairs ($D^{+\bullet}/A^{\bullet-}$) if the rates of reactions (4) and (5) are higher than the rate of the singlet–triplet transition. To monitor the spin state of this pair using recombination luminescence, the electron donor or acceptor should be a luminophore with a rather short fluorescence time. Then, recombination (6) of the singlet radical pair resulting in a singlet-excited product A^* (or D^*) will be followed by emission of a fluorescence quan-

tum. As a consequence, the dynamic singlet–triplet transitions responsible for the oscillations of the singlet state population will induce modulation of the kinetics of recombination fluorescence. The recombination products of triplet pairs usually show no intense phosphorescence in solution.

Solutions in non-polar solvents are the most convenient systems for carrying out these experiments. The reasons are as follows. First, the separation between radical ions in the primary RPs generated in a non-polar medium is shorter than the Onsager radius. Therefore, they mainly recombine in a geminate fashion, *i.e.*, with the spin-correlated partners. Second, the solvation energy of the recombining radical ions in the non-polar medium is minimum, which favours the release of energy sufficient for recombination luminescence.²⁴ In addition, recombination immediately follows the first collision between radical ions irrespective of their spin state due to strong Coulomb attraction. Therefore, the effects of secondary collisions almost do not manifest themselves,¹ and the rate of formation of the singlet-excited products of recombination (6) can be represented by the product of the recombination rate to the singlet state population of the RP. This essentially simplifies the analysis of the kinetics of recombination luminescence in order to detect the quantum beats due to the singlet–triplet transitions in the spin state of the RP. Finally, the partners emerge and spend most time at a long distance from each other. Under these conditions the effect of the dipole–dipole and exchange interactions between partners can be ignored, which also essentially simplifies the theoretical description of the spin evolution in radical pairs.

3. Methods and instruments

Advances in detection of quantum beats were to a great extent due to the use of the single photon counting technique²⁵ for detection of recombination fluorescence. The method permits detection of fluorescence with high temporal resolution in high dynamic range of intensities ($>10^5$). Quantum beats are detected using radioactive sources of fast electrons^{13, 14, 17, 26–48} and controllable sources of ionising radiation,^{13, 14, 17, 41, 49–66} the latter providing a much higher performance of experimental installations.

At rather short excited-state lifetimes of recombination products, the experimental procedures involving detection of recombination fluorescence in fact detect the derivative of the accumulation kinetics of the product of the spin-dependent reaction. This improves the detection of quantum beats. An analogy is provided by radiospectroscopy. Namely, going to phase-sensitive detection (here, the derivative of the signal is recorded) provides enhanced resolution and improves the signal-to-noise ratio. Clearly, relevant mathematical processing of the data obtained by other methods will also allow quantum beats in reactions of spin-correlated RPs to be observed. Analysis of the temporal dependence of the fluorescence intensity ratio in nonzero and in zero magnetic field rather than the kinetics of recombination fluorescence offers additional advantages in the interpretation of experimental results (see below). This ratio was called the time-resolved magnetic field effect (TRMFE).

As an example of experimental setup for TRMFE studies, Figure 3 presents a block diagram of an X-ray fluorimeter designed at the same Institute, Siberian Branch of the Russian Academy of Sciences. This instrument was used to obtain many of the results discussed below. The electron gun was also designed at the Institute of Chemical Kinetics and Combustion, Siberian Branch of the Russian Academy of Sciences and is used to generate X-ray pulses in the ~ 20 keV energy range. X-Ray radiation incident on the sample placed between the poles of an electromagnet causes fluorescence, which passes through the light guide and light filter to the photomultiplier

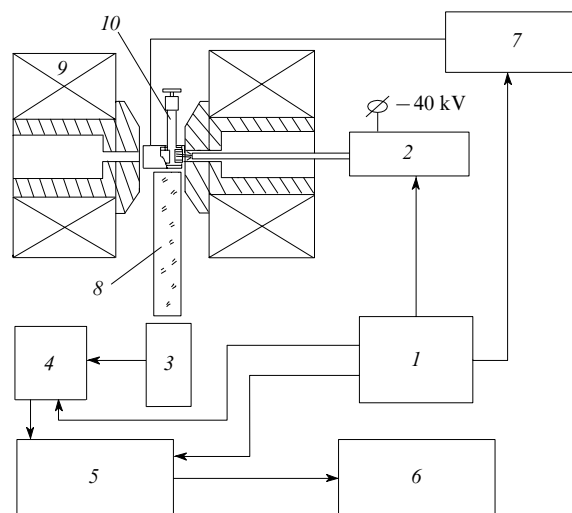


Figure 3. Blok diagram of a nanosecond X-ray fluorimeter.⁴⁹

Synchronisation and control unit (1), electron gun (2), fluorescence detection unit (3), converter of time intervals (4), multichannel analyser (5) coupled with a computer (6), magnetic field and temperature control unit (7), light guide (8), electromagnet (9), and sample (10).

and the fluorescence detection unit. The fluorimeter makes it possible to detect the kinetics of radiofluorescence on the time scale from 10 to 10^4 ns at the magnetic field induction ranging from 0 to 1.1 T and provides temperature stabilization in the 223–353 K range.

4. First observations of quantum beats

Quantum beats due to hyperfine coupling were first observed by Klein and Voltz^{26, 27} in 1976 and independently by Brocklehurst.^{28, 29} Klein and Voltz^{26, 27} measured the kinetics of recombination fluorescence induced by irradiating a cyclohexane solution of a dye [2,5-bis(4-butylphenyl)-1,3,4-oxadiazole, bPPD] with fast electrons in magnetic field by the single photon counting technique at times up to 700 ns. Having plotted the TRMFE curve, the authors revealed a kink. The nonmonotonic character of the TRMFE curve was associated with magnetic-field-dependent singlet–triplet transitions in the secondary radical ion pairs $\text{bPPD}^{+\bullet}/\text{bPPD}^{-\bullet}$. These transitions determine the multiplicity of the RP at the instant of recombination and, as a consequence, the multiplicity of the recombination product, *i.e.*, an excited bPPD molecule. As a result, fluorescence due to emission of singlet-excited molecules of this dye is modulated, the modulation frequencies being equal to the singlet–triplet transition frequencies.

Brocklehurst reported similar experiments with other luminophores (*p*-terphenyl and biphenyl) in various non-polar solvents.^{28, 29} Researchers from both groups used radicals with complex hyperfine structures characterised by a number of different HFC constants. As a result the TRMFE curves exhibited a single peak of oscillations (Fig. 4), thus providing a little information on the phenomenon under study.¹¹ The authors of the pioneering and subsequent studies (see a review¹¹) clearly demonstrated the possibility of observation of the spin evolution in RPs using the TRMFE technique.

Studies reported by Anisimov *et al.*^{30, 31} in 1983 gave a new impetus to the development of the method of quantum beats in recombination fluorescence. Anisimov *et al.* observed a number of quantum beat peaks in the kinetics of recombination luminescence of the solutions of tetramethylethylene

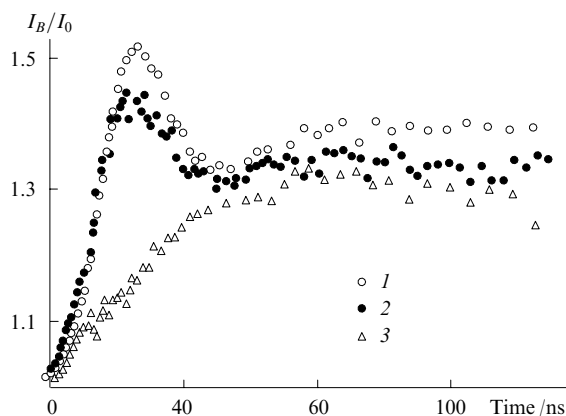


Figure 4. Magnetic field effect ($B = 100$ mT) in recombination fluorescence for squalane solutions of *p*-terphenyl (curves 1 and 2) and *p*-terphenyl- d_{14} (curve 3). Solute concentration: $5 \text{ mmol litre}^{-1}$ (1) and $1 \text{ mmol litre}^{-1}$ (2, 3).¹¹

(2,3-dimethylbut-2-ene) and *p*-terphenyl- d_{14} in *trans*-decalin, *cis*-decalin, squalane and pentadecane in strong (Fig. 5) and zero magnetic field.

Tetramethylethylene chosen as hole scavenger forms a radical cation containing twelve equivalent protons. Therefore, the pattern of quantum beats in a strong magnetic field is formed by oscillations with the multiple frequencies and looks quite simple. Similar results were obtained^{30,31} in studies of a solution of durene (its radical cation also contains twelve equivalent protons) and *p*-terphenyl- d_{14} in *trans*-decalin. Both the shape and period of oscillations corresponded to the theoretically predicted ones, but the amplitude of beats observed in the experiments was much smaller than it follows from theory.

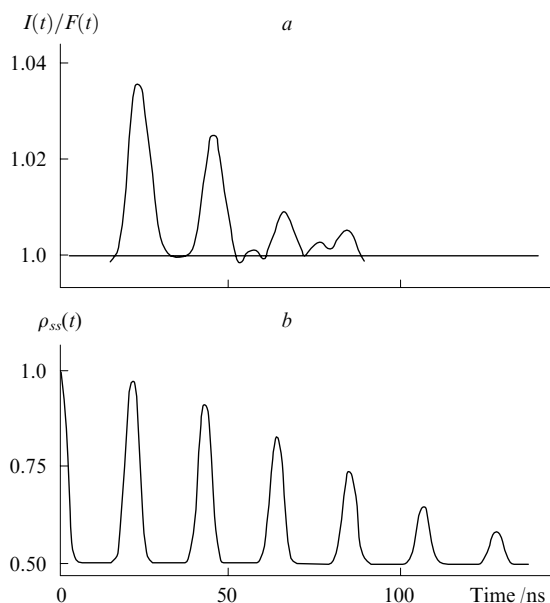


Figure 5. Quantum beats in recombination fluorescence of tetramethylethylene and *p*-terphenyl- d_{14} solutions in *trans*-decalin in a magnetic field of 0.33 T, detected as the ratio of the fluorescence kinetics to the smooth function $F(t)$ simulating the recombination kinetics (a) and theoretical curve for the singlet state population of the RP (b).³⁰

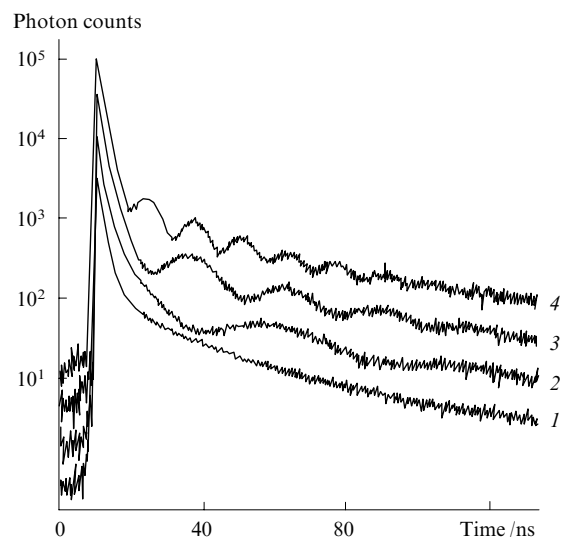


Figure 6. Recombination fluorescence kinetics of a isoctane solution of mixture of *p*-terphenyl- d_{14} ($1 \text{ mmol litre}^{-1}$) with diphenyl sulfide- d_{10} ($30 \text{ mmol litre}^{-1}$) in magnetic field of 0.017 (1), 0.24 (2), 0.48 (3) and 0.96 T (4).³⁶ For clarity, the curves are arbitrarily shifted along the Y axis.

Researchers from this group also detected quantum beats due to the g -factor differences between radicals in the solutions of diphenyl sulfide- d_{10} and *p*-terphenyl- d_{14} in various solvents (Fig. 6).^{32,33,35–38}

The (diphenyl sulfide- d_{10})⁺⁺ and (*p*-terphenyl- d_{14})^{–•} radical ions produced in such solutions are characterised by negligible HFC constants and significantly different g -factors. The amplitude of beats was found to be much larger compared to the results of the earlier studies.^{30,31} In this case the frequency of beats is proportional to the induction of external magnetic field.

III. Theory of quantum beats in recombination luminescence of spin-correlated radical ion pairs

Theory of quantum beats in the spin states of radical pairs has been well developed for isotropic HFC.² No analytical solution for the general case of arbitrary magnitudes of HFC constants and magnetic fields is available. However, most of experimental data can be approximately described using analytical solutions derived for some particular cases. These analytical results are of paramount value because the computational cost of the available algorithms of numerical solution to this problem is very high. This strongly complicates calculations and makes them of limited use in simulating experimental curves.

The possibility of manifestation of singlet–triplet transitions in recombination of radical pairs was first reported by Brocklehurst in 1969.⁶⁷ He analysed a radiation-chemical process of geminate recombination of an electron (or radical anion) with the parent radical cation and assumed that in this case the S–T transitions in the pair can affect the product ratio and that these transitions are induced by paramagnetic relaxation of electron spins. In the mid-1970s, interest in the singlet–triplet evolution in RPs increased after carrying out the pioneering experiments on observation of recombination fluorescence.^{26,27,43} At that time, Brocklehurst^{44,68} and Schulten and Wolynes⁶⁹ calculated the effect of HFC on the singlet–triplet transitions for some particular cases. Further development of the theory of singlet–triplet evolution is associated with the studies by Salikhov, his followers and colleagues who succeeded in deriving analytical solutions for

a broader range of hyperfine interactions (key results were reported in a monograph²). Some practically valuable relationships were derived recently.^{42, 70–72}

A salient feature of radical ion pairs produced in solution upon the action of a pulse of ionising radiation is that only a fraction of them is in the spin-correlated singlet state. Theoretical models usually assume that recombination of both correlated and uncorrelated pairs obeys the same kinetic law and that fluorescence of the excited molecules of recombination products occurs instantaneously. Then, the experimentally observed kinetics of the fall-off of recombination fluorescence intensity $I(t)$ is given by^{42, 50, 51}

$$I(t) \propto F(t) \left[\theta \rho_{ss}(t) + \frac{1}{4}(1 - \theta) \right].$$

Here $F(t)$ is the rate of pair recombination, θ is the fraction of singlet-correlated pairs, $\rho_{ss}(t)$ is the temporal dependence of the singlet state population of the spin-correlated pair, which is determined by both dynamic spin processes and the spin relaxation and strongly depends on the strength of the applied magnetic field. The second term in the square brackets includes the contribution of the singlet component of spin-uncorrelated pairs to fluorescence.

As mentioned above, the $I_B(t)/I_0(t)$ ratio (time-resolved magnetic field effect) is more convenient for analysis. This ratio is independent of the function $F(t)$, being determined only by the evolution of the spin state.

$$\frac{I_B(t)}{I_0(t)} = \frac{\theta \rho_{ss}^B(t) + 1/4(1 - \theta)}{\theta \rho_{ss}^0(t) + 1/4(1 - \theta)} \quad (7)$$

Here the superscripts ‘B’ and ‘0’ indicate that the system is in external nonzero and zero magnetic field, respectively. This simplifies the situation and allows the spectral parameters to be determined by fitting relation (7) to the experimentally measured TRMFE using the singlet state populations $\rho_{ss}(t)$ calculated in the framework of a particular model for hyperfine coupling in radical ions of the pair.

When calculating the singlet state population $\rho_{ss}(t)$, one should allow for the fact that the initial spin state of the radical pair is correlated (sometimes, it is called ‘entangled’ state), *i.e.*, the corresponding density matrix cannot be represented as the product of the density matrices of subsystems. This means that, generally, it is impossible to write the solution as the product of the functions, each of them corresponding to a single radical. At the same time the absence of interactions between electron spins of radicals in the pair, which is characteristic of the examples considered in this review, simplifies the solution and it can be written in the form reported by Schulten and Wolynes,⁶⁹

$$\rho_{ss}(t) = \frac{1}{4} + \sum_{i,k} T_{ik}^{(1)}(t) T_{ik}^{(2)}(t), \quad (8)$$

where $i, k = \{x, y, z\}$, and the components of the correlation tensor are

$$T_{ik}^{(1)}(t) = \langle \text{Tr}_e \{ \hat{S}_{1i}(t) \hat{S}_{1k}(0) \} \rangle, \quad (9)$$

$$T_{ik}^{(2)}(t) = \langle \text{Tr}_e \{ \hat{S}_{2i}(t) \hat{S}_{2k}(0) \} \rangle.$$

Here $\hat{S}(t)$ are the operators of the electron spins of the radicals in the Heisenberg representation. The superscripts ‘1’ and ‘2’ in the tensors and the subscripts ‘1’ and ‘2’ in the spin operators correspond to different radicals in the RP; Tr_e denotes the trace over electron spin variables and the angle brackets denote the averaging over projections of the magnetic nuclei. Equa-

tion (8) makes it possible to obtain the solution to the problem of the spin evolution of the RP using the components of the correlation tensor, each of them depending only on the Hamiltonian of one radical.

As mentioned above, there is no general analytical solution for the components of the correlation tensor at arbitrary HFC in each radical in the RP and arbitrary magnetic field. Now we will consider some particular cases of isotropic HFC with the known analytical solutions.

1. One magnetic nucleus or equal HFC constants for all magnetic nuclei in arbitrary external magnetic field

The results for the case of HFC with one magnetic nucleus were reported earlier;^{2, 68} the corresponding expressions written in a more convenient form⁷⁰ are as follows:

$$T_{xx} = T_{yy} = \frac{1}{2} \text{Re}(h(t)), \quad (10)$$

$$T_{xy} = -T_{yx} = \frac{1}{2} \text{Im}(h(t)),$$

$$T_{zz} = \frac{1}{2} g(t),$$

where

$$g(t) = 1 - \frac{a^2}{2I+1} \sum_{m=-I}^I \frac{I(I+1) - m(m+1)}{(2R_m)^2} [1 - \cos(2R_m t)],$$

$$h(t) = \frac{1}{4(2I+1)} \sum_{m=-I}^I \left[(1 + D_m) e^{iR_m t} + (1 - D_m) e^{-iR_m t} \right] \times$$

$$\times \left[(1 + D_{m-1}) e^{iR_{m-1} t} + (1 - D_{m-1}) e^{-iR_{m-1} t} \right] \quad (11)$$

and

$$2R_m = \sqrt{\omega_0^2 + a\omega_0(2m+1) + a^2 \left(I + \frac{1}{2} \right)^2},$$

$$D_m = \frac{\omega_0 + a(m+1/2)}{2R_m}.$$

In the last two relationships $\omega_0 = g\beta B/\hbar$ is the Larmor precession frequency of electron spin in external field, g is the g -factor of the radical, β is the Bohr magneton, B is the magnetic field induction, \hbar is the Planck constant, a is the isotropic HFC constant expressed in circular frequency units, m is the nuclear spin projection on the magnetic field direction and I is the spin of the magnetic nucleus in the radical.

This result can also be used in the case of a group of nuclei with equal HFC constants. Here, expressions (10) and (11) should be averaged over the spin I treated as the total spin of the magnetic nuclei. The weight P_I of each I value can be found by adding the spins of magnetic nuclei characterised by equal HFC constants. In particular, for n nuclei with the spin 1/2 (see Ref. 42) one has

$$P_{n,I} = \frac{(2I+1)^2 n!}{2^n [(n/2) - I]! [(n/2) + I + 1]!}.$$

In weak magnetic fields, a specific situation of weak HFC in one and strong HFC in the other radical in the pair is also possible (for both radicals the HFC constant is compared to the induction of external magnetic field). It was theoretically predicted and experimentally confirmed that in this case quantum beats at a frequency similar to the frequency of Larmor precession of electron spin manifest themselves in recombination fluorescence.^{64, 65}

2. The singlet state population of a radical pair in zero magnetic field

In zero external magnetic field we deal with the diagonal tensor (9) having equal principal values. Therefore, in zero magnetic field one gets

$$\rho_{ss}^0(t) = \frac{1}{4} + 3T_{zz}^{(1)}(t)T_{zz}^{(2)}(t). \quad (12)$$

In the presence of a HFC with only one nucleus with the spin I (HFC constant a) in zero magnetic field one has²

$$T_{zz}(t) = \frac{3 + 4I(I+1) + 8I(I+1)\cos[a(I+1/2)t]}{6(2I+1)^2}. \quad (13)$$

In the case of several magnetic nuclei with equal HFC constants, expression (13) should be averaged over the total nuclear spin I . For instance, the expression for a group of n nuclei with the spin $1/2$ and equal HFC constants a , has the form⁴²

$$T_{zz}(t) = \frac{1}{6} \left[\frac{n+3}{n+1} + \frac{2n(n+2)}{n+1} \left(\cos \frac{at}{2} \right)^{n+1} - 2n \left(\cos \frac{at}{2} \right)^{n-1} \right]. \quad (14)$$

Schulten and Wolynes derived⁶⁹ an approximate solution for the case of a large number of magnetic nuclei characterised by small, but not necessarily equal, HFC constants; this corresponds to an unresolved EPR spectrum of a radical. To allow for zero magnetic field in this approximation, expression (12) should be written using the quantity

$$T_{zz} = \frac{1}{6} [1 + 2C(\sigma t)],$$

where

$$C(x) = (1 - x^2)e^{-0.5x^2},$$

and the parameter σ^2 is the second moment of the EPR spectrum of the radical:

$$\sigma^2 = \frac{1}{3} \sum_n a_n^2 I_n(I_n + 1). \quad (15)$$

An approximate solution to the problem of the spin evolution in a singlet-correlated pair of noninteracting radicals in zero magnetic field was derived for the case where one nucleus (or a group of equivalent nuclei) in the radical is involved in isotropic HFC characterised by a large HFC constant and other nuclei have relatively small (not necessary equal) HFC constants.⁷¹ In EPR and NMR spectroscopy this is called ‘inhomogeneous line broadening’. Simulation⁷¹ showed that this type of broadening affects the spin dynamics similarly to phase relaxation.

An analytical solution for $T_{zz}(t)$ in the case of isotropic HFC with two groups of equivalent nuclei in zero magnetic field is also available.⁷² In the two last-named cases, the solutions are cumbersome, so we have to address the reader to the original studies.^{71, 72}

3. The singlet state population of a radical pair in a strong magnetic field

Considering the case of a strong magnetic field whose strength much exceeds the HFC constants of the radicals in the RP, one can use the high-field approximation² to simplify the Hamiltonian of the RP. Here, assuming an isotropic HFC tensor and g -tensor, expression (8) takes the form

$$\rho_{ss}(t) = \frac{1}{2} + \frac{1}{2} \cos[(\omega_{01} - \omega_{02})t] G_1(t) G_2(t), \quad (16)$$

where ω_{01} and ω_{02} are the frequencies of Larmor precession of electron spins in the magnetic field and the functions $G(t)$ are determined by the HFC constants (a_n) and the spins of the magnetic nuclei (I_n) in each radical in the RP

$$G(t) = \prod_n \left\{ \frac{1}{(2I_n + 1)} \frac{\sin[a_n(2I_n + 1)t/2]}{\sin(a_n t/2)} \right\}. \quad (17)$$

Here the subscript n enumerates the magnetic nuclei.

The solution (16), (17) was first reported by Brocklehurst⁶⁸ in the form of a relation for the singlet state population at particular I values. In a particular case where one radical contains n_1 and the other radical contains n_2 equivalent nuclei with the spin $I = 1/2$ and the HFC constants a_1 and a_2 , respectively, one gets

$$\rho_{ss}(t) = \frac{1}{2} + \frac{1}{2} \cos[(\omega_{01} - \omega_{02})t] \left(\cos \frac{a_1 t}{2} \right)^{n_1} \left(\cos \frac{a_2 t}{2} \right)^{n_2}.$$

In the quasi-classical approximation,⁶⁹ which is valid for many magnetic nuclei having small HFC constants, the functions (17) take the form

$$G(t) = e^{-(\sigma^2 t^2)/2},$$

where the second moment of the EPR spectrum σ^2 is given by Eqn (15).

4. Taking into account the effect of paramagnetic relaxation

The effect of paramagnetic relaxation on the singlet state population of RPs in a strong and zero magnetic field was also included as follows.^{13, 17, 42, 45, 46, 50–61} Let $\rho'_{ss}(t)$ be the singlet state population calculated ignoring paramagnetic relaxation. The singlet state population with allowance for relaxation in a strong magnetic field is given by

$$\rho_{ss}(t) = \frac{1}{4} + \frac{1}{4} e^{-t/T_1} + e^{-t/T_2} \left(\rho'_{ss}(t) - \frac{1}{2} \right), \quad (18)$$

and the corresponding expression for zero magnetic field has the form

$$\rho_{ss}(t) = \frac{1}{4} + e^{-t/T_0} \left(\rho'_{ss}(t) - \frac{1}{4} \right), \quad (19)$$

where T_1 and T_2 are, respectively, the longitudinal and transverse paramagnetic relaxation times in the strong magnetic field and T_0 is the transverse paramagnetic relaxation time in zero magnetic field.

Although some theoretical background substantiating relations (18) and (19) is available,^{5, 11, 45} one must admit that these equations are based on semiempirical considerations only. Namely, in the strong magnetic field the transverse relaxation mixes the singlet state of the RP with only one of the three triplet states in which the spin projection on the magnetic field direction is zero. This means that the asymptotic $\rho_{ss}(t)$ value in the presence of transverse relaxation is $1/2$. In Eqn (18), this is included by the exponent e^{-t/T_2} . At the same time longitudinal relaxation equilibrates the populations of the singlet state and all the three triplet states [see the exponent e^{-t/T_1} in Eqn (18)]. In zero magnetic field there is no preferred axis and the rates of longitudinal and transverse relaxation should be equal to each other.

This approach usually provides a satisfactory description of experimental results using a minimum number of relaxation rate parameters, namely, two and one for the case of a strong and zero magnetic field, respectively. At the same time this may appear to be insufficient for rigorous treatment of a particular physical mechanism of paramagnetic relaxation.⁷³

IV. Spectroscopy of quantum beats in radical pairs

Spectroscopic information on the partners of a radical pair extracted by the method of quantum beats is similar to that obtained in EPR studies. The key advantages of the title method are much higher sensitivity and the possibility of detecting species characterised by the lifetimes of up to a few nanoseconds. Development of this technique made it possible to study short-lived radical ion species in liquid solutions at ambient temperatures.

1. Determination of hyperfine coupling constants and g -factors of radical ions

The simple TRMFE curves for the case of hyperfine coupling with a number of equivalent protons in one partner of the radical pair were analysed.⁴² It was shown that in this case quantum beats manifest themselves as a sequence of peaks in the TRMFE curve. The position of the first peak on the time scale is determined by the second moment of the EPR spectrum of this radical. For even number of protons, the next peak is more intense and its position is determined by the HFC constant. If the number of protons is odd, a trough occurs instead of the peak. Then the beats show a periodic damping pattern due to relaxation. These predictions were checked in the same study⁴² taking radical cations of nine compounds (alkanes, alkenes and aromatics) with equivalent protons. The p -terphenyl- d_{14} radical anion, whose HFC constants are small and make a negligible contribution to the spin evolution of the pair, served as the geminate partner. Figure 7 presents some examples of the TRMFE curves. The HFC constants determined from the instants corresponding to the appearance of the second peak are listed in Table 1. It should be noted that the obtained HFC constants coincided with the published data measured by other methods.

The possibility of determining both the HFC constants and the g -factor differences between radical ions was demon-

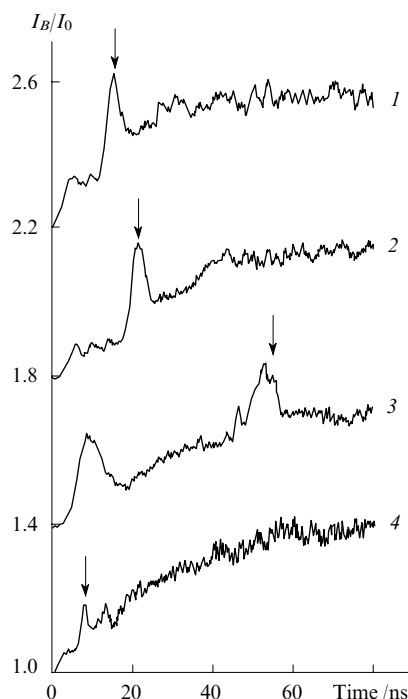


Figure 7. TRMFE curves for dilute cyclohexane solutions of mixtures of p -terphenyl- d_{14} with 9,10-octalin (1), tetramethylethylene (2), octamethylcyclohexa-1,4-diene (3) and *cis*-decalin (4).⁴² The arrows show the theoretical positions of the second (main) peak.

Table 1. HFC constants (a) for radical cations of various electron donors in nonpolar solutions measured by quantum beats technique.

Donor	a /mT ^a	Ref.
<i>cis</i> -Decalin	4.5 (4H)	42
9,10-Octalin	2.4 (8H)	42
Tetramethylethylene	1.6 (12H)	42
Octamethyl-1,4-cyclohexadiene	0.7 (12H)	42
<i>p</i> -Xylene	1.7 (6H)	42
<i>p</i> -Diethylbenzene	1.7 (4H)	42
1,2,4,5-Tetramethylbenzene	1.0 (12H)	42
Hexamethylbenzene	0.6 (18H)	42
Hexamethylethane	1.24 (18H)	52
2,3-Dimethylbutane	1.66 (12H)	72
	0.65 (2H)	72
2,2,6,6-Tetramethylpiperidine	−1.85 (1H)	72
	1.78 (1N)	72
Diisopropylamine	2.1 (1N)	72
	2.1 (2H)	72
	−2.4 (2H)	72
2,2,3-Trimethylbutane	1.24 (9H)	66
	1.55 (6H)	66
2,2,4-Trimethylpentane	1.3 (10H)	66
	0.37 (6H)	66
2,2-Dimethylpentane	1.33 (11H)	66
	0.39 (3H)	66
2,2,4,4,6,8,8-Heptamethylnonane	$\sigma = 1.6$ ^b	66

^a Figures in parentheses denote the number and types of nuclei. ^b Parameter of the second moment of the EPR spectrum of the radical cation.

strated⁵² taking the hexamethylethane (2,2,3,3-tetramethylbutane) radical cation as an example. The EPR spectrum of this species is governed by isotropic HFC with eighteen equivalent protons. The HFC constant was calculated from positions of peaks in the TRMFE curve, and the g -factor difference between the (hexamethylethane)⁺⁺ and (p -terphenyl- d_{14})^{−−} radical ions was determined from analysis of the dependence of the shape of the TRMFE curve (Fig. 8) on the magnetic field strength. These results coincided with the data obtained in the same study by the optically detected EPR (OD EPR) technique and with the published data.

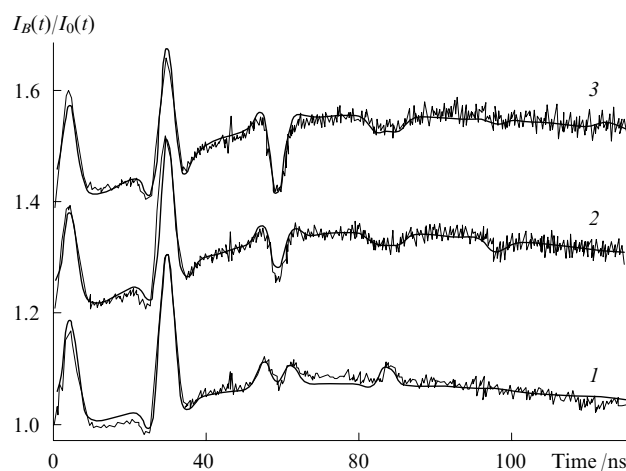
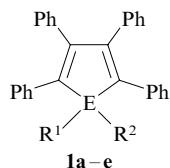


Figure 8. TRMFE curves of dilute *n*-hexane solutions of mixture of hexamethylethane with p -terphenyl- d_{14} in magnetic field of 0.1 (1), 0.5 (2) and 0.7 T (3).⁵² Smooth solid curves represent the results of simulation of experimental data.

The TRMFE method was used to study radical anions of 1,2,3,4-tetraphenylcyclopenta-1,3-diene (**1a**) and its heteroorganic analogues containing silicon (**1b**) and germanium (**1c–e**) in *n*-decane solutions.^{50, 51}



- E = C, R¹ = R² = H (**a**);
 E = Si, R¹ = R² = H (**b**);
 E = Ge, R¹ = R² = H (**c**);
 R¹ = R² = Cl (**d**);
 R¹ = Me, R² = Cl (**e**).

Simulation of experimental curves (Fig. 9) gave the following HFC constants:

Compound 1	<i>a</i> /mT
a	2.50 ± 0.04 (2H)
b	1.56 ± 0.03 (2H)
c	1.50 ± 0.03 (2H)
d	0.7 ± 0.1 (2Cl)
e	1.14 ± 0.1 (Cl)

Reliable detection of this type of radical anions by the TRMFE method indicates that their lifetimes in solution are at

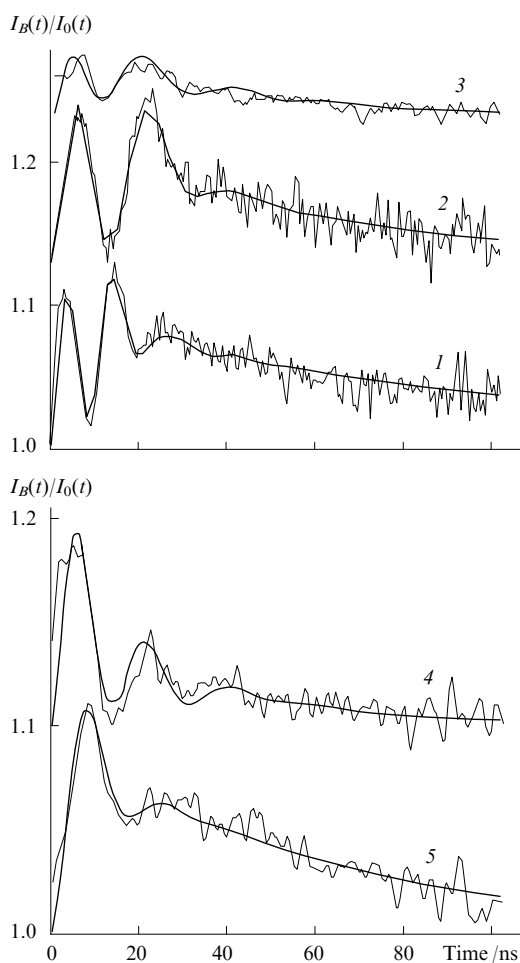


Figure 9. TRMFE curves of solutions of 1,2,3,4-tetraphenylcyclopenta-1,3-diene (**1a**) and its heteroorganic analogues **1b** (**2**) and **1c–e** (**3–5**) in *n*-decane.⁵¹ Smooth solid curves represent the results of simulation of experimental data.

least of the order of tens of nanoseconds. This is of great importance for chemistry of such compounds, because attempts to detect these species (except for radical anion **1a**) by other methods failed and the possibility of their formation in solutions cast some doubts.

The contributions of each radical in the pair to the spin evolution [see Eqns (14) and (16)] can be separated.⁵³ Figure 10 shows the TRMFE curves obtained for an *n*-octane solution of mixture of hexamethylethane (0.1 mol litre^{−1}) with tetraphenylcyclopentadiene (3 × 10^{−4} mol litre^{−1}) at a magnetic field induction of 0.1 and 0.7 T at room temperature. The spin evolution is determined by the hyperfine coupling in the (hexamethylethane)⁺·/(tetraphenylcyclopentadiene)[−]· pair. The former species is involved in HFC with eighteen equivalent protons (HFC constant *a*₁ = 1.24 mT), while the latter has two equivalent protons (HFC constant *a*₂ = 2.46 mT). The smooth curves in Fig. 10 represent the results of approximation of experimental data by a relevant model. Although the pattern of beats is more complicated, experimental data are well described by the theory.

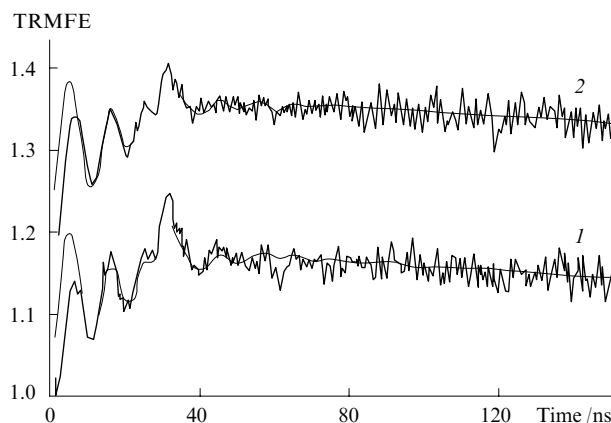


Figure 10. TRMFE curves of solutions of hexamethylethane and tetraphenylcyclopentadiene in *n*-octane [*B* = 0.1 (**1**) and 0.7 T (**2**)].⁵³ Smooth solid curves represent the results of simulation of experimental data.

The 2,3-dimethylbutane, 2,2,4,4-tetramethylpiperidine and diisopropylamine radical cations containing two groups of magnetically equivalent nuclei were studied.⁷² In addition to the calculation of absolute values of the HFC constants, the authors of this study confirmed the theoretically predicted possibility of determining the signs of the HFC constants for groups of nuclei. In Fig. 11 we present the experimental curve

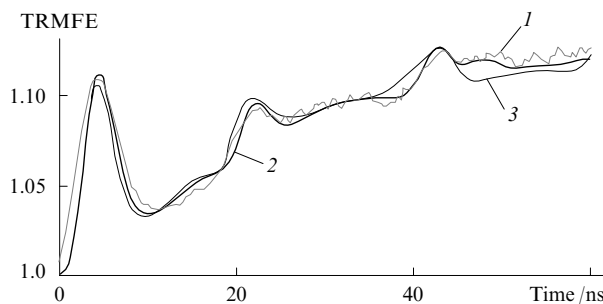


Figure 11. TRMFE curve for an *n*-hexane solution of mixture of 2,3-dimethylbutane with *p*-terphenyl-d₁₄ (**1**) and best fits of experimental data using a model with the HFC constants *a* (12H) and *a* (2H) of the same sign (**2**) and of different signs (**3**).⁷²

of TRMFE due to hyperfine coupling in the 2,3-dimethylbutane radical cation. The best approximation of experimental data with the '12H + 2H' model gave the same signs of the HFC constants for these groups of protons, which was confirmed by quantum chemical calculations. Calculations with the HFC constants of different sign led to poorer agreement with the experiments.

Radical cations of branched alkanes and their heteroorganic analogues Me_4E and Me_3EEMe_3 ($\text{E} = \text{C}, \text{Si}, \text{Ge}, \text{Sn}$) in hexane were studied by the TRMFE method⁵⁴ and the g -factors and HFC constants of the heteroorganic radical cations were obtained. Fast degenerate electron exchange (DEE) was observed in the Me_4E compounds, whereas this was not observed in the Me_3EEMe_3 compounds. It was found that, in contrast to the alkane radical cations, the heteroorganic ones are characterised by short phase relaxation time of the order of 10 ns. The authors believed that a large contribution to relaxation comes from the spin-rotational interaction and degenerate electron exchange. The last-mentioned mechanism is particularly efficient due to a considerable proportion of magnetic isotopes ^{29}Si , ^{73}Ge , ^{117}Sn and ^{119}Sn .

A number of radical cations of branched alkanes were studied.⁶⁶ The formation of such species upon radiolysis of solutions was confirmed and their HFC constants were also determined (see Table 1).

2. Studies of fast chemical reactions involving radical ions by the method of time-resolved magnetic field effect

Along with spectroscopic data, monitoring of quantum beats in recombination luminescence makes it possible to obtain spectroscopic data and information on reactions of short-lived radical ions in solutions. The reaction causes changes in the spin Hamiltonian of the pair, which leads to changes in the character of quantum beats and in the shape of the TRMFE curve. In the text below we present some examples of the reactions of electron transfer and degenerate electron exchange in solutions.

To determine the rate of the transfer of the solvent hole (or an electron) to acceptor, the acceptor concentration should not be too high. In this case the secondary pairs are generated not instantaneously and the scatter of the corresponding formation times should cause a decrease in the amplitude and the appearance of phase shifts of quantum beats. By analysing the changes in the TRMFE pattern it is possible to determine the rate constant for charge transfer.

This approach was first employed in measuring the phase shift of the Δg beats as function of the concentration of diphenyl sulfide- d_{10} used as hole trap.^{35–38} This dependence was used to determine the rate constant for solvent (isooctane) hole scavenging by the diphenyl sulfide molecule, which was found to be similar to the value corresponding to the diffusion-controlled process.

A study of alkane solutions of 9,10-octalin revealed a rather strong peak of quantum beats due to hyperfine couplings in the 9,10-octalin radical cations even at rather low concentrations of this compound.⁴⁶ The large peak amplitude was explained by the contribution of fast non-stationary stage of electron transfer [reaction (4)] from the 9,10-octalin molecule to the primary radical cation and by the fact that the electron-transfer radius exceeds the geometric radius. The electron-transfer radii determined for three n -alkanes from experimental data using the model proposed are 15.1, 13.9 and 10 Å for octane, decane and dodecane, respectively. A decrease in the electron transfer radii for hydrocarbons C_8 , C_{10} , C_{12} was associated with the decrease in the ionisation potential difference between the alkane and 9,10-octalin in this series, which is consistent with the predictions based on the Marcus theory.⁷⁴

The degenerate electron exchange



between n -alkane, norbornane and tetramethylsilane molecules and their radical cations was studied by the method of quantum beats.^{54–57} In EPR spectroscopy, slow degenerate electron exchange causes broadening of spectral lines, whereas fast degenerate electron exchange leads to the exchange narrowing of the spectrum. These changes in the EPR spectra correspond to characteristic features in the TRMFE curves; by simulating such curves one can determine the rate constant for the exchange reaction.

Figure 12 shows the transformation of the TRMFE curves measured in hexane solutions of n -nonane with an increase in the n -nonane concentration from 0.07 to 3 mol litre⁻¹ and in neat n -nonane. The shift of the maximum in the MFE curves following an increase in the nonane concentration is due to the narrowing of the EPR spectrum of the nonane radical cation with an increase in the DEE rate [reaction (20)]. This was also confirmed by calculations (smooth lines in Fig. 12). The theoretical curves were obtained using a mathematical model developed by Schulten and Wolynes.⁶⁹ Details of simulation were documented.⁵⁵

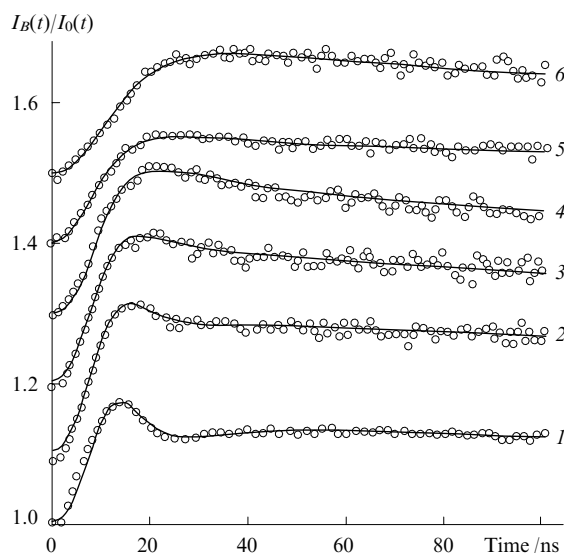


Figure 12. Time-resolved magnetic field effect obtained in hexane solutions of n -nonane at a concentration of 0.07 (1), 0.3 (2), 0.6 (3), 1 (4) and 3 mol litre⁻¹ (5) and in neat n -nonane.⁵⁵ Smooth curves represent the results of simulation using the DEE rates shown in Fig. 13.

The dependence of the DEE rate (τ^{-1}) on the concentration of n -nonane established in Ref. 55 is shown in Fig. 13. Linear character of the rate–concentration plot confirms the bimolecular character of the DEE reaction for n -nonane. n -Alkanes are characterised by much lower DEE rates (two orders of magnitude lower than the rate of diffusion-controlled process). This was explained by the effect of numerous conformations of neutral n -alkane molecules and a rather high activation barrier to electron transfer in the collisional complex between the radical cation and the molecule.⁵⁵

Modulation of the HFC constants due to DEE can induce not only the phase relaxation, but also noticeable spin–lattice relaxation even in a relatively strong magnetic field.⁵⁷ The DEE reaction involving the norbornane radical cation containing four equivalent protons with non-negligible HFC constants was studied. The authors reported exact calculations

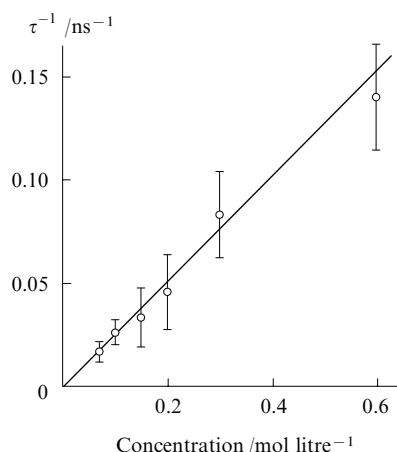


Figure 13. DEE rate for n-nonane radical cation plotted vs. n-nonane concentration in hexane solution.⁵⁵ The straight line is the best linear approximation obtained at a rate constant of $2.6 \times 10^8 \text{ litre mol}^{-1} \text{ ns}^{-1}$.

of the evolution of the spin state of the radical pair under DEE conditions. The asymptotic behaviour of the exact dependence of the singlet state population is satisfactorily described by an exponent with a single time parameter, which can be treated as the spin–lattice relaxation time T_1 . The T_1 value obtained was similar to that calculated in the framework of the Redfield theory.⁷⁵

Figure 14 shows the TRMFE curves for an n-hexane solution of mixture of norbornane ($0.2 \text{ mol litre}^{-1}$) with *p*-terphenyl- d_{14} ($30 \mu\text{mol litre}^{-1}$) plotted vs. magnetic field induction. The fall-off of the TRMFE curves is determined by the rate of spin–lattice relaxation of the norbornane radical cation. Analysis of the dependence of spin–lattice relaxation rate on the magnetic field induction at different norbornane concentrations (Fig. 15) showed that the magnetic field-dependent contribution to relaxation is due to DEE in the norbornane radical cation. The rate constant for DEE was $1.5 \times 10^{10} \text{ litre mol}^{-1}$, which is similar in magnitude to the

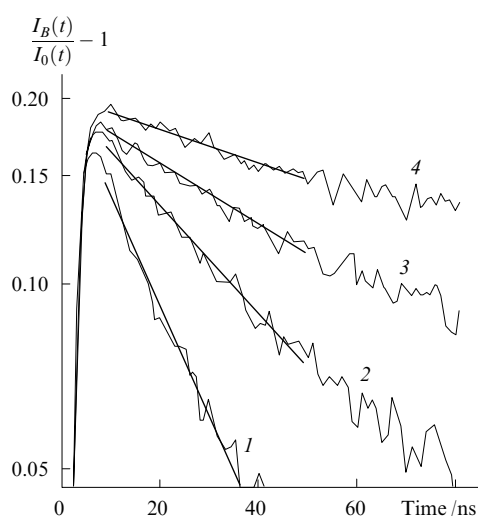


Figure 14. TRMFE curves for an n-hexane solution of mixture of norbornane ($0.2 \text{ mol litre}^{-1}$) with *p*-terphenyl- d_{14} ($30 \mu\text{mol litre}^{-1}$) at a magnetic field induction of 0.05 (1), 0.1 (2), 0.2 (3) and 1 T (4).⁵⁷ Straight lines are the exponential approximation of the TRMFE curves in the range of 10 to 50 ns.

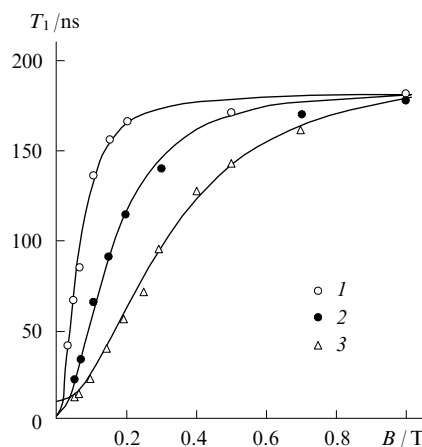


Figure 15. Spin–lattice relaxation time of norbornane radical cation plotted vs. magnetic field induction at a norbornane concentration of 0.04 (1), 0.2 (2) and 0.6 mol litre^{-1} (3).⁵⁷ Solid lines represent the results of approximation in the framework of the Redfield theory.

diffusion-controlled rate constant. The relaxation time of the norbornane radical cation in the strong magnetic field tended to a value of $\sim 180 \text{ ns}$. The nature of the magnetic field independent contribution remains unknown. Probably, it is due to the spin–orbit interaction, as in the case of some cycloalkanes (see below).

The DEE reaction involving the tetramethylsilane (TMS) radical cation in n-hexane was studied.⁵⁴ The TRMFE curves obtained for the solution of TMS are shown in Fig. 16. Good agreement between theory and experiment (curve 1) was attained only assuming that hyperfine coupling in the TMS radical cation is averaged almost to zero due to DEE that occurs under diffusion control.

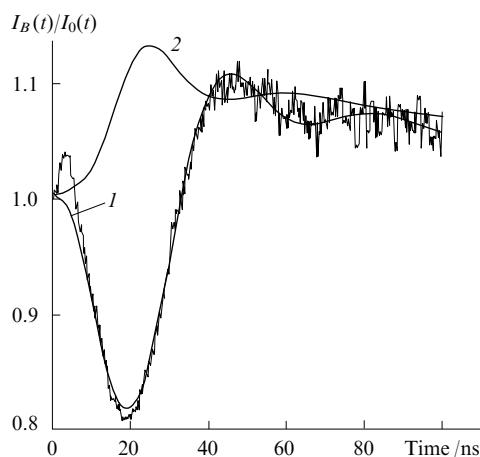


Figure 16. Experimental and theoretical TRMFE curves for a solution of tetramethylsilane and *p*-terphenyl- d_{14} in n-hexane.⁵⁴ Calculated for fast DEE (1) and no exchange (2).

A radical cation of alicyclic amine, namely, 2,2,4,4-tetramethylpiperidine was studied by the TRMFE and quantum chemistry methods.⁵⁸ Based on the changes in the spectra observed upon an increase in the amine concentration and temperature variation, the formation of dimeric radical cations of unusual structure was suggested. A collision between the amine radical cation and the amine molecule is accompanied by proton transfer to the molecule and results in the formation

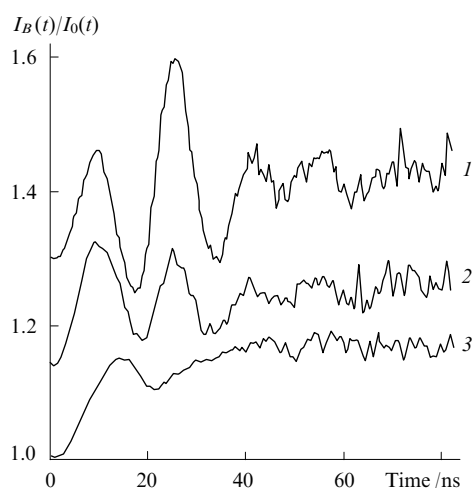


Figure 17. Experimental TRMFE curves obtained for a solution of 2,2,4,4-tetramethylpiperidine and *p*-terphenyl- d_{14} in *n*-octane ($B = 0.1$ T).⁵⁸ Amine concentration/mmole litre⁻¹: 30 (1), 10 (2) and 3 (3).

of a rather stable distonic dimer in which the charge and spin are localised on different molecules. The rate constant for dimerisation reaction determined by simulating the changes in the shape of quantum beats pattern with an increase in the amine concentration (Fig. 17) was similar to the diffusion-controlled rate constant.

3. Studies of paramagnetic relaxation in radical ions

The TRMFE technique has unique potential for measuring the spin–lattice relaxation rates of short-lived radical ions in solutions over a wide range of change in the magnetic field induction. Some examples were considered above. Mention can be made of a pioneering study⁴⁷ in which the relaxation times of a number of aromatic radical ions (about 1 μ s) were measured. Most results can be satisfactorily described in the framework of the relaxation mechanisms known from EPR spectroscopy.

Unusually fast spin–lattice relaxation in the cyclohexane and adamantane radical cations and their alkyl-substituted analogues detected recently by the TRMFE technique appeared to be a surprising exception.^{59–61} Figure 18 shows the TRMFE curves obtained for solutions of some cycloalkanes. The exponential decay of the TRMFE curves is determined by the T_1 -relaxation. In all cases a three-fold change in the cycloalkane concentration and temperature variation in the 250–320 K range had almost no effect on the rate of T_1 -relaxation. The T_1 -relaxation times of various cycloalkanes are listed in Table 2.

Using the known data on the EPR spectrum of cyclohexane radical cation and the Redfield theory,⁷⁵ it was shown that the relaxation time $T_1 = 9$ ns obtained for the cyclohexane radical cation at a magnetic field induction of 1 T is due to neither modulation of HFC constants or the g -tensor anisotropy nor degenerate electron exchange involving the radical cations. Earlier, unusually fast relaxation was observed by EPR spectroscopy in radical anions of some symmetrical aromatic molecules.⁷⁶

Although quantitative theory of unusually fast relaxation has not been developed so far, it is believed^{76,77} that the phenomenon can be due to strong spin–orbit interaction in symmetrical radical ions. The unusually fast relaxation in some cycloalkane radical cations provides an explanation for unsuccessful attempts to record their OD EPR spectra.⁷⁸

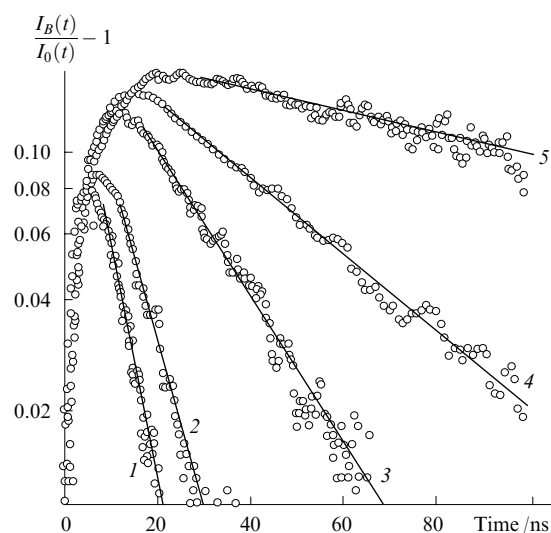


Figure 18. Experimental TRMFE curves ($B = 1$ T) obtained for C_6F_6 solutions in *n*-hexane in the presence of adamantane (1), cyclohexane (2), ethylcyclohexane (3), methylcyclohexane (4) and *cis*-decalin (5).⁵⁹ Solid lines represent the results of exponential approximations.

Table 2. Paramagnetic relaxation times of radical ions generated from corresponding compounds in nonpolar solvents.^{59–61}

Compound	T_1 /ns	$T_2 = T_0$ /ns
Hexafluorobenzene ^a	350 ± 15	15 ± 5
<i>cis</i> -Decalin	390 ± 15	10 ± 5
Cyclohexane	9 ± 2	9 ± 2
Methylcyclohexane	57 ± 10	5 ± 2
Ethylcyclohexane	21 ± 3	10 ± 5
Propylcyclohexane	38 ± 4	7 ± 3
Isopropylcyclohexane	280 ± 20	20 ± 5
<i>cis</i> -1,2-Dimethylcyclohexane	280 ± 20	20 ± 5
Adamantane	6.5 ± 1	5 ± 3
1,3-Dimethyladamantane	8.2 ± 1	5 ± 3

^a A radical anion is produced in this case; all other entries in this Table correspond to radical cations.

4. Manipulation of the spin state of a radical pair

As mentioned above, the character of the spin evolution in a radical pair depends strongly on the external magnetic field. The spin evolution can also be affected by the resonance alternating magnetic field. Pulsed switching-on and(or) switching-off of the magnetic field makes it possible to immediately tamper with the elementary step of RP recombination. The TRMFE technique involving detection of recombination fluorescence permits real-time observation of these effects.

The procedure and results of the first experiments (Fig. 19) on observation of the dynamics of the spin state of a radical ion pair upon fast (~ 20 ns) switching-off of external magnetic field (initial magnetic field induction 4 mT) were reported.⁶² Prior to switching the magnetic field off the system shows a conventional TRMFE pattern determined by the spin evolution in the pair in both zero or nonzero external magnetic field. The fall-off of the TRMFE curves after switching the magnetic field off depends only on the spin evolution in zero field. As should be expected, the fall-off rate is determined by the second moment of the EPR spectrum of radical ions. Deuterated *p*-terphenyl- d_{14} is characterised by a much longer fall-off time compared to non-deuterated *p*-terphenyl.

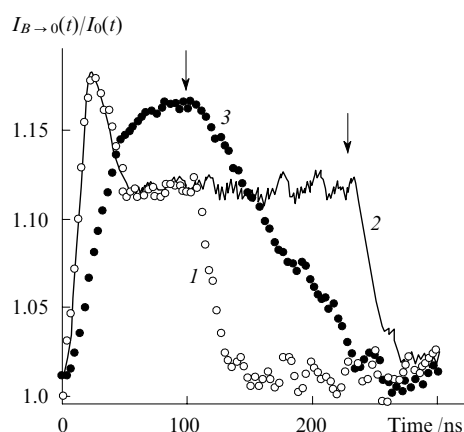


Figure 19. Curves of $I_{B \rightarrow 0}(t)/I_0(t)$ ratio obtained for a solution of *p*-terphenyl (10^{-3} mol litre $^{-1}$) in *n*-decane at field switching-off delays of 100 (1) and 225 ns (2) and for a solution of *p*-terphenyl- d_{14} (10^{-3} mol litre $^{-1}$) in decane at 100-ns delay of the field switching-off (3).⁶²

The arrows denote the instants of the magnetic field switching-off.

A procedure for control of the course of a spin-dependent reaction using the pulses of alternating resonance magnetic field was studied taking radical ion pair $(C_8H_{18})^{+ \cdot}/(p\text{-terphenyl})^{- \cdot}$ as an example.⁶³ The relative change in the fluorescence intensity (Fig. 20) characterises the change in the singlet state population in the pair in the resonance field. Prior to switching the resonance field off, damping oscillations are observed (see Fig. 20), the oscillation frequency being determined by the amplitude of the magnetic field in the rotating frame.⁶³ At the instants corresponding to the switching-off of the resonance field (arrowed), the spin state of the pair is 'frozen'. Then, the spin populations are equilibrated at the rate determined by spin–lattice relaxation.

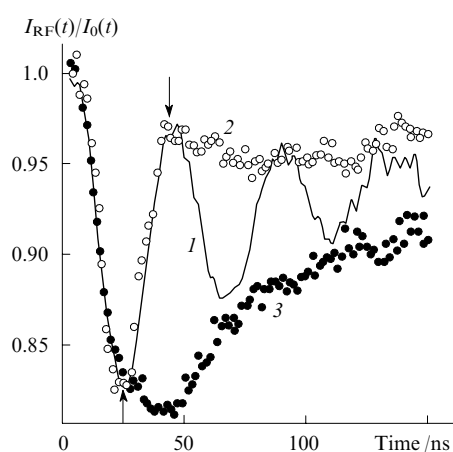


Figure 20. Effect of microwave field, $I_{RF}(t)/I_0(t)$, obtained for a solution of 2,2,4-trimethylpentane and *p*-terphenyl- d_{14} in *n*-hexane at the resonance UHF field switching-off delays of 300 (1), 45 (2) and 25 ns (3).⁶³

5. Radiation chemistry applications

In the examples considered above, ionising radiation only served a convenient instrument of pulsed generation of spin-correlated radical ion pairs. Meanwhile, from the very beginning it was clear that TRMF studies can provide valuable

information on specific features of fast reactions in tracks of ionising particles.

The key role in the development of this avenue of research was played by the studies by Brocklehurst who used the TRMF technique in recombination luminescence to solve some stubborn problems in radiation chemistry and physics of non-polar solutions. These include the structure of tracks, the origin of superdiffusion mobility of positive charges (solvent holes), the role of excited states in delayed luminescence, the possibility of spin correlation of non-geminate RP in radiation tracks, *etc.* The results obtained by Brocklehurst were summarised in reviews.^{11, 14} Due to complexity of the problems under study, some of these results are ambiguous. However, in the cited reviews, Brocklehurst touches upon almost all significant details of the processes the radical pairs in radiation tracks are involved in. A thorough study of the dependence of the fraction of the RPs recombining in the spin-correlated state (geminate pairs in the track) on the type and energy of ionising radiation deserves particular attention.

The fraction of geminate radical ion pairs in radiation tracks was determined from the amplitude of quantum beats.^{39–41} When different non-polar solutions were irradiated with fast electrons, this quantity was 1.3–2.8 times higher than that found for irradiation with X-rays.⁴¹

The kinetics of recombination luminescence of non-polar solutions and the magnetic field effect on these kinetics were reported in a study⁴⁸ aimed at investigating the formation of radical ion pairs under the action of vacuum ultraviolet; the magnetic field effect observed was used for substantiation of his statement that the primary radical pair is formed from singlet-excited solvent molecule.

6. Quantum beats in laser generation of radical pairs

Laser photolysis undoubtedly belongs to the most widely used methods of pulsed generation of spin-correlated radical pairs and radical ion pairs. However, data on observation of quantum beats in recombination of pairs under laser irradiation are scarce. Most experiments were characterised by low temporal resolution and a complex structure of EPR spectra of the pair partners, which excluded the possibility of obtaining a clearly seen pattern of quantum beats.

Clearly observed beats were reported in a study of time-resolved magnetic field effect on the delayed fluorescence of *N,N,N',N'*-tetramethyl-1,4-phenylenediamine (TMPD) in alcoholic solutions.⁷⁹ Fluorescence was excited by a pulse of a UV laser operating at 308 nm. Irradiation with light resulted in ionisation of TMPD and generation of a spin-correlated pair $(TMPD)^{+ \cdot}/e^{- \cdot}$. The spin evolution in this pair caused oscillations at times shorter than 150 ns; at longer times, a magnetic field effect due to triplet–triplet annihilation of excited TMPD molecules was observed.

Real-time observations of manifestations of the spin dynamics of radical pairs were also reported in fast switched magnetic field CIDNP studies.^{80–82} A solution irradiated with a laser pulse was placed in a Helmholtz coil that allowed the magnetic field to be switched within the limits of ± 2 mT (switching time 1 ns) with variable delay between the pulse and the switching of magnetic field. Then, the solution was rapidly transferred to the magnet of an NMR spectrometer for CIDNP measurements. In the experiments with radical ion pairs $(naphthalene-d_8)^{+ \cdot}/(1,2\text{-}cis\text{-dicyanoethylene})^{- \cdot}$, switching of the magnetic field from 2.3 to 0 mT was followed by oscillations of the CIDNP plotted *vs.* delay time due to the hyperfine interactions in the radical anion. The shapes of these curves (Fig. 21) depend on the concentration of the electron acceptor, which was explained by the effect of degenerate electron exchange.

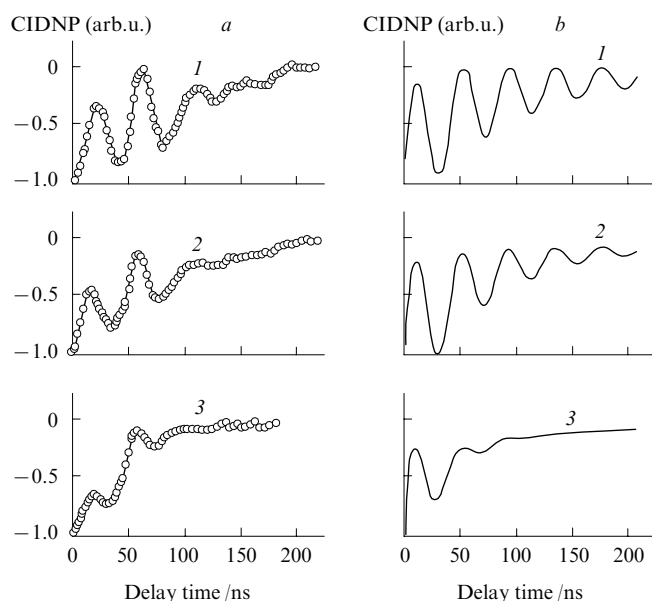


Figure 21. Magnetic field switch CIDNP kinetics observed in photolysis of solutions containing different concentrations of 1,2-*cis*-dicyanoethylene (a) and simulation with allowance for DEE (b).⁸¹ Concentration /mmol litre⁻¹: 1 (1), 2 (2) and 8 (3); DEE time /ns: 220 (1), 110 (2) and 28 (3).

V. Conclusion

The method of quantum beats in recombination luminescence proved itself as a powerful tool in the solution studies of short-lived radical ions (lifetimes up to a few nanoseconds). Theoretical foundations of extraction of unique information on these species from experimental data were developed and relevant experimental approaches were implemented. Using the quantum beats technique, one can determine the magnitudes and, in some cases, the signs of the HFC constants of radical ions, the *g*-factors, the paramagnetic relaxation times and the fraction of spin-correlated radical pairs in radiation tracks. The main advantages of the method of quantum beats over conventional EPR spectroscopy consist in the high sensitivity and temporal resolution. The former factor is due to the possibility of carrying out light intensity measurements on the single-photon scale. Therefore, the quantum beats technique makes it possible to study very low concentrations of radical ion pairs (up to about 100 pairs per sample), being enormously more sensitive than EPR spectroscopy. Compared to the OD EPR technique, which is based on the same properties of radical ion pairs, the method of quantum beats provides the possibility of monitoring the course of the chemical reactions involving RPs on the nanosecond time scale.

An apparent limitation of the title method is the necessity of tuning the conditions for a rather high quantum yield of recombination fluorescence and short fluorescence time (it should be shorter than the desired temporal resolution in the experiments). In most cases the radical ions of interest are produced from molecules that do not possess the properties of luminophores. This limitation can be eliminated with ease by choosing an appropriate luminophore as partner (*i.e.*, acceptor of the opposite charge). One can face some difficulties in studies of radical ions in polar solvents. For instance, in this case the energy released in recombination of radical ions may appear to be too low to form an excited luminophore molecule owing to high polarisation energy. These problems are still to be studied, because almost no experiments in polar solvents were carried out as yet.

Prospects for the use of the method of quantum beats are first of all associated with an increase in the number of those radical ions that cannot be studied in solution by other methods due to the short lifetimes. These can be radical ions of heteroorganic or halogen-containing compounds, spin traps, biologically active substances, *etc.*

Yet another promising avenue of research involves the use of laser methods for generation of radical ion pairs. Photoionisation processes attract considerable attention of chemists and physicists and the methods considered above could find wider application. The results of photochemical experiments involving photogeneration of pairs may appear to be simpler to interpret because of the lack of cross-recombination effects typical of radiation tracks. Here, the method of quantum beats could provide additional information on the primary act of formation of radical pairs in solutions upon photoionisation, because many details of this key step remain unknown so far.

This review has been written with financial support from the Chemistry and Materials Science Division of the Russian Academy of Sciences (in the framework of the Basic Research Programme No.1) and the Federal Programme for State Support of Leading Scientific Schools in the Russian Federation (Grant NSh-5078.2006.3)

References

1. A L Buchachenko, R Z Sagdeev, K M Salikhov *Magnitnye i Spinovye Effekty v Khimicheskikh Reaktsiyakh* (Magnetic and Spin Effects in Chemical Reactions) (Novosibirsk: Nauka, 1978)
2. K M Salikhov, Yu N Molin, R Z Sagdeev, A L Buchachenko *Spin Polarization and Magnetic Effects in Chemical Reactions* (Amsterdam: Elsevier, 1984)
3. *Dynamic Spin Chemistry: Magnetic Controls and Spin Dynamics of Chemical Reactions* (Eds S Nagakura, H Hayashi, T Azumi) (Tokyo: Wiley, Kodansha, 1998)
4. H Hayashi *Introduction to Dynamic Spin Chemistry. Magnetic Field Effects on Chemical and Biochemical Reactions*. (World Scientific Lecture and Course Notes in Chemistry) Vol. 8 (River Edge, NJ: World Sci. Publ., 2004)
5. U E Steiner, T Ulrich *Chem. Rev.* **89** 51 (1989)
6. Y Tanimoto, Y Fujiwara *Handbook of Photochemistry and Photobiology. Inorganic Photochemistry* Vol. 1 (Ed. H S Nalwa) (Stevenson Ranch: American Sci. Publ., 2003) p. 413
7. K Schulten *Advances in Solid State Physics* Vol. 22 (Ed. J Treusch) (Braunschweig: Vieweg, 1982) p. 61
8. N J Turro *Proc. Natl. Acad. Sci. USA* **80** 609 (1983)
9. S G Boxer, C E D Chidsey, M G Roelofs *Annu. Rev. Phys. Chem.* **34** 389 (1983)
10. A L Buchachenko *Usp. Khim.* **62** 1139 (1993) [*Russ. Chem. Rev.* **62** 1073 (1993)]
11. B Brocklehurst *Radiat. Phys. Chem.* **50** 213 (1997)
12. A L Buchachenko *Pure Appl. Chem.* **72** 2243 (2000)
13. Yu N Molin *Bull. Korean Chem. Soc.* **20** 7 (1999)
14. B Brocklehurst *Chem. Soc. Rev.* **31** 301 (2002)
15. S Tero-Kubota, A Katsuki, Y Kabori *J. Photochem. Photobiol., C* **2** 17 (2001)
16. H Murai *J. Photochem. Photobiol., C* **3** 183 (2003)
17. Yu N Molin *Mendeleev Commun.* **85** (2004)
18. C R Timmel, K B Henbest *Philos. Trans. R. Soc. London, Ser. A* **362** 2573 (2004)
19. H Hayashi, Y Sakaguchi *J. Photochem. Photobiol., C* **6** 25 (2005)
20. R Bittl, S Weber *Biochim. Biophys. Acta* **1707** 117 (2005)
21. H Hayashi *J. Chin. Chem. Soc. (Taipei)* **49** 137 (2002)
22. E B Aleksandrov, G I Khvostenko, M P Chaika *Interferentsiya Atomnykh Sostoyanii* (Interference of Atomic States) (Moscow: Nauka, 1991)
23. R T Carter, J R Huber *Chem. Soc. Rev.* **29** 305 (2000)
24. D W Werst *Chem. Phys. Lett.* **251** 315 (1996)
25. L M Bollinger, G E Thomas *Rev. Sci. Instrum.* **32** 1044 (1961)
26. J Klein, R Voltz *Phys. Rev. Lett.* **36** 1214 (1976)
27. J Klein, R Voltz *Can. J. Chem.* **55** 2102 (1977)

28. B Brocklehurst *Chem. Phys. Lett.* **44** 245 (1976)
29. B Brocklehurst *Faraday Discuss. Chem. Soc.* **63** 96 (1977)
30. O A Anisimov, V L Bizyaev, N N Lukzen, V M Grigoryants, Yu N Molin *Chem. Phys. Lett.* **101** 131 (1983)
31. O A Anisimov, V L Bizyaev, N N Lukzen, V M Grigoryants, Yu N Molin *Dokl. Akad. Nauk SSSR* **272** 383 (1983)^a
32. A V Veselov, V I Melekhov, O A Anisimov, Yu N Molin *Chem. Phys. Lett.* **136** 263 (1987)
33. A V Veselov, V I Melekhov, O A Anisimov, Yu N Molin *Dokl. Akad. Nauk SSSR* **297** 1399 (1987)^a
34. A V Veselov, V L Bizyaev, V I Melekhov, O A Anisimov, Yu N Molin *Radiat. Phys. Chem.* **34** 567 (1989)
35. V M Grigoryants, B M Tadjikov, O M Usov, Yu N Molin *Dokl. Akad. Nauk* **346** 478 (1996)^a
36. V M Grigoryants, B M Tadjikov, O M Usov, Yu N Molin *Chem. Phys. Lett.* **246** 392 (1995)
37. O M Usov, D V Stass, B M Tadjikov, Yu N Molin *J. Phys. Chem. A* **101** 7711 (1997)
38. O M Usov, V M Grigoryants, B M Tadjikov, Yu N Molin *Dokl. Akad. Nauk* **349** 780 (1996)^a
39. O M Usov, Candidate Thesis in Chemical Sciences, Institute of Chemical Kinetics and Combustion, Siberian Branch of the Russian Academy of Sciences, Novosibirsk, 1997
40. O M Usov, V M Grigoryants, B M Tadjikov, Yu N Molin *Radiat. Phys. Chem.* **49** 237 (1997)
41. S V Anishchik, O M Usov, O A Anisimov, Yu N Molin *Radiat. Phys. Chem.* **51** 31 (1998)
42. V A Bagryansky, O M Usov, V I Borovkov, T V Kobzeva, Yu N Molin *Chem. Phys.* **255** 237 (2000)
43. B Brocklehurst, R S Dixon, E M Gardy, V J Lopata, M J Quinn, A Singh, F P Sargent *Chem. Phys. Lett.* **28** 361 (1974)
44. B Brocklehurst *Chem. Phys. Lett.* **28** 357 (1974)
45. V A Bagryansky, O M Usov, N N Lukzen, Yu N Molin *Appl. Magn. Reson.* **12** 505 (1997)
46. T V Kobzeva, V A Bagryansky, Yu N Molin *Dokl. Akad. Nauk* **387** 506 (2002)^a
47. B Brocklehurst *J. Chem. Soc., Faraday Trans.* **93** 1079 (1997)
48. J M Jung *Chem. Phys. Lett.* **380** 190 (2003)
49. S V Anishchik, V M Grigoryants, I V Shebolaev, Yu D Chernousov, O A Anisimov, Yu N Molin *Pribory Tekh. Eksperim.* (4) 74 (1989)
50. V A Bagryansky, V I Borovkov, Yu N Molin, M P Egorov, O M Nefedov *Mendeleev Commun.* 132 (1997)
51. V A Bagryansky, V I Borovkov, Yu N Molin, M P Egorov, O M Nefedov *Chem. Phys. Lett.* **295** 230 (1998)
52. V A Bagryansky, V I Borovkov, Yu N Molin *Phys. Chem. Chem. Phys.* **6** 924 (2004)
53. V A Bagryansky, Doctoral Thesis in Physical and Mathematical Sciences, Kazan Physical Technical Institute, Russian Academy of Sciences, Kazan, 2006
54. V I Borovkov, V A Bagryansky, Yu N Molin, M P Egorov, O M Nefedov *Phys. Chem. Chem. Phys.* **5** 2027 (2003)
55. V I Borovkov, N P Gritsan, I V Yeletskikh, V A Bagryansky, Yu N Molin *J. Phys. Chem. A* **110** 12752 (2006)
56. V I Borovkov, N P Gritsan, V A Bagryansky, Yu N Molin *Dokl. Akad. Nauk* **413** 202 (2007)^a
57. V I Borovkov, K L Ivanov, V A Bagryansky, Yu N Molin *J. Phys. Chem. A* **110** 4622 (2006)
58. V A Bagryansky, M M Vyushkova, I V Beregovaya, L N Shchegoleva, V I Borovkov, P A Potashov, N N Lukzen, Yu N Molin *The 5th Asia-Pacific EPR/ESR Symposium (APES 2006) (Book of Abstracts)*, Novosibirsk, 2006 p. 43
59. V I Borovkov, Yu N Molin *Phys. Chem. Chem. Phys.* **6** 2119 (2004)
60. V I Borovkov, Yu N Molin *Chem. Phys. Lett.* **398** 422 (2004)
61. V I Borovkov, Yu N Molin *Dokl. Akad. Nauk* **396** 633 (2004)^a
62. V I Borovkov, I V Yeletskikh *Pribory Tekh. Eksperim.* (1) 90 (2005)
63. S V Anishchik, V I Borovkov, V I Ivannikov, Yu D Chernousov, I V Shebolaev *Pribory Tekh. Eksperim.* (2007) (in the press)
64. V A Bagryansky, V I Borovkov, Yu N Molin *Dokl. Akad. Nauk* **382** 794 (2002)^a
65. V A Bagryansky, V I Borovkov, Yu N Molin *Mol. Phys.* **100** 1071 (2002)
66. V I Borovkov, P A Potashov, L N Shchegoleva, V A Bagryansky, Yu N Molin *J. Phys. Chem. A* **111** 5839 (2007)
67. B Brocklehurst *Nature (London)* **221** 921 (1969)
68. B Brocklehurst *J. Chem. Soc., Faraday Trans.* **2** **72** 1869 (1976)
69. K Schulten, P G Wolynes *J. Chem. Phys.* **68** 3292 (1978)
70. D V Stass, N N Lukzen, B M Tadjikov, V M Grigoryantz, Yu N Molin *Chem. Phys. Lett.* **243** 533 (1995)
71. V A Bagryansky *Dokl. Akad. Nauk* **402** 781 (2005)^a
72. V A Bagryansky, K L Ivanov, V I Borovkov, N N Lukzen, Yu N Molin *J. Chem. Phys.* **122** 224503 (2005)
73. M V Fedin, P A Purtov, E G Bagryanskaya *Chem. Phys. Lett.* **339** 395 (2001)
74. R A Marcus *Annu. Rev. Phys. Chem.* **15** 155 (1964)
75. Ch Slichter *Principles of Magnetic Resonance* (Heidelberg: Springer, 1978)
76. M G Townsend, S I Weissman *J. Chem. Phys.* **32** 309 (1960)
77. M R Das Stephen, B Wagner, J H Freed *J. Chem. Phys.* **52** 5404 (1970)
78. B M Tadjikov, D V Stass, Yu N Molin *J. Phys. Chem. A* **101** 377 (1997)
79. Y Iwasaki, K Maeda, H Murai *J. Phys. Chem. A* **105** 2961 (2001)
80. E G Bagryanskaya, V R Gorelik, R Z Sagdeev *Chem. Phys. Lett.* **264** 655 (1997)
81. S R Shakirov, T N Makarov, E G Bagryanskaya, R Z Sagdeev *Phys. Chem. Chem. Phys.* **3** 3672 (2001)
82. T N Makarov, E G Bagryanskaya, S R Shakirov, N N Lukzen, R Z Sagdeev *Chem. Phys. Lett.* **317** 252 (2000)

^a — *Dokl. Phys. Chem. (Engl. Transl.)*

Acetylene: new prospects of classical reactions

B A Trofimov, N K Gusarova

Contents

I. Introduction	507
II. Acetylene reactions in superbasic media	508
III. Chemistry of acetylenic hydroxy acids and their derivatives	514
IV. Acetylene- and allene-derived carbanions	515
V. New reactions involving pyrrole	516
VI. The use of acetylenes in the synthesis of phosphines and phosphine chalcogenides	517
VII. Acetylene derivatives of silicon and germanium	519
VIII. New acetylene-based technologies	520
IX. Conclusion	521

Abstract. The latest results in the field of classical reactions of acetylene are analysed. Attention is focused on reactions catalysed by strong bases (vinylation, alkynol synthesis, acetylene–allene isomerisation) and related syntheses. The bibliography includes 347 references.

I. Introduction

Chemistry of acetylene, a versatile building block of the organic synthesis, is continued to be rapidly developed.¹ As compared with ethylene, highly reactive acetylene and its derivatives better match the trends in the development of chemical industry, which is more and more oriented to the production of science intensive chemicals for modern technologies, medicine and agriculture. Acetylene can be considered as an accumulator of high-density energy, *i.e.*, the heat consumed in its formation is liberated in chemical reactions thus promoting them and providing the shortest and the least power-consuming way to the target products.

Although quite recently, acetylene was virtually beyond competition as the basic chemical used in the industry, now it has lost its leading position. At the same time, according to certain analysts, acetylene might again become the leader.^{2–7} Future will show whether or not this happens and to the full extent or only partly, however, there are objective prerequisites for this to happen.

Acetylene is mainly produced from oil and natural gas by oxidative pyrolysis in an electric discharge, in plasma, by laser technologies and using solar energy. Moreover, acetylene is the main side product in the ethylene synthesis.² At the same time, acetylene can also be produced from coal. Accounts of natural

energy resources show that oil and natural gas fields are being rapidly exhausted, while the coal resources may last for centuries. Hence, the return to coal-based technologies seems quite likely.^{2,5,6} Acetylene is obtained from coal by both the traditional carbide method and the modern plasma technologies as well as by hydrogenation, gasification or *via* the synthesis gas. Moreover, different types of biomass such as lignine and various carbon-containing industrial and domestic waste may be transformed into acetylene by their fast pyrolysis in plasma. The latter method seems especially attractive, being associated with the solution of environmental problems.

Long-term economical prognoses allow one to assume that new, constantly modernised plasma technologies for the production of acetylene from coal have a sufficient potential for making acetylene once again the chief chemical in the manufacturing of commercial products such as vinyl chloride, vinyl acetate, acrylates, chloroprene and chlorinated solvents.^{2,5–7}

To make the quest for new synthetic approaches to the chemistry of acetylene more effective, the theoretical studies based on high-level *ab initio* quantum-chemical calculations are invoked with increasing frequency.^{8,9}

Among the popular synthetic methods actively elaborated today, classical reactions of the addition of nucleophiles to the triple bond, the acetylene–allene–diene isomerisation and the transformations of acetylene and allene-derived carbanions deserve mention. Recent reviews^{10,11} show numerous examples of syntheses of heterocyclic and carbocyclic compounds by the addition of different nucleophiles to acetylenes.

The quest for new reactions of the formation of C–C bonds that involve acetylene-derived carbanions (metal acetylenides) and especially those based on the addition of acetylene to the carbonyl group (the Favorsky alkynol synthesis and its analogues) is carried on.¹² Numerous studies on transition metal acetylenides were summarised in several reviews.^{13,14}

Unconventional prospects for the organic synthesis are opened up by acetylenic sugars, which were the subject of hundreds of publications (*e.g.*, for a review, see Ref. 15).

The progressively greater efforts are directed to the quest for new organic semiconductors and optoelectronic materials based on acetylene polymers and oligomers. Today, high expectations are placed on polyarylene ethynyls, *i.e.*, polymers containing alternating triple bonds and arene

B A Trofimov, N K Gusarova A E Favorsky Irkutsk Institute of Chemistry, Siberian Branch of the Russian Academy of Sciences, ul. Favorskogo 1, 664033 Irkutsk, Russian Federation. Fax (7-3952) 41 93 46, tel. (7-3952) 42 44 11, e-mail: boris_trofimov@iriokh.irk.ru (B A Trofimov), tel. (7-3952) 42 24 36, e-mail: gusarova@iriokh.irk.ru (N K Gusarova)

Received 3 April 2007

Uspekhi Khimii 76 (6) 550–570 (2007); translated by T Ya Safonova

groups,^{16–19} and unique polyne structures, which can be synthesised through alkylidenecarbenes and -carbenoids.^{20, 21} The interest in polyynes^{22, 23} and arylene–ethynylene systems²⁴ is explained by their prospects as the molecular wires and also in the context of studies of carbyne and its analogues as the allotropic forms of carbon.

The appearance of new synthetic approaches to the design of new acetylenic structures, which are based on cross-coupling reactions catalysed by transition metal complexes, has revolutionised the assembling of different acetylene-containing systems and ensembles.^{25–27}

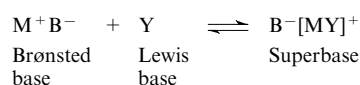
In the recent decades, systematic studies were carried out aimed at further development of classical reactions of acetylene with the use of superbasic catalysts and reagents. The present review is devoted to the brief analysis of achievements in this field. At the same time, due to the limited volume, it chiefly deals with the addition reactions to the triple bond (vinylation), addition of acetylene-derived carbanions (alkynol synthesis) and acetylene–allene–diene isomerisation, which serve as the basis for the most popular synthetic methods in the acetylene chemistry and are used most widely in laboratories and the industry.

The elaboration of a new approach to the enhancement of the reactivity of nucleophilic reagents, which is associated with the use of superbasic catalysts, have led not only to the refining of most important base-catalysed reactions of acetylene but also to the discovery of new reactions involving the triple bond and the development of synthetic methods based on them.^{7, 28–43}

II. Acetylene reactions in superbasic media

The concept of superbasicity was first formulated by Trofimov⁴⁴ in 1977: ‘a medium consisting of a strong base and a solvent or a reagent that specifically binds cations thus ‘stripping’ the conjugated anions is considered superbasic...’. Later, this concept was systematically used in the refinement of classical reactions involving triple carbon–carbon bonds (Refs 7, 28–30, 33, 41 and 43).

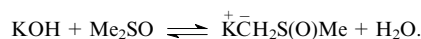
Obviously, within the framework of this concept, the definition of superbasicity is the ‘mirror image’ of superacidity, *i.e.*, a superbase is a complex of a strongly ionised base (the Brønsted base) with a ligand that can specifically interact with the cation of this base (the Lewis base) in a medium capable of weak solvation of anions (as a rule, in a medium of a polar hydroxyl-free solvent).^{33, 41}



M = Li, Na, K, Rb, Cs; B is a carbanion, H, OH, OR, NH₂, NR₂; Y correspond to ethers (polyethers), amines (polyamines), NH₃, cryptands, sulfoxides, sulfones, amides, phosphine oxides, *etc.*

Systems with the Hammett acidity function (*H*₀) higher than 18.5, *i.e.*, the systems with the basicity unattainable in hydroxyl-containing solvents (water and alcohols) due to the limitations imposed by the intrinsic acidity of the medium, were assigned^{33, 41} to superbases.

Among diverse superbasic systems, the system KOH–DMSO proved to be the most suitable for the systematic application in the acetylene chemistry as the simplest, most easily prepared and versatile system.^{7, 28–30, 32, 33, 41–46} Its upper basicity limit is determined by the DMSO acidity (*pK*_a = 35.1); however, the acidity does not usually exceed 32 (in the *H*₀ scale) unless special measures have been undertaken for the removal of water liberated in the formation of dimethylpotassium.



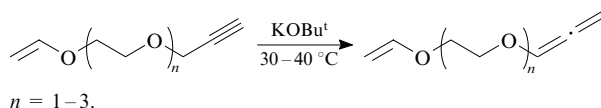
A great advantage of the system KOH–DMSO is its controllable basicity. As the water content in DMSO decreases to 25%, the system passes to the superbasicity region (*H*₀ > 20). With further decrease in the water concentration, the value of *H*₀ sharply increases approaching 30–32 for 99% DMSO.⁴¹

Yet another advantage of the system KOH–DMSO is its ability for autostabilisation (self-adjustment), *i.e.*, its basicity is maintained on a constant level due to the absorption of water (if water is liberated in the reaction) by the solid phase (KOH); the KOH concentration in the liquid phase is low (~0.04 mol litre⁻¹ in pure DMSO) and the consumed KOH is replenished from the solid phase, *i.e.*, its concentration is automatically kept constant. Thus, the reactions in this system often acquire the features of the phase-transfer catalysis.⁴¹

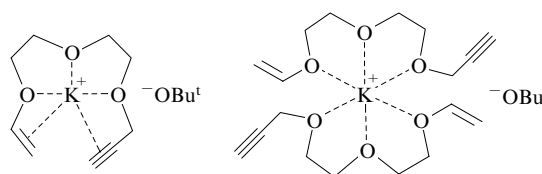
1. Development of classical acetylene reactions

a. The Favorsky acetylene–allene isomerisation

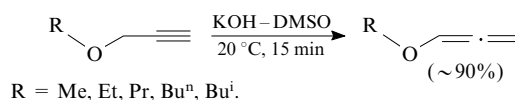
The selective isomerisation of propargyl ethers to allenyl ethers was first carried out under the action of KOBu^t on propargyl vinyl ethers of ethylene glycol oligomers.^{47, 48}



The superbasicity of the reaction mixture was achieved due to the formation of chelate complexes of potassium cations with the polyether chain.

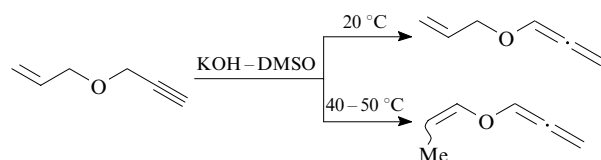


The use of the superbasic system KOH–DMSO in the isomerisation of propargyl ethers have led to the development of an efficient and highly selective method for the synthesis of alkyl allenyl ethers.⁴⁹

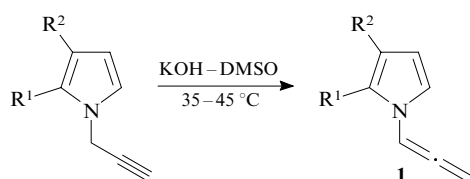


This reaction made accessible the alkyl allenyl ethers, which so far pertained to the insufficiently explored class of substances.^{7, 50–52} Obviously, their synthetic potential as the reactive monomers and building blocks is more multifaceted as compared with the corresponding vinyl ethers that have found wide application in both the organic synthesis^{2, 28, 53–58} and polymer chemistry.^{59–67}

It was shown that the system KOH–DMSO allows one to selectively isomerise the propargyl group of an allyl propargyl ether to the allenyl group, leaving intact the allyl fragment. When carried out at higher temperatures, this reaction can shift the double bond to afford allenyl prop-1-enyl ether.⁴¹

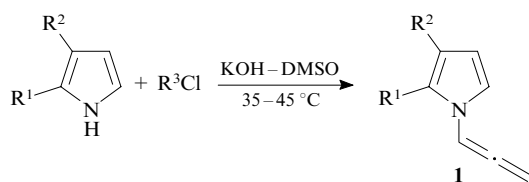


N-Allenylpyrroles **1**, the promising monomers⁶⁸ and building blocks in synthetic chemistry, which were difficult to synthesise until recently, were easily obtained in high yields by the isomerisation of *N*-propargylpyrroles catalysed by the system KOH–DMSO.⁶⁹



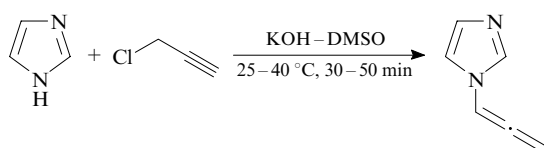
R ¹	R ²	Yield of 1 (%)	R ¹	R ²	Yield of 1 (%)
H	H	63	Me	Me	49
Me	H	68		(CH ₂) ₄	88
Ph	H	70			

N-Allenylpyrroles **1** can be synthesised in a one-pot procedure using both propargyl chloride⁷⁰ (which is sufficiently obvious) and much cheaper 2,3-dichloroprop-1-ene⁷¹ and 1,2,3-trichloropropane,⁷² which are the side products of the industrial synthesis of epichlorohydrin. In this case, the system KOH–DMSO serves not only as the catalyst, but also as the reagent and, hence, should be taken in a superstoichiometric amount.

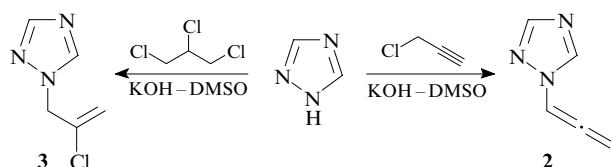


R¹ = H, Me, Ph; R² = H, Me; R¹–R² = (CH₂)₄;
R³ = CH₂C≡CH, CH₂CCl=CH₂, CH₂CHClCH₂Cl.

The same superbases and the same reagents allowed the one-pot allenylation of other azoles to be carried out.^{73, 74} For example, *N*-allenylimidazole was synthesised from imidazole and propargyl chloride in the yield of 75%.



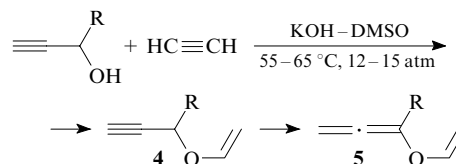
1,2,4-Triazole behaves in a similar way, namely, its reaction with propargyl chloride produces *N*-allenyl-1,2,4-triazole (**2**) in the yield of 31%.^{73, 74} The use of trichloropropane in allenylation allows one to stop the reaction after the formation of *N*-chloroallyl derivative **3** (yield 21%).⁷³



b. Nucleophilic addition to a triple bond (vinylation)

Superbasic catalysts have extended in principle the potentials of the classical Favorsky reaction of vinylation.⁷⁵ For example, vinylation of acetylenic alcohols with acetylene is impossible in the presence of common bases (alkali metal hydroxides or alkoxides); however, in superbasic systems such as KOH–DMSO this reaction proceeds sufficiently smoothly.⁴¹

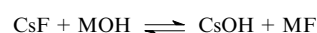
As a rule, it is rather difficult to stop this reaction in a stage of the formation of a vinyl ether of acetylenic alcohol **4** (this requires special measures to be undertaken). Usually, the acetylene–allene isomerisation proceeds simultaneously to afford the corresponding allenyl vinyl ethers **5** (yields up to 80%).^{76, 77}



R = H, Me, Et, Prⁿ, Prⁱ, Bu^t.

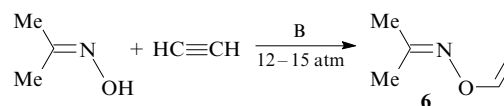
This reaction is the most promising for the transformation of commercially available propargyl alcohol into vinyl-oxyallene.

A new generation of superbases, the catalytic systems CsF–MOH–DMSO (M = Li, Na, K) have been developed recently. As a rule, they are more active^{41, 78–83} than the system KOH–DMSO. In a simple way, their enhanced activity can be explained by the formation of caesium hydroxide (a base stronger than potassium hydroxide) due to the shift of the equilibrium to the formation of poorly soluble fluorides, particularly, lithium fluoride.⁴¹



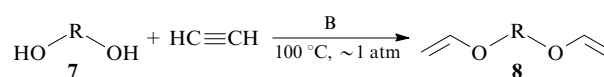
M = Li, Na, K.

A comparison of the activity of two superbasic catalytic systems, namely, KOH–DMSO and CsF–NaOH–DMSO, in the vinylation of acetone oxime shows that the caesium system is much more active. In the presence of this system, the optimum reaction temperature was lower (by ~10 °C) and the yield of *O*-vinyl acetone oxime (**6**) was higher (by 20%)^{78, 80} as compared with the system KOH–DMSO.



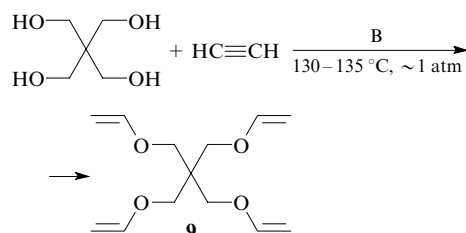
B	T / °C	Yield of 6 (%)
CsF–NaOH–DMSO	70–72	85
KOH–DMSO	78–80	65

Yet more impressive difference in the activities of these two superbasic catalytic systems was observed in the vinylation of polyhydric alcohols. Thus the vinylation of glycols **7** at 100 °C and atmospheric pressure in the presence of the system CsF–NaOH–DMSO afforded divinyl ethers **8** in the yields from 45% to 90% (depending on the glycol structure), whereas in the KOH–DMSO system, the yield of divinyl ethers was at the level of 10%.^{41, 83}



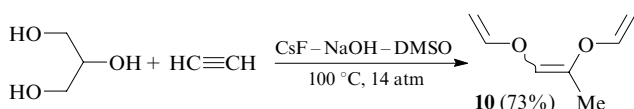
R = (CH₂)₃, (CH₂)₄, MeCH(CH₂)₂, (CH₂)₇;
B = CsF–NaOH–DMSO, KOH–DMSO.

In the reaction of acetylene with pentaerythritol carried out at 130–135 °C and the atmospheric pressure in the system CsF–NaOH–DMSO, the yield of tetravinyl ether of pentaerythritol (**9**) exceeded 60%, whereas in the system KOH–DMSO, its yield was 5%.⁴¹

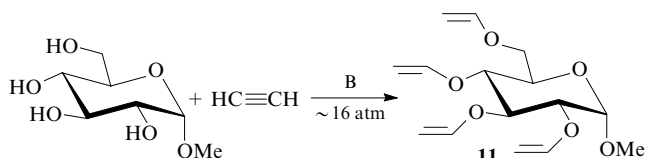


B = CsF–NaOH–DMSO, KOH–DMSO.

The reaction of glycerol with acetylene in the system CsF–NaOH–DMSO produced 1,2-bis(vinyl)oxyprop-1-ene (**10**) rather than the expected trivinyl ether of glycerol.⁸¹ Thus, this reaction represents a new type of vinylation, namely, the eliminative vinylation.⁸⁴ In the presence of the system KOH–DMSO as the catalyst, only traces of compound **10** were obtained.

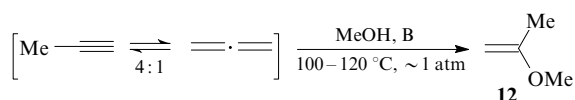


Recently, tetravinyl ether **11** was synthesised from methyl α -D-glucoside in the presence of superbasic catalysts KOH–DMSO and KOH–THF.⁸⁵



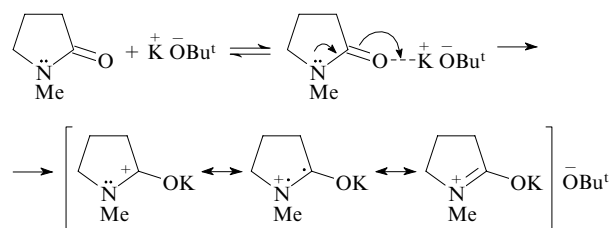
B	<i>T</i> / °C	<i>t</i> / h	Yield of 11 (%)
KOH–DMSO	85–87	1	75
KOH–THF	135–140	6	52

Superbasic catalytic systems that allow one to perform isopropenylation of methanol with methylacetylene (the second most readily accessible acetylenic hydrocarbon) at the atmospheric pressure and 100–120 °C have been developed.⁸⁶ This made it possible to synthesise⁸⁶ 2-methoxyprop-1-ene (**12**), a valuable monomer and reagent, which has found its application in the industrial syntheses of fragrant compounds, vitamins and carotenoids.^{87–90} Complexes of potassium and caesium *tert*-alkoxides with *N*-methylpyrrolidone (NMP) proved to be the most active in this reaction.

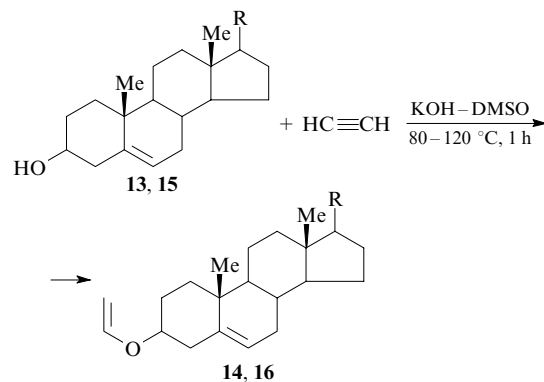


B = KOBu^t–NMP (the yield of compound **12** is 87 %), CsOCMe₂Et–NMP (87%), KOH–DMSO (60%), CsOMe–NMP (22%), CsF–NaOH–NMP (11%), 2 KOH·H₂O–NMP (6%).

Apparently, this is associated with the formation of a charge-transfer complex between NMP and alkoxides. This is evidenced by the presence of the charge transfer bands (283, 543, 580 nm; bright purple colour) in the UV spectrum of a KOBu^t solution in NMP and also by the high-frequency shift of vibrations of the C=O group (1683 cm^{–1} → 1693 cm^{–1}, probably due to the contribution of the vibrations of the ⁺N=C group) observed in the IR spectrum.⁴¹

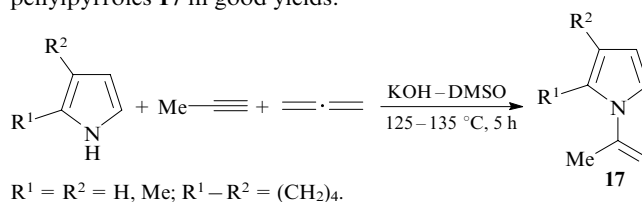


At present, the superbasic catalytic system KOH–DMSO is the most versatile for the vinylation reactions.^{7, 41, 43} Thus this allowed the vinylation of cholesterol **13** to be carried out under mild conditions (without epimerisation and migration of the double bond) to afford the quantitative yield of optically active liquid-crystalline vinyl ether **14**, which is used as a monomer and a highly reactive intermediate in the synthesis of new compounds of the steroid series.⁹¹ In the presence of the same catalytic pair, pregnenolone **15** and acetylene gave vinyl ether **16** with retention of the keto group and configurations of all asymmetric centres. This is the first example of the successful vinylation of a hydroxy ketone.^{41, 92}



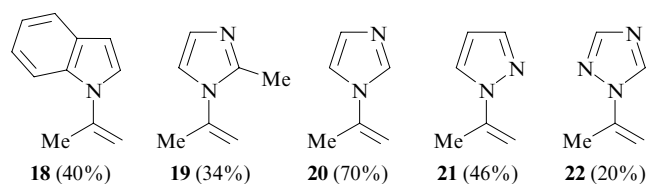
R = C₈H₁₇ (**13**, **14**), Ac (**15**, **16**).

In the presence of the system KOH–DMSO, pyrroles were vinylated for the first time under relatively mild conditions with a methylacetylene–allene mixture to produce *N*-isopropenylpyrroles **17** in good yields.⁹³



R¹ = R² = H, Me; R¹–R² = (CH₂)₄.

This catalyst can also be used in the isopropenylation of other azoles (105–145 °C, 5–15 h), namely, indoles, imidazoles, pyrazoles, triazoles. The corresponding *N*-isopropenyl derivatives **18–22** were obtained in yields of 20%–70% (non-optimised yields).⁹⁴

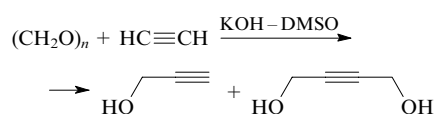


The above (hardly exhaustive) examples illustrate the impressive advances in the studies of vinylation with acetylenes, which were observed in the past decades due to the use of superbasic catalytic systems.^{7, 41}

c. The Favorsky alkynol synthesis and its analogues

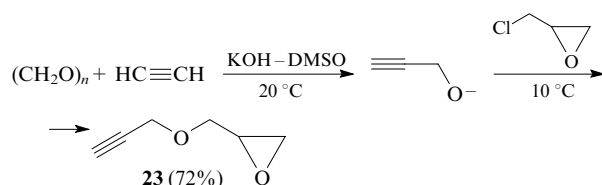
The quantum-chemical analysis^{95–97} shows that in the gas phase or a weakly solvating medium the formation of acetylide anions from acetylene under the action of superbases at low temperatures is more preferential than the alternative nucleophilic addition of anions to the triple bond. Hence, superbases should accelerate the Favorsky ethynylation of aldehydes and ketones (the addition of acetylide anions to the C=O bond).

Indeed, it was shown that in the superbasic medium KOH–DMSO, acetylene reacts quickly and quantitatively with paraform at the atmospheric pressure and room temperature to form propargyl alcohol^{98–100} and/or but-2-yn-1,4-diol.^{33,41} In contrast to the classical vinylation of formaldehyde, which proceeds in the presence of an explosive copper acetylide under a pressure of up to 70 atm and at a temperature of 90–130 °C, the new method allows one to make, if required, propargyl alcohol the main reaction product (yield up to 90%).⁹⁹

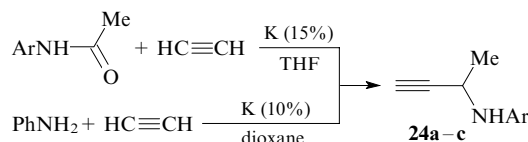


Other aldehydes and ketones also react with acetylene more actively in the presence of the system KOH–DMSO than under conventional conditions; moreover, different acetylenic alcohols and glycols can be synthesised in high yields with no recourse to high pressures, cooling and large volumes of solvents,^{7,33,101} *i.e.*, in the absence of all attributes inherent in the classical ethynylation.

In the system KOH–DMSO, the one-pot synthesis of glycidyl propargyl ether (**23**) was carried out from paraform, acetylene and epichlorohydrin.¹⁰²

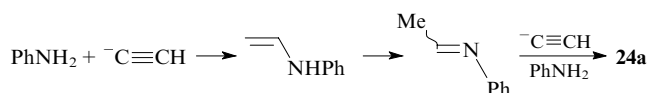


Acetylide anions generated from acetylene in superbasic media add to the C=N bond. Thus anilides^{103–105} and anilines¹⁰⁶ react with acetylene in the presence of their potassium derivatives (at 160 °C, under enhanced pressure, in THF or dioxane) to form 3-arylaminoabutynes **24a–c**.



Ar = Ph (**a**), 2-MeC₆H₄ (**b**), 4-MeC₆H₄ (**c**).

It was proved that these reactions proceed through the intermediate formation of the Schiff base that adds the acetylide anion to the C=N bond (the aza analogue of the Favorsky reaction).^{103,105}

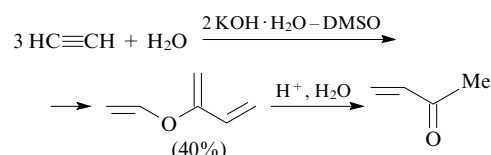


2. New reactions

Several new general reactions of acetylene that occur in superbasic media and produce promising monomers and synthons for the fine organic synthesis have been discovered.^{7,28–36,40–43}

a. Hydrative trimerisation of acetylene

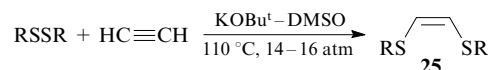
It was found that in the presence of the complex 2 KOH·H₂O–DMSO (80–115 °C, 10–15 atm), three acetylene molecules and one water molecule undergo a single-stage formation of 2-vinyloxybuta-1,3-diene that simultaneously contains a 1,3-diene fragment and a vinyl group.^{107,108}



Mild acid-catalysed hydrolysis of 2-vinyloxybuta-1,3-diene (1% HCl, 20 °C) affords methyl vinyl ketone in the quantitative yield.³³

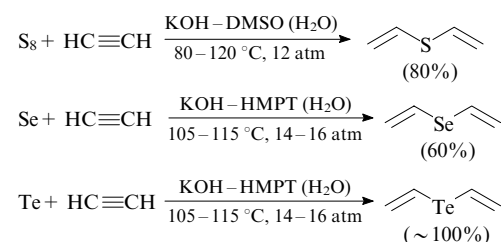
b. Direct vinylation of chalcogens and elemental phosphorus

The use of superbasic systems made it possible to carry out a series of unconventional acetylene reactions, particularly, the direct vinylation of chalcogens and elemental phosphorus in the presence of a minimum amount of a proton donor (usually, water). These studies were initiated by the discovery of a reaction of acetylene incorporation into the S–S bond of disulfides in the system KOBu^t–DMSO. The reaction is stereoselective and produces *Z*-isomers of 1,2-bis(alkylthio)-ethenes **25**.^{109–111}



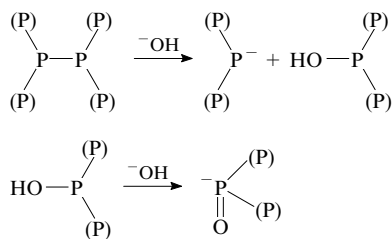
R = Me, Et, Buⁿ, Bu^t.

As was found later, this reaction is general and may be extended to dialkyl diselenides¹¹² and elemental S₈, Se and Te.^{111,113–115} Being a supernucleophile, the polysulfide anion formed from the cyclic octamer S₈ is easily captured by acetylene. As a result of subsequent transformations, the polysulfide anion transforms into divinyl sulfide in the presence of proton donors.^{111,113,114} Selenium and tellurium are vinylated to divinyl selenide and divinyl telluride, respectively, in the presence of the system KOH–HMPT (HMPT is hexamethylphosphotriamide).^{111,114,115} In this reaction, superbases act not only as the catalysts but also as the reagents, being involved in the redox disproportionation of selenium or tellurium.

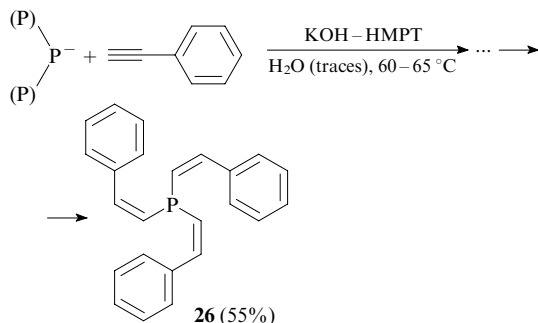


Under these conditions, elemental phosphorus behaves in a similar way. Under the action of an activated hydroxide

ion, the P–P bonds of both white and red phosphorus are easily cleaved to form phosphide and phosphinite anions,[†] which react with the appropriate electrophile (complementary with respect to symmetry and population of unoccupied valence molecular orbitals).^{35, 116–120}

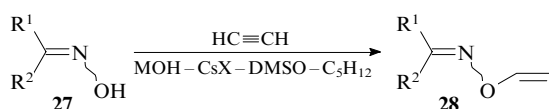


For phosphide anions, acetylenes proved to be these complementary electrophiles. Thus the reaction of phosphide anion with phenylacetylene at 60–65 °C proceeds by a stereoselective mechanism to form a *Z,Z,Z*-isomer of tristyrylphosphine (**26**).^{35, 117–119}



c. Synthesis of *O*-vinylketoximes

Nucleophilic addition of ketoximes **27** to acetylene in superbasic media to form *O*-vinylketoximes **28** made the latter easily accessible.^{42, 121–124}

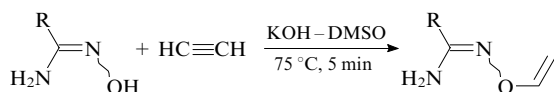


R¹, R² = Alk, Ar, Het; M = Li, Na, K; X = Cl, F.

The highest yield of vinyloximes **28** was reached due to the modification of the superbasic system MOH–DMSO by the addition of a non-polar solvent (pentane) and caesium halides. Pentane extracts the *O*-vinyloximes formed and thus prevents their further transformation to pyrroles, while caesium salts are converted to CsOH due to the exchange processes thus providing the high basicity of the system.^{121–123}

d. Synthesis of *O*-vinylamidoximes

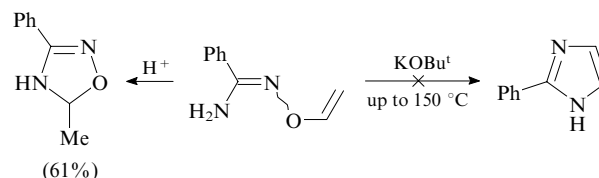
The use of superbasic catalysts made it possible to vinylate amidoximes, which are prone to tautomeric transformations under ordinary conditions.^{125, 126}



R = Me (46%), Ph (89%).

[†] In the first stages, phosphide and phosphinite anions represent super-nucleophilic anionic clusters.

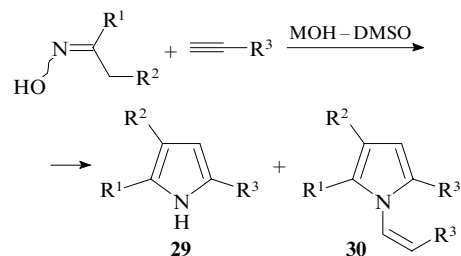
Chemoselective vinylation at the hydroxyl group occurs at a temperature unusually low for this reaction (75 °C) very quickly, virtually instantaneously (it takes about 5 min for the reaction to be completed).^{125, 126} The resulting *O*-vinylamidoximes form a new class of promising monomers and synthons, particularly, for designing heterocycles. For example, they are easily cyclised to oxodiazolines,⁴¹ although the attempts to rearrange them into imidazoles (analogously to the rearrangement of *O*-vinyloximes to pyrroles^{42, 127}) failed so far.



e. Acetylene reactions with ketoximes: synthesis of pyrroles

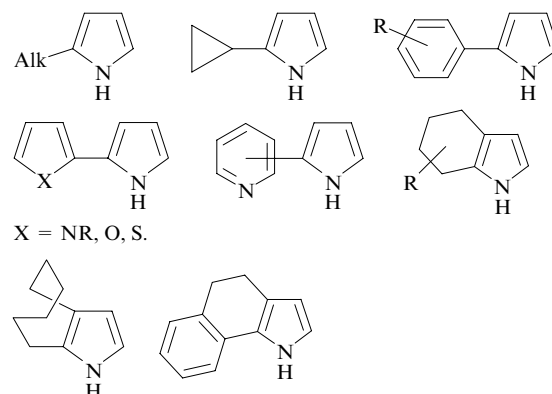
A new general reaction of ketoximes with acetylenes, which proceeds in superbasic media such as MOH–DMSO (M is an alkali metal) and afford pyrroles **29** and *N*-vinylpyrroles **30**, was discovered.^{30, 32–34, 37, 41, 42 127–144} An excess of acetylene favours direct formation of *N*-vinylpyrroles **30**. Actually, this reaction represents a two-stage transition from ketones to diverse pyrroles.

By this reaction, virtually any ketone that has at least one methylene or methyl group in the α-position with respect to the carbonyl function and contains no strong base-sensitive substituents can be transformed into the corresponding pyrrole or *N*-vinylpyrrole. If necessary, a one-pot synthesis can be carried out in the system MOH–DMSO. For this purpose, a ketone is treated first with hydroxylamine (or its hydrochloride) and then with acetylene.¹⁴³



R¹, R² = Alk, Ar, Het; R³ = H, Me, Ph; M = Li, Na, K, Rb, Cs.

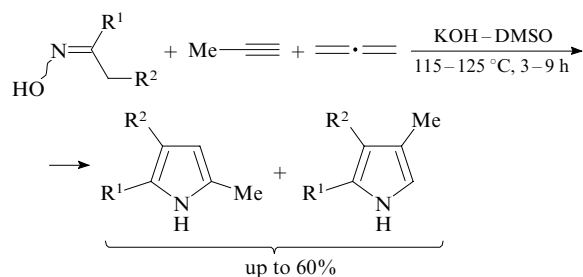
This reaction has provided a facile route to pyrroles with alkyl, cycloalkyl, aryl and hetaryl substituents and pyrroles annulated with common rings, macrocycles and fused systems.^{7, 30, 41, 140–146}



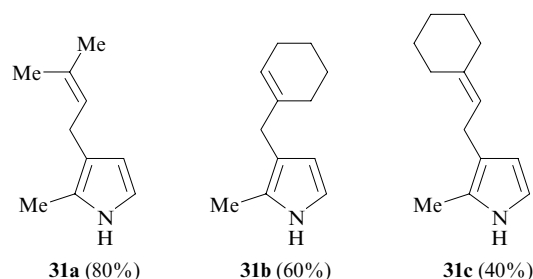
At present, this reaction is widely referred to in the literature as the Trofimov reaction (*e.g.*, see Refs 147–157).

Alkali metal hydroxides were used as the MOH component of the superbasic catalytic system MOH–DMSO. Rubidium and caesium hydroxides are more active than KOH but the latter is much cheaper; this is why the system KOH–DMSO is used, as a rule. Lithium and sodium hydroxides are less active; however, they allow one to obtain NH pyrroles more selectively, because they virtually do not catalyse their vinylation. In the absence of DMSO, pyrroles are not formed, *i.e.*, the intrinsic basicity of alkali metal hydroxides is insufficient and this reaction requires superbasicity.⁴¹

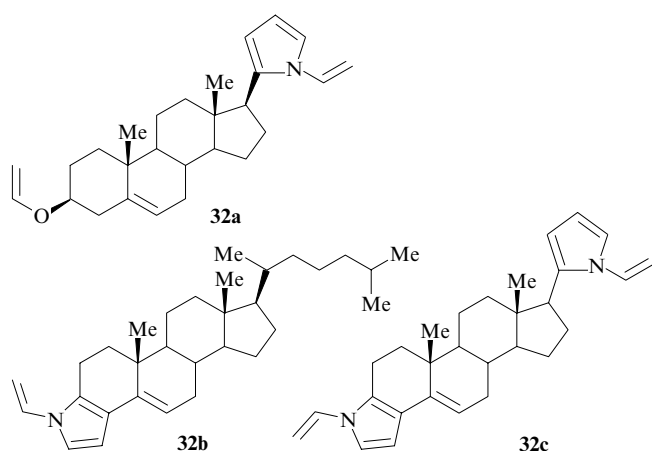
In place of acetylene, methylacetylene and allene can be employed.⁹³



This reaction was successfully used for the synthesis of pyrroles **31a–c** with terpenoid substituents.^{7,41,131} For this purpose, terpenoid ketones were treated first with hydroxylamine and then with acetylene in the system KOH–DMSO.

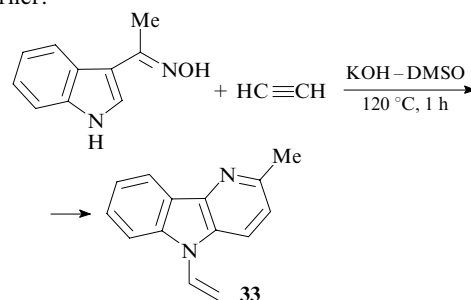


This reaction was also used to prepare recently unknown steroid pyrrole compounds including those containing highly reactive *O*- (compound **32a**) and *N*-vinyl (**32a–c**) groups capable of polymerisation and further chemical modification.^{41,134,136,137}

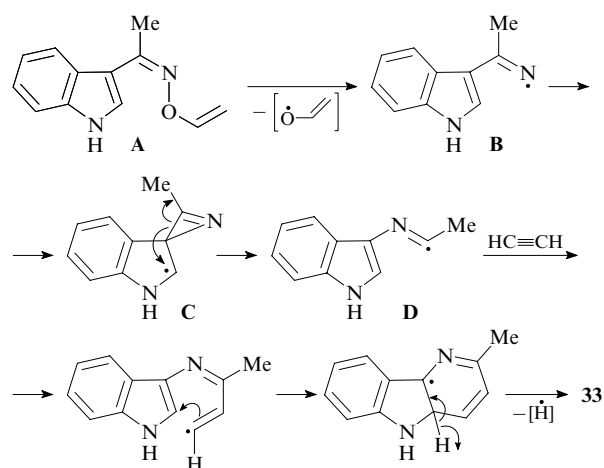


f. Synthesis of δ -carboline from 3-acetylindole oxime and acetylene
The reaction 3-acetylindole oxime with acetylene in the superbasic catalytic system KOH–DMSO opened up a new way

(one-pot assembling) to the synthesis of δ -carboline system, namely, pyridoindole **33**, which was difficult to synthesise earlier.¹⁵⁸



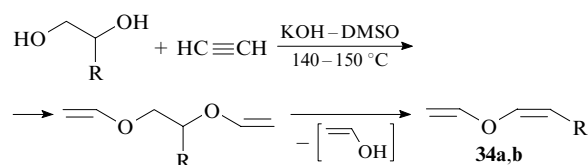
Apparently, this reaction proceeds through the homolytic cleavage of the N–O bond in the intermediate *O*-vinoxime **A** followed by the intramolecular attack of iminyl radical **B** on the pyrrole ring. After this, the homolytic opening of the spiroazirine intermediate **C** and the addition of the second acetylene molecule to radical **D** complete closure of the pyridine ring.¹⁵⁸



Carboline structures are present in many natural compounds and medicinal drugs; however, so far the synthesis of δ -carbolines remained an unsolved problem in the chemistry of indole alkaloids. An important advantage of this reaction is the possibility of the one-stage synthesis of the hitherto unknown *N*-vinyl- δ -carbolines.⁴² The latter combine the properties of an *NH*-protected δ -carboline with those of highly reactive synthons and monomers, which opens up wide prospects for the development of the fundamental and synthetic chemistry of indole alkaloids and high-molecular-weight compounds of the carboline series.

g. Eliminative vinylation of 1,2-diols and polyols

The eliminative vinylation of 1,2-diols and polyols opened up a rational way to divinyl ethers, namely, vinyloxyalkenes **34**.³³ The formal elimination of vinyl alcohol from the intermediate divinyl ethers proceeds only in the presence of superbases such as KOH–DMSO; moreover, the elimination proceeds more smoothly in the presence of acetylene.^{159,160}

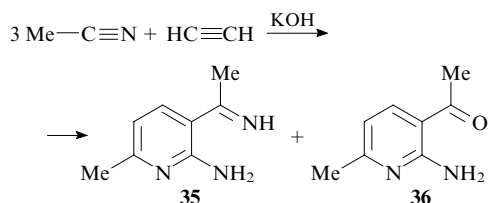


R = H (**a**), Me (**b**).

Due to this reaction, divinyl ethers, the promising monomers and synthons, have become accessible for the first time and the reaction itself, being general, has supplemented the arsenal of methods of organic chemistry.³³

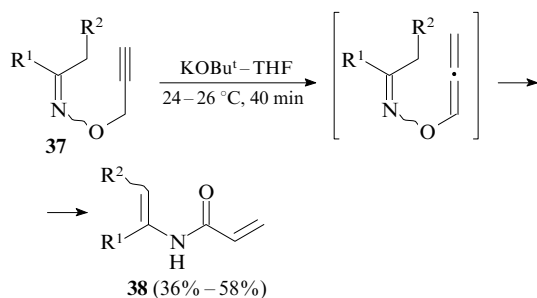
h. Cyclo-co-oligomerisation of acetylene with acetonitrile

The cyclisation of acetylene with three acetonitrile molecules pertains to the new reactions of acetylene that proceed in superbasic media. The cyclisation occurs under mild conditions (from -10 to 20 °C, atmospheric pressure, a superbasic system KOH–MeCN) and leads to 2-amino-3-(2-iminoethyl)-6-methylpyridine (**35**), the first representative of pyridines that simultaneously contains an imine and an amine functions, and 3-acetyl-2-amino-6-methylpyridine (**36**).¹⁶¹



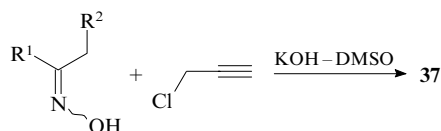
i. Rearrangement of *O*-propargylketoximes

In the presence of a specific superbasic system KO^tBu –THF, propargyl ethers of ketoximes **37** are rearranged to *N*-vinylacrylamides **38** rather than to the expected allenyl ethers (room temperature, exothermic process). This rearrangement is general.¹⁶²



$\text{R}^1 = \text{Alk, Ar}; \text{R}^2 = \text{H, Alk.}$

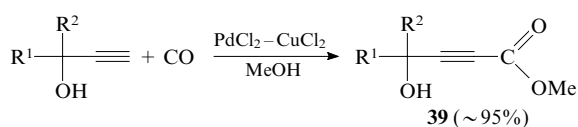
In turn, *O*-propargylketoximes **37** are obtained in quantitative yields from oximes and propargyl chloride in the superbasic system KOH–DMSO.^{41, 163} It is amazing that this virtually universal catalytic system fails to induce the rearrangement of *O*-propargylketoximes formed.



III. Chemistry of acetylenic hydroxy acids and their derivatives

1. Oxidative methoxycarbonylation of acetylenic alcohols

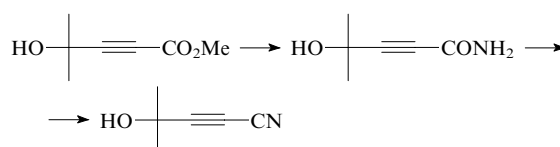
The direct catalytic synthesis of methyl esters of acetylenic hydroxy acids **39** was carried out by the reaction of acetylenic alcohols with carbon monoxide in methanol in the presence of



$\text{R}^1, \text{R}^2 = \text{Alk, cyclo-Alk, Ar.}$

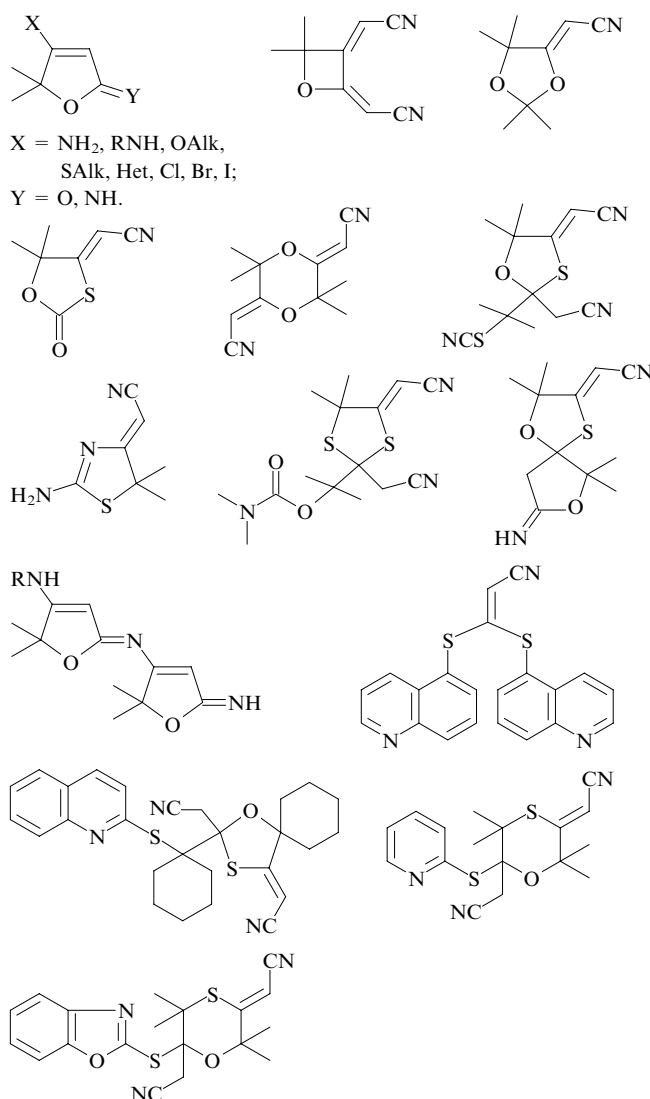
palladium and copper chlorides.^{31, 33} In contrast to the classical Reppe carbonylation, which affords the acrylic systems, in this case, the triple bond remains intact. The presence of an acceptor group near the triple bond in compounds **39** dramatically enhances the reactivity of this bond, which makes these compounds the promising reagents for the fine organic synthesis.

The reaction of oxidative methoxycarbonylation of acetylenic alcohols provided reliable synthetic grounds to the chemistry of acetylenic hydroxy acids and their derivatives.^{31, 38}



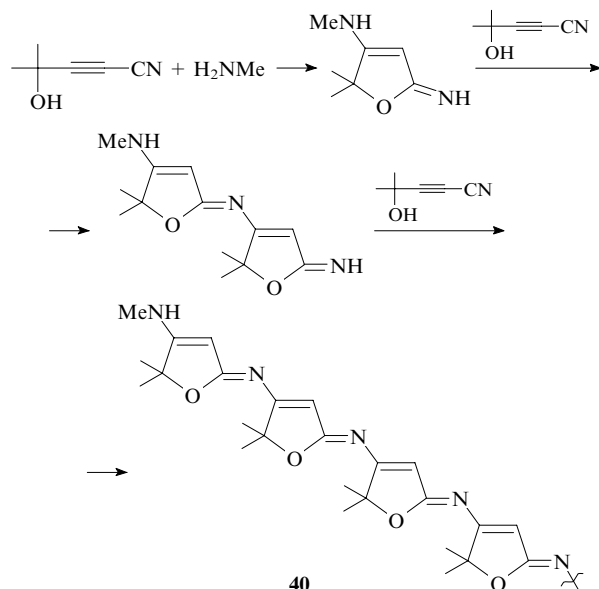
2. Addition of nucleophiles

The addition of different nucleophiles (alcohols, thiols, amines, cyanide anion) to esters and nitriles of α, β -acetylenic γ -hydroxy acids followed by the cyclisation under biomimetic conditions (room temperature, aqueous medium) opened up new approaches to the synthesis of functionalised heterocycles, which were difficult to prepare. Below, the examples of compounds synthesised by this approach are shown.^{7, 31, 38, 164–172}



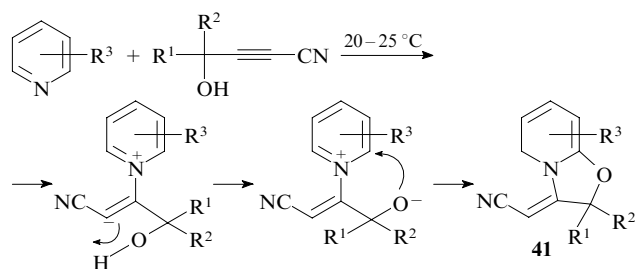
This strategy can be applied to the directed synthesis of biologically important derivatives of tetrone, ascorbic and penicillic acids and other antibiotics of this series, particularly, the promising anti-HIV drugs.³⁸

The nucleophilic addition of amines to nitriles of hydroxy acetylenic acids affords conjugated poly(iminodihydrofurans) **40** with unusual electrophysical properties.^{173–178}



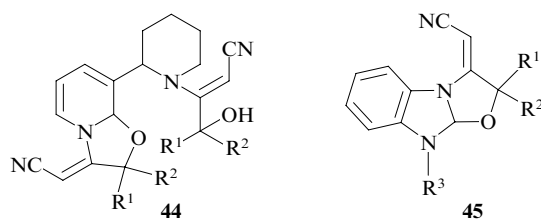
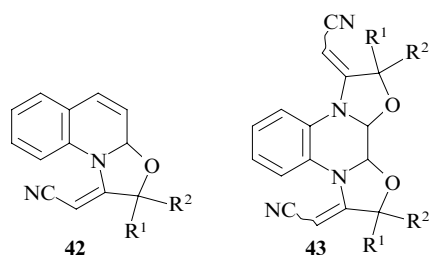
3. Synthesis of fused pyridine systems

An unexpected regiospecific cyclisation of nitriles of hydroxy acetylenic acids with pyridine and its methyl derivatives (α -, β - and γ -picolines), which occurs at room temperature in the absence of catalysts and solvents, leads to the formation of (*Z*)-cyanomethylidene-1,3-oxazolidino[3,2-*a*]-1,2-dihydropyridines **41** in high yield. The latter compounds serve as the reactive building blocks in the fine organic synthesis, the promising biologically active compounds and polydentate ligands for the design of metal-complex catalysts.¹⁷⁹



$R^1 = R^2 = \text{Me}$, $R^1 - R^2 = (\text{CH}_2)_5$; $R^3 = \text{H}$, 2-Me, 3-Me, 4-Me.

Later, this reaction was extended to the functional pyridine derivatives^{180–184} and 1-substituted benzimidazoles.¹⁸⁵ Hence, this is a general reaction. It was used for the syntheses of oxazolidinoquinolines **42**,¹⁸¹ bis(oxazolidino)quinoxalines

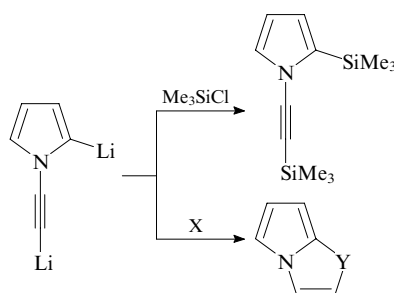


43,¹⁸¹ substituted (oxazolidinopyridinyl)piperidines **44**,¹⁸³ oxazolidinobenzimidazoles **45**.¹⁸⁵

IV. Acetylene- and allene-derived carbanions

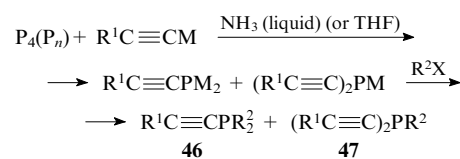
In the past decade, a considerable contribution was made to the chemistry of carbanions of the acetylene and allene series.^{186–192}

The functionalisation of the pyrroloacetylene dianion with trimethylchlorosilane and chalcogens afforded 2-trimethylsilyl-1-trimethylsilylthiopyrrole, pyrrolo[2,1-*b*]thiazole and the hitherto unknown fused heterocyclic systems, namely, pyrrolo[2,1-*b*]selenazole and pyrrolo[2,1-*b*]tellurazole.¹⁸⁶



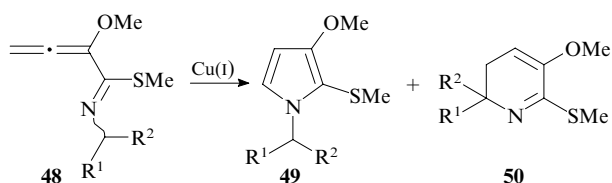
$X = \text{S}, \text{Se}, \text{Te}$; $Y = \text{S}, \text{Se}, \text{Te}$.

A direct reaction of elemental phosphorus with the acetylenide ions generated from acetylenes under the action of a strong base served as the basis of a new convenient approach to the formation of the $\text{C}_{\text{sp}}-\text{P}$ bond and the synthesis of acetylenic phosphines **46** and **47**, the promising monomers, reagents, intermediates and ligands for the production of effective metal-complex catalysts, which were difficult to synthesise.^{187, 188, 190}

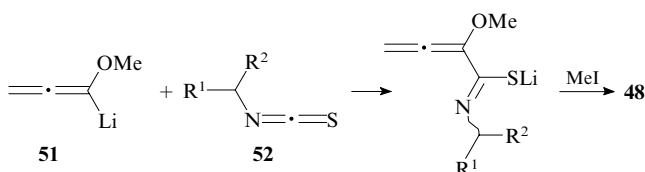


$R^1 = \text{Alk}, \text{Ph}$; $R^2 = \text{Alk}$; $M = \text{Li}, \text{Na}$; $X = \text{Br}, \text{Cl}$.

A new direction in the organic and organometallic chemistry has been developed. This concerns the low-temperature reactions of carbanions derived from alkynes and allenes with isothiocyanates.^{7, 189, 191, 192} Based on these reactions, new convenient approaches to the synthesis of fundamental heterocyclic systems, namely, derivatives of pyrrole, pyridine, quinoline and thiophene, were developed.^{189, 191–204} Thus the copper salt-catalysed cyclisation of azatrienes **48** produced 1-alkyl-3-methoxy-2-methylthiopyrroles **49** and their isomers, 2,3-dihydropyridines **50** in the total yield of 80%.



Azatrienes **48** are easily formed from 1-lithio-1-methoxyallene (**51**) and alkyl thiocyanates **52**.^{189, 191–193, 203}



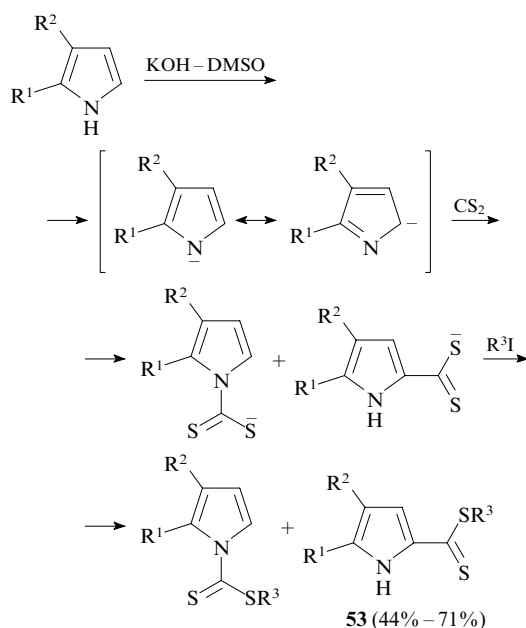
$R^1, R^2 = \text{Alk.}$

V. New reactions involving pyrrole

The systematic elaboration of acetylene reactions with ketoximes (the Trofimov reaction) made accessible a virtually unlimited series of substituted pyrroles, which served as a new impetus for further development of the chemistry of pyrrole compounds.^{7, 30, 32–34, 37, 39–46, 129, 205–208} Although the discussion of pyrroles is beyond the frames of this review, we, nonetheless, decided to discuss several new reactions involving these compounds.

1. Ambident pyrrole anions in the synthesis of alkyl pyrrole-2-dithiocarboxylates

A method was developed for the synthesis of alkyl pyrrole-2-dithiocarboxylates **53** by the pyrrole reaction with carbon disulfide and alkyl halides at room temperature in the superbasic system KOH–DMSO.^{209–211}



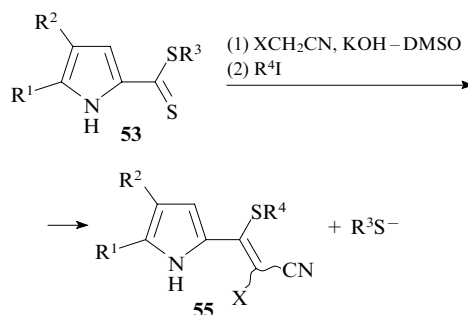
$R^1 = \text{Me, Ph; } R^2 = \text{H, Me; } R^1 - R^2 = (\text{CH}_2)_4;$
 $R^3 = \text{Et, Bu, CH}_2=\text{CHCH}_2.$

In the presence of substituents in both α -positions of the pyrrole ring, pyrrole-3-carbodithioates **54a–g** are exclusively formed in yields of 36%–61%.²¹²

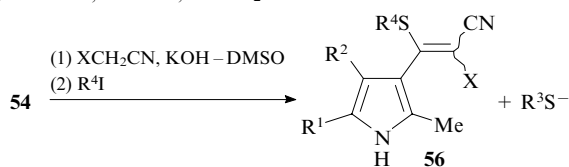
Compound	R^1	R^2	R^3
54a	Me	H	Et
54b	Me	Me	Et
54c		$(\text{CH}_2)_4$	Et
54d		$(\text{CH}_2)_4$	Bu
54e	Ph	H	Et
54f	2-furyl	H	Et
54g	2-thienyl	H	Et

2. Synthesis of functional 2- and 3-vinylpyrroles

A simple, general and reliable approach to the synthesis of 2-(**55**) and 3-(1-alkylthio-2-cyanovinyl)pyrroles (**56**) has been found, which is based on the reaction of pyrrole-2- (**53**) and pyrrole-3-carbodithioates (**54**) with nitriles containing an active methylene function (with malononitrile and cyanoacetamide) followed by alkylation of the intermediate thiolate.^{39, 40, 213–216}



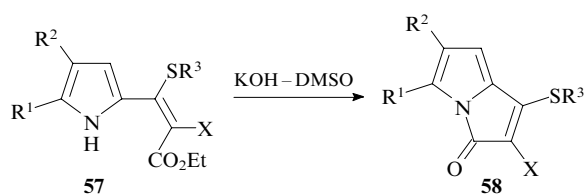
$R^1 = \text{Me, Ph; } R^2 = \text{H, Me; } R^1 - R^2 = (\text{CH}_2)_4;$
 $R^3, R^4 = \text{Alk; } X = \text{CN, CONH}_2.$



$R^1 = \text{Me, Ph, 2-furyl, 2-thienyl; } R^2 = \text{H, Me; } R^1 - R^2 = (\text{CH}_2)_4;$
 $R^3, R^4 = \text{Alk; } X = \text{CN, CONH}_2.$

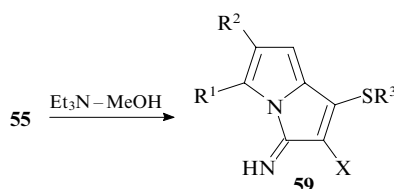
3. Cyclisation of functionally substituted 2-vinylpyrroles to 3H-pyrrolizin-3-ones and 3H-iminopyrrolizines

On heating (55–100 °C) in the system KOH–DMSO, the functionally substituted 2-vinylpyrroles **57** undergo intramolecular cyclisation to form earlier unknown 3H-pyrrolizin-3-ones **58**.^{217, 218}



$R^1 = \text{Ph, } R^2 = \text{H; } R^1 - R^2 = (\text{CH}_2)_4; R^3 = \text{Alk; } X = \text{CN, COMe, CO}_2\text{Et.}$

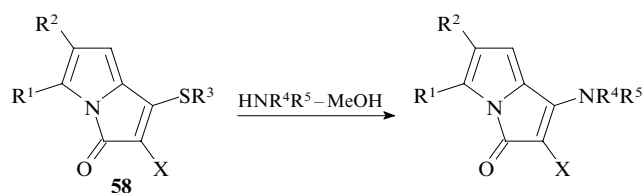
By the example of 2-[(alkylthio)cyanovinyl]pyrroles **55**, it was shown that cyclisation in the system $\text{Et}_3\text{N} - \text{MeOH}$ leads to 3H-iminopyrrolizines **59**.^{218, 219}



$R^1 = \text{Ph, } R^2 = \text{H; } R^1 - R^2 = (\text{CH}_2)_4; R^3 = \text{Alk; } X = \text{CN, CONH}_2.$

4. Nucleophilic substitution of an amino group for the alkylthio group in 3H-pyrrolizin-3-ones

Under mild conditions (20–25 °C, 15 min), 3H-pyrrolizin-3-ones **58** react quickly and quantitatively with secondary amines to form aminopyrrolizin-3-ones.²¹⁸

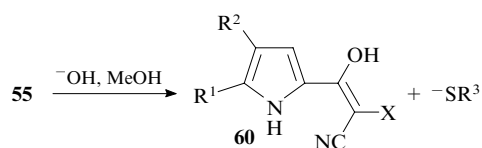


$R^1 = \text{Ph}$, $R^2 = \text{H}$; $R^1 - R^2 = (\text{CH}_2)_4$; $R^3 - R^5 = \text{Alk}$;
 $X = \text{CN}$, CONH_2 , CO_2Et .

A similar exchange was observed for 3-imino-4,5,6,7-tetrahydrocyclohexa[*c*]-3*H*-pyrrolizines.^{219–222}

5. Enols of the pyrrole series

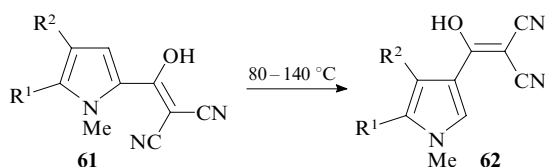
On treatment with NaOH, the alkylthio group in 2-[(alkylthio)cyanovinyl]pyrroles **55** is easily (40–45 °C, 1 h) displaced by a hydroxide ion to form stable enols, namely, 2-(1-hydroxy-2-cyanovinyl)pyrroles **60** in the yield of up to 90%.²²³



$R^1 = \text{Me}$, Ph ; $R^2 = \text{H}$, Me ; $R^1 - R^2 = (\text{CH}_2)_4$; $R^3 = \text{Alk}$;
 $X = \text{CN}$, CONH_2 .

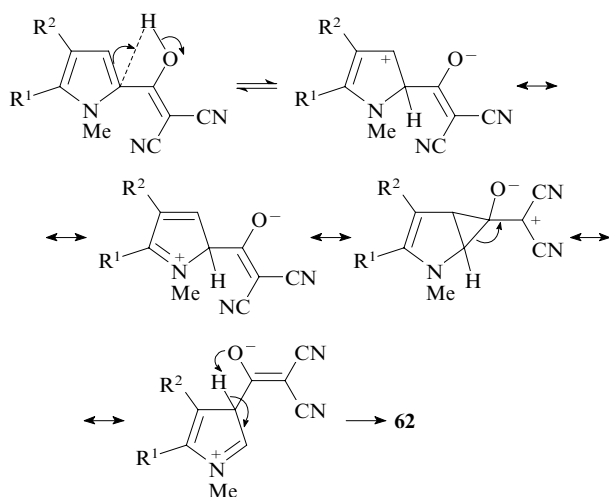
This reaction opened up a new way to the new class of stable enols with pyrrole substituents, which are the promising subjects for studying the fundamental problems of reactivity, the theory of chemical bonds, the electron transfer in conjugated systems, the hydrogen bond and tautomerism. The synthesised enols are also highly reactive building blocks for targeted synthesis of new medicinal drugs and materials.

On heating, enols **61** are rearranged into 3-isomers **62**. This is the first example of the migration of a functional substituent from the α - to β -position in the pyrrole ring.²²⁴



$R^1 = R^2 = \text{H}$; $R^1 - R^2 = (\text{CH}_2)_4$.

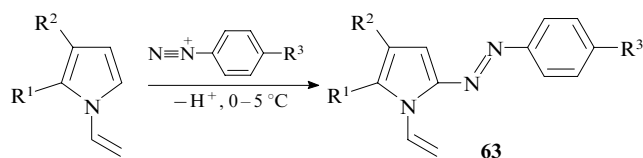
Obviously, the easy migration of the enol fragment is due to the enhanced acidity of the hydroxyl function (the effect of two strong electron-withdrawing CN groups in the conjugated



system) and the sensitivity of the pyrrole ring with respect to protonation.²²⁴

6. 2-Arylazo-1-vinylpyrroles

To extend the synthetic potential of 1-vinylpyrroles and assess the relative reactivity of the vinyl group and the pyrrole ring with respect to different cations, the reaction of 1-vinylpyrroles with aryldiazonium salts was studied. The use of this reaction made possible a highly efficient synthesis of 2-arylazo-1-vinylpyrroles **63**,^{225,226} which are promising compounds for the development of electrochromic devices, optical switches and materials for non-linear optics.

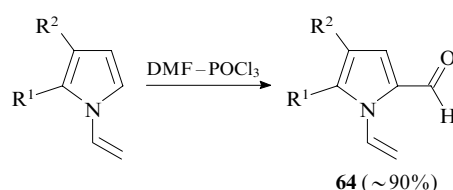


$R^1 = \text{H}$; $R^2 = \text{H}$, Me , Ph , 4- MeOC_6H_4 , 2-furyl, 2-thienyl;
 $R^1 - R^2 = (\text{CH}_2)_4$; $R^3 = \text{H}$, Br , Me , OEt , NO_2 , 4- $\text{N}_2\text{C}_6\text{H}_4$.

Based on 2-arylazo-1-vinylpyrroles, coloured polymers were synthesised as well as palladium complexes, which are promising catalysts of cross-coupling reactions.²²⁵

7. 1-Vinylpyrrole-2-carbaldehydes

The efficient formylation of *N*-vinylpyrroles was carried out under mild conditions (0–20 °C) according to the modified Vilsmeier–Haack reaction to produce a new, previously unknown class of functional pyrroles, namely, 1-vinylpyrrole-2-carbaldehydes **64**.²²⁷



$R^2 = \text{H}$; $R^1 = \text{Me}$, Ph ; $R^1 - R^2 = (\text{CH}_2)_4$.

The simultaneous presence of two reactive groups (vinyl and aldehyde) in vinylpyrrolecarbaldehydes **64** makes them promising reagents for the fine organic synthesis.²²⁸

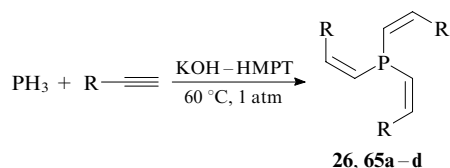
VI. The use of acetylenes in the synthesis of phosphines and phosphine chalcogenides

A new approach to the formation of the C–P bond, which was discovered by the example of the reaction of phenylacetylene with elemental phosphorus, has been systematically developed.^{35, 116–119, 229} This approach is based on the use of phosphorus-centred anions generated from elemental phosphorus in heterogeneous superbasic media such as KOH–DMSO or KOH–H₂O–organic solvent–phase-transfer catalyst. These studies allowed the commercially manufactured electrophiles to be directly phosphorylated with elemental phosphorus (or with a phosphine generated from phosphorus) and also the highly efficient syntheses of phosphines and phosphine chalcogenides.^{230–240} The thus obtained primary and secondary phosphines and phosphine chalcogenides are the promising PH-addends for the addition to multiple bonds.

1. Nucleophilic addition of primary and secondary phosphines to acetylenes

Superbases proved to be good catalysts for the vinylation of phosphines under the action of aryl- and hetarylacetylenes.

At 60 °C and atmospheric pressure, the reaction is stereo-selective to afford *Z,Z,Z*-isomers of tristyrylphosphine (**26**) and its analogues **65a–d** in the yields of up to 80%.^{36, 117, 119, 240–243}



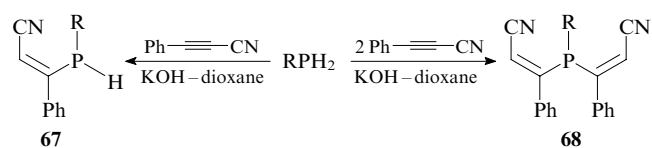
R = Ph (**26**), 4-FC₆H₄ (**65a**), 2-Py (**65b**), 2-furyl (**65c**), 2-thienyl (**65d**).

Primary alkyl- and arylphosphines add to phenylacetylene in the system KOH–DMSO (60 °C, 1–4 h) to form *Z,Z*-isomers of distyrylphosphines **66**.²⁴⁴



R = n-C₆H₁₃, Ph(CH₂)₂, PhCH(Me)CH₂.

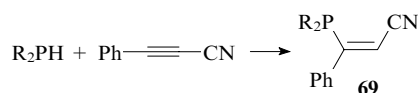
An activated alkyne [cyano(phenyl)acetylene] reacts with alkylphosphines under mild conditions (KOH–dioxane, 20–22 °C) to form either secondary (compound **67**) or tertiary (compounds **68**) phosphines in the *Z*-configuration (yield 70%–91%) depending on the reactant ratio.²⁴⁵



R = Alk.

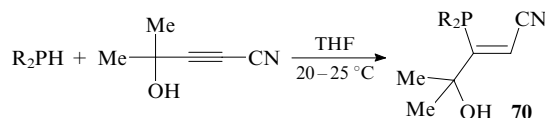
It was experimentally proved (based on the EPR and UV spectroscopic data) that the reaction proceeds through a single-electron transfer.²⁴⁵

Secondary phosphines readily react with cyano(phenyl)acetylene in the absence of catalysts to form monoadducts **69** preferentially in the *Z*-configuration.²⁴⁶ According to the results of EPR and UV spectroscopic studies, this reaction also involves the single-electron transfer stage.²⁴⁶



R = Ph(CH₂)₂, PhCH(Me)CH₂.

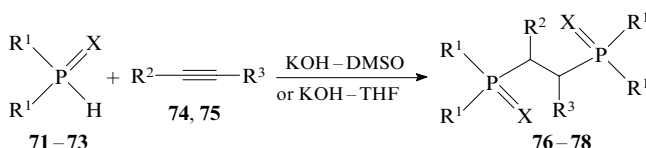
Based on the reaction of secondary phosphines with 4-hydroxy-4-methylpent-2-ynonitrile, a convenient, efficient and stereo-controlled method for the synthesis of functionally substituted tertiary phosphines **70** containing hydroxyl and nitrile groups has been developed.^{245, 247}



R = Bu, Ph(CH₂)₂, 2-Py(CH₂)₂.

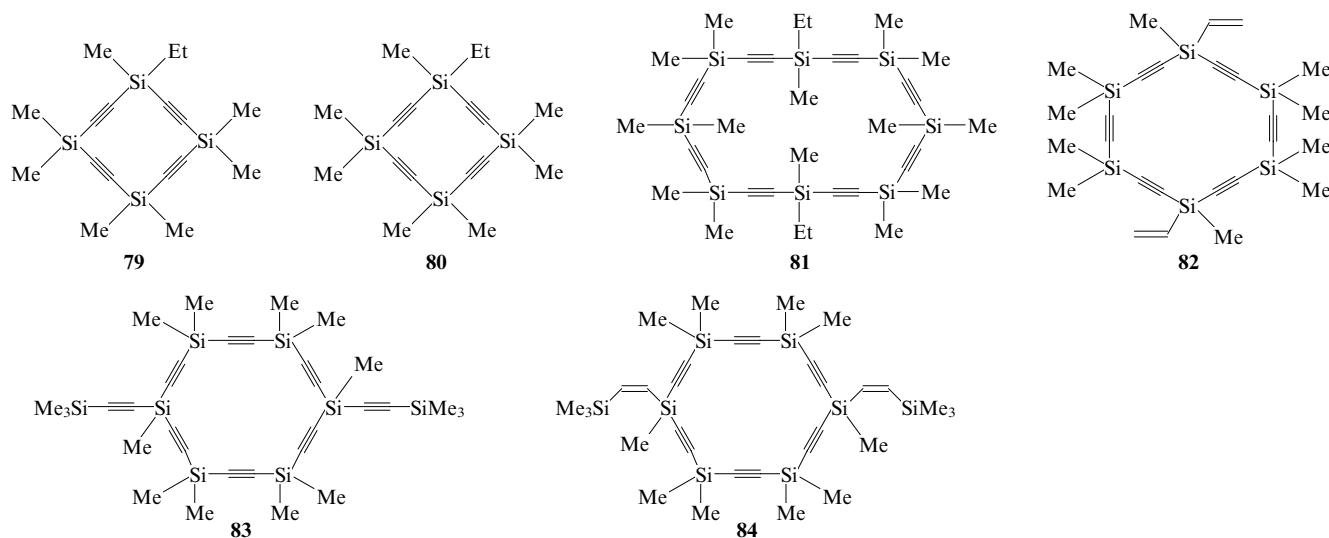
2. Nucleophilic addition of primary and secondary phosphine chalcogenides to acetylenes

Secondary phosphine oxides **71** [X = O, R¹ = Ph(CH₂)₂], **72** (X = O, R¹ = Ph) and phosphine sulfides **73** [X = S, R¹ = Ph(CH₂)₂] react virtually quantitatively with methylacetylene (**74**) (R² = H, R³ = Me)²⁴⁸ and cyano(phenyl)acetylene (**75**) (R² = Ph, R³ = CN)²⁴⁹ in the presence of superbases KOH–DMSO (Ref. 248) or KOH–THF (Ref. 249) to form phosphine oxides **76**, **77** and phosphine sulfide **78** containing chiral carbon centres.



Compound	X	R ¹	R ²	R ³
76	O	Ph(CH ₂) ₂	H	Me
77	O	Ph	Ph	CN
78	S	Ph(CH ₂) ₂	Ph	CN

Compounds **76–78** are the promising intermediates for the synthesis of optically active phosphine ligands, which are widely used in the catalytic stereospecific synthesis.



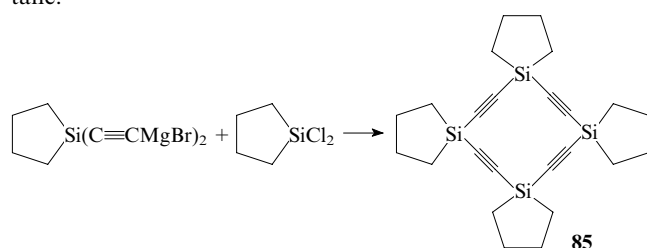
VII. Acetylene derivatives of silicon and germanium

M G Voronkov and co-workers have developed the synthetic approaches to macrocyclic silaalkynes^{250–273} and silicon-and-chalcogen-containing heterocyclic compounds.^{274–277}

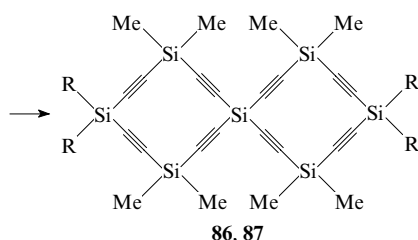
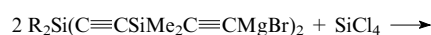
1. Synthesis of acetylene- and silicon-containing macrocycles

Based on the condensation reaction of the bromomagnesio derivatives of dimethyldiethynyl- and methyl(vinyl)diethynylsilane, bis(dimethylethynylsilyl)ethyne, dimethylbis(dimethylethynylsilyl)ethynylsilane, *etc.* with dialkyl-, ethyl(methyl)-, methyl(trimethylsilyl)ethynyl- and methyl(2-trimethylsilylvinyl)dichlorosilanes, a general method of synthesis of methyl-organylcyclosilaalkynes **79–84** ($\text{MeRSiC}\equiv\text{C}$)_{*n*} (*n* = 4–8) containing exocyclic substituents (*R* = H, Me, Et, $\text{CH}_2=\text{CH}$, $\text{Me}_3\text{SiC}\equiv\text{C}$, $\text{Me}_3\text{SiCH}=\text{CH}$) was developed.^{257–259, 261, 263}

12-Membered cyclosilaethyne **85** of the propellane type was synthesised by the reaction of 1,1-bis(bromomagnesioethynyl)silacyclopentane with 1,1-dichlorosilacyclopentane.²⁶⁵

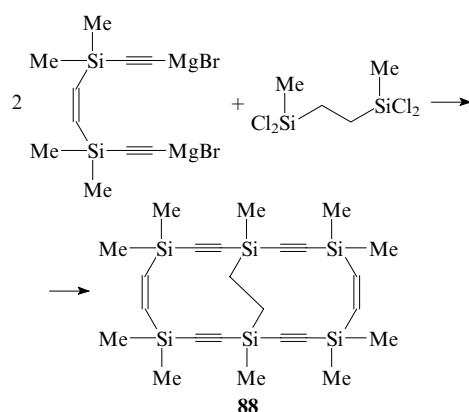


Spiromacrocylic polysilaalkynes **86** and **87** were synthesised by the condensation of bromomagnesio derivatives of dialkylbis(dimethylethynylsilyl)ethynylsilane with silicon tetrachloride.²⁶⁴



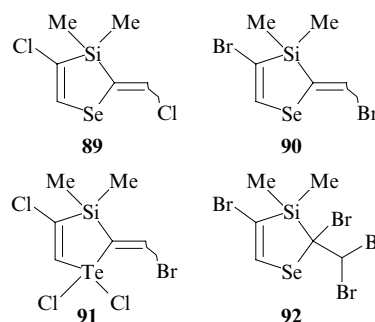
R = Me (**86**), Et (**87**).

The (*E*)-1,2-bis(bromomagnesioethynyldimethylsilyl)ethene reaction with 1,2-bis(methyldichlorosilyl)ethane produced an unusual macrobiocyclic compound **88**, which contained both unsaturated and saturated endocyclic groups ($\text{SiC}\equiv\text{CSi}$, $\text{SiCH}=\text{CHSi}$, $\text{SiCH}_2\text{CH}_2\text{Si}$).²⁷⁰



2. New five-membered silicon-and-chalcogen-containing heterocycles

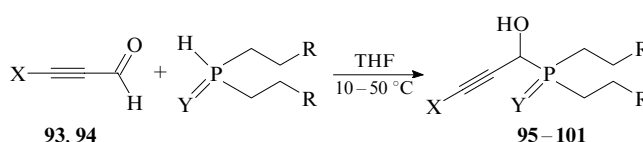
New unsaturated heterocycles of the fulvene (compounds **89–91**) or cyclopentene (compound **92**) types, which contain silicon, selenium and tellurium atoms, were synthesised from dimethyldiethynylsilane and selenium and tellurium tetrahalides under mild conditions (20–25 °C, CHCl_3) in good or moderate yields.^{274–277}



3. Silicon- and germanium-containing acetylene aldehydes

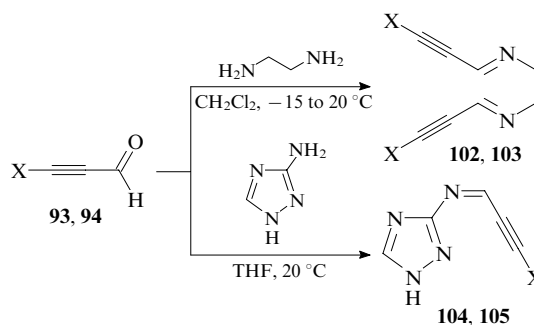
The reactivity of 3-(trimethylsilyl)- (**93**, *X* = Me_3Si) and 3-(triethylgermyl)prop-2-ynals (**94**, *X* = Et_3Ge), which are easily prepared by the oxidation of the corresponding 3-trimethylsilyl- and 3-(triethylgermyl)prop-2-ynols^{278–285} with the activated system MnO_2 – SiO_2 ²⁸⁶ or pyridinium chlorochromate²⁸⁷ under microwave radiation in the absence of a solvent, was studied. Being ambident 1,3-biselectrophiles, propynals **93** and **94** react with nucleophiles chemoselectively involving the triple bond, the carbonyl group or both reaction centres.^{288–298}

By the example of secondary phosphine chalcogenides, it was shown that the chemoselective addition of P-centred nucleophiles to the carbonyl groups in propynals **93** and **94** can efficiently proceed under mild conditions (10–50 °C, THF, without catalyst) to afford earlier unknown multifunctional chiral tertiary phosphine chalcogenides **95–101** containing ethynyl and hydroxyl functions.^{290, 296}



Compound	X	Y	R	Compound	X	Y	R
95	SiMe_3	O	Ph	99	GeEt_3	O	Ph
96	SiMe_3	O	2-Py	100	GeEt_3	S	Ph
97	SiMe_3	S	Ph	101	GeEt_3	Se	Ph
98	SiMe_3	Se	Ph				

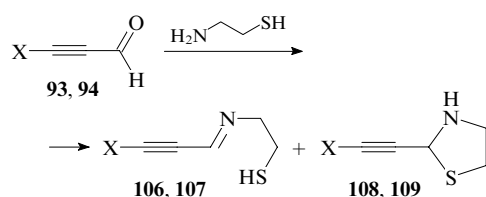
The reactions of propynals **93** and **94** with ethylenediamine and 1*H*-1,2,4-triazol-3-ylamine to afford the corresponding



X = Me_3Si (**93**, **102**, **104**), Et_3Ge (**94**, **103**, **105**).

bis(azomethines) **102**, **103** and triazolylaldimines **104**, **105** also involve the carbonyl group.²⁹⁷

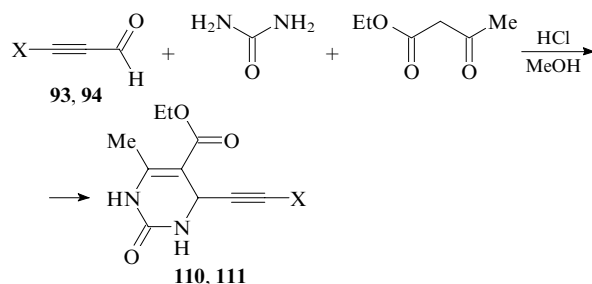
Azomethines **106**, **107** and their cyclisation products, namely, 1,3-thiazolidines **108**, **109**, were prepared from propynals **93**, **94** and 2-aminoethanethiol.²⁹⁷



X = Me₃Si (**93**, **106**, **108**), Et₃Ge (**94**, **107**, **109**).

Under microwave radiation (420 W, 12 min), the reaction can be directed to the exclusive formation of heterocycles **108**, **109**.²⁹⁷

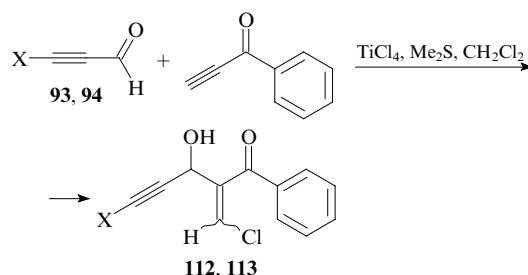
By the example of the same propynals, the possibility of using acetylenic aldehydes in the Biginelli reaction was demonstrated. Thus, on refluxing with urea and ethyl acetoacetate in methanol in the presence of HCl (5 mol %), polyfunctional tetrahydropyrimidines **110** and **111** were obtained in high yields.²⁹⁸



X = Me₃Si (**93**, **110**), Et₃Ge (**94**, **111**).

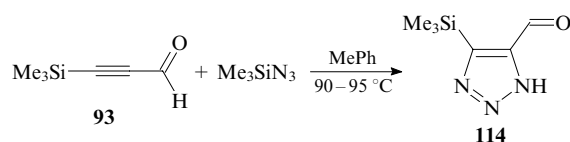
The use of LiClO₄ (20 mol %) instead of HCl led to the selective formation of the Knoevenagel adducts, *i.e.*, ethyl 2-acetyl-5-(trimethylsilyl)- and ethyl 2-acetyl-5-(triethylgermyl)pent-2-en-4-ynoates.²⁹⁸

Under the conditions of the Baylis–Hillman reaction (TiCl₄, Me₂S), propynals **93** and **94** react with 1-phenylprop-2-yn-1-one to form 3-hydroxy-1-phenyl-2-[(*Z,E*)-chloromethylidene]-5-X-pent-4-yn-1-ones **112**, **113**.²⁸⁹

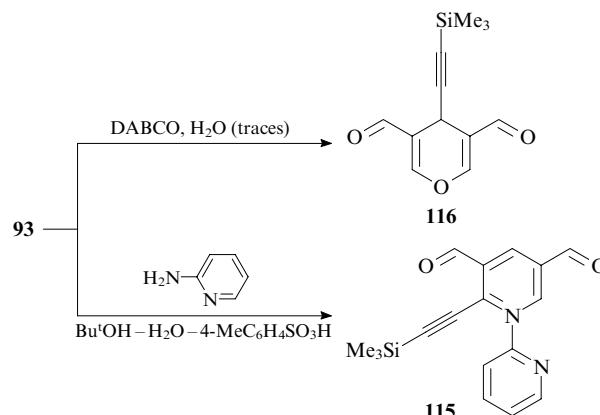


X = Me₃Si (**93**, **112**), Et₃Ge (**94**, **113**).

Regiospecific 1,3-dipolar cycloaddition of trimethylsilyl azide involves the triple bond of propynal **93** and produces 4-trimethylsilyl-1*H*-1,2,3-triazole-5-carbaldehyde (**114**).²⁹²

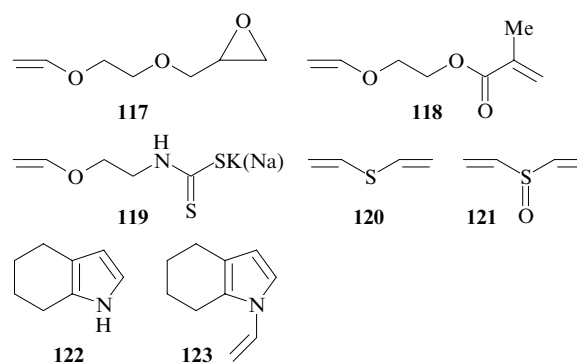


By the example of propynal **93**, unusual cascade assembling of new multifunctional heterocyclic compounds were developed. Thus under microwave radiation, the propynal **93** reacts with 2-aminopyridine in the system Bu^tOH–H₂O–4-MeC₆H₄SO₃H (5 mol %) to produce *N*-(2-pyridinyl)-2-(trimethoxyylethynyl)-1,2-dihydropyridine-3,5-dicarbaldehyde (**115**) in the yield of 75%.²⁹³ In the presence of a basic catalyst [5 mol % of diazabicyclooctane (DABCO)] and trace amounts of water, propynal **93** is quantitatively trimerised to 4-trimethylsilylethynyl-4*H*-pyran-3,5-dicarbaldehyde (**116**).²⁹⁵



VIII. New acetylene-based technologies

New modifications of classical acetylene reactions made it possible to develop simple and commercially feasible methods of the synthesis of unique monomers and intermediates that were implemented in laboratory and in pilot plants.³³ As a result, commercially feasible technologies were developed for the synthesis of pentaerythritol tetravinyl ether (**9**),^{33, 299–301} ethylene glycol glycidyl vinyl ether (**117**) ('Vinylux'),^{53, 302, 303} 2-vinylxyethyl methacrylate (**118**),^{33, 304, 305} potassium (sodium) *N*-[2-(vinylxy)ethyl]dithiocarbamate (biocide 'Vinditat') (**119**),^{33, 306} divinyl sulfide (**120**),^{29, 111, 307} divinyl sulfide (**121**),^{308, 309} tetrahydroindole (**122**) and *N*-vinyltetrahydroindole (**123**).^{30, 32, 310, 311}



New effective methods were developed for the preparation of certain other valuable monomers and intermediates, namely, methyl vinyl and ethyl vinyl ethers,^{312–314} propargyl alcohol,^{99, 315} *N*-vinylcarbazole,^{33, 316, 317} 3-methylbut-1-yn-3-ol,^{318, 319} 1-ethynylcyclohexanol,³¹⁹ dehydrolinalool^{33, 320} and other acetylenic alcohols and their derivatives.⁴³

Based on the developed technologies, ethylene glycol monovinyl ether (2-vinylxyethanol),^{28, 33} 2-methyl-1,3-dioxolane divinyl ether,^{28, 33, 43} diethylene glycol^{28, 33, 160} and ethanolamine vinyl ether (2-vinylxyethylamine)^{314, 321} were produced on a pilot scale ('Karbid', Temirtau).

IX. Conclusion

In this review, the progress in the studies on several classical acetylene reactions in the past 10–15 is surveyed, although it is evident that certain new modifications of these reactions rely on the achievements of earlier decades. From this review, it is evident that the interest in many directions developed by the Favorsky school is quickened. First of all, this concerns the field of base-catalysed reactions of vinylation, ethynylation and prototropic migration of a triple bond through the allene and diene structures. The systematic use of superbasic catalysts and the development of a concept of superbasicity made it possible to develop new, in principle, versions of the classical Favorsky reactions and convert them into more efficient and practically feasible synthetic methods. New processes that employ acetylene at the atmospheric or reduced pressure were carried out on the experimental and commercial scales (the vinylation of alcohols, glycols, glycerol, pentaerythritol, carbazole and ethanolamines; the preparation of divinyl sulfide; the synthesis of acetaldehyde *via* vinyl ethers).⁴³

Together with the development of classical reactions, new base-catalysed reactions of acetylene, which are genetically linked to their classical prototypes, were discovered. These are the vinylation of sulfur, selenium, tellurium and phosphorus, the hydrative trimerisation of acetylene (vinylation of water), the synthesis of pyrroles and *N*-vinylpyrroles from ketones and acetylene *via* ketoximes, *etc.*⁴³ These reactions substantially extend the synthetic potential of acetylene.

Methods for the synthesis of macrocyclic silaalkynes that utilise the corresponding sodium and bromomagnesium derivatives of acetylene (the Iotsich complexes) were developed. Based on bis(ethynylsilanes), new unsaturated heterocyclic compounds that contain silicon and chalcogen atoms in their rings were prepared. Chemistry of silicon and germanium-containing acetylenic aldehydes has been developed further.

Some of these directions have a considerable effect on the development of the chemistry of acetylene all over the world, although, naturally, hardly embrace the whole vast field of chemistry of compounds with triple carbon–carbon bonds. The best studies carried out within the scope listed above are actively cited and many research groups successfully explore these directions.

The studies on the modification of classical acetylene reactions are in progress. In addition to superbases (KOBu^t) conventionally used in the synthesis of acetylenic alcohols (*e.g.*, from ferrocenylacetylene³²²), the current attention is focused on the alkynol synthesis (the addition of acetylenes to the C=O bond) in the presence of either metal complexes particularly those with chiral ligands (the asymmetric version of the Favorsky reaction),^{323–326} or zinc salts and organozinc compounds,³²⁷ triphenylphosphine,³²⁸ organic catalysts.³²⁹ The recently published review³³⁰ is devoted to alkynylation of chiral aldehydes (including those with alkoxy, amino and thio groups) under the action of metal acetylides.

The addition of amines to a triple bond successfully employs the catalysis with metal complexes.^{331–336} Recently, the addition of hydroselenides and diselenides to acetylenes in the presence of InBr₃ was accomplished.³³⁷

Superbases (KOH–DMSO,³³⁸ KOBu^t–THF,³³⁹ KOH–THF³⁴⁰) are successfully used in the synthesis of amides of the allene series and the corresponding propargyl compounds. The base-catalysed acetylene–allene isomerisation (acetylene ‘zipper’), which employs lithium 2-aminoethylamide, is the easy way for the synthesis of 1,3-alkadiynes and their internal isomers.³⁴¹

It should be stressed that the metal-complex catalysis now becomes the main trend in the modification of classical acetylene reactions and opens up new horizons in the tradi-

tional chemistry of acetylene;³⁴² however, its discussion is beyond the scope of this review.

The popularity of chemistry of acetylene increases, which is associated with the progressive extension of the use of acetylenic compounds in the organic synthesis, particularly, in the synthesis of medicinal drugs (*e.g.*, enediyne antibiotics),³⁴³ optoelectronic materials,^{344–346} molecular machines and other nanostructured objects,^{27, 347} including porphyrins with acetylene bonds.

The authors hope that this review will help a wide circle of chemists and technologists in solving the topical problems of the organic synthesis and modern technologies based on the use of acetylene and its derivatives.

References

1. *Acetylene Chemistry: Chemistry, Biology, and Material Science*. (Eds F Diederich, P J Stang, R R Tykwinski) (Wiley-VCH: Weinheim, 2005)
2. R J Tedeschi *Acetylene-Based Chemicals from Coal and Other Natural Resources* (New York: Marcel Dekker, 1982)
3. L S Polak, R A Kalinenko *Neftekhimiya* **25** 271 (1985)^a
4. H-G Beiers, H Baumann, D Bittner, J Klein, H Juntgen *Fuel* **67** 1012 (1988)
5. A M Tikhvatullin, Yu V Izinger *Tekhniko-ekonomicheskije Otsenki Plazmokhimicheskikh Protseessov Pererabotki Uglei i Uglevodorodov* (Feasibility Assessment of Plasma- Chemical Processing of Coals and Hydrocarbons) (Irkutsk: Siberian Energetic Institute, Siberian Branch of the Russian Academy of Sciences, 1989) p. 56
6. V Neverov, A Igolkin *Ekonom. Zhizn'* **41** 1 (1992)
7. B A Trofimov *Curr. Org. Chem.* **6** 1121 (2002)
8. D A Plattner, Y Li, K N Houk *Modern Acetylene Chemistry* (Eds P J Stang, F Diederich) (Weinheim: Wiley-VCH, 1995)
9. R Chauvin, C Lepetit *Acetylene Chemistry: Chemistry, Biology, and Material Science* (Eds F Diederich, P J Stang, R R Tykwinski) (Weinheim: Wiley-VCH, 2005) p. 1
10. O Kitagawa, T Inoue, T Taguchi *Rev. Heteroat. Chem.* **15** 243 (1996)
11. R C Larock *Acetylene Chemistry: Chemistry, Biology, and Material Science* (Eds F Diederich, P J Stang, R R Tykwinski) (Weinheim: Wiley-VCH, 2005) p. 51
12. P Aschwanden, E M Carreira *Acetylene Chemistry: Chemistry, Biology, and Material Science* (Eds F Diederich, P J Stang, R R Tykwinski) (Weinheim: Wiley-VCH, 2005) p. 101
13. N J Long, C K Williams *Angew. Chem., Int. Ed.* **42** 2586 (2003)
14. U Rosenthal *Acetylene Chemistry: Chemistry, Biology, and Material Science* (Eds F Diederich, P J Stang, R R Tykwinski) (Weinheim: Wiley-VCH, 2005) p. 139
15. B Bernet, A Vasella *Acetylene Chemistry: Chemistry, Biology, and Material Science* (Eds F Diederich, P J Stang, R R Tykwinski) (Weinheim: Wiley-VCH, 2005) p. 173
16. R Giesa *J. Macromol. Sci., Rev. Macromol. Chem. Phys.* **C36** 631 (1996)
17. U N F Bunz *Chem. Rev.* **100** 1605 (2000)
18. T M Swager *Acetylene Chemistry: Chemistry, Biology, and Material Science* (Eds F Diederich, P J Stang, R R Tykwinski) (Weinheim: Wiley-VCH, 2005) p. 233
19. D J Armit, G T Crisp *J. Org. Chem.* **71** 3417 (2006)
20. Y Tobe, R Umeda, N Iwasa, M Sonoda *Chem.–Eur. J.* **9** 5549 (2003)
21. S Eisler, R Tykwinski *Acetylene Chemistry: Chemistry, Biology, and Material Science* (Eds F Diederich, P J Stang, R R Tykwinski) (Weinheim: Wiley-VCH, 2005) p. 259
22. R B Heimann, S E Evsyukov, L Kavan *Carbyne and Carbonyl Structures* (Dordrecht: Kluwer Academic, 1999)
23. Y Tobe, T Wakabayashi *Acetylene Chemistry: Chemistry, Biology, and Material Science* (Eds F Diederich, P J Stang, R R Tykwinski) (Weinheim: Wiley-VCH, 2005) p. 387
24. C Wang, A S Batsanov, M R Bryce, I Sage *Org. Lett.* **6** 2181 (2004)

25. *Metal-Catalyzed Cross-Coupling Reactions* (Eds F Diederich, P J Stang) (Weinheim: Wiley-VCH, 1998)
26. E-i Negishi, L Anastasia *Chem. Rev.* **103** 1979 (2003)
27. C S Jones, M J O'Connor, M M Haley *Acetylene Chemistry: Chemistry, Biology, and Material Science* (Eds F Diederich, P J Stang, R R Tykwinski) (Weinheim: Wiley-VCH, 2005) p. 303
28. B A Trofimov *Geteroatomnye Proizvodnye Atsetilena. Novye Polifunktsional'nye Monomery, Reagenty i Poluprodukty* (Heteroatomic Derivatives of Acetylene. New Polyfunctional Monomers, Reagents and Intermediates) (Moscow: Nauka, 1981)
29. B A Trofimov, S V Amosova *Divinilsul'fid i ego Proizvodnye* (Divinyl Sulfide and Its Derivatives) (Novosibirsk: Nauka, 1983)
30. B A Trofimov, A I Mikhaleva *N-Vinilpirroly (N-Vinylpyrroles)* (Novosibirsk: Nauka, 1984)
31. B A Trofimov, A G Mal'kina, Yu M Skvortsov *Zh. Org. Khim.* **29** 1268 (1993)^b
32. B A Trofimov, A I Mikhaleva *Heterocycles* **37** 1193 (1994)
33. B A Trofimov *Zh. Org. Khim.* **31** 1368 (1995)^b
34. B A Trofimov, A I Mikhaleva *Zh. Org. Khim.* **32** 1127 (1996)^b
35. B Trofimov, N Gusarova, L Brandsma *Main Group Chem. News* **4** 18 (1996)
36. B A Trofimov, S N Arbuzova, N K Gusarova *Usp. Khim.* **68** 240 (1999) [*Russ. Chem. Rev.* **68** 215 (1999)]
37. S E Korostova, A I Mikhaleva, B A Trofimov *Usp. Khim.* **68** 506 (1999) [*Russ. Chem. Rev.* **68** 459 (1999)]
38. B A Trofimov, A G Mal'kina *Heterocycles* **51** 2485 (1999)
39. L N Sobenina, A P Demenev, A I Mikhaleva, B A Trofimov *Usp. Khim.* **71** 641 (2002) [*Russ. Chem. Rev.* **71** 563 (2002)]
40. B A Trofimov, L N Sobenina, A P Demenev, A I Mikhaleva *Chem. Rev.* **104** 2481 (2004)
41. B A Trofimov *Sov. Probl. Org. Khim.* **14** 131 (2004)
42. A I Mikhaleva, A B Zaitsev, B A Trofimov *Usp. Khim.* **75** 884 (2006) [*Russ. Chem. Rev.* **75** 797 (2006)]
43. A I Mikhaleva, N K Gusarova *Atsetilen: Reaktsii i Proizvodnye (Bibliografiya Nauchnykh Trudov B A Trofimova)* [Acetylene: Reactions and Derivatives (Bibliography of Scientific Works of B A Trofimov)] (Irkutsk: Izd-vo Ottisk, 2006)
44. B A Trofimov, S V Amosova, A I Mikhaleva, N K Gusarova, E P Vyalykh *Fundamental'nye Issledovaniya. Khimicheskie Nauki* (Fundamental Research. Chemical Sciences) (Novosibirsk: Nauka, 1977) p. 174
45. B A Trofimov *Usp. Khim.* **50** 248 (1981) [*Russ. Chem. Rev.* **50** 138 (1981)]
46. B A Trofimov *Zh. Org. Khim.* **22** 1991 (1986)^b
47. B A Trofimov, A S Atavin, V I Lavrov, M F Shostakovskii *Zh. Obshch. Khim.* **37** 743 (1967)^c
48. USSR P. 210129; *Byull. Izobret.* (6) (1968)
49. USSR P. 1444334; *Byull. Izobret.* (46) (1988)
50. R Zimmer *Synthesis* 165 (1993)
51. O Flögel, J Dash, I Brüdgam, H Hartl, H-U Reißig *Chem. – Eur. J.* **10** 4283 (2004)
52. M A Chowdhury, H-U Rensing *Synlett* 2383 (2006)
53. B A Trofimov, N A Nedolya *Rev. Heteroat. Chem.* **9** 205 (1993)
54. D A Evans, J S Johnson *J. Am. Chem. Soc.* **120** 4895 (1998)
55. S C Ennis, A J Fairbanks, C A Slinn, R J Tennant-Eyles, H S Yeates *Tetrahedron* **57** 4221 (2001)
56. L A Oparina, O V Vysotskaya, L N Parshina, N K Gusarova, B A Trofimov *Phosphorus, Sulfur Silicon Relat. Elem.* **178** 2087 (2003)
57. B A Trofimov, B G Sukhov, S F Malysheva, N A Belogorlova, A P Tantsirev, L N Parshina, L A Oparina, S P Tunik, N K Gusarova *Tetrahedron Lett.* **45** 9143 (2004)
58. N K Gusarova, N I Ivanova, M V Bogdanova, S F Malysheva, N A Belogorlova, B G Sukhov, B A Trofimov *Mendeleev Commun.* 216 (2004)
59. B A Trofimov, L V Morozova, A I Mikhaleva, M V Markova *Vysokomol. Soedin., Ser. A* **35** 119 (1993)^d
60. L V Morozova, A I Mikhaleva, M V Markova, B A Trofimov *Zh. Prikl. Khim.* **68** 341 (1995)^e
61. W G S Reyntjens, E J Goethals *Polym. Adv. Technol.* **12** 107 (2001)
62. L Ding, S E Evsyukov *J. Macromol. Sci., Part A: Pure Appl. Chem.* **38** 307 (2001)
63. B A Trofimov, L V Morozova, I V Tatarinova, M Ya Khil'ko, N I Ivanova, A I Mikhaleva, T A Skotheim *Vysokomol. Soedin., Ser. A* **44** 2048 (2002)^d
64. A I Vorob'eva, S A Onina, R R Muslukhov, S V Kolesov, L N Parshina, M Ya Khil'ko, B A Trofimov, Yu B Monakov *Vysokomol. Soedin., Ser. B* **45** 700 (2003)^d
65. A I Vorob'eva, S A Onina, I D Musina, S V Kolesov, R R Muslukhov, L N Parshina, L A Oparina, B A Trofimov, Yu B Monakov *Vysokomol. Soedin., Ser. B* **46** 364 (2004)^d
66. A I Vorob'eva, S A Onina, S V Kolesov, L N Parshina, L A Oparina, B A Trofimov, Yu B Monakov *Vysokomol. Soedin., Ser. B* **46** 1239 (2004)^d
67. B A Trofimov, L V Morozova, M V Markova, A I Mikhaleva, G F Myachina, I V Tatarinova, T A Skotheim *Vysokomol. Soedin., Ser. B* **47** 695 (2005)^d
68. L V Morozova, O A Tarasova, A I Mikhaleva, M V Markova, G F Myachina, B A Trofimov *Izv. Akad. Nauk, Ser. Khim.* 1958 (1997)^f
69. O A Tarasova, L Brandsma, B A Trofimov *Synthesis* 571 (1993)
70. O A Tarasova, B A Trofimov, A I Mikhaleva, M V Sigalov, L M Sinegovskaya *Zh. Org. Khim.* **27** 1798 (1991)^b
71. O A Tarasova, A I Mikhaleva, T L Markova, B A Trofimov *Khim. Geterotsikl. Soedin.* 125 (1992)^g
72. O A Tarasova, T L Markova, B A Trofimov *Izv. Akad. Nauk SSSR, Ser. Khim.* 2161 (1991)^f
73. O A Tarasova, E Yu Shmidt, L V Baikalova, A I Mikhaleva, B A Trofimov *Izv. Akad. Nauk, Ser. Khim.* 2005 (1997)^f
74. O A Tarasova, E Yu Shmidt, L V Klyba, L M Sinegovskaya, A I Mikhaleva, L B Krivdin, B A Trofimov *Zh. Org. Khim.* **34** 730 (1998)^b
75. M F Shostakovskii *Prostye Vinilovye Efiiry* (Vinyl Ethers) (Moscow: Academy of Sciences of the USSR, 1952)
76. O A Tarasova, B A Trofimov, A V Afonin, L M Sinegovskaya, N A Kalinina, S V Amosova *Zh. Org. Khim.* **27** 1172 (1991)^b
77. O A Tarasova, B A Trofimov, V V Keiko, S V Amosova *Zh. Org. Khim.* **27** 1180 (1991)^b
78. B A Trofimov, A I Mikhaleva, A M Vasil'tsov, E Yu Schmidt, O A Tarasova, L V Morozova, L N Sobenina, T Preiss, J Henkelmann *Synthesis* 1125 (2000)
79. L N Parshina, Doctoral Thesis in Chemical Sciences, Irkutsk Institute of Chemistry, Siberian Branch of the Russian Academy of Sciences, Irkutsk, 2005
80. A B Zaitsev, A M Vasil'tsov, E Yu Schmidt, A I Mikhaleva, L V Morozova, A V Afonin, I A Ushakov, B A Trofimov *Tetrahedron* **58** 10043 (2002)
81. B A Trofimov, S F Malysheva, N K Gusarova, A A Tatarinova, J Henkelmann *Zh. Org. Khim.* **39** 1428 (2003)^b
82. L A Oparina, S I Shaikhudinova, L N Parshina, O V Vysotskaya, Th Preiss, J Henkelmann, B A Trofimov *Zh. Org. Khim.* **41** 672 (2005)^b
83. L A Oparina, M Ya Khil'ko, N A Chernysheva, S I Shaikhudinova, L N Parshina, T Preiss, J Henkelmann, B A Trofimov *Zh. Org. Khim.* **41** 677 (2005)^b
84. B A Trofimov, S F Malysheva, M V Sigalov, E P Vyalykh, G A Kalabin *Tetrahedron Lett.* **25** 4257 (1984)
85. B A Trofimov, L A Oparina, L B Krivdin, N K Gusarova, K A Chernyshev, L M Sinegovskaya, L V Klyba, L N Parshina, A P Tantsyrev, O N Kazheva, G G Alexandrov, O A D'yachenko *J. Mol. Struct.* **791** 1 (2006)
86. B A Trofimov, L A Oparina, N K Gusarova, M Ya Khil'ko, L N Parshina, J Henkelmann *Mendeleev Commun.* 13 (2006)
87. E M Carreira, W Lee, R A Singer *J. Am. Chem. Soc.* **117** 3649 (1995)
88. L F Tietze, J Grolitzer *Synthesis* 877 (1997)
89. J M Kim, J Shin, P Shum, D H Thompson *J. Dispersion Sci. Technol.* **22** 399 (2001)
90. R T Ruck, E N Jacobsen *J. Am. Chem. Soc.* **124** 2882 (2002)
91. B A Trofimov, A M Vasil'tsov, E Yu Schmidt, A B Zaitsev, A I Mikhaleva, A V Afonin *Synthesis* 1521 (2000)
92. A B Zaitsev, A M Vasil'tsov, E Yu Shmidt, A I Mikhaleva, A V Afonin, L N Il'icheva *Zh. Org. Khim.* **39** 1479 (2003)^b
93. B A Trofimov, O A Tarasova, A I Mikhaleva, N A Kalinina, L M Sinegovskaya, J Henkelmann *Synthesis* 1585 (2000)

94. B A Trofimov, O A Tarasova, M A Shemetova, A V Afonin, L V Klyba, L V Baikalova, A I Mikhaleva *Zh. Org. Khim.* **39** 437 (2003)^b
95. N M Vitkovskaya, O Yu Dolgunicheva, F S Dubnikova, B A Trofimov *Izv. Akad. Nauk SSSR, Ser. Khim.* 1339 (1988)^f
96. N M Vitkovskaya, O Yu Dolgunicheva, F S Dubnikova, B A Trofimov *Izv. Akad. Nauk SSSR, Ser. Khim.* 1343 (1988)^f
97. N M Vitkovskaya, V B Kobychiev, N Yu Matveenko, F S Dubnikova, O Yu Dolgunicheva, B A Trofimov *Izv. Akad. Nauk SSSR, Ser. Khim.* 1793 (1990)^f
98. B A Trofimov, L N Sobenina, A I Mikhaleva, R N Nesterenko, M G Voronkov *Zh. Org. Khim.* **25** 1110 (1989)^b
99. A I Moiseev, V K Stankevich, G K Balakhchi, A I Mikhaleva, R N Nesterenko, B A Trofimov *Dokl. Akad. Nauk SSSR* **321** 524 (1991)^h
100. Russ. P. 2004542; *Byull. Izobret.* (45–46) (1993)
101. B A Trofimov, L N Sobenina, S E Korostova, A I Mikhaleva, N I Shishov, V D Fel'dman, S G Shevchenko, A N Vasil'ev *Zh. Prikl. Khim.* **60** 1366 (1987)^e
102. V K Stankevich, G R Klimenko, B F Kukharev, B A Trofimov *Zh. Prikl. Khim.* **73** 163 (2000)^e
103. B A Trofimov, E P Vyalykh, S F Malysheva *Zh. Org. Khim.* **12** 2469 (1976)^e
104. USSR P. 633856; *Byull. Izobret.* (43) (1978)
105. B A Trofimov, S N Istomina, S F Malysheva, E P Vyalykh *Izv. Akad. Nauk SSSR, Ser. Khim.* 2402 (1978)^f
106. B A Trofimov, S F Malysheva, E P Vyalykh *Zh. Org. Khim.* **15** 880 (1979)^b
107. B A Trofimov, S V Amosova, M L Al'pert, O A Tarasova *Zh. Org. Khim.* **13** 2230 (1977)^b
108. B A Trofimov *Z. Chem.* **26** 41 (1986)
109. N K Gusarova, B A Trofimov, A S Atavin, S V Amosova, A V Gusarov *Zh. Org. Khim.* **7** 1780 (1971)^b
110. USSR P. 387982; *Byull. Izobret.* (28) (1973)
111. B A Trofimov *Sulfur Rep.* **11** 207 (1992)
112. V A Potapov, S V Amosova, V Yu Shestakova, A A Starkova, A R Zhnikin *Sulfur Lett.* **21** 105 (1997)
113. USSR P. 568638; *Byull. Izobret.* (30) (1977)
114. B A Trofimov, S V Amosova, N K Gusarova, G K Musorin *Tetrahedron* **38** 713 (1982)
115. N K Gusarova, A A Tatarinova, L M Sinogovskaya *Sulfur Rep.* **11** 1 (1991)
116. B A Trofimov, T N Rakhmatulina, N K Gusarova, S F Malysheva *Usp. Khim.* **60** 2619 (1991) [*Russ. Chem. Rev.* **60** 1360 (1991)]
117. N K Gusarova, S F Malysheva, S N Arbuzova, B A Trofimov *Izv. Akad. Nauk, Ser. Khim.* 1695 (1998)^f
118. B G Sukhov, N K Gusarova, S F Malysheva, B A Trofimov *Izv. Akad. Nauk, Ser. Khim.* 1172 (2003)^f
119. S F Malysheva, S N Arbuzova *Sovremennyyi Organicheskii Sintez* (Modern Organic Synthesis) (Moscow: Khimiya, 2003) p. 160
120. B A Trofimov, B G Sukhov, S F Malysheva, N K Gusarova *Kat. Prom-sti* (4) 18 (2006)
121. B A Trofimov, A I Mikhaleva, A N Vasil'ev, M V Sigalov *Izv. Akad. Nauk SSSR, Ser. Khim.* 695 (1979)^f
122. BRD P. 19834654; *Chem. Abstr.* **132** 109750 (2000)
123. A M Vasil'tsov, Doctoral Thesis in Chemical Sciences, Irkutsk Institute of Chemistry, Siberian Branch of the Russian Academy of Sciences, Irkutsk, 2001
124. E Yu Schmidt, Doctoral Thesis in Chemical Sciences, Irkutsk Institute of Chemistry, Siberian Branch of the Russian Academy of Sciences, Irkutsk, 2005
125. B A Trofimov, E Yu Schmidt, A I Mikhaleva, A M Vasil'tsov, A V Afonin *Mendeleev Commun.* 29 (2000)
126. B A Trofimov, E Yu Schmidt, A M Vasil'tsov, A I Mikhaleva, A B Zaitsev, L V Morozova, A G Gorshkov, J Henkelmann, J-D Arndt *Synthesis* 2427 (2001)
127. B A Trofimov *Adv. Heterocycl. Chem.* **51** 177 (1990)
128. B A Trofimov, S E Korostova, S G Shevchenko, E A Polubentsev, A I Mikhaleva *Zh. Org. Khim.* **26** 1110 (1990)^b
129. B A Trofimov *The Chemistry of Heterocyclic Compounds. Pyrroles* (Ed. R A Jones) (New York: Wiley-Interscience, 1992) Vol. 48, Pt. 2, p. 131
130. B A Trofimov, L V Sokolyanskaya, R N Kudyakova *Sulfur Lett.* **18** 27 (1994)
131. B A Trofimov, A M Vasil'tsov, E Yu Schmidt, O V Petrova, A I Mikhaleva *Zh. Org. Khim.* **30** 576 (1994)^b
132. O V Petrova, A I Mikhaleva, L N Sobenina, E Yu Schmidt, E I Kositsyna *Mendeleev Commun.* 162 (1997)
133. O V Petrova, A I Mikhaleva, L N Sobenina, E Yu Schmidt, E I Kositsyna *Zh. Org. Khim.* **33** 1078 (1997)^b
134. A M Vasil'tsov, E Yu Schmidt, A I Mikhaleva, A V Afonin, A B Zaitsev *Khim. Geterotsikl. Soedin.* 1641 (2001)^g
135. A M Vasil'tsov, A B Zaitsev, E Yu Schmidt, A I Mikhaleva, A V Afonin *Mendeleev Commun.* 74 (2001)
136. A M Vasil'tsov, A B Zaitsev, A I Mikhaleva, E Yu Schmidt, A V Afonin *Khim. Geterotsikl. Soedin.* 66 (2002)^g
137. A B Zaitsev, Candidate Thesis in Chemical Sciences, Irkutsk Institute of Chemistry, Siberian Branch of the Russian Academy of Sciences, Irkutsk, 2003
138. B A Trofimov, A B Zaitsev, E Yu Schmidt, A M Vasil'tsov, A I Mikhaleva, I A Ushakov, A V Vashchenko, N V Zorina *Tetrahedron Lett.* **45** 3789 (2004)
139. E Yu Schmidt, N V Zorina, A B Zaitsev, A I Mikhaleva, A M Vasil'tsov, P Audebert, G Clavier, R Méallet-Renault, R B Pansu *Tetrahedron Lett.* **45** 5489 (2004)
140. A B Zaitsev, R Méallet-Renault, E Yu Schmidt, A I Mikhaleva, S Badré, C Dumas, A M Vasil'tsov, N V Zorina, R B Pansu *Tetrahedron* **61** 2683 (2005)
141. A M Vasil'tsov, E Yu Schmidt, A I Mikhaleva, N V Zorina, A B Zaitsev, O V Petrova, L B Krivdin, K B Petrushenko, I A Ushakov, C Pozo-Conzalo, J A Pomposo, H-J Grande *Tetrahedron* **61** 7756 (2005)
142. B A Trofimov, A M Vasil'tsov, E Yu Schmidt, N V Zorina, A V Afonin, A I Mikhaleva, K B Petrushenko, I A Ushakov, L B Krivdin, V K Belsky, L I Bryukvina *Eur. J. Org. Chem.* 4338 (2005)
143. E Yu Schmidt, A I Mikhaleva, A M Vasil'tsov, A B Zaitsev, N V Zorina *Arkivoc* (vii) 11 (2005)
144. A B Zaitsev, E Yu Schmidt, A M Vasil'tsov, A I Mikhaleva, A V Afonin, I A Ushakov *Khim. Geterotsikl. Soedin.* 839 (2005)^g
145. A I Mikhaleva, E Yu Schmidt *Izbrannyye Metody Sintez i Modifikatsii Geterotsiklov* (Selected Methods of Synthesis and Modification of Heterocycles) (Moscow: IBS Press, 2003) Vol. 1, p. 349
146. A B Zaitsev, E Yu Schmidt, A M Vasil'tsov, A I Mikhaleva, O V Petrova, A V Afonin, N V Zorina *Khim. Geterotsikl. Soedin.* 39 (2006)^g
147. A P Pozharskii, V A Anisimova, E B Tsupak *Prakticheskie Raboty po Khimii Geterotsiklov* (Practical Works on the Chemistry of Heterocycles) (Rostov: Rostov University, 1988) p. 159
148. G P Bean *The Chemistry of Heterocyclic Compounds. Pyrroles* (Ed. R A Jones) (New York: Wiley-Interscience, 1992) Vol. 48, Pt. 2, p. 105
149. R J Tedeschi *Encyclopedia of Physical Science and Technology* Vol. 1 (San Diego, CA: Academic Press, 1992) p. 27
150. A Gossauer *Methoden der Organischen Chemie. Heterene I. (Houben-Weyl)* Teil 1 (Stuttgart, New York: Georg Thieme, 1994) p. 556
151. M Puciova, P Ertl, S Toma *Collect. Czech. Chem. Commun.* **59** 175 (1994)
152. A V Varlamov, L G Voskresenskii, T N Borisova, A I Chernyshev, A N Levov *Khim. Geterotsikl. Soedin.* 683 (1999)^g
153. J Chen, A Burghart, A Derecskei-Kovacs, K Burgess *J. Org. Chem.* **65** 2900 (2000)
154. E Abele, E Lukevics *Heterocycles* **53** 2285 (2000)
155. T L Gilchrist *J. Chem. Soc., Perkin Trans. 1* 2491 (2001)
156. L-X Wang, X-G Li, Y-L Yang *React. Funct. Polym.* **47** 125 (2001)
157. E Abele, E Lukevics *Khim. Geterotsikl. Soedin.* 156 (2001)^g

158. B A Trofimov, E Yu Schmidt, A I Mikhaleva, N V Zorina, I A Ushakov, A V Afonin, A M Vasil'tsov *Mendeleev Commun.* 40 (2007)
159. B A Trofimov, L A Oparina, L N Parshina, V V Vins, V I Lavrov *Izv. Akad. Nauk SSSR, Ser. khim.* 2873 (1989)^f
160. B A Trofimov, R N Kudyakova, L A Oparina, L N Parshina, V V Vins *Zh. Prikl. Khim.* 64 873 (1991)^e
161. B A Trofimov, A G Mal'kina, A V Afonin, I A Ushakov, V V Nosyreva, V K Bel'skii *Zh. Org. Khim.* 39 1430 (2003)^b
162. B A Trofimov, O A Tarasova, M V Sigalov, A I Mikhaleva *Tetrahedron Lett.* 36 9181 (1995)
163. O A Tarasova, E Yu Schmidt, L M Sinogovskaya, O V Petrova, L N Sobenina, A I Mikhaleva, L Brandsma, B A Trofimov *Zh. Org. Khim.* 35 1614 (1999)^b
164. B A Trofimov, Yu M Skvortsov, E I Moshchevitina, A G Mal'kina, V K Bel'skii *Zh. Org. Khim.* 25 221 (1989)^b
165. B A Trofimov, Yu M Skvortsov, A G Mal'kina, A I Gritsa *Sulfur Lett.* 11 209 (1990)
166. B A Trofimov, A G Mal'kina, Yu M Skvortsov, V K Bel'ski, E I Moshchevitina *Sulfur Lett.* 13 63 (1991)
167. A G Mal'kina, Yu M Skvortsov, E I Moshchevitina, V K Bel'skii, B A Trofimov *Khim. Geterotsikl. Soedin.* 335 (1992)^g
168. B A Trofimov, L V Andriankova, A G Mal'kina, A V Afonin, T I Vakul'skaya *Sulfur Lett.* 20 23 (1996)
169. A G Mal'kina, E I Moshchevitina, Yu M Skvortsov, L V Sokolyanskaya, B A Trofimov *Zh. Org. Khim.* 35 1637 (1999)^b
170. A G Mal'kina, R N Kudyakova, B A Trofimov *Zh. Org. Khim.* 37 737 (2001)^b
171. B A Trofimov, A G Mal'kina, O A Shemyakina, R N Kudyakova, L V Sokolyanskaya, L M Sinogovskaya, A I Albanov, V I Smirnov, O N Kazheva, A N Chekhlov, O A D'yachenko *Zh. Org. Khim.* 41 903 (2005)^b
172. A G Mal'kina, O A Shemyakina, V V Nosyreva, A I Albanov, L V Klyba, E R Zhanchipova, B A Trofimov *Synthesis* 637 (2006)
173. Yu M Skvortsov, O M Fartysheva, A G Mal'kina, B A Trofimov *Khim. Geterotsikl. Soedin.* 1689 (1985)^g
174. Yu M Skvortsov, O M Fartysheva, A G Mal'kina, E I Kositsyna, T V Kashik, S M Ponomareva, M V Sigalov, B A Trofimov *Zh. Org. Khim.* 22 255 (1986)^b
175. Yu M Skvortsov, A G Mal'kina, O M Fartysheva, M V Sigalov, B A Trofimov *Zh. Org. Khim.* 22 260 (1986)^b
176. B A Trofimov, A G Mal'kina, Yu M Skvortsov, L V Sokolyanskaya, V I Smirnov, E I Kositsyna *Dokl. Akad. Nauk SSSR* 318 1395 (1991)^h
177. B A Trofimov, A G Mal'kina, Yu M Skvortsov, L V Sokolyanskaya, V I Smirnov, E I Kositsyna *Zh. Org. Khim.* 28 881 (1992)^b
178. A G Mal'kina, L V Sokolyanskaya, R N Kudyakova, L M Sinogovskaya, A I Albanov, O A Shemyakina, B A Trofimov *Zh. Org. Khim.* 41 64 (2005)^b
179. B A Trofimov, L V Andriankova, S A Zhivet'ev, A G Mal'kina, V K Voronov *Tetrahedron Lett.* 43 1093 (2002)
180. B A Trofimov, L V Andriankova, S I Shaikhudinova, T I Kazantseva, A G Mal'kina, S A Zhivet'ev, A V Afonin *Synthesis* 853 (2002)
181. L V Andriankova, A G Mal'kina, A V Afonin, B A Trofimov *Mendeleev Commun.* 186 (2003)
182. L V Andriankova, A G Mal'kina, L P Nikitina, K V Belyaeva, I A Ushakov, A V Afonin, M V Nikitin, B A Trofimov *Tetrahedron* 61 8031 (2005)
183. B A Trofimov, L V Andriankova, R T Tlegenov, A G Mal'kina, A V Afonin, L N Il'icheva, L P Nikitina *Mendeleev Commun.* 33 (2005)
184. B A Trofimov, L V Andriankova, A G Mal'kina, L P Nikitina, A V Afonin, I A Ushakov, L M Sinogovskaya, T I Vakul'skaya *Eur. J. Org. Chem.* 1581 (2006)
185. B A Trofimov, L V Andriankova, A G Mal'kina, K V Belyaeva, L P Nikitina, O A Dyachenko, O N Kazheva, A N Chekhlov, G V Shilov, A V Afonin, I A Ushakov, L V Baikalova *Eur. J. Org. Chem.* 1018 (2007)
186. A G Mal'kina, R Besten, A C H T M Kerk, L Brandsma, B A Trofimov *J. Organomet. Chem.* 493 271 (1995)
187. B A Trofimov, L Brandsma, S N Arbuzova, N K Gusarova *Zh. Obshch. Khim.* 67 343 (1997)^c
188. B A Trofimov, L Brandsma, S N Arbuzova, N K Gusarova *Izv. Akad. Nauk, Ser. Khim.* 884 (1997)^f
189. B A Trofimov *J. Heterocycl. Chem.* 36 1469 (1999)
190. S N Arbuzova, L Brandsma, N K Gusarova, M V Nikitin, B A Trofimov *Mendeleev Commun.* 66 (2000)
191. L Brandsma, N A Nedolya, O A Tarasova, B A Trofimov *Khim. Geterotsikl. Soedin.* 1443 (2000)^g
192. L Brandsma, N A Nedolya *Synthesis* 735 (2004)
193. N A Nedolya, L Brandsma, B A Trofimov *Dokl. Akad. Nauk* 350 68 (1996)^h
194. L Brandsma, N A Nedolya, R-J Lang, B A Trofimov *Izv. Akad. Nauk, Ser. Khim.* 3024 (1996)^f
195. N A Nedolya, R-J Lang, L Brandsma, B A Trofimov *Zh. Org. Khim.* 33 87 (1997)^b
196. N A Nedolya, L Brandsma, R-J Lang, B A Trofimov *Zh. Org. Khim.* 33 637 (1997)^b
197. N A Nedolya, L Brandsma, R-J Lang, B A Trofimov *Zh. Org. Khim.* 33 1437 (1997)^b
198. L Brandsma, N A Nedolya, R-J Lang, B A Trofimov *Khim. Geterotsikl. Soedin.* 571 (1997)^g
199. L Brandsma, N A Nedolya, V Heerma, A C H T M Kerk, E T H G Lutz, R-J Lang, A V Afonin, B A Trofimov *Khim. Geterotsikl. Soedin.* 572 (1997)^g
200. L Brandsma, N A Nedolya, O A Tarasova, L V Klyba, L M Sinogovskaya, B A Trofimov *Dokl. Akad. Nauk* 357 350 (1997)^h
201. L Brandsma, N A Nedolya, H D Verkruijsse, N L Owen, L Du, B A Trofimov *Tetrahedron Lett.* 38 6905 (1997)
202. O A Tarasova, N A Nedolya, V Yu Vvedensky, L Brandsma, B A Trofimov *Tetrahedron Lett.* 38 7241 (1997)
203. L Brandsma, N A Nedolya, O A Tarasova, L V Klyba, L M Sinogovskaya, B A Trofimov *Zh. Org. Khim.* 35 953 (1999)^b
204. L Brandsma, N A Nedolya, B A Trofimov *Eur. J. Org. Chem.* 2663 (1999)
205. B A Trofimov, A I Mikhaleva, L V Morozova *Usp. Khim.* 54 1034 (1985) [*Russ. Chem. Rev.* 54 609 (1985)]
206. B A Trofimov *Phosphorus, Sulfur Silicon Relat. Elem.* 95–96 145 (1994)
207. B A Trofimov, M V Sigalov *Main Group Chem. News* 6 30 (1998)
208. B A Trofimov *Khimiya i Biologicheskaya Aktivnost' Sinteticheskikh i Prirodnikh Soedinenii. Kislorod- i Serusoderzhashchie Geterotsikly* (The Chemistry and Biological Activity of Synthetic and Natural Compounds. Oxygen- and Sulfur-containing Heterocycles) (Moscow: IBS Press, 2003) Vol. 1, p. 119
209. B A Trofimov, L N Sobenina, A I Mikhaleva, M P Sergeeva, N I Golovanova, R I Polovnikova, A N Vavilova *Khim. Geterotsikl. Soedin.* 1176 (1992)^g
210. B A Trofimov, L N Sobenina, A I Mikhaleva, M P Sergeeva, R I Polovnikova *Sulfur Lett.* 15 219 (1992)
211. L N Sobenina, L E Protasova, M P Sergeeva, O V Petrova, T N Aksamentova, O B Kozyreva, R I Polovnikova, A I Mikhaleva, B A Trofimov *Khim. Geterotsikl. Soedin.* 47 (1995)^g
212. B A Trofimov, L N Sobenina, A I Mikhaleva, A P Demenev, O A Tarasova, I A Ushakov, S V Zinchenko *Tetrahedron* 56 7325 (2000)
213. B A Trofimov, L N Sobenina, A I Mikhaleva, M P Sergeeva, N I Golovanova *Zh. Org. Khim.* 28 1766 (1992)^b
214. L N Sobenina, A I Mikhaleva, M P Sergeeva, O V Petrova, T N Aksamentova, O B Kozyreva, D-S D Toryashinova, B A Trofimov *Tetrahedron* 51 4223 (1995)
215. B A Trofimov, A P Demenev, L N Sobenina, A I Mikhaleva, O A Tarasova *Tetrahedron Lett.* 44 3501 (2003)
216. A P Demenev, L N Sobenina, A I Mikhaleva, B A Trofimov *Sulfur Lett.* 26 95 (2003)

217. B A Trofimov, L N Sobenina, A I Mikhaleva, M P Sergeeva, M V Sigalov, N I Golovanova *Khim. Geterotsikl. Soedin.* 998 (1992)^g
218. L I Sobenina, A I Mikhaleva, M P Sergeeva, D-S D Toryashinova, O B Kozyreva, B A Trofimov *Khim. Geterotsikl. Soedin.* 919 (1996)^g
219. L N Sobenina, A I Mikhaleva, D-S D Toryashinova, O B Kozyreva, B A Trofimov *Sulfur Lett.* **20** 205 (1997)
220. L N Sobenina, A I Mikhaleva, B A Trofimov *Khim. Geterotsikl. Soedin.* 418 (1995)^g
221. L N Sobenina, A I Mikhaleva, D-S D Toryashinova, B A Trofimov *Sulfur Lett.* **20** 9 (1996)
222. L N Sobenina, A I Mikhaleva, B A Trofimov *Russ. Khim. Zh.* **49** (6) 97 (2005)ⁱ
223. B A Trofimov, O V Petrova, L N Sobenina, V N Drichkov, A I Mikhaleva, I A Ushakov, O A Tarasova, O N Kazheva, A N Chekhlov, O A Dyachenko *Tetrahedron* **62** 4146 (2006)
224. B A Trofimov, O V Petrova, L N Sobenina, I A Ushakov, A I Mikhaleva, Yu Yu Rusakov, L B Krivdin *Tetrahedron Lett.* **47** 3645 (2006)
225. B A Trofimov, E Yu Schmidt, A I Mikhaleva, A M Vasil'tsov, A B Zaitsev, N S Smolyanina, E Yu Senotrusova, A V Afonin, I A Ushakov, K B Petrusenko, O N Kazheva, O A Dyachenko, V V Smirnov, A F Schmidt, M V Markova, L V Morozova *Eur. J. Org. Chem.* 4021 (2006)
226. Yu Yu Rusakov, L B Krivdin, E Yu Senotrusova, E Yu Schmidt, A M Vasil'tsov, A I Mikhaleva, B A Trofimov, O A Dyachenko, A N Chekhlov, O N Kazheva *Magn. Reson. Chem.* **45** 142 (2007)
227. A I Mikhaleva, A B Zaitsev, A V Ivanov, E Yu Schmidt, A M Vasil'tsov, B A Trofimov *Tetrahedron Lett.* **47** 3693 (2006)
228. A M Vasil'tsov, A V Ivanov, I A Ushakov, A I Mikhaleva, B A Trofimov *Synthesis* 452 (2007)
229. B G Sukhov, S F Malysheva, T I Vakul'skaya, V V Tirskey, E F Martynovich, Yu V Smetannikov, N P Tarasova *Arkivoc* (xiii) 196 (2003)
230. B A Trofimov, L Brandsma, S N Arbuzova, S F Malysheva, N K Gusarova *Tetrahedron Lett.* **35** 7647 (1994)
231. S N Arbuzova, L Brandsma, N K Gusarova, B A Trofimov *Recl. Trav. Chim. Pays-Bas* **113** 575 (1994)
232. L Brandsma, N K Gusarova, A V Gusarov, H D Verkruijsse, B A Trofimov *Synth. Commun.* **24** 3219 (1994)
233. L Brandsma, J A Doorn, R-J Lang, N K Gusarova, B A Trofimov *Mendeleev Commun.* 14 (1995)
234. B A Trofimov, N K Gusarova, L Brandsma *Phosphorus, Sulfur Silicon Relat. Elem.* **109** – **110** 601 (1996)
235. S N Arbuzova, N K Gusarova, S F Malysheva, L Brandsma, A I Albanov, B A Trofimov *Zh. Obshch. Khim.* **66** 56 (1996)^c
236. B A Trofimov, S I Shaikhudinova, V I Dmitriev, K V Nepomnyashchikh, T I Kazantseva, N K Gusarova *Zh. Obshch. Khim.* **70** 43 (2000)^c
237. N K Gusarova, S I Shaikhudinova, T I Kazantseva, S F Malysheva, B G Sukhov, N A Belogorlova, V I Dmitriev, B A Trofimov *Zh. Obshch. Khim.* **72** 399 (2002)^c
238. N K Gusarova, M V Bogdanova, N I Ivanova, N A Chernysheva, B G Sukhov, L M Sinegovskaya, O N Kazheva, G G Alexandrov, O A D'yachenko, B A Trofimov *Synthesis* 3103 (2005)
239. B G Sukhov, N K Gusarova, N I Ivanova, M V Bogdanova, O N Kazheva, G G Aleksandrov, O A D'yachenko, L M Sinegovskaya, S F Malysheva, B A Trofimov *Zh. Strukt. Khim.* **46** 1103 (2005)^j
240. S N Arbuzova, N K Gusarova, B A Trofimov *Arkivoc* (v) 12 (2006)
241. N K Gusarova, S F Malysheva, S N Arbuzova, L Brandsma, B A Trofimov *Zh. Obshch. Khim.* **64** 2062 (1994)^c
242. B A Trofimov, N K Gusarova, S N Arbuzova, S F Malysheva, R Besten, L Brandsma *Synthesis* 387 (1995)
243. N Gusarova, L Brandsma, S Malysheva, S Arbuzova, B Trofimov *Phosphorus, Sulfur Silicon Relat. Elem.* **111** 174 (1996)
244. S F Malysheva, B G Sukhov, L I Larina, N A Belogorlova, N K Gusarova, B A Trofimov *Zh. Obshch. Khim.* **71** 2012 (2001)^c
245. N K Gusarova, S I Shaikhudinova, S N Arbuzova, T I Vakul'skaya, B G Sukhov, L M Sinegovskaya, M V Nikitin, A G Mal'kina, N A Chernysheva, B A Trofimov *Tetrahedron* **59** 4789 (2003)
246. B A Trofimov, S N Arbuzova, A G Mal'kina, N K Gusarova, S F Malysheva, M V Nikitin, T I Vakul'skaya *Mendeleev Commun.* 163 (1999)
247. S N Arbuzova, S I Shaikhudinova, N K Gusarova, M V Nikitin, A G Mal'kina, B G Sukhov, M V Bogdanova, B A Trofimov *Zh. Obshch. Khim.* **75** 552 (2005)^c
248. B A Trofimov, B G Sukhov, S F Malysheva, N A Belogorlova, S N Arbuzova, S P Tunik, N K Gusarova *Zh. Org. Khim.* **40** 138 (2004)^b
249. S N Arbuzova, N K Gusarova, M V Bogdanova, N I Ivanova, I A Ushakov, A G Mal'kina, B A Trofimov *Mendeleev Commun.* 183 (2005)
250. M G Voronkov, O G Yarosh, G Yu Turkina, V Yu Vitkovskii, T I Albanov *J. Organomet. Chem.* **389** 1 (1990)
251. M G Voronkov, O G Yarosh, V K Roman, A I Albanov *Metalloorg. Khim.* **3** 1423 (1990)^k
252. Yu E Ovchinnikov, V A Igonin, I A Zamaev, V E Shklover, Yu T Struchkov, O G Yarosh, M G Voronkov, G Yu Turkina *Zh. Strukt. Khim.* **32** 116 (1991)^j
253. Yu E Ovchinnikov, V A Igonin, I A Zamaev, V E Shklover, Yu T Struchkov, O G Yarosh, M G Voronkov, G Yu Turkina, T M Orlova *Metalloorg. Khim.* **4** 1011 (1991)^k
254. M Voronkov, O Yarosh, L Zhilitskaya *Phosphorus, Sulfur Silicon Relat. Elem.* **65** 33 (1992)
255. Yu E Ovchinnikov, Yu T Struchkov, M G Voronkov, O G Yarosh, G Yu Turkina, T M Orlova *Metalloorg. Khim.* **5** 1280 (1992)^k
256. Yu E Ovchinnikov, Yu T Struchkov, O G Yarosh, G Yu Turkina, M G Voronkov *Zh. Strukt. Khim.* **34** 139 (1993)^j
257. M G Voronkov, O G Yarosh, L V Zhilitskaya, A I Albanov, V Yu Vitkovskii *Metalloorg. Khim.* **6** 77 (1993)^k
258. O G Yarosh, L V Zhilitskaya, A I Albanov, L V Klyba, M G Voronkov *Zh. Obshch. Khim.* **64** 281 (1994)^c
259. O G Yarosh, L V Zhilitskaya, A I Albanov, L V Klyba, M G Voronkov *Zh. Obshch. Khim.* **64** 1801 (1994)^c
260. O G Yarosh, L V Zhilitskaya, A I Albanov, T D Burnashova, M G Voronkov *Zh. Obshch. Khim.* **65** 609 (1995)^c
261. O G Yarosh, M G Voronkov, E I Brodskaya *Usp. Khim.* **64** 896 (1995) [*Russ. Chem. Rev.* **64** 839 (1995)]
262. M G Voronkov, L V Zhilitskaya, O G Yarosh, A I Albanov, L V Klyba *Zh. Obshch. Khim.* **67** 2006 (1997)^c
263. L V Zhilitskaya, O G Yarosh, A I Albanov, L V Klyba, T D Burnashova, M G Voronkov *Zh. Obshch. Khim.* **69** 1456 (1999)^c
264. M G Voronkov, O G Yarosh, L V Zhilitskaya, A I Albanov *Zh. Obshch. Khim.* **70** 1650 (2000)^c
265. M G Voronkov, L V Zhilitskaya, O G Yarosh, T D Burnashova, A I Albanov, L V Klyba *Zh. Obshch. Khim.* **71** 578 (2001)^c
266. O G Yarosh, V V Bystrova, A I Albanov, L V Klyba, M G Voronkov *Zh. Obshch. Khim.* **71** 1974 (2001)^c
267. O G Yarosh, L V Zhilitskaya, N K Yarosh, A I Albanov, M G Voronkov *Zh. Obshch. Khim.* **73** 1645 (2003)^c
268. O G Yarosh, L V Zhilitskaya, N K Yarosh, A I Albanov, L V Klyba, M G Voronkov *Zh. Obshch. Khim.* **74** 1282 (2004)^c
269. O G Yarosh, L V Zhilitskaya, N K Yarosh, E E Istomina, A I Albanov, Yu A Chuvashov, M G Voronkov *Zh. Obshch. Khim.* **74** 1612 (2004)^c
270. O G Yarosh, L V Zhilitskaya, E E Istomina, N K Yarosh, A I Albanov, M G Voronkov *Zh. Obshch. Khim.* **75** 1157 (2005)^c
271. O G Yarosh, L V Zhilitskaya, N K Yarosh, A I Albanov, M G Voronkov *Zh. Obshch. Khim.* **75** 1299 (2005)^c
272. L V Zhilitskaya, E E Istomina, O G Yarosh, M G Voronkov *Zh. Obshch. Khim.* **76** 1315 (2006)^c

273. L V Zhilitskaya, E E Istomina, N K Yarosh, M G Voronkov, A I Albanov, O G Yarosh *Zh. Obshch. Khim.* **76** 1952 (2006)^c
274. V A Potapov, S V Amosova, O V Belozerova, A I Albanov, O G Yarosh, M G Voronkov *Khim. Geterotsikl. Soedin.* 633 (2003)^g
275. V A Potapov, S V Amosova, O V Belozerova, A I Albanov, O G Yarosh, M G Voronkov *Khim. Geterotsikl. Soedin.* 634 (2003)^g
276. L V Klyba, S V Amosova, O V Belozerova, V A Potapov, E R Zhanchipova, O G Yarosh, M G Voronkov *Izv. Akad. Nauk, Ser. Khim.* 639 (2005)^f
277. O V Belozerova, Candidate Thesis in Chemical Sciences, Irkutsk Institute of Chemistry, Siberian Branch of the Russian Academy of Sciences, Irkutsk, 2006
278. M M Demina, A A Velikanov, A S Medvedeva, M G Voronkov *Zh. Obshch. Khim.* **63** 2274 (1993)^c
279. A S Medvedeva, V V Novokshonov, M M Demina, M G Voronkov *Zh. Obshch. Khim.* **64** 1224 (1994)^c
280. V V Novokshonov, A S Medvedeva, M M Demina, L V Sherstyannikova, M G Voronkov *Zh. Org. Khim.* **32** 1828 (1996)^b
281. M M Demina, A A Velikanov, A S Medvedeva, M G Voronkov *J. Organomet. Chem.* **553** 129 (1998)
282. A S Medvedeva, V V Novokshonov, M M Demina, M G Voronkov *J. Organomet. Chem.* **553** 481 (1998)
283. A S Medvedeva, I A Yazovtsev, L P Safronova, M M Demina *Zh. Org. Khim.* **34** 141 (1998)^b
284. A S Medvedeva, V V Novokshonov *Zh. Org. Khim.* **34** 1412 (1998)^b
285. V V Novokshonov, A S Medvedeva, A V Mareev *Zh. Org. Khim.* **37** 626 (2001)^b
286. A S Medvedeva, A V Mareev, A I Borisova, A V Afonin *Arkivoc* (xiii) 157 (2003)
287. A V Mareev, A S Medvedeva, A V Khatashkeev, A V Afonin *Mendeleev Commun.* 263 (2005)
288. A S Medvedeva *Zh. Org. Khim.* **32** 289 (1996)^b
289. A S Medvedeva, M M Demina, P S Novopashin, G I Sarapulova, A V Afonin *Mendeleev Commun.* 110 (2002)
290. N K Gusarova, A M Reutskaya, N I Ivanova, A S Medvedeva, M M Demina, P S Novopashin, A V Afonin, A I Albanov, B A Trofimov *J. Organomet. Chem.* **659** 172 (2002)
291. A S Medvedeva, V V Novokshonov, A V Mareev, A I Borisova *Zh. Org. Khim.* **39** 368 (2003)^b
292. M M Demina, P S Novopashin, G I Sarapulova, L I Larina, A S Smolin, V S Fundamenskii, A A Kashaev, A S Medvedeva *Zh. Org. Khim.* **40** 1852 (2004)^b
293. A S Medvedeva, A V Mareev, A V Afonin, I A Ushakov *Zh. Org. Khim.* **41** 478 (2005)^b
294. A V Mareev, A V Tikhonov, A V Afonin, I A Ushakov, A S Medvedeva *Zh. Org. Khim.* **41** 1425 (2005)^b
295. A S Medvedeva, A V Khatashkeev, A V Mareev, A V Afonin, I A Ushakov *Zh. Org. Khim.* **41** 1740 (2005)^b
296. N K Gusarova, N I Ivanova, N A Konovalova, B G Sukhov, L V Balkalova, L M Sinegovskaya, D V Pavlov, B A Trofimov *Synthesis* 4159 (2006)
297. M M Demina, P S Novopashin, T V Kon'kova, G I Sarapulova, A V Afonin, A S Medvedeva *Khim. Geterotsikl. Soedin.* 1697 (2006)^g
298. V V Novokshonov, I A Novokshonova, I A Ushakov, A S Medvedeva *Khim. Geterotsikl. Soedin.* 1734 (2006)^g
299. Russ. P. 1504968; *Byull. Izobret.* (21) (1994)
300. B A Trofimov, S F Malysheva, E P Vyalykh, L M Sinegovskaya, N K Gusarova *Zh. Org. Khim.* **34** 507 (1998)^b
301. B A Trofimov, S F Malysheva *Nauka — Proizvodstvu* (6) 12 (2003)
302. USSR P. 1129208; *Byull. Izobret.* (46) (1984)
303. V K Stankevich, L E Belozerov, B F Kukharev, B A Trofimov *Nauka — Proizvodstvu* (1) 19 (2004)
304. B A Trofimov, V I Lavrov, L N Parshina, V N Alekankin, V K Stankevich, V I Grigorenko *Zh. Org. Khim.* **18** 528 (1982)^b
305. B A Trofimov, O V Vysotskaya, L A Oparina, L N Parshina, N K Gusarova *Nauka — Proizvodstvu* (6) 16 (2003)
306. L T Stroganova, S A Bol'shakova, T N Tuzhilkova, S V Amosova, N I Ivanova, O A Tarasova, M L Al'pert *Khim.-Farm. Zh.* **24** (2) 143 (1990)¹
307. A M Vasil'tsov, B A Trofimov, S V Amosova, V K Stankevich, I S Zhikharev, V V Kuzin *Izv. Sib. Otd. Akad. Nauk, Ser. Khim. Nauk* 127 (1982)
308. N K Gusarova, M G Voronkov, B A Trofimov *Sulfur Rep.* **9** 95 (1989)
309. N A Chernysheva, N K Gusarova, B A Trofimov *Zh. Org. Khim.* **36** 11 (2000)^b
310. A I Mikhaleva, B A Trofimov, A N Vasil'ev, P M Alkhimenkov, I S Zhikharev, L I Sineva, N P Vasil'ev *Izv. Sib. Otd. Akad. Nauk, Ser. Khim. Nauk* 150 (1981)
311. A I Mikhaleva, A M Vasil'tsov, L N Sobenina, V K Stankevich, B A Trofimov *Nauka — Proizvodstvu* (6) 27 (2003)
312. B A Trofimov, L A Oparina, V I Lavrov, L N Parshina *Zh. Org. Khim.* **31** 647 (1995)^b
313. US P. 6504064; *Chem. Abstr.* **136** 69592 (2002)
314. B A Trofimov, L N Parshina, L A Oparina *Nauka — Proizvodstvu* (6) 2 (2003)
315. Russ. P. 1832674; *Byull. Izobret.* (6) (1995)
316. Russ. P. 1536761; *Byull. Izobret.* (21) (1994)
317. A I Mikhaleva, A M Vasil'tsov, L N Sobenina, V K Stankevich, B A Trofimov *Tekh. Mashinost. Khim.* (4) 42 (2004)
318. Russ. P. 2059597; *Byull. Izobret.* (13) (1996)
319. A I Mikhaleva, A M Vasil'tsov, L N Sobenina, V K Stankevich, B A Trofimov *Nauka — Proizvodstvu* (6) 28 (2003)
320. A I Mikhaleva, A M Vasil'tsov, L N Sobenina, V K Stankevich, B A Trofimov *Nauka — Proizvodstvu* (6) 18 (2003)
321. V I Lavrov, L A Oparina, L N Parshina, V V Vins, B A Trofimov *Zh. Prikl. Khim.* 835 (1990)^c
322. M Son, Q Shi, G Huang, Y Liang, Y Ma *Synthesis* 2482 (2005)
323. Z-J Han, R Wang, Y-F Zhou, L Liu *Eur. J. Org. Chem.* 934 (2005)
324. Y-F Kang, L Lie, R Wang, Y-F Zhou, W-J Yan *Adv. Synth. Catal.* **347** 393 (2005)
325. M Yamashita, K Yamada, K Tomioka *Adv. Synth. Catal.* **347** 1649 (2005)
326. M Ni, R Wang, Z-J Ban, B Mao, C-S Da, L Lie, C Chen *Adv. Synth. Catal.* **347** 1656 (2005)
327. P G Cozzi, J Rudolph, C Bolm, P-O Norrby, C Tomasini *J. Org. Chem.* **70** 5733 (2005)
328. S Xue, Q-F Zhou, L-Z Li, Q-X Guo *Synlett* 2990 (2005)
329. T Weil, P R Schreiner *Eur. J. Org. Chem.* 2213 (2005)
330. S Guillaume, K Plé, A Banchet, A Liard, A Haudrechy *Chem. Rev.* **106** 2355 (2006)
331. A Heutling, R Severin, S Doye *Synthesis* 1200 (2005)
332. A Heutling, F Pohlki, I Bytschkov, S Doye *Angew. Chem., Int. Ed.* **44** 2951 (2005)
333. T Shimade, G B Bajracharya, Y Yamamoto *Eur. J. Org. Chem.* 59 (2005)
334. J-S Herrmann, P W Roesky, S Blechert *Angew. Chem., Int. Ed.* **44** 7794 (2005)
335. K Marcsekova, B Wegener, S Doye *Eur. J. Org. Chem.* 4843 (2005)
336. A Tillack, V Khedkar, H Jiao, M Beller *Eur. J. Org. Chem.* 5001 (2005)
337. C Peppe, E S Lang, G N Ledesma, L B de Castro, O S D Barros, P de Azevedo Mello *Synlett* 3091 (2005)
338. R P Hsung, C A Zifcsak, L-L Wei, C J Douglas, H Xiong, J A Mulder *Org. Lett.* **1** 1237 (1999)
339. L L Wei, J A Mulder, H Xiong, C A Zifcsak, C J Douglas, R P Hsung *Tetrahedron* **57** 459 (2001)
340. I Fernandez, M I Monterde, J Plumet *Tetrahedron Lett.* **46** 6029 (2005)
341. I A Balova, V N Sorokoumov, S N Morozkina, O V Vinogradova, D W Knight, S F Vasilevsky *Eur. J. Org. Chem.* 882 (2005)
342. *Metal-Catalyzed Cross-Coupling Reactions* (Eds A de Meijere, F Diederich) (Weinheim: Wiley-VCH, 2004)
343. I A Maretina, B A Trofimov *Usp. Khim.* **75** 913 (2006) [*Russ. Chem. Rev.* **75** 825 (2006)]

344. S P McIlroy, E Clo, L Nikolajsen, P K Frederiksen, C B Nielsen, K V Mikkelsen, K V Gothelf, P R Ogilby *J. Org. Chem.* **70** 1134 (2005)
345. J W Y Lam, B Z Tang *Acc. Chem. Res.* **38** 745 (2005)
346. E H van Dijk, D J T Myles, M H van der Veen, J C Hummelen *Org. Lett.* **8** 2333 (2006)
347. K Li, Q Wang *Chem. Commun.* 4786 (2005)

^a — *Petrol. Chem. (Engl. Transl.)*

^b — *Russ. J. Org. Chem. (Engl. Transl.)*

^c — *Russ. J. Gen. Chem. (Engl. Transl.)*

^d — *Polym. Sci. (Engl. Transl.)*

^e — *Russ. J. Appl. Chem. (Engl. Transl.)*

^f — *Russ. Chem. Bull., Int. Ed. (Engl. Transl.)*

^g — *Chem. Heterocycl. Compd. (Engl. Transl.)*

^h — *Dokl. Chem. (Engl. Transl.)*

ⁱ — *Mendeleev Chem. J. (Engl. Transl.)*

^j — *J. Struct. Chem. (Engl. Transl.)*

^k — *Russ. J. Organomet. Chem. (Engl. Transl.)*

^l — *Pharm. Chem. J. (Engl. Transl.)*

Chalcogenide clusters of Group 5–7 metals

V E Fedorov, Yu V Mironov, N G Naumov, M N Sokolov, V P Fedin

Contents

I. Introduction	529
II. Main structural types of chalcogenide clusters	530
III. Methods of synthesis of chalcogenide clusters	539
IV. Reactivity of chalcogenide clusters	541
V. Potential applications of chalcogenide clusters	546
VI. Conclusion	547

Abstract. The state-of-the-art and prospects of the development of chemistry of chalcogenide clusters of Group 5–7 metals of the Periodic Table are discussed. The main structural types, methods of synthesis, the reactivity and possible applications of vanadium, niobium, tantalum, chromium, molybdenum, tungsten and rhenium chalcogenide clusters with nuclearity of three and larger are considered. The bibliography includes 363 references.

I. Introduction

The achievements of chemistry in the second half of the 20th century are mostly associated with the foundation of basics of cluster chemistry. In 1964, F Cotton introduced the term ‘cluster’ for compounds the molecules of which contain a core of metal atoms linked by metal–metal bonds.¹ The development of cluster chemistry was a revolutionary step in coordination chemistry.² The complexes in which metal clusters are coordinated by chalcogenide or polychalcogenide ligands occupy a special place among numerous types of cluster compounds. Chalcogenide clusters are a typical example of so-called inorganic or high-valence clusters and are most characteristic of 4d- and 5d-metals of Groups 5–7. The present review discusses methods of synthesis, structures and properties of sulfide, selenide and telluride cluster compounds of vanadium, niobium, tantalum, chromium, molybdenum, tungsten and rhenium. The review includes only the metal clusters with nuclearity equal, to or larger than, three.

The present review is dedicated to the 50th anniversary of the A V Nikolaev Institute of Inorganic Chemistry, Siberian Branch of the Russian Academy of Sciences (NIIC) and it is

not a coincidence: from the date of its foundation and up to now systematic studies of chalcogenide clusters of transition metals have been carried out in the Institute and several new key types of chalcogenide clusters have been discovered here. In the mid-1960s, trinuclear molybdenum complexes $\text{Mo}_3\text{Q}_7\text{X}_4$ ($\text{Q} = \text{S}, \text{Se}; \text{X} = \text{Cl}, \text{Br}, \text{I}$)^{3,4} were synthesised in NIIC, which became a beginning of massive studies of triangular chalcogenide clusters. At the same time lower molybdenum chalcogenides of the Mo_6Q_8 ($\text{Q} = \text{Se}, \text{Te}$) type have been found,^{5,6} which turned out to be predecessors of a group of numerous closely related ternary cluster compounds later called the Chevrel phases (these compounds were also intensively studied because of their properties as superconductors).⁷ The studies of hexa- and tetranuclear rhenium clusters $\text{Re}_6\text{Te}_{15}$,⁸ $\text{Re}_6\text{Q}_4\text{X}_{10}$,⁹ $\text{Re}_4\text{Q}_4(\text{TeX}_2)_4\text{X}_8$ (Ref. 10) and chalcocyanide complexes $[\text{Re}_6\text{Q}_8(\text{CN})_6]^{4-}$ (Ref. 11) and $[\text{Re}_4\text{Q}_4(\text{CN})_{12}]^{4-}$ (Ref. 12) should be noted among the pioneering investigations of NIIC. Recently, new types of square vanadium and tantalum clusters $\text{V}_4\text{S}_9\text{Br}_4$ (Ref. 13) and $\text{Ta}_4\text{Q}_9\text{X}_8$ ($\text{Q} = \text{S}, \text{Se}; \text{X} = \text{Br}, \text{I}$)¹⁴ were discovered in NIIC and the unique 12-nuclear rhenium clusters $[\text{Re}_{12}\text{CS}_{17}(\text{CN})_6]^{8-/6-}$ (Ref. 15) containing an interstitial carbon atom were synthesised.

Chalcogenide clusters of Group 5–7 transition metals are typically obtained by high-temperature synthesis. Such clusters usually possess polymeric structures and therefore they are insoluble, low-reactive and their chemical properties could not be studied for a long period. The breakthrough in this area occurred after the discovery¹⁶ of synthetic methods of transformation of polymeric cluster complexes into soluble molecular complexes by introduction of new ligands. In addition, the substitution of atoms of the cluster core was performed, including preparation of heterometallic clusters. Inorganic ligands (SSe^{2-} , STe^{2-} , TeCl_2 , TeBr_2 , TeI_2 , Te_6), previously unknown in coordination chemistry were discovered. Most of the studies of tellurium containing cluster complexes were also performed in NIIC.^{11, 17–20}

In the present review we summarise the forty years of development of chemistry of chalcogenide clusters of early transition metals. A particular attention is paid to the new advances in chemistry of this class of compounds that emerged during the last years and to the prospects of development of basic studies and practical applications of these compounds.

V E Fedorov, Yu V Mironov, N G Naumov, M N Sokolov, V P Fedin
A V Nikolaev Institute of Inorganic Chemistry, Siberian Branch of the Russian Academy of Sciences, prosp. Acad. Lavrentieva 3, 630090 Novosibirsk, Russian Federation. Fax (7-383) 330 94 89, tel. (7-383) 330 92 53, e-mail: fed@che.nsk.su (V E Fedorov), yuri@che.nsk.su (Yu V Mironov), naumov@che.nsk.su (N G Naumov), tel. (7-383) 339 18 45, e-mail: caesar@che.nsk.su (M N Sokolov), tel. (7-383) 330 94 90, e-mail: cluster@che.nsk.su (V P Fedin)

Received 2 April 2007

Uspekhi Khimii 76 (6) 571–595 (2007); translated by D S Yufit

II. Main structural types of chalcogenide clusters

1. Triangular clusters with the cluster core M_3Q_4

The cluster core $M_3(\mu_3-Q)(\mu_2-Q)_3$ contains a triangular metal cluster M_3 , which coordinates four chalcogenide ligands Q (one μ_3-Q and three μ_2-Q). Cluster complexes with the core M_3Q_4 are most typical of molybdenum, tungsten and rhenium, while for Group 5 metals (V, Nb, Ta) such complexes are uncommon and are represented only by sulfide clusters of vanadium $[V_3S_4(edt)_3]^{3-}$ (H_2edt is ethane-1,2-dithiol)²¹ and niobium $[Nb_3SO_3(NCS)_9]^{6-}$ (Ref. 22). Numerous examples of sulfide and selenide clusters of molybdenum and tungsten are known, but so far only one telluride cluster, $\{Mo_3Te_4[(Pr^iO)_2PS_2]_3(\mu-o-NH_2C_6H_4CO_2)(PBu_3^t)\}$, has been described.²³

Metal ions in triangular clusters with the number of valence electrons available for metal–metal bond formation (N_e) equal to 6 (*i.e.*, there are three two-electron bonds) possess d^2 electron configuration. Accordingly, the charge of the cluster core $M_3Q_4^{n+}$ is determined by the position of the metal in the Periodic Table: for V and Nb, $n = 1$, for Mo and W $n = 4$, for Re, $n = 7$. The $M-M$ metal bond lengths correspond to those of single bonds. Besides, in the case of monodentate ligands each metal atom coordinates three ligands. Anionic complexes with single-charged anionic ligands $[M_3Q_4L_9]^{5-}$, where L is cyanide,²⁴ thiocyanate,^{25–29} formate,³⁰ *etc.*, are typical examples of such clusters. There are two types of ligands L in such complexes: *cis*- and *trans*-oriented relative to the μ_3-Q ligand. The well-known aqua complexes of molybdenum and tungsten $[M_3Q_4(H_2O)_9]^{4+}$ ($M = Mo, W; Q = S, Se$) (Fig. 1)^{25, 31, 32} are examples of cluster complexes with neutral ligands.

The cluster complexes $[Mo_3S_4(C_2O_4)_3(H_2O)_3]^{2-}$ contain simultaneously both bidentate ($C_2O_4^{2-}$) and monodentate (H_2O) ligands; the monodentate ligands in these complexes occupy only *trans*-positions relative to μ_3-Q (Fig. 2).^{33–35} The complexes with chelating O-, N-, P- and S-donor ligands are most abundant among triangular cluster compounds. The complexes with oxalate,^{33–35} iminodiacetate,³⁶ nitrilotriacetate,^{25, 37, 38} triethylenetetraaminohexaacetate³⁹ and other ligands belong to this class. A number of complexes with

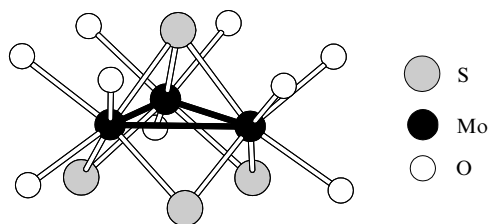


Figure 1. Structure of the complex $[Mo_3(\mu_3-S)(\mu_2-S)_3(H_2O)_9]^{4+}$.

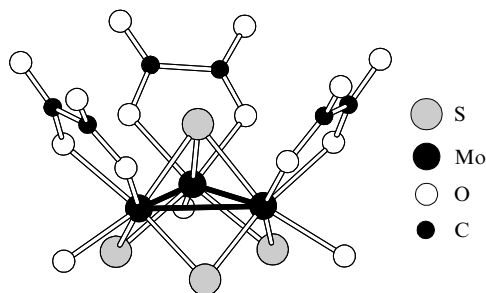


Figure 2. Structure of the complex $[Mo_3S_4(C_2O_4)_3(H_2O)_3]^{2-}$.

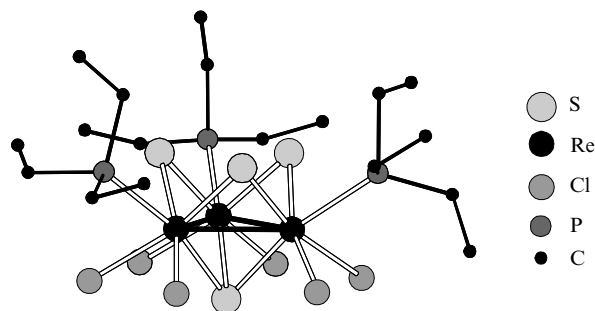


Figure 3. Structure of the complex $[Re_3S_4Cl_6(PEt_3)_3]^-$.

phosphine ligands are also known. Usually the bulky monodentate phosphine ligands occupy *trans*-positions relative to the chalcogenide μ_3 -ligand as, for instance, in $(HPEt_3)_3[Re_3S_4Cl_6(PEt_3)_3]^{40}$ (Fig. 3). In contrast to oxalate complexes, one phosphorus atom in complexes with bidentate phosphine ligands is in *trans*-position and another in *cis*-position relative to the chalcogenide μ_3 -ligand. This results in the chirality of the cluster cations formed $[M_3S_4X_3(dmpe)_3]^+$ and $[M_3S_4X_3(dppe)_3]^+$ [$M = Mo, W; X = Cl, Br$; $dmpe$ is 1,2-bis(dimethylphosphino)ethane, $dppe$ is 1,2-bis(diphenylphosphino)ethane] (Fig. 4).^{18, 41}

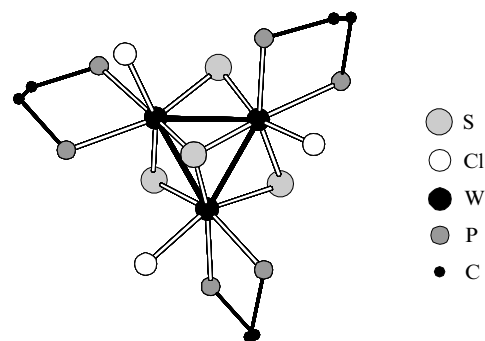


Figure 4. Structure of the complex $[W_3S_4Cl_3(dppe)_3]^+$ (the phenyl groups are omitted).

The $Mo-Mo$ bond lengths (2.807 Å) in the cluster $Mo_3S_4^{3+}$ of the paramagnetic reduced electron-rich complex $[Mo_3S_4Cl_3(dppe)_2(PEt_3)]$ ($N_e = 7$) are slightly longer than those in its phosphine analogues with the cluster core $Mo_3S_4^{4+}$ (2.776 Å).^{42, 43}

There is also a significant number of compounds with S-donor ligands, including dithiophosphate, dithiolate, dithiophosphate and dithiocarbamate complexes.¹⁸ The tetrasulfide ligand in compound $(NH_4)_2[W_3S_4(S_4)(NH_3)_3] \cdot H_2O$ is bidentate and an ammonia molecule is also coordinated to the tungsten atom (Fig. 5).⁴⁴

2. Triangular clusters with the cluster core M_3Q_7

This structural type is most typical of molybdenum and tungsten compounds; here the metal cluster M_3 coordinates one chalcogenide μ_3 -ligand and three dichalcogenide μ_2 -ligands $M_3(\mu_3-Q)(\mu_2-Q)_3$ (Fig. 6).

Bidentate bridged dichalcogenide ligands asymmetrically coordinate metal–metal bonds according to the $\mu_2-\eta^2:\eta^2$ -mode, which results in structural and chemical non-equivalence of the chalcogen atoms of these ligands. Thus, the distances $Mo-S_{eq}$ and $Mo-S_{ax}$ complex $(Ph_4P)_2[Mo_3S_7Cl_6]$ are equal to 2.485 and 2.391 Å, respectively.⁴⁵ The bond force

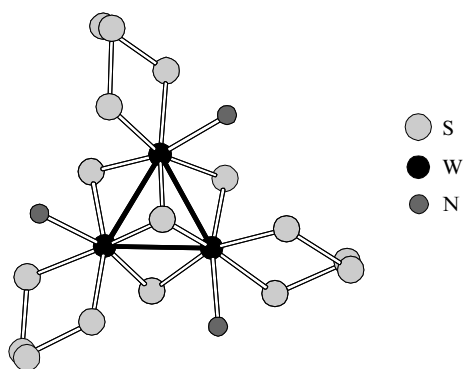


Figure 5. Structure of the complex $[\text{W}_3\text{S}_4(\text{S}_4)_3(\text{NH}_3)_3]^{2-}$.

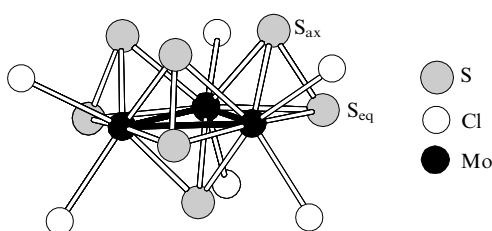


Figure 6. Structure of the complex $[\text{Mo}_3(\mu_3\text{-S})(\mu_2\text{-S}_2)_3\text{Cl}_6]^{2-}$.

constant of the $\text{Mo}-\text{S}_{\text{eq}}$ bond is also smaller⁴⁶ and the equatorial sulfur atoms are quite labile in chalcogen substitution and elimination reactions.^{44, 47–49} This makes possible their selective substitution by selenium atoms resulting in the formation of the cluster core $\text{Mo}_3(\mu_3\text{-S})(\mu_2\text{-SSe})_3$.⁴⁷ Another feature of the M_3Q_7 core is its predisposition to the formation of specific non-valence interactions of the $\text{M}_3\text{Q}_7\cdots\text{Y}$ type with short contacts between axial chalcogen atoms and atom Y (Y may be a halide or chalcogenide ion). These interactions may be described as electrostatic or as a charge transfer from $\mu_3\text{-Y}$ to the σ^* -orbital of the dichalcogenide ligand Y_2^{2-} (Ref. 50).

For the first time, compounds with the core M_3Q_7 were synthesised as polymeric chalcogenides $\text{Mo}_3\text{Q}_7\text{X}_4$ (Q = S, Se; X = Cl, Br, I).^{3, 4} The cluster cores M_3Q_7 in these compounds are linked together into infinite zigzag chains by bridging halogen atoms (Fig. 7). A number of complexes containing anions $[\text{M}_3\text{Q}_7\text{X}_6]^{2-}$ (M = Mo, W; Q = S, Se; X = Cl, Br, I, NCS) is known nowadays.¹⁸ However, there are very few complexes with N-donor ligands. Complexes with aniline $[\text{Mo}_3\text{S}_7\text{Br}_3(\text{PhNH}_2)_3]^+$,⁵¹ pyridine,⁵² 1,10-phenanthroline $[\text{M}_3\text{Se}_7(\text{phen})_3]^{4+}$ (Ref. 53) and ethylenediamine⁵⁴ were synthesised. On the contrary, the cluster compounds in which the

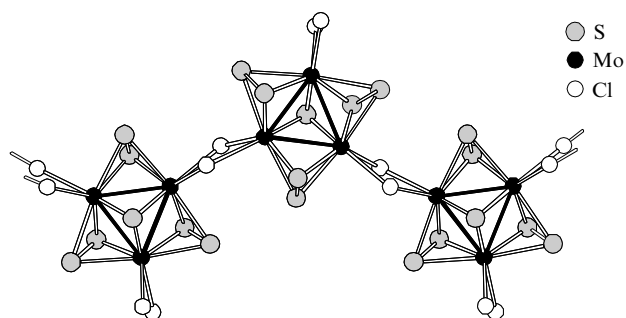


Figure 7. Structure of the polymer $\text{Mo}_3\text{S}_7\text{Cl}_4$.

cores M_3Q_7 coordinate S-donor ligands are fairly numerous and include complexes with various thio-ligands: polysulfide $[\text{Mo}_3\text{S}_7(\text{S}_2)_3]^{2-}$, dithiophosphate $[\text{Mo}_3\text{S}_7(\text{dtp})_3]^+$, dithiocarbamate $[\text{M}_3\text{Se}_7(\text{dte})_3]^+$, dithiophosphinate $[\text{Mo}_3\text{S}_7(\text{R}_2\text{PS}_2)_3]^+$ (R = Et, Prⁿ, Buⁿ) and other.^{55–58}

Triangular clusters of molybdenum and tungsten with the core M_3Q_7 are well studied; similar complexes of vanadium and rhenium are also known. The metal–metal bond lengths in $[\text{V}_3^{\text{III}}\text{S}_7(\text{bipy})_3]\text{PF}_6$ (Fig. 8) are equal to 2.75–2.78 Å;⁵⁹ the cluster fragment $\text{V}_3\text{S}_7^{2+}$ corresponding to the oxidised form is found in $(\text{Et}_4\text{N})[\text{V}_3\text{S}_7(\text{Me}_2\text{NCS}_2)_3]$, where the V–V distances are slightly shorter (2.74–2.75 Å).⁶⁰

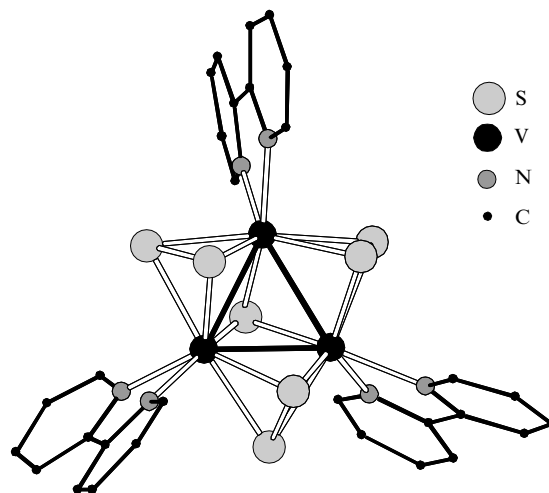


Figure 8. Structure of the complex $[\text{V}_3(\mu_3\text{-S})(\mu_2\text{-S}_2)_3(\text{bipy})_3]^+$.

A series of isostructural rhenium complexes $\text{Re}_3\text{Q}_7\text{X}_4$ (Q = S, Se; X = Cl, Br, I) were synthesised.^{61–63} In these compounds, the cluster core $\text{Re}_3\text{Q}_7^{7+}$ is isoelectronic to that of $\text{Mo}_3\text{Q}_7^{4+}$, but the distance $\text{Re}-\text{Re}$ in $\text{Re}_3\text{S}_7\text{Cl}_4$ (2.698 Å) is slightly shorter than the distance $\text{Mo}-\text{Mo}$ in $\text{Mo}_3\text{S}_7\text{Cl}_4$ (2.758 Å) probably because of the difference in atomic radii of Re^{V} and Mo^{IV} .

There are very few telluride complexes M_3Q_7 . The complexes $\text{Mo}_3\text{Te}_{10}\text{I}_{10}$, $[\text{Mo}_3\text{Te}_7(\text{CN})_6]^{2-}$, $[\text{W}_3\text{Te}_7(\text{CN})_6]^{2-}$ and $[\text{Mo}_3\text{Te}_7((\text{EtO})_2\text{PS}_2)_3]\text{I}$ containing the $\text{M}_3(\mu_3\text{-Te})(\mu_2\text{-Te}_2)_3^{4+}$ core were synthesised and their structures were established.^{50, 64–67}

3. Other examples of triangular chalcogenide clusters

There are some mixed chalcogenide compounds among M_3Q_4 clusters.⁶⁸ In the triangular cluster $[\text{Nb}_3(\mu_3\text{-S})(\mu_2\text{-O})_3(\text{NCS})_9]^{6-}$, only the sulfur atom occupies the μ_3 -position.²² Compounds $[\text{M}_3(\mu_3\text{-S})(\mu_2\text{-O})_x(\mu_2\text{-S})_{3-x}(\text{H}_2\text{O})_9]^{4+}$ (M = Mo, W; $x = 1–3$) and $[\text{Mo}_3(\mu_3\text{-Se})(\mu_2\text{-O})_x(\mu_2\text{-Se})_{3-x}(\text{H}_2\text{O})_9]^{4+}$ are also known.^{18, 69–71} Dithiophosphate derivatives of the cluster $\text{Mo}_3(\mu_3\text{-O})(\mu_2\text{-S})_3^{4+}$ were described as well.⁷² Recently the complex $[\text{W}_3(\mu_3\text{-Te})(\mu_2\text{-Se})_3(\text{CN})_9]^{5-}$ has been synthesised.⁶⁷ Mixed-chalcogen clusters M_3Q_7 are more diverse, they include $\text{Mo}_3(\mu_3\text{-O})(\mu_2\text{-S}_2)_3^{4+}$, $\text{Mo}_3(\mu_3\text{-S})(\mu_2\text{-Se}_2)_3^{4+}$, $\text{M}_3(\mu_3\text{-S})(\mu_2\text{-SSe})_3^{4+}$, $\text{M}_3(\mu_3\text{-Se})(\mu_2\text{-SSe})_3^{4+}$ (M = Mo, W), $\text{Mo}_3(\mu_3\text{-S})(\mu_2\text{-Te}_2)_3^{4+}$, $\text{Mo}_3(\mu_3\text{-O})(\mu_2\text{-Te}_2)_3^{4+}$ and $\text{W}_3(\mu_3\text{-Te})(\mu_2\text{-TeSe})_3^{4+}$ (Refs 47, 49, 50, 54, 67, 73 and 74). The substitution of the μ_3 -chalcogen atom by an atom of lighter chalcogen results in significant shortening of metal–metal bonds in the M_3 triangle. This shortening corresponds approximately to the difference in size of the bridged chalcogen atoms. For example, the shortening in dithiophosphate complexes $[\text{Mo}_3\text{Q}(\text{S}_2)_3\{(\text{EtO})_2\text{PS}_2\}_3]\text{X}$

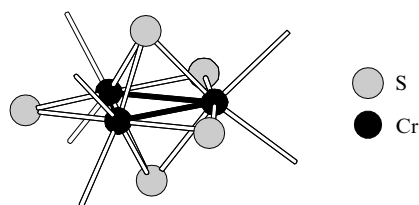


Figure 9. Cluster core in the complex $[\text{Cr}_3(\mu_3\text{-S})_2(\mu_2\text{-S})_3(\text{dmpe})_3]$ (the dmpe ligands are omitted).

($\text{X} = \text{Cl}, \text{I}, \text{I}_3$) is equal to $\sim 0.1 \text{ \AA}$: from 2.723 \AA for $\text{Q} = \text{S}$ to 2.626 \AA for $\text{Q} = \text{O}$.⁷³

Along with most typical triangular clusters M_3Q_4 and M_3Q_7 , a number of other metal chalcogenide clusters are known. The cluster $[\text{Cr}_3(\mu_3\text{-S})_2(\mu_2\text{-S})_3(\text{dmpe})_3]$ contains two μ_3 -bridging chalcogen atoms (Fig. 9).⁷⁵ Similar ‘double-capped’ coordination was also observed in $(\text{Et}_4\text{N})_2[\text{Cr}_3(\mu_3\text{-Se})_2(\text{CO})_{10}]$ and $[\text{Re}_3(\mu_3\text{-S})_2(\mu_2\text{-S})_2(\mu_2\text{-Cl})\text{Cl}_3(\text{PET}_3)_3]$.^{76, 77} An equilateral triangle Nb_3 in compound $[(\eta^5\text{-C}_5\text{EtMe}_4)_3\text{Nb}_3\{\mu_3\text{-BS}_3(\text{SH})\}(\mu_2\text{-S})_3]$ is symmetrically ‘covered’ by the $[\text{BS}_3(\text{SH})]^{4-}$ ligand.⁷⁸ Only two electrons are available for metal–metal bonding in this cluster. Very similar tantalum cluster was found in the compound $[(\eta^5\text{-C}_5\text{EtMe}_4)_3\text{Ta}_3.(\mu_3\text{-BS}_3(\text{H}))(\mu_2\text{-S})_3]$. In this cluster the ‘cap’ is represented by the hydridotriethioborato anion $[\text{BS}_3(\text{H})]^-$.⁷⁹

Polymeric chalcogenides of niobium and tantalum M_3QX_7 contain the cluster core $\text{M}_3(\mu_3\text{-Q})(\mu_2\text{-X})_3^{4+}$.^{80–83} The structure consists of parallel planes containing triangular clusters Nb_3 (the Nb–Nb bond length is 2.776 \AA). The triangles are linked together into a two-dimensional network by bridging halogen atoms (Fig. 10).

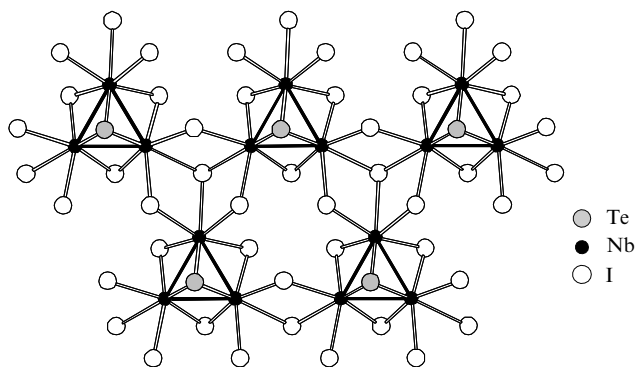


Figure 10. Fragment of the polymer Nb_3TeI_7 .

4. Tetrahedral metal clusters with the core M_4Q_4

Each face of the M_4 tetrahedron in tetrahedral clusters with the core $\text{M}_4(\mu_3\text{-Q})_4$ coordinates μ_3 -chalcogen atoms in such a way that the metal and chalcogen atoms form a distorted cubane structure. The cubane clusters are topologically (and often genetically) related to previously discussed clusters of the $\text{M}_3(\mu_3\text{-Q})(\mu_2\text{-Q})_3$ type, which may be regarded as defective cubane clusters (without one metal atom). Such type of cluster compounds is known for all discussed transition metals. Twelve valence electrons ($N_e = 12$) are required for the formation of six two-electron two-centre covalent metal–metal bonds in a tetrahedral cluster M_4 . The stoichiometry of most of the stable complexes with d^3 electronic configuration of metal ions supports this rule. However, there are numerous examples of clusters where this simple model does not work and these compounds are formally electron-deficient.

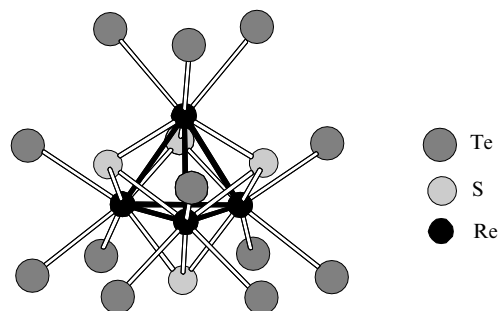


Figure 11. Structure of the cluster fragment $\text{Re}_4\text{S}_4\text{Te}_{12/3}$ in the compound $\text{Re}_4\text{S}_4\text{Te}_4$.

Polymeric ternary chalcogenides and chalcogenides of the types $\text{M}_4\text{Q}_4\text{X}_4$ ($\text{M} = \text{Nb}, \text{Mo}$; $\text{Q} = \text{S}, \text{Se}$; $\text{X} = \text{Cl}, \text{Br}, \text{I}$),^{84–86} $\text{Re}_4\text{S}_4\text{Te}_4$ (Fig. 11)⁸⁷ and MMo_4Q_8 ($\text{M} = \text{Al}, \text{Ga}$)^{88–91} are an abundant group of tetrahedral cluster compounds. All these compounds are isostructural and form spinel-type cubic crystal structures. The cubane cluster groups are linked into a three-dimensional framework by bridging halogen atoms or by excess chalcogen atoms according to the $[\text{M}_4\text{Q}_4\text{X}_{12/3}]_{\infty\infty\infty}$ -type. Interestingly, only sulfur atoms occupy μ_3 -positions in the cluster core of rhenium telluride $\text{Re}_4\text{S}_4\text{Te}_4$. Part of rhenium atoms of this cluster may be replaced by molybdenum atoms, which results in the formation of heterometallic cluster $\text{Re}_{4-x}\text{Mo}_x\text{S}_4\text{Te}_4$ ($0 \leq x \leq 1.25$).⁹² The metal–metal distances in these clusters are correlated with N_e values (Table 1). The electronic and magnetic properties are determined by the successive filling of the d shell.

Table 1. Number of metal–metal bonding valence electrons and the metal–metal distances in tetrahedral metal clusters.

Compound	N_e	M–M bond length / \AA
GaNb_4Se_8	7	3.03
$\text{Nb}_4\text{Se}_4\text{I}_4$	8	2.96
GaMo_4Se_8	11	2.89
$\text{Mo}_4\text{S}_4\text{Br}_4$	12	2.80
$\text{Re}_4\text{S}_4\text{Te}_4$	12	2.78

The rhenium atoms of the cluster core Re_4Q_4 of molecular rhenium chalcogenide complexes $[\text{Re}_4\text{Q}_4(\text{TeX}_2)_4\text{X}_8]$ ($\text{Q} = \text{S}, \text{Se}, \text{Te}$; $\text{X} = \text{Cl}$ and $\text{Q} = \text{Te}, \text{X} = \text{Br}$; $N_e = 12$) additionally coordinate two halide ligands and the ligand TeX_2 .^{10, 93} The tetrahedral chalcogenide clusters $[(\eta^5\text{-C}_5\text{H}_4\text{R})_4\text{M}_4\text{Q}_4]$ with monosubstituted cyclopentadienyl ligands are known for some metals discussed: V ($\text{Q} = \text{S}, \text{R} = \text{Me}$),⁹⁴ Cr ($\text{Q} = \text{S}, \text{Se}, \text{Te}$; $\text{R} = \text{Me}$),^{95–100} Mo ($\text{Q} = \text{S}, \text{Se}$; $\text{R} = \text{Pr}^i$).¹⁰¹ The cyclopentadienyl cluster complexes of the Group 5 elements are represented only by vanadium cyclopentadienyl(thio) complexes $[(\eta^5\text{-C}_5\text{H}_4\text{R})_4\text{V}_4\text{S}_4]$ ($\text{R} = \text{H}, \text{Me}$).⁹⁴ The N_e value in neutral complexes is equal to 8 for vanadium and 12 for chromium and molybdenum.

A large number of chalcocyanide cluster complexes $[\text{M}_4\text{Q}_4(\text{CN})_{12}]^{n-}$, where $\text{M} = \text{Mo}, \text{W}, \text{Re}$; $\text{Q} = \text{S}, \text{Se}, \text{Te}$ (Fig. 12) is studied in detail.^{102–107} The cluster core of the complexes $[\text{Re}_4\text{Q}_4(\text{CN})_{12}]^{4-}$ coordinates terminal cyano groups through the carbon atom. The cluster M_4 becomes electron-deficient in the corresponding molybdenum complexes $[\text{Mo}_4\text{Q}_4(\text{CN})_{12}]^{6-}$. The cyano complexes $[\text{M}_4\text{OTe}_4(\text{CN})_{12}]^{6-}$ containing the metal core $\text{M}_4(\mu_4\text{-O})$. $(\mu_3\text{-Te})_4^{5+}$ with an interstitial oxygen atom were obtained for niobium and tantalum.¹⁰⁸ In these clusters, $N_e = 4$, and the M–M distances are significantly longer than those in the

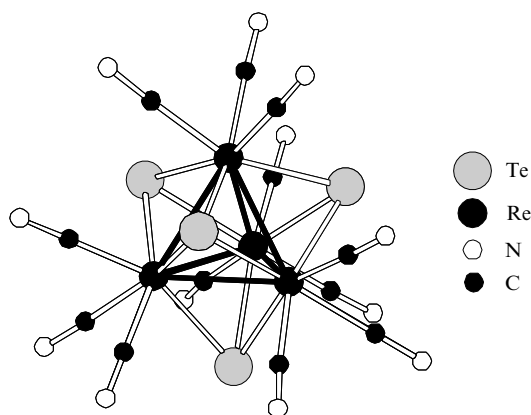


Figure 12. Structure of the complex $[\text{Re}_4\text{Te}_4(\text{CN})_{12}]^{4-}$.

corresponding metals or in the compounds containing single M–M bond.

A series of the complexes $\text{M}_4\text{Q}_4\text{L}_{12}$ with various terminal ligands L such as H_2O ($\text{M} = \text{Mo}, \text{W}$; $\text{Q} = \text{S}, \text{Se}$),^{109–111} Cl ($\text{M} = \text{Re}, \text{Q} = \text{Te}$; $\text{M} = \text{Mo}, \text{Q} = \text{S}$),^{22, 70, 112–119} NCS ($\text{M} = \text{Re}$; $\text{Q} = \text{S}, \text{Se}, \text{Te}$; $\text{M} = \text{Mo}, \text{Q} = \text{S}$)^{111, 116, 120} are known for the cubane clusters of molybdenum, tungsten and rhenium. Complexes $[\text{Re}_4\text{S}_4(\text{S}_3)_6]^{4-}$ and $[\text{Re}_4\text{Q}_4(\text{S}_3)_4(\text{S}_4)_2]^{4-}$ with polysulfide ligands are known for rhenium.^{121–123} The edges of the tetrahedron Re_4 in the complex $[\text{Re}_4\text{Se}_4(\text{S}_3)_4(\text{S}_4)_2]^{4-}$ coordinate four bidentate polysulfide ligands S_3 and two S_4 ligands in *trans*-position relatively to each other (Fig. 13).

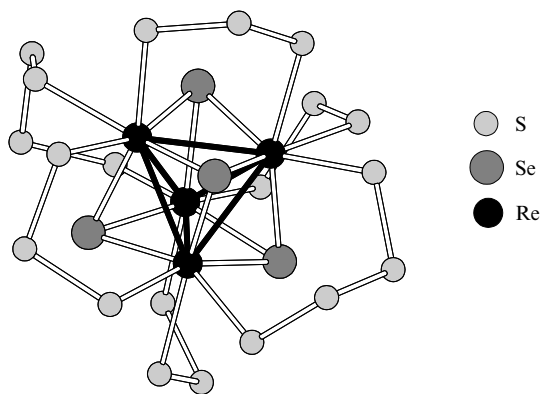


Figure 13. Structure of the complex $[\text{Re}_4\text{Se}_4(\text{S}_3)_4(\text{S}_4)_2]^{4-}$.

Sulfur-containing ligands stabilise the electron-deficient cluster core $\text{Mo}_4\text{S}_4^{6+}$ ($N_e = 10$): this cluster core was found in dithiophosphate $[\text{M}_4\text{S}_4(\mu_2\text{-dtp})_2(\text{dtp})_4]$ ($\text{M} = \text{Mo}, \text{W}$; $\text{Q} = \text{S}$)^{115, 124} and in dithiocarbamate $[\text{Mo}_4\text{S}_4(\mu_2\text{-Et}_2\text{NCS}_2)_2 \cdot (\text{Et}_2\text{NCS}_2)_4]$ ¹¹⁵ complexes.

A unique series of high-valence cubane clusters based on *p*-tolylimide (tolN^{2-}) derivatives of $\text{Mo}(\text{V})$ and $\text{W}(\text{V})$, were synthesised.^{125, 126} Each metal atom in the structure of $[\text{Mo}_4\text{S}_4(\text{tolN})_4(\text{S}_2\text{P}(\text{OEt})_2)_4]$ is bound to one terminal $=\text{NC}_6\text{H}_4\text{Me-}p$ group, to one chelating dithiophosphate and to three bridging sulfide ligands of the cluster core. Four electrons available for M–M-bonding are localised in such a way that two single Mo–Mo (2.862 Å) bonds are located at the opposite edges of the tetrahedron. The four remaining metal–metal distances are significantly longer (3.69 Å). The complex $[\text{W}_4\text{S}_4(\text{en})_4(\text{S}_4)]\text{S}$ (en is ethylenediamine) containing a

distorted metal cluster ($N_e = 6$; W–W 2.801–2.878 Å) is another example.¹²⁷ Alternatively, one can regard this compound as $[\text{W}_4\text{S}_4(\text{en})_4(\text{SH})_4]\text{S}$ with a more conventional cluster core $\text{W}_4\text{S}_4^{6+}$.

5. Square metal M_4 clusters

The complex $\text{Li}_4[\text{Nb}_4\text{S}_2(\text{SPh})_{12}]$ in which the square metal cluster coordinates two $\mu_4\text{-S}$ -ligands was the first discovered compound of this rare type.¹²⁸ Four Nb^{III} atoms in this diamagnetic compound provide eight electrons for the formation of four metal–metal bonds with distances Nb–Nb equal to 2.83 Å. Another example is the $[\text{Nb}_4\text{S}_2(\text{SPh})_8(\text{PMe}_2\text{R})_4]$ complex ($\text{R} = \text{Me}, \text{Ph}$).¹²⁹

The polymeric vanadium compound $\text{V}_4\text{S}_9\text{Br}_4$ contains the metal core $\text{V}_4(\mu_4\text{-S})(\mu_2\text{-S}_2)_4^{4+}$ (Fig. 14).¹³ Four ligands S_2 are coordinated asymmetrically. The bridging bromine atoms link the clusters into the layer $[\text{V}_4(\mu_4\text{-S})(\mu_2\text{-S}_2)_4\text{Br}_{8/2}]_{\infty}$. The vanadium oxidation state in this complex is equal to +3.5 and only two electrons take part in the metal–metal bonding (the distances V–V are equal to 3.01 Å). The remaining four non-bonded electrons are located at the metal centres (one per each metal atom), which makes the compound paramagnetic. The oxidation state of tantalum atoms in the cluster core $\text{Ta}_4(\mu_4\text{-Q})(\mu_4\text{-Q}_2)_4^{8+}$ of molecular diamagnetic compounds

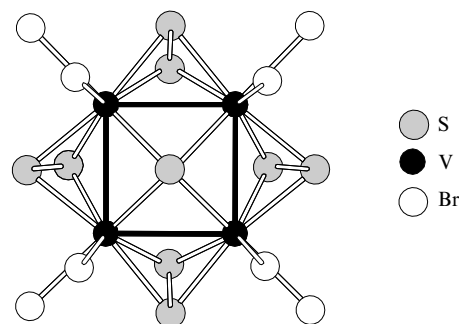


Figure 14. Structure of the cluster fragment $\text{V}_4(\mu_4\text{-S})(\mu_2\text{-S}_2)_4\text{Br}_8$ in the compound $\text{V}_4\text{S}_9\text{Br}_4$.

$\text{Ta}_4\text{Q}_9\text{X}_8$ ($\text{Q} = \text{S}, \text{Se}$; $\text{X} = \text{Br}, \text{I}$) is +4.5 and therefore only two electrons are available for bonding in the metal cluster.¹⁴ Long distances Ta–Ta (3.30–3.39 Å) are typical of such electron-deficient square clusters.

6. Other examples of tetranuclear chalcogenide clusters

Tetranuclear complexes containing the cluster core $\text{M}_4(\mu_3\text{-S})_2(\mu_2\text{-S})_4^{2+}$ with planar arrangement of metal atoms were synthesised. The complexes $[\text{Mo}_4(\mu_3\text{-S})_2(\mu_2\text{-S})_4 \cdot (\text{SH})_2(\text{PMe}_3)_6]$ (Fig. 15)¹³⁰ and $[\text{W}_4(\mu_3\text{-S})_2(\mu_2\text{-S})_4(\text{SH})_2 \cdot (\text{PMe}_2\text{Ph})_6]$ belong to this class.¹³¹ These clusters provide ten electrons for the formation of five localised metal–metal bonds; the bond lengths lie in the narrow interval (Mo–Mo 2.83–2.85 Å; W–W 2.81–2.84 Å). The two-electron oxidation of the complex $[\text{W}_4(\mu_3\text{-S})_2(\mu_2\text{-S})_4\text{Cl}_2(\text{PMe}_2\text{Ph})_6]$ yields the salt of double-charged cationic cluster $[\text{W}_4(\mu_3\text{-S})_2(\mu_2\text{-S})_4\text{Cl}_2 \cdot (\text{PMe}_2\text{Ph})_6](\text{CF}_3\text{SO}_3)_2$.¹³¹ The reduction of the same cluster by excess of sodium amalgam results in the formation of the tungsten(III) complex $[\text{W}_4(\mu_2\text{-S})_6(\text{PMe}_2\text{Ph})_6]$, containing tetrahedral metal cluster W_4 ($N_e = 12$, the distances W–W are equal to 2.634 Å).¹³¹

The cluster M_4 core of a ‘butterfly’ type with two $\mu_3\text{-S}$ -ligands was found in the complex $[\text{Mo}_4(\mu_3\text{-S})_2(\mu\text{-CO})_4 \cdot (\eta^5\text{-C}_5\text{H}_5\text{CO}_2\text{Me})_4]$; the edges also coordinate four $\mu_2\text{-carbonyl}$ groups (Fig. 16).¹³²

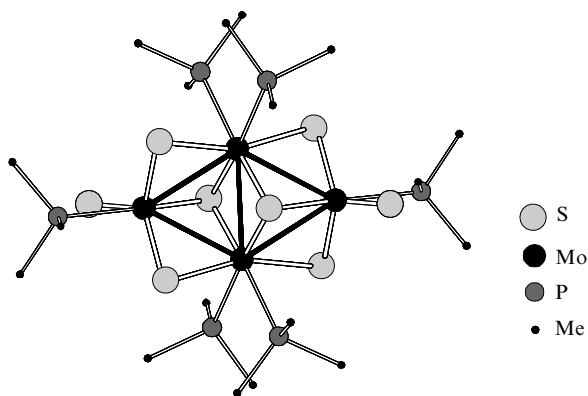


Figure 15. Structure of the complex $[\text{Mo}_4(\mu_3\text{-S})_2(\mu_2\text{-S})_4(\text{SH})_2(\text{PMe}_3)_6]$.

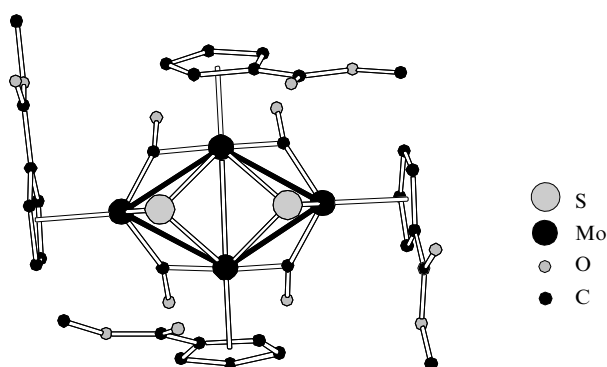


Figure 16. Structure of the complex $[\text{Mo}_4(\mu_3\text{-S})_2(\mu\text{-CO})_4.(\eta^5\text{-C}_5\text{H}_4\text{CO}_2\text{Me})_4]$.

7. Octahedral clusters

The octahedral clusters (Fig. 17) are the most numerous among hexanuclear cluster complexes. The metal cluster M_6 in these complexes is surrounded by eight $\mu_3\text{-L}^i$ ligands coordinated to triangular faces of the metal octahedron. Additionally, the metal atoms coordinate the terminal ligands L^a producing a cluster complex $[\{\text{M}_6\text{L}_8^i\}\text{L}_6^a]$. [The indices i and a were introduced by Schäfer and Schnering¹³³ and derived from German words inner (inner) and ausser (outer); the ligands of the $\mu_2\text{-L}$ type, coordinated to the edges of metal cluster, were classified as inner.] Then the cluster core may be regarded as a combination of the metal cluster and L^i ligands. The total

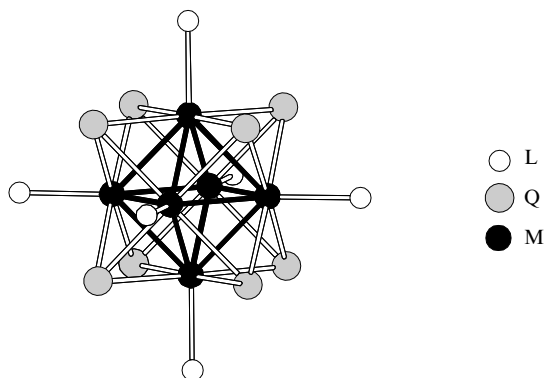


Figure 17. Structure of the octahedral cluster complex $[\text{M}_6\text{Q}_8]\text{L}_6^a$.

number of the ligands surrounding the M_6 octahedron is equal to 14. Accordingly, the cluster compounds with $\text{L}:\text{M} = 14:6$ possess the molecular structure with isolated cluster complexes {for example, $[\text{Re}_6\text{S}_4\text{Br}_{10}]$, $\text{Cs}_4[\text{Mo}_6\text{S}_2\text{Br}_{12}]$,¹³⁴ $[\text{W}_6\text{S}_8(\text{py})_6]$,¹³⁵ *etc.*}. When the ratio $\text{L}:\text{M}$ is smaller, the polymeric structures are formed. In these structures, both L^i and L^a may play the role of bridging ligands. The examples of such structures are given below.

Twenty-four valence electrons ($N_e = 24$) are required for the filling of 12 bonding molecular orbitals (MO) corresponding to metal–metal bonds in a metal cluster M_6 . This situation exists in compounds in which the metal ions possess the d^4 electron configuration, for instance, in the octahedral Re^{III} complexes that contain the $\text{Re}_6\text{Q}_8^{2+}$ cluster core.¹³⁶ Compounds with electron-deficient cluster cores ($N_e = 20\text{--}22$) are stable in the case of chromium, molybdenum and tungsten chalcogenide complexes; the most spectacular examples of such compounds are molybdenum chalcogenides, Mo_6Se_8 ($N_e = 20$) and PbMo_6S_8 ($N_e = 22$).

The octahedral chalcogenide clusters of the Group 5 metals are virtually unknown, probably, because of the considerable deficit of electrons required for the formation of the $\text{M}–\text{M}$ bonds in the cluster. The complex $[\text{V}_6\text{Se}_8(\text{O})(\text{PMe}_3)_6]$ (Fig. 18), in which the metal cluster V_6 contains an interstitial (μ_6) oxygen atom, is the only example of such chalcogenide clusters.¹³⁷ The octahedral geometry of this electron-deficient cluster ($N_e = 12$) is retained due to the formation of $\text{V}–\text{O}$ bonds.

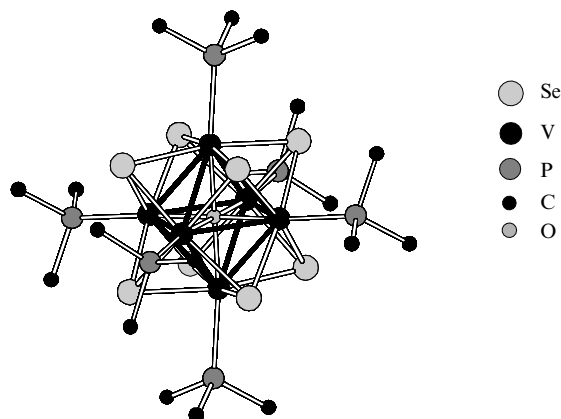


Figure 18. Structure of the complex $[\text{V}_6\text{Se}_8(\text{O})(\text{PMe}_3)_6]$.

Isocharged or non-isocharged substitution of chalcogenide ligands in the cluster core M_6Q_8 results in the formation of isomers which are very hard to separate. Thus in the case of $\text{M}_6\text{Q}_6\text{Q}'_2$ three geometric isomers are possible (Fig. 19), and in the case of $\text{M}_6\text{Q}_4\text{Q}'_4$ the number of isomers is six. Typically, the heteroatoms in the solid state structure of the clusters with mixed ligands are disordered over all possible positions. However, there are some examples of ordered structures. These compounds are usually formed in the cases of significant difference in atomic radii of the ligands L^i : Te and Cl in $\text{Re}_6\text{Te}_8\text{Cl}_{10}$ (Ref. 138) or Se and O in $[\text{Re}_6\text{Se}_4\text{O}_4\text{Cl}_6]^{4-}$.¹³⁹ The metal cluster Re_6 in compound $\text{Cs}_{11}(\text{H}_3\text{O})$. $[\text{Re}_6\text{Se}_4\text{O}_4\text{Cl}_6]_3 \cdot 4\text{H}_2\text{O}$ is surrounded by four oxygen atoms and four selenium atoms, localised at the opposite faces of the Se_4O_4 cube (Fig. 20).¹³⁹ Such ligand environment results in a significant distortion of the metal cluster and the $\text{Re}–\text{Re}$ distances in this compound vary from 2.46 Å (in the faces coordinating the $\mu_3\text{-oxygen}$ atoms) to 2.62 Å (in the faces coordinating the $\mu_3\text{-selenium}$ atoms).

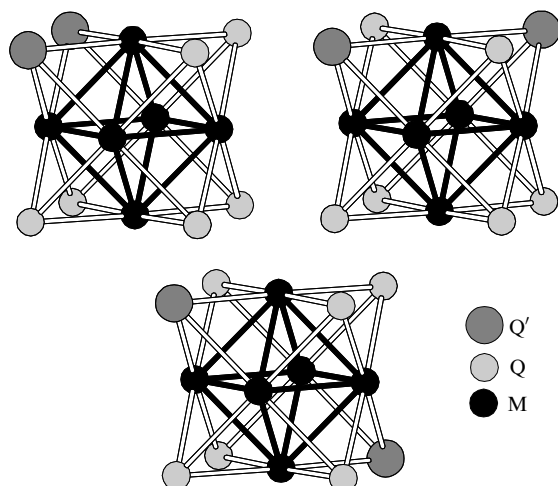


Figure 19. Geometrical isomers of the cluster core $[M_6Q_6Q'_2]$.

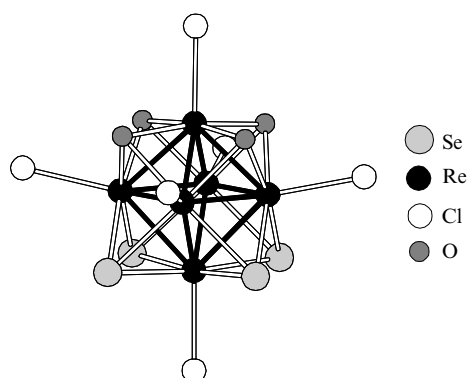


Figure 20. Structure of the complex $[Re_6Se_4O_4Cl_6]^{4-}$.

There are several examples of heterometallic octahedral clusters: $Mo_{6-x}M_xQ_8$ ($M = Re$: $Q = S, Se, Te, x = 4$; $M = Ru$: $Q = Se, Te, 0 \leq x \leq 2$; $M = Rh$, $Q = Te, x = 0.5, 1.33$),¹⁴⁰ $Nb_{6-x}Ru_xTe_8$ ($2.50 \leq x \leq 3.17$),¹⁴¹ $Cs_5[Re_{6-x}Mo_xS_8(CN)_6]$,¹⁴² $Cs_3[Re_5OsS_{11}]$,¹⁴³ $Cs_3[Re_{6-x}Os_xSe_8Cl_6]$ ($x = 1, 2$) and $K_2[Re_3Os_3Se_8Cl_6][Re_4Os_2Se_7Cl_7]$.¹⁴⁴ The phosphine and cyanide complexes were studied for rhenium–osmium clusters.^{144, 145}

A great number of molecular complexes of molybdenum, tungsten and rhenium with the cluster core M_6Q_8 were studied. Ions (halides, cyanide, thiocyanate, hydroxide) or neutral molecules (phosphines, pyridines, *etc.*) play the role of ligands L^a in these complexes.^{19, 135, 136, 139, 146–178} Usually, the terminal ligands are coordinated in a monodentate mode or as bridging ligands linking adjacent clusters. The study of coordination of diphosphine $Ph_2P(CH_2)_nPPH_2$ with octahedral rhenium clusters has shown that the chelate complexes are formed if $n \geq 6$.¹⁵³

8. Miscellaneous hexanuclear clusters

The metal cluster V_6 in compound $(Et_4N)_3[V_6S_4(edt)_6(O)_2]$ is essentially planar. Nine valence electrons take part in the formation of five V–V bonds (2.82–2.86 Å) (Fig. 21).¹⁷⁹ Four triangles Mo_3 with shared edges in the topologically related hexanuclear molybdenum clusters $[Mo_6S_{10}(SH)_2.(PET_3)_6]$ coordinate four μ_3 - and six μ_2 -chalcogen atoms (Fig. 22).¹³⁰ There are 14 electrons per nine Mo–Mo bonds in this cluster, which results in the shortening (in comparison

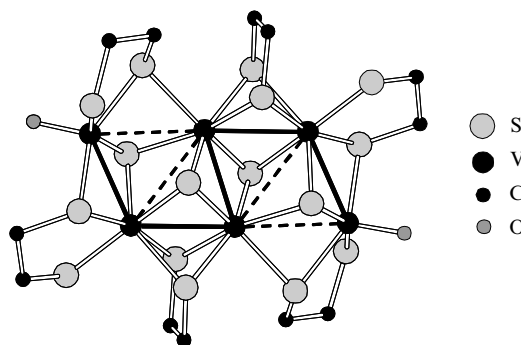


Figure 21. Structure of the complex $[V_6(\mu_3-S)_4(edt)_6(O)_2]^{3-}$.

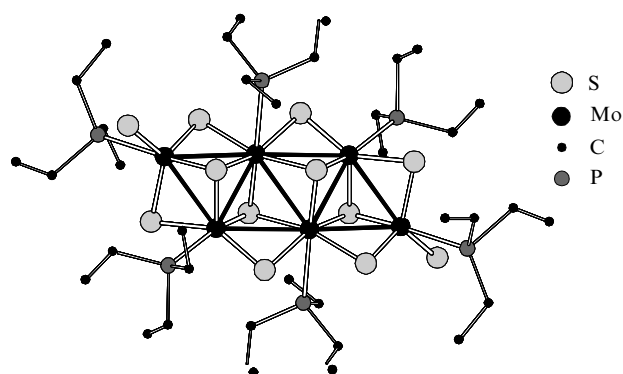


Figure 22. Structure of the complex $[Mo_6(\mu_3-S)_4(\mu-S)_6(SH)_2(PET_3)_6]$.

with the vanadium structure) of the distances Mo–Mo (2.73–3.06 Å). Similar structure of the cluster core was also observed in compounds $[Mo_6Q_8Cl_6(PET_3)_6]$.¹⁸⁰

The metal cluster Mo_6 in an unusual complex $[Mo_6S_6(CN)_{16}]^{8-}$ (Fig. 23) may be represented by two edge-sharing tetrahedrons. Four edges coordinate sulfur atoms according to the μ_3 -type and two pairs of fused faces (*i.e.* those with the shared edge) coordinate sulfur atoms according to the μ_4 -type.¹⁸¹

Two triangles Nb_3 in the hexanuclear cluster $[Nb_6SBr_{17}]^{3-}$ (Fig. 24) are linked together by a μ_6 -sulfur atom.¹⁸² The Nb–Nb bond lengths in the triangles are in the range of 2.95–2.98 Å, the distances between the triangles are longer and equal to 3.276 Å.

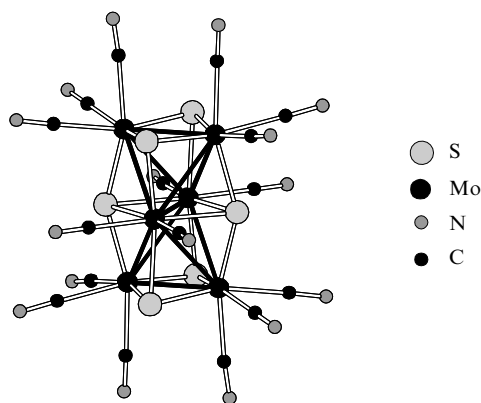


Figure 23. Structure of the complex $[Mo_6S_6(CN)_{16}]^{8-}$.

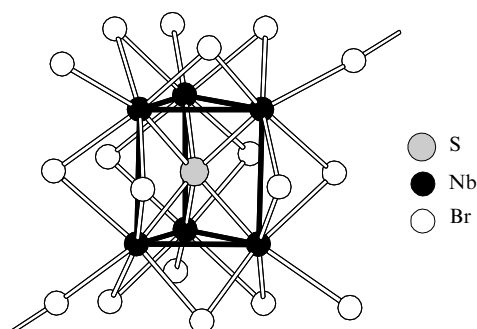


Figure 24. Structure of the complex $[\text{Nb}_6\text{SBr}_{17}]^{3-}$.

9. Compounds based on polymeric octahedral cluster complexes

The decrease of the number of ligands in molecular complexes $[\text{M}_6\text{L}_8]\text{L}_6^a$ results in the formation of polymeric-bridged structures. According to Schäfer,¹³³ the inter-cluster bridging ligands are designated as L^{a-a} , L^{i-a} and L^{a-i} depending on their structural role in each of the metal clusters linked by them.

a. Linking of the octahedral cluster cores through bridging halide ligands L^{a-a}

One of the most common methods of linking of cluster cores M_6L_8 into polymeric chains, layers and frameworks (when the ratio $\text{L}:\text{M}$ is decreasing) is the linking through apical halide ligands which become bridging between two cluster cores (Table 2). If all six apical ligands are bridging, then the compounds form 3D frameworks (Fig. 25), if four equatorial ligands are bridging then layered 2D polymers are formed and in the case of two bridging ligands 1D chains are formed.

The ternary systems $\text{Re}-\text{Q}-\text{Y}$ ($\text{Q} = \text{S}, \text{Se}; \text{Y} = \text{Cl}, \text{Br}$) are models in the studies of the influence of the number of shared ligands on the polymeric structure type. Depending on the ratio $\text{Q}:\text{Y}$, all possible types of structures are formed in these systems: the frameworks in $\{(\text{Re}_6\text{Q}_7^i\text{Y}^i)\text{Y}_{6/2}^{a-a}\}$,¹⁸⁴ the layers in $\{(\text{Re}_6\text{Q}_6^i\text{Y}_2^i)\text{Y}_4^{a-a}\}$,¹⁸⁴ the chains in $\{(\text{Re}_6\text{Q}_5^i\text{Y}_3^i)\text{Y}_4^{a-a}\}$ ¹⁸⁴ and isolated cluster complexes in $(\text{Re}_6\text{Q}_4^i\text{Y}_4^i)\text{Y}_6^a$.¹⁸⁶⁻¹⁹⁰ The structures and properties of these compounds are discussed in details in reviews.^{16, 136, 191}

Table 2. Octahedral clusters with inter-cluster halide ligands.

Compound	Structural type	Crystallochemical formula	Ref.
$\text{Mo}_6\text{QCl}_{10}$	framework (3D)	$\{(\text{Mo}_6\text{Q}^i\text{Cl}_7^i)\text{Cl}_{6/2}^{a-a}\};$ $\text{Q} = \text{S}, \text{Se}, \text{Te}$	183
$\text{Re}_6\text{Q}_7\text{X}_4$	"	$\{(\text{Re}_6\text{S}_7^i\text{Br}^i)\text{Br}_{6/2}^{a-a}\}$	184
$\text{Re}_6\text{Q}_6\text{X}_6$	layer (2D)	$\{(\text{Re}_6\text{Se}_6^i\text{Cl}_2^i)\text{Cl}_2^{a-a}\},$ $\{(\text{Re}_6\text{S}_6^i\text{Br}_2^i)\text{Br}_2^{a-a}\}$	184
$\text{Re}_6\text{Q}_5\text{X}_8$	chain (1D)	$\{(\text{Re}_6\text{Se}_5^i\text{Cl}_3^i)\text{Cl}_4^{a-a}\},$ $\{(\text{Re}_6\text{S}_5^i\text{Br}_3^i)\text{Br}_4^{a-a}\}$	184
$\text{AgRe}_6\text{Se}_6\text{Cl}_7$	"	$\text{Ag}\{(\text{Re}_6\text{Se}_6^i\text{Cl}_2^i)\text{Cl}_4^{a-a}\}$	185
$\text{ZnRe}_6\text{Se}_7\text{Cl}_6$	"	$\text{Zn}\{(\text{Re}_6\text{Se}_7^i\text{Cl}^i)\text{Cl}_3^{a-a}\}$	185

b. Linking of the octahedral cluster cores through chalcogenide and polychalcogenide inter-cluster ligands

The compounds with bridging chalcogenide and polychalcogenide ligands were obtained only for rhenium and technetium;¹⁹² some crystal data on these compounds are listed in Table 3. The examples of the compounds with unusual bridging ligands, viz., spiro- Te_7^{2-} and Te_6 , are shown in Figs 26 and 27.^{8, 206}

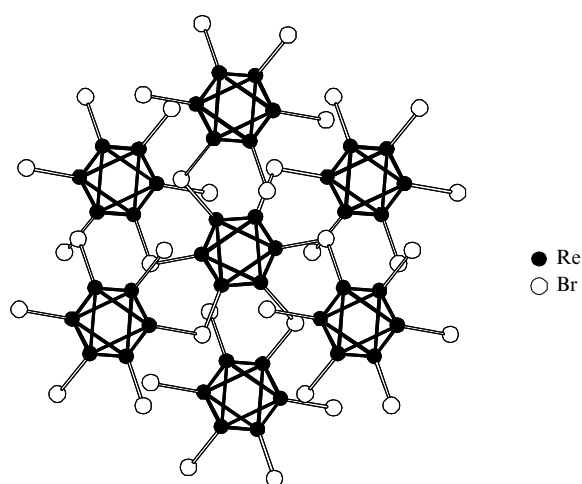


Figure 25. Fragment of the structure of $\text{Re}_6\text{Se}_7\text{Br}_4$ (the 'inner' ligands are omitted).

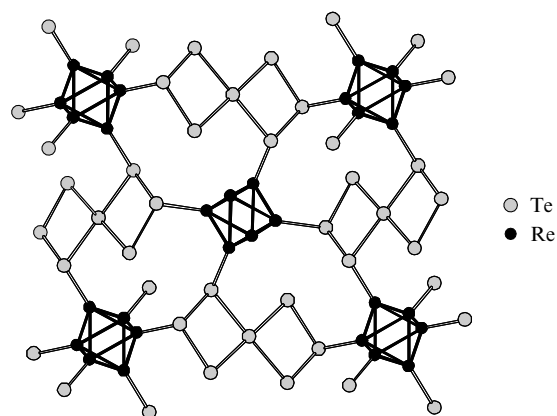


Figure 26. Linking of the metal clusters Re_6 through Te_7 ligands in the structure of $\text{Re}_6\text{Te}_{15}$.

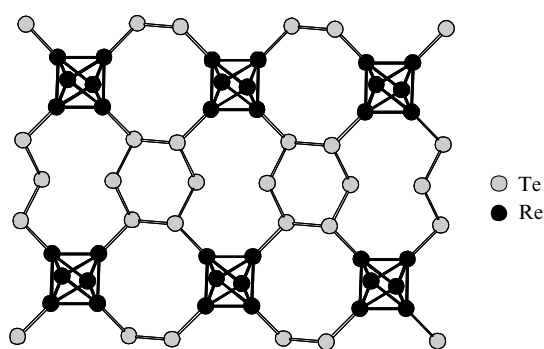


Figure 27. Linking of the metal clusters Re_6 through Te_6 ligands in the structure of $\text{Re}_6\text{Te}_{16}\text{Cl}_{18}$.

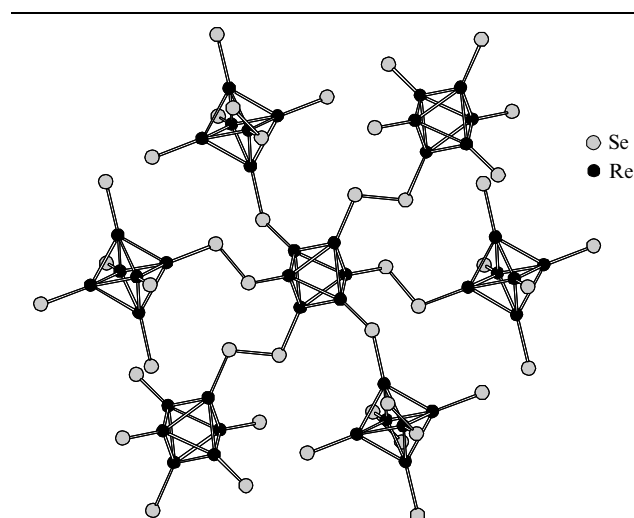
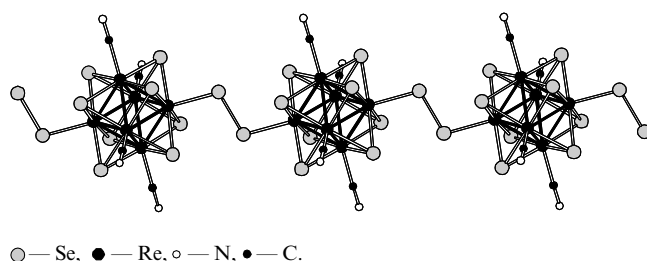
Linking of the cluster cores into layered or 3D-framework structures through chalcogen atoms is typical of ternary rhenium sulfides and selenides. The cluster cores in $\text{Cs}_4[(\text{Re}_6\text{Se}_8^i)\text{Se}_{2/2}^{a-a}(\text{Se}_2)_{4/2}^{a-a}]$ are linked together by two selenide and four diselenide bridges yielding a 3D structure (Fig. 28).²⁰¹

Recently, octahedral rhenium chalcocyanide complexes with bridging chalcogenide ligands have been obtained: the layered structure of $\text{K}_4[\text{Re}_6\text{S}_{10}(\text{CN})_2]$ and chain structures of

Table 3. Octahedral clusters with chalcogenide and polychalcogenide inter-cluster ligands.

Compound	Structural type	Crystallochemical formula	Ref.
Compounds containing only the chalcogenide bridges			
Cs ₄ Re ₆ S ₉ (CN) ₄	chain (1D)	Cs ₄ {(Re ₆ S ₈ ⁱ)(CN) ₄ (S) _{2/2} ^{a-a} }	193
K ₄ Re ₆ S ₁₀ (CN) ₂	layer (2D)	K ₄ {(Re ₆ S ₈ ⁱ)(CN) ₂ (S) _{4/2} ^{a-a} }	194
Cs ₆ Re ₆ S ₁₂	"	Cs ₆ {(Re ₆ S ₈ ⁱ)(S) _{4/2} ^{a-a} S ₂ ^a }	195
Li ₄ Re ₆ S ₁₁	framework (3D)	Li ₄ {(Re ₆ S ₈ ⁱ)(S) _{6/2} ^{a-a} }	196
M ₂ Re ₆ S ₁₁ , M = Sr, Ba, Eu	"	M ₂ {(Re ₆ S ₈ ⁱ)(S) _{6/2} ^a }	197, 198
Compounds containing polychalcogenide bridges			
K ₄ Re ₆ Se ₁₀ (CN) ₄	chain (1D)	K ₄ {(Re ₆ S ₈ ⁱ)(CN) ₄ (Se ₂) _{2/2} ^a }	194
M ₄ Re ₆ S ₁₂ , M = Na, K, Rb	framework (3D)	M ₄ {(Re ₆ S ₈ ⁱ)(S) _{4/2} ^{a-a} (S ₂) _{2/2} ^{a-a} }	199, 200
M ₄ Re ₆ Se ₁₂ , M = K, Rb	"	M ₄ {(Re ₆ Se ₈ ⁱ)(Se) _{4/2} ^{a-a} (Se ₂) _{2/2} ^{a-a} }	201
M ₄ Re ₆ S ₁₃ , M = (K,Rb), Rb, Cs	"	M ₄ {(Re ₆ S ₈ ⁱ)(S) _{2/2} ^{a-a} (S ₂) _{4/2} ^{a-a} }	201, 202
Cs ₄ Re ₆ Se ₁₃	"	Cs ₄ {(Re ₆ Se ₈ ⁱ)(Se) _{2/2} ^a (Se ₂) _{4/2} ^{a-a} }	201
Cs ₄ Re ₆ S _{13.5}	"	Cs ₄ {(Re ₆ S ₈ ⁱ)(S) _{2/2} ^{a-a} (S ₂) _{3/2} ^{a-a} (S ₃) _{1/2} ^{a-a} }	202, 203
Cs ₆ Re ₆ S ₁₅	"	Cs ₄ {(Re ₆ S ₈ ⁱ)(S) _{2/2} ^{a-a} (S ₂) _{6/2} ^{a-a} } · Cs ₂ S	204
Cs ₆ Re ₆ Se ₁₅	"	Cs ₄ {(Re ₆ Se ₈ ⁱ)(Se ₂) _{6/2} } · Cs ₂ Se	205
Re ₆ Te ₁₅	"	{(Re ₆ Te ₈ ⁱ)(Te ₇) _{6/6} ^a }	8
Re ₆ Te ₈ (Te ₈ Cl ₁₈)	"	{(Re ₆ Te ₈ ⁱ)(Te ₈ Cl ₁₈) _{6/6} ^a }	206
Re ₆ Te ₈ (Te ₆)(TeCl ₃) ₂	layer (2D)	{(Re ₆ Te ₈ ⁱ)(TeCl ₃) ₂ ^a (Te ₆) _{4/4} ^a }	206

K₄[Re₆Se₁₀(CN)₄] and Cs₄[Re₆S₉(CN)₄] contain bridging sulfide and diselenide ligands (Fig. 29).^{193, 194}

**Figure 28.** Fragment of polymer layer $[\{\text{Re}_6\text{Se}_8\}(\text{Se}_{2/2}^{\text{a-a}})(\text{Se}_2)_{4/2}^{\text{a-a}}]_{\infty}^{4-}$ in the structure of Cs₄[Re₆Se₁₃] (the μ₃-Se ligands are omitted).**Figure 29.** Fragment of polymer chain $[\{\text{Re}_6\text{Se}_8\}(\text{Se}_2)_{2/2}(\text{CN})_4]_{\infty}^{4-}$ in the structure of K₄[Re₆Se₁₀(CN)₄].

c. Linking of the octahedral cluster cores through ‘inner’ ligands

The metal coordination sphere of lower chalcogenides contains the ligands of an adjacent cluster core which thus become the inter-cluster bridges. The less is the L : M ratio the more ‘inner’ ligands are involved in the formation of these inter-cluster bridges. Examples of such compounds are given in Table 4.

Each molybdenum atom in the compound Mo₆Se₈ is bonded to the inner ligand of the adjacent cluster, which thus may be regarded as an apical ligand.^{213, 214} As a result, the clusters are strongly linked together due to the formation of rhombic fragments Mo₂Se₂ⁱ (Fig. 30) and the Mo–Mo distances between the molybdenum atoms of the neighbouring metal clusters are shortened (3.266 Å).

Other compounds with strong inter-cluster bridges are represented by rhenium chalcogenides Re₆S₈Cl₂, Re₆Se₈Cl₂, Re₆S₈Br₂ and Re₆Se₈Br₂.^{207–209} The cores Re₆S₈ⁱ in crystals of Re₆S₈Cl₂ are linked in chains by two centrosymmetrical Re–S

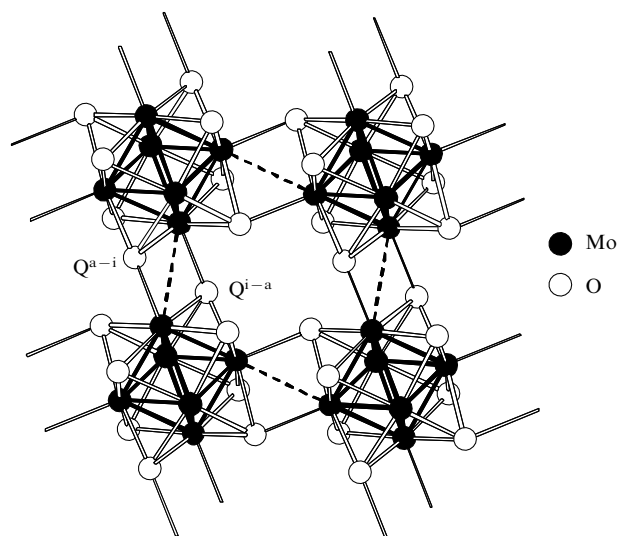
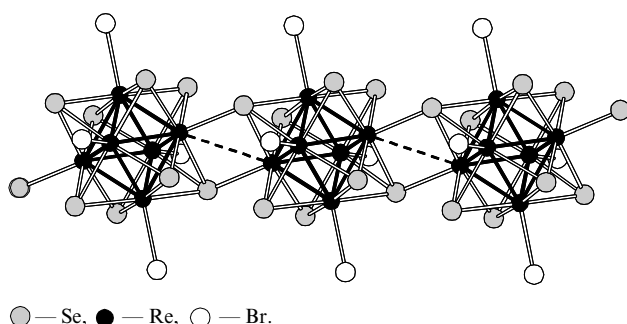
**Figure 30.** Fragment of the structure of Mo₆Q₈ in the Chevrel phases. The inter-cluster Mo–Mo contacts are shown by dashed lines.

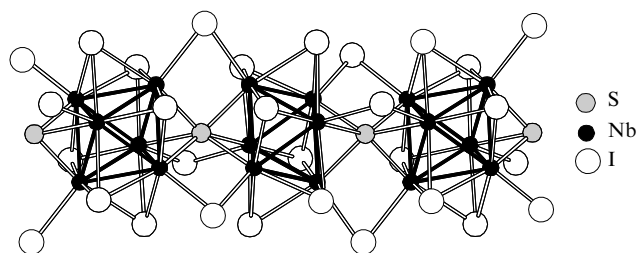
Table 4. Octahedral clusters with additional coordination of the 'inner' ligands of cluster core.

Compound	Structural type	Crystallochemical formula	Ref.
Re ₆ S ₈ Cl ₂ , Re ₆ S ₈ Br ₂ , Re ₆ Se ₈ Br ₂	framework (3D)	{(Re ₆ Q ₆ ^{i-a} Q _{2/2} ^{i-a} Q _{2/2} ^{i-a} Y _{4/2} ^{a-a}); Q = S, Se; Y = Cl, Br}	207–209
Re ₆ Se ₈ Cl ₂	layer (2D)	{(Re ₆ Se ₄ ^{i-a} Se _{4/2} ^{i-a} Se _{4/2} ^{i-a} Cl ₂ ^a)}	210
Cs ₂ Re ₆ Se ₈ Br ₄	chain (1D)	Cs ₂ {(Re ₆ Se ₆ ^{i-a} Se _{2/2} ^{i-a} Br ₄ ^a Se _{2/2} ^{i-a})}	211
TlRe ₆ Se ₈ Cl ₃	layer (2D)	Tl{(Re ₆ Se ₅ ^{i-a} Se _{3/2} ^{i-a} Cl ₃ ^a Se _{3/2} ^{i-a})}	212
CsRe ₆ Se ₈ I ₃	"	Cs{(Re ₆ Se ₆ ^{i-a} Se _{2/2} ^{i-a} I ₂ ^a I _{2/2} ^{i-a} Se _{2/2} ^{i-a})}	211
M ₂ Re ₆ Q ₈ Cl ₄ , M = Tl: Q = S, Se; M = Cs, Q = S	chain (1D)	M ₂ [Re ₆ Q ₆ ^{i-a} Q _{2/2} ^{i-a} Cl ₄ ^a Q _{2/2} ^{i-a}]	211, 212
Re ₄ Os ₂ Se ₈ Cl ₄	framework (3D)	{(Re ₄ Os ₂ Se ₈ ^{i-a} Se _{2/2} ^{i-a} Cl ₂ ^a Cl _{2/2} ^{i-a} (Re ₄ Os ₂ Se ₆ ^{i-a} Se _{2/2} ^{i-a} Cl ₂ ^a Cl _{2/2} ^{i-a})}	144
Mo ₆ Q ₈	"	{(Mo ₆ Q ₆ ^{i-a} Q _{2/2} ^{i-a} Q _{2/2} ^{i-a}); Q = S, Se}	213, 214
Mo ₆ S ₆ Br ₂	"	{(Mo ₆ Br ₂ ^{i-a} S _{6/2} ^{i-a} S _{6/2} ^{i-a})}	215
Mo ₆ I ₈ Se ₂	"	{(Mo ₆ I ₅ ^{i-a} Se ₃ ^{i-a} I _{6/2} ^a I _{6/2} ^{i-a})}	216
Nb ₆ I ₉ S	chain (1D)	{Nb ₆ I ₆ ^{i-a} S _{2/2} ^{i-a} I _{6/2} ^a I _{6/2} ^{i-a} }	217

bonds. The chains are combined into a 3D structure by Re—Cl^{a-a}—Re bridges. The rhombic bridges Re₂Q₂ were also found in some other compounds. The structure TlRe₆.Se₈Cl₃, *i.e.* Tl{(Re₆Se₅^{i-a}Se_{3/2}^{i-a}Se_{3/2}^{i-a}Cl₃^a)}, consists of layers linked by three Re₂Se₂ bridges.²¹² The cores Re₆Se₈ in crystals of Cs₂Re₆Se₈Br₄ are *trans*-linked in chains by rhombuses Re₂Se₂ (Fig. 31).²¹¹

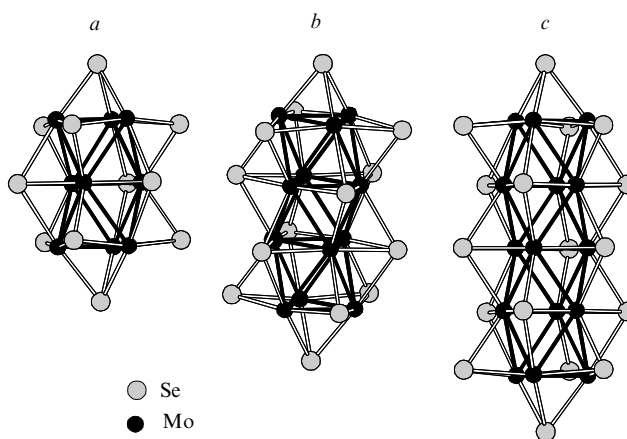
**Figure 31.** Fragment of polymer chain {Re₆Se₈Br₄}_∞²⁻ in the structure of Cs₂Re₆Se₈Br₄.

The complex Nb₆I₉S containing the electron-deficient 19-electron cluster core Nb₆I₆^{i-a}S₂^{i-a} occupies a special place among the polymeric chalcogenides. The sulfide ligands Lⁱ in this compound are shared between adjacent clusters (Fig. 32). In addition, the apical iodine atoms also make bridges between the clusters; this results in the formation of unusual linear chains [Nb₆I₆^{i-a}S_{2/2}^{i-a}I_{6/2}^aI_{6/2}^{i-a}].²¹⁷

**Figure 32.** Fragment of a polymeric chain {Nb₆I₆^{i-a}S_{2/2}^{i-a}I_{6/2}^aI_{6/2}^{i-a}} in the structure of Nb₆I₉S.

10. High nuclearity clusters

A homologous series of the clusters Mo_{6+3x}Q_{8+3x} (Q = S, Se; x = 1–3), which was found in ternary molybdenum chalcogenides, may be described as a product of the progressive condensation of triangles Mo₃. The first member of the series, Mo₉Se₁₁, contains a dioctahedral metal cluster Mo₉.²¹⁸ Eight selenium atoms are bonded to the metal cluster according to the μ₃-mode, and three selenium atoms, which are located in the plane of the middle Mo₃ triangle, are μ₄-mode coordinated. The metal atoms of the outer triangles Mo₃ of the cluster core Mo₉Q₁₁ in a crystal are additionally coordinated by six bridging Se atoms, which link together the adjacent cluster fragments Mo₉Q₁₁. The structures of clusters Mo₉Q₁₁, Mo₁₂Q₁₄ and Mo₁₅Q₁₇ are shown in Fig. 33.^{218–221} The condensation continues up to joining together 11 octahedra in the structure of Rb₁₀Mo₃₆S₃₈.²²² The ultimate case of the condensation of the triangles Mo₃ is represented by compounds M[Mo₃Q₃] (M = Li, In, Tl; Q = Se, Te) containing infinite chains [Mo₃Q₃]_∞.²²³

**Figure 33.** Structures of the cluster cores Mo₉Se₁₁ (a), Mo₁₂Se₁₄ (b), Mo₁₅Se₁₈ (c).

The mixed-valence cluster complex [Re₉Se₁₁Br₆]²⁻ consists of eight Re^{III} atoms and one Re^{II} atom. This is the only example of a rhenium cluster in the family of condensed octahedral clusters.²²⁴ The complex contains a cluster core similar to that of the Mo₉Se₁₁ and only the bromine ligands occupy terminal positions.

The unique twelve-nuclear cluster complex [Re₁₂CS₁₇(CN)₆]⁸⁻ (Fig. 34) consists of two Re₆ octahedra

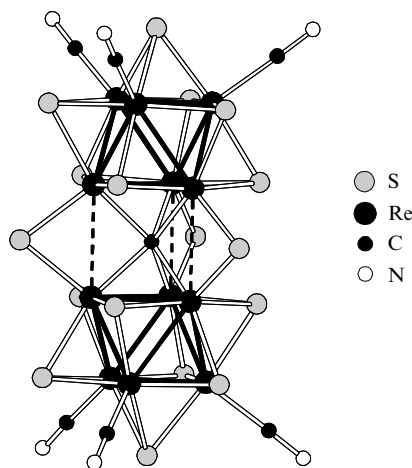


Figure 34. Structure of the complex $[\text{Re}_{12}\text{CS}_{17}(\text{CN})_6]^{8-}$.

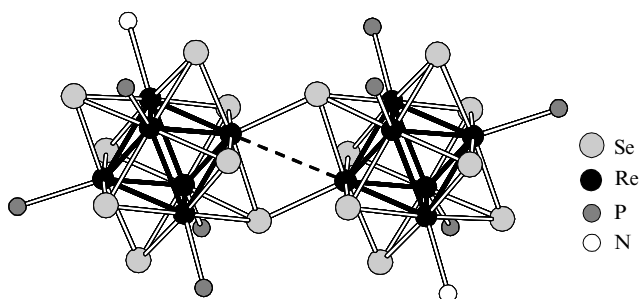


Figure 35. Structure of the complex $\text{trans-}[\text{Re}_{12}\text{Se}_{16}(\text{PEt}_3)_8(\text{MeCN})_2]^{4+}$ (the ethyl and MeC groups are omitted).

linked by three μ_2 -S-bridges and a μ_6 -carbon atom.¹⁵ Each Re_6 -cluster coordinates seven μ_3 -S-atoms and a μ_6 -C-ligand attaining environment typical of octahedral Re clusters Re_6Q_8 . The Re_6 prism formed by 'inner' triangles and centred by the μ_6 -carbon atom is an important part of the structure. The mean distance between metal clusters in the anion $[\text{Re}_{12}\text{CS}_{17}(\text{CN})_6]^{8-}$ is equal to 3.17 Å. This distance is very sensitive to the charge of the cluster anion and decreases to 2.90 Å after two-electron oxidation of the cluster.¹⁵ The cluster $\text{Mo}_{12}\text{S}_{18}$, which was found in the compound $\text{Ba}_4\text{Mo}_{12}\text{S}_{18}$, possesses a similar structure.²²⁵

The dodecanuclear clusters of a different type are formed in the condensation of the octahedral clusters with labile apical ligands. Thus thermolysis of $\text{cis-}[\text{Re}_6\text{Se}_8(\text{PEt}_3)_4(\text{MeCN})_2]$ containing two labile MeCN ligands results in the formation of dimers of $\text{trans-}[\text{Re}_{12}\text{Se}_{16}(\text{PEt}_3)_8(\text{MeCN})_2]^{4+}$ (Fig. 35).^{152, 226}

III. Methods of synthesis of chalcogenide clusters

The methods of synthesis of the cluster compounds may be divided into two main groups: the high-temperature synthesis, which is carried out in closed systems (usually, in sealed evacuated tubes), and the solution synthesis. The high-temperature reactions are extremely important for the synthesis of clusters of the Group 5–7 metals because quite often a chalcogenide cluster core, especially a high-nuclear one, cannot be formed in solution. Further chemical modifications of a cluster compound obtained by high-temperature synthesis may be carried out in solutions or in melts.

1. High-temperature synthesis

The method is based on the fact that a phase that is thermodynamically stable under certain experimental conditions may be obtained from different starting compounds taken in the appropriate ratio. The elements and compounds (for example, metal halides, chalcogenides and chalcogenides) are used as the starting compounds in the synthesis of chalcogenide clusters. In addition to the ratio of the starting compounds in the reaction mixture, the right choice of temperature of the synthesis is very important. A standard procedure for the synthesis of cluster chalcogenides is as follows: a quartz tube is loaded with starting compounds and then evacuated and sealed. If necessary, the tube is cooled down by liquid nitrogen prior to evacuation in order to avoid the loss of volatile components. The sealed tube is placed into a furnace and heated according to the chosen protocol. The reaction mixture is kept at certain temperature for the required period, usually from several tens of hours up to several days, in order to complete the reaction. Such processes, particularly in the case of chalcogenide systems, are accompanied sometimes by mass-transfer processes, which results in the concentration of a solid phase in a cool area. Usually, such gas-transport reactions produce crystals of high quality suitable for X-ray crystallographic and other physicochemical studies.

The chalcogenides of niobium Nb_3QX_7 ($\text{Q} = \text{S}, \text{Se}, \text{Te}$; $\text{X} = \text{Cl}, \text{Br}, \text{I}$)^{80, 83, 227} and tantalum Ta_3QI_7 ($\text{Q} = \text{Se}, \text{Te}$)²²⁸ Ta_3SBr_7 ,⁸² $\text{Ta}_4\text{SI}_{11}$,²²⁹ $\text{Ta}_4\text{S}_9\text{Br}_8$, $\text{Ta}_4\text{Se}_9\text{I}_8$ (Ref. 14) were obtained from the elements at 450–550 °C.

Trinuclear molybdenum and tungsten complexes $\text{M}_3\text{Q}_7\text{X}_4$ ($\text{Q} = \text{S}, \text{Se}, \text{Te}$; $\text{X} = \text{Cl}, \text{Br}, \text{I}$) were synthesised at 350–400 °C. The choice of this temperature interval is caused by both kinetic and thermodynamic factors because these compounds are unstable at higher temperatures. Wide variety of compounds that ensure the correct stoichiometry may be used as the starting components: elementary compounds, lower halides (MoCl_3 or $\text{Mo}_6\text{Cl}_{12}$, W_6Cl_{12}) with sulfur or selenium, sulfides MS_3 ($\text{M} = \text{Mo}, \text{W}$) with PCl_5 as well as other systems.^{3, 230, 231}

High-temperature synthesis affords the telluride complexes $[\text{Mo}_3\text{Te}_7(\text{TeI}_3)_3]$,⁶⁶ $[\text{Mo}_3\text{Te}_7(\text{TeI}_3)_3]_2(\text{TeI}_3)_1$, $[\text{Mo}_3\text{Se}_7(\text{TeI}_3)_2]\text{I}$ and $[\text{Mo}_3\text{Se}_7(\text{TeBr}_3)\text{Br}_2]_2[\text{Te}_2\text{Br}_{10}]$ as single crystals in which the cluster fragments are coordinated by TeX_3^- ligands.²³² The triangular clusters $\text{Re}_3\text{Q}_7\text{X}_7$ ($\text{Q} = \text{S}, \text{Se}$; $\text{X} = \text{Cl}, \text{Br}$) were synthesised from ReX_4 or ReOCl_4 , elemental sulfur or selenium and the corresponding sulfur and selenium halides Q_2X_2 or SeX_4 ($\text{Q} = \text{S}, \text{Se}$; $\text{X} = \text{Cl}, \text{Br}$) at 130–250 °C.⁶¹ Compounds $\text{Re}_3\text{S}_7\text{Br}_7$ and $[\text{Re}_3\text{S}_7\text{Cl}_6][\text{AlCl}_4]$ were obtained in the reaction of Re_2O_7 with S_2Br_2 and with the solution of AlCl_3 and S_2Cl_2 , respectively.^{62, 63}

The high-temperature synthesis is used for the preparation of various types of tetranuclear cluster compounds: rhombic, square and tetrahedral clusters. The rhenium dichalcogenides ReQ_2 ($\text{Q} = \text{S}, \text{Se}$) containing rhombic clusters were obtained by the high-temperature synthesis from elements at 600–800 °C.^{233, 234} The vanadium and tantalum chalcogenides $\text{V}_4\text{S}_9\text{Br}_4$ (Ref. 13) and $\text{Ta}_4\text{Q}_9\text{X}_8$ ($\text{Q} = \text{S}, \text{Se}$)^{14, 235} containing square clusters were synthesised by the same method but at lower temperatures (400–450 °C).

The cubane clusters form the most abundant group of tetranuclear chalcogenide clusters. A series of Mo and Nb chalcogenides $\text{M}_4\text{Q}_4\text{X}_4$ ($\text{Q} = \text{S}, \text{Se}$; $\text{X} = \text{Cl}, \text{Br}, \text{I}$) was obtained by high-temperature synthesis (880–1000 °C) from various starting compounds providing the required proportion of the metal, chalcogen and halogen.^{84, 85} The isostructural rhenium mixed chalcogenide $\text{Re}_4\text{S}_4\text{Te}_4$ was synthesised by heating a stoichiometric mixture of metallic rhenium, sulfur and tellurium for three weeks at 900 °C.⁸⁷ A series of ternary chalcogenides AM_4Q_8 ($\text{A} = \text{Al}, \text{Ga}$; $\text{M} = \text{Mo}, \text{Nb}, \text{Ta}$; $\text{Q} = \text{S}, \text{Se}$), $\text{GaMo}_4(\text{Q}, \text{Q}')_8$ ($\text{Q}, \text{Q}' = \text{S}, \text{Se}, \text{Te}$) and $\text{MMo}_2\text{Re}_2\text{S}_8$ ($\text{M} = \text{Zn}$,

Ni, Co, Fe) belong to the same group of compounds (Refs 88–91, 236–238).

The synthesis of $\text{Re}_4\text{Te}_4(\text{TeBr}_2)_4\text{Br}_8$ from elements at 550 °C was also described.⁹³ The tetrahedral cluster-type rhenium chalcogenides $\text{Re}_4\text{Q}_4(\text{TeCl}_2)_4\text{Cl}_8$ were obtained from ReCl_5 by the reaction either with tellurium or with a mixture S–Te or Se–Te at 350–400 °C:¹⁰



Chalcocyanide cluster complexes can also be prepared by high-temperature synthesis. The niobium and tantalum tellurocyanide tetrahedral complexes $[\text{M}_4\text{OTe}_4(\text{CN})_{12}]^{6-}$ are formed in the reaction of higher tellurides NbTe_4 and TaTe_4 with KCN at 440–460 °C and 340–360 °C, respectively.^{108, 239} The tetrahedral tellurocyanides $[\text{Mo}_4\text{Te}_4(\text{CN})_{12}]^{7-}$ and $[\text{W}_4\text{Te}_4(\text{CN})_{12}]^{6-}$ were obtained from the ditellurides of these metals by heating with KCN at 400 °C.¹⁰² Interestingly, the interaction of trinuclear chalcogenides $\text{M}_3\text{Q}_7\text{X}_4$ (M = Mo, W) with KCN at 400 °C also yields the clusters $[\text{M}_4\text{Q}_4(\text{CN})_{12}]^{n-}$ of higher nuclearity.¹⁰²

The high-temperature synthesis is the main method for the preparation of octahedral chalcogenide clusters of Mo, W, Re. The binary and ternary molybdenum chalcogenides Mo_6Q_8 (Q = Se, Te) and $\text{M}_x\text{Mo}_6\text{Q}_8$ (M is a transition or post-transition metal) as well as phases with condensed clusters containing two, three, four and more fused octahedra up to the phase MMo_3Q_3 (M is an alkali metal), which consists of infinite chains $(\text{Mo}_3\text{Q}_3)^-$, were synthesised from the simple compounds.^{214, 223} The temperature of the synthesis of these compounds is in the range of 900–1500 °C. The synthesis of clusters of higher nuclearity usually requires higher temperatures. The octahedral chalcogenide complexes of the type $\text{A}_4\text{M}_6\text{S}_x$ (A is an alkali metal or thallium; M = Tc, Re; $x = 11, 12, 13, 13.5$) were synthesised at 800–1400 °C. Hydrogen sulfide or hydrogen selenide were used as sources of chalcogen, which were passed over the mixture of a powder metallic rhenium with an alkali metal carbonate.^{192, 196, 197, 199, 201, 203, 240} The cluster-type rhenium telluride $\text{Re}_6\text{Te}_{15}$ was obtained by heating metallic rhenium with tellurium for two weeks at 900 °C.⁸ The reaction rate increases significantly if highly reactive highly-dispersed rhenium powder is used. The chalcogenides $\text{Re}_6\text{Q}_{8-n}\text{X}_{2+2n}$, where Q = S, Se; $n = 1, 2, 3, 4$, were synthesised from elements or from the corresponding compounds at 800–900 °C. ReCl_5 is typically used as a source of chlorine in the synthesis of chalcogenides.¹³⁶ The tellurohalide complexes $\text{Re}_6\text{Te}_8(\text{Te}_8\text{Cl}_{18})$, $\text{Re}_6\text{Te}_8(\text{Te}_6)(\text{TeCl}_3)_2$ and $\text{Re}_6\text{Te}_8(\text{TeBr}_2)_6\text{Br}_2$ with unusual ligands TeX_2 , Te_6 , $\text{Te}_8\text{Cl}_{18}^{2-}$ were obtained from ReCl_5 or Re_3Br_9 at 450–500 °C.^{138, 189, 206, 241} It should be noted that the octahedral rhenium chalcogenides are formed exclusively in the high-temperature reactions. Besides the synthesis from simple compounds, the octahedral rhenium chalcogenides are formed in the condensation of triangular clusters: in the reaction of rhenium bromide Re_3Br_9 with cadmium or lead chalcogenides at 500–550 °C.¹⁹⁰ The nonanuclear dioctahedral complex $[\text{Re}_9\text{Se}_{11}\text{Br}_6]^{2-}$ is also formed.²²⁴ The dodecanuclear sulfido-carbide cluster $[\text{Re}_{12}\text{S}_{17}\text{C}(\text{CN})_6]^{8-/6-}$ was obtained by the reaction of ReS_2 with KCN at 750 °C.¹⁵

2. Methods of solution synthesis

The methods of synthesis in aqueous solutions or in organic solvents are mainly used for chemical modifications of cluster-type complexes obtained by high-temperature synthesis. The reactions in solutions used specially for the synthesis of chalcogenide clusters are significantly less common, as the yields in these reactions are usually low and are well developed only for a limited number of clusters. Solution syntheses are used most often for the preparation of thio complexes, less

often for seleno complexes and only in very few cases for telluro complexes. Mononuclear tetrathiomallate complexes, metal halides or organometallic compounds are used as starting components of these reactions. In some cases, reductive condensation of bi- or trinuclear complexes into cluster complexes of higher nuclearities are also carried out in solutions.

a. Synthesis of triangular cluster complexes

At present, trinuclear vanadium complexes are obtained only in solutions. Usually, VCl_3 or $(\text{NH}_4)_3\text{VS}_4$ are used as the starting compounds. For instance, the compound $(\text{Et}_4\text{N})[\text{V}_3\text{S}_7(\text{Me}_2\text{NCS}_2)_3]$ was obtained in low yield in the reaction of $(\text{NH}_4)_3\text{VS}_4$ with CuCl , PhSNa , $\text{Na}(\text{Me}_2\text{NCS}_2)$ and Et_4NCl in DMF,⁶⁰ and the complex $(\text{Et}_4\text{N})[\text{V}_3\text{S}_7.(\text{Et}_2\text{NCS}_2)_3]$ was synthesised from $(\text{NH}_4)_3\text{VS}_4$, $\text{Na}(\text{Et}_2\text{NCS}_2)$ and Et_4NCl in methanol with passage of H_2S through the reaction mixture.²⁴² The reaction of $[\text{V}(\text{SPh})_2(\text{bipy})_2]\text{PF}_6$ with sulfur in MeCN furnishes $[\text{V}_3\text{S}_7(\text{bipy})_3]\text{PF}_6$ in 35%–40% yield.⁵⁹ The unique cluster-type complex $(\text{Et}_4\text{N})_3[\text{V}_3\text{S}_4.(\text{edt})_3] \cdot 2 \text{MeCN}$ with the core $\text{V}_3\text{S}_4^{3+}$ was isolated in 20% yield from a multicomponent reaction mixture containing $\text{Na}_2(\text{edt})$, Et_4NBr , VCl_3 and sulfur.²¹

The cluster-type niobium complex $[\text{Nb}_3\text{SO}_3(\text{NCS})_9]^{6-}$ was obtained by dissolution of $[\text{Nb}_2\text{Cl}_6(\text{THT})_3]$ (THT is tetrahydrothiophene) in hydrochloric acid followed by treatment with NH_4NCS .²² The triangular complex $[\text{Cr}_3\text{S}_5(\text{dmpe})_3]$ was synthesised in the reaction of anhydrous CrCl_2 with NaSH (78 °C, methanol) with subsequent addition of the phosphine.⁷⁵ The selenide cluster $(\text{Et}_4\text{N})_2[\text{Cr}_3(\mu_3\text{-Se})_2(\text{CO})_{10}]$ was obtained in 52% yield by the reaction of SeO_2 with $\text{Cr}(\text{CO})_6$ in a methanolic alkaline solution with subsequent addition of Et_4NBr .⁷⁶

The cluster aqua complexes, obtained preliminarily by reductive condensation of mono- or binuclear chalcogenide complexes, are used in the synthesis of triangular Mo and W complexes. In most cases these reactions are non-selective and result in mixtures of products that can be separated by chromatography with difficulty. Thus, the aqua complex $[\text{Mo}_3\text{S}_4(\text{H}_2\text{O})_9]^{4+}$ was obtained in 15% yield alongside with $[\text{Mo}_4\text{S}_4(\text{H}_2\text{O})_{12}]^{5+}$ (20%) in the reaction of $[\text{Mo}(\text{CO})_6]$ with anhydrous Na_2S in acetic anhydride.³⁵ The cluster $[\text{Mo}_3\text{S}_4(\text{H}_2\text{O})_9]^{4+}$ was synthesised with the yield of 20% by the reduction of $(\text{NH}_4)_2[\text{Mo}_2(\text{S}_2)_2\text{Cl}_8]$ with Pb or In in concentrated HCl.²⁴³ The compound $(\text{NH}_4)_2\text{MoS}_4$ can be reduced with NaBH_4 in aqueous hydrochloric acid yielding $[\text{Mo}_4\text{S}_4(\text{H}_2\text{O})_{12}]^{5+}$. Oxidation of the latter with atmospheric oxygen results in $[\text{Mo}_3\text{S}_4(\text{H}_2\text{O})_9]^{4+}$ isolated by ion-exchange chromatography in 50% yield.²⁵ The selenium analogue $[\text{Mo}_3\text{Se}_4(\text{H}_2\text{O})_9]^{4+}$ is difficult to obtain and it was synthesised by the reduction of $[\text{Mo}_2\text{O}_2\text{Se}_2(\text{cys})_2]^{2-}$ (cysH is L-cysteine) with NaBH_4 in a solution of hydrochloric acid. Cation-exchange chromatography afforded a mixture of species, viz., $[\text{Mo}_3\text{O}_2\text{Se}_2(\text{H}_2\text{O})_9]^{4+}$, $[\text{Mo}_3\text{OSe}_3(\text{H}_2\text{O})_9]^{4+}$, $[\text{Mo}_3\text{Se}_4.(\text{H}_2\text{O})_9]^{4+}$ and $[\text{Mo}_4\text{Se}_4(\text{H}_2\text{O})_{12}]^{5+}$ in a total yield of 10%. The cluster $[\text{Mo}_3\text{O}_2\text{Se}_2(\text{H}_2\text{O})_9]^{4+}$ was obtained in 70% yield by the reaction of $[\text{Mo}_2\text{O}_2\text{Se}_2(\text{cys})_2]^{2-}$ with $[\text{MoCl}_6]^{3-}$ (90 °C, 1 h, 1 M HCl), and the complex $[\text{Mo}_3\text{O}_3\text{Se}(\text{H}_2\text{O})_9]^{4+}$ was synthesised by electrochemical reduction of $[\text{Mo}_2\text{O}_4(\text{cys})_2]^{2-}$ in the presence of grey selenium powder in 3% yield or by treatment of $[\text{Mo}_3\text{O}_2\text{Se}_2(\text{H}_2\text{O})_9]^{4+}$ with a 30-fold excess of NaBH_4 .^{28, 29} The cationic complex $[\text{W}_3\text{S}_4(\text{H}_2\text{O})_9]^{4+}$ was obtained in the reduction of a solution of $(\text{NH}_4)_2[\text{WS}_4]$ with NaBH_4 in the presence of HCl. The reaction produces a mixture of complexes, viz., $[\text{W}_3\text{O}_2\text{S}_2(\text{H}_2\text{O})_9]^{4+}$ (0.3%), $[\text{W}_3\text{OS}_3(\text{H}_2\text{O})_9]^{4+}$ (5%) and $[\text{W}_3\text{S}_4(\text{H}_2\text{O})_9]^{4+}$ (25%).²⁵ The complex $(\text{NH}_4)_2[\text{Mo}_3\text{S}_7(\text{S}_2)_3]$, which is a starting compound in the synthesis of other $\text{Mo}_3\text{S}_4^{4+}$ derivatives, was obtained by the reaction of $(\text{NH}_4)_6[\text{Mo}_7\text{O}_{24}]$ with $(\text{NH}_4)_2\text{S}_x$ at 90 °C,²⁴⁴ and the selenide analogue $[\text{Mo}_3\text{Se}_7(\text{Se}_2)_3]^{2-}$, by the hydrothermal

synthesis from Mo or MoO₃ and a polyselenide.²⁴⁵ The cluster [Mo₃O(Te₂)₃·(en)₃]In₂Te₆ was synthesised by heating the mixture of Li₂Te, K₂Te, MoCl₅, InCl₃ and Te in ethylenediamine (180 °C, 7 days).⁵⁴

b. Synthesis of tetranuclear cluster complexes

The solution synthesis is extremely important for the preparation of vanadium and chromium tetrahedral complexes because the high-temperature methods of synthesis of these compounds are yet to be developed. The vanadium cyclopentadienyl complexes [(η⁵-C₅H₄R)₄V₄S₄] were obtained from the corresponding mononuclear vanadium complexes by the reactions with thiols (as a source of sulfur) in hydrocarbon solvents. Thus refluxing of [(η⁵-C₅H₄Me)₂V] with Bu^tSH in heptane yields [(η⁵-C₅H₄Me)₄V₄S₄] (with a small amount of pentanuclear [(η⁵-C₅H₄Me)₅V₅S₆]).²⁴⁶ The compound [Cp₄V₄S₄] was obtained from the vanadocene and MeC(S)SH or H₂S.^{247, 248} The cluster V₄S₄⁵⁺ was isolated as the dithiocarbamate complex (Et₄N)[V₄S₄(C₄H₈NCS₂)₆] in 67% yield from (NH₄)₃VS₄, ammonium pyrrolidinodithiocarbamate and PPh₃ in the presence of Et₃N.²⁴⁹

Tetranuclear vanadium clusters can be synthesised by reductive dimerisation of binuclear complexes. For example, the complex [(η⁵-C₅H₄Me)₄V₄S₄] was obtained by the reaction of [(η⁵-C₅H₄Me)₂V₂S₂] with Bu₃P.²⁴⁷ The selenide [Cp₂V₂Se₂] also reacts with PBu₃ in CH₂Cl₂ yielding [Cp₄V₄Se₄] (72% yield).⁹⁴ The tellurides [(η⁵-C₅H₄R)₄V₄Te₄] (R = H, Me) were obtained by thermolysis of [(η⁵-C₅H₄R)₂V₂(CO)₄(μ-Te)₂] in toluene at 50–60 °C in virtually quantitative yields.⁹⁴

Only the cyclopentadienyl derivatives of the cubane-type clusters Cr₄Q₄ⁿ⁺ (n = 4, 5) are known. The compounds [(η⁵-C₅H₄R)₄Cr₄S₄] (R = H, Me) were obtained from the corresponding chromocenes [(η⁵-C₅H₄R)₂Cr] and elemental sulfur or Bu^tSH by heating in high-boiling organic solvents.^{250, 251} Thermolysis of [Cp₂Cr₂(μ-S)₂(CO)₅] in toluene at 100 °C yields [Cp₄Cr₄S₄].^{95–97} The cluster [(η⁵-C₅H₄Me)₄·Cr₄S₄] was obtained upon thermolysis of [(η⁵-C₅H₄Me)₂·Cr₂(SBu^t)₂S] or upon its reaction with CuBr₂ in THF in the presence of triethylamine.²⁵² The complexes [(η⁵-C₅H₄R)₄·Cr₄Se₄] (R = H, Me) were formed upon heating [Cp₂Cr₂(CO)₆] or [(η⁵-C₅H₄Me)₂Cr] with grey selenium.^{95, 97} The reaction of [(η⁵-C₅H₄Me)₂Cr] with H₂Se in toluene produces complex [(η⁵-C₅H₄Me)₄Cr₄Se₄] in the yield of 90%.^{252, 253} The cluster [Cp₄Cr₄Se₄] was obtained from [Cp₂Cr₂(CO)₆] and Ph₂Se.^{98, 99} For tellurium, only mixed oxide-telluride clusters [Cp₄Cr₄Te₃O], [Cp₄Cr₄Te₂O₂] and [Cp₄Cr₄TeO₃], obtained by thermolysis of [CpCr(CO)₃TePh], are known.¹⁰⁰

In contrast to the derivatives of the Group 5 metals and chromium, the tetrahedral clusters of Mo and W are so resistant against oxygen and water that they can also be obtained in aqueous solutions. Mononuclear carbonyls, halides or chalcogenides are used as the starting compounds. Reductive condensation of binuclear chalcogenide complexes and the addition of a mononuclear fragment to a triangular cluster are also potentially very important as the synthetic methods. The methods of synthesis of tetrahedral Mo and W complexes are numerous, well developed and described in detail in several reviews.^{18, 19} It should be noted that in most cases the solution syntheses of the cubane-type cluster are non-selective and afford complex mixtures of products requiring laborious separations.

There is an example of synthesis of the complex [W₄S₄(en)₄(S₄)S] by a reaction of [W(CO)₆] with K₂S₄ in supercritical ethylenediamine at 300 °C.¹²⁷ The complex [(η⁵-C₅H₄Prⁱ)MoCl₂]₂ reacts with LiHS or LiHSe producing [(η⁵-C₅H₄Prⁱ)₄Mo₄Q₄] (Q = S, Se) in high yield.^{101, 253}

A unique method of synthesis of Cs₆[Mo₄S₄(S_x)₆] (x = 3, 4) by the reaction of Mo₆Br₁₂ with Cs₂S₃ in water was found. So

far this is the only example of the transformation of a hexanuclear halide cluster into a tetranuclear chalcogenide cluster.²⁵⁴

The tetrahedral polysulfide cluster complex [Re₄(μ₃-S)₄·(μ-S₃)₆]^{4–} was obtained by heating a solution of NH₄ReO₄ with an aqueous solution of ammonium polysulfide.^{122, 123} The cyanide complex [Re₄S₄(CN)₁₂]^{4–} was prepared by the reaction of trinuclear thiobromide Re₃S₇Br₇ with KCN in aqueous solution at room temperature.¹⁰⁴

c. Synthesis of octahedral cluster complexes

The molecular octahedral vanadium complex [V₆Se₈O(PMe₃)₆] with an interstitial oxygen atom was obtained from [CpVCl₂(PMe₃)₂] and (Me₃Si)₂Se.¹³⁷ Octahedral clusters with the Cr₆(μ₃-Te)₈ core were synthesised by either the reaction of [CrCl₂(PET₃)₂] with alkyl magnesium chloride and TePET₃ (the source of tellurium) or the reaction of bis(2,4-dimethylpentadienyl)chromium with TePET₃ in the presence of excess PET₃.²⁵⁵ The reaction of anhydrous CrCl₂ with Na₂Se or NaSH followed by treatment with PET₃ in methanol yields a mixture of complexes [Cr₆Q₈(PET₃)₆] and [Cr₆Q₈(H)(PET₃)₆].²⁵⁶

The first molecular octahedral molybdenum clusters [Mo₆S₈(PET₃)₆] and [Mo₆Se₈(PET₃)₆] stable in air were obtained by the reductive dimerisation of trinuclear clusters [Mo₃Q₄Cl₄(PET₃)_x] (x = 3, 4; Q = S, Se) with Mg.^{257–259} The substitution of halogen atoms in octahedral molybdenum dihalide is yet another approach to the synthesis of chalcogenide clusters. The cluster [Mo₆S₈(py)₆] was obtained by the reaction of Mo₆Cl₁₂ with NaSH and NaOBU^t in pyridine,¹⁷⁶ and complexes Cs₅[Mo₆Se_{3,6}Cl_{4,4}(CN)₆] and Cs₅[Mo₆Se_{3,4}·Br_{4,6}(CN)₆], by refluxing metal dihalides and Cs₂Se₃ in water followed by the addition of KCN to the reaction mixture.²⁶⁰

The methods of solution synthesis are particularly important for the preparation of octahedral chalcogenide tungsten clusters. The reaction of W₆Cl₁₂ with NaSH and NaOBU^t in pyridine yields [W₆S₈(py)₆] via complexes [W₆Cl₆S₂Cl₂(py)₆] and [W₆S₆Cl₂(py)₆].¹³⁵ The octahedral tungsten telluride clusters [Na(py)₆][W₆Te₈(py)₆]·py and [W₆Te₈(pip)₆]·6(pip) were obtained by the reaction of Na₂Te with W₆Cl₁₂ [3 days, refluxing in pyridine (py) or piperidine (pip)].^{175, 178}

IV. Reactivity of chalcogenide clusters

Diverse chemical transformations of the chalcogenide cluster complexes may be divided into two large groups, *viz.*, transformations occurring with and without changes in the metal chalcogenide cluster core. The reactions of the former type for the clusters of various nuclearity have much in common but the changes in cluster cores are highly specific for different types of clusters.

1. Substitution of terminal ligands

Similarly to the classic coordination chemistry, the reactions of ligand substitution in clusters are the most abundant and allow an access to compounds with virtually any cluster–ligand combinations. In the present review, we will discuss general features of these reactions for each cluster type, specially highlighting only the most important or unusual cases.

The substitution of halide or aqua ligands proceeds most easily. Therefore, it is not surprising that the chemistry of clusters stable in such environment is the most well studied. Three main classes of compounds belong to such clusters: the triangular chalcogenide clusters M₃Q₄ and M₃Q₇ (M = Mo, W), the tetrahedral clusters M₄Q₄ (M = Mo, W, Re) and the octahedral clusters M₆Q₈ (M = Mo, Re). However, in some cases as, for example, for [Mo₃(μ₃-S)₂(μ-Cl)₃Cl₆]^{2–},¹⁸ such studies have not been carried out yet. The octahedral clusters [M₆S₈L₆] containing highly labile inorganic (hydroxide and

halide) and organic (acetonitrile, amines, *etc.*) ligands that can easily be substituted by other ligands (for example, phosphines) are quite perspective in studies of the ligand substitution reactions.¹⁸

a. Triangular clusters M_3Q_4

The substitution of water molecules in aqua complexes $[M_3Q_4(H_2O)_9]^{4+}$ is studied in detail.²⁶¹ The exchange of the coordinated water in $[Mo_3S_4(H_2O)_9]^{4+}$ was studied by ^{17}O NMR spectroscopy. Different exchange rates were observed for the ligands in non-equivalent positions. The exchange rate of the molecules in *trans*-positions relative to the μ_3 -sulfur atom (*c*- H_2O) is approximately 10^5 times slower than that for the water molecules in the *cis*-position relative to μ_3 -S and therefore in the *trans*-position relative to the bridging sulfur atom (*d*- H_2O). It was suggested that the conjugated base $[Mo_3S_4(H_2O)_8(OH)]^{3+}$ is formed in which the positions *d* rather than *c* are activated. The dissociation constant value (K_a) of $[Mo_3S_4(H_2O)_9]^{4+}$ was equal to $0.18 \text{ mol litre}^{-1}$ ($25^\circ C$, ionic strength $I = 2.00 \text{ mol litre}^{-1}$) when the formation of this conjugated base was taken into account.²⁶¹ Depending on the concentration of HCl in the solution, equilibrium mixtures of aqua chloride complexes are produced up to $[Mo_3S_4 \cdot (H_2O)_2Cl_7]^{3-}$, which can be isolated by the formation of supramolecular systems of hydrogen bonds with the macrocyclic cavitands cucurbit[*n*]urils. So far, all attempts to isolate the complexes with completely substituted anions $[M_3Q_4Cl_9]^{5-}$ were unsuccessful.²⁶² The small value of the formation constant for the complex $[Mo_3S_4(H_2O)_8Cl]^{3+}$ (3.0) indicates low competitiveness of the chloride ligands in aqueous solutions.²⁶²

The substitution of thiocyanate for coordinated water was studied in detail for a series of complexes $[Mo_3O_xQ_{4-x}(H_2O)_9]^{4+}$ and $[W_3O_xQ_{4-x}(H_2O)_9]^{4+}$. The following regularities were found: the substitution of μ_3 -S and further of μ_3 -Se for μ_3 -O in the series from $[Mo_3O_4(H_2O)_9]^{4+}$ to $[Mo_3Se_4(H_2O)_9]^{4+}$ decreases the rate of *d*-ligand, substitution by 6 and 11 orders of magnitude for S and Se, respectively. At the same time, the substitution of μ_2 -bridging ligands increases the substitution rate by 10 (for S) and 20 (for Se) orders of magnitude per bridging atom.⁶⁹ In the mixed-metal complexes $[Mo_2WS_4(H_2O)_9]^{4+}$ and $[MoW_2S_4(H_2O)_9]^{4+}$, the substitution of the ligands bonded to the molybdenum atom is faster than of those bonded to the tungsten atom.²⁶⁴ The kinetic data of the reaction of $[W_3S_4(H_2O)_9]^{4+}$ with NCS^- were explained by the formation of an intermediate complex with S-coordinated thiocyanate ligand and its subsequent transformation into more stable N-bonded isomer.²⁶³ The complexes $[M_3Q_4(NCS)_9]^{5-}$ are easily formed upon the treatment of thiocyanate aqua complexes, and in all isolated solid products the ligand is coordinated by nitrogen atom.^{25–28, 265, 266} The substitution of formate for water results in the formation of η^1 -formate complexes, which were isolated and structurally characterised in the form of salts $K_4[Mo_3S_4(HCO_2)_8(H_2O)]$ and $K_6[W_3S_4(HCO_2)_9](HCO_2) \cdot 3 H_2O$.³⁰ No complexes of this type with other carboxylate ligands are known. The anion pts^- in the known toluene-*p*-sulfonates is always located in the outer coordination sphere as follows from structural studies of the corresponding aqua complexes $[M_3Q_4(H_2O)_9](pts)_4 \cdot x H_2O$.^{31, 118, 267} The cyclopentadienyl derivatives $[Cp_3M_3S_4](pts)$ and their analogues with substituted cyclopentadienyl ligands were synthesised from the complex $Mo_3S_4(pts)_4 \cdot THF$ obtained *in situ* by its reaction with $TiCp$ and $Ti(\eta^5-C_5H_4Me)$.²⁶⁸

The substitution of oxalate or acetylacetonate for water molecules yields the complexes $[M_3Q_4(C_2O_4)_3(H_2O)_3]^{2-}$ and $[M_3Q_4(acac)_3L_3]^+$ ($L = py, NH_3$; $M = Mo, W$; $Q = S, Se$), respectively.^{33, 34} The complexes $[Mo_3S_4(dtp)_3(\mu-dtp)(H_2O)]$ and $[Mo_3OS_3(dtp)_3(\mu-dtp)(H_2O)]$ (*dtp* is diethyldithiophos-

phate) are formed in the reactions of the corresponding aqua complexes with $(EtO)_2PS_2H$. The remaining water molecule is easily substituted by other neutral ligands and the bridging diethyl dithiophosphate, by carboxylate.^{269, 270} A number of complexes obtained from $[Mo_3S_4(dtp)_3(\mu-dtp)(H_2O)]$ and related compounds by substitution of various (predominantly, nitrogen-containing heterocycles and carboxylates) ligands for coordinated water and bridging dithiophosphate have been described.¹⁸ The complex $[Mo_3Se_4(dtp)_3(\mu-AcO)(py)]$ was obtained from the aqua complex $[Mo_3Se_4(H_2O)_9]^{4+}$ similarly.²⁷¹ The attempt to synthesise the dithiophosphate complexes $[M_3Se_4(\mu-dtp)(dtp)_3(H_2O)]$ ($M = Mo, W$) from solutions of $[M_3Se_4(H_2O)_9]^{4+}$ in hydrochloric acid by the addition of P_4S_{10} in the corresponding alcohol yielded the complexes $[M_3(\mu_3-Se)(\mu-Se_qSe_{ax})_3(dtp)_3]Cl$ as a result of sulfur addition to the cluster core $M_3(\mu_3-Se)(\mu-Se_{ax})_3$.²⁷¹

Quite complicated molecules can be obtained on the basis of polynuclear carboxylates, such as the complexes $[\{ Mo_3S_4(dtp)_3L \}_2(\mu-COO(CH_2)_nCOO)]$ ($n = 3, 4$) containing two cluster units linked by bridging glutarate or adipinate ligands.²⁷² Two bridging ligands, glutarate and 1,3-bis(4-pyridyl)propane, link simultaneously two cluster units in $[\{ Mo_3(\mu_3-O)S_3(dtp)_3 \}_2(\mu-COO(CH_2)_3COO)(\mu-py'(CH_2)_3py')]$ (py' is 4-pyridyl).²⁷³

The tridentate ligand diethylenetriamine (*dien*) reacts with $[Mo_3S_4(H_2O)_9]^{4+}$ and $[Mo_3OS_3(H_2O)_9]^{4+}$ yielding $[Mo_3S_4 \cdot (dien')(dien)_2]Cl_3 \cdot 4 H_2O$ and $[Mo_3OS_3(dien')(dien)_2]Cl_3 \cdot 3 H_2O$ where one of three ligands (*dien*) is deprotonated (*dien'*).²⁷⁴ The reaction of $[Mo_3S_4(H_2O)_9]^{4+}$ and $[Mo_3OS_3(H_2O)_9]^{4+}$ with $KHB(pz)_3$ (*pz* is pyrazolo) results in the formation of the corresponding pyrazoloborate complexes $[Mo_3Q_4\{HB(pz)_3\}_3]^+$.²⁷⁵ Due to partial hydrolysis of the ligand, the compound $[\{ (HB(pz)_3)_2Mo_3S_4 \}_2(\mu-O)(\mu-pz)_2]$ is also formed. Two cluster fragments of this compound are linked by a bridging oxygen atom and two pyrazolyl ligands.²⁷⁶

Of the ligands containing both nitrogen oxygen donor atoms only polyaminocarboxylates were the subject of fairly detailed studies. A series of iminodiacetate (*H_2ida*) and nitrilotriacetate (*H_3nta*) complexes $[Mo_3S_xO_{4-x}(ida)_3]^{2-}$ and $[M_3S_xO_{4-x}(Hnta)_3]^{2-}$ were synthesised.¹⁸ The nitrilotriacetate is a tridentated ligand leaving one CH_2COOH group free. In all cases, the nitrogen atoms occupy the *trans*-positions with respect to the μ_3 -sulfur atom. Complexes of $W_3S_4^{4+}$ and $W_3O_3S^{4+}$ with polyaminocarboxylate ligands [ethylenedioxybis(ethylenenitrilo)tetraacetate, triethylenetetramine hexaacetate, oxybis(ethylenenitrilo)tetraacetate, 1,4-butylenediaminotetraacetate, 1,3-propylenediaminotetraacetate and its 2-methyl-, 2-methoxy- and 2-carboxymethyl derivatives] were suggested as X-ray contrast diagnostic agents of a new generation.^{39, 277, 278}

Complexes of $Mo_3S_4^{4+}$ with 1,3,5-triamino-1,3,5-trideoxy-*cis*-inositol (*taci*) and its hexa-*N*-methyl derivative were synthesised. Three bond isomers with ligands coordinated in the *N,N,N*-, *N,N,O*-, and *N,O,O*-mode are present in aqueous solution of $[Mo_3S_4(taci)_3]^{4+}$.²⁷⁹

The lacunar anions $[SiW_{11}O_{39}]^{6-}$ and $[P_2W_{17}O_{61}]^{10-}$ can also serve as the ligands to form, with $[Mo_3S_4(H_2O)_9]^{4+}$, nanosized hybrid polyoxometallate cluster complexes $[\{ (SiW_{11}O_{39})Mo_3S_4(H_2O)_3(\mu-OH) \}_2]^{10-}$ and $[\{ (P_2W_{17}O_{61})Mo_3S_4(H_2O)_3(\mu-OH) \}_2]^{14-}$. In these structures, the polyoxometallate ligands are coordinated around the central core, which consists of two fragments $Mo_3S_4(H_2O)_3^{4+}$ linked by two hydroxyl bridges (both are in the *cis*-positions with respect to μ_3 -S). These complexes are stable in solutions in the pH range of 1–7, but in more acidic solutions form $[Mo_3S_4(H_2O)_9]^{4+}$ quantitatively.²⁸⁰

The halide ligands in the phosphine complexes $[W_3Q_4Cl_3(dmpe)_3]^+$ and $[W_3Q_4Br_3(dppe)_3]^+$ may be substituted by the hydride by the reaction with $NaBH_4$ to yield the

salts $[\text{W}_3\text{Q}_4\text{H}_3(\text{dmpe})_3]^+$ and $[\text{W}_3\text{Q}_4\text{H}_3(\text{dppe})_3]^+$.²⁷⁶ The halide complexes can be recovered upon treatment with hydrohalide acids. According to the kinetic data, in the presence of water the reaction proceeds through several stages and the dihydrogen complex $[\text{W}_3\text{Q}_4(\text{H}_2)\text{H}_2(\text{dmpe})_3]^+$ is formed initially. In the absence of water, this does not happen and the bond $\text{H}\cdots\text{H}$ is formed between the hydride complex and the dimer $(\text{HCl})_2$.^{281–283} The reaction with NaOH in acetonitrile yields $[\text{W}_3\text{Q}_4(\text{OH})_3(\text{dmpe})_3]^+$.^{281, 283}

b. Triangular clusters M_3Q_7

In the presence of sources of halide ions, the coordination polymers $\text{M}_3\text{Q}_7\text{X}_4$ can be transformed into discrete anionic complexes $[\text{M}_3\text{Q}_7\text{X}_6]^{2-}$ under rather drastic conditions: in melt, upon mechanochemical treatment or upon radiolysis.^{45, 53, 231, 284, 285} The salts $[\text{M}_3\text{Q}_7\text{X}_6]^{2-}$ in turn can be transformed into aqua complexes $[\text{M}_3\text{Q}_7(\text{H}_2\text{O})_6]^{4+}$ that are quite stable in an aqueous solution of TsOH , but could not be isolated in the solid state.^{24, 32} The rate constants of substitution of the halide ion for the coordinated water in the molybdenum aqua complexes $[\text{Mo}_3\text{Q}_7(\text{H}_2\text{O})_6]^{4+}$ do not depend on $[\text{H}^+]$ [for Cl^- : 1.83×10^{-4} ($\text{Q} = \text{S}$); 6.7×10^{-4} ($\text{Q} = \text{Se}$); for Br^- : 2.07×10^{-4} ($\text{Q} = \text{S}$); 33×10^{-4} litre $\text{mol}^{-1} \text{s}^{-1}$ ($\text{Q} = \text{Se}$)].³² The observed kinetic data agree with the suggestion that the replacement of the water molecule in *cis*-position relative to $\mu_3\text{-Q}$ proceeds in one step yielding $[\text{Mo}_3\text{Q}_7\text{Cl}_3(\text{H}_2\text{O})_3]^+$. The halide complexes $[\text{M}_3\text{Q}_7\text{Br}_6]^{2-}$ are convenient starting materials for the synthesis of other $\text{Mo}_3\text{S}_7^{4+}$ derivatives by the ligand substitution reactions. The complexes $[\text{Mo}_3\text{Q}_7(\text{NCS})_6]^{2-}$ [$\text{Q} = \text{S}$,^{51, 286} Se (Ref. 44)] are formed in the reactions with thiocyanate and the reaction with aniline furnishes the complex $[\text{Mo}_3\text{S}_7\text{Br}_3(\text{PhNH}_2)_3]\text{Br} \cdot \text{Et}_4\text{NBr}$.^{51, 286} The ligand exchange reactions were used for the synthesis of dithiocarbamates $[\text{Mo}_3\text{S}_7(\text{Et}_2\text{NCS}_2)_3]\text{X}$, $[\text{Mo}_3\text{S}_7(\text{pdtc})_3]\text{X}$ (pdtc is piperidine-1-dithiocarboxylate), dithiophosphates and diselenophosphates.^{53, 287–290} The compounds $[\text{Mo}_3\text{Q}_7\{\text{N}(\text{QPPH}_2)_2\}_3]\text{Br}$ containing six-membered chelate rings were synthesised from $(\text{Et}_4\text{N})_2[\text{Mo}_3\text{Q}_7\text{Br}_6]$ and $\text{K}\{\{\text{Ph}_2\text{P}(\text{Q})\}_2\text{N}\}$ ($\text{Q} = \text{S}$, Se).^{287, 291} The complex $(\text{Et}_4\text{N})_2 \cdot [\text{Mo}_3\text{S}_7(\text{MeC}_6\text{H}_4\text{S}_2)_3]$ with toluene-3,4-dithiolate as a ligand was synthesised and its structure was studied.²⁹² Catecholate complexes are also known.^{293, 294} Trischelate complexes of Mo_3S_7 with bidentate ligands [2-mercaptosuccinic acid (H_3msa), *meso*-2,3-dimercaptosuccinic acid (H_4dsa), 2-mercaptobenzoic acid, 3,4-dihydroxybenzoic acid, 8-hydroxyquinoline and 6-mercaptopurine] were obtained by exchange reactions from $(\text{Et}_4\text{N})_2[\text{Mo}_3\text{S}_7\text{Br}_6]$ in acetonitrile or DMF.^{293–295} Although the presence of only one isomer of the compound $(\text{Et}_3\text{NH})_2[\text{Mo}_3\text{S}_7(\text{Hmsa})_3]$ in which the sulfur atoms of the three ligands are coordinated in *cis*-positions with respect to $\mu_3\text{-S}$ was established, the results of potentiometric titration of $[\text{Mo}_3\text{S}_7(\text{dsa})_3]^{2-}$ better correspond to the behaviour of less symmetric isomer in which two chelate rings are closed through the sulfur atoms (S, S') and the third one through the S and O atoms.²⁹³ The coordination of the redox-active ligands 4,5-dimercapto-1,3-dithiole-2-thione (dmit) and dimercaptomaleonitrile (mnt) results in the complexes $[\text{Mo}_3\text{S}_7(\text{dmit})_3]^{2-}$ and $[\text{Mo}_3\text{S}_7(\text{mnt})_3]^{2-}$.^{296, 297}

The oxalate complexes $[\text{M}_3\text{Q}_7(\text{C}_2\text{O}_4)_3]^{2-}$ ($\text{M} = \text{Mo}$; $\text{Q} = \text{S}$, Se ; $\text{M} = \text{W}$, $\text{Q} = \text{S}$) were obtained by mechanochemical synthesis from the corresponding coordination polymers and potassium oxalate or the solution synthesis from the bromide complexes and oxalate.^{34, 297} The oxalate ligands can subsequently coordinate ions of other transition metals, lanthanides and actinides yielding in some cases nanosized complexes and porous coordination polymers.²⁹⁸

Melting of selenobromides $\text{M}_3\text{Se}_7\text{Br}_4$ ($\text{M} = \text{Mo}$, W) with 1,10-phenanthroline produces very stable complexes $[\text{M}_3\text{Se}_7(\text{phen})_3]^{4+}$ isolated as salts with anions X^- or ZnX_4^{2-}

($\text{X} = \text{Cl}$, Br) after the extraction of the melt with hot concentrated solutions of HCl or HBr .⁵³

The chalcogenides $\text{Mo}_3\text{Te}_7\text{I}_4$ and $\text{W}_3\text{Te}_7\text{Br}_4$ produce the cyanide complexes $[\text{M}_3\text{Te}_7(\text{CN})_6]^{2-}$ when heated with aqueous solution of KCN . The cluster $[\text{Mo}_3\text{Te}_7(\text{TeI}_3)_3]\text{I}$ forms $[\text{Mo}_3\text{Te}_7\{(\text{RO})_2\text{PS}_2\}_3]\text{I}$ in a solid-state reaction with dithiophosphates $\text{KS}_2\text{P}(\text{OR})_2$ ($\text{R} = \text{Et}$, Pr^i) at 100°C . The mechanochemical reactions of $\text{Mo}_3\text{Te}_7\text{I}_4$ or $\text{W}_3\text{Te}_7\text{Br}_4$ with $(\text{EtO})_2\text{PS}_2\text{K}$ also result in the ‘cutting out’ of the M_3Te_7 cluster fragment and formation of $[\text{Mo}_3\text{Te}_7\{(\text{EtO})_2\text{PS}_2\}_3]\text{I}$ or $[\text{W}_3\text{Te}_7\{(\text{EtO})_2\text{PS}_2\}_3]\text{Br}$ in low yields.^{50, 64, 67, 299, 300}

c. Cubane-type clusters M_4Q_4

The cubane-type molybdenum aqua complexes $[\text{Mo}_4\text{S}_4(\text{H}_2\text{O})_{12}]^{n+}$ exist in three oxidation states with $n = 4, 5$ (the most stable state) and 6. The chloride ion is weakly coordinated to $[\text{Mo}_4\text{S}_4(\text{H}_2\text{O})_{12}]^{5+}$ ($K_1 = 1.98$, which is approximately 1000 times less than the corresponding value for thiocyanate). According to the kinetic data, the rate of substitution of thiocyanate for water molecule increases by several orders of magnitude in the series $5+ < 4+ < 6+$. The substitution of Se for S in the aqua complex $[\text{Mo}_4\text{S}_4(\text{H}_2\text{O})_{12}]^{5+}$ increases the rate of substitution approximately tenfold. In all cases, the full substitution is accompanied by oxidation of the cluster core to the state $\text{M}_4\text{Q}_4^{6+}$ and the formation of isothiocyanate complexes $[\text{M}_4\text{Q}_4(\text{NCS})_{12}]^{6-}$, although the kinetic data indicate probability of the intermediate formation of an S-coordinated isomer.⁷⁰ The salts $[\text{Mo}_4\text{S}_4(\text{NCS})_{12}]^{6-}$, $[\text{Mo}_4\text{Se}_4(\text{NCS})_{12}]^{6-}$, $[\text{W}_4\text{Q}_4(\text{NCS})_{12}]^{6-}$, $[\text{MoW}_3\text{Q}_4(\text{NCS})_{12}]^{6-}$ ($\text{Q} = \text{S}$, Se), $[\text{Mo}_3\text{WS}_4(\text{NCS})_{12}]^{6-}$ were synthesised and their structures were studied.^{22, 116–118} The oxidation of the cluster $\text{M}_4\text{Q}_4^{5+}$ into $\text{M}_4\text{Q}_4^{6+}$ also occurs upon addition of the dithiophosphates $(\text{RO})_2\text{PS}_2^-$ ($\text{R} = \text{Et}$, Pr^i) to solutions of aqua complexes in HCl . This results in the dithiophosphate complexes $[\text{M}_4\text{Q}_4(\text{dtp})_6]$, which exist in the form of two isomers $[\text{M}_4\text{Q}_4(\mu\text{-dtp})_2(\text{dtp})_4]$ and $[\text{M}_4\text{Q}_4(\mu\text{-dtp})_3(\text{dtp})_3]$.¹¹⁶ Similarly to the triangular clusters M_3Q_4 , the bridging dithiophosphate ligand in $[\text{Mo}_4\text{S}_4(\mu\text{-dtp})_2(\text{dtp})_4]$ is rather labile and can be easily replaced by other bidentate ligands such as, for example, acetate or benzoate. As a result, the paramagnetic complexes $[\text{Mo}_4\text{S}_4(\mu\text{-OOCR})_2(\text{dtp})_4]$ are formed.^{114, 124} The bridging dithiocarbamate ligands can be selectively substituted by xanthate producing a mixture of $[\text{Mo}_4\text{S}_4(\mu\text{-Et}_2\text{NCS}_2)(\mu\text{-EtOCS}_2)(\text{Et}_2\text{NCS}_2)_4]$ and $[\text{Mo}_4\text{S}_4(\mu\text{-EtOCS}_2)_2(\text{Et}_2\text{NCS}_2)_4]$.¹¹⁵ On the contrary, treatment of the aqua complex $[\text{Mo}_4\text{S}_4(\text{H}_2\text{O})_{12}]^{5+}$ with concentrated aqueous ammonia results in the reduction of the cluster core and formation of the complex $[\text{Mo}_4\text{S}_4(\text{NH}_3)_{12}]^{4+}$.¹¹³ Reaction of the aqua complex $[\text{Mo}_4\text{S}_4(\text{H}_2\text{O})_{12}]^{5+}$ with potassium tris(pyrazolo)borate proceeds without any redox processes in the cluster core and yields $[\text{Mo}_4\text{S}_4\{\text{HB}(\text{pz})_3\}_4(\text{pz})]$.³⁰¹ An attempt to coordinate oxalate to $[\text{Mo}_4\text{S}_4(\text{H}_2\text{O})_{12}]^{5+}$ resulted in the isolation of the triangular cluster $[\text{Mo}_3\text{S}_4(\text{C}_2\text{O}_4)_3(\text{H}_2\text{O})_3]^{2-}$ as the only product.³⁵

The molecular complexes $[\text{Re}_4\text{Q}_4(\text{TeCl}_2)_4\text{Cl}_8]$ ($\text{Q} = \text{S}$, Se , Te) are very convenient starting compounds in the chemistry of tetranuclear rhenium complexes:¹²¹ the coordinated TeCl_2 molecules and chloride ions can easily be substituted for other ligands.^{106, 107, 120, 302–304}

d. Octahedral clusters Re_6Q_8

The halide complexes $[\text{Re}_6\text{S}_8\text{X}_6]^{4-}$ ($N_e = 24$) and $[\text{Re}_6\text{Se}_8\text{I}_6]^{3-}$ ($N_e = 23$) are the most common starting compounds for the substitution reactions.¹³⁶ The substitution rarely proceeds completely and even in the excess of the ligand di- and trisubstituted products are often formed. The addition of Ag^+ ions for binding of the halide ions allows complete substitution of the terminal ligands. This method was used for the synthesis of the complexes $[\text{Re}_6\text{S}_8(\text{H}_2\text{O})_6]^{2+}$ (from $[\text{Re}_6\text{S}_8\text{X}_6]^{4-}$ and AgClO_4 in HClO_4),¹⁴⁷ $[\text{Re}_6\text{Se}_8(\text{MeCN})_6]^{2+}$

(from $[\text{Re}_6\text{Se}_8\text{Br}_6]^{3-}$ and AgBF_4 in MeCN; in this case the substitution is accompanied by the cluster reduction).¹⁴⁶ The reaction of $\text{Cs}_3[\text{Re}_6(\text{S}_7\text{Br})\text{Br}_6]$ (the 'inner' ligands L^i of the cluster complex are given in parentheses) with aqueous ammonia results in step-by-step substitution of NH_3 for all terminal ligands and in the formation of $[\text{Re}_6(\text{S}_7\text{Br})(\text{NH}_3)_6]^{3+}$.¹⁴⁸ The reactions of $[\text{Re}_6\text{S}_8\text{Cl}_6]^{3-}$ with pyridine affords a mixture of *cis*- and *trans*-isomers of $[\text{Re}_6\text{S}_8\text{Cl}_4(\text{py})_2]^{2-}$ as well as facial isomers of trisubstituted complexes $[\text{Re}_6\text{S}_8\text{Cl}_3(\text{py})_3]^{n-}$ ($n = 0, 1$).^{149, 150} In the case of phosphines, more complete substitution is possible. Thus in the reaction of $[\text{Re}_6\text{Se}_8\text{I}_6]^{3-}$ with PET_3 the following complexes were obtained: *fac*- and *mer*- $[\text{Re}_6\text{Se}_8(\text{PET}_3)_3\text{I}_3]^-$, *cis*- and *trans*- $[\text{Re}_6\text{Se}_8(\text{PET}_3)_4\text{I}_2]$, $[\text{Re}_6\text{Se}_8(\text{PET}_3)_5\text{I}]^+$ and completely substituted $[\text{Re}_6\text{Se}_8(\text{PET}_3)_6]^{2+}$. The reaction of $[\text{Re}_6\text{Se}_8\text{I}_6]^{3-}$ with a bidentate 1,6-bis(diphenylphosphino)hexane ligand also results in the monochelate, *cis*- and *trans*-bischelate and trischelate complexes and is accompanied as usual, by one-electron reduction of the cluster core.¹⁵³ The remaining unsubstituted halogen atoms in the mixed-ligand phosphine complexes can be substituted by other ligands. For example, the solvolysis of $[\text{Re}_6\text{Se}_8(\text{PET}_3)_4\text{I}_2]$ in donor solvents yields cationic complexes $[\text{Re}_6\text{Se}_8(\text{PET}_3)_4\text{L}_2]^{2+}$ ($\text{L} = \text{MeCN}$, DMF, DMSO).^{152, 154} The bicluster derivatives $\{[\text{Re}_6\text{Se}_8(\text{PET}_3)_5]_2(\text{L}-\text{L})\}^{4+}$ were obtained from $[\text{Re}_6\text{Se}_8(\text{PET}_3)_5(\text{MeCN})]^{2+}$ using the bidentate bridging (ditopic) ligands [4,4'-bipyridyl and 1,2-disubstituted ethane, ethylene and acetylene with 4-pyridyl substituents ($\text{L}-\text{L}$)].¹⁵⁴ These reactions with $[\text{Re}_6\text{Se}_8(\text{PET}_3)_4(\text{MeCN})_2]^{2+}$ result in the formation of tetrakiscluster complexes in which the clusters and bipyridyl bridges form molecular squares.¹⁵⁵ The substitution of 4-(3,4,6-tribenzyloxy)benzyloxy pyridine for acetonitrile molecules in the complex $[\text{Re}_6\text{Se}_8(\text{MeCN})_6]^{2+}$ is the first step in the synthesis of dendrimers based upon redox-active sixnuclear clusters.¹⁴⁶

Highly nucleophilic cyanide ion is able of substituting all bridging ligands even in the three-dimensional structures $[\text{Re}_6\text{Q}_8\text{Br}_2]$ ($\text{Q} = \text{S}, \text{Se}$) and $\text{Re}_6\text{Te}_{15}$ yielding $[\text{Re}_6\text{Q}_8(\text{CN})_6]^{4-}$ (Refs 156, 157 and 305). Similarly compound $[\text{Re}_6\text{Q}_8(\text{OH})_8]^{4-}$ is formed in a melt of KOH .¹⁵⁸ In the case of $[\text{Re}_6\text{Se}_8\text{Br}_2]$, the reaction can also result in partial substitution of oxide bridges for the selenide yielding $\text{Re}_6\text{Se}_4\text{O}_4^{2+}$ derivatives. Remarkably, the selective substitution of selenium atoms of just one face of the Se_8 cube takes place.¹³⁹ Another method for the synthesis of hexacyanide complexes is based on the reactions of the salts $[\text{Re}_6\text{Se}_8\text{I}_6]^{4-}$ and $[\text{Re}_6\text{S}_8\text{Br}_6]^{4-}$ with a melt of NaCN .³⁰⁶ The telluride $[\text{Re}_6\text{Te}_8(\text{Te}_7)]$ forms $[\text{Re}_6\text{Te}_8(\text{CN})_6]^{4-}$ in the cyanide melt.¹⁶³ Similarly, the chalcogenides ZnMo_6S_8 and Mo_6Se_8 give $[\text{Mo}_6\text{S}_8(\text{CN})_6]^{7-}$ and $[\text{Mo}_6\text{Se}_8(\text{CN})_6]^{7-}$ in a sodium cyanide melt, the latter complex is readily oxidised to $[\text{Mo}_6\text{Se}_8(\text{CN})_6]^{6-}$.^{162, 307}

The interaction of the cluster complexes $\text{Cs}_4[\text{Re}_6\text{S}_8\text{Br}_6] \cdot 2\text{H}_2\text{O}$, $\text{Cs}_3[\text{Re}_6\text{S}_8\text{Br}_6] \cdot 2\text{H}_2\text{O}$, $\text{Cs}_3[\text{Re}_6(\text{Q}_7\text{Br})\text{Br}_6] \cdot \text{H}_2\text{O}$ and $\text{K}_2[\text{Re}_6(\text{S}_6\text{Br}_2)\text{Br}_6]$ with the melts of 3,5-dimethylpyrazole (3,5-Me₂pzH) and triphenylphosphine results in complete or partial substitution of the halide ligands. The complexes $[\text{Re}_6\text{Q}_8(3,5\text{-Me}_2\text{pzH})_6]\text{Br}_2 \cdot 2(3,5\text{-Me}_2\text{pzH})$, $[\text{Re}_6(\text{Q}_7\text{O})(3,5\text{-Me}_2\text{pzH})_6]\text{Br}_2 \cdot (3,5\text{-Me}_2\text{pzH})$ (with the substitution of $\mu_3\text{-O}$ for $\mu_3\text{-Br}$), *trans*- $[\text{Re}_6\text{Q}_8(\text{PPh}_3)_4\text{Br}_2]$, *fac*- $[\text{Re}_6(\text{Q}_7\text{Br})(\text{PPh}_3)_3\text{Br}_3]$, *cis*- $[\text{Re}_6(\text{S}_6\text{Br}_2)(\text{PPh}_3)_2\text{Br}_4]$ and *trans*- $[\text{Re}_6(\text{S}_6\text{Br}_2)(\text{PPh}_3)_2\text{Br}_4] \cdot 4\text{H}_2\text{O}$ were isolated and their structures were studied.^{159–161}

2. Redox reactions

Cyclic voltammetry (CV) of triangular clusters $\text{M}_3\text{Q}_4^{4+}$ shows two waves of reduction, which can be explained as sequential reduction $\text{M}_3^{\text{IV}}\text{O}_4^{4+} \rightarrow \text{M}_2^{\text{IV}}\text{M}^{\text{III}}\text{Q}_4^{3+} \rightarrow \text{M}^{\text{IV}}\text{M}_2^{\text{III}}\text{Q}_4^{2+}$. The reduction ability decreases in the series $\text{Mo}_3\text{S}_4^{4+} > \text{Mo}_3\text{Se}_4^{4+} > \text{W}_3\text{Se}_4^{4+} > \text{W}_3\text{S}_4^{4+}$ (Refs 24, 38, 269 and 308). In some cases the one-electron reduction products may be isolated and their structures can be established.^{42, 309, 310} Usually,

the reduction of the clusters $\text{Mo}_3\text{S}_7^{4+}$ is irreversible and is accompanied by elimination of sulfur yielding $\text{Mo}_3\text{S}_4^{4+}$ (Ref. 293).

Cyclic voltammetry revealed the possibility of reversible one-electron reduction (to $n = 4$) and oxidation (to $n = 6$) of the clusters $[\text{Mo}_x\text{W}_{4-x}\text{Q}_4(\text{H}_2\text{O})_{12}]^{n+}$ ($x = 0-4$).^{116, 117} For both of the pairs $5+/4+$ and $6+/5+$, the value of half-wave potential ($E_{1/2}$) almost linearly decreases with the increase in the number of tungsten atoms in the cluster: each additional tungsten atom causes a negative potential shift of approximately 0.2 V. It reflects the predisposition of tungsten to higher oxidation states. The effect of the substitution of selenium for sulfur in the cluster core is less pronounced: the substitution of four Se atoms for S decreases the potential by less than 0.1 V.^{116, 117} Two waves of one-electron reduction of the cyanide clusters $[\text{M}_4\text{Q}_4(\text{CN})_{12}]^{6-}$ ($\text{M} = \text{Mo}, \text{W}$; $\text{Q} = \text{S}, \text{Se}, \text{Te}$) were also observed by CV. Interestingly, the substitution of the cyanide ions for coordinated water molecules results in a significant positive shift of the potentials (0.6–0.7 V), which makes possible the reduction of $[\text{W}_4\text{Q}_4(\text{CN})_{12}]^{7-}$ to $[\text{W}_4\text{Q}_4(\text{CN})_{12}]^{8-}$ ($\text{Q} = \text{S}, \text{Se}, \text{Te}$). The cyanide ligands damp the effect of the metal change on the electrode potential: while for the pair $[\text{Mo}_4\text{S}_4(\text{H}_2\text{O})_{12}]^{6+}/[\text{W}_4\text{S}_4(\text{H}_2\text{O})_{12}]^{6+}$ $\Delta E_{1/2}$ is equal to 825 mV, it is only 411 mV for the pair $[\text{Mo}_4\text{S}_4(\text{CN})_{12}]^{6-}/[\text{W}_4\text{S}_4(\text{H}_2\text{O})_{12}]^{6-}$. Presumably, this is caused by the participation of the cyanide ion π -orbitals in the charge redistribution within the cluster core. The transition from $\text{Q} = \text{S}$ to Se and Te regularly (by approximately 100 mV) decreases the redox potential stabilising the most oxidised state of the cluster ($\text{M}_4\text{Q}_4^{6+}$).¹⁰² However, in the case of $[\text{Mo}_4\text{Q}_4(\text{edta})_2]^{n-}$ ($n = 2-4$), the substitution of Se for S does not affect the $E_{1/2}$ value.³¹¹ The reversible two-electron oxidation was also observed in the case of cyclopentadienyl clusters $[(\eta^5\text{-C}_5\text{H}_4\text{Pr})_4\text{Mo}_4\text{Q}_4]$ ($\text{Q} = \text{S}, \text{Se}$); the selenium clusters undergo oxidation at significantly more negative potentials.^{101, 253} In contrast to the molybdenum and tungsten analogues, no reversible redox transformations were observed for rhenium tetrahedral clusters.

One-electron oxidation proceeds relatively easily in the case of the chalcogenide clusters Re_6Q_8 ($N_e = 24$).¹³⁶ The reversible one-electron reduction at the negative potentials was detected by CV for the compounds $[\text{Re}_6(\text{Q}_5\text{Cl}_3)\text{Cl}_6]^-$ ($\text{Q} = \text{S}, \text{Se}$), but no oxidation occurs.¹⁸⁸ Such behaviour is in keeping with both the increase in the negative charge of the cluster anion with the increase in the number of chalcogen atoms in the cluster core and lower electronegativity of the chalcogen atoms. In some cases, stable oxidation products, such as $(\text{Bu}^t\text{N})_3[\text{Re}_6\text{S}_8\text{Cl}_6]$, $(\text{Ph}_4\text{P})_3[\text{Re}_6\text{S}_8(\text{CN})_6]$, $(\text{Ph}_4\text{P})_2(\text{H}) \cdot [\text{Re}_6\text{Se}_8(\text{CN})_6] \cdot 8\text{H}_2\text{O}$ and $(\text{Et}_4\text{N})_2(\text{H})[\text{Re}_6\text{Te}_8(\text{CN})_6] \cdot 2\text{H}_2\text{O}$, can be isolated.^{312, 313} It was found that the oxidation potential of complexes with heterocyclic amines increases in accord with the basicity of the ligand. The reduction of heterocyclic ligands takes place in the region of negative potentials and the electronic interaction of two heterocyclic ligands through the cluster was observed.¹⁴⁹ The oxidation of the cyanide complexes $[\text{Re}_6\text{Q}_8(\text{CN})_6]^{4-}$ occurs at significantly lower potential than that of their halide analogues. The transition from a sulfide cluster to the telluride drastically (by 0.5 V) reduces the oxidation potential.³¹⁴

Both reversible one-electron reduction and one-electron oxidation are possible for the electron-deficient molybdenum clusters $[\text{Mo}_6\text{Q}_8(\text{PET}_3)_6]$ ($\text{Q} = \text{S}, \text{Se}$; $N_e = 20$). In spite of a strong electron-deficient character of the clusters, reduction occurs at highly negative potentials. Both electrode processes occur at virtually the same potentials for sulfide and selenide clusters.²⁵⁹ On the contrast, the monochalcogenide clusters $[\text{Mo}_6(\text{QX}_7)\text{X}_6]^{3-}$ ($\text{Q} = \text{S}, \text{Se}$; $\text{X} = \text{Cl}, \text{Br}$) can reversibly lose one or two electrons. The introduction of the second chalcogen atom results in a strong negative shift of the potentials, as in the

case of the cyanide clusters $[\text{Mo}_6\text{Q}_2\text{X}_6(\text{CN})_6]^{4-}$ ($\text{Q} = \text{S}, \text{Se}$).¹³⁴ It should be noted that there is virtually no difference in $E_{1/2}$ values for $[\text{Mo}_6(\text{QCl}_7)\text{X}_6]^{3-/2-}$, whereas for two geometrical isomers of $[\text{Mo}_6(\text{Se}_2\text{Cl}_6)\text{Cl}_6]^{4-/3-/2-}$, the difference in $E_{1/2}$ values is as large as $\sim 0.1 \text{ V}$.^{164, 165}

3. Clusters of clusters, coordination polymers and supramolecular compounds

Cyanide derivatives of chalcogenide clusters attract attention as ‘building blocks’ in the synthesis of coordination polymers, particularly those with big cavities and high porosity. Both tetrahedral clusters $\text{M}_4\text{Q}_4(\text{CN})_{12}$ and octahedral clusters $\text{M}_6\text{Q}_8(\text{CN})_6$ ($\text{M} = \text{Mo}, \text{W}, \text{Re}$; $\text{Q} = \text{S}, \text{Se}, \text{Te}$) are used for these purposes.^{11, 12, 315–330} Recently, coordination polymers based on the aqua complexes $[\text{Re}_6\text{Q}_8(\text{OH})_6]^{4-}$ ($\text{Q} = \text{S}, \text{Se}$) have been synthesised.³³¹

The condensation of clusters takes place during thermolysis of $[\text{Re}_6\text{Se}_8(\text{PEt}_3)_5(\text{MeCN})_2]^{2+}$ and *cis*- $[\text{Re}_6\text{Se}_8(\text{PEt}_3)_4.(\text{MeCN})_2]^{2+}$. Here, the labile acetonitrile molecules are substituted by the μ_3 -Se atom of the other cluster core yielding $[\text{Re}_{12}\text{Se}_{16}(\text{PEt}_3)_{10}]^{4+}$ and *trans*- $[\text{Re}_{12}\text{Se}_{16}(\text{PEt}_3)_8(\text{MeCN})_2]^{4+}$ (Ref. 152). Similar process resulting in the formation of $[\text{Mo}_{12}\text{Q}_{16}(\text{PEt}_3)_{10}]$ was observed in the elimination of coordinated triethylphosphine from the complex $[\text{Mo}_6\text{Q}_8(\text{PEt}_3)_6]$ under the action of sulfur.³³²

Due to the formation of complementary bonds between the carbonyl groups of the macrocyclic cavitand cucurbit[6]uril and water molecules of aquachloride complexes, the isolation of the cluster complexes $[\text{M}_3\text{Q}_4(\text{H}_2\text{O})_{9-x}\text{Cl}_x]^{(4-x)+}$ ($x = 1–3$) in the form of supramolecular adducts with cucurbit[6]uril from solutions in 2–4 M HCl and studies of their structures become possible. The size and the symmetry of six carbonyl groups of cucurbituril correspond well to six aqua ligands in *cis*-positions with respect to μ_3 -bridging chalcogen atom in the triangular cluster aqua complexes. In the case of bulkier and less water-soluble cucurbit[8]uril, the aquachloride complexes with higher chloride content (up to $x = 7$) were isolated in spite of the loss of complementarity, because the cluster aquachloride complexes occupied the voids between differently packed large cucurbit[8]uril molecules and the hydrogen bonds provided additional stabilisation of the structure.^{262, 333, 334}

4. Substitution of ‘inner’ bridging ligands

The reactions of the sulfohalides $[\text{M}_3\text{S}_7\text{X}_6]^{2-}$ with PPh_3Se or KNCS result in the selective substitution of selenium for the equatorial sulfur atom of the disulfide ligand. This reaction is irreversible and even the excess of KNCS or PPh_3S does not transform the clusters $\text{Mo}_3\text{S}(\text{SSe})_3^{4+}$ back into $\text{Mo}_3\text{S}_7^{4+}$. The synthesis of the compound $[\text{Mo}_3\text{S}_4\text{Se}_3(\text{Et}_2\text{NCS}_2)_3]^{+}$ from $[\text{Mo}_3\text{S}_7(\text{Et}_2\text{NCS}_2)_3]^{+}$ and KNCS in MeCN at room temperature is an example of such reaction.^{47, 49} High lability of the equatorial sulfur atom was confirmed by selective isotope exchange in the reaction of $(\text{NH}_4)_2[\text{Mo}_3\text{S}_7(\text{S}_2)_3]$ with a solution of ammonium polysulfide containing the isotope ^{34}S .^{44, 48} The substitution of chalcogen atoms of $\text{Mo}_3\text{S}_7\text{Br}_4$ in KNCS melt at 200–220 °C proceeds further *via* $[\text{Mo}_3\text{S}_4\text{Se}_3(\text{CN})_6]^{2-}$ and $[\text{Mo}_3(\mu_3\text{-S})\text{Se}_6(\text{CN})_6]^{2-}$ and yields finally $[\text{Mo}_3\text{Se}_7(\text{CN})_6]^{2-}$.⁶⁷ The relative lability of the chalcogen atoms in three different positions of the cores $\text{M}_3(\mu_3\text{-Q})(\mu\text{-Q}_{\text{ax}}\text{Q}_{\text{eq}})_3^{4+}$ decreases in following order $\text{Q}_{\text{eq}} > \text{Q}_{\text{ax}} > \mu_3\text{-Q}$. Seleno cyanate serves simultaneously as a source of selenium for the formation of selenide clusters and a source of cyanide ions. A similar order of substitution of Se for Te was found in the reaction of $\text{M}_3\text{Te}_7\text{Br}_4$ with KNCS . The complex $[\text{W}_3(\mu_3\text{-Te}).(\mu_2\text{-TeSe})_3(\text{CN})_6]^{2-}$, containing a new inorganic ligand TeSe^{2-} was isolated and its structure was studied.⁶⁷ The molten KNCS transforms the chalcobromides $\text{W}_3\text{S}_7\text{Br}_4$ and

$\text{W}_3\text{Se}_7\text{Br}_4$ into $[\text{W}_3\text{S}_4(\text{NCS})_9]^{5-}$ *via* $[\text{W}_3\text{S}_2\text{Se}_{4-x}(\text{NCS})_9]^{5-}$ ($x = 1–3$).³³⁵ The transformation of the cluster $\text{Mo}_3\text{Se}_7^{4+}$ into $\text{Mo}_3\text{S}_7^{4+}$ was also observed in the reaction of $\text{Mo}_3\text{Se}_7\text{Br}_4$ with $(\text{NH}_4)_2\text{S}_x$ under hydrothermal conditions.⁴⁴

The substitution of ions Q^{2-} ($\text{Q} = \text{O}, \text{S}, \text{Se}, \text{Te}$), NR^{2-} , P^{3-} , As^{3-} for μ_3 -bridging halogen atoms is typical of octahedral rhenium complexes. This reaction proceeds more easily in the case of the most halogen-rich cluster cores. Thus $[\text{Re}_6(\text{Se}_4\text{O}_2\text{Cl}_2)\text{Cl}_6]^{2-}$ is formed upon mere heating of the compound $[\text{Re}_6(\text{Se}_4\text{Cl}_4)\text{Cl}_6]$ in wet DMF, both isomers, which differ in mutual position of the oxygen atoms, being isolated. $[\text{Re}_6(\text{S}_7\text{Br})\text{Br}_6]^{3-}$ is one of the products of a complex reaction of the sulfobromide $[\text{Re}_6(\text{S}_4\text{Br}_4)\text{Br}_6]$ with KNCS in a melt.³³⁶

The clusters $[\text{Re}_6(\text{Q}_5\text{Cl}_3)\text{Cl}_6]^{-}$ ($\text{Q} = \text{S}, \text{Se}$) are studied in most details. They readily form the complexes $[\text{Re}_6(\text{Q}_5\text{Q}'\text{Cl}_2)\text{Cl}_6]^{2-}$ ($\text{Q}' = \text{O}, \text{S}, \text{Se}, \text{Te}$) in the reactions with the silylated chalcogen carriers $[(\text{Me}_3\text{Si})_2\text{Q}]$.³³⁷ With the silylamide reagents $[(\text{Me}_3\text{Si})_2\text{NR}]$, where $\text{R} = \text{H}, \text{Me}, \text{Bu}^n$, the complexes $[\text{Re}_6(\text{Q}_5\text{EX}_2)\text{Cl}_6]^{2-}$ ($\text{E} = \text{NSiMe}_3, \text{NMe}, \text{NBu}^n$) are formed. The trimethylsilyl group can be removed by treatment of the reaction mixture with Bu_4^+NF^- yielding $[\text{Re}_6(\text{Q}_5(\text{NH})\text{X}_2)\text{Cl}_6]^{2-}$. The nitrogen atom in this cluster remains nucleophilic and can be alkylated by butyl chloride in the presence of a base yielding the complex $[\text{Re}_6(\text{Q}_5(\text{NBu}^n)\text{X}_2)\text{Cl}_6]^{2-}$.³³⁸ In the case of the oxide cluster, the substitution of one of the terminal chloride ligands also takes place and the complex $[\{\text{Re}_6(\text{S}_5\text{OCl}_2)\text{Cl}_5\}_2\text{O}]^{4-}$ is formed.³³⁹ The substitution of O, S, NH for two μ_3 -chlorine atoms in the chalcogenide clusters $[\text{Re}_6(\text{S}_6\text{Cl}_2)\text{Cl}_6]^{2-}$ is possible in the reactions with silyl reagents. The clusters $[\text{Re}_6(\text{S}_6\text{E}_2)(\text{PPR}_3)_6]^{2+}$ ($\text{E} = \text{P}, \text{As}$) containing μ_3 -atoms of Group 15 elements in the cluster core were obtained when $\text{PhAs}(\text{SiMe}_3)_2$ or $\text{P}(\text{SiMe}_3)_3$ were used.¹³⁶

The bridging chalcogenide ligands are less labile and can be substituted only under drastic conditions. For instance, the reaction of $[\text{Re}_6\text{Te}_8(\text{Te}_7)]$ with a melt of KNCS results in the substitution of sulfur for μ_3 -tellurium atoms and produces a mixture of $[\text{Re}_6\text{S}_8(\text{CN})_6]^{4-}$ and $[\text{Re}_6\text{S}_6\text{Te}_2(\text{CN})_6]^{4-}$.^{163, 340} The formation of the mixed-chalcogen clusters was confirmed by ^{77}Se and ^{125}Te NMR spectroscopy.³⁴¹ The reaction of $[\text{Re}_6\text{Te}_8(\text{Te}_7)]$ with bromine yields $[\text{Re}_6(\text{Te}_4\text{Br}_4)\text{Br}_6]$.^{8, 187} Iodine, being a weaker oxidant, transforms the *spiro*-anion Te_7^{2-} into the ligand TeI_2 without affecting the cluster core to give the cluster $[\text{Re}_6\text{Te}_8(\text{TeI}_2)_6]\text{I}_2$.³⁴²

In the series of the octahedral molybdenum chalcogenide clusters Mo_6Q_8 ($\text{Q} = \text{S}, \text{Se}, \text{Te}$), the telluride possesses the highest reactivity and can be transformed into $\text{Mo}_6\text{Cl}_{12}$ with chlorine or other chlorinating reagents. The experiments with isotopomeric compounds have shown that the octahedron of Mo_6 remains intact.^{343, 344}

5. Elimination of chalcogens from the clusters M_3Q_7

A well studied transformation of triangular clusters M_3Q_7 into M_3Q_4 in the reaction with such reagents as cyanide ion or phosphines belongs to this class of processes.¹⁸ It was shown by isotope exchange method that it is the equatorial atom of dichalcogenide ligand that is eliminated.^{46, 48} The selenium atom is eliminated from the clusters $\text{Mo}_3(\mu_3\text{-S}).(\mu\text{-S}_{\text{ax}}\text{Se}_{\text{eq}})_3^{4+}$.^{32, 47} The proneness to chalcogen elimination decreases in the order $\text{Mo}_3\text{S}_7 > \text{Mo}_3\text{Se}_7 > \text{Mo}_3\text{Te}_7$. In the case of telluride clusters, no elimination of tellurium atom in reactions with cyanides or phosphines usually occurs. The only exception is the reaction of $[\text{Mo}_3\text{Te}_7\{(\text{Pr}^i\text{O})_2\text{PS}_2\}_3]\text{I}$ with tributylphosphine (in the presence of benzoic acid), which results in the formation of the complex $[\text{Mo}_3\text{Te}_4. \{(\text{Pr}^i\text{O})_2\text{PS}_2\}_3(\mu\text{-C}_6\text{H}_4\text{CO}_2)(\text{PBu}_3^i)]$.²³

The aqua complex $[\text{Mo}_3\text{S}_7(\text{H}_2\text{O})_6]^{4+}$ quantitatively yields $[\text{Mo}_3\text{S}_4(\text{H}_2\text{O})_9]^{4+}$ in the reaction with water-soluble phosphine PR_3^{3-} ($\text{R} = \text{C}_6\text{H}_4\text{SO}_3$). The following equation describes the dependence of the rate of this reaction on $[\text{H}^+]$

$$k = k_1[\text{H}^+] + k_{-1}[\text{H}^+]^{-1}$$

($k_1 = 3.14 \times 10^4 \text{ litre}^2 \text{ mol}^{-2} \text{ s}^{-1}$; $k_{-1} = 2.78 \times 10^4 \text{ s}^{-1}$). It was thus suggested that both the $\mu\text{-S}_2$ -protonated form of $[\text{Mo}_3\text{S}_5(\text{HS}_2)(\text{H}_2\text{O})_6]^{5+}$ and the conjugated base $[\text{Mo}_3\text{S}_7 \cdot (\text{H}_2\text{O})_5(\text{OH})]^{3+}$ are involved. The rate of this reaction in the case of the selenide complex $[\text{Mo}_3\text{Se}_7(\text{H}_2\text{O})_6]^{4+}$ is approximately 1000 times lower than for the sulfide analogue.³² The reactions with cyanide and phosphines usually produce the corresponding cyanide or phosphine complexes.^{18, 24, 308, 345} Even coordination polymers react in this way.^{24, 53} The complexes $[\text{M}_3\text{Q}_4(\text{dmpe})_3\text{X}_3]^+$ obtained in the reaction with dmpe are convenient starting compounds for the synthesis of heterometallic cubane-type clusters.³⁴⁶ Recently, complexes with chiral phosphines have been obtained.³⁴⁷ The isotope labelling studies suggest that the formation of $[\text{Mo}_3\text{S}_7(\text{S}_2)_3]^{2-}$ from $\text{Mo}_3\text{S}_7\text{Br}_4$ and $(\text{NH}_4)_2\text{S}_x$ proceeds as the elimination–addition in the equatorial position, *i.e.*, *via* the cluster Mo_3S_4 .^{44, 48} In the case of $\text{W}_3\text{S}_7\text{Br}_4$ and $(\text{NH}_4)_2\text{S}_x$ the complex $[\text{W}_3\text{S}_4(\text{S}_4)_3(\text{NH}_3)_3]^{2-}$ is the reaction product.^{44, 231} Generally, the tungsten clusters W_3Q_7^+ are less stable and readily eliminate three chalcogen atoms yielding the clusters $\text{W}_3\text{Q}_4^{4+}$, for example, in the synthesis of oxalate complexes.³³ The complex $[\text{W}_3\text{S}_7\text{Br}_6]^{2-}$ yields $[\text{W}_3\text{S}_4(\text{NCS})_9]^{5-}$ even upon heating with KNCs in acetonitrile.²³¹ The sulfobromide $\text{Mo}_3\text{S}_7\text{Br}_4$ eliminates sulfur atoms from the disulfide ligands in a melt of KHF_2 furnishing $[\text{Mo}_3\text{S}_4\text{F}_7(\text{FHF})_2]^{5-}$.³⁴⁸

The reaction of $[\text{Re}_3\text{S}_7\text{Cl}_6]\text{Cl}$ with an ionic liquid (a mixture of 1-ethyl-3-methyl-imidazolium bromide and AlBr_3) results in the formation of the anionic complex $[\text{Re}_3\text{S}_4\text{Br}_9]^{2-}$.³⁴⁹ The reactions with phosphines are accompanied by reduction and transformation of the cluster core.³⁵⁰

6. Reactions with the change in of the number of metal atoms

The incorporation of Group 6–15 metals (more than 20 elements) in low oxidation states into the cluster core is typical of triangular clusters M_3Q_4 and results in the formation of heterometallic cubane-type clusters. These reactions were intensively studied and the results were summarised in several reviews.^{18, 19, 346} In the case of a transition metal (Cr, Mo, W, Re, Fe, Ru, Os, Co, Rh, Ir, Ni, Pd, Pt, Cu) that is incorporated, this is involved in bonding Mo (W) to form a metallotetrahedron. Group 12–15 metals do not form metal–metal bonds. In the case of transition metals, the clusters in which the total number of valence electrons (NVE) including those provided by the ligand is equal to 60 are the most stable. This corresponds to the scheme of MO of tetrahedral clusters. The derivatives of $\text{Mo}_3\text{CuQ}_4^{4+}$ (NVE = 61), $\text{Mo}_3\text{CoQ}_4^{4+/3+}$ (NVE = 58 and 59), $\text{Mo}_3\text{FeS}_4^{4+}$ (NVE = 58) are exceptions to the rule. When an atom of post-transition element is incorporated, the heterometallic clusters are formed only if the metal is in the formally zero oxidation state (Zn, Cd, Hg, In, Tl, Ge, Sn, Pb, As, Sb, Bi) or possesses a lone pair of electrons (Ga^{I} , In^{I} , Ge^{II} , Sn^{II} , Pb^{II} , Sb^{III} , Bi^{III}). The tendency towards the formation of heterometallic clusters decreases in the order $\text{Mo}_3\text{S}_4^{4+} > \text{Mo}_3\text{Se}_4^{4+} > \text{W}_3\text{Se}_4^{4+} > \text{W}_3\text{S}_4^{4+}$, *i.e.* similarly to the order of decrease in the rate of cluster core reduction.^{18, 19, 346}

Oxidation of heterometallic cubane-type clusters recovers readily the starting triangular clusters $\text{M}_3\text{Q}_4^{4+}$.¹⁹ The ease of oxidation increases in the same order as the tendency to reduction of a triangular cluster decreases. In the case of heterocubane clusters $[\text{Mo}_x\text{W}_{4-x}\text{Q}_4(\text{H}_2\text{O})_{12}]^{6+}$ ($x = 1-3$), oxidation always proceeds with elimination of the tungsten atom. This reaction can be used for selective synthesis of

otherwise hardly accessible mixed heterometallic triangular clusters $[\text{Mo}_x\text{W}_{3-x}\text{Q}_4(\text{H}_2\text{O})_9]^{4+}$ ($\text{Q} = \text{S}, \text{Se}$; $x = 1, 2$).^{116, 117} The first heterometallic clusters Re_3MS_4 ($\text{M} = \text{Ni}, \text{Co}, \text{Cu}$) were obtained.^{40, 351, 352}

In some cases the cubane-type clusters M_4S_4 are formed from triangular clusters as a result of complicated reactions in attempted reduction or ligand exchange reactions. Thus, the reduction of the aqua complex $[\text{Mo}_3\text{S}_4(\text{H}_2\text{O})_9]^{4+}$ affords a mixture of a cubane-type and a heptanuclear bis-cubane clusters $[\text{Mo}_4\text{S}_4(\text{H}_2\text{O})_{12}]^{4+}$ and $[\text{Mo}_7\text{S}_8(\text{H}_2\text{O})_{18}]^{8+}$,³⁵³ and an attempt to synthesise Re_3S_4 derivatives from $[\text{Re}_3\text{S}_7\text{Cl}_6]\text{Cl}$ by the reaction with KCN unexpectedly yields $[\text{Re}_4\text{S}_4(\text{CN})_{12}]^{4-}$.⁸⁷ The cyanide cluster complexes $[\text{M}_4\text{Q}_4(\text{CN})_{12}]^{6-}$ were obtained by high-temperature reactions of triangular coordination polymers $\text{M}_3\text{Q}_7\text{X}_4$ ($\text{Q} = \text{S}, \text{Se}, \text{Te}$; $\text{X} = \text{Br}, \text{I}$) with KCN.¹⁰²

The reduction of phosphine complexes $[\text{Mo}_3\text{Q}_4 \cdot (\text{PET}_3)_{3-4}\text{X}_4(\text{MeOH})_{1-2}]$ ($\text{Q} = \text{S}, \text{Se}$) with magnesium results in the reductive fusion of two metal triangles into an octahedron and the formation of phosphine cluster complexes $[\text{Mo}_6\text{Q}_8(\text{PET}_3)_6]$, which are molecular analogues of the Chevrel phases.²⁵⁷ Formally, octahedral clusters M_6Q_8 are the dimerisation products of reduced triangular clusters M_3Q_4 . If the reaction takes place at low temperatures, then the dimerisation of two triangular clusters happens at the stage of one-electron reduction. This reaction affords the compounds $[\text{Mo}_6\text{Q}_8\text{Cl}_6 \cdot (\text{PET}_3)_6]$ in which two metal triangles are linked by one metal–metal bond.¹⁷⁹ The cluster $[\text{Mo}_6\text{S}_{10}(\text{SH})_2(\text{PET}_3)_6]$ of a similar structure was obtained from $(\text{NH}_4)_2[\text{Mo}_3\text{S}_7(\text{S}_2)_3]$ and triethylphosphine.¹³⁰

The cases of transformation of tetrahedral clusters into octahedral clusters are extremely rare. One example is the formation (simultaneously with the chalcogen atom replacement in the cluster core) of the complex $[\text{Re}_6\text{Se}_8(\text{CN})_6]^{4-}$ from $[\text{Re}_4\text{Te}_4(\text{TeCl}_2)_4\text{Cl}_8]$ and KNCSe (the latter is the reducing agent as well as the source of selenium and cyanide ions) in acetonitrile at 200 °C. The cluster $\text{Re}_4\text{S}_4\text{Te}_4$ reacts with KCN at 850 °C yielding the octahedral cluster complex $[\text{Re}_6\text{S}_6(\text{S}_{0.34}\text{Te}_{0.66})_2(\text{CN})_6]^{4-}$. This reaction was used for the synthesis of heterometallic clusters $[\text{Re}_5\text{MoS}_8(\text{CN})_6]^{5-}$ and $[\text{Re}_4\text{Mo}_2\text{S}_8(\text{CN})_6]^{5-}$ from $\text{Re}_3\text{MoS}_4\text{Te}_4$.¹⁴²

V. Potential applications of chalcogenide clusters

The progress in chemistry of chalcogenide clusters of early transition metal is very important for better understanding of the processes that occur in living systems with involvement of transition metals. It is well known that at least seven metals (V, Mo, W, Fe, Ni, Cu and Zn) in living systems are bonded quite often to sulfur (and/or selenium) atoms and are vital for various biological functions. Among the early transition metals, molybdenum is particularly important as a part of different enzymes. Tungsten is the heaviest element with reliably determined biological role. Chalcogenide clusters are also of interest as models of solid-state metal chalcogenides; besides they are used in the synthesis of new catalysts and advanced materials (superconductors, X-ray contrast diagnostic agents and non-linear optic materials).

Catalysis. Supported transition metal sulfides are catalysts of hydrorefining of crude oil.³⁵⁴ CoMoS and NiMoS supported onto alumina are widely used in industry for desulfurisation. Traditionally they are prepared by impregnation of $\gamma\text{-Al}_2\text{O}_3$ with ammonium heptamolybdate and cobalt or nickel nitrate with subsequent calcination and transformation of oxides into sulfide phases by heating in an atmosphere of H_2S and H_2 at 400 °C. More effective catalysts were obtained in the reactions of the sulfide cluster $[\text{Mo}_3\text{S}_{13}]^{2-}$ with various salts, including those with complex nickel- or cobalt-containing cations.³⁵⁵ The metal ratio in the heterometallic cubane-type clusters M_3NiS_4 and M_3CoS_4 corresponds to the composition

of the best hydrotreating catalysts and the coordination of heterometal is thought to be similar to that of cobalt or nickel atom in the active site of such catalysts.³⁵⁶ The triangular and heterometallic cubane-type cationic aqua complexes $[\text{Mo}_3\text{S}_4(\text{H}_2\text{O})_9]^{4+}$ and $[\text{Mo}_3\text{NiS}_4(\text{H}_2\text{O})_{10}]^{4+}$ were incorporated into zeolites by an ion-exchange reaction.^{357–359} It was shown that the activity of such catalysts in hydrogenation of thiophene strongly depends on the zeolite type. The complex $[\text{Mo}_3\text{NiS}_4(\text{H}_2\text{O})_{10}]^{4+}$ incorporated into the zeolite cavity catalyses also the synthesis of ethane and ethylene in the hydrogenation of CO.

The triangular pentamethylcyclopentadienyl cluster $[\text{Cp}^*\text{Mo}_3\text{S}_4]^+$ reacts with $[\text{Ni}(\text{cod})_2]$ (cod is cycloocta-1,5-diene) in dichloromethane at room temperature yielding the cubane-type heterometallic cluster $[(\text{Cp}^*\text{Mo}_3\text{NiS}_4)_2(\text{cod})]^{2+}$, which is a highly effective catalyst of intramolecular cyclisation of alkynoic acids into the corresponding enolactones in the presence of Et_3N . Presumably, an intermediate nickel alkyne complex is formed in this reaction.³⁶⁰

The 1,4,7-triazacyclononane (tacn) heterometallic cluster $[\text{Mo}_3(\text{PdCl})\text{S}_4(\text{tacn})]^{3+}$ possesses a unique ability of coordinating and activating such π -acidic ligands as CO, isonitriles, alkenes and alkynes under very mild conditions. Thus the solution reaction with CO proceeds even at room temperature and yields the brown complex $[\text{Mo}_3(\text{PdCO})\text{S}_4(\text{tacn})_3]^{3+}$. Activated alkynes (for example, $\text{HC}\equiv\text{CCO}_2\text{Me}$ and $\text{MeO}_2\text{CC}\equiv\text{CCO}_2\text{Me}$) also coordinate only the palladium atom of the cluster, but form very labile complexes, which could not be isolated. However, selective nucleophilic addition of methanol to methyl propiolate result in (Z)- $\text{MeOCH}=\text{CHCO}_2\text{Me}$ in virtually quantitative yield takes place in the presence of methanol. It is important that the reactions of nucleophilic addition are catalytic processes and more effective than the catalytic reactions of mononuclear palladium complexes.³⁶¹

Unique catalysts possessing a chiral metal chalcogenide cores can be obtained from chalcogenide clusters.³⁴⁷ Each diphosphine ligand in the triangular molybdenum and tungsten diphosphine complexes $[\text{M}_3\text{Q}_4(\text{diphosphine})_3\text{X}_3]^+$ ($\text{M} = \text{Mo}, \text{W}$; $\text{Q} = \text{S}, \text{Se}$; $\text{X} = \text{Cl}, \text{Br}$) links to only one metal atom, while the phosphorus atoms are located in *cis*- and *trans*-positions with respect to the μ_3 -chalcogen atom. These diphosphine clusters are chiral. From the chiral diphosphine (+)-1,2-bis[(2*R*,5*R*)-2,5-(dimethylphospholan-1-yl)]ethane [(*R,R*)-MeBPE], the chiral triangular cluster $[\text{Mo}_3\text{S}_4\{(\text{R,R})\text{-MeBPE}\}_3\text{Cl}_3]^+$ and heterometallic derivative $[\text{Mo}_3\text{CuS}_4\{(\text{R,R})\text{-MeBPE}\}_3\text{Cl}_3]^+$ were obtained. This heterometallic cluster turned out to be an effective catalyst of two reactions: the intramolecular cyclisation of 1-diazohex-5-en-2-one and the intermolecular cyclopropanation of styrene or 2-phenylpropene with ethyl diazoacetate. The reactions proceed in high yields of the corresponding cyclopropanes (up to 95%), the enantiomeric excess being in the range from 12% to 25%.³⁴⁷

Conductors and superconductors. A unique substance was obtained by two-electron oxidation of the anionic molybdenum cluster $[\text{Mo}_3\text{S}_7(\text{dmit})_3]^{2-}$.³⁶² Electrochemical oxidation of its *tert*-butylammonium salt yields deep-violet needle-shaped crystals stable in air. Chemical oxidation with iodine in dichloromethane is yet another method of its synthesis in quantitative yield. The neutral cluster molecules crystallise in a hexagonal space group and the structure is built of chains. The molecules in the chains are linked by short $\text{S}\cdots\text{S}$ contacts between axial sulfur atoms of the bridging disulfide ligands and μ_3 -sulfur atoms. The $\text{S}\cdots\text{S}$ contacts between the sulfur atoms of the cluster complexes of different chains combine the chains into honeycomb-like framework with spacious vacant channels ~ 10 Å in diameter. The room-temperature conductivity measurements have shown that $[\text{Mo}_3\text{S}_7(\text{dmit})_3]$ is a quasi-one-

dimensional semiconductor with a very low value of activation energy. The magnetic susceptibility measurements reveal the presence of antiferromagnetic exchange interactions between unpaired electrons of the neutral clusters $[\text{Mo}_3\text{S}_7(\text{dmit})_3]$. It is expected that chemical modification of this unique cluster (for example, by the replacement of the metal, chalcogen or redox-active ligand) and application of high pressure will eventually result in the stabilisation of the metal state.

Non-linear optical properties. The triangular molybdenum and tungsten chalcogenide clusters and their heterometallic cubane derivatives were systematically studied in this respect. All triangular clusters $[\text{M}_3\text{Q}_4\text{L}_3\text{X}_4]^+$ ($\text{M} = \text{Mo}, \text{W}$; $\text{Q} = \text{S}, \text{Se}$; $\text{L} = \text{dmpe}, \text{dppe}$) and their copper-containing cubane-type derivatives $[\text{M}_3\text{CuQ}_4\text{L}_3\text{X}_4]^+$ turned out to be promising optical limiters and the value of threshold limiting flux decreases on going from the cubane-type clusters to triangular ones and from tungsten clusters to molybdenum analogues.^{296, 308, 346}

X-Ray contrast agents. The cluster-type tungsten thio complexes ($\text{W}_3\text{S}_4^{4+}$ derivatives) represent a new class of X-ray contrast diagnostic agents. The cluster compounds of heavy metals ($Z > 50$) possess a high X-ray absorption coefficient, which results in a significant improvement of the image quality and/or reduction of X-ray irradiation dose. Triangular tungsten thio clusters are highly soluble in water, do not hydrolyse in aqueous solutions and form stable chelate complexes with various ligands. It is very important that the $\text{W}_3\text{S}_4^{4+}$ derivatives are significantly less toxic in comparison with water-soluble tungsten heteropolyanions.³⁶³

VI. Conclusion

The data presented show that the chemistry of chalcogenide cluster complexes of Group 5–7 metals is extensive and diverse. Many specific properties of cluster compounds are determined by the structure, geometry and electronic features of the cluster core. The possibility of modifying the cluster core by isovalent and non-isovalent substitution of both 'inner' ligands and metal atoms allows one to change the properties of cluster complexes. Such approach underlies the directed synthesis of materials with preset properties in which the cluster complexes are used as building blocks with predetermined spatial, electronic, optical or magnetic characteristics. The list of useful properties of chalcogenide cluster compounds is already quite remarkable and will undoubtedly be extended with the further studies of this class of compounds. More and more, not only synthetic chemists, but also physicists, theoreticians, materials scientists are involved in these studies and, owing to their efforts, the first steps towards the design of new materials and better understanding of the principles which control the properties of these compounds are being made.

The data presented show the progress in the studies of cluster chalcogenide complexes of transition metals. Quite interesting is the evolution of studies of such systems. Whereas after the discovery of the key compounds, they were studied predominantly by the methods of solid state chemistry the set of which was rather small, nowadays the main attention is paid to the chemistry of solutions due to the development of methods of transformation of polymeric cluster compounds into molecular complexes. New research groups became involved into this field of chemistry, which increases the ability to detect specific properties of cluster complexes.

At the first glance, it seems that, as a result of intensive studies, the chemistry of chalcogenide cluster complexes of Group 5–7 metals has been exhausted. However, recent syntheses of cluster metal complexes of unexpected types, such as square vanadium $\text{V}_4\text{S}_9\text{Br}_4$ and tantalum $\text{Ta}_4\text{Q}_9\text{X}_8$ ($\text{Q} = \text{S}, \text{Se}$) clusters, dodecanuclear rhenium complexes $[\text{Re}_{12}\text{CS}_{17}(\text{CN})_6]^{8-/6-}$ with interstitial carbon atom, indicate that further discoveries are awaiting.

References

1. F A Cotton *Inorg. Chem.* **3** 1217 (1964)
2. F A Cotton *J. Chem. Soc., Dalton Trans.* 1961 (2000)
3. A A Opalovskii, V E Fedorov, K A Kholdoyanidi *Dokl. Akad. Nauk SSSR* **182** 1095 (1968)^a
4. A V Nikolaev, A A Opalovsky, V E Fedorov *Thermal Analysis* Vol. 2 (New York: Academic Press, 1969)
5. A A Opalovskii, V E Fedorov *Izv. Akad. Nauk SSSR, Neorg. Mater.* **2** 447 (1966)^b
6. A A Opalovskii, V E Fedorov *Izv. Akad. Nauk SSSR, Neorg. Mater.* **2** 443 (1966)^b
7. *Superconductivity in Ternary Compounds I. Structural, Electronic and Lattice Properties* (Eds F Fisher, M Maple) (Heidelberg: Springer, 1982)
8. V E Fedorov, N V Podberezskaya, A V Mishchenko, G F Khudorozko, I P Asanov *Mater. Res. Bull.* **21** 1335 (1986)
9. A A Opalovskii, V E Fedorov, E U Lobkov, B G Erenburg *Zh. Neorg. Khim.* **16** 3175 (1971)^c
10. Yu V Mironov, T E Albrecht-Schmitt, J A Ibers *Inorg. Chem.* **36** 944 (1997)
11. N G Naumov, A V Virovets, V E Fedorov *Zh. Strukt. Khim.* **41** 609 (2000)^d
12. O A Efremova, Yu V Mironov, V E Fedorov *Eur. J. Inorg. Chem.* 2533 (2006)
13. Yu V Mironov, S S Yarovoi, D Yu Naumov, S G Kozlova, V N Ikorsky, R K Kremer, A Simon, V E Fedorov *J. Phys. Chem. B* **109** 23804 (2005)
14. M N Sokolov, A L Gushchin, P A Abramov, A V Virovets, E V Peresypkina, S G Kozlova, B A Kolesov, C Vicent, V P Fedin *Inorg. Chem.* **44** 8756 (2005)
15. Yu V Mironov, N G Naumov, S G Kozlova, S J Kim, V E Fedorov *Angew. Chem., Int. Ed.* **44** 6867 (2005)
16. V E Fedorov, A V Mishchenko, V P Fedin *Usp. Khim.* **54** 694 (1985) [*Russ. Chem. Rev.* **54** 408 (1985)]
17. V E Fedorov, N G Naumov, Yu V Mironov, A V Virovets, S B Artemkina, K A Brylev, S S Yarovoi, O A Efremova, U H Paek *Zh. Strukt. Khim.* **43** 721 (2002)^d
18. M N Sokolov, V P Fedin, A G Sykes, in *Comprehensive Coordination Chemistry II* Vol. 4 (Amsterdam: Elsevier, 2003) p. 761
19. R Hernandez-Molina, M N Sokolov, A G Sykes *Acc. Chem. Res.* **34** 223 (2001)
20. M N Sokolov, V P Fedin *Coord. Chem. Rev.* **248** 925 (2004)
21. J K Money, J C Huffman, G Christou *Inorg. Chem.* **27** 507 (1988)
22. F A Cotton, M P Diebold, R Llusar, W J Roth *J. Chem. Soc., Chem. Commun.* 1276 (1986)
23. X Lin, H Y Chen, L S Chi, C Z Lu, H H Zhuang *Polyhedron* **19** 925 (2000)
24. V P Fedin, G J Lamprecht, T Kohzuma, W Clegg, M R J Elsegood, A G Sykes *J. Chem. Soc., Dalton Trans.* 1747 (1997)
25. T Shibahara, M Yamasaki, G Sakane, K Minami, T Yabuki, A Ichimura *Inorg. Chem.* **31** 640 (1992)
26. T Shibahara, T Yamada, H Kuroya, E F Hills, P Kathirgamanathan, A G Sykes *Inorg. Chim. Acta* **113** L19 (1986)
27. V P Fedin, M N Sokolov, A V Virovets, N V Podberezskaya, V Ye Fedorov *Polyhedron* **11** 2973 (1992)
28. M Nasreldin, G Henkel, G Kampmann, B Krebs, G J Lamprecht, C A Routledge, A G Sykes *J. Chem. Soc., Dalton Trans.* 737 (1993)
29. G J Lamprecht, M Martinez, M Nasreldin, C A Routledge, N Alshatti, A G Sykes *J. Chem. Soc., Dalton Trans.* 747 (1993)
30. M Brorson, A Hazell, C J H Jacobsen, I Schmidt, J Villadsen *Inorg. Chem.* **39** 1346 (2000)
31. H Akashi, T Shibahara, H Kuroya *Polyhedron* **9** 1671 (1990)
32. D M Saysell, V P Fedin, G J Lamprecht, M N Sokolov, A G Sykes *Inorg. Chem.* **36** 2982 (1997)
33. M N Sokolov, A L Gushchin, D Yu Naumov, O A Gerasko, V P Fedin *J. Cluster Sci.* **16** 309 (2005)
34. M N Sokolov, A L Gushchin, D Yu Naumov, O A Gerasko, V P Fedin *Inorg. Chem.* **44** 2431 (2005)
35. F A Cotton, Z Dori, R Llusar, W Schwotzer *J. Am. Chem. Soc.* **107** 6734 (1985)
36. T Shibahara, S Yoshida, M Maeyama, M Kojima *Bull. Chem. Soc. Jpn.* **72** 2271 (1999)
37. M Yamasaki, T Shibahara *Anal. Sci.* **8** 727 (1992)
38. T Shibahara, M Yamasaki, T Watase, A Ichimura *Inorg. Chem.* **33** 292 (1994)
39. S-B Yu, M Droegge, B Segal, S-H Kim, T Sanderson, A D Watson *Inorg. Chem.* **39** 1325 (2000)
40. N Miyake, H Imoto, T Saito *Chem. Lett.* 913 (1997)
41. F A Cotton, R Llusar *Inorg. Chem.* **27** 1303 (1988)
42. J Mizutani, H Imoto, T Saito *J. Cluster Sci.* **6** 523 (1995)
43. F Estevan, M Feliz, R Llusar, J A Mata, S Uriel *Polyhedron* **20** 527 (2001)
44. V P Fedin, M N Sokolov, O S Kibirev, A V Virovets, N V Podberezskaya, V E Fedorov *Zh. Neorg. Khim.* **36** 3089 (1991)^c
45. A V Virovets, Yu L Slovokhotov, Yu T Struchkov, V E Fedorov, N G Naumov, O A Geras'ko, V P Fedin *Koord. Khim.* **16** 332 (1990)^c
46. V P Fedin, M N Sokolov, Yu V Mironov, B A Kolesov, S V Tkachev, V Ye Fedorov *Inorg. Chim. Acta* **167** 39 (1990)
47. V P Fedin, Yu V Mironov, M N Sokolov, B A Kolesov, V Ye Fedorov, D S Yufit, Yu T Struchkov *Inorg. Chim. Acta* **174** 275 (1990)
48. V P Fedin, B A Kolesov, Yu V Mironov, V Ye Fedorov *Polyhedron* **8** 2419 (1989)
49. V P Fedin, M N Sokolov, A V Virovets, N V Podberezskaya, V Ye Fedorov *Polyhedron* **11** 2395 (1992)
50. A V Virovets, A L Gushchin, P A Abramov, N I Alferova, M N Sokolov, V P Fedin *Zh. Strukt. Khim.* **47** 332 (2006)^d
51. V P Fedin, Yu V Mironov, A V Virovets, N V Podberezskaya, V Ye Fedorov *Polyhedron* **11** 2083 (1992)
52. J Mizutani, H Imoto, T Saito *Chem. Lett.* 2117 (1994)
53. V P Fedin, M N Sokolov, O A Geras'ko, A V Virovets, N V Podberezskaya, V Ye Fedorov *Inorg. Chim. Acta* **187** 81 (1991)
54. J Li, Z Chen, T J Emge, D M Proserpio *Inorg. Chem.* **36** 1437 (1997)
55. H Keck, W Kuelhen, J Mathow, B Meyer, D Mootz, H Wunderlich *Angew. Chem., Int. Ed. Engl.* **20** 975 (1981)
56. G Borgs, H Keck, W Kuchen, D Mootz, R Wiskemann, H Wunderlich *Z. Naturforsch., B* **46** 1525 (1991)
57. R Yu, S Lu, X Huang, Q Wu, J Huang *Chin. J. Struct. Chem. (Jiegou Huaxue)* **17** 137 (1998); *Chem. Abstr.* **128** 330305 (1998)
58. X Lin, J Lu, J Huang, J Huang *Chin. J. Struct. Chem. (Jiegou Huaxue)* **9** 236 (1990); *Chem. Abstr.* **114** 177119 (1991)
59. N S Dean, K Folting, E Lobkovsky, G Christou *Angew. Chem., Int. Ed. Engl.* **32** 594 (1993)
60. Y Yang, Q T Liu, D X Wu *Inorg. Chim. Acta* **208** 85 (1993)
61. J Beck, K Muller-Buschbaum *Z. Anorg. Allg. Chem.* **625** 1212 (1999)
62. N N Timoshchenko, V L Kolesnichenko, S V Volkov, Yu L Slovokhotov, Yu T Struchkov *Koord. Khim.* **16** 1062 (1990)^c
63. L A Aslanov, S V Volkov, V L Kolesnichenko, V B Mischanchuk, V B Rybakov, N N Timoshchenko *Ukr. Khim. Zh.* **57** 675 (1991)
64. V P Fedin, H Imoto, T Saito, W McFarlane, A G Sykes *Inorg. Chem.* **34** 5097 (1995)
65. N V Pervukhina, N V Podberezskaya, I V Kalinina, V P Fedin *Zh. Strukt. Khim.* **41** 1027 (2000)^d
66. V P Fedin, H Imoto, T Saito *J. Chem. Soc., Chem. Commun.* 1559 (1995)
67. M N Sokolov, P A Abramov, A L Gushchin, I V Kalinina, D Yu Naumov, A V Virovets, E V Peresypkina, C Vicent, R Llusar, V P Fedin *Inorg. Chem.* **44** 8116 (2005)
68. J-Q Huang, J-L Huang, M-Y Shang, S-F Lu, X-T Lin, Y-H Lin, M-D Huang, H-H Zhuang, J-X Lu *Pure Appl. Chem.* **60** 1185 (1988)
69. D T Richens, in *The Chemistry of Aqua Ions* (Chichester: Wiley, 1997) p. 302

70. R Hernandez-Molina, A G Sykes *J. Chem. Soc., Dalton Trans.* 3137 (1999)
71. T Shibahara, G Sakane, S Mochida *J. Am. Chem. Soc.* **115** 10408 (1993)
72. J-Q Huang, S-F Lu, X-Y Huang, Q-J Wu, R-M Yu *J. Cluster Sci.* **8** 47 (1997)
73. Y Peng, S-F Lu, H-J Fan, Q-J Wu, R-M Yu, J-Q Huang *Polyhedron* **19** 733 (2000)
74. J Hu, H H Zhuang, S X Liu, J L Huang *Trans. Met. Chem.* **23** 547 (1998)
75. A M Arif, J G Hefner, A Jones, T A Albright, S-K Kang *J. Am. Chem. Soc.* **108** 1701 (1986)
76. M Shie, L-F Ho, L-F Jang, C-H Ueng, S-M Peng, Y-H Liu *Chem. Commun.* 1014 (2001)
77. S Yamada, N Miyake, H Imoto, T Saito *Chem. Lett.* 671 (1997)
78. H Brunner, G Gehart, J Wachter, B Nuber, M L Ziegler *Angew. Chem., Int. Ed. Engl.* **31** 1021 (1992)
79. H Kawaguchi, K Tatsumi *Organometallics* **16** 307 (1997)
80. G V Khvorykh, A V Shevelkov, V A Dolgikh, B A Popovkin *J. Solid State Chem.* **120** 311 (1995)
81. M D Smith, G J Miller *J. Alloys Compd.* **281** 202 (1998)
82. M Smith, G J Miller *J. Solid State Chem.* **140** 226 (1998)
83. P J Schmidt, G Thiele *Acta Crystallogr., Sect. C* **53** 1743 (1997)
84. V E Fedorov, V K Evstaf'ev, S D Kirik, A V Mishchenko *Zh. Neorg. Khim.* **26** 2701 (1981)^c
85. C Perrin, R Chevrel, M Sergent *C.R. Seances Acad. Sci., Ser. C* **280** 949 (1975)
86. C Perrin, R Chevrel, M Sergent *C.R. Seances Acad. Sci., Ser. C* **281** 23 (1975)
87. V E Fedorov, Yu V Mironov, V P Fedin, H Imoto, T Saito *Acta Crystallogr., Sect. C* **52** 1065 (1996)
88. H Barz *Mater. Res. Bull.* **8** 983 (1973)
89. D Brasen, J M Vandenberg, M Robbins, R H Willens, W A Reed, R C Sherwood, X J Pinder *J. Solid State Chem.* **13** 298 (1975)
90. J M Vandenberg, D Brasen *J. Solid State Chem.* **14** 203 (1975)
91. J M Vandenberg, B T Matthias *Mater. Res. Bull.* **9** 1085 (1974)
92. G F Khudorozhko, E A Kravtsova, L N Mazalov, V E Fedorov, L G Bulusheva, I P Asanov, G K Paroshina, Yu V Mironov *Zh. Strukt. Khim.* **37** 901 (1996)^d
93. E S Lang, U Abram, J Strähle *Z. Anorg. Allg. Chem.* **622** 251 (1996)
94. M Herberhold, M Schrepfermann, J Darkwa *J. Organomet. Chem.* **430** 61 (1992)
95. W Chen, L Y Goh, E Sinn *Organometallics* **7** 2020 (1988)
96. L Y Goh, T W Hambley, G B Robertson *Organometallics* **6** 1051 (1987)
97. I L Eremenko, A A Pasynskii, A S Katugin, B Orazsakhmatov, V E Shklover, Yu T Struchkov *Metalloorg. Khim.* **1** 166 (1988)^f
98. I L Eremenko, S E Nefedov, A A Pasynskii, B Orazsakhmatov, O G Ellert, Yu T Struchkov, A I Yanovsky, D V Zagorevsky *J. Organomet. Chem.* **368** 185 (1989)
99. L Y Goh, M S Tay, T C W Mak, R-G Wang *Organometallics* **11** 1712 (1992)
100. L Y Goh, W Chen *J. Chem. Soc., Dalton Trans.* 2697 (1994)
101. J A Bandy, C E Davies, J C Green, M L H Green, K Prout, D P S Rodgers *J. Chem. Soc., Chem. Commun.* 1395 (1983)
102. V P Fedin, I V Kalinina, D G Samsonenko, Yu V Mironov, M N Sokolov, S V Tkachev, A V Virovets, N V Podberezskaya, M R J Elsegood, W Clegg, A G Sykes *Inorg. Chem.* **38** 1956 (1999)
103. V P Fedin, D G Samsonenko, A V Virovets, N V Kalinina, D Yu Naumov *Izv. Akad. Nauk, Ser. Khim.* **18** (2000)^g
104. V P Fedin, M R J Elsegood, W Clegg, A G Sykes *Polyhedron* **15** 485 (1996)
105. Yu V Mironov, T E Albrecht-Schmitt, J A Ibers *Z. Kristallogr. New Cryst. Struct.* **212** 308 (1997)
106. Yu V Mironov, A V Virovets, W S Sheldrick, V E Fedorov *Polyhedron* **20** 969 (2001)
107. Yu V Mironov, A V Virovets, S B Artemkina, V E Fedorov *Zh. Strukt. Khim.* **40** 374 (1999)^d
108. V P Fedin, I V Kalinina, A V Virovets, N V Podberezskaya, I S Neretin, Yu L Slovokhotov *Chem. Commun.* 2579 (1998)
109. M Martinez, B L Ooi, A G Sykes *J. Am. Chem. Soc.* **109** 4615 (1987)
110. T C W Mak, K S Jasim, C Chieh *Inorg. Chem.* **24** 1587 (1985)
111. M N Sokolov, D N Dybtsev, A V Virovets, V P Fedin, P Esparza, R Hernandez-Molina, D Fenske, A G Sykes *Inorg. Chem.* **41** 1136 (2002)
112. Yu V Mironov, V E Fedorov *Izv. Akad. Nauk, Ser. Khim.* 529 (2002)^g
113. T Shibahara, E Kawano, M Okano, M Nishi, H Kuroya *Chem. Lett.* 827 (1986)
114. H-H Zhuang, D-M Wu, J-Q Huang, J-L Huang *Chin. Chem. Lett.* **2** 553 (1991)
115. C L Coyle, K A Eriksen, S Farina, J Francis, Y Gea, M A Greaney, P J Guzi, T R Halbert, H H Murray, E I Stiefel *Inorg. Chim. Acta* **198–200** 565 (1992)
116. M Sokolov, P Esparza, R Hernandez-Molina, J G Platas, A Mederos, J A Gavin, R Llugar, C Vicent *Inorg. Chem.* **44** 1132 (2005)
117. I J McLean, R Hernandez-Molina, M N Sokolov, M-S Seo, A V Virovets, M R J Elsegood, W Clegg, A G Sykes *J. Chem. Soc., Dalton. Trans.* 2557 (1998)
118. T Shibahara, H Kuroya, H Akashi, K Matsumoto, S Ooi *Inorg. Chim. Acta* **212** 251 (1993)
119. F A Cotton, Z Dori, R Llugar, W Schwotzer *Inorg. Chem.* **25** 3654 (1986)
120. Yu V Mironov *Polyhedron* **19** 437 (2000)
121. Yu V Mironov, M A Pell, T E Albrecht-Schmitt, J A Ibers *Inorg. Chem.* **40** 5472 (2001)
122. A Müller, E Krickemeyer, H Bögge *Angew. Chem., Int. Ed. Engl.* **25** 272 (1986)
123. A Müller, E Krickemeyer, H Bögge *Z. Anorg. Allg. Chem.* **554** 61 (1987)
124. S-F Lu, J-Q Huang, H-H Zhuang, J-Q Li, D-M Wu, Z-X Huang, C-Z Lu, J-L Huang, J-X Lu *Polyhedron* **10** 2203 (1991)
125. A W Edelblut, K Folting, J C Huffman, R A D Wentworth *J. Am. Chem. Soc.* **103** 1927 (1981)
126. M L Sampson, J F Richardson, M E Noble *Inorg. Chem.* **31** 2726 (1992)
127. P T Wood, W T Pennington, J W Kolis, B Wu, C J O'Connor *Inorg. Chem.* **32** 129 (1993)
128. J L Seela, J C Huffman, G Christou *J. Chem. Soc., Chem. Commun.* 1258 (1987)
129. E Babaian-Kibala, F A Cotton, P A Kibala *Polyhedron* **9** 1689 (1990)
130. K Tsuge, H Imoto, T Saito *Inorg. Chem.* **31** 4715 (1992)
131. S Kuwata, Y Mizobe, M Hidai *J. Chem. Soc., Dalton Trans.* 1753 (1997)
132. L-C Song, J-Q Wang, Q-M Hu, X-Y Huang *Polyhedron* **15** 2453 (1996)
133. H Schäfer, H G Schnering *Angew. Chem.* **76** 833 (1964)
134. S Cordier, N G Naumov, D Salloum, F Paul, C Perrin *Inorg. Chem.* **43** 219 (2004)
135. X Zhang, R E McCarley *Inorg. Chem.* **34** 2678 (1995)
136. J C P Gabriel, K Boubekeur, S Uriel, P Batail *Chem. Rev.* **101** 2037 (2001)
137. D Fenske, A Grissinger, M Loos, J Magull *Z. Anorg. Allg. Chem.* **598** 121 (1991)
138. Yu V Mironov, M A Pell, J A Ibers *Inorg. Chem.* **35** 2709 (1996)
139. S S Yarovoi, Yu V Mironov, S F Solodovnikov, D Yu Naumov, N K Moroz, S G Kozlova, A Simon, V E Fedorov *Chem. Commun.* 719 (2005)
140. A Perrin, R Chevrel, M Sergent, Ø Fischer *J. Solid State Chem.* **33** 43 (1980)
141. J Neuhausen, E W Finckh, W Tremel *Inorg. Chem.* **35** 5622 (1996)
142. N G Naumov, K A Brylev, Yu V Mironov, A V Virovets, D Fenske, V E Fedorov *Polyhedron* **23** 599 (2004)
143. W Bronger, C Koppe, M Loevenich, D Schmitz, T Schuster *Z. Anorg. Allg. Chem.* **623** 695 (1997)
144. E G Tulskey, J R Long *Inorg. Chem.* **40** 6990 (2001)
145. K Ramaswamy, E G Tulskey, J R Long, J L F Kao, S E Hayes *Inorg. Chem.* **46** 1177 (2007)
146. R Wang, Z Zheng *J. Am. Chem. Soc.* **121** 3549 (1999)

147. V P Fedin, A A Virovets, A G Sykes *Inorg. Chim. Acta* **271** 228 (1998)
148. Yu V Mironov, N G Naumov, S S Yarovoi, S Cordier, C Perrin, V E Fedorov *Izv. Akad. Nauk, Ser. Khim.* 1766 (2002)^g
149. T Yoshimura, K Umakoshi, Y Sasaki, A G Sykes *Inorg. Chem.* **38** 5557 (1999)
150. T Yoshimura, S Ishizaka, K Umakoshi, Y Sasaki, H-B Kim, N Kitamura *Chem. Lett.* 697 (1999)
151. M W Willer, J R Long, C C McLauchlan, R H Holm *Inorg. Chem.* **37** 328 (1998)
152. Z P Zheng, R H Holm *Inorg. Chem.* **36** 5173 (1997)
153. Z-N Chen, T Yoshimura, M Abe, Y Sasaki, S Ishizaka, H-B Kim, N Kitamura *Angew. Chem., Int. Ed.* **40** 239 (2001)
154. Z P Zheng, T G Gray, R H Holm *Inorg. Chem.* **38** 4888 (1999)
155. H D Selby, Z P Zheng, T G Gray, R H Holm *Inorg. Chim. Acta* **312** 205 (2001)
156. N G Naumov, A V Virovets, N V Podberezhskaya, V E Fedorov *Zh. Strukt. Khim.* **38** 1018 (1997)^d
157. Kh Imoto, N G Naumov, A V Virovets, T Saito, V E Fedorov *Zh. Strukt. Khim.* **39** 885 (1998)^d
158. S S Yarovoi, Yu V Mironov, D Yu Naumov, Yu V Gatilov, S G Kozlova, S J Kim, V E Fedorov *Eur. J. Inorg. Chem.* 3945 (2005)
159. M A Shestopalov, Yu V Mironov, K A Brylev, S G Kozlova, V E Fedorov, H Spies, H-J Pietzsch, H Stephan, G Geipel, G Bernhard *J. Am. Chem. Soc.* **129** 3714 (2007)
160. Yu V Mironov, K A Brylev, M A Shestopalov, S S Yarovoi, V E Fedorov, H Spies, H-J Pietzsch, H Stephan, G Geipel, G Bernhard, W Kraus *Inorg. Chim. Acta* **359** 1129 (2006)
161. Yu V Mironov, M A Shestopalov, K A Brylev, S S Yarovoi, G V Romanenko, V E Fedorov, H Spies, H-J Pietzsch, H Stephan, G Geipel, G Bernhard, W Kraus *Eur. J. Inorg. Chem.* 657 (2005)
162. Yu V Mironov, A V Virovets, N G Naumov, V N Ikorskii, V E Fedorov *Chem. – Eur. J.* **6** 1361 (2000)
163. Yu V Mironov, J A Cody, T E Albrecht-Schmitt, J A Ibers *J. Am. Chem. Soc.* **119** 493 (1997)
164. M Ebihara, K Isobe, Y Sasaki, K Saito *Inorg. Chem.* **31** 1644 (1992)
165. M Ebihara, K Toriumi, Y Sasaki, K Saito *Gazz. Chim. Ital.* **125** 87 (1995)
166. S Jin, D Venkataraman, F J DiSalvo *Inorg. Chem.* **39** 2747 (2000)
167. D Venkataraman, L L Rayburn, L I Hill, S Jin, A-S Malik, K J Turneau, F J DiSalvo *Inorg. Chem.* **38** 828 (1999)
168. G M Ehrlich, C J Warren, D A Vennos, D M Ho, R C Haushalter, F J DiSalvo *Inorg. Chem.* **34** 4454 (1995)
169. L I Hill, S Jin, R Zhou, D Venkataraman, F J DiSalvo *Inorg. Chem.* **40** 2660 (2001)
170. S Jin, R Zhou, E M Scheuer, J Adamchuk, L L Rayburn, F J DiSalvo *Inorg. Chem.* **40** 2666 (2001)
171. S Jin, F J DiSalvo *Chem. Commun.* 1586 (2001)
172. S Jin, J Adamchuk, B Xiang, F J DiSalvo *J. Am. Chem. Soc.* **124** 9229 (2002)
173. S Jin, F Popp, S W Boettcher, M Yuan, C M Oertel, F J DiSalvo *J. Chem. Soc., Dalton Trans.* 3096 (2002)
174. S Jin, F J DiSalvo *Chem. Mater.* **14** 3448 (2002)
175. T Yoshimura, Z N Chen, A Itasaka, M Abe, Y Sasaki, S Ishizaka, N Kitamura, S S Yarovoi, S F Solodovnikov, V E Fedorov *Inorg. Chem.* **42** 4857 (2003)
176. S J Hilsenbeck, V G Young, R E McCarley *Inorg. Chem.* **33** 1822 (1994)
177. X Xie, R E McCarley *Inorg. Chem.* **35** 2713 (1996)
178. X Xie, R E McCarley *Inorg. Chem.* **36** 4665 (1997)
179. K A York, K Folting, G Christou *J. Chem. Soc., Chem. Commun.* 1563 (1993)
180. J Mizutani, S Yamada, H Imoto, T Saito *Inorg. Chem.* **35** 244 (1996)
181. N G Naumov, K A Brylev, S Kordier, O Khernandez, K Perrin, V E Fedorov *Zh. Strukt. Khim.* **44** 760 (2003)^d
182. H Womelsdorf, H-J Meyer *Angew. Chem., Int. Ed. Engl.* **33** 1943 (1994)
183. C Perrin, M Sergeant, F Le Traon, A Le Traon *J. Solid State Chem.* **25** 197 (1978)
184. A Perrin, L Leduc, M Sergeant *Eur. J. Solid State Inorg. Chem.* **28** 919 (1991)
185. L Leduc Ph D Thesis University of Rennes, Rennes, France, 1983
186. A A Opalovskii, V E Fedorov, E U Lobkov *Zh. Neorg. Khim.* **16** 790 (1971)^c
187. A A Opalovskii, V E Fedorov, E U Lobkov *Zh. Neorg. Khim.* **16** 1685 (1971)^c
188. J C Gabriel, K Boubekeur, P Batail *Inorg. Chem.* **32** 2894 (1993)
189. Yu V Mironov, J A Cody, J A Ibers *Acta Crystallogr., Sect. C* **52** 281 (1996)
190. S S Yarovoi, Yu I Mironov, Yu V Mironov, A V Virovets, V E Fedorov, U-H Paek, S C Shin, M-L Seo *Mater. Res. Bull.* **32** 1271 (1997)
191. A Perrin, M Sergeant *New J. Chem.* **12** 337 (1988)
192. W Bronger, M Kanert, M Loevenich, D Schmitz, K Schwochau *Angew. Chem., Int. Ed. Engl.* **32** 576 (1993)
193. N G Naumov, S J Kim, A V Virovets, Yu V Mironov, V E Fedorov *Bull. Korean Chem. Soc.* **27** 635 (2006)
194. Yu V Mironov, V E Fedorov, C C McLauchlan, J A Ibers *Inorg. Chem.* **39** 1809 (2000)
195. W Bronger, M Loevenich, D Schmitz *J. Alloys Compd.* **216** 25 (1994)
196. W Bronger, H J Miessen, P Mueller, R Neugröschel *J. Less-Common Met.* **105** 303 (1985)
197. W Bronger, H J Miessen, D Schmitz *J. Less-Common Met.* **95** 275 (1983)
198. W Bronger, H J Miessen *J. Less-Common Met.* **83** 29 (1982)
199. W Bronger, M Loevenich *J. Alloys Compd.* **216** 29 (1994)
200. W Bronger, M Spangenberg *J. Less-Common Met.* **76** 73 (1980)
201. W Bronger, H J Miessen, R Neugröschel, D Schmitz, M Spangenberg *Z. Anorg. Allg. Chem.* **525** 41 (1985)
202. W Bronger, M Loevenich, D Schmitz, T Schuster *Z. Anorg. Allg. Chem.* **587** 91 (1990)
203. M Spangenberg, W Bronger *Angew. Chem.* **90** 382 (1978)
204. W Bronger, T Schuster *Z. Anorg. Allg. Chem.* **587** 74 (1990)
205. W Bronger, C Koppe, D Schmitz *Z. Anorg. Allg. Chem.* **623** 239 (1997)
206. Yu V Mironov, M A Pell, J A Ibers *Angew. Chem., Int. Ed. Engl.* **35** 2854 (1996)
207. C Fischer, N Alonso-Vante, S Fiechter, H Tributsch, G Reck, W Schulz *J. Alloys Compd.* **178** 305 (1992)
208. C Fischer, S Fiechter, H Tributsch, G Reck, B Schultz *Ber. Bunsen-Ges. Phys. Chem.* **96** 1652 (1992)
209. N L Speziali, H Berger, G Leicht, R Sanjines, G Chapuis, F Lévy *Mater. Res. Bull.* **23** 1597 (1988)
210. L Leduc, A Perrin, M Sergeant *Acta Crystallogr., Sect. C* **39** 1503 (1983)
211. J R Long, L S McCarty, R H Holm *J. Am. Chem. Soc.* **118** 4603 (1996)
212. J R Long, A S Williamson, R H Holm *Angew. Chem., Int. Ed. Engl.* **34** 226 (1995)
213. R Chevrel, M Sergeant, J Prigent *J. Solid State Chem.* **3** 515 (1971)
214. R Chevrel, M Sergeant, J Prigent *Mater. Res. Bull.* **9** 1487 (1974)
215. C Perrin, R Chevrel, M Sergeant, Ø Fischer *Mater. Res. Bull.* **14** 1505 (1979)
216. C Perrin, M Sergeant *J. Chem. Res.* 38 (1983)
217. H J Meyer, J D Corbett *Inorg. Chem.* **30** 963 (1991)
218. R Chevrel, M Potel, M Sergeant, M Decroux, Ø Fischer *J. Solid State Chem.* **34** 247 (1980)
219. S Picard, P Gougeon, M Potel *Inorg. Chem.* **45** 1611 (2006)
220. R Gautier, S Picard, P Gougeon, M Potel *Mater. Res. Bull.* **34** 93 (1999)
221. S Picard, P Gougeon, M Potel *Acta Crystallogr., Sect. C* **57** 335 (2001)
222. S Picard, M Potel, P Gougeon *Angew. Chem., Int. Ed.* **38** 2034 (1999)
223. W Hoenle, H G von Schnering, A Lipka, K Yvon *J. Less-Common Met.* **71** 135 (1980)
224. V E Fedorov, S S Yarovoi, Yu V Mironov, M R J Elsegood *Chem. Commun.* 1861 (1998)
225. D Salloum, R Gautier, M Potel, P Gougeon *Angew. Chem., Int. Ed.* **44** 1363 (2005)

226. Z Zheng, J R Long, R H Holm *J. Am. Chem. Soc.* **119** 2163 (1997)
227. G J Miller *J. Alloys Compd.* **229** 93 (1995)
228. M D Smith, G J Miller *J. Am. Chem. Soc.* **118** 12238 (1996)
229. M D Smith, G J Miller *Inorg. Chem.* **42** 4165 (2003)
230. V P Fedin, Yu V Mironov, V E Fedorov *Zh. Neorg. Khim.* **33** 2531 (1988)^c
231. V P Fedin, M N Sokolov, O A Geras'ko, B A Kolesov, V Ye Fedorov, A V Mironov, D S Yufit, Yu L Slovokhotov, Yu T Struchkov *Inorg. Chim. Acta* **175** 217 (1990)
232. M N Sokolov, A L Gushchin, P A Abramov, A V Virovets, E V Peresypkina, V P Fedin *Inorg. Chem.* **46** 4677 (2007)
233. H H Murray, S P Kelty, R R Chianelli, C S Day *Inorg. Chem.* **33** 4418 (1994)
234. N W Alcock, A Kjekshus *Acta Chem. Scand.* **19** 79 (1965)
235. M N Sokolov, A L Gushchin, A V Virovets, E V Peresypkina, S G Kozlova, V P Fedin *Inorg. Chem.* **43** 7966 (2004)
236. C Perrin, R Chevrel, M Sergent *J. Solid State Chem.* **19** 305 (1976)
237. H Ben Yaich, J C Jegaden, M Potel, M Sergent, A K Rastogi, R Tournier *J. Less-Common Met.* **102** 9 (1984)
238. H Ben Yaich, J C Jegaden, M Potel, R Chevrel, M Sergent, A Berton, J Chaussy, A K Rastogi, R Tournier *J. Solid State Chem.* **51** 212 (1984)
239. V P Fedin, I V Kalinina, A V Virovets, D Fenske *Izv. Akad. Nauk, Ser. Khim.* 892 (2001)^g
240. W Bronger, M Kanert, M Loevenich, D Schmitz *Z. Anorg. Allg. Chem.* **619** 2015 (1993)
241. Yu V Mironov, S J Kim, V E Fedorov *Bull. Korean Chem. Soc.* **27** 939 (2006)
242. H Zhu, Q Liu, Y Deng, T Wen, C Chen, D Wu *Inorg. Chim. Acta* **286** 7 (1999)
243. M N Sokolov, O A Geras'ko, V A Fedorov *Zh. Neorg. Khim.* **43** 407 (1998)^c
244. A Muller, E Krickemeyer *Inorg. Synth.* **27** 47 (1990)
245. J -H Liao, J Li, M G Kanatzidis *Inorg. Chem.* **34** 2658 (1995)
246. A A Pasynskii, I L Eremenko, A S Katugin, G S Gasanov, E A Turchanova, O G Ellert, Yu T Struchkov, V E Shklover, N T Berberova, A G Sogomonova, O Y Okhlobystin *J. Organomet. Chem.* **344** 195 (1988)
247. C M Bolinger, J Darkwa, G Gammie, S D Gammon, J W Lyding, T B Rauchfuss, S R Wilson *Organometallics* **5** 2386 (1986)
248. C E Davies, J C Green, N Kaltsoyannis, M A MacDonald, J Qiu, T B Rauchfuss, C M Redfern, G H Stringer, M G Woolhouse *Inorg. Chem.* **31** 3779 (1992)
249. H Zhu, Q Liu, C Chen, D Wu *Inorg. Chim. Acta* **306** 131 (2000)
250. A A Pasynskii, I L Eremenko, Yu V Rakitin, V M Novotortsev, O G Ellert, V T Kalinnikov, V E Shklover, Yu T Struchkov, S V Lindeman, T Kh Kurbanov, G S Gasanov *J. Organomet. Chem.* **248** 309 (1983)
251. A A Pasynskii, I L Eremenko, V T Kalinnikov *Izv. Akad. Nauk SSSR, Ser. Khim.* 2843 (1976)^g
252. Yu L Slovokhotov, M Yu Antipin, R G Gerr, A I Yanovskii, Yu T Struchkov *Dokl. Akad. Nauk SSSR* **285** 1413 (1985)^h
253. P Baird, J A Bandy, M L H Green, A Hamnett, E Marsegli, D S Obertelli, K Prout, J Qin *J. Chem. Soc., Dalton Trans.* 2377 (1991)
254. Yu V Mironov, A S Gardberg, J A Ibers *Inorg. Chem.* **41** 1333 (2002)
255. B Hessen, T Siegrist, T Palstra, S M Tanzler, M L Steigerwald *Inorg. Chem.* **32** 5165 (1993)
256. S Kamiguchi, H Imoto, T Saito, T Chihara *Inorg. Chem.* **37** 6852 (1998)
257. T Saito, N Yamamoto, T Yamagata, H Imoto *J. Am. Chem. Soc.* **110** 1646 (1988)
258. J Mizutani, S Amari, H Imoto, T Saito *J. Chem. Soc., Dalton Trans.* 819 (1998)
259. T Saito, N Yamamoto, T Nagase, T Tsuboi, K Kobayashi, T Yamagata, H Imoto, K Unoura *Inorg. Chem.* **29** 764 (1990)
260. Yu V Mironov, V N Ikorskii, V E Fedorov, J A Ibers *Eur. J. Inorg. Chem.* 214 (2005)
261. D T Richens, P A Pittet, A E Merbach, M Humanes, G J Lamprecht, B-L Ooi, A G Sykes *J. Chem. Soc., Dalton Trans.* 2305 (1993)
262. E V Chubarova, M N Sokolov, D G Samsonenko, C Vicent, V P Fedin *Zh. Strukt. Khim.* **47** 948 (2006)^d
263. Y J Li, C A Routledge, A G Sykes *Inorg. Chem.* **30** 5043 (1991)
264. J E Varey, A G Sykes *J. Chem. Soc., Dalton Trans.* 3293 (1993)
265. Z Dori, F A Cotton, R Llusar, W Schwotzer *Polyhedron* **5** 907 (1986)
266. P Kathirgamanathan, M Martinez, A G Sykes *J. Chem. Soc., Chem. Comm.* 953 (1985)
267. R Hernandez-Molina, M R J Elsegood, W Clegg, A G Sykes *J. Chem. Soc., Dalton Trans.* 2173 (2001)
268. B Rink, M Brorson, I J Scowen *Organometallics* **18** 2309 (1999)
269. R Hernandez-Molina, M Sokolov, W Clegg, P Esparza, A Mederos *Inorg. Chim. Acta* **331** 52 (2002)
270. Y Yao, H Akashi, G Sakane, T Shibahara, H Ohtaki *Inorg. Chem.* **34** 42 (1995)
271. R Hernandez-Molina, M Sokolov, P Núñez, A Mederos *J. Chem. Soc., Dalton Trans.* 1072 (2002)
272. Y H Tang, Y-G Yao, L-Wu, Y-Y Qin, Y Kang, Z J Li *Chem. Lett.* 542 (2001)
273. Y-B Chen, Y-H Wen, Y-Y Qin, Y Kang, Z-J Li, J-K Cheng, Y-G Yao *Inorg. Chem. Commun.* **7** 718 (2004)
274. T Shibahara, N Kurimoto, S Kiyoda, Y Kobayashi, G Sakane *J. Cluster Sci.* **11** 333 (2000)
275. T Yamauchi, H Takagi, T Shibahara, H Akashi *Inorg. Chem.* **45** 5429 (2006)
276. F A Cotton, R Llusar, W Schwotzer *Inorg. Chim. Acta* **155** 231 (1989)
277. S -B Yu, M Droege, S Downey, B Segal, W Newcomb, T Sanderson, S Crofts, S Suravajjala, E Bacon, W Earley, D Delecki, A D Watson *Inorg. Chem.* **40** 1576 (2001)
278. S-B Yu, M Droege, B Segal, S Downey, T Sanderson, J Fellmann, A Watson *Inorg. Chim. Acta* **263** 61 (1997)
279. K Hegetschweiler, M Wörle, M D Meienberger, R Nesper, H W Schmalle, R D Hancock *Inorg. Chim. Acta* **250** 35 (1996)
280. A Müller, V P Fedin, C Kuhlmann, H Bögge, B Hauptfleisch, H-D Fenske, G Baum *Chem. Commun.* 1189 (1999)
281. M G Basallote, F Estevan, M Feliz, M J Fernandez-Trujillo, D A Hoyos, R Llusar, S Uriel, C Vicent *Dalton Trans.* 530 (2004)
282. M G Basallote, M Feliz, M J Fernandez-Trujillo, R Llusar, V S Safont, S Uriel *Chem. – Eur. J.* **10** 1463 (2004)
283. A G Algarra, M G Basallote, M Feliz, M J Fernandez-Trujillo, R Llusar, V S Safont *Chem. – Eur. J.* **12** 1413 (2006)
284. V P Fedin, A Müller, K Filipek, R Rohlfing, H Bögge, A V Virovets, J O Dziejewski *Inorg. Chim. Acta* **223** 5 (1994)
285. K G Myakishev, V P Fedin, M N Sokolov, G S Voronina, V V Volkov *Zh. Neorg. Khim.* **44** 223 (1999)^c
286. V P Fedin, M N Sokolov, V Ye Fedorov, D S Yufit, Yu T Struchkov *Inorg. Chim. Acta* **179** 35 (1991)
287. V Bureau, J A Ibers *C.R. Acad. Sci., Ser. II, Chim.* **3** 123 (2000)
288. V P Fedin, A Myuller, G Bege, A Armatazh, M N Sokolov, S S Yarovoi, V E Fedorov *Zh. Neorg. Khim.* **38** 1677 (1993)^c
289. M N Sokolov, S S Yarovoi, V P Fedin, V E Fedorov *Zh. Neorg. Khim.* **41** 1862 (1996)^c
290. V P Fedin, M N Sokolov, O A Geras'ko, A V Virovets, N V Podbereskaya, V Ye Fedorov *Polyhedron* **11** 3159 (1992)
291. V Bureau, C G Pernin, J A Ibers *Inorg. Chem.* **39** 854 (2000)
292. S Lu, Q Wu, H Chen, R Yu, J Huang *Chin. J. Struct. Chem. (Jiegou Huaxue)* **13** 389 (1994); *Chem. Abstr.* **122** 95147 (1995)
293. K Hegetschweiler, T Keller, W Amrein, W Schneider *Inorg. Chem.* **30** 873 (1991)
294. H Zimmermann, K Hegetschweiler, T Keller, V Gramlich, H W Schmalle, W Petter, W Schneider *Inorg. Chem.* **30** 4336 (1991)
295. K Hegetschweiler, T Keller, M Baeumle, G Rihs, W Schneider *Inorg. Chem.* **30** 4342 (1991)
296. J M Garriga, R Llusar, S Uriel, C Vicent, A J Usher, N T Lucas, M G Humphrey, M Samoc *Dalton Trans.* 4546 (2003)
297. R Llusar, S Triguero, C Vicent, M N Sokolov, B Domercq, M Fourmigué *Inorg. Chem.* **44** 8937 (2005)

298. M N Sokolov, A L Gushchin, K A Kovalenko, E V Peresypkina, A V Virovets, J Sanchiz, V P Fedin *Inorg. Chem.* **46** 2115 (2007)
299. H Chen, X Lin, L S Chi, C Lu, H Zhuang, J Huang *Inorg. Chem. Commun.* **3** 331 (2000)
300. X Lin, H-Y Chen, L-S Chi, H-H Zhuang *Polyhedron* **18** 217 (1999)
301. F A Cotton, Z Dori, R Llusar, W Schwotzer *Inorg. Chem.* **25** 3529 (1986)
302. Yu V Mironov, S S Yarovoi, D Yu Naumov, N V Kuratieva, S G Kozlova, A Simon, V E Fedorov *Eur. J. Inorg. Chem.* 2476 (2005)
303. Yu V Mironov *Eur. J. Inorg. Chem.* 997 (1999)
304. Yu V Mironov, T E Albrecht-Schmitt, D M Smith, J A Ibers *Z. Kristallogr. – New Cryst. Struct.* **216** 517 (2001)
305. N G Naumov, A V Virovets, Yu I Mironov, S B Artemkina, V E Fedorov *Ukr. Khim. Zh.* **65** 21 (1999)
306. L G Beauvais, M P Shores, J R Long *Chem. Mater.* **10** 3783 (1998)
307. K A Brylev, A V Virovets, N G Naumov, Yu V Mironov, D Fenske, V E Fedorov *Izv. Akad. Nauk, Ser. Khim.* 1088 (2001)^g
308. M Feliz, R Llusar, S Uriel, C Vicent, M G Humphrey, N T Lucas, M Samoc, B Luther-Davies *Inorg. Chim. Acta* **349** 69 (2003)
309. R E Cramer, K Yamada, H Kawaguchi, K Tatsumi *Inorg. Chem.* **35** 1743 (1996)
310. W Beck, W Danzer, G Thiel *Angew. Chem.* **85** 625 (1973)
311. W McFarlane, M Nasreddin, D M Saysell, Z-S Jia, W Clegg, M R J Elsegood, K S Murray, B Moubaraki, A G Sykes *J. Chem. Soc., Dalton Trans.* 363 (1996)
312. C Guilbaud, A Deluzet, B Domercq, P Molinié, K Boubekur, P Batail, C Coulon *Chem. Commun.* 1867 (1999)
313. N G Naumov, E V Ostanina, A V Virovets, M Shmidtman, A Müller, V E Fedorov *Izv. Akad. Nauk, Ser. Khim.* 799 (2002)^g
314. T Yoshimura, S Ishizaka, Y Sasaki, H-B Kim, N Kitamura, N G Naumov, M N Sokolov, V E Fedorov *Chem. Lett.* 1121 (1999)
315. I V Kalinina, A V Virovets, F M Dolgushin, M Yu Antipin, R Llusar, V P Fedin *Inorg. Chim. Acta* **357** 3390 (2004)
316. V P Fedin, I V Kalinina, A Gerasimenko, A V Virovets *Inorg. Chim. Acta* **331** 48 (2002)
317. V P Fedin, A V Virovets, I V Kalinina, V N Ikorskii, M R J Elsegood, W Clegg *Eur. J. Inorg. Chem.* 2341 (2000)
318. V P Fedin, I V Kalinina, A V Virovets, D Fenske *Izv. Akad. Nauk, Ser. Khim.* 119 (2003)^g
319. Yu V Mironov, A V Virovets, S B Artemkina, V E Fedorov *Angew. Chem., Int. Ed.* **37** 2507 (1998)
320. Yu V Mironov, O Oeckler, A Simon, V E Fedorov *Eur. J. Inorg. Chem.* 2751 (2001)
321. Yu V Mironov, V E Fedorov, I Ijjaali, J A Ibers *Inorg. Chem.* **40** 6320 (2001)
322. Yu V Mironov, O A Efremova, D Yu Naumov, W S Sheldrick, V E Fedorov *Eur. J. Inorg. Chem.* 2591 (2003)
323. Yu V Mironov, N G Naumov, K A Brylev, O A Efremova, V E Fedorov, K Hegetschweiler *Angew. Chem., Int. Ed.* **43** 1297 (2004)
324. K A Brylev, Yu V Mironov, N G Naumov, V E Fedorov, J A Ibers *Inorg. Chem.* **43** 4833 (2004)
325. Yu V Mironov, O A Efremova, D Yu Naumov, V E Fedorov *Izv. Akad. Nauk, Ser. Khim.* 718 (2006)^g
326. N G Naumov, A V Virovets, M N Sokolov, S B Artemkina, V E Fedorov *Angew. Chem., Int. Ed.* **37** 1943 (1998)
327. N G Naumov, S B Artemkina, A V Virovets, V E Fedorov *J. Solid State Chem.* **153** 195 (2000)
328. N G Naumov, D V Soldatov, J A Ripmeester, S B Artemkina, V E Fedorov *Chem. Commun.* 571 (2001)
329. M S Tarasenko, N G Naumov, A V Virovets, D Yu Naumov, N V Kurat'eva, Yu V Mironov, V N Ikorskii, V E Fedorov *Zh. Strukt. Khim.* **46** S134 (2005)^d
330. N G Naumov, M S Tarasenko, A V Virovets, Y Kim, S J Kim, V E Fedorov *Eur. J. Inorg. Chem.* 298 (2006)
331. Yu V Mironov, V E Fedorov, H J Bang, S J Kim *Eur. J. Inorg. Chem.* 553 (2006)
332. S Amari, H Imoto, T Saito *Chem. Lett.* 967 (1997)
333. D N Dybtsev, M N Sokolov, V P Fedin *Izv. Akad. Nauk, Ser. Khim.* 987 (2003)^g
334. O A Gerasko, M N Sokolov, V R Fedin *Pure Appl. Chem.* **76** 1633 (2004)
335. O M Yaghi, M J Scott, R H Holm *Inorg. Chem.* **31** 4778 (1992)
336. V P Fedin, H Imoto, T Saito, V E Fedorov, Yu V Mironov, S S Yarovoi *Polyhedron* **15** 1229 (1996)
337. S Uriel, K Boubekur, P Batail, J Orduna, E Canadell *Inorg. Chem.* **34** 5307 (1995)
338. S Uriel, K Boubekur, P Batail, J Orduna *Angew. Chem., Int. Ed. Engl.* **35** 1544 (1996)
339. F Simon, K Boubekur, J-C P Gabriel *Chem. Commun.* 845 (1998)
340. Yu V Mironov, A V Virovets, V E Fedorov, N V Podberezhskaya, O V Shishkin, Yu T Struchkov *Polyhedron* **14** 3171 (1995)
341. V E Fedorov, S V Tkachev, N G Naumov, Yu V Mironov, Yu I Mironov *Zh. Neorg. Khim.* **43** 1683 (1998)^c
342. V P Fedin, V E Fedorov, H Imoto, T Saito *Polyhedron* **16** 1615 (1997)
343. M Sheer, V P Fedin, Yu V Mironov, V E Fedorov *Zh. Neorg. Khim.* **36** 138 (1991)^c
344. A Müller, V Fedin, K Hegetschweiler, W Amrein *J. Chem. Soc., Chem. Commun.* 1795 (1992)
345. M N Sokolov, V P Fedin, A Müller, K Hegetschweiler, W Amrein, V E Fedorov *Zh. Neorg. Khim.* **38** 891 (1993)^c
346. R Llusar, S Uriel *Eur. J. Inorg. Chem.* 1271 (2003)
347. M Feliz, E Guillaumon, R Llusar, C Vicent, S E Stiriba, J Perez-Prieto, M Barberis *Chem. – Eur. J.* **12** 1486 (2006)
348. Yu V Mironov, S S Yarovoi, S F Solodovnikov, V E Fedorov *J. Mol. Struct.* **656** 195 (2003)
349. H Sakamoto, Y Watanabe, T Saito *Inorg. Chem.* **45** 4578 (2006)
350. T Saito *J. Chem. Soc., Dalton Trans.* 97 (1999)
351. N Sakai, T Saito *Polyhedron* **23** 2611 (2004)
352. K Iijima, T Sunaga, M Hirose, T Saito *Inorg. Chem.* **45** 3452 (2006)
353. M N Sokolov, N Coichev, H D Moya, R Hernandez-Molina, C D Borman, A G Sykes *J. Chem. Soc., Dalton Trans.* 1863 (1997)
354. T Kabe, A Ishihara, W Qian *Hydrodesulfurization and Hydrodenitrogenation* (Weinheim: Wiley-VCH, 1999)
355. V P Fedin, J Czyzniewska, R Prins, T Weber *Appl. Catal. A: General* **213** 123 (2001)
356. *Transition Metal Sulfur Chemistry. Biological and Industrial Significance* (Eds E I Stiefel, K Matsumoto) (Washington, DC: American Chemical Society, 1996)
357. M Taniguchi, D Imamura, H Ishige, Y Ishii, T Murata, M Hidai, T Tatsumi *J. Catal.* **187** 139 (1999)
358. T Tatsumi, M Taniguchi, H Ishige, Y Ishii, T Murata, M Hidai *Appl. Surf. Sci.* **121** 500 (1997)
359. M Taniguchi, Y Ishii, T Murata, T Tatsumi, M Hidai *J. Chem. Soc., Chem. Commun.* 2533 (1995)
360. I Takei, Y Wakebe, K Suzuki, Y Enta, T Suzuki, Y Mizobe, M Hidai *Organometallics* **22** 4639 (2003)
361. M Hidai, S Kuwata, Y Mizobe *Acc. Chem. Res.* **33** 46 (2000)
362. R Llusar, S Uriel, C Vicent, J M Clemente-Juan, E Coronado, C J Gómez-García, B Braña, E Canadell *J. Am. Chem. Soc.* **126** 12076 (2004)
363. S B Yu, A D Watson *Chem. Rev.* **99** 2353 (1999)

^a — *Dokl. Chem. (Engl. Transl.)*

^b — *Inorg. Mater. (Engl. Transl.)*

^c — *Russ. J. Inorg. Chem. (Engl. Transl.)*

^d — *J. Struct. Chem. (Engl. Transl.)*

^e — *Russ. J. Coord. Chem. (Engl. Transl.)*

^f — *Russ. J. Organomet. Chem. (Engl. Transl.)*

^g — *Russ. Chem. Bull., Int. Ed. (Engl. Transl.)*

^h — *Dokl. Phys. Chem. (Engl. Transl.)*

Modern trends in the development of surface science as applied to catalysis. The elucidation of the structure – activity relationships in heterogeneous catalysts

V I Bukhtiyarov

Contents

I. Introduction	553
II. The ‘pressure gap’ problem	555
III. The ‘material gap’ problem	564
IV. Investigations into the structure of active sites in porous catalysts	570
V. Development of methods of the purposeful synthesis of highly active catalysts	575
VI. Conclusion	578

Abstract. A fundamental approach to the development of heterogeneous catalysts consisting of the study of the structure – activity relationships using surface science methods and techniques is proposed. According to this approach, a study should start with an investigation into well-ordered single crystals under ultrahigh vacuum conditions and then move along the way of both increasing the gas phase pressure (to address the ‘pressure gap’ problem) and complicating the samples under study from single crystals to supported clusters (to address the ‘material gap’ problem). The case studies cited in the review prove the efficacy of the proposed approach to investigations into the reactivity of active component particles for the subsequent molecular design of catalysts with improved performance (activity, selectivity and stability) and demonstrate that it conforms with the modern trends in the development of surface science as applied to heterogeneous catalysis. The bibliography includes 198 references.

I. Introduction

Traditionally, the term ‘Surface Science’ implies the application of specific instrumental techniques that are intrinsically surface sensitive to studies of the surface structure and composition of solids. In contrast to standard analytical techniques, such methods yield information on a few surface layers (with a thickness of up to 10 nm) of a sample rather than on its total bulk. The tremendous progress in this field started in the 1970s when serial ultrahigh vacuum spectrometers equipped with one or several surface science techniques appeared on the market. That time, Auger electron spectroscopy (AES), low-energy electron diffraction (LEED), X-ray and UV photoelectron spectroscopy (XPS and UPS, respectively), electron energy loss spectroscopy (EELS) were among the most popular techniques. Their wide utilisation in the practice of the experimental studies of solid surfaces enabled the retrieval of

important information at the atomic or molecular level. Fundamentals of instrumental techniques for surface studies (ITSS) as well as specific examples of their application, which demonstrate general trends in this field by the end of the 20th century are nicely described in a series of reviews published in 1994 in a special issue of the journal ‘Surface Science’ devoted to its 30th anniversary.¹

As applied to catalysis, it is the interactions between simple gases (*e.g.*, CO, O₂, NO, C₂H₄, *etc.*) and clean single-crystalline metal surfaces (Pt, Pd, Ag, Cu) that were the central problem of surface science in that period (see Refs 2–4 and references therein). These studies gave rise to the identification of a large number of adsorbed species, which helped to rationalise diverse surface phenomena, such as physical and chemical adsorption, lateral interactions in adsorbed monolayers and chemical interactions on surfaces.

The results obtained were immediately appreciated by specialists in catalysis such that the knowledge gathered on the ‘intimate’ life of atoms and molecules became a basis for the improvement on the performance of catalysts. Since then, attempts at the molecular design of catalysts with improved characteristics were often preceded by in-depth elucidations of the interactions between the reaction media and smooth solid surfaces in order to understand the nature of the catalytic action of specific active components in specific catalytic reactions. Recently, such an approach referred to as the fundamental one in contrast to the empirical approach became very popular.

Despite the fact that ITSS provide detailed information at the atomic and molecular levels, their efficient application to the description of real catalytic processes is hindered by two major factors commonly referred to as ‘pressure gap’ and ‘material gap’. The former problem consists of the difference in pressures typical of the majority of surface science studies ($P \leq 10^{-6}$ mbar) and of real catalytic processes ($P \geq 1$ mbar). As a result, concentrations of important intermediates as well as rates of certain reaction steps under the measurement conditions can appear substantially lower than the sensitivity threshold of the instrumental techniques applied. In this case, the information gathered often inadequately reflects the chemistry behind the processes on the surface of a functioning catalyst.

Yet another problem encountered by many surface science researchers refers to the use of metal single crystals as subjects of catalysis-related studies instead of small metal particles

V I Bukhtiyarov G K Borekov Institute of Catalysis, Siberian Branch of the Russian Academy of Sciences, prosp. Acad. Lavrentieva 5, 630090 Novosibirsk, Russian Federation. Fax (7-383) 330 80 56, tel. (7-383) 330 67 71, e-mail: vib@catalysis.nsk.su

Received 17 April 2007

Uspekhi Khimii 76 (6) 596–627 (2007); translated by Ya V Zubavichus

supported on an inert matrix, which represent real catalysts in most cases. Since all heterogeneous reactions proceed on the surface of a solid, the surface/volume ratio has to be increased in order to enhance the utilisation coefficient of the active metal. Therefore, metal particles in real practically applicable catalysts are often so small (3–5 nm) that deviations in their properties from those of the bulk metal have to be taken into account, which is referred to as the size effect and gives rise to the ‘material gap’ problem.

Starting from the end of the 1980s, these two problems were seriously addressed. In particular, high-pressure reactors and cells integratable into standard ultrahigh vacuum (UHV) equipment were designed, which enabled measurements of catalytic reaction rates at atmospheric pressures followed by an *ex situ* analysis of the catalyst composition avoiding its contact with air. Thus it became possible to systematically compare the surface composition and morphology of catalysts before and after the reaction with the respective changes in the catalytic activity. Such a combined *ex situ* approach was applied by Over *et al.*^{5–7} to address the ‘pressure gap’ problem in the case of CO oxidation on the Ru(0001) surface. By using temperature-programmed desorption (TPD), scanning tunneling microscopy (STM), LEED and XPS, they demonstrated that the clean Ru(0001) surface, which is inert under UHV conditions, is oxidised to RuO_x under the action of the reaction medium. The latter proved to be even more reactive with respect to the CO oxidation than platinum, which is a prototypical catalyst for this reaction. Such an oxidised surface cannot be formed spontaneously under UHV conditions. Another example of the efficiency of this approach to the studies of model catalytic systems was demonstrated by Campbell *et al.*^{8–10} for the oxygen and ethylene adsorption on single-crystalline (111) and (110) faces of silver. In this study, a special design of the electron spectrometer was used, which made it possible to transfer samples from a high-pressure microreactor to an UHV analytical chamber for the characterisation of the preprocessed surfaces with various instrumental techniques very fast (in less than 20 s). Still, such experiments are not free from the major drawback of the post-reaction analysis: evacuation of the reaction medium effectively eliminates weakly bound adsorbed species that could act as key species governing the catalyst reactivity under the reaction conditions.

A different in principle approach to address the ‘pressure gap’ problem was utilised by the British company ‘Vacuum Generators’, which is a recognised world-leading manufacturer of UHV equipment. This company designed and put into production a ‘high-pressure’ electron spectrometer,[†] which enabled the *in situ* registration of photoelectron spectra at pressures of up to 1 mbar,¹¹ *i.e.*, 6 orders of magnitude higher than in serial spectrometers. With such spectrometers that operate at pressures close to that of typical catalytic reactions, the quantitative determination of the relationships between the composition of the surface layer of a sample and its catalytic performance became possible. It is apparent that this approach to the solution of the ‘pressure gap’ problem is very promising.

The necessity to address the size effects within the context of the ‘material gap’ problem became apparent in the end of the 20th century, when studies of catalytic properties of supported metal catalysts as a function of the size of the active component (see Refs 14, 15 and references therein) revealed that the rates of many catalytic reactions normalised to the number of surface atoms vary upon changes in the size of supported metal particles. Boudart¹⁴ introduced the term structure-sensitive reactions to designate this phenomenon and distinguish it from structure-insensitive reactions, the rates of which

were independent of the size of catalytic metal particles. Interestingly, the size effect can be both positive (*i.e.*, the reaction rate increases with a decrease in the size of supported metal particles) and negative (*i.e.*, the reaction rate decreases). It was size effects that encouraged extensive investigations into the electronic, structural and adsorption properties of small metal clusters in comparison with those of bulk metals.

However, only low efficiency and slow progress in this field were achieved with traditional supported catalysts. Indeed, real catalysts that are usually prepared by impregnation of a support with a large specific surface area with aqueous solutions of salts of the active component followed by the drying and reduction of the salt to the metal state refer to colloidal systems. The collection of fully reproducible data on such systems is naturally very difficult. This fact together with possible contamination of the catalytic systems by undesired admixtures either coming from the substrate material or introduced at the steps of catalyst synthesis likely explain the large contradiction in data on catalytic activities of nominally identical catalytic systems reported by different authors.¹⁵ Poor reproducibility of the results can be overcome if the synthesis of supported catalysts and their subsequent characterisation are repeated many times. Furthermore, it has to be taken into account that the preparation of a series of catalysts with a systematically varying mean size of metal particles is a time-consuming procedure by itself.

As an alternative, model supported catalysts can be prepared in a reproducible way by vacuum deposition of disperse metal particles onto the surface of a planar substrate. Thin oxide films grown on the surface of metal single crystals or surfaces of oxide single crystals can be used as the substrates.^{16,17} Indeed, the preparation of metal nanoparticles directly in a UHV spectrometer makes it possible, first, to carefully pre-clean the substrate and deposition system and, second, to transfer the sample into an analytical chamber without its contact with air. This preparation scheme avoids introduction of undesired contaminants and enables quick production of series of samples with variable sizes of metal clusters. This way of the simulation of real catalysts is widely applied to the analysis of the electronic properties and morphology of metal nanoparticles as a function of their size (for example, see Refs. 16–20). Several attempts have been undertaken to study the specificity of adsorption on disperse metal particles.^{18–21} It is of note that the inconsistency between the model and real substrates intrinsic to the preparation method has not only negative, but also positive aspects, since it allows a wider choice of the substrate material. For instance, an oxide substrate can be replaced by a carbon-based one. This makes it possible to appeal to supplementary instrumental techniques to probe the adsorption properties of metal clusters. With graphite substrates instead of oxide ones, XPS can be efficiently applied to study the oxygen adsorption on metal clusters since in this case relatively weak O1s signal from the adsorbate is not superimposed on the prevailing background signal from Al₂O₃ or SiO₂ substrates. And thus adsorbed oxygen species can be identified based on an analysis of the O1s spectra.

The low specific surface area of single crystals prevents measurements of the specific catalytic activity of single crystal-based model systems in many catalytic reactions. Nevertheless, the chemistry underlying the catalytic action of metals cannot be understood without comparison of the results on model objects with the catalytic properties of real catalysts. Investigations into the reactivity of small clusters towards the reactants and reaction products, necessarily as a function of their size, can help to fill the gap between surface science studies and the real catalysis.

Therefore, the nature of the catalytic action of metals can efficiently be analysed using an approach depicted schemati-

[†] Two such spectrometers were purchased by Cardiff University (UK)¹² and G K Boreskov Institute of Catalysis (Novosibirsk, Russia).¹³

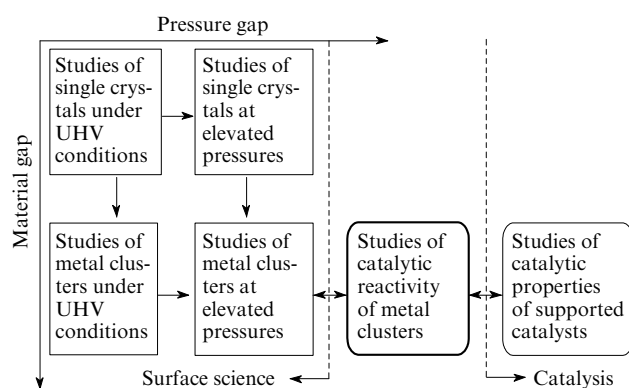


Figure 1. A scheme of the suggested approach aimed at establishing the structure–activity relationship in heterogeneous catalysts.

cally in Fig. 1. A study should start with well-ordered single crystals under UHV conditions and then move along both increasing the pressure of the reaction medium (*i.e.*, from left to right) and complicating the object under study (*i.e.*, from top to bottom). The movement from left to right implies the elimination of the ‘pressure gap’ problem, whereas that from top to bottom addresses the ‘material gap’ problem. Finally, instrumental techniques for surface studies have to be applied to elucidate the structure of the active sites in real catalysts during their formation, activation and deactivation and these data are to be compared to the results of model studies.

It is evident that in order to retrieve reliable data on the structure of functioning catalysts, not only ITSS but also bulk-sensitive techniques, such as transmission electron microscopy (TEM), X-ray diffraction and X-ray absorption methods (EXAFS, XANES), have to be applied.

Examples of studies accomplished over recent years in the Laboratory of surface science of the G K Boreskov Institute of Catalysis as well as in other world-renowned research centres specialised in the field, which are described in detail below, demonstrate that the above approach conforms with the modern trends in surface science as applied to catalysis by helping to establish the structure–activity relationship in heterogeneous catalysts and advancing towards purposeful design of highly active, selective and deactivation-resistant catalysts.

It has to be however noted that several methodological problems non-typical of traditional surface science, which hinder the retrieval of required information, emerge in the implementation of this approach in practice. Possible solutions of these problems are often highly specific and cannot be generalised and standardised. With this regard, in the description of experimental results below, we shall put an emphasis (somewhat greater than in traditional reviews) on relevant technical details of the respective measurements.

II. The ‘pressure gap’ problem

As has been stated in the Introduction, the development or optimisation of surface science techniques capable of *in situ* monitoring of processes directly in the course of a chemical reaction represents the most promising way to address the ‘pressure gap’ problem.^{22–38} Among techniques working at pressures close to those of real catalytic reactions ($P > 0.1$ mbar), Infrared Reflection-Absorption Spectroscopy (IRAS),^{22–24} in particular, in the polarisation modulation mode, Sum-Frequency Generation (SFG) spectroscopy,^{25–28} X-ray Absorption Near-Edge Structure (XANES),^{29–31} X-ray

Photoelectron Spectroscopy (XPS)^{11–13, 32–36} and scanning tunneling microscopy^{37, 38} are of special note.

X-Ray photoelectron spectroscopy occupies a special place in this list being one of the best analytical techniques for studies of the chemical composition and electronic structure of solid surfaces. The physical limit of pressure at which an XPS spectrum can still be measured is determined by the photoelectron mean-free path. The latter value is of the order of a few millimetres at a pressure of 1 mbar. Meanwhile, the typical pressure in the vast majority of XPS spectrometers is $\sim 10^{-9}$ mbar, which required for the safe operation of an X-ray source, an electron energy analyser and a secondary electron multiplier. Due to fundamental difficulties in combining these two requirements in one spectrometer design, the *in situ* mode of XPS data collection had been inaccessible for a long time. The situation has changed only recently and there are currently several research groups worldwide running XPS spectrometers capable of measuring spectra at a pressure range from 10^{-9} mbar to 1 mbar.^{11–13, 32–36} One of such dedicated high-pressure machines manufactured by ‘Vacuum Generators’ is installed at the Boreskov Institute of Catalysis in Novosibirsk. Its preliminary adaptation to the *in situ* studies of catalytic reactions at pressures of up to 10^{-2} mbar was accomplished in the Laboratory of metal catalysts.¹³ The additional cycle of spectrometer optimisation enabled the extension of the operational pressure range to 0.2–0.3 mbar (Refs 34–36). This value is only severalfold lower than the maximum achievable operational pressure realised in advanced spectrometers installed at the synchrotron radiation beamlines[‡] in ALS (Berkeley, USA)³³ and BESSY (Berlin, Germany).³⁵

A few illustrative examples of the application of XPS in the *in situ* mode to the elucidation of mechanisms of catalytic reactions are given below.

1. Interaction of CO with the Pd surface

As the first example, let us consider the combined application of XPS and SFG to the elucidation of interactions of CO and CH_3OH with the palladium surface in a wide range of temperatures and pressures. Simultaneous utilisation of several complementary instrumental techniques, which increases the reliability of conclusions derived from the experimental results, reflects one of the trends in contemporary surface science. Sum-frequency generation spectroscopy based on the irradiation of a sample surface with two pulse lasers operated in visible and IR spectral ranges is a rather complicated but still very promising non-linear optical technique suitable for the *in situ* studies of adsorbed complexes. The physical background of this method is described in detail elsewhere.^{25–28} During the measurements, the frequency of the visible-light laser is kept constant ($\lambda = 532$ nm), whilst that of the IR laser is scanned over a certain range, which gives rise to the appearance of characteristic SFG resonances under specific conditions associated with the vibrational excitations of adsorbed molecules.^{25, 26} The SFG is a second-order non-linear optical process, which has a non-vanishing probability exclusively in a non-centrosymmetrical medium. The requirement of the absence of the local inversion symmetry is always met for an interface and, as a rule, violated for an isotropic gas and the bulk of a solid, which provides the ultimate surface sensitivity of this method. According to the selection rules, both IR- and Raman-active vibrations are manifested in the SFG spectra. With SFG, vibrational spectra of adsorbed species can be collected in the *in situ* mode at high pressures up to the

‡ The extreme brilliance of synchrotron radiation makes it possible to approach to the theoretical limit of pressures in the *in situ* experiments (1–2 mbar).

atmospheric pressure, which is an evident advantage of this technique.

On the other hand, XPS provides direct quantitative information on chemical composition of the adsorbed and near-surface layers of the catalyst under study and its variation under high pressures (*vide supra*).

The mechanism of activation of the C–O bonds on the surfaces of transition metals attracts keen attention from specialists working in the field of heterogeneous catalysis. It plays a key role in the carbon monoxide hydrogenation as well as methanol oxidation and dehydrogenation, which are the important steps of large-scale industrial processes of production of hydrocarbons, aldehydes, alcohols and hydrogen.^{39–44} In particular, the C–O bond activation (followed by its cleavage) is a necessary step in the synthesis of hydrocarbons according to the Fischer–Tropsch process. Meanwhile, the progressive carbon deposition on the catalyst surface as a result of the CO dissociation often reduces its catalytic activity due to the shielding of active surface sites. Actually, the activity and selectivity of all of the above reactions is governed by the activation of the C–O bonds depending on the catalyst nature, gaseous medium composition and reaction conditions. With this regard, deep understanding of the mechanism of the C–O activation on the surface of transition metals is a prerequisite to the prediction of the catalytic action and consequently to the purposeful design of catalysts with improved efficiencies for specific reactions.

Figure 2 shows SFG and XPS spectra measured *in situ* during the CO adsorption on atomically smooth Pd(111) single-crystalline face at 400 K. At low pressure ($P_{\text{CO}} = 10^{-6}$ mbar), the SFG spectrum reveals a single line at 1910 cm^{-1} attributable to stretching vibrations of bridge-bonded CO molecules. At the same time, a narrow symmetrical line centred at 285.6 eV emerges in the C1s XPS spectrum (Fig. 2b), which can thus also be ascribed to adsorbed CO molecules in bridging positions. Upon an increase in pressure, a new SFG resonance at $2075\text{--}2080\text{ cm}^{-1}$ appears, which is indicative of the appearance of terminally bound species due to the higher surface concentration of CO_{ads} . Meanwhile, the C1s XPS line broadens due to the emergence of a new component of terminally bound CO with $E_{\text{b}} = 286.3\text{ eV}$ (according to the deconvolution of the spectra into the components I' and I''). Such an attribution of the C1s components agrees with the results of high-resolution XPS obtained by Surnev *et al.*,⁴⁵ who demonstrated that the three-fold hollow, bridge-bonded and on-top CO molecules on Pd(111) are characterised by similar C1s binding energies of $285.6 \pm 0.1\text{ eV}$, 285.85 eV and 286.3 eV , respectively. The C1s feature at around 290 eV appearing at even higher pressures $P_{\text{CO}} > 5 \times 10^{-2}$ mbar (the component I in Fig. 2b) can be assigned to gaseous carbon monoxide.⁴⁶

SFG and XPS spectra registered *in situ* during the CO adsorption on the atomically smooth Pd(111) crystal face at 200 K and $P_{\text{CO}} = 1\text{ mbar}$ (SFG) or 0.1 mbar (C1s) are shown in Fig. 3. These experimental conditions (*viz.*, high pressure and low temperature) provided the maximum possible coverage of palladium surface with CO molecules of 0.75 monolayers. The respective SFG spectrum reveals two vibrational bands at 1895 cm^{-1} and 2107 cm^{-1} assigned to three-fold and on-top species, respectively. The conclusion on the presence of terminally coordinated CO molecules on Pd(111) is supported by the comparison of the C1s XPS spectrum measured under similar conditions with that measured at $T = 400\text{ K}$ and $P_{\text{CO}} = 10^{-6}\text{ mbar}$, *i.e.* where such species are surely absent (see the SFG spectrum in Fig. 3a). The difference spectrum (spectrum 3 in Fig. 3b) obtained by subtracting the contribution of the three-fold CO species from the total C1s spectrum is characteristic of the terminal adsorbed CO species. This conclusion is supported by the quantitative estimation of relative

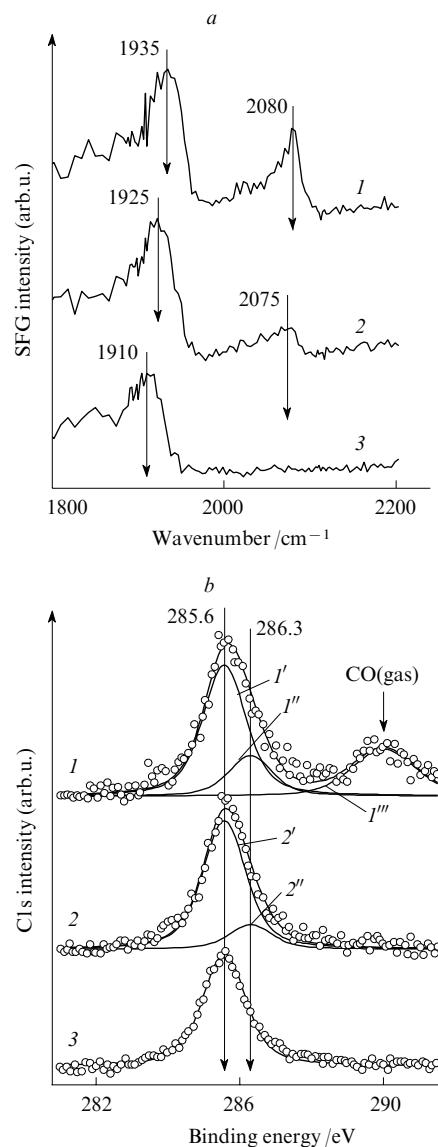


Figure 2. SFG (a) and C1s XPS (b) spectra measured *in situ* during CO adsorption on the atomically smooth Pd(111) surface at 400 K as a function of P_{CO} .

P_{CO} /mbar: (a) 1 (1), 10^{-3} (2), 10^{-6} (3); (b) 0.1 (1), 5×10^{-3} (2), 10^{-6} (3). Lines (1–3) are experimental data, (I' , I'') and ($2'$, $2''$) are deconvolution of the experimental curve into two components corresponding to bridge-bonded (I' and $2'$) and on-top (I'' and $2''$) CO molecules; (I''') is a component attributed to gaseous CO. Hereinafter, all C1s spectra are normalised to the integral intensity of the respective Pd3d lines.

surface concentrations of the three-fold (spectrum 2) and on-top (spectrum 3) CO_{ads} . The respective ratio of ~ 1.9 obtained from the experimental XPS spectra is close to the value 2 determined earlier for the $(2 \times 2)\text{-}3\text{CO}$ surface structure, which corresponds to the maximum coverage of Pd(111) with the CO molecules ($\theta = 0.75$ monolayers). It is also of note that this clear separation of the C1s spectral component responsible for the terminally coordinated CO species ($E_{\text{b}} = 286.3\text{ eV}$) validates the spectral deconvolution procedure utilised in the analysis of the XPS spectra shown in Fig. 2.

The application of XPS to the *in situ* studies of the CO adsorption on Pd(111) helped to answer the important question whether the dissociation of C–O bonds can proceed on palladium. In a number of earlier publications (for instance, see Refs 47–50), a dissociative character of the CO adsorption

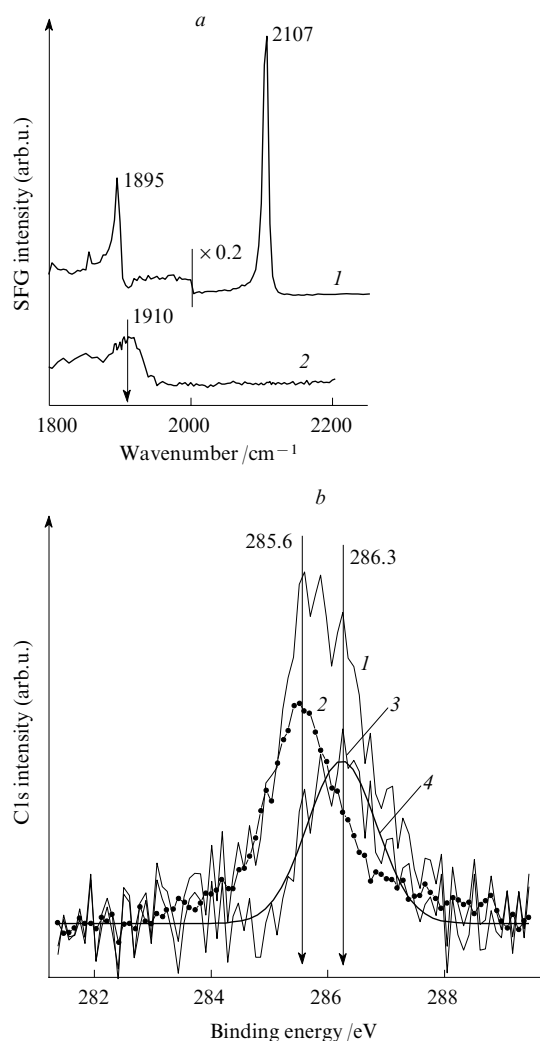


Figure 3. SFG (a) and C1s XPS (b) spectra measured *in situ* during CO adsorption on the atomically smooth Pd(111) surface at 200 K and 1 mbar (curve 1) and at 400 K and 10^{-6} mbar (curve 2). The curve (3) is calculated by the direct subtraction of the respective C1s spectra, (4) is the averaged spectrum (3).

on the surface of highly disperse palladium particles was suggested. On the other hand, no CO dissociation was observed in other studies,^{51–53} despite the detection of weakly bound adsorbed CO species on palladium particles with a size of 2–3 nm. A strong influence of pressure on the adsorption process can be a reason for this apparent discrepancy. The rate of the CO disproportionation under UHV conditions is quite low, such that very often no respective products can be detected. Indeed, the probability of CO dissociation on the palladium surface is very low according to theoretical calculations.^{53–55} However, the combined application of SFG and XPS decisively rules out this explanation since only lines of molecularly adsorbed CO are observed in all the C1s XPS spectra, including those measured *in situ* at pressures of up to 1 mbar.⁴⁶ In the cases of CO dissociation or formation of carbonyl structures [e.g., Pd(CO)₂], the appearance of additional photoemission components at about 284 eV and 287 eV, respectively, is expected.^{56,57} Thus, no indication of the CO dissociation or the formation of other adsorbed species on the Pd(111) surface was found by *in situ* measurements over the pressure range from 10^{-6} mbar to 1 mbar and temperature range from 200 K to 400 K.

2. Interaction of CH₃OH with the Pd surface

Despite the fact that the interaction of methanol with the palladium surface has been the subject of intense investigations by many research groups for a long time, the mechanism of catalytic methanol decomposition remains disputable.^{58–70} The majority of specialists have a consensus that it is the dehydrogenation of methanol to CO and H₂ that is the predominant pathway of this reaction.^{58–62} As has been established,⁵⁸ at low temperature, methanol is adsorbed on the palladium surface molecularly through the oxygen lone pair. A layer of adsorbed methanol and formaldehyde molecules as well as methoxy groups is formed following methanol adsorption at 170 K.^{59,60} An investigation into the decomposition of methanol on Pd(111) by means of Secondary-Ion Mass Spectrometry (SIMS)⁶¹ and EELS⁶² revealed that the cleavage of the O–H bond in an adsorbed methanol molecule occurs as the first step of the reaction to yield the CH₃O groups, which further decompose to CO and H₂ by the stepwise detachment of the hydrogen atoms upon heating. The reaction proceeds *via* CH₂O and CHO. Such a mechanism is supported by the TPD and EELS data.^{59,60}

Nevertheless, some authors believe that the methanol decomposition on Pd(111) occurs as the C–O bond cleavage to yield adsorbed CH_x ($x = 0–3$) species.^{54,63–65} The probable dissociation of the C–O bond in a methanol molecule upon its adsorption on the Pd(111) surface has been suggested by Winograd *et al.*^{54,63} based on the XPS, SIMS and TPD data. Species CH_{3,ads} were detected on Pd(111) (in a concentration of $\theta = 0.04$ monolayers) after methanol adsorption at 110 K (to $\theta \approx 0.5$ monolayers) followed by annealing *in vacuo* at 175 K. Further annealing resulted in the dehydrogenation of the CH₃ species to CH_{2,ads}, CH_{ads} and C_{ads}.

Notwithstanding, no cleavage of the C–O bond in methanol molecules upon adsorption on Pd(111) was detected in a TPD study of isotopically labelled compounds ¹³CH₃¹⁶OH and ¹²CH₃¹⁸OH over a wide temperature range (87–265 K), which provided a very high sensitivity of ~ 0.01 monolayers.⁶⁴ It was suggested that this apparent discrepancy is due to different rates of competing pathways of the methanol decomposition on the palladium surface. For instance, the rate of methanol dehydrogenation to CO is approximately two orders of magnitude higher than the decomposition through the C–O bond cleavage,⁶⁶ and thus it is nearly impossible to detect the formation of CH_{x,ads} species under UHV conditions at low temperatures and small methanol exposures.

This hypothesis was verified in a combined XPS and SFG study of the methanol interaction with the atomically smooth Pd(111) surface at variable temperatures and pressures.^{67,68} The SFG (a) and C1s XPS (b) spectra measured *in situ* during the methanol decomposition on Pd(111) is shown in Fig. 4. The methanol adsorption at room temperature and 10^{-6} mbar gives rise to the emergence of a vibrational SFG resonance at 1915 cm^{−1} corresponding to bridging adsorbed CO molecules at a coverage of $\theta \approx 0.5$ monolayers.^{27,28,45,46,69} Meanwhile, the C1s XPS spectra reveal two components with binding energies of 284 eV and 285.6 eV, which can be assigned to hydrocarbon CH_{x,ads} ($x = 0–3$) and oxygen-containing CH_xO_{ads} ($x = 0–3$) species based on an analysis of the literature data.^{45,46,56} Quantitative agreement between the coverages ($\theta \approx 0.5$ monolayers) estimated from the relative intensity of the C1s line at $E_b = 285.6$ eV and from the SFG data allowed the authors to limit the range of potential species and assign the C1s component with $E_b = 285.6$ eV to adsorbed CO.⁶⁷ This assignment is supported by numerous studies indicating that the decomposition of the CH₃O groups to CO_{ads} on palladium proceeds efficiently already at 200–250 K.^{60,62,70} With an increase in residence time, the intensity of the XPS signal at 284 eV progressively increases, whereas that of the component at 285.6 eV remains virtually constant.

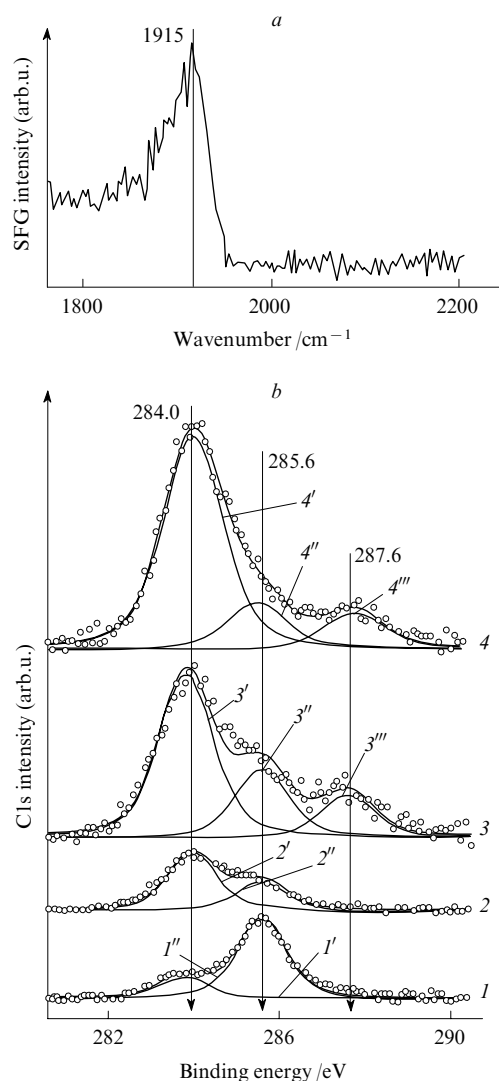


Figure 4. SFG (a) and C1s XPS (b) spectra measured *in situ* during the methanol decomposition on the atomically smooth Pd(111) surface.

(1) $P = 10^{-6}$ mbar and $T = 300$ K; (2) $P = 10^{-6}$ mbar and $T = 400$ K; (3) $P = 0.1$ mbar and $T = 300$ K; (4) $P = 0.1$ mbar and $T = 400$ K. The SFG spectrum was registered at 300 K and a methanol pressure of 10^{-6} mbar. The experimental C1s spectra (curves 1–4) and their deconvolution into components (1', 1'', 2', 2'', 3', 3'', 3''') and (4', 4'', 4''') are shown.

An increase in temperature up to 400 K or in the methanol pressure up to 0.1 mbar results in an abrupt increase in the surface concentration of the CH_x species (see Fig. 4b). In

particular, the absolute intensity of the C1s component with $E_b = 283.8$ eV corresponds to $\Theta \approx 1.0$ monolayer at 300 K and $P_{\text{MeOH}} = 0.1$ mbar (the spectrum 3). Despite this large apparent coverage of the Pd(111) surface with the CH_x species, a part of the surface remains covered with adsorbed CO molecules ($\Theta \approx 0.4$ –0.5 monolayers). The total concentration of adsorbed species (including both CH_x and CO) exceeding one monolayer was explained by either partial dissolution of carbon in the near-surface region of palladium⁷¹ or formation of three-dimensional carbon structures. The amount of carbon-like species further increases at 400 K ($\Theta \approx 1.5$ monolayers), which is accompanied by a small shift of the respective line towards higher binding energies ($E_b = 284.0$ eV). This change probably reflects some chemical transformations of the carbon particles.

These results clearly demonstrate that the C–O bond of the methanol molecule is activated on the atomically smooth Pd(111) surface at a measurable rate even at 300–400 K. The methanol decomposition rate and the amount of deposited carbon increases with an increase in methanol pressure. Carbon particles formed as the methanol decomposition product lead to the progressive coking of the metal surface and ultimately to its complete deactivation. Due to this process, no products of the catalytic methanol decomposition on Pd(111) (*i.e.*, CO and H_2) were detected by means of gas chromatography at elevated pressures (15–30 mbar of methanol in a helium atmosphere) and temperatures (300–600 K) even after their accumulation for several hours.⁶⁸ On the other hand, the introduction of oxygen into the reaction mixture immediately resulted in the appearance of the methanol total oxidation products, *viz.*, CO_2 and H_2O .

Based on these experimental results, the following scheme of the methanol interaction with the Pd(111) surface can be proposed. The first step of the decomposition is cleavage of the O–H bond to yield the methoxy groups.^{59, 60, 62, 64} The adsorbed methoxy groups as well as methanol molecules are bound to the palladium surface through the oxygen lone pairs. They are oriented nearly perpendicular to the surface.⁶² As the dehydrogenation proceeds, the molecular axis of the adsorbed complex is rotated by 90° , such that formaldehyde molecules ($\text{CH}_2\text{O}_{\text{ads}}$) and formyl groups (CHO_{ads}) are oriented parallel to the palladium surface.^{65, 66} The final dehydrogenation product, CO, is oriented again perpendicular to the surface but it is bound to the metal atoms through the carbon atom.^{72, 73}

The formation of carbon deposits on the atomically smooth Pd(111) surface observed experimentally^{67, 68} supports the activation mechanism of the C–O bonds upon the methanol interaction with the palladium surface schematically depicted in Fig. 5. It is evident that an increase in the lifetime of the reaction intermediates should give rise to a higher probability of the C–O bond dissociation. Likely, this is a reason for the experimentally observed increase in the rate of carbon accumulation on the Pd(111) surface at high reaction pressures

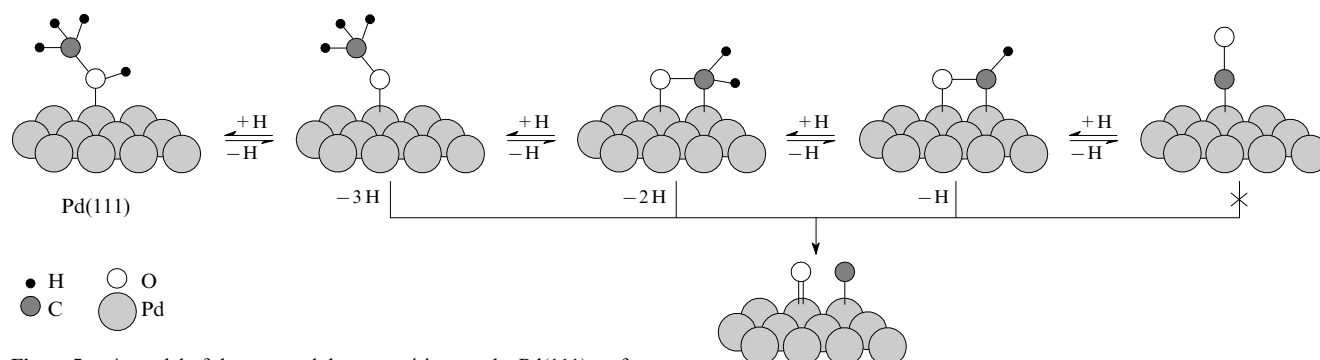


Figure 5. A model of the methanol decomposition on the Pd(111) surface.

(see Fig. 4) and in the presence of defects on the surface of supported palladium clusters.⁶⁶

Taking into account the principle of microscopic reversibility of reaction steps, it might be assumed that the CO hydrogenation on palladium



can also be accompanied by the C–O bond dissociation and catalyst deactivation due to the accumulation of carbon deposits. The emergence of the respective C1s signal with ($E_b \approx 284$ eV) was indeed detected in the XPS spectra measured *in situ* during the interaction of CO + H₂ mixtures with Pd(111) surfaces.⁷⁴

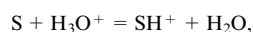
All these results are well explained within the Blyholder model, which describes the interaction of CO with transition metal surfaces as an electron density exchange between the metal d orbitals and $5\sigma/2\pi^*$ molecular orbitals of CO. Presumably, the geometry of the adsorption complex is the key factor governing this interaction, especially, the electron back donation from the metal d orbitals to the $2\pi^*$ -antibonding molecular orbitals of CO. In the case of an adsorbed CO molecule, the orientation perpendicular to the palladium surface suppresses the back donation contribution and thus provides the inertness of palladium towards the C–O bond dissociation. The formation of intermediates like CH_xO ($x = 1-3$) in the course of the methanol dehydrogenation (or CO hydrogenation) promotes the electron transfer from the metal to the $2\pi^*$ -antibonding orbital of CO, which weakens the C–O bond and ultimately gives rise to its dissociation and formation of carbon deposits on the palladium surface.

3. Ethylene epoxidation over silver

It has to be stressed that the collection of spectral data in the presence of a reaction medium over the sample (at $P = 0.1-1$ mbar) in the *in situ* mode does not *a priori* provides information on the mechanism of catalytic reactions. Indeed, adsorbed species detected on the surface of a catalyst at high pressure are not necessarily catalytically active species or reaction intermediates. This issue can be effectively solved by combining the studies of the state of a catalyst surface with measurements of its catalytic properties (such as activity and selectivity) by means of mass spectrometry or gas chromatography. The efficiency of such an approach is demonstrated below by the example of a combined study of the ethylene epoxidation reaction on silver using mass spectrometry and a number of spectral techniques (including XPS, UPS, AES and XANES).^{30, 75-77}

Despite numerous studies devoted to the ethylene epoxidation on silver by diverse instrumental techniques,^{8-10, 12, 13, 78-82} a number of key questions on the mechanism of this reaction remain disputable in the literature. Recent kinetics measurements have clarified some important points, but due to the lack of direct experimental data, there are still a few issues unaddressed. In particular, neither the nature of actual oxygen species driving the epoxidation,^{8-10, 78-79} nor the structure of the key intermediate⁷⁸⁻⁸² yielding ethylene oxide were unambiguously established. Ethylene coordinated in a way similar to π -complexes⁷⁸⁻⁸⁰ or an oxametallacycle^{81, 82} were regarded as such intermediates. This stipulates the necessity of *in situ* measurements during the reaction to establish direct quantitative correlations between the yield of ethylene oxide and surface composition. Recently, the results of a series of studies on the ethylene epoxidation on silver using XPS and Proton-Transfer Reaction Mass Spectrometry (PTR-MS) jointly conducted by specialists from the G K Boreskov Institute of Catalysis SB RAS and the Department of Inorganic Chemistry, the Fritz Haber Institute (Berlin, Germany) have been published.⁷⁵⁻⁷⁷

Figure 6 shows ethylene and ethylene oxide partial pressures in the reaction cell of a photoelectron spectrometer as a function of temperature and reaction duration. The final regions of the plots were measured in the flow of pure ethylene (no O₂ was supplied) at $T = 470$ K (a) and 520 K (b), respectively. The partial pressure values were calculated from the respective PTR-MS signals corresponding to $m/z = 45$. The ionisation of gaseous species for the subsequent separation in a mass analyser in this relatively uncommon variant of mass spectrometry, was achieved through the proton transfer from H₃O⁺ ions generated in a special source to the molecules subject to analysis. The reaction



where S is the substrate, yields a molecular ion SH⁺ with a mass larger (due to a surplus proton) than that registered by traditional mass spectrometry by 1 a.m.u.. This specific ionisation mechanism guarantees that only substances with proton affinities higher than that of hydroxonium ions (*e.g.*, ethylene oxide but not CO₂) contribute to the mass spectra. Furthermore, this ionisation method virtually completely avoids the fragmentation of the molecular ion into lower-molecular-mass fragments, which greatly facilitates quantitative analysis of the experimental data. The high sensitivity of PTR-MS technique to organic molecules, such as ethylene oxide, is yet another its advantage. A detailed description of this modification of mass spectrometry can be found elsewhere.⁸³

The PTR-MS data presented in Fig. 6a indicate that the signal of ethylene oxide is negligible at ≤ 370 K but is reliably detected at $T = 420$ K. Further increase in temperature results in an abrupt increase in the ethylene oxide partial pressure, whereas a slow but continuous decrease in the partial pressure of C₂H₄O starts above $T \geq 470$ K, which is explained by the deactivation of the catalyst at these temperatures. After stop of

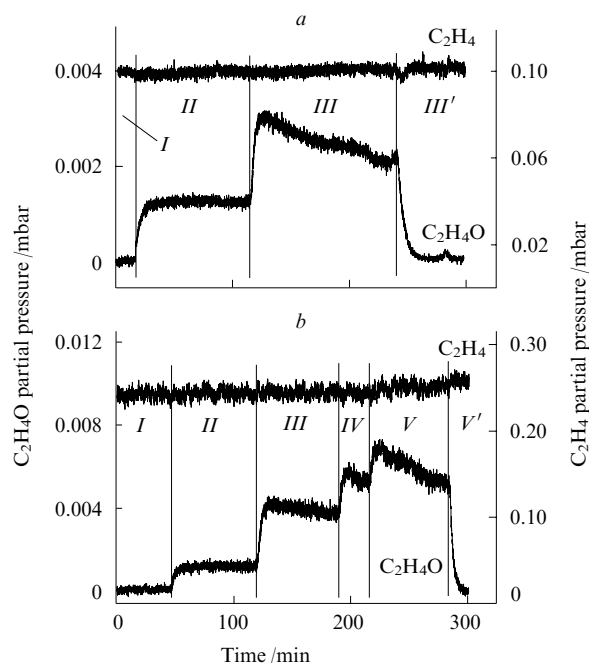


Figure 6. Changes in partial pressures of ethylene oxide and ethylene at $P_{\text{C}_2\text{H}_4} = 0.1$ (a) and $P_{\text{C}_2\text{H}_4} = 0.24$ mbar (b) (the oxygen pressure is 0.25 mbar in both cases) as a function of temperature. T/K : 370 (I), 420 (II), 470 (III), 500 (IV), 520 (V). The last regions of the spectra (regions III' and V') were collected after cessation of the oxygen supply. The partial pressures were recalculated from ion currents measured by mass spectrometry (see text).

the oxygen flow, the PTR-MS signal of ethylene oxide rapidly drops down to the background value. These results imply that ethylene oxide forms as a product of the direct catalytic ethylene oxidation on silver at a pressure in the range of 0.1–0.5 mbar, and the epoxidation rate increases with an increase in temperature. This conclusion is supported by test measurements, which showed that no ethylene oxide is formed upon heating of ethylene in the temperature range of 300–600 K in the absence of silver. In order to analyse the composition of adsorbed layers, full sets of XPS spectra were collected in the regions of constant temperatures (see Fig. 6).⁷⁷

The respective O1s and C1s XPS spectra measured *in situ* at $P_{\text{C}_2\text{H}_4} = 0.1$ mbar and $P_{\text{O}_2} = 0.25$ mbar are plotted in Fig. 7. All O1s spectra are normalised to the integral intensity of the

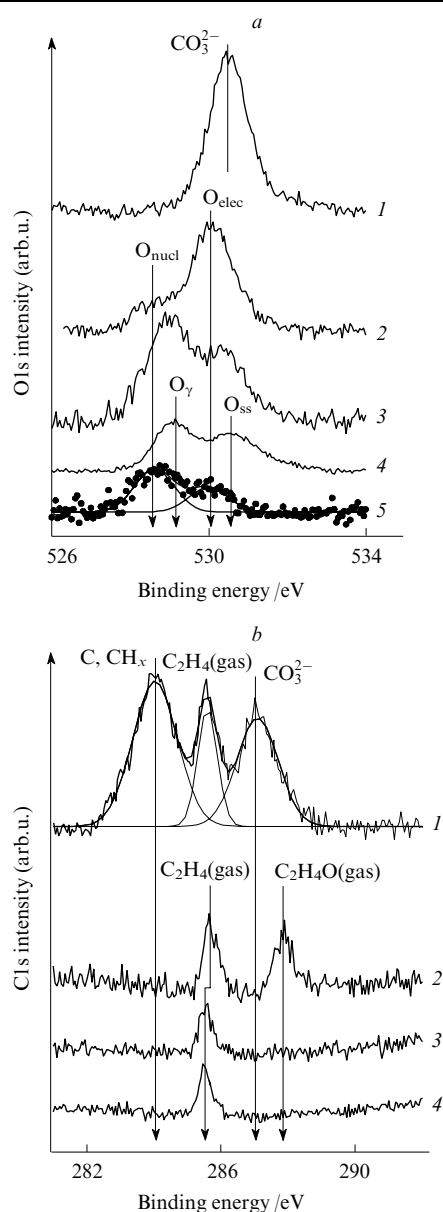


Figure 7. O1s (a) and C1s (b) XPS spectra measured *in situ* in $\text{C}_2\text{H}_4 + \text{O}_2$ reaction mixtures at $P_{\text{C}_2\text{H}_4} = 0.1$ mbar and $P_{\text{O}_2} = 0.25$ mbar as a function of temperature.

T/K : 370 (1), 420 (2), 470 (3). The spectrum 4 was measured at 470 K in a flow of pure ethylene after cessation of the O_2 supply. The difference O1s spectrum (curve 5 and its components) exhibit only signals of species present on the Ag surface under reaction conditions.

$\text{Ag}3d_{5/2}$ spectra. At 370 K, the XPS spectra reveal only one O1s component with $E_b = 530.5$ eV and three types of carbon-containing species corresponding to the C1s components with $E_b = 284.2$ eV, 285.8 eV and 287.3 eV, respectively (spectra 1 in Figs 7a and b). The spectra change dramatically upon heating of the sample to 420 K: the dominant component in the O1s spectrum shifts to 530.0 eV and a shoulder appears at 528.5 eV. Meanwhile, two components with $E_b = 285.8$ eV and 287.9 eV (spectra 2 in Figs 7a and b) are observed in the C1s spectrum. Upon further increase in temperature 470 K, the shape of the O1s signal becomes more complicated, which implies the emergence of additional components from other types of oxygen-containing species (spectrum 3 in Fig. 7a). After removal of oxygen from the gas mixture, two components with $E_b = 529.1$ eV and 530.6 eV appear in the O1s spectrum (spectrum 4 in Fig. 7a). The difference spectrum (spectrum 5 in Fig. 7a) indicates that two O1s peaks with $E_b = 530.0$ eV and 528.5 eV present in the spectra under reaction conditions at a lower temperature disappear. In the C1s spectrum measured in a flow of pure ethylene (spectrum 4 in Fig. 7b), a single peak at 285.8 eV is revealed.

It has to be noted that the large number of spectral components and the resultant ambiguities in their assignment is a common problem of the interpretation of spectra registered *in situ*. This problem can be solved by making use of supplementary reference data from traditional adsorption experiments, which in some cases requires additional measurements on special model systems. The ethylene epoxidation reaction clearly demonstrates why this supplementary information is needed.

Indeed, despite the apparent complexity of the pattern of temperature changes in the XPS spectra, numerous experimental data available in the literature^{8–10, 78–81, 84–86} make it possible to quite reliably assign the components observed in the XPS spectra to different surface and gaseous species. The XPS signals coming from gas molecules, which start to make appreciable contribution at $P > 0.05$ mbar,^{33–36} can be differentiated from those of adsorbed species by their significantly smaller FWHM (full width at the half maximum). It is for this reason, as well as taking into account possible compositions of the mixture under the catalytic reaction, that the components with $E_b = 285.7$ eV and 287.9 eV observed in the C1s spectrum (spectrum 2) were attributed to gaseous ethylene and ethylene oxide, respectively.⁷⁷ Indeed, rather similar binding energies of free ethylene and ethylene oxide ($\Delta E_b \approx 2$ eV) were reported earlier by Siegbahn *et al.*⁸⁵ This assignment is additionally supported by the spectral changes following cessation of the oxygen supply. The signal of gaseous ethylene ($E_b = 285.8$ eV) remains virtually unaffected, whereas that of ethylene oxide rapidly drops down to the background value (spectrum 4 in Fig. 7b), which is in keeping with the disappearance of one of the reactants. The direct observation of gaseous ethylene oxide in the XPS spectra is a significant merit of the *in situ* measurements, since it solidly confirms the assignment of the PTR-MS signal with $m/z = 45$ to ethylene oxide rather than its isomer, acetaldehyde, which was reported by some authors.^{8–10, 12, 13}

Other signals in the C1s and O1s spectra (see Fig. 7) were assigned to adsorbed species.⁷⁷ Temperature ranges of their existence can be used as a supplementary criterion for their assignment. In particular, the peaks at ~ 530.5 eV (O1s) and ~ 287.5 eV (C1s) observed at $T = 370$ K were attributed to surface carbonates CO_3^{2-} , not only based on the binding energy values, but also taking into account that they disappear upon heating to 420 K.⁸ Furthermore, the atomic ratio

§ Carbonate anions adsorbed on silver are known to be stable only below 420 K.^{13, 78, 84}

O : C = 2.8–2.9 calculated from the absolute intensities of the respective components corresponds to the stoichiometric value expected for carbonates (3.0). The low-binding energy peak observed in the C1s spectrum measured at 370 K ($E_b = 284.2$ eV) was attributed to carbon deposits (elementary carbon or hydrocarbon residues), which can accumulate on the silver surface at moderately low temperatures. It was concluded⁷⁷ that the screening of the silver surface with carbon deposits and adsorbed carbonate groups is primarily responsible for the lack of catalytic activity of silver below 370 K (see Fig. 6).

The O1s signals observed in the XPS spectra measured at $T > 370$ K were assigned to atomic oxygen, taking into account the absence of any Cs1 signal from adsorbed carbon species. The attribution of lines with $E_b = 528.5$ eV and 530.0 eV to the nucleophilic and electrophilic forms of adsorbed oxygen was made on the basis of earlier publications devoted to the studies of surface interactions of polycrystalline silver foil with reaction media.^{75, 76, 79} The line with $E_b \approx 529.0$ eV was ascribed to the so-called O_γ form, which has been elucidated in detail by Schlögl *et al.*^{86, 87} within the context of partial methanol oxidation over silver. This species was formulated as a strongly bound atomic oxygen substituting the silver atoms in the fcc lattice. An additional O1s signal that emerges at $T > 470$ K was attributed to the near-surface oxygen O_{ss} (or O_β)[†] incorporated into the octahedral cavities of the silver fcc lattice near the surface. The subsurface location of the O_γ and O_β oxygen species explains their inertness towards ethylene. It is these forms of oxygen that remain on the silver surface after the oxygen supply is stopped. In contrast, the nucleophilic (O_{nuc}) and electrophilic (O_{elec}) oxygen species (see the difference spectrum 5 in Fig. 7a) rapidly disappear from the silver surface in the absence of O_2 in the reaction mixture, which clearly indicates their high reactivity towards the ethylene oxidation.

To clarify the roles played by the nucleophilic and electrophilic oxygen species in the ethylene oxidation reaction, a quantitative comparison of the XPS and PTR-MS data collected at variable $C_2H_4 : O_2$ ratios in the gaseous reaction mixture has been carried out. The absolute intensities of the respective peaks normalised to that of the $Ag3d_{5/2}$ line were used as measures of the surface concentrations of these species. This procedure was necessary to account for the decrease in the XPS absolute line intensities for different compositions and pressures of the gas phase. The partial pressure of ethylene oxide was taken as a measure of the reaction yield. The ethylene oxide yield is correlated with the relative amounts of the nucleophilic and electrophilic oxygen species (Fig. 8). A dependence of the ethylene oxide yield on the concentration of the electrophilic oxygen is apparent: the larger the $O1s/Ag3d_{5/2}$ ratio for the component with $E_b(O1s) = 530.0$ eV, the higher the partial pressure of C_2H_4O . This dependence can readily be approximated by a straight line passing through the point of origin. This correlation clearly proves the involvement of the electrophilic form of the adsorbed oxygen in the ethylene oxide formation, which supports the epoxidation mechanism proposed by Bukhtiyarov *et al.*⁷⁹



Note that the linear dependence of the ethylene oxide yield on the surface concentration of the electrophilic oxygen species was also observed at other temperatures (470 K and 520 K),⁷⁷ the slopes of the respective lines being increased for higher temperatures. These slopes were used to calculate the activa-

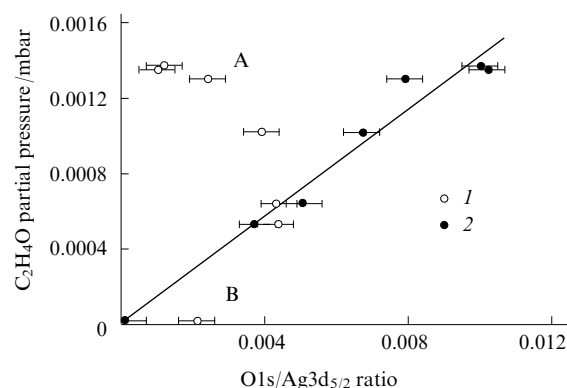


Figure 8. The yield of ethylene oxide as a function of surface concentrations of the nucleophilic (1) and electrophilic (2) oxygen species.⁷⁷ The measurements were performed at $T = 420$ K and variable partial pressures of oxygen and ethylene.

tion energy of the epoxidation reaction, which appeared in excellent agreement with the known E_{act} values measured for the epoxidation reaction over real $Ag/\alpha-Al_2O_3$ catalysts.^{8–10, 78, 82} Even a decrease in the E_{act} value from 14 kcal mol^{–1} to 11.3 kcal mol^{–1} with an increase in temperature from 450 K to 500 K is reproduced.^{77, 82}

The surface concentration of the nucleophilic oxygen species correlates with the ethylene oxide yield in a more complex way (see Fig. 8). As has been found, in different experiments silver can demonstrate dramatically different catalytic activities at nearly identical surface concentrations of the nucleophilic oxygen. In particular, for $I(O1s)/I(Ag3d_{5/2}) \approx 0.02$ the partial pressure of ethylene oxide is 0.0013 mbar (which is still a reliably measured value) in one experimental point A (Fig. 8), but drops far below the detection threshold ($< 10^{-5}$ mbar) in another point B. It has to be noted that the latter case was realised at low pressure and thus the concentration of the electrophilic oxygen was negligible. If only data point in the pressure range of 0.1–1 mbar are taken into account, then a negative correlation of the ethylene oxide yield with the surface concentration of nucleophilic oxygen species is observed. Such a correlation can be rationalised by assuming that the nucleophilic oxygen catalyses the total ethylene oxidation. A similar conclusion was derived in earlier studies^{3, 8–10, 78, 79, 88} based on the results of titration of this type of adsorbed oxygen species with ethylene. Only CO_2 and H_2O were registered as the titration products in numerous experiments. However, other authors^{75, 76, 79} recognised the positive role played by the nucleophilic oxygen in the ethylene epoxidation, since it is involved in the formation of the $Ag^\delta+$ ions,^{89, 90} which further act as adsorption sites for ethylene. According to this scheme, adsorbed ethylene then reacts with the electrophilic oxygen species to yield ethylene oxide.

The possible co-existence of two forms of oxygen atomically adsorbed on the silver surface has been substantiated for the first time by Carter and Goddard.^{91, 92} Using quantum chemical calculations, they demonstrated stability of two distinct states of atomically adsorbed oxygen, *viz.*, oxide-like and oxyradical-like. The electronic structures of these forms depend on the coordination of the oxygen atom to the silver atoms. The oxyradical anion is active towards the selective alkene oxidation and is essentially equivalent to the electrophilic form of the adsorbed oxygen. The oxide oxygen, as will be shown below, can be associated with the nucleophilic oxygen form.

The specificity of chemical interactions of silver atoms with the electrophilic and nucleophilic adsorbed oxygen species were studied using X-ray Absorption Near-Edge Structure

[†] This form of oxygen is referred to as O_β , according to the classification adopted in earlier publications.^{86, 87}

spectroscopy (XANES, the term NEXAFS is also frequently used in the literature^{75,76}). This method provides direct information on vacant orbitals of atoms and molecules with element sensitivity. According to the dipole selection rules ($\Delta l = \pm 1$), the oxygen *K*-edge XANES spectra are formed by the electron transitions from the O1s core level to vacant oxygen p-orbitals.⁹³

Figure 9*a,b* shows the oxygen *K*-edge XANES spectra collected under conditions providing the selective formation of either nucleophilic (spectrum 1) or electrophilic (spectrum 4) oxygen species. In the case of O_{nuc} , the XANES spectrum reveals two distinct resonances at ~ 531 eV and ~ 539 eV (Fig. 9*a*). According to the literature data,^{94,95} the presence of a narrow low-energy resonance below the main absorption edge at ~ 531 eV indicates the effective hybridisation between the oxygen 2p and silver 4d electrons. The broader signal just above the main absorption edge is due to the hybridisation of oxygen p and silver 5sp electrons. The presence of a narrow absorption pre-edge peak in the spectrum of O_{nuc} clearly indicates that its 2p shell is not filled completely. In fact, in the case of a purely ionic Ag–O bond,

the transfer of two electrons from the silver atoms to the oxygen atom should give rise to the electronic configuration $O1s^2 2s^2 2p^6$, and the transition $1s \rightarrow 2p$ responsible for the pre-edge peak in the XANES spectrum will be formally forbidden. With this regard, a value of the partial negative charge on the oxygen atom estimated from the Auger spectra^{75,76} (~ 1.65 e per oxygen atom) is in complete accordance with its nucleophilic nature, and the involvement of the silver 4d electrons into the formation of the Ag–O bonds explains its high ionicity and the observed shift of the Ag3d line by 0.5 eV.⁷⁵

The oxygen XANES spectrum of bulk Ag_2O is very similar, which suggests similar electronic structures of $O(Ag_2O)$ and O_{nuc} (Fig. 9*a*). The involvement of the silver 4d electrons into the formation of the Ag–O bonds in Ag_2O is also supported by the emergence of a ‘white line’ in the Ag *L*₃-edge XANES spectrum (3.352 keV, see inset to Fig. 9*a*), which corresponds to the dipole-allowed electron transition $2p_{3/2} \rightarrow 4d$ ($\Delta l = 1$). An increase in the intensity of this line with an increase in the ionicity of the bond reflects the degree of the actual involvement of the silver 4d electrons in its formation.^{96,97} The transition $2p_{3/2} \rightarrow 4d$ is forbidden for an Ag^+ ion characterised by the electronic configuration $4d^{10}5s^0$. However, the formation of the chemical bond Ag–O results in electron density transfer from the 4d to the 5s orbitals. As a result, the electronic configuration of the Ag^+ ion can be formulated as $4d^{10-\delta}5s^\delta$, which features partly vacant 4d states near the Fermi level responsible for the emergence of a narrow X-ray absorption resonance at 3.352 keV.

The conclusions derived from the experimental XANES spectra are fully supported by quantum chemical calculations of the electronic structure of Ag_2O .⁹⁸ Indeed, the weak population of the Agd_{z^2} and $Ag5s$ states indicates appreciable charge transfer from the Ag atom to the O atom associated with the Ag–O ionic bond formation. It is of note that this type of hybridisation (*viz.*, sd_{z^2}) is rather frequently observed for metals but rarely for ionic semiconductors like Ag_2O due to the wide energy gap between the occupied d-band and vacant sp-states. In terms of the molecular orbital theory, this can be reformulated in the following way. The O2p and Agd_{z^2} states are hybridised to form the $pd\sigma$ bond, whereas the hybridisation of the O2p and Agd_{xz}, d_{yz} yields the $pd\pi$ bonds. These interacting orbitals are split into bonding and antibonding states with partial p- and d-characters. The $Agd_{x^2-y^2}$ and Agd_{xy} orbitals remain essentially non-bonding.⁹⁸

The *K*-edge XANES spectrum of electrophilic oxygen species displays a broad peak around 541 eV (spectrum 3 in Fig. 9*b*). The absence of distinct pre-edge peaks (around 531 eV) strongly implies that the Ag–O bonds are formed by the hybridisation of the oxygen 2p and silver 5sp electrons, whereas the metal 4d electrons remain unaffected. The respective $Ag3d_{5/2}$ spectrum does not show additional ‘ionic’ lines, such that the electronic state of the silver atoms is similar to that in the bulk metal⁷⁵ (the electronic configuration of silver atoms is $4d^{10}5s^1$). In the metallic state, the 5s electrons of silver are delocalised in the conduction band. Most likely, it is these delocalised conductivity electrons that participate in the formation of Ag– O_{elec} bonds.

According to the literature data, a similar oxygen XANES spectrum is characteristic of oxygen adsorbed on the copper surface in the suboxide state.⁹⁹ The respective Cu *L*_{2,3}-edge XANES spectra reveal no characteristic ‘white line’ in contrast to the spectra of CuO or Cu₂O (which are similar to that of Ag_2O), which means that the copper atoms in this structure indeed preserve essentially metal-like properties and only outermost 4sp electrons are involved in the Cu–O bond formation. Therefore, in both these cases, the M–O bonds are formed by the interaction of the oxygen 2p and metal outermost sp orbitals and characterised by the essentially covalent character.

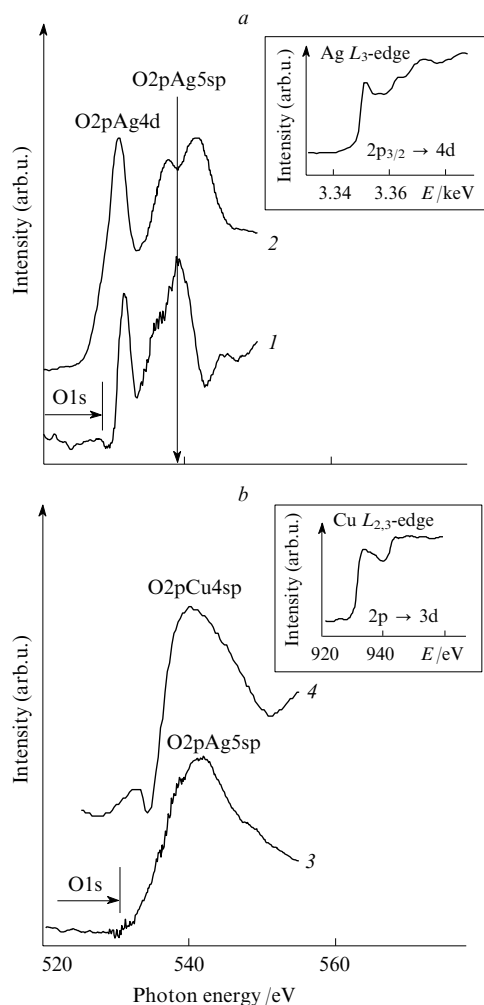


Figure 9. *K*-Edge XANES spectra of the nucleophilic form of adsorbed oxygen (O_{nuc}) (a, spectrum 1) and oxygen within Ag_2O (a, spectrum 2), electrophilic form of adsorbed oxygen (O_{elec}) (b, spectrum 3) and oxygen adsorbed on the copper surface (b, spectrum 4).

Insets: *L*-edge spectrum of Ag_2O (a) and *L*-edge spectrum of the copper surface with adsorbed oxygen (b).^{2,3} The O1s binding energies from the XPS measurements for the respective samples are shown with horizontal arrows.

Then another important question arises, what geometries can be ascribed to the adsorption complexes of O_{nuc} and O_{elec} . According to the literature data, the binding energy of O_{nuc} is $E_b(O1s) = 528.4 \pm 0.1$ eV (calibrated against the $Ag3d_{5/2}$ line with $E_b = 368.2$ eV) independent of the type of the silver surface [different polycrystalline foils, single-crystalline faces $Ag(111)$, $Ag(110)$ or $Ag(100)$ and even graphite-supported silver particles]. The small scatter of the experimental data suggests the common character of the nucleophilic oxygen species adsorbed on different silver faces. The majority of researchers agree that the formation of the nucleophilic oxygen state is directly related to silver surface reconstruction. In particular, the oxygen adsorption on the $Ag(110)$ crystal face at 300–500 K can give rise to the superstructures of the type $Ag(110)-(n \times 1)-O$, where n decreases from 7 to 2 with an increase in the O_2 exposure.^{78, 100, 101} The $Ag(110)-(2 \times 1)-O$ reconstruction due to the appearance of supplementary atomic rows going along the $[001]$ direction with the oxygen atoms residing nearly in the plane of the supplementary rows has been reliably established with scanning tunneling microscopy and photoelectron diffraction. The $Ag-O$ bond length is 2.044 Å, which is nearly identical to the respective value typical of bulk Ag_2O (2.05 Å).¹⁰² The formation of such a surface structure with $\theta = 0.5$ monolayers results in a substantial (by 0.8 eV) increase of the work function as compared to clean silver surface, which indicates a significant charge transfer from the metal to oxygen atoms.¹⁰⁰ The linear increase in the work function with an increase in coverage implies that the surface dipole moment per adsorbed oxygen species is independent of coverage,¹⁰¹ i.e., the electronic structure of nucleophilic oxygen adsorbed on $Ag(110)$ remains constant over the entire coverage range and is close to that in oxide. The adsorption of oxygen in the nucleophilic form on the densely packed $Ag(111)$ face gives rise to the $p(4 \times 4)$ surface reconstruction. The nature of the $Ag-O$ bonds in this surface structure is also believed (for instance, see Refs 10, 103 and 104) to be similar to that in bulk Ag_2O .

Thus, the nucleophilic form of oxygen is formed on the silver surface as a result of the reconstructive adsorption giving rise to linear fragments $Ag-O-Ag$ (Fig. 10a). Indeed, the angle $Ag-O-Ag$ in both the bulk Ag_2O oxide and in the $Ag-O_{\text{nuc}}-Ag$ surface structure are close to 180° . Such a geometry favours the rather strong interaction between the silver 4d and oxygen 2p orbitals associated with the substantial

charge transfer. The high ionicity of the $Ag-O$ bonds in such a structure, on the one hand, provides the conversion of the silver atoms into the ionic form Ag^+ required for the ethylene adsorption and, on the other hand, determines the nucleophilic properties of the oxygen atoms in the ethylene epoxidation.

The geometry of the electrophilic oxygen state is less elucidated. It is only known from the experimental data that oxygen in the electrophilic form is adsorbed directly on the silver surface.^{76, 79, 103} Most likely, the adsorption does not induce surface reconstruction and the oxygen atom is located above the triangle of silver atoms (three-fold hollow, Fig. 10b). For instance, the adsorbed oxygen species with $E_b(O1s) = 530.1$ eV have been detected on the $Ag(111)$ face.¹⁰³ The absence of a surface reconstruction in that case was evidenced by LEED, whereas surface location of the oxygen atoms was confirmed by angular-resolved XPS. The absence of additional components in the $Ag3d$ spectrum was consistent with the covalent character of the $Ag-O_{\text{elec}}$ bonds.

This model agrees well with the results of quantum chemical calculations. Zilberberg *et al.*^{105, 106} found a stable state of atomically adsorbed oxygen on the non-reconstructed $Ag(111)$ surface. The oxygen atoms are located symmetrically above a three-centre cavity and bound to three silver atoms [the three-fold axial symmetry is governed by the symmetry of the $Ag(111)$ face]. The $Ag-O$ bond length is 2.109 Å (note that the $Ag-O_{\text{nuc}}$ is 2.044 Å). The charge transfer from the metal to the adsorbate in this case should be much smaller than that in the binding of Ag to O_{nuc} . The aforementioned oxyradical oxygen adsorbed on $Ag(110)$ is characterised by a similar geometry.^{91, 92} In this case, oxygen is also localised on the three-centre position of the non-reconstructed surface, i.e., the oxygen adsorption on $Ag(110)$ proceeds dissociatively without reconstruction. Such a geometry of the adsorption complex determines the essential covalency of the $Ag-O$ bond and consequently the electrophilic properties of this oxygen form in the ethylene epoxidation to ethylene oxide.

The experimental efforts aimed at the elucidation of the structure of the active site and the mechanism of the ethylene epoxidation have been described in so much detail to demonstrate that the *in situ* measurements provide correlation dependences sufficient to establish the structure–activity relationship in heterogeneous catalysis, despite they are associated with greater difficulties and ambiguities in data interpretations as compared to traditional UHV measurements. It is also evident that it is the application of several instrumental techniques to one system that gives a chance of success in establishing this relationship.

4. Reaction of partial methanol oxidation into formaldehyde over copper

As another example of efficient determination of the mechanism of a catalytic reaction using *in situ* measurements, we describe the methanol oxidation into formaldehyde over the copper surface studied by XANES, XPS and mass-spectrometry.^{29, 35, 107} A brief survey of experimental facts available in the literature indicates that:

- a Cu catalyst has to be activated prior to use;
- the methanol conversion pathway depends on the ratio of methanol/oxygen partial pressures in the reaction mixture and on the sequence of the reactants supply;
- stoichiometric copper oxides (Cu_2O and CuO) demonstrate low selectivity in the formaldehyde synthesis;
- Cu catalysts are transformed into Cu_2O after evacuation of the reaction medium or its fast cooling aimed at the freezing of the active state of the copper surface.

This means that the forms of adsorbed oxygen responsible for the copper activity towards the selective methanol oxidation are formed directly under the reaction conditions. Thus, the catalytic system represents a dynamic system, which exists only

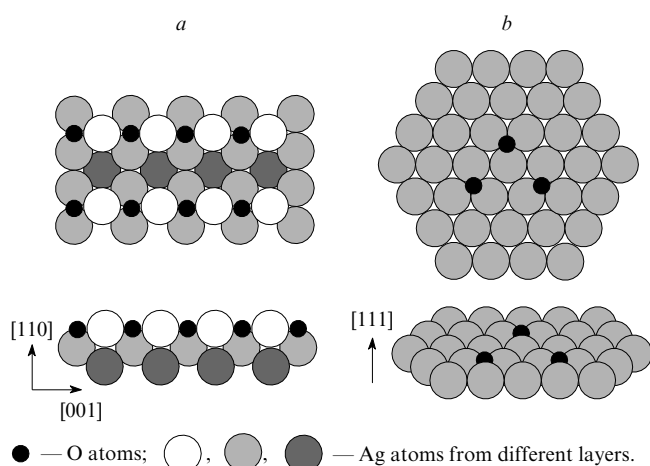


Figure 10. A structural model of adsorbed oxygen species. (a) Nucleophilic oxygen on the reconstructed $Ag(110)$ surface, (b) electrophilic oxygen on the unreconstructed $Ag(111)$ surface. Top panels is top view, bottom panels is side view.

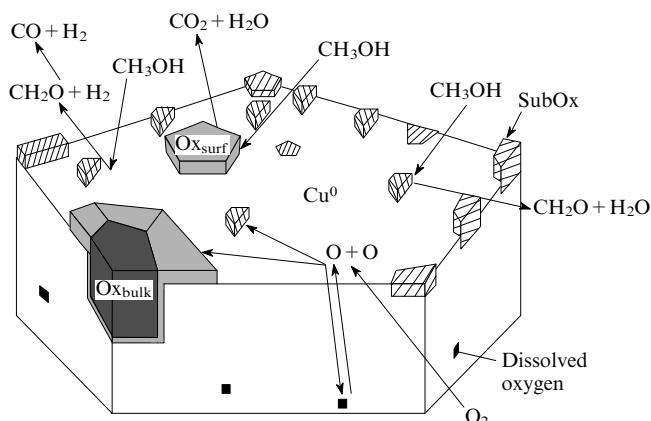


Figure 11. A model of the active surface of a copper catalyst with various co-existing oxygen species.¹⁰⁷

The arrows indicate routes of mutual transformations of various oxygen species and interaction paths of $\text{CH}_3\text{OH}(\text{gas})$ with the copper surface. Bulk (Ox_{bulk}) and surface (Ox_{surf}) oxide forms of oxygen catalyse the total methanol oxidation into CO_2 and H_2O . Formaldehyde is formed upon the interaction of methanol with weakly bound oxygen species (SubOx) adsorbed on the copper surface.

in the contact with the reaction medium and thus the ‘pressure gap’ problem is very important for this system.

As a result of studies, various forms of adsorbed oxygen have been identified and correlations between their concentrations and yields of respective products of the methanol oxidation via different pathways (*i.e.*, total or partial oxidation, *etc.*) have been determined. The surface oxygen species identified include two oxide forms (a surface and a bulk forms) and one suboxide form. The assignment of the latter to the a suboxide oxygen state was based on the absence of a characteristic $\text{O}1s \rightarrow \text{O}2p\text{Cu}3d$ peak in the oxygen K-edge XANES spectra. Judging from the linear correlation between the surface concentration of suboxide oxygen and formaldehyde yield, it was concluded that it is this form that catalyses the partial methanol oxidation.^{29, 107} Similar dependences of the formaldehyde yield on the concentration of the oxide forms were far from the linear character, which allowed a conclusion that these forms catalyse the total methanol oxidation.

A generalised scheme of various species present on the copper surface in the course of the catalytic methanol oxidation and responsible for different reaction pathways is shown in Fig. 11.¹⁰⁷ It is of note that the suboxide oxygen form on the copper surface was detected by means of XANES only in the presence of the reaction medium, which additionally demonstrates the importance of *in situ* studies.

A great interest of researchers to the state of active catalyst surfaces during their operation (even in the case of model systems) is reflected in the appearance over recent years of numerous monographs and special issues of scientific journals devoted to the application of instrumental techniques to studies of the catalytic activity in the *in situ* mode with surface-sensitive techniques occupying a notable place among them.^{107–111}

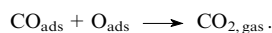
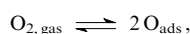
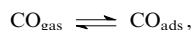
III. The ‘material gap’ problem

The intermediate state occupied by nanoparticles in the row metal–atom determines their unique physicochemical properties (electronic, magnetic, optical, *etc.*) clearly distinguishable from those of both bulk metals and isolated atoms. No doubt, it is the changes in the surface structures and electronic properties of metal catalysts upon transition from bulk samples to nanoparticles that are of primary interest for catalysis

specialists,^{18–20} since it is these characteristics that govern the features of the interaction of reactants with the active component, the nature and reactivity of adsorbed species and ultimately the activity and selectivity of nanostructures in heterogeneous catalysis.

1. CO oxidation over nanoparticles of the platinum-group metals

According to investigations into the catalytic activity of palladium particles supported on $\alpha\text{-Al}_2\text{O}_3$ with respect to the CO oxidation as a function of the mean particle size,¹¹² a decrease in the particle size from 30 nm to 5 nm accelerates the reaction three fold. This experimental fact was explained within the Langmuir–Hinshelwood mechanism, which assumes that any adsorption–desorption steps of a heterogeneous catalytic reaction are in equilibrium and the total rate is limited by the reaction between the adsorbed species:



In the case of CO oxidation of single-crystalline surfaces, the validity of this mechanism has been established earlier.^{1, 113} An increase in the rate of the CO oxidation on Pd particles was explained by weaker binding of the CO molecules to the Pd atoms of small clusters. This conclusion was derived from a comparative TPD analysis of the CO adsorption on Pd(111) single crystal and disperse palladium samples.^{1, 49} In the case of Pd nanoparticles with a size of 2.5 nm, the TPD spectrum of carbon monoxide reveals additional weakly bound states that are characterised by lower desorption temperatures as compared to adsorption states on the single-crystalline surface. Meanwhile, in the case of large particles with $d = 27$ nm, the TPD spectrum was identical to that measured with the single crystal.

A different in principle picture was observed for Pt particles supported on alumina⁴⁷ or mica:¹¹⁴ the TPD spectra of CO desorption showed that a weakly bound state typical of a single-crystalline surface or large supported particles virtually disappears for Pt particles smaller than 3 nm. This observation is in accord with a more than seven fold deceleration of the CO oxidation on small Pt nanoparticles.¹¹⁵ According to TPD studies of the CO adsorption on supported platinum and rhodium particles,¹¹⁶ relative populations of weakly and strongly bound CO_{ads} is virtually independent of the mean size of rhodium dispersed particles. This explains why the reaction of $\text{CO} + \text{O}_2$ on the rhodium surface is structure-insensitive.¹¹⁷

The above example demonstrates that the use of model catalysts prepared by the thermal deposition of a metal on planar substrates is extremely efficient for the analysis of size effects for reactions catalysed by supported metal particles. This statement can be most spectacularly illustrated with a study of the CO oxidation on gold particles. Presently, this reaction became a canonical example of the ‘nanosize’ effect.

2. CO oxidation over gold nanoparticles

For a long time, gold was considered as one of the most inert metals. Nevertheless, as was discovered in the 1990s, gold nanoparticles with a size of <5 nm supported on titania manifested high catalytic activity in a series of practically important reactions exceeding that of platinum catalysts traditionally applied in the field (the CO oxidation was the first reaction of this series^{118, 119}). Figure 12 plots the atomic catalytic activity of nanosized gold particles for the CO oxidation reaction as a function of the mean particle size.^{120, 121} It is clearly seen that the reaction rate rapidly increases with a decrease in the mean size of gold particles to

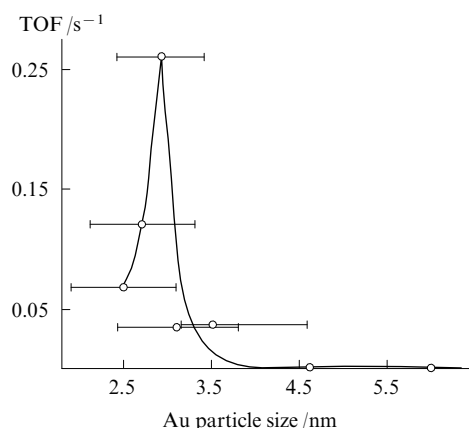


Figure 12. Turnover frequency (TOF) of the supported Au/TiO₂ catalysts with high specific surface areas in the CO oxidation at 300 K as a function of the mean Au particle size.¹²¹

3.5 nm. Further decrease in the particle size results in a decrease in the catalytic activity. Such an unusual catalytic behaviour of ultrasmall Au particles remained unexplained at the atomic level for a long time despite enormous efforts put forth. The understanding of the size effect has been achieved owing to a transition to Au/TiO₂ model systems.^{122–127} These brilliant results have been obtained by a group of researchers from the A&M University (Texas, USA) headed by Prof. Goodman.

A typical STM pattern for a model sample composed of gold nanoparticles with a diameter of 2.6 nm and a height of 0.7 nm (which constitutes only 2–3 atomic layers) dispersed on the TiO₂(110)-1 × 1 single-crystalline face and covering

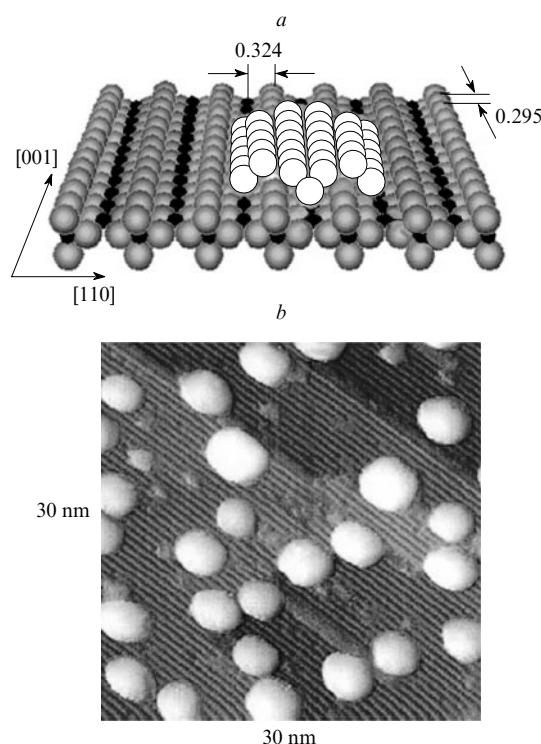


Figure 13. A structural model of bilayer Au islets on the TiO₂(110) surface (a) and STM image of the Au/TiO₂(110)-(1 × 1) surface at $\Theta(\text{Au}) = 0.25$ monolayers (b).¹²⁷

25% of its surface is shown in Fig. 13. Such a morphology of the gold particles is explained by the fact that the growth proceeds in two steps: first two-dimensional (2D) islets are formed and only then as the surface concentration of gold increases, the particles start to grow in the third dimension.^{128, 129} By changing the surface concentration of deposited gold, a series of model samples was prepared with the mean particle size systematically varying from 1.5 nm to 6 nm.

These model catalysts Au/TiO₂(110)-1 × 1 were assayed in the catalytic activity in the CO oxidation. The reaction rate as a function of the gold particle size obtained (Fig. 14) was nearly identical to that measured for real supported catalysts, which justifies the utilisation of model systems in the analysis of the size effects. The apparent activation energy in the temperature range of 350–450 K increases from 1.7 kcal mol⁻¹ to 5 kcal mol⁻¹ with an increase in the mean Au particle size from 2.5 nm to 6 nm.

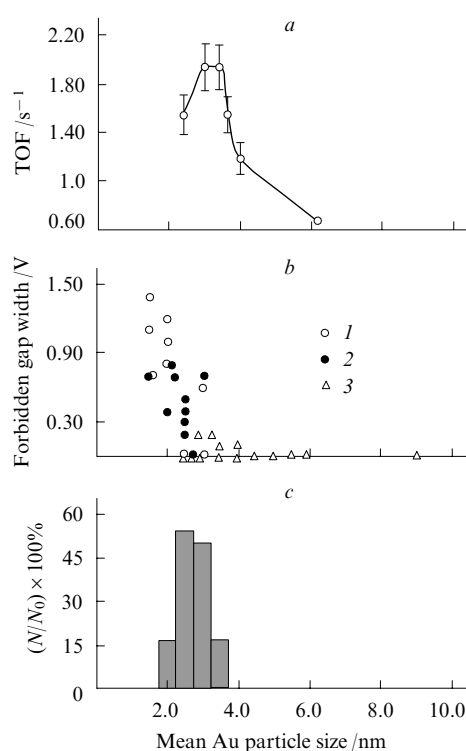


Figure 14. Turnover frequency (TOF) of the Au/TiO₂(100) catalyst in the CO oxidation as a function of the mean Au particle size assuming their dispersion (a); changes in the band gap widths according to the STM measurements (b); relative coverage of the TiO₂(100) surface with bilayer Au particles (c) as functions of the mean Au particle size. The data points 1–3 correspond to three samples with different gold concentrations.

These measurements on model samples helped to shed light upon the reasons for the extraordinary activity of gold nanoparticles. Variations in the mean size of particles in a range from 2 nm to 4 nm are accompanied by changes in the band gap (Fig. 14b).^{122, 127} With a decrease in the mean Au particle size below < 3.5 nm, a metal–insulator transition occurs:[†] particles with a height of one atomic layer are characterised by

[†] The metal–insulator transition, which is a particular case of the quantum size effect, was observed earlier for many metal catalysts.^{124, 130, 131}

a rather wide band gap, whereas particles with heights of 3 layers and more are essentially metallic.

Furthermore, the strength of the CO–Au bond was shown to be dependent on the Au particle size. This conclusion was derived based on IR absorption spectroscopy of CO molecules adsorbed on gold nanoparticles with a size from 1.8 nm to 3.1 nm.^{125, 126} The specific heat of absorption abruptly increased from 12.5 kcal mol^{−1} to 18.3 kcal mol^{−1} with a decrease in the particle size, and the maximum is observed at the same size (~3 nm) as the catalytic activity maximum and the onset of the metal–insulator transition.¹²² The final conclusion about the structure of active sites was made based on an analysis of the relative distribution of bilayer gold particles as a function of the mean particle size, which is also shown in Fig. 14c. The maximum of this distribution falls on the same mean size (2.5–3.0 nm) as the maximum strength of the CO–Au bonds and activity of model catalyst in the CO oxidation.

Further arguments in favour of the suggestion that it is the bilayer gold particles that are active in the CO oxidation^{33, 101} were gathered in an LEED study of gold particles deposited into an ultrathin single-crystalline film of TiO₂. The film was prepared by mild oxidation of a titanium monolayer grown on a Mo(112) single crystal.¹²⁷ The surface was characterised by a distinct (8 × 2) LEED pattern. Two-dimensional gold islets and bilayer particles were identified by the appearance of (1 × 1) and (1 × 2) LEED patterns, respectively. The sample containing bilayer gold particles manifested an unprecedented catalytic activity in the CO oxidation (Fig. 15). Thus, it was demonstrated that in order to provide high activity of nanosized gold catalysts in the low-temperature CO oxidation, gold particles composed of exactly two layers of Au atoms have to be selectively prepared. This finding initiated extended experiments aimed at the development of methods for the synthesis of nanoparticles supported on porous alumina and design of advanced catalysts on their base (see Section V).

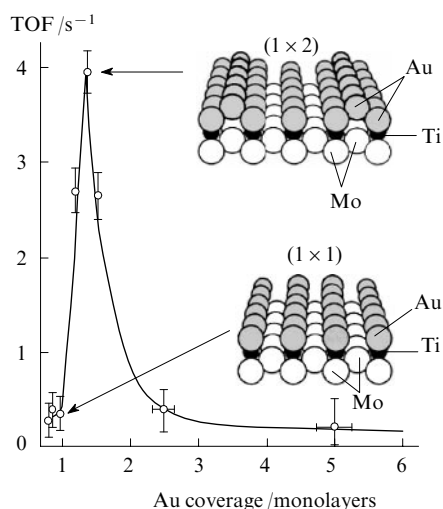


Figure 15. Turnover frequency (TOF) of the Au/Mo(112)-(8 × 2)-TiO_x catalysts in the CO oxidation at 300 K as a function of coverage of the surface with gold nanoparticles.

Model samples synthesised by the UHV deposition of metals on planar supports were used to study many aspects of the catalytic action of supported metal catalysts. Only a few of them will be addressed in the present review, including the catalytic synergism in the CO oxidation on bimetallic Pt–Rh

catalysts,^{132–135} the size effects[‡] in the ethylene epoxidation on silver catalysts^{20, 136–138} and the deactivation mechanism of Pt/Al₂O₃ catalysts for neutralisation of exhaust gases in the presence of SO₂.^{139, 140}

3. CO oxidation on bimetallic Pt–Rh catalysts

The synergism in the CO oxidation on supported Pt–Rh/Al₂O₃ catalysts used for the exhaust gases neutralisation has been reported for the first time by Oh and Carpenter,¹⁴¹ who studied this reaction under conditions of excess of oxygen. They showed that catalysts prepared by successive impregnation of alumina with solutions of platinum and rhodium salts manifest significantly higher activities than mechanical mixtures of two catalysts with individual metals. This result was later reproduced by Cai *et al.*¹⁴²

On the other hand, Nieuwenhuys *et al.*^{143, 144} observed no synergistic effect in the Pt–Rh/Al₂O₃ catalytic system. They noted only a monotonic change in the catalytic properties between two limiting points represented by monometallic platinum and rhodium systems. This apparent discrepancy was likely due to variations in the nature of studied samples, experimental conditions and procedures used for the catalysts preparation.^{141–144} Nieuwenhuys *et al.*^{143, 144} employed simultaneous impregnation of alumina with a solution of platinum and rhodium salts, whereas Oh and Carpenter¹⁴¹ and Cai *et al.*¹⁴² performed the impregnation successively in two steps. It would be reasonable to assume that a statistical distribution of alloy particles over the alumina surface is realised in the case of the simultaneous impregnation and subsequent reduction, whereas isolated Pt and Rh particles are generated upon successive impregnation.

In order to verify this assumption, Bukhtiyarov *et al.*^{132–135} carried out a comparative analysis of the CO oxidation on continuous polycrystalline films of Pt and Rh, their alloy and heterophase Pt–Rh bimetallic surfaces at a reaction mixture pressure below 10^{−5} mbar. The high-vacuum conditions were necessary to exclude surface oxidation of the catalysts, which cannot be avoided with porous supports.^{141, 142} Continuous polycrystalline films of Pt and Rh were prepared by UHV deposition of the respective metals on a Ta foil. In order to suppress the diffusion of the noble metals into tantalum, the surface of clean Ta foil was covered with a thin alumina film prior to metal deposition.¹³²

The alloy with a composition of 56 at.% of Pt and 44 at.% of Rh was prepared by successive deposition of platinum and rhodium from two independent sources. Prior to experiments, the alloy was annealed at 800 °C for 10 min under UHV to equilibrate the atomic distribution.

The preparation of heterophase Pt–Rh surfaces included several steps: (a) vacuum deposition of a continuous rhodium film on the Al₂O₃/Ta substrate; (b) total oxidation of rhodium to Rh₂O₃ by exposure to oxygen for 30 min at *P* = 10 mbar and *T* = 400 °C; (c) vacuum deposition of Pt on the oxidised rhodium surface until the Pt4f_{7/2}/Rh3d_{5/2} line intensity ratio in the XPS spectrum becomes equal to 0.38 and (d) subsequent reduction of the surface in hydrogen at *P* = 10^{−6} mbar and *T* = 300 °C. The heterophase surface prepared in this way can be regarded as a model of catalysts synthesised by successive impregnation, whereas the alloy surface mimics the catalysts produced by simultaneous impregnation.

According to an STM study of these samples, the heterophase surface is composed of platinum particles with a size of

[‡] As has been demonstrated earlier, the rate of ethylene oxide formation decreases by more than one order of magnitude with a decrease in the mean size of supported silver particles below 50 nm.

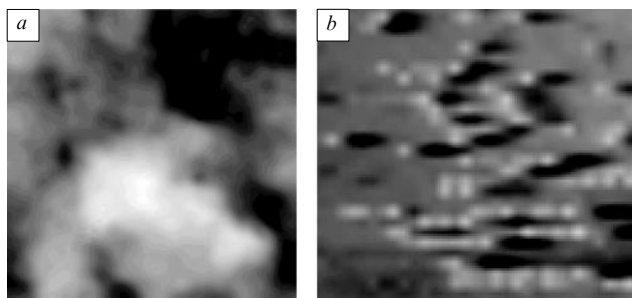


Figure 16. STM Images of the Pt–Rh alloy (a) and the Pt–Rh heterophase surface (b) prepared by the UHV Pt and Rh co-deposition on a thin alumina film grown on a Ta foil (see text).

10–20 nm dispersed on a flat rhodium substrate and covering 50% of its surface; the alloy is characterised by a smooth surface with a roughness of < 1 nm (Fig. 16). The heterophase surface is stable against heating up to 350 °C but converts into the homogeneous alloy at higher temperatures.

Typical plots of the CO oxidation rates (measured as a CO_2 partial pressure) for the platinum sample measured at a constant O_2 pressure (10^{-6} mbar) and variable CO pressures as a function of temperature are shown in Fig. 17. All curves reveal three distinct regions. At low temperatures, the reaction is very slow and the CO_2 concentration is below the detection limit of the mass spectrometer. With an increase in temperature up to a certain threshold value, CO_2 appears in the gas phase, then the reaction rate rapidly increases reaching the maximum value. After that, the reaction rate smoothly decreases. Similar dependences were obtained for all the samples under study.

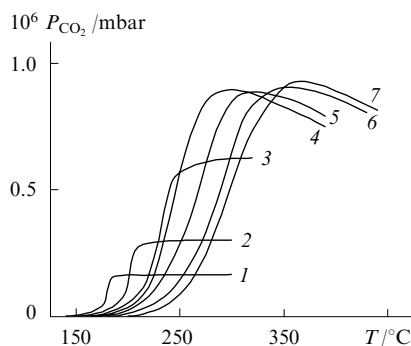


Figure 17. Temperature dependences of the CO oxidation rates (expressed as CO_2 partial pressures) on Pt as a function of P_{CO} at a constant oxygen pressure ($P_{\text{O}_2} = 10^{-6}$ mbar). $10^7 P_{\text{CO}}$ /mbar: 0.07 (1), 0.17 (2), 0.35 (3), 0.47 (4), 0.96 (5), 3.6 (6), 8.6 (7).

Such a character of the reaction rate vs. temperature plots is typical of platinum metals and explained by the adsorption mechanism of the CO oxidation (the Langmuir–Hinshelwood mechanism), which involves steps of reversible molecular adsorption of CO, dissociative adsorption of O_2 and a reaction between the adsorbed species on the metal surface.¹ At low temperature, the metal surface is covered by adsorbed CO molecules, which screen surface areas accessible to the O_2 adsorption. As a consequence, the reaction rate is low.

With an increase in temperature, CO_{ads} species partly desorb freeing adsorption sites for O_2 . Under these conditions, the reaction rate is limited by the carbon monoxide desorption, i.e., CO inhibits the reaction. With further increase in temperature, the reaction rate rapidly increases reaching the maximum value, which is accompanied by a change in the

composition of the adsorbed layer from purely CO_{ads} to $\text{CO}_{\text{ads}} + \text{O}_{\text{ads}}$.¹⁴⁵ Further smooth decrease in the reaction rate with increasing temperature is usually attributed to the screening effects of adsorbed oxygen. At high temperatures, the reaction is characterised by the zero order with respect to the concentration of the excess of the reactant and nearly first order with respect to the concentration of the deficient reactant.¹

Due to the validity of the Langmuir–Hinshelwood mechanism for the CO oxidation, the temperature dependences of the CO conversion known as the ‘light-off curves’ came in use as an industrial test of properties of catalysts for the after-burning of exhaust gases. Typically, the light-off curve has a shape similar to the above curves of the CO oxidation rates measured in a chamber of an XPS spectrometer serving as a catalytic reactor (see Fig. 17): the CO conversion is negligible at low temperature but rapidly increases reaching 100% when temperature is increased above the critical value. This fact can easily be rationalised taking into account that CO_2 is the only product of the CO oxidation. A catalyst that provides the minimum temperature of the 100% CO conversion is considered to be the best one (the half-conversion temperature is routinely used in quantitative comparisons).

In order to verify the probable synergistic effects for the heterophase surfaces, the temperature dependences of the CO oxidation rates were compared for different model surfaces, including monometallic Pt and Rh films, the Pt–Rh alloy and the Pt–Rh heterophase surface (Fig. 18). For the sake of comparison, Fig. 18 also shows a calculated temperature dependence of the CO oxidation rate on a bimetallic Pt–Rh sample with two independent platinum and rhodium domains with areas twice smaller than those in the individual monometallic samples (curve 5). The number of platinum and rhodium surface sites in the case of the calculated curve was adjusted to be the same as in the heterophase surface. All experimental curves were measured under identical conditions for equimolar CO and O_2 mixtures ($P \approx 10^{-6}$ mbar).

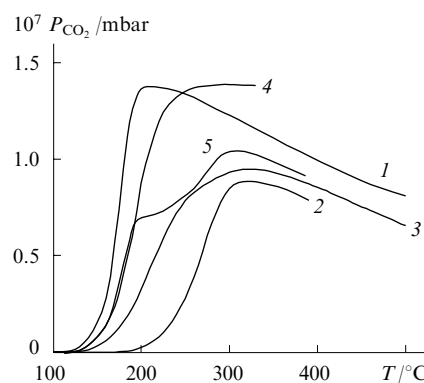


Figure 18. Temperature dependences of the CO_2 formation rates at $P_{\text{CO}} = P_{\text{O}_2} = 10^{-6}$ mbar on Rh (curve 1), Pt (2), Pt–Rh alloy (3), Pt–Rh heterophase surface (4).

The simulated dependence for a heterophase Pt–Rh surface assuming independent Pt and Rh domains with relative coverages of 0.5 (curve 5, see text).

As it becomes clear from Fig. 18, rhodium manifests much higher activity than platinum. Importantly, high oxidation rates are observed on the Rh catalyst at relatively low temperature. In particular, the activity of rhodium is maximum at $T = 200$ °C where platinum exhibits nearly zero activity. The activity of the alloy is intermediate between those of individual Rh and Pt. The CO oxidation rate on the heterophase surface is

close to that on rhodium at low temperatures and exceeds that on rhodium above 250 °C. Nevertheless, it has to be taken into account that the accessible area of rhodium in the case of the heterophase samples is twice smaller than in the case of the purely rhodium sample. Therefore, a comparison of the activity of the heterophase sample (curve 4 in Fig. 18) with the calculated curve (curve 5) would be more informative. The calculated curve has a kink at $T = 200$ °C corresponding to the maximum reaction rate on pure rhodium and a maximum at $T = 300$ °C (corresponding to the maximum reaction rate on platinum).

The curves 4 and 5 are nearly identical at $T < 200$ °C, while the CO oxidation rate on the heterophase Pt–Rh surface starts to significantly exceed the respective value expected for the bimetallic surface under assumption of the independent behaviour of Pt and Rh domains at higher temperatures, *i.e.*, there is a prominent synergistic effect. This result was explained by a specific structure of the adsorption layer and its evolution in the course of the reaction (Fig. 19). At the ignition temperature, the adsorbed CO molecules are oxidised by O_{ads} species adsorbed on the rhodium regions that become vacant due to the CO desorption. The CO oxidation rate is maximum at $T = 200$ °C, which corresponds to the T_{max} for pure Rh. At this temperature, the reaction rate on platinum is low (since Pt particles are covered with CO_{ads}). At $T > 200$ °C, the reaction between CO_{ads} (on platinum) and O_{ads} (on rhodium) takes place (see Fig. 19). The experimentally observed synergism in this case is due to the involvement of the Pt particles into the overall process as a supplier of one of the reactants (*i.e.*, CO_{ads}).

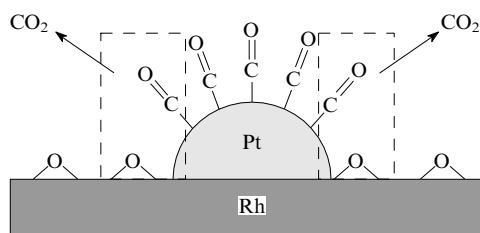


Figure 19. A structural model for the active Pt/Rh surface explaining the synergism in the CO oxidation.

In summary, the enhanced activity of the bimetallic catalyst can be explained by the selective adsorption of the reactants on different surface sites (O_{ads} preferably on rhodium whilst CO_{ads} preferably on platinum) and a reaction between the O_{ads} and CO_{ads} proceeding at the interface between Pt and Rh.

4. Interaction of oxygen with silver nanoparticles

The size effects in the ethylene epoxidation on silver catalysts were elucidated on model catalysts prepared by vacuum deposition of silver on the graphite substrate.^{20, 136–138} The use of the carbon substrate instead of the oxide (Al_2O_3) helped to suppress the charging effects, which hampers studies of the electronic properties of supported metals by means of XPS for dielectric samples, and get rid of the masking O1s signal from the substrate. The absence of the spurious O1s from the substrate makes the XPS method highly informative for the elucidation of O_2 adsorption on the surface of supported silver particles.^{137, 146} Sputtering of silver and subsequent oxygen adsorption on model Ag/C specimens was performed directly in a UHV chamber of a photoelectron spectrometer avoiding air exposure of the specimens. Only the STM characterisation of the supported silver particles was performed in a vacuum chamber of the tunneling microscope

following transfer of the samples from the chamber of the photoelectron spectrometer.

A typical STM pattern of the graphite surface after the silver deposition (relative coverages were estimated according to ratios of the silver and carbon line intensities in the XPS spectra; the current sample corresponds to $I_{Ag3d}/I_{C1s} = 0.13$) is shown in Fig. 20. The originally rather smooth graphite surface becomes substantially rough after the silver deposition due to the formation of three-dimensional silver nanoparticles with a mean size of 1–3 nm. A statistical treatment of several (> 10) STM pictures afforded a size distribution histogram of silver particles depicted in Fig. 20b. This sample is characterised by a mean silver particle size of 1–1.2 nm. Samples with larger mean particle sizes were prepared using longer deposition times, although this necessarily resulted in broadening of the size distribution.

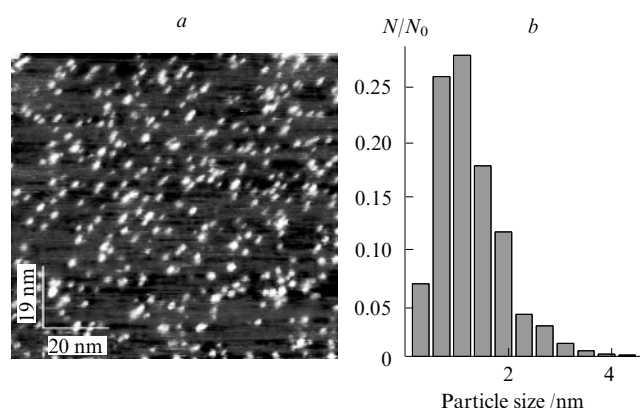


Figure 20. A typical STM image of the highly oriented pyrolytic graphite surface with deposited silver particles (a) and the respective size distribution histogram of the silver particles (b).

The O1s XPS spectra recorded just after the O_2 adsorption on Ag particles (within 10 min) at $P_{O_2} = 0.1$ mbar and $T = 420$ K are shown in Fig. 21. Only nucleophilic O_{ads} species are formed under these conditions on the bulk silver

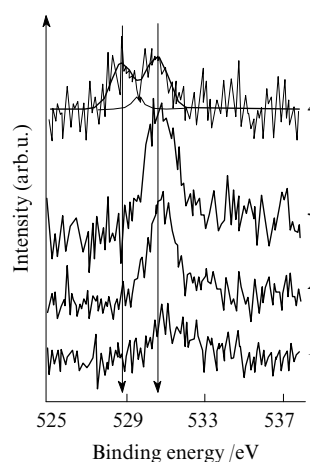


Figure 21. O1s XPS Spectra after exposure of graphite-supported silver particles to O_2 for 10 min at $T = 420$ K and $P_{O_2} = 0.1$ mbar as a function of coverage (estimated as the I_{Ag3d}/I_{C1s} line intensity ratio). Coverage (particle size): (1) 0.13 (1–2 nm), (2) 1.5 (5–7 nm), (3) 2.4 (~10 nm), (4) 13.1 (>20 nm). The mean size of Ag particles (in parentheses) was estimated from STM.

surface, whereas the electrophilic species are found on the nanoparticles, which is evidenced by the appearance of the O1s component with $E_b \approx 530.5$ eV in the XPS spectra. The electrophilic form of adsorbed oxygen remains prevailing for silver nanoparticles with sizes of up to 30 ± 10 nm. Only for larger Ag particles, the line characteristic of the nucleophilic oxygen species emerges in the spectra.

This result indicates that the same two species of adsorbed oxygen (*viz.*, the nucleophilic and electrophilic ones) can be detected on the surface of supported silver nanoparticles as on bulk samples. They are formed directly upon adsorption of pure O_2 rather than of a mixture of oxygen and ethylene, which was necessary for the formation of the O_{elec} species in the case of bulk silver. This enables the collection of reliable TPD data for the electrophilic oxygen to estimate the strength of the Ag– O_{elec} bonds. This was impossible for bulk silver due to a parasitic desorption contribution from oxygen dissolved in silver and O_{elec} elimination through the interaction with near-surface carbon (both dissolved oxygen and near-surface carbon are generated upon the activation of the bulk silver surface by the reaction medium).

The procedure used for the preparation of Ag/C samples was slightly modified for the determination of the strength of the Ag–O bonds by means of TPD. A thin film of graphite (with a thickness of a few hundred nm) was deposited on a Ta foil by pyrolysis of ethylene at $T = 1100$ K and $P = 50$ mbar.¹³⁷ The Ta foil was used as a resistive heater, which provided a sample heating rate of $2–3$ K s^{-1} sufficient for the TPD data acquisition. The time of ethylene pyrolysis was monitored by repeating survey XPS scans: the pyrolysis was stopped when the tantalum line was completely suppressed. The graphite-like nature of the carbon deposit was confirmed by XPS: the position of the C1s line and the appearance of a characteristic shake-up satellite were fully consistent with the respective features in the spectrum of bulk graphite.¹⁴⁶ The graphite layer was prepared in the same UHV chamber where subsequent vacuum deposition of silver and oxygen adsorption were carried out.

Figure 22 shows the curves of temperature-programmed desorption of electrophilic oxygen measured using mass spectrometry by the appearance of O_2 in the gas phase (heavy line) and as changes in the intensity of the O1s component with $E_b = 530.5$ eV (fine line) after its differentiation and inversion (the procedure used for the conversion of XPS data into TPD spectra is described in detail elsewhere¹⁴⁷). The full agreement

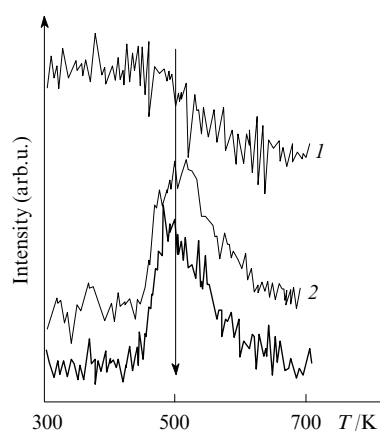


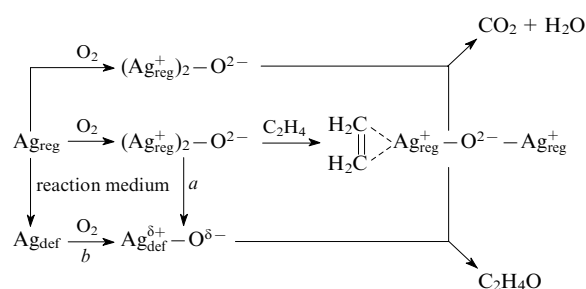
Figure 22. TPD Spectra of electrophilic oxygen adsorbed on Ag particles measured by mass spectrometry (heavy line) and as changes in the XPS O1s line intensity for a relative coverage $I_{Ag3d}/I_{C1s} = 2.4$ [thin lines; (1) after differentiation, (2) after inversion].

of the TPD spectra obtained by mass spectrometry with that calculated from the XPS data confirms that the signal in both cases is due to the desorption of the electrophilic oxygen. According to these results, the electrophilic form of atomically adsorbed oxygen is characterised by a lower desorption temperature as compared to the nucleophilic form (500 K vs. 580 K), which means that this form responsible for the ethylene epoxidation is bound to the silver surface less strongly than the nucleophilic form, which is active in the total ethylene oxidation to CO_2 and H_2O . This conclusion is of great importance, since it confirms the compliance with the thermodynamical requirement of the possible participation of electrophilic oxygen in the formation of ethylene oxide: the upper limit of the bond strength for an oxygen species driving the epoxidation was estimated to $25–27$ kcal mol^{-1} (Refs 148 and 149).

The changes in relative amounts of the electrophilic and nucleophilic forms of O_{ads} on Ag/C catalysts dependent on the silver particle size is yet another feature of these catalysts. The character of this dependence (*i.e.*, the disappearance of O_{nuc} with a decrease in the Ag particle size below 200–300 Å) explains within a common mechanism the decrease in the rate of the ethylene epoxidation on Ag/ α - Al_2O_3 catalysts by more than an order of magnitude with a decrease in the mean size of silver particles down to 50 nm.¹³⁶ Indeed, the disappearance of the nucleophilic form of adsorbed oxygen on silver particles with a size < 50 nm results in a decrease in the concentration of adsorbed ethylene, which in turn results in deceleration of the key step of the epoxidation reaction, according to the active surface law. This result is another illustration that both the electrophilic and nucleophilic forms of oxygen adsorbed on silver are involved into the ethylene epoxidation.^{136–138}

Based on the results of fundamental investigations into the nature and reactivity of adsorbed oxygen species on supported silver particles, a mechanism of the ethylene epoxidation reaction was proposed (Scheme 1), which takes into account the silver surface morphology ensuring the formation of two forms of adsorbed oxygen.

Scheme 1



(a) Ag surface restructuring; (b) oxygen diffusion; Ag_{reg} and Ag_{def} are regular and defect domains of the supported silver particle surface.

The oxygen adsorption on a regular surface yields the nucleophilic adsorbed oxygen species, which promotes ethylene adsorption but is active only with respect to the total ethylene oxidation. Only transformation of regular surface domains into defect ones due to the silver activation under the action of the reactants enables the formation of the electrophilic form of O_{ads} , which upon interaction with adsorbed ethylene, affords the target partial oxidation product, ethylene oxide. Alternatively, the formation of the electrophilic form is also possible upon the direct adsorption of O_2 on defect sites of the silver surface. In particular, the surface of supported silver nanoparticles with a size of < 50 nm consists of electron density-deficient low-coordinated Ag atoms.¹³⁸

The understanding of the molecular mechanisms of catalytic reactions makes it possible to predict catalytic properties of specific catalysts and suggest possible ways of the improve-

ment of the existing catalytic systems. In particular, the yield of the target product, ethylene oxide, is one of the key characteristics of the epoxidation reaction on the industrial scale. In order to optimise the catalytic system as regards this parameter, the factors affecting the selectivity of the overall process have to be analysed. The selectivity of the reaction (S) with respect to ethylene oxide

$$S = \frac{R(\text{C}_2\text{H}_4\text{O})}{R(\text{C}_2\text{H}_4\text{O}) + R(\text{CO}_2)}$$

is determined by the rate ratio of two competing reaction pathways, *viz.*, epoxidation [$R(\text{C}_2\text{H}_4\text{O})$] and total oxidation [$R(\text{CO}_2)$].

In the case of bulk silver samples, the nucleophilic oxygen species are formed efficiently, while the rate of the electrophilic form formation due to the modification of surface by components of the reaction medium is rather low. This favours the total oxidation pathway of the reaction. As a result, the selectivity of the epoxidation reaction rarely exceeds 30%–40% with silver single crystals, despite its relatively high rate.^{8–10, 150}

When supported catalysts are used, the epoxidation reaction is decelerated by two orders of magnitude due to the low concentration of sites suitable for the ethylene chemisorption. But at the same time, the rate of the ethylene total oxidation by nucleophilic oxygen species also decreases and decreases more abruptly than that of the epoxidation. This is due to different stoichiometries of the two oxidation pathways: the total oxidation of a C_2H_4 molecule to CO_2 and H_2O requires six oxygen atoms, whereas only one oxygen atom is needed for the partial oxidation. This results in a substantially enhanced selectivity of the partial oxidation of C_2H_4 in the case of supported catalysts¹⁵¹ (S drops below 50% only in rare cases). If the mechanism of the ethylene oxidation reaction described above is valid, further decrease in the mean silver particle size (especially down to 50 nm and smaller) should further enhance the selectivity of the partial C_2H_4 oxidation (>86%, which is the maximum possible value realisable for molecular oxygen as the ethylene epoxidising agent; $S < 6/7$).^{9, 10}

Notwithstanding, several authors (for instance, see Ref. 152) reported on a decrease in the selectivity on going to very small silver particles, which cannot be rationalised without postulated secondary reactions of ethylene oxide after-oxidation on the alumina surface. Ethylene oxide is formed exclusively on the silver surface (see above). Meanwhile, the total oxidation products, CO_2 and H_2O , can be generated in at least two pathways, *viz.*, the interaction of C_2H_4 with the nucleophilic oxygen species adsorbed in silver and the after-oxidation of ethylene oxide. It is well known that it is the reaction proceeding on the alumina surface that makes the dominant contribution to the afteroxidation pathway. Its rate is independent of the mean size of supported silver particles. This implies that the side reaction of the ethylene oxide after-oxidation has to be suppressed in order to increase the selectivity of the partial ethylene oxidation. Taking into account that this reaction is catalysed by acidic OH-sites present on the alumina surface,¹⁵³ the use of surfaces devoid of such sites can serve as a possible solution of the problem. Indeed, Balzhinimaev *et al.*¹⁵⁴ achieved the selectivity of the ethylene epoxidation as high as 85%–88% by using a carbon substrate (sibunit) instead of alumina. Even higher selectivity (>90%) was achieved by the utilisation of utradispersed silver particles with a mean size close to the optimum (50–100 nm).¹⁵⁴ This results are the best confirmation of the validity of the proposed reaction mechanism and consequently of the efficiency of the fundamental approach to the design of

catalysts based on experimental studies of model systems with surface science techniques discussed in the present review.

IV. Investigations into the structure of active sites in porous catalysts

The elucidation of the formation and evolution of active sites during the preparation, activation and deactivation of porous catalysts with surface science techniques constitutes an important part of the proposed investigation scheme (see Introduction), since it enables the transition from model objects to real catalytic systems. However this task is very demanding from the experimental viewpoint. First of all, difficulties in the interpretation of the experimental results have to be taken into account, which are due to the complex stoichiometry and phase composition of real catalysts, low concentrations of the active component and high concentrations of promoters therein. In our opinion, a rational compromise between catalytic characteristics of a model catalyst and the relative simplicity of its structure is needed to make an advance in these investigations. Although preparation of such catalyst results in a decrease in its activity (however, this should not be dramatic), this is compensated for by more straightforward interpretation of the experimental results. In order to improve the reliability of structural information provided, one should supplement surface science techniques with traditional techniques of catalyst characterisation, such as TEM, X-ray diffraction, *etc.*

The history of ITSS application to the characterisation of porous catalysts is nearly as long as their utilisation for studies of chemical interactions on the surface of model samples; pioneering works in both directions date back to the 1970s. The number of studies in this field is so large that any their systematic analysis is near to impossible. Often the experimental results are reported as a mere characteristics of specific catalyst samples without recourse to respective results on appropriate model objects. Nevertheless, even these results are in some cases valuable for establishing the structure–activity relationships in heterogeneous catalysts within the fundamental approach discussed in the present review. First of all, this concerns systems where model catalysts do not possess sufficient catalytic activity under conditions accessible to instrumental characterisation (even in the *in situ* mode), *i.e.*, where a catalytic reaction proceeds at a measurable rate only on a catalyst with high specific surface area. Ruthenium catalysts of the ammonia synthesis are typical examples of such systems. Indeed, all attempts at the elucidation of the structure of possible ruthenium active sites with traditional model experiments failed due to the negligible activity of Ru single crystals with respect to N_2 adsorption (the respective N_2 sticking probabilities reported in the literature lie in the range of 10^{-12} – 10^{-9}).^{155–157} Meanwhile, catalytic, structural and spectral studies performed on porous Ru/MO_x , $\text{Ru}-\text{Cs}^+/\text{MO}_x$ ($\text{MO}_x = \text{MgO}$, Al_2O_3 or SiO_2) catalytic systems revealed important details of the promoter–metal and promoter–support interactions and helped to determine the active site structure.^{158–160}

1. The promotion mechanism of ruthenium catalysts in the ammonia synthesis

Ruthenium-containing supported systems are widely recognised as the most promising and practical catalysts of the gas-phase ammonia synthesis at moderate pressures and temperatures. It is known that the activity of such catalysts in the ammonia synthesis is dependent on the chemical nature of the support: higher activity is provided by supports with prominent basic properties. The highest activity was achieved with magnesia.¹⁶¹ The use of technologically more suitable supports, such as alumina or carbonaceous materials, instead of MgO results in a dramatic decrease in the activity of ruthenium

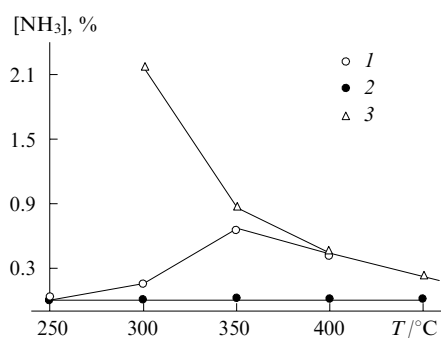


Figure 23. Steady ammonia concentration in the reaction mixture at the reactor outlet for the $\text{Ru}-\text{Cs}^+/\text{MgO}$ (curve 1) and $\text{Ru}-\text{Cs}^+/\text{Al}_2\text{O}_3$ (curve 2) catalysts as a function of temperature. Equilibrium of the ammonia curve yield (3) calculated for the reaction conditions used in the experiment.

catalysts.^{162, 163} The activity of supported ruthenium catalysts can be enhanced to a level sufficient for industrial applications by doping with alkali metals or their compounds. The activity of ruthenium catalysts increases with an increase in the basicity of the dopant along the series $\text{Na}^+ < \text{K}^+ < \text{Rb}^+ < \text{Cs}^+$.¹⁶⁴

The reasons and mechanisms underlying the influence of the support material and dopant type on the activity of supported ruthenium catalysts in the ammonia synthesis remains a subject of vivid scientific discussions, but no consensus has been reached so far. In order to make progress in this field, three types of interactions have to be considered: (1) between the catalytically active metal and promotor, (2) between the metal and support and (3) between the promotor and support.^{158–160} Within the context of this study, magnesia, alumina and silica were tested as support materials, $\text{Ru}(\text{OH})\text{Cl}_3$ and Cs_2CO_3 were chosen as precursors of the active component and promotor, respectively.

Studies of catalytic properties of promoted and non-promoted supported ruthenium systems differing in supports and precursors revealed $\text{Ru}-\text{Cs}^+/\text{MgO}$ samples to be the most active. Al_2O_3 -Supported ruthenium is significantly less active than MgO -supported. Temperature dependences of the catalytic activities of two catalysts, *viz.*, $\text{Ru}-\text{Cs}^+/\text{MgO}$ and $\text{Ru}-\text{Cs}^+/\text{Al}_2\text{O}_3$, expressed as steady-state ammonia concentrations in the reaction mixtures are presented in Fig. 23 together with the equilibrium curve of ammonia yield calculated for the reaction conditions. In the presence of the $\text{Ru}-\text{Cs}^+/\text{MgO}$ catalyst, the yield of ammonia nearly reaches

Table 1. Performance of the ruthenium catalysts in the ammonia synthesis measured at ambient pressure and a ratio of $\text{H}_2:\text{N}_2$ partial pressures of 3:1.

Temperature / °C	$\text{Ru}-\text{Cs}^+/\text{Al}_2\text{O}_3$ /ml(NH_3) g(cat) ⁻¹ h ⁻¹	$\text{Ru}-\text{Cs}^+/\text{MgO}$ /ml(NH_3) g(cat) ⁻¹ h ⁻¹
250	0 ^a	0.4
300	0	4.4
350	0	19.8
400	0	12.7

^a The lowest detection limit was less than 0.1 ml(NH_3) g(cat)⁻¹ h⁻¹ (the volume of NH_3 under normal conditions).

its equilibrium value at $T = 350^\circ\text{C}$, whereas the $\text{Ru}-\text{Cs}^+/\text{Al}_2\text{O}_3$ catalyst is inert under these conditions. The performances of these two catalysts in the ammonia synthesis expressed as the amount of ammonia (ml) per g of the catalyst in 1 hour are listed in Table 1. The tabulated data also clearly confirm that $\text{Ru}-\text{Cs}^+/\text{MgO}$ is characterised by a significantly higher activity than $\text{Ru}-\text{Cs}^+/\text{Al}_2\text{O}_3$. A combination of instrumental techniques was used to analyse the reasons for the so different catalytic properties of the samples.

The results of XPS and AES studies on the electronic states of different ruthenium catalysts are given in Table 2. The binding energy of the ruthenium core level $E_b(\text{Ru}3d_{5/2})$ changes from 280.2 eV typical of bulk ruthenium to 279.0 eV or 280.4 eV in the $\text{Ru}-\text{Cs}^+/\text{MgO}$ and $\text{Ru}/\text{Al}_2\text{O}_3$ catalysts, respectively. The shift of $\text{Ru}3d$ binding energies in MgO -supported catalysts (279.2–279.5 eV) with respect to bulk ruthenium suggests that the high activity of these samples is due to the charge transfer from the basic support (MgO) to the ruthenium nanoparticles.¹⁶³ The access of electron density on the ruthenium atoms facilitates the activation of a nitrogen molecule owing to the electron transfer from the 3d orbitals of Ru to the antibonding orbitals of N_2 (which is the first step of the dissociative N_2 adsorption). It is generally accepted that it is the nitrogen activation that is the rate-limiting step in the ammonia synthesis. In contrast to the Ru/MgO catalysts, the $\text{Ru}/\text{Al}_2\text{O}_3$ and Ru/SiO_2 samples are characterised by standard (normal) values of the binding energy close to that in bulk ruthenium (280.2–280.5 eV).^{160, 163, 165}

Although the negative shift in the position of the core-level line in XPS spectra can indeed indicate an excessive electron density on the supported metal due to its interaction with the support, there are several other reasons (including non-chemical ones), which could be responsible for the effect observed. These include a change in the relaxation energy (which is the

Table 2. Relevant XPS parameters of the ruthenium catalysts.

Sample	$E_b(\text{Ru}3d_{5/2})_{\text{exp}}/\text{eV}$	$E_{\text{kin}}(\text{Ru}MNN)/\text{eV}$	α/eV	$\Delta E_{\text{relax}}/\text{eV}$	$\Delta E_{\text{dif}}/\text{eV}$	$E_b(\text{Ru}3d_{5/2})_{\text{corr}}/\text{eV}$
Ru_{bulk}	280.2	274.5	554.7	0	0	280.2
Ru/MgO	279.5	275.3	554.8	0	+1.0	280.5
$\text{Ru}/\text{Al}_2\text{O}_3$	280.4	274.3	554.7	0	+0.1	280.5
$\text{Ru}-\text{s}^+/\text{MgO}$	279.0	274.6	553.6	−0.6	+1.3	279.7
$\text{Ru}-\text{Cs}^+/\text{Al}_2\text{O}_3$	280.2	274.5	554.7	0	+0.4	280.6

Notations adopted: $E_b(\text{Ru}3d_{5/2})_{\text{exp}}$ is the $\text{Ru}3d_{5/2}$ core-level binding energy observed experimentally; $E_{\text{kin}}(\text{Ru}MNN)$ is the kinetic energy corresponding to the $\text{Ru}MNN$ Auger peak (with the AlK_{α} excitation at 1488.6 eV); α is the modified Auger parameter calculated as $\alpha = E_b(\text{Ru}3d_{5/2}) + E_{\text{kin}}(\text{Ru}MNN)$; ΔE_{relax} is a change in the relaxation energy calculated as $\Delta E_{\text{relax}} = 0.5\Delta\alpha$, where $\Delta\alpha$ is a difference in α between a supported catalyst and bulk Ru; ΔE_{dif} is a differential charging value determined from a comparison of the valence-band spectra as a difference between the Fermi edge positions for a supported catalyst and bulk Ru; $E_b(\text{Ru}3d_{5/2})_{\text{corr}}$ is the $\text{Ru}3d_{5/2}$ core-level binding energy corrected for the final state effects, *i.e.*, $E_b(\text{Ru}3d_{5/2})_{\text{corr}} = E_b(\text{Ru}3d_{5/2})_{\text{exp}} + \Delta E_{\text{relax}} + \Delta E_{\text{dif}}$.

energy of the electron redistribution in the presence of a core hole generated upon photoemission, it is also referred to as the final-state effect) and a differential charging,[§] *i.e.*, a smaller positive electrostatic potential of the surface of metal particles with respect to that of the dielectric support, which gives rise to different shifts of the respective core-level lines (a sample surface during XPS measurements is always charged positively to a certain steady value dependent on the dielectric properties of the material due to the constant emission of photoelectrons).

Neither relaxation nor differential charging effects can be estimated using the internal standard method (the positions of XPS lines in the spectra of supported catalysts are usually referenced to a selected line of an element from the support material). The change in the relaxation energy (ΔE_{relax}) can be determined from the change in the modified Auger parameter α for the supported metal with respect to the bulk metal. The modified Auger parameter α is calculated as the sum of the binding energy of a metal core-level and the kinetic energy of the respective Auger peak:¹⁶⁶

$$\Delta E_{\text{relax}} = \frac{1}{2} \Delta \alpha = \frac{1}{2} \Delta [E_b(\text{Ru}3d_{5/2}) + E_{\text{kin}}(\text{RuMNN})].$$

The extent of the differential charging (ΔE_{dif}) can be determined from the Fermi edge shift in the valence-band spectrum of supported metal particles with respect to its position in the spectrum of the bulk metal.^{167, 168}

The values of parameters α , ΔE_{relax} and ΔE_{dif} determined for the Ru/MO_x and Ru–Cs⁺/MO_x supported systems from the XPS spectra are compiled in Table 2. The values of α for Ru/MO_x and Ru_{bulk} are identical to within 0.1 eV (554.7–554.8 eV), which implies that $\Delta E_{\text{relax}} \approx 0$ for non-promoted systems. Non-zero differential charging of Ru particles was observed only in the case of Ru/MgO ($\Delta E_{\text{dif}} = +1.0$ eV), whereas it equals to zero for Ru/Al₂O₃ and Ru/SiO₂. Thus the original experimental values of $E_b(\text{Ru}3d_{5/2})$ for Ru/Al₂O₃ and Ru/SiO₂ are correct, whereas the respective value for Ru/MgO has to be corrected to the differential charging:

$$\begin{aligned} E_b(\text{Ru}3d_{5/2})_{\text{corr}} &= E_b(\text{Ru}3d_{5/2})_{\text{exp}} + \Delta E_{\text{dif}} = \\ &= 279.5 + 1.0 = 280.5 \text{ eV.} \end{aligned}$$

Therefore, taking into account the necessary corrections, the binding energy of the Ru atoms in the Ru/MgO system is essentially the same as in other Ru/MO_x systems studied exceeding the respective value of bulk ruthenium by $\Delta E = 0.3 \pm 0.1$ eV. The latter value means that the surface ruthenium atoms in the Ru/MO_x systems are slightly oxidised, which disproves the earlier assumption of the excess electron density on the MgO-supported Ru particles.

In the case of promoted samples (see Table 2), the experimental ruthenium binding energies $E_b(\text{Ru}3d_{5/2})$ are 279.0 eV and 280.2 eV for Ru–Cs⁺/MgO and Ru–Cs⁺/Al₂O₃, respectively. The modified Auger parameter α for Ru–Cs⁺/MgO differs from that of bulk ruthenium by -1.2 eV, *i.e.*, in this case, $\Delta E_{\text{relax}} = -0.6$ eV. Furthermore, a non-zero differential charging was identified for both promoted systems Ru–Cs⁺/MgO ($\Delta E_{\text{dif}} = +1.3$ eV) and Ru–Cs⁺/Al₂O₃ ($\Delta E_{\text{dif}} = +0.4$ eV). The true binding energies after all corrections, $E_b(\text{Ru}3d_{5/2})_{\text{corr}}$, are 279.7 eV and 280.6 eV for Ru–Cs⁺/MgO and Ru–Cs⁺/Al₂O₃, respectively. Thus, a negative shift in the ruthenium binding energy with respect to bulk metal is observed for the promoted MgO-supported catalyst.

§ This possible reason for negative shifts of XPS lines is most frequently ignored, which is not actually justified.

The reasons for the negative shifts of the Ru3d_{5/2} binding energy in this sample were found in additional studies, primarily, using TEM. Histograms of the size distributions of Ru particles revealed that, in both supported Ru/MO_x systems and promoted samples, ruthenium particles are characterised by sizes in the range of 2–10 nm¹⁶⁰ or several nanometres, respectively, which rules out the possible assignment of the Ru3d line shift to a change in the mean Ru particle size. More details on the structure of the active component have been obtained using high-resolution TEM. The respective micrographs of promoted catalysts are shown in Fig. 24. In the case of Ru–Cs⁺/MgO (Fig. 24a), it is clearly seen that the Ru particles are coated with a thin layer of a substance, while the Ru particles in the Ru–Cs⁺/Al₂O₃ sample are devoid of such a coating (Fig. 24b).

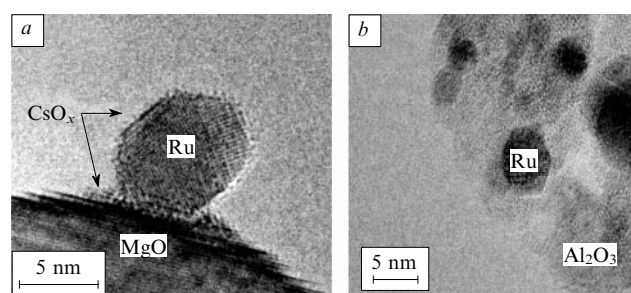


Figure 24. Electron micrographs of the surface of the Ru–Cs⁺/MgO (a) and Ru–Cs⁺/Al₂O₃ (b) catalysts.

The nature of the surface coating of the Ru particles was identified by the Energy-Dispersive X-ray fluorescence analysis (EDX) implemented in an attachment to a transmission electron microscope (it provides a spatial resolution of <100 nm).¹⁶⁰ The EDX spectra measured in the proximity of ruthenium particles for the Ru–Cs⁺/MgO and Ru–Cs⁺/Al₂O₃ catalysts are compared in Fig. 25. In the case of Ru–Cs⁺/MgO, the EDX spectrum reveals a weak peak attributed to Cs in addition to the dominant ruthenium signal, whereas no additional signal was detected for Ru–Cs⁺/Al₂O₃. This result was consistently reproduced for a larger number of ruthenium particles.¹⁶⁰

Data on CO chemisorption provide another experimental evidence for the formation of a Cs-compound on the surface of Ru particles in the catalyst Ru–Cs⁺/MgO. It was

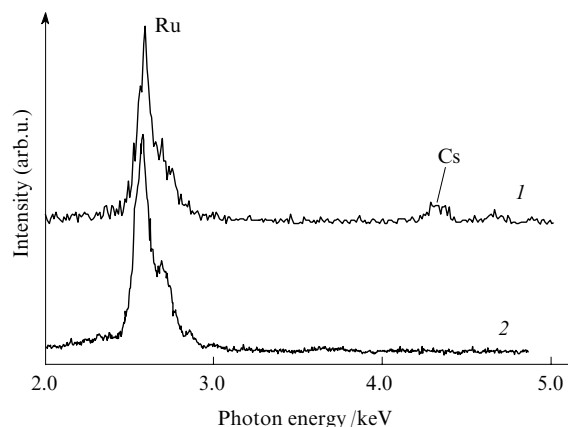


Figure 25. EDX Spectra from areas in the proximity of ruthenium particles for the Ru–Cs⁺/MgO (spectrum 1) and Ru–Cs⁺/Al₂O₃ (spectrum 2) catalysts (see Fig. 24).

found that the degrees of dispersion D defined as $D = (N_{\text{surf}}/N_{\text{tot}}) \times 100\%$, where N_{surf} is the number of surface Ru atoms and N_{tot} is the total number of Ru atoms, in the promoted and non-promoted Al_2O_3 -supported samples are nearly identical ($D = 25.0\%$ and 23.6% , respectively). Meanwhile, a totally different picture is observed for the analogous MgO -supported catalysts: the degree of dispersion D in the promoted sample decreases to 9.9% from 27.3% in the non-promoted sample despite no significant changes in the mean size of ruthenium particles is detected by TEM. This observation suggests that the surface of Ru particles accessible for CO adsorption in the latter sample is partly screened by the promotor. Presumably, this interaction between ruthenium and the promotor plays a key role in the formation of the active catalytic state, which is manifested in the negative shift of the $\text{Ru}3d_{5/2}$ line.^{158–160}

The speciation of the promotor chemical state was accomplished based on the $\text{Cs}3d_{5/2}$ XPS data. Figure 26 shows the respective core-level spectra for $\text{Ru}-\text{Cs}^+/\text{MgO}$ (a) and $\text{Ru}-\text{Cs}^+/\text{Al}_2\text{O}_3$ (b) measured both immediately after loading of the samples into the spectrometer and after their reduction with hydrogen directly in the spectrometer. The efficiency of XPS for the identification of the caesium chemical state is demonstrated by Table 3, which compiles the $E_b(\text{Cs}3d_{5/2})$ values for various caesium compounds with oxygen.^{169–171} The data given in Table 3 indicate that inverse chemical shifts in the binding energy are typical of caesium, as well as for some other metals (Ag, Cd, Ba, etc.), i.e., the binding energy decreases rather than increases upon oxidation. The reasons for this phenomenon lie beyond the scope of this review and will not be discussed here. It is important that the data from Table 3 help to assign the experimentally observed $\text{Cs}3d$ spectral features to specific states of the caesium atoms or caesium compounds.

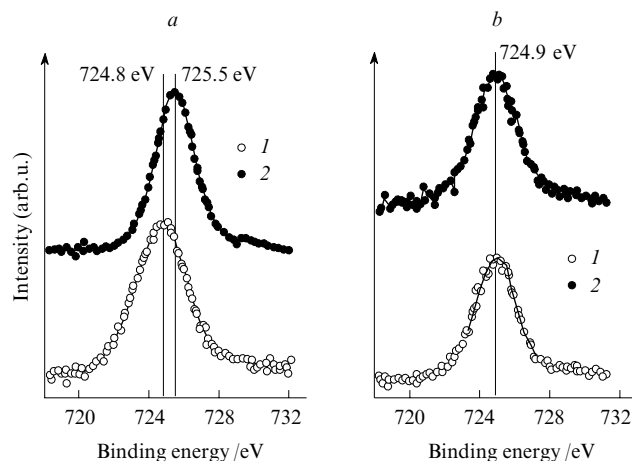


Figure 26. The $\text{Cs}3d_{5/2}$ XPS spectra of the $\text{Ru}-\text{Cs}^+/\text{MgO}$ (a) and $\text{Ru}-\text{Cs}^+/\text{Al}_2\text{O}_3$ (b) before (1) and after (2) hydrogen treatment directly in the spectrometer.

The XPS spectra of the $\text{Ru}-\text{Cs}^+/\text{MgO}$ and $\text{Ru}-\text{Cs}^+/\text{Al}_2\text{O}_3$ catalysts measured immediately after their loading into the spectrometer reveal nearly identical positions of the $\text{Cs}3d_{5/2}$ lines with binding energies of 724.8 eV and 724.9 eV , respectively (see Fig. 26). This caesium state can be attributed to Cs^+ (suggestedly, as caesium peroxide). Caesium in caesium oxide Cs_2O is characterised by a similar binding energy $E_b(\text{Cs}3d_{5/2}) = 725.0\text{ eV}$, but it is known that caesium oxide readily converts into peroxide upon exposure to oxygen

Table 3. $E_b(\text{Cs}3d_{5/2})$ and $E_b(\text{O}1s)$ values for various caesium compounds.^{166–170}

Binding energy / eV	Cs compound					
	Cs_{met}	Cs_{2+x}O	Cs_2O	Cs_2O_2	Cs_2O_4	CsOH
$E_b(\text{Cs}3d_{5/2})$	726.1	725.5	725.0	724.5	724.2	724.1
$E_b(\text{O}1s)$	—	531	528.2	530.6	532.9	—

(exposure doses of $(5-10) \times 10^{-6}\text{ Torr s}$),¹⁷⁰ which quite decisively rules out its presence in the catalysts under study.

The reduction of the $\text{Ru}-\text{Cs}^+/\text{MgO}$ sample with hydrogen directly in the spectrometer leads to a shift of the $\text{Cs}3d_{5/2}$ line to larger binding energy, which is indicative of caesium reduction, whereas the spectrum of $\text{Ru}-\text{Cs}^+/\text{Al}_2\text{O}_3$ remains unchanged upon similar treatment. Meanwhile, the $\text{Cs}3d_{5/2}$ binding energy in promoted ruthenium-free samples on different supports shows no shifts due to oxidative or reductive treatments. The shift of $\text{Cs}3d$ lines upon reduction of $\text{Ru}-\text{Cs}^+/\text{MgO}$ also supports the existence of direct caesium–ruthenium interactions.¹⁶⁰ Presumably, during the reduction, hydrogen molecules dissociate on the surface of ruthenium particles, which enables the subsequent reduction of caesium ions with atomic hydrogen.

The details of the interaction of caesium with ruthenium were established by XPS studies of model samples prepared by the deposition of caesium onto a polycrystalline ruthenium foil either in vacuum or in an oxygen flow. The $\text{Cs}3d_{5/2}$ and $\text{O}1s$ binding energies and the $\text{Cs}:\text{O}$ atomic ratios were determined. An analysis of these spectral data and, especially of the $E_b(\text{O}1s)$ values, which are highly specific for different caesium compounds with oxygen^{170,171} revealed that the vacuum deposition yields caesium suboxide Cs_{2+x}O , whereas that in an oxygen flow affords caesium peroxide Cs_2O_2 . Some deviations of the experimental $\text{Cs}:\text{O}$ atomic ratios from the stoichiometric values were attributed¹⁶⁰ to a partial oxidation of the suboxide due to an insufficiently high vacuum or concomitant formation of caesium superoxide Cs_2O_4 (in the cases of the $\text{Cs}_{2+x}\text{O}/\text{Ru}$ and $\text{Cs}_2\text{O}_2/\text{Ru}$ layers, respectively). The presence of superoxide in the sample is evidenced by the emergence of an additional component with $E_b = 533.5\text{ eV}$ in the $\text{O}1s$ XPS spectrum.^{172,173}

Taking these results of model studies into account, it might be concluded that the $\text{Cs}3d_{5/2}$ binding energy in the range of $725.4-725.8\text{ eV}$ can be attributed to caesium suboxide (although its partial contamination with oxide cannot be ruled out), whereas the values in the range of $724.7-725.2\text{ eV}$ are due to caesium peroxide.

However, it has to be noted that, for the suboxide, this assignment means only the formation of surface species rather than an individual phase. Otherwise it would have been possible to observe these compounds by X-ray diffraction. At the same time, only metallic ruthenium and the respective support (MgO or Al_2O_3) were identified in the diffraction patterns of both non-promoted and promoted samples.^{158–160} In earlier works devoted to Cs -promoted silver catalysts of the ethylene epoxidation, Podgornov *et al.*¹⁷³ suggested that silver atoms are capable of substituting for the Cs atoms in the $\text{Cs}-\text{Cs}$ fragment present in the bulk structure of caesium suboxide to form the $\text{Cs}-\text{Ag}$ bond.

Following this analogy, it might be suggested that bonds between the caesium and ruthenium atoms are formed in the catalyst $\text{Ru}-\text{Cs}^+/\text{MgO}$. This suggestion is further supported by the fact that the $E_b(\text{Cs}3d_{5/2})$ binding energy in promoted ruthenium blacks (i.e., in support-free materials) increases from 725.0 eV to 725.5 eV upon their reduction in the spectrometer. Similar results were observed for thin films of caesium on the surface of bulk ruthenium. At the same time,

in the alumina-based systems, the $\text{Cs}3d_{5/2}$ binding energy remains constant irrespective of the oxidative or reductive treatment applied.

The experimental evidence presented above indicate that it is the ruthenium–promotor rather than ruthenium–support interactions that are responsible for the observed shift of the $\text{Ru}3d_{5/2}$ line to a smaller E_b .^{158,160} The formation of a thin alkali metal film on the surface of a transition metal is known to decrease the work function (*e.g.*, S1 caesium–silver photocathodes are formed in a similar way).¹⁷¹ Thus, the downshift of the binding energy can also be due to a decrease in the work function of the electron escape from the surface of Ru particles covered with a promotor layer.

If this suggestion is valid, a next question arises, why ruthenium effectively interacts with caesium only with magnesia as a support, whereas no such interaction occurs on alumina. An answer to this question was given by an X-ray diffraction study of the $\text{Ru}-\text{Cs}^+/\text{Al}_2\text{O}_3$ and $\text{Ru}/\text{Al}_2\text{O}_3$ samples. The diffraction pattern of the promoted catalyst reveals some increase in the scattering background in the angle range of $20-40^\circ$,¹⁶⁰ which is typical of caesium aluminate. Most likely, caesium cations in this sample are incorporated into the aluminate structure due to a chemical reaction of the promotor with Al_2O_3 . The $E_b(\text{Cs}3d_{5/2})$ value of 724.9 eV found for $\text{Ru}-\text{Cs}^+/\text{Al}_2\text{O}_3$ also does not contradict to its assignment to caesium aluminate.

The following important conclusion can be derived from the above extensive studies^{158–160} of supported ruthenium catalysts of the ammonia synthesis. An analysis of the mechanisms of the formation of active sites schematically depicted in Fig. 27 has to take into account the promotor–ruthenium and promotor–support interactions in addition to more common support–ruthenium interactions. Indeed, magnesia, due to its prominent basicity, is expected to be quite inert as regards its reaction with caesium oxides, which are themselves strong bases. This largely facilitates the migration of caesium over the magnesia surface to react with ruthenium particles thus generating active sites for the $\text{N}_2 + \text{H}_2$ reaction (Fig. 27*a*). The dissociative adsorption of N_2 should be accelerated on such sites due to a decrease in the electron escape work function.

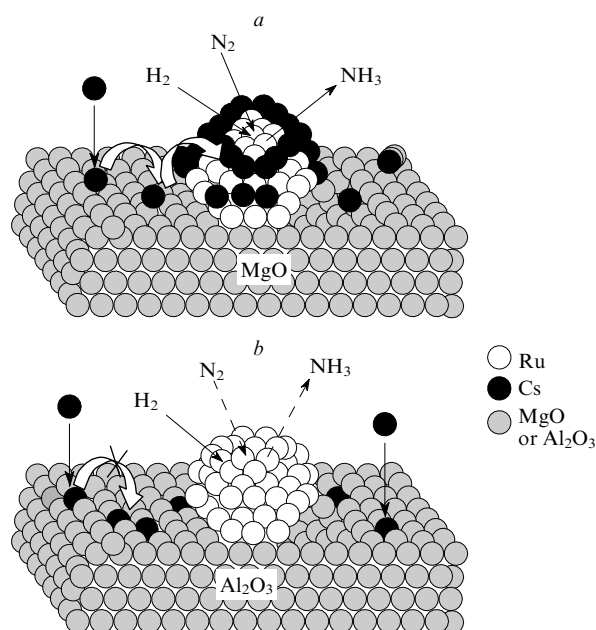


Figure 27. A scheme of interaction of the promotor with the support and active component in the catalysts $\text{Ru}-\text{Cs}^+/\text{MgO}$ and $\text{Ru}-\text{Cs}^+/\text{Al}_2\text{O}_3$.

On the contrary, acidic sites present on the alumina surface strongly bind the promotor thus preventing them from the reaction with ruthenium particles (Fig. 27*b*). Consequently, non-promoted ruthenium particles manifest a lower activity in the dissociative nitrogen adsorption, which determines to the overall low activity of such catalysts in the ammonia synthesis. It is of note that alumina-based catalytic systems can manifest high activity in the ammonia synthesis, but only at high promotor content (promotor: metal ≥ 3.0).¹⁷⁴ Very likely, at high concentrations, a fraction of the promotor remains unbound to the support and thus capable of ruthenium activation.

Despite the prominent success of the post-reaction analysis of the mechanism of formation of active component in porous catalysts with surface-sensitive techniques, future progress in this field relates to the extensive usage of *in situ* measurements. For instance, the structure of active sites of barium-promoted ruthenium catalysts supported on BN has been determined by *in situ* TEM studies.¹⁷⁶ In the as-prepared catalysts, ruthenium particles were incorporated into boron nitride. TEM micrographs measured under the reaction conditions of the ammonia synthesis reveal restructured catalyst surfaces and support-free ruthenium particles covered with the barium promotor in the form of either amorphous particles or a monolayer coating. It was concluded that barium is an electron promotor for ruthenium.¹⁷⁶

Additional examples of highly efficient *in situ* XPS investigations into the state of active components in porous catalysts can be found in recent publications by Schlögl *et al.*^{177–179}

2. Hydrogen sulfide oxidation of iron-based catalysts

The use of model objects instead of real catalysts for monitoring the formation of active sites becomes inefficient for catalytic reactions involving aggressive reaction media. The inadmissibility of aggressive gases into UHV chambers due to safety reasons prevents *in situ* measurements thus eliminating one of the most important merits of model experiments, *viz.*, the absence of exposure to air of samples after their activation. This limits the research capabilities to the traditional post-reaction analysis with a necessary comparison of as-prepared, activated and sometimes deactivated catalysts. It is always desirable to avoid exposure to air of the samples upon their transfer from a catalytic reactor to the analytical UHV chamber. This requirement was fulfilled in a study of the formation of active sites of supported iron catalysts for the H_2S oxidation, such as $\text{Fe}_2\text{O}_3/\text{SiO}_2$ and $\text{Fe}_2\text{O}_3/\text{Al}_2\text{O}_3$.^{180,181}

According to the XPS data, the reaction of the iron-containing catalysts with gas mixtures containing a large fraction of water vapour in addition to hydrogen sulfide and oxygen, gives rise to the sulfidation of surface layers of iron oxide(III) particles.^{180,181} Such a change in the chemical state of the active component was identified by the appearance of a $\text{Fe}2p_{3/2}$ component with a binding energy of 708.8 eV, which is typical of FeS_2 .^{182,183} At the same time, an intense signal of sulfide ions emerges in the $\text{S}2p$ XPS spectra ($E_b \approx 163$ eV). The spectral line attributable to Fe_2O_3 with $E_b(\text{Fe}2p_{3/2}) = 711.2$ eV remains dominant in the spectra, which suggests the surface sulfidation of the active component.

A comparison of the XPS results with data on the catalytic activity revealed that oxide forms of the active site catalyse the selective oxidation of H_2S to sulfur, whereas the formation of FeS_2 alters the oxidation pathway. The total oxidation product, SO_2 , becomes dominant in this case. It is of note that both the selective and total hydrogen sulfide oxidation are of practical interest, although for different applications. The application of instrumental techniques, such as XPS, to the elucidation of the sulfidation process revealed important details regarding the effects of the support type, precursor

nature, annealing temperature and amount of water on the rate of formation and depth of FeS₂ formation.^{180, 181}

V. Development of methods of the purposeful synthesis of highly active catalysts

The purposeful design of catalysts based on the knowledge of the structure of active sites gathered in model studies is an extremely important task, since it allows the easiest verification of the performance of intuitively envisaged active site structures in practice. Indeed, the correctness of the structure–activity relationship adopted in the molecular design enables the development of convenient methods for the synthesis of highly active and selective catalysts with a prolonged service life. Without this knowledge, such methods affording advanced practical catalysts will remain elusive. Instrumental techniques of surface studies within this approach are necessary to control the results of the molecular design aimed at the preparation of active sites with a desirable composition and structure. The productivity of this approach is demonstrated below with some examples.

1. Bimetallic Ni–Au catalyst for the steam reforming of hydrocarbons

The purposeful improvement of Ni catalysts for the steam reforming of hydrocarbons is one of the most striking examples of the efficacy of the fundamental approach to the improvement of the catalyst performance.^{184–186} Nickel is widely used as a component of industrial catalysts of the steam reforming of natural gas (primarily, methane). As has been shown, the steam reforming starts with the methane activation on nickel. This is accompanied by the progressive deposition of graphite on the surface of Ni catalyst followed by the growth of filamentous carbon and ultimately by the catalyst deactivation.^{187, 188}

The deactivation of Ni catalysts due to the formation of graphite layers on early steps of the catalytic reaction was established unambiguously using TEM. The deactivation of Ni catalysts can be suppressed by introducing minor amounts of hydrogen sulfide into the reaction mixture. Sulfur adsorbed on the Ni particles poisons the catalyst, which, on the one hand, decelerates the overall steam conversion reaction but, on the other hand, inhibits the graphite formation, thus significantly prolonging the service life of the catalyst. Despite some promise of this approach, it has not found wide application since sulfur-containing compounds poison various catalytic reactions, in particular those combined with the steam reforming into technological scheme, such as ammonia synthesis.

Another possible approach to overcome the problem of the fast deactivation of Ni catalysts in the steam reforming relates to a modification of the active component by, for example, alloying nickel with another metal. The best results are expected for metals forming only surface rather than bulk alloys with nickel. As has been shown by Besenbacher *et al.*^{190–192} in an STM study of model objects, nickel indeed forms surface alloys in a series of binary systems, such as nickel–gold. The reason for the formation of this surface alloy is a decrease in the surface tension energy of nickel due to the electron density transfer from the gold atoms to the low-coordinated nickel atoms at the surface. These simple qualitative speculations were supported by quantum chemical calculations at the DFT level, which demonstrated that the bonding of carbon to the nickel atoms having adjacent Au atoms is much weaker than that to Ni atoms in the exclusively nickel environment.

As a result of these model studies,^{190–192} the porous Ni–Au catalysts were suggested. They were prepared by depositing 16.5 mass.% of a nickel–gold mixture (0.3% of gold) on the surface of magnesium aluminate.¹⁹³ The incorpo-

ration of gold atoms in the surface layers of nickel particles yielding a surface alloy was unambiguously confirmed by EXAFS. Further assay of these Ni(Au)/MgAl₂O₄ catalysts in the steam reforming of *n*-butane demonstrated a stably high activity of the bimetallic systems in contrast to the standard nickel catalysts.¹⁹³ Butane was used rather than methane due to its easier graphitisation.

Thus, the understanding of the structure–activity relationships indeed enabled the molecular design of advanced nickel-based catalysts for the steam reforming of hydrocarbons characterised by significantly improved stability against deactivation.

2. Nanosized Au/Al₂O₃ catalysts for the low-temperature CO oxidation

The synthesis of Au/Al₂O₃ catalysts for the low-temperature CO oxidation represents yet another example of the purposeful design of an advanced catalyst for specific catalytic processes.^{194–196} The molecular design of this system was based on the results of fundamental investigations into the reasons governing the catalytic activity of gold nanoparticles,^{120–123} which revealed a pronounced size effect in the activity of Au/TiO₂ catalysts. Taking into account some technological inconvenience of TiO₂ as a support for industrial applications, alumina was chosen as the support material. Therefore, it became necessary to develop efficient methods for the preparation of nanosized gold particles on the surface of alumina particles, including γ - (microspherical particles) and θ -Al₂O₃ (fine powder).^{194–196} Three major synthetic procedures were tested: the Deposition-Precipitation (DP), Chemical Liquid-Phase Grafting (CLPG) and Chemical Vapour Deposition (CVD) from volatile gold complexes.

Hexachloroauric acid was selected as a precursor of the active component in the DP synthesis, whereas dimethylgold acetylacetonate was used for CLPG and CVD due to its high volatility, thermal stability [the saturated vapour pressure of (CH₃)₂Au(acac) is 5.5×10^{-4} Torr at 25 °C, while the decomposition point in the solid state is 54 °C] and accessibility.¹⁹⁴

The mean sizes of gold particles in the catalysts were determined using X-ray diffraction and TEM. X-ray diffraction was also used to control the phase composition of the samples. Since the most intense diffraction peaks of bulk gold (*i.e.*, 111, 200 and 220) overlap with the reflexes of Al₂O₃, the sizes of Au crystallites were determined from the width of the Au(311) peak at $2\theta \approx 78^\circ$ using the Selyakov–Scherrer equation.

Preliminary TEM study of the Au/Al₂O₃ catalysts showed that standard procedures of TEM images measurement appeared unsatisfactory: the Au particles with a diameter smaller than ≤ 5 nm were nearly undistinguishable on the background of the support. Therefore, special techniques of the contrast enhancement were applied. In particular, the use of Fresnel scattering suppression on the Al atoms helped to decrease the brightness of the Al₂O₃ surface background with respect to that Au particles. Furthermore, the TEM micrographs used for the size distribution analysis of the Au particles were obtained in the so-called Z-contrast mode, *i.e.*, at a specific electron collection angle providing that only electrons scattered on the Au atoms contribute to the image. In this mode, the gold particles occur in the micrographs as bright spots on the uniform black background coming from the support and thus the particle size can be determined quite precisely. Typical micrographs of the catalysts prepared by the DP method and annealed at 673 K are shown in Figs. 28 and 29. From a series of TEM micrographs, histograms of the gold particle size distribution were obtained in both cases, which are also shown in Figs 28 and 29.

It is apparent that the Au/ θ -Al₂O₃ catalyst (sample 1, Fig. 28a) mainly contains gold particles with a size of

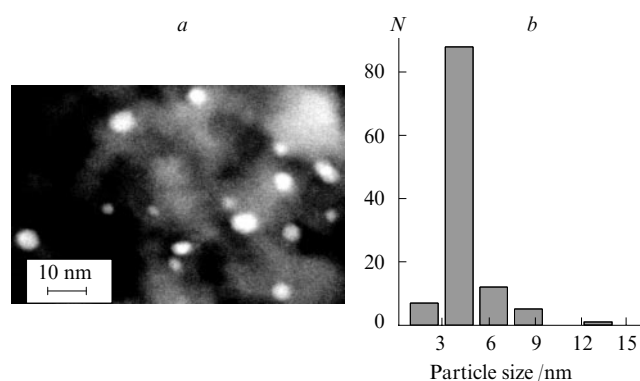


Figure 28. TEM Image of the Au/ θ - Al_2O_3 catalyst (sample 1) (a) and the respective Au particle size distribution (b) (hereinafter, N is the number of particles).

The catalyst was prepared by the deposition precipitation method from Au(III) hydroxo complexes. The image was acquired in the Z-contrast mode. The mean linear diameter of the Au particles is 3.8 nm.

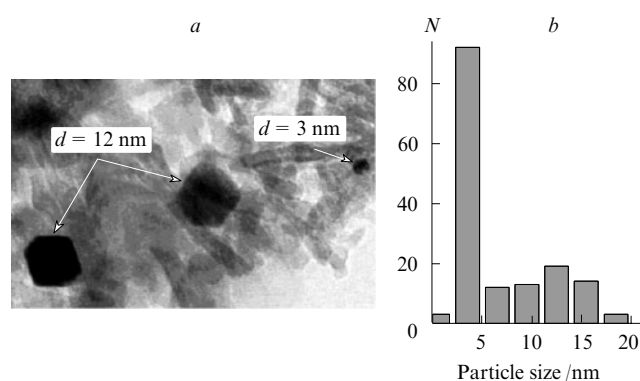


Figure 29. TEM Image of the Au/ γ - Al_2O_3 catalyst (sample 2) (a) and the respective Au particle size distribution (b).

The catalyst was prepared by the deposition precipitation method from Au(III) hydroxo complexes. The image was acquired in the normal contrast mode. The mean linear diameter of the Au particles is 6.6 nm.

2–4 nm and single particles with a size from 5 nm to 8 nm. The particles are characterised by a nearly spherical shape. The size distribution is relatively narrow and has a Gaussian shape; the mean linear diameter of the Au particles $\langle d_{\text{Au}} \rangle = 3.8$ nm (Fig. 28 b). In the case of the Au/ γ - Al_2O_3 catalyst (sample 2, Fig. 29 a), the TEM micrographs reveal microaggregates composed of primary globules of the support covered with mainly small gold particles with a size of 2–4 nm. At the same time, larger particles of up to 10–15 nm are also present in the sample. As a result, the size distribution of Au particles in this case is bimodal with two maxima at 4 nm and 12 nm (Fig. 29 b).

The mean sizes of Au particles in the Au/ Al_2O_3 catalysts determined from TEM and X-ray diffraction data are compared in Table 4. In the case of samples prepared by deposition-precipitation, the mean volume-surface diameter ($\langle d_{\text{vs}} \rangle$) of Au particles estimated from TEM was larger than that calculated from the broadening of the Au(311) diffraction line. The maximum discrepancy between the TEM and diffraction estimates is observed for sample 2. In this case, the contribution of relatively large metal particles into the diffraction broadening is small, although total numbers of small and large particles are comparable according to the TEM estimate.

Table 4. The mean diameters of supported gold particles in the Au/ Al_2O_3 catalysts estimated from X-ray diffraction (XRD) and TEM data.

Sample	Preparation method	Support	Au content (mass %)		Mean diameter of Au particles /nm		
					XRD	TEM ^a	
						$\langle d_l \rangle$	$\langle d_s \rangle$ $\langle d_{\text{vs}} \rangle$
1	DP	θ - Al_2O_3	1.4	≤ 3	3.8 ± 1.3	4.1	4.5
2	DP	γ - Al_2O_3	1.3	6.6	6.6 ± 4.7	8.1	12.5
3	CLPG	γ - Al_2O_3	3.8	12	13.3 ± 2.8	13.6	14.5
4	CVD	γ - Al_2O_3	1.2	> 5	20–25		5.6
5	CVD	γ - Al_2O_3	0.7	≤ 3	2.9 ± 0.9		3.5

$$^a \langle d_l \rangle = \frac{\sum_i f_i d_i}{\sum_i f_i}, \langle d_s \rangle = \sqrt{\frac{\sum_i f_i d_i^2}{\sum_i f_i}} \text{ and } \langle d_{\text{vs}} \rangle = \frac{\sum_i f_i d_i^3}{\sum_i f_i d_i^2},$$

where f_i is the number of particles with a diameter d_i encountered in TEM images.

Sample 3 prepared by the CLPG method from $(\text{CH}_3)_2\text{Au}(\text{acac})$ and annealed at 673 K in air contained predominantly Au particles with a size of 8–18 nm characterised by a normal distribution and single particles with a larger size of ~ 20 nm (Fig. 30 b). This sample was nearly devoid of metal particles with a size ≤ 5 nm. The mean diameters of Au particles estimated by TEM and X-ray diffraction were nearly identical (see Table 4).

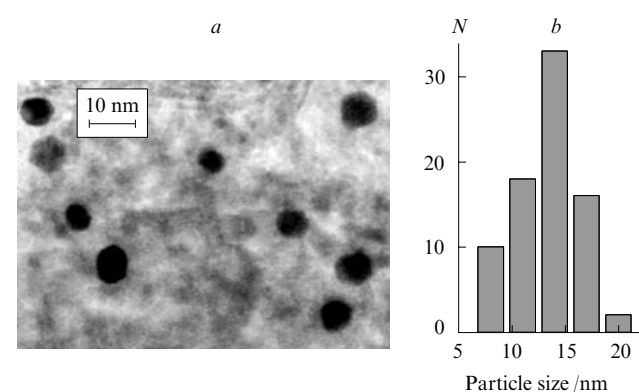


Figure 30. TEM Image of the Au/ γ - Al_2O_3 catalyst (sample 3) (a) and the respective Au particle size distribution (b).

The catalyst was prepared by the chemical liquid-phase grafting of $(\text{CH}_3)_2\text{Au}(\text{acac})$ on the γ - Al_2O_3 surface. The mean linear diameter of the Au particles is 13 nm.

The chemical vapour deposition was performed according to two procedures. Sample 4 was synthesised by passing $(\text{CH}_3)_2\text{Au}(\text{acac})$ vapour through an immobile layer of γ - Al_2O_3 kept at room temperature. The process was accompanied by a change in the vapour colour indicative of a partial decomposition of the complex by water molecularly adsorbed on the support surface. A chemical analysis of several probes of the sample 4 taken in different places of the reactor showed that the Au concentration progressively decreases along the direction of the gas flow. This gradient indicates that the interaction of $(\text{CH}_3)_2\text{Au}(\text{acac})$ with the surface of γ - Al_2O_3 is too strong. Thus, the CVD procedure was modified in order to prevent the uncontrollable decomposition of the organometallic precursor and provide the uniform distribution of the active component over the support. This modified procedure was

used for the preparation of sample 5. First, the support was carefully dehydrated by annealing *in vacuo* ($\sim 10^{-7}$ Torr) at 300–350 °C prior to its contact with vapourised $(\text{CH}_3)_2\text{Au}(\text{acac})$. Second, the deposition was accomplished in a constantly rotating reactor under the quasistationary conditions. The resultant sample was uniformly coloured and the Au concentrations in several probes taken from different places were nearly identical.

According to the TEM studies, sample 4 contained gold particles characterised by a very broad size distribution (from 5 nm to 35 nm), whereas TEM micrographs of sample 5 typically revealed microaggregates of primary $\gamma\text{-Al}_2\text{O}_3$ globules covered with mainly small Au particles of spherical or semispherical shapes with sizes from 2 nm to 4 nm (Fig. 31 *a*), although single larger particles with a diameter 5–10 nm were also present. The size distribution is rather narrow and has a Gaussian shape with a maximum at 2.5–3.0 nm (Fig. 31 *b*).

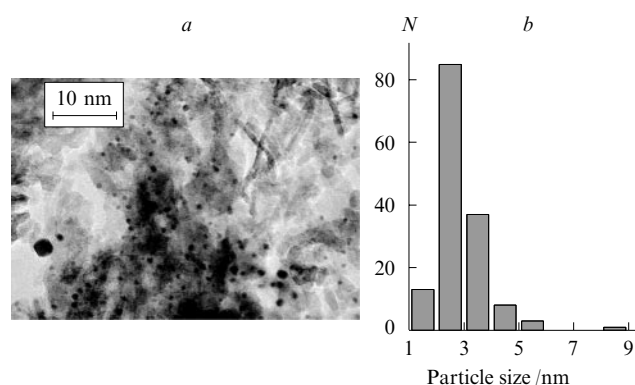


Figure 31. TEM Image of the Au/ $\gamma\text{-Al}_2\text{O}_3$ catalyst (sample 5) (*a*) and the respective Au particle size distribution (*b*).

The catalyst was prepared by the chemical vapour deposition of $(\text{CH}_3)_2\text{Au}(\text{acac})$ on the $\gamma\text{-Al}_2\text{O}_3$ surface. The mean linear diameter of the Au particles is 3.3 nm.

These Au/ Al_2O_3 catalysts prepared by different synthetic routes were assayed in terms of their catalytic activity towards the CO oxidation. The catalytic studies were performed in a plug-flow reactor at 313 K and ambient pressure. The testing conditions were chosen so as to approach the realistic oxidation conditions in a closed room with ordinary humidity and slightly elevated temperature. The composition of the initial reaction medium (IRM) corresponded to air purified from CO. The results obtained are listed in Table 5.

Under the conditions used, samples 1 and 2 demonstrated high catalytic activities in the CO oxidation. The most active Au/ $\theta\text{-Al}_2\text{O}_3$ catalyst (sample 1) taken in an amount as small as 40–50 mg provided the degree of CO conversion of $\sim 45\%$ at the maximum possible SRM supply rate (400 ml min^{-1}). It was impossible to realise the process for this sample under differential conditions, which resulted in somewhat underestimated reaction rates (see Table 5). The Au/ $\gamma\text{-Al}_2\text{O}_3$ catalyst (sample 2) demonstrated a lower activity probably due to a significantly larger mean size of gold particles in this sample ($\langle d_{\text{vs}} \rangle = 12.5 \text{ nm}$) as compared to sample 1.

Sample 3 did not demonstrate any measurable catalytic activity in the CO oxidation over the temperature range of 313–523 K; in the presence of this catalyst, CO_2 lines were detected in the Raman spectra only when temperature was increased to 773 K (the degree of CO conversion was then $\sim 2\%$). Since the mean size of Au particles ($\langle d_{\text{vs}} \rangle$) in sample 3 is virtually the same as in sample 2 (according to TEM), the observed dramatic difference in the catalytic activity could be attributed to different size distributions of Au particles in these

Table 5. Activities of the Au/ Al_2O_3 catalysts prepared by different methods in the CO oxidation measured in a plug-flow reactor at 313 K.

Sample	$\langle d_{\text{vs}} \rangle^a / \text{nm}$	CO conversion level (%) in		Reaction rate ^b
		1 h	7 h	
1	4.5	89	85	47
2	12.5	19	31	7.4
3	12.0 ^c	< 1	< 1	< 0.05
4	5.6	< 1	< 1	< 0.05
5	3.5	24	55	18.7

Notes. The initial reaction mixture compositions: 1 vol.% CO, 2.2 vol.% H_2O , 20 vol.% O_2 , the rest is N_2 ; the volume rate of the initial reaction mixture supply is 100 ml min^{-1} .

^a Mean volume surface diameter of the Au particles calculated from the TEM data (see Table 4). ^b The unit of measure is $\text{mol CO (mol Au)}^{-1} \text{ s}^{-1}$. ^c The mean particle diameter calculated from the XRD data.

two samples (see Figs 29 *b* and 30 *b*). Sample 2 is characterised by a broad distribution encompassing particles with sizes from 3 nm to 20 nm. Meanwhile, the distribution for sample 3 is much narrower and includes virtually no Au particles smaller than 5 nm. This strongly suggests that in the case of Au/ Al_2O_3 , the specific catalytic activity exhibits the same size effect as was observed earlier for the Au/ TiO_2 , Au/ Co_3O_4 and Au/ Fe_2O_3 systems: the catalytic activity abruptly increases (by several orders of magnitude) with a decrease in the size of Au crystallites down to $d \leq 5 \text{ nm}$.

Studies on the catalytic activity of samples 4 and 5 also demonstrates the size effect. Sample 4 containing only Au particles with a diameter $\geq 5 \text{ nm}$ demonstrated no measurable activity. In contrast, sample 5 composed of mainly small gold particles of $< 5 \text{ nm}$ showed a relatively high activity in the CO oxidation. The starting level of CO conversion in the presence of this catalyst at an Au content of 0.7 mass % was 15%. In three hours, the degree of conversion increased to 35% and remained constant at this level until the end of testing. The apparent activation energy (E_a) of the CO oxidation on the catalyst 5 calculated from the experimental temperature dependence of the reaction rate assuming the Arrhenius-type function is 9.5 kJ mol^{-1} , which is only slightly larger than the respective value of 7 kJ mol^{-1} found by Goodman for model catalysts.¹²⁷ (This again proves the close correspondence between model and real catalytic experiments.)

A change in the electronic state of gold atoms during the preparation of the Au/ $\theta\text{-Al}_2\text{O}_3$ catalysts (sample 1) was studied using Diffuse Reflectance UV-Vis Spectroscopy (DR-UV-Vis).¹⁹⁵ In addition, the plasmon resonance features in the electronic spectra of gold particles with the bulk structure and the electronic spectra of some model Au(III) complexes with the Au–O–Au bonds were simulated theoretically. A colloid suspension of gold containing spherical Au particles with a mean diameter of $\sim 50 \text{ nm}$ was used, as the reference sample, which was prepared by heating of an aqueous HAuCl_4 solution ($0.05 \text{ mg Au ml}^{-1}$) with a 1% solution of sodium citrate. The respective spectra are shown in Fig. 32.¹⁹⁵

The spectrum of an alkalinised HAuCl_4 solution (spectrum 1, Fig. 32) shows an absorption band centred at 48000 cm^{-1} . Such spectra with one weak ligand–metal charge transfer line in the UV range are characteristic of mononuclear complexes $[\text{AuCl}_{4-x}(\text{OH})_x]^-$ with $x = 2$ and 3. According to the literature data, upon treatment of Al_2O_3 with alkalinised HAuCl_4 solutions, the complexes $[\text{AuCl}_2(\text{OH})_2]^-$ and $[\text{AuCl}(\text{OH})_3]^-$ react with the surface OH groups of the support resulting in the immobilisation of the Au(III) ions due to the

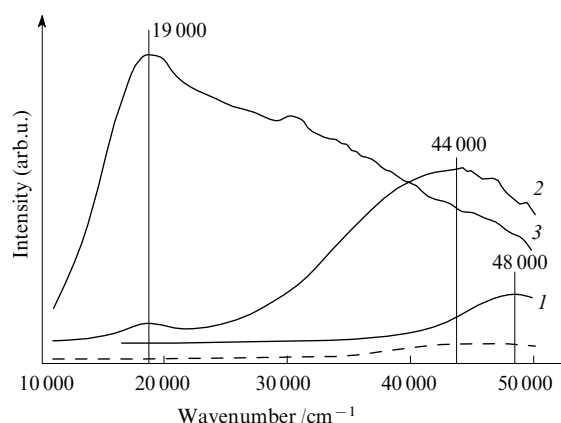


Figure 32. Transmission (1) and diffusion reflectance (2, 3) UV-Vis spectra for the Au/ θ -Al₂O₃ catalyst and reference samples; (1) alkalified aqueous solution of HAuCl₄ ([Au] = 0.013 mol litre⁻¹, [OH]/[Au] = 3.8 mol mol⁻¹); (2) θ -Al₂O₃ support after treatment with the HAuCl₄ solution (conditions 1) at 70 °C, thorough washing with water and drying; (3) sample (2) after calcination in air at 400 °C for 4 h (1.5% Au/ θ -Al₂O₃ catalyst). The DR-UV-Vis spectrum of the original θ -Al₂O₃ is shown with a dashed line.

formation of the Al–O–Au bonds. A subsequent thorough washing with warm water leads to the removal of the Au(III) ions weakly bound to the support and the hydrolysis of the Au–Cl bonds in the immobilised complexes. The residual Cl content in samples prepared in this way is < 0.01 mass %, according to X-ray fluorescence analysis.¹⁹⁵

The DR-UV-Vis spectrum of the θ -Al₂O₃ sample treated with an alkalified HAuCl₄ solution reveals a new broad absorption band over 35 000–50 000 cm⁻¹ centred at 44 000 cm⁻¹ (spectrum 2, Fig. 32), which is probably due to chemisorbed Au(III) complexes. The so large width of this band indicates heterogeneous composition of the surface compounds. A shift in the position of the absorption band maximum to lower wavenumber with respect to the spectrum of parent alkalified HAuCl₄ solution can be due to exchange interactions between the Au(III) ions immobilised on the Al₂O₃ surface. The exchange interaction implies that the sorbed Au(III) ions are associated, for instance into ‘islets’ with a high local concentration of grafted complexes with neighbouring metal ions located at a distance of 0.5–1 nm from each other.

In addition to the absorption band at 44 000 cm⁻¹, the DR-UV-Vis spectrum of θ -Al₂O₃ treated with an alkalified HAuCl₄ solution exhibits an additional weak band at 19 000 cm⁻¹ attributed to the plasmon absorption band from gold metal nanoparticles. The appearance of the resonance plasmon line for this sample means that metallic gold is partly formed already upon adsorption or during the washing and/or drying steps. The absorption band at 19 000 cm⁻¹ abruptly increases after annealing of the sample in air at 400 °C and a new band at 25 000–32 000 cm⁻¹ emerges. Since resonance plasmon features cannot be shifted so far to larger wavenumbers, the observation of the band at 25 000–32 000 cm⁻¹ indicates that the Au/ θ -Al₂O₃ sample contains ‘ionic’ species of gold in addition to metal particles.¹⁹⁵

The formation of metal oxide clusters and their co-existence with metallic gold was observed earlier in Au/MgO catalysts manifesting high activity in the low-temperature CO oxidation.^{197, 198} The application of X-ray absorption techniques EXAFS and XANES to probe the chemical state of gold nanoparticles revealed that both cationic and zero-valence (i.e., metallic) gold co-exist in the functioning catalysts and

relative amounts of these two forms depend on the composition of the reaction mixture. Simultaneous measurements of X-ray absorption spectra and the catalytic activity of Au/MgO catalysts in the CO oxidation for reaction media with different reactant ratios made it possible to correlate the reaction rate and relative fractions of the cationic and zero-valence gold. The results of these measurements are shown in Fig. 33. The maximum activity is achieved in the case of Au/MgO catalysts with nearly equal fractions of the ionic and metallic gold.

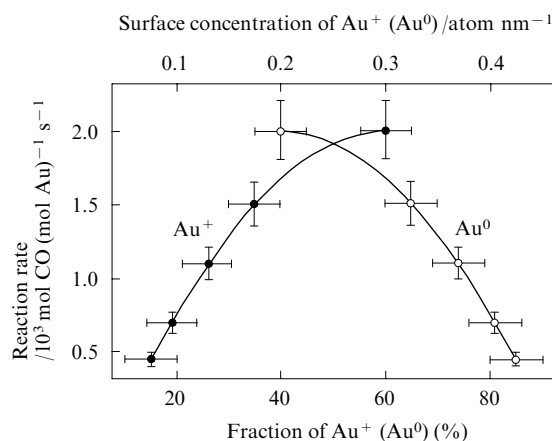


Figure 33. Catalytic activity of the Au/MgO catalyst in the CO oxidation as a function of surface concentrations of cationic and zero-valence gold in the sample.¹⁹⁷

These results suggest that the activity of the Au/Al₂O₃ catalysts in the low-temperature CO oxidation is due to the associative mechanism of the process similar to that used earlier to rationalise the catalytic action of some metal oxides in this reaction. The associative mechanism of the CO oxidation assumes that a decrease in the apparent activation energy of the catalytic reaction is achieved due to energy-coupled oxidation and reduction of surface oxide metal clusters accompanied by the formation of carbonate structures as key intermediates.

The above data demonstrate a practical potential of the Au/Al₂O₃ catalysts. Indeed, possible areas of application of catalysts providing the low-temperature CO oxidation are extremely broad. These catalysts are of importance for the air purification in closed spaces, solution of the ‘cold start’ problem in the exhaust gas neutralisation, purification of hydrogen from CO for the use in fuel cells based on proton-conducting membranes, etc.

VI. Conclusion

The examples discussed in the present review clearly demonstrate that instrumental techniques for surface studies remain essential for catalytic investigations, since they yield detailed information on the structure of surface sites driving specific catalytic reactions thus helping to establish the structure–activity relationships in heterogeneous catalysts. In parallel, modern trends in surface science require several novel approaches to be included into everyday practice of scientific investigations. In particular, these include:

- *in situ* methods of catalyst characterisation enabling studies exactly under conditions of catalytic reactions (a new term Operando spectroscopy appeared recently to designate this type of experiments);
- techniques for the analysis of nanosized and nanostructured materials (primarily, with a low concentration of an

active component) sensitive to the metal–support interactions (it is the efficient interaction of metal nanoparticles with the support that provides the optimum, from the catalytic perspective size of the active component and its stability against aggregation and deactivation upon sintering);

— methods for the synthesis of nanosized and nanostructured catalysts with a controlled narrow particle size distribution, including both model catalysts on single-crystalline substrates and real catalysts with high specific surface area.

The first approach offers one possible way to address the ‘pressure gap’ problem, whereas two latter approaches address the ‘material gap’ problem. The experimental information on the structure of active sites retrieved by instrumental methods for surface science will be reliable and relevant to specialists in catalysis for the design of highly active and selective catalysts only provided that both these problems are properly addressed. The costs for the development of so expensive direction as surface science are well warranted by the ultimate practical success in the invention of novel advanced catalysts. Essentially, this concerns research efforts that can result in the establishment of a totally new material and technical basis of chemical and petrochemical industry, where 80% of all processes are nowadays catalytic.

Due to the complexity and expensiveness of the surface science instrumentation, further progress in the field is only possible with a wide cooperation of scientists from diverse disciplines (physicists and chemists, theoreticians and experimentalists, surface scientists and catalysis experts), integration of research capabilities of different centres and laboratories, including international collaborations.

The author is grateful to the personnel of the Surface Science Laboratory at the G K Boreskov Institute of Catalysis, Siberian Branch of the Russian Academy of Sciences V V Kaichev, A V Kalinkin, R I Kvon, Yu V Larichev, B L Moroz, A V Pashis, I P Prosvirin, P A Pyryaev, A M Sorokin and M Yu Smirnov as well as to colleagues from other laboratories and foreign colleagues (see references) for the help in the discussion and implementation of experiments bridging surface science and catalysis. The author also thanks the Russian Foundation for Basic Research for the long-term financial support of the work (Project Nos 96-03-33 891, 01-03-32 853, 03-03-89 012-NWO, 06-03-33 020 and 07-03-00 931).

References

1. *Surf. Sci.* **299/300** 837 (1994)
2. T Engel, G Ertl *Adv. Catal.* **28** 1 (1979)
3. M W Roberts, C S McKee *Chemistry of the Metal–Gas Interface* (Oxford: Clarendon Press, 1978)
4. G A Somorjai *Surface Chemistry and Catalysis* (New York: Wiley, 1994)
5. A Böttcher, H Niehus, S Schwegmann, H Over, G Ertl *J. Phys. Chem. B* **101** 11185 (1997)
6. H Over, Y D Kim, A P Seitsonen, S Wendt, E Lundgren, M Schmid, P Varga, A Morgante, G Ertl *Science* **287** 1474 (2000)
7. H Over, A P Seitsonen, E Lundgren, M Wiklund, J N Andersen *Chem. Phys. Lett.* **342** 467 (2001)
8. C T Campbell, M T Paffett *Surf. Sci.* **139** 396 (1984)
9. C T Campbell, M T Paffett *Surf. Sci.* **143** 517 (1984)
10. C T Campbell *Surf. Sci.* **157** 43 (1985)
11. R W Joyner, M W Roberts, K Yates *Surf. Sci.* **87** 501 (1979)
12. R W Joyner, M W Roberts *Chem. Phys. Lett.* **60** 459 (1979)
13. A I Boronin, V I Bukhtiyarov, A L Vishnevskii, G K Boreskov, V I Savchenko *Surf. Sci.* **201** 195 (1988)
14. M Boudart *Adv. Catal.* **20** 153 (1969)
15. M Che, C O Bennett *Adv. Catal.* **36** 55 (1989)
16. H Poppa *Catal. Rev. Sci. Eng.* **35** 359 (1993)
17. M Bäumer, H-J Freund *Prog. Surf. Sci.* **61** 127 (1999)
18. C R Henry *Surf. Sci. Rep.* **31** 231 (1998)
19. A A Kolmakov, D W Goodman, in *Chapter in Quantum Phenomena in Clusters and Nanostructures* (Eds S V Khann, A W Castleman) (Berlin: Springer-Verlag Physics Series in Cluster Physics, 2003) p. 159
20. V I Bukhtiyarov, M G Slin'ko *Usp. Khim.* **70** 167 (2001) [*Russ. Chem. Rev.* **70** 147 (2001)]
21. V I Bukhtiyarov, in *Interfacial Science 'Chemistry for the 21st Century Monograph'* (Ed. M W Roberts) (Oxford: Blackwell, 1997) p. 109
22. J Szanyi, W K Kuhn, D W Goodman *J. Vac. Sci. Technol., A* **11** 1969 (1993)
23. E Ozensoy, D C Meier, D W Goodman *J. Phys. Chem. B* **106** 9367 (2002)
24. O Rodríguez de la Fuente, M Borasio, P Galletto, G Rupprechter, H-J Freund *Surf. Sci.* **566–568** 740 (2004)
25. P S Cremer, B J McIntyre, M Salmeron, Y-R Shen, G A Somorjai *Catal. Lett.* **34** 11 (1995)
26. G A Somorjai, G Rupprechter *J. Phys. Chem. B* **103** 1623 (1999)
27. G Rupprechter, T Dellwig, H Unterhalt, H-J Freund *J. Phys. Chem. B* **105** 3797 (2001)
28. G Rupprechter *Phys. Chem. Chem. Phys.* **3** 4621 (2001)
29. A Knop-Gericke, M Hävecker, Th Shedel-Niedrig, R Schlögl *Top. Catal.* **15** 27 (2001)
30. V I Bukhtiyarov, M Hävecker, V V Kaichev, A Knop-Gericke, R W Mayer, R Schlögl *Catal. Lett.* **74** 121 (2001)
31. H Bluhm, M Hävecker, E Kleimenov, A Knop-Gericke, A Liskowski, R Schlögl, D S Su *Top. Catal.* **23** 99 (2003)
32. H J Ruppender, M Grunze, C W Kong, M Wilmers *Surf. Interface Anal.* **15** 245 (1990)
33. D F Ogletree, H Bluhm, G Lebedev, C S Fadley, Z Hussain, M Salmeron *Rev. Sci. Instrum.* **73** 3872 (2002)
34. I P Prosvirin, E P Tikhomirov, A M Sorokin, V V Kaichev, V I Bukhtiyarov *Kinet. Catal.* **44** 724 (2003)^a
35. H Bluhm, M Hävecker, A Knop-Gericke, E Kleimenov, R Schlögl, D Teschner, V I Bukhtiyarov, D F Ogletree, M Salmeron *J. Phys. Chem. B* **108** 14340 (2004)
36. V I Bukhtiyarov, V V Kaichev, I P Prosvirin *Top. Catal.* **32** 3 (2005)
37. B J McIntyre, M Salmeron, G A Somorjai *Science* **265** 1415 (1994)
38. B L M Hendriksen, J W M Frenken *Phys. Rev. Lett.* **89** 46101 (2002)
39. M A Vannice *J. Catal.* **37** 449 (1975)
40. P Biloen, W M H Sachtler *Adv. Catal.* **30** 165 (1981)
41. A T Bell *Catal. Rev. Sci. Eng.* **23** 203 (1981)
42. G Henrici-Olive, S Olive *The Chemistry of the Catalysed Hydrogenation of Carbon Monoxide* (Berlin: Springer, 1984)
43. R B Anderson *The Fischer–Tropsch Synthesis* (London: Academic Press, 1984)
44. E V Slivinskii, Yu P Voitsekhovskii *Usp. Khim.* **58** 94 (1989) [*Russ. Chem. Rev.* **58** 57 (1989)]
45. S Surnev, M Sock, M G Ramsey, F P Netzer, M Wiklund, M Borg, J N Anderson *Surf. Sci.* **470** 171 (2000)
46. V V Kaichev, I P Prosvirin, V I Bukhtiyarov, H Unterhalt, G Rupprechter, H-J Freund *J. Phys. Chem. B* **107** 3522 (2003)
47. D L Doering, H Poppa, J T Dickinson *J. Catal.* **73** 104 (1982)
48. V Matolin, E Gillet *Surf. Sci.* **238** 75 (1990)
49. I Stará, V Matolin *Surf. Sci.* **313** 99 (1994)
50. H Dropsch, M Baerns *Appl. Catal., A* **158** 163 (1997)
51. K Christmann, J E Demuth *J. Chem. Phys.* **76** 6308 (1982)
52. J L Davis, M A Barteau *Surf. Sci.* **235** 235 (1990)
53. F Solymosi, A Berkó, Z Tóth *Surf. Sci.* **285** 197 (1993)
54. J-J Chen, Z-C Jaing, Y Zhou, B R Chakraborty, N Winograd *Surf. Sci.* **328** 248 (1995)
55. M Rebholz, V Matolin, R Prins, N Kruse *Surf. Sci.* **251** 1117 (1991)
56. N M Rodriguez, P E Anderson, A Wootsch, U Wild, R Schlögl, Z Paal *J. Catal.* **197** 365 (2001)
57. M Barber, J A Connor, M F Guest, M B Hall, I H Hillier, W N E Meredith *Faraday Discuss. Chem. Soc.* **54** 219 (1972)
58. H Lüth, G W Rubloff, W D Grobmann *Surf. Sci.* **63** 325 (1977)

59. J L Davis, M A Barteau *Surf. Sci.* **187** 387 (1987)
60. N Kruse, M Rebholz, V Matolin, G K Chuah, J H Block *Surf. Sci.* **238** L457 (1990)
61. M Rebholz, N Kruse *J. Chem. Phys.* **95** 7745 (1991)
62. A K Bhattacharya, M A Chesters, M E Pemble, N Sheppard *Surf. Sci.* **206** L845 (1988)
63. R J Levis, J Zhicheng, N Winograd *J. Am. Chem. Soc.* **111** 4605 (1989)
64. X Guo, L Hanley, J T Yates Jr *J. Am. Chem. Soc.* **111** 3155 (1989)
65. C J Zhang, P Hu *J. Chem. Phys.* **115** 7182 (2001)
66. S Schauermaun, J Hoffmann, V Johánek, J Hartmann, J Libuda, H-J Freund *Angew. Chem., Int. Ed.* **41** 2532 (2002)
67. M Morkel, V V Kaichev, G Rupprechter, H-J Freund, I P Prosvirin, V I Bukhtiyarov *J. Phys. Chem. B* **108** 12955 (2004)
68. V V Kaichev, V I Bukhtiyarov, G Rupprechter, H-J Freund *Kinet. Katal.* **46** 288 (2005)^a
69. J Szanyi, W K Kuhn, D W Goodman *J. Phys. Chem.* **98** 2978 (1994)
70. J A Gates, L L Kesmodel *J. Catal.* **83** 437 (1983)
71. S K Desai, M Neurock, K Kourtakos *J. Phys. Chem. B* **106** 2559 (2002)
72. R D Ramsier, K-W Lee, J T Yates Jr *Surf. Sci.* **322** 243 (1995)
73. P Schilbe, D Farias, K H Rieder *Chem. Phys. Lett.* **281** 366 (1997)
74. G Rupprechter, V V Kaichev, H Unterhalt, M Morkel, V I Bukhtiyarov *Appl. Surf. Sci.* **235** 26 (2004)
75. V V Kaichev, V I Bukhtiyarov, M Hävecker, A Knop-Gericke, R W Mayer, R Schlögl *Kinet. Katal.* **44** 471 (2003)
76. V I Bukhtiyarov, M Hävecker, V V Kaichev, A Knop-Gericke, R W Mayer, R Schlögl *Phys. Rev. B* **67** 235422 (2003)
77. V I Bukhtiyarov, A I Nizovskii, H Blum, M Hävecker, E Kleimenov, A Knop-Gericke, R Schlögl *J. Catal.* **238** 260 (2006)
78. R A van Santen, H P C E Kuipers *Adv. Catal.* **35** 265 (1987)
79. V I Bukhtiyarov, A I Boronin, I P Prosvirin, V I Savchenko *J. Catal.* **150** 262 (1994)
80. F J Williams, D P C Bird, A Palermo, A K Santra, R M Lambert *J. Am. Chem. Soc.* **126** 8509 (2004)
81. S Linic, M A Barteau *J. Am. Chem. Soc.* **124** 310 (2003)
82. C Stegelmann, N C Schiødt, C T Campbell, P Stoltze *J. Catal.* **221** 630 (2004)
83. W Lindinger, A Hansel, A Jordan *Chem. Soc. Rev.* **27** 347 (1998)
84. M A Barteau, R J Madix *The Chemical Physics of Solid Surfaces and Heterogeneous Catalysis* Vol. 4. (Eds D A King, D P Woodruff) (Amsterdam: Elsevier, 1982) Ch. 4
85. K Siegbahn, C Nordling, G Johansson, J Hedman, P F Hedén, K Hamrin, U Gelius, T Bergmark, L O Werme, R Manne, Y Baer *ESCA Applied to Free Molecules* (Amsterdam: North-Holland, 1969)
86. X Bao, M Muhler, Th Schedel-Niedrig, R Schlögl *Phys. Rev. B* **54** 2249 (1996)
87. Th Schedel-Niedrig, X Bao, M Muhler, R Schlögl *Ber. Bunsen-Ges. Phys. Chem. Chem. Phys.* **101** 994 (1997)
88. C T Campbell *J. Catal.* **94** 436 (1985)
89. V I Bukhtiyarov, I P Prosvirin, R I Kvon *Surf. Sci.* **320** L47 (1994)
90. W M H Sachtler, C Backx, R A van Santen *Catal. Rev. Sci. Eng.* **23** 127 (1981)
91. E A Carter, W A Goddard III *J. Catal.* **112** 80 (1988)
92. E A Carter, W A Goddard III *Surf. Sci.* **209** 243 (1989)
93. J Stöhr *Springer Series in Surface Sciences* Vol. 25 (Berlin, Heidelberg, New York: Springer, 1992)
94. F M F de Groot, M Grioni, J C Fuggle, J Ghijsen, G A Sawatzky, H Petersen *Phys. Rev. B* **40** 5715 (1989)
95. J Purans, A Kuzmin, Ph Parent, C Laffon *Physica B* **259–261** 1157 (1999)
96. P Behrens *Solid State Commun.* **81** 235 (1992)
97. P Behrens, S Aßmann, U Bilow, C Linke, M Jansen *Z. Anorg. Allg. Chem.* **625** 111 (1999)
98. A Deb, A K Chatterjee *J. Phys.: Condens. Matter* **10** 11719 (1998)
99. A Knop-Gericke, M Hävecker, Th Shedel-Niedrig, R Schlögl *Top. Catal.* **10** 187 (2000)
100. G Rovida, F Pratesi *Surf. Sci.* **52** 542 (1975)
101. H A Engelhardt, D Menzel *Surf. Sci.* **57** 591 (1976)
102. M Pascal, C L A Lamont, P Baumgärtel, R Terborg, J T Hoeft, O Schaff, M Polcik, A M Bradshaw, R L Toomes, D P Woodruff *Surf. Sci.* **464** 83 (2000)
103. V I Bukhtiyarov, V V Kaichev, I P Prosvirin *J. Chem. Phys.* **111** 2169 (1999)
104. C I Carlisle, T Fujimoto, W S Sim, D A King *Surf. Sci.* **470** 15 (2000)
105. I L Zilberberg, M A Milov, G M Zhidomirov *Zh. Strukt. Khim.* **40** 422 (1999)^b
106. M A Milov, I L Zilberberg, S Ph Ruzankin, G M Zhidomirov *J. Mol. Catal. A: Chem.* **158** 309 (2000)
107. A Knop-Gericke, F M F de Groot, J A van Bookhoven, T Ressler *In Situ Spectroscopy of Catalysis* (Ed. B M Weckhuysen) (New York: American Sci. Publ., 2006) Ch. 8
108. P L Hansen, S Helveg, A K Datye *Adv. Catal.* **50** 77 (2006)
109. J V Lauritsen, F Besenbacher *Adv. Catal.* **50** 97 (2006)
110. C Lamberti, E Groppo, G Spoto, S Bordiga, A Zecchina *Adv. Catal.* **51** 1 (2007)
111. G Rupprechter *Adv. Catal.* **51** 133 (2007)
112. F Rumpf, H Poppa, M Boudart *Langmuir* **4** 722 (1988)
113. T Engel, G Ertl *J. Chem. Phys.* **69** 1267 (1978)
114. E I Altman, R J Gorte *Surf. Sci.* **195** 392 (1988)
115. M Herskowitz, R Holliday, M B Cutlip, C N Kenney *J. Catal.* **74** 408 (1982)
116. E I Altman, R J Gorte *Surf. Sci.* **172** 71 (1986)
117. S H Oh, C C Eickel *J. Catal.* **128** 526 (1991)
118. M Haruta *Catal. Today* **36** 153 (1997)
119. G C Bond, D T Thomson *Catal. Rev. Sci. Eng.* **41** 319 (1999)
120. M Haruta, S Tsubota, T Kobayashi, H Kageyama, M J Genet, B Delmon *J. Catal.* **144** 175 (1993)
121. G R Bamwenda, S Tsubota, T Nakamura, M Haruta *Catal. Lett.* **44** 83 (1997)
122. M Valden, X Lai, D W Goodman *Science* **281** 1647 (1998)
123. M Valden, S Pak, X Lai, D W Goodman *Catal. Lett.* **56** 7 (1998)
124. C Xu, X Lai, G W Zajac, D W Goodman *Phys. Rev. B* **56** 13464 (1997)
125. D C Meier, V Bukhtiyarov, D W Goodman *J. Phys. Chem. B* **107** 12668 (2003)
126. D C Meier, D W Goodman *J. Am. Chem. Soc.* **126** 1892 (2004)
127. M S Chen, D W Goodman *Catal. Today* **111** 22 (2006)
128. F Cosandey, T E Madey *Surf. Rev. Lett.* **8** 73 (2001)
129. C T Campbell, S C Parker, D E Starr *Science* **298** 811 (2002)
130. H Hovel, B Grimm, M Bodecker, K Fieger, B Reihl *Surf. Sci.* **463** L603 (2000)
131. N Nilius, M Kulawik, H P Rust, H J Freund *Surf. Sci.* **572** 347 (2004)
132. A V Kalinkin, A V Pashis, V I Bukhtiyarov *React. Kinet. Catal. Lett.* **77** 255 (2002)
133. A V Kalinkin, A V Pashis, V I Bukhtiyarov *React. Kinet. Catal. Lett.* **78** 107 (2003)
134. A V Kalinkin, A V Pashis, V I Bukhtiyarov *React. Kinet. Catal. Lett.* **78** 121 (2003)
135. A V Kalinkin, A V Pashis, V I Bukhtiyarov *Kinet. Katal.* **48** 314 (2007)^a
136. V I Bukhtiyarov, I P Prosvirin, R I Kvon, S N Goncharova, B S Bal'zhinimaev *J. Chem. Soc., Faraday Trans. 2* **2323** (1997)
137. V I Bukhtiyarov, V V Kaichev *J. Mol. Catal. A: Chem.* **158** 167 (2000)
138. V I Bukhtiyarov *Kinet. Katal.* **44** 457 (2003)^a
139. M Yu Smirnov, A V Kalinkin, A V Pashis, A M Sorokin, A S Noskov, V I Bukhtiyarov, K S Kharas, M A Rodkin *Kinet. Katal.* **44** 629 (2003)^a
140. M Yu Smirnov, A V Kalinkin, A V Pashis, A M Sorokin, A S Noskov, K C Kharas, V I Bukhtiyarov *J. Phys. Chem. B* **109** 11712 (2005)
141. S H Oh, J E Carpenter *J. Catal.* **98** 178 (1986)
142. Y Cai, H G Stenger, C E Lyman *J. Catal.* **161** 123 (1996)
143. J Siera, F Rutten, B E Nieuwenhuys *Catal. Today* **10** 353 (1991)

144. F C M van Delft, J Siera, B E Nieuwenhuys *Surf. Sci.* **208** 365 (1989)
145. S B Schwartz, L D Schmidt, G B Fisher *J. Phys. Chem.* **90** 6194 (1986)
146. V I Bukhtiyarov, A F Carley, L A Dollard, M W Roberts *Surf. Sci.* **381** L605 (1997)
147. V I Bukhtiyarov, V V Kaichev, E A Podgornov, I P Prosvirin *Catal. Lett.* **57** 233 (1999)
148. R A van Santen, C P M de Groot *J. Catal.* **98** 530 (1986)
149. A V Khasin *Kinet. Katal.* **34** 42 (1993)^a
150. R B Grant, R M Lambert *J. Catal.* **92** 364 (1985)
151. D J Sajkowski, M Boudart *Catal. Rev. Sci. Eng.* **29** 325 (1987)
152. S N Goncharova, E A Paukshtis, B S Balzhinimaev *Appl. Catal., A* **126** 67 (1995)
153. D A Bulushev, E A Paukshtis, Yu N Nogin, B S Balzhinimaev *Appl. Catal., A* **123** 301 (1995)
154. B S Balzhinimaev, V I Zaikovskii, L G Pinaeva, A V Romanenko, G V Ivanov *Kinet. Katal.* **39** 775 (1998)^a
155. H Dietrich, P Geng, K Jakobi, G Ertl *J. Chem. Phys.* **104** 375 (1996)
156. K Jakobi, H Dietrich, G Ertl *Appl. Surf. Sci.* **121** 558 (1997)
157. K Jakobi *Phys. Status Solidi A* **177** 37 (2000)
158. Yu V Larichev, B L Moroz, I P Prosvirin, V A Likhobolov, V I Bukhtiyarov *Chem. Sust. Develop.* **11** 155 (2003)
159. Yu V Larichev, I P Prosvirin, D A Shlyapin, N B Shitova, P G Tsyrl'nikov, V I Bukhtiyarov *Kinet. Katal.* **46** 635 (2005)^a
160. Yu V Larichev, B L Moroz, E M Moroz, V I Zaikovskii, S M Yunusov, E S Kalyuzhnaya, V B Shur, V I Bukhtiyarov *Kinet. Katal.* **46** 940 (2005)^a
161. P Moggi, G Predieri, A Maione *Catal. Lett.* **79** 7 (2002)
162. F Rosowski, A Hornung, O Hinrichsen, D Herein, M Muhler, G Ertl *Appl. Catal., A* **151** 443 (1997)
163. K Aika, K Shimazaki, Y Hattori, A Ohya, S Ohshima, K Shirota, A Ozaki *J. Catal.* **92** 305 (1985)
164. T Hikita, K-i Aika, T Onishi *Catal. Lett.* **4** 157 (1990)
165. M G Cattania, F Parmigiani, V Ragani *Surf. Sci.* **211**–**212** 1097 (1989)
166. C D Wagner, in *Practical Surface Analysis* Vol. 1 (Eds D Briggs, M P Seach) (New York: Wiley, 1990) p. 602
167. T L Barr *Crit. Rev. Anal. Chem.* **22** 229 (1991)
168. V I Bukhtiyarov, I P Prosvirin, R I Kvon *J. Electron. Spectrosc. Relat. Phenom.* **77** 7 (1996)
169. C C Hwang, K S An, R J Park, J S Kim, J B Lee, C Y Park, S B Lee, A Kimura, A Kakizaki *J. Electron. Spectrosc. Relat. Phenom.* **88** 733 (1998)
170. G Ebbinghaus, A Simon *Chem. Phys.* **43** 117 (1997)
171. S J Yang, C W Bates *Appl. Phys. Lett.* **36** 675 (1980)
172. J Hrbek, Y W Yang, J A Rodriguez *Surf. Sci.* **296** 164 (1993)
173. E A Podgornov, I P Prosvirin, V I Bukhtiyarov *J. Mol. Catal. A: Chem.* **158** 337 (2000)
174. P Moggi, G Albanesi, G Predieri, G Spoto *Appl. Catal., A* **123** 145 (1995)
175. C J H Jacobsen, S Dahl, P L Hansen, E Törnqvist, L Jensen, H Topsøe, D V Prip, P B Møenhaug, I Chorkendorf *J. Mol. Catal. A: Chem.* **163** 19 (2000)
176. T W Hansen, J B Wagner, P L Hansen, S Dahl, H Topsøe, C J H Jacobsen *Science* **294** 1508 (2001)
177. D Teschner, A Pestryakov, E Kleimenov, M Hävecker, H Bluhm, H Sauer, A Knop-Gericke, R Schlögl *J. Catal.* **230** 186 (2005)
178. E Kleimenov, H Bluhm, M Hävecker, A Knop-Gericke, A Pestryakov, D Teschner, J A Lopez-Sanchez, J K Bartley, G J Hutchings, R Schlögl *Surf. Sci.* **575** 181 (2005)
179. O Pozdnyakova, D Teschner, A Wootsch, J Krohnert, B Steinhauer, H Sauer, L Toth, F C Jentoft, A Knop-Gericke, Z Paal, R Schlögl *J. Catal.* **237** 1 (2006)
180. G A Bukhtiyarova, N S Sakaeva, V A Varnek, E B Burgina, L M Plyasova, V I Bukhtiyarov, V V Kaichev, B P Zolotovskii *Khim. Interes. Ustoich. Razvitiya* **7** 359 (1999)^c
181. G A Bukhtiyarova, V I Bukhtiyarov, N S Sakaeva, V V Kaichev, B P Zolotovskii *J. Mol. Catal. A: Chem.* **158** 251 (2000)
182. P C J Graat, M A J Somers *Appl. Surf. Sci.* **100**–**101** 36 (1996)
183. M Descostes, F Mercier, N Thoromat, C Beaucaire, M Gautier-Soyer *Appl. Surf. Sci.* **165** 288 (2000)
184. J R Rostrup-Nielsen, J Sehested, J K Nørskov *Adv. Catal.* **47** 65 (2002)
185. J R Rostrup-Nielsen, in *Catalysis: Science and Technology* Vol. 5 (Eds J R Anderson, M Boudart) (Berlin: Springer, 1984) p. 1
186. J R Rostrup-Nielsen, T Rostrup-Nielsen *CATTECH* **6** 150 (2002)
187. S Helveg, C López-Cartes, J Sehested, P L Hansen, B S Clausen, J R Rostrup-Nielsen, F Abild-Pedersen, J K Nørskov *Nature (London)* **427** 426 (2004)
188. H S Bengaard, J K Nørskov, J Sehested, B S Clausen, L P Nielsen, A M Molenbroek, J R Rostrup-Nielsen *J. Catal.* **209** 365 (2002)
189. J R Rostrup-Nielsen *J. Catal.* **85** 31 (1984)
190. L P Nielsen, F Besenbacher, I Stensgaard, E Lægsgaard, C Engdahl, P Stoltze, K W Jacobsen, J K Nørskov *Phys. Rev. Lett.* **71** 754 (1993)
191. F Besenbacher, L P Nielsen, P T Springer *Chemical Physics of Solid Surfaces and Heterogeneous Catalysis* (Amsterdam: Elsevier, 1997) Ch. 10
192. F Besenbacher, I Chorkendorff, B S Clausen, B Hammer, A M Molenbroek, J K Nørskov, I Stensgaard *Science* **279** 1913 (1998)
193. J V Lauritsen, R T Vang, F Besenbacher *Catal. Today* **111** 34 (2006)
194. P P Semyannikov, B L Moroz, S V Trubin, G I Zharkova, P A Pyryaev, M Yu Smirnov, V I Bukhtiyarov *Zh. Strukt. Khim.* **47** 473 (2006)^b
195. V F Anufrienko, B L Moroz, T V Larina, S F Ruzankin, V I Bukhtiyarov, V N Parmon *Dokl. Akad. Nauk* **413** 493 (2007)^d
196. S B Erenburg, B L Moroz, N V Bausk, V I Bukhtiyarov, S Nikitenko *Nucl. Instrum. Methods Phys. Res., Sect. A* **575** 105 (2007)
197. J Guzman, B C Gates *J. Am. Chem. Soc.* **126** 2672 (2004)
198. J Guzman, B C Gates *J. Phys. Chem. B* **106** 7659 (2002)

^a — *Kinet. Catal. (Engl. Transl.)*

^b — *J. Struct. Chem. (Engl. Transl.)*

^c — *Chem. Sust. Develop. (Engl. Transl.)*

^d — *Dokl. Chem. (Engl. Transl.)*

Multinuclear magnetic resonance imaging as a multifunctional tool for the investigation of the properties of materials, transport processes and catalytic reactions

I V Koptug, A A Lysova, K V Kovtunov, V V Zhivonitko, A V Khomichev, R Z Sagdeev

Contents

I. Introduction	583
II. Multinuclear magnetic resonance imaging of solids	583
III. Multinuclear magnetic resonance imaging of transport processes	585
IV. Magnetic resonance imaging of chemical reactions	588
V. Conclusion	595

Abstract. New physicochemical applications of multinuclear magnetic resonance imaging that will determine the development of the method in the near future are considered. These include studies of solids, investigations of mass transfer processes in multiphase systems, studies on *in situ* reactors, heterogeneous hydrogenation with para-hydrogen and spectroscopy of long-lived singlet states. It is noted that in addition to an extension of the range of objects and processes of interest, the magnetic resonance imaging technique itself undergoes considerable changes. The bibliography includes 204 references.

I. Introduction

Magnetic resonance imaging (MRI) formerly referred to as nuclear magnetic resonance (NMR) tomography is known primarily as a method of medical diagnostics. This method is also widely used in biological studies. At the same time, MRI has found increasing and fruitful application in studies of non-living objects, including investigations in chemistry, chemical engineering, materials science, *etc.*^{1–4} Both the fundamentals of MRI and its physicochemical applications were considered in the reviews.^{5–7} In the last five years, this method has gained new applications due to its extensive development, resulting in a considerable expansion of the range of objects and processes studied by MRI. This range includes catalytic reactors and biofilm reactors, fuel cells, microreactors, polymers, drug delivery systems, gas hydrates, rock cores, building materials, film coatings, cultural heritage objects, plants, food products, *etc.* This, in turn, stimulates the further development of MRI technique itself. Efforts of researches in this field of science led

to fundamentally new applications, including those, which have been considered to be impossible or impracticable. In particular, these are MRI of gas transport, single-spin magnetic resonance, NMR spectroscopy and MRI in highly inhomogeneous or very low magnetic fields, MRI of solids and high-temperature processes, the diffusion coefficient and flow rate measurements at time intervals that are substantially longer than the spin relaxation times, and many other.

Unfortunately, these investigations have received little attention in Russia. The present review summarises recent achievements and trends in the development of MRI, including results obtained in recent years at the International Tomography Centre of the Siberian Branch of the Russian Academy of Sciences. In the present review, we do not try to cover the results of all investigations. This is practically impossible taking into account the progress achieved in this field in the last 5–10 years. Our aim is to attract the attention of researchers to this field of science by presenting the most remarkable applications, which apparently will determine the progress in MRI in the nearest future.

II. Multinuclear magnetic resonance imaging of solids

In biomedical applications, the MRI technique is mainly used for investigations of soft tissues and fluid transport (blood and lymph fluid) in living organisms. Until recently, scientific and technical applications of MRI have been limited mainly to investigations of objects containing considerable amounts of liquids. The progress in MRI of gases is hampered mainly by a low density of gases (*i.e.*, a low concentration of nuclear spins) and, as a consequence, low sensitivity and low spatial resolution. As a result, MRI of gases has found limited use although methods for the preparation of hyperpolarised gases with a considerable degree of nuclear spin polarisation have been extensively developed in recent years to overcome limitations associated with low sensitivity. At the same time, in spite of a relatively high density of solid materials, their investigations by MRI also present difficulties due mainly to the characteristic features of magnetic resonance of solids. However, it is evident that the use of MRI for investigations of solid materials would substantially extend the scope of this method.

In the solid phase (unlike in liquids), anisotropic interactions involving nuclear spins are not averaged to zero because of low molecular mobility. This is responsible for a large linewidths in NMR spectra of solids. For example, the line-

I V Koptug, A A Lysova, K V Kovtunov, V V Zhivonitko, A V Khomichev, R Z Sagdeev International Tomography Centre, Siberian Branch of the Russian Academy of Sciences, ul. Institutskaya 3a, 630090 Novosibirsk, Russian Federation. Fax (7-383) 333 13 99, tel. (7-383) 333 35 61, e-mail: koptug@tomo.nsc.ru (I V Koptug), lysova@tomo.nsc.ru (A A Lysova), kovtunov@tomo.nsc.ru (K V Kovtunov), v_zhivonitko@tomo.nsc.ru (V V Zhivonitko), khomichev@tomo.nsc.ru (A V Khomichev), tel. (7-383) 333 14 48, e-mail: itc@tomo.nsc.ru (R Z Sagdeev)

Received 2 April 2006

Uspekhi Khimii 76 (6) 628–645 (2007); translated by T N Safonova

widths for quadrupolar nuclei are often > 1 MHz. An exception are soft solids, such as polymers and elastomers, which can often be studied by conventional MRI techniques.^{8,9} For rigid solids, a large linewidths lead to a very fast NMR signal decay, resulting in a substantial decrease in the sensitivity of the technique. Moreover, the NMR signals cannot be detected at all in some cases. In addition, magnetic field gradients, which are far beyond the possibilities of commonly used 'liquid-phase' instruments, may be required to achieve a satisfactory spatial resolution. For example, separate two-dimensional images of powdered alumina and zeolite^{10,11} and one-dimensional projections of ceramic samples¹² were obtained from ^{27}Al NMR signals with the use of magnetic field gradients amplitude of $225\text{--}350\text{ G cm}^{-1}$. However, even such values are beyond the possibilities of modern NMR tomographs.

Several research teams are currently developing approaches to MRI of solids based on solid-state NMR techniques,⁷ such as magic-angle sample spinning,¹³ the use of multiple-pulse sequences,¹⁴ large magnetic field gradients,^{15–18} single point imaging (SPI), single point ramped imaging with T_1 enhancement (SPRITE),^{19–21} continuous wave NMR,²² *etc.* However, the wide application of MRI of solids is substantially hampered by the necessity (actual or implied) of the use of specialised instruments and complex techniques;²³ the vast majority of commercial or homebuilt instruments are oriented towards procedures conventionally used in NMR and MRI of liquids.

It is known that a line broadening in NMR spectra of solids is inhomogeneous, *i.e.*, broadened signals are virtually sets of overlapping signals with a substantially smaller own width. This fact can be used in different ways. For example, the use of long frequency-selective pulses can allow excitation of only a part of the inhomogeneously broadened resonances. In this case, the time of transverse magnetisation decay T_2^* is substantially increased and it becomes possible to use liquid-phase techniques in MRI of solids.^{24,25} The obvious drawback of this approach is that only a small part of nuclear magnetisation is used in experiments, resulting in low sensitivity.

In our studies,^{26–30} we used another approach. Originally, the choice of a solid material ($\gamma\text{-Al}_2\text{O}_3$) and, consequently, the magnetic nucleus (^{27}Al) was determined by our MRI studies of heterogeneous hydrogenation of unsaturated compounds on $\text{Pt}/\gamma\text{-Al}_2\text{O}_3$ or $\text{Pd}/\gamma\text{-Al}_2\text{O}_3$ catalysts and by the fact that alumina is a commonly used support for catalysts. However, we found that this approach is also applicable to many magnetic nuclei involved in rigid solid materials. Our investigations were based on a number of concepts well-known in the field of NMR. First, a large difference between homogeneous and inhomogeneous widths of the signals is essentially a large difference between the characteristic decay time of the observed signal T_2^* (the time of transverse magnetisation decay or free induction decay) and the true transverse magnetisation relaxation time T_2 . After the application of the first non-selective radio frequency (RF) pulse, a rapid signal decay with the characteristic time T_2^* is observed. However, the application of the second RF pulse can substantially reverse the decay and refocus magnetisation.¹² Second, the central transition ($1/2 \rightleftharpoons -1/2$) in the spectrum of half-integer quadrupolar nuclei $I = (2n + 1)/2$, $n = 1, 2, \dots$, including ^{27}Al ($I = 5/2$), is much narrower than the satellite transitions.^{18,31} Therefore, the detection of the central band in the spectra of quadrupolar nuclei in many cases poses no big problems,^{32,33} in particular if combined with the phase encoding of the spatial information.

The above approach was used with advantage for two-dimensional imaging of cylindrical alumina pellets and alumina or cordierite monolithic honeycomb supports with ^{27}Al NMR signal detection.^{26,27,29} The images were acquired within ~ 15 min. To demonstrate the potential of this method, a series of composite samples of complex composition con-

taining various materials (Al_2O_3 , V_2O_5 , KMnO_4 , NaHCO_3 , glass, *etc.*) were prepared. Images of the corresponding parts of the composite samples at a spatial resolution of $150\text{--}300\text{ }\mu\text{m}$ were obtained by detecting signals of different nuclei (^{27}Al , ^{23}Na , ^{51}V , ^{55}Mn).^{28–30}

The observation of a signal from a glass tube in images obtained from the ^{27}Al NMR signal is evidence that multi-nuclear MRI shows promise for investigation of glass samples. The studies were based on the detection of NMP signals of ^{27}Al , ^{11}B , ^{23}Na , and ^{29}Si NMR nuclei.^{26,29,30} This can be used, for example, in studies of the macrostructures of catalysts and supports, glass and ceramic materials and the structures of granular layers and containers in which they are located. In particular, the structure of a reactor can be visualised in studies of catalytic processes occurring in the reactor. This, along with studies of transport processes, will allow investigation of the correlation between the structure of the reactor and the processes that take place in it. For this purpose, the MRI technique was used for three-dimensional imaging of model granular layers composed of glass beads (^{23}Na MRI, Fig. 1) or spherical alumina grains (^{27}Al MRI).

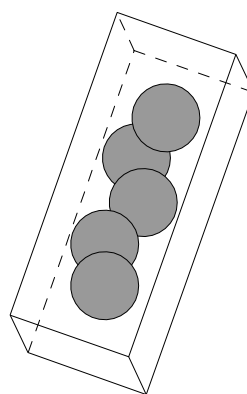


Figure 1. Three-dimensional image of the packing of glass beads with a diameter of 3.5 mm in a glass tube with an inner diameter of 4.2 mm . The image was acquired within 9 h by detecting the ^{23}Na NMR signal. The image of the tube has been removed.

The merit of the MRI method is that it not only provides structural information but, which is more important, also gives spatially resolved maps of properties of the objects of interest (velocity, temperature, chemical composition, *etc.*). Hence, the further progress in MRI of solids will be directed towards the use of this method with different image contrast mechanisms. An evident field of application involves studies of the motion of solids and granulated materials.

The development of spatially resolved NMR thermometry is another promising area of investigation. Heat transport processes are of primary importance in the design and use of catalytic reactors. Nuclear magnetic resonance tomography is rather widely applied in thermometry of liquids.^{7,34–37} However, none of the available approaches based on the signal detection of a liquid phase can be used for thermometry of heterogeneous catalytic processes. This is associated with the fact that all parameters used in NMR thermometry (signal intensity, chemical shifts, relaxation times, diffusion coefficients) substantially depend on other factors, for example, on the amount of a liquid in pores. Therefore, it is impossible to relate unambiguously the changes in these parameters to the changes in temperature.

At the same time, the detection of a signal from a solid matrix, which is much less subjected to changes during operation of a reactor, allows the use of MRI for thermometry of reactors. This possibility was documented almost exclusively for soft solids. For example, the pronounced temperature dependence of the longitudinal (spin–lattice) and transverse (spin–spin) nuclear relaxation times (T_1 and T_2 , respectively) was used to construct three-dimensional temper-

ature maps for a *cis*-polybutadiene block, through which cold and hot water was pumped using two pipes,³⁸ and for vulcanisates of butadiene – styrene rubber under dynamic mechanical load.^{8,9,39} Two-dimensional MRI of a KBr crystal,⁴⁰ for which the time T_1 of the ^{81}Br NMR signal shows a pronounced temperature dependence, is an example of thermometry of rigid solids. As mentioned above, alumina is widely used for the preparation of catalysts and supports. Investigations demonstrated that both the time T_1 and the amplitude of the ^{27}Al signal of alumina are characterised by a pronounced temperature dependence.²⁶ In the future, it can be used for the development of procedures for spatially resolved NMR thermometry of solids.

III. Multinuclear magnetic resonance imaging of transport processes

Magnetic resonance imaging has long been advantageously used in investigations of transport processes.⁶ In particular, liquid flow, filtration, dispersion and diffusion in various geometries, including transport in model granular layers,^{41–44} plants,^{45,46} electroosmotic flow,^{47,48} turbulent flows,⁴⁹ etc., were considered in a vast number of publications.

Nowadays, MRI is being increasingly used in studies of structures of bioreactors and transport processes in them. The development of new technologies based on the use of various bioreactors is of importance, for example, in such fields as waste water treatment, food industry, construction of artificial tissues, etc. The MRI technique allows the non-invasive determination of the amount and spatial distribution of a biomass in a reactor and location of inhomogeneities in biofilm structures. For example, studies of the growth of biopolymers based on *Staphylococcus epidermidis* in a capillary bioreactor showed the presence of clusters of biomass, in which channels and cavities were distinguished.⁵⁰ The use of relaxation time contrast made it possible to obtain separate three-dimensional MRI images of water and biopolymers.⁵¹

Another approach to the separate visualisation of water and biofilms was used in the study,⁵² where the differences in the diffusion coefficients were employed. The MRI method was applied also to investigate the structures of methanogenic aggregates from an anaerobic purification system of waste water.⁵³ The contrast of MRI images is substantially enhanced upon absorption of paramagnetic compounds by a biofilm.^{54–56} In model studies, the removal of metal ions (La^{3+} and/or Cu^{2+}) from aqueous solutions with biopolymers based on the bacterium *Citrobacter* sp. was investigated.^{55,56} Considerable attention was focussed on the flow and diffusive transport in bioreactors.^{50,54,57,58} The flow in a new coaxial bioreactor based on hollow fibre permeable membranes was studied.⁵⁹ The relationship between the structure and transport properties of biopolymers was considered in several publications.^{50,58} Mammalian cell-based bioreactors have found increasing use for the production of antibodies, hormones and proteins for therapeutic and clinical application, the tissue growth for transplantation and the design of artificial tissues and organs. The distribution and transport of paramagnetic gadolinium complexes in such reactors were investigated.^{60,61} Aspects of application of MRI in studies of transport and biological activity in biofilms and bioreactors were considered in several reviews (see, for example, Refs 62 and 63).

In recent years, considerable attention has been given to application of MRI in studies of two-phase (liquid – gas) flows in various geometries,⁶⁴ in particular, of gas and liquid trickle flow in model granular beds. In this case, MRI experiments provide information on the residual and dynamic liquid holdup in a reactor, the presence of liquid streamlets in the bed and wetting of the catalyst surface. For example, it was

demonstrated⁶⁵ that the flow pattern can remain unchanged for many hours for a co-current trickle flow of water and air in a model granular bed at constant gas and liquid flow rates. An analysis of the results of investigation was used for the determination of the above-mentioned parameters and their dependence on the liquid flow rate. Changes in the gas flow rate do not lead to substantial changes in the liquid distribution in the layer. However, the initial state of the granular bed was found to have a substantial effect on the gas and liquid distribution in the bed.^{65,66} A study of the dependence of the liquid holdup in the reactor and wetting of the surface of cylindrical alumina pellets in a granular bed on the liquid flow rate⁶⁷ showed that smaller grains are characterised by higher values of these parameters. After the flow is turned on as well as after the temporary interruption of the liquid feed, a few minutes^{64,68} to several hours⁶⁹ are required for the establishment of the stationary liquid and gas distribution in the bed.

Investigations of fast dynamic processes under two-phase flow conditions require fast MR imaging. The imaging at a rate of 10 images per second revealed liquid slugs passing through the imaged slice at a high liquid flow rate.^{64,68} Ultrafast imaging (20 ms for two-dimensional images and 0.3 s for three-dimensional images) allows MRI studies of gas – liquid two-phase flows in the trickle, pulsing and transient flow regimes.^{70,71} Most likely, the pulsing regime begins with the appearance of local fluctuations and is characterised by the co-existence of regions with constant and fluctuating contents of a liquid. The sizes of the regions with an unstable flow increase with the liquid flow rate and finally the regions coalesce. In the transient flow regime, the instability regions in the bed are shifted, which is apparently responsible for a hysteresis in the plot of the pressure drop vs. the liquid flow rate. In the pulsing flow regime, changes in the intensity of most of elements of an MR image are observed. To characterise the periodicity of changes in the local liquid content in the bed, the time autocorrelation function was calculated from these data. A preliminary study of the periodic mode with a modulated liquid feed to the bed was documented.⁷⁰ In spite of changes in the liquid distribution in the bed after the liquid flow rate returns to the starting value, no changes in the wetting of the catalyst and the liquid holdup in the bed were observed.

It should be noted that the character of transport and its quantitative characteristics can be radically changed if the mass transfer is coupled with heat transfer and/or a chemical reaction (see Section IV.2). A comparative study of a two-phase flow of a diesel oil and N_2 in a bed of glass beads or alumina trilobes was carried out under normal conditions and at high temperature and pressure (398 K, 10 atm).⁷² The liquid holdup in the bed was determined from MR images. The results obtained in the trickle flow mode showed a considerable influence of the temperature on the dynamic liquid holdup in the bed, which decreases with temperature.

To study a two-phase flow in channels of honeycomb monolithic supports, for example, in a bubble-train flow with alternating liquid slugs and gas bubbles, it is also necessary to use fast magnetic resonance imaging because, unlike a steady-state pattern in the trickle flow mode, the gas and liquid distribution pattern is continuously changed. The possibility of acquiring 4–8 successive two-dimensional images in ~ 0.6 s was demonstrated in studies of air – water two-phase bubble-train flow in a thin pipe⁷³ and a cordierite monolithic honeycomb support.^{74,75} These experiments allow one to determine the size of gas bubbles and liquid slugs and to follow their motion in time. A fast NMR signal decay provides indirect evidence for liquid recirculation in the case of two-phase bubble-train flow.⁷³ The same approach was used in studies of ascending gas bubbles in channels of a monolith placed in a static liquid.^{64,66,67,76}

Studies of the filtration of liquid–liquid two-phase systems in porous media, for example, of water and silicon oil embedded in glass beads, are presently underway.^{77, 78}

The possibility of investigating gas flow and filtration by the MRI technique has been demonstrated earlier.^{79–82} The results of these studies gave impetus to further progress in MRI techniques as applied to investigations of gas transport. For example, a methane flow and accumulation of solid particles in soot filters of diesel engines was considered.⁸³ A relatively high spatial resolution (100–250 μm) was achieved by increasing the gas pressure to 10 MPa. The measured maps of gas flow velocity showed that the flow distribution through a porous filter wall is relatively uniform along the channel length. The next series of experiments was concerned with the accumulation of small carbon particles, which were introduced into a gas flow, in a filter.

Until recently, it has been believed that the turbulent gas flow in an inhomogeneous magnetic field should lead to fast NMR signal decay and, consequently, this flow cannot be studied by MRI. However, recently it has been demonstrated that this is not true. The maps of flow velocity and turbulent diffusivity for SF_6 flowing at velocities $> 10 \text{ m s}^{-1}$ ($\text{Re} > 10^5$) above a step or about a wing model were reported.⁸⁴ The experimental results are in rather good agreement with calculations by computational fluid dynamics methods.

Even at high pressure, the sensitivity in experiments on MRI of gases remains substantially lower than that of MRI of water. Hence, velocity maps can be obtained only in channels of a rather large diameter and, in contrast to MRI of liquids, cannot be obtained in granular beds. However, studies of gas filtration in porous media are of considerable interest in many fields of science and technology. The use of pulsed field gradient NMR (PFG NMR) for measuring an average propagator (the velocity distribution of molecules) holds promise as an approach to studying gas flow and filtration.^{79, 81, 85} This method was used to obtain average propagators for axial and transverse directions of propane or butane flows in different granular beds.^{86, 87} If the time between gradient pulses (Δ), during which the molecular motion is determined, is short, the Gaussian distribution with a maximum for the zero displacement is observed. A relatively large width of this distribution is associated with a large gas diffusion coefficient. As Δ increases, an extended wing on the side of larger displacements appears in the axial displacement distribution. Then a Gaussian distribution is formed again but with a maximum near the average displacement due to gas flow. The widths of the axial and transverse distributions for large Δ are determined by the corresponding dispersion coefficients, which are substantially larger than the gas diffusion coefficient. In experiments, the dependence of the axial and transverse dispersion coefficients on Δ , the gas flow rate and the grain size in the bed was studied. The Gaussian distribution at large Δ for the axial transport indicates that dead zones are absent in the layer. In the case of gas filtration through a bed of porous particles [for example, of poly(vinyl chloride)],⁸⁷ the axial distribution shows the second peak at zero displacements in the limit of large Δ . This peak corresponds to the gas present in grain pores, which is rather slowly exchanged with the free flowing gas. In addition, the characteristic autocorrelation times of the velocity of gas molecules were experimentally studied for filtration through model granular bed.⁸⁸

In spite of the progress in application of MRI in studies of gas transport, low sensitivity is still the main obstacle to such investigations. Hence, considerable recent attention has been focussed on the production of hyperpolarised gases with a considerable increase (by several orders of magnitude) in nuclear spin polarisation compared to thermal equilibrium polarisation in a spectrometer or tomograph magnet field.⁸⁹ Laser procedures were developed for the continuous genera-

tion of hyperpolarised noble gases (^{129}Xe , ^3He , ^{83}Kr).^{90–92} It is convenient to use these procedures to study gas flow and filtration by MRI.^{80, 93}

The use of hyperpolarised gases, particularly combined with highly sensitive methods for the signal detection (for example, with a superconducting quantum interferometer) allows the detection of NMR signals and MR imaging at very low magnetic fields using extremely small field gradients. For example, experiments⁹⁴ were carried out at a magnetic field of 2.3 mT, which is approximately 3 orders of magnitude lower than those used in most of MRI studies of non-living objects. In the cited study, the filtration of hyperpolarised $^{129}\text{Xe}^*$ through an aerogel and a bed of powdered polypropylene was considered. In the latter case, due to a large chemical shift difference (200 ppm or 5 Hz), bulk xenon and adsorbed xenon were distinguished in spite of a very low magnetic field. Ultra-low frequency magnetic fields allow investigation of samples inside a metal container.⁹⁵ In strong magnetic fields, these investigations are in principle impossible because high-frequency electromagnetic radiation does not penetrate into conducting screens (skin-effect).

In recent years, methods of the so-called remote-detection NMR and MRI have been developed based on the use of continuous generation systems of hyperpolarised gases and their delivery.^{96–99} The remote detection is a new method, in which spatial information is encoded into an NMR signal with the use of radiofrequency pulses and field gradients at the moment when molecules (information carriers) are present in the object of interest, while the signal is detected at a different site. This provides delay for the time of molecule transport from the object to the site of detection. The distance between the object of interest and the site of detection can vary from several millimetres to several metres if the transport time is no longer than the spin relaxation time, which determines the lifetime of the encoded information. An obvious advantage of this approach is that conditions of signal detection can be optimised regardless of the properties and size of the object of interest. Preliminary studies using remote-detection NMR have demonstrated an enhancement of sensitivity and spatial resolution for hyperpolarised $^{129}\text{Xe}^*$ in model objects and real porous materials.^{96, 97} The remote signal detection was applied in MRI of transport in model microreactors.^{98, 99} This made it possible to perform detailed studies on the role of flow, diffusion and mixing processes and reveal dead zones.⁹⁹

The transport of solid granulated materials is used in many industrial processes, including fluidised granular beds, granulation, drying, pneumatic transport, *etc.* Magnetic resonance imaging is widely used for investigating such processes. However, all MRI studies of the transport of solids are based on the detection of the NMR signal of a liquid phase. Hence, liquid-containing solid particles are required. Plant seeds (poppy or mustard) with high oil and moisture content, pharmaceutical pellets with a liquid core, and liquid-saturated porous grains are often used for this purpose.^{4, 6, 100, 101}

Three-dimensional images of a granular bed fluidised with an air stream¹⁰² clearly show low-density regions (as vertical columns) of the particle distribution above each orifice of the gas-distribution plate. Interestingly, these regions were observed at a gas velocity lower than the minimum fluidisation velocity ($U < U_{\text{mf}}$). At $U > U_{\text{mf}}$, these regions coalesce into a single low-density region in the upper part of the bed. The images also clearly show dead zones between adjacent orifices. Mixing of particles in a fluidised bed was studied using two types of particles, which give and do not give NMR signals.¹⁰³ Different modes of fluidisation were examined by recording axial profiles of the particle density distribution, the particle velocity distribution and the effective dispersion coefficient.¹⁰⁴ In somewhat more complex MRI experiments, the contributions of coherent (differences in particle velocity) and incoher-

ent (velocity modulation due to collisions) particle motion to the dispersion coefficients can be distinguished.¹⁰⁵ In particular, the dispersion coefficients for the transverse transport with and without considering the coherent contribution differ by a factor of 3–4; for the axial transport, this difference is substantially smaller. Local information on the particle velocity averaged over the time and an element of an MR image can be obtained by combining MRI sequences and velocity encoding methods.^{102, 105} Velocity distribution maps reflect the upward particle motion in the central part of the bed and downward motion in the near-wall region at a much lower velocity. The transport of a gas used for fluidisation of a granular bed can be studied by MRI. The gas exchange between different phases (gas bubbles and emulsions) was studied and gas velocity distributions at different gas flow rates were obtained with the use of hyperpolarised xenon.^{106, 107}

Magnetic resonance imaging is applied also to study fluidisation of a granular bed in vibrating containers.^{108–111} In addition, the particle transport in Couette flow^{112, 113} and in horizontal rotating cylinders was investigated^{114–117} and filtration of mineral oil-containing Al_2O_3 particles through a bead pack, which serves as a model of a catalytic reactor, was studied.^{85, 118, 119}

The drawback of the above-considered applications of MRI in studies of the transport of solids is that it is necessary to detect the signal of a liquid phase. This largely limits the range of materials and processes, which can be studied by this method. Until recently, the possibility of detecting the NMR signal of a solid phase in such studies has not been considered. The successful use of multinuclear MRI allowed us to study for the first time the motion of solids by the direct detection of the NMR signal of a solid phase. We used³⁰ the MRI method for visualising the rotation of a cylinder filled with an alumina powder. Three-dimensional velocity maps of the two velocity components perpendicular to the cylinder axis were constructed by detecting the ^{27}Al NMR signal. These data are in good agreement with the results of calculations based on the known parameters, *viz.*, the rotation velocity and the diameter of the sample. Propagators for motion of finely grained alumina under the force of gravity were also obtained (Fig. 2).

The further progress in applications of MRI is greatly hampered by the sensitivity of the method. This is also true for the MRI of solids, especially when the signals of nuclei with a low natural abundance of a magnetic isotope or a low magnetogyric ratio are detected. Hence, we made considerable efforts to enhancing the sensitivity of detection of the ^{27}Al NMR signal and signals of other nuclei. One of approaches in

NMR of half-integer quadrupolar nuclei is based on an increase in the level population difference of the central transition as a result of a inversion of satellite transitions by means of adiabatic sweep of the radiofrequency field.¹²⁰ This made it possible to double the intensity of the ^{27}Al NMR signal in MR imaging of a glass tube with a wall thickness of 1.5 mm.³⁰ The use of a narrower spectral band in the signal detection^{19, 121} led to a further increase in the signal-to-noise ratio by a factor of 3.5. Nowadays, we use another approach based on the development and construction of higher-sensitivity resonator-type radio frequency detectors.

Multinuclear MRI can be useful not only in studying the transport of solids but also in investigating the transport of different dissolved compounds. From a methodological viewpoint, this obviates problems associated with the detection of signals of a solid phase because a fast molecular motion in solutions averages anisotropic nuclear spin interactions, resulting in a narrowing of NMR lines by several orders of magnitude. Due to this, all liquid-phase MRI techniques are fully applicable for multinuclear MRI of solutes.

Transport processes of dissolved substances have attracted interest of researchers in different fields of science and technology. For example, the transport of salts in porous building materials is of primary importance. In recent years, multinuclear MRI has found application in studies of such processes.^{122, 123} The design of functional porous materials is often based on impregnation of a porous matrix with various substances. For example, efficient sorbents were prepared by introducing different salts into pores of alumina, silica gel or another porous matrix.¹²⁴ It will be possible in future to characterise both transport processes of dissolved substances in impregnation and drying steps and the final distribution of a solid-phase component introduced into a porous matrix after complete removal of the solvent by combining MRI of dissolved compounds and MRI of solids.^{29, 125, 126}

The transport of dissolved substances is of great importance also in the preparation of supported catalysts by impregnation of a porous support with the corresponding solutions. The diffusive transport rate of substances into a porous support substantially depends on the character of interactions between these substances and the support, the presence of modifying additives in solution, pH of the medium and other factors. In some case, this rate can be very low, but in this case uniform distribution of an active component over a support cannot be achieved. In some cases, a non-uniform distribution of egg-shell, egg-white, *etc.* types are required. In earlier studies, we have found that platinum hexachloride (PtCl_6^{2-}) deposited onto an extended surface of alumina can increase the proton spin relaxation times of liquids filling the pore space of supports.^{127, 128} As a result, MRI images reflecting the macro-distribution of platinum in grains was obtained by detecting signals of a liquid (cyclohexane or water) in grain pores. Analogous experiments were performed for palladium tetrachloride (PdCl_4^{2-}). Moreover, the non-destructive character of MRI allowed, for the first time, the observation of the dynamics of redistribution of adsorbed platinum hexachloride in real time in one grain in the course of competitive adsorption from a solution together with oxalic acid.^{127, 128} Unlike PtCl_6^{2-} and PdCl_4^{2-} , paramagnetic adsorbates lead to a decrease in the spin relaxation times of contacting liquids. This allows the use of MRI in studies of simultaneous adsorption of two active components of different nature (for example, PtCl_6^{2-} and Cu^{2+}) upon simultaneous deposition onto an alumina grain.^{118, 129}

More recently, studies of practical importance were carried out. The corresponding procedures were developed using alumina-supported (Ni/Co)Mo catalysts for hydrodesulfurisation. These catalysts are often prepared with the addition of other components, *viz.*, co-promoters and modifying agents

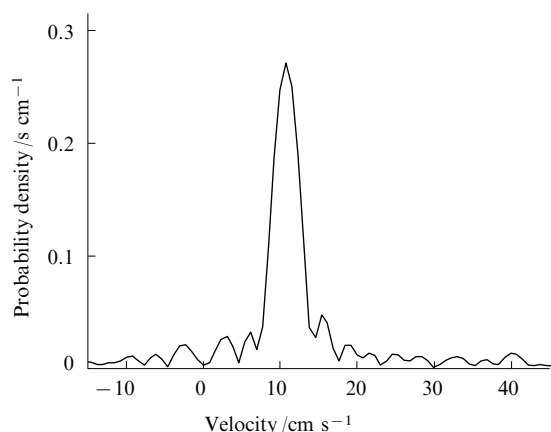


Figure 2. Particle velocity distribution of finely grained Al_2O_3 in a vertical pipe obtained by detecting the ^{27}Al NMR signal.

(for example, phosphates and citrates). The transport of phosphate in an alumina grain upon impregnation of the latter in an aqueous H_3PO_4 solution was studied in the first step. Magnetic resonance imaging with ^{31}P NMR signal detection provided dynamic visualisation of the phosphate transport in a grain in the course of impregnation.^{125, 126} To confirm the reliability of this method, maps of the spatial distribution of phosphate in the solid phase were recorded after termination of impregnation at various stages of impregnation and the subsequent drying of the granules. This became possible due to the development of the above-considered (see Section II) multi-nuclear MRI of solids. The distribution of phosphate in a dry grain was demonstrated to correlate with the distribution of phosphate in the liquid phase during impregnation. In addition, an investigation with the use of the initially dry grain combined with an alternating detection of ^{31}P (phosphate) and ^1H (water) images demonstrated fast capillary ingress of water from a solution, the penetration of phosphate inside the grain being much slower due to a strong interaction between the phosphate and the surface of alumina pores.

In the next step, the cobalt transport during impregnation of an alumina pellet with an aqueous solution of a cobalt salt was investigated. The dynamics of the process was studied by MR imaging by detecting ^1H NMR signal of water because paramagnetic cobalt ions (Co^{2+}) have a substantial effect on the intensity of the NMR signal of water. The addition of citric acid to an impregnation solution was demonstrated to have a substantial effect on the impregnation process: the cobalt concentration at the periphery of the grain decreases due to a stronger interaction between citric acid and the pore surface and the displacement of cobalt further into the granule (Fig. 3). The influence of the impregnation conditions on the character of cobalt transport and the final distribution of cobalt over the grain of the support was studied in detail. For example, the redistribution of cobalt in the course of impregnation at high and low pH (8 and 1, respectively) of an impregnation solution for a grain with a diameter of 3.5 mm is completed in ~ 2 h. At pH 1, the final distribution has an egg-yolk type. At pH 8, cobalt is uniformly distributed over a granule in spite of the presence of citrate. At intermediate pH (for example, 5), the

impregnation time exceeds 15 h. Images obtained by MRI in studies of the transport of Co^{2+} ions were converted into concentration profiles with the use of calibration curves, *i.e.*, it was demonstrated that quantitative information on transport processes in the course of supported catalysts preparation can be obtained.

In the next step, the transport of molybdenum ($\text{Mo}_7\text{O}_{24}^{6-}$) was studied. Granules were impregnated with an aqueous solution of ammonium heptamolybdate. Diamagnetic molybdenum ions (Mo^{6+}) were found to lead to a substantial increase in the spin relaxation times of water in the pores. This effect is analogous to the effect used earlier in studies of impregnation of support grains with an aqueous solution of H_2PtCl_6 or H_2PdCl_4 (see above). Based on the results of these investigations, approaches were developed for selective visualisation of the regions of grains containing (or not containing) Mo^{6+} , and a procedure was devised for observing the dynamics of molybdenum transport in grains during impregnation. However, it is necessary to use MRI in combination with other physicochemical methods for complete characterisation of such multicomponent systems. For example, spatially resolved optical spectroscopy can be used for determining the nature of ionic metal complexes.^{126, 130}

In the above-described investigations, the transport of a diamagnetic precursor of an active component in grains of a support in the course of the preparation of supported catalysts by impregnation was for the first time monitored by detecting directly the NMR signal of the metal atom. This was exemplified¹²⁵ by the preparation of a $\text{Pt}/\gamma\text{-Al}_2\text{O}_3$ catalyst with the observation the dynamics of the process by detecting the ^{195}Pt NMR signal. The approaches developed in the latter study were used for investigating the preparation of catalysts on other supports, for example, for studying the distribution of an active component in different samples of monolithic honeycomb supports both after calcination and in freshly prepared samples.¹³¹ To visualise the spatial distribution of an active component, T_1 -weighted images were generated. Therefore, approaches were devised for the first time to using MRI for the non-destructive control of the preparation of supported catalysts by dynamic visualisation of the distribution of active components and compounds promoting catalytic activity.

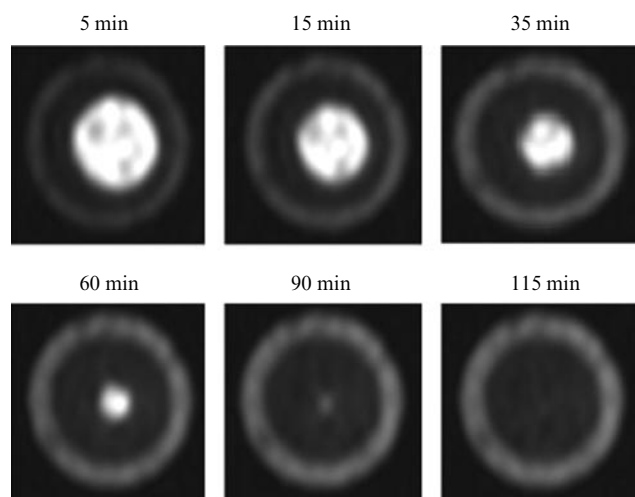


Figure 3. Two-dimensional ^1H MRI images reflecting the dynamics of transport of Co^{2+} ions into a $\gamma\text{-Al}_2\text{O}_3$ grain in the course of its impregnation with a solution of 0.2 M $\text{Co}(\text{NO}_3)_2$ and 0.4 M citric acid at pH 1.

The images were acquired by detecting the ^1H NMR signal; the dark ring corresponds to the part of the grain with the highest concentration of Co^{2+} ions; the spatial resolution was $(139 \times 231) \mu\text{m}^2$.

IV. Magnetic resonance imaging of chemical reactions

1. Homogeneous reactions

Under homogeneous conditions, a liquid-phase reaction or related mass-transfer processes can give rise to non-uniform spatial distributions of reactants, products, intermediates and other important parameters. In these cases, MRI can provide useful information on processes occurring in systems. An example is MRI studies of the Belousov–Zhabotinsky (BZ) reaction, metal ion-catalysed oxidation of organic substrates by bromate anions.¹³² A series of interesting MRI investigations were carried out in this field^{133, 134} (see the review⁷). In the last three to four years, after a hiatus, interest in this problem was rekindled. For example, the reaction alternative to the classical BZ reaction, *viz.*, the non-catalytic cyclohexane-1,4-dione + bromate + acid reaction, was studied.¹³⁵ However, since the MR image contrast in all previous studies of the BZ reaction has been based on the periodic change in the oxidation state of metal ions (catalyst), the latter investigation was performed with the addition of manganese ions as a passive indicator of the processes occurring in the system. This allowed investigation of the appearance and evolution of wave structures in this system. The concentrations of the reactants, products and intermediates at different instants of time were determined by NMR monitoring of the reaction, which partially confirmed the reaction mech-

anism proposed earlier. Later,¹³⁶ spatial maps of the concentrations of Mn(II) and Mn(III) ions were obtained directly in the course of the BZ reaction.

The BZ reaction is homogeneous. However, its behaviour can be substantially changed by performing this reaction in thin capillaries or in an inert porous medium. The behaviour of the BZ system in glass bead or quartz sand packs was investigated.^{88, 137, 138} In particular, the concentration wave velocity in a glass bead pack with a bead diameter of 0.5 mm was demonstrated to decrease by a factor of ~ 2.5 after passing through the interface between the bulk liquid and the granular layer filled with the liquid. The wave velocity is proportional to the square root of the diffusion coefficient of an autocatalyst.¹³² The diffusion coefficient in a porous medium decreases by a factor of ε/T (ε is the porosity of the medium and T is the tortuosity of the pore space) compared to the diffusion coefficient in the liquid bulk.¹³⁹ Estimates demonstrated that changes in the concentration wave front velocity after passing through the interface between these phases are associated primarily with this factor.

The concentration wave propagation velocity decreases as the curvature of the front increases.^{140, 141} As the critical curvature is achieved, the formal velocity becomes negative, resulting in the disappearance of wave activity of the medium. The local (on the length scale of individual pores) curvature of the wave front is determined by the pore size in a granular layer. Hence, the propagation of the concentration front can be influenced by varying the grain size. In particular, at fixed concentrations of the key reactants, there is a critical pore size, below which no wave activity is observed. In addition, the wave propagation velocity depends on the bromate anion concentration.¹³² These investigations actually demonstrated that each granular layer is characterised by a particular concentration range, where the wave activity can be observed. For porous materials with small pores, such as alumina, the wave activity was not found at all.

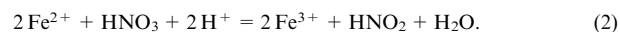
Considerable attention is given to characteristic features of coupling of a non-linear chemical reaction with transport processes in open systems. In particular, very interesting effects are observed in the course of filtration of a BZ reaction medium through inert granular layers. The descending wave velocity (*i.e.*, the wave propagating in the direction of flow) in a porous medium was demonstrated to be substantially larger than the sum of the flow velocity and the wave velocity in the stationary medium, whereas the ascending wave can remain steady-state in a laboratory reference system in a wide range of flow velocities.^{137, 142, 143} Spatially resolved periodic-in-time concentration oscillations were studied¹⁴⁴ by pumping the BZ reaction medium through a glass bead pack. To create constant boundary conditions at the layer inlet, the reaction mixture was introduced from a continuously stirred tank reactor. After the initial transition period, stationary wave structures were observed in the system over a long period of time. Evidently, it is impossible to detect three-dimensional wave structures by optical methods in a non-transparent system.

Since the detailed mechanism of the BZ reaction is rather complex, this unusual behaviour of wave fronts in a granular layer in the presence of a reactant flow remains to be explained.

The concentration wave propagation is observed also in different non-oscillating autocatalytic reactions, which often have a much simpler mechanism than the BZ reaction. In this connection, we performed a series of investigations of such reactions to reveal the common features of coupling of transport processes with a non-linear reaction. For experiments in a reactor containing a stationary granular layer, we chose two autocatalytic systems suitable for MRI studies: oxidation of the Co^{2+} ethylenediaminetetraacetate (EDTA) complex by hydrogen peroxide¹⁴⁵ (OH^- ions act as the autocatalyst)

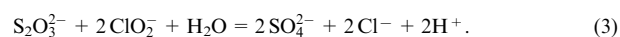


and oxidation of Fe^{2+} with nitric acid (NO_2^- ions act as the autocatalyst)



In addition to the above-mentioned advantages, an advantage of these systems over the BZ system is that the initiation of chemical waves can easily be controlled. Owing to changes in paramagnetic properties of metal ions in the course of the above transformations, it is easy to acquire MR images with T_1 contrast. For reaction (1), a qualitative pattern for the chemical wave front propagation was obtained. In experiments with reaction (2), the quantitative dependence of the wave propagation velocity on the flow velocity of the reactants through a stationary granular layer was measured. These experiments demonstrated that the wave velocity linearly depends on the flow velocity of reactants, but the slope of the plot differs from unity, *i.e.*, the wave velocity in the moving medium is not a simple sum of the wave velocity in a stationary medium and the flow velocity. For comparison, reaction (2) was performed in a thin capillary. The latter process is characterised by a liquid flow velocity distribution, but the dependence of the wave propagation velocity on the average reactant flow velocity is analogous to that observed for reaction (2) in a reactor with a stationary granular layer. The experiments demonstrated that the wave front propagation can be accompanied by a spontaneous change in velocity from slow to fast and back. This unusual behaviour is apparently attributed to the exothermic character of the chemical reaction and, consequently, to changes in the density of the reaction solution.

In these experiments, considerable efforts were made to develop MRI techniques for studying the chemical wave propagation under different conditions. For example, the chemical wave propagation in polymeric media is of interest as a model, which can be used to study living biological tissues, where different specific transformations can proceed. To perform experiments in polymeric media, we chose oxidation of thiosulfate with chlorite ions



This reaction shows a wave activity at low ($< 0.1 \text{ mol litre}^{-1}$) concentrations of the reactants (autocatalysis by H^+ ions). Isopropylacrylamide gel was used as a polymer matrix. We found that the nuclear spin relaxation times of water vary with pH. For example, the chemical wave propagation in the gel impregnated with the chlorite–thiosulfate reaction solution led to a change in pH by 7 units, resulting in an increase in the relaxation time T_1 by $\sim 200 \text{ ms}$. This allowed us to acquire MR images with pH contrast of the propagating wave front at different instants of time.

The spatially resolved NMR thermometry for visualisation of the chemical wave propagation is another area of methodological development. Since reaction (3) is exothermic, the concentration front propagation can in principle be observed from changes in the local temperature of the medium. Magnetic resonance imaging is rather widely used for measuring the local temperature in different samples.⁷ For systems containing large amounts of water, including living objects, the temperature determination is often based on an almost linear temperature dependence of the chemical shift of a water molecule in a wide temperature range. For the first time, we used MRI thermometry for measuring the local temperature in the course of concentration wave propagation.¹⁴⁶ The reaction was performed in a vertical glass cell with an inner diameter of 9 mm, and two-dimensional images of a 2-mm thick slice were acquired at three-second intervals for central longitudinal or transverse sections. As a result, temperature profiles for this colourless reaction were obtained (Fig. 4). According to the

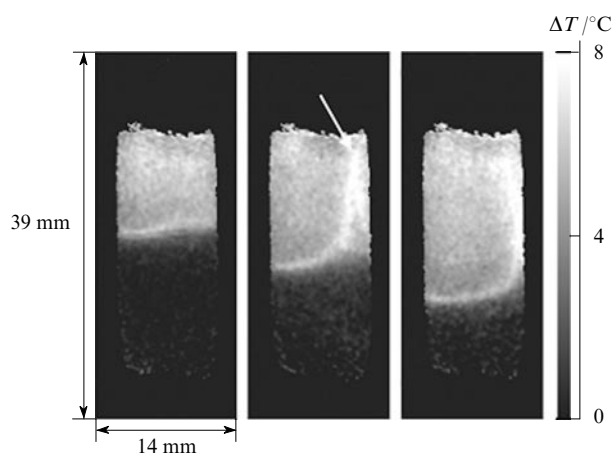


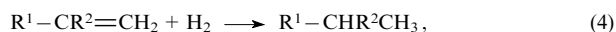
Figure 4. Temperature profiles obtained in the course of chemical wave propagation in a chlorite – thiosulfate system. Longitudinal sections of the cell are shown; the images were acquired at 25-s intervals; the convective flow is indicated by an arrow.

MRI data, an increase in the temperature of the solution in the course of reaction front propagation was $\sim 8^\circ\text{C}$, which is in good agreement with the results of thermocouple measurements performed separately. The accuracy of MRI measurements of the temperature in these experiments was estimated at 1°C . After the front propagation, the temperature of the solution gradually decreases to the initial level, which is reflected in the temperature profiles. These profiles also demonstrate the presence of convective flows in the cell, resulting from heating of the medium in the vicinity of the reaction front. Therefore, the above-described procedures are applicable to studies of the influence of reactant transport in polymeric media and the temperature on the chemical wave propagation.

2. Heterogeneous reactions

The application of MRI in the *in situ* studies of operating reactors is a relatively new field that made its appearance in the 21st century.¹⁴⁷ Nevertheless, numerous data were obtained during this short period of time. Investigations carried out in the course of a reaction are of great importance because coupling of transport processes with reactions and attendant processes (heat transfer and phase transformation) can fundamentally change the situation.

First *in situ* MRI investigations of heterogeneous catalytic reactions proceeding at high temperature were carried out at the International Tomography Centre of the Siberian Branch of the Russian Academy of Sciences in collaboration with the Institute of Catalysis of the Siberian Branch of the Russian Academy of Sciences. Heterogeneous hydrogenation of unsaturated compounds (α -methylstyrene, heptene, and octene) on supported metal catalysts ($\text{Pt}/\gamma\text{-Al}_2\text{O}_3$ and $\text{Pd}/\gamma\text{-Al}_2\text{O}_3$) were chosen as model reactions



$\text{R}^1 = \text{C}_6\text{H}_5$, $\text{R}^2 = \text{CH}_3$; $\text{R}^2 = \text{H}$: $\text{R}^1 = \text{n-C}_5\text{H}_{11}$, $\text{n-C}_6\text{H}_{13}$.

To perform reactions inside an NMR magnet, a NMR-compatible reactor was designed, which allowed an increase in the temperature of the reaction zone to $\sim 100^\circ\text{C}$ due to external heating by a hot air stream. The reaction zone and the hot-air jacket were placed in an evacuated glass Dewar to prevent overheating of gradient coils of the instrument. The catalyst is placed in the reaction zone; both the liquid reagent which is fed through a capillary and the preheated

hydrogen gas which can be additionally saturated with the reagent vapour are supplied from above.

Early studies^{28, 88, 148–150} addressed the spatial distribution of a liquid phase in a single cylindrical pellet of the 15% $\text{Pt}/\gamma\text{-Al}_2\text{O}_3$ catalyst in the course of hydrogenation of α -methylstyrene (AMS). At that time, one two-dimensional image was acquired during ~ 260 s. Nevertheless, this first experiment, where the operation of a model three-phase reactor was directly observed, revealed the presence of considerable concentration gradients of the liquid phase in the catalyst grain under conditions of the simultaneous endothermic evaporation of the liquid reactant and exothermic hydrogenation of its vapour.^{88, 149, 150} Presumably, fast evaporation of the reactant occurs at the interface between the filled and dry parts of the catalyst grain, whereas its vapour is efficiently hydrogenated in the dry part of the grain.

Evidently, to study dynamic processes in a reactor, it was necessary to decrease the MR acquisition time for each image, which is determined primarily by the spin relaxation time of the liquid phase. Hence, subsequent experiments were carried out with grains of the 1 mass % $\text{Pd}/\gamma\text{-Al}_2\text{O}_3$ catalyst containing 0.1 mass % Mn.^{27, 28, 85, 151, 152} This made it possible to acquire two-dimensional images in 34 s. As a result, a number of interesting dynamic processes, such as redistribution of the liquid phase in the granule upon 'ignition' of the catalyst grain, were observed. It is worthy of note that in some experiments, 'ignition' started when the pellet was virtually completely wetted and it led to drying of the grain by more than a half. Most likely, the optimal conditions for the beginning of the process are provided in the near-surface region of the grain, because the temperature directly on the surface is lower due to continuous heat removal by a gaseous reactant flow, while the diffusive transport to inner parts of the grain through pores filled with the liquid is hindered. As a result, 'ignition' begins in the grain at a particular distance from the surface, whereas the near-surface and inner regions of the grain remain filled with the liquid during a much longer period of time. As the liquid reagent is evaporated, the inner wetted region of the grain shrinks, resulting in a decrease in the rate of hydrogen transport to the evaporation – reaction zone. At a particular instant of time, inhibition becomes the main process, the temperature of the grain decreases, and a new cycle of filling of the grain with the liquid begins. Based on these results, a hypothesis can be made that hydrogenation efficiently proceeds in the region under the grain surface, where the optimal balance between the temperature of the grain and the diffusive supply of hydrogen through the pore space is provided.

In longer experiments, numerous grain 'ignitions' giving rise to quasiperiodic oscillations of the liquid that was present in the grain and the back-and-forth motion of the liquid front were observed. These oscillations were observed when the grain was filled with the liquid by more than a half and were accompanied by changes in the amount of the liquid in the grain and its temperature, large gradients of the liquid phase in the grain in the radial direction and the liquid front propagation in a radial direction. The nature of these oscillation is associated with the mutual influence of several processes, such as heat transfer, mass transfer, phase transitions and the chemical reaction itself. This is confirmed by the results of mathematical simulation.¹⁵³

Another type of behaviour is observed when a grain is initially filled with a liquid by less than a half. In this case, the concentration wave propagation along the axis of a cylindrical grain occurs in a plug-like fashion. The largest amount of liquid was detected in the upper part of the grain, where the liquid reactant was delivered. The size of this region and its boundaries continuously oscillated. The remaining part of the grain was filled with a vapour – gas mixture and did not contain the liquid. Evaporation of AMS and the gas-phase reaction led

to temperature oscillations, which were detected in the lower dry part of the grain by a thermocouple located in this region. In the course of oscillations, the instant of time when the largest (smallest) amount of the liquid in the grain was observed did not coincide with the instant of time when the lowest (highest) temperature was detected. In addition, the amounts of the liquid in the upper and lower parts of the grain change out of phase. These observations provide evidence for the delayed feedback between the temperature of the grain and the amount of the liquid in pores.

The oscillating liquid front propagation in a catalyst grain suggests that, under particular conditions, a steady-state reaction can become unstable because of its exothermic character. Subsequent experiments demonstrated considerable sensitivity of the oscillating mode to external conditions. In particular, the existence of oscillations and their periodicity and regularity were found to depend on the activity of the catalyst, the flow rate of liquid AMS and the temperature of the supplied gas.

Experiments with single grains provide information on dynamic processes at a characteristic single-grain size scale. To study processes at larger scales and to investigate interactions and the collective behaviour of grains, experiments were performed with clusters consisting of a small number of spherical catalyst grains with a diameter of 4.2 mm, which form an approximately regular packing containing 3–4 grains in each horizontal layer. Two-dimensional MR images of horizontal sections of the grain packing were obtained. These experiments showed the possibility of ‘ignition’ of individual grains in a layer. These grains can act as microreactors remaining dry after ‘ignition’ due to the efficiency of the reaction in spite of the fact that these grains contact with grains filled with a liquid. In addition, the mutual influence of adjacent grains in the layer was revealed. In particular, it was demonstrated that dry grains can be replenished with the liquid from adjacent wet grains.

In the practice, beds consisting of a huge number of catalyst grains are used. The operation efficiency of a catalytic reactors substantially depends on the liquid phase distribution in a granular bed. It is highly probable that the appearance of hot spots in a bed is also associated with the character of the liquid phase distribution. Hence, it is very important to map the liquid phase distribution in a catalytic reactor for different operation modes. Finally, these investigations will allow establishment of the mechanisms responsible for the development of critical phenomena both at the micro- and macroscale. We carried out a series of investigations of the liquid phase distribution in a granular bed of spherical catalyst grains with a diameter of either 1 or 2–3 mm directly in the course of hydrogenation. In particular, it was found that the liquid phase distribution in a catalyst layer substantially depends on the conditions of reactor start-up. For example, essentially different liquid phase distributions are observed when a liquid reactant is supplied to a dry layer or a layer initially saturated with a liquid.

In subsequent studies, we succeeded in obviating the need for impregnation of catalyst grains with paramagnetic ions to reduce the image acquisition time. Procedures were developed for three-dimensional imaging of the whole catalyst bed with a submillimetre spatial resolution in 20–30 s and for acquiring a set of five two-dimensional sections in 2–3 s each. This, in turn, enabled us to perform the detailed study of the dynamics of the liquid phase redistribution in regular layers of spherical catalyst grains. The results of these investigations confirmed the existence of partially wet catalyst grains over long periods of time, replenishment of dry or partially wet grains with a liquid from adjacent grains and the fluctuating liquid front propagation in partially wet grain (Fig. 5). Evidently, the observation of such effects, which are impossible in a ‘cold’

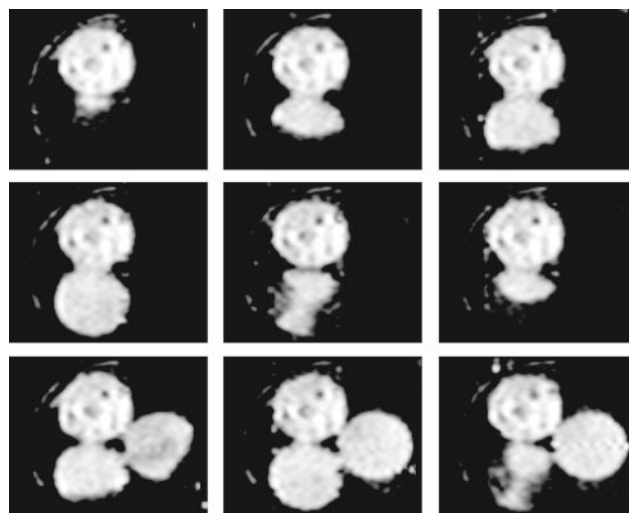


Figure 5. Liquid phase distribution in a regular bed of a catalyst (1% Pd/ γ -Al₂O₃, catalyst bed diameter is 4.2 mm) directly in the course of octene hydrogenation.

Each image was acquired for 3 s at 0.5–3.5-min intervals; the images show a non-steady-state operation of the reactor; lighter shades of gray correspond to a higher local concentration of the liquid phase.

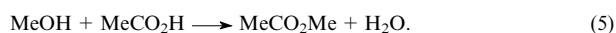
reactor (in the absence of reaction), is a manifestation of the non-linear coupling of heat and mass transfer processes, phase transformations and a chemical reaction proceeding in the reactor. In the absence of the reaction, the liquid is approximately uniformly distributed as a result of capillary imbibition of the liquid in porous grains. The above-described approaches allow individual imaging of both a liquid phase in porous grains and a liquid filling the space between grains. Experiments demonstrated that the liquid phase transport occurs primarily through film flow over the surface of catalyst grains and showed the possible disturbance of the local phase equilibrium in an exothermic reaction, which creates conditions for the reactor to deviate from a stable operation mode.¹⁵⁴

Images obtained in the above-described experiments reflect the total liquid (both the reactant and the product) distribution. However, NMR is primarily a powerful spectroscopic method. Many available applications are based on a combination of NMR spectroscopy and imaging, which give either spatially localised NMR spectra, *i.e.*, spectra reflecting the local chemical composition, or tomographic images (the spatial distribution of the substance in question). These data are necessary for characterisation of the reactor operation because they provide spatially resolved information on the degree of conversion of the reactants. Undoubtedly, an improvement of combined NMR/MRI techniques for chemical engineering will be one of the main directions of further development in this field.

Unlike high-resolution NMR spectra of bulk solutions, in which the linewidth is often < 1 Hz, NMR spectra of pore-filling liquids are characterised by substantially broader lines. Nevertheless, in room-temperature NMR spectra with a spatial resolution of $2 \times 0.5 \times 0.12$ mm³ of a mixture of AMS and cumene, which fills pores of an alumina grain, the ¹H linewidth is not so large, and at least semiquantitative analysis of the composition of the reaction mixture can be performed.¹⁴⁹ Subsequent experiments were carried out for an operating reactor with a packed bed of catalyst grains with a diameter of 1 mm.¹⁵¹ In three-dimensional experiments (one spectral and two spatial coordinates), NMR spectra were measured for each element of a two-dimensional image. The reactant-to-

product ratios in different regions of the granular layer were determined directly in the course of the reaction by comparing these spectra with the spectra for pure AMS and cumene. The NMR spectrum detected in the upper part, where the liquid reactant is supplied, corresponds to virtually pure AMS; the NMR spectrum detected in the lower part, to the virtually pure product (cumene); the spectrum detected in the middle part corresponds to a mixture of the reactant and the product. Their ratio gradually changes along the height of the layer. In addition, the degree of conversion in the radial direction also varies.

A number of other catalytic reactions (liquid–solid and gas–liquid–solid) were studied by MRI. For example, esterification of methanol and acetic acid giving rise to methyl acetate and water in a reactor with a granular bed composed of small grains of the acidic form of an ion-exchange resin was documented.¹⁵⁵



The spatial pattern of the degree of conversion in a reactor was obtained by combining the spectroscopic and MRI methods. It was found that the concentration of the product along the length of the reactor increases and the degree of conversion decreases as the flow rate increases. The variations of the conversion in the radial direction are as high as $\sim 20\%$. All experiments were carried out under stationary conditions, because the signal acquisition time was long. Later, investigations aimed at revealing correlations between the degree of conversion and the transport characteristics of the reactor with a granular bed were performed.^{68, 156} For example, the plot of the local conversion *vs.* the local rate showed a good correlation between these two parameters in spite of the fact that the degree of conversion is not a local characteristic. An approach used in the studies^{68, 155, 156} is based on the detection of ^1H NMR signals of the OH groups of acetic acid, methanol and water, which coalesce into one broadened line as a result of fast proton exchange. The position of this line in the spectrum depends on the relative concentrations of all three compounds. This approach is limited to a particular class of reactions. A more common approach, which is based on the use of MRI with a spectroscopic resolution, was successfully used¹⁵⁷ for catalytic esterification of propionic acid and butan-1-ol giving rise to butyl propionate and water with the use of an enzyme immobilised on a single calcium alginate grain,



Experiments with the use of one spatial coordinate and one spectroscopic coordinate made it possible to trace the increase in the intensity of the signals of water and butyl propionate and the decrease in the intensity of the signal of butanol in the grain in the course of the reaction.

Multinuclear MRI produces images from not only the ^1H NMR signal but also from signals of other magnetic nuclei. In particular, the ^{13}C nucleus is characterised by a substantially broader range of chemical shifts than the ^1H nucleus, which, in principle, enables one to obtain substantially more accurate quantitative spectral information even in the case of substantial line broadening in NMR spectra. However, since the natural isotopic abundance of ^{13}C is very low (1.1%), the quality of images is poor and, consequently, a long time is required for image acquisition or it is necessary to use isotope-labelled compounds. Nevertheless, such investigations were documented. The competitive transformation of 2-methylbut-2-ene into *tert*-amyl methyl ether and *tert*-amyl alcohol at 40°C catalysed by ion-exchange resin grains ($600\text{--}850\ \mu\text{m}$) in a reactor with a diameter of $15\ \text{mm}$ was studied.¹⁵⁸



Two-dimensional integrated images of a reactor were acquired, and a ^{13}C NMR spectrum was measured for each element. The conversion of 2-methylbut-2-ene into ether and alcohol was found to be gradually increased in the axial direction, the selectivity to ether being retained at $\sim 75\text{--}80\%$. Both the selectivity and the conversion fluctuate in the transverse direction, the variation of the conversion for a fixed axial coordinate being $\sim 15\%$. The equilibrium magnetisation transfer from ^1H to ^{13}C nuclei was used to compensate, in part, for the loss of sensitivity in experiments with a natural isotopic abundance of ^{13}C . However, even in this case, a moderate spatial resolution ($2.5 \times 3.75\ \text{mm}$, without slice selection) was achieved at the acquisition time of one image of 16 h. The ^{13}C NMR signal detection was used also in investigations of hydrogenation and isomerisation of oct-1-ene.¹⁵⁹ To record spectra with a spatial resolution of $2.8\ \text{mm}$ along one coordinate integrated over two other coordinates, more than a quarter of an hour was required.

In spite of considerable difficulties in performing MRI of gases and problems associated with the use of high temperatures in a probe of a microimaging instrument, some research teams designed special apparatus and proceeded to studies of high-temperature gas-phase reactions. For example, to perform MRI studies of combustion processes, a probe with water cooling and a system for removing combustion products was designed.¹⁶⁰ In the experiments, the behaviour of gas streams before and after methane ignition was compared. A stream of the unignited gas was visualised a flow rate of up to $2\ \text{m s}^{-1}$ from an orifice with a diameter of $1\ \text{mm}$. In the presence of flame, an NMR signal gradually disappears at a distance of $\sim 3\ \text{mm}$ from the orifice. The acquisition time of each image was several hours.

One possible way of enhancing the sensitivity in gas-phase MRI experiments is based on the use of hyperpolarised gases (see Section III). In particular, this approach was applied in studies of non-catalytic methane combustion over the surface of a granular layer of partially dehydrated zeolite NaX.¹⁶¹ A mixture of hyperpolarised $^{129}\text{Xe}^*$ and methane was supplied to the layer together with air from the bottom, and the process was studied by recording ^{129}Xe NMR spectra without spatial resolution. Due to very high sensitivity of the ^{129}Xe chemical shift to the environment, the authors succeeded in visualising different regions in the cell, which differ in the concentration of xenon, the composition of the mixture and the temperature. The exchange between these regions in the course of combustion was studied by two-dimensional exchange NMR spectroscopy.

3. Hydrogenation with parahydrogen

Hyperpolarised gases and liquids can be prepared by hydrogenation. Molecular hydrogen (H_2) is a mixture of two spin isomers, *viz.*, orthohydrogen ($o\text{-H}_2$, the total nuclear spin $I = 1$) and parahydrogen ($p\text{-H}_2$, $I = 0$). Only orthohydrogen gives an observable NMR signal due to RF-induced transitions between three spin sublevels. The spin relaxation times of the ^1H NMR signal under normal conditions are rather short ($T_1 = 3\ \text{ms}$, $T_2 = 0.4\ \text{ms}$). However, states with different multiplicities are not mixed in relaxation process, and the time of the ortho–para conversion for hydrogen under normal conditions can be as long as one year. Hence ortho- and parahydrogen can be considered as two different gases, one of which ($p\text{-H}_2$) is generally not involved in NMR experiments because it has the zero nuclear spin.

At room temperature, the $o\text{-H}_2 : p\text{-H}_2$ equilibrium ratio is close to a random value (3 : 1). At lower temperatures, the equilibrium is shifted to $p\text{-H}_2$. At the liquid hydrogen temperature, the equilibrium mixture consists virtually exclusively of $p\text{-H}_2$. At $77\ \text{K}$, the equilibrium ratio is approximately 1 : 1. Taking into account the low rate of spontaneous ortho–para

conversion, normal hydrogen is cooled over a catalyst for ortho–para conversion to achieve the equilibrium. Paramagnetic compounds [FeO(OH), activated carbon, *etc.*] are commonly used as catalysts for this process. An advantage of a low rate of spontaneous conversion is that, after the establishment of the equilibrium at low temperature, hydrogen can be stored at room temperature over a long period of time, no substantial changes in the o-H₂:p-H₂ ratio being observed.

Non-equilibrium mixtures of ortho- and parahydrogen are characterised by the presence of an overall correlation of nuclear spins in an ensemble of molecules. For this correlation to be observed in NMR spectra, it is necessary to break the magnetic equivalence of nuclear spins of two hydrogen atoms. Evidently, this can be achieved by using parahydrogen in hydrogenation, as a result of which two hydrogen atoms in the reaction product are in non-equivalent positions. It is important that two atoms of one hydrogen molecule be added to one substrate molecule, which retains the initial correlation of nuclear spins. In this case, the intensity of the NMR signal of the reaction product increases by a factor of 4×10^4 for a spectrometer with a magnetic field of 7 T and this signal is even more enhanced in weak fields. The spectral manifestation of parahydrogen-induced polarisation depends on the experimental scheme. If hydrogenation is performed directly in an NMR probe, the spectrum shows two antiphase multiplets (the PASADENA effect, parahydrogen and synthesis allow dramatically enhanced nuclear alignment). If the reaction is performed in magnetic field of the Earth followed by the transfer of a sample to a probe of a spectrometer, a net enhancement of two multiplets having opposite signs is observed (ALTADENA, adiabatic longitudinal transport and dissociation engender net alignment).^{162, 163}

During 15 years, hydrogenation with parahydrogen was used primarily in studies of the reaction mechanisms of homogeneous hydrogenation with transition metal complexes (for example, with the Wilkinson and Vaska catalysts). The reaction mechanism implies the formation of a metal dihydride complex as a short-lived intermediate. The use of parahydrogen in hydrogenation allows an increase in the intensity of the NMR signal by several orders of magnitude and, consequently, it is possible to detect ¹H NMR spectra of intermediate dihydride complexes.¹⁶⁴ Parahydrogen-induced polarisation was observed in homogeneous processes involving different Rh, Ir, Ru, Pt and Os complexes. Detailed studies of the kinetics and mechanism of homogeneous hydrogenation reactions involving such complexes were carried out with the use of parahydrogen as a spin label, and in some cases the new intermediate species were detected.^{165–168} As a result of polarisation transfer from protons to other nuclei (¹³C, ³¹P, ¹⁵N, ¹⁹F), a much more detailed spectroscopic information can be obtained.^{169–172}

Interest in the use of parahydrogen for enhancement of the NMR signal was rekindled after the publication of the study,¹⁷³ where hydrogenation with parahydrogen was used for the first time to enhance the signal in MRI. In this study, hydrogenation was followed by polarisation transfer to ¹³C nuclei by varying the external magnetic field. Then the solution was injected into a blood vessel of a laboratory animal and an MR image was recorded. The use of this procedure and its subsequent modifications^{169, 174} allowed the authors to acquire two-dimensional images of a blood vessels (angiograms) from the ¹³C NMR signal of the reaction product in less than 1 s with a natural isotopic abundance of ¹³C.

The presence of a catalyst in solution is a drawback of the approach used in the studies,^{169, 173, 174} which substantially limits its application in studies of living organisms and makes it impossible to perform these investigations in medical purposes. In addition, this fact hampers the development of technical applications of MRI. For example, the construction

of systems with a continuous polarised fluid (liquid or gas) flow for MRI of different objects with the use of homogeneous hydrogenation requires large amounts of an expensive catalyst. In principle, the catalyst can be removed from solution with an appropriate adsorbent.¹⁷⁵ However, the polarisation relaxation time is equal to a few seconds and is additionally decreased in the case of a contact between the product and a porous material.

Up to 2007, data on parahydrogen-induced polarisation in heterogeneous reactions were lacking. It should be noted that polarisation was observed¹⁷⁶ when performing hydrogenation on colloidal (Pd)_x[N(n-C₈H₁₇)₄Cl]_y particles in a liquid. However, it cannot be ruled out that the solution simultaneously contained the dissolved metal complex, which was responsible for the observed polarisation. In addition, the authors of this study mentioned the commonly accepted view that polarisation of the product is impossible in heterogeneous catalytic hydrogenation with parahydrogen. Actually, many industrial hydrogenation catalysts are highly dispersed metal (Pt or Pd) particles deposited on a porous support (for example, Al₂O₃). It is commonly accepted that hydrogenation on these catalysts involves dissociative chemisorption of hydrogen on metal particles, hydrogen migration over the particle surface and spillover onto the support. Under these conditions, the probability that the correlation of nuclear spins of the starting parahydrogen molecule will be retained and that two hydrogen atoms of one H₂ molecule will be present in one product molecule is negligibly small. Hence, until recently, it was believed that parahydrogen-induced polarisation can be observed only in homogeneous catalytic processes with all attendant problems and drawbacks.

In recent years, experts in catalysis have made great efforts to establish bridges between homogeneous and heterogeneous catalytic processes.¹⁷⁷ In many cases, homogeneous catalysts exhibit much higher activity and selectivity; however, the unbeatable advantage of heterogeneous catalysts is that the latter can easily be removed from the reaction mixture. Presently, the latter fact is of key importance not only in view of strengthening of environmental requirements for industrial processes, but also because the catalysts become considerably more expensive as their structure gets progressively more complex. In this connection, a combination of the advantages of homogeneous and heterogeneous catalysis by immobilisation of homogeneous catalysts on an appropriate porous support is one of increasing trends in modern catalysis.^{178, 179} Nowadays, several procedures are available for immobilisation based on formation of hydrogen bonds, ion pairs, covalent attachment to organic or inorganic supports, *etc.* Many of these procedures were used also in the design of new hydrogenation catalysts^{180–185} characterised by high stability, efficiency and selectivity in heterogeneous hydrogenation under mild conditions. It is important that, in many cases, the chemical structure of metal complexes does not undergo substantial changes upon their immobilisation. Consequently, the reaction mechanism presumably remains unchanged upon immobilisation. However, it is difficult to obtain direct evidence for this fact.

Polarisation in heterogeneous hydrogenation with parahydrogen was observed for the first time in the study by Koptug *et al.*¹⁸⁶ (Fig. 6). For this purpose the following three catalysts were used: the Wilkinson catalyst (**1**) immobilised on a styrene–divinylbenzene copolymer (**1**/polymer), the same catalyst immobilised on modified silica gel RhCl(PPh₃)₂PPh₂(CH₂)₂–SiO₂ (**1**/SiO₂) and the immobilised tridentate complex Rh(cod)(sulfos)–SiO₂ (**2**/SiO₂; cod is cycloocta-1,5-diene; sulfos is –O₃S(C₆H₄)CH₂C(CH₂PPh₂)₃). In one series of experiments, hydrogenation was carried out in magnetic field of an NMR spectrometer. For this purpose, a tube with a solution of the substrate (styrene) and the catalyst

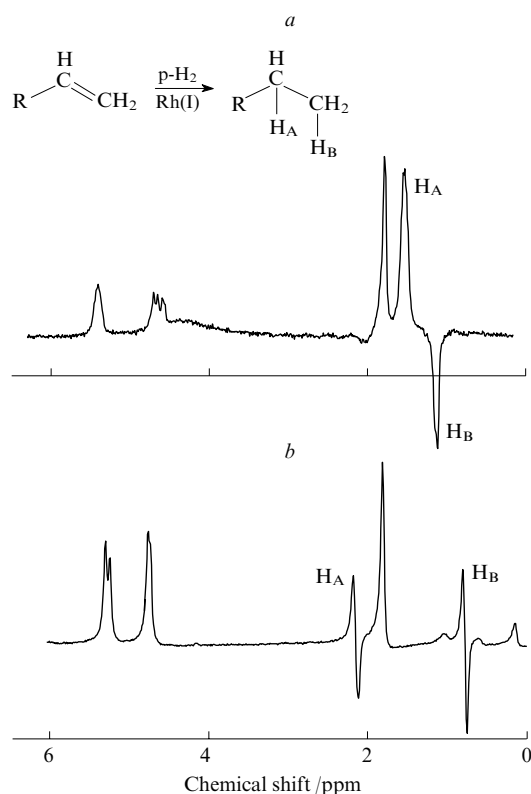


Figure 6. Parahydrogen-induced polarisation of nuclear spins in heterogeneous hydrogenation of unsaturated compounds.

(a) ALTADENA for propylene hydrogenation ($R = \text{Me}$) in weak field at $130\text{ }^{\circ}\text{C}$, (b) PASADENA for styrene hydrogenation ($R = \text{Ph}$) in strong field at $60\text{ }^{\circ}\text{C}$. In both cases, equilibrium NMR signals of the reaction product are negligibly small.

($1/\text{SiO}_2$ or $1/\text{polymer}$) was placed in a probe of the spectrometer and heated to $65\text{--}80\text{ }^{\circ}\text{C}$. Both catalysts efficiently hydrogenate styrene to ethylbenzene. In reactions with the use of enriched parahydrogen, both catalysts lead to substantial polarisation of nuclear spins in the reaction product and give rise to the characteristic antiphase structure of multiplets in the NMR spectrum (PASADENA, see Fig. 6b). The NMR spectra of the product, which was prepared by hydrogenation outside a magnet followed by the transfer of the sample to a probe of an NMR spectrometer, show multiplets with net polarisation of opposite signs (ALTADENA). It was also found that after removal of the catalyst from the solution, bubbling with hydrogen did not lead to either the formation of the product or polarisation. These results confirm that polarisation upon hydrogenation with parahydrogen was observed in a heterogeneous process for the first time.

Besides, hydrogenation with parahydrogen was applied for the first time¹⁸⁶ to generate nuclear spin polarisation in gases. For this purpose, catalysts immobilised on a porous support ($1/\text{SiO}_2$ or $2/\text{SiO}_2$) were used. To observe the PASADENA effect, the tube with a dry catalyst was placed in an NMR probe and heated to $80\text{ }^{\circ}\text{C}$. A mixture of propylene and enriched parahydrogen was continuously introduced into a tube through thin capillaries. The nuclear spin polarisation of the reaction product, *viz.*, propane, was determined from NMR spectra. To observe the ALTADENA effect, the reaction was carried out outside a magnet. For this purpose, a mixture of propylene and enriched parahydrogen was continuously purged through a copper tube packed with a catalyst heated to $130\text{ }^{\circ}\text{C}$ and then passed to an NMR probe (see Fig. 6a). The observation of polarisation upon hydrogenation of a gas is

unambiguous evidence for the fact that nuclear spin polarisation can be produced not only in homogeneous but also in heterogeneous processes. Later, polarisation in hydrogenation of propylene with parahydrogen was achieved with the use of the silica gel-immobilised $\text{RhCl}(\text{POMe}_3)_3$ complex.

In further investigations,¹⁸⁷ the possibility of the preparation of a hyperpolarised gas in heterogeneous hydrogenation was used for MR imaging of model objects; NMR tubes with cross-shaped partitions or capillary bundles mounted inside the tubes were used as such objects. As in the earlier experiments,¹⁸⁶ hydrogenation of propylene was performed using a continuous flow of a gas mixture through a heated catalyst. Then the polarised product (propane) was delivered through a system of tubes to the model object, and the MR image was obtained by detecting the NMR signal of the polarised gas. Until recently, the preparation of hyperpolarised gases was limited primarily by laser polarisation of noble gases (see Section III). Therefore, the results of the studies^{186, 187} substantially extended the range of gases, for which the signal-to-noise ratio in MRI experiments can be substantially improved by producing nuclear spin polarisation.

The above-described results are of importance for several reasons. First, the observation of polarisation of the product with the use of parahydrogen is direct evidence for the pair-wise addition of two hydrogen atoms of an H_2 molecule to one substrate molecule. Therefore, these results confirm that the reaction mechanism of hydrogenation by metal complexes remains unchanged upon their immobilisation onto a support. Second, the pair-wise addition is a necessary but not sufficient condition for observation of polarisation. After the formation of the dihydride complex, two hydrogen atoms become non-equivalent and their spin correlation decays due to spin relaxation.¹⁸⁸ Immobilisation of the complex leads to a substantial decrease in molecular mobility, and the spin relaxation times can be substantially shorter than the spin relaxation times of complexes in solution. The observation of polarisation indicates that the lifetime of intermediate dihydride cannot be substantially longer than its spin relaxation time.

The preparation of pure fluids with polarised nuclear spins opens a broad spectrum of new possible applications, particularly, those associated with the NMR signal detection in low and ultra-low magnetic fields,^{189, 190} where the equilibrium differences in the populations of spin energy sublevels are very small. The possibility of creating continuous flows of polarised fluids is particularly attractive. This possibility was exemplified by heterogeneous hydrogenation of propylene. Efficiency of biomedical experiments with parahydrogen-induced polarisation can be increased using solid catalysts. In addition, many studies based on homogeneous hydrogenation with parahydrogen are characterised by an uncertain duration of this process because the termination of bubbling of a solution with parahydrogen does not lead to the immediate termination of the reaction. This substantially complicates the interpretation of the results.^{170, 191} It is important to obtain pure quantum states in experiments with the use of parahydrogen-induced polarisation aimed at designing quantum computers.^{192, 193}

In view of the results of recent investigations, hydrogenation with parahydrogen has yet another important potential application in NMR. Many modern NMR and MRI experiments are based on the creation of particular perturbation of a spin system, which then undergoes evolution over a particular period of time. The evolution is followed by the 'read-out' of the new state of the spin system. This principle provides the basis for the diffusion coefficient and flow rate measurements,^{139, 194} different two-dimensional NMR spectroscopic experiments,¹⁹⁵ *etc.* If the evolution period is substantially longer than the spin relaxation times, the detection of the final state of the spin system does not give useful information on the

processes in question. Hence, until recently, researchers have believed that the maximum evolution time is comparable with the spin–lattice relaxation time (T_1) of the spin system. However, recently it has been demonstrated^{196,197} that this limitation can be overcome by using the unique properties of singlet spin states. Actually, for pairs of equivalent nuclei with spin 1/2, the states with a certain total spin of the pair are the eigenstates of the Hamiltonian: singlet ($I = 0$) and triplet ($I = 1$). This is also the case with a hydrogen molecule (see above). The spinless singlet state is not involved in relaxation processes which affect the NMR spectra, and the interconversion time between states with different total spins can be longer than the spin relaxation times by an order of magnitude or larger.^{196,197} As in the above-considered NMR of parahydrogen, the singlet state of a pair of nuclei is not directly involved in NMR experiments. Hence, to use the unique properties of singlet states, it is necessary to construct a molecular system in which the magnetic equivalence of a pair of nuclei could be ‘switched on’ and ‘switched off’ under the external action on the spin system. So far, the two different ways of performing this switching have been suggested: the physical transfer of a sample from a weak magnetic field to a strong field and back¹⁹⁷ or prolonged RF irradiation of the spin system in a strong field of a spectrometer.¹⁹⁶ For example, the measured lifetime of the singlet state (T_s) of 2,3-dibromothiophene in DMSO- d_6 in weak field was 104 s ($T_1 = 17$ s).¹⁹⁷ For 2-chloroacrylonitrile in DMSO- d_6 , $T_s = 141$ s ($T_1 = 7.8$ s) in the case of continuous RF irradiation.¹⁹⁶

Practical outputs of these investigations hold considerable promise. A substantial increase in the lifetime of spin coherence can be useful in studies of slow transport processes. For example, the use of long-lived singlet states in experiments on measurements of molecular diffusion coefficients (D) by PFG NMR at $T_s = 10 T_1$ allows a decrease of the lower detection limit of D by an order of magnitude, all other factors being the same. An example of the application of this approach was described in the study,¹⁹⁸ where the diffusion coefficients of 2-chloroacrylonitrile in a DMSO- d_6 –D $_2$ O mixture were measured in the temperature range from -46 to $+25$ °C. Long-lived spin states hold promise also in investigations of very slow dynamic processes, such as chemical exchange, conformational transformations, protein and RNA refolding, etc. Two-dimensional exchange spectroscopy with the use of long-lived singlet states was proposed in the study.¹⁹⁹ This study dealt with conformational transformations of monosaccharide, in which all hydrogen atoms, except for two atoms, were replaced by deuterium. The lifetime of the singlet state for this pair of protons was demonstrated to be 37 times longer than T_1 . In an exchange experiment, the mixing time allotted for a conformational change of the molecules was 12 s ($T_1 = 0.7$ s).

The extensive development of the theory of long-lived spin states is presently underway.^{200–204} Evidently, the use of states with lifetimes substantially longer than T_1 also shows promise for imaging applications, particularly, for liquid and gas flows, for example in the remote imaging (see Section III). A combination of the properties of long-lived singlet states and nuclear polarisation produced by hydrogenation with parahydrogen is also promising.^{170,191} The initially produced state of a pair of nuclear spins in the reaction product is singlet, and an additional advantage is that an excess of these states in an ensemble of molecules increases by several orders of magnitude.

V. Conclusion

In recent years, the number of studies in the area of physico-chemical applications of the MRI technique has rapidly increased. In addition to a substantial extension of the range of objects and processes, the MRI technique itself underwent

considerable changes. This stage of investigations is characterised by the development of new applications, which have been considered to be impossible to implement in practice until recently. These are studies of solids without the use of solid-state NMR techniques, investigations of gas transport, studies of high-temperature reactions, etc. In addition, the development of methods of nuclear spin hyperpolarisation and spectroscopy of singlet spin states opens new prospects for the further progress in MRI.

We thank our colleagues engaged in these investigations and particularly our co-authors working at the Borskoy Institute of Catalysis of the Siberian Branch of the Russian Academy of Sciences. The research has been performed with the financial support of the Russian Foundation for Basic Research (Project No. 05-03-32472), the Division of Chemistry and Materials Science of the Russian Academy of Sciences (Project Nos 5.2.3 and 5.1.1), the Siberian Branch of the Russian Academy of Sciences (Integration Grant 11), the Programme for State Support of Leading Scientific Schools of the Russian Federation (Grant NSH-4821.2006.3), the Russian Science Support Foundation (I V Koptug and A A Lysova), the Council on Grants of the President of the Russian Federation (Grant MK-5135.2007.3) and the Global Energy Foundation (A A Lysova).

References

1. *NMR Imaging in Chemical Engineering* (Eds S Stapf, S Han) (Weinheim: Wiley-VCH, 2005)
2. *Appl. Magn. Reson. (Special Issue)* **32** 1 (2007)
3. L F Gladden *AIChE J.* **49** 2 (2003)
4. M D Mantle, A J Sederman *Prog. Nucl. Magn. Reson. Spectrosc.* **43** 3 (2003)
5. I V Koptug, R Z Sagdeev *Usp. Khim.* **71** 672 (2002) [*Russ. Chem. Rev.* **71** 593 (2002)]
6. I V Koptug, R Z Sagdeev *Usp. Khim.* **71** 899 (2002) [*Russ. Chem. Rev.* **71** 789 (2002)]
7. I V Koptug, R Z Sagdeev *Usp. Khim.* **72** 183 (2003) [*Russ. Chem. Rev.* **72** 165 (2003)]
8. P Blumler, B Blumich *Rubber Chem. Technol.* **70** 468 (1997)
9. B Blumich, P Blumler, K Saito, in *Solid State NMR of Polymers. Studies in Physical and Theoretical Chemistry* Vol. 84 (Eds I Ando, T Asakura) (Amsterdam: Elsevier, 1998) p. 123
10. J R Moore, L Garrido, J L Ackerman *Ceram. Eng. Sci. Proc.* **11** 1302 (1990)
11. J L Ackerman, L Garrido, J R Moore, B Pfeleiderer, Y Wu, in *Magnetic Resonance Microscopy. Methods and Applications in Materials Science, Agriculture and Biomedicine* (Eds B Blumich, W Kuhn) (Weinheim: VCH, 1992) p. 237
12. M S Conradi *J. Magn. Reson.* **93** 419 (1991)
13. W S Veeman, in *Magnetic Resonance Microscopy. Methods and Applications in Materials Science, Agriculture and Biomedicine* (Eds B Blumich, W Kuhn) (Weinheim: VCH, 1992) p. 29
14. S Matsui, M Nonaka, T Nakai, T Inouye *J. Magn. Reson.* **138** 220 (1999)
15. P J McDonald, B Newling *Rep. Prog. Phys.* **61** 1441 (1998)
16. E W Randall, in *Encyclopedia of Nuclear Magnetic Resonance* Vol. 9 (Eds D M Grant, R K Harris) (Chichester: Wiley, 2002) p. 150
17. P Bodart, T Nunes, E W Randall *Solid State NMR* **8** 257 (1997)
18. V S Swaminathan, B H Suits *J. Magn. Reson.* **132** 274 (1998)
19. S Choi, X-W Tang, D G Cory *Int. J. Imaging Syst. Technol.* **8** 263 (1997)
20. I V Mastikhin, B J Balcom, P J Prado, C B Kennedy *J. Magn. Reson.* **136** 159 (1999)
21. C B Kennedy, B J Balcom, I V Mastikhin *Can. J. Chem.* **76** 1753 (1998)
22. G R Davies, D J Lurie, J M S Hutchison, S J McCallum, I Nicholson *J. Magn. Reson.* **148** 289 (2001)
23. J B Miller *Prog. Nucl. Magn. Reson. Spectrosc.* **33** 273 (1998)

24. V Antochshuk, M-J Kim, A K Khitrin *J. Magn. Reson.* **167** 133 (2004)
25. M J Kim, A K Khitrin *Magn. Reson. Imaging* **23** 865 (2005)
26. I V Koptug, D R Sagdeev, E Gerkema, H Van As, R Z Sagdeev *J. Magn. Reson.* **175** 21 (2005)
27. I V Koptug, A A Lysova, R Z Sagdeev, V A Kirillov, A V Kulikov, V N Parmon *Catal. Today* **105** 464 (2005)
28. I V Koptug, A A Lysova, in *NMR Imaging in Chemical Engineering* (Eds S Stapf, S Han) (Weinheim: Wiley-VCH, 2005) p. 570
29. I V Koptug, A A Lysova *Bruker Spin Rep.* **157–158** 22 (2006)
30. I V Koptug, A V Khomichev, A A Lysova, R Z Sagdeev *Appl. Magn. Reson.* (2007) (in the press)
31. D D Laws, H M L Bitter, A Jerschow *Angew. Chem., Int. Ed.* **41** 3096 (2002)
32. F H Larsen, H J Jakobsen, P D Ellis, N C Nielsen *J. Magn. Reson.* **131** 144 (1998)
33. P R Bodart, J-P Amoureux, Y Dumazy, R Lefort *Mol. Phys.* **98** 1545 (2000)
34. W Wlodarczyk, R Boroschewski, M Hentschel, P Wust, G Monich, R Felix *J. Magn. Reson. Imaging* **8** 165 (1998)
35. D German, P Chevallier, A Laurent, H Saint-Jalmes *Magn. Reson. Mater. Phys., Biol. Med.* **13** 47 (2001)
36. K P Nott, L D Hall *Trends Food Sci. Technol.* **10** 366 (1999)
37. N Hosten, R Felix, P Wust, W Wlodarczyk, M Hentschel, R Noeske, H Rinneberg *Phys. Med. Biol.* **44** 607 (1999)
38. S J Doran, T A Carpenter, L D Hall *Rev. Sci. Instrum.* **65** 2231 (1994)
39. D Hauck, P Blumler, B Blumich *Macromol. Chem. Phys.* **198** 2729 (1997)
40. B H Suits, D White *J. Appl. Phys.* **60** 3772 (1986)
41. J Goetz, K Zick, C Heinen, T Koenig *Chem. Eng. Process.* **41** 611 (2002)
42. C Heinen, J Tillich, H Buggisch, T Zeiser, H Freund *Magn. Reson. Imaging* **23** 369 (2005)
43. M L Johns, A J Sederman, A S Bramley, L F Gladden, P Alexander *AIChE J.* **46** 2151 (2000)
44. A Feinauer, S A Altobelli, E Fukushima *Magn. Reson. Imaging* **15** 479 (1997)
45. T W J Scheenen, D van Dusschoten, P A de Jager, H Van As *J. Magn. Reson.* **142** 207 (2000)
46. T W J Scheenen, F J Vergeldt, C W Windt, P A de Jager, H Van As *J. Magn. Reson.* **151** 94 (2001)
47. B R Locke, M Acton, S J Gibbs *Langmuir* **17** 6771 (2001)
48. U Tallarek, T W J Scheenen, H Van As *J. Phys. Chem. B* **105** 8591 (2001)
49. A J Sederman, M D Mantle, C Buckley, L F Gladden *J. Magn. Reson.* **166** 182 (2004)
50. J D Seymour, S L Codd, E L Gjersing, P S Stewart *J. Magn. Reson.* **167** 322 (2004)
51. B C Hoskins, L Fevang, P D Majors, M M Sharma, G Georgiou *J. Magn. Reson.* **139** 67 (1999)
52. K Potter, R L Kleinberg, F J Brockman, E W McFarland *J. Magn. Reson., Ser. B* **113** 9 (1996)
53. G Gonzalez-Gil, P N L Lens, A Van Aelst, H Van As, A I Versprille, G Lettinga *Appl. Environ. Microbiol.* **67** 3683 (2001)
54. B Manz, F Volke, D Goll, H Horn *Biotechnol. Bioeng.* **84** 424 (2003)
55. K P Nott, M Paterson-Beedle, L E Macaskie, L D Hall *Biotechnol. Lett.* **23** 1749 (2001)
56. M Paterson-Beedle, K P Nott, L E Macaskie, L D Hall *Methods Enzymol.* **337** 285 (2001)
57. E E Beuling, D van Dusschoten, P Lens, J C van den Heuvel, H Van As, S P P Ottengraf *Biotechnol. Bioeng.* **60** 283 (1998)
58. E L Gjersing, S L Codd, J D Seymour, P S Stewart *Biotechnol. Bioeng.* **89** 822 (2005)
59. S P Wolfe, E Hsu, L M Reid, J M Macdonald *Biotechnol. Bioeng.* **77** 83 (2001)
60. P E Thelwall, A A Neves, K M Brindle *Biotechnol. Bioeng.* **75** 682 (2001)
61. C Planchamp, M K Ivancevic, C M Pastor, J-P Vallee, S Pochon, F Terrier, J M Mayer, M Reist *Biotechnol. Bioeng.* **85** 656 (2004)
62. P N L Lens, M A Hemminga *Biodegradation* **9** 393 (1998)
63. H Van As, P Lens *J. Ind. Microbiol. Biotechnol.* **26** 43 (2000)
64. L F Gladden *Top. Catal.* **24** 19 (2003)
65. A J Sederman, L F Gladden *Chem. Eng. Sci.* **56** 2615 (2001)
66. L F Gladden, M D Mantle, A J Sederman, E H L Yuen *Appl. Magn. Reson.* **22** 201 (2002)
67. L F Gladden, M H M Lim, M D Mantle, A J Sederman, E H Stitt *Catal. Today* **79** 203 (2003)
68. L F Gladden, P Alexander, M M Britton, M D Mantle, A J Sederman, E H L Yuen *Magn. Reson. Imaging* **21** 213 (2003)
69. M D Mantle, A J Sederman, L Gladden *Chem. Eng. Sci.* **56** 523 (2001)
70. M H M Lim, A J Sederman, L F Gladden, E H Stitt *Chem. Eng. Sci.* **59** 5403 (2004)
71. L D Anadon, M H M Lim, A J Sederman, L F Gladden *Magn. Reson. Imaging* **23** 291 (2005)
72. N L Nguyen, V van Buren, A von Garnier, E H Hardy, R Reimert *Chem. Eng. Sci.* **60** 6289 (2005)
73. A J Sederman, M D Mantle, L F Gladden *J. Magn. Reson.* **161** 15 (2003)
74. M D Mantle, A J Sederman, L F Gladden, S Raymahasay, J M Winterbottom, E H Stitt *AIChE J.* **48** 909 (2002)
75. J J Heras, A J Sederman, L F Gladden *Magn. Reson. Imaging* **23** 387 (2005)
76. A J Sederman, M D Mantle, L F Gladden *Magn. Reson. Imaging* **21** 359 (2003)
77. A A Khrapitchev, S Han, S Stapf, B Blumich *J. Magn. Reson.* **159** 36 (2002)
78. I Okamoto, S Hirai, K Ogawa *Meas. Sci. Technol.* **12** 1465 (2001)
79. I V Koptug, L Yu Ilyina, A V Matveev, R Z Sagdeev, V N Parmon, S A Altobelli *Catal. Today* **69** 385 (2001)
80. L G Kaiser, J W Logan, T Meersmann, A Pines *J. Magn. Reson.* **149** 144 (2001)
81. I V Koptug, S A Altobelli, E Fukushima, A V Matveev, R Z Sagdeev *J. Magn. Reson.* **147** 36 (2000)
82. E Brunner, M Haake, L Kaiser, A Pines, J A Reimer *J. Magn. Reson.* **138** 155 (1999)
83. S Tsushima, S Hirai, Y Yamamoto, Y Nakasuji *Magn. Reson. Imaging* **21** 430 (2003)
84. B Newling, C C Poirier, Y Zhi, J A Rioux, A J Coristine, D Roach, B J Balcom *Phys. Rev. Lett.* **93** 154503-1 (2004)
85. I V Koptug, A A Lysova, A V Matveev, R Z Sagdeev, V N Parmon *Katal. Prom-sti* (Spec. Issue) **60** (2004)
86. I V Koptug, A V Matveev, S A Altobelli *Appl. Magn. Reson.* **22** 187 (2002)
87. S L Codd, S A Altobelli *J. Magn. Reson.* **163** 16 (2003)
88. I V Koptug, A A Lysova, A V Matveev, L Yu Ilyina, R Z Sagdeev, V N Parmon *Magn. Reson. Imaging* **21** 337 (2003)
89. R W Mair, R L Walsworth *Appl. Magn. Reson.* **22** 159 (2002)
90. K Knagge, J Prange, D Raftery *Chem. Phys. Lett.* **397** 11 (2004)
91. R Seydoux, A Pines, M Haake, J A Reimer *J. Phys. Chem. B* **103** 4629 (1999)
92. G E Pavlovskaya, Z I Cleveland, K F Stupic, R J Basaraba, T Meersmann *Proc. Natl. Acad. Sci. USA* **102** 18275 (2005)
93. R W Mair, R Wang, M S Rosen, D Candela, D G Cory, R L Walsworth *Magn. Reson. Imaging* **21** 287 (2003)
94. A Wong-Foy, S Saxena, A J Moule, H-M L Bitter, J A Seeley, R McDermott, J Clarke, A Pines *J. Magn. Reson.* **157** 235 (2002)
95. M Mossle, S-I Han, W R Myers, S-K Lee, N Kelso, M Hatridge, A Pines, J Clarke *J. Magn. Reson.* **179** 146 (2006)
96. A J Moule, M M Spence, S-I Han, J A Seeley, K L Pierce, S Saxena, A Pines *Proc. Natl. Acad. Sci. USA* **100** 9122 (2003)
97. J A Seeley, S Han, A Pines *J. Magn. Reson.* **167** 282 (2004)
98. E E McDonnell, S-I Han, C Hilty, K L Pierce, A Pines *Anal. Chem.* **77** 8109 (2005)
99. C Hilty, E E McDonnell, J Granwehr, K L Pierce, S-I Han, A Pines *Proc. Natl. Acad. Sci. USA* **102** 14960 (2005)
100. E Fukushima, in *NMR Imaging in Chemical Engineering* (Eds S Stapf, S Han) (Weinheim: Wiley-VCH, 2005) p. 490
101. E Fukushima *Adv. Complex Syst.* **4** 503 (2001)
102. A C Rees, J F Davidson, J S Dennis, P S Fennell, L F Gladden, A N Hayhurst, M D Mantle, C R Muller, A J Sederman *Chem. Eng. Sci.* **61** 6002 (2006)

103. P S Fennell, J F Davidson, J S Dennis, L F Gladden, A N Hayhurst, M D Mantle, C R Muller, A C Rees, S A Scott, A J Sederman *Chem. Eng. Sci.* **60** 2085 (2005)
104. R Savelsberg, D E Demco, B Blumich, S Stapf *Phys. Rev. E* **65** 020301 (2002)
105. S Harms, S Stapf, B Blumich *J. Magn. Reson.* **178** 308 (2006)
106. R Wang, M S Rosen, D Candela, R W Mair, R L Walsworth *Magn. Reson. Imaging* **23** 203 (2005)
107. R Wang, M S Rosen, D Candela, R W Mair, R L Walsworth *Chem. Eng. Technol.* **23** 203 (2005)
108. A Caprihan, E Fukushima, A D Rosato, M Kos *Rev. Sci. Instrum.* **68** 4217 (1997)
109. X Yang, D Candela *Phys. Rev. Lett.* **85** 298 (2000)
110. X Y Yang, C Huan, D Candela, R W Mair, R L Walsworth *Phys. Rev. Lett.* **88** 44301 (2002)
111. C Huan, X Y Yang, D Candela, R W Mair, R L Walsworth *Phys. Rev. E* **69** 41302 (2004)
112. D M Mueh, G F Debregeas, G S Karczmar, P J Eng, S R Nagel, H M Jaeger *Nature (London)* **406** 385 (2000)
113. D M Mueh *Phys. Rev. E* **67** 011304 (2003)
114. M T Hardin, T Howes, D A Mitchell, A K Whittaker *Biotechnol. Lett.* **24** 521 (2002)
115. K M Hill, A Caprihan, J Kakalios *Phys. Rev. Lett.* **78** 50 (1997)
116. K M Hill, A Caprihan, J Kakalios *Phys. Rev. E* **56** 4386 (1997)
117. G Metcalfe, L Graham, J Zhou, K Liffman *Chaos* **9** 581 (1999)
118. I V Koptiyug, L Yu Ilyina, A V Matveev, V N Parmon, R Z Sagdeev *Khim. Fiz.* **21** 68 (2002)^a
119. A V Matveev, L V Barysheva, I V Koptiyug, V M Khanaev, A S Noskov *Chem. Eng. Sci.* **61** 2394 (2006)
120. A F McDowell, M S Conradi, J Haase *J. Magn. Reson., Ser. A* **119** 211 (1996)
121. Y Cheng, Q L Huang, M Eic, B J Balcom *Langmuir* **21** 4376 (2005)
122. L Pel, K Kopinga, E F Kaasschieter *J. Phys. D: Appl. Phys.* **33** 1380 (2000)
123. F D Cano, T W Bremner, R P McGregor, B J Balcom *Cem. Concr. Res.* **32** 1067 (2002)
124. I V Koptiyug, L Yu Khitrina, Yu I Aristov, M M Tokarev, K T Isakov, V N Parmon, R Z Sagdeev *J. Phys. Chem. B* **104** 1695 (2000)
125. A A Lysova, I V Koptiyug, R Z Sagdeev, V N Parmon, J A Bergwerff, B M Weckhuysen *J. Am. Chem. Soc.* **127** 11916 (2005)
126. J A Bergwerff, L G A van der Water, A A Lysova, I V Koptiyug, T Visser, K P de Jong, B M Weckhuysen *Stud. Surf. Sci. Catal.* **162** 175 (2006)
127. L Yu Khitrina, I V Koptiyug, N A Pakhomov, R Z Sagdeev, V N Parmon *J. Phys. Chem. B* **104** 1966 (2000)
128. Yu I Aristov, N N Bukhavtsova, N V Vernikovskaya, V P Voloshin, V N Glaznev, L Yu Ilyina, I V Koptiyug, Yu G Korobeinikov, I N Korotkikh, V A Luchnikov, N N Medvedev, N M Ostrovskii, V N Parmon, A D Simonov, M M Tokarev, V B Fenelonov, V M Fomin, N A Chumakova, N A Yazykov *Sovremennye Podkhody k Issledovaniyu i Opisaniyu Protessov Sushki Poristyykh Tel* (Modern Approaches to Investigation and Description of the Drying of Porous Solids) (Ed. V N Parmon) (Novosibirsk: Siberian Branch of the Russian Academy of Sciences, 2001)
129. I V Koptiyug, L Yu Khitrina, V N Parmon, R Z Sagdeev *Magn. Reson. Imaging* **19** 531 (2001)
130. J A Bergwerff, T Visser, B R G Leliveld, B D Rossenaar, K P de Jong, B M Weckhuysen *J. Am. Chem. Soc.* **126** 14548 (2004)
131. Z R Ismagilov, S A Yashnik, A V Matveev, I V Koptiyug, J A Moulijn *Catal. Today* **105** 484 (2005)
132. *Oscillations and Travelling Waves in Chemical Systems* (Eds R J Field, M Burger) (New York: Wiley, 1985)
133. Y Gao, A R Cross, R L Armstrong *J. Phys. Chem.* **100** 10159 (1996)
134. A L Cross, R L Armstrong, C Gobrecht, M Paton, C Ware *Magn. Reson. Imaging* **15** 719 (1997)
135. M M Britton *J. Phys. Chem. A* **107** 5033 (2003)
136. M M Britton *J. Phys. Chem. A* **110** 2579 (2006)
137. I V Koptiyug, A A Lysova, A V Matveev, V N Parmon, R Z Sagdeev *Top. Catal.* **32** 83 (2005)
138. I V Koptiyug, A A Lysova, V N Parmon, R Z Sagdeev *Kinet. Katal.* **44** 436 (2003)^b
139. J Kärgner, D M Ruthven *Diffusion in Zeolites and Other Microporous Solids* (New York: Wiley, 1992)
140. A Toth, K Showalter *J. Chem. Phys.* **103** 2058 (1995)
141. O Steinbock, P Kettunen, K Showalter *J. Phys. Chem.* **100** 18970 (1996)
142. M Kaern, M Menzinger *J. Phys. Chem. B* **106** 3751 (2002)
143. M Kaern, M Menzinger *J. Phys. Chem. A* **106** 4897 (2002)
144. M M Britton, A J Sederman, A F Taylor, S K Scott, L F Gladden *J. Phys. Chem. A* **109** 8306 (2005)
145. R Evans, C R Timmel, P J Hore, M M Britton *Chem. Phys. Lett.* **397** 67 (2004)
146. V V Zhivonitko, I V Koptiyug, R Z Sagdeev *J. Phys. Chem. A* (2007) (in press)
147. *Nuclear Magnetic Resonance. A Specialist Periodical Report* Vol. 33 (Cambridge: RSC Publishing, 2004)
148. I V Koptiyug, A V Kulikov, A A Lysova, V A Kirillov, R Z Sagdeev, V N Parmon *Dokl. Akad. Nauk* **385** 205 (2002)^c
149. I V Koptiyug, A V Kulikov, A A Lysova, V A Kirillov, V N Parmon, R Z Sagdeev *J. Am. Chem. Soc.* **124** 9684 (2002)
150. I V Koptiyug, A V Kulikov, A A Lysova, V A Kirillov, V N Parmon, R Z Sagdeev *Chem. Sust. Dev.* **11** 109 (2003)
151. I V Koptiyug, A A Lysova, A V Kulikov, V A Kirillov, V N Parmon, R Z Sagdeev *Appl. Catal. A* **267** 143 (2004)
152. I V Koptiyug, A A Lysova, A V Kulikov, V A Kirillov, V N Parmon, R Z Sagdeev *Magn. Reson. Imaging* **23** 221 (2005)
153. V A Kirillov, I V Koptiyug, A V Kulikov, N A Kuzin, A A Lysova, A B Shigarov, V N Parmon *Teor. Osnovy Khim. Tekhnol.* **39** 27 (2005)^d
154. V A Kirillov, I V Koptiyug *Ind. Eng. Chem. Res.* **44** 9727 (2005)
155. E H L Yuen, A J Sederman, L F Gladden *Appl. Catal. A* **232** 29 (2002)
156. E H L Yuen, A J Sederman, F Sani, P Alexander, L F Gladden *Chem. Eng. Sci.* **58** 613 (2003)
157. M Kuppers, C Heine, S Han, S Stapf, B Blumich *Appl. Magn. Reson.* **22** 235 (2002)
158. B S Akpa, M D Mantle, A J Sederman, L F Gladden *Chem. Commun.* 2741 (2005)
159. A J Sederman, M D Mantle, C P Dunkley, Z Huang, L F Gladden *Catal. Lett.* **103** 1 (2005)
160. P M Glover, B Newling, C Poirier, B J Balcom *J. Magn. Reson.* **176** 79 (2005)
161. S Anala, G E Pavlovskaya, P Pichumani, T J Dieken, M D Olsen, T Meersmann *J. Am. Chem. Soc.* **125** 13298 (2003)
162. J Natterer, J Bargon *Prog. Nucl. Magn. Reson. Spectrosc.* **31** 293 (1997)
163. S B Duckett, C J Sleight *Prog. Nucl. Magn. Reson. Spectrosc.* **34** 71 (1999)
164. C R Bowers, D P Weitekamp *J. Am. Chem. Soc.* **109** 5541 (1987)
165. P Hubler, J Bargon *Angew. Chem., Int. Ed.* **39** 3701 (2000)
166. J P Dunne, S Aiken, S B Duckett, D Konya, K Q A Lenero, E Drent *J. Am. Chem. Soc.* **126** 16708 (2004)
167. C R Bowers, in *Encyclopedia of Nuclear Magnetic Resonance* Vol. 9 (Eds D M Grant, R K Harris) (Chichester: Wiley, 2002) p. 750
168. S B Duckett, S A Colebrooke, in *Encyclopedia of Nuclear Magnetic Resonance* Vol. 9 (Eds D M Grant, R K Harris) (Chichester: Wiley, 2002) p. 598
169. H Johannesson, O Axelsson, M Karlsson *C. R. Phys.* **5** 315 (2004)
170. T Jonischkeit, U Bommerich, J Stadler, K Woelk, H G Niessen, J Bargon *J. Chem. Phys.* **124** 201109-1 (2007)
171. S Aime, R Gobetto, F Reineri, D Canet *J. Chem. Phys.* **119** 8890 (2003)
172. L T Kuhn, U Bommerich, J Bargon *J. Phys. Chem. A* **110** 3521 (2006)
173. K Golman, O Axelsson, H Johannesson, S Mansson, C Olofsson, J S Petersson *Magn. Reson. Med.* **46** 1 (2001)
174. M Goldman, H Johannesson, O Axelsson, M Karlsson *Magn. Reson. Imaging* **23** 153 (2005)

175. P Bhattacharya, K Harris, A P Lin, M Mansson, V A Norton, W H Perman, D P Weitekamp, B D Ross *Magn. Reson. Mater. Phys., Biol. Med.* **18** 245 (2005)
176. A Eichhorn, A Koch, J Bargon *J. Mol. Catal. A* **174** 293 (2001)
177. *Catalysis by Metal Complexes. Catalyst Separation, Recovery and Recycling. Chemistry and Process Design* Vol. 30 (Eds D J Cole-Hamilton, R P Tooze) (Dordrecht: Springer, 2006)
178. P Barbaro, C Bianchini *Top. Catal.* **19** 17 (2002)
179. D J Cole-Hamilton *Science* **299** 1702 (2003)
180. C Bianchini, D G Burnaby, J Evans, P Frediani, A Meli, W Oberhauser, R Psaro, L Sordelli, F Vizza *J. Am. Chem. Soc.* **121** 5961 (1999)
181. C Merckle, S Haubrich, J Blumel *J. Organomet. Chem.* **627** 44 (2001)
182. C P Mehnert, E J Mozeleski, R A Cook *Chem. Commun.* 3010 (2002)
183. J Huang, T Jiang, B Han, T Mu, Y Wang, X Li, H Chen *Catal. Lett.* **98** 225 (2004)
184. C Simons, U Hanefeld, I W Arends, A J Minnaard, T Maschmeyer, R A Sheldon *Chem. Commun.* 2830 (2004)
185. P Barbaro, C Bianchini, G Giambastiani, W Oberhauser, L M Bonzi, F Rossi, V Dal Santo *Dalton Trans.* 1783 (2004)
186. I V Koptug, K V Kovtunov, S R Burt, M S Anwar, C Hilty, S Han, A Pines, R Z Sagdeev *J. Am. Chem. Soc.* **129** 5580 (2007)
187. L-S Bouchard, K V Kovtunov, S R Burt, M S Anwar, I V Koptug, R Z Sagdeev, A Pines *Angew. Chem., Int. Ed.* **46** 4064 (2007)
188. G Buntkowsky, B Walaszek, A Adamczyk, Y Xu, H-H Limbach, B Chaudret *Phys. Chem. Chem. Phys.* **8** 1929 (2006)
189. S Xu, V V Yashchuk, M H Donaldson, S M Rochester, D Budker, A Pines *Proc. Natl. Acad. Sci. USA* **103** 12668 (2006)
190. R McDermott, S-K Lee, B ten Haken, A H Trabesinger, A Pines, J Clarke *Proc. Natl. Acad. Sci. USA* **101** 7857 (2004)
191. D Canet, S Bouguet-Bonnet, C Aroulanda, F Reineri *J. Am. Chem. Soc.* **129** 1445 (2007)
192. P Hubler, J Bargon, S J Glaser *J. Chem. Phys.* **113** 2056 (2000)
193. M S Anwar, D Blazina, H A Carteret, S B Duckett, J A Jones *Chem. Phys. Lett.* **400** 94 (2004)
194. P T Callaghan *Principles of Nuclear Magnetic Resonance Microscopy* (Oxford: Clarendon Press, 1991)
195. R R Ernst, G Bodenhausen, A Wokaun *Principles of Nuclear Magnetic Resonance in One and Two Dimensions* (Oxford: Clarendon Press, 1987)
196. M Carravetta, M H Levitt *J. Am. Chem. Soc.* **126** 6228 (2004)
197. M Carravetta, O G Johannessen, M H Levitt *Phys. Rev. Lett.* **92** 153003 (2004)
198. S Cavadini, J Dittmer, S Antonijevic, G Bodenhausen *J. Am. Chem. Soc.* **127** 15744 (2005)
199. R Sarkar, P R Vasos, G Bodenhausen *J. Am. Chem. Soc.* **129** 328 (2007)
200. M Carravetta, M H Levitt *J. Chem. Phys.* **122** 214505 (2005)
201. G Pileio, M Concistre, M Carravetta, M H Levitt *J. Magn. Reson.* **182** 353 (2006)
202. K Gopalakrishnan, G Bodenhausen *J. Magn. Reson.* **182** 254 (2006)
203. R Kimmich, D E Demco, S Hafner, in *Magnetic Resonance Microscopy. Methods and Applications in Materials Science, Agriculture and Biomedicine* (Eds B Blumich, W Kuhn) (Weinheim: VCH, 1992) p. 59
204. N Luger, F De Luca, B Maraviglia, in *Magnetic Resonance Microscopy. Methods and Applications in Materials Science, Agriculture and Biomedicine* (Eds B Blumich, W Kuhn) (Weinheim: VCH, 1992) p. 103

^a — *Chem. Phys. Rep. (Engl. Transl.)*

^b — *Kinet. Catal. (Engl. Transl.)*

^c — *Dokl. Phys. Chem. (Engl. Transl.)*

^d — *Theor. Found. Chem. Eng. (Engl. Transl.)*

Spin chemistry of enzymatic processes

M S Afanasyeva, P A Purtov, M B Taraban, T V Leshina

Contents

I. Introduction	599
II. Phenomenological description of the magnetic field and spin effects in enzymatic systems	600
III. Theory of the magnetic field and spin effects in enzymatic multispin systems	602
IV. Magnetic field effects in enzymatic reactions catalysed by horseradish peroxidase	604
V. Conclusion	612

Abstract. The results of spin chemistry studies of the single electron transfer step and the role of spin states of paramagnetic intermediates in the enzymatic oxidation of organic substrates induced by horseradish peroxidase are generalised. Detailed theoretical description of the approach used to analyse the magnetic field effects in enzymatic multispin systems is presented. Prospects for the use of spin chemistry techniques for elucidation of the mechanisms of radical steps of enzymatic processes are considered. The bibliography includes 80 references.

I. Introduction

Spin chemistry methods are used in studies of radical reactions the rates and, often, directions of which depend on the orientation of the electron and nuclear spins of transient radical species and on the strength of external and local magnetic fields. Spin chemistry became an individual avenue of chemical research nearly twenty-five years ago and currently there is no need to introduce it to the reader. The term ‘spin chemistry’ refers to the chemistry of the radical processes mentioned above and to the methods employed. The latter comprise the methods based on the phenomena of chemically induced dynamic electron and nuclear polarisation (CIDEP and CIDNP, respectively), magnetic field effect (MFE), magnetic isotope effect (MIE) and related techniques that have been comprehensively described in a number of reviews and monographs (see, e.g., Refs 1 and 2).

After completion of theoretical description of the magnetic field effects detected in model systems, the last decade was marked by the trend to practical application of this knowledge to the studies of complex chemical and biochemical processes by spin chemistry. This avenue of research seems to be quite

important because elucidation of the structure and properties of short-lived intermediates in chemical reactions belongs to the key problems in modern chemistry. Spin chemistry methods make it possible to study paramagnetic intermediates with lifetimes from a few nanoseconds to a few microseconds, viz., radical ions and neutral free radicals, biradicals, carbenes and carbene analogues and triplet-excited molecules.

The involvement of radical ions, radicals and biradicals in some reactions was only postulated; remarkable examples of successful use of the CIDNP and MFE techniques for elucidation of the mechanisms of these processes have been reported.^{3–5} Of particular interest are recent spin chemistry studies in biology⁶ including investigations of oscillatory enzymatic reactions,⁷ structural features of reversible protein folding,⁸ type of the intermediates in the reactions of B₁₂-dependent enzymes⁹ and simulation of protein–nucleic acid interactions.¹⁰

Recently, the experimental data suggesting that free-radical states initiate processes that damage cell structures, certain proteins and nucleic acids have been accumulated increasingly.¹¹ It is believed that free radicals are responsible for the development of cardiovascular diseases,¹² compromised immune response,¹³ cataract development,¹⁴ development of Parkinson’s disease,¹⁵ schizophrenia,¹⁶ and Alzheimer’s disease,^{15, 17} as well as accelerated ageing and higher risk of cancer.¹⁸ According to modern concepts, destructive changes in living organisms are most probably due to the processes involving reactive oxygen species and oxygen-containing radicals (O₂^{•−}, HO₂[•], HO[•] and ¹O₂) that induce oxidative stress, diseases and senilism.¹⁹ In this connection, a demand arose for spin chemistry studies of reactive paramagnetic intermediates in biological systems.

Paramagnetic species play an important role in some processes that are responsible for normal activity of mammalian cells.²⁰ The involvement of radical species in many biological processes was reviewed.^{21, 22} Enzymatic processes in living systems are sources of various free radicals, in particular, HO₂[•] (Ref. 23). The present review is devoted to reaction mechanisms of horseradish peroxidase (HRP), which is the source of intermediates that react with many free radicals; of note is the appearance of the expression ‘the free-radical chemistry of peroxidase’.²⁴ Peroxidase is present both in mammalian organisms and plants, where it decomposes toxic hydrogen peroxide and can serve as a scavenger of free radicals. It should be noted that at present researchers are far from

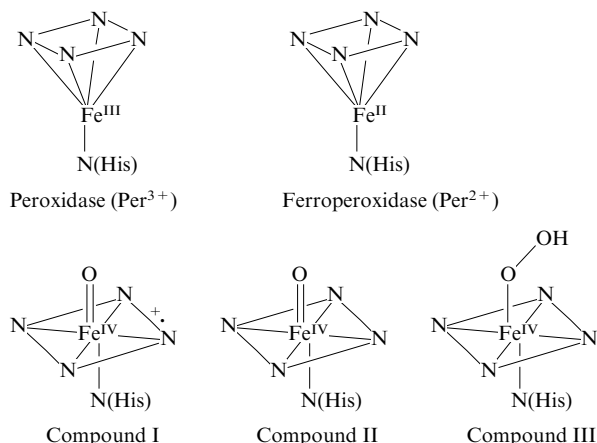
M S Afanasyeva, P A Purtov, M B Taraban, T V Leshina Institute of Chemical Kinetics and Combustion, Siberian Branch of the Russian Academy of Sciences, ul. Institutskaya 3, 630090 Novosibirsk, Russian Federation. Fax (7-383) 330 73 50, tel. (7-383) 333 14 05, e-mail: afanasieva@ns.kinetics.nsc.ru (M S Afanasyeva), taraban@ns.kinetics.nsc.ru (M B Taraban), leshina@ns.kinetics.nsc.ru (T V Leshina), tel. (7-383) 333 11 02, e-mail: purtov@ns.kinetics.nsc.ru (P A Purtov)

Received 5 April 2007

Uspekhi Khimii 76 (7) 651–668 (2007); translated by A M Raevskiy

knowing all sources of free radicals in the living systems in health and disease.

Taking into account the aforesaid, studies on the elementary processes resulting in emergence of free radicals, in particular, enzymatic reactions, are of considerable interest. The mechanisms of enzymatic reactions are studied by various modern physicochemical methods. Identification of paramagnetic species often faces severe difficulties.²⁵ Problems concerned with detection of free radicals by EPR spectroscopy (low steady-state concentrations of radicals in biological systems) are well known.²⁶ Using the spin trap technique in EPR spectroscopy, one can solve the 'concentration' problem, but some new problems often arise, *e.g.*, the need of suppression of EPR signals corresponding to further transformations of spin traps and stable radicals that formed.²⁶ In addition, when observing the EPR signal of a free radical, it is unclear whether the radical is involved in the process under study or it is the side reaction product. Spin chemistry studies of radical intermediates in biological processes could answer this question. Clearly, enzymatic processes are also promising subjects for spin chemistry studies, because chemical transformations in the active sites of many metal-containing enzymes involve spin-change reactions and interconversions of the intermediates existing in different spin states; it is the oxidation states of such metals as Fe, Cu, Zn, *etc.* that are dealt with. For instance, the catalytic cycle of HRP involves reliably characterised reactive intermediates, the so-called HRP-Compounds the active sites of which contain iron atoms in different oxidation and spin states (high-spin state in native HRP and ferroperoxidase and low-spin state in Compounds I–III).²⁴



N(His) is the nitrogen atom of histidine.

However, until very recently the lack of comprehensive theoretical description of multispin systems precluded the extension of spin chemistry studies of enzymatic processes. Even a few years ago a relevant theoretical description (radical pair theory) was only developed for the cases where reaction products were formed from radical pairs with half-integer spins ($S = 1/2$). Meanwhile, iron-containing intermediates in the high-spin states are paramagnetic intermediates in many biological processes (*e.g.*, in reactions involving iron ions or haem-containing enzymes including HRP and cytochromes). Usually, in such systems a multi-electron atom having several unpaired electrons serves as the radical centre.²⁷ Here, analysis of the MFE requires knowledge of the specific features of the evolution of spin states in multispin systems. At present, intensive experimental research of multispin systems has been carried out taking the processes in radical pairs (RP) induced by the so-called third or fourth spin (usually, the spins of stable radicals or biradicals) as examples.^{28,29} Progress in this field of research, which is in the early stage of development (accumu-

lation of experimental results), was stimulated by the studies^{30,31} in which a novel phenomenon called 'spin catalysis' was discovered.

The magnetic field effects treated in a broad sense, *i.e.*, the effects of external magnetic fields on various processes in living organisms, from migratory orientation of birds to the effect of the so-called magnetic storms on human health, belong to popular subjects of research.³² Since such effects undoubtedly have a complex nature, detection of the changes occurring in the presence of a magnetic field usually provides no information on the mechanisms of generation of the MFE signals and on the magnetic field-sensitive steps of the processes under study.

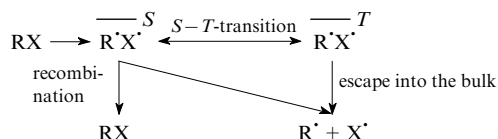
Mechanistic studies of the magnetic field effect on particular stages of *in vitro* processes using spin chemistry techniques are much more informative. These methods were used for comprehensive treatment of enzymatic processes involving magnetic field sensitive steps with participation of the pairs of paramagnetic species generated in single-electron transfer reactions.^{33–35} Conclusions about the involvement of radical pairs in an enzymatic process are based on a comparison of the experimental and calculated dependences of the rate constants for transformations of paramagnetic intermediates on the magnetic field strength. Such studies were carried out for transformations of reactive paramagnetic intermediates in the catalytic cycle of the oxidation of some HRP substrates in the steady-state^{33–35} and oscillatory regimes.⁷ An important result of these investigations consists of the demonstration of the role of spin states of the paramagnetic intermediates in the catalytic cycle of the enzymatic process.

The magnetic field effects in biological systems were considered in a review,⁶ which also summarised the data on possible biological effects under the action of static and alternating magnetic fields. In the present review, we make an attempt at systematisation and interpretation of the available material concerning theoretical description of the spin and magnetic field effects in multispin enzymatic systems and the results obtained in experimental studies of the dependences of the rates for enzymatic oxidation of organic substrates by horseradish peroxidase on the strength of the external magnetic field.

II. Phenomenological description of the magnetic field and spin effects in enzymatic systems

Reactions the rates and, sometimes, directions of which depend on the orientation of the electron and nuclear spins of the paramagnetic precursors of reaction products are the major subject of spin chemistry studies. An example of such a reaction is shown in Scheme 1.

Scheme 1



A radical pair emerged in, *e.g.*, photochemical or thermal decomposition of a molecule exists in one of the two correlated spin states, namely, in a singlet (S) or a triplet (T) state. The total electron spin of the radicals is equal to zero in the former state and unity in the latter. Usually, the triplet state of the radical pair is non-reactive (or low reactive),¹ and the RP recombination mainly occurs from the singlet state. Magnetic and spin interactions induce transitions between the non-reactive T -state and reactive S -state (the so-called $T \rightarrow S$ -transitions responsible for the change in the fraction of the reactive species). These singlet–triplet transitions represent the

physical essence of the spin and magnetic field effects in chemical processes. The most important magnetic interactions that induce the singlet–triplet transitions and affect their efficiency include the Zeeman interaction of the unpaired electrons in the RP with the external magnetic field, hyperfine coupling (HFC) between the electron spins and the magnetic nuclei (nuclei with a non-zero nuclear spin I) of the radicals and electron exchange interaction between the unpaired electrons in the RP. Figure 1 schematically presents two limiting cases of singlet–triplet mixing. For instance, in weak magnetic fields (Fig. 1 *a*) the hyperfine interaction induces S – T -transitions between all the three triplet Zeeman sublevels (T_0 , T_{+1} and T_{-1}) and the recombining singlet state (HFC-mechanism of singlet–triplet transitions). In strong external magnetic fields that exceed substantially the local magnetic fields due to HFC, a large splitting between the T_{+1} and T_{-1} sublevels leads to the situation where the hyperfine interaction only affects the transitions between the singlet state and one triplet state (T_0). Isotropic hyperfine interaction does not involve the other two triplet states (T_{+1} and T_{-1}) in the S – T -transition (Fig. 1 *b*). Mixing of the S and T_0 states of a radical pair can also be due to the g -factor difference between the radicals (Δg -mechanism of singlet–triplet transitions). Thus, even weak (*e.g.*, Zeeman and hyperfine) magnetic interactions the constants of which are 5–6 orders of magnitude lower than kT can increase the fraction of the reactive state of the radical pair owing to the S – T -transition.

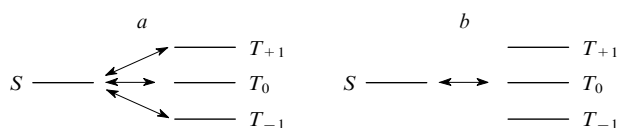


Figure 1. Energy levels of a radical pair and allowed transitions between the S - and T -states in weak (*a*) and strong (*b*) magnetic fields.

The manifestation of singlet–triplet transitions requires that the RP lifetime be rather long. In a condensed medium, this can be attained due to the cage effect. This effect determines two key features of the reactions under study, namely, the relatively long time of contact between partners and the possibility of repeated contacts of the same pair of reactants in the course of diffusion motion. The characteristic cage size (R) and the residence time (τ) of the reactants in the cage are governed by the kinematics of the relative motion, interaction between the reactants and some other properties. For instance, the hyperfine coupling constant between the unpaired electrons and magnetic nuclei (ω , in frequency units) in organic free radicals is of the order of about 10^8 – 10^9 rad s $^{-1}$ and the probability of singlet–triplet transitions on the time scale $\tau \sim 10^{-9}$ – 10^{-10} s is

$$\omega\tau \sim 0.01\text{--}0.1.$$

The probability of S – T -transitions increases with an increase in the viscosity of the solution (as τ increases) or in the reactions involving radical ion pairs (due to the Coulomb interaction between the partner radicals).

The singlet–triplet conversion depends on the orientation of electron and nuclear spins of the partners in the RP and the singlet–triplet conversion rate is affected by the HFC, Δg and external magnetic field. An important consequence is the possibility of manifestation of the magnetic field and spin effects (MIE and CIDNP) in chemical and biochemical reactions.

The MIE is due to the T – S conversion rate difference between the radical pairs containing magnetic nuclei and the RP devoid of such nuclei. The MIE provides the isotopic selectivity in different reaction products. Chemically induced dynamic nuclear polarisation is a manifestation of the α - and β -spin selection in different reaction products. When carrying out the reaction in the probe of an NMR spectrometer, the lines observed in the NMR spectra at the very beginning of the process correspond to the distribution of the spin sublevel population that differs from the Boltzmann (equilibrium) distribution. A detailed description of the spin and magnetic field effects can be found in a monograph.¹

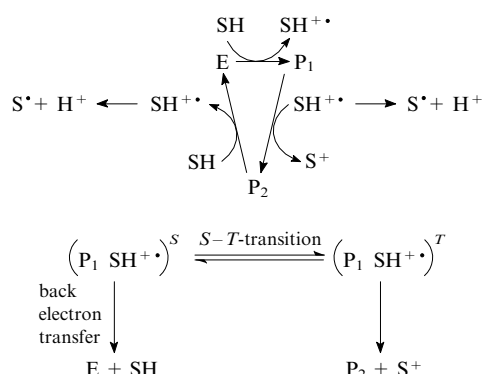
At present, the effect of the external magnetic field and CIDNP were detected for a number of chemical processes, such as single-electron transfer steps in the reactions previously treated as nucleophilic substitution;³ *cis*–*trans*-isomerisation of alkenes including biologically valuable polyenes (retinal and carotenoids);³⁶ donor-acceptor interactions of synthetic analogues of nicotinamide adenine dinucleotide (NADH), namely, 1,4-dihydropyridines containing electron-withdrawing groups^{37–40} and many other processes.

Now we will consider the specific features of manifestation of the magnetic field and spin effects in biochemical systems. In homogeneous solutions, a strong cage effect is most probably due to a high viscosity of the solvent and to the electrostatic interaction between partners in radical ion pairs. Pronounced cage effects are also characteristic of the reactions occurring in molecularly organised media, *e.g.*, liposomes, micelles, ‘guest–host’ inclusion complexes, *etc.* (here, the time spent by radical pairs in the contact zone due to the so-called weak interactions is longer than in non-viscous systems). Weak interactions also include the enzyme–substrate interactions (enzyme–substrate binding) in the active site of enzyme, which is usually considered as the main factor responsible for the high selectivity of enzymatic processes.⁴¹ By analogy with well-studied processes in complexes or micelles,⁴² one can expect that the radical intermediates formed in an enzymatic process will also form quite a long-lived enzyme–substrate complex. Binding of the partners in the active site of enzyme gives grounds to expect manifestations of rather strong electron exchange interaction between paramagnetic species in the enzyme–substrate complexes, which can be detected by spin chemistry techniques.

Now we have to dwell on basic differences between manifestations of the magnetic field and spin effects in homogeneous radical and enzymatic processes. In a radical reaction, the magnetic field effects consist of a change in the ratio of the recombination probability of free radicals to the probability of their escape into the bulk.¹ In enzymatic reactions, where the paramagnetic intermediates are involved in the catalytic cycle, two different spin states of a pair of paramagnetic species (corresponding to recombination and escape to the bulk, see Scheme 1) can characterise different steps in the catalytic cycle. Thus, the magnetic field will affect the ratio of recombination probabilities (or back electron transfer in the case of single-electron transfer) and transition to the next step in the catalytic cycle. As an example, we will consider a model catalytic cycle shown in Scheme 2.

The cycle begins with the formation of an enzyme–substrate complex $[E\cdots SH]$ in which an electron is transferred from the donor (substrate) to acceptor (enzyme) to form the $(P_1 SH^+)$ radical pair in, *e.g.*, the singlet state. Magnetic interactions induce the singlet–triplet conversion; when the RP is in the singlet state, back electron transfer (recombination) and regeneration of the starting enzyme (E) and substrate (SH) are possible. The triplet RP is a precursor of the next stage of the catalytic cycle, which involves the formation of the intermediate P_2 . Thus, this example clearly demonstrated the possibility of the effect of the spin states of paramagnetic

Scheme 2



intermediates on the rates of the processes occurring in the catalytic cycle of the enzyme.

The effect of the magnetic field on an enzymatic process will manifest itself as the dependence of particular steps of the catalytic cycle on the strength of external magnetic field. In this case, the magnetic field effect can be defined as the ratio of the rate constants for the reactions carried out in a magnetic field of specified strength to the corresponding rate constants measured in zero (geomagnetic) field. Analysis of the magnetic field effects detected in enzymatic processes involves measurements of the dependences of the rates of particular steps of the catalytic cycle or the overall process on the strength of the external magnetic field (magnetic field dependence) and a comparison of the experimental and calculated dependences on the magnetic field. In the case of enzymatic processes, the recombination (back electron transfer) probabilities are calculated for a pair of paramagnetic species with specified magnetic resonance parameters (HFC constants, g -factors of radicals, effective electron exchange interaction constant J) with allowance for the lifetimes of the paramagnetic pair and the multiplicity of the initial and recombining states. Now we will consider an approach to the calculation of a recombination probability in multispin systems including enzymes.

III. Theory of the magnetic field and spin effects in enzymatic multispin systems

A model of a multispin system differs from that model used in the radical pair theory in the number of unpaired electrons (> 2). For instance, the spin catalysis³⁰ deal with systems comprising three radicals (triads) or pairs of species with spins $I > 1/2$. Thus, the description of multispin systems requires taking account of possible correlated doublet, quartet, quintet and higher spin states. Recombination probability calculations for such multispin pairs should be carried out with allowance for a large number of subensembles of radical pairs, each corresponding to particular configurations of electron and nuclear spins. The interaction of RP spins with external magnetic fields and the spin–spin interactions induce transitions of a given RP from one subensemble to another. These interactions are described by systems of a large number of coupled kinetic equations. In addition, description of the dynamics of the RP spin state requires the use of quantum mechanics. The density matrix formalism is the most appropriate for simultaneous consideration of the spatial motion and spin dynamics of a radical pair. Now we will calculate the recombination probability in the framework of this method.

If the density matrix, $\rho(\vec{r}, t)$, of a pair of paramagnetic species separated by the distance r depends on r , changes in $\rho(\vec{r}, t)$ with time (t) are governed by three factors, *viz.*, the spin evolution of the unpaired electrons due to the spin–spin interactions and spin interactions with external and local

magnetic fields, the relative motion of reactants and recombination of radicals¹

$$\frac{\partial \rho(\vec{r}, t)}{\partial t} = \left(\frac{\partial \rho}{\partial t} \right)_{\text{spin}} + \left(\frac{\partial \rho}{\partial t} \right)_{\text{motion}} + \left(\frac{\partial \rho}{\partial t} \right)_{\text{recomb}}. \quad (1)$$

This equation is usually written as follows:⁴³

$$\frac{\partial \rho(\vec{r}, t)}{\partial t} = i\hat{L}(\vec{r})\rho(\vec{r}, t) + \hat{R}(\vec{r})\rho(\vec{r}, t) - \hat{U}(\vec{r})\rho(\vec{r}, t), \quad (2)$$

where $\hat{L}(\vec{r}) = \hat{\Omega} + i\hat{R} + \hat{J}(\vec{r})$ is the Liouville operator (Liouvillian), which allows for the coordinate-independent spin evolution due to isotropic HFC and the Zeeman interaction with external magnetic fields ($\hat{\Omega}$), the spin relaxation processes (\hat{R}), and the coordinate-dependent spin evolution induced by the exchange interaction [$\hat{J}(\vec{r})$]. The operator $\hat{U}(\vec{r})$ describes the spin-dependent RP recombination, and its matrix elements characterise the rate of transformation of different components of the density matrix to the reaction product (or products). The functional operator $\hat{R}(\vec{r})$ specifies the motion of reactants, which is usually treated in the framework of classical mechanics.

The probability of RP recombination from a certain spin state at the instant t is given by the corresponding components of the vector $\hat{w}(t)$

$$\hat{w}(t) = \int_0^t \int \hat{U}(\vec{r})\rho(\vec{r}, \tau) d\tau d\vec{r}. \quad (3)$$

Among a large number of methods for solving Eqn (2), the Green function formalism is most often used. The Green functions specify the character of the relative motion of other paramagnetic species in the pair.⁴⁴ This method makes use of a physically substantiated admission that the reaction zone is always a rather narrow region in the space of motion of reactants. In this case, the general matrix expression for the probability of recombination of a pair of paramagnetic species from a certain spin state has the form:⁴³

$$\hat{w} = \hat{U}_0 \hat{g} \left(1 + \hat{U}_0 \hat{g} \right)^{-1} \rho_0, \quad (4)$$

where \hat{U}_0 is the matrix of recombination constants for different spin states (generally, recombination from any electron spin state is possible, but at different rate); \hat{g} is the operator (averaged over the reaction zone) characterising the relative motion and the spin dynamics in the pair. The matrix of this operator is the matrix of characteristic ‘times’. For instance, the matrix element $g_{nm, kk}$ is the mean lifetime of the RP in the spin state $|nm\rangle$ provided that the system initially was in the electron spin state $|kk\rangle$. All elements of this matrix are expressed through the one and only function $g(s)$ characterising the relative motion (changes in the mutual position) in the pair of recombining paramagnetic species.

Carrying out particular calculations often requires knowledge of only certain elements of the matrix \hat{g} , *i.e.*, one or several of characteristic ‘times’. Consider a typical case where the RP can recombine only in a particular electron spin state, *e.g.*, a doublet or singlet state. Let the spin evolution in the RP occur in such a way that no transitions between different recombining states of the radicals occur. Then, the whole ensemble of radical pairs can be divided into subensembles with a particular configuration, $\{m\}$, of nuclear spins in the doublet (or singlet) state. Calculations for each subensemble are performed independently; the recombination probability for a specified subensemble is given by

$$w_m = \frac{U_0 \tau_m}{1 + U_0 \tau_m}, \quad (5)$$

where the quantity τ_m is the mean residence time of the radical pair in the reaction zone in the doublet state with the specified spin configuration $\{m\}$ provided that the pair was born in the reaction zone in the doublet state with the same spin configuration $\{m\}$.

In some cases, transitions between doublet states can play an important role. Suppose that a transition from the doublet state with the nuclear spin configuration $\{m\}$ to the doublet state with the spin configuration $\{m'\}$ is possible. We thus obtain a more general expression compared to Eqn (5)

$$w_m = U_0 \frac{\tau_m + \tau_{mm'} + U_0(\tau_m \tau_{m'} - \tau_{mm'} \tau_{m'm})}{1 + U_0(\tau_m + \tau_{m'}) + U_0^2(\tau_m \tau_{m'} - \tau_{mm'} \tau_{m'm})}. \quad (6)$$

Here $\tau_{mm'}$ is the mean residence time of the RP in the reaction zone in the doublet state with the preset spin configuration $\{m\}$ provided the start is from the doublet state with the preset spin configuration $\{m'\}$. The parameter $\tau_{m'm}$ has a similar meaning.

Further calculations require specifying of the spin Hamiltonian of the RP to describe the spin evolution and choosing an appropriate model for the relative motion to describe the spatial motion of the species. Changes in the mutual position of the species in the enzyme-substrate complex can be described using a rather simple two-position model,⁴⁵ according to which two states of an RP in the cage are possible: (i) radicals contact each other and can recombine and (ii) radicals do not contact each other but can return to the contact state. The state (i) is characterised by the time τ_1 necessary for transition of RP from this state to the state (ii). The state (ii) is characterised by two parameters, namely, the time τ_2 of back transition from the state (ii) to the state (i) and the time τ_c of irreversible decomposition of the RP. The singlet–triplet transitions occur in the state (ii) of the RP.

In the framework of the two-position model, the function $g(s)$ characterising the changes in the mutual position in a pair of recombining paramagnetic species is given by:⁴⁵

$$g(s) = \frac{\tau_p}{n+1} \left(1 + \frac{n}{1+s\tau_c} \right), \quad (7)$$

where n is the number of repeated contacts and $\tau_p = n\tau_1$.

The spin evolution is described using appropriate basis spin states φ_i . For instance, the singlet–triplet basis is suitable for the description of a pair of species with $I = 1/2$. If a pair comprises two species with $I = 1/2$ and 1, the resultant spin state can be doublet or quartet. The spin functions of these states have the form

$$|D\rangle = \begin{cases} \sqrt{\frac{2}{3}}\beta T_{+1} - \sqrt{\frac{1}{3}}\alpha T_0 \\ \sqrt{\frac{2}{3}}\alpha T_{-1} - \sqrt{\frac{1}{3}}\beta T_0 \end{cases}, \quad (8)$$

$$|Q\rangle = \begin{cases} \alpha T_{+1} \\ \sqrt{\frac{1}{3}}\beta T_{+1} + \sqrt{\frac{2}{3}}\alpha T_0 \\ \sqrt{\frac{1}{3}}\alpha T_{-1} + \sqrt{\frac{2}{3}}\beta T_0 \\ \beta T_{-1} \end{cases}.$$

By specifying the spin Hamiltonian of the system it is possible to determine the stationary energy levels (E_i) and the eigenfunctions (wavefunctions) of the system (ψ_i). The stationary wavefunctions in the φ_i basis set are represented by

$$\psi_i = \sum_j (\hat{Q})_{ij} \varphi_j,$$

where $(\hat{Q})_{ij}$ is the matrix that describes transition from the initial spin basis set to the basis of eigenfunctions. The dependence of the wavefunctions on time is as follows:

$$|\psi(t)\rangle = \exp(-i\hat{H}t)|\psi(0)\rangle.$$

Now we will write the density matrix in the basis of the φ_i functions. The action of the operator \hat{Q} on the functions φ_i leads to

$$\begin{aligned} |\varphi(t)\rangle &= \hat{Q}^{-1}|\psi(t)\rangle = \hat{Q}^{-1}\exp(-i\hat{H}t)|\psi(0)\rangle = \\ &= \hat{Q}^{-1}\exp(-i\hat{H}t)\hat{Q}|\varphi(0)\rangle; \end{aligned} \quad (9)$$

since

$$\hat{\rho}(t) = |\varphi(t)\rangle\langle\varphi(t)|,$$

one gets

$$\hat{\rho}(t) = \hat{Q}^{-1}\exp(-i\hat{H}t)\hat{Q}|\varphi(0)\rangle\langle\varphi(0)|\hat{Q}^{-1}\exp(i\hat{H}t)\hat{Q}. \quad (10)$$

For instance, the probability for the RP to exist in a doublet state at any instant is given by:

$$\rho_{DD}(t) = \langle D|\hat{Q}^{-1}\exp(-i\hat{H}t)\hat{Q}|D\rangle\langle D|\hat{Q}^{-1}\exp(i\hat{H}t)\hat{Q}|D\rangle. \quad (11)$$

Here \hat{Q} represents the matrix coefficients; therefore, the expression for $\rho_{DD}(t)$ can be transformed as follows:

$$\begin{aligned} \rho_{DD}(t) &= \sum_i Q_{i1}^4 + \sum_{i,j} Q_{i1}^2 Q_{j1}^2 \exp[-i(E_i - E_j)t] + \\ &+ \sum_{i,j} Q_{i1}^2 Q_{j1}^2 \exp[i(E_i - E_j)t]. \end{aligned} \quad (12)$$

The average lifetime of an RP in a doublet state provided that the RP was born in the same state can be determined from the following expression

$$\begin{aligned} \tau = (\hat{g})_{DD,DD} &= \sum_i Q_{i1}^4 g(0) + \sum_{i,j} Q_{i1}^2 Q_{j1}^2 g[-i(E_i - E_j)] + \\ &+ \sum_{i,j} Q_{i1}^2 Q_{j1}^2 g[i(E_i - E_j)]. \end{aligned} \quad (13)$$

For the two-position model, the equation for τ takes the form

$$\tau = \tau_p \left[\sum_i Q_{i1}^4 + 2 \sum_{i>j} \frac{Q_{i1}^2 Q_{j1}^2}{n+1} \left(\frac{1+n}{1+[(E_i - E_j)\tau_c]^2} \right) \right]. \quad (14)$$

The probability of recombination from the doublet state provided that the RP was formed in the doublet and quartet state, respectively, can be calculated using the following relationships:

$$w^D = \frac{1}{2} \frac{U_0 \tau}{1 + U_0 \tau}, \quad (15)$$

$$w^Q = \frac{1}{4} \frac{U_0(\tau_p - \tau)}{1 + U_0 \tau}. \quad (16)$$

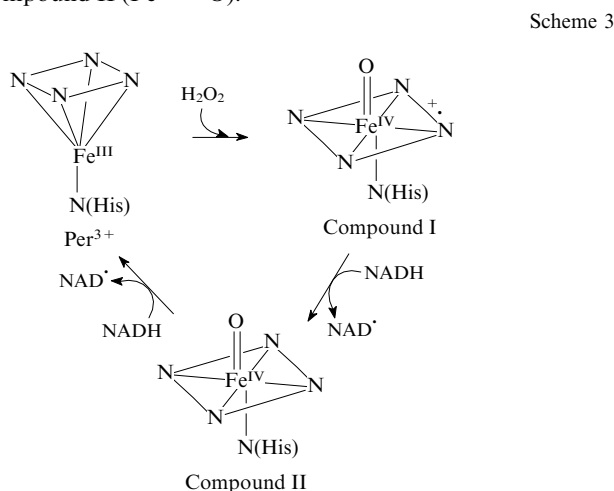
Recombination probability calculations for such systems are exemplified by the reactions catalysed by horseradish

peroxidase containing an iron atom in the active site (see below).

IV. Magnetic field effects in enzymatic reactions catalysed by horseradish peroxidase

1. Modern concepts of the mechanisms of horseradish peroxidase-catalysed oxidation of substrates

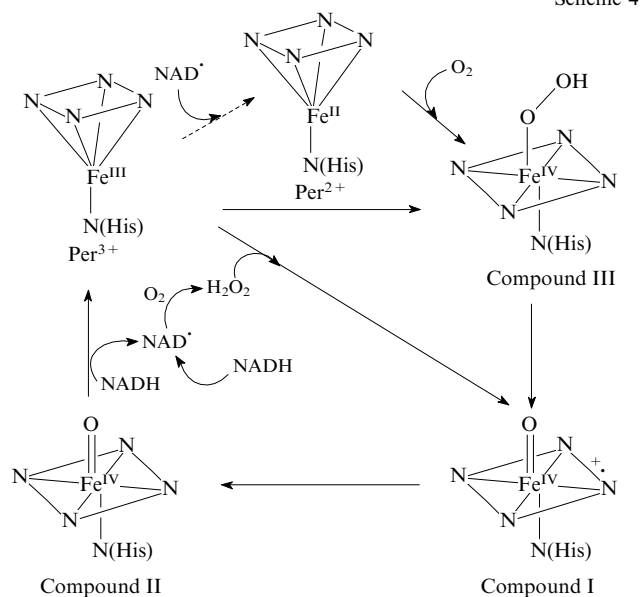
Two models for the mechanism of the HRP catalytic cycle are available in the literature, a 'simplified' model²⁷ and a 'chemically realistic' one.²⁴ The former model (Scheme 3) was proposed as a possible mechanism of the oxidation of the natural peroxidase substrate (NADH) in the presence of an initiator (hydrogen peroxide) and involves successive transformation of native HRP (Per^{3+} , Fe^{III}) into reactive paramagnetic HRP intermediates, namely, Compound I containing a haem oxoform π -radical cation ($\text{Fe}^{\text{IV}}=\text{O}^+$) in the active site and Compound II ($\text{Fe}^{\text{IV}}=\text{O}$).



The second model (Scheme 4) was used to describe the NADH oxidation in the absence of H_2O_2 . It is based on the assumption that slow oxidation of NADH with oxygen present in the buffer solution in an acid medium results in the formation of H_2O_2 and that the amount of H_2O_2 formed is sufficient for initiation of the catalytic cycle,⁴⁶ which includes interconversions of native HRP (Per^{3+} , Fe^{III}), Compound I ($\text{Fe}^{\text{IV}}=\text{O}^+$), Compound II ($\text{Fe}^{\text{IV}}=\text{O}$), Compound III ($\text{Fe}^{\text{IV}}-\text{O}-\text{OH}$) and ferropoxidase (Per^{2+} , Fe^{II}).

However, the efficiency of the hypothetical step of H_2O_2 generation casts some doubts. The authors of the present review believe that single-electron transfer between the native HRP and substrate (NADH) is much more probable, because this is a commonly accepted starting point of oxidation in the reactions catalysed by other haem-containing enzymes.^{47, 48} Indeed, according to published data on HRP-catalysed oxidation of substrates,^{49, 50} the binding of a substrate in the active site of enzyme occurs near the haem plane, which permits direct electron transfer from the substrate to the haem. Here, the rate of single-electron transfer from the substrate to the haem in the enzyme-substrate complex should be much higher than the rate of the substrate oxidation by dissolved oxygen (for NADH, $k = 3.0 \times 10^{-6} \text{ s}^{-1}$).²⁴ It should be noted that high probability of single-electron transfer is also due to the donor properties of NADH ($E^0 = -320 \text{ mV}$) and acceptor properties of HRP ($E^0 = -306 \text{ mV}$).⁵¹

However, in spite of these arguments, the concept considering the formation of H_2O_2 as the starting point of the peroxidase-catalysed substrate oxidation still dominates in the literature.^{24, 47} Nevertheless, the aforesaid suggests^{34, 35} that the single-electron transfer step can occur in the $[\text{Per}^{3+} \dots \text{NADH}]$ enzyme-substrate complex. It should be noted that the possibility of electron transfer between HRP and NADH to



give ferropoxidase (Per^{2+}) was discussed in a study of HRP-catalysed oxidation of photoexcited NADH.⁵²

Thus, the possibility of electron transfer between the native HRP and NADH requires experimental proof. Of particular interest are the experimental proofs of the involvement of the $\text{NADH}^{+\cdot}$ radical cation in the enzymatic oxidation processes. Discussion of whether the multistep mechanism involving electron transfer is possible in biological systems



or the oxidation occurs as the hydride transfer remains topical.⁵³ It should be emphasised that the radical steps were proposed for almost all processes involving HRP, that is, hydrogen peroxide utilisation, initiation of polymerisation in the synthesis of plant cell membranes, *etc.*⁴⁷ Meanwhile, only reactive paramagnetic intermediates of the native HRP, *i.e.*, Compounds I–III, were experimentally detected to date.⁴⁶ Since the involvement of paramagnetic intermediates (Per^{3+} , Per^{2+} , Compounds I–III) in the catalytic cycle of HRP can be considered proven (see Schemes 3 and 4), it was quite natural to expect that the use of spin chemistry methods will provide reliable information on hypothetical reactive paramagnetic substrate species generated in these processes.

Further, we briefly outline the methodology of experiments and analysis of the magnetic field effects, which permits reliable establishment of manifestations of the radical steps in the HRP-catalysed oxidation of organic substrates.

2. Methodology of studies on the magnetic field effects in the substrate oxidation catalysed by horseradish peroxidase

To date, detailed magnetic-field-effect-based spin chemistry studies were carried out of the HRP-catalysed oxidation of organic substrates, namely, 2-methyl-1-(trimethylsilyloxy)-prop-1-ene ($\text{Me}_2\text{C}=\text{CHOSiMe}_3$) in the presence of H_2O_2 ,³³ NADH³⁴ and its synthetic analogue, 3,5-di(methoxycarbonyl)-2,3-dimethyl-4-nitrophenyl-1,4-dihydropyridine (nifedipine, NF), in the absence of H_2O_2 .³⁵ In all the three cases, the effective rate constants for transformations of particular intermediates of the catalytic cycle of HRP (Per^{3+} , Per^{2+} , Compounds I–III) were measured using a rapid-scanning stopped-flow spectrophotometer. Since the intermediates listed above show different absorption spectra⁴⁶ (Fig. 2), it is possible to monitor the kinetics of corresponding interconversions. For instance, in the study of $\text{Me}_2\text{C}=\text{CHOSiMe}_3$

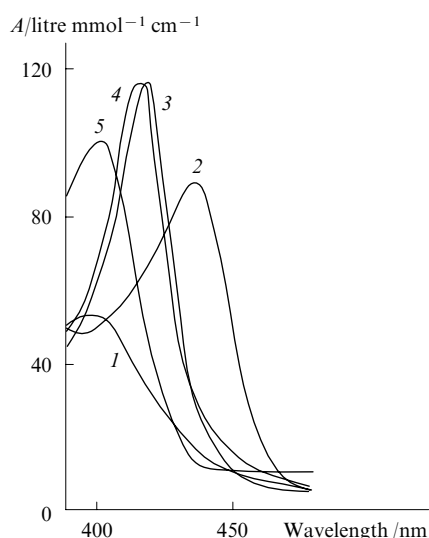


Figure 2. Absorption spectra of horseradish peroxidase and peroxidase reactive intermediates.⁴⁷ Compound I (1), Per^{2+} (2), Compound III (3), Compound II (4) and Per^{3+} (5).

oxidation, the changes in the absorbance (A) of the reactive HRP intermediates were detected at 418 nm (maximum absorption of Compounds II and III, see Fig. 2) over a period of 1 s with a time resolution of 1 ms.³³ The time resolution was 16 ms in the NADH oxidation³⁴ and 32 ms in the NF oxidation,³⁵ because the reactions with these substrates took much longer time to complete (up to 500 s). To study the effect of external magnetic field, the mixing cell in which the reaction of the substrate with HRP occurred, was placed between the poles of an electromagnet and the magnetic field strength was varied from 0 to 4500 G. The kinetic traces recorded in each case were compared with the corresponding traces obtained in zero magnetic field (to this end, the residual magnetisation of the electromagnet was compensated up to a value of 0.3 to 0.5 G). The effective rate constants for interconversions of the HRP intermediates were determined using the Levenberg–Marquardt non-linear regression algorithm. The analytical solution to the system of differential equations describing successive transformations of intermediates of the catalytic cycle of HRP with allowance for their molar extinction coefficients at 418 nm^{24,47} was used as the fitting function. The magnetic field effects were detected as the dependence of the ratio of the effective rate constant in a particular magnetic field to the corresponding rate constant determined in terrestrial magnetic field on the strength of the external magnetic field.

3. Analysis of magnetic field effects in the oxidation of 2-methyl-1-(trimethylsilyloxy)prop-1-ene by horseradish peroxidase

The oxidation of $\text{Me}_2\text{C}=\text{CHOSiMe}_3$ by horseradish peroxidase in the presence of hydrogen peroxide³³ was the first example of the substrate oxidation by a haem-containing enzyme, in which the effect of magnetic field on transformations of paramagnetic intermediates was detected.

The kinetic curves (Fig. 3) with allowance for absorption of reactive peroxidase intermediates at 418 nm (see Fig. 2) can be explained by a sequence of conversions of the paramagnetic species. The initial decrease in the absorbance (see Fig. 3, region 1) can be explained by the formation of Compound I (extinction coefficient $\epsilon_{418} = 35 \text{ litre mmol cm}^{-1}$) in the reaction of the native HRP with H_2O_2 . The subsequent reaction of

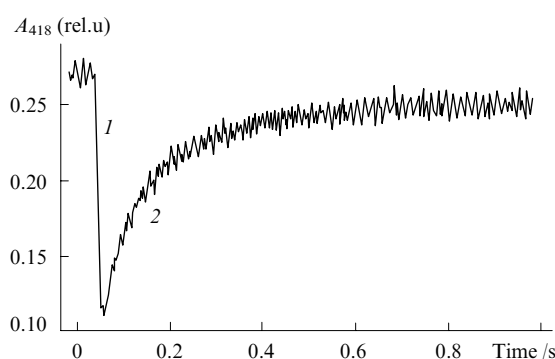
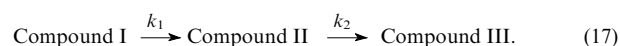


Figure 3. Kinetic curve of chemical transformations of reactive paramagnetic peroxidase intermediates observed at 418 nm.

Reaction conditions (all concentrations after mixing): 100 mM phosphate buffer (pH 7.4), $[\text{Per}^{3+}] = 4 \mu\text{mol litre}^{-1}$, $[\text{H}_2\text{O}_2] = 0.1 \text{ mmol litre}^{-1}$, [2-methyl-1-(trimethylsilyloxy)prop-1-ene] = $16 \text{ mmol litre}^{-1}$; 25 °C.

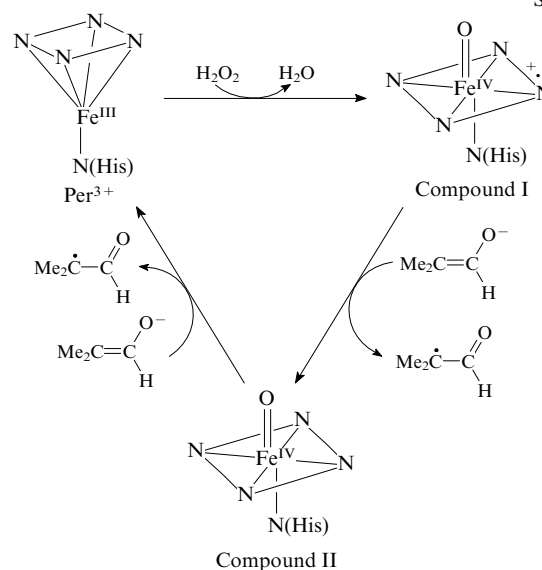
Compound I with the first substrate molecule results in Compound II ($\epsilon_{418} = 115 \text{ litre mmol cm}^{-1}$) and, consequently, in an increase in the absorbance (see Fig. 3, region 2). Then Compound II reacts with the second substrate molecule to regenerate the native HRP.

The reaction of HRP with hydrogen peroxide is too fast to be treated correctly under the experimental conditions and at the time resolution mentioned above. In this connection the initial region of the fall-off of the kinetic curve was ignored in the design of the kinetic model for theoretical description of the process. Therefore, changes in the optical absorption can be described, in the framework of the sequence of conversions shown in Scheme 5, using the kinetic model for two successive unimolecular reactions



Since the extinction coefficient of HRP at 418 nm is much lower than that of Compound II (see Fig. 2), the overall function for the description of the experimentally observed kinetics of changes in the optical absorption (A_{418}) is given by:

Scheme 5



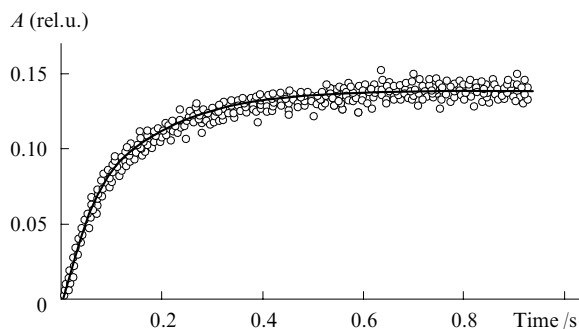


Figure 4. Fitting of the experimental kinetic curve using the Levenberg–Marquardt non-linear regression algorithm and analytical solution (18).

Experimental data are shown by open circles and the fitting results are shown by the solid line.

$$A_{418} = [\text{compound II} + \text{Per}^{3+}] \approx \quad (18)$$

$$\approx \frac{[\text{compound I}]_0}{2} \left[1 - \frac{(k_2 - 2k_1) \exp(-k_1 t)}{k_2 - k_1} - \frac{k_1 \exp(-k_2 t)}{k_2 - k_1} \right].$$

To determine the effective rate constants k_1 and k_2 , the analytical solution (18) is used for constructing a corresponding kinetic plot with allowance for the sequence of conversions of reactive paramagnetic intermediates of the peroxidase catalytic cycle (see Scheme 5) using the Levenberg–Marquardt non-linear regression algorithm. Figure 4 illustrates

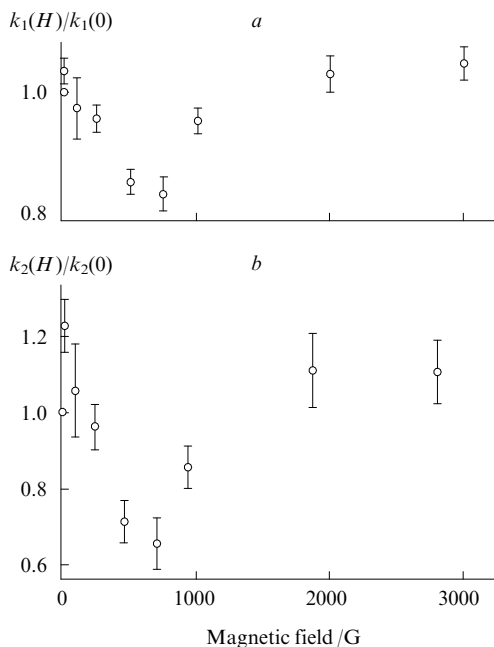
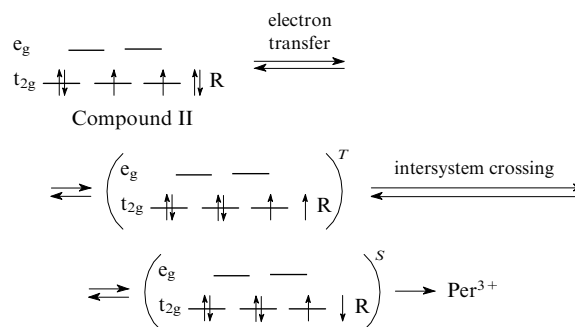


Figure 5. Magnetic field effect on the rate constants k_1 (a) and k_2 (b) of the oxidation of 2-methyl-1-(trimethylsilyloxy)prop-1-ene catalysed by horseradish peroxidase. Shown are the standard deviations (averaging over three experimental series including 5 or 6 measurements each). Reaction conditions (all concentrations are reported after mixing): 100 mM phosphate buffer (pH 7.4), $[\text{Per}^{3+}] = 4 \mu\text{mol litre}^{-1}$, $[\text{H}_2\text{O}_2] = 0.1 \text{ mmol litre}^{-1}$, $[\text{2-methyl-1-(trimethylsilyloxy)prop-1-ene}] = 16 \text{ mmol litre}^{-1}$; 25 °C.

excellent agreement between the experimental kinetic curve and calculated function (18). The magnetic field effects were calculated as the ratio of the rate constants k_1 and k_2 measured in non-zero external magnetic fields to the corresponding rate constants determined in the zero magnetic field. The magnetic field dependences of the magnetic field effects determined for k_1 and k_2 are shown in Fig. 5. In Section III, we showed that the shape of the magnetic field dependence of the magnetic field effect and positions of extrema are determined by the magnetic resonance parameters of two paramagnetic species.¹ By comparing the experimental magnetic field dependence (see Fig. 5) and the results of calculations using the known semi-classical approximation,⁵⁴ one can determine the magnetic field-sensitive step of the process, namely, the second stage of the catalytic cycle, which involves the interaction of Compound II with the substrate. In this stage, the event of single-electron transfer is followed by the formation of the radical form of Compound II and the radical anion of the enol form of 1-isobutylaldehyde ($\text{Me}_2\text{C}=\text{CHO}^\cdot$). In this case the magnetic field effect is due to the probability difference between back electron transfer in the radical pair in weak and strong magnetic fields. Here, the reversible electron transfer event in the collective triplet state of the RP is accompanied by regeneration of Compound II, whereas the singlet state eventually results in the starting HRP (Per^{3+}) (Scheme 6).

Scheme 6



Thus, manifestation of the magnetic field effect confirms the assumption of involvement of the paramagnetic intermediates in the catalytic cycle of HRP. This also indicates the possibility for a new, non-studied, short-lived radical form of Compound II to exist.^{24, 27, 47}

4. Magnetic field effects in the oxidation of NADH and its synthetic analogues by horseradish peroxidase

a. Enzymatic oxidation of NADH catalysed by horseradish peroxidase

Yet another example of manifestation of the magnetic field effect in the reactions catalysed by HRP is provided by the oxidation of NADH, a natural HRP substrate. In the above discussion of modern concepts of the mechanisms of oxidation of organic substrates catalysed by HRP, mention was made that the initiation step of the catalytic cycle in the absence of hydrogen peroxide requires additional studies. Electron transfer from the donor molecule (NADH) to acceptor (e.g., haem of the active site of HRP) can be a highly probable starting point of the catalytic cycle. The use of spin chemistry methods to prove this assumption seems to be correct.

The oxidation of NADH catalysed by HRP in the absence of H_2O_2 was studied by the stopped-flow spectrophotometric technique (see above). The reactive HRP intermediates (Compounds I, II and III) were also detected at the wavelength of maximum absorption of Compounds II and III (418 nm). Based on the known sequences of interconversions of HRP intermediates⁴⁶ and their molar extinction coefficients²⁴ (see

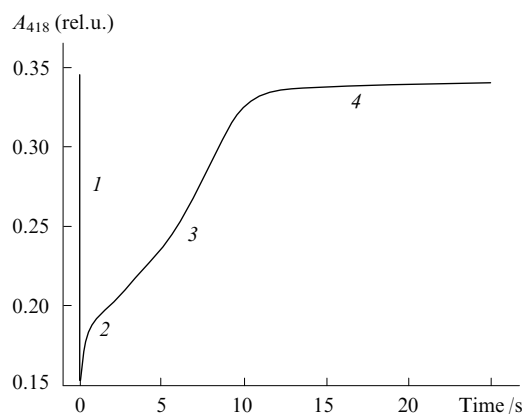
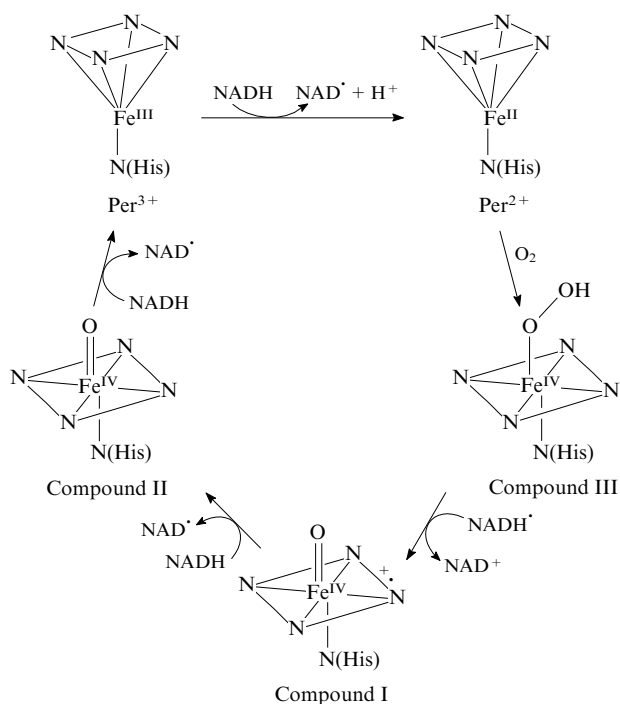


Figure 6. Kinetic curve of chemical transformations of horseradish peroxidase reactive paramagnetic intermediates observed at 418 nm in the NADH oxidation catalysed by peroxidase.

Reaction conditions (all concentrations after mixing): 100 mM MES buffer, pH 5.6; $[\text{Per}^{3+}] = 1 \mu\text{mol litre}^{-1}$, $[\text{NADH}] = 100 \mu\text{mol litre}^{-1}$; 25 °C.

Fig. 2), the characteristic kinetic curve of this process (Fig. 6) was explained as follows:³⁴ a decrease in absorption in the first step (see Fig. 6, region 1) is associated with the transformation of native HRP ($\epsilon_{418} = 62 \text{ litre mmol}^{-1} \text{ cm}^{-1}$) to ferropoxidase (Per^{2+}) ($\epsilon_{418} = 62 \text{ litre mmol}^{-1} \text{ cm}^{-1}$) upon electron transfer event from the substrate (NADH) to the starting HRP, which results in the formation of the reduced form (Per^{2+}). This is followed by the reactions of ferropoxidase with oxygen dissolved in the buffer solution (Scheme 7), which leads to rapid conversion of Per^{2+} ($k = 5.8 \times 10^4 \text{ litre mol}^{-1} \text{ s}^{-1}$) to Compound III ($\epsilon_{418} = 115 \text{ litre mmol}^{-1} \text{ cm}^{-1}$)²⁴ and subsequent increase in absorption (see Fig. 6, region 2). Fast deprotonation of the $\text{NADH}^{+\cdot}$ radical cation ($k = 3.6 \times 10^6 \text{ s}^{-1}$) (Ref. 55) produces the NAD^{\cdot} radical, which reacts with Compound III to give Compound I ($\epsilon = 35 \text{ litre mmol}^{-1} \text{ cm}^{-1}$) (see Scheme 7). This process

Scheme 7



corresponds to the ‘deflection’ region of the kinetic curve (see Fig. 6, region 3). Then, the single-electron reduction of Compound I produces Compound II ($\epsilon_{418} = 115 \text{ litre mmol}^{-1} \text{ cm}^{-1}$), which leads to an increase in the absorption at 418 nm (Fig. 6, region 4).

The initial portion of the kinetic curve of ferropoxidase formation was too fast for quantitative treatment; therefore, the corresponding rate constant was excluded from the theoretical kinetic model. Therefore, in accordance with the proposed sequence of reactions (see Scheme 7), an increase in the absorption (see Fig. 6, regions 2–4) was described using a kinetic model that assumes three unimolecular reactions



Compounds II and III are characterised by equal extinction coefficients that are about three times higher than the molar extinction of Compound I and twice as high as that of Per^{2+} ; therefore, the overall fitting function for the description of the experimental changes in absorbance with time can be written as follows:

$$\begin{aligned} A_{418} &= [\text{compound III}] + [\text{compound II}] + \\ &+ \frac{[\text{compound I}]}{3} + \frac{[\text{Per}^{2+}]}{2} = \\ &= [\text{Per}^{2+}]_0 - \frac{2[\text{compound I}]}{3} - \frac{[\text{Per}^{2+}]}{2}. \end{aligned} \quad (20)$$

The curve calculated using experimental data and the Levenberg–Marquardt non-linear regression algorithm for the overall analytical solution (20) to the system of equations that describe the sequence of reactions in the catalytic cycle of HRP (19) virtually coincides with the experimental kinetic curve shown in Fig. 7. It should be noted that kinetic simulation with allowance for ferropoxidase formation allowed one to obtain the best fit of the experimental and theoretical curves. This made it possible to determine the rate constants k_1 , k_2 and k_3 for the reactions (19).

Yet another proof of occurrence of single-electron transfer between HRP and NADH in the enzymatic oxidation was obtained by analysing the magnetic field dependences of the magnetic field effect detected in this process. The magnetic field effect calculated as the ratio of the effective rate constants in a magnetic field to the corresponding rate constants in the zero magnetic field was found only for the constant k_1 (Fig. 8). The most probable magnetic field sensitive step is electron transfer

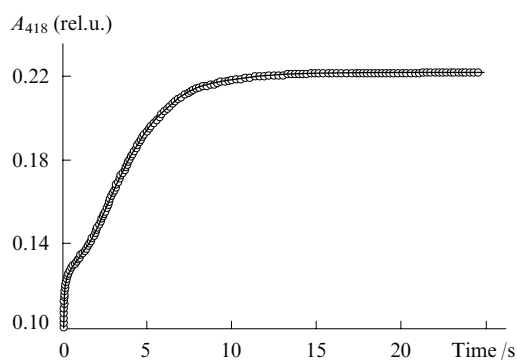


Figure 7. Fitting of the experimental kinetic curve for the reaction of peroxidase with NADH using the Levenberg–Marquardt non-linear regression algorithm and analytical solution (20).

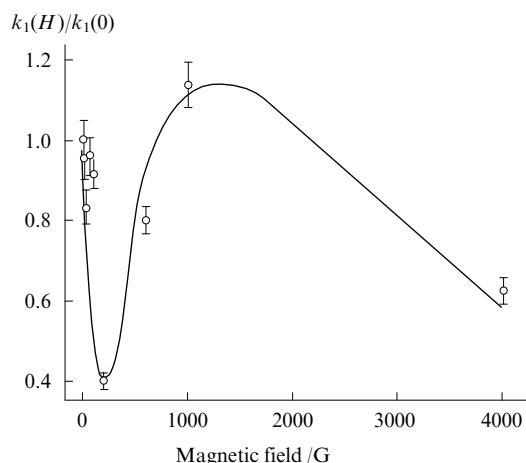


Figure 8. Magnetic field effect on the rate constant k_1 of the oxidation of NADH catalysed by horseradish peroxidase.

The error bars show the sum of the instrumental error (3.5%) and the standard error of averaging over three experimental series including 5 or 6 measurements each. Reaction conditions (all concentrations after mixing): 100 mM MES buffer (pH 5.6); $[\text{Per}^{3+}] = 1 \mu\text{mol litre}^{-1}$, $[\text{NADH}] = 100 \mu\text{mol litre}^{-1}$; 25 °C.

between the native HRP and NADH. Subsequent conversion of ferropoxidase in the reaction with oxygen occurs under kinetic control ($k = 6 \times 10^4 \text{ litre mol}^{-1} \text{ s}^{-1}$);^{24, 47} therefore, the rate of formation of Compound III will be much lower than the rate of spin conversion in the pair ($\text{Per}^{2+} \text{ O}_2$) and the process will most probably be spin-independent. The interaction of Compound III with the radical NAD^\bullet also cannot be the source of a strong magnetic field effect, if a collision of this radical with the radical NAD^\bullet in the bulk produces the so-called F-pair (strong magnetic field effects are not characteristic of this species).⁵⁶ However, is it possible to consider enzymatic reactions as bulk processes? The issue has not been answered so far. As to the subsequent steps of the catalytic cycle, the interaction of Compound I with NADH produces no RP and the formation of peroxidase as a result of the reaction between Compound II and NADH was not included in the analytical function at all, because this step was not observed on the time scale studied. Thus, we have formulated a hypothesis that the dependence of the rate constant k_1 on the strength of the external magnetic field is due to the effect of the magnetic field on the rate of ferropoxidase formation in the event of single-electron transfer between HRP and NADH.

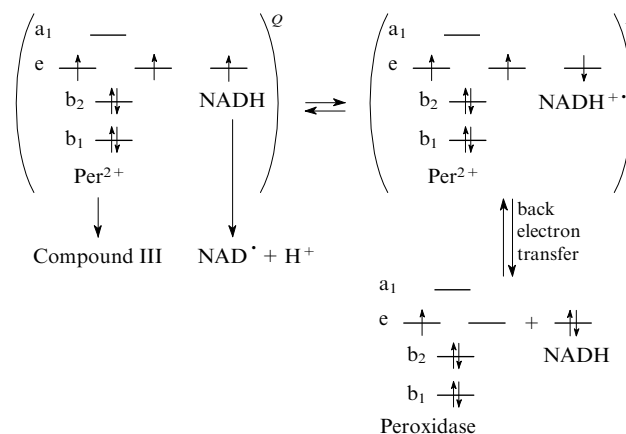
To check the assumption that the magnetic field effect is formed in the first step of the catalytic cycle, the magnetic field dependence of the magnetic field effect for the paramagnetic pair ($\text{Per}^{2+} \text{ NADH}^{+\bullet}$) was calculated. The RP multiplicity was established in the framework of the theory of crystal field by analysing³⁴ the spin state of the central iron atom in the ferropoxidase haem.⁵⁷

According to modern concepts, the inorganic complex (ferropoxidase, Per^{2+}) can be treated as a stable polyatomic system in which the effect of ligands [porphyrin (N) and histidine (N_{His})] on the central ion Fe(II) is electrostatic in nature. It was established that in a free iron atom five d-states (d_{xy} , d_{xz} , d_{yz} , d_{z^2} and $d_{x^2-y^2}$) with the same energy are split into four groups with different energies in the pyramidal field of ferropoxidase ligands (N and N_{His}), *i.e.*, the quintuply degenerate ^5D -term of free ion is split in the ligand field of the pyramidal complex into four terms, namely, b_1 ($d_{x^2-y^2}$), b_2 (d_{xy}), a doubly degenerate e (d_{xz} , d_{yz}) and a (d_{z^2}).

The electron states of the RP are shown in Scheme 8. Donation of a single electron from NADH to the native HRP

causes the formation of the ($\text{Per}^{2+} \text{ NADH}^{+\bullet}$) RP in the quartet and doublet states. Owing to intersystem crossing, the non-reactive quartet spin state becomes a reactive doublet state. Recombination of the latter (back electron transfer) maintains the possibility of regeneration of the starting HRP and NADH.

Scheme 8



The recombination probability for the RP under study was calculated in the framework of the density matrix formalism for the two-position model. The basics of this approach have been considered above (see Section III). It was assumed³⁴ that the observed quartet–doublet spin evolution of the RP is governed by the electron spin interaction with the constant external magnetic field, isotropic hyperfine interaction between the unpaired electrons and magnetic nuclei in the system and by the exchange interaction between the unpaired electrons, which causes splitting of the RP terms into a doublet and a quartet.

The Hamiltonian of this system of interactions has the form:

$$\hat{H} = \omega_1 \hat{S}_1 + \omega_2 \hat{S}_2 + a \hat{S}_1 \hat{I} + J \hat{S}_1 \hat{S}_2, \quad (21)$$

where $\omega_1 = g_1 \beta \hbar^{-1} H_0$ and $\omega_2 = g_2 \beta \hbar^{-1} H_0$ are the spin precession frequencies of the radicals in the pair of species with the electron spins 1 and 1/2, respectively; the g -factors are $g_1 = 3.25$ (for ferropoxidase)⁵⁸ and $g_2 = 2.003$ (for the substrate radical cation);⁵⁵ $a = 32.9 \text{ G}$ (Ref. 55) is the constant of isotropic hyperfine interaction between the unpaired electron of the radical cation $\text{NADH}^{+\bullet}$ and the magnetic nucleus in this radical cation ($I = 1/2$); and J is the exchange integral between the doublet and quartet terms of the radical pair. It should be noted that in the general case the exchange interaction constant depends on the distance between the radicals (r) and the orientation angles (θ and φ), *i.e.*, $J = f(r, \theta, \varphi)$. For simplicity, only two possible conformational states of the complex $[\text{Per}^{2+} \dots \text{NADH}^{+\bullet}]$ characterised by the quartet–doublet ($Q-D$) evolution with the corresponding exchange integrals J_1 and J_2 varied from 200×10^7 to $300 \times 10^7 \text{ rad s}^{-1}$ were analysed.³⁴ The best agreement between the calculated and experimental dependences on the magnetic field applied was attained at $J_1 = 200 \times 10^7$ and $J_2 = 265 \times 10^7 \text{ rad s}^{-1}$.

The spin Hamiltonian (21) commutes with the projection of the total spin of the electrons and nucleus on the direction of the external magnetic field H_0 , the total projection being equal to

$$\hat{\Sigma}_Z = \hat{S}_{1Z} + \hat{S}_{2Z} + \hat{I}_Z. \quad (22)$$

Because only the states with the same total projection participate in quantum transitions, all spin states of the radical pair

can be divided into the following subensembles: $\Sigma_Z = \pm 2$, $\Sigma_Z = \pm 1$ and $\Sigma_Z = 0$, only the subensembles with the total spin projections equal to $+1$, -1 and 0 contributing to the RP recombination. The behaviour of the stationary energy levels obtained by solving the Schrödinger equation with the Hamiltonian given by expression (21) for the subensembles mentioned above is illustrated in Fig. 9. Recombination probability calculations were carried out for each of the three subensembles. The final recombination probability for the RP ($\text{Per}^{2+} \text{NADH}^{+\bullet}$) was calculated as the sum of the probabilities for each subensemble with allowance for the statistical weights. The recombination probability $W(Q)$ thus calculated for the radical pair ($\text{Per}^{2+} \text{NADH}^{+\bullet}$) born in the quartet state is plotted vs. magnetic field in Fig. 10.

The magnetic field dependence of the recombination probability first calculated for the multispin system was interpreted as follows.³⁴ According to the classical radical pair theory, a radical pair born in the non-reactive quartet state is characterised by a minimum recombination probability in zero magnetic field, which is confirmed by calculations. Further increase in the recombination probability $W(Q)$ in weak magnetic fields corresponds to removal of degeneracy of the Zeeman energy levels on going from the zero to a non-zero magnetic field. Interpretation of the remaining regions of the magnetic field dependence requires consideration of the behaviour of the stationary energy levels of the subensembles with the spin projections equal to $+1$, 0 and -1 (see Fig. 9) in different magnetic fields. A decrease in separation between the energy levels in the range 200–250 G indicates that here one should expect manifestation of specific features of the recombination probability behaviour. Indeed, the theoretical curve (see Fig. 10) shows an extremum at 250 G the position of which unambiguously indicates manifestation of electron exchange interaction (J). The role of J is clearly illustrated in

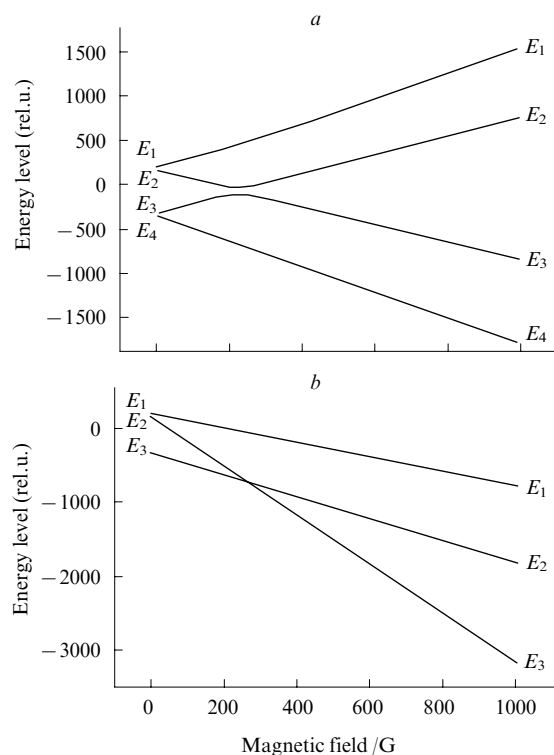


Figure 9. $Q-D$ transitions in the paramagnetic pair ($\text{Per}^{2+} \text{NADH}^{+\bullet}$) Q . Splitting of stationary energy levels with the total spin projection equal to 0 (a) and -1 (b) in an external magnetic field.

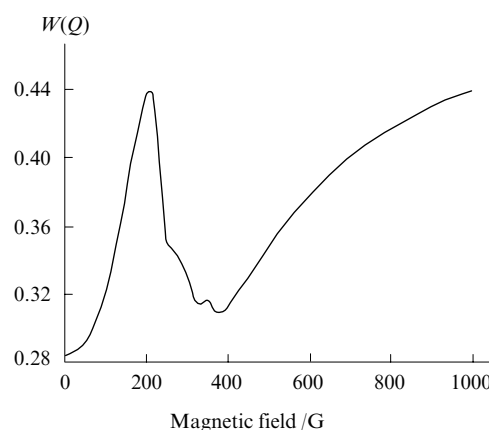


Figure 10. Calculated recombination probability $W(Q)$ for the paramagnetic pair ($\text{Per}^{2+} \text{NADH}^{+\bullet}$) Q plotted vs. the magnetic field induction.

the scheme of the RP terms in the magnetic field (Scheme 9). Effective quartet–doublet mixing is possible in the external magnetic field equal to

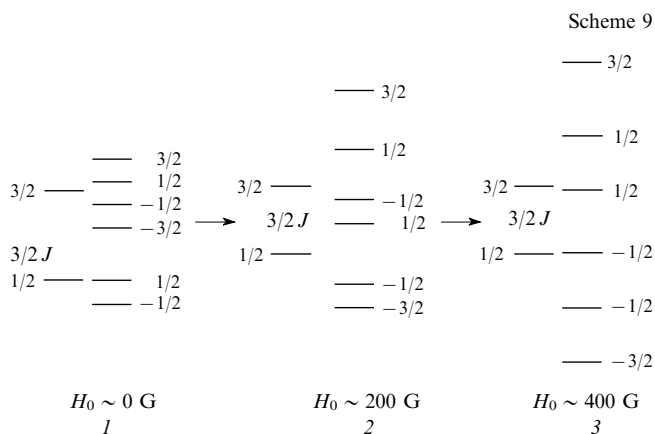
$$H_0 = \frac{(3/2)J}{(g_1 + g_2)\beta}.$$

Then, after passage of the local maximum of the magnetic field dependence, the splitting between the energy levels (see Scheme 9, lines 2, 3) increases again due to the Zeeman interaction. As a result, transitions from the quartet state to the doublet state occur at lower rates and the recombination probability decreases (see Fig. 10). Since the frequency of transitions between states is determined by the Larmor frequency difference between the radicals in the pair

$$\omega_{QD} = \omega_1 - \omega_2 = (g_1 - g_2)\beta\hbar^{-1}H_0,$$

the efficiency of transitions between the non-reactive quartet state and reactive doublet state will increase again with an increase in the magnetic field. Therefore, the recombination probability increases in strong magnetic fields (400–1000 G).

The calculated recombination probability characterises the magnetic field effect on the $Q-D$ transition in the radical pair ($\text{Per}^{2+} \text{NADH}^{+\bullet}$), resulting in regeneration of the starting HRP. Therefore, the experimentally detected formation of Compound III in the bimolecular reaction between ferroperoxidase and oxygen molecule with the rate constant k_1 is described by the dependence of $[1 - W(Q)]$ on the magnetic field applied (Fig. 11). A comparison of the calculated (see



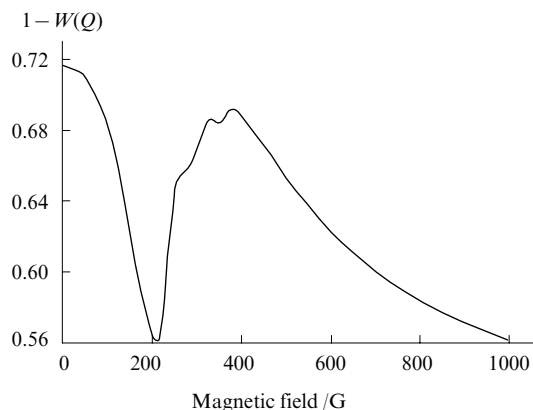


Figure 11. Escape probability $[1 - W(Q)]$ calculated for the paramagnetic pair $(\text{Per}^{2+} \text{NADH}^{+\bullet})$ plotted vs. the external magnetic field (simulation of experimental dependence of the rate constant k_1 in the NADH oxidation catalysed by horseradish peroxidase on the external magnetic field).

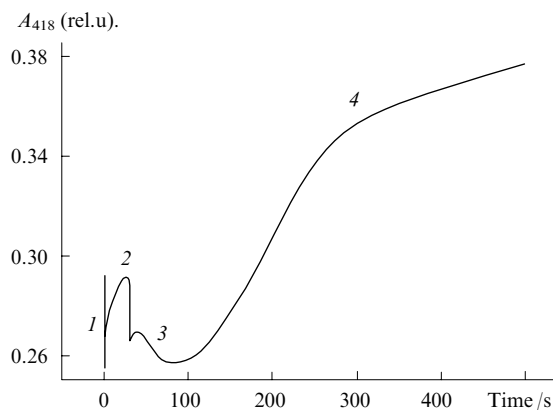


Figure 12. Kinetic curve of chemical transformations of the peroxidase reactive intermediates observed in the oxidation of nifedipine. Reaction conditions (all concentrations after mixing): 100 mM phosphate buffer (pH 7.0); $[\text{Per}^{3+}] = 1 \mu\text{mol litre}^{-1}$; $[\text{NF}] = 15 \mu\text{mol litre}^{-1}$; 15 vol.% EtOH; 25 °C.

Fig. 11) and experimental (see Fig. 8) magnetic field dependences of the magnetic field effect revealed qualitative agreement between them.

Thus, manifestation of the magnetic field effect, the magnetic field dependence of which is described in the framework of the radical pairs theory, indicates involvement of two paramagnetic species in the NADH oxidation catalysed by HRP. Agreement between the experimental and calculated magnetic field dependences is attained assuming formation of the magnetic field effect in the pair $(\text{Per}^{2+} \text{NADH}^{+\bullet})$. It should be emphasised that the conclusion about the presence of single-electron transfer step in the catalytic cycle of HRP also follows from the analysis of the experimental kinetic curves (see, *e.g.*, Fig. 6).

b. Magnetic field effect in the enzymatic oxidation of nifedipine, a synthetic analogue of NADH

The presence of the single-electron transfer step in the catalytic cycle of HRP was additionally substantiated in the studies of the enzymatic oxidation of nifedipine [3,5-di(methoxycarbonyl)-2,3-dimethyl-4-nitrophenyl-1,4-dihydropyridine], a synthetic analogue of NADH, which were also carried out using the stopped-flow technique.³⁵

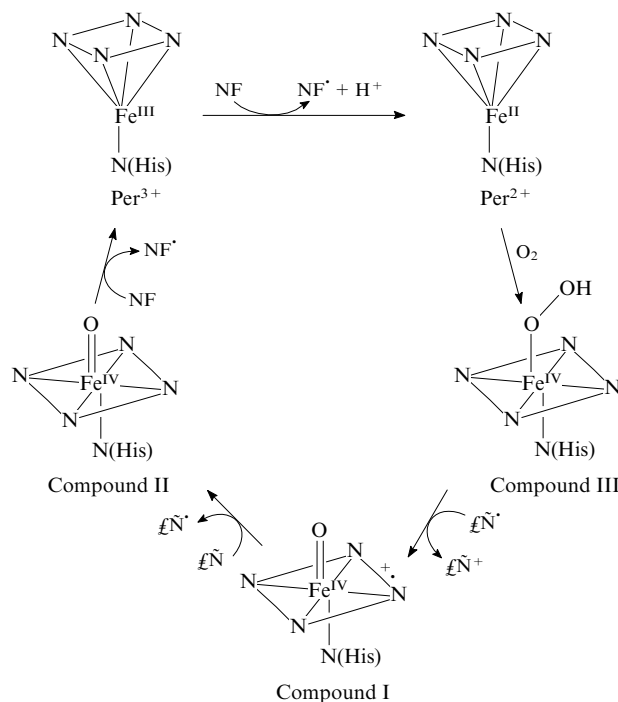
The characteristic kinetic curve of the formation and decay of the peroxidase reactive intermediates in the oxidation of NF observed at 418 nm (maximum absorption wavelength of Compounds II and III) is shown in Fig. 12. The kinetic curve was analysed using the approach similar to that described above for the enzymatic oxidation of NADH. It was found that the NF oxidation kinetics can be explained by a sequence of elementary steps³⁵ identical to that proposed³⁴ for the description of the enzymatic NADH oxidation (Scheme 10).

A decrease in the absorbance in the initial portion of the kinetic curve (see Fig. 12, region 1) is associated³⁵ with the formation of ferroperoxidase ($\epsilon_{418} = 62 \text{ litre mmol}^{-1} \text{ cm}^{-1}$) upon electron transfer from NF to the haem iron atom of the enzyme, which also leads to formation of the radical cation $\text{NF}^{+\bullet}$. Further increase in absorbance (see Fig. 12, region 2) occurs during the reaction of ferroperoxidase with the dissolved oxygen to give Compound III ($\epsilon_{418} = 115 \text{ litre mmol}^{-1} \text{ cm}^{-1}$). In the next stage, a neutral nifedipine radical (NF^{\bullet}) formed as a result of deprotonation of the $\text{NF}^{+\bullet}$ radical cation is involved in the reaction. A CIDNP study³⁵ of the transformations of $\text{NF}^{+\bullet}$ in a model process showed that the deprotonation takes a few nanoseconds. The radical thus formed reacts with Compound III, which causes a dramatic

decrease in absorbance (see Fig. 12, region 3) due to the formation of Compound I ($\epsilon_{418} = 35 \text{ litre mmol}^{-1} \text{ cm}^{-1}$). Single-electron reduction of Compound I by the second NF molecule results in the formation of Compound II ($\epsilon_{418} = 115 \text{ litre mmol}^{-1} \text{ cm}^{-1}$); as a result, absorbance increases (see Fig. 12, region 4). No rapid regeneration of the native HRP occurs in the course of the reaction between NF and Compound II; this seems to be due to inactivation of the enzyme in the reactions with radicals.³⁵

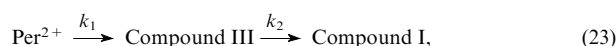
At the same time, a comparison of the kinetic curves of the HRP-catalysed oxidation of NADH and NF (*cf.* Figs. 6 and 12) clearly demonstrates significant differences between these processes. For instance, it should be noted that each step of the NF oxidation is much slower than the corresponding step of the reaction of HRP with NADH. This can be explained by several factors, in particular, a lower concentration of NF compared to the NADH concentration (15 and 100 μmol

Scheme 10



litre⁻¹, respectively) and by the use of the phosphate buffer (pH 7.0) instead of the MES buffer (pH 5.6) in which HRP is more reactive.²⁴ The activity of the enzyme is also affected by the addition of EtOH (15%) necessary for solubilisation of NF, because ethanol acts as an inhibitor of HRP.

The effective rate constants for the formation of Compounds III and I were determined by treating the kinetic curves measured at different strengths of external constant magnetic field using the Levenberg–Marquardt non-linear regression algorithm. In this case, the kinetic model for two successive unimolecular stages was considered



and fitting was performed only for the portion of the kinetic curve that describes the kinetics of formation and consumption of Compound III (see Fig. 12,2). It turned out that, similarly to the NADH oxidation, only the rate constant k_1 is magneto-sensitive. The experimental magnetic field dependence of the magnetic field effect (Fig. 13) agrees with the theoretical curve (see Fig. 11) assuming that the magnetic field effect is formed in the pair ($\text{Per}^{2+} \text{NF}^{+\cdot}$) (Scheme 11).

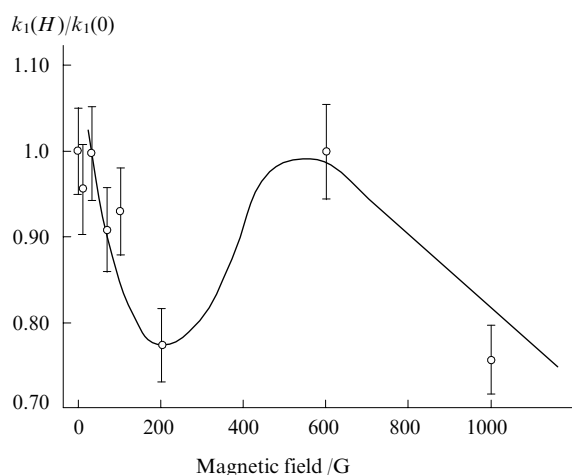
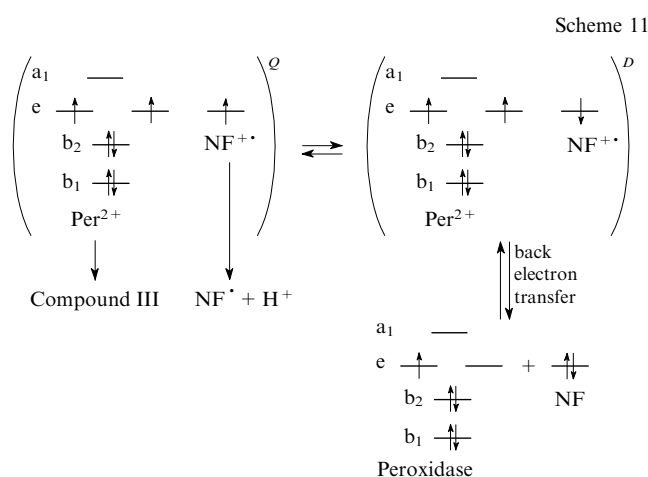


Figure 13. Magnetic field effect on the rate constant k_1 for oxidation of nifedipine catalysed by horseradish peroxidase.

The error bars show the sum of the instrumental error (3.5%) and the standard error of measurements (averaged over three experimental series including 5–6 measurements each). Reaction conditions (all concentrations after mixing): 100 mM phosphate buffer (pH 7.0); $[\text{Per}^{3+}] = 1 \mu\text{mol litre}^{-1}$, $[\text{NF}] = 15 \mu\text{mol litre}^{-1}$; 15 vol.% EtOH; 25 °C.

Thus, we can conclude that, similarly to the case of NADH, back electron transfer in the pair ($\text{Per}^{2+} \text{NF}^{+\cdot}$) occurs in the doublet state of the RP, whereas the quartet spin state is the source of Compound III (see Schemes 8 and 11).

An important conclusion that can be drawn based on the analysis of the magnetic field effects detected in the enzymatic oxidation of the natural substrate of horseradish peroxidase, NADH and its synthetic analogue nifedipine, is as follows. In the absence of hydrogen peroxide, the enzymatic oxidation begins with electron transfer between the native HRP and substrate rather than the reaction with trace amounts of hydrogen peroxide formed as a result of NADH (NF) oxidation by dissolved oxygen, which was earlier considered as the initiation step.^{24, 47}



5. Studies of the magnetic field effect on the NADH oxidation by horseradish peroxidase in an oscillatory reaction

Of particular interest is the oscillatory reaction of NADH with O_2 catalysed by HRP, which has been a subject of intensive studies. The reaction dynamics shows a number of specific features dependent on the reaction conditions.⁵⁹ The peroxidase–oxidase system exhibits bistability (*i.e.*, two different dynamic states can exist under identical experimental conditions).²⁴ Examples are provided by two coexisting stable states⁶⁰ and a stable state that coexists with periodic oscillations.⁶¹

It should be noted that oscillations in an enzymatic system are complex biochemical processes that often involve up to 10–20 coupled elementary reactions associated with either generation or consumption of free radicals. To study the oscillatory oxidation reaction, NADH and oxygen are continuously added to a stirred aqueous buffer solution (pH 5.0–6.5) containing HRP and an initiator (usually, an aromatic compound, such as 4-hydroxybenzoic acid, melatonin or Methylene Blue). Under such conditions one can observe oscillatory processes.^{62, 63} Reaction products include hydrogen peroxide and a number of oxygen-containing free radicals.²⁴ The formation of reactive oxygen species is undesired for cell metabolism due to their destructive properties; additionally, too high concentrations of H_2O_2 cause inactivation of HRP in the reaction of peroxide with Compound I.^{64, 65} A mechanism of inactivation of the enzyme by free-radical species is described⁶⁶ and the role of aromatic initiators in this process was discussed. It was assumed that inactivation is a result of the interaction between reactive oxygen species and the side chains of amino acid molecules and peroxidase sugar residues.⁶⁷ It was shown that reduction of inactivation of the enzyme in the oscillatory system is followed by an increase in the concentration of melatonin, which rapidly reacts with the oxygen radical species formed, *e.g.*, OH^\cdot .

Studies of the effect of external magnetic field on the rate of oscillatory processes are of particular interest. It is quite important to answer the question whether or not does the enzymatic oxidation retain its magnetic field sensitivity in the oscillatory reaction and what is the role of its initiator?

The effect of external magnetic field on the consumption of oxygen in the oscillatory reaction of NADH with O_2 catalysed by horseradish peroxidase was first observed by Olsen *et al.*⁷ The oxygen concentrations in the solution during the reaction in a magnetic field of strength varied from 0 to 4000 G were measured with a Clark-type oxygen electrode. The frequency and amplitude of $[\text{O}_2]$ -oscillations are plotted vs. magnetic field in Fig. 14. The plots exhibit characteristic extrema at about

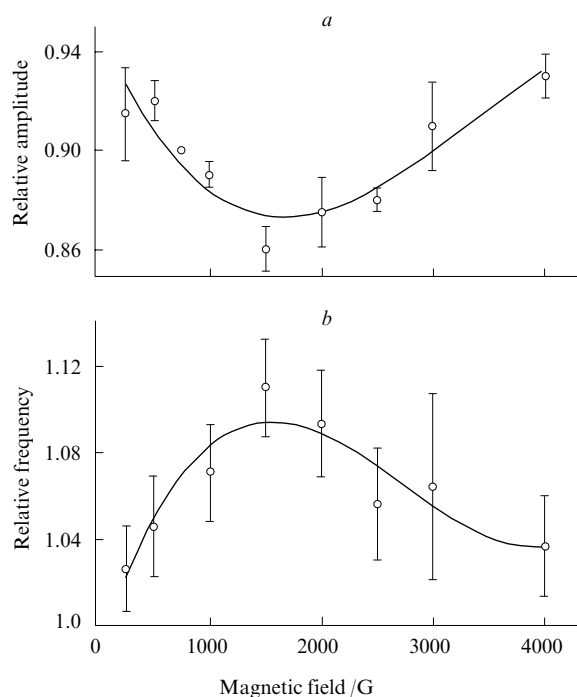


Figure 14. Effect of the magnetic field on the [O₂]-oscillation amplitude (a) and frequency (b).

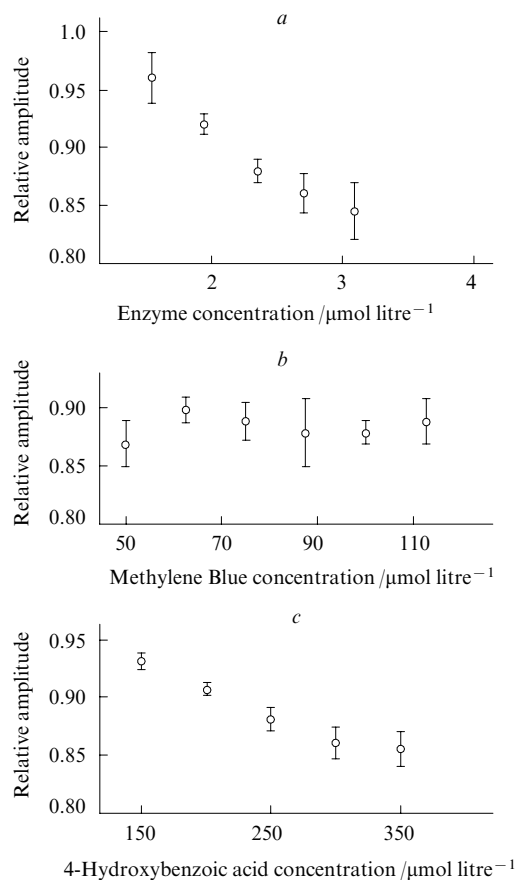
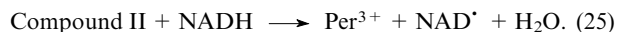
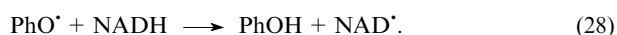


Figure 15. Effect of the concentrations of peroxidase (a), Methylene Blue (b) and 4-hydroxybenzoic acid (c) on the [O₂]-oscillation amplitude.

1500 G. The magnetic field effect is independent of the pH value, NADH and methylene blue concentrations, being sensitive to the change in the concentrations of HRP and initiator, 4-hydroxybenzoic acid (Fig. 15).⁷ It was assumed that the magnetic field sensitive steps of the oxidase oscillatory reaction can involve radical pairs including Compounds I and II.



The dependence of the magnetic field effects observed on the concentration of phenolic compounds can be explained⁷ by participation of the latter in electron transfer between Compounds I and II in the course of the reactions



Note that the lack of a theoretical magnetic field dependence⁷ precludes drawing unambiguous conclusions about the magnetic field sensitive step of the process. We can only point to significant differences between the magnetic field dependences obtained for the steady-state HRP-catalysed oxidation of organic substrates [Me₂C=CH(OSiMe₃), NADH and NF] (see above) and measured in the course of oscillatory NADH oxidation by peroxidase (*cf.* Figs 5, 8, 13 and 14). These differences can be explained taking into account the fact that in the course of the steady-state substrate oxidation catalysed by HRP the magnetic field effects were detected in particular stages of the catalytic cycle, whereas in the case of oscillatory oxidase reaction⁷ the effect of the magnetic field on the rate of the overall process was studied. The observed dependence of the magnetic field effect on the concentration of phenol⁷ gives grounds to assume the presence of a number of magnetic field sensitive steps in the reaction under study, which can be a possible reason for the differences between the magnetic field dependences (see above).

V. Conclusion

The material presented in this review demonstrates the applicability of spin chemistry methods to studies of paramagnetic species involved in the enzymatic oxidation. Manifestation of the magnetic field effects in enzymatic reactions points to a relationship between the reactivity and spin states of paramagnetic intermediates of the catalytic cycle of HRP. For instance, it was shown that in the absence of hydrogen peroxide the enzymatic oxidation is initiated by electron transfer between the native enzyme and substrate. In addition, observation of the CIDNP effect⁶⁸ in the interaction of photoexcited NADH with horseradish peroxidase not only substantiates the conclusion about the possibility of electron transfer between the peroxidase haem and NADH, but also proves the formation of the radical cation NADH^{•+}, which was postulated in the analysis of the magnetic field effect.³⁴

Agreement between the experimental magnetic field dependences of the magnetic field effects detected in studies of the oxidation catalysed by horseradish peroxidase and the results of calculations in the approximations used in the radical pair theory makes it possible to draw some conclusions on the subtle mechanisms of the processes occurring in the catalytic cycle.

For instance, the molecular dynamics of partners in the enzyme–substrate complex should meet key requirements of the radical pair theory, namely, the rates of electron transfer in

enzymatic processes should be similar to the diffusion rates (otherwise, manifestation of the magnetic field effect is impossible), and the lifetimes of reactive intermediates should not exceed a few microseconds. The calculated magnetic field dependence³⁴ showed the best agreement with experimental data at submicrosecond lifetimes of the pair of paramagnetic species. Since the theoretical model is based on the concept of diffusion of partners, one should assume that reactants to some extent retain their mobilities in the enzymatic processes. In addition, extrema present in the magnetic field dependences at a magnetic fields strength of the order of hundreds of Gauss attest unambiguously to electron exchange interaction between partners in the catalytic cycle of horseradish peroxidase. This is most probably due to the substrate binding in the active site of the enzyme. One can hope that analysis of positions of the extrema in the plots of the magnetic field dependences of the magnetic field effects in the enzymatic oxidation of different substrates in combination with the data obtained by other methods for detection of enzyme–substrate interactions will in the future allow one to formulate criteria for evaluation of binding.

An important result is also the observation of the magnetic field effect in the oscillatory reaction of NADH oxidation by peroxidase. To draw unambiguous conclusions about changes in the processes occurring in the catalytic cycle of peroxidase in the course of oscillatory oxidation in the presence of additional sources of free radicals (Methylene Blue, phenol, *etc.*), one should study the effect of magnetic field on interconversions of HRP-Compounds, as was done for the steady-state oxidation. Differences in the character of the magnetic field dependences of the magnetic field effects detected in particular steps of the steady-state oxidation and in the oscillatory reaction (overall reaction) suggest the presence of non-identified magnetic field-sensitive steps of the oscillatory process.

Summing up, it seems useful to list other enzymatic processes that are most promising for spin chemistry studies in order to establish the mechanisms of elementary reactions. These are first of all the processes involving cytochrome P450 and cytochrome *c* oxidase,⁶⁹ which have well-established paramagnetic intermediates and are structurally similar to the peroxidase Compounds.

Cytochrome P450 plays an important role in enzymatic catalysis by metal-containing enzymes:⁴⁷ it participates in hydroxylation of xenobiotics, such as saturated and unsaturated fatty acids,⁷⁰ steroid hormones,⁷¹ cholesterol,⁷² bile acids⁷³ and prostaglandins.⁷⁴ Despite the fact that the mechanism of substrate oxidation catalysed by cytochrome P450 has been studied for two decades, it is still to be clarified. The catalytic cycle of hydroxylation by cytochrome P450 involves radical steps (Scheme 12).⁴⁷ For instance, it was assumed that

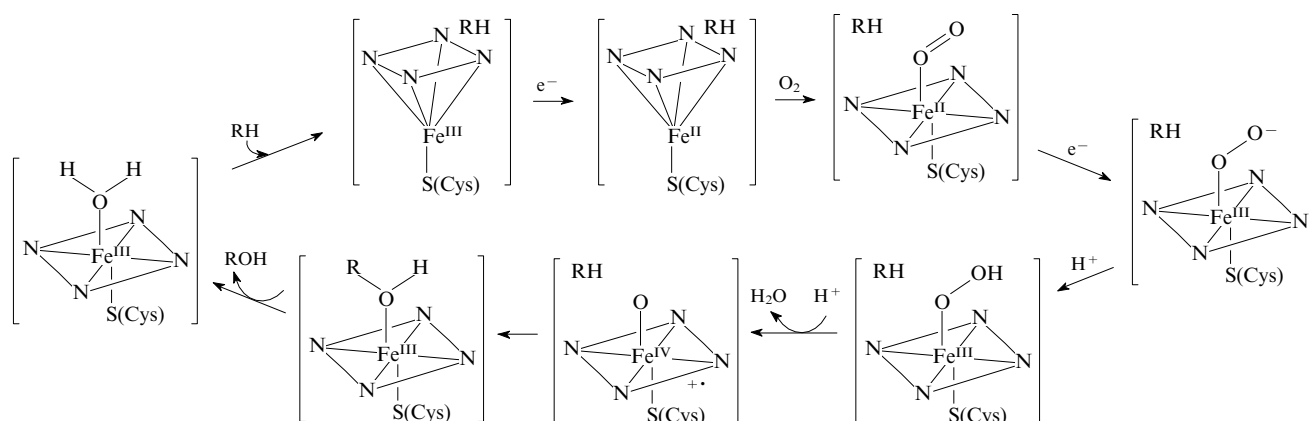
the substrate oxidation starting with the binding by the $\text{Fe}^{\text{IV}}=\text{O}$ group can proceed by either a radical ('radical clock' of norcaradiene and spiro-2,5-octane) or cationic mechanism. This results in different reaction products.⁷⁵

In addition, the state (high-spin or low-spin) of the active site of enzyme in the enzyme–substrate complex and the changes in this spin state upon reduction as a result of single-electron transfer are still unclear.⁴⁸

Spin chemistry methods can be useful in studies of the mechanism of hydroxylation by cytochrome P450. Indeed, by analysing the magnetic field dependences of the effective rates of the interconversions of reactive intermediates in the catalytic cycle of cytochrome and the dependences of the product ratio of substrate oxidation on the strength of external magnetic field it is possible to determine the spin state of iron in the enzyme active site and the spin configurations of the cytochrome reactive intermediates. Analysis of the magnetic field effects also permits monitoring of the effect of electron spins of the cytochrome P450 intermediates on the ratio of the radical and cationic oxidation pathways.

Yet another enzymatic system that can (potentially) be studied by spin chemistry methods is the cytochrome *c*–cytochrome *c* oxidase system. The role of electron-transfer steps in this system has been a subject of considerable discussion.⁷⁶ The case in point is the generation of the chemical potential within a mitochondrion in the respiratory chain, which produces most of the free energy necessary for life processes in aerobic organisms by combining electron transfer and the synthesis of adenosine triphosphate (ATP).⁷⁷ The electron transfer steps involving proteins and highly reactive paramagnetic cytochrome intermediates in the mitochondrial chain is the key to this process. At present, we know that the cytochrome *c*–cytochrome *c* oxidase system contains four cofactors, namely, two copper atoms, a low-spin haem group and a haem group that is a constituent of the protein containing haem iron and copper.⁷⁸ During the reaction, the system adds four electrons in four successive single-electron steps, thus reducing oxygen to water, and at the same time creates a proton gradient across the inner mitochondrial membrane (see Scheme 12). Recently,⁷⁶ the reactive paramagnetic intermediates of cytochrome *c* oxidase were determined spectroscopically. These are peroxide linkers (Compounds P_M and P_R), ferryl intermediate (Compound F), ground state (Compound O), a singly reduced form (Compound E) and a doubly reduced form (Compound R). Interconversions of these species involve single-electron transfer between the paramagnetic intermediates of the enzyme.⁶⁹ Based on the results of structural studies of cytochrome *c*,^{79, 80} possible pathways of electron transfer in the enzyme and a mechanism involving interconversion of cytochrome *c* intermediates were proposed; however, all these assumptions

Scheme 12



require additional proofs. It is desired to prove them in studies of the dynamics of the processes occurring in the cytochrome *c*–cytochrome *c* oxidase system. One can expect that spin chemistry methods, such as the magnetic field effect and chemically induced dynamic nuclear polarisation, will provide the possibility of establishing the role of the electron spin states in different paramagnetic intermediates and obtaining information on the subtle mechanism of functioning of the system of mitochondrial breath, namely, the cytochrome *c*–cytochrome *c* oxidase system.

References

1. K M Salikhov, Yu N Molin, R Z Sagdeev, A L Buchachenko *Spin Polarization and Magnetic Effects in Radical Reactions* (Amsterdam: Elsevier, 1984)
2. U Steiner, T Ulrich *Chem. Rev.* **89** 51 (1989)
3. I P Gragerov, L A Kiprianova, A F Levit *Khimicheskaya Polyarizatsiya Yader v Issledovaniyakh Mekhanizma Reaktsii Organicheskikh Soedinenii* (Chemically Induced Nuclear Polarisation in the Mechanistic Studies of Organic Reactions) (Kiev: Naukova Dumka, 1985)
4. M B Taraban, V I Rakhlin, T V Leshina *Russ. Khim. Zh.* **43** 80 (1999)^a
5. T V Leshina, O S Volkova, M B Taraban *Izv. Akad. Nauk, Ser. Khim.* 1830 (2001)^b
6. C B Grissom *Chem. Rev.* **95** 3 (1995)
7. A C Möller, A Lunding, L F Olsen *Phys. Chem. Chem. Phys.* **2** 3443 (2000)
8. P J Hore, S L Winder, C H Roberts, C M Dobson *J. Am. Chem. Soc.* **119** 5049 (1997)
9. T T Harkins, C B Grissom *Science* **263** 958 (1994)
10. O A Snytnikova, Yu P Tsentalovich, R Z Sagdeev *Appl. Magn. Reson.* **26** 183 (2004)
11. C E Cross, B Halliwell, E T Borish *Ann. Intern. Med.* **107** 526 (1987)
12. S Matsuzaki, L I Szveda *Biochemistry* **46** 1350 (2007)
13. G R Castro, B Panilaitis, E Bora, D L Kaplan *Mol. Pharm.* **4** 33 (2007)
14. C Brady, S E J Bell, C Parsons, S P Gorman, D S Jones, C P McCoy *J. Phys. Chem. B* **111** 527 (2007)
15. E Gaggelli, H Kozlowski, D Valensin, G Valensin *Chem. Rev.* **106** 1995 (2006)
16. A Zhang, J L Neumeyer, R J Baldessarini *Chem. Rev.* **107** 274 (2007)
17. D P Smith, G D Cicotosto, D L Tew, M T Fodero-Tavolotti, T Johansson, C L Masters, K J Barnham, R Cappai *Biochemistry* **46** 2881 (2007)
18. M Lukin, C de los Santos *Chem. Rev.* **106** 607 (2006)
19. C J Burrows, J G Muller *Chem. Rev.* **98** 1109 (1998)
20. B Halliwell, J M C Gutteridge *Methods of Enzymology* Vol. 186 (Eds L Parker, A N Glazer) (San Diego, CA: Academic Press, 1990) p. 1
21. A R Cross *The Molecular Basis of Oxidative Damage by Leukocytes* (Eds A J Jesaitis, E A Dratz) (Boca Raton, FL: CRC Press, 1992) p. 215
22. *The Respiratory Burst and Its Physiological Significance* (Eds A J Sbarra, R R Strauss) (New York: Plenum Press, 1988)
23. T M Penning, S T Ohnishi, T Ohnishi, R G Harvey *Chem. Res. Toxicol.* **9** 84 (1996)
24. A Scheeline, D L Olson, E P Williksen, G A Horras, M L Klein, R Larter *Chem. Rev.* **97** 739 (1997)
25. R P Mason, M B Kadiiska *Biological Magnetic Resonance. Biomedical EPR. Part A: Free Radicals, Metals, Medicine and Physiology* Vol. 23 (Eds S S Eaton, G R Eaton, L J Berliner) (New York: Kluwer Academic, Plenum, 2005) p. 93
26. H Hirata, H Fujii *Curr. Org. Chem.* **10** 521 (2006)
27. J H Dawson *Science* **240** 433 (1988)
28. O S Volkova, M B Taraban, V F Plyusnin, T V Leshina, M P Egorov, O M Nefedov *J. Phys. Chem. A* **107** 4001 (2003)
29. I M Magin, P A Purtov, A I Kruppa, T V Leshina *J. Phys. Chem. A* **109** 7395 (2005)
30. A L Buchachenko, V L Berdinsky *J. Phys. Chem.* **100** 18292 (1996)
31. A L Buchachenko, V L Berdinsky *Chem. Rev.* **102** 603 (2002)
32. *Biological Effects of Electromagnetic Fields* (Ed. P Stavroulakis) (Berlin: Springer, 2003)
33. M B Taraban, T V Leshina, M A Anderson, C B Grissom *J. Am. Chem. Soc.* **119** 5768 (1997)
34. M S Afanasyeva, M B Taraban, P A Purtov, T V Leshina, C B Grissom *J. Am. Chem. Soc.* **128** 8651 (2006)
35. M S Afanasyeva, M B Taraban, N E Polyakov, P A Purtov, T V Leshina, C B Grissom *J. Phys. Chem. B* **110** 21232 (2006)
36. N E Polyakov, T V Leshina, L Kispert *RIKEN Rev.* **44** 140 (2002)
37. M B Taraban, A I Kruppa, N E Polyakov, T V Leshina, V Lüs, D Muceniece, G Duburs *J. Photochem. Photobiol., A* **73** 151 (1993)
38. A I Kruppa, M B Taraban, N E Polyakov, T V Leshina, V Lüs, D Muceniece, G Duburs *J. Photochem. Photobiol., A* **73** 159 (1993)
39. N E Polyakov, M B Taraban, A I Kruppa, N I Avdievich, V V Mokrushin, P V Schastnev, T V Leshina, V Lüs, D Muceniece, G Duburs *J. Photochem. Photobiol., A* **74** 75 (1993)
40. N E Polyakov, A I Kruppa, T V Leshina, V Lüs, D Muceniece, G Duburs *J. Photochem. Photobiol., A* **111** 61 (1997)
41. V P Komov, V N Shvedova *Biokhimiya* (Moscow: Drofa, 2004)
42. S S Petrova, A I Kruppa, T V Leshina *Chem. Phys. Lett.* **385** 40 (2004)
43. P A Purtov, A B Doktorov *Chem. Phys.* **178** 47 (1993)
44. P A Purtov, Doctoral Thesis in Physical and Mathematical Sciences, Institute of Chemical Kinetics and Combustion, Siberian Branch of the Russian Academy of Sciences, Novosibirsk, 2000
45. S A Mikhailov, P A Purtov, A B Doktorov *Chem. Phys.* **166** 35 (1992)
46. K Yokota, I Yamazaki *Biochemistry* **16** 1913 (1977)
47. I Schlichting, J Berendzen, K Chu, A M Stock, S A Maves, D E Benson, R M Sweet, D Ringe, G A Petsko, S G Sligar *Science* **287** 1615 (2000)
48. H A Harbury *J. Biol. Chem.* **225** 1009 (1957)
49. S Colonna, N Gaggero, C Richelmi, P Pasta *Trends Biotechnol.* **17** 163 (1999)
50. L Casella, M Gullotti, R Ghezzi, S Poli, T Beringhelli, S Colonna, G Carrea *Biochemistry* **31** 9451 (1992)
51. G Battistuzzi, M Borsari, A Ranieri, M Sola *J. Am. Chem. Soc.* **124** 26 (2002)
52. F I Ataullakhanov, A M Zhabotinskii *Biofizika* **20** 596 (1975)^c
53. J Gebicki, A Marcinek, J Zielonka *Acc. Chem. Res.* **37** 379 (2004)
54. K Schulten, P G Wolynes *J. Chem. Phys.* **68** 3293 (1978)
55. S Fukuzumi, T Tanaka *Photoinduced Electron Transfer Reactions. Part C. Photoinduced Electron Transfer Reactions: Organic Substrates* (Eds M A Fox, M Chanon) (Amsterdam: Elsevier, 1988) Ch. 4.10
56. A L Buchachenko, R Z Sagdeev, K M Salikhov *Magnitnye i Spinovye Effekty v Khimicheskikh Reaktsiyakh* (Magnetic and Spin Effects in Chemical Reactions) (Novosibirsk: Nauka, 1978)
57. I B Bersuker *Elektronnoe Stroenie i Svoistva Koordinatsionnykh Soedinenii* (Electronic Structure and Properties of Coordination Compounds) (Leningrad: Khimiya, 1986)
58. E G Pavel, N Kitajima, E I Solomon *J. Am. Chem. Soc.* **120** 3949 (1998)
59. M J B Hauser, L F Olsen *Transport and Structure — Their Competitive Role in Biophysics and Chemistry* (Eds S C Müller, J Parisi, W Zimmermann) (Berlin: Springer, 1999)
60. H Degn *Nature (London)* **217** 1047 (1968)
61. B D Aguda, L-L H Frisch, L F Olsen *J. Am. Chem. Soc.* **112** 6652 (1990)
62. S Nakamura, K Yokota, I Yamazaki *Nature (London)* **222** 794 (1969)
63. L F Olsen, H Degn *Biochim. Biophys. Acta* **523** 321 (1978)
64. J N Rodriguez-Lopez, J Hernández-Ruiz, F García-Cárnovas, R N F Thorneley, M Acosta, M B Arnao *J. Biol. Chem.* **272** 5469 (1997)
65. J Hernández-Ruiz, M B Arnao, A N P Hiner, F García-Cárnovas, M Acosta *Biochem. J.* **354** 107 (2001)
66. L F Olsen, M J B Hauser, U Kummer *Eur. J. Biochem.* **270** 2796 (2003)
67. C L Hawkins, M J Davies *Biochim. Biophys. Acta* **1504** 196 (2001)
68. M S Afanas'eva, P A Purtov, M B Taraban, T V Leshina, Ch B Grissom *Izv. Akad. Nauk, Ser. Khim.* 1090 (2006)^b

69. P R Rich, S E J Rigby, P Heathcote *Biochim. Biophys. Acta* **1554** 137 (2002)
70. M L Das, S Orrenius, L Ernster *Eur. J. Biochem.* **4** 519 (1968)
71. R I Salganik, S V Nedel'kina, S V Argutinskaya,
L P Kusmartseva *Voprosy Med. Khim.* **20** 135 (1974)
72. G S Boyd, A C Brownie, C R Jefcoate, E R Simpson *Biochem. J.* **125** 1 (1971)
73. K Einarason, G Johansson *FEBS Lett.* **4** 177 (1969)
74. U Israelsson, H Hamberg, B Samuelsson *Eur. J. Biochem.* **11** 390 (1969)
75. M Newcomb, R Shen, Y Lu, M J Coon, P F Hollenberg,
D A Koop, S J Lippard *J. Am. Chem. Soc.* **124** 6879 (2002)
76. B G Malmstrom *Chem. Rev.* **90** 1247 (1990)
77. H S Carr, D R Winge *Acc. Chem. Res.* **36** 309 (2003)
78. M Hartmut *Proc. Natl. Acad. Sci. USA* **95** 12819 (1998)
79. T Tsukihara, H Aoyama, E Yamashita, T Tomazaki,
H Yamaguchi, K Shinzawa-Itoh, R Nakashima, R Yaono,
S Yoshikawa *Science* **272** 1136 (1996)
80. S Iwata, C Ostermeier, B Ludwig, H Michel *Nature (London)* **376** 660 (1995)

^a — *Mendeleeev Chem. J. (Engl. Transl.)*

^b — *Russ. Chem. Bull., Int. Ed. (Engl. Transl.)*

^c — *Biophysics (Engl. Transl.)*

Advances in the development of new catalysts for ethylene and α -olefin polymerisation

S S Ivanchev

Contents

I. Introduction	617
II. Catalyst systems based on late transition metal α -diimine and bis(imino)pyridine complexes	619
III. Phenoxy-imine catalysts for olefin polymerisation	627
IV. Conclusion	633

Abstract. The role of catalyst systems in the perfection of polymerisation processes and the improvement of the performance characteristics of polyethylene and other polyolefins is considered. The scope of application of post-metallocene catalysts based on transition metal α -diimine, bis(imino)pyridine and phenoxy imine complexes designed in the last decade is analysed. The structures of complexes depending on the type of ligands are described systematically. The development of research into these catalyst systems is discussed, the optimal structures as regards the activity and selectivity are mentioned, and the mechanism of their action and the prospects for industrial use are demonstrated. The bibliography includes 207 references.

I. Introduction

In the early 21st century, the annual production of polymers exceeded hundred million tons ('*World Polymer Products*' issued by the Chemical Marketing Association, Inc., on September 2005) due to the universal use of these materials in industry and other fields of human activity. Among various classes of polymers, there are leaders in both the amount of production and the width of consumption. For example, the percentage of polyolefins in the total annual production of plastic materials (180–190 million tons) is higher than 50% (105 mil. tons, including ~64 mil tons of polyethylene and ~41 mil tons of polypropylene). Consequently, polyethylene (PE) and polypropylene (PP) are the most widely used polymer materials, whose production increases annually by 3%–7%.

Polyolefins attract great attention of both manufacturers and consumers because these materials are produced from inexpensive and readily available sources and are characterised by an attractive combination of their properties and the ease of processing. The advantages of polyolefins are also their hydrocarbon composition and, consequently, the ease of utilisation by recycling or burning. Polyolefins have wide and various

applications due to rather high melting points [up to 135 °C for polyethylene, ~160 °C for propylene and ~200 °C for poly-(4-methylpentene)] combined with a low weight, transparency, corrosion resistance, rigidity, shock resistance and ability to be modified.

The history of the development of research into polymerisation processes of ethylene, propylene and other α -olefins and the development and commercialisation of polyolefin production processes dates back approximately 70 years. After the first successful technological solutions on procedures for ethylene polymerisation under high pressure, ICI Plc (UK) began commercial production of PE in the late 1930s. More recently, in addition to the autoclave process, a procedure for ethylene polymerisation in tubular reactors was developed and commercialised.¹ These processes hold industrial importance to the present day.

The Nobel Laureates K Ziegler and G Natta laid the scientific foundation for catalytic ethylene and propylene polymerisation at moderate pressure and temperature.^{2–7} These scientists have designed catalysts based on titanium chloride and alkylaluminium compounds, which are commonly known as Ziegler–Natta catalysts. The application of these catalysts and their analogues on the industrial scale took great efforts and years because of difficulties in elucidating the mechanism of action of catalysts, choosing the optimal structures of components of catalyst systems and finding conditions for the preparation of polymers with required properties and performance characteristics.

Montagna and Floyd⁸ suggested a graphical interpretation of the evolution of catalytic olefin polymerisation as an S-shaped step curve (Fig. 1). This curve reflects the relationship between the level of technological solutions and the molecular architecture (structure) control of polymers, on the one hand, and the structural features of polymerisation catalysts and the time of their design, on the other hand. This plot was published in the recent handbook⁹ of polyolefins for characterisation of the steps of perfection of olefin polymerisation processes.

An analysis of the plot presented in Fig. 1 shows that the progress in the control of the polymer structure is always associated with advances in the design of new high-performance and highly selective commercial catalysts.

In the first step of investigations of olefin polymerisation corresponding to the first step in the curve presented in Fig. 1, high-pressure ethylene polymerisation was performed in autoclave reactors. The technology of ethylene polymerisation (1500 atm, 200 °C) by the radical mechanism developed in

S S Ivanchev St Petersburg Department of G K Boreskov Institute of Catalysis, Siberian Branch of the Russian Academy of Sciences, prosp. Dobrolyubova 14, 197198 St Petersburg, Russian Federation.
Fax (7-812) 323 05 57, tel. (7-812) 323 09 85,
e-mail: ivanchev@SM2270.spb.edu

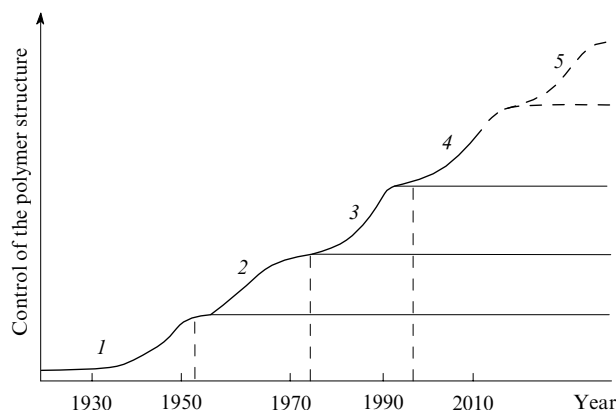


Figure 1. Evolution of olefin polymerisation catalysts.

(1) Low-density PE (non-catalytic radical process); (2) high-density PE and PP (Ziegler–Natta catalysts); (3) gas-phase polymerisation (supported catalysts); (4) preparation of homo- and copolymers with different microstructures (single-site catalysts and metallocenes); (5) copolymerisation of olefins with polar monomers, functionalised polymers and block copolymers (post-metallocene catalysts).

the late 1930s allowed the preparation of polyethylene with a specific structure. Macromolecules of this polymer contain both long-chain and short-chain branches (Fig. 2a). The process equipment was improved to increase the performance and the degree of control over the structure of high-molecular-weight products with the use of a wider range of initiators (in addition to oxygen, peroxides with different structures). This led to an improvement of the properties and an extension of the assortment of PEs.

The second step in the PE production started in 1950s, when the Standard Oil Company (USA) began the commercial production of PE at moderate pressure (~ 40 atm) and temperature of ~ 100 °C in the presence of an alumina-supported molybdenum oxide catalyst.¹⁰ A new class of complex organometallic catalysts discovered by Ziegler and co-workers² in 1953 made a revolution in this technology, resulting in an increase in the efficiency of ethylene polymerisation under moderate pressure. Natta and co-workers^{4–6} developed a procedure for stereospecific propylene polymerisation.

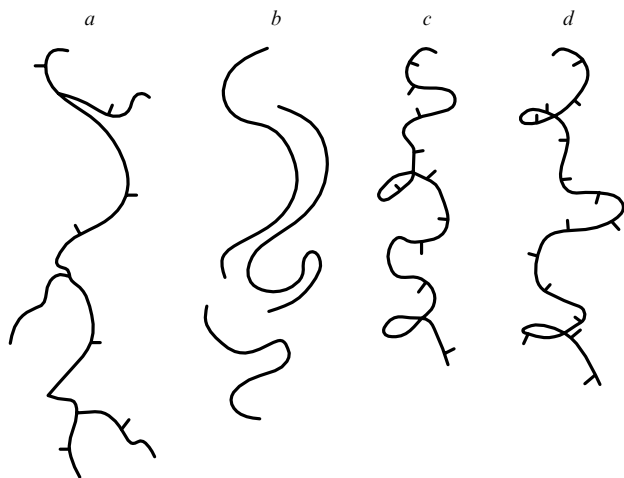


Figure 2. Structures of different types of polyethylene:

(a) Long-chain branches combined with short-chain branches; (b) unbranched polymer; (c) short-chain branches, whose regularity depends on MW; (d) short-chain branches (or the insertion of a comonomer) with a regular distribution in the chain.

There are three factors responsible for the unique technological and industrial advances in the improvement of properties and extension of the scope of application of polyolefins:

— strategy of the control over promising technologies to form materials with improved performance characteristics and an extension of the fields of their rational use;

— permanent perfection of the production processes and the improvement of the structure and properties of polymers, the design of new types of polyolefins;

— dynamism of the development of convenient technologies and the efficiency of introduction of modern technological solutions, which is a prerequisite for the design of materials with new properties and new possibilities of their application.

As mentioned above, the design of new-generation catalysts for olefin polymerisation, in-depth investigations of the mechanism of their action and the determination of conditions for their optimal use were and remain the driving force of the progress in studies in this field. Discoveries of higher-performance catalyst systems always led to the perfection of polyolefin production and new advances in the control of the molecular structures of polymers.

For example, the modification of Ziegler–Natta catalysts by electron-donor additives resulted in an increase in the activity and selectivity of the catalysts by two orders of magnitude.¹¹ The use of such catalysts allowed the simplification of the flow scheme for the polyethylene production (the polymer washing step is excluded) and the improvement of the efficiency of copolymerisation of ethylene with higher α -olefins. As a result, linear low-density polyethylene (LLDPE) was prepared.^{11–23} This polymer consists of linear molecules with short-chain branches (see Fig. 2c), and this is the difference from PE prepared earlier, which has a linear structure without branches and is characterised by a high density (see Fig. 2b).

The design of catalyst systems supported on inorganic adsorbents (SiO_2 , Al_2O_3 or MgCl_2) and, more recently, on polymer supports was an important breakthrough in the perfection of olefin polymerisation catalysts. This gives rise to a new version of the flow scheme, *viz.*, gas-phase polymerisation. The Union Carbide Corporation (USA) was the first to employ this scheme in industry. Later on, this process was used also by other companies [British Petroleum, BASF (Germany), *etc.*]. Studies of the characteristic features of the behaviour of supported catalyst systems, primarily of MgCl_2 -supported catalysts, which were independently performed by the Mitsui Chemical (Japan) and Montedison (Italy) Companies resulted in the design of catalysts allowing the control over the properties and polymer morphology. It appeared that these systems are able to replicate (reproduce the shape) the starting catalyst particles by the resulting polymer particles. This allowed the synthesis of granular polymers directly in a polymerisation reactor.^{11, 23–28}

A new step in the perfection of olefin polymerisation catalysts (1980s) was associated with investigations of so-called ‘metallocene’ catalysts based on coordination organometallic compounds. In these complexes, one or two cyclopentadienyl rings (including substituted rings) form a π bond with the central Group IVB, VB or VIB transition metal atom.^{11, 20, 29–39} A new type of organoaluminium compounds, *viz.*, poly(methylalumoxane) ($[\text{—Al(Me)O—}]_n$, MAO), was used for activation.⁴⁰

In the 25-year metallocene epoch, about 700 patents were granted and more than 10 reviews and monographs devoted to this problem were published (see, for example, Refs 20, 29–31 and 33–39). The following aspects were considered: the evolution of the design of new structures of metallocene complexes, the mechanism of action of catalyst systems based on these complexes with the use of cocatalysts of different nature and the possibility of application of these complexes in

olefin polymerisation and copolymerisation. A detailed analysis of problems associated with the mechanism of olefin polymerisation in the presence of metallocene catalysts and the related publications are beyond the scope of the present review. Let us only note the most important aspects due to which this type of catalysts attracts great interest of researchers.

Metallocene catalyst systems are characterised by a number of important features:

- high activity[†] in ethylene polymerisation (up to 40 tons of PE per gram of transition metal for 1 h);
- the single-site character of the catalysis process;
- the similarity of the constants of copolymerisation of ethylene and higher α -olefins, which provides the uniform incorporation of α -olefins into the polymer chain regardless of the molecular mass of the copolymer (see Fig. 2 d);
- high performance in polymerisation and copolymerisation of a wide range of monomers;
- lower oxophilicity compared to Ziegler–Natta catalysts allowing polymerisation of monomers containing functional groups remote from double bonds.

Judging by numerous predictions, metallocene catalyst systems would replace Ziegler–Natta catalysts in the polyolefin production. However, their introduction occurred much more slowly than expected due primarily to a high price of the components of these catalysts and problems associated with processing of polyolefins.^{41, 42}

To summarise the aforesaid, it can be stated that, in spite of great progress in studies of olefin polymerisation catalysts, a number of problems associated with the technology of these processes remain to be solved. For example, copolymers of ethylene and other olefins with various available comonomers containing polar groups cannot be prepared because of the oxophilic character of the components of metallocene catalyst systems. A search for ways for increasing the performance and selectivity of catalysts and controlling the morphology of the resulting polyolefins as well as the improvement of methods for stereochemical control of the growing chain are still important.

Many research teams were engaged in solving these problems. This gave rise to the subsequent step in the history of evolution of olefin polymerisation processes associated with the design of a radically new generation of catalysts. This step is represented by dashed line 5 at the top of Fig. 1 and corresponds to more perfect catalyst systems characterised by high performance and selectivity, a wider range of conditions (temperature and pressure), the possibility to control the catalytic properties by varying the oxophilicity of the ligand and the ability to control the polymerisation process. These catalysts should solve the problem of copolymerisation of ethylene with polar monomers and should be characterised by high efficiency, accessibility and the safe storage and use. In addition, the use of these catalysts provides the possibility of improving the structural characteristics of polyolefins, thus ensuring better recycling and performance characteristics of polymer materials.

First publications on new catalyst systems meeting the above-mentioned requirements date back only 10 years. Nevertheless, numerous papers, patents and reviews have been published during these years.^{43–52} A new class of high-performance non-metallocene catalyst systems is referred to as ‘post-metallocene catalysts’.[‡]

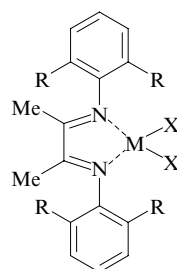
Most of the studies of olefin polymerisation catalysts published in the last decade are related to systems based on late transition metal complexes with nitrogen-containing ligands (‘the nitrogen skeleton’). These are primarily nickel and palladium diimine complexes as well as iron and cobalt-bis(imino)pyridine complexes (see, for example, Refs 44, 45, 48, 49 and 51). A new type of post-metallocene catalysts based on phenoxy imine complexes of titanium, zirconium, hafnium and some other transition metals has attracted attention more recently.^{47, 50, 52}

In Russia, investigations of post-metallocene catalyst systems started somewhat later. In this connection, the publication of a Russian review devoted to an analysis of the progress in this field will apparently attract interest of researchers concerned with catalytic olefin polymerisation.

II. Catalyst systems based on late transition metal α -diimine and bis(imino)pyridine complexes

1. α -Diimine complexes as catalysts for olefin polymerisation

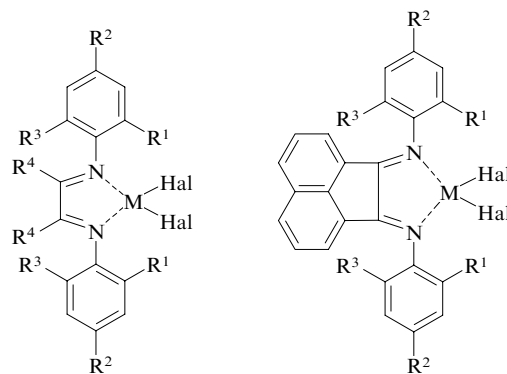
In 1995, the US research team headed by Brookhart obtained first successful results in the design and application of post-metallocene catalyst systems.^{53–56} The authors demonstrated that ethylene, propylene and hex-1-ene polymerisation can be performed in the presence of nickel or palladium complexes (**1** and **2**, respectively) with bis(arylimine) ligands.



1, 2

M = Ni (**1**), Pd (**2**); R = Me, Prⁱ; X = Cl, Br, Me.

The results of investigations of these systems obtained in the first five years were summarised in the review.⁴⁵ α -Diimine fragments most often contain aryl substituents at the nitrogen atoms and are involved in an aliphatic or complex polyaromatic system (for example, the acenaphthylene system). The general structures of nickel and palladium α -diimine complexes can be represented as follows:



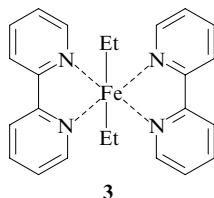
M = Ni, Pd; Hal = Cl, Br; R¹, R², R³ = H, Alk, Ar; R⁴ = H, Alk.

[†] Hereinafter, the activities of catalysts are given in units of (amount of a polymer) [mole (or gramme) of a catalyst]^{−1} h^{−1}.

[‡] The term ‘post-metallocene catalysts’ has been used for the first time in the review by Britovsek *et al.*⁴⁴

A sophisticated analysis of the published data on the synthesis and studies of late transition metal complexes with ligands containing the nitrogen skeleton demonstrated that studies by Brookhart were preceded by earlier investigations in

this field. For example, Yamamoto *et al.* reported⁵⁷ the results of tests of catalysts based on cobalt and iron alkyl complexes with bipyridine ligands (for example, compound **3**), in polymerisation of acrylic acid derivatives, as early as in 1970. It is evident that these catalysts are similar to late transition metal α -diimine complexes.



Later on, it was demonstrated⁵⁷ that bipyridine complexes **3** are characterised by relatively weak coordination of the iron atom by bipyridine ligands. This facilitates side processes, such as β -hydride migration and reductive elimination. The termination of the polymer chain growth leads to fast deactivation of the catalyst⁵⁸ and, consequently, to a decrease in its activity. Because of these drawbacks, researchers have lost interest in this type of complexes.

It should be emphasised that the newly synthesised catalysts based on late transition metal complexes containing ligands with the nitrogen skeleton were covered by numerous patents. In the period from 1994 to 2001, 742 patents were issued (cited from the monograph,⁵¹ p. 59), which is comparable only with the number of patents on the design of metallocene systems.

To perform olefin polymerisation, it is necessary to transform α -diimine complexes into the active form. Methylalumoxane or perfluoroaryl boron compounds (the latter are more suitable for complexes with the central palladium atom) are commonly used as activators (or cocatalysts). Somewhat later, it was demonstrated that simple alkyl derivatives of aluminium can also be used for these purposes.^{59,60}

Depending on the structure of the ligand and the reaction conditions, nickel and palladium α -diimine complexes can exhibit high activity in ethylene polymerisation to give PE with molecular weight (MW) varying in a wide range. For example, the performance of up to 11 (kg PE) mmol⁻¹ h⁻¹ bar⁻¹ was observed for some nickel derivatives,⁵³ PE with MW of up to 1 million was obtained at low temperatures. On the whole, nickel α -diimine complexes provide higher activity of catalysts in ethylene polymerisation and form polymers with higher MW compared to analogous palladium complexes.

Studies of the PE structures showed that new catalyst systems allow the preparation of polymers with short-chain (methyl, ethyl, butyl or longer) branches.

Based on low-temperature NMR spectroscopic data, the branch migration mechanism for ethylene polymerisation in the presence of nickel or palladium α -diimine complexes was suggested (Scheme 1).^{45,61,62} The reactions of the complexes with cocatalysts and coordination with ethylene afford the inactive (latent) cationic form **A** and the polymer chain begins to grow. The formation of the growing linear chain can alternate with β -elimination of a hydride ion and the formation of alkenyl hydride complex **B**, whose transformation gives rise to methyl branching in the growing chain. The formation of the whole macrochain is a result of a combination or alternation of the chain growth and β -elimination of a hydride ion in the alkenyl hydride complex, resulting in the next branching.

According to this mechanism, catalyst systems based on Ni and Pd α -diimine complexes afford polymers with methyl branches. Several successive β -hydride transfer reactions give rise to short-chain ethyl, propyl or other (longer) α -alkyl branches. These catalysts are very promising because they allow the preparation of short-chain branched polyethylenes without the use of comonomers.

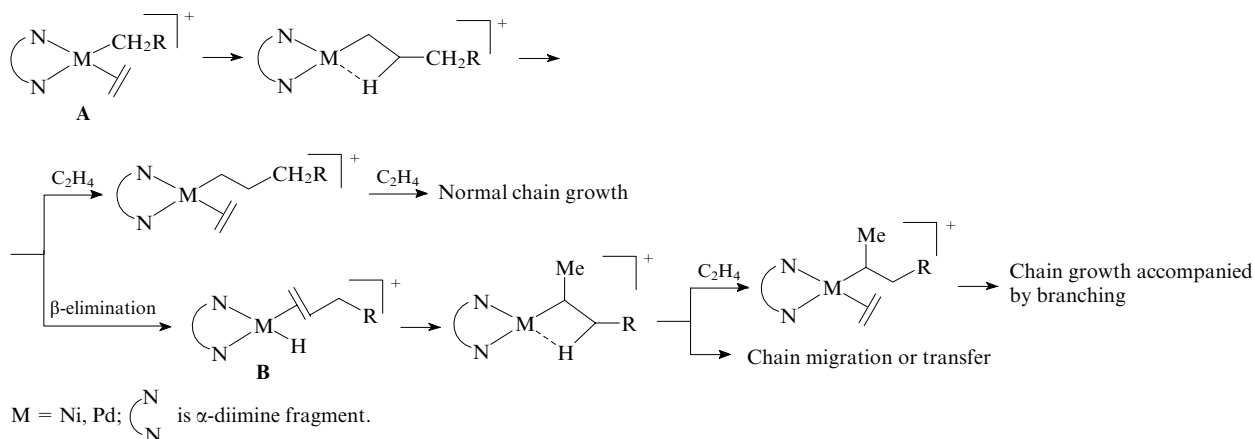
For palladium systems, the barrier to ethylene insertion by the migration mechanism was estimated^{53,63} at 17–18 kcal mol⁻¹ (the lowest barrier is observed for the bulkiest imine ligands), whereas this barrier for nickel systems is substantially lower (13–14 kcal mol⁻¹). Therefore, the energy difference of 4–5 kcal mol⁻¹ is consistent with higher activity of nickel complexes observed in experiments.

In the presence of palladium catalysts, the branching of PE is independent of the monomer pressure in the polymerisation process. However, the ethylene pressure influences the polymer morphology. At moderate pressures, polymerisation affords viscous amorphous oils; at high pressures, amorphous rubber-like solids, plastomers (Fig. 3).

In the case of nickel complexes, the degree of branching of PE is always lower than that obtained with the use of palladium analogues, and this degree decreases with increasing ethylene pressure. The sensitivity of the degree of branching of the product to the pressure is a result of a competition between two processes, *viz.*, trapping of ethylene by the active complex and the chain transfer. High pressures are favourable for trapping of ethylene, resulting in a lower degree of branching.

Polymerisation on diimine catalysts giving high-molecular-mass polymers is characterised by a much higher chain growth rate compared to the chain transfer rate. An increase in steric crowding of the axial regions in the square plane of the complex is the key factor responsible for a decrease in the chain transfer rate.⁴⁵ The crystallographic data show that the benzene rings in square-planar palladium α -diimine complexes are located approximately perpendicular to the plane of the square, and the *ortho* substituents are located above and below this plane.

Scheme 1



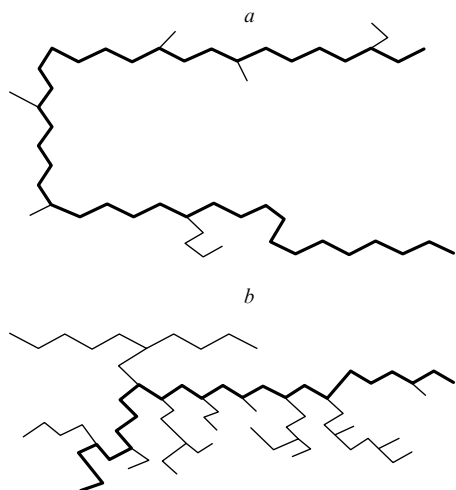


Figure 3. Branched structures formed upon ethylene polymerisation: plastomers (a) and hyperbranched low-molecular-weight compounds (oils) (b).

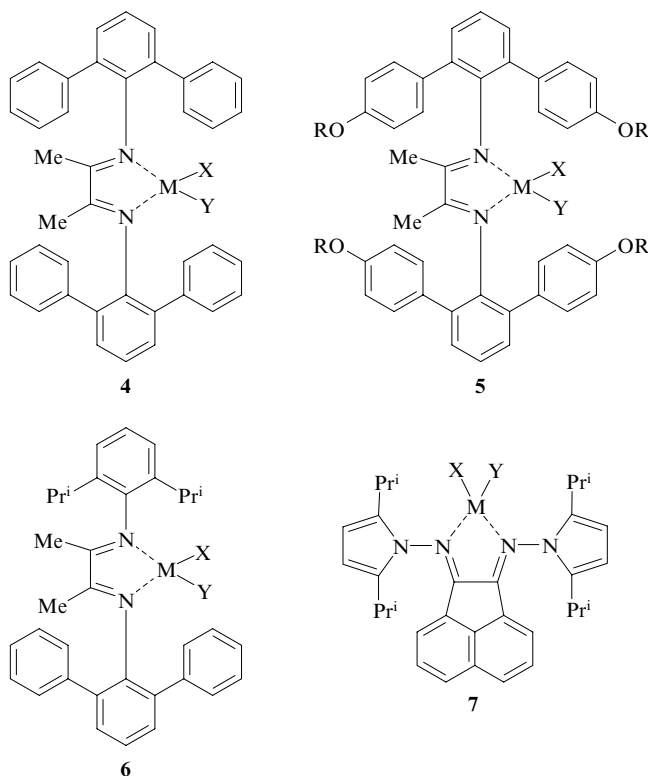
Important investigations aimed at optimising the structures of diimine catalyst systems involve variations of the nature of substituents in the ligand and the elucidation of their influence on the characteristics of the resulting polymers. For example, the detailed theoretical investigation of nickel complexes with various diimine ligands was carried out.⁶⁴ An increase in the bulkiness of substituents at the nitrogen atom was demonstrated to play a dual role. First, these groups block the access to the transition metal atom in the axial direction. This destabilises the inactive (latent) state of the catalyst and the chain termination transition state, in which both axial positions are occupied. Second, the aryl rings in nickel complexes, unlike those in palladium analogues, are located in one plane with the diimine fragment, which is favourable for stabilisation of the transition state of ethylene insertion compared to the latent state of the catalyst. An increase in the bulkiness of substituents either at the carbon atoms or in the *ortho* positions of the aryl groups at the nitrogen atoms of diimine results in a more rigid fixation of the plane of the aromatic ring perpendicular to the metal–ligand coordination plane. In this case, *ortho* substituents more efficiently block the axial directions.⁶⁵

In particular, the 2,3-bis(2,6-dimethylphenyl)butanediimine nickel dichloride complex (**1**, R = Me, X = Cl) is one of the most active catalysts in this class.⁶⁶ Ethylene polymerisation on this catalyst activated by MAO affords PE characterised by the number average MW (M_n) in the range of $(1.7–6) \times 10^5$ and a rather narrow molecular weight distribution (MWD) of 2.0–3.5. The degree of branching increases, whereas MW decreases as the temperature of the process is increased. The polymer branching is virtually independent of the Al : Ni molar ratio and the concentration of the catalyst.

Therefore, the main structural feature of ligands in late transition metal α -diimine [as well as bis(imino)pyridine, see below] complexes and catalysts based on these complexes is that the active cationic centre is sterically shielded by bulky *ortho*-substituted aryl groups at the nitrogen atom, resulting in suppression of side processes of chain termination (elimination of the hydrogen atom from the β position and the associative substitution of olefins) during polymerisation. The ability to provide efficient stabilisation of organometallic complexes that are formed in the reactions with monomers is another

important property of these ligands. The electronic structure of ligands is rather flexible because it is determined primarily by the nature of substituents in *N*-aryl groups. These characteristic features were observed in many experimental^{45, 48, 49, 51, 53–58, 67–70} and theoretical^{60, 64, 65, 71, 72} investigations.

Therefore, the activity of α -diimine catalysts based on nickel and palladium complexes in olefin polymerisation was substantially increased by changing the structure of the ligand, to be more precise, by introducing bulky aryl substituents at the *ortho* positions of the phenyl rings at the nitrogen atoms of the imine fragments.⁵¹ Recently, new Ni and Pd complexes with the use of various types of ligand variation were synthesised.^{73–75} For example, complexes having symmetric (**4** and **5**) or non-symmetric (**6**) structures and complexes with heteroaromatic substituents (**7**) were prepared.

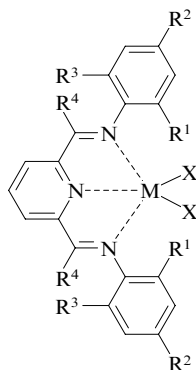


M = Ni, Pd; X, Y = Hal, Me; R = Alk.

The activity of catalyst systems based on compounds **4–7** in ethylene polymerisation and MW of polymerisation products appeared to be similar to the corresponding characteristics for complexes, which have been studied earlier by Brookhart. The highest performance was observed for the catalyst based on compound **5**. These systems are characterised by the dependence of the degree of branching of PE and, consequently, of its glass-transition temperature (T_g) on the structure of ligands. For example, complexes **4**, **5** and **7** allow the synthesis of virtually linear PE. In addition, polymerisation in the presence of complex **6** containing unsymmetrical ligands affords PE characterised by a lower degree of branching compared to a polymer prepared with the use of structurally similar Brookhart's complexes. Polymerisation in the presence of catalyst systems based on complexes **7** with peripheral heterocyclic substituents affords polymers with lower MW. It should be noted that an analogous situation is observed for complexes containing other heteroaromatic substituents (for example, indoles, *etc.*) instead of the pyrrole rings.

2. Bis(imino)pyridine complexes as olefin polymerisation catalysts

Several years after the discovery of α -diimine catalysts for olefin polymerisation, Brookhart and co-workers^{45,76,77} in USA and the research group headed by Gibson^{48,78–84} in UK simultaneously and independently published data on the design and examination of iron and cobalt 2,6-bis(aryliminoalkyl)pyridine [hereinafter, referred to as bis(imino)pyridine] complexes.

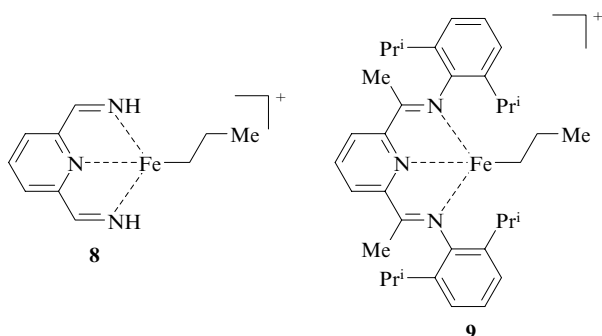


M = Fe, Co; X = Cl, Br; R¹, R², R³ = H, Alk, Ar; R⁴ = H, Alk.

Iron complexes with R¹ = R³ = Me, Prⁱ or Bu^t, R² = H, R⁴ = Me and X = Cl, Br or NO₃ were the first representatives of this type of compounds.⁷⁷ A short time later, other researchers were also engaged in the synthesis of complexes with *N*-tridentate ligands (see, for example, Ref. 85).

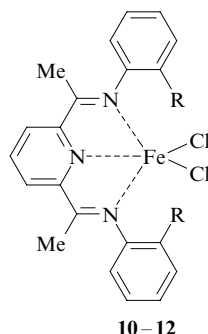
The characteristic structural feature of these complexes is that the metal atom in them has the coordination number 5 and a pseudosquare-pyramidal coordination geometry with the phenyl rings being virtually perpendicular to the plane of the square. High-molecular-weight polyethylene (*M_w* up to 7 × 10⁵) was prepared on these catalysts in high yield upon activation by modified methylalumoxane (MAO) in the presence of ethylene in toluene. As opposed to Ni(II) and Pd(II) diimine catalysts, linear (without branches) PE is formed under analogous conditions even in the presence of bulky ligands in the complexes and at low ethylene pressure. The molecular weight of the polymer varies in a wide range depending on the type of the ligand, the nature of the central metal atom and the concentration of the cocatalyst. As in the above-considered diimine complexes, the bulkiness of the aryl fragments at the imine nitrogen atoms in the ligands in Fe and Co bis(imino)pyridine catalysts plays an important role. Thus, an increase in the bulkiness of the *ortho* substituents also leads to an increase in the activity of the catalyst system.

The mechanism of ethylene polymerisation with the use of catalysts based on Fe(II) bis(imino)pyridine complexes was analysed in detail⁸⁶ using quantum chemical calculations by the density functional theory (DFT) method and in combination with the molecular mechanics method. The calculations were carried out for the active state of the catalysts, *viz.*, for the model (8) and real (9) cationic complexes.



The trapping of ethylene by the cationic metal alkyl complex was demonstrated⁸⁶ to be the rate-determining step of both the chain growth and termination. The mechanism of chain termination involves the β -hydride transfer of the growing chain to the monomer in the active centre as the major process (see Scheme 1). As in the case of α -diimine ligands, the presence of bulky aryl groups containing substituents in the *ortho* positions at the imine nitrogen atom (for example, 2,6-Prⁱ₂C₆H₃) is desirable for the highest performance. In the presence of complexes with such substituents, the chain termination is suppressed and the rate of monomer insertion into the growing chain increases.

The group headed by Brookhart found⁴⁵ that bis(aryl-iminoethyl)pyridine complexes 10–12 containing only one *ortho* substituent in each benzene ring are superactive catalysts for ethylene oligomerisation.

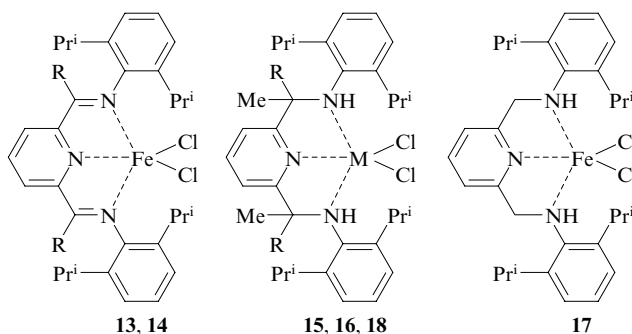


R = Me (10), Et (11), Prⁱ (12).

It should be noted that this fact is consistent with the results of our investigation⁶⁸ of ethylene oligomerisation with the use of substituted diimine complexes.

In the study,⁸³ the dependence of the kinetic activity of bis(imino)pyridine complexes in ethylene polymerisation on their structure (primarily, on the size of substituents in the *ortho* position of the arylimino fragment) was found and the molecular characteristics of PE were determined. These characteristics are also not contradictory to the above-considered data.

Ethylene polymerisation in the presence of iron complexes with various tridentate nitrogen-containing ligands, such as 2,6-bis(aryliminoalkyl)pyridine (13, 14), 2-arylaminoalkyl-6-aryliminoalkylpyridine (15, 16) and 2,6-bis(arylaminoethyl)pyridine (17), and cobalt complex 18 combined with the cocatalyst MAO was investigated.⁸⁴ Compounds containing bis(imine) fragments were demonstrated to have higher catalytic activity than bis(amine) and aminoimine derivatives; complexes with ketimine ligands are more active than complexes with aldimine ligands. Cobalt complex 18 is less active than its iron analogue 15.

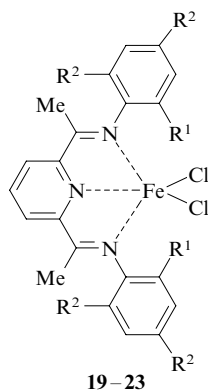


M = Fe: R = H (13, 15), Me (14, 16); M = Co, R = H (18).

It was noted that lower activity of amine complexes compared to bis(imino)pyridine analogues is possibly attributed to a relatively weak bond between amine and the iron atom, whose cleavage results in dissociation of the amine fragment. In addition, insufficiently strong conjugation of the ligand environment and the spatial orientation of the amino-aryl substituent, which hinders access of the monomer to the catalyst active site and, correspondingly, the growth of the polymer chain, can also play a particular role.

On the whole, ethylene polymerisation catalysts based on transition metal bis(imino)pyridine complexes are attractive because they are synthetically accessible and inexpensive,⁸⁷ allow the synthesis of products with both narrow and wide MWD and can be activated by various alkyl derivatives of aluminium.^{59,60} The main drawbacks are relatively low thermal stability, which is manifested in a considerable decrease in the catalytic activity of the system as the temperature rises (by a factor of two and nine as the temperature rises to 50 and 70 °C, respectively, compared to the activity at the optimal temperature of 35–40 °C). In addition, an increase in the polymerisation temperature leads to a sharp decrease in the MW of polyethylenes prepared with the use of these catalysts. Attempts to eliminate this drawback were made in several studies.

Our research team made a considerable contribution to the solution of this problem.^{88,89} For example, we demonstrated that the temperature range, where catalysts based on complexes **19–22** containing cycloalkyl substituents in the *ortho* position of the arylimine group exhibit high performance, can be shifted to higher temperatures.



$R^2 = \text{Me}$, $R^1 = \text{cyclo-}C_nH_{2n-1}$ [$n = 5$ (**19**), 6 (**20**), 8 (**21**), 12 (**22**)];
 $R^1 = R^2 = \text{Pr}^i$ (**23**).

Ethylene polymerisation was performed in toluene using the catalyst:activator (MAO) ratio of 1:1500 at ethylene pressure of 0.3 MPa; the reaction time was 1 h.⁸⁹ The curves of the temperature dependence of the activity of catalyst systems based on iron bis(imino)pyridine complexes with cycloalkyl substituents **19–22** and reference complex **23** containing isopropyl substituents at positions 2, 4 and 6 of the arylimine groups are presented in Fig. 4. It can be seen that the activity of catalyst **23** sharply decreases at temperatures higher than 50 °C, whereas the optimal temperatures for cycloalkyl-substituted complexes are higher, this effect being more pronounced as the number of the methylene groups in the ring is increased. The experimental results were confirmed by quantum chemical calculations for the complexes in question.^{88,89}

A generalised analysis of the influence of the structure of transition metal complexes with α -diimine and bis(imino)pyridine ligands on the activity of catalyst systems based on these ligand was performed in the Polymer Research Laboratory of the BASF Company (see the monograph,⁵¹ pp. 59–98). The authors confirmed that the key feature of the ligand

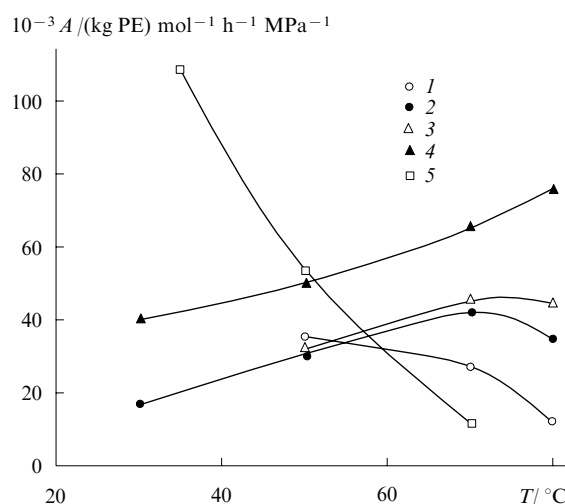
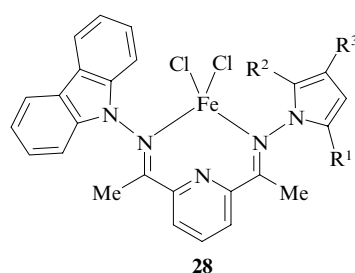
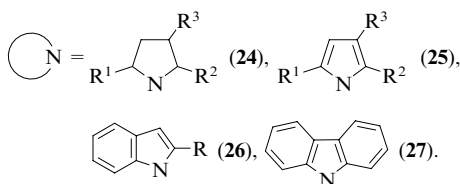
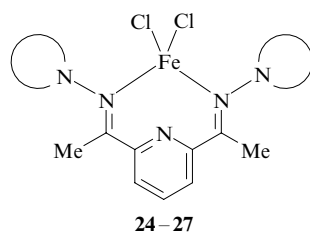


Figure 4. Plot of the activity of complexes **19–23** (curves **1–5**, respectively) vs. the temperature of ethylene polymerisation.⁸⁹

structure of these catalysts is that the active cationic centre is sterically shielded to an extent sufficient to suppress undesirable chain termination processes (primarily, β -hydride elimination and associative substitution of olefins in active complexes). Steric shielding can be provided, for example, by bulky *ortho*-substituted aryl groups bound to the peripheral donor centres (imine nitrogen atoms).

The results of studies of nontraditional substituents at the imine nitrogen atoms of α -diimine and bis(imino)pyridine ligands, for example, of nitrogen-containing heteroaromatic groups, made a substantial contribution to knowledge about the influence of the structure of complexes on their activity. Earlier, when considering the catalytic activity of α -diimine systems containing *N*-pyrrole rings, we have demonstrated that the degree of branching of PE in polymerisation can be changed (decreased or completely suppressed). An similar effect was observed also in the presence of symmetrical (**24–27**) or unsymmetrical (**28**) iron bis(imino)pyridine complexes with peripheral *N*-heterocyclic substituents.⁵¹



A comparison of the polymerisation activity of systems based on complexes **24–28** in ethylene polymerisation with that of the most active classical Brookhart–Gibson catalysts showed that the activity of the former catalyst systems is rather high, but MW of PE prepared with their use is substantially lower. The molecular mass was increased by increasing the bulkiness of the peripheral *N*-azolyl substituents in the catalyst, but this led to a decrease in activity. However, the most substantial difference is that the reaction mechanism changes. Polymerisation with the use of complexes **24–28** affords branched polymeric or oligomeric products, whereas polymerisation with the use of Brookhart–Gibson complexes studied earlier gives linear products.

The above-considered data show that there is a fine equilibrium between the following two processes that occur during ethylene polymerisation catalysed by transition metal bis(imino)pyridine complexes: the monomer insertion resulting in the formation of linear PE and β -hydride elimination with the repeated addition of the isomerised chain giving rise to branched structures. This equilibrium substantially depends on the steric and electronic effects of peripheral substituents in catalytic complexes, whose nature (for example, the introduction of the *N*-azolyl fragment instead of the *N*-phenyl group) determines the mechanism of polymer formation. The chain growth can give rise to either linear or branched structures with the use of both α -diimine and bis(imino)pyridine complexes.

When analysing new complexes containing ligands with the nitrogen skeleton, the recently synthesised oligomeric nickel α -diimine complexes⁹⁰ and iron bis(imino)pyridine complexes⁹¹ deserve note. Unfortunately, the results of examination of these complexes in ethylene polymerisation were not reported in the study cited.⁹⁰ However, in the presence of polyfunctional oligomeric bis(imino)pyridine complexes **29** and **30** (these complexes were synthesised by our group⁹¹) activated by MAO, polyethylenes with high MW were obtained at high temperatures (70–90 °C), *i.e.*, the temperature range of high performance of the catalyst system was extended.

Bis(imino)pyridine complexes not only with the central divalent iron atom but also with other transition metals, such as cobalt, nickel, vanadium, copper, zinc, chromium and manganese, were synthesised. The results of research into the activity of catalyst systems based on various metals were considered.^{92–96} Divalent iron complexes exhibited the highest activity in ethylene polymerisation, whereas Fe(III) complexes proved to have low activity. Divalent cobalt complexes, which were synthesised virtually simultaneously with the iron ana-

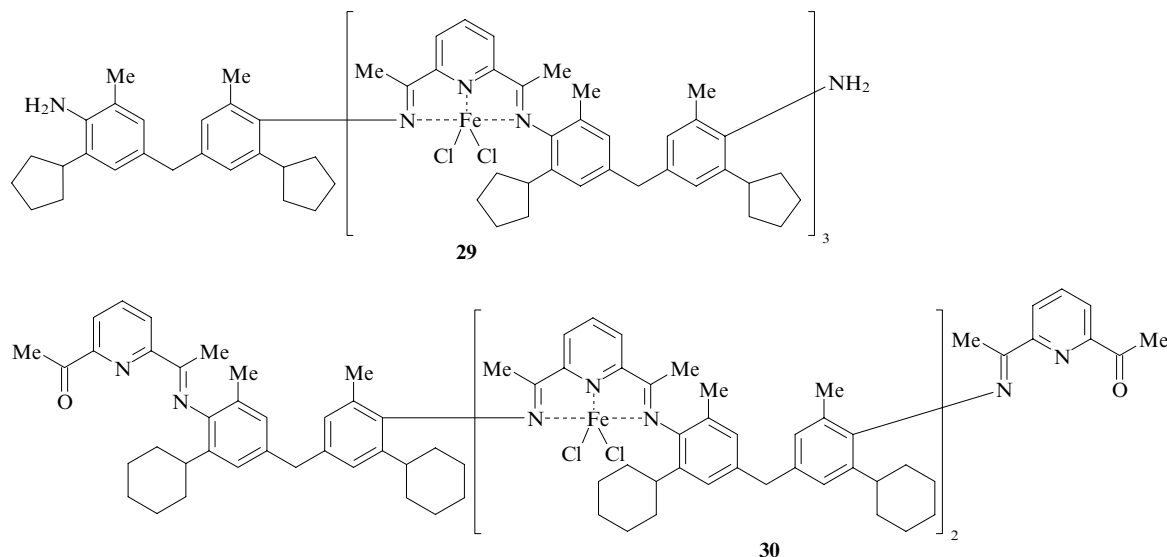
logues, are generally substantially less active than the latter. However, Co(II) complexes in the presence of MAO show higher activity in polymerisation of vinyl ethers than the corresponding iron complexes.⁹⁷ Divalent cobalt complexes containing electron-accepting substituents exhibit high activity also in selective dimerisation and oligomerisation of α -olefins.⁹⁸

Vanadium bis(imino)pyridine complexes were documented.⁹⁹ Detailed studies of the influence of the structure of complexes on the properties of the reaction products demonstrated^{100,101} that olefin polymerisation in the presence of vanadium systems gives mainly oligomeric products.

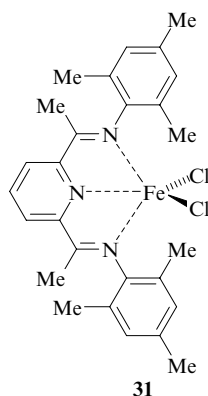
Chromium complexes analogous to iron bis(imino)pyridine complexes have received little study as olefin polymerisation catalysts. As a rule, these complexes exhibit lower activity than the above-considered iron, cobalt and vanadium complexes and often form low-molecular-weight products.^{101,102}

The differences in the behaviour of iron and cobalt 2,6-bis(imino)pyridine complexes activated by modified methylalumoxane in ethylene polymerisation under homogeneous conditions were noted in the recent publication by Kissin *et al.*¹⁰³ Cobalt complexes form virtually single-site catalysts with MMAO, whereas iron complexes give multisite (polyfunctional) catalysts, whose character depends on the Al:Fe ratio, the ethylene pressure, the temperature and the nature of substituents in the ligands.

In recent years, great attention has been given to the mechanism of action of Fe(II) 2,6-bis(imino)pyridine complexes in ethylene polymerisation, including the determination of key intermediates. For example, based on the results of ¹H and ¹³C NMR spectroscopic studies of the structures of intermediates formed in homogeneous systems in the reactions of the complexes with an activator, it was concluded¹⁰⁴ that individual Fe(II) complexes rather than cationic intermediates are active components of the catalyst system. In more recent studies,^{105–108} this conclusion was reviewed and it was hypothesised that neutral complexes in these systems are precursors of active sites for ethylene polymerisation. The schemes of the transformations of these complexes into active sites were proposed. The influence of activators, *viz.*, various alkyl derivatives of aluminium, on both the activity of the Fe(II) 2,6-bis(imino)pyridine complex and the characteristics of the resulting polyethylene (MW, MWD and the molecular structure) was analysed.¹⁰⁸ In this study, data on the number of active sites and the rate constants of chain growth in ethylene polymerisation were obtained.



New views of the mechanism of influence of alkylaluminum cocatalysts AlR_3 ($\text{R} = \text{Et}$, Bu^i or $n\text{-C}_6\text{H}_{13}$) on the activity of iron bis(imino)pyridine complex **31** were reported in the recent publication.¹⁰⁹

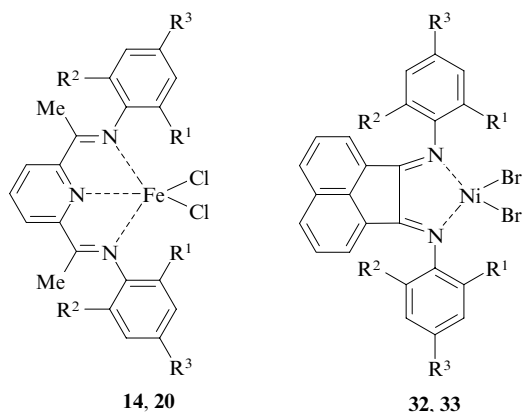


It was found that the activity of catalyst systems and the structure, MW and MWD of PE depend on the polymerisation temperature and the $\text{Al}:\text{Fe}$ molar ratio. The analysis of *in situ* UV-Vis spectra suggested the formation of two types of catalytic species, *viz.*, LFeRCl and LFeR_2 (L is 2,6-bis-[1-(2,4,6-trimethylphenylimino)ethyl]pyridine), the predominant formation of which being determined by the $\text{Al}:\text{Fe}$ molar ratio. The LFeR_2 compound has lower activity and favours the formation of low-molecular-mass branched polyethylenes.

It should be noted that catalysts with the nitrogen skeleton, in particular, α -diimine complexes, can be involved in two-component catalyst systems for olefin polymerisation (the method of reactor mixing). These mixtures (provided that the components are compatible and the catalytic activity is not decreased) are synthesised with the aim of changing the structure and molecular characteristics of PE. Reactor mixtures of PE were prepared by combining two catalyst systems, which provide the modification of polymers in the course of the synthesis, with the possibility of controlling their MW and achieving wider MWD.¹¹⁰

The reactor mixtures of PE have been prepared earlier with the use of two-component systems based on Ziegler–Natta catalysts and late transition metal complexes, as well as of metallocene and α -diimine systems.^{111,112}

For these purposes, our research group used two-component heterobimetallic catalyst systems consisting of α -diimine and bis(imino)pyridine complexes.¹¹³ The kinetic features of ethylene polymerisation on methylalumoxane-activated catalysts involving 2,6-bis(imino)pyridyl complexes of iron dichloride **14** and **20** and 1,2-bis(imino)acenaphthyl complexes



$\text{R}^1 = \text{cyclo-C}_6\text{H}_{11}$, $\text{R}^2 = \text{R}^3 = \text{Me}$ (**20**, **32**);

$\text{R}^1 = \text{R}^2 = \text{Pr}^i$, $\text{R}^3 = \text{H}$ (**14**, **33**).

of nickel dibromide **32** and **33** were studied at different ratios of the components in the temperature range of 50–70 °C.

These components were confirmed to be compatible in one reactor, and it was demonstrated that they can be efficiently used (at high rates) to synthesise polyethylene with different MW and short-chain branches. A mixture of complexes **14** and **32** proved to be an optimal combination of the components of a binary catalyst system, which retains high activity and gives rise to branched polyethylenes with satisfactory molecular characteristics.

3. Copolymerisation of ethylene with polar monomers in the presence of catalysts based on α -diimine and bis(imino)pyridine complexes

The structures and low oxophilicity of late transition metal complexes containing ligands with the nitrogen skeleton hold promise for their use as catalysts for copolymerisation of ethylene with polar monomers.

For example, catalyst systems based on palladium α -diimine complexes were successfully used by Brookhart and co-workers^{53,54,56} for copolymerisation of ethylene and propylene with monomers containing functional groups. Methyl acrylate, *tert*-butyl acrylate, methyl vinyl ketone and fluoro-octyl acrylate served as polar comonomers; the process was carried out in the presence of the $[\text{LPdMeCl}] - \text{NaBAR}_4$ systems (L is the α -diimine ligand) using the catalyst in an amount of 0.1 mmol per mole of the monomer in CH_2Cl_2 at 25–35 °C for 18–37 h. High-molecular-mass random polymers, which are amorphous highly branched structures with approximately 100 branches per 1000 carbon atoms, were synthesised. These polymers are characterised by the predominant arrangement of the ester groups at branches or at the ends of the chain (Fig. 5). The glass-transition temperature of these products varies from –67 to –77 °C. The maximum degree of introduction of the comonomer was 12.1%, 0.7%, 1.3% and 5.6% for methyl acrylate, *tert*-butyl acrylate, methyl vinyl ketone and fluoro-octyl acrylate, respectively.

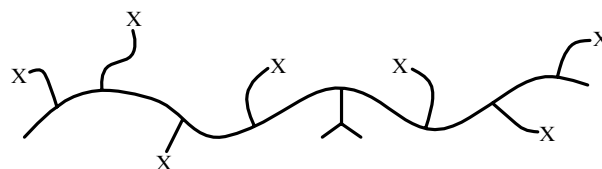


Figure 5. Structure of copolymers of ethylene with acrylates prepared with the use of $\text{Pd}(\alpha\text{-diimine})$ catalysts (X are acrylate groups).

The introduction of functional groups of amines and nitriles into the polymer chain of polyolefins was reported.¹¹⁴ The efficiency of binding of the metal centre of the catalyst to the fragments of the $\text{CH}_2=\text{CH}(\text{CH}_2)_n\text{X}$ monomers ($\text{X} = \text{CN}$, NH_2 or NMe_2), *viz.*, the N -containing polar group and the π -system of the double bond, was compared¹¹⁵ by the density functional theory method. The energies of stabilisation of π - and N -complexes of monomers with Ni(II) - and Pd(II) -based catalysts containing diimine and salicylaldimine ligands were calculated, and the energy diagrams of their decomposition were constructed. It appeared that π coordination of a monomer to metal is more favourable for systems with the central palladium atom, which provides the further growth of the polymer chain. In the presence of nickel catalysts, stronger metal–nitrogen bonds are formed and the latter hinder efficient copolymerisation, which accounts for the lack of success in ethylene copolymerisation with the use of this type of systems.

Chien *et al.*¹¹⁶ successfully performed copolymerisation of ethylene with a series of polar monomers, such as hex-5-en-1-ol, undec-10-enoic acid, methyl vinyl ketone, vinyl acetate and ϵ -caprolactam. The authors modified the catalyst system by activating bis(imino)acenaphthene nickel(II) dihalide with a mixture of methylalumoxane (or diethylaluminium chloride) and dibutylmagnesium.

In the review,¹¹⁷ the optimal structures of nickel and palladium diimine complexes were proposed for copolymerisation of ethylene with polar monomers and the mechanism of formation of copolymers with polar functional groups was analysed based on the results obtained by the research teams headed by Brookhart and Chien. As a result of the electron distribution in the complexes, these palladium catalysts are polar compounds due to which they readily form highly branched PE, and provide the introduction of polar (in particular, acrylate) fragments into the ends of branches in copolymerisation reactions (see Fig. 5).

It should be noted that the possibility of polymerisation of methyl methacrylate in *o*-xylene at 90 °C in the presence of divalent iron complexes with tetradentate nitrogen-containing ligands, for example, with [*N,N'*-diphenyl-*N,N'*-di(quinolin-2-ylmethyl)]-1,2-ethylenediamine (using ethyl 2-bromoisobutyrate as the initiator) was demonstrated for the first time in the recent publication by Seppälä and co-workers.¹¹⁸ In this case, iron complexes catalyse the so-called atom transfer radical polymerisation (ATRP).

4. Supported catalyst systems based on α -diimine and bis(imino)pyridine complexes

As mentioned above, catalyst systems based on α -diimine and bis(imino)pyridine complexes are characterised by relatively low thermal stability and, as a consequence, rapidly lose activity during high-temperature polymerisation. The use of catalysts adsorbed on the surface of inorganic supports is a way to overcome this drawback.¹¹⁹ Experiments with supported catalyst systems demonstrated that they not only have high thermal stability but also allow the synthesis of polymers with substantially higher MW, improve their morphology and density and prevent adsorption of polymers on the walls of the reactor.

Patents^{120, 121} on the preparation of supported α -diimine and bis(imino)pyridine complexes were issued shortly after the discovery of post-metallocene catalysts. These supported catalyst systems were studied in detail.^{122, 123} A comparison of the efficiency of ethylene polymerisation in the presence of the MAO-activated 2,6-bis[1-(2,6-diisopropylphenylimino)ethyl]pyridine complex of iron dihalide under homogeneous conditions and in the presence of the SiO₂-supported complex showed¹²³ that the activity of the supported system is 5 times lower. However, the polymer formed on the supported catalyst has higher MW and better morphology.

Our research group¹²⁴ studied the kinetic features of ethylene polymerisation in the suspension and gas-phase modes in the presence of SiO₂-supported 2,6-bis(arylimino)pyridine complexes of iron chloride and 1,2-bis(arylimino)acenaphthyl complexes of nickel bromide containing cycloalkyl substituents in the *ortho* positions of the aryl groups. We prepared supported catalysts under the conditions described in the patents.^{120, 121} It was found that supported catalyst systems based on iron bis(imino)pyridine complexes **19–22** allow a decrease in the amount of the required activator (the optimal Al:Fe ratio is 110). The kinetic characteristics of polymerisation were steady in time (during > 1 h), whereas a sharp decrease in the polymerisation rate during the process was observed for the analogous homogeneous catalyst. For supported systems, the pattern of the dependence of the catalytic activity on the bulkiness of the cycloalkyl substituent in the *ortho* position of the aryl ring also changes. In the latter

case, complex **20** with the cyclohexyl group showed the highest performance, whereas the activity of the corresponding homogeneous analogues increases with increasing bulkiness of the substituent in the series cyclopentyl (**19**) < cyclohexyl (**20**) < cyclooctyl (**21**).

In the presence of substituted 1,2-bis(imino)acenaphthyl complexes of nickel bromide (for example, compound **32**), polymerisation proceeds without the additional (except for the step of catalyst deposition) introduction of a cocatalyst. The kinetic profile of the process is generally similar to that observed with the use of bis(imino)pyridine systems.

In the very recent study by Zakharov and co-workers,¹²⁵ the characteristic features of ethylene polymerisation in the presence of the 2,6-[(2,6-Me₂C₆H₃N=CMe)₂C₅H₃N]FeCl₂ (**34**) complex activated by various alkyl derivatives of aluminium, such as MAO, AlMe₃, AlBu₃¹ and Al(*n*-C₈H₁₇)₃, were investigated. The catalytic behaviour of these systems under homogeneous conditions was compared with that of the systems supported on SiO₂, Al₂O₃ or MgCl₂. The supported catalysts showed high activity, retained stability up to 70–80 °C and gave higher-molecular-mass products. The polymers synthesised with the use of both homogeneous and supported systems were characterised by rather wide MWD. The authors also compared the number of active sites and determined the rate constants for chain growth in the presence of both types of catalysts. It should be noted that these constants for the homogeneous and heterogeneous systems were of the same order in the beginning of the process. However, in the presence of the supported catalysts, these constants remained virtually unchanged with time, whereas they were decreased by a factor of three already within 5 min of polymerisation in the presence of the homogeneous catalysts. The absolute values of the effective rate constants for chain growth¹²⁵ for the homogeneous systems (2.6 × 10⁴ litre mol⁻¹ s⁻¹) are rather similar to those for the supported systems [(1.2–2.4) × 10⁴ litre mol⁻¹ s⁻¹], whereas the numbers of the active sites are substantially different. In the case of the supported systems (0.028–0.032 mol per mole of Fe), this number is lower than that for the homogeneous systems (0.41 mol per mole of Fe). Unfortunately, this fact remained unexplained.

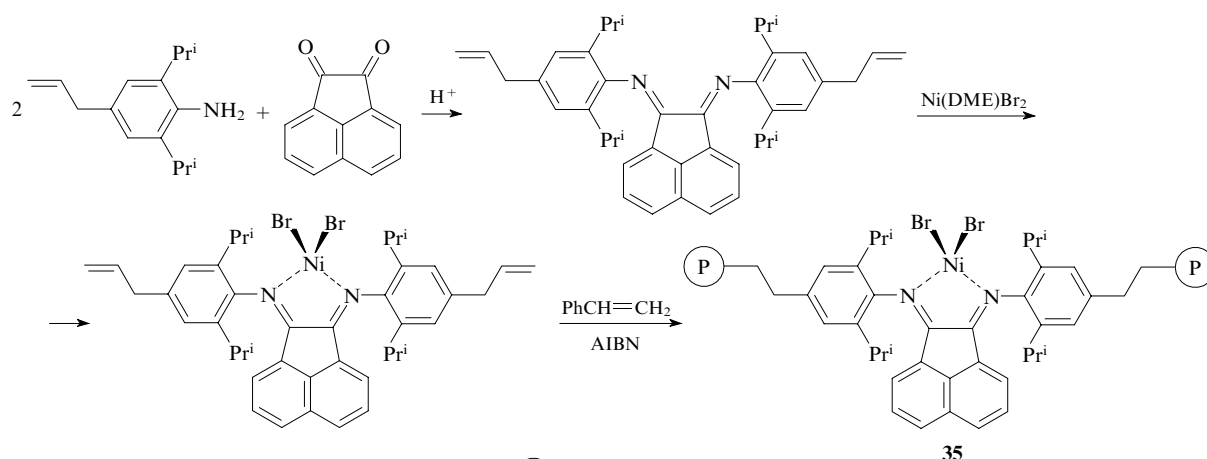
The interaction of the bis(imino)pyridine complex of divalent iron with oxide supports was studied by diffuse reflectance IR spectroscopy.¹²⁶ This study showed that the complex was strongly fixed possibly as a result of interactions of the ligand with several hydroxyl groups on the oxide surface, the geometric arrangement of these groups favours a multisite (according to the nomenclature used by the authors) contact. In aluminium oxide, both hydroxyl groups and Lewis acid sites are located on the surface, which provides stronger binding of the nitrogen-containing ligand to the support.

In the case of formation of supported catalysts on the surface of MgCl₂, the LFeCl₂ complex [L is the bis(imino)pyridine ligand] interacts only with Lewis acid sites of activated magnesium chloride.¹²⁷ Consequently, when choosing the conditions for deposition of the catalyst system, it is necessary to take into account the character of its interaction with the support. A characteristic feature of the behaviour of nickel α -diimine complexes immobilised on MgCl₂ is that the particle shape of the dispersed catalyst system is replicated by the polymer formed on this system.¹²⁸

The scope of action and the elucidation of the optimal conditions for the preparation of SiO₂-supported two-component catalyst systems based on α -diimine and bis(imino)pyridine complexes were described in our study.¹²⁹

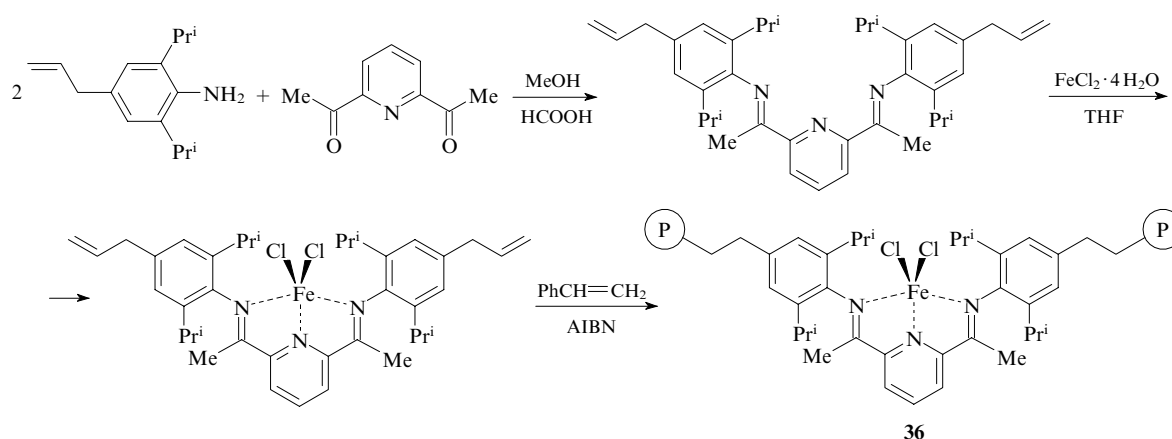
Recently, an original procedure for immobilisation of nickel α -diimine complex **35** (Scheme 2) and iron bis(imino)pyridine complex **36** (Scheme 3) on a polymeric support (polystyrene) has been published.¹³⁰ These catalysts were

Scheme 2



DME is dimethoxyethane, AIBN is azobis(isobutyronitrile), (P) is polystyrene.

Scheme 3



called polymerised catalysts. Copolymerisation of an excess of styrene with comonomer complexes in toluene afforded copolymers with low molecular weight (MW \sim 10 000) involving the catalytic complex.

Procedures for the synthesis of the corresponding ligands and complexes containing alkenyl groups, capable of polymerisation, were reported.^{131–134} A procedure was developed for the preparation of an SiO₂-supported polymerised catalyst as spherical particles with a core–shell structure.¹³⁰

The resulting polymerised systems were examined as ethylene polymerisation catalysts in the suspension mode using activation by MMAO. These catalysts showed high activity and gave good results as regards the replication ability in the formation of polymer particles, which confirms the prospects of this field of investigation.

III. Phenoxy-imine catalysts for olefin polymerisation

1. General views

A new generation of post-metallocene catalysts for olefin polymerisation based on transition metal phenoxy-imine[§] complexes was discovered by the research group from the Mitsui Chemical, Inc., Company (Japan) in the framework of the Project 'Ligand-Oriented Catalyst Design' started in the mid-1990s.

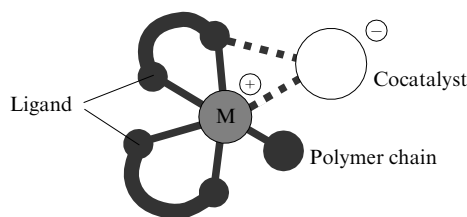
[§] The term phenoxy-imine complexes is generally referred to complexes containing salicylaldimine ligands and their analogues.

First patents^{135, 136} and articles (see, for example, Ref. 137) on phenoxy-imine catalyst systems, which were issued less than 10 years ago, marked the beginning of a large series of publications on this problem in different journals.

As the authors noted, the concept of the above-mentioned project was based on the analysis of advances in the design of high-performance single-site olefin polymerisation catalysts and was aimed at searching for systems satisfying the following main criteria:

- catalyst systems should provide an efficient insertion of structurally different olefins, including sterically hindered olefins, as well as polar monomers, into the polymer chain;
- stability of catalysts under standard conditions of the polymerisation process;
- the possibility to control the chain transfer reaction, the achievement of the uniform distribution of the comonomer and stereochemical control of the product;
- extension of the range of the produced polymers by performing copolymerisation with the previously unused monomers.

An important principle of this concept was that olefin polymerisation is accompanied by extensive electron exchange between transition metal and ligands. In this case, it is necessary that the ligands should contain heteroatoms (as a rule, oxygen and/or nitrogen atoms), coordinate metal atoms in a bidentate fashion and have an unsymmetrical structure with mobile electrons (the so-called electron-flexible structure). The ability of transition metals to coordinate olefins and to be introduced into the polymer chain combined with such oriented ligands would provide high activity of the system in



M is metal.

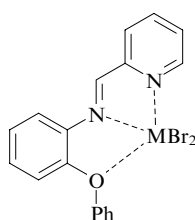
Figure 6. Schematic representation of catalysts discovered based on ligand-oriented catalyst design.⁵²

polymerisation. Figure 6 schematically shows a catalyst system based on ligand-oriented catalyst design.⁵²

It was demonstrated that polydentate electron-flexible unsymmetrical ligands, which are capable of chelating and forming five- or six-membered rings, satisfy the above-mentioned conditions. These are primarily ligands containing phenoxy, pyridine and/or conjugated imine fragments. These ligands are characterised by stability under the reaction conditions, have required electron-donating properties for the efficient olefin insertion and stabilisation of the transition state and contain accessible coordination sites necessary for polymerisation.

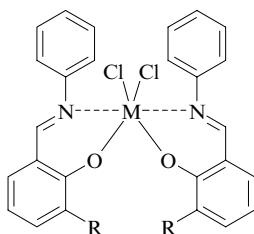
However, in my opinion, the authors of this concept, when designing a new class of high-performance phenoxy-imine catalysts, did not give proper attention to studies of the Shell Company on the development of SHOP (Shell Higher Olefin Process) catalysts and improvement of nickel catalyst systems for ethylene oligomerisation and polymerisation.^{138–143}

Initially, the research group headed by Fujita^{135–137} synthesised catalytic complexes with unsymmetrical electron-flexible ligands based on *N*-(*o*-phenoxyphenyl)pyridylaldimine (37, 38) and salicylaldiminate (39–41) derivatives.



37, 38

M = Co (37), Ni (38).



39–41

R = Bu^t, M = Zr (39);
R = H: M = Ti (40), Hf (41).

Studies of the catalytic activity of cobalt complex (37) and nickel complex (38) in MAO-mediated ethylene polymerisation in toluene showed that the former complex is inactive and the latter complex has lower activity than Ni catalysts with α -diimine ligands. Zirconium complex 39 in toluene at 25 °C exhibited activity of 519 (t PE) mol⁻¹ h⁻¹ (the molecular mass of the polymer was $\sim 10^4$), which is 20 times higher than the activity of the metallocene catalyst Cp₂ZrCl₂ (Cp = η -C₅H₅). In addition, this zirconium complex is characterised by rather high stability in a wide temperature range (the activity gradually decreases as the temperature is raised).

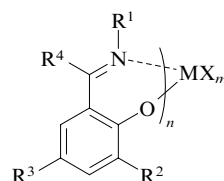
Over a rather short period of time, this research group synthesised a large number of structurally different phenoxy-imine complexes containing substituents of different nature both at the imine nitrogen atom and the phenoxy group,^{144, 145} including those with perfluorinated fragments.^{146–149} Conceptually similar derivatives based on nitrogen-containing heterocycles, viz., indolyl-imine¹⁵⁰ and pyrrolyl-imine¹⁵¹ complexes, were also synthesised.

Shortly thereafter, the results of investigations in this field were summarised and systematised, which showed considerable progress in the design of this new class of post-metallocene catalysts.^{52, 149, 152, 153} For example, the classification of different catalysts, which were developed based on the ligand-oriented catalyst design concept, was proposed in the review.⁵² Table 1 summarises the general structures of phenoxy-imine and analogous chelate complexes. It should be noted that not only complexes, in which metal atoms are coordinated by heteroatoms (oxygen and nitrogen), but also titanium phenoxy-cyclopentadienyl complexes with similar properties are referred to this class.^{160, 161}

Many complexes listed in Table 1 proved to be high-performance catalysts for the synthesis of a number of special polymers and copolymers. For example, particular phenoxy-cyclopentadienyl complexes of Group IV transition metals showed high activity in copolymerisation of ethylene with sterically hindered monomers. In the presence of titanium bis(pyrrolyl-imine) complexes, living copolymerisation of ethylene with norbornene giving rise to high-molecular-weight copolymers and block copolymers can be performed at room temperature. The titanium indolyl-imine complex allows living polymerisation of ethylene and propylene and their living block copolymerisation at room temperature.

Among the above-mentioned structures, phenoxy-imine catalysts (or FI catalysts according to the nomenclature by Fujita¹³⁷) are most promising due to high catalytic activity, the possibility of varying substituents in the ligand and the simplicity of the synthesis. These catalysts are considered in more detail below.

The general structure of FI complexes consists of two bidentate unsymmetrical phenoxy-imine ligands coordinated to transition metal.



M = Ti, Zr, Hf, V, Cr, etc.; R¹, R², R³ and R⁴ = Alk, Ar and other groups; X = Hal.

As can be seen in Fig 7, the complexes with $n = m = 2$ can exist in five isomeric forms having an octagonal coordination

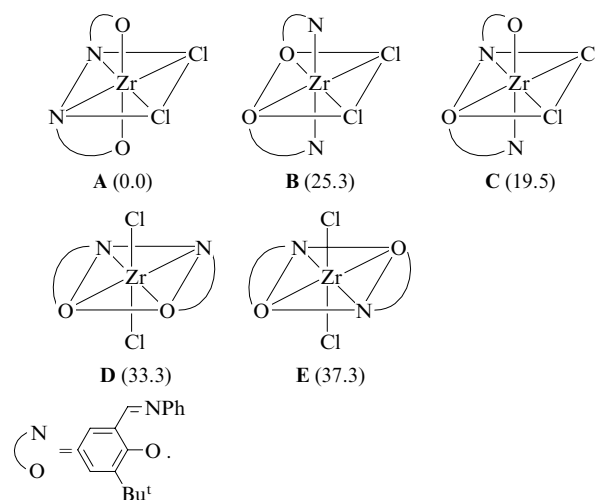
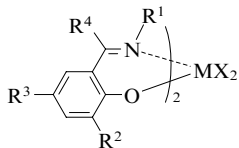
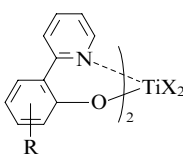
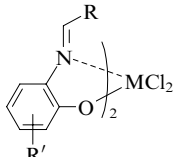
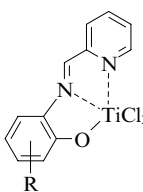
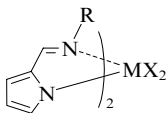
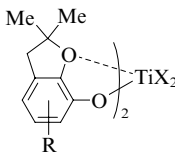
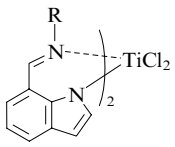
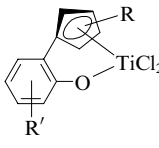
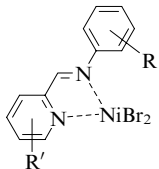
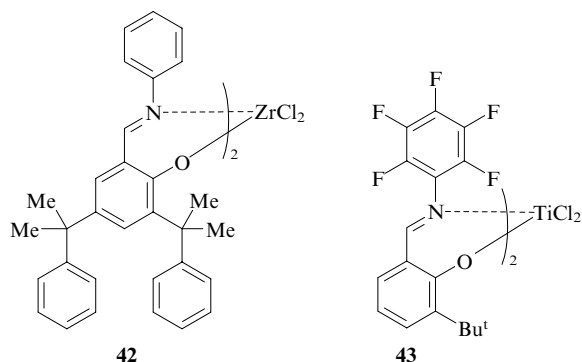


Figure 7. Possible isomeric forms of the octagonal coordination of FI catalysts [the energies of their formation (kJ mol⁻¹) for complex 39 are given in parentheses].⁵²

Table 1. Ligand-oriented olefin polymerisation catalysts.

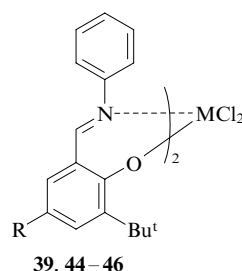
Complex	Structure	Ref.	Complex	Structure	Ref.
Bis(phenoxy-imine)	 <p>$M = \text{Ti, Zr, Hf, V, Cr, etc.}$</p>	135–137, 144, 145	Bis(phenoxy-pyridine)		158
	 <p>$M = \text{Ti, Zr}$</p>	135–137, 154	Phenoxyimino-pyridine		149
Bis(pyrrolyl-imine)	 <p>$M = \text{Ti, Zr, Hf}$</p>	151, 155, 156	Bis(phenoxy-ether)		149, 159
Bis(indolyl-imine)		150, 157	Phenoxy-cyclopentadienyl		160, 161
Phenylimino-pyridine		149			

(depending on the arrangement of the ligand). According to the ^1H NMR spectroscopic data,⁵² FI catalysts with the central Ti, Zr or Hf atom exist in solution as mixtures of isomers. Quantum chemical calculation (the density functional theory) of the corresponding energies of the formation of isomers showed that isomers **A** and **B** are most often present in solution (see Fig. 7). It should be noted that for some FI complexes the formation of only one isomer is favourable. For example, Zr complex **42** exists predominantly as isomer **B**, whereas Ti complex **43** containing the perfluoroaryl fragment at the imine nitrogen atom exists exclusively as isomer **A**.



The coexistence of different isomeric forms of FI catalysts can be responsible for deviation from the single-site character of the catalyst system formed on their basis.

The structural characteristics and stereochemistry of FI complexes have been extensively studied, including by X-ray diffraction. The geometric parameters of four FI complexes **39** and **44–46**, in which the natures of metal and the substituent in the phenoxy group were varied, were determined.^{52, 162}



$M = \text{Zr: R} = \text{H}$ (**39**), Me (**44**); $M = \text{Ti: R} = \text{H}$ (**45**), Me (**46**).

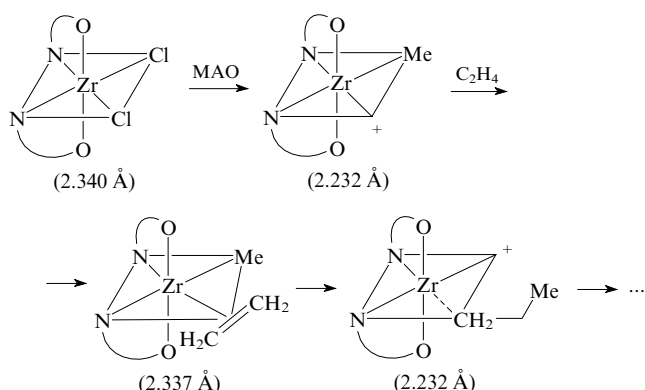
The X-ray diffraction study demonstrated⁵² that these complexes in the solid state contain the metal centre (Zr or Ti) in a nearly octahedral coordination environment characterised by the space group C_2 with the O, N and Cl atoms being in *trans*, *cis* and *cis* positions, respectively. The bond lengths and bond angles in complexes **39** and **44** and in their homologues **45** and **46** determined by different research groups^{52, 162} are given in Table 2. It can be seen that these results are in good agreement with each other. Small differences in the bond angles are attributed to the presence of the methyl substituent in complexes **45** and **46**.

Table 2. Geometric parameters of FI complexes **39** and **44–46**.

Complex	Bond lengths /Å			Bond angles /deg			Ref.
	M–O	M–N	M–Cl	OMO	NMN	ClMCl	
39	1.985(2)	2.355(2)	2.423(5)	165.5(1)	74.0(1)	100.3(8)	52
44	1.980(3)	2.351(4)	2.428(8)	157.9(9)	84.3(3)	94.6(1)	52
45	1.852(4)	2.236(4)	2.305(2)	171.6(2)	76.4(2)	103.1(1)	162
46	1.844(3)	2.212(5)	2.306(2)	164.0(3)	86.0(3)	94.08(1)	162

The results of quantum chemical calculations⁵² (the density functional theory) for the structures of the precursors of the ethylene-coordinated methyl cationic catalyst, which is generated in the reaction of highly active Zr complex **39** with MAO (the calculated Zr–N bond lengths are given in parentheses), are presented in Scheme 4. The cationic complex has a distorted octahedral coordination, the Zr–N bonds and the polymerisation site being located in one plane. The interaction with a monomer leads to an increase in the length of this bond from 2.232 to 2.337 Å, whereas the Zr–O bond lengths remains unchanged. The change in the Zr–N bond length is indicative of a flexible exchange between the metal atom and the ligands, and the *cis* arrangement of the active site combined with the nature of the ligands is, apparently, responsible for high activity of this FI system [519 (t PE) mol^{−1} h^{−1}].

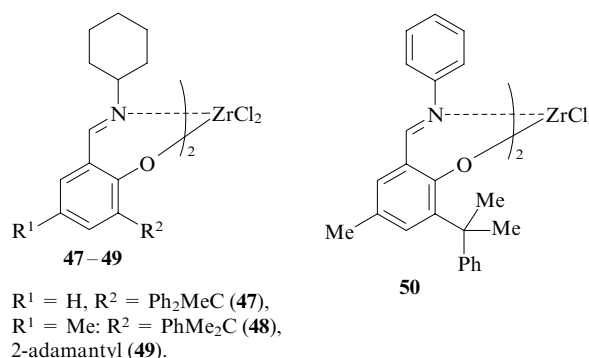
Scheme 4



New FI catalyst systems synthesised by Fujita and co-workers^{163,164} were studied as ethylene polymerisation catalysts. The authors analysed the dependence of the catalytic activity on the nature of transition metal and the nature and size of substituents at the imine nitrogen atom and in the *ortho* and *para* positions of the phenoxy group. For example, after the replacement of Zr by Ti, Hf, V or Cr in complex **39** combined with the cocatalyst MAO, the catalytic activity was 3, 26, 4 and 1 (t PE) mol^{−1} h^{−1}, respectively.

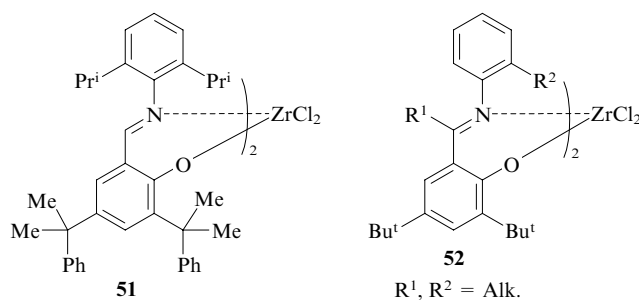
The first conclusions about the influence of the bulky substituents in the *ortho* position of the phenoxy group and the small substituent at the imine carbon atom were made in the publications.^{163,164} The steric hindrance caused by the bulky substituent adjacent to the oxygen atom of the phenoxy group protects the latter from the electrophilic attack of a Lewis acid, which is present in the polymerisation system, and facilitates the efficient separation of the cationic active species and the anionic species of the cocatalyst. Small substituents in the imine fragment leave sufficient space for the approach of the monomer to the active site of the growing chain. Hence, the presence of the aldimine fragment in the complex provides high activity of the catalyst, whereas ketimine-type FI systems (for example, those containing the substituted RC=N fragment, where R = Me, Et or Ph) are substantially less active.¹⁶⁵

Complexes **47–50** are ethylene polymerisation catalysts of exceptionally high efficiency.



For example, MAO-activated FI system **47** exhibits the surprisingly high activity [6552 (kg PE) mmol^{−1} h^{−1}, 25 °C, MW of the polymer was $\sim 1 \times 10^4$] and is characterised by the record turnover frequency of 64 900 s^{−1} atm^{−1}.⁵² The activities of bis[*N*-(3-cumyl-5-methylsalicylidene)phenylamino]ZrCl₂ (**50**) and bis[*N*-(3-cumyl-5-methylsalicylidene)cyclohexylamino]ZrCl₂ (**48**) are as high as 2 (t PE) mol^{−1} h^{−1} and are increased as the concentration of the catalyst is slightly decreased. For bis[*N*-(3-(2-adamantyl)-5-methylsalicylidene)cyclohexylamino]ZrCl₂ (**49**), the yield of the polymer is 0.7 t min^{−1} (Refs 144 and 145). It was noted^{166,167} that FI complex **42** shows the unusual behaviour, which is manifested in that MWD of the product varies with the temperature. At 0 and 25 °C, the monomodal curve is observed, whereas the curve at 75 °C is bimodal, which was attributed to a change in the ratio between the coordination isomers in the FI system.

Zirconium complexes (for example, **51**), in which the phenyl group at the imine nitrogen atom contains substituents in both *ortho* positions, were also reported.¹⁶⁸ The use of these systems generally results in a decrease in the activity of catalysts. Catalysts **52** are exceptions to the general rule.



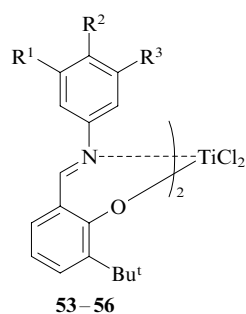
In spite of the facts that ketimine complexes are less active than aldimine complexes¹⁶⁵ and that the presence of an *ortho* substituent in the aniline fragment does not lead to an increase in the activity of the system, complexes **52** showed high catalytic activity, and high MW of the resulting polyethylene were achieved.¹⁶⁹

Our research group revealed the relationship between the structure of such catalysts and their activity in ethylene polymerisation using the density functional theory method.¹⁷⁰ The influence of the structure of complexes on the energy effects of the formation of catalytically active species, the formation of π complexes of the catalysts with ethylene, the chain growth and chain transfer and deactivation of the system was analysed for five titanium and zirconium phenoxy-imine complexes. The results of investigation provided an explanation for the different behaviour of Ti and Zr complexes and the dependence of the activity of the catalyst system on the ligand structure.

In the recent study,¹⁷¹ an attempt was made to systematise the results of research into the influence of substituents in phenoxy-imine complexes on their catalytic activity in ethylene polymerisation by analysing FI systems, in which the substituents either at the imine nitrogen atom or in the phenoxy group were varied. An investigation of ten structurally different FI complexes demonstrated that the substituents at the imine nitrogen atom influence not only the activity of the catalyst system but also the temperature range of the efficient catalyst functioning. Sterically hindered substituents in the *ortho* position of the phenoxy group should have the optimal volume; otherwise, the activity of the catalyst system decreases.

In the presence of particular FI catalysts in polymerisation systems, polymerisation can proceed according to the living polymerisation mechanism. Initially, this mechanism was established for structures containing perfluorinated aryl groups at the imine nitrogen atom.^{146–148} For example, living polymerisation of not only ethylene but also of propylene was successfully performed in the presence of complex **43**. In the latter case, syndiotactic polypropylene (SPP) with narrow MWD ($M_w : M_n = 1.11$) was obtained.

Polyethylene was synthesised by living polymerisation with the use of complexes **53–56** combined with MAO [the activity was 43.3 (kg PE) mmol⁻¹ h⁻¹, $M_n = 1.36 \times 10^6$].¹⁴⁷



$R^1 = R^3 = \text{H}, R^2 = \text{F}$ (**53**); $R^1 = R^3 = \text{F}, R^2 = \text{H}$ (**54**);

$R^1 = R^2 = R^3 = \text{F}$ (**55**); $R^1 = R^3 = \text{CF}_3, R^2 = \text{H}$ (**56**).

Quantum chemical molecular orbital calculations demonstrated that the characteristic features of the mechanism of living polymerisation with the use of these systems are associated with the electron-accepting effect of the fluorine atoms, resulting in an increase in the electrophilicity of the metal centre and a decrease in the activation energy for ethylene insertion.

The possibility of living ethylene and propylene polymerisation was demonstrated by Bulychev and co-workers¹⁷² using dinuclear fluorine-containing titanium bis(salicylidene)-imine complexes. According to the results of calculations (the density functional theory), fluorine-substituted phenyl groups at the imine nitrogen atom provide the living polymerisation mechanism. In the course of polymerisation, the fluorine atom in the active state of the catalyst interacts with the hydrogen atom in the β position of the polymer chain thus preventing β hydride transfer.

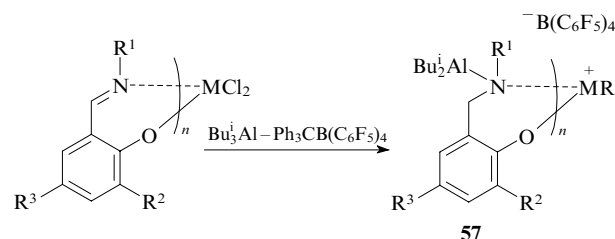
Living ethylene and propylene polymerisation is successfully used for the preparation of a number of unique block copolymers (both diblock and multiblock copolymers).

We were the first to perform living ethylene polymerisation with the use of non-fluorinated titanium FI systems. For example, it was demonstrated^{162, 173} that ethylene polymerisation on the MAO-activated bis[*N*-(3-(*tert*-butyl)-5-methylsalicylidene)anilinato]TiCl₂ complex (**46**) affords the polymer, whose molecular mass linearly increases with time. After termination of feeding of ethylene and subsequent introduction of hex-1-ene into the polymerisation system, polyethylene–block–poly(hex-1-ene) was obtained. This confirms that polymerisation proceeds according to the living polymerisation mechanism. The detailed analysis of living olefin polymerisation in the presence of various catalyst systems, including phenoxy-imine complexes, was performed in the recent review.¹⁷⁴

2. Influence of activators on catalytic activity and selectivity of FI complexes

The influence of the nature of the cocatalyst on the activity and selectivity of Ziegler–Natta catalysts, as well as of metallocene systems, in olefin polymerisation was considered in-depth in numerous monographs and reviews (see, for example, Refs 8, 12, 16, 17, 22, 36 and 40). Taking into account that FI ligands contain heteroatoms, it could be expected that these complexes would be activated with a larger number of structurally different cocatalysts compared to metallocenes.

Earlier, the successful use of MAO or its modified derivatives as activators of FI complexes has been documented. In addition, the $\text{Bu}_3\text{Al}–\text{Ph}_3\text{CB}(\text{C}_6\text{F}_5)_4$ systems can serve this purpose.^{144, 175–179} It was found that the mechanism of activation of FI catalysts by this system is based on the formation of amino-ligated complex **57** catalysing polymerisation.



$M = \text{Ti, Zr, Hf, etc.}; R^1, R^2, R^3 = \text{Alk or Ar.}$

The use of FI complexes combined with the $\text{Bu}_3\text{Al}–\text{Ph}_3\text{CB}(\text{C}_6\text{F}_5)_4$ system in olefin polymerisation results in a decrease in the activity compared to that observed in the presence of MAO; nevertheless, the activity remains at a satisfactory level, MW of the polymers being substantially increased.

Taking into account the specific mechanism of activation, the structure of FI complexes substantially influences the efficiency and selectivity of this type of catalyst systems. For example, polymerisation with the use of FI complex **39** activated with $\text{Bu}_3\text{Al}–\text{Ph}_3\text{CB}(\text{C}_6\text{F}_5)_4$ at 50 °C affords polyethylene with $\text{MW} \sim 5 \times 10^6$, and the activity of the catalyst was 11 (kg PE) mmol⁻¹ h⁻¹, while the same system combined with MAO exhibited activity of 519 (kg PE) mmol⁻¹ h⁻¹, and MW of the resulting polyethylene was as low as $\sim 1 \times 10^4$. It should be emphasised that the application of the $\text{Bu}_3\text{Al}–\text{Ph}_3\text{CB}(\text{C}_6\text{F}_5)_4$ system as the activator proved to be very useful.

Magnesium chloride-supported organic derivatives of aluminium, for example, $\text{R}'_n\text{Al}(\text{OR})_{3-n}/\text{MgCl}_2$ (R and $R' = \text{Et or Bu}^t$), were proposed as promising cocatalysts for FI systems. These activating systems simultaneously serve as supports for FI complexes. Earlier attempts^{180, 181} to use these systems

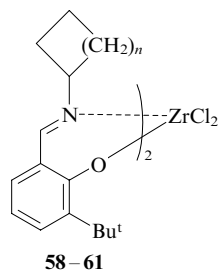
combined with metallocene catalysts have failed. Recently, it has been demonstrated^{182–184} that the efficiency of the use of specially treated MgCl_2 as the cocatalyst for olefin polymerisation is determined by the presence of heteroatoms in FI systems.

The latest advances in research into the FI complex– $\text{R}'_n\text{Al}(\text{OR})_{3-n}/\text{MgCl}_2$ catalyst systems were considered in the publication.¹⁸⁵ For example, the activity of catalyst **49** in ethylene polymerisation in the presence of $\text{R}'_n\text{Al}(\text{OR})_{3-n}/\text{MgCl}_2$ amounts up to 1819 (kg PE) $\text{mmol}^{-1} \text{h}^{-1}$ (50 °C, 0.9 MPa).¹⁸⁵ The use of vanadium-based FI systems in the presence of this type of activators makes it possible to perform polymerisation with high efficiency at high temperatures (75 °C). Modified MgCl_2 serves as the active cocatalyst for living olefin polymerisation with the use of fluorinated FI ligands.¹⁸⁶

Substantial advantages of activators based on modified MgCl_2 are that the polymer morphology is improved (replication of spherical, including ultradisperse, particles of the supported catalyst) and the polymer has a high bulk density and is not deposited on the walls of the reactor.¹⁸⁵ The characteristic features of immobilisation of complexes on modified MgCl_2 and the coordination mode of ligands in supported catalyst systems were reported.^{187, 188}

3. Use of FI catalyst systems for the preparation of non-traditional polyolefins

The use of FI catalysts can allow the preparation of polymers with a nonconventional topology. For example, MAO-mediated complexes **58** and **59** catalyse the formation of low-molecular-mass polyethylenes with terminal vinyl groups (the percentage of vinyl groups at one of the ends of the polymer chain is no lower than 90%).¹⁸⁹ High reactivity of the terminal groups is combined with rather high melting points of these polymers (> 120 °C). Polymerisation in the presence of complex **58** affords a product with the weighted-average molecular weight (M_w) of 2100 and the ratio $M_w : M_n = 1.52$; in the case of compound **59**, $M_w = 3800$ and $M_w : M_n = 1.82$.



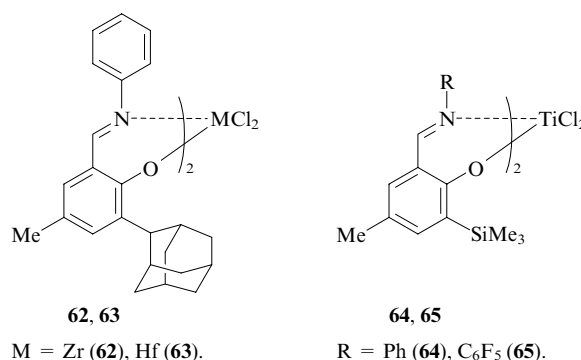
$n = 1$ (**58**), 2 (**59**), 3 (**60**), 4 (**61**).

The steric factors rather than the electronic nature of substituents play the key role in the formation of the terminal vinyl groups of the polymers when polymerisation is catalysed by complexes containing lower cycloalkyl (cyclobutyl or cyclopentyl) substituents in the imine fragment. Recently,¹⁹⁰ the structures of zirconium bis(phenoxy)imine complexes **58–61** containing various cycloalkyl groups at the imine nitrogen atom were studied by X-ray diffraction. It was noted that the substituents greatly influence the kinetic behaviour of these complexes in ethylene polymerisation (MAO as the cocatalyst, 25 °C). Complexes **58–61** were demonstrated to have identical coordination geometry irrespective of the number of CH_2 groups in the ring. Nevertheless, the cyclic substituent strongly influences the steric environment of the potential active sites of polymerisation and, consequently, the catalytic activity of complexes **58–61** depends on the bulkiness of the cycloalkyl substituent. Both low- and high-molecular-weight polyethylenes containing unsaturated vinyl groups at the ends of the

polymer chain can be prepared with the use of these phenoxy-imine complexes due to the fact that the β -hydride transfer to monomers prevails over the transfer to the metal centre. This character of the transfer process was confirmed by quantum chemical calculations and experiments on the effect of the ethylene pressure on the polymerisation process. Thus, the influence of substituents in phenoxy-imine complexes on the mechanism of elementary steps of chain transfer in olefin polymerisation was demonstrated for the first time in the study.¹⁹⁰

Polymers containing terminal vinyl groups can find use as macromers for the preparation of copolymers with long-chain branches. Various modifying additives as well as graft and block copolymers can be synthesised by functionalisation of vinyl fragments in these polymers.

Propylene polymerisation catalysed by FI complexes **62** and **63** afforded highly isotactic polypropylene.¹⁷⁹ Isotactic polypropylene (IPP) with $M_w = 172\,000$ and the ratio $M_w : M_n = 2.1$ was synthesised with the use of zirconium complex **62** combined with the $\text{Bu}_3^i\text{Al}-\text{Ph}_3\text{CB}(\text{C}_6\text{F}_5)_4$ system. This polymer is characterised by a high percentage of *mm* triads[†] (98%) and the relatively high melting point (164 °C). The catalyst based on analogous hafnium complex **63** facilitates the formation of IPP with $M_w = 364\,000$, $M_w : M_n = 3.5$, [*mm*] = 98% and $T_m = 165$ °C.



Syndiotactic polypropylene was synthesised on MAO-activated titanium FI complexes **64** and **65**.^{191, 192} Polymerisation with the use of complex **64** containing the phenyl substituent at the imine nitrogen atom at 1 °C afforded SPP containing 91% of *rr* triads with $T_m = 140$ °C. The replacement of this substituent by the perfluorinated phenyl group (complex **65**) resulted in the formation of SPP with [*rr*] = 94% and $T_m = 156$ °C. Polymerisation in the presence of $\text{Bu}_n^i\text{Al}(\text{OR})_{3-n}/\text{MgCl}_2$ -activated catalyst **65** at 25 °C gave SPP with [*rr*] = 97%, $T_m = 155$ °C and $M_w = 32\,000$. The characteristic features of the formation of SPP were discussed.^{192–196}

It is generally very difficult to synthesise stereo- and regioregular higher α -olefins because of the difficulties in performing stereocontrol of the process (exclusion of 'regio errors'). Another problem is associated with a decrease in the activity of the catalyst because of steric hindrance to the approach of the monomer to the active site. These difficulties were successfully overcome with the use of $\text{Bu}_3^i\text{Al}-\text{Ph}_3\text{CB}(\text{C}_6\text{F}_5)_4$ -activated titanium phenoxy-imine complex **40** as a catalyst for hex-1-ene polymerisation.¹⁷⁶ In this case, atactic (non-regioregular) polyhexene with $M_w = 720\,000$, $M_w : M_n = 1.68$ and the regio error of ~50% was obtained at

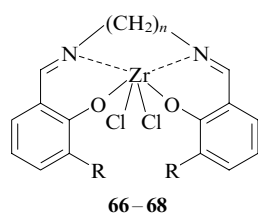
[†] Isotactic diads (*m*-diads) are characterised by an identical arrangement of the methyl groups with respect to the plane of the carbon chain of the macromolecules, as opposed to syndiotactic (*r*) diads, in which the methyl groups of propylene are located on the opposite sides of this plane.³⁹

25 °C. Under analogous conditions, polyoctene, poly(4-methylpentene) and other higher polyolefins were prepared. The catalytic activity decreases in the following series of monomers: 4-methylpentene > dodec-1-ene > oct-1-ene > hex-1-ene.

Recently, the advances in the synthesis of isotactic polypropylene have been demonstrated with the use of titanium phenoxy-alimine and -ketimine complexes containing *ortho*-phenoxyhalide substituents.¹⁹⁷

4. Non-standard phenoxy-imine and structurally similar complexes

Group IV metal complexes with tetradentate ligands containing hydrocarbon-bridged phenoxy-imine fragments are of particular interest as high-performance olefin polymerisation catalysts.¹⁹⁸



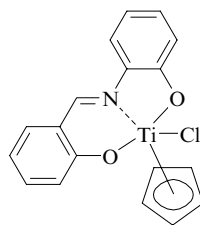
66–68

$m = 1$, $R = H$, $n = 2$ (**66**);
 $m = 0$; R is 2-adamantyl, $n = 2–6$ (**67**); $R = CH_2Ph$, $n = 4$ or 6 (**68**).

The rigidly organised structure of these complexes is responsible for their high thermal stability and provides stereospecificity in polymerisation reactions. For example, the activity of SiO_2 -supported compound **66** in the presence of MAO is 3.53 (kg PE) $mmol^{-1} h^{-1}$, which is 30 times higher than the activity of an analogous catalyst under homogeneous conditions.¹⁹⁸

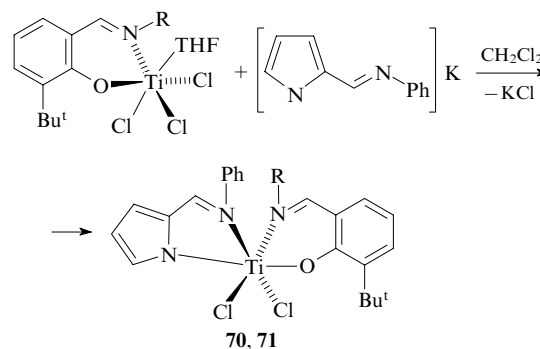
The catalytic activity of tetradentate bis(phenoxy-imine) complexes **67** and **68** was studied.^{199–201} These catalysts are characterised by high stability and can function at high temperatures [for example, in the course of solution ethylene polymerisation at 150 °C, the activity of compound **67** was 143 (kg PE) $mmol^{-1} h^{-1}$]. It should be noted that the activity of such catalyst systems increases with the number of CH_2 groups in the bridge between the imine nitrogen atoms.²⁰⁰

Tridentate titanium complexes containing simultaneously the phenoxy-imine and cyclopentadienyl ligands were synthesised;²⁰² however, their activity in ethylene polymerisation appeared to be low. For example, the activity of compound **69** was 15.6 (g PE) $mmol^{-1} h^{-1}$, the molecular weight of the resulting polymer being 1 630 000.



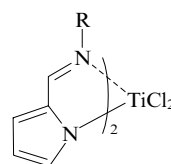
69

In 2005, hybrid titanium (phenoxy-imino-pyrrolyl-imine) complexes **70** and **71** were described.²⁰³ These complexes showed high activity in MAO-mediated ethylene polymerisation. The complexes were prepared by the reaction of the titanium mono(salicylaldimine) complex with the metallated pyrrolylaldimine ligand.



$R = Ph$ (**70**), C_6F_5 (**71**).

Bis(pyrrolyl-imine) complexes of Group IV metals, which are structurally similar to FI systems and were synthesised by Fujita and co-workers,^{204,205} are of great interest in both theoretical and commercial aspects.



$R = Et$, $n-C_6H_{13}$, cyclo- C_6H_{11} , Ph .

Such complexes with the central titanium atom proved to be better ethylene polymerisation catalysts than zirconium complexes. As in the case of phenoxy-imine ligands, methylalumoxane is a more efficient cocatalyst for these compounds than the $Bu_3Al-Ph_3CB(C_6F_5)_4$ system, with MW of the resulting polymers being of the same order of magnitude.

Further investigations^{151,206} demonstrated an interesting possibility of living copolymerisation of ethylene with norbornene in the presence of these systems. This process gives copolymers whose composition is similar to that of alternating copolymers. It should be emphasised that these catalysts are inactive in living homopolymerisation of both norbornene and ethylene. It was found²⁰⁷ that the introduction of substituents into the pyrrolidine ring does not change the activity of the catalyst system.

Pyrrolyl-imine catalysts are very efficient in copolymerisation of ethylene with propylene and α -olefins providing a high degree of comonomer insertion.

A search for and investigation of new structures of phenoxy-imine catalysts and their analogues having unusual and sometimes exotic structures are presently underway. Unfortunately, it is impossible to mention all results obtained by numerous research groups in this important and interesting field of investigation. Nevertheless, the present review hopefully provides insight into the advances and prospects in the design of post-metallocene catalysts for olefin polymerisation.

IV. Conclusion

The fifty-year history of the large-scale production of the most important polymers, *viz.*, polyethylene and polypropylene, which are widely used in various fields of human activity, shows a tremendous role of catalysts in the perfection of the polymerisation process. The use of Ziegler–Natta catalysts, catalyst systems for gas-phase polymerisation and transition metal metallocene complexes made a considerable contribution to the perfection of polyolefin production processes and improvement of their performance characteristics.

The chronology of the design and introduction of new catalysts showed that the search for active and selective catalyst systems for olefin polymerisation is a high-priority field in polymer chemistry. In recent years, the design of these catalysts has become more extensive. It took 30 years to change over Ziegler–Natta catalysts to metallocene catalysts, whereas the last decade witnessed the discovery of a new type of catalysts, *viz.*, transition metal post-metallocene complexes, which hold considerable promise for commercial olefin polymerisation and copolymerisation.

Over a short period of time, the characteristics of post-metallocene polymerisation catalysts, such as activity, selectivity, sensitivity to the reaction conditions, availability, safety and the range of monomers used in polymerisation, became as good as and even better than those of metallocene complexes. The use of these catalysts becomes preferable also from the economical point of view. Post-metallocene systems are characterised by a wide range of activators and supports ensuring their functioning. A wide range of ligands for these systems and prospects for solving the problems of monitoring (NMR method) and controlling the structures of the resulting polymer systems (molecular weight, branching and block structure) substantially extend the scope of their commercial application. The experimentally established possibility of the synthesis of superhigh-molecular-weight polymers and copolymers by the living polymerisation mechanism, the synthesis of block copolymers of different composition, an increase in the percentage of sterically hindered monomers in copolymers and the formation of low-molecular-weight polymers with unsaturated reactive groups are some of the characteristic features of new post-metallocene systems demonstrating their great potentialities. Great prospects for their use are associated also with high performance of heterogeneous complexes, in which modified MgCl_2 serves as the activator and support.

Post-metallocene catalyst systems have been discovered rather recently. Nevertheless, the main aim of investigations of these systems would be expected to be changed, the research into commercial applications of catalysts will be more intensive, interest in the design of new complexes being retained, as well as the mechanism of polymerisation with the use of these catalysts will be refined. The immobilisation of catalyst systems, an increase in the temperature range of their steady activity, the extension of the possibilities to control the structure and performance characteristics of the resulting polymers, simulation of polymerisation processes and tailoring of pilot devices to real industrial conditions will likely receive more attention.

I thank Academician G A Tolstikov and Dr. N I Ivancheva for helpful discussion of some aspects of the present review and Dr S V Myakin for help in preparing this review.

References

1. *Polietilen Vysokogo Davleniya. Nauchno-tehnicheskie Osnovy Promyshlennogo Sintez* (Low-Density Polyethylene. Scientific and Technological Foundations of Industrial Synthesis) (Ed. A V Polyakov) (Leningrad: Khimiya, 1988)
2. K Ziegler, H G Gellert, K Zosel, W Lehmkuhl, W Pfohl *Angew. Chem.* **67** 424 (1955)
3. K Ziegler, E Holzkamp, H Breil, H Martin *Angew. Chem.* **67** 541 (1955)
4. G Natta, P Pino, P Corradini, F Danusso, E Mantica, G Mazzanti, G Moraglio *J. Am. Chem. Soc.* **77** 1708 (1955)
5. G Natta, P Corradini, G Allegra *J. Polym. Sci.* **51** 399 (1961)
6. *Stereoregular Polymers and Stereospecific Polymerizations* (Eds G Natta, F Danusso) (Oxford: Pergamon Press, 1967)
7. J Boor Jr *Ziegler–Natta Catalysts and Polymerizations* (New York: Academic Press, 1979)
8. A A Montagna, J C Floyd *Hydrocarbon Process.* **73** (3) 57 (1994)
9. *Handbook on Polyolefins* (2nd Ed.) (Ed. C Vasile) (New York, Basel: Marcel Dekker, 2000) p. 41
10. *Polietilen Nizkogo Davleniya. Nauchno-tehnicheskie Osnovy Promyshlennogo Sintez* (High-Density Polyethylene. Scientific and Technological Foundations of Industrial Synthesis) (Ed. A V Polyakov) (Leningrad: Khimiya, 1980)
11. S S Ivanchev *Katal. Prom-sti* (6) 15 (2002)
12. N M Chirkov, P E Matkovskii, F S D'yachkovskii *Polimerizatsiya na Kompleksnykh Metalloorganicheskikh Katalizatorakh* (Polymerisation on Complex Organometallic Catalysts) (Moscow: Khimiya, 1976)
13. J C W Chen *Preparation and Properties of Stereoregular Polymers* (Eds R W Lenz, F Ciardelli) (Dordrecht: Reidel, 1980) p. 113
14. T E Nowlin *Prog. Polym. Sci.* **11** 29 (1985)
15. Yu V Kissin *Transition Metal Catalyzed Polymerizations: Alkenes and Dienes Pt. B* (Ed. R P Quirk) (New York: Harwood Academic Publ., 1985) p. 597
16. A Zambelli, M C Sacchi, P Locatelli *Transition Metal Catalyzed Polymerizations: Alkenes and Dienes Pt. B* (Ed. R P Quirk) (New York: Harwood Academic Publ., 1985) p. 83
17. Yu V Kissin *Isospecific Polymerization of Olefins with Heterogeneous Ziegler–Natta Catalysts* (New York: Springer, 1985)
18. V A Zakharov, Yu I Yermakov *Catal. Rev. Sci. Eng.* **19** 67 (1979)
19. A V Kryzhanovskii, S S Ivanchev *Vysokomol. Soedin., Ser. A* **32** 1383 (1990)^a
20. B A Krentsel, Yu V Kissin, V Y Kleiner, L L Stotskaya *Polymers and Copolymers of Higher α -Olefins. Chemistry, Technology, Applications* (Munich, Vienna, New York: Hanser Publ., 1997)
21. B A Krentsel', F S D'yachkovskii *Vysokomol. Soedin., Ser. A* **31** 1123 (1989)^a
22. *Ziegler Catalysts* (Eds G Fink, R. Mülhaupt, H H Brintzinger) (Berlin: Springer, 1995)
23. G Di Drusco, R Rinaldini *Hydrocarbon Process.* **63** (11) 113 (1984)
24. P C Barbe, G Cecchin, L Norish *Adv. Polym. Sci.* **81** 1 (1986)
25. *Chem. Week* **147** (25) 13 (1990)
26. P Galli, G Vecellio *Prog. Polym. Sci.* **26** 1287 (2001)
27. N Kashiwa, T Tsutsui *Macromol. Rapid Commun.* **4** 491 (1983)
28. S-i Kojoh, N Kashiwa *Chem. Rec.* **3** 342 (2004)
29. S S Reddy, S Sivaram *Prog. Polym. Sci.* **20** 309 (1995)
30. J Huang, G L Rempel *Prog. Polym. Sci.* **20** 459 (1995)
31. W Kaminsky *Macromol. Chem. Phys.* **197** 3907 (1996)
32. M Bochman *J. Chem. Soc., Dalton Trans.* 255 (1996)
33. A E Hamielec, J B P Soares *Prog. Polym. Sci.* **21** 651 (1996)
34. O Olabisi, M Atiqullah, W Kaminsky *J. Macromol. Sci., Part C: Polym. Rev.* **37** 519 (1997)
35. K Soga, T Shiono *Prog. Polym. Sci.* **22** 1503 (1997)
36. *Metalorganic Catalysts for Synthesis and Polymerization* (Ed. W Kaminsky) (Berlin, Heidelberg: Springer, 1999)
37. H G Alt, A Koppl *Chem. Rev.* **100** 1205 (2000)
38. G G Hlatky *Chem. Rev.* **100** 1347 (2000)
39. N M Bravaya, P M Nedorezova, V I Tsvetkova *Usp. Khim.* **71** 57 (2002) [*Russ. Chem. Rev.* **71** 49 (1002)]
40. E Y-X Chen, T J Marks *Chem. Rev.* **100** 1391 (2000)
41. *GAK* **51** 64 (1998)
42. D Rottman *Chem. Week* **159** (20) 23 (1997)
43. A L McKnight, R M Waymouth *Chem. Rev.* **98** 2587 (1998)
44. G J P Britovsek, V C Gibson, D F Wass *Angew. Chem., Int. Ed.* **38** 428 (1999)
45. S D Ittel, L K Johnson, M Brookhart *Chem. Rev.* **100** 1169 (2000)
46. L Bourget-Merle, M F Lappert, J R Severn *Chem. Rev.* **102** 3031 (2002)
47. H Makio, N Kashiwa, T Fujita *Adv. Synth. Catal.* **344** 477 (2002)
48. V C Gibson, S K Spitzmesser *Chem. Rev.* **103** 283 (2003)
49. R Mülhaupt *Macromol. Chem. Phys.* **204** 289 (2003)
50. Y Suzuki, H Terao, T Fujita *Bull. Chem. Soc. Jpn.* **76** 1493 (2003)

51. *Late Transition Metal Polymerization Catalysis* (Eds B Rieger, L S Baugh, S Kacker, S Striegler) (Weinheim: Wiley, 2003)
52. M Mitani, J Saito, S-i Ishii, Y Nakayama, H Makio, N Matsukawa, S Matsui, J-i Mohri, R Furuyama, H Terao, H Bando, H Tanaka, T Fujita *Chem. Rec.* **4** 137 (2004)
53. L K Johnson, C M Killian, M Brookhart *J. Am. Chem. Soc.* **117** 6414 (1995)
54. L K Johnson, S Mecking, M Brookhart *J. Am. Chem. Soc.* **118** 267 (1996)
55. C M Killian, D J Tempel, L K Johnson, M Brookhart *J. Am. Chem. Soc.* **118** 11664 (1996)
56. S Mecking, L K Johnson, L Wang, M Brookhart. *J. Am. Chem. Soc.* **120** 888 (1998)
57. A Yamamoto, T Shimizu, S Ikeda *Makromol. Chem.* **136** 297 (1970)
58. A Yamamoto *J. Chem. Soc., Dalton Trans.* 1027 (1999)
59. K R Kumar, S Sivaram *Macromol. Chem. Phys.* **201** 1513 (2000)
60. R J Maldanis, J S Wood, A Chandrasekaran, M D Rausch, J C W Chien *J. Organomet. Chem.* **645** 158 (2002)
61. S A Svejda, L K Johnson, M Brookhart *J. Am. Chem. Soc.* **121** 10634 (1999)
62. L C Simon, C P Williams, J B P Soares, R F de Souza *J. Mol. Catal. A: Chem.* **165** 55 (2001)
63. D J Tempel, M Brookhart *Organometallics* **17** 2290 (1998)
64. L Deng, T K Woo, L Cavallo, P M Margl, T Ziegler *J. Am. Chem. Soc.* **119** 6177 (1997)
65. T Schleis, T P Spaniol, J Okuda, J Heinemann, R Mülhaupt *J. Organomet. Chem.* **569** 159 (1998)
66. F Zhu, W Xu, X Liu, S Lin *J. Appl. Polym. Sci.* **84** 1123 (2002)
67. D Pappalardo, M Mazzeo, C Pellicchia *Macromol. Rapid Commun.* **18** 1017 (1997)
68. S S Ivanchev, G A Tolstikov, V K Badaev, N I Ivancheva, I I Oleinik, S Ya Khaikin, I V Oleinik *Vysokomol. Soedin., Ser. A* **44** 1478 (2002) ^a
69. M E Bluhm, C Folli, M Döring *J. Mol. Catal. A: Chem.* **212** 13 (2004)
70. S S Ivanchev, G A Tolstikov, V K Badaev, I I Oleinik, N I Ivancheva, D G Rogozin, I V Oleinik, S V Myakin *Kinet. Katal.* **45** 192 (2004) ^b
71. L Deng, P Margl, T Ziegler *J. Am. Chem. Soc.* **119** 1094 (1997)
72. P Margl, L Deng, T Ziegler *Organometallics* **18** 5701 (1999)
73. M Schmid, R Eberhardt, J Kukral, B Rieger *Z. Naturforsch., B* **57** 1141 (2002)
74. M Schmid, Dissertation, Universität Ulm, Germany, 2001
75. B Lindner, Dissertation, Universität Ulm, Germany, 2001
76. B L Small, M Brookhart, A M A Bennett *J. Am. Chem. Soc.* **120** 4049 (1998)
77. B L Small, M Brookhart *Macromolecules* **32** 2120 (1999)
78. G J P Britovsek, V C Gibson, S J McTavish, G A Solan, A J White, D J Williams, B S Kimberley, P J Maddox *Chem. Commun.* 849 (1998)
79. G J P Britovsek, M Bruce, V C Gibson, B S Kimberley, P J Maddox, S Mastroianni, S J McTavish, C Redshaw, G A Solan, S Strömberg, A J P White, D J Williams *J. Am. Chem. Soc.* **121** 8728 (1999)
80. G J P Britovsek, S Mastroianni, G A Solan, S P D Baugh, C Redshaw, V C Gibson, A J P White, D J Williams, M R J Elsegood *Chem. – Eur. J.* **6** 2221 (2000)
81. G J P Britovsek, V C Gibson, B S Kimberley, S Mastroianni, C Redshaw, G A Solan, A J P White, D J Williams *J. Chem. Soc., Dalton Trans.* 1639 (2001)
82. V C Gibson, M J Humphries, K P Tellmann, D F Wass, A J P White, D J Williams *Chem. Commun.* 2252 (2001)
83. G J P Britovsek, S P D Baugh, O Hoarau, V C Gibson, D F Wass, A J P White, D J Williams *Inorg. Chem. Acta* **345** 279 (2003)
84. G J P Britovsek, V C Gibson, S Mastroianni, D C H Oakes, C Redshaw, G A Solan, A J P White, D J Williams *Eur. J. Inorg. Chem.* 431 (2001)
85. T M Kooistra, Q Knijnenburg, J M M Smits, A D Horton, P H M Budzelaar, A W Gal *Angew. Chem.* **113** 4855 (2001)
86. L Deng, P Margl, T Ziegler *J. Am. Chem. Soc.* **121** 6479 (1999)
87. G Marsh *Mater. Today* **1** 6 (1998)
88. S S Ivanchev, A V Yakimanskii, D G Rogozin *Dokl. Akad. Nauk* **393** 504 (2003) ^c
89. S S Ivanchev, A V Yakimanskii, D G Rogozin *Polymer* **45** 6453 (2004)
90. H-K Luo, H Schumann *J. Mol. Catal. A: Chem.* **227** 153 (2005)
91. G A Tolstikov, S S Ivanchev, I I Oleinik, N I Ivancheva, I V Oleinik *Dokl. Akad. Nauk* **404** 1 (2005) ^c
92. B de Bruin, E Bill, E Bothe, T Weyhermüller, K Wieghardt *Inorg. Chem.* **39** 2936 (2000)
93. I Kim, B H Han, Y-S Ha, C-S Ha, D-W Park *Catal. Today* **93** 281 (2004)
94. J-Y Liu, Y Zeng, Y-G Li, L Pan, Y-S Li, N-H Hu *J. Organomet. Chem.* **690** 1233 (2005)
95. F Pelascini, F Peruch, P J Lutz, M Wesolek, J Kress *Eur. Polym. J.* **41** 1288 (2005)
96. I Kim, Y S Ha, C-S Ha *Macromol. Rapid Commun.* **25** 1069 (2004)
97. K P Tellmann, V C Gibson, A J P White, D J Williams *Organometallics* **24** 280 (2005)
98. D Reardon, F Conan, S Gambarotta, G Yap, Q Wang *J. Am. Chem. Soc.* **121** 9318 (1999)
99. R Schmidt, M B Welch, R D Knudsen, S Gottfried, H G Alt *J. Mol. Catal. A: Chem.* **222** 9 (2004)
100. B L Small, M J Carney, D M Holman, C E O'Rourke, J A Halfen *Macromolecules* **37** 4375 (2004)
101. Y Nakayama, K Sogo, H Yasuda, T Shiono *J. Polym. Sci., Part A: Polym. Chem.* **43** 3368 (2005)
102. M J Carney, N J Robertson, J A Halfen, L N Zakharov, A L Rheingold *Organometallics* **23** 6184 (2004)
103. Yu V Kissin, C Qian, G Xie, Y Chen *J. Polym. Sci., Part A: Polym. Chem.* **44** 6159 (2006)
104. E P Talsi, D E Babushkin, N V Semikolenova, V N Zudin, V A Zakharov *Kinet. Katal.* **42** 165 (2001) ^b
105. E P Talsi, D E Babushkin, N V Semikolenova, V N Zudin, V N Panchenko, V A Zakharov *Macromol. Chem. Phys.* **202** 2046 (2001)
106. K P Bryliakov, N V Semikolenova, V N Zudin, V A Zakharov, E P Talsi *Catal. Commun.* **5** 45 (2004)
107. I I Zakharov, V A Zakharov *Macromol. Theory Simul.* **13** 583 (2004)
108. A A Barabanov, G D Bukatov, V A Zakharov, N A Semikolenova, T B Mikenas, L G Echevskaja, M A Matsko *Macromol. Chem. Phys.* **207** 1368 (2006)
109. S Wang, D Liu, R Huang, Yu Zhang, B Mao *J. Mol. Catal. A: Chem.* **245** 122 (2006)
110. L A Utracki *Polymer Alloys and Blends* (Munich: Hanser, 1989)
111. S Mecking *Macromol. Rapid Commun.* **20** 139 (1999)
112. F A Kunrath, R S Mauler, R F de Souza, O I Casagrande Jr *Macromol. Chem. Phys.* **203** 2058 (2002)
113. S S Ivanchev, V K Badaev, N I Ivancheva, E V Sviridova, D G Rogozin, S Ya Khaikin *Vysokomol. Soedin., Ser. B* **46** 1959 (2004) ^a
114. S G Correia, M M Marques, J R Ascenso, A F G Ribeiro, P T Gomes, A R Dias, M Blais, M D Rausch, J C W Chien *J. Polym. Sci., Part A: Polym. Chem.* **37** 2471 (1999)
115. D V Deubel, T Ziegler *Organometallics* **21** 1603 (2002)
116. J C W Chien, S Fernandes, S G Correia, M D Rausch, L C Dickson, M M Marques *Polym. Int.* **51** 729 (2002)
117. L S Boffa, B M Novak *Chem. Rev.* **100** 1479 (2000)
118. K Ibrahim, K Yliheikkilä, A Abu-Surrah, B Löfgren, K Lappalainen, M Leskelä, T Repo, J Seppälä *Eur. Polym. J.* **40** 1095 (2004)
119. *Khimiya Privitykh Poverkhnostnykh Soedinenii* (The Chemistry of Graft Surface Compounds) (Ed. G V Lisichkin) (Moscow: Fizmatlit, 2003) p. 481
120. WO PCT 99/12981A1 (1999)
121. WO PCT 99/62968A1 (1999)
122. V F V Marques, C C Pombo, R A Silva, A Conte *Eur. Polym. J.* **39** 561 (2003)
123. Z Ma, Y Ke, H Wang, C Guo, M Zhang, W-H Sun, Y Hu *J. Appl. Polym. Sci.* **88** 466 (2003)

124. S S Ivanchev, V K Badaev, N I Ivancheva, E V Sviridova, S Ya Khaikin, D G Rogozin, A S Abakunchik *Vysokomol. Soedin., Ser. A* **47** 934 (2005)^a
125. V A Zakharov, N V Semikolenova, T B Mikenas, A A Barabanov, G D Bukatov, L G Echevskaya, M A Mats'ko *Kinet. Katal.* **47** 303 (2006)^b
126. N V Semikolenova, V A Zakharov, E A Paukshtis, I G Danilova *Top. Catal.* **32** 77 (2005)
127. T B Mikenas, V A Zakharov, L G Echevskaya, M A Matsko *J. Polym. Sci., Part A: Polym. Chem.* **43** 2128 (2005)
128. J C Chadwick, J R Severn *Kinet. Katal.* **47** 186 (2006)^b
129. S S Ivanchev, N I Ivancheva, S Ya Khaikin, E V Sviridova, D G Rogozin *Vysokomol. Soedin., Ser. A* **48** 423 (2006)^a
130. J Zhang, X Wang, G-X Jin *Coord. Chem. Rev.* **250** 95 (2006)
131. H B Zhu, G-X Jin, N H Hu *J. Organomet. Chem.* **655** 167 (2002)
132. C-K Liu, G-X Jin *New J. Chem.* **26** 1485 (2002)
133. D Zhang, G-X Jin *Appl. Catal. A: General* **262** 13 (2004)
134. D Zhang, G-X Jin, L-H Weng, F Wang *Organometallics* **23** 3270 (2004)
135. Eur. P. 0874005; *Chem. Abstr.* **129** 331166 (1998)
136. WO PCT 01/55231A1; *Chem. Abstr.* **135** 137852 (2001)
137. S Matsui, T Fujita *Catal. Today* **66** 63 (2001)
138. W Keim, F H Kowaldt, R Goddard, C Krüger *Angew. Chem., Int. Ed. Engl.* **17** 466 (1978)
139. U Müller, W Keim, C Krüger, P Betz *Angew. Chem., Int. Ed. Engl.* **28** 1011 (1989)
140. K Hirose, W Keim *J. Mol. Catal.* **73** 271 (1992)
141. U Klabunde, S D Itten *J. Mol. Catal.* **41** 123 (1987)
142. C Wang, S Friedrich, T R Younkin, R T Li, R H Grubbs, D A Bansleben, M W Day *Organometallics* **17** 3149 (1998)
143. T R Younkin, T F Connor, J I Henderson, S K Friedrich, R H Grubbs, D A Bansleben *Science* **287** 460 (2000)
144. S Matsui, M Mitani, J Saito, Y Tohi, H Makio, N Matsukawa, Y Tagaki, K Tsuru, M Nitabar, T Nakano, H Tanaka, N Kashiwa, T Fujita *J. Am. Chem. Soc.* **123** 6847 (2001)
145. N Matsukawa, S Matsui, M Mitani, J Saito, K Tsuru, N Kashiwa, T Fujita *J. Mol. Catal. A: Chem.* **169** 99 (2001)
146. J Saito, M Mitani, J-i Mohri, S-i Ishii, Y Yosida, T Matsugi, S-i Kojoh, N Kashiwa, T Fujita *Chem. Lett.* 576 (2001)
147. S-i Ishii, J Saito, M Mitani, J-i Mohri, N Matsukawa, Y Tohi, S Matsui, N Kashiwa, T Fujita *J. Mol. Catal. A: Chem.* **179** 11 (2002)
148. M Mitani, J-i Mohri, Y Yoshida, J Saito, S-i Ishii, K Tsuru, S Matsui, R Furuyama, T Nakano, H Tanaka, S-i Kojoh, T Matsugi, N Kashiwa, T Fujita *J. Am. Chem. Soc.* **124** 3327 (2002)
149. S-i Ishii, R Furuyama, N Matsukawa, J Saito, M Mitani, H Tanaka, T Fujita *Macromol. Rapid Commun.* **24** 452 (2003)
150. T Matsugi, S Matsui, S-i Kojoh, Y Takagi, Y Inoue, T Fujita, N Kashiwa *Chem. Lett.* 566 (2001)
151. Y Yoshida, J-i Mohri, S-i Ishii, M Mitani, J Saito, S Matsui, H Makio, T Nakano, H Tanaka, M Onda, Y Yamamoto, A Mizuno, T Fujita *J. Am. Chem. Soc.* **126** 12023 (2004)
152. J Saito, M Mitani, J-i Mohri, Y Yoshida, S Matsui, S-i Ishii, S-i Kojoh, N Kashiwa, T Fujita *Angew. Chem., Int. Ed.* **40** 2918 (2001)
153. H Makio, T Fujita *Bull. Chem. Soc. Jpn.* **78** 52 (2005)
154. Y Suzuki, N Kashiwa, T Fujita *Chem. Lett.* 358 (2002)
155. S Matsui, T P Spaniol, Y Takagi, Y Yoshida, Y Okuda *J. Chem. Soc., Dalton Trans.* 4529 (2002)
156. S Matsui, Y Yoshida, Y Tagaki, T P Spaniol, J Okuda *J. Organomet. Chem.* **689** 1155 (2004)
157. T Matsugi, S Matsui, S-i Kojoh, Y Takagi, Y Inoue, T Nakano, T Fujita, N Kashiwa *Macromolecules* **35** 4880 (2002)
158. Y Inoue, T Nakano, H Tanaka, N Kashiwa, T Fujita *Chem. Lett.* 1060 (2001)
159. L E Turner, M G Thorn, R D Swartz II, R W Chesnut, P E Fanwick, I P Rothwell *Dalton Trans.* 4580 (2003)
160. Y Zhang, Y Mu, C Lu, G Li, J Xu, Y Zhang, D Zhu, S Feng *Organometallics* **23** 540 (2004)
161. Y Suzuki, Y Inoue, H Tanaka, T Fujita *Macromol. Rapid Commun.* **25** 493 (2004)
162. S S Ivanchev, V A Trunov, V B Rybakov, D V Al'bov, D G Rogozin *Dokl. Akad. Nauk* **404** 57 (2005)^c
163. S Matsui, M Mitani, J Saito, J Tohi, H Makio, H Tanaka, T Fujita *Chem. Lett.* 1263 (1999)
164. S Matsui, M Mitani, J Saito, N Matsukawa, H Tanaka, T Nakano, T Fujita *Chem. Lett.* 554 (2000)
165. S Reinartz, A F Mason, E B Lobkovsky, G W Coates *Organometallics* **22** 2542 (2003)
166. Y Tohi, H Makio, S Matsui, M Onda, T Fujita *Macromolecules* **36** 523 (2003)
167. Y Tohi, T Nakano, H Makio, S Matsui, T Fujita, T Yamaguchi *Macromol. Chem. Phys.* **205** 1179 (2004)
168. A Pärssinen, T Luhtanen, M Klinga, T Pakkanen, M Leskeli, T Repo *Eur. J. Inorg. Chem.* 2100 (2005)
169. S Chen, X Zhang, H Ma, Y Lu, Z Zhang, H Li, Z Lu, N Cui, Y Hu *J. Organomet. Chem.* **690** 4184 (2005)
170. A V Yakimanskii, S S Ivanchev *Dokl. Akad. Nauk* **410** 217 (2006)^c
171. N I Ivancheva, M Yu Malinskaya, S S Ivanchev, I I Oleinik, A I Kochnev, G A Tolstikov *Kinet. Katal.* **48** (6) (2007) (in the press)^b
172. S K Gagieva, T A Sukhova, D B Savinov, N M Bravaya, Yu N Belokon', B M Bulychev *Russ. Khim. Vest.* **53** 2763 (2004)
173. S S Ivanchev, V K Badaev, N I Ivancheva, S Ya Khaikin *Dokl. Akad. Nauk* **394** 639 (2004)^c
174. G J Domski, J M Rose, G W Coates, A D Bolig, M Brookhart *Progr. Polym. Sci.* **32** 30 (2007)
175. J Saito, M Mitani, S Matsui, Y Tohi, H Makio, T Nakano, H Tanaka, N Kashiwa, T Fujita *Macromol. Chem. Phys.* **203** 59 (2002)
176. J Saito, M Mitani, S Matsui, N Kashiwa, T Fujita *Macromol. Rapid Commun.* **21** 1333 (2000)
177. J Saito, M Onda, S Matsui, M Mitani, R Furuyama, H Tanaka, T Fujita *Macromol. Rapid Commun.* **23** 1118 (2003)
178. J Saito, Y Suzuki, T Fujita *Chem. Lett.* 236 (2003)
179. A V Prasad, H Makio, J Saito, M Onda, T Fujita *Chem. Lett.* 250 (2004)
180. K Soga, T Uozumi, M Saito, T Shiono *Macromol. Chem. Phys.* **195** 1503 (1994)
181. Yu V Kissin, T E Nowlin, R I Mink, A J Brandolini *Macromolecules* **33** 4599 (2000)
182. Y Nakayama, H Bando, Y Sonobe, H Kaneko, N Kashiwa, T Fujita *J. Catal.* **215** 171 (2003)
183. Y Nakayama, H Bando, Y Sonobe, T Fujita *J. Mol. Catal. A: Chem.* **213** 141 (2004)
184. Y Nakayama, J Saito, H Bando, T Fujita *Macromol. Chem. Phys.* **206** 1847 (2005)
185. Y Nakayama, J Saito, H Bando, T Fujita *Chem. – Eur. J.* **12** 7546 (2006)
186. Y Nakayama, H Bando, Y Sonobe, T Fujita *Bull. Chem. Soc. Jpn.* **77** 617 (2004)
187. J R Severn, J C Chadwick *Macromol. Chem. Phys.* **205** 1987 (2004)
188. J R Severn, J C Chadwick, V Van Axel Castelli *Macromolecules* **37** 6258 (2004)
189. S-i Ishii, M Mitani, J Saito, S Matsuura, S-i Kojoh, N Kashiwa, T Fujita *Chem. Lett.* 740 (2002)
190. H Terao, S-i Ishii, J Saito, S Matsuura, M Mitani, N Nagai, H Tanaka, T Fujita *Macromolecules* **39** 8584 (2006)
191. R Furuyama, J Saito, S-i Ishii, M Mitani, S Matsui, Y Tohi, H Makio, N Matsukawa, H Tanaka, T Fujita *J. Mol. Catal. A: Chem.* **200** 31 (2003)
192. M Mitani, R Furuyama, J-i Mohri, J Saito, S-i Ishii, H Terao, T Nakano, H Tanaka, T Fujita *J. Am. Chem. Soc.* **125** 4293 (2003)
193. G Milano, L Cavallo, G Guerra *J. Am. Chem. Soc.* **124** 13368 (2002)
194. V Busico, R Cipullo, F Cutillo, N Friederichs, S Ronca, B Wang *J. Am. Chem. Soc.* **125** 12402 (2003)
195. M Lamberti, D Pappalardo, A Zambelli, C Pellecchia *Macromolecules* **35** 658 (2002)
196. G Talarico, V Busico, L Cavallo *J. Am. Chem. Soc.* **125** 7172 (2003)

197. M Mazzeo, M Strianese, M Lamberti, I Santoriello, C Pellecchia *Macromolecules* **39** 7812 (2006)
198. T Repo, M Klinga, P Pietikainen, M Leskeli, A-M Uusitalo, T Pakkanen, K Hakala, P Aaltonen, B Lofgren *Macromolecules* **30** 171 (1997)
199. J P Corden, W Errington, P Moore, M G H Wallbridge *Chem. Commun.* 323 (1999)
200. S-i Ishii, M Mitani, J Saito, S Matsuura, R Furuyama, T Fujita *Science and Technology in Catalysis (Studies in Surface Science and Catalysis)* (Eds M Ango, M Onaka, H Yamashita) (Amsterdam: Elsevier, 2003) Vol. 145, p. 49
201. P D Knight, A J Clarke, B S Kimberley, R A Jackson, P Scott *Chem. Commun.* 352 (2002)
202. J Huang, B Lian, Y Qian, W Zhou, W Chen, G Zheng *Macromolecules* **35** 4871 (2002)
203. D A Pennington, S J Coles, M B Hursthouse, M Bochman, S J Lancaster *Chem. Commun.* 3150 (2005)
204. Y Yoshida, S Matsui, Y Tagaki, M Mitani, M Nitabaru, T Nakano, H Tanaka, T Fujita *Chem. Lett.* 1270 (2000)
205. Y Yoshida, S Matsui, Y Tagaki, M Mitani, T Nakano, H Tanaka, N Kashiwa, T Fujita *Organometallics* **20** 4793 (2001)
206. Y Yoshida, J Saito, M Mitani, Y Takagi, S Matsui, S-i Ishii, T Nakano, N Kashiwa, T Fujita *Chem. Commun.* 1298 (2002)
207. Y Yoshida, S Matsui, T Fujita *J. Organomet. Chem.* **690** 4382 (2005)

^a — *Polym. Sci. (Engl. Transl.)*

^b — *Kinet. Catal. (Engl. Transl.)*

^c — *Dokl. Phys. Chem. (Engl. Transl.)*

Unsteady catalytic processes and sorption-catalytic technologies

A N Zagoruiko

Contents

I. Introduction	639
II. Theoretical basis and methods for organisation of unsteady-state conditions in catalyst beds	640
III. Catalytic processes that utilise the unsteady states of catalyst	642
IV. Conclusion	650

Abstract. Catalytic processes that occur under conditions of the targeted unsteady state of the catalyst are considered. The highest efficiency of catalytic processes was found to be ensured by a controlled combination of thermal non-stationarity and unsteady composition of the catalyst surface. The processes based on this principle are analysed, in particular, catalytic selective reduction of nitrogen oxides, deep oxidation of volatile organic impurities, production of sulfur by the Claus process and by hydrogen sulfide decomposition, oxidation of sulfur dioxide, methane steam reforming and anaerobic combustion, selective oxidation of hydrocarbons, *etc.* The bibliography includes 234 references.

I. Introduction

Catalytic processes operating under targeted unsteady state conditions receive considerable attention in both the scientific research and industry. The reason for such keen interest lies in the fact that unsteady-state conditions allow one to enhance the efficiency of catalytic technologies, namely, accelerate reactions, enhance their selectivity, increase the yields of the target products, decrease the energy consumption and reduce the operational expenses and the cost of reactors.

None of the known heterogeneous catalysts represent a true unsteady system during its operation. At the very least, this is associated with their inevitable deactivation, which shortens their service life and necessitates their replacement or regeneration once the service life is overrun. Nonetheless, two conceptually opposite approaches are distinguished, namely, a steady-state approach that postulates the time invariability (as far as possible) of all process parameters and the unsteady approach based on the targeted dynamic variation of these parameters. The present review is exclusively devoted to catalytic technologies that employ catalysts under the targeted unsteady-state conditions and demonstrate substantial advantages over analogous stationary processes.

A N Zagoruiko G K Borekov Institute of Catalysis, Siberian Branch of the Russian Academy of Sciences, prosp. Acad. Lavrentieva 5, 630090 Novosibirsk, Russian Federation. Fax (7-383) 330 68 78, tel. (7-383) 330 94 91, e-mail: zagor@catalysis.ru

Received 13 September 2006

Uspekhi Khimii 76 (7) 691–706 (2007); translated by T Ya Safonova

In the recent decades, the most significant progress in unsteady catalysis was associated with the reverse-flow processes. The latter are based on concepts of the thermal non-stationarity that arises in a fixed adiabatic catalyst bed as the parameters of the reaction mixture flowed through this bed are modulated. However, it is evident that the progress in this field lies in the development of processes with not only the modulated catalyst temperature but also with the modulated chemical composition of the surface.

The present review considers mainly the gas-phase reactions that occur on the solid catalyst surface. Apparently, the formulated approach can also be applied to multiphase catalytic processes; however, this field is very wide and deserves special consideration.

Insofar as the periodic changes in the catalyst state are directly associated with the sorption, most of processes considered below can be described as sorption-catalytic processes, which implies that it is joint sorption and catalytic processes that occur within one catalyst bed or a single process vessel. This approach does not embrace the combinations of catalytic and sorption processes that are carried out separately and independently in different reactors even within one flow scheme.

In this study, sorption is understood in the general sense, *i.e.*, as the reversible physical adsorption of reactants, their reversible (irreversible) chemisorption associated with chemical reactions and the formation of stable intermediates on the active surface or even as the absorption of reactants in a liquid film of the active component melt.

The first studies of cyclic catalytic processes that involved the periodically modulated catalyst state date back to the 19th century. The analysis of the development of these studies leads to a paradoxical idea that in a certain sense, the first catalytic processes studied were cyclic unsteady processes.

This can be illustrated by several examples. Thus the English chemist Claus^{1,2} studied the reaction of hydrogen sulfide oxidation to sulfur, which opened up the way to the recovery of elemental sulfur from hydrogen sulfide, in fact, first under the adsorption-catalytic conditions (with the adsorption of liquid sulfur on the catalyst). Somewhat earlier, his compatriot Deacon^{3–5} discovered the reaction of hydrogen chloride oxidation with oxygen, which marked the beginning of the catalytic processes for the commercial synthesis of chlorine. Unlike Claus, he did not deal with unsteady technologies but, on the contrary, proposed and carried out a stationary

catalytic process. However, this very fact indicates that the periodic processes preceded his studies.

The same year that his patent was issued,³ the unsteady methane steam reforming in the presence of a sorbent that absorbed CO₂ was described.⁶ This study is considered as the pioneering in the catalytic steam reforming of hydrocarbons.

Many other examples of similar studies carried out since the end of the 19th century to the first half of the 20th century can be mentioned.

Such a development, which, at the first glance, looks paradoxical, however does not lack logics. In their early stage, the studies of the periodical combination of the known chemical reactions could be reduced to the closed reaction cycles, actually, to the stationary catalysis, which, at that time, was of significant interest for practice. Scientific research was also directed towards the stationary catalytic processes as more predictable, reproducible and hence more attractive for their exploration and building up the relevant theories.

Later, with the accumulation of knowledge on the catalytic processes, the limitations inherent in the stationary catalysis and narrowing the freedom of developers of new technologies were revealed. That is why attention was redirected to the 'origins', *i.e.*, the unsteady catalytic processes but with the new insight into the already known phenomena.

Systematic studies of the unsteady phenomena in catalysis date back to the second half of the 20th century. After the first publications on the unsteady modes of operation of catalytic reactors, which appeared in the 1960s,^{7–11} the rapid progress in this field (both experimental^{12–16} and theoretical^{17–20}) was observed.

The studies^{21–29} carried out under supervision of academician G K Boreskov and Yu Sh Matros at the Institute of Catalysis of the Siberian Branch of the Russian Academy of Science have made a considerable contribution into the theory and practice of unsteady catalysis. These studies have given the first physical explanation and substantiation to the observed phenomena, being particularly based on the Boreskov's concept of the changes in the catalyst state under the reaction conditions.

II. Theoretical basis and methods for organisation of unsteady-state conditions in catalyst beds

Any heterogeneous catalytic reaction includes several separate stages that can be associated with successive chemical and sorption processes. Obviously, under steady-state conditions, the rates of these stages are related by rigid balance relationships, which sometimes limit the efficiency of the process.

Under unsteady-state conditions, a set of stages can be represented as separate cycles, which are technologically isolated in the space and/or time. Such conditions make it possible to weaken or violate, at least theoretically, the local balance relationships mentioned above. This eliminates a part of restrictions and opens up additional possibilities for the development of new technologies.

Obviously, the disintegration of reactions into individual cycles implies that the latter form a closed system. In other words, a series of cycles should provide the return of the catalytic system into its original state in order to ensure their repetition. Otherwise, the system cannot be considered as catalytic. Moreover, the closed nature implies the observance of the integral mass and energy balances in the overall process cycle.

The rates of reaction and sorption processes involved in the catalytic cycle and their ratio are determined by the nature of the active catalyst surface and reaction mixture components and also by the external conditions (reaction mixture compo-

sition, temperature, pressure). Hence, the realisation of unsteady-state conditions is associated with the choice of an appropriate catalyst–sorbent and with the cyclic time variations of at least one of external factors.

1. Temperature modulation

The effect of temperature modulation as a source of the unsteady state in catalytic systems was discussed in numerous scientific studies. Their most important result was the development of catalytic reverse-flow processes,^{22, 25, 30, 31} which have found wide use in the industry. Reverse processes involve no direct control over the temperature, and their thermal non-stationarity is caused by the motion of thermal waves in the motionless adiabatic catalyst beds under the conditions of the periodic reversal of the direction of the initial filtrating gas mixture with a low inlet temperature.

Figure 1 shows examples of flow schemes of reverse processes. In the simplest case (Fig. 1 *a*), a system of switching valves changes the flow direction of the reaction mixture in the catalyst bed. In a modified scheme shown in Fig. 1 *b*, the catalyst in the edge parts of the bed is partially replaced by a heat-regenerating material (inert), which is catalytically inactive. Figure 1 *c* shows a multibed scheme (for the sake of simplicity, only two beds are shown) in which the inlet or outlet of both heat and mass (heating/cooling of the flow, inlet/outlet of additional flows and reagents) takes place between the fragments of the catalyst bed. A valve-free version of the reverse process is known, which includes the rotating beds packed with the catalyst and the inert material (Fig. 1 *d*).

Figure 2 shows certain interesting flow schemes in which the thermal non-stationarity in the catalyst beds may be created without the reversal of the reaction flow.²²

It is important to understand that for processes involving the thermal non-stationarity of the catalyst, one faces the problem of the basic approach to the development of such technologies rather than of the unsteady chemical composition of the catalyst.

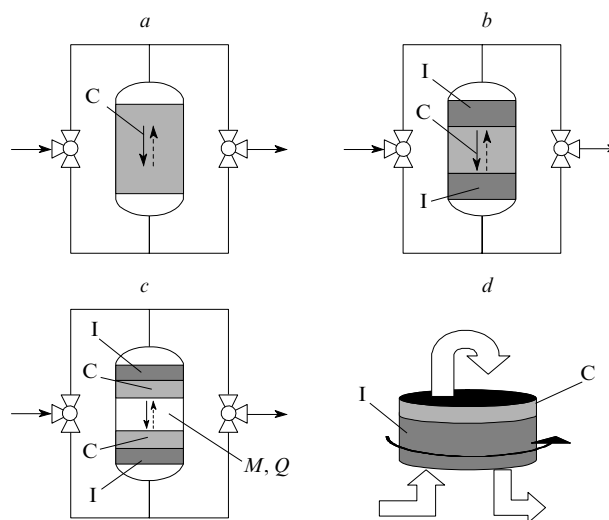


Figure 1. Flow schemes of reverse processes.

(*a*) A one-bed scheme, (*b*) a scheme inert–catalyst–inert, (*c*) a multibed scheme with intermediate heat exchange and inlet/outlet of flows, (*d*) a scheme with rotating beds; dark arrow shows the direction of rotation of the catalyst bed, light arrows show the directions of the reactant flows. Here and in Fig. 2, solid and dashed arrows show the directions of the reaction flow in different phases of the cycle; C is the catalyst; I is an inert heat-regenerating material; M, Q are the inlet/outlet of reactants and heat, respectively.

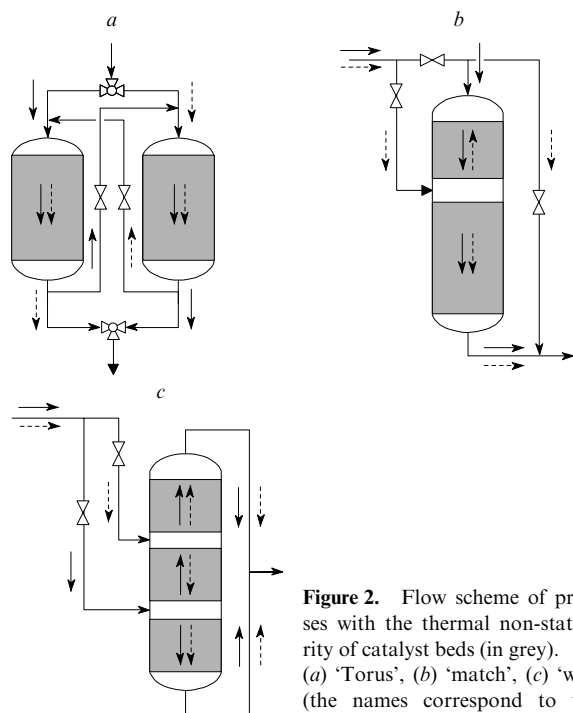


Figure 2. Flow scheme of processes with the thermal non-stationarity of catalyst beds (in grey). (a) 'Torus', (b) 'match', (c) 'wings' (the names correspond to those given in Ref. 22).

2. Modulation of the reaction mixture composition

A comprehensive review of the studies on unsteady isothermal modes under forced modulation of the reaction mixture composition is given in Ref. 32. As a rule, the effectiveness of periodic modes is compared with the parameters of equivalent stationary modes in which the reactant concentrations are equal to the cycle-averaged concentrations in the unsteady mode.

In simple reaction mixtures with virtually one reaction route (CO oxidation,^{33–47} hydrogenation of ethylene^{15, 48} and aromatic hydrocarbons,^{49–51} methanation of carbon oxides,^{52–54} syntheses of methanol^{55–57} and ammonia,^{58–63} SO₂ oxidation,^{16, 64} the Claus reaction,⁶⁵ synthesis of ethyl acetate from ethylene and acetic acid,^{66–68} deamination of primary amines and dehydration of alcohols,^{69–72} etc.), the main positive effect of the optimum unsteady mode lies in the increase in the cycle-averaged reaction rate. However, for the majority of simple reaction systems, the rate increase was no more than 1.5–2-fold, which can hardly be considered quantitatively significant. At the same time, it should be noted that for the SO₂ oxidation under isothermal conditions with periodic alteration of the SO₂-containing mixture and air feeding,⁶⁴ the average yield of sulfur trioxide can exceed the equilibrium limit in the equivalent stationary mode.

Modes with periodic modulation of the reactant concentrations in systems with complicated parallel-sequential processes are more interesting.

According to theoretical studies, for the periodic modulation of the mixture composition in a model system of two parallel reactions, the selectivity of the target conversion can change if the reactions have different orders with respect to reactants,¹⁷ whereas in a model system of three sequential reactions in a perfect-mixing reactor, the selectivity with respect to the intermediate product can increase.⁷³ Matros *et al.*^{21–28} carried out a comprehensive systematic analysis of unsteady modes of complex reactions. They have found that the gain in the selectivity of processes carried out in unsteady cyclic modes substantially depends on the reaction mechanism and the type and parameters of unsteady modes. Moreover, they have shown that the adequate description of such systems

requires the use of unsteady kinetic models that take into account the dynamics of adsorption processes and the changes in the catalyst surface state under the reaction conditions.

The possibility of the enhancement of the reaction selectivity and the increase in the yield of the target products and of the reduction of the side-product yields was experimentally demonstrated by the example of several complex processes such as the NO reduction under the action of CO,^{74–80} selective hydrogenation of butadiene⁸¹ and acetylene,^{82, 83} oligomerisation of methane and ethylene,^{84–88} oxidative dimerisation of methane,^{89–92} oxidation of ethylene to ethylene oxide^{93, 94} and propylene to propylene oxide,⁹⁵ oxidative and steam reforming of methane into the synthesis gas,^{96–98} oxidation of propylene to acrolein,^{99–102} anaerobic oxidative dehydrogenation of hydrocarbons (propane to propylene, butane to butene and butadiene, butene to butadiene),^{46, 103–109} oxidation of butane to maleic anhydride, of aromatic hydrocarbons to maleic and phthalic anhydrides, synthesis of aromatic nitriles, the Fischer–Tropsch reaction,³² etc.

For all these reactions, the positive effect was observed only in a limited range of characteristics of unsteady modes (cycle duration, amplitude of concentration oscillations, phase shift in the supply of reactants, etc.). As an example, a system for the catalytic purification of automotive exhausts can be considered. Its peculiarity consists of the fact that the unsteady composition of the original reaction mixture is determined by the specifics of the engine operation. Under the conditions that did not allow one to control the system and optimise the parameters of unsteady modes, both positive and negative effects of the non-stationarity could be observed,^{110–113} and its overall effect was ambiguous.³²

Figure 3 shows flow schemes that makes it possible to realise periodic modulation of the reaction mixture composition and/or the separate delivery of reactants. In the simplest case (Fig. 3a), the modulation of the composition was achieved by the alternating supply of individual reactants or reaction mixtures of different composition. Such a process is basically periodic. To provide the overall continuity in the composition modulation, a scheme that includes two (and more) reactors (Fig. 3b) with the alternating cyclic supply of reactants and the processes with moving or rotating catalyst beds (Figs 3c,d) were used. In the latter case, different reactants are permanently delivered into different reactors and transported in their sorbed state by the catalyst, which permanently travels between the reactors.

3. Chromatographic mode of catalytic reactions

Reactive chromatographic processes with the periodically varied composition of the mixture form a subclass of unsteady processes.^{114–117} They were pioneered by Roginskii back in the early 1960s.^{7–9} In these processes, advantage was taken of the adsorption properties of catalysts, which allow one to carry out chromatographic separation of the reaction mixture simultaneously with chemical transformations. The merits of these technologies include the possibility of separate extraction of individual products and the achievement of superequilibrium degrees of conversion due to the dynamic separation of components in the catalyst bed.

The chromatographic mode is based on the pulsed supply of the reaction mixture (pulsed delivery of reactants into the inert-gas flow or pulsed introduction of one component into the flow of another reactant) and can be implemented in a one-reactor scheme (see Fig. 3a). A multibed scheme with the constant direction of the reaction mixture flow in beds and the periodical shift of the points of the reactant inlet and the product outlet, which provides the permanent circulation of the adsorption and reaction waves in catalyst beds, deserves attention¹¹⁸ (Fig. 4). Such a system, which received the name

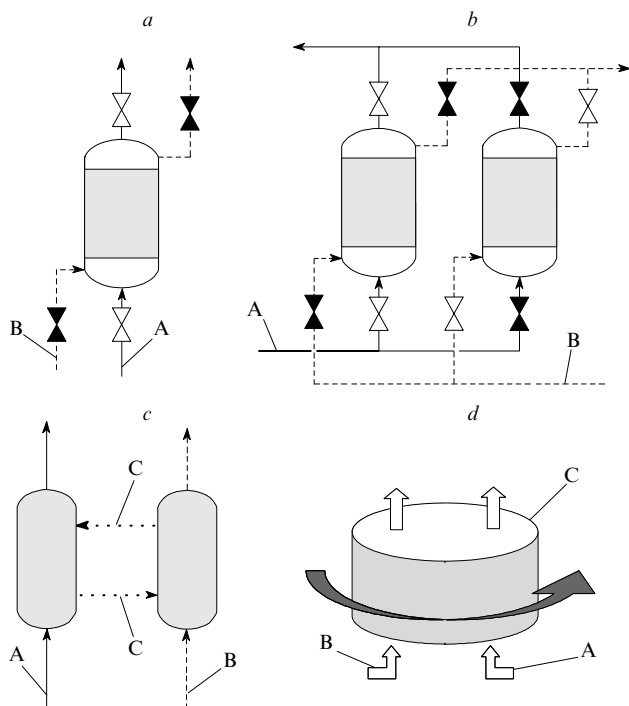


Figure 3. Flow schemes of modes with modulation of the reaction mixture composition.

(a) One-reactor periodic process; (b) two-reactor continuous process, valves in different positions that correspond to different phases of the process are marked in white and black; (c) two-reactor process with the moving catalyst bed; (d) process with rotating catalyst bed. A and B are different reactants or mixtures of different composition, C is catalyst.

Simulated Moving Bed Reactor (SMBR), holds much promise for carrying out certain practically important reactions.¹¹⁴

It should be noted that a reactive chromatography process is efficient under the high residence time of the reaction mixture in the reactor, *i.e.*, in case of high loading volume of a catalyst with low specific productivity. Obviously, it is economically more reasonable to use the reactive chromatography only in small-scale processes of fine organic synthesis, where the highly

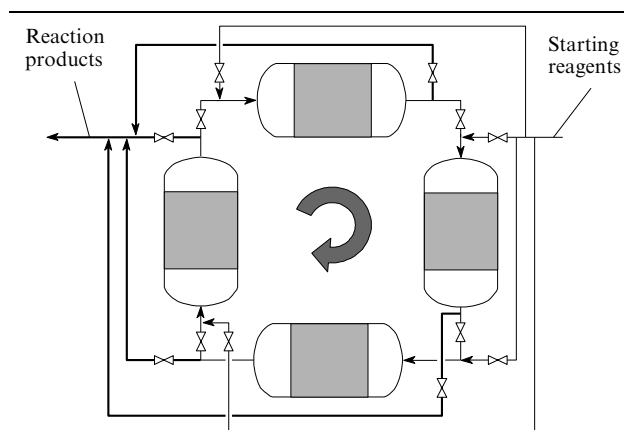


Figure 4. Flow scheme for a reactive chromatography process with pseudomoving catalyst beds.

The arrow in the centre shows the direction of shift of inlet points of reagents and outlet points of reaction products.

expensive reactants and products determine the high capital and production costs.

4. Periodic pressure modulation

Periodic pressure modulation or the impact of periodic pressure pulses on the reaction system represent an alternative method for the creation of unsteady-state conditions in catalytic reactions. Here, two groups of processes should be distinguished, namely, at low and high frequencies of pressure oscillations.

The first group includes the processes with the cycle duration from several tens of seconds to several minutes. They combine the pressure swing adsorption (PSA) process, which was known since the early 1960s,¹¹⁹ and a catalytic reaction. Such processes are called pressure swing reactions (PSR) processes. Their efficiency was demonstrated in model studies^{120,121} and also by the example of methane steam reforming in the presence of substances that absorb CO₂.¹²²

The second group includes the processes generated by high-frequency pressure pulses (from tenth fractions to several tens and hundreds of Hz). Studies of such processes were surveyed by Silveston and Hudgins.¹²³ Pressure oscillations intensify mass transfer in the catalyst pores, which, on the one hand, can accelerate the reactions in simple reaction systems and, on the other hand, change the selectivities and yields of products and the other parameters in complex systems. Presumably, such pulses can induce oscillations in the reactant concentrations on the catalyst surface, which may affect the reaction rate and selectivity.

Pressure pulses can be generated both by an external source or be induced by mechanical oscillations in catalytic systems. Particularly, as was shown theoretically, the periodic pressure modulation with a frequency of an order of magnitude of several hundreds and thousands of Hz can arise in the channels of a block catalyst as a result of spontaneous turbulisation of the gas flow at the entry of channels in the presence of surface irregularities on the frontal panel of the unit.¹²⁴

III. Catalytic processes that utilise the unsteady states of catalyst

In this Section, attention is focused on the technologies that purposefully utilise the unsteady state of a catalyst. The described processes are based on the combined action of thermal and adsorption unsteady factors.

1. Selective catalytic reduction of nitrogen oxides

As the example of the targeted use of the unsteady state of a catalyst, the NO_x reverse process can be mentioned, which was developed^{30,125,126} at the Institute of Catalysts of the Siberian Branch of the Russian Academy of Sciences based on the principle of the periodic reversal of the reaction mixture flow for the reduction of nitrogen oxides according to the reaction



At the Biysk Oleum Plant, a commercial-scale unit has been developed for the reduction of nitrogen oxides from the exhaust gases of the production of dilute nitric acid. Insofar as ammonia water cannot be evaporated in the 'hot' part of the bed, it was supplied into the central part of the catalyst bed (see Fig. 1 c).

The commercial application of this system showed that this way of ammonia feeding enhances the efficiency of this process above the theoretical estimates. Particularly, the gases were purified from nitrogen oxides to a very high extent and virtually no 'breakthrough' of ammonia was observed.[†]

The detailed kinetic studies of this process and its mathematical simulation^{128–131} have shown that ammonia strongly

sorbs on the catalyst surface and reacts in its chemisorbed state with nitrogen oxides. In the reverse-flow process, ammonia sorbs in the exit part of the bed. Simultaneously, in its entry part, NO_x introduced with the inlet gases react with ammonia sorbed in the previous cycle to form molecular nitrogen. After the flow reversal, this process is repeated. The adsorbed NH_3 is concentrated in the central part of the bed, which virtually totally prevents the loss of ammonia as a result of its desorption from the bed edges. The introduction of ammonia water into the middle part of the bed produces a positive side effect, namely, the direct contact between NH_3 and NO_x becomes possible only in the preheated parts of the reactor, which prevents the formation of explosive ammonium salts in the unit.

2. Deep oxidation of impurities volatile organic compound

Decontamination of exhaust gases of industrial plants from the impurities of volatile organic compounds (VOC), namely, hydrocarbons, alcohols, acids, ethers, esters, aldehydes, ketones, *etc.*, is an important environmental problem.

If the exhausts contain high VOC concentrations, their decontamination may well involve the procedures of extraction and recycling of impurities, which are based on the absorption, adsorption, condensation and membrane processes.³¹ For dilute gases, it is reasonable to use the thermal and catalytic oxidation of VOC with oxygen (usually, atmospheric oxygen) to harmless products, namely, carbon dioxide and water vapour; moreover, in the treatment of low-concentration exhausts, the catalytic reverse-flow processes that provide the autothermal (*i.e.*, without additional supply of energy or fuel) processing of gases with the VOC content from 0.6 to 0.8 g m⁻³ and higher proved to be the method of choice from the economical and environmental viewpoints. Purification of gases with lower VOC contents requires additional energy to be supplied.

Thus, a pressing problem of the treatment of large volumes of vent gases with a very low concentration of harmful impurities (below 0.1 g m⁻³) should be mentioned. This enhances the specific power consumption and increases the cost of decontamination systems. Moreover, such systems should be simple and safe in operation due to the abundance of exhaust sources at different kinds of plants and the quite probable lack of skilled staff.

The decontamination technologies that include the adsorption-catalytic processes meet the criteria mentioned. Their realisation usually requires a simple combination of adsorbents and catalytic reactors, *i.e.*, VOC are first absorbed in a sorbent layer, which is followed by the sorbent regeneration (usually with water vapour or hot air) and the catalytic oxidation of impurities in a separate unit. However, in the framework of this review we are interested in adsorption-catalytic processes based on the VOC adsorption immediately on the surface of a deep-oxidation catalyst at low temperature with periodic regeneration of the catalyst by oxidation of sorbed impurities at elevated temperatures.^{132–141}

Adsorption-catalytic processes exhibit substantial advantages over the conventional catalytic technologies of deep oxidation of VOC, especially in the processing of low-concentration gases. In this case, the use of such processes allows one to avoid permanent heating of gases to be cleaned, which reduces substantially power consumption. Their high technological flexibility makes it possible to decontaminate gases with the initial VOC concentration varying over a wide range and

quickly put units into operation without preliminary heating. Such processes can be implemented within a one-reactor scheme (Fig. 5a) with the periodic elevation of the temperature of the gas to be decontaminated at the reactor inlet in order to initiate the catalyst regeneration.

However, the practical experience and the results of mathematical simulation^{142–145} revealed certain drawbacks of adsorption-catalytic processes. Thus partial desorption of non-oxidised VOC or the products of their incomplete oxidation is possible on heating of the catalyst, which reduces the degree of decontamination and necessitates additional purification of desorbed gases; there is also the risk of the reactor overheating during the regeneration.

These drawbacks can be overcome by the optimisation of flow schemes, operation conditions and parameters of the catalyst-adsorbent. Particularly, one of the ways to minimise desorption losses is the use of a procedure of stepwise heating of the catalyst during its regeneration.¹³⁶ In this version, the gradual heating in the beginning of the regeneration cycle allows one to transform a considerable part of weakly sorbed reactant into its strongly chemisorbed form. However, this approach is effective for a limited number of VOC and, moreover, substantially complicates the regeneration process and makes it more lengthy.

In addition, the losses can be reduced by using relatively coarse-grained catalysts-sorbents (*i.e.*, by creating internal diffusion hindrances for the desorption).¹⁴⁶

The reduction in the efficiency of decontamination due to the desorption of non-oxidised VOC can be avoided by using more sophisticated flow schemes that include, *e.g.*, a post-reactor¹³⁴ (Fig. 5b), which is preliminarily heated before the catalyst regeneration where final oxidation of the desorbed impurities occurs. Yet another version represents an adsorption-catalytic reverse process^{142–144, 147, 148} (Fig. 5c) where the adsorption phase involves the delivery of the original gases into

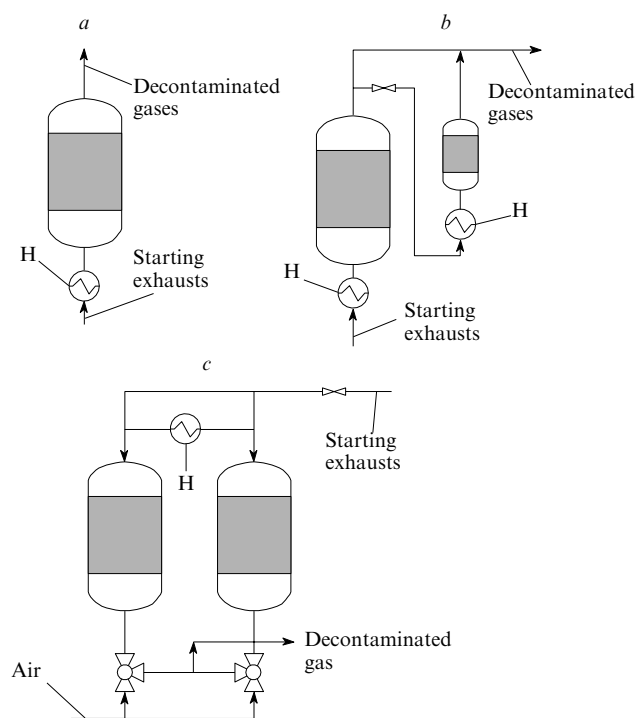


Figure 5. Flow schemes of adsorption-catalytic processes of deep oxidation of VOC.

(a) One-reactor scheme, (b) scheme with additional post-reactor, (c) adsorption-catalytic reverse process. From hereon, H is a heater.

† In other versions of the reverse process (*e.g.*, with the ammonia delivery into the original mixture), the breakthrough caused by the ammonia desorption from the edges of the catalyst bed after the flow reversal posed a serious problem.¹²⁷

two parallel reactors, and the regeneration occurs due to the heating of gases with simultaneous supply of air and periodic changes in the flow direction. In this case, VOC impurities are preferentially sorbed in the catalyst-bed parts adjacent to the point of inlet of the original gases, which allows one to minimise their losses in the desorption. Moreover, the efficient heat regeneration in the mode with the flow reversal makes it possible to considerably reduce the power consumed in the regeneration of the catalyst-sorbent.

It is of note that the developed model of adsorption-catalytic process allows one to cast a fresh glance on the conventional reverse process of deep oxidation of VOC (see Fig. 1*b*). The results of simulation¹⁴⁹ have shown that at moderate temperatures in the inlet of the catalyst bed, before the flow reversal, the admixtures are adsorbed and a substantial part of them is sorbed reversibly. After the reversal of the flow, this part of the bed becomes the outlet and its temperature begins to increase. As a result, a part of sorbed substance can be sorbed to be flown away with the exit gas flow, which substantially decreases the overall degree of decontamination. To avoid this, it is necessary to use sufficiently long beds packed with an inert heat-regenerating material (the choice of this material is also important; in the ideal case, it should have the zero adsorption capacity with respect to VOC), and apply a reasonable strategy of the control over the process (particularly, it is important to choose the correct temperature of flow reversal at the catalyst–inert interface).

Of interest is a flow scheme of an adsorption-catalytic process according to which the catalyst is regenerated by a combustion wave of sorbed VOC that moves towards the gas flow due to the heat conduction of the catalyst bed.^{140, 145} A feature of this mode is that the desorbed substances get into the preheated part of the catalyst bed where they can be efficiently oxidised. However, according to mathematical simulations and experimental studies,¹⁴⁵ the motion of the counter-current heat front is possible only for the low linear filtration rates of the regenerating air. Under these conditions, it is possible to achieve complete conversion of oxygen present in the air flow and, as a consequence, the formation of partial oxidation products, including CO. It was proposed¹⁴⁵ to solve this problem by the installation of an additional post-reactor at the outlet main unit which substantially complicated the scheme and made it more expensive. At the same time, it cannot be ruled out that the use a catalyst-sorbent with a reduced adsorption capacity would be sufficient.

A process is known in which the catalyst regeneration and the oxidation of sorbed VOC occur upon simultaneous increase in the temperature and pressure in the closed space of the reactor-adsorber by delivery of compressed air.¹⁵⁰ The efficiency of this process is due to the fact that no flows at all exit before the end of regeneration and the VOC losses are impossible in principle. However, this process is technologically complicated and requires sufficiently high skill of the staff, which may limit its practical application.

An advantageous version of the adsorption-catalytic processes of VOC oxidation employs a spiral reactor (Fig. 6*a*) consisting of two concentric metal spirals of which one is covered with a thin catalyst layer and the other is coated with a thin sorbent layer.¹⁵¹ The original gas travels along one system of spiral channels to the spiral centre and then along the second system of channels from the centre to the exit. The gas is decontaminated by the adsorption. The periodic regeneration of the sorbent is performed by switching on a heater located in the centre of the spiral. The active heat exchange between the inlet and outlet gases provides the fast heating of the sorbent and the catalyst (due to the heat produced by the heater and

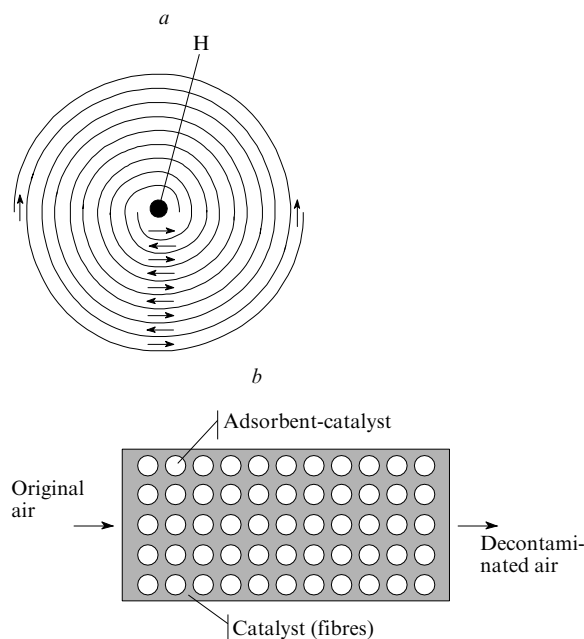


Figure 6. Promising schemes of adsorption-catalytic systems for decontamination of gases from VOC.

(*a*) Spiral adsorber-reactor, (*b*) multidispersed adsorption-catalytic system.

released in the VOC oxidation) with the minimum energy consumption. The high heating rate of the catalyst provides the high efficiency of oxidation of desorbed VOC to harmless products. Due to the complexity of spiral reactors, their practical implementation is hardly possible for high gas flow rates; however, they can be used in compact systems for local decontamination of air.

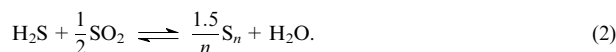
For the effective decontamination of gases from VOC, a multidispersed adsorption-catalytic system can be used¹⁵² (Fig. 6*b*), which consists of a relatively coarse-grain adsorbent-catalyst with the spaces between the grains filled with a microfibre catalyst. The typical geometric size of catalyst microfibrils ($< 10 \mu\text{m}$) is substantially smaller than the grain size ($> 1 \text{ mm}$); hence, the specific surface of fibres substantially exceeds that of grains. During the regeneration, the catalyst microfibrils are heated in contact with the hot gas flow much more quickly than the grains of the catalyst-sorbent. Correspondingly, VOC desorbed during the regeneration phase come in contact with the preheated catalyst and are efficiently oxidised.

Returning to the second problem of adsorption-catalytic processes of deep oxidation, *i.e.*, the possible overheat of a catalyst above the threshold of its thermal stability, it should be noted that this problem might be solved by the optimisation of the maximum adsorption capacity of the sorbent-catalysts. For example, according to the results of simulations,^{142, 144} this capacity should be from 1 to 2 mass % for the oxidation of aromatic hydrocarbons on the aluminium–chromium–copper catalyst (with the operation temperature limit of 750°C).

In the development of adsorption-catalytic processes, attention was often focused on the elaboration and the use of catalysts and sorbents with the maximum possible adsorption capacity. However, in the general case, the optimum capacity for a process does not coincide with the maximum capacity of the catalyst.

3. Claus sulfur recovery process

The commercial production of elemental sulfur from acid waste gases of certain industrial processes is based on the Claus reaction



This reaction is reversible and exothermic; hence the maximum degree of sulfur recovery from gases is, as a rule, limited by thermodynamic parameters. The catalytic process usually involves several stages. Between the stages, the gases are cooled and the sulfur formed is removed. However, even this does not help in reaching the required degree of sulfur recovery. Obviously, the equilibrium in the Claus reaction can be shifted to the products upon removal of one component of the gas mixture (sulfur or water) directly in the course of reaction.

a. Sulfur condensation and adsorption

According to one version, the Claus reaction is carried out at a temperature below the dew point of sulfur vapour and its condensation occurs directly in the catalyst bed. The transfer of sulfur from the gas to the condensed state can substantially shift equilibrium (2), although this requires the timely cleaning of the catalyst from liquid sulfur by its evaporation. The basics of this approach were formulated by Claus back in the 19th century.^{1,2} Later, the concept of Cold Bed Adsorption was formulated, which gave rise to the development of the commercial CBA¹⁵³ and Sulfreen¹⁵⁴ processes, which are widely used in the modern industrial practice of Claus units tail gas cleanup and make it possible to increase the total degree of sulfur recovery from 96%–98% (the theoretical limit for two- and three-stage stationary Claus units) to 99.5% and higher. For the comprehensive review and the analysis of these technologies, see Ref. 155. It should be noted that sulfur vapour is removed from the gas mixture by both their condensation and the adsorption in the catalyst pores; therefore, the use of the term ‘adsorption-catalytic’ process is justified in this case.

The realisation of such processes requires the use of multi-reactor parallel schemes (see Fig. 3 b) containing, as a rule, two or three reactors in which, in turn, the following stages alternate: reaction/sulfur adsorption, catalyst regeneration (evaporation of sulfur at elevated temperature of the catalyst in a flow of a hydrogen sulfide-containing gas) and reactor cooling.

Moreover, schemes are known in which the catalyst regeneration and the removal of sulfur are carried out using the hot reaction gas delivered from the Claus furnace; as an example, a process¹⁵⁶ in which the unsteady-state conditions in three successive catalyst beds are realised by the periodic shift of the position of the inlet and outlet points of the reaction mixture and, correspondingly, by the change in the succession of catalyst beds the gas flow passes through. Conceptually, this scheme is close to the ‘torus’ scheme (see Fig. 2 a) and also to a scheme with the pseudomoving catalyst beds (see Fig. 4). According to the results of modelling, such a scheme allows up to 99.9% of sulfur to be recovered; moreover, whereas the aforementioned conventional technologies such as Sulfreen serve only for the cleanup of tail gases from stationary Claus units, the proposed scheme is an alternative for the complete combination of the Claus and Sulfreen methods (with virtually the same capital and operational costs as in the Sulfreen process).

b. The Claus reverse processes

Yet another version of processes that include sulfur condensation and evaporation is the Claus reverse process,^{157–165} which due to the periodic reversal of the flow, allows one to carry out

the reaction at a low inlet gas temperature, *i.e.*, under the conditions of sulfur condensation.

Mathematical models of this process have shown^{161–164} that under these conditions, a zone with a temperature above the sulfur dew point is formed in the central part of the catalyst bed. In this zone, the Claus reaction occurs, while in the cooler edge zones, sulfur is condensed and evaporated. In the reverse process, the maximum temperature in the reaction zone that defines the equilibrium yield of sulfur can exceed the sulfur dew point merely by several degrees; as a result, this temperature is substantially lower as compared with the stationary process (the maximum temperature of the latter is determined by both the dew point as the minimum inlet gas temperature and the adiabatic heat of the Claus reaction). This allows one to reach higher degrees of conversion of the starting reactants.

Particularly, the one-stage Claus reverse process, which is carried out by the schemes shown in Fig. 1 a,b, is equivalent to the two-stage stationary process as regards the total degree of sulfur recovery (up to 96%), whereas the reverse process with intermediate heat removal¹⁵⁹ (see Fig. 1 c) is equivalent to the conventional three-stage process with the degree of sulfur recovery approaching 98%. Moreover, the reverse process does not require heat exchangers and the preliminary heating of gases, which makes this technology substantially cheaper.

The one-stage reverse process has the following drawbacks: the degree of sulfur recovery is <96%; a part of sulfur is lost as a result of the incomplete hydrolysis of CS₂ and COS usually present in the reaction gas; sulfur is lost due to the formation of a fog from its vapour. These disadvantages can be overcome by using the Claus ‘double’ reverse process¹⁶⁰ (Fig. 7). The unit includes three reactors, of which the first operates at high temperature of the gas delivered from the Claus furnace (300–400 °C), while the second and third reactors operate at temperatures below the sulfur dew point (120–160 °C). Continuous operation of the second reactor is provided by periodic reversals of the gas flow in the internal circuit, while the catalyst regeneration in the third bed occurs when the order of reactors the gas passes through is changed upon the reversal of the flow direction in the external circuit. High temperature in the first (with respect to the gas flow) reactor favours the efficient hydrolysis of CS₂ and COS and also the efficient regeneration of the catalyst (due to the evaporation of liquid sulfur accumulated in the previous phase of the external cycle). The high overall degree of conversion and also the condensation and adsorption of non-condensed sulfur vapour are

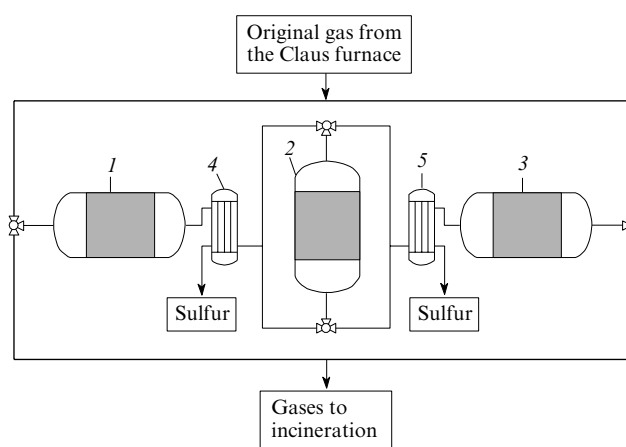


Figure 7. Flow scheme of the Claus ‘double’ reverse process. (1–3) Catalytic reactors, (4, 5) units for sulfur condensation.

favoured by the low temperature in the third reactor (with respect to the gas flow).

According to the results of modelling,¹⁶⁴ the 'double' reverse process provides a high degree of mixture conversion, efficient hydrolysis of COS and CS₂ and elimination of sulfur losses with non-condensed fog (the total level of sulfur extraction was 99.6%–99.8%). This process is advantageous due to the absence of strict requirements to the quick response of switching valves. This is associated with the fact that the switches in the external cycle are rare (about once in a day) and the losses in the switch are insignificant, while the gas breakthroughs in the switches in the internal circle (the characteristic switch frequency is several times per hour) is damped by the protective action of the third bed. The units for the 'double' reverse process do not require complex equipment and thus are very compact.

Pilot-plant tests of the Claus reverse process¹⁶⁵ confirmed its feasibility.

c. Adsorption of water vapour

As was noted above, the equilibrium in the Claus reaction can be shifted by the removal of water vapour from the reaction mixture. The Claus process in a combined bed containing catalyst grains and a zeolite sorbent was described.^{166–169} The scheme of this version provides for a two-stage reverse process (see Fig. 1c) with the intermediate heat exchange and the intermediate sulfur removal. The original gas is fed to the reactor at a temperature that exceeds the dew point of sulfur vapour (e.g., at 250 °C). In the first bed, the Claus reaction and the adsorption of water vapour on the sorbent (zeolite) occur simultaneously. The gases that exit from the second bed are first cooled for sulfur condensation and then heated to higher temperature before entering the second bed where the water vapour is desorbed. As the sorbent is saturated with water, the flows in the first bed are reversed and the process is carried out in the same mode.

According to theoretical and experimental studies,^{166–169} removal of water vapour by adsorption provides a substantial shift of the reaction equilibrium and ensures virtually 100% conversion of the mixture even for high initial contents of reactants and the cycle time between reversals of no less than 1 h. However, it was noted¹⁶⁹ that such a scheme has certain drawbacks, particularly, it does not rule out a decrease in the efficiency of the hydrolysis of COS, which may be present in the gases. At the same time, they assumed that these drawbacks can presumably be minimised or eliminated provided the optimum combination of the time-dependent concentration and temperature fields in the catalyst beds will be found.

4. Low-temperature decomposition of hydrogen sulfide

Direct decomposition of H₂S is one of the methods for the production of elemental sulfur from hydrogen sulfide



This method attracts attention due to the possibility of the production of hydrogen (in place of water in the Claus process) in addition to sulfur, which is important in view of the development of hydrogen energetics.

However, all attempts to develop a commercial process of decomposition of hydrogen sulfide faced serious thermodynamic limitations, namely, reaction (3) is reversible and the equilibrium degree of hydrogen sulfide dissociation is virtually zero under ordinary conditions. To achieve the equilibrium H₂S conversion of about 10%, the temperature should be elevated to 700 °C, while its complete dissociation requires temperatures of nearly 2000 °C. It is difficult to carry out such a process; moreover, recombination of sulfur and hydrogen to H₂S during the cooling of the reaction products is probable,

and the elimination of this route would require additional efforts.

In the industry, acidic gases produced upon refining of natural gas and oil and containing, as a rule, considerable amounts of hydrocarbons and carbon oxides in addition to H₂S are the main source of hydrogen sulfide. At high temperatures, there is a high probability for the pyrolysis of these compounds, which may substantially complicate the technology, viz., necessitate the use of rather intricate and expensive equipment for the separation and purification of H₂S before its utilisation.

The use of the adsorption-catalytic process proved to be an effective (and interesting within the framework of this review) way for overcoming the equilibrium limitations of the degree of dissociation of hydrogen sulfide and also for the decrease in the reaction temperature.

The known methods of H₂S decomposition^{170–172} involve hydrogen sulfide chemisorption on the surface of sulfides of transition metals (iron, nickel, cobalt, copper, etc.), which is accompanied by the formation of surface polysulfides of metals and hydrogen, and periodic thermolysis of polysulfides to the original sulfides and sulfur. Chemisorption proceeds at relatively low temperatures (200–550 °C), which, nonetheless, allows one to achieve high degrees of H₂S decomposition. The sorbent is regenerated by heating to 700–800 °C in a gas flow containing no hydrogen or hydrogen sulfide, which results in the release of elemental sulfur.

Startsev *et al.*^{173–176} have shown experimentally that the stage of hydrogen sulfide chemisorption can proceed at a sufficiently high rate even at room temperature, whereas the regeneration occurs at temperatures not exceeding 200–300 °C provided the supported sulfide catalysts or certain catalytically active systems are taken as the chemisorbents.

Figure 8 shows the dynamics of hydrogen evolution in the stage of hydrogen sulfide chemisorption where the gas mixture is fed to the sulfide catalyst bed. In the beginning of the experiment, almost 100% adsorption of hydrogen sulfide was observed; moreover, even at room temperature, considerable amount of hydrogen evolved. If relatively short cycles (<10 min) were used, the process involved no discharge of hydrogen sulfide into the gas phase and the degree of H₂S decomposition was 100%. Periodic regeneration of the catalyst-chemisorbent at moderate temperatures (200 °C) allowed complete recovery of its chemisorption properties. This was confirmed in multiple chemisorption–regeneration cycles.

At the first glance, the possibility of achievement of that high degree of hydrogen sulfide decomposition to sulfur and

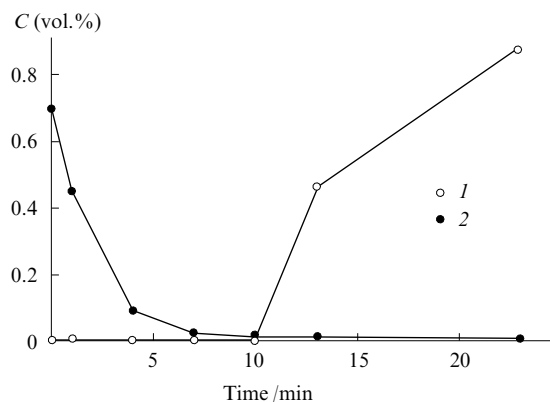
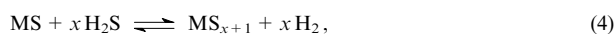


Figure 8. Time changes in the outlet concentrations of H₂S (1) and H₂ (2) at the feeding of a gas mixture containing 1 vol.% H₂S to the sulfide catalyst bed. *T* = 20 °C, *P* = 1 atm, contact time is 1 s.

hydrogen at low temperatures contradicts the thermodynamic limitations. This is rationalised as being due to different states of a catalyst in a periodic adsorption-catalytic process, which enables the spatial and temporal separation of the reaction stages and allows one to substantially shift the equilibria.

In the general case, the sequence of stages is as follows:



A simplified scheme includes the transformation of iron sulfide into disulfide in the chemisorption stage



and the reverse transformation in the regeneration stage¹⁴³

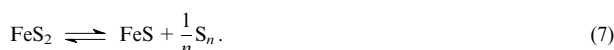


Figure 9 shows the equilibrium degrees of conversion of sulfides according to reactions (6) and (7). Reaction (6) is exothermic and virtually irreversible in the low-temperature range. Decomposition of FeS₂ to sulfur proceeds with the absorption of a large amount of heat [which ensures the total endothermic effect in the overall reaction (3)] and is thermodynamically less advantageous (which explains the low equilibrium degree of H₂S dissociation under steady-state conditions at low temperatures).

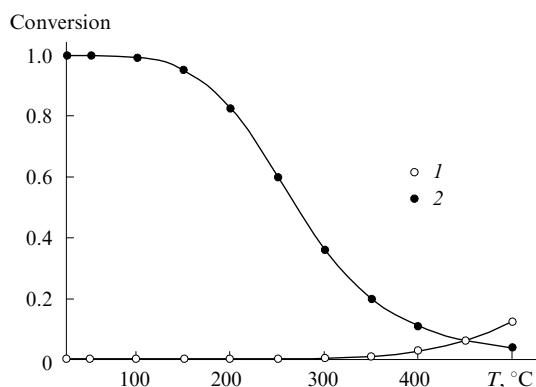


Figure 9. Equilibrium degrees of conversion of sulfides according to the reactions (7) (1) and (6) (2).

However, the equilibrium degree of sulfide dissociation concerns only steady-state modes of reactions and imposes no direct limitations on the operation of a flow-through reactor with the variable catalyst state. Continuous removal of sulfur vapour from the reaction zone with a flow of a regenerating gas gradually enables complete regeneration of the chemisorbent-catalyst surface. Under these conditions, the equilibrium degree of dissociation determines the regeneration time rather than its maximum degree. It is of fundamental significance that the regeneration occurs in the absence of hydrogen in the gas flow, which eliminates the reverse process, *i.e.*, the H₂S formation.

Obviously, the above description is quite simplified. A much more comprehensive study with involvement of the quantum chemical simulation¹⁷⁶ has shown that the formation of complex compounds comprising hydrogen atoms in addition to the metal and sulfur occurs in the chemisorption of hydrogen sulfide on the surface of a sulfide catalyst.

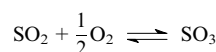
It should be emphasised that the attainment of super-equilibrium degrees of H₂S dissociation is only possible in a periodic chemisorption-catalytic process with the well-defined separation of the chemisorption and regeneration stages in space and time

The low-temperature decomposition of hydrogen sulfide can be carried out in a multireactor system (see Fig. 3b) with the periodically alternating delivery of a cold gas containing hydrogen sulfide and a heated regeneration gas (*e.g.*, commercial nitrogen, carbon dioxide, natural gas, *etc.*) to each reactor. Such a technology allows one to achieve the 100% conversion of hydrogen sulfide at quite moderate temperatures. At low temperatures, the requirements to construction materials and to the heat removal from the reactor become less severe, in addition, complex sour gases containing hydrogen sulfide can be processed without preliminary extraction and purification of H₂S. Moreover, this reduces the energy consumption due to not only the minimisation of the heat loss as a result of the lower operation temperatures, but also the substantial shift of the heat balance of this reaction. Thus at $T > 600^\circ\text{C}$, the endothermic effect of the sulfur formation as the molecules S₂ was 90 kJ mol⁻¹, while at $T \sim 200^\circ\text{C}$, where S₆ and S₈ are the dominant allotropic forms of sulfur, the effect decreased to 35–40 kJ mol⁻¹. This decrease was caused by strongly exothermic reactions of sulfur molecule growth in the series $\text{S}_2 \rightarrow \text{S}_6 \rightarrow \text{S}_8$.

The chemisorption-catalytic processes are advantageous in a situation where the volume of produced hydrogen is of importance. Particularly, their use is promising in the processing of sour natural gases, *e.g.*, the gas from the Astrakhan gas field, which contains 30% H₂S. The obtained hydrogen can be utilised in fuel cells for the electric power production.

5. Oxidation of sulfur dioxide

Sulfur dioxide oxidation



is a reversible reaction the equilibrium in which can be shifted by adsorption effects. There are two adsorption-catalytic approaches that can substantially enhance the efficiency of the conventional version of this reaction.

a. Water flushing of the catalyst

The first way of shifting the reaction equilibrium is the oxidation of sulfur dioxide at low temperatures in the presence of water vapour. Under such conditions, sulfur trioxide reacts with water to form a sulfuric acid condensate, thus shifting the equilibrium of the target reaction.

The processes of SO₂ oxidation at 35–80 °C on activated carbon (this catalyst was chosen because the conventional vanadium catalysts are inactive at low temperatures) with the initial concentrations of sulfur dioxide of 0.1 vol.%–0.5 vol.% were studied.^{177–179} Under these conditions, the acid formed was condensed and sorbed in the catalyst pores. The catalyst was regenerated by flushing it with water.

The described processes, which were characterised by rather lengthy operation cycles, namely, up to 100–200 min, made it possible to reach very high degrees of sulfur dioxide conversion (the residual concentration of SO₂ in gases was about 50 ppm). However, the use of water flushing leads to the formation of vast amounts of off-grade (low-concentration) acid, which substantially limits the practical application of this technology.

b. Flushing of catalyst beds with air

Yet another method aimed at the shift of the equilibrium to enhance the efficiency of SO₂ oxidation takes advantage of the

adsorption properties of the molten active component of conventional vanadium catalysts.

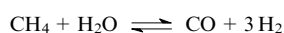
It was shown¹⁸⁰ that the alternating feeding of the reaction mixture and air to the vanadium catalyst bed can substantially increase the degree of sulfur dioxide conversion. Presumably, flushing of the catalyst bed with air leads to the supersaturation of a film of the molten active component on the catalyst surface with oxygen so that in the next reactant feeding cycle, the oxygen concentration in the melt substantially exceeds its equilibrium value (with respect to the reaction mixture composition); and, hence, the degree of SO₂ conversion can also exceed the equilibrium limit reached in the steady-state mode.

This process can be implemented in a two-reactor scheme (see Fig. 3b) with separate delivery of air and the reaction mixture according to two main versions, namely, with direct flow¹⁸⁰ and counter flow.¹⁸¹ The calculations¹⁸² carried out within the framework of a one-dimensional model of an adiabatic catalyst bed that operates under the plug flow conditions¹⁸³ together with a comprehensive unsteady-state kinetic model of this process,¹⁸⁴ have shown that both versions allow one to reach extremely high degrees of SO₂ conversion (>99.9%). However, the counterflow version provides stable operation of the system in much wider ranges of initial concentrations of sulfur dioxide and inlet gas temperatures and, hence, can be carried out at technologically favourable parameters (cycle duration, catalyst load, initial temperature of gases, *etc.*) in the second stage of the sulfuric acid contacting schemes DC/DA (double contacting/double adsorption). In this case, the total degree of sulfur dioxide conversion in the contact unit can reach 99.999%, which corresponds to the final SO₂ concentration on a level of 50 ppm and meets the most severe environmental requirements. These theoretical conclusions were successfully confirmed by the pilot tests.¹⁴³

6. Steam reforming of methane and CO

The reforming of methane and other hydrocarbons aimed at the production of hydrogen, which is utilised in the syntheses of ammonia and methanol and in the petroleum industry and hydrogen energetics, is among the most important directions of chemical technology.

In these technologies, the most important stages are the methane steam reforming



and the CO steam reforming (water gas shift-reaction)



In both cases, the formation of hydrogen is limited by the equilibrium factors. According to the thermodynamic analysis, the hydrogen yield can be substantially increased if carbon dioxide is removed from the reaction zone. The removal of CO₂ can be accomplished by its adsorption, particularly, on metal oxides, to form carbonates.

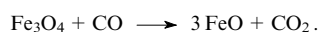
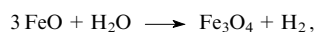
Attention is focused on the reaction of methane steam reforming, the equilibrium of which can be shifted due to the absorption of carbon dioxide^{185–193} by various sorbents (CO, MgO, hydrotalcite, dolomite, lithium zirconate, *etc.*). In a single-stage process, hydrogen with the purity grade from 85% to 98% is produced; moreover, the residual mixture mainly contains methane with the minimum amounts of carbon oxides.

Analogous studies have also confirmed the possibility of a substantial shift of the chemical equilibrium in water gas shift reaction by the adsorption of CO₂ on CaO.¹⁹⁴ In this case, hydrogen with the purity grade of 99.5% was formed.

The reverse reaction, namely, the carbon dioxide reduction with hydrogen to CO and water, also deserves mention.¹⁹⁵ In this case, the virtually 100% CO yield was reached due to the adsorption of water on a zeolite sorbent.

It should be stressed that the developments mentioned above were based on a concept of the catalyst steady state, whereas the non-stationarity of the process was entirely attributed to the sorbent effect. Particularly, the well-known steady-state model¹⁹⁶ was used in the simulation of the processes of methane steam reforming. However, the correctness of this approach was not substantiated and is not self-evident.

An interesting scheme was proposed,¹⁹⁷ in which cyclic feeding alternation of steam and the synthesis gas was used in the production of hydrogen on an iron oxide catalyst



This process, which was named the Reformer Sponge Iron Cycle (RESC), can be employed in the production of hydrogen from the natural gas, liquid hydrocarbon fuels and coal gasification products. Similar schemes were proposed recently.^{198, 199}

The production of hydrogen by the catalytic pyrolysis of hydrocarbons with the simultaneous production of valuable types of activated coal is actively studied.^{200–209} In this method, carbon is deposited and accumulated on the catalyst surface, and the processes involved are basically unsteady.

7. Anaerobic oxidation of methane

At present, the processes of cyclic oxidation of methane under anaerobic conditions, where nickel and iron oxides are used as the catalysts, are actively studied.^{210–213} These processes are called Chemical-Looping Combustion (CLC). They are aimed at the deep oxidation, which is achieved by the correct choice of the reaction temperature (1000 °C) and the catalyst composition. Natural gas is passed through a catalyst bed to oxidise hydrocarbons to CO₂ and water vapour; the catalyst is periodically reoxidised with air.

This processes is meant particularly for energy purposes, *e.g.*, for the electric power production. What is its main advantage over the conventional combustion of natural gas consists, is that in the hydrocarbon delivery cycle, the gas mixture at the outlet from the reactor contains only carbon dioxide and water vapour. Due to relative simplicity of water removal from this flow, highly concentrated CO₂ can be produced and extracted later in the pure form and utilised without its emission to the atmosphere. The latter factor is currently the topical problem in view of the Kyoto Protocol requirements. The second advantage of this process is the relatively low temperature in both phases of the cycle, which allows substantial reduction of the emission of nitrogen oxides to the atmosphere.

8. Anaerobic processes of oxidative dehydrogenation of hydrocarbons

The quest for the ways of increasing the selectivity of target reactions in complex reaction systems is among the currently topical problems of catalysis. These reactions include numerous processes of selective catalytic oxidation of hydrocarbons (propane to propylene, butane to butylene and butadiene, *etc.*).

As was shown above, the way of enhancing the selectivity of conversion and the yield of target products as compared with steady-state processes lies in the use of the unsteady state of a catalyst, which can be generated by the cyclic separate feeding of hydrocarbons and the oxidant (air). Oxygen chemisorbed on the catalyst surface acts as the oxidant, whereas

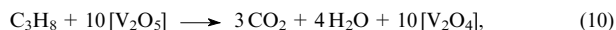
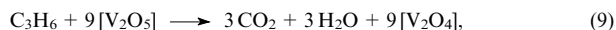
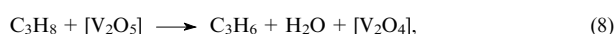
molecular oxygen is not present in the hydrocarbon flow (this explains the term 'anaerobic process').

Reactions of selective oxidation of hydrocarbons with oxygen are, as a rule, exothermic and the selectivity of most of them decreases as the temperature increases. As a consequence, the maximum concentrations of reactants are limited in a steady-state adiabatic process, which has a negative effect on the efficiency. Apparently, the effective coupling of heat and concentration fronts in the catalyst bed is the key problem in the elaboration of selective oxidation processes.

Model studies of parallel adiabatic endothermic reactions have shown^{143, 214–216} that under adiabatic conditions the cyclic feeding of a preheated hydrocarbon into a cold bed of a preliminarily oxidised catalyst leads to substantially lower maximum temperatures as compared with the steady-state process. This is associated with the fact that, in the former case, a considerable portion of heat released in oxidation reactions is consumed for the catalyst heating. The lower temperatures, in turn, favour the higher reaction selectivity. Moreover, this allows one to feed concentrated hydrocarbons into the reactor, which makes it possible to substantially enhance the efficiency of the process.

Model studies also showed the possibility of the existence of a reversed heat front, which, due to the heat conduction of the bed, can move in the catalyst bed counter-currently the reaction gas flow. This allows one to additionally decrease the maximum temperature and enhance the oxidation selectivity.

In the studies^{142, 217} devoted to the processes of selective oxidation of hydrocarbons with the separate delivery of reactants, propane oxidative dehydrogenation to propylene on a vanadium-oxide catalyst was considered. The system of reactions can be written as follows:¹⁰⁴



According to rough estimates, the stage of selective oxidation (8) produces a virtually zero (within the calculation error) heat (about -4.6 kJ per mole of propane), while the total exothermic effect of the overall selective oxidation of propane (116.8 kJ mol⁻¹) is largely due to a sufficiently high exothermic effect in the catalyst reoxidation stage (11), namely, 121.4 kJ per mole of V_2O_4 . At the same time, the stages of deep oxidation of propylene (9) and propane (10) are characterised by pronounced heat evolution (840 kJ mol⁻¹) approximately the same for both these reactions.

Based on these results, a very important conclusion can be drawn, *viz.*, the temperature conditions of the process depend not only on the catalyst activity and selectivity, but also on its thermodynamic properties, particularly, the energy of the bond between chemisorbed oxygen and the surface, which determines the redistribution of the released heat between the stages of catalyst reduction (8)–(10) and reoxidation (11).

According to model studies,²¹⁷ feeding of pure propane with a temperature of 300°C into a cold bed of a preliminarily oxidised catalyst gives rise to a thermal front that travels toward the filtrating gas flow. In the front, due to the virtually zero thermal effect of the main reaction and the insignificant extent of deep oxidation reactions, the catalyst is not heated above the outlet gas temperature.

In addition, such a process can be carried out in a continuous mode with a cyclic separate feeding of cold propane and air in counterflows, *e.g.*, according to the two-reactor scheme (see Fig. 3*b*), into the preliminarily heated catalyst bed. As a result, a stable autothermal unsteady mode is

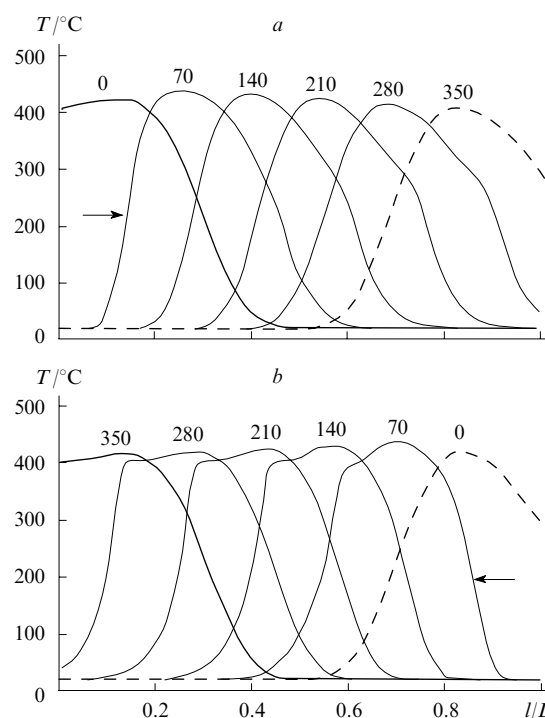


Figure 10. Temperature profiles of a catalyst along the bed length in the established cyclic mode with separate counter-current feeding of propane and air.

(a) Propane feeding cycle (catalyst reduction), (b) air feeding cycle (catalyst reoxidation). Arrows show the direction of the reaction mixture flow, numbers over the curves show time (in s) from the beginning of each cycle. The inlet gas temperature was 20°C in both cycles, the cycle duration was 350 s.

generated in this bed (Fig. 10), which eliminates the necessity of the energy supply and the preheating of reaction flows.

According to estimates, the use of concentrated propane makes it possible to increase the efficiency as compared with steady-state technologies and also noticeably enhance the selectivity of propane oxidation. Among the other advantages of this process, the following factors deserve mention.

1. Technological simplicity and low costs required for its implementation, which is associated with the use of simple and inexpensive reactors with steady-state adiabatic beds of catalyst grains and with the minimum use of the heat-exchange infrastructure.

2. Safety of the process, which is due to the absence of direct contact between hydrocarbons and oxygen.

3. A possibility of utilising air as the oxidant in place of pure oxygen.

4. The possibility of prolongation of the catalyst service life due to the effective suppression of the coke formation in the stage of propane conversion (as a consequence of low temperatures) and to the burning out of coke with oxygen in each cycle of catalyst reoxidation.

The processes under consideration also include the dehydrogenation of paraffins to alkenes, which involves the selective anaerobic oxidation of hydrogen over transition metal oxides and periodic reoxidation of the latter with air,^{218, 219} the partial oxidation of *n*-butane to maleic anhydride²²⁰ (implemented on the commercial scale by DuPont company) and of *o*-xylene to phthalic anhydride²²¹ in moving catalyst beds and also the oxidation of paraffins to alkenes²²² with separate feeding of hydrocarbons and oxygen.

9. Purification of automotive exhaust

The currently topical problems include the problem of 'cold start', which concerns the idle start of an engine when the catalyst temperature is too low.

A solution to this problem lies in the corporation of adsorption traps into the catalytic neutralisers. These traps can adsorb toxic impurities (CO, hydrocarbons, NO_x) and soot particles from the exhaust gases.^{223–226} However, although the sorbed hydrocarbons and soot can be oxidised to the higher or lesser extent, removal of nitrogen oxides poses certain difficulties associated with the fact that these oxides are desorbed during heating of the neutraliser much sooner than the temperature necessary for their efficient reduction is reached.

An original solution to this problem was patented.²²⁷ In essence, the patent describes a procedure for the reversal of flows in a multibed system inert–catalyst–sorber–catalyst–inert, where the reversal is carried out by a mechanical rotation of this system.

At a low temperature, the impurities are accumulated in the sorber located between two catalyst beds. As the temperature increases, the catalyst beds are first to be heated, while the sorber layer is heated later. Thus, the desorption of impurities begins only when the catalyst temperature becomes sufficient for its effective decontamination. This process may be a good illustration of the effective interrelation between the adsorption properties of the system and the dynamics of thermal fields in it.

10. Miscellaneous processes

Among the other processes actively employing the sorption properties of catalysts, the following processes can be singled out:

- direct synthesis of HCN from CO and ammonia with sorption of CO₂ formed on lithium zirconate;¹⁶⁶

- the unsteady Deacon process^{228, 229} of complete oxidation of HCl to elemental chlorine, which includes separate stages, namely, chemisorption of hydrogen chloride on copper oxide to form CuCl₂ and water vapour and the regeneration of the sorber due to the copper chloride oxidation to form CuO and Cl₂;

- a cyclic process of alkene synthesis from methane through transient bromination of methane, which includes the stages of chemisorption of molecular HBr on oxide sorbents used in this process and periodic regeneration of the sorber to form elemental bromine;²³⁰

- synthesis of methanol with removal of the product formed by its absorption with a fine-grain sorber continuously filtered through a fixed catalyst bed;²³¹

- dehydrogenation of cyclohexane to benzene over a metal-hydride catalyst with chemisorption removal of hydrogen;²³²

- unsteady processes of hydrodesulfurisation and hydrodearomatisation of fuels, which take advantage of high adsorption capacity of the catalyst with respect to sulfur compounds^{233, 234} and include reverse processes for hydro-treatment.

All the processes listed above are based on the sorption properties of the catalytic surface and could be carried out in unsteady-state modes with the efficiency enhanced as compared with steady-state processes and particularly afforded superequilibrium yields of the reaction products.

IV. Conclusion

The studies of sorption-catalytic processes described above showed that the purposeful use of sorption (adsorption and chemisorption) properties of heterogeneous catalysts allows one to substantially enhance the efficiency of many catalytic reactions. The highest technological effect can be achieved for

a controlled combination of the thermal non-stationarity with the composition non-stationarity of the catalyst surface.

In the elaboration of a new process, when choosing the main active factor (*e.g.*, concentration modulation), it is necessary to take into account the other factors (dynamic changes in the temperature and the pressure). Otherwise, instead of the expected improvement in the characteristics as compared with steady-state processes, one may obtain a zero and even negative effect.

It should be borne in mind that unsteady catalytic processes are cyclic or periodic, and certain technological efforts may be necessary to ensure their recurrence and, in most cases, the uninterrupted operation of the system as a whole. This complicates practical implementation of such technologies and makes them less attractive; hence, their development is reasonable only if the unsteady-state mode offers substantial advantages over the steady-state processes. Correspondingly, this entails high requirements to the skill of developers and the quality of their service, while the success is determined by the deep insight into the phenomena observed and the use of modern experimental techniques and the methods of comprehensive mathematical simulation.

The diversity of methods for the development of unsteady-state conditions and their combinations is even reflected in the yet unsettled terminology used in the literature. The term 'unsteady catalysis' is often used, although it is too wide and, in certain cases, ambiguous. Insofar as the technologies with modulating catalyst state actively utilise the adsorption phenomena, the term 'sorption-enhanced catalytic processes' is often used. Other popular terms are 'multifunctional processes', which reflects simultaneous occurrence of different types of phenomena (*e.g.*, adsorption and catalysis), and 'chemical looping', which characterises the cyclic nature of processes. The latter are sometimes called (however, not always correctly) the 'reactive chromatographic' processes.

The development of unsteady and adsorption-catalytic processes is a very sophisticated task, which requires that a large number of different factors and their combined action on different-scale levels of the process be understood and taken into account. It should be noted that many relationships typical of steady-state processes do not in principle valid the unsteady catalytic processes.

Particularly, in unsteady processes, even in formally adiabatic catalyst beds, the conditions are realised where the temperature in the bed substantially deviates from the adiabatic value. This difference is determined, in addition to the dynamic effects associated with the regenerative heat exchange and the motion of thermal fronts in the catalyst bed (a property typical of conventional reverse processes with the thermal non-stationarity of the catalyst), by the possible dynamic redistribution of released heat, which occurs in different reaction stages and phases, in both space and time (this is a unique property of systems with the sorption non-stationarity). Depending on the chosen strategy of the realisation of the unsteady mode, the maximum temperature in the process can be either substantially lower (*e.g.*, as in the anaerobic oxidation of hydrocarbons, see Section III.8) or higher (as in the adsorption-catalytic process of VOC oxidation, see Section III.2) than the adiabatic temperature in an equivalent steady-state process.

The use of the sorption capacity of the catalyst allows one to carry out individual reaction stages within certain phases of the technological cycle, which opens up wide prospects for the modulation of the reactant concentrations on the catalyst surface. In many cases, the correct organisation of this process in combination with the temperature factor allows one to overcome the equilibrium limitations and reach higher yields of the target products as compared with analogous steady-state processes.

It is of note that in many cases the parameters of unsteady modes substantially depend on the factors that play a minor role or have an indirect effect on the steady-state technologies. These factors include the bond energy of the reactant with the catalyst surface, the heat capacity of the catalyst, its specific surface, *etc.*

Summarising, the following advantages of the sorption-catalytic technologies over the steady-state methods can be mentioned:

— a decrease in the energy consumption in the processing of low-concentration gases (deep oxidation of VOC);

— an increase in the efficiency of decontamination of exhaust gases (NO_x reduction and purification of automotive exhausts);

— superequilibrium yields of target products in thermodynamically limited reactions (the Claus process, H₂S decomposition, SO₂ oxidation, steam reforming of methane and CO, the Deacon process, *etc.*);

— the enhanced selectivity of partial oxidation processes provided by the use of chemisorbed oxygen as a 'soft' oxidant (oxidation of n-butane to maleic anhydride, o-xylene to phthalic anhydride, paraffins to alkenes, *etc.*).

In many cases, these advantages may include the reduction in the capital costs in the realisation of these processes and also, paradoxical as this may look at the first glance, the simplification of flow schemes and the enhancement of their operation stability.

However, it should be stressed that the aforementioned improvements are achieved only in the case of optimally organised processes. Otherwise, the utilisation of catalyst sorption properties may have a negative effect. Particularly, as was demonstrated above by the example of reactions of deep oxidation of VOC and of the reduction of nitrogen oxides and the oxidation of sulfur dioxide, the sorption-desorption phenomena in a conventional reverse process reduce its efficiency; and, hence, different technological approaches are required in order to achieve positive effects. This is why the key factor of the successful development of sorption-catalytic processes is the correct choice of the process scheme and the search for the optimum strategy for its dynamic control.

The author wants to express his deep gratitude to academician V N Parmon and to A S Noskov, M V Dmitrienko, B S Bal'zhinimaev, V O Strots, P G Tsurul'nikov, A G Okunev, and I A Zolotarskii for valuable discussions and the assistance in the preparation of this publication.

References

1. C F Claus *Chem. Ber.* **15** 744 (1882)
2. US P. 349981 (1886)
3. US P. 85370 (1868)
4. US P. 118209 (1871)
5. US P. 165802 (1875)
6. M Tessie du Motay, M Marechal *Bull. Soc. Chim. Fr.* **9** 334 (1868)
7. S Z Roginskii, M I Yanovskii, G A Gaziev *Kinet. Katal.* **3** 529 (1962)^a
8. S Z Roginskii, M I Yanovskii, G A Gaziev *Dokl. Akad. Nauk SSSR* **146** 152 (1962)^b
9. S Z Roginskii, E I Semenenko, M I Yanovskii *Dokl. Akad. Nauk SSSR* **153** 383 (1963)^b
10. J M Douglas, D W T Rippin *Chem. Eng. Sci.* **21** 305 (1966)
11. J M Douglas *Ind. Eng. Chem. Proc. Des. Dev.* **6** (5) 42 (1967)
12. C Wandrey, A Renken *Chem.-Ing.-Tech.* **45** 854 (1973)
13. C Wandrey, A Renken *Proceedings GVC/AIChE Joint Meeting* Vol. 1 (Weinheim: Verlag Chemie GmbH, 1974) p. A 3–3
14. C Wandrey, A Renken *Chem. Eng. Sci.* **32** 448 (1977)
15. H Helmrich, A Renken, K Schirgerl *Chem.-Ing.-Tech.* **46** (15) 647 (1974)
16. M P Unni, R R Hudgins, P L Silveston *Can. J. Chem. Eng.* **31** 623 (1973)
17. J E Bailey, F J M Horn *J. Optim. Theory Appl.* **2** 441 (1968)
18. J E Bailey, F J M Horn *AIChE J.* **17** 550 (1971)
19. J E Bailey, F J M Horn *Chem. Eng. Sci.* **21** 109 (1972)
20. J E Bailey, F J M Horn, R C Lin *AIChE J.* **17** 818 (1971)
21. Yu Sh Matros *Nestatsionarnye Protsessy v Khimicheskikh Reaktorakh* (Unsteady Processes in Chemical Reactors) (Novosibirsk: Nauka, 1982)
22. Yu Sh Matros *Kataliticheskie Protsessy v Nestatsionarnykh Usloviyakh* (Catalytic Processes under Unsteady-State Conditions) (Novosibirsk: Nauka, 1987)
23. G K Boreskov, Yu Sh Matros, O V Kiselev, G A Bunimovich *Dokl. Akad. Nauk SSSR* **237** 160 (1977)^b
24. Yu Sh Matros *Unsteady Processes in Catalytic Reactors* (Amsterdam: Elsevier, 1985)
25. Yu Sh Matros *Catalytic Processes under Unsteady-State Conditions* (Amsterdam: Elsevier, 1989)
26. I A Zolotarskii, Yu Sh Matros *React. Kinet. Catal. Lett.* **3–4** 321 (1982)
27. A I Oruzhenikov, Yu V Ivanov, Yu Sh Matros, A P Gerasev *Kinet. Katal.* **27** 954 (1986)^a
28. I A Zolotarskii, S M Bogdashev, Yu Sh Matros *Kinet. Katal.* **30** 1310 (1989)^a
29. G K Boreskov *Geterogennyye Kataliz* (Heterogeneous Catalysis) (Novosibirsk: Nauka, 1986)
30. Yu Sh Matros, G A Bunimovich *Catal. Rev. Sci. Eng.* **38** (1) 1 (1996)
31. Yu Sh Matros, A S Noskov, V A Chumachenko *Kataliticheskoe Obezvrezhivanie Otkhodyashchikh Promyshlennykh Gazov* (Catalytic Deactivation of Exhaust Industrial Gas) (Novosibirsk: Nauka, 1991)
32. P L Silveston *Composition Modulation of Catalytic Reactors* (New York: Gordon and Breach, 1998)
33. M M Slin'ko, N I Jaeger *Oscillating Heterogeneous Catalytic Systems* (Amsterdam: Elsevier, 1994)
34. M B Cutlip *AIChE J.* **25** 502 (1979)
35. Y Barshad, E Gulari *AIChE J.* **31** 649 (1985)
36. Y Barshad, E Gulari *J. Catal.* **94** 468 (1985)
37. X Zhou, E Gulari *Chem. Eng. Sci.* **41** 883 (1986)
38. X Zhou, E Gulari *Langmuir* **2** 709 (1986)
39. X Zhou, Y Barshad, E Gulari *Chem. Eng. Sci.* **41** 1277 (1986)
40. G Vaporciyan, A Annapragada, E Gulari *Chem. Eng. Sci.* **43** 2957 (1988)
41. B K Cho *Ind. Eng. Chem. Fundam.* **22** 410 (1983)
42. W R C Graham, D T Lynch *Catalysis on the Energy Scene, Studies in Surface Science and Catalysis* Vol. 19 (Amsterdam: Elsevier, 1984) p. 197
43. F Qin, E E Wolf *Chem. Eng. Sci.* **50** 117 (1995)
44. S C Capsaskis, C N Kenney *J. Phys. Chem.* **90** 4631 (1986)
45. H K Abdul-Kareem, A K Jain, P L Silveston, R R Hudgins *Chem. Eng. Sci.* **35** 273 (1980)
46. S A Ven'yaminov *Mekhanizmy Geterogenno-kataliticheskikh Reaktsii Okisleniya* (Mechanisms of Heterogeneous and Catalytic Oxidation) (Novosibirsk: Institute of Catalysis, Siberian Branch of the Russian Academy of Sciences, 1993) p. 73
47. V N Tomilov, A N Zagoruiko, S A Ven'yaminov *Tezisy Mezhdunarodnoi Konferentsii 'Khimreaktor-13', Novosibirsk, 1996* (Abstracts of Reports of the International Conference 'Khimreaktor-13', Novosibirsk, 1996) Vol. 2, p. 175
48. M R Prairie, J E Bailey *Chem. Eng. Sci.* **42** 2085 (1987)
49. A Baiker, M Bergougnan *Can. J. Chem. Eng.* **63** 138 (1985)
50. A Baiker, M Bergougnan *Can. J. Chem. Eng.* **63** 146 (1985)
51. A S Rao, K B S Prasad, M B Rao *J. Catal.* **136** 242 (1992)
52. V Stuchly, K Klusacek *Unsteady State Processes in Catalysis* (Utrecht: VSP, 1990) p. 422
53. N L Jaeger, P J Plath, P Svensson *Spatial Inhomogeneities and Transient Behavior in Chemical Kinetics* (Manchester: Manchester University Press, 1990) p. 593
54. M Marwood, F Van Vyve, R Doepper, A Renken *Catal. Today* **20** 437 (1994)
55. A Nappi, L Fabbicino, R R Hudgins, P L Silveston *Can. J. Chem. Eng.* **63** 963 (1985)

56. K G Chanchlani, R R Hudgins, P L Silveston *Can. J. Chem. Eng.* **72** 657 (1994)
57. M A McNeil, R G Rinker *Chem. Eng. Commun.* **127** 137 (1994)
58. H D Wilson, R G Rinker *Chem. Eng. Sci.* **37** 43 (1982)
59. L Chiao, F K Zack, J Thullie, R G Rinker *Chem. Eng. Commun.* **49** 273 (1987)
60. A K Jain, R R Hudgins, P L Silveston *Proceedings of the 7th ISCRE (ACS Symp. Ser.)* Vol. 196 (Washington, DC: American Chemical Society, 1982) p. 97
61. A K Jain, R R Hudgins, P L Silveston *Can. J. Chem. Eng.* **61** 824 (1983)
62. G Rambeau, H Amariglio *Appl. Catal.* **1** 291 (1981)
63. G Rambeau, A Jorti, H Amariglio *Appl. Catal.* **3** 273 (1982)
64. V O Strots, Yu Sh Matros, G A Bunimovich *Chem. Eng. Sci.* **47** 2701 (1992)
65. H A El Masry *Appl. Catal.* **16** 301 (1985)
66. E L Leupold, A Renken *Ger. Chem. Eng.* **1** 218 (1978)
67. BRD P. 2545845; *Chem. Abstr.* **87** 38924 (1977)
68. M A Truffer, A Renken *AICHE J.* **32** 1612 (1986)
69. J Koubek, J Pasek, V Ruzicka *Proceedings of the 7th International Congress on Catalysis, Tokyo, 1980* p. 852
70. J Koubek, J Pasek, V Ruzicka *Catalyst Deactivation* (Amsterdam: Elsevier, 1980) p. 251
71. S Su, P Zasa, A Renken *Chem. Eng. Technol.* **17** 34 (1994)
72. P Zasa, H Randall, R Doepper, A Renken *Catal. Today* **20** 233 (1994)
73. A Renken *Chem. Eng. Sci.* **27** 1925 (1972)
74. H Muraki, Y Fujitani *Ind. Eng. Chem. Prod. Res. Dev.* **25** 414 (1986)
75. B K Cho, B H Shanks, J E Bailey *J. Catal.* **115** 486 (1989)
76. R R Sadhankar, D T Lynch *J. Catal.* **149** 278 (1994)
77. J-P Dath, T Fink, R Imbihl, G Ertl *J. Chem. Phys.* **92** 1582 (1992)
78. T Fink, J-P Dath, M R Bassett, R Imbihl, G Ertl *Surf. Sci.* **245** 96 (1991)
79. S B Schwartz, L D Schmidt *Surf. Sci.* **183** L269 (1987)
80. S B Schwartz, L D Schmidt *Surf. Sci.* **206** 169 (1988)
81. A S Al-Taie, L S Kerschenbaum *Chemical Reaction Engineering-Houston (ACS Symp. Ser.)* Vol. 65 (Washington, DC: American Chemical Society, 1978) p. 512
82. M R Bilimoria, J E Bailey *Chemical Reaction Engineering-Houston (ACS Symp. Ser.)* Vol. 65 (Washington, DC: American Chemical Society, 1978) p. 526
83. C K Lee, J E Bailey *Ind. Eng. Chem. Prod. Res. Dev.* **19** 160 (1980)
84. A Renken *Chem.-Ing.-Tech.* **46** (3) 113 (1974)
85. F Solymosi, A Erdohelyi, A Szeke *Catal. Lett.* **32** 43 (1995)
86. F Solymosi, J Csereenyi *Catal. Lett.* **34** 343 (1995)
87. H Amariglio, P Pareja, A Amariglio *Catal. Today* **25** 113 (1995)
88. L Lefort, A Amariglio, H Amariglio *Catal. Lett.* **29** 125 (1994)
89. G E Keller, M M Bhasin *J. Catal.* **73** 9 (1982)
90. C A Jones, J J Leonard, J A Sofranko *Energy Fuels* **1** 72 (1987)
91. Y Mortazavi, R R Hudgins, P L Silveston *Proceedings of the 12th Canadian Symposium on Catalysis, Banff, Alberta, 1992* p. 104
92. Y Mortazavi, R R Hudgins, P L Silveston *Can. J. Chem. Eng.* **74** 683 (1996)
93. A Renken, M Mueller, C Wandrey *Proceedings of the 4th International Symposium on Chemical Reaction Engineering, Dechema, Frankfurt, Germany, 1976* Vol. 3, p. 107
94. D W Park, S Ghazali, G Gau *Appl. Catal.* **6** 175 (1983)
95. B S Balzhinimaev, D W Park, G Gau *React. Kinet. Catal. Lett.* **24** 59 (1984)
96. T Kodama, T Shimizu, T Satoh, K I Shimizu *Energy* **11** 1055 (2003)
97. Y Zeng, S Tamhankar, N Ramprasad, F Fitch, D Acharya, R Wolf *Chem. Eng. Sci.* **58** 577 (2003)
98. V A Sadykov, T G Kuznetsova, S A Veniaminov, D I Kochubey, B N Novgorodov, E B Burgina, E M Moroz, E A Paukshtis, V P Ivanov, S N Trukhan, S A Beloshapkin, Y V Potapova, V V Lunin, E Kemnitz, A Aboukais *React. Kinet. Catal. Lett.* **76** 83 (2002)
99. M Niwa, Y Murakami *J. Catal.* **26** 359 (1972)
100. P L Silveston *Influence of Composition Modulation on Product Yields and Selectivity in the Partial Oxidation of Propylene (Preprint of the 73rd Annual Meeting of American Institute of Chemical Engineers), Chicago, 1980* p. 54
101. P L Silveston, M Forriessier *Ind. Eng. Chem. Prod. Res. Dev.* **24** 320 (1985)
102. Y A Salah-Alhahamed, R R Hudgins, P L Silveston *Chem. Eng. Sci.* **47** 2885 (1992)
103. F Genser, S Pietrzyk *Chem. Eng. Sci.* **54** 4315 (1999)
104. R Grabowski, S Pietrzyk, J Sloczynski, F Genser, K Wcislo, B Grzybowska-Swierkosz *Appl. Catal. A* **232** 277 (2002)
105. V A Doroshenko, L P Shapovalova, L P Dolya *Zh. Prikl. Khim.* **59** 1176 (1986)^c
106. V P Luk'yanenko, L P Shapovalova, M Yu Kutnaya, V S Solodkaya *Zh. Prikl. Khim.* **60** 1169 (1987)^c
107. O Rubio, J Herguido, M Menendez *Chem. Eng. Sci.* **58** 4619 (2003)
108. D Creaser, B Andersson, R R Hudgins, P L Silveston *Appl. Catal. A* **187** 147 (1999)
109. V V Sinelnikov, A Yu Stakheev, N N Tolkachev *Proceedings of International Conference 'Chemreactor-17', Athens, 2006* p. 562
110. R K Herz, J B Kleta, J A Sell *Ind. Eng. Chem. Prod. Res. Dev.* **22** 387 (1983)
111. R K Herz *Catalysis Under Transient Conditions (ACS Symp. Ser.)* Vol. 178 (Washington, DC: American Chemical Society, 1982) p. 59
112. R K Herz *Catalysis and Automotive Pollution Control* (Amsterdam: Elsevier, 1987) p. 427
113. L L Hegedus, C C Chang, D J McEwen, E M Sloan *Ind. Eng. Chem. Fundam.* **19** 367 (1980)
114. F Lode, M Houmar, C Migliorini, M Mazotti, M Morbidelli *Chem. Eng. Sci.* **56** 269 (2001)
115. V G Gomes, K W K Yee *Chem. Eng. Sci.* **57** 3839 (2002)
116. G Strohlein, Y Assuncao, R Proplesch, M Mazotti, M Morbidelli *Chem.-Ing.-Tech.* **77** 1819 (2005)
117. S Grüner, A Kienle *Chem. Eng. Sci.* **59** 901 (2004)
118. Can. P. 631882; *Chem. Abstr.* **55** 25158 (1961)
119. US P. 2944627; *Chem. Abstr.* **54** 23491 (1960)
120. E Alpay, C N Kenney, D M Scott *Chem. Eng. Sci.* **48** 3173 (1993)
121. D Chatsiriwech, E Alpay, L S Kerschenbaum, C P Hull, N F Kirkby *Catal. Today* **20** 351 (1994)
122. G-h Xiu, P Lia, A E Rodrigues *Chem. Eng. Sci.* **18** 3893 (2002)
123. P L Silveston, R R Hudgins *Chem. Eng. Sci.* **59** 4055 (2004)
124. V P Zakharov, I A Zolotarskii, V A Kuzmin *Chem. Eng. J.* **91** 249 (2003)
125. A S Noskov, L N Bobrova *Proceedings of International Conference on Unsteady-State Processes in Catalysis (Utrecht: VSP, 1990)* p. 665
126. A S Noskov, L N Bobrova, Yu Sh Matros *Catal. Today* **17** 293 (1993)
127. J D Snyder, B Subramaniam *Chem. Eng. Sci.* **53** 727 (1998)
128. D W Agar, W Ruppel *Chem. Eng. Sci.* **43** 2073 (1988)
129. E S Borisova, A S Noskov, L N Bobrova *Catal. Today* **38** 97 (1997)
130. W R Smith, L N Bobrova *Chem. Eng. Sci.* **57** 393 (2002)
131. A S Noskov, L N Bobrova, G A Bunimovich, O V Goldman, A N Zagoruiko, Yu Sh Matros *Catal. Today* **27** 315 (1996)
132. Br. P. 1582441; *Chem. Abstr.* **88** 196888 (1978)
133. US P. 4234549; *Chem. Abstr.* **94** 38453 (1981)
134. Br. P. 2051761; *Chem. Abstr.* **94** 213666 (1981)
135. V M Orlyk, A D Tereshenko, M G Martcenyuk-Kucharuk, A S Vorobey, I A Farafonova *Proceedings of the 1st World Congress on Environmental Catalysis, Roma, 1995* p. 671
136. O S Rabinovich, I G Gurevich, V M Kisarov, G N Toropkina, L I Kalinkina *Materialy Mezhdunarodnoi Konferentsii po Teplomassobmenu, Minsk, 1988* (Proceedings of the International Conference on Heat-mass Exchange, Minsk, 1988) p. 80

137. V M Brovtseva, S M Iolkina, L I Kalinkina, E M Kvashnina, L V Labzova, G N Toropkina *Tezisy Dokladov 5-oi Vsesoyuznoi Konferentsii 'Kataliticheskaya Ochistka Gazov', Tbilisi, 1989* (Abstracts of Reports of the 5th All-Union Conference 'Catalytic Purification of Gases', Tbilisi, 1989) p. 75
138. V E Suprunov *Tezisy Dokladov 4-oi Vsesoyuznoi Konferentsii po Mekhanizmu Kataliticheskikh Reaktsii, Moskva, 1986* (Abstracts of Reports of the 4th All-Union Conference on Mechanism of Catalytic Reactions, Moscow, 1986) Pt. 2, p. 401
139. V E Suprunov *Tezisy Dokladov 3-ei Konferentsii 'Nestatsionarnye Protessy v Katalize', Novosibirsk, 1986* (Abstracts of Reports of the 3rd Conference 'Unsteady-State Processes in Catalysis', Novosibirsk, 1986) Pt. 1, p. 170
140. L I Kalinkina, V M Kisarov, S M Iolkina, G N Toropkina, E M Kvashnina, I G Gurevich, G A Fateev *Proceedings of International Conference on Unsteady-State Processes in Catalysis, Novosibirsk, Utrecht, 1990* p. 525
141. USSR P. 1674933; *Byull. Izobret.* (33) 40 (1991)
142. A N Zagoruiko, O V Kostenko, A S Noskov *Chem. Eng. Sci.* **51** 2989 (1996)
143. A N Zagoruiko, Doctoral Thesis in Engineering Sciences, Institute of Catalysis, Siberian Branch of the Russian Academy of Sciences, Novosibirsk, 2006
144. A N Zagoruiko, O V Kostenko, P G Tsyul'nikov, V N Tomilov, V S Sal'nikov, A S Noskov *Khim. Prom-st* **4** 278 (1997)^d
145. A Salden, G Eigenberger *Chem. Eng. Sci.* **56** 1605 (2001)
146. N V Vernikovskaya, A N Zagoruiko, N A Chumakova, A S Noskov *Chem. Eng. Sci.* **54** 4639 (1999)
147. Russ. P. 2102119; *Byull. Izobret.* (2) 187 (1998)
148. Russ. P. 2147457; *Byull. Izobret.* (11) 131 (2000)
149. A N Zagoruiko *Tezisy Mezhdunarodnoi Konferentsii 'Khimrektor-14', Tomsk, 1998* (Abstracts of Reports of the International Conference 'Khimrektor-14', Tomsk, 1998) p. 61
150. Russ. P. 2176618; *Byull. Izobret.* (34) 247 (2001)
151. US P. 5487869; *Chem. Abstr.* **124** 298450 (1996)
152. Russ. P. 2263539; *Byull. Izobret.* (31) 449 (2005)
153. *Hydrocarbon Process.* **63** 74 (1984)
154. *Hydrocarbon Process.* **58** 140 (1979)
155. J Wieckowska *Catal. Today* **24** 405 (1995)
156. Russ. P. 2041162; *Byull. Izobret.* (22) 154 (1995)
157. USSR P. 911852; *Byull. Izobret.* (46) 211 (1984)
158. A N Zagoruiko, Candidate Thesis in Chemical Sciences, Institute of Catalysis, Siberian Branch of the Russian Academy of Sciences, Novosibirsk, 1991
159. USSR P. 1701625; *Byull. Izobret.* (48) 78 (1991)
160. USSR P. 1701626; *Byull. Izobret.* (48) 78 (1991)
161. Yu Sh Matros, A N Zagoruiko *Dokl. Akad. Nauk SSSR* **294** 1424 (1987)^b
162. O V Kiselev, Yu Sh Matros, G A Bunimovich, A S Noskov, A N Zagoruiko, A G Ivanov *Rasprostraneniye Teplovyykh Voln v Geterogennykh Sredakh* (Heat-Wave Transmission in Heterogeneous Media) (Novosibirsk: Nauka, 1988) p. 203
163. A N Zagoruiko, A S Noskov, V I Drobyshevich, L V Yausheva, I V Malakhova, Yu Sh Matros *Teor. Osnovy Khim. Tekhnol.* **23** 209 (1989)^c
164. A N Zagoruiko, Yu Sh Matros *Chem. Eng. J.* **87** 73 (2002)
165. G I Brolinskii, O I Sytyak *Razrabotka Tekhnologii Polucheniya Sery Metodom Klausia v Nestatsionarnom Rezhime (Otchet po NIR)* [Development of Technology of Synthesis of Sulfur by the Claus Method in Unsteady Regime (Report on Research Work)]; the article deposited in VINITI, No. 0288.0005770, L'vov, 1987
166. M P Elsner, C Dittrich, D W Agar *Chem. Eng. Sci.* **57** 1607 (2002)
167. M Grunewald, D W Agar *Chem. Eng. Sci.* **59** 5519 (2004)
168. D W Agar *Chem. Eng. Sci.* **54** 1299 (1999)
169. M P Elsner, M Menge, C Mmiller, D W Agar *Catal. Today* **79–80** 487 (2003)
170. US P. 2979384; *Chem. Abstr.* **55** 21510 (1961)
171. US P. 4439412; *Chem. Abstr.* **98** 128594 (1983)
172. Russ. P. 2088516; *Byull. Izobret.* (24) 298 (1997)
173. Russ. P. 2216506; *Byull. Izobret.* (32) 462 (2003)
174. WO PCT 2004103895; *Chem. Abstr.* **141** 426067 (2004)
175. Russ. P. 2261838; *Byull. Izobret.* (28) 853 (2005)
176. A N Startsev, I I Zakharov, O V Voroshina, A V Pashigreva, V N Parmon *Dokl. Akad. Nauk* **399** 217 (2004)^b
177. J K Lee, R R Hudgins, P L Silveston *Chem. Eng. Sci.* **16** 2523 (1995)
178. A N Stegasov, V A Kirillov, P L Silveston *Chem. Eng. Sci.* **49** 3699 (1994)
179. Y X Li, Z M Cheng, L H Liu, W K Yuan *Chem. Eng. Sci.* **10** 1571 (1999)
180. J P Briggs, R R Hudgins, P L Silveston *Chem. Eng. Sci.* **32** 1087 (1977)
181. Russ. P. 2085481; *Byull. Izobret.* (21) 263 (1997)
182. N V Vernikovskaya, A N Zagoruiko, A S Noskov *Chem. Eng. Sci.* **54** 4475 (1999)
183. G A Bunimovich, N V Vernikovskaya, V O Strots, B S Balzhinimaev, Yu Sh Matros *Chem. Eng. Sci.* **50** 565 (1995)
184. B S Balzhinimaev, A A Ivanov, O B Lapina, V M Mastikhin, K I Zamaraev *Faraday Discuss. Chem. Soc.* **87** 133 (1989)
185. A R Brun-Tsekhovoi, Doctoral Thesis in Chemical Sciences, Institute of Petrochemical Synthesis, Moscow, 1990
186. S S Kurdyumov, A R Brun-Tsekhovoi, A L Rosental *Pet. Chem.* **36** 139 (1996)
187. B Balasubramanian, A Lopez Ortiz, S Kaytakoglu, D P Harrison *Chem. Eng. Sci.* **15–16** 3543 (1999)
188. Y Ding, E Alpay *Chem. Eng. Sci.* **18** 3929 (2000)
189. G-h Xiua, P Lia, A E Rodrigues *Chem. Eng. J.* **1–3** 83 (2003)
190. E Ochoa-Fernandez, H K Rusten, H A Jakobsen, M Ronning, A Holmen, D Chen *Catal. Today* **106** 41 (2005)
191. D K Lee, I H Baek, W L Yoon *Chem. Eng. Sci.* **59** 931 (2004)
192. K Johnsen, H J Ru, J R Grace, C J Lim *Chem. Eng. Sci.* **61** 1195 (2006)
193. A G Okunev, V E Sharonov, Yu I Aristov *Tezisy Dokladov II Vserossiiskogo Seminara 'Toplivnye Elementy i Energoustanovki na ikh Osnove', Novosibirsk, 2003* (Abstracts of Reports of IIInd All-Union Seminar 'Fuel Cells and Energy Installations Based on Them'), Novosibirsk, 2003) p. 124
194. Ch Han, D P Harrison *Chem. Eng. Sci.* **24** 5875 (1994)
195. B T Carvill, J R Hufton, M Anand, S Sircar *AIChE J.* **42** 2756 (1996)
196. J Xu, G F Froment *AIChE J.* **35** 89 (1989)
197. V Hacker *J. Power Sources* **118** 311 (2003)
198. V Galvita, K Sundmacher *Proceedings of International Conference 'Chemreactor-17', Athens, 2006* p. 132
199. M Ryden, A Lyngfelt *Int. J. Hydrogen Energy* **31** 1271 (2006)
200. F J Derbyshire, D L Trimm *Carbon* **13** 189 (1975)
201. R T K Baker, M A Barber, P S Harris, F S Feates, R J Waite *J. Catal.* **26** 51 (1972)
202. A Sacco, P Thacker, T N Chang, A T S Chiang *J. Catal.* **85** 224 (1984)
203. P K de Bokx, A J H M Kock, E Boellaard, W Klop, J W Geus *J. Catal.* **96** 454 (1985)
204. L B Avdeeva, O V Goncharova, D I Kochubey, V I Zaikovskii, L M Plyasova, B N Novgorodov, Sh K Shaikhutdinov *Appl. Catal. A* **141** 117 (1996)
205. Z R Ismagilov, N V Shikina, V N Kruchinin, N A Rudina, V A Ushakov, N T Vasenin, H J Veringa *Catal. Today* **102–103** 85 (2005)
206. N Muradov, F Smith, A T Raissi *Catal. Today* **102–103** 225 (2005)
207. M A Ermakova, D Yu Ermakov, G G Kuvshinov *Appl. Catal. A* **201** 61 (2000)
208. T V Reshetenko, L B Avdeeva, Z R Ismagilov, A L Chuvilin, V B Fenelonov *Catal. Today* **102–103** 115 (2005)
209. T V Reshetenko, L B Avdeeva, Z R Ismagilov, V V Pushkarev, S V Cherepanov, A L Chuvilin, V A Likholobov *Carbon* **41** 1605 (2003)
210. H J Richter, K F Knocke *Inositol Phosphates and Derivatives (ACS Symp. Ser.)* (Washington, DC: American Chemical Society, 1983) Vol. 235, p. 71
211. M Ishida, D Zheng, T Akehata *Energy* **12** 147 (1983)
212. M Ishida, J Hin *Ind. Eng. Chem. Res.* **35** 2469 (1996)

213. R Villa, C Cristiani, G Groppi, L Lietti, P Forzatti, U Coronaro, S Rossini *J. Mol. Catal. A* **204–205** 637 (2003)
214. A N Zagoruiko *Proceedings of International Conference 'Chemreactor-16', Berlin, 2003* p. 202
215. A N Zagoruiko *Teor. Osnovy Khim. Tekhnol.* **39** 72 (2005)^c
216. A N Zagoruiko *Chem. Eng. J.* **107** 133 (2005)
217. A N Zagoruiko *Proceedings of International Conference 'Chemreactor-17', Athens, 2006* p. 169
218. US P. 5530171; *Chem. Abstr.* **125** 11415 (1996)
219. R K Grasselli, D L Stern, G G Tsykoyannis *Appl. Catal. A* **189** 9 (1999)
220. R M Contractor *Chem. Eng. Sci.* **22** 5627 (1999)
221. A A Ivanov *Mekhanizmy Geterogenno-kataliticheskikh Reaktsii Okisleniya* (Mechanisms of Heterogeneous and Catalytic Reactions of Oxidation) (Novosibirsk: Institute of Catalysis, Siberian Branch of the Russian Academy of Sciences, 1993) p. 103
222. US P. 6291686; *Chem. Abstr.* **132** 153651 (2001)
223. R M Heck, R J Farrauto *Appl. Catal. A* **221** 443 (2001)
224. M Shelef, R W McCabe *Catal. Today* **26** 35 (2000)
225. T V Pavlova, N V Vernikovskaya, N A Chumakova, A S Noskov *Trudy Pervoi Shkoly-konferentsii 'Dizain Katalizatorov', Novosibirsk, 2006* (Proceedings of the First School-Conference 'Design of Catalysts', Novosibirsk, 2006) p. 244
226. W S Epling, L E Campbell, A Yezerets, N W Currier, J E Parks *Catal. Rev. Sci. Eng.* **46** 163 (2004)
227. US P. 6314722; *Chem. Abstr.* **135** 361806 (2001)
228. D Agar *Proceedings of International Conference 'Recovery, Recycling, Reintegration', Geneva, 1997* Vol. 4, p. 45
229. U Nieken, O Watzenberger *Chem. Eng. Sci.* **54** 2619 (1999)
230. A Breed, M F Doherty, S Gadewar, P Grosso, I M Lorkovic, E W McFarland, M J Weiss *Catal. Today* **106** 301 (2005)
231. M Kuczynski, M H Oyevaar, R T Pieters, K R Westerterp *Chem. Eng. Sci.* **42** 1887 (1987)
232. S Goto, T Tagawa, T Oomiya *Chem. Eng. Essay* **19** 978 (1993)
233. E A Ivanov, S I Reshetnikov, M V Sidiyakin, A N Startsev *React. Kinet. Catal. Lett.* **2** 389 (2003)
234. K S Gulyaev, Candidate Thesis in Chemical Sciences, Omsk Branch of Institute of Catalysis, Siberian Branch of the Russian Academy of Sciences, Omsk, 1997

^a — *Kinet. Catal. (Engl. Transl.)*

^b — *Dokl. Phys. Chem. (Engl. Transl.)*

^c — *Russ. J. Appl. Chem. (Engl. Transl.)*

^d — *Ind. Chem. (Engl. Transl.)*

^e — *Theor. Found. Chem. Eng. (Engl. Transl.)*

Plant metabolites of the Siberian flora. Chemical transformations and the scope of practical application

E E Shults, V A Raldugin, K P Volcho, N F Salakhutdinov, G A Tolstikov

Contents

I. Introduction	655
II. Results of the resource and structural analytical studies	655
III. Chemical transformations of terpenoids and alkaloids	658
IV. Practical applications of natural compounds and their derivatives	667

Abstract. The results of studies of some terpenoids, alkaloids and phenolic derivatives isolated from Siberian plants are summarised. The structures of the compounds studied are presented and the chemical transformations of the available terpenoids and alkaloids are considered. Examples of practical application of natural compounds and their derivatives are given. The bibliography includes 131 references.

I. Introduction

Natural compounds of plant origin, namely, secondary plant metabolites, are of interest from the scientific and practical standpoints. A fundamental basis for resource studies lies in taxonomy, determination of the chemical composition of plants and elucidation of the structure of particular components. Often, chemical compounds isolated from plants represent novel classes of chemical compounds, which favours the progress in new fields of organic chemistry. At the same time, many plant metabolites and products of their transformations possess practically useful properties, first of all, various biological activities.

At present, a great body of information on plants as sources of valuable compounds has been collected. Many of these compounds can easily be produced in amounts that meet current demands. The development of efficient methods for the isolation of natural compounds in individual form stimulates the design of new pharmaceuticals and agricultural preparations based on them.

Plant metabolites themselves can be the active principles of drugs. For instance, oriental medicine has long used camphor, which was recommended as an inhalation remedy during plague epidemic in the Middle Ages in Europe. A number of individual natural compounds were introduced into medicinal

practice in the 19th century. These are quinine, morphine, strophanthin, *etc.* In the 1950s, drugs based on alkaloids vinblastine and vincristine were introduced into antitumour therapy.

However, at present the search for biologically active compounds is mainly associated with modification of the known plant metabolites aimed at either enhancing the original activity of the chemical compound or obtaining derivatives that exhibit other activities.

For a long time, researchers working at the N N Vorozhtsov Novosibirsk Institute of Organic Chemistry, Siberian Branch of the Russian Academy of Sciences, have been investigating the chemical composition of compounds isolated from forest trees and landscape plants of Siberia and Altai. The resource and structural analytical studies are being carried out to reveal plant producers of valuable metabolites and to develop new methods of processing of plant raw materials to isolate individual compounds that are either used in practice or are of interest for the design of chemical structures with novel properties. The structures of the compounds isolated are determined using all available modern physicochemical methods. In the last two decades, the research carried out at the Institute follows a programme that is aimed, on the one hand, at obtaining basic knowledge on the reactivity of three important classes of plant metabolites, namely, terpenoids, alkaloids and phenolic compounds and, on the other hand, at searching biologically valuable derivatives of these classes of compounds. The ultimate goal of these studies is the development of novel pharmaceuticals and environmentally safe pesticides.

The present review reports on the most important results obtained in the studies of secondary plant metabolites of the Siberian flora.

II. Results of the resource and structural analytical studies

In the 1960s, N N Vorozhtsov, the founder of the Novosibirsk Institute of Organic Chemistry (NIOCh), Siberian Branch of the Russian Academy of Sciences, initiated organisation of the laboratory for wood chemistry. The first two decades of studies headed by V A Pentegova gave a great deal of information on coniferous plants growing in Siberia and Far East (pine, cedar, abies, *etc.*) as unique sources of terpene compounds. Chemical compositions of oleoresins, turpentine and extracts including mono-, sesqui- and diterpenoids from several species of coniferae were determined. The results obtained in these studies

E E Shults, V A Raldugin, K P Volcho, N F Salakhutdinov, G A Tolstikov
N N Vorozhtsov Novosibirsk Institute of Organic Chemistry, Siberian Branch of the Russian Academy of Sciences, prosp. Acad. Lavrentieva 9, 630090 Novosibirsk, Russian Federation. Fax (7-383) 330 97 52, tel. (7-383) 330 85 33, e-mail: schultz@nioch.nsc.ru (E E Shults), raldugin@nioch.nsc.ru (V A Raldugin), volcho@nioch.nsc.ru (K P Volcho), tel. (7-383) 330 97 33, e-mail: anvar@nioch.nsc.ru (N F Salakhutdinov), tel. (7-383) 330 49 80, e-mail: gtolstik@nioch.nsc.ru (G A Tolstikov)

Received 10 April 2007

Uspekhi Khimii 76 (7) 707–723 (2007); translated by A M Raevskiy

were summarised in a monograph¹ and by right became part of the treasury of knowledge in the domestic and world science of resources and served as the basis of a new research avenue, which is rapidly developed at present.

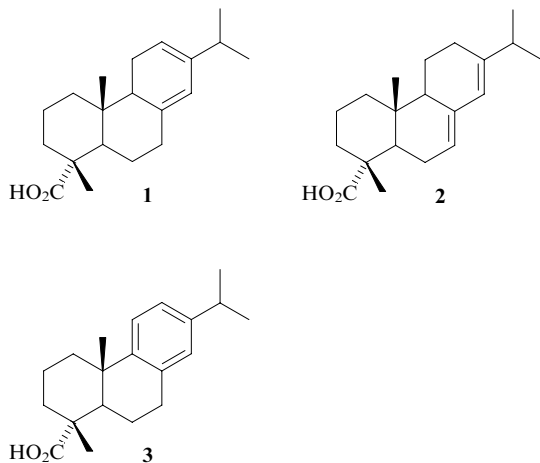
Particular attention is paid to Siberian plants containing di- and triterpenoids. The interest of chemists and pharmacologists in these compounds is indicated by a number of publications.^{2–7} In addition to terpenoids, researchers at the NIOCh study readily available alkaloids and phenolic metabolites present in some landscape plants. The resource and structural analytical studies of the Siberian flora included search for sources of promising plant metabolites, investigations of variation of the composition of the components depending on the species of plants, identification and structural elucidation of individual compounds and the development of optimum isolation procedures. As a result, researchers at the NIOCh created a database that includes the metabolites characterised by the following major features:

- availability of the plant source;
- efficiency of the isolation procedures;
- chemical structure providing great potential for synthetic modification; and
- putative biological activity.

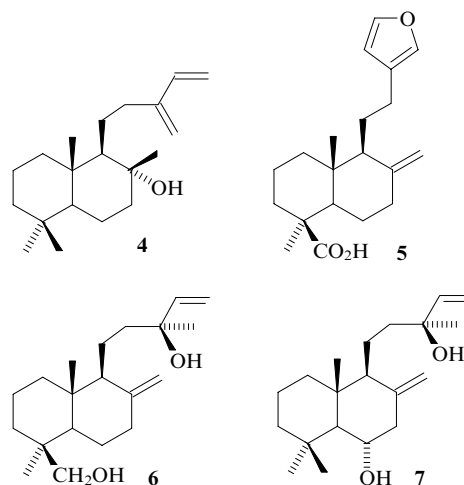
Here we shall consider a number of compounds that are of interest for further investigations isolation of which from Siberian plants relies on well-developed procedures.

1. Diterpenoids

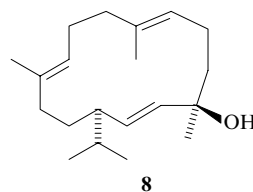
Undoubtedly, levopimaric acid (**1**), abietic acid (**2**) and their derivative, dehydroabietic acid (**3**) are the most available tricyclic diterpenoids. These compounds are isolated from pine resin and oleoresin, being of interest as substrates for targeted chemical transformations and pharmacological studies.⁸



One of the key components of the extractives of pine needles is a labdane-type diterpenoid isoabienol (**4**). Labdanoids containing a conjugated diene system in the side chain are of interest as the starting compounds for the synthesis of fragrances⁹ and pharmaceuticals.¹⁰ Yet another labdanoid, lambertianic acid (**5**),^{11,12} which can readily be isolated from cedar oleoresin and needles, also exhibits physiological activity. Labdanoids epitorusolol (**6**) and larixol (**7**) can be obtained from oleoresins of the Siberian and Gmelin larch.

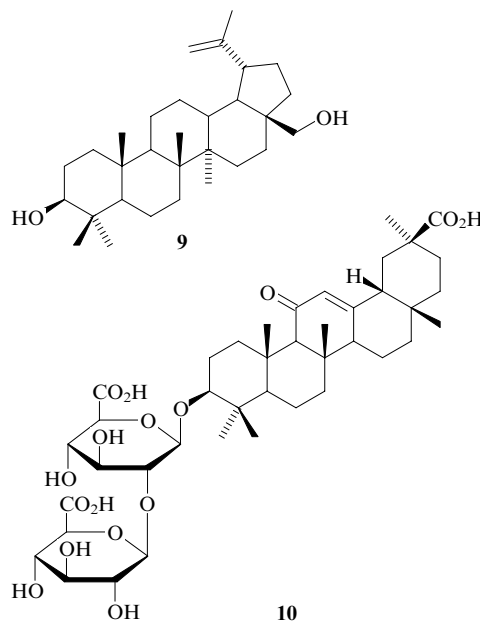


Among monocyclic diterpenoids isolated from the oleoresin of Siberian cedar, macrocyclic cembranoid isocembrol (**8**), a structural analogue of metabolites of marine organisms possessing high antitumour activity,¹³ deserves attention.

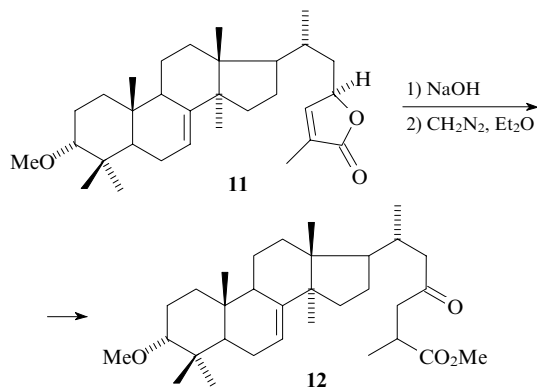


2. Triterpenoids

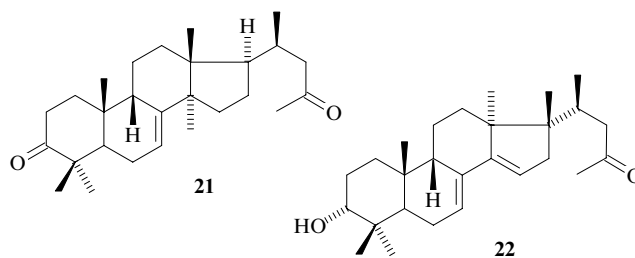
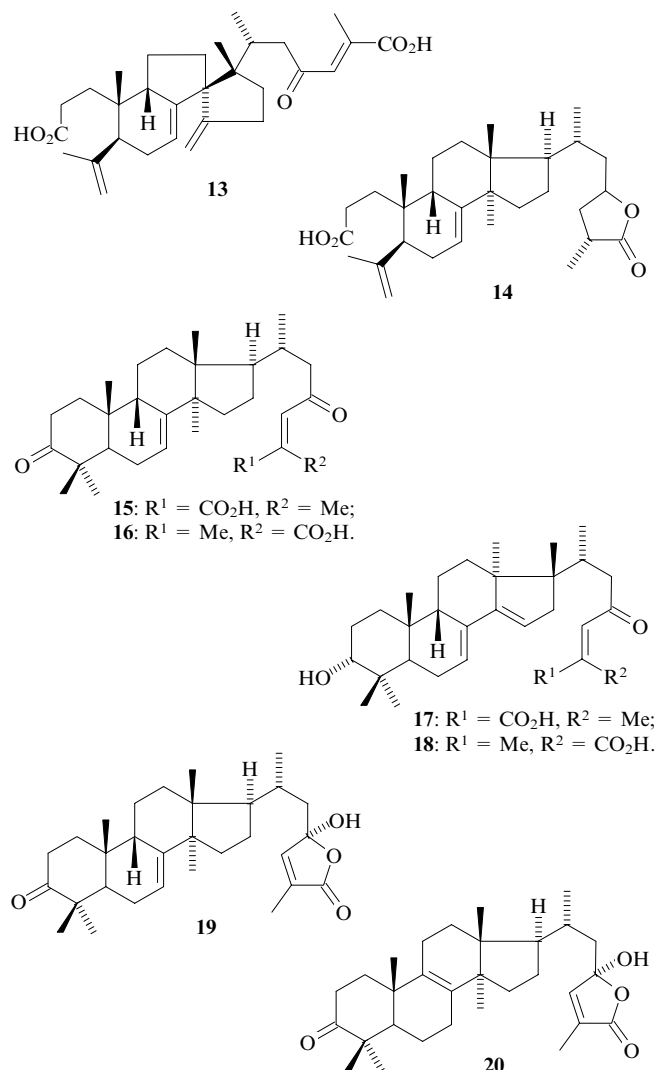
As to triterpene compounds, betulin (**9**) isolated from birch bark^{5,14} and glycyrrhizic acid (**10**), a metabolite of licorice⁶ belonging to oleanane-type glycosides, should undoubtedly be ranked first in the availability and pharmacological potential.



From the standpoint of plant physiology, Firs (*Abies* genus) differ from Pines, Spruces and Larches belonging to the same botanical family in production of triterpenoids having a modified lanostane carbon skeleton. One of them, namely, abieslactone (**11**) present in bark of many species of Firs, can readily be isolated from extracts of plant raw materials by crystallisation.^{15, 16} Of particular interest is also an abieslactone derivative **12** with an antitumour activity.¹⁷



Triterpenoids **13–22** produced by Siberian fir (*Abies sibirica* Ledeb.) show structural diversity.^{18–31} These compounds can affect the immune status of agricultural plants, thus enhancing their resistance against fungi.

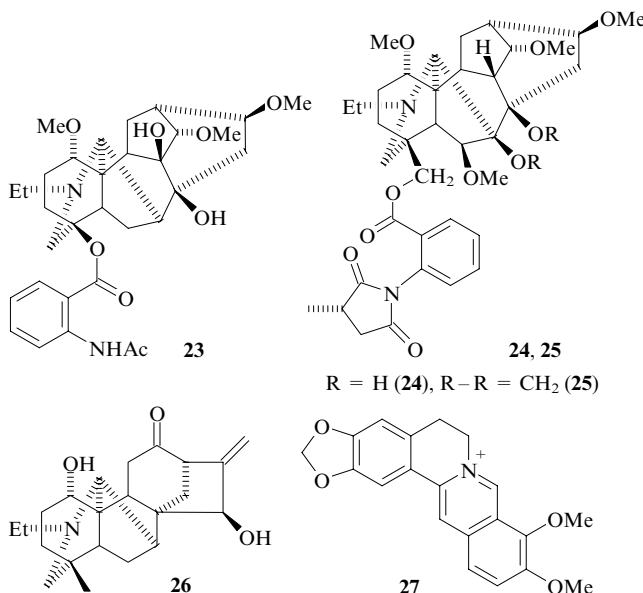


3. Alkaloids

Classical investigations on alkaloids carried out by researchers from the scientific school headed by academician S Yu Yunusov (Uzbekistan) demonstrate a fruitful combination of the resource, taxonomic, structural analytical and processing studies that enabled the progress in medicinal chemistry and pharmaceutical industry. Despite the fact that most of these studies were carried out using Middle-Asian plant raw materials (see, *e.g.*, a review³²), they played an important role in the studies of Russian alkaloid-containing flora.

The first results of studies on the chemistry, isolation techniques and pharmacological properties of alkaloids from Siberian and Altai plants carried out at the NIOCh clearly demonstrated that the methods and strategies developed by the researchers from Uzbekistan are well applicable for progress in this research avenue. Plants of West Siberia and Gornyi Altai are rich sources of alkaloids many of which also grow in mountain regions of the Middle Asian.

To date, the field and processing investigations made a number of alkaloids including lappaconitine (**23**), methyllicaconitine (**24**), elatine (**25**), songorine (**26**) and berberine (**27**) available for extensive studies.^{33–35} For instance, the pilot plant at the NIOCh can produce several kilogrammes of lappaconitine (**23**) annually.

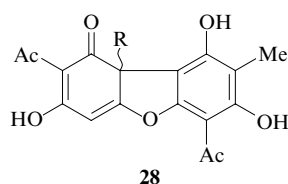


Lappaconitine (**23**) isolated from *Aconitum septentrionale* Koelle is the active principle of the anti-arrhythmic drug allapinine.³⁶ Alkaloids **24** and **25** isolated from *Delphinium retropilosum* Sambuk³⁴ and *Delphinium elatum* L (Ref. 33), respectively, are agonists of neuronal acetylcholine receptors (N-AChRs);³⁷ the former compound also shows insecticide activity.³⁸ The antiarrhythmic activity of songorine (**26**) produced by *Aconitum barbatum* Pers.³⁵ was reported by research-

chers from Uzbekistan in the 1970s³⁹ and berberine (**27**) isolated from *Berberis sibirica* Pall. is known as choleric and antimalarial agent.⁴⁰

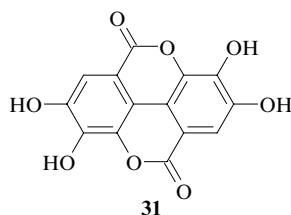
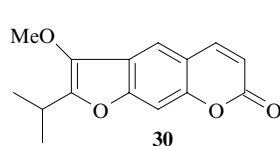
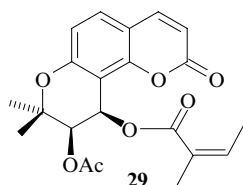
4. Phenolic compounds

Phenolic plant metabolites represent one of the most important classes of natural bioregulators that can have beneficial effect on the vital functions of organisms.^{41–43} Many of them inhibit tumorigenesis and exhibit antiviral (including anti-HIV) and antitubercular activities. Phenolic metabolites of the Siberian flora show a diversity of structural types and have a great resource potential. According to the data obtained by researchers from the Irkutsk Institute of Chemistry, Siberian Branch of the Russian Academy of Sciences,⁴⁴ the total amount of larch wastewood permits large-scale production of phenolic metabolites used as substances for biologically active additives. Recent studies carried out at the NIOCh made many phenolic metabolites available,^{45,46} first of all, the (+)- and (–)-usnic acids (**28**) isolated from lichens.

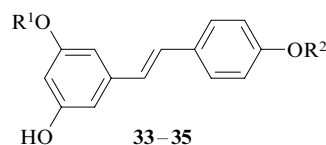
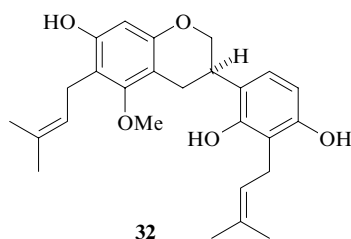


R = β-Me [(+)-**28**], α-Me [(–)-**28**].

Phenolic compounds also include linear and angular coumarins, which are internal phenol esters. Some Umbelliferae plants produce (+)-pterixin (**29**)⁴⁵ and peucedanin (**30**);⁴⁶ *Myricaria dahurica* is a producer of ellagic acid (**31**), a strong protein kinase inhibitor.⁴⁷



Licorice roots are a source of licoricidine (**32**), which exhibits antiulcer and antitumour activity.⁴⁸ Cedar bark contains readily extractable resveratrol (**33**), pinostilbene (**34**) and their glycoside derivatives, namely, resveratrolsides (**35a**) and pinostilbensides (**35b**).⁴⁹ The therapeutic action of stilbenes **33–35** has been comprehensively reviewed.⁵⁰



R¹ = R² = H (**33**), Me (**34**); R² = Glc: R¹ = H (**35a**), Me (**35b**).

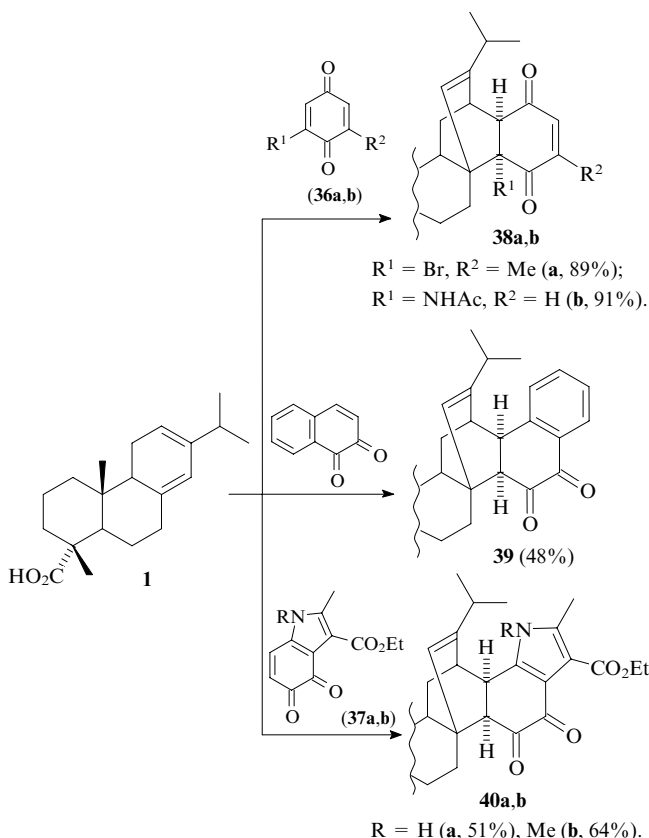
All these phenolic metabolites are considered as promising agents for further modification.

III. Chemical transformations of terpenoids and alkaloids

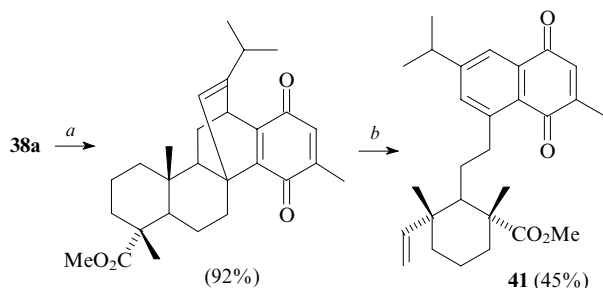
1. The Diels–Alder (retro-Diels–Alder) reactions

The availability of levopimaric acid (**1**) has made it a subject of synthetic studies. This diterpenoid has two conjugated double bonds and readily reacts with activated alkenes.⁵¹ (Note that the Diels–Alder reaction adducts can be obtained from pine oleoresin containing up to 20% of levopimaric acid). Compound **1** readily reacts with quinone-type dienophiles to give high yields of adducts of unique structures.^{52,53} The effect of the dienophile structure on the selectivity of [4+2]-cycloaddition was studied taking levopimaric acid as an example. It was established that 2,6-disubstituted benzoquinones **36a,b**, 1,2-naphthoquinone and indoloquinones **37a,b** add to diene **1** regioselectively. Regioselectivity of the cycloaddition of asymmetric benzoquinones **36a,b** can be explained by the presence of electron-donor substituents (NHAc, Br) in their molecules; this favours the formation of a hydrogen bond between the carboxyl group and the carbonyl oxygen atom in position 1 of the quinone molecule. In addition, stabilisation of this transition state is also due to the shielding effect of the isopropyl group. Levopimaric acid derivatives **38–40** can be of interest as the starting compounds for the synthesis of pharmacologically valuable products (Scheme 1).

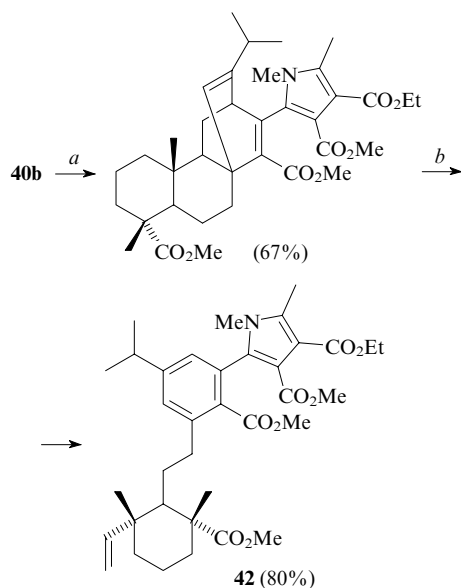
Scheme 1



Of particular interest is the ability of adducts, *i.e.*, bicyclooctadienes, to undergo a retro-diene cleavage. This reaction offers efficient ways for the synthesis of derivatives containing terminal vinyl groups, *e.g.*, 1,4-naphthoquinone (**41**) and pyrrole (**42**).⁵³



(a) 1) CH_2N_2 ; 2) Al_2O_3 , HO^- ; (b) DMF, 150 °C.

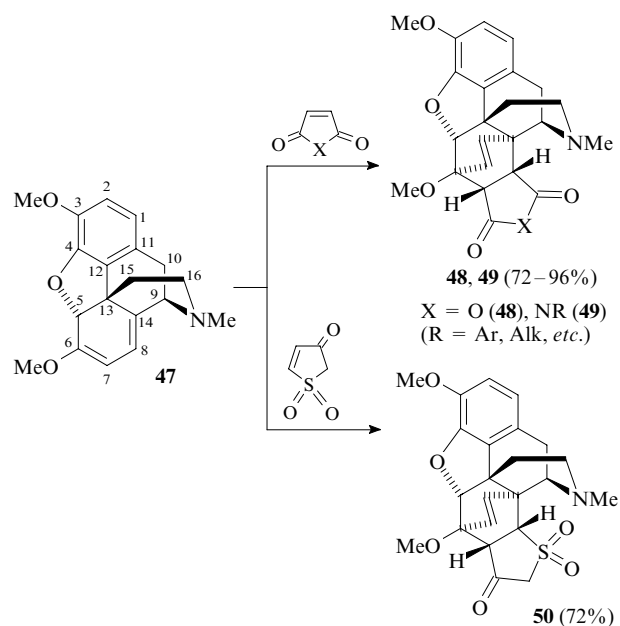


(a) 1) H_2O_2 , HO^- , 50 °C; 2) CH_2N_2 ; (b) 260 °C.

Quinopimaric acid (**43**) turned out to be a highly reactive dienophile, which readily reacts with silyloxy- and sulfur-containing butadienes and their aza analogues.⁵⁴ For instance, the reactions of acid **43** with 5-alkoxyoxazoles (the Kondra-

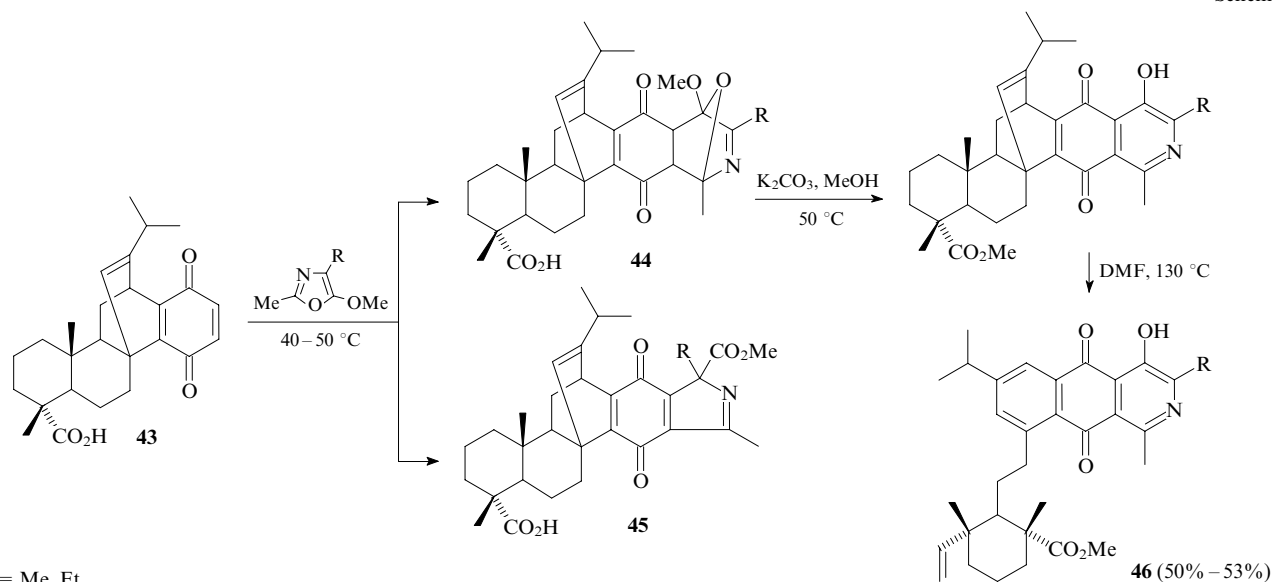
tyeva reagents) result in two compounds, *viz.*, a Diels–Alder adduct **44** and a 1,3-dipolar cycloadduct **45**.⁵⁵ In the latter case, the dipole is likely to be formed upon thermal decomposition of 5-alkoxyoxazole. The results of the reactions of quinopimaric acid (**43**) with alkoxyoxazoles depend on the nature of the solvent. In acetic acid, compounds **44** are the major products (yields 58%–67%), whereas the reactions in an AcOH–MeCN mixture afford adducts **44** (yields 40%–42%) and isoindole derivatives **45** (yields 25%–35%). Further transformations of compound **44** give terpenylazaanthraquinones **46** (Scheme 2).

The behaviour of a morphinan-type alkaloid thebaine (**47**) in the Diels–Alder reaction was studied.⁵⁶ A new group of thebaine derivatives was synthesised, which includes compounds **48**–**54** containing additional carbocyclic and hetero-

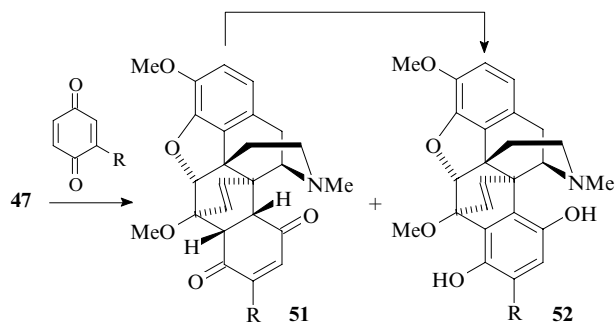


cyclic units.^{57–63} Maleimides and maleic anhydride, 2,3-dihydrothiophen-3-one 1,1-dioxide, substituted benzoquinones (or the corresponding hydroquinones in the presence of Ag_2O) and indoloquinones **37a,b** served as the dienophiles. The cycloaddition of thebaine (**47**) to cyclic dienophiles results in 7,8-fused derivatives **46** of 6 α ,14 α -ethnoisomorphinans; the reaction is regioselective in the case of non-symmetric dienophiles.

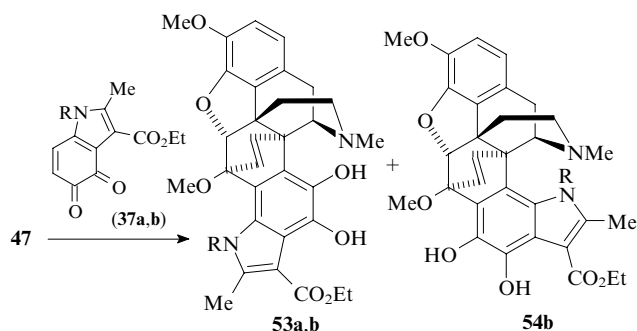
Scheme 2



R = Me, Et.



R = NHAc, SCH₂X (X = CH₂OH, CO₂H, CO₂Me, CH(NH₂)CH₂OH).

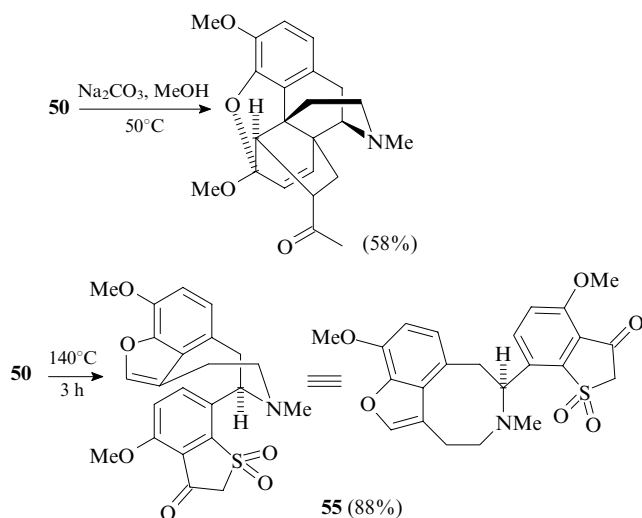


R = H (a), Me (b).

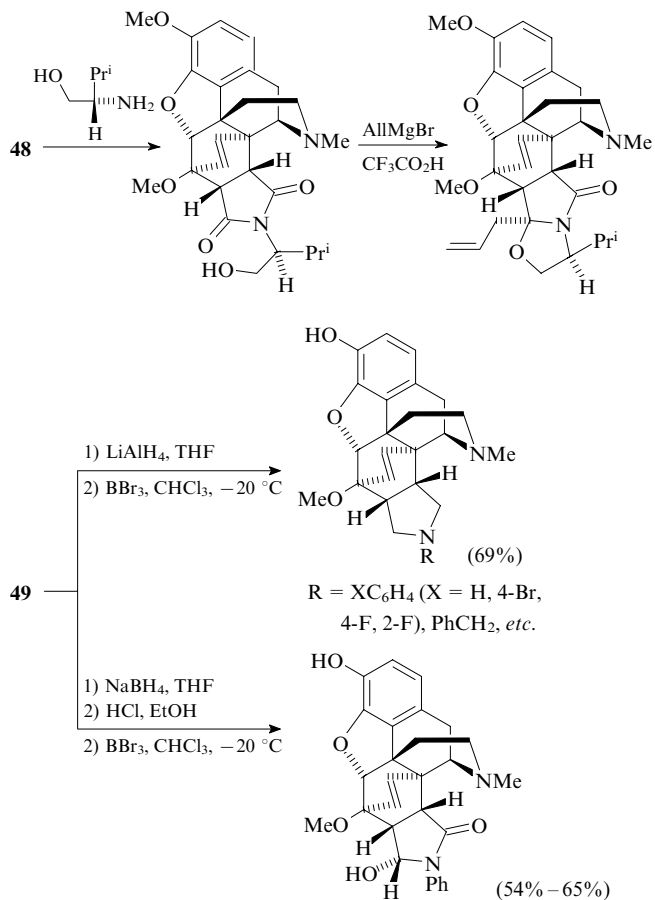
Thebaine (47) reacts with substituted benzoquinones (aqueous dioxane, 20 °C) or with a system hydroquinone–silver oxide (MeOH, 20 °C) to give adducts 51 and subsequent fused hydroquinones 52 (yields 75%–90%). The product ratio varies from 1 : 8 to 1 : 10. Compounds 51 readily isomerise to hydroquinone derivatives 52 under the action of alkaline alumina in CH₂Cl₂ (yields 92%–98%).

Indoloquinone 37a adds to thebaine (47) in aqueous dioxane with simultaneous aromatisation to a dihydro derivative 53a (yield 62%). Regioselectivity of the reaction is probably due to stabilisation of the transition state upon the interaction of the NH group in the pyrrole fragment with the methoxy group in position 6. The reaction of *N*-methylindoloquinone 37b with diene 47 results in products 53b and 54b in a 3 : 2 ratio (overall yield 75%).

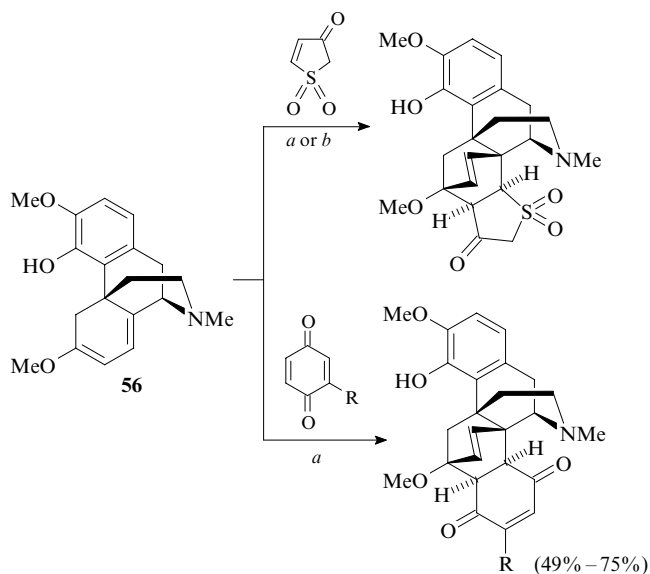
A thebaine adduct 50 is prone to skeletal rearrangements with elimination of SO₂.^{57, 60, 61, 64} For the mechanism of this reaction, see Ref. 57. The retro-Diels–Alder cleavage of compound 50 results in a furobenzoazocine derivative 55.^{58, 61, 64}



Here we present some transformations^{62, 63} of adducts 48 and 49, which made it possible to synthesise oripavines (promising psychotropic agents) from natural alkaloids.^{61, 63}



Reactions of morphinandiene 56 with a number of dienophiles were also studied. Taking the Diels–Alder reactions of dienes 47 and 56 as examples, the factors affecting the regio- and stereoselectivity of these processes were studied. It was found that introduction of morphinandiene 56 devoid of the dihydrofuran fragment into the reaction changes the stereochemistry of the cycloaddition. This results in 6β,14β-ethenomorphinans.^{59, 64}



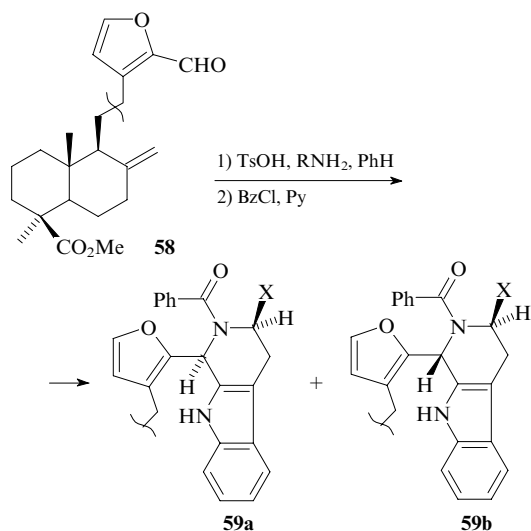
(a) aqueous dioxane; (b) Al₂O₃, CH₂Cl₂, 20 °C.

R = NHAc, SCH₂X [X = CH₂OH, CO₂H, CO₂Me, CH(NH₂)CH₂OH].

2. Diterpenoids in the synthesis of alkaloid-like compounds

Alkaloid-like compounds can be synthesised from structures that can be readily transformed to nitrogen-containing heterocycles. These are, *e.g.*, methyl lambertianate (**57**) and related derivatives.

For instance, terpenocarbolines **59a,b** were synthesised from methyl 16-formyllambertianate (**58**) using the Pictet–Spengler reaction.⁶⁵

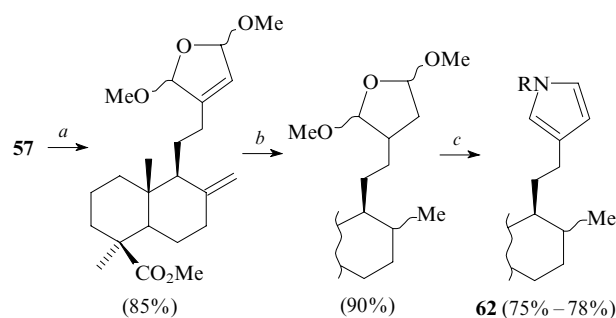


RNH₂ is triptamine, X = H; RNH₂ is L-tryptophan, X = CO₂H.

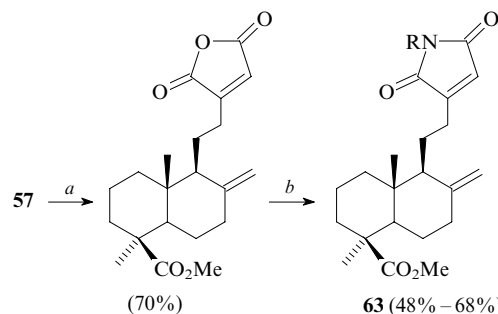
By choosing selective oxidants affecting different fragments of the molecule of lambertianic acid (**5**), it is possible to obtain various oxygen-containing derivatives suitable for further structural modifications. For instance, the oxidation of methyl lambertianate (**57**) followed by aminomethylation involving the furan ring led to *N*-heterocycles **60** and **61** (Scheme 3).^{66, 67}

The synthesis of pyrrolyllabdanoids **62** and **63** from compound **5** has been reported.^{68, 69} In the first stage lambertianic

acid (**5**) is converted to methyl ester **57** under the action of dimethyl sulfate in ethanol; ester **57** is then oxidised using various reagents. Note that compound **62** was isolated as a 1 : 1 mixture of C(8)-epimers.



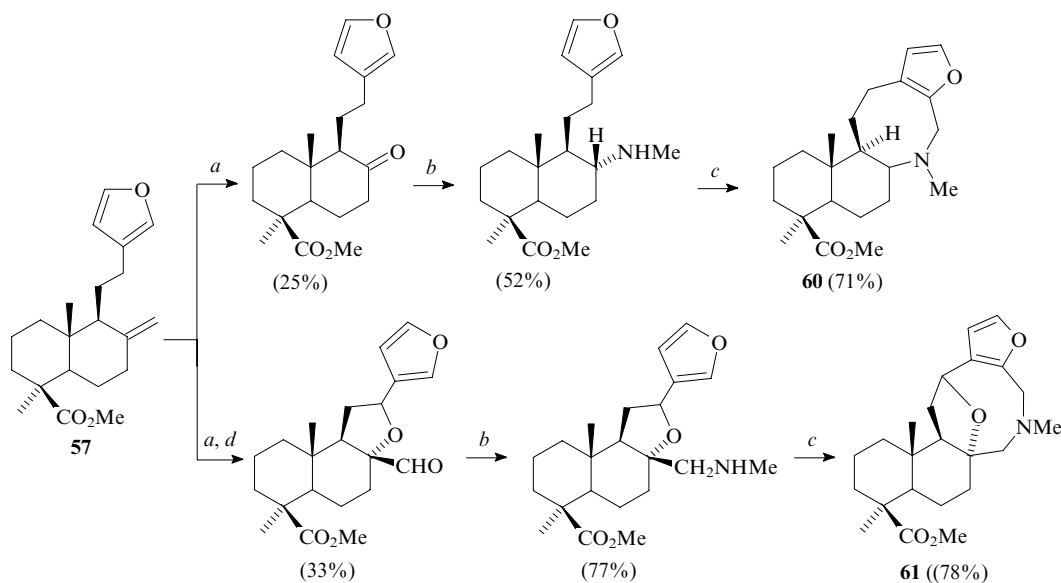
(a) PhSO₂NHCl, MeOH, 0–5 °C; (b) H₂/Ni-Ra, MeOH, 20 °C; (c) RNH₂, AcOH, H₂O, 90 °C, 15 min. R = Me, Et, cyclo-Pr, Bn.



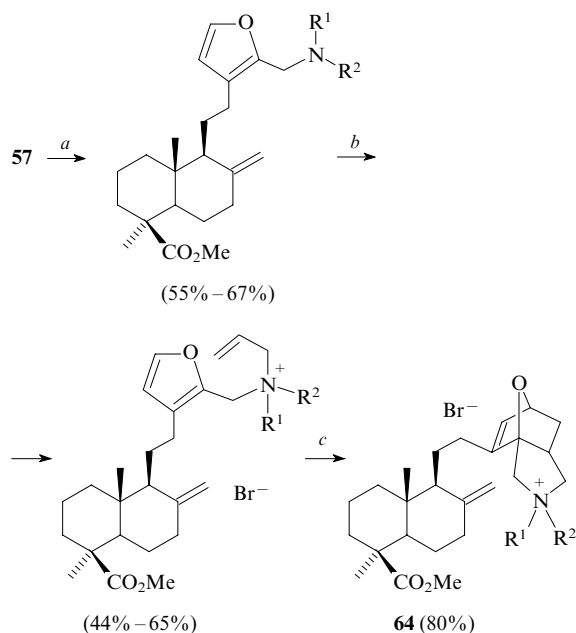
(a) CrO₃, H₂SO₄, Me₂CO, 0–20 °C; (b) RNH₂, AcOH, 100 °C, 5–8 h. R = Bn, (CH₂)₂Ph, (CH₂)₂C₆H₄OH-4, CH(CO₂H)Et, (CH₂)₃CO₂H.

Synthetic routes to labdane derivatives **64** and **65** containing tricyclic nitrogen-containing fragments starting from lambertianic acid were developed.^{70, 71}

Scheme 3

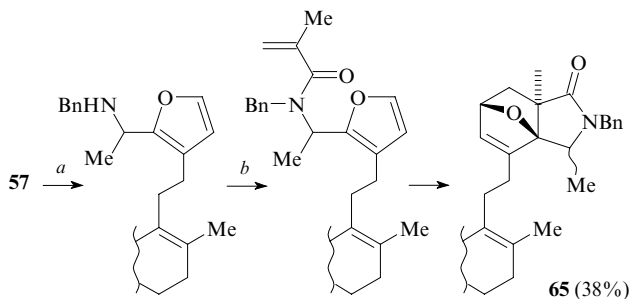


(a) KMnO₄–MgSO₄, PhH, H₂O, Bu₄NBr, 50 °C; (b) 1) MeNH₂, MeOH; 2) NaBH₄; (c) (CH₂O)_n, CF₃CO₂H, PhH, 80 °C; (d) PCC, CH₂Cl₂, 20 °C; PCC is pyridinium chlorochromate.



(a) $(\text{Me}_2\text{N})_2\text{CH}_2$ or *N*-bis(piperidino)methane, AcCl , CH_2Cl_2 , $0 \rightarrow 20^\circ\text{C}$;
 (b) AlI_3 , PhH , KOH , K_2CO_3 , Me_3BnNCl , 80°C ; (c) PhH , 80°C .
 $\text{R}^1 = \text{R}^2 = \text{Me}$; $\text{R}^1 - \text{R}^2 = (\text{CH}_2)_5$.

Alkylation of the amino derivative (step *b*) in acetonitrile as a solvent results in products **64** (yields 54%–58%) without isolation of salt. All stages of the synthesis of compound **65** are characterised by good yields (68%–84%), the last step, heterocyclisation, occurs spontaneously.

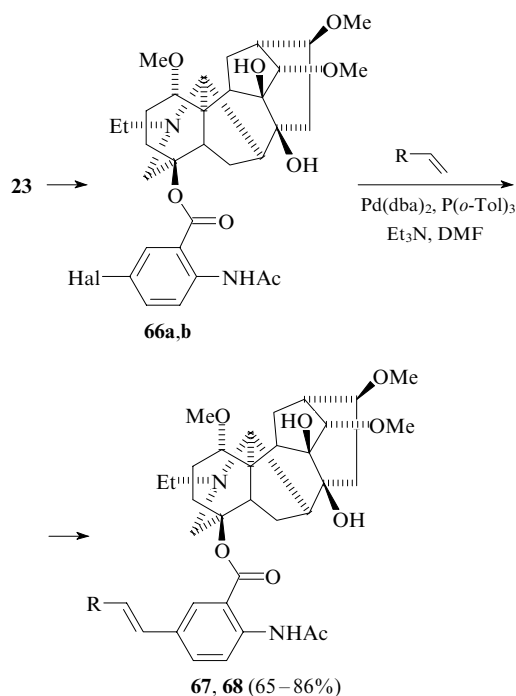


(a) 1) TsOH , PhH , 80°C ; 2) $\text{Mg}(\text{ClO}_4)_2$, Ac_2O , 20°C ; 3) BnNH_2 , NaBH_4 , $(\text{Pr}^i\text{O})_4\text{Ti}$, $0 \rightarrow 20^\circ\text{C}$; (b) Et_3N , CHCl_3 .

3. Reactions involving metal complex catalysis

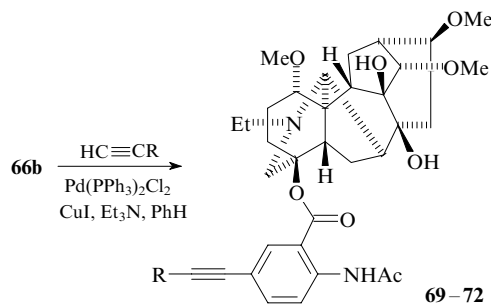
The programme of studies on synthetic transformations of some available alkaloids carried out at the NIOCh^{72–79} involves metal complex catalysis as a particular research avenue.

For instance, the aromatic fragment of lappaconitine (**23**) was modified using cross-coupling reactions.^{80, 81} Procedures for lappaconitine bromination and iodination were also developed, which made it possible to obtain the corresponding 5'-halogeno derivatives **66a,b**. Lappaconitine derivatives **67** and **68** containing alkenyl substituents conjugated with the benzene ring were first synthesised by condensation of these halides with ethyl acrylate or 5-vinyl-2-methylpyridine under the Heck reaction conditions.



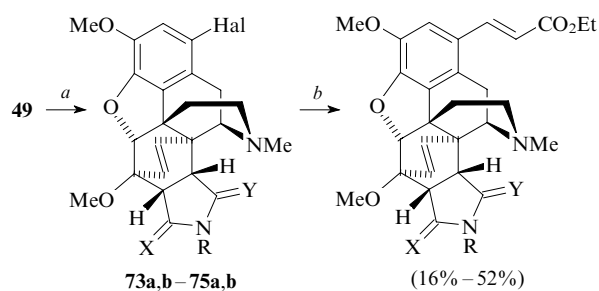
$\text{Hal} = \text{Br}$ (**66a**), I (**66b**); $\text{R} = \text{EtO}_2\text{C}$ (**67**), Me (**68**);
 dba is dibenzylidene acetone.

Condensation of 5'-iodolappaconitine **66b** with terminal acetylenes, namely, prop-2-yn-1-ol, 2-methylbut-3-yn-2-ol, phenylacetylene and 5-ethynylpyrimidine under the Sonogashira reaction conditions affords lappaconitine derivatives **69–72** containing alkynyl fragments.



$\text{R} = \text{CH}_2\text{OH}$ (**69**), CM_2OH (**70**), Ph (**71**), N -substituted pyrimidine (**72**).

Halogeno derivatives of *endo*-ethenotetrahydrothebaine (**73a,b–75a,b**) and dihydrothebainohydroquinone (**76a,b**) also react with various alkenes in the presence of palladium complex catalysts.^{82, 83} This strategy was used for the synthesis of some C(1)-substituted thebaine derivatives. Succinimido-annulated 1-iodotetrahydrothebaines **73b** are more reactive than pyrrolidine derivatives **74b** in the Heck reaction with ethyl acrylate; the reactions of the former compounds occur under milder conditions and in higher yields.



(a) Br₂ (or ICl), HCO₂H; (b) CH₂=CHCO₂Et, Pd(OAc)₂, P(*o*-Tol)₃,

Et₃N, DMF.

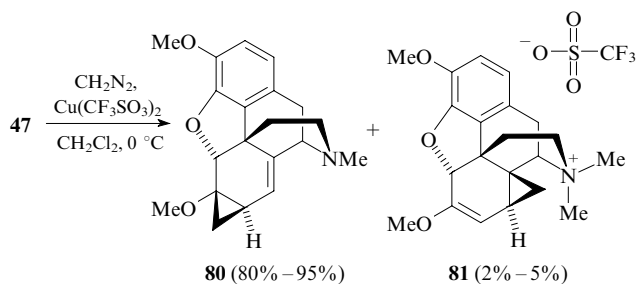
X = Y = O (**73**); X = Y = H₂ (**74**); X = , Y = O (**75**);

Hal = Br (**a**), I (**b**); R = H, Me, Ph, 4-BrC₆H₄.

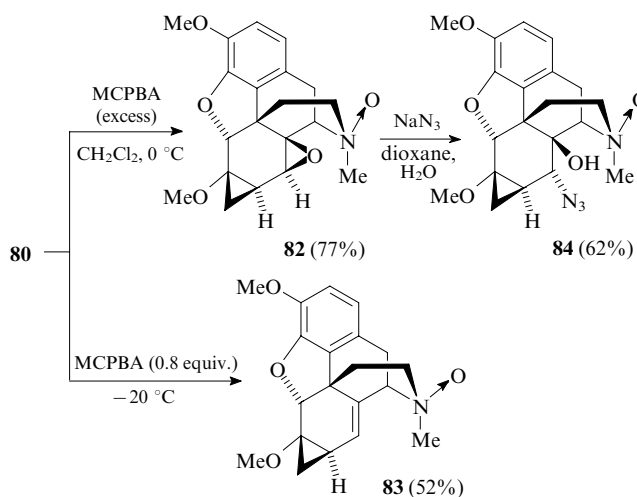
The effect of the structure of alkenes (acrylates, 2-methyl-5-vinylpyridine, styrene, alkyl vinyl ethers) on the yield of 1-ethenyl-substituted dihydrothebainohydroquinones was studied. It was found that the reaction of 7,8-(1-acetoxy-4-hydroxybenzo)-1-iodo-6,14-*endo*-ethenodihydrothebaine (**76b**) with ethyl vinyl ether results in an arylation product at α -position of the ethyl vinyl ether molecule, but work up of the reaction mixture gives 1-acetyl-7,8-(1-acetoxy-4-hydroxybenzo)-6,14-*endo*-ethenodihydrothebaine (**77b**) as a result of hydrolysis. 1-[(*E*)-Pyridinylethenyl]dihydrothebainohydroquinone **78b** was used in the synthesis of hybrid structures **79b** containing fragments of indolizine- and isoquinoline-type alkaloids (Scheme 4).

Structural modification of thebaine (**47**) and its 7,8-annulated derivatives (e.g., compounds **49** and **52**) using organo-metallic compounds made it possible to synthesise novel morphinan derivatives containing substituents at the C(8) and C(1) atoms. For instance, thebaine adds diazomethane in the presence of copper triflate (0.02–0.04 mol) to give 6 β ,7 β -methylene-6,7-dihydrothebaine (**80**), a carbene addition product of to the C(6)–C(7) bond. A side reaction product, *N,N*-dimethyl-*N*-nor-8 β ,14 β -methylene-8,14-dihydrothebainium trifluoromethanesulfonate (**81**), formed upon addition of two diazomethane molecules to the C(8)–C(14) bond and the tertiary nitrogen atom was also isolated. The structure of

compound **81** was established by spectral data and confirmed by X-ray diffraction analysis.^{84, 85}

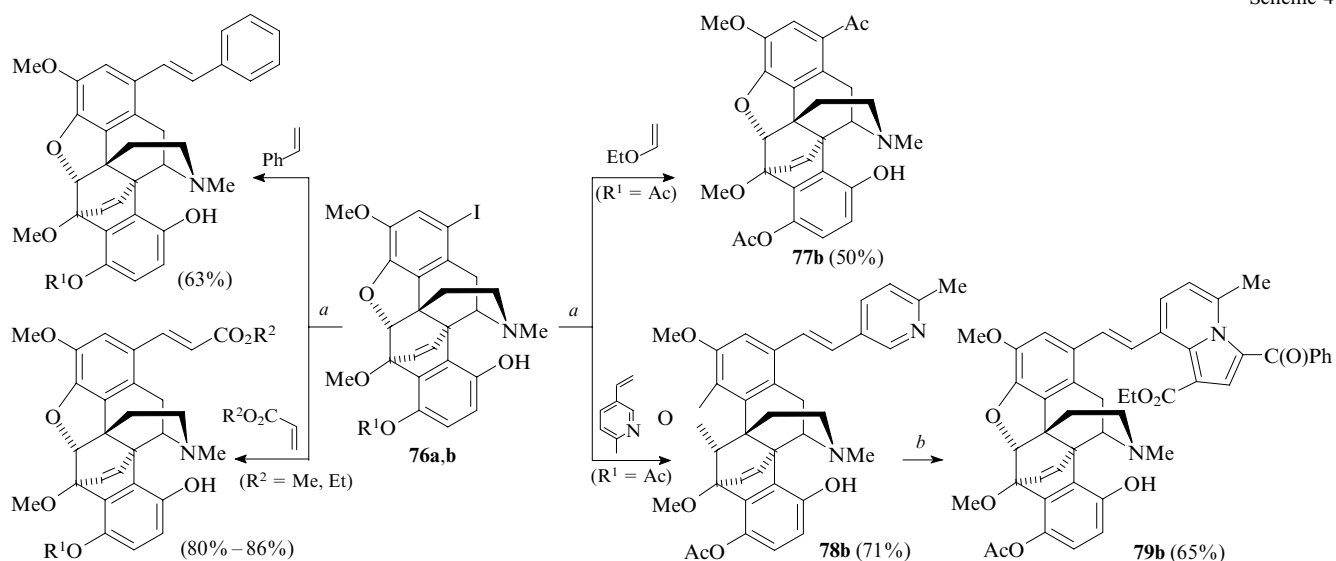


We studied the possibility of synthesis of 8 α -substituted derivatives of 14 β -hydroxy-6 β ,7 β -methylenedihydrocodeine. For instance, the oxidation of compound **80** with excess *m*-chloroperoxybenzoic acid (MCPBA) in dichloromethane gives 8 β ,14 β -epoxy-6 β ,7 β -methylene-6,7,8,14-tetrahydrothebaine *N*-oxide (**82**).



The reaction occurs under kinetic control. *N*-Oxide **83** can be isolated from the reaction mixture at a reduced temperature using 0.8 equiv. of the oxidant. The epoxide ring opening in

Scheme 4

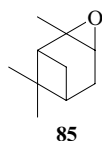


(a) Pd(OAc)₂, P(*o*-Tol)₃, Et₃N, DMF; (b) 1) BrCH₂COPh, Et₂O; 2) HC \equiv CCO₂Et, Et₃N, CH₂Cl₂. R¹ = H (**a**), Ac (**b**).

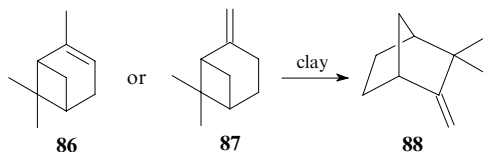
compound **82** under the action of sodium azide in aqueous dioxane gave the 8 α -azido derivative of 6 β ,7 β -methylene-7,8-dihydrocodein-14 β -ol (**84**).⁸⁵

4. Reactions of monoterpenoids in the presence of crystalline aluminosilicate catalysts

Monoterpenoids are widespread in nature. They are produced by Coniferous plants and constitute their oleoresins, turpentine and resins, being also the major components of essential oils extracted from many other plants. Most monoterpenoids are highly reactive compounds and readily undergo various acid-catalysed cyclisation reactions and rearrangements. This often makes selective transformations difficult. For instance, isomerisation and polymerisation reactions occurring upon storage of α -pinene epoxide (**85**) in acid media can result in the formation of more than 200 different products.⁸⁶



It turned out that the problem can be solved by carrying out the process under heterogeneous conditions, namely, on crystalline aluminosilicates (zeolites and clays). The first successful example of the use of aluminosilicates in the chemistry of monoterpenes is provided by the development, in the first half of the 20s century, of a large-scale method for isomerisation of α - (**86**) and β -pinenes (**87**) to camphene (**88**) in the presence of clays.⁸⁷



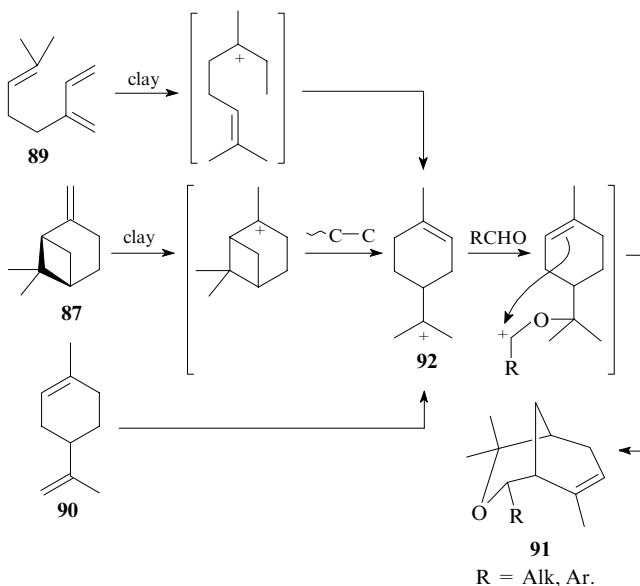
However, systematic studies of the behaviour of terpenoids on crystalline aluminosilicates began only in the early 1990s.⁸⁸ It was found that the use of zeolites and clays as catalysts of acid transformations of terpenoids made it possible not only to carry out reactions under milder conditions, enhance reaction selectivity, simplify work up of reaction mixtures and solve the acid waste problem, but also often allows the reactions to follow unusual pathways, which cannot be realised under conditions of conventional homogeneous catalysis.

Intramolecular reactions of terpenoids in the presence of aluminosilicate catalysts have been reviewed in detail;^{88–90} therefore, here we only present some examples of intermolecular reactions of monoterpenoids on zeolite and clay supports that were first carried out at the NIOCh. We present the most unusual reactions that demonstrate that the laws of homogeneous catalysis cannot always be directly applied to reactions of labile polyfunctional compounds (including monoterpenoids) in the presence of crystalline aluminosilicate catalysts.

a. Reactions of monoterpenes with carbonyl compounds

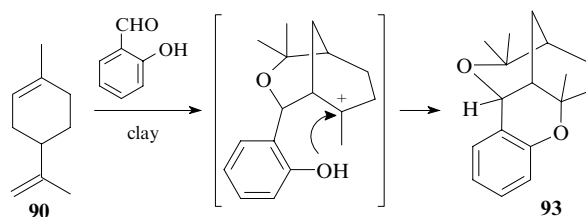
Studies of the reactions of some monoterpenes, namely, mircene (**89**), dipentene [(\pm)-limonene] (**90**) and β -pinene (**87**) with aliphatic and aromatic aldehydes in the presence of natural montmorillonite (askanite–bentonite) clay made it possible to develop a simple and efficient method of synthesis of bicyclic ethers **91** with the 3-oxabicyclo[3.3.1]nonane skeleton.^{91,92} The interest in these compounds is due to, *e.g.*,

recently found selectivity of binding to estrogen α - and β -receptors.⁹³ The highest yield of the target product (up to 56%) was attained in the case of β -pinene (**87**).



A possible mechanism of transformations of the three monoterpenes involves the formation of the same intermediate *p*-menthane carbocation **92**, which then interacts with the aldehyde molecule. It should be noted that α -pinene (**86**), which also forms a tertiary carbocation upon protonation, does not react with aldehydes under these conditions. This is apparently due to specific features of adsorption of monoterpenes **86** and **87** on aluminosilicate.

The reaction of dipentene (**90**) with salicylic aldehyde on clay does not stop after the formation of bicyclic ether.⁹⁴ Favourable spatial arrangement of the hydroxyl group in the intermediate carbocation leads to double heterocyclisation resulting in compound **93** with a new tricyclic skeleton.

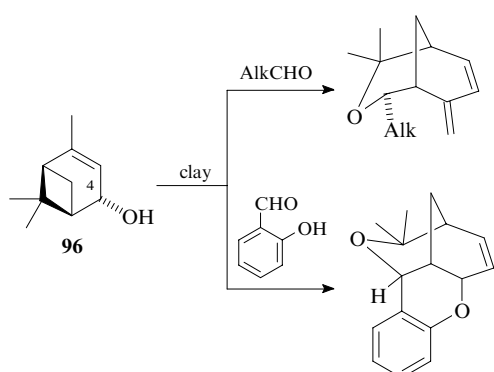
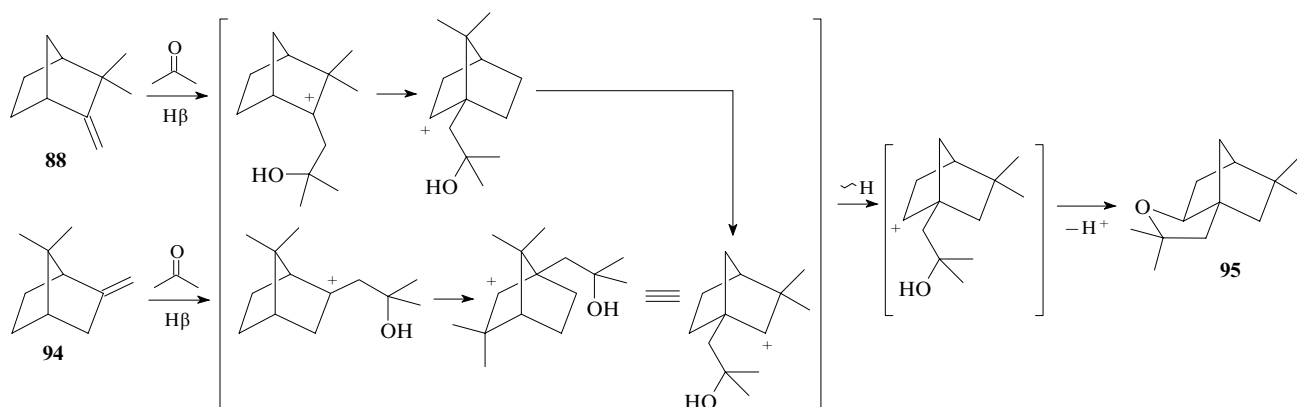


Reactions of (–)-camphene (**88**) and (+)- α -fenchene (**94**) with acetone in the presence of β -zeolite (H β) mainly give the same enantiomer of tricyclic compound **95**.⁹⁵ The yield and optical activity of the product depend on the solvent used. The best results were obtained for the reaction in CH₂Cl₂ (Scheme 5).

b. Reactions of monoterpene alcohols with aldehydes

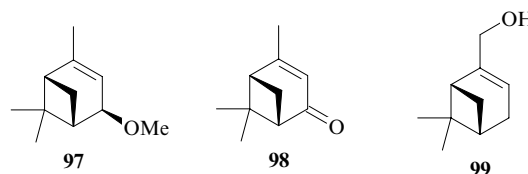
Reactions of aldehydes with natural monoterpene alcohols or hydroxymethylated monoterpenes in the presence of aluminosilicate catalysts result in polycyclic ethers. In particular, *trans*-verbenol (**96**) reacts with aldehydes on montmorillonite to give compounds that are structurally similar to products of β -pinene reactions with aldehydes (see Section III.4.a).⁹⁶

Scheme 5



Reactions of *cis*-verbenol and *trans*-verbenol methyl ether (**97**) with aldehydes occur similarly. Therefore, the stereochemistry of the hydroxyl group (including alkylated one) has no effect on the direction of intermolecular reactions; only position of the hydroxyl group in the molecule does matter. Indeed, neither α -pinene (**86**) having no oxygen-containing substituents nor verbenone (**98**) (carbonyl group in position 4)

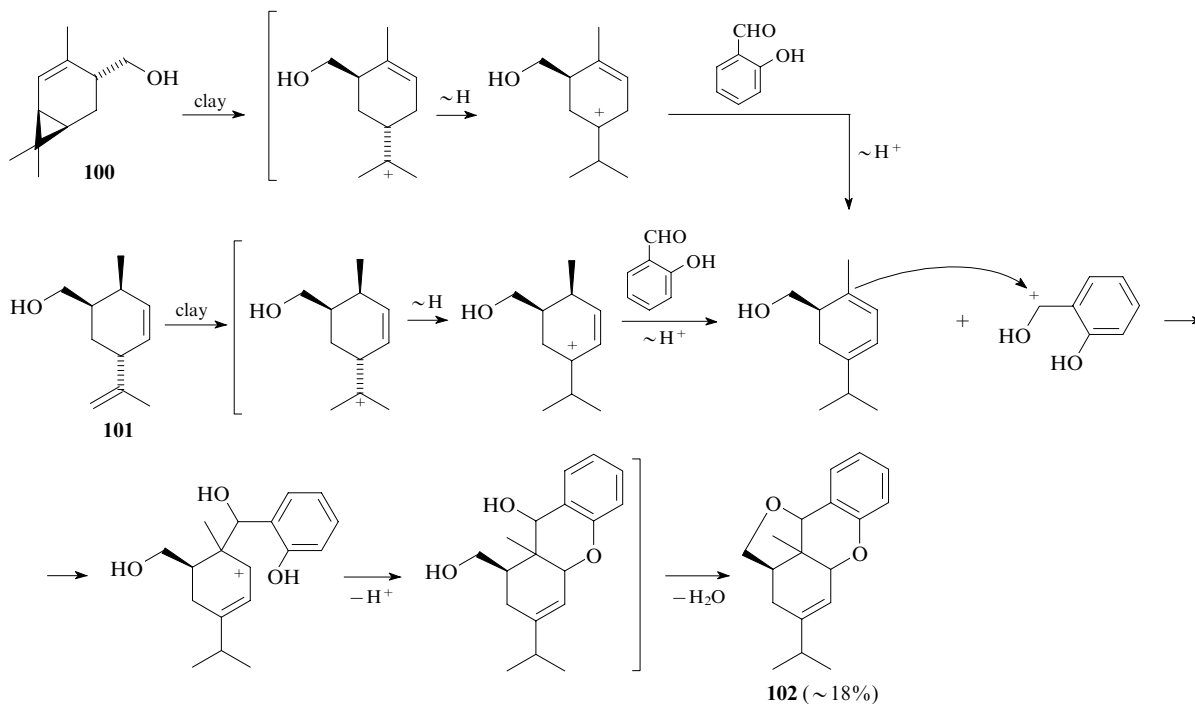
nor myrtenol (**99**) (hydroxyl group in position 10) react with aldehydes on clays.^{96,97}



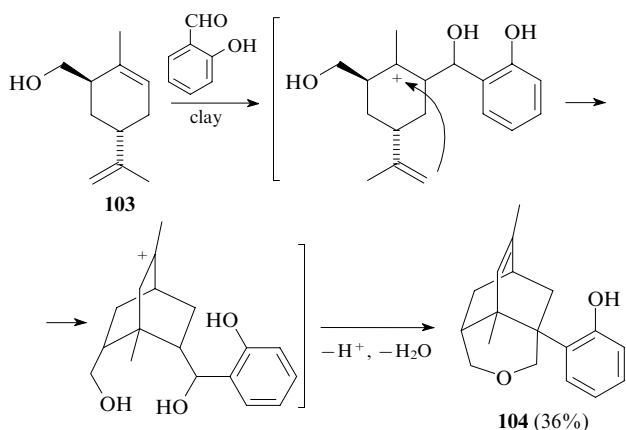
Reactions of 3-hydroxymethyl-2-carene (**100**) or 6-hydroxymethylisolimonene (**101**) with salicylaldehyde in the presence of clay gave a tetracyclic compound **102** with a furo[4,3,2-*k*]xanthene skeleton.⁹⁸ The mechanism of formation of this compound involves a number of carbocationic rearrangements (Scheme 6).

At the same time, the reaction of 6-hydroxymethylislimonene (**103**), a double bond regio isomer of compound **101**, with salicylic aldehyde on clay affords product **104** having a 5-oxatricyclo[5.3.1.0^{3,8}]undecene skeleton.⁹⁸ Thus, monoterpenes **103** and **90** containing the same *p*-mentha-1,8-diene

Scheme 6



skeleton react with salicylaldehyde in different manner because they bear different functional groups.

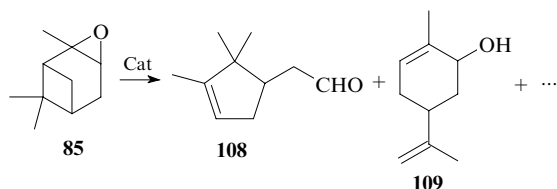


The reaction products of 3-hydroxymethyl-2-carene (**100**) with other aldehydes (α -methylacrolein and butyraldehyde) were also obtained in the presence of clay.⁹⁹ It was found that the direction of these reactions depended on the structure of the aldehyde. For instance, the reaction with α -methylacrolein resulted in indeno[1,7-*bc*]furan **105** as the major product. In the case of Pr^nCHO , the reaction involves the addition of two aldehyde molecules to give 6,10-dioxatricyclo[5.4.0.0^{4,8}]undecane **106** (Scheme 7). Unlike alcohol **100**, attempts to introduce compound **101** into reactions with other aldehydes failed.

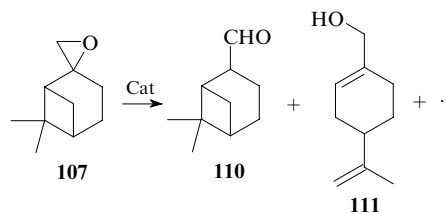
Thus, structurally similar, conformationally labile molecules form different products in the presence of montmorillonite clays.

c. Transformations of monoterpenoid epoxides

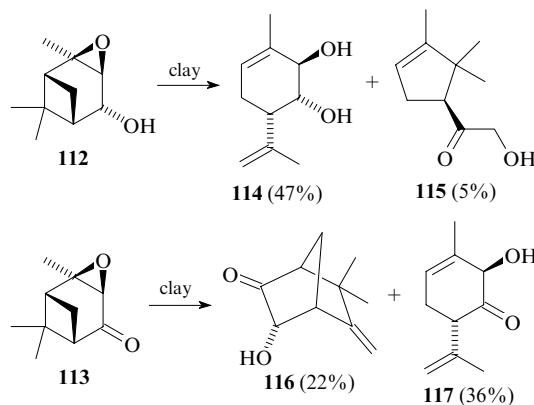
The behaviour of α -pinene epoxide (**85**) and β -pinene epoxide (**107**) in the presence of crystalline aluminosilicates was studied in detail.^{88, 100} This is associated with both the availability of the starting compounds and the fact that many reaction products (*e.g.*, campholenic aldehyde (**108**), carveol (**109**),



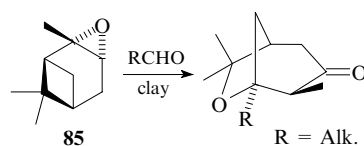
myrtenal (**110**), perillyl alcohol (**111**), *etc.*) are commercially valuable products. The product ratio depends strongly on the nature of the catalysts used (zeolites and clays) and varies over a rather broad range.



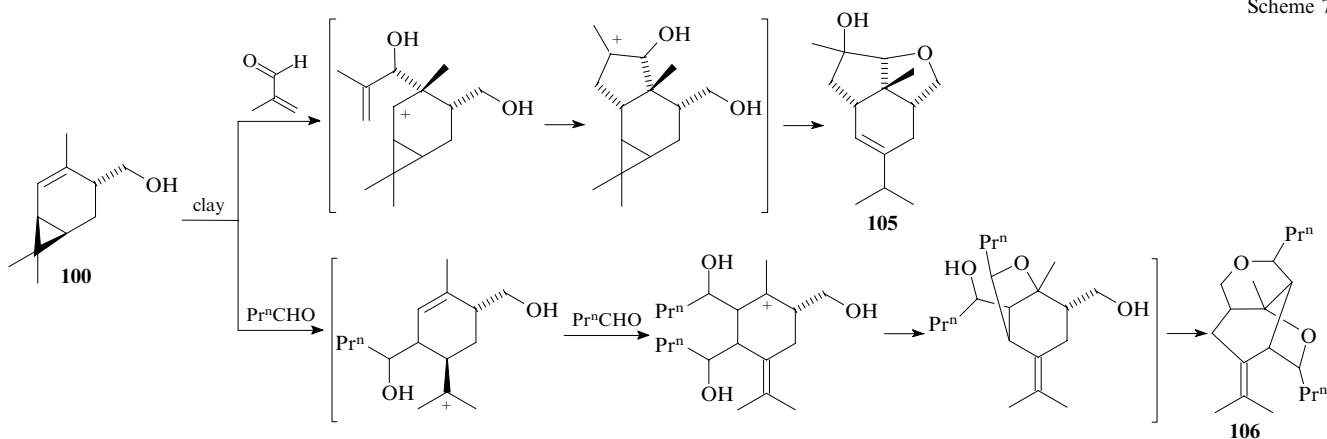
Recently,^{97, 101} it has been shown that transformations of verbenol epoxide (**112**) and verbenone epoxide (**113**) in the presence of montmorillonite clays gives different products. Moreover, they significantly differ from the products synthesised using conventional homogeneous catalysts (analogues of campholenic aldehyde). For instance, isomerisation of verbenol epoxide (**112**) results in *trans*-diol **114** as the major product, whereas an analogue of campholenic aldehyde **115** was isolated as the minor product.⁹⁷ Isomerisation of verbenone epoxide (**113**) on clay afforded α -hydroxyketones with the camphane (**116**) and *p*-menthane (**117**) structures, whereas no campholenic-type products were detected.¹⁰¹

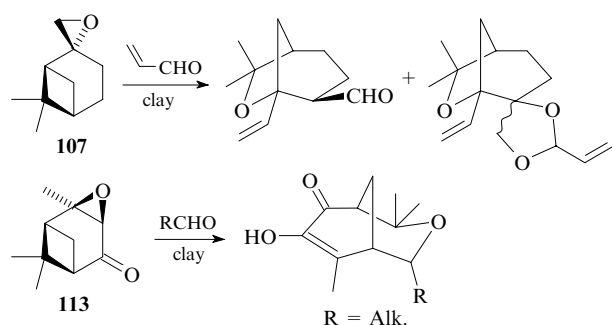


Some epoxides of the pinane series undergo intermolecular reactions with aldehydes in the presence of montmorillonite clays. The products formed on clay in the reactions of α -pinene, β -pinene and verbenone epoxides (compounds **85**, **107** and **113**, respectively) with aliphatic aldehydes^{96, 101} have



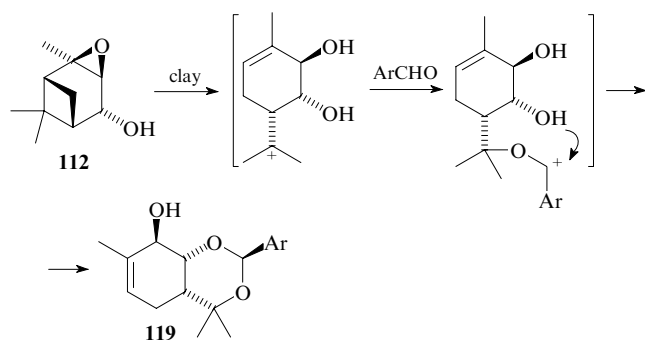
the 3-oxabicyclo-[3.3.1]nonane skeleton [see reactions of β -pinene (**87**) with aldehydes] with different reactive functional groups.





The reaction of α -pinene epoxide (**85**) with salicylaldehyde⁹⁶ led to unexpected results; namely, an unusual tetracyclic ether **118** was isolated as the only product. The reaction scheme proposed to explain the mechanism of formation of compound **118** involves more than ten stages (Scheme 8).

Reactions of epoxide **112** with aromatic aldehydes in the presence of clay result not only in products of substrate isomerisation, compounds **114** and **115**, but also heterocycle **119**; the product ratio depends on the structure of the aldehyde.⁹⁷ Product **119** has the benzo[1,3-*d*]dioxine skeleton in contrast to the reaction products of other terpenoids with aldehydes (see Section III.4.a), which have the 3-oxabicyclo[3.3.1]nonane skeleton. This can be explained by different reaction mechanisms, namely, heterocyclisation in the last step of formation of compound **119** rather than carbocyclisation in the case of other terpenoids.^{96, 97, 99, 101}



Thus, the use of crystalline aluminosilicate catalysts (clays and zeolites) for performing diverse reactions of monoterpenoids significantly extends the synthetic potential of these compounds and allows easy access to heterocyclic systems that are difficult to obtain. In addition, transformations of terpenoids occur with retention of optical purity under these conditions.^{88, 97, 101}

Note that most reactions presented above do not occur in the presence of conventional homogeneous catalysts. Therefore, the aluminosilicate catalysts not only play the role of the acidic reagent, but also determine the mutual arrangement of the reactants and the site where the cationic centre appears. Because of this, even relatively small changes in the structure of the terpenoid or reagent can cause significant changes in the direction of the reaction.

IV. Practical applications of natural compounds and their derivatives

Studies in the properties of plant metabolites gave practically valuable results. Both natural compounds and their derivatives have found applications in agriculture and medicine.

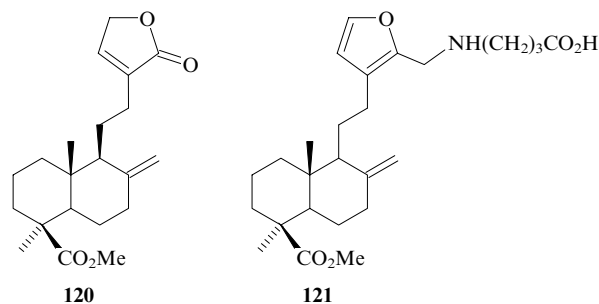
1. Triterpene acids isolated from fir as the basis for fungicides

Triterpene acids isolated from fir wood green enhance the stability of cotton-plant, crops and vegetables. A mixture of triterpene acids produced in a pilot plant^{102–104} served as the basis for the preparation 'Novosil'. This has passed the Russian Federation State tests and was certified in 1995 as a plant growth regulator.^{105–107} Its positive complex effect on plants consists in an increase in yield by 10%–30%, 2–4-fold enhancement of plant resistance to bacterial and fungal diseases, enhancement of freezing tolerance and drought resistance of plants and acceleration of ripening.¹⁰⁸

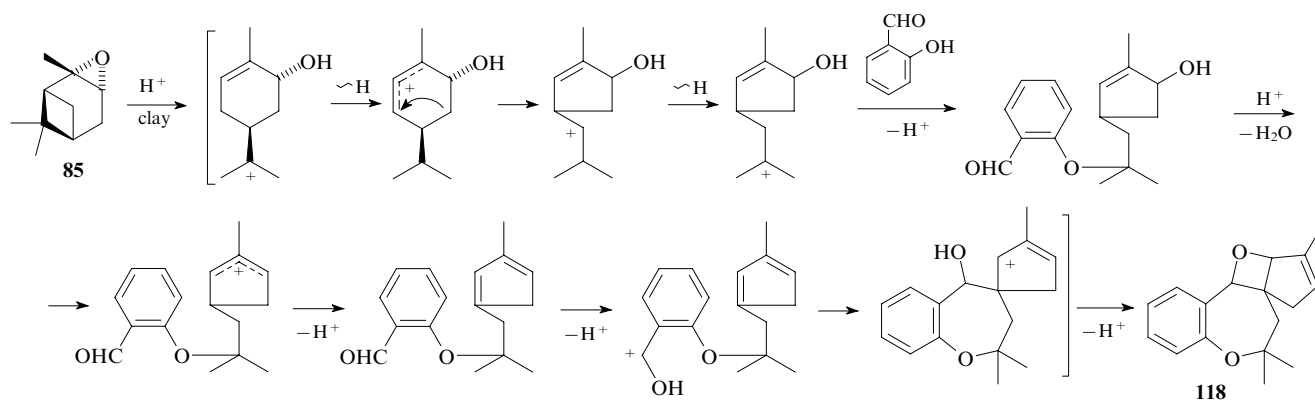
2. Pharmacological properties

a. Diterpenoids

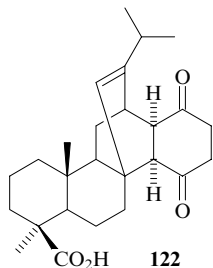
Two derivatives of lambertianic acid (**5**), namely, pinusolide (**120**) and a diterpene derivative of γ -aminobutyric acid **121** show pronounced physiological action. Pinusolide, an inducer of apoptosis, is active towards cells of juvenile lymphoblastic and mieloid leukemia,¹⁰⁹ while compound **121** exhibits nootropic activity determined from the rate of dissipation of conditioned passive avoidance reflex and from the degree of the anxiolytic effect.^{110, 111}



Scheme 8



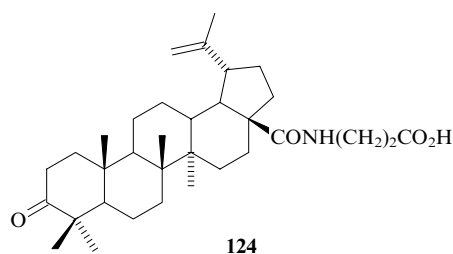
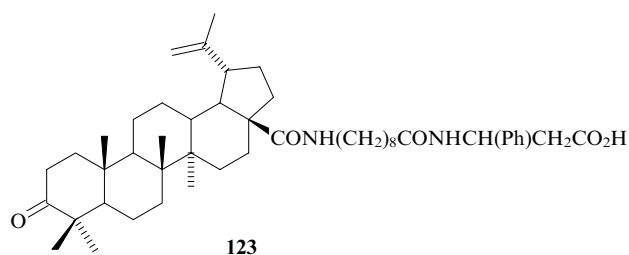
Levopimaric acid is the starting material for the synthesis of dihydroquinopimaric acid (**122**), which shows antiulcer activity, which compares well with modern drugs (*e.g.*, Venter).



b. Triterpenoids

Among triterpene compounds, the most active are betulonic acid derivatives. For instance, betulonic acid-derived dipeptide **123** is a new HIV integrase inhibitor¹¹² and inducer of apoptosis of malignant cells.¹¹³ At present, pre-clinical anti-HIV trials of this preparation are in progress.^{114, 115}

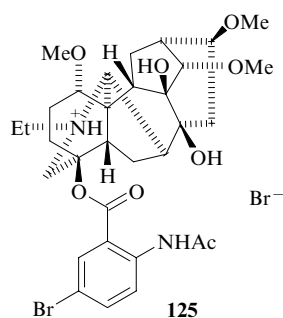
Betulonic acid alanylamide **124** shows antioxidant action and is considered to be a promising corrector of toxic effects in cytostatic chemotherapy.^{116–118}



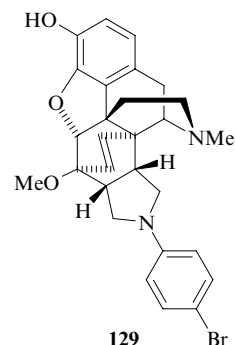
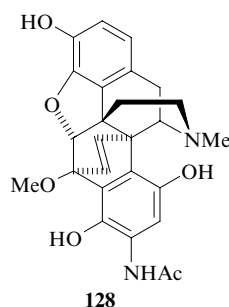
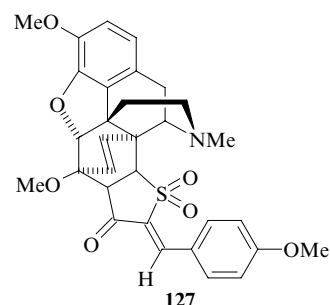
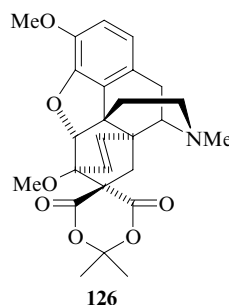
Glycyrrhizic acid (**10**) has been the subject of considerable attention of researchers for long. A particular manifestation of the physiological activity is the complexation with various drugs, which ensures reduction of the therapeutic dose of the drug.^{119–122}

c. Alkaloids

Modification of diterpene alkaloids made it possible to synthesise novel derivatives of lappaconitine (**23**), which exhibit a much higher anti-arrhythmic activity compared to the well-known drug allapinine.^{123, 124} An example is provided by 5'-bromolappaconitine hydrobromide (**125**). When introduced in a dose equal to one-tenth of the therapeutic dose of allapinine, compound **125** prevents the development of calcium chloride- and adrenaline-induced arrhythmia, being 4.8 times less toxic than allapinine.¹²⁴



A number of highly efficient analgesics possessing no adverse effects typical of morphinans^{63, 125–127} were synthesised from thebaine (**47**). Among the annulated morphinan derivatives, mention may be made of compounds **126–129**.



Compound **126**, in a lipophilic transport form, acts as blocker of pain caused by all types of stimulators. The ED_{50} value was 0.02 mg kg^{-1} for the electric pain stimulation model, 0.07 mg kg^{-1} for the hot-plate model and 0.009 mg kg^{-1} for the acetic acid writhing (AAW) model. These data characterise compound **126** as a μ -receptor agonist.¹²⁶ Compound **127** is a threefold times more efficient pain blocker for the AAW model. The effect of physical and visceral pain control was also observed upon introduction of compound **128**. In the dose corresponding to ED_{50} it only slightly changes the heart rate and has no effect on the bronchomotor tone in cats.¹²⁷ A morphinan derivative **129** shows a prolonged analgesic action on physical pain models.⁶³

* * *

The material presented above shows that intensive development of chemistry of low-molecular-mass plant metabolites is being continued. These compounds are important not only as

representatives of various structural types and information carriers in chemotaxonomic studies, but also as precursors for the synthesis of many valuable products and design of original drugs, cosmetics and agricultural preparations. At present, the available terpenoids and phenolic compounds are first of all used for directed synthesis of complex carbocyclic and heterocyclic structures. Recently, there have been increasing studies on transformations of those alkaloids, which in the native forms are of limited use in medicine owing to high toxicity or pronounced adverse effects. Considerable attention is paid to medicinal chemistry-oriented transformations of the metabolite classes described above (search for novel leader compounds and optimisation of their structures; fragment-oriented ligand design), as reported in recently published reviews, 2, 128–131

References

1. V A Pentegova, Zh V Dubovenko, V A Raldugin, E N Shmidt *Terpenoidy Khvoynykh Rastenii* (Terpenoids of Coniferous Plants) (Novosibirsk: Nauka, 1987)
2. M S Butler *Nat. Prod. Rep.* **22** 162 (2005)
3. W N Setzer, M C Setzer *Mini Rev. Med. Chem.* **3** 540 (2003)
4. P Dzubak, M Hajdich, D Vydra, A Hustova, M Kvasnica, D Biedermann, L Markova, M Urban, J Sarek *Nat. Prod. Rep.* **23** 394 (2006)
5. T G Tolstikova, I V Sorokina, G A Tolstikov, A G Tolstikov, O B Flekhter *Bioorg. Khim.* **32** 42 (2006)^a
6. G A Tolstikov, L A Baltina, E E Shults, A G Pokrovskii *Bioorg. Khim.* **23** 691 (1997)^a
7. D Yu, S L Morris-Natschke, K-H Lee *Med. Res. Rev.* **27** 108 (2007)
8. M Dakir, F El Hanbali, F Mellouki, M Akssira, A Benharref, J F Quilez del Moral, A F Barrero *Nat. Prod. Res.* **19** 719 (2005)
9. R F Vlad, M N Koltza *Sintez i Primenenie Dushistykh Veshchestv iz Labdanovykh Diterpenoidov* (Synthesis and Applications of Fragrance Compounds from Labdanum Diterpenoids) (Kishinev: Shtiintsa, 1988)
10. I Chinou *Curr. Med. Chem.* **12** 1295 (2005)
11. B H Han, H O Yang, Y-H Kang, D-Y Suh, H J Go, W-J Song, Y C Kim, M K Park *J. Med. Chem.* **41** 2626 (1998)
12. T G Tolstikova, S V Chernov, E E Shults, M P Dolgikh, L N Popova, G A Tolstikov *The 3rd International Symposium on the Chemistry of Natural Compounds (Abstracts of Papers)*, Bukhara, Uzbekistan, 1998 p. 13
13. K H Altmann, J Gertsch *Nat. Prod. Rep.* **24** 327 (2007)
14. G A Tolstikov, O B Flekhter, E E Shults, L A Baltina, A G Tolstikov *Khim. Inter. Ustoich. Razvitiya* **13** 1 (2005)^b
15. T Takahashi *J. Pharm. Soc. Jpn.* **58** 888 (1938)
16. J P Kutney, N D Westcott, F H Allen, N W Isaacs, O Kennard, W D S Motherwell *Tetrahedron Lett.* **12** 3463 (1971)
17. J Takayasu, R Tanaka, S Matsunaga, H Ueyama, H Tokuda, T Hasegawa, A Nishino, H Nishino, A Iwashima *Cancer Lett.* **53** 141 (1990)
18. V A Raldugin, Yu V Gatilov, I Yu Bagryanskaya, N I Yaroshenko *Khim. Prirod. Soedin.* 584 (1986)^c
19. V A Raldugin, Yu V Gatilov, T V Rybalova, Ya V Rashkes *Khim. Prirod. Soedin.* 688 (1986)^c
20. V I Roshchin, V A Raldugin, R A Baranova, V A Pentegova *Khim. Prirod. Soedin.* 648 (1986)^c
21. S A Shevtsov, V A Raldugin *Khim. Prirod. Soedin.* 364 (1988)^c
22. V A Raldugin, S A Shevtsov, V I Roshchin, V A Pentegova *Khim. Prirod. Soedin.* 816 (1988)^c
23. V A Raldugin, M M Shakirov, T V Leibyuk, S A Shevtsov *Khim. Prirod. Soedin.* 511 (1991)^c
24. S A Shevtsov, V A Raldugin *Khim. Prirod. Soedin.* 212 (1989)^c
25. V A Raldugin, S A Shevtsov, M M Shakirov, V I Roshchin, V A Pentegova *Khim. Prirod. Soedin.* 207 (1989)^c
26. V V Grishko, A G Druganov, M M Shakirov, V A Raldugin *Izv. Akad. Nauk, Ser. Khim.* 519 (1998)^d
27. V A Raldugin, S A Shevtsov, T V Leibyuk *Khim. Prirod. Soedin.* 206 (1991)^c
28. V V Grishko, I Yu Bagryanskaya, Yu V Gatilov, M M Shakirov, V A Raldugin *Izv. Akad. Nauk, Ser. Khim.* 748 (1996)^d
29. I Yu Bagryanskaya, Yu V Gatilov, V V Grishko, V A Raldugin *Izv. Akad. Nauk, Ser. Khim.* 1314 (1997)^d
30. S A Osadchii, E E Shults, G A Tolstikov *Izv. Akad. Nauk, Ser. Khim.* 2094 (1997)^d
31. A G Druganov, V A Raldugin, M M Shakirov, S A Nekhoroshev, A P Koskin, G A Tolstikov *Khim. Inter. Ustoich. Razvitiya* **8** 699 (2000)^b
32. I A Bessonova, S F Aripova, R Shakirov *Khim. Prirod. Soedin.* 3 (1993)^c
33. S A Osadchii, E E Shults, G A Tolstikov *Khim. Prirod. Soedin. (Spec. Issue)* 18 (1999)^c
34. S A Osadchii, E Yu Yakovleva, M M Shakirov, E E Shults, G A Tolstikov *Izv. Akad. Nauk, Ser. Khim.* 800 (1999)^d
35. I Yu Bagryanskaya, Yu V Gatilov, Zh Ganbaatar, S A Osadchii, M M Shakirov, E E Shults, G A Tolstikov *Izv. Akad. Nauk, Ser. Khim.* 2000 (2001)^d
36. M D Mashkovskii *Lekarstvennye Sredstva* (Drugs) (Ed. 15) (Moscow: Novaya Volna, 2006)
37. D J Hardick, I S Blagbrough, G Cooper, B V L Potter, T Critchley, S A Wonnacott *J. Med. Chem.* **39** 4860 (1996)
38. J M Jacyno, J S Harwood, N-H Lin, J E Campbell, J P Sullivan, M W Holladay *J. Nat. Prod.* **59** 707 (1996)
39. N Tulyaganov, F N Dzhakhangirov, F S Sadritdinov, V Khamdamov *Farmakologiya Rastitel'nykh Veshchestv* (Pharmacology of Vegetal Substances) (Tashkent: FAN, 1976) p. 76
40. A I Potopal'skii, L I Petlichnaya, S V Ivasivka *Barbaris i ego Preparaty v Biologii i Meditsine* (Barberry and Its Preparations in Biology and Medicine) (Kiev: Naukova Dumka, 1989)
41. M N Zaprometov *Fenol'nye Soedineniya. Rasprostraneniye, Metabolizm i Funktsii v Rastenyakh* (Phenol Compounds. Occurrence, Metabolism and Functions in Plants) (Moscow: Nauka, 1993)
42. L C Chang, A D Kinghorn *Bioactive Compounds from Natural Sources: Isolation, Characterisation and Biological Properties* (Ed. C Tringali) (London: Taylor and Francis, 2001) p. 161
43. *Flavonoids: Chemistry, Biochemistry and Applications* (Eds Ø M Andersen, K R Markham) (London: Taylor and Francis, 2006)
44. V A Babkin, L A Ostroukhova, S G D'yachkova, Yu K Svyatkin, D V Babkin, N A Onuchina *Khim. Inter. Ustoich. Razvitiya* **5** 105 (1997)^b
45. J Ganbaatar, Ya Yamyansan, S A Osadchii, E E Shults, G A Tolstikov, M M Shakirov *Ann. Sci. Rep.* **32** 20 (2006)
46. E E Shults, T N Petrova, M M Shakirov, E I Chernyak, L M Pokrovskii, S V Nekhoroshev, G A Tolstikov *Khim. Inter. Ustoich. Razvitiya* **11** 683 (2003)^b
47. G Cozza, P Bonvini, E Zorzi, G Poletto, M A Pagano, S Sarno, A Donella-Deana, G Zagotto, A Rosolen, L A Pinna, F Meggio, S Moro *J. Med. Chem.* **49** 2363 (2006)
48. E E Shults, T N Petrova, M M Shakirov, E I Chernyak, G A Tolstikov *Khim. Prirod. Soedin.* 296 (2000)^c
49. Russ. P. 2294919; *Byull. Izobret.* (7) 123 (2007)
50. B B Aggarwal, A Bhardwaj, R S Aggarwal, N P Seeram, S Shishodia, Y Takada *J. Anticancer Res.* **24** 713 (2004)
51. W Herz, R S Blackstone, M G Nair *J. Org. Chem.* **32** 2992 (1967)
52. G A Tolstikov, E E Shults, T Sh Mukhametyanova, I P Baikova, L V Spirikhin *Zh. Org. Khim.* **29** 698 (1993)^c
53. S V Chernov, E E Shults, M M Shakirov, Yu V Gatilov, I Yu Bagryanskaya, G A Tolstikov *Zh. Org. Khim.* **36** 1671 (2000)^c
54. G A Tolstikov, E E Shults, G F Vafina, L V Spirikhin *Zh. Org. Khim.* **28** 192 (1992)^c
55. G A Tolstikov, E E Shults, T Sh Mukhametyanova, V S Sultanova, L V Spirikhin *Zh. Org. Khim.* **28** 1310 (1992)^c

56. L Maat *Drugs of Abuse: Chemistry, Pharmacology, Immunology and AIDS (NIDA Research Monographs)* Vol. 96 (Eds P T K Phan, K Rice) (Washington, DC: U.S. National Institute on Drug Abuse, 1990) p. 35
57. G A Tolstikov, E E Shults, L V Spirikhin *Tetrahedron* **42** 591 (1986)
58. G A Tolstikov, E E Shults, T Sh Mukhametyanova, L V Spirikhin *Zh. Org. Khim.* **27** 273 (1991)^e
59. E E Shults, T Sh Malikova, I A Shafifgaliev, L V Spirikhin, G A Tolstikov *Zh. Org. Khim.* **29** 938 (1993)^e
60. G A Tolstikov, E E Shults, T Sh Malikova, L V Spirikhin *Mendeleev Commun.* **4** 60 (1994)
61. E E Shults, G A Tolstikov, M M Shakirov, T G Tolstikova *Nitrogen Containing Heterocycles and Alkaloids* Vol. 1 (Eds V G Kartsev, G A Tolstikov) (Moscow: Iridium Press, 2001) P. 161
62. E E Shults, M M Shakirov, G A Tolstikov, V N Kalinin, G Shmidkhammer *Zh. Org. Khim.* **41** 1155 (2005)^e
63. E E Shults, T G Tolstikova, S E Tolstikov, V T Daibova, M M Shakirov, A V Bolkunov, G A Tolstikov *Khim.-Farm. Zh.* (2) 15 (2007)^f
64. E E Shults, T Sh Mukhametyanova, L V Spirikhin, V S Sultanova, G A Tolstikov *Zh. Org. Khim.* **29** 1149 (1993)^e
65. S V Chernov, E E Shults, M M Shakirov, G A Tolstikov *Zh. Org. Khim.* **38** 703 (2002)^e
66. S V Chernov, E E Shults, M M Shakirov, I Yu Bagryanskaya, Yu V Gatilov, G A Tolstikov *Arkivoc* (xiii) 172 (2003)
67. S V Chernov, E E Shults, M M Shakirov, I Yu Bagryanskaya, Yu V Gatilov, G A Tolstikov *Zh. Org. Khim.* **41** 547 (2005)^e
68. S V Chernov, E E Shults, M M Shakirov, G A Tolstikov *Zh. Org. Khim.*, **42** 852 (2006)^e
69. Yu V Kharitonov, E E Shults, M M Shakirov, G A Tolstikov *Zh. Org. Khim.* **39** 67 (2003)^e
70. Yu V Kharitonov, E E Shults, M M Shakirov, G A Tolstikov *Zh. Org. Khim.* **41** 1167 (2005)^e
71. Yu V Kharitonov, E E Shults, M M Shakirov, G A Tolstikov *Zh. Org. Khim.* **42** 725 (2006)^e
72. S A Osadchii, N A Pankrushina, M M Shakirov, E E Shults, G A Tolstikov *Izv. Akad. Nauk, Ser. Khim.* 552 (2000)^d
73. N A Pankrushina, I A Nikitina, N V Anferova, S A Osadchii, M M Shakirov, E E Shults, G A Tolstikov *Izv. Akad. Nauk, Ser. Khim.* 2354 (2003)^d
74. N V Anferova, I Yu Bagryanskaya, Yu V Gatilov, S A Osadchii, M M Shakirov, E E Shults, G A Tolstikov *Izv. Akad. Nauk, Ser. Khim.* 2363 (2003)^d
75. N V Malykhina, S A Osadchii, M M Shakirov, E E Shults, G A Tolstikov *Dokl. Akad. Nauk* **394** 343 (2004)^g
76. S A Osadchii, E E Shults, G A Tolstikov *Izv. Akad. Nauk, Ser. Khim.* 868 (2001)^d
77. Zh Ganbaatar, D Batsuren, S A Osadchii, E E Shults, G A Tolstikov *Izv. Akad. Nauk, Ser. Khim.* 493 (2002)^d
78. Zh Ganbaatar, S A Osadchii, E E Shults, T G Tolstikova, M P Dolgikh, G A Tolstikov *Khim.-Farm. Zh.* (9) 20 (2002)^f
79. Zh Ganbaatar, S A Osadchii, E E Shults, G A Tolstikov *Izv. Akad. Nauk, Ser. Khim.* 2127 (2002)^d
80. S A Osadchii, E E Shults, E V Polukhina, M M Shakirov, G A Tolstikov *Izv. Akad. Nauk, Ser. Khim.* 1038 (2006)^d
81. S A Osadchii, E E Shults, S F Vasilevskii, E V Polukhina, A A Stepanov, G A Tolstikov *Izv. Akad. Nauk, Ser. Khim.* 344 (2007)^d
82. V T Bauman, E E Shults, G A Tolstikov *Tezisy Dokladov IX Nauchnoi Shkoly-konferentsii po Organicheskoi Khimii, Moskva, 2006* (Abstracts of Reports of the IXth Research School-Conference on Organic Chemistry, Moscow, 2006) p. 71
83. V T Bauman, E E Shults, M M Shakirov, G A Tolstikov *Zh. Org. Khim.* **43** 529 (2007)^e
84. S Z Sultanov, V A Dokichev, E E Shults, U M Dzhemilev, G A Tolstikov, O M Nefedov *Izv. Akad. Nauk, Ser. Khim.* 550 (1994)^d
85. E E Shults, M M Shakirov, I Yu Bagryanskaya, Yu V Gatilov, G A Tolstikov, V N Kalinin, G Shmidkhammer *Zh. Org. Khim.* **39** 1154 (2003)^e
86. W F Hölderich, U Barsnick *Fine Chemicals through Heterogeneous Catalysis* (Eds R A Sheldon, H van Bekkum) (Weinheim: Wiley-VCH, 2001) p. 223
87. G A Rudakov *Kamfora* (Camphor) (Moscow: Goslesbumizdat, 1961)
88. N F Salakhutdinov, V A Barkhash *Usp. Khim.* **66** 376 (1997) [*Russ. Chem. Rev.* **66** 343 (1997)]
89. J L F Monteiro, C O Veloso *Top. Catal.* **27** 169 (2004)
90. K A D Swift *Top. Catal.* **27** 143 (2004)
91. K P Volcho, L E Tatarova, D V Korchagina, N F Salakhutdinov, I S Aul'chenko, K G Ione, V A Barkhash *Zh. Org. Khim.* **30** 641 (1994)^e
92. I V Il'ina, D V Korchagina, N F Salakhutdinov, V A Barkhash *Zh. Org. Khim.* **35** 491 (1999)^e
93. L G Hamann, J H Meyer, D A Ruppar, K B Marschke, F G Lopez, E A Allegretto, D S Karanewsky *Bioorg. Med. Chem. Lett.* **15** 1463 (2005)
94. K P Volcho, D V Korchagina, N F Salakhutdinov, V A Barkhash *Tetrahedron Lett.* **37** 6181 (1996)
95. V V Fomenko, K P Volcho, D V Korchagina, N F Salakhutdinov, V A Barkhash *Zh. Org. Khim.* **38** 392 (2002)^e
96. I V Il'ina, D V Korchagina, N F Salakhutdinov, V A Barkhash *Zh. Org. Khim.* **36** 1483 (2000)^e
97. I V Il'ina, K P Volcho, D V Korchagina, V A Barkhash, N F Salakhutdinov *Helv. Chim. Acta* **90** 353 (2007)
98. K P Volcho, D V Korchagina, Yu V Gatilov, N F Salakhutdinov, V A Barkhash *Zh. Org. Khim.* **33** 666 (1997)^e
99. N F Salakhutdinov, K P Volcho, I V Il'ina, D V Korchagina, L E Tatarova, V A Barkhash *Tetrahedron* **54** 15619 (1998)
100. P J Kunkeler, J C van der Waal, J Bremmer, B J Zuurdeeg, R S Downing, H van Bekkum *Catal. Lett.* **53** 135 (1998)
101. I V Il'ina, K P Volcho, D V Korchagina, V A Barkhash, N F Salakhutdinov *Helv. Chim. Acta* **89** 507 (2006)
102. Russ. P. 2025976; *Chem. Abstr.* **123** 332736 (1995)
103. Russ. P. 2108803; *Byull. Izobret.* (11) 171 (1998)
104. Russ. P. 2108107; *Byull. Izobret.* (10) 153 (1998)
105. Russ. P. 2083110; *Chem. Abstr.* **128** 1208 (1998)
106. Russ. P. 2147400; *Chem. Abstr.* **135** 222845 (2001)
107. *Zashchita Karantin Rastenii* (5) 26 (1995)
108. *Spisok Pestitsidov i Agrokhimikatov, Razreshennykh k Primeneniiu na Territorii Rossiiskoi Federatsii (Prilozhenie k Zhurnalu 'Zashchita i Karantin Rastenii')* [List of Pesticides and Agrochemicals Registered in the Russian Federation (Appendix to Journal 'Protection and Quarantine of Plants')] (Moscow: Kolos, 2001)
109. E E Shults, J Velder, H-G Schmalz, S V Chernov, T V Rubalova, Yu V Gatilov, G Henze, G A Tolstikov, A Prokop *Bioorg. Med. Chem. Lett.* **16** 4228 (2006)
110. T G Tolstikova, I V Sorokina, M P Dolgikh, Yu V Kharitonov, S V Chernov, E E Shults, G A Tolstikov *Khim.-Farm. Zh.* (10) 13 (2004)^f
111. T G Tolstikova, M P Dolgikh, G A Tolstikov *Dokl. Akad. Nauk* **374** 268 (2000)^g
112. E A Semenova, O A Plyasunova, N I Petrenko, N V Uzenkova, E E Shults, G A Tolstikov, A G Pokrovskii *Dokl. Akad. Nauk* **391** 556 (2003)^g
113. A G Pokrovskii, A B Shintyapina, N V Pronkina, V S Kozhevnikov, O A Plyasunova, E E Shults, G A Tolstikov *Dokl. Akad. Nauk* **407** 698 (2006)^g
114. A G Pokrovskii, O A Plyasunova, T N Il'icheva, O A Borisova, N V Feduk, N I Petrenko, V Z Petukhova, E E Shults, G A Tolstikov *Khim. Inter. Ustoich. Razvitiya* **9** 485 (2001)^b
115. Russ. P. 2211843; *Byull. Izobret.* (25) 152 (2003)
116. I V Sorokina, T G Tolstikova, N A Zhukova, N I Petrenko, E E Shults, N V Uzenkova, O R Grek, S V Pozdnyakova, G A Tolstikov *Dokl. Akad. Nauk* **399** 274 (2004)^g
117. N A Zhukova, D E Semenov, I V Sorokina, T G Tolstikova, S V Pozdnyakova, O R Grek *Byull. Eksperim. Biol. Med.* **140** 348 (2005)^h

118. I V Sorokina, N A Zhukova, T G Tolstikova, S V Pozdnyakova, O R Grek, N A Popova, E M Andreeva, V A Kaledin, V P Nikolin *Vopr. Biol. Med. Farm. Khim.* (1) 29 (2006)
119. T G Tolstikova, I V Sorokina, I L Kovalenko, A G Tolstikov *Dokl. Akad. Nauk* **394** 707 (2004) ^g
120. G T Shishkina, N N Dygalo, A M Yudina, T S Kalinina, T G Tolstikova, I V Sorokina, I L Kovalenko, L V Anikina *Zh. Vyssh. Nervn. Deyat.* **55** 207 (2005) ⁱ
121. T G Tolstikova, A O Bryzgalov, I V Sorokina, E A Morozova, S E Tolstikov, A V Al'fonsov, A G Tolstikov *Dokl. Akad. Nauk* **403** 274 (2005) ^g
122. T G Tolstikova, I V Sorokina, A O Bryzgalov, M P Dolgikh, G I Lifshits, M V Khvostov *Ratsional. Farmakoterap. Kardiol.* (1) 55 (2006)
123. Russ. P. 2180583; *Byull. Izobret.* (8) 148 (2002)
124. Russ. P. 2295524; *Byull. Izobret.* (8) 68 (2007)
125. G A Tolstikov, T G Tolstikova, E E Shults, T Sh Mukhametyanova, V G Popov, V A Davydova, D N Lazareva, F S Zarudii *Khim.-Farm. Z.* (11–12) 39 (1992) ^f
126. T G Tolstikova, V A Davydova, D N Lasareva, F S Zarudiy, E E Shults, G A Tolstikov *Eur. J. Pharmacol.* **183** 2336 (1990)
127. T G Tolstikova, E E Shults, M P Dolgikh, G A Tolstikov *Dokl. Akad. Nauk* **394** 280 (2004) ^g
128. A D Buss, B Cox, R D Waigh *Burger's Medicinal Chemistry and Drug Discovery* Vol. 35 (Ed. D J Abraham) (New York: Wiley, 2003) p. 847
129. P A Krasutsky *Nat. Prod. Rep.* **23** 919 (2006)
130. B R Copp, A N Pearce *Nat. Prod. Rep.* **24** 278 (2007)
131. D J Newman, G M Cragg *J. Nat. Prod.* **70** 461 (2007)

^a — *Russ. J. Bioorg. Chem. (Engl. Transl.)*

^b — *Chem. Sust. Develop. (Engl. Transl.)*

^c — *Chem. Nat. Compd. (Engl. Transl.)*

^d — *Russ. Chem. Bull., Int. Ed. (Engl. Transl.)*

^e — *Russ. J. Org. Chem. (Engl. Transl.)*

^f — *Pharm. Chem. J. (Engl. Transl.)*

^g — *Dokl. Chem. (Engl. Transl.)*

^h — *Bull. Exp. Biol. Med. (Engl. Transl.)*

ⁱ — *J. High. Nerv. Activ. (Engl. Transl.)*

Methods for the synthesis of polycyclic nitramines

S V Sysolyatin, G V Sakovich, V N Surmachev

Contents

I. Introduction	673
II. Synthesis of polycyclic nitramines by condensation of amines and their derivatives with formaldehyde	673
III. Synthesis of polycyclic nitramines by condensation of amines and their derivatives with glyoxal	674
IV. Miscellaneous methods for the synthesis of polycyclic nitramines	677

Abstract. Published data on the methods of synthesis of polycyclic nitramines are analysed. The advantages, drawbacks and prospects of two main approaches to the formation of the molecular cage, namely, amine or amide condensation with carbonyl compounds and consecutive formation of the polycyclic cage with introduction of reactive terminal substituents, are discussed. The bibliography includes 64 references.

I. Introduction

Currently, polycyclic nitramines (PCNA) are becoming significant as promising high-energy compounds, which are superior to other explosives in some properties. They have high density, which improves the explosive characteristics without increasing the sensitivity to mechanical action. High content of hydrogen in PCNA (unlike aromatic heterocyclic compounds) results in an increase in the heat of explosive transformation and a decrease in the average molecular mass of the detonation products.

Polycyclic nitramines meet the requirements imposed on promising components of high-energy compositions: they have the optimum oxygen balance, moderate enthalpy of formation and high density.

There are rather few studies devoted to the synthesis of PCNA, most being concerned with the methods of synthesis of 2,4,6,8,10,12-hexanitro-2,4,6,8,10,12-hexaazatetracyclo-[5.5.-0.0^{3,11}.0^{5,9}]dodecane (hexanitrohexaazaisowurtzitane, CL-20, HNIW).¹ The present review describes systematically the known methods for the synthesis of PCNA, including approaches to the formation of the polycyclic cage and ways of substitution of nitro groups for functional groups at the nitrogen atoms.

The cages of most polycyclic nitramines are synthesised in one step. This way is most convenient for industrial implementation and, as a rule, represents the condensation of amines or amides with carbonyl compounds.

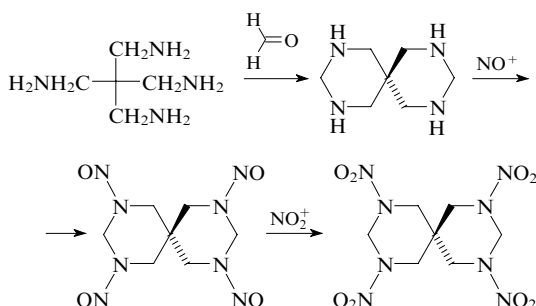
The second stage is introduction of nitro groups. This is accomplished by substituting them for *N*-alkyl and functional (*N*-acyl, *N*-sulfonyl) groups.^{2–6} Nitrolysis of protected secondary amines for the synthesis of cyclic nitramines is fairly well studied.⁷ Of the alkyl substituents, the *tert*-butyl group is replaced most easily. In the series of acyl substituents (CHO, Ac, EtCO, Me₂NCO, ROCO, ArCO), acetyl group is replaced most easily by the nitro group, while the replacement of formyl and propionyl groups requires more drastic conditions. The sulfo group, which undergoes nitrolysis under very mild conditions, is the substituent of choice for the introduction of the nitro group.

Thus, the main problem in PCNA synthesis is construction of a polycyclic cage with *N*-substituents appropriate for substitution of nitro groups. The simplest method for the construction of the hexaazaisowurtzitane cage is condensation of glyoxal with benzylamine or its derivatives. Direct nitrolysis of hexabenzylhexaazaisowurtzitane does not result in HNIW; the major part of investigations on this subject are devoted to the transformation of benzyl groups into substituents suitable for the replacement by the nitro groups.¹

II. Synthesis of polycyclic nitramines by condensation of amines and their derivatives with formaldehyde

The polycyclic cage of nitramines can be formed by condensation of tetramines with formaldehyde. The condensation products are labile compounds, and they are usually converted into the corresponding nitroso derivatives, which are readily nitrated to nitramines.

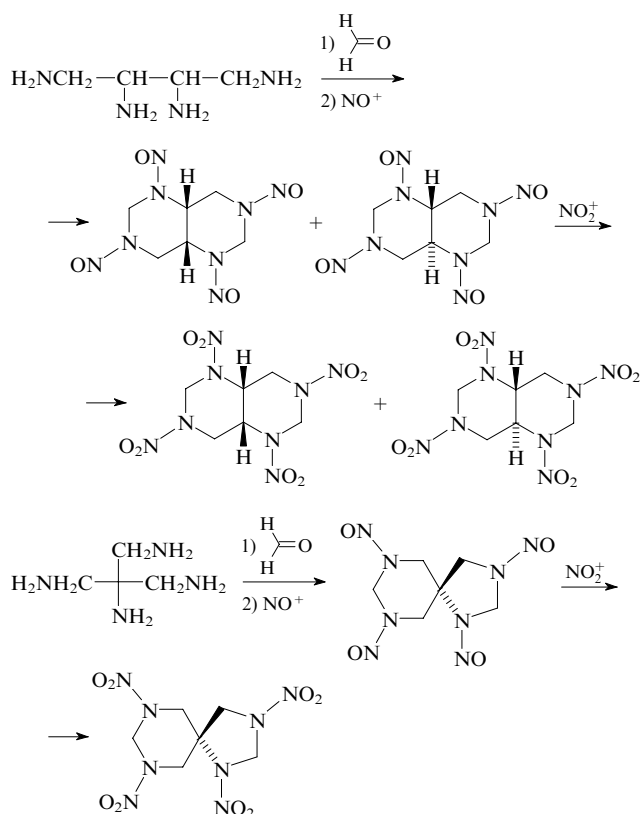
This method was used to synthesise^{8–10} a number of bicyclic nitramines.



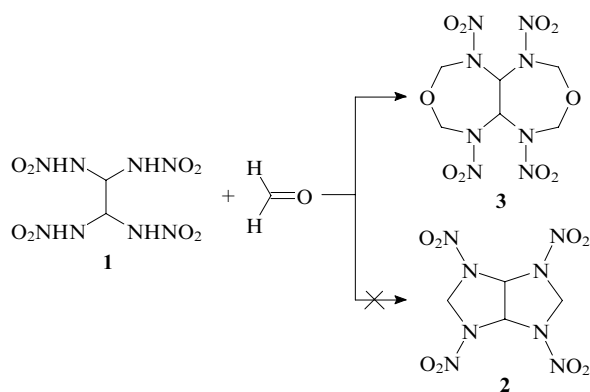
S V Sysolyatin, G V Sakovich, V N Surmachev Institute for Problems of Chemical and Energetic Technologies, Siberian Branch of the Russian Academy of Sciences, ul. Sotsialisticheskaya 1, 659322 Biysk, Altai Territory, Russian Federation. Fax (7-3854) 30 47 25, tel. (7-3854) 30 46 72, e-mail: cherry@yourline.ru (S V Sysolyatin), tel. (7-3854) 30 59 98, e-mail: ipcet@mail.ru (G V Sakovich), tel. (7-3854) 35 60 59 (V N Surmachev)

Received 10 April 2007

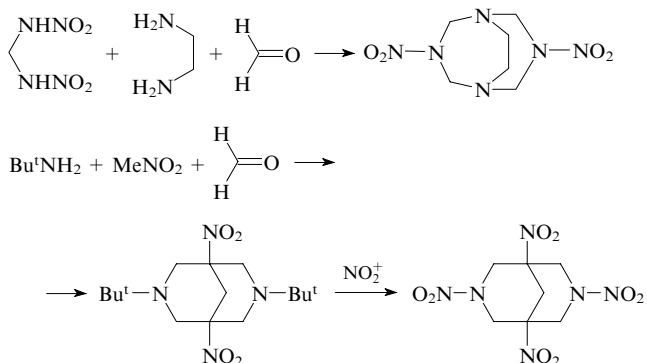
Uspekhi Khimii 76 (7) 724–731 (2007); translated by Z P Bobkova



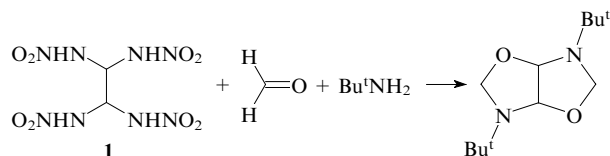
The reaction of 1,1,2,2-tetrakis(nitramino)ethane (**1**) with formalin gives, instead of the expected 2,4,6,8-tetranitro-2,4,6,8-tetraazabicyclo[3.3.0]octane (**2**), bicyclic compound **3** containing nitrogen and oxygen atoms in the seven-membered heterocycles.¹¹



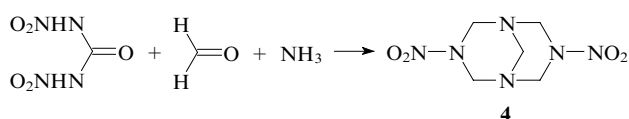
The cage of bicyclic nitramines can be prepared by aminomethylation of compounds with an active hydrogen atom (the Mannich condensation):^{2, 12}



The reaction of nitraminoethane **1** with formalin and *tert*-butylamine results unexpectedly in elimination of nitramine groups.¹³



The reaction of *N,N'*-dinitrourea with ammonia and formaldehyde gives dinitropentamethylenetetramine **4**, which is the starting compound for the synthesis of octogen.¹⁴ It is assumed that *N,N'*-dinitrourea is hydrolysed to nitramide during the synthesis.

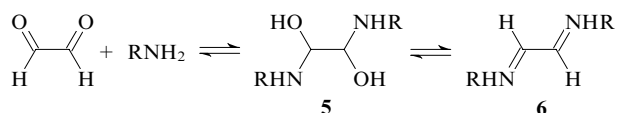


Despite the simplicity and, hence, attractiveness of the PCNA synthesis by condensation of amine derivatives with formaldehyde, it should be noted that compounds with high explosion characteristics cannot be obtained in this way.

III. Synthesis of polycyclic nitramines by condensation of amines and their derivatives with glyoxal

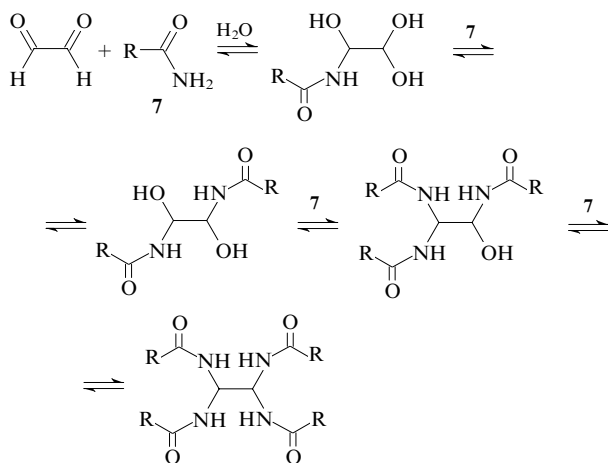
Glyoxal is widely used to prepare nitrogen-containing heterocyclic compounds.^{15, 16} In an aqueous solution of glyoxal, glyoxal hydrate exists in equilibrium with its hydrated oligomeric derivatives.¹⁷

The condensation of glyoxal with primary amines affords mainly 1,2-diaminoethylene glycols **5**, which readily eliminate water being converted into conjugated diimines **6**.^{18, 19}



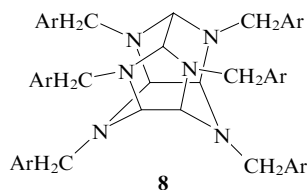
R = Buⁿ, Buⁱ, Bu^t, cyclo-C₆H₁₁, 4-MeC₆H₄, 4-MeOC₆H₄, 4-HOC₆H₄.

The reactions of glyoxal with primary amides **7** afford products with different degrees of substitution depending on the reactant ratio and reaction conditions.^{20–25}



R = Me, Et, OMe, OEt, OPri, All, Bn, Ph.

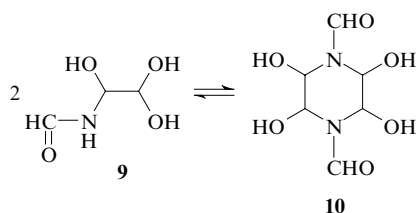
Compounds **5** and **6** where R is the benzyl or substituted benzyl group ($R = \text{ArCH}_2$) usually serve as precursors of hexaazaisowurtzitane derivatives **8**.¹



$\text{Ar} = \text{Ph}, \text{XC}_6\text{H}_4$ ($X = 4\text{-Me}, 2\text{-Me}, 4\text{-MeO}, 2\text{-MeO}, 4\text{-Pr}^i, 4\text{-Cl}, 2\text{-Cl}, 2\text{-F}, 2\text{-Br}, 3,4\text{-(MeO)}_2\text{C}_6\text{H}_3$).

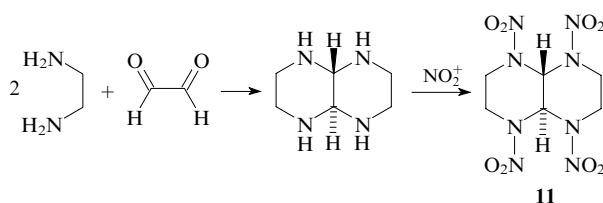
Recently, similar hexaazaisowurtzitanes were synthesised²⁶ using other amines (R is furfuryl, allyl, propargyl, 3-pyridylmethyl, cinnamyl, 2-thienylmethyl, 1-naphthylmethyl).

Dimerisation of compound **9** gives rise to piperazine derivative **10**.²⁷

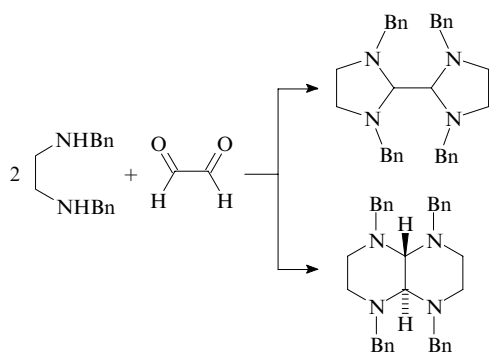


No polycyclic structures are formed in this case.

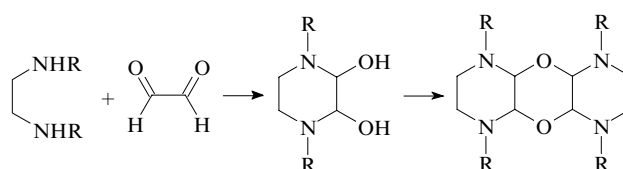
The reaction of ethylenediamine with glyoxal follows different routes depending on the reactant ratio and reaction conditions. When the molar ratio is 2:1, the reaction gives *trans*-fused tetraazadecalin; its nitration results in 2,5,7,10-tetranitro-2,5,7,10-tetraazabicyclo[4.4.0]decane (**11**).²⁸



The reaction of *N,N'*-dibenzylethylenediamine with glyoxal in 2:1 ratio yields cyclic products containing fused and non-fused heterocycles.²⁹

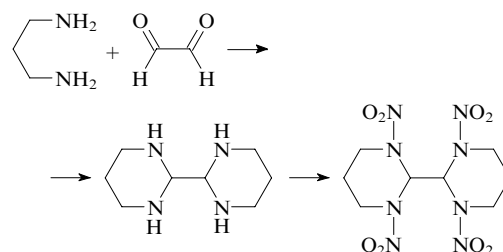


In the case of 1:1 molar ratio of the reactants, a tricyclic compound is formed in a relatively low yield (< 10%).^{30, 31}

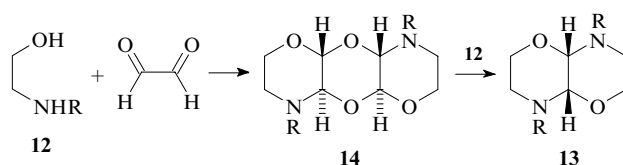


$R = \text{Me}, \text{Pr}^i, \text{Bn}$.

The use of a longer hydrocarbon chain between the amino groups in the diamine results in compounds with non-fused 1,3-diazacycles.³²

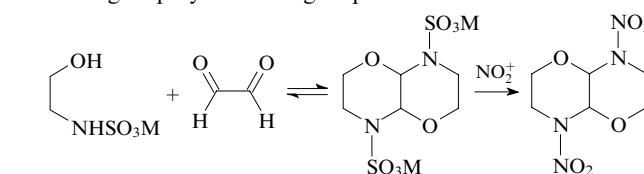


Glyoxal reacts with aminoethanols **12** to give oxazabicyclic (**13**) and -tricyclic (**14**) compounds.³³



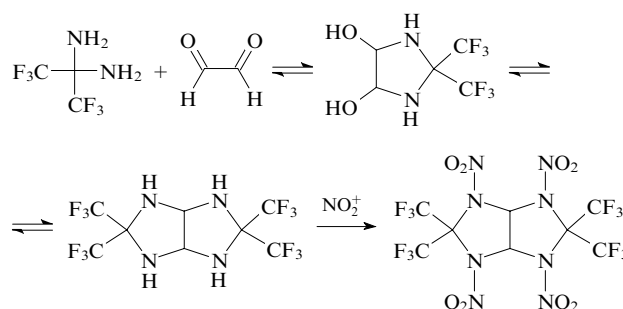
$R = \text{Me}, \text{Et}, \text{Bu}^n, \text{Ph}$.

The use of *N*-(2-hydroxyethyl)sulfamate in the condensation allows one to obtain the bicyclic cage and easily replace the sulfo group by the nitro group.³⁴

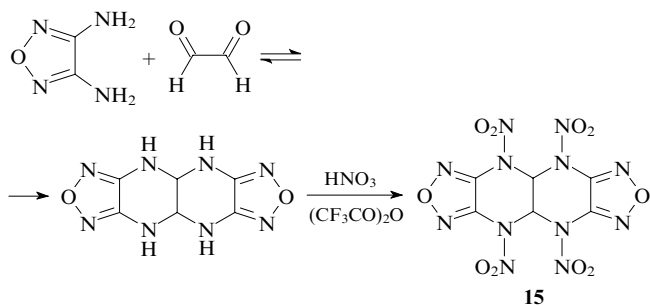


$M = \text{Na}, \text{K}$.

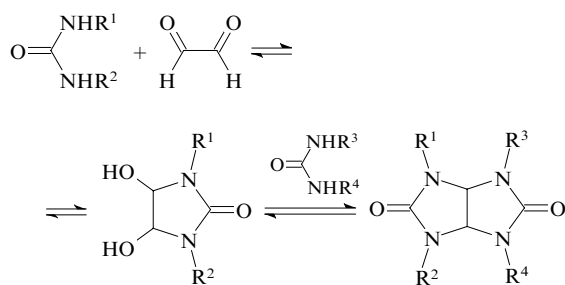
2,2-Diaminohexafluoropropane is a stable compound (unlike diaminomethane); it reacts with glyoxal to afford a bicyclic product, which is nitrated to give bicyclic nitramines.³⁵



Weakly basic diaminofurazan is also readily coupled with glyoxal.^{36, 37} Nitration of the coupling product results in a series of nitro derivatives, including the fully nitrated compound **15**.

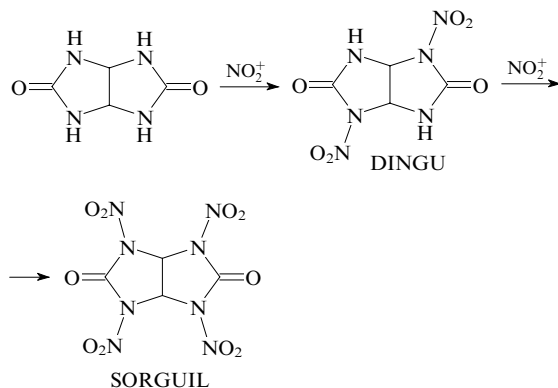


The reactions of glyoxal with urea derivatives proceed very easily to afford glycoluril.^{38–41}

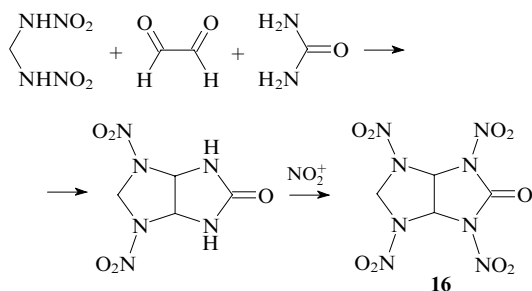


$R^1, R^2, R^3, R^4 = H, Me, Et, Ph, CH_2OH$.

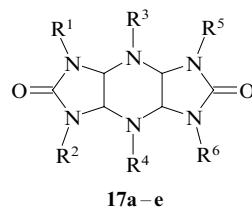
Nitration of glycoluril gave a series of its nitro derivatives, among which DINGU and SORGUIL (TENGU) are distinguished as regards explosion characteristics.^{42, 43}



In order to prepare 2,4,6,8-tetranitro-2,4,6,8-tetraazabicyclo[3.3.0]octane, attempts at multicomponent condensation of amines with amides and glyoxal or formaldehyde have been undertaken.^{38, 44} Thus condensation of *N,N'*-dinitromethylenediamine with urea and glyoxal afforded⁴⁵ 2,4,6,8-tetranitro-2,4,6,8-tetraazabicyclo[3.3.0]octan-3-one (**16**).

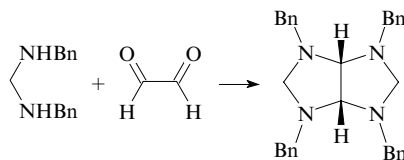


A series of tricyclic derivatives of urea **17a–e** were synthesised in a similar way.⁴⁶

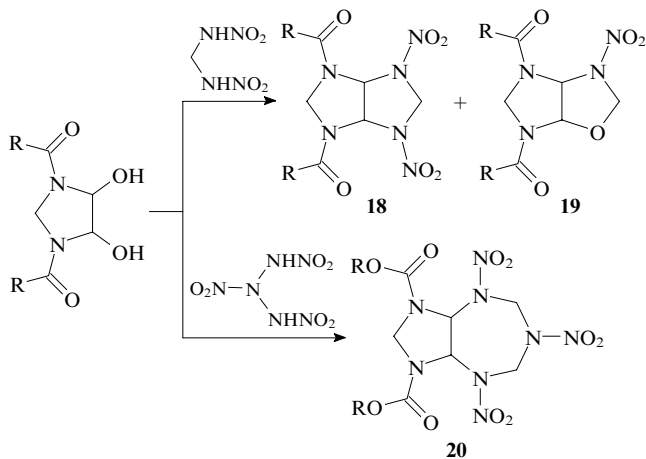


Compound 17	R^1	R^2	R^3	R^4	R^5	R^6
a	H	H	H	H	H	H
b	NO ₂	H	NO ₂	NO ₂	NO ₂	H
c	NO ₂	H	NO ₂	NO ₂	H	NO ₂
d	NO ₂	NO ₂	NO ₂	NO ₂	H	NO ₂
e	NO ₂	NO ₂	NO ₂	NO ₂	NO ₂	NO ₂

In the search for synthetic routes to bicyclic nitramines, coupling of methylenediamine derivatives with glyoxal was studied. The condensation of *N,N'*-dibenzylidiaminomethane with glyoxal resulted⁴⁷ in a *cis*-fused bicyclic system.



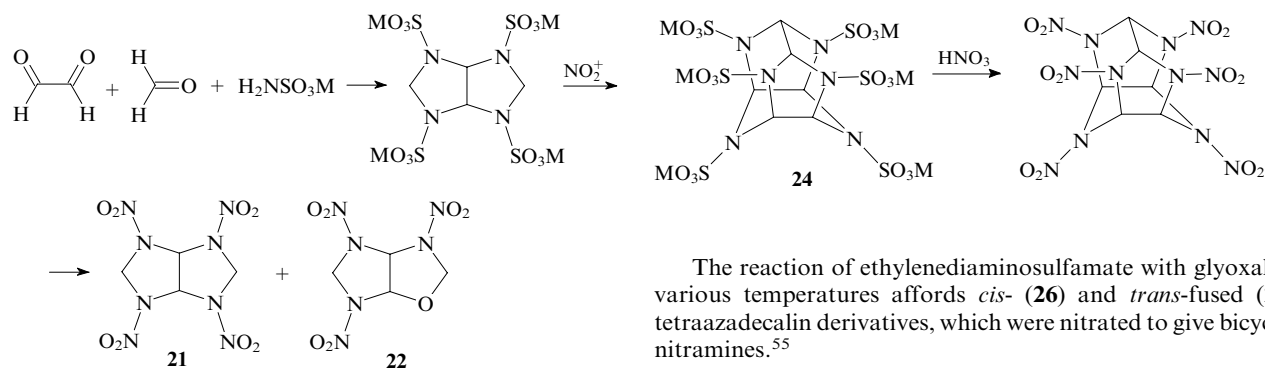
The reaction of *N,N'*-diacyl-4,5-dihydroxyimidazolidine (obtained by condensation of methylenediamide with glyoxal) with dinitramines resulted^{48–51} in a number of bicyclic structures **18–20**. However, attempts to replace the acyl substituents at the nitrogen atoms by the nitro groups failed.



$R = Me, Et$.

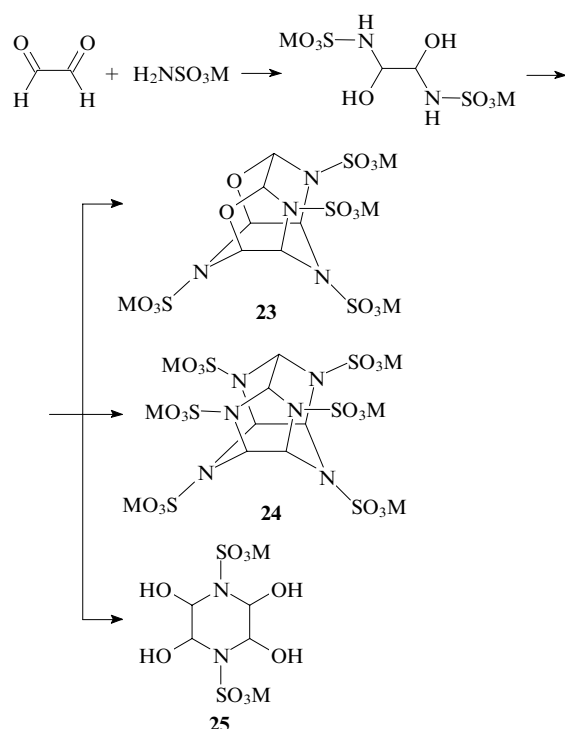
The coupling of glyoxal with metal sulfamates deserves special attention. The sulfo group is easily replaced by the nitro group, which makes it the protecting group of choice among those used for the synthesis of polycyclic nitramines. The coupling sulfamates with carbonyl compounds forms not only mono- and bi-, but also tetracyclic products.

The multicomponent condensation of glyoxal with formaldehyde and sulfamates followed by nitration of the bicyclic product with concentrated nitric acid at $-30^\circ C$ affords 2,4,6,8-tetranitro-2,4,6,8-tetraazabicyclo[3.3.0]octane (**21**) (or, at $0^\circ C$, its oxo analogue **22**).⁵²



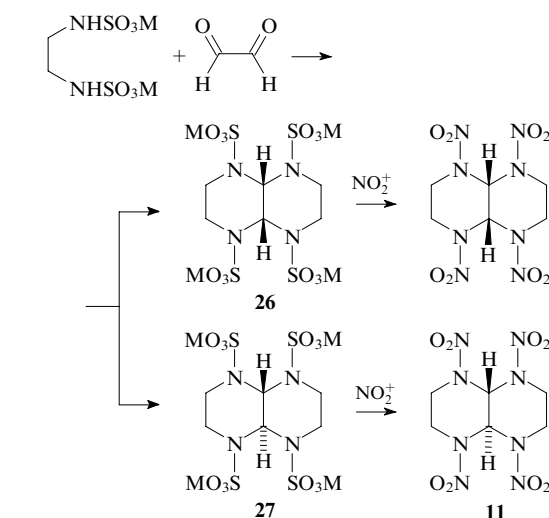
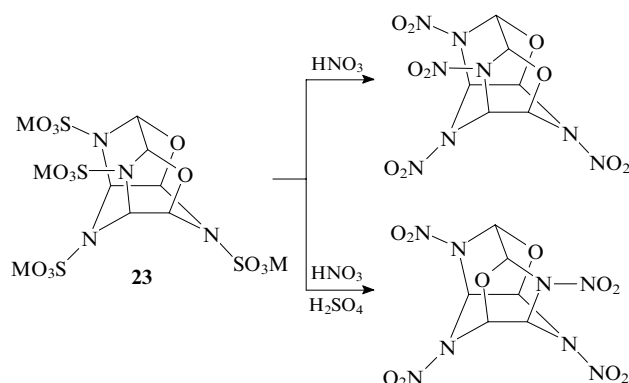
M = Na, K.

The reaction of glyoxal with sulfamates proceeds in different ways,^{52, 53} depending on the reactant ratio and reaction conditions.



Compound **23** and **24** with the isowurtzitane structure are formed in an acid medium (pH 2.8–4.0) at 50–65 °C. At lower temperature and acidity, salts of 2,3,5,6-tetrahydroxypiperazine-1,4-disulfonic acid (**25**) are mainly formed.

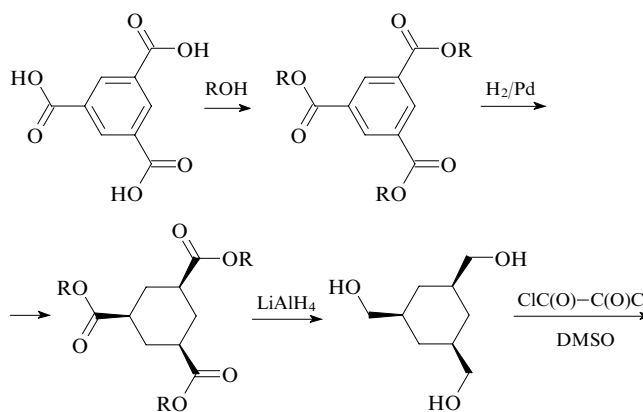
Nitrolysis of sulfonates **23** and **24** with nitric acid–based mixtures proceeds under relatively mild conditions and results in nitramines with the isowurtzitane structure.^{52–54}

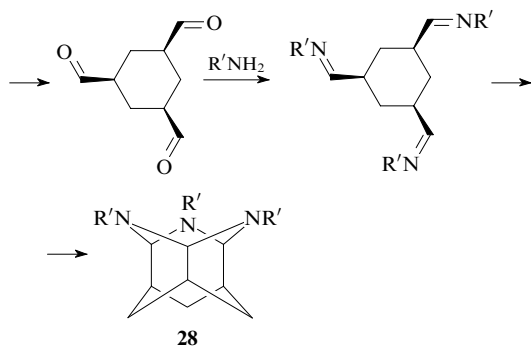


Thus, the reactions of amines and their derivatives with glyoxal provide a broad range of PCNA with different structures. Some of them present practical interest and are produced in industry. The main trend of future works would involve the search for economical two-step methods for the synthesis of hexanitrohexaazaisowurtzitane, the most powerful explosive among the PCNA synthesised and the study of application of PCNA and their precursors as biologically active compounds.

IV. Miscellaneous methods for the synthesis of polycyclic nitramines

The following method for the construction of the 3,5,12-triazawurtzitane cage **28** has been proposed:^{56, 57}

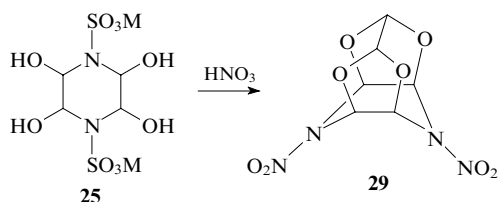




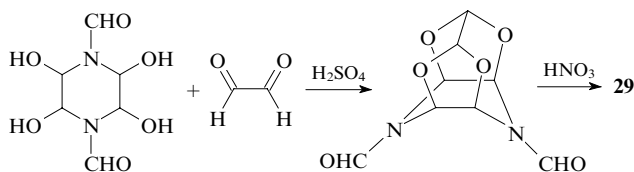
R = Me, Et, Prⁿ; R' = Me, Et, Bn, 4-MeOC₆H₄CH₂, 4-Me₂NC₆H₄CH₂.

However, the attempts to carry out substitution at the nitrogen atoms in compound **28** failed.

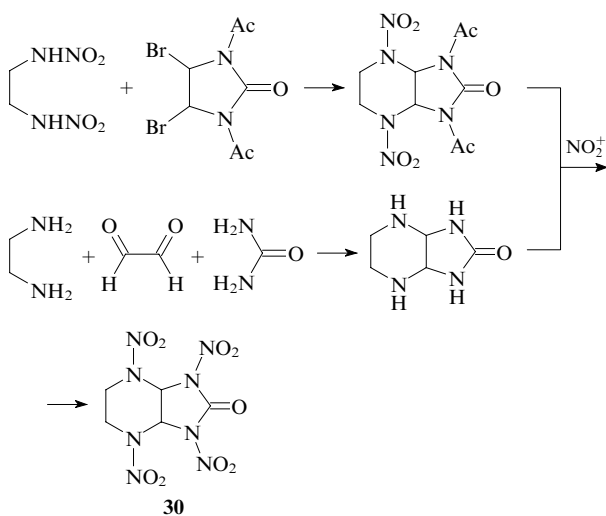
Nitration of the condensation product of the sulfamate salts with glyoxal (**25**) gave 4,10-dinitro-2,6,8,12-tetraoxa-4,10-diazatetracyclo[5.5.0.0^{3,11}.0^{5,9}]dodecane (**29**).^{53, 54}



This compound can also be prepared in a different way.⁵⁸

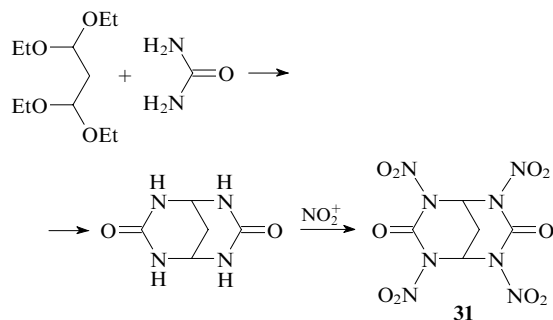


Alkylation of ethylenedinitramine with 1,3-diacetyl-4,5-dibromimidazolidin-2-one with subsequent nitrolysis results in bicyclic urea derivative **30**. This compound was also prepared by nitration of the condensation product of ethylenediamine with urea and glyoxal.^{59, 60}

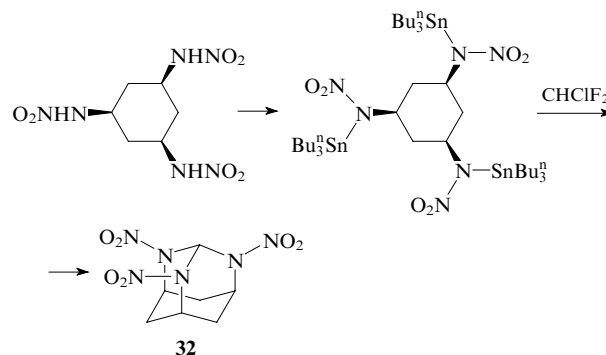


Polycyclic structures called cucurbiturils were prepared by condensation of glycoluril with formaldehyde,⁶¹ and hexacyclic systems were formed upon the reaction of glycoluril, formaldehyde, and diamines.⁶² The attempts to introduce nitro groups in these compounds were unsuccessful.

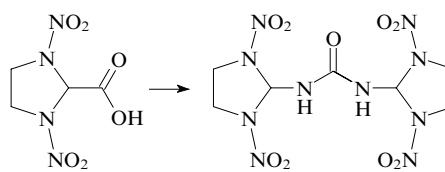
The reaction of urea with 1,1,3,3-tetraethoxypropane and subsequent nitration yielded 2,4,6,8-tetranitro-2,4,6,8-tetraazabicyclo[3.3.1]nonane-3,7-dione (**31**).⁶⁰



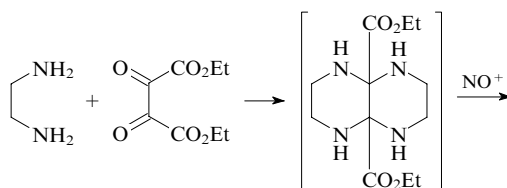
Alkylation of a stannyl derivative of tris(nitramino)cyclohexane was used to synthesise 2,4,10-trinitro-2,4,10-triazaadamantane (**32**).⁵⁶

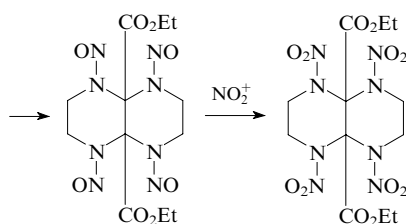


The possibility of attachment of an amino group at the carbon atom already containing two nitramino groups would give a broad range of PCNA with a tris(nitramino)methane fragment in the molecule, for example, hexanitrohexaazaadamantane. According to calculations, the introduction of terminal amino groups into the PCNA structure would sharply increase the density and explosion characteristic of the compound. Due to the ability of the carboxy group to be replaced by the amino group, the former is a preferable terminal group for the PCNA synthesis.⁶³



The reaction of ethylenediamine with dioxosuccinate, the fixation of the reaction product as the nitrosamine and subsequent nitration with dinitrogen pentoxide in nitric acid gives rise to a bicyclic nitramine containing carboxy groups.⁶³





The methods of synthesis of polycyclic structures by consecutive formation of the molecular skeleton have not been adequately developed as yet, but they are quite promising for the design of diverse PCNA.

* * *

Analysis of published data allows one to distinguish two main methods for the synthesis of PCNA: one-step construction of the polycyclic core of the molecule by condensation of amines and their derivatives with carbonyl compounds and the consecutive formation of the polycyclic cage. Most of PCNA described in the literature were prepared by the former method. The second method is not adequately developed as yet but holds much promise and may yield PCNA of different structures.

The chemistry of high-energy materials, in particular, methods for their synthesis is a topical field of research being actively developed, as indicated by regular publication of new studies (see, for example, the monograph⁶⁴).

References

- S V Sysolyatin, A A Lobanova, Yu T Chernikova, G V Sakovich *Usp. Khim.* **74** 830 (2005) [*Russ. Chem. Rev.* **74** 757 (2005)]
- J H Robson, J Reinhart *J. Am. Chem. Soc.* **77** 2453 (1955)
- Y Ogata, Y Sawaki, Y Kuriyama *Tetrahedron* **24** 3425 (1968)
- W P Norris *J. Org. Chem.* **25** 1244 (1960)
- D A Levins, C D Bedford, S J Staats *Propellants, Explos. Pyrotech.* **8** 74 (1983)
- R L Willer, R L Atkins *J. Org. Chem.* **49** 5147 (1984)
- L L Kuznetsov, B V Gidasov *Nitrovanie Aromaticheskikh Soedinenii* (Nitration of Aromatic Compounds) (Leningrad: Leningrad Technology Institute, 1977)
- R L Willer *J. Org. Chem.* **49** 5150 (1984)
- A Edwards, G A Webb *J. Chem. Soc., Perkin Trans. I* 1989 (1977)
- Y Zheng, J Zhou, M Zhang *Acta Armamentarii* **1** 24 (1988)
- D A Cichra, H G Adolph *J. Org. Chem.* **47** 2474 (1982)
- S S Novikov, A Dudinskaya, N V Makarov, L I Khmel'nitskii *Izv. Akad. Nauk SSSR, Ser. Khim.* 1839 (1967)^a
- A L Kovalenko, Yu V Serov, I V Tselinskii *Zh. Obshch. Khim.* **61** 2778 (1991)^b
- S G Il'yasov, A A Lobanova, N I Popov, R R Sataev *Zh. Org. Khim.* **38** 1800 (2002)^c
- G Mattioda, B Metivier, J P Guette *Chem.-Tech. (Heidelberg)* **13** 478 (1983)
- J P Guette, G Mattioda, B Metivier *Actual. Chim.* **23** (1982)
- E B Whipple *J. Am. Chem. Soc.* **92** 7183 (1970)
- J M Kliegman, R K Barnes *Tetrahedron* **26** 2555 (1970)
- J M Kliegman, R K Barnes *Tetrahedron Lett.* 1953 (1969)
- S L Vail, C M Moran, R H Barker *J. Org. Chem.* **30** 1195 (1965)
- E E Gilbert *J. Chem. Eng. Data* **19** 182 (1974)
- S L Vail, A G Pierce Jr *J. Org. Chem.* **37** 391 (1972)
- G F Whitfield, R Johnson, D Swern *J. Org. Chem.* **37** 95 (1972)
- P M Quan *J. Org. Chem.* **33** 3937 (1968)
- J M Kliegman, R K Barnes *J. Heterocycl. Chem.* **7** 1153 (1970)
- H Gregoire, J Guy, G Roger *Chem. - Eur. J.* **12** 3339 (2006)
- A C Currie, A H Dinwoodie, J M C Thompson *J. Chem. Soc.* **491** (1967)
- R L Willer *Propellants, Explos. Pyrotech.* **8** 65 (1983)
- R L Willer, D W Moore, D J Vanderah *J. Org. Chem.* **50** 2365 (1985)
- R L Willer, D W Moore, C K Lowe-Ma, D J Vanderah *J. Org. Chem.* **50** 2368 (1985)
- A T Nielsen, R A Nissan, D J Vanderah, C L Coon, R D Gilardi, C F George, J Flippen-Anderson *J. Org. Chem.* **55** 1459 (1990)
- D S Black, D C Craig, O Giitsidis, R W Reed, A Salek, M A Safton *J. Org. Chem.* **54** 4771 (1989)
- A Le Rouzic, D Raphalen, D Papillon, M Kefranto *Tetrahedron Lett.* **26** 1853 (1985)
- A S Ermakov, E Yu Petrov, Yu A Strelenko, D B Vinogradov, V A Tartakovskii *Zh. Org. Khim.* **41** 1219 (2005)^c
- W M Koppes, M Chaykovsky, H G Adolph, R Gilardi, C George *J. Org. Chem.* **52** 1113 (1987)
- R L Willer *J. Org. Chem.* **50** 5123 (1985)
- R L Willer *Armada Int.* **5** 78 (1983)
- S L Vail, C M Moran, H B Moore, R M H Kullman *J. Org. Chem.* **27** 2071 (1962)
- J Nematollahi, R Ketcham *J. Org. Chem.* **28** 2378 (1963)
- S L Vail, R H Barker, P G Mennitt *J. Org. Chem.* **30** 2179 (1965)
- A N Kravchenko, O V Lebedev, E Ya Marsareva *Mendelev Commun.* **27** (2000)
- J Boileau, E Wimmer, M Carail, R Gallo *Bull. Soc. Chim. Fr.* 465 (1986)
- J Boileau, M Carail, E Wimmer, R Gallo, M Pierrot *Propellants, Explos. Pyrotech.* **10** 118 (1985)
- S L Vail, R H Barker, C M Moran *J. Org. Chem.* **31** 1642 (1966)
- L Wenjie, H Guifen, C Miaohong *Proceedings of International Symposium on Pyrotechnics and Explosives* (Beijing: China Academic Publ., 1987) p. 187
- V F Zhilin, G F Rudakov, A V Ladonin, V P Sinditskii, V Yu Egorshv, M V Berezin *The 34th Annual Conference of ICT, Karlsruhe, 2003* p. 141/1; *Chem. Abstr.* **140** 341679 (2004)
- A T Nielsen, R A Nissan, A P Chafin, R D Gilardi, C F George *J. Org. Chem.* **57** 6756 (1992)
- R D Gilardi, J L Flippen-Anderson, C F George *Acta Crystallogr., Sect. C* **48** 1872 (1992)
- R D Gilardi, C F George, J L Flippen-Anderson *Acta Crystallogr., Sect. C* **48** 1528 (1992)
- J L Flippen-Anderson, C F George, R D Gilardi *Acta Crystallogr., Sect. C* **48** 1530 (1992)
- R D Gilardi, C F George, J L Flippen-Anderson *Acta Crystallogr., Sect. C* **48** 1532 (1992)
- S V Sysolyatin, G V Sakovich, Yu T Chernikova, V N Surmachev, A A Lobanova *The 37th Annual Conference of ICT, Karlsruhe, 2006* p. 141/1
- S V Sysolyatin, V N Surmachev, A A Lobanova, Yu T Chernikova, G V Sakovich *The 5th International High Energy Materials Conference and Exhibit, DRDL, Hyderabad, 2005* p. 67
- Yu V Gatilov, T V Rybalova, O A Efimov, A A Lobanova, G V Sakovich, S V Sysolyatin *Zh. Strukt. Khim.* **46** 579 (2005)^d
- S V Sysolyatin, A A Lobanova, Yu T Chernikova *Sovremennye Problemy Organicheskoi Khimii (Tezisy Dokl. Nauchnoi Konferentsii), Novosibirsk, 2001* [Today's Problems of Organic Chemistry (Abstracts of Reports of the Research Conference), Novosibirsk, 2001] p. SD51
- A T Nielsen, A P Chafin, S L Christian, D W Moore, M P Nadler, R A Nissan, D J Vanderah, R D Gilardi, C F George, J L Flippen-Anderson *Tetrahedron* **54** 11793 (1998)
- A T Nielsen, S L Christian, D W Moore, R D Gilardi, C F George *J. Org. Chem.* **52** 1656 (1987)
- V T Ramakrishnan, M Vedachalam, J H Boyer *Heterocycles* **31** 479 (1990)
- P F Pagoria, A R Mitchell, E S Jessop *Propellants, Explos. Pyrotech.* **21** 14 (1996)
- A K Sidker, G M Bhokare, D B Sazwade, J P Agraval *Propellants, Explos. Pyrotech.* **26** 63 (2001)
- W A Freeman, W L Mock, N-Y Shih *J. Am. Chem. Soc.* **103** 7367 (1981)

62. W L Mock, T Manimaran, W A Freeman, R M Kuksuk, J E Maggio, D H Williams *J. Org. Chem.* **50** 60 (1985)
63. S V Sysolyatin, A A Lobanova, V N Surmachev, Yu T Chernikova *Sovremennye Problemy Tekhnicheskoi Khimii (Materialy Dokl. Nauchno-tekhn. Konferentsii), Kazan', 2004* [Today's Problems of Technical Chemistry (Proceedings of the Scientific and Technical Conference), Kazan, 2004] p. 333
64. J P Agrawal, R D Hodgson *Organic Chemistry of Explosives* (New York: Wiley, 2006)

^a — *Russ. Chem. Bull., Int. Ed. (Engl. Transl.)*

^b — *Russ. J. Gen. Chem. (Engl. Transl.)*

^c — *Russ. J. Org. Chem. (Engl. Transl.)*

^d — *Russ. J. Struct. Chem. (Engl. Transl.)*

Non-symmetrically substituted phthalocyanines: synthesis and structure modification

A Yu Tolbin, L G Tomilova, N S Zefirov

Contents

I. Introduction	681
II. Methods for the synthesis of non-symmetrically substituted phthalocyanines	681
III. Structure modification of non-symmetrically substituted phthalocyanines	684
IV. Prospects for the use of non-symmetrically substituted phthalocyanines	690

Abstract. The presently known approaches to the synthesis of non-symmetrically substituted phthalocyanines of the A_3B and A_2B_2 types are surveyed. The prospects for the use of these compounds for the synthesis of binuclear and heteronuclear complexes and phthalocyanine oligomers and polymers are demonstrated. The bibliography includes 84 references.

I. Introduction

Phthalocyanines, being synthetic analogues of porphyrins wide spread in nature attract attention of many researchers owing to their prominent chemical and thermal non-stability. Over the last decade, non-symmetrically substituted phthalocyanines bearing different types of substituents came into the focus of interest. These compounds manifest a number of valuable properties enabling their application as advanced materials, in particular in non-linear optics.^{1–12} Non-symmetrically substituted phthalocyanines readily form ordered single layers (*i.e.*, the Langmuir–Blodgett films)^{11–14} and linear polymers.¹⁵ Furthermore, their zinc complexes are promising substrates in the photodynamic anticancer therapy.^{16, 17}

It is of note that the synthesis of non-symmetrical phthalocyanines is a very labourious task, which hinders their studies and practical applications. In the vast majority of cases, non-symmetrically substituted phthalocyanines are synthesised by random cyclisation of phthalogens, which gives rise, naturally, to mixtures of phthalocyanines that are difficult to separate in extremely low yields of the target products.

Non-symmetrically substituted phthalocyanines are of interest from both theoretical and practical standpoints. The presence of different functional substituents in these macrocyclic compounds enables the design of novel supramolecular structures with unique physicochemical properties.^{18–21} That is why the development of methods for the directed synthesis of this class of

compounds is one of the topical directions in the chemistry of phthalocyanines.

In the present review, the emphasis is placed on the methods for the synthesis of non-symmetrically substituted phthalocyanines and their modifications aimed at the introduction of new functional substituents required for the design of bi- and poly-nuclear assemblies of any complexity.

II. Methods for the synthesis of non-symmetrically substituted phthalocyanines

As has been noted above, the directed synthesis of non-symmetrically substituted phthalocyanines remains a challenging problem. The known methods of synthesis do not provide sufficiently high yields^{15–17, 22–41} comparable to those achievable in the synthesis of symmetrical phthalocyanines.

There are two major approaches to the synthesis of non-symmetrically substituted phthalocyanines, *viz.*, the random cyclisation of different phthalonitriles and their synthetic analogues, 1,3-diiminoisindolines,^{15–17, 22–32, 40, 42–50} and the macrocycle ring expansion in subphthalocyanines, *i.e.*, compounds with three rather than four isoindole fragments.^{33–39, 51–56}

1. Methods of synthesis based on the phthalogen random cyclisation

The random cyclisation is presently used the most often for the synthesis of different types of non-symmetrically substituted phthalocyanines, despite its intrinsically low selectivity. Thus the joint cyclisation of two phthalogens **A** and **B** may theoretically afford six products, *viz.*, **AAAA** (A_4), **BBBB** (B_4), **AABB**, **ABAB** (two isomers with the A_2B_2 stoichiometry), **AAAB** (A_3B) and **ABBB** (AB_3) (Scheme 1).

The separation of the resultant random mixture requires the application of sophisticated chromatographic techniques. Due to the high proneness of phthalocyanine molecules to self-aggregation, the isolation of the target product represents a rather difficult problem.^{23, 57} Typically, it can be solved with the use of phthalogens with substituents of different nature. In particular, bulky substituents prevent the self-aggregation and increase the solubility thus facilitating the chromatographic isolation and purification of the target product.^{43, 58, 59}

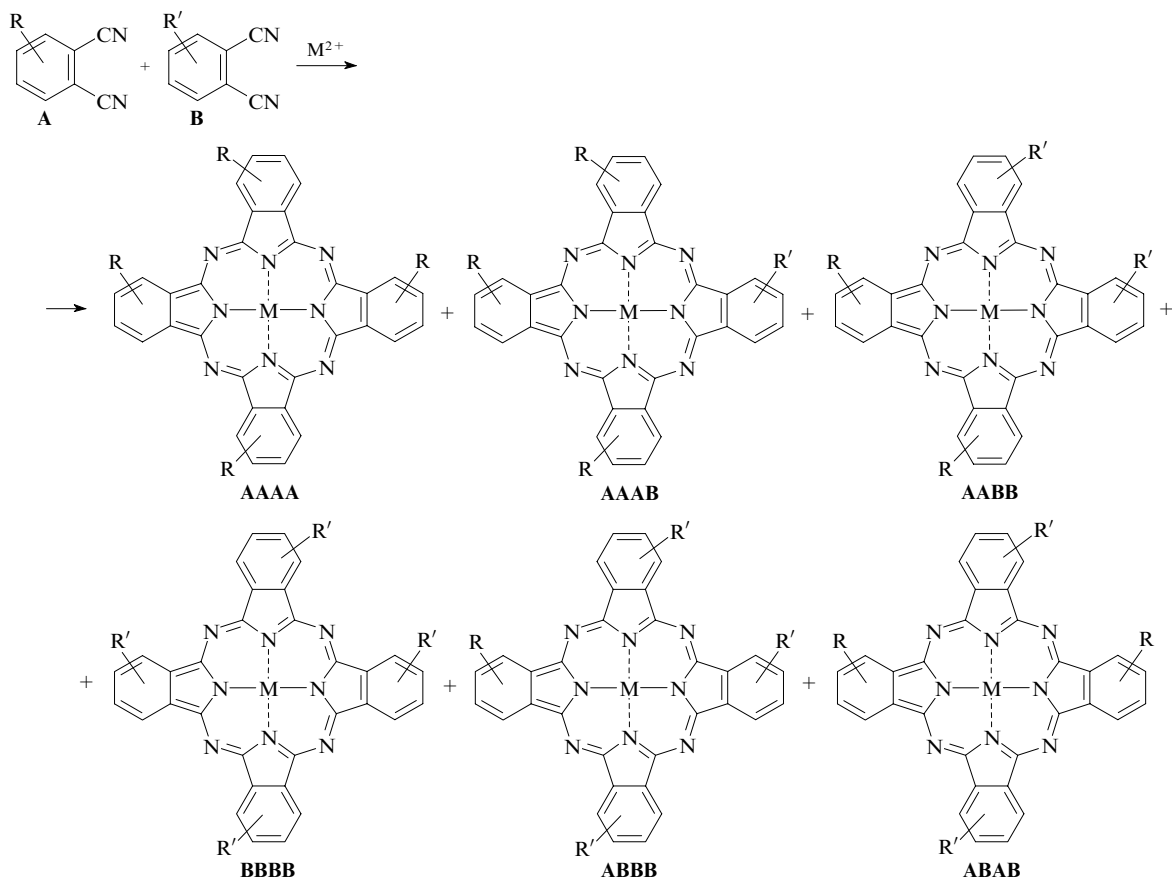
The yield of a target product is strongly affected by the ratio of the reactants.^{16, 17, 22–27} According to a theoretical analysis, the reaction of phthalogens **A** and **B** with similar reactivities taken in a molar ratio of 3 : 1 yields a mixture containing phthalocyanines A_4 and A_3B in a ratio of 3 : 4.⁵⁸ The total yield of the A_3B products does not exceed 10%–20%. Leznoff and co-workers¹⁷ noted that

A Yu Tolbin, L G Tomilova, N S Zefirov Department of Chemistry, M V Lomonosov Moscow State University, Leninskie Gory, 119992 Moscow, Russian Federation. Fax (7-495) 939 02 90, tel. (7-495) 939 12 43, e-mail: tolbin@newmail.ru (A Yu Tolbin), tom@org.chem.msu.ru (L G Tomilova), tel. (7-495) 939 16 20, e-mail: zefirov@org.chem.msu.ru (N S Zefirov)

Received 14 February 2007

Uspekhi Khimii 76 (7) 732–744 (2007); translated by Ya V Zubavichus

Scheme 1

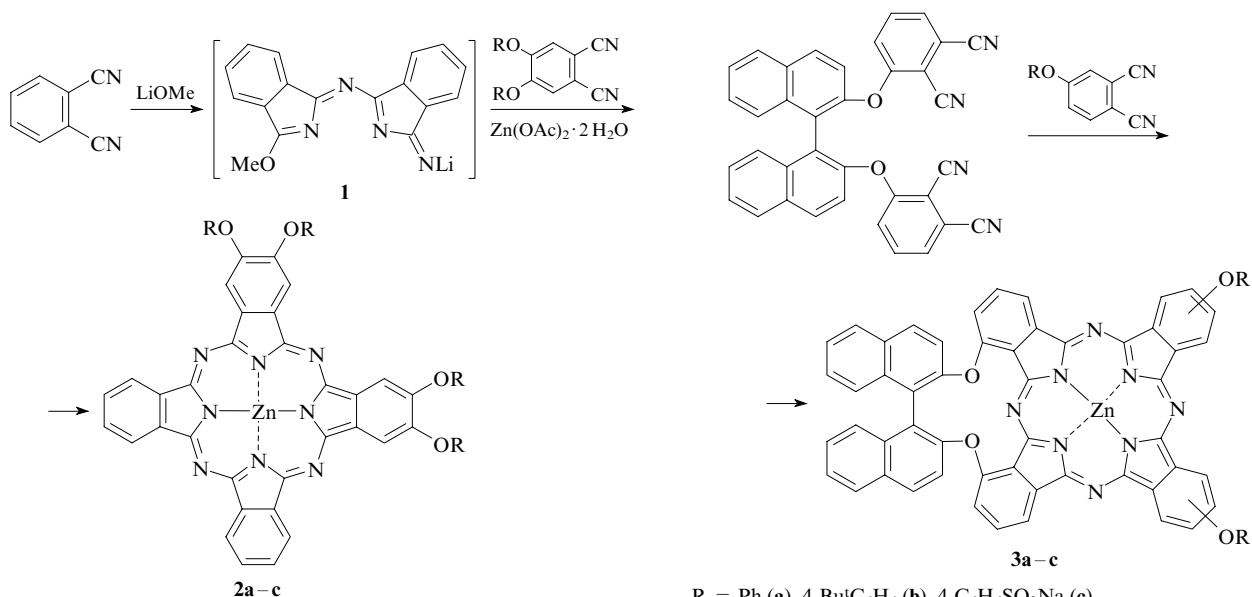


the content of the product A_3B in the reaction mixture can be increased with respect to other possible phthalocyanines by increasing the amount of the phthalogen **A** to 9–10 equivalents. But even in this case, the yield of the target product rarely exceeds 20%.

In the synthesis of the A_2B_2 type phthalocyanines, the formation of two isomers with the identical fragments arranged either next to (**AABB**), or opposite to (**ABAB**), each other is possible.^{15–17, 27, 28, 43–45} These isomers cannot be separated by adsorption chromatography, thus a two-step process has been elaborated¹⁷ for the selective synthesis of the isomer **AABB**.

The reaction of lithium methoxide with phthalonitrile taken in the equimolar ratio in methanol at 40–60 °C yields mainly intermediate **1**. Its subsequent cyclisation with alkoxy-substituted phthalonitriles in *n*-octanol affords complexes **2**.

An alternative approach to the synthesis of structures **AABB** consists of the use of the mixed cyclisation of bis(phthalonitriles) prepared from 3-nitrophthalonitrile and diols with closely arranged OH groups.^{7, 8, 27, 60, 61} Such phthalocyanines synthesised for the first time in the mid 1990s⁶¹ are commonly referred to as side-strapped.



$R = \text{Me}$ (**a**), CH_2Ph (**b**), CHPh_2 (**c**).

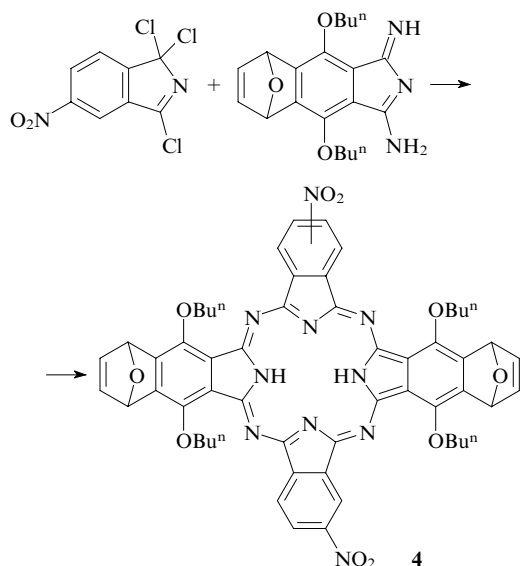
$R = \text{Ph}$ (**a**), $4\text{-Bu}^t\text{C}_6\text{H}_4$ (**b**), $4\text{-C}_6\text{H}_4\text{SO}_3\text{Na}$ (**c**).

Since in the starting compound the phthalonitrile groups are located close to each other, the probability of the oligomerisation and formation of binuclear products is rather low, such that non-symmetrically substituted phthalocyanines of the **AABB** type are preferably formed. Nevertheless, the possible formation of a phthalocyanine with two cross-links at the opposite sides is not totally ruled out even in the presence of phthalonitrile.²⁷

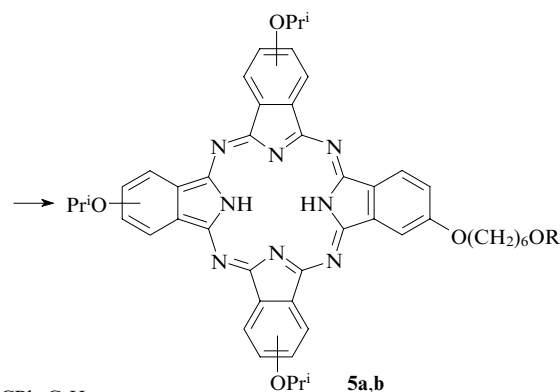
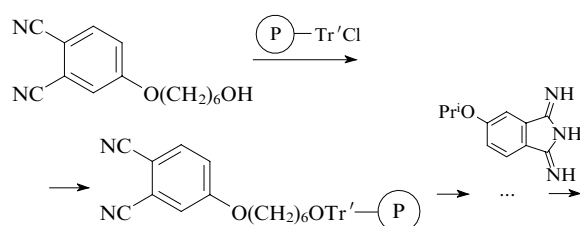
Young and Onyebuagu²⁸ proposed a method for the selective synthesis of phthalocyanines **ABAB** based on the cyclisation of 6-nitro-1,3,3-trichloroisindole and substituted 1,3-diiminoisindoline taken in an equimolar ratio.

The target product **4** is formed in 50% yield, which is record high for non-symmetrically substituted phthalocyanines. However, other authors who employed this method^{15,62} observed the formation of the phthalocyanine **AAAB** as a by-product with the total yield of the target phthalocyanine **ABAB** not exceeding 15%–25%. It was also noted⁶³ that the selectivity of the reaction increases with an increase in the bulk of substituents in one of the phthalogens.

Therefore, the random cyclisation as a method for the synthesis of non-symmetrically substituted phthalocyanines provides low selectivity, which weakly depends on the nature and ratio of the starting phthalogens.



The synthesis on a polymer support (**P**) represents a promising modification of the random cyclisation method. This approach involves grafting of a phthalonitrile containing an OH group in a substituent to a polymer, converting the thus modified phthalogen into the respective 1,3-diiminoisindoline analogue followed by its mixed cyclisation with another substituted 1,3-diiminoisindoline.^{40,49}



$\text{Tr}' = \text{CPh}_2\text{C}_6\text{H}_4$;

$\text{R} = \text{Tr}' - \text{P}$ (**a**), **H** (**b**).

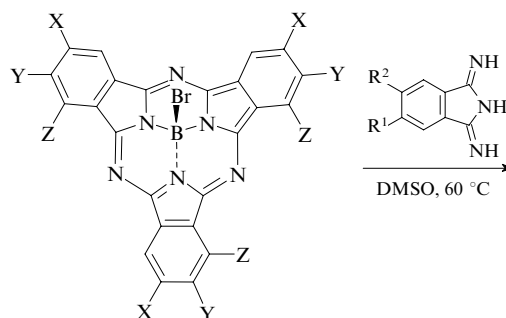
An acid treatment of the immobilised phthalocyanine **5a** afforded compound **5b** in 20% yield. The simplicity of the isolation of the target product is an evident advantage of this method — it is sufficient to wash the immobilised phthalocyanine with an appropriate solvent to remove concomitant symmetrical phthalocyanine. Wöhrle and co-workers⁵⁰ proposed to use modified silica gel as a support for the assembly of the target phthalocyanine.

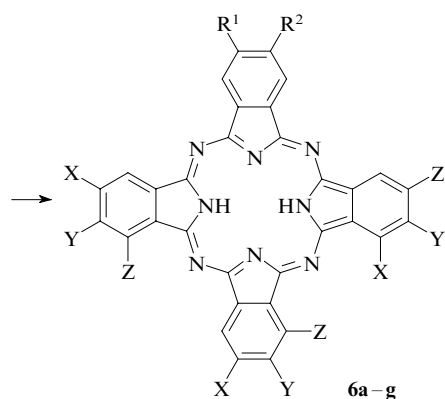
The synthesis on a polymeric support requires that substituents in the starting phthalonitriles should contain suitable reactive groups, which limits the diversity of substituted phthalocyanines that can be synthesised by this method.

2. A method of synthesis based on the ring expansion in subphthalocyanine macrocycles

A rather convenient and elegant method for the synthesis of A_3B -type phthalocyanines has been suggested by Kobayashi *et al.*⁵³ and further developed by Torres and co-workers,^{37,38,51} van Lier and co-workers^{33,54,56} and Wöhrle and co-workers.⁵² These studies showed that energetically strained subphthalocyanines undergo ring opening in the presence of 1,3-diiminoisindolines giving rise to phthalocyanines. In a recent paper, van Lier and co-workers⁵⁶ reported on the synthesis of a number of functionally substituted phthalocyanines **6a–g** by this method. This method provides a substantial advantage over the statistical cyclisation: the reaction selectivity can be finely controlled.

The ring expansion reaction is shown^{64,65} to be of the first order with respect to subphthalocyanine and its selectivity is mainly governed by the nature of substituents in the reactants. The reaction proceeds with the maximum selectivity and the target products are obtained in the maximum yields (>20%) provided that the subphthalocyanine is either non-substituted⁵¹ or bears acceptor substituents,³⁹ whereas the 1,3-diiminoisindoline bears electron-releasing substituents.^{35,38,51,52} Highly reactive 1,3-diiminoisindolines with electron-withdrawing groups yield random mixtures of products.^{36,37}





Compound 6	R ¹	R ²	X	Y	Z
a	H	H	I	H	H
b	H	Bu ^t	I	H	H
c	CH=CHCH=CH	I	H	H	H
d	H	H	H	H	I
e	H	Bu ^t	H	H	I
f	CH=CHCH=CH	H	H	H	I
g	H	H	I	I	H

Mixtures of DMSO with α -chloronaphthalene or *o*-dichlorobenzene are typically used as solvents for the subphthalocyanine ring expansion.^{33–39, 51–54} Dimethyl sulfoxide is the optimum medium for the reaction, but subphthalocyanines are only moderately soluble in DMSO and thus co-solvents are necessary. The use of such solvents as DMF or alcohols results exclusively in the decomposition of subphthalocyanines.³⁹

Torres and co-workers^{37, 38, 66} suggested a mechanism of this reaction. In the first step, an ‘open’ phthalocyanine, which is an intermediate with four isoindole fragments, is formed. Then the intermediate undergoes either ring closure to yield phthalocyanine or fragmentation to a random mixture of products. However, the

mechanism of the attack at subphthalocyanine, which is central, in our opinion, for the selection of optimum conditions for the subphthalocyanine ring expansion, remains largely unexplored.

3. A comparison of the methods for the synthesis of non-symmetrically substituted phthalocyanines

A comparison of yields of non-symmetrically substituted phthalocyanines with the stoichiometry A₃B provided by the subphthalocyanine ring expansion and random cyclisation reveals their similar efficiencies. In both cases, the total yields do not exceed 20%. Thus since the former method requires an additional step of synthesis and purification of subphthalocyanines, the random cyclisation is considered as the method of choice by the majority of researchers despite the laborious isolation of the target products. Furthermore, the random cyclisation of phthalogens with bulky substituents seems to be preferable for the synthesis of A₂B₂-type phthalocyanines.

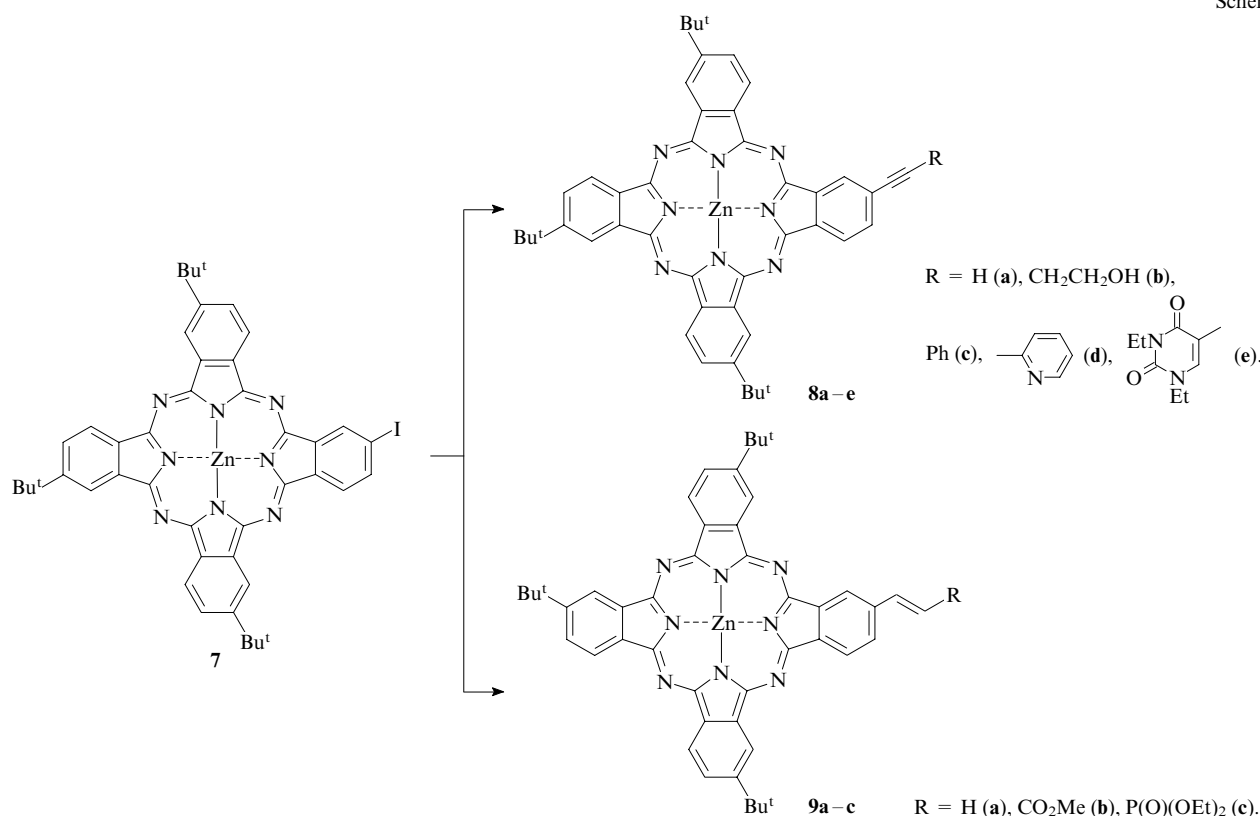
III. Structure modification of non-symmetrically substituted phthalocyanines

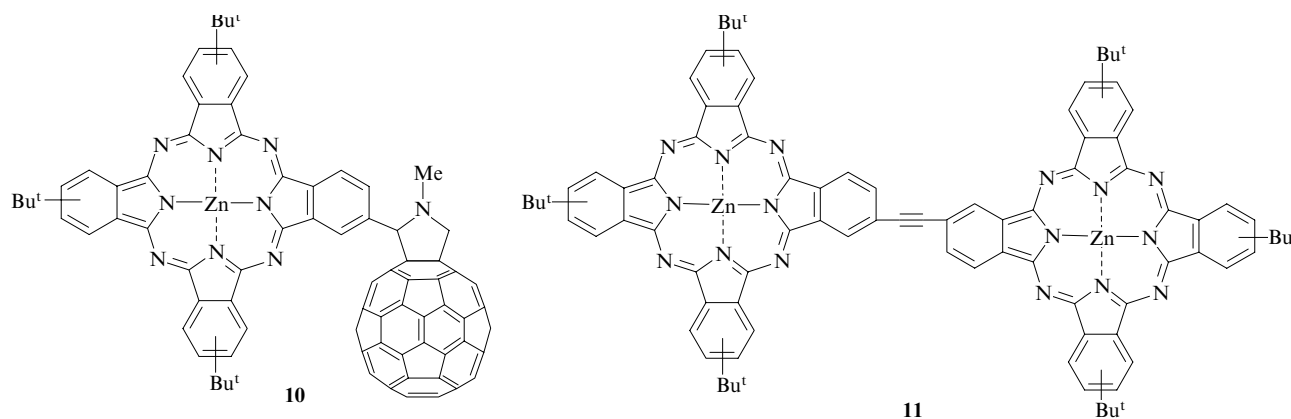
The majority of non-symmetrically substituted phthalocyanines described in the literature bear functional groups, which allow their post-synthetic modifications.^{2–6, 9, 13, 18, 26, 31, 67–70} In particular, a selective method for the synthesis of planar bi- and trinuclear phthalocyanines with the macrocycles linked by ethylene,^{71, 72} ethynyl,^{67, 68, 73} ferrocenediethynyl,^{3, 4} dehydroannulene^{20, 70} or anthraquinone² spacers has been developed. These phthalocyanines are of great potential as new-generation functional materials due to their extended conjugated π -systems providing efficient interactions between the phthalocyanine macrocycles.

1. Structure modification of halogen-substituted phthalocyanines

In the late 1990s, Ali and van Lier⁷⁴ found that zinc 9,16,23-tri(*tert*-butyl)-2-iodophthalocyanine (**7**) readily undergoes the Heck and Stille reactions affording products **8a–e**, **9b,c** and **9a**, respectively, in preparative yields (Scheme 2).

Scheme 2

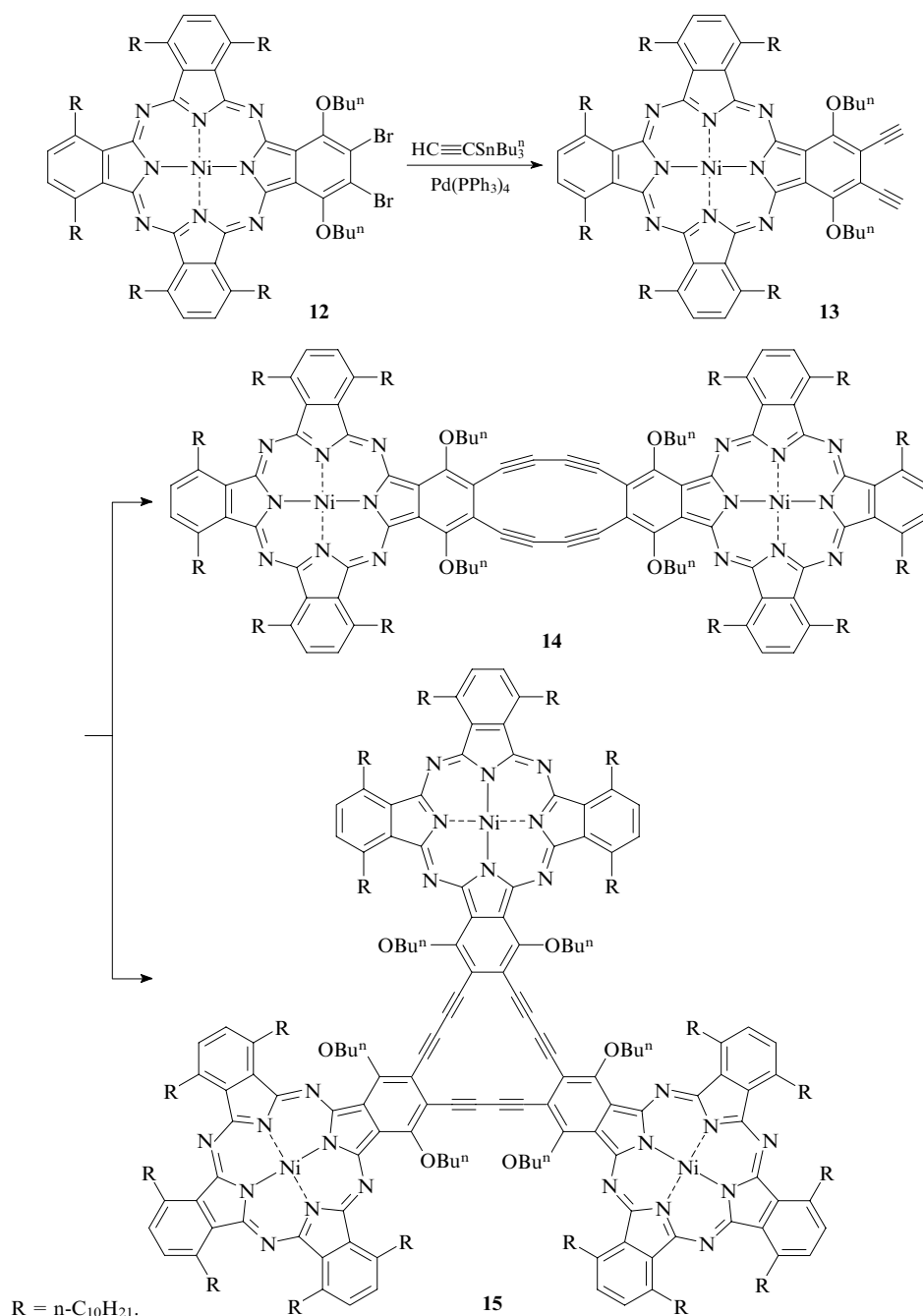




Later, other cross-coupling products were synthesised²⁶ based on the phthalocyanine **7**. Thus, halogen-substituted phthalocyanines can be regarded as the basic synthetic precursors of both other non-

symmetrically substituted phthalocyanines (with the composition A_3B) and binuclear phthalocyanines.^{2–4, 18, 26, 67–69, 73–75}

Scheme 3



In this way, a fullerene-substituted phthalocyanine (**10**) and a planar binuclear phthalocyanine (**11**) have been prepared. Both compounds manifest unique photophysical properties owing to the efficient intramolecular interaction between the macrocycles.^{70, 73}

The starting phthalocyanine **7** is usually synthesised by co-cyclisation of 4-(*tert*-butyl)phthalonitrile and 4-iodonaphthonitrile,^{26, 73} although an alternative more complex two-step modification of the respective nitro-substituted phthalocyanine has been reported.⁶⁹

Phthalocyanine **12** with two bromine atoms in the *ortho*-position is no less important from the synthetic viewpoint. Its cross-coupling with tributylstannylacetylene yields diethynylphthalocyanine **13**. This compound can also be prepared from the respective diiodo-substituted complex.¹⁸

Starting from phthalocyanine **13**, bi- and trinuclear phthalocyanines **14** and **15** can be synthesised, which can well be regarded as supramolecular structures: the phthalocyanine macrocycles therein are fused through the dehydroannulene spacers (Scheme 3).^{20, 70} This fusion provides even more efficient intramolecular conjugation, which is important for the practical utilisation.

o-Dihalogen-substituted phthalocyanines can be synthesised by co-cyclisation using respective 4,5-dibromo- or 4,5-diiodo-substituted phthalonitriles as one of the phthalogens.^{18, 20, 70}

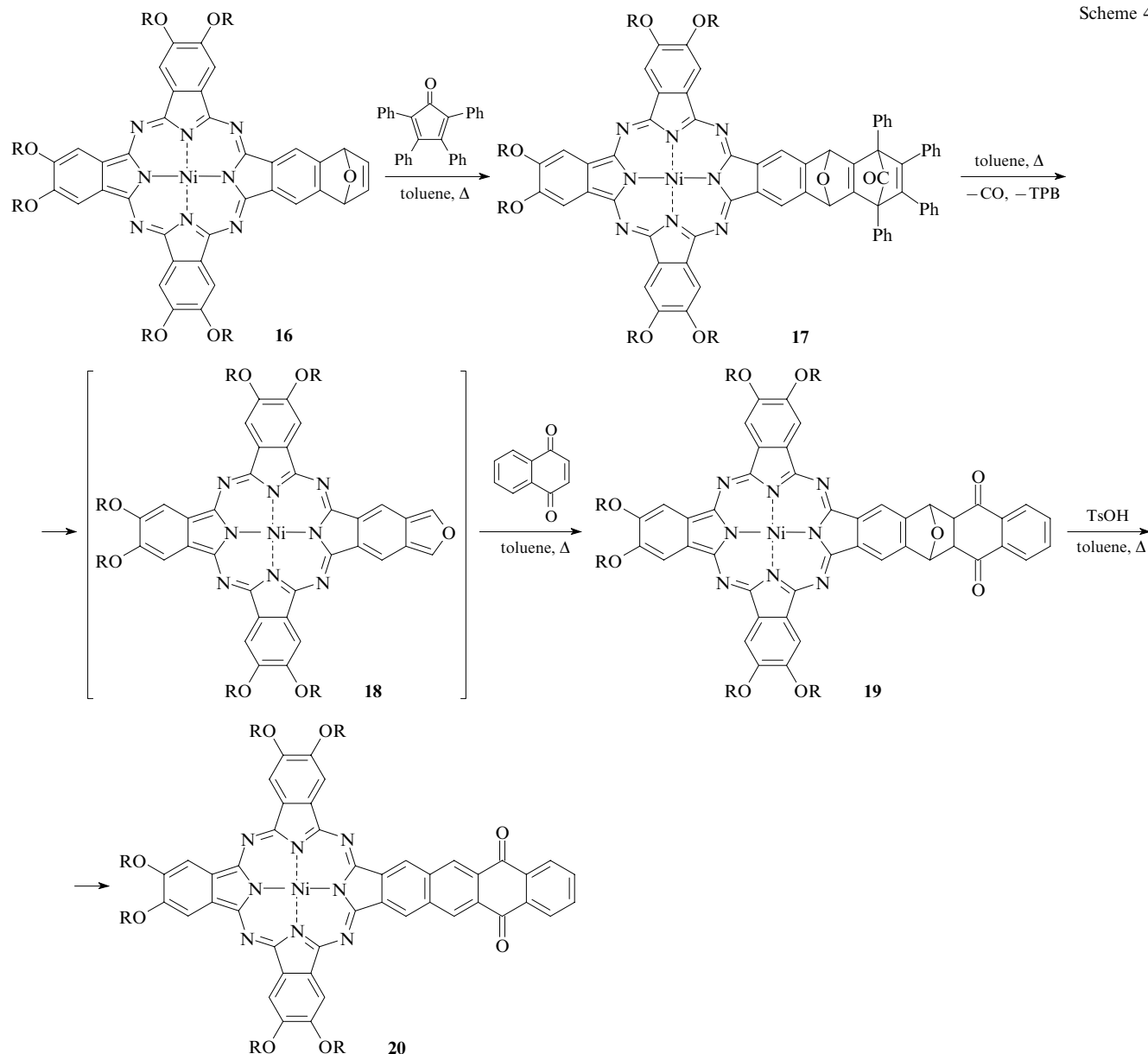
2. Structure modification of phthalocyanines using the Diels–Alder and Wittig reactions

The Diels–Alder and Wittig reactions are among few classical organic reactions that enable the stereo- and regioselective construction of compounds with specified structures under mild conditions in high yields. The possibility of utilisation of phthalocyanines in these reactions opens broad synthetic prospects.^{71, 72, 76, 77}

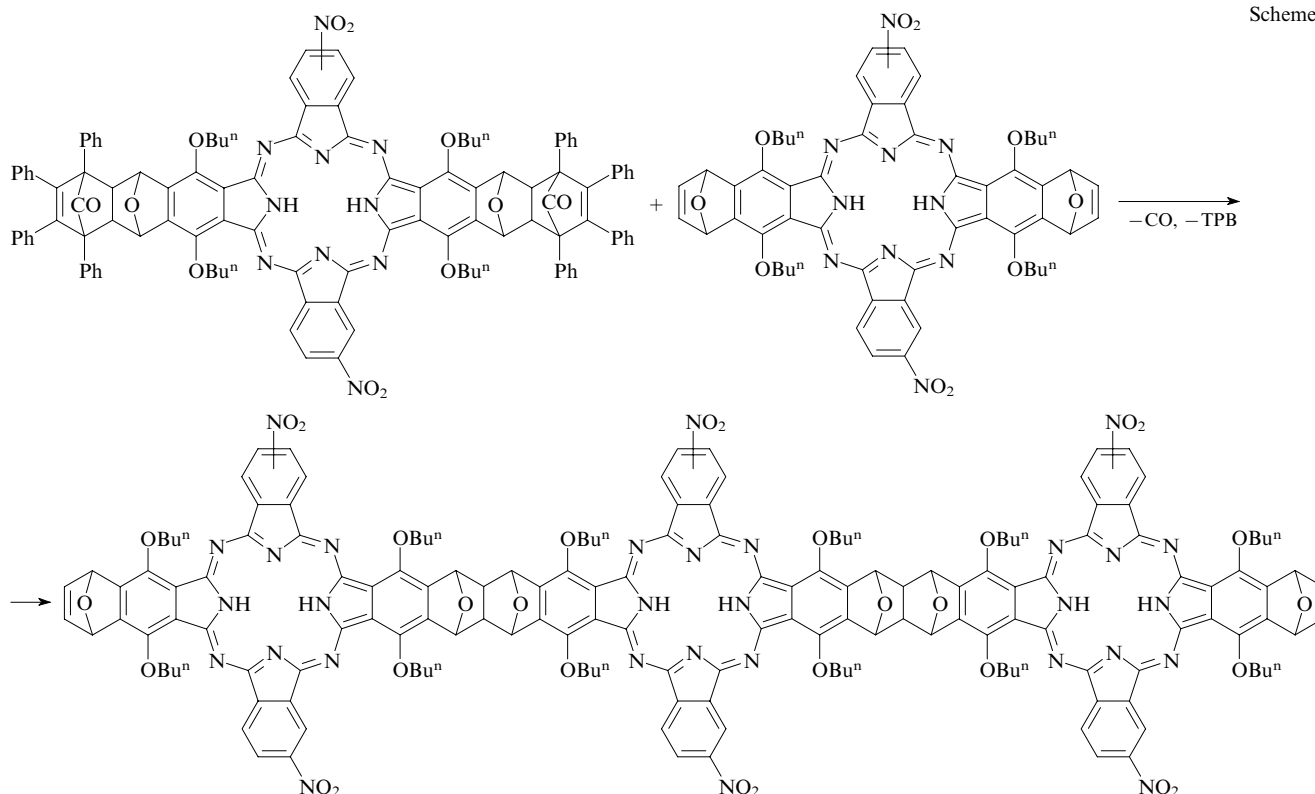
The Diels–Alder reaction of non-symmetrically substituted phthalocyanines has been realised for the first time by Hanack and co-workers^{72, 76} aimed at the preparation of linear phthalocyanine-based oligomers and polymers. It was demonstrated first for symmetrically and then for non-symmetrically substituted phthalocyanines (*e.g.*, **16**) that the isobenzofuran fragments in peripheral substituents in phthalocyanine macrocycles readily react as dienophiles with 2,3,4,5-tetraphenylpentadienone as a diene (Scheme 4).

Complex **17** loses CO and tetraphenylbenzene (TPB) molecules upon boiling in toluene yielding an unstable intermediate **18**

Scheme 4



Scheme 5

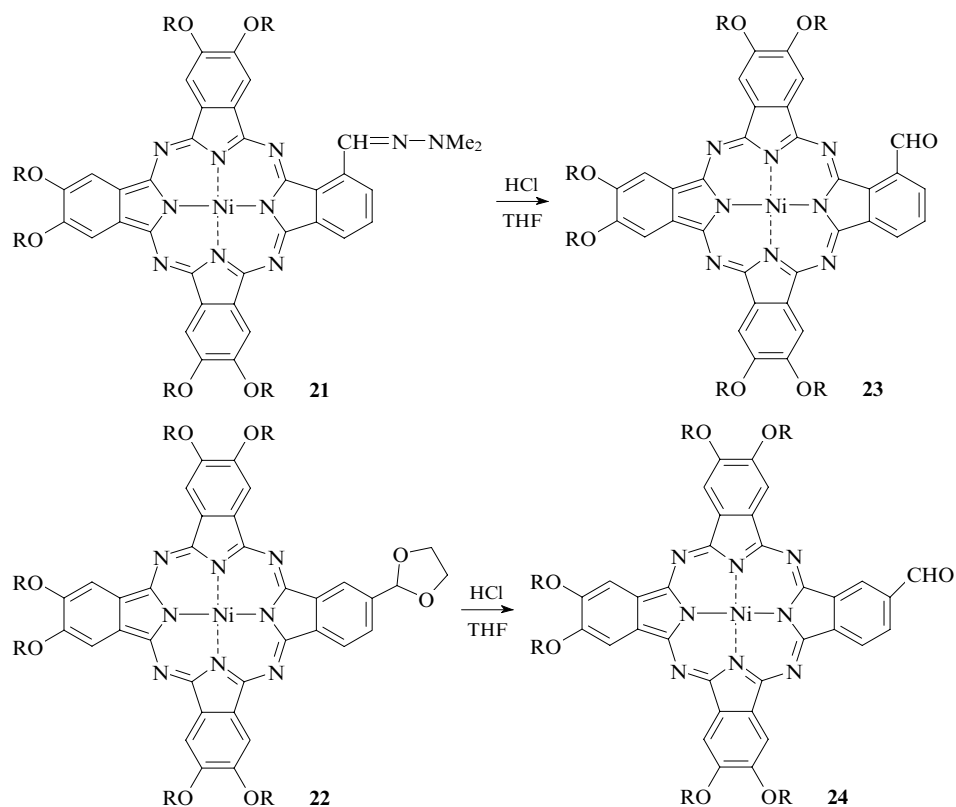


with a diene structure capable of reacting with dienophiles, *e.g.*, with 1,4-naphthoquinone. Product **19** has to be only aromatised to afford the target phthalocyanine **20**. However, standard reagents used for similar naphthalocyanine substrates (*e.g.*, TsOH) react with phthalocyanines, as a rule, with partial decom-

position of the macrocycles. Therefore, the use of a mild Lewis acid, trimethylsilyl triflate is more appropriate.

The Diels–Alder reaction was also successfully applied to prepare ordered polymeric structures. Non-symmetrically substituted phthalocyanines **ABAB** can be converted into linear polymers (Scheme 5).^{15, 62}

Scheme 6



R is 2-ethylhexyl.

The Wittig reaction necessitates a phthalocyanine to bear at least one aldehyde group. Such phthalocyanines cannot be directly synthesised by the standard method based on the random cyclisation since dicyanobenzaldehydes yield no phthalocyanine products.^{72,77} Therefore, the required aldehyde-functionalised phthalocyanines should be synthesised by a structure modification of other non-symmetrically substituted phthalocyanines (Scheme 6).

Hydrolysis of hydrazone **21** or acetal **22** yields phthalocyanines **23** and **24**, respectively. The starting derivatives **21** and **22** can easily be prepared by the random cyclisation of the corresponding phthalogens.⁷⁷

The Wittig reaction makes it possible not only to modify the structure of non-symmetrically substituted phthalocyanines but also to synthesise planar binuclear phthalocyanines. The structure of the target product in this case is governed by the number of ylide groups in the selected spacer (Scheme 7).

The simple control over the structure of the target products and nearly quantitative yields make this method very useful for both the modification of monophthalocyanines and the preparation of bi- and polynuclear phthalocyanines with a specified spatial orientation of the macrocycles.

The phthalocyanines synthesised by the Diels–Alder or Wittig reactions are characterised by extended conjugated electron systems, which results in bathochromic shifts of the Q band in their UV-Vis absorption spectra.^{71,72,76,77}

3. Functionalisation of nitro-substituted phthalocyanines

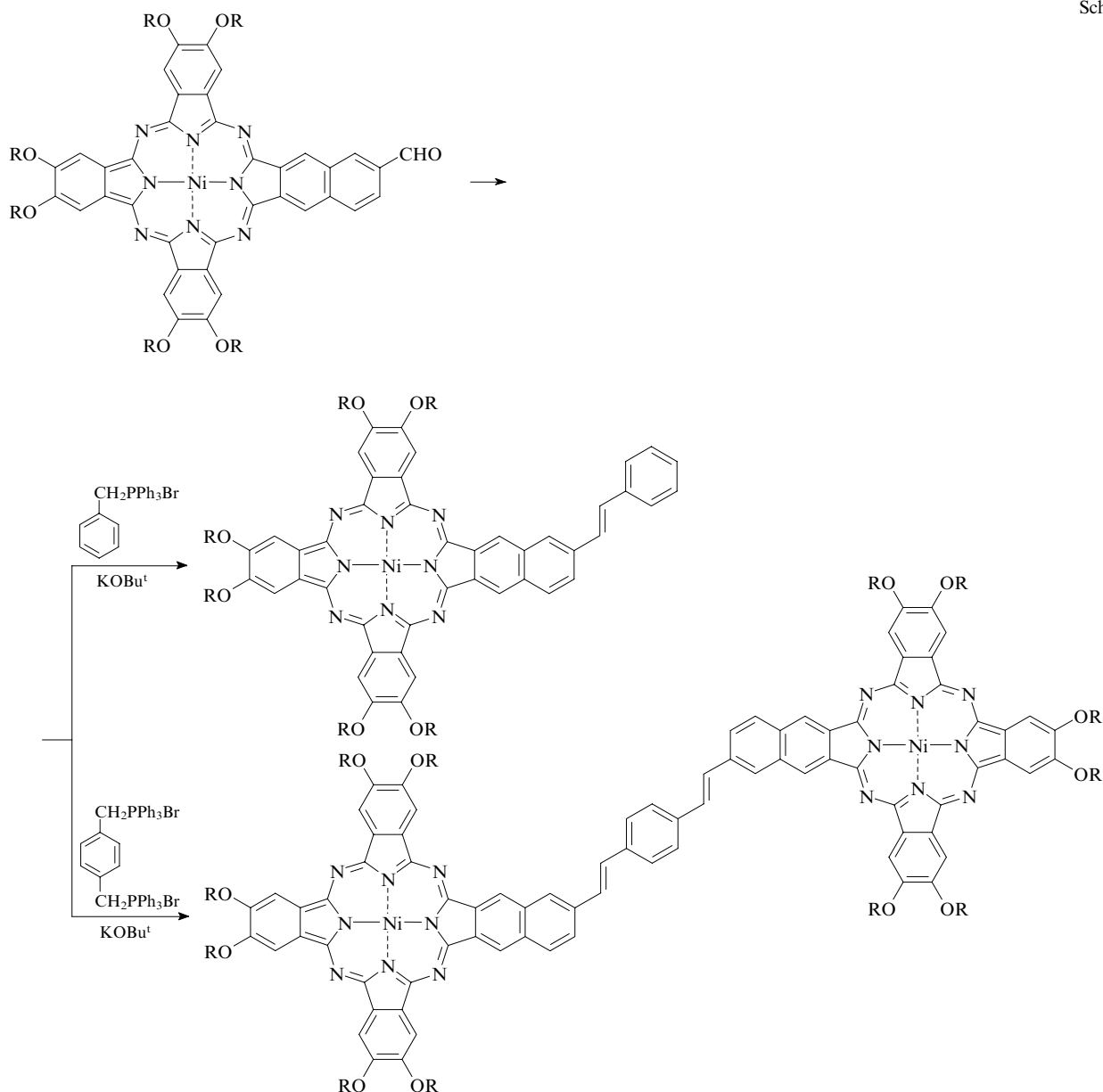
A nitro group as an electron-withdrawing substituent activates the aromatic nucleophilic substitution. Furthermore, it can readily be reduced to amino and diazo groups, which can further be involved in the preparation of various alkylation and coupling products.

One possible way to modify nitro groups in non-symmetrically substituted phthalocyanines, *viz.*, the reduction to the amino group, has been mentioned above in the description of the synthesis of moniodo-substituted phthalocyanine **7**. A unique synthesis of planar trinuclear phthalocyanine **25** (Scheme 8) is based on the easy alkylation of the amino group.¹⁹

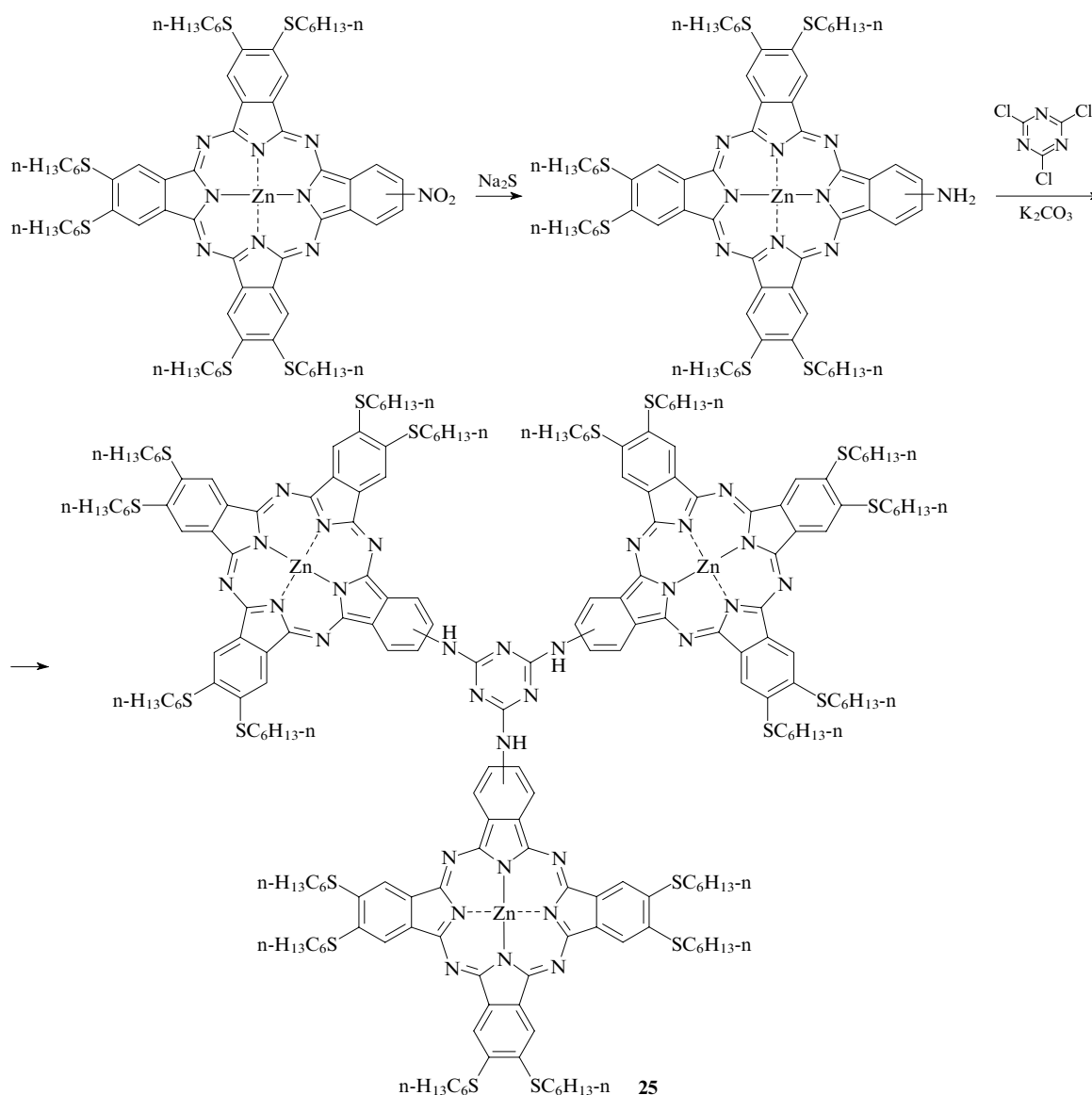
A similar alkylation reaction has been realised for monohydroxy-substituted phthalocyanine.²¹

Yet another method for the structure modification of mononitrophthalocyanines, *viz.*, the nucleophilic substitution of the nitro group, has been developed^{78,79} for the synthesis of new functionally substituted phthalocyanines, which served as precur-

Scheme 7

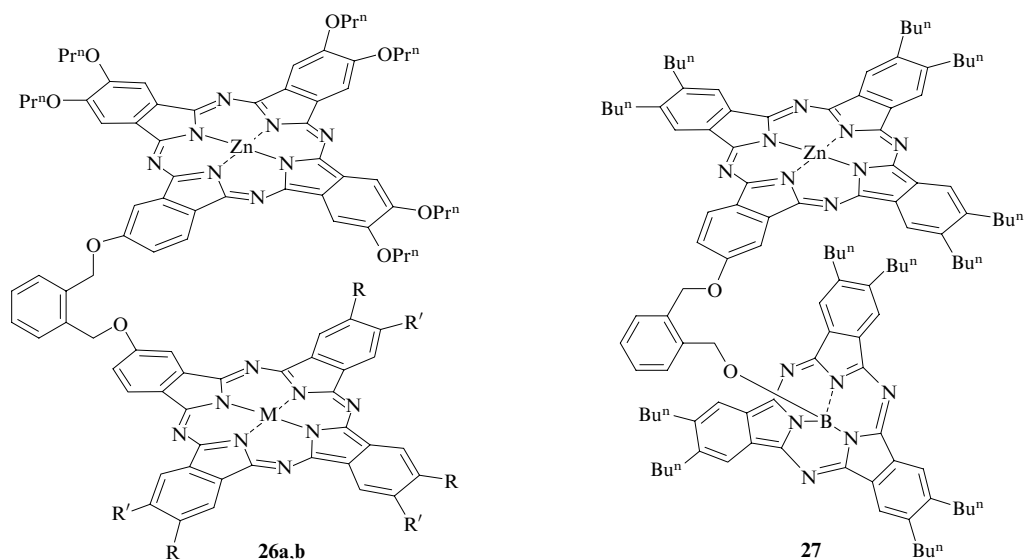


Scheme 8



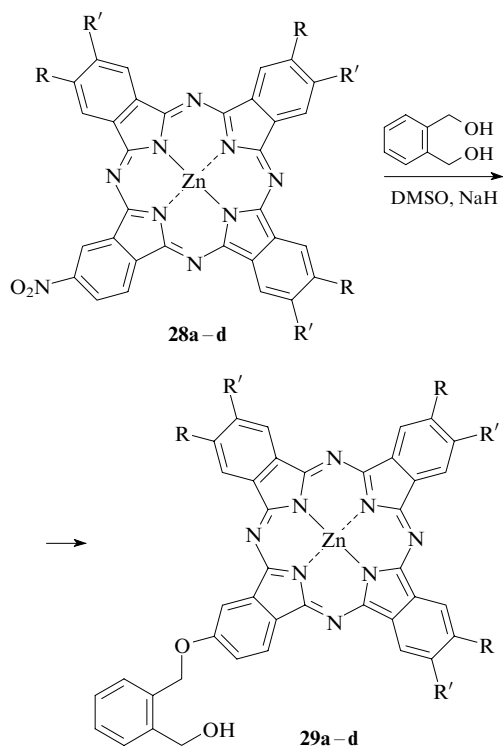
sors of binuclear clamshell phthalocyanines **26a,b**⁸⁰ and a heteronuclear complex phthalocyanine–spacer–subphthalocyanine **27**.^{81, 82}

The *ipso*-substitution of the nitro group is typically accomplished in substrates with strong electron-withdrawing substituents, such as CN groups. Such an approach is used



$\text{R} = \text{Bu}^t$, $\text{R}' = \text{H}$, $\text{M} = \text{Zn}$ (**a**); $\text{R} = \text{R}' = \text{OPr}^n$, $\text{M} = \text{Cu}$ (**b**).

for the synthesis of bis(phthalonitriles)⁸³ and the majority of alkoxy-substituted phthalonitriles.^{27, 84} However, this reaction has not been applied to phthalocyanines so far. The feasibility of the nucleophilic substitution of a nitro group in non-symmetrically substituted phthalocyanines **28a–d** has been demonstrated for the first time and the optimum reaction conditions have been found by our group.⁷⁸ The target complexes **29a–d** containing a benzyl alcohol fragment in a peripheral substituent were isolated in preparative yields.

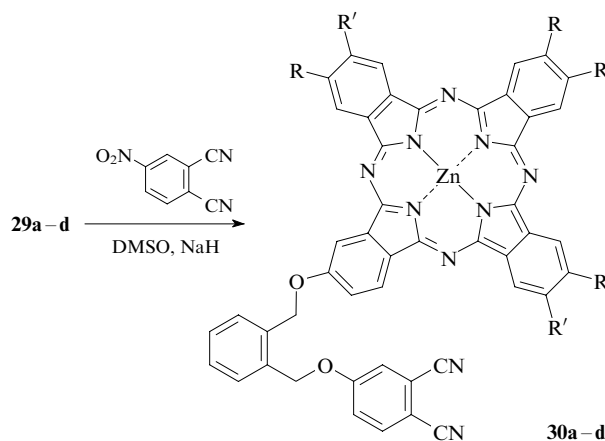


R = R' = Et (**a**), Buⁿ (**b**), OPrⁿ (**c**); R = Bu^t, R' = H (**d**).

When K₂CO₃ was used as the base, the reaction was completed in 50 h and the products **29a–d** formed in trace concentrations. The use of a stronger base, *viz.*, sodium hydride, made it possible to both accelerate the reaction and increase the yields of the target products **29a–d**. The course of the reaction can conveniently be monitored by means of UV-Vis absorption spectroscopy (Fig. 1). The starting nitrophthalocyanines **28a–d** manifest split Q bands. The products **29a–d** devoid of both electron-releasing and -withdrawing substituents should be characterised by spectra typical of mononuclear metal complexes, which is indeed observed experimentally.

As the nucleophilic substitution reaction proceeds, the splitting of the Q band gradually disappears. Meanwhile, it was found that a prolonged contact of phthalocyanines with a strong base should be avoided, since it results in a gradual decomposition, which was confirmed by control experiments.

A similar reaction of the aromatic nucleophilic *ipso*-substitution was utilised for the synthesis of phthalocyanines **30a–d** containing reactive phthalonitrile fragment.⁷⁸



R = R' = Et (**a**), Buⁿ (**b**), OPrⁿ (**c**); R = Bu^t, R' = H (**d**).

Phthalocyanines **30a–d** are synthetic precursors of non-symmetric binuclear clamshell phthalocyanines. The feasibility of the synthesis of such compounds has been demonstrated with complex **30c** as an example.⁸⁰ The co-cyclisation of phthalocyanine **30c** with substituted phthalonitriles in the presence of copper and zinc acetates afforded binuclear phthalocyanines **26a,b**.

The presence of a benzylic OH group in complexes **29a–d** enables the synthesis of heteronuclear complexes and supramolecular structures. In particular, the reaction of phthalocyanine **29b** with boron μ -chlorohexabutylsubphthalocyanine yields complex **27** involving a phthalocyanine and a subphthalocyanine moieties.

Therefore, the functionalisation of monosubstituted phthalocyanines together with the structure modification of non-symmetrically substituted phthalocyanines considered above make it possible to prepare diverse bi- and polynuclear (including heteronuclear) macrocyclic compounds.

IV. Prospects for the use of non-symmetrically substituted phthalocyanines

Non-symmetrically substituted phthalocyanines attract attention not only from synthetic chemists but also from physicists. Primarily, this concerns complexes of the push–pull type. The

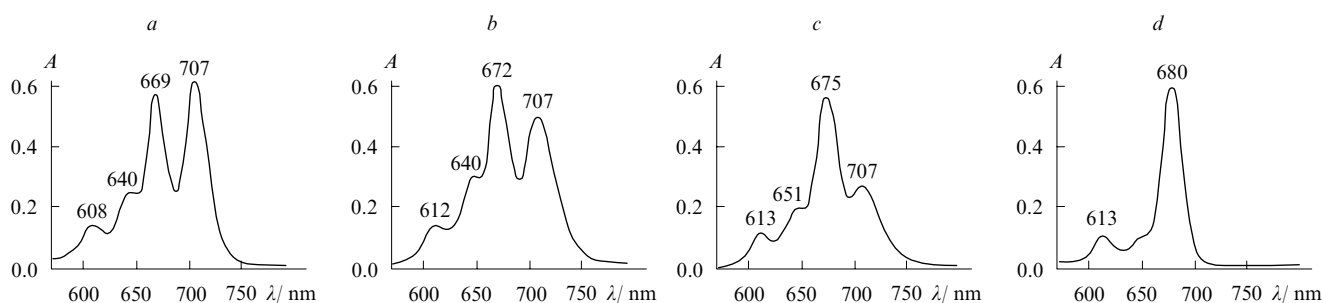
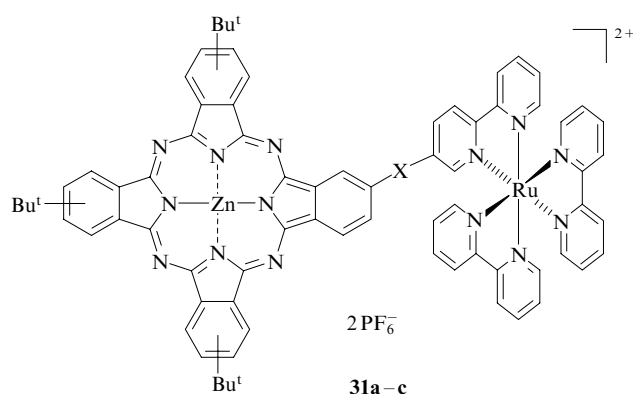


Figure 1. Changes in the UV-Vis absorption spectra (in DMSO) in the course of the nucleophilic substitution of the nitro group in phthalocyanine **28d** in the presence of NaH at 25 °C. Reaction time (min): 5 (**a**), 15 (**b**), 30 (**c**), 45 (**d**).

simultaneous presence of substituents of the opposite character modifies, first of all the spectral properties of these macrocyclic compounds.^{31, 46, 78} In particular, an intramolecular electron transfer from a donating to a withdrawing substituent has been observed in A₃B phthalocyanines.^{11, 14, 47}

Non-symmetrically substituted phthalocyanines possess no inversion centre and thus they are prone to the formation of oriented dipoles upon irradiation with coherent light. They manifest non-linear optical properties and thus can be used for the second harmonic generation.^{11, 12} Furthermore, it was found that these phthalocyanines readily form Langmuir–Blodgett films,^{11–14} which significantly facilitates the above studies.

Recently, the capability of fullerene-substituted A₃B phthalocyanines to separate and accumulate for a long time electric charges in a solid phase has attracted considerable attention. A possible application of such compounds as components of solar cells has already been demonstrated.^{6, 9} The chemical conversion of solar energy was achieved with heteronuclear complexes zinc phthalocyanine–ruthenium(II) tris(bipyridine) **31a–c**.⁵



X = CH=CH (a), NHCO (b), C≡C (c).

Thus, non-symmetrically substituted phthalocyanines are very promising compounds and the progress in the methods for their synthesis will certainly extend fields of their practical utilisation.

* * *

The well-known methods for the formation of a phthalocyanine macrocycle has recently been supplemented with regioselective reactions giving rise to new classes of macrocyclic compounds and unveiling new avenues in the synthesis of supramolecular structures for emerging areas of science and technology. The methods for the synthesis and structure modification of non-symmetrically substituted phthalocyanines are being successfully developed, which makes the macrocyclic compounds accessible for the investigations and practical applications. We hope that the number of structurally diverse non-symmetrically substituted phthalocyanines will expand substantially in the nearest future and some day they will come into practice as advanced functional materials.

References

1. Y J Zhang, L S Li, J Jin, S M Jiang, Y Y Zhao, T J Li, X G Du, S O Yang *Langmuir* **15** 2183 (1999)
2. A Gouloumis, S G Liu, P Vazquez, L Echegoyen, T Torres *Chem. Commun.* 399 (2001)
3. A Gonzalez-Cabello, P Vazquez, T Torres *J. Organomet. Chem.* **637–639** 751 (2001)
4. A de la Escosura, M V Martinez-Diaz, P Thordarson, A E Rowan, R J M Nolte, T Torres *J. Am. Chem. Soc.* **125** 12300 (2003)
5. A Gonzalez-Cabello, P Vazquez, T Torres, D M Guldi *J. Org. Chem.* **68** 8635 (2003)
6. D M Guldi, I Zilbermann, A Gouloumis, P Vazquez, T Torres *J. Phys. Chem. B* **108** 18485 (2004)
7. I Seotsanyana-Mokhosi, T Nyokong *J. Porphyrins Phthalocyanines* **9** 476 (2005)
8. I Seotsanyana-Mokhosi, J Y Chen, T Nyokong *J. Porphyrins Phthalocyanines* **9** 316 (2005)
9. M A Loi, P Denk, H Hoppe, H Neugebauer, C Winder, D Meissner, C Brabec, N S Sariciftci, A Gouloumis, P Vazquez, T Torres *J. Mater. Chem.* **13** 700 (2003)
10. S Makarov, C Litwinski, E A Ermilov, O Suvorova, B Roder, D Wöhrle *Chem.–Eur. J.* **12** 1468 (2006)
11. Y Q Liu, Y Xu, D B Zhu, T Wada, H Sasabe, X S Zhao, X M Xie *J. Phys. Chem.* **99** 6957 (1995)
12. Y Liu, Y Xu, D Zhu, X Zhao *Thin Solid Films* **289** 282 (1996)
13. Y Liu, W Hu, W Qiu, Y Xu, S Zhou, D Zhu *Sens. Actuators, B* **80** 202 (2001)
14. S Zhou, Y Liu, Y Xu, W Hu, D Zhu, X Qiu, C Wang, C Bai *J. Chem. Phys. Lett.* **297** 77 (1998)
15. P Stihler, B Hauschel, M Hanack *Chem. Ber.* **130** 801 (1997)
16. K Oda, S Ogura, I Okura *J. Photochem. Photobiol. B* **59** 20 (2000)
17. M Hu, N Brasseur, S Z Yildiz, J E van Lier, C C Leznoff *J. Med. Chem.* **41** 1789 (1998)
18. E M Garcia-Frutos, F Fernandez-Lazaro, E M Maya, P Vazquez, T Torres *J. Org. Chem.* **65** 6841 (2000)
19. N Ozan, O Bekaroglu *Polyhedron* **22** 819 (2003)
20. M J Cook, M J Heeney *Chem.–Eur. J.* **6** 3958 (2000)
21. S Makhseed, A Bumajdad, B Ghanem, K Msayib, N B McKeown *Tetrahedron Lett.* **45** 4865 (2004)
22. A Kalkan, A Koca, Z A Bayir *Polyhedron* **23** 3155 (2004)
23. D M Guldi, A Gouloumis, P Vazquez, T Torres, V Georgakilas, M Prato *J. Am. Chem. Soc.* **127** 5811 (2005)
24. M V Martinez-Diaz, S Esperanza, A de la Escosura, M Catellani, S Yunus, S Luzzati, T Torres *Tetrahedron Lett.* **44** 8475 (2003)
25. S Makhseed, A Cook, N B McKeown *Chem. Commun.* 419 (1999)
26. A Gouloumis, S G Liu, A Sastre, P Vazquez, L Echegoyen, T Torres *Chem.–Eur. J.* **6** 3600 (2000)
27. I Seotsanyana-Mokhosi, T Nyokong *J. Porphyrins Phthalocyanines* **8** 1214 (2004)
28. J G Young, W Onyebuagu *J. Org. Chem.* **55** 2155 (1990)
29. M Q Tian, T Wada, H Sasabe *J. Heterocycl. Chem.* **34** 171 (1997)
30. S V Kudrevich, H Ali, J E van Lier *J. Chem. Soc., Perkin Trans. 1* 2767 (1994)
31. M Q Tian, T Wada, H Sasabe *Dyes Pigm.* **52** 1 (2002)
32. M Q Tian, T Wada, H Kimura-Suda, H Sasabe *J. Mater. Chem.* **7** 861 (1997)
33. H Ali, S K Sim, J E van Lier *J. Chem. Res.* 496 (1999)
34. P L Chen, X B Wang, D H Tang, Z Zhen, J C Zhang, X H Liu *Dyes Pigm.* **48** 85 (2001)
35. E Musluoglu, A Gurek, V Ahsen, A Gul, O Bekaroglu *Chem. Ber.* **125** 2337 (1992)
36. S Dabak, A Gul, O Bekaroglu *Chem. Ber.* **127** 2009 (1994)
37. A Sastre, B del Rey, T Torres *J. Org. Chem.* **61** 8591 (1996)
38. A Sastre, T Torres, M Hanack *Tetrahedron Lett.* **36** 8501 (1995)
39. S Kudrevich, N Brasseur, C La Madeleine, S Gilbert, J E van Lier *J. Med. Chem.* **40** 3897 (1997)
40. C C Leznoff *Can. J. Chem.* **78** 167 (2000)
41. G de la Torre, T Torres *J. Porphyrins Phthalocyanines* **6** 274 (2002)
42. C Piechocki, J Simon *J. Chem. Soc., Chem. Commun.* 259 (1985)
43. T G Linssen, M Hanack *Chem. Ber.* **127** 2051 (1994)
44. J Yang, T C Rogers, M R van De Mark *J. Heterocycl. Chem.* **30** 571 (1993)
45. C C Leznoff, S Greenberg, B Khouw, A B P Lever *Can. J. Chem.* **65** 1705 (1987)
46. Y Q Liu, D B Zhu *Synth. Met.* **71** 1853 (1995)
47. Y Q Liu, D B Zhu, T Wada, H Sasabe *Synth. Met.* **71** 2283 (1995)
48. Y Liu, D Zhu, T Wada, A Yamada, H Sasabe *J. Heterocycl. Chem.* **31** 1017 (1994)
49. C C Leznoff, T W Hall *Tetrahedron Lett.* **23** 3023 (1982)
50. A Hirth, A K Sobbi, D Wöhrle *J. Porphyrins Phthalocyanines* **1** 275 (1997)
51. M Geyer, F Plenzig, J Rauschnabel, M Hanack, B del Rey, A Sastre, T Torres *Synthesis* 1139 (1996)
52. A Weitemeyer, H Kliesch, D Wöhrle *J. Org. Chem.* **60** 4900 (1995)

53. N Kobayashi, R Kondo, S Nakajima, T Osa *J. Am. Chem. Soc.* **112** 9640 (1990)
54. S V Kudrevich, S Gilbert, J E van Lier *J. Org. Chem.* **61** 5706 (1996)
55. P Matlaba, T Nyokong *Polyhedron* **21** 2463 (2002)
56. W M Sharman, J E van Lier *J. Porphyrins Phthalocyanines* **9** 651 (2005)
57. C F van Nostrum, R J M Nolte *Chem. Commun.* 2385 (1996)
58. J Bakboord, M J Cook, E Hamuryudan *J. Porphyrins Phthalocyanines* **4** 510 (2000)
59. T Fukuda, T Ishiguro, N Kobayashi *Tetrahedron Lett.* **46** 2907 (2005)
60. H Miwa, N Kobayashi *Chem. Lett.* 1303 (1999)
61. C C Leznoff, D M Drew *Can. J. Chem.* **74** 307 (1996)
62. M Hanack, P Stihler *Eur. J. Org. Chem.* 303 (2000)
63. R Polley, T G Linssen, P Stihler, M Hanack *J. Porphyrins Phthalocyanines* **1** 169 (1997)
64. K Kasuga, T Idehara, M Handa, K Isa *Inorg. Chim. Acta* **196** 127 (1992)
65. N Kobayashi, T Ishizaki, K Ishii, H Konami *J. Am. Chem. Soc.* **121** 9096 (1999)
66. F Fernandez-Lazaro, E M Maya, M Nicolau, T Torres *Uspekhi Khimii Porfirinov* (Progress in the Chemistry of Porphyrins) (St Petersburg: St Petersburg State University, 1999) Vol. 2, p. 279
67. M Q Tian, Y D Zhang, T Wada, H Sasabe *Dyes Pigm.* **58** 135 (2003)
68. E M Maya, P Vazquez, T Torres, L Gobbi, F Diederich, S Pyo, L Echegoyen *J. Org. Chem.* **65** 823 (2000)
69. J M Sutton, R W Boyle *Chem. Commun.* 2014 (2001)
70. M J Cook, M J Heeney *Chem. Commun.* 969 (2000)
71. R Jung, K H Schweikart, M Hanack *Eur. J. Org. Chem.* 1687 (1999)
72. R Jung, K H Schweikart, M Hanack *Synth. Met.* **111** 453 (2000)
73. E M Maya, P Vazquez, T Torres *Chem. – Eur. J.* **5** 2004 (1999)
74. H Ali, J E van Lier *Tetrahedron Lett.* **38** 1157 (1997)
75. E M Maya, P Vazquez, T Torres *Chem. Commun.* 1175 (1997)
76. B Hauschel, R Jung, M Hanack *Eur. J. Inorg. Chem.* 693 (1999)
77. K H Schweikart, M Hanack *Eur. J. Org. Chem.* 2551 (2000)
78. A Yu Tolbin, L G Tomilova, N S Zefirov *Izv. Akad. Nauk, Ser. Khim.* 2036 (2005)^a
79. A Yu Tolbin, A V Ivanov, L G Tomilova, N S Zefirov *J. Porphyrins Phthalocyanines* **8** 866 (2004)
80. A Yu Tolbin, V E Pushkarev, E V Shulishov, A V Ivanov, L G Tomilova, N S Zefirov *Mendeleev Commun.* 24 (2005)
81. L G Tomilova, A Yu Tolbin, V E Pushkarev, M O Breusova, N S Zefirov *J. Porphyrins Phthalocyanines* **10** 516 (2006)
82. A Yu Tolbin, M O Breusova, V E Pushkarev, L G Tomilova *Izv. Akad. Nauk, Ser. Khim.* 2020 (2005)^a
83. T M Keller, T R Price, J R Griffith *Synthesis* 613 (1980)
84. M Kandaz, A R Ozkaya, O Bekaroglu *Monatsh. Chem.* **132** 1013 (2001)

^a — *Russ. Chem. Bull., Int. Ed. (Engl. Transl.)*

Bibliometric analysis of the journal *Uspekhi Khimii* (Russian Chemical Reviews)

I V Zibareva, T N Teplova, O M Nefedov

Scientific journals, which first appeared in the second half of the 17th century (the oldest of the currently existing journals, *Philosophical Transactions of the Royal Society*, has been published since 1665),¹ made a great contribution to the formation and development of science. At that time, scientific journals did not publish review articles, as there was no need in them. However, the subsequent avalanche-like increase in the amount of primary scientific information made impossible 'tracing' of the necessary publications in the rapidly growing number of scientific periodicals. It became necessary to generalise the scientific knowledge either as monographs or as scientific reviews, which are much faster responding and available than monographs. In the early 20th century, special review journals were founded for publishing review articles. In chemistry, these journals were represented by *Chemical Reviews*, *Accounts of Chemical Research*, *Chemical Society Reviews* and so on; in the USSR, the *Uspekhi Khimii* (Russian Chemical Reviews) journal was created for this purpose.

Uspekhi Khimii was founded in 1932 by the decision of the USSR Narkompros (Ministry of Education) for publishing review papers in theoretical and experimental chemistry and chemical engineering that were of great methodological and integrating value. Currently, this is a leading periodical of the Russian Academy of Sciences concerned with chemistry and related sciences. In 2007, *Uspekhi Khimii* marked its 75th birthday. This is a serious age for a journal and a worthy occasion for its bibliometric analysis. The bibliometric (scientometric) methods² using statistical data on publications, references, citation and some other parameters have come in wide use in the second half of the 20th century to characterise the state-of-the-art and the trends in the development of science and to evaluate scientific journals. At present, bibliometric analysis of scientific journals has become routine practice for both foreign and Russian periodicals, including those dealing with chemistry.^{3–10}

Modern bibliometric studies use most often databases (DB) of scientific and technical information as the source of primary data.^{2, 11} Despite the fact that bibliometry is mainly a retrospective descriptive science, systematically described bibliometric data form the quantitative base for analysis. In some cases, this analysis reveals hidden features and trends of a

particular field of research covered by the journal and allows one to formulate proposals for increasing the efficiency and professional image of the journal.

The bibliometric analysis of the journal *Uspekhi Khimii* over the 75-year period of existence was carried out using reliable global DB, viz., Chemical Abstracts (CA) and SCISearch (a version of the Science Citation Index, SCI), i.e., the International Scientific and Technical Network (STN International),¹² through which the journal is perceived by most of the world chemical community (the STN provides the access to the CA DB retrospect down to 1907¹³ and the SCI DB, down to 1974¹⁴). The journal *Uspekhi Khimii* (Russian Chemical Reviews) is included in the core journals list of the authoritative international DB — CA and SCI. It has been abstracted in the CA database from the first issue of 1932; overall, this DB keeps records of 99% of the journal's original publications.

By the search date (February to March 2007), the CA DB has contained 4281 papers of *Uspekhi Khimii* where the publications of 1932–1998 (starting with the first published review 'New problems in the investigation of mineral raw materials' by Academician A E Fersman) were recorded based on the original Russian-language edition *Uspekhi Khimii* (USP), while the 1999–2006 publications were taken from the translated version *Russian Chemical Reviews* (RCR), which has been published since 1960. The SCI database was found to contain 2324 papers published in *Uspekhi Khimii* in 1973–2006.

The joint search through both CA DB and SCI DB resulted in 4403 non-identical publications of the journal for 1932–2006, which is about 90% of the total number of publications (the original and translated versions of a paper were regarded as one publication). The difference between the total number of publications in USP/RCR and their number included in the DBs is due to the fact that from the early years of existence (1932–1950) and up to 1980 the journal published not only submitted papers but also translations of the reviews and survey papers written by most prominent world scientists (J Bernal, L Hammett, C Ingold, K Kohlrusch, E Rutherford, E Schrödinger, G Seaborg and others), which were not abstracted by the DB producers. During the period from 1932 to 1942 the numbers of original and translated articles in the journal were almost equal. Apart from translated articles, the journal also published historical and biographical as well as information articles, in particular, those dealing with the activities of scientific laboratories and institutes of the USSR Academy of Sciences. Figure 1a presents the year-by-year variation of the journal's original publications abstracted in the DB and Fig. 1b shows the same plot for the whole set of journal's publications.

The CA and SCI databases have records of 4766 authors of the journal USP/RCR. The average number of authors per review is two; the average number of reviews per author is less than two. About 75% of authors had only one publication in *Uspekhi Khimii*.

I V Zibareva N N Vorozhtsov Novosibirsk Institute of Organic Chemistry, Siberian Branch of the Russian Academy of Sciences, prosp. Akad. Lavrentieva 9, 630090 Novosibirsk, Russian Federation. Fax (7-383) 330 97 52, tel. (7-383) 330 96 62, e-mail: zib@nioch.nsc.ru
T N Teplova, O M Nefedov N D Zelinsky Institute of Organic Chemistry, Russian Academy of Sciences, Leninsky prosp. 47, 119991 Moscow, Russian Federation. Fax (7-495) 135 53 59, tel. (7-495) 135 87 97, e-mail: ukh@ioc.ac.ru (T N Teplova), tel. (7-495) 135 93 70 (O M Nefedov)

Received 6 June 2007

Uspekhi Khimii 76 (8) 747–751 (2007); translated by Z P Bobkova

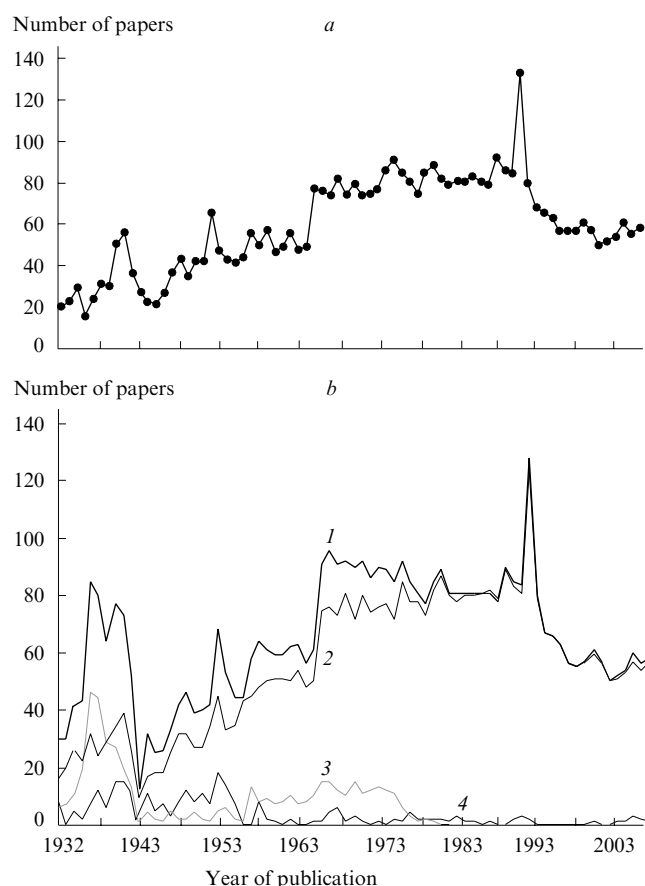


Figure 1. Year-by-year variation of the journal publications abstracted in the CA DB (a) and found by examining all journal issues (b). (1) Total number of papers, (2) original reviews, (3) translated papers, (4) other.

The small difference between the curve shown in Fig. 1 a and curve 2 in Fig. 1 b is due to the fact that not all of the original papers published in *Uspekhi Khimii* were abstracted in the DB.

The authors' addresses kept in the DBs can be used to investigate their geographic and departmental distributions. The CA database cites the addresses for all authors. Table 1 summarises the institutions the employees of which appear most often in the journal (based on the data for 1978–2006), and Table 2 presents the departmental affiliations of the authors. It can be seen that the Academy of Sciences predominates among the departments and Moscow predominates among the cities.

Subject classification and controlled terminology of the CA DB allow one to characterise, although roughly, the main subject matter of journal publications. In the CA database, every abstract is placed in a particular subject section corresponding to the publication contents. The primary (1907) 30 sections were transformed in 1962–1967 into 80 subject sections, which were combined in 1974 into five gross categories: Biochemistry (BIO, sections 1–20), Organic chemistry (ORG, sections 21–34), Macromolecular chemistry (MAC, sections 35–46), Applied Chemistry and Chemical Engineering (APP, sections 47–64) and Physical, Inorganic and Analytical Chemistry (PIA, sections 65–80).¹⁵

The distributions of journal publications according to the CA DB subject sections and categories are presented in Fig. 2 (the publications of 1932–1966 were assigned to the currently existing categories taking into account the known prehistory of the sections¹⁵). These results indicate, in particular, that organic and physical chemistry prevail among branches of chemistry. Up to the mid-1960s, the attention has been

Table 1. Most productive scientific institutions in 1978–2006 (more than 25 reviews).

Institution	City	The number of papers in the DB	
		CA	SCI
A N Nesmeyanov Institute of Organoelement Compounds of the RAS	Moscow	169	164
M V Lomonosov Moscow State University	Moscow	165	158
N N Semenov Institute of Chemical Physics of the RAS	Moscow	138	133
N D Zelinsky Institute of Organic Chemistry of the RAS	Moscow	103	101
Institute of Problems of Chemical Physics of the RAS	Chernogolovka	79	75
Institute of Physical Chemistry of the RAS ^a	Moscow	54	54
G K Borekov Institute of Catalysis, Siberian Branch of the RAS	Novosibirsk	46	39
Rostov State University	Rostov-on-Don	44	44
N I Lobachevskii Nozhnii Novgorod State University	Nizhnii Novgorod	39	34
St Petersburg State University	St Petersburg	39	42
A E Favorsky Irkutsk Institute of Chemistry, Siberian Branch of the RAS	Irkutsk	37	33
L Ya Karpov Institute of Physical Chemistry	Moscow	37	34
Kazan State University	Kazan	35	34
A V Topchiev Institute of Petrochemical Synthesis of the RAS	Moscow	31	24
D I Mendeleev University of Chemical Technology of Russia	Moscow	29	27
A N Frumkin Institute of Electrochemistry of the RAS ^a	Moscow	27	24

^a Since 2006, A N Frumkin Institute of Physical Chemistry and Electrochemistry of the RAS.

Table 2. Department affiliations of journal authors.

Department	Database	
	CA	SCI
USSR Academy of Sciences/ Russian Academy of Sciences	1574	1096
Universities	1003	633
Research Institutes	379	142
Other	16	18

focussed on the physical, inorganic and analytical chemistry, and in subsequent years, on organic chemistry (in the last decade, *Uspekhi Khimii* published many reviews on the chemical foundations of materials science). Since the mid-1960, the quantitative relations between the subjects distinguished in Fig. 2 for decade periods have been generally retained.

Analogous data for the journal *Chemical Reviews*⁵ published by the American Chemical Society demonstrate that the majority of papers in this journal are also concerned with organic and physical chemistry. However, in recent years *Chemical Reviews* have published increasing number of reviews related to biological and biomedical sciences.⁵

The renown of any scientific journal is evaluated, among other factors, based on the amount of citation of papers

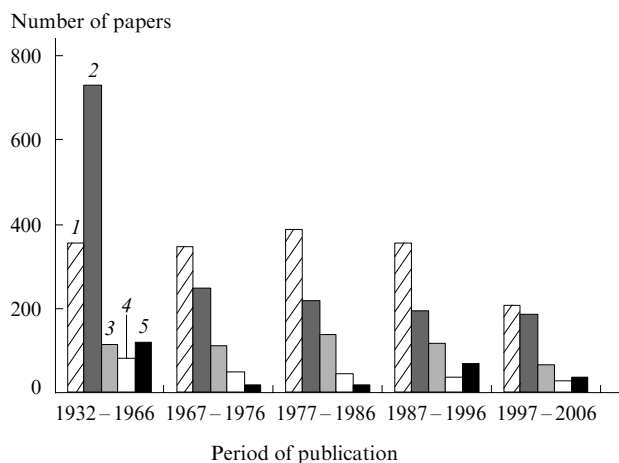


Figure 2. Distribution of *Uspekhi Khimii* (Russian Chemical Reviews) publications among the subject sections of the CA DB. (1) ORG, (2) PIA, (3) MAC, (4) BIO, (5) APP.

published in this journal by other periodicals; this is reflected, in particular, by the impact factor (IF) of the journal. In terms of this parameter, *Uspekhi Khimii* has held the first or second position among all Russian scientific journals during the last 10 years. According to the Journal Citation Reports (JCR) DB, in 1996–2006 the impact factor of the journal varied from 0.983 (in 1997) to 2.392 (in 2004) (Fig. 3).^{16,17}

The citation search for the journal publications was carried out by two standard procedures:^{6–10} (i) using special search terms created on the basis of journal publications found; (ii) using full and abbreviated names of original (USP) and translated (RCR) versions of the journal. According to the SCI DB, 4403 publications of the journal were cited 66 350 times in 1974–2006; the original version was cited 47 827 times, while the English-translated one (since 1960) was cited 18 523 times.

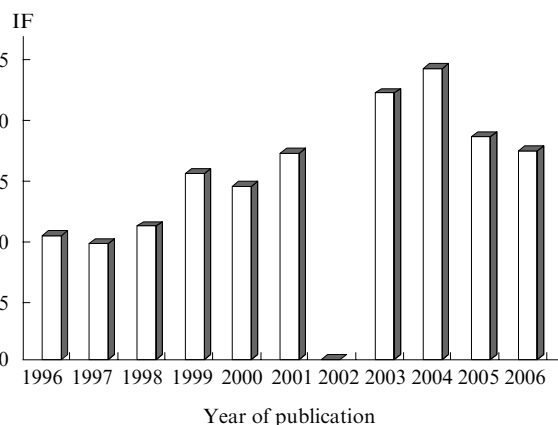


Figure 3. Impact factor of the journal *Uspekhi Khimii* for 1996–2006 (no data for 2002 are available).

According to the CA DB, 4403 publications of the journal were cited 22 857 times in 1996–2006; of these, the original version was cited 12 303 times, while the English-language one, 10 556 times. A comparison of the list of publications in USP/RCR with the obtained list of references to these publications revealed journal's papers not included in the DB and, hence, not found during the primary search. This is due to the facts that *Uspekhi Khimii* published translated reviews from other journals not covered by the DB and that the original papers references to which contained mistakes in the digital part (year, volume, the first page), precluding their unambiguous identification, were also missing from the DB. The subsequent discussion takes into account only unambiguously identified original publications in USP/RCR. As a result, the number of citations of these identified publications in the SCI DB in 1974–2006 amounted to 61 540, while that in the CA DB was 22 401. Table 3 presents 15 most cited journal publications in the period of 1993–2006 according to the SCI

Table 3. Most cited publications in *Uspekhi Khimii* (Russian Chemical Reviews) in 1993–2006.

The number of references in the database		Publication				
SCI	CA ^a	authors, title	year	volume	page	
159	131	Yu V Zefirov, P M Zorky. New applications of van der Waals radii in chemistry	1995	64	415	
116	128	V I Ovcharenko, R Z Sagdeev. Molecular ferromagnets	1999	68	345	
108	77	V I Sokolov, I V Stankevich. The fullerenes — new allotropic forms of carbon: molecular and electronic structure, and chemical properties	1993	62	419	
96	111	D V Konarev, R N Lyubovskaya. Donor–acceptor complexes and radical ionic salts based on fullerenes	1999	68	19	
91	106	Yu V Pleskov. Synthetic diamond in electrochemistry	1999	68	381	
89	73	A P Polishchuk, T V Timofeeva. Metal-containing liquid–crystal phases	1993	62	291	
87	86	G I Koldobskii, V A Ostrovskii. Tetrazoles	1994	63	797	
83	63	I V Kozhevnikov. Fine organic synthesis with the aid of heteropolycompounds	1993	62	473	
83	86	V L Ermolaev, E B Sveshnikova. The application of luminescence-kinetic methods in the study of the formation of lanthanide ion complexes in solution	1994	63	905	
71	63	O I Kolodiaznyi. Methods of preparation of C-substituted phosphorus ylides and their application in organic synthesis	1997	66	225	
70	75	I.Yu. Galaev. 'Smart' polymers in biotechnology and medicine	1995	64	471	
64	58	R Sh Vartapetyan, A M Voloshchuk. The mechanism of the adsorption of water molecules on carbon adsorbents	1995	64	985	
64	67	A Ya Sychev, V G Isak. Iron compounds and the mechanisms of the homogeneous catalysis of the activation of O ₂ , H ₂ O ₂ and the oxidation of organic substrates	1995	64	1105	
63	78	A F Pozharskii. Naphthalene 'proton sponges'	1998	67	1	
55	66	A D Garnovskii, B I Kharisov, G Gojon-Zorrilla, D A Garnovskii. Direct synthesis of coordination compounds from zerovalent metals and organic ligands	1995	64	201	

^a The CA DB considers citations only since 1996.

Table 4. Most cited (more than 150 citations) publications of the journal of 1974–2006 (SCI DB).

Publication	The number of references in the SCI BD		
	version		USP + RCR
	USP	RCR	
I V Berezin, K Martinek, A K Yatsimirskii. Physicochemical foundations of micellar catalysis 1973, Vol. 42, P. 787	142	347	489
T A Masrtyukova, M I Kabachnik. The application of the Hammett equation with the constants σ^{PH} in the chemistry of organophosphorus compounds, 1969, Vol. 38, P. 795	232	40	272
E A Paukshtis, E N Yurchenko. Study of the acid – base properties of heterogeneous catalysts by infrared spectroscopy, 1983, Vol. 52, P. 242	178	89	267
Yu V Zefirov, P M Zorky. Van der Waals radii and their application in chemistry, 1989, Vol. 58, P. 421	205	36	241
I V Kozhevnikov. Advances in catalysis by heteropolyacids, 1987, Vol. 56, P. 811	80	158	238
V V Dunina, O A Zalevskaya, V P Potapov. General principles and characteristics of cyclopalladation reactions, 1988, Vol. 57, P. 250	48	181	229
I V Kozhevnikov, K I Matveev. Heteropolyacids in catalysis, 1982, Vol. 51, P. 1075	81	96	177
M I Vinnik. Acidity functions of aqueous solutions of strong acids, 1966, Vol. 35, P. 802	167	6	173
M I Stankevich, I V Stankevich, N S Zefirov. Topological indices in organic chemistry, 1988, Vol. 57, P. 191	117	43	160
Yu V Zefirov, P M Zorky. New applications of van der Waals radii in chemistry, 1995, Vol. 64, P. 415	127	32	159
A L Buchachenko. Organic and molecular ferromagnetics: advances and problems, 1990, Vol. 59, P. 307	57	100	157

and CA DBs and Table 4 shows the most cited publications of the journal (more than 150 citations) for 1974–2006 (according to the SCI DB data) with indication of the journal version that is cited.

It can be seen from Table 3 that the numbers of citations according to the SCI DB and CA DB do not coincide, but nevertheless, they allow one to evaluate the popularity of a particular paper. (It should, however, be borne in mind that the amount of citation does not say anything about other features of the papers, *i.e.*, the originality and reliability, information value and the contribution to the scientific progress.¹⁸) It follows from Table 4 that both Russian- and English-language versions of the journal are cited. When comparing the citation data with data on downloading of full papers from the journal's Internet site (Table 5, statistical data from the

journal's DB), one can see that the request rate for the electronic versions of the papers does not correlate with the citation rate. Note that of the 17 publications presented in Table 5, nine are related to nanomaterials.

Analysis of the citation dynamics makes sense for comparing rather long periods of time, for example, 10-year periods of publications and 12-year citation periods. Table 6 presents the citation data for these periods, which demonstrate that the number of citations of journal publications for corresponding 12-year periods was only 40%–50% of the total number of citations by the search instant (the end of 2006). Thus it follows that the reviews published by *Uspekhi Khimii* (Russian Chemical Reviews) remain topical for long.

The reviews published in *Uspekhi Khimii* (Russian Chemical Reviews) are often cited by both Russian and foreign

Table 5. Statistical data on downloading of the electronic versions of papers from the *Uspekhi Khimii* (Russian Chemical Reviews) internet site for 1996–2006.

The number of down-loadings	Publication	year	volume	page
	authors, title			
203	T V Vernitskaya, O N Efimov. Polypyrrole: a conducting polymer; its synthesis, properties and applications	1997	66	443
108	A L Ivanovskii. Non-carbon nanotubes: synthesis and simulation	2002	71	175
105	G B Sergeev. Nanochemistry of metals	2001	70	809
104	A D Pomogailo. Hybrid polymer-inorganic nanocomposites	2000	69	53
102	S P Gubin, Yu A Koksharov, G B Khomutov, G Yu Yurkov Magnetic nanoparticles: preparation, structure and properties	2005	74	520
87	V A Tarasevich, N G Kozlov. Reductive amination of oxygen-containing organic compounds	1999	68	55
85	E G Rakov. Methods for preparation of carbon nanotubes	2000	69	35
83	R F Khairutdinov. Chemistry of semiconductor nanoparticles	1998	67	109
78	V V Rozanov, O V Krylov Hydrogen spillover in heterogeneous catalysis	1997	66	107
76	E G Rakov. The chemistry and application of carbon nanotubes	2001	70	827
66	E M Zubin, E A Romanova, T S Oretskaya. Modern methods for the synthesis of peptide – oligonucleotide conjugates	2002	71	239
65	V N Korotchenko, V G Nenajdenko, E S Balenkova, A V Shastin. Olefination of carbonyl compounds: modern and classical methods	2004	73	957
63	V I Roldugin. Self-assembly of nanoparticles at interfaces	2004	73	115
58	B V Timokhin, V A Baransky, G D Eliseeva. Levulinic acid in organic synthesis	1999	68	73
52	A D Pomogailo. Polymer-immobilised nanoscale and cluster metal particles	1997	66	679
51	L M Bronstein, S N Sidorov, P M Valetsky. Nanostructured polymeric systems as nanoreactors for nanoparticle formation	2004	73	501
50	N A Bragina, V V Chupin. Methods of synthesis of deuterium-labelled lipids	1997	66	975

Table 6. Citation of Uspekhi Khimii (Russian Chemical Reviews) according to periods (10-year publication periods and 12-year citation periods).

Database	Publication period	The number of publications	The number of citations	
			in 12 years (% of the total number of citations)	during 1975–2006
SCI	1975–1984	828	8862 (41)	21 615
	1985–1994	853	6780 (51)	13 214
SCI	1995–2004	568	7070	—
CA			7759	—

periodicals; according to the SCI DB, in the last decade (1996–2006), among the citing periodicals, about 48% are Russian journals and 52% are foreign journals. According to the CA DB, these values are 38% and 62%, respectively.

Table 7. Journals that cite most often papers from Uspekhi Khimii (Russian Chemical Reviews).

Journal	Database			
	SCI, references		CA, references	
	number	%	number	%
Russian Chemical Bulletin, International Edition (Izvestiya Akademii Nauk. Seriya Khimicheskaya)	379	6.1	345	5.8
Russian Journal of General Chemistry (Zhurnal Obshchei Khimii)	245	3.9	222	3.7
Russian Chemical Reviews (Uspekhi Khimii)	244	3.9	204	3.4
Russian Journal of Organic Chemistry (Zhurnal Organicheskoi Khimii)	217	3.5	199	3.4
Polymer Science (Vysokomolekulyarnye Soedineniya)	201	3.2	—	—
Russian Journal of Physical Chemistry (Zhurnal Fizicheskoi Khimii)	146	2.3	28	0.5
Russian Journal of Inorganic Chemistry (Zhurnal Neorganicheskoi Khimii)	144	2.3	—	—
Russian Journal of Applied Chemistry (Zhurnal Prikladnoi Khimii)	131	2.1	92	1.5
Kinetics and Catalysis (Kinetika i Kataliz)	118	1.9	106	1.8
Doklady of Chemistry (Doklady Akademii Nauk)	112	1.8	64	1.1
Tetrahedron	85	1.4	80	1.3
Journal of Organic Chemistry	72	1.2	76	1.3
Journal of the American Chemical Society	71	1.1	73	1.2
Phosphorus, Sulfur and Silicon and the Related Elements	64	1.0	51	0.9
Inorganic Chemistry	59	1.0	60	1.0
Synthesis	57	0.9	53	0.9
European Journal of Organic Chemistry	50	0.8	47	0.8
Journal of Organometallic Chemistry	45	0.7	47	0.8
Angewandte Chemie, International Edition	46	0.7	43	0.7
Journal of Applied Polymer Science	45	0.7	45	0.8
Chemical Reviews	39	0.6	37	0.6
Journal of Physical Chemistry A	39	0.6	38	0.6
Organometallics	38	0.6	38	0.6

Table 7 presents quantitative data on citation of reviews published by USP/RCR by Russian and foreign periodicals. The journal self-citation is low: from 3.4% to 3.9%.

In conclusion, we would like to note that in recent years, owing to crucial changes in the editorial policy of the journal Uspekhi Khimii (Russian Chemical Reviews), transfer of the whole body of preparatory work for the edition of Russian- and English-language versions to the editorial office and recruiting highly skilled research personnel from the chemical institutes of the Russian Academy of Sciences for participation in editorial work, it became possible to increase the quality of selection of reviews and preparation for publication, to improve the appearance of the journal and attain almost simultaneous publication of the Russian and English versions.

The range of the journal authors and the staff of the Editorial Board headed by Academician O M Nefedov since 1995 were substantially extended; the international Advisory Board was founded. The journal started to practice the publication of invited reviews and subject-related issues devoted to topical trends of chemical science as well as the publication of special issues composed of reviews by leading scientists of particular centres of chemical science such as the Siberian Branch of the RAS, Moscow, St Petersburg and Kiev Universities, the Institute of Problems of Chemical Physics of the RAS and other.

Currently, both versions of the journal (Uspekhi Khimii and Russian Chemical Reviews) appear as both printed and electronic editions. Since 1995, the following information about the journal is available free on the Internet (<http://www.uspkhim.ru>): general information, subscription terms, the contents of the journal for a year and brief abstracts of all papers. In 2004, in cooperation with the British company Turpion Ltd (a partner in publishing English version of the journal), the electronic archive of the English version starting with the first issue (1960) was composed and an up-to-date integrated system for preparation, publication and distribution of the electronic version of the journal with the on-line submission and refereeing options was elaborated. By now, the first stage of composing the electronic archive of the Russian version of the journal for 1990–2006 has been completed.

All this helps to maintain the subscribers' and readers' interest in the journal and to ensure its high rating.

References

- W Hellemans, B Bunch *Timetables of Science* (New York: Simon and Schuster, 1988) p. 146
- I Wormell *Encyclopedia of Library and Information Science (Suppl. 33)* Vol. 70 (New York: Marcel Dekker, 2000) p. 77
- H P Moed, T N Van Leeuwen, J Reekijk *Scientometrics* **37** 105 (1996)
- A Schubert *Inorg. Chim. Acta* **253** 111 (1996)
- J Michl, J A Gladysz, R D Kuchta *Chem. Rev.* **100** 1 (2000)
- W Marx *Angew. Chem., Int. Ed.* **40** 139 (2001)
- W Marx, M Cardona *Solid State Commun.* **127** 323 (2003)
- V M Buznik, I V Zibareva, V N Piottukh-Peletsii, N I Sorokin *Zh. Strukt. Khim.* **45** 1142 (2004)^a
- I V Zibareva, B G Derendyaev *Khim. Inter. Ustoich. Razvitiya* **121** (2004)^b
- V M Buznik, I V Zibareva *Khim. Tekhnol.* **40** (2006)
- W W Hood, C S Wilson *Scientometrics* **58** 587 (2003)
- STN International URL: <http://www.stn-international.de>
- CA Database Summary Sheet URL: http://www.stn-international.de/stdatabases/sum_sheet/CA.pdf
- SciSearch Database Summary Sheet URL: <http://www.cas.org/ONLINE/DBSS/scisearchss.html>
- D B Baker, J W Horisznay, W V Metanonski *J. Chem. Inf. Comput. Sci.* **20** 193 (1980)

16. JCR® on CD-ROM, Science Edition
17. Impact Factor Trend Graph: USPEKHI KHIMII Journal
Citation Reports URL: <http://portal.isiknowledge.com/portal.cgi?DestApp=JCR&Func=Frame>
18. E D Sverdlov *Vestn. Ross. Akad. Nauk* 1073 (2006)^c

^a — *J. Struct. Chem. (Engl. Transl.)*

^b — *Chem. Sust. Develop. (Engl. Transl.)*

^c — *Herald Russ. Acad. Sci. (Engl. Transl.)*

Pulsed EPR in the method of spin labels and probes

S A Dzuba

Contents

I. Introduction	699
II. EPR spectroscopy of nitroxide radicals — the fundamentals	699
III. Pulsed EPR techniques	702
IV. Structural studies of spin-labelled systems	706
V. Studies of the dynamics of spin-labelled systems	709
VI. Conclusion	711

Abstract. Various pulsed EPR in the method of spin labels and probes based on electron spin echo spectroscopy (spin echo envelope modulation through electron–nuclear interactions, electron–electron double resonance, echo detected EPR, *etc.*) are considered. These methods provide information on the conformations of complex biomolecules, nanostructure of matter, depth of water penetration into biological membranes, supramolecular structure of multicomponent systems (membrane–peptide, *etc.*), co-operative orientational dynamics of molecules and dynamic low-temperature transitions in disordered molecular media and biosystems. The bibliography includes 130 references.

I. Introduction

The method of spin labels and probes has been widely used in physicochemical and biophysical studies since the 1970s.^{1–3} Spin probes are stable paramagnetic molecules (usually, nitroxyl radicals^{4,5}) that are introduced into the system under study as a minor additive. Spin labels represent nitroxide radicals covalently bound to macromolecules. The method of spin labels and probes is used in studies of the local structure of molecules and molecular dynamics, for identification of particular functional groups, measurement of oxygen concentration and proton content, determination of polarity, acceleration of nuclear spin relaxation in MRI studies and for solving some other problems.[†]

The method makes use of unpaired electrons present in radicals, which permits utilisation of electron paramagnetic resonance (EPR) spectroscopy. Despite the fact that EPR spectroscopy emerged more than six decades ago, the state-of-the-art in this field is characterised by continuous progress and improvement of various experimental techniques. Quite recently, pulsed EPR spin label–spin probe studies began using, in particular, pulsed electron–electron double resonance (PELDOR), electron spin echo envelope modulation

(ESEEM), pulsed electron–nuclear resonance, echo-detected EPR, *etc.* All of them are based on the ESE technique.^{6,7}

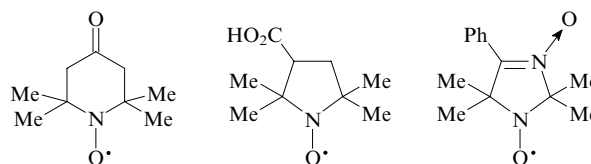
Pulsed EPR spectroscopy significantly extended the potential of the method of spin labels and probes. It allows one to investigate the nanostructure of matter including large biomolecules, supramolecular structure of complex systems, *e.g.*, membranes and their peptide components as well as co-operative small-amplitude orientational motions of molecules in disordered media and biological liquids.

There are a number of reviews^{8–15} concerning particular aspects of pulsed EPR spin label–spin probe studies. The main goal of this review was to briefly outline the fields of application of the method, to summarise the results of recent investigations and to highlight new experimental techniques.

II. EPR spectroscopy of nitroxide radicals — the fundamentals

1. Nitroxide radicals. Site-directed spin labelling technique

Nitroxide radicals are stable paramagnetic molecules containing a paramagnetic NO fragment bearing an unpaired electron.^{4,5} This fragment is surrounded by the shielding substituents (usually, methyl groups). To date, a few hundreds of nitroxide radicals have been synthesised. A few simple examples are given below:



The so-called site-directed spin labelling (SDSL) technique appeared to be of particular importance for obtaining information on the molecular level.^{16–18} The method involves attachment of a spin label to the molecular fragment of interest in a complex biomolecule or supramolecular system. In protein studies, a cysteine residue in the amino acid sequence is most often labelled using a methanethiosulfonate spin label, namely,

S A Dzuba Institute of Chemical Kinetics and Combustion, Siberian Branch of the Russian Academy of Sciences, ul. Institutskaya 3, 630090 Novosibirsk, Russian Federation. Fax (7-383) 330 73 50, tel. (7-383) 330 91 50, e-mail: dzuba@kinetics.nsc.ru

Received 17 April 2007

Uspekhi Khimii 76 (8) 752–767 (2007); translated by A M Raevskiy

[†] According to the IUPAC Compendium of Chemical Terminology (2nd Edition, 1997), the use of the prevailing terms ‘nitroxyl radicals’ and ‘nitroxides’ as a class name for ‘aminoxyl radicals’ is not desirable.

(1-oxyl-2,2,5,5-tetramethylpyrrolin-3-yl)methyl methanethio-sulfonate (MTSL). Artificial protein analogues containing this residue are also studied. It is possible to label some other amino acid residues, *e.g.*, lysine, aminoisobutyric acid, *etc.* Small spin-labelled peptides containing less than 50 amino acids and bearing spin labels at desired positions of the amino acid sequence can directly be synthesised. Not only peptides and proteins, but also other biomolecules (*e.g.*, lipids) can be site-directed spin labelled.

2. EPR spectra of nitroxide radicals. Electron – nuclear interactions. The effects of motion

In the framework of the first-order perturbation theory, the X-band (wavelength about 3 cm, frequency ~ 10 GHz) EPR condition for nitroxide radicals can be quite correctly approximated by¹⁹

$$g(\theta, \varphi)\beta B + a(\theta, \varphi)M = \hbar\omega, \quad (1)$$

where

$$g(\theta, \varphi) = g_{XX} \sin^2 \theta \cos^2 \varphi + g_{YY} \sin^2 \theta \sin^2 \varphi + g_{ZZ} \cos^2 \theta,$$

$$a(\theta, \varphi) = \sqrt{A_{XX}^2 \sin^2 \theta \cos^2 \varphi + A_{YY}^2 \sin^2 \theta \sin^2 \varphi + A_{ZZ}^2 \cos^2 \theta},$$

β is the Bohr magneton; B is the magnetic field induction; M is the nuclear spin projection on the quantisation axis; \hbar is the Planck constant; ω is the frequency of the alternating magnetic field; g_{XX} , g_{YY} and g_{ZZ} are the principal values of the g -tensor; and A_{XX} , A_{YY} and A_{ZZ} are the principal values of the hyperfine coupling tensor. Usually, the molecular system of coordinates is used, in which the X axis is aligned with the N–O bond and the Z axis is normal to the plane in which the \geq N–O fragment is situated. The angles θ and φ define the direction of the magnetic field in the spherical system of coordinates. Typical values of the components of the magnetic tensors of nitroxide radicals are as follows: $g_{XX} \approx 2.0090$, $g_{YY} \approx 2.0060$, $g_{ZZ} \approx 2.0025$, $A_{XX}/g_e\beta \approx A_{YY}/g_e\beta \approx 5$ G, $A_{ZZ}/g_e\beta \approx 35$ G (g_e is the g -factor of free electron). In the case of high-field

EPR, Eqn (1) should be augmented with a term corresponding to the Zeeman interaction between atomic nuclei.

The overall shift of the resonance due to unresolved hyperfine coupling (HFC) of the unpaired electron with other nuclei in the radical and matrix is about 3 G. In the c.w. EPR spectrum, these couplings remain unresolved due to superposition of many lines with small splittings; it should be noted that signals from radicals characterised by different $g(\theta, \varphi)$ values may appear in the same spectral region.

The c.w. EPR technique involves sweep of the field B under continuous action of alternating microwave field at a constant frequency ω . Figure 1 shows a typical shape of the EPR spectrum of a nitroxide radical. Usually, the first derivative of the absorption lineshape with respect to the magnetic field is measured. The parallel and perpendicular orientations of the molecule are also shown; this can be done assuming axial symmetry of the magnetic tensors (see above) and ignoring unresolved hyperfine coupling.

Orientalional motions cause averaging of magnetic interactions. In the X-band, the characteristic frequency variation due to different molecular orientations is $\sim 10^9$ rad s⁻¹. Therefore, in the case of fast motions of the whole molecule at frequencies much higher than 10^9 rad s⁻¹ the EPR spectrum should exhibit three lines of equal intensity corresponding to three projections of the nitrogen spin on the direction of the external magnetic field. Here, the g -tensor and the HFC tensor are averaged to the scalar values equal to 1/3 of the spurs of the tensors.

Biological and other supramolecular systems are usually characterised by slow molecular motions at frequencies lower than 10^9 rad s⁻¹. As a consequence, no complete averaging occurs; therefore, the results obtained in conventional c.w. EPR experiments are often ambiguous. Pulsed methods based on the ESE technique are sensitive to motion even under glass transition conditions.

3. Electron – electron dipole – dipole interactions between radicals

At present, the dipole–dipole (d–d) interaction between electron spins in spin labels is widely used in studies of the nanostructure of spin-labelled systems. This interaction is of the order of $g_e^2\beta^2/r^3$ in magnitude, where r is the distance between two radicals. Pulsed EPR methods based on the ESE technique are highly sensitive to d–d-interaction. The characteristic times of transverse relaxation in organic solids are about 10^{-6} s and thus the upper bound of the measured distances is nearly 5 to 7 nm. The lower bound obtained from the ‘dead time’ of an instrument ($\sim 10^{-7}$ s) is close to 1.5 nm. The advantage of ESE spectroscopy consists of high accuracy of measurements in this range of distances. At $r \sim 3$ nm, the error is at most 0.1 nm.^{8–10} This is a record spatial resolution among all known physical methods, which allows one to reveal subtle effects in the nanostructure of matter that cannot be disclosed by other methods. It should also be noted that ESE studies do not require special treatment of samples (*e.g.*, crystallisation, high degree of purification, *etc.*)

The Hamiltonian of magnetic dipole–dipole interactions between the magnetic moments of two electrons has the form

$$H_d = g_1 g_2 \beta^2 \frac{r^2 \mathbf{S}_1 \mathbf{S}_2 - (\mathbf{S}_1 \mathbf{r})(\mathbf{S}_2 \mathbf{r})}{r^5}, \quad (2)$$

where g_1 and g_2 are the g -factors of two particles; \mathbf{S}_1 , \mathbf{S}_2 are the spin operators; \mathbf{r} is the radius vector connecting the particles. Almost all long-chain biradicals can be studied in the point dipole approximation, which assumes that the spin density of the unpaired electron is localised at some point.¹⁰

When studying nitroxide biradicals, one can use the perturbation theory, which treats the Hamiltonian (2) as a small

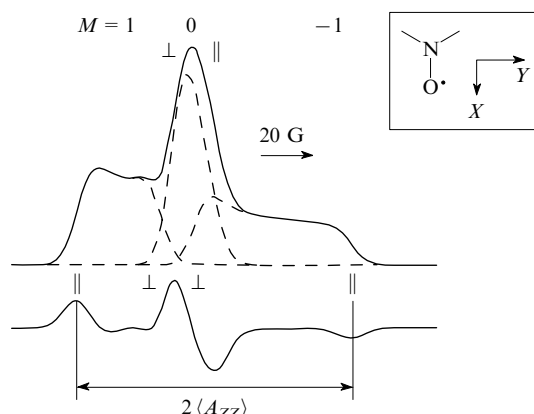


Figure 1. EPR spectrum of a nitroxide radical.

The lower curve represents the EPR spectrum as the first derivative of the absorption lineshape with respect to the magnetic field. Dashed lines denote particular components of HFC; for each component, approximate positions of the parallel and perpendicular orientations are shown. The inset specifies the molecular system of coordinates. The splitting between the outermost peaks in the lower curve approximately equals the doubled A_{ZZ} principal value of the HFC tensor [averaged value is $\langle A_{ZZ} \rangle$ in the presence of librations].

perturbation compared to expression (1). In the case of weak d–d-interactions, where

$$\varepsilon_d \ll |g_1 - g_2|\beta B$$

(this is always valid at $r > 0.15$ nm), the transition frequencies for each of the two spins are given by¹⁰

$$\omega_{1,2} = \frac{g_{1,2}\beta}{\hbar}B \pm \frac{1}{2}\varepsilon_d, \quad (3)$$

where

$$\varepsilon_d = \frac{g_1 g_2 \beta^2}{r^3 \hbar} (1 - 3 \cos^2 \Theta),$$

(Θ is the angle between the direction of the external magnetic field and the line connecting two radicals). The sign \pm means that for each spin the resonance is shifted due to the d–d-interaction with the partner spin depending on the projection of the latter on the direction of the external magnetic field.

Considering pulsed EPR methods, expression (3) leads to temporal dependences of the type $\cos(\varepsilon_d t)$ (see below).¹⁰ The Fourier-transformed EPR spectrum exhibits a doublet at the frequencies $\pm \varepsilon_d$. In a polyoriented system, the frequency (ω)-dependent intensities of the dipolar doublet lines are averaged over all spatial orientations of the pair. At

$$\omega_{\perp} = \pm \frac{g_1 g_2 \beta^2}{r^3 \hbar},$$

singularities appear ($\Theta = \pi/2$, perpendicular orientation of the pair). Often, only the singularity due to the relatively low intensity of other lines can be observed experimentally. Its position permits immediate determination of the distance r .

4. Electron spin echo of nitroxide radicals

Excitation of transitions between spin energy levels by intensive microwave pulses causes the appearance of a free induction signal, *i.e.*, an oscillating macroscopic transverse magnetisation.^{6,7} Optimum conditions for observation of the free induction signal are attained by applying a pulse that causes a $\pi/2$ (90°) flip of the magnetisation vector. Typical microwave pulse durations in ESE spectrometers are 10 to 100 ns. Signal decay is due to the scatter of precession frequencies (this determines the shape of the EPR spectrum).

The resolution of ESE spectrometers is limited by the characteristic time of transient processes in the cavity upon application of microwave pulses (usually, it is of the order of 100 ns),^{6,7} which is called the ‘dead’ time. In the case of nitroxide radicals, the nonzero ‘dead’ time makes observation of the free induction signal impossible owing to fast signal decay. The free induction signal can only be observed after some hardware improvements aimed at shortening the ‘dead time’, *e.g.*, on going to the Ku-band (resonance frequency 17 GHz, not to be confused with the Q-band!) and to elevated temperatures (this is required for line narrowing).

Two pulses applied with a time delay cause the appearance of an echo signal (see Fig. 2a). The time delay after the second pulse equals the time delay between two pulses, τ . The optimum flip angle of the magnetisation vector upon application of the second pulse is π . The formal notation for the pulse sequence and the echo signal is given below:

$$\pi/2 - \tau - \pi - \tau - \text{echo}.$$

The mechanism of the appearance of the echo signal is as follows. The second pulse follows the first one after the time delay τ and changes the phase of spin precession in the plane normal to the external magnetic field. Now the precessing spins

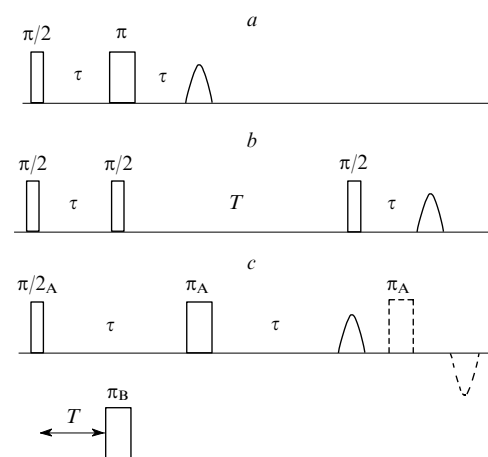


Figure 2. Electron spin echo pulse sequences.

Basic two-pulse sequence (a), three-pulse stimulated echo sequence (b) and two-frequency double resonance (PELDOR) (c). PELDOR experimental conditions: detection at the A spin frequency and an additional pump pulse at the B spin frequency. Dashed lines show an additional refocusing pulse and echo (see text).

have the same velocities but different initial phases. At the instant τ after the second pulse, refocussing occurs (all spins have the same phase) and the echo signal appears (then, defocussing will occur again). The echo signal decays with increase in τ due to spin relaxation.

Yet another method for ESE detection is the three-pulse stimulated echo pulse sequence (Fig. 2b)

$$\pi/2 - \tau - \pi/2 - T - \pi/2 - \tau - \text{echo}.$$

The first pulse creates a precessing transverse magnetisation and the second pulse creates the projection of the magnetisation vector on the Z axis (longitudinal magnetisation), which retains its magnitude during the time T in the absence of relaxation. This pulse creates a nuclear coherence, *i.e.*, the system is described by a non-stationary superposition of various electron–nuclear states upon application of the second pulse. The third pulse again creates the transverse magnetisation, which refocusses at the instant

$$t = 2\tau + T,$$

i.e., the echo signal appears.

A feature of the ESE studies of nitroxide radicals consists in incomplete (or selective) excitation of the EPR spectrum by microwave pulses. In most experiments, the pulse amplitudes reach 3–5 G, whereas the overall width of the EPR spectrum is of the order of 70–80 G. In some cases (*e.g.*, in studies of spectral diffusion, *i.e.*, stochastic fluctuations of the resonance frequency due to orientational motion), this feature is of crucial importance.

If orientational motions cause fluctuations of the resonance frequencies with the root-mean-square $\langle \Delta\omega^2 \rangle$ and the correlation time τ_c , theory predicts that at

$$\langle \Delta\omega^2 \rangle \tau_c^2 \ll 1,$$

the relaxation rate is given by $\langle \Delta\omega^2 \rangle \tau_c$.²⁰ The $\Delta\omega$ value can be estimated with ease from Eqn (1). For simplicity, suppose an axial symmetry

$$g_{XX} = g_{YY} = g_{\perp}, A_{XX} = A_{YY} = A_{\perp}.$$

Let us denote

$$g_{zz} = g_{\parallel}, A_{zz} = A_{\parallel}.$$

In the case of small-amplitude motions the angle θ fluctuates by $\Delta\theta$. Then, in a constant magnetic field B , expansion of the resonance frequency fluctuations $\Delta\omega$ in terms of $\Delta\theta$ has the form²¹

$$\Delta\omega = 2 \sin \theta \cos \theta \times \left[(g_{\perp} - g_{\parallel}) \frac{\beta B}{\hbar} + M \frac{A_{\perp}^2 - A_{\parallel}^2}{2\hbar \sqrt{A_{\perp}^2 \sin^2 \theta + A_{\parallel}^2 \cos^2 \theta}} \right] \Delta\theta. \quad (4)$$

At $\theta = 0, \pi$ and $\pi/2$, the $\Delta\omega$ value equals zero, *i.e.*, spin relaxation near the canonical orientations (parallel and perpendicular) should be slow.

Fast small-amplitude orientational motions also manifest themselves in c.w. EPR spectra, because they cause partial averaging of anisotropic magnetic interactions. In the case of orientational motion about an axis lying in the XY plane of the molecular system of coordinates, the parameter A_{\parallel} is averaged²²

$$\langle A_{\parallel} \rangle = A_{\parallel} - (A_{\parallel} - A_{\perp}) \langle \alpha^2 \rangle, \quad (5)$$

where the angular deviation, α , from the equilibrium position is related to $\Delta\theta$ as follows: $\Delta\theta = \alpha \sin \phi$. The parameter $\langle A_{\parallel} \rangle$ can be measured with ease from the splitting between the outermost peaks in the EPR spectrum (see Fig. 1).

III. Pulsed EPR techniques

1. ESEEM through electron – nuclear interactions

If an electron spin interacts with a nuclear spin, application of microwave pulses at the EPR resonance frequency causes simultaneous excitation of both allowed and forbidden spin transitions (without and with nuclear spin flip, respectively) in a solid.^{6,7} Interference of the resonance frequencies of these transitions upon ESE decay induces beats (oscillations) of the signal, which are called electron – nuclear modulation or the electron spin echo envelope modulation (ESEEM) effect.^{6,7} A few examples of the ESEEM effect are shown in Fig. 3 *a*, which corresponds to the interaction between the unpaired electron of the spin label and deuterons from the surrounding heavy water. The Fourier-transformed frequency spectrum of the beats exhibits peaks (see Fig. 3 *b*), the positions of which are determined by the electron – nuclear interactions. In the case of interactions with the nearest nuclei in the matrix, these peaks are centred around the resonance (Larmor) frequency of a given nucleus in the magnetic field of the ESE spectrometer (2.2 MHz for deuterons). These peaks cannot be resolved in c.w. EPR experiments (see above).

The ESEEM through electron – nuclear interactions represents a convenient tool of structural studies in the nearest environment of spin labels; it can be used for identification of the types of the nuclei in the nearest environment and determination of their spatial arrangement relative to the unpaired electron.

This approach has long been used in pulsed EPR spectroscopy, where it can be considered classical. Most related methodological problems have been solved to date. The fundamentals of the ESEEM technique have been comprehensively treated in monographs.^{6,7} Recently, this method has found increasing application in studies of the local environment of spin labels.

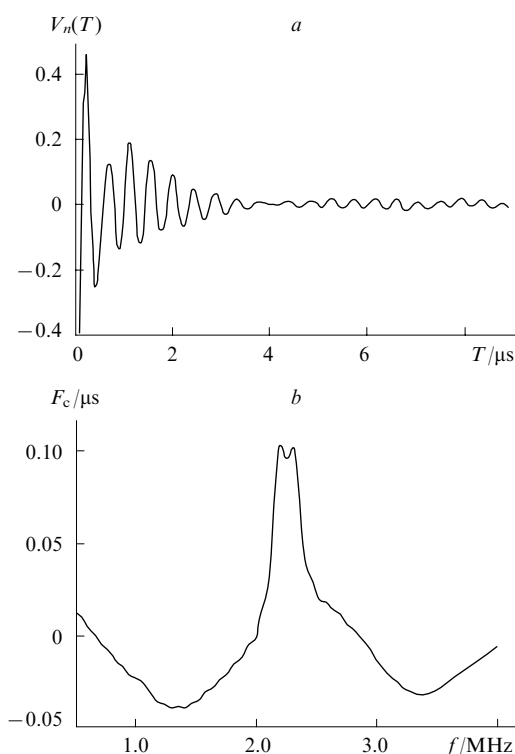


Figure 3. Typical signal oscillations (ESEEM) induced by electron – nuclear interactions (*a*) and Fourier-transformed frequency spectrum (*b*) of a spin label in D_2O -containing matrix.

From original experimental ESEEM a smooth non-oscillating function (result of averaging) was subtracted; the resulting $V_n(T)$ signal is normalised to this function at $T = 0$. F_c denotes the Fourier transform amplitude.

2. Pulsed electron – electron double resonance in studies of d – d-interactions between radicals

As mentioned above, the d – d-interaction between radicals is now widely used in studies of the nanostructure of spin-labelled systems. Most of them are carried out by pulsed double electron – electron resonance (PELDOR).^{8–10,13} The method was proposed in the 1980s.^{23,24} It allows one to determine the distances between radicals on the nanometre scale, draw conclusions on the conformations of doubly spin-labelled biomolecules and estimate the size of the aggregate (cluster) of spin-labelled molecules in the case of their aggregation (clusterisation).

In the PELDOR experiments the echo signal appears upon application of a conventional two-pulse sequence and an additional 180° pump pulse at the other resonance frequency (Fig. 2 *c*). The spins responsible for the appearance of the echo signal are called A spins while their partner spins (in our case, they are influenced by the additional pulse) are called B spins. The phase of the A spins at $t = 2\tau$ equals

$$\varphi_A = \pi \pm \varepsilon_d T$$

(the ‘plus’ or ‘minus’ sign depends on the projection of the B spin).

The echo signal is proportional to $\cos(\varepsilon_d T)$, which means that the signal is modulated at the frequency ε_d as the time T changes. Note that here modulation is due to electron – electron rather than electron – nuclear interactions (see above). The Fourier transform of the modulated ESE decay in a polyoriented system leads to the appearance of a peak at the singularity frequency

$$\omega_{\perp} = \pm \frac{g_1 g_2 \beta^2}{r^3 \hbar}.$$

The separation between spin labels can be determined from the position of this peak.

The effect of finite pulse duration (theory assumes infinitely short pulses) can be eliminated using an additional refocussing pulse.¹³

Pulsed ELDOR technique also allows study on clusterisation of spin-labelled molecules. Actually, the pump pulse excites only a fraction, P_B , of the partner spins of a given A spin. If a cluster comprises N particles and the probability of simultaneous excitation of more than one B spin is low (*i.e.*, $P_B N \ll 1$), the ESE signal is given by⁸

$$V(T) = [1 - P_B \langle 1 - \cos(\varepsilon_d T) \rangle]^{N-1}. \quad (6)$$

It follows that at $t \rightarrow \infty$ the $V(T)$ value tends to the limiting value equal to $(1 - P_B)^{N-1}$. This asymptotic value can experimentally be measured with ease and thus one can estimate the number of particles, N , in the cluster.

The same effect can be attained not only by irradiating B spins at the other resonance frequency, but also by changing the magnetic field in a pulsed (jumpwise) manner. This experimental technique was practically implemented in the X-band²⁵ and W-band²⁶ EPR experiments. The A spins are excited using the three-pulse stimulated echo sequence. In the time between the second and third pulses, the magnetic field is changed in a jumpwise manner and a 180° pump pulse is applied. Due to shift of the resonance, this pulse affects only the B spins. The approach assumes the time delay τ between the first and second pulses to be varied. Here, electron–nuclear modulation also appears in addition to modulation through electron–electron interactions. The two mechanisms can be distinguished by separating the overall decay signal into the decay signal observed in the presence and in the absence of pump (no pump pulse). These mechanisms are independent of each other and should therefore contribute multiplicatively to the observed envelope modulation.

The advantage of the field-step PELDOR over the two-frequency PELDOR technique consists in the possibility of using a scanning pump²⁵ owing to an increase in the proportion of spins P_B to be excited, which leads to an increase in the modulation depth. A drawback of the technique is the effect of transverse relaxation on the echo decay observed.

Various methodological aspects of the PELDOR technique have been considered in a number of recent studies. Mention may be made of the problem of correct inclusion of the spin label structure and binding to a biomolecule in modelling the structure of the biomolecule from PELDOR data.²⁷ Methodological aspects concerned with extraction of information from PELDOR data and optimisation of experimental design have been considered.^{28–30} A comparative PELDOR study of biradicals in two (X and S) EPR bands was carried out.³¹ Since the electron–nuclear modulation depends on the particular microwave band while the electron–electron modulation is independent of it, the approach can be employed to determine the contribution of the electron–electron modulation. It was reported³² that the quality of information extracted from the PELDOR frequency spectra can be improved using isotopic substitution, namely, by replacing (i) ^{14}N atom by ^{15}N atom and (ii) hydrogen atom by deuterium atom in one radical of the pair. Here, the 2D version of the four-pulse PELDOR was proposed as the experimental technique. The potential of PELDOR studies of biradicals in the high-frequency EPR band (frequencies higher than 95 GHz) was discussed.³³ Orientational selectivity effects due to high spectral resolution were demonstrated.

3. Miscellaneous methods of investigation of d–d-interactions

Complications in PELDOR experiments (need for an additional source of microwave radiation, a special cavity, *etc.*) gave an impetus to the development of miscellaneous experimental techniques for studying d–d-interactions.

The ‘2 + 1’ method³⁴ is similar to the PELDOR technique except for the fact that all pulses are applied at the same resonance frequency. The pulse sequence is as follows:

$$\text{pulse 1} - T - \text{pulse } (+1) - (\tau - T) - \text{pulse 2} - \tau - \text{echo}.$$

The echo signal is created by two pulses (pulse 1 and pulse 2); an additional pulse (it is this pulse that is called +1) is necessary to achieve alternation of the d–d-interaction. Experiments involve variation of the time T at constant τ . A drawback of the ‘2 + 1’ method is that it is not free from electron–nuclear ESEEM. Moreover, the dipole–dipole interaction alternates under the action of not only pulse +1, but also the second pulse. Correct allowance for interference between these two effects is not always possible. As a result, information on the d–d-interaction can be significantly distorted.

Method based on double-quantum coherence. Using an appropriately designed pulse sequence, it is possible to excite a double-quantum coherence in the spin level system of a biradical.³⁵ A commonly used pulse sequence for this experiment includes four pulses. Three of them ($\pi/2$ pulses) create a stimulated echo signal. An additional π pulse is applied at the midpoint of the time interval between the second and third pulses. The contribution of the double-quantum coherence is selected using the pulse phase cycling from one series to another. Experiments involve variation of the time τ ; the signal is modulated at the ε_d frequency.

In order to avoid the loss of signal during the ‘dead’ time, an additional refocussing (fifth) pulse is applied. One can also use the six-pulse sequence, in which the double-quantum coherence is created by three rather than two pulses.

$$\pi/2 - \tau/2 - \pi - \tau/2 - \pi/2.$$

The advantage of this approach consists in the absence of the interference effects characteristic of the ‘2 + 1’ method. However, in this case the electron–nuclear ESEEM occurs too.³⁶ The drawbacks of the double-quantum coherence technique also include the large number of phase change cycles (a total of sixty-four cycles), which can introduce an additional error, and high demands to experimental equipment, namely, the amplitudes of microwave pulses should be higher than the pulse amplitudes for commercially available spectrometers. Finally, the phenomenon is characterised by a rather complicated theoretical description and the lack of a clear picture. Nevertheless, a number of double-quantum coherence studies of the d–d-interaction of spin probes are available in the literature. Methodological aspects of application of the method have been considered.³⁷ ESEEM suppression techniques were also proposed.³⁸

A method based on the solid-state NMR pulse sequences³⁹ is based on the known ‘solid echo’ and Jeener–Broekaert pulse sequences. The ‘solid echo’ pulse sequence is as follows:

$$(\pi/2)_x - \tau - (\pi/2)_y - \tau - \text{echo}.$$

Compared to the double-quantum coherence method, here the experimental design is much simpler (smaller number of phase change cycles is required). However, theoretical description remains complicated and no clear representation of the phenomenon is available.

The aforesaid suggests that at present PELDOR is the most convenient method of investigation of d–d-interactions. It provides a clear picture of the phenomenon and essentially simplified theoretical description and is almost free from the ESEEM effects. These advantages were demonstrated in a comparative double-quantum coherence and PELDOR study³⁶ of a doubly spin-labelled protein with a label-to-label separation of 3.55 nm.

4. Relaxation-induced enhancement of electron–electron ESEEM induced by in d–d-interaction

The drawback of all the methods described above including PELDOR is low portion of excited spins (at most 10%–15%) due to a large width of the EPR spectra of nitroxide radicals compared to the amplitude of microwave pulses; as a consequence, the ESEEM effect is weak. This drawback becomes particularly pronounced on going to high-field EPR. An approach⁴⁰ based on the use of spin–lattice (longitudinal) relaxation in the spin pair makes it possible to overcome these difficulties. The Larmor frequency of the resonance A spin coupled with an off-resonance B spin

$$\omega_A^* = \omega_A + m_B \varepsilon_d,$$

where m_B is the B spin projection, can be changed by B spin flips induced by longitudinal relaxation. In this case the probability for an odd number of the B spin flips to occur during the time interval T is $0.5[1 - \exp(-T/T_1)]$, where T_1 is the longitudinal relaxation time. With scanning τ , the stimulated ESE is modulated at the dipolar frequency ε_d . The modulation amplitude increases with the ‘evolution’ period T . Relaxation-induced dipolar modulation enhancement (RIDME) was observed experimentally.⁴⁰ The RIDME method is free from the drawbacks associated with the low portion of excited spins, because up to 50% of all off-resonance spins can be involved in dipolar modulation. Therefore, RIDME is a quite promising method of high-field ESE studies, as was shown by, *e.g.*, a 130-GHz (4.4 T) ESE.⁴¹

5. ESEEM modulation due to spontaneous intramolecular motions and nuclear spin relaxation

Modulation phenomena in conventional ESE methods are due to coherent dynamic effects caused by simultaneous excitation of two and more transitions in the EPR spectrum under the action of microwave pulses. In the case of RIDME, the ESE modulation is due to spontaneous changes in the magnetic parameters of radicals under the action of the pulse sequence. However, spontaneous changes can also be induced by intramolecular motions⁴² and nuclear spin relaxation in the nearest environment.⁴³ Such effects are studied using the three-pulse stimulated echo sequence. It includes scanning the time delay τ between the first and second pulses at the fixed time delay T between the second and third pulses. The ESEEM is due to a spontaneous change in the Larmor precession frequency of electron spin in the course of system evolution between the pulses during the time T , induced by longitudinal nuclear spin relaxation in the nearest environment. The longer the time T the more probable the event. Manifestation of spontaneous processes in the ESEEM have been considered in a review.⁴⁴

6. Pulsed high-field/high-frequency EPR

High-field (high-frequency) EPR is observed in magnetic fields higher than 3 T (frequencies higher than 95 GHz). Continuous-wave high-field/high-frequency EPR has long been used in studies of spin-labelled systems. The main advantage of the technique consists of orientation selectivity due to the g -factor anisotropy, which permits investigation of particular (dif-

ferent) orientations of spin probes and spin labels. Therefore, research on polyoriented systems provides information identical to that obtained in studies of oriented single crystals. Recently, a number of pulsed high-field/high-frequency EPR studies of the molecular structure and dynamics of spin-labelled systems have been reported (see, *e.g.*, Refs 26, 33, 41, 45, 46). High-field/high-frequency EPR spectrometers are commercially available.

7. Echo-detected EPR in studies of orientational dynamics

In echo-detected EPR, the echo signal is recorded as the function of the magnetic field at different times τ (2D experiment).²¹ Different resonance fields correspond to different orientations of the radical relative to the external magnetic field direction (see Fig. 1); therefore, the method allows one to obtain information on the orientational dependence of the relaxation rate or relaxation anisotropy. The relaxation anisotropy is related to the mechanism and rate of motion.

For convenience, a number of echo-detected EPR spectra are recorded at different τ normalised to the same magnetic field corresponding to the spectral maximum and then plotted together as shown in Fig. 4. This allows one to exclude the magnetic field independent isotropic relaxation governed by some processes not related to motions and to clarify the character of the relaxation anisotropy. For instance, Fig. 4 shows that relaxation near the spectral edges (they correspond to the parallel orientation of the molecule, see Fig. 1) is slower.

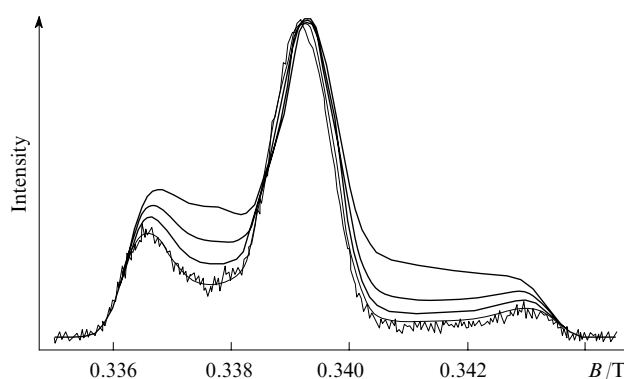


Figure 4. Typical echo-detected spectra recorded at different time intervals τ between pulses and normalised to the maximum intensity. The thin solid line denotes the results of calculations using the model of fast small-amplitude motions (see text).

Echo-detected EPR of spin probes is sensitive to fast small-amplitude stochastic motions of the spin probe and spin label molecules near equilibrium positions. Such orientational motions are called stochastic librations; they are only characteristic of disordered molecular (including biological) media. The technique is sensitive to very small motion amplitudes (down to $0.1-1^\circ$).⁴⁷ Note that stochastic motions are different from dynamic orientational oscillations that are characteristic of any phase state of matter.

8. Two-dimensional pulsed electron–electron double resonance in studies of orientational dynamics

The pulse sequence of 2D pulsed electron–electron double resonance^{12, 48, 49} is the same as the PELDOR pulsed sequence. The difference is that here the free induction signal appeared after application of the last pulse is measured. The Fourier transform is performed over two times, the time T and the time

delay after the last pulse in the pulse sequence. The 2D spectra allow one to differentiate the homogeneous broadening due to the motion and the inhomogeneous broadening caused by microscopic ordering, *i.e.*, to obtain information on structural dynamic heterogeneity of the system. In this case, observation of the free induction signal requires the use of short-‘dead-time’ instruments, *e.g.*, Ku-band EPR spectrometers (17 GHz). Line narrowing can be attained at elevated temperatures.

9. Pulsed double electron – nuclear resonance

In addition to ESEEM EPR, electron – nuclear interactions can be studied by c.w. electron – nuclear double resonance (ENDOR) and by pulsed ENDOR according to Mims and Davies. A comparative study⁵⁰ of the interaction of spin labels with ³¹P nuclear spins carried out by different experimental techniques showed that the most reliable data can be obtained using the Mims pulsed ENDOR method, which allows small splittings (to 0.03 MHz; this corresponds to a distance of 1 nm) to be measured. In studies of spin-labelled lipids in a completely hydrated membrane these measurements permit determination of the tilt angles of lipid chains with respect to the membrane plane.

High-field pulsed ENDOR/EPR studies are also possible.⁵¹ Orientation selectivity allows one to obtain more detailed information on the structure of the nearest environment of the molecule under study. This method was used to study the geometry of complexes of spin probes with solvent molecules (*e.g.*, complexes of 5-doxylosteoric acid with deuterated alcohols).⁵¹

10. ‘Saturation – recovery’ technique in time-resolved EPR

Time-resolved EPR⁵² is not a pulsed technique, because the EPR signal is detected using c.w. microwave field. Considering relaxation time measurements, the ‘saturation – recovery’ technique occupies an intermediate position between the pulsed and c.w. EPR, because it combines pulsed saturation of the EPR spectrum (usually, the saturation pulse is a few microseconds long) and continuous recording of the EPR signal. The method was employed to study acceleration of the spin label relaxation in biosystems induced by the fluctuating magnetic dipole – dipole interaction with the neighbouring metal ion. The results obtained were used for estimating the distance in a pair spin label – ion.^{53–55}

The ‘saturation – recovery’ technique is used for the determination of local concentrations of molecular oxygen (so-called oximetry) in biological objects.⁵⁶ It is based on acceleration of spin label relaxation by collisions with molecular oxygen.

EPR has an advantage over than the ESE spectroscopy-based techniques, when the ESE (or free induction) signal cannot be observed due to the problems related to the ‘dead’ time of the spectrometer and short relaxation times. However, the technique is not free from drawbacks including a lower temporal resolution, a complex and ambiguous theoretical description and lower functionality.

There are some interesting applications of time-resolved EPR spectroscopy for solving spin chemistry problems. An example is provided by spin polarisation transfer to the spin label in the molecule of a model hexapeptide from photo-excited chromophore located in the same molecule.⁵⁷ Yet another example is the effect of spin labels on the formation of spin polarisation in spin-correlated radical pairs generated upon photoexcitation of photosynthetic reaction centres in plants.⁵⁸ The results obtained may be useful in studies of electron transfer in these systems. Pulsed EPR spectroscopy also seems to be useful in this case.

IV. Structural studies of spin-labelled systems

1. Conformations of long-chain biradicals and doubly spin-labelled biomolecules

Different conformations of a molecule have different length. Therefore, the conformational structure of biradicals or doubly spin-labelled biomolecules can be determined by measuring the distances between two unpaired electrons in them. Details of relevant measuring techniques including PELDOR and some other methods have been reviewed (see, *e.g.*, Refs 8–10). Now we will discuss the state-of-the-art in the field and recent literature.

Long-chain biradicals can adopt a large number of possible conformations; therefore, one should consider a distance distribution function of paramagnetic fragments. If the distance distribution is expected to be rather narrow, its width can be directly estimated from the ESEEM decay. In particular, a magnetic field jump PELDOR study of two long-chain (~2 nm long) biradicals (a rigid-chain and a flexible one) was reported.²⁵ The distance distribution width estimated from the ESEEM decay for the flexible biradical was found to be about 0.3 nm.

Conformations of a biradical containing two nitroxide fragments separated by a chain comprising from 8 to 20 methylene groups ($n = 8, \dots, 20$) were studied by the PELDOR method.^{59,60} A large scatter of distances between the two radicals was expected. The data extracted from the frequency spectra were compared with the results of calculations of (i) fully stretched *trans*-conformation (limiting case) and (ii) conformational statistics at a specified temperature. The results of distance measurements and conformational statistics calculations coincided within the limits of experimental error. At $n = 10$ and $r = 2.1$ nm (average distance), the distribution function width at half-height was 0.5 nm.

The PELDOR technique permits measurements of spin – spin interactions not only in nitroxide biradicals, but also in biradicals containing a paramagnetic metal ion as the spin partner.⁶¹

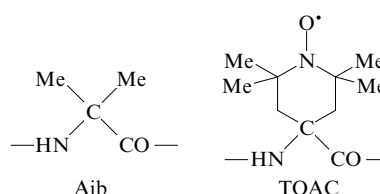
Doubly spin-labelled peptides can also be studied in a similar manner. If the spin labels are separated by a short distance (< 1.5 nm), c.w. EPR spectroscopy is employed.⁶² If the label – label distance exceeds 1.5 nm, pulsed EPR techniques should be used.

PELDOR studies of conformations of a doubly spin-labelled peptide Trichogin GA IV in organic glasses are available.^{63–65} This linear peptide isolated from the fungus *Trichoderma longibrachiatum* is a rich source of aminoisobutyric (Aib) acid



(n-Oct is n-octanoyl and Lol is leucinol). Trichogin GA IV possesses antibacterial and antifungal properties. Such peptides can create ionic channels in membranes, thus making them permeable, which may cause cell death. A distinctive feature of Trichogin GA IV is that its molecule is short. It comprises only 10 amino acids, which is much smaller than the membrane thickness; therefore, the mechanism of membrane permeability is unclear as yet.

The Aib residues are replaced by structurally similar nitroxide spin labels (TOAC) in the course of chemical synthesis.⁶⁶



For convenience, the peptide terminal groups could be replaced by other residues. This does not change the membrane-modifying properties of the peptides.⁶⁷ The peptides synthesised were doubly labelled at positions 1 and 4, 4 and 8 or 1 and 8. The first two types of biradicals can be studied by c.w. EPR spectroscopy, whereas the third type can only be studied by pulsed EPR methods due to long spin–spin separations.

Conformations of doubly spin-labelled peptide were studied at 77 K in different glass-forming solvents (methanol, ethanol, trifluoroethanol) and in chloroform–DMSO mixtures with different component ratios.^{63,64} PELDOR studies in all matrices revealed modulation effects at different oscillation frequencies. The distances between the spin labels in positions 1 and 8 vary from 1.53 (in trifluoroethanol) to 2.18 nm (in ethanol). It was concluded that the peptide adopts the 3_{10} -helical conformation in trifluoroethanol and the 2_7 -helical conformation in other matrices.

Conformation of spin-labelled Trichogin-1,8 in biological membranes was studied.^{68,69} The distance distribution function in egg L- α -phosphatidylcholine membranes exhibits two maxima at 1.3 and 1.8 nm.⁶⁸ The authors suggested that the peptide conformations represent combinations of the α -helical conformation, 3_{10} -helical conformation and more stretched conformations. Similar results were obtained for this peptide in model phospholipid membranes.⁶⁹

PELDOR studies of doubly-nitroxide-labelled RNA were reported.^{70–72} The label–label distances were found to lie between 2 and 5 nm. The results of measurements were in agreement with the results of molecular dynamics calculations. Based on the results obtained, the conformations of the biomolecules were determined.

Changes in the conformation of a protein (BtuB) upon binding to a substrate (TonB) in a membrane have been a subject of a joint SDSL–PELDOR study.⁷³ The protein binds and carries vitamin B₁₂ across the outer membrane of Gram-negative bacteria such as *Escherichia coli*. The protein was doubly spin labelled. In the absence of the substrate, the results of measurements showed a narrow interspin distance distribution for the number of pairs (number of pairs from r to $r + dr$). In the presence of the substrate, the distance distributions broadened. This indicates a substrate-induced transition of the protein from the ordered to disordered state.

Singly labelled Na⁺/H⁺ regulators, namely, NhaA from *Escherichia coli* were studied.⁷⁴ Residues situated in domains undergoing pH-dependent structural changes were chosen for site-directed spin labelling. PELDOR experiments revealed modulation of the echo signal, which showed that NhaA exists in the dimeric form. The modulation depth reversibly decreased with the decrease in the pH value, thus indicating an increase in the distance in the dimer. Relation between these results and the mechanism of NhaA activity was considered.

The structure of different-size [2]catenanes was studied by the PELDOR method.⁷⁵ Each of the two macrocycles was spin labelled. The molecular conformation distribution and size were evaluated by comparing the experimental data and theoretical estimates.

The arrangement of the b -subunits in the holo-enzyme F₀F₁-ATP synthase from *E. coli* was investigated by the SDSL and PELDOR methods.⁷⁶ Based on the interspin distances, parallel orientation of two helices and other structural features were revealed.

A double-quantum coherence study of model peptide helices was carried out.⁷⁷ The intramolecular distances were determined and the folding of the helices was studied.

The possibility of SDSL and PELDOR studies of the global structure of nucleic acids was considered.⁷⁸ Spin labelled duplexes of DNA dodecamers with known structure were used as model systems. The distances measured by PELDOR

(2 to 4 nm) were in agreement with those obtained from NMR data.

2. Peptide aggregation in molecular glasses and biomembranes

There are reasons to assume that peptide aggregation in biomembranes significantly affects their functional properties, e.g., formation of ionic channels. The sizes of peptide aggregates are on the nanometre scale, which points to the possibility of using the PELDOR method.

To clarify possible mechanisms of peptide aggregation in biomembranes, peptides in simpler model systems were studied. The results of the PELDOR studies of aggregation of spin-labelled peptide Trichogin GA IV in organic molecular glasses were considered in detail in reviews.^{8,10,14} No aggregation was observed in polar media, whereas in glasses of low polarity the number of molecules in aggregates (N) varied from 3.1 to 4.3 depending on the type of the system. For spin-labelled Trichogin dimers (two molecules covalently bound in 'head-to-tail' fashion) in a chloroform–toluene mixture, the number N varies from 2 to 3 and the interspin distance varies from 3.0 to 4.5 nm.⁷⁹ As the concentration increases, the formation of tetramers occurs.⁸⁰

A PELDOR study of aggregation of spin-labelled zervamycin IIA (fungal hexadecapeptide) in a glassy toluene–methanol mixture at 77 K revealed the presence of aggregates with antiparallel orientation of the peptide molecules.⁸¹

Aggregation of spin-labelled peptide alamethicin in polar and non-polar molecular glasses was studied.⁸² The peptide molecule contains 20 amino acid residues.

Act-Aib-Pro-Aib-Ala-Aib-Ala-Glu-Aib-Val-Aib-Gly-

-Leu-Aib-Pro-Val-Aib-Glu-Gln-Phol.

The compound possesses the properties of an antibiotic. Samples spin-labelled at position 16 by replacing the amino-isobutyric acid residue by the TOAC spin label were studied. No aggregation was observed in the polar glass, in contrast to the glass of low polarity (chloroform–toluene mixture). It was found that the number of molecules in the aggregate is rather large and varies from 6 to 8.

Aggregation of spin-labelled peptides Trichogin GA IV in biological membranes was studied.^{68,69} At a concentration of 2.2 mol.%, the peptide is uniformly distributed in egg L- α -phosphatidylcholine membrane.⁶⁸ The addition of cholesterol (up to 16.5 mol.%) led to an increase in the local peptide concentration. No peptide aggregation occurred at low peptide concentration in model phospholipid membranes (peptide:lipid ratio lower than 1:100).⁶⁹ An increase in the peptide concentration in the model phospholipid membranes to a peptide:lipid ratio of 1:20 caused the formation of dimeric aggregates with an average interspin distance of nearly 2.5 nm.

Peptide aggregation with an increase in the peptide concentration seems to be of fundamental importance for the appearance of membrane channels. A unique advantage of the PELDOR technique consists in the possibility of determining the number and characteristic size of molecules in aggregates.

3. Nanostructure of ionomers

Ionomers are polymers bearing ionic end groups.^{83,84} The ionomer structure comprises ionic clusters a few nanometres in size. The intercluster distance is of the same order of magnitude. These parameters of the nanostructure of ionomers based on a polyisoprene/polystyrene copolymer were estimated in a PELDOR study using ionic spin probes.^{85–87} The surface of ion clusters is accessible to such probes. The characteristic interparticle distance in the cluster was about

2 nm and the characteristic cluster – cluster distance was nearly 5 nm. The results obtained were considered in more detail in reviews.^{10, 13}

4. Detection of structural transformations in materials

The mechanism of formation of mesoporous materials (MCM-41 and SBA-15) from the starting micellar compounds in the presence of spin probes was studied by the method of ESEEM through electron – nuclear interactions.^{88–91} In different stages of the reaction the sample was cooled to 77 K and the ESEEM through the interaction of the spin-probe unpaired electron with deuterium present in the starting compounds was recorded. A number of stages of the formation of the materials were observed and interpreted.

5. Profile of water penetration into biomembranes

The depth of water penetration into a biomembrane is an important characteristic that governs transport of polar and charged particles across membranes and the energy characteristics of protein embedding in them.^{92–95} The content of water in the local environment of the spin label was measured using the ESEEM effect due to hyperfine interaction of the spin-label unpaired electron with deuterium nuclei in the molecules of heavy water used for hydration of membranes.^{96–99} The use of heavy water is due to the fact that, first, the amplitude of deuterium modulation much exceeds that of proton modulation. Second, this allows the contribution of the protons of biomolecules to the ESEEM effect to be separated. Using the SDSL technique, one can determine the local concentration of water in the nearest environment of the spin label by the ESEEM method. The estimated spatial resolution of the method was about 0.5 nm.

Studies were carried out using either lipids spin-labelled at different positions of the aliphatic chain in DL- α -dipalmitoyl phosphatidylcholine (DPPC) model phospholipid membranes^{96, 99} or spin probes based on *p*-doxylstearic acid ($n = 5, 7, 12, 16$) in multilayered egg phosphatidylcholine liposomes.^{97, 98} The experimental techniques employed were two-pulse echo^{96–98} and stimulated echo,⁹⁹ the latter being much more accurate.

The experimental temporal oscillations of stimulated ESEEM signals and the corresponding cosine-Fourier-transformed spectra are similar to those shown in Fig. 3. The

spectrum exhibits a narrow line and a broad background component (see Fig. 3 *b*). According to theoretical analysis,⁹⁹ the narrow line is due to the interaction with free water, whereas the broad component arises from the interaction with bound water that forms a complex with the nitroxide radical. For samples labelled at different positions of the lipid chain, the amplitudes (spectral density) of the deuterium line are appreciably different. In Fig. 5 this amplitude is plotted vs. label position (amplitudes of the narrow line and broad component appeared to be in proportion to each other). As the label ‘moves’ into membrane’s interior, the amplitude (and, hence, water concentration) decreases. In the presence of cholesterol, the concentration of water near the membrane surface is higher and decreases much more abruptly on ‘moving’ into the membrane interior. The drop occurs near the C(8) atom in the lipid chain. The smooth decrease in the absence of cholesterol can be explained by ‘entanglement’ of lipid chains (cholesterol favours ordering of lipid molecules).

The results mentioned above were also considered in a review.¹⁰⁰

6. Localisation of peptides and other biomolecules in membranes

A series of spin probes, namely, *p*-doxylstearic acid ($n = 5, 7, 10, 12, 16$) in DPPC and dihexadecyl prosthate (DHP) vesicles were studied by the ESEEM method.¹⁰¹ The ESEEM effect was induced by the interaction between the unpaired electron in the doxyl group and ³¹P nuclei of the polar heads of the lipid vesicles. Based on the results obtained, one can draw conclusions about localisation of the spin probe relative to the membrane surface. It was found that the spin probe penetrates about 0.5 nm into the DHP vesicles.

At present, considerable attention is given to studies of the supramolecular structure of membrane – peptide systems. A ‘classical’ object of such studies is peptide Trichogin GA IV. The peptide helix is 1.6 nm long, which is about half the membrane thickness. Most studies were carried out using fluorescent labels.^{102–104} However, this technique has a significant drawback, namely, the labels are too bulky and can be displaced towards the membrane surface along with the peptide.¹⁰³ Therefore, it is interesting to perform corresponding spin label studies because spin labels are much more compact.

The localisation and orientation of peptide Trichogin GA IV in a phospholipid membrane were studied⁶⁷ using the effect of polarity on the parameters of HFI in c.w. EPR spectra. However, molecular motions also contribute to these interactions, thus introducing errors in experimental data. The methods based on ESEEM are free from this drawback.

The ESEEM profile of water concentration in a model phospholipid membrane⁹⁹ was used for the determination of localisation of spin-labelled peptide Trichogin GA IV in this membrane.¹⁰⁵ Three peptide analogues spin-labelled at different positions (1, 4 and 8) were studied.

Fmoc-TOAC-Gly-Leu-Aib⁴-Gly-Gly-Leu-

-Aib⁸-Gly-Ile-Leu-OMe,

Fmoc-Aib¹-Gly-Leu-TOAC-Gly-Gly-Leu-

-Aib⁸-Gly-Ile-Leu-OMe,

Fmoc-Aib¹-Gly-Leu-Aib⁴-Gly-Gly-Leu-

-TOAC-Gly-Ile-Leu-OMe.

Figure 6 presents the ESEEM spectra of the three samples. The peak amplitudes obtained should be compared with the amplitudes obtained for the spin labels in lipids measured

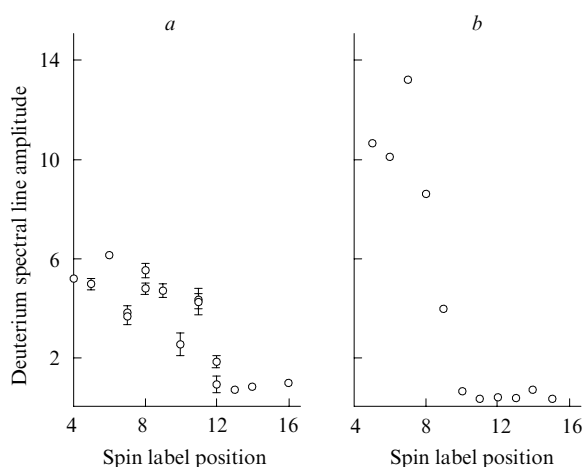


Figure 5. Spectral line amplitudes at 2.2 MHz (see Fig. 3) plotted vs. label position in the lipid chain in model phospholipid membranes hydrated with deuterium water. Cholesterol-free DPPC membrane (*a*) and cholesterol-containing DPPC membrane (*b*).

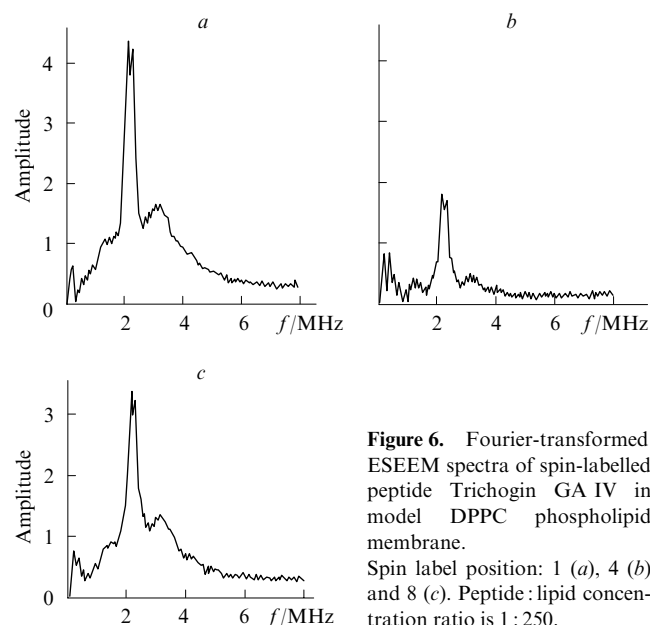


Figure 6. Fourier-transformed ESEEM spectra of spin-labelled peptide Trichogin GA IV in model DPPC phospholipid membrane. Spin label position: 1 (a), 4 (b) and 8 (c). Peptide:lipid concentration ratio is 1 : 250.

under identical conditions (see Fig. 5, data in the absence of cholesterol). A comparison shows that the amplitudes for positions 1 and 8 (4.2 and 3.3 arbitrary units, see Fig. 6) are similar to those for the spin label positions in the lipids that are closer to the membrane surface than position 10 with respect to the polar head, *i.e.*, positions 1 and 8 of the spin labels in the peptide molecule are closer to the membrane surface than the spin label in position 10 in the lipid. At the same time, a comparison of the two types of data showed that position 4 in the peptide molecule is similar to position 10 in the lipid molecule. This suggests that the peptide molecule is oriented parallel to the membrane surface.

This situation is observed at small peptide:lipid concentration ratios (lower than 1 : 100). As this ratio increases to 1 : 20, the saturation changes significantly (Fig. 7), namely, the peak amplitude for the spin-labelled position 1 appreciably decreases. Thus, as the peptide concentration increases, the peptide *N*-terminus moves deeper into the membrane interior and now the orientation of the whole molecule is similar to transmembrane one. As mentioned above, this is accompanied

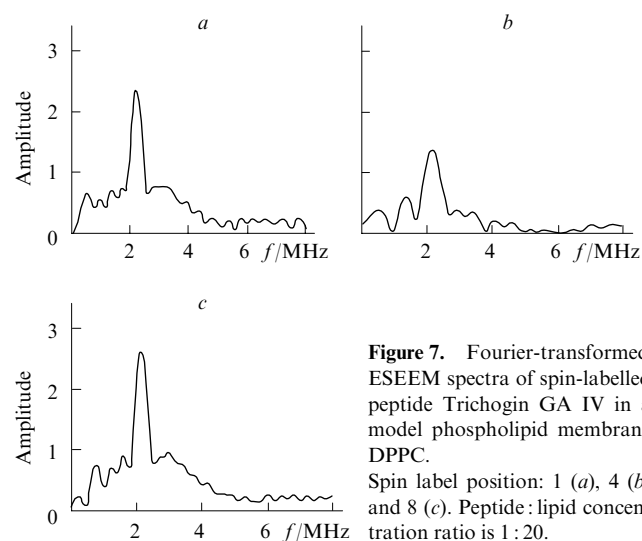


Figure 7. Fourier-transformed ESEEM spectra of spin-labelled peptide Trichogin GA IV in a model phospholipid membrane DPPC. Spin label position: 1 (a), 4 (b) and 8 (c). Peptide:lipid concentration ratio is 1 : 20.

by peptide aggregation into dimers with a broad interspin distance distribution.

Probably, it is these changes in the supramolecular structure of a membrane with embedded peptides that are responsible for the membrane permeability. Probably, the formation of the transmembrane dimer can lead to formation of a channel in the membrane.

A similar approach was employed in a study¹⁰⁶ of localisation of two peptides antibiotics, a natural peptide melittin (26-mer) and a synthetic peptide (15-mer) using model membranes. The spin label was attached to the *N*-termini of the peptides (here, peptides were labelled only in one position¹⁰⁵). Either D₂O-hydrated membranes or H₂O-hydrated membranes containing deuterium-substituted lipids were used. A comparison of the deuterium ESEEM peaks with the peaks of the lipids spin-labelled at different positions showed that the peptide *N*-terminus is on the membrane surface. An increase in the concentration of non-labelled peptides caused a noticeable water penetration into the membrane, which was detected from the increase in the deuterium peaks for the labelled lipids. This suggests that membrane permeability is governed by the peptide concentration.

7. Structural studies of spin-labelled photosynthetic reaction centres

The SDSL and pulsed EPR studies of the supramolecular structure of photosynthetic reaction centres of plants and bacteria began quite recently. In a PELDOR study,¹⁰⁷ the MTSL spin label was attached to a cysteine residue at position 156 of protein *H* in the reaction centre of the bacteria *Rhodobacter sphaeroides* R26. The distance between the spin label and the primary quinone electron acceptor Q_A was found to be 3.05 ± 0.05 nm. The results of measurements were compared with the results of molecular dynamics calculations. It was concluded that the accuracy of measurements is sufficient for detection of structural changes that can be expected upon transfer of an electron.

V. Studies of the dynamics of spin-labelled systems

1. Rotation of methyl groups in nitroxide radicals

The paramagnetic fragment NO in the nitroxide radicals is most often shielded by four methyl groups. Generally, rotation of methyl groups has little effect on the EPR spectral shape; however, in some cases this influence can be significant. Therefore, proper use of EPR spectroscopy in the method of spin labels and probes requires information on the parameters of this motion. Studies of nitroxide radicals aimed at determining the rotational correlation times and the amplitudes of accompanying HFC fluctuations in a wide temperature range have been reported only very recently. They were carried out by the ESEEM method (see above); here the ESEEM effect is due to spontaneous changes in the magnetic parameters of radicals induced by the three-pulse stimulated ESE sequence.^{42–44}

The Fourier transformed stimulated ESE spectra of some nitroxide radicals in glassy toluene, ethanol and water–glycerol (1 : 1) mixture at 77 and 90 K revealed⁴² the appearance of intense peaks in a broad frequency range from 0 to 15 MHz. The peak at 15 MHz, which is due to the interaction with the matrix protons, showed no temperature dependence, whereas the peaks at lower frequencies became much more intense with an increase in *T*. The effect was attributed to rotation of methyl groups. The Fremy salt nitroxide radical contains no methyl groups; a reference experiment with this compound showed no effect.

A study⁴³ of nitroxide radicals in *o*-terphenyl and glycerol in the temperature range 120–260 K also revealed intense peaks that became more intense with increasing *T*. This effect was attributed to relaxation of methyl protons. The nuclear

relaxation rate was determined from the kinetics of peak growth. The rotational correlation time of methyl groups was determined from the relaxation rate using the Redfield theory.²⁰ The Arrhenius parameters of this rotation are as follows: the energy barrier lies in the range 1300–1500 K and the pre-exponent is about 10^{12} s^{-1} .

2. Fast small-amplitude orientation mobility of spin probes in molecular glasses

Spectral transformations with an increase in τ (see Fig. 4) correspond to the model of small-amplitude stochastic librations. In this case, the relaxation anisotropy is determined using expression (4). The results of these calculations and the experimental data are in excellent agreement.²² The whole set of the spectra recorded at different τ was calculated using only one fitting parameter, namely, the product $\langle \alpha^2 \rangle \tau_c$, which is proportional to the relaxation rate $\langle \Delta \omega^2 \rangle \tau_c$.

The c.w. EPR spectra are also consistent with the model of fast small-amplitude motions.¹⁰⁸ Note that c.w. EPR experiments with glassy liquids and other disordered systems are often treated in terms of such motion models as continuous Brownian diffusion in the angular space or discrete rotation by an arbitrary or fixed angle (accounting or ignoring the motion anisotropy).¹⁰⁹ These models assume an infinite molecular motion in the angular space. However, there are data that contradict the infinite character of motion. For instance, if polarised light ‘burns out’ a particular orientation of photosensitive molecules, one can monitor how the spectral ‘hole’ broadens with time.¹¹⁰ These experiments permit immediate measurements of the rate of the infinite angular motion. It was found that the rate determined is many orders of magnitude lower than the rate determined by analysing the EPR spectra of spin probes of similar size. Therefore, the models of infinite motions are inappropriate for the description of the motion in highly viscous media and molecular glasses, often despite good agreement between theory and experiment.¹⁰⁹

The behaviour of the echo-detected EPR spectra with an increase in τ (see Fig. 4) is typical of spin labels and spin probes in disordered media including biosystems. Moreover, it is also characteristic of other types of paramagnetic species that exhibit anisotropic EPR spectra, namely, metal complexes,¹¹¹ semiquinone radicals in high-field EPR¹¹² and molecules in triplet excited states.¹¹³ Thus, it becomes clear that here we deal with some universal basic regularities of the molecular dynamics in such systems. Unusual character of the molecular dynamics in disordered media has long been reported in studies carried out by various physical methods, namely, light scattering,¹¹⁴ single-molecule spectroscopy,¹¹⁵ dielectric relaxation,¹¹⁶ neutron scattering,¹¹⁷ Mössbauer absorption,¹¹⁸ etc. Despite numerous experimental data, the nature of the phenomena is still to be clarified.

Interesting information on the properties of this motion can be obtained using echo-detected EPR spectroscopy. Observation of anisotropic relaxation in echo-detected EPR spectroscopy indicates that orientational motion of the whole molecule occurs in the system. A study of the dynamics of spin probes of different structure and in different glassy solvents¹¹⁹ allowed one to establish with certainty that the motion depends on the nature of the solvent rather than the type of the spin probe. Probes used in these studies were 0.3 to 5 nm in size; therefore, it is clear that it is co-operative molecular dynamics, *i.e.*, the motion occurs by collective rearrangements in the molecular structure, being supramolecular in character. The size of the molecular cluster is a few nanometres. In the case of simple low-molecular-mass glasses the motion is also supramolecular in character.

The principal value of the HFC tensor $\langle A_{ZZ} \rangle$ averaged by fast motions can be determined with ease from c.w. EPR spectra (see Fig. 1). Typical results obtained for molecular

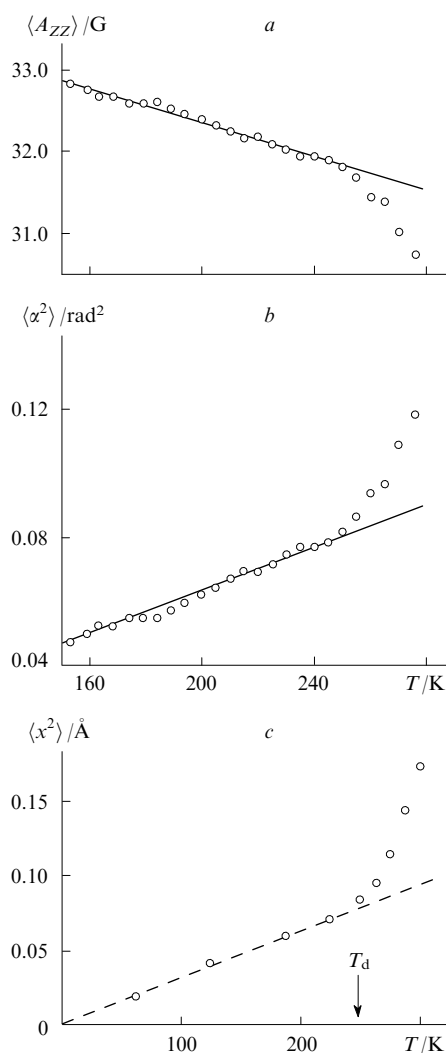


Figure 8. Typical temperature dependences of the spectral splitting $\langle A_{ZZ} \rangle$ (see Fig. 1) obtained for nitroxide spin probes in *o*-terphenyl (a), root-mean-square angles of deviation from equilibrium position obtained from relationship (5) (b) and root-mean-square fluctuations of atomic positions relative to the equilibrium position $\langle x^2 \rangle$ obtained from neutron scattering studies (c). T_d is dynamic transition temperature.

glasses are shown in Fig. 8a. The temperature dependence of $\langle A_{ZZ} \rangle$ is linear at low temperatures and becomes much steeper above a certain temperature. Using these data and relation (5), it is possible to obtain the temperature dependence of $\langle \alpha^2 \rangle$ (Fig. 8b).

3. Dynamic low-temperature transition in disordered media

Neutron scattering^{117, 120} and Mössbauer absorption¹¹⁸ studies of atomic vibrations in molecular disordered (including biological) media (in the latter case the substance under study contains ^{57}Fe ions) revealed a clearly defined transition from harmonic to anharmonic motion on raising the temperature. The effect manifests itself as transition from the linear temperature dependence of the root-mean-square atomic displacement $\langle x^2 \rangle$ (this is characteristic of harmonic motion) to a steeper dependence with an increase in temperature. The transition is only characteristic of the disordered media. A feature of the crystalline state is a linear temperature dependence in the whole temperature range. This transition is

called the dynamic transition; the transition temperature is denoted by T_d (Fig. 8c).

Biosystems have the T_d temperatures lying in the range 200–230 K.¹²⁰ The physiological activity of biosystems manifests itself only above T_d . At present, the nature of this transition and its importance for biosystems have been subjects of intensive studies. Interestingly, these T_d values are similar to the minimum air temperatures on the Earth.

Valuable information on the molecular dynamics can be obtained by echo-detected EPR spectroscopy of spin labels and spin probes. Noteworthy is an analogy between the EPR data and the neutron scattering data shown in Figs 8b and 8c, respectively. Neutron scattering is sensitive to motions at frequencies higher than 10^9 s^{-1} (Mössbauer absorption is sensitive to motions at frequencies higher than 10^7 s^{-1}). These frequencies are of the same order of magnitude as that required for librational narrowing of EPR spectra (10^8 s^{-1}). The characteristic motion amplitudes $\langle x^2 \rangle$ (see Refs 117, 118 and 120) are also similar in magnitude to the $\langle \alpha^2 \rangle$ values shown in Fig. 8b (numerical values of $\langle \alpha^2 \rangle$ expressed in squared radians and of $\langle x^2 \rangle$ expressed in squared Ångströms can be compared with allowance for the fact that the characteristic size of the molecule is $\sim 1 \text{ Å}$). These quantitative relations suggest that different methods deal with the same type of motion.

The applicability of c.w. EPR for measuring $\langle \alpha^2 \rangle$ is limited to non-polar media. In polar media, the measured A_{ZZ} value is additionally affected by the change in the matrix polarity, which may introduce rather large errors. In the case of echo-detected EPR, information on the motion is extracted from the rate of anisotropic relaxation, which is not affected by the polarity of the matrix.

A typical temperature dependence of the characteristic changes in the echo-detected EPR spectra in molecular glasses is shown in Fig. 9. These changes can be characterised by the relative intensity at the centre of the high-field component. At low temperatures, no changes occur, but raising the temperature causes a marked decrease in the intensity, which may be assigned to the dynamic transition.

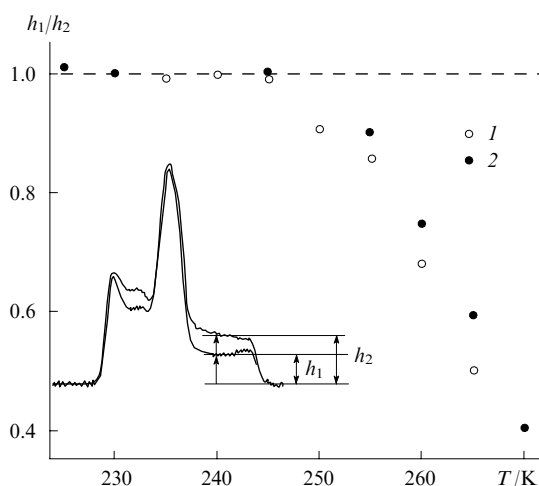


Figure 9. Typical temperature dependences of characteristic changes in echo-detected EPR spectrum induced by unfreezing of stochastic librations (nitroxide spin probe in *o*-terphenyl); h_1/h_2 is the height ratio of the EPR spectra recorded at different temperatures and normalised to maximum amplitudes; h_2 corresponds to a temperature of 230 K (no spectral changes occur at lower temperatures). The open (1) and solid (2) circles denote data obtained for different nitroxide radicals.

The T_d values determined for molecular glasses (glycerol and *o*-terphenyl) are 195 and 245 K, respectively.^{121, 122} It was found that these temperatures coincide with the T_d values determined for these glasses from neutron scattering data.^{117, 123}

Thus, echo-detected EPR is a sensitive tool for determination of the temperature of the dynamic transition from harmonic to anharmonic (or stochastic) motion. Other important advantages of this technique are the relative, compared to neutron scattering and Mössbauer absorption, accessibility of measurements and the possibility of SDSL studies of different fragments in complex supramolecular systems.

A rather steep decrease in the temperature dependence shown in Fig. 9 prompts that the potential of this motion seems to be temperature dependent and changes its shape above a certain temperature. Different versions are possible, namely, the potential can be essentially anharmonic or it may become a stochastic function of time.

Since the potential is determined by the structure of matter, we can say that the so-called mean order in this structure (correlations in the arrangement of atoms and molecules on the nanometre scale) changes above T_d .

4. Dynamic low-temperature transition in spin-labelled model biomembranes

Echo-detected EPR spectroscopy studies of the dynamics of DPPC lipids spin-labelled at different positions of the lipid chain in model phospholipid membranes with high content of cholesterol (50 mol.%) revealed¹²⁴ a dynamic transition, common to all positions, with T_d lying in the range 200–230 K. This is in agreement with the results obtained in a neutron scattering study.⁹³ A new phenomenon was disclosed in comparing the data for different positions in the spin label, namely, in the membrane interior the dynamic transition spans a wide temperature range and begins at 100–120 K.

A dynamics study of cholestane spin probe (this compound is structurally similar to cholesterol, an important membrane component)¹²⁵ also showed low-temperature motions in the membrane interior.

Different-type dynamics at different distances from the membrane surface and low-temperature motions may appear to be important for understanding the mechanisms of membrane functioning. These data may also be of interest for the development of fundamental concepts of possible mechanisms of biological tissue cryoconservation.

5. Dynamic low-temperature transition in spin-labelled complex biosystems and its interrelation with functional activity

Seed and pollen cells are interesting subjects for studies using the method of spin labels and probes. They show a remarkable ability to be stored for years without loss of vital activity. A possible explanation for this ability involves intracellular glass formation. An echo-detected EPR study of spin probes introduced into the seed and pollen cells revealed a marked anisotropic relaxation at $T > 200 \text{ K}$, which itself indicates glass formation.¹²⁶ These effects depend strongly on the water content in the samples. These studies are important for understanding the processes that govern the storage period of seeds and other biological objects.

Echo-detected EPR was also used to study SDSL reaction centres isolated from the photosynthetic centre of purple bacteria.¹²⁷ These objects are often used in studies of fundamental processes in photosynthesis. Cysteine residues in these centres were labelled with the MTSL spin label. A clearly defined dynamic transition was detected near 200 K. At this temperature, transfer of a photo-induced electron along the electron acceptor chain is blocked,^{128–130} namely, electron back transfer occurs followed by recombination with the

'hole' (radical cation of bacteriochlorophyll dimer) instead of direct electron transfer from the primary quinone acceptor to the secondary one. The nature of the reversal of electron transfer direction is still to be clarified. Moreover, no correlations between this effect and the properties of complex supramolecular structure of the reaction centre were reported so far. The results of echo-detected EPR studies indicate the correlation of this effect with the dynamic transition near 200 K in the system.

6. Dynamic structure of vesicular membranes

The motion of cholestane spin probes in multilayered phospholipid vesicles in the presence of cholesterol was studied by the 2D PELDOR method.⁴⁹ At present, it is accepted that a liquid ordered phase appears in cholesterol-containing membranes in addition to conventional liquid-crystalline phase (which also exists in the absence of cholesterol). The ordered domains are called rafts. The two phases are in equilibrium; their investigations are of considerable interest from the standpoint of research on the membrane operation mechanisms. Visual studies of 2D spectra did allow one to distinguish two phases differing in the rotational diffusion rate and degree of molecular ordering (these parameters were higher in the ordered domains).

VI. Conclusion

The use of pulsed EPR in the method of spin labels and probes have been started quite recently. Spectroscopic methods appeared to be useful in conformational and aggregation studies of large biomolecules, nanostructure of matter, supramolecular structure of multicomponent systems and co-operative orientational dynamics of molecules. In some cases they show a record resolution compared to other physicochemical methods of investigation. For instance, the PELDOR technique is highly sensitive to distance measurements in the nanometre range and provides a 0.1-nm accuracy of measurements at distances of about 3 nm. Echo-detected EPR spectroscopy is a sensitive tool of investigation of small-amplitude stochastic orientational motions (down to amplitudes of 0.1–1°). Using this method, the temperature of dynamic transition from harmonic to anharmonic (or stochastic) motion in disordered molecular media and biosystems can be determined with ease. More and more data reported in the literature indicate that this transition is a crucially important characteristic of living systems.

Pulsed EPR techniques are continuously developed and improved. It is of great importance that the vast majority of the results discussed above were (or could be) obtained using commercially available spectrometers.

The review has been written with the financial support from the Russian Foundation for Basic Research and NWO (Joint Project No. 06-03-89 400-HBO_a), the U.S. Civilian Research and Development Foundation (Grant RUC1-2635-NO-05) and the Siberian Branch of the Russian Academy of Sciences (Integration Project No. 51).

References

1. *Spin Labeling. Theory and Application* (Ed. L J Berliner) (New York: Academic Press, 1976)
2. *Spin Labeling. Theory and Applications, Biological Magnetic Resonance* Vol. 8 (Ed. L J Berliner) (New York: Plenum, 1989)
3. *Spin Labeling. The Next Millennium, Biological Magnetic Resonance* Vol. 14 (Ed. L J Berliner) (New York: Plenum, 1998)
4. A L Buchachenko, A M Vasserman *Stabil'nye Radikaly* (Stable Radicals) (Moscow: Khimiya, 1973)
5. L B Volodarskii, I A Grigor'ev, S A Dikanov *Imidazolinovye Nitroksil'nye Radikaly* (Imidazoline Nitroxide Radicals) (Novosibirsk: Nauka, 1988)
6. K M Salikhov, A G Semenov, Yu D Tsvetkov *Elektronnoe Spinovoe Ekho i Ego Primenenie* (Electron Spin Echo and Its Applications) (Novosibirsk: Nauka, 1976)
7. A Schweiger, G Jeschke *Principles of Pulsed Electron Paramagnetic Resonance* (Oxford: Oxford University Press, 2001)
8. A D Milov, A G Maryasov, Yu D Tsvetkov *Appl. Magn. Reson.* **15** 107 (1998)
9. *Distance Measurements in Biological Systems by EPR Biological Magnetic Resonance* Vol. 19 (Eds G R Eaton, S S Eaton, L J Berliner) (New York: Kluwer Academic, Plenum, 2000)
10. S A Dzuba *Usp. Khim.* **74** 686 (2005) [*Russ. Chem. Rev.* **74** 619 (2005)]
11. T Prisner, M Rohrer, F MacMillan *Annu. Rev. Phys. Chem.* **52** 279 (2001)
12. J H Freed *Annu. Rev. Phys. Chem.* **51** 655 (2000)
13. G Jeschke *ChemPhysChem* **3** 927 (2002)
14. Yu D Tsvetkov *EPR Instrumental Methods, Biological Magnetic Resonance* Vol. 21 (Eds C L Bender, L J Berliner) (New York: Kluwer Academic, Plenum, 2004) p. 385
15. H J Steinhoff *Biol. Chem.* **385** 913 (2004)
16. C Altenbach, T Marti, H Khorana, W L Hubbell *Science* **248** 1088 (1990)
17. W L Hubbell, A Cross, R Langen, M A Lietzov *Curr. Opin. Struct. Biol.* **8** 649 (1998)
18. G E Fanucci, D S Cafiso *Curr. Opin. Struct. Biol.* **16** 644 (2006)
19. L J Libertini, O H Griffith *J. Chem. Phys.* **53** 1359 (1970)
20. C P Slichter *Principles of Magnetic Resonance* (Berlin: Springer, 1996)
21. S A Dzuba, Yu D Tsvetkov, A G Maryasov *Chem. Phys. Lett.* **188** 217 (1992)
22. E P Kirilina, S A Dzuba, A G Maryasov, Yu D Tsvetkov *Appl. Magn. Reson.* **21** 203 (2001)
23. A D Milov, K M Salikhov, M D Shchirov *Fiz. Tv. Tela* **23** 975 (1981)^a
24. A D Milov, A B Ponomarev, Yu D Tsvetkov *Chem. Phys. Lett.* **110** 67 (1984)
25. L V Kulik, Yu A Grishin, S A Dzuba, I A Grigoryev, S V Klyatskaya, S F Vasilevsky, Yu D Tsvetkov *J. Magn. Reson.* **157** 61 (2002)
26. A A Dubinskii, Yu A Grishin, A N Savitsky, K Mobius *Appl. Magn. Reson.* **22** 369 (2002)
27. K Sale, L K Song, Y S Liu, E Perozo, P Fajer *J. Am. Chem. Soc.* **127** 9334 (2005)
28. M K Bowman, A G Maryasov, N Kim, V J DeRose *Appl. Magn. Reson.* **26** 23 (2004)
29. G Jeschke, G Panek, A Godt, A Bender, H Paulsen *Appl. Magn. Reson.* **26** 223 (2004)
30. G Jeschke, A Bender, H Paulsen, H Zimmermann, A Godt *J. Magn. Reson.* **169** 1 (2004)
31. A Weber, O Schiemann, B Bode, T Prisner *J. Magn. Reson.* **157** 277 (2002)
32. G Jeschke, H Zimmermann, A Godt *J. Magn. Reson.* **180** 137 (2006)
33. Ye Polyhach, A Godt, C Bauer, G Jeschke *J. Magn. Reson.* **185** 118 (2007)
34. V V Kurshev, A M Raitsimring, Yu D Tsvetkov *J. Magn. Reson.* **81** 441 (1989)
35. S Saxena, J H Freed *Chem. Phys. Lett.* **251** 102 (1996)
36. H Hara, T Tenno, M Shirakawa *J. Magn. Reson.* **184** 78 (2007)
37. Y W Chiang, P P Borbat, J H Freed *J. Magn. Reson.* **172** 279 (2005)
38. M Bonora, J Becker, S Saxena *J. Magn. Reson.* **170** 278 (2004)
39. G Jeschke, M Pannier, A Godt, H W Spiess *Chem. Phys. Lett.* **331** 243 (2000)
40. L V Kulik, S A Dzuba, I A Grigoryev, Yu D Tsvetkov *Chem. Phys. Lett.* **343** 315 (2001)
41. L V Kulik, S V Paschenko, S A Dzuba *J. Magn. Reson.* **159** 237 (2002)
42. L V Kulik, I A Grigor'ev, E S Salnikov, S A Dzuba, Yu D Tsvetkov *J. Phys. Chem. A* **107** 3692 (2003)

43. L V Kulik, E S Salnikov, S A Dzuba *Appl. Magn. Reson.* **28** 1 (2005)
44. L V Kulik, S A Dzuba *Zh. Strukt. Khim.* **45** 313 (2004)^b
45. M M Hertel, V P Denysenkov, V Bennati, T F Prisner *Magn. Reson. Chem.* **43** 248 (2005)
46. E P Kirilina, T F Prisner, M Bennati, B Endeward, S A Dzuba, M R Fuchs, K Möbius, A Schnegg *Magn. Reson. Chem.* **43** S119 (2005)
47. S A Dzuba, E P Kirilina, E S Salnikov, L V Kulik *J. Chem. Phys.* **122** 094702 (2005)
48. P P Borbat, A J Costa-Filho, K A Earle, J Moscicki, J H Freed *Science* **291** 266 (2001)
49. A J Costa-Filho, Y Shimoyama, J H Freed *Biophys. J.* **84** 2619 (2003)
50. P P Zanker, G Jeschke, D Goldfarb *J. Chem. Phys.* **122** 024515 (2005)
51. T I Smirnova, A I Smirnov, S V Paschenko, O G Poluektov *J. Am. Chem. Soc.* **129** 3476 (2007)
52. R W Quine, S S Eaton, G R Eaton *Rev. Sci. Instrum.* **63** 4252 (1992)
53. M Huber, M Lindgren, P Hammarstrom, L G Martensson, U Carlsson, G R Eaton, S S Eaton *Biophys. Chem.* **94** 245 (2001)
54. C S Klug, S S Eaton, G R Eaton, J B Feix *Biochemistry* **37** 9016 (1998)
55. J S Hyde, J J Yin, W K Subczynski, T G Camenisch, J J Ratke, W Froncisz *J. Phys. Chem. B* **108** 9524 (2004)
56. W K Subczynski, A Wisniewska, J S Hyde, A Kusumi *Biophys. J.* **92** 1573 (2007)
57. F Formaggio, E Sartori, A Toffoletti, C Corvaja, L Moroder, C Toniolo *Adv. Exp. Med. Biol.* **527** 731 (2003)
58. K M Salikhov, S G Zech, D Stehlik *Mol. Phys.* **100** 1311 (2002)
59. G Jeschke, A Koch, U Jonas, A Godt *J. Magn. Reson.* **155** 72 (2002)
60. V Pfannebecker, H Klos, M Hubrich, T Volmer, A Heuer, U Wiesner, H W Spiess *J. Phys. Chem.* **100** 13428 (1996)
61. E Narr, A Godt, G Jeschke *Angew. Chem., Int. Ed.* **41** 3907 (2002)
62. J C McNulty, G L Millhauser *Distance Measurements in Biological Systems by EPR Biological Magnetic Resonance* Vol. 19 (Eds G R Eaton, S S Eaton, L J Berliner) (New York: Kluwer Academic, Plenum, 2000) p. 277
63. A D Milov, A G Maryasov, Yu D Tsvetkov, J Raap *Chem. Phys. Lett.* **303** 135 (1999)
64. A D Milov, A G Maryasov, R I Samoilova, Yu D Tsvetkov, J Raap, V Monaco, F Formaggio, M Crisma, C Toniolo *Dokl. Akad. Nauk* **370** 265 (2000)^c
65. A D Milov, Yu D Tsvetkov, F Formaggio, M Crisma, C Toniolo, J Raap *J. Am. Chem. Soc.* **123** 3784 (2001)
66. M Crisma, V Monaco, F Formaggio, C Toniolo, C George, J-L Flippen-Anderson *Lett. Pept. Sci.* **4** 213 (1997)
67. V Monaco, F Formaggio, M Crisma, C Toniolo, P Hanson, G L Millhauser *Biopolymers* **50** 239 (1999)
68. A D Milov, R I Samoilova, Yu D Tsvetkov, F Formaggio, C Toniolo, J Raap *Appl. Magn. Reson.* **29** 703 (2005)
69. A D Milov, D A Erilov, E S Salnikov, Yu D Tsvetkov, F Formaggio, C Toniolo, J Raap *Phys. Chem. Chem. Phys.* **7** 1794 (2005)
70. O Schiemann, A Weber, T E Edwards, T Prisner, S T Sigurdsson *J. Am. Chem. Soc.* **125** 3434 (2003)
71. N Piton, O Schiemann, Y G Mu, G Stock, T Prisner, J W Engels *Nucleosides, Nucleotides and Nucleic Acids* **24** 771 (2005)
72. O Schiemann, N Piton, Y G Mu, G Stock, J W Engels, T F Prisner *J. Am. Chem. Soc.* **126** 5722 (2004)
73. Q Xu, J F Ellena, M Kim, D S Cafiso *Biochemistry* **45** 10847 (2006)
74. D Hilger, H Jung, E Padan, C Wegener, K P Vogel, H J Steinhoff, G Jeschke *Biophys. J.* **89** 1328 (2005)
75. G Jeschke, A Godt *ChemPhysChem* **4** 1328 (2003)
76. S Steigmiller, M Borsch, P Graber, M Huber *Biochim. Biophys. Acta, Bioenergetics* **1708** 143 (2005)
77. A T Fafarman, P P Borbat, J H Freed, R Kirshenbaum *Chem. Commun.* 377 (2007)
78. Q Cai, A K Kuznetsov, W L Hubbell, I S Haworth, G P C Gacho, N Van Eps, K Hideg, E J Chambers, P Z Qin *Nucleic Acids Res.* **34** 4722 (2006)
79. A D Milov, Yu D Tsvetkov, F Formaggio, S Oancea, C Toniolo, J Raap *J. Phys. Chem. B* **107** 13719 (2003)
80. A D Milov, Yu D Tsvetkov, F Formaggio, M Crisma, C Toniolo, J Raap *J. Pept. Sci.* **9** 690 (2003)
81. A D Milov, Yu D Tsvetkov, E Yu Gorbunova, L G Mustaeva, T V Ovchinnikova, J Raap *Biopolymers* **64** 326 (2002)
82. A D Milov, R I Samoilova, Yu D Tsvetkov, C Peggion, F Formaggio, C T Toniolo, J Raap *Dokl. Akad. Nauk* **406** 341 (2006)^c
83. S Schlick *Ionomers: Characterization Theory and Applications* (Boca Raton, FL: CRC Press, 1996)
84. A Eisenberg, J-S Kim *Introduction to Ionomers* (New York: Wiley-Interscience, 1998)
85. M Pannier, V Schadler, M Schops, U Wiesner, G Jeschke, H W Spiess *Macromolecules* **33** 7812 (2000)
86. M Pannier, M Schops, V Schadler, U Wiesner, G Jeschke, H W Spiess *Macromolecules* **34** 5555 (2001)
87. G Jeschke *Macromol. Rapid Commun.* **23** 227 (2002)
88. D Baute, V Frydman, H Zimmermann, S Kababya, D Goldfarb *J. Phys. Chem. B* **109** 7807 (2005)
89. S Ruthstein, V Frydman, D Goldfarb *J. Phys. Chem. B* **108** 9016 (2004)
90. S Ruthstein, V Frydman, S Kababya, M Landau, D Goldfarb *J. Phys. Chem. B* **107** 1739 (2003)
91. J Y Zhang, P J Carl, H Zimmermann, D Goldfarb *J. Phys. Chem. B* **106** 5382 (2002)
92. K Aman, E Lindahl, O Edholm, P Hakansson, P-O Westlund *Biophys. J.* **84** 102 (2003)
93. J Fitter, R E Lechner, N A Dencher *J. Phys. Chem. B* **103** 8036 (1999)
94. J Milhaud *Biochim. Biophys. Acta, Biomembranes* **1663** 19 (2004)
95. S Y Bhidé, M L Berkowitz *J. Chem. Phys.* **123** 224702 (2005)
96. R Bartucci, R Guzzi, D Marsh, L Sportelli *Biophys. J.* **84** 1025 (2003)
97. V Noethig-Laslo, P Cevc, D Arcon, M Sentjerc *Origins Life Evol. Biosphere* **34** 237 (2004)
98. V Noethig-Laslo, P Cevc, D Arcon, M Sentjerc *Appl. Magn. Reson.* **27** 303 (2004)
99. D A Erilov, R Bartucci, R Guzzi, A A Shubin, A G Maryasov, D Marsh, S A Dzuba, L Sportelli *J. Phys. Chem. B* **109** 12003 (2005)
100. R Bartucci, D A Erilov, R Guzzi, L Sportelli, S A Dzuba, D Marsh *Chem. Phys. Lipids* **141** 142 (2006)
101. V V Kurshev, L Kevan *J. Phys. Chem.* **99** 10616 (1995)
102. R F Epand, R M Epand, V Monaco, S Stolia, F Formaggio, M Crisma, C Toniolo *Eur. J. Biochem.* **266** 1021 (1999)
103. R D Kaiser, E London *Biochim. Biophys. Acta* **1375** 13 (1998)
104. C Mazzuca, L Stella, M Venanzi, F Formaggio, C Toniolo, B Pispisa *Biophys. J.* **88** 3411 (2005)
105. E S Salnikov, D A Erilov, A D Milov, Yu D Tsvetkov, C Peggion, F Formaggio, C Toniolo, J Raap, S A Dzuba *Biophys. J.* **91** 1532 (2006)
106. R Carmieli, N Papo, H Zimmermann, A Potapov, Y Shai, D Goldfarb *Biophys. J.* **90** 492 (2006)
107. I V Borovykh, S Ceola, P Gajula, P Gast, H J Steinhoff, M Huber *J. Magn. Reson.* **180** 178 (2006)
108. S V Paschenko, Yu V Toropov, S A Dzuba, Yu D Tsvetkov, A Kh Vorobiev *J. Chem. Phys.* **110** 8150 (1999)
109. J S Hwang, R P Mason, L-P Hwang, J H Freed *J. Phys. Chem.* **79** 489 (1975)
110. A K Vorobiev, V S Gurman, T A Klimenko *Phys. Chem. Chem. Phys.* **2** 379 (2000)
111. R Husted, J L Du, S S Eaton, G R Eaton *Magn. Reson. Chem.* **33** S66 (1995)
112. A Schnegg, M Fuhs, M Rohrer, W Lubitz, T F Prisner, K Möbius *J. Phys. Chem. B* **106** 9454 (2002)
113. A Barbon, M Bortolus, M Brustolon, A Comotti, A L Maniero, U Segre, P Sozzani *J. Phys. Chem. B* **107** 3325 (2003)

114. N V Surovtsev, J A H Wiedersich, V N Novikov, E Rössler
Phys. Rev. B **58** 14888 (1998)
115. E Barkai, A V Naumov, Yu G Vainer, M Bauer, L Kador
Phys. Rev. Lett. **91** 075502 (2003)
116. J P Johari *Ann. N.Y. Acad. Sci.* **279** 117 (1976)
117. A Tölle, H Zimmermann, F Fujara, W Petry, W Schmidt,
W Schober, J Wuttke *Eur. Phys. J., B* **16** 73 (2000)
118. F G Parak *Curr. Opin. Struct. Biol.* **13** 552 (2003)
119. E P Kirilina, I A Grigoriev, S A Dzuba *J. Chem. Phys.* **121**
12465 (2004)
120. G Galiskan, R M Briber, D Thirumalai, V Garein-Sakai,
S A Woodson, A P Sokolov *J. Am. Chem. Soc.* **128** 32 (2006)
121. S A Dzuba, E P Kirilina, E S Salnikov *J. Chem. Phys.* **125**
054502 (2006)
122. S A Dzuba, E S Salnikov, L V Kulik *Appl. Magn. Reson.* **30** 637
(2006)
123. J Wuttke, W Petry, G Coddens, F Fujara *Phys. Rev. E* **52** 4026
(1995)
124. D A Erilov, R Bartucci, R Guzzi, D Marsh, S A Dzuba,
L Sportelli *Biophys. J.* **87** 3873 (2004)
125. S A Dzuba, H Watari, Y Shimoyama, A G Maryasov,
Y Kodera, A Kawamori *J. Magn. Reson., Ser. A* **115** 80 (1995)
126. J Buitink, S A Dzuba, F A Hoekstra, Yu D Tsvetkov *J. Magn.
Reson.* **142** 364 (2000)
127. I V Borovykh, P Gast, S A Dzuba *Appl. Magn. Reson.* **31** 159
(2007)
128. Q Xu, M R Gunner *Biochemistry* **40** 3232 (2001)
129. M Bixon, J Jortner *J. Phys. Chem.* **90** 3795 (1986)
130. G Feher, M Y Okamura, D Kleinfeld *Protein Structure:
Molecular and Electronic Reactivity* (Eds R Austin, E Buhks,
B Chance, D De Vault, P L Dutton, H Frauenfelder,
V I Goldanskii) (New York: Springer, 1987) p. 399

^a — *Phys. Solid. State (Engl. Transl.)*

^b — *J. Struct. Chem. (Engl. Transl.)*

^c — *Dokl. Chem. (Engl. Transl.)*

The formation of [5,6]- and [6,6]-open fulleroid structures

M V Reinov, M A Yurovskaya

Contents

I. Introduction	715
II. Reactions of diazo compounds with fullerene	715
III. Reactions of azides with fullerene	720
IV. Reactions of nitrile ylides with fullerene	724
V. The formation of fulleroid structures with an open [6,6] bond	725
VI. The formation of miscellaneous fulleroid structures	726
VII. The formation of open homo[70]fullerenes	728
VIII. Theoretical investigations into the possible formation of open adducts in the cycloaddition reactions	728
IX. Conclusion	728

Abstract. The experimental and theoretical data concerning the formation of open fulleroid structures (homofullerenes) upon chemical modifications of the fullerene spheroid are generalised. The bibliography includes 88 references.

I. Introduction

Cycloaddition is one of the best studied types of reactions in organic chemistry of fullerenes. The results of detailed studies of cycloaddition reactions involving fullerenes such as the Diels–Alder, 1,3-dipolar, [2+1] and others have been described in numerous publications. In the vast majority of cases, these reactions afford addition products at the fullerene C=C double bond, the so-called [6,6]-closed adducts. As expected for the normal cycloaddition, a π -bond is cleaved and all σ -bonds are maintained in these products. Meanwhile, many examples of the formation of [5,6]-open and [6,6]-open fulleroid structures in parallel, or in addition, to the expected [6,6]-closed adducts are presently available, which implies that it is σ -bonds between the carbon atoms of the fullerene sphere that are cleaved. In some particular cases, open fulleroids can spontaneously isomerise into closed fullerenes and *vice versa*. Various types of the cycloaddition reactions yield fulleroids, and the reasons for the formation of these unexpected structures among reaction products have not yet been completely established. Several authors speculated upon possible reasons for the formation of open adducts, whereas other authors merely described the experimental data obtained. Despite the fact that the formation of open fulleroid structures is undoubtedly of theoretical interest, no systematic review on this topic has been published so far.

M V Reinov 'New Scientific Technology' Co. Ltd.
Tverskaya ul. 10/1, 103009 Moscow, Russian Federation,
e-mail: reinov2@mail.ru

M A Yurovskaya Department of Chemistry, M V Lomonosov Moscow State University, Leninskie Gory, 119992 Moscow, Russian Federation.
Fax (7-495) 932 88 46, tel. (7-495) 939 53 76,
e-mail: yumar@org.chem.msu.ru

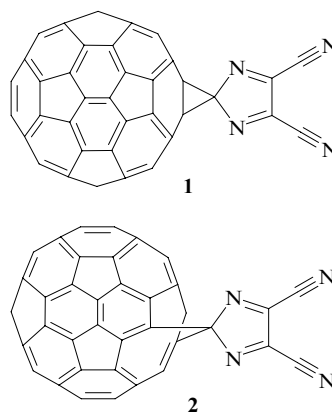
Received 30 January 2007

Uspekhi Khimii 76 (8) 768–783 (2007); translated by Ya V Zubavichus

II. Reactions of diazo compounds with fullerene

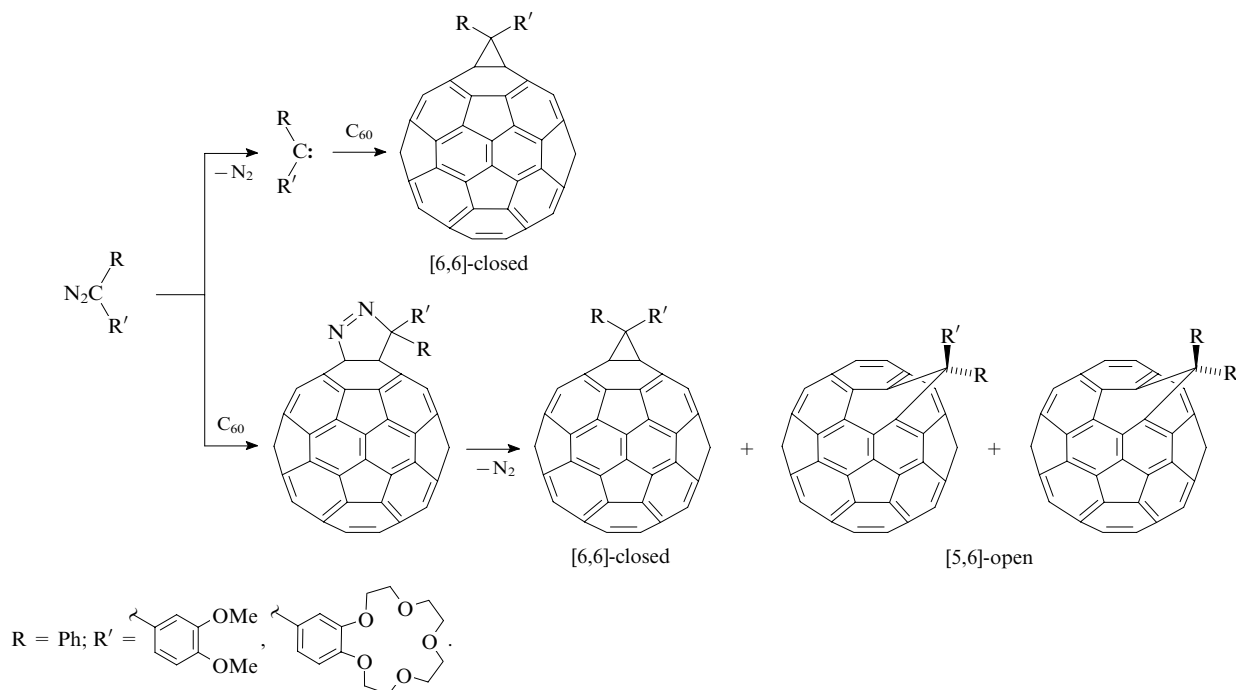
Carbenes are known to readily add to the double bonds C=C to yield cyclopropanes. Diazo compounds are widely used as synthetic precursors of carbenes. However, the thermally induced addition of diazo compounds to C₆₀ fullerene proceeds in a more complex way than the addition of singlet carbenes generated by other methods and affords mixtures of [6,6]-closed (fullerene) and [5,6]-open (fulleroid) isomeric cycloadducts. This is due to two possible mechanisms of the cyclopropane fragment formation in the thermally induced reactions of C₆₀ with diazo compounds: the thermal decomposition of a diazo compound to a carbene followed by its synchronous addition to the [6,6] bond of fullerene giving rise to closed products and the 1,3-dipolar cycloaddition to fullerene followed by the extrusion of nitrogen from the pyrazoline intermediate, which can yield both isomers (Scheme 1).¹

However, thermolysis of 2-diazo-4,5-dicyanoimidazole, which can afford two electrophilic intermediates, *viz.*, carbene-type and zwitter-ionic species stabilised by two electron-withdrawing substituents in the heterocyclic ring in the presence of C₆₀ does not yield isomeric fullerene and fulleroid spiromethanofullerenes (**1** and **2**, respectively),



but rather an adduct **3**.² In our opinion, the radical 1,4-addition is a probable mechanism, since it is quite common in fullerene chemistry,³ whereas no nucleophilic 1,4-addition to

Scheme 1



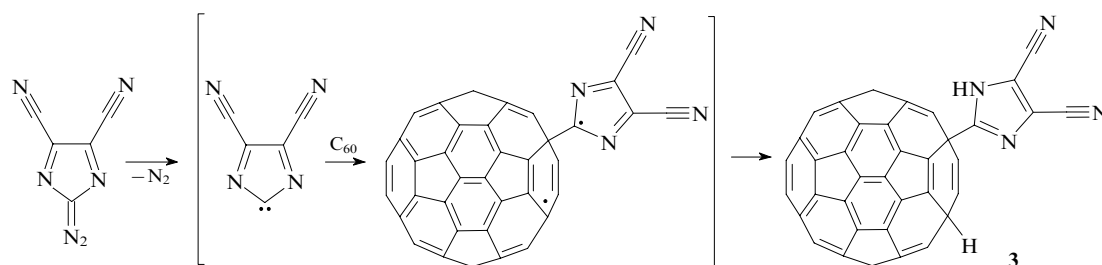
C_{60} has been described so far in the literature. Furthermore, the conversion of 2-diazo-4,5-dicyanoimidazole into a radical is by far more probable than into an anion, which requires the presence of a reducing agent (Scheme 2).

The thermal attachment of dimethyl diazomethylphosphonate $\text{N}_2\text{CHP}(\text{O})(\text{OMe})_2$ to C_{60} (110 °C, toluene) also yields a mixture of isomeric fullerene and fulleroid cycloadducts in a 3 : 1 ratio.⁴

Pellicciari *et al.*⁵ reported the first addition of carbenoids to C_{60} catalysed by transition metals. In particular, the reaction of C_{60} with alkoxycarbonylcarbenoids generated from diethyl diazomalonate with $\text{Rh}_2(\text{OAc})_4$ as a catalyst provides higher product yields and selectivity as compared to ordinary thermal reactions (Scheme 3, Table 1).

Unstable diazo compounds can be generated *in situ* from stable hydrazones and their derivatives using oxidation of hydrazones, *e.g.*, with MnO_2 .^{6,7} It was suggested^{8,9} that the reaction proceeds through the initial 1,3-dipolar cycloaddition of the diazo compound to C_{60} followed by the extrusion of a nitrogen molecule from the pyrazoline intermediate formed. As a result, a mixture of [6,6]-closed (fullerene) and [5,6]-open (fulleroid) derivatives is obtained. This method was successfully used to introduce methylene bridges containing benzocrown ether fragments⁶ or 3,5-bis[(dimethylamino)methyl]-phenyl (dmmph) group⁷ aimed at studying the complexation properties of new fullerene derivatives. It is of note that the formation of only one of two possible [5,6]-open stereoisomers (**8** and **9**) in addition to [6,6]-closed adduct **7** is feasible for specific asymmetric methanofullerenes, according to calcula-

Scheme 2



Scheme 3

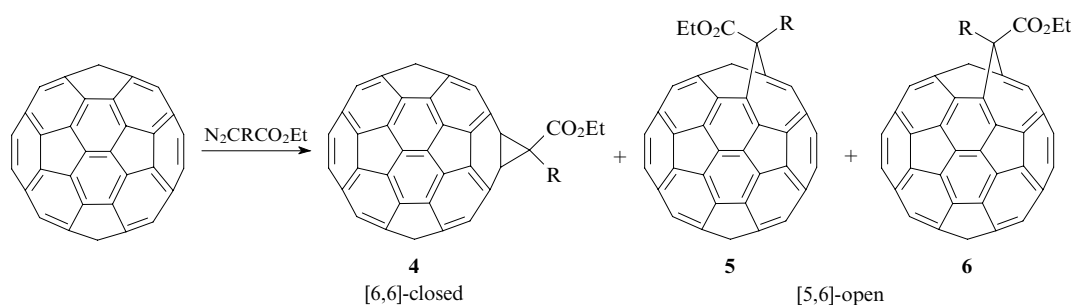
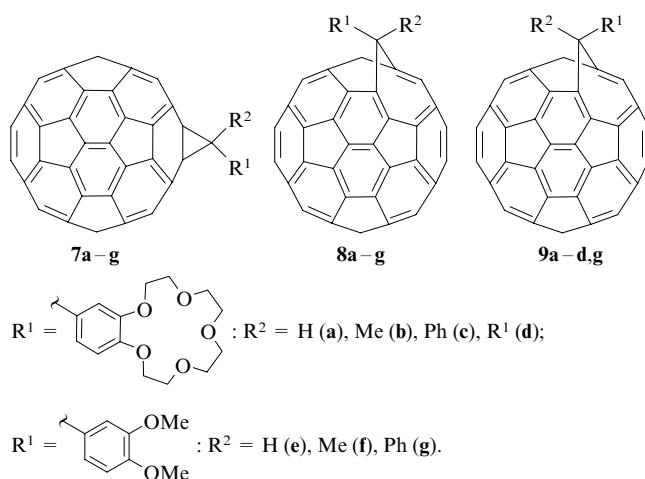


Table 1. Conditions, yields and product ratios for the reaction of C₆₀ with diethyl diazomalonate.

Catalyst	R	Solvent	T/°C	Reaction time/h	Yield (%)	Ratio of isomers		
						4	5	6
—	H	toluene	110	7	35	1	4	2
Rh ₂ (OAc) ₄	H	toluene	20	20	21	14	1	1
Rh ₂ (OAc) ₄	H	1-methylnaphthalene	20	8	42	52	1	—
—	CO ₂ Et	toluene	110	20	10	not determined		
Rh ₂ (OAc) ₄	CO ₂ Et	1-methylnaphthalene	80	32	9	1	—	—

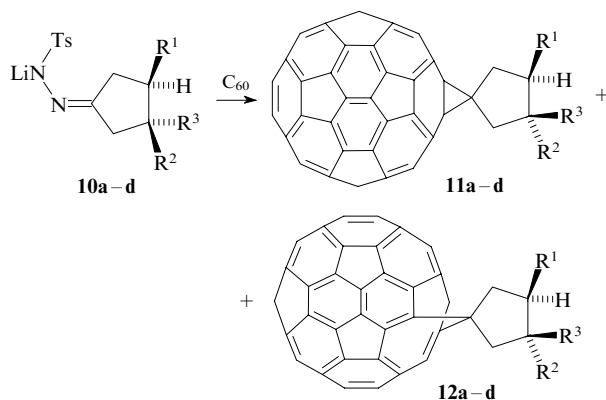
tions. In particular, isomers **8e,f** are feasible, whereas isomers **9e,f** are not.⁶



For all other non-symmetrical methanofullerenes, both [5,6]-open isomers have been isolated. No rationale for this experimental fact has been given.⁶

Initially, the reaction of fullerene with diazo compounds bearing a dmmph group was found⁷ to yield a mixture of [5,6]-open fulleroids and [6,6]-closed methanofullerene in a 9 : 1 ratio.

In addition to the aforementioned oxidation of unsubstituted hydrazones, thermolysis of *N*-tosylhydrazone anions **10** can be employed for the generation of diazo compounds.^{8, 10–16} Their addition also yields a mixture of [6,6]-closed and [5,6]-open isomeric cycloadducts (compounds **11** and **12**, respectively). Conditions of the thermolysis of the corresponding *N*-tosylhydrazone lithium salts in boiling toluene could be tuned so as to enable the preferred formation of fulleroid derivatives. This was accomplished by shortening the reaction time, which favours the formation of a kinetically controlled product.

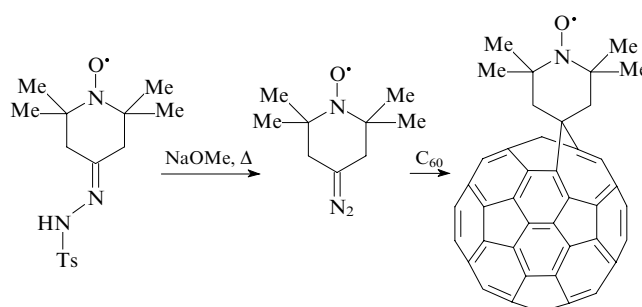


$R^1 = R^2 = R^3 =$ H (a); $R^1 = R^2 =$ CO₂Et, $R^3 =$ H (b);
 $R^1 = R^3 =$ CO₂Me, $R^2 =$ H (c); $R^1 = R^3 =$ CO₂Et, $R^2 =$ H (d).

The maximum yield of 67% and the maximum isomer ratio of [5,6]-open to [6,6]-closed (13.3 : 1) were achieved for compound **10c** and a reaction time of 25 min. With an increase in the reaction time to 90 min, the yield of monoadducts drops down to 23% and the isomer ratio, to 1.7 : 1. Most probably, such a change in the product ratio is due to the progressive accumulation of the product of thermal rearrangement of the initially formed [5,6]-open isomer into the [6,6]-closed isomer.

In contrast, the reaction of C₆₀ with 4-[bis(4'-*tert*-butylphenyl-4-yl)]benzaldehyde *N*-tosylhydrazone in *o*-dichlorobenzene in the presence of sodium methoxide even at a relatively low temperature (40 °C) yields selectively the thermodynamically more stable [6,6]-closed isomer.¹⁷

The reaction of fullerene C₆₀ with 2,2,6,6-tetramethyl-4-oxopiperidine-1-oxyl *N*-tosylhydrazone affords only the open isomer in a ~25% yield.¹⁰



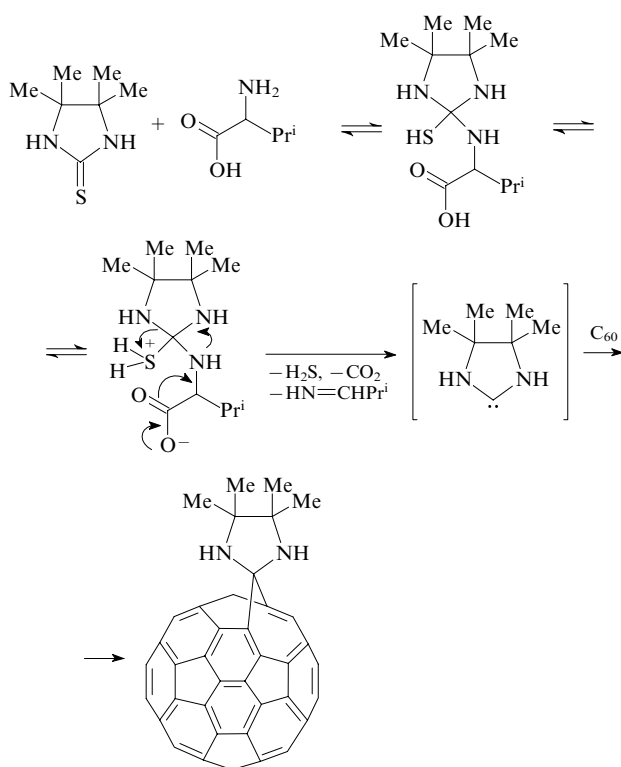
The kinetically controlled products, *viz.*, [5,6]-fulleroids, were obtained in the reaction of fullerene with a diazo compound bearing a tetrathiafulvalene substituent¹³ and a diazo compound generated *in situ* from 4-benzoylbutyric acid *N*-tosylhydrazone.¹⁸

An unusual method for the carbene generation has been found in the reaction of C₆₀ with DL-valine and 4,4,5,5-tetramethylimidazoline-2-thione.¹⁹ This reaction yields the respective spiro-fused fulleroid (Scheme 4).

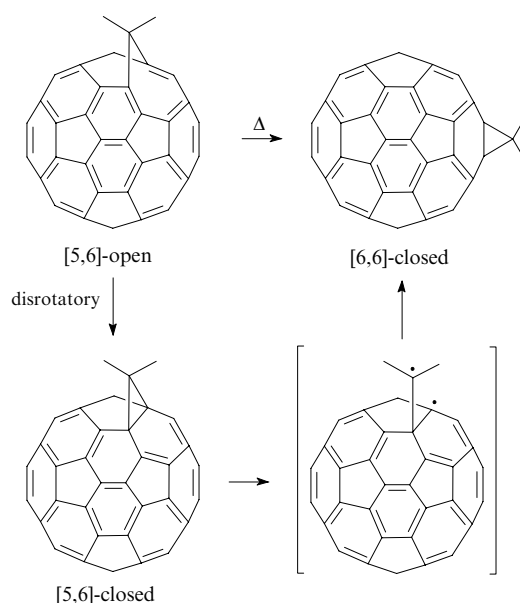
As has been noted above, the reactions of C₆₀ with carbenes afford [6,6]-closed methanofullerenes, whereas those with diazo compounds yield fulleroids (*i.e.*, [5,6]-open isomers). This allows fullerenes to be used as specific probes to distinguish carbenes and diazo compounds. The nature of the adducts formed provides information on the reaction mechanism.²⁰

However, it has to be noted that the thermal reaction of C₆₀ with a dibromo derivative **13**, which involves a carbene intermediate, yields a symmetrical fullerene adduct **14**, dimers formed upon the reaction of two molecules of the carbene intermediate and an isomeric non-symmetrical adduct **15** comprising fullerene and fulleroid fragments in one molecule.²¹ It was shown that the fulleroid **15** was the major reaction product (its yield varies from 5% to 10%), but no explicit ratio between the adducts **14** and **15** was given. According to calculations,²¹ the isomer **15** is more stable than **14** (Scheme 5).

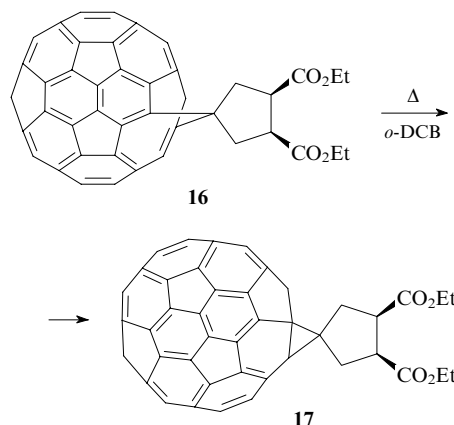
Scheme 4



Scheme 6



from light failed and the starting fulleroid **16** remained quantitatively intact.²⁵



As has been shown by different groups,^{6–8, 13, 18} [5,6]-open fulleroids synthesised in this way undergo a thermal rearrangement into thermodynamically more stable [6,6]-closed isomers. A number of [5,6]-open fulleroids bearing substituents stabilising radical species in the methylene bridge was proven to rearrange into [6,6]-closed fullerenes both in the zero-order (in terms of kinetics) photochemical process and in the high-energy unimolecular route, which involves the disrotatory ring closure into a [5,6]-closed fullerene followed by its rearrangement into the [6,6]-closed isomer *via* biradical intermediates.²² Generally, this process is depicted in Scheme 6 (omitting substituents in the bridge). The energy parameters of various isomers of methanofullerenes and fulleroids calculated by the MNDO method are reported.²³

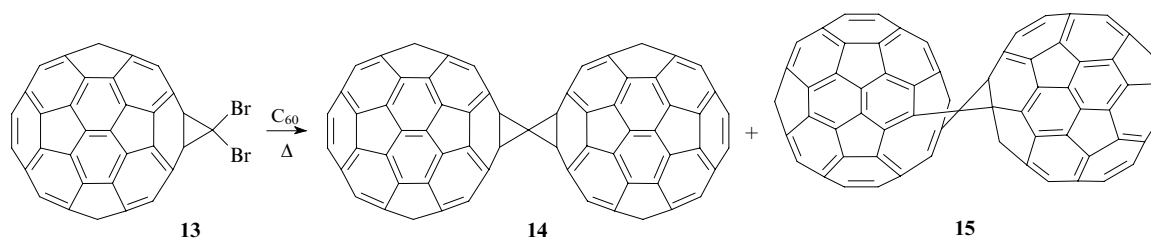
It has to be stressed that unsubstituted [5,6]-methanofulleroid is not thermally converted into methanofullerene.²⁴ This agrees with the radical mechanism of the rearrangement suggested above, since the formation of a biradical intermediate becomes thermodynamically unfavourable due to the absence of radical-stabilising substituents in the bridge.

The rearrangement of fulleroid **16** into methanofullerene **17** occurs in *o*-dichlorobenzene (*o*-DCB) at 153 °C, but all attempts to perform it in an NMR tube carefully protected

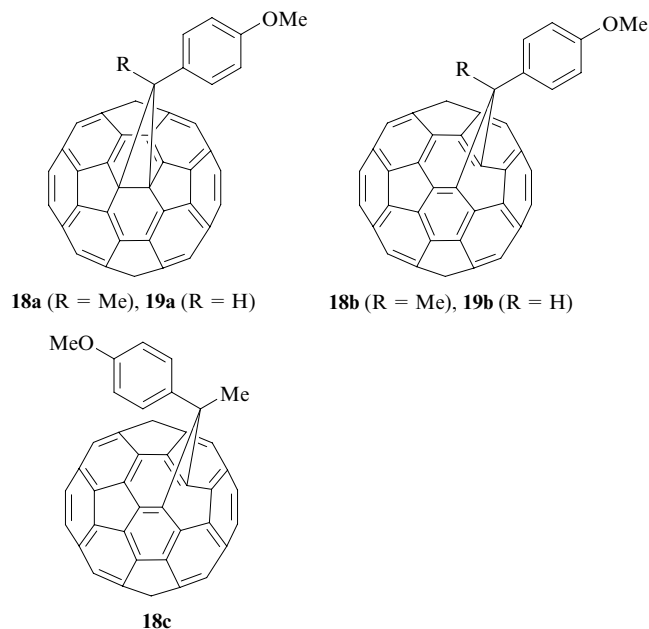
Thus, this rearrangement requires illumination. Indeed, compound **16** is converted into methanofullerene **17** quantitatively upon illumination of its solution with filtered light ($\lambda > 500$ nm, 200 W) for 16 h. Oxygen inhibits the reaction, which supports the suggested biradical mechanism of the isomerisation.

Prato *et al.*²³ also described experiments on the thermal rearrangement of fulleroids into methanofullerenes and presented calculations demonstrating higher thermodynamic

Scheme 5

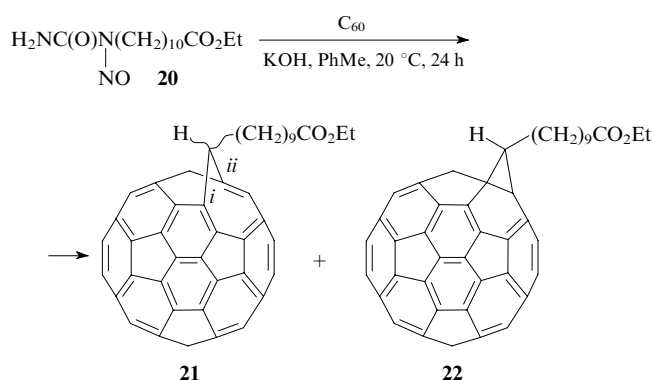


stability of methanofullerenes. It is of note that the reaction of fullerene with 1-(*p*-methoxyphenyl)diazoethane affords a mixture of [6,6]-closed (**18a**) and two [5,6]-open (**18b,c**) isomers in a 4 : 2 : 1 ratio, whereas the reaction with *p*-methoxyphenyldiazomethane yields only two isomers, *viz.*, [6,6]-closed (**19a**) and one [5,6]-open (**19b**) adducts.



According to calculations for a series of model systems containing fused six- and five-membered rings similar to those in the fullerene molecule (using MMPI, RHF/AM1 and UHF/AM1 methods with the geometry optimisation),⁹ [5,6]-open isomers can become more stable than their [6,6]-closed counterparts with an increase in the degree of convexity.

The known instability of aliphatic diazo compounds makes the control over the process of their addition to C_{60} very difficult, the more so that the reaction occurs in extremely low yields. Zhu *et al.*²⁶ generated diazo compounds *in situ* from a stable precursor, compound **20**, which allowed them to overcome this problem.



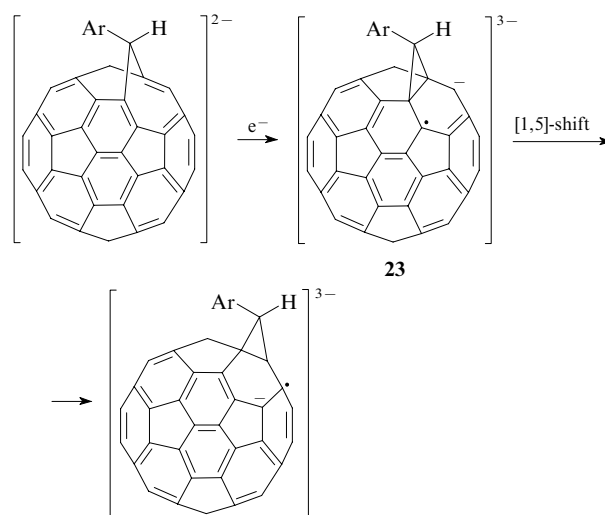
Since the addition of KOH to the nitroso compound results in the immediate nitrogen evolution and pyrazoline intermediates have never been observed among the reaction products, it was suggested that the reaction follows the carbene mechanism.

In this case, the [5,6]-open isomer **21** proves thermodynamically more stable. It is formed upon rearrangement of initially formed [6,6]-closed cycloadduct **22** (according to the data from NMR spectra), which was rationalised by the effect

of a bulky aliphatic substituent in the bridge. On the one hand, the sp^2 carbon atoms *i* and *ii* of the fullerene cage in the open adduct are characterised by localised double bonds, which should induce strains in the cyclic structure, according to the Bredt rule. In the closed adduct, these carbon atoms are sp^3 -hybridised and thus the total structural strain is substantially lower. On the other hand, the closed adduct contains a strained cyclopropane fragment, the strain in which is proportional to the steric bulk of the substituent in the methylene bridge. The distance between the carbon atoms *i* and *ii* is larger in the open adduct than in the closed one and thus the strain in the attached molecular fragment is lower. The relative stability of the two isomers, open and closed, is exactly determined by the interplay of these two factors. In the present case, the [5,6]-open adduct is more stable. Zhu *et al.*²⁶ stressed that the adduct isomerisation is strongly affected by solvents. They concluded that temperature, solvent and the nature of substituents are the three key factors governing the formation of a specific isomer. This conclusion on the reasons for a higher stability of open adducts with bulky substituents in the bridge agrees with the aforementioned experimental data²¹ on higher stability of the open isomer with the fullerene molecule serving as the bulky substituent. This explanation, however, contradicts the results of other authors,²⁷ who showed that methanofullerenes bearing substituents of a comparable size [*viz.*, $\text{C(R)CH}_2\cdot\text{C(O)OCH}_2\text{CMe}_2\text{CH}_2\text{OH}$, $R = \text{H, Et, Ph}$] do not rearrange into open fulleroids even upon heating to 200 °C.

Eiermann *et al.*²⁸ reported the electrochemical isomerisation of a [5,6]-open fullerene synthesised by the addition of (*p*-methoxycarbonylphenyl)diazomethane to C_{60} into the respective [6,6]-closed methanofullerene. In this case, the generation of a radical anion **23** favours the isomerisation. The tentative mechanism is shown in Scheme 7.

Scheme 7

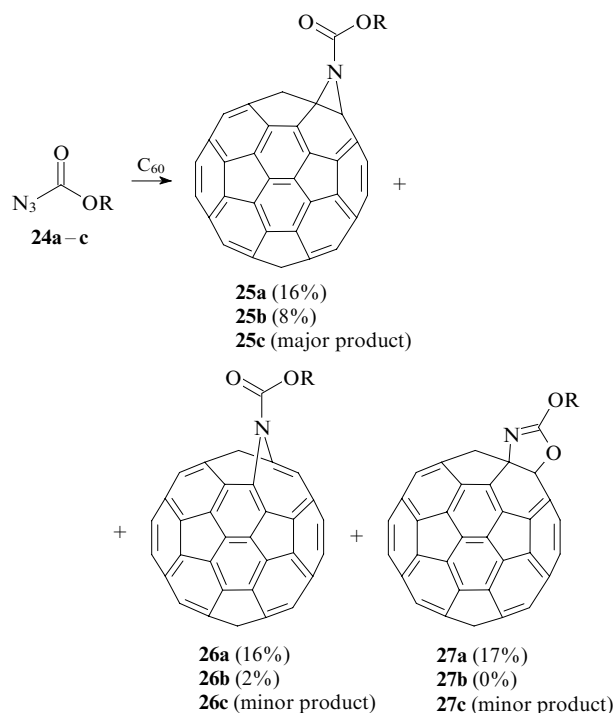


$\text{Ar} = 4\text{-MeO}_2\text{CC}_6\text{H}_4$.

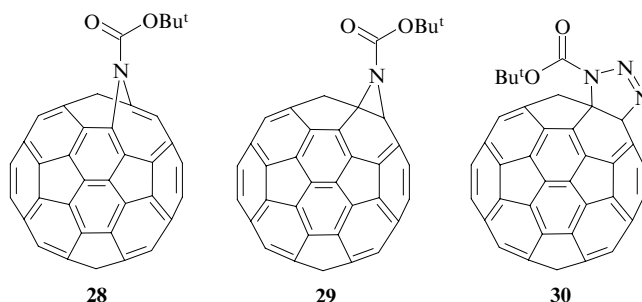
As has been mentioned above, there are two possible mechanisms of the cyclopropanation upon thermal reactions of C_{60} with diazo compounds.^{1,9} Wallenborn *et al.*²⁹ theoretically studied the possibility of the formation of methanofullerenes with the thermal extrusion of N_2 from the pyrazoline intermediate. According to *ab initio* calculations (using the B3LYP/6-31G* method) on benzene and pyracene as mimics for the fullerene core, the extrusion of a nitrogen molecule proceeds as a synchronous process with an energy barrier of 15–20 kcal mol^{−1}. The energy of biradical transition states corresponding to potential stepwise mechanism of the reaction is much higher, which makes this mechanism hardly probable.

III. Reactions of azides with fullerene

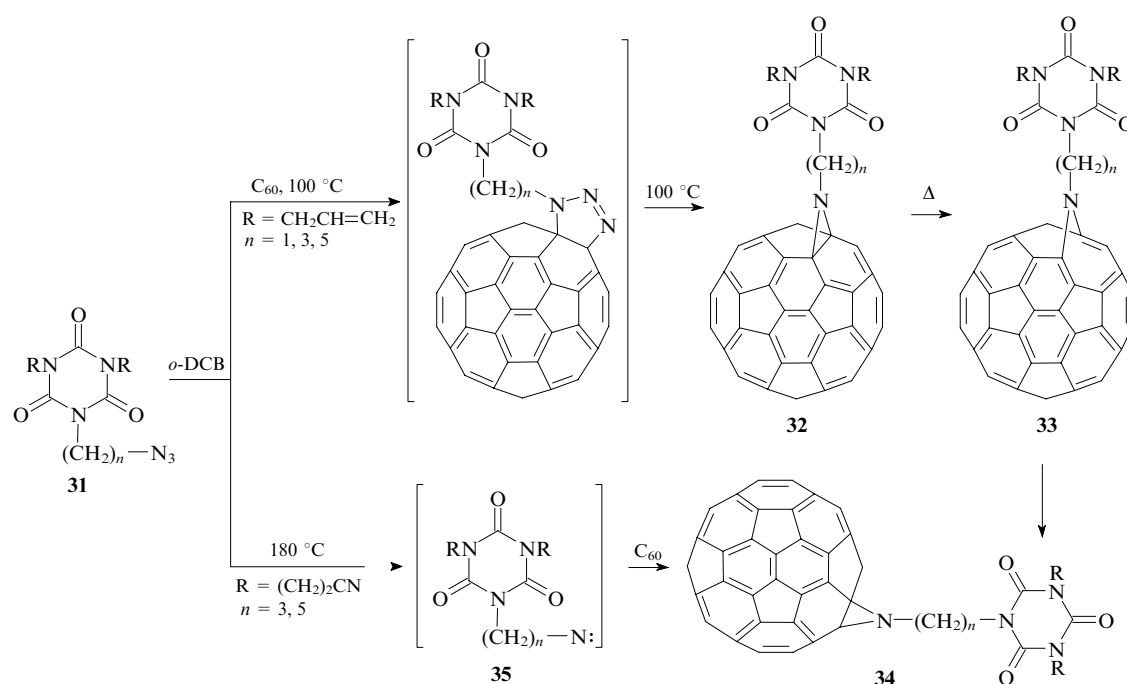
Aza analogues of carbenes, *i.e.*, nitrenes, which can be generated *in situ* by the thermal decomposition of azides behave similarly in cycloaddition reactions, resulting in [6,6]-closed fulleraziridines. However, it was found³⁰ that the reaction of fullerene with azidoformates **24** yields closed adducts **25** together with an appreciable amount of [5,6]-open isomers **26** (the reactions were accomplished under drastic conditions where azidoformates undergo thermal decomposition to nitrenes). Additionally, fullerooxazolines **27**, which are the thermal rearrangement products of alkoxy carbonyl fulleraziridines, were isolated.



Schick *et al.*³¹ reported the following synthesis. A concentrated solution of fullerene C_{60} in 1-chloronaphthalene was heated at 60 °C in the presence of $N_3CO_2Bu^t$ (1 equiv.); such conditions are typical of the formation of fullerotriazolines. Then the reaction mixture was diluted tenfold with toluene and heated at 120 °C to give a mixture of [5,6]-open and [6,6]-closed adducts (**28** and **29**, respectively) in a ratio 16:3. This result clearly demonstrates the preferred formation of the open fulleroid upon the thermal decomposition of fullerotriazoline **30**. Under the conditions of nitrene generation (*i.e.*, thermal decomposition of N_3CO_2Et), the [6,6]-closed aziridinofullerene is the major reaction product with fullerene.



The reactions with alkyl azides typically afford [5,6]-open adducts, which can further rearrange into more stable [6,6]-closed isomers. Less stable acyl azides preferably yield [6,6]-closed adducts. This can be explained by the fact that the reaction of alkyl azides with fullerene follows the 1,3-dipolar cycloaddition mechanism giving rise to unstable triazolines that further decompose to [5,6]-open adducts. The thermal decomposition of acyl azides proceeds more readily, the resultant nitrenes react with fullerene to yield the [6,6]-closed adducts. Most probably, the nitrene attack occurs to the shortest and most reactive [6,6] bond of fullerene. This conclusion is supported by the fact that the addition of singlet carbenes and silylenes always occurs to the [6,6] bond yielding the respective closed adducts.^{32,33} Nevertheless, the reasons for the formation of [5,6]-open isomers in some reactions of fullerene with oxycarbonylnitrenes remain unclear.³⁴ Banks *et al.*³⁵ formulated two hypotheses. According to one of them,



Scheme 8

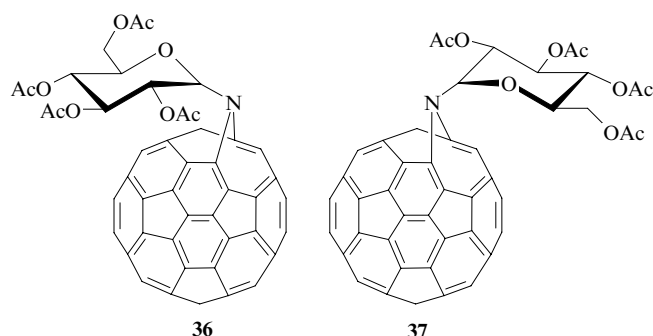
R = CH₂CH=CH₂, (CH₂)₂CN.

open adducts are formed directly upon the addition of a singlet nitrene to the [5,6] bond. According to another hypothesis, the addition of the remaining triplet nitrene to fullerene can result in a mixture of [5,6] and [6,6] regioisomers. The former hypothesis is supported by calculations,³⁶ which demonstrated that the [5,6] and [6,6] bonds are comparable in reactivities from both thermodynamic and kinetic viewpoints under the conditions of the nitrene addition to fullerene.

Within the context of investigations into the cycloaddition reactions of isocyanurate-substituted alkyl azides (**31**) to fullerene (Scheme 8), [5,6]-closed isomer **32** has been detected for the first time and convincing spectroscopic evidence for its existence has been gathered: in particular, its ¹³C NMR spectrum revealed two signals assigned to the two sp³-hybridised carbon atoms of the fullerene core.^{37, 38}

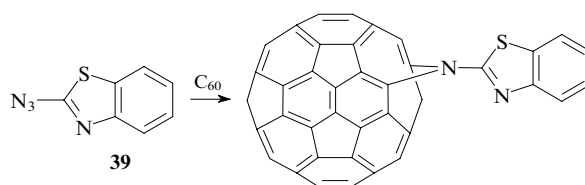
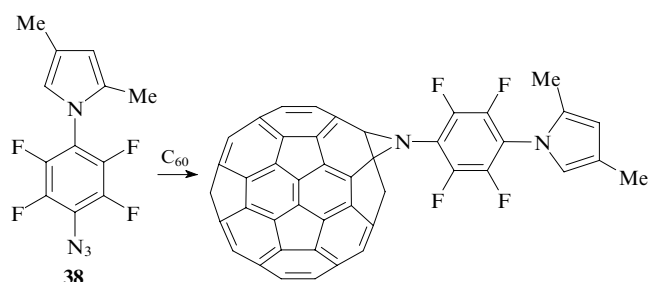
The reaction of C₆₀ with 5-(5-azidopentyl)-1,3-diallyl-1*H*,3*H*,5*H*-1,3,5-triazine-2,4,6-trione (*n* = 5) at 100 °C affords in a preparative yield [5,6]-closed isomer **32**, which is successively converted first into [5,6]-open isomer **33** and then into the thermodynamically most stable [6,6]-closed aziridinofullerene **34**. Under more drastic conditions (180 °C), the reaction with 1,3-bis(cyanoethyl)-substituted azide affords closed adduct **34** alongside with the dimerisation product of the intermediate nitrene **35**, which strongly supports the dominance of the nitrene mechanism at high temperature.

The cycloaddition of per-*O*-acetylglycosyl azides to C₆₀ was used³⁹ for the preparation of fullerene glycoconjugates; this reaction yielded a mixture of open stereoisomers **36** and **37** in a ratio 2 : 1.



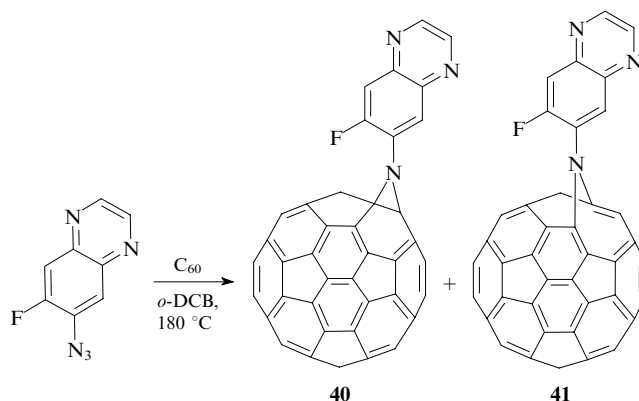
Compounds with fullerene and porphyrin moieties linked by a polyether linker were synthesised in a similar way.⁴⁰ The cycloaddition of azides was used to introduce a pharmacophore acridine group (known by its activity with respect to DNA) into fullerene.⁴¹ Fulleroid cycloadducts were obtained in all these cases.

Jagerovic *et al.*⁴² considered the dependence of the direction of cycloaddition on the azide structure using aryl and hetaryl azides. It is known that the nitrene addition occurs to the double [6,6] bond to yield closed fulleroaziridines, whereas the initial 1,3-dipolar cycloaddition yields triazoline intermediate, which converts into [5,6]-open π -azafulleroids upon subsequent extrusion of nitrogen. The [6,6]-closed and [5,6]-open cycloadducts are formed from aromatic and heterocyclic



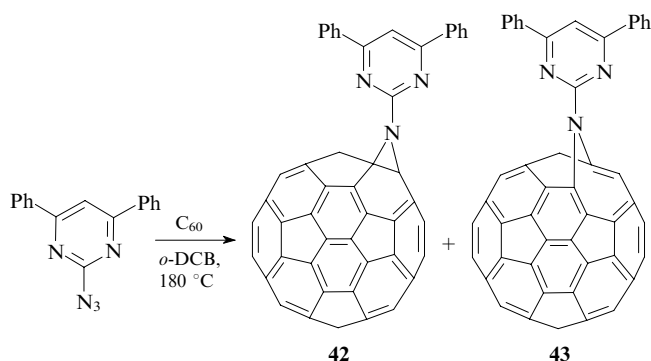
azides **38** and **39**, respectively. However, the authors did not comment this experimental result.

The reaction of C₆₀ with 7-azido-6-fluoroquinoxaline in *o*-DCB at 180 °C yields a mixture of [6,6]-closed (**40**) and [5,6]-open (**41**) isomers with predominance of the former one.⁴³



The structure of [6,6]-closed isomer **40** was reliably established by ¹³C NMR spectroscopy. Unfortunately, the available amount of compound **41** was insufficient for the collection of NMR spectra and thus its assignment to the [5,6]-open isomer was made on the basis of the UV spectrum that revealed no narrow weak band at λ_{max} = 425 nm typical of the closed isomer **40**.

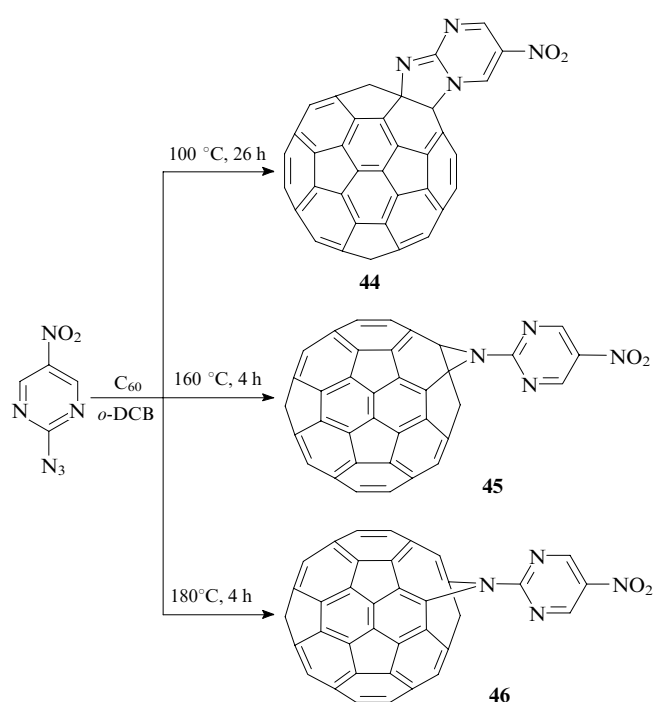
Similar results were obtained for the reaction of fullerene with 2-azido-4,6-diphenylpyrimidine.⁴⁴



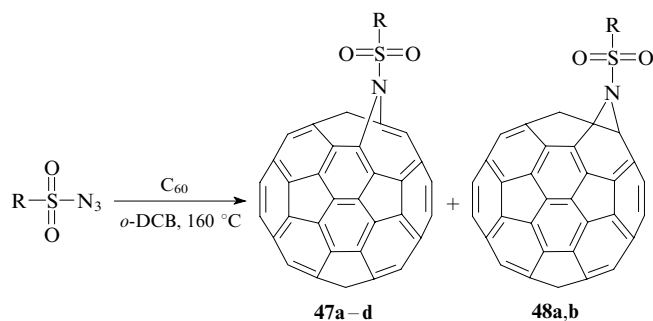
Studies of the electrochemical reduction of compounds **40–43** bearing quinoxaline and pyrimidine fragments by means of cyclic voltammetry revealed that they represent first fulleroaziridines that are stronger electron acceptors than the parent fullerene.^{43, 44}

Different products can be obtained in the reaction of fullerene C₆₀ with 2-azido-5-nitropyrimidine, depending on the reaction conditions.^{45, 46} In particular, 4-nitro[60]fullero[1',2':4,5]imidazo[1,2-*b*]pyrimidine (**44**) was obtained upon heating at 100 °C in *o*-DCB; [6,6]-closed 5-nitro-2-[[60]fullereno[1,2-*b*]aziridino]pyrimidine (**45**) was obtained in a 13% yield at 160 °C; and azahomofullerene **46** is formed at a higher temperature (Scheme 9). It is of note that the reaction products do not undergo thermal interconversions.

Scheme 9

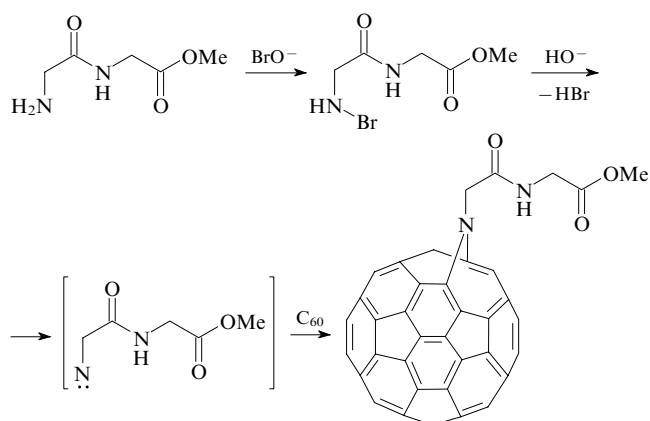


The reaction of alkylsulfonyl azides with fullerene yields a mixture of open (**47a,b**) and closed (**48a,b**) adducts, whereas that with arylsulfonyl azides affords exclusively open fulleroids **47c,d**. All open fulleroids synthesised in this way undergo the photochemical rearrangement into [6,6]-closed fulleroaziridines.⁴⁷

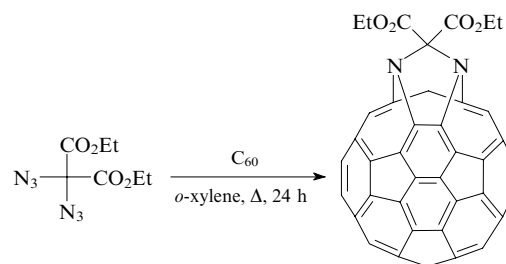


R = Me (**a**), Bn (**b**), 4-MeC₆H₄ (**c**), 4-MeOC₆H₄ (**d**).

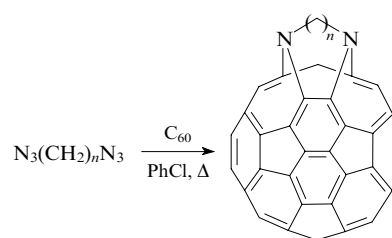
The possibility of oxidative generation of nitrene from glycylglycine methyl ester enabled the synthesis of a dipeptide with a fulleroid substituent.⁴⁸



Bisazides are added to two fullerene [5,6] bonds giving rise to fulleroid structures. In particular, the reaction of C₆₀ with diethyl diazidomalonate in boiling xylene affords a 1 : 1 adduct representing a bis(aza)fulleroid in a 65% yield.⁴⁹

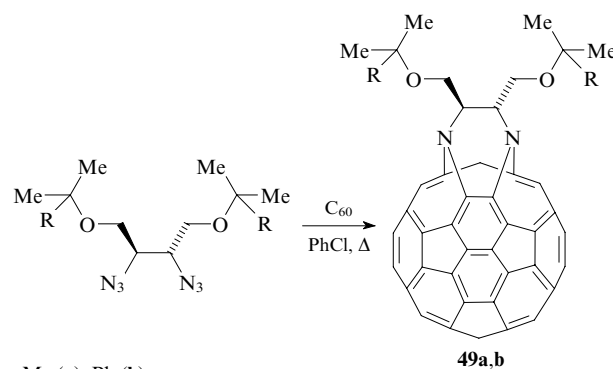


The bis-addition proceeds regioselectively: it still involves two [5,6] bonds of the same five-membered ring of fullerene even when the azido groups are separated by two or three methylene units.⁵⁰



n = 2, 3.

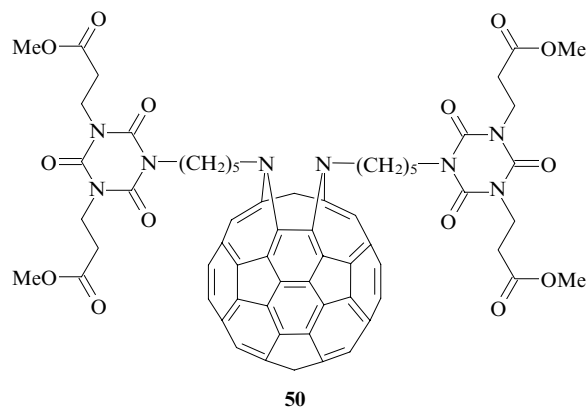
The reaction of C₆₀ with chiral 1,4-di(*tert*-alkoxy)-2,3-bis(azido)butanes affords the respective chiral bis(aza)fulleroids (2*R*,3*R*)-**49a**, (2*S*,3*S*)-**49a**, (2*R*,3*R*)-**49b** and (2*S*,3*S*)-**49b** in yields of 54%, 49%, 56% and 51%, respectively.⁵¹



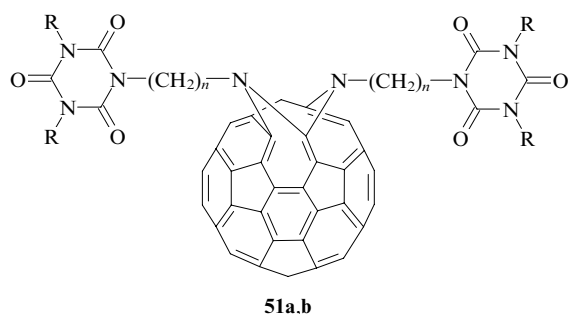
R = Me (**a**), Ph (**b**).

It turned out that the regioselective synthesis of aza-homofullerene bisadducts is possible even with monoazides. In particular, the addition of isocyanurate-substituted alkyl azides to fullerene C₆₀ can result in the regioselective formation of diverse azahomofullerene adducts, depending on the bulk and structure of organic substituents.⁵² For instance, in the case of isocyanurate groups with methoxycarbonyl ethyl substituents at the nitrogen atom, an open bisadduct **50** similar to those described above is obtained owing to the azide addition to two [5,6] bonds.

Bisadducts with different structures were unexpectedly formed upon changes in the substituent R at the nitrogen atom in the isocyanurate-substituted alkyl azides virtually independent of the length of the methylene spacer between the azido group and the heterocycle. The structure of adducts **51a,b** was postulated⁵² due to the presence of a signal at



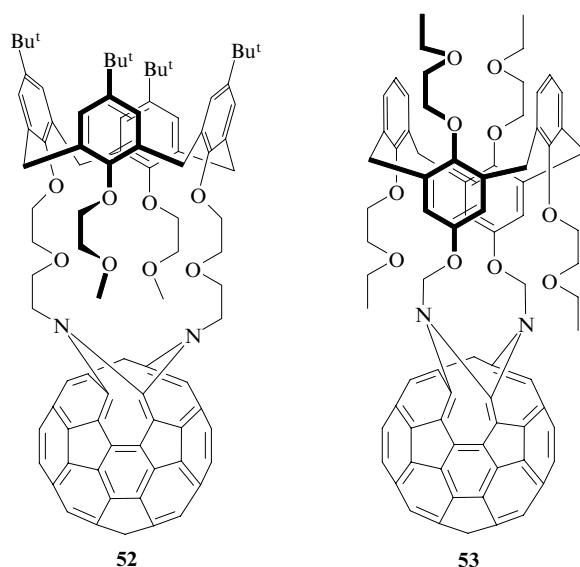
$\delta = 160$ in their ^{13}C NMR spectra, which is typical of carbon atoms bonded to two nitrogen atoms.



$\text{R} = \text{CH}_2\text{CH}=\text{CH}_2$; $n = 2, 3, 5$ (a); $\text{R} = (\text{CH}_2)_2\text{CN}$, $n = 5$ (b).

In our opinion, this single argument is insufficient for the unambiguous determination of the structure that has to be confirmed by X-ray crystallography. The possible pathway to various azahomofullerene bisadducts proposed by the researchers cited is shown in Scheme 10.

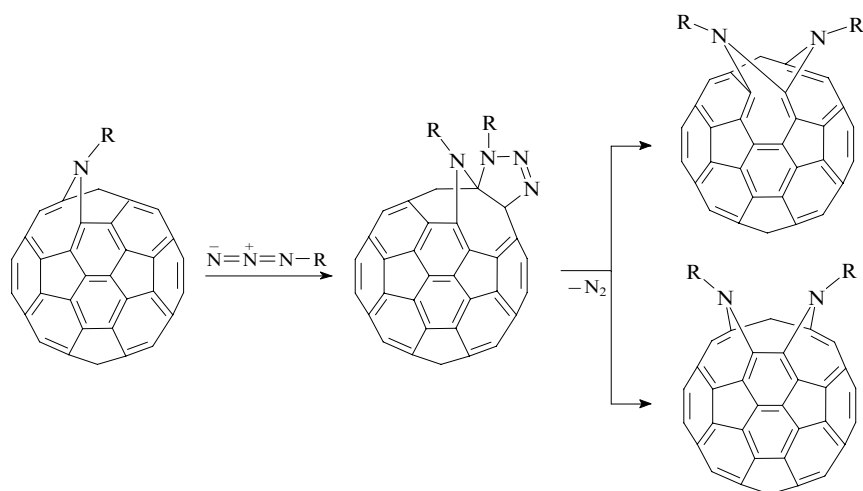
The similar bis(aza)fulleroid structure was proposed for fullerene-containing calix[4]arene derivatives (*e.g.*, compounds **52** and **53**) capable of exohedral complex formation with Li^+ , Na^+ and Ag^+ cations. In the [5,6]-open structures formed, one carbon atom of the fullerene part of the adduct is bonded to two nitrogen atoms.^{49, 53}



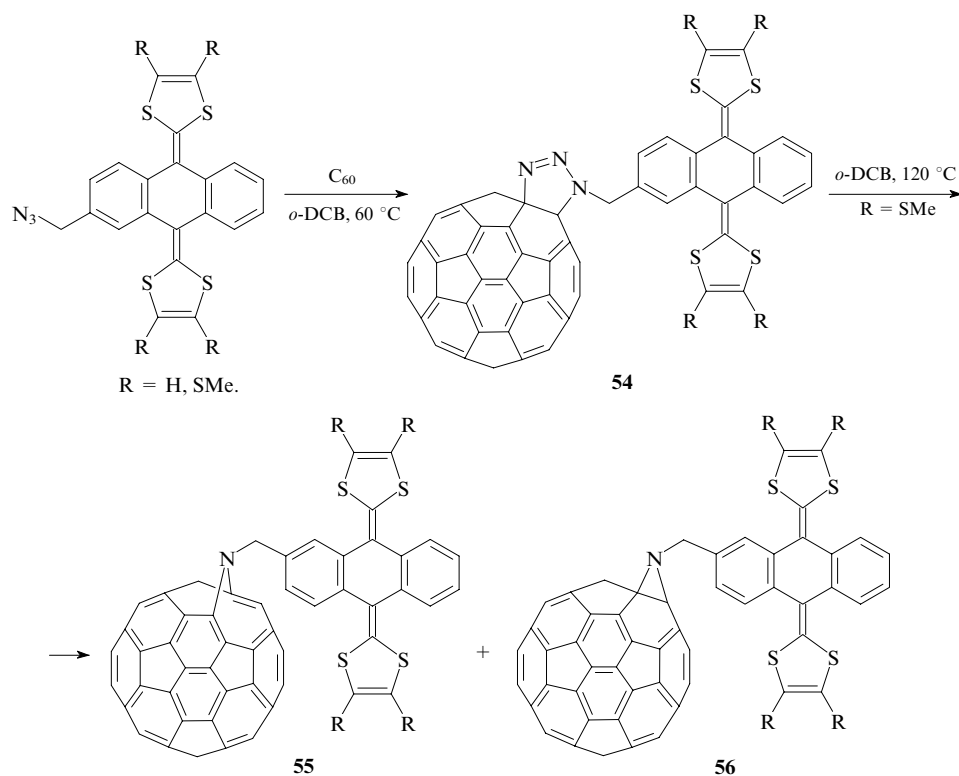
The reaction of C_{60} with tetrathiafulvalene-substituted methyl azides in *o*-dichlorobenzene with heating in an argon atmosphere for 4 h yields [60]fullero[1,2-*e*]-triazolines stable in the solid state at room temperature; the products include initially formed triazoline **54**, azafulleroid **55** (20%) and traces of fulleroaziridine **56** (Scheme 11).⁵⁴

The mechanism of the reaction involving the 1,3-dipolar cycloaddition of methyl azide to fullerene C_{60} followed by the extrusion of a nitrogen molecule was theoretically substantiated using quantum chemical calculations at the semiempirical level and within the density functional theory.⁵⁵ According to the results obtained, the azide addition occurs to the [6,6] double bond to yield the triazoline intermediate, which is characterised by the energy barrier of $\sim 20 \text{ kcal mol}^{-1}$ and an exothermic effect of $\sim 2 \text{ kcal mol}^{-1}$ (according to B3LYP/6-31G*//AM1 calculations). The subsequent thermal extrusion follows the stepwise mechanism with the cleavage of an N–N single bond followed by the cleavage of a C–N bond with an overall activation energy of $\sim 45 \text{ kcal mol}^{-1}$. The N_2 elimination occurs simultaneously with the formation of a new C–N bond. During this process, the steric influence of the outgoing N_2 molecule prevents the nitrene addition to the [6,6]

Scheme 10

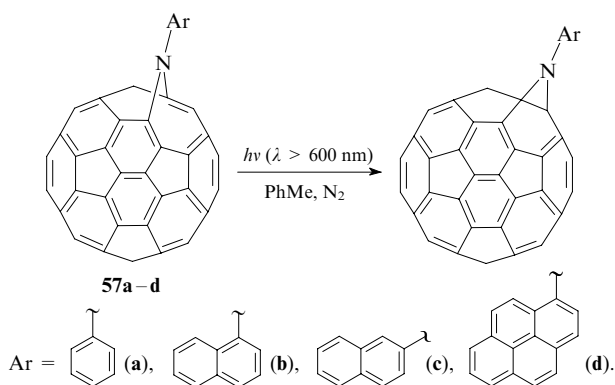


Scheme 11



bond thus enhancing the probability of the addition to the [5,6] bond.

It turned out that substituents at the azafulleroid nitrogen atom strongly affect the rate of the photochemical rearrangement into fulleroaziridines.⁵⁶



In particular, times for the completion of the reaction are 1440 : 1 : > 2160 : 360 for a series of derivatives **57a–d**. Thus, the rates of the photochemical rearrangement differ by a factor

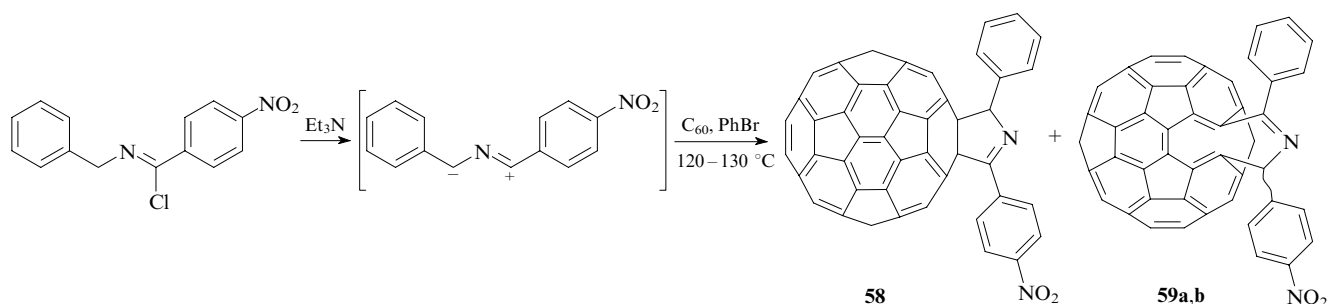
of more than 2000 between the most (**57b**) and least (**57c**) reactive compounds. Photolysis of compounds **57a–d** in air-saturated solutions proceeds much more slowly, which implies intermediacy of the triplet state of the starting azafulleroid.

IV. Reactions of nitrile ylides with fullerene

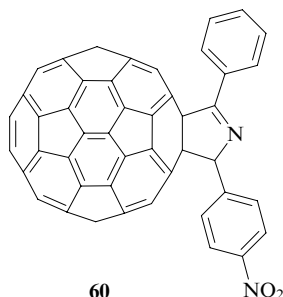
In all cases described in the early literature, only [6,6]-closed cycloadducts were obtained with fragments of five-membered heterocycles annulated to the fullerene spheroid. Unexpectedly, it was found⁵⁷ that the 1,3-dipolar cycloaddition of nitrile ylides to C_{60} can also yield [5,6]-open fulleroid isomers. Indeed, the cycloaddition of 1-(4-nitrophenyl)-3-phenylnitrile ylide generated *in situ* from *N*-benzyl-4-nitrophenylimidoyl chloride under the action of triethylamine at 130 °C yields [6,6]-closed [60]fullero[1,2-*c*]-5-(4-nitrophenyl)-2-phenyl-2*H*-3,4-dihydropyrrole (**58**) along with a mixture of diastereomeric [5,6]-open fulleroid cycloadducts **59a,b** in a ratio 2 : 1 (Scheme 12). The $\text{C}=\text{N}$ double bond in the open cycloadducts **59** is in the α -position with respect to the unsubstituted phenyl group, whereas it is in the α -position with respect to the nitrophenyl substituent in the [6,6]-closed isomer.

Under milder conditions (toluene, room temperature), this reaction yields another set of cycloadducts with no open

Scheme 12



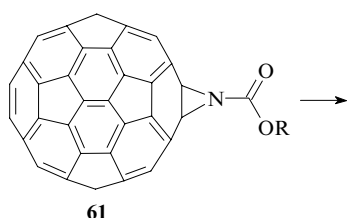
isomers.⁵⁸ In that case, isomeric compounds **58** and **60** differing in the position of a double bond were isolated.



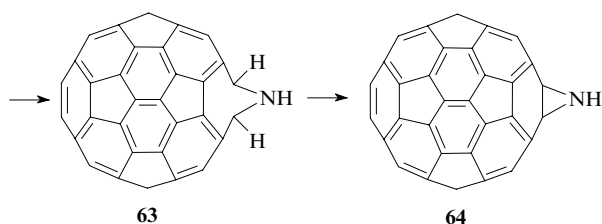
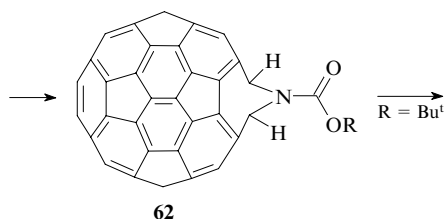
In our opinion, the nitro group can stabilise the biradical mesomeric form of the ylide, which enables the stepwise addition of the radical form to fullerene yielding open structures in addition to the concerted [6,6]-addition of the dipolar form yielding the closed adduct at high temperature.

V. The formation of fulleroid structures with an open [6,6] bond

The unusual opening of the fullerene sphere has been discovered for the first time⁵⁹ in the reduction of *N*-alkoxycarbonyl[60]fullero[1,2-*b*]-aziridines (**61**) with zinc or magnesium in glacial acetic acid. This reaction yields fulleroids **62** with an open [6,6] bond. In the case of R = Bu^t, the removal of the *tert*-butoxycarbonyl protection with 50% aqueous CF₃CO₂H provides a convenient synthetic route to C₆₀H₂NH (**63**), which is a parent compound of a new class of fulleroids. Under the action of a base (e.g., 1,4-diazabicyclo[2.2.2]octane), compound **63** converts in several minutes into fullero-aziridine **64**.

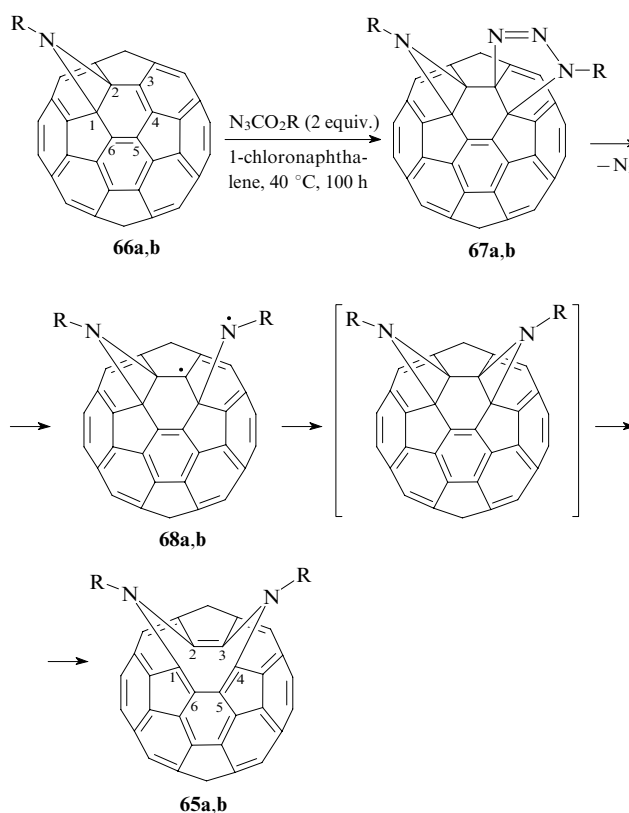


R = Et, Bu^t, CCl₃CH₂, 9-fluorenylmethyl



This reaction is of general character, compounds **61** bearing diverse substituents (R = Bu^t, Et, CCl₃CH₂ or 9-fluorenylmethyl) can readily be reduced to derivatives **62** in yields of > 90%.

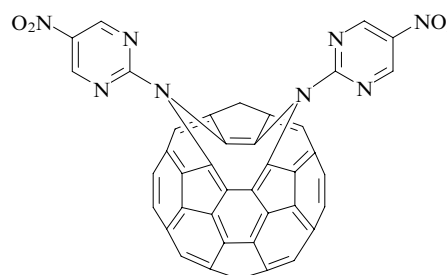
In addition to regioisomeric [6,6]-closed bis(imino)fullerenes, *cis*-1-isomeric bisadducts **65**, which represent the first example of fullerene derivatives with open [6,6]-transannular bonds, were isolated in the bisfunctionalisation of C₆₀ with monoazides (e.g., ethyl and *tert*-butyl azidoformates).⁶⁰



R = Et (a), Bu^t (b).

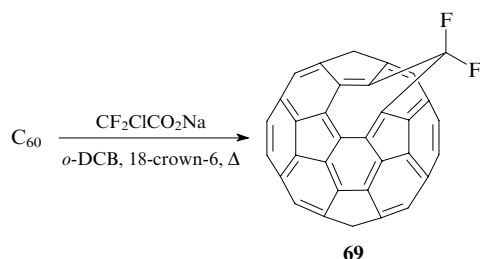
A relatively regioselective synthesis of compounds **65** was accomplished starting from monoiminofullerenes **66** via highly reactive intermediates **67** generated upon [3 + 2]-cycloaddition with a negatively polarised (R)N atom attached to a positively polarised C(4) atom of the adjacent non-functionalised [6,6] bond. Such a polarisation of bonds in the carbon cages of molecules **66** is supported by calculations using the AM1 method. The thermal extrusion of nitrogen gives rise to biradical intermediates **68**. Due to the localisation of the first addend at the same six-membered ring, normal spin density delocalisation over this ring [*i.e.*, spin density transfer to the C(5) atom] becomes impossible and thus the radical recombination can occur only for the radical site localised at the C(3) atom. Consequently, the formation of 1,2;3,4-bis(imino)[60]-fullerene isomer prevails. The subsequent retro-Diels-Alder reaction (or 2π-2σ isomerisation) results in compounds **65**.

Similar formation of a bisadduct with [6,6]-open transannular bonds was also observed in the reaction of C₆₀ with 2-azido-5-nitropyrimidine.⁶¹



It is of note that this adduct undergoes the electrochemical oxidation more readily than fullerene C_{60} .

It is well known that the reaction of C_{60} with dihalocarbenes (CCl_2 and CBr_2) yields closed [6,6]-dihalomethanofullerenes.^{62–64} Nevertheless, as has been found recently,⁶⁵ [6,6]-difluoromethylene-homo[60]fullerene (**69**) can be synthesised by the reaction of C_{60} with CF_2ClCO_2Na in *o*-DCB in the presence of 18-crown-6.

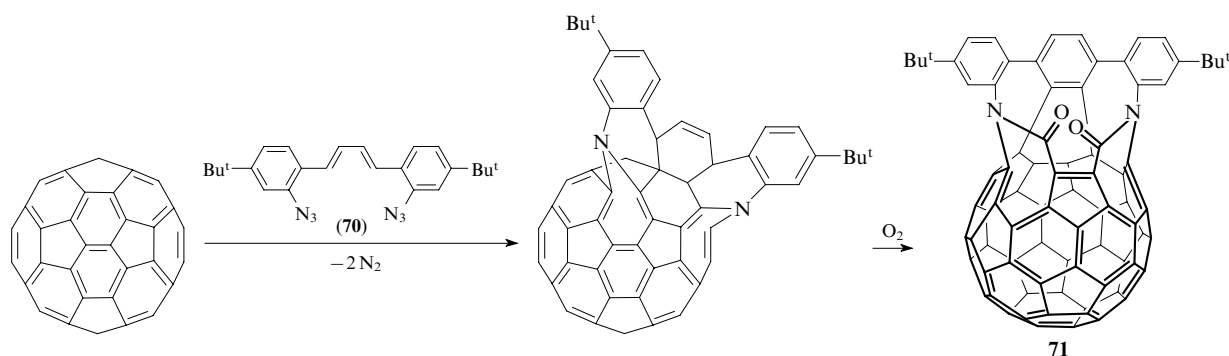
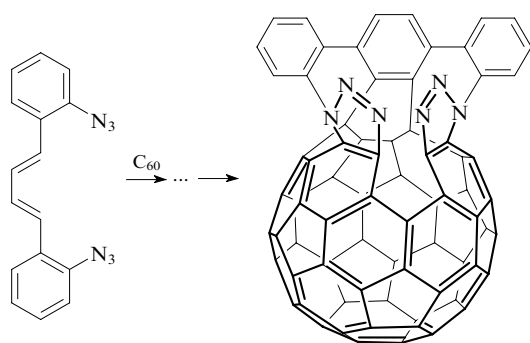


This open monoadduct is the major reaction product (the yield of pure compound is 19%), whereas polyadducts $C_{60}(CF_2)_n$ ($n = 2, 3$) and minor [5,6]-open isomeric monoadduct are formed as by-products. The structure of the adduct **69** was reliably established by mass spectrometry (MALDI), ^{19}F and ^{13}C NMR, UV and IR spectroscopy and further confirmed by quantum chemical calculations.

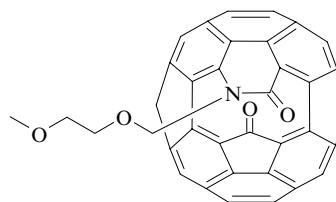
VI. The formation of miscellaneous fulleroid structures

The reaction of C_{60} with diazide **70** is also accompanied by the opening of the fullerene sphere. The oxidation of the intermediate yields bislactam **71** with an open carbon cage capable of accommodating foreign small molecules (He or H_2) (Scheme 13).^{66, 67}

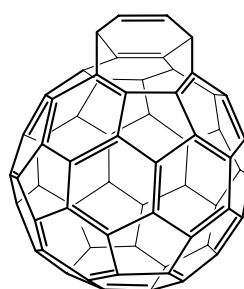
The addition of 1,4-bis(2-azidophenyl)buta-1,3-diene to fullerene is accompanied by complex rearrangements of both the fullerene cage and the addend finally resulting in an open derivative with two fused triazole rings.⁶⁸



A fulleroid keto lactam containing an 11-membered ring was synthesised⁶⁹ by the reaction of C_{60} with methoxyethoxymethyl azide.



A fulleroid with an eight-membered ring in the fullerene cage is obtained from the fullerene adduct with 1,3-cyclohexadiene by the photochemical intramolecular [4+4]-cycloaddition followed by the ring opening.^{70, 71}



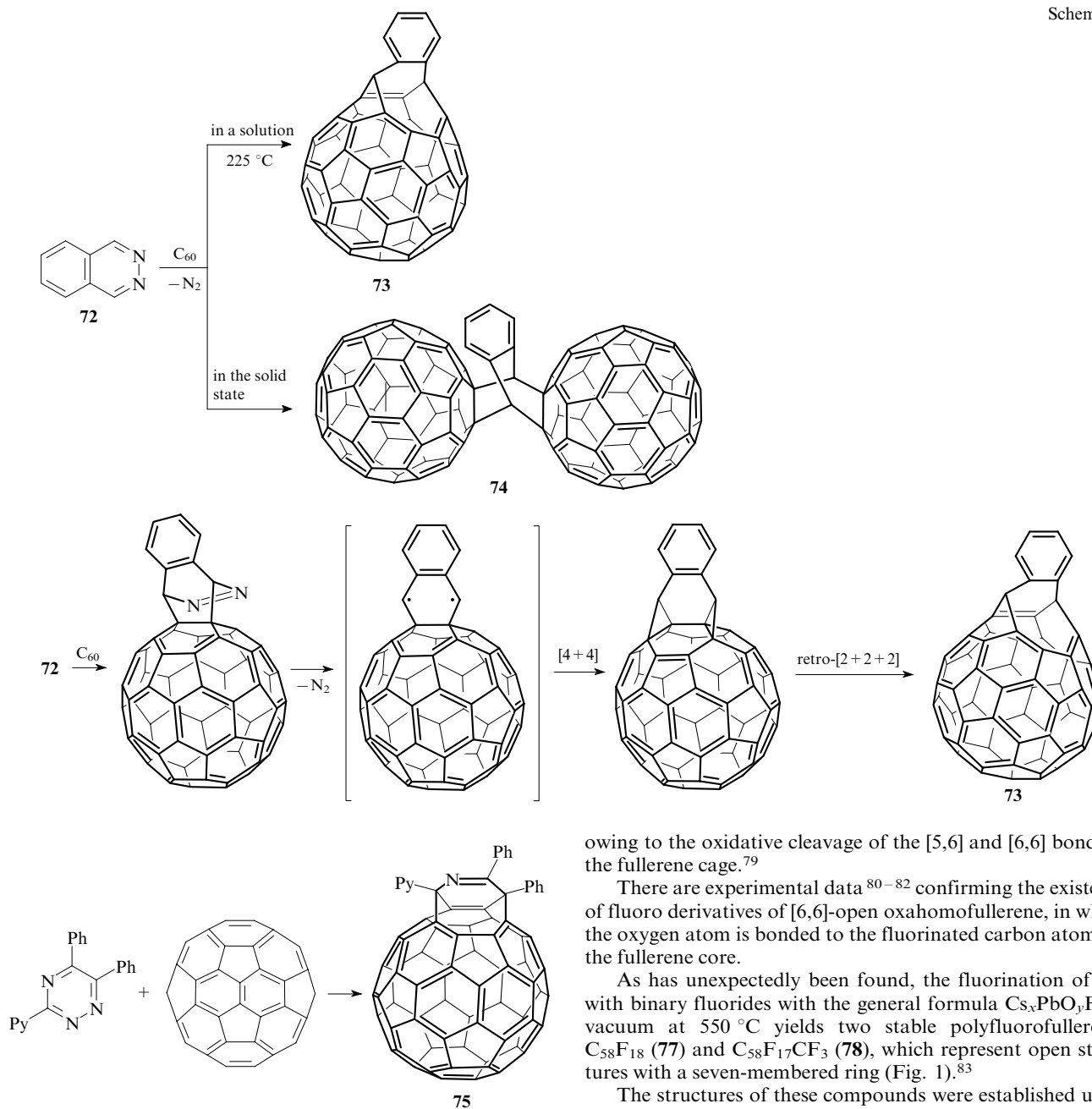
Fulleroid structures with eight-membered rings in the fullerene cages were synthesised in a similar way by the reaction of C_{60} with nickel-⁷² and palladacyclopentadiene⁷³ derivatives and phthalazine.⁷⁴ The direction of the reaction of C_{60} with phthalazine (**72**) depends on the reaction conditions. In particular, a fulleroid structure **73** with an eight-membered ring in the fullerene cage is formed in 1-chloronaphthalene at 225 °C, whereas the mechanochemical solid-state synthesis yields fullerene dimer **74**. The authors argue that both processes start with the [4+2]-cycloaddition stage.^{74, 75} A tentative mechanism of these reactions for di- and triazines is depicted in Scheme 14.^{74–76} It involves the following principal stages: the [4+2]-cycloaddition of azines to the [6,6] bond of fullerene, the elimination of a nitrogen molecule, the radical [4+4]-cycloaddition⁷⁴ and finally the retro-[2+2+2]-process giving rise to the eight-membered ring.

Similarly, the thermal reaction of C_{60} with a 1,2,4-triazine derivative yields an open fulleroid **75** with an eight-membered ring.⁷⁵

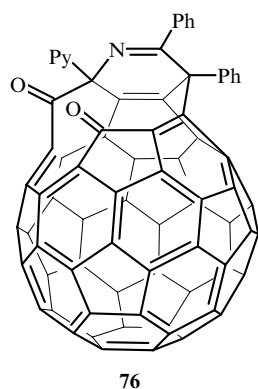
Oxidation of all aforementioned open fulleroids with an eight-membered ring in the cage gives rise to open structures

Scheme 13

Scheme 14



with 12-membered rings^{75–78} (compound **76** can serve as an example). In addition, open structures with 11- and 13-membered rings in the fullerene core were obtained as oxidation products.⁷⁵



The reaction of fulleroperoxide $C_{60}(O)(OOBu^t)_4$ with aluminium chloride yields [5,6]- and [6,6]-oxahomo[60]fullerenes

owing to the oxidative cleavage of the [5,6] and [6,6] bonds in the fullerene cage.⁷⁹

There are experimental data^{80–82} confirming the existence of fluoro derivatives of [6,6]-open oxahomofullerene, in which the oxygen atom is bonded to the fluorinated carbon atoms of the fullerene core.

As has unexpectedly been found, the fluorination of C_{60} with binary fluorides with the general formula $Cs_xPbO_yF_z$ in vacuum at $550\text{ }^{\circ}\text{C}$ yields two stable polyfluorofullerenes $C_{58}F_{18}$ (**77**) and $C_{58}F_{17}CF_3$ (**78**), which represent open structures with a seven-membered ring (Fig. 1).⁸³

The structures of these compounds were established using mass spectrometry and ^{19}F NMR spectroscopy. The authors suggested that the C_{60} molecules lose a carbon atom through the steps of fluorine atom addition to the single C–C and the

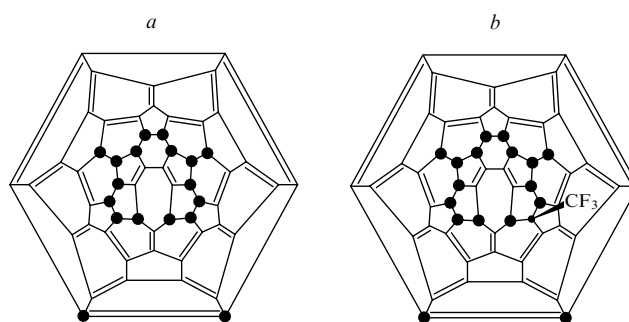


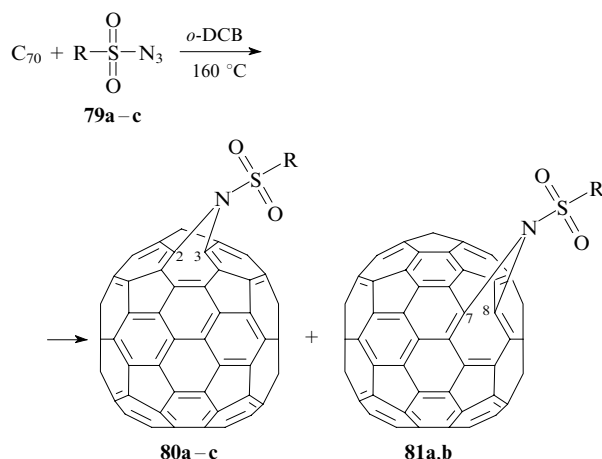
Figure 1. The Schlegel diagrams of open fullerene derivatives $C_{58}F_{18}$ (**77**) (a) and $C_{58}F_{17}CF_3$ (**78**) (b). Black circles denote the addition sites of F atoms.

conjugated double C=C bonds followed by elimination of difluorocarbene.

VII. The formation of open homo[70]fullerenes

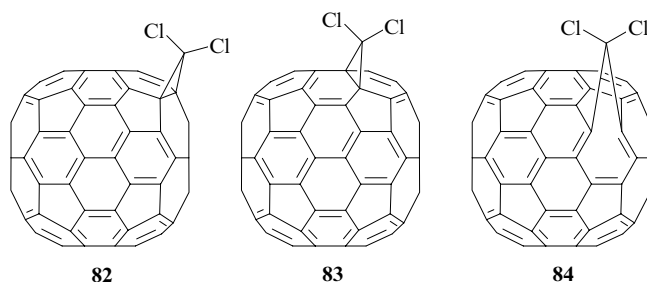
Chemistry of fullerene C₇₀ is studied in much less detail than that of fullerene C₆₀ due to its lower accessibility. Nevertheless, there are some examples of the formation of open structures derived from fullerene C₇₀.

In contrast to fullerene C₆₀, even monofunctionalisation of C₇₀ gives rise to mixtures of regioisomers due to its lower symmetry and larger differences in the reactivity of bonds. Four [6,6]-closed and four [5,6]-open isomeric adducts are possible.



Ulmer and Mattay⁴⁷ studied the reaction of C₇₀ with sulfonyl azides. It is of note that in this case, in contrast to the analogous reaction with C₆₀, only open adducts are formed. These reactions with azides **79a,b** afford two [5,6]-open isomers **80a,b** (in yields of 9% and 10%, respectively) and **81a,b** (in yields of 6% and 7%, respectively). Meanwhile, the reaction with azide **79c** yields only one fulleroid **80c** (12%).

The reaction of C₇₀ with PhHgCCl₂Br, which produces dichlorocarbene upon heating, affords⁸⁴ three monoadducts (**82**, **83**, **84**) in a ratio of 35:37:29 along with polyadducts. Among the products, the adduct **84** is a [5,6]-open fulleroid.



The reaction of C₆₀ with carbenes yields exclusively [6,6]-closed methanofullerenes, in contrast to the situation with C₇₀.

It is known that it is the [5,6] bond between the atoms C(7) and C(8) of fullerene C₇₀ that is involved in the addition of dehydrobenzene resulting in a [5,6]-closed adduct.⁸⁵ The authors suggested that the reaction of C₇₀ with dichlorocarbene begins with the carbene addition to the [5,6] bond to form a [5,6]-closed methanofullerene, which subsequently undergoes the norcaradiene rearrangement to afford a [5,6]-open fulleroid.

VIII. Theoretical investigations into the possible formation of open adducts in the cycloaddition reactions

The mechanisms of the 1,3-dipolar cycloaddition of diazo-methane, nitrile oxide and nitrene to fullerene C₆₀ have been simulated⁸⁶ by *ab initio* calculations at the B3LYP/6-31G(d,p)//AM1 level. All four possible types of the addition giving rise to [6,6]-closed, [6,6]-open, [5,6]-closed and [5,6]-open adducts have been considered. According to the calculations, the cycloaddition processes resulting in [5,6]-closed and [6,6]-open adducts are endothermic, whereas those resulting in [6,6]-closed and [5,6]-open adducts are exothermic. Among all the aforementioned dipolar ylides, the formation of [6,6]-closed adducts is most favourable from both the kinetic and thermodynamic viewpoints. This process has to follow the concerted mechanism. Qualitatively, this theoretical result can be explained by three factors:

- open structures are more strained than closed ones;
- three and two double bonds in five-membered rings appear in [5,6]-closed and [6,6]-open adducts, respectively, which is energetically unfavourable;
- the [6,6] bonds are characterised by higher electron density than the [5,6] bonds, which enables more efficient overlap of the frontier orbitals upon the [6,6]-addition.

Similar to the case of methanofullerenes and their open isomers, [6,6]-closed aziridinofullerenes are calculated to be more stable than [5,6]-azafulleroids, whereas [6,6]-open and [5,6]-closed isomers should be least stable.^{36, 87, 88}

IX. Conclusion

The literature data summarised in the present review suggest that the presently available experimental results and theoretical studies are insufficient for comprehensive understanding of the mechanisms governing the formation of fulleroids. Furthermore, some experimental facts and rationales for the formation of open structures contradict each other. Nevertheless, certain common regularities behind the cycloaddition processes resulting in open adducts can be revealed, which allows us to make some suggestions on the mechanism of the fulleroid formation.

1. With a high level of confidence it can be assumed that open structures are produced as a result of rearrangement or decomposition of an initially formed closed adduct in the majority of systems studied except for nitrile ylides and a few other nitrenes.

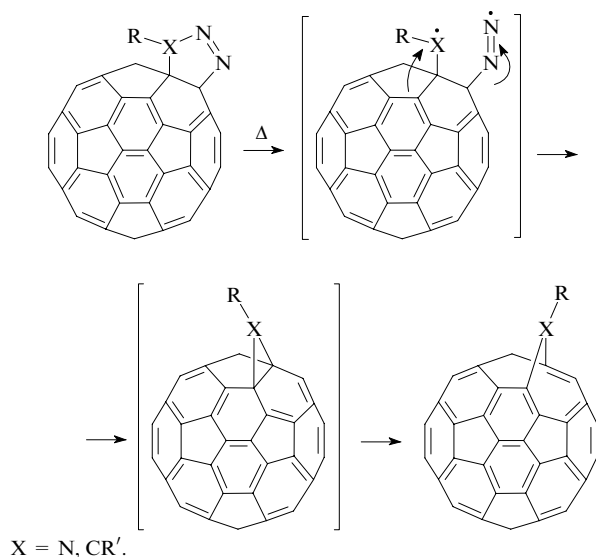
2. Very likely, synchronous addition to the [6,6] bond typically occurs, to yield closed fullerene adducts. This suggestion is supported by both theoretical calculations and numerous experimental data. The available data on the formation of open structures upon the addition of nitrenes, carbenes, diazo compounds, azides and dienes to fullerene suggest that a [6,6]-closed adduct is formed initially but then it is transformed into a fulleroid structure. Nevertheless, some theoretical calculations^{35, 36} point to possible direct addition of nitrenes to the [5,6] bond to yield an open adduct.

3. Open and closed isomers are prone to interconversions, which often do not follow simple structure–stability relationships. In the majority of cases, [6,6]-closed isomers are thermodynamically most stable. Open adducts can transform into closed ones by thermal, photochemical or electrochemical isomerisations; for the opposite process, only thermal rearrangements have been described.

4. Hardly there is a single mechanism explaining the formation of any open structure; several routes to fulleroids can be envisaged.

The first, most common mechanism consists of the thermal decomposition of fulleropyrazolines and fullerotriazolines initially formed upon cycloaddition. The extrusion of a nitrogen molecule proceeds simultaneously with the formation of a new C—X bond, three-membered rings involving a [5,6] bond being preferably formed due to the steric effects of the outgoing nitrogen molecule, *i.e.*, [5,6]-closed adducts are formed. They undergo rapid rearrangements into more stable [5,6]-open fulleroids (Scheme 15).

Scheme 15



An alternative is represented by thermal rearrangements of [6,6]-closed methanofullerenes bearing bulky substituents that induce substantial steric strains in the three-membered ring thus making [5,6]-open isomers thermodynamically more stable. The mechanism of such rearrangements remains unclear.

The third route consists of the formation of [5,6]-open adducts directly as a result of the 1,3-dipolar cycloaddition of specific nitrile ylides to fullerene. Probably, this reaction proceeds as successive addition of nitrile ylide in the biradical form, which gives rise to fulleroids.

There are a number of reactions resulting in the cleavage of a [6,6] bond in the fullerene sphere or even a few σ -bonds at once. These transformations follow different mechanisms that cannot be unified within a single principle. The C—C σ -bonds in a fullerene cage can be cleaved upon the oxidation, reduction or rearrangements.

References

1. J Osterodt, M Nieger, P-M Windscheif, F Vögtle *Chem. Ber.* **126** 2331 (1993)
2. P G Rasmussen, T S Fabre, P A Beck, M J Eissa, J Escobedo, R M Strongin *Tetrahedron Lett.* **42** 6823 (2001)
3. J R Morton, K F Preston, P J Krusic, S A Hill, E Wasserman *J. Phys. Chem.* **96** 3576 (1992)
4. R Pellicciari, B Natalini, L Amori, M Marinozzi, R Seraglia *Synlett* 1816 (2000)
5. R Pellicciari, D Annibali, G Costantino, M Marinozzi, B Natalini *Synlett* 1196 (1997)
6. J Osterodt, A Zett, F Vögtle *Tetrahedron* **52** 4949 (1996)
7. M D Meijer, M Rump, R A Gossage, J H T B Jastrzebski, G van Koten *Tetrahedron Lett.* **39** 6773 (1998)
8. Z Z Li, K H Bouhadir, P B Shevlin *Tetrahedron Lett.* **37** 4651 (1996)
9. P M Warner *J. Am. Chem. Soc.* **116** 11059 (1994)
10. T Ishida, K Shinozuka, T Nogami, M Kubota, M Ohashi *Tetrahedron* **52** 5103 (1996)
11. K-Y Kay, I C Oh *Tetrahedron Lett.* **40** 1709 (1999)
12. K-Y Kay, L H Kim, I C Oh *Tetrahedron Lett.* **41** 1397 (2000)
13. N Martin, L Sanchez, D M Guldi *Chem. Commun.* 113 (2000)
14. A G Avent, P R Birkett, F Paolucci, S Roffia, R Taylor, N K Wachter *J. Chem. Soc., Perkin Trans. 2* 1409 (2000)
15. M T Rispens, L Sanchez, J Knol, J C Hummelen *Chem. Commun.* 161 (2001)
16. L Sanchez, M T Rispens, J C Hummelen *Angew. Chem., Int. Ed.* **41** 838 (2002)
17. T Ohno, K Moriwaki, T Miyata *J. Org. Chem.* **66** 3397 (2001)
18. J C Hummelen, B W Knight, F L Lepeq, F Wudl, J Yao, C L Wilkins *J. Org. Chem.* **60** 532 (1995)
19. J-H Xu, Y-L Li, D-G Zheng, J-K Yang, Z Mao, D-B Zhu *Tetrahedron Lett.* **38** 6613 (1997)
20. T Wakahara, Y Niino, T Kato, Y Maeda, T Akasaka, M T H Liu, K Kobayashi, S Nagase *J. Am. Chem. Soc.* **124** 9465 (2002)
21. N Dragoe, H Shimotani, J Wang, M Iwaya, A de Bettencourt-Dias, A L Balch, K Kitazawa *J. Am. Chem. Soc.* **123** 1294 (2001)
22. M H Hall, H Lu, P B Shevlin *J. Am. Chem. Soc.* **123** 1349 (2001)
23. M Prato, V Lucchini, M Maggini, E Stimpfl, G Scorrano, M Eiermann, T Suzuki, F Wudl *J. Am. Chem. Soc.* **115** 8479 (1993)
24. A B Smith, R M Strongin, L Brard, G T Furst, W J Romanov, K G Owens, R C King *J. Am. Chem. Soc.* **113** 5829 (1993)
25. Z Z Li, P B Shevlin *J. Am. Chem. Soc.* **119** 1149 (1997)
26. C C Zhu, Y Xu, Y Q Liu, D B Zhu *J. Org. Chem.* **62** 1996 (1997)
27. H Tokuyama, M Nakamura, E Nakamura *Tetrahedron Lett.* **34** 7429 (1993)
28. M Eiermann, F Wudl, M Prato, M Maggini *J. Am. Chem. Soc.* **116** 8364 (1994)
29. E-U Wallenborn, R F Haldimann, F-G Klärner, F Diederich *Chem. – Eur. J.* **4** 2258 (1998)
30. A B Smith, H Tokuyama *Tetrahedron* **52** 5257 (1996)
31. G Schick, T Grosser, A Hirsch *J. Chem. Soc., Chem. Commun.* 2289 (1995)
32. F Diederich, L Isaacs, D Philp. *Chem. Soc. Rev.* **23** 243 (1994)
33. A Hirsch *Synthesis* 895 (1995)
34. C K-F Shen, H H Yu, C-G Juo, K-M Chien, G-R Her, T-Y Luh *Chem. – Eur. J.* **3** 744 (1997)
35. M R Banks, J I G Cadogan, I Gosney, P K G Hodgson, P R R Langridge-Smith, J R A Millar, J A Parkinson, D W H Rankin, A T Taylor *J. Chem. Soc., Chem. Commun.* 885 (1995)
36. M Cases, M Duran, M Sola *J. Mol. Model.* **6** 205 (2000)
37. O G Sinyashin, I R Romanova, G G Yusupova, V I Kovalenko, V V Yanilkin, N M Azanchev *Mendeleev Commun.* 96 (2000)
38. I P Romanova, G G Yusupova, S G Fattakhov, A A Nafikova, V I Kovalenko, V V Yanilkin, V E Kataev, N M Azanchev, V S Reznik, O G Sinyashin *Izv. Akad. Nauk, Ser. Khim.* 426 (2001)^a
39. A Yashiro, Y Nishida, M Ohno, S Eguchi, K Kobayashi *Tetrahedron Lett.* **39** 9031 (1998)
40. P S Baran, R R Monaco, A U Khan, D I Schuster, S R Wilson *J. Am. Chem. Soc.* **119** 8363 (1997)
41. Y N Yamakoshi, T Yagami, S Sueyoshi, N Miyata *J. Org. Chem.* **61** 7236 (1996)
42. N Jagerovic, J Elguero, J-L Aubagnac *Tetrahedron* **52** 6733 (1996)
43. I P Romanova, G G Yusupova, O A Larionova, D G Yakhvarov, N N Mochul'skaya, L P Sidorova, V V Zverev, V N Charushin, O G Sinyashin *Izv. Akad. Nauk, Ser. Khim.* 650 (2005)^a
44. I P Romanova, G G Yusupova, D G Yakhvarov, O A Larionova, N N Mochul'skaya, L P Sidorova, V N Charushin, V V Zverev, O G Sinyashin *Izv. Akad. Nauk, Ser. Khim.* 2056 (2003)^a

45. I P Romanova, V V Kalinin, A A Nafikova, D G Yakhvarov, V V Zverev, V I Kovalenko, G L Rusinov, P V Plekhanov, V N Charushin, O G Sinyashin *Izv. Akad. Nauk, Ser. Khim.* **163** (2003)^a
46. I P Romanova, V V Kalinin, D G Yakhvarov, A A Nafikova, V I Kovalenko, P V Plekhanov, G L Rusinov, O G Sinyashin *Mendeleev Commun.* **51** (2002)
47. L Ulmer, J Mattay *Eur. J. Org. Chem.* **2933** (2003)
48. N Wang, J Li, D Zhu, T H Chan *Tetrahedron Lett.* **36** 431 (1995)
49. M Kawaguchi, A Ikeda, S J Shinkai *J. Chem. Soc., Perkin Trans. 1* **179** (1998)
50. L-L Shiu, K-M Chien, T Y Liu, T-I Lin, G-R Her, T-Y Luh *J. Chem. Soc., Chem. Commun.* **1159** (1995)
51. C K-F Shen, K-M Chien, C-G Juo, G-R Her, T-Y Luh *J. Org. Chem.* **61** 9242 (1996)
52. I P Romanova, G G Yusupova, O A Larionova, A A Balandina, Sh K Latypov, D G Yakhvarov, V V Zverev, O G Sinyashin *Izv. Akad. Nauk, Ser. Khim.* **672** (2006)^a
53. C Chen, J Li, G Ji, Q Zheng, D Zhu *Tetrahedron Lett.* **39** 7377 (1998)
54. S González, M Martin, A Swartz, D M Guldi *Org. Lett.* **5** 557 (2003)
55. M Cases, M Duran, J Mestres, N Martin, M Sola *J. Org. Chem.* **66** 433 (2001)
56. A Ouchi, R Hatsuda, B Z S Awen, M Sakuragi, R Ogura, T Ishii, Y Araki, O Ito *J. Am. Chem. Soc.* **124** 13364 (2002)
57. A A Ovcharenko, V A Chertkov, A V Karchava, M A Yurovskaya *Tetrahedron Lett.* **38** 6933 (1997)
58. S-H Wu, G-W Wang, L-H Shu, H-M Wu, K Jiang, J-F Xu *Synth. Commun.* **27** 1415 (1997)
59. M R Banks, J I G Cadogan, I Gosney, A J Henderson, P K G Hodgson, W G Kerr, A Kerth, P R R Langridge-Smith, J R A Millar, A R Mount, J A Parkinson, A T Taylor, P Thornburn *Chem. Commun.* **507** (1996)
60. G Schick, A Hirsch, H Mauser, T Clark *Chem. – Eur. J.* **2** 935 (1996)
61. I P Romanova, G G Yusupova, O A Larionova, A A Nafikova, D G Yakhvarov, V V Zverev, Yu Ya Efremov, O G Sinyashin *Mendeleev Commun.* **309** (2006)
62. Z Yinghuai *J. Phys. Chem. Solids* **65** 349 (2004)
63. M Tsuda, T Ishida, T Nogami, S Kurono, M Ohashi *Tetrahedron Lett.* **34** 6911 (1993)
64. J Osterodt, F Vögtle *Chem. Commun.* **547** (1996)
65. A S Pimenova, A A Kozlov, A A Goryunkov, V Yu Markov, P A Khavrel, S M Avdoshenko, I N Ioffe, S G Sakharov, S I Troyanov, L N Sidorov *Chem. Commun.* **374** (2007)
66. Y Rubin, T Jarrosson, G-W Wang, M D Bartberger, K N Houk, G Schick, M Saunders, R J Cross *Angew. Chem., Int. Ed.* **40** 1543 (2001)
67. J-F Nierengarten *Angew. Chem., Int. Ed.* **40** 2973 (2001)
68. G Schick, T Jarrosson, Y Rubin *Angew. Chem., Int. Ed.* **38** 2360 (1999)
69. J C Hummelen, M Prato, F Wudl *J. Am. Chem. Soc.* **117** 7003 (1995)
70. M-J Arce, A L Viado, Y-Z An, S I Khan, Y Rubin *J. Am. Chem. Soc.* **118** 3775 (1996)
71. W Qian, M D Bartberger, S J Pastor, K N Houk, C L Wilkins, Y Rubin *J. Am. Chem. Soc.* **122** 8333 (2000)
72. T-Y Hsiao, K C Santhosh, K-F Liou, C-H Cheng *J. Am. Chem. Soc.* **120** 12232 (1998)
73. H Inoue, H Yamaguchi, T Suzuki, T Akasaka, S Murata *Synlett* **1178** (2000)
74. Y Murata, N Kato, K Komatsu *J. Org. Chem.* **66** 7235 (2001)
75. Y Murata, M Murata, K Komatsu *Chem. – Eur. J.* **9** 1600 (2003)
76. Y Murata, M Murata, K Komatsu *J. Org. Chem.* **66** 8187 (2001)
77. Y Murata, K Komatsu *Chem. Lett.* **896** (2001)
78. H Inoue, H Yamaguchi, S Iwamatsu, T Uozaki, T Suzuki, T Akasaka, S Nagase, S Murata *Tetrahedron Lett.* **42** 895 (2001)
79. S H Huang, Z Xiao, F D Wang, J Zhou, G Yuan, S W Zhang, Z F Chen, W Thiel, P von R Schleyer, X Zhang, X Q Hu, B C Chen, L B Gan *Chem. – Eur. J.* **11** 5449 (2005)
80. O V Boltalina, B de La Vaissiere, P W Fowler, A Y Lukonin, A K Abdul-Sada, J M Street, R Taylor *J. Chem. Soc., Perkin Trans. 2* **2212** (2000)
81. O V Boltalina, A D Darwish, J M Street, R Taylor, X-W Wei *J. Chem. Soc., Perkin Trans. 2* **251** (2002)
82. R Taylor *J. Fluorine Chem.* **125** 359 (2004)
83. P A Troshin, A G Avent, A D Darwish, N Martsinovich, A K Abdul-Sada, J M Street, R Taylor *Science* **309** 278 (2005)
84. A F Kiely, R C Haddon, M S Meier, J P Selegue, C P Brock, B O Patrick, G W Wang, Y Chen *J. Am. Chem. Soc.* **121** 7971 (1999)
85. M S Meier, G W Wang, R C Haddon, C P Brock, M A Lloyd, J P Selegue *J. Am. Chem. Soc.* **120** 2337 (1998)
86. K Kavitha, P Venunalingam *J. Org. Chem.* **70** 5426 (2005)
87. K Raghavachari, C Sosa *Chem. Phys. Lett.* **209** 223 (1993)
88. F Diederich, L Isaacs, D Philp *J. Chem. Soc., Perkin Trans. 2* **391** (1994)

^a — *Russ. Chem. Bull., Int. Ed. (Engl. Transl.)*

Processes for obtaining linear block copolymers

T B Zheltonozhskaya, S V Fedorchuk, V G Syromyatnikov

Contents

I. Introduction	731
II. Sequential polymerisation of monomers by the same mechanism	731
III. Combination of different mechanisms of monomer polymerisation	748
IV. Matrix effects in block copolymerisation processes	759

Abstract. The advantages and disadvantages of modern methods of synthesis of linear block copolymers using identical and different mechanisms of monomer polymerisation are considered. The attention is focussed on the synthesis of block copolymers with a controlled molecular structure and narrow molecular-mass distribution. The matrix effects that appear in block copolymerisation due to chemical complementarity of the blocks are considered. The bibliography includes 393 references.

I. Introduction

Block type copolymers include a broad spectrum of heteropolymer compounds comprised of two (A, B), three (A, B, C) and more components. There are linear block copolymers, graft copolymers, star-like block copolymers and block copolymers of complex molecular architecture.¹ During the last fifteen years the synthesis of block copolymers has been considered in reviews and monographs (see, *e.g.*, Refs 2–11). This is due to considerable interest of researchers in such compounds and the development of new polymerisation techniques (first of all, controlled, or ‘pseudoliving’, radical polymerisation¹²) that open new possibilities for macromolecular design. Block copolymers are widely used in nanotechnologies;^{13–19} therefore, obtaining of almost monodisperse products with specified length and position of particular blocks requires improvement of relevant synthetic procedures.

Various methods of synthesis of linear di-, three- and multiblock copolymers of the types A-b-B, A-b-B-b-A, B-b-A-b-B, A-b-B-b-C, [A-b-B]_n, [A-b-B-b-C]_n and gradient (tapered) block copolymers of the A-b-(B-co-A)-b-B type are available at the moment. All of them can be divided into three main groups, namely, (i) sequential polymerisation of monomers by the same mechanism; (ii) monomer polymerisation by some mechanism; and (iii) interaction between reactive end groups of oligomers.

T B Zheltonozhskaya, S V Fedorchuk, V G Syromyatnikov Department of Chemistry, Kiev National Taras Shevchenko University, ul. Vladimirska 64, 01033 Kiev, Ukraine. Fax (38-044) 239 31 00, tel. (38-044) 239 34 11, e-mail: zheltonozhskaya@ukr.net (T B Zheltonozhskaya), sergey_fedorchuk@ukr.net (S V Fedorchuk), tel. (38-044) 239 33 00, e-mail: svg@univ.kiev.ua (V G Syromyatnikov)

Received 31 January 2007

Uspekhi Khimii 76 (8) 784–820 (2007); translated by A M Raevskiy

This review concerns the first two groups of the methods of synthesis of linear block copolymers and manifestations of the matrix effects in block copolymerisation, where the first block already formed and the growing second block in the macromolecules of di- or triblock copolymers are chemically complementary. In each case we begin with a brief survey of the corresponding polymerisation mechanism and provide references to comprehensive sources.

II. Sequential polymerisation of monomers by the same mechanism

One-stage (or one-pot) synthesis of linear block copolymers is the most preferable method. The approach involves sequential introduction of different monomers into the reaction without changing external conditions (temperature, solvent, *etc.*) and leads to copolymers of necessary composition, with the desired block lengths and narrow molecular mass distribution (MMD). This can be done provided a correct choice of monomers using the ‘living’ ionic, ion-coordinative and ‘pseudoliving’ radical polymerisation.

1. Homogeneous and microheterogeneous radical polymerisation

Sequential free radical polymerisation was the first method used for the synthesis of linear block copolymers. A PMMA-b-PS block copolymer [PMMA is poly(methyl methacrylate) and PS is polystyrene] was synthesised in the early 1940s by adding styrene to PMMA macroradicals.²⁰ The technique was then used for preparation of various block copolymers of the A-b-B and A-b-B-b-A types.²¹ The mechanism, advantages and drawbacks of free radical polymerisation are well known.^{22, 23} The advantages of this block copolymer synthesis were found to be simplicity of practical implementation, high reaction rate and versatility, a great choice of the monomer pairs and weak dependence on the solvent nature and a presence of impurities.^{22, 23} However, poor controllability of the process owing to its high rate and various chain termination reactions leads to broad MMD and compositional inhomogeneity of resulting block copolymers and to the presence of homopolymer impurities. This makes the method unpromising compared to other techniques.

At the same time the advantages of the process (see above) still attract the attention of researchers, as indicated by studies of so-called ‘micellar’ radical polymerisation.^{24–27} At present, this technique is used only in aqueous medium for the synthesis of multiblock copolymers from polyacrylamide (PAA) or

polyacrylic acid (PAAc) and their hydrophobically modified derivatives. However, the one-stage synthesis and some degree of self-control in the system allow one to hope for progress of research in this field. Since only a few reviews of the method are available,^{24, 27} we will dwell on it in more detail.

The main idea of 'micellar' polymerisation, as applied to the synthesis of block copolymers rather than random ones from a mixture of monomers in the presence of radical initiators, is to separate the chemically different monomers in such a fashion that the system be characterised by micro-heterogeneity and no phase separation. This can be done using a mixture of amphiphilic monomers in water in the presence of surfactants (surfactant concentration should be higher than the critical micelle concentration).^{24–31} The mechanism of 'micellar' polymerisation is shown in Fig. 1. One (soluble) monomer is dissolved in the reaction medium and the other (insoluble) monomer is present in the hydrophobic core of surfactant micelles. The introduction of a soluble initiator (potassium or ammonium persulfate) causes polymerisation of the hydrophilic monomer and the hydrophilic block is thus formed. If the growing chain 'meets' a surfactant micelle, polymerisation of the hydrophobic monomer occurs and the hydrophobic block is formed. A multiblock copolymer is a final product.

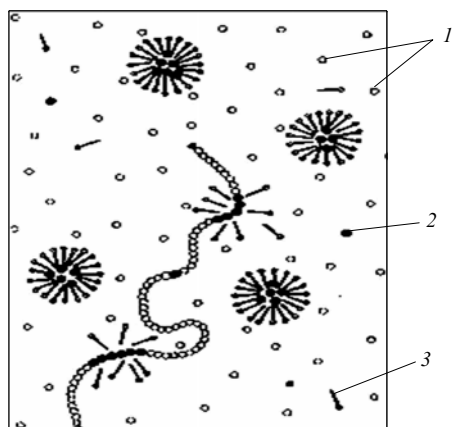
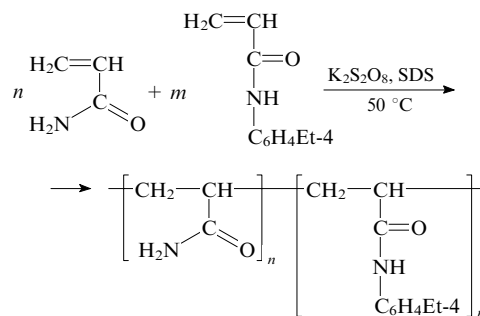


Figure 1. Schematic representation of micellar radical polymerisation.³² Hydrophilic monomer molecules (1), hydrophobic monomer molecules (2) and surfactant micelles (3).

The authors of the pioneering studies (see, *e.g.*, Ref. 33) assumed that copolymers thus synthesised are comprised of randomly distributed hydrophilic and hydrophobic monomers. However, the properties of these copolymers were different from those of the random copolymers synthesised from the same monomers in a common solvent; therefore, a microblock structure of the copolymers was proposed.³⁰ This hypothesis was confirmed by the results of fluorescence studies of the copolymers containing acrylamide derivatives with styryl or pyrenyl groups as hydrophobic co-monomers.^{34, 35} These studies revealed one of the basic regularities of 'micellar' polymerisation, namely, the higher the hydrophobic monomer to surfactant ratio the longer the hydrophobic blocks.²⁴ The structure of micelles was determined. It was shown that the hydrophilic fragments of hydrophobic monomers are located in the hydrophilic 'corona', which also contains a small amount of hydrophilic monomers.^{24, 34} Hence, it was assumed that chain propagation through addition of hydrophobic monomers begins proceeds in the hydrophilic 'corona' of micelles.

Kinetic studies^{32, 36} of the reaction of acrylamide with *N*-(4-ethylphenyl)acrylamide in the presence of sodium

dodecyl sulfate (SDS) as surfactant revealed some additional features of 'micellar' polymerisation.



Solubilisation of hydrophobic monomers into micelles does not reduce their accessibility to the growing chains formed in the aqueous medium. Hydrophobic monomers are more rapidly added to the propagating chain in the initial steps of the process (the larger the hydrophobic monomer : surfactant ratio the higher the addition rate). This effect was explained by migration of the hydrophobic monomers between micelles that occurs three orders of magnitude faster than the addition of these monomers to the PAA' radical. As a result, during polymerisation of the hydrophobic monomer in one micelle the delivery of this monomer from other micelles is also possible. Therefore, in the initial stages of the process the number of monomer units in the hydrophobic blocks, which determines the lengths of such blocks, can be larger than the average number of hydrophobic monomers in the micelle. As the monomer in the micelles is consumed, the hydrophobic blocks become shorter. The major distinction between 'micellar' polymerisation and conventional emulsion polymerisation consists in the high surfactant to hydrophobic monomer ratio (from 15 : 1 to 70 : 1 by mass, see Ref. 32).

Pioneering studies on 'micellar' polymerisation were carried out using pairs of monomers with hydrophilic acrylamide (AAm) and hydrophobic *N*-mono-substituted AAm. In addition to *N*-(4-ethylphenyl)acrylamide (see the reaction shown above), *N*-benzylacrylamide³⁷ and *N*-octyl-, *N*-decyl- and *N*-dodecylacrylamide were used as hydrophobic co-monomers.³⁸ The hydrophilic/hydrophobic balance in the system was changed using not only insoluble *N*-(*n*-decyl)acrylamide or *N*-[4-(*n*-butyl)phenyl]acrylamide and soluble AAm, but also ionogenic monomers, such as sodium acrylate, sodium 3-acrylamido-3-methylbutanoate and sodium 2-acrylamido-2-methylpropanesulfonate.^{39, 40} Therefore, multiblock copolymers comprised blocks built of random copolymers of AAm with ionogenic co-monomers. Recently, alkyl methacrylates⁴¹ and *N,N*-dialkyl acrylamides^{42, 43} with growing hydrocarbon 'tails' have been used as hydrophobic monomers. Surfactants used in 'micellar' polymerisation include not only anionic SDS and sodium hexadecyl sulfate,^{32, 41–43} but also cationic surfactants, *e.g.*, hexadecyltrimethylammonium bromide.³⁷

2. 'Living' anionic polymerisation

Sequential 'living' anionic polymerisation is the most widely used method of synthesis of linear block copolymers of specified composition, molecular masses of constituent blocks and narrow MMD. Generally, 'living' polymerisation involves no chain termination and chain transfer stages, *i.e.*, the rate constants for these reactions are equal to zero ($k_t = 0$, $k_{tr} = 0$, see Refs 22, 23, 44 and 45). However, the 'living' mechanism is also retained if k_t and k_{tr} are much lower than the rate constant for chain propagation in accordance with the following criteria⁴⁶

$$\frac{k_p}{k_t} \geq \frac{\ln([M]_0/[M]_\infty)}{[I]_0}$$

$$\frac{k_p}{k_{tr}} \geq 10 \frac{[M]_0}{[I]_0} \sim 10 \bar{P}_n.$$

Here $[M]_0$ and $[I]_0$ are the initial concentrations of the monomer and initiator, respectively; $[M]_\infty$ is the concentration of monomer at the end of polymerisation and \bar{P}_n is the degree of polymerisation.

These relations represent two important conditions for 'livingness' of the system and obtaining of polymers with predictable structure and molecular mass. The third condition is fast initiation of the process.²² Exactly in this case the polymer chains are formed and grow simultaneously and the degree of polymerisation rises linearly with the monomer conversion (q)

$$\bar{P}_n = \frac{q[M]_0}{f_i[I]_0},$$

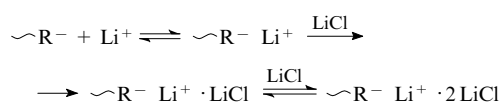
where f_i is the efficiency of initiation. In actual experiments, the condition $k_i = \infty$ (k_i is the rate constant for initiation) is not necessary for control of the molecular mass of a polymer; it is sufficient that inequality $k_i \geq k_p$ be valid.⁴⁶ Obtaining a narrow MMD requires that the following additional conditions be met: (i) equal activity of the growing chains or fast exchange between their active sites; (ii) irreversible chain growth (rate constant for chain propagation should be much higher than the rate constant for depolymerisation). Under these conditions the MMD of the polymer depends only on the degree of polymerisation (according to the Poisson distribution) and the M_w/M_n ratio (*i.e.*, polydispersity index) near to unity.

The 'livingness' of a system may be determined provided that individual or relative rate constants for chain growth, chain termination and chain transfer are known.^{47,48} These principles of retention of the 'living' mechanism mainly concern ionic processes characterised by long lifetimes of active species (this makes it possible to create the fast initiation mode) and by the absence of bimolecular chain termination reactions. Practical implementation of controlled, or 'pseudoliving', radical polymerisation is based on other principles (see below Sections II.5–II.7).

The mechanism of anionic polymerisation and the problems related to the activity of monomers, stability of macro-radicals, choice of initiators, solvents and temperature have been subjects of intensive research and discussion.^{22,23,44,46,49} We remind that anionic polymerisation assumes a nucleophilic attack of carbanion on the double bond of the monomer. Therefore, the monomer which has the most electrophilic double bond and provides greater stabilisation of the negative charge is the most reactive. The nucleophilicity of initiator should be high enough to initiate the process, but not too high to preclude the occurrence of side reactions. The formal criterion for sufficiently high nucleophilicity of the initiator is as follows: the pK_a of corresponding conjugate acid is equal to or higher than the pK_a value of the macroanion.^{22,50} Different forms of active species, namely, ion pairs, separated ion pairs and free ion pairs are in equilibrium. The rate of anionic polymerisation (k_p^-) in the free ion regime increases dramatically⁴⁴

$$k_p^- \approx 10^5 k_p^\pm.$$

To reduce this parameter and thus obtain a narrower MMD, lithium chloride is introduced into the system (this salt shifts the equilibrium from free ions to ion pairs).^{46,51,52}



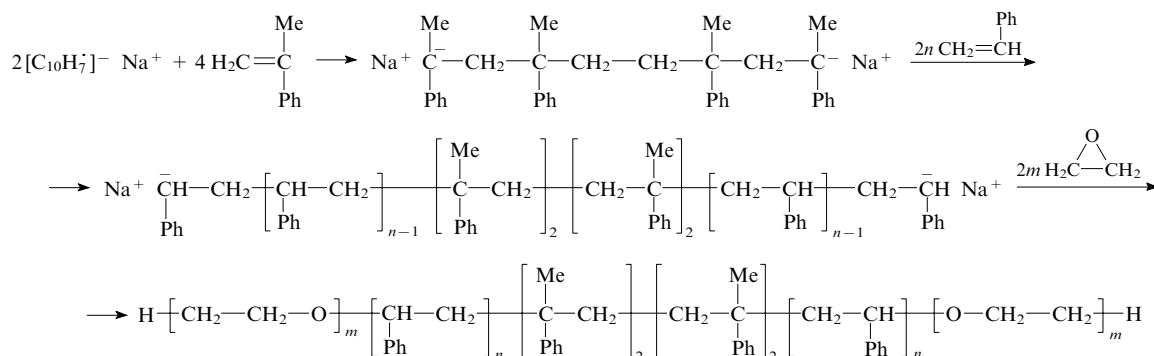
Solvents used in anionic polymerisation processes include hydrocarbons and ethers. Protic and halogen-containing solvents that favour chain transfer or termination are not used. The 'living' anionic polymerisation requires pure reagents, inert atmosphere and correct choice of temperature conditions. Polymerisation of nonpolar monomers in nonpolar solvents is well controllable at moderate positive temperatures (from 0 to 50 °C). Anionic polymerisation of polar monomers in polar solvents occurs at much higher rates, being controllable at low temperatures (as rule, –78 °C). Chain termination is most often attained by adding methanol.

To obtain a copolymer of specified composition, particular block lengths and narrow MMD by 'living' anionic polymerisation, some additional problems should be solved. The main problem is the relative reactivity of monomers, which determines the possibility or impossibility of initiation of polymerisation of the second (and then third) monomer by macroanions formed in the polymerisation of the first (and the second) monomer.^{22,44,46} To this end, a series of monomers with increasing (electrophilic) reactivity are chosen. The process begins with polymerisation of the least reactive monomer that produces the most reactive macroanion; then increasingly more reactive monomers are added. The second problem is the side reactions occurring upon nucleophilic attack of macroanions on other reactive groups of the second (or third) monomer rather than the double bond. This is true for polymerisation of polar monomers containing hydroxyl, carbonyl, ester, amino and other groups.^{22,46} To prevent the process, the 'living' ends of a preceding block are protected by monomers with bulky groups in α -position (α -methylstyrene, α -diphenylethylene, *etc.*). In addition, only protected derivatives of common functional monomers, in particular, (meth)acrylic acids are employed instead of ordinary functional monomers.^{9,53,54} The protective groups include *tert*-butyl, trimethylsilyl, benzyl, alkoxyalkyl and other groups that are removed by polymer-analogous transformations of the block copolymer.⁹ Sequential anionic polymerisation requires a correct choice of reaction conditions (solvent and temperature) to avoid a heterogeneous process. This is particularly important in the synthesis of block copolymers with thermodynamically incompatible blocks. In this connection we will now consider particular syntheses of block copolymers.

a. Binary nonpolar/nonpolar block copolymers

Nonpolar monomers (styrene, dienes, *etc.*) and their macroanions formed in nonpolar solvents show almost identical reactivity in anionic polymerisation. The similarity of nucleophilicities of the styrene and diene macroanions is confirmed by almost equal pK_a values of conjugate acids (40–42 for styrenes and 43 for dienes).⁴⁶ Therefore, the order in which monomers are introduced is of no concern for the synthesis of corresponding di-, tri- and multiblock copolymers. Copolymers with nonpolar blocks were among the first copolymers synthesised.^{55–57} Among them, copolymers based on polystyrene (PS) and polybutadiene (PB) are best known. These are the first representatives of thermoplastic elastomers⁵⁸ that can absorb radiation.⁵⁹ Di-, tri- and multiblock copolymers of predictable structure and narrow MMD were synthesised by sequential addition of styrene (St) and butadiene (B) (*or vice versa*) in nonpolar solvents (hexane, benzene, *etc.*) in the presence of initiators (organolithium compounds). Moreover, by sequentially introducing (i) one monomer, (ii) an equivalent mixture of two monomers and (iii) the other monomer into the reaction one can obtain the so-called gradient triblock copolymers.^{60–62} Here, the PS and PB blocks are separated by a 'mixed' block characterised by a compositional gradient (transition from pure PS to pure PB) owing to the features of copolymerisation of the monomers.

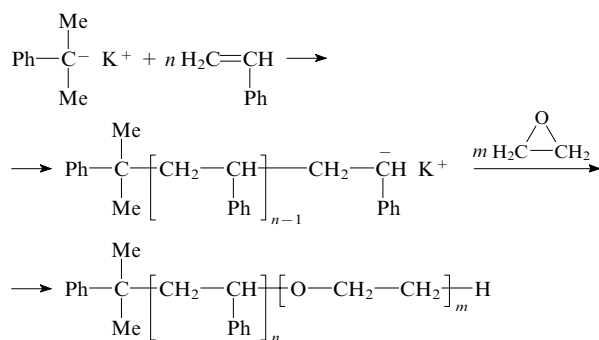
Scheme 1



b. Binary nonpolar/polar block copolymers

Polar monomers are much more reactive than nonpolar ones in anionic polymerisation in contrast to the reactivity ratio of corresponding macroanions. Therefore, anionic polymerisation of polar and nonpolar monomers only leads to two types of block copolymers, namely, A-b-B and B-b-A-b-B (A is the hydrophobic block, which is formed first). Multiblock copolymers based on such pairs of monomers are synthesised using other techniques, *e.g.*, by the reaction between the end functional groups.

The block copolymers in question first of all include amphiphilic block copolymers based on nonpolar PS, PB and polyisoprene (PI) and on polar poly(ethylene oxide) (PEO). When comparing the nucleophilicities of the St and ethylene oxide (EO) macroanions using the $\text{p}K_{\text{a}}$ values of conjugate acids (41–42 and 16–18, respectively),⁴⁶ it is clear that sequential polymerisation of St and EO should develop very actively. The authors of Ref. 63 were among the first to obtain a PS-b-PEO diblock copolymer by sequential introduction of St and EO into the reactor in the presence of cumyl potassium as initiator.



This copolymer was also synthesised using toluene as solvent and 1-phenylethyl potassium as initiator.⁶⁴ Polymerisation of the first block was carried out at 10 °C. The kinetic curves showed an induction period of about 1 h, which reduced as the temperature increased and upon introduction of tetrahydrofuran (THF). Polymerisation of the second block was conducted at a higher temperature (30 °C); as a result, the EO conversion increased to 92%. To study the self-assembly of block copolymers into micelles, PS-b-PEO copolymers containing intermediate units bearing pyrene, anthracene and phenanthrene groups were synthesised.^{65,66} To improve the controllability of sequential polymerisation of St and EO, in the 1990s it was proposed to carry out the process in a polar solvent (THF) at low temperatures (−78 °C).^{67,68}

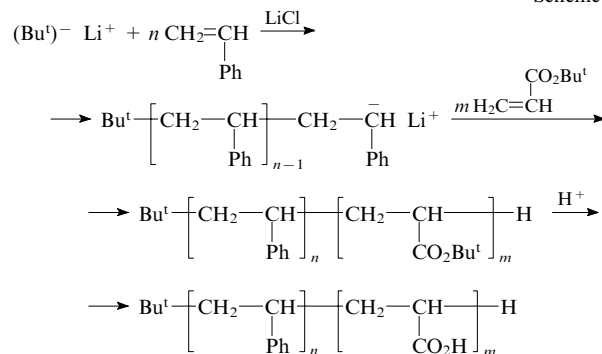
PEO-b-PS-b-PEO triblock copolymers were first prepared using sodium naphthalene as initiator and THF as solvent.⁶⁹ An analogous initiator (potassium naphthalene) was used in polymerisation of styrene and ethylene oxide.⁷⁰ However, in a series of other works^{64,71,72} the dimeric or tetrameric adducts

of sodium (potassium) naphthalene with α -methylstyrene were applied as initiators (Scheme 1). It was found that the reactivities of metal naphthalenes in block copolymerisation decrease as follows: potassium naphthalene > sodium naphthalene > lithium naphthalene. The last-named compound is a very poor initiator for the block copolymerisation of styrene and ethylene oxide.⁶⁴

Di- and triblock copolymers based on polydienes and PEO were synthesised by the same method using mono- and bifunctional organopotassium initiators. In this case the lithium initiator was inefficient. For instance, a PB-b-PEO copolymer was obtained in a polar medium (THF) in the presence of cumyl potassium as initiator,⁷³ while a PEO-b-PI-b-PEO triblock copolymer was synthesised by sequential polymerisation of isoprene and EO in THF with potassium naphthalene as initiator.⁷⁴ Polymerisation of the first block was carried out at −40 °C for 6 h and that of the second block was performed at 25 °C for 3 days. Raising the temperature was due to low solubility of PEO in THF.

The copolymers in question also include copolymers with PS, PB or PE (polyethylene) nonpolar blocks and polar blocks of polyalkyl (meth)acrylates and products of their hydrolysis [PAAc and polymethacrylic acid (PMAAc) or their salts]. Note that methacrylates treated as conjugate acids with respect to macroanions formed from them are characterised by $\text{p}K_{\text{a}}$ values of 27–28,⁴⁶ which is much lower than the $\text{p}K_{\text{a}}$ values of styrene and dienes. Therefore, macroanions based on alkyl(meth)acrylates are incapable of initiating anionic polymerisation of nonpolar monomers. The first syntheses of di- and triblock copolymers based on PS and poly(*tert*-butyl acrylate) (PTBA) were reported in the 1990s.⁷⁵ Sequential anionic polymerisation was conducted in THF in the presence of LiCl at −78 °C.

Scheme 2



The block copolymer precursors were then hydrolysed in toluene at 80 °C in the presence of *p*-toluenesulfonic acid as catalyst to obtain the PS-b-PAAc and PAAc-b-PS-b-PAAc polyacid blocks. The synthesis of PS-b-PAAc and PS-b-PMAAc copolymers with controlled molecular structure and narrow MMD following Scheme 2 was simultaneously

reported by three research groups.^{68,76,77} The side reactions characteristic of 'living' PS chains in the polymerisation of (meth)acrylates were avoided by 'capping' the ends of macroanions by 1,1-diphenylethylene^{76,77} or α -methylstyrene.⁶⁸ This synthetic procedure is used to change the hydrophilic/hydrophobic balance in block copolymers; this is a basic technique in the design of micellar structures sensitive to the pH value of the medium and to salt additives.^{78,79} The lengths of the PS and PAAc blocks varied over a rather wide range, but the polydispersity index of the block copolymers was low ($M_w/M_n = 1.05-1.21$).⁸⁰ An alternative procedure of PTBA transformation into PAAc involves prolonged (more than 10 h) hydrolysis in dioxane at 100 °C in the presence of HCl.⁷⁹ PAAc or PMAAc can also be converted to polyacrylates or polymethacrylates by adding alkali.⁷⁹

PE-b-PMAAc and PMAAc-b-PE-b-PMAAc block copolymers were synthesised by sequential anionic polymerisation involving two polymer-analogous reactions.⁸¹ First, anionic polymerisation of butadiene and *tert*-butyl methacrylate (TBMA) in the presence of mono- or bifunctional initiators resulted in PB-b-PTBMA and PTBMA-b-PB-b-PTBMA copolymers. This was followed by hydrogenation of PB using Wilkinson's catalyst and hydrolysis of PTBMA.

Sequential anionic polymerisation of styrene and alkoxyethyl methacrylates, namely, 1-(ethoxy)ethyl methacrylate (EEMA) and 1-(*tert*-butoxy)ethyl methacrylate (TBEMA), was carried out not only at -78 °C and -35 °C, but also at 0 °C.⁸² A well-controlled process resulted in PS-b-PEEMA and PS-b-PTBEMA copolymers of predictable molecular architecture.

Yet another group of copolymers belonging to this class comprises diblock copolymers based on PS or poly(*tert*-butylstyrene) (PTBS) and cationic polyelectrolytes, namely, poly(2-vinylpyridine) (P2VP), poly(4-vinylpyridine) (P4VP), poly[5-(*N,N*-diethylamino)isoprene] and their quaternised derivatives. They are of interest as stabilisers of colloidal dispersions,⁸³ however, the attention was focussed on their micellar structures^{84,85} and films showing microphase separation.⁸⁶ It should be noted that the pK_a values of 2-vinylpyridine and 4-vinylpyridine treated as conjugate acids with respect to corresponding macroanions are much lower (29 and 26, respectively) than the pK_a values of styrene and dienes.⁴⁶ Therefore, polyvinylpyridine macroanions cannot initiate polymerisation of the nonpolar monomers mentioned above. A typical synthetic route to PS-b-P2VP, PS-b-P4VP and PTBS-b-P2VP assumes sequential introduction of nonpolar and polar monomers in THF, the presence of *n*-butyllithium or *sec*-butyllithium as initiator and a low temperature (-78 °C).^{86,87} Yet another initiator, namely, an adduct of *sec*-butyllithium with 1-methylstyrene, was used⁸⁴ to obtain block copolymers with $M_w/M_n = 1.13-1.14$. When needed, the polyvinylpyridine block was treated with methyl iodide in ethanol, which resulted in a strong cationic polyelectrolyte.⁸⁴

Basic monomers, namely, 5-(*N,N*-dialkylamino)isoprenes, have been synthesised quite recently.^{88,89} Two new amphiphilic block copolymers having poly[5-(*N,N*-diethylamino)isoprene] (PDEAI) blocks, PS-b-PDEAI and PDEAI-b-PS-b-PDEAI, were prepared and studied.⁹⁰⁻⁹² The procedure for the synthesis of the triblock copolymer consisting of sequential introduction of diethylaminoisoprene, styrene and again diethylaminoisoprene⁹¹ points to almost equal reactivities of the monomers. The polymerisation was carried out in benzene at 10 °C using *sec*-butyllithium as initiator. The copolymers had narrow MMDs ($M_w/M_n = 1.2-1.4$, $M_n = 1.36 \times 10^4-2.68 \times 10^4$).^{91,92} Quaternisation of the copolymers with dimethyl sulfate gave copolymers having strong cationic polyelectrolyte blocks.

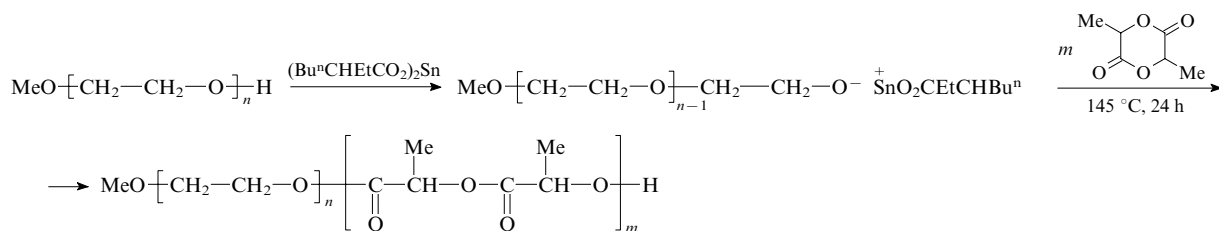
c. Binary polar/polar block copolymers

This group comprises block copolymers based on PEO and poly[alkyl (meth)acrylates]. Comparison of the pK_a values of alkyl (meth)acrylates and oxiranes showed that alkyl (meth)acrylate macroanions should be more reactive than PEO macroanions. Indeed, 'living' poly[alkyl (meth)acrylates] readily initiate the polymerisation of EO.⁹³ However, when using methyl methacrylate (MMA), one can obtain inhomogeneous PMMA-b-PEO copolymers due to side reactions between the 'living' end groups of PEO and the methyl ester groups of PMMA. The monomers can also be introduced in the reverse order. For instance, efficient polymerisation of MMA in THF using PEO disodium alkoxide was reported.⁹⁴ This was explained by the fact that the nucleophilicity of the macroanions is higher than that of the anions at one chain end. Sequential anionic polymerisation of EO and MMA faces two problems.⁹⁵ One of them consists in low solubility of PEO in THF. To avoid the formation of a heterogeneous system, polymerisation of the second block should be carried out at $T > 20$ °C. Under these conditions for polymerisation of MMA the chain termination and chain transfer reactions seem to be unavoidable. The second problem is transesterification between the PEO macroanion and MMA. It was found that by protecting the ester groups of (meth)acrylates with *tert*-butyl groups it is possible to preclude the formation of side products and to obtain copolymers with a desired structure and narrow MMD irrespective of the order of introduction of the monomers. In particular, polymerisation of EO and TBMA in THF at room temperature using cumyl potassium as initiator led not only to diblock copolymers characterised by narrower MMD ($M_w/M_n = 1.4-1.7$) compared to the polymerisation of EO and MMA, but also to multiblock copolymers.⁹⁶ Analogously, sequential anionic polymerisation of the same monomers was used for the synthesis of all possible di- and triblock copolymers, that is, PEO-b-PTBMA, PTBMA-b-PEO, PEO-b-PTBMA-b-PEO and PTBMA-b-PEO-b-PTBMA⁹⁷ with diphenylmethyl potassium and potassium naphthalene as initiators. The synthetic procedure involved polymerisation of TBA at -78 °C; after introduction of ethylene oxide the temperature was raised to 35 °C. Analysis of the reaction products by gel-permeation chromatography and by NMR and IR spectroscopies revealed no side processes and no homopolymers. Quantitative hydrolysis of *tert*-butyl ester groups of PTBMA led to formation of new block copolymers containing PMAAc.

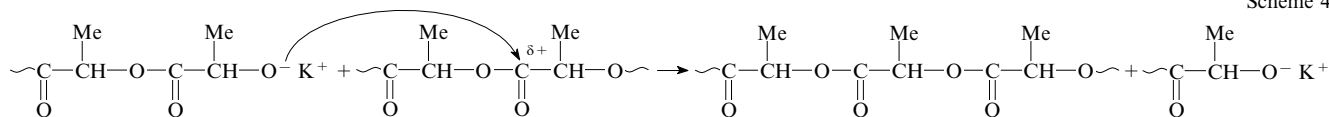
The known non-ionogenic di- and triblock copolymers based on hydrophilic PEO and hydrophobic poly(propylene oxide) (PPO) should be pointed out. They are produced on a large-scale basis under the trademarks 'Proxanols', 'Plurionics' and 'Poloxamers' mainly by sequential anionic polymerisation.²² These amphiphilic block copolymers can form micelles⁹⁸ and complexes with many organic substances^{99,100} including pharmaceuticals.¹⁰¹

A quite interesting group of copolymers is built of PEO and cationic P2VP or P4VP blocks. There are few studies on the synthesis of such compounds, although their micelle-forming properties in aqueous solutions have been a subject of intensive research.¹⁰² Since 2-vinylpyridine and 4-vinylpyridine (VP) are characterised by much higher pK_a values than oxiranes (29 and 26 vs. 16-18, respectively),⁴⁶ one can assume that PVP macroanions will be more reactive than PEO macroanions. This requires that the basic monomer be polymerised first. This order of introduction of the monomers was used in the synthesis of P2VP-b-PEO diblock copolymer.^{102,103} The polymerisation was carried out in THF at -78 °C with cumyl potassium/18-crown-6 ether complex as initiator.¹⁰³ In spite of a narrow MMD of the P2VP blocks, not all 'living' P2VP chain ends initiated the polymerisation of EO. As a result, the

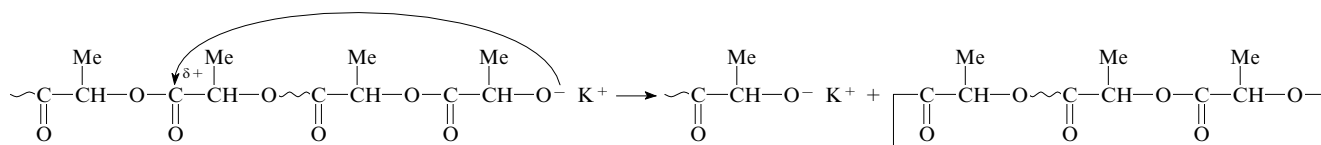
Scheme 3



Scheme 4



Scheme 5



reaction product contained up to 30 mass% of P2VP homopolymer.

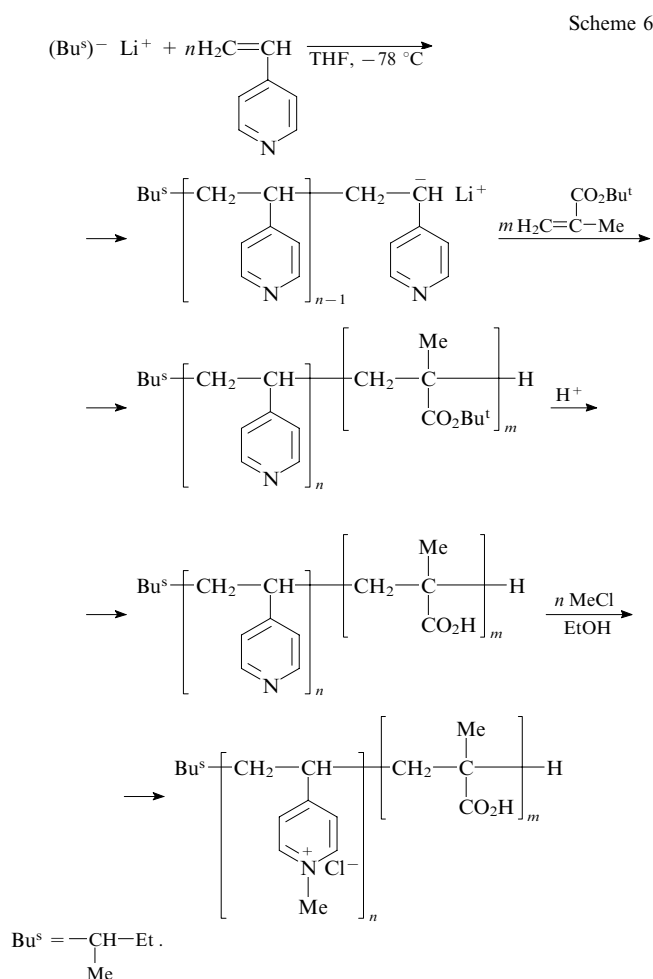
Recently, there has been search for new polar hydrophobic polymer blocks to obtain micelle-forming biocompatible and biodegradable materials by copolymerisation with PEO. One of such polymers is poly(ϵ -caprolactone) (PCL). Copolymers PEO-b-PCL that were synthesised and studied recently^{104,105} are promising for the design of macromolecular therapeutic systems.¹⁰⁶ It should be noted that among the monomers listed in Ref. 46, lactones have the lowest $\text{p}K_a$ values in the range from 6 to 8, *i.e.*, their macroanions have the lowest nucleophilicity. Yet another biodegradable hydrophobic polymer is poly-L(or DL)-lactide (PL),¹⁰⁷ which is also widely used as a constituent of block copolymers. For instance, copolymers PEO-b-PL and PL-b-PEO-b-PL were synthesised and studied.^{108,109} However, the synthetic procedure did not involve sequential anionic polymerisation; macroinitiators based on commercially available polyethylene glycol (PEG) ($M_n = 4 \times 10^3$) or PEG monomethyl ether (PEGME, $M_n = 5 \times 10^3$) were employed. The hydroxyl groups of PEG or PEGME were activated by metallic potassium (in THF)¹⁰⁸ or tin 2-ethylhexanoate,¹⁰⁹ converted to mono- or bifunctional initiators and then anionic ring-opening polymerisation of DL- or L-lactide (Scheme 3) was carried out.

Copolymers PEO-b-PL and PL-b-PEO-b-PL were characterised by M_n of $(5.8-19.2) \times 10^3$ and $(6.0-17.4) \times 10^3$, respectively.¹⁰⁹ Analogous triblock copolymers¹⁰⁸ had similar molecular masses; however, the MMD was broad ($M_w/M_n = 3.04-4.21$) due to intermolecular (Scheme 4) and intramolecular (Scheme 5) re-esterification reactions during the polymerisation of D,L-lactide.

By combining sequential anionic polymerisation and polymer-analogous transformations it is possible to form copolymers containing anionic PAAc or PMAAc blocks and non-ionogenic thermally sensitive *N*-mono- or *N,N*-dialkyl-substituted acrylamide blocks.⁹ They are called the double stimuli-responsive copolymers, because the state of the polyacid blocks is determined by the pH value, while the state of the substituted PAA blocks is governed by temperature. The first stage involved block copolymerisation of protected *tert*-butyl acrylate (TBA) with *N,N*-diethylacrylamide (DEAA)⁹ initiated by a mixture of diphenylhexyl lithium with LiCl. The polymerisation of the first block was followed by introducing triethylaluminium into the system. In the second stage the PTBA-b-PDEAA copolymer was hydrolysed to obtain the PAAc-b-PDEAA copolymer. A similar technique was used for the

synthesis of PTBMA-b-PDMAA copolymers [PDMAA is poly(*N,N*-dimethylacrylamide)] with different block lengths.¹¹⁰ First, *tert*-butyl methacrylate was polymerised under the action of an oligostyryllithium adduct with 1,1-diphenylethylene in the presence of LiCl ($T = -30$ °C). Then, the active centres were modified with an excess of diethylzinc at -40 °C, the temperature was reduced to -78 °C, *N,N*-dimethylacrylamide was introduced and the process continued. Block copolymers thus obtained had $M_n = 3.7 \times 10^4$ ($M_w/M_n = 1.33$) and 1.542×10^5 ($M_w/M_n = 1.28$) and contained 48.7 mass % and 14.3 mass % of PDMAA, respectively.

Amphoteric block copolymers, or copolyampholytes, containing acid (PAAc or PMAAc) and basic {poly[*p*-(*N,N*-dimethylamino)styrene] (PDAS), PVP and poly[2-(dimethylamino)alkyl methacrylates]} blocks occupy a special position. They are synthesised by sequential anionic polymerisation of the basic monomers and protected alkyl (meth)acrylates followed by acid hydrolysis of the polyester blocks. Amphoteric diblock copolymers P2VP-b-PMAAc and P2VP-b-PAAc were first obtained¹¹¹ by sequential polymerisation of 2-VP and trimethylsilyl methacrylate (TMSMA) or TBA followed by hydrolysis of the protected ester groups. A P4VP-b-PMAAc copolymer synthesised in a similar fashion was converted to poly(4-vinyl-1-methylpyridinium chloride)-b-PMAAc copolymer by quaternisation of pyridine groups (Scheme 6).^{112,113} When obtaining the PTMSMA-b-PDAS and PTBMA-b-PDMAEMA copolymers {PDMAEMA is poly[2-(dimethylamino)ethyl methacrylate]},^{114,115} the order of introduction of the acid and basic monomers was reversed. Therefore, the macroanions formed by the basic monomers and protected alkyl (meth)acrylates have similar nucleophilicities. Note that the PTBMA-b-PDMAEMA copolymer¹¹⁵ had a desired molecular mass ($M_{n,\text{exp}} = 5.4 \times 10^3$ from gel-permeation chromatography data, *cf.* $M_{n,\text{theor}} = 5.5 \times 10^3$) and a narrow MMD ($M_w/M_n = 1.08$). The initiation efficiency of the polymerisation of 2-(dimethylamino)ethyl methacrylate by PTBMA macroanions was $f_i = 0.92$. Copolyampholytes PMAAc-b-PDMAEMA were also synthesised and studied.¹¹⁶⁻¹¹⁸ A similar synthesis of the di- and triblock copolymers A-b-B, A-b-B-b-A and B-b-A-b-B with poly[2-(dimethylamino)alkyl methacrylate] (alkyl = ethyl, propyl and 1-ethylmethyl) groups as the A component and sodium polymethacrylate as the B component was reported.¹¹⁹ Polymerisation was carried out in THF at -78 °C with diphenylmethyl lithium as initiator and LiCl as regulator.



d. Nonpolar/polar block terpolymers

One of the first reviews concerning the synthesis of linear block terpolymers by sequential anionic polymerisation was reported in 1980.¹²⁰ In the last decade, considerable advances in the design of A-b-B-b-C copolymers with controlled molecular structures were made using this technique. As previously, the key factor in the design of the synthetic procedure is the relative reactivity of monomers and their macroanions.

A few studies on the synthesis of A-b-B-b-C-terpolymers containing two nonpolar blocks have been reported so far. Recently, PS-b-PB-b-PMAAc terpolymers were obtained by hydrolysing PS-b-PB-b-PTBMA terpolymers synthesised by sequential polymerisation of St, butadiene and TBMA.¹²¹ It was found that the presence of a polar (ionogenic) and two nonpolar blocks ('hard' PS and 'soft' PB) in the same macromolecule leads to a specific morphology of triblock copolymer films, which is different from that of diblock copolymer films. To study the morphology of terpolymers with two nonpolar blocks, a PB-b-PS-b-PEO terpolymer was synthesised by sequential polymerisation with *sec*-butyllithium as initiator.¹²² Hydrogenation of the PB block in the presence of Wilkinson's catalyst gave a PE-b-PS-b-PEO terpolymer with two crystallisable end blocks.

Terpolymers having one nonpolar PS or PB block are of much greater interest. The simplest task is to synthesise terpolymers with a side nonpolar block, which in this case is polymerised first and its highly reactive 'living' chain end initiates the polymerisation of a broad spectrum of polar monomers. This method was employed to obtain a PS-b-PMMA-b-PTBA terpolymer.¹²³ The polymerisation of St in cyclohexane was initiated by *sec*-butyllithium. Once formed,

the PS block was 'capped' with α -methylstyrene to avoid side reactions in the polymerisation of MMA. Then, the third monomer was added. Subsequent hydrolysis of TBA units with *p*-toluenesulfonic acid in toluene (at 100 °C for 5 h) afforded the PS-b-PMMA-b-PAAc terpolymer. It was shown that no hydrolysis of MMA units occurs in the polymer-analogous reaction. This polymerisation scheme was implemented in the synthesis of PS-b-PMMA-b-PEEMA terpolymer⁸² with MAAc protected by 1-(ethoxy)ethyl groups as the third monomer. It was possible to introduce the second and third monomers in any order and thus to change the position of the PMAAc ionogenic block formed upon hydrolysis of the protected units. Terpolymers thus obtained had desired compositions and narrow MMDs. PS-b-PMAAc-b-PMMA terpolymers with central ionogenic block and similar chemical structure were also synthesised.¹²⁴ The ability of the A-b-B-b-C terpolymers comprised of one nonpolar, one polar hydrophobic and one polar hydrophilic (ionogenic) block to form specific micellar structures in aqueous and non-aqueous media attracts the attention of researchers. Such block copolymers may be used as nanoreactors and nanocontainers.^{13, 14, 17, 18}

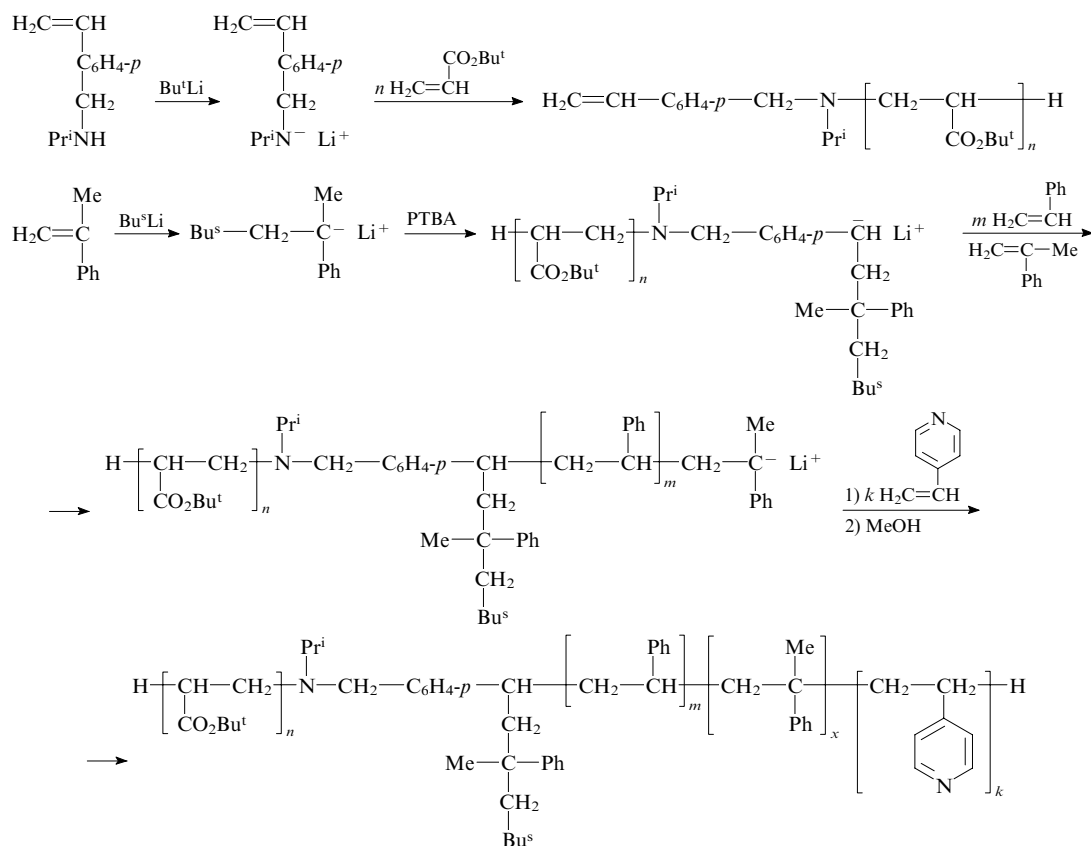
Recently, the synthesis of terpolymers with one nonpolar and two polar hydrophilic blocks by sequential anionic polymerisation has been part of research on novel micellar structures. A number of studies in this field concern the synthesis and investigation of PS-b-P2VP-b-PEO terpolymers with the polybasic central block.^{125–129} Monitoring of changes in the molecular masses and MMDs of the blocks in the course and after the synthesis by gel-permeation chromatography and ¹H NMR spectroscopy gave $M_{n\text{PS}} = 2 \times 10^4$ ($M_w/M_n = 1.07$), $M_{n\text{P2VP}} = 1.4 \times 10^4$ and $M_{n\text{PEO}} = 2.6 \times 10^4$, the polydispersity index of the terpolymer was 1.1 (Ref. 128). The terpolymers formed specific core-shell-corona aqueous micelles.^{127, 130}

A series of studies is devoted to the synthesis of ampholytic block terpolymers. The PS-b-P2VP(P4VP)-b-PMAAc block copolyampholytes were prepared by conventional technique.¹³¹ Sequential polymerisation of St, VP and protected MA gave a precursor of terpolymer and subsequent acid hydrolysis of the protected units resulted in the copolyampholyte. Attempts to synthesise a triblock copolyampholyte with the nonpolar central PS block were reported.^{132, 133} This is a severe problem because P2VP (or P4VP) and protected polymethacrylate macroanions cannot initiate the polymerisation of St. To overcome the difficulty, 5-(*N,N*-dimethylamino)isoprene (DMAI) was used instead of 2-VP (or 4-VP).¹³² The reactivity of DMAI in anionic polymerisation is similar to that of St; therefore, no bifunctional initiator was used in the synthesis of the PDMAI-b-PS-b-PMAAc terpolymer with the central PS block. Sequential polymerisation of the necessary monomers in the reactor afforded a precursor, PDMAI-b-PS-b-PTBMA terpolymer, which was hydrolysed to obtain the PDMAI-b-PS-b-PMAAc copolyampholyte. Another procedure was employed for the synthesis of a copolyampholyte with the side P4VP block.¹³³ In the first stage, a PTBA-based macromonomer with the terminal double bond was prepared. Then, initiation of the macromonomer and anionic polymerisation of St and P4VP (Scheme 7) were carried out.

The process was performed in THF at -78°C using an adduct of *sec*-butyllithium with α -methylstyrene as initiator in the presence of LiCl. The copolyampholyte samples were characterised by narrow MMD ($M_w/M_n = 1.09–1.11$, $M_n = 5.26 \times 10^4–9.86 \times 10^4$).

e. Polar block terpolymers

Presently, a few terpolymers formed by various methacrylates are available. The monomers used are similar in reactivity; therefore, by varying the order of their introduction one can form hydrophilic and hydrophobic blocks at necessary positions. In particular, terpolymers comprised of



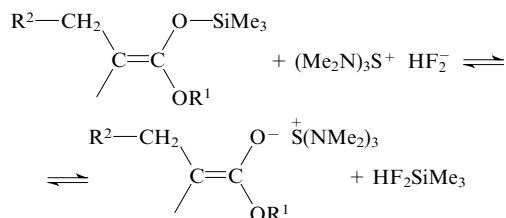
x is the number of molecules of the capping agent (α -methylstyrene) added.

poly[2-(perfluorobutyl)ethyl methacrylate], PTBMA and poly[2-(trimethylsilyloxy)ethyl methacrylate] (PTMSOEMA) were synthesised; the monomers were introduced in different order.¹³⁴ Poly[2-(hydroxy)ethyl methacrylate] blocks were prepared by selective hydrolysis of protected PTMSOEMA units. The microphase structure of terpolymer films was studied.¹³⁵

3. Anionic group transfer polymerisation

Anionic group transfer polymerisation (GTP) discovered in 1983 (Ref. 136) is widely used for the synthesis of di- and triblock copolymers based on polyacrylates and polymethacrylates at room temperature or at somewhat higher temperatures. The key condition for practical implementation of a sequential process is to use monomers with similar reactivities. Opinions differ on the mechanism of this kind of polymerisation.^{22, 23, 137–139} Researchers who proposed the GTP technique explained the ‘living’ mechanism of the polymerisation of methacrylates in the presence of initiators (*O*-silyl ketene ketals) and catalysts [strong nucleophiles, *e.g.*, HF_2^- with tris(dimethylamino)sulfonium or tetrabutylammonium counterions] by the formation of intermediate eight-membered ring accompanied by transfer of the trimethylsilyl group.^{22, 46} This is the so-called associative mechanism.

However, more recently yet another (dissociative) mechanism was proposed with allowance for a lower rate of the process compared to the classical anionic polymerisation of methacrylates, a narrower MMD of polymers and nearly identical stereochemical structure of polymers synthesised by both methods (instead of predominant isotacticity expected for GTP).^{140, 141} It assumes that GTP occurs as anionic polymerisation in which a small amount of enolate anions is in equilibrium with the vast majority of silyl ketene ketal end groups.⁴⁶



Owing to this equilibrium the lifetime of the enolate anions is shortened, which favours retardation of GTP compared to the classical anionic polymerisation. The equilibrium (see Scheme 8) and its shift towards a particular type of active centres also provides an explanation for the lower polydispersity of GTP products. Since here the role of counter-ions is played by tris(dimethylamino)sulfonium or tetrabutylammonium cations, solvent-stabilised free anions should act as the chain growth centres.

At present, GTP is treated as classic anionic polymerisation controlled by reversible chain termination (dissociative mechanism) and/or degenerate chain transfer.⁴⁶ Note that direct group transfer polymerisation of AAc and MAAC is also impossible; the PAAc and PMAAC blocks are prepared by GTP of corresponding protected derivatives followed by removal of the protective groups using relevant chemical reactions.⁹ Now we will consider some examples of the GTP-synthesis of block copolymers.

a. Binary block copolymers

Amphiphilic diblock copolymers PMMA-*b*-PMAAC were synthesised¹⁴² using GTP and a polymer-analogous reaction. Sequential polymerisation of MMA and benzyl methacrylate (BMA) was followed by hydrolysis of the protected units. Diblock copolymers PMMA-*b*-PAAc were prepared in a

similar fashion to study the micelle-forming properties.¹⁴³ The AAc units were protected with *tert*-butyl groups. Triblock copolymer PTBMA-*b*-PMMA-*b*-PTBMA was synthesised from the same monomers (MMA and TBMA) by the GTP method.¹⁴⁴ The copolymer with the central hydrophobic block surrounded by hydrophilic blocks was isolated upon hydrolysis of PTBMA.

New diblock copolymers with various basic blocks were synthesised by sequential GTP of 2-(imidazol-1-yl)ethyl methacrylate and DMAEMA at 25 °C using the 1-methoxy-1-trimethylsiloxy-2-methylpropene–tetrabutylammonium benzoate system as initiator.¹⁴⁵ The basic block containing imidazole groups showed high catalytic activity in the hydrolysis of *p*-nitrophenyl acetate. Two more copolymers with the basic blocks, namely, PDMAEMA-*b*-PDEAEMA {PDEAEMA is poly[2-(ethylamino)ethyl methacrylate]} and PDEAEMA-*b*-PMEMA {PMEMA is poly[2-(morpholino)ethyl methacrylate]} were obtained by the GTP technique.^{146, 147}

Diblock copolyampholytes containing PDMAEMA and PMAAc were synthesised by the same method using protected benzyl methacrylate monomer¹⁴⁸ and tetrahydropyranyl methacrylate (THFMA).¹⁴⁹ In the latter case, poly-THFMA blocks were readily hydrolysed at room temperature.

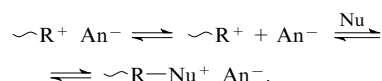
b. Block terpolymers

Model block terpolymers poly[(2-ethylhexyl acrylate)-*b*-PMMA-*b*-PAAc with gradually increasing hydrophilicity of the blocks were synthesised by sequential polymerisation of 2-ethylhexyl acrylate with MMA and TBA followed by hydrolysis of the PTBA block.¹⁵⁰ The GTP technique was used for the synthesis of not only diblock, but also triblock copolyampholytes containing two unlikely charged blocks (PDMAEMA and PMAAc) and a hydrophobic PMMA block.¹⁴⁸ The position of the hydrophobic block strongly affected the micelle-forming properties of the copolyampholytes.¹⁵¹ Triblock copolyampholytes containing the same polymeric components were also obtained using THFMA as the protected monomer and all possible types of introduction of the monomers.¹⁵² Polymerisation was followed by hydrolysis of the PTHFMA block in a weak acid medium.

4. 'Living' cationic polymerisation

'Living' cationic polymerisation makes the design of the chemical structure of block copolymers more versatile, because there exist monomers (isobutylene, alkyl vinyl ethers, *etc.*) that are better polymerised by the cationic mechanism.^{22, 23, 44, 45} Specific features of cationic polymerisation and the stages, kinetics and conditions for carrying out the process have been well documented;^{22, 45, 46} because of this, we will only dwell on the key steps. Cationic polymerisation represents a sequential addition of monomers possessing the properties of nucleophiles and capable of stabilising the positive charge to carbocations.^{22, 23, 45} The development of the process requires that the double bond be the most nucleophilic fragment of the monomer molecule. Traditionally used initiators of 'living' cationic polymerisation include protic acids and products of the interaction of Lewis acids with water, alcohols, ethers and alkyl halides. High reactivity of carbocations predetermines a high rate of chain growth, which makes the process poorly controllable. In addition, β -H atoms become highly mobile; therefore, chain transfer by abstraction of β -protons from the growing carbocations is a typical side reaction occurring in the course of cationic polymerisation of α -olefins.⁴⁶ However, the side reactions can be suppressed by carrying out polymerisation at low temperatures in hydrocarbons and in chlorine- and nitrogen-containing solvents.¹⁵³ Protic solvents and amines that favour chain transfer and chain termination should not be used.

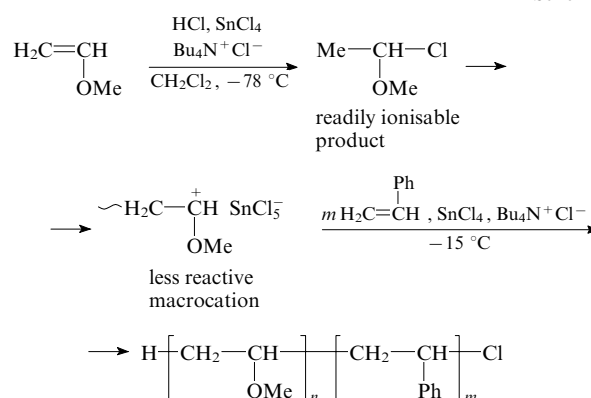
In cationic polymerisation the active centres include the contact and free ion pairs that coexist in equilibrium. The solvent separated ion pairs are not involved in polymerisation processes.⁴⁶ The reactivities of ion pairs and free ions in cationic polymerisation are almost equal ($k_p^\pm \approx k_p^+$), but these species have different lifetimes.^{154, 155} This leads to products of higher polydispersity compared to anionic polymerisation products. An important condition for providing the 'livingness' of the process is reduction of the polymerisation rate. This is achieved by shift of the equilibrium between the active centres towards the contact ion pairs. The growth centres are 'deactivated' by introducing salts (containing the same counterion as the active centre)¹⁵⁶ and nucleophiles (Nu)⁴⁶ that interact with carbocations and form stable ion pairs.



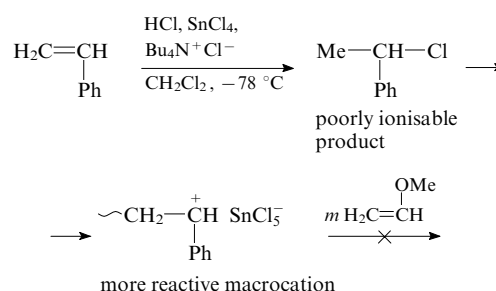
Binding of carbocations to salts or nucleophiles under fast exchange between the active and 'sleeping' centres causes the rate of the process and the polydispersity of macrochains to decrease. Yet another important condition is the reversible character of chain termination. In cationic polymerisation, in the absence of impurities and chain termination agents, the chain growth is mainly ceased owing to collapse of the ion pair,⁴⁶ namely, formation of a covalent bond between the carbocation and counterion (or its fragment²²). However, in some cases the reaction is reversible due to, *e.g.*, the addition of halide ions from the $SnCl_5^-$, $SbCl_6^-$, $SnBr_5^-$, BCl_4^- and BBr_4^- counterions. In such systems, one can hope for controllable character of polymerisation.

The design of a sequential chain in the synthesis of block copolymers using cationic polymerisation has a number of specific features. In particular, the most reactive (most nucleophilic) monomer is most often polymerised first (Scheme 9). This favours fast and quantitative initiation. The polymerisation of the more reactive monomer requires a lower temperature. To activate the polymerisation of the other (less reactive) monomer, the temperature and/or concentration of the co-initiator is increased (Scheme 10).⁴⁶

Scheme 9



Scheme 10



Numerous examples of the synthesis of the A-b-B, A-b-B-b-A, B-b-A-b-B and A-b-B-b-C copolymers by sequential cationic polymerisation are available in the literature. In the early studies, sequential polymerisation of THF and 3,3-bis(chloromethyl)oxetane was carried out.¹⁵⁷ More recently, poly(*p*-methoxystyrene)-*b*-poly(isobutyl vinyl ether) diblock copolymers were prepared.¹⁵⁸ Now we will consider the synthesis of particular block copolymers.

a. Binary nonpolar block copolymers

Studies^{159–162} on the synthesis of block copolymers by sequential cationic polymerisation revealed the possibility of introducing the monomers in the reversed order starting from the less reactive monomer provided that the first block is ‘capped’ with a readily ionisable monomer that cannot be polymerised. This technique was used to obtain almost monodisperse ($M_w/M_n < 1.1$) di- and triblock copolymers containing polyisobutylene (PIB) and poly(1-methylstyrene) (PMS) or other styrene derivatives. Initially, HCl and TiCl_4 were used as initiator and co-initiator, respectively. The polymerisation of IB was followed by ‘capping’ the PIB block with 1,1-diphenylethylene and deactivation of the first Lewis acid (TiCl_4) with titanium isopropoxide or butoxide [$\text{Ti}(\text{OR})_4$]. Then, the second Lewis acid (SnBr_4) was added and the styrene derivative was polymerised. The efficiency of polymerisation initiation of the second monomer approached 100%. At the same time a study on the synthesis of PS-*b*-PMS-*b*-PS copolymers from styrene and *p*-methylstyrene (*p*-MS) characterised by similar reactivities using a bifunctional initiator showed that the resulting triblock copolymer had a narrower MMD ($M_w/M_n = 1.15$) if the more reactive *p*-MS was polymerised first.¹⁶³ When styrene was polymerised first, the product was characterised by $M_w/M_n = 1.34$.

Sequential cationic polymerisation was used for the synthesis of PS-*b*-PIB-*b*-PS triblock copolymers with nonpolar components, which possessed the properties of thermoelastic elastomers.^{164–168}

b. Binary nonpolar/polar block copolymers

Syntheses of block copolymers based on PS, PMS or PB (nonpolar blocks) and on various poly(vinyl ethers) (polar blocks) have been reported. Cationic polymerisation of the following pairs of monomers was studied: *p*-MS–isobutyl vinyl ether (IBVE),¹⁶⁹ St–methyl vinyl ether (MVE), St–chloroethyl vinyl ether (CEVE)¹⁷⁰ and α -MS–CEVE.¹⁷¹ The best results (narrower MMD) were obtained where more reactive monomers, namely, IBVE and MVE, were polymerised first. The technique was used to obtain¹⁷⁰ a PMVE-*b*-PS copolymer with controlled molecular structure and a polydispersity index of 1.33, although the temperature and the Lewis acid concentration were increased in the second stage (see Scheme 9). Polymerisations of the less reactive monomers in the first stage led to mixtures of block copolymers with homopolymers formed by the more reactive monomers in second stage.^{169, 170} Since α -MS and CEVE had almost identical reactivities, their block copolymerisation could be performed in any order.¹⁷¹

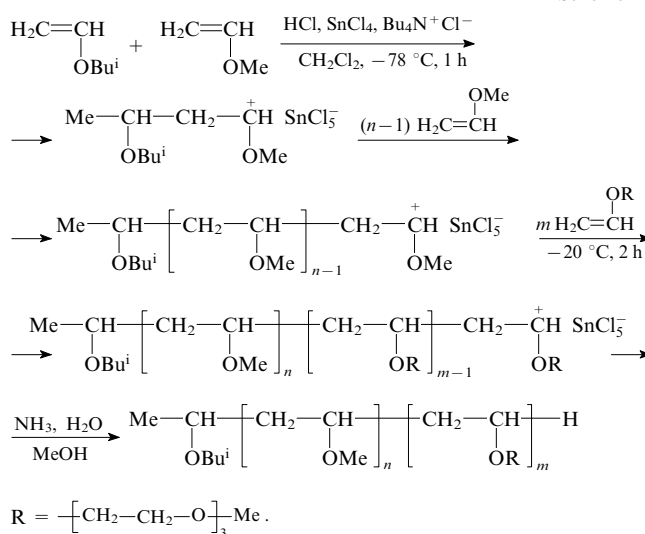
Sequential cationic polymerisation starting with the less reactive monomer was employed for the synthesis of PIB-*b*-PMVE copolymers with a very narrow MMD ($M_w/M_n < 1.1$).¹⁷²

c. Binary polar/polar block copolymers

Typical representatives of this group are diblock copolymers based on various polyethers. Copolymers PMVE-*b*-PCVE [poly(cetyl vinyl ether)] having two polyether blocks ($M_n < 3.5 \times 10^3$), a narrow MMD and controllable composition were obtained¹⁷³ using a HI/ZnI_2 mixture as initiator in the early stage of research in this field.¹⁷³ Sequential cationic

polymerisation starting from the most nucleophilic monomer was employed for the synthesis of diblock copolymers comprised of poly(isobutyl vinyl ether) and poly(*p*-methoxystyrene) (PMOS),¹⁶⁹ PMVE and PMOS¹⁷⁴ and poly[*p*-(*tert*-butoxy)-styrene] (PTBOS) and PIBVE.¹⁶⁹ Copolymers PMVE-*b*-PMTEGVE (PMTEGVE is poly(methyltriethylene glycol vinyl ether) were prepared in a similar fashion (Scheme 11)¹⁷⁵ using an adduct of HCl with isobutyl vinyl ether and SnCl_4 as initiating system. The addition of tetrabutylammonium chloride enhanced the ‘livingness’ of the system. Seven samples of copolymers were obtained in a yield of 99 mass % (no homopolymers). They had molecular masses ($M_n = 1.58 \times 10^3 - 1.40 \times 10^4$) similar to theoretical values and narrow MMDs ($M_w/M_n = 1.14 - 1.29$).

Scheme 11



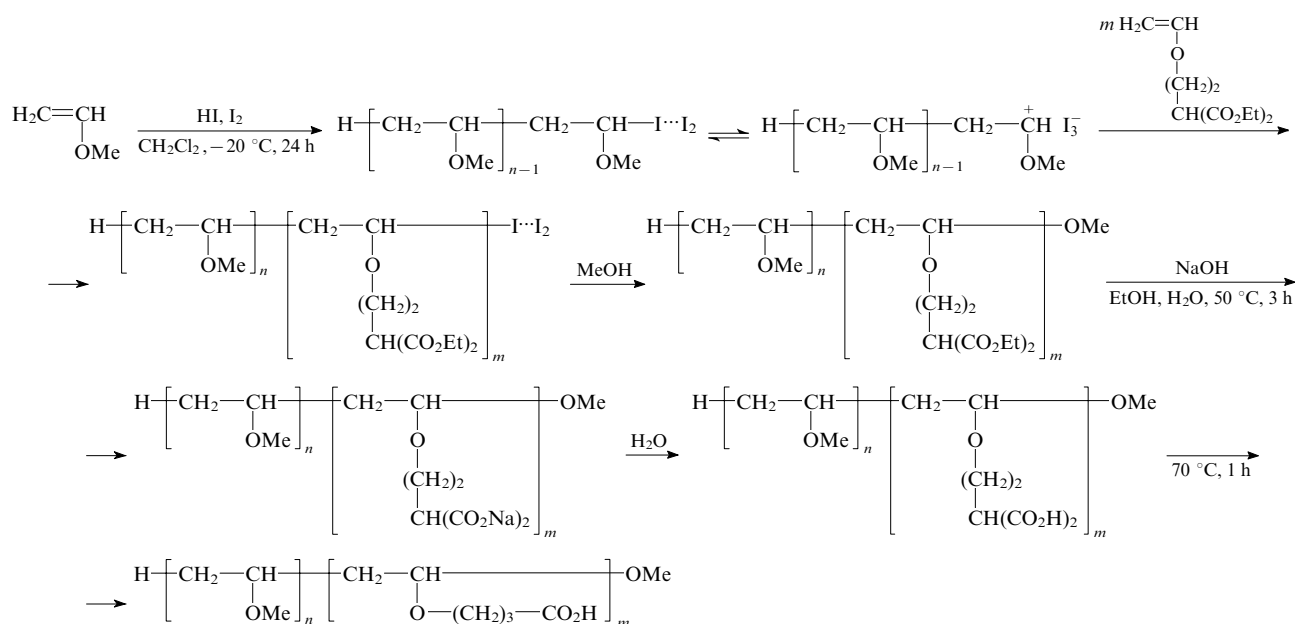
Sequential cationic polymerisation of MVE and ethyl [2-(vinyl)oxyethyl]malonate (EVOEM) to prepare PMVE-*b*-PVOBA diblock copolymers [PVOBA is poly(vinyl-4-butoxy-4-butanoic acid)] (Scheme 12) was reported.¹⁷⁶ Polymerisation of the first block of variable length was followed by introduction of a constant amount of the second monomer and the process was continued. The diblock copolymers thus obtained were involved in two polymer-analogous reactions, namely, alkaline hydrolysis followed by decarboxylation after dialysis. According to size exclusion chromatography and ^1H NMR spectroscopy data, five specimens of PMVE-*b*-PVOBA were characterised by variation of the molecular mass of the first block over a wide range ($M_n = 5.86 \times 10^3 - 3.55 \times 10^4$) and by small variations of the molecular mass of the second block [$M_n = (4.94 - 6.37) \times 10^3$]. The copolymers had narrow MMDs ($M_w/M_n = 1.1 - 1.3$) and served as efficient stabilisers of aqueous and organic iron oxide dispersions.

This polymerisation technique also appeared to be efficient in the synthesis of diblock copolymers based on poly(2-ethyl-2-oxazoline) and poly(L-lactide).¹⁷⁷ Such copolymers attract increasing interest of researchers because they contain two biocompatible blocks.

d. Block terpolymers

The search for new methods of control of the micellar and microphase structures of copolymers predetermines an increase in the number of components in block copolymers, which in turn requires improvement of synthetic procedures. ‘Living’ cationic polymerisation, which is also employed in this case, is of limited use compared to ‘living’ anionic polymerisation. Among the small range of block terpolymers synthesised by this method, mention may be made of model triblock copolymers based on poly(ethyl vinyl ether) (PEVE), PMVE

Scheme 12



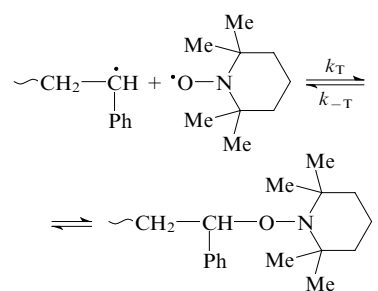
and PMTEGVE containing an equal number of each type of monomer units ($N = 20$).¹⁷⁸ These terpolymers attract the attention of researchers owing to combination of a water-insoluble (PEVE), poorly water-soluble (PMTEGVE) and readily water-soluble (PMVE) blocks in the same macromolecule. Interestingly, the terpolymer dissolved in water (less than 1 mass %) possessed the micelle-forming properties only upon addition of a low-molecular-mass salt.

5. 'Pseudoliving' radical polymerisation involving stable radicals

A fundamental problem in polymer chemistry is to develop methods of controlled radical synthesis of polymers. This problem was solved by the end of the XXth century. At present, there are three commonly accepted types of 'pseudoliving' radical process. These are the stable free radical polymerisation (SFRP), atom transfer radical polymerisation (ATRP) and reversible addition–fragmentation transfer (RAFT) radical polymerisation. Mention may also be made of the molecular design *via* interchange to xanthates (MADIX). At the same time all the methods are based on common principles that allow one to carry out a controlled 'pseudoliving' radical process. From the standpoint of control, the drawbacks of free radical polymerisation include (i) high reactivity of radicals and, as a consequence, a very high rate of the process and (ii) bimolecular chain termination reactions. Therefore, it was proposed to 'divide' the overall polymerisation process into a large number of 'short-term' stages by choosing such reversible chain termination reactions (SFRP and ATRP) or chain transfer reactions (RAFT and MADIX) that their equilibrium constants be rather low and provide a long 'sleep' period. Thus, the main idea of 'pseudoliving' radical polymerisation is to provide conditions for reversible chain termination (inhibition) or chain transfer provided that these reversible reactions are faster than the recombination reaction ($k_{\text{in(tr)}} \gg k_t$).^{23, 179–183} Reversible chain termination or chain transfer reactions characterised by low equilibrium constants play the role of a 'valve' that 'opens' the polymerisation process and 'closes' it upon adding a few monomer units. The characteristic features of a 'pseudoliving' radical process include a linear dependence of the molecular mass of the polymer on the monomer conversion and a narrow MMD.^{22, 180–184} The kinetic laws of various types of 'pseudoliving' polymerisation have been comprehensively treated in reviews.^{185, 186} An original method of determi-

nation of the kinetic parameters of controlled radical processes by linearising the polymer chain length distribution was proposed.¹⁸⁷ Presently, all types of 'pseudoliving' polymerisation are widely used in the synthesis of block copolymers; therefore, we will consider the key features of each type separately.

Otsu and Yoshita¹⁸⁸ were the first to report the significance of reversible chain termination in radical polymerisation. In the mid-1980s, the SFRP technique was developed.^{189, 190} The best results were obtained for the polymerisation and copolymerisation of St-based monomers. Reversibility of the process was maintained by the chain termination reaction involving the growing chains and stable nitroxides [*e.g.*, 2,2,6,6-tetramethylpiperidine-*N*-oxyl (TEMPO)], which became reversible at $T > 100\text{ }^\circ\text{C}$.



The equilibrium constant for C–O bond cleavage in the polymeric alkoxyamine formed is^{23, 191}

$$K = \frac{k_{-T}}{k_T} = 2.1 \times 10^{-11} \text{ mol litre}^{-1}.$$

Here k_T and k_{-T} are the rate constants for chain termination and re-initiation (TEMPO addition and elimination), respectively. In the presence of TEMPO a controlled radical polymerisation of St is thermally initiated using a conventional radical initiator (*e.g.*, benzoyl peroxide) and low-molecular-mass alkoxyamines (AOA) that are products of the interaction of the initiator, TEMPO and (in some cases) monomer molecule.^{23, 179, 180} The rate of 'pseudoliving' polymerisation of St in the presence of AOA obeys the first-order equation with respect to the monomer concentration

$$-\frac{d[M]}{dt} = k_p K \beta [M],$$

where K is the equilibrium constant and $\beta = [\text{AOA}]/[\text{T}^*]$ is the alkoxyamine:TEMPO concentration ratio (this ratio is a constant for a steady-state process).^{23, 179} In addition, up to $q \sim 90\%$ the process is characterised by a linear dependence of the molecular mass on conversion and by narrow MMD ($1.05 < M_w/M_n < 1.2$)

$$\frac{\bar{M}_w}{\bar{M}_n} = 1 + \frac{2}{tk_{-T}}.$$

A feature of ‘pseudoliving’ polymerisation of styrene is alternation of short ($\sim 10^{-4}$ – 10^{-3} s) addition steps of some monomer molecules to the growing chains and long (~ 40 min) ‘sleep’ periods. In the late stages of SFRP polymerisation the rate of the process decreased and the polydispersity of the product increased because of the decomposition of the polymeric alkoxyamine due to disproportionation reaction between the nitroxide radical and the growing macroradical resulting in hydroxyamine and the polymer with the double bond at the chain end.¹⁸⁶

In addition to TEMPO, stable radicals *N,N*-di(*tert*-butyl)-*N*-oxyl (DBN), *N*-(*tert*-butyl)-*N*-(isopropylphenyl)methyl-*N*-oxyl (TIPNO), *N*-(*tert*-butyl)-*N*-(*tert*-butyldiethylphosphonyl)methyl-*N*-oxyl (DEPN), *etc.* were also used in the SFRP processes.^{185, 186} The structure of the nitroxide radical strongly affects the kinetic parameters of the SFRP process. In particular, the more sterically hindered the nitroxide the easier the C–O bond cleavage in alkoxyamines and the higher the rate constants for their dissociation (k_{-T}) and the equilibrium constants (K). For instance, the polymerisation of styrene in the presence of DEPN was characterised by an equilibrium constant K of 6×10^{-9} mol litre⁻¹ (see Refs 185 and 192), which is two orders of magnitude higher than in the case of TEMPO. This makes it possible to reduce the temperature of the SFRP process.¹⁸⁶

SFRP of acrylic monomers (especially methacrylates) in the presence of TEMPO is complicated by the accumulation of nitroxide in the system, which slow down or even prevent the polymerisation.⁹ The degree of control and the rate of polymerisation of these monomers considerably increase in the presence of sterically hindered nitroxide compounds, such as TIPNO, DBN and DEPN. The reason is a higher dissociation rate of the corresponding alkoxyamines compared to that of the TEMPO-based ones.^{185, 186} In addition, a kinetic study of SFRP of *tert*-butyl acrylate in the presence of DBN showed that the rate of the process increases upon addition of a radical initiator dicumyl peroxide.¹⁹³ No significant MMD broadening occurs in this case. In addition, polymerisation of *n*-butyl acrylate under the action of DEPN occurred even without decomposition of polymeric alkoxyamine and was well controlled.¹⁹² At the same time the polymerisation of methacry-

lates was poorly controlled even using sterically hindered nitroxides because polymeric alkoxyamines tend to undergo disproportionation involving abstraction of a proton from α -methyl group.^{186, 194}

Recently, an interesting avenue of research on *in situ* formation of nitroxide radicals in the polymerisation system emerged.^{195, 196} High-molecular-mass spin adducts are formed in the reactions of chain growth radicals with nitrones and nitroso compounds,^{197–202} triazines,²⁰³ sterically hindered secondary amines,²⁰⁴ a nitrogen monoxide/nitrogen dioxide mixture¹⁹⁶ and other compounds. Controlled syntheses of PS, PMMA, poly(vinyl chloride) (PVC), poly(*N*-vinylpyrrolidone) (PVPD) and copolymers of VPD with MMA in the presence of these stable radicals were carried out at low temperatures (50–120 °C) and at rather high rates.^{196–199, 205} However, inhomogeneous structure of the *in situ* formed nitroxides was reported.¹⁹⁶

A new interesting approach to involvement of inactive monomers (MMA and vinyl acetate (VA) in controlled SFRP process by copolymerisation with an active monomer (St) was proposed.^{194, 206} Yet another procedure for practical implementation of a ‘pseudoliving’ SFRP process in the presence of an alternative stable radical, namely, a product of oxidation of alkyl-9-borobicyclo[3.3.1]nonane, will be considered below (see Section III.1).

a. Binary nonpolar block copolymers

Pioneering studies on SFRP of styrene and its derivatives (under the action of benzoyl peroxide in the presence of TEMPO) aimed at preparing block copolymers date back to the early 1990s.^{184, 207–210} The method was used for the synthesis of A-b-B and A-b-B–b-A type block copolymers.^{211–214} More recently, SFRP was also employed in the synthesis of copolymers with polar blocks.

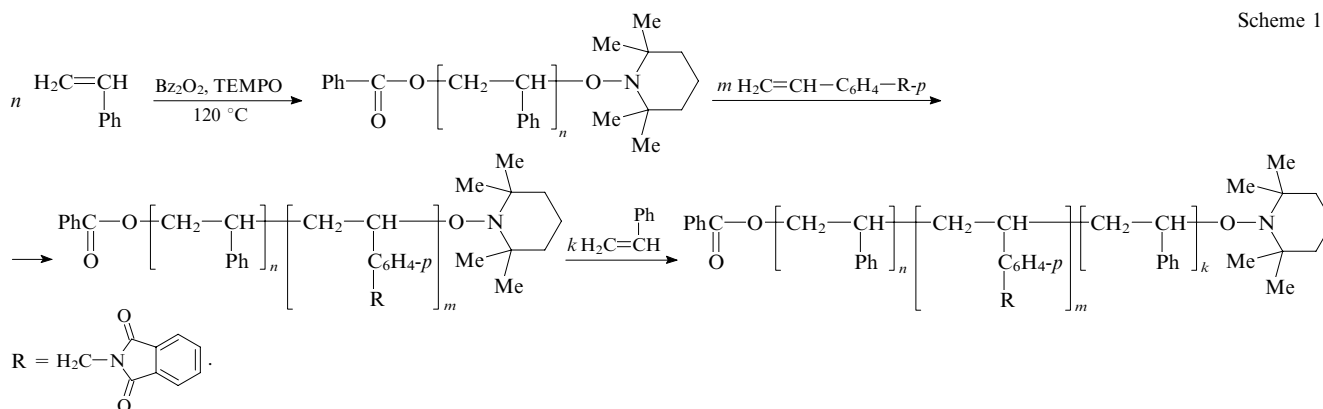
b. Binary nonpolar/polar block copolymers

Quite interesting copolymers PS-*b*-PPhIMS {PPhIMS is poly-*[p*-(phthalimidomethyl)styrene]} and PS-*b*-PPhIMS-*b*-PS were prepared by the SFRP method.²¹⁵ Initially, the polymerisation of styrene under the action of benzoyl peroxide in the presence of TEMPO resulted in PS bearing a nitroxide end group. Then it was used as macroinitiator of the polymerisation of PhIMS, and diblock copolymers with the same end group were thus synthesised. The third, PS, block was obtained using the diblock copolymer as macroinitiator (Scheme 13).

The molecular masses of the PS blocks increased in proportion to conversion and the M_w/M_n ratio was 1.15–1.25. The number-average molecular masses, M_n , of the copolymers varied between 1.9×10^4 and 3×10^4 . Under the action of hydrazine the phthalimide groups were converted to amino groups and thus di- and triblock copolymers containing basic poly[*p*-(aminomethyl)styrene] blocks were prepared.

Diblock copolymers containing the first PS block and PMMA, poly(ethyl methacrylate) (PEMA), poly(butyl meth-

Scheme 13



acrylate) (PBMA), poly(octyl methacrylate) (POMA), PDMAEMA, poly(vinyl acetate) (PVA) and PDMAA as the second block were synthesised analogously using the same initiator (benzoyl peroxide) in the presence of TEMPO radical at higher temperature ($T = 130\text{ }^{\circ}\text{C}$).²¹⁶ The copolymers were thoroughly characterised by gel permeation chromatography and ^1H NMR spectroscopy. The first stage involved the synthesis of PS blocks with nitroxide group ($M_n = 5 \times 10^2 - 2.6 \times 10^3$), which played the role of macro-initiators in the next step. In all cases, except the polymerisation of DMAEMA and VA, the diblock copolymers were obtained in high yields, the molecular masses increased in proportion to conversion and the polydispersity was $M_w/M_n = 1.2 - 1.5$. The end nitroxide groups were detected for all the copolymers. Interestingly, an earlier attempt²¹⁷ to attain controlled homopolymerisation of DMAA in the presence of TEMPO also failed. Controlled homo- and block copolymerisation of this monomer is only possible in the presence of sterically hindered nitroxides TIPNO.²¹⁸ (Co)polymers thus obtained were characterised by $M_n = 4 \times 10^3 - 4.8 \times 10^4$ and a narrow MMD ($M_w/M_n = 1.10 - 1.21$).

It should be noted that the polydispersity indices of the diblock copolymers obtained by SFRP of PS and poly(meth)acrylates are much higher than those of the identical copolymers synthesised by sequential anionic polymerisation. This is quite natural because the efficiency of nitroxide-bearing PS in SFRP of acrylates is low ($f_i < 0.6$ at 125 °C), being even lower for the polymerisation of methacrylates ($f_i < 0.4$).²¹⁰ Therefore, such diblock copolymers have a broader MMD.

Nitroxide-controlled radical polymerisation was successfully used for the synthesis of diblock copolymers from sodium poly(styrene sulfonate) (PSSNa) and polyvinyl naphthalene²¹⁹ and a copolymer with PS blocks and alternating copolymer of St with maleic anhydride (MA).²²⁰ *N*-(*tert*-Butyl)-*N*-(2-methyl-1-phenylpropyl)-*o*-(1-phenylethyl)hydroxylamine was used instead of TEMPO and the poly(St-alt-MA)-*b*-PS copolymer was synthesised in one step.²²⁰ Styrene and MA were taken in a 9 : 1 ratio; the process began with alternating copolymerisation of styrene with MA, which was followed by homopolymerisation of excess styrene upon consumption of MA. A linear increase in M_n with conversion and a narrow MMD ($M_w/M_n \leq 1.2$) were observed.

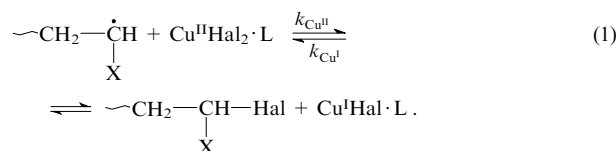
c. Binary polar/polar block copolymers

Only a few studies on the synthesis of polar/polar block copolymers using the SFRP technique have been reported so far. In particular, a PTBA-*b*-PDMAA diblock copolymer was obtained by the SFRP method; subsequent hydrolysis of TBA units afforded PAAc blocks.²¹⁸ Studies^{221–223} carried out to selectively modify the microphase structure of polymer films were based on an original idea. Block copolymers containing protected poly(*p*-hydroxystyrene) blocks were synthesised by the SFRP method in the presence of alkoxyamine. To this end, *p*-acetoxystyrene (AOS), *p*-(*tert*-butoxy)styrene (TBOS), *p*-[di(*tert*-butyl)methylsiloxy]styrene and *p*-(tetrahydropyranyloxy)styrene (THPOS) were used. The main goal was not only to improve the polymerisation process using protected monomers, but also to selectively remove the protective groups from particular blocks of the copolymers by a chemical or thermal method, thus affecting the microphase structure of polymer films. In particular, the protective groups were removed from the PAOS blocks by treatment of the films with hydrazine hydrate and from the PTHPOS blocks by heat treatment.

6. Controlled atom transfer radical polymerisation

6. Controlled atom transfer radical polymerisation
Controlled atom transfer radical polymerisation (ATRP) is an alternative to 'pseudoliving' radical polymerisation. The

method developed by two independent research groups in the mid-1990s^{224–229} differs from the SFRP technique in that chain growth is controlled by a reversible termination redox reaction. The growing chain reversibly interacts with a metal (copper^{224, 226} or ruthenium^{227, 228}) halide fragment of a complex with an organic base, donates an electron to the metal and adds the halogen atom. In the case of a copper catalyst the equilibrium is as follows:



Hal = Cl or Br, L is organic ligand; X is substituent.

Since in the course of polymerisation the halogen atom is transferred along the chain, this ‘pseudoliving’ mechanism was named ATRP. The equilibrium constant for chain growth activation is ^{23, 181}

$$K = \frac{k_{\text{Cu}^{\text{I}}}}{k_{\text{Cu}^{\text{II}}}} = \frac{[\text{M}_n^{\cdot}][\text{Cu}^{\text{II}}]}{[\text{M}_n\text{Hal}][\text{Cu}^{\text{I}}]},$$

where $[M_n]$ and $[M_n\text{Hal}]$ are the concentrations of the ‘living’ and ‘sleeping’ radicals. The polymerisation is initiated by low-molecular-mass organic compounds containing a mobile halogen atom, *e.g.*, 1-phenylethyl halides. Most often, complex-forming organic ligands include 2,2′-bipyridyl and its derivatives, namely, 4,4′-di-(hept-1-yl)-2,2′-bipyridyl; 4,4′-di(non-5-yl)-2,2′-bipyridyl (DNBP) and *N,N,N′,N″,N″′*-pentamethyldiethylenetriamine, *N,N,N′,N″,N″′,N″″*-hexamethyltriethylenetetraamine, *etc.*^{181, 186} The reversible termination mode is attained at high temperatures ($T > 100^\circ\text{C}$). However, lower-temperature ATRP were also reported. For instance, the ATRP of styrene, MA and MMA in the presence of $\text{Cu}^{\text{I}}\text{Cl}(\text{Br})$ complexes with sterically hindered DNBP was carried out at 90°C ; the corresponding equilibrium constants K being rather high, namely, $(1-2) \times 10^{-8}$ (Ref. 230), 1.2×10^{-9} (Ref. 231) and 7×10^{-7} (Ref. 232). With nickel and rhodium halide complexes with triphenylphosphine $[\text{NiBr}_2(\text{PPh}_3)_2]$ and $\text{RhBr}(\text{PPh}_3)_3$ as catalysts the temperature of the ATRP polymerisation of MMA was reduced to 75°C ²³³ with retention of MM control and a narrow MMD of PMMA.

The ATRP method has been well documented in monographs and research communications^{12, 181, 186, 234–237} that provide comprehensive treatment of the mechanism of this process and criteria for the choice of each component of the system (monomer, initiator, transition metal, organic ligands and solvent). When carrying out an ATRP process, the initiator, regulator, solvent and other conditions should be chosen for each monomer in such a fashion that the equilibrium constant ($K = 10^{-8 \pm 2}$) and the rate constant for deactivation of radicals ($k_{\text{da}} = 10^{7 \pm 1} \text{ litre mol}^{-1} \text{ s}^{-1}$) be optimum [for reaction (1) $k_{\text{da}} = k_{\text{CuI}}$].²³⁸ The method does its best in the polymerisation of St- and (meth)acrylate-based monomers, but can also be used for polymerisation of acrylamide, (meth)acrylamides and dienes.²³⁸ It should be noted that ATRP polymerisation can be performed not only in organic solvents (most studies),^{232, 239–241} but also in the bulk,²⁴² in emulsion,²⁴³ in suspension²⁴⁴ and even in aqueous solutions.^{245, 246} However, an attempt to use this approach for polymerisation of (meth)acrylamides failed;²⁴⁷ the process was poorly controlled and the resulting polymers were characterised by a broad MMD. Similar results were obtained for ATRP of DMAA, which led to $M_w/M_n > 1.6$ for the resulting PDMAA.^{248, 249} It was shown that ATRP requires the use of protected acid monomers that cannot be coordinated to the

transition metal and thus poison the catalyst.⁹ In addition, the best catalytic systems are obtained using protonated basic ligands, because this precludes strong complexation with the metal.

In contrast to 'living' anionic polymerisation the ATRP technique is quite tolerant to the nature of monomers and solvents. This makes it possible to synthesise the A-b-B-b-A, B-b-A-b-B and A-b-B-b-C type copolymers from polar and nonpolar monomers starting in any order. Each ATRP synthesised polymer has a mobile halogen atom at the chain end. Therefore, it can act as macroinitiator of polymerisation of other monomers under the action of the same catalytic system. Some examples of the use of ATRP for the synthesis of binary and ternary block copolymers are presented below.

a. Binary nonpolar/polar block copolymers

In this group the most popular objects of synthetic studies are di- and triblock copolymers of PS with protected poly(meth)acrylates. As mentioned above, the (meth)acrylic monomers are protected to prevent the poisoning of catalyst. Di- and triblock copolymers of PS with poly(butyl acrylate) (PBA) of well-defined molecular structure were obtained.²⁵⁰ Similar PBA-b-PS copolymers were synthesised in a water-hexane-Brij98 dispersion.²⁵¹ The process was initiated by ethyl-2-bromoisobutyrate and a complex of CuBr with DNBP was used for reversible termination. The block copolymers thus obtained were characterised by $M_n = 1 \times 10^4 - 4 \times 10^4$ and $M_w/M_n = 1.12 - 1.25$. Amphiphilic di- and triblock copolymers of PS with PAAc were obtained as follows:²⁵²⁻²⁵⁶ di- or triblock precursors (with PTBA) were synthesised by ATRP and subsequent acid hydrolysis of the TBA units gave the PAAc blocks. Studies^{252,253} were carried out using methyl 2-bromopropionate as initiator and a complex of CuBr with PDMETA as catalyst. A 'pseudoliving' mechanism of the process with a linear increase in M_n depending on conversion was observed at 60 °C only in polar solvent (acetone).

A similar scheme was also used to obtain block copolymers of PS with PMAAc in other studies;^{257,258} however, the protected monomer was *p*-nitrophenyl methacrylate in the former study and TBMA in the latter.

Examples of successful use of ATRP in the synthesis of highly hydrophobic diblock copolymers based on PS and polyfluorinated polyalkoxystyrenes have been reported.^{259,260} First, polyfluorinated monomers, namely, 2,3,5,6-tetrafluoro-4-(2,2,3,3,3-pentafluoropropoxy)styrene [TF(F₅)S] and 2,3,5,6-tetrafluoro-4-(2,2,3,3,4,4,5,5,6,6,7,7,8,8,8-pentadecafluorooctoxy)styrene [TF(F₁₅)S] were synthesised and their ability to undergo controlled ATRP was checked and confirmed.²⁶⁰ The products synthesised were characterised by a narrow MMD ($M_w/M_n \leq 1.3$). Oligomers with $M_n = 6.5 \times 10^3$ were then used as macroinitiators of the polymerisation of styrene, which resulted in A-b-B type copolymers [poly-TF(F₅)S-b-PS and polyTF(F₁₅)S-b-PS] of well-defined molecular structure and narrow MMD. In addition, the polymerisation in a xylene solution (owing to poor solubility of the fluorinated blocks) was performed using the reverse order of introduction of the monomers and led to B-b-A type copolymers characterised by M_{nPS} of 4×10^3 and 9.7×10^3 , PS content of 36 and 90 mol.%, respectively, and $M_w/M_n \leq 1.37$.

An ATRP synthesised diblock copolymer of poly(4-fluorostyrene) (PFS) and poly(methyl acrylate) (PMA) was converted to PFS-b-PAAc amphiphilic copolymer by hydrolysis of the PMA blocks and used for the synthesis of micellar nanoparticles with cross-linked 'corona' comprised of the PAAc blocks.²⁶¹

b. Binary polar/polar block copolymers

ATRP was used for preparation of amphiphilic diblock copolymers containing hydrophobic PMA or PMMA blocks.

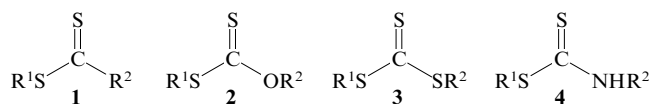
A block copolymer precursor synthesised by sequential polymerisation of MMA with TBMA was selectively hydrolysed,²⁶² which resulted in PMMA-b-PMAAc copolymer. This scheme was also employed in the synthesis of amphiphilic diblock copolymer PAAc-b-PMA²⁶³ with TBA as the protected monomer in the first stage. The micelle-forming properties of the copolymers were the most interesting.

c. Block terpolymers

In recent years, the ATRP method has been used for the synthesis of copolymers containing three chemically different blocks (terpolymers). For instance, not only diblock copolymers, but also terpolymers of composition PTBA-b-PS-b-PMA were synthesised in the study mentioned above.²⁶³ Sequential introduction of TBA, PS and PMA faced no problems, unlike the case of 'living' anionic polymerisation (see Section II.2). The ATRP polymerisation of TBA, MA and styrene led to a PTBA-b-PMA-b-PS terpolymer, which was converted to the PAAc-b-PMA-b-PS terpolymer with increasing block hydrophobicities by hydrolysis of the PTBA block.²⁵² The micelle-forming properties of these compounds and the possibility of nanoparticle formation with a chemically cross-linked 'corona' was studied.

7. 'Pseudoliving' radical polymerisation with reversible chain transfer

The third type of 'pseudoliving' radical polymerisation, namely, reversible addition-fragmentation chain transfer (RAFT) polymerisation was developed in the 1998-1999s.²⁶⁴⁻²⁶⁷ It is characterised by the lowest sensitivity to the nature of monomers, solvents and external polymerisation conditions. The method was even used for controlled synthesis of PAAc ($M_w/M_n = 1.23$) using unprotected AAc [$T = 60$ °C, dimethylformamide (DMF) as solvent and azobis(isobutyronitrile) (AIBN) as initiator].²⁶⁴ A feature of the RAFT polymerisation is the presence of dithioester chain transfer agents (CTA) of the general structure 1-4



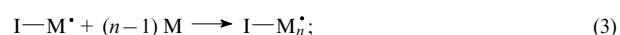
which readily react with either the initiator radical (e.g., AIBN) or the growing polymer chain, thus forming a new CTA, or with the macroCTA, and the reactive radical (R^1), which re-initiates the polymerisation:

initiation

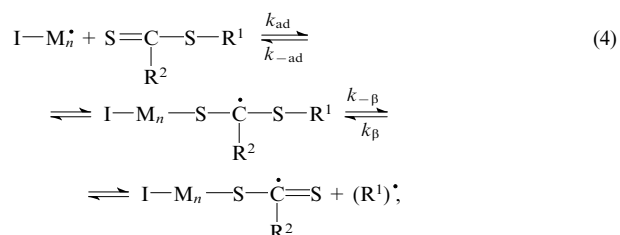


where k_d is the rate constant for decomposition of the initiator;

chain growth



addition-fragmentation reaction

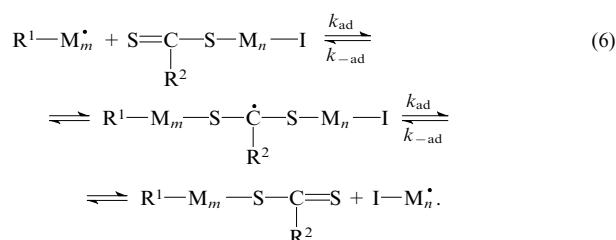


where k_{ad} and $k_{-\text{ad}}$ are the rate constants for addition of (macro)CTA molecules to the growing chains and for elimination of the (macro)CTA molecules, respectively, and k_{β} and $k_{-\beta}$ are the rate constants for addition of $(\text{R}^1)^\bullet$ radicals to the macroCTA molecules and for their fragmentation, respectively;

re-initiation/chain growth



chain alignment(degenerative chain transfer)



'Pseudoliving' polymerisation mode provides a reversible chain transfer.^{264, 265, 268} Reversible (degenerative) chain transfer occurs until the MMs of the growing chains become almost equal to one another, thus providing a narrow MMD.

The rate constant for degenerative chain transfer, *i.e.*, the rate constant for radical exchange in the CTA molecules [stage (6)], is defined as follows:

$$C_{\text{ex}} = \frac{k_{\text{ex}}}{k_{\text{p}}} = 0.5 \frac{k_{\text{ad}}}{k_{\text{p}}},$$

where k_{ex} and k_{p} are the rate constant for degenerative chain transfer and the rate constant for chain growth, respectively.^{185, 186} At $C_{\text{ex}} \geq 100$ and at low conversions, the starting CTA is completely transformed into macroCTA following reaction (4) and then the macroCTA participates in degenerative chain transfer following reaction (6). The highest C_{ex} values are characteristic of the RAFT polymerisation of *n*-alkyl acrylates, they are somewhat lower for the polymerisation of styrene and even more lower for that of MMA.²⁶⁹ For instance, the polymerisation of styrene ($T = 40^\circ\text{C}$) and MMA ($T = 60^\circ\text{C}$) under the action of macroCTA (polystyryl dithiobenzoate) was characterised by $C_{\text{ex}} = 6000 \pm 2000$ and 140, respectively.²⁷⁰ The existence of radical intermediates [see stages (4) and (6)] in the RAFT polymerisation of styrene, *n*-butyl acrylate (nBA), *N*-vinylpyrrolidone, VA and other monomers was proved by EPR spectroscopy.^{271, 272} No proof was obtained only for MMA owing to high $k_{-\text{ad}}$ value.²⁷¹ The first CTAs used in the synthesis of PAAc were 1-phenylethyl dithiobenzoate²⁶⁴ and 1-cyanoethyl-2-pyrrolidone-1-carbodithioate.²⁷³

Practical implementation of a RAFT process requires that the rates of radical addition to the $\text{C}=\text{S}$ double bond and subsequent abstraction of reactive radicals be higher than the chain propagation rate. Therefore, the choice of the R^1 and R^2 radicals in the CTA molecule matters. To provide fast radical addition to CTA, the R^2 substituent should act as stabiliser. Usually, this role is played by the phenyl group.²⁶⁸ Rapid abstraction of the R^1 radical requires that R^1 have a rather long lifetime, be active in the re-initiation reaction and be surrounded by bulky groups to avoid recombination. With allowance for these requirements, good results were obtained using a tertiary radical of 4-cyanopentanoic acid.^{268, 273, 274} By appropriately choosing the R^2 substituent one can also eliminate the well-known effect of a strong decrease in the chain propagation rate in the presence of RAFT agents.^{186, 267}

Yet another reaction proposed²⁷⁵ to control radical polymerisation processes is the reaction of chain transfer to dithiocarbonates (xanthates) of general formula represented by structure 2. This type of controlled radical polymerisation was named the 'molecular design *via* interchange to xanthates' (MADIX). Among other CTAs used for reversible chain transfer, mention may be made of trithiocarbonates 3 and dithiocarbamates 4.^{273, 276–278} For instance, dibenzyl and bis(1-phenylethyl) trithiocarbonates provided well-controlled polymerisation of AAc²⁷⁹ and benzyl and cumyl dithiocarbamates provided well-controlled polymerisation of *N*-isopropylacrylamide.²⁷⁷

The number-average MM of a polymer obtained by RAFT polymerisation is given by²⁸⁰

$$\bar{M}_n = q \frac{M_{\text{M}}[\text{M}]_0}{[\text{CTA}]_0 + 2f_{\text{i}}[\text{I}]_0(1 - e^{-k_{\text{at}}t})} + M_{\text{CTA}},$$

where M_{M} and M_{CTA} are, respectively, the molecular masses of the monomer and CTA, and $[\text{M}]_0$ and $[\text{CTA}]_0$ are the initial concentrations of the corresponding reactants. For an ideal RAFT process the number of polymer chains emerged from the initiator molecules should be minimum. In this case the second term in the denominator becomes small compared to $[\text{CTA}]_0$. In addition, the parameter M_{CTA} can be neglected at a high molecular mass of the polymer. Therefore, in most studies on RAFT polymerisation the value \bar{P}_n was estimated from the relationship

$$\bar{P}_n = q \frac{[\text{M}]_0}{[\text{CTA}]_0}.$$

Once synthesised, polymers contain dithioester, xanthate, trithiocarbonate or dithiocarbamate end groups, which permits continuation of controlled radical polymerisation of other monomers to obtain linear block copolymers. The method allows one to carry out controlled synthesis of anionic and cationic polyelectrolytes and polyelectrolyte block copolymers in aqueous medium. Below we present some examples of the synthesis of block copolymers using different versions of the technique. All of them concern diblock copolymers containing at least one polar block.

a. Nonpolar/polar diblock copolymers

These block copolymers were synthesised by the RAFT method. For instance, a PS-*b*-PEA [PEA is poly(ethyl acrylate)] copolymer was obtained by the MADIX technique in emulsion.²⁸¹ By hydrolysis of the ethyl acrylate units it was converted to amphiphilic copolymer PS-*b*-PAAc. A PS-*b*-PEA copolymer ($M_{\text{nPS}} = 2 \times 10^3$, $M_{\text{nPEA}} = 1.95 \times 10^4$; $M_{\text{w}}/M_{\text{n}} \sim 2.0$) was synthesised in a similar fashion and the effect of the degree of hydrolysis of PEA on the character of the micelle-forming properties of the diblock copolymer in aqueous medium was studied.²⁸² A series of poly(St-*alt*-MA)-*b*-PS copolymers with variable length of both blocks [$M_{\text{n}} = (3.11 - 3.52) \times 10^4$] and narrow MMD ($M_{\text{w}}/M_{\text{n}} = 1.09 - 1.16$) was synthesised by the RAFT method.²⁸³

b. Polar (including ionogenic) block copolymers

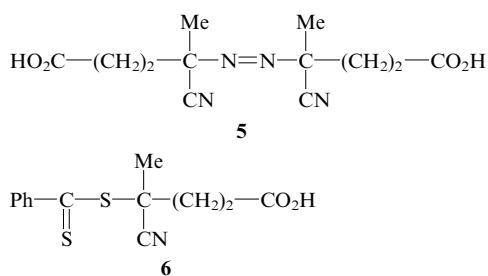
The RAFT method was used for the synthesis of diblock copolymers involving PAAc and PMAAc, namely, PBA-*b*-PAAc, PMMA-*b*-PMAAc and PBMA-*b*-PMAAc, where PBMA is poly(benzyl methacrylate).²⁶⁵ The polymerisation was carried in DMF with 1-phenylethyl dithiobenzoate as CTA. The copolymers obtained were characterised by low polydispersity. More recently, block copolymers of PAAc with poly(*N*-isopropylacrylamide) (PAAc-*b*-PIPA) were synthesised using 1-cyanoethyl 2-pyrrolidone-1-carbodithioate as

CTA.²⁷³ The first block to synthesise was PAAc, which then played the role of macroCTA in the polymerisation of *N*-isopropylacrylamide. Diblock copolymers with the same components were also obtained with benzyl and cumyl dithiocarbamates as CTA.²⁷⁷ The presence of dithiocarbamate groups at the end is important for subsequent transformation to thiols and conjugation with proteins or pharmaceuticals.

In some studies on the synthesis of polar block copolymers by 'pseudoliving' RAFT polymerisation (see above) and in most related studies to be considered below it was pointed that the best results (narrower MMD) can be obtained if the more rigid block is synthesised first. This indicates an important role of the conformation of the first block in the initiation and growth of the second block. For instance, amphiphilic block copolymers PAAc-*b*-PTBA with well-controlled molecular structure were obtained by polymerisation of acrylic acid followed by the polymerisation of TBA using trithiocarbonate or xanthate as CTA.²⁸⁴ The synthetic route to the block copolymers based on poly(meth)acrylonitrile (PMAN and PMA) involving the RAFT polymerisation starting with the rigid block (PMAN) was patented.²⁸⁵ Chain-transfer agents of general formula $R-S-C(=S)Z$ (R is a mobile group capable of easy elimination by the radical mechanism and Z is a hydrogen or halogen atom or a low-molecular-mass or polymer group) were proposed for the synthesis of linear block copolymers.

Block copolymers having two hydrophilic blocks, PAA and PAAc, were synthesised by the MADIX method using mono- or bifunctional xanthates as CTA.²⁸⁶ The A-*b*-B and A-*b*-B-*b*-A type copolymers were characterised by $M_w/M_n \leq 1.5$.

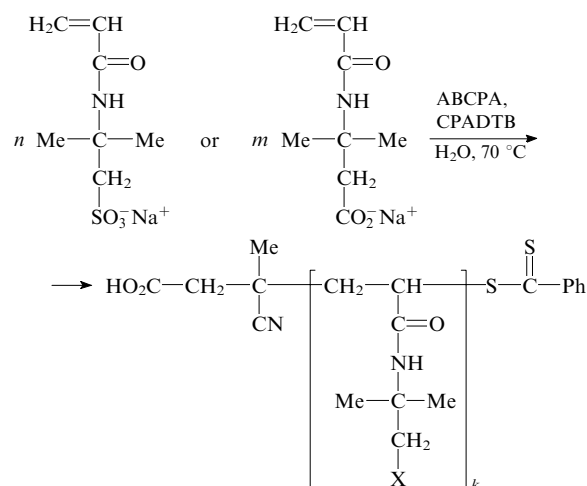
Interesting studies on the synthesis of polyelectrolyte block copolymers using an improved RAFT technique are available.^{268, 287} The polymerisation was initiated by 4,4'-azobis(4-cyanopentanoic acid) (ABCPA) (**5**), which gave the same tertiary radicals of 4-cyanopentanoic acid upon thermal decomposition as those formed upon abstraction from the CTA molecule [4-cyanopentanoic acid dithiobenzoate (CPADTB) (**6**)] in the course of chain transfer reactions.



This methodology was employed for controlled synthesis of three diblock copolymers containing various polyanionic or polycationic blocks in aqueous solution *via* RAFT. These were PSSNa-*b*-PVBNa based on poly(sodium 4-styrenesulfonate) and poly(sodium 4-vinyl benzoate), PVTMAC-*b*-PDMVBA based on poly(vinyltrimethylammonium chloride) and poly(*N,N*-dimethylvinylbenzylamine) and PNaAAMPS-*b*-PNaAAMB based on poly(sodium 2-acrylamido-2-methylpropane sulfonate) and poly(sodium 3-acrylamido-3-methylbutanoate). The first two copolymers were obtained in two steps.²⁶⁸ The first step (sealed tubes, 70 °C, 8 h) afforded almost monodisperse PSSNa and PVTMAC containing dithioester end groups. The molecular masses of the blocks monotonically increased with conversion. In the second stage (reactor, 70 °C, inert atmosphere, 24 h) both blocks played the role of the macroCTA in 'pseudoliving' radical polymerisation

of sodium vinyl benzoate and *N,N*-dimethylvinylbenzylamine. The copolymer containing polyanionic blocks was characterised by $M_n = 1.86 \times 10^4$ and $M_w/M_n = 1.18$ while the copolymer with polycationic blocks had $M_n = 5.1 \times 10^4$ and $M_w/M_n = 1.37$.

The third copolymer, PNaAAMPS-*b*-PNaAAMB, was synthesised from *N*-substituted acrylamides in two stages using the same reactor²⁸⁷



$\text{X} = \text{SO}_3^- \text{Na}^+ \text{ or } \text{CO}_2^- \text{Na}^+, k = (n + m) \text{ or } (m + n)$.

The monomers were introduced in different order and the overall polymerisation processes were studied, because the polymerisation of acrylamide monomers by the SFRP and ATRP methods is problematic (see above). The polymerisation of the first block (PNaAAMPS or PNaAAMB) was accompanied by a linear increase in M_n with increasing conversion, the reaction being first-order with respect to the monomer concentration; the first-order rate plot showed an induction period (~ 1 h). This was attributed²⁸⁷ to the slow initiation by the initiator used. Unlike the SFRP and ATRP methods for which the polydispersity of products usually decreases with conversion, here the polydispersity M_w/M_n somewhat increased with conversion but remained below 1.3. Because of high viscosities of strong polyelectrolytes in aqueous solutions (this can reduce the reaction rate) in the second stage of polymerisation the concentration of the second monomer was halved. Simultaneously, the duration of the polymerisation of the second block was doubled. The molecular masses M_n of the PNaAAMPS-*b*-PNaAAMB and PNaAAMB-*b*-PNaAAMPS copolymers (6.97×10^4 and 5.79×10^4 , respectively) were in excellent agreement with the theoretical values; the polydispersities M_w/M_n were also low (1.14 and 1.16, respectively).

c. Multiblock copolymers

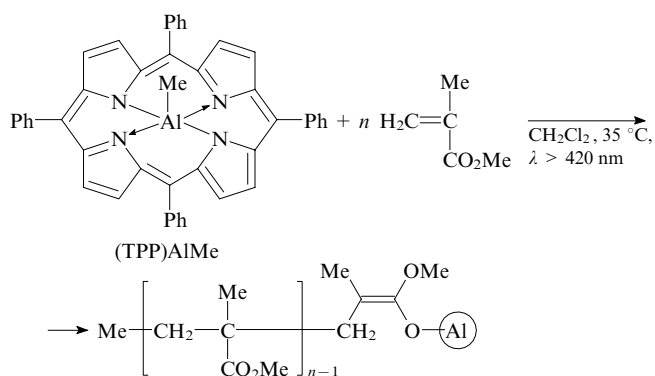
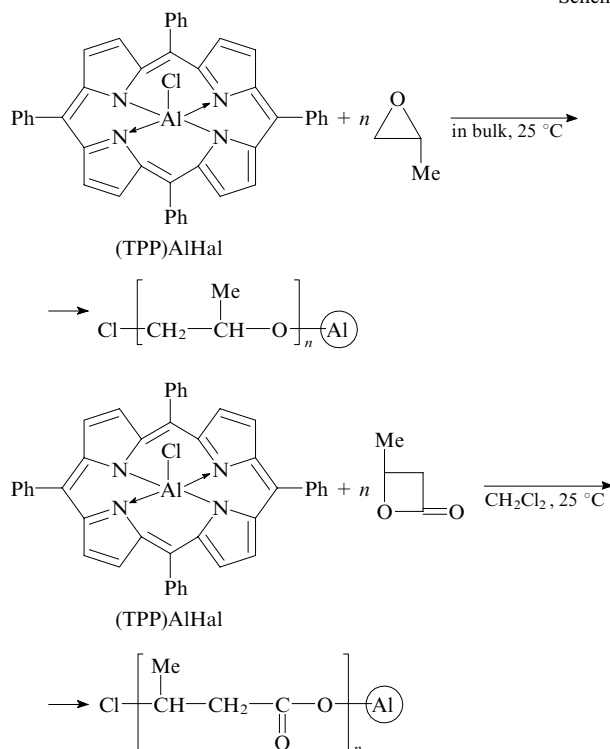
Prospects for the synthesis of block polyelectrolytes in aqueous solutions offered by the RAFT and MADIX methods are clouded by some circumstances. First, most CTAs are insoluble in water. Second, the synthesis of copolymers containing only one polyelectrolyte block often causes an abrupt increase in the medium viscosity. This complicates the RAFT polymerisation of tri- and multiblock copolymers or makes the process impossible. Therefore, now considerable attention is paid to industrial implementation of this polymerisation technique. In particular, prospects for the synthesis of homopolymers and copolymers using emulsion/mini-emulsion RAFT polymerisation technique were studied.^{288–292} The advantages of the RAFT process under conditions of emulsion/mini-emulsion polymerisation compared to the same process in a homo-

geneous medium consist in a higher chain propagation rate (due to segregation of radicals) and a better processability of products owing to low viscosity in solution at high polymer content. To improve the process, it was proposed to use a train of continuous tank reactors instead of a single reactor.²⁹³ This allows one to achieve higher monomer conversions in smaller reaction volumes and to obtain narrow-MMD multiblock copolymers of specified architecture. Taking the synthesis of gradient multiblock copolymers of St with *n*-butyl acrylate as an example, it was shown that the composition and length of any block can easily be varied by varying the temperature, flow rate in the reactor train and the injection point. The polymerisation was carried out at 72–77 °C with Na₂S₂O₈ as initiator, 1-phenylethyl phenyldithioacetate as CTA and SDS as emulsifier).

8. Other methods

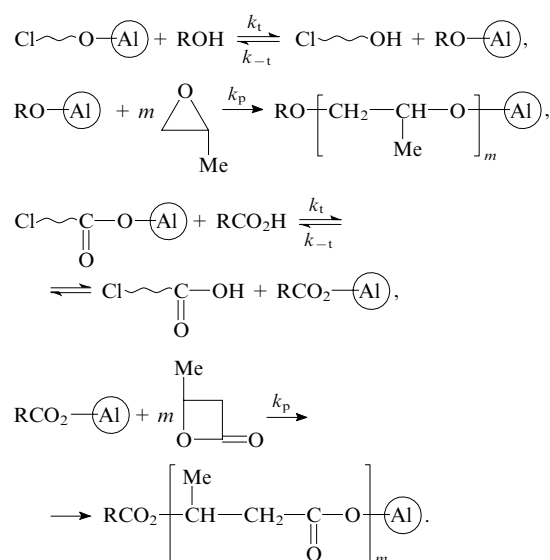
Now we will dwell on yet another, rarely used, method of 'living' polymerisation, namely, sequential anion-coordination polymerisation in the presence of metalloporphyrins, which permits the synthesis of certain block copolymers of specified molecular architecture. It has been comprehensively treated in a review⁴⁶ and concerns controlled room-temperature, ring-opening polymerisation of oxiranes, β -lactones, δ -valerolactones, ϵ -caprolactones, D-lactide, methacrylates and methacrylonitrile. The role of polymerisation initiators and nanoreactors, where a next monomer molecule is added to a growing chain by the anion-coordination mechanism, is played by (5,10,15,20-tetraphenylporphyrinato)aluminium chlorides, (5,10,15,20-tetraphenylporphyrinato)(methyl)aluminium and (5,10,15,20-tetraphenylporphyrinato)(methoxy)aluminium.⁴⁶ The growth centres include aluminium alkoxides for the polymerisation of oxiranes, δ -valerolactones, ϵ -caprolactones and D-lactide; aluminium carboxylate for the polymerisation of β -lactones and aluminium enolate for the polymerisation of methacrylates (see the processes shown in Scheme 14).

Scheme 14



Reversible chain termination reactions of the alcohol or carboxylic acid protons (for the polymerisation of oxiranes and lactones) represent important elements of control of the polymerisation of heterocyclic compounds (see the first and third processes in Scheme 15).^{46, 294}

Scheme 15



The reversible chain termination reactions are much faster compared to chain propagation, namely, $k_t/k_p = 10$ (Ref. 294). Therefore, the polydispersity index of polymers remains very low ($M_w/M_n \approx 1.1$). The number-average degree of polymerisation in these processes is given by the ratio⁴⁶

$$\bar{P}_n = q \frac{[M]_0}{[(\text{TPP})\text{AlHal}] + [\text{H}]},$$

where [H] is the concentration of the compound containing a mobile proton (alcohol or acid). Owing to fast reversible chain termination by the alcohol or acid protons these processes take a few days or weeks until complete consumption of the heterocyclic compounds.⁴⁶ However, they can be accelerated by introducing sterically hindered Lewis acids, e.g., methylaluminium bis[2,6-di(*tert*-butyl)-4-methylphenolate].²⁹⁵

Unlike heterocyclic compounds, (TPP)AlHal do not initiate the polymerisation of methacrylates and methacrylonitrile. Polymerisation of these monomers in the presence of (TPP)AlMe is only possible upon irradiation of the system with visible light (see the last reaction in Scheme 14). These slow processes can also be accelerated by introducing solid Lewis acids, such as methylaluminium bis[2,6-di(*tert*-butyl)phenolate], triphenylphosphine and organoboron compounds.⁴⁶ The Lewis acids are coordinated by the monomer carbonyl groups and enhance their electrophilicity. Successful polymerisation of non-irradiated methacrylates can be performed using more

nucleophilic porphyrins, such as (propylthio)- and (phenylthio)(5,10,15,20-tetraphenylporphyrinato)aluminium with methylaluminium bis[2,6-di(*tert*-butyl)-4-methylphenolate].⁴⁶ In these processes the degree of polymerisation (up to $P_n = 300$) is determined by the ratio

$$P_n = \frac{q[M]_0}{[I]_0},$$

and the MMD is very narrow ($M_w/M_n = 1.05 - 1.2$).⁴⁶

Aluminium porphyrinates were used in the synthesis of diblock copolymers from two oxiranes,^{296, 297} two β -lactones,²⁹⁸ β -lactone and oxirane.²⁹⁸ In the last (mixed) case, β -lactone was polymerised first because aluminium carboxylate at the chain end initiated the polymerisation of oxiranes, whereas the corresponding aluminium alkoxide was incapable of initiating the polymerisation of β -lactone. Diblock copolymers were also obtained by sequential polymerisation of EO and ϵ -caprolactone,⁸³ propylene oxide and D-lactide²⁹⁹ and various methacrylates.³⁰⁰ It should be noted that, in contrast to carbochain polymers, products of polymerisation of heterocycles (in particular, polyethers and polyesters) possess a unique ability to undergo biodegradation.³⁰¹ Therefore, considerable attention has been paid recently to the design of block copolymers containing these specific blocks.^{104 - 109}

III. Combination of different mechanisms of monomer polymerisation

This Section concerns alternative methods of synthesis of block copolymers. Common to all of them is the involvement of different polymerisation techniques in the course of synthesis. This strategy of synthesis of block copolymers is called multimode polymerisation.⁹ The new avenue of research began with a study³⁰² whose authors reported for the first time a transition from 'living' cationic polymerisation of THF to 'living' anionic polymerisation of St. Short after this publication the subject has attracted considerable attention of researchers.^{303, 304} The major impetus to the development of multimode polymerisation techniques came from the need of the synthesis of copolymers from blocks of different chemical nature that are difficult or hard to synthesise by sequential polymerisation of monomers by the same mechanism. The idea of using polymeric products of large-scale synthesis for preparation of block copolymers also played its role. At present, three strategies of multimode polymerisation of linear block copolymers are developed. These are (i) formation of macroinitiators for radical, ionic or other types of polymerisation at the ends of ready polymers; (ii) combination of various mechanisms of controlled ('living' ionic and 'pseudoliving' radical) polymerisation and (iii) use of bifunctional initiators. Consider now each strategy in more detail.

1. Formation of macroinitiators based on ready blocks

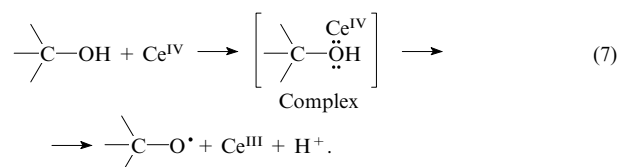
Transformation of the end groups of polymers into macroinitiators of polymerisation requires that they bear active

groups of particular chemical nature. In some polymers, such groups are formed in the course of synthesis. An example is provided by PEG containing active hydroxyl groups at the chain ends. In other polymers, especially in practically important polyolefins [PE, polypropylene (PP), PS, poly(4-methylpent-1-ene), *etc.*] the formation of active groups occurs during the synthesis or follows it.^{8, 305}

a. Macroinitiators based on poly(ethylene glycol)

The use of the OH groups of PEG and PEGME to obtain macroinitiators of radical polymerisation and prepare A-b-B, A-b-B-b-A and B-b-A-b-B block copolymers has been a subject of considerable literature (see, *e.g.*, Refs 306 - 310). These problems have been treated in most detail in a review.⁶ There are two main methods of conversion of PEG into macroinitiators. One of them involves direct 'activation' of the OH groups of PEG in the presence of other monomers followed by synthesis of block copolymers. The other technique involves modification of the end groups of PEG, their 'activation' in the presence of monomers and synthesis of di- or triblock copolymers. Now we will consider some examples.

Direct activation of PEG is possible in a redox reaction of formation/breakup of complexes between hydroxyl groups and mixed-valence metal ions (Co^{III} , Ce^{IV} , Mn^{III} , *etc.*).³¹¹ The mechanism of a reaction of isolated OH groups with a Ce^{IV} salt is as follows:^{311, 312}

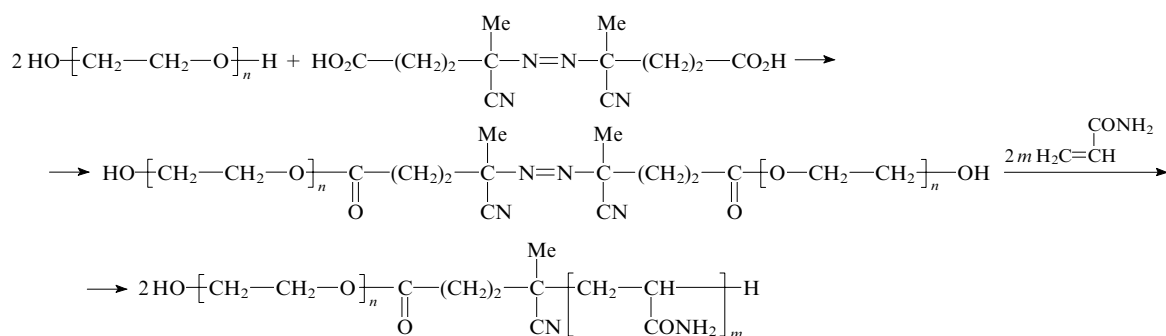


The lifetime of the intermediate complex varies from tens of seconds to a few hours depending on the structure of the hydroxyl-containing compound.³¹²

Novitskaya and Konkin³⁰⁶ were the first who used reaction (7) for the synthesis of PAN-b-PEO-b-PAN copolymers (PAN is polyacrylonitrile). The starting PEG had a molecular mass of 4.4×10^3 . The PEO content in the resulting triblock copolymer varied from 12% to 20 % by mass. More recently, this technique was employed for the synthesis of PAA-b-PEO-b-PAA, PEO-b-PIPAA, PIPAA-b-PEO-b-PIPAA and PAAC-b-PEO-b-PAAC copolymers with variable molecular mass of the PEO block.^{307, 308} A PMMA-b-PEO-b-PMMA copolymer was synthesised in a similar fashion in the presence of Mn^{III} .³⁰⁹

Yet another method was used for modification of the hydroxyl groups of PEG and formation of thermal macroinitiators, which form free radicals upon a change in temperature. In particular, the reaction of PEG with 4,4-azobis(4-cyanopentanoic acid) gave a polyazo ester, which was used in the synthesis of PEO-b-PAA diblock copolymers (Scheme 16).³¹⁰

The same thermal macroinitiator was obtained as intermediate product in the synthesis of the PEO-b-PS, PEO-b-PMA, PEO-b-PMMA, PEO-b-PVA and PEO-b-PAN copoly-



Scheme 16

mers.³¹³ The reactivities of monomers were compared at the same macroinitiator concentration under identical conditions (60 °C, 24 h). The rates of polymerisation of MA and MMA were higher and, therefore, higher q values and molecular masses of blocks were observed in these cases (q 80%–85% for MA and MMA vs. at most 20% for styrene). This macroinitiator was also obtained³¹⁴ by the interaction of PEG with 4,4-azobis(4-cyanopentanoic acid) anhydride. Then, it was thermally ‘activated’ in the presence of styrene and the PEO-b-PS copolymer was obtained.

A macroinitiator with ester end groups was synthesised in the reaction of PEG ($M_n = 400$) with azobis(cyanopentanoic) acid chloride in the presence of benzoyl chloride or acetyl chloride (Scheme 17)³¹⁵ and used in the polymerisation of St to obtain a liquid block copolymer PEO-b-PS with $M_n = 2.2 \times 10^4 - 2.9 \times 10^4$.

Yet another polyazo ester was synthesised by the interaction of PEG with AIBN in acidic medium (Scheme 18).³¹⁶ Its heating in aqueous acrylonitrile solution caused the formation of polydisperse PEO-b-PAN block copolymer (maximum yield 40 mass % at 85 °C) containing a soluble (6%–12% of PAN) and insoluble (86%–92% of PAN) fractions.

A more complex method³¹⁷ of synthesis of PEG-based macroinitiators of styrene polymerisation involves³¹⁷ the formation of macroazocarbamate in the reaction of PEG with aliphatic diisocyanate and then with 4,4-azobis(4-cyanopen-

tan-1-ol). Heat treatment of the macroazocarbamate in the presence of styrene led to PEO-b-PS copolymer (Scheme 19).

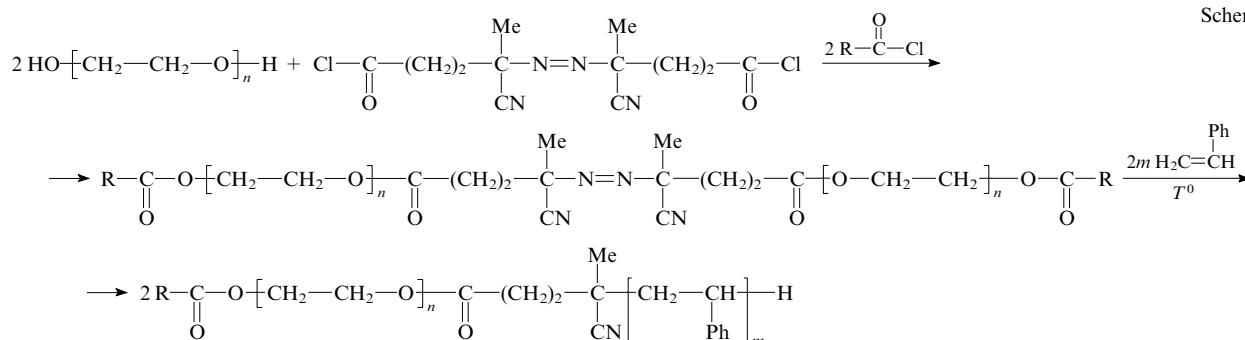
Macroazocarbamate was synthesised analogously using isophorone diisocyanate and initiated polymerisation of MMA.³¹⁸ The final product, a PMMA-b-PEO-b-PMMA copolymer, had $M_w = (2-7) \times 10^5$.

Yet another type of modification of the OH groups of PEG to obtain a PS-b-PEO-b-PS triblock copolymers is shown in Scheme 20.^{319, 320} PEG was mixed with isophorone diisocyanate and then with dihydroperoxides of general formula $\text{HOO}-\text{R}-\text{OOH}$ or with monoperoxide Bu^tOOH . This resulted in yet another thermal macroinitiator, PEO diperoxycarbamate. The final triblock copolymer had a broad MMD and contained the homopolymer due to occurrence of the chain transfer reaction.³¹⁹

Direct ‘activation’ of the OH groups of a PEG-based polyazo ester in the interaction with Ce^{IV} or Mn^{III} followed by thermal initiation was used³²¹ for the synthesis of PMMA-b-PEO-b-PMMA and PMMA-b-PEO-b-PS block copolymers (Scheme 21). A bifunctional polyazo ester was treated with Ce^{IV} or Mn^{III} salts in MMA solution at room temperature. The resulting tetrablock copolymer with the central azo group was heated in the presence of styrene or MMA.

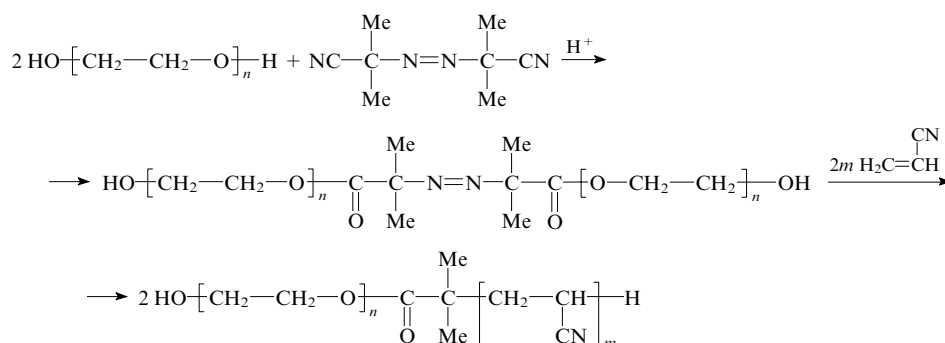
Of course, the block copolymers obtained by radical polymerisation of monomers under the action of PEG-based macroinitiators had broader MMDs compared to the block

Scheme 17

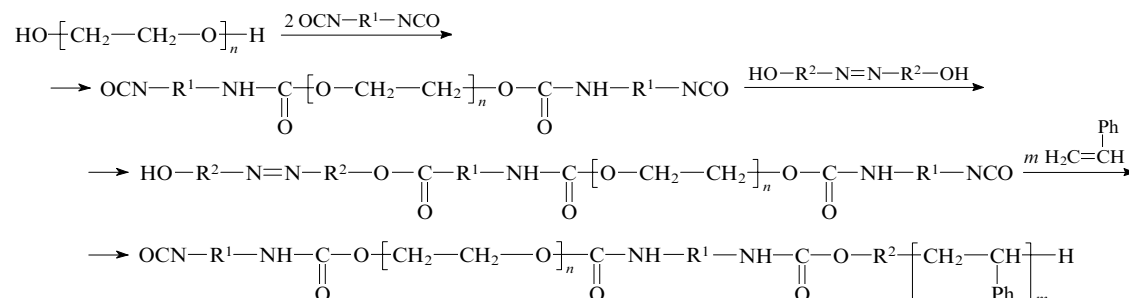


R = Ph or Me.

Scheme 18

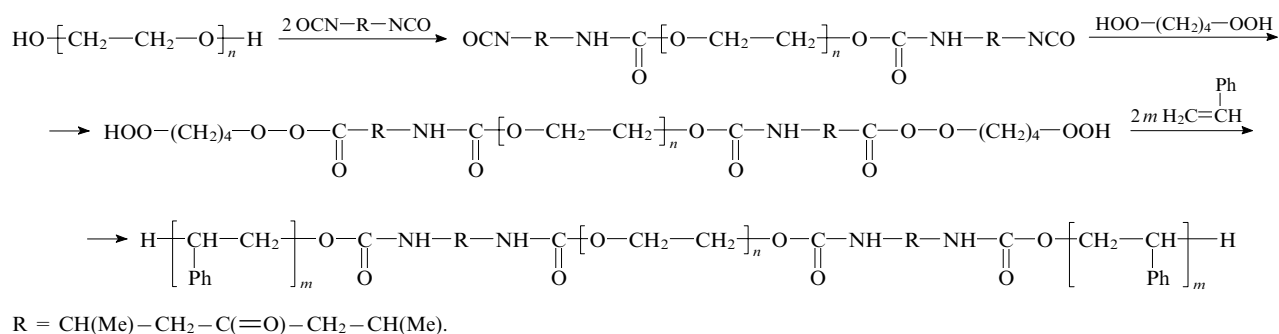


Scheme 19

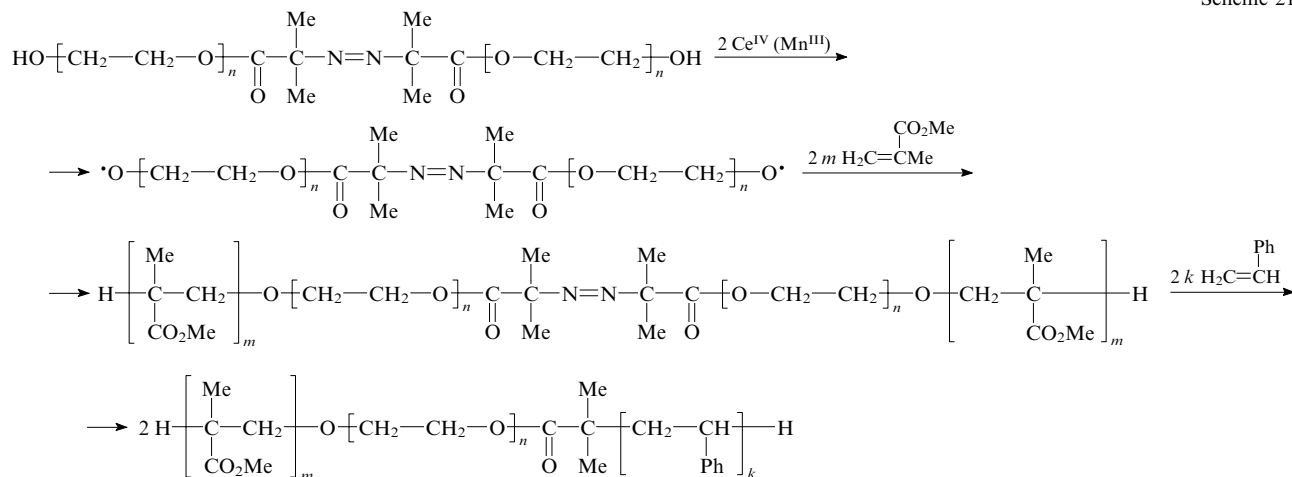


$\text{R}^1 = \text{Alk}$, $\text{R}^2 = -(\text{CH}_2)_3-\text{CMe}-\text{CN}$.

Scheme 20



Scheme 21



copolymers obtained by controlled sequential polymerisation. Nevertheless, in the former case the number of partners for PEG was larger.

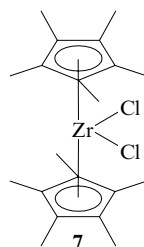
Recently, various transformations of PEG into mono- and bifunctional macroinitiators of anionic ring-opening polymerisation of lactones and lactides to synthesise biodegradable block copolymers^{108,109} (see Section II.2) and studies on the formation of PEG-based macroinitiators of controlled radical polymerisation were reported. For instance, the bromo derivatives of PEG and random copolymers of ethylene glycol and propylene glycol [poly(EG-co-PG)] were used in ATRP of 2,3,4,5,6-pentafluorostyrene (PFSt).^{322,323} PEG chains ($M_n = 2 \times 10^3 - 1 \times 10^4$) and poly(EG-co-PG) ($M_n \sim 1 \times 10^3$, EG content 74 mass %) were converted into macroinitiators by esterification of OH groups with bromoisobutanoic acid bromide. ¹H NMR spectroscopy studies confirmed the limiting degree of functionalisation of the end groups ($F_n = 1$). The ATRP of PFSt at both ends of polyethers afforded triblock copolymers PPFSt-b-PEG-b-PPFSt and PPFSt-b-P(EG-co-PG)-b-PPFSt. The molecular masses of the central blocks increased by 15%–84 % by mass and the polydispersity index M_w/M_n was less than 1.22. The triblock copolymers formed films with well-defined microphase separation and complexes with Li^+ salts.

A unique synthesis of diblock polyelectrolyte PEO-b-P(NaMA) by ATRP in aqueous solution was reported.³²⁴ The polymerisation of NaMA performed with a PEG bromo derivative as macroinitiator and the $\text{Cu}^{\text{I}}\text{Br}-2,2'$ -bipyridyl system as catalyst resulted in a high yield of narrow-MMD copolymer. A feature of the synthesis consisted in an optimal pH value (pH 8–9) that allowed one to maintain a balance between the possible reduction of P(NaMA) chain propagation rate at too high pH and competing protonation of 2,2'-bipyridyl at too low pH.

b. Macroinitiators based on polyolefins

Polyolefins are polymeric materials produced on a large-scale basis. Due to the lack of polar groups they are poorly compatible with inorganic fillers, polar polymers, glass fibre, pigments and metals. An efficient method of improving the compatibility of polyolefins with other materials is the synthesis of polyolefin-based block copolymers containing polar blocks. Therefore, in the last decade researchers undertook considerable efforts to develop methods of functionalisation of polyolefins. These methods were most comprehensively treated in reviews.^{8,305} In the text below we present the most promising techniques used for the synthesis of linear block copolymers. In this connection we will first dwell on the synthesis of polyolefins.

At present, stereoregular polyolefins are synthesised on a large scale using ionic-coordination polymerisation in the presence of heterogeneous or homogeneous Ziegler–Natta catalysts [*e.g.*, $\text{TiCl}_3 + \text{AlR}_n\text{Cl}_{3-n}$ ($n = 1-3$) on MgCl_2 powder].^{22,305} The mechanism of the process is well known.^{22,23} Recently, new homogeneous metallocene and post-metallocene catalysts have been widely used in the field. The major components of the metallocene catalysts are sandwich complexes of Group IV transition metals (Ti, Zr or Hf) with two cyclopentadienyl ligands (**7**). In some cases ligands may be linked by bridging groups involving carbon or silicon atoms.³⁰⁵



Cp_2ZrCl_2 ($\text{Cp} = \eta\text{-C}_5\text{H}_5$)

Complex with unsubstituted ligands

$\text{Cp}_2^*\text{ZrCl}_2$ ($\text{Cp}^* = \eta\text{-C}_5\text{Me}_5$)

Complex with substituted ligands

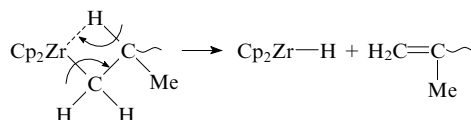
Active co-catalyst of metallocenes is methylalumoxane (MAO) of general formula $[-\text{Al}(\text{Me})-\text{O}]_n$ with a molecular mass of 8×10^2 to 1.5×10^3 (Ref 305), which is formed upon partial hydrolysis of trimethylaluminium. The post-metallocene catalysts may contain unsubstituted and substituted indene (Ind) or fluorene (Flu) ligands, in particular, $(\text{Ind})_2\text{ZrCl}_2$ and $(\text{Flu})_2\text{ZrCl}_2$, instead of cyclopentadienyls.³⁰⁵ The ability of the ligands to donate electrons to the transition metal increases in the order $\text{Cp} < \text{Ind} < \text{Flu}$.³²⁵ By varying the electronic and steric effects by changing the ligand structure one can control the polymerisation, stereoregularity and the MM of polyolefins, as well as modify their end groups.

To prepare macroinitiators, the end groups of homo- or copolyolefins are functionalised in the course of metallocene-catalysed synthesis of these compounds (to make the products cheaper) using two main procedures involving formation of (i) unsaturated end groups to be chemically modified and (ii) end groups capable of directly initiating block copolymerisation when activated.

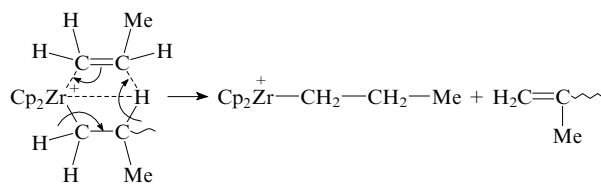
The formation of terminal double bonds in polyolefins is due to transfer of β -H atoms or β -alkyl groups (if exist), which occur in the active centres of chain growth (see the reactions shown in Scheme 22) and reduce the molecular mass of the polymer.^{8,305} The first type of transfer resulting in metal hydrides and alkenes (first reaction) was observed in the active centres of neutral or positively charged alkylmetallocenes.³⁰⁵ The second type of transfer (second reaction) was detected in the polymerisation of propylene on heterogeneous metallocene catalysts and in the copolymerisation of propylene with ethylene on $\text{Cp}_2\text{ZrCl}_2 + \text{MAO}$.³⁰⁵ Transfer of β -alkyl (methyl) groups to the transition metal (third reaction) was observed in a study of propylene oligomerisation with Cp_2^*LaMe as catalyst.³²⁶

Scheme 22

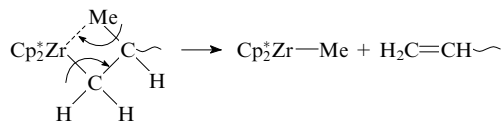
β -H transfer to transition metal



β -H transfer to monomer



β -Alkyl transfer to transition metal

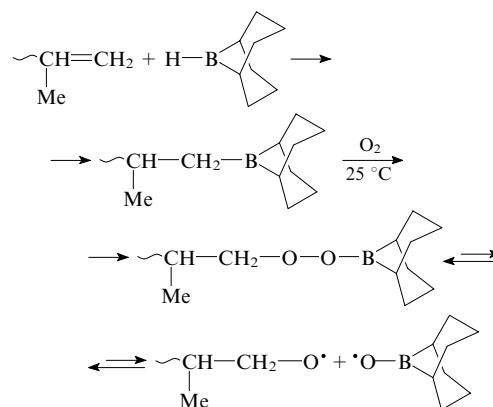


The transfer reactions can be controlled with ease by varying the metallocene structure (electronic and steric factors) and conditions of polymerisation (temperature and pressure).³⁰⁵ The more readily the ligands donate electrons to the metal the lower (i) the thermodynamic affinity of the metal to the β -proton in the growing chain and (ii) the probability of β -proton transfer. A similar effect can be attained by increasing the volume and number of substituents in the ligands, because this is accompanied by an increase in steric hindrances to the orientation of a single polymer chain (see the first process in Scheme 22) or to that of a polymer chain and a monomer molecule (see the second process in Scheme 22) in the active

centre that are necessary for β -proton transfer. In addition, reduction of the pressure and temperature causes the transfer rate to decrease; at $T < -20^\circ\text{C}$, the chain transfer reactions can be suppressed at all.

Further modification of unsaturated polyolefin end groups can be done in various fashions.³⁰⁵ One of the most promising methods is to form macroinitiators by, *e.g.*, quantitative ($F_n = 1$) hydroboration of unsaturated end groups using 9-borabicyclo[3.3.1]nonane (9-BBN) (Scheme 23). Alkylborane groups thus obtained are readily oxidised at room temperature and form two radicals.³⁰⁵

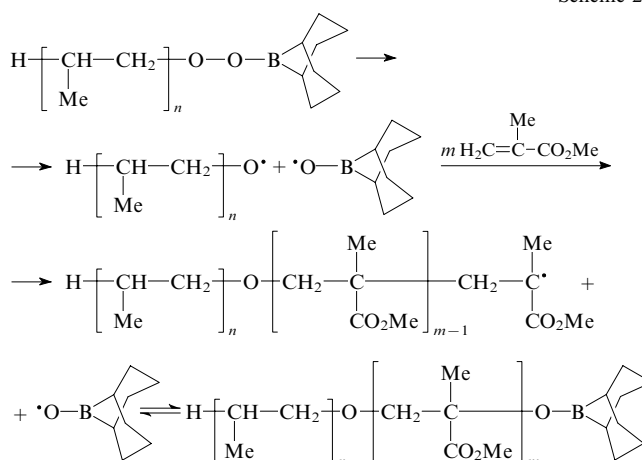
Scheme 23



The alkoxy radical is reactive and readily initiates the polymerisation of α -olefins. The borinate radical is more stable, being incapable of initiating polymerisation. In fact, alkyl-9-BBN peroxide, which is in equilibrium with the reactive ($\text{C}-\text{O}^\bullet$) and stable ($\text{B}-\text{O}^\bullet$) radicals, forms an initiating and control system, which can maintain the 'pseudoliving' character of radical polymerisation³²⁶ and is similar to alkoxyamines based on the TEMPO stable radicals in the mechanism of action.

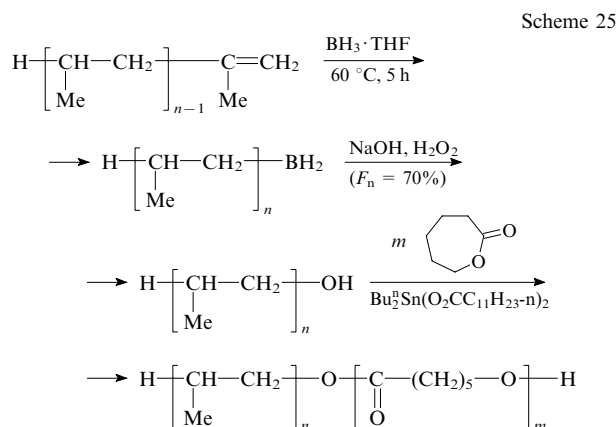
This method of formation of macroinitiators at the ends of unsaturated polyolefins was first used for the synthesis of the following diblock copolymers: PP-b-PMMA and PP-b-PMA,³²⁷ PP-b-PBA, PP-b-PS and PP-b-PVA³²⁸ and PP-b-poly(St-alt-MA).³²⁹ For the first copolymer the 'pseudoliving' polymerisation of MMA is described by Scheme 24.

Scheme 24



In this step, the molecular mass of the polymer increased from 1.3×10^4 (for the starting PP) to 2.9×10^4 (for the PP-b-PMMA copolymer) and the polydispersity index varied insignificantly, from 1.5 to 1.7 (Ref. 327). High efficiency of the initiation with alkylborane groups ($f_i = 1$) was pointed.

Hydroboration of unsaturated polyolefins (isotactic PP) followed by oxidation of the product (Scheme 25) was used to form hydroxyl end groups.³³⁰ Quantitative addition of the borane groups to the double bonds was characterised by lower oxidation efficiency (final value $F_n = 0.7$). The modified PP was activated by dibutyl tin dilaurate [$\text{Bu}_2\text{Sn}(\text{O}_2\text{CC}_{11}\text{H}_{23-n})_2$] and used as macroinitiator of anionic ring-opening polymerisation of ϵ -caprolactone.^{331,332} Based on PP with $M_n = 1.0 \times 10^3$, a PP-b-PCL copolymer with $M_n = 4.6 \times 10^3$ (see Ref. 332) was obtained; the monomer conversion was 70%.

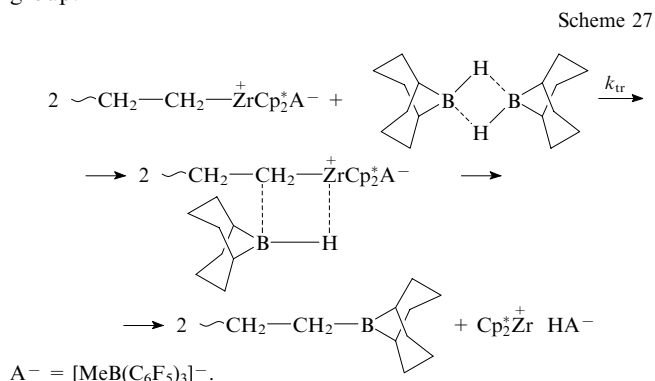


A more complex procedure for conversion of unsaturated polyolefins to macroinitiators by hydroboration (Scheme 26) was also reported.³³³ Treatment of isotactic PP ($M_n = 2.2 \times 10^3$) with a borane/dimethyl sulfide complex led to replacement of all protons by PP chains. Subsequent addition of an organomagnesium reagent resulted in quantitative yield of a macroinitiator of 'living' anionic polymerisation, which was used for the synthesis of PP-b-PMMA block copolymer ($M_n = 2.5 \times 10^3 - 3 \times 10^3$). The 'living' mechanism of polymerisation of the PMMA blocks was confirmed by a linear increase in their molecular mass with time.

Consider two recently developed methods of *in situ* formation of active end groups in polyolefins in the course of metallocene-catalysed synthesis.⁸ They are based on the reaction of chain transfer to specific chain transfer agents (CTA) that do not affect the chain propagation rate. One method uses 9-BBN, while the other uses *p*-methylstyrene as CTA.

In situ modification of polyolefin end groups with 9-BBN appeared to be a complicated task. A proton of the 9-BBN group can be exchanged with ease with alkyl groups of metal alkyls and simultaneously react with unsaturated α -olefins. Therefore, polymerisation of olefins on metallocene catalysts can involve not only chain transfer to 9-BBN, but also side exchange reactions (between borane and aluminium alkyl groups of MAO) and hydroboration of monomers. Nevertheless, these problems were solved and the side reactions avoided.^{8,305} It was shown that the 9-BBN molecules form stable dimers in the conventional nonpolar solvents (hexane, toluene) used for carrying out metallocene-catalysed polymerisation and do not react with olefins. In this case, a perfluoroborate co-initiator, which does not react with most

alkylboranes, was used instead of MAO. This made it possible to develop a rather efficient polymerisation process (Scheme 27) resulting in polyolefins bearing one 9-BBN end group.



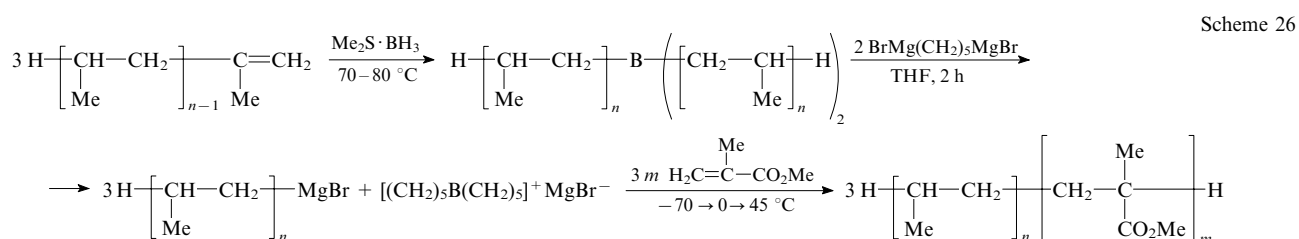
A narrow-MMD polymer was obtained³³⁴ by the polymerisation of ethylene in the presence of 9-BBN on the $[\text{Cp}_2\text{ZrMe}]^+[\text{MeB}(\text{C}_6\text{F}_5)_3]^-$ and $[\text{Cp}_2^*\text{ZrMe}]^+[\text{B}(\text{C}_6\text{F}_5)_4]^-$ catalysts. A linear dependence of $P_n(\text{PE})$ on the monomer: 9-BBN concentration ratio was established:

$$P_n = \frac{k_p[\text{M}]}{k_{tr}[\text{CTA}]}$$

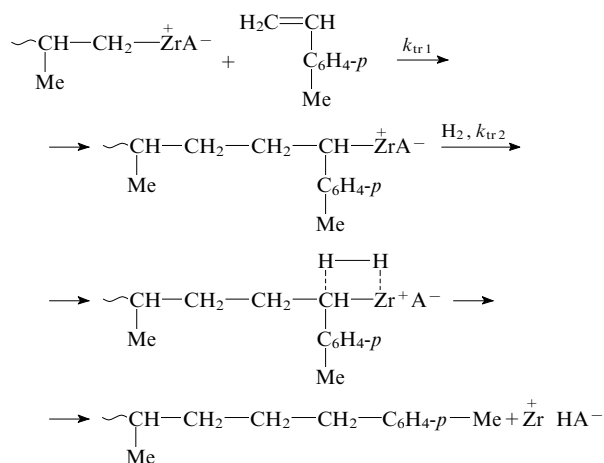
The k_p/k_{tr} ratio determined from the slope of the straight line thus obtained equals 75. The presence of borane end groups in PE was confirmed by NMR spectroscopy. 9-BBN was used as CTA in the synthesis of syndiotactic PS on $[\text{Cp}_2^*\text{TiMe}_2]^+[\text{MeB}(\text{C}_6\text{F}_5)_3]^-$ catalyst.³³⁵ As the 9-BBN concentration increased, the molecular mass of PS decreased. 9-BBN has almost no effect on the stereotacticity of PS; however, the catalyst activity reduced, which was explained by competitive coordination of St and 9-BBN to the catalyst.

Borane-modified PE and PS were used as macroinitiators of controlled radical polymerisation of MMA and benzyl methacrylate.³³⁴⁻³³⁶ The macroinitiators were 'activated' using the known oxidation reaction of alkyl-9-BBN (see Scheme 23). The kinetics of MMA polymerisation ($T = 25^\circ\text{C}$) under the action of oxidised PE chains (PE: $M_n = 1.94 \times 10^4$ and 4.27×10^4 ; $M_w/M_n = 2.1$ and 2.2 , respectively) was studied.³³⁴ The linear increase in the molecular mass of PMMA with time confirmed the 'pseudoliving' mechanism of radical polymerisation. The resulting PE-b-PMMA copolymers had $M_n = 9.03 \times 10^4$ and 9.76×10^4 and similar MMDs ($M_w/M_n = 2.0$ and 2.9). An analogous picture was observed in a study³³⁵ of MMA and BMA polymerisation under the action of oxidised PS ($M_n = 1.5 \times 10^4$, $M_w/M_n = 2.2$). The molecular masses of the PMMA and PBMA blocks linearly increased with time, which indicated correctness of the polymerisation mechanism proposed. After 24 h, the PS-b-PMMA and PS-b-PBMA copolymers were characterised by M_n of 2.9×10^4 and 3.33×10^4 , respectively.

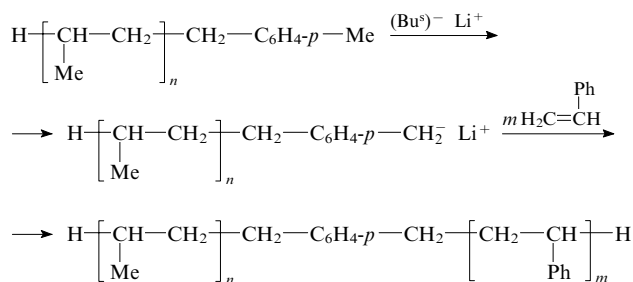
Yet another example of efficient CTA is provided by *p*-methylstyrene.⁸ Introduction of this compound and molec-



ular hydrogen in metallocene-catalysed polymerisation of olefins led to chain termination and formation of terminal *p*-methylphenyl groups. To make the reaction mechanism efficient and avoid the copolymerisation of olefins with MS, it was proposed to use a sterically hindered metallocene catalyst with bridging ligands. For instance, the problem of chain transfer to MS in the propylene polymerisation in toluene ($T = 30\text{ }^{\circ}\text{C}$) was solved using the *rac*-Me₂Si[2-Me-4-Ph(Ind)]₂ZrCl₂ + MAO system as catalyst.³³⁷ Owing to steric hindrances in the active centre, one *p*-MS molecule added to PP and after that, the polymerisations of all monomers ceased. To cleave the Zr–C bonds and restore the Zr–H bonds responsible for continuation of the polymerisation cycle, hydrogen was added.



The terminal character of *p*-methylphenyl groups was confirmed by ¹H and ¹³C NMR spectroscopies and by the involvement of PP in 'living' anionic polymerisation of styrene.³³⁷ The *p*-methylphenyl groups were 'activated' using the metallation reaction.



The modified PP was suspended in cyclohexane in the presence of excess Bu^sLi at room temperature for 5 h. The product was filtered off and used in the polymerisation of styrene. An increase in the molecular mass of PS with time confirmed the 'living' mechanism of polymerisation. Two samples of the PP-*b*-PS copolymer with $M_n = 5.4 \times 10^4$ and 1.175×10^5 ($M_w/M_n = 2.34$ and 2.25) were prepared (cf. $M_n = 2.59 \times 10^4$ and $M_w/M_n = 2.3$ for the initial modified PP).

The last-named two methods of functionalisation of polyolefins and formation of macroinitiators seem to be the best. They provide a convenient transition from metallocene catalysed polymerisation of the first block to controlled radical or ionic polymerisation of the second block. This offers prospects for attachment of blocks of different chemical nature to the polyolefin blocks and for the design of copolymers of specified molecular structure.

c. Macroinitiators based on another polymers

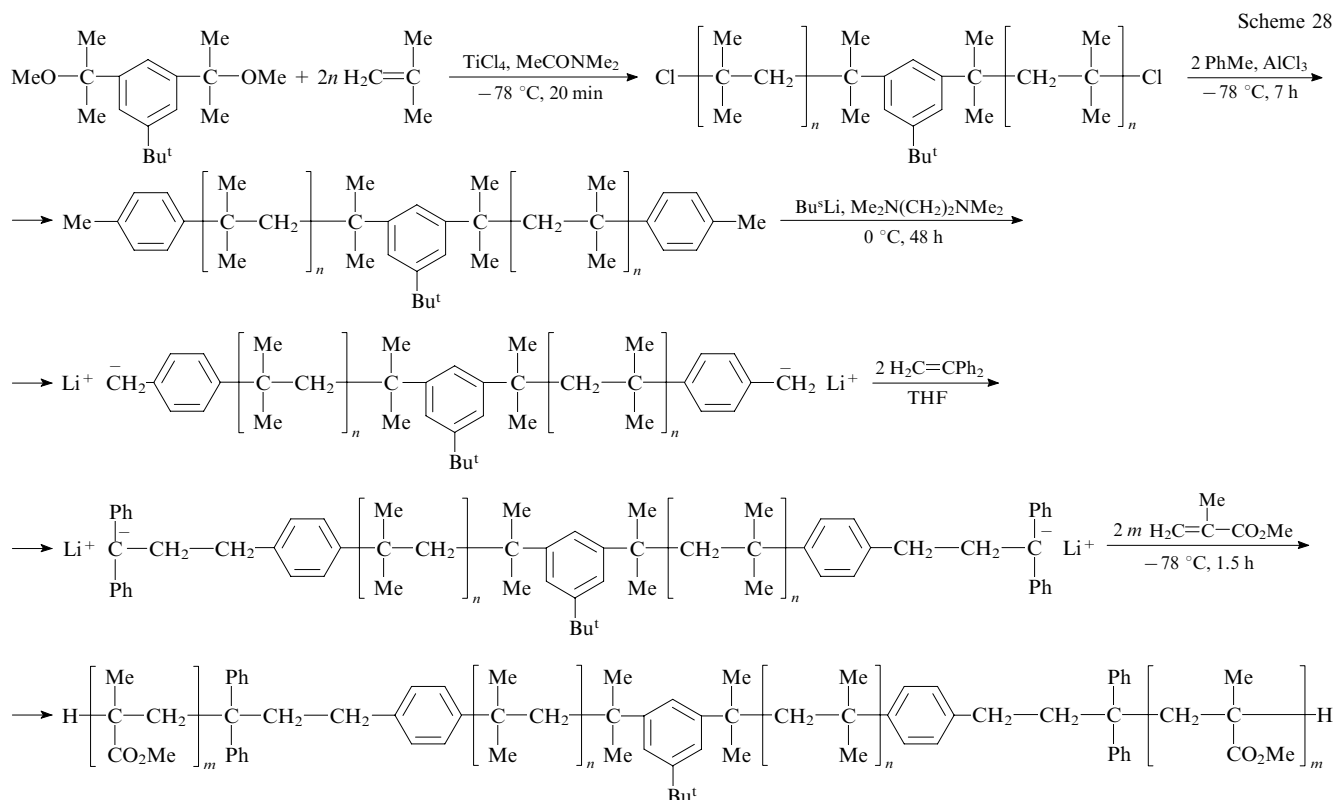
Polydimethylsiloxane (PDMS) containing flexible hydrophobic chains is produced on a large-scale basis and attracts considerable interest of researchers as a component of block copolymers. The compound is widely used as macroinitiator of polymerisation of various monomers in both the native (with silanol end groups) and end-group-modified forms. Remind that usually PDMS is synthesised on a large-scale basis by anionic polymerisation of cyclic dimethylsiloxanes accompanied by partial polycondensation.²² The modification of SiOH groups in PDMS can be best exemplified by the etherification reaction. PDMS containing one or two silyl ketene acetal groups was used as macroinitiator of GTP of (meth)acrylic acids protected with *tert*-butyl or dimethylsilyl groups.^{338–340} The initiation efficiency was low and therefore the di- and triblock copolymers contained an impurity of the starting PDMS.³³⁸ Hydrolysis of the protected blocks gave amphiphilic copolymers of PDMS and PAAc (or PMAAc) of the A-*b*-B and B-*b*-A-*b*-B types. The copolymers possessed the properties of a surfactant and stabilised the polymerisation dispersions even in supercritical carbon dioxide.^{339,340} PDMS was also used as macroinitiator of 'pseudoliving' radical polymerisation.^{341,342} To this end, halogen derivatives of PDMS were first obtained and the 'pseudoliving' ATRP was carried out.

Recently, yet another method of formation of macroinitiators of radical polymerisation was developed. This is ultrasonic destruction of polymer chains in the presence of monomers. The technique is of particular importance for the synthesis of block copolymers based on natural polymers, *e.g.*, chitosan {poly[β(1–4)-2-amino-2-deoxy-D-glucose]} belonging to polysaccharides.³⁴³ Chitosan is a cationic polyelectrolyte characterised by high reactivity and sorption capacity and also radiation resistance. Ultrasonic destruction of chitosan ($M_v = 1.44 \times 10^5$, frequency 22 kHz, electric current 40 mA, $T = 0\text{ }^{\circ}\text{C}$) in an acetic acid solution in the presence of VPD, AA, acrylonitrile and DMAEMA salt causes the formation of block copolymers containing almost no homopolymers.³⁴³ Only in the case of AAm did the final product contain about 2 mass % of PAA. Clearly, the products of synthesis should be polydisperse with respect to molecular mass and composition. Indeed, ultrasonic destruction of polymers takes some time to complete; the limiting value of the molecular mass is attained at the end of this time interval.³⁴⁴ For chitosan, the limiting molecular mass is 2×10^3 after 15–20 min.³⁴³ As a result, in the initial step of ultrasonic destruction the macroradicals initiating the polymerisation of monomers are longer than in, *e.g.*, 20 min; this is the reason for polydispersity of the product.

2. Combination of 'living' cationic and 'living' anionic polymerisation

Synthetic procedures involving a combination of several types of 'living' ionic and/or 'pseudoliving' radical polymerisation open new prospects for the design of block copolymers; however, this requires considerable experimental efforts. The main problem consists in quantitative conversion of one type of active centres into another type of polymerisation centres. Studies on conversion of 'living' carbocations into 'living' carbanions began in the early 1990s.^{345–353} They were aimed at obtaining block copolymers of nonpolar PIB (elastomer highly resistant to external factors) with rigid poly(meth)acrylate, poly(meth)acrylic acid, polyacrylamide and polyester polar blocks. A number of methods of modification of PIB macrocations were proposed.

Cationic polymerisation of IB was initiated with bifunctional cumyl ether, namely, 1,3-bis(1-methoxyisopropyl)-5-(*tert*-butyl)benzene in the presence of dimethylacetamide and TiCl₄.^{348,349} Therefore, the polymerisation carried out in a methyl chloride–*n*-hexane mixture [40 : 60 (vol.%)] with heating in the last step immediately gave a dichloro derivative of



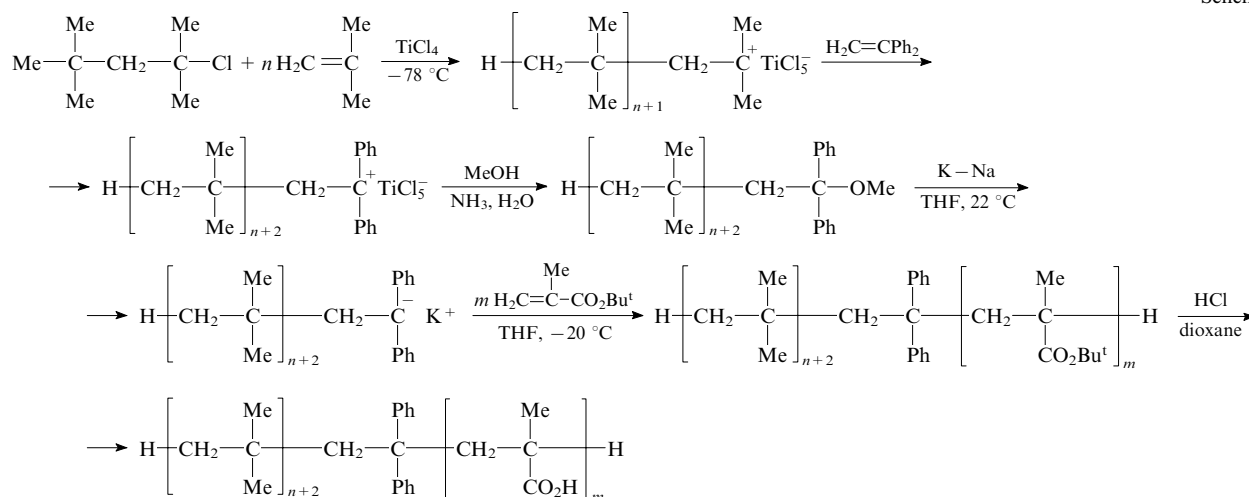
PIB (Scheme 28),²² Cl-PIB-Cl, which had the expected molecular mass and showed a narrow MMD ($M_n = 6.1 \times 10^4$, $M_w/M_n = 1.15$). In the second stage it was used in the toluene alkylation according to Friedel-Crafts and a ditolyl derivative of PIB was obtained ($F_n = 1$).

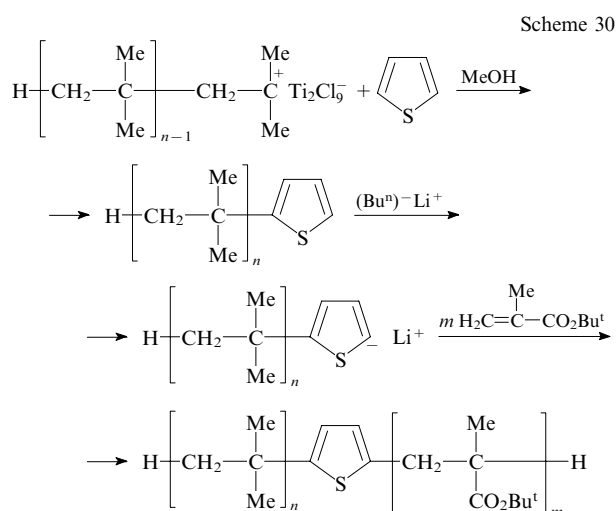
In the third stage, MePh-PIB-PhMe was transformed into a 'living' polydianion by the reaction of *sec*-butyllithium (in *n*-hexane) in the presence of *N,N,N',N'*-tetramethylethylenediamine (TMEDA) followed by the reaction with 1,1-diphenylethylene in THF. Then, the monomer (MMA) was introduced, the temperature was reduced and PMMA-*b*-PIB-*b*-PMMA copolymers were obtained (see Scheme 28). The copolymers were characterised by $M_{n\text{PMMA}} = 7 \times 10^3 - 1.65 \times 10^4$ and a narrow MMD ($M_w/M_n = 1.23 - 1.30$) and contained almost no homopolymers.³⁴⁹ The PMMA blocks showed a high stereoregularity (content of syndiotactic units was about 75%).

A simpler procedure for quantitative conversion of PIB macrocations to macroanions was also proposed.^{9, 354-356} In the first step cationic polymerisation of IB in a MeCl-*n*-hexane mixture was initiated by TiCl_4 with 2,4,4-trimethyl-2-chloropentane (Scheme 29). 'Living' PIB chains were 'capped' with diphenylethylene, terminated with methanol and diphenylmethoxyl terminal fragments were thus obtained. In the second step they were quantitatively converted to carbanions by the reaction of methoxy groups with alkali metals. Then, the polar monomer (TBMA) was introduced, the temperature was reduced and 'living' anionic polymerisation was carried out. This resulted in PIB-*b*-PTBMA copolymers with controlled molecular mass and a narrow MMD; subsequent hydrolysis gave a block polyacid PIB-*b*-PMAAc (see Scheme 29).

Yet another method of transformation of PIB macrocations into macroanions to obtain PIB-*b*-PTBMA

Scheme 29





(Scheme 30)⁹ differs from the technique considered above in that (i) macroanions are 'capped' with thiophene in the last step of IB polymerisation and (ii) thiophenelithium derivative of PIB ($F_n = 1$) should be synthesised to initiate anionic polymerisation of polar monomers, such as TBMA.

3. Combination of 'living' anionic and 'pseudoliving' radical polymerisation

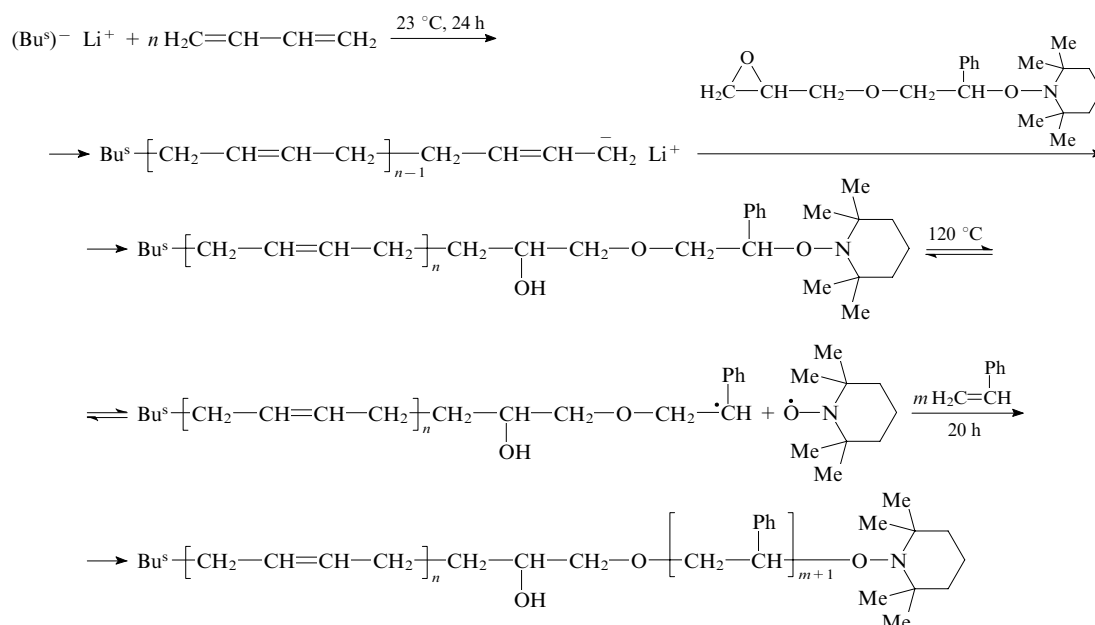
The discovery of various types of 'pseudoliving' radical polymerisation was followed by intensive use of these techniques in multimode polymerisation. The most promising method of synthesis of block copolymers with controlled molecular structure and low polydispersity is a combination of controlled radical polymerisation and 'living' ionic polymerisation.¹⁸¹ At the same time, attempts to obtain, *e.g.*, PS-*b*-PBA, PS-*b*-PMMA and PS-*b*-PI copolymers with rather broad MMDs by 'pseudoliving' polymerisation (SFRP) following the free radical process have also been reported.³⁵⁷

A specific feature of the multimode process involving a 'pseudoliving' (radical mechanism) and a 'living' (ionic mechanism) polymerisation consists in performing the ionic polymerisation first. The reason is not only the higher temperatures of controlled radical processes, but also easier conversion of ionic active centres into the groups necessary for

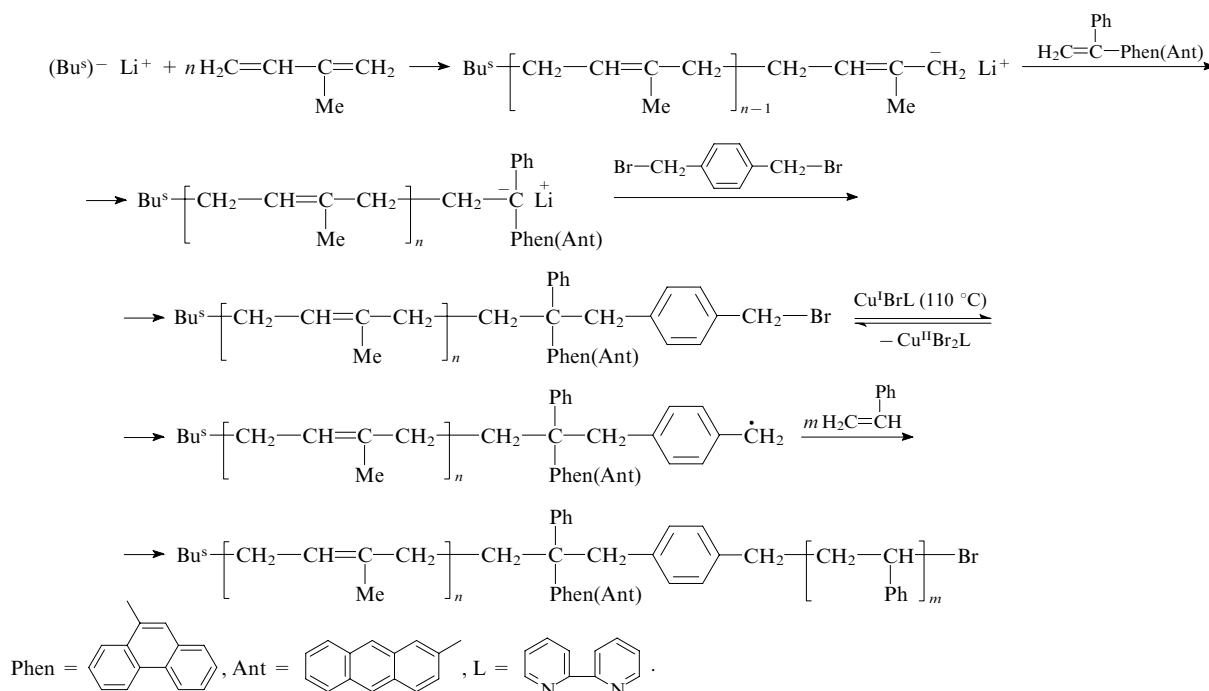
initiation and control of 'pseudoliving' radical polymerisation. These groups are different for different types of polymerisation, namely, nitroxides for SFRP, mobile halogen atoms for ATRP, dithioester groups for RAFT and dithiocarbonate (or trithiocarbonate and trithiocarbamate) groups for MADIX.

There are strong proofs of the synthesis of linear block copolymers of well-defined structure and narrow MMD by combining 'living' anionic polymerisation with SFRP or ATRP. A PB-*b*-PS copolymer was synthesised using anionic polymerisation followed by SFRP.^{358,359} The process (see Scheme 31) began with 'living' anionic polymerisation of butadiene in cyclohexane. Termination of PB macroanions to change the polymerisation mechanism was done with an epoxy-functionalised alkoxyamine, namely, 2,2,6,6-tetramethyl-1-(2-glycidyloxy-1-phenylethoxy)piperidine.³⁵⁸ The nitroxide-'capped' PB block had $M_n = 3.84 \times 10^3$ (this is in agreement with the calculated values) and a narrow MMD ($M_w/M_n = 1.02$). High degree of functionalisation of PB ($F_n > 0.95$) was established by ¹H NMR spectroscopy. In the second stage, the nitroxide-'capped' PB served a macroinitiator of 'pseudoliving' polymerisation (SFRP) of styrene in the bulk (see Scheme 31) with the initiation efficiency $f_i = 1$. After 20 h, styrene conversion was 65%. The PB-*b*-PS copolymer was characterised by $M_n = 1.74 \times 10^4$, which was in agreement with the calculated value ($M_n = 1.5 \times 10^4$), and a low polydispersity index ($M_w/M_n = 1.22$).

Considerable literature devoted to combination of 'living' anionic polymerisation with ATRP is available. Now we will dwell on some typical examples. Nonpolar block copolymers PI-*b*-PS were synthesised using a multimode process involving anionic polymerisation and ATRP.³⁶⁰ The synthesis involved not only the polymerisation of particular blocks and transformation of active centres, but also the formation of fluorescent phenanthryl or anthryl linkers between the blocks (Scheme 32) to study the structure and properties of the copolymers. The polymerisation of isoprene in cyclohexane was followed by sequential addition of 1-(9-phenanthryl)- or 1-(2-anthryl)-1-phenylethylene and α, α' -dibromo-*p*-xylene to 'living' PI. The product was isolated and used in 'pseudoliving' radical polymerisation of styrene in the presence of the CuBr-2,2'-bipyridyl system (see Scheme 32). Gel-permeation chromatography and NMR studies revealed good agreement between the experimental [$M_n = (5-45) \times 10^3$] and calculated



Scheme 32



molecular mass and a low polydispersity ($M_w/M_n = 1.1-1.2$) of the PI-*b*-PS copolymers.

A combination of 'living' anionic polymerisation with ATRP was used³⁶¹ for preparation of PS-*b*-P2VP block copolymer containing nonpolar and polar (polybasic) blocks. Anionic polymerisation of St (first stage) in benzene was initiated by Bu^sLi and followed by modification of the PS chain ends to 'cap' them with mobile chlorine atoms (Scheme 33). The product was isolated and dissolved in toluene. The catalyst ($\text{Cu}^{\text{I}}\text{Cl}-2,2'$ -bipyridyl) was introduced followed by the second monomer (2VP) and the mixture was heated to 120°C . Gel-permeation chromatography and NMR data showed that the molecular mass of PS-*b*-PVP was insignificantly different from the calculated MM and that the MMD was also narrow ($M_w/M_n = 1.05-1.14$).

A combination of anionic ring-opening polymerisation with ATRP was used in the synthesis of diblock copolymers containing polar non-ionogenic and polyacid blocks. In particular, anionic ring-opening polymerisation of ϵ -caprolactone (similar to the process shown in Scheme 3) followed by ATRP of TBA resulted in a precursor (PCL-*b*-PTBA copolymer). Subsequent hydrolysis of the PTBA blocks (see the process in Scheme 6) gave a PCL-*b*-PAAc copolymer.³⁶² As another example, copolymers PEO-*b*-PTBA were synthesised by anionic ring-opening polymerisation of EO followed by mod-

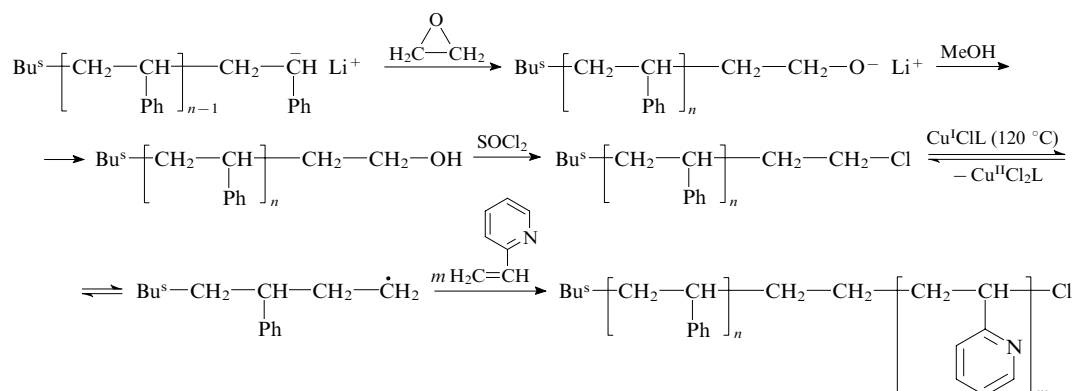
ification of the OH groups of PEG with α -halo esters and subsequent ATRP of TBA.³⁶³ The resulting copolymers were then converted to PEO-*b*-PAAc.

Since 'living' ionic and 'pseudoliving' radical polymerisations themselves allow one to synthesise a broad range of binary and ternary block copolymers, combination of the techniques offers additional prospects for the design of block copolymers. In this connection, noteworthy is a study³⁶⁴ on the synthesis of PDMS-*b*-PS-*b*-PDMOMSPA terpolymers {PDMOMSPA is poly[3-(dimethoxymethylsilyl)propyl acrylate]}. An appropriately chosen multimode process involved anionic ring-opening polymerisation of cyclic dimethylsiloxane, transformation of the SiOH groups of PDMS into 2-bromoisobutylsilyl groups and two consecutive ATRPs of styrene and 3-dimethoxymethylsilylpropyl acrylate. The resulting terpolymer was characterised by high affinity to the surface of the silicon plate where it formed a 'brush'-like layer.

4. Combination of 'living' cationic and 'pseudoliving' mechanisms

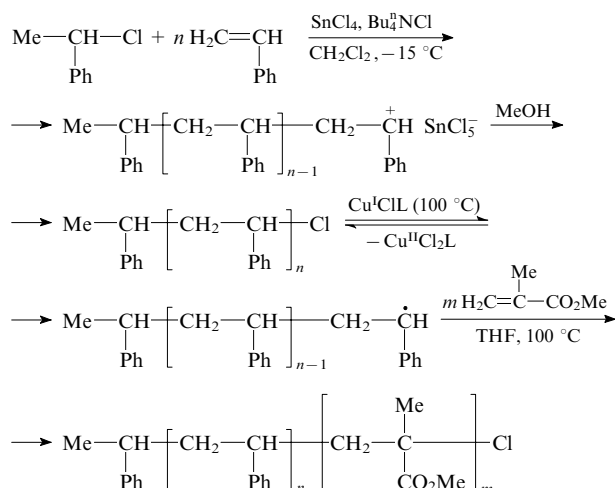
Controlled synthesis of block copolymers using 'living' cationic and 'pseudoliving' radical (ATRP) polymerisation was first reported in 1997.³⁶⁵ Earlier, 'living' cationic polymerisation to obtain poly(vinyl ethers) was combined with free radical polymerisation of methacrylonitrile³⁶⁶ and benzyl

Scheme 33



methacrylate.³⁶⁷ The lack of control in the second stage led to polydisperse final products containing homopolymers. The authors of study³⁶⁵ synthesised the PS-*b*-PS, PS-*b*-PMA and PS-*b*-PMMA copolymers (with two nonpolar blocks and with nonpolar and polar blocks) of controlled structure and narrow MMD. 'Living' cationic polymerisation of St was carried out using the SnCl₄–1-phenylethyl chloride initiating system in the presence of Bu₄ⁿNCl as nucleophile (Scheme 34).

Scheme 34



The chloro derivative of PS, isolated upon reprecipitation in methanol ($M_n = 2.1 \times 10^3$, $M_w/M_n = 1.17$), served as a macro-initiator of ATRP of styrene, MA and MMA in toluene using the Cu^ICl–4,4'-di(non-5-yl)-2,2'-bipyridyl catalytic system. The molecular masses of the PS-*b*-PS, PS-*b*-PMA and PS-*b*-PMMA copolymers ($M_n = 5.08 \times 10^3$, 6.33×10^3 and 1.109×10^4 , respectively) were in agreement with the calculated values (at $f_i = 1$). This means that the unmodified chloro derivative of PS is a highly efficient macroinitiator of ATRP of styrene and (meth)acrylates. The polydispersity indices of the copolymers were also low ($M_w/M_n = 1.10$, 1.20 and 1.57, respectively).

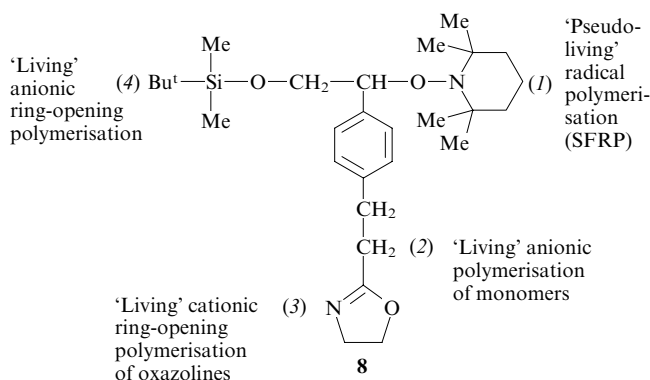
An important advantage made by the authors of study³⁶⁵ is the one-pot polymerisation of, *e.g.*, the PS-*b*-PMA copolymers. To this end, the chloro derivative of PS was deactivated by methyl methacrylate introduced at -15°C . Then the temperature was increased and the solvent, the Lewis acid and the ester were distilled off, a solution of the catalytic system in toluene and the monomer were added, the temperature was raised to 100°C and ATRP of methyl methacrylate was carried out. One-pot multimode process resulted in the PS-*b*-PMA copolymer characterised by almost the same parameters ($M_n = 6.3 \times 10^3$, $M_w/M_n = 1.21$) as the copolymer obtained *via* isolation of intermediate product.

Similar syntheses of PS-*b*-PIB-*b*-PS and PAOS-*b*-PIB-*b*-PAOS copolymers [PAOS is poly(*p*-acetoxystyrene)] containing three nonpolar blocks, as well as one nonpolar and two polar blocks, were reported.³⁶⁸ Here, 'living' PIB chains propagating along both directions were 'capped' with styrene at both ends. This resulted in a dichloro derivative of PIB, which efficiently initiated ATRP of various monomers (styrene and AOS). This combination of polymerisation processes was also used for the synthesis of block copolymers of PIB with PMAAc.³⁶⁹ 'Living' cationic polymerisation led to mono-chloro and dichloro derivatives of PIB, while ATRP of protected MAAc monomers in the presence of the Cu^ICl(Cu^IBr)–*N,N,N',N',N''*-pentamethyldiethylenetriamine catalytic system followed by acid hydrolysis gave di- and triblock copolymers PIB-*b*-PMAAc and PMAAc-*b*-PIB-*b*-PMAAc. The molecular masses of the blocks varied as follows: $M_{n\text{PIB}} = 2.8 \times 10^3$ – 5.6×10^4 and $M_{n\text{PMAAc}} =$

4.3×10^2 – 1.72×10^3 . Thus, the authors reached the main goal, namely, they synthesised model block copolymers of variable length of the elastomeric and rigid ionic blocks. The mechanical and rheological properties of the block copolymers were determined by aggregation of macrocoils governed by hydrogen and ionic bonds.³⁷⁰

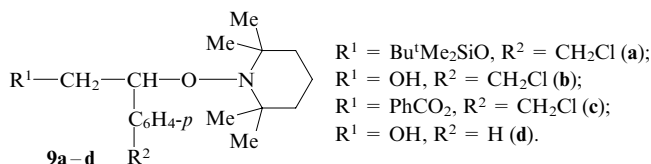
5. Application of bifunctional initiators

Design of selective multifunctional initiators is a new promising approach to implementation of multimode (including one-pot) polymerisation processes. Only a few studies on the subject are available at the moment; however, researchers point to great prospects for this strategy of synthesis of block copolymers. Unlike a simple combination of various polymerisation mechanisms, here the main advantage consists in the possibility of carrying out sequential and concurrent multimode processes that do not include additional chain end functionalisation stages. Puts and Sogah^{371–374} pioneered in formulating the problem and doing research in this field. Initially, the global challenge was to design a universal initiator capable of initiating the most important types of controlled polymerisation processes.³⁷¹ It was assumed that corresponding functional groups of the initiator will act independently. Puts and Sogah greatly succeeded in solving the problem posed. They synthesised a multifunctional initiator 1-[(*tert*-butyl)dimethylsiloxy]-2-[4-[2-(4,5-dihydrooxazol-2-yl)ethyl]-phenyl]-2-(2,2,6,6-tetramethyl-1-piperidineoxy)ethane (**8**).



The compound was designed to allow for the following: (i) alkyl adducts of nitroxides (**1**) can initiate a SFRP process; (ii) C–H bonds (**2**) in α -position to the oxazoline group can form carbanions and initiate 'living' anionic polymerisation;³⁷⁵ (iii) oxazoline ring (**3**) can be a monomer in cationic ring-opening polymerisation;³⁷⁶ (iv) neutral oxazolines are stable to free radicals and ionic reactions; (v) oxazolines are good protective groups for carboxylic acids and can be readily removed;³⁷⁷ (vi) alkylsiloxy group (**4**) can initiate anionic ring-opening polymerisation of heterocycles;³⁷⁸ (vii) by removal of oxazoline protection from CO₂H groups (**3**) and *tert*-butyldimethylsilyl protection from OH groups (**4**) the polymerisation centres can be converted into polycondensation centres.³⁷⁹ Thus, initiator **8** includes four polymerisation centres and allows one to obtain linear, graft and star-like block copolymers. Since only a [poly(2-oxazoline)-*g*-PS] graft copolymer was synthesised using this initiator,³⁷¹ analysis of the synthetic procedure goes beyond the scope of this review.

Then, the multifunctional initiators **9a–d** and tribromoethanol (**10**) were proposed.^{372–374} Using some of them, not only one-pot, but also concurrent multimode syntheses of linear block copolymers were developed. Consider these results in more detail. A bifunctional initiator 1-hydroxy-2-phenyl-2-(2,2,6,6-tetramethylpiperidin-1-yloxy)ethane containing a nitroxide and an OH group (**9a**) was used³⁷⁴ for the synthesis of A-*b*-B and B-*b*-A copolymers from poly(ϵ -caprolactone)



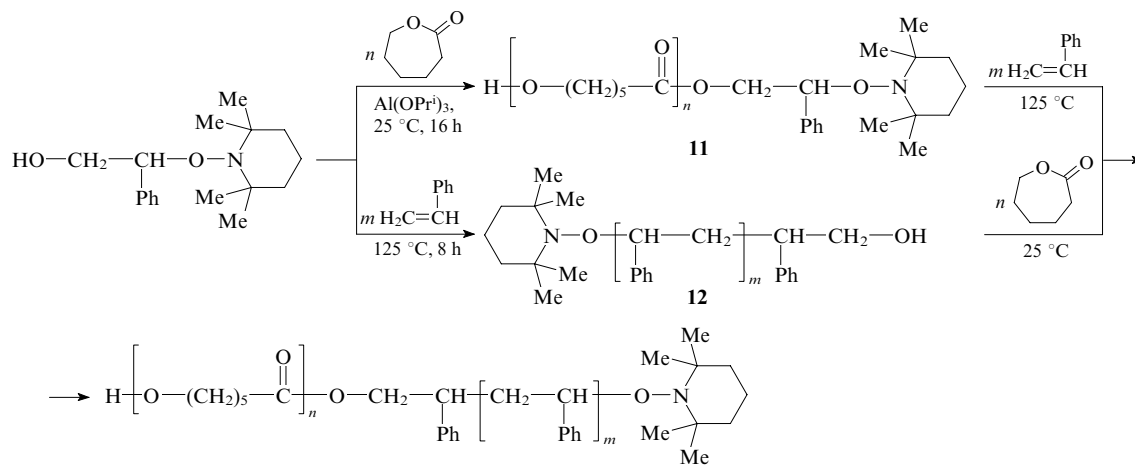
and PS. The role of the order in which the multimode process is carried out (anionic polymerisation of ϵ -caprolactone (CL) followed by 'pseudoliving' SFRP of styrene, or *vice versa*) and the relative reactivities of nitroxide radicals attached to the initiator and to the PCL chain end in the polymerisation of styrene was studied. Anionic ring-opening polymerisation of CL under the action of the OH groups of the initiator in the presence of catalyst $Al(OPr^i)_3$ readily occurred in toluene at 25 °C. However, the nitroxide group of initiator initiated bulk SFRP of styrene only at a high temperature ($T = 125$ °C). Due to significant differences between polymerisation conditions various multimode processes (Scheme 35) involving isolation of intermediate products (**11** or **12**) could be performed with ease. There was no need for additional chain end modification steps. Gel-permeation chromatography and 1H NMR studies revealed full control of the MM of the PCL and PS blocks (linear increase in MM with monomer conversion) irrespective of the order in which they were synthesised; the MMDs of particular blocks and the whole copolymer also remained narrow ($M_w/M_n = 1.07-1.4$). It was found that the nitroxide radicals at the PCL chains are more reactive than those attached to initiator; this manifested itself in acceleration of the polymerisation of styrene in the presence of macroinitiator **11** compared with the homopolymerisation of styrene under the action of the unmodified initiator. In addition, the molecular mass of PS in the block copolymer was controlled up to high values ($M_n = 1.5 \times 10^5$). The authors provided no explanation

for this effect, but the assumption of a change in the medium polarity in the presence of PCL as the sole factor affecting the system under study was ruled out (SFRP of styrene with covalently nonbonded PCL of various molecular mass showed no acceleration of the polymerisation process).

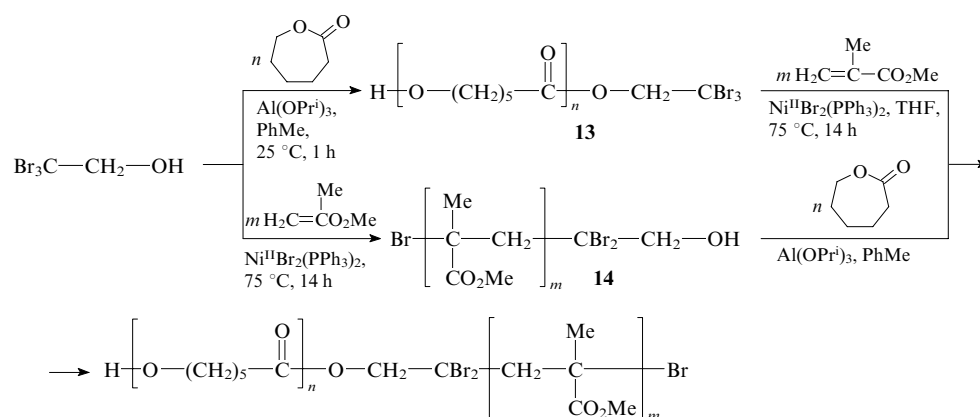
The activity of a simpler commercially available and cheap bifunctional initiator **10** in another multimode process involving 'living' anionic polymerisation and ATRP was checked.³⁷⁴ First, high efficiency of the initiator in (i) anionic ring-opening polymerisation of ϵ -caprolactone [in toluene in the presence of catalytic amounts of $Al(OPr^i)_3$]; (ii) ATRP of styrene (in toluene with $Cu^I Cl-2,2'$ -bipyridyl as catalyst); and (iii) ATRP of MMA in THF in the presence of $NiBr_2(PPh_3)_2$ or $RhBr(PPh_3)_3$ complexes was proved. Then, multimode synthesis of A-b-B and B-b-A copolymers based on PS (or PMMA) and PCL were carried out using the reverse strategy, where polymerisation of CL was followed by polymerisation of styrene (MMA) (see example in Scheme 36). According to 1H NMR data, macroinitiators **13** and **14** and hydroxyl-terminated PS showed high efficiency in polymerisation of the second block ($f_i = 1$). This excluded additional chain-end functionalisation stages from the synthetic procedure. The molecular masses of the PS, PMMA and PCL blocks in the copolymers were in agreement with the calculated values. The polydispersities of particular blocks and the copolymer were also low ($M_w/M_n = 1.21$ and 1.17 for PS-b-PCL with $M_{nPS} = 2.25 \times 10^3$ and $M_{nPS-b-PCL} = 4.45 \times 10^4$, respectively). Taking into account the fact that one end of the diblock copolymer obtained after ATRP of the second block contained chlorine atoms capable of initiating ATRP of the third block, a PCL-b-PBA-b-PMMA copolymer of specified molecular structure was synthesised.³⁷⁴

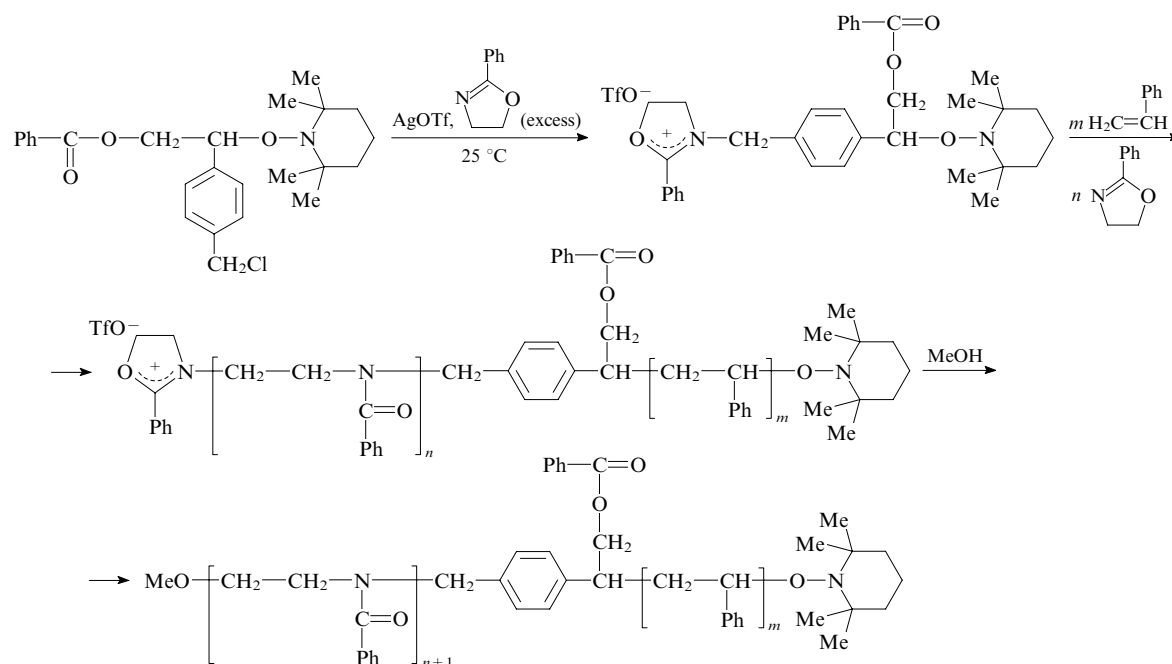
The possibility of concurrent multimode synthesis of diblock copolymers using bifunctional initiators was first

Scheme 35



Scheme 36





reported by Sogah and co-workers.³⁷³ Using 1-benzoyl-2-[4-(chloromethyl)phenyl]-2-(2,2,6,6-tetramethyl-1-piperidinoxy)-ethane (**9c**) as initiator, the authors carried out concurrent ‘pseudoliving’ SFRP of styrene and ‘living’ cationic polymerisation of 2-phenyl-2-oxazoline (PhOx) (Scheme 37). This unique synthesis was performed in the bulk as follows. The reactor was charged with anhydrous initiator and anhydrous silver triflate (silver trifluoromethanesulfonate, AgOTf), purged with an inert gas, an excess PhOx was added at 25 °C; this resulted in a cationic derivative of the initiator in excess of the monomer. Then, styrene was introduced, the temperature was raised to 125 °C and polymerisation was carried out for 44 h. The rigid block copolymer was cooled, dissolved in CH_2Cl_2 and methanol was added to convert the charged phenyloxazoline group of PPhOx-b-PS to methyl ether group. The AgCl precipitate was filtered off. The PPhOx-b-PS diblock copolymers were characterised by $P_{n \text{ PPhOx}}$ ranging from 29 to 198. The copolymers contained almost no homopolymers (according to gel-permeation chromatography and ^1H NMR spectroscopy data) and had a narrow MMD ($M_w/M_n = 1.27 - 1.40$). Subsequent hydrolysis of the oxazoline units led to copolymers of PEI-b-PS with linear polyethyleneimine (PEI).

Questions posed by Sogah and co-workers.³⁷³ remain unanswered as yet. In particular, the authors confirmed the formation of block copolymers, but gave no proofs of concurrent character of ‘living’ cationic and ‘pseudoliving’ SFRP polymerisation throughout the whole 44 h. An unambiguous answer can be obtained by investigating the kinetics and mechanisms of this and other multimode processes. At the moment, it should be emphasised that this study opens a new avenue of research on polymer synthesis, which involves concurrent and competing polymerisation processes.

IV. Matrix effects in block copolymerisation processes

Now we will consider yet another important aspect, which was ignored for long in studies on the synthesis and properties of block copolymers. Most studies on the subject concern block copolymers whose components are thermodynamically incompatible or show a limited compatibility; macromolecules of such components form ‘supercrystal’ structures in the bulk^{15, 19, 380, 381} and various micellar and vesicular structures

in solution.^{1, 7, 9, 13, 382} However, block copolymers with highly compatible, chemically complementary components are also of considerable interest. Such components can form a system of co-operative noncovalent bonds between blocks, namely, electrostatic bonds, as in ampholytic (or zwitter-ionic) block copolymers,^{112, 113} or hydrogen bonds, as in the block and graft copolymers synthesised from non-ionogenic polymers and polyacids.^{6, 383} This type of block copolymers is treated as intramolecular polymer complexes (IntraPC). They can be used as binders in biotechnology and medicine, membranes, as flocculants and drag reducing agents in the case of turbulent flow.³⁸⁴ Taking into account specific properties of the block and graft copolymers that form IntraPC, the formation of a system of noncovalent bonds between the components in the course of synthesis was hypothesised (in other words, the case in point is manifestation of matrix effects that are well known for polymerisation of monomers in the presence of chemically complementary polymer chains, matrices, in the block and graft copolymerisation).³⁸⁵ The fruitfulness of this hypothesis was first confirmed in the kinetic studies of the synthesis of starch-g-PAA and PVS-g-PAA graft copolymers. Namely, it was shown that the rate of graft copolymerisation of PAA with starch³⁸⁶ and PVS³⁸⁷ substantially increases compared to the rate of homopolymerisation of acrylamide under identical conditions. These results were considered in a review.³⁸⁴

Since investigations of the matrix phenomena in block copolymerisation processes are in the early stage of development, we will dwell on them in more detail. Studies^{388, 389} concern the kinetics of radical block copolymerisation of PAA with different-MM PEG whose terminal groups were activated in the reaction of OH groups with Ce^{IV} ions [see reaction (7)]. Block copolymerisation was carried out in aqueous solution at 25 °C. For comparison, homopolymerisation of AAm initiated with ethanol instead of PEG was performed under similar conditions. Chemical complementarity of PAA and PEG was preliminarily confirmed in the complexation studies of covalently nonbonded polymers³⁹⁰ and a system of H-bonds in the resulting InterPC³⁹¹ in water.

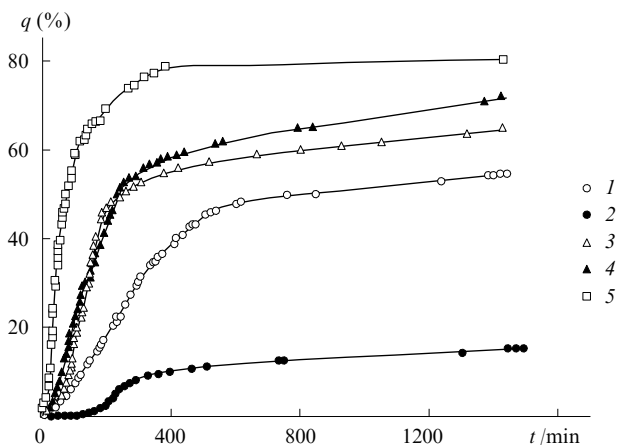
The results of dilatometric studies are presented in Fig. 2. All kinetic curves show an induction period. The authors believed that it is governed by the ‘lifetime’ of the intermediate complex formed by Ce^{IV} ions with the OH groups of PEG. The rate of block copolymerisation of PAA with the lowest-molecular-mass sample (PEG1) and the yield of the PAA-b-

Table 1. Kinetic parameters of block copolymerisation of PAA with PEG of different molecular mass and homopolymerisation of AA.

Polymer	$10^{-4} M_{\text{vPEG}}$	τ/min	$10^5 V_{\text{p}}^{20}/\text{mol dm}^{-3} \text{ s}^{-1}$	$10^5 V_{\text{p}}^{40}/\text{mol dm}^{-3} \text{ s}^{-1}$	$10^5 V_{\text{p}}^{60}/\text{mol dm}^{-3} \text{ s}^{-1}$	q (%)
PAA	—	15.5	1.6	1.02	—	53.5
TBC1	0.1	168.0	0.6 ^a	—	—	14.2
TBC3	0.6	54.9	5.76	5.62	0.16	63.4
TBC4	1.5	31.4	4.62	4.19	0.34	69.5
TBC5	4.0	25.0	15.5	7.92	2.87	80.3

Note. τ_0 is the induction period; V_{p}^{20} , V_{p}^{40} , V_{p}^{60} are the block copolymerisation rates at a monomer conversion, q , of 20%, 40% and 60%, respectively; and q is the monomer conversion after 20 h.

^a Listed is the value for V_{p}^{10} .

**Figure 2.** Conversion for homopolymerisation of AA (1) and block copolymerisation of PAA with PEG with a molecular mass of 1×10^3 (2), 6×10^3 (3), 1.5×10^4 (4) and 4×10^4 (5) at 25 °C plotted vs. time.

PEO-b-PAA1 triblock copolymer (TBC1) were very low, whereas the induction period τ_0 was very long compared to τ_0 for homopolymerisation of AAm (see Fig. 2, curves 1 and 2). Another situation was observed in block copolymerisation of PAA with longer-chain PEG ($M_{\text{v}} > 1 \times 10^3$). Namely, the induction period shortened and the copolymerisation rate and the yield of the final product increased (curves 3–5). This is quantitatively characterised by the data listed in Table 1.

Significant acceleration of the block copolymerisation and an increase in AAm conversion in the synthesis of the TBC3, TBC4 and TBC5 copolymers compared to the synthesis of PAA points to a positive kinetic matrix effect due to the interaction of the PEO blocks (matrices) with the growing daughter PAA blocks that are covalently bonded through a system of hydrogen bonds (see Fig. 2).^{388, 389} The effect became more pronounced with elongation of the PEG block. Indeed, a change in M_{vPEG} from 6×10^3 to 4×10^4 caused the rate of block copolymerisation (V_{p}^{20}) to increase by an order of magnitude compared to the homopolymerisation rate of AAm (see Tabl. 1). This is consistent with the well-known increase in the energy of the interaction between partners and stability of the polycomplex with elongation of polymer chains. Unlike similar matrix processes that occur in water due to formation of a system of H-bonds between the covalently nonbonded matrix and the daughter chain and lead to high compaction of InterPC,³⁹² matrix block copolymerisation of PAA with PEO resulted in water-soluble IntraPC. This is a manifestation of the effect of the third hydrophilic block (PAA), which prevented high hydrophobisation and compaction of macroglobules.

A characteristic feature of the PAA-b-PEO-b-PAA triblock copolymers is a nearly linear increase in the molecular

mass of the PAA blocks (from 4.5×10^4 to 9.07×10^5) with an increase in the molecular mass of the PEO central block.^{388, 389} It was established that the interblock interaction strongly affects both the synthesis and the molecular structure of the block copolymers.

Yet another type of matrix effects was observed³⁹³ in a comparative study of the RAFT polymerisation of monomer mixtures, namely, *N,N*-dimethylacrylamide (DMAA) and 2-(*N*-butyl perfluorooctane-fluorosulfonamido)ethyl acrylate (BPFOFSAEA), in the presence of both low-molecular-mass CTA (3-benzylsulfonylethylthiocarbonylpropionic acid) and a macroCTA obtained by etherification of the low-molecular-mass CTA with PDMS ($M_{\text{n}} = 1.8 \times 10^4$). Polymerisation was carried out under identical conditions at 60 °C. The DMAA content was constant and the content of the second monomer was varied; azobis(isobutyronitrile) was used as initiator. α, α, α -Trifluorotoluene was chosen as the common solvent with allowance for high hydrophobicity of macroCTA. RAFT polymerisation of a mixture of monomers resulted in poly(DMAA-co-BPFOFSAEA) copolymer in the presence of the low-molecular-mass CTA and in poly(DMAA-co-BPFOFSAEA)-b-PDMS-b-poly(DMAA-co-BPFOFSAEA) copolymer in the presence of the macroCTA. In both cases the RAFT process showed some common features, namely, a linear increase in the molecular mass of the polymers with conversion and narrow MMDs for all products ($M_{\text{w}}/M_{\text{n}} = 1.12$ –1.26). However, the compositions of the side blocks in the triblock copolymers were basically different from the compositions of the copolymers obtained in the presence of the low-molecular-mass CTA. Namely, the triblock copolymers contained a large excess of BPFOFSAEA. In fact, the hydrophobic matrix (PDMS block) ‘selected’ the most hydrophobic monomer (BPFOFSAEA) from the mixture, to which it has a higher thermodynamic affinity, this is the reason for the effect observed. Shortening of the induction period in the kinetic curves for the RAFT polymerisation in the presence of macroCTA was also pointed out.

* * *

In this review we considered new methods of synthesis of block copolymers and new aspects of the investigations of the regularities of polymerisation processes, with allowance for chemical complementarity of the blocks formed. This may be useful for further research in this field.

References

1. G Riess *Prog. Polym. Sci.* **28** 1107 (2003)
2. I Piirma *Polymeric Surfactants (Surfactant Science Series)* Vol. 42 (New York: Marcel Dekker, 1992) p. 1
3. P Alexandridis, T A Hatton *Block Copolymers. Polymeric Materials Encyclopedia 1* (Boca Raton, FL: CRC Press, 1996) p. 743

4. V M Nace *Nonionic Surfactants: Polyoxyalkylene Block Copolymers (Surfactant Science Series)* Vol. 60 (New York: Marcel Dekker, 1996) p. 1
5. S Poser, H Fischer, M Arnold *Prog. Polym. Sci.* **23** 1337 (1998)
6. H-Q Xie, D Xie *Prog. Polym. Sci.* **24** 275 (1999)
7. P Alexandridis, B Lindman *Amphiphilic Block Copolymers: Self-Assembly and Applications* (Amsterdam: Elsevier, 2000)
8. T C Chung *Prog. Polym. Sci.* **27** 39 (2002)
9. H Mori, A H E Müller *Prog. Polym. Sci.* **28** 1403 (2003)
10. K Ishizu, K Tsubaki, A Mori, S Uchida *Prog. Polym. Sci.* **28** 27 (2003)
11. J Bohrisch, C D Eisenbach, W Jaeger, H Mori, A H E Müller, M Rehahn, C Schaller, S Traser, P Wittmeyer *Adv. Polym. Sci.* **165** 1 (2004)
12. K A Davis, K Matyjaszewski *Adv. Polym. Sci.* **159** 1 (2002)
13. M Moffitt, H Vali, A Eisenberg *Chem. Mater.* **10** 1021 (1998)
14. N S Cameron, A Eisenberg, R G Brown *Biomacromolecules* **3** 124 (2002)
15. I Hamley *Block Copolymers* (Oxford: Oxford University Press, 1999)
16. M Li, C K Ober *Mater. Today* **9** 30 (2006)
17. P L Soo, A Eisenberg *J. Polym. Sci., Part B* **42** 923 (2004)
18. H Rainer *Angew. Chem., Int. Ed.* **43** 278 (2004)
19. S Krishnamoorthy, C Hinderling, H Heinzlmann *Mater. Today* **9** 40 (2006)
20. H W Melville *J. Chem. Soc.* 414 (1941)
21. M K Mishra, Y Yagci *Block Copolymers. Comprehensive Polymer Science* 7 (Oxford: Pergamon Press, 1989) p. 808
22. Yu P Get'manchuk *Polimerna Khimiya* (Polymeric Chemistry) (Kiev: Kiev University, 1999)
23. Yu D Semchikov *Vysokomolekulyarnye Soedineniya* (High-Molecular Compounds) (Moscow: Academia, 2003)
24. A Hill, F Candau, J Selb *Prog. Colloid Polym. Sci.* **84** 61 (1991)
25. J Selb, S Biggs, D Renoux, F Candau *Hydrophilic Polymers. Performance with Environmental Acceptability (Adv. Chem. Ser.)* Vol. 248 (Ed. J E Glass) (Washington, DC: American Chemical Society, 1996) p. 251
26. E Volpert, J Selb, F Candau *Polymer* **39** 1025 (1998)
27. F Candau, J Selb *Adv. Colloid Interface Sci.* **79** 85 (1999)
28. Eur. P. 57875; *Chem. Abstr.* **98** 5109 (1983)
29. US P. 4528348; *Chem. Abstr.* **102** 7279 (1985)
30. W Peer *Polymers in Aqueous Media (Adv. Chem. Ser.)* Vol. 223 (Ed. J E Glass) (Washington, DC: American Chemical Society, 1989) Ch. 20, p. 381
31. S A Ezzell, C L McCormick *Water-Soluble Polymers. Synthesis, Solution Properties and Applications (ACS Symp. Ser.)* Vol. 467 (Eds S Shalaby, C L McCormick, G B Butler) (Washington, DC: American Chemical Society, 1991) p. 130
32. A Hill, F Candau, J Selb *Macromolecules* **26** 4521 (1993)
33. J Bock, P L Valint Jr, C J Pace, D B Siano, D N Schulz, S R Turner *Water-Soluble Polymers for Petroleum Recovery* (Eds G A Stahl, D N Schulz) (New York: Plenum, 1988) p. 147
34. K C Dowling, J K Thomas *Macromolecules* **23** 1059 (1990)
35. S A Ezzell, C E Hoyle, D Creed, C L McCormick *Macromolecules* **25** 1887 (1992)
36. S Biggs, A Hill, J Selb, F Candau *J. Phys. Chem.* **96** 1505 (1992)
37. G O Yahaya, A A Ahdab, S A Ali, B F Abu-Sharkh, E Z Hamad *Polymer* **42** 3363 (2001)
38. C L McCormick, T Nanaka, C B Johnson *Polymer* **29** 731 (1988)
39. C L McCormick, J C Middleton, C E Grady *Polymer* **33** 4184 (1992)
40. C L McCormick, J C Middleton, D F Cummins *Macromolecules* **25** 1201 (1992)
41. L Z Rogovina, V G Vasil'ev, N A Churochkina, T A Pryakhina, A R Khokhlov *Vysokomol. Soedin., Ser. A* **46** 644 (2004)^a
42. G L Smith, C L McCormick *Macromolecules* **34** 918 (2001)
43. G L Smith, C L McCormick *Macromolecules* **34** 5579 (2001)
44. M Szwarc *Ionic Polymerization Fundamentals* (New York: Hanser Publishers, 1996)
45. *Cationic Polymerizations* (Ed. K Matyjaszewski) (New York: Marcel Dekker, 1996)
46. C Pugh, A L Kiste *Prog. Polym. Sci.* **22** 601 (1997)
47. K Matyjaszewski *J. Polym. Sci., Part A* **31** 995 (1993)
48. K Matyjaszewski *Macromolecules* **26** 1787 (1993)
49. H L Hsieh, R P Quirk *Anionic Polymerization: Principles and Practical Applications* (New York: Marcel Dekker, 1996)
50. R P Quirk, D J Kinning, L J Fetters *Comprehensive Polymer Science* Vol. 7 (Eds S K Aggarwal, S Russo) (Oxford: Pergamon Press, 1992) Ch. 1
51. S K Varshney, J P Hautekeer, R Fayt, R Jérôme, P Teyssie *Macromol. Chem., Macromol. Symp.* **23** 2618 (1990)
52. D Kunkel, A H E Müller, M Janata, L Lochmann *Macromol. Chem., Macromol. Symp.* **60** 315 (1992)
53. S Nakahama, A Hirao *Prog. Polym. Sci.* **15** 299 (1990)
54. A Hirao, S Nakahama *Acta Polym.* **49** 133 (1998)
55. W Burlant, A Hoffman *Graft and Block Copolymers* (New York: Reinold, 1960)
56. R Ceresa *Block and Graft Copolymers* (London: Butterworths, 1962)
57. J Fetters *J. Polym. Sci., Part C* **26** 1 (1969)
58. A Noshay, J McGrath *Block Copolymers* (New York: Academic Press, 1977)
59. N M Bol'bit, Yu N Korneev, A L Izyumnikov, E R Klinshpont *Vysokomol. Soedin., Ser. A* **31** 147 (1989)^a
60. T Hashimoto, Y Tsukahara, K Tachi, H Kawai *Macromolecules* **16** 648 (1983)
61. G Kraus, C W Childers, J T Gruver *J. Appl. Polym. Sci.* **11** 1581 (1967)
62. G Kraus, K W Rollmann *Angew. Makromol. Chem.* **16–17** 271 (1971)
63. J J O'Malley, R G Crystal, P F Erhardi *Macromol. Syn.* **4** 35 (1972)
64. H Q Xie, P G Zhou, *Multicomponent Polymer Materials (Adv. Chem. Ser.)* Vol. 211 (Eds D R Paul, C H Sperling) (Washington, DC: American Chemical Society, 1986) p. 139
65. R P Quirk, J Kim, K Rodrigues, W L Mattice *Polym. Prepr. (Am. Chem. Soc., Div. Polym. Chem.)* **31** 87 (1990)
66. F Calderara, Z Hruska, G Hurtrez, T Nagay, G Riess, M A Winnik *Makromol. Chem.* **194** 1411 (1993)
67. Z Hruska, G Hurtrez, S Walter, G Riess *Polymer* **33** 2447 (1992)
68. X F Zhong, S K Varshney, A Eisenberg *Macromolecules* **25** 7160 (1992)
69. D H Richard, M Szwarc *Trans. Faraday Soc.* **55** 1644 (1959)
70. V N Zgonnik, L A Shibaev, N I Nikolaev *Int. Symp. Macromol. Chem. Prepr.* **4** 319 (1969)
71. G P Finaz, P Rempp, J Parrod *Bull. Soc. Chim. Fr.* 262 (1962)
72. S Marti, J Nervo, G Riess *Prog. Colloid Polym. Sci.* **58** 114 (1975)
73. M Gervais, B Gallot *Makromol. Chem.* **178** 1577 (1977)
74. C Robitaille, J Prud'homme *Macromolecules* **16** 605 (1983)
75. J P Hautekeer, S K Varshney, R Fayt, C Jacobs, R Jérôme, P Teyssie *Macromolecules* **23** 3893 (1990)
76. H Zhang, H Ishikawa, M Ohata, T Kazama, Y Isono, T Fujimoto *Polymer* **33** 828 (1992)
77. C Ramireddy, Z Tuzar, K Prochazka, S E Webber, P Munk *Macromolecules* **25** 2541 (1992)
78. K Khougaz, D Nguyen, C E Williams, A Eisenberg *Can. J. Chem.* **73** 2086 (1995)
79. I Astafieva, K Khougaz, A Eisenberg *Macromolecules* **28** 7127 (1995)
80. O Terreau, L Luo, A Eisenberg *Langmuir* **19** 5601 (2003)
81. S Pispas, E Siakali-Kioulafa, N Hadjichristidis, T Mavromoustakos *Macromol. Chem. Phys.* **203** 1317 (2002)
82. E Ruckenstein, H Zhang *Macromolecules* **31** 9127 (1998)
83. M A Ansarifar, P F Luckham *Polymer* **29** 329 (1988)
84. Z Gao, S K Varshney, S Wong, A Eisenberg *Macromolecules* **27** 7923 (1994)
85. J P Spatz, S Sheiko, M Möller *Macromolecules* **29** 3220 (1996)
86. R Saito, S Okamura, K Ishizu *Polymer* **33** 1099 (1992)
87. K Ishizu, K Inagaki, K Bessho, T Fukutomi *Makromol. Chem.* **185** 1169 (1984)
88. C L Petzhold, R Stadler, H Frauenrath *Makromol. Chem., Rapid Commun.* **14** 33 (1993)

89. C L Petzhold, R Morschhäuser, H Kolshorn, R Stadler *Macromolecules* **27** 3707 (1994)
90. C L Petzhold, R Stadler *Macromol. Chem. Phys.* **196** 2625 (1995)
91. I C Riegel, A Eisenberg *Langmuir* **18** 3358 (2002)
92. I C Riegel, D Samios, C L Petzhold, A Eisenberg *Polymer* **44** 2117 (2003)
93. P K Seow, Y Gallot, A Skoulios *Makromol. Chem.* **176** 3135 (1975)
94. T Suzuki, Y Murakami, Y Takegami *Polym. J. (Tokio)* **12** 183 (1980)
95. D Gary, S Horing, J Ulbricht *Makromol. Chem., Rapid Commun.* **5** 615 (1984)
96. H Reuter, I V Berlinova, S Hoering, J Ulbricht *Eur. Polym. J.* **27** 673 (1991)
97. J S Wang, S V Varshney, R Jérôme, P Teyssie *J. Polym. Sci., Part A* **30** 2251 (1992)
98. J Waton, B Michels, R Zana *Macromolecules* **34** 907 (2001)
99. I N Topchieva, E L Kolomnikova, M I Banatskaya, V A Kabanov *Vysokomol. Soedin., Ser. A* **35** 395 (1993)^a
100. I N Topchieva, A L Blyumenfel'd, A A Klyamkin, V A Polyakov, V A Kabanov *Vysokomol. Soedin.* **36** 271 (1994)^a
101. S R Sroy, G S Kwon *J. Controlled Release* **95** 161 (2004)
102. L V Vinogradova, V N Sgonnik, A A Ilina, D T Dotcheva, C B Tsvetanov *Macromolecules* **25** 6733 (1992)
103. T J Martin, K Prochazka, P Munk, S E Webber *Macromolecules* **29** 6071 (1996)
104. Y Yu, A Eisenberg *Polym. Mater. Sci. Eng.* **79** 288 (1998)
105. P L Soo, L Luo, D Maysinger, A Eisenberg *Langmuir* **18** 9996 (2002)
106. *Amphiphilic Block Copolymers: Self-Assembly and Applications* (Eds P Alexandridis, B Lindman) (Amsterdam: Elsevier, 2000)
107. H M Burt, X Zhang, P Toleikis, L Embree, W L Hunter *Colloids Surf., B* **16** 161 (1999)
108. Z Zhu, C Xiong, L Zhang, M Yuan, X Deng *Eur. Polym. J.* **35** 1821 (1999)
109. J-S Yoon, W-S Lee, K-S Kim, I-J Chin, M-N Kim, C Kim *Eur. Polym. J.* **36** 435 (2000)
110. L V Vinogradova, V V Shamanin, D Kuckling, H-J P Adler *Vysokomol. Soedin., Ser. A* **47** 2070 (2005)^a
111. M Kamachi, M Kurihara, J K Stille *Macromolecules* **5** 161 (1972)
112. E A Bekturov, S E Kudaibergenov, R E Khamzamalina, V A Frolova, D E Nurgalieva, R C J Schulz, J Zöller *Makromol. Chem., Rapid Commun.* **13** 225 (1992)
113. E A Bekturov, V A Frolova, S E Kudaibergenov, R C Schulz, J Zöller *Makromol. Chem.* **191** 457 (1990)
114. Y Morishima, T Hashimoto, Y Itoh, M Kamachi, S Nozakura *J. Polym. Sci., Polym. Chem. Ed.* **20** 299 (1982)
115. S Creutz, P Teyssie, R Jérôme *Macromolecules* **30** 6 (1997)
116. B Mahltig, J F Gohy, R Jérôme, C Bellmann, M Stamm *Colloid Polym. Sci.* **278** 502 (2000)
117. B Mahltig, R Jérôme, M Stamm *Phys. Chem. Chem. Phys.* **3** 4371 (2001)
118. B Mahltig, P Müller-Buschbaum, M Wolkenhauer, O Wunnicke, S Wiegand, J F Gohy, R Jérôme, M Stamm *J. Colloid Interface Sci.* **242** 36 (2001)
119. S Creutz, J Van Stam, P C De Schryver, R Jérôme *Macromolecules* **31** 681 (1998)
120. G Riess, M Schlienger, S Marti *J. Macromol. Sci., Part B* **17** 355 (1980)
121. V Abetz, K Markgraf, V Rebizant *Macromol. Symp.* **177** 139 (2002)
122. A B De Fierro, G Reiter, A Mueller, V Abetz *Extended Abstracts of European Polymer Congress 2005, Moscow 2005 CD* P. 3.2-5 3594
123. G E Yu, A Eisenberg *Macromolecules* **31** 5546 (1998)
124. P Guegan, J J Cernohouse, A K Khandpur, T R Hoye, C W Macosko *Macromolecules* **29** 4605 (1996)
125. J F Gohy, N Willet, S Varshney, J X Zhang, R Jérôme *Angew. Chem., Int. Ed.* **40** 3214 (2001)
126. J F Gohy, N Willet, S Varshney, J X Zhang, R Jérôme *e-Polymers* **35** (2002)
127. L Lei, J F Gohy, N Willet, S Varshney, J X Zhang, R Jérôme *Macromolecules* **37** 1089 (2004)
128. L Lei, J F Gohy, N Willet, J X Zhang, S Varshney, R Jérôme *Polymer* **45** 4375 (2004)
129. M Stepanek, J Humpolíčková, K Prochazka, M Hof, Z Tuzar, M Spirkova, T Wolff *Collect. Czech. Chem. Commun.* **68** 121 (2003)
130. C-A Fastin, V Abetz, J-F Gohy *Eur. Polym. J., E* **16** 291 (2005)
131. E Giebler, R Stadler *Macromol. Chem. Phys.* **198** 3815 (1997)
132. R Bieringer, V Abetz, A H E Müller *Eur. Phys. J., E* **5** 5 (2001)
133. F Liu, A Eisenberg *Angew. Chem., Int. Ed.* **42** 1404 (2003)
134. T Ishizone, K Sugiyama, Y Sakano, H Mori, A Hirao, S Nakahama *Polym. J. (Tokio)* **31** 983 (1999)
135. Y Tanaka, H Hasegawa, T Hashimoto, A Ribbe, K Sugigama, A Hirao, S Nakahama *Polym. J. (Tokio)* **31** 989 (1999)
136. O W Webster, W R Hertler, D Y Sogah, W B Farnham, T V Rajanbabu *J. Am. Chem. Soc.* **105** 5706 (1983)
137. P M Mai, A H E Müller *Makromol. Chem., Rapid Commun.* **8** 99 (1987)
138. P M Mai, A H E Müller *Makromol. Chem., Rapid Commun.* **8** 247 (1987)
139. I B Dicker, G M Cohen, W B Farnham, W R Hertler, E D Laganis, D Y Sogah *Macromolecules* **23** 4034 (1990)
140. A H E Müller *Makromol. Chem., Macromol. Symp.* **32** 87 (1990)
141. K Matyjaszewski, C Pugh *Makromol. Chem., Macromol. Symp.* **67** 67 (1993)
142. S P Rannard, N C Billingham, S P Armes, J Mykytiuk *Eur. Polym. J.* **29** 407 (1993)
143. J Kriz, B Masar, H Pospišil, J Pleštil, Z Tuzar, M A Kiselev *Macromolecules* **29** 7853 (1996)
144. W J Choi, Y B Kim, S K Kwon, K T Lim, S K Choi *J. Polym. Sci., Part A* **30** 2143 (1992)
145. M R Simmons, C S Patrickios *Macromolecules* **31** 9075 (1998)
146. V Bütün, N C Billingham, S P Armes *J. Am. Chem. Soc.* **120** 11818 (1998)
147. V Bütün, N C Billingham, S P Armes *J. Am. Chem. Soc.* **120** 12135 (1998)
148. C S Patrickios, W R Hertler, N L Abbott, T A Hatton *Macromolecules* **27** 930 (1994)
149. A B Lowe, N C Billingham, S P Armes *Macromolecules* **31** 5991 (1998)
150. J Kriz, B Masar, J Pleštil, Z Tuzar, H Pospišil, D Doskocilova *Macromolecules* **31** 41 (1998)
151. W-Y Chen, P Alexandridis, C-K Su, C S Patrickios, W R Hertler, T A Hatton *Macromolecules* **28** 8604 (1995)
152. C S Patrickios, A B Lowe, S P Armes, N C Billingham *J. Polym. Sci., Part A* **36** 617 (1998)
153. K Matyjaszewski, C-H Lin, C Pugh *Macromolecules* **26** 2649 (1993)
154. T Kunitake, K Takarabe *Macromolecules* **12** 1067 (1979)
155. H Mayr, R Schneider, C Schade, J Bartl, R Bederke *J. Am. Chem. Soc.* **112** 4446 (1990)
156. K Matyjaszewski, C-H Lin, A Bon, J S Xiang *Makromol. Chem., Macromol. Symp.* **85** 65 (1994)
157. M P Dreyfuss, P Dreyfuss *Polymer* **6** 93 (1965)
158. T Higashimura, M Mitsuhashi, M Sawamoto *Macromolecules* **12** 178 (1979)
159. Z Fodor, R Faust *J. Macromol. Sci., Part A* **31** 1985 (1994)
160. Z Fodor, R Faust *J. Macromol. Sci., Part A* **32** 575 (1995)
161. D Li, R Faust *Macromolecules* **28** 1383 (1995)
162. R Faust *Polym. Prepr. (Am. Chem. Soc., Div. Polym. Chem.)* **40** 960 (1999)
163. J-M Oh, S-J Kang, O-S Kwon, S-K Choi *Macromolecules* **28** 3015 (1995)
164. J P Kennedy *J. Polym. Sci., Part A* **37** 2285 (1999)
165. US P. 4946897; *Chem. Abstr.* **111** 116319 (1989)
166. G Kaszas, J E Puskas, W Hager, J P Kennedy *J. Polym. Sci., Part A* **29** 427 (1991)
167. J E Puskas, G Kaszas *Rubber Chem. Technol.* **69** 462 (1996)
168. J E Puskas, G Kaszas *Prog. Polym. Sci.* **25** 403 (2000)
169. K Kojima, M Sawamoto, T Higashimura *Macromolecules* **24** 2658 (1991)

170. T Ohmura, M Sawamoto, T Higashimura *Macromolecules* **27** 3714 (1994)
171. M Sawamoto, T Hasebe, M Kamigaito, T Higashimura *J. Macromol. Sci., Part A* **31** 937 (1994)
172. S Hadjikyriakon, R Faust *Macromolecules* **29** 526 (1996)
173. M Miyamoto, M Sawamoto, T Higashimura *Macromolecules* **18** 123 (1985)
174. K Kojima, M Sawamoto, T Higashimura *Polym. Bull. (Berlin)* **23** 149 (1990)
175. C Forder, C S Patrickios, S P Armes, N C Billingham *Macromolecules* **29** 8160 (1996)
176. A W M De Laat, H F M Schoo *Colloid Polym. Sci.* **276** 176 (1998)
177. C Kim, S C Lee, Y Chang, J S Yoon, I J Chin, I C Kwon, Y H Kim *Polym. Prepr. (Am. Chem. Soc., Div. Polym. Chem.)* **37** 159 (1996)
178. C S Patrickios, C Forder, S P Armes, N C Billingham *J. Polym. Sci., Part A* **35** 1181 (1997)
179. E V Malmström, C J Hawker *Macromol. Chem. Phys.* **199** 923 (1998)
180. C J Hawker, A W Bosman, E Harth *Chem. Rev.* **101** 3661 (2001)
181. K Matyjaszewski, J Xia *Chem. Rev.* **101** 2921 (2001)
182. M Yu Zaremskii, V B Golubev *Vysokomol. Soedin., Ser. C* **43** 1689 (2001)^a
183. G V Korolev, A P Marchenko *Usp. Khim.* **69** 447 (2000) [*Russ. Chem. Rev.* **69** 409 (2000)]
184. C J Hawker *J. Am. Chem. Soc.* **116** 11185 (1994)
185. A Goto, T Fukuda *Prog. Polym. Sci.* **29** 329 (2004)
186. A V Yakimanskii *Vysokomol. Soedin., Ser. C* **47** 1241 (2005)^a
187. M Yu Zaremskii *Vysokomol. Soedin., Ser. A* **48** 404 (2006)^a
188. T Otsu, M Yoshita *Makromol. Chem., Rapid Commun.* **3** 127 (1982)
189. US P. 4581429; *Chem. Abstr.* **102** 221335 (1985)
190. Eur. P. 135280; *Chem. Abstr.* **102** 221335 (1985)
191. T Fukuda, T Terauchi, A Goto, K Ohno, Y Tsujii, T Miyamoto, S Kobatake, B Yamada *Macromolecules* **29** 6393 (1996)
192. D Benoit, S Grimaldi, S Robin, J-P Finet, P Tordo, Y Gnanou *J. Am. Chem. Soc.* **122** 5929 (2000)
193. A Goto, T Fukuda *Macromolecules* **32** 618 (1999)
194. M Yu Zaremskii, A B Zhaksylykov, A P Orlova, E S Garina, G A Badun, M B Lachinov, V B Golubev *Vysokomol. Soedin., Ser. A* **47** 886 (2005)^a
195. D F Grishin, L L Semenycheva *Usp. Khim.* **70** 486 (2001) [*Russ. Chem. Rev.* **70** 425 (2001)]
196. C Detrembleur, M Claes, R Jérôme, *Advances in Controlled/Living Radical Polymerization (ACS Symp. Ser.)* Vol. 854 (Ed. K Matyjaszewski) (Washington, DC: American Chemical Society, 2003) Ch. 35, p. 496
197. D F Grishin, L L Semenycheva, E V Kolyakina *Dokl. Akad. Nauk* **362** 634 (1998)^b
198. M Yu Zaremskii, A P Orlova, E S Garina, A V Olenin, M B Lachinov, V B Golubev *Vysokomol. Soedin., Ser. A* **45** 871 (2003)^a
199. C Detrembleur, V Sciannamea, C Koulic, M Claes, M Hoebeke, R Jérôme *Macromolecules* **35** 7214 (2002)
200. K Matyjaszewski, S Gaynor, D Greszta, D Mardare, T Shigemoto *Macromol. Symp.* **98** 83 (1995)
201. D F Grishin, S K Ignatov, A G Razuvaev, E V Kolyakina, A A Shchepalov, M V Pavlovskaya, L L Semenycheva *Vysokomol. Soedin., Ser. A* **43** 1742 (2001)^a
202. D F Grishin, M V Pavlovskaya, E V Kolyakina, L L Semenycheva *Zh. Prikl. Khim.* **75** 1500 (2002)^c
203. D F Grishin, M V Pavlovskaya, L L Semenycheva *Vysokomol. Soedin., Ser. A* **43** 1913 (2001)^a
204. E V Kolyakina, D F Grishin *Vysokomol. Soedin., Ser. B* **47** 2197 (2005)^a
205. D F Grishin, E V Kolyakina, V V Polyanskova *Vysokomol. Soedin., Ser. A* **48** 764 (2006)^a
206. M Yu Zaremskii, A L Reznichenko, Yu V Grinevich, E S Garina, M B Lachinov, V B Golubev *Vysokomol. Soedin., Ser. A* **37** 898 (2005)^a
207. M K Georges, R P N Veregin, P K Kazmaier, G K Hamer *Polym. Prepr. (Am. Chem. Soc., Div. Polym. Chem.)* **35** 582 (1994)
208. P M Kazmaier, K Daimon, M K Georges, G K Hamer, R P N Veregin *Macromolecules* **30** 2228 (1997)
209. S O Hammouch, J M Catala *Macromol. Rapid Commun.* **17** 149 (1996)
210. M Steenbock, M Klapper, K Mullen, M Pinhal *Acta Polym.* **47** 276 (1996)
211. I Q Li, B A Howell, R A Koster, D B Priddy *Macromolecules* **29** 8554 (1996)
212. S Jousset, S O Hammouch, J M Catala *Macromolecules* **30** 6685 (1997)
213. E Yoshida *J. Polym. Sci., Part A* **34** 2937 (1996)
214. E Yoshida, T Fujii *J. Polym. Sci., Part A* **35** 2371 (1997)
215. M Mariani, M Lelli, K Sparnacci, M Laus *J. Polym. Sci., Part A* **37** 1237 (1999)
216. Y Zhou, J Lin, R Zhuang, J Ye, L Dai, L Zheng *Macromolecules* **33** 4745 (2000)
217. D Li, W J Brittain *Macromolecules* **31** 3852 (1998)
218. D Benoit, V Chaplinski, R Braslau, C J Hawker *J. Am. Chem. Soc.* **121** 3904 (1999)
219. M Nowakowska, S Zapotoczny, A Karewicz *Macromolecules* **33** 7345 (2000)
220. D Benoit, C J Hawker, E Huang, Z Lin, T P Russell *Macromolecules* **33** 1505 (2000)
221. A Leuteritz, M Messerschmidt, B Voit, M Yin, T Krause, W D Habicher *Polym. Prepr. (Am. Chem. Soc., Div. Polym. Chem.)* **43** 283 (2002)
222. M Messerschmidt, L Häubler, B Voit, T Krause, W D Habicher *Macromol. Symp.* **210** 111 (2004)
223. B Voit, M Messerschmidt, A Leuteritz *Extended Abstracts of European Polymer Congress 2005, Moscow, 2005 CD i.1.4.1* 4998
224. J-S Wang, K Matyjaszewski *Macromolecules* **28** 7572 (1995)
225. J-S Wang, K Matyjaszewski *Macromolecules* **28** 7901 (1995)
226. J-S Wang, K Matyjaszewski *J. Am. Chem. Soc.* **117** 5614 (1995)
227. M Kato, M Kamigaito, M Sawamoto, T Hihashimura *Polym. Prepr. Jpn.* **43** 1792 (1994)
228. M Kato, M Kamigaito, M Sawamoto, T Hihashimura *Macromolecules* **28** 1721 (1995)
229. Y Kotani, M Kato, M Kamigaito, M Sawamoto *Macromolecules* **29** 6979 (1995)
230. K Matyjaszewski, T E Patten, J Xia *J. Am. Chem. Soc.* **119** 674 (1997)
231. K A Davis, H-J Paik, K Matyjaszewski *Macromolecules* **32** 1767 (1999)
232. J Wang, T Grimaud, K Matyjaszewski *Macromolecules* **30** 6507 (1997)
233. C Granel, G Moineau, P Lecomte, P Dubois, R Jérôme, T Tessie *Polym. Prepr. (Am. Chem. Soc., Div. Polym. Chem.)* **38** 450 (1997)
234. S Hvilsted, S Borkar, H W Siesler, K Jankova, *Advances in Controlled/Living Radical Polymerization (ACS Symp. Ser.)* Vol. 854 (Ed. K Matyjaszewski) (Washington, DC: American Chemical Society, 2003) Ch. 17, p. 236
235. K Matyjaszewski, S G Gaynor, J Qiu, K Beers, S Coca, K Davis, A Mühlebach, J Xia, X Zhang *Associative Polymers in Aqueous Media. (ACS Symp. Ser.)* Vol. 765 (Ed. J E Glass) (Washington, DC: American Chemical Society, 2000) p. 52
236. X S Wang, S P Armes *Polym. Prepr. (Am. Chem. Soc., Div. Polym. Chem.)* **41** 413 (2000)
237. X S Wang, F L G Malet, S P Armes, D M Haddleton, S Perrier *Macromolecules* **34** 162 (2001)
238. T E Patten, K Matyjaszewski *Adv. Mater.* **10** 901 (1998)
239. J Xia, K Matyjaszewski *Macromolecules* **30** 7697 (1997)
240. J Wang, K Matyjaszewski, T Grimaud *Macromolecules* **31** 1527 (1998)
241. Y Shen, S Zhu, F Zeng, R Pelton *Macromolecules* **33** 5399 (2000)
242. G Moineau, Ph Dubois, R Jérôme, T Senninger, P Teyssie *Macromolecules* **31** 545 (1998)
243. S Jousset, J Qiu, K Matyjaszewski *Macromolecules* **34** 6641 (2001)

244. C Zhu, F Sun, M Zhang, J Jin *Polymer* **45** 1141 (2004)
245. E J Ashford, V Naldi, R O'Dell, N C Billingham, S P Armes *Chem. Commun.* 1285 (1999)
246. X-S Wang, R A Jackson, S P Armes *Macromolecules* **33** 255 (2000)
247. M Teodorescu, K Matyjaszewski *Macromolecules* **32** 4826 (1999)
248. M Senoo, Y Kotani, M Kamigaito, M Sawamoto *Macromolecules* **32** 8005 (1999)
249. J T Rademacher, M Baum, M E Pallack, W J Brittain, W J Simonsick *Macromolecules* **33** 284 (2000)
250. M Cassebras, S Pascual, A Pelton, M Tardi, J P Vairon *Macromol. Rapid Commun.* **20** 261 (1999)
251. K Matyjaszewski, D A Shipp, J Qiu, S G Gaynor *Macromolecules* **33** 2296 (2000)
252. K A Davis, K Matyjaszewski *Macromolecules* **33** 4039 (2000)
253. K A Davis, B Charleux, K Matyjaszewski *J. Polym. Sci., Part A* **38** 2274 (2000)
254. C Burguiere, S Pascual, C Bui, J-P Vairon, B Charleux, K A Davis, K Matyjaszewski, I Betremieux *Macromolecules* **34** 4439 (2001)
255. C Burguiere, C Chassenieux, B Challeux *Polymer* **44** 509 (2003)
256. S Gravano, M Borden, A Chen, E Doerffler, T E Patten, M Longo *Polym. Prepr. (Am. Chem. Soc., Div. Polym. Chem.)* **42** 549 (2001)
257. Y Liu, L Wang, C Pan *Macromolecules* **32** 8301 (1999)
258. G Wang, D Yan *J. Appl. Polym. Sci.* **82** 2381 (2001)
259. S Hvilsted *Extended Abstracts of European Polymer Congress 2005, Moscow, 2005* CD i.1.1.2 5177
260. S Borkar, K Jankova, H W Siesler, S Hvilsted *Macromolecules* **37** 788 (2004)
261. M L Becker, E E Remsen, K L Wooley *J. Polym. Sci., Part A* **39** 4152 (2001)
262. P Ravi, C Wang, K C Tam, L H Gan *Macromolecules* **36** 173 (2003)
263. Q Ma, K L Wooley *J. Polym. Sci., Part A* **38** 4805 (2000)
264. J Chiefari, Y K Chong, F Ercole, J Krstina, T P Le, R T A Mayadunne, G F Meijs, G Moad, C L Moad, E Rizzardo, S H Thang *Macromolecules* **31** 5559 (1998)
265. Y K Chong, T P T Le, G Moad, E Rizzardo, S H Thang *Macromolecules* **32** 2071 (1999)
266. E Rizzardo, J Chiefari, B Y K Chong, F Ercole, J Krstina, J Jeffery, T P T Le, R T A Mayadunne, G F Meijs, G Moad, C L Moad, S H Thang *Macromol. Symp.* **143** 291 (1999)
267. G Moad, J Chiefari, Y K Chong, J Krstina, R T A Mayadunne, A Postma, E Rizzardo, S H Thang *Polym. Int.* **49** 993 (2000)
268. Y Mitsukami, M S Donovan, A B Lowe, C L McCormick *Macromolecules* **34** 2248 (2001)
269. J Chiefari, R T A Mayadunne, C L Moad, G Moad, E Rizzardo, A Postma, M A Skidmore, S H Thang *Macromolecules* **36** 2273 (2003)
270. A Goto, K Sato, Y Tsujii, T Fukuda, G Moad, E Rizzardo, S H Thang *Macromolecules* **34** 402 (2001)
271. D G Hawthorne, G Moad, E Rizzardo, S H Thang *Macromolecules* **32** 5457 (1999)
272. V B Golubev, E V Chernikova, E A Leonova, A V Morozov *Vysokomol. Soedin., Ser. A* **47** 1115 (2005)^a
273. C Schilli, A H E Müller, S H Thang, E Rizzardo, B Chong *Controlled/Living Radical Polymerization. (ACS Symposium Ser.)* Vol. 854 (Ed. K Matyjaszewski) (Washington, DC: American Chemical Society, 2003) p. 603
274. S H Thang, Y K Chong, R T A Mayadunne, G Moad, E Rizzardo *Tetrahedron Lett.* **40** 2435 (1999)
275. WO PCT 9858974; *Chem. Abstr.* **130** 82018 (1999)
276. C Ladaviere, N Dörr, J P Claverie *Macromolecules* **34** 5370 (2001)
277. C Schilli, M G Lanzendörfer, A H E Müller *Macromolecules* **35** 6819 (2002)
278. M Destarac, D Charnot, X Franck, S Z Zard *Macromol. Rapid Commun.* **21** 1035 (2000)
279. J Loiseau, N Doeerr, J M Suau, J B Egraz, M F Llauro, C Ladaviere, J Claverie *Macromolecules* **36** 3066 (2003)
280. D B Thomas, A J Convertine, L J Myrick, C W Scales, A E Smith, A B Lowe, Y A Vasilieva, N Ayres, C L McCormick *Macromolecules* **37** 8941 (2004)
281. D Bendejacq, V Ponsinet, M Joanicot, Y L Loo, R A Register *Macromolecules* **35** 6645 (2002)
282. M A Crichton, S R Bhatia *J. Appl. Polym. Sci.* **93** 490 (2004)
283. O E Bogomolova, E B Chernikova, D V Pergushov, A B Zézin *Sbornik Tezisov Dokladov i Soobshchenii na Vserossiiskoi Konferentsii 'Yal'chik-2004'* (Abstracts of Reports of the All-Russian Conference 'Yalchik-2004') (Moscow: Institute of Chemical Physics, 2004) p. 38
284. N Gaillard, A Guyot, J Claverie *J. Polym. Sci., Part A* **41** 684 (2003)
285. Appl. Eur. 1411070; *Ref. Zh. Khim.* 328P (2005)
286. D Taton, A-Z Wilezewska, M Destarac *Macromol. Rapid Commun.* **22** 1497 (2001)
287. B S Sumerlin, M S Donovan, Y Mitsukami, A B Lowe, C L McCormick *Macromolecules* **34** 6561 (2001)
288. H De Brower, J G Tsavalas, F J Schork, M J Monteiro *Macromolecules* **33** 9239 (2000)
289. J G Tsavalas, F J Schork, H De Brower, M J Monteiro *Macromolecules* **34** 3938 (2001)
290. W Smulders, R G Gilbert, M J Monteiro *Macromolecules* **36** 4309 (2003)
291. S W Prescott, M J Ballard, E Rizzardo, R G Gilbert *Macromolecules* **35** 5417 (2002)
292. C J Ferguson, R J Hughes, B T T Pham, B S Hawket, R G Gilbert, A K Setelis, C H Such *Macromolecules* **35** 9243 (2002)
293. W W Smulders, C W Jones, F J Schork *Macromolecules* **37** 9345 (2004)
294. T Aida, Y Maekawa, S Asano, S Inoue *Macromolecules* **21** 1195 (1988)
295. M Akatsuka, T Aida, S Inoue *Macromolecules* **27** 2820 (1994)
296. T Aida, S Inoue *Makromol. Chem., Rapid Commun.* **1** 677 (1980)
297. T Aida, S Inoue *Macromolecules* **14** 1162 (1981)
298. T Yasuda, T Aida, S Inoue *Macromolecules* **17** 2217 (1984)
299. L Trofimoff, T Aida, S Inoue *Chem. Lett.* 991 (1987)
300. M Kuroki, T Aida, S Inoue *J. Am. Chem. Soc.* **109** 4737 (1987)
301. M Okada *Prog. Polym. Sci.* **27** 87 (2002)
302. P Cohen, M J Abadie, F Schue, D H Richards *Polymer* **23** 1105 (1982)
303. G Riess, G Hurtrez, P Bahadur *Encyclopedia of Polymer Science and Engineering (Second Edition)* (New York: Wiley, 1985) Vol. 2, p. 324
304. Y Yağci, M K Mishra *Polymeric Materials Encyclopedia* (Ed. J C Salamone) (Boca Raton, FL: CRC Press, 1996) Vol. 1, p. 789
305. M J Yanjarappa, S Sivaram *Prog. Polym. Sci.* **27** 1347 (2002)
306. M A Novitskaya, A A Konkin *Vysokomol. Soedin.* **7** 1719 (1965)^a
307. S Nagarayan, K Srinivasan, V Sabdham *Makromol. Chem., Rapid Commun.* **17** 281 (1996)
308. M D C Topp, P J Dijkstra, H Talsma, J Feijen *Macromolecules* **30** 8518 (1997)
309. I Cakmak *Angew. Makromol. Chem.* **224** 1 (1995)
310. H R Dicke, M Heitz *Makromol. Chem., Rapid Commun.* **2** 83 (1981)
311. B A Dolgoplosk, E I Tinyakova *Okislitel'no-Vosstanovitel'nye Sistemy kak Istochniki Svobodnykh Radikalov* (Redox Systems as Sources of Free Radicals) (Moscow: Nauka, 1972)
312. R Shriner, R Fuson, D Curtin *Systematic Identification of Organic Compounds* (New York: Wiley, 1980)
313. A Ueda, S Nagai *J. Polym. Sci., Part A* **25** 3498 (1987)
314. A Ueda, S Nagai *J. Polym. Sci., Polym. Chem. Ed.* **24** 405 (1986)
315. B Hazer, B Erdan, R W Lenz *J. Polym. Sci., Part A* **32** 1739 (1994)
316. T K Wodka *J. Appl. Polym. Sci.* **47** 407 (1993)
317. H Yuruk, A B Ozdemir *J. Appl. Polym. Sci.* **31** 2171 (1986)
318. H Yuruk, S Ulupiner *Angew. Makromol. Chem.* **213** 197 (1993)
319. E H Orhan, I Yilgor, B M Baysal *Polymer* **18** 286 (1977)
320. N Uyanik, B M Baysal *J. Appl. Polym. Sci.* **41** 1981 (1990)
321. I Cakmak *Angew. Makromol. Chem.* **224** 49 (1995)

322. K Jankova, P Jannash, S Hvilsted *J. Mater. Chem.* **14** 2902 (2004)
323. K Jankova, S Hvilsted *J. Fluorine Chem.* **126** 241 (2005)
324. E J Ashford, V Naldi, R O'Dell, N C Billingham, S P Armes *Chem. Commun.* 1285 (1999)
325. A R Siedle, W M Lamanna, R A Newmark, J Stevens, D E Richardson, M Ryan *Makromol. Chem., Macromol. Symp.* **66** 215 (1993)
326. T C Chung, W Janvikul, H L Lu *J. Am. Chem. Soc.* **118** 705 (1996)
327. T C Chung, H L Lu, W Janvikul *Polymer* **38** 1495 (1997)
328. T C Chung, H L Lu *J. Mol. Catal. A* **115** 115 (1997)
329. B Lu, T C Chung *Macromolecules* **31** 5943 (1998)
330. R Mulhaupt, T Duschek, B Rieger *Makromol. Chem., Macromol. Symp.* **48–49** 317 (1991)
331. S Sosnowski, S Slomkowski, S Penczek, Z Florjanczyk *Macromol. Chem.* **192** 1457 (1991)
332. R Mulhaupt, T Duschek, D Fischer, S Setz *Polym. Adv. Technol.* **4** 439 (1993)
333. T Shiono, Y Akino, K Soga *Macromolecules* **27** 6229 (1994)
334. G Xu, T C Chung *Macromolecules* **32** 8689 (1999)
335. G Xu, T C Chung *J. Am. Chem. Soc.* **121** 6763 (1999)
336. G Xu, J Y Dong, T C Chung *Polym. Prepr. (Am. Chem. Soc., Div. Polym. Chem.)* **41** 1926 (2000)
337. T C Chung, J Y Dong *J. Am. Chem. Soc.* **123** 4871 (2001)
338. K T Lim, S E Webber, K P Johnston *Macromolecules* **32** 2811 (1999)
339. M Z Yates, G Li, J J Shim, S Maniar, K P Johnston, K T Lim, S Webber *Macromolecules* **32** 1018 (1999)
340. P A Psathas, S R P Da Rocha Jr, C T Lee, K P Johnston, K T Lim, S Webber *Ind. Eng. Chem. Res.* **39** 2655 (2000)
341. S Perrier, C Barner-Kowollik, J F Quinn, P Vana, T P Davis *Macromolecules* **35** 8300 (2002)
342. K Huan, L Bes, D M Haddleton, E Khoshdel *J. Polym. Sci., Part A* **39** 1833 (2001)
343. L A Smirnova, Yu D Semchikov, N A Andriyanova, N V Pastukhova, S D Zaitsev *Vysokomol. Soedin., Ser. B* **45** 1359 (2003)^a
344. *Chemistry with Ultrasound* (Ed. T J Mason) (New Nork: Elsevier, 1990)
345. A Gadkari, J P Kennedy *J. Appl. Polym. Sci., Appl. Polym. Symp.* **44** 19 (1989)
346. S Nemes, J P Kennedy *J. Macromol. Sci., Part A* **28** 311 (1991)
347. T Kitayama, T Nishiura, K Hatada *Polym. Bull. (Berlin)* **26** 513 (1991)
348. J P Kennedy, J L Price *Polym. Mater. Sci. Eng.* **64** (1991)
349. J P Kennedy, J L Price, K Koshimura *Macromolecules* **24** 6567 (1991)
350. Q Liu, M Konas, R M Davis, J S Riffle *J. Polym. Sci., Part A* **31** 1709 (1993)
351. J Ruth, C Moore, W J Brittain, J Si, J P Kennedy *Polym. Prepr. (Am. Chem. Soc., Div. Polym. Chem.)* **34** 479 (1993)
352. R Nomura, M Narita, T Endo *Macromolecules* **27** 4853 (1994)
353. R Nomura, M Narita, T Endo *Macromolecules* **28** 86 (1995)
354. J Feldthusen, B Ivan, A H E Müller *Macromolecules* **30** 6989 (1997)
355. J Feldthusen, B Ivan, A H E Müller *Functional Polymers (ACS Symp. Ser.)* Vol. 704 (Eds B M Novak, A O Patil, D N Schultz) (Washington, DC: American Chemical Society, 1998) p. 121
356. J Feldthusen, B Ivan, A H E Müller *Macromolecules* **31** 578 (1998)
357. I Q Li, B A Howell, M T Dineen, P E Kastl, J W Lyons, D M Meunier, P B Smith, D B Priddy *Macromolecules* **30** 5195 (1997)
358. S Kobatake, H J Harwood, R P Quirk, D B Priddy *Macromolecules* **30** 4238 (1997)
359. S Kobatake, H J Harwood, R P Quirk, D B Priddy *Macromolecules* **31** 3735 (1998)
360. J-D Tong, S Ni, M A Winnik *Macromolecules* **33** 1482 (2000)
361. A Ramakrishnan, R Dhamodharan *J. Macromol. Sci., Part A* **37** 621 (2000)
362. Q Zhang, E E Remsen, K L Wooley *J. Am. Chem. Soc.* **122** 3642 (2000)
363. M Bednarek, T Biedron, P Kubisa *Macromol. Rapid Commun.* **20** 59 (1999)
364. J Pyun, S Jia, T Kowalewski, K Matyjaszewski *Macromol. Chem. Phys.* **205** 411 (2004)
365. S Coca, K Matyjaszewski *Macromolecules* **30** 2808 (1997)
366. O Nuyken, H Kroner, S Aechtner *Makromol. Chem., Rapid Commun.* **9** 671 (1988)
367. O Nuyken, H Kroner, S Aechtner *Polym. Bull. (Berlin)* **24** 513 (1990)
368. X Chen, B Ivan, J Kops, W Batsberg *Macromol. Rapid Commun.* **19** 585 (1998)
369. Z Fang, J P Kennedy *J. Polym. Sci., Part A* **40** 3662 (2002)
370. Z Fang, S Wang, S Q Wang, J P Kennedy *J. Appl. Polym. Sci.* **88** 1516 (2003)
371. R Puts, D Sogah *Macromolecules* **30** 7050 (1997)
372. D Sogah, R Puts, A Trimble, O Scherman *Polym. Prepr. (Am. Chem. Soc., Div. Polym. Chem.)* **38** 731 (1997)
373. M Weimer, O Scherman, D Sogah *Macromolecules* **31** 8425 (1998)
374. C Hawker, J Hedrick, E Malmström, M Trollsas, D Mecerreyes, G Moineau, P Dubois, R Jérôme *Macromolecules* **31** 213 (1998)
375. R S Velichkova, D C Christova *Prog. Polym. Sci.* **20** 819 (1995)
376. S Kobayashi *Prog. Polym. Sci.* **15** 751 (1990)
377. T G Gant, A I Meyers *Tetrahedron* **50** 2297 (1994)
378. S Baileau *Comprehensive Polymer Chemistry* (Ed. G Allen) (New York: Pergamon Press, 1989) Ch. 12
379. C J Hawker *Trends Polym. Sci.* **4** 183 (1996)
380. T M Birshtein, V M Amoskov *Vysokomol. Soedin., Ser. C* **42** 2286 (2000)^a
381. R J Spontak, P Alexandridis *Curr. Opin. Colloid Interface Sci.* **4** 140 (1999)
382. I W Hamley, V Castelletto *Prog. Polym. Sci.* **29** 909 (2004)
383. T Zheltonozhskaya, O Demchenko, I Rakovich, J-M Guenet, V G Syromyatnikov *Macromol. Symp.* **203** 173 (2003)
384. T B Zheltonozhskaya, N E Zagdanskaya, O V Demchenko, L N Momot, N M Permyakova, V G Syromyatnikov, L R Kunitskaya *Usp. Khim.* **73** 877 (2004) [*Russ. Chem. Rev.* **73** 811 (2004)]
385. I M Papisov *Vysokomol. Soedin., Ser. B* **39** 562 (1997)^a
386. P Aravindakshan, A Bhatt, V G Kumar *J. Appl. Polym. Sci.* **66** 397 (1997)
387. N E Zagdanskaya, T B Zheltonozhskaya, V G Syromyatnikov *Voprosy Khim. Khim. Tekhnol.* **3** 53 (2002)
388. N Permyakova, S Fedorchuk, T Zheltonozhskaya, N Zagdanskaya, V Syromyatnikov *Scientific Conference Reviews of the IVth Ukrainian–Polish Scientific Conference 'The Polymers of Special Application', Dnepropetrovsk, Ukraine, 2006* p. 25
389. N M Permyakova, S V Fedorchuk, T B Zheltonozhskaya, N E Zagdanskaya, V G Syromyatnikov *Voprosy Khim. Khim. Tekhnol.* **8** 108 (2007)
390. L N Momot, T B Zheltonozhskaya, N M Permyakova, S V Fedorchuk, V G Syromyatnikov *Macromol. Symp.* **222** 209 (2005)
391. N M Permyakova, T B Zheltonozhskaya, V V Shilov, N E Zagdanskaya, L N Momot, V G Syromyatnikov *Macromol. Symp.* **222** 135 (2005)
392. I M Papisov, V A Kabanov, E Osada, M Leskano Brito, J Reimont, A N Gvozdetkii *Vysokomol. Soedin., Ser. A* **14** 2462 (1972)^a
393. T S C Pai, C Barner-Kowollik, T P Davis, M H Stenzel *Polymer* **45** 4383 (2004)

^a — *Polym. Sci. (Engl. Transl.)*^b — *Dokl. Chem. (Engl. Transl.)*^c — *Russ. J. Appl. Chem. (Engl. Transl.)*

Rigid aromatic dendrimers

M S Rajadurai, Z B Shifrina, N V Kuchkina, A L Rusanov, K Müllen

Contents

I. Introduction	767
II. Rigid aromatic dendrimers synthesised by the convergent method	768
III. Rigid aromatic dendrimers synthesised by the divergent method	772
IV. Possible areas of application of rigid dendrimers	779
V. Conclusion	781

Abstract. Rigid aromatic dendrimers synthesised by convergent, divergent and combined methods are considered. The potential of practical application of rigid aromatic dendrimers is analysed. The bibliography includes 121 references.

I. Introduction

In the last decades, data on dendrimers have been covered in numerous reviews,^{1–28} which suggests continuing interest in this unique class of monodisperse highly branched macromolecules with a highly ordered controllable and regular structure. Unlike conventional polymers, dendrimers incorporate the following three main structural components: the central fragment (core), internal branched units and terminal units (Fig. 1). Two main strategies, divergent and convergent, were developed for the synthesis of dendrimers.

The divergent approach is based on iterative coupling and activation steps starting from the polyfunctional core, the growth of molecules proceeding from the centre to the periphery. In the first step (the growth step), monomers (building blocks) are attached to the core to form first-generation dendrimers (Fig. 2). Monomers (A_nB) containing functional groups of different nature are generally used as building blocks. In these monomers, one group (B) is reactive and can be involved in the reaction, whereas other groups (A_n , their number depends on the nature of the monomer) are deactivated. In the next step (the activation step), the passive groups are activated by deprotection or in other ways, after which these groups are ready to be involved in the growth of dendrimers. Therefore, dendrimers grow layer by layer. Theo-

retical calculations demonstrated that this growth is, however, not infinite.²⁹ The density of the periphery of the molecule increases from generation to generation, and the resulting steric hindrance limits the growth of dendrimers. As a result of steric restrictions, the molecule assumes a nearly spherical shape. The packing density at the periphery achieved in this step is called the De Gennes dense packing.²⁹ According to this model, attempts to grow the subsequent layer should lead to the formation of irregular dendrimers (due to the incomplete substitution of functional groups). This problem is particularly acute for rigid aromatic dendrimers.

The functionalisation of dendrimers in the final step of the molecule formation can be performed with the use of monomers containing the necessary functional groups. The difficulties of controlling the transformations of the functional groups are often considered as a drawback of the divergent approach to the synthesis of dendrimers. Not all functional groups of the growing macromolecule can be involved in the growth of a new layer, which in turn can result in defects in the structure of the final product. This problem can be obviated by using excess of the monomer A_nB , which creates difficulties in the step of purification of the final product. Nevertheless, the divergent approach is a method of choice for the synthesis of high-

M S Rajadurai, Z B Shifrina, N V Kuchkina, A L Rusanov

A N Nesmeyanov Institute of Organoelement Compounds, Russian Academy of Sciences, ul. Vavilova 28, 119991 Moscow.

Fax (7-495) 135 50 58, tel. (7-495) 135 93 17,

e-mail: marina_averina@yahoo.com (M S Rajadurai),

shifrina@ineos.ac.ru (Z B Shifrina),

n_firsova@yahoo.com (N V Kuchkina),

tel. (7-495) 135 63 72, e-mail: alrus@ineos.ac.ru (A L Rusanov)

K Müllen Max Planck Institute for Polymer Research, Ackermannweg 10, 55128 Mainz, Germany. Fax (49-6131) 37 93 50, tel. (49-6131) 37 91 50, e-mail: muellen@mpip-mainz.mpg.de

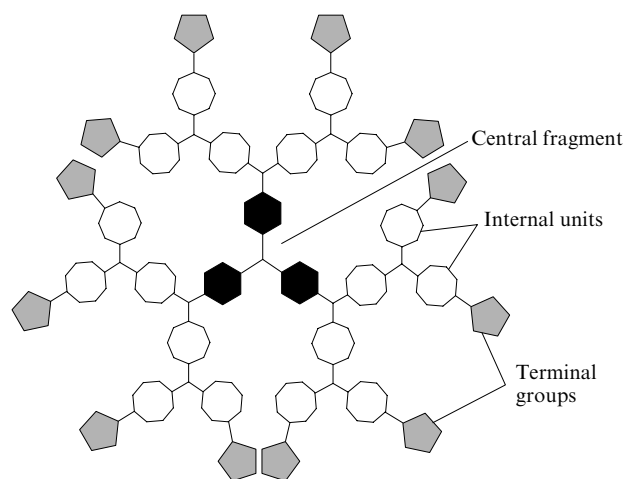


Figure 1. Schematic representation of the dendritic macromolecule.

Received 2 March 2007

Uspekhi Khimii 76 (8) 821–838 (2007); translated by T N Safonova

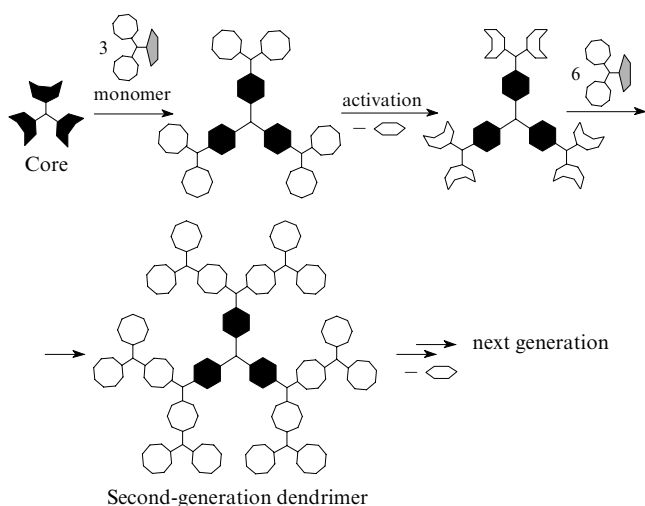


Figure 2. Schematic representation of the synthesis of dendrimers by the divergent method.

generation dendrimers if coupling reactions are selective and efficient.

The convergent approach is also based on the alternation of growth and activation steps. However, the growth of macromolecules occurs from the periphery to the centre, which is achieved due to formation of branched monomers called dendrons, which are attached to the core in the final step of the synthesis. In the first step, a monomer A_nB is attached to the monomer containing peripheral groups of the future dendrimer (the growth step) giving rise to the first-generation dendron (Fig. 3). The activation and coupling of the dendron to the monomer A_nB gives the next-generation dendron. In the

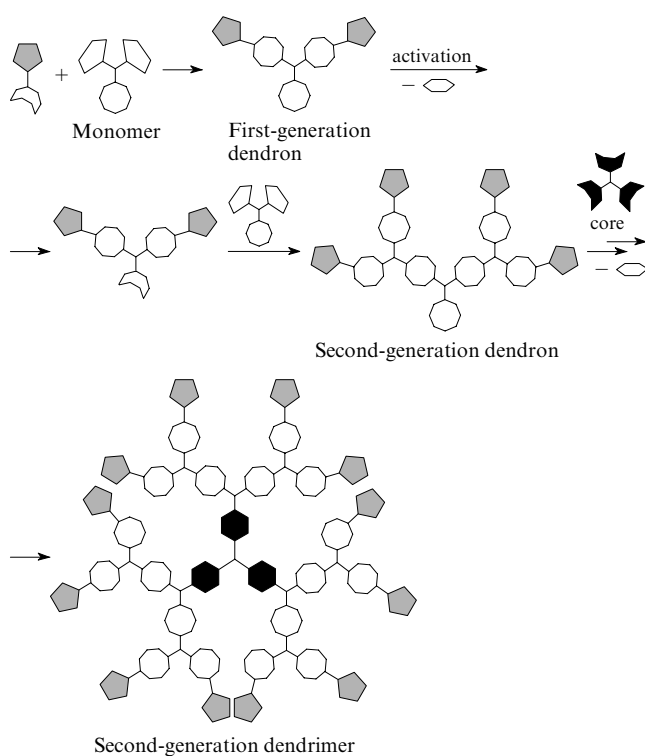


Figure 3. Schematic representation of the synthesis of dendrimers by the convergent method.

last step, the dendrons are attached to the central polyfunctional fragment (core) to form the final dendrimer.

The convergent approach also has advantages and disadvantages. The number of reactive functional groups of each molecule involved in the reaction is small and remains constant regardless of the number of generations and the size of the dendron, thus allowing minimisation of the amount of unconsumed groups. The reaction can be brought to completion using a small excess of the monomer (unlike the divergent method). It is much easier to purify the reaction products synthesised according to the convergent approach, because the reaction mixture contains smaller amounts of by-products. The difference in physical properties of the components of the reaction mixture allows the efficient use of chromatographic purification, thus providing the access to individual macromolecules. However, the convergent approach does not allow the formation of high-generation dendrimers (*i.e.*, dendrimers composed of a large number of layers) because of steric hindrance in the step of coupling of the dendron to the core.¹

An advantage of the convergent method is that it can be used for the preparation of dendrimers containing different functional groups at the periphery of the molecule. To this end, building blocks containing various substituents are used.

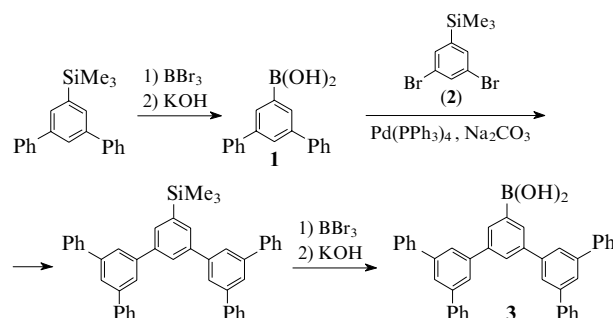
Therefore, the divergent approach is the method of choice for the formation of high-molecular-mass monodisperse dendrimers composed of a large number of layers, whereas the convergent approach is suitable when it is necessary to synthesise monodisperse macromolecules containing a small number of layers and different functional groups at the periphery.¹

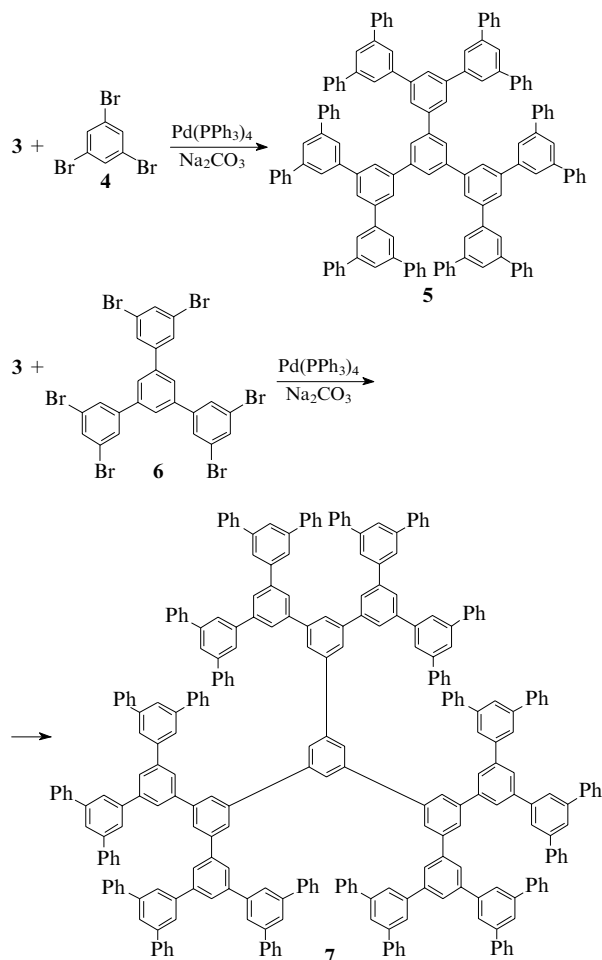
The potential of the synthesis of macromolecules with different architecture and chemical composition can be extended by combining the divergent and convergent schemes.^{23, 30–33} For example, a versatile procedure for the synthesis of organosilicon dendrimers³¹ is based on the grafting of dendrons, which are prepared according to the convergent scheme onto an oligomeric dendrimer constructed by the divergent method.

In the present review, emphasis is given to rigid dendrimers, because these macromolecules have received little attention in the literature.^{34–38} However, these compounds belong to one of the most interesting classes of dendrimers, are characterised by high chemical and thermal stability and are soluble in conventional organic solvents. Rigid aromatic dendrimers of controlled size hold promise in high-temperature catalysis. In addition, aromatic dendrimers with a π -conjugated system can find use in optoelectronic devices.^{26, 28, 33, 34, 39–41}

II. Rigid aromatic dendrimers synthesised by the convergent method

Polyphenylene dendrimers have been synthesised for the first time^{42, 43} by the convergent method using the Suzuki coupling of substituted phenylboronic acid **1** with aryl bromides.⁴⁴ This was used for the synthesis of dendrimers based on 1,3,5-triphenyl-substituted monomers.



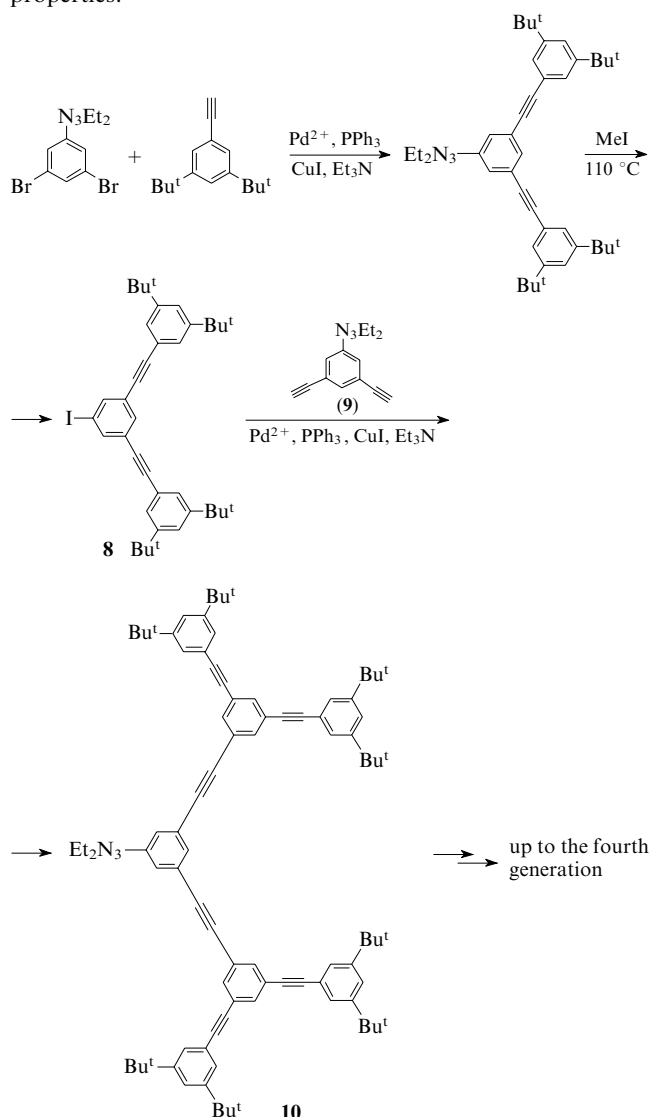


A first-generation dendron was prepared by coupling of 3,5-dibromo-1-(trimethylsilyl)benzene (**2**) with substituted phenylboronic acid **1**. The trimethylsilyl protecting group was removed by treating with boron tribromide followed by hydrolysis, and then activated dendrons **3** were attached to the central fragment, *viz.*, to 1,3,5-tribromobenzene (**4**), giving rise to dendrimer **5**. More branched central fragment **6** was used for the synthesis of dendrimer **7**.⁴³ Monitoring of the reaction of compound **3** with **6** by chromatography demonstrated that the first three bromine atoms are replaced very rapidly, whereas the replacement of other bromine atoms occurs much more slowly due to steric effects. This situation is typical of the convergent synthesis. Due to the presence of a 'rigid' repeating fragment in the dendrimer structure, the shape and size of molecules remain unchanged under different external conditions.

The synthesis of macromolecules based on arylalkyne and phenylacetylene fragments was documented.^{26,45} 4-(*tert*-Butyl)phenyl substituents were used as groups increasing the solubility of the final dendrimer; however, their influence on solubility was extended only up to third-generation dendrimers. Fourth-generation dendrimers with 3,5-di(*tert*-butyl)-phenyl terminal groups proved to be somewhat better soluble.⁴⁶

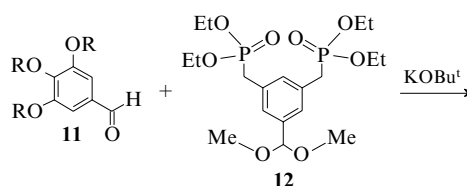
Poly(phenylacetylene) dendrimers were synthesised using dendrons that have been prepared based on the diethynyl monomer containing a triazene protecting group. This dendron is easily activated for the subsequent coupling reaction by replacing the protecting group by a halogen.⁴⁷

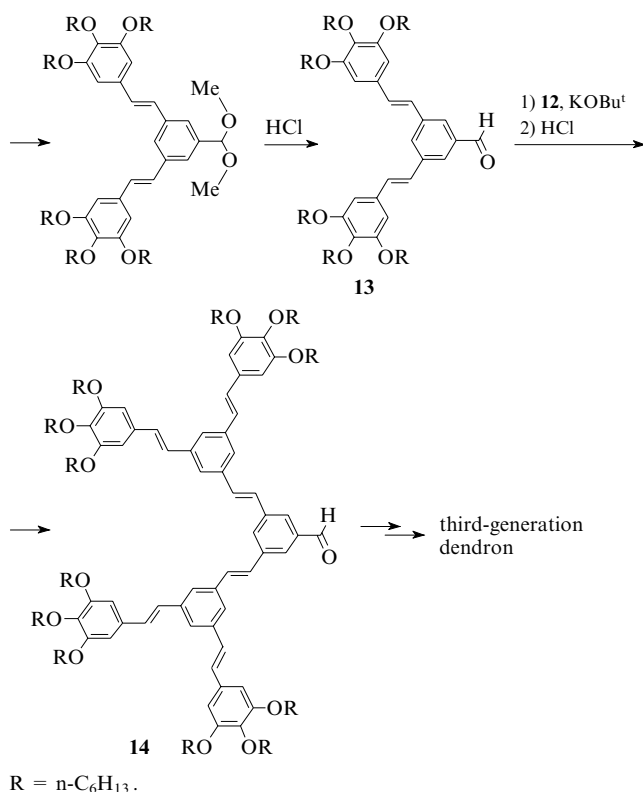
The cross-coupling reaction of first-generation halogen-containing dendron **8** with compound **9** catalysed by a palladium complex afforded second-generation dendron **10**. Due to the rigid defect-free structures of such dendrimers containing conjugated fragments, they possess promising photophysical properties.



Phenylacetylene dendrimers containing Bu^tCO_2 peripheral groups were synthesised by the modified convergent method. Solid-state thermolysis of these systems resulted in the conversion of the Bu^tCO_2 groups into carboxy groups.⁴⁸ Since thermolysis of high-generation dendritic molecules is accompanied by partial cross-linking, an alternative procedure for the synthesis of phenylacetylene dendrimers containing carboxy terminal groups was developed. Dendrimers prepared by this method in high yields (up to 90%) are water-soluble compounds.

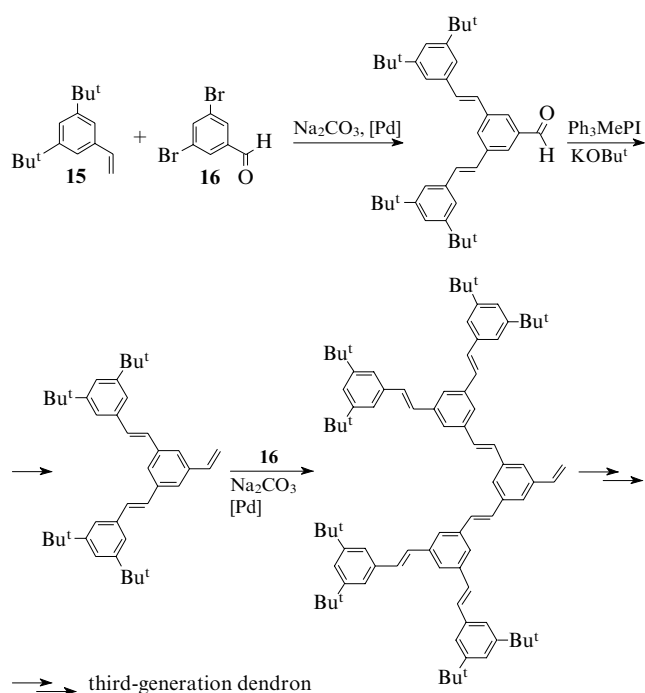
A first-generation dendron was synthesised⁴⁹ by coupling of aldehyde **11** with monomer **12** containing two phosphate groups.



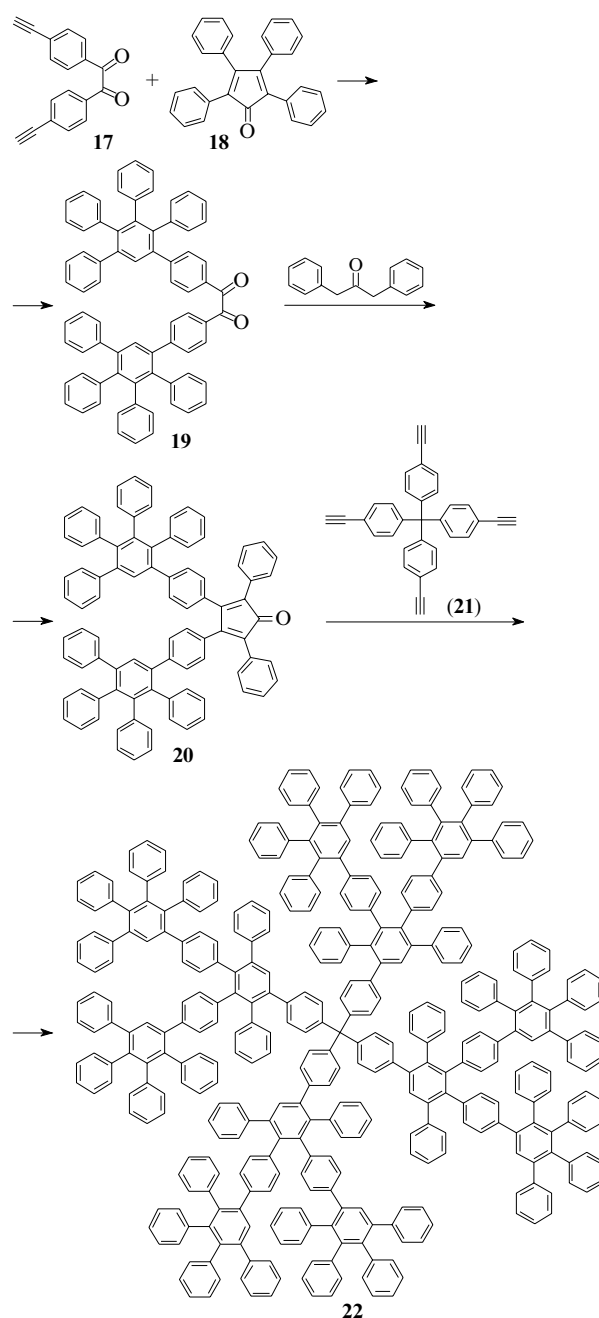


Acid hydrolysis leads to the conversion of the acetal group into the aldehyde (compound **13**), which can be involved in the Horner–Wadsworth–Emmons coupling reaction giving rise to second-generation dendron **14**. However, only third-generation dendrons were synthesised by this procedure. The synthesis of the fourth-generation dendron was considered unreasonable because of low yields and long reaction times.

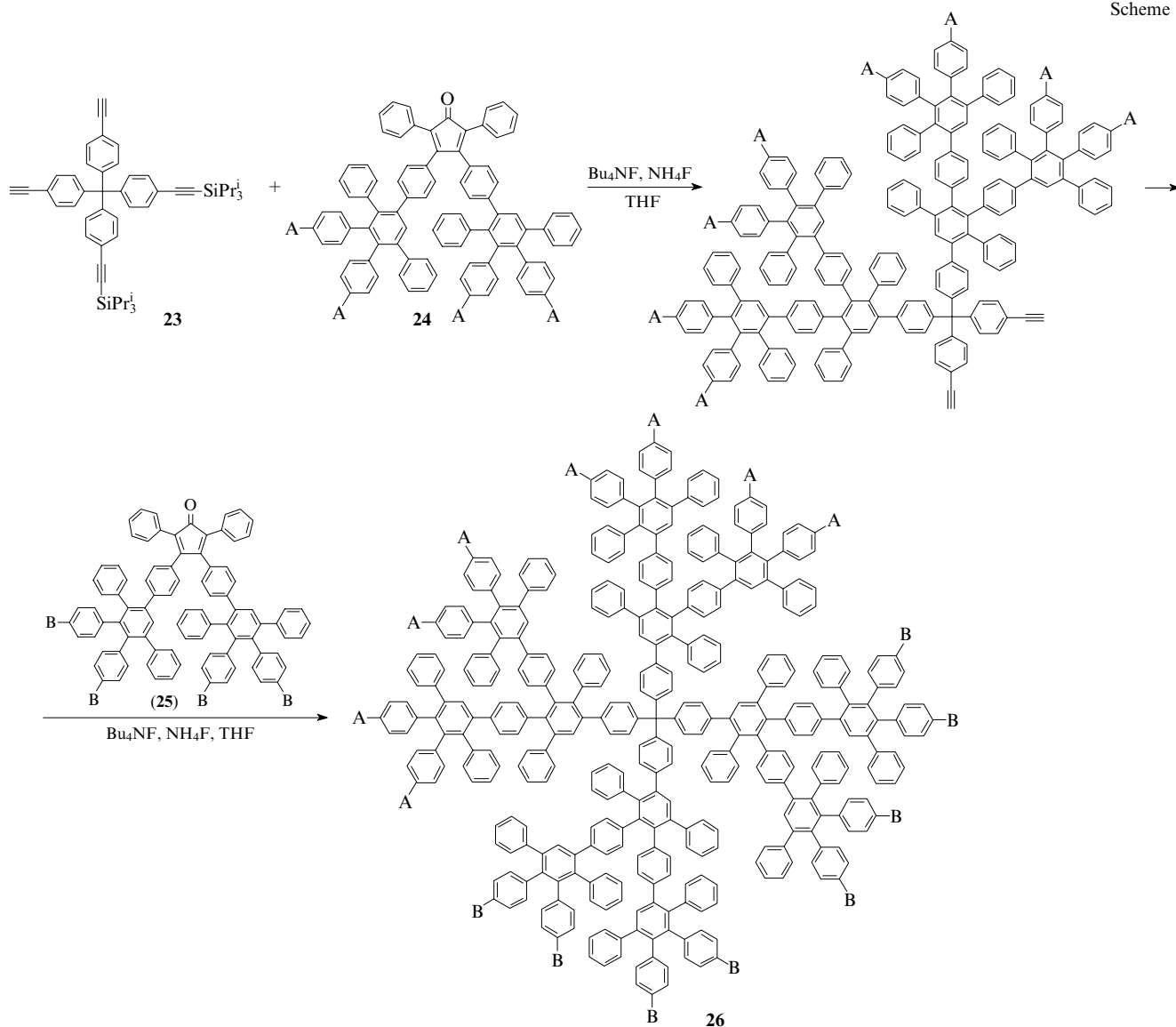
Analogous dendrons were synthesised⁵⁰ by Heck coupling^{51,52} of substituted styrene **15** with 3,5-dibromobenzaldehyde (**16**) followed by the Wittig reaction with methylenetriphenylphosphorane iodide. Unfortunately, dendrons of only three generations could be synthesised by this procedure.



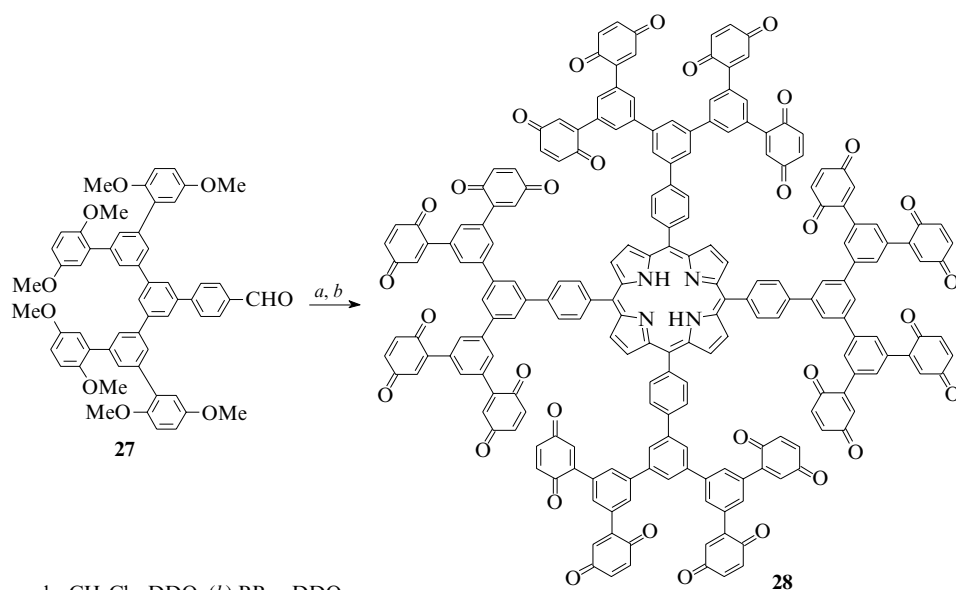
The convergent method was developed⁵³ for the synthesis of polyphenylene-type dendrimers based on the Diels–Alder reaction. This starts with coupling of 4,4'-diethynylbenzil (**17**) with an excess of 2,3,4,5-tetraphenylcyclopentadienone (**18**). 4,4'-Diethynylbenzil is a monomer A₂B-type because it contains two dienophilic ethynyl groups, which can be involved in the Diels–Alder reaction with dienes, and one ethanedione group, which is inactive in the [2+4]-cycloaddition but is helpful for further transformations. Dendron **19** formed in the growth step is converted by the Knoevenagel reaction with diphenylacetone into reactive second-generation dendron **20**. This undergoes the Diels–Alder reaction with the central fragment, *viz.*, tetrakis(4-ethynylphenyl)methane (**21**), to form phenylated rigid second-generation dendrimer **22**. First-, second- and third-generation dendrons were prepared in rather high yields (85%–89%). Nevertheless, all attempts to make the third-generation dendron react failed because steric hindrance did not allow it to undergo condensation with diphenylacetone. However, identical dendrimers of not only



Scheme 1



Scheme 2



(a) $\text{BF}_3 \cdot \text{OEt}_2$, pyrrole, CH_2Cl_2 ; DDQ; (b) BBr_3 , DDQ.

the third, but also the fourth generation can be synthesised using the divergent approach, as will be demonstrated in the next section.

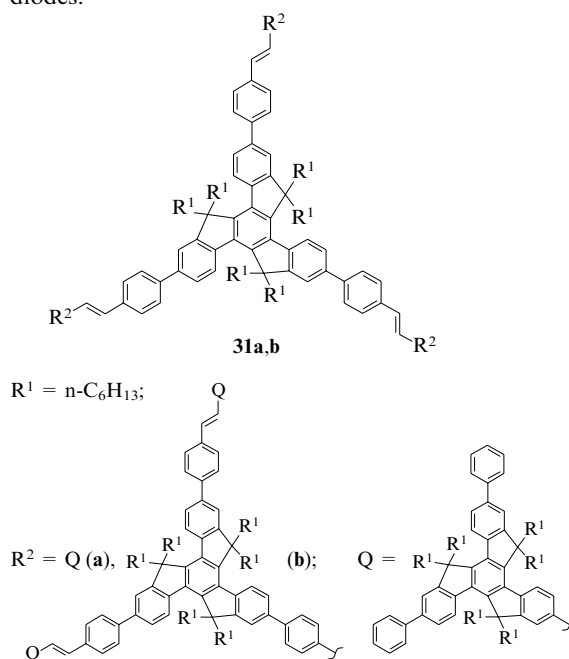
The convergent method was successfully applied to the synthesis of polyphenylene dendrimers containing peripheral substituents of different nature.³⁸ For this purpose, the central fragment, *viz.*, bis(4-ethynylphenyl)bis[4-(triisopropylsilyl)-ethynylphenyl]methane (**23**), with two protected triple bonds was synthesised using a deficient amount of desilylating agents from a tetrasilyl precursor. Then the Diels–Alder reaction with dendrons **24** containing substituents A was carried out. After desilylation, the liberated ethynyl groups were involved in the Diels–Alder reaction with dendrons **25** containing substituents B to give finally dendrimer **26** containing different substituents in one molecule (Scheme 1).

Dendrimers based on porphyrin fragments have attracted interest because of their valuable photophysical properties.^{17, 54–57} For example, rigid polyphenylene dendrimers containing the porphyrin fragment as the central group have recently been synthesised.³⁶ Dendron **27**, which has been prepared by the convergent method using the Suzuki reaction, was coupled with pyrrole. The further demethylation with boron tribromide and oxidation with 2,3-dichloro-5,6-dicyano-*p*-quinone (DDQ) produced dendrimer **28** containing peripheral benzoquinone groups (Scheme 2).

The synthesis of luminescent dendrimers **29** and **30** containing the porphyrin core and carbazole peripheral fragments was documented.⁵⁸ Initially, aldehyde precursors were synthesised by a multistep procedure using the Ullmann reaction or the palladium-catalysed Suzuki reaction. Further condensation with pyrrole was carried out under the Lindsey conditions.^{59, 60}

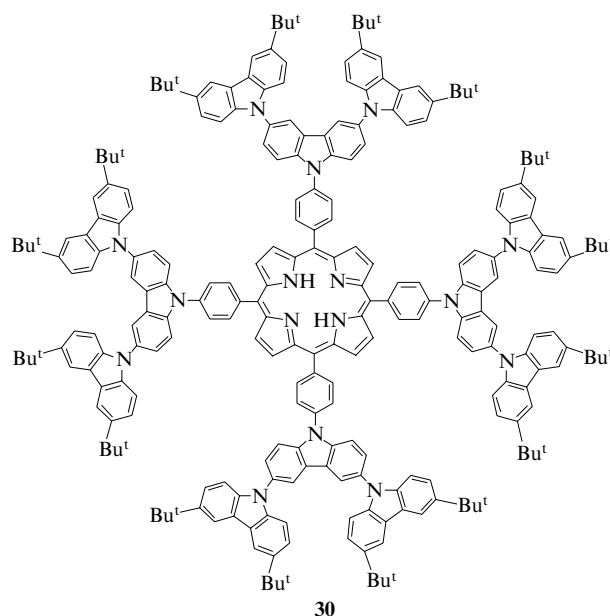
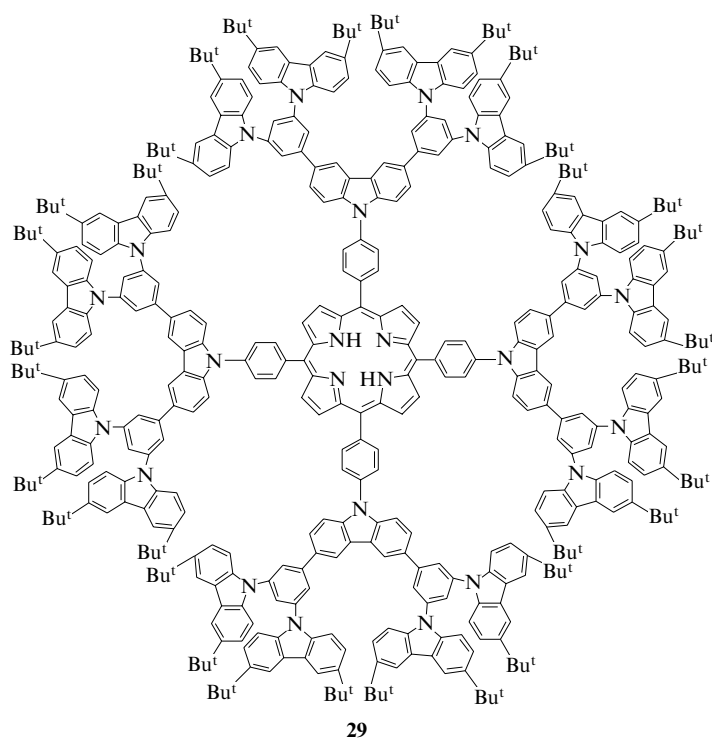
Due to the presence of large hyperbranched blocks, π -conjugated dendritic molecules possess characteristic three-dimensional architecture, which imparts qualitatively new properties to these molecules compared to linear semiconducting oligomers and polymers.²⁸ π -Conjugated aromatic dendrimers **31a,b** containing stilbene-like groups as bridging fragments were synthesised by the convergent method using the Suzuki

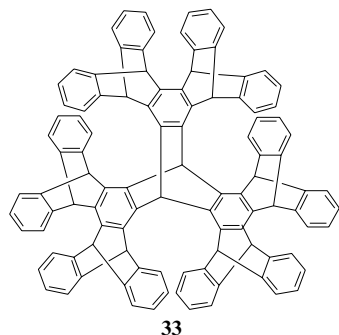
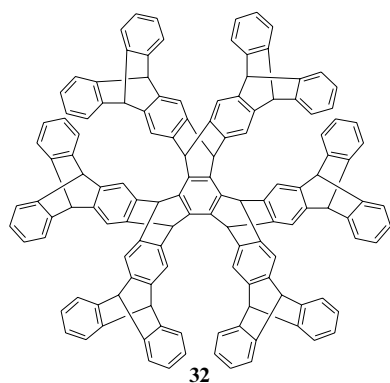
reaction and the Horner–Wadsworth–Emmons reaction.⁶¹ These dendrimers show luminescence in the blue region with high quantum yield, which led the authors to conclude that these compounds can be used as materials for light-emitting diodes.



III. Rigid aromatic dendrimers synthesised by the divergent method

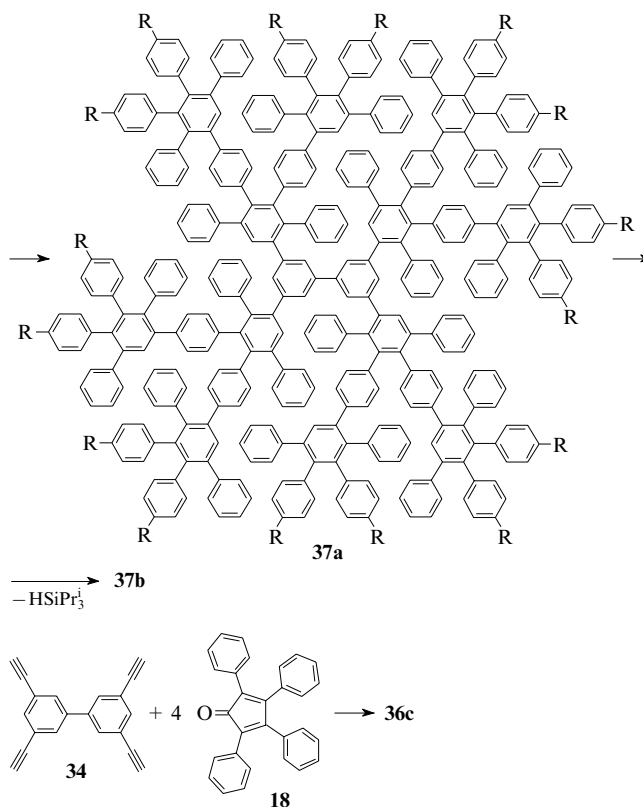
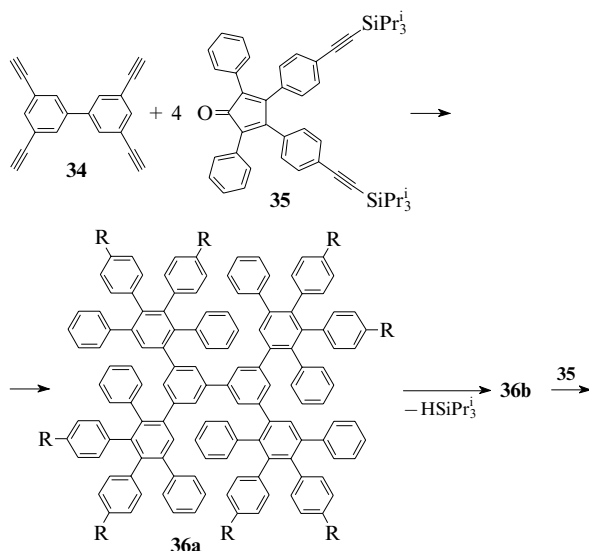
The so-called iptycenes were among the first characterised rigid dendrimers, which were synthesised by the divergent method (using the Diels–Alder reaction).⁶² These unique molecules based on the benzene or iptycene cores (compounds **32** and **33**, respectively) are characterised by high thermal stability.





Very simple but stringent requirements are imposed on the chemical reactions involved in the main cycle including growth and activation of a molecule: the reactions should be unambiguous, enable complete conversion of the substrates and be feasible. One of the most efficient synthetic schemes for the preparation of polyphenylene dendrimers by the divergent method was developed by Müllen and co-workers.^{34, 38, 63–71} This is based on two iterative reactions, *viz.*, the Diels–Alder cycloaddition of tetraphenylcyclopentadienones to substituted ethynyl compounds⁷² (the growth step) and desilylation of tri(isopropylsilyl)-substituted alkynes (the activation step).

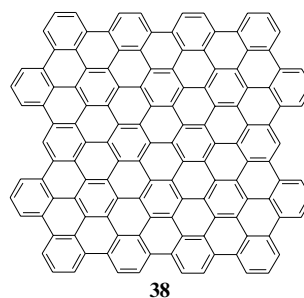
The reaction of 3,3',5,5'-tetraethynylbiphenyl (**34**) with cyclopentadienone derivative **35** afforded first-generation dendrimer **36a** containing tri(isopropyl)silyl-substituted ethynyl groups. Activated first-generation dendrimer **36b** with eight ethynyl terminal groups was obtained after removal of tri(isopropyl)silyl protection. The reaction of compound **36b** with cyclopentadienone **35** afforded second-generation dendrimer **37a**. As a result, dendrimer **36a** with a molecular mass of 3119 (220 carbon atoms) was transformed into dendrimer **37a** with a



R = —SiPr_3^i (**a**), — (**b**), H (**c**).

molecular mass of 7606 (548 carbon atoms) by the two-step reaction. In spite of the high molecular masses, compounds **36** and **37** are readily soluble in organic solvents.

Graphite-like highly fused system **38** was prepared by dehydrocyclisation of dendrimer **36c**.



A series of dendritic polyphenylenes were synthesised based on compound **21** as the core using A_2B -type monomer **35** as the building block (Scheme 3). These dendrimers of four generations exhibit good chemical stability, thermal stability and solubility in many organic solvents. In addition, a series of dendrimers were synthesised⁶⁸ using an A_2B block, an A_4B block and various cores [compounds **21**, **34**, 1,3,5-triethynylbenzene (**39**) and 1,2,3,4,5,6-hexakis(4-ethynylphenyl)benzene (**40**)], and their spatial organisation was studied. In the case of an A_2B monomer and cores **21** and **34**, the ability of a dendrimer to grow was demonstrated to be independent of the nature of the core, and the nearly globular shape is achieved only in the fourth generation. On the contrary, the globular shape is achieved very rapidly with the use of an A_4B monomer; however, it is impossible to prepare defect-free dendrimers of generations higher than two.

Alkyl-substituted polyphenylene dendrimers, which are capable of self-assembly on solid surfaces (for example, on graphite), were synthesised^{64, 66, 73} starting from 1,3,5-triethy-

Scheme 3

(21)

(39)

SiPr_3

Pr_3Si

Bu_4NF

R^1

R^2

$$R^1 = n\text{-C}_{12}\text{H}_{25}, \text{H}; R^2 = \text{H}, n\text{-C}_{12}\text{H}_{25}.$$

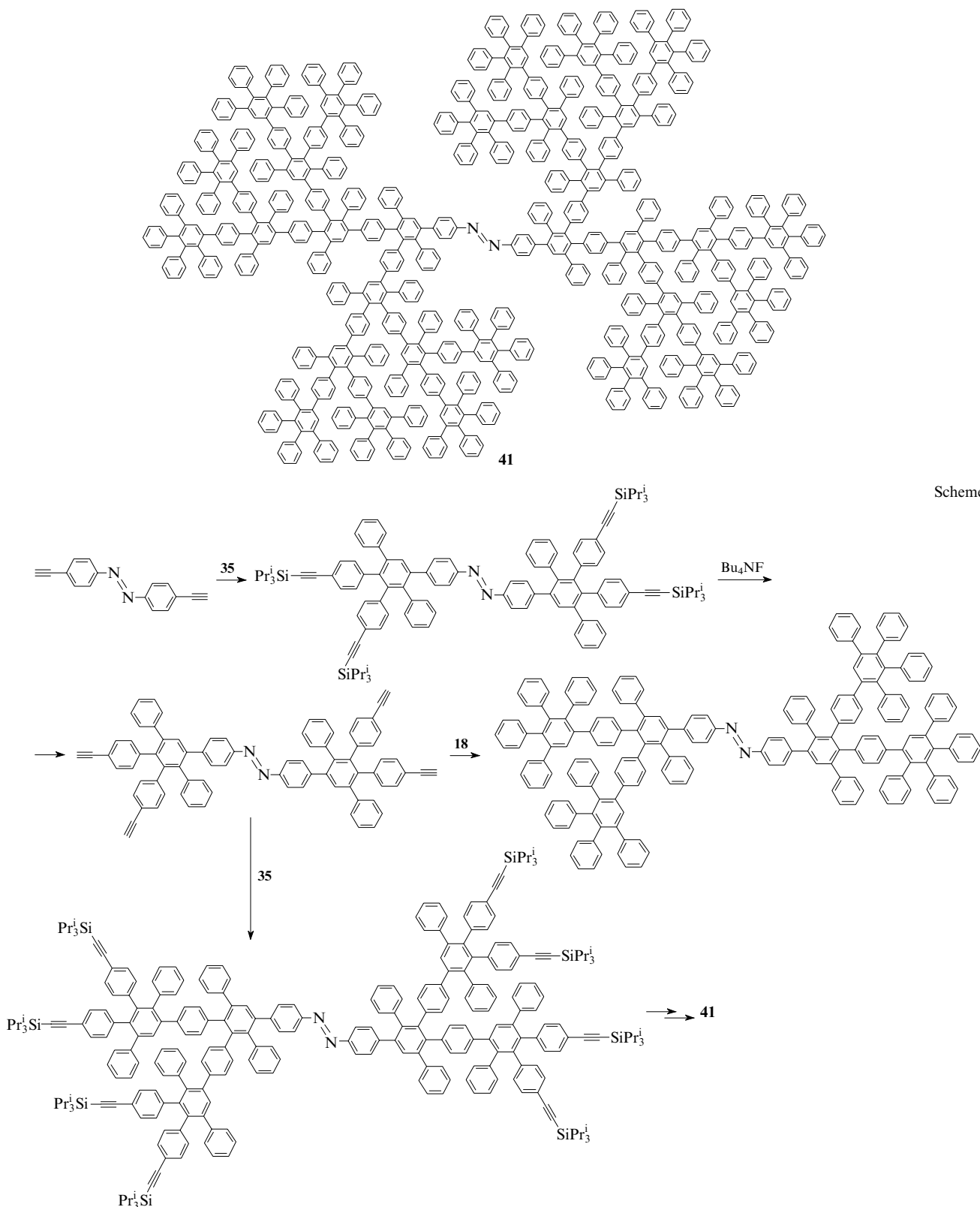
nylbenzene and tetrakis(4-ethynylphenyl)methane (see Scheme 3).

First- and second-generation dendrimers containing the 1,3,5-triethynylbenzene fragment as the core were studied by the molecular dynamics method.⁷⁴ It was demonstrated that only four of six possible conformations of second-generation dendritic molecules are stable, and the dendrimer sizes can vary only within 10%.

A series of dendrimers containing 4, 10 and 22 symmetrically arranged fluorine-substituted aromatic rings were syn-

thesised.⁴³ The surface layers of the molecular structures of dendrimers consist of perfluorinated phenyl groups. Dendrimers are rather thermally stable, monodisperse and readily soluble in organic solvents (THF, CH_2Cl_2 or CHCl_3). In addition, these dendrimers have good electron-conducting properties and chemical stability. Due to the above-mentioned characteristics, these dendrimers are attractive materials for the design of light-emitting diodes.⁷⁵

A series of polyphenylene dendrimers of four generations (compound **41** is a fourth-generation dendrimer) containing



the azobenzene cores were synthesised starting from 4,4'-bis(4-ethynylphenyl)azobenzene (Scheme 4).⁷¹ The resulting dendrimers exhibit reversible photosensitivity under UV-Vis irradiation, which reflects reversible structural changes in the molecule. The influence of the number of the dendrimer generation and the degree of branching of the dendrimers on the kinetic characteristics of photoisomerisation was studied.

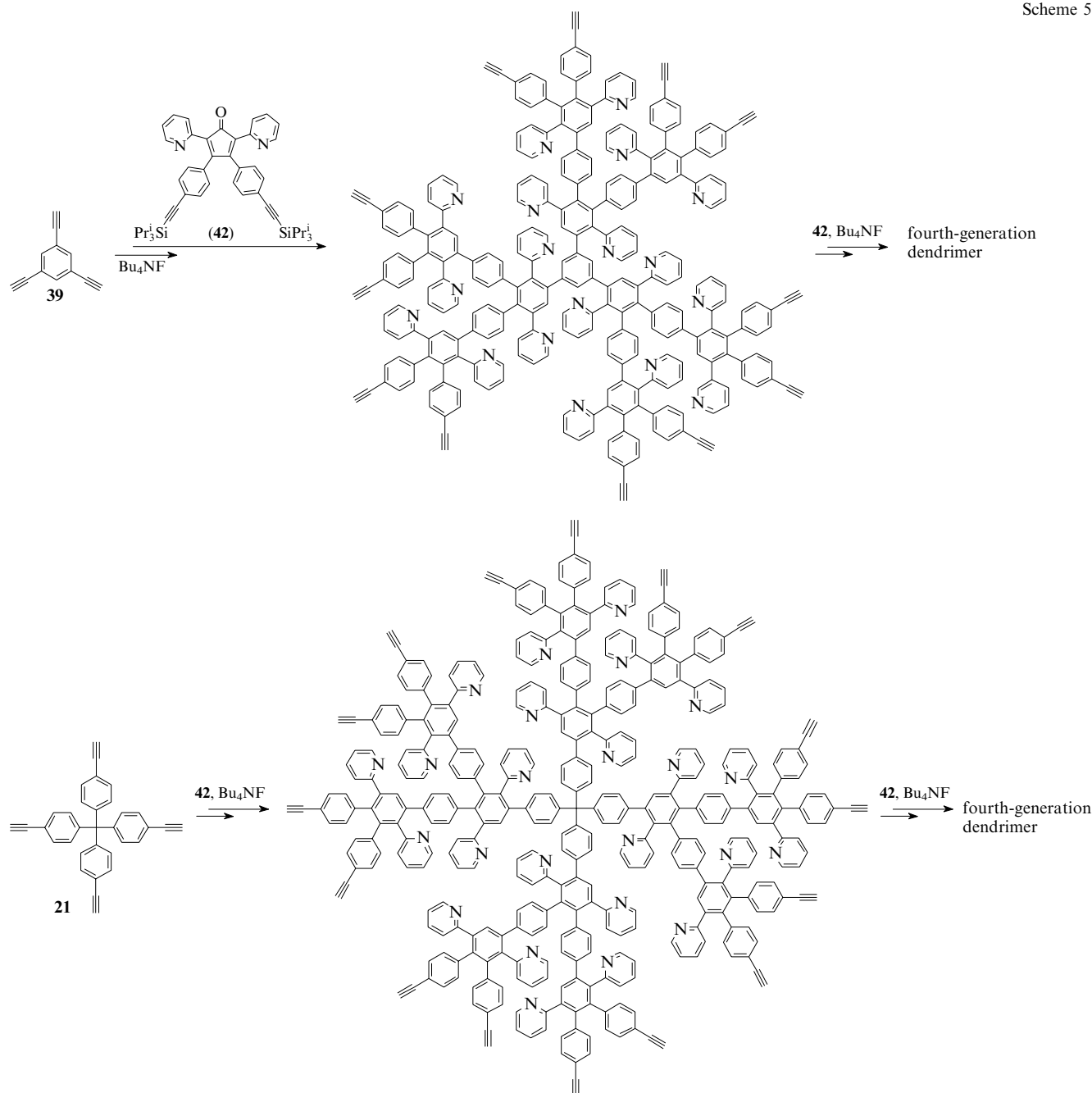
In addition to polyphenylene dendrimers containing different functional groups at the periphery and/or in the centre of the macromolecule, dendrimers with different arrangement and compositions of functional groups in the inner sphere were synthesised. Studies aimed at designing polyphenylene dendrimers based on new pyridine-containing monomers, such as 3,4-bis{4-[tri(isopropyl)silylethynyl]phenyl}-2,5-di(pyridin-2-yl)cyclopenta-2,4-dienone (**42**), 3,4-di(pyridin-2-yl)-2,5-

diphenylcyclopenta-2,4-dienone (**43**) and 2,3,4,5-tetrakis(pyridin-2-yl)cyclopenta-2,4-dienone, have been carried out.^{76–78}

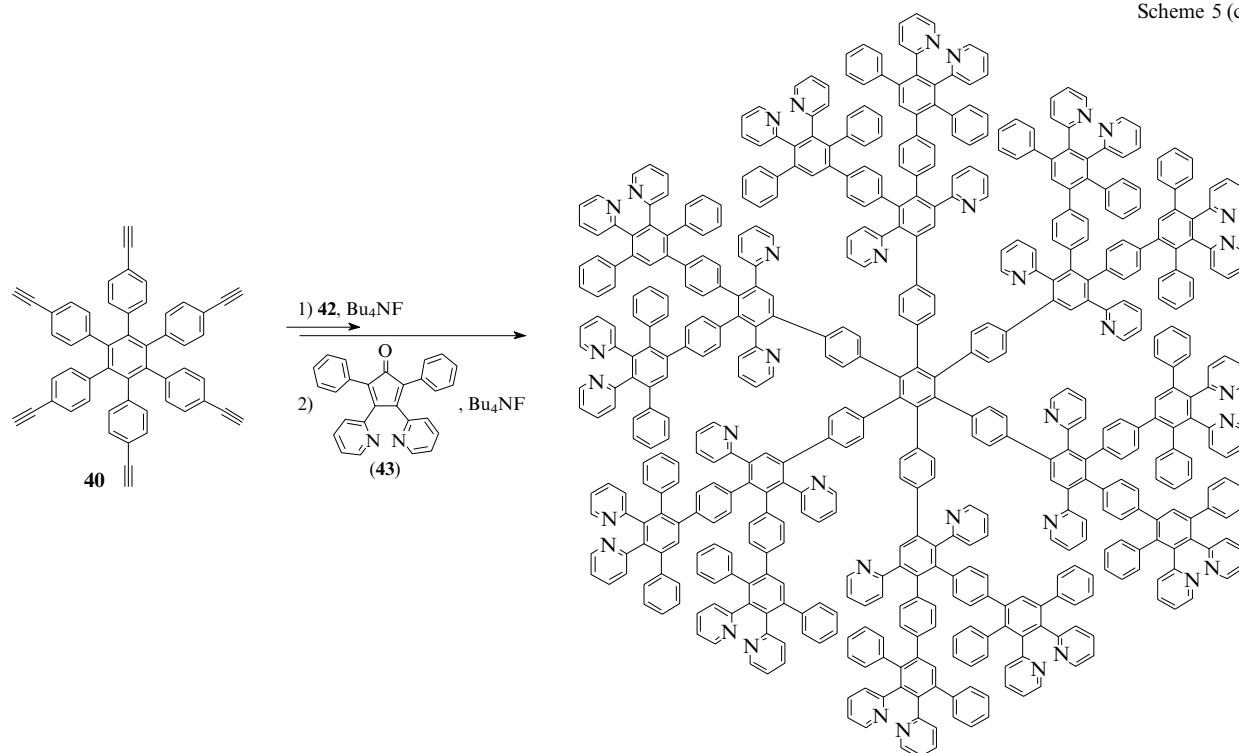
The introduction of pyridine fragments into polyphenylene dendrimers can impart new properties to the latter. The presence of pyridine rings not only at the periphery, but also in the inner sphere of macromolecules extends the potential of functionalisation. Pyridine-containing dendrimers of four generations were prepared using synthetic routes based on the Diels–Alder reaction; however, steric hindrance appears already in the synthesis of the third-generation dendrimer with substituted benzene **40** as the dendrimer core (Scheme 5).

The synthesis of dendrimers of four generations based on core **39** is presented in detail in Scheme 6. In the last step, the third-generation dendrimer containing ethynyl peripheral

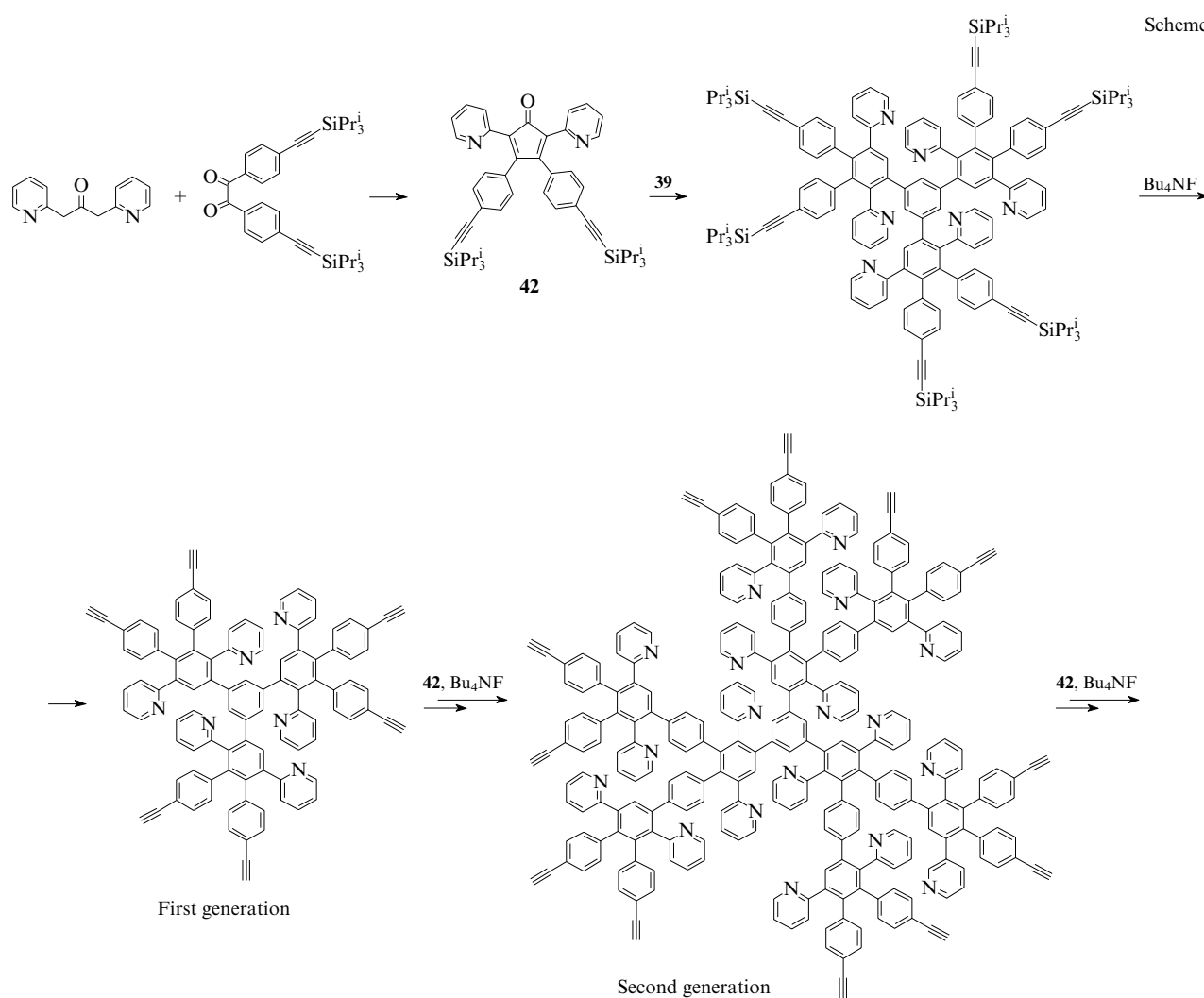
Scheme 5



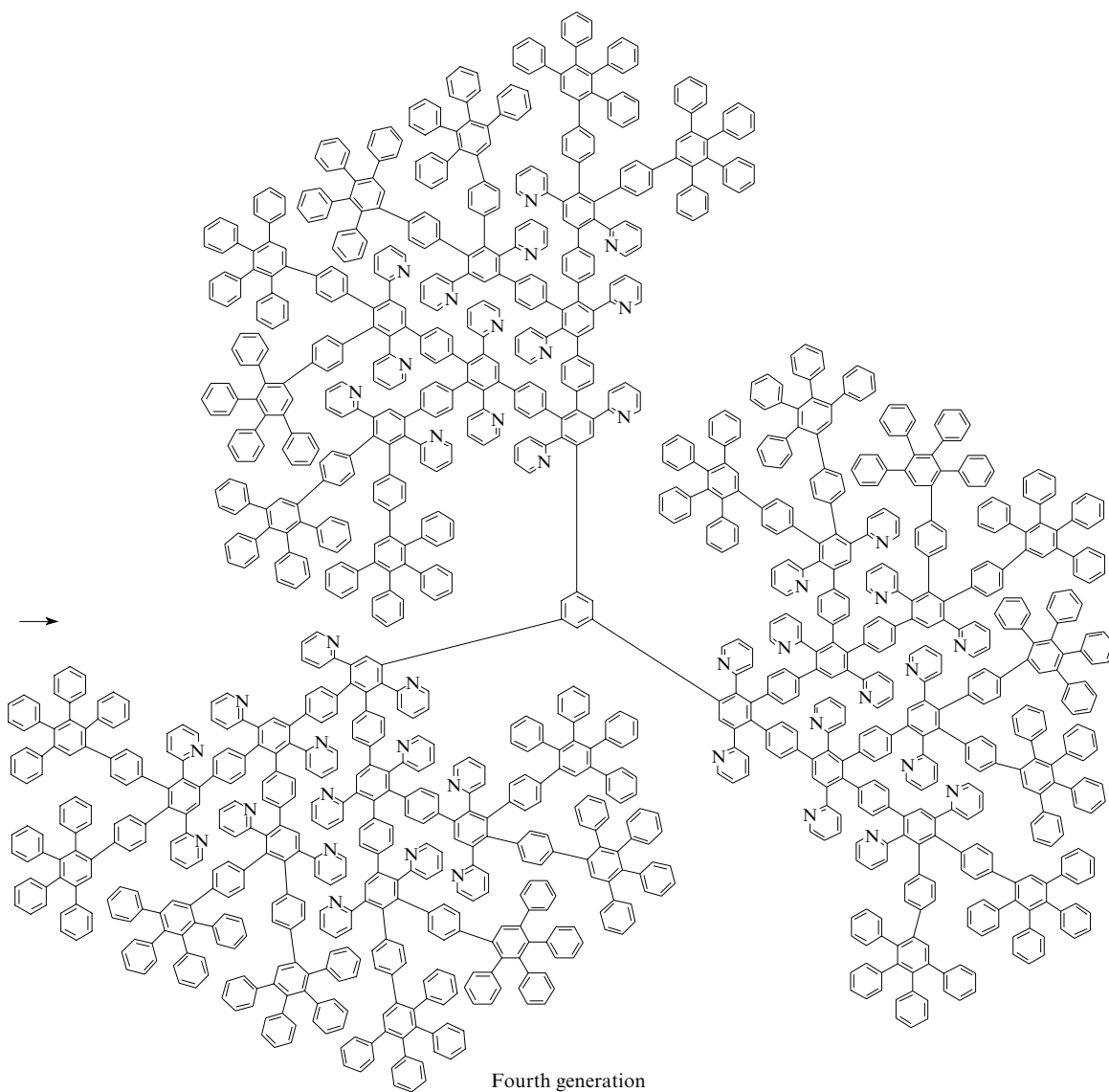
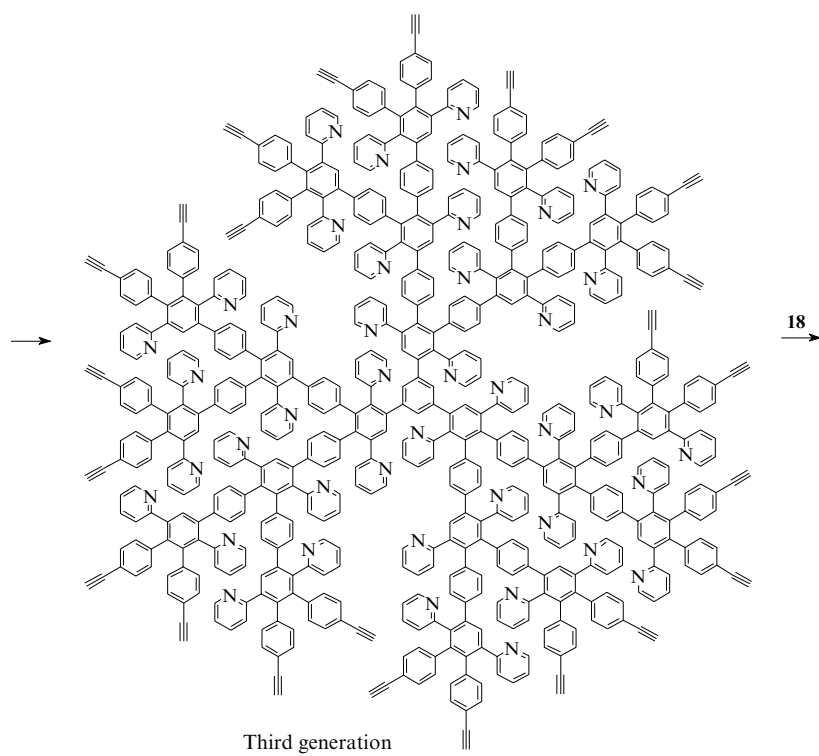
Scheme 5 (continued)

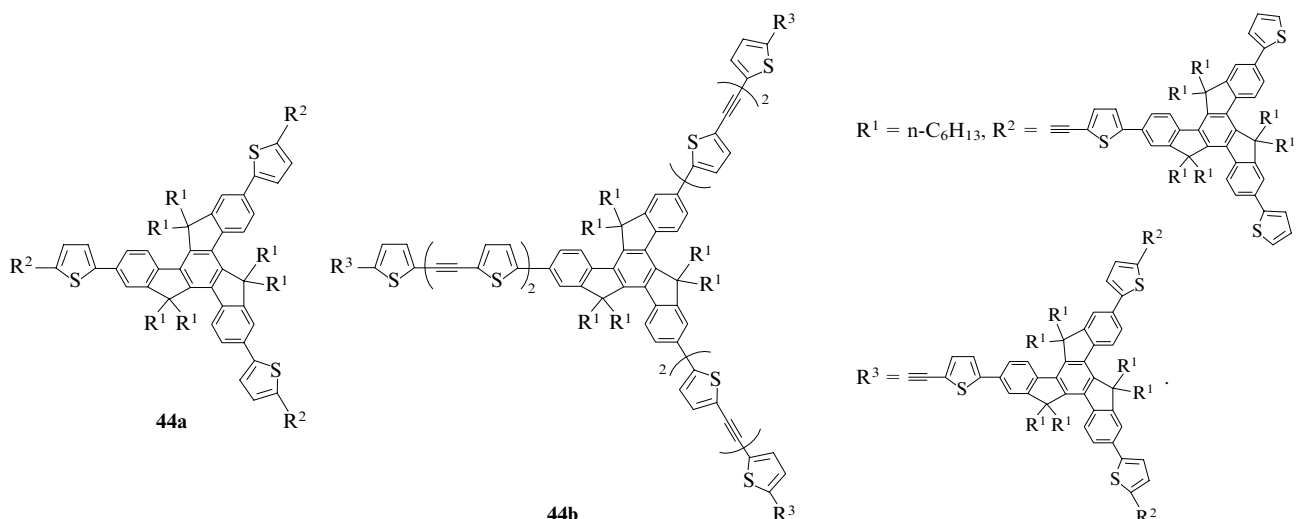


Scheme 6



Scheme 6 (continued)





groups is transformed into the fourth-generation dendrimer containing phenyl peripheral groups.

According to the thermogravimetric analysis, all the dendrimers under study are characterised by rather high thermal stability. Thus, a 10% mass loss in air for second–fourth generation dendrimers was observed at temperatures above 480 °C. According to the differential scanning calorimetry, no phase transitions occur in samples of dendrimers up to the decomposition temperature. The structures of the above-mentioned dendrimers are not destroyed even upon treatment with acids or alkalis over a long period of time. Due to high chemical and thermal stability, the resulting macromolecules are unique compounds among other known dendrimers containing the pyridine or amine (imine) functional groups, and these compounds can be used in corrosive media and/or at high temperatures. In addition, these dendrimers can be used in the design of new hybrid (dendrimer–metal) nanostructured systems having catalytic properties.⁷⁷

The efficient combined divergent/convergent synthesis of new conjugated zero-generation (**44a**) and first-generation (**44b**) dendrimers containing oligo(ethynylthiophene) fragments was documented.³³ This method is based on the iterative Sonogashira and Wittig reactions. The dendrimers prepared in high yields (72%–82%) are readily soluble in organic solvents, which made it possible to study in detail the dependence of their properties on the structure. Due to the ability to absorb light in a very broad frequency range, these dendrimers hold promise for the design of light-absorbing materials analogous to natural substances.

The above-considered results show considerable progress in the synthesis of rigid aromatic dendrimers by both the convergent and divergent methods. It is expected that further investigations will be aimed at extending the range of these dendrimers and searching for fields of their practical application.

IV. Possible areas of application of rigid dendrimers

The development of procedures for the synthesis of versatile dendritic matrices, which can be used for the design of special materials for different fields of application (catalysts, optical materials, magnetic nanoparticles and drug delivery agents), is one of the most interesting and important areas in chemistry of dendrimers. Due to predictable, controlled and highly reproducible molecular sizes, dendrimers are ideal standards for mass spectrometry, electronic and atomic spectroscopy and ultrafiltration. The presence of channels and pores in dendritic macromolecules allows their use for encapsulation and immobilisation of small-molecular-mass guest molecules. The possi-

bility of incorporation of guest molecules into dendrimers has been demonstrated,⁷⁹ which gave impetus to numerous investigations in this field and the design of new composites of dendrimers with guest molecules.^{80, 81} Such host–guest composites can find use in biology, medicine, pharmacology and catalysis.^{14, 23, 82, 83}

The use of dendrimers as host molecules for the encapsulation of guest metal nanoparticles holds considerable promise. Pioneering investigations in this field date back to 1994.⁹ First essential results were published in the late 1990s. The formation of copper nanoparticles in a dendrimeric template was documented.^{84, 85} Reduction of copper ions in the presence of dendrimers gave rise to colloidal solutions stable at room temperature for more than 90 days. The formation of nanoparticles stabilised by a dendrimeric template was confirmed by UV spectroscopy and electron microscopy. Gold nanoparticles in a dendrimeric template were synthesised by an analogous procedure.⁸⁶ It was found that the size of the resulting nanoparticles can be controlled using dendrimers of different generations (from zero to fifth). It was demonstrated that the strategy of the formation of metal nanoparticles inside a dendrimeric nanoreactor can be successfully applied to all transition metals. The introduction of monometallic, bimetallic⁹⁰ and semiconducting⁸⁷ nanoparticles into dendrimers was examined.^{19, 83, 84, 87–93} In this case, dendritic macromolecules are used for efficient stabilisation of supersmall metal particles.

The growing interest in the synthesis of metal nanosized particles in dendrimeric templates was dictated not only by the novelty and simplicity of the procedure, but also by the possible practical applications of nanocomposites, in particular, as catalysts. It was noted⁹⁴ that dendrimers allow combination of advantages of homogeneous and heterogeneous catalysis and can provide the control over the structure and size of catalytic particles. For example, Pd and Pt nanoparticles stabilised by a dendrimeric template are characterised by excellent catalytic activity in hydrogenation of simple (for example, allyl alcohol) and electron-deficient (*N*-isopropylacrylamide) alkenes in an aqueous medium.⁸⁹ Bimetallic nanoparticles synthesised in the presence of dendrimers are also active in the Heck and Suzuki coupling reactions.⁸⁸

The choice of rigid dendrimers as templates for the formation of metal nanoparticles provides better control over the particle growth and morphology. New hybrid (dendrimer–metal) nanostructured systems based on poly(pyridylphenylene) dendrimers, which have catalytic properties, were studied.^{76, 77} The catalytic mono- and bimetallic nanoparticles thus synthesised proved to be rather active catalysts for hydrogenation of the triple bond in acetylenic alcohols.^{95, 96}

Rigid dendritic macromolecules with a strictly defined structure and predictable properties have a high potential for

the design of optical and electronic devices. Conjugated phenylacetylene dendrimers⁹⁷ containing optically pure 4,4',6,6'-tetrabromo-1,1'-bi(2-naphthol) diacetate were among the first rigid dendrimers having optical properties, which hold promise for the design of enantioselective fluorescent sensors. Such optically active dendrimers can also be used in the asymmetric synthesis.

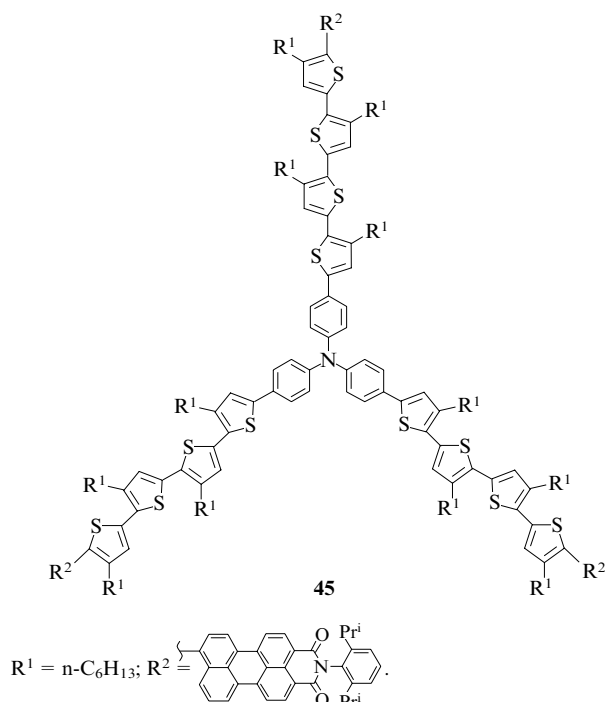
Perfluorinated first- and second-generation polyphenylene dendrimers were investigated as materials for organic light-emitting diodes.⁹⁸ These systems can be used for the design of blue-light-emitting diodes; however, perfluorinated dendrimers are inferior to linear or branched analogues because of a low degree of conjugation of dendrimers (due to the presence of bulky fluorine atoms) and low electron affinity.

The efficiency of natural light-harvesting systems in plants and bacteria performing the visible light harvesting and conversion of visible light energy into chemical energy stimulated many researchers to design analogous artificial systems. Due to the unique features, conjugated dendrimers are attractive materials for such systems. Numerous dendrimers of different architecture with efficient light-harvesting properties have already been synthesised. For example, the synthesis of conjugated phenylacetylene dendrimers and dendrons,^{26, 99–103} phenylenevinylene dendrimers¹⁰⁴ and dendrimers with porphyrin^{105, 106} and perylene groups^{107–109} was documented.

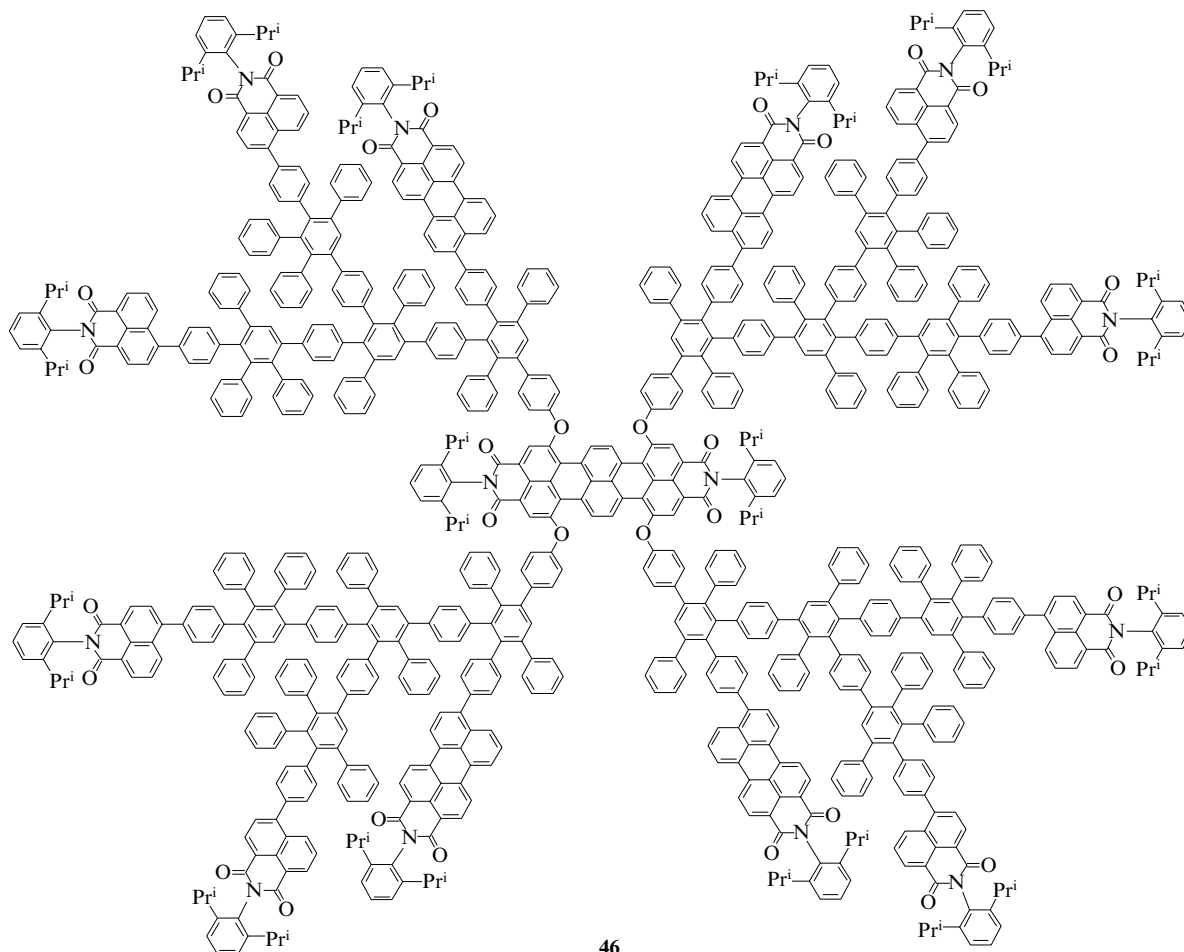
The above-mentioned conjugated dendrimers³³ containing oligo(ethynylthiophene) fragments are highly promising light-absorbing materials due to the efficient inter- and intramolecular energy transfer and a broad absorption spectrum.

Efficient donor–acceptor systems **45** containing the triarylamine core, oligothiophene side branches and peryleneimide terminal groups were studied.¹¹⁰ These systems also showed high photochemical activity. The photochemically stable peryleneimide terminal group acts as an electron acceptor; the

triphenylamine core, as an electron donor. In different solvents (THF, chloroform or toluene), the luminescence quantum yield decreases with an increase in the solvent polarity due apparently to better stabilisation of the donor–acceptor pair.



Porphyrin-containing dendrimers are of interest as synthetic analogues of biological systems.^{16, 111, 112} Porphyrin-type

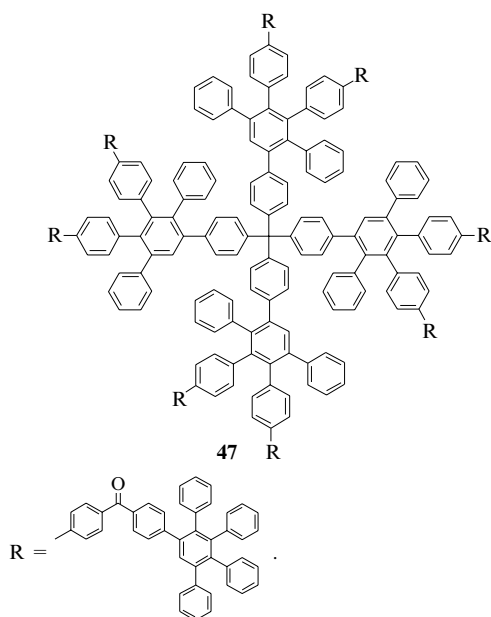


dendrimers **29** and **30** with carbazole peripheral groups can be used as efficient light-harvesting antennas.⁵⁸ The porphyrin core acts as an energy trap. In addition, porphyrin-containing dendrimers can be involved in various redox reactions.

Multichromophoric system **46** based on rigid polyphenylene dendrimers was studied.¹¹³ The specified spatial arrangement of chromophore groups and their spectroscopic characteristics provide efficient light absorption throughout the visible region and the energy transfer to the central terrylene diimide fragment, which converts this energy into the IR radiation energy.

The growing interest in the synthesis of dendrimers with unique photophysical properties requires a deeper insight into charge transfer mechanism in these systems. Investigations of symmetrical dendritic molecules did not give an unambiguous answer to these questions. Investigations of phenyleneethynylene dendrimers with asymmetric architecture^{100, 101} provided the partial solution to this problem. Intramolecular interactions and the charge transfer mechanism in the systems were considered in more detail.¹⁰³ Phenylethynylene dendrimers exhibit highly efficient energy transfer from dendrons to the core, an increase in the generation number of dendrimers having no negative effect on the fluorescent properties of the system. The fluorescence dynamics was studied for symmetrical and non-symmetrical dendrimers both in the presence and absence of an energy trap. The ~50% energy transfer was found to proceed according to a multistep mechanism. Nevertheless, the process is completed in less than one picosecond.

In recent years, bulky macromolecules bearing charged functional groups and having magnetic properties have attracted growing interest. From this point of view, polyphenylene dendrimers are promising nanoobjects.¹¹⁴ In addition to such advantages as the regular structure and high thermal and chemical stability, polyphenylene dendrimers can stabilise active radical groups with very short lifetimes. In addition to the electronic effects (for example, the resonance effects), dendrimers stabilise radicals due to steric effects by retaining the distance between individual radical groups and preventing them from interacting with each other.^{115, 116} The synthesis of a series of dendrimers containing radicals both at the periphery^{117, 118} and as the core was documented.^{119, 120} In addition, a series of polyphenylene dendrimers (for example, compound **47**) containing definite number of carbonyl groups uniformly distributed in the macromolecular structure were synthesised.



These dendrimers were modified with organolithium reagents with the aim of preparing different types of radicals.¹²¹

V. Conclusion

Polyaromatic dendrimers have various unique properties different from those of aliphatic analogues. The synthesis of such dendrimers is rather simple and unambiguous because monodisperse dendritic molecules are, as a rule, produced in high yields. Due to the rigid molecular shape, the desired arrangement of functional groups in dendrimers can be achieved with the use of appropriate building blocks. This approach facilitates the introduction of functional groups both into the core of dendrimers or dendritic branches and at the periphery. Some of the above-mentioned features, in particular, the presence of numerous functional groups at the periphery, allows the use of dendrimers as nanosupports for catalysts and chromophore groups. Therefore, polyaromatic dendrimers are attractive as objects of investigation for both organic chemists and experts in the fields of materials science and nanotechnology.

Due to a constant shape, rigid dendrimers are used in studies of electron transfer processes between different redox centres. If one centre is located in the core and another centre is present at the periphery of a dendrimer, the distances, which are necessary to overcome for the electron transfer, can be calculated. In addition, dendrimers containing fragments of two different types of fluorescent dyes at the periphery are of interest in studies of energy transfer processes between these dyes (light-harvesting antennas).

The introduction of fluorescent dye labels into dendritic molecules bearing an active receptor allows the use of such systems in biological objects to determine the degree of binding of the receptor to a biological substrate.

Based on the analysis of the published data, it can be concluded that the development of procedures for the synthesis of dendritic systems and a search for new fields of their application are of great importance. Due to the unique properties, dendrimers are interesting objects of investigation for both fundamental science and various fields of applied studies. Virtually defect-free structures of polyaromatic dendrimers hold promise for the design of various materials having optical, catalytic and magnetic properties. Due to high chemical and thermal stability, such dendrimers are particularly attractive materials for the use in corrosive media and/or at high temperatures.

This review has been written with the financial support of the Russian Foundation for Basic Research (Project Nos. 07-03-00220 and 07-03-00228).

References

1. S M Grayson, J M J Fréchet *Chem. Rev.* **101** 3819 (2001)
2. C J Hawker, J M J Fréchet *J. Am. Chem. Soc.* **112** 7638 (1990)
3. *Advances in Dendritic Macromolecules* (Ed. G R Newkome) (Greenwich: JAI Press, 1994)
4. G R Newkome, Z Yao, G R Baker, V K Gupta *J. Org. Chem.* **50** 2003 (1985)
5. G R Newkome, C N Moorefield, F Vögtle *Dendritic Molecules: Concepts, Syntheses, Perspectives* (Weinheim: VCH, 1996)
6. D A Tomalia, H Baker, J Dewald, M Hall, G Kallos, S Martin, J Roeck, J Ryder, P Smith *Polym. J.* **17** 117 (1985)
7. D A Tomalia, A M Naylor, W A Goddard III *Angew. Chem., Int. Ed. Engl.* **29** 138 (1990)
8. D A Tomalia, H D Durst *Supramolecular Chemistry I: Directed Synthesis and Molecular Recognition (Topics in Current Chemistry)* Vol. 165 (Ed. E Weber) (Berlin: Springer, 1993) p. 133
9. D A Tomalia, P R Dvornic *Nature (London)* **372** 617 (1994)
10. C Schlenk, H Frey *Monatsh. Chem.* **130** 3 (1999)

11. F Vögtle, S Gestermann, R Hesse, H Schwierz, B Windisch *Prog. Polym. Sci.* **25** 987 (2000)
12. S Yokoyama, A Otomo, T Nakahama, Y Okuno, S Mashiko *Dendrimers V: Functional and Hyperbranched Building Blocks, Photophysical Properties, Applications in Materials and Life Sciences (Topics in Current Chemistry)* Vol. 228 (Eds C A Schally, F Vögtle) (Berlin: Springer, 2003) p. 205
13. S C Zimmerman, L J Lawless *Dendrimers IV: Metal Coordination, Self Assembly, Catalysis (Topics in Current Chemistry)* Vol. 217 (Eds F Vögtle, C A Schally) (Berlin: Springer, 2001) p. 95
14. I P Beletskaya, A V Chuchurjukin *Usp. Khim.* **69** 699 (2000) [*Russ. Chem. Rev.* **69** 639 (2000)]
15. A M Muzafarov, E A Rebrov *Vysokomol. Soedin., Ser. C* **42** 2015 (2000)^a
16. V Balzani, P Ceroni, A Juris, M Venturi, S Campagna, F Puntoriero, S Serroni *Coord. Chem. Rev.* **219** 545 (2001)
17. V Balzani, P Ceroni, M Maestri, C Saudan, V Vicinelli *Dendrimers V: Functional and Hyperbranched Building Blocks, Photophysical Properties, Applications in Materials and Life Sciences (Topics in Current Chemistry)* Vol. 228 (Eds C A Schally, F Vögtle) (Berlin: Springer, 2003) p. 159
18. A W Bosman, H M Janssen, E W Meijer *Chem. Rev.* **99** 1665 (1999)
19. R M Crooks, M Zhao, L Sun, V Chechik, L K Yeung *Acc. Chem. Res.* **34** 181 (2001)
20. M Fischer, F Vögtle *Angew. Chem., Int. Ed.* **38** 884 (1999)
21. J M J Fréchet *Science* **263** 1710 (1994)
22. H Frey, C Lach, K Lorenz *Adv. Mater.* **10** 279 (1998)
23. K Inoue *Prog. Polym. Sci.* **25** 453 (2000)
24. J Issberner, R Moors, F Vögtle *Angew. Chem., Int. Ed. Engl.* **33** 2413 (1994)
25. J-P Majoral, A-M Caminade *Chem. Rev.* **99** 845 (1999)
26. J S Moore *Acc. Chem. Res.* **30** 402 (1997)
27. O A Matthews, A N Shipway, J F Stoddart *Prog. Polym. Sci.* **23** 1 (1998)
28. G R Newkome, C N Moorefield, F Vögtle *Dendrimers and Dendrons: Concepts, Syntheses, Applications* (Weinheim: Wiley-VCH, 2001)
29. P G De Gennes, H Hervet *J. Phys. Lett.* **44** 351 (1983)
30. H Ihre, A Hult, J M J Fréchet, I Gitsov *Macromolecules* **31** 4061 (1998)
31. A M Muzafarov, E A Rebrov, V S Papkov *Usp. Khim.* **60** 1596 (1991) [*Russ. Chem. Rev.* **60** 807 (1991)]
32. K L Wooley, C J Hawker, J M J Fréchet *Angew. Chem., Int. Ed. Engl.* **33** 82 (1994)
33. J-L Wang, J Luo, L-H Liu, Q-F Zhou, Y Ma, J Pei *Org. Lett.* **8** 2281 (2006)
34. A J Berresheim, M Müller, K Müllen *Chem. Rev.* **99** 1747 (1999)
35. R E Bauer, A C Grimsdale, K Müllen *Functional Molecular Nanostructures. (Topics in Current Chemistry)* Vol. 245 (Ed. A D Schlüter) (Berlin: Springer, 2005) p. 253
36. G J Capostoti, C D Guerrero, D E Binkley Jr, C S Rajesh, D A Modarelli *J. Org. Chem.* **68** 247 (2003)
37. D Liu, S De Feyter, M Cotlet, A Stefan, U-M Wiesler, A Herrmann, D Grebel-Koehler, J Q Qu, K Müllen, F C De Schryver *Macromolecules* **36** 5918 (2003)
38. U M Wiesler, T Weil, K Müllen *Dendrimers III: Design, Dimension, Function (Topics in Current Chemistry)* Vol. 212 (Ed. F Vögtle) (Berlin: Springer, 2001) p. 1
39. F C De Schryver, T Vösch, M Cotlet, M Van der Auweraer, K Müllen, J Hofkens *Acc. Chem. Res.* **38** 514 (2005)
40. H Meier, M Lehmann *Angew. Chem., Int. Ed.* **37** 643 (1998)
41. M Lehmann, I Fischbach, H W Spiess, H Meier *J. Am. Chem. Soc.* **126** 772 (2004)
42. T M Miller, T X Neenan *Chem. Mater.* **2** 346 (1990)
43. T M Miller, T X Neenan, R Zayas, H E Bair *J. Am. Chem. Soc.* **114** 1018 (1992)
44. N Miyauchi, T Yanagi, A Suzuki *Synth. Commun.* **11** 513 (1981)
45. J S Moore, Z Xu *Macromolecules* **24** 5893 (1991)
46. Z F Xu, J S Moore *Angew. Chem., Int. Ed. Engl.* **32** 246 (1993)
47. P Bharathi, U Patel, T Kawaguchi, D J Pesak, J S Moore *Macromolecules* **28** 5955 (1995)
48. D J Pesak, R Moor, T E Wheat *Macromolecules* **30** 6467 (1997)
49. M Lehmann, B Schartel, M Hennecke, H Meier *Tetrahedron* **55** 13377 (1999)
50. J N G Pillow, M Halim, J M Lupton, P L Burn, I D W Samuel *Macromolecules* **32** 5985 (1999)
51. R E Heck *Pure Appl. Chem.* **53** 2323 (1981)
52. R E Heck *Palladium Reagents in Organic Synthesis* (New York: Academic Press, 1985)
53. U-M Wiesler, K Müllen *Chem. Commun.* 2293 (1999)
54. D Gust, T A Moore, A L Moore *Acc. Chem. Res.* **34** 40 (2001)
55. A K Burrell, D L Officer, P G Plieger, D C W Reid *Chem. Rev.* **101** 2751 (2001)
56. D Holten, D F Bocian, J S Lindsey *Acc. Chem. Res.* **35** 57 (2002)
57. S Campagna, S Serroni, F Puntoriero, C Di Pietro, V Ricevuto *Electron Transfer in Chemistry* Vol. 5 (Ed. V Balzani) (Weinheim: Wiley-VCH, 2001) p. 186
58. F Loiseau, S Campagna, A Hameurlaine, W Dehaen *J. Am. Chem. Soc.* **127** 11352 (2005)
59. A Hameurlaine, W Dehaen *Tetrahedron Lett.* **44** 957 (2003)
60. J S Lindsey, I C Schreyman, H C Hsu, P S Kearney, P C Marguerettaz *J. Org. Chem.* **52** 827 (1987)
61. Y Jiang, J Y Wang, Y G Ma, Y X Cui, Q F Zhou, J Pei *Org. Lett.* **8** 4287 (2006)
62. H Hart *Pure Appl. Chem.* **65** 27 (1993)
63. F Morgenroth, K Müllen *Tetrahedron* **53** 15349 (1997)
64. F Morgenroth, C Kubel, K Müllen *J. Mater. Chem.* **7** 1207 (1997)
65. F Morgenroth, C Kubel, M Müller, U-M Wiesler, A J Berresheim, M Wagner, K Müllen *Carbon* **36** 833 (1998)
66. F Morgenroth, A J Berresheim, M Wagner, K Müllen *Chem. Commun.* 1139 (1998)
67. A J Berresheim, F Morgenroth, U-M Wiesler, K Müllen *Polym. Prepr. (Am. Chem. Soc., Div. Polym. Chem.)* **39** 721 (1998)
68. U-M Wiesler, A J Berresheim, F Morgenroth, G Lieser, K Müllen *Macromolecules* **34** 187 (2001)
69. C D Simpson, D J Brand, A J Berresheim, L Przybilla, H J Räder, K Müllen *Chem. – Eur. J.* **8** 1424 (2002)
70. S Loi, U-M Wiesler, H-J Butt, K Müllen *Macromolecules* **34** 3661 (2001)
71. D Grebel-Koehler, D J Liu, S De Feyter, V Enkelmann, T Weil, C Engels, C Samyn, K Müllen, F C De Schryver *Macromolecules* **36** 578 (2003)
72. M A Ogliaruso, M G Romanelli, E I Becker *Chem. Rev.* **65** 261 (1965)
73. F Morgenroth, E Reuther, K Müllen *Angew. Chem., Int. Ed. Engl.* **36** 631 (1997)
74. P Carbone, A Calabretta, M Di Stefano, F Negri, K Müllen *J. Phys. Chem. A* **110** 2214 (2006)
75. Y Sakamoto, T Suzuki, A Miura, H Fujikawa, S Tokito, Y Taga *J. Am. Chem. Soc.* **122** 1832 (2000)
76. Z B Shifrina, M S Averina, N V Firsova, A L Rusanov, K Müllen *Dokl. Akad. Nauk* **400** 774 (2005)^b
77. Z B Shifrina, M S Rajadurai, N V Firsova, L M Bronstein, X Huang, A L Rusanov, K Müllen *Macromolecules* **38** 9920 (2005)
78. N V Tsvetkov, S K Filippov, T M Kudryavtseva, V O Ivanova, Z B Shifrina, M S Averina, N V Firsova, A L Rusanov *Vysokomol. Soedin., Ser. A* **48** 692 (2006)^a
79. J F G A Jansen, E M M de Brabander-van den Berg, E W Meijer *Science* **266** 1226 (1994)
80. A M Naylor, W A Goddard, G E Kiefer, D A Tomalia *J. Am. Chem. Soc.* **111** 2339 (1989)
81. J F G A Jansen, E W Meijer *J. Am. Chem. Soc.* **117** 4417 (1995)
82. F Grohn, B J Bauer, E J Amis *Macromolecules* **34** 6701 (2001)
83. F Grohn, B J Bauer, Y A Akpalu, C L Jackson, E J Amis *Macromolecules* **33** 6042 (2000)
84. M Zhao, L Sun, R M Crooks *J. Am. Chem. Soc.* **120** 4877 (1998)
85. L Balogh, D A Tomalia *J. Am. Chem. Soc.* **120** 7355 (1998)
86. K Esumi, A Suzuki, N Aihara, K Usui, K Torigoe *Langmuir* **14** 3157 (1998)
87. B I Lemon III, R M Crooks *J. Am. Chem. Soc.* **122** 12886 (2000)
88. Y Niu, R M Crooks *C. R. Acad. Sci., Ser. II: Chim.* **6** 1049 (2003)
89. M Zhao, R M Crooks *Angew. Chem., Int. Ed.* **38** 364 (1999)

90. R W J Scott, A K Datye, R M Crooks *J. Am. Chem. Soc.* **125** 3708 (2003)
91. K Esumi, A Suzuki, A Yamahira, K Torigoe *Langmuir* **16** 2604 (2000)
92. O Varnavski, R G Ispasoiu, L Balogh, D Tomalia *J. Chem. Phys.* **114** 1962 (2001)
93. J Zheng, R M Dickson *J. Am. Chem. Soc.* **124** 13982 (2002)
94. J W J Knapen, A W Vandermade, J C Dewilde, P W N M Vanleeuwen, P Wijkens, D M Grove, G Vankoten *Nature (London)* **372** 659 (1994)
95. Z Shifrina, M Averina, A Rusanov, K Müllen *International Conference 'Polycondensation 2004' (Abstracts of Reports)*, Roanoke, VA, 2004 Abstr. 7
96. Z Shifrina, M Rajadurai, N Firsova, A Rusanov, K Müllen, L Bronstein *Proceedings of European Polymer Congress, Moscow, 2005* p. 37
97. Q S Hu, V Pugh, M Sabat, L Pu *J. Org. Chem.* **64** 7528 (1999)
98. A P Kulkarni, C J Tonzola, A Babel, S A Jenekhe *Chem. Mater.* **16** 4556 (2004)
99. C Devadoss, P Bharathi, J S Moore *J. Am. Chem. Soc.* **118** 9635 (1996)
100. Y C Pan, M Lu, Z H Peng, J S Melinger *J. Org. Chem.* **68** 6952 (2003)
101. Y C Pan, Z H Peng, J S Melinger *Tetrahedron* **59** 5495 (2003)
102. E Atas, C Mair, J S Mellinger, Z H Peng, V Kleiman *Abstracts of Papers of the 228th American Chemical Society National Meeting, Philadelphia, PA, 2004* U52
103. E Atas, Z H Peng, V D Kleiman *J. Phys. Chem. B* **109** 13553 (2005)
104. S C J Meskers, M Bender, J Hubner, Yu V Romanovskii, M Oestreich, A P H J Schenning, E W Meijer, H Bassler *J. Phys. Chem. A* **105** 10220 (2001)
105. E K L Yeow, K P Ghiggino, J N H Reek, M J Crossley, A W Bosman, A P H J Schenning, E W Meijer *J. Phys. Chem. B* **104** 2596 (2000)
106. M S Choi, T Aida, T Yamazaki, I Yamazaki *Chem. – Eur. J.* **8** 2668 (2002)
107. K Tomizaki, R S Loewe, C Kirmaier, J K Schwartz, J L Retsek, D F Bocian, D Holten, J S Lindsey *J. Org. Chem.* **67** 6519 (2002)
108. R Metivier, F Kulzer, T Weil, K Müllen, T Basche *J. Am. Chem. Soc.* **126** 14364 (2004)
109. T Weil, E Reuther, C Beer, K Müllen *Chem. – Eur. J.* **10** 1398 (2004)
110. A Petrella, M Tamborra, M L Curri, P Cosma, M Striccoli, P D Cozzoli, A Agostiano *J. Phys. Chem. B* **109** 1554 (2005)
111. P Weyermann, J P Gisselbrecht, C Boudon, F Diederich, M Gross *Angew. Chem., Int. Ed.* **38** 3215 (1999)
112. A Juris *Electron Transfer in Chemistry* Vol. 3 (Ed. V Balzani) (Weinheim: Wiley-VCH, 2001) p. 655
113. M Cotlet, T Vosch, S Habuchi, T Weil, K Müllen, J Hofkens, F De Schryver *J. Am. Chem. Soc.* **127** 9760 (2005)
114. S Rajca, A Rajca, J Wongsriratanakul, P Butler, S M Choi *J. Am. Chem. Soc.* **126** 6972 (2004)
115. W P Neumann, W Uzick, A K Zarkadis *J. Am. Chem. Soc.* **108** 3762 (1986)
116. W P Neumann, A Penenory, U Stewen, M J Lehnig *J. Am. Chem. Soc.* **111** 5845 (1989)
117. S Fuchs, T Kapp, H Otto, T Schoneberg, P Franke, R Gust, A D Schluter *Chem. – Eur. J.* **10** 1167 (2004)
118. J M J Fréchet *J. Polym. Sci., Part A: Polym. Chem.* **41** 3713 (2003)
119. K R Gopidas, J K Whitesell, M A Fox *J. Am. Chem. Soc.* **125** 14168 (2003)
120. E M Harth, S Hecht, B Helms, E E Malmstrom, J M J Fréchet, C J Hawker *J. Am. Chem. Soc.* **124** 3926 (2002)
121. S Bernhardt, M Baumgarten, M Wagner, K Müllen *J. Am. Chem. Soc.* **127** 12392 (2005)

^a — *Polym. Sci. (Engl. Transl.)*

^b — *Dokl. Chem. (Engl. Transl.)*

Synthesis of azomethine macrocycles by condensation of dicarbonyl compounds with diamines without using metal ions as template agents

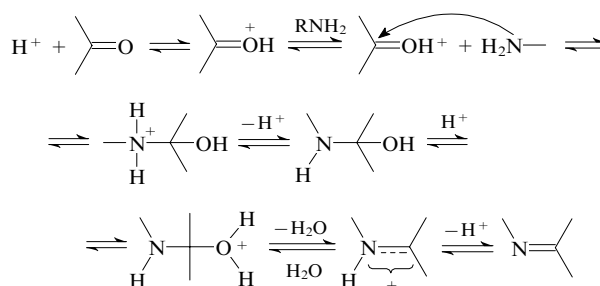
N E Borisova, M D Reshetova, Yu A Ustynyuk

Contents

I. Introduction	785
II. Symmetrical macrocyclic Schiff bases	786
III. Unsymmetrical macrocyclic Schiff bases	808
IV. Anion template effect in the synthesis of macrocyclic azomethines	815
V. Acyclic condensation products of dicarbonyl compounds with diamines	819
VI. Conclusion	821

Abstract. Different strategies for the synthesis of symmetrical and unsymmetrical macrocyclic Schiff bases in the absence of metal ions are considered. General methods for performing macrocyclisation under thermodynamic or kinetic control are analysed. The key factors influencing the structure of macrocyclic azomethines are discussed. The bibliography includes 215 references.

Scheme 1



I. Introduction

Schiff bases (azomethines) contain the $\text{RC}=\text{N}$ group and are widely used in organic synthesis, for example, as intermediates in the synthesis of amines. Some azomethines have high biological activities, including antitumour,^{1,2} bactericidal³ or antiviral activity.⁴ Schiff bases containing additional electron-donating groups belong to an important class of heteropolycyclic ligands involved in mono- or polynuclear complexes with metals. Macrocyclic azomethines can trap metal ions with large radii and high coordination numbers, including lanthanides and actinides, in their cavities and form bi- and polynuclear complexes, in which two or more metal atoms are located in one cavity in close proximity to each other and which are characterised by unusual magnetic properties⁵ and catalytic activity.⁶ Some azomethine complexes have non-linear optical properties.⁷ Macrocyclic azomethines are prone to form discotic liquid crystals.⁸ In recent years, it has been demonstrated⁹ that macrocyclic Schiff bases can also recognise and selectively bind anions, thus acting as artificial anionic receptors.

The most general procedure for the synthesis of azomethines is based on acid-catalysed condensation of carbonyl compounds with primary amines discovered by Schiff¹⁰ in 1864. The classical Schiff reaction generally proceeds with high yield (Scheme 1).

Since all steps in this transformation sequence are reversible, the process performed under thermodynamic control affords an equilibrium mixture of products, which can be considered as a dynamic combinatorial library.¹¹ An understanding of the factors determining the equilibrium in this system is of key importance for the achievement of chemoselectivity.

The reactions of dicarbonyl compounds with diamines are much more complicated and can afford a large set of cyclic and acyclic condensation products (Scheme 2). In the first step, one molecule of a dicarbonyl compound reacts with one diamine molecule to give the acyclic [1 + 1]-condensation product **A**, which can then form either the [2 + 1] product **B** with the second molecule of the dicarbonyl compound or the [1 + 2] product **C** with the second diamine molecule. In addition, compound **A** can undergo either cyclisation to give the [2 + 2] macrocycle **D** or polycondensation to form linear oligomers **E** with different molecular mass. In turn, bis-azomethines **B** and **C** can give the macrocyclic [2 + 2]-condensation product **D** in the subsequent reaction with diamine or the dicarbonyl compound, respectively.

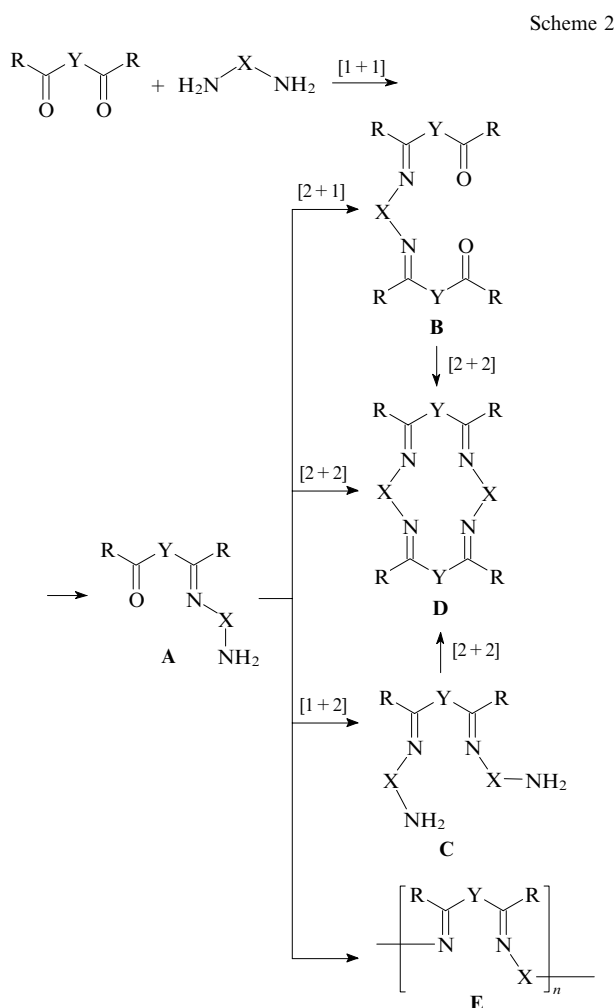
The rate-determining step of the reaction depends on the acidity of the medium and it is either the addition of amine at the double bond of the carbonyl group in acidic medium or elimination of the water molecule in neutral medium. Hence, the proton-donor properties of the solvent have a substantial effect on the composition of the products, particularly, in the case of the assembly of large rings or if the starting compounds have complex geometry.

The classical scheme of processes involved in the reaction of diamines with dicarbonyl compounds was reported in several reviews (see, for example, Refs 12 and 13).

N E Borisova, M D Reshetova, Yu A Ustynyuk Department of Chemistry, M V Lomonosov Moscow State University, Leninskie Gory, 119992 Moscow, Russian Federation. Fax (7-495) 939 26 77, tel. (7-495) 939 26 47, e-mail: borisova.nataliya@gmail.ru (N E Borisova), mres@nmr.chem.msu.ru (M D Reshetova), tel. (7-495) 939 26 77, e-mail: ustynyuk@nmr.chem.msu.ru (Yu A Ustynyuk)

Received 20 March 2007

Uspekhi Khimii 76 (9) 843–884 (2000); translated by T N Safonova



In the synthesis of macrocycles, the addition of a template agent is the most efficient way of preventing polycondensation. Systematic studies of the template effect were initiated by Busch and co-workers^{14–17} in the early 1960s. Template agents are generally classified into several types depending on the nature of dominant interactions with the starting compounds (donor-acceptor, electrostatic or hydrophobic interactions, π, π stacking, hydrogen bonding). The principal studies on the template synthesis were covered in sufficient detail in two volumes of *Topics in Current Chemistry*.^{18,19} The anionic template effect was considered in depth in several review articles^{20–22} included in the special issue of *Coordination Chemistry Reviews* and also in reviews.^{23,24} In the last decade, investigations on the synthesis of macrocyclic Schiff bases in the presence of metal ions and the properties of the resulting complexes were summarised in more than ten publications (see, for example, reviews^{13,25–28} and monographs²⁹). The metal template synthesis has been covered in depth in publications by Vigato and co-workers.^{30,31} Recently, Sessler and co-workers³² have published a review on the synthesis of pyrrole-containing macrocyclic Schiff bases by different methods.

The metal template synthesis of macrocyclic Schiff bases has been studied in most detail. However, this method has two substantial drawbacks. First, the reactions with dicarbonyl compounds and diamines as the starting components generally produce symmetrical complexes. Hence, the template synthesis is unsuitable for the preparation of unsymmetrical macrocyclic Schiff bases. Second, metal-free compounds cannot be synthesised by this method. The selective condensation in the presence of a template agent is provided by strong binding of a metal ion in the cavity of the macrocycle. In many cases,

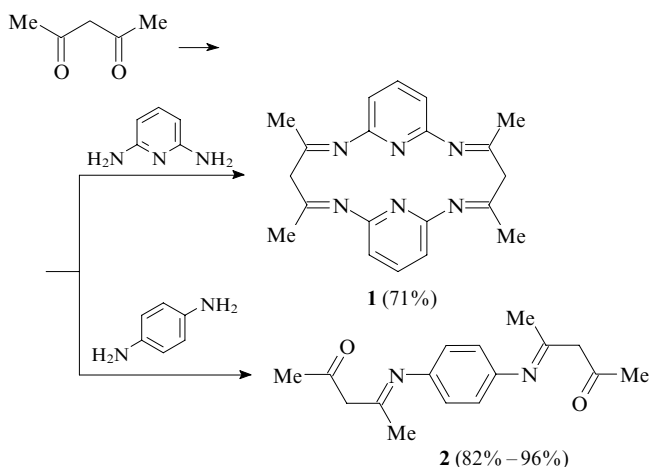
demetallation of complexes can be performed only with the use of simultaneous reduction of imino groups to amino groups.

In the last two decades, considerable efforts were made to develop template-free methods for the synthesis of Schiff bases. In the present review, we analyse main approaches to the synthesis of macrocyclic azomethines by the self-assembly method in the absence of template agents. These data are considered from other points of view and are substantially extended and revised compared to the data published in our earlier review.³³

II. Symmetrical macrocyclic Schiff bases

Symmetrical macrocyclic Schiff bases are generally synthesised by $[n+n]$ -condensation reactions, where $n = 2, 3$ or 4.

Schiff bases prepared from diamines and carbonyl compounds of the aliphatic series are unstable and readily undergo hydrolysis. These macrocyclic ligands are usually synthesised by the template method. On the contrary, azomethines generated from aromatic or heteroaromatic diamines and aliphatic dicarbonyl compounds are rather stable and can be isolated as free ligands. For example, the condensation of acetylacetone with equimolar amount of 2,6-diaminopyridine in methanol in the presence of catalytic amounts of hydrochloric acid affords the corresponding $[2+2]$ macro-cycle **1**.³⁴



The $[2+1]$ -condensation product of acetylacetone with *p*-phenylenediamine, *viz.*, compound **2**, was prepared in high yield in the presence of a large excess of the dicarbonyl compound.³⁵

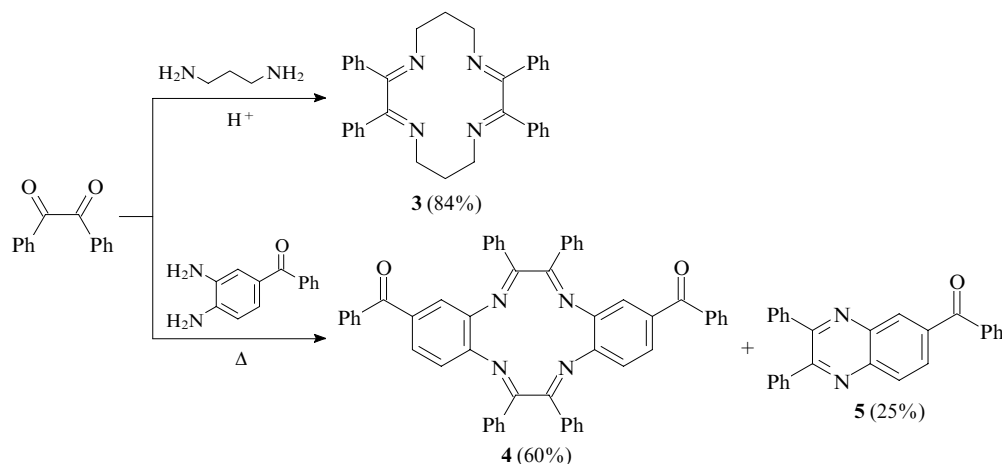
Even more stable Schiff bases can be synthesised from aliphatic or aromatic diamines and dicarbonyl derivatives of aromatic and heteroaromatic series. These compounds are used in the synthesis of polydentate ligands by self-assembly reactions more often than other reagents.

Aromatic diketones generally react with aliphatic diamines in ethanol in the presence of catalytic amounts of acids to form the corresponding $[2+2]$ -condensation products. For example, the reaction of benzil with 1,3-diaminopropane produces macrocyclic Schiff base **3**.³⁶

This reaction with aromatic diamines proceeds under prolonged reflux and gives not only macrocyclic $[2+2]$ -condensation product **4** but also quinoxaline derivative **5** as a $[1+1]$ -condensation product (Scheme 3).³⁷

The composition of the products synthesised by the reactions of dicarbonyl compounds with diamines is determined by several factors, among which the nature of the starting compounds is of most importance. As a rule, the target products can be prepared in good yields by varying the concentration and the ratio of the reagents, the nature of the solvent, the temperature and the catalyst. The reactions of dicarbonyl

Scheme 3



compounds with aliphatic α,ω -diamines were studied in most detail. For these reactions, the conditions of the synthesis of stoichiometrically controlled condensation products were found.

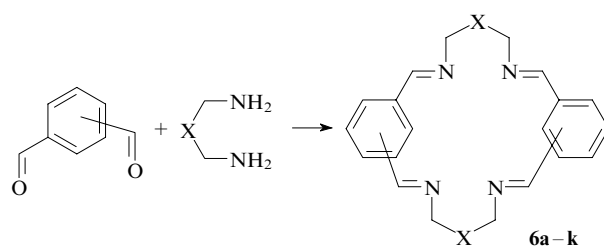
Two amino groups of aliphatic diamines separated by a hydrocarbon bridge react independently of each other. Hence, the reactions involving these groups cannot, as a rule, be terminated after the formation of acyclic [1 + 1]-condensation products. In the absence of metal salts, most of these reactions produce oligomeric compounds.^{38,39} However, [2 + 2] macrocyclic compounds can be prepared as the major products by carefully choosing the ratio and the concentration of the reactants and the nature of the solvent.⁴⁰

Intermolecular reactions giving oligomers are generally suppressed using high-dilution conditions (the concentration is 10^{-2} – 10^{-3} mol litre⁻¹ or lower) and stoichiometric amounts of the components. The solvent is chosen such that the starting reagents are readily soluble, whereas the target product is poorly soluble. Taking into account the fact that the resulting macrocyclic Schiff bases are less polar than the starting compounds, polar solvents, such as methanol, ethanol and acetonitrile, are the solvents of choice. The reactions can be performed either at room temperature over a long period of time (> 12 h) or by refluxing for 0.5–4 h. Many efficient syntheses of [2 + 2] macrocycles based on aromatic and hetero-aromatic dicarbonyl compounds, which were performed under these conditions, were documented. The composition of the reaction products depends primarily on the nature of the aromatic moiety of dicarbonyl compounds and the presence of substituents in these compounds, whereas the geometry and conformations of the fragments involved in the reaction are insignificant.

The macrocyclisation reactions systematised according to the type of the starting dicarbonyl compounds are considered below.

1. Cyclocondensation of diamines with aromatic dicarbonyl derivatives

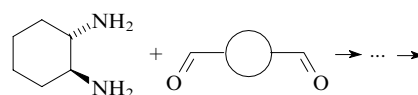
The condensation of isophthalaldehyde and terephthalaldehyde with diamines in dilute solutions ($\sim 10^{-2}$ – 10^{-3} mol litre⁻¹) of lower alcohols or acetonitrile affords [2 + 2]-macrocyclic Schiff bases **6a–k**. (Most of macrocyclic compounds based on phthalaldehyde were synthesised by the template method.²⁹)

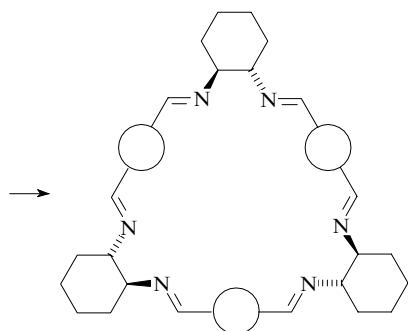


Compound 6	X	Isomer	Yield (%)	Ref.
a	absent	1,3	88	41
b	CH ₂ NMeCH ₂	1,3	10	42
c	CH ₂ NHCH ₂	1,3	60–70	40
d	CH ₂ NHCH ₂	1,4	—	43
e	CH ₂ NTsCH ₂	1,3	87	42
f	(CH ₂ SCH ₂) ₂	1,3	71	41
g	(CH ₂ SCH ₂) ₂	1,4	48	44
h	1,2-C ₆ H ₄ (CH ₂ SCH ₂) ₂	1,3	86	45
i	1,2-C ₆ H ₄ (CH ₂ SCH ₂) ₂	1,4	96	45
j	1,3-phenylene	1,3	—	46
k	1,3-phenylene	1,4	—	43

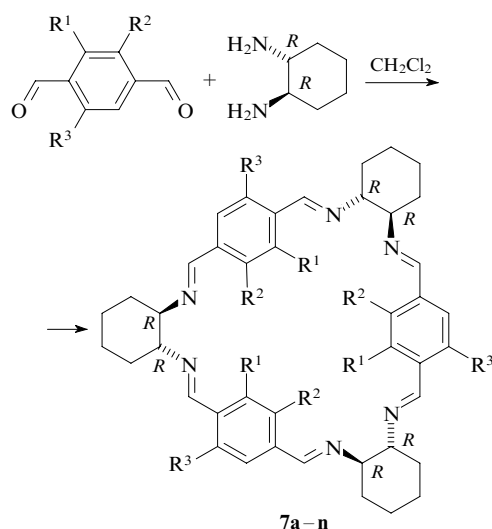
X-Ray diffraction studies showed that, in the crystals, such macrocyclic compounds adopt a stair-like conformation with the parallel arrangement of the aromatic rings. The [2 + 2]-condensation product of isophthalaldehyde with 1,3-bis(aminomethyl)benzene, *viz.*, compound **6j**, contains two pairs of mutually parallel aromatic rings, which form a cavity inside the ligand (Fig. 1).⁴⁶ The azomethine groups in this compound are in the *cis,trans* conformation with respect to the aromatic ring.

Unlike acyclic aliphatic diamines, diaminocyclohexanes have a rather rigidly fixed configuration. In *trans*-1,2-diaminocyclohexane, both amino groups are in equatorial positions, and the H₂N–C–C–NH₂ dihedral angle is close to 60°. Because of this, *trans*-1,2-diaminocyclohexane behaves like an almost planar building block, which is prone to form [3 + 3] macrocycles in the reactions with structurally rigid dicarbonyl compounds with the linear arrangement of carbonyl groups.





For example, the reactions of *trans*-(*R,R*)-1,2-diaminocyclohexane with terephthalaldehyde and its derivatives afford [3 + 3]-condensation products **7a–i**. Low yields of some macrocyclic compounds are attributed to the necessity of performing repeated reprecipitation of the resulting compounds to isolate analytically pure samples, although the yields determined from the spectroscopic data are no lower than 80%–85%.



Compound 7	R ¹	R ²	R ³	Yield (%)	Ref.
a	H	H	H	90	47
b	H	Me	Me	97	48
c	H	OMe	OMe	90	48, 49
d	H	OEt	OEt	18	50
e	H	OPr ⁿ	OPr ⁿ	17	50
f	H	OBu ⁿ	OBu ⁿ	32	50
g	H	OBn	OBn	23	50
h	H	OCH ₂ C ₆ H ₄ F-4	OCH ₂ C ₆ H ₄ F-4	29	50
i	OMe	OMe	H	25	49
j	H	OMe	Et	8	50
k	H	OMe	Bu ⁿ	13	50
l	H	OMe	Bn	15	50
m	H	OMe	(CH ₂) ₂ OMe	5	50
n	H	OMe	Me	46	50

The use of a low-polarity aprotic solvent (dichloromethane) made it possible to perform reactions at high concentrations of the reactants (~ 0.1 mol litre⁻¹) and obviate oligomerisation. According to the results of calculations by the molecular mechanics method, the position of the conformational equilibrium for model compound **8**, which differs from macrocycles **7** by the absence of one azomethine group, is favourable for the closure of the [3 + 3] macrocycle.⁴⁷ Apparently, the cyclic structure is generated from this conformation of the acyclic [3 + 3] precursor.

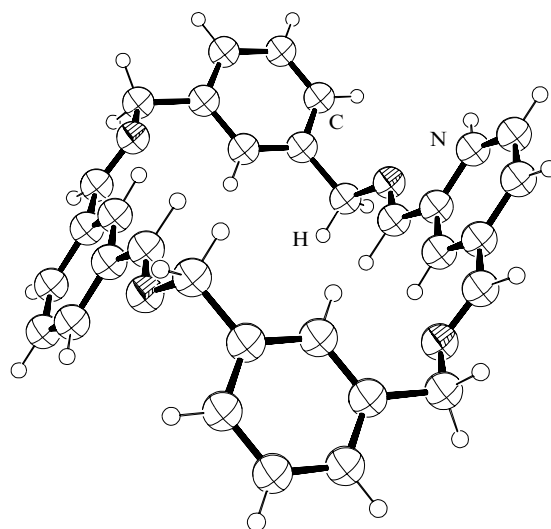
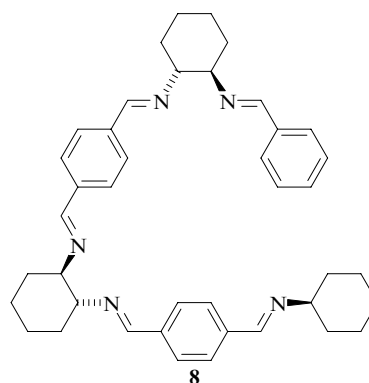


Figure 1. X-Ray diffraction structure of compound **6j**.⁴⁶ (All structures shown in the figures in the present review were retrieved from the Cambridge Structural Database.)



The X-ray diffraction data for compound **7a** show that the cyclohexane fragments in [3 + 3] azomethine molecules are in one plane, whereas the benzene rings are virtually perpendicular to this plane and form a trihedral prism (Fig. 2).^{47, 51}

A detailed study of this reaction of a series of 2,5-disubstituted terephthalaldehydes showed that their condensation

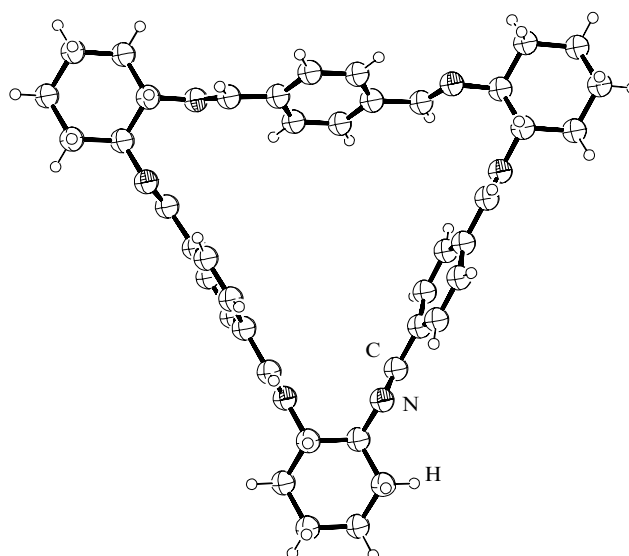
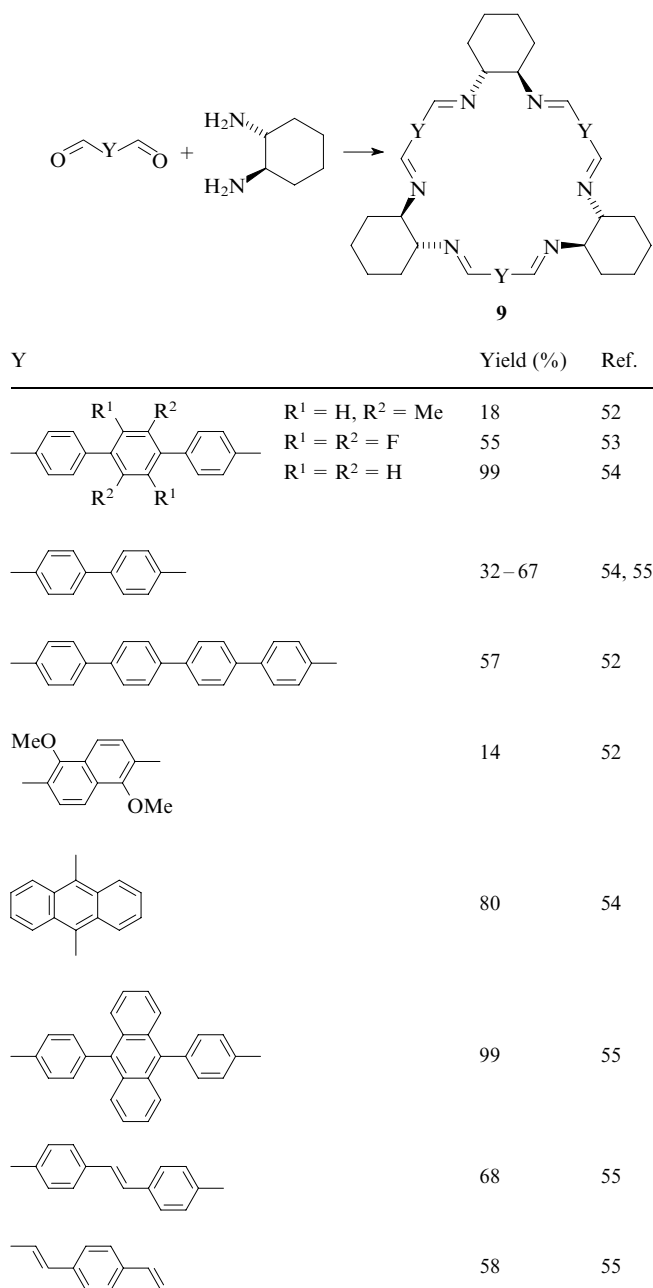


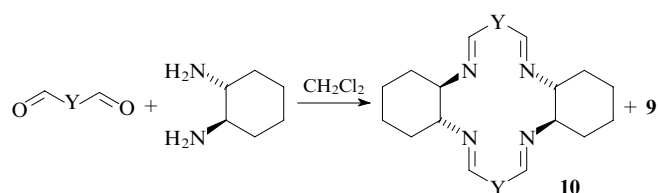
Figure 2. Structure of [3 + 3] azomethine **7a**.⁴⁷

with *trans*-(*R,R*)-1,2-diaminocyclohexane is stereospecific and affords only one of two possible stereoisomeric macrocycles. As a result, only highly symmetrical [3 + 3]-condensation products **7j–n** are formed.⁵⁰

The reaction with *trans*-(*R,R*)-1,2-diaminocyclohexane was successfully extended to other aromatic dicarbonyl compounds containing formyl groups in the *para* positions with respect to each other. For example, [3 + 3] macrocycles **9** were synthesised in yields from moderate to high.

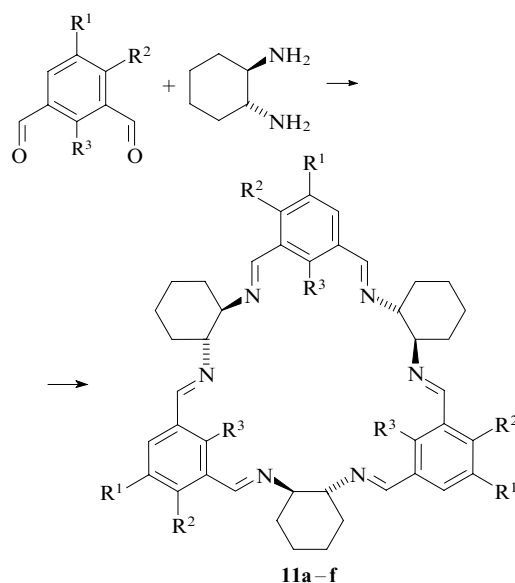


A consideration of the results of macrocyclisation in terms of geometry of the starting compounds (the geometric approach) leads to the conclusion that changes in the mutual orientation of the carbonyl groups in dialdehydes should determine the direction of the process. Actually, the deviation of the angle between the formyl substituents from 180° results in mixtures of cyclic compounds **9** and **10**, [2 + 2] macrocycles being the major reaction products, upon reactions of such dialdehydes with *trans*-(*R,R*)-1,2-diaminocyclohexane.



Y	10 : 9	Yield 10 (%)	Ref.
	97 : 3	67	53
	98 : 2	72	53
	95 : 5	72	53
	98 : 2	66	53
	A = B = CH: 90 : 10	79	53
	A = N, B = CH: 90 : 10	78	53
	A = CH, B = N: 88 : 12	81	53
	85 : 15	34	53
	—	42	52
	—	68	56
	—	42	56
	—	30	48

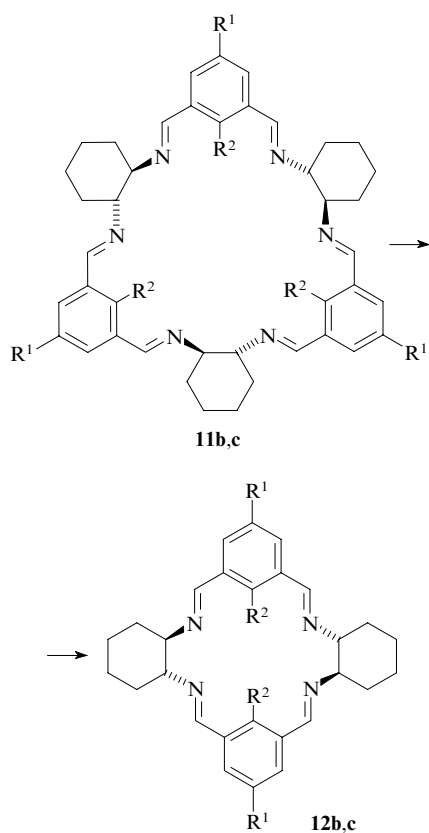
By contrast, the condensation of substituted isophthalaldehydes, in which the mutual arrangement of the carbonyl groups seemingly hinders the formation of [3 + 3] macrocycles, with *trans*-(*R,R*)-1,2-diaminocyclohexane in concentrated (0.1 mol litre^{−1}) solutions in dichloromethane gives [3 + 3]-macrocyclic azomethines **11a–f** in good yields.



Compound 11	R ¹	R ²	R ³	Yield (%)	Ref.
a	H	H	H	90	47
b	Me	H	H	75	48, 49
c	H	H	Me	67	48

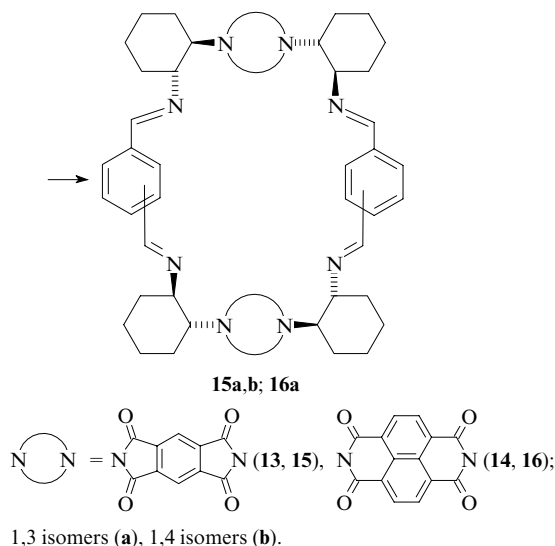
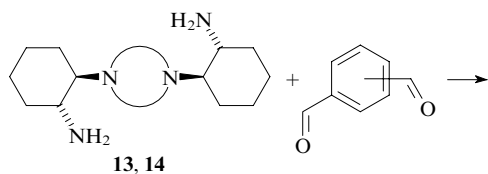
Compound 11	R ¹	R ²	R ³	Yield (%)	Ref.
d	OMe	OMe	OMe	70	48
e	Me	OH	H	78	57
f	Me	H	OTs	59	50

Under these conditions, [3 + 3]-macrocyclic products **11** are formed under kinetic control, but the reaction mixtures contain also [2 + 2] Schiff bases as the products formed under thermodynamic control. The latter were detected in the ESI (electrospray ionisation) mass spectra of the reaction mixtures produced in the synthesis of compounds **11b,c**.⁴⁸ In addition, the [3 + 3]-condensation products can undergo the rearrangement into the corresponding [2 + 2] macrocycles **12b,c** in quantitative yield upon prolonged refluxing (12–72 h) in dichloromethane.⁴⁸

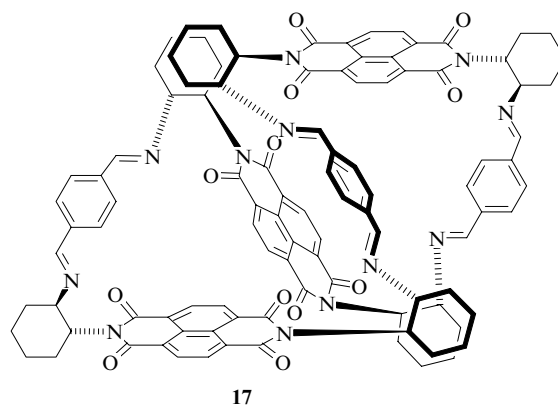


R¹ = Me, R² = H (**b**); R¹ = H, R² = Me (**c**).

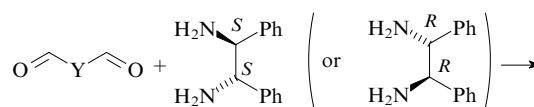
This geometric approach does not operate in the reactions of tetramines **13** and **14** with aromatic dicarbonyl compounds. For example, the reactions of diamine **13** with iso- and terephthalaldehydes give [2 + 2]-condensation products **15a** and **15b**, respectively.⁵⁸

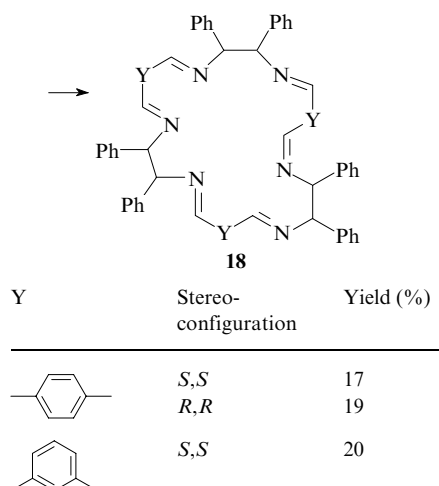


However, the reaction of geometrically similar diamine **14** with terephthalaldehyde afforded [3 + 3]-condensation product **17**, whereas isophthalaldehyde gave, as expected, [2 + 2] macrocycle **16a**.⁵⁸ The results of molecular simulation (PM3 method) show that [3 + 3]-condensation product **17** adopts a figure eight-like conformation due to the π, π -stacking interaction between the benzene ring of the terephthalate fragment and the naphthalene system.⁵⁸ Apparently, this interaction determines the reaction pathway.



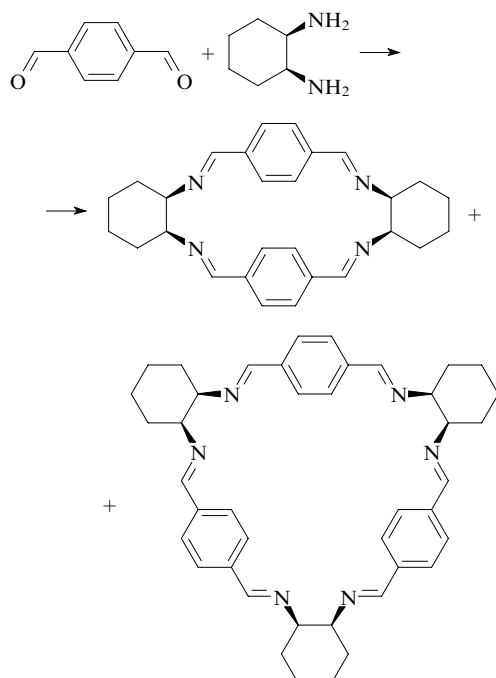
Stereoisomeric (*R,R*)- and (*S,S*)-1,2-diamino-1,2-diphenylethanes contain two bulky benzene rings serving as conformational anchors. These substituents rather rigidly fix the mutual arrangement of the amino groups. The angle between these groups, like that in *trans*-1,2-diaminocyclohexanes, is close to 60°. Because of this, the reactions of these diamines with dicarbonyl compounds proceed analogously to the reactions of *trans*-1,2-diaminocyclohexanes. For example, the reactions of these diamines with iso- or terephthalaldehyde in dichloromethane at room temperature produce [3 + 3] macrocycles **18**.⁴⁹



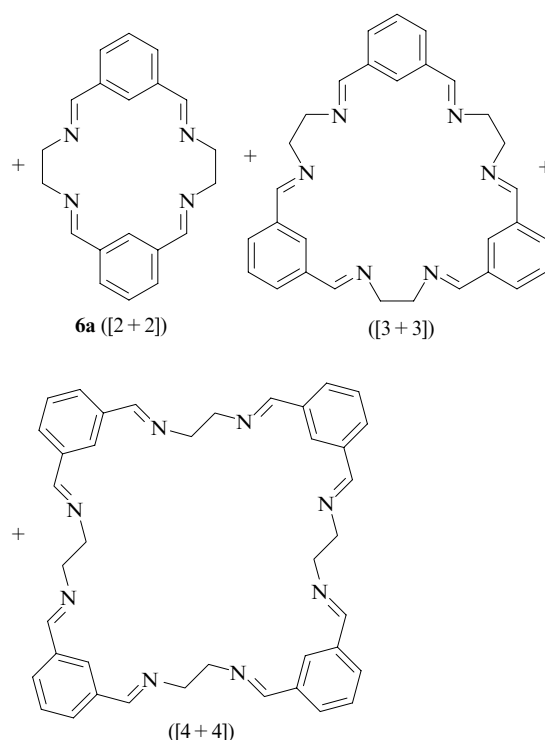
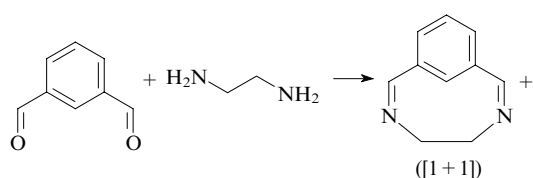


An investigation of the behaviour of [3 + 3] macrocycles **18** demonstrated that these compounds are decomposed in chloroform to give oligomeric condensation products. Apparently, [3 + 3] azomethines are generated under kinetic control, whereas oligomers are produced under thermodynamic control. It cannot be ruled out that thermodynamic stability is determined by the solvation effect, *i.e.*, it depends on the nature of the solvent.

The amino groups in *cis*-1,2-diaminocyclohexane are in the equatorial and axial positions. This change in the geometry leads to changes in the reactivity with respect to dicarbonyl compounds. *cis*-1,2-Diaminocyclohexane, unlike the *trans* isomer, reacts with terephthalaldehyde to give a mixture of [2 + 2]- and [3 + 3]-condensation products (mass spectrometric data), with the latter greatly predominating.⁵⁹



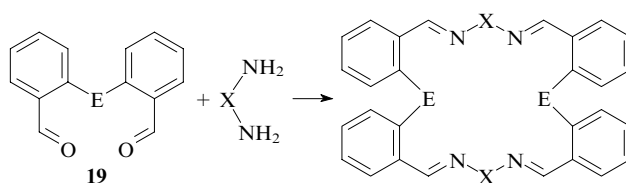
Complex mixtures are also produced in the reactions of acyclic 1,2-ethylenediamine.



The field desorption (FD) mass spectrometric study demonstrated⁶⁰ that the reaction of isophthalaldehyde with ethylenediamine in methanol gives a combinatorial library of [1 + 1]-, [2 + 2]-, [3 + 3]- and even [4 + 4]-condensation products.

By contrast, these reactants afford only one reaction product, *viz.*, [2 + 2] macrocycle **6a** (see above), in acetonitrile. Presumably, the use of protic methanol instead of aprotic acetonitrile leads to an increase in the condensation rate and, as a consequence, to a decrease in the selectivity of the reaction.

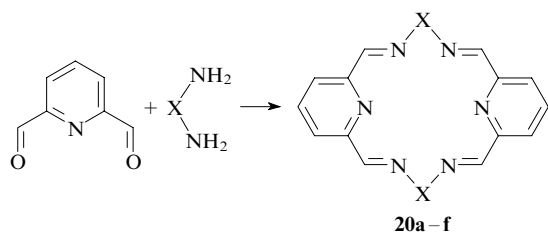
Dicarbonyl derivatives containing several benzene rings, including those linked to each other through heteroatoms, react analogously to monocyclic compounds. For example, the reactions of bis(2-formylphenyl) chalcogenides **19** (E = Se or Te) with aliphatic diamines in boiling acetonitrile produce the corresponding macrocyclic Schiff bases.^{61, 62}



E = Se, Te; X = (CH₂)_n (n = 3, 6) (yield for E = Se is 61%), CH₂CHMe (71%), (CH₂)₂NH(CH₂)₂ (32%), CH₂(CH₂NHCH₂)₂CH₂ (60%).

2. Cyclocondensation of diamines with pyridine dicarbonyl derivatives

On the whole, pyridine dicarbonyl derivatives are very reactive in nucleophilic addition reactions to the carbonyl group because of the electron-withdrawing character of the pyridine ring, due to which they readily form Schiff bases. However, the selectivity of such reactions is, as a rule, low. Examples of the selective formation of macrocyclic systems from pyridine dicarbonyl derivatives in the absence of template agents are few in number, whereas products of their template condensation in the presence of metal ions are widely known.¹³ As a rule, diformylpyridines react with various diamines in dilute solutions in acetonitrile (more rarely, in methanol) to form [2 + 2] macrocycles **20a–f** in satisfactory yields.



Compound 20	X	Solvent	Yield (%)	Ref.
a	(CH ₂) ₃	MeCN	62	63
b	CH ₂ C≡CCH ₂	MeOH	86	64
c	(CH ₂) ₂ NMe(CH ₂) ₂	MeCN	60	42
d	(CH ₂) ₂ NH(CH ₂) ₂	MeCN	60–70	40, 43
e		MeOH	45	65
f		—	—	66

Data on the three-dimensional structures of macrocyclic Schiff bases based on pyridine derivatives are scarce. According to the available data, two pyridine rings in [2 + 2] macrocycle **20f**, which was synthesised from 2,6-diformylpyridine and *trans*-4,5-bis[(1-amino-1,1-diphenyl)methyl]-2,2-dimethyldioxolane, are linked to each other by the π, π -stacking interaction and are spaced by 3.3 Å (Fig. 3).⁶⁶ The azomethine groups of the macrocycle are in the *trans,trans* conformation, resulting in the lipophilic character of the cavity.

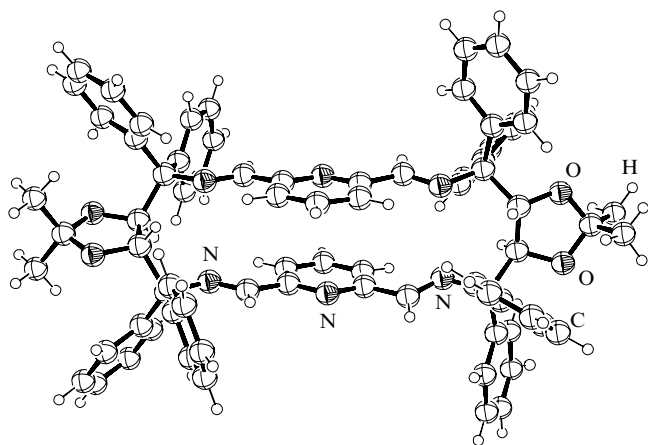
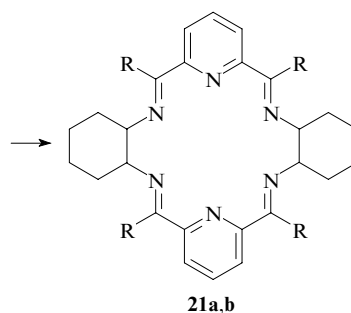
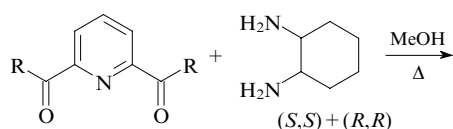


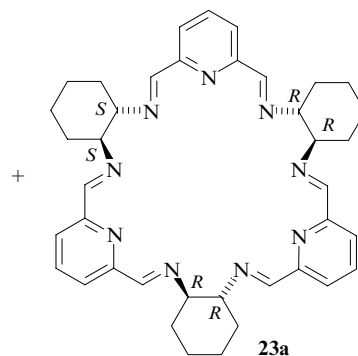
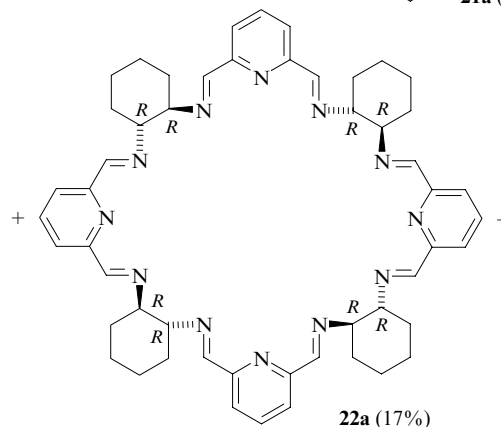
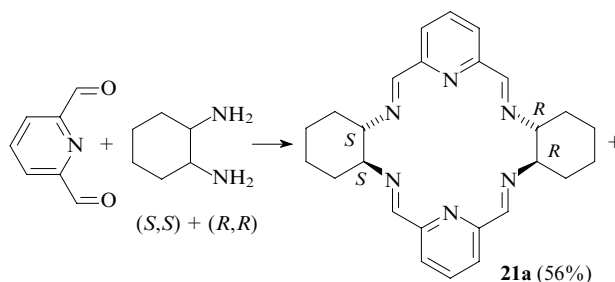
Figure 3. Structure of [2 + 2] macrocycle **20f**.⁶⁶

The condensation of *trans*-1,2-diaminocyclohexane with 2,6-diformyl- or 2,6-diacetylpyridine (refluxing in methanol) gives [2 + 2]-macrocyclic Schiff bases **21a,b** in both dilute and concentrated solutions.⁶⁷



R = H (**a**, 68%), Me (**b**, 57%).

The detailed study of this reaction with diformylpyridine and racemic *trans*-diamine demonstrated that this reaction gave a mixture of [2 + 2]- (**21a**) and [4 + 4]-condensation products (**22a**),⁶⁸ which were isolated and characterised by different physicochemical methods, and [3 + 3] macrocycle **23a**, which was detected by the NMR method. No formation of macrocycles diastereomeric with macrocycles **21a**, **22a** and **23a** was observed. The self-organisation of the achiral and racemic starting compounds gives rise to the only stereoisomer even in the case of [4 + 4] macrocyclisation.



The reaction of 2,6-diformylpyridine with *trans*-(R,R)-1,2-diaminocyclohexane also yields a mixture of [2 + 2]-, [3 + 3]- and [4 + 4]-condensation products, with the [3 + 3]-condensation product substantially predominating.⁶⁸

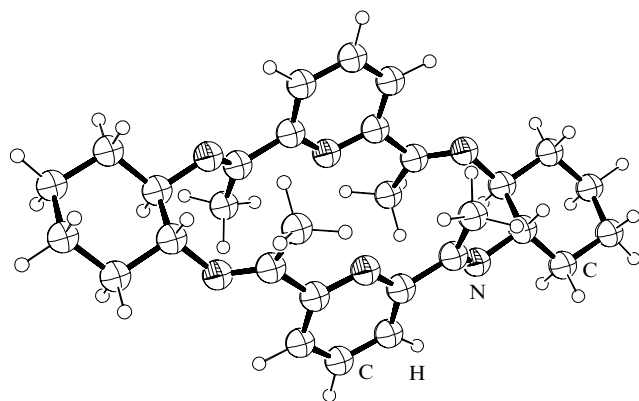
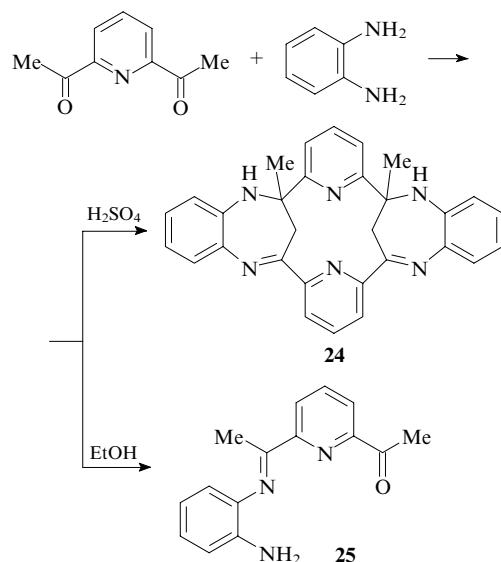


Figure 4. Structure of [2 + 2] macrocycle **21b**.⁶⁷

The structures of [2 + 2] macrocycles **21** containing the *trans*-(*R,R*)-1,2-diaminocyclohexane fragments substantially differ from those of azomethines containing aliphatic diamine fragments because the cyclohexane ring is geometrically more rigid. Macrocycle **21b** adopts a stair-like conformation with the coplanar pyridine rings (Fig. 4).⁶⁷ The pyridine nitrogen atoms are spaced by 3.6 Å due to the fact that all azomethine groups are in the *trans,trans* conformation.

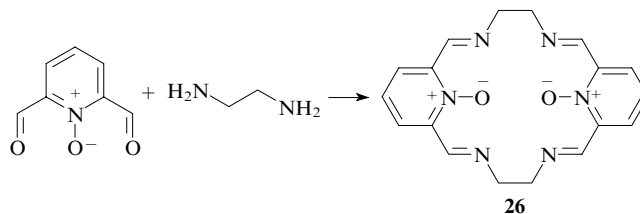
The reactions of *o*-phenylenediamine with pyridine dicarbonyl derivatives in the presence of sulfuric acid also produce macrocycles. Initially, the [2 + 2]-macrocyclic structure has been assigned to the condensation product of 2,6-diacetylpyridine with *o*-phenylenediamine.⁶⁹ However, a more detailed investigation showed that the closure of the macrocycle in this product is followed by intramolecular alkylation at the C=N bond to give product **24**.⁷⁰



In the absence of acids, pyridine dicarbonyl derivatives behave abnormally in the reactions with *o*-phenylenediamines. For example, the reaction of 2,6-diacetylpyridine with *o*-phenylenediamine in ethanol in the absence of acid catalysts affords only [1 + 1]-condensation product **25**, which reacts with neither the dicarbonyl compound nor diamine.⁷⁰

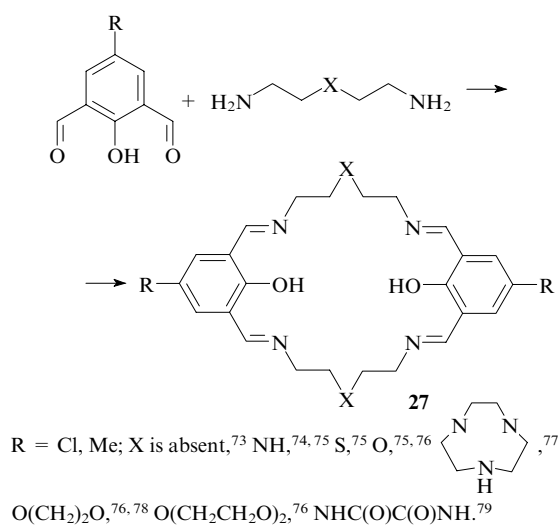
This inertness of bifunctional derivatives can be explained, for example, in terms of the electron-withdrawing properties of the pyridine ring. Since the carbonyl group in the resulting [1 + 1]-Schiff bases **25** is involved in the chain of direct polar conjugation with the amino group, the reactivity of each group substantially decreases.

From this point of view, investigations of the behaviour of 2,6-diformylpyridine *N*-oxide under analogous conditions are of obvious interest. However, the reaction of this compound only with 1,2-ethylenediamine was documented.⁷¹ This reaction proceeds under reflux in methanol and gives [2 + 2] macrocycle **26**.

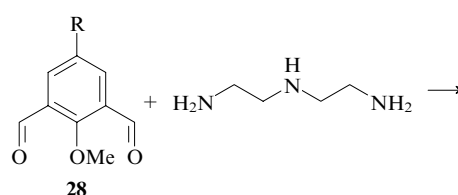


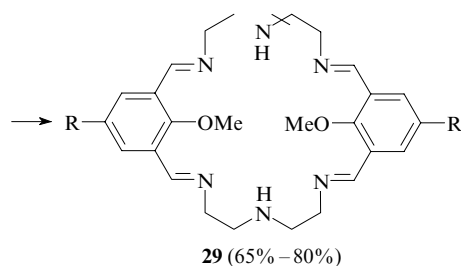
3. Cyclocondensation of diamines with dicarbonyl derivatives of phenols and their thio analogues

The reactions of diamines with dicarbonyl derivatives of phenols were studied in most detail. Due to the presence of the proton-donating hydroxy group, such dicarbonyl compounds can catalyse self-condensation with diamines. Although the acidity of dicarbonyl derivatives of phenols is not too high (pK_a of salicylaldehyde is 8.37),⁷² the autocatalytic reactions of phenol derivatives with diamines in alcohols proceed easily. The corresponding macrocycles are formed in high yields, although with low selectivity. The reactions of long-chain aliphatic and heteroaliphatic diamines with 4-substituted 2,6-diformylphenols readily proceed in dilute ($\sim 10^{-2}$ mol litre⁻¹) methanolic or ethanolic solutions to give [2 + 2]-macrocyclic Schiff bases **27** in quantitative yields.^{73–79}



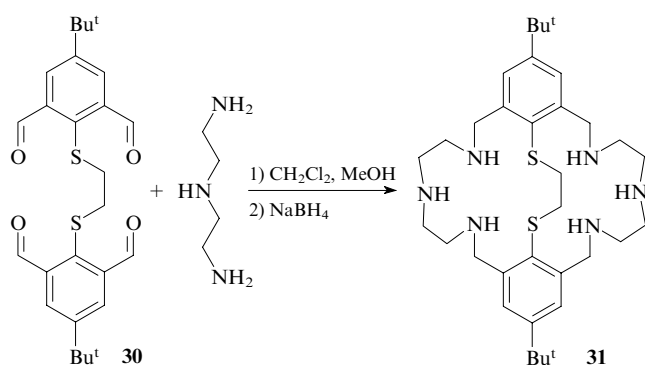
As demonstrated above (see Section II.1), dicarbonyl derivatives of phenol ethers react similarly to benzene analogues containing no OR groups. This is the basic difference between derivatives of phenol ethers and phenols. However, the reaction of 2,6-diformylanisoles **28** with ethylenetriamine produces [2 + 2]-macrocyclic Schiff bases **29**.⁸⁰



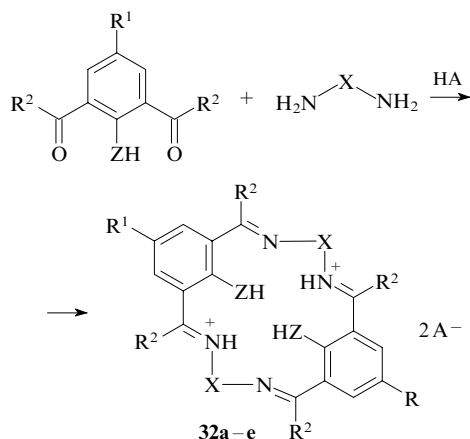


R = Br, Cl, Me, OMe.

The condensation proceeds more easily if two dicarbonyl fragments are linked to each other by a bridge of an appropriate length to form one molecule. For example, diethylenetriamine reacted with bis-sulfide **30** to give the corresponding macrobicyclic Schiff base, which was reduced to the corresponding polyamine **31** in a total yield of >90%.⁸¹



Under standard conditions (heating in alcohols), dicarbonyl derivatives of phenols do not form macrocyclic Schiff bases in the reactions with ethylene- and propylenediamines.^{41, 43} However, these compounds can be synthesised by performing the reaction in dilute methanolic solutions ($\sim 10^{-2}$ mol litre⁻¹) in the presence of two equivalents of a strong protic acid (HBr). Macrocyclic [2 + 2] Schiff bases **32a–f** thus synthesised were isolated as salts.^{82, 83}



Compound 32	X	R ¹	R ²	Z	A
a	(CH ₂) ₂	Me	H	O	Br
b	(CH ₂) ₂	Bu ^t	Me	O	Br
c	(CH ₂) ₃	Me	H	O	Br
d	(CH ₂) ₃	Me	Me	S	Br
e	CH ₂ CH(OH)CH ₂	Me	H	S	Br
f	(CH ₂) ₄	Me	H	O	ClO ₄

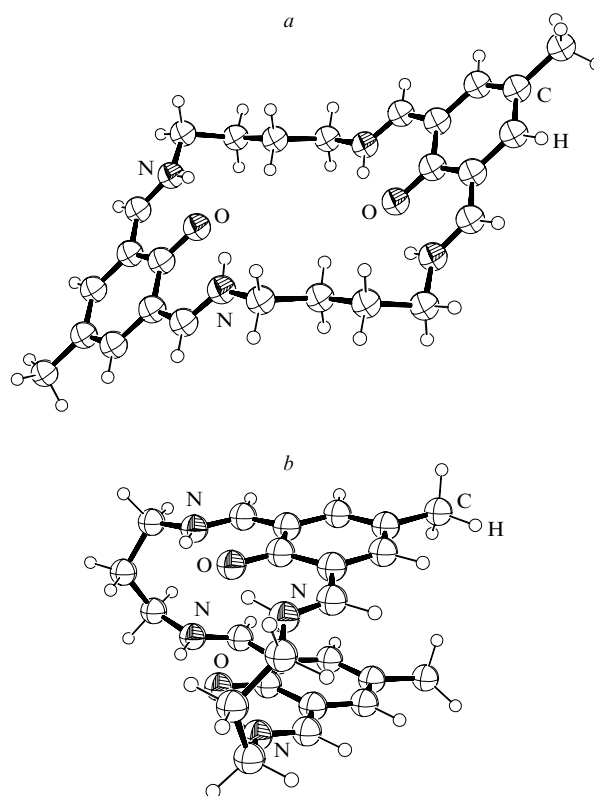
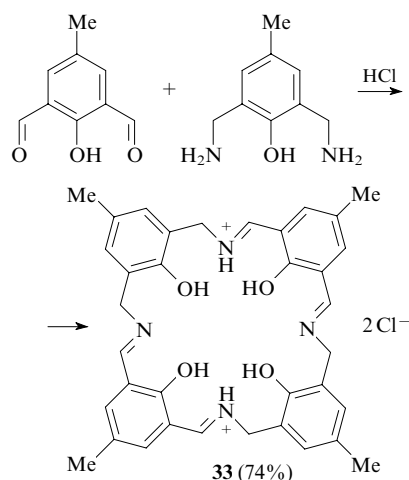


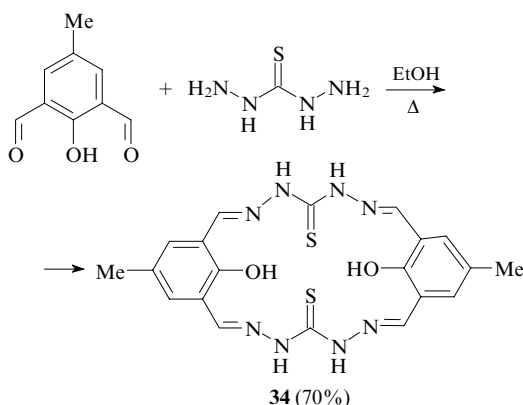
Figure 5. Molecular structures of doubly protonated macrocycles **32f** (a)⁸⁴ and **32c** (b).⁸⁵

The structures of dications **32a–e** depend on the number of the carbon atoms (n) in aliphatic α,ω -diamines. If $n = 2$ or 4 , the molecules adopt a stair-like conformation. Macrocyclic **32f** [$\text{R}^1 = \text{Me}$, $\text{R}^2 = \text{H}$, $\text{Z} = \text{O}$, $\text{X} = (\text{CH}_2)_4$, $\text{A} = \text{ClO}_4$] formed from 1,4-diaminobutane (Fig. 5a) is an example.⁸⁴ Macrocyclic **32c** containing an odd number of carbon atoms ($n = 3$) adopts a horseshoe conformation because of the close proximity of two aromatic rings of the phenolic fragments located at a distance of 3.6–4.1 Å (Fig. 5b).^{85, 86} Under conditions of acid catalysis, 2,6-bis(aminomethyl)-4-methylphenol reacts with 2,6-diformyl-4-methylphenol to give [2 + 2] macrocycle **33**.⁸⁷



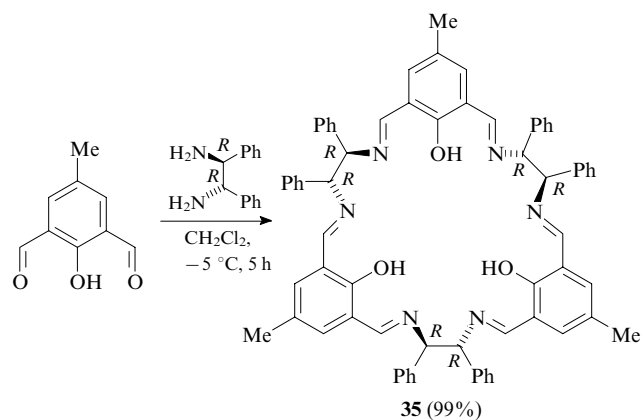
In the reactions with dicarbonyl compounds, thiocarbohydrazide behaves like aliphatic diamines. For example, the condensation of this compound with an equimolar amount of

2,6-diformyl-4-methylphenol in boiling ethanol affords [2 + 2] macrocycle **34**.⁸⁸

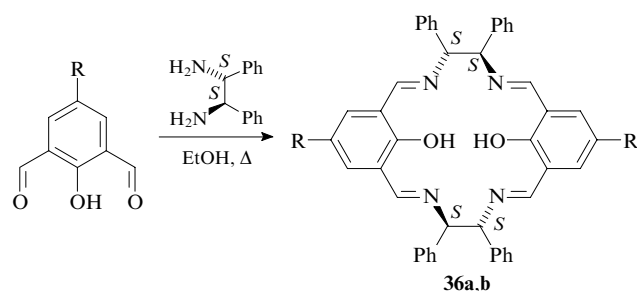


The reactions of dicarbonyl derivatives of phenols with 1,2-diaminoalkanes in dichloromethane instead of ethanol produce lower cyclooligomers. As mentioned in the Introduction, the addition of amine at the carbonyl group is the rate-determining step of the reactions giving azomethines in acidic medium. Hence, the use of a less polar aprotic solvent, which prevents dissociation of the hydroxy group of phenol, instead of polar ethanol readily performing the proton solvation is an appropriate solution.

The reaction of 2,6-diformyl-4-methylphenol with (*R,R*)-1,2-diamino-1,2-diphenylethane in dichloromethane at -5°C produced [3 + 3] macrocycle **35**, which was isolated in 99% yield uncontaminated with other azomethines (mass spectrometric data).⁸⁹ The structure of compound **35** is shown in Fig. 6.



By contrast, the reaction of 4-substituted 2,6-diformylphenols with (*S,S*)-1,2-diamino-1,2-diphenylethane in boiling ethanol produces [2 + 2] macrocycles **36a,b**.⁹⁰



R = H (**a**), Bu^t (**b**).

From the above it follows that enantiomerically pure 1,2-diphenylethylenediamines give [3 + 3] macrocycles as the major products under kinetic control and [2 + 2] products under thermodynamic control. An analogous situation is observed

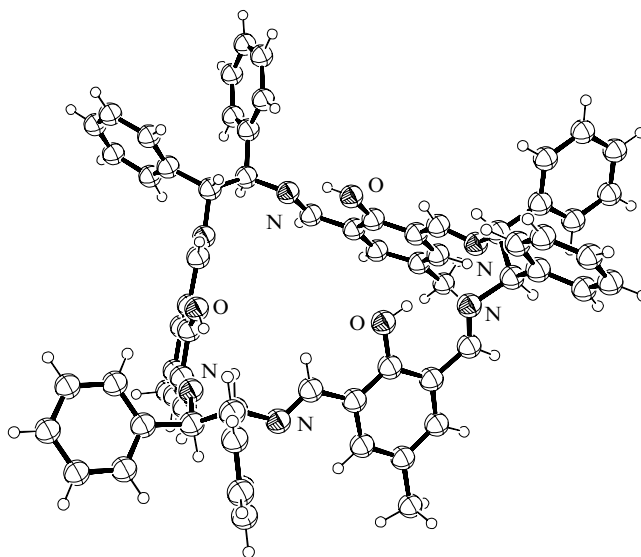
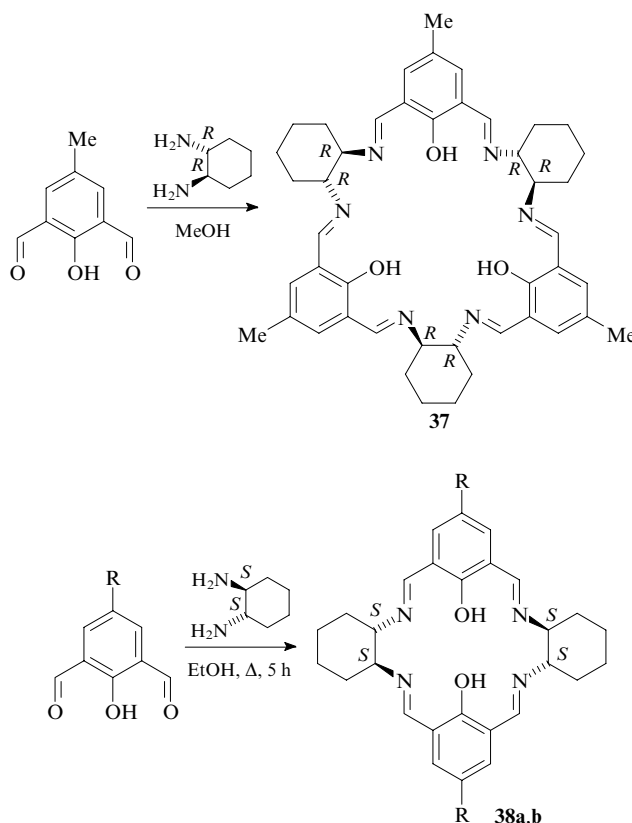


Figure 6. Structure of [3 + 3] macrocycle **35**.⁸⁹

in the reactions of diformylphenols with *trans*-1,2-diaminocyclohexanes even when carried out in alcohols.

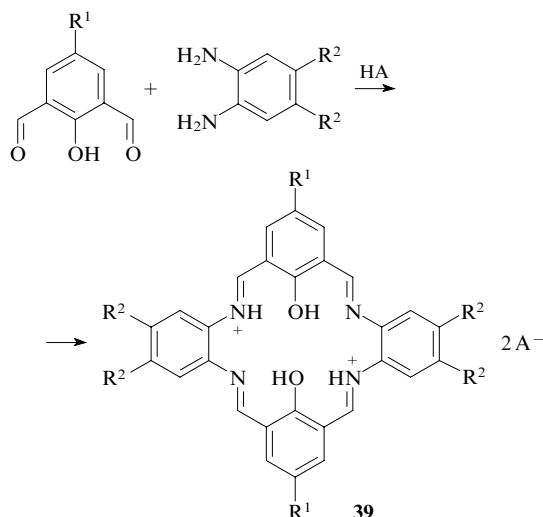
For example, the reaction of *trans*-(*R,R*)-1,2-diaminocyclohexane with 2,6-diformyl-4-methylphenol in a concentrated (0.1 mol litre⁻¹) methanolic solution at -5°C or at room temperature produces [3 + 3]-macrocyclic azomethine **37** in quantitative yield.^{57,89,91,92} However, according to the results of the study,⁹⁰ *trans*-(*S,S*)-1,2-diaminocyclohexane reacts with 4-substituted 2,6-diformylphenols under reflux in ethanol for 5 h to give [2 + 2] products **38a,b**. This is circumstantial evidence that the formation of [2 + 2]-condensation products is thermodynamically controlled.



R = H (**a**), Bu^t (**b**).

The structures of the [3 + 3] macrocycles synthesised by the reactions of 1,2-diaminocyclohexane with diformylphenols substantially differ from those obtained in the reactions with diformylbenzenes containing no OH groups (see Fig. 2). In the former case, the molecules adopt a bowl conformation due to which they can be considered as analogues of calix[3]arenes.⁸⁹

The reactions of *o*-phenylenediamine and its derivatives with 2,6-diformylphenols in alcohols easily proceed only in the presence of acids and give salts of [2 + 2] macrocycles **39**, like the reactions with 1,2-ethylenediamine.³⁹



The X-ray diffraction data show that structures of macrocycles **39** are planar, and the hydrogen atoms are localised at the oxygen atoms of the phenolic groups and the nitrogen atoms of the azomethine fragments (Fig. 7).³⁹ Consequently, the macrocycles prepared by the reactions of diformylphenols with aromatic diamines are structurally different from their aliphatic analogues (see above), in which all endocyclic hydrogen atoms are located at the nitrogen atoms of the azomethine groups.

Different, in principle, macrocycles were synthesised by the reactions of 2,6-diformylphenols with *o*-phenylenediamine in the absence of acids. These reactions afford mixtures of [2 + 2]-macrocylic Schiff bases **40**, in which two of four imino groups are reduced, as well as 2,6-bis(benzimidazol-2-yl)phenols **41**.^{74, 93, 94} Macrocylic compound **40** ($R^1 = \text{Me}$, $R^2 = \text{H}$) was synthesised in 60% yield by the reaction of *o*-phenylenediamine with 2,6-diformyl-4-methylphenol in the presence of catalytic amounts of hydrochloric acid (Scheme 4).³⁹

The theoretical investigation of the mechanism of formation of macrocycles **40** by the density functional theory method⁹⁴ demonstrated that the first step of this reaction

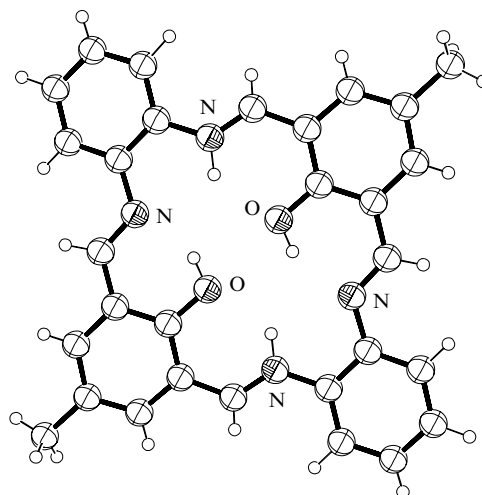
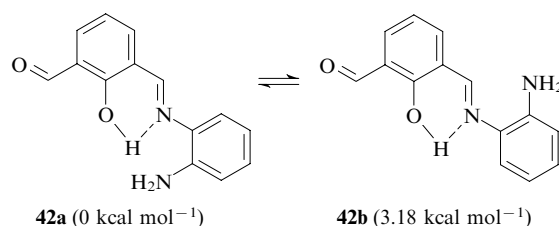
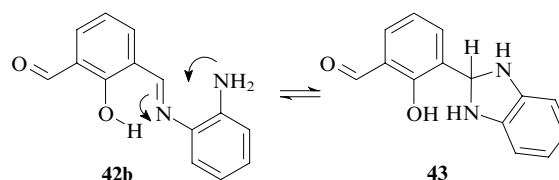


Figure 7. Structure of dication **39** ($R^1 = \text{Me}$, $R^2 = \text{H}$).³⁹

(like the reaction of 2,6-diacetylpyridine with *o*-phenylenediamine) gives the [1 + 1]-condensation product, which can be represented as two rotamers **42a** and **42b**.

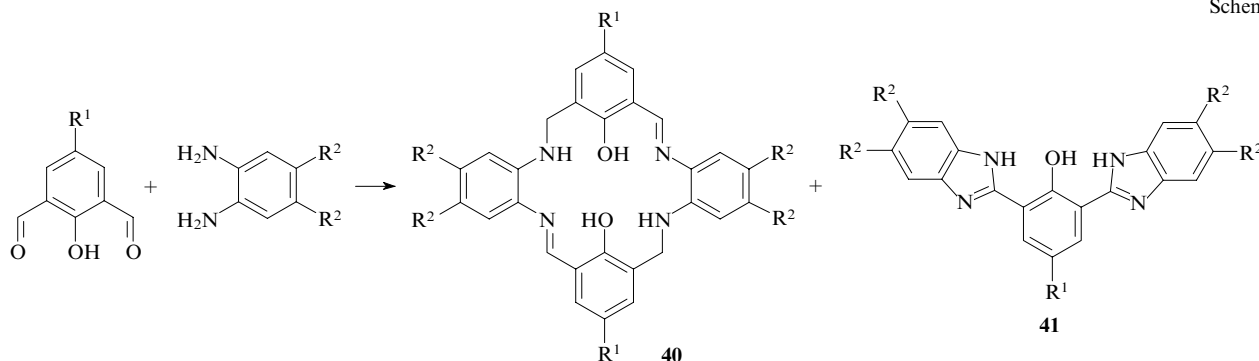


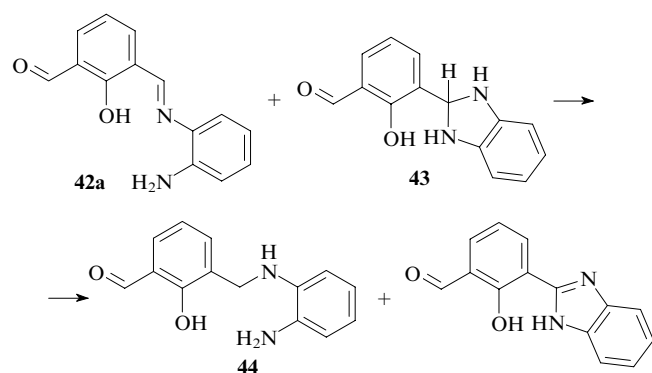
The most stable conformer **42a** exists in equilibrium with isomer **42b**, whose energy is 3.18 kcal mol⁻¹ lower. In the latter isomer, the distance between the nitrogen atom of the amino group and the carbon atom of the imino group is about 3.5 Å, which is favourable for intramolecular cyclisation.



The resulting benzimidazole **43** is a strong reducing agent. The reaction of **43** with [1 + 1] Schiff base **42a** leads to reduction of the latter to diamine **44**. According to the results of calculation, this process is exothermic (27.3 kcal mol⁻¹).

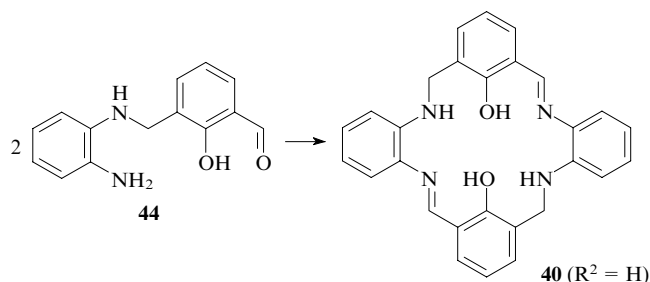
Scheme 4





Two molecules of diamine **44**, in which the carbonyl and amino groups are separated from each other, are readily involved in the usual Schiff condensation yielding compound **40** ($R^1 = R^2 = H$). This reaction is exothermic ($\Delta H^\circ = -0.12 \text{ kcal mol}^{-1}$, $\Delta G^\circ = -9.15 \text{ kcal mol}^{-1}$).

The X-ray diffraction structure of macrocyclic compound **40** ($R^1 = \text{Bu}^t$, $R^2 = H$) is planar (Fig. 8). In the crystal structure, the molecules are disordered so that the CH_2NH and $\text{CH}=\text{N}$ groups randomly replace each other,



due to which the differences in the lengths of the double and single CN bonds are not observed (the standard $\text{HC}=\text{N}$ and $\text{H}_2\text{C}-\text{N}$ bond lengths are 1.303 and 1.460 Å, respectively).⁹³ Apparently, the crystal structure contains several tautomeric forms, in which the hydrogen atoms are in the vicinity of different nitrogen atoms. In addition, the crystal structure can contain zwitterions, in which all three or four nitrogen atoms are protonated and the negative charges are located on one or two oxygen atoms [the $\text{C}-\text{O}$ bond lengths are 1.33(1) and

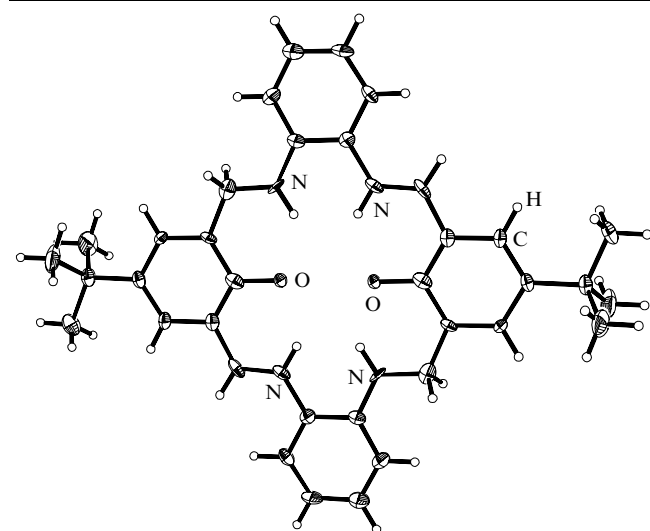
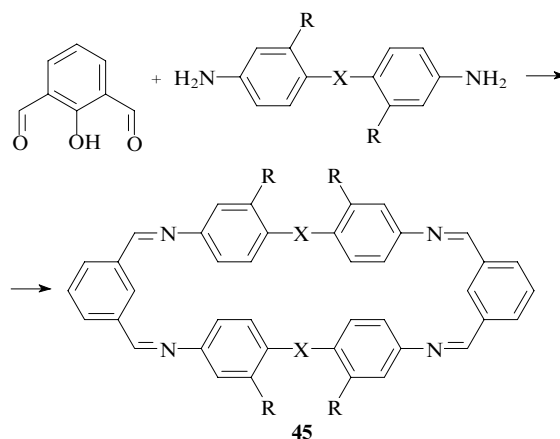


Figure 8. X-Ray diffraction structure of macrocycle **40** ($R^1 = \text{Bu}^t$, $R^2 = H$).⁹³

1.34(1) Å and are similar to the standard $\text{C}(\text{sp}^2)-\text{OH}$ and $\text{C}(\text{sp}^2)-\text{O}^-$ bond lengths, respectively].

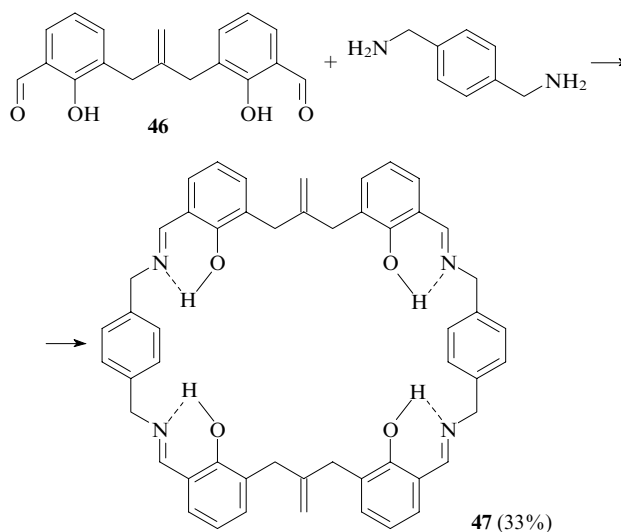
In the reactions with dicarbonyl compounds, polycyclic aromatic diamines containing amino groups in different aromatic rings behave like aliphatic α,ω -diamines. For example, the condensation of 2,6-diformylphenol in methanol with equimolar amounts of diamino derivatives of biphenyl, diphenylmethane and 1,2-diphenylethane afforded the expected [2 + 2] macrocycles **45**.^{95, 96}



X is absent: $R = \text{Me}$, OMe ; $X = (\text{CH}_2)_n$ ($n = 1, 2$), $R = H$.

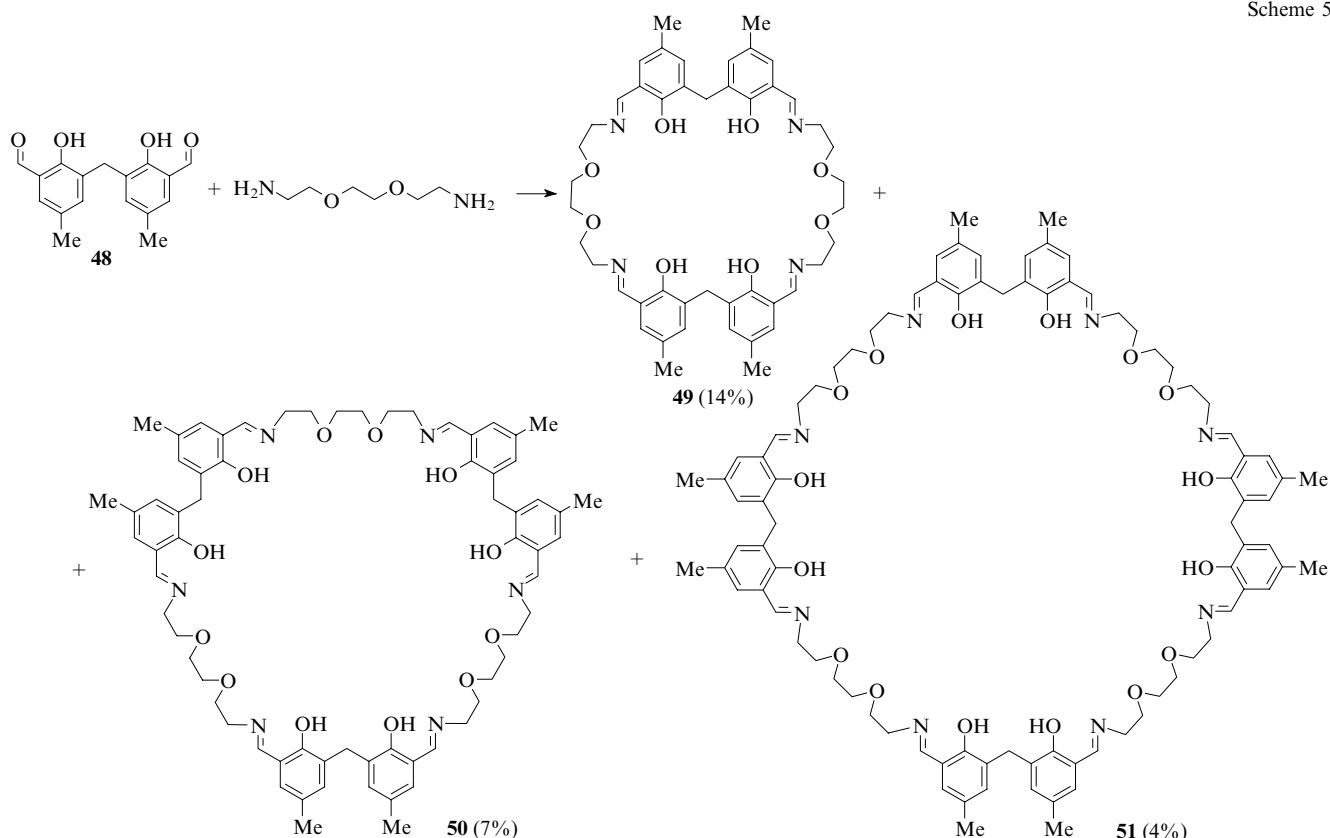
Schiff bases that are formed in reactions of diformyl derivatives of polyphenols or their thio analogues with diamines, are of great interest as ligands. Unexpected results were obtained in the reaction with dicarbonyl compounds containing the hydroxy group that undergoes deprotonation, particularly, if the hydroxy and carbonyl groups are in the *ortho* positions with respect to each other. In this case, there are conditions favourable for the formation of strong hydrogen bonds both in the starting dicarbonyl compound and its cyclocondensation products with diamines, resulting in an increase in thermodynamic stability of such compounds. In addition, the absence of the direct polar conjugation between the carbonyl groups in dicarbonyl compounds results in an increase in their reactivity with respect to diamines.

The reaction of diformyl derivative **46** with 1,4-bis(amino-methyl)benzene in THF at room temperature affords [2 + 2]-macrocyclic Schiff base **47**.⁹⁷



The condensation of bis-phenol **48** with 3,6-dioxo-1,8-diaminooctane in a chloroform-methanol mixture under high-dilution conditions affords a mixture of [2 + 2], [3 + 3],

Scheme 5

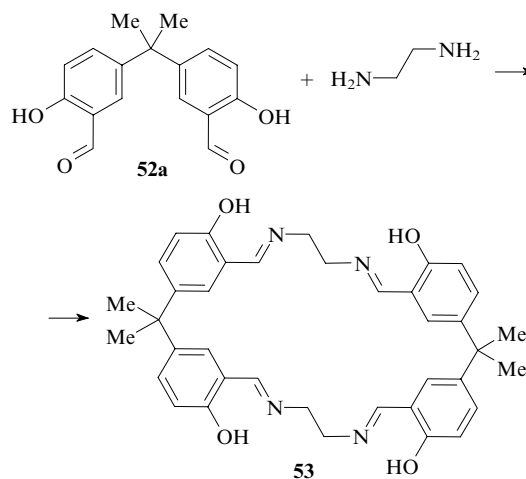


[4 + 4], [5 + 5], [6 + 6] and even [7 + 7] macrocycles. Some of these products (compounds **49**–**51**) were isolated in the individual state. The high-molecular-mass products were detected by MALDI-TOF mass spectrometry.⁹⁸ It should be noted that the [1 + 1]-condensation product was not found in the mixture (Scheme 5).

The X-ray diffraction data for [2 + 2]-condensation product **49** show that, in the crystal, this macrocycle adopts a twisted, figure eight-like, conformation due to the π, π -stacking interaction between two of four phenol fragments (Fig. 9).⁹⁸ This suggests that the template reaction in which the π, π -stacking plays the organising role is possible, because cycloligomer **49** is produced in the maximum yield.

In the reactions with aliphatic diamines, polyphenols containing the salicylaldehyde fragments linked to each other by

bridges in the *para* position with respect to the hydroxy group show reactivity similar to that of monophenols. For example, the reaction of bis-phenol **52a** with ethylenediamine produces [2 + 2]-macrocyclic Schiff base **53**.⁹⁹



The reactions of bis-phenols **52** with salts of chiral diamines in alcohols in the presence of potassium carbonate under microwave irradiation also afford [2 + 2] macrocycles.¹⁰⁰

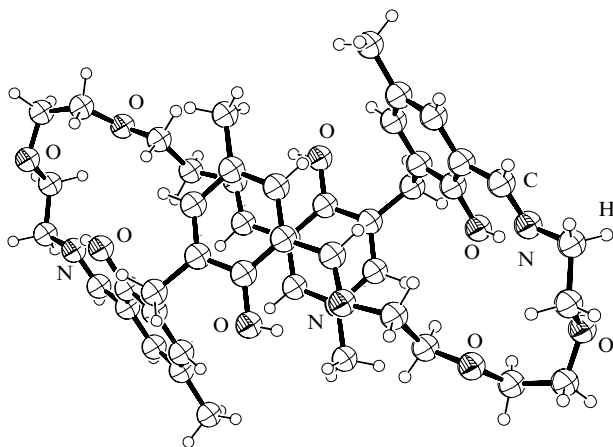
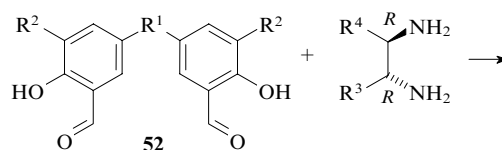
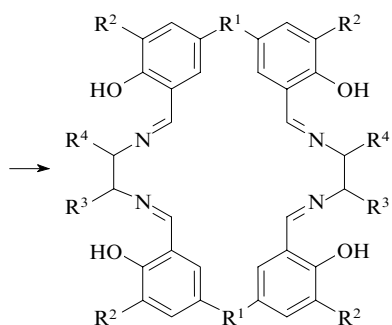


Figure 9. X-Ray diffraction structure of [2 + 2] macrocycle **49**.⁹⁸

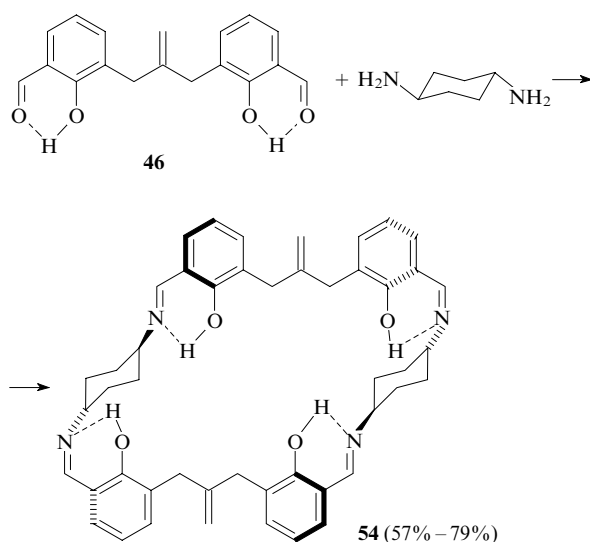


$R^1 = \text{CH}_2$; $R^2 = \text{H, Br, NO}_2, \text{Bu}^t$; $R^1 = \text{CMe}_2$; $R^2 = \text{H, Br}$;

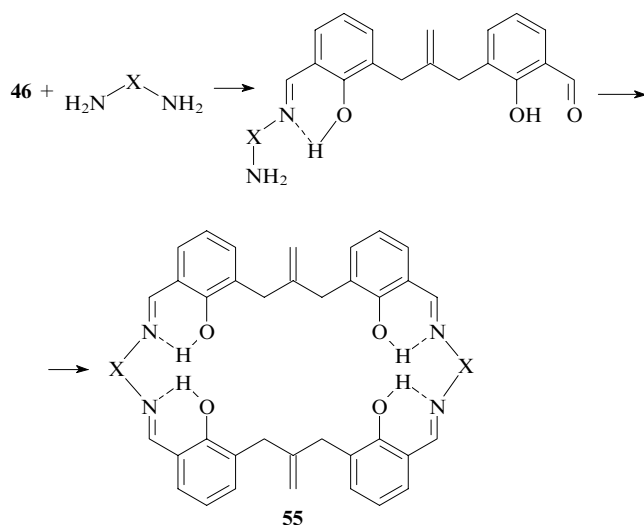
$R^1 = \text{SO}_2$, $R^2 = \text{H}$; R^1 is absent, $R^2 = \text{H}$;

$R^3-R^4 = (\text{CH}_2)_4, \text{CH}_2\text{NBnCH}_2$; $R^3 = R^4 = \text{CO}_2\text{Bn}$.

The reaction of *trans*-1,4-diaminocyclohexane with a dicarbonyl derivative of bis-phenol **46**, in which the carbonyl groups are fixed by strong hydrogen bonding, produced [2 + 2]-macrocyclic Schiff base **54**.⁹⁷



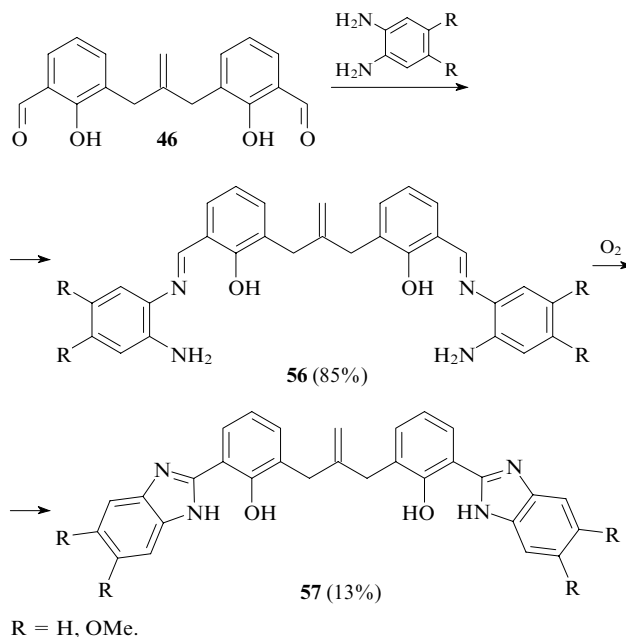
Because of the absence of direct polar conjugation between the carbonyl groups in dicarbonyl compound **46**, these groups are involved in the reactions with diamines independently of



X is 1,2-phenylene (90%–97%), 1,3-phenylene (58%–64%),
1,4-phenylene (76%–98%), 1,5-naphthylene (90%–97%).

each other, which allows the synthesis of stoichiometrically controlled products. The reaction of 0.1 M solutions of dialdehyde **46** with aromatic diamines (in a ratio of 1 : 1) in THF or DMF at room temperature afforded the corresponding [2 + 2] macrocycles **55**.⁹⁷ The reaction was demonstrated to give initially [1 + 1]-condensation products. The ¹H NMR spectroscopic study showed that these compounds are stabilised (like the final products) by strong hydrogen bonding between the phenolic hydroxy groups and the azomethine nitrogen atoms.⁹⁷

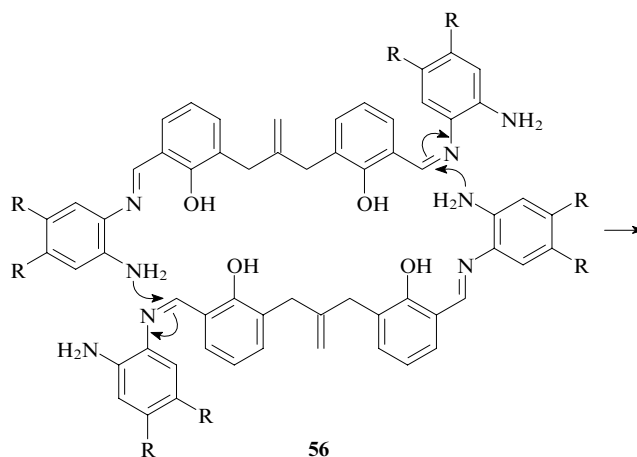
The reactions of dilute (0.04 mol litre⁻¹) methanolic solutions of dialdehyde **46** with an excess of *o*-phenylenediamine or its 4,5-dimethoxy derivative at room temperature yielded acyclic [1 + 2]-condensation products **56**.¹⁰¹

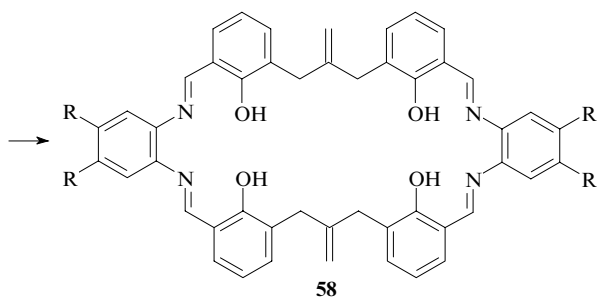


R = H, OMe.

Diamines **56** thus synthesised are very sensitive to atmospheric oxygen and, like the [1 + 1]-condensation products involving 1-R-2,6-diformylphenols (see above), are oxidised to the corresponding benzimidazole derivatives **57**. This process is the major side reaction in the synthesis of these azomethines.¹⁰¹

The X-ray diffraction study showed that two molecules of [1 + 2] azomethine **56** in the unit cell are located so that the nitrogen atoms of the amino groups of one molecule are located close to the carbon atoms of the azomethine fragments of the adjacent molecule.

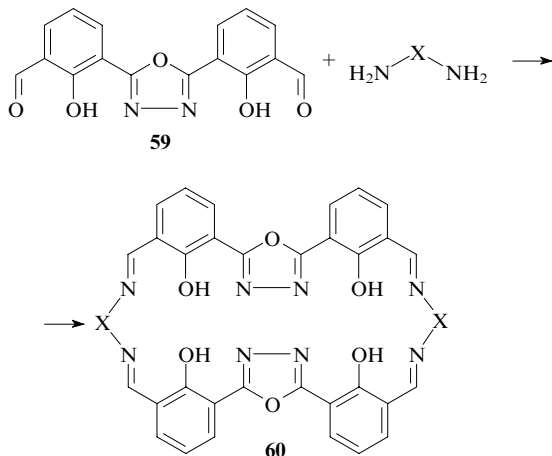




R = H (71%), OMe (37%).

It was hypothesised that the dimeric structure is retained in solution. Upon prolonged storage of solutions, two molecules of compound **56** undergo condensation to form [2 + 2] macrocyclic Schiff base **58**, which is accompanied by elimination of two *o*-phenylenediamine molecules.¹⁰¹

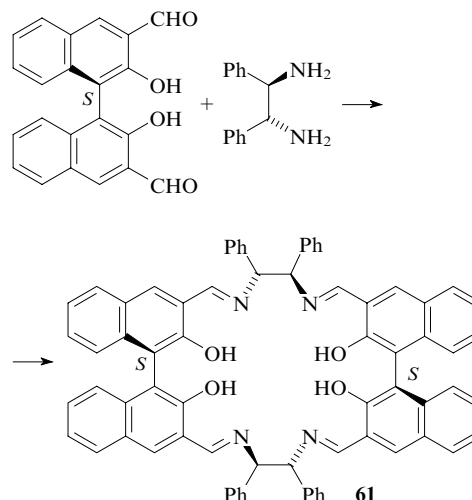
The condensation of dicarbonyl derivatives of polyphenols with diamines proceeds analogously even if two fragments of salicylaldehyde are linked to each other by a rigid bridge. For example, the reaction of equimolar amounts of dialdehyde **59** with diamines in dilute acetonitrile solution (0.01 mol litre⁻¹) produces [2 + 2]-macrocyclic azomethines **60**.¹⁰²



X = CH₂CH₂, *o*-phenylene.

Important results giving a new insight into the formation of macrocycles were obtained in the study of the reaction of 3,3'-diformyl-2,2'-dihydroxybinaphthyl with (*R,R*)-1,2-diamino-1,2-diphenylethane. For example, dialdehyde having the *R*

configuration forms only oligomers,^{103, 104} whereas the *S* enantiomer undergoes [2 + 2] condensation to give macrocycle **61**.¹⁰⁵

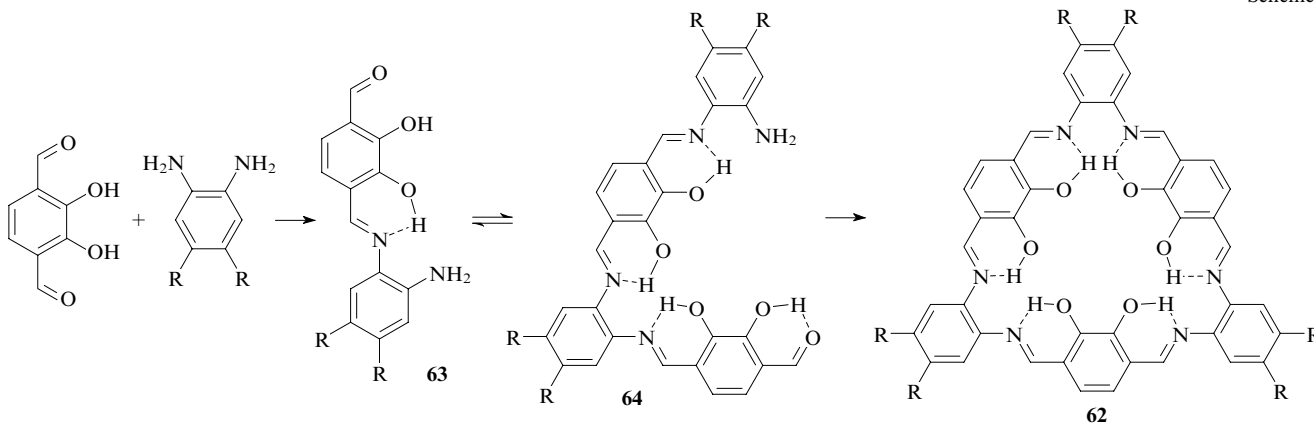


The selective reaction of the *S* enantiomer of dialdehyde with optically pure diamine allowed the resolution of racemic 3,3'-diformylbinaphthyl and the isolation of the pure *S* enantiomer in 50% – 60% yield (with respect to theoretical).¹⁰⁵

Unlike dicarbonyl derivatives of polyphenols, diformylpyrocatechols react with aromatic dialdehydes to form only [3 + 3]-condensation products. Apparently, this is a consequence of the rigid structural preorganisation of the reactants. In some sense, the same factor of self-organisation of macrocycles, which was responsible for the predominant formation of [3 + 3] macrocycles in the reaction of terephthalaldehyde with *trans*-1,2-diaminocyclohexanes (see Section II.1), plays the decisive role.

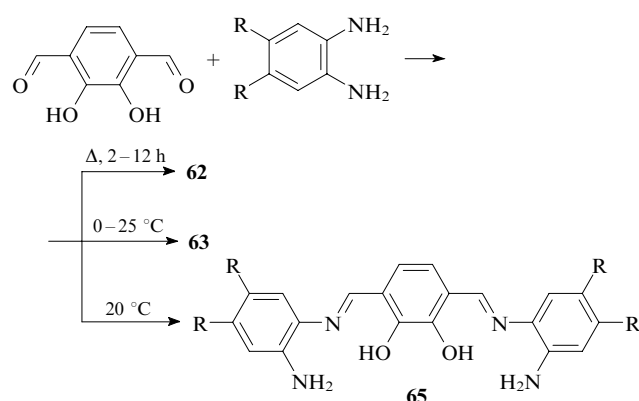
The reaction of 3,6-diformylpyrocatechol with *o*-phenylenediamines in acetonitrile in the absence of catalysts proceeds in complete agreement with the geometry of the reaction components and affords [3 + 3]-condensation products **62**. The reaction proceeds through the formation of acyclic [1 + 1]- (**63**) and [2 + 2]-condensation products (**64**). In this case, the macrocycles are stabilised by hydrogen bonds, which was demonstrated by ¹H NMR spectroscopy.^{106, 107} Thermodynamically most stable [3 + 3] macrocycle **62** precipitates from the reaction mixture, resulting in the shift of the equilibrium toward the formation of this product (Scheme 6).

Scheme 6



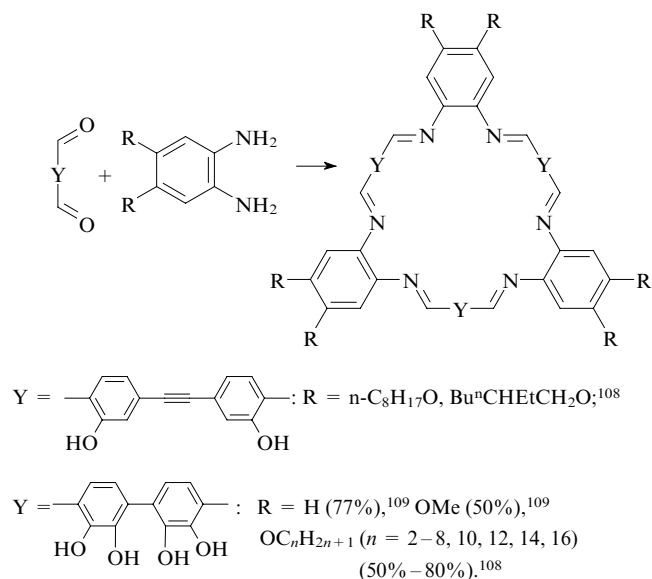
R = H (91%);¹⁰⁶ OC₆H_{13-n} (70%).¹⁰⁷

This reaction in a boiling chloroform–acetonitrile mixture also produces [3 + 3] macrocycles **62**, a much longer reaction time being required for the reactions with long-chain amines [1,2-diamino-4,5-di(hexyloxy)benzene].⁸ In this case, [1 + 1]-, [1 + 2]- and [2 + 1]-condensation products were also detected in the reaction mixture. The position of the equilibrium in this dynamic combinatorial library substantially depends on the reaction conditions. Since [3 + 3] macrocycle **62** is the thermodynamically controlled reaction product, it is formed as the major product upon prolonged refluxing of the reaction mixture. The reaction under kinetic control (low temperature and short reaction time) gives predominantly [1 + 1]-condensation product **63** and at room temperature, [1 + 2]-condensation product **65**. All these compounds were demonstrated⁸ to be intermediates in the reaction affording the [3 + 3] macrocycle.



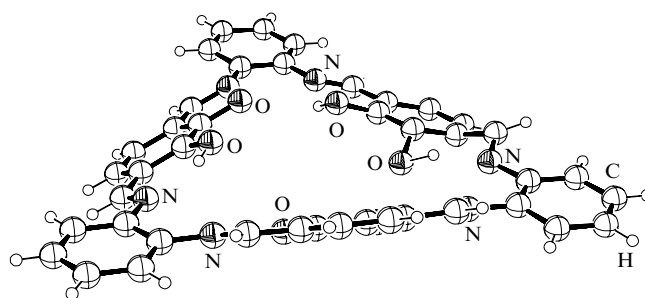
Other diformylphenols with analogous arrangement of the carbonyl groups are also involved in the reactions with *o*-phenylenediamines. Their reactions with *o*-phenylenediamines in a chloroform–acetonitrile mixture yield [3 + 3]-condensation products (Scheme 7).^{108, 109}

Scheme 7

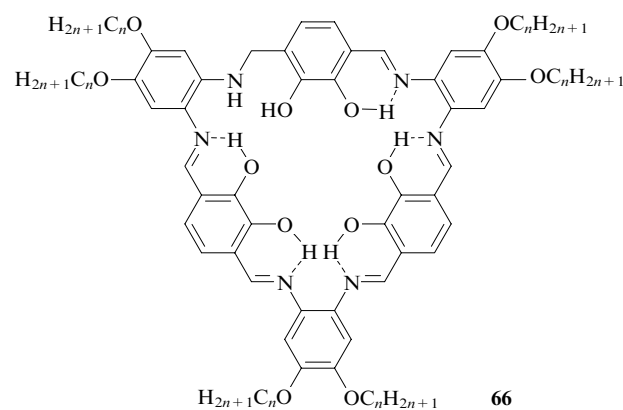


X-Ray diffraction studies showed that the resulting anti-aromatic 48p-electron macrocycles are non-planar (Fig. 10).^{106, 109} Due to this geometry, the conjugation between the aromatic rings is absent, the antiaromaticity is violated, and these compounds become unstable.

The analogous reaction in commercial chloroform produces [3 + 3] macrocycles **62** along with partially reduced derivatives **66** in low yields (10%–20%). The reduction products

Figure 10. Structure of macrocycle **62** (R = H).¹⁰⁶

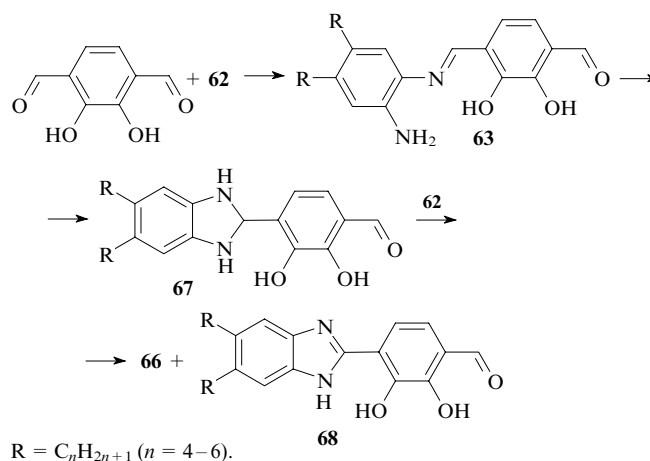
were not detected if the reaction was carried out in chloroform purified from traces of moisture and acids.^{8, 110}



n = 4–6.

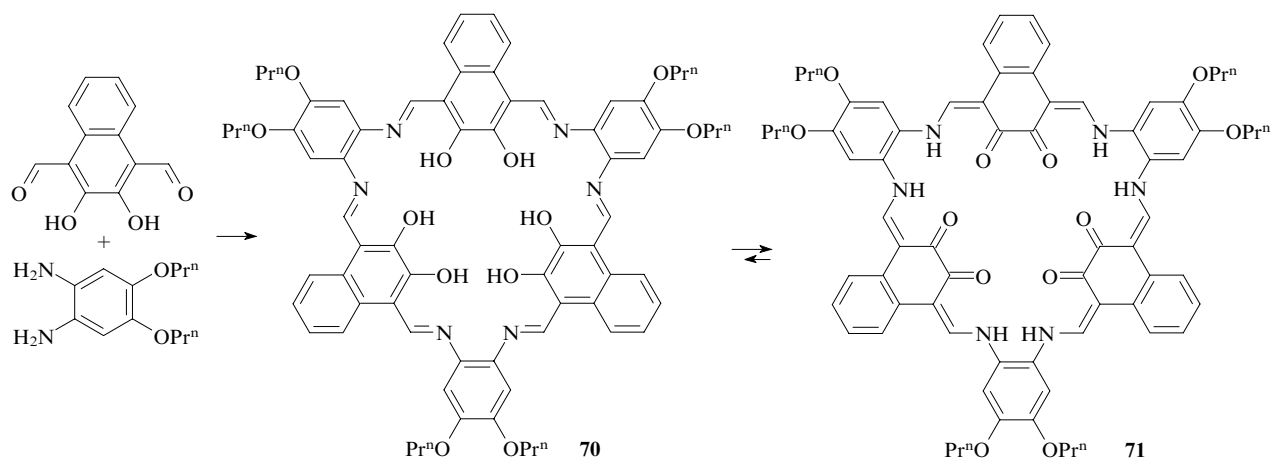
The mechanism of formation of reduced product **66** is presented in Scheme 8.¹¹⁰ The reaction of [3 + 3] macrocycle **62** with the starting dialdehyde in commercial chloroform affords products of the macrocycle cleavage, including [1 + 1]-condensation product **63**. The latter can undergo intramolecular cyclisation analogous to that described above for phenol derivatives to form benzimidazoline derivative **67**, which is involved in reduction of [3 + 3] macrocycle **62** yielding compound **66**. The transfer of the hydrogen atom to the carbon atom of the imino group occurs from the carbon atom of benzimidazoline, which was confirmed experimentally with the use of an isotope label.¹¹⁰

Scheme 8

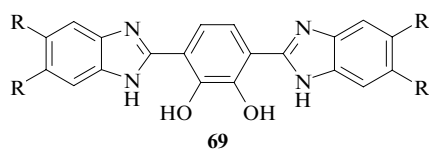


Reduction of [3 + 3] macrocycles **62** is accompanied by oxidation of benzimidazoline **67** to benzimidazole **68**, which

Scheme 9

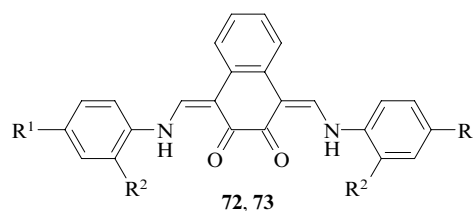


was detected in the reaction mixture along with reduced macrocycle **66** and bis(benzimidazoline) derivative **69**.^{8, 110}

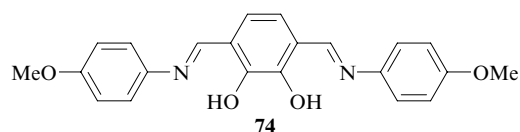


The extension of [3 + 3]-condensation of *o*-phenylenediamines with aromatic 1,4-dialdehydes to naphthalene derivatives resulted in macrocycle **70**, which exists in equilibrium with keto-enamine tautomeric form **71** (Scheme 9).¹¹¹

Tautomerisation of azomethine to the corresponding enamine leads to the removal of antiaromaticity of [3 + 3] macrocyclic Schiff base, the second aromatic ring in naphthalene remaining intact. Studies of model compounds by quantum chemical methods and X-ray diffraction showed¹¹¹ that azomethine derivatives of 1,4-diformyl-2,3-dihydroxynaphthalene, *viz.*, compounds **72** and **73**, unlike their pyrocatechol analogue **74**, exist in the keto-enamine form.

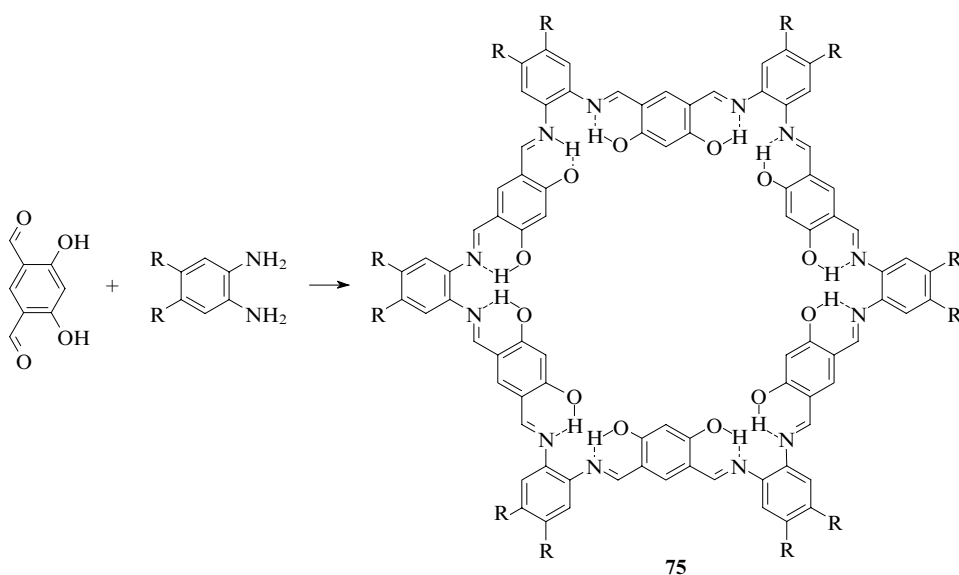


$R^1 = \text{OMe}, R^2 = \text{H}$ (**72**); $R^1 = \text{H}, R^2 = \text{NHBoc}$ (**73**), Boc is *tert*-butoxycarbonyl.



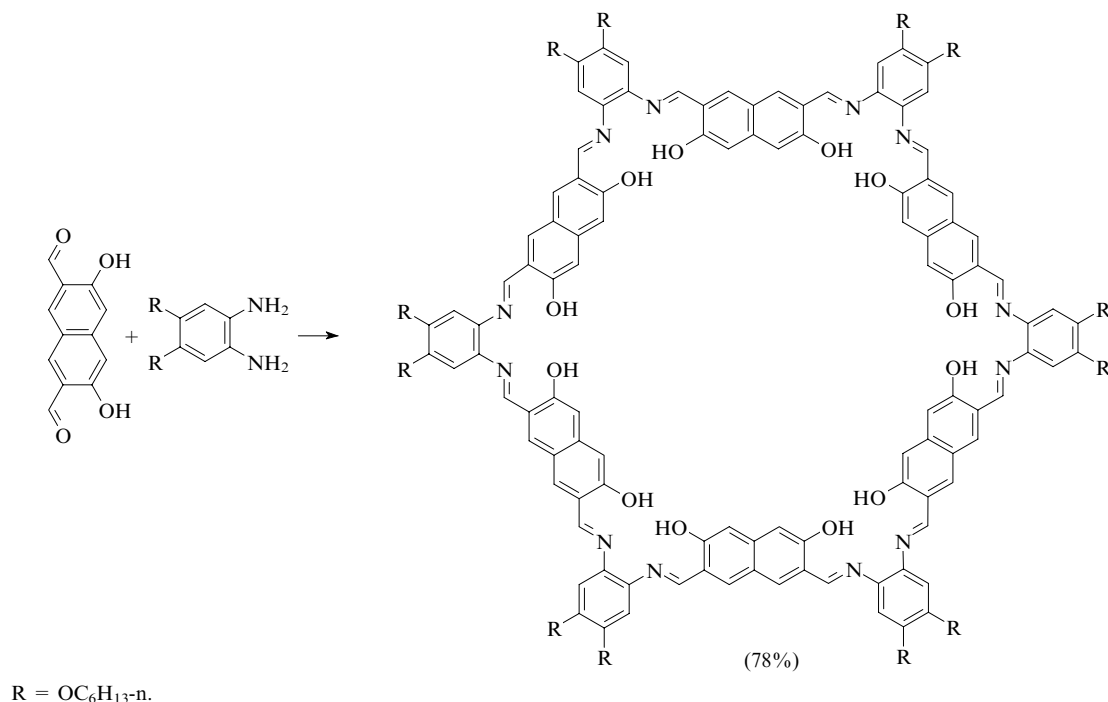
The formation of hydrogen bonds is a powerful driving force for the self-organisation of macrocycles. This is most clearly illustrated by the formation of macrocycles **75** as a result of [6 + 6] condensation of diformylresorcinol with *o*-phenylenediamine (Scheme 10).¹¹²

Scheme 10



$R = \text{OC}_6\text{H}_{13-n}$ (19%), $\text{OC}_5\text{H}_{11-n}$ (25%).

Scheme 11



The fact that the analogous reaction of 2,7-diformyl-3,6-dihydroxynaphthalene was successful suggests that this [6 + 6] macrocyclisation for rigidly preorganised dihydroxydiformyl derivatives of polycyclic aromatic compounds has the general character (Scheme 11).¹¹²

4. Cyclocondensation of diamines with dicarbonyl derivatives of five-membered carbo- and heterocycles

a. 2,5-Diformyl derivatives of furan and thiophene

2,5-Diformylfuran and -thiophene readily react with aliphatic diamines to form [2 + 2]-macrocyclic Schiff bases **76a,b** and **77a–g** if the amino groups are separated by a chain of three or more atoms. Dilute solutions of these compounds in acetonitrile or methanol are used. The behaviour of these dicarbonyl compounds is completely analogous to that of related benzene derivatives (Scheme 12).

The three-dimensional structure of one of these compounds, *viz.*, the reaction product of 2,5-diformylthiophene with 3-oxapentane-1,5-diamine **77e**, was established (Fig. 11).¹¹⁸

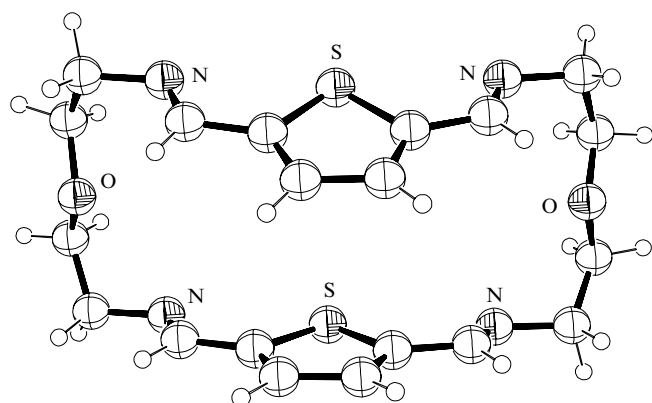
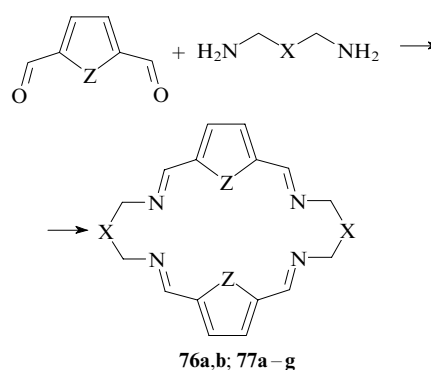


Figure 11. Structure of [2 + 2] macrocycle **77e** ($n = 1$).¹¹⁸

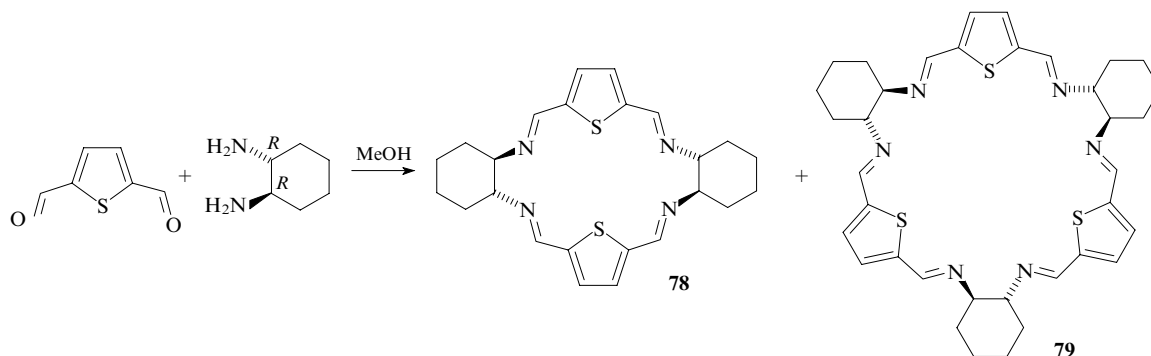
Scheme 12



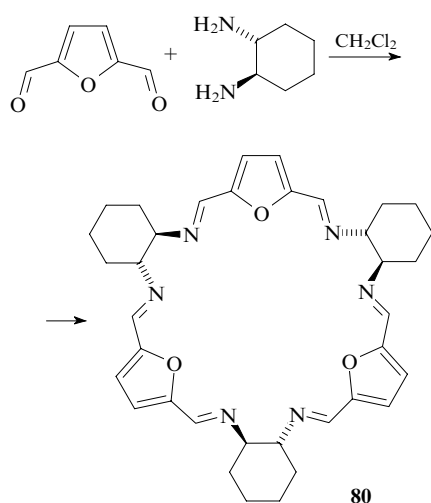
Compound	X	Z	Yield (%)	Ref.
76a	CH_2NHCH_2	O	—	43
76b	$(\text{CH}_2\text{OCH}_2)_n$ ($n = 1-3$)	O	60–70	40
77a	CHOH	S	50–55	113
77b	CH_2NHCH_2	S	—	114
77c	$\text{CH}_2\text{NBu}^t\text{CH}_2$	S	48	115, 116
77d	CH_2SCH_2	S	70	114, 117
77e	$(\text{CH}_2\text{OCH}_2)_n$ ($n = 1-3$)	S	60–70	114, 117
77f	$(\text{CH}_2)_n$ ($n = 1-3$)	S	50–90	117
77g	$(\text{CH}_2)_2\text{NH}(\text{CH}_2)_2$	S	50–90	117

With a geometrically more rigid diamine, *viz.*, *trans*-(*R,R*)-1,2-diaminocyclohexane, more complex processes occur compared to the reactions with flexible aliphatic amines. For example, the reactions of 2,5-diformylthiophene in methanol at room temperature produce [2 + 2] (**78**) and [3 + 3] macrocycles (**79**). Studies by mass spectrometry showed that these products are present in a mixture in equal amounts.¹¹⁹ The replacement of methanol by dichloromethane results in the formation of only one reaction product, *viz.*, [3 + 3] macrocycle **79** (35% yield) (Scheme 13).⁴⁸

Scheme 13



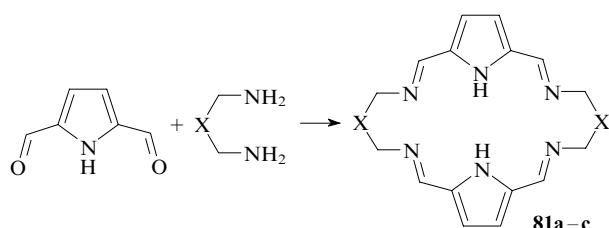
The condensation of 2,5-diformylfuran with *trans*-(*R,R*)-1,2-diaminocyclohexane at room temperature in dichloromethane gives [3 + 3] azomethine **80** in quantitative yield.⁵²



Such different results obtained for related 2,5-diformyl derivatives of furan and thiophene provide conclusive evidence that the formation of [3 + 3] macrocycles depends on the nature of the solvent. In weakly polar dichloromethane, the reactions afford only [3 + 3]-condensation products, whereas a series of products are formed in polar methanol.

b. Diformyl derivatives of pyrrole and compounds with several pyrrole rings

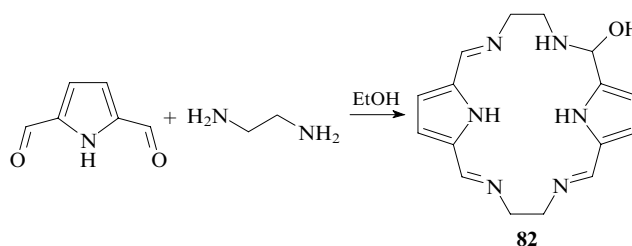
Unlike oxa and thia analogues, α,α' -dicarbonyl derivatives of pyrrole are less reactive toward amines. Hence, the synthesis of pyrrole-containing macrocycles requires the use of a catalyst (acids). A rather few azomethine macrocyclic compounds (for example, compounds **81a–c**) were synthesised by direct reactions of 2,5-diformylpyrrole with aliphatic diamines.



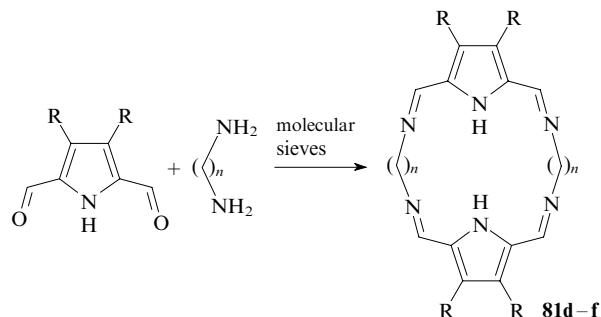
$X = \text{CHOH}$ (**a**, 50%–55%),¹²³ CH_2NHCH_2 (**b**),^{43, 114} CH_2 (**c**, 66%).⁶³

However, not all reactions yield macrocyclic azomethines. For example, the reaction of ethylenediamine with 2,5-diformylpyrrole in ethanol stops at the formation of hemiaminal **82**,

which is the intermediate of the [2 + 2]-condensation reaction.³⁸

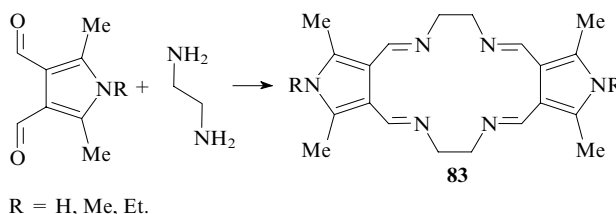


The addition of molecular sieves to the reaction mixture favours the completion of the reaction giving rise to macrocycles. Under these conditions, the reactions of diformylpyrrole derivatives with ethylenediamine and propylenediamine produced compounds **81d–f**.¹²⁰



$n = 2$: $R = \text{H}$ (**d**), Me (**e**); $n = 3$, $R = \text{Me}$ (**f**).

Unlike the 2,5 isomers, 3,4-diformylpyrroles react with diamines in the absence of acids and molecular sieves to give [2 + 2] macrocycles **83** in high yields.¹²¹

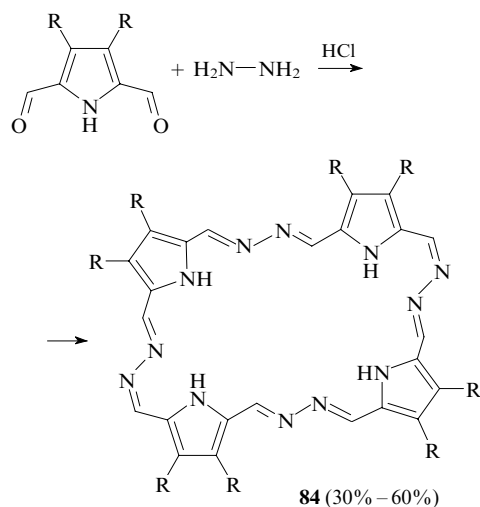


$R = \text{H}, \text{Me}, \text{Et}$.

The reactions of 3,4-dialkoxy-2,5-diformylpyrroles with hydrazine,[†] which can, in principle, be considered as the simplest diamine, yielded unexpected results. The reactions in

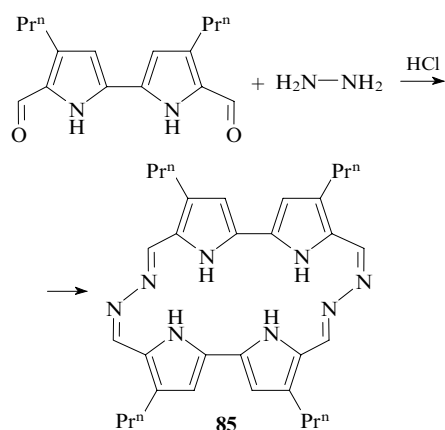
[†] The template synthesis affords the corresponding [2 + 2] macrocycles.

methanol in the presence of HCl afford [4 + 4] macrocycles **84** as the condensation products.¹²²

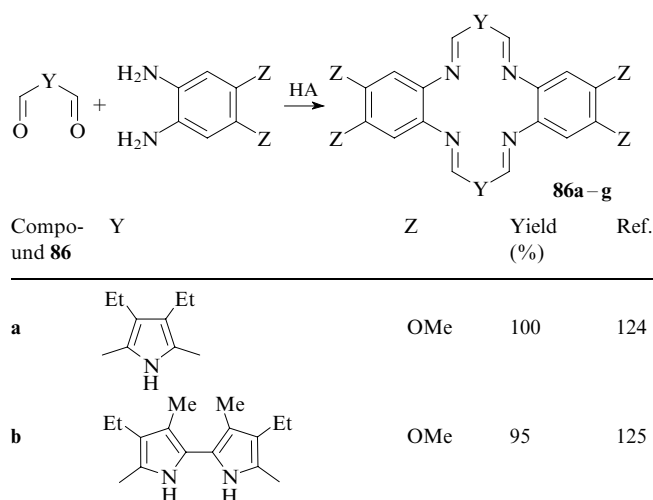


$R = OC_nH_{2n+1}$ ($n = 1, 6, 10, 14$).

By contrast, the reaction of hydrazine with 5,5'-diformyl-4,4'-dipropyl-2,2'-bipyrrole gives [2 + 2]-condensation product **85**.¹²³

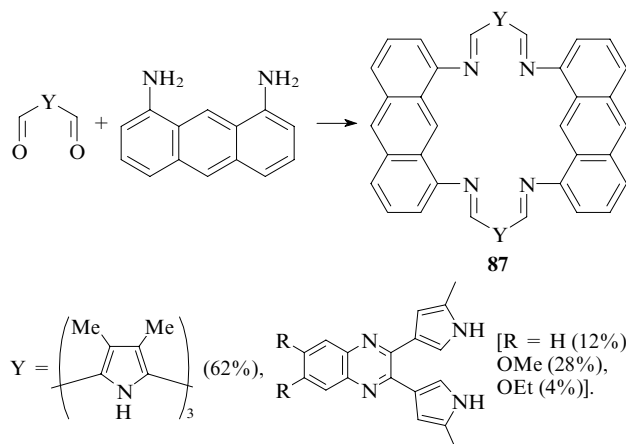


Since aromatic diamines are much less nucleophilic than aliphatic diamines, the reactions of the former with diformyl derivatives of pyrrole proceed only in the presence of acid catalysts. As a rule, the reactions give [2 + 2]-condensation products, *i.e.*, compounds **86a–g**, in good yields.

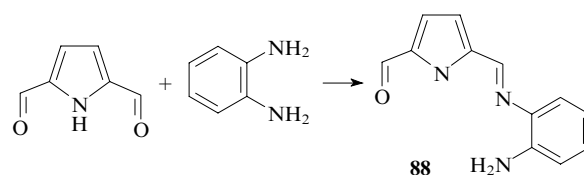


Compo- und 86	Y	Z	Yield (%)	Ref.
c		OMe	60	126
d	$R^1 = R^2 = H, R^3 = Me$	H	98	127, 128
e	$R^1 = R^2 = H, R^3 = Me$	OMe	66	127
f	$R^1 = Me, R^2 = Et, R^3 = H$	H	91	127
g	$R^1 = R^2 = H, R^3 = Ph$	H	48	128, 129

The reactions of 1,8-diaminoanthracene with diformyl derivatives of the pyrrole series in methanol in the presence of acids also produce [2 + 2]-macrocyclic Schiff bases **87**.^{126, 130}



In the absence of acids, 2,5-diformylpyrrole reacts with *o*-phenylenediamine in ethanol to give only [1 + 1]-condensation product **88**, which is involved in reactions with neither the dicarbonyl compound nor the diamine without additional activation.¹³¹



Since the carbonyl group in the resulting [1 + 1] Schiff base **88** is also involved in the chain of direct polar conjugation with the amino group, both groups become substantially less reactive. Two azomethine molecules in the crystal of **88** are linked to each other to form a stable dimer through four hydrogen bonds between the amino groups and the hydrogen atoms of the pyrrole rings and the oxygen atoms of the carbonyl groups (Fig. 12).¹³¹ The energy of formation of this dimer estimated by quantum chemical calculations in terms of density functional theory¹³¹ is 15.4 kcal mol^{−1}. Apparently, the dimeric structure is retained in solution, which additionally decreases the ability of this azomethine to be involved in further condensation.

c. Diformyl derivatives of pyrazole

Data on macrocyclic azomethine derivatives of five-membered heterocycles containing more than one heteroatoms are scarce. Only several successful syntheses of macrocycles from 3,5-

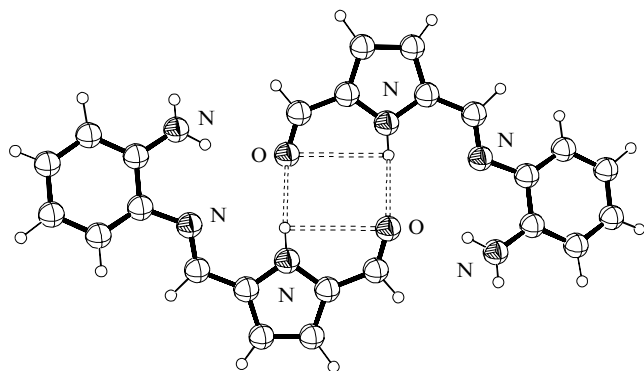
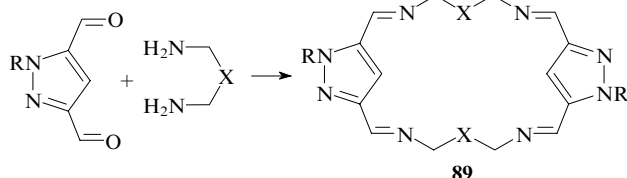


Figure 12. Structure of the dimer of product **88**.¹³¹

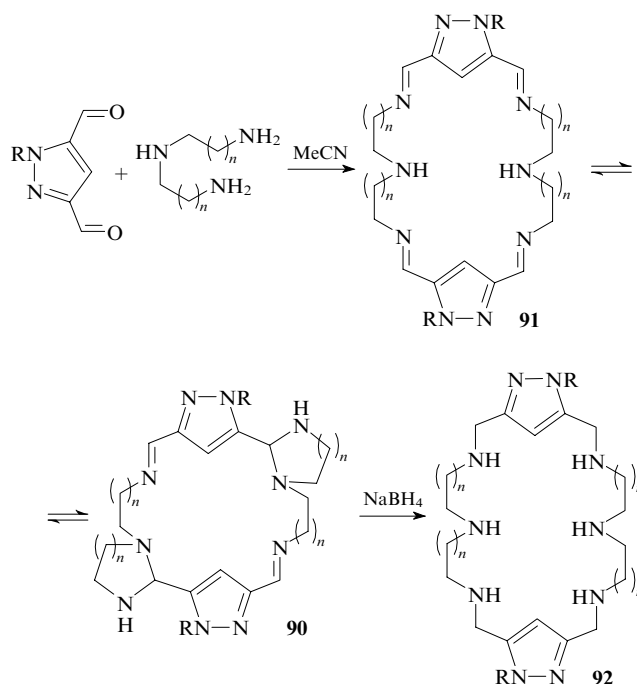
diformylpyrazoles in the absence of metal ions were documented. In alcohols or acetonitrile, the reactions of 1-substituted 3,5-diformylpyrazoles with diamines containing no additional nitrogen atoms produce macrocyclic Schiff bases **89**.^{132, 133}



R = H, Me, Bn; X is *m*-phenylene (30%), CH₂OCH₂ (90%–94%).

Under the same conditions, the reaction of diethylenetriamine or dipropylenetriamine gave pentacyclic products **90** in 80% yield.¹³² Presumably, the reaction initially produces [2 + 2]-macrocyclic azomethine **91**, which undergoes intramolecular cyclisation, *viz.*, the nucleophilic addition of the secondary amino group at the C=N bond.^{132, 133} Most likely, this process is reversible because reduction of Schiff bases **90** to compounds **92** is accompanied by the opening of both imidazolidine rings.^{133, 134}

The intramolecular nucleophilic addition at the C=N bond was observed also in the template condensation of diformyl derivatives of pyrazole with diamines containing additional donor atoms (for example, with 1,3-diamino-2-hydroxypropane, diethylenetriamine, *etc.*).^{135–138} This process was demonstrated to be reversible, and the equilibrium can be shifted by adding ions of various metals or performing transmetallation of the resulting complexes.

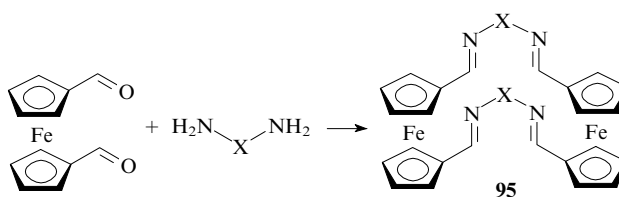


R = Me, Bn; *n* = 1, 2.

d. Diformyl derivatives of azulene and ferrocene

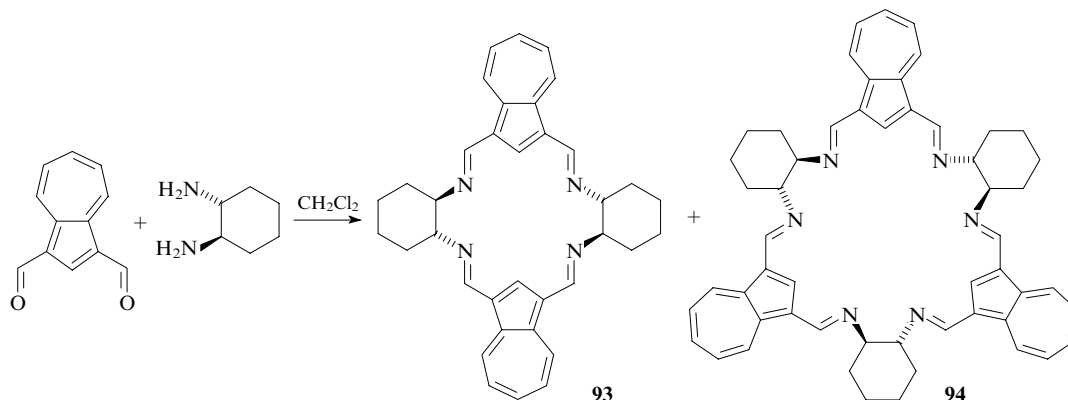
The reactions of compounds containing two carbonyl groups in a five-membered carbocycle with diamines have received little study. Only one synthesis of macrocycles by condensation of 1,3-diformylazulene with *trans*-(*R,R*)-1,2-diaminocyclohexane in dichloromethane at room temperature giving rise to a mixture of [2 + 2]- (**93**) and [3 + 3]-condensation products (**94**) in a ratio of 1 : 4 (Scheme 14) was documented.⁴⁸

The reactions of 1,1'-diformylferrocene were studied in more detail. Due to the unique properties, this dicarbonyl organometallic compound is widely studied in supramolecular chemistry. The reactions of 1,1'-diformylferrocene with diamines in acetonitrile or chloroform at concentrations lower than 0.1 mol litre^{−1} generally produce [2 + 2]-macrocyclic Schiff bases **95**.^{139, 140}



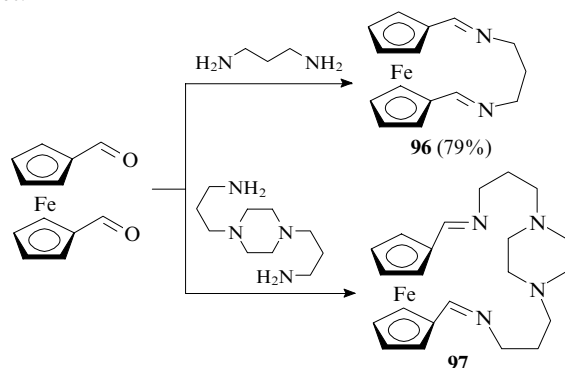
X = CM₂CH₂, CH₂CM₂CH₂, CH₂C₆H₄CH₂-3, NHC(Z)NH (Z = O, S).

Scheme 14



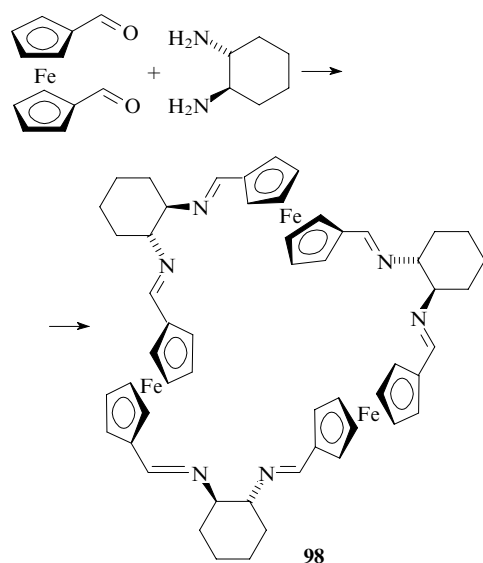
The reaction pathway substantially depends on the nature of the diamine. Aliphatic diamines and 1,3-bis(aminomethyl)benzene give [2+2]-cyclocondensation products, whereas 1,4-di(aminomethyl)benzene forms only oligomeric products (Ref. 139).

The carbonyl groups in 1,1'-diformylferrocene are located in different planes and can occupy different positions with respect to each other due to free rotation of the cyclopentadienyl rings. This allows the synthesis of [1+1] macrocycles based on this aldehyde even by the reactions of the latter with lower aliphatic diamines. For example, the reaction of 1,1'-diformylferrocene with 1,3-diaminopropane in ethanol instead of acetonitrile gives [1+1] macrocycle **96** as the major product.¹⁴¹



The reactions of diamines containing amino groups at a longer distance give [1+1] macrocycles as the major products regardless of the nature of the solvent. For example, compound **97** was synthesised by the reaction of 1,1'-diformylferrocene with 1,4-bis(3-aminopropyl)piperazine in a mixture of ethanol and chloroform at a dialdehyde concentration of 6×10^{-3} mol litre⁻¹ (Ref. 139).

Due to ability of two cyclopentadienyl rings in 1,1'-diformylferrocene to rotate about the common axis, the reaction of this compound with *trans*-(*R,R*)-1,2-diaminocyclohexane gave rise to [3+3] azomethine **98**; however, the yield of this product was as low as 13.8%.⁵² Nuclear Overhauser effect (NOE) experiments showed that the cyclopentadienyl rings in each ferrocene moiety of compound **98** in solution are turned round so that the angle between the $\text{C}_{\text{ipso}}-\text{C}(=\text{N})$ bonds is 180°.⁵²

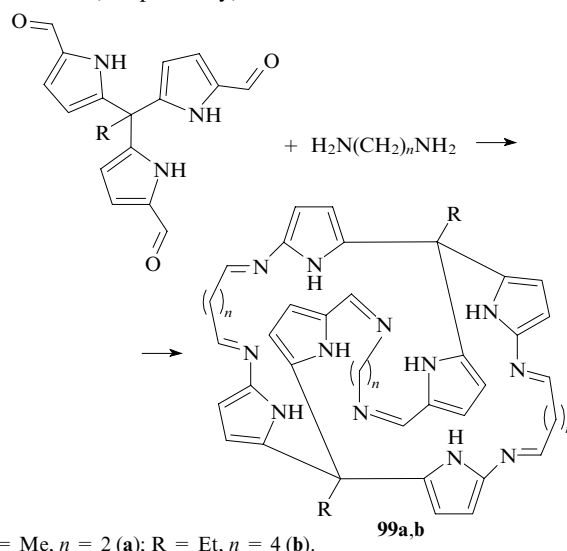


e. Synthesis of cryptands by condensation of diformyl compounds with triamines

Cryptands can be assembled by the Schiff reaction of dicarbonyl compounds with triamines ([3+2] condensation) or of

tricarbonyl compounds with diamines ([2+3] condensation). Only the former reaction has gained wide acceptance.

A unique example of the formation of a cryptand by the latter of condensation type was described in 2001.¹⁴² Compounds **99a,b** were synthesised by the reactions of triformyl derivatives of tripyrromethanes with ethylenediamine or butylenediamine, respectively, in THF.¹⁴²



Regardless of the nature of diformyl compounds, their reactions with polyamines generally produce cryptands. The reactions in dilute solutions ($\sim 2 \times 10^{-2}$ mol litre⁻¹) in different solvents (alcohols or acetonitrile) give [3+2]-condensation products, *viz.*, compounds **100**¹⁴³ and **101a–g**, in moderate or high yields. The cryptands produced in these reactions are structurally similar. Their molecules have a trihedral prismatic shape, the prisms being bound by three aromatic fragments of the dialdehyde and the nitrogen atoms of the polyamine.^{154–157} Figure 13 shows the structure of cryptand **101a** prepared from 2,5-diformylfuran and tris-(2-aminoethyl)amine.¹⁵⁴

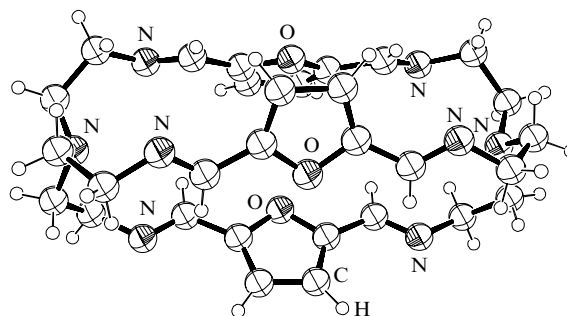
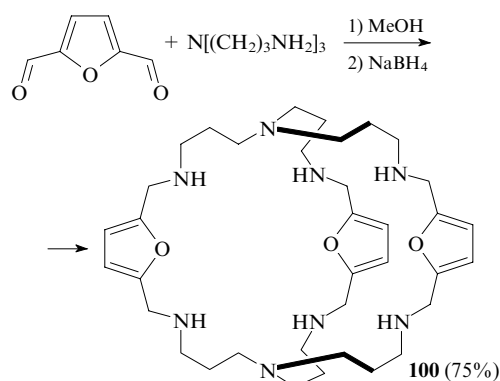


Figure 13. Structure of cryptand **101a**.¹⁵⁴

Scheme 15

$\text{O}=\text{C}-\text{Y}-\text{C}=\text{O} + \text{N}[(\text{CH}_2)_2\text{NH}_2]_3 \rightarrow \text{Y} \begin{array}{c} \diagup \text{N} \diagdown \\ \diagdown \text{N} \diagup \end{array} \text{N} \begin{array}{c} \diagup \text{N} \diagdown \\ \diagdown \text{N} \diagup \end{array} \text{N} \begin{array}{c} \diagup \text{N} \diagdown \\ \diagdown \text{N} \diagup \end{array} \text{Y} \\ \text{101a-i}$				
Compound 101	Y	R	Yield (%)	Ref.
a		—	62	43, 144
b		—	—	43
c		—	60	43, 145
d		—	47–56	43, 73, 145
e		OMe	42	146
		Me	63	147
f		Me	55–65	148, 149
		n-C ₆ H ₁₃	50	148
		H	—	30, 150
g		—	64	151
h		—	60	152
i		—	60	153

The condensation of 2,6-diformyl-4-methylphenol with 2,6-bis[1,1-bis(aminomethyl)ethyl]pyridine in the presence of

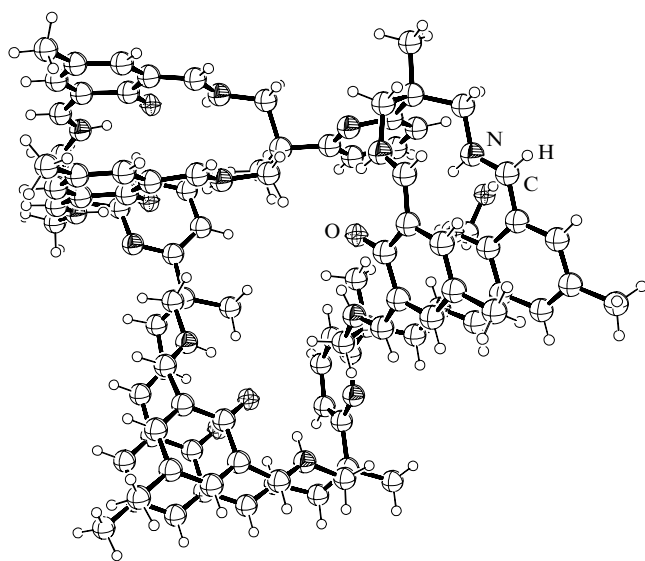
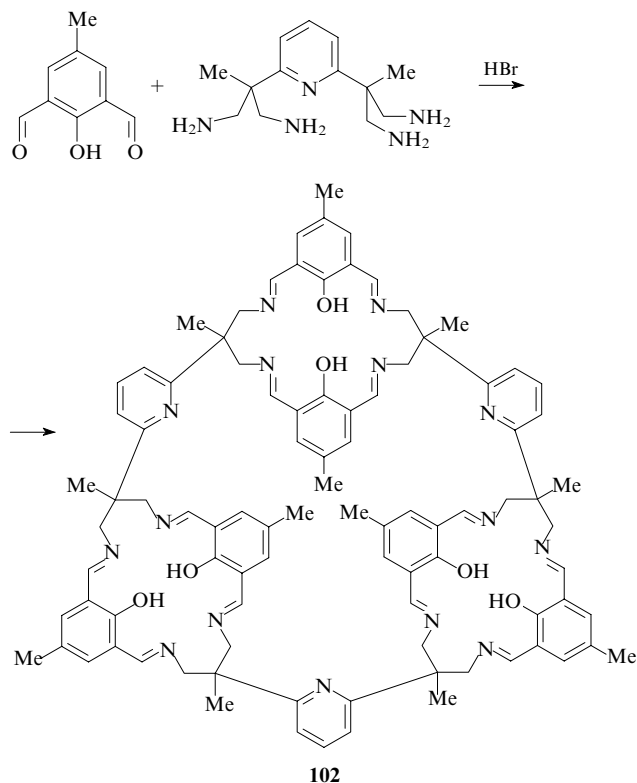


Figure 14. Structure of macrocycle **102**.¹⁵⁹



HBr affords polycycle **102** as the [6 + 3]-condensation product in a yield higher than 90% (Scheme 15).^{158, 159}

Macrocycle **102** contains three [2 + 2] macrocyclic fragments formed by 2,6-diformyl-4-methylphenol and 1,3-propylenediamine, which are linked to each other by pyridine bridges. All three fragments, like free protonated [2 + 2] macrocycles (see Fig. 5b), adopt a horseshoe conformation (Fig. 14).¹⁵⁹

To generalise the results considered in the present section, it should be noted that the following two methods are used most widely for the synthesis of azomethine macrocycles from dicarbonyl compounds and diamines: the condensation of $\sim 10^{-2}$ M solutions of equimolar amounts of the starting compounds in acetonitrile at room temperature and the condensation of more dilute solutions ($\sim 10^{-3}$ M) by refluxing in alcohols. The results of the reactions with aliphatic diamines are determined primarily by the reactant ratio. The synthesis according to most of other procedures affords a library of products. The isolation of individual compounds from this library can be based on low solvation of certain macrocyclic azomethines in low-polarity solvents.

The nature of diamines has the main effect on the ratio of the components. If the amino groups in diamines are separated by a long aliphatic or heteroatomic chain, these groups react independently of each other because they are spatially distant and the conjugation is absent. In reactions with monocyclic dicarbonyl compounds in the absence of acids, diamines in which the amino groups are in rather close proximity (α,β and α,γ diamines), as a rule, form oligomers. In the presence of strong acids (HCl or HBr), these reactions give salts of [2 + 2] macrocycles as the major products.

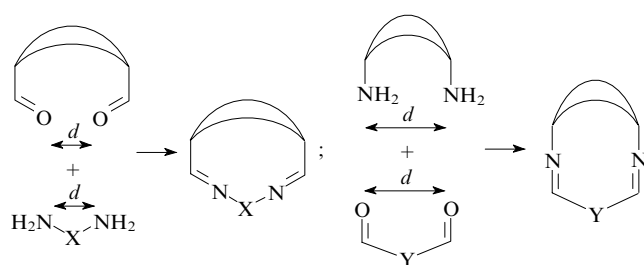
III. Unsymmetrical macrocyclic Schiff bases

An analysis of the published data shows that the condensation of dicarbonyl compounds with diamines offers great scope for the synthesis of various polydentate Schiff bases. In this class of

compounds, unsymmetrical macrocyclic compounds containing at least two coordination units of different nature (a soft unit for binding late transition metals and a hard unit for binding early transition metals) inside the macrocycle have attracted considerable attention in recent years. Heterobinuclear complexes belonging to this class are of exceptional interest for catalysis. Quantum chemical calculations demonstrated that these complexes can bind low-reactivity compounds (alkenes, carbon monoxide and dioxide, nitrogen and even alkanes) and activate them for further chemical transformations as a result of the concerted push-pull effect of two metals of radically different nature on the substrate molecule.¹⁶⁰ The structures and properties of heterobinuclear complexes were covered in the reviews.^{29, 30, 161}

In the previous sections, we considered several special examples of the synthesis of unsymmetrical macrocyclic Schiff bases. The optimal strategy for the construction of such structures is based on the idea of the fragment assembly involving the [1 + 1] condensation of large bifunctional blocks presynthesised in the previous steps. The diamine and dicarbonyl components are most often synthesised independently, although blocks containing one amino group and one carbonyl group can, in principle, be used. The structure complementarity of the fragments, including their ability to adopt conformations favourable for cyclisation, is the main prerequisite for the last step of the macrocyclic ring closure (Scheme 16).

Scheme 16



The choice of an appropriate solvent capable of stabilising such conformations plays an exceptionally important role. The reactions can proceed both under acid catalysis and in the absence of acids. In some cases, the nature of the anion has a considerable effect on the reaction pathway in the presence of acids, which indicates that anions can act as template agents (see Section IV).

Numerous [1 + 1] condensations of bifunctional blocks with the use of metal ions as template agents were documented. In these reactions, metal ions provide preliminary coordination of the both starting polydentate building blocks by fixing the conformation favourable for cyclisation, which proceeds in the inner coordination sphere of the ion. Its coordination number determines also the size of the resulting ring. In most of the characterised reactions of this type, diamine and one of the presynthesised dicarbonyl precursors were used for the template assembly of macrocyclic Schiff bases. However, many examples of the use of mononuclear metal complexes with a dicarbonyl precursor and a diamine molecule in condensation reactions were documented. In these reactions, the metal ion located in the cavity distant from the reaction centres serves the function of retaining the dicarbonyl fragment in the conformation favourable for cyclisation. Although the carbonyl and amino groups involved in the reaction are not included in the coordination sphere of the metal ion, these transformations are always considered in depth in reviews on the template synthesis.

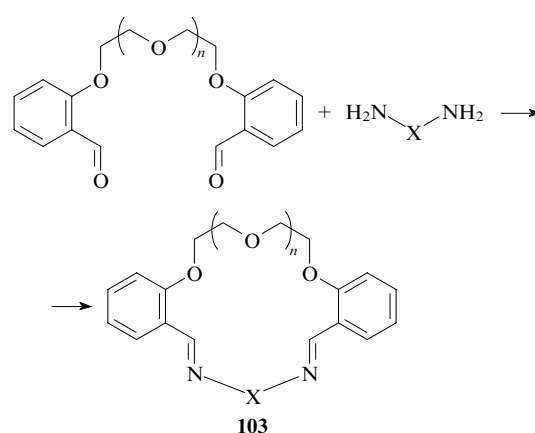
The assembly of macrocycles based on diamines has found little use because these compounds are difficult to synthesise. Template-free reactions of dicarbonyl compounds with di-

amines giving macrocyclic structures are considered in detail below.

1. Template-free fragment assembly in the absence of acids

As mentioned above, the nature of the solvent has a substantial effect on the [1 + 1] cyclocondensation pathway. The assembly of macrocycles from enlarged blocks is performed in aprotic solvents (acetonitrile, chloroform or dioxane), which rather weakly solvate polar carbonyl and amino groups of the starting compounds without hindering hydrogen bonding between these groups. Hydrogen bonds provide the organisation of the prereaction complex, in which the carbonyl and amino groups of two reactants involved in the reaction are in spatial proximity.

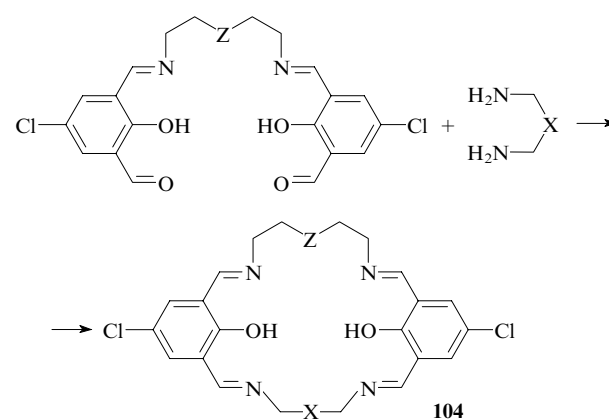
As an example of such condensations, let us refer to the synthesis of oxazamacrocyclic ligands **103**. In the case of *trans*-1,2-diaminocyclohexane, the yields of the products were 89%–95%.



X = (CH₂)₂N(CH₂CH₂NH₂)(CH₂)₂ (n = 1);¹⁶²

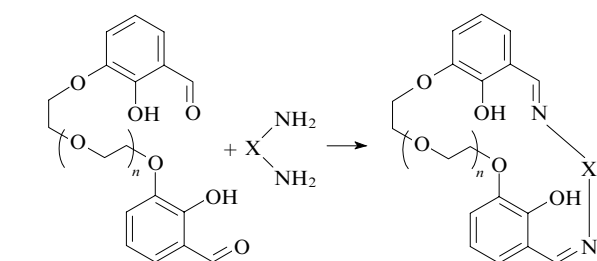
X = , n = 0–4.¹⁶³

The reactions of dicarbonyl precursors with aliphatic diamines in chloroform at room temperature under kinetic control produce unsymmetrical compounds **104**.⁷⁵



Z = S, NH; X is absent, CH₂ZCH₂.

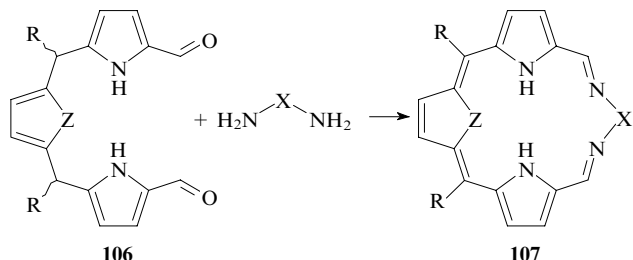
The condensation in polar aprotic solvents (chloroform or acetonitrile) also affords [1 + 1] macrocycles (for example, compounds **105a–h**) as the major products if the reactions of aliphatic α,ω -diamines are performed with dicarbonyl derivatives, in which two salicylaldehyde fragments are separated by a flexible oligo(oxyethylene) chain.



$n = 1, 2$.

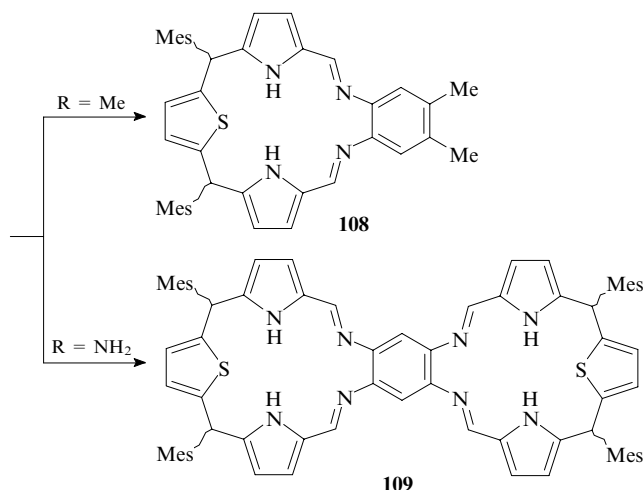
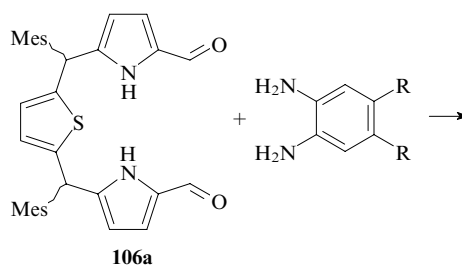
Compound 105	X	Yield (%)	Ref.
a	(CH ₂) ₂	62–65	164, 165
b	(CH ₂) ₃	42	166
c	(CH ₂) ₂ NMe(CH ₂) ₂	55–60	165, 167
d	(CH ₂) ₂ NH(CH ₂) ₂	60–70	165
e	(CH ₂) ₂ N(CH ₂) ₂	54–59	164
	C ₁₁ H _{23-n}		
f	(CH ₂) ₃ NH(CH ₂) ₃	54–59	164
g	CH ₂ CHCO ₂ H	69–70	164
h	(CH ₂) ₂ CHCO ₂ H	69–70	164

High dilution is yet another prerequisite for the synthesis of [1 + 1]-condensation products. The reactions of dicarbonyl blocks **106**, in which the carbonyl groups located in different parts of the molecules are in spatial proximity, with 1,2-diamines and hydrazine afford [1 + 1]-condensation products **107** in moderate yields only in chloroform at concentrations of 2×10^{-3} mol litre⁻¹ in the presence of molecular sieves. Under these conditions, the condensation is accompanied by dehydrogenation of the macrocyclic system.



Diamine	Z	R	Yield (%)	Ref.
H ₂ N(CH ₂) _n NH ₂ ($n = 2-4$)	S	2,4,6-Me ₃ C ₆ H ₂ (Mes)	—	167
	S	Mes	—	168
	S	Mes	—	168
H ₂ NCH ₂ CH ₂ NH ₂	S	Ph	20	169
	S	Ph	40	169
	S	Mes	50	169
H ₂ N-NH ₂	O	Mes	43	170

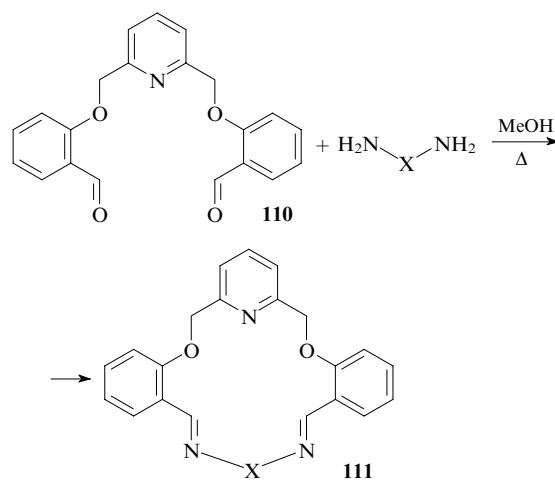
The reactions of *o*-phenylenediamine with such dicarbonyl compounds also produce [1 + 1] macrocycles. For example, the reaction of dicarbonyl derivative **106a** with *o*-phenylenediamine in chloroform in the presence of molecular sieves gives the expected [1 + 1] macrocycle **108**.¹⁶⁸



Interestingly, unlike the condensation with aliphatic diamines and hydrazine, the latter reaction is not accompanied by dehydrogenation to form a conjugated system. Apparently, this is associated with the fact that the completely conjugated macrocycle, which could be formed in this transformation, is antiaromatic.

The analogous condensation of compound **106a** with 1,2,4,5-tetraaminobenzene affords [2 + 1]-condensation product **109**.¹⁶⁸

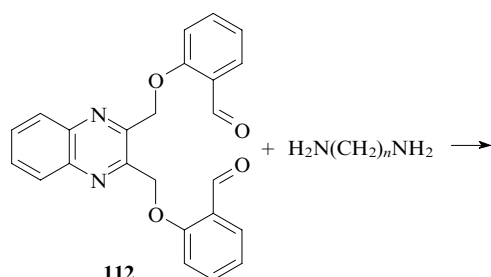
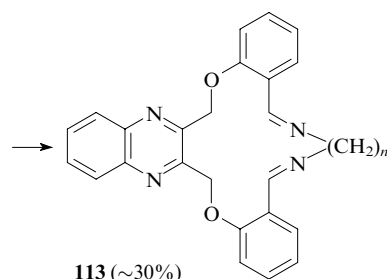
The assembly of macrocyclic Schiff bases can be performed also in methanol under thermodynamic control. For example, [1 + 1] macrocycles **111** were synthesised by the reaction of dicarbonyl compound **110** with 1,2-diaminoalkanes in boiling methanol.^{163, 171}



X = (CH₂)₂,

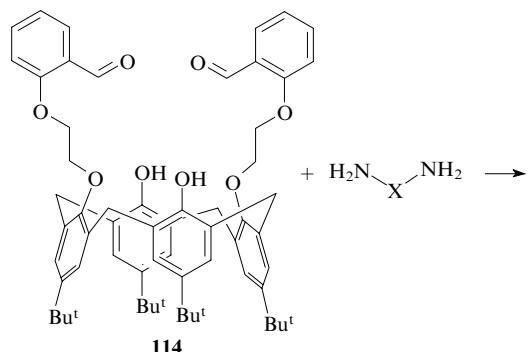
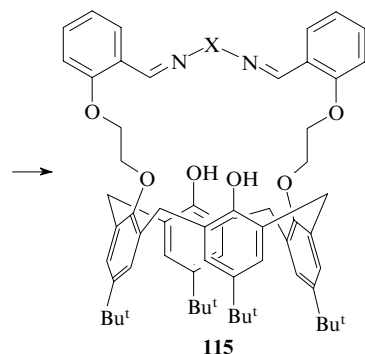
However, if the dicarbonyl block and diamine are non-complementary, the reactions give, as a rule, mixtures of products. For example, dicarbonyl derivative **112** reacted

with ethylenediamine to form [1 + 1]- and [2 + 2]-condensation products, which were not isolated in the individual state. By contrast, the reactions of this compound with other diamines (1,3-diaminopropane and 1,4-diaminobutane) gave only [1 + 1]-condensation products **113**.¹⁷²


112

113 (~30%)

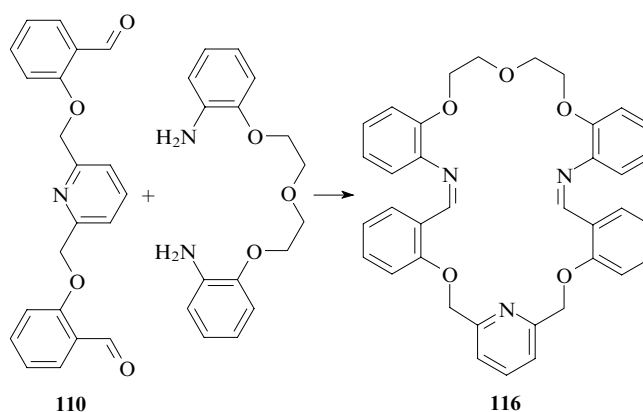
$n = 3, 4$.

Under prolonged reflux in a methanol–acetonitrile mixture, the dicarbonyl derivative of calixarene (**114**) reacts with diamines to form [1 + 1] macrocycles **115**.¹⁷³

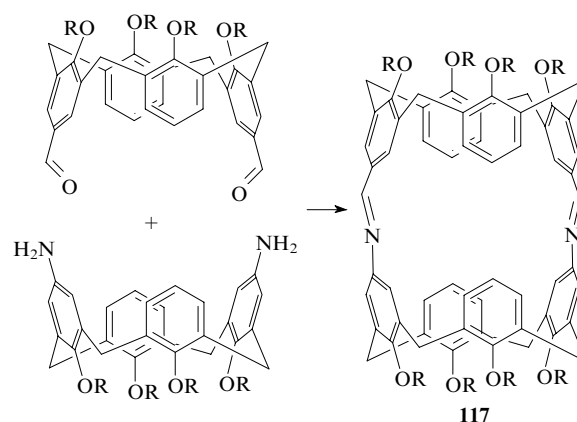

114

115

$X = (CH_2)_n$ ($n = 2$ (56%), 3 (86%), 4 (54%)), 1,2-phenylene (14%), $CH_2C_6H_4CH_2$ -4 (96%)

Enlarged precursor blocks can react with each other to give large rings. For example, salicylaldehyde derivative **110** reacts in boiling ethanol with diamine containing the oxyethylene chain to form [1 + 1] macrocycle **116**.¹⁷⁴

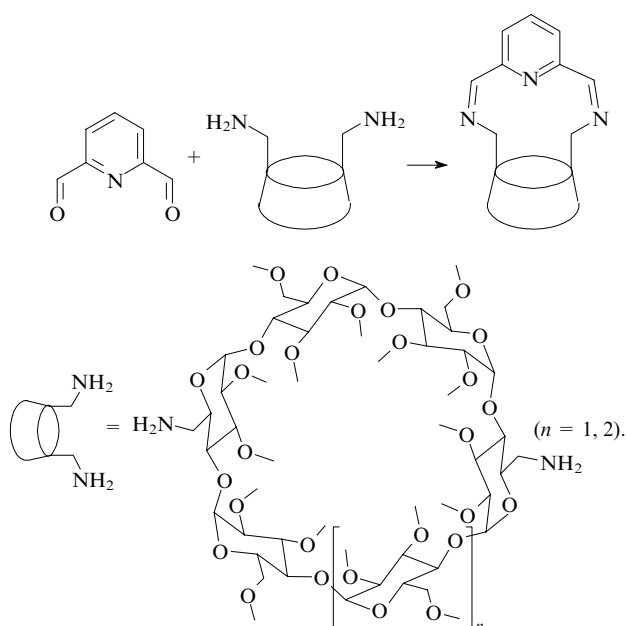

110
116

The reactions of dicarbonyl derivatives of calixarenes with complementary diamines produce [1 + 1] macrocycles **117** in high yields (74%–92%).¹⁷⁵


117

$R = Pr^n, (CH_2)_2OEt$.

Even more complex supramolecular aggregates can be synthesised by condensation of dicarbonyl compounds with per-*O*-methylamino derivatives of α - and β -cyclodextrins.¹⁷⁶ The reaction proceeds at room temperature in acetonitrile in the presence of molecular sieves A4.



The condensation products of 2,6-diformylpyridine with diaminocyclodextrins contain a hemispherical hydrophilic

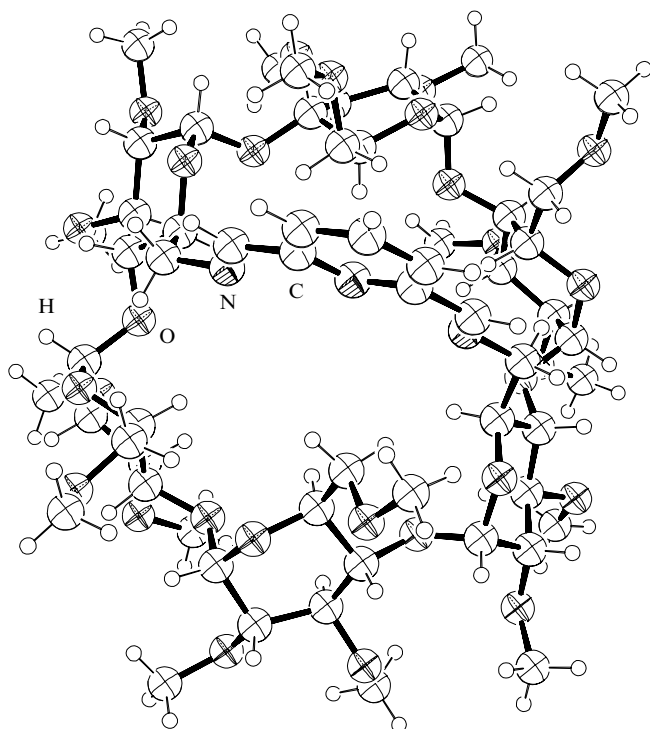
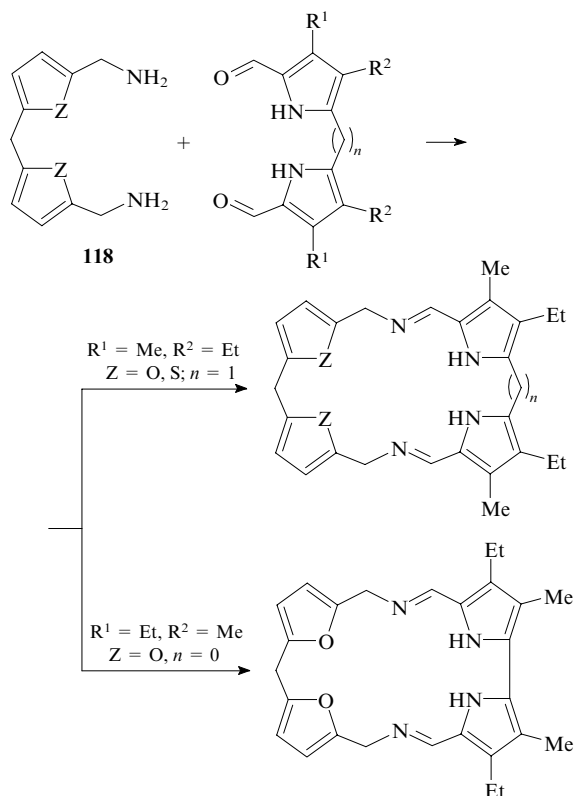


Figure 15. Structure of modified α -cyclodextrin.¹⁷⁶

cavity bound by a fragment of the dicarbonyl compound (Fig. 15).¹⁷⁶

The use of blocks containing two amino groups for the fragment assembly is limited by the fact that they are less widespread and are difficult to synthesise.

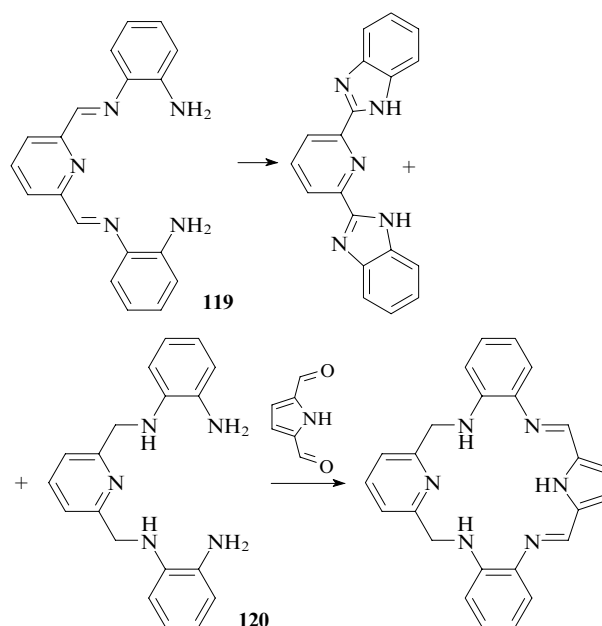
Scheme 17



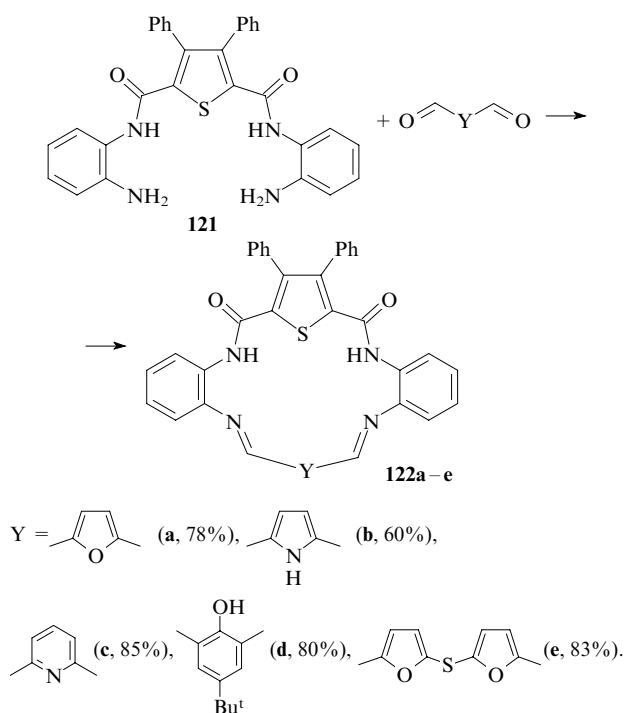
Z = O, S; R¹, R² = Me, Et; n = 0, 1.

For example, the condensation of compounds **118** with dicarbonyl derivatives of bis-pyrroles (Scheme 17) can be assigned to this type of reactions.[‡]

It should be noted that diamine **119**, which was synthesised by demetallation of the template [1 + 2]-condensation product of 2,6-diformylpyridine with *o*-phenylenediamine,⁶³ does not react with dicarbonyl compounds due to the electron-withdrawing effect of the azomethine fragments conjugated with the amino groups (see Sections II.3 and II.4). However, its reduction product **120**, which is synthesised by refluxing in toluene as a result of redox disproportionation, reacts with 2,5-diformylpyrrole to form an unsymmetrical macrocycle.¹⁷⁷



On the contrary, aromatic diamines acylated at one of the amino groups by dicarboxylic acid readily form macrocycles.

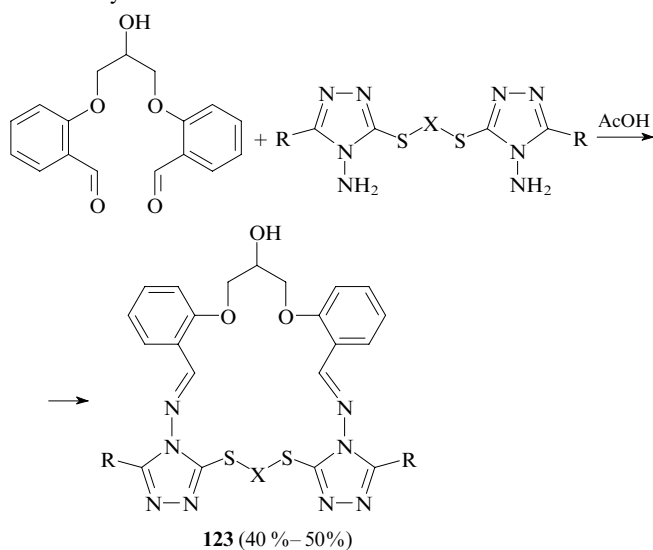


[‡] The data from the graduate study by A M Jasat, University of British Columbia, Vancouver, Canada, 1995.

For example, diamine **121** reacts in an aprotic polar solvent (1,4-dioxane) with various dicarbonyl compounds to give [1 + 1] macrocycles **122a–e**.¹⁷⁸ In this case, the geometry of the starting diamine imposes strict restrictions on the second reaction component (dialdehyde). Diamine **121** is planar, and dicarbonyl compounds, which can adopt planar conformations, are most active in reactions with this diamine resulting in the closure of the macrocycle because only this can give rise to a system containing a long chain of conjugation.

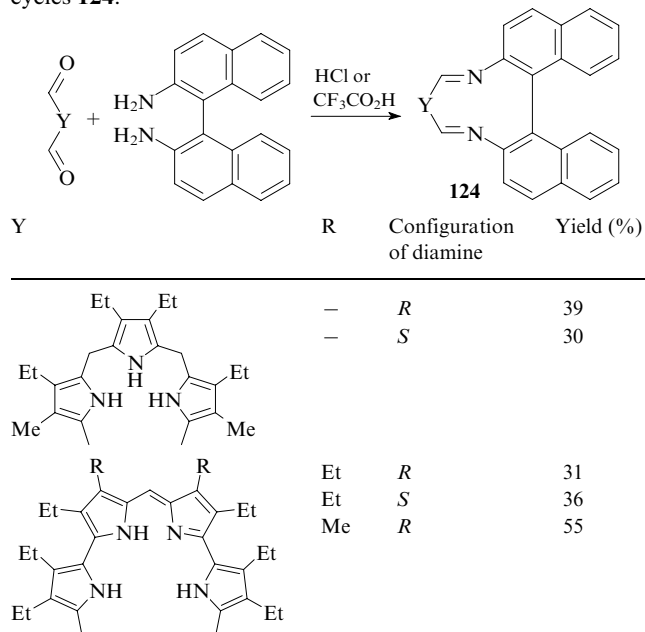
2. Fragment assembly in the presence of protic acids

Numerous syntheses of macrocycles from dicarbonyl compounds and diamines in the presence of protic acids were documented. For example, the reaction with excess acetic acid produced 13-membered azathiacycrown macrocycles **123**.¹⁷⁹ In this case, the acid acts as both the solvent and the acid catalyst.

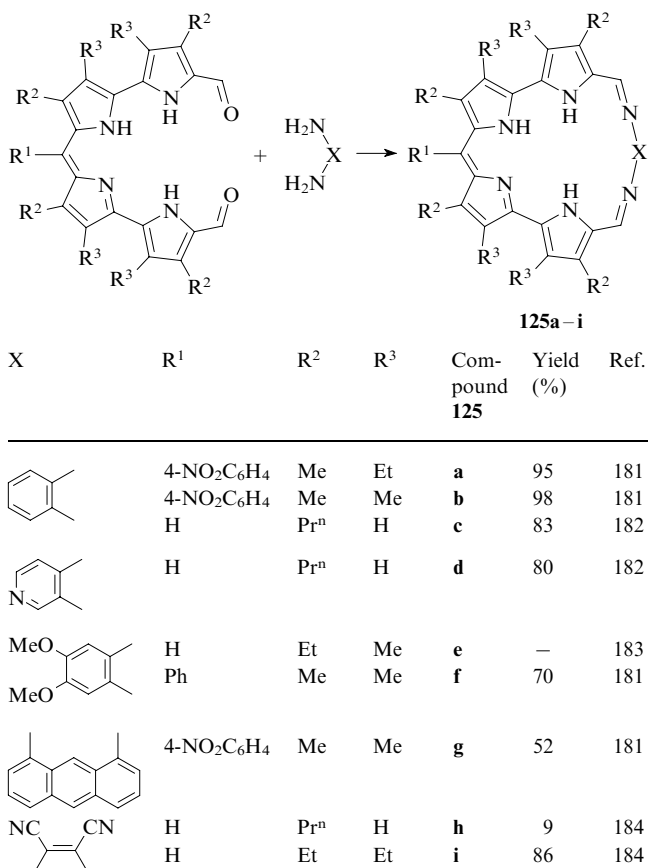


R = Ph, CH₂Ph; X = (CH₂)_n (n = 3, 4).

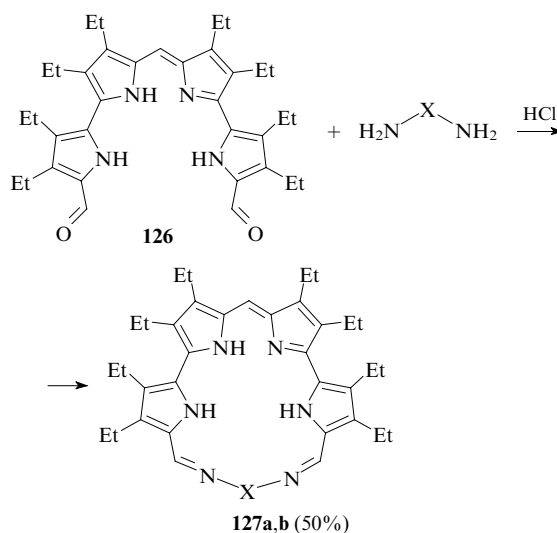
In polar protic solvents, which readily solvate amino groups (for example, in methanol), dicarbonyl derivatives of the pyrrole series are involved in condensation only in the presence of strong protic acids. For example, the condensation of dicarbonyl derivatives of the pyrrole series with optically active 2,2'-diamino-1,1'-binaphthyls in methanol in the presence of hydrochloric or trifluoroacetic acid affords macrocycles **124**.¹⁸⁰



Under acid catalysis, dicarbonyl compounds react with weakly nucleophilic diamines, even with 2,3-diaminomaleonitrile, to form macrocycles **125a–i**.



Polypyrrole dialdehyde **126** reacts with hydrazine and 1,3-diaminoguanidine in methanol in the presence of hydrochloric acid to form the corresponding macrocycles **127a,b**.¹⁸⁴



X is absent (**a**), NHC(=NH)NH (**b**).

Macrocycles obtained from polypyrrole derivatives, which are close analogues of extended porphyrins,¹⁸⁵ are of interest for supramolecular chemistry because they contain a cavity inside the macrocycle, which can include substrates of various nature. For example, X-ray diffraction data show that a methanol molecule is fixed in the cavity of compound **125e** by five hydrogen bonds (Fig. 16).¹⁸³ The structures of other inclusion compounds are similar to that described above.¹⁸¹

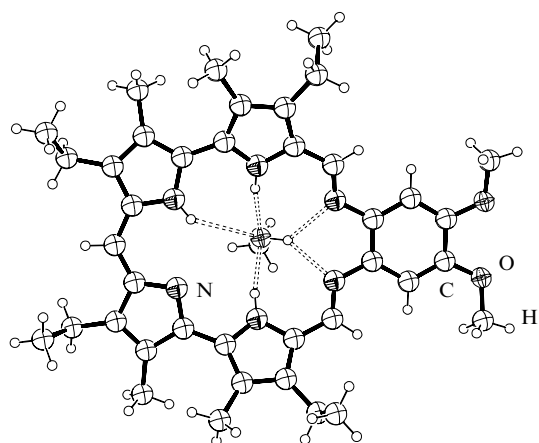
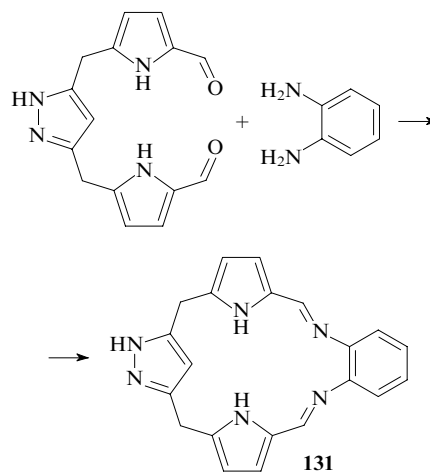


Figure 16. Structure of the inclusion complex based on macrocycle **125e**.¹⁸³

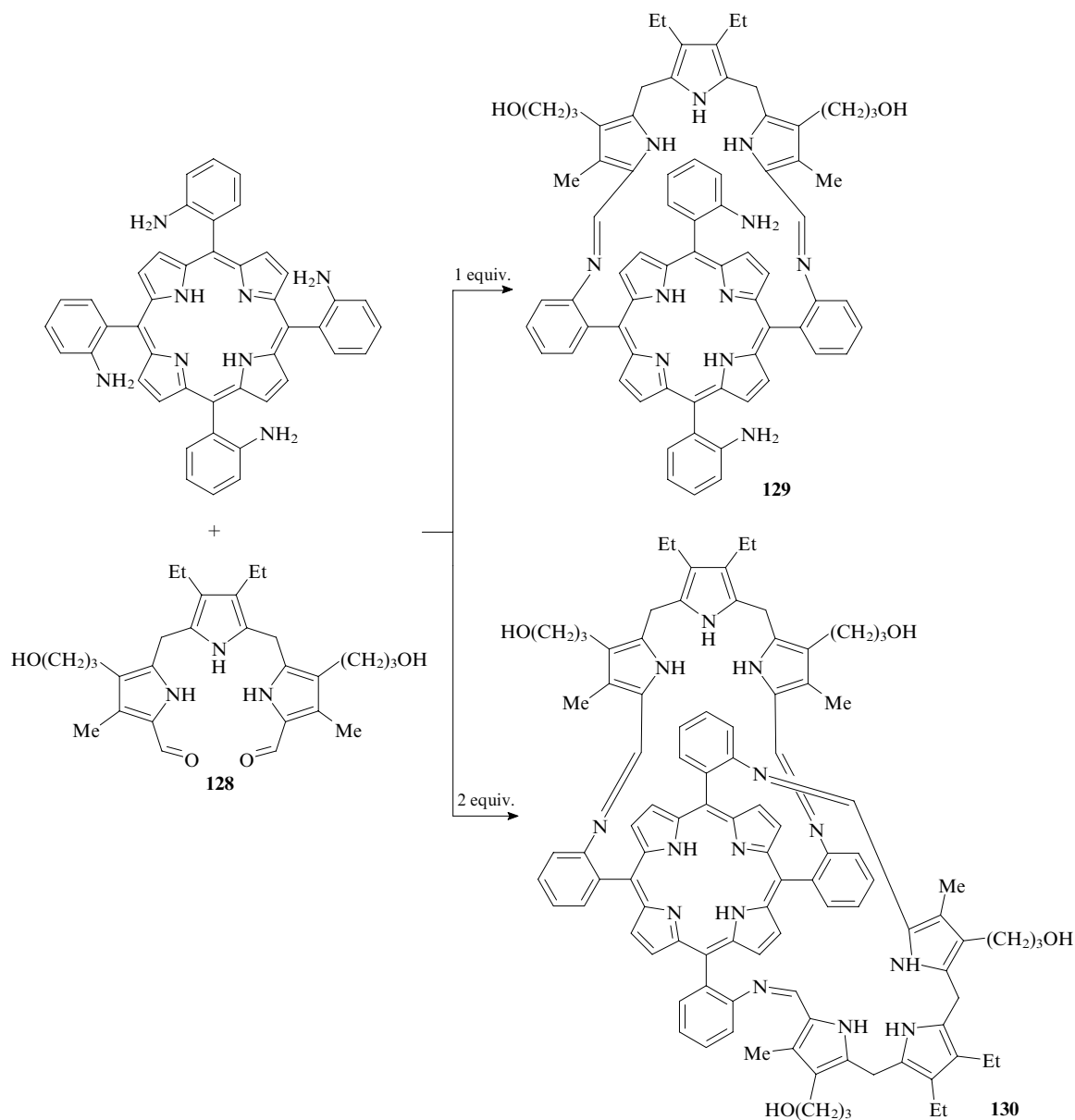
The strategy of the fragment assembly can be used for the synthesis of three-dimensional structures. The condensation of *meso*-(2-aminophenyl)porphyrin with one or two equivalents

of dialdehyde **128** in the presence of trifluoroacetic acid affords the corresponding three-dimensional polycyclic systems **129** and **130** in moderate yields (30% – 45%) (Scheme 18).¹⁸⁶

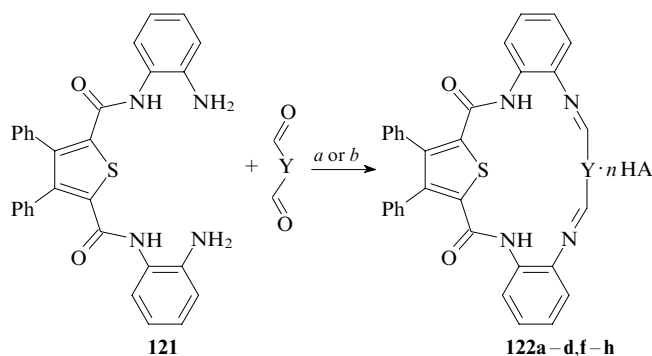
Catalysis is required also in the synthesis of heterocyclic analogues of polypyrrole macrocycles, in particular, of pyrazolepyrrole system **131**.¹⁸⁷



Scheme 18



Examples of the successful assembly of macrocycles by condensation of diamines in the presence of protic acids are few in number. For instance, compound **121** reacts with various dicarbonyl derivatives in methanol only in the presence of protic acids to form salts of [1 + 1] macrocycles **122a–c,f** or free Schiff bases **122d,g,h**.^{178, 188} Free macrocyclic azomethines can be isolated by treating the salts with triethylamine. Interestingly, the yield of some macrocycles in these reactions substantially depends on the nature of the acid used in the reaction.



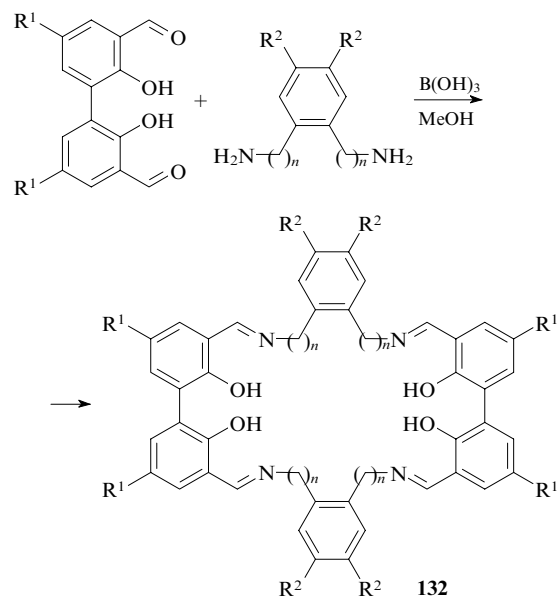
(a) HA, MeOH; (b) (1) HA, MeOH; (2) Et₃N, CH₂Cl₂.

Compound 122	Y	HA	Conditions	n	Yield (%)
a		HCl	a	2	73
b		HCl	a	2	73
c		HCl	a	3	42
d		HCl	b	0	88
f		H ₃ PO ₄ CF ₃ CO ₂ H	a a	2/3 2	85 70
g		H ₂ SO ₄ HCl	b b	0 0	95 65
h		HCl	b	0	83

IV. Anion template effect in the synthesis of macrocyclic azomethines

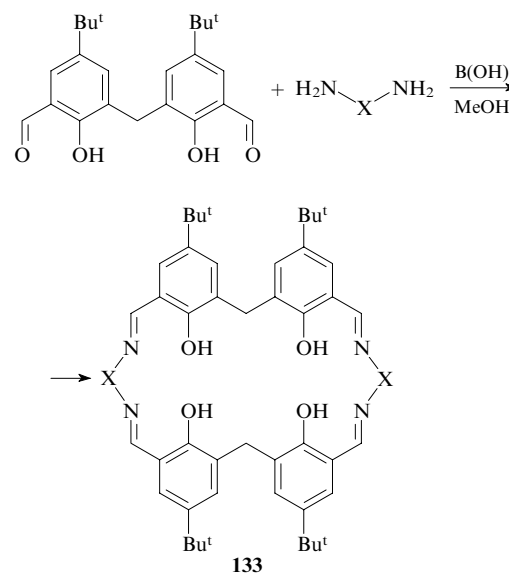
For most of the above-described reactions of dicarbonyl compounds with diamines, the nature of the Brønsted acid anion has no effect on the structure of the reaction products or their yield. However, in 1982 Corey¹⁸⁹ found that the cyclocondensation in the synthesis of the boron-containing antibiotic aplasmomycin efficiently proceeds only in the presence of boric acid. Corey was the first to hypothesise that the borate anion acts in this reaction as the template agent. In 1985, it was found that boric acid serves as a good catalyst for the [2 + 2] condensation of 3,3'-diformyl-2,2'-dihydroxybiphenyl with 1,4-bis(aminomethyl)benzene in methanol. In more recent

years, this approach has been extended to the condensation of this dialdehyde with *o*-phenylenediamine, which allowed the synthesis of macrocycles **132**.



R¹ = H, R² = H, n = 1;¹⁹⁰ R¹ = Bu^t, R² = H, n = 0 (66%);
R² = Me, n = 0 (86%).¹⁹¹

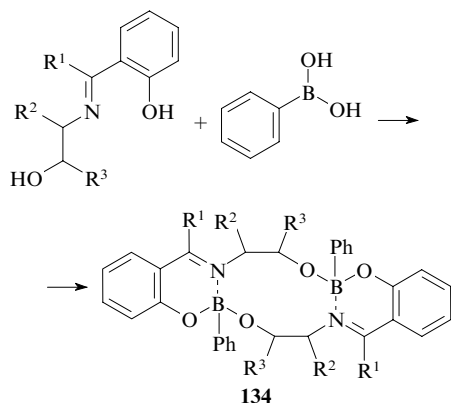
Analogously, boric acid can direct the condensation of other bis-phenol dialdehydes as well. For example, [2 + 2] macrocycles **133** were generated from various diamines in the presence of boric acid.¹⁹²



X = (CH₂)_n (n = 2, 3), , *o*-phenylene.

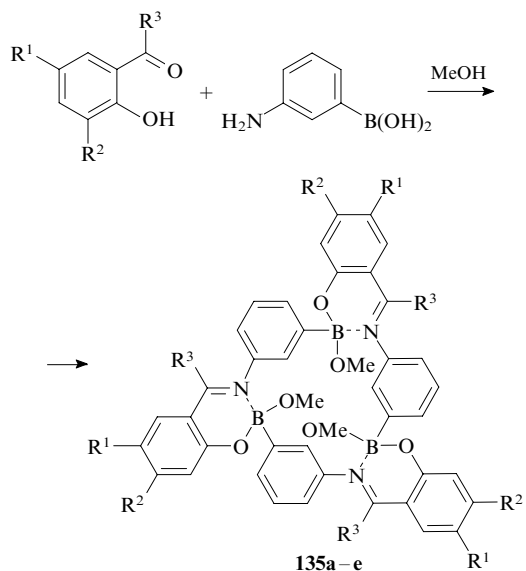
Apparently, borate with two molecules of the diformyl derivative of bis-phenol is produced as an intermediate in this reaction. Intermediate tetrahedral borate fixes the relative arrangement of the dicarbonyl fragments favourable for the closure of a macrocycle, but renders the oligomerisation impossible. Hence, the role of boric acid as a template agent is limited only to phenol derivatives. This reaction with the use of phenylboronic acid affords boron-containing macrocycles **134**. In this case, the covalent template, *viz.*, phenylboronic

acid, remains in the molecule and forms a macrocycle through ester bonds and additional coordination with the azomethine nitrogen atom.^{193, 194}



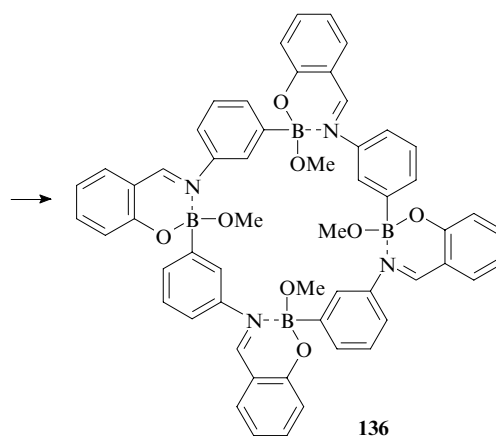
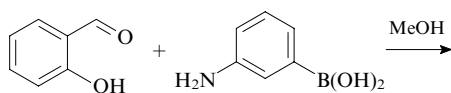
$R^1, R^2 = \text{H, Me}; R^3 = \text{H, Me, Ph.}$

The presence of the borate group in amine molecules is favourable for the autotemplate reactions with aldehydes. The reaction of 3-aminophenylboronic acid with substituted salicylaldehydes leads to the autotemplate [3 + 3] macrocyclisation giving rise to compounds **135a–e**.

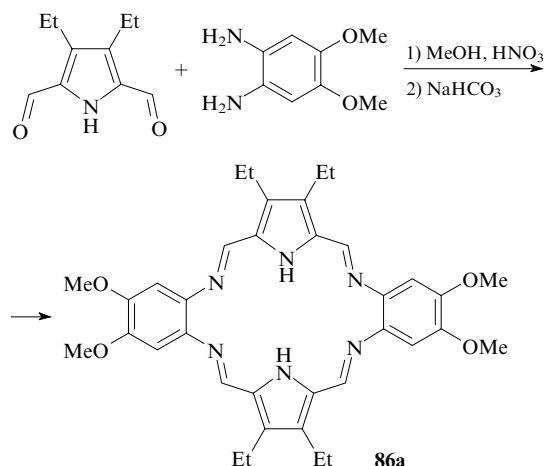


Compound 135	R^1	R^2	R^3	Yield (%)	Ref.
a	Bu ^t	Bu ^t	H	92	195
b	I	I	H	56	196
c	OH	H	H	57	196
d	H	H	Me	48	197
e	H	H	Ph	65	197

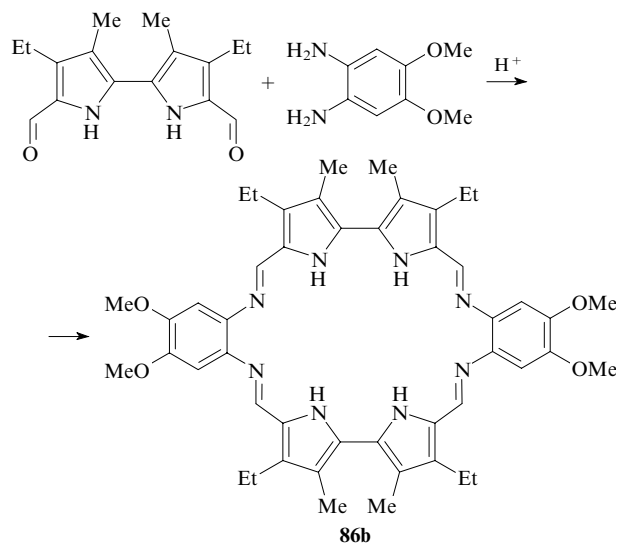
As opposed to the above-described reactions, the reaction of unsubstituted salicylaldehyde with 3-aminophenylboronic acid produces [4 + 4] macrocycle **136**.¹⁹⁷



The possible involvement of acid anions, which are incapable of binding with dicarbonyl compounds or diamines by a strong covalent bond, has long been an open question. Sessler *et al.*¹²⁴ were among the first to find the influence of the nature of anions on the reaction pathway of dicarbonyl compounds with diamines (see Section II.4.b). It appeared that the [2 + 2] cyclisation of 3,4-diethylpyrrole-2,5-dicarbaldehyde with *o*-phenylenediamine produces compound **86a** in quantitative yield only in the presence of nitric acid.



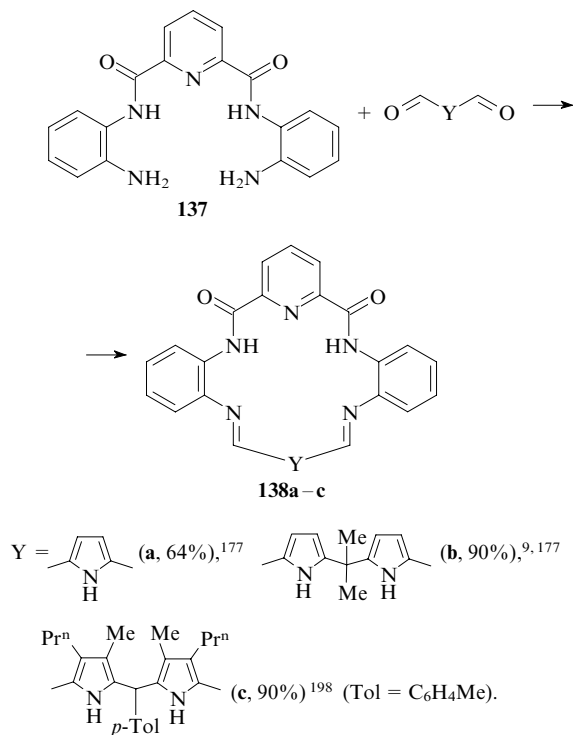
A detailed study of the reaction of 2,2'-diformylbipyrrole with *o*-phenylenediamine in the presence of various acids demonstrated that the reactions of these compounds proceed



$\text{H}^+ = \text{HNO}_3$ (95% yield), H_2SO_4 (84%), HClO_4 (81%), $\text{CF}_3\text{CO}_2\text{H}$ (74%), HCl (47%), HI (37%), $\text{HCl} + \text{Bu}_4\text{NNO}_3$ (> 80%).

in the presence of nitric acid to give product **86b** in a yield of up to 95%, whereas the reactions in the presence of other acids produce the macrocycle in substantially lower yields.¹²⁵

Recently, it has been found that diamide of pyridine-2,6-dicarboxylic acid and *o*-phenylenediamine (**137**) reacts with dialdehydes in the presence of trifluoroacetic or sulfuric acid to form [1 + 1]-condensation products **138a–c**. The reactions in the presence of other acids (HCl, AcOH, HNO₃ or H₃PO₄) afford mixtures of [1 + 1] macrocycles and oligomeric products.



It was demonstrated^{9, 177, 198} that macrocycles containing the dipyrromethane fragment can bind tetrahedral anions. The binding constants of template agents are known to correlate with the molar fraction of the receptor in a dynamic combinatorial library.¹⁹⁹ As mentioned in the Introduction, the synthesis of azomethines from polyfunctional derivatives gives mixtures of products. Therefore, high affinity of receptors for tetrahedral anions accounts for the template function of the latter in the macrocyclisation. However, the role of trifluoroacetic acid remains unclear. This acid can also efficiently

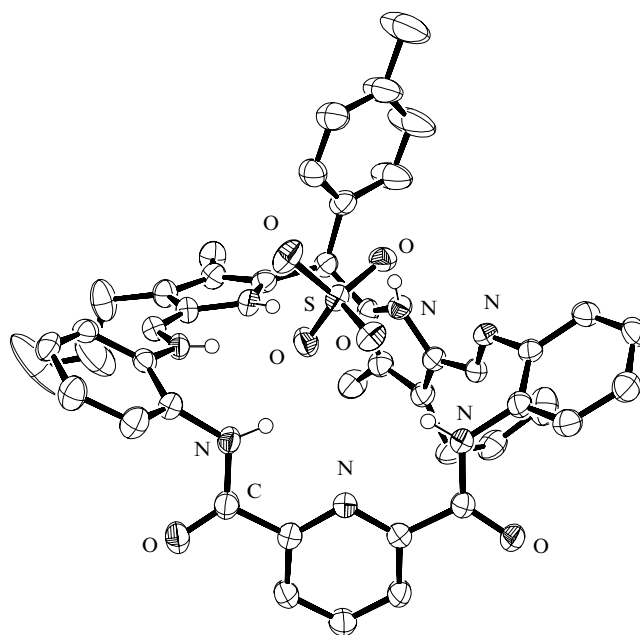


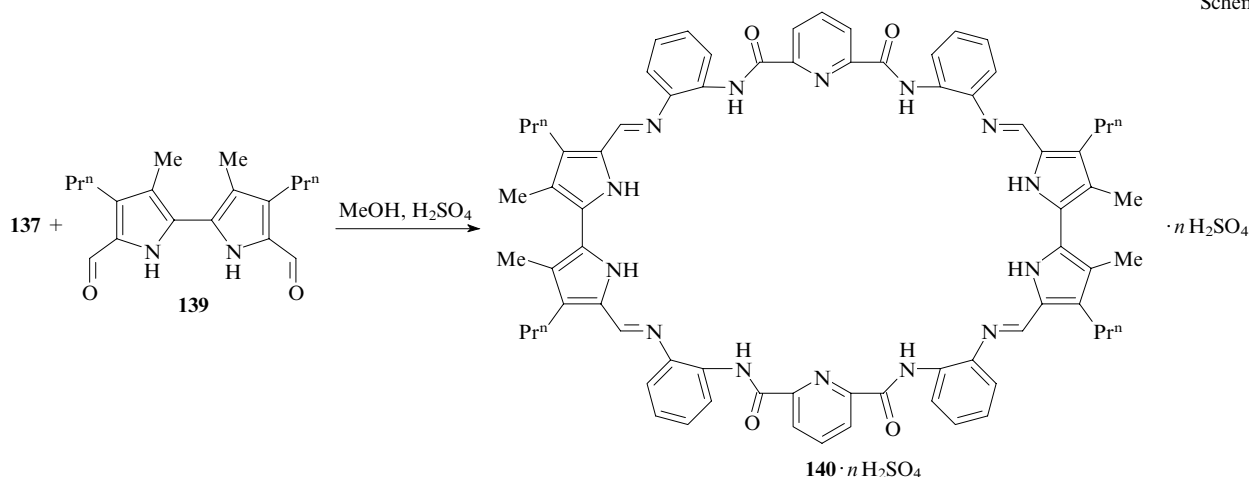
Figure 17. Structure of complex **138c** · H₂SO₄ (for clarity, the hydrogen atoms at the C atoms are omitted).¹⁹⁸

catalyse the macrocyclisation despite that the binding constants of the resulting macrocycles with acetate ions are low.

The structure of the complex of ligand **138c** with sulfuric acid was determined by X-ray diffraction (Fig. 17).¹⁹⁸ As can be seen from Fig. 17, H₂SO₄ occurs in the complex as the dianion; macrocyclic azomethine is present as a derivative doubly protonated at the azomethine nitrogen atoms. This suggests that the synthesis of such systems requires the treatment of the reaction mixture with a base for deprotonation of azomethines.

Further study of the reactions of diamine **137** with dicarbonyl derivatives of the pyrrole series showed that the reaction of compound **137** with 2,2'-diformylbipyrrole (**139**), with carbonyl groups more remote from each other, in methanol in the presence of various acids gives different products.²⁰⁰ Studies by mass spectrometry demonstrated that the reaction in the presence of nitric acid produces only oligomers. Oligomers are also the major products in the reactions catalysed by HCl or HBr, although these reactions produce small amounts of [1 + 1] macrocycles. In the presence of acetic or trifluoroacetic acids, the reaction gives the salt of [2 + 2] macrocycle **140**

Scheme 19



as the major product along with a small amount of oligomers. The salt of [2 + 2] macrocycle **140** containing two H_2SO_4 molecules was isolated without traces of oligomerisation products only in the presence of sulfuric acid as the catalyst.²⁰⁰ This result deserves notice. It indicates that the reaction of **137** with **139** in the presence of tetrahedral anions proceeds according to the template scheme (Scheme 19).

The structure of dihydrate of compound **140**, which was isolated upon the treatment with triethylamine, was determined by X-ray diffraction (Fig. 18).²⁰⁰

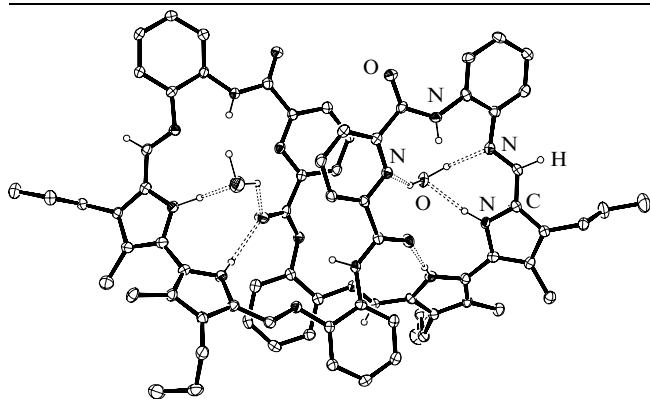
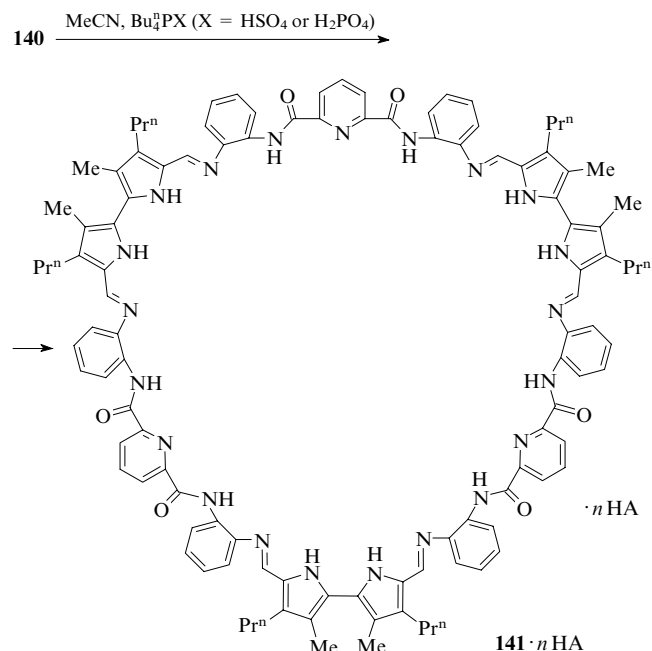


Figure 18. X-Ray diffraction structure of macrocycle **140** · 2 H_2O (aromatic and aliphatic H atoms are omitted).²⁰⁰

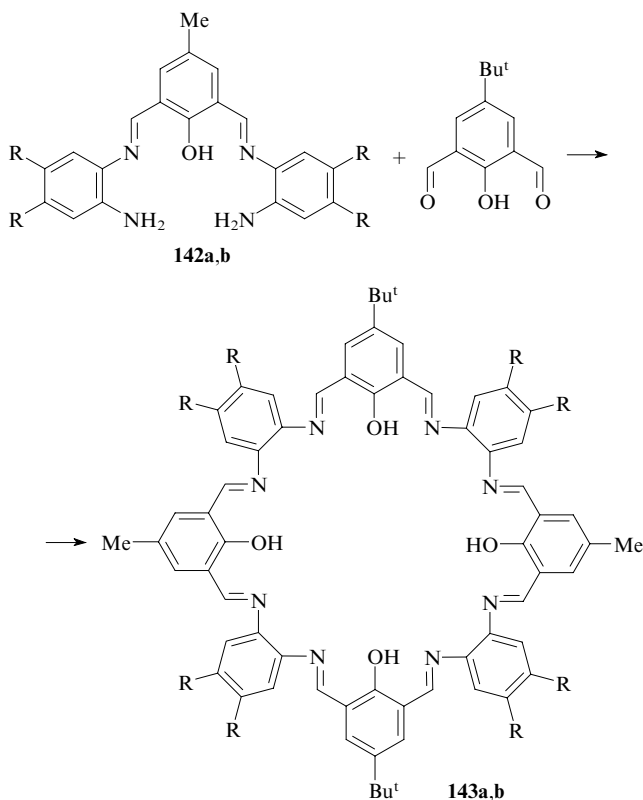
Macrocycle **140** is quite stable under standard conditions. However, storage of this compound in acetonitrile in the presence of tetrabutylphosphonium hydrosulfate or dihydrophosphate leads to its rearrangement into sulfate of macrocycle **141** in quantitative yield as a result of [3 + 3] condensation.²⁰⁰



Apparently, sulfate of [2 + 2] macrocycle **140** is formed in methanol; sulfate of [3 + 3] macrocycle **141**, in acetonitrile. Evidently, the nature of the solvent has a substantial influence on the formation of macrocycles due to solvation of the anion and macrocyclic products formed in the course of the reaction.

The anion template effect is not the only factor determining the pathway of these reactions giving rise to macrocycles. As demonstrated in Section II, the results of macrocyclisation depend also on π, π -stacking interactions. The formation of macrocycles in $[n + n]$ -template condensations governed by π, π interactions was documented for dicarbonyl derivatives, primarily of benzene and phenol (see Sections II.1 and II.2).

Phenolic azomethines **142a,b** react with 4-*tert*-butyl-2,6-diformylphenol²⁰¹ analogously to related pyridine derivative **137**. However (unlike the anion template reaction of compounds **137** and **139**), the reactions of azomethines **142a,b** with this phenol proceed in the absence of template agents to give [2 + 2] macrocycles **143a,b** without traces of oligomerisation products.²⁰¹ The reaction in the presence of metal ions as the template agent affords a radically different macrocycle, viz., the [1 + 1]-condensation product.²⁰¹



R = H (a), Me (b).

X-Ray diffraction data show that [2 + 2] macrocycle **143a** adopts a figure eight conformation due to pairwise stacking interactions between two phenolic fragments and two *o*-phenylenediamine fragments (Fig. 19).²⁰¹ In addition, this system is stabilised by numerous hydrogen bonds between the phenol hydrogen atoms and the azomethine nitrogen atoms. Evidently, the successful macrocyclisation is attributed to π, π interactions.

From the above it follows that both hydrogen bonds and other weak nonbonding interactions can be efficiently used for controlling the condensation of dicarbonyl compounds with diamines under thermodynamic control. These interactions provide the selective binding of one of the products from the dynamic combinatorial library, thus shifting the equilibrium toward the most stable complex. This phenomenon lies at the basis of an efficient approach to the design of artificial cationic and anionic receptors.

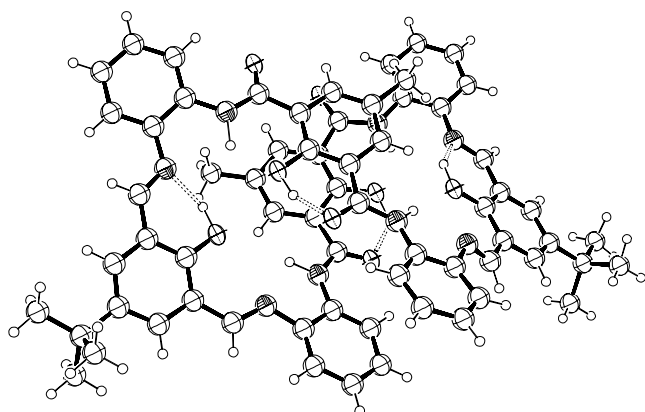
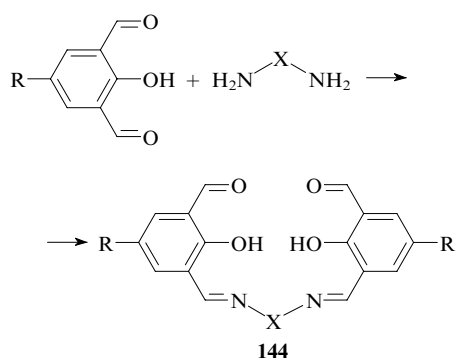


Figure 19. Structure of [2 + 2] macrocycle **143a**.²⁰¹

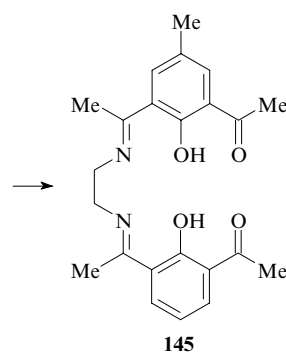
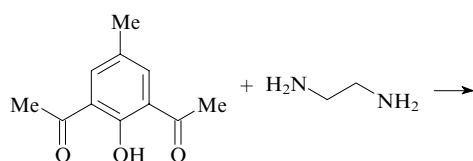
V. Acyclic condensation products of dicarbonyl compounds with diamines

Investigations of the pathways of formation of acyclic condensation products of dicarbonyl compounds with diamines are of importance primarily in the synthesis of enlarged blocks used in the further fragment assembly of macrocycles. [2 + 1]-Condensation products are of great interest as building blocks for the assembly of unsymmetrical macrocycles by performing their reactions with diamines of different structure. Several successful syntheses of these compounds by the reactions of diformyl derivatives of phenols with aliphatic diamines (the reactant ratio was 2 : 1) were documented. The condensation can be performed in boiling acetonitrile or methanol. Products **144** are formed in nearly quantitative yields.

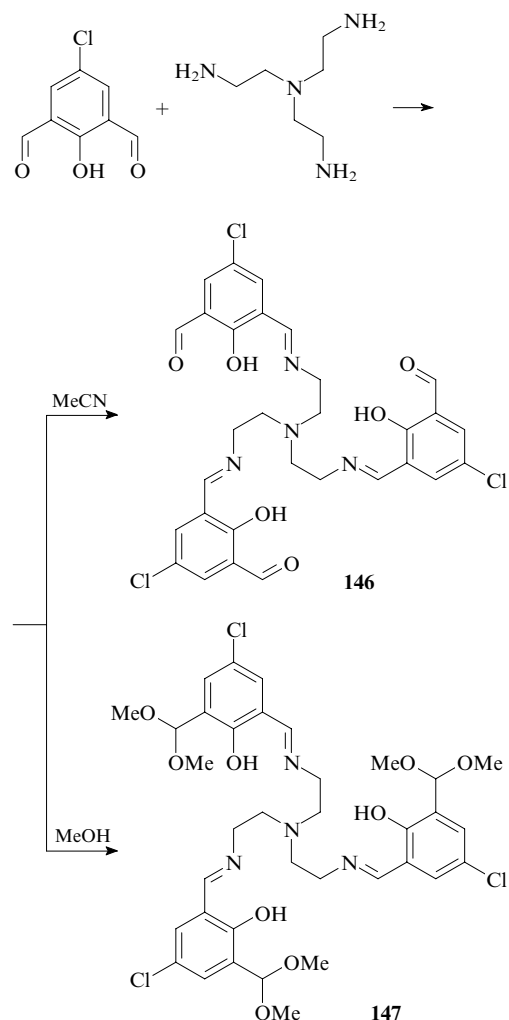


R = Cl, Me; X = (CH₂)_n (n = 2, 3),²⁰² (CH₂)₂NH(CH₂)₂,
(CH₂)₂S(CH₂)₂,⁷⁵ CH₂(CH₂OCH₂)₂CH₂,²⁰²
(CH₂)₂NHC(O)C(O)NH(CH₂)₂,⁷⁹ NHC(S)NH.⁸⁸

2,6-Diacetyl-4-methylphenol reacts analogously yielding azomethine **145**.²⁰³

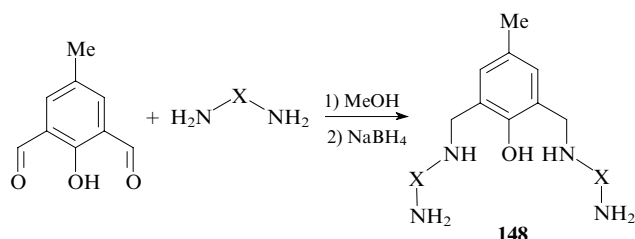


The condensation of diformyl derivatives of phenols with tris(2-aminoethyl)amine in a ratio of 3 : 1 in anhydrous acetonitrile affords [3 + 1]-condensation product **146**.^{147, 202, 204, 205} Acyclic condensation product **146** is formed only if the reactants are used in a stoichiometric ratio; otherwise, the macrocyclisation giving cryptands is the main reaction pathway (see Section II.4.e).



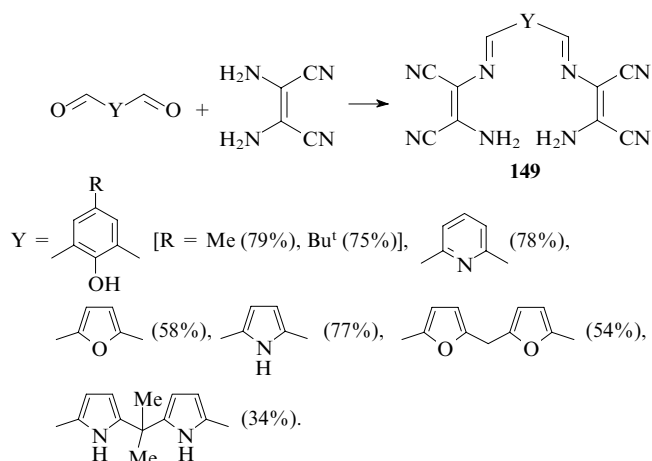
The reaction in methanol results not in the triformyl derivative but in its acetal **147**.²⁰⁶

All attempts to perform the stoichiometrically controlled [1 + 2] condensation of dicarbonyl compounds with two equivalents of aliphatic diamines failed. The reactions afford [1 + 2]-condensation products only in the presence of a 50–100-fold excess of diamines. However, attempts to isolate azomethines in the pure form were also unsuccessful because of hydrolytic instability of these compounds. The corresponding stable amines **148** are formed only after reduction of Schiff bases with sodium borohydride.



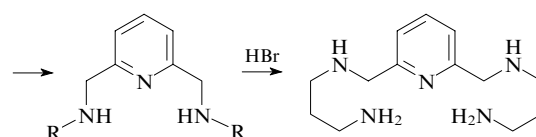
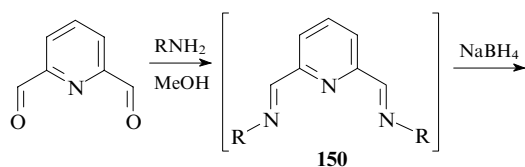
X = (CH₂)₂ (80%),²⁰⁷ (CH₂)₃ (64%),^{208, 209} (CH₂)₂NH(CH₂)₂.²¹⁰

2,3-Diaminomaleonitrile existing (like *o*-phenylenediamine) in the enediamine form has low basicity and nucleophilicity due to the strong electron-withdrawing effect of two nitrile groups conjugated with the amino groups. The reactions of this compound with dicarbonyl compounds give [1 + 2]-condensation products **149** in high yields.^{211, 212}

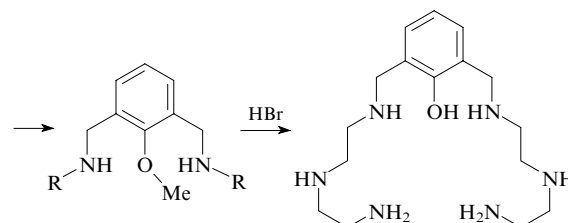
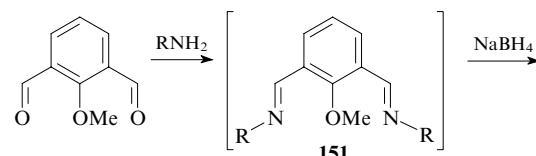


After completion of the reaction at the first amino group, the nucleophilicity of the second amino group decreases so that the process is terminated. Regardless of the nature of the dicarbonyl compound and the reactant ratio, diamines **149** were isolated as the only products.

Special procedures were developed for the controlled synthesis of [1 + 2]-condensation products. In these procedures, one of two amino groups in diamines is preliminarily protected. After condensation and reduction of the imine function, the protecting group is removed. For example, the monoacetyl¹⁹⁹ derivative of 1,3-diaminopropane and the monobenzyloxycarbonyl²⁰⁰ derivative of diethylenetriamine gave [1 + 2]-condensation products with diformylpyridine and diformylanisole, respectively, in high yields (the reactants were used in a stoichiometric ratio). The resulting Schiff bases **150** and **151** were immediately (without isolation) reduced to amines followed by deprotection.^{213, 214}

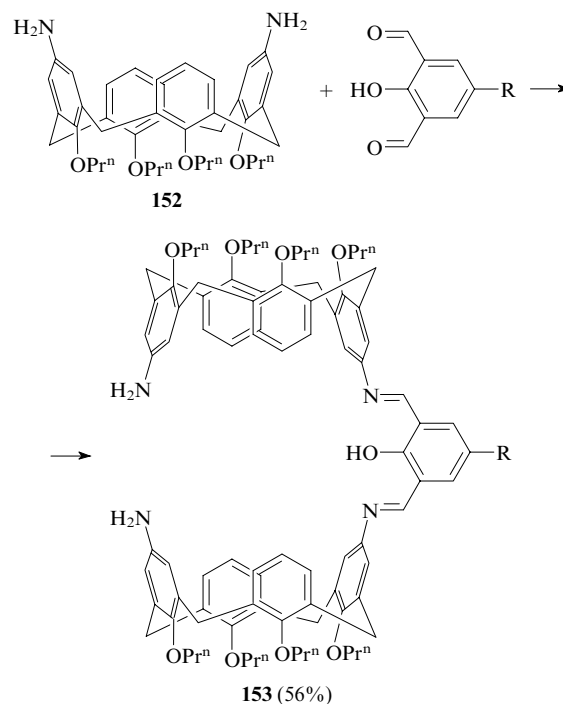


R = (CH₂)₃NHAc.



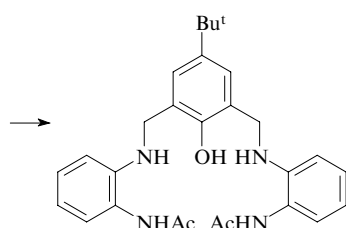
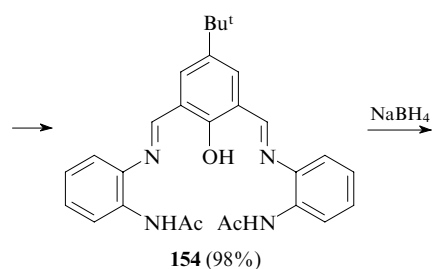
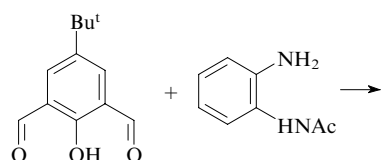
R = (CH₂)₂NH(CH₂)₂NHCbz (Cbz is benzyloxycarbonyl).

The reactions of 2,6-diformyl-4-R-phenols (R = H or Cl) with a twofold excess of the diamino derivative of calixarene **152** in methanol afford the stoichiometrically controlled [1 + 2]-condensation product **153**.¹⁵² In this case, the aromatic diamine gives the [1 + 2]-condensation product without the formation of the corresponding macrocycle.

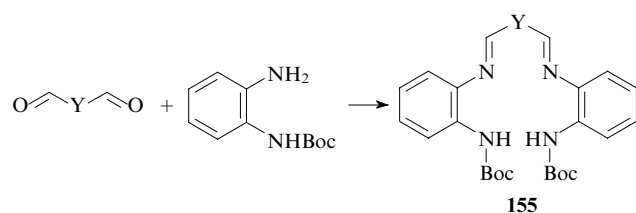


R = H, Cl.

To perform the target [1 + 2] condensation of dicarbonyl compounds with *o*-phenylenediamine, one of the amino groups is protected, as in the case of aliphatic diamines (see above). *N*-Acetyl-*o*-phenylenediamine reacts with 4-*tert*-butyl-2,6-diformylphenol in methanol at room temperature to form [1 + 2]-condensation product **154**, which is then reduced with NaBH₄ to yield the corresponding tetramine.²¹⁵

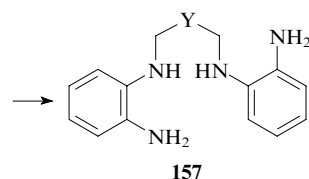
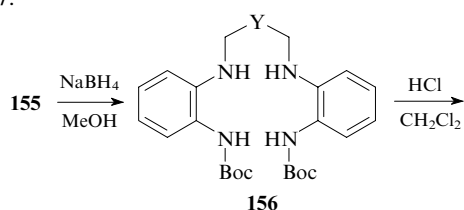


Under analogous conditions (methanol, room temperature), the reaction of *N*-(*tert*-butoxycarbonyl)-*o*-phenylenediamine produces [1 + 2]-Schiff bases **155**.



Y	Z	R	Yield (%)
	COH	Bu ^t	70
	N	H	60
	O	—	71
	NH	—	75
	NH	CMe ₂	69
	O	S	90
	—	—	10

Reduction of the C=N bond in azomethines **155** with NaBH₄ followed by treatment of tetramines **156** with gaseous HCl in dichloromethane afforded salts of acyclic diamines **157**.²¹⁵



Y	Yield of 156 (%)	Yield of 157 (%)
	98	90
	98	75
	95	80
	76	80

These condensations allow the synthesis of diamines and dicarbonyl derivatives containing additional functional groups of different nature. The resulting compounds can be used as building blocks for the construction of more complex macrocycles, which are of interest as polydentate ligands.

VI. Conclusion

The data summarised in the present review show that the condensation of dicarbonyl compounds with diamines under thermodynamic equilibrium conditions gives dynamic combinatorial libraries, which can contain numerous products, due to reversibility of all steps of series-parallel reactions involved in the condensation process. A careful choice of the conditions (the solvent, the concentration and the ratio of the reactants, the temperature and acid catalysis) allows the equilibrium to be shifted toward the target product, and free Schiff bases can be synthesised in good yields in the absence of metal cations, which are traditionally used as template agents. The most complex problem of the formation of unsymmetrical macrocycles can be successfully solved by performing fragment assembly from enlarged building blocks as precursors. In the final step of the synthesis, not only metal ions but also anions can be used as template agents. The latter are particularly efficient in the assembly of macrocycles containing a large number of proton-donor groups capable of hydrogen bonding inside the cavity. Such template condensations provide an approach to the design of artificial anionic and cationic receptors. Polydentate Schiff bases play an important role in coordination and supramolecular chemistry, organic synthesis and various biological and medical applications, resulting in the extensive development of this field of chemistry.

This review has been written with the financial support of the Russian Foundation for Basic Research (Project Nos 06-03-07017, 05-03-32684 and 05-03-08017).

References

- V E Kuz'min, V P Lozitsky, G L Kamalov, R N Lozitskaya, A I Zheltvay, A S Fedtchouk, D N Kryzhanovskiy *Acta Biochim. Polonica* **47** 867 (2000)
- J Gao, F R Woolley, R A Zingaro *J. Med. Chem.* **48** 7192 (2005)

3. D E Burton, K Clarke, G W Gray *J. Chem. Soc.* 438 (1965)
4. R Lozyska, D Kryzhanovsky, A Mazepa, V Gorodniuk, V Kuz'min, V Lozitsky, A Fedchuck, S Rybalko, S Diadiun, J J V Eynde *ARKIVOC* (xiv) 118 (2004)
5. S Brooker *Eur. J. Inorg. Chem.* 2535 (2002)
6. A E Martell, J Perutka, D Kong *Coord. Chem. Rev.* **216**–217 55 (2001)
7. S Di Bella *Chem. Soc. Rev.* **30** 355 (2001)
8. A J Gallant, J K-H Hui, F E Zahariev, Y A Wang, M J MacLachlan *J. Org. Chem.* **70** 7936 (2005)
9. J L Sessler, E Katayev, G D Pantos, Yu A Ustynyuk *Chem. Commun.* 1276 (2004)
10. H Schiff *Ann. Chem. Pharm.* **131** 118 (1864)
11. C Godoy-Alcántar, A K Yatsimirsky, J-M Lehn *J. Phys. Org. Chem.* **18** 979 (2005)
12. S M Nelson *Pure Appl. Chem.* **52** 2461 (1980)
13. W Radecka-Paryzek, V Patroniak, J Lisowski *Coord. Chem. Rev.* **249** 2156 (2005)
14. M C Thompson, D H Busch *Chem. Eng. News* **40** 57 (1962)
15. D H Busch, J A Burke, D C Jicha, M C Thompson, M L Morris *Advances in Chemistry* (Ed. R E Gould) (Washington, DC: American Chemical Society, 1963) Vol. 37, p. 125
16. G A Melson, D H Busch *Proc. Chem. Soc.* 223 (1963)
17. G A Melson, D H Busch *J. Am. Chem. Soc.* **87** 1706 (1965)
18. *Templates in Chemistry I (Topics in Current Chemistry)* Vol. 248 (Eds C A Schalley, F Vögtle, K H Dötz) (Berlin, Heidelberg: Springer, 2004)
19. *Templates in Chemistry II (Topics in Current Chemistry)* Vol. 249 (Eds C A Schalley, F Vögtle, K H Dötz) (Berlin, Heidelberg: Springer, 2005)
20. M D Lankshear, P D Beer *Coord. Chem. Rev.* **250** 3142 (2006)
21. N Gimeno, R Vilar *Coord. Chem. Rev.* **250** 3161 (2006)
22. P A Gale, R Quesada *Coord. Chem. Rev.* **250** 3219 (2006)
23. R Vilar *Angew. Chem., Int. Ed.* **42** 1460 (2003)
24. P D Beer, M R Sambrook, D Curiel *Chem. Commun.* 2105 (2006)
25. S R Collinson, D E Fenton *Coord. Chem. Rev.* **148** 19 (1996)
26. U Beckmann, S Brooker *Coord. Chem. Rev.* **245** 17 (2003)
27. S Brooker *Coord. Chem. Rev.* **222** 33 (2001)
28. S Brooker, T C Davidson, S J Hay, R J Kelly, D K Kennepohl, P G Plieger, B Moubaraki, K S Murray, E Bill, E Bothe *Coord. Chem. Rev.* **216**–217 3 (2001)
29. N V Gerbeleu, V B Arion, J Burgess *Template Synthesis of Macrocyclic Compounds* (Weinheim, New York, Chichester, Brisbane, Singapore, Toronto: Wiley-VCH, 1999)
30. P Guerriero, S Tamburini, P A Vigato *Coord. Chem. Rev.* **139** 17 (1995)
31. P A Vigato, S Tamburini *Coord. Chem. Rev.* **248** 1717 (2004)
32. W B Callaway, J M Veauthier, J L Sessler *J. Porphyrins Phthalocyanines* **8** 1 (2004)
33. N E Borisova, M D Reshetova, Yu A Ustynyuk *Chem. Rev.* **107** 46 (2007)
34. S Chandra, L K Gupta *Spectrochim. Acta, Part A* **60** 1751 (2004)
35. N M Shauib, A-Z A Elassar, A El-Dissouky *Spectrochim. Acta, Part A* **63** 714 (2006)
36. S Chandra, L K Gupta *Spectrochim. Acta, Part A* **62** 307 (2005)
37. M Shakir, S Khatoun, S Parveen, Y Azim *Transition Met. Chem.* **32** 42 (2007)
38. H Adams, N A Bailey, D E Fenton, S Moss, C O Rodriguez de Barbarin, G Jones *J. Chem. Soc., Dalton Trans.* 693 (1986)
39. Y Tian, J Tong, G Frenzen, J-Z Sun *J. Org. Chem.* **64** 1442 (1999)
40. A E Martell, R J Motekaitis, Q Lu, D A Nation *Polyhedron* **18** 3203 (1999)
41. R Gupta, R Mukherjee *Inorg. Chim. Acta* **263** 133 (1997)
42. H Fenniri, C Dallaire, D P Funeriu, J-M Lehn *J. Chem. Soc., Perkin Trans. 2* 2073 (1997)
43. D Chen, A E Martell *Tetrahedron* **47** 6895 (1991)
44. P Comba, A Fath, T W Hambley, A Vielfort *J. Chem. Soc., Dalton Trans.* 1691 (1997)
45. G Wei, G A Lawrance, D T Richens, T W Hambley, P Turner *J. Chem. Soc., Dalton Trans.* 623 (1998)
46. M Allmendinger, P Zell, A Amin, U Thewalt, M Klinga, B Rieger *Heterocycles* **60** 1065 (2003)
47. J Gawronski, H Kolbon, M Kwit, A Katrusiak *J. Org. Chem.* **65** 5768 (2000)
48. N Kuhnert, G M Rossignolo, A Lopez-Periago *Org. Biomol. Chem.* **1** 1157 (2003)
49. N Kuhnert, A M Lopez-Periago *Tetrahedron Lett.* **43** 3329 (2002)
50. N Kuhnert, A M Lopez-Periago, G M Rossignolo *Org. Biomol. Chem.* **3** 524 (2005)
51. M Chadim, M Budesinský, J Hodacová, J Závada, P C Junk *Tetrahedron: Asymmetry* **12** 127 (2001)
52. N Kuhnert, N Burzlaff, C Patel, A Lopez-Periago *Org. Biomol. Chem.* **3** 1911 (2005)
53. N Kuhnert, C Patel, F Jami *Tetrahedron Lett.* **46** 7575 (2005)
54. M Kwit, P Skowronek, H Kolbon, J Gawronski *Chirality* **17** S93 (2005)
55. N Kuhnert, C Straßnig, A M Lopez-Periago *Tetrahedron: Asymmetry* **13** 123 (2002)
56. J Gawronski, M Brzostowska, M Kwit, A Plutecka, U Rychlewska *J. Org. Chem.* **70** 10147 (2005)
57. M Kwit, J Gawronski *Tetrahedron: Asymmetry* **14** 1303 (2003)
58. M Kaik, J Gawronski *Org. Lett.* **8** 2921 (2006)
59. J Gao, A E Martell *Org. Biomol. Chem.* **1** 2795 (2003)
60. D Utz, F W Heinemann, J Mukherjee, R Mukherjee, S Schindler *Z. Anorg. Allg. Chem.* **629** 2211 (2003)
61. S C Menon, A Panda, H B Singh, R P Patel, S K Kulshreshtha, W L Darby, R J Butcher *J. Organomet. Chem.* **689** 1452 (2004)
62. A Panda, S C Menon, H B Singh, C P Morley, R Bachman, T M Cocker, R J Butcher *Eur. J. Inorg. Chem.* 1114 (2005)
63. E A Kataev, M D Reshetova, Yu A Ustynyuk *Izv. Akad. Nauk, Ser. Khim.* 322 (2004)^a
64. S Warzeska, R Krämer *Chem. Ber.* **128** 115 (1995)
65. Z Wang, J Reibenspies, A E Martell *Inorg. Chem.* **36** 629 (1997)
66. D A Plattner, A K Beck, M Neuburger *Helv. Chim. Acta* **85** 4000 (2002)
67. S W A Bligh, N Choi, W J Cummins, E G Evagorou, J D Kelly, M McPartlin *J. Chem. Soc., Dalton Trans.* 3369 (1994)
68. J Gregoliński, J Lisowski, T Lis *Org. Biomol. Chem.* **3** 3161 (2005)
69. R W Stotz, R C Stouffer *J. Chem. Soc. D* 1682 (1970)
70. F Benetollo, G Bombieri, L De Cola, A Polo, D L Smailes, L M Vallarino *Inorg. Chem.* **28** 3447 (1989)
71. A B Blake, E Sinn, A Yavari, B Moubaraki, K S Murray *Inorg. Chim. Acta* **229** 281 (1995)
72. *Svoistva Organicheskikh Soedinenii* (Properties of Organic Compounds) (Ed. A A Potekhin) (Leningrad: Khimiya, 1984)
73. W Schilf, B Kameński, B Kolodziej, E Grech, Z Rozwadowski, T Dziembowska *J. Mol. Struct.* **615** 141 (2002)
74. A Aguiari, E Bullita, P Casellato, S Tamburini, P A Vigato *Inorg. Chim. Acta* **202** 157 (1992)
75. U Casellato, D Fregona, S Sitran, S Tamburini, P A Vigato *Inorg. Chim. Acta* **110** 181 (1985)
76. A Aguiari, N Brianese, S Tamburini, P A Vigato *Inorg. Chim. Acta* **235** 233 (1995)
77. L Tei, A J Blake, F A Devillanova, A Garau, V Lippolis, C Wilson, M Schröder *Chem. Commun.* 2582 (2001)
78. P Guerriero, P A Vigato, J-C G Bünzli, E Moret *J. Chem. Soc., Dalton Trans.* 647 (1990)
79. A Aguiari, S Tamburini, P Tomasin, P A Vigato *Inorg. Chim. Acta* **256** 199 (1997)
80. C-Y Shen, M-F Hu, Q-H Luo, M-C Shen *J. Inorg. Biochem.* **68** 195 (1997)
81. B Kersting, G Steinfeld *Chem. Commun.* 1376 (2001)
82. A J Atkins, D Black, A J Blake, A Marin-Becerra, S Parsons, I Ruiz-Ramirez, M Schröder *Chem. Commun.* 457 (1996)
83. D Black, A J Blake, R L Finn, L F Lindoy, A Nezhadali, G Rognaghi, P A Tasker, M Schröder *Chem. Commun.* 340 (2002)

84. B Dutta, P Bag, B Adhikary, U Flörke, K Nag *J. Org. Chem.* **69** 5419 (2004)
85. A J Atkins, A J Blake, M Schröder *J. Chem. Soc., Chem. Commun.* 353 (1993)
86. S S Tandon, V McKee *J. Chem. Soc., Dalton Trans.* 19 (1989)
87. M Bell, A J Edwards, B F Hoskins, E H Kachab, R Robson *J. Am. Chem. Soc.* **111** 3603 (1989)
88. A D Naik, S M Annigeri, U B Gangadharmath, V K Revankar, V B Mahale *J. Inclusion Phenom. Macrocycl. Chem.* **43** 291 (2002)
89. J Gao, J H Reibenspies, R A Zingaro, F R Woolley, A E Martell, A Clearfield *Inorg. Chem.* **44** 232 (2005)
90. G-J Kim, D-W Park, Y-S Tak *Catal. Lett.* **65** 127 (2000)
91. S R Korupoju, N Mangayarkarasi, S Ameerunisha, E J Valente, P S Zacharias *J. Chem. Soc., Dalton Trans.* 2845 (2000)
92. S R Korupoju, P S Zacharias *Chem. Commun.* 1267 (1998)
93. Yu A Ustynyuk, N E Borisova, V M Nosova, M D Reshetova, S S Talismanov, S E Nefedov, G G Aleksandrov, I L Eremenko, I I Moiseev *Izv. Akad. Nauk, Ser. Khim.* 454 (2002)^a
94. N E Borisova, Yu A Ustynyuk, M D Reshetova *Izv. Akad. Nauk, Ser. Khim.* 174 (2004)^a
95. D S Kumar, V Alexander *Inorg. Chim. Acta* **238** 63 (1995)
96. B Srinivas, N Aruslami, P S Zacharias *Polyhedron* **10** 731 (1991)
97. H Houjou, S-K Lee, Y Hishikawa, Y Nagawa, K Hiratani *Chem. Commun.* 2197 (2000)
98. H Shimakoshi, T Kai, I Aritome, Y Hisaeda *Tetrahedron Lett.* **43** 8261 (2002)
99. S Abe, J Mochizuki, T Sone *Anal. Chim. Acta* **319** 387 (1996)
100. S Srimurugan, B Viswanathan, T K Varadarajan, B Varghese *Tetrahedron Lett.* **46** 3151 (2005)
101. H Houjou, Y Nagawa, K Hiratani *Tetrahedron Lett.* **42** 3861 (2001)
102. M A Perez, J M Bermejo *J. Org. Chem.* **58** 2628 (1993)
103. E J Corey, R Imwinkelried, S Pikul, Y B Xiang *J. Am. Chem. Soc.* **111** 5493 (1989)
104. K Saigo, N Kubota, S Takebayashi, M Hasegawa *Bull. Chem. Soc. Jpn.* **59** 931 (1986)
105. H Brunner, H Schiessling *Angew. Chem., Int. Ed. Engl.* **33** 125 (1994)
106. S Akine, T Taniguchi, T Nabeshima *Tetrahedron Lett.* **42** 8861 (2001)
107. A J Gallant, M J MacLachlan *Angew. Chem., Int. Ed.* **42** 5307 (2003)
108. C T L Ma, M J MacLachlan *Angew. Chem., Int. Ed.* **44** 4178 (2005)
109. S Akine, D Hashimoto, T Saiki, T Nabeshima *Tetrahedron Lett.* **45** 4225 (2004)
110. A J Gallant, B O Patrick, M J MacLachlan *J. Org. Chem.* **69** 8739 (2004)
111. A J Gallant, M Yun, M Sauer, C S Yeung, M J MacLachlan *Org. Lett.* **7** 4827 (2005)
112. J K-H Hui, M J MacLachlan *Chem. Commun.* 2480 (2006)
113. D E Fenton, R Moody *J. Chem. Soc., Dalton Trans.* 219 (1987)
114. N A Bailey, M M Eddy, D E Fenton, S Moss, A Mukhopadhyay, G Jones *J. Chem. Soc., Dalton Trans.* 2281 (1984)
115. H Adams, N A Bailey, S R Collinson, D E Fenton, J C Hawley, S J Kitchen *J. Organomet. Chem.* **550** 20 (1998)
116. H Adams, N A Bailey, P Bertrand, S R Collinson, D E Fenton, S J Kitchen *Inorg. Chim. Acta* **250** 139 (1996)
117. A Lavery, S M Nelson, M G B Drew *J. Chem. Soc., Dalton Trans.* 2975 (1987)
118. N A Bailey, M M Eddy, D E Fenton, G Jones, S Moss, A Mukhopadhyay *J. Chem. Soc., Chem. Commun.* 628 (1981)
119. J Gao, A E Martell *Org. Biomol. Chem.* **1** 2801 (2003)
120. R A Jones, G Quintanilla-Lopes, O Ozturk, S A N Taheri, G B Karatepe, R O Jones *J. Chem. Res.* 309 (2001)
121. S A N Taheri, R A Jones, S S Badesha, M M Hania *Tetrahedron* **45** 7717 (1989)
122. J L Sessler, W Callaway, S P Dudek, R W Date, V Lynch, D W Bruce *Chem. Commun.* 2422 (2003)
123. M R Johnson, C Slebodnick, J A Ibers *J. Porphyrins Phthalocyanines* **1** 87 (1997)
124. J L Sessler, T D Mody, V Lynch *Inorg. Chem.* **31** 529 (1992)
125. J L Sessler, T D Mody, V Lynch *J. Am. Chem. Soc.* **115** 3346 (1993)
126. C Givaja, A J Blake, C Wilson, M Schröder, J B Love *Chem. Commun.* 2508 (2003)
127. J M Veauthier, W -S Cho, V M Lynch, J L Sessler *Inorg. Chem.* **43** 1220 (2004)
128. S Meyer, B Andrioletti, J L Sessler, V Lynch *J. Org. Chem.* **63** 6752 (1998)
129. J L Sessler, W-S Cho, S P Dudek, L Hicks, V M Lynch, M T Huggins *J. Porphyrins Phthalocyanines* **7** 97 (2003)
130. J L Sessler, H Maeda, T Mizuno, V M Lynch, H Furuta *J. Am. Chem. Soc.* **124** 13474 (2002)
131. A Yu Chernyad'ev, Yu A Ustynyuk, O V Yazev, E A Kataev, M D Reshetova, A A Sidorov, G G Aleksandrov, V M Novotortsev, V N Ikorskii, S E Nefedov, I L Eremenko, I I Moiseev *Izv. Akad. Nauk, Ser. Khim.* 2334 (2001)^a
132. M Kumar, V S N Bhalla, V Kumar, M Singh, G Singh *J. Inclusion Phenom. Macrocycl. Chem.* **39** 241 (2001)
133. V J Aran, M Kumar, J Molina, L Lamarque, P Navarro, E Garcia-Espana, J A Ramirez, S V Luis, B Escuder *J. Org. Chem.* **64** 6135 (1999)
134. L Lamarque, P Navarro, C Miranda, V J Aran, C Ochoa, F Escarti, E Garcia-Espana, J Latorre, S V Luis, J F Miravet *J. Am. Chem. Soc.* **123** 10560 (2001)
135. S Aime, M Botta, U Casellato, S Tamburini, P A Vigato *Inorg. Chem.* **34** 5825 (1995)
136. J Liu, Y Masuda, E Sekido *Bull. Chem. Soc. Jpn.* **63** 2516 (1990)
137. H Adams, N A Bailey, P Bertrand, S R Collinson, D E Fenton, S J Kitchen *J. Chem. Soc., Dalton Trans.* 1181 (1996)
138. S M Nelson, F S Esho, M G B Drew *J. Chem. Soc., Dalton Trans.* 407 (1982)
139. E Bullita, U Casellato, F Ossola, P Tomasin, P A Vigato, U Russo *Inorg. Chim. Acta* **287** 117 (1999)
140. Z H Chohan, K M Khan, C T Supuran *Appl. Organomet. Chem.* **18** 305 (2004)
141. M J L Tendero, A Benito, J M Lloris, R Martinez-Manez, J Soto, J Payá, A J Edwards, P R Raithby *Inorg. Chim. Acta* **247** 139 (1996)
142. O D Fox, T D Rolls, M G B Drew, P D Beer *Chem. Commun.* 1632 (2001)
143. K E Krakowiak, A V Bordunov, J S Bradshaw *J. Heterocycl. Chem.* **35** 169 (1998)
144. Q Lu, J-M Latour, C J Harding, N Martin, D J Marrs, V McKee, J Nelson *J. Chem. Soc., Dalton Trans.* 1471 (1994)
145. D McDowell, J Nelson *Tetrahedron Lett.* **29** 385 (1988)
146. J-J Zhang, W Zhang, Q-H Luo, Y-H Mei *Polyhedron* **18** 3637 (1999)
147. F Avecilla, R Bastida, A de Blas, D E Fenton, A Macias, A Rodriguez, T Rodriguez-Blas, S Garsia-Granada, R Corzo-Suarez *J. Chem. Soc., Dalton Trans.* 409 (1997)
148. M Kumar, V Sharma, J N Babu *J. Inclusion Phenom. Macrocycl. Chem.* **42** 247 (2002)
149. M Kumar, V J Aran, P Navarro *Tetrahedron Lett.* **36** 2161 (1995)
150. L Lamarque, C Miranda, P Navarro, F Escarti, E Garcia-Espana, J Latorre, J A Ramirez *Chem. Commun.* 1337 (2000)
151. S Brooker, J D Ewing, J Nelson *Inorg. Chim. Acta* **317** 53 (2001)
152. S Tamburini, P Tomasin, P A Vigato, A Casnati, L Domiano *Inorg. Chim. Acta* **254** 209 (1997)
153. J Jazwinski, J-M Lehn, D Lilienbaum, R Ziessel, J Guilhem, C Pascard *J. Chem. Soc., Chem. Commun.* 1691 (1987)
154. D McDowell, J Nelson, V McKee *Polyhedron* **8** 1143 (1989)
155. V McKee, W T Robinson, D McDowell, J Nelson *Tetrahedron Lett.* **30** 7453 (1989)
156. M G B Drew, V Felix, V McKee, G Morgan, J Nelson *Supramol. Chem.* **5** 281 (1995)
157. M G B Drew, D Marrs, J Hunter, J Nelson *J. Chem. Soc., Dalton Trans.* 11 (1992)

158. A Grohmann, H Lanig, W Bauer, S Schmidt, F W Heinemann *J. Mol. Model.* **6** 119 (2000)
159. S Schmidt, W Bauer, F W Hienemann, H Lanig, A Grohmann *Angew. Chem., Int. Ed.* **39** 913 (2000)
160. Yu A Ustynyuk, O V Yazev, I P Gloriozov, D N Laikov *Proceedings of Humboldtian Conference on Biomedical Science, Moscow, 2001* P. 7
161. H Okawa, H Furutachi, D E Fenton *Coord. Chem. Rev.* **174** 51 (1998)
162. M Vicente, R Bastida, A Macias, L Valencia, C F G C Geraldes, C D Brondino *Inorg. Chim. Acta* **358** 1141 (2005)
163. W H Correa, J L Scott *Molecules* **9** 513 (2004)
164. N Brianese, U Casellato, S Tamburini, P Tomasin, P A Vigato *Inorg. Chim. Acta* **293** 178 (1999)
165. U Casellato, S Tamburini, P Tomasin, P A Vigato *Inorg. Chim. Acta* **357** 4191 (2004)
166. U Casellato, S Tamburini, P Tomasin, P A Vigato *Inorg. Chim. Acta* **341** 118 (2002)
167. U Casellato, S Tamburini, P Tomasin, P A Vigato *Inorg. Chim. Acta* **262** 117 (1997)
168. D-H Won, C-H Lee *Tetrahedron Lett.* **42** 1969 (2001)
169. C-H Lee, K-T Oh *Tetrahedron Lett.* **40** 1921 (1999)
170. C-H Lee, J-W Ka, D-H Won *Tetrahedron Lett.* **40** 6799 (1999)
171. E Bertolo, R Bastida, A de Blas, D E Fenton, C Lodeiro, A Macias, A Rodriguez, T Rodriguez-Blas *J. Inclusion Phenom. Macrocycl. Chem.* **35** 191 (1999)
172. A H M Elwahy *Tetrahedron* **56** 897 (2000)
173. R Seangprasertkij, Z Asfari, F Arnaud, J Vicens *J. Org. Chem.* **59** 1741 (1994)
174. C Lodeiro, R Bastida, A de Blas, D E Fenton, A Macias, A Rodriguez, T Rodriguez-Blas *Inorg. Chim. Acta* **267** 55 (1998)
175. O Struck, L A J Christoffels, R J W Lugtenberg, W Verboom, G J van Hummel, S Harkema, D N Reinhoudt *J. Org. Chem.* **62** 2487 (1997)
176. D Armspach, D Matt, F Peruch, P Lutz *Eur. J. Inorg. Chem.* 805 (2003)
177. E A Kataev, G D Pantos, J L Sessler, M D Reshetova, Yu A Ustynyuk *Izv. Akad. Nauk, Ser. Khim.* 161 (2005)^a
178. V V Roznyatovskii, N E Borisova, M D Reshetova, A G Buyanovskaya, Yu A Ustynyuk *Izv. Akad. Nauk, Ser. Khim.* 2152 (2005)^a
179. A A Abbas *Tetrahedron* **60** 1541 (2004)
180. K Gunst, S Seggewies, E Breitmaier *Synthesis* 1856 (2001)
181. S Meyer, M C Hoehner, V Lynch, J L Sessler *J. Porphyrins Phthalocyanines* **3** 148 (1999)
182. S Seggewies, T Schönameier, E Breitmaier *Synthesis* 565 (1999)
183. J L Sessler, A E V Gordon, D Seidel, S Hannah, V Lynch, P L Gordon, R J Donohoe, C D Tait, D W Keogh *Inorg. Chim. Acta* **341** 54 (2002)
184. A Drews, T Schönameier, S Seggewies, E Breitmaier *Synthesis* 749 (1998)
185. A Jasat, D Dolphin *Chem. Rev.* **97** 2267 (1997)
186. J L Sessler, R M Dávila, V Král *Tetrahedron Lett.* **37** 6469 (1996)
187. S Katsiaouni, S Dechert, C Brückner, F Meyer *Chem. Commun.* 951 (2007)
188. J L Sessler, V Roznyatovskiy, G D Pantos, N E Borisova, M D Reshetova, V M Lynch, V N Khrustalev, Yu A Ustynyuk *Org. Lett.* **7** 5277 (2005)
189. E J Corey, B-C Pan, D H Hua, D R Deardorff *J. Am. Chem. Soc.* **104** 6816 (1982)
190. W Moneta, P Baret, J-L Pierre *J. Chem. Soc., Chem. Commun.* 899 (1985)
191. L Salmon, P Thuery, E Riviere, S Miyamoto, T Yamato, M Ephritikhine *New J. Chem.* **30** 1220 (2006)
192. H Shimakoshi, H Takemoto, I Aritome, Y Hisaeda *Tetrahedron Lett.* **43** 4809 (2002)
193. H Höpfl, M Sanchez, V Barba, N Farfán, S Rojas, R Santillan *Inorg. Chem.* **37** 1679 (1998)
194. H Höpfl, N Farfán *J. Organomet. Chem.* **547** 71 (1997)
195. V Barba, H Höpfl, N Farfán, R Santillan, H I Beltran, L S Zamudio-Rivera *Chem. Commun.* 2834 (2004)
196. V Barba, R Villamil, R Luna, C Godoy-Alcantar, H Höpfl, H I Beltran, L S Zamudio-Rivera, R Santillan, N Farfan *Inorg. Chem.* **45** 2553 (2006)
197. V Barba, E Gallegos, R Santillan, N Farfán *J. Organomet. Chem.* **622** 259 (2001)
198. J L Sessler, E A Katayev, D G Pantos, P Scherbakov, M D Reshetova, V N Khrustalev, V M Lynch, Yu A Ustynyuk *J. Am. Chem. Soc.* **127** 11442 (2005)
199. P T Corbett, S Otto, J K M Sanders *Chem. – Eur. J.* **10** 3139 (2004)
200. E A Katayev, G D Pantos, M D Reshetova, V N Khrustalev, V M Lynch, Yu A Ustynyuk, J L Sessler *Angew. Chem., Int. Ed.* **44** 7386 (2005)
201. S Brooker, G S Dunbar, T Weyhermuller *Supramol. Chem.* **13** 601 (2001)
202. N Brianese, U Casellato, S Tamburini, P Tomasin, P A Vigato *Inorg. Chim. Acta* **272** 235 (1998)
203. X Chen, S Zhan, C Hu, Q Meng, J Shun *Inorg. Chim. Acta* **260** 95 (1997)
204. M D Timken, W A Marritt, D N Hendrickson, R A Gagne, E Sinn *Inorg. Chem.* **24** 4202 (1985)
205. U Casellato, S Tamburini, P Tomasin, P A Vigato, M Botta *Inorg. Chim. Acta* **247** 143 (1996)
206. S J Archibald, A J Blake, S Parsons, M Schröder, R E P Winpenny *J. Chem. Soc., Dalton Trans.* 173 (1997)
207. I E Dickson, R Robson *Inorg. Chem.* **13** 1301 (1974)
208. S Brooker, P D Croucher, T C Davidson, P D Smith *Polyhedron* **19** 1887 (2000)
209. S Brooker, P D Croucher *J. Chem. Soc., Chem. Commun.* 2075 (1995)
210. S Brooker, P D Croucher *J. Chem. Soc., Chem. Commun.* 1278 (1993)
211. N E Borisova, Yu A Ustynyuk, M D Reshetova, G G Aleksandrov, I L Eremenko, I I Moiseev *Mendeleev Commun.* 202 (2003)
212. N E Borisova, V V Roznyatovskii, M D Reshetova, Yu A Ustynyuk *Zh. Org. Khim.* **41** 1028 (2005)^b
213. S Brooker, T J Simpson *J. Chem. Soc., Dalton Trans.* 1151 (1998)
214. G Ambrosi, M Formica, V Fusi, L Giorgi, A Guerri, M Micheloni, R Pontellini, P Rossi *Polyhedron* **22** 1135 (2003)
215. N E Borisova, M D Reshetova, M V Kuznetsov, Yu A Ustynyuk *Synthesis* 1169 (2007)

^a — *Russ. Chem. Bull., Ent. Ed. (Engl. Transl.)*^b — *Russ. J. Org. Chem. (Engl. Transl.)*

Hypervalent silicon-containing organosilicon derivatives of nitrogen heterocycles

M G Voronkov, O M Trofimova, Yu I Bolgova, N F Chernov

Contents

I. Introduction	825
II. Intramolecular organosilicon complexes of nitrogen heterocycles	826
III. Silatranyl derivatives of nitrogen-containing heterocycles	836

Abstract. The published data on the methods of synthesis, properties and transformations of organosilicon derivatives of nitrogen heterocycles containing a hypervalent silicon atom are generalised and described systematically. The bibliography includes 173 references.

I. Introduction

Most of the known organosilicon compounds contain a tetracoordinate silicon atom. However, the coordination number of silicon can increase to 5 or 6, especially when the silicon atom is surrounded by electronegative substituents. Intermolecular complexes containing a hexacoordinate silicon atom have been known since the early 19th century when Gay-Lussac and Thenard¹ obtained the addition product of ammonia to tetrafluorosilane, $2\text{H}_3\text{N} \cdot \text{SiF}_4$. In the second half of the 20th century, the attention of scientists was attracted by intramolecular complexes of pentacoordinate silicon. Of particular interest among these are silatranes studied in detail by Academician M G Voronkov and his co-workers.^{2–16} Studies on silatranes made a valuable contribution to the theoretical, synthetic, medical and applied chemistry. Organosilicon intramolecular complexes are considered in reviews.^{17–22} These compounds have an unusual molecular structures, high reactivities and specific biological activities.

During the same period, many researchers were interested in organosilicon derivatives of nitrogen heterocycles,^{23–27} which came into use as synthons in organic chemistry for the preparation of biologically active compounds, sorbents, *etc.* It is known that nitrogen-containing rings such as pyrrole, imidazole, pyrazole, pyrimidine, indole, carbazole, *etc.*, form the core of alkaloids, natural and synthetic antibiotics and

other pharmaceuticals. The introduction of an organosilicon substituent containing a hypervalent silicon atom into nitrogen heterocycle molecules changes considerably their electronic structure and reactivity. The most pronounced changes are observed upon introduction of a silatranyl [inductive constants $\sigma_1 = -0.56$,²⁸ $\sigma^* = -3.49$ (Ref. 29)] and silatranylmethyl [$\sigma_1 = -0.36$,³⁰ $\sigma^* = -2.24$ (Ref. 29)] groups exhibiting strong electron-donating inductive effect and having a high dipole moment. This modification of heterocyclic compounds gives rise to new classes of biologically active products promising for medicine and agriculture.

Hypervalent silicon-containing organosilicon derivatives of nitrogen heterocycles can be classified into three groups.

1. Intermolecular complexes of heterocyclic compounds with tetrahalosilanes and organylhalosilanes, for example, complexes of pyridine, picolines, 2,2'- and 4,4'-bipyridines and 1,10-phenanthroline with tetrafluorosilane and organylfluorosilanes which have been described in detail in a review.³¹

2. Heterocyclic compounds in which the silicon atom becomes hypervalent due to intramolecular coordination with endo- (or exo-)cyclic heteroatom N or O.

3. Heterocyclic compounds in which the hypervalent silicon atom is a part of an exocyclic substituent. The main representatives of this group are silatrane derivatives in which the silicon atom is bound to the heterocycle either directly or through a $(\text{CH}_2)_n$, CH_2NR , CH_2S , O or another bridge.

This review deals with organosilicon derivatives of nitrogen heterocycles of the last two groups, except for *N*-(dialkylchlorosilylmethyl)lactams with an $\text{O} \rightarrow \text{Si}$ bond and their derivatives, which were studied in detail by Baukov's group (Russia),^{25,32} and zwitter-ionic spirocyclic $\lambda^5\text{-Si}$ -silicates with an $\text{Si}-\text{C}-\text{N}(\text{Het})$ fragment described by Tacke and co-workers (Germany).^{33–35} Some data concerning compounds of the second and third groups obtained by the authors of the present review have been briefly surveyed before.^{36–38} The organosilicon compounds considered below that contain simultaneously a nitrogen heterocycle and a hypervalent silicon atom are of substantial theoretical interest for organic chemists. The knowledge of the molecular structure and physical properties of these compounds would extend the existing views on both the stereoelectronic structure of the hypervalent silicon derivatives and the specific influence of organosilicon substituents containing a penta- or hexacoordinate Si atom on the character of the heterocycle and its reactivity. In addition, many of these compounds possess high and specific biological activities and are potential pharmaceutical or agricultural agents.

M G Voronkov, O M Trofimova, Yu I Bolgova

A E Favorsky Irkutsk Institute of Chemistry, Siberian Branch of the Russian Academy of Sciences, ul. Favorskogo 1, 664033 Irkutsk, Russian Federation. Fax (7-3952) 39 60 46, tel. (7-3952) 42 64 00, e-mail: voronkov@irioch.irk.ru (M G Voronkov), tel. (7-3952) 42 75 45, e-mail: omtrof@irioch.irk.ru (O M Trofimova, Yu I Bolgova)

N F Chernov Irkutsk State Pedagogical University, ul. Nizhnaya Naberezhnaya 6, 664011 Irkutsk, Russian Federation. Fax (7-3952) 33 63 97

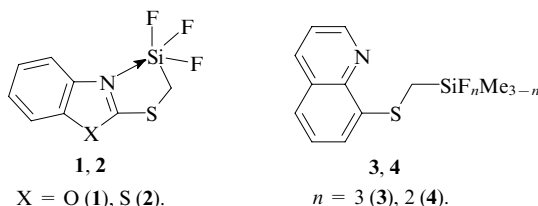
Received 30 March 2007

Uspekhi Khimii 76 (9) 885–906 (2007); translated by Z P Bobkova

II. Intramolecular organosilicon complexes of nitrogen heterocycles

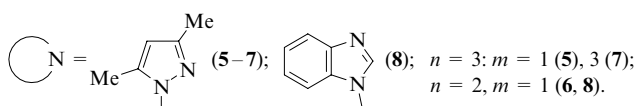
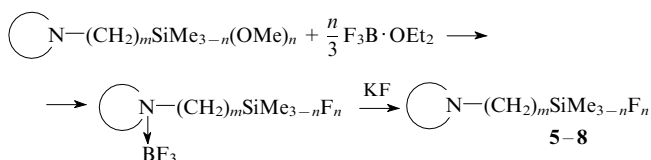
1. Methods of synthesis

The presence of an organosilicon substituent $\text{YSiX}_n\text{Me}_{3-n}$ ($\text{X} = \text{Cl}, \text{F}$; $n = 1-3$; Y is a hydrocarbon or heteroatomic group) in a nitrogen heterocycle may produce, at a certain molecular structure, a pentacoordinate silicon atom through the donor–acceptor interaction with the endocyclic heteroatom, either nitrogen or oxygen. This is observed, for example, in trifluorosilylmethyl derivatives of 2-mercaptobenzoxazole (1) or 2-mercaptobenzothiazole (2).³⁹



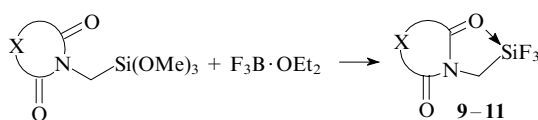
This type of compounds were synthesised by reactions of *S*-trimethoxysilylmethyl derivatives of heterocycles with boron trifluoride etherate. Trifluoro(8-quinolylthiomethyl)- (3) and difluoro(methyl)(8-quinolylthiomethyl)silanes (4) were obtained in a similar way.⁴⁰ However, UV and IR spectroscopic data did not support the assumption about the presence of intramolecular $\text{N} \rightarrow \text{Si}$ donor–acceptor bonds closing six-membered chelate rings in these compounds.

The reaction of *N*-trimethoxysilylalkyl or *N*-dimethoxy(methyl)silylmethyl derivatives of 3,5-dimethylpyrazole and benzimidazole with an excess of boron trifluoride etherate involves not only the replacement of methoxy groups by fluorine atoms but also coordination of nitrogen to the BF_3 molecule to give *B*-trifluoroborazane.^{37, 38}



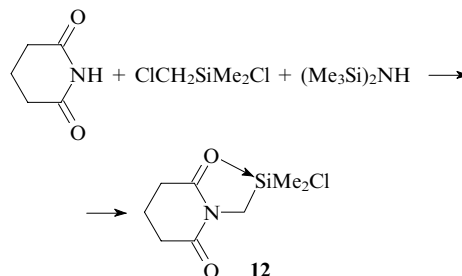
On treatment with potassium fluoride or carbamide, borazanes lose BF_3 being converted into compounds 5–8.

The reaction of *N*-(trimethoxysilylmethyl)imides of dicarboxylic acids, namely, succinic, glutaric and phthalic acids, with boron trifluoride etherate without a solvent at 35–40 °C afforded intramolecular complexes: *N*-(trifluorosilylmethyl)succinimide (9),^{41–43} -glutarimide (10)^{43, 44} and -phthalimide (11).⁴⁵ In these compounds, the silicon atom is pentacoordinated due to the formation of an additional transannular $\text{O} \rightarrow \text{Si}$ donor–acceptor bond; the presence of this bond was confirmed by X-ray crystallography and multinuclear NMR and IR spectroscopy.^{41, 43–45} These compounds refer to the group of so-called dragonoids.¹³

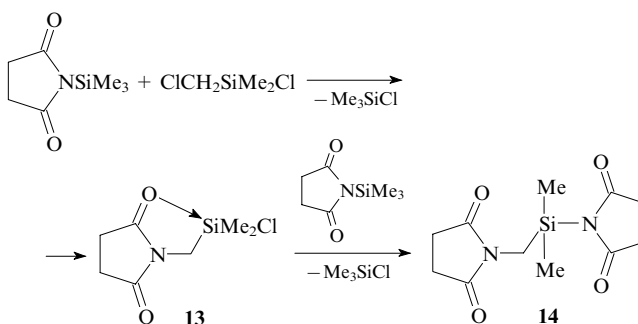


X = $(\text{CH}_2)_n$ ($n = 2$ (9), 3 (10)), *o*-phenylene (11).

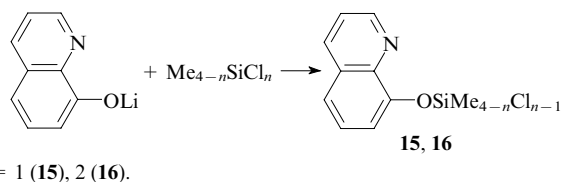
N-(Chlorodimethylsilylmethyl)glutarimide (12) was prepared by the reaction of *N*-(trimethylsilyl)glutarimide with chloro(chloromethyl)dimethylsilane or by the reaction of unsubstituted glutarimide with a mixture of hexamethyldisilazane and chloro(chloromethyl)dimethylsilane.⁴⁶ The presence of a pentacoordinate silicon in compound 12 was demonstrated both in solutions and in crystals



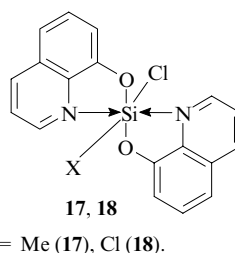
In the case of *N*-(trimethylsilyl)succinimide, the formation of the expected *N*-(chlorodimethylsilylmethyl)succinimide (13) was accompanied by the formation of organosilicon diimide 14, resulting from substitution of the imide fragment for chlorine. According to NMR and X-ray diffraction data, the silicon atom in compound 14 is tetracoordinated.



Hensen and Klebe⁴⁷ demonstrated that the reaction of *O*-lithio-8-hydroxyquinoline with chloro(methyl)silanes $\text{Cl}_n\text{SiMe}_{4-n}$ ($n = 1, 2$) results in substitution of the quinolyloxy group for chlorine to give compounds 15 ($n = 1$) and 16 ($n = 2$) with tetracoordinate silicon atoms.

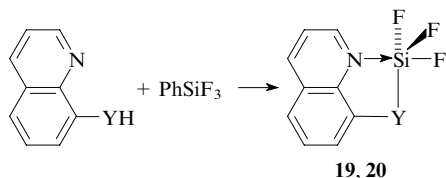


In an analogous reaction with more chlorinated silanes ($n = 3$ and 4), two chlorine atoms are replaced, because two molecules of lithiated 8-hydroxyquinoline are involved. In the compounds 17 and 18 thus formed, the silicon atom is linked by $\text{N} \rightarrow \text{Si}$ donor–acceptor bonds to both heterocyclic molecules.



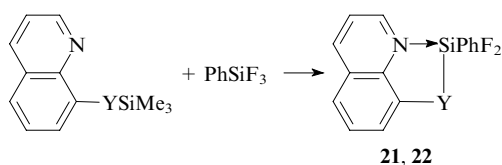
It was found⁴⁸ that the silicon coordination polyhedron in (chloro)methyl[bis(8-quinolyloxy)]silane (**17**) is a distorted octahedron.

We proposed a new original method for the synthesis of organosilicon intramolecular complexes of quinoline **19** and **20** containing a pentacoordinate silicon atom by protolytic cleavage of the Si–C bond in trifluoro(phenyl)silane under the action of 8-hydroxy- or 8-mercaptoquinoline:^{38, 49}



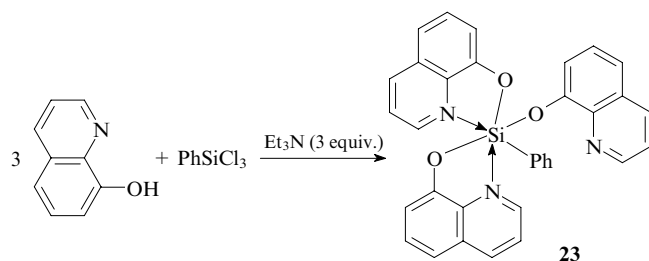
Y = O (**19**), S (**20**).

The reaction of trifluoro(phenyl)silane with 8-(trimethylsiloxy)quinoline and its thio analogue occurs as transsilylation with elimination of fluoro(trimethyl)silane to give intramolecular complexes **21** and **22** containing an N → Si donor–acceptor bond.⁴⁹

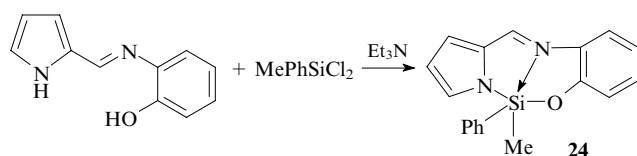


Y = O (**21**), S (**22**).

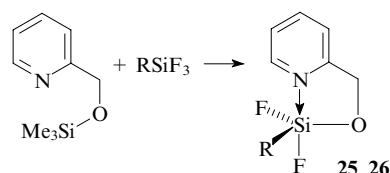
Trichloro(phenyl)silane can be used to prepare organosilicon derivatives of nitrogen heterocycles. When made to react with 3 equivalents of 8-hydroxyquinoline in the presence of triethylamine as HCl acceptor, this compound produces complex **23** containing a hexacoordinate silicon atom.⁵⁰



The reaction of pyrrole-2-*N*-(*o*-hydroxyphenyl)carbalimine with dichloro(methyl)phenylsilane results in compound **24**. In this case, the additional coordination of silicon is accomplished through the formation of the donor–acceptor bond with the imine nitrogen.⁵¹

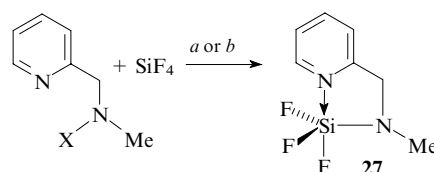


2-(Trimethylsiloxy)methylpyridine reacts with trifluorophenyl- and tetrafluorosilanes to give compounds **25** and **26**, which also contain intramolecular N → Si coordination bonds.⁵²



R = Ph (**25**), F (**26**).

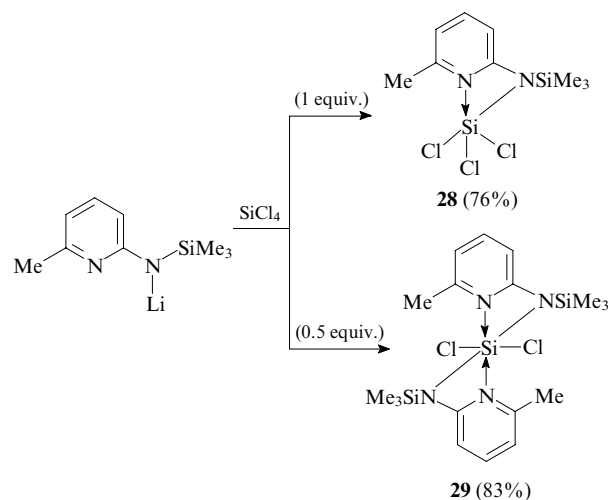
The reaction of lithium methyl(2-pyridylmethyl)amide with SiF₄ in ether gives intramolecular complex **27** with pentacoordinate silicon in 20% yield.⁵³



(a) Et₂O, X = Li; (b) CH₂Cl₂, –25 °C, X = Me₃Si.

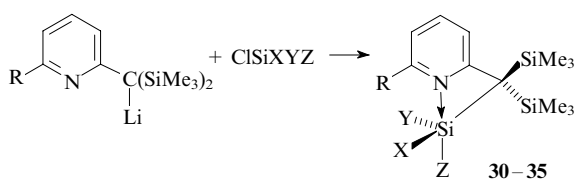
Note that compound **27** is also formed on treatment of 2-[methyl(trimethylsilyl)aminomethyl]pyridine with tetrafluorosilane in dichloromethane at –25 °C (yield 62%).⁵³

Lithium trimethylsilyl(6-methylpyridin-2-yl)amide reacts with tetrachlorosilane in ether giving rise to intramolecular complexes **28** or **29**, depending on the reactant molar ratio (1 : 1 or 2 : 1), in good yields.⁵⁴



Compound **28** contains pentacoordinate silicon, while dimer **29** contains a hexacoordinate silicon atom. Dimer **29** is stable on heating to 100 °C, whereas compound **28** decomposes even at 50 °C.

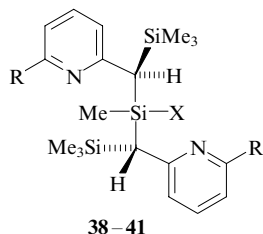
It was found^{55, 56} that reactions of chloromethylsilanes Me_{4–n}SiCl_n (*n* = 2, 3) or HSiCl₃ with 2-[lithiobis(trimethylsilyl)]methylpyridine or its 6-methyl derivative afford compounds **30–35**. These intramolecular complexes contain a pentacoordinate silicon atom incorporated in a four-membered (!) coordination ring through the N → Si bond.



X = H, Y = Z = Cl: R = H (**30**), Me (**31**); X = Me, Y = Z = Cl: R = H (**32**), Me (**33**); X = Y = Me, Z = Cl: R = H (**34**), Me (**35**).

It is noteworthy that no N→Si coordination bond was found in related compounds **36** (X = Y = Z = Me, R = H) and **37** (X = Y = Z = R = Me) obtained from chlorotrimethylsilane.

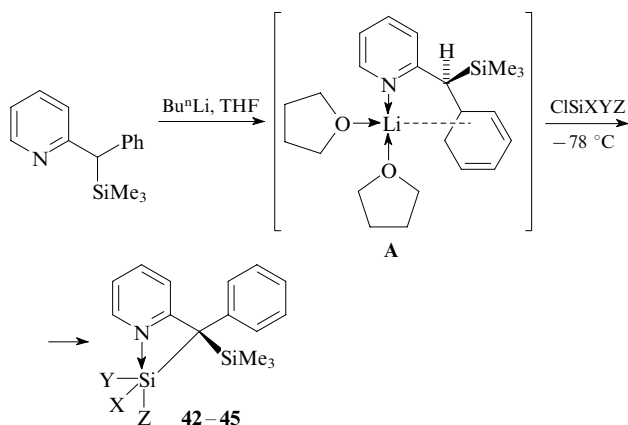
However, when analogous lithio derivatives of picoline and lutidine containing one trimethylsilyl group are made to react with trichloro(methyl)- or dichloro(dimethyl)-silane, crystalline racemates with tetracoordinate silicon, compounds **38–41**, are formed.⁵⁶



38–41

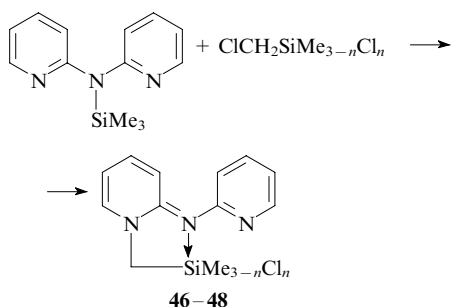
X = Cl: R = H (**38**), Me (**39**); X = Me: R = H (**40**), Me (**41**).

The metallation of 2-[(trimethylsilyl)phenyl]methylpyridine with *n*-butyllithium in tetrahydrofuran gives a red-coloured solution of complex **A**. Its subsequent reaction with $\text{SiX}_{4-n}\text{Cl}_n$ (X = H, *n* = 3; X = Me, *n* = 1–3) in THF at -78°C leads to compounds **42–45** containing pentacoordinate silicon; the THF solutions of these products are dark-red.⁵⁶



X = H, Y = Z = Cl (**42**); X = Me, Y = Z = Cl (**43**);
X = Y = Me, Z = Cl (**44**); X = Y = Z = Me (**45**).

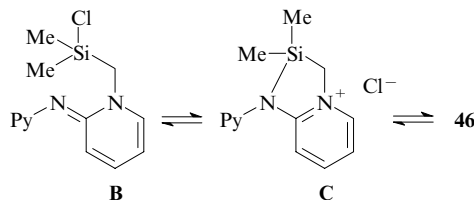
Intramolecular organosilicon complexes **46–48** were synthesised by the reaction of bis(2-pyridyl)(trimethylsilyl)amine with chloro(halomethyl)methylsilanes $\text{XCH}_2\text{SiMe}_{3-n}\text{Cl}_n$ (X = Cl, Br; *n* = 1–3).⁵⁷ For X = Cl, the reaction proceeds as shown below



n = 1 (**46**), 2 (**47**), 3 (**48**).

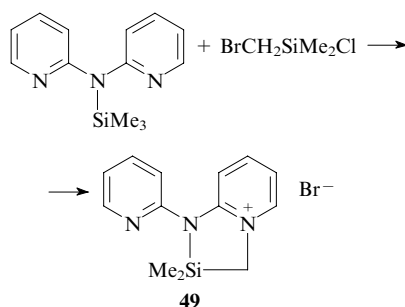
Evidently, the reaction starts with quaternisation and isomerisation of the pyridine fragment accompanied by elimination of chlorotrimethylsilane. Formally, the SiMe_3 group is substituted by $\text{CH}_2\text{SiMe}_2\text{Cl}$ (*i.e.*, the reaction occurs as transilylation²⁵) (Scheme 1).

Scheme 1

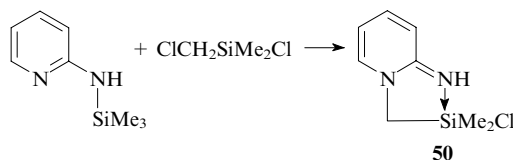


The compound **B** thus formed isomerises to give pyridinium salt **C**. The silicon atom in intermediates **B** and **C** is tetracoordinated. However, in product **46** containing an N→Si donor–acceptor bond, the silicon atom is pentacoordinated.

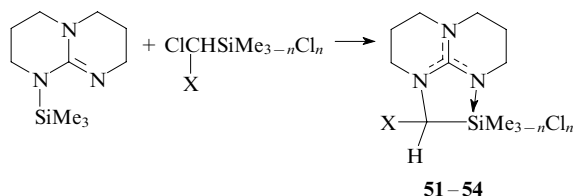
As opposed to this mechanism, for X = Br, the pyridinium nitrogen atom becomes the reaction site; therefore, the reaction yields stable pyridinium bromide **49**.⁵⁷



Compound **50** was prepared in a similar way from *N*-trimethylsilyl-2-pyridylamine and chloro(chloromethyl)dimehylsilane.²⁷

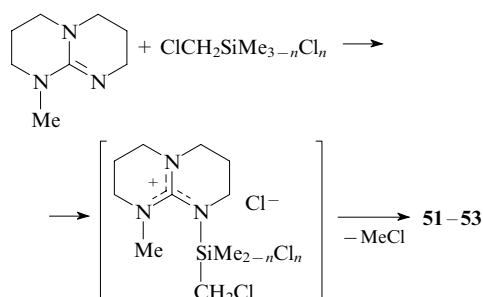


The reactions of chloro(chloromethyl)methylsilanes, trichloro(1-chloroethyl)silane and trichloro(chloromethyl)silane with 1-trimethylsilyl-2*H*-1,3,4,6,7,8-hexahydropyrimido[1,2-*a*]pyrimidine have been studied.⁵⁸ These reactions give crystalline intramolecular complexes **51–54** containing a pentacoordinate silicon atom in nearly quantitative yields (88%–94%).

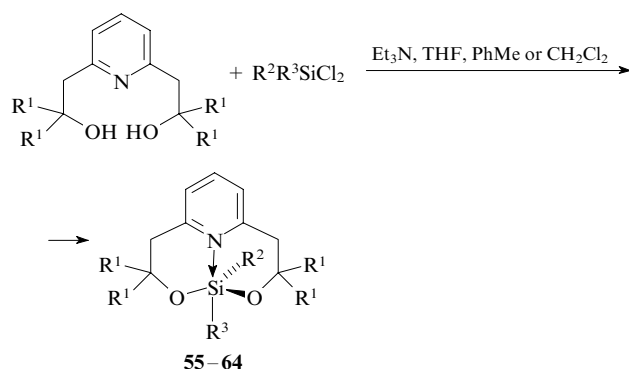


X = H: *n* = 1 (**51**), 2 (**52**), 3 (**53**); X = Me, *n* = 3 (**54**).

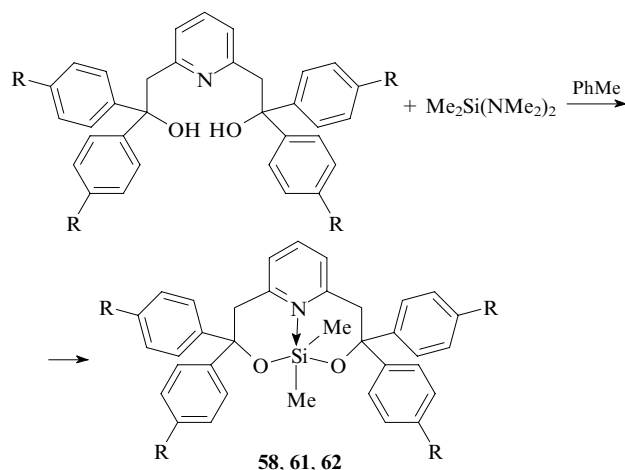
Compounds **51–53** were also obtained (yields 86%–92%) from 1-methyl-2*H*-1,3,4,6,7,8-hexahydropyrimido[1,2-*a*]pyrimidine and appropriate chloro(chloromethyl)silanes.⁵⁸



The reactions of substituted 2,6-bis(2-hydroxyethyl)pyridines with dimethyl-, diphenyl- and methylphenyl-dichlorosilanes and with bis(dimethylamino)dimethylsilane yield compounds **55–64**.^{59–63}



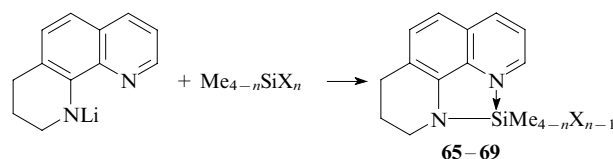
$\text{R}^1 = \text{Ph}$; $\text{R}^2 = \text{R}^3 = \text{Me}$ (**55**), Ph (**56**); $\text{R}^2 = \text{Me}$, $\text{R}^3 = \text{Ph}$ (**57**);
 $\text{R}^1 = \text{C}_6\text{H}_4\text{F-4}$; $\text{R}^2 = \text{R}^3 = \text{Me}$ (**58**), Ph (**59**); $\text{R}^2 = \text{Me}$, $\text{R}^3 = \text{Ph}$ (**60**);
 $\text{R}^1 = \text{C}_6\text{H}_4\text{Br-4}$, $\text{R}^2 = \text{R}^3 = \text{Me}$ (**61**);
 $\text{R}^1 = \text{C}_6\text{H}_4\text{Bu}^t\text{-4}$, $\text{R}^2 = \text{R}^3 = \text{Me}$ (**62**);
 R_2^1COH is 2-hydroxyadamantan-2-yl; $\text{R}^2 = \text{R}^3 = \text{Me}$ (**63**), Ph (**64**).



$\text{R} = \text{F}$ (**58**), Br (**61**), Bu^t (**62**).

Compound **63** was the first example of a 1,3-dioxa-7-aza-2-silacyclodecane system incorporating a heterocycle (pyridine) and containing a weak transannular $\text{N} \rightarrow \text{Si}$ coordination bond (length 2.727 Å).⁵⁹ The structure of this compound was confirmed by ^{29}Si NMR spectroscopy [the silicon chemical shift $\delta(^{29}\text{Si})$ was -41.9]. The silicon atom geometry in molecule **63** is much closer to tetrahedral than to trigonal-bipyramidal (see Section II.2.a). The silicon atom in compound **55** also has a geometry intermediate between a tetrahedron and a trigonal bipyramid.⁶⁰

The reaction of *N*-lithio-1,2,3,4-tetrahydro-1,10-phenanthroline with halo(methyl)silanes $\text{Me}_{4-n}\text{SiX}_n$ ($\text{X} = \text{F}, \text{Cl}$; $n = 1-4$) follows the route shown below:^{47, 64}

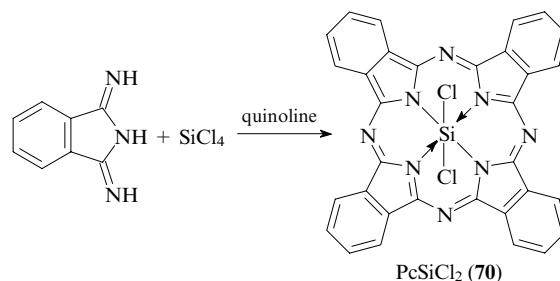


$\text{X} = \text{Cl}$: $n = 1$ (**65**), 2 (**66**), 3 (**67**); $n = 4$: $\text{X} = \text{F}$ (**68**), Cl (**69**).

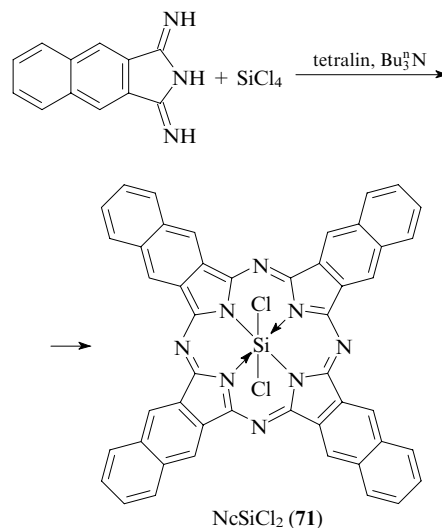
According to X-ray diffraction data,^{64–68} and ^{15}N , ^{29}Si (Ref. 69) and ^{19}F (Ref. 70) NMR spectroscopy, the silicon atom in compounds **66–69** is pentacoordinated due to the formation of the intramolecular $\text{N} \rightarrow \text{Si}$ coordination bond. The same is true for the isostructural compound containing an SiF_2Cl group.⁶⁷ Meanwhile, intramolecular $\text{N} \rightarrow \text{Si}$ interaction in 1-trimethylsilyl-1,2,3,4-tetrahydro-1,10-phenanthroline (**65**) is absent or very weak.⁶⁷

Organosilicon intramolecular complex derivatives of phthalocyanine (Pc), naphthalocyanine (Nc), porphyrin, *etc.* containing a hexacoordinated central silicon atom attracted attention of researchers back in the beginning of the second half of the 20th century.^{71, 72} These compounds can be regarded as siliconium(VI) derivatives. Over the period from 1960 to 1965, a dozen of publications were devoted to these compounds, the studies by Joyner *et al.*^{73, 74} being pioneering. In this review we dwell only on the compounds studied over the last two decades.

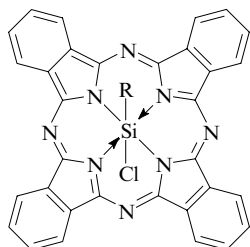
A key method for the synthesis of phthalocyanino- or naphthalocyanino- λ^6 -siliconium dichlorides is the reaction of silicon tetrachloride with 1,3-diiminoisoindoline.⁷⁵



or 1,3-diiminobenzoisoindoline.⁷⁶

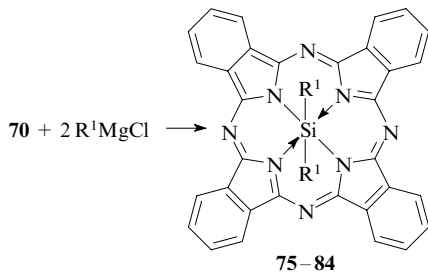


Organosilicon phthalocyanines have received much more attention than phthalocyanino- λ^6 -siliconium dichlorides. Chloroorganylsilyl phthalocyanine derivatives **72–74** were obtained by the reaction of chloroorganylsilanes with 1,3-diiminoisoindoline (yields up to 80%).^{77,78}

**72–74**

R = Me (**72**), Ph (**73**), n-C₈H₁₇ (**74**).

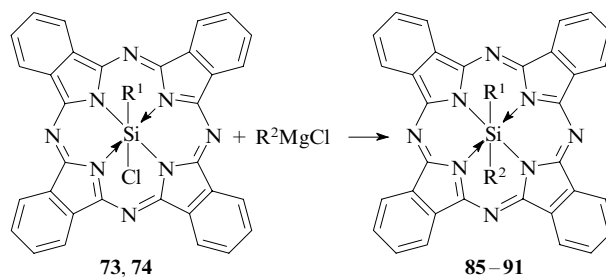
Phthalocyanino- λ^6 -siliconium chlorides can also serve as the starting compounds for the synthesis of organosilicon phthalocyanines. For example, symmetric phthalocyanino- λ^6 -siliconium derivatives **75–84** were prepared from dichloride **70** by the reaction with Grignard reagents.^{78,79}

**75–84**

R¹ = Me (**75**), R²C₆H₄ [R² = H (**76**), 4-Me (**77**), 4-MeO (**78**), 3-CF₃ (**79**)], n-C₈H₁₇ (**80**), R³C \equiv C [R³ = H (**81**), Me (**82**), Bu^t (**83**), Ph (**84**)].

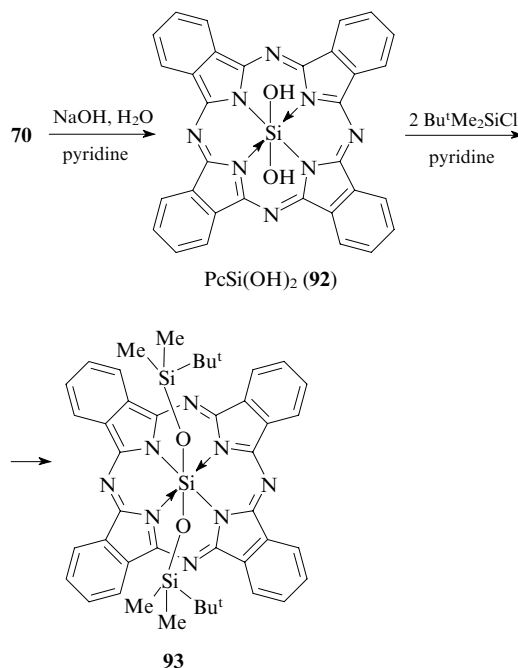
Similarly, chlorine-containing precursors PcSiR¹Cl were converted into unsymmetrical organosilicon phthalocyanine derivatives **85–91**.⁷⁸

Dichloride PcSiCl₂ (**70**) is hydrolysed on treatment with an aqueous solution of pyridine or NaOH to give silanediol



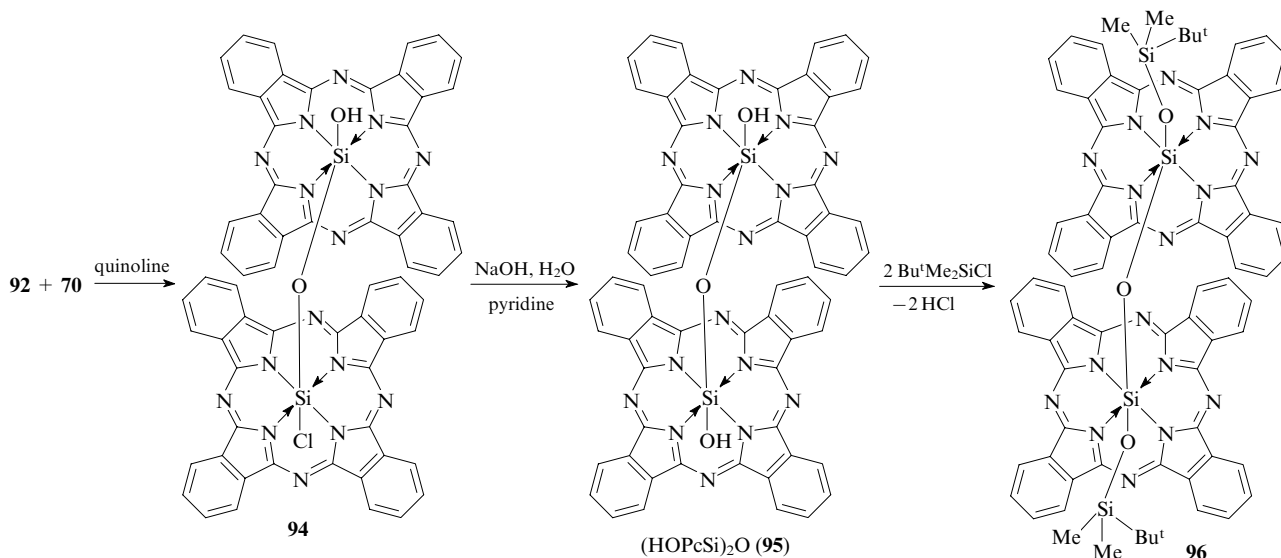
R¹ = Ph: R² = R³C₆H₄ [R³ = 4-Me (**85**), 4-MeO (**86**), 3-CF₃ (**87**)],
R¹ = n-C₈H₁₇: R² = R⁴C₆H₄ [R⁴ = H (**88**), 4-Me (**89**), 4-MeO (**90**), 3-CF₃ (**91**)].

PcSi(OH)₂ (**92**).⁸⁰ The reaction of this product with *tert*-butyl(chloro)dimethylsilane results in siloxy derivative **93**.



The reaction of phthalocyanine **92** with an excess of PcSiCl₂ (**70**) followed by hydrolysis of product **94** (Scheme 2)

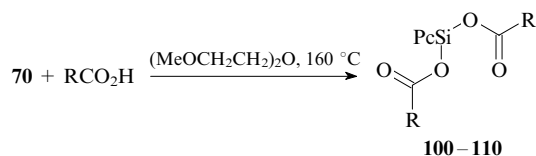
Scheme 2



affords $[\text{HOPcSi}]_2\text{O}$ (**95**), which reacts with $\text{Bu}^t\text{Me}_2\text{SiCl}$ in dry pyridine giving rise to compound **96**.⁸⁰

The reaction of chlorotrihexylsilane with $\text{PcSi}(\text{OH})_2$ (**92**) in the presence of tributylamine in dry γ -picoline furnished phthalocyanine $\text{PcSi}[\text{OSi}(\text{n-C}_6\text{H}_{13})_3]_2$ (**97**). An analogous transformation has also been described for naphthalocyanino- λ^6 -siliconium derivative. For example, treatment of dichloride **71** with concentrated H_2SO_4 yields diol $\text{NcSi}(\text{OH})_2$ (**98**), which reacts with $(\text{n-C}_6\text{H}_{13})_3\text{SiCl}$ to be converted into bis(trihexylsiloxynaphthalocyanino)- λ^6 -siliconium $\text{NcSi}[\text{OSi}(\text{n-C}_6\text{H}_{13})_3]_2$ (**99**).⁷⁶

Organosilicon phthalocyanino- λ^6 -siliconium derivatives **100–110** were formed upon reaction of dichloride **70** with appropriate carboxylic acids.⁸¹



$\text{R} = 4\text{-Bu}^t\text{C}_6\text{H}_4$ (**100**), 3-CH=CHSCH=CCH_2 (**101**), $2\text{-MeOC}_6\text{H}_4\text{CH}_2$ (**102**), $3\text{-MeOC}_6\text{H}_4\text{CH}_2$ (**103**), $4\text{-MeOC}_6\text{H}_4\text{CH}_2$ (**104**), $2,5\text{-(MeO)}_2\text{C}_6\text{H}_3\text{CH}_2$ (**105**), $3,4\text{-(MeO)}_2\text{C}_6\text{H}_3$ (**106**), $3,4\text{-(MeO)}_2\text{C}_6\text{H}_3\text{CH}_2$ (**107**), $3,4,5\text{-(MeO)}_3\text{C}_6\text{H}_2\text{CH}_2$ (**108**), $3,4\text{-(MeO)}_2\text{C}_6\text{H}_3(\text{CH}_2)_2$ (**109**), $3,4\text{-(MeO)}_2\text{C}_6\text{H}_3(\text{CH}_2)_3$ (**110**).

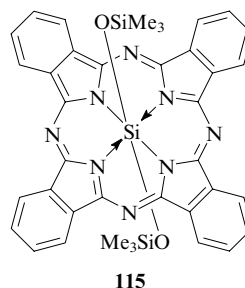
At $\text{R} = 4\text{-Bu}^t\text{C}_6\text{H}_4$, compound **100** with a rigid orthogonal arrangement of the aryloxy groups is produced. Bis(3-thienylcarboxylate) **101** is conformationally more flexible. The change in the nature of the aromatic substituent in phthalocyanino- λ^6 -siliconium induces a change in its spectroscopic properties, which are related to the energies of excited states, while elongation of the aliphatic chain causes changes in the luminescence time and the quantum yield.⁸¹

Dichlorosilylphthalocyanine (**70**) reacts with 4-hydroxy-4'-nitroazobenzene in the presence of sodium hydride to give organosilicon bis(azobenzophthalocyanine) **111** with a hexacoordinate central silicon atom. Compound **111** is the first example of azobenzophthalocyanino- λ^6 -siliconium (Scheme 3).⁸² The electrochemical properties of this compound indicate that it is promising for the use in devices such as photoelectric relays.

The synthesis of *Si*-disubstituted phthalocyanino- λ^6 -siliconium derivatives containing two 1,3-bis(dimethylamino)isopropoxy groups (compound **112**)⁸³ or one (**113**) or two (**114**) 1,2,3,4-di-*O*-isopropylidene- α -D-galactopyranose fragments at the central silicon atom was reported.⁸⁴ Organosilicon phthalocyanine derivatives, especially unsymmetrical ones, proved to be highly efficient carcinostatics with respect to

human carcinoma cells HepG2 and were captured by the mouse macrophage J774. The photodynamic activity of these compounds is due to their absorption by cancer cells and efficient generation of singlet oxygen.

The reaction of $\text{PcSi}(\text{OH})_2$ (**92**) with *N,O*-bis(trimethylsilyl)acetamide in the presence of pyridine gives $\text{PcSi}(\text{OSiMe}_3)_2$ (**115**).⁸⁵ Similarly, compounds $\text{Me}_3\text{SiO}(\text{PcSiO})_n\text{SiMe}_3$ ($n = 2\text{--}5$) were prepared from $\text{HO}(\text{PcSiO})_n\text{H}$.



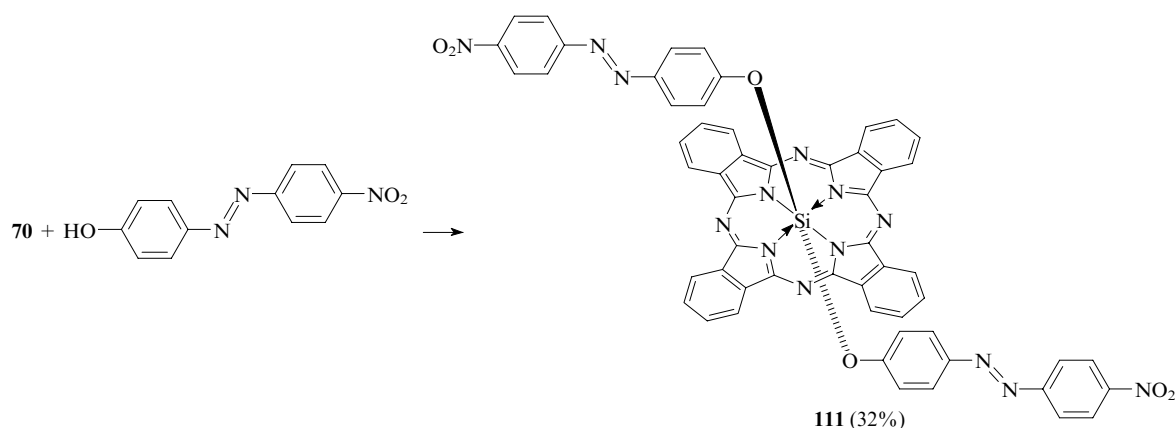
More than 100 papers published during the last 30 years were devoted to the methods of preparation, structure, and properties (chemical, physical, optical and electronic) of organosilicon phthalocyanine polymers and the scope of their applications in advanced fields of engineering and medicine.^{86–94}

Axially disubstituted phthalocyanino- λ^6 -siliconium derivatives with ester groups at the silicon atoms and with phenyl, terphenyl, thienyl, pyrenyl^{95,96} and fullerene⁹⁷ substituents have been synthesised. Electrochemical, absorption and film-forming characteristics of these compounds and dependence of properties on the nature of substituents at the hexacoordinate silicon atom were studied.

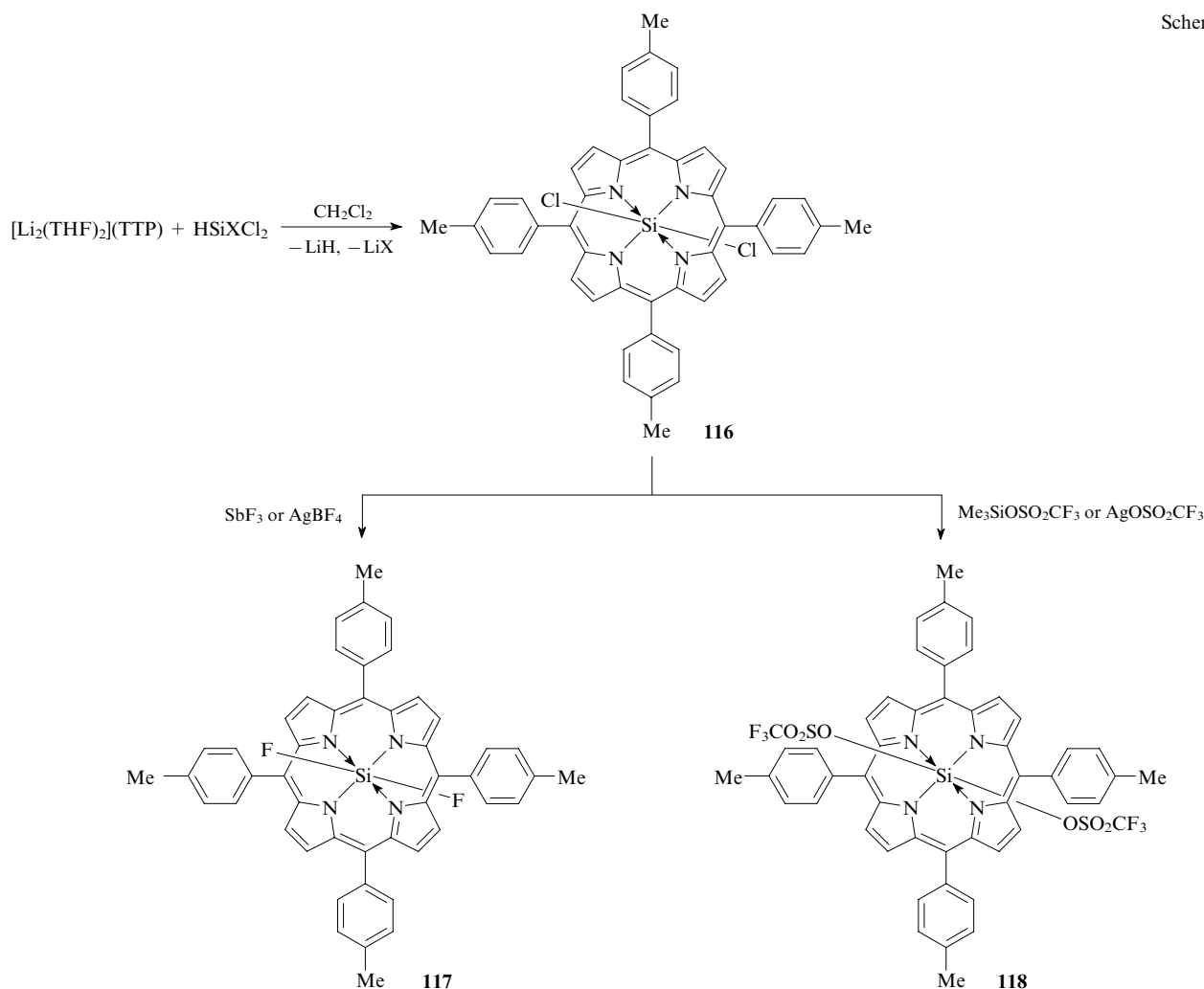
Phthalocyanino- λ^6 -siliconium oligomers $\text{R}_3\text{SiO}(\text{SiPcO})_n\text{SiR}_3$ ($n = 2\text{--}4$) comprising two, three or four monomers cross-linked by siloxane bridges have also been described. The spatial and electronic structures of these compounds were investigated by NMR and UV/Vis absorption spectroscopy and by other physical, kinetic and computational methods.^{98–103}

As a conclusion of this Section, consider examples of silicon-containing derivatives of tetra(*p*-tolyl)porphyrin (TTP). The reduction of $\text{Si}(\text{TTP})\text{Cl}_2$ (see Ref. 104) with the $\text{Na/Hg}\text{--THF}$ system afforded tetratolylporphyrino- λ^6 -siliconium $\text{Si}(\text{TTP})(\text{THF})_2$.¹⁰⁵ The reaction of the lithium derivative of TTP with trichlorosilane in dichloromethane at -78°C gave compound **116**.¹⁰⁴ The reactions of compound **116** with SbF_3 (or AgBF_4) and with $\text{Me}_3\text{SiOSO}_2\text{CF}_3$ (or $\text{AgOSO}_2\text{CF}_3$) in CH_2Cl_2 gave difluoride **117** and ditriflate **118** in quantitative yields (Scheme 4).

Scheme 3



Scheme 4



2. Studies of the molecular structure

a. X-Ray diffraction method

The pentacoordinate silicon atom present in organosilicon intramolecular complex derivatives of nitrogen heterocycles containing an endocyclic $N \rightarrow Si$ coordination bond exists in a trigonal-bipyramidal environment. The lengths of the bonds between silicon and two apical ligands for some of these molecules are presented in Table 1.

The $N \rightarrow Si$ dative bond and the $Si-X$ bond ($X = F, Cl, O, N$) usually occupy axial positions. If two or three electronegative atoms are attached to silicon, then the apical position is occupied by the atom with a higher apical activity (the ability to occupy this site and ensure *trans*-coordination of the ligands), which decreases in the sequence $Cl, OCOR > F \approx SR > OR, NR_2 > Ar > Alk > H$.^{108, 109} The position of an atom or an atomic group in this sequence is correlated with their electronegativity and the polarisability of their bonds with silicon.

The displacement of the silicon atom (ΔSi) from the central plane formed by three equatorial ligands toward the axial vertex Z (see Table 1) varies from 0.01 to 0.380 Å.

The compounds of pentacoordinate silicon contain most often a five-membered chelate ring. Compounds with four-membered (**28**,⁵⁴ **30–35**,^{55, 56} **42–44**)⁵⁶ and six-membered (**55–64**)^{59–63} coordination rings are also known.

The variations of the $N \rightarrow Si$ and $Si-Z$ interatomic distances are antiparallel. In molecules **46**, **50**, **51** and **66**, shortening of the $Si-Cl$ bond in the $N \rightarrow Si-Cl$ axial fragment from 3.908 to 2.269 Å is accompanied by elongation of the $Si-N$ bond from 1.766 to 2.028 Å. This is in good agreement with the

Table 1. Bond lengths $N \rightarrow Si$ and $Si-Z$ in the $N \rightarrow Si-Z$ fragment of intramolecular silicon heterocyclic complexes.

Compound	X	Y	Z	$N \rightarrow Si$ /Å	$Si-Z$ /Å	ΔSi /Å	Ref.
1	F	F	F	1.967	1.624		106
2	F	F	F	1.988	1.632		106
9	F	F	F	2.096 ^a	1.607	0.290	41
10	F	F	F	1.977 ^{a, b}	1.619	0.160	107
				1.992		0.180	
11	F	F	F	2.654 ^a	1.576	0.380	45
12	Me	Me	Cl	2.171	2.210	0.190	46
27	F	F	F	1.974	1.621		53
28	Cl	Cl	Cl	1.975	2.107		54
30	H	Cl	Cl	2.066	2.167		55
31	H	Cl	Cl	2.072	2.163		56
46	Me	Me	Cl	1.898	2.598	0.167	57
48	Cl	Cl	Cl	1.901	2.238	0.010	57
50	Me	Me	Cl	1.766	3.908		27
				1.777	4.111		
51	Me	Me	Cl	1.852	2.679	0.166	58
66	Me	Me	Cl	2.028	2.269		68
67	Me	Cl	Cl	2.027	2.207		68
68	F	F	F	1.969	1.621	0.195	64
69	Cl	Cl	Cl	1.984	2.150		65, 66, 68

^a The $O \rightarrow Si$ bond length is given; ^b bond lengths for two conformers, namely, with an envelope (α) and planar (β) geometries of the six-membered heterocycle are given.

hypervalence theory proposed by Musher¹¹⁰ and developed later by Pestunovich, Sidorkin, and Voronkov.^{14, 15, 111} According to this concept, the axial atoms are bound to the silicon p_z -orbital by a system of three-centre four-electron ($3c-4e$) molecular orbitals.

The equatorial substituents interact with the axial fragment, thus shortening the $N \rightarrow Si$ bond and lengthening the $Si-Cl$ bond.¹⁴ This effect is not very pronounced but evidently significant. However, in molecules **66**, **67** and **69** differing in the number of equatorial chlorine atoms (1, 2 and 3, respectively), the $N \rightarrow Si$ bond length and the axial $Si-Cl$ bond length decrease as the number of chlorine atoms increases (see Table 1).⁶⁸ The equatorial bonds in an ideal trigonal bipyramid (TBP) with the silicon atom in the equatorial plane ($\Delta Si = 0$) are orthogonal to the three-centre MOs. Shortening of the bonds is apparently caused by the electron-withdrawing effect of silicon, which makes the silicon atom approach the axial substituents.

In molecule **51**, the silicon atom is located at the centre of a disordered TBP the axial positions of which are occupied by the heterocycle nitrogen atom and the chlorine atom (the $N-Si-Cl$ angle is 167.9°).⁵⁸ The length of the very short $N \rightarrow Si$ bond (1.852 \AA) is close to a covalent bond length (1.796 \AA), while the length of the very long $Si-Cl$ bond (2.679 \AA) attests to a substantial polarisation.

The two interatomic distances $N-Si$ in 2-[methyl(trifluorosilyl)aminomethyl]pyridine (**27**)⁵³ are non-equivalent, the $N \rightarrow Si$ coordination bond being much longer than the covalent bond. In the TBP of molecule **27**, the pyridine nitrogen atom and the fluorine atom are in the axial positions (the $NSiF$ angle is 178.0°). The $Si-F_{ax}$ bond (1.621 \AA) is longer than $Si-F_{eq}$ (1.603 \AA).

Attention is attracted by the considerable difference between the $O \rightarrow Si$ bond lengths in the *N*-(trifluorosilylmethyl)succinimide (**9**) and -glutarimide (**10**) molecules and that in the *N*-(trifluorosilylmethyl)phthalimide (**11**) molecule, indicating much stronger bonds in the case of compounds **9** and **10** than in compound **11**.^{41, 43–45, 107} This is due to the fact that the five-membered pyrrolidine-2,5-dione ring in the molecule of organosilicon phthalimide derivative **11** is aromatic, as it has a closed six- π -electron shell. Therefore, the nucleophilicity of the carbonyl oxygen atoms in compound **11** is lower than that in non-aromatic molecules **9** and **10**.

The $C=O$ bond incorporated in the five-membered coordination ring of molecules **9–11** (see Table 1) is 0.04 , 0.038 and 0.02 \AA longer than the exocyclic $C=O$ bond (1.202 , 1.202 and 1.210 \AA , respectively) in which the oxygen atom is not coordinated.⁴³ Due to the donor–acceptor bonding of the O and Si atoms in molecules **9–11**, the lengths of the two endocyclic $N-C$ bonds in the heterocycle are different. The $N-C$ bond in compounds **9–11** incorporated in the coordination ring (1.323 , 1.357 and 1.367 \AA , respectively) is much shorter than the $N-C$ bond at the second carbonyl group (1.400 , 1.409 and 1.393 \AA , respectively). These data suggest a higher degree of p, π -conjugation of nitrogen with the carbonyl group incorporated in the coordination heterocycle in molecules **9–11**.

The surrounding of the silicon atom in the 2-diphenyl(methyldichlorosilyl)methylpyridine molecule is nearly tetrahedral, whereas in the 2-[dichlorobis(trimethylsilyl)silylmethyl]pyridine molecule (**30**), the silicon atom of the dichlorosilyl group is located at the centre of the TBP, the $N \rightarrow Si$ bond length being 2.066 \AA .⁵⁵

According to X-ray diffraction^{64–66} and neutron diffraction⁶⁴ data, the lengths of the $N \rightarrow Si$ coordination bonds in 1-trifluoro- and 1-trichlorosilyl-1,2,3,4-tetrahydro-1,10-phenanthroline (**68**) and (**69**) (see Table 1) are much longer than the length of the $Si-N$ valence bond (1.732 and 1.737 \AA , respectively). The replacement of one or two chlorine atoms in molecule **69** by methyl group(s) results in a slight increase in the

$N \rightarrow Si$ distance (see Table 1).⁶⁸ However, when all three Cl atoms are replaced by methyl groups (trimethylsilyl phenanthroline derivative **65**), the $N \rightarrow Si$ donor–acceptor bond is substantially elongated (2.689 \AA). The environment of the silicon atom in molecule **65** can be defined as a highly disordered tetrahedron, unlike that in analogous molecules **68** and **69** where the silicon atom is located at the center of a TBP.⁶⁷

The structures of 2-(trifluorosilylmethyl)thiobenzoxazole (**1**) and -benzothiazole (**2**) resemble each other in many respects. The silicon atom polyhedron is a TBP in both molecules and the lengths of the $N \rightarrow Si$ donor–acceptor bonds are equal to 1.967 and 1.988 \AA , respectively. The $Si-F_{ax}$ bonds in compounds **1** and **2** (1.624 and 1.632 \AA , respectively) are longer than the equatorial $Si-F_{eq}$ bonds (1.594 and 1.589 \AA , respectively).¹⁰⁶

In molecule **28**, the silicon atom is pentacoordinated and has a distorted trigonal-bipyramidal geometry.⁵⁴ The axial positions of the bipyramid are occupied by the $N(Py)$ and Cl atoms (the $NSiCl$ angle is 167.9°). The equatorial $N_{eq}-Si$ valence bond (1.753 \AA) is much shorter than the $N_{ax}-Si$ bond (1.975 \AA), which attests to the presence of $N(Py) \rightarrow Si$ dative interaction.

In the molecule of compound **56**, the axial $N \rightarrow Si-C$ angle is 170° , which implies a distorted TBP.⁶¹ The equatorial $Si-C$ bond is 0.1 \AA shorter than chemically the same axial bond (Table 2), which is a typical feature of this geometry. The $N \rightarrow Si$ bond in **56** is somewhat longer than those in compounds **55** and **63** (by 0.087 and 0.063 \AA , respectively) (see Table 2), which is attributable to a higher positive charge of the silicon atom in the $SiPh_2$ group compared with $SiMe_2$.^{59–61}

In the molecule of compound **61**, which is a bromophenyl analogue of compound **56**, the pentacoordinate silicon atom is at the vertex of a square pyramid. This type of geometry is seldom encountered in hypervalent silicon compounds.⁶² The $N \rightarrow Si$ interatomic distance in molecule **61** (1.950 \AA , see Table 2) is shorter than this distance in any of the studied silatranes (see Section III.2).¹⁵

Unlike compound **56**, the silicon polyhedron in molecules **58** and **60** is a distorted TBP in which the apical positions are occupied by the nitrogen atom and the phenyl group.⁶³ The $N \rightarrow Si$ interatomic distance (see Table 2) is rather long but it is still markedly shorter than the sum of the van der Waals radii of these elements (3.65 \AA). Structural studies of compound **58** have shown^{59, 60} that the $N \rightarrow Si$ distance is somewhat shorter than those found in compounds **55** and **63**.

The silicon atom in molecule **17** has a distorted octahedral geometry. The two bidentate ligands in chloro(methyl)bis-(8-quinolyloxy)silane (**17**) are nearly mutually orthogonal and occur in the *cis*-positions, hence, the silicon atom becomes a chiral centre.⁴⁸ The $Si-O$ bonds form an angle of 168.7° and the $NSiN$ angle is close to right angle (85.3°). The $N \rightarrow Si$ coordination bonds (see Table 2) are much longer than the $N-Si$ covalent bond, *i.e.*, they are the same as in many compounds of penta- and hexacoordinate silicon.

The disordered structure of $Si(TTP)(THF)_2$ has been studied by X-ray diffraction.¹⁰⁴ Four nitrogen atoms and one silicon atom are coplanar, the Si atom being situated in a slightly distorted octahedral environment, while the *meso*-carbon atoms are located above or below the SiN_4 plane. The oxygen atoms of tetrahydrofuran are in axial positions and are bound to silicon by a dative bond.

The silicon atom in the molecule $(TTP)Si(OSO_2CF_3)_2$ (**118**) has a slightly distorted octahedral geometry with triflate groups in the *trans*-position. In this molecule, the porphyrin rings have a corrugated geometry favourable for the incorporation of a small silicon atom. The $O-Si-O$ angle (178°) is nearly linear. The average $Si-N$ distance in molecule **118** is shorter than in molecules **17**⁴⁸ or **115**⁸⁵ (by 0.145 and 0.050 \AA ,

Table 2. Bond lengths N→Si and Si–X (or Si–Y) in the N→Si–X fragment of intramolecular complex silicon heterocycles.

Com- pound	X	Y	N→Si, /Å	Si–X or Si–Y /Å	Ref.
17	Cl	Me	2.014 2.016	1.94 (C) 2.199 (Cl)	48
23	Ph	OC ₉ H ₆ N	2.034	1.966 1.754	50
55	Me	Me	2.703	1.859 1.852	60
56	Ph	Ph	2.790	1.970 1.871	61
58	Me	Me	2.665	1.862 1.856	63
60	Ph	Me	2.570	1.886 1.867	63
61	Me	Me	1.950	1.896 1.868	62
63	Me	Me	2.727	1.871 1.854	59
100	O ₂ CC ₆ H ₄ Bu ^t -4	O ₂ CC ₆ H ₄ Bu ^t -4	1.914 1.909	1.754	81
101	CH ₂ O ₂ C. .C ₄ H ₃ S-3	CH ₂ O ₂ C. .C ₄ H ₃ S-3	1.906 1.912	1.762	81
109	(CH ₂) ₂ O ₂ C. .C ₆ H ₃ (OMe) ₂	(CH ₂) ₂ O ₂ C. .C ₆ H ₃ (OMe) ₂	1.904 1.913 1.924	1.756	81
115	OSiMe ₃	OSiMe ₃	1.922 1.918 1.915 1.873	1.678 1.680	85
118	OSO ₂ CF ₃	OSO ₂ CF ₃	1.848 1.887 1.874	1.842 1.821	105

respectively). The molecule [Bu^tMe₂SiO(Pc)Si]₂O (**96**) represents a dimer with PcSi units linked by an oxygen atom.⁸⁰ In the molecule PcSi(OSiMe₃)₂ (**115**), the central silicon atom is located in a distorted octahedral environment. Two symmetrically independent Si(Pc)–O–Si(Me) bond angles are 157.8 and 156.6°.⁸⁵

b. ²⁹Si NMR spectroscopy

In the ²⁹Si NMR spectra of hypervalent silicon compounds, typical upfield shifts of the ²⁹Si signals compared to those of tetracoordinate silicon are observed. The chemical shifts in the ²⁹Si NMR spectra of heterocyclic derivatives of pentacoordinate silicon are summarised in Table 3.

According to ²⁹Si NMR data, the N→Si coordination interaction in Si(V) or Si(VI) organosilicon compound considered here is either missing or very weak if the coordination-induced change in the chemical shift (Δδ) defined as

$$\Delta\delta = \delta[^{29}\text{Si}(\text{V or VI})] - \delta[^{29}\text{Si}(\text{VI})]$$

is close to zero.

Yet another feature of the ²⁹Si NMR spectra of heterocyclic derivatives of hypervalent silicon is the clear-cut temperature dependence of the δ(²⁹Si) value. As temperature decreases, the ²⁹Si signal shifts upfield, indicating an increase in the strength of the N→Si coordination bond. The low-temperature change in δ(²⁹Si) may be caused by two processes taking place on decreasing the temperature:

(1) shift of the equilibrium between the tetra- and pentacoordinate states of silicon toward the latter;

(2) shortening of the N→Si coordination bond in the coordination polyhedron of hypervalent silicon.^{112–114}

Nevertheless, in some cases, the ²⁹Si chemical shift changes in the opposite direction upon decrease in the temperature. For example, in the ²⁹Si NMR spectrum of compound **46**, the chemical shift is –6.2 ppm at 100 °C and –18.4 ppm at –80 °C.⁵⁷ This is due to the equilibrium interconversion of compounds **B** and **C** (see Scheme 1), which decreases the silicon coordination number to 4 *via* the stable iminium chloride **C**.

Attention is attracted by the fact that the pentacoordinate state of Si in *N*-trifluorosilylmethylsuccinimide (**9**), -glutarimide (**10**) and -phthalimide (**11**) in solutions is much less pronounced than in most dragonoids studied by ²⁹Si NMR.^{41–45} The presence of intramolecular O→Si coordination bond in organosilicon derivatives of cyclic imides **9–11** is indicated by lower shielding constants of ¹⁹F nuclei [δ(¹⁹F) = –133.5 (for compound **9**), –134.19 (**10**), –134.6 (**11**)] and the ¹J(²⁹Si–¹⁹F) spin-spin coupling constants [248.8 (for compound **9**), 224.5 (**10**) and 256.3 Hz (**11**)] compared to those for tetracoordinate (chloromethyl)trifluorosilane [δ(¹⁹F) = –143.99, ¹J(²⁹Si–¹⁹F) = 267 Hz]. In the ²⁹Si NMR spectra, the silicon signal [–75.7 (**9**), –94.2 (**10**), –72.0 ppm (**11**)] is shifted upfield relative to that for (chloro-

Table 3. Chemical shifts (δ) in the ²⁹Si NMR spectra of heterocyclic derivatives with pentacoordinate silicon Het–SiXYZ.

Com- pound	X	Y	Z	δ(²⁹ Si)	Ref.
9	F	F	F	–75.7	41, 43
10	F	F	F	–94.2	43, 44
11	F	F	F	–72.0	45
12	Me	Me	Cl	6.1	46
16	Cl	Me	Me	–21.0	47
22	F	F	Ph	–79.8	49
23	Ph	OC ₉ H ₆ N	OC ₉ H ₆ N	–149.8	50
30	H	Cl	Cl	–18.0	55, 56
31	H	Cl	Cl	–30.90	56
32	Me	Cl	Cl	–64.82	56
33	Me	Cl	Cl	–33.06	56
34	Me	Me	Cl	–14.72	56
35	Me	Me	Cl	–11.18	56
42	H	Cl	Cl	–27.03	56
43	Me	Cl	Cl	5.32	56
44	Me	Me	Cl	15.59	56
46	Me	Me	Cl	6.4	57
51	Me	Me	Cl	17.1	58
52	Me	Cl	Cl	–19.3	58
53	Cl	Cl	Cl	–81.9	58
54	Cl	Cl	Cl	–77.6	58
55	–	Me	Me	–32.4	60
56	–	Ph	Ph	–63.8	61
57	–	Ph	Me	–49.4	62
58	–	Me	Me	–31.7	63
59	–	Ph	Ph	–60.9	63
60	–	Ph	Me	–48.9	63
61	–	Me	Me	–56.5	62
62	–	Me	Me	–58.0	62
63	–	Me	Me	–41.6	59
64	–	Ph	Ph	–72.6	62
65	Me	Me	Me	–1.5	69
66	Cl	Me	Me	–53.6	69
67	Cl	Cl	Me	–75.9	69
68	F	F	F	–125.2	69
70	–	Cl	Cl	–217	71

methyl)trifluorosilane ($\delta = -71.3$) containing a tetracoordinate silicon atom. This difference, which is most pronounced in low-temperature spectra, allows one to detect the enhanced shielding of ^{29}Si nuclei typical of trigonal-bipyramidal silicon derivatives. However, even at $-100\text{ }^\circ\text{C}$, the NMR spectra of compound **11** attest to equivalence of the ^{13}C nuclei of both carbonyl groups [$\delta(^{13}\text{C}) = -168.4$] and the axial and equatorial fluorine atoms. Altogether, this suggests substantial weakening of the $\text{O} \rightarrow \text{Si}$ coordination bond in the organosilicon phthalimide derivative **11** in low-polarity media and fast (on the NMR time scale) transcoordination of silicon from one oxygen atom to another (pendulum effect).⁴⁵ A similar pendulum effect was found in the molecules of *N*-trifluorosilylmethylsuccinimide (**9**), -glutarimide (**10**) and *N*-(dimethylchlorosilylmethyl)glutarimide (**12**).^{41,43,44,46} The substantial difference $\Delta\delta$ (relative to $\text{ClCH}_2\text{SiF}_3$) for compound **10** (-23 ppm) compared to that for compound **9** (-4 ppm) attests to stronger $\text{O} \rightarrow \text{Si}$ interaction in the former.

According to ^{29}Si NMR spectra, compound **30** contains two magnetically non-equivalent trimethylsilyl groups at ambient temperature, which is in line with the sterically more rigid structure in the crystal.⁵⁵ This confirms the assumption that the nitrogen atom in a distorted TBP of molecule **30** is apically bonded to the silicon atom by an intramolecular coordination bond, which closes a four-membered ring. The carbon atom of the 2-substituent in the pyridine ring bears two SiMe_3 groups located in the *cis*- and *trans*-positions with respect to the equatorial H and Cl atoms, respectively.⁵⁵ Unlike this compound, derivative **31** exhibits temperature-dependent ^{29}Si NMR chemical shifts. The lowest-frequency signal of the central silicon atom is observed at $-70\text{ }^\circ\text{C}$. An increase in intensities of the two resonance signals due to the SiMe_3 groups⁵⁵ attests to fast equilibrium between tetra- and pentacoordinate states of the silicon atom at this temperature.

The ^{29}Si chemical shifts of the central silicon atom in compounds **30–35** (see Table 3) with two trimethylsilyl groups at the exocyclic carbon atom are negative.⁵⁶ Meanwhile, in the NMR spectra of isostructural derivatives **42–44** in which one SiMe_3 group has been replaced by phenyl group, the ^{29}Si chemical shifts may be either negative or positive. In the former case, they correspond to a pentacoordinate silicon atom and in the latter case, to a tetracoordinate silicon atom.⁵⁶ The negative ^{29}Si chemical shifts in the spectra of compound **42** indicate that silicon is pentacoordinate. However, in molecules **43** and **44**, it is apparently tetracoordinate. Thus, NMR data imply that the Si atom passes from the tetracoordinate into the

pentacoordinate state. The coordination environment of the central silicon atom depends on the chemical nature and the bulk of the substituents attached. In organosilicon pyridine derivatives **42–44**, silicon is most often pentacoordinate; however, an increase in the bulk of substituents at the central silicon atom results in its tetracoordination.⁵⁶

The presence of a highly basic ligand at the silicon atom in molecules **51** and **52** changes considerably its coordination with respect to that in compounds **46** and **47** containing weakly basic ligands.⁵⁸ Compounds **51–54** contain pentacoordinate silicon in the crystalline state (compounds **53** and **54**, also in solution). In the crystal structure of molecule **51**, the TBP coordination of silicon is highly distorted towards tetrahedral with ionisation of the $\text{Si}-\text{Cl}$ bond (2.679 \AA) as compared with compound **46**. The ratio of structures containing tetra- or pentacoordinate silicon atom in compounds **51–54** in solutions depends on temperature and the solvent nature. An increase in temperature shifts the equilibrium to the pentacoordinate structure and *vice versa* (the entropy effect). The effect of the solvent nature on the ratio of penta- to tetracoordinate Si atoms ($\text{Si}-\text{Cl}$ bond ionisation) correlates with the electron-withdrawing properties of the Si-substituents.⁵⁸

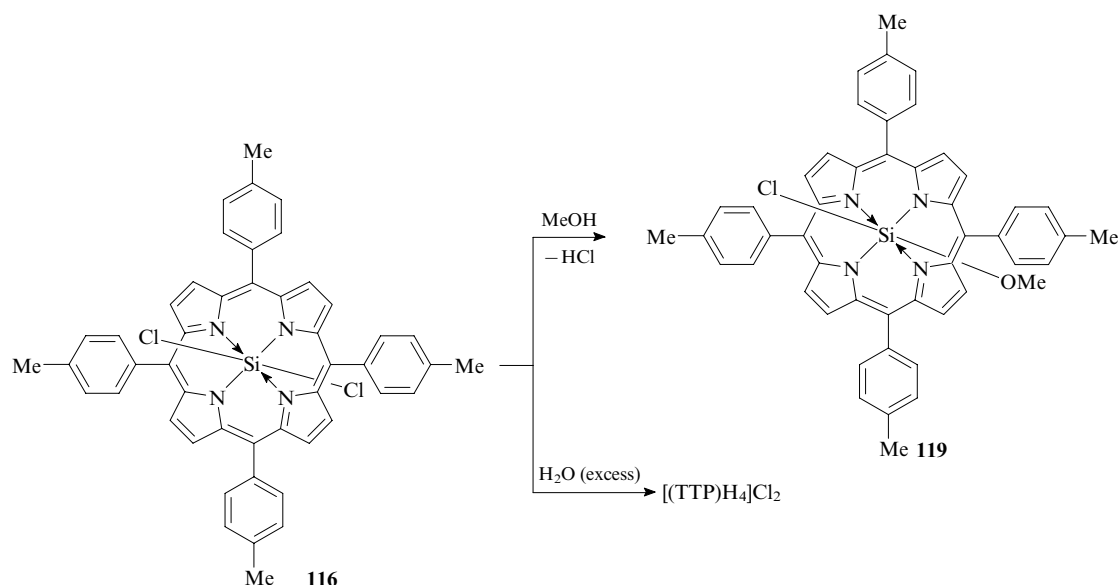
The NMR spectra of organosilicon 1,2,3,4-tetrahydro-1,10-phenanthroline derivatives **65–68** with methyl groups at the central Si atom being replaced by halogen atoms (see Table 3) also show transition from the tetra- to pentacoordinate state of silicon.⁶⁹

The $\delta(^{29}\text{Si})$ value (-217) in the ^{29}Si NMR spectrum of organosilicon tetrakis(4-tolyl)porphyrin derivative (**116**) is indicative of a hexacoordinate state of silicon.¹⁰⁴ The absence of a low-field signal in the ^1H NMR spectrum and the $J_{\text{Si}-\text{H}}$ value in the ^{29}Si NMR spectrum of compound **116** correspond to a *trans*- SiCl_2 group.

A study of the photophysical and voltammetric properties of organosilicon phthalocyanines containing $\text{OSi}(\text{n-C}_6\text{H}_{13})_3$ and $\text{OSiBu}_2(\text{n-C}_{18}\text{H}_{37})$ groups has shown⁷⁶ that they possess the maximum first oxidation potentials due to the highest steric hindrance in their molecules. Meanwhile, the first reduction potential depends little on the spatial structure.

3. Chemical properties

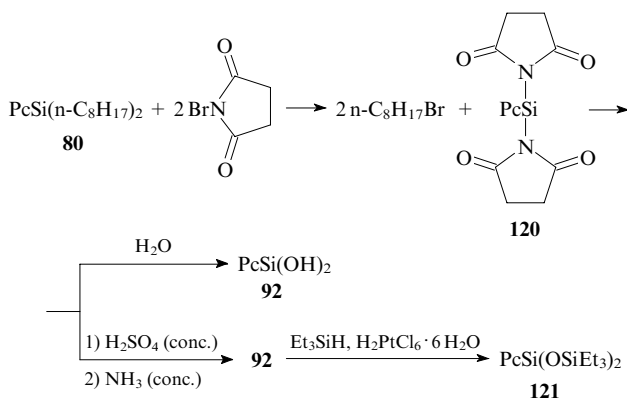
Strange as it may seem, the chemical properties of organosilicon intramolecular complexes of nitrogen heterocycles received relatively little interest from researchers, who paid attention mainly to their synthesis and molecular and stereo-electronic structures. The works devoted to the reactivity of



these compounds were focussed on Si—C and Si—X bond cleavage in organosilicon porphyrin and phthalocyanine complexes (hydrolysis, alcoholysis and halogenolysis).

Organosilicon porphyrin complex **116** containing a central SiCl₂ group reacts with protic solvents.¹⁰⁴ When this compound is treated with methanol, only one chlorine atom is replaced by a methoxy group to give (TTP)Si(OMe)Cl (**119**) (Scheme 5). Hydrolysis of compound **116** results in the loss of the central silicon atom.

When phthalocyanino-λ⁶-siliconium **80** containing two octyl groups reacts with an excess of *N*-bromosuccinimide in benzene (20 °C), the colour of the reaction mixture gradually changes from dark green to deep blue-violet.⁷⁸ According to GLC, the reaction is complete in 2 h giving rise to 1-bromooctane (yield 60%). As a result, both Si—C bonds are cleaved. After being washed with water, methanol, and diethyl ether, the blue-violet precipitate proved to be dihydroxy derivative PcSi(OH)₂ (**92**). Treatment of intermediate **120** with conc. H₂SO₄, NH₄OH and then Et₃SiH in the presence of H₂PtCl₆·6H₂O resulted the phthalocyanine PcSi(OSiEt₃)₂ (**121**). This product results evidently from the reaction of Et₃SiH with diol **92**.



The Si—C bonds in phthalocyanino-λ⁶-siliconium derivatives **76–80** are cleaved by halogens or iodine monochloride even at room temperature.⁷⁸ The Si—C(Octyl) bond in compound **80** cleaves more readily under the action of bromine than under the action of chlorine or iodine. The reactivities of the Si—Ar bonds in organosilicon phthalocyanine complexes **76–80** depend on the nature of the aromatic substituent, decreasing in the sequence 4-MeOC₆H₄ > 4-MeC₆H₄ > Ph ≫ 3-CF₃C₆H₄.

The cleavage of Si—C(Alk) and Si—C(Ar) bonds with iodine chloride occurs in different ways. In the former case, a mixture of chloroalkane and iodoalkane is formed, while in the latter case, aryl iodide is produced.⁷⁸ The Si—C(Alk) bond in phthalocyanino-λ⁶-siliconium derivatives cleaves with greater difficulty than the Si—C(Ar) bond. Halogen induced cleavage of the Si—C(Alk) bond affords alkyl radicals, whereas the Si—C(Ar) bond is cleaved according to the common electrophilic substitution mechanism.

The Si—C bonds in organosilicon Pc complexes **76–80** are cleaved in reactions with CuCl₂ or CuBr₂ (THF, 50 °C) to form the Si—X bond (X = Cl, Br).⁷⁸



76–80

X = Cl, Br.

Organosilicon phthalocyanine complexes **78** and **80** do not react with peroxybenzoic acid.⁷⁸ This fact was attributed to high stability of these complexes with hexacoordinate silicon atom caused by the macrocycle rigidity.

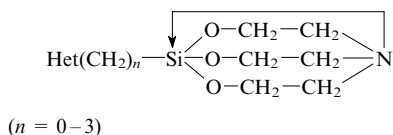
Particular attention is devoted to silicon phthalocyanine polysiloxanes.^{100, 115–117} These polymers are regarded as precursors of conducting polymers. The possibility of the radiation-induced synthesis,¹⁰⁰ the ability to form liquid crystals,¹¹⁶ dark electrical conductivity, electrochemical properties and conduction of microwave radiation were studied in detail for these compounds.

Studies on the chemical properties of hexacoordinate silicon compounds provide valuable information on the mechanisms of Si—C and Si—X bond cleavage and formation. This knowledge helps determining the routes of similar reactions also for Si(VI)-organic complexes with simpler structure.

III. Silatranyl derivatives of nitrogen-containing heterocycles

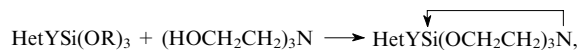
1. Methods of synthesis

The first representatives of silatranyl derivatives of nitrogen heterocycles, 1-(heterylalkyl)silatrane with the general formula



were synthesised in the 1970s.^{118–124} Since 1993, we have carried out systematic investigations into these compounds.^{36–40}

1-(Heterylalkyl)silatrane are synthesised most often by transesterification of (heterylalkyl)trialkoxysilanes on treatment with tris(2-hydroxyethyl)amine (TEA):^{5, 8, 10, 13, 15}

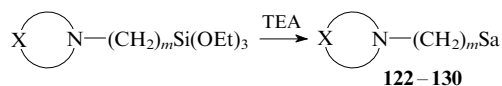


where Het is the heterocyclic fragment, Y is a hydrocarbon bridge (CH₂)_{*n*} (*n* = 0–3) or a heteroatom (S, O, N) connecting the heterocycle to the silicon atom of the silatranyl group (Sa)



The reaction is carried out in the presence of a basic catalyst (AlkONa, KOH, *etc.*) or without a catalyst, usually with distillation of ethanol.

This method was employed to carry out the first syntheses of 1-[(*N*-azacycloalkyl)alkyl]silatrane **122–130** (yields 70%–79%) in which the Si atom and the heterocycle N atom are linked through one, two or three methylene units. The reactions were carried out in chloroform, benzene or *o*-xylene^{118–121} without a catalyst.

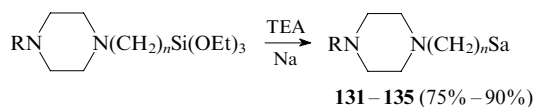


X = (CH₂)_{*n*} [*n* = 2 (**122**), 4 (**123**, **124**), 5 (**125**, **126**), 6 (**127**, **128**)], (CH₂)₂O(CH₂)₂ (**129**, **130**); *m* = 1 (**123**, **125**, **127**, **129**), 2 (**122**), 3 (**124**, **126**, **128**, **130**).

Note that (pyrrolidinomethyl)- (**123**) and (piperidinomethyl)silatrane (**125**) with *m* = 1 have higher melting points than the homologues with *m* = 3 (compounds **124** and **126**, respectively).¹²⁰ However, low-melting (perhydroazepinoalkyl)silatrane (**127**, **128**) do not follow this regularity.

1-(Piperazinoalkyl)silatrane and their *N'*-derivatives (**131–135**) were synthesised by the reaction of the corres-

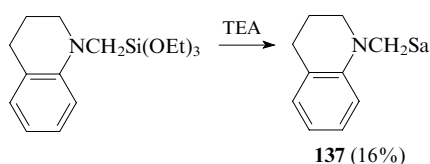
ponding (piperazinoalkyl)triethoxysilanes with tris(2-hydroxyethyl)amine in boiling xylene in the presence of a catalytic amount of metallic sodium.¹²²



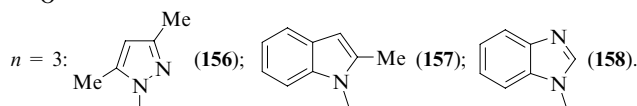
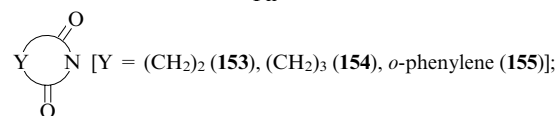
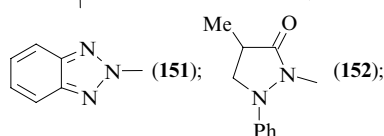
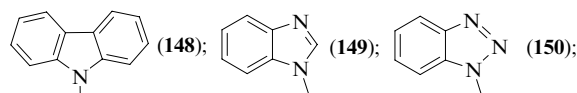
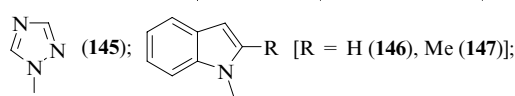
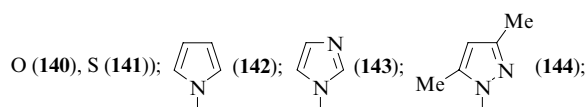
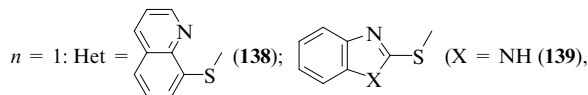
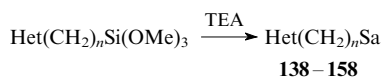
$n = 1$: R = H (**131**), Me (**132**); $n = 3$: R = H (**133**), Me (**134**), Ph (**135**).

The same route was used to convert *N,N'*-bis[3-(triethoxysilyl)propyl]piperazine into 1,4-bis(3-silatranylpropyl)piperazine (**136**) (yield 40%).¹²²

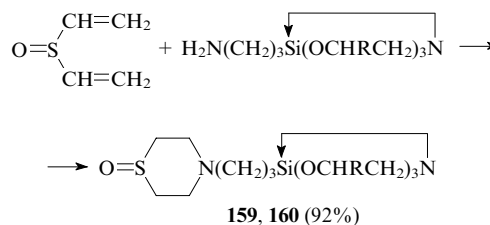
Heating tetrahydroquinoline with (chloromethyl)triethoxysilane in xylene followed by transesterification of the resulting *N*-(triethoxysilylmethyl)tetrahydroquinoline with tris(2-hydroxyethyl)amine affords 1-(tetrahydroquinolinomethyl)silatrane (**137**) in a moderate yield.^{123, 124}



Transesterification of the corresponding (8-quinolylthiomethyl)-, (2-heterylthiomethyl)- and (*N*-heterylalkyl)trimethoxysilanes with tris(2-hydroxyethyl)amine carried out without a solvent or a catalyst resulted in 1-(8-quinolylthiomethyl)- (**138**), 1-(2-heterylthiomethyl)- (**139–141**) and 1-(*N*-heterylalkyl)silatrane (**142–158**) (yields 73%–92%) (Refs 37, 39, 40 and 125).

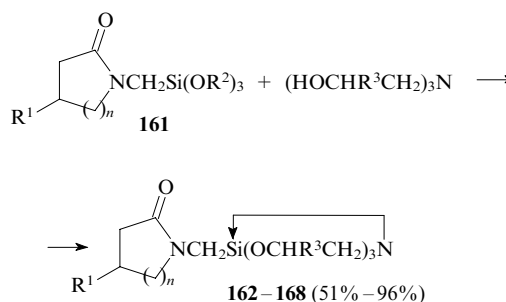


The reaction of 4-(3-triethoxysilylpropyl)thiomorpholine 1-oxide with tris(2-hydroxyethyl)amine in the presence of a catalytic amount of a saturated methanolic sodium methoxide gives 4-[3-(1-silatranyl)propyl]thiomorpholine 1-oxide (**159**) in 40% yield.¹²⁶ 1-(3-Aminopropyl)silatrane or its 3,7,10-trimethyl derivative reacts with divinyl sulfoxide in ethanol at 45–65 °C to give *N*-[3-(1-silatranyl)propyl] derivatives of thiomorpholine 1-oxide **159**, **160**.¹²⁷



R = H (**159**), Me (**160**).

N-(Trialkoxysilylmethyl)lactams **161** react with tris(2-hydroxyethyl)- or tris(2-hydroxypropyl)amines in boiling xylene in the presence of KOH giving rise to *N*-(silatranylmethyl)lactams **162–168**.¹²⁸



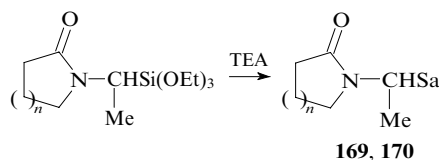
$\text{R}^1 = \text{R}^3 = \text{H}$: $n = 1$ (**162**), 2 (**163**), 3 (**164**);

$\text{R}^1 = \text{H}$, $\text{R}^3 = \text{Me}$: $n = 1$ (**165**), 2 (**166**), 3 (**167**);

$\text{R}^1 = \text{Ph}$, $\text{R}^3 = \text{H}$, $n = 1$ (**168**); $\text{R}^2 = \text{Me}$, Et.

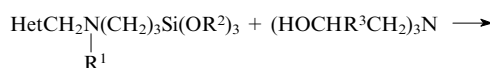
These silatranylactams have also been prepared by a one-pot procedure involving the reaction of *N*-(trimethylsilyl)lactams with (chloromethyl)trimethoxysilane and tris(2-hydroxyethyl)amine without intermediate isolation of *N*-(trimethoxysilyl)methyl derivatives (yields 30%–63%).¹²⁸

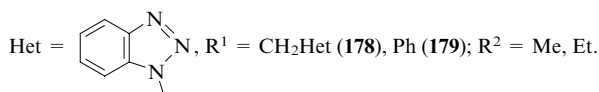
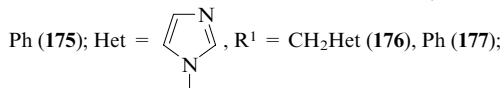
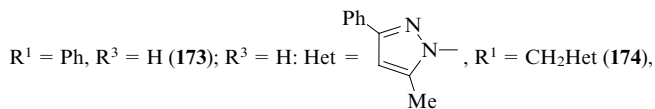
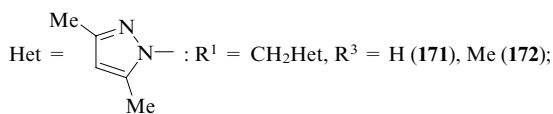
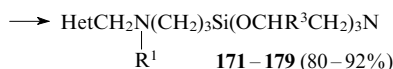
Transesterification of *N*-(triethoxysilyl)lactams with tris(2-hydroxyethyl)amine in boiling xylene without a catalyst afforded, 1-[1-(2-oxoperhydroazepino)ethyl]- (**169**) and 1-[1-(2-oxopyrrolidino)ethyl]silatrane (**170**).^{129, 130}



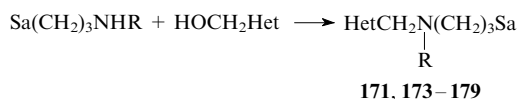
$n = 1$ (**169**), 3 (**170**).

Transesterification of *N*-(trialkoxysilylpropylamino)-methyl derivatives of imidazole, 3,5-dimethylpyrazole, 5-methyl-3-phenylpyrazole and benzotriazole with tris(2-hydroxyethyl)amine or tris(2-hydroxypropyl)amine furnished silatrane derivatives **171–179**.¹³¹

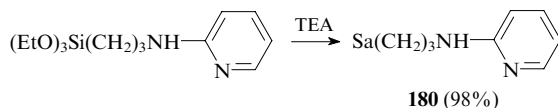




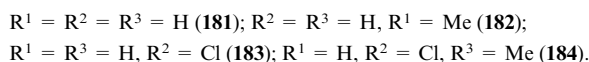
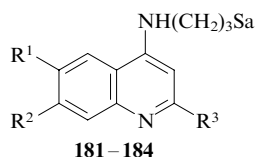
Another synthetic route to compounds **171**, **173–179** is based on anhydrocondensation of the corresponding 1-(3-aminopropyl)silatrane with 1-hydroxymethylated 3,5-dimethylpyrazole, 5-methyl-3-phenylpyrazole, imidazole or benzotriazole in dichloroethane at room temperature.¹³²



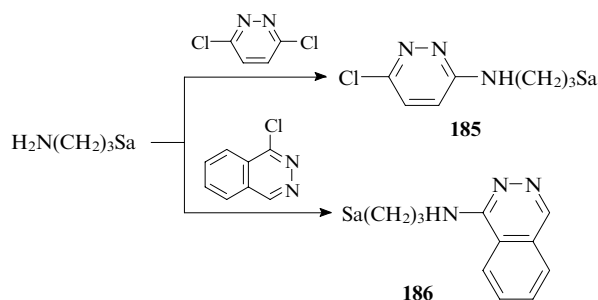
The condensation of (3-aminopropyl)triethoxysilane with 2-aminopyridine yielded 2-[3-(triethoxysilyl)propyl]amino-2-pyridine, which was then converted into 2-[3-(1-silatranyl)propyl]aminopyridine (**180**) by transesterification.¹³³



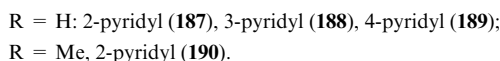
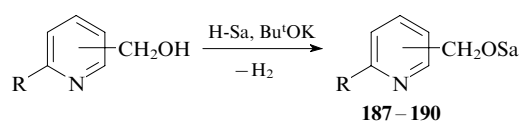
1-(Quinolylaminoalkyl)silatrane **181–184** were synthesised by two routes: transesterification of 4-[3-(triethoxysilyl)propyl]aminoquinolines on treatment with tris(2-hydroxyethyl)amine or by heating of 4-chloroquinoline with 1-(3-aminopropyl)silatrane in diglyme (yields 51%–65%).¹²⁴



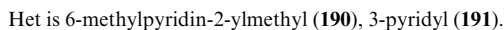
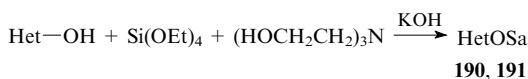
When [3-(*N*-heterylamino)propyl]triethoxysilanes are heated with tris(2-hydroxyethyl)amine in benzene or xylene, 1-{3-[(6-chloropyridazin-3-yl)amino]propyl}- (**185**) and 1-{3-[(phthalazin-1-yl)amino]propyl} silatrane (**186**) are formed.¹²¹ Low yields of the products (20%–30%) were attributed to the fact that the triethoxy derivatives were not isolated from the reaction mixture. No increase in the yields of compounds **185** and **186** was achieved by preparing them by the reaction of 1-(3-aminopropyl)silatrane with 3,6-dichloropyridazine or 1-chlorophthalazine in the presence of K₂CO₃:



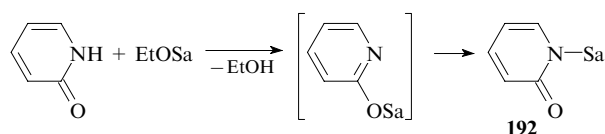
Silatrane **187–191** containing pyridyloxy or pyridylmethoxy group can be prepared by two methods.^{134, 135} Dehydrocondensation of isomeric pyridylmethanols with 1-hydroxysilatrane in xylene at 130 °C in the presence of 5 mol % Bu^tOK yielded 1-(pyridylmethoxy)silatrane **187–190** (yields 44%–56%). (Note that NaOH, KOH or NaOEt do not catalyse this reaction.)



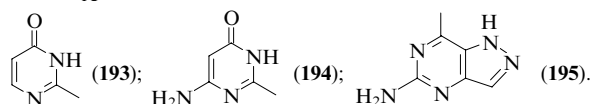
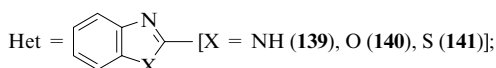
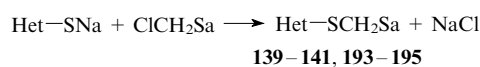
A more efficient method for the synthesis of 1-(6-methylpyridin-2-ylmethoxy)- (**190**) and 1-(3-pyridyloxy)silatrane (**191**) is based on the reaction of hydroxy(methyl)pyridines with tetraethoxysilane and tris(2-hydroxyethyl)amine in xylene in the presence of 3.5 mol % KOH with distillation of ethanol.¹³⁵



Transesterification of 1-ethoxysilatrane under the action of 2-hydroxypyridine follows an unusual route resulting in 1-silatranyl-2-pyridone (**192**).¹³⁶ This compound is the first silatrane that contains an axial N→Si–N fragment and the mechanism of its formation is the first example of a silatranotropic rearrangement.

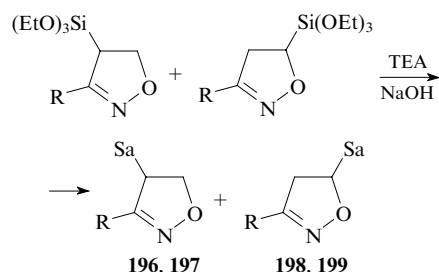


The reactions of sodium hetarenethiolates with 1-(chloromethyl)silatrane in DMF furnished (4-hydroxypyrimidin-2-yl)thiomethyl- (**193**), (6-amino-4-hydroxypyrimidin-2-yl)thiomethyl- (**194**), (2-aminopurin-6-yl)thiomethylsilatrane (**195**) and 2-(1-silatranylmethylthio)benzimidazole (**139**), -benzoxazole (**140**) and -benzothiazole (**141**) in 60%–85% yields.¹³⁷



As regards the reactivity toward 1-(chloromethyl)silatrane, sodium hetarenethiolates occupy an intermediate position between EtSNa and Et₂NCS₂Na.

Refluxing of a mixture of 3-substituted 4(5)-(triethoxysilyl)-2-isoxazolines with tris(2-hydroxyethyl)amine in toluene in the presence of NaOH as the catalyst results in silatranes **196–199** in yields of ~70%.^{138, 139} Compounds **196** and **197** can be isolated by recrystallisation from chloroform.



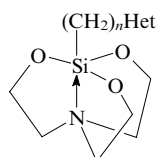
R = Me (**196**, **198**), Ph (**197**, **199**).

2. Studies of the molecular and electronic structures

a. X-Ray diffraction method

The molecular structures of silatranyl derivatives of nitrogen heterocycles in which the Het and Sa groups are linked either by a (CH₂)_n bridge (*n* = 1, 3) or directly have been comprehensively studied by X-ray diffraction.^{11, 12, 15, 18, 22}

Data from numerous X-ray diffraction studies of these compounds indicate that the silatrane cage has a distorted trigonal-bipyramidal structure with a nearly equatorial arrangement of three oxygen atoms and with axial N and C atoms of the (CH₂)_nHet substituent at silicon.



The N→Si–C angle amounts to 174–179°, *i.e.*, it is close to the straight angle in an ideal TBP (180°). The O–Si–O and O–Si–C bond angles are in the ranges of 119.0–119.2 and 95.0–95.8°, respectively. The shift (ΔSi) of the silicon atom from the equatorial plane through three oxygen atoms towards the (CH₂)_nHet substituent is 0.11–0.18 Å. The average length of the Si–O equatorial bond (1.66–1.67 Å) is greater than in organyltrialkoxysilanes containing a tetrahedral silicon atom

[for example, in the MeSi(OMe)₃ molecule, this is 1.63 Å].¹⁴⁰ In the crystalline state, the length of the dative N→Si bond in silatranes is usually in the range of 1.965–2.24 Å, which is much shorter than the sum of the van der Waals radii of the silicon and nitrogen atoms (3.65 Å).

The N→Si interatomic distances in silatranes Het(CH₂)_nSa fall into a rather narrow range (2.09–2.15 Å), being a linear function of the inductive constant σ* of the substituent Het.²⁹ The same range covers the N→Si bond length in the molecules HetSa, which is 2.12 Å. The Si–C bond length in these molecules (1.89–1.94 Å) is much greater than in compounds of tetracoordinate silicon or in silatranes containing a saturated or unsaturated substituent comprising two carbon atoms at the silicon atom (1.77–1.78 Å).¹⁴¹ Since the lengths of the transannular N→Si bond and the Si–C bond in the molecules Het(CH₂)_nSa do not differ much, one should admit that irrespective of the nature, the substituent Het affects the structure of the axial N→Si–C fragment in the same way.

Selected geometric parameters of silatranyl derivatives of nitrogen heterocycles are summarised in Table 4.

The length of the transannular N→Si bond in the *N*-(1-silatranylalkyl)pyrazole molecules Het(CH₂)_nSa for *n* = 1 (compound **144**) is 0.036 Å shorter than that for *n* = 3 (**156**). Conversely, the Si–C bond is 0.026 Å longer for *n* = 1 (compound **144**) than for *n* = 3 (**156**). This is caused by the decrease in the inductive effect of the substituent Het on the Sa group following an increase in the number of methylene groups separating them.¹⁴⁶

In the 8-(1-silatranylmethylthio)quinoline molecule (**138**), the S–CH₂ bond occurs in a nearly ideal crossed position with respect to the silatrane fragment, the SCSiO torsion angle being 179° (Ref. 40). In addition, the *trans*-configuration of the SiCSC bridge is nearly ideal (the torsion angle is 178°). The bridge is approximately in the same plane as the quinoline ring (the CSCC angle is 3°).

In 1-(2-benzothiazolylthiomethyl)silatrane (**141**),¹⁴² the bond lengths of the silatranyl group, except for the Si–C bond length, are similar to the standard values for the XCH₂Sa molecule.¹⁵³ As in other silatranes of this type, the exocyclic Si–C bond is elongated (1.912 Å).¹⁴¹ The geometric parameters of the trigonal-bipyramidal coordination of Si are similar to those established for molecule **138**.⁴⁰ The orientation of the planar benzothiazolylthiomethyl substituent in compound **141** is crossed with respect to the Si–O bonds and also resembles that observed in molecule **138**. The full difference Fourier synthesis shows a clear-cut 0.25 e Å^{–3}-high electron density peak in the line of the transannular N→Si bond at a 0.65 Å distance from the N atom. In the crystals of 1-halosilatranes

Table 4. Geometric parameters of the Het(CH₂R)_nSa molecules (*n* = 0, 1, 3).

Compound	Bond length/Å			Bond angle/deg			ΔSi/ Å	Ref.
	N→Si	Si–C	Si–O	C–Si–N	C–Si–O	O–Si–O		
138	2.111	1.893	1.667	175.0	95.8	119.0	0.169	40
141	2.100	1.912	1.663	176.7	95.2	119.2	—	142
142	2.089	1.902	1.665	177.9	95.4	119.1	0.16	143, 144
143	2.088	1.898	1.664	176.1	95.6	119.2	0.15	145
144	2.118	1.913	1.663	178.0	—	—	—	146
145	2.095	1.906	1.661	177.4	95.2	119.2	0.15	147
146	2.11	1.910	1.657	176.8	95.2	119.2	0.11–0.12	144, 148
148	2.097	1.897	1.664	177.8	95.4	119.1	0.16	144, 149
149	2.088	1.909	1.667	177.2	95.2	119.2	—	150
151	2.089	1.908	1.658	176.2	95.0	119.2	0.14	151, 152
156	2.154	1.887	1.664	179.7	—	—	—	146
170	2.122	1.909	1.665	177.3	—	—	0.176	129
196	2.119	1.920	1.644	177.5	—	119.0	0.170	139
197	2.118	1.897	1.657	176.1	—	119.0	0.168	139

XSa (X = F, Cl), this delocalised electron density peak, which reflects the strength of the N→Si donor-acceptor interaction, is located at approximately the same distance from the nitrogen atom.¹⁵⁴

It is worthy of note that all carbon–carbon bonds in the pyrrole ring of the *N*-(1-silatranylmethyl)pyrrole molecule (**142**) [especially the C(3)–C(4) bond] are equalised and are shorter than those in unsubstituted pyrrole or *N*-methylpyrrole and in the *N*-(1-silatranylmethyl)indole (**146**) or -carbazole (**148**).^{143, 144, 148, 149} The N–C bond lengths (1.37 Å) are nearly the same as those in pyrrole or *N*-methylpyrrole. The difference between the C(3)–C(4) and C(2)=C(3), C(4)=C(5) bonds in molecule **142** and in pyrrole or *N*-methylpyrrole can be regarded as a measure of electron density delocalisation in the pyrrole ring. The equalisation of all bonds in the pyrrole ring of *N*-(1-silatranylmethyl)pyrrole (**142**) is also indicated by equal bond angles in the pyrrole ring (~108°). These data imply that the pyrrole ring in molecule **142** is more aromatic than in pyrrole or *N*-methylpyrrole, which prompts a comparison of compound **142** with the cyclopentadiene rather than 1-azacyclopentadiene anion. This is also confirmed by quantum-chemical calculations.¹⁵⁵

On going from *N*-(1-silatranylmethyl)pyrrole (**142**) to *N*-(1-silatranylmethyl)indole (**146**) and -carbazole (**148**), equalisation of the bond lengths in the pyrrole heterocycle disappears, indicating a lower aromaticity of the pyrrole fragment in these molecules. Conversely, the average length of the bonds between the benzene-ring carbon atoms in compounds **146** and **148** [1.390 (α), 1.386 (β) and 1.390, 1.393 Å, respectively][†] is smaller than in benzene. This means that the attachment of an *N*-silatranylmethyl group to the indole and carbazole nitrogen atom increases the aromaticity of the benzene rings.^{148, 149}

b. Miscellaneous physicochemical methods

The presence of an intramolecular N→Si bond in *N*-(1-silatranylmethyl)azacycloalkanes **123**–**128** is also supported by ¹H NMR spectra.¹²⁰ Specifically, the proton chemical shifts of the SiCH₂ group in compounds with *m* = 1 (**123**, **125**, **127**) and *m* = 3 (**124**, **126**, **128**) are lower than those in the initial trialkoxysilyl derivatives. The difference between the chemical shifts of the NCH₂- and CH₂O-group protons in derivatives **123**–**128** almost does not depend on the size of the heterocycle, being nearly constant and equal, on average, to 0.97 ppm. This implies transfer of the electronic effect of the substituent (CH₂)_{*n*}N to the whole silatranyl group, *i.e.*, the electronic states of both Si and N atoms are changed. Relying on the change in the chemical shift differences Δδ(SiCH₂) and Δδ(NCH₂) in the spectra of (CH₂)_{*n*}NCH₂Si(OCH₂CH₂)₃N (**123**, **125**, **127**) and (CH₂)_{*n*}NCH₂Si(OR)₃, the extent of the (*p*–*d*)σ interaction in the N→Si–C fragment increases with an increase in the negative inductive effect of the (CH₂)_{*n*}NCH₂ group.

The change in the NMR chemical shifts of the exocyclic NCH₂ protons of the heterocyclic (CH₂)_{*n*}N fragments of silatrane derivatives **123**, **125** and **127** confirms that the basicity of the endocyclic nitrogen atom increases with *n* in the following sequence: 5 < 4 < 6. The basicity of the heterocycle nitrogen atom increases on going from (CH₂)_{*n*}NCH₂Si(OR)₃ to (CH₂)_{*n*}NCH₂Si(OCH₂CH₂)₃N.¹²⁰

The ¹H NMR chemical shifts of solutions of 1-[(*N*-azacycloalkyl)methyl]silatrane (CH₂)_{*n*}NCH₂SiSa (*n* = 4–6) (**123**, **125**, **127**) depend on the nature of the solvent.¹²⁰ On going from

CCl₄ to DCCl₃, hydrogen bonds of the ODCCl₃ and NDCCl₃ types are formed, the latter being stronger. This is confirmed by the frequency shifts Δν(C–D⋯N) and Δν(C–D⋯O) of DCCl₃ in the IR spectra of solutions of compounds **123**, **125** and **127** (~70 and 10 cm^{–1}, respectively). The assumption about hydrogen bonding between chloroform and silatrane molecules in which the oxygen atoms act as donor centres is consistent with the increase in the dipole moments of alkyl-, alkoxy- and aryloxy-silatrane in chloroform¹⁵⁶ compared with those in ethyl acetate or benzene. 1-[(*N*-Azacycloalkyl)methyl]silatrane **123**, **125** and **127** form strong hydrogen bonds with proton donors through the heterocycle nitrogen atom. Meanwhile, no hydrogen bond exists between the deuteriochloroform D atom and silatrane nitrogen since the electron pair of nitrogen is involved in the transannular interaction with silicon and is hence inaccessible.

The ¹H NMR spectra of *N*-(1-silatranylmethyl)lactams contain, apart from the proton signals of the lactam rings and the Si(OCH₂CH₂)₃N group, singlets for the NCH₂Si methylene protons at δ = 2.39–2.98.¹²⁸

In the ¹H NMR spectra of unsubstituted (**187**–**189**) and 6-methyl-substituted (**190**) pyridylmethoxysilatrane, the proton signals for the exocyclic CH₂ group are shifted downfield with respect to these signals in the spectra of initial pyridylmethanols. This is due to interaction of the oxygen atom with silicon of the silatranyl group.¹³⁴

In the ¹⁵N NMR spectra of *N*-(1-silatranylmethyl) derivatives of imidazole (**143**), 3,5-dimethylpyrazole (**144**), 1,2,4-triazole (**145**), 2-methylindole (**147**), benzimidazole (**149**) and phthalimide (**155**), the CH₂Si group has little effect on the chemical shifts of the heterocycle nitrogen with respect to the corresponding *N*-methylazoles.¹⁵⁷ Enhancement of the electron-withdrawing effect of the heterocycle (depending on the number, positions and type of bonding of endocyclic nitrogen atoms) increases the shielding of the ²⁹Si nucleus and deshielding of the ¹⁵N nucleus in the silatrane cage. These dependences of δ(¹⁵N) and δ(²⁹Si) are typical of *Si*-substituted silatrane XCH₂Si.¹⁵

A comparison of the ¹H, ¹³C and ¹⁵N NMR spectra of 1- and 2-substituted (trimethoxysilylmethyl)benzotriazole and 1- (**150**) and 2-(1-silatranylmethyl)benzotriazole (**151**) indicates that the nature of the organosilicon substituent affects only slightly the electron density of the nitrogen atoms, but the nitrogen electron density markedly depends on the substituent position (1 or 2). The difference between the ¹⁵N chemical shifts of 1- (**150**) and 2-isomers (**151**) is more than 100 ppm.^{152, 158}

IR spectroscopy is often used to confirm the structures of silatranyl derivatives of nitrogen heterocycles. The silatrane cage is responsible for the following absorption bands in the IR spectra of compounds Het(CH₂)_{*n*}SiSa (ν): 340–390 (N→Si bond), 730–790 cm^{–1} (CH₂ rocking vibrations), 2870–3000 cm^{–1} (CH₂ stretching vibrations), 1020–1250 cm^{–1} (NC₃ asymmetric stretching vibrations), 750–820, 1040–1180 and 1270–1280 cm^{–1} (Si–O–C skeletal vibrations with predominance of the C–O and Si–C vibrations).¹⁵⁹ The absorption of Si–C vibrations is typical of most silatrane. These are shifted to lower frequencies relative to the corresponding signals observed for tetracoordinate silicon compounds. The bathochromic shift is indicative of a higher positive charge on the silicon atom and polarisation of the Si–C bond. The skeletal vibrations ν(C–C) produce bands at 1020, 940, 1050 cm^{–1}. The two last-mentioned bands are usually doublets.

The mutual influence of the organosilicon substituent and heterocyclic fragment on the exocyclic sulfur atom in 1-silatranylmethylthio derivatives of quinoline **138**, benzoxazole **140** and benzothiazole **141** containing an SCH₂–Sa group in heterocycle positions 8, 2 and 2, respectively, was studied by UV and IR spectroscopy.¹⁶⁰ In the IR spectra of these com-

[†] The unit cell of the *N*-(1-silatranylmethyl)indole (**146**) single crystal contains 4 pairs of crystallographically independent molecules of α- and β-modifications; in the case of *N*-(1-silatranylmethyl)carbazole (**148**), the average bond length for each benzene ring of the carbazole ring is given.

pounds, the absorption bands of the silatrane cage do not depend on the nature of the heterocycle. The UV spectra of compounds **138**, **140** and **141** exhibit a considerable bathochromic shift of the bands corresponding to the heterocycle (quinoline, benzoxazole and benzothiazole) with respect to the absorption spectra of their analogues in which the substituent contains a tetracoordinate silicon atom. This shift is due to high positive inductive effect of the silatranylmethyl group with a pentacoordinate silicon atom.

1- (**150**) and 2-(1-silatranylmethyl)benzotriazoles (**151**) differ in both the number and intensity of UV bands.^{152, 161} The UV spectra of a solution of **150** (benzenoid structure) in MeCN show two absorption peaks at 270–290 and 250–270 nm. Their positions are the same as the positions of peaks in the spectra of unsubstituted and 1-methyl-substituted benzotriazoles. The UV spectrum of a solution of compound **151** (quinonoid structure) contains only one peak at 270–285 nm, like the UV spectra of unsubstituted and 2-methyl and 2-sodium derivatives of benzotriazole.^{152, 161} The benzenoid and quinonoid structures of benzotriazoles **150**, **151** are also manifested in their IR spectra. The spectra of 1-substituted benzotriazole **150** display bands for ring vibrations at 665–670, 1565–1590, 1614–1616 cm⁻¹, while in the case of 2-substituted benzotriazole **151**, these bands occur at 620–630, 1567–1569 cm⁻¹. The IR absorption frequencies of the substituent CH₂Si(OCH₂CH₂)₃N in compounds **150**, **151** almost do not depend on its position (1 or 2).

In the IR spectra of compounds O=S(CH₂CH₂)₂N.(CH₂)₃Si(OCHRCH₂)₃N (R = H, Me) (**159** and **160**), the strong bands at 830 and 1035–1130 cm⁻¹ refer to the Si–O–C groups. This range (1040–1060 cm⁻¹) contains also strong bands for S=O. The medium bands at 489 cm⁻¹ are due to the S=O bending vibrations. The bands at 570–580 cm⁻¹ represent the bending vibrations of the silatrane cage.¹²⁷

In the IR spectra of *N*-(1-silatranylmethyl)lactams (**162**–**167**),¹²⁸ the carbonyl absorption is shifted to longer wavelengths by 20–40 cm⁻¹ relative to that in the spectra of the *N*-(trialkoxysilyl)- and *N*-(trimethylsilyl)methyl derivatives. This effect is enhanced if the silatranyl group bears three methyl groups in positions 3, 7 and 10. For example, in the spectra of compounds **165**–**167**, ν(C=O) is recorded at 1610 cm⁻¹, which is 25–80 cm⁻¹ higher than that for unsubstituted analogues. The lack, in the IR spectra of *N*-(1-silatranylmethyl)lactams, of a band at 1500–1520 cm⁻¹, typical of *Si*-substituted *N*-(dimethylsilylmethyl)lactams with intramolecular O→Si coordination confirms the absence of this coordination bond.

High dipole moments (μ) of silatranes (5–7 D) indicate that the charge transfer from nitrogen to silicon equals 0.1–0.3 e.^{5, 8} In line with this, the dipole moments of (CH₂)_nN(CH₂)_mSi(OCH₂CH₂)₃N (*n* = 4–6; *m* = 1, 3) (**123**–**128**) are in the range of μ = 5.0–5.6 D.¹²⁰ These values are 3.2–3.4 D higher than the dipole moments of the respective (*N*-azacycloalkyl)triethoxysilanes (CH₂)_nN(CH₂)_mSi(OEt)₃ (*n* = 4–6; *m* = 1, 3).

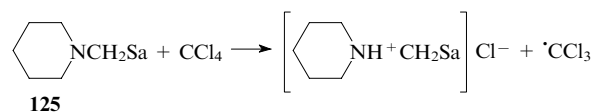
The dipole moments of *N*-(1-silatranylmethyl) derivatives of pyrrole (**142**), indole (**146**), 2-methylindole (**147**) and carbazole (**148**) depend on the structure of the heterocyclic substituent.¹⁴⁴ The dipole moments of the silatranylmethyl derivatives increase in the sequence **148** < **146** < **147** < **142**, which is not the case for *N*-(trimethoxysilylmethyl) derivatives of pyrrole, indole and 2-methylindole, the parent heterocycles (pyrrole, indole, carbazole), 2-methylindole or their *N*-methyl derivatives. This effect is due most likely to specific features of the electronic interaction of the Het and Sa fragments in

compounds **142**, **146**–**148**. The role of their specific spatial structure in solution cannot be ruled out either.

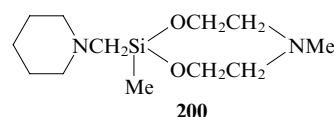
3. Chemical properties

Specific reactivities of 1-(*N*-heterylmethyl)silatranes Het(CH₂)_nSa with polarised Si–C bond are of particular interest.

Indeed, the reaction of 1-(piperidinomethyl)silatrane (**125**) with CCl₄ in benzene gives the corresponding hydrochloride even under daylight [(18–20) 10³ lux].¹⁶² The hydrogen atom is readily split off from the methylene group attached to silicon to give hydrogen chloride, which adds to another molecule **125**. The subsequent behaviour of the Cl₃C[•] radicals and the dehydrogenated initial silatrane as well as the composition and structure of the resulting polymeric products or the exact mechanism of this reaction are still obscure. The induction period of this photochemical process is 0.2 h.



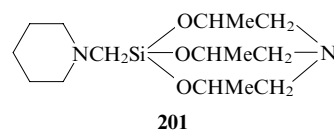
The induction period of a similar reaction with 5-methyl-(*N*-piperidinomethyl)-1-methylquasisilatrane (**200**)



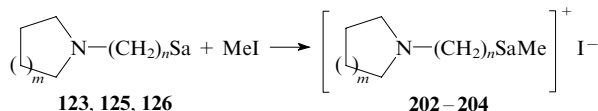
is 96 h at the same luminous intensity. The photochemical reaction of CCl₄ with (CH₂)₅NCH₂Si(OEt)₃ or Et₃N at the luminous intensity of (18–20) × 10³ lux starts only after 120 or 144 h, respectively.

The basicity of nitrogen in 1-(*N*-heterylmethyl)silatranes Het(CH₂)_nSa is much higher than in R₂NCH₂Si(OEt)₃ or in aliphatic amines. This is a result of strong electron-releasing effect of the CH₂Sa^{29, 30} group and n,σ-hyperconjugation in the NCH₂Si fragment.^{162–167}

In molecules such as NCH₂Si(OR)₃, the n,σ-interaction decreasing the nitrogen basicity exists in parallel with the electron-releasing effect of the CH₂Si(OR)₃ group.^{168–170} The enhanced basicity of nitrogen in the NCH₂Sa fragment is also indicated by the ionisation potential (7.46 eV) of the nitrogen lone pair in 1-piperidinomethyl-3,7,10-trimethylsilatrane (**201**),



which is much lower than that in *N*-methylpiperidine (8.30 eV).^{162, 168} The ionisation potentials of the molecules (CH₂)₅NCH₂Si(OEt)₃ and (CH₂)₅NCH₂SiMe(OCH₂CH₂)₂.NMe (**200**) are also increased (7.95 and 8.15 eV, respectively). This is confirmed by equilibrium constants of the phenol complexes with (CH₂)₅NCH₂Si(OCHMeCH₂)₃N (1100 litre mol⁻¹), (CH₂)₅NCH₂Si(OEt)₃ (110 litre mol⁻¹), (CH₂)₅NCH₂SiMe(OCH₂CH₂)₂NMe (**200**) (150 litre mol⁻¹) and Et₃N (52 litre mol⁻¹).^{162, 171} Note that the basicity of the N atom in methylbis(1-silatranylmethyl)amine is even higher. (Pyrrolidinomethyl)- (**123**) and (piperidinoalkyl)silatranes (**125**, **126**) react with methyl iodide in ethanol or toluene to give methiodides **202**–**204** with melting points above 200 °C.¹¹⁸

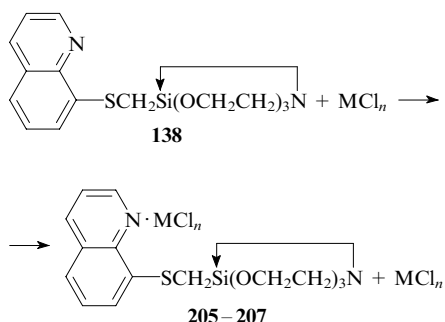


$m = 1, n = 1$ (**123, 202**);

$m = 2: n = 1$ (**125, 203**), 3 (**126, 204**).

(Silatranylalkyl)tetrahydro-1,4-thiazine 1-oxides react with MeI in a similar way to give quaternary ammonium salts.¹²⁶

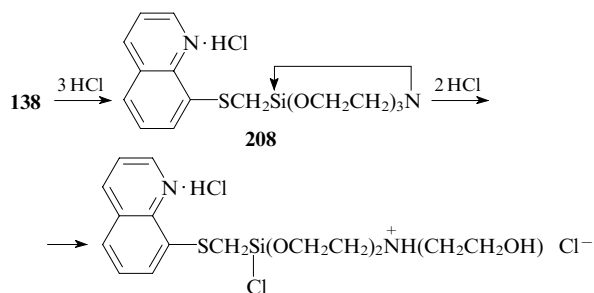
The reaction of 1-(8-quinolylthiomethyl)silatrane (**138**) with copper(II), zinc(II) and tin(IV) chlorides in chloroform affords 1 : 1 complexes **205–207**.^{172, 173}



$\text{MCl}_n = \text{CuCl}_2$ (**205**), ZnCl_2 (**206**), SnCl_4 (**207**).

The complex of silatrane **138** with SnCl_4 (**207**) contains a strong $\text{N} \rightarrow \text{Sn}$ donor–acceptor bond. The complex with ZnCl_2 (**206**) has a chelate structure (the zinc atom forms a donor–acceptor bond with nitrogen and sulfur atoms). The reaction product of compound **138** with CuCl_2 , viz., complex **205**, exists in solutions as two species: a complex with the $\text{N} \rightarrow \text{Cu}$ bond and a chelate in which Cu is coordinated to N and S atoms.

1-(8-Quinolylthiomethyl)silatrane (**138**) reacts with an equimolar amount of HCl in ether giving 1 : 1 hydrochloride **208**. When an excess of hydrogen chloride is used, one endocyclic Si–O bond is cleaved in the Sa fragment.^{172, 173}



Note that in the silatrane derivatives of nitrogen heterocycles $\text{Het}(\text{CH}_2)_n\text{Sa}$, the negatively charged oxygen atoms of the silatrane fragment are more prone to form hydrogen bonds than the heterocycle nitrogen atom. In the crystal hydrate of *N*-[1-(1-silatranyl)ethyl]pyrrolidone (**169**), water molecule is connected by $\text{O} \cdots \text{HO}$ hydrogen bonds to the oxygen atom of the silatranyl group.¹³⁰ Unfortunately, the formation of hydrogen bonds by silatrane nitrogen heterocycles has been scarcely studied.

* * *

Silatrane as compounds possessing a cage structure and containing a trace substance, silicon, exert a physiological action on all living organisms, existing at different stages of evolution (from microbes to humans).¹⁶ The biological action

of silatranyl nitrogen heterocycles is due to both the presence of a heterocyclic system and the presence of hypervalent silicon atom in appropriate environment. Unfortunately, the biological activity of 1-(*N*-heterylalkyl)silatrane has not been adequately studied as yet. However, we are confident that in the near future valuable pharmaceutical agents or protection means for agricultural plants will be found among this class of compounds.

References

1. J L Gay-Lussac, L J Thenard *Mem. Phys. Chim. Soc. d'Arcueil* **2** 317 (1809)
2. M G Voronkov *Organosilicon Chemistry* (Ed. V Bazhant) (London: Butterworths, 1966) p. 35
3. M G Voronkov *Pure Appl. Chem.* **19** 399 (1969)
4. M G Voronkov, G I Zelchan, E Ya Lukevics *Kremnii i Zhizn'* (Silicon and Life) (Riga: Zinatne, 1978)
5. M G Voronkov, V M D'yakov *Silatrany* (Silatrane) (Novosibirsk: Nauka, 1978)
6. M G Voronkov *Top. Curr. Chem.* **84** 77 (1979)
7. V F Sidorkin, V A Pestunovich, M G Voronkov *Usp. Khim.* **49** 789 (1980) [*Russ. Chem. Rev.* **49** 414 (1980)]
8. M G Voronkov, V M Dyakov, S V Kirpichenko *J. Organomet. Chem.* **233** 1 (1982)
9. S N Tandura, M G Voronkov, N V Alekseev *Structural Chemistry of Boron and Silicon (Topics in Current Chemistry)* Vol. 131 (Berlin, Heidelberg: Springer, 1986) p. 99
10. M G Voronkov, V P Baryshok, L P Petukhov, V I Raklin, R G Mirskov, V A Pestunovich *J. Organomet. Chem.* **358** 39 (1988)
11. V E Shklover, Yu T Struchkov, M G Voronkov *Main Group Met. Chem.* **11** 109 (1988)
12. V E Shklover, Yu T Struchkov, M G Voronkov *Usp. Khim.* **58** 353 (1989) [*Russ. Chem. Rev.* **58** 211 (1989)]
13. M G Voronkov *Izv. Akad. Nauk SSSR, Ser. Khim.* 2664 (1991)^a
14. V A Pestunovich, V F Sidorkin, M G Voronkov *Progress in Organosilicon Chemistry* (Eds B Marciniak, J Chojnowski) (New York: Gordon and Breach, 1995) p. 9
15. V Pestunovich, S Kirpichenko, M Voronkov *The Chemistry of Organic Silicon Compounds* (Eds Z Rappoport, Y Apeloig) (New York: Wiley, 1998) Vol. 2, p. 1447
16. M G Voronkov, V P Baryshok *Silatrany v Meditsine i Sel'skom Khozyaistve* (Silatrane for Medicine and Agriculture) (Novosibirsk: Siberian Branch of Russian Academy of Sciences, 2005)
17. P Hencsei, L Parkanyi *Kgm. Klzl.* **61** 319 (1984); *Chem. Abstr.* **103** 105019 (1985)
18. E Ya Lukevics, O A Pudova, R Ya Sturkovich *Molekulyarnaya Struktura Kremniorganicheskikh Soedinenii* (Molecular Structure of Organosilicon Compounds) (Riga: Zinatne, 1988)
19. C Chuit, R J P Corriu, C Reye, J C Young *Chem. Rev.* **93** 1371 (1993)
20. J G Verkade *Acc. Chem. Res.* **26** 483 (1993)
21. J G Verkade *Coord. Chem. Rev.* **137** 233 (1994)
22. E Ya Lukevics, O A Pudova *Khim. Geterotsikl. Soedin.* 1605 (1996)^b
23. E Ya Lukevics, A E Pestunovich *Usp. Khim.* **41** 1994 (1972) [*Russ. Chem. Rev.* **41** 938 (1972)]
24. E Lukevics, I D Segal *Organomet. Chem. Rev.* 69 (1988)
25. M G Voronkov, V A Pestunovich, Yu I Baukov *Metalloorg. Khim.* **4** 1210 (1991)^c
26. A R Katritzky, X Lan, J Z Yang, O V Denisko *Chem. Rev.* **98** 409 (1998)
27. D Kost, I Kalikhman *The Chemistry of Organic Silicon Compounds* (Eds Z Rappoport, Y Apeloig) (New York: Wiley, 1998) Vol. 2, p. 1339
28. V I Glukhikh, M G Voronkov, O G Yarosh, S N Tandura, N V Alekseev, N Yu Khromova, T K Gar *Dokl. Akad. Nauk SSSR* **258** 387 (1981)^d

29. M G Voronkov, V V Belyaeva *Zh. Obshch. Khim.* **72** 2012 (2002)^c
30. A Daneshrad, C Eaborn, D R M Walton *J. Organomet. Chem.* **85** 35 (1975)
31. M G Voronkov, L I Gubanov *Main Group Met. Chem.* **10** 209 (1987)
32. V V Negrebetskii, Yu I Baukov *Izv. Akad. Nauk, Ser. Khim.* 1912 (1997)^a
33. R Tacke, M Pülm, B Wagner *Adv. Organomet. Chem.* **44** 221 (1999)
34. D Kost, I Kalikhman, S Krivonos, R Bertermann, C Burschka, R E Neugebauer, M Pülm, R Willeke, R Tacke *Organometallics* **19** 1083 (2000)
35. R Tacke, R Bertermann, C Burschka, S Dragota, M Penka, I Richter *J. Am. Chem. Soc.* **126** 14493 (2004)
36. O M Trofimova, N F Chernov, M G Voronkov *Usp. Khim.* **68** 318 (1999) [*Russ. Chem. Rev.* **68** 287 (1999)]
37. M G Voronkov, O M Trofimova, Yu I Bolgova, N F Chernov *Khim. Geterotsikl. Soedin.* 1487 (2001)^b
38. M G Voronkov, O M Trofimova, N F Chernov *Uspekhi Organicheskogo Kataliza i Khimii Geterotsiklov* (Progress in Organic Catalysis and Chemistry of Heterocycles) (Moscow: Khimiya, 2006) p. 110
39. M G Voronkov, N F Chernov, O M Trofimova, T N Aksamentova *Izv. Akad. Nauk, Ser. Khim.* 1965 (1993)^a
40. M G Voronkov, N F Chernov, O M Trofimova, Yu E Ovchinnikov, Yu T Struchkov, G A Gavrilova *Izv. Akad. Nauk, Ser. Khim.* 758 (1993)^a
41. M G Voronkov, E A Zel'bst, Yu V Katkevich, A A Kashaev, V S Fundamenskii, Yu I Bolgova, O M Trofimova, N F Chernov, A I Albanov, Yu I Baukov, V A Pestunovich *Dokl. Akad. Nauk* **402** 344 (2005)^d
42. T N Aksamentova, M G Voronkov, O M Trofimova, N N Chipanina, Yu I Bolgova, N F Chernov, E A Zel'bst, V K Turchaninov *Zh. Strukt. Khim.* **46** 257 (2005)^f
43. M G Voronkov, O M Trofimova, N F Chernov, Yu I Bolgova, A I Albanov, N N Chipanina, E A Zelbst *Heteroat. Chem.* **17** 567 (2006)
44. M G Voronkov, A I Albanov, N F Chernov, O M Trofimova, Yu I Bolgova, L V Sherstyannikova *Zh. Obshch. Khim.* **76** 1948 (2006)^c
45. M G Voronkov, E A Zel'bst, A A Kashaev, Yu V Katkevich, V S Fundamenskii, Yu I Bolgova, O M Trofimova, A I Albanov, N F Chernov, V A Pestunovich *Dokl. Akad. Nauk* **393** 493 (2003)^d
46. S A Pogozhikh, Yu E Ovchinnikov, E P Kramarova, V V Negrebetskii, A G Shipov, A I Albanov, M G Voronkov, V A Pestunovich, Yu I Baukov *Zh. Obshch. Khim.* **74** 1617 (2004)^c
47. K Hensen, G Klebe *J. Organomet. Chem.* **209** 17 (1981)
48. G Klebe, D T Qui *Acta Crystallogr., Sect. C* **40** 476 (1984)
49. M G Voronkov, O M Trofimova, N F Chernov, A I Albanov, N N Chipanina, E A Grebneva *Appl. Organomet. Chem.* **19** 538 (2005)
50. J Wagler, D Gerlach, G Roewer *Khim. Geterotsikl. Soedin.* 1826 (2006)^b
51. D Gerlach, E Brendler, T Heine, J Wagler *Organometallics* **26** 234 (2007)
52. R Krebs, D Schomburg, R Schmutzler *Z. Naturforsch., B* **40** 282 (1985)
53. G Klebe, M Nix, K Hensen *Chem. Ber.* **117** 797 (1984)
54. C Jones, P C Junk, S G Leary, N A Smithies, J W Steed *Inorg. Chem. Commun.* **5** 533 (2002)
55. T van den Ancker, B S Jolly, M F Lappert, C L Raston, B W Skelton, A H White *J. Chem. Soc., Chem. Commun.* 1006 (1990)
56. T van den Ancker, C L Raston, B W Skelton, A H White *Organometallics* **19** 4437 (2000)
57. D Kummer, S C Chaudhry, J Seifert, B Deppisch, G Mattern *J. Organomet. Chem.* **382** 345 (1990)
58. D Kummer, S H A Halim, W Kuhs, G Mattern *J. Organomet. Chem.* **446** 51 (1993)
59. J J H Edema, R Libbers, A Ridder, R M Kellogg, A L Spek *J. Organomet. Chem.* **464** 127 (1994)
60. T K Prakasha, A Chandrasekaran, R O Day, R R Holmes *Inorg. Chem.* **35** 4342 (1996)
61. E Gómez, V Santes, V de la Luz, N Farfán *J. Organomet. Chem.* **590** 237 (1999)
62. E Gómez, V Santes, V de la Luz, N Farfán *J. Organomet. Chem.* **622** 54 (2001)
63. E Gómez, Z Hernández, C Alvarez-Toledano, R A Toscano, V Santes, P Sharma *J. Organomet. Chem.* **648** 280 (2002)
64. G Klebe, K Hensen, H Fuess *Chem. Ber.* **116** 3125 (1983)
65. G Klebe, J W Bats, K Hensen *Z. Naturforsch., B* **38** 825 (1983)
66. G Klebe, J W Bats, H Fuess *J. Am. Chem. Soc.* **106** 5202 (1984)
67. G Klebe *J. Organomet. Chem.* **293** 147 (1985)
68. G Klebe, J W Bats, K Hensen *J. Chem. Soc., Dalton Trans.* 1 (1985)
69. G Klebe, K Hensen, J Von Jouanne *J. Organomet. Chem.* **258** 137 (1983)
70. G Klebe, K Hensen *J. Chem. Soc., Dalton Trans.* 5 (1985)
71. J E Falk *Porphyrins and Metalloporphyrins* (Amsterdam, London, New York: Elsevier, 1964)
72. *The Porphyrins. Structure and Synthesis* (Ed. D Dolphin) (London, New York: Academic Press, 1978) Vol. 1, Pt. A
73. R D Joyner, J Cekada, R G Linck, M E Kenney *J. Inorg. Nucl. Chem.* **15** 387 (1960)
74. R D Joyner *Diss. Abstr.* **22** 731 (1961)
75. M K Lowery, A J Starshak, J N Esposito, P C Krueger, M E Kenney *Inorg. Chem.* **4** 128 (1965)
76. B L Wheeler, G Nagasubramanian, A J Bard, L A Schechtman, D R Dininny, M E Kenney *J. Am. Chem. Soc.* **106** 7404 (1984)
77. J N Esposito, J E Lloyd, M E Kenney *Inorg. Chem.* **5** 1979 (1966)
78. K Tamao, M Akita, H Kato, M Kumada *J. Organomet. Chem.* **341** 165 (1988)
79. M Hanack, K Mitulla, G Pawlowski, L R Subramanian *J. Organomet. Chem.* **204** 315 (1981)
80. E Ciliberto, K A Doris, W J Pietro, G M Reisner, D E Ellis, I Fragala, F H Herstein, M A Ratner, T J Marks *J. Am. Chem. Soc.* **106** 7748 (1984)
81. C Farren, S Fitzgerald, M R Bryce, A Beeby, A S Batsanov *J. Chem. Soc., Perkin Trans. 2* 59 (2002)
82. J L Rodríguez-Redondo, Á Sastre-Santos, F Fernández-Lázaro, D Soares, G C Azzellini, B Elliott, L Echegoyen *Chem. Commun.* 1265 (2006)
83. P-C Lo, J-D Huang, D Y Y Cheng, E Y M Chan, W-P Fong, W-H Ko, D K P Ng *Chem. –Eur. J.* **10** 4831 (2004)
84. P P S Lee, P-C Lo, E Y M Chan, W-P Fong, W-H Ko, D K P Ng *Tetrahedron Lett.* **46** 1551 (2005)
85. J R Mooney, C K Choy, K Knox, M E Kenney *J. Am. Chem. Soc.* **97** 3033 (1975)
86. M A Brook *Silicon in Organic, Organometallic and Polymer Chemistry* (New York: Wiley, 2000) p. 466
87. N B McKeown *J. Mater. Chem.* **10** 1979 (2000)
88. R Bonnett, D G Buckley, T Burrow, A B B Galia, B Saville, S P Songca *J. Mater. Chem.* **3** 323 (1993)
89. H L Anderson *Chem. Commun.* 2323 (1999)
90. E M Maya, P Vázquez, T Torres *Chem. –Eur. J.* **5** 2004 (1999)
91. A Gonzvlez, P Vázquez, T Torres *Tetrahedron Lett.* **40** 3263 (1999)
92. E M Maya, P Haisch, P Vázquez, T Torres *Tetrahedron* **54** 4397 (1998)
93. E M Maya, P Vázquez, T Torres *Chem. Commun.* 1175 (1997)
94. R Jung, K H Schweikart, M Hanack *Eur. J. Org. Chem.* 1687 (1999)
95. G Cheng, X Peng, G Hao, V O Kennedy, I N Ivanov, K Knappenberger, T J Hill, M A J Rodgers, M E Kenney *J. Phys. Chem. A* **107** 3503 (2003)
96. C A Barker, K S Findlay, S Bettington, A S Batsanov, I F Perepichka, M R Bryce, A Beeby *Tetrahedron* **62** 9433 (2006)
97. K N Kim, C S Choi, K-Y Kay *Tetrahedron Lett.* **46** 6791 (2005)

98. E Orthmann, G Wegner *Makromol. Chem., Rapid Commun.* **7** 243 (1986)
99. D W DeWulf, J K Leland, B L Wheeler, A J Bard, D A Batzel, D R Dininny, M E Kenney *Inorg. Chem.* **26** 266 (1987)
100. P G Schouten, J M Warman, M P De Haas, J F Van der Pol, J W Zwikker *J. Am. Chem. Soc.* **114** 9028 (1992)
101. J Kleinwächter, M Hanack *J. Am. Chem. Soc.* **119** 10684 (1997)
102. T Gunaratne, V O Kennedy, M E Kenney, M A J Rodgers *J. Phys. Chem. A* **108** 2576 (2004)
103. A N Cammidge, F Nekelson, M Helliwell, M J Heeney, M J Cook *J. Am. Chem. Soc.* **127** 16382 (2005)
104. K M Kane, F R Lemke, J L Petersen *Inorg. Chem.* **34** 4085 (1995)
105. J A Cissell, T P Vaid, A L Rheingold *J. Am. Chem. Soc.* **127** 12212 (2005)
106. Yu E Ovchinnikov, Yu T Struchkov, N F Chernov, O M Trofimova, M G Voronkov *J. Organomet. Chem.* **461** 27 (1993)
107. M G Voronkov, E A Zel'bst, A A Kashaev, A V Katkevich, V S Fundamenskii, O M Trofimova, N F Chernov *Zh. Strukt. Khim.* **48** 394 (2007)^f
108. R R Holmes *Chem. Rev.* **90** 17 (1990)
109. R R Holmes *Chem. Rev.* **96** 927 (1996)
110. J I Musher *Angew. Chem.* **81** 68 (1969)
111. V F Sidorkin, V A Pestunovich, M G Voronkov *Dokl. Akad. Nauk SSSR* **235** 1363 (1977)^d
112. B J Helmer, R West, R J P Corriu, M Poirier, G Royo, A De Saxe *J. Organomet. Chem.* **251** 295 (1983)
113. V A Pestunovich, B Z Shterenberg, E T Lippmaa, Ya Myagi, M A Alla, S N Tandura, V P Baryshok, L P Petukhov, M G Voronkov *Dokl. Akad. Nauk SSSR* **258** 1410 (1981)^d
114. V A Pestunovich, B Z Shterenberg, S N Tandura, V P Baryshok, E I Brodskaya, N G Komalenkova, M G Voronkov *Dokl. Akad. Nauk SSSR* **264** 632 (1982)^d
115. C W Dirk, T Inabe, K F Schoch Jr, T J Marks *J. Am. Chem. Soc.* **105** 1539 (1983)
116. C Sirlin, L Bosio, J Simon *J. Chem. Soc., Chem. Commun.* 236 (1988)
117. P Gättinger, H Rengel, D Neher, M Gurka, M Buck, A M van de Craats, J M Warman *J. Phys. Chem. B* **103** 3179 (1999)
118. E Ya Lukevics, L I Libert, M G Voronkov *Izv. Akad. Nauk Latv. SSR, Ser. Khim.*, 451 (1972)
119. USSR P. 321120; *Ref. Zh. Khim.* 8N94P (1974)
120. E Ya Lukevics, R Ya Moskovich, E Liepin'sh, I S Yankovskaya *Zh. Obshch. Khim.* **46** 604 (1976)^e
121. E Ya Lukevics, A F Lapsinya, G I Zelchan, A Zh Dauvarte, A A Zidermane *Izv. Akad. Nauk Latv. SSR, Ser. Khim.*, 338 (1978)
122. E Ya Lukevics, E P Popova *Izv. Akad. Nauk Latv. SSR, Ser. Khim.* 207 (1978)
123. USSR P. 579275; *Byull. Izobret.* (41) 86 (1977)
124. E Ya Lukevics, A A Ziderman, A Zh Dauvarte, T V Lapina, L N Khokhlova, I D Segal *Khim.-Farm. Zh.* (12) 62 (1978)^g
125. N F Chernov, Yu I Bolgova, O M Trofimova, M G Voronkov *Zh. Obshch. Khim.* **69** 1453 (1999)^e
126. M G Voronkov, A E Pestunovich, N N Vlasova, T V Kashik, T I Nikiforova, A I Albanov, Yu N Pozhidaev, S V Amosova *Zh. Obshch. Khim.* **63** 869 (1993)^e
127. USSR P. 722913; *Byull. Izobret.* (11) 82 (1980)
128. V P Kramarova, A G Shipov, Yu I Baukov *Zh. Obshch. Khim.* **62** 2559 (1992)^e
129. V E Shklover, Yu E Ovchinnikov, Yu T Struchkov, V M Kopylov, T G Kovyazina, M G Voronkov *Dokl. Akad. Nauk SSSR* **284** 131 (1985)^d
130. Yu E Ovchinnikov, V E Shklover, Yu T Struchkov, V M Kopylov, T G Kovyazina, M G Voronkov *Zh. Strukt. Khim.* **27** 133 (1986)^f
131. M Nasim, P Tharmaraj, P S Venkataramani *Synth. React. Inorg. Met.-Org. Chem.* **29** 1249 (1999)
132. S C Verma, M Nasim, P S Venkataramani *Synth. React. Inorg. Met.-Org. Chem.* **31** 527 (2001)
133. L I Belousova, N N Vlasova, Yu N Pozhidaev, M G Voronkov *Zh. Obshch. Khim.* **71** 1984 (2001)^e
134. E Lukevics, I Shmukste, I Iovel, L Ignatovich *Khim. Geterotsikl. Soedin.* 839 (1998)^b
135. I Iovel, L Golomba, Yu Popelis, S Grinberga, E Lukevics *Khim. Geterotsikl. Soedin.* 1203 (1999)^b
136. M G Voronkov, Yu A Lukina, S N Tandura, V K Voronov, V M D'yakov *Zh. Obshch. Khim.* **49** 1278 (1979)^d
137. M S Sorokin, V A Lopyrev, M G Voronkov *Zh. Obshch. Khim.* **69** 407 (1999)^d
138. E Lukevics, V Dirnens, N Pokrovskaya, J Popelis, A Kemme. *Main Group Met. Chem.* **18** 337 (1995)
139. E Lukevics, V Dirnens, A Kemme, J Popelis *J. Organomet. Chem.* **521** 235 (1996)
140. È Gergö, I Hargittai, G Schultz *J. Organomet. Chem.* **112** 29 (1976)
141. M G Voronkov, E A Zel'bst, A A Kashaev, A V Katkevich, V S Fundamenskii, V A Bruskov, P F Abumov, V V Belyaeva *Dokl. Akad. Nauk* **414** 49 (2007)^d
142. Yu E Ovchinnikov, Yu T Struchkov, N F Chernov, O M Trofimova, M G Voronkov *Dokl. Akad. Nauk* **328** 330 (1993)^d
143. M G Voronkov, E A Zel'bst, A A Kashaev, Yu V Katkevich, V S Fundamenskii, Yu I Bolgova, O M Trofimova, N F Chernov *Dokl. Akad. Nauk* **386** 56 (2002)^d
144. M G Voronkov, O M Trofimova, V K Turchaninov, E A Zel'bst, Yu I Bolgova, V V Belyaeva, L I Larina, T N Aksamentova, A I Mikhaleva, N F Chernov *Zh. Org. Khim.* **39** 1527 (2003)^h
145. M G Voronkov, V S Fundamenskii, E A Zel'bst, Yu V Katkevich, O M Trofimova, Yu I Bolgova, N F Chernov *Dokl. Akad. Nauk* **401** 41 (2005)^d
146. M G Voronkov, E A Zel'bst, A A Kashaev, Yu V Katkevich, V S Fundamenskii, Yu I Bolgova, O M Trofimova, N F Chernov *Dokl. Akad. Nauk* **397** 57 (2004)^d
147. M G Voronkov, E A Zel'bst, A A Kashaev, O M Trofimova, Yu I Bolgova, V S Fundamenskii, N F Chernov *Dokl. Akad. Nauk* **376** 204 (2001)^d
148. M G Voronkov, E A Zel'bst, A A Kashaev, Yu V Katkevich, V S Fundamenskii, V A Bruskov, Yu I Bolgova, O M Trofimova, N F Chernov *Dokl. Akad. Nauk* **391** 772 (2003)^d
149. M G Voronkov, E A Zel'bst, A A Kashaev, Yu V Katkevich, V S Fundamenskii, Yu I Bolgova, O M Trofimova, V V Belyaeva, N F Chernov *Dokl. Akad. Nauk* **389** 478 (2003)^d
150. M G Voronkov, E A Zel'bst, V S Fundamenskii, Yu V Katkevich, Yu I Bolgova, O M Trofimova, N F Chernov *Zh. Strukt. Khim.* **46** 1165 (2005)^f
151. M G Voronkov, E A Zel'bst, V S Fundamenskii, A A Kashaev, O M Trofimova, Yu I Bolgova, N F Chernov *Dokl. Akad. Nauk* **381** 348 (2001)^d
152. M G Voronkov, O M Trofimova, E I Brodskaya, Yu I Bolgova, L I Larina, L V Klyba, E A Zelbst, N F Chernov *Arkivoc* (xiii) 125 (2003)
153. F H Allen, O Kennard, D G Watson, L Brammer, A G Orpen, R Taylor *J. Chem. Soc., Perkin Trans. 2* S1 (1987)
154. L Párkányi, P Hencsei, L Bihátsi, T Müller *J. Organomet. Chem.* **269** 1 (1984)
155. M G Voronkov, B A Shainyan, O M Trofimova *Dokl. Akad. Nauk* **396** 779 (2004)^d
156. V A Chetverikova, V A Kogan, G I Zelchan, M G Voronkov, O A Osipov *Khim. Geterotsikl. Soedin.* 446 (1969)^b
157. M G Voronkov, L I Larina, Yu I Bolgova, O M Trofimova, N F Chernov, V A Pestunovich *Khim. Geterotsikl. Soedin.* 1857 (2006)^b
158. M G Voronkov, O M Trofimova, Yu I Bolgova, L V Klyba, L I Larina, A I Albanov, V A Pestunovich, N F Chernov, K B Petrushenko *Khim. Geterotsikl. Soedin.* 1861 (2003)^b

159. M G Voronkov, S G Shevchenko, E I Brodskaya, V P Baryshok, V M D'yakov, Yu L Frolov, P Raikh, I L Anisimova *Atlas Spektrov Organicheskikh Soedinenii* (Atlas of Spectra of Organic Compounds) (Ed. V A Koptug) (Novosibirsk: Novosibirsk Institute of Organic Chemistry, Siberian Branch of Academy of Sciences of the SSSR, 1985)
160. E I Brodskaya, V V Belyaeva, O M Trofimova, N F Chernov, V B Pukhnarevich, M G Voronkov *Zh. Obshch. Khim.* **70** 1139 (2000)^e
161. O M Trofimova, E I Brodskaya, Yu I Bolgova, N F Chernov, M G Voronkov *Dokl. Akad. Nauk* **388** 208 (2003)^d
162. N F Lazareva, E I Brodskaya, V V Belyaeva, M G Voronkov *Zh. Obshch. Khim.* **70** 1645 (2000)^e
163. C Eaborn *Organosilicon Compounds* (London: Butterworth, 1960)
164. L H Sommer, J Rockett *J. Am. Chem. Soc.* **73** 5130 (1951)
165. H Bock, W Kaim, M Kira, H Osawa, H Sakurai *J. Organomet. Chem.* **164** 295 (1979)
166. E Hasegawa, W Xu, P S Mariano, U C Yoon, J-U Kim *J. Am. Chem. Soc.* **110** 8099 (1988)
167. W Xu, Y T Jeon, E Hasegawa, U C Yoon, P S Mariano *J. Am. Chem. Soc.* **111** 406 (1989)
168. E I Brodskaya, M G Voronkov, V V Belyaeva, V P Baryshok, N F Lazareva *Zh. Obshch. Khim.* **63** 2252 (1993)^e
169. E I Brodskaya, V V Belyaeva, N F Lazareva, M G Voronkov *Zh. Obshch. Khim.* **69** 403 (1999)^e
170. V Fialova, V Bazant, V Chvalovsky *Coll. Czech. Chem. Commun.* **38** 3837 (1973)
171. E I Brodskaya, N F Lazareva, G V Ratovskii *Zh. Obshch. Khim.* **73** 1123 (2003)
172. N N Chipanina, L V Sherstyannikova, O M Trofimova, N F Chernov, V M Turchaninov, M G Voronkov *Zh. Obshch. Khim.* **70** 1147 (2000)^e
173. M G Voronkov, N F Chernov, O M Trofimova, N N Chipanina, L V Sherstyannikova, V K Turchaninov *J. Organomet. Chem.* **642** 91 (2002)

^a — *Russ. Chem. Bull., Int. Ed. (Engl. Transl.)*

^b — *Chem. Heterocycl. Compd. (Engl. Transl.)*

^c — *Russ. J. Organomet. Chem. (Engl. Transl.)*

^d — *Dokl. Chem. (Engl. Transl.)*

^e — *Russ. J. Gen. Chem. (Engl. Transl.)*

^f — *J. Struct. Chem. (Engl. Transl.)*

^g — *Pharm. Chem. J. (Engl. Transl.)*

^h — *Russ. J. Org. Chem. (Engl. Transl.)*

Chemistry of metallasiloxanes. Current trends and new concepts

M M Levitsky, B G Zavin, A N Bilyachenko

Contents

I. Introduction	847
II. Synthetic methods in the chemistry of metallasiloxanes	847
III. The structure of metallasiloxanes	855
IV. Rearrangements of metallasiloxanes	858
V. Metallasiloxanes in catalysis	860
VI. Conclusion	863

Abstract. The current status of the chemistry of metallasiloxanes is surveyed. Synthetic methods affording the metallasiloxane fragments and specific transformations of metallasiloxanes governed by the coordination properties of the metal site are analysed. The emphasis is placed onto the formation of compounds with the metallasiloxane fragments and rearrangements of these fragments. Principles of the design of catalytic systems based on metallasiloxanes, in particular, containing low-coordinated metal sites, are generalised. The bibliography includes 174 references.

I. Introduction

Chemistry of metallasiloxanes (hereinafter, MS), *viz.*, compounds containing a >Si(R)OM fragment, where M is a metal atom, initially emerged as a subfield within chemistry of organosilicon compounds, but then gradually grew into an independent scientific direction. The vast majority of transformations of MS directly involves the SiOM fragment, and the structure of MS is largely governed by the coordination properties of the constituent metal.

Intensive investigations into individual metallasiloxanes started in the 1950s. The major results of these studies are summarised in a number of reviews and monographs.^{1–8} In parallel, oligomeric^{9–11} and polymeric MS containing metallasiloxane fragments in the main organosiloxane chain became a subject of numerous studies. Some of these compounds came into industrial-scale production within literally years of their first synthesis.¹²

The following directions in the chemistry of metallasiloxanes have proven most fruitful over the last 15 years:

— the development of novel methods for the creation of the metallasiloxane fragment, which has led to the discovery of new structural types of MS and extended the range of metal atoms that can be incorporated in the metallasiloxane fragment;

— investigations into highly specific chemical transformations of MS;

— the development of general concepts that describe the formation of the MS structure;

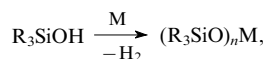
— the elaboration of concepts that rationalise the regularities of rearrangements of metallasiloxane fragments in the structure of MS;

— the application of MS as catalysts in various processes of organic synthesis.

II. Synthetic methods in the chemistry of metallasiloxanes

Methods used to create the metallasiloxane fragment are rather diverse. Some early methods have been modified and are used nowadays.

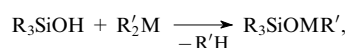
The reaction of organosilanols with reactive metals, such as alkali metals,¹³ zinc¹⁴ or aluminium,¹⁵ represents one of the historically first methods.



M = K, Na, Zn, Al; *n* is the metal oxidation state.

Presently, this method retains its preparative importance mainly for the synthesis of alkali metal organosilanolates.

The reaction of organosilanols with organometallic compounds is a less common method.^{16–18}



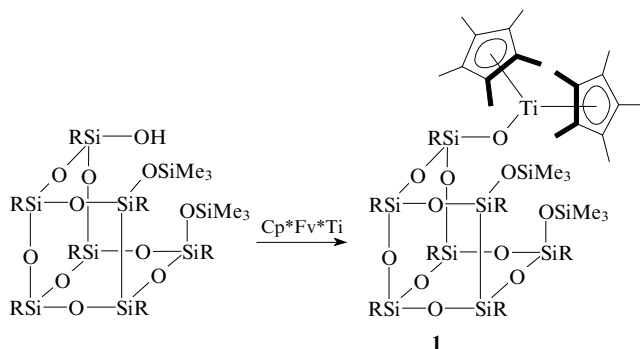
R = Me, Et, Ph; R' = Me, Et; M = Zn, Cd.

Typically, this reaction is accompanied by the liberation of the corresponding hydrocarbon. However, according to recent studies,¹⁹ in some cases hydrocarbon ligands at the metal atom undergo rearrangements (*e.g.*, fulvene converts into cyclopentadienyl giving rise to compound **1**).

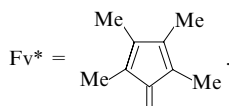
M M Levitsky, B G Zavin, A N Bilyachenko A N Nesmeyanov Institute of Organoelement Compounds, Russian Academy of Sciences, ul. Vavilova 28, 119991 Moscow, Russian Federation. Fax (7-499) 135 50 85, tel. (7-499) 135 93 71, e-mail: levitsk@ineos.ac.ru (M M Levitsky), zavin@ineos.ac.ru (B G Zavin), xeloff@mail.ru (A N Bilyachenko)

Received 12 April 2007

Uspekhi Khimii 76 (9) 907–926 (2007); translated by Ya V Zubavichus

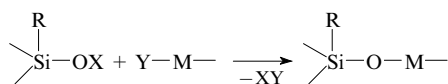


R = cyclo-C₆H₁₁; Cp* = η-C₅Me₅,

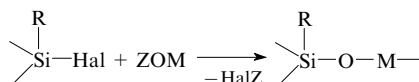


The heterofunctional condensation is the most common method for the synthesis of MS; this reaction can be accomplished in different ways to afford both individual and oligomeric MS (R, R' and R'' are organic substituents) (Scheme 1).

Scheme 1

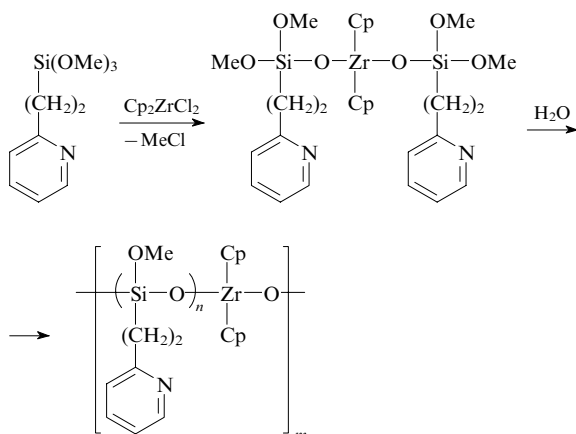


X = H: Y = Hal, R'O; X = R': Y = Hal, AcO; X = Ac, Y = Hal.

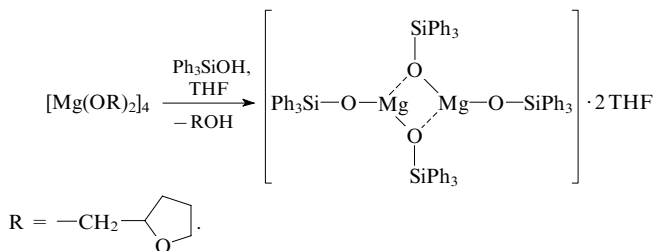


Z = H, R.

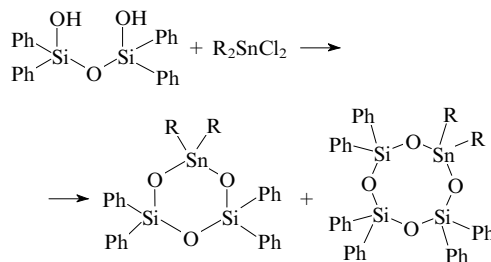
Below we consider only those versions of the heterofunctional condensation that are widely applied in modern studies. A combination X = R'' and Y = Hal (see Scheme 1) is especially suitable for the synthesis of polymeric MS, since the low-molecular-mass condensation product (R''Hal) does not destroy the main chain of the product.²⁰



Organometallic derivatives with Y = OR' should be utilised provided the self-condensation of a silanol R₃SiOH is hindered, for instance:²¹

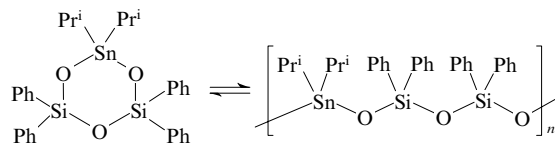


The heterofunctional condensation of silanols with metal halides (X = H and Y = Hal in Scheme 1) is useful in those cases where a silicon (or metal) atom bears a bulky branched substituent (e.g., isopropyl or *tert*-butyl group).²²

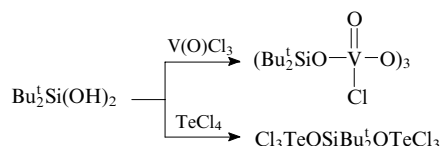


R = Prⁱ, Bu^t.

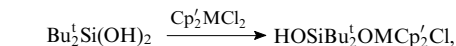
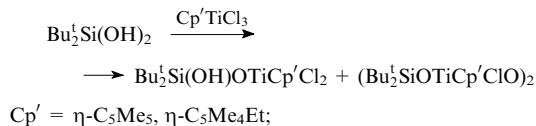
If the Sn atom bears isopropyl (but not *tert*-butyl) groups, cyclic organostannasiloxanes can undergo polymerisation.



Often, the reaction of organosilanedioles with metal halides results in only partial substitution of organosiloxy groups for the Cl⁻ ions.²³

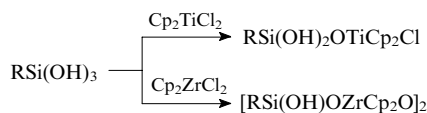


Derivatives with one or two Cp groups at the metal atom can be obtained provided the Si atom in the starting organosilicon compound bears the Bu^t group; this reaction is impossible with Et or Ph substituents at the silicon atom.²⁴

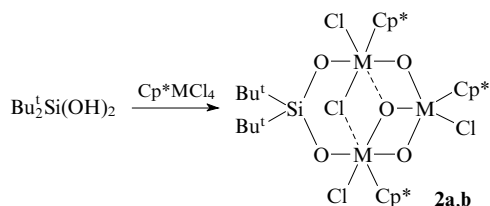


M = Ti, Zr: Cp' = η-C₅H₄Me; M = Hf, Cp' = η-C₅H₅.

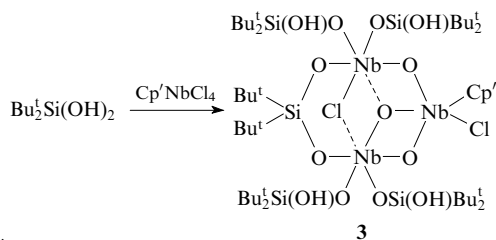
The presence of a bulky branched group at the silicon atom allows the use of organosilaneetriols in addition to diorganosilanedioles in these reactions, since their self-condensation is hindered.²⁵


$$R = 2,6\text{-Pr}_2\text{C}_6\text{H}_3\text{NSiMe}_3.$$

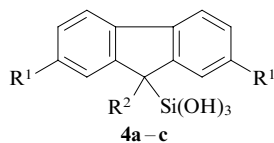
It must be noted that the synthesis of Nb- and Ta-containing MS (for instance, compounds **2a,b**) is accompanied by the formation of metal oxide fragments $M-O-M$,²⁶ which cannot be explained by the heterofunctional condensation mechanism. This fact suggests a rearrangement to occur during the synthesis (this is described in more detail in Section IV).


$$\mathbf{M} = \text{Nb } (\mathbf{a}), \text{Ta } (\mathbf{b}).$$

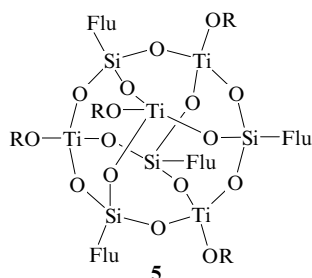
In some cases, the reaction is additionally complicated by a competing process, *viz.*, organosiloxy group substitution for the π -coordinated ligand.²⁶ Synthesis of compound **3** may serve as an example.


$$\text{Cp}' = \eta\text{-C}_5\text{Me}_4\text{Et}.$$

The strongest shielding effect among organic substituents studied is exerted by the fluorenyl group, which allows complete suppression of the self-condensation of the organosilane-triol upon its reaction with metal alkoxides. The heterofunctional condensation of fluorenyl-substituted organosilane-triols **4a–c**

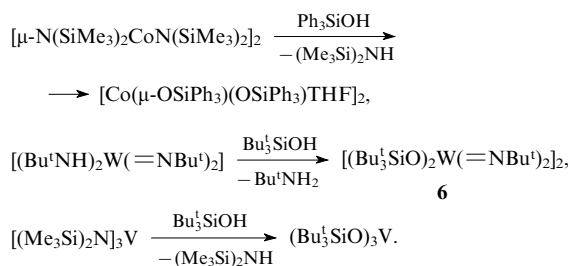

$$\text{R}^1 = \text{H}; \text{R}^2 = \text{SiMe}_3 \text{ (a), Me (b); R}^1 = \text{Bu}^t, \text{R}^2 = \text{SiMe}_3 \text{ (c).}$$

with titanium alkoxides $\text{Ti}(\text{OR})_4$ yields cage titanasiloxanes **5**.^{27, 28}

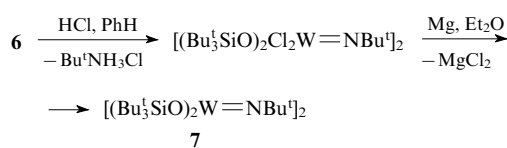


Flu is a substituted fluorenyl; R = Et, Prⁱ.

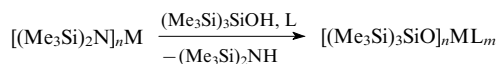
Another relatively rare method for the synthesis of MS, *viz.*, the reaction of organosilanols with metal amides or imides can also be classified as the heterofunctional condensation.^{29–31}



Owing to the presence of bulky substituents at the silicon atom in compound **6**, a novel tricoordinate tungsten compound **7** was synthesised.³⁰

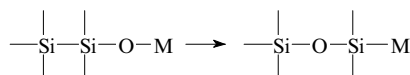


An analogous reaction of metal silylamides with organosilanols yields MS with the disilane bridges Si—Si; the tris(trimethylsilyl)silyl fragment (Me₃Si)₃Si acts as a bulky substituent in this case.^{32, 33}

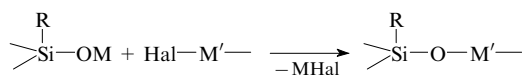


M	<i>n</i>	L
Co	2	THF, DME, MeCN, PhCN, 2,2'-bipy, 4,4'-bipy, Ph ₃ P
Fe	2	2,2'-bipy, 4,4'-bipy
La	3	THF
Gd	3	THF, MeCN, 4,4'-bipy

The Si—Si bonds in these compounds are highly reactive. They are very sensitive to oxidation and are easily converted into the siloxane fragments Si—O—Si under the action of O₂ (Ref. 32); pyrolysis in the absence of O₂ results in the migration of an O atom, which is accompanied by a rearrangement and formation of the bond Si—M.^{34, 35}



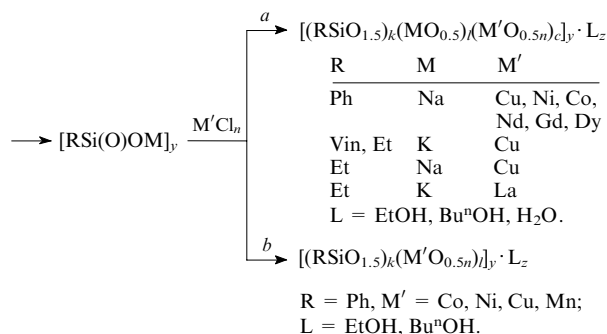
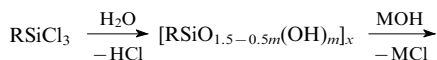
The reaction of alkali metal organosilanolates with polyvalent metal halides (M') is yet another popular version of the heterofunctional condensation; it is commonly referred to as the exchange reaction in the literature.



This reaction is most versatile. It was successfully used to synthesise MS containing Mg, Zn, Al, Ga, Ti, Zr, Fe, Co, Ni, Cu and some other metals,^{8, 11} which substantially extended the range of metal atoms incorporated in the metallasiloxane fragment.^{36–40} The use of bulky organic groups at the silicon atom played the key role in the development of the synthetic potential of this method.

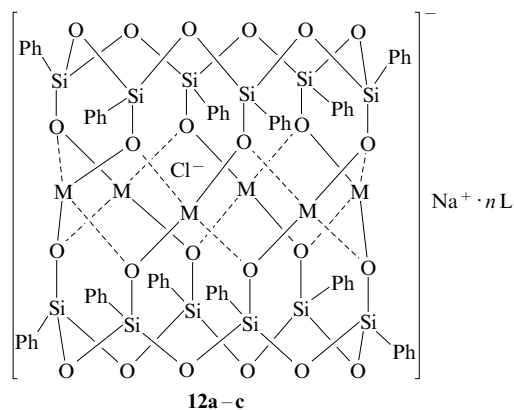
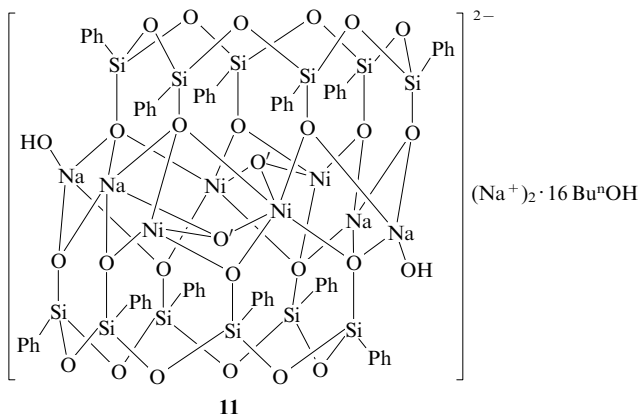
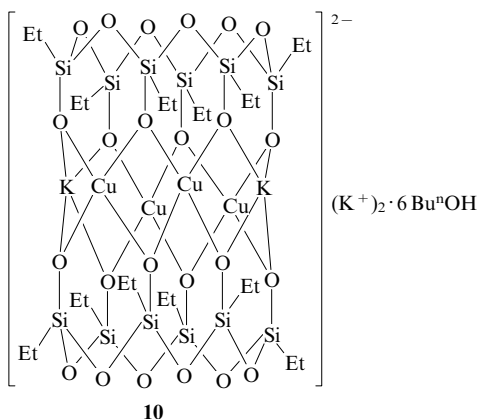
of the metal from the reaction medium in the form of hydroxide. Therefore, for alkali-assisted cleavage of the polysiloxane, definite amount of sodium (not shown in the reaction scheme below), which reacts with the silanol groups, has been added to the reaction medium in addition to alkali to maximally suppress the potential self-condensation of the silanol groups.

Two versions of this reaction have been studied,^{44–49} viz., partial (*a*) and complete (*b*) substitution of the polyvalent metal atoms M' for the silanolate groups SiOM .



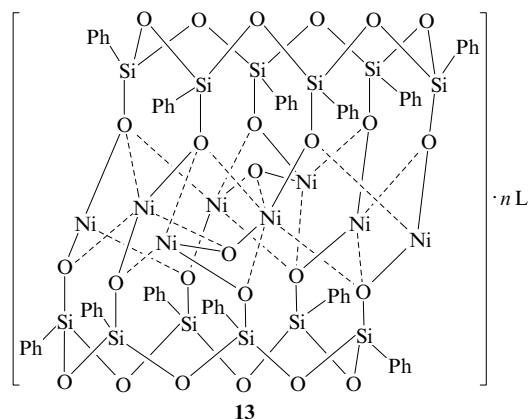
For *a*, *b* see text; *n* is the oxidation state of M' ; Vin is vinyl.

The majority of compounds synthesised according to the above scheme irrespective of partial or complete substitution of the silanolate groups have prism-shaped structures (sometimes, skewed prisms) with the cyclosiloxane fragments at the base (compounds **10–14**) (in the structure of compound **11**, the O' atoms belong to coordinated water molecules).

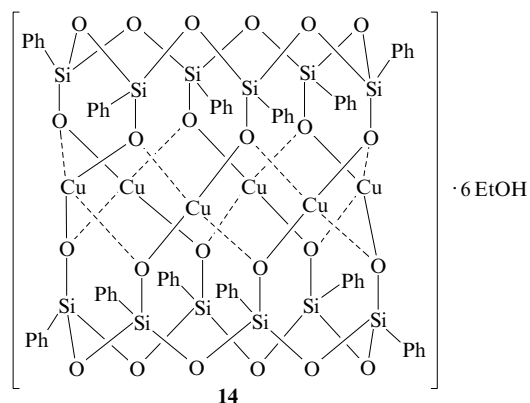


$M = \text{Co (a)}, \text{Mn (b)}, \text{Ni (c)};$

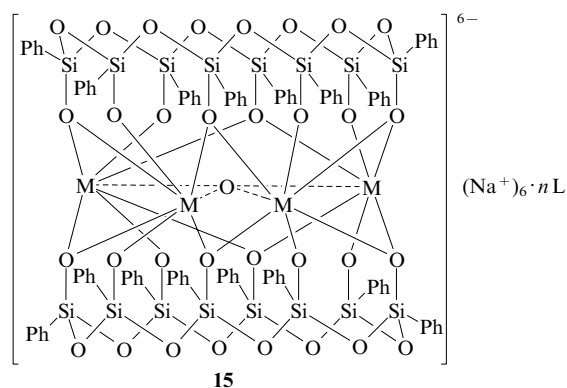
$L = \text{Bu}^n\text{OH}, \text{EtOH}, \text{H}_2\text{O}, \text{Me}_2\text{CO}, \text{CHCl}_3.$



$L = \text{Bu}^n\text{OH}, \text{H}_2\text{O}, \text{Me}_2\text{CO}.$

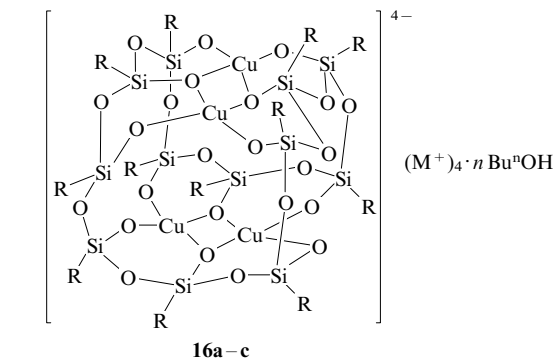


The cyclic fragments at the base of the prism are expanded from six- to eight-membered rings when lanthanides are introduced into MS^{50–53} (compounds **15**).



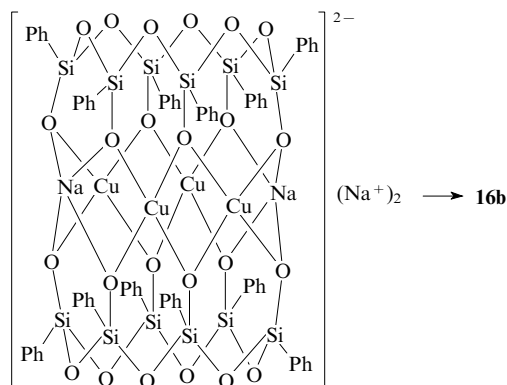
$M = \text{Nd}, \text{Gd}, \text{Dy}; L = \text{EtOH}, \text{H}_2\text{O}.$

In some rather rare cases of Cu-containing MS **16a–c** also incorporating alkali metal cations, the cage is characterised by a globular shape.^{54, 55}

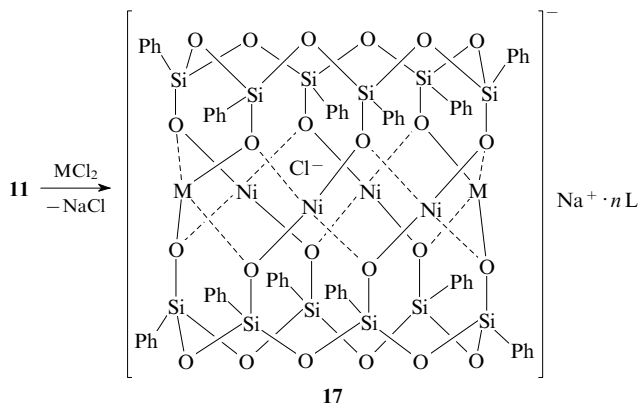


Compound 16	M	R	n
a	Na	Et	4
b	Na	Ph	8
c	K	Vin	4

It was possible to convert the prismatic structure into the globular type cage upon prolonged heating of the compound in an organic solvent (butanol or dioxane).⁵⁶



In those case where MS simultaneously contain transition (polyvalent) and alkali metals (in unsubstituted silanolate groups), other transition metals can substitute the alkali metal ions. Here, partial structural transformation of the metal–oxygen part of the cage occurs to yield bimetallic MS **17**, which are also characterised by prismatic structures.^{57–59}

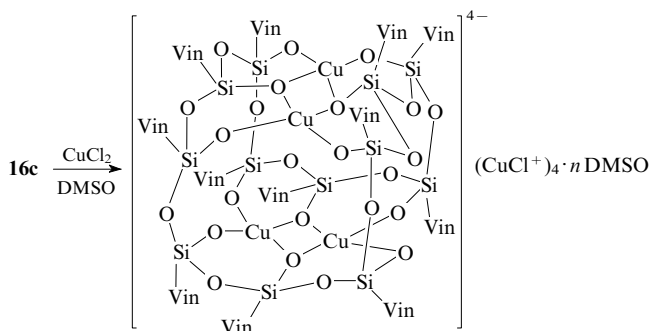


M = Co, Cu, FeOH, FeOMe; L = H₂O, DMSO.

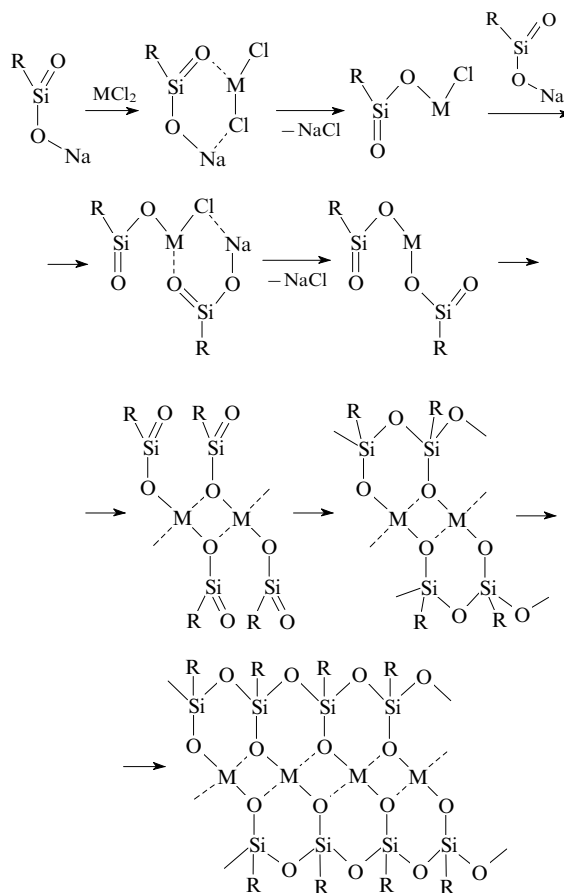
The reaction of Cu-, Co-, Ni- and Mn-containing prismatic MS with acetylacetonate gives rise to a partial removal of the

metal ions from the cage in the form of the respective acetylacetonates.⁶⁰

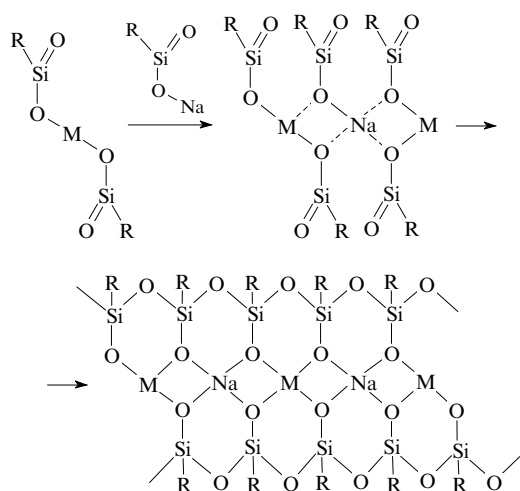
Substitution of the copper ion for an alkali metal ion in the outer sphere of the globular MS **16c** results in the incorporation of an unusual cation MCl^+ (Ref. 61).



Spirocyclic fragments assembled from the units $\text{M}–\text{O}–\text{M}$ linked to siloxane rings are common to both types of structures (*i.e.*, prismatic and globular). The synthesis of this novel class of the cage MS stimulated chemists to try to rationalise the mechanism of their formation. A suggested general scheme of the formation of such structures postulated the presence of alkali metal silanates in the form of associated silanone derivatives in the reaction medium. These associates rearrange to yield building blocks of the prismatic cages considered above.⁶²

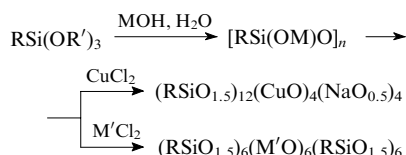


The formation of MS containing unsubstituted organo-silanolate groups can be described in a similar way.



The above method for the synthesis of cage MS has several disadvantages. Thus the yields of target products are low due to the presence of free OH groups in the starting organosiloxane (despite the use of metallic sodium as described above). In addition, no cage MS with small organic substituents at the silicon atoms (*e.g.*, methyl) can be synthesised by this method, since the respective starting siloxanes are insoluble.

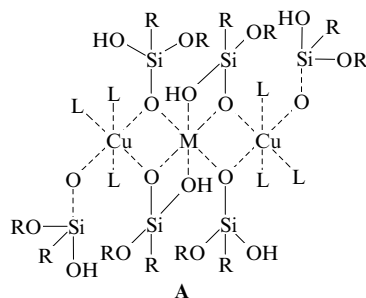
The idea of modification of the method for the synthesis of polyhedral MS has been inspired by the above scheme of the cage 'assembly'. It was the first step of the process, *viz.*, the generation of silanolates that has been modified. It was suggested to assemble a cage structure from monomeric units rather than cleave the organosiloxane into separate fragments under the action of a base. The polyvalent metal atoms were thought to act as nuclei that would arrange components of the future polyhedron. Trialkoxyorganosilanes were selected as a source of the monomeric units.^{63–67}



R = Me, Et, Vin, Ph, (CH₂)₃NH₂; R' = Me, Et, Buⁿ;
M = K, Na; M' = Mn, Ni.

The new version provided higher yields in the syntheses of all the above cage structures, this also enabled the synthesis of cage Na,Cu-vinyl-, K,Cu-phenyl- and Na,Cu-methylsiloxanes inaccessible earlier.^{68, 69}

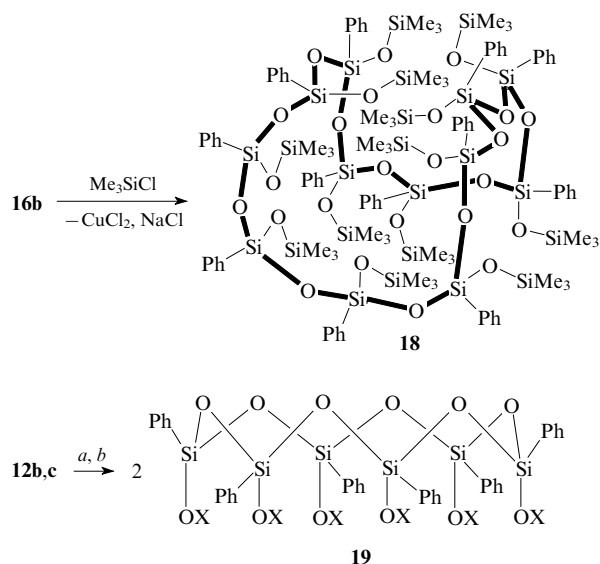
The mechanism of the cage formation considered above was somewhat changed, as applied to trialkoxyorganosilanes. The modified mechanism assumed the generation of metallasiloxane associates **A** followed by the condensation of functional groups at the silicon atom giving rise to spirocyclic fragments around the metal atoms.⁶⁷



R = Me, Vin, Ph; M = K, Na; L = ROH, H₂O.

It must be noted that such a mechanism is equally applicable to the formation of cage MS according to the previous method (*i.e.*, without alkoxyorganosilanes) and seems more preferable, since it does not presume the formation of extremely unstable silanones as intermediates.

The idea of exploiting different reactivities of the fragments Si–O–Si and Si–O–M in polyhedral MS proved to be the most fruitful: the fragment Si–O–Si is sensitive to the action of nucleophilic agents, whereas the fragment Si–O–M is rather susceptible to electrophiles. The reaction of cage MS with Me₃SiCl results in the cleavage of the fragments Si–O–M to yield macrocyclic organosiloxanes, in which the configuration of the starting MS is preserved.^{64, 70, 71} Globular structures are transformed into 12-membered rings with the *cis*–*trans* configuration (*e.g.*, compound **18**; bonds forming a closed macrocycle are shown as thick lines), whereas prismatic structures are transformed into six-membered siloxane rings in the *cis* configuration. The reaction with a mineral acid (H₂S or dilute HCl with cooling) instead of Me₃SiCl yields Si-function-alised stereoregular hydroxycyclosiloxanes **19**.^{66, 72}



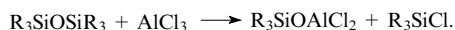
(a) is Me₃SiCl (–MCl); (b) is HCl or H₂S (–MCl or M₂S);
X = SiMe₃, H; M = Ni, Mn.

Metal sulfides, which are by-products of the reaction, form nanocomposite aggregates dispersed in the siloxane matrix, which is promising for the design of new materials. Furthermore, the highly reactive hydroxycyclosiloxanes can be regarded as active precursors of structurally organised systems.

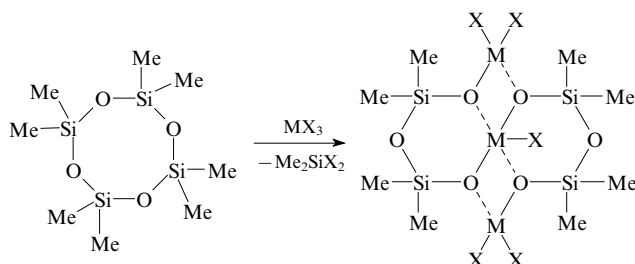
Stereoregular organosiloxane rings with smaller sizes, *e.g.* [PhSi(OSiMe₃)O]₄, have been synthesised⁶⁵ in a similar way by the reaction of cyclic organosilanolate [PhSi(ONa)O]₄ with Me₃SiCl.

Presently, it is the only method that makes it possible to synthesise stereoregular cyclosiloxanes with variable sizes. Moreover, it provides wide capabilities for further syntheses. In particular, if the organotrichlorosilane bears functional groups in the organic substituents at the silicon atom, the reaction yields stereoregular cyclosiloxanes, such as (PhSiO)₁₂[OSiMe₂CH₂OCH₂O₂CMe]₁₂, which can be incorporated in polymeric siloxane chains.^{73, 74}

In addition to the methods for the creation of fragments Si–O–M considered above, yet another method is of particular interest. It is based on the cleavage of siloxane chains under the action of metal compounds. For the first time, this reaction has been carried out⁷⁵ with metal halides.

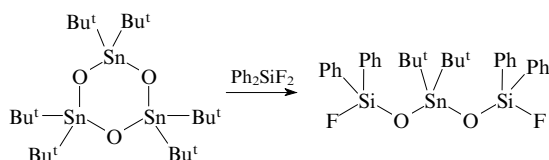


Later, it has been shown^{76–80} that some metal halides as well as alkyl derivatives are capable of cleaving the siloxane bonds in organosiloxane rings.

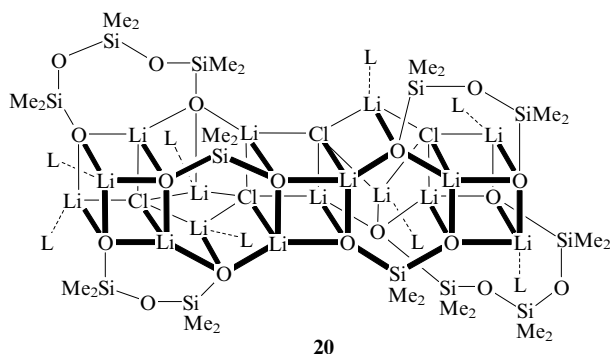


M = Al, Ga; X = Hal, Alk.

The introduction of tin atoms into MS inverts the roles played by the silicon and tin atoms, *viz.*, the metallasiloxane ring is opened under the action of silicon halides.²²

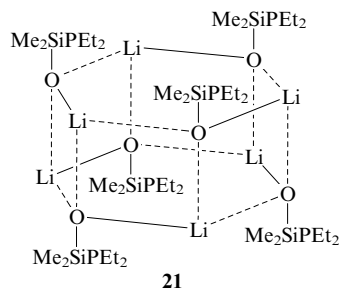


In the modifications considered above, this reaction is of limited use. However, it became widespread after the discovery of the fact that organometallic compounds can cleave polymeric organosiloxanes. Now that this fact has been reliably established it comes as no surprise. But for a long time, the very idea of a reaction of an organometallic compound with a polymeric organosiloxane seemed a nonsense. An occasional observation gave an impetus to the reconsideration of this issue: MS derivatives were detected upon storage of certain organometallic compounds in a contact with an organosilicon grease (which is often used for a ground joint sealing). In particular, a mixture of Me_2GaCl and Bu^tAsLi_2 in a contact with polydimethylsiloxane $(Me_2SiO)_n$ readily affords polynuclear lithium complex **20** containing neither Ga nor As in a yield of 48%.⁸¹

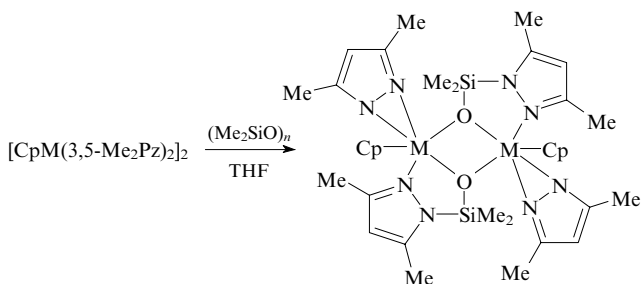
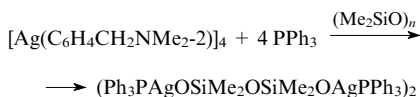
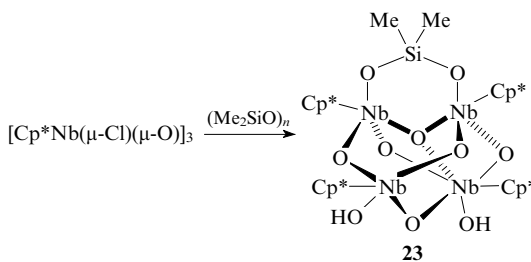
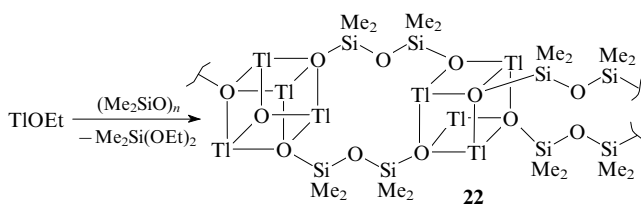
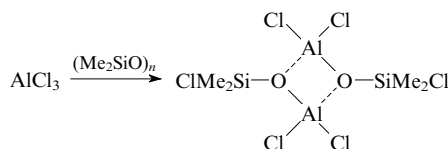


L = THF.

Similarly, a prolonged storage of a solution of $LiPEt_2$ in diethyl ether at 20 °C in a contact with a silicone polymer gave rise to the formation of Li-containing MS **21** with the hexagonal prismatic structure.⁸²

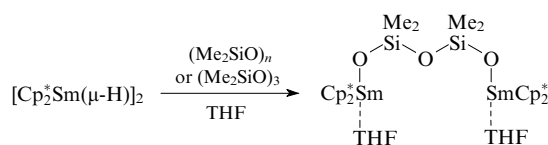


In the modern version of this method, a diorganosiloxane polymer rather than an individual compound [such as $Me_3SiO \cdot SiMe_3$ or $(Me_2SiO)_4$] is used as the organosilicon component. This allows the introduction (under mild conditions) of the groups Me_2SiO , which are involved in the construction of metallasiloxane cages and can be incorporated as mono-, di- or trisiloxane units. In addition to the metal halides,⁸³ organic derivatives of the main group^{84,85} and transition^{86,87} metals as well as lanthanides^{88,89} can be used as the metal-containing component in this reaction. The structural features of the resultant MS (*e.g.*, **22** and **23**) are considered in detail in the next section.

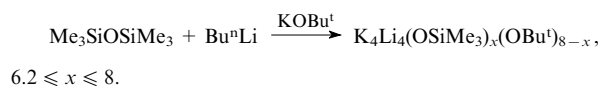


M = Yb, Tb, Dy, Ho; HPzMe₂ is 3,5-dimethylpyrazole.

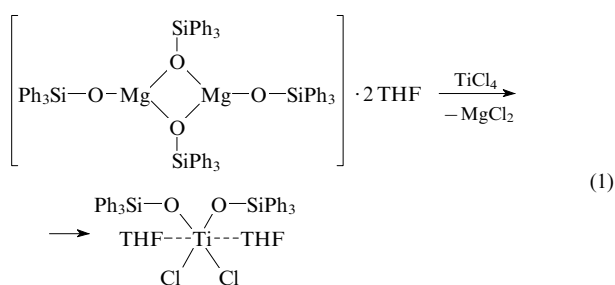
We note that in some cases, the reactions of an organometallic compound with a polyorganosiloxane and the respective individual cyclosiloxane yield identical products.⁹⁰



This method is versatile and can be used for the synthesis of alkali metal-containing MS. For instance, the reactions of disiloxanes with organometallic compounds (alkali metal derivatives) (also in the presence of alkoxides) yield mixed silanolates – alkoxides with variable composition.⁹¹



Yet another method for the synthesis of MS consists of the exchange of polyvalent metal ions. Typically, the reaction results in a change in the molecular structure.²¹



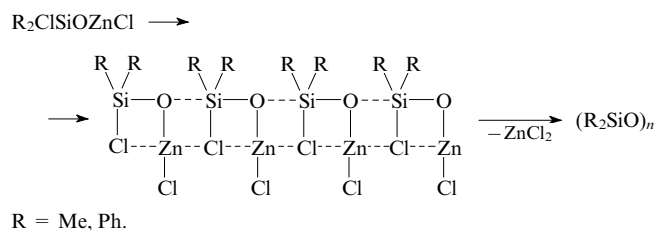
This recently discovered transformation stimulated the development of concepts underlying the structure formation in MS (this subject is addressed in more detail in subsequent sections).

Zavin and co-workers^{92, 93} reported a non-traditional method for the formation of metallasiloxane fragments based on the reaction of organochlorosilanes with zinc oxide.

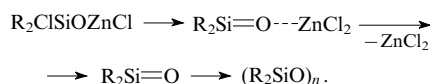


The resultant MS are intermediates in the synthesis of polysiloxanes. Two mechanisms of the transformation were considered.

1. The formation of polymeric zincasiloxane involving bridging coordination bonds:



2. The formation of an intermediate zinc complex with the organosilanone followed by its decomposition:



According to quantum chemical calculations, the former mechanism is more probable from the thermodynamical point of view. This reaction allows the formation of siloxane fragments in a non-hydrolytic way. In particular, completely soluble polymethylsilsesquioxane ($\text{MeSiO}_{1.5}$)_n with a molecular mass as large as ~25 000 has been successfully obtained

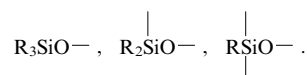
from MeSiCl_3 , which was nearly impossible with other methods.

Concluding the section devoted to synthetic methods of MS chemistry we note that the possibility of MS synthesis under conditions of the mechanochemical activation has been demonstrated quite recently; this makes it possible to accomplish a solvent-free process. The reaction of copper acetylacetonate with diphenylsilanediol can serve as an example.⁹⁴



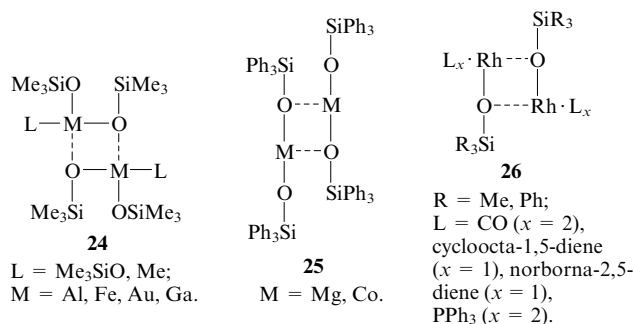
III. The structure of metallasiloxanes

The methods for the synthesis and transformations of MS considered in the previous section are difficult to systematise. On the contrary, the classification of structures of individual MS is rather straightforward. Most conveniently, all the MS synthesised can be divided into three large groups according to the type of the constituent organosilicon fragment:

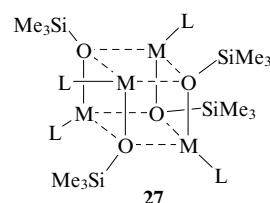


Similar structures within this classification would fall into the same group. Meanwhile, the general principles of the formation of the coordination sphere of the metal atom remain common for all these groups.

In the vast majority of cases, the coordination sphere of the metal atom is filled by bridging oxygen atoms from the neighbouring fragments $\text{Si}-\text{O}-\text{M}$. The formation of coordination dimers is typical of MS containing monofunctionalised fragments R_3SiO (compounds **24–26**). Similar structures occur for a variety of main group and transition metals,^{21, 29, 95–98} including Ru, Rh and Pd.^{99–104}

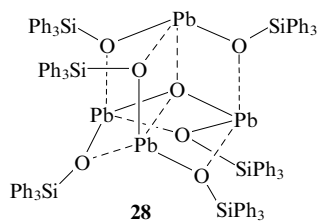


In a few cases, coordination tetramers (e.g., compound **27**)^{16, 105} or hexamers (compound **21**) are formed.

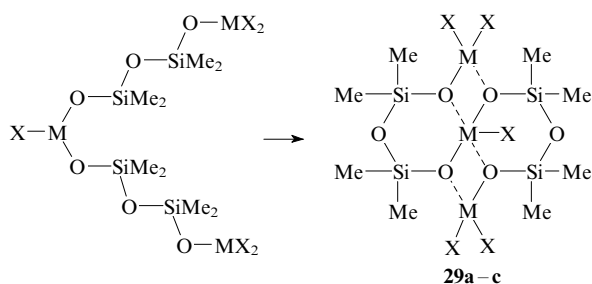


L = Me: M = Cd, Zn; L = PPh_3 , M = Cu.

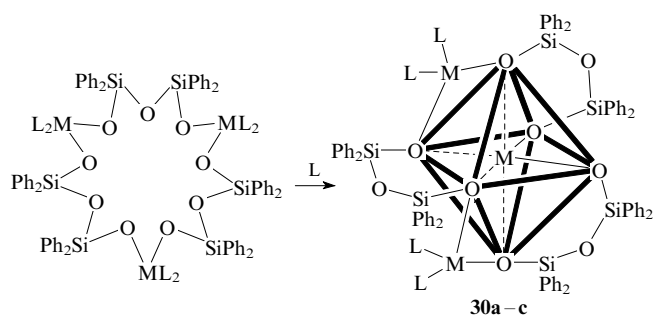
In addition to the oxygen atoms from the $\text{Si}-\text{O}-\text{M}$ groups, highly basic O atoms from the $\text{M}-\text{O}-\text{M}$ groups can be involved in the coordination sphere of the metal atoms [as, for instance, in Nb (**23**) and Pb organosiloxanes (**28**)]¹⁰⁶ as well as anions, usually halides (as in compounds **2** and **3**).



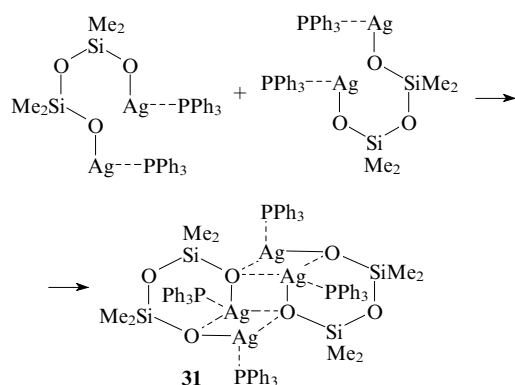
In MS bearing flexible difunctionalised organosilicon fragments $\text{SiR}_2\text{--O--SiR}_2$, the filling of the metal coordination sphere requires the respective change in the molecular conformation. The major driving force of the change, *viz.*, the coordination unsaturation of the metal atom, sometimes makes molecules fold in intricate way. The coordination sphere of the metal atoms involves O atoms of the Si--O--M groups. This can be seen in metallasiloxanes containing aluminium or gallium (compounds **29a–c**),^{76–80} alkali-earth metals (compounds **30a–c**)^{107, 108} or silver (compound **31**).⁸⁷



M = Al: X = Cl (**a**), Br (**b**); M = Ga, X = Cl (**c**).



M = Ca (**a**), Sr (**b**), Ba (**c**); L = Py, tetraglyme.

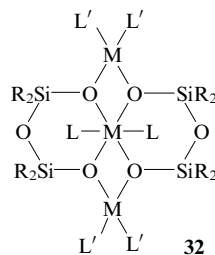


Trifunctionalised fragments $\text{RSiO}_{1.5}$ give rise to MS with totally different structures, although the basic principle of the metal coordination sphere formation, *viz.*, the involvement of

the O atoms from the fragments Si--O--M and M--O--M and sometimes stabilising Hal^- anions, is preserved. This can be seen in cage structures **12–14**.

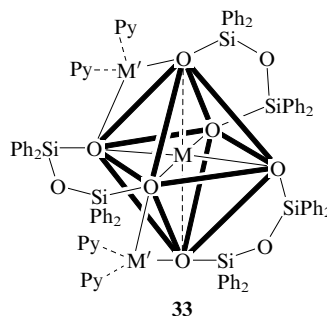
It is noteworthy that there are only a few types of the coordination polyhedra of the metal atom; in the majority of cases, the polyhedron is close to either tetrahedron [the coordination number (CN) is 4] or tetragonal bipyramid (CN = 6).

Among ligands that fill the coordination sphere of the metal atom in MS, one ligand takes a special place. This is the silanolate anion, SiO^- . This appears in the structures of MS containing a polyvalent metal and the silanolate groups Si--O--M , where M is an alkali metal. As a result, mixed-metal MS involving metal atoms of different nature (*i.e.*, polyvalent and alkali metals) are formed, the alkali metal atoms being not incorporated in the cage. The existence of anions in these systems was confirmed by electrochemical techniques.¹⁰⁹ The majority of individual crystalline MS obtained so far fall into this type of compounds. They are obtained in high yields (> 90% in some cases)⁶³ and are rather stable and do not change composition upon subsequent recrystallisations. Different structures involving the silanolate anion have been synthesised with a variety of metal atoms. For instance, a series of compounds **32** with Mg,¹¹⁰ Cr,¹¹¹ Co,¹¹² Cu,¹¹³ Gd,¹¹⁴ V,¹¹⁵ and Sn,¹¹⁶ which are characterised by a structure similar to the tetracyclic Al- and Ga-containing MS (*e.g.*, structures **29a–c**), have been synthesised.



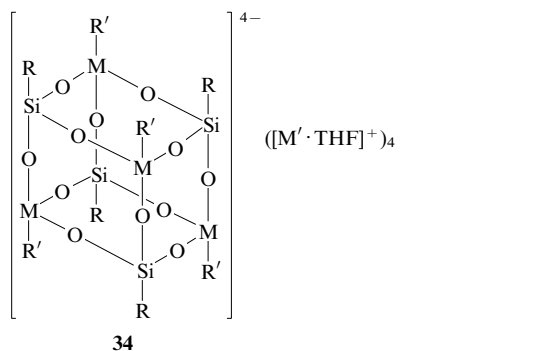
M = Mg, Cr, Co, Cu, Gd, V, Sn; R = Me, Ph; L, L' = Py, THF.

Similarly, transition metals, such as Ti,¹¹⁷ Zr,¹¹⁸ Hf¹¹⁹ and Ta¹¹⁶ (compounds **33**), have been successfully incorporated into octahedral MS structures closely related to the Ca, Sr and Ba organosiloxanes (compounds **30a–c**) owing to the silanolate anions.



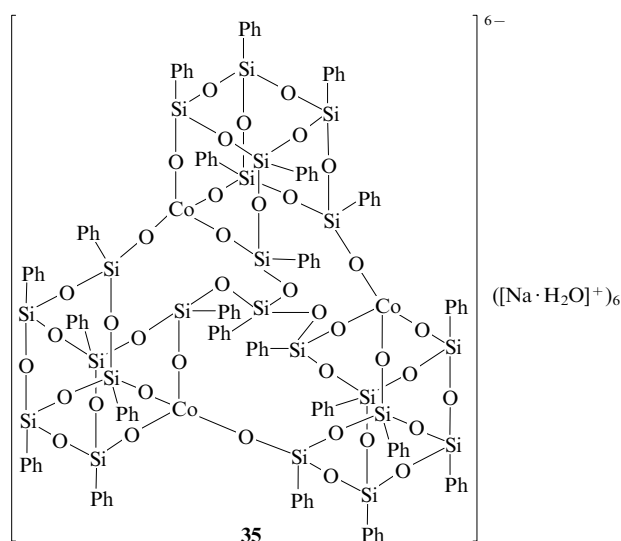
M = Ti, Zr, Hf, Ta; M' = Na, Li.

MS based on trifunctional fragments $\text{RSiO}_{1.5}$ and containing the silanolate anions are equally numerous. Prismatic Cu, K (**8**), Mn, Co and Cu organosiloxanes (**12a–c**) as well as cubane-like Al¹²⁰ and Ga(In) organosiloxanes¹²¹ (compounds **34**) can be given as examples.

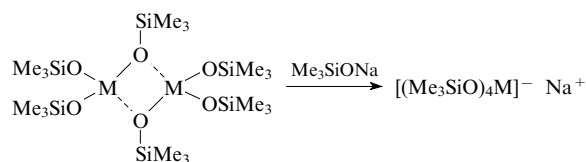
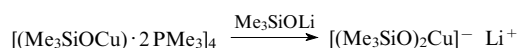


M = Al, Ga, In; M' = Li, Na; R = 2,6-Prⁱ₂C₆H₃NSiMe₃; R' = Me, Et.

Some cage molecules with the silanolate anions specific to this group of compounds have been synthesised, for instance, basket-like Co organosiloxane **35**⁴⁸ and globular structures **16a–c**.

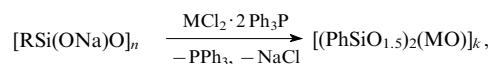
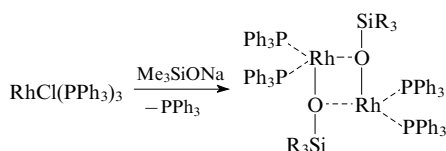


The coordination ability of the silanolate anion is so high that it can replace other ligands in the coordination sphere of the metal atom, in particular, n-donor ligands¹⁰⁵ and the O atoms of the fragments Si–O–M, which are typical ligands for MS.^{97, 122}

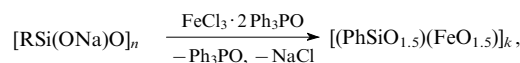


M = Al, Fe, Au.

It is worth noting that the O atoms of the fragments Si–O–M can replace n-donor ligands in the coordination sphere of the metal atom both in individual¹⁰² and oligomeric MS.¹²³



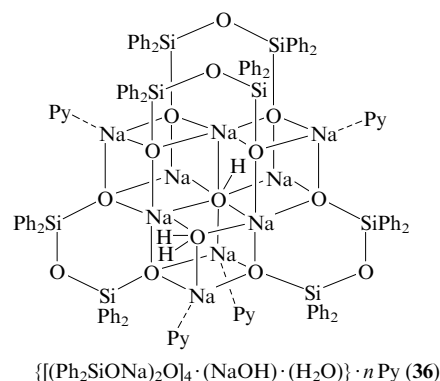
R = Ph, Bu^t; M = Co, Ni; n = 3, 4; k ≠ n;



R = Ph, Bu^t; n = 3, 4; k ≠ n.

Therefore, the coordination environment of the metal atom becomes most stable with the introduction of the silanolate anions. For some transition metals (Cr, Co, Cu, V, Ti, Zr and Hf), only MS containing the silanolate anions have been synthesised so far.

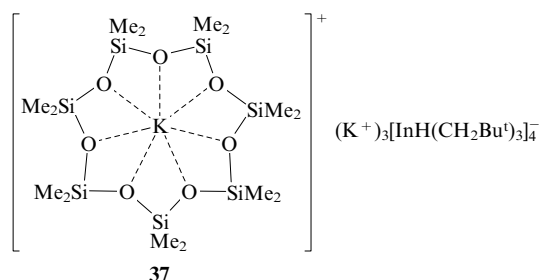
Several general regularities not mentioned above that are somewhat hidden by the multitude of structural types of siloxanes can be revealed. First, oxygen atoms located between two silicon atoms, *i.e.*, in the siloxane units Si–O–Si, virtually never enter into the coordination sphere of the metal atom. This can clearly be seen in the structures **20**, **29** and **30**. In sodium diphenylsilanolate **36**, the O atoms of the disiloxane fragments are also located outside the coordination cluster.¹²⁴

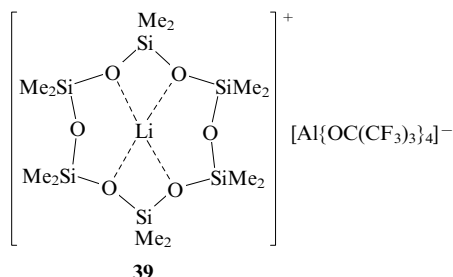
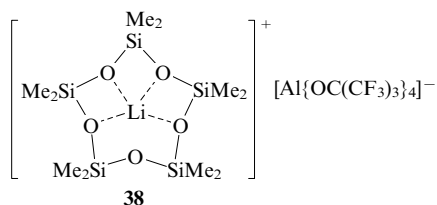


A similar situation is observed in the structure of tallasiloxane **22** where metal oxide cubic fragments are linked together into a chain with disiloxane bridges.

This regularity is also strictly obeyed in prismatic structures built up of trifunctionalised fragments RSiO_{1.5} (*e.g.*, compounds **12–14**). This behaviour of the siloxane fragments in MS is due to the ultimately low basicity of the O atom in the unit Si–O–Si. This fact is nearly completely ignored in the literature devoted to MS but it is actually of no surprise. Independently of MS studies, this property of the siloxane bonds has been established for organosiloxanes.¹²⁵ Diorganocyclosiloxanes (Me₂SiO)_n (n = 6–8) cannot be used as crown ethers for the same reason.¹²⁶

Nevertheless, there are examples of structures violating this rule: in complex **37**, the K⁺ cation is coordinated to a seven-membered organosiloxane ring,¹²⁷ in complexes **38** and **39**, the cations Li⁺ are coordinated to five- and six-membered organosiloxane rings, respectively.¹²⁸





These results however should not be interpreted as a manifestation of increased basicity of the O atoms of the fragments Si—O—Si, especially taking into account that the cations are located not exactly in the plane of the ring but rather above it.

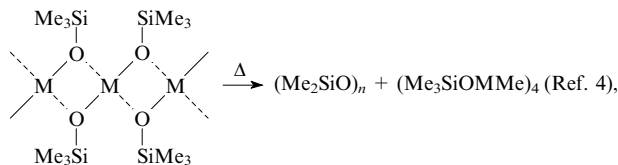
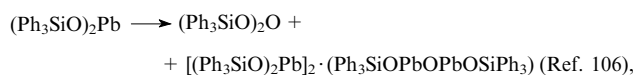
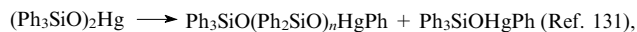
Another structural feature of MS nearly completely missed by researchers consists of the formation of metal oxide fragments M—O—M in some cases (*e.g.*, compounds **2**, **3**, **4**, **13**, **23** and **28**). This concerns units linked by σ -bonds rather than coordination interactions. The appearance of such fragments cannot be explained by the schemes of synthesis of these MS and is due to the secondary process, *viz.*, the rearrangement of metallasiloxane chains. It has to be emphasised that no formation of the fragments M—O—M occurs in structures containing the silanolate anions.

IV. Rearrangements of metallasiloxanes

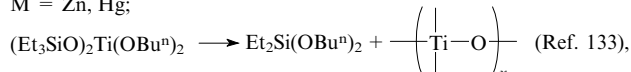
The structural diversity of synthesised MS raised questions on basic principles of their structure formation. The influence exerted by the nature of organic and alkoxy groups at the silicon atom in trialkoxysilanes $\text{RSi}(\text{OR}')_3$ as well as by conditions of synthesis on the selective formation of a certain type of cage (prismatic *vs.* globular) in the synthesis of individual Na,Cu and K,Cu organosiloxanes has been thoroughly studied.⁵⁷

Wide potential of the synthesis of some inaccessible MS provided by the use of bulky R_3SiO groups is now adopted as a specific concept, which considers these groups as an alternative to the cyclopentadienyl ligand due to their rather similar sizes and electron donor properties.¹²⁹

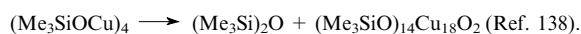
In the majority of studies, the emphasis is placed onto regularities of the synthesis and structural features of the target MS, whereas possible side reactions and post-synthetic transformations of MS have eluded the appropriate consideration for a long time. Nevertheless, from experimental evidence gathered, it gradually became apparent that the as-synthesised compounds partly or sometimes completely rearrange into other compounds with increased or decreased metal content (with respect to the parent compound). Some syntheses ultimately afforded metal-free or silicon-free compounds. Such rearrangements are often accompanied by the formation of metal oxide M—O—M chains (in the reaction equations below, reaction products enriched with silicon are indicated first and those enriched with metal are indicated second).



M = Zn, Hg;



M = Ni, Co;



As has been established upon the extension of the range of compounds under study, similar transformations also occur with oligomeric MS.^{139–144}

In the majority of cases considered in the previous section, the rearrangements are suppressed (typically, due to the presence of stabilising anions). In the absence of suppressing factors, the rearrangements of oligomeric MS can be detected using fractionation. The fractions isolated differ in the metal content, *i.e.*, the M : Si atomic ratio, which gradually decreases from the first fractions to successive ones, rather than in the molecular mass, which is typical of the majority of polymers (Table 1).

In the case of individual MS, the influence of the metal nature (transition *vs.* main group metal) is somewhat masked except for the fact that the synthesis of MS with several transition metals (*viz.*, Cr, Co, Cu, V, Ti, Zr and Hf) was possible only in the presence of the silanolate ions. Meanwhile,

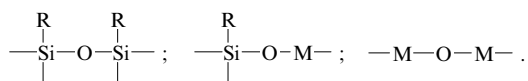
Table 1. Rearrangement products of oligomeric metallasiloxanes.

Monomeric unit	Range of the M : Si ratios in fractions	Ref.
$\text{Ph}-\text{Si}-\text{O}-\text{Cu}-\text{O}-$	0.5–1	139
$\text{Ph}-\text{Si}-\text{O}-\text{Cu}-\text{O}-\text{Si}(\text{Ph})-\text{O}-\text{Al}-\text{O}-$	0.27–0.32 ^a 0.05–0.28 ^b	139
$\text{Me}-\text{Si}(\text{Me})-\text{O}-\text{Cu}-\text{O}-$	0.31–2.0	140, 143
$\text{Ph}-\text{Si}-\text{O}-\text{Cu}-\text{O}-$	0.21–2.5	140, 143
$\text{Ph}-\text{Si}-\text{O}-\text{Fe}-\text{O}-$	0.18–1.6	142, 144
$\text{Ph}-\text{Si}-\text{O}-\text{Co}-\text{O}-$	0.14–0.9	142, 144

^a Al : Si; ^b Cu : Si.

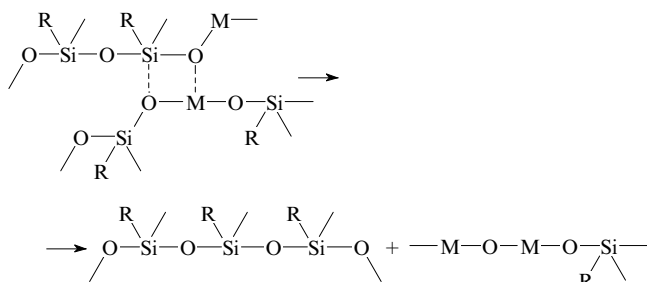
this is not required for main group metals. It can be assumed that the syntheses of MS with the transition metals listed above in the absence of the silanolate anions were accompanied by rearrangements to yield products that were of low importance for synthetic chemists. Thus, these results were not reported and the rearrangements eluded the discussion.

In contrast, in the case of oligomeric MS, the influence of the metal nature is more prominent: the rearrangements are manifested more clearly with transition metals. According to the current concepts,^{142, 143} the rearrangements are driven by coordination unsaturation of the metal atoms in siloxane structures. In oligomeric MS, there are three inequivalent types of the oxygen atoms, *viz.*, those present in siloxane, metallasiloxane and metal oxide units:

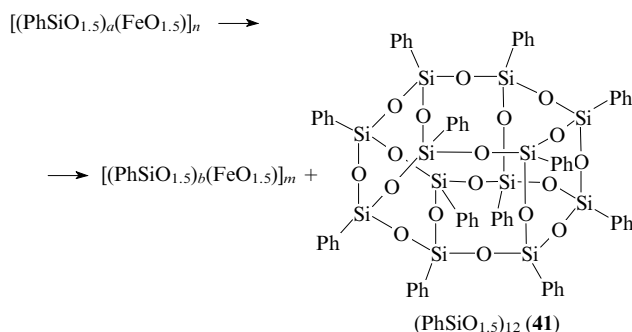
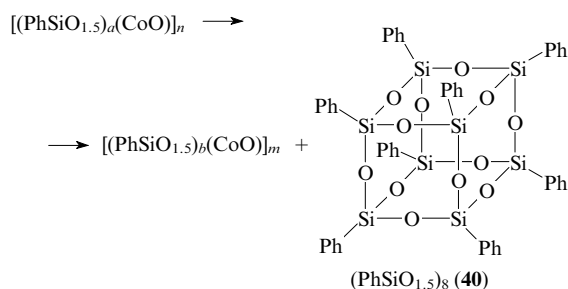


As has been noted above, the oxygen atoms of the siloxane fragments cannot be involved into the coordination sphere of the metal atom due to their ultimately low basicity. On the contrary, the O atoms of the metallasiloxane (Si—O—M) and metal oxide (M—O—M) units are sufficiently basic and thus readily occupy the coordination sphere of the metal atom.

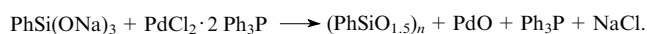
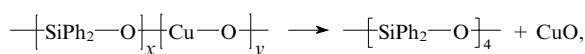
Thus the driving force of rearrangements consists of the formation of compounds with increased amount of such fragments. They proceed *via* intermediate complexes and further give rise to metal oxide fragments,¹⁴² which cannot be explained by the mechanism of the MS synthesis.



Under certain conditions (primarily, with an appropriate solvent), one of the rearrangement products (either the one enriched with metal or that enriched with silicon) is eliminated from the reaction medium due to its lower solubility. In such cases, the rearrangement can be observed even without fractionation. Two different processes are possible, depending on the composition of the reaction medium, *viz.*, precipitation of poorly soluble crystalline metal-free organosilsesquioxanes (RSiO_{1.5})_n (*e.g.*, compounds **40** and **41**)^{141, 145}

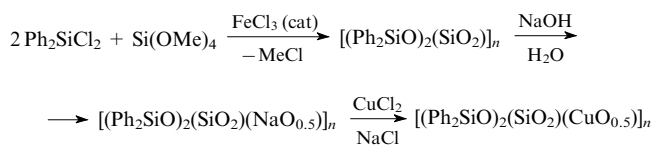


or, alternatively, of poorly soluble fractions enriched with metal. Sometimes, the process results in complete removal of metal in the form of the respective oxide from siloxane chains:¹⁴⁶



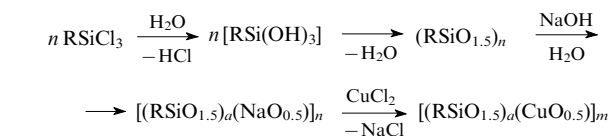
In order to gain a deeper insight into the rearrangement of MS, the kinetics of this process was studied using UV spectroscopy. Co-containing oligophenylsiloxanes were selected as the subjects of this study.¹⁴⁷ It was found that the rearrangement obeys the first-order law with a mean apparent reaction rate constant $k_{\text{app}} = (4.5 \pm 0.5) \times 10^{-6} \text{ s}^{-1}$. The first order of the reaction implies that the total rate of the rearrangement is limited by the decomposition of the intermediate complex to yield compounds with increased metal content with respect to the original MS.

According to studies of the MS rearrangement as a function of the number of identical organic groups at the silicon atom,¹⁴⁸ branched structures containing fragments RSiO_{1.5} suppress the rearrangement to a larger extent than linear structures with the fragments R₂SiO. This observation pointed to a possible means to suppress the rearrangement, *viz.*, an increase in the steric hindrance of the molecule with the introduction of sildioxane fragments SiO₂ (Ref. 149).



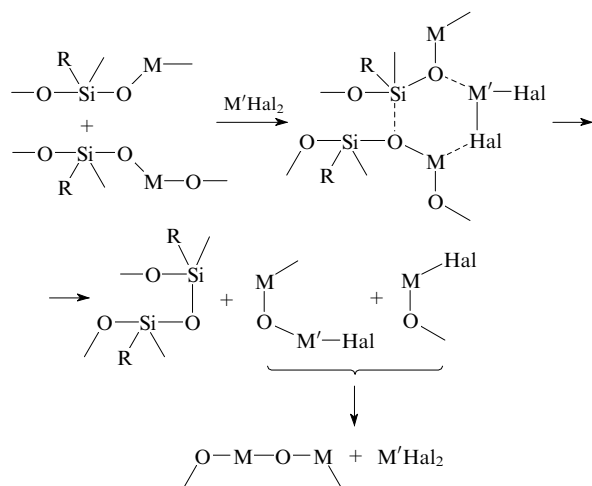
It has been established¹⁴⁹ that the introduction of sildioxane fragments into oligomeric MS impedes the formation of an intermediate complex, which appears in the course of the rearrangement.

Alternatively, the rearrangement can be suppressed by using bulky aliphatic groups at the silicon atom, which sterically hinder the interchain coordination of MS.¹⁵⁰



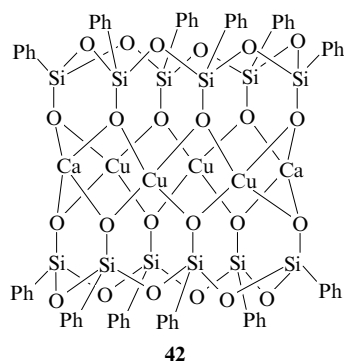
R = n-C₉H₁₉, Bu^t.

Conditions accelerating the rearrangement have also been found. It has been established that the presence of a catalytic amount of metal halides promotes rapid rearrangement towards compounds enriched with metal.¹⁴⁹ Presumably, the rearrangement proceeds *via* a six-membered ring intermediate, which is most typical of organosiloxane compounds.

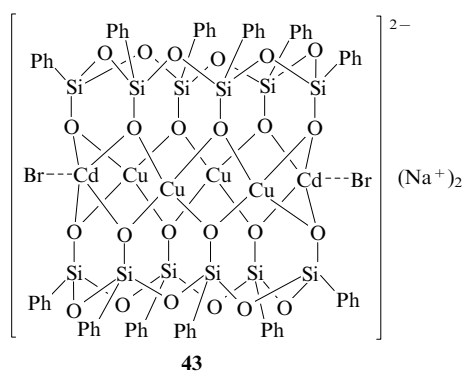


M = Cu, Co; M' = Co, Fe.

The reaction (1) discussed in Section II, in which the Ti atom substitutes the Mg atom in the MS structure, indicates that magnesium can act as an alkali metal as regards the exchange reaction. The electronegativity of Mg (1.2) is close to the respective values for alkali metals (0.91–0.97), which naturally leads to a conclusion that the Mg ion is capable of generating the stabilising silanolate anions in the MS structure. A bimetallic Cu,Ca organosiloxane **42** has been synthesised to verify this suggestion.¹⁵¹ The choice of the alkaline-earth metal was dictated by the fact that calcium, in terms of electronegativity (1.04), is rather more similar to alkali metals and thus a prominent stabilising effect could be expected. Another bimetallic Cu,Cd organosiloxane **43** has been synthesised for comparison¹⁵¹ (for both structures, coordinated solvent molecules are omitted for clarity).



42



43

A comparison of the two structures, **42** and **43**, indicates that the silanolate anions introduced into the structure together with two calcium ions are accommodated in the coordination spheres of four Cu ions. Meanwhile, the cadmium ions, which are characterised by a substantially higher

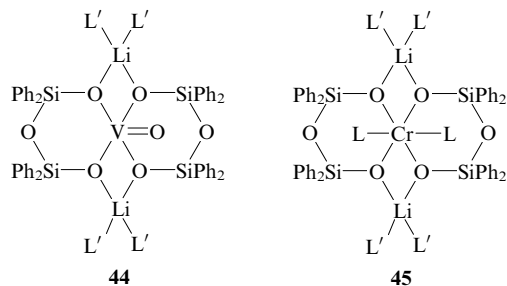
electronegativity (1.46) as compared to calcium, cannot bring the silanolate ions into the structure. As a result, a stable crystalline structure can be formed only with the assistance of additional coordinated anions (Br^- in the present case).

V. Metallasiloxanes in catalysis

Alkali metal organosilanolates are traditional catalysts of the anionic polymerisation of organocyclosiloxanes aimed at the production of linear organosiloxane polymers.⁸ More recently, it was found that the use of mixed silanolates–alkoxides $\text{K}_4\text{Li}_4(\text{OSiMe}_3)_{6-8}(\text{OBu}^t)_{1-2}$ allows the synthesis of high-molecular-mass organosiloxanes with a low polydispersity.⁹¹

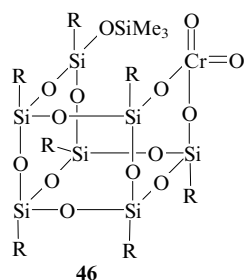
In the majority of cases, the catalytic properties of MS are caused by the nature of the metal atom, which acts as the catalytically active site. As a rule, the siloxy groups play only a secondary role forming a specific environment of the catalytic site. Nevertheless, the involvement of the siloxane matrix becomes decisive in certain cases.

A series of studies have been devoted to the catalytic activity of MS towards the alkene conversion. Catalysts mimicking the Ziegler–Natta catalysts have been developed. In these systems, a transition metal complex is combined with AlR_3 . In particular, it has been demonstrated^{111, 115} that spirocyclic V(IV) and Cr(II) organosiloxanes (compounds **44** and **45**, respectively) combined with AlMe_3 efficiently catalyse the ethylene and propylene polymerisation.



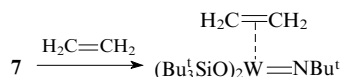
L, L' = Py, THF.

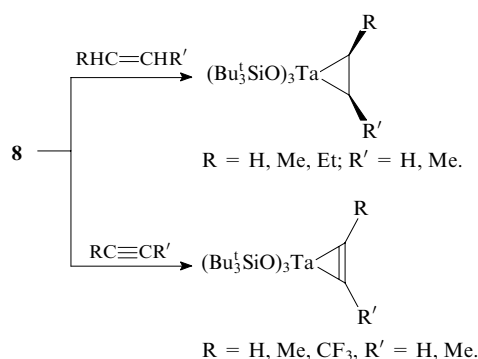
According to an original idea,¹⁵² organosiloxane cage can be used as a support for catalytic sites instead of traditional inorganic silicate matrix. For instance, polyhedral Cr(VI) organosiloxane **46** possesses¹⁵³ as high activity as the classical Philips catalyst (Cr/SiO_2).



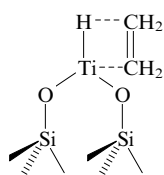
R = cyclo- C_6H_{11} .

Modern investigations into the MS-based catalysts of the alkene conversion are dominantly focused on the utilisation of low-coordinate complexes. Several metal triorganosiloxy derivatives (in particular, a tricoordinate tungsten complex **7**) are promising catalysts for the alkene and alkyne activation:

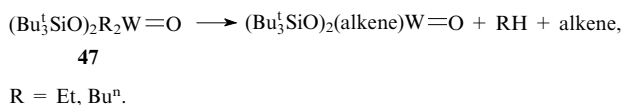




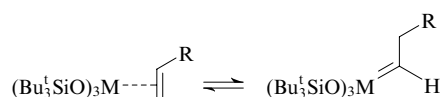
Diorganosiloxyhydridotitanium (promoted with trimethylphosphine) forms an intermediate with ethylene¹⁵⁴ and thus catalyses its conversion into but-1-ene and higher ethylene oligomers.



In specific cases, an alkene is generated upon the conversion of a metal (alkyl)siloxy derivative: for instance, thermolysis of tungsten compound **47** yields alkenes upon β -elimination of the alkyl groups in parallel to alkene complexes.⁴⁰

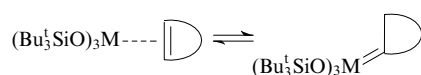


The advantage of bulky triorganosiloxy substituents at the metal atom is manifested most prominently in studies of catalytic properties of Nb and Ta organosiloxanes. It has to be emphasised that it is with these two metals that Richard Shrock (the 2005 Nobel Prize winner in chemistry) started his search for metathesis catalysts by introducing the *tert*-butoxy groups into the coordination environment of the metal sites in order to impart stability to metallacarbenes generated from them. According to more recent studies,¹⁵⁵ this purpose can alternatively be achieved with *tert*-butylsiloxy groups and it is even more efficient since a larger number of bulky organic groups can be attached to the catalytic site in this case. It has been established¹⁵⁵ that niobium and tantalum triorganosiloxy derivatives add alkenes with the generation of the respective metallacarbenes that catalyse the metathesis reaction.



$\text{M} = \text{Nb}; \text{R} = \text{H, Me, Et, Bu}^t, \text{Ph, 4-MeOC}_6\text{H}_4;$

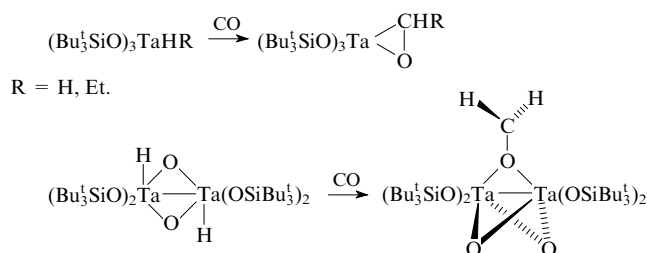
$\text{M} = \text{Ta}; \text{R} = \text{H, Me, Et, Ph, 4-MeOC}_6\text{H}_4, 4\text{-CF}_3\text{C}_6\text{H}_4.$



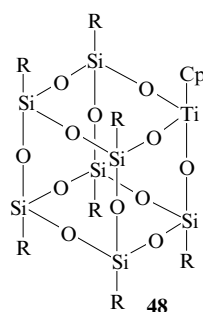
$\text{M} = \text{Nb, Ta};$.

Triorganosiloxy-substituted tantalum hydrides represent another type of catalysts. They efficiently bind CO, which

makes them promising catalysts of the Fischer–Tropsch reaction.^{156–159}

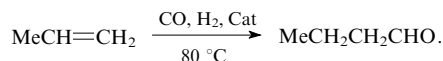


Polyhedral Ti^{III} and Ti^{IV} silsesquioxanes, which are characterised by closed (compound **48**) or partly closed (compound **1**) structures,^{160, 161} are used as either homogeneous or heterogeneous alkene epoxidation catalysts.



$\text{R} = \text{cyclo-C}_6\text{H}_{11}.$

Triorganosiloxy derivatives of platinum metals traditionally find wide applications determined by the nature of the metal. The organosiloxy groups increase the stability of these catalysts in the repeated use. Rhodium triorganosiloxy derivative $[\text{Ph}_3\text{SiORh}(\text{CO})_2]_2$ performs as a highly efficient hydroformylation catalyst.¹⁰⁰



Complexes $\text{RMSiPh}_3 \cdot 2\text{L}$ ($\text{M} = \text{Pt or Pd}; \text{R} = \text{Me, Et or Ph}; \text{L}$ is cycloocta-1,5-diene) provide a higher catalytic activity towards the CO hydrogenation than compounds $\text{R}_2\text{M} \cdot 2\text{L}$ or supported catalysts $\text{H}_2\text{PtCl}_6/\text{SiO}_2$ (Ref. 162).

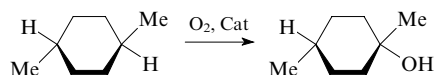
The formation of fragments $\text{Si}-\text{O}-\text{Pd}$ in intermediates is postulated¹⁶³ for the Pd-catalysed cross-coupling processes involving organosilicon reactants.

Oligomeric MS are also applicable in catalysis. It has to be noted that their use as a binder for supported catalysts shows little promise due to the fact that they form most often polymeric systems with a relatively low molecular mass (2000–5000), which are characterised by a low mechanical strength. Nevertheless, studies of their catalytic properties gave rise to interesting and sometimes surprising results.

These compounds were primarily tested in processes of petrochemical synthesis due to their close analogy to inorganic silicates. It has been found that oligomeric MS gradually lose organic substituents being converted into inorganic silicates upon the high-temperature polycondensation, although structural features of the starting MS are preserved. These compounds successfully compete with inorganic silicates with similar compositions, but they possess higher catalytic activities and selectivities in a number of processes, including cracking, halogenation, dehydration, alkylation, *etc.*¹¹

More recently, oligomeric MS found application as catalysts for other reactions where metal silicates were inactive. These include, for instance, the stereoselective oxidation of

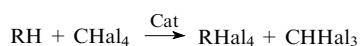
hydrocarbons (e.g., 1,4-dimethylcyclohexane) in the presence of oligophenylferrasiloxane.^{164, 165}



Probably, the most important catalytic application of oligomeric MS relates to the halohydrocarbon conversion. A number of large-scale industrial processes are based on these reactions (e.g., the production of polyvinyl chloride, dichloroethane, chlorobenzene, chloroalkanes, etc.). Halohydrocarbons are poor ligands for the majority of metal complexes, which complicates the choice of a proper catalyst. This selection was however made on the basis of the following idea: the most efficient catalysis is expected in those cases where the chain-radical mechanism involving a variable-valence metal atom becomes possible. Transition metals incorporated in the structure of the organosiloxane matrix can change their oxidation state (this is the key step for the catalysis of this type of reactions) remaining within the siloxane cage. Of other advantages of the utilisation of oligomeric MS, their solubility in organic solvents enables their application as homogeneous catalysts. In the case of heterogeneous catalysts, they can be chemically grafted to widely adopted inorganic supports (SiO₂, Al₂O₃ and so on). Furthermore, diverse systems incorporating nearly any transition metals and their combinations in specified ratios are now available. Their properties can be additionally adjusted by varying parameters of the high-temperature condensation processes, which strongly affect surface characteristics of the target catalysts.

Oligomeric Cu, Co and Fe organosiloxanes have been tested¹⁶⁶ as catalysts of the isomerisation of non-symmetric 3,4-dichlorobut-1-ene into symmetric 1,4-dichlorobut-2-ene (it is the key step in the industrial production of chloroprene rubber). The Cu-containing MS manifested the highest activity, which confirmed the current concept assuming the partial reduction of the metal ions in the course of the catalytic reaction: the copper ions undergo the reduction most readily among the compounds studied. Still, the Co- and Fe-containing MS are also of interest, since they provide higher selectivity: no *cis*-1,4-dichlorobut-2-ene is formed in their presence. The major difference of the oligomeric MS from traditional catalysts (i.e., copper naphthenate or halides) consists of their prominent stability: even repeated use (6–10 cycles) does not lead to any significant decrease in activity, whereas traditional catalysts are nearly completely deactivated after the first cycle.

Oligomeric MS have been tested as catalysts in the exchange halogenation processes, which enable the production of halohydrocarbons avoiding the use of halogens as elementary substances.

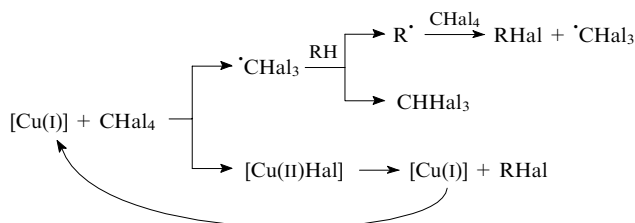


R = Alk, Ar; Hal = Cl, Br.

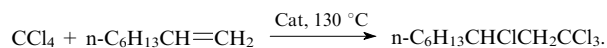
In the case of chlorohydrocarbons, a more environmentally friendly industrial process can be implemented using this method. This is especially important for brominated derivatives, since the direct bromination with molecular bromine usually proceeds with difficulty and non-selectively; furthermore, syntheses of bromides are usually multi-step processes.

Detailed investigations^{148, 167, 168} into the exchange halogenation of hydrocarbons, including n-C₁₀H₂₂, n-C₁₂H₂₆, cyclo-C₆H₁₂, *p*-Me₂C₆H₄ and C₆H₅Me, with CCl₄ or CBr₄ (in the presence of a catalytic amount of oligomeric Cu phenylsiloxane) shed light on the mechanism of the process. The reaction follows the radical mechanism: the transfer of the

radical centre along the chain from the [•]CCl₃ radical to the hydrocarbon molecule is shown in the upper half of the scheme, whereas transformations of the catalytic site are shown in the lower half (according to classical view, the catalyst returns to the initial state after the catalytic cycle, which is indicated by the bent arrow). The activity of oligomeric Cu phenylsiloxane remains nearly constant over five catalytic cycles, whereas the standard catalyst CuCl₂·(DMF)_n is deactivated within one cycle.

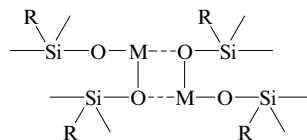


The above exchange halogenation reaction yields a mixture of monohalogenated derivatives with different locations of the halogen atom. The addition of halohydrocarbons to alkenes proceeds more selectively, since the location of the double bond determines the sites of attachment of the Cl atom and CCl₃ fragment.



Oligomeric monophenyl and diphenyl Cu-containing organosiloxanes have been tested as catalysts in this reaction.¹⁶⁹ The process follows the radical mechanism detailed above. The only difference is that the formation of a radical site is facilitated due to the involvement of the alkene double bond. Structured monophenyl derivatives (i.e., molecules with cage fragments) bearing trifunctional fragments RSiO_{1.5} are characterised¹⁶⁹ by a poorer accessibility of the active site and thus lower catalytic activity with respect to diphenyl derivatives built up of linear fragments.

As has been shown by kinetic studies of the two aforementioned types of halogenation, a substantial fraction of potential catalytic sites is 'switched off' the catalytic process since they are involved into the formation of interchain coordination clusters. The metal atoms tend to complete their coordination spheres by coordinating oxygen atoms from the neighbouring fragments Si—O—M (as has been discussed in previous sections).



As a result, these metal atoms become coordinatively saturated and structurally inaccessible for the interaction with CCl₄. Therefore, the main task is to prevent the formation of the interchain metal oxide clusters. If a metal atom is screened by a ligand, this effectively suppresses the interchain coordination, but does not solve the main problem, since the additional ligand equally hinders the approach of the reactant. A rather easily realisable solution of the problem consists of¹⁵⁰ the use of nonyl instead of phenyl groups at the silicon atoms. According to UV spectroscopy, the Cu ion in the oligononylsiloxane remains coordinatively unsaturated.

Thus, the bulky aliphatic group efficiently suppresses the coordinative interactions between the copper atoms of neighbouring chains by screening the metal sites. In solutions, it

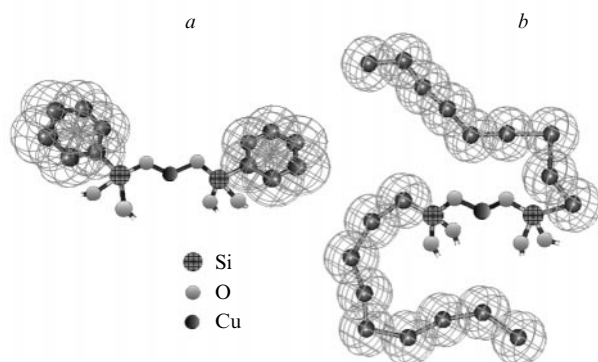


Figure 1. The structure of fragments $(-O)_2RSi-O-Cu-O-SiR(O-)_2$; $R = Ph$ (a), $n-C_9H_{19}$ (b). Contour lines schematically indicate van der Waals surfaces around the molecules.

possesses the mobility of a polymer segment and does not prevent the approach of the organic reactant (CCl_4) to the catalytic site (Fig. 1).

The implementation of this idea gives quite impressive results:¹⁷⁰ the activity of nonyl-containing polymeric Cu MS with respect to the addition of CCl_4 to oct-1-ene is twice larger than that of phenylcuprasiloxanes.

VI. Conclusion

The experimental data considered above clearly demonstrate that metallasiloxanes are very interesting from both theoretical and practical points of view. This explains the multitude of studies devoted to their synthesis and consequent diversity of synthetic approaches to the formation of the fragment $Si-O-M$. The method based on the cleavage of the siloxane bonds with organometallic compounds has been developed to the large extent. The utilisation of bulky aliphatic groups as substituents at the silicon atom has proven its practical usefulness. Many niobium, tantalum, tungsten, *etc.* MS inaccessible earlier have been successfully synthesised, including low-coordinate complexes of these metals.

Metallasiloxanes themselves can be regarded as precursors in the synthesis of siloxanes that cannot be obtained by other methods. In particular, the cleavage of cage MS with electrophilic reagents yields stereoregular organocyclosiloxanes.

From the theoretical point of view, problems related to the structural features of MS are of particular importance, including the factors governing the formation of specific structural types of MS. As has been reliably established to date, the products of many reactions are actually formed due to rearrangements of the initially generated MS. These rearrangements give rise to compounds enriched with either metal or silicon (ultimately, the metal can be completely excluded from the siloxane matrix in the form of the respective oxide). A number of efficient methods for the suppression or *vice versa* facilitation of the rearrangements have been elaborated, depending on the specific goal of the synthesis. Structures stable against the rearrangements emerge in those cases where anions and, primarily, silanolate anions, are involved into the coordination sphere of the transition metal atom.

Spherical fullerene-like organosiloxane molecules can be assembled from cage MS, which can hardly be synthesised by other methods.^{171, 172} According to quantum chemical calculations,^{173, 174} nanotube-like assemblies are also possible for certain combinations of structural parameters.

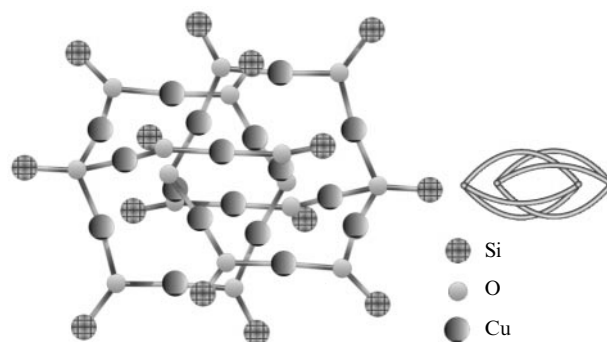


Figure 2. The structure of metallasiloxane $Cu_{18}O_2(OSiMe_3)_{14}$ (Ref. 138).

Catenane MS should be anticipated in the nearest future. The first representative of this class has already been synthesised:³⁸ it is characterised by an unusual topology built up of two interpenetrating bicyclic fragments (Fig. 2, methyl groups at the Si atoms are omitted for clarity).

Practical applications of metallasiloxanes primarily relates to catalysis. As a rule, the catalytic properties are determined by the nature of the constituent transition metal. Low-coordinate metal (in particular, tungsten) complexes bearing bulky organic substituents at the silicon atom have been attracting much attention from researchers over the recent years.

Oligomeric MS has a huge potential as catalytic systems. Initially, they were considered exclusively as analogues of inorganic silicates for the petrochemical synthesis. But their prominent catalytic activities in other industrially important reactions, in particular, halohydrocarbon conversion and exchange halogenation, have been discovered recently. It has to be emphasised that the type of the siloxane matrix plays equally important role as the nature of the metal in the case of oligomeric MS, since it determines the accessibility of the catalytic site.

The present review is written with a partial financial support from the Grant Council at the President of Russian Federation (the Programme of Federal Support of Young Scientists with the PhD degree, Grant MK-126.2007.3) and Russian Foundation for Basic Research (Project Nos 06-03-32347 and 08-03-00026).

References

1. S N Borisov *Usp. Khim.* **28** 63 (1959)
2. A L Suvorov, S S Spasskii *Usp. Khim.* **28** 1267 (1959)
3. H Schmidbaur *Angew. Chem.* **77** 206 (1965)
4. F Schindler, H Schmidbaur *Angew. Chem.* **79** 697 (1967)
5. D C Bradley *Coord. Chem. Rev.* **2** 299 (1967)
6. S N Borisov, M G Voronkov, E Ya Lukevics *Kremnii elementoorganicheskie Soedineniya* (Organosilicon Compounds) (Leningrad: Khimiya, 1966)
7. G E Coates, B I Aylett, L H Green *Organometallic Compounds. Groups IV and V* (London: Chapman and Hall, 1979)
8. M G Voronkov, E A Maletina, V K Roman *Heterosiloxany* (Heterosiloxanes) (Novosibirsk: Nauka, 1984)
9. K A Andrianov, A A Zhdanov *J. Polym. Sci.* **30** 513 (1958)
10. K A Andrianov *Polimery s Neorganicheskimi Glavnymi Tsepyami Molekul* (Polymers with Inorganic Backbones) (Moscow: Academy of Sciences of the USSR, 1962)
11. A A Zhdanov, M M Levitsky *Uspekhi v Oblasti Sintezy Elementoorganicheskikh Polimerov* (Progress in Synthesis of Organoelement Polymers) (Ed. V V Korshak) (Moscow: Nauka, 1988) p. 143

12. K A Andrianov, L M Khananashvili *Tekhnologiya Elemento-organicheskikh Monomerov i Polimerov* (Industrial Production of Organoelement Monomers and Polymers) (Moscow: Khimiya, 1973)
13. W S Tatlock, E G Rochow *J. Org. Chem.* **17** 1555 (1952)
14. E D Hornbaker, F Conrad *J. Org. Chem.* **24** 1858 (1959)
15. K A Andrianov, A A Zhdanov *Izv. Akad. Nauk SSSR, Otd. Khim. Nauk* 1076 (1958)
16. F Schindler, H Schmidbaur, U Kruger *Angew. Chem.* **77** 865 (1965)
17. G G Petukhov, R F Galiullina, Yu N Krasnov, A D Chernova *Zh. Obshch. Khim.* **42** 1046 (1972)^a
18. V V Pankratova, L P Stepovik, I V Lomakova, L A Pogodina *Zh. Obshch. Khim.* **42** 1752 (1972)^a
19. F T Edelmann, S Gießmann, A Fischer *Chem. Commun.* 2153 (2000)
20. T Sugama, N Carciello, S L Rast *Thin Solid Films* **258** 174 (1995)
21. P Sobota, S Przybylak, J Ejfler, M Kobylka, L B Jerzykiewicz *Inorg. Chim. Acta* **334** 159 (2002)
22. J Beckmann, K Jurkschat *Coord. Chem. Rev.* **215** 267 (2001)
23. H J Gosink, H W Roesky, M Noltemeyer, H G Schmidt, C Freire-Erdbrugger, G M Sheldrick *Chem. Ber.* **126** 279 (1993)
24. F Q Liu, I Uson, H W Roesky *J. Chem. Soc., Dalton Trans.* 2453 (1995)
25. A Voigt, R Murugavel, H W Roesky, H G Schmidt *J. Mol. Struct.* **437** 49 (1997)
26. H G Gosink, H W Roesky, H G Schmidt, M Noltemeyer, E Irmer, R Herbst-Irmer *Organometallics* **13** 3420 (1994)
27. H M Lindeman, M Schneider, B Neumann, H-G Stammler, A Stammler, P Jutzi *Organometallics* **21** 3009 (2002)
28. J-O Nolte, M Schneider, B Neumann, H-G Stammler, P Jutzi *Organometallics* **22** 1010 (2003)
29. G A Sigel, R A Bartlett, D Decker, M M Olmstead, P P Power *Inorg. Chem.* **26** 1773 (1987)
30. D F Eppley, P T Wolczanski, G D Van Duyne *Angew. Chem., Int. Ed. Engl.* **30** 584 (1991)
31. A S Veige, LeGrande M Slaughter, E B Lobkovsky, P T Wolczanski, N Matsunaga, S A Decker, T R Cundari *Inorg. Chem.* **42** 6204 (2003)
32. T A Chesnokova, E V Zhezlova, A N Kornev, Ya V Fedotova, L N Zakharov, G K Fukin, Yu A Kursky, T G Mushtina, G A Domrachev *J. Organomet. Chem.* **642** 20 (2002)
33. A N Kornev, T A Chesnokova, E V Zhezlova, L N Zakharov, G K Fukin, Yu A Kursky, G A Domrachev, P D Lickiss *J. Organomet. Chem.* **587** 113 (1999)
34. V V Semenov, N F Cherepennikova, A N Kornev, E V Naumova, N P Makarenko, S Ya Khorshev, G A Domrachev, O A Bochkova *Izv. Akad. Nauk, Ser. Khim.* 2561 (1996)^b
35. A N Kornev, T A Chesnokova, V V Semenov, E V Zhezlova, L N Zakharov, L G Klapshina, G A Domrachev, V S Rusakov *J. Organomet. Chem.* **547** 113 (1997)
36. K J Covert, D R Neithamer, M C Zonneville, R E La Pointe, C P Schaller, P T Wolczanski *Inorg. Chem.* **30** 2494 (1991)
37. A R Chadeayne, P T Wolczanski, E B Lobkovsky *Inorg. Chem.* **43** 3421 (2004)
38. R L Miller, K A Lawler, J L Bennet, P T Wolczanski *Inorg. Chem.* **35** 3242 (1996)
39. O L Sydora, P T Wolczanski, E B Lobkovsky, C Buda, T R Cundari *Inorg. Chem.* **44** 2606 (2005)
40. D C Rosenfeld, D S Kuiper, E B Lobkovsky, P T Wolczanski *Polyhedron* **25** 251 (2006)
41. J B Bonanno, A S Veige, P T Wolczanski, E B Lobkovsky *Inorg. Chim. Acta* **345** 173 (2003)
42. R Murugavel, V S Shete, K Baheti, P Davis *J. Organomet. Chem.* **625** 195 (2001)
43. I Kownacki, M Kubicki, B Marciniak *Polyhedron* **20** 3015 (2001)
44. M M Levitsky, O I Shchegolikhina, A A Zhdanov, V A Igonin, Yu E Ovchinnikov, V E Shklover, Yu T Struchkov *J. Organomet. Chem.* **401** 199 (1991)
45. V A Igonin, S V Lindeman, K A Potekhin, V E Shklover, Yu T Struchkov, O I Shchegolikhina, A A Zhdanov, I V Razumovskaya *Metalloorg. Khim.* **4** 790 (1991)^c
46. V A Igonin, O I Shchegolikhina, S V Lindeman, M M Levitsky, Yu T Struchkov, A A Zhdanov *J. Organomet. Chem.* **423** 351 (1992)
47. O I Shchegolikhina, A A Zhdanov, V A Igonin, Yu E Ovchinnikov, V E Shklover, Yu T Struchkov *Metalloorg. Khim.* **4** 74 (1991)^c
48. Yu E Ovchinnikov, A A Zhdanov, M M Levitsky, V E Shklover, Yu T Struchkov *Izv. Akad. Nauk SSSR, Ser. Khim.* 1206 (1986)^b
49. V A Igonin, S V Lindeman, Yu T Struchkov, Yu A Molodtsova, I V Razumovskaya, O I Shchegolikhina, A A Zhdanov *Izv. Akad. Nauk, Ser. Khim.* 752 (1993)^b
50. V I Igonin, S V Lindeman, Yu T Struchkov, O I Shchegolikhina, Yu A Molodtsova, Yu A Pozdnyakova, A A Zhdanov *Izv. Akad. Nauk, Ser. Khim.* 184 (1993)^b
51. V I Igonin, S V Lindeman, Yu T Struchkov, Yu A Molodtsova, Yu A Pozdnyakova, O I Shchegolikhina, A A Zhdanov *Izv. Akad. Nauk, Ser. Khim.* 193 (1993)^b
52. G Palyi, C Zucchi, M Borsari, A Fabretti, Yu A Pozdnyakova, S V Lindeman, A A Zhdanov, E Rentschler, D Gatteschi, R Ugo, R Psaro, G Gavioli, A Cornia, O I Shchegolikhina *J. Mol. Catal. A: Chem.* **107** 313 (1996)
53. O I Shchegolikhina, Yu A Pozdnyakova, S V Lindeman, A A Zhdanov, R Psaro, R Ugo, G Gavioli, R Battistuzzi, M Borsari, T Ruffer, C Zucchi, G Palyi *J. Organomet. Chem.* **514** 29 (1996)
54. C Zucchi, M Mattioli, G Gavioli, M Moret, A Sironi, R Ugo, M Pizzotti, O I Shchegolikhina, G Palyi *Eur. J. Inorg. Chem.* 1327 (2000)
55. V I Igonin, S V Lindeman, Yu T Struchkov, O I Shchegolikhina, A A Zhdanov, Yu A Molodtsova, I V Razumovskaya *Metalloorg. Khim.* **4** 1355 (1991)^c
56. B G Zavin, N V Sergienko, E V Gorodnichev, V D Myakushev, A A Korlyukov, M Yu Antipin *Mendeleev Commun.* 245 (2005)
57. G Gavioli, R Battistuzzi, P Santi, C Zucchi, G Palyi, R Ugo, A Vizi-Orosz, O I Shchegolikhina, Yu A Pozdnyakova, S V Lindeman, A A Zhdanov *J. Organomet. Chem.* **485** 257 (1995)
58. C Zucchi, M Mattioli, A Cornia, A C Fabretti, G Gavioli, M Pizzotti, R Ugo, Yu A Pozdnyakova, O I Shchegolikhina, A A Zhdanov, G Palyi *Inorg. Chim. Acta* **280** 282 (1998)
59. A Cornia, A C Fabretti, G Gavioli, C Zucchi, M Pizzotti, A Vizi-Orosz, O I Shchegolikhina, Yu A Pozdnyakova, G Palyi *J. Cluster Sci.* **9** 295 (1998)
60. N V Cherkun, N V Sergienko, B G Zavin *Nauka o Polimerakh 21-mu Veku (Tez. Ustnykh i Stendovykh Dokl. Chetvertoi Vserossiiskoi Karginskoi Konf.)*, Moskva, 2007 [Polymer Science to the 21st Century (Abstracts of Orally and Poster Reports of the Forth Kargin Conference), Moscow, 2007] Vol. 2, p. 307
61. N V Sergienko, E S Trankina, V I Pavlov, A A Zhdanov, K A Lysenko, M Yu Antipin, E I Akhmet'eva *Izv. Akad. Nauk, Ser. Khim.* 337 (2004)^b
62. A A Zhdanov, O I Shchegolikhina, Yu A Molodtsova *Izv. Akad. Nauk, Ser. Khim.* 957 (1993)^b
63. A A Zhdanov, N V Sergienko, E S Trankina *Izv. Akad. Nauk, Ser. Khim.* 2530 (1998)^b
64. Yu A Molodtsova, Yu A Pozdnyakova, K A Lyssenko, I V Blagodatskikh, D Katsoulis, O I Shchegolikhina *J. Organomet. Chem.* **571** 31 (1998)
65. O I Shchegolikhina, Yu A Pozdnyakova, M Yu Antipin, D Katsoulis, N Auner, B Herrschaft *Organometallics* **19** 1077 (2000)
66. O I Shchegolikhina, Yu A Pozdnyakova, Yu A Molodtsova, S D Korkin, S S Bukalov, L A Leites, K A Lyssenko, A S Peregodov, N Auner, D Katsoulis *Inorg. Chem.* **41** 6892 (2002)

67. Yu A Molodtsova, Yu A Pozdnyakova, I V Blagodatskikh, A S Peregodov, O I Shchegolikhina *Izv. Akad. Nauk, Ser. Khim.* **2577** (2003)^b
68. Yu A Pozdnyakova, Yu A Molodtsova, O I Shchegolikhina *Peterburgskie Vstrechi (Tez. Dokl. 3-go Mezhdunar. Simp. po Khimii Fosfor-, Sera- i Kremniorganicheskikh Soedinenii), Sankt-Peterburg 1998* [Petersburg Meetings (Abstracts of Reports of the Third International Symposium on the Chemistry of Organophosphorus, Organosulfur and Organosilicon Compounds), St Petersburg, 1998] p. 155
69. Yu A Molodtsova, Yu A Pozdnyakova, I V Blagodatskikh, K A Lyssenko, O I Shchegolikhina *Modern Trends in Organometallic and Catalytic Chemistry (Abstracts of Mark Vol'pin Memorial International Symposium)*, Moscow, 2003 p. 133
70. A A Zhdanov, O I Shchegolikhina, Yu A Molodtsova, T I Strelkova *Dokl. Akad. Nauk* **325** 1186 (1992)^d
71. V A Igonin, A A Zhdanov, Yu A Pozdnyakova, S V Lindeman, T V Strelkova, O I Shchegolikhina, Yu A Molodtsova *J. Organomet. Chem.* **562** 141 (1998)
72. A A Zhdanov, N V Sergienko, E S Trankina *Dokl. Akad. Nauk* **370** 50 (2000)^d
73. L I Makarova, N V Sergienko, E S Trankina, A A Zhdanov, E I Akhmet'eva *Izv. Akad. Nauk, Ser. Khim.* **160** (2002)^b
74. A A Zhdanov, L I Makarova, N V Sergienko *Izv. Akad. Nauk, Ser. Khim.* **2527** (1998)^b
75. M G Voronkov, Yu I Khudobin *Izv. Akad. Nauk SSSR, Otd. Khim. Nauk* **713** (1956)
76. V E Shklover, Yu T Struchkov, M M Levitsky, A A Zhdanov *Zh. Strukt. Khim.* **27** (6) 120 (1986)^e
77. A W Apblett, A H Barron *Organometallics* **9** 2137 (1990)
78. C C Landry, J A Davis, A W Apblett, A R Barron *J. Mater. Chem.* **3** 597 (1993)
79. A W Apblett, A C Warren, A R Barron *Chem. Mater.* **4** 167 (1992)
80. E Mulhaupt, J Calabrese, S D Ittel *Organometallics* **10** 3403 (1991)
81. E Irvani, A Dashti-Mommertz, B Neumuller *Z. Anorg. Allg. Chem.* **629** 1136 (2003)
82. R A Jones, S U Koschmieder, J L Atwood, S G Bott *J. Chem. Soc., Chem. Commun.* **726** (1992)
83. M R Alexander, F S Mair, R G Pritchard, J E Warren *Appl. Organomet. Chem.* **17** 730 (2003)
84. M L Cole, C Jones, P C Junk *New J. Chem.* **26** 89 (2002)
85. S Harvey, M F Lappert, C L Raston, B W Skeltoii, G Srivastava, A H White *J. Chem. Soc., Chem. Commun.* **1216** (1988)
86. F Bottomley, S Karsioğlu *Organometallics* **11** 326 (1992)
87. D A Edwards, M Harker, M F Mahon, K C Molloy *J. Chem. Soc., Dalton Trans.* **3509** (1997)
88. X Zhou, Z X Huang, X Z You *J. Chem. Soc., Chem. Commun.* **2483** (1995)
89. X Zhou, Z X Huang, R Cai, L Zhang, Y Liu, C Duan *Synth. React. Inorg. Met.-Org. Chem.* **30** 649 (2000)
90. W J Evans, T A Ulibarri, J W Ziller *Organometallics* **10** 134 (1991)
91. K B Renkema, R J Matthews, T L Bush, S K Hendges, R N Redding, F W Vance, M E Silver, S A Snow, J C Huffman *Inorg. Chim. Acta* **244** 185 (1996)
92. A Yu Rabkina, L I Kuteinikova, M N Il'ina, I I Dubovik, B G Zavin, V S Papkov *Vysokomol. Soedin., Ser. A* **45** 562 (2003)^f
93. Yu A Borisov, V S Papkov, A Yu Rabkina, B G Zavin *J. Mol. Struct. (THEOCHEM)* **664–665** 157 (2003)
94. A A Kapustina, N P Shapkin, N I Gavrilova, M Yu Kalugina, V I Bessonova *Zh. Obshch. Khim.* **70** 258 (2000)^a
95. H Schmidbaur *Chem. Ber.* **96** 2696 (1963)
96. H Schmidbaur, W Richter *Chem. Ber.* **107** 2427 (1974)
97. H Schmidbaur, M Bergfeld *Inorg. Chem.* **5** 2069 (1966)
98. H Schmidbaur, B Armer, M Bergfeld *Z. Chem.* **8** 254 (1968)
99. L Marko, A Vizi-Orosz *Trans. Met. Chem.* **7** 216 (1982)
100. G Palyi, C Zucchi, R Ugo, R Psaro, A Sironi, A Vizi-Orosz *J. Mater. Catal.* **74** 51 (1992)
101. A J Vizi-Orosz, R Ugo, R Psaro, A Sironi, M Moret, C Zucchi, F Ghelfi, G Palyi *Inorg. Chem.* **33** 4600 (1994)
102. B Marciniak, P Krzyzanowski *J. Organomet. Chem.* **493** 261 (1995)
103. P Krzyzanowski, M Kubicki, B Marciniak *Polyhedron* **15** 1 (1996)
104. B Marciniak, P Krzyzanowski, M Kubicki *Polyhedron* **15** 4233 (1996)
105. H Schmidbaur, J Adlkofer, A Shiotani *Chem. Ber.* **105** 3389 (1972)
106. C Gaffney, P Harrison, T King *J. Chem. Soc., Chem. Commun.* **1251** (1980)
107. I Baxter, J Darr, S Drake, M Hursthouse *J. Chem. Soc., Dalton Trans.* **2875** (1997)
108. J Darr, S Drake, D Williams, A Slawin *J. Chem. Soc., Chem. Commun.* **866** (1993)
109. M Borsari, G Gavioli, C Zucchi, G Palyi, R Psaro, R Ugo, O I Shchegolikhina, A A Zhdanov *Inorg. Chim. Acta* **258** 139 (1997)
110. M Motevalli, D Shah, S Shah, A Sullivan *J. Chem. Soc., Chem. Commun.* **2427** (1994)
111. M Motevalli, M Sanganee, P Savage, S Shah, A Sullivan *J. Chem. Soc., Chem. Commun.* **1132** (1993)
112. M Hursthouse, M Mazid, M Motevalli, M Sanganee, A Sullivan *J. Organomet. Chem.* **381** C43 (1990)
113. M Hursthouse, M Motevalli, M Sanganee, A Sullivan *J. Chem. Soc., Chem. Commun.* **1709** (1991)
114. V Lorenz, A Fischer, K Jacob, W Bruser *Chem. Commun.* **2217** (1998)
115. M Motevalli, D Shah, S Shah, A Sullivan *Organometallics* **13** 4109 (1994)
116. I Abrahams, M Motevalli, S Shah, A Sullivan *J. Organomet. Chem.* **492** 99 (1995)
117. M Lazelli, M Motevalli, S A A Shah, C K S Simon, A C Sullivan *J. Chem. Soc., Dalton Trans.* **1449** (1996)
118. M A Hossain, M B Hursthouse, A Ibrahim, M Mazid, A C Sullivan *J. Chem. Soc., Dalton Trans.* **2347** (1989)
119. M Motevalli, D Shah, A C Sullivan *J. Chem. Soc., Dalton Trans.* **2849** (1993)
120. M L Montero, A Voigt, M Teichert, I Uson, H W Roesky *Angew. Chem., Int. Ed. Engl.* **34** 2504 (1995)
121. A Voigt, A Murugavel, E Parisini, H W Roesky *Angew. Chem., Int. Ed. Engl.* **35** 748 (1996)
122. H Schmidbaur, H Hussek, F Schindler *Chem. Ber.* **97** 255 (1964)
123. A N Bilyachenko, M M Levitsky, B G Zavin, A Yu Rabkina, L M Sidorova, V E Evshov *Organosilicon Compounds: Synthesis, Properties, Application (Abstracts of Reports of the 10th All-Russian Conference)*, Moscow, 2005 1S5
124. I Abrahams, M Lazelli, M Motevalli, S A A Shah, A C Sullivan *J. Organomet. Chem.* **553** 23 (1998)
125. M G Voronkov, V P Mileshekevich, Yu A Yuzhelevskii *Siloksanovaya Svyaz' (Silicone Bond)* (Novosibirsk: Nauka, 1976)
126. Yu A Yuzhelevskii, V V Pchelintsev, N N Fedoseeva *Vysokomol. Soedin., Ser. B* **18** 873 (1976)^f
127. M R Churchill, C H Lake, S H L Chao, O T Beachley *J. Chem. Soc., Chem. Commun.* **1577** (1993)
128. A Decken, J Passmore, X Wang *Angew. Chem., Int. Ed.* **45** 2773 (2006)
129. P T Wolczanski *Polyhedron* **14** 3335 (1995)
130. R Okawara *J. Am. Chem. Soc.* **83** 1342 (1961)
131. A Ghosh, C E Hansing, A I Stutz, A G MacDiarmid *J. Chem. Soc.* **403** (1962)
132. M G Voronkov, S V Vlasenko, V Yu Vitkovskii, S M Yuzdrina, R G Mirskov *Metalloorg. Khim.* **2** 310 (1989)^c
133. L I Fridman, E L Khrustaleva, A L Suvorov *Zh. Obshch. Khim.* **56** 2103 (1986)^a
134. M Schmidt, H Schmidbaur *Angew. Chem.* **71** 220 (1959)
135. D Brandes, A Blaschette *J. Organomet. Chem.* **49** C6 (1973)
136. D Brandes, A Blaschette *J. Organomet. Chem.* **73** 217 (1974)

137. H-F Klein, H H Karsch *Chem. Ber.* **108** 944 (1975)
138. T Greiser, O Jarchow, K-H Klaska, E Weiss *Chem. Ber.* **111** 3360 (1978)
139. M M Levitsky, A I Kokorin, V V Smirnov, N V Karpilovskaya, A V Kudryashov, S M Nevskaya, E N Golubeva *Izv. Akad. Nauk, Ser. Khim.* 1946 (1998)^b
140. M M Levitsky, A I Kokorin, V V Smirnov *Izv. Akad. Nauk, Ser. Khim.* 1813 (2000)^b
141. A A Zhdanov, M M Levitsky, O Yu Shilkloper *Izv. Akad. Nauk, Ser. Khim.* 958 (1985)^b
142. A A Zhdanov, M M Levitsky, A Yu D'yakov, O I Shchegolikhina, A D Kolbanovskii, R A Stukan, A G Knizhnik, A L Buchachenko *Izv. Akad. Nauk, Ser. Khim.* 2512 (1990)^b
143. M M Levitsky, A R Arutyunyan, B G Zavin, V V Erokhin, A L Buchachenko *Izv. Akad. Nauk, Ser. Khim.* 1691 (1999)^b
144. A Yu Dyakov, B J McCormick, P K Kahol, N Pinto, M M Levitsky, A L Buchachenko *Mol. Cryst. Liq. Cryst.* **274** 199 (1995)
145. V E Shklover, Yu E Ovchinnikov, Yu T Struchkov, M M Levitsky, A A Zhdanov *Metalloorg. Khim.* **1** 1273 (1988)^c
146. M M Levitsky, N V Karpilovskaya, A N Gavrilova, B G Zavin, E S Shubina *Izv. Akad. Nauk, Ser. Khim.* 782 (1996)^b
147. A N Bilyachenko, B G Zavin, E S Shubina, A M Filin, M M Levitsky *Izv. Akad. Nauk, Ser. Khim.* 1912 (2004)^b
148. V V Smirnov, E N Golubeva, O A Zagorskaya, S M Nevskaya, M M Levitsky, V Yu Zufman *Kinet. Katal.* **41** 439 (2000)^g
149. A N Bilyachenko, B G Zavin, M M Levitsky *International Conference Dedicated to 50th Anniversary of A N Nesmeyanov Institute of Organoelement Compounds, Moscow, 2004 P.* 8
150. M M Levitsky, B G Zavin, A N Bilyachenko *Vysokomol. Soedin., Ser. A* **46** 1680 (2004)^f
151. A N Bilyachenko, N V Sergienko, A A Korlyukov, M Yu Antipin, B G Zavin, M M Levitsky *Izv. Akad. Nauk, Ser. Khim.* 909 (2006)^b
152. O A Beliakova, Ya V Zubavichus, Yu L Slovokhotov, O I Shchegolikhina, A A Zhdanov *Phys. Condens. Matter* **208–209** 655 (1995)
153. F J Feher, R L Blanski *J. Chem. Soc., Chem. Commun.* 1614 (1990)
154. M Taoufic, A de Mallmann, E Prouzet, G Saggio, J Thirivolle-Cazat, J M Basset *Organometallics* **20** 5518 (2001)
155. K F Hirsekorn, A S Veige, M P Marshak, Ye Koldobskaya, P T Wolczanski, T R Cundari, E B Lobkovsky *J. Am. Chem. Soc.* **127** 4809 (2005)
156. R L Miller, R Toreki, R E La Pointe, P T Wolczanski, G D Van Duyne, D C Roe *J. Am. Chem. Soc.* **115** 5570 (1993)
157. R E La Pointe, P T Wolczanski *J. Am. Chem. Soc.* **108** 3535 (1986)
158. R E La Pointe, P T Wolczanski, J F Mitchell *J. Am. Chem. Soc.* **108** 6382 (1986)
159. R Toreki, R E La Pointe, P T Wolczanski *J. Am. Chem. Soc.* **109** 7558 (1987)
160. H C L Abbenhuis, S Krijnen, R A van Santen *Chem. Commun.* 331 (1997)
161. S Krijnen, H C L Abbenhuis, R W J M Hansen, J H C van Hooff, R A van Santen *Angew. Chem., Int. Ed.* **37** 356 (1998)
162. A Fukuoka, A Sato, K Kodama, M Hirano, S Komiya *Inorg. Chim. Acta* **294** 266 (1999)
163. S E Denmark, J D Baird *Chem. – Eur. J.* **12** 4954 (2006)
164. V S Kulikova, M M Levitsky, A L Buchachenko *Izv. Akad. Nauk, Ser. Khim.* 3021 (1996)^b
165. V S Kulikova, M M Levitsky, A F Shestakov, A E Shilov *Izv. Akad. Nauk, Ser. Khim.* 450 (1998)^b
166. V V Smirnov, M M Levitsky, S M Nevskaya, E N Golubeva *Kinet. Katal.* **40** 86 (1999)^g
167. V V Smirnov, V M Zelikman, I P Beletskaya, M M Levitsky, M A Kazankova *Mendeleev Commun.* 175 (2000)
168. V V Smirnov, M M Levitsky, I G Tarkhanova, S M Nevskaya, E N Golubeva *Kinet. Katal.* **42** 560 (2001)^g
169. V V Smirnov, M M Levitsky, I G Tarkhanova, A I Kokorin, S N Lanin *Kinet. Katal.* **42** 737 (2001)^g
170. V V Smirnov, M M Levitsky, I G Tarkhanova, B G Zavin, A N Bilyachenko *Kinet. Katal.* **44** 625 (2003)^g
171. E Rikowski, H C Marsmann *Polyhedron* **16** 3357 (1997)
172. R P Kruger, H Much, G Schulz, E Rikowski *Monatsh. Chem.* **130** 163 (1999)
173. D Wichmann, K Jug *J. Phys. Chem. B* **103** 10087 (1999)
174. K Jug, D Wichmann *J. Comput. Chem.* **16** 1549 (2000)

^a — *Russ. J. Gen. Chem. (Engl. Transl.)*

^b — *Russ. Chem. Bull., Int. Ed. (Engl. Transl.)*

^c — *Russ. J. Organomet. Chem. (Engl. Transl.)*

^d — *Dokl. Chem. (Engl. Transl.)*

^e — *J. Struct. Chem. (Engl. Transl.)*

^f — *Polym. Sci. (Engl. Transl.)*

^g — *Kinet. Catal. (Engl. Transl.)*

Kinetics of ‘blue’ flames in the gas-phase oxidation and combustion of hydrocarbons and their derivatives

V Ya Basevich, S M Frolov

Contents

I. Introduction	867
II. Cool and blue flames	867
III. Modelling of gas-phase oxidation of acetaldehyde and hydrocarbons C ₁ –C ₇	870
IV. Conclusion	883

Abstract. Experimental and calculated data on the kinetics of ‘blue’ flame observed in the gas-phase oxidation and combustion of hydrocarbons and their derivatives are considered. It is shown that blue flames arise due to the decomposition of hydrogen peroxide that forms in the oxidation of hydrocarbons. They manifest themselves by light emission, are identified by partial heat release (the appearance of a step in the time dependences of temperature and pressure observed in closed-vessel experiments) and propagate as conventional hot flames. The bibliography includes 43 references.

I. Introduction

Oxidation and combustion of hydrocarbons play an important role in chemical engineering, power production in thermal machines of various types and in environmental control. Being started quite long ago, their studies achieved considerable progress only in the second half of the 20th century. By that time, it was reliably stated that slow gas-phase oxidation of hydrocarbons represents a radical-chain reaction with degenerate branches. Kinetic studies of low-temperature oxidation of hydrocarbons have demonstrated its multistage nature. It is assumed that low-temperature oxidation and combustion of hydrocarbons involves the stages of cool, blue and hot flames. All these stages were observed experimentally. Thus cool flames were observed back in 1882 for the hydrocarbon oxidation in heated vessels.¹ Further studies of low-temperature oxidation of hydrocarbons demonstrated that this process represents partial oxidation to afford valuable oxygen-containing products such as alcohols, aldehydes, acids and peroxides. This explains the keen attention drawn to the cool-flame oxidation of hydrocarbons (*e.g.*, see monographs^{2–4} and references therein). However, whereas to date the mechanism of the appearance of cool flame can be considered as understood with a large degree of confidence, the mechanism of the emergence of blue flames is still largely unknown.

V Ya Basevich, S M Frolov N N Semenov Institute of Chemical Physics, Russian Academy of Sciences, ul. Kosygina 4, 119991 Moscow, Russian Federation. Fax (7-495) 137 61 30, tel. (7-495) 939 74 52, e-mail: basevich@center.chph.ras.ru (V Ya Basevich), tel. (7-495) 939 72 28, e-mail: smfrol@center.chph.ras.ru (S M Frolov)

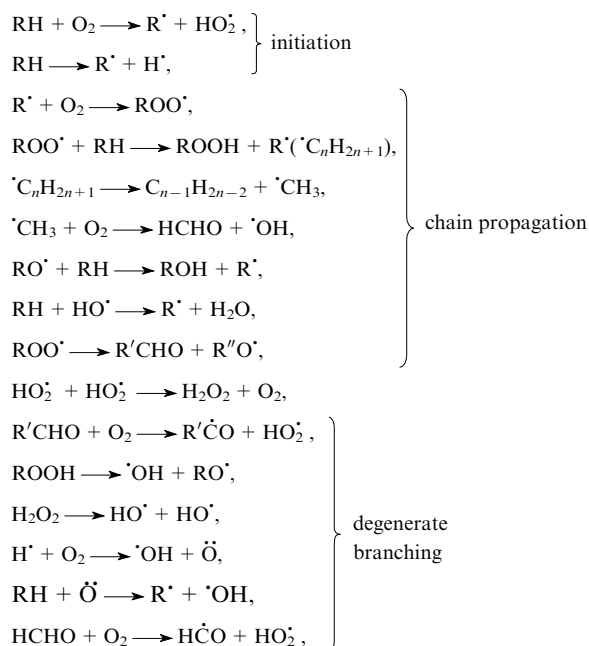
Received 7 March 2007

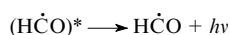
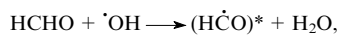
Uspekhi Khimii 76 (9) 927–944 (2007); translated by T Ya Safonova

Blue flames manifest themselves by light emission and can be identified by a partial heat release (the appearance of a step in curves that describe the time dependences of pressure and temperature in closed-vessel experiments). They can propagate like conventional hot flames. Blue flames were observed in the gas-phase oxidation and combustion of methane, ethane, n-heptane, isooctane and benzene as well as of acetaldehyde and diethyl ether. Experimental and theoretical studies of blue flames observed in the low-temperature oxidation of hydrocarbons and their derivatives are closely associated with the studies of cool flames; hence, the latter will also be briefly considered in this review, especially as both cool and blue flames pertain to low-temperature flames and their separation is a difficult task.

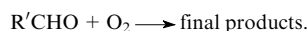
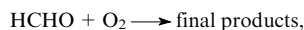
II. Cool and blue flames

It is well known that low-temperature oxidation of hydrocarbons follows the radical-chain mechanism with degenerate branching, where the branching is due to either the decomposition of hydroperoxides formed in the reaction or the interaction of aldehydes formed with oxygen. The main steps of this reaction are as follows:





and *etc.*,



The appearance of cool flame in hydrocarbon oxidation is due to the glow of excited formaldehyde. Blue flame arises as a result of further conversion of hydrocarbons owing to the glow of both excited formaldehyde and formyl radicals. Cool flames are observed at both low and high pressures typical of internal combustion engines (ICE).

The majority of scientists who studied the low-temperature oxidation of hydrocarbons assumed that cool flame arises as a result of explosive decomposition of organic hydroperoxides after their concentration has exceeded a certain critical value (*e.g.*, see Ref. 5). (As a rule, the decomposition is caused by the temperature increase in the course of the reaction). Due to the degenerate branching of the reaction as a result of the hydroperoxide decomposition and also due to the appearance of active species $\cdot\text{OH}$, the process sharply accelerates, heat is released, the temperature and the pressure increase, which leads to the appearance of cool flame.

Figure 1 shows typical kinetic curves of pentane cool-flame oxidation that represent the changes in the overall pressure during the reaction as a result of branching.² Cool flame is identified as a small pressure peak in the $\Delta P(t)$ curve, particularly, at the lowest initial pressure $P_0 = 225$ mm Hg, cool flame appears with a delay $t_i = 120$ s. As the initial pressure increases, the cool-flame delay shortens and the intensity (the pressure peak height) increases. Ultimately, at a pressure $P_0 = 340$ mm Hg, the cool-flame step is followed by hot autoignition, which is accompanied by a strong increase in the pressure (marked by an arrow). This is the so-called two-stage autoignition.

If the cool flame has failed to be transformed into the hot flame so that the reaction mixture is cooled from the vessel walls and also if the initial concentrations of fuel and oxidant have changed insignificantly in the cool flame, the autoignition can be repeated. This is the mechanism of origination of multiple (periodic) cool flames.

Figure 2 shows kinetic curves of cool-flame oxidation of ethyl methyl ketone.⁶ As is seen, cool flames appear twice during the oxidation (1 cf and 2 cf). Figure 3 shows a cool flame region confined by the first cool flame region (light circles) on the one side and a region of hot autoignition (dark

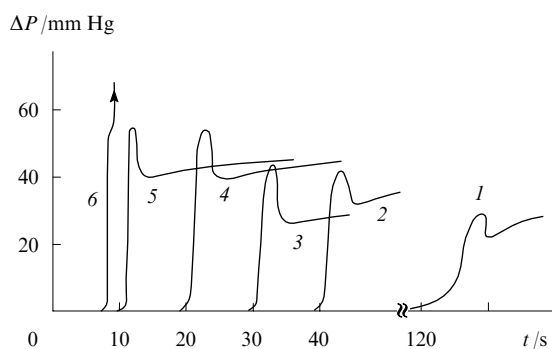


Figure 1. Kinetic curves of cool-flame oxidation of pentane (mixture composition: $\text{n-C}_5\text{H}_{12} + 4\text{O}_2$) for initial temperature $T_0 = 591$ K. Initial pressure P_0 /mm Hg: (1) 225, (2) 250, (3) 280, (4) 320, (5) 330, (6) 340.

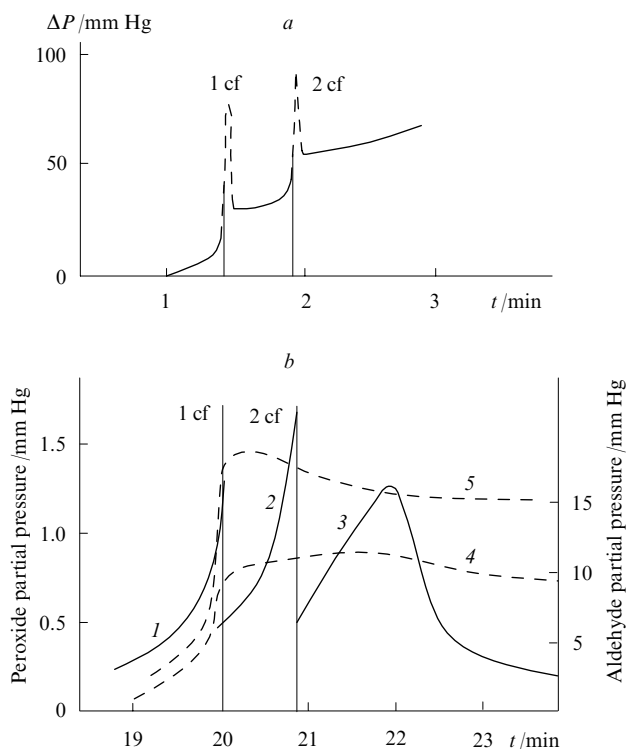


Figure 2. Kinetic curves of cool-flame oxidation of ethyl methyl ketone (mixture composition: $\text{CH}_3\text{COC}_2\text{H}_5 + \text{O}_2$).⁶

(a) Increase in the overall pressure (ΔP); (b) increase in partial pressures of peroxides (curves 1–3), formaldehyde (4) and higher aldehydes (5) in periodic cool flames.

Initial conditions: (a) $P_0 = 32$ kPa, $T_0 = 563$ K (in the presence of acetaldehyde $P_{\text{CH}_3\text{CHO}} = 0.27$ kPa); (b) $P_0 = 40$ kPa, $T_0 = 556$ K.

circles) on the other side in the coordinates 'initial temperature vs. initial pressure'.⁶

As the temperature increases, the formation of peroxides is hindered and, if the concentrations of initial hydrocarbon and oxygen have decreased significantly during the reaction, the oxidation process may be decelerated and even stop but may also continue (depending on conditions) by other reaction channels.

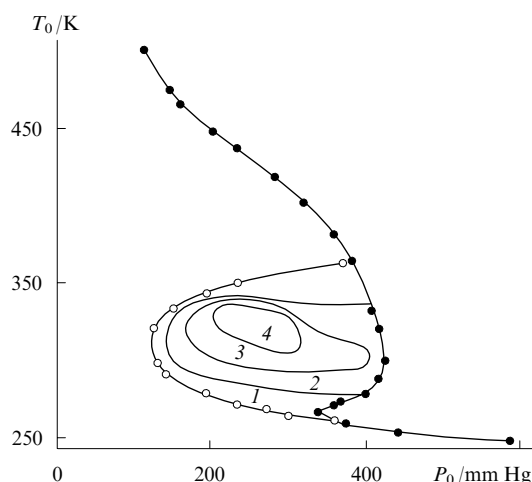


Figure 3. Region of periodic cool flames in equimolar methyl ethyl ketone mixtures with oxygen (numbers within the cool-flame region designate the number of flames).⁶

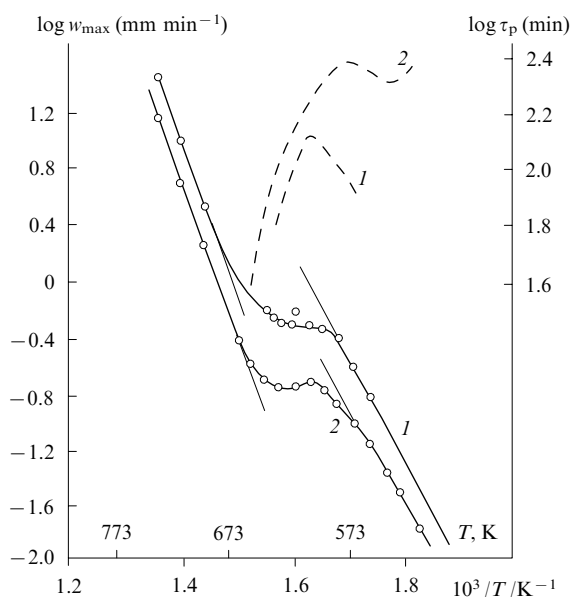


Figure 4. Logarithms of maximum oxidation rate w_{\max} (solid lines) and delay period τ_p (dash lines) for different temperatures.⁷ Mixture $\text{C}_2\text{H}_6 + 0.5\text{O}_2$; (1) $E = 30.0\text{--}33.6 \text{ kcal mol}^{-1}$, $P_0 = 67 \text{ kPa}$; (2) $E = 55.6 \text{ kcal mol}^{-1}$, $P_0 = 83 \text{ kPa}$.

Cold flames are associated with yet another peculiarity of the oxidation kinetics of hydrocarbons and their derivatives, *viz.*, the presence of a region of the negative temperature coefficient (NTC) in which the reaction rate decreases (or remains unchanged) rather than increases with the increase in temperature (Fig. 4).⁷ This phenomenon is associated with the fact that with the increase in temperature in the course of the reaction (or at an elevated initial temperature), the peroxide formation is hindered and the earlier formed peroxides easily decompose. In this case, the reaction branching that involves peroxides ceases to be dominant and the oxidation continues by other channels, which are not so efficient in the NTC region. As a result, in this temperature range, the rate turns out to be

lower at higher temperatures than at lower temperatures. Below, this phenomenon will be considered in more detail.

The first records of blue flames can be found in the studies by Townend *et al.* (*e.g.*, see Ref. 8 and a monograph² and references therein). They studied cool flames that arise at the ignition of fuel–air mixtures with a heated spiral and observed that the cool flame was followed by the appearance of a second brighter flame that propagated through the vessel. They named this phenomenon blue flame. Blue flames were accompanied by a higher (50–250 °C) warming up of the reaction mixture and brighter glow of excited formaldehyde as compared with cool flames.

Blue flames immediately precede the hot autoignition of hydrocarbons. It is assumed that in blue flame hydrocarbons undergo more extensive transformations as compared with cool flame. In addition to the glow of excited formaldehyde, which is inherent in cool flame, the glow at the wavelength of the formyl radical HC^*O is observed. Figure 5 shows experimental data obtained in the studies of autoignition of isooctane–air mixtures in closed vessels.³ In Fig. 5e, three pressure waves are well distinguishable, namely, the first cool-flame wave, the second blue-flame wave and the third wave of the hot explosion. The blue flame period (second wave) corresponds to the delay (induction period) of the hot explosion. In Fig. 5e, this delay is designated as τ_3 .

One piece of evidence for the multistage mechanism of the low-temperature autoignition of hydrocarbons is the appearance of blue flame in the experiments on the autoignition of 'lean' methane–air and isooctane–air mixtures carried out in ICE at temperatures and pressures near the autoignition point. However, no blue flame was observed in the subsequent experiments in a static bomb at the same temperatures and pressures. The later experiments with ICE also demonstrated the appearance of blue flames in the autoignition region of lean methane–air mixtures and benzene mixtures with oxygen. Hence, it seems that the appearance of blue flames during the autoignition processes in fuel–air mixtures in ICE is reliably ascertained (*e.g.*, see Ref. 3 and references therein).

In contrast to multistage high-temperature autoignition of hydrocarbons, the high-temperature autoignition develops continuously without any intermediate stages and ends with hot flame.

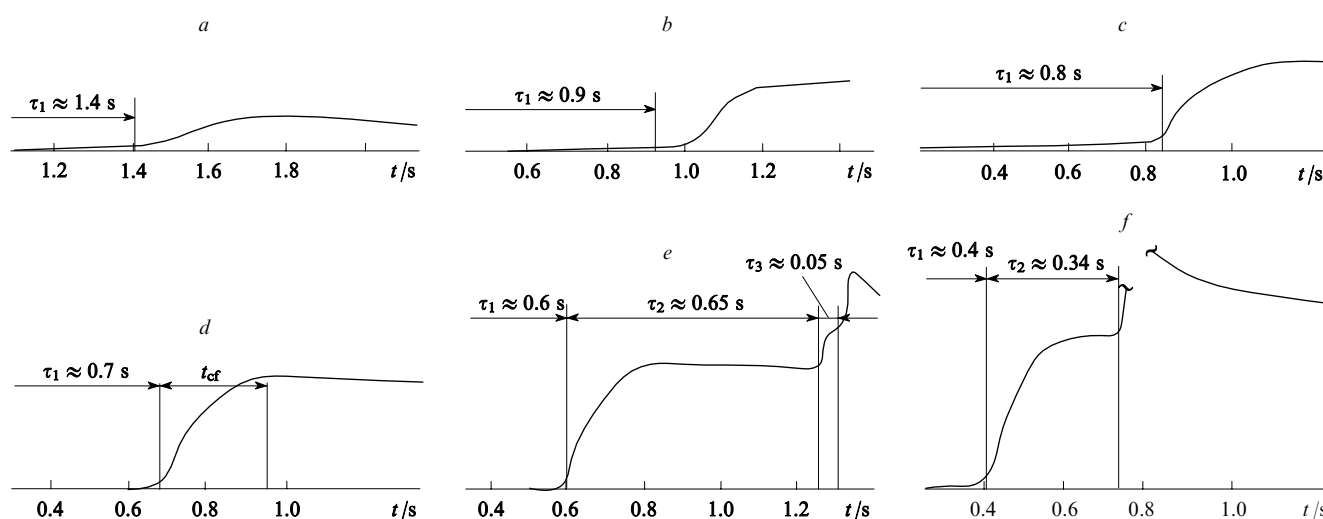


Figure 5. Pressure variation at autoignition of isooctane–air mixtures (stoichiometric ratio $\phi = 1.25$).³ The gain in pressure in the course of the reaction was measured for $T_0 = 643 \text{ K}$ and different initial pressures.

(a) $P_0 = 80 \text{ kPa}$, $P_{\text{ct}}/P_0 = 1.8$; (b) $P_0 = 105 \text{ kPa}$, $P_{\text{ct}}/P_0 = 1.09$; (c) $P_0 = 140 \text{ kPa}$, $P_{\text{ct}}/P_0 = 1.1$; (d) $P_0 = 180 \text{ kPa}$, $P_{\text{ct}}/P_0 = 1.13$; (e) $P_0 = 230 \text{ kPa}$, $P_{\text{ct}}/P_0 \approx 1.14$; (f) $P_0 = 320 \text{ kPa}$, $P_{\text{ct}}/P_0 \approx 1.2$.

Experimental results on the gas-phase oxidation of different hydrocarbons obtained in the mid-20th century are thoroughly described in several monographs.^{2–4}

III. Modelling of gas-phase oxidation of acetaldehyde and hydrocarbons C₁–C₇

For a long time, a concept on the multistage autoignition mechanism of hydrocarbons was not discussed in the literature. The first publications^{9,10} on the oxidation of hydrocarbons at elevated temperatures and pressures, which merely mentioned cool and blue flames but did not establish any new facts, appeared only in the 1980s.

In the long period during which the hydrocarbon oxidation and combustion were studied, numerous kinetic schemes were proposed that described sufficiently comprehensively the oxidation and combustion of particular hydrocarbons, for instance, radical-chain schemes of oxidation and combustion of methane,^{2,4,11,12} ethane,¹³ propane,^{14–16} n-butane,^{17,18} n-pentane,^{19,20} n-heptane,^{21–23} n-octane and isooctane.²⁴ These schemes adequately describe many aspects of hydrocarbon oxidation and combustion, agree with experimental data and allow one to model the corresponding processes. However, if a process can be modelled, then it is sufficiently understood and can be reproduced on the quantitative level. The simultaneous consideration of the known kinetic schemes of oxidation of hydrocarbons and their derivatives allowed the general comprehensive kinetic mechanism of oxidation and combustion of hydrocarbons to be proposed (Table 1 shows such a mechanism for hydrocarbons C₁–C₂; for simplicity, the radical signs in this and the subsequent Table are omitted); however, even incomplete knowledge of all reaction channels and the use of very approximate reaction rate constants often allows one to adequately describe the experimentally observed kinetics of oxidation and combustion using appropriate calculations.

For oxidation of hydrocarbons with ≥ 3 carbon atoms, the cool flames were modelled and the calculations were carried

out that perfectly described the characteristics of these flames.^{14–24} However, none of these studies considered blue flames and the mechanism of their origination. Papers on the modelling of blue flames were absent in the literature, which stimulation us to dwell into this issue.

As was mentioned above, blue flames are experimentally identified by glow and a stepwise gain in pressure observed in closed-vessel experiments. The detection of the blue-flame glow apparently provides little information on the chemical reactions responsible for its appearance; hence, the data on the variations of pressure and, correspondingly, temperature in the course of oxidation attract keen attention for the identification of blue flames. This information can be retrieved from calculations on the simulation of oxidation and combustion processes, which allows one to determine the temperature, the pressure and the concentrations of all products.

Calculations based on kinetic schemes constructed for the low-temperature oxidation of hydrocarbons involve an uncertainty associated with the necessity of taking into account the wall reactions, which are insufficiently studied. For long times and low pressures, the wall reactions can be represented in calculations as unimolecular reactions of the decay of species [reactions (140)–(143)].

1. Acetaldehyde

a. Two regions of the negative temperature coefficient

Acetaldehyde is a convenient subject for studying individual stages of the oxidation processes because its oxidation involves the appearance of intense cool and blue flames. Separate propagation of the latter was even observed at the initial room temperature.

Acetaldehyde oxidation was discussed in many studies (e.g., see monographs^{2–4} and references therein and also a recent paper²⁵); however, none of these publications described blue flames and the more so considered the possibility of their quantitative interpretation.

Kinetic schemes describing the oxidation of hydrocarbons C₁–C₂ were used²⁶ in modelling blue flames at the multistage

Table 1. Kinetic mechanism of oxidation and combustion of acetadehyde and hydrocarbons C₁–C₂.

Reaction number	Reaction	<i>H</i> /kJ mol ^{–1}	Forward reaction			Reverse reaction		
			<i>A</i> ^a	<i>n</i>	<i>E</i> /kJ mol ^{–1}	<i>A</i> ^a	<i>n</i>	<i>E</i> /kJ mol ^{–1}
1	OH + H ₂ ⇌ H + H ₂ O	62.80	2.2 × 10 ⁵	1.5	14.65	1.00 × 10 ⁶	1.5	77.87
2	OH + O ⇌ H + O ₂	66.99	2.8 × 10 ¹²	–0.8	–0.42	1.90 × 10 ¹¹	0.0	68.66
3	OH + H ⇌ O + H ₂	8.37	6.9 × 10 ⁹	0.0	29.31	1.50 × 10 ¹⁰	0.0	37.26
4	OH + OH ⇌ O + H ₂ O	71.18	6.0 × 10 ⁵	1.3	0.00	6.30 × 10 ⁶	1.3	71.18
5	H + H + M ⇌ H ₂ + M	431.24	2.0 × 10 ¹⁰	–0.3	0.00	1.00 × 10 ¹⁷	–1.3	438.78
6	O + O + M ⇌ O ₂ + M	494.04	3.6 × 10 ⁹	–0.6	0.00	1.60 × 10 ¹⁷	–1.6	502.42
7	OH + H + M ⇌ H ₂ O + M	494.04	3.6 × 10 ¹³	–1.0	0.00	8.70 × 10 ¹⁷	–2.0	502.42
8	O + H + M ⇌ OH + M	422.87	4.7 × 10 ⁹	0.0	0.00	1.1 × 10 ¹³	0.0	435.43
9	H + HO ₂ ⇌ H ₂ + O ₂	234.46	6.0 × 10 ⁹	0.0	0.00	1.1 × 10 ⁹	0.0	234.46
10	H + O ₂ + M ⇌ HO ₂ + M	196.78	4.1 × 10 ⁹	0.0	0.00	5.7 × 10 ¹²	0.0	204.32
11	H + HO ₂ ⇌ OH + OH	154.91	2.0 × 10 ¹⁰	0.0	0.00	1.6 × 10 ⁹	0.0	157.42
12	O + HO ₂ ⇌ O ₂ + OH	226.09	6.0 × 10 ¹⁰	0.0	0.00	9.4 × 10 ¹⁰	0.0	226.09
13	OH + HO ₂ ⇌ O ₂ + H ₂ O	297.26	6.0 × 10 ⁹	0.0	0.00	1.0 × 10 ¹¹	0.0	298.10
14	H + HO ₂ ⇌ H ₂ O + O	226.09	6.0 × 10 ⁸	0.0	0.00	5.3 × 10 ⁸	0.0	227.76
15	OH + H ₂ O ₂ ⇌ HO ₂ + H ₂ O	129.79	1.8 × 10 ⁹	0.0	1.26	1.9 × 10 ⁹	0.0	130.63
16	H + H ₂ O ₂ ⇌ H ₂ O + OH	276.13	7.1 × 10 ⁹	0.0	17.58	6.4 × 10 ⁸	0.0	303.96
17	OH + OH + M ⇌ H ₂ O ₂ + M	209.34	1.6 × 10 ⁸	0.0	–40.19	4.1 × 10 ¹³	0.0	175.85
18	O + H ₂ O ₂ ⇌ O ₂ + H ₂ O	355.88	2.8 × 10 ¹⁰	0.0	26.80	4.8 × 10 ¹⁰	0.0	382.67
19	H + H ₂ O ₂ ⇌ H ₂ + HO ₂	66.99	7.00 × 10 ⁹	0.0	17.58	1.6 × 10 ⁹	0.0	83.74
20	HO ₂ + HO ₂ ⇌ H ₂ O ₂ + O ₂	167.47	2.4 × 10 ¹⁰	0.0	6.28	3.7 × 10 ¹¹	0.0	175.01
21	O + H ₂ O ₂ ⇌ HO ₂ + OH	58.62	2.8 × 10 ¹⁰	0.0	26.80	2.9 × 10 ⁹	0.0	85.41
22	CO + OH ⇌ CO ₂ + H	108.86	1.2 × 10 ⁴	1.4	–1.67	4.6 × 10 ⁶	1.4	101.32
23	CO + HO ₂ ⇌ CO ₂ + OH	259.58	1.3 × 10 ¹¹	0.0	96.30	4.3 × 10 ¹²	0.0	355.88
24	CO + O + M ⇌ CO ₂ + M	531.72	6.2 × 10 ⁸	0.0	12.56	4.7 × 10 ¹⁴	0.5	548.47

Table 1 (continued).

Reaction number	Reaction	$H/\text{kJ mol}^{-1}$	Forward reaction			Reverse reaction		
			A^a	n	$E/\text{kJ mol}^{-1}$	A^a	n	$E/\text{kJ mol}^{-1}$
25	$\text{CO} + \text{O}_2 \rightleftharpoons \text{CO}_2 + \text{O}$	37.68	2.5×10^9	0.0	200.97	5.1×10^{10}	0.0	234.46
26	$\text{HCHO} + \text{OH} \rightleftharpoons \text{HCO} + \text{H}_2\text{O}$	121.42	7.5×10^9	0.0	0.84	2.2×10^9	0.0	121.42
27	$\text{HCHO} + \text{H} \rightleftharpoons \text{HCO} + \text{H}_2$	58.62	6.0×10^{10}	0.0	6.28	3.7×10^9	0.0	64.90
28	$\text{HCHO} + \text{O} \rightleftharpoons \text{HCO} + \text{OH}$	50.24	1.8×10^{10}	0.0	12.98	5.0×10^8	0.0	63.64
29	$\text{HO}_2 + \text{HCO} \rightleftharpoons \text{HCHO} + \text{O}_2$	171.66	3.5×10^8	0.0	52.34	2.0×10^{10}	0.0	222.32
30	$\text{H} + \text{CO} + \text{M} \rightleftharpoons \text{HCO} + \text{M}$	62.80	1.2×10^8	0.0	2.51	1.9×10^{14}	-1.0	71.18
31	$\text{H}_2\text{O}_2 + \text{HCO} \rightleftharpoons \text{HCHO} + \text{HO}_2$	12.56	1.6×10^8	0.0	20.93	6.0×10^8	0.0	33.49
32	$\text{HCO} + \text{O}_2 \rightleftharpoons \text{HO}_2 + \text{CO}$	142.35	6.0×10^{10}	0.0	30.14	5.5×10^{10}	0.0	173.75
33	$\text{O} + \text{HCO} \rightleftharpoons \text{H} + \text{CO}_2$	468.92	1.2×10^9	0.0	0.00	6.8×10^{11}	0.0	468.92
34	$\text{HCO} + \text{H} + \text{M} \rightleftharpoons \text{HCHO} + \text{M}$	376.81	3.8×10^4	1.0	0.00	3.2×10^{12}	0.0	314.01
35	$\text{OH} + \text{HCO} \rightleftharpoons \text{CO} + \text{H}_2\text{O}$	435.43	6.0×10^{10}	0.0	0.00	8.9×10^{11}	0.0	435.43
36	$\text{H} + \text{HCO} \rightleftharpoons \text{H}_2 + \text{CO}$	372.63	6.0×10^{10}	0.0	0.00	1.9×10^{11}	0.0	372.63
37	$\text{O} + \text{HCO} \rightleftharpoons \text{OH} + \text{CO}$	364.25	6.0×10^8	0.0	0.00	8.5×10^8	0.0	364.25
38	$\text{OH} + \text{CH}_4 \rightleftharpoons \text{CH}_3 + \text{H}_2\text{O}$	71.18	1.6×10^4	1.8	11.72	1.8×10^3	1.8	79.13
39	$\text{CH}_3 + \text{H}_2 \rightleftharpoons \text{H} + \text{CH}_4$	4.19	1.9×10^9	0.0	46.05	7.6×10^{10}	0.0	50.24
40	$\text{OH} + \text{CH}_3 \rightleftharpoons \text{O} + \text{CH}_4$	8.37	7.6×10^3	1.6	25.12	6.9×10^5	1.6	35.59
41	$\text{HO}_2 + \text{CH}_3 \rightleftharpoons \text{O}_2 + \text{CH}_4$	226.09	4.3×10^8	0.0	-1.67	6.0×10^{10}	0.0	230.27
42	$\text{H} + \text{CH}_3 + \text{M} \rightleftharpoons \text{CH}_4 + \text{M}$	422.87	2.3×10^6	1.0	-45.64	4.7×10^{14}	0.0	391.88
43	$\text{CH}_3 + \text{H}_2\text{O}_2 \rightleftharpoons \text{HO}_2 + \text{CH}_4$	58.62	6.5×10^7	0.0	18.00	6.0×10^8	0.0	79.55
44	$\text{CH}_3 + \text{HCHO} \rightleftharpoons \text{HCO} + \text{CH}_4$	62.80	1.0×10^9	0.0	18.84	2.5×10^9	0.0	79.97
45	$\text{HCO} + \text{CH}_3 \rightleftharpoons \text{CO} + \text{CH}_4$	376.81	6.0×10^{10}	0.0	0.00	7.8×10^{12}	0.0	374.72
46	$\text{O} + \text{CH}_3\text{O} \rightleftharpoons \text{CH}_3 + \text{O}_2$	117.23	1.7×10^{11}	0.0	12.14	2.3×10^{10}	0.0	128.95
47	$\text{OH} + \text{CH}_3 \rightleftharpoons \text{CH}_2 + \text{H}_2\text{O}$	37.68	6.0×10^9	0.0	11.72	2.2×10^{10}	0.0	50.24
48	$\text{O} + \text{CH}_2 \rightleftharpoons \text{H} + \text{HCO}$	376.81	6.0×10^9	0.0	0.00	4.5×10^{10}	0.0	376.81
49	$\text{CH}_2 + \text{H}_2\text{O} \rightleftharpoons \text{H}_2 + \text{HCHO}$	263.77	6.0×10^9	0.0	10.47	3.5×10^{11}	0.0	273.82
50	$\text{CH}_2 + \text{O}_2 \rightleftharpoons \text{OH} + \text{H} + \text{CO}$	247.02	6.0×10^9	0.0	14.65	1.5×10^3	1.0	256.23
51	$\text{CH}_2 + \text{O}_2 \rightleftharpoons \text{H} + \text{H} + \text{CO}_2$	351.69	1.8×10^8	0.0	0.00	1.8×10^4	1.0	343.32
52	$\text{CH}_3 + \text{O}_2 \rightleftharpoons \text{OH} + \text{HCHO}$	213.53	4.0×10^9	0.0	75.36	3.8×10^9	0.0	288.89
53	$\text{O} + \text{CH}_3 \rightleftharpoons \text{H} + \text{HCHO}$	284.70	7.2×10^{10}	0.0	0.00	1.5×10^{12}	0.0	285.54
54	$\text{CH}_3 + \text{O}_2 \rightleftharpoons \text{CH}_3\text{O}_2$	117.23	6.0×10^8	0.0	0.00	5.0×10^{13}	0.0	131.47
55	$\text{OH} + \text{CH}_3\text{O} \rightleftharpoons \text{CH}_3\text{O}_2\text{H}$	180.03	6.0×10^{10}	0.0	0.00	1.0×10^{15}	0.0	180.03
56	$\text{HO}_2 + \text{CH}_3 \rightleftharpoons \text{H}_2\text{O} + \text{HCHO}$	510.79	1.2×10^9	0.0	0.00	1.2×10^9	0.0	510.79
57	$\text{CH}_3\text{O}_2\text{H} + \text{CH}_3 \rightleftharpoons \text{CH}_3\text{O}_2 + \text{CH}_4$	62.80	6.0×10^8	0.0	19.68	6.0×10^8	0.0	83.74
58	$\text{OH} + \text{CH}_2 \rightleftharpoons \text{H}_2\text{O} + \text{CH}$	75.33	6.0×10^9	0.0	29.30	1.4×10^{10}	0.0	104.63
59	$\text{H} + \text{CH}_2 \rightleftharpoons \text{H}_2 + \text{CH}$	12.56	6.0×10^9	0.0	46.05	3.1×10^9	0.0	56.52
60	$\text{O} + \text{CH}_2 \rightleftharpoons \text{OH} + \text{CH}$	4.19	6.0×10^9	0.0	46.05	1.4×10^9	0.0	50.24
61	$\text{OH} + \text{CH} \rightleftharpoons \text{H}_2 + \text{CO}$	741.06	6.0×10^9	0.0	0.00	6.2×10^{11}	0.0	749.44
62	$\text{O} + \text{CH} \rightleftharpoons \text{H} + \text{CO}$	732.69	6.0×10^9	0.0	0.00	2.8×10^{11}	0.0	741.06
63	$\text{OH} + \text{CH}_3 \rightleftharpoons \text{CH}_3\text{OH}$	385.19	9.4×10^6	1.0	-9.21	9.4×10^{15}	0.0	376.81
64	$\text{HO}_2 + \text{CH}_3\text{O} \rightleftharpoons \text{CH}_3\text{OH} + \text{O}_2$	226.09	2.6×10^8	0.0	0.00	6.0×10^9	0.0	217.71
65	$\text{CH}_3\text{O} + \text{CH}_4 \rightleftharpoons \text{CH}_3\text{OH} + \text{CH}_3$	0.00	4.7×10^8	0.0	37.26	1.4×10^8	0.0	46.89
66	$\text{OH} + \text{CH}_3\text{OH} \rightleftharpoons \text{H}_2\text{O} + \text{CH}_3\text{O}$	71.18	6.0×10^9	0.0	30.14	4.7×10^9	0.0	96.30
67	$\text{H} + \text{CH}_3\text{OH} \rightleftharpoons \text{H}_2 + \text{CH}_3\text{O}$	8.37	1.3×10^{10}	0.0	22.19	2.2×10^9	0.0	25.54
68	$\text{O} + \text{CH}_3\text{OH} \rightleftharpoons \text{OH} + \text{CH}_3\text{O}$	0.00	4.3×10^9	0.0	8.37	3.2×10^8	0.0	4.19
69	$\text{CH}_3\text{O} + \text{O}_2 \rightleftharpoons \text{HO}_2 + \text{H}_2\text{CO}$	104.67	6.6×10^7	0.0	10.89	2.8×10^8	0.0	125.60
70	$\text{H} + \text{H}_2\text{CO} + \text{M} \rightleftharpoons \text{CH}_3\text{O} + \text{M}$	92.11	1.2×10^5	1.0	26.80	6.0×10^{11}	0.0	92.11
71	$\text{OH} + \text{CH}_3\text{O} \rightleftharpoons \text{H}_2\text{O} + \text{HCHO}$	401.93	6.0×10^9	0.0	0.00	8.3×10^9	0.0	401.93
72	$\text{H} + \text{CH}_3\text{O} \rightleftharpoons \text{H}_2 + \text{HCHO}$	339.13	6.0×10^{10}	0.0	0.00	1.8×10^{10}	0.0	339.13
73	$\text{O} + \text{CH}_3\text{O} \rightleftharpoons \text{OH} + \text{HCHO}$	330.76	6.0×10^9	0.0	0.00	7.9×10^8	0.0	332.43
74	$\text{O}_2 + \text{C}_2\text{H}_2 \rightleftharpoons \text{HCO} + \text{HCO}$	138.16	1.9×10^{11}	0.0	138.16	2.7×10^9	0.0	276.33
75	$\text{C}_2\text{H} + \text{H} + \text{M} \rightleftharpoons \text{C}_2\text{H}_2 + \text{M}$	523.35	6.8×10^5	1.0	-54.43	4.2×10^{13}	0.0	447.99
76	$\text{C}_2\text{H} + \text{H}_2 \rightleftharpoons \text{C}_2\text{H}_2 + \text{H}$	92.11	3.5×10^8	0.0	-2.51	6.0×10^9	0.0	83.74
77	$\text{C}_2\text{H} + \text{O}_2 \rightleftharpoons \text{CO} + \text{HCO}$	665.70	6.0×10^9	0.0	0.00	5.4×10^9	0.0	665.70
78	$\text{OH} + \text{C}_2\text{H}_2 \rightleftharpoons \text{CH}_3 + \text{CO}$	234.46	7.8×10^9	0.0	19.26	5.9×10^9	0.0	259.58
79	$\text{O} + \text{C}_2\text{H}_2 \rightleftharpoons \text{CH}_2 + \text{CO}$	192.59	2.2×10^1	2.8	20.93	5.8	2.8	334.94
80	$\text{H} + \text{C}_2\text{H}_2 \rightleftharpoons \text{C}_2\text{H}_3$	167.47	5.5×10^9	0.0	10.05	2.6×10^{16}	-1.0	194.27
81	$\text{H}_2 + \text{C}_2\text{H}_2 \rightleftharpoons \text{C}_2\text{H}_4$	171.66	1.6×10^3	1.0	46.05	3.1×10^{11}	0.0	231.95
82	$\text{OH} + \text{CO} + \text{CH}_3 \rightleftharpoons \text{O}_2 + \text{C}_2\text{H}_4$	20.93	2.8×10^1	1.0	133.98	6.0×10^{10}	0.0	146.54
83	$\text{OH} + \text{C}_2\text{H}_4 \rightleftharpoons \text{H}_2\text{O} + \text{C}_2\text{H}_3$	62.80	6.0×10^9	0.0	3.77	1.4×10^9	0.0	72.85
84	$\text{H}_2 + \text{C}_2\text{H}_3 \rightleftharpoons \text{H} + \text{C}_2\text{H}_4$	4.19	5.8×10^8	0.0	53.59	6.0×10^9	0.0	50.24
85	$\text{O} + \text{C}_2\text{H}_4 \rightleftharpoons \text{HCO} + \text{CH}_3$	113.04	6.0×10^9	0.0	2.93	5.0×10^7	0.0	113.04
86	$\text{O}_2 + \text{C}_2\text{H}_3 \rightleftharpoons \text{HO}_2 + \text{C}_2\text{H}_2$	29.31	6.0×10^9	0.0	41.87	1.8×10^9	0.0	62.80

Table 1 (continued).

Reaction number	Reaction	$H/\text{kJ mol}^{-1}$	Forward reaction			Reverse reaction		
			A^a	n	$E/\text{kJ mol}^{-1}$	A^a	n	$E/\text{kJ mol}^{-1}$
87	$\text{OH} + \text{C}_2\text{H}_3 \rightleftharpoons \text{HCO} + \text{CH}_3$	138.16	6.0×10^9	0.0	0.00	1.5×10^9	0.0	150.72
88	$\text{OH} + \text{C}_2\text{H}_3 \rightleftharpoons \text{H}_2\text{O} + \text{C}_2\text{H}_2$	326.57	6.0×10^9	0.0	0.00	2.3×10^{10}	0.0	318.20
89	$\text{H} + \text{C}_2\text{H}_3 \rightleftharpoons \text{H}_2 + \text{C}_2\text{H}_2$	263.77	6.0×10^9	0.0	0.00	6.3×10^{10}	0.0	259.58
90	$\text{O} + \text{C}_2\text{H}_3 \rightleftharpoons \text{CH}_3 + \text{CO}$	489.86	6.0×10^9	0.0	0.00	2.1×10^9	0.0	485.67
91	$\text{O} + \text{C}_2\text{H}_3 \rightleftharpoons \text{OH} + \text{C}_2\text{H}_2$	255.39	6.0×10^9	0.0	0.00	2.8×10^9	0.0	251.21
92	$\text{CH}_4 + \text{C}_2\text{H}_3 \rightleftharpoons \text{CH}_3 + \text{C}_2\text{H}_4$	12.56	6.0×10^8	0.0	46.05	2.0×10^9	0.0	58.62
93	$\text{CH}_3 + \text{CH}_3 \rightleftharpoons \text{C}_2\text{H}_4 + \text{H}_2$	230.27	2.0×10^{13}	0.0	159.94	3.0×10^{15}	0.0	381.00
94	$\text{C}_2\text{H}_4 + \text{H} + \text{H} \rightleftharpoons \text{CH}_3 + \text{CH}_3$	200.97	1.8×10^6	1.0	-41.87	6.0×10^{10}	0.0	174.17
95	$\text{HCHO} + \text{C}_2\text{H}_3 \rightleftharpoons \text{HCO} + \text{C}_2\text{H}_4$	75.36	6.0×10^{10}	0.0	0.00	6.0×10^{10}	0.0	75.36
96	$\text{HCO} + \text{CH}_3 \rightleftharpoons \text{CH}_3\text{CHO}$	355.88	6.6×10^8	1.0	0.00	1.2×10^{16}	0.0	341.22
97	$\text{HO}_2 + \text{CH}_3\text{CO} \rightleftharpoons \text{CH}_3\text{CHO} + \text{O}_2$	154.91	5.3×10^7	0.0	0.00	1.0×10^9	0.0	163.29
98	$\text{OH} + \text{CH}_3\text{CHO} \rightleftharpoons \text{H}_2\text{O} + \text{CH}_3\text{CO}$	138.16	3.3×10^9	0.0	6.70	2.9×10^9	0.0	146.54
99	$\text{H} + \text{CH}_3\text{CHO} \rightleftharpoons \text{H}_2 + \text{CH}_3\text{CO}$	75.36	1.4×10^{10}	0.0	13.82	1.2×10^9	0.0	89.18
100	$\text{O} + \text{CH}_3\text{CHO} \rightleftharpoons \text{OH} + \text{CH}_3\text{CO}$	66.99	7.2×10^9	0.0	8.37	6.0×10^8	0.0	75.36
101	$\text{HO}_2 + \text{CH}_3\text{CHO} \rightleftharpoons \text{H}_2\text{O}_2 + \text{CH}_3\text{CO}$	4.19	6.0×10^8	0.0	41.87	4.9×10^8	0.0	46.05
102	$\text{CH}_3 + \text{CO} + \text{M} \rightleftharpoons \text{CH}_3\text{CO} + \text{M}$	58.62	1.1×10^8	0.0	15.91	6.0×10^{12}	0.0	59.45
103	$\text{H} + \text{CH}_3\text{CO} \rightleftharpoons \text{HCO} + \text{CH}_3$	4.19	6.0×10^9	0.0	20.10	6.6×10^7	0.0	26.38
104	$\text{O} + \text{CH}_3\text{CO} \rightleftharpoons \text{CO} + \text{CH}_3\text{O}$	322.38	6.0×10^9	0.0	0.00	1.6×10^{10}	0.0	322.38
105	$\text{C}_2\text{H}_5 + \text{O}_2 \rightleftharpoons \text{OH} + \text{CH}_3\text{CHO}$	255.39	4.0×10^9	0.0	75.36	3.0×10^9	0.0	330.76
106	$\text{HO}_2 + \text{C}_2\text{H}_5 \rightleftharpoons \text{O}_2 + \text{C}_2\text{H}_6$	213.53	3.2×10^8	0.0	-5.02	6.0×10^9	0.0	209.34
107	$\text{CH}_3 + \text{CH}_3 \rightleftharpoons \text{C}_2\text{H}_6$	376.81	8.4×10^9	0.0	0.00	1.3×10^{16}	0.0	364.25
108	$\text{OH} + \text{C}_2\text{H}_6 \rightleftharpoons \text{H}_2\text{O} + \text{C}_2\text{H}_5$	83.74	1.8×10^{11}	0.0	16.75	1.6×10^{11}	0.0	100.48
109	$\text{H} + \text{C}_2\text{H}_6 \rightleftharpoons \text{H}_2 + \text{C}_2\text{H}_5$	20.93	7.4×10^{10}	0.0	40.19	1.4×10^{10}	0.0	59.45
110	$\text{O} + \text{C}_2\text{H}_6 \rightleftharpoons \text{OH} + \text{C}_2\text{H}_5$	12.56	4.6×10^9	0.0	16.75	3.8×10^8	0.0	29.31
111	$\text{H}_2\text{O}_2 + \text{C}_2\text{H}_5 \rightleftharpoons \text{HO}_2 + \text{C}_2\text{H}_6$	46.05	4.9×10^8	0.0	33.49	6.0×10^8	0.0	79.55
112	$\text{H} + \text{C}_2\text{H}_4 \rightleftharpoons \text{C}_2\text{H}_5$	138.16	8.8×10^{10}	-0.5	5.86	1.1×10^{14}	-0.6	160.35
113	$\text{C}_2\text{H}_5 + \text{O}_2 \rightleftharpoons \text{HO}_2 + \text{C}_2\text{H}_4$	58.62	6.0×10^8	0.0	33.49	4.5×10^7	0.0	75.36
114	$\text{C}_2\text{H}_5 + \text{O}_2 \rightleftharpoons \text{HCHO} + \text{CH}_3\text{O}$	230.27	6.0×10^8	0.0	41.87	1.7×10^8	0.0	259.58
115	$\text{OH} + \text{C}_2\text{H}_5 \rightleftharpoons \text{CH}_3 + \text{CH}_3\text{O}$	16.75	3.0×10^{10}	0.0	0.00	8.0×10^9	0.0	5.86
116	$\text{OH} + \text{C}_2\text{H}_5 \rightleftharpoons \text{H}_2\text{O} + \text{C}_2\text{H}_4$	355.88	6.0×10^9	0.0	0.00	7.2×10^9	0.0	334.94
117	$\text{H} + \text{C}_2\text{H}_5 \rightleftharpoons \text{CH}_3 + \text{CH}_3$	62.80	4.8×10^{10}	0.0	4.61	8.2×10^7	0.0	53.59
118	$\text{H} + \text{C}_2\text{H}_5 \rightleftharpoons \text{CH}_2 + \text{CH}_4$	20.93	6.0×10^9	0.0	25.12	7.1×10^7	0.0	40.19
119	$\text{H} + \text{C}_2\text{H}_5 \rightleftharpoons \text{C}_2\text{H}_6$	410.31	3.6×10^{10}	0.0	0.00	1.0×10^{15}	0.0	410.31
120	$\text{H} + \text{C}_2\text{H}_5 \rightleftharpoons \text{H}_2 + \text{C}_2\text{H}_4$	293.08	6.0×10^9	0.0	0.00	1.6×10^9	0.0	276.33
121	$\text{O} + \text{C}_2\text{H}_5 \rightleftharpoons \text{CH}_3 + \text{H}_2\text{CO}$	347.50	6.0×10^{10}	0.0	0.00	2.1×10^8	0.0	334.94
122	$\text{O} + \text{C}_2\text{H}_5 \rightleftharpoons \text{OH} + \text{C}_2\text{H}_4$	284.70	6.0×10^9	0.0	0.00	6.9×10^8	0.0	267.96
123	$\text{H}_2 + \text{C}_2\text{H} \rightleftharpoons \text{H} + \text{C}_2\text{H}_2$	117.23	3.5×10^8	0.0	-20.93	6.0×10^9	0.0	83.74
124	$\text{CH}_3\text{O}_2 + \text{CH}_3 \rightleftharpoons \text{CH}_3\text{O} + \text{CH}_3\text{O}$	142.35	1.3×10^9	0.0	0.00	2.9×10^9	0.0	142.35
125	$\text{CH}_3\text{O}_2 + \text{HO}_2 \rightleftharpoons \text{CH}_3\text{O}_2\text{H} + \text{O}_2$	167.47	5.0×10^7	0.0	12.56	6.8×10^8	0.0	180.03
126	$\text{CH}_3 + \text{HO}_2 \rightleftharpoons \text{CH}_3\text{O} + \text{OH}$	108.86	2.0×10^8	0.0	0.00	2.0×10^9	0.0	117.23
127	$\text{C}_2\text{H}_5 + \text{O}_2 \rightleftharpoons \text{C}_2\text{H}_5\text{O}_2$	117.23	2.8×10^7	0.0	-4.19	2.0×10^{14}	-1.0	104.67
128	$\text{C}_2\text{H}_5\text{O}_2\text{H} + \text{C}_2\text{H}_5 \rightleftharpoons \text{C}_2\text{H}_5\text{O}_2 + \text{C}_2\text{H}_6$	20.93	1.8×10^7	0.0	50.24	6.3×10^8	0.0	71.18
129	$\text{C}_2\text{H}_5\text{O} + \text{OH} \rightleftharpoons \text{C}_2\text{H}_5\text{O}_2\text{H}$	180.03	5.5×10^7	1.0	16.33	4.0×10^{15}	0.0	180.03
130	$\text{C}_2\text{H}_4 + \text{OH} \rightleftharpoons \text{C}_2\text{H}_5\text{O}$	100.48	9.1×10^6	1.0	8.37	1.3×10^{13}	0.0	108.86
131	$\text{CH}_3 + \text{HCHO} \rightleftharpoons \text{C}_2\text{H}_5\text{O}$	46.05	5.0×10^7	1.0	41.87	1.0×10^{14}	0.0	87.92
132	$\text{C}_2\text{H}_5\text{O}_2 + \text{C}_2\text{H}_5 \rightleftharpoons \text{C}_2\text{H}_5\text{O} + \text{C}_2\text{H}_5\text{O}$	129.79	6.3×10^8	0.0	0.00	1.1×10^8	0.0	126.02
133	$\text{C}_2\text{H}_5\text{O}_2 + \text{HO}_2 \rightleftharpoons \text{C}_2\text{H}_5\text{O}_2\text{H} + \text{O}_2$	163.29	7.9×10^7	0.0	8.37	3.7×10^8	0.0	171.66
134	$\text{C}_2\text{H}_5 + \text{HO}_2 \rightleftharpoons \text{C}_2\text{H}_5\text{O} + \text{OH}$	104.67	2.0×10^8	0.0	0.00	1.2×10^7	0.0	104.67
135	$\text{CH}_3\text{CO} + \text{O}_2 \rightleftharpoons \text{CH}_3\text{CO}_3$	117.23	1.0×10^9	0.0	0.00	1.0×10^{14}	0.0	117.23
136	$\text{CH}_3\text{CO}_3 + \text{CH}_3\text{CHO} \rightleftharpoons \rightleftharpoons \text{CH}_3\text{CO} + \text{CH}_3\text{CO}_3\text{H}$	8.37	6.3×10^8	0.0	35.59	1.8×10^7	0.0	43.96
137	$\text{CH}_3 + \text{CO}_2 + \text{OH} \rightleftharpoons \text{CH}_3\text{CO}_3\text{H}$	138.16	5.5×10^4	2.0	0.00	6.0×10^{14}	0.0	138.16
138	$\text{CH}_3\text{CO}_3 + \text{HO}_2 \rightleftharpoons \text{CH}_3\text{CO}_3\text{H} + \text{O}_2$	167.47	7.9×10^7	0.0	0.00	3.7×10^8	0.0	167.47
139	$\text{CH}_3\text{O}_2 + \text{CH}_3\text{CHO} \rightleftharpoons \rightleftharpoons \text{CH}_3\text{CO} + \text{CH}_3\text{O}_2\text{H}$	12.56	6.0×10^8	0.0	62.80	6.8×10^8	0.0	75.36
140	$\text{H}_2\text{O}_2 \longrightarrow \text{H}_2\text{O} + 0.5\text{O}_2$	0.00	3.0	0.0	0.00			
141	$\text{CH}_3\text{OOH} \longrightarrow \text{H}_2 + \text{H}_2\text{O} + \text{CO}$	0.00	6.0	0.0	0.00			
142	$\text{CH}_3\text{COOOH} \longrightarrow \text{CO} + \text{O}_2 + \text{CH}_4$	0.00	6.0	0.0	0.00			
143	$\text{C}_2\text{H}_5\text{OOH} \longrightarrow \text{H}_2\text{O} + \text{O}_2 + \text{CH}_4$	0.00	6.0	0.0	0.00			

^a A is the pre-exponential factor in equation describing the unimolecular (in s^{-1}), bimolecular ($\text{litre mol}^{-1} \text{s}^{-1}$) and trimolecular ($\text{litre}^2 \text{mol}^{-2} \text{s}^{-1}$) reactions.

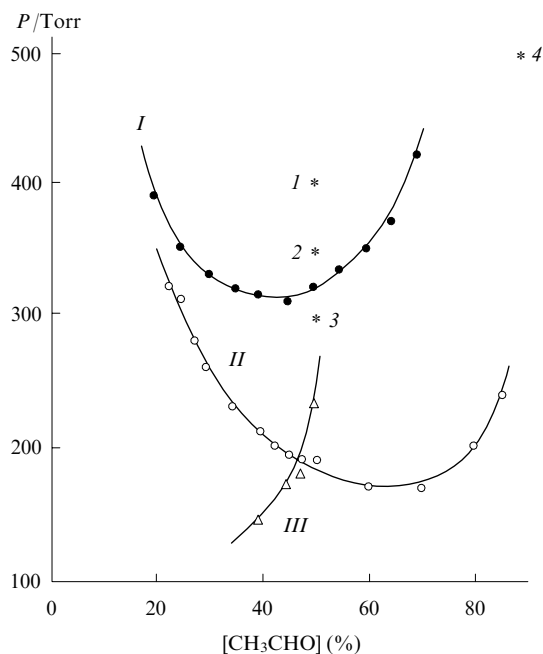


Figure 6. Regions of propagation of cool and blue flames (region I), only cool flame (II) and normal hot flame (III) in $\text{CH}_3\text{CHO} + \text{O}_2$ mixtures.⁸

Arabic numerals correspond to the conditions (pressure and mixture composition) under which solutions of the problem of propagation of normal hot flame (1, 2), cool flame (3) and combined propagation of cool and blue flame (4) were found.

autoignition of acetaldehyde mixtures with oxygen. Townend *et al.*⁸ have shown that in the induced ignition of 'rich' mixtures of diethyl ether and acetaldehyde with oxygen, one can observe cool and blue flames at reduced (subatmospheric) pressures and ambient or relatively low temperatures (Fig. 6), which involves only insignificant heating in the flames (50–250°) (cited according to Ref. 2). This is why before embarking on the kinetic modelling of blue flame, it is necessary to elucidate whether the region of acetaldehyde autoignition corresponds to the region of propagation of cool and blue flames upon ignition, how these flames are characterised and what are the calculated conditions of their origination. For these purposes, a kinetic scheme of the hydrocarbon C_1 – C_2 oxidation²⁷ supplemented by the data on acetaldehyde oxidation was taken.²⁸ Table 1 shows all the proposed elementary steps of acetaldehyde oxidation.

A homogeneous reaction (*i.e.*, a reaction that simultaneously proceeds in the whole reactor volume) in a closed vessel was modelled. A system of equation describing the material and heat balance in this reaction is as follows:

$$\frac{dn_j}{dt} = \sum_j w_{ij}, \quad (1)$$

$$\rho c_v \frac{dT}{dt} = \sum_j h_{ij} w_{ij} + \frac{\kappa S}{V} (T - T_w), \quad (2)$$

where n_j is the concentration of species; t is the time; T is the temperature; w_{ij} and h_{ij} are the rate and heat of the i th reaction (elementary step) involving the j th species; ρ is the density; c_v is the heat capacity at a constant volume; κ is the coefficient of heat-transfer to the walls of the reaction vessel; S and V are the surface and volume of the reaction vessel or a combustion chamber; T_w is the vessel wall temperature. The first term in Eqn (2) corresponds to the heat release due to the reaction, the second term corresponds to the heat exchange with the wall. The density was calculated using the equation of gas state. The

solution of this equation for the initial conditions $t = 0$, $n_j = [n_j]_0$, $T = T_0$ allows one to describe the kinetics of homogeneous reactions, *i.e.* find the time dependences of the temperature and concentrations of all substances involved in this reaction.

Figure 7 shows the calculated kinetic dependences of temperature (a) and concentrations of starting compounds (b), most important intermediate compounds and radicals

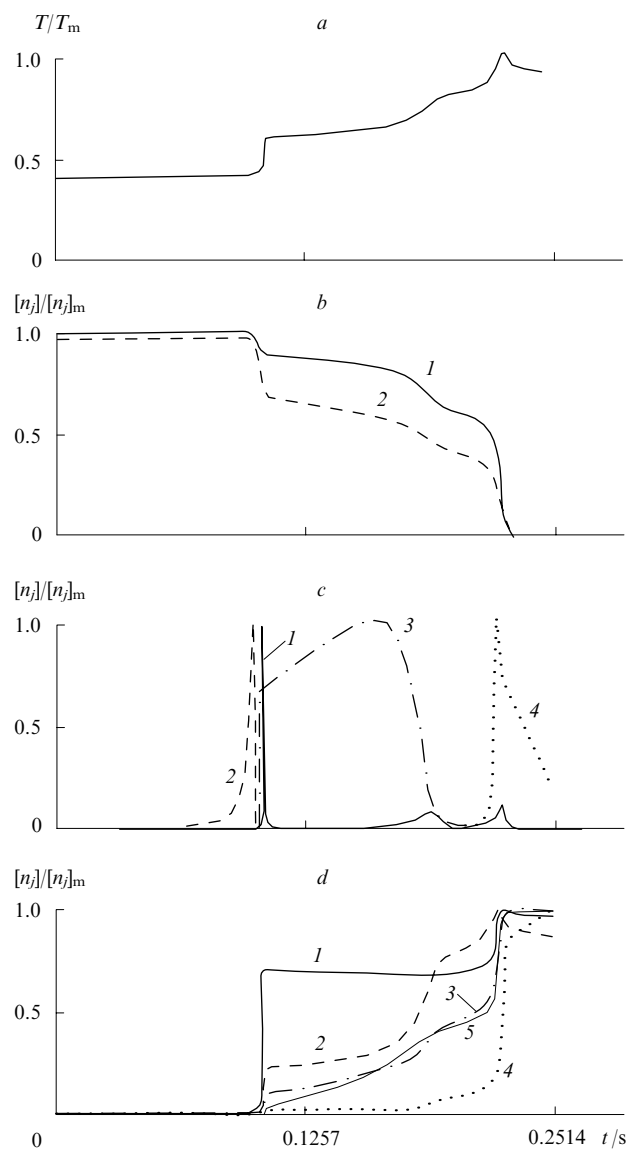


Figure 7. Time profiles of relative temperature (T/T_m , a) and concentrations $[n_j]/[n_j]_m$ (subscript m corresponds to the maximum values) of initial compounds (b), intermediate compounds and radicals (c) and also final products (d) at the autoignition of an acetaldehyde–oxygen mixture.²⁸ Initial conditions: $T_0 = 537$ K, $P_0 = 64.1$ kPa, $[\text{CH}_3\text{CHO}]_0 = 75\%$, $[\text{O}_2]_0 = 25\%$.

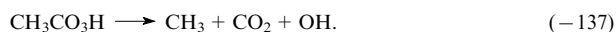
(a) T/T_m , $T_m = 1343$ K;

(b) (1) $[\text{CH}_3\text{CHO}]/[\text{CH}_3\text{CHO}]_m$, $[\text{CH}_3\text{CHO}]_m = 0.75$ (here and further, the maximum concentrations are given in volume fractions); (2) $[\text{O}_2]/[\text{O}_2]_m$, $[\text{O}_2]_m = 0.25$;

(c) (1) $[\text{OH}]/[\text{OH}]_m$, $[\text{OH}]_m = 8.55 \times 10^{-6}$; (2) $[\text{CH}_3\text{CO}_3\text{H}]/[\text{CH}_3\text{CO}_3\text{H}]_m$, $[\text{CH}_3\text{CO}_3\text{H}]_m = 1.27 \times 10^{-2}$; (3) $[\text{H}_2\text{O}_2]/[\text{H}_2\text{O}_2]_m$, $[\text{H}_2\text{O}_2]_m = 2.61 \times 10^{-2}$; (4) $[\text{H}]/[\text{H}]_m$, $[\text{H}]_m = 1.88 \times 10^{-5}$;

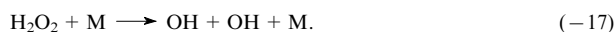
(d) (1) $[\text{CO}_2]/[\text{CO}_2]_m$, $[\text{CO}_2]_m = 3.67 \times 10^{-2}$; (2) $[\text{H}_2\text{O}]/[\text{H}_2\text{O}]_m$, $[\text{H}_2\text{O}]_m = 1.63 \times 10^{-1}$; (3) $[\text{CO}]/[\text{CO}]_m$, $[\text{CO}]_m = 4.02 \times 10^{-1}$; (4) $[\text{H}_2]/[\text{H}_2]_m$, $[\text{H}_2]_m = 2.33 \times 10^{-1}$; (5) $[\text{CH}_4]/[\text{CH}_4]_m$, $[\text{CH}_4]_m = 8.83 \times 10^{-2}$.

$[\text{CH}_3\text{CO}_3\text{H}, \text{H}_2\text{O}_2, \text{H}, \text{OH}]$ (c) and final products $[\text{CO}_2, \text{CO}, \text{H}_2, \text{H}_2\text{O}, \text{CH}_4]$ (d) on time in the blue flame region for the autoignition of an acetaldehyde mixture ($[\text{CH}_3\text{CHO}]_0 = 75\%$) with oxygen ($[\text{O}_2]_0 = 25\%$). The calculations were carried out for the following initial conditions: $T_0 = 537$ K and $P_0 = 64.1$ kPa. The temperature curve (Fig. 7a) demonstrates three steps, which correspond to the temperature rise in cool, blue and conventional hot flames. The temperature rise in cool flame (at $t \approx 0.1$ s) is explained by a sharp increase in the reaction rate due to branching associated with the decomposition of hydroperoxide $\text{H}_3\text{CO}_3\text{H}$ (hereinafter, the reaction number corresponds to that shown in Table 1).



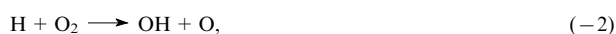
The same time corresponds to the appearance of a maximum in the $[\text{OH}]/[\text{OH}]_{\text{m}}$ vs. t curve (curve 1 in Fig. 7c).

In cool flame, a great deal of H_2O_2 is formed (curve 3 in Fig. 7c) the concentration of which first increases and then, after a certain period, starts to sharply decrease due to the H_2O_2 decomposition by the reaction



The second temperature jump due to the reaction acceleration as a result of the H_2O_2 decomposition is also accompanied by an increase in the concentration of OH radicals (the second peak in curve 1 in Fig. 7c). It is the chemical processes accompanying this temperature jump that are identified as the blue flame. The identification of blue flame and its mechanism as a local maximum of the reaction rate that arises due to the hydrogen peroxide decomposition was proposed in the study²⁹ dealing with analysis of the kinetics of ethane oxidation. The decomposition reaction of hydrogen peroxide is present in virtually all detailed kinetic schemes of hydrocarbon oxidation. However, before the appearance of the above publication,²⁹ the authors of these schemes never studied blue flames nor analysed their mechanism and the role of hydrogen peroxide decomposition in the appearance of blue flame.

Ultimately, as the reaction mixture is self-heated during the reaction, the conditions arise for the intense reaction branching typical of hot flames



which is accompanied by a new increase in the reaction rate and in the temperature. The concentrations of OH radicals (the third peak in curve 1, Fig. 7c) and hydrogen atoms H (curve 4 in Fig. 7c) increase again and the concentrations of acetaldehyde and oxygen decrease (curves 1 and 2 in Fig. 7b). Figure 7d shows the concentration profiles of several products of acetaldehyde oxidation and combustion, which are formed in the highest yields.

Presumably, the above description of the chemical process of acetaldehyde oxidation reflects the general phenomenological pattern and the essence of the three-stage autoignition of a $\text{CH}_3\text{CHO} + \text{O}_2$ mixture with the formation of cool, blue and hot flames.

Computations made it possible to follow the effect of the initial conditions ($\text{CH}_3\text{CHO} + \text{O}_2$ mixture composition, pressure and temperature) on the form of a $T(t)$ function, which describes most comprehensively the external aspects of a chemical reaction, in the t range from 0 to 0.5 s.²⁶ On the one hand, as the acetaldehyde concentration increases from 75% to 85%, the reaction rate decreases and the $T(t)$ function transforms from three-stage into two-stage due to the disappearance of the hot flame stage. On the other hand, the decrease in the $[\text{CH}_3\text{CHO}]_0$ concentration to 65% increases the reaction rate, and the three-step mechanism remains unchanged. With the

further decrease in the acetaldehyde concentration to 50%, the $T(t)$ function corresponds to a two-stage reaction that involves cool and hot flames. Thus, the form of the $T(t)$ function does not always one to conclude on the presence or absence of different stages during the acetaldehyde oxidation and also on the mechanism of relevant elementary reactions.

As the initial pressure of the gas mixture decreases from 64.1 to 25 kPa and the overall reaction decelerates, the function $T(t)$ transforms from three-stage into two-stage due to the disappearance of the hot-flame stage. At the pressure rise from 64.1 to 100 and 200 kPa, the function $T(t)$ still remains three-stage; however, further increase in the pressure to 400 and then to 1000 kPa results in the reaction acceleration and function $T(t)$ is no step-wise any longer.

The theory of oxidation and combustion of hydrocarbons uses the notion of induction period, which is the time during which the reaction rate increases to explosive without any visible indications. The description of a three-stage process³ involves the concepts of induction periods of cool (τ_1), blue (τ_2) and hot (τ_3) flames, where each period precedes a new increase in the temperature, and also a concept of the overall induction period $\tau_\Sigma = \tau_1 + \tau_2 + \tau_3$. The inflection points in the temperature curve $T(t)$ can be assumed conditionally to correspond to the end of period τ_1 and the beginning of period τ_2 and also the end of period τ_2 and the beginning of τ_3 . The values of τ_1 , τ_2 and τ_3 are largely qualitative estimates. To qualitatively assess the overall induction period τ_Σ , one may assume that it is equal to the time from the beginning of the process to the attainment of the maximum of function $T(t)$.

Basevich *et al.*²⁶ considered the dependence of calculated τ_Σ values on the initial temperature T_0 (Fig. 8). This Figure shows that in the range $T_0 = 500$ –1000 K, the $\tau_\Sigma(T)$ curve has two maxima (at $T_0 = 650$ and 900 K) and two minima (at $T_0 = 537$ and 775 K), *i.e.*, there are two NTC regions ($T_0 = 537$ –650 K and $T_0 = 775$ –900 K) in which the reaction rate decreases with an increase in the temperature.

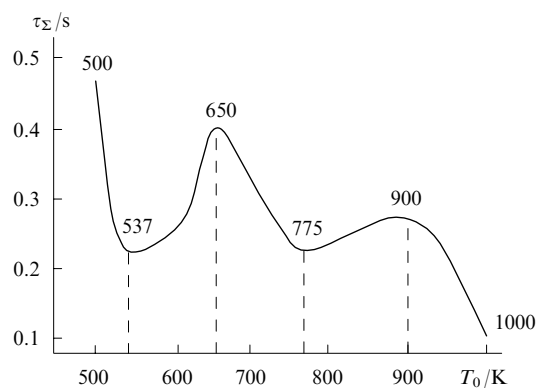


Figure 8. Dependences of the induction period on the initial temperature for autoignition of acetaldehyde mixtures with air at different temperatures.²⁶

Initial conditions: $P_0 = 64.1$ kPa, $[\text{CH}_3\text{CHO}]_0 = 75\%$.

Figure 9 shows functions $T(t)$ obtained for different initial temperatures corresponding to such extrema in the τ_Σ vs. T_0 curve (see Fig. 8). It is evident that functions $T(t)$ are three-stage for $T_0 = 500$, 537 and 650 K, *i.e.*, in the vicinity of the first minimum (curves 1–3), two-stage without any apparent cool-flame stage for $T_0 = 775$ K (in the vicinity of the second minimum) (curve 4) and monotonically increase without any visible stages for $T_0 = 900$ and 1000 K (curves 5 and 6).

Such a shape of curves is explained by the fact that in the vicinity of the first minimum, three branching reactions occur,

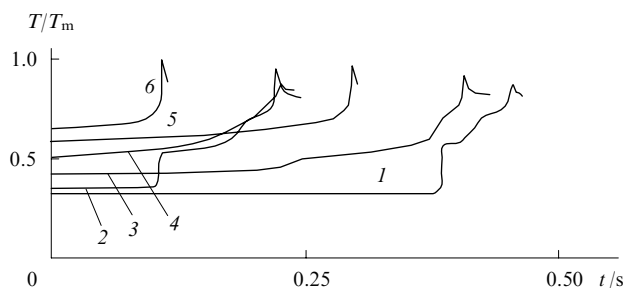
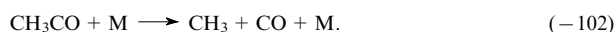


Figure 9. Time dependences of relative temperature for autoignition of acetaldehyde–oxygen mixtures at different initial temperatures.²⁶
 T_0/K : (1) 500, (2) 537, (3) 650, (4) 775, (5) 900, (6) 1000.
 Initial conditions: $P_0 = 64.1$ kPa and $[\text{CH}_3\text{CHO}]_0 = 75\%$.

i.e., three-stage autoignition is observed. Hydroperoxide $\text{CH}_3\text{CO}_3\text{H}$ is formed in the reactions

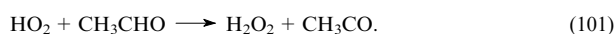


As the temperature increases (in the temperature range $T_0 = 537\text{--}650$ K), the equilibrium of reaction (135) shifts to the left and active decomposition of CH_3CO radicals by the following reaction begins:



As a result, the hydroperoxide concentration decreases, its decomposition by reaction (–137) does not play a significant role any longer, the rate of acetaldehyde oxidation decreases and the first NTC region appears.

A similar situation takes place in the temperature range $T_0 = 775\text{--}900$ K. At these initial temperatures, a large amount of hydrogen peroxide is formed



As the temperature increases, the equilibrium of reaction (10) shifts to the left. In this temperature range, reactions of consumption of hydrogen atoms start to prevail, the H_2O_2 concentration decreases, the branching of the acetaldehyde oxidation reaction due to the hydrogen peroxide decomposition [reaction (–17)] becomes insignificant and the process decelerates again, which is manifested by the appearance of the second NTC region.

With the further increase in the initial temperature, only one branching reaction remains, namely, the hydrogen atom reaction with oxygen (–2), which is typical of all high-temperature processes of hydrocarbon combustion. Now, function $T(t)$ increases monotonically.

Thus, the existence of two regions of the negative temperature coefficient of the reaction rate was theoretically proved for the first time.²⁶ Their existence was explained by the fact that the temperature range of the formation and decomposition of acetyl hydroperoxide (cool flames) is located much below the temperature range of hydrogen peroxide decomposition (blue flames) so that the cool and blue flames are well separated in time in the acetaldehyde autoignition.

b. Propagation of cool and blue flames

Data on the modelling of the propagation of cool flames through fresh unheated acetaldehyde mixtures with oxygen are available.²⁸ The calculations involved the use of a computer code³⁰ for solving the following system of equations that

describes the one-dimensional stationary propagation of the oxidation and combustion wave to be solved:³¹

$$\frac{\partial}{\partial x} \left[\rho D_j \frac{\partial (n_j/\rho)}{\partial x} \right] - \rho_0 u_n \frac{\partial (n_j/\rho)}{\partial x} + \sum_j w_{ij} = 0, \quad (3)$$

$$\frac{\partial}{\partial x} \left(\lambda \frac{\partial T}{\partial x} \right) - c_p \rho_0 u_n \frac{\partial T}{\partial x} + \sum_{ij} h_{ij} w_{ij} = 0, \quad (4)$$

where x is the coordinate along which the oxidation and combustion wave propagates; ρ , ρ_0 are the currently observed and initial densities, $\rho = \rho_0(T_0/T)(P/P_0)$; D_j is the diffusion coefficient of the j th species of the chemical reaction, $D_j = D_j^*(T/T^*)^{\gamma^2} (P/P^*)$ (the asterisk marks the parameters at normal conditions, $T^* = 293$ K and $P^* = 100$ kPa); u_n is the stationary velocity of wave propagation; λ is the molecular heat conductivity coefficient, $\lambda = \lambda^*(T/T^*)^{\gamma^1}$; c_p is the specific heat, $c_p = c^* + c^{**}T$, where c^* , c^{**} , γ^1 , γ^2 are constants.

The wave propagation velocity was determined based on the condition that the system of equations (3) and (4) has a solution at the following boundary conditions:

$$x \rightarrow -\infty: T \rightarrow T_0, \quad n_j \rightarrow [n_j]_0;$$

$$x \rightarrow +\infty: \frac{dT}{dx} \rightarrow 0, \quad \frac{d(n_j\rho)}{dx} \rightarrow 0.$$

All the necessary coefficients were taken from reference editions.

The problem was solved using the relaxation method where the terms with derivative with respect to time (t) were added artificially to equations (3) and (4). After setting certain initial functions $T(t=0, x)$ and $n_j(t=0, x)$, the calculations were carried on up to a t value at which the temperature and concentration profiles and the u_n value no longer depended on time. As a result, a stationary solution to the non-stationary problem was found. This stationary solution is in fact quasistationary, because the calculations were stopped when the criteria of sufficiently small changes in temperature and concentration with time were fulfilled.

For a conventional 'hot' laminar flame, the stationarity means approaching the thermodynamic equilibrium. For cool and blue flames, there is no thermodynamic equilibrium: there is also no equilibrium in the initial fuel–oxidant mixture, but there exists a quasi-equilibrium that can be retained infinitely long. Apparently, depending on the form of initial functions [mainly depending on the function $T(t=0, x)$ at the right boundary], under conditions close to experimental,⁸ it is possible to find solutions that well describe both cool flame or cool and blue flames, on the one hand [if function $T(t=0, x)$ corresponds to the temperature of cool flame or cool and blue flames], and hot flame, on the other hand [if function $T(t=0, x)$ corresponds to the final equilibrium temperature of combustion].

Calculations²⁸ were carried out for different fuel–oxygen mixtures, the initial temperature $T_0 = 293$ K and several pressures. Profiles of temperature and substance concentrations in the propagating cool flame were reported²⁸ for an equimolar $\text{CH}_3\text{CHO} + \text{O}_2$ mixture at a pressure of 40 kPa (300 mm Hg). For this pressure, the flame propagation velocity was found to be equal to 2.4 cm s^{-1} . In cool flame, the temperature increased from 293 to 772 K. There, nearly 23% of starting reactants were consumed to afford a certain amount of stable products such as H_2 , H_2O , CO , CH_4 , etc. The rapid temperature increase in cool flame corresponds to a considerable increase in the concentration of the OH radical, one of the main active species in this reaction. This jump in the OH concentration coincides with a sharp decrease in the concentration of acetyl hydroperoxide $\text{CH}_3\text{CO}_3\text{H}$. The subsequent

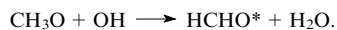
deceleration of the reaction with the decrease in the $[\text{OH}]$ was associated with the decomposition of secondary peroxides $\text{C}_2\text{H}_5\text{O}_2\text{H}$ and $\text{CH}_3\text{O}_2\text{H}$, which are more stable than $\text{CH}_3\text{CO}_3\text{H}$.

The appearance and joint propagation of cool and blue flames in a $\text{CH}_3\text{CHO} + \text{O}_2$ mixture was modelled.³² The first attempts to model blue flames failed due to the instability of the solution. However, this instability was overcome by refining the computation procedure.

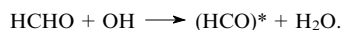
The calculations were carried out for $\text{CH}_3\text{CHO} + \text{O}_2$ mixtures with different composition, the initial temperature $T_0 = 293$ K and several pressures. In Fig. 6, the mixture compositions and pressures used in calculations are marked with asterisks. By selecting the initial functions for calculations, it was possible to simulate the flame types observed in experiments.

Let us consider a solution that corresponds to the joint propagation of cool and blue flames during the combustion of the 85% $\text{CH}_3\text{CHO} + 15\%$ O_2 mixture at a pressure of 67 kPa (point 4 in Fig. 6). Figure 10 shows the profiles of the temperature wave (T/T_m , *a*) and the concentration waves ($[n_i]/[n_i]_m$) of initial compounds (*b*), most important intermediate products and radicals (*c*) and final products (*d*), which contain separate zones of cool and blue flames. Under these initial conditions, the velocity of wave propagation was found to be 2.42 cm s^{-1} . Two temperature waves could be distinguished (see Fig. 10*a*). In cool flame, the temperature increased from 293 to 800 K, whereas in blue flame, it increased from 800 to 1267 K. The first temperature wave coincided with the decomposition of acetyl hydroperoxide $\text{CH}_3\text{CO}_3\text{H}$ to form OH radical and demonstrated a local maximum in the decay range. This maximum corresponds to the decomposition of secondary peroxides $\text{C}_2\text{H}_5\text{O}_2\text{H}$ and $\text{CH}_3\text{O}_2\text{H}$, which are somewhat more stable. The second temperature wave is associated with the decomposition of hydrogen peroxide H_2O_2 and HO_2 radicals to form OH radicals [due to the relatively large step of calculations over space, the resulting hydroxyl concentration curve is lumped rather than smooth (curve 4 in Fig. 7*c*)]. The following stable compounds were observed among the combustion products (in the order of decreasing concentration): H_2 , CH_4 , CO , H_2O , C_2H_4 , C_2H_6 , CO_2 , CH_3OH , *etc.* and the following radicals: CH_3 , HO_2 , CH_3O , C_2H_5 , CHO , OH , *etc.* Beyond the combustion zone, $\sim 10\%$ of acetaldehyde and more than 1% of oxygen remain non-consumed.

As was mentioned above, cool flame corresponds to the glow of excited HCHO^* . Apparently, this species is formed by the reaction



As is seen from Fig. 10*c*, the concentration profiles of methoxyl radical CH_3O and hydroxyl OH partly overlap, which corresponds to a certain probability that this reaction occurs in the cool flame zone. According to the same data, the blue flame glow owes its existence to the $(\text{HCO})^*$ radical. Presumably, this radical is formed by the reaction



Concentration profiles of HCHO and OH also overlap in the blue flame reaction zone, which shows that such a reaction can occur in this flame zone with a certain degree of probability.

The acetaldehyde oxidation mechanism assumed in a study²⁸ mentioned above includes none of these reactions, because the appearance of these species and their glow do not affect the main chemical process of heat release. In principle, the HCHO^* glow may be masked by the more intense $(\text{HCO})^*$ glow. The foregoing is nothing but the possible external manifestations of multistage mechanism of the acetaldehyde

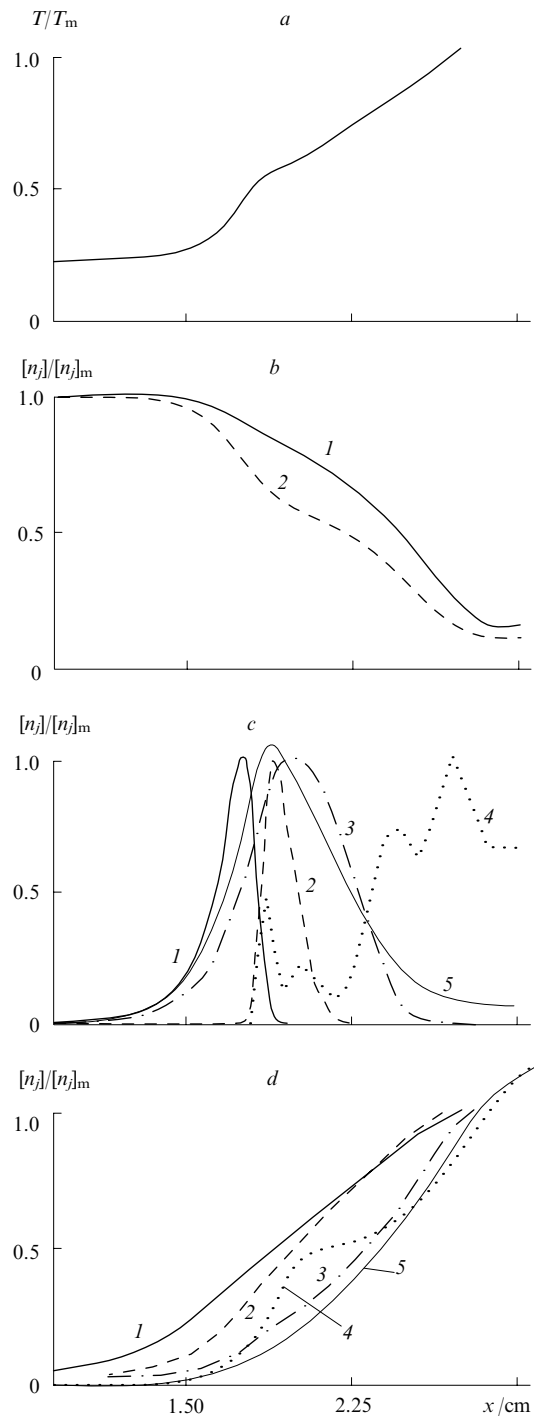


Figure 10. Profiles of relative temperature (T/T_m , *a*) and concentrations $[n_i]/[n_i]_m$ of initial compounds (*b*), most significant intermediate compounds and radicals (*c*) and final products (*d*) in the cool-flame reaction zone.³²

Initial conditions: $[\text{CH}_3\text{CHO}]_0 = 85\%$, $[\text{O}_2]_0 = 15\%$, $T_0 = 293$ K, $P_0 = 67$ kPa (~ 500 Torr).

(*a*) T/T_m , $T_m = 1267$ K;

(*b*) (1) $[\text{CH}_3\text{CHO}]/[\text{CH}_3\text{CHO}]_m$, $[\text{CH}_3\text{CHO}]_m = 0.85$; (2) $[\text{O}_2]/[\text{O}_2]_m$, $[\text{O}_2]_m = 0.15$;

(*c*) (1) $[\text{CH}_3\text{CO}_3\text{H}]/[\text{CH}_3\text{CO}_3\text{H}]_m$, $[\text{CH}_3\text{CO}_3\text{H}]_m = 1.7 \times 10^{-3}$; (2) $[\text{CH}_3\text{O}]/[\text{CH}_3\text{O}]_m$, $[\text{CH}_3\text{O}]_m = 4.5 \times 10^{-5}$; (3) $[\text{H}_2\text{O}_2]/[\text{H}_2\text{O}_2]_m$, $[\text{H}_2\text{O}_2]_m = 8.1 \times 10^{-3}$; (4) $[\text{OH}]/[\text{OH}]_m$, $[\text{OH}]_m = 1.4 \times 10^{-7}$; (5) $[\text{HCHO}]/[\text{HCHO}]_m$, $[\text{HCHO}]_m = 6.0 \times 10^{-3}$;

(*d*) (1) $[\text{H}_2]/[\text{H}_2]_m$, $[\text{H}_2]_m = 0.15$; (2) $[\text{H}_2\text{O}]/[\text{H}_2\text{O}]_m$, $[\text{H}_2\text{O}]_m = 0.0729$; (3) $[\text{CO}]/[\text{CO}]_m$, $[\text{CO}]_m = 0.401$; (4) $[\text{CO}_2]/[\text{CO}_2]_m$, $[\text{CO}_2]_m = 0.024$; (5) $[\text{CH}_4]/[\text{CH}_4]_m$, $[\text{CH}_4]_m = 0.135$.

oxidation and joint propagation of cool and blue flames. The presence of branching reactions in the decomposition of $\text{CH}_3\text{CO}_3\text{H}$ and H_2O_2 also points to the multistage nature of the acetaldehyde oxidation.

It can be stated that when cool and blue flames propagate in fresh unheated $\text{CH}_3\text{CHO} + \text{O}_2$ mixtures, the cool-flame and blue-flame reactions follow the same route as in the appearance of conventional bulk homogeneous cool and blue flames, with a difference that these reactions are initiated by the heat transfer and diffusion and such a double flame propagates over initially unheated mixtures.

The solutions corresponding to the propagating hot flame were not analysed in the mentioned study.²⁸

2. n-Heptane

Well-pronounced blue flame was observed in the combustion of n-heptane. Sokolik and Yantovskii³ experimentally (by recording the pressure) proved the multistage mechanism of the combustion of an n-heptane–air mixture in a closed vessel. The experiment was carried out at the relatively low initial temperature $T_0 = 573$ K and pressure $P_0 = 150$ kPa. The authors observed three pressure waves, namely, the first cool-flame wave, the second blue-flame wave and the third wave corresponding to the hot explosion (Fig. 11). In Fig. 11, the waves of cool and blue flames are united in a single delay τ_2 . This is associated with the fact that the authors have not yet brought forth a concept of multistage autoignition and

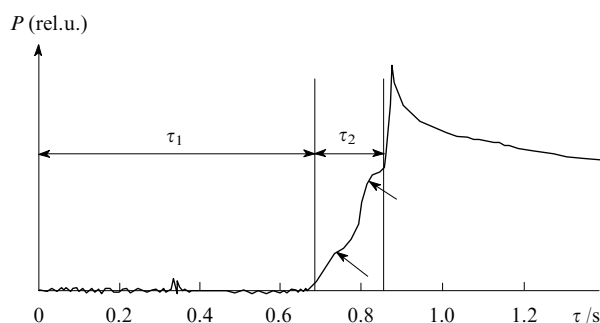


Figure 11. Pressure changes at autoignition of an n-heptane–air mixture with stoichiometric ratio $\phi = 1.25$. Initial conditions: $T_0 = 573$ K, $P_0 = 150$ kPa.³

explained the observed pressure jumps based on another idea.

A semi-empirical mechanism of n-heptane oxidation and combustion at the higher initial temperature (700–1300 K) and pressure (1200–10 000 kPa) was proposed and checked in a series of calculations that modelled the autoignition and combustion of n-heptane in propagating flame.³³ Figure 12 shows the autoignition delay times, both experimental and calculated based on the kinetic mechanism of n-heptane autoignition (for the experimental data on the overall autoignition delays $\tau_\Sigma = \tau_1 + \tau_2 + \tau_3$, see Ref. 33). It is evident that the results of calculations adequately agree with experimental data. Modelling of n-heptane oxidation and combustion has shown³⁴ that the proposed³³ kinetic mechanism of this process describes rather adequately the multistage autoignition of n-heptane with the appearance of cool and blue flames. The conditions taken in calculations corresponded to experimental conditions (stoichiometric amounts of n-heptane and air, $P_0 = 1500$ kPa) and the temperature range embraced an interval from 680 to 1000 K (the temperature corresponding to the beginning of high-temperature oxidation). Figure 13 shows the results of calculations. The calculations demonstrated the time dependences (in the range of the overall

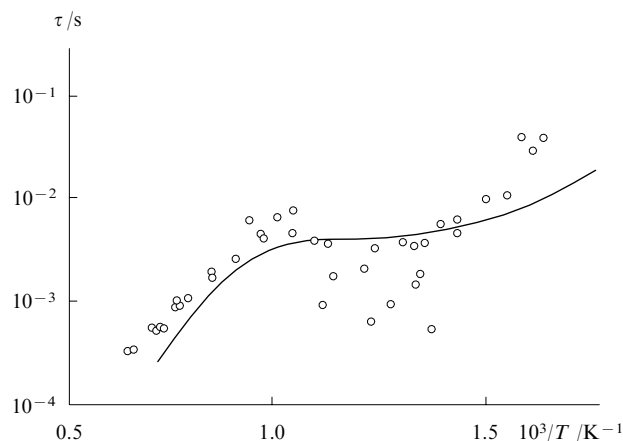
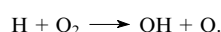


Figure 12. Comparison of calculated (line) and measured (points) delays in the ignition of a stoichiometric n-heptane–air mixture at $P_0 = 1500$ kPa.³³

autoignition delay) of the relative temperature (T/T_m) and concentrations ($[n_i]/[n_j]_m$) of key intermediates such as $\text{C}_7\text{H}_{15}\text{O}_2\text{H}$, H_2O_2 , OH and H, which were formed in the autoignition of a stoichiometric n-heptane–air mixture at different initial temperatures. These results show that at $T_0 = 680$ K, the multistage autoignition occurs (curves 4 in Fig. 13 a–d). In the temperature profile (Fig. 13 a), two waves are present. The first wide wave (amplitude of 150°) corresponds to the temperature rise due to the cool flame, the second shorter wave appears at the end of the induction period. Its amplitude is approximately 250° and the temperature reaches as high as ~ 1350 K. This wave corresponds to blue flame. Subsequently, the reaction transforms into hot explosion. The first temperature wave is caused by the reaction acceleration due to the stepwise increase in the concentration of OH radicals formed in the thermal decomposition of hydroperoxide $\text{C}_7\text{H}_{15}\text{O}_2\text{H}$, whereas the second wave is caused by the reaction acceleration with the next sharp increase in the OH concentration due to the thermal decomposition of more stable H_2O_2 molecules. The first slight increase in the concentration of H atoms (curve 4 in Fig. 13 e) is observed at the end of cool flame region, the second is observed in the blue flame region. After the complete decomposition of hydrogen peroxide (the end of the blue flame region), the concentrations of hydroxyl and hydrogen atoms first decrease and then sharply increase due to the branched chain reaction



Due to the vigorous progress of the reaction, the temperature begins to sharply increase and reaches its maximum, i.e., the combustion temperature (is not shown in the Figure).

Figure 13 also shows the time dependences of the relative temperatures and concentrations at higher initial temperatures T_0 : 800 (curve 3), 900 (2) and 1000 K (1). These dependences provide an insight into the dynamics of variations in the temperature and concentrations of the main substances involved in the autoignition on the transition from multistage to single-stage oxidation. As the initial temperature increases to $T_0 = 900$ and 1000 K, the relative concentration of $\text{C}_7\text{H}_{15}\text{O}_2\text{H}$ (Fig. 13 c) decreases by several orders of magnitude and cannot be seen in the plot (shown by arrows), the H_2O_2 concentration decreases less sharply and the concentration of hydrogen atoms is very low during the delay at high initial

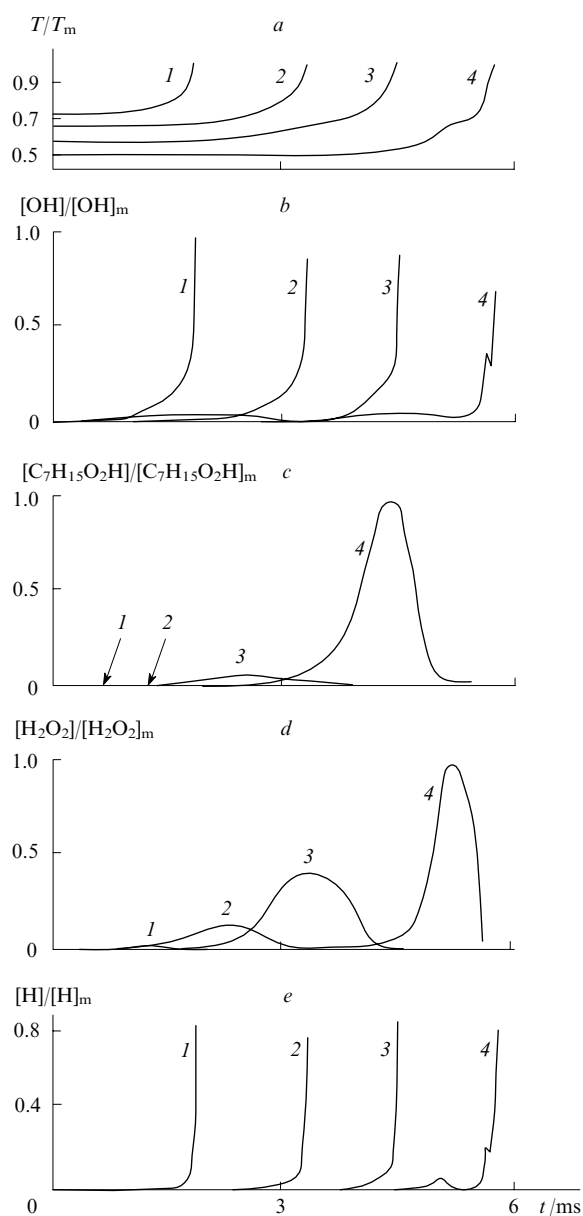


Figure 13. Dependences of relative temperatures (a) and concentrations (b–e) on time for autoignition of a stoichiometric n-heptane–air mixture at $P_0 = 1500$ kPa, $[C_7H_{16}]_0 = 1.87\%$ and different temperatures.³⁴ T_0/K : (1) 1000, (2) 900, (3) 800, (4) 680. (a) T/T_m , $T_m = 1363$ K; (b) $[OH]/[OH]_m$, $[OH]_m = 3.025 \times 10^{-4}$; (c) $[C_7H_{15}O_2H]/[C_7H_{15}O_2H]_m$, $[C_7H_{15}O_2H]_m = 8.176 \times 10^{-5}$; (d) $[H_2O_2]/[H_2O_2]_m$, $[H_2O_2]_m = 8.176 \times 10^{-5}$; (e) $[H]/[H]_m$, $[H]_m = 1.283 \times 10^{-7}$.

temperatures but quickly increases at the hot explosion to a quite considerable value for all temperatures.

Due to the fact that the temperature regions of the formation and decomposition of n-heptyl hydroperoxide are considerably lower than the regions of the formation and decomposition of hydrogen peroxide, the cool and blue flames observed at the n-heptane autoignition are well separated as in the case of acetaldehyde.

3. Propane

No blue flame was observed in the propane combustion. However, in view of similar mechanisms of oxidation and combustion of paraffin hydrocarbons, it can be assumed that propane combustion, like n-heptane combustion, may feature

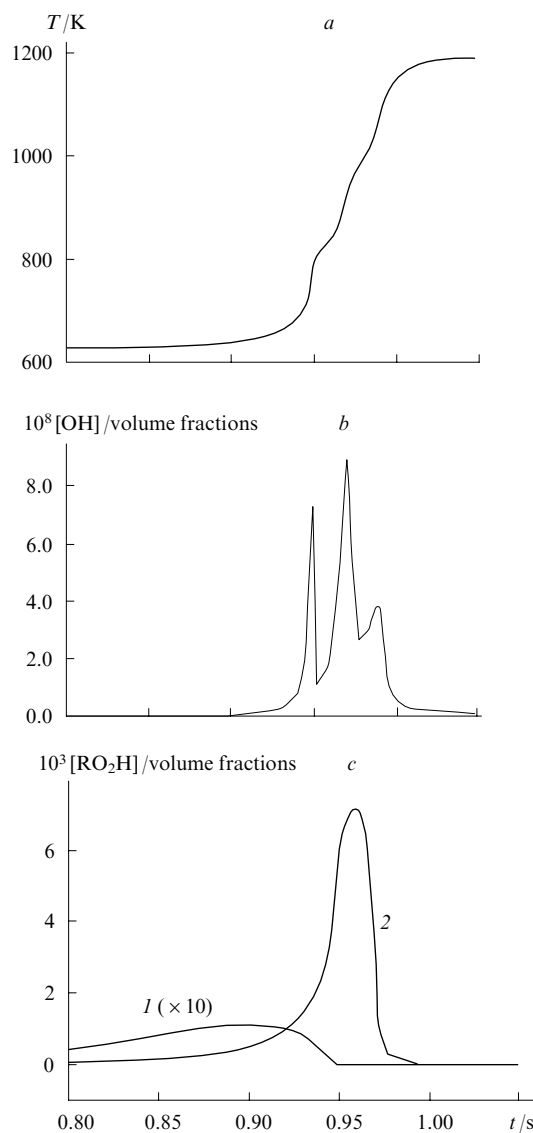


Figure 14. Calculation of autoignition of a propane–air mixture 15.5% C_3H_8 –10.5% O_2 –74% N_2 for initial conditions $T_0 = 625$ K, $P_0 = 550$ kPa.

Variations of temperature (a) and concentrations of hydroxyl (b) and hydroperoxides $C_3H_7O_2H$ (1) and H_2O_2 (2) (c).

the appearance of blue flame under appropriate conditions. As follows from the abundant experimental data on the propane oxidation and combustion that can be found in the literature (e.g., see a monograph² and references therein), its oxidation features cool flame, regions of the negative temperature coefficient (NTC) and other phenomena typical of the oxidation of higher hydrocarbons. This is why an attempt was undertaken to theoretically determine the conditions for the appearance of blue flame during low-temperature propane oxidation by modelling. The kinetic mechanism of propane oxidation and combustion was taken from Ref. 16.

Typical calculated temperature vs. time records for the autoignition of a propane–air mixture corresponds to two-stage autoignition, namely, demonstrates delays in the appearance of cool (τ_1) and hot (τ_2) flames (Fig. 14). For example, for $T_0 = 650$ K, the overall delay in the autoignition of a propane (6.5%)–air mixture was ~ 2.48 s (varied from 2.1 to 3.5 s in different experiments). Such a form of hydrocarbon autoignition is typical of low temperatures. Cool flame appears at

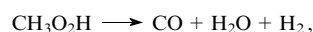
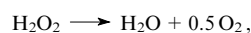
the decomposition of propyl hydroperoxide $C_3H_7O_2H$ as a result of chain branching, which leads to a sharp increase in the hydroperoxide concentration and accelerates C_3H_8 oxidation. As all accumulated hydroperoxide is consumed, the reaction decelerates and, in the next period (during the τ_2 delay) hydrogen peroxide H_2O_2 is accumulated. Its decomposition, *i.e.*, the second branching of the reaction, leads to an increase in the reaction rate and, ultimately, to hot explosion (reaction of H with O_2). Immediately before the hot explosion, a local break is observed in the smooth increase of the OH concentration, which, however, does not cause any apparent changes in the temperature growth rate. When richer propane–air mixtures are used, the irregular changes in the OH concentration manifest themselves by the appearance of the second maximum in the $[OH]$ vs. T curve. As a result, the curve demonstrates a break that corresponds to blue flame. Figures 14 *a–c* show the results of calculations of autoignition of a propane–air mixture with the 15.5% C_3H_8 –10.5% O_2 –74% N_2 ratio at $T_0 = 625$ K and $P_0 = 550$ kPa. Three inflections in the $T(t)$ curve and three maxima in the $[OH]$ vs. T curve correspond to the multistage autoignition with the appearance of cool, blue and hot flames.

4. Ethane

Until recently, no blue flame was observed in the ethane oxidation and combustion and even cool flames were discovered not long ago. The analysis of the staged mechanism of the ethane autoignition²⁹ was based on the assumption that its oxidation involves the same reactions as the oxidation of higher hydrocarbons, *i.e.*, the process includes three stages, namely, cool flame, blue flame and hot autoignition. Cool-flame phenomena may be associated with both the ethane oxidation and the oxidation of stable products and radicals that are formed in the later stages and are typical of methane oxidation.

Let us dwell on calculations²⁹ performed using a kinetic mechanism of oxidation of hydrocarbons C_1 – C_2 , which was proposed in Ref. 27 and extended by the introduction of additional reactions necessary for modelling of the cool-flame phenomena at the ethane oxidation (see Table 1). First of all, it was selectively checked whether this model adequately describes certain phenomenological characteristics of the ethane oxidation and combustion in the low and high-temperature ranges. This was necessary because the multistage ethane oxidation was never modelled earlier.

Calculations of the ethane oxidation at low temperatures and moderate pressures (*i.e.*, when the reaction time is long and the diffusion rate is sufficiently high) took into account the following effective wall reactions of the decay of active species:



In calculations, the rate constants k_w used for these reactions were the same and were close to their maximum value in the diffusion approximation. The heat-transfer coefficient was taken equal to $0.126 \text{ J litre}^{-1} \text{ s}^{-1} \text{ K}^{-1}$ in all cases.

The calculations of the low-temperature process were accomplished for different conditions (different mixture compositions, initial temperatures and pressures) described in the experimental study.³⁵ The experiments carried out under these conditions revealed the multiple appearance of one, two or three cool flames, where the number of cool flames increased with the diameter of the reaction vessel. On the qualitative level, the calculations²⁹ adequately described the experimentally observed cool-flame phenomena³⁵ as regards both the

time (minutes) and heating (tens of degrees). Thus at $k_w = 1 \text{ s}^{-1}$, no cool flame was observed at all (this rate constant value corresponds to the highest possible diffusion rate constant under these conditions). For a rate constant $k_w = 0.35 \text{ s}^{-1}$, a single cool flame was observed (manifested by an NTC). Two and three cool flames were observed for $k_w = 0.25 \text{ s}^{-1}$ and $k_w = 0.12 \text{ s}^{-1}$, respectively. For $k_w = 0$ (in the absence of peroxide decay on the wall), the calculations pointed to the autoignition process. The authors of experimental studies³⁵ did not observe the autoignition because they did not deal with pressures above 118 kPa.

Insofar as the calculations described rather adequately the experimental data on cool flames, the next step was the analysis and modelling of the multistage mechanism of ethane combustion under autoignition conditions. Based on the fact that $k_w = 0.353 \text{ s}^{-1}$ at a pressure of 100 kPa and a temperature of 600 K, the authors calculated k_w for other pressures and temperatures. According to calculations, the autoignition begins as soon as a pressure of 150 kPa and a temperature of 560 K ($k_w = 0.23 \text{ s}^{-1}$) are reached (at lower temperatures, no autoignition was observed).

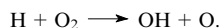
In view of the multistage autoignition mechanism, the authors of calculations considered the combustion of an ethane–oxygen equimolar mixture at $T_0 = 560$ K and $P_0 = 150$ kPa. Under these conditions, a two-stage process is observed, namely, a cool-flame flash occurs with a delay $\tau_1 = 390$ s and is accompanied by a partial energy release and a temperature rise by 104° ; after a time $\tau_2 = 9$ s, hot autoignition occurs so that the overall delay turns out to be $\tau_\Sigma = \tau_1 + \tau_2 = 399$ s. As the temperature is increased from 560 to 600 K, the cool flame delay τ_1 becomes shorter and the flame intensity expressed as a temperature rise (ΔT) becomes lower. Delay τ_2 and overall delay τ_Σ increase.

Note the specific features of the autoignition kinetics in the cool-flame region. According to the analysis, during the induction period that precedes the appearance of cool flame, the accumulation of ethyl hydroperoxide $C_2H_5O_2H$ occurs and the decomposition of the latter leads to the low-temperature branching of the combustion reaction. The branching causes a temperature jump, namely, the cool-flame flash. Methyl hydroperoxide and hydrogen peroxide are also involved in the later stages of ethane combustion. In cool flame, as the temperature increases, the equilibrium in the formation of peroxide radicals $C_2H_5O_2$ shifts to the left (*i.e.*, the formation of $C_2H_5O_2$ radicals is hindered), the reaction is slowed down and the temperature stops to increase. The concentrations of CH_3O and OH radicals in the reaction mixture sharply increase 390 s after the beginning of the reaction. The increase in $[OH]$ reflects the increase in the reaction rate in cool flame. Then, the OH concentration begins to decrease, which entails a decrease in the overall reaction rate after the cool flame.

Based on the shape of kinetic curves obtained with a low resolution, one can infer on a typical two-stage mechanism of autoignition (cool flame and hot autoignition). However, at a higher time resolution, the multistage autoignition can be deduced, *i.e.*, the presence of an additional stage before the hot flame. Thus immediately before the hot autoignition, one can observe an increase in the H_2O_2 concentration and also an increase in the concentrations of C_2H_5O , CH_3O , HO_2 and HCO radicals. This violates the monotonic nature of the first derivative of $T(t)$. At the same time, a new considerable increase in the OH concentration is observed, which points to the acceleration of the ethane oxidation. Modelling makes it possible to find the factor responsible for this acceleration. Thus, if in the middle of the considered time interval, the rate constants of each branching reaction, namely, the rate constants for the decomposition of $C_2H_5O_2H$, CH_3O_2H and H_2O_2 are in turn put to zero, this will not affect the increase in the OH concentration for the case of alkyl peroxides, whereas for

H_2O_2 , this will lead to a decrease in the OH concentration and, hence, to the increase in the reaction rate and the temperature. Hence, one can unambiguously conclude that the reaction branching due to the H_2O_2 decomposition is the main reason for the reaction acceleration. This very increase in the ethane oxidation rate prior to hot flame is defined as the blue flame and allows one to assume the multistage mechanism of the ethane autoignition.

In hot flame (the third stage of autoignition), the chief role in the reaction branching is played by the process



Within the framework of a concept of multistage autoignition of paraffin hydrocarbons, a kinetic scheme of ethane combustion was proposed,²⁹ which contains the following stages: (1) cool-flame stage (reaction branching occurs due to the decomposition of hydroperoxides $\text{C}_2\text{H}_5\text{O}_2\text{H}$, $\text{CH}_3\text{O}_2\text{H}$ and also of a part of H_2O_2), (2) blue-flame stage, which precedes hot autoignition (reaction branching due to the decomposition of hydrogen peroxide) and (3) hot-flame stage (reaction branching due to the reaction of H radicals with oxygen).

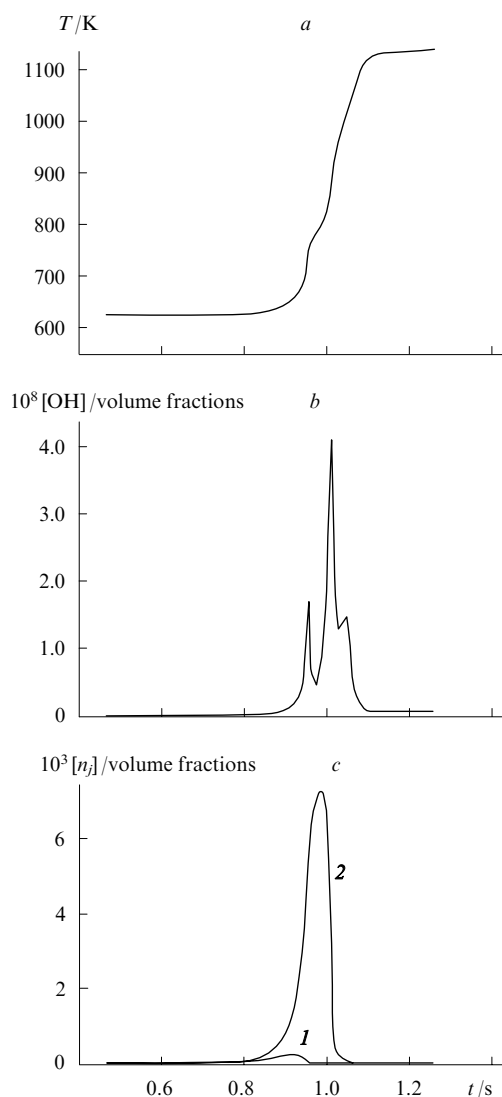


Figure 15. Calculated time dependences of temperature (a) and concentrations [OH] (b), $[\text{C}_2\text{H}_5\text{O}_2\text{H}]$ (c, curve 1) and of H_2O_2 (c, curve 2) for autoignition of an ethane–air mixture 16.5% C_2H_6 –9.5% O_2 –74% N_2 for initial conditions $T_0 = 625$ K and $P_0 = 550$ kPa.

In mixtures richer in ethane, the break of the smooth increase in the concentration [OH] manifests itself by the appearance of the second maximum in the [OH] vs. t curves and a bend in the T vs. t curve, which correspond to blue flame (later calculations¹⁶). As the example, Fig. 15 *a–c* shows the results of calculations of the autoignition of an ethane–air mixture with the composition 16.5% C_2H_6 –9.5% O_2 –74% N_2 for $T_0 = 625$ K at $P_0 = 550$ kPa. Here, as for the propane oxidation, three bends are present in the temperature curve and three maxima appear in the [OH] vs. t curve, which correspond to the multistage autoignition with generation of cool, blue and hot flames.

In the case of ethane, ethyl hydroperoxide plays the chief role in the appearance of cool flames. The closeness of the temperature interval of its decomposition to the temperature interval of hydrogen peroxide decomposition complicates the separation of the cool-flame and blue-flame stages.

5. Methane

The first mention³⁶ of the multistage mechanism of low-temperature oxidation of methane dates back to 1956. In this study, two stages in this process, namely, cool-flame oxidation and autoignition, were observed experimentally.

The first attempt to model the methane autoignition within the framework of a relatively simple kinetic scheme was undertaken in 1982 (Ref. 37) and, although the kinetic scheme used in calculations was developed for modelling of the combustion processes and was supplemented by merely few reactions typical of the low-temperature range of methane oxidation, the results obtained demonstrated the possibility of describing the staged nature of the methane oxidation.

The later calculations employed a kinetic scheme specially developed for the description of low-temperature oxidation of rich methane mixtures.³⁸ Figure 16 shows the results of such calculations.³⁹ As is seen, at the initial temperatures $T_0 < 710$ K, the staged nature of the reaction was not manifested (curve 1). For $T_0 > 758$ K (curves 5–7), ignition occurred (arrows at the ends of curves point to the further increase in the temperature). In the temperature range $T_0 = 728$ –753 K, flashes with incomplete heat release were observed which were followed by reaction inhibition accompanied by a temperature decrease due to the cooling of the reaction mixture by the reactor walls. As a whole, the calculated data corresponded to experimental results described,³⁶ which made it possible to use this kinetic scheme in predicting the behaviour of this reaction under high-pressure conditions

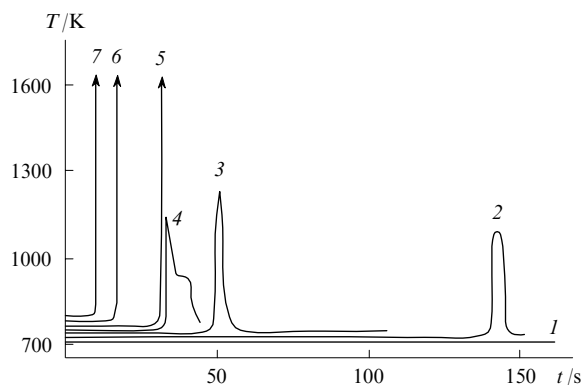


Figure 16. Time dependences of temperature during the oxidation of methane–oxygen mixtures for different initial temperatures.³⁹ Initial conditions: $[\text{CH}_4]_0 = 67\%$, $[\text{O}_2]_0 = 33\%$, $P_0 = 92$ kPa, $\kappa S/V = 6.61 \text{ J cm}^{-3} \text{ s}^{-1} \text{ K}^{-1}$; T_0/K : (1) 710, (2) 728, (3) 748, (4) 753, (5) 758, (6) 768 and (7) 788.

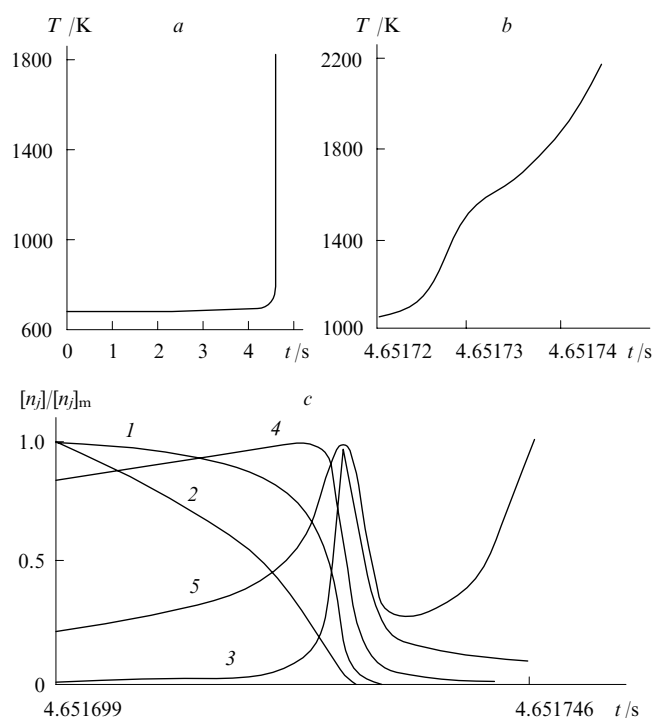


Figure 17. Dependences of (a, b) temperature and (c) concentrations on the reaction time on time scales of (a) seconds and (b, c) microseconds during the oxidation of a methane–oxygen mixture.³⁹

Initial conditions: $[\text{CH}_4]_0 = 67\%$, $[\text{O}_2]_0 = 33\%$, $T_0 = 710 \text{ K}$, $P_0 = 7000 \text{ kPa}$.

(c) (1) $[\text{H}_2\text{O}_2]/[\text{H}_2\text{O}_2]_m$, $[\text{H}_2\text{O}_2]_m = 2.279 \times 10^{-6}$; (2) $[\text{CH}_3\text{O}_2\text{H}]/[\text{CH}_3\text{O}_2\text{H}]_m$, $[\text{CH}_3\text{O}_2\text{H}]_m = 1.412 \times 10^{-8}$; (3) $[\text{HO}_2]/[\text{HO}_2]_m$, $[\text{HO}_2]_m = 1.619 \times 10^{-6}$; (4) $[\text{CH}_3\text{O}_2]/[\text{CH}_3\text{O}_2]_m$, $[\text{CH}_3\text{O}_2]_m = 2.156 \times 10^{-7}$; (5) $[\text{H}]/[\text{H}]_m$, $[\text{H}]_m = 1.420 \times 10^{-8}$.

for which no experimental data could be obtained in static setups.

Calculations were carried out for the mixture 67% CH_4 –33% O_2 at the initial temperature of 710 K and different initial pressures (from 180 to 10 000 kPa). It was found that as the pressure increases, the transition from oxidation to autoignition occurs and the latter is reached in shorter times. Even active heat transfer from the gas to the reactor walls (within reasonable heat transfer coefficients) fails to stop the ignition and reverse the temperature increase, although the heat transfer increases the time the oxidation reaction develops to the autoignition. Figure 17a shows the

typical temperature dependence for the methane oxidation on a time scale of seconds.³⁹ With this resolution, the curve shows no indications of the multistage mechanism. Based on the shape of this curve, the methane oxidation can be assigned to conventional single-stage autoignition processes. However, curve $T(t)$ recorded at a rapid temperature-vs.-time scanning (on a microsecond time scale, Fig. 17b) has a bend, which suggests that the temperature rise to $T = 1400 \text{ K}$ is followed by the reaction retardation with the subsequent hot flash in approximately 15 μs , i.e., the multistage nature of the reaction is evident. In this case, the duration of the first combustion stage was $\sim 4.6 \text{ s}$, and the duration of the second stage was 15 μs (it is very difficult to experimentally observe two stages within such times). The staged nature is evident most clearly in the concentration profiles of hydroperoxides $\text{CH}_3\text{O}_2\text{H}$ and H_2O_2 , and also of radicals HO_2 , CH_3O_2 and H shown on a microsecond scale (see Fig. 17c).

A similar situation was also observed at 750 K and higher, at which the autoignition process that looks as a single-stage process occurs. Calculations of the oxidation of methane–air mixtures were also carried out for the lower oxygen contents, a pressure $P_0 = 10\,000 \text{ kPa}$ and temperatures $T_0 = 683$ –750 K. It was shown that with a decrease in the oxygen content, the indications of the staged mechanism become less pronounced and totally disappear at $[\text{O}_2]_0 = 5\%$.

In the calculations of oxidation processes under high-pressure conditions, the limiting values of reaction rate constants for the infinitely high pressure were taken (the corresponding data can be found in Table 2).

The detection of blue flames in experiments carried out in ICE near the autoignition limits of lean methane–air mixtures served as evidence for the multistage mechanism of hydrocarbon autoignition.⁴⁰

An attempt⁴¹ was made to model blue flames experimentally observed in ICE⁴⁰ by using a kinetic scheme of the process and a computer code that takes into account the piston motion. The analysis of methane oxidation in ICE made it possible to explain the illusory contradiction between the experimental data obtained in ICE⁴⁰ and in a static setup.⁴² Methane oxidation was frozen on the piston back stroke, which makes it possible to establish the initial conditions corresponding to the cessation of the relatively slow initial reaction. In a static bomb, such conditions favourable for the reaction suppression are absent.

For calculations, the same conditions as in the ICE experiments⁴³ were taken (the compression ratio $\varepsilon = 14.7$ for a speed $n = 1000 \text{ rpm}$) (the calculations were carried out according to a kinetic scheme that can be found in Ref. 26 and Table 1). According to calculations, as the compression temperature changes, in the range of low methane concentration, there is a

Table 2. Kinetic parameters of high-pressure oxidation of C_1 – C_2 hydrocarbons.

Reaction number ^a	Reactions	$H/\text{kJ mol}^{-1}$	Forward reaction			Reverse reaction		
			A^b	n	$E/\text{kJ mol}^{-1}$	A^b	n	$E/\text{kJ mol}^{-1}$
7	$\text{OH} + \text{H} \rightleftharpoons \text{H}_2\text{O}$	494.04	6.8×10^{10}	0.1	0.00	1.6×10^{15}	−0.9	502.42
10	$\text{H} + \text{O}_2 \rightleftharpoons \text{HO}_2$	196.78	1.2×10^9	0.6	0.00	1.6×10^{12}	−0.4	204.32
17	$\text{OH} + \text{OH} \rightleftharpoons \text{H}_2\text{O}_2$	209.34	3.4×10^7	1.0	0.00	1.0×10^{16}	0.0	209.34
24	$\text{CO} + \text{O} \rightleftharpoons \text{CO}_2$	531.72	1.0×10^4	1.0	10.47	9.0×10^{12}	0.0	544.28
34	$\text{HCO} + \text{H} \rightleftharpoons \text{HCHO}$	305.64	7.1×10^5	1.6	62.80	5.9×10^{13}	0.6	376.81
42	$\text{H} + \text{CH}_3 \rightleftharpoons \text{CH}_4$	422.87	8.4×10^7	0.0	0.00	1.8×10^{16}	0.0	439.61
71	$\text{H} + \text{HCHO} \rightleftharpoons \text{CH}_3\text{O}$	92.11	2.8×10^7	1.0	10.05	3.0×10^{14}	0.0	108.86
76	$\text{C}_2\text{H} + \text{H} \rightleftharpoons \text{C}_2\text{H}_2$	523.35	1.4×10^5	1.0	−54.43	8.5×10^{12}	0.0	447.99
81	$\text{H} + \text{C}_2\text{H}_2 \rightleftharpoons \text{C}_2\text{H}_3$	167.47	5.5×10^9	0.0	10.05	2.6×10^{16}	−1.0	194.27

^a The reaction number corresponds to that in Table 1. ^b The pre-exponential factor A is expressed in s^{-1} for unimolecular reactions, in $\text{litre mol}^{-1} \text{s}^{-1}$ for bimolecular reactions and in $\text{litre}^2 \text{mol}^{-2} \text{s}^{-1}$ for trimolecular reactions.

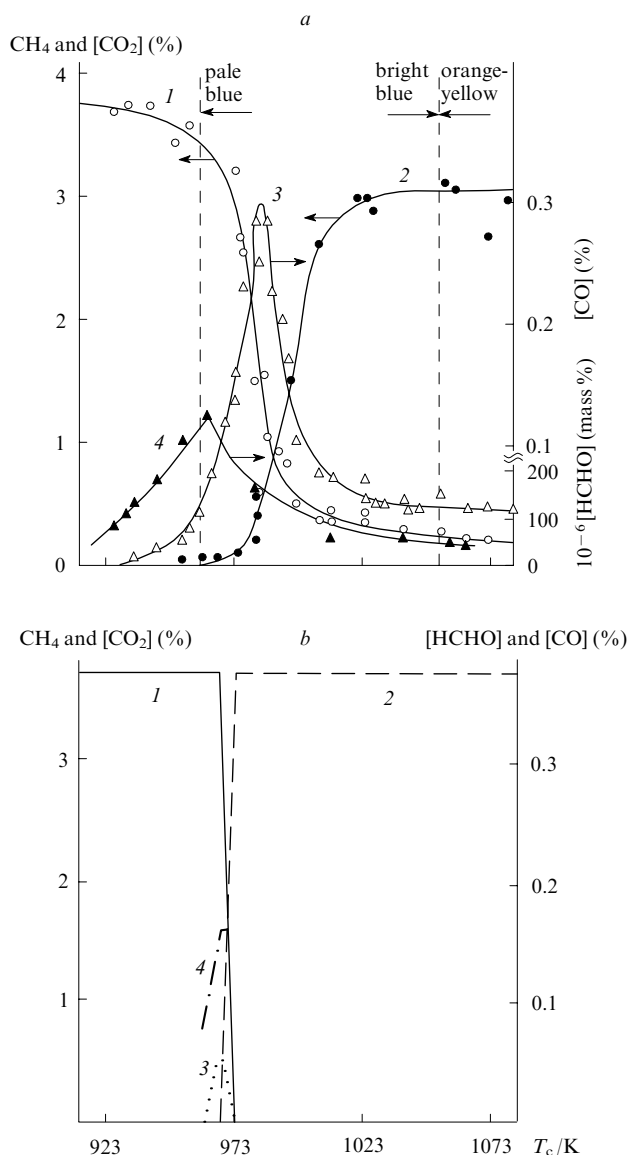


Figure 18. Experimental (a)⁴³ and calculated (b)⁴¹ dependences of relative concentrations of CH₄ (curve 1), CO₂ (2), CO (3) and HCHO (4) on the final compression temperature T_c during the oxidation of a methane–air mixture.

Initial conditions: $[\text{CH}_4]_0 = 3.7\%$, $\varepsilon = 14.7$, $n = 1000$ rpm.

transition from the reaction absence to the complete combustion through the region of incomplete heat release typical of cool and blue flames. In Fig. 18, the dashed lines mark the transition region of the methane incomplete oxidation and combustion, which was experimentally obtained for $[\text{CH}_4]_0 = 3.7\%$. This region extends from 963 to 1053 K, *i.e.*, approximately for 90°. This region revealed experimentally in Ref. 43 was assigned to blue flames. In the calculations (see Fig. 18b) with the same methane concentrations, the blue flame region was merely 1°. As the $[\text{CH}_4]_0$ decreased, the blue flame region extended to 10°. Thus Fig. 19 shows the changes in pressure (curve 1), temperature (curve 2) and concentrations of CH₄, OH, HCHO, CO and CO₂ (curves 3–7) in this transition region. It is evident that methane is partially oxidised to form a certain amount of CO and a very small amount of CO₂. The heat released in the process does not considerably increase the pressure or the temperature.

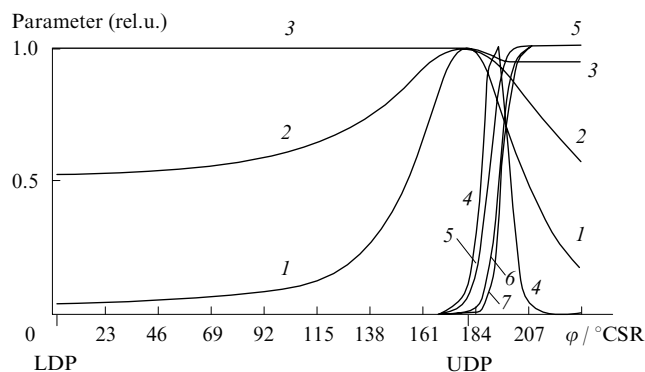
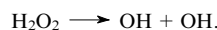


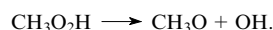
Figure 19. Diagram of autoignition of a methane–air mixture containing 3.7% CH₄, for $T_c = 968$ K, $\varepsilon = 14.7$, $n = 1000$ rpm. Here, LDP and UDP are the lower (0°) and upper (180°) dead points, CSR are crankshaft rotations.

(1) P/P_m , $P_m = 3510$ kPa; (2) T/T_m , $T_m = 968$ K; (3) $[\text{CH}_4]/[\text{CH}_4]_m$, $[\text{CH}_4]_m = 3.7\%$; (4) $[\text{OH}]/[\text{OH}]_m$, $[\text{OH}]_m = 6.3 \times 10^{-4}\%$; (5) $[\text{HCHO}]/[\text{HCHO}]_m$, $[\text{HCHO}]_m = 0.16\%$; (6) $[\text{CO}]/[\text{CO}]_m$, $[\text{CO}]_m = 5.5 \times 10^{-2}\%$; (7) $[\text{CO}_2]/[\text{CO}_2]_m$, $[\text{CO}_2]_m = 2.5 \times 10^{-4}\%$.

The reason for the staged mechanism of methane oxidation and the incomplete heat release in the transition region is sequence of poorly separated main branching processes that arise in the decomposition of methyl hydroperoxide and hydrogen peroxide. Thus the analysis of the oxidation kinetics of a lean methane–air mixture under the conditions described in Ref. 43 showed that the branching of active sites takes place mainly due to the reaction



In this case, the OH concentration first increases and then, after the consumption of all accumulated H_2O_2 , starts to decrease. This is why only a part of methane is consumed in the reaction. A hypothetical mathematical experiment in which the rate constant for the H_2O_2 decomposition is set equal to zero in the very beginning shows that virtually no methane can be oxidised under ICE conditions.⁴³ Methyl hydroperoxide $\text{CH}_3\text{O}_2\text{H}$ is the main branching product in the cool-flame oxidation of methane; its decomposition yields hydroxyl



Under the chosen conditions, due to the relatively high initial temperature, only a small amount of $\text{CH}_3\text{O}_2\text{H}$ is formed. Nonetheless, if we set the rate constant for the $\text{CH}_3\text{O}_2\text{H}$ decomposition equal to zero, the methane oxidation is slowed and the yield of products becomes several times lower. Thus, non-separated mixed cool and blue flames were observed in the methane oxidation under these conditions.

All studies devoted to the stepwise mechanism and the pre-flame reactions in the methane oxidation described either cool or blue flames; however, no publications reported on the separate observation of these stages in one experiment. Apparently, it can be concluded that these flames exist only as a united ‘cool-blue flame’ that features the peculiarities of both stages.

Figure 20 shows calculated time dependences of the relative temperature (a) and relative concentrations of hydroxyl (b) and hydroperoxides (c) in the oxidation of rich methane–oxygen mixtures. One can see the regions of the origination of the pre-flame reaction (from 1 to 2.5–3 s) and hot autoignition (at ~ 7.5 s). As seen, the ranges where the temperature rises and the OH concentration increases are situated in the regions

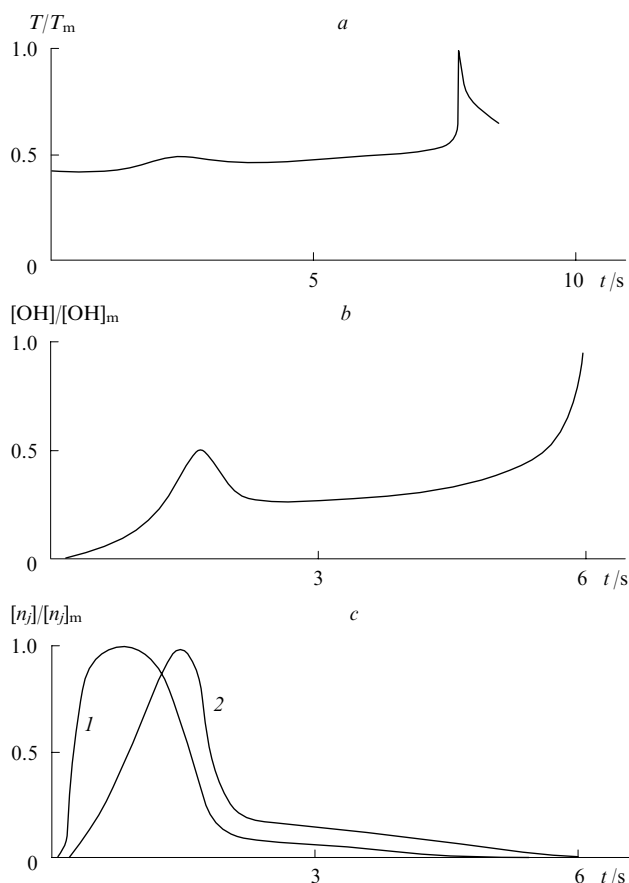


Figure 20. Time dependences of relative temperature T/T_m (a) and relative concentrations of OH (b), $\text{CH}_3\text{O}_2\text{H}$ (c, curve 1) and H_2O_2 (c, curve 2) in the oxidation of a methane-oxygen mixture. Initial conditions: $[\text{CH}_4]_0 = 67\%$, $[\text{O}_2]_0 = 33\%$, $P_0 = 122 \text{ kPa}$, $\kappa S/V = 6.61 \text{ J cm}^{-3} \text{ s}^{-1} \text{ K}^{-1}$, $T_m = 1849 \text{ K}$, $[\text{OH}]_m = 5.43 \times 10^{-9}$, $[\text{CH}_3\text{O}_2\text{H}]_m = 4.19 \times 10^{-5}$, $[\text{H}_2\text{O}_2]_m = 8.60 \times 10^{-2}$.

corresponding to the decomposition of $\text{CH}_3\text{O}_2\text{H}$ (1.3 s) and H_2O_2 (2.6–3 s). Modelling of a process during which the rate constants for the $\text{CH}_3\text{O}_2\text{H}$ and H_2O_2 decomposition decreased one after another has led to a dramatically different pattern of the overall autoignition process, which reflects the effects of both branching reactions on the pre-flame processes. This substantiates a conclusion that the separation of cool and blue flames in the methane oxidation reaction is a difficult and even impossible task and these processes occur simultaneously (with a very short time lag).

IV. Conclusion

Experimental and calculated data obtained based on the detailed kinetic mechanisms of the oxidation of hydrocarbons and their derivatives demonstrate that blue flame arises due to the decomposition of hydrogen peroxide formed in the hydrocarbon oxidation. This is typical of all reactions of oxidation and combustion of hydrocarbons and their derivatives. Blue flame was observed in the gas-phase oxidation and combustion of methane, ethane, n-heptane, isooctane, benzene, acetaldehyde and diethyl ether. Blue flames were clearly observed in the oxidation of acetaldehyde and n-heptane and less clearly in the ethane oxidation. In the methane oxidation, mixed 'cool-blue flame' was observed.

The division of the oxidation process at autoignition into stages is not always possible. Depending on the fuel type, the mixture composition, temperature and pressure, the contribu-

tions of individual stages into the overall oxidation rate can change. These contributions may overlap, which makes impossible their separation. However, the essence of the stepwise mechanism, *i.e.*, the involvement of different reaction groups that make their own contributions to the branching and oxidation, remains unchanged. For example, in the ethane oxidation, the stages corresponding to individual contributions of the $\text{C}_2\text{H}_5\text{O}_2\text{H}$ and $\text{CH}_3\text{O}_2\text{H}$ decomposition reactions could not be separated probably due to their very close kinetic characteristics. In connection with this, it is interesting to analyse the oxidation of heavy paraffin hydrocarbons with the larger number of carbon atoms in molecules for which the kinetic characteristics of the decomposition of the main ($\text{C}_n\text{H}_{2n+1}\text{O}_2\text{H}$) and secondary hydroperoxides are not so similar. At present, when the scientists have at their disposal such fast-response analytical instruments that allow them to study the reactions of hydrocarbon oxidation, the implementation of such a study would be extremely desirable.

References

1. H Perkin *J. Chem. Soc.* **41** 363 (1882)
2. V Ya Shtern *Mekhanizm Okisleniya Uglevodorodov v Gazovoi Faze* (Mechanism of Gas-Phase Oxidation of Hydrocarbons) (Moscow: Izd. Akad. Nauk SSSR, 1960)
3. A S Sokolik *Samovosplamnenie, Plamya i Detonatsiya v Gazakh* (Autoignition, Flame and Detonation of Gases) (Moscow: Izd. Akad. Nauk SSSR, 1960)
4. B Lewis, G Elbe *Combustion, Flames and Explosions of Gases* (Orlando: Academic Press, 1987)
5. M B Neiman *Usp. Khim.* **7** 341 (1938)
6. J Bardwell, C N Hinshelwood *Proc. R. Soc. London, Ser. A* **205** 375 (1951)
7. N M Chirkov, S G Entelis *Kinetika Tsepnykh Reaktsii Okisleniya* (Kinetics of Chain Oxidation Reactions) (Moscow: Izd. Akad. Nauk SSSR, 1950) p. 118
8. J E C Topps, D T A Townend *Trans. Faraday Soc.* **42** 345 (1946)
9. Y Ohta, H Takahashi *Progress in Astronautics and Aeronautics* Vol. 88 (Reston, VA: AIAA, 1983) p. 38
10. Y Ohta, H Takahashi *Progress in Astronautics and Aeronautics* Vol. 95 (Reston, VA: AIAA, 1984) p. 236
11. L V Karmilova, N S Enikolopyan, A B Nalbandyan, N N Semenov *Zh. Fiz. Khim.* **34** 1177 (1960)^a
12. B Natarajan, F V Bracco *Combust. Flame* **57** 179 (1984)
13. C T Bowman *Combust. Sci. Technol.* **2** 161 (1970)
14. S Refael, E Sher *Combust. Flame* **78** 326 (1989)
15. J S Hoffman, W Lee, T A Litzinger, D A Santavica, W J Pitz *Combust. Sci. Technol.* **77** 95 (1991)
16. V Ya Basevich, V I Vedenev, S M Frolov, L B Romanovich *Khim. Fiz.* **25** (11) 87 (2006)^b
17. W J Pitz, C K Westbrook *Combust. Flame* **63** 113 (1986)
18. S Kojima *Combust. Flame* **99** 87 (1994)
19. C K Westbrook *AIAA J.* **24** 2002 (1986)
20. A Chakir, M Belumam, J C Boettner, M Cathonnet *Combust. Sci. Technol.* **77** 239 (1991)
21. M Bui-Pham, K Seshadri *Combust. Sci. Technol.* **79** 293 (1991)
22. E Ranzi, T Faravelli, P Gaffuri, A Sogaro *Combust. Flame* **102** 179 (1995)
23. H J Curran, P Gaffuri, W J Pitz, C K Westbrook *Combust. Flame* **114** 149 (1998)
24. H J Curran, P Gaffuri, W J Pitz, C K Westbrook *Combust. Flame* **129** 253 (2002)
25. L L Skrumeda, J Ross *J. Phys. Chem.* **99** 12835 (1995)
26. V Ya Basevich, V I Vedenev, L B Romanovich *Khim. Fiz.* **22** (7) 60 (2003)^b
27. V Ya Basevich *Handbook of Heat and Mass Transfer* Vol. 4 (Ed. N Chermisinoff) (Houston: Gulf, 1990) p. 769
28. V Ya Basevich, V I Vedenev, V S Arutyunov *Khim. Fiz.* **18** (6) 40 (1999)^b
29. V Ya Basevich, V I Vedenev, V S Arutyunov *Khim. Fiz.* **17** (5) 73 (1998)^b

30. A A Belyaev, V S Posvyanskii *Gosudarstvennyi Fond Algoritmov i Programm SSSR. Algoritmy i Programmy. Informatsionnyi Byulleten'* (Consolidated Fund of Algorithms and Programmes of the USSR. Algorithms and Programmes. Information Bulletin) (Moscow: VNTITsENTR, 1985) No. 3, p. 35
31. V N Kondrat'ev, E E Nikitin *Kinetika i Mekhanizm Gazofaznykh Reaktsii* (Kinetics and Mechanism of Gas Reactions) (Moscow: Nauka, 1974)
32. V Ya Basevich, V I Vedeneev, V S Arutyunov *Khim. Fiz.* **19** (11) 94 (2000)^b
33. V Ya Basevich, A A Belyaev, V Brandstetter, M G Neigauz, R Taschl, S M Frolov *Fiz. Goren. Vzryva* **30** (6) 15 (1994)^c
34. V Ya Basevich, V I Vedeneev, S M Frolov, L B Romanovich *Khim. Fiz.* **24** (2) 77 (2005)^b
35. J H Knox, R G W Norrish *Trans. Faraday Soc.* **50** 928 (1954)
36. M Vanpee *C. R. Acad. Sci.* **243** 804 (1956)
37. V Ya Basevich, S M Kogarko *Izv. Akad. Nauk SSSR, Ser. Khim.* 2658 (1982)^d
38. V I Vedeneev, M Ya Gol'denberg, N I Gorban', M A Teitel'boim *Kinet. Katal.* **29** 7 (1988)^e
39. V Ya Basevich, V I Vedeneev, V S Arutyunov *Khim. Fiz.* **13** (8–9) 157 (1994)^b
40. F C Egerton, N P W Moor, W T Lyn *Nature (London)* **167** 191 (1951)
41. V Ya Basevich, V I Vedeneev *Khim. Fiz.* **20** (5) 119 (2001)^b
42. J D Broatch, A C Egerton *Fuel* **31** 494 (1952)
43. A G Gaydon, N P W Moore, J R Simonson *Proc. R. Soc. London, Ser. A* **230** 1 (1955)

^a — *Russ. J. Phys. Chem. (Engl. Transl.)*

^b — *Chem. Phys. Rep. (Engl. Transl.)*

^c — *Comb. Explos. Shock Waves (Engl. Transl.)*

^d — *Russ. Chem. Bull., Int. Ed. (Engl. Transl.)*

^e — *Kinet. Catal. (Engl. Transl.)*

Chemical functionalisation of polychloroarenes

A A Vasil'ev, A S Burukin, S G Zlotin

Contents

I. Introduction	885
II. Reactions with S- and Se-nucleophiles	886
III. Reactions with N-nucleophiles	893
IV. Reactions with O-nucleophiles	897
V. Reactions with F-nucleophiles	900
VI. Reactions with C-nucleophiles	903
VII. Catalytic carbonylation and carboxylation	904
VIII. Catalytic C–C cross-coupling	905
IX. Metallation	909

Abstract. Methods for the replacement of chlorine atoms in polychloroarenes upon treatment with various reagents are surveyed. Considerable attention is given to catalytic methods and elucidation of the structure–reactivity relationships for polychloroarenes. The bibliography includes 322 references.

I. Introduction

According to the long-term environmental protection strategy of the EU countries, the production and utilisation of environmentally hazardous chemical compounds will be ceased by 2020. Polychlorinated aromatic compounds (polychloroarenes, PCA) are among such compounds. The disposal of toxic PCA produced on the industrial scale, such as first-generation insecticides polychlorobiphenyls and polychlorodioxins formed as their biodegradation products, remains an unsolved problem. Its solution requires information on the reactivity of these compounds, which would suggest promising approaches to their conversion into ecologically safe products or substances with useful properties. Catalytic hydrogenolysis of the C–Cl bond in PCA has been studied in sufficient detail.^{1–8} However, the resulting products are, as a rule, of little practical significance because many hydrogenolysis products can be prepared according to simpler and cheaper procedures. Other reactions of PCA containing from two to six chlorine atoms in the aromatic nuclei have been documented to a lesser extent. Of these reactions, reduction-type processes, including metallation and electron-transfer reactions, as well as reactions with nucleophilic reagents, deserve notice. In addition, the development of procedures for the formation of new C–C and C–heteroatom bonds instead of poorly reactive C–Cl bonds

is a good challenge for processing PCA into practically useful compounds of the aromatic series.

The chemical properties of PCA often differ from those of monochloro derivatives due to the mutual influence of the chlorine atoms. Polychloroarenes are characterised by high acidity of the aromatic protons and high electron affinity. The shift of the first half-wave reduction potential ($E_{1/2}$) to more positive values, on the average, by 0.2–0.3 V, upon the introduction of every next chlorine atom into the aromatic nucleus can serve as the criterion of the electron affinity.^{9, 10} For example, this parameter for hexachlorobenzene is –1.44 V (relative to a saturated calomel electrode), as opposed to monochloroarenes, which are reduced at potentials equal or close to the values of supporting electrolyte discharge. At the same time, a negative charge on the chlorine atoms (for example, in hexachlorobenzene), the small C–Cl bond length (1.7 Å) and the rather large van der Waals radius of the chlorine atoms (1.8 Å) hinder the attack of nucleophiles on the electron-deficient carbon atoms in PCA.

The present review summarises the main reactions of PCA (containing from two to six carbon atoms in the aromatic core) resulting in the replacement of chlorine atoms by other elements. These include:

- (1) nucleophilic substitution reactions,
- (2) reactions accompanied by the C–C bond formation through metallation of PCA,
- (3) transition metal-catalysed cross-coupling reactions.

The only monograph summarising the reactions of PCA was published in 1974.¹¹ The reactions of perchloroalkylarenes that involve the side aliphatic chains with retention of chlorine atoms in the aromatic moieties were considered in a more recent review.¹² In a chapter of a multivolume monograph¹³ devoted to organic halogen-containing compounds, the properties of polyhaloarenes are not considered separately. In this connection, in our opinion, it is reasonable to discuss not only the results of studies published in the last decade, but also the earlier data. The present review includes data on low-chlorinated arenes in particular, because dioxins containing two chlorine atoms in the aromatic nuclei belong to environmentally hazardous compounds. In addition, certain reactions, which have been studied only for arenes containing two or three chlorine atoms, would be useful also for chemical

A A Vasil'ev, A S Burukin, S G Zlotin N D Zelinsky Institute of Organic Chemistry, Russian Academy of Sciences, Leninsky prosp. 47, 119991 Moscow, Russian Federation. Fax (7-499) 135 53 28, tel. (7-499) 135 89 61, e-mail: vasiliev@ioc.ac.ru (A A Vasil'ev), tel. (7-916) 664 24 37, e-mail: scander@inbox.ru (A S Burukin), tel. (7-499) 137 13 53, e-mail: zlotin@ioc.ac.ru (S G Zlotin)

Received 23 April 2007

Uspekhi Khimii 76 (10) 947–978 (2007); translated by T N Safonova

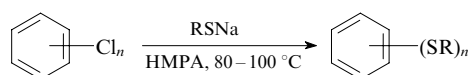
modifications of highly chlorinated PCA. Since the physico-chemical properties and the structures of polychloroarenes have been covered in detail in the earlier monograph,¹¹ various chemical transformations of these compounds are only considered below.

II. Reactions with S- and Se-nucleophiles

Aromatic thiols, sulfides and their derivatives have found wide use as rubber vulcanisation promoters and modifiers of polymeric compositions. They also serve as intermediates in the synthesis of organic conductors, biologically active compounds and other valuable compounds. The main procedure for their synthesis is based on the nucleophilic substitution of chlorine atoms in chloroaromatic compounds under the action of sulfur-containing nucleophiles.

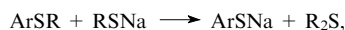
1. Characterisation of reactions of non-activated polychloroarenes with S- and Se-nucleophiles

Reactions of polychlorobenzenes with sodium alkanethiolates RSNa in hexamethylphosphoramide (HMPA) resulting in high yields of poly(alkylthio)benzenes were documented.^{14–16}



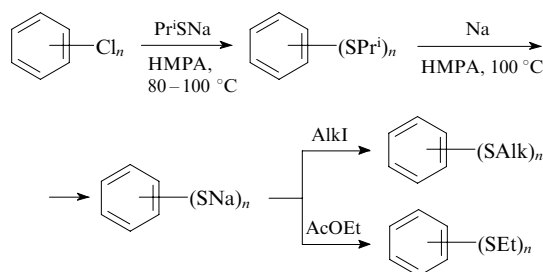
$n = 2–6$; $R = \text{Me, Et, Pr}^i$.

The course of the reactions with sodium ethanethiolate and with sodium methanethiolate especially should be thoroughly controlled^{16,17} because alkylthiobenzenes formed in the first step can undergo dealkylation induced by an excess of sodium alkenethiolate to give alkali metal arenethiolates (see the review¹⁸).



$R = \text{Me, Et}$.

It is more convenient to use Pr^iSNa as the sulfur-containing reagent. Under the reaction conditions, the resulting aryl isopropyl sulfides are stable. After completion of the reaction, these compounds can be transformed into benzenethiols and then into other alkyl aryl sulfides. The latter can be prepared by one-pot reactions with metallic sodium and then with alkylating agents (alkyl iodides or esters). The isopropyl groups can be removed by the reaction with sodium in HMPA or pyridine at $\sim 100^\circ\text{C}$.¹⁹



$n = 2–6$.

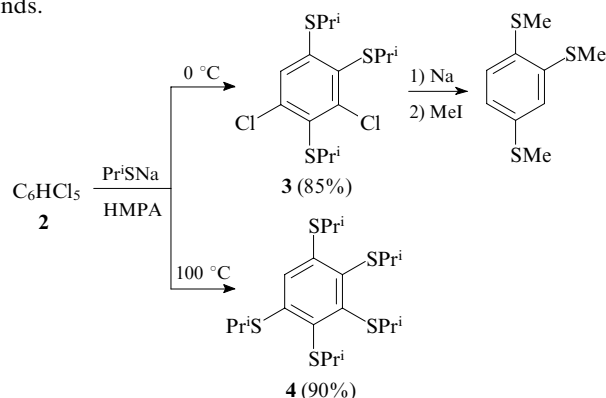
Dichlorobenzenes **1a–c**[†] react with sodium alkanethiolates in HMPA to form bis(alkylthio)arenes and their transformation products.¹⁷ For example, the reactions of 1,4-dichlorobenzene (**1c**) with EtSNa and MeSNa afford 1,4-bis(ethylthio)benzene (85%) and 4-(methylthio)benzene-

thiol (52%), respectively, as the major products. The reactions with sodium propane-2-thiolate are not accompanied by S-dealkylation. However, these reactions afford mixtures of mono- and bis(isopropylthio)benzenes. The composition of the products depends on the amount of the reagent. The disubstitution products are the major products in the reactions of Pr^iSNa with 1,3- and 1,4-dichlorobenzenes (**1b,c**); for steric reasons, the reaction with 1,2 isomer **1a** gives 2-chloro(isopropylthio)benzene as the major product even in the presence of an excess of thiolate (Table 1).¹⁵

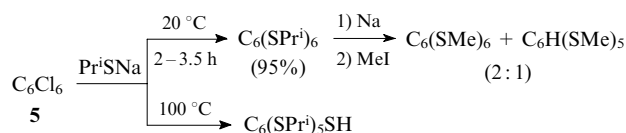
Table 1. Reactions of isomeric dichlorobenzenes **1a–c** with Pr^iSNa in HMPA at 80°C .¹⁵

Compound	Number of equiv. of Pr^iSNa	Reaction time/h	Products	Yield (%)
1,2- $\text{Cl}_2\text{C}_6\text{H}_4$ (1a)	1	0.5	2- $\text{ClC}_6\text{H}_4\text{SPr}^i$	92
	3	36	2- $\text{ClC}_6\text{H}_4\text{SPr}^i$, 1,2- $(\text{Pr}^i\text{S})_2\text{C}_6\text{H}_4$	68 11
1,3- $\text{Cl}_2\text{C}_6\text{H}_4$ (1b)	1	0.5	3- $\text{ClC}_6\text{H}_4\text{SPr}^i$	60
	3	36	1,3- $(\text{Pr}^i\text{S})_2\text{C}_6\text{H}_4$	5
1,4- $\text{Cl}_2\text{C}_6\text{H}_4$ (1c)	1	0.5	1,4- $(\text{Pr}^i\text{S})_2\text{C}_6\text{H}_4$	56
	3	4	4- $\text{ClC}_6\text{H}_4\text{SPr}^i$, 1,4- $(\text{Pr}^i\text{S})_2\text{C}_6\text{H}_4$	72 7
	3	4	1,4- $(\text{Pr}^i\text{S})_2\text{C}_6\text{H}_4$	96

Thiolate anions react also with highly chlorinated arenes.^{14,17} For example, the reactions of isomeric tri- and tetrachlorobenzenes with an excess of Pr^iSNa in HMPA at 100°C resulted in products of complete substitution of chlorine atoms in yields of up to 95%.¹⁹ The degree of substitution in the reaction with pentachlorobenzene (**2**) can be controlled by varying the temperature. At 0°C , three chlorine atoms are replaced to give compound **3**; at 100°C , five chlorine atoms are replaced to form compound **4**. It should be noted that the removal of the isopropyl groups in dichloroarene **3** with metallic sodium is accompanied by reduction of the $\text{C}–\text{Cl}$ bonds.



The product of the complete replacement of chlorine atoms in hexachlorobenzene (**5**) by Pr^iS groups is formed at room temperature.^{17,20} The increase in the reaction temperature to 100°C results in the elimination of one isopropyl group and the formation of pentakis(isopropylthio)benzenethiol. The reaction of $\text{C}_6(\text{SPr}^i)_6$ with metallic sodium is accompanied by the replacement of one sulfur-containing group by hydrogen.¹⁴

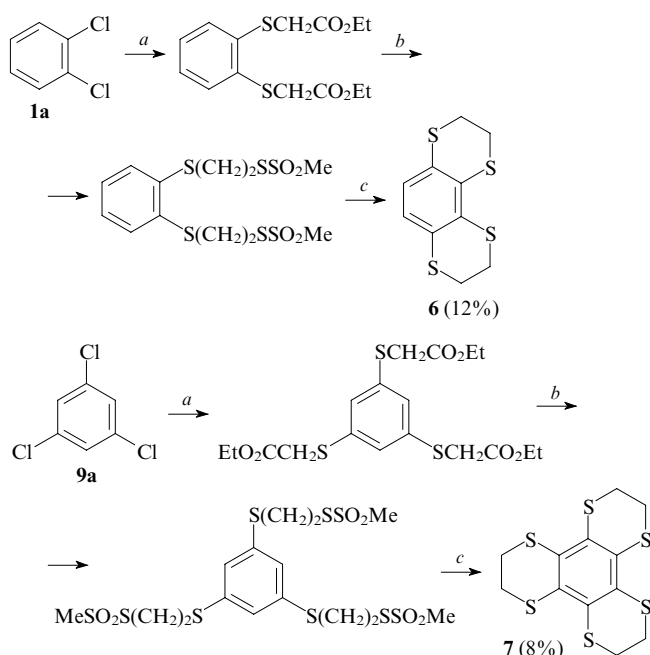


[†] Hereinafter, isomeric PCA have identical numbers but are denoted by different letters.

The reaction of hexachlorobenzene (**5**) with PhCH_2SNa produced hexakis(benzylthio)benzene, whose benzyl groups can be removed under the action of sodium in liquid ammonia.²¹

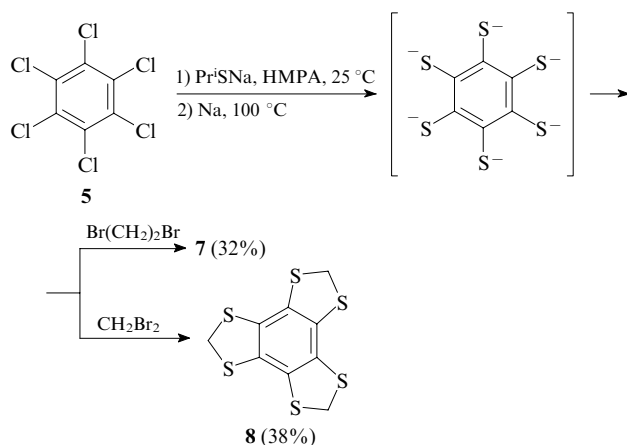
It should be noted that compounds $\text{C}_6(\text{SAlk})_6$ are produced by nucleophilic substitution only in the case of hexachlorobenzene (**5**). Attempts to obtain this type of compounds by the reactions of copper mercaptides with tetra-, penta- or hexabromobenzenes failed.^{17, 22}

Polychloroarenes were used as the starting compounds for the synthesis of fused heterocycles containing the 1,4-dithiane (**6**, **7**) or 1,3-dithiolane (**8**) fragments.²⁰ Two approaches to the synthesis of these products were developed. One approach is based on the substitution of isopropylthio groups for chlorine atoms in 1,2-dichlorobenzene (**1a**) and 1,3,5-trichlorobenzene (**9a**) followed by the transformation of the resulting compounds into the target heterocycles in six experimental steps. Compounds **6** and **7** are formed in low yields (12% and 8%, respectively, based on the starting chloroarenes).



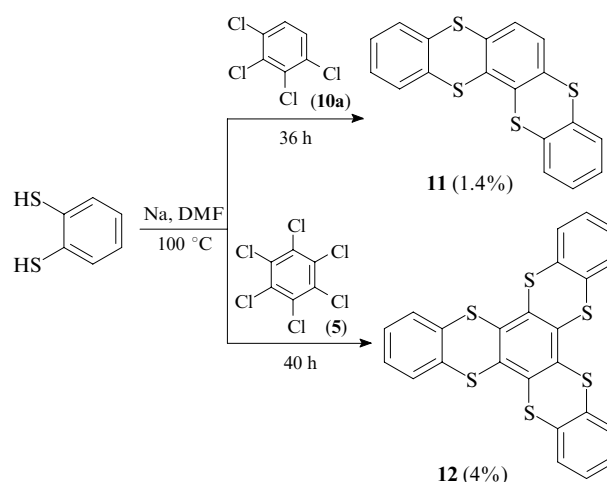
(a) (1) Pr^iSNa , HMPA, 25 °C, 2 h; (2) Na, 100 °C, 2 h; (3) $\text{BrCH}_2\text{CO}_2\text{Et}$, 50 °C, 2 h; (b) (1) LiAlH_4 , THF; (2) SOCl_2 , PhH, 2 h; (3) MeSO_2SK , EtOH, 18 h; (c) AlCl_3 , MeNO_2 .

Another, more efficient, approach is based on the treatment of the *in situ* generated benzenehexathiolate with dibromoalkanes.²⁰ Reaction products **7** and **8** were synthesised in two steps in satisfactory yields.

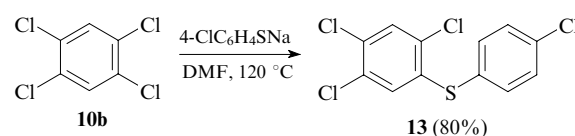


The nucleophilic substitution of sulfur for the chlorine atoms was carried out also in other solvents, for example, in DMF,^{23–26} methanol,²⁷ *etc.* Not only alkali metal alkanethiolates, but less nucleophilic alkali metal arenethiolates were also used as the reagents. The reactions of 1,3- and 1,4-dichlorobenzenes (**1b,c**) with potassium benzenethiolate in DMF, dimethylacetamide (DMA), *N*-methylpyrrolidone (NMP), diglyme and ethylene glycol were investigated.^{28, 29} As a rule, both chlorine atoms are replaced in these reactions. The best results (high yields of products) were obtained in DMA and NMP, whereas the reactions in diglyme and ethylene glycol did not virtually take place. Such solvents as water and toluene were used primarily in combination with phase-transfer catalysts (see below).

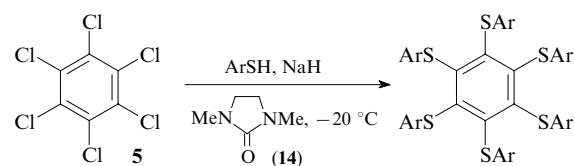
The substitution of benzene-1,2-dithiolate for the chlorine atoms in 1,2,3,4-tetrachloro- (**10a**) and hexachlorobenzene (**5**) gave polycyclic dithianes **11** and **12**, respectively; however, their yields did not exceed 4%.²⁴



The reaction of 1,2,4,5-tetrachlorobenzene (**10b**) with an excess of $4\text{-ClC}_6\text{H}_4\text{SNa}$ in DMF at 120 °C affords only monosubstitution product **13** due apparently to the insufficiently high nucleophilicity of the 4-chlorobenzenethiolate anion.³⁰

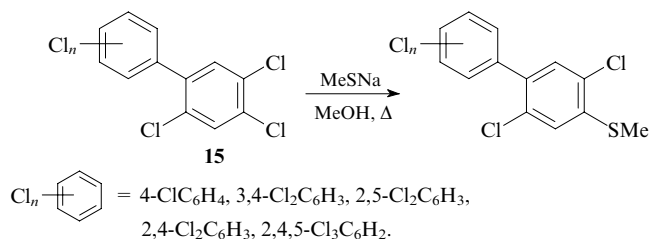


Sodium benzenethiolates (prepared from benzenethiols and NaH) react with 1,2,4-trichlorobenzene (**9b**) in 1,2-dimethoxyethane to give the complete substitution product in 94% yield.³¹ Under these conditions, hexachlorobenzene (**5**) gave hexakis(phenylthio)benzene. 1,3-Dimethylimidazolidin-2-one (**14**) is a solvent of choice for such reactions. In this solvent, the reactions proceed even at room temperature to form hexakis(arylthio)benzenes in high yields.^{32, 33}



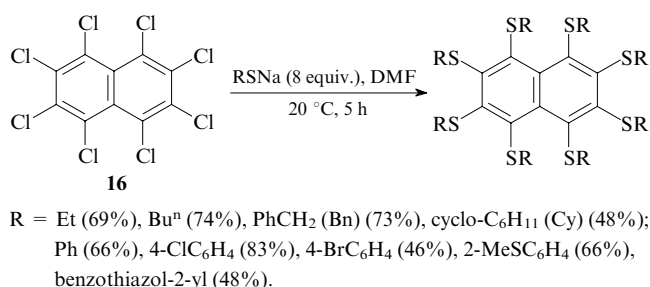
Ar = Ph (96%), 4-MeC₆H₄ (91%), 4-Bu^tC₆H₄ (76%), 4-BrC₆H₄ (48%), 2-naphthyl (72%).

Not only mononuclear PCA, but also compounds containing several aromatic rings, react with S-nucleophiles. In polychlorobiphenyls **15**, one chlorine atom at position 4 is generally replaced.²⁷

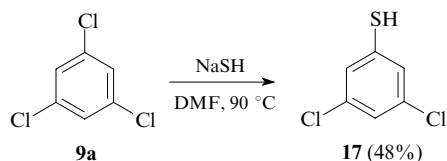


The substitution product of two chlorine atoms (at positions 4 and 4') was detected only in the case of symmetrical 2,2',4,4',5,5'-hexachlorobiphenyl.

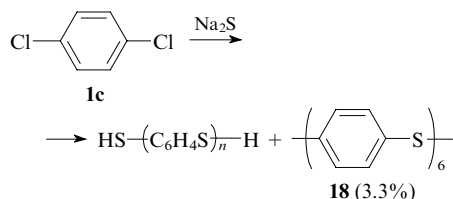
In octachloronaphthalene (**16**), all chlorine atoms can be replaced by sulfur-containing groups in DMF at room temperature.³⁴



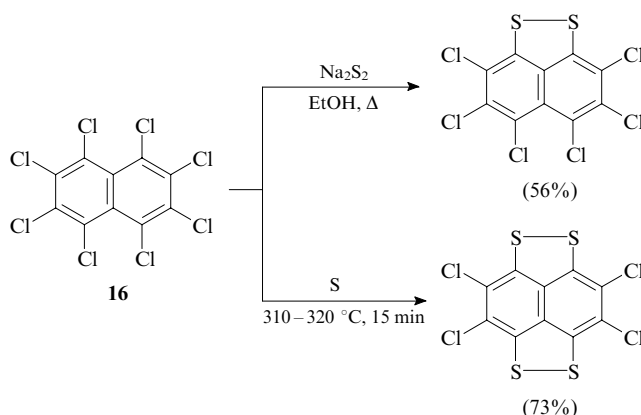
In addition to alkane- and arenethiolates, the reactions of PCA were carried out also with other sulfur-containing nucleophiles, including hydrogen sulfide, metal sulfides, isothiurea derivatives, heterocyclic thiones, dimethyl sulfoxide, carbon disulfide and dialkyl sulfides.^{30, 35–39} For example, the reaction of 1,3,5-trichlorobenzene (**9a**) with sodium hydrosulfide produced 3,5-dichlorobenzenethiol (**17**).³⁰



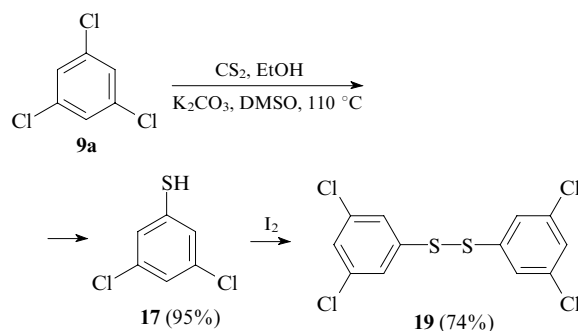
The reaction of 1,4-dichlorobenzene (**1c**) with Na_2S in NMP is of industrial significance as a procedure for the production of poly(1,4-phenylene sulfide). After the completion of the reaction in NMP, small amount of macrocyclic hexamer **18** was isolated from low-molecular-mass fractions.³⁹



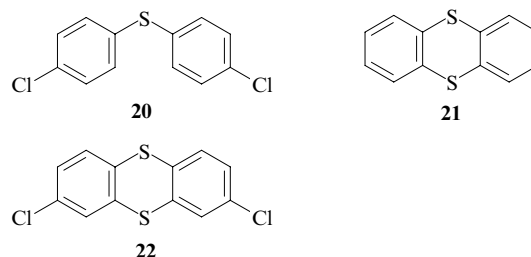
The chlorine atoms at positions 1 and 8 in octachloronaphthalene (**16**) were replaced by the disulfide fragment upon refluxing with Na_2S_2 in ethanol.⁴⁰ Fusion of compound **16** with elemental sulfur at 310–320 °C under nitrogen allows the introduction of two disulfide bridges into the molecule.



Carbon disulfide can be used as the S-nucleophile.⁴¹ Oxidation of the reaction product, viz., 2,4-dichlorobenzenethiol (**17**), afforded the corresponding disulfide **19**. Analogously, the reaction of hexachlorobenzene (**5**) with the $\text{CS}_2\text{–Bu}^t\text{OK–DMSO}$ system at 110 °C produced pentachlorobenzenethiol in 72% yield.



The chlorine atom in chloroarenes is replaced by the sulfur atom also in the gas-phase reaction with hydrogen sulfide in a flow reactor at 500–700 °C.^{35, 36} The reaction afforded a complex mixture of products consisting mainly of benzenethiols and diaryl sulfides and was accompanied by the partial dehalogenation of arenes. 1,4-Dichlorobenzene (**1c**) reacts much more easily than chlorobenzene. The yields of 4-chlorobenzenethiol and bis(4-chlorophenyl) sulfide (**20**) are 15% and 56%, respectively. Under these conditions, the reaction of 1,2-dichlorobenzene (**1a**) gives 2-chlorobenzenethiol (30%) and thianthrene **21** (61%); the reaction of 1,2,4-trichlorobenzene (**9b**) produces dichlorobenzenethiol (15%–56%) and 2,7-dichlorothianthrene **22** (26%–45%).



Dialkyl sulfides and dialkyl disulfides can also serve as a source of sulfur at high temperature. 1,4-Dichlorobenzene (**1c**) reacts with diethyl disulfide to form a mixture of 4-chlorobenzenethiol (55%), bis(4-chlorophenyl) sulfide (16%), benzene (9%) and thiophene (14%).³⁸ Presumably, the reaction involves thermal decomposition of dialkyl disulfides accompanied by elimination of hydrogen sulfide, which reacts with PCA. Dialkyl disulfides are reagents of choice for the synthesis of benzenethiols, while hydrogen sulfide, for the synthesis of diaryl sulfides.^{35, 36, 38}

The replacement of chlorine atoms in PCA in the reaction with thiourea under electroreduction conditions in liquid ammonia ($-40\text{ }^{\circ}\text{C}$, with KBr or Bu'OK as the additives) was documented.⁴² The reaction afforded a mixture of sulfur-containing products, *viz.*, ArSH, ArSSAr and ArSAr. The ion-radical $\text{S}_{\text{RN}}1$ mechanism was proposed for this reaction.

Selenation reactions of PCA were less studied. For example, the reaction of PCA with lithium methaneselenolate produces aryl methyl selenides,⁴³ which readily undergo demethylation with an excess of methaneselenolate (analogously to methanethiolates). The resulting areneselenolates can be alkylated with alkyl iodides to give alkyl aryl selenides **23**.⁴⁴ Examples of such products are given in Table 2.

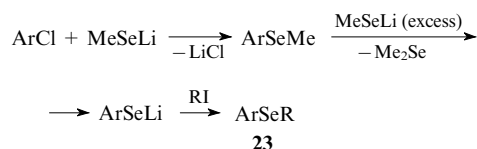
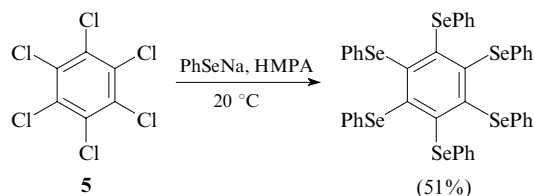


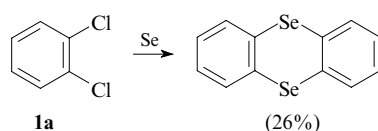
Table 2. Reactions of isomeric dichlorobenzenes **1a–c** with lithium methaneselenolate (4 equiv. MeSeLi, DMF, $120\text{ }^{\circ}\text{C}$) followed by alkylation with RI.⁴³

Compound	Time/h	R	Products 23	Yield (%)
1,2- $\text{C}_6\text{H}_4\text{Cl}_2$ (1a)	16	Me	2- $\text{ClC}_6\text{H}_4\text{SeMe}$	87
1,3- $\text{C}_6\text{H}_4\text{Cl}_2$ (1b)	8	Me	3- $\text{ClC}_6\text{H}_4\text{SeMe}$	86
1,4- $\text{C}_6\text{H}_4\text{Cl}_2$ (1c)	8	Me	4- $\text{ClC}_6\text{H}_4\text{SeMe}$	72
	8	Et	4- $\text{ClC}_6\text{H}_4\text{SeEt}$	81
	8	Pr ⁱ	4- $\text{ClC}_6\text{H}_4\text{SePr}^i$	76

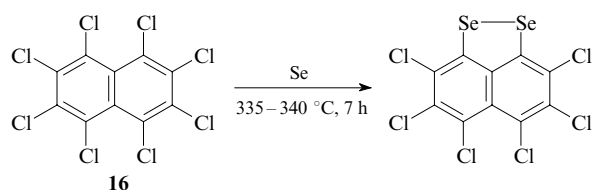
The reaction of hexachlorobenzene (**5**) with sodium benzeneselenolate in HMPA proceeds at room temperature to give hexakis(phenylseleno)benzene.³²



The reaction of 1,2-dichlorobenzene (**1a**) with elemental selenium affords 9,10-diseleno-9,10-dihydroanthracene in moderate yield.⁴⁵



A heterocycle containing the diselenide bridge between positions 1 and 8 of the naphthalene fragment was synthesised by the fusion of perchloronaphthalene (**16**) with selenium at $335\text{--}340\text{ }^{\circ}\text{C}$ in an inert atmosphere.⁴⁰

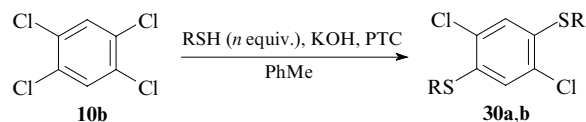


2. Reactions of activated polychloroarenes with S-nucleophiles

The reactions of PCA containing electron-withdrawing groups in the *ortho* or *para* positions with respect to chlorine atoms generally proceed under milder conditions, in some cases, at room or reduced temperatures. Data on the formation of the reaction products of activated PCA, including compounds **24–29**, with S-nucleophiles are presented in Table 3.^{46–64}

3. Reactions of polychloroarenes with S-nucleophiles under conditions of phase-transfer catalysis

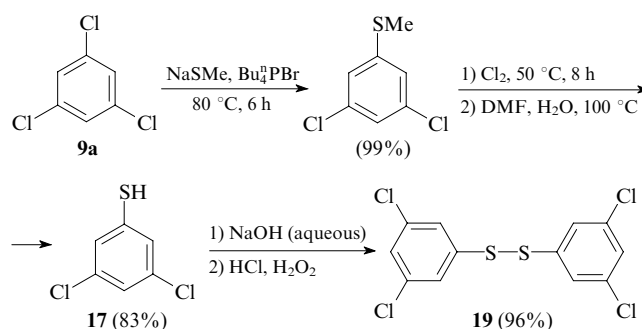
The reactions of PCA with S-nucleophiles can be promoted, in particular, by phase-transfer catalysts (PTC). Crown ethers, ammonium salts and phosphonium salts were used as PTC.^{65,66} Under these conditions, it became possible to perform the reaction of 1,2,4,5-tetrachlorobenzene (**10b**) with an alkanethiol–KOH system in toluene, which does not proceed in the absence of catalysts (Table 4).⁶⁷ The reaction produces 1,4-dialkylthio-2,5-dichlorobenzenes (**30a,b**). The highest yield of the products was achieved with the use of dodecyltricyclohexylphosphonium bromide as the catalyst. The reactions of 1,3,5- and 1,2,4-trichlorobenzenes (**9a,b**) with alkanethiols in the presence of PTC proceed at higher temperatures.



R = $n\text{-C}_7\text{H}_{15}$ (**a**), $n\text{-C}_{12}\text{H}_{25}$ (**b**).

The reactions of dichlorobenzenes require even more drastic conditions ($110\text{ }^{\circ}\text{C}$).⁶⁸ The reactivity of the compounds decreases in the following sequence: 1,2 isomer (**1a**) > 1,3 isomer (**1b**) > 1,4 isomer (**1c**); the reactivity of nucleophiles decreases in the following sequence: primary thiols > tertiary thiols > benzenethiols (Table 5).

The reactions of sodium methanethiolate with dichloro- and trichlorobenzenes in the presence of tetrabutylphosphonium bromide resulted in the replacement of one chlorine atom to yield (methylthio)chlorobenzenes. The latter were transformed into the corresponding disulfides by demethylation and oxidation, for example, as shown below:⁶⁵



3-Chloro-2-(isopropylthio)nitrobenzene was obtained in quantitative yield by the reaction of 2,3-dichloronitrobenzene (**24a**) with the PrⁱSH–KOH system in water in the presence of PTC (the quaternary ammonium salt Adogen 464).⁶⁹

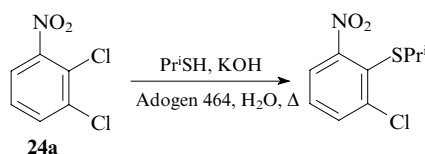


Table 3. Reactions of polychloroarenes bearing electron-withdrawing groups with S-nucleophiles.

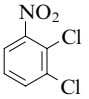
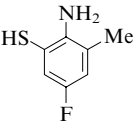
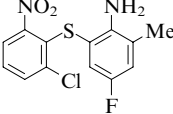
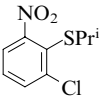
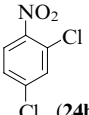
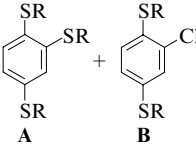
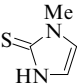
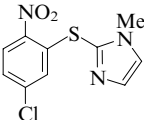
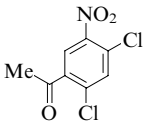
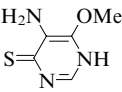
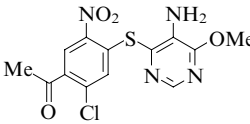
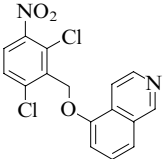
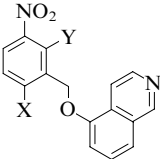
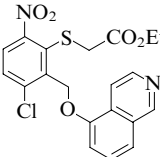
Compound	S-Nucleophile	Reaction conditions	Products	Yield (%)	Ref.
 (24a)		AcONa, EtOH, Δ		85	46
	Pr ⁱ SH	H ₂ O – organic solvent Bu ₄ NBr, 65 °C		97	47
 (24b)	RSNa (R = Et, Bu ^t)	HMPA, 80 °C	 A B	R = Et: A (65%); R = Bu ^t : A (21%) + B (42%)	48
		—		99	49
		KOH, MeOH		67	50
	MeSNa	DMF, 0 °C		60 (X = Y = SMe) 24 (X = SMe, Y = Me) 7 (X = Me, Y = SMe)	51
	HSCH ₂ CO ₂ Et	Et ₃ N, DMF, 0 °C		60	51

Table 3 (continued).

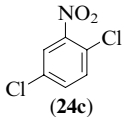
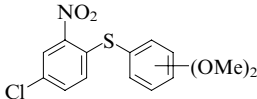
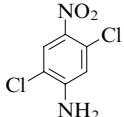
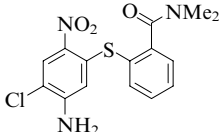
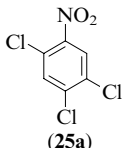
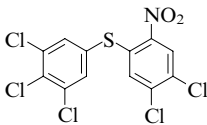
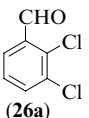
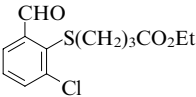
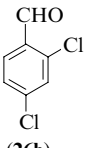
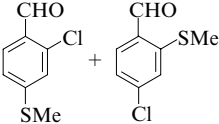
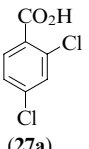
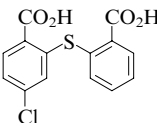
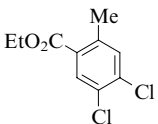
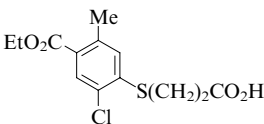
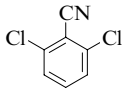
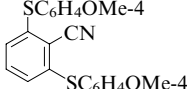
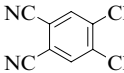
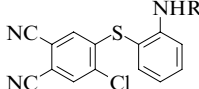
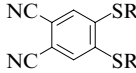
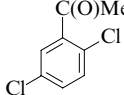
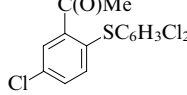
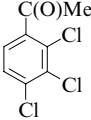
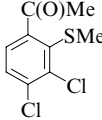
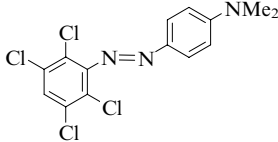
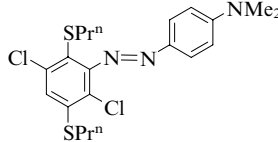
Compound	S-Nucleophile	Reaction conditions	Products	Yield (%)	Ref.
 (24c)	2,5-, 2,4- and 3,5-(MeO) ₂ C ₆ H ₃ SH	—		91 – 99	52
	2-HSC ₆ H ₄ C(O)NMe ₂	K ₂ CO ₃ , DMF, Δ		75	53
 (25a)	1,2,3-Cl ₃ C ₆ H ₂ SH	AcONa, EtOH, Δ		6 (see ^a)	54
 (26a)	HS(CH ₂) ₃ CO ₂ Et	K ₂ CO ₃ , DMF, 20 °C		70	55
 (26b)	see ^b	KF, DMSO, sulfolane, 180 °C		71	56
 (27a)	2-HSC ₆ H ₄ CO ₂ H	K ₂ CO ₃ , PhCH ₂ OH, Cu, 110 °C		70	57
	HS(CH ₂) ₂ CO ₂ H	K ₂ CO ₃ , DMF, 120 – 125 °C		60	58

Table 3 (continued).

Compound	S-Nucleophile	Reaction conditions	Products	Yield (%)	Ref.
 (28a)	4-MeOC ₆ H ₄ SH	1) Bu ^t OK, DMSO 2) MeCN, Δ		9	59
	2-RNHC ₆ H ₄ NSH (R = Alk)	K ₂ CO ₃ , THF		—	60
	RSH (R = Pr ⁿ , Ph)	K ₂ CO ₃ , DMSO, 90 °C		51 (R = Pr ⁿ), 55 (R = Ph)	61
 (29)	2,5- and 3,4-Cl ₂ C ₆ H ₃ SH	K ₂ CO ₃ , Cu, 125–155 °C		37–77	62
	MeSNa	THF, 25 °C		82–94	63
	Pr ⁿ SH	NaH, DMSO, 120 °C		—	64

Note. The dash means that the reaction conditions or the yields were not reported. ^a The yield of the product of reduction to the corresponding amine is given. ^b The MeS[−] ions generated *in situ* from DMSO were used as the reagent.

Table 4. Reactions of polychloroarenes **9a,b** and **10b** with thiols (RSH) under phase-transfer catalysis.⁶⁷

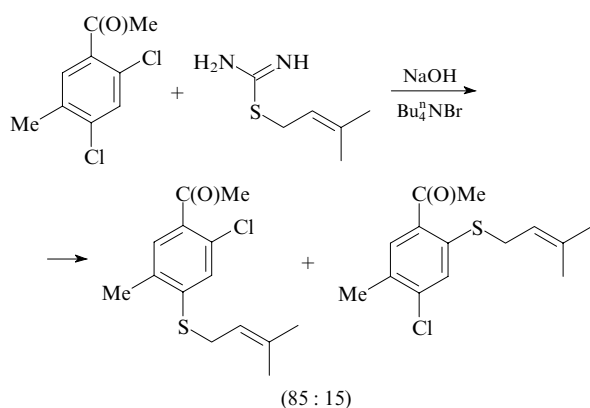
Compound	R	Equiv. of thiol, <i>n</i>	PTC	Time /h	Temperature /°C	Product	Yield (%)
1,2,4,5-Cl ₄ C ₆ H ₂ (10b)	n-C ₇ H ₁₅	3	18-Crown-6	2	25	30a	70
			PEG-300 ^a	2	25	30a	62
			n-C ₁₂ H ₂₅ PCy ₃ Br	2	25	30a	99
	n-C ₁₂ H ₂₅	3	—	24	50	—	—
			Bu ₄ NBr	24	25	—	—
			Bu ₄ PBr	2	25	30b	78
1,3,5-Cl ₃ C ₆ H ₃ (9a)	Pr ⁱ	0.3	Bu ₄ NBr ^b	5.5	140	see ^c	85
	n-C ₇ H ₁₅	1.5	n-C ₁₂ H ₂₅ PCy ₃ Br	3	50	see ^c	93
1,2,4-Cl ₃ C ₆ H ₃ (9b)	n-C ₇ H ₁₅	1.5	n-C ₁₂ H ₂₅ PCy ₃ Br	3	50	see ^d	92

^a PEG is poly(ethylene glycol); ^b aqueous NaOH was used;⁶⁶ ^c 3,5-Cl₂C₆H₃SR is formed; ^d 2,5-Cl₂C₆H₃SR is formed.

Table 5. Reactions of isomeric dichlorobenzenes **1a–c** with thiols under phase-transfer catalysis (110 °C, 60% KOH, dicyclohexano-18-crown-6).⁶⁸

Compound	Thiol	Time /h	Composition of substitution products (GLC data) (%)		Yield of the isolated monosubstitution product (%)
			mono-	di-	
1,2-Cl ₂ C ₆ H ₄ (1a)	Pr ⁱ SH	16	93	0	89
	Bu ⁿ SH	14	92	5	88
	Bu ⁱ SH	75	94	0	84
1,3-Cl ₂ C ₆ H ₄ (1b)	Pr ⁱ SH	24	86	6	79
	Bu ⁿ SH	24	87	6	81
	Bu ⁱ SH	125	86	12	73
1,4-Cl ₂ C ₆ H ₄ (1c)	Pr ⁱ SH	150	54	35	43
	Bu ⁿ SH	90	76	14	65
	Bu ⁱ SH	250	31	53	27

The Bu₄NBr-catalysed reaction of 2,4-dichloro-5-methylacetophenone with *S*-prenylisothiourea allowed the introduction of the prenylthio group into the aromatic nucleus.⁷⁰

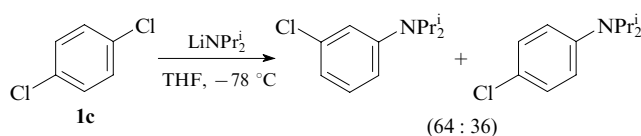


III. Reactions with N-nucleophiles

Since amines are much less reactive than S-nucleophiles, the reactions of the former with PCA are performed under more drastic conditions or in the presence of catalysts. In some cases, metal amides are used as aminating agents.

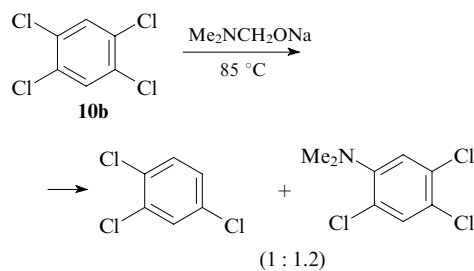
1. Amination of non-activated polychloroarenes

The reaction of 1,4-dichlorobenzene (**1c**) with lithium diisopropylamide at -78°C affords a mixture of isomeric amination products,⁷¹ with 3-chloro-*N,N*-diisopropylaniline predominating. This can be attributed to the fact that the reaction proceeds *via* 4-chlorobenzene.

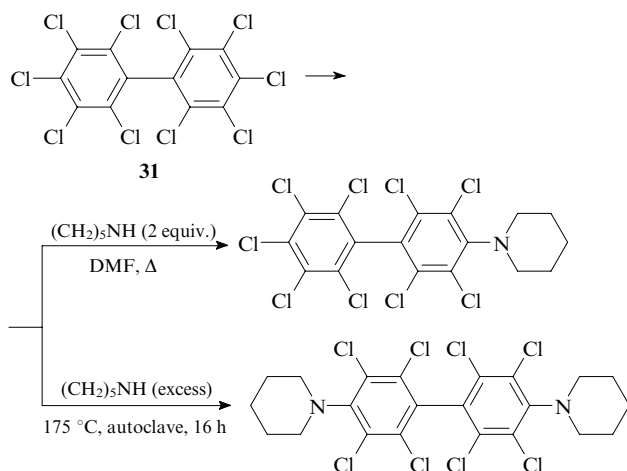


The reaction of an excess of 1,2-dichlorobenzene (**1a**) with diphenylamine and KOH in the presence of polyethylene glycol dimethyl ether at $160-165^{\circ}\text{C}$ produced *N*-(3-chlorophenyl)-*N,N*-diphenylamine in 53% yield,⁷² which is also evidence for the intermediate formation of 3-chlorobenzene. The reaction of 1,3,5-trichlorobenzene (**9a**) with hydrazine hydrate at $180-200^{\circ}\text{C}$ in pyridine produced 3,5-dichlorophenylhydrazine in 60%–82% yield.⁷³

1,2,4,5-Tetrachlorobenzene (**10b**) reacts with a strong reducing agent, Me₂NCH₂ONa, which is prepared from NaBH₄ and DMF in the presence of Cp₂TiCl₂ (Cp = η -C₅H₅). The complete conversion of the starting compound (GLC data) affords 2,4,5-trichloro-*N,N*-dimethylaniline along with the reduction product.⁷⁴

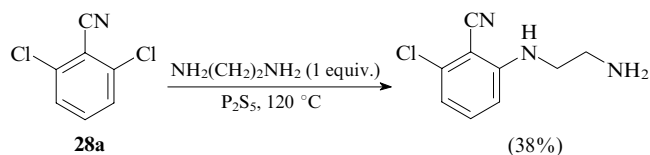


In the reaction of piperidine with decachlorobiphenyl (**31**), one or two chlorine atoms are replaced.⁷⁵ The degree of conversion depends on the reaction conditions. Thus the monosubstitution at position 4 is achieved upon refluxing in DMF, whereas prolonged heating with an excess of piperidine in an autoclave gives the 4,4'-disubstituted product.

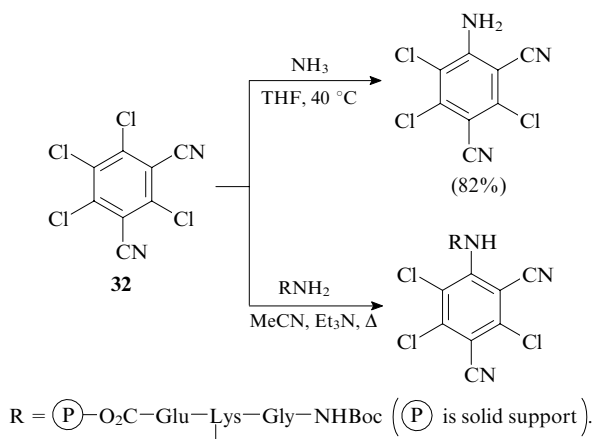


2. Substituent effect on the reactivity and regioselectivity of amination of polychloroarenes

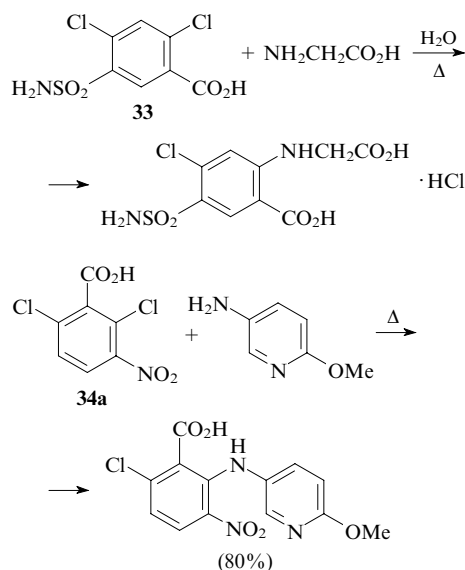
The reactivity of PCA and the pathway of amination depend on the nature and position of the substituent. For example, 2,6-dichlorobenzonitrile (**28a**) reacts with ethylenediamine at 120°C resulting in the replacement of one chlorine atom.⁷⁶ The reaction was performed in the presence of catalytic amounts of P_2S_5 to ensure the attack of ethylenediamine at the nitrile group with the aim of providing the route to the corresponding imidazolidine; however, the electrophilicity of the aromatic C—Cl fragment proved to be higher.



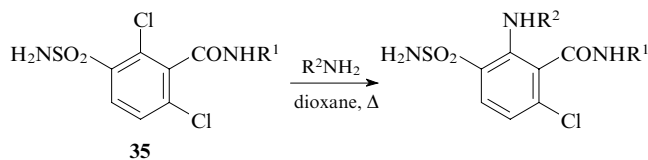
The reaction of perchloroisophthalonitrile (**32**) with ammonia proceeds under milder conditions⁷⁷ to give 3,5,6-trichloro-2,4-dicyanoaniline. In the reaction of compound **32** with an oligopeptide, it is the amino group of the lysine fragment that is involved in the replacement.⁷⁸



In the reactions of dichlorobenzoic acid derivatives **33** and **34a** with amines, one chlorine atom in the *ortho* position with respect to the carboxy group is replaced.^{79–82}

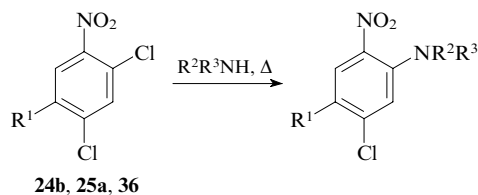


The reactions of polychlorobenzoic esters or amides with amines and hydrazines proceed analogously.⁸² For example, methyl 2,6-dichloro-3-nitrobenzoate reacts with 1 equiv. of alkylamine or hydrazine in aqueous ethanol resulting in the replacement of the chlorine atom at position 2 (82%–97% yields). In the presence of an excess of amine, both chlorine atoms are replaced to give the corresponding products in virtually quantitative yield. In the reactions of 3-aminosulfonyl-2,6-dichlorobenzamides **35** with alkyl- and benzylamines in EtOH, also one or two chlorine atoms are replaced depending on the conditions; in dioxane, the major products result from the replacement of the chlorine atom at position 2.⁸³



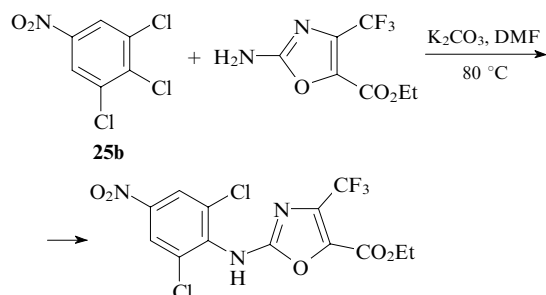
R^1	R^2	Yield (%)
H	Bn	62
	Bu ⁿ	86
2-MeC ₆ H ₄	Bn	67
	Bu ⁿ	82
Ph(CH ₂) ₂	EtO(CH ₂) ₂	88

The nitro group is a good activating substituent in the nucleophilic substitution reactions involving PCA.^{84–93} In 2,4-dichloronitrobenzene derivatives **24b**, **25a** and **36**, the chlorine atom in the *ortho* position with respect to the nitro group is replaced.^{85, 86, 88}



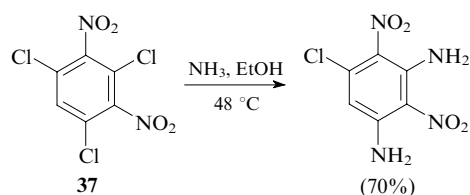
$\text{R}^1 = \text{H}$ (**24b**), Me (**36**), Cl (**25a**);
 $\text{R}^2\text{R}^3\text{N} = \text{AlkNH}$, NH_2 , $\text{N}(\text{CH}_2)_4$, N (morpholine).

In the reaction of 3,4,5-trichloronitrobenzene (**25b**) with a heterocyclic amine, the replacement occurs primarily at the chlorine atom in the *para* position with respect to the nitro group.⁹⁴

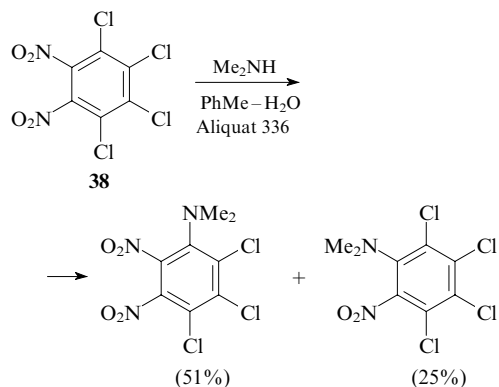


The reactions of PCA with amines proceed more rapidly at high pressure (0.6–1.0 GPa).⁹⁵ For example, 2,3,5,6-tetrachloronitrobenzene reacts with primary amines under these conditions to form the substitution product of the nitro group; in the reactions with secondary amines, the chlorine atom in the *ortho* position with respect to the nitro group is replaced. In some cases, the reactions afford mixtures of isomeric mono- and diamines. The reactions with diamines produce annelated compounds.

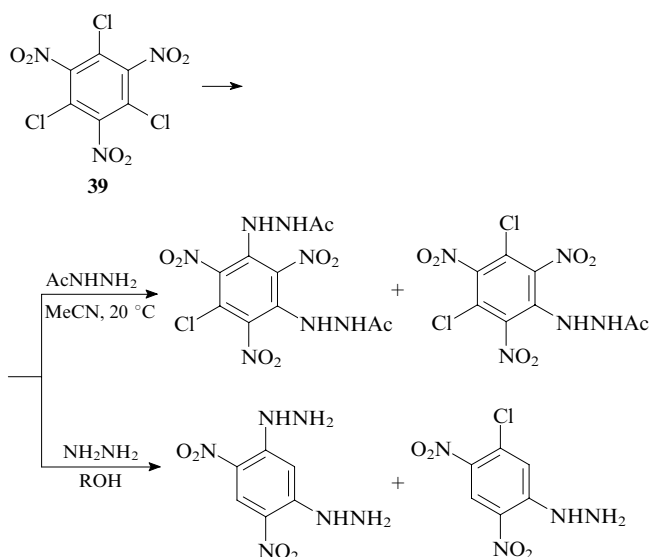
Polychloroarenes containing two nitro groups react at substantially lower temperatures. For example, ammonolysis of 2,4,6-trichloro-1,3-dinitrobenzene (**37**) proceeds at 48 °C and results in the replacement of two chlorine atoms.⁹⁶



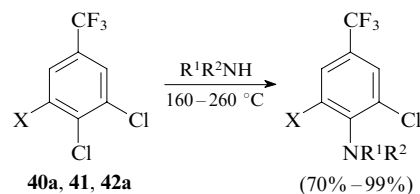
In the reactions of 1,2,3,4-tetrachlorodinitrobenzene (**38**) with amines, not only chlorine atoms, but also nitro groups are replaced.⁹⁷ As a rule, primary amines replace one of the nitro groups, whereas secondary amines replace the chlorine atom in the *ortho* position with respect to the nitro group. High yields of the substitution products were achieved in the reactions performed in the two-phase toluene–water system in the presence of tetraalkylammonium salts (for example, Aliquat 336).



Trichlorotrinitrobenzene **39** reacts with hydrazine derivatives at room temperature.⁹⁸ The reaction with acetylhydrazine affords a mixture of monosubstitution products. The reaction with unsubstituted hydrazine is accompanied by dehalogenation and denitration.

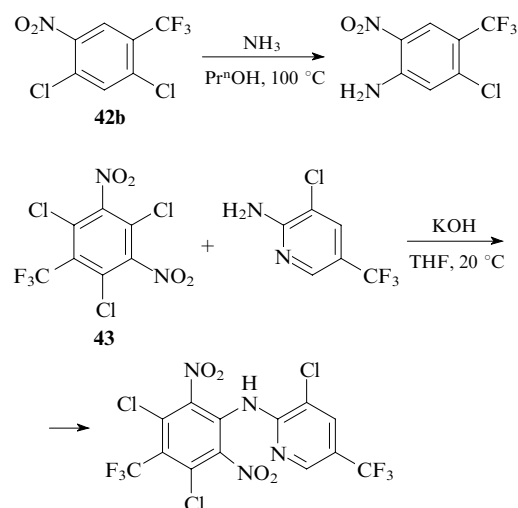


The trifluoromethyl group having a strong $-I$ effect also facilitates the replacement of the chlorine atom in PCA. However, its activating effect is weaker than the effect of $-M$ groups. The reactions of trifluoromethyl derivatives of PCA **40a**, **41** and **42a** with amines proceed, as a rule, only at high temperature.^{99–104}



X = H (**40a**), Cl (**41**), NO₂ (**42a**).

Due to the simultaneous presence of the CF₃ and NO₂ groups in chloroarenes **42b** and **43**, the reactions can be performed under milder conditions.^{105, 106}

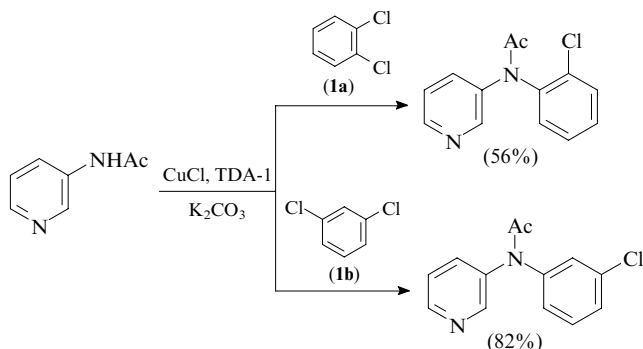


The relative reactivity of chlorine atoms in PCA depends not only on the activating substituents, but also on the polarisability of the nucleophile.¹⁰⁷ For example, 2,4,6-trichloro-3,5-bis(trifluoromethylsulfonyl)nitrobenzene reacts with sodium azide (a soft nucleophile) in methanol at -80 °C to form a mixture of substitution products. However, harder nucleophiles, such as piperidine and 4-acetylaminobenzene, selectively replace one chlorine atom in the *ortho* position with respect to the nitro group.

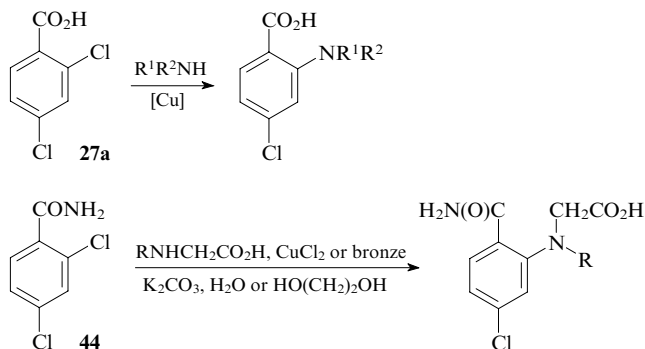
3. Catalytic amination of polychloroarenes

Copper salts and oxides catalyse amination of non-activated PCA. The reactions of 1,3-dichloro-substituted tetrafluoro- and 2,4,6-trifluorobenzenes with aqueous ammonia in the presence of CuCl in an autoclave at 140 °C were found to proceed non-selectively to give mixtures of amination and hydrodechlorination products.¹⁰⁸ The reactions of 1,2- and 1,4-dichlorobenzenes (**1a,c**) with ammonia in the presence of copper oxide at 180–240 °C produce the corresponding phenylenediamines.¹⁰⁹

Ultradispersed (nanosized) copper, which is formed *in situ* by the reaction of tris(3,6-dioxaheptyl)amine (TDA-1) with copper salts, proved to be an efficient catalyst for the reaction of *N*-(3-pyridyl)acetamide with dichlorobenzenes **1a,b**.¹¹⁰ The solvent-free reaction was carried out by refluxing the reactants with azeotropic distillation of water.

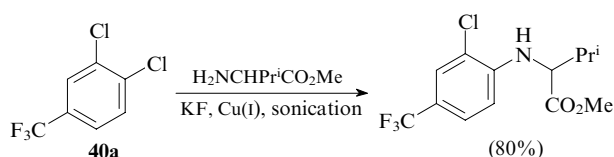


In some cases, it is reasonable to perform the amination of PCA bearing electron-withdrawing substituents in the presence of copper or its salts as the catalyst. For example, 2,4-dichlorobenzoic acid (**27a**) and its amide (**44**) react with amines in the presence of copper or its salts resulting in the replacement of the *ortho*-chlorine atom with respect to the electron-withdrawing group.^{111–119}

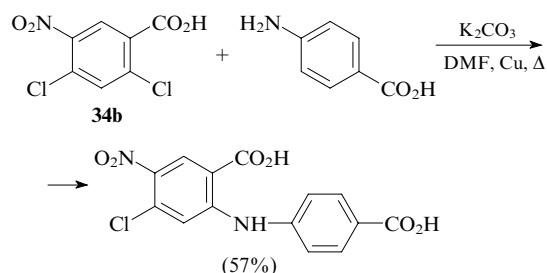


R = H (55%), 4-FC₆H₄ (80%).

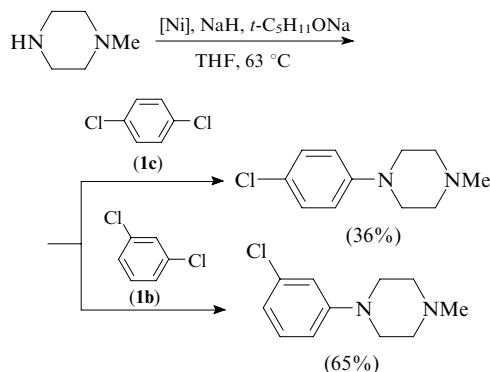
In the reaction of valine methyl ester with 3,4-dichloro(trifluoromethyl)benzene (**40a**) catalysed by Cu(I) salts using sonication, the chlorine atom in the *para* position with respect to the CF₃ group is replaced to give the corresponding substitution product in high yield.¹²⁰ Without sonication, the yield is as low as 10%.



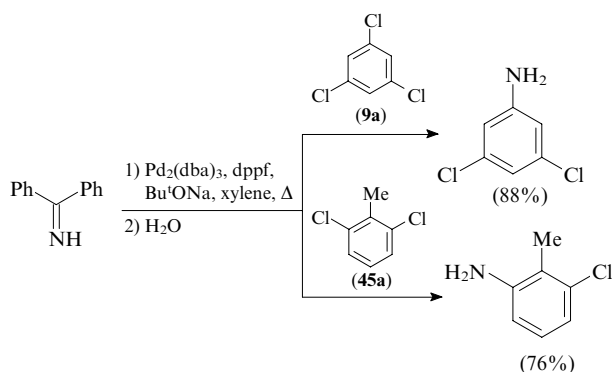
4-Aminobenzoic acid in which the nucleophilicity of the amino group is lower than that in aniline reacts with 2,4-dichloro-5-nitrobenzoic acid (**34b**) in boiling DMF in the presence of copper powder to give 2-(4-carboxyanilino)-4-chloro-5-nitrobenzoic acid.¹²¹



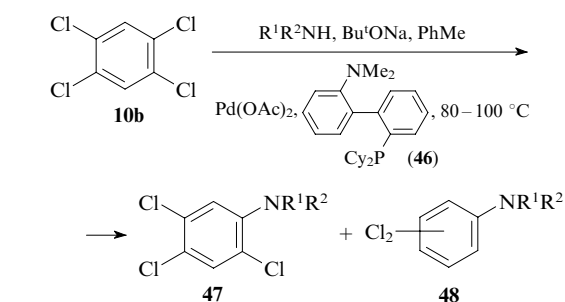
Nickel complexes with the 1,1'-bis(diphenylphosphino)ferrocene (dppf), 1,10-phenanthroline (phen) and 2,2'-bipyridyl (bipy) ligands were examined as catalysts for amination of PCA.¹²² Under these conditions, 1-methylpiperazine reacts with 1,3- and 1,4-dichlorobenzenes (**1b,c**), resulting in the replacement of only one chlorine atom.



Amination of PCA (for example, of compounds **9a** and **45a**) with benzophenone imine can be performed with the use of the catalytic Pd₂(dba)₃–dppf system (dba is dibenzylideneacetone).¹²³ After hydrolysis in the final step, the corresponding aniline derivatives are obtained in good yields.



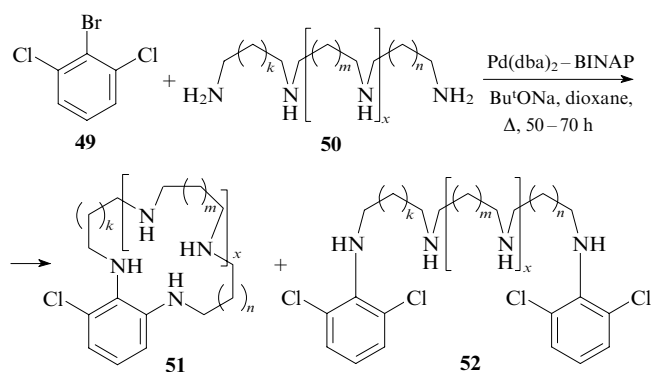
Cross-coupling of 1,2,4,5-tetrachlorobenzene (**10b**) with primary and secondary amines in the presence of Pd(OAc)₂ and ligand **46** according to a developed procedure¹²⁴ afford compounds **47** as a result of the replacement of one chlorine atom.^{125, 126} The reaction is accompanied by reductive dechlorination to dichloroaniline derivatives **48**. Hexachlorobenzene (**5**) does not react with amines under the above-mentioned conditions.



R¹R²N	Yield (%)	
	47	48
(CH₂)₄N	26	10
O(CH₂CH₂)₂N	25	41
BuⁱNH	72	4

Amination of chloroarenes with *trans*-di(μ -acetato)bis{2-[di(*tert*-butyl)phosphino]-2-methylpropyl-C,P}dipalladium (which was prepared by heating Pd(OAc)₂ with Bu₃P in toluene) was covered by the patent.¹²⁷ This method was used for the synthesis of *N*-(4-chlorophenyl)piperidine (59% yield) and 1,4-bis(dibutylamino)benzene (77% yield) by the reactions of 1,4-dichlorobenzene (**1c**) with piperidine or dibutylamine, respectively.

Cross-coupling of 1-bromo-2,6-dichlorobenzene (**49**) with polyamines **50** catalysed by the Pd(dba)₂–BINAP system [BINAP is 2,2'-bis(diphenylphosphino)-1,1'-binaphthyl] proceeds slowly.¹²⁸ However, cyclisation products **51** were prepared by refluxing the reactants in dioxane over a long period of time (50–70 h), the yields being dependent on the length and conformational flexibility of the polyamine chain. The structures of linear by-products **52** provide evidence that the bromine atom is replaced in the first step of the reaction. No cyclisation products are formed in the reaction with the diamino ether H₂N(CH₂CH₂O)₂CH₂CH₂NH₂.



<i>k</i>	<i>m</i>	<i>n</i>	<i>x</i>	Yield (%)	
				51	52
1	0	1	1	47	—
0	0	0	1	27	—
0	1	0	1	17	—
0	0	0	2	12	17
0	0	0	3	10	21

The results of studies on the reactions of mono- and polynuclear chloroarenes in the presence of catalytic systems

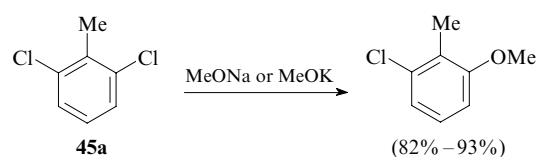
containing a source of palladium combined with BINAP,^{129–131} 1-diphenylphosphino-2-(1-methoxyethyl)ferrocene¹³² or tri(*tert*-butyl)phosphine¹³³ may be useful for performing the C–N cross-coupling reactions of PCA.

IV. Reactions with O-nucleophiles

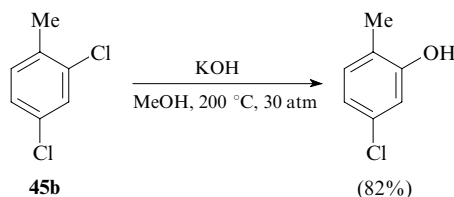
Chlorine atoms in PCA can be replaced by O-nucleophiles to form phenols or their ethers.

1. Reactivity of polychloroarenes towards O-nucleophiles in the presence of bases

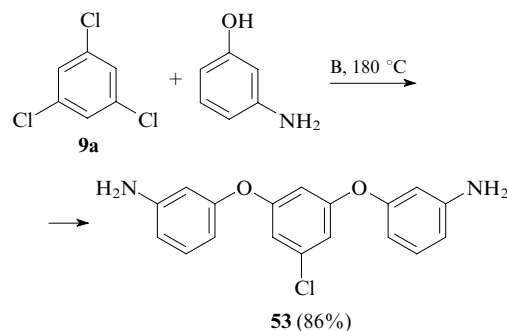
Isomeric dichlorobenzenes react with NaOMe in HMPA to form the corresponding chloroanisoles.¹³⁴ In the reactions of 2,6-dichlorotoluene (**45a**) with potassium or sodium methoxides in aprotic solvents, one chlorine atom is replaced.^{135–138} The reaction rate can be increased by addition of copper compounds; however, the resulting aryl methyl ether undergoes partial demethylation.



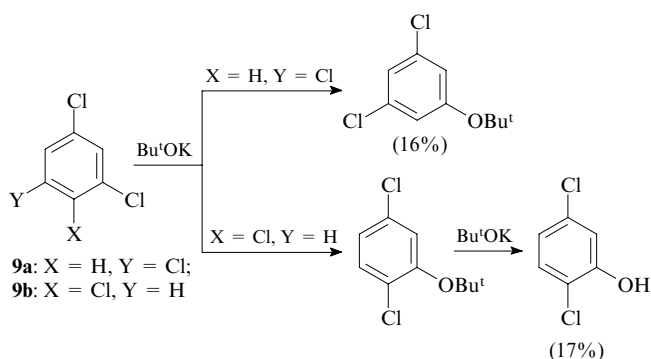
The reaction of 2,4-dichlorotoluene (**45b**) with KOH in methanol at 200 °C and 30 atm produced 5-chloro-2-methylphenol.¹³⁹ At lower pressure (12 atm), the product was obtained in substantially lower yield (12%).



3-Aminophenol reacts with 1,3,5-trichlorobenzene (**9a**) as the O-nucleophile to give diether **53**.¹⁴⁰ In this reaction, K₂CO₃ or NaOMe was used as the base (B) and HMPA or NMP as the solvent.

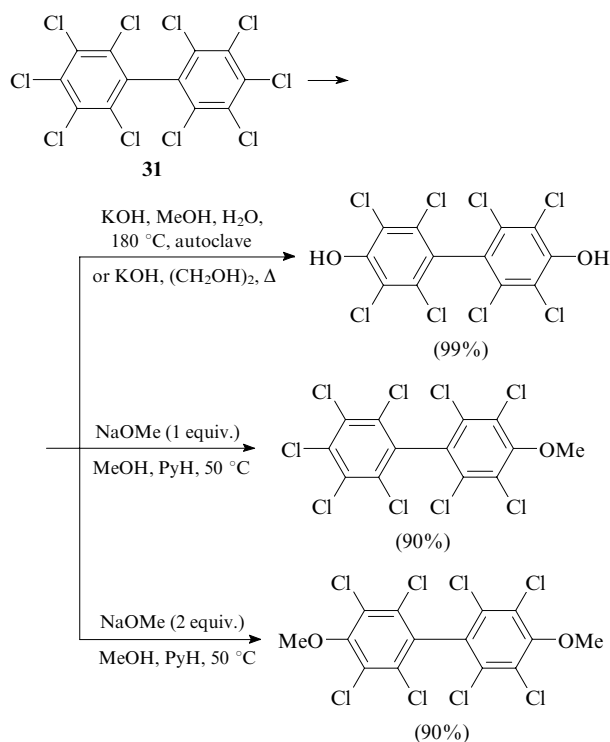


The reactions of 1,3,5- (**9a**) and 1,2,4-trichlorobenzenes (**9b**) with BuⁱOK in HMPA¹⁴¹ resulted in the replacement of one chlorine atom to give the corresponding substitution products in low yields. In the case of isomer **9b**, the initially formed ether undergoes dealkylation to give 2,5-dichlorophenol.



Unlike compounds **9a,b**, 1,2,3,5-tetrachlorobenzene (**10c**) undergoes disproportionation under these conditions to form a mixture of 1,2,4,5-tetrachlorobenzene (**10b**), pentachlorobenzene (**2**) and isomeric trichlorobenzenes.¹⁴¹

Hexachlorobenzene (**5**) reacts with potassium *tert*-butoxide in THF¹⁴² or with the $Pr^iOH-NaOH$ system¹⁴³ to give the corresponding alkyl pentachlorophenyl ethers in 67% and 92% yields, respectively. The reaction of decachlorobiphenyl (**31**) with KOH in aqueous methanol (autoclave, 180 °C) or in boiling ethylene glycol produces 4,4'-dihydroxyoctachlorobiphenyl in quantitative yield.¹⁴⁴ In the reaction of decachlorobiphenyl (**31**) with sodium methoxide in a $MeOH$ –pyridine mixture (PyH), one or two chlorine atoms at positions 4 and 4' are replaced depending on the amount of the nucleophile.⁷⁵



The reactions of octachloronaphthalene (**16**) with alkali metal hydroxides and alkoxides were investigated.^{142, 145} Although the reaction conditions are substantially different, it should be noted that the attack of the alkoxide ion occurs predominantly on position 1 of the naphthalene ring; the attack of the hydroxide ion, on position 2. These reactions produce compounds **54a** and **54b**, respectively (Table 6).

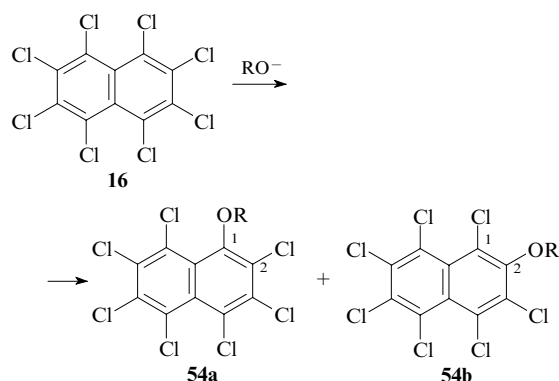
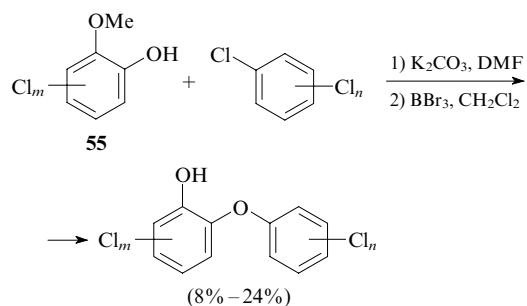


Table 6. Reactions of octachloronaphthalene (**16**) with alkali metal derivatives.^{142, 145}

R	Reagent	Solvent	Temperature / °C	Yield (%)	54a : 54b
Me	MeONa	pyridine	115	25 ^a	90 : 10
Me	MeOH, NaOH		~ 100	63	99 : 1
Bu ^t	Bu ^t OK	THF	20	82	85 : 15
H	KOH	DMSO	120	90	30 : 70

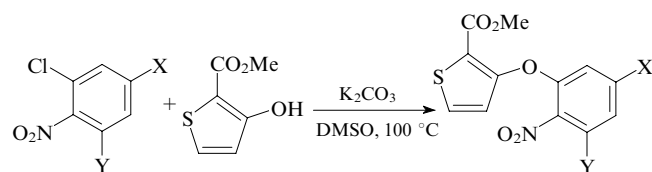
^a Disubstituted (25% yield) and trisubstituted (20%) products were also isolated.

Polychlorinated *o*-hydroxylated diphenyl oxides were synthesised by the reactions of polychlorobenzenes with (poly)chloroguaiaacols **55** in the K_2CO_3 –DMF system followed by demethylation of the substitution products with boron tribromide.¹⁴⁶



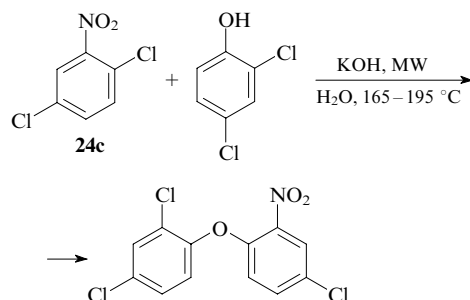
$m = 0-4; n = 2-5$.

As mentioned above, the presence of an electron-withdrawing substituent in the aromatic ring increases the reactivity of PCA, due to which the reactions with O-nucleophiles can be performed under milder conditions. In these reactions, it is the chlorine atom in the *ortho* position with respect to the electron-withdrawing group that, as a rule, undergoes replacement. For example, the reaction of 2,4-dichlorobenzoic acid (**27a**) with chlorophenols in pyridine in the presence of K_2CO_3 afforded *ortho*-substitution products (in approximately 70% yields).¹⁴⁷ In the reactions of 2,4- (**24b**) and 2,6-dichloronitrobenzenes (**24d**) with hydroxythiophene derivatives in DMSO at 100 °C, the chlorine atom in the *ortho* position with respect to the nitro group is replaced to give the products in 57% and 84% yields, respectively.¹⁴⁸

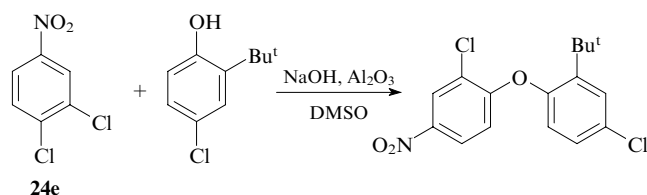


24b: X = Cl, Y = H;
24d: X = H, Y = Cl

The reactions of 2,5-dichloronitrobenzene (**24c**) with substituted phenols,^{149, 150} including the microwave (MW)-promoted reactions, are characterised by analogous regioselectivity.¹⁵¹

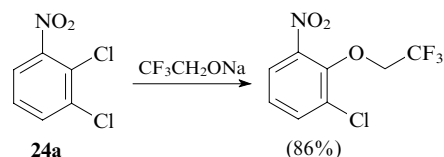


In the reactions of 3,4-dichloronitrobenzene (**24e**)^{152, 153} and 3,4-dichloro-1-trifluoromethylbenzene (**40a**)¹⁵⁴ containing no chlorine atoms in the *ortho* position with respect to the electron-withdrawing group, the attack of O-nucleophiles occurs on the *para* position; for example:



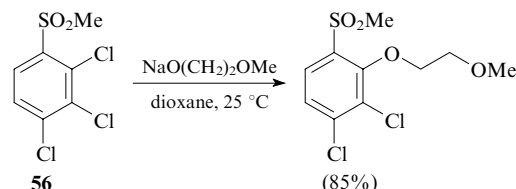
The *para* position in the aromatic ring is more active in hydrolysis of 1-substituted 3,4-dichlorobenzenes. For example, hydrolysis of 3,4-dichloronitrobenzene (**24e**) (15% NaOH in MeOH, 72 °C) affords 2-chloro-4-nitrophenol with the regioselectivity of >99%.¹⁵⁵ The reaction of 3,4-dichlorotrifluoromethylbenzene (**40a**) with the Bu^tOH–KOH system in DMSO at 75 °C produces 2-chloro-4-trifluoromethylphenol in 27% yield.¹⁵⁶ Interestingly, the hydroxy group replaces the Cl atom in the *meta* position with respect to the nitro group in 2,5-dichloronitrobenzene (**24c**) upon hydrolysis of the latter with aqueous NaOH.¹⁵⁷

The reactions of dichloronitrobenzenes **24** with sodium 2,2,2-trifluoroethoxide proceed under more drastic conditions (in DMF or HMPA at 150 °C under N₂).¹⁵⁸ The reactivity of the chlorine atoms increases in the following sequence: *ortho* position > *para* position > *meta* position. For example, under these reaction conditions, the chlorine atom in the *ortho* position with respect to the nitro group is replaced in 2,3- and 2,5-dichloronitrobenzenes (**24a,c**), the reaction of 2,4 isomer **24b** affords a mixture of the *ortho*- and *para*-substituted products in a ratio of 3 : 1, and 3,4 isomer **24e** gives the *para*-substituted product.

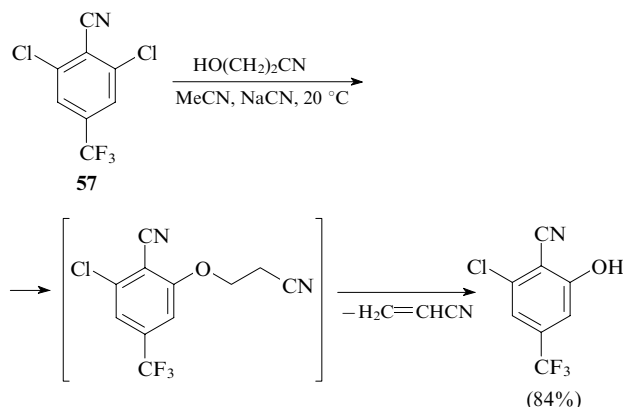


The reactions of sodium 2,2,2-trifluoroethoxide with dichlorobenzonitriles proceed analogously to form products in higher yields.

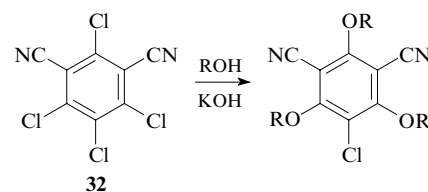
The reactions of trichloroarenes containing electron-withdrawing substituents proceed analogously. For example, the replacement of the chlorine atom in sulfone **56** in the reaction with sodium 2-methoxyethoxide also occurs at the *ortho* position.^{159, 160}



The reactions of dichlorobenzenes containing two or more electron-withdrawing groups with O-nucleophiles were documented.^{161, 162} The product of the replacement at the *para* position with respect to the trifluoromethyl group was prepared in 75% yield by refluxing 3,4-dichloro-2-nitro-6-trifluoromethylbenzene (**42c**) with 3-hydroxybenzoate in acetone in the presence of potassium carbonate. In the reaction of 2,4-dichloro-3,5-dinitrotrifluoromethylbenzene (**43**) with ethyl 3-hydroxybenzoate in acetone at room temperature, the chlorine atom at position 4 is also replaced,¹⁶¹ and the subsequent nitration affords ethyl 5-(3-chloro-2,6-dinitro-4-trifluoromethylphenoxy)-2-nitrobenzoate in a total yield of 83%. 2,6-Dichloro-4-trifluoromethylbenzonitrile (**57**) reacts with HOCH₂CH₂CN and NaCN in acetonitrile at room temperature. In this case, acrylonitrile is eliminated from the initially formed β-cyanoethyl ether to give the corresponding phenol.¹⁶²



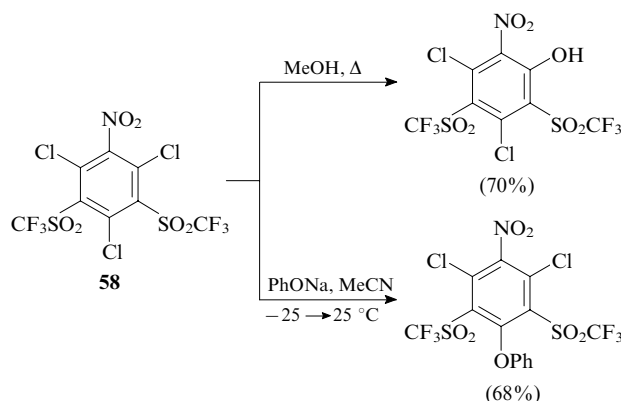
Three chlorine atoms are replaced in perchloroisophthalonitrile (**32**) by refluxing it in alcoholic solutions of KOH.¹⁶³



R = Me (79% yield), Et (58%).

Due to high electrophilicity, the chlorine atom at position 2 in 2,4,6-trichloro-1-nitro-3,5-bis(trifluoromethylsulfonyl)benzene (**58**) is replaced by the hydroxy group upon refluxing in methanol even in the absence of bases (apparently, due to the presence of water in methanol).¹⁰⁷ In the reaction of compound

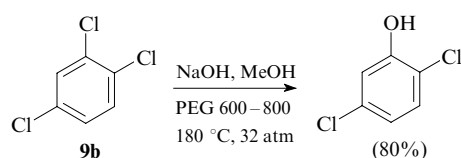
58 with sodium phenoxide in acetonitrile, it is the chlorine atom at position 4 that is replaced.



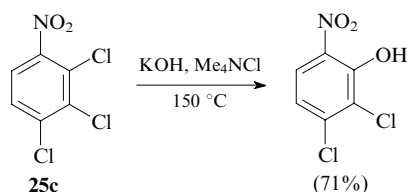
2. Reactions of polychloroarenes with O-nucleophiles in the presence of catalysts

In some cases, the reactions of PCA with O-nucleophiles are notably promoted by phase-transfer catalysts, metal complex catalysts or enzymes. Let us consider several reactions performed in the presence of phase-transfer catalysts. The reaction of 1,2-dichlorobenzene (**1a**) with the KOH–MeOH system in the presence of 18-crown-6 at 0 °C afforded 2-chloroanisole in 60% yield.¹⁶⁴ 2,4-Dichlorotoluene (**45b**) reacts with KOH in ethylene glycol at 200 °C and 30 atm in the presence of dibenzo-18-crown-6 to give 5-chloro-2-methylphenol in 78% yield.¹³⁹ The reaction of 1,2,3-trichlorobenzene (**9c**) with methanolic KOH at 140 °C in the presence of TDA-1 as the PTC affords a mixture of dichloroanisoles in a total yield of 97%;¹⁶⁴ in the absence of PTC, the yields of the products decrease to 8%.

Hydrolysis of 1,2,4-trichlorobenzene (**9b**) with methanolic NaOH in the presence of poly(ethylene glycol) (PEG 600–800) gives 2,5-dichlorophenol.¹⁶⁵

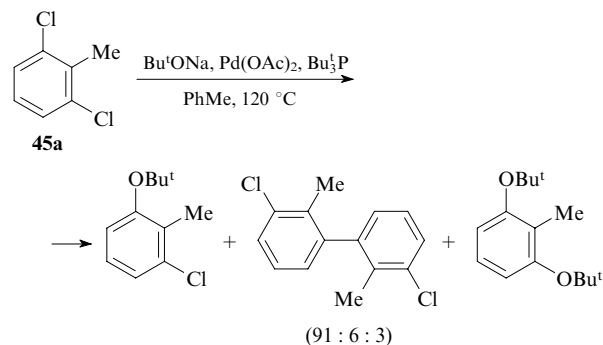


The replacement of the chlorine atom mainly in the *ortho* position with respect to an electron-withdrawing group is observed also in catalytic reactions. 2,3,4-Trichloronitrobenzene (**25c**) reacts with KOH in DMSO in the presence of tetramethylammonium chloride at 150 °C in an autoclave to form 2,3-dichloro-6-nitrophenol.¹⁶⁶

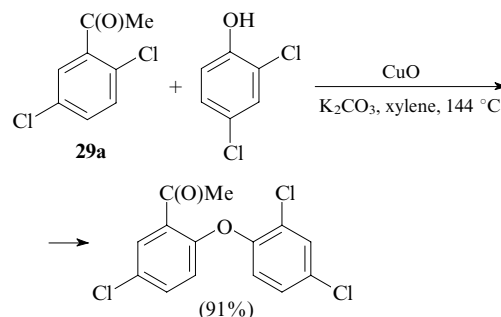


In addition to PTC, the C–O bond formation in the reactions of PCA is promoted by transition metal compounds. For example, 2,6-dichlorotoluene (**45a**), which is poorly reactive in the absence of catalysts, reacts with sodium *tert*-butoxide in toluene in the presence of the Pd(OAc)₂–Bu₃P system¹⁶⁷ to form 2-(*tert*-butoxy)-6-chlorotoluene. In this reaction, the homodimerisation product of PCA and

2,6-bis(*tert*-butoxy)toluene were isolated as the by-products. The use of the PCy₃ and dppf ligands combined with a palladium salt proved to be less efficient.

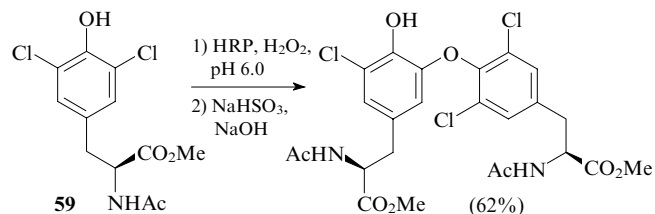


Copper compounds are used as catalysts for the C–O cross-coupling involving dichlorobenzenes with electron-withdrawing groups. For example, the reaction of 2,5-dichloroacetophenone (**29a**) with 2,4-dichlorophenol in the presence of CuO resulted in the replacement of the chlorine atom in the *ortho* position of the benzene ring of ketone.¹⁶⁸ In the absence of catalysts (heating of compound **29a** with KOH in xylene), the yield of the product decreases to 82%.¹⁶⁹



In the reactions of 2,5-dichlorobenzoic acid with 3- and 4-chlorophenols (Cu, CuI, NaOMe, MeOH, 200 °C), the chlorine atom at position 2 was replaced to give the products in 78%–82% yield.¹⁷⁰

Enzymatic dimerisation of dichlorotyrosine (**59**) catalysed by horseradish peroxidase (HRP) formally proceeds as the nucleophilic substitution of one chlorine atom to yield an isodityrosine derivative.^{171–173}



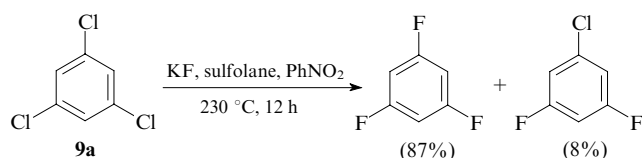
V. Reactions with F-nucleophiles

A convenient procedure for the synthesis of fluorine-containing aromatic compounds is based on the replacement of chlorine atoms in PCA under the action of metal fluorides. Considerable data on fluorodechlorination reactions of arenes were covered by patents, which is evidence that this approach is of practical importance. Data on this problem were summarised in the review¹⁷⁴ and monographs.^{175, 176}

1. Reactivity of polychloroarenes in fluorodechlorination

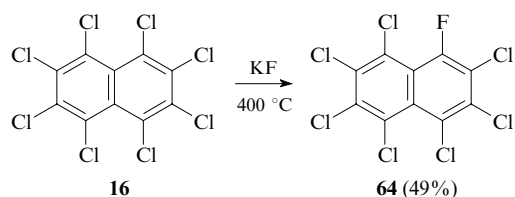
The fact that it is possible, in principle, to transform PCA into polyfluoroarenes was demonstrated for the first time in 1947.¹⁷⁷ The reaction of hexachlorobenzene (**5**) with BrF_3 followed by the successive treatment of the resulting mixture of perhalocyclohexanes $\text{C}_6\text{Br}_2\text{Cl}_4\text{F}_6$ with SbF_5 and zinc dust produced a mixture of chlorofluorobenzenes $\text{C}_6\text{Cl}_n\text{F}_{6-n}$ ($n = 0-6$). Individual reaction products, including hexafluorobenzene (**60**, ~10% yield), were isolated by rectification.

Later, available alkali and alkaline-earth fluorides have been used as fluorination agents. The reactions of non-activated PCA, for example, of 1,3,5-trichlorobenzene (**9a**), with metal fluorides are performed in polar aprotic solvents (sulfolane, DMF, *etc.*) under rather drastic conditions.^{178, 179} The necessity of using high temperatures is determined by low solubility of inorganic fluorides in organic solvents and their ability to form stable weakly nucleophilic hydrates.



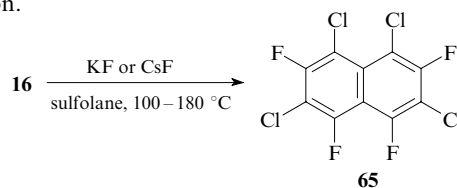
The reaction of hexachlorobenzene (**5**) with KF in an autoclave at 460–470 °C for 20 h and then at 490–510 °C for 10 h produced a mixture containing hexafluorobenzene (**60**) and chloropentafluorobenzene (**61**).^{180, 181} At lower temperatures (400–480 °C, 19–35 h), the yield of hexafluorobenzene (**60**) was at most 6%.¹⁸² In the presence of water vapour,¹⁸³ fluorodechlorination is accompanied by the replacement of one chlorine atom with hydrogen to form a large set of polyhalobenzenes, including compounds **60–63** (Scheme 1).

Heating of octachloronaphthalene (**16**) with KF in an autoclave (300–330 °C, 25 h) gave a mixture of products, from which octafluoronaphthalene (24%) was isolated by rectification.¹⁸⁴ According to the data of another study,¹⁸⁵ this reaction at 400 °C, even in the presence of a tenfold excess of KF, afforded heptachloro-1-fluoronaphthalene (**64**) as the major product.

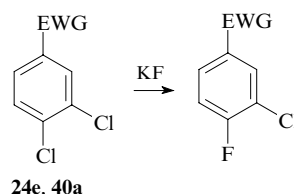


The increase in the temperature to 420 °C resulted in the formation of a mixture of higher fluorodechlorinated products from which 1- and 2-chloro-substituted heptafluoronaphtha-

lenes were isolated in 14.5% and 9.5% yields, respectively. The reaction of octachloride **16** in sulfolane affords a mixture of fluorodechlorination products containing from 1 to 4 fluorine atoms.¹⁸⁶ Individual 2,4,5,7-tetrachloro-1,3,6,8-tetrafluoronaphthalene (**65**) was isolated from the mixture by sublimation.

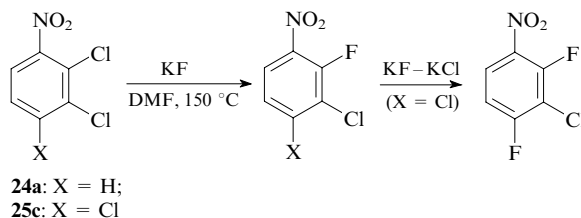


Polychloroarenes containing additional electron-withdrawing substituents in the aromatic nucleus are more reactive in fluorodechlorination compared to polychlorobenzenes, the reaction often being regioselective. For example, fluorodechlorination of *o*-dichlorobenzenes **24e** and **40a** containing electron-withdrawing groups at position 1 gives 4-fluoro derivatives.^{187–189} The reactions with KF are carried out in aprotic solvents (DMSO, DMF, NMP, sulfolane or DMAA) at 190–250 °C; the products are formed in yields of up to 90%.



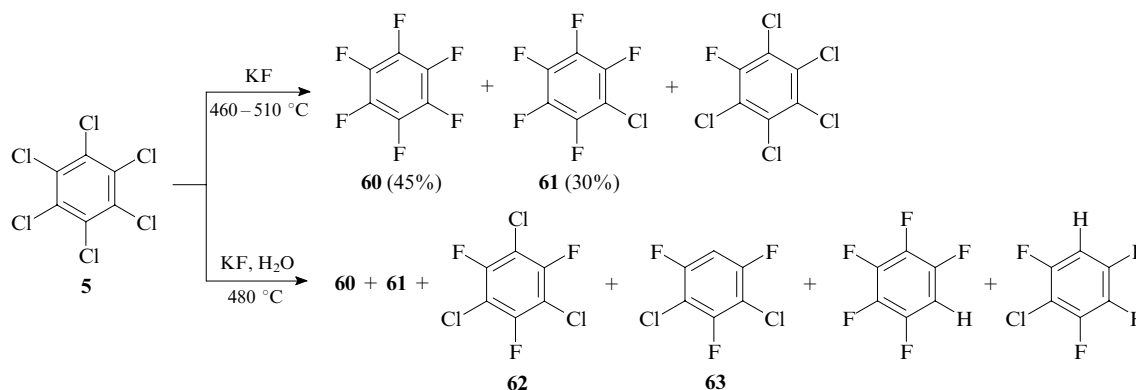
EWG = NO_2 (**24e**), CF_3 (**40a**).

The chlorine atom in the *ortho* position with respect to the electron-withdrawing substituent is, as a rule, replaced in 1-nitro-substituted chlorobenzenes **24a**^{190–192} and **25c**.¹⁹³ However, it has been possible to replace the chlorine atoms in the *ortho* and *para* positions by refluxing compound **25c** in DMF in the presence of a mixture of KF and KCl.¹⁹⁴

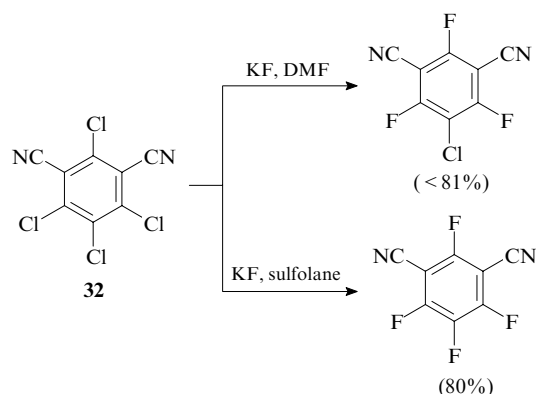


The cyano group serves as a good activating substituent in polychloroarenes. For example, fluorodechlorination of pentachlorobenzonitrile with KF at 350 °C in an autoclave results in pentafluorobenzonitrile in 70% yield.¹⁹⁵ An analogous

Scheme 1

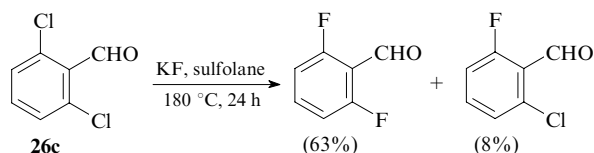


reaction of tetrachlorophthalonitrile proceeds at 300 °C (the yield of the tetrafluoro derivative is 74%).¹⁹⁶ The reaction of 2,3,4,5-tetrachlorobenzonitrile with KF in sulfolane affords a mixture of fluorodechlorination products, including 2,3,4,5-tetrafluorobenzonitrile.¹⁹⁷ The reaction of tetrachloroisophthalonitrile (**32**) with KF in DMF resulted in the replacement of three chlorine atoms in the *ortho* positions with respect to the cyano groups.^{198–201} All four chlorine atoms in compound **32** can be replaced by performing the reaction in sulfolane.²⁰²



It should be noted that the reaction of 2,4-dichloro-5-fluorobenzoyl fluoride with KF in aprotic solvents gives 2,4,5-trifluorobenzoyl fluoride as the major product.²⁰³

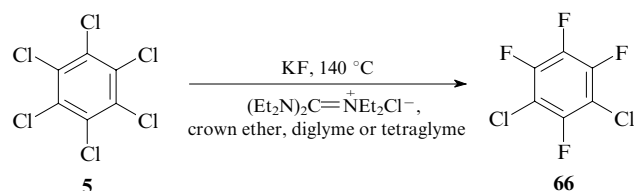
In spite of drastic conditions, PCA containing the labile aldehyde group undergo fluorodechlorination. For example, the reaction of 2,6-dichlorobenzaldehyde (**26c**) with KF in sulfolane at 180 °C affords 2,6-difluorobenzaldehyde in good yield, while the monofluoro derivative is formed as a by-product.¹⁷⁹



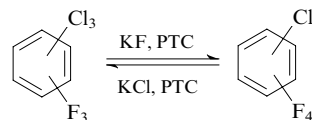
2. The means for activation of fluorodechlorination

The use of PTC (quaternary ammonium or phosphonium salts) facilitating the transfer of fluoride anions to an organic phase is one of ways of promoting fluorodechlorination of PCA.²⁰⁴ The use of salts of HF with organic bases, for example, $\text{Ph}_4\text{P}^+(\text{HF}_3)^-$,²⁰⁵ or fluorides with organic cations, such as Me_4NF , as fluorination agents was documented.²⁰⁶

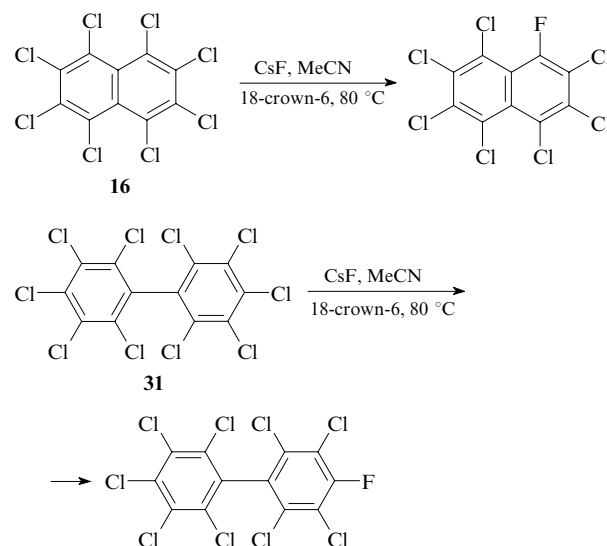
Fluorodechlorination of hexachlorobenzene (**5**) with KF supported on CaF_2 or BaF_2 in the presence of $(\text{Et}_2\text{N})_4\text{PBr}$ as the catalyst at 230 °C in an autoclave affords a mixture of arenes C_6ClF_5 (**61**, 25% yield), $\text{C}_6\text{Cl}_2\text{F}_4$ (**45**) and $\text{C}_6\text{Cl}_3\text{F}_3$ (**62**, 30%).²⁰⁷ Under the above-mentioned conditions, no reaction proceeds in the absence of catalysts. Hexaethylguanidium chloride in combination with crown ethers, diglyme or tetraglyme can be used as PTCs.²⁰⁸ The reaction of hexachlorobenzene (**5**) in the presence of this catalytic system gave a mixture of isomeric products, resulting from the substitution of four chlorine atoms, 1,2,3,5-tetrafluoro derivative **66** being the major product (> 90%).



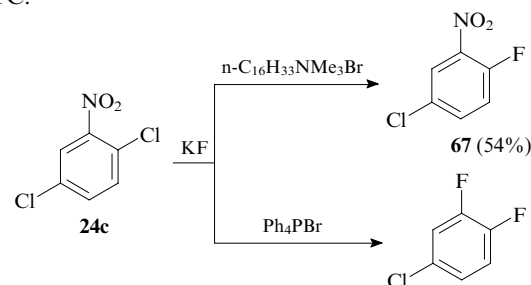
The inhibition of the subsequent fluorodechlorination of compound **66** is, apparently, attributed to an increase in the concentration of chloride ions with rather high nucleophilicity. The suggestion that the fluorodechlorination is reversible was confirmed in the study,²⁰⁹ where the possibility of transforming $\text{C}_6\text{Cl}_2\text{F}_4$ into trichlorotrifluorobenzene was demonstrated.



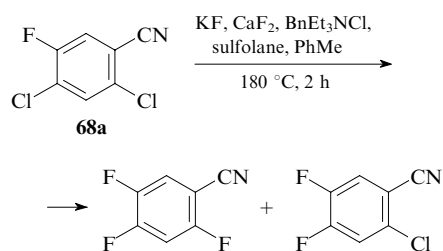
The 18-crown-6-catalysed fluorodechlorination of binuclear PCA **16** and **31** with CsF under mild conditions (MeCN , 80 °C)²¹⁰ allows the selective introduction of one fluorine atom at positions 1 and 4, respectively.



Phase-transfer catalysts are successfully used for fluorodechlorination of PCA containing additional electron-withdrawing substituents. In these reactions, the chlorine atoms in the *ortho* and *para* positions with respect to these substituents are generally replaced. For example, the reaction of 2,3-dichloronitrobenzene (**24a**) with KF in xylene in the presence of trimethyl(ethoxypolyoxypropyl)ammonium chloride produced 3-chloro-2-fluoronitrobenzene in 72% yield.²¹¹ Under these conditions, both chlorine atoms are replaced in 2,6-dichlorobenzonitrile (**28a**)²¹² and 2,4-dichloronitrobenzene (**24b**).²¹³ The fluorodechlorination of 2,5-dichloronitrobenzene (**24c**) in the presence of trimethylcetylammmonium bromide at 140–150 °C affords product **67**.^{214, 215} The nitro group is also replaced in the reaction with the use of Ph_4PBr as the PTC.²¹⁶



The reaction of 2,4-dichloro-5-fluorobenzonitrile (**68a**) with KF supported on CaF_2 in the presence of BnEt_3NCl produces a mixture of 2,4,5-trifluoro- and 2-chloro-4,5-difluorobenzonitriles in a total yield of 82%.^{198, 217}



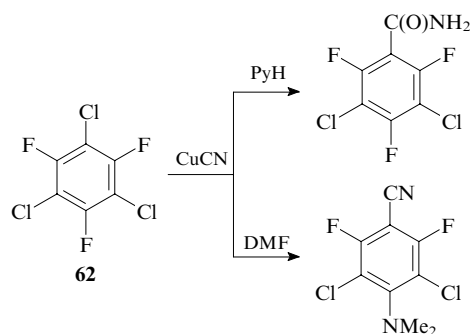
Fluorodechlorination of 3,4-dichlorobenzonitrile (**28b**) with KF in DMSO in the presence of PTCs of the iminium series, such as $(R_2^1N)_2C=N^+=C(NR_2^2)_2Hal^-$, $(R_2^1N)_2C=N^+=P(NR_2^2)_3Hal^-$ or $(R_2^1N)_3P=N^+=P(NR_2^2)_3Hal^-$ ($R^1, R^2 = Alk$), occurs exclusively at position 4 (the yield of the product is 81%–92%).²¹⁸ Polychloroarenes containing chlorine atoms in the *meta* position with respect to an electron-withdrawing substituent are much less reactive. For example, only one chlorine atom is replaced in 3,5-dichloro-4-fluorobenzonitrile (**68b**) or 3,5-dichloro-4-fluoro-1-trifluoromethylbenzene in the reaction with KF in sulfolane in the presence of PTC.²¹⁹

Fluorodechlorination of PCA is promoted by sonication.^{187, 220} For example, the reaction of 3,4-dichloronitrobenzene (**24e**) with KF and *N*-(2-ethylhexyl)-4-(*N,N*-dimethylamino)pyridinium bromide on polystyrene in DMSO promoted by sonication produced 3-chloro-4-fluoronitrobenzene in 95% yield.²²⁰

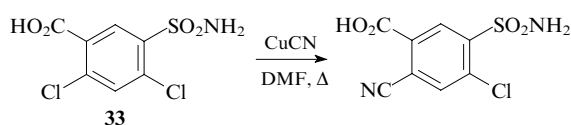
VI. Reactions with C-nucleophiles

1. Cyanation reactions

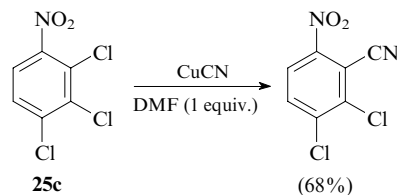
The reactions of PCA with copper cyanide produce the corresponding chlorobenzonitriles generally in low yields. For example, the yield of pentachlorobenzonitrile in the reaction of hexachlorobenzene (**5**) with CuCN was only 4%.²²¹ 3,5-Dichloro-2,4,6-trifluorobenzamide and 3,5-dichloro-2,6-difluoro-4-dimethylaminobenzonitrile were synthesised by the reaction of 2,4,6-trichloro-1,3,5-trifluorobenzene (**62**) with CuCN in pyridine and DMF, respectively.²²²



In 5-aminosulfonyl-2,4-dichlorobenzoic acid (**33**), the chlorine atom at position 2 is replaced upon heating with CuCN in DMF to give the derivative of phthalic acid mononitrile.²²³



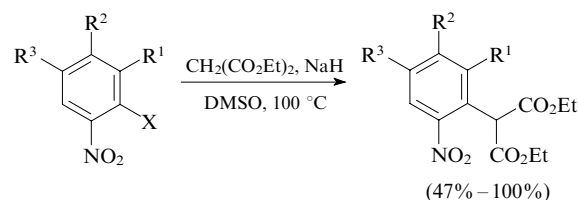
2,3,4-Trichloronitrobenzene (**25c**) is transformed into 5,6-dichloro-2-nitrobenzonitrile in the reaction with CuCN in the presence of 1 equiv. of DMF.²²⁴



The yield of the cyanation product can be increased in the presence of transition metal complexes as catalysts. For example, the reaction of 1,4-dichlorobenzene (**1c**) with KCN catalysed by Pd or Ni complexes at 100–250 °C produces terephthalonitrile in 87% yield.²²⁵

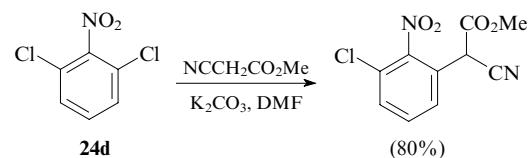
2. Reactions of polychloroarenes with carbanions

Polychloroarenes activated by the nitro group readily react with anions of CH acids (malonic and cyanoacetic esters, *etc.*) on heating in aprotic solvents. As a rule, it is the halogen atom in the *ortho* position with respect to an electron-withdrawing substituent that is replaced.^{226–228} The reaction with diethyl malonate can serve as an example:



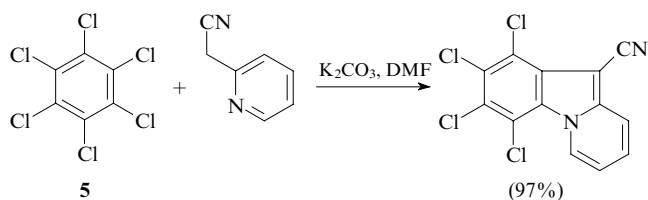
X = Cl, F; $R^1, R^2 = Cl, H$; $R^3 = Cl, H, ArC(O)$.

Methyl (3-chloro-2-nitrophenyl)cyanoacetate was prepared by the reaction of 2,6-dichloronitrobenzene (**24d**) with methyl cyanoacetate in DMF in the presence of K_2CO_3 .^{229, 230}

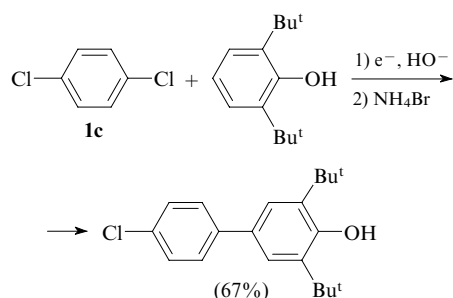


If a PCA contains no chlorine atoms in the *ortho* position with respect to the activating group, the chlorine atom in the *para* position is replaced. For example, *para*-substitution products were obtained in 80%–85% yields from 3,4-dichloronitrobenzene (**24e**) and 3,4,5-trichloronitrobenzene (**25b**).²²⁸

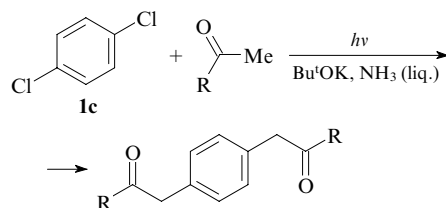
The reaction of the 2-(cyanomethyl)pyridine anion with hexachlorobenzene (**5**) affords the pyrido[1,2-*a*]indole derivative in nearly quantitative yield.²³¹



The electrochemically generated 2,6-di(*tert*-butyl)-phenolate anion reacts with 1,4-dichlorobenzene (**1c**) as the C-nucleophile.²³²



The reactions of methyl ketone enolates with 1,4-dichlorobenzene (**1c**) in liquid ammonia were studied.²³³ Under photochemical conditions, the ion-radical mechanism operates.



R = Me, Bu^t.

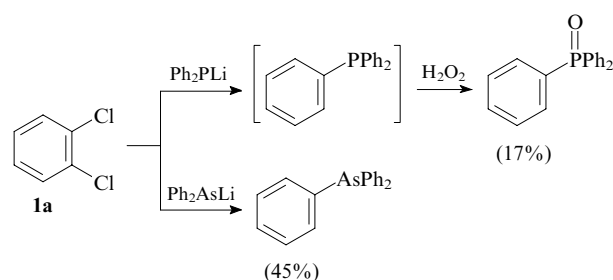
Irradiation of PCA with the light from a mercury lamp (254- or 185-nm) in benzene for 40 h at 25 °C under nitrogen resulted in the replacement of chlorine atoms by phenyl groups, the solvent serving as the source of the latter (Table 7).²³⁴ The reaction, which proceeds apparently by the radical mechanism, is accompanied by partial hydrodechlorination of both the starting arenes and products, particularly, of highly chlorinated compounds.

Table 7. Photochemical transformations of polychloroarenes in benzene.²³⁴

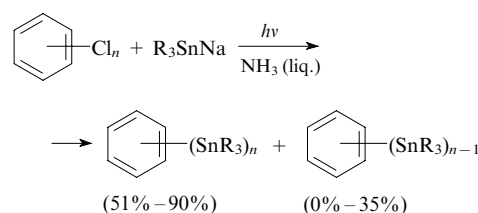
Compounds	Products (yield, %)
1,2-Cl ₂ C ₆ H ₄ (1a)	2-ClC ₆ H ₄ Ph (43) + Ph ₂ (14) + 1,2-Ph ₂ C ₆ H ₄ (1)
1,3-Cl ₂ C ₆ H ₄ (1b)	3-ClC ₆ H ₄ Ph (41) + Ph ₂ (1)
1,4-Cl ₂ C ₆ H ₄ (1c)	4-ClC ₆ H ₄ Ph (26) + Ph ₂ (1)
1,3,5-Cl ₃ C ₆ H ₃ (9a)	3,5-Cl ₂ C ₆ H ₃ Ph (31) + 1,3-Cl ₂ C ₆ H ₄ (1)
1,2,3-Cl ₃ C ₆ H ₃ (9c)	2,5-Cl ₂ C ₆ H ₃ Ph (22) + 3-ClC ₆ H ₄ Ph (3) + 4-ClC ₆ H ₄ Ph (1) + 1,4-Cl ₂ C ₆ H ₄ (1)
1,2,3,4-Cl ₄ C ₆ H ₂ (10a)	2,3,6-Cl ₃ C ₆ H ₂ Ph (21) + 1,2,4-Cl ₃ C ₆ H ₃ (3) + 4-Cl-1,2-Ph ₂ C ₆ H ₃ (2) + 2,5-Cl ₂ C ₆ H ₃ Ph (1) + 3,6-Cl ₂ -1,2-Ph ₂ C ₆ H ₂ (1) + Ph ₂ (1)
1,2,4,5-Cl ₄ C ₆ H ₂ (10b)	2,4,5-Cl ₃ C ₆ H ₂ Ph (9) + 3,4-Cl ₂ C ₆ H ₃ Ph (9) + 1,2,4-Cl ₃ C ₆ H ₃ (2)
1,2,3,5-Cl ₄ C ₆ H ₂ (10c)	2,4,6-Cl ₃ C ₆ H ₂ Ph (7) + 2,3,5-Cl ₃ C ₆ H ₂ Ph (5) + 1,3,5-Cl ₃ C ₆ H ₃ (2)

3. Reactions with anions of heteroorganic compounds

In the reactions of 1,2-dichlorobenzene (**1a**) with lithium diphenylphosphide and diphenylarsenide, one of the chlorine atoms is replaced by a heteroorganic substituent and another chlorine atom is replaced by hydrogen to give the corresponding products in low yields.²³⁵ The hypothesis that this reaction proceeds *via* benzyne was not confirmed, since experiments with furan as a scavenger were unsuccessful.



UV irradiation ($\lambda = 350$ nm) of some PCA in the presence of Me₃SnNa^{236, 237} or Ph₃SnNa²³⁸ in liquid ammonia affords substitution products. The reaction proceeds by the anion-radical mechanism and only under irradiation.



$n = 2, 3$; R = Me, Ph.

1,4-Bis(triphenylstannyl)benzene was obtained in 90% yield by the reaction of 1,4-dichlorobenzene (**1c**) with SnPh₄ in DMSO or acetonitrile under photochemical conditions.²³⁹

VII. Catalytic carbonylation and carboxylation

Catalytic carbonylation of polychloroarenes in the CO–Co₂(CO)₈–NaOH–H₂O system proceeds under UV irradiation (Table 8).²⁴⁰ In some cases, the reaction is accompanied by partial dechlorination (see, for example, the transformation of compound **69**). The selectivity of the reaction is determined by the number and arrangement of substituents in the starting arene.

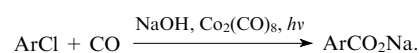
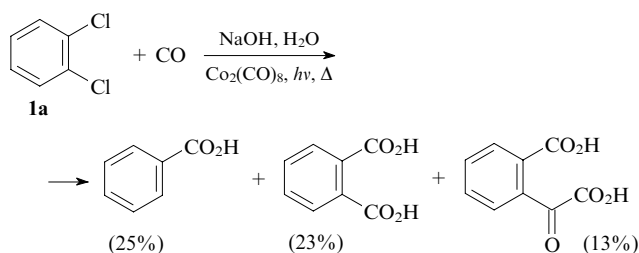


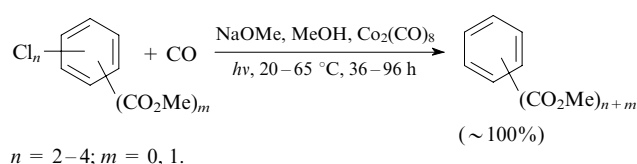
Table 8. Carbonylation of PCA [conditions: 1) $h\nu$, CO, Co₂(CO)₈, NaOH, H₂O; 2) H⁺] with the 100% conversion of the substrate.²⁴⁰

Compound	Time/h	Products	Yield (%)
1,2-Cl ₂ C ₆ H ₄ (1a)	24	PhCO ₂ H 2-ClC ₆ H ₄ CO ₂ H 1,2-(HO ₂ C) ₂ C ₆ H ₄ PhCl	24 40 2 7
1,3-Cl ₂ C ₆ H ₄ (1b)	20	1,3-(HO ₂ C) ₂ C ₆ H ₄	92
1,4-Cl ₂ C ₆ H ₄ (1c)	20	1,4-(HO ₂ C) ₂ C ₆ H ₄	88
1,3,5-Cl ₃ C ₆ H ₃ (9a)	20	1,3,5-(HO ₂ C) ₃ C ₆ H ₃	86
3,5-Cl ₂ C ₆ H ₃ CO ₂ H (27b)	20	1,3,5-(HO ₂ C) ₃ C ₆ H ₃	89
3,4-Cl ₂ C ₆ H ₃ CO ₂ H (27c)	6	4-ClC ₆ H ₄ CO ₂ H 1,4-(HO ₂ C) ₂ C ₆ H ₄ 2-Cl-C ₆ H ₃ (CO ₂ H) ₂ -1,4 1,2,4-(HO ₂ C) ₃ C ₆ H ₃	15 14 57 11
4,5-Cl ₂ C ₆ H ₂ (CO ₂ H) ₂ -1,2 (69)	24	1,2,4-(HO ₂ C) ₃ C ₆ H ₃ 1,2,4,5-(HO ₂ C) ₄ C ₆ H ₂	53 30

Carbonylation of 1,2-dichlorobenzene (**1a**) affords, along with benzoic and phthalic acids, 2-carboxyphenylglyoxalic acid.²⁴¹

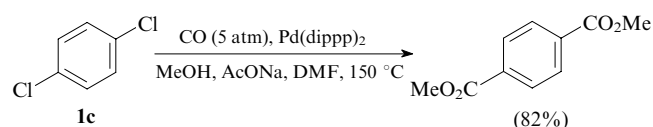


The reaction of polychloroarenes with carbon monoxide in methanol in the presence of MeONa produces methyl arene-polycarboxylates.²⁴² The reaction time varies from 36 to 95 h. Compounds containing vicinal chlorine atoms react much more slowly.



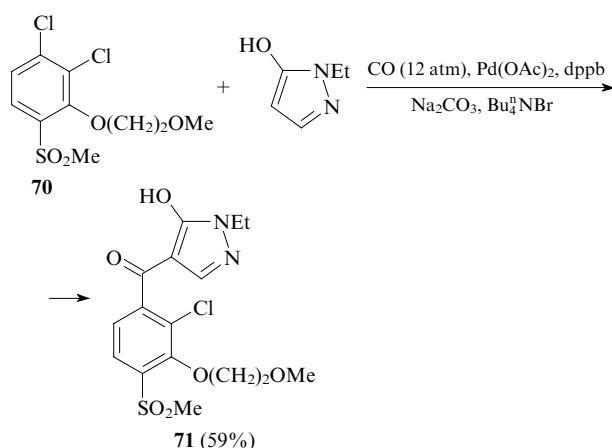
Carbonylation of 1,4-dichloro- (**1c**) and 1,3,5-trichlorobenzenes (**9a**) in EtOH affords ethyl benzenedi- and tricarboxylates.²⁴³

Palladium(0) complexes can be used as catalysts for these reactions.²⁴⁴



dppp is 1,3-bis(diisopropylphosphino)propane.

The use of Pd catalysts in combination with PTC allowed the carbonylation of dichloroarene **70** in the presence of 1-ethyl-5-hydroxypyrazole giving rise to aryl pyrazolyl ketone derivative **71**.¹⁶⁰



dppb is 1,4-bis(diphenylphosphino)butane.

The reactions of PCA with CO₂ proceed less selectively. Electrochemical carboxylation of 3,4-dichloro-1-trifluoromethylbenzene (**40a**) in aprotic polar solvents (Bu₄NBr as the supporting electrolyte, 15 °C, the current density $j = 5-50 \text{ mA cm}^{-2}$) affords 2-chloro-4-trifluoromethylben-

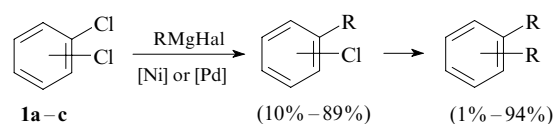
zoic acid as the major product.²⁴⁵ Electrochemical carboxylation of 1,2,4,5-tetrachlorobenzene (**10b**) and hexachlorobenzene (**5**) is accompanied by reductive hydrodechlorination.²⁴⁶

VIII. Catalytic C–C cross-coupling

Aryl chlorides are, as a rule, less reactive than the corresponding bromides and iodides in cross-coupling reactions catalysed by Pd or Ni complexes. The following approaches are used to accelerate these reactions: (1) the introduction of electron-withdrawing groups into the aromatic nucleus, (2) an increase in the nucleophilicity of the cross-counterpart or (3) the use of efficient catalytic systems. In recent years, considerable progress has been achieved in the design of new catalysts, particularly, in combination with sterically hindered phosphine^{247–257} and *N*-heterocyclic^{258–266} ligands. Data on some other types of ligands were reported elsewhere.^{267–272}

1. Reactions of polychloroarenes with organometallic compounds (M = Mg, Al or Zn)

Cross-coupling of PCA, unlike the analogous reactions with monochloroarenes, have been little studied. Most attention was focused on the transition metal complex-catalysed reactions of dichlorobenzenes **1a–c** with the Grignard reagents containing primary or secondary alkyl substituents (the Kumada reaction).^{273–277}



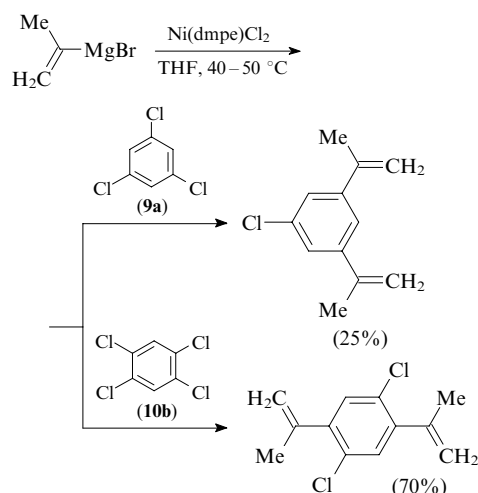
R = Alk, Ph.

The nickel complexes Ni(dppp)Cl₂ [dppp is 1,3-bis(diphenylphosphino)propane] and Ni(dppe)Cl₂ [dppe is 1,2-bis(diphenylphosphino)ethane] are the catalysts of choice allowing the replacement of both chlorine atoms.²⁷³ The high activity of these complexes is attributed to the fact that, after the replacement of the first chlorine atom, the catalyst tends to migrate intramolecularly to the second chlorine atom rather than to escape into solution. This reaction catalysed by the complex Ni(PPh₃)₂Cl₂ with the monodentate phosphine ligand affords products in much lower yields.

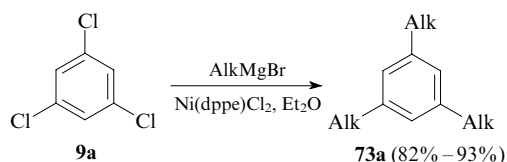
The reaction can be terminated after the replacement of one chlorine atom in the case of the complex Ni(triphos)ClPF₆ [triphos is the tridentate ligand *P,P*-bis(2-diphenylphosphinoethyl)phenylphosphine].²⁷⁷ In the cross-coupling reactions of 2,5-dichloro-1-trifluoromethylbenzene (**40b**) and 2,3-dichloroanisole (**72a**) with EtMgBr, the chlorine atom in the *meta* position with respect to the electron-withdrawing substituent is predominantly replaced.²⁷⁷ The selectivity is particularly high in the reaction with compound **72a** (the yields of 2-chloro-3-ethyl- and 3-chloro-2-ethylanisoles are 70% and 4%, respectively).

The reaction can be terminated at the monoalkylation step also in the presence of palladium catalysts [the complex Pd(dppf)Cl₂ is the catalyst of choice] in the dichlorobenzene:Grignard reagent molar ratio of ~2:1.²⁷⁶ In some cases, it is advantageous to add 0.5–1 equiv. (with respect to the catalyst) of the corresponding free ligand. The reactions efficiently proceed in THF at 85–105 °C. The Pd(PPh₃)₄-catalysed reaction of 1,4-dichlorobenzene (**1c**) with MeMgBr affords 4-chlorotoluene as the major product (92%).²⁷⁸

Several cross-coupling reactions of higher chlorinated PCA with the Grignard reagents were documented. The reactions of 1,3,5-trichlorobenzene (**9a**) and 1,2,4,5-tetrachlorobenzene (**10b**) with isopropenylmagnesium bromide in THF in the presence of Ni(dmpe)Cl₂ [dmpe is bis(dimethylphosphino)ethane] resulted in the replacement of two chlorine atoms.²⁷³

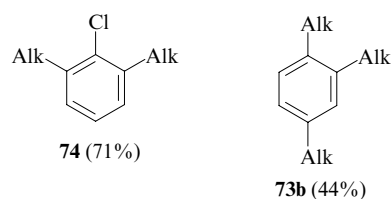


The use of the complex $\text{Ni}(\text{dppe})\text{Cl}_2$ allowed the replacement of all chlorine atoms in 1,3,5-trichlorobenzene (**9a**),²⁷⁹ 1,3,5-trialkylbenzenes **73a** being produced in yields of up to 93%.

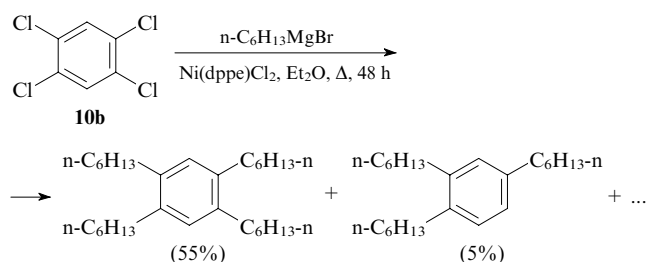


$\text{Alk} = n\text{-C}_n\text{H}_{2n+1}$ ($n = 6-10$).

Polychloroarenes containing vicinal chlorine atoms are less reactive towards alkylmagnesium bromides. For example, only 'lateral' chlorine atoms are replaced in 1,2,3-trichlorobenzene (**9c**) to give monochlorides **74**. The reaction of 1,2,4-trichlorobenzene (**9b**) affords a mixture of complete substitution products, *viz.*, compounds **73b** (44%), along with dialkylchlorobenzene (22%), the positions of the substituents in the latter remaining unknown.

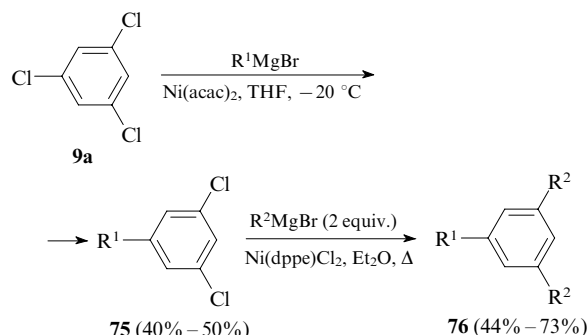


The reaction of 1,2,4,5-tetrachlorobenzene (**10b**) with *n*-hexylmagnesium bromide in the presence of $\text{Ni}(\text{dppe})\text{Cl}_2$ affords tetrahexylbenzene along with by-products, one of which was identified as 1,2,4-tri(*n*-hexyl)benzene.²⁷⁹



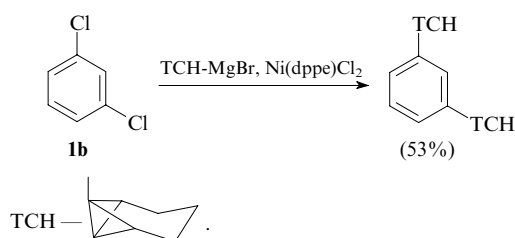
The use of various catalysts allowed the synthesis of 1,3,5-trialkylbenzenes containing different alkyl substituents starting from 1,3,5-trichlorobenzene (**9a**).²⁷⁹ The reaction in THF at -20°C in the presence of $\text{Ni}(\text{acac})_2$ as the catalyst afforded compounds **75** as a result of the replacement of the first

chlorine atom by the group R^1 . The latter compounds were used in the $\text{Ni}(\text{dppe})\text{Cl}_2$ -catalysed reaction with an excess of another alkylmagnesium bromide R^2MgBr . The preparative yields of trialkylbenzenes **76** were achieved only after refluxing in diethyl ether for 7–10 days.

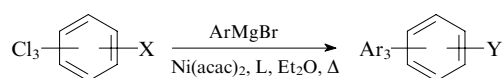


$\text{R}^1, \text{R}^2 = \text{Alk}$.

The reactions of di- (**1a,b**) and trichlorobenzenes (**9a**) with the tricyclic Grignard reagent, *viz.*, tricyclo[4.1.0.0.2,7]hept-1-ylmagnesium bromide (TCH-MgBr), in the presence of $\text{Ni}(\text{dppe})\text{Cl}_2$ were documented.²⁸⁰ The satisfactory yield of the substitution product (53%) was achieved only in the reaction with 1,3-dichlorobenzene (**1b**).



Cross-coupling of tri- and tetrachloroarenes with aromatic Grignard reagents (Table 9) were performed with the use of the catalytic system $\text{Ni}(\text{acac})_2$ –diphenyl[2-(1-hydroxyethyl)phenyl]phosphine (**L**).²⁸¹ Under these conditions, complete substitution of trichlorobenzenes **9a,b,d** and **77** occurred to give the corresponding products in high yields. In the case of 1,2,4,5-tetrachlorobenzene (**10b**), incomplete conversion is accompanied by partial dechlorination.



$\text{X} = \text{H, Cl, OMe}; \text{Y} = \text{H, Ar, OMe}; \text{Ar} = \text{Ph, 4-MeC}_6\text{H}_4$ (Tol);

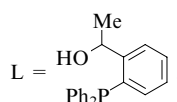
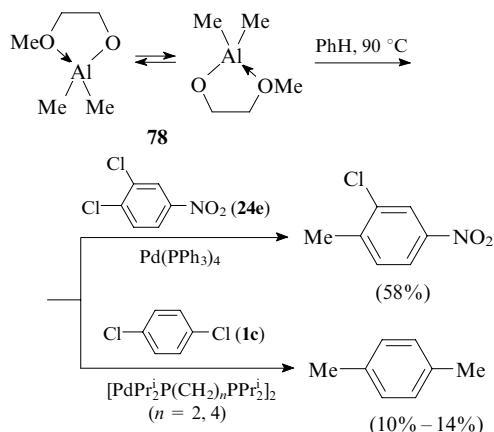


Table 9. Cross-coupling of tri- and tetrachlorobenzenes with ArMgBr .²⁸¹

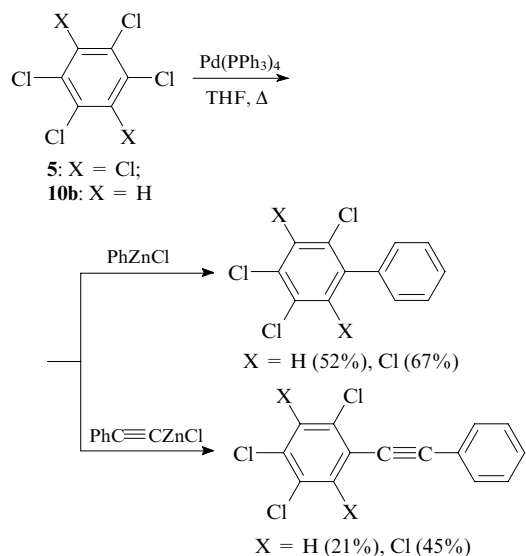
Compound	Ar	Time/h	Product	Yield (%)
1,3,5- $\text{Cl}_3\text{C}_6\text{H}_3$ (9a)	Tol	2	1,3,5- $\text{ToI}_3\text{C}_6\text{H}_3$	91
1,2,4- $\text{Cl}_3\text{C}_6\text{H}_3$ (9b)	Ph	48	1,2,4- $\text{Ph}_3\text{C}_6\text{H}_3$	89
1,2,3- $\text{Cl}_3\text{C}_6\text{H}_3$ (9d)	Tol	24	2,6- $\text{ToI}_2\text{C}_6\text{H}_4$	85
1,2,4,5- $\text{Cl}_4\text{C}_6\text{H}_2$ (10b)	Ph	96	1,2,4,5- $\text{Ph}_4\text{C}_6\text{H}_2$	58 ^a
2,4,6- $\text{Cl}_3\text{C}_6\text{H}_2\text{OMe}$ (77)	Tol	20	2,4,6- $\text{ToI}_3\text{C}_6\text{H}_2\text{OMe}$	80

^a By-products: 1-Cl-2,4,5- $\text{Ph}_3\text{C}_6\text{H}_2$ and 1,2,4- $\text{Ph}_3\text{C}_6\text{H}_3$ (2 : 3).

Reactions of PCA with complex organoaluminium compounds were documented.²⁸² For example, compound **24e** containing the nitro group reacts with derivative **78** in the presence of $\text{Pd}(\text{PPh}_3)_4$. The reaction with non-reactive 1,4-dichlorobenzene (**1c**) required the use of a Pd complex with electron-rich phosphine ligands; however, the yield of *p*-xylene was at most 14%.

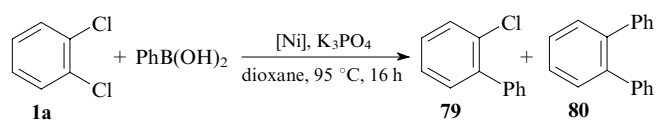


In the $\text{Pd}(\text{PPh}_3)_4$ -catalysed reactions of 1,2,4,5-tetrachlorobenzene (**10b**) and hexachlorobenzene (**5**) with organozinc compounds (1.6 mol per mole of arene) in boiling THF, one chlorine atom is replaced to give the corresponding products in moderate yields.²⁸³ The conversion of PCA varies from 58% to 89% and is accompanied by side processes, such as homocoupling of the nucleophilic and electrophilic components and reductive dechlorination.



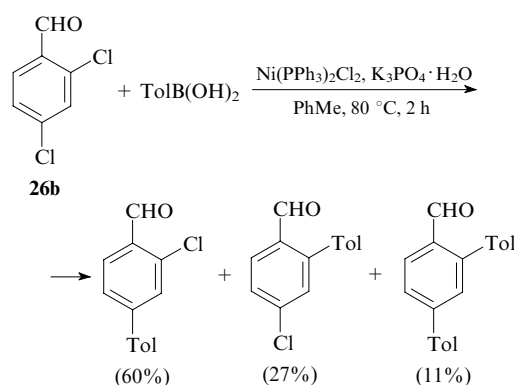
2. Reactions of polychloroarenes with arylboronic acids

Transition metal-catalysed cross-coupling reaction of PCA with arylboronic acids (the Suzuki reaction) can serve as a convenient one-pot procedure for the synthesis of polyarylbenzenes. However, this reaction is far from being always selective. For example, the reaction of 1,2-dichlorobenzene (**1a**) with 4.4 equiv. of $\text{PhB}(\text{OH})_2$ in the presence of the nickel complexes $\text{Ni}(\text{dppf})\text{Cl}_2$ or $\text{Ni}(\text{PPh}_3)_2\text{Cl}_2$ affords a mixture of 2-chlorobiphenyl (**79**) and *o*-terphenyl (**80**).²⁸⁴



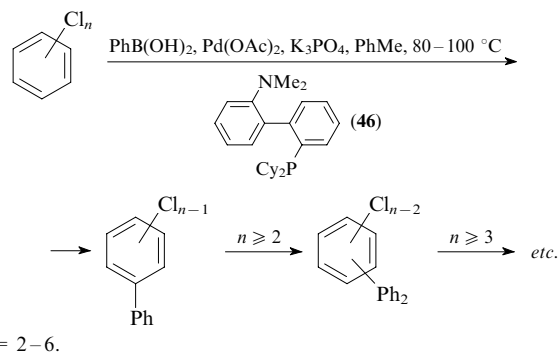
[Ni]	Yield (%)	
	79	80
$\text{Ni}(\text{dppf})\text{Cl}_2$	4	69
$\text{Ni}(\text{PPh}_3)_2\text{Cl}_2$	34	28

Cross-coupling of 2,4-dichlorobenzaldehyde (**26b**) with *p*-tolylboronic acid with a nickel catalyst also affords a mixture of compounds, with the *para*-substitution product predominating (the *para* isomer : *ortho* isomer ratio ~ 2 : 1).²⁸⁵ On the contrary, the *ortho* isomer is formed in higher yield with the palladium catalyst $\text{Pd}(\text{dba})_2\text{-L}$ (L = PPh_3 , PCy_3 , dppb or dppf).



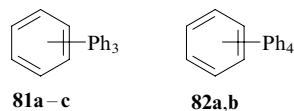
The reaction of 1,2-dichlorobenzene (**1a**) with $\text{PhB}(\text{OH})_2$ on a heterogeneous nanocluster catalyst with the composition Cu/Pd/Ru in DMF at 110 °C in the presence of K_2CO_3 as a base affords the monoarylated product in 25% yield.²⁸⁶ In the reaction of 1,4-dichlorobenzene (**1c**) with 4-tolylboronic acid in the presence of the catalytic system $\text{PdCl}_2\text{-PCy}_3\text{-Na}_2\text{CO}_3$ in NMP at 150 °C, also only one chlorine atom is replaced.²⁸⁷

We demonstrated²⁸³ that highly chlorinated PCA, such as C_6Cl_6 (**5**) and $\text{C}_6\text{Cl}_5\text{Ac}$, do not react with phenylboronic acid in the presence of $\text{Pd}(\text{PPh}_3)_4$ under the conditions typical of the reaction of aryl bromides. Unexpectedly, pentachloroiodobenzene also appeared to be inert under these conditions due apparently to steric hindrance of the reactive C–I bond by the adjacent chlorine atoms. The target products were synthesised with the use of modern catalytic systems designed in recent years for the cross-coupling of monochloroarenes, including deactivated compounds. For example, the cross-coupling of $\text{PhB}(\text{OH})_2$ with equimolar amounts of 1,2,4,5-tetrachlorobenzene (**10b**) and hexachlorobenzene (**5**) in the presence of the system $\text{Pd}(\text{dba})_2\text{-Bu}_3\text{P-K}_3\text{PO}_4\text{-PhMe}$ (Ref. 248) gave the

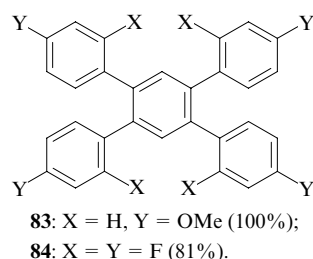


products in 82% and 37% yields, respectively.²⁸³ The Buchwald ligands containing the 2-phosphinobiphenyl fragment, particularly, 2-dicyclohexylphosphino-2'-dimethylaminobiphenyl (**46**),^{125, 126} proved to be very efficient in these reactions.^{247, 252, 253}

The cross-coupling of tri- and tetrachlorobenzenes with arylboronic acids ArB(OH)_2 ($\text{Ar} = \text{Ph}$, 4-MeOC₆H₄ or 4-FC₆H₄) under Buchwald conditions resulted in the complete replacement of the chlorine atoms to give compounds **81–84** in high yields.

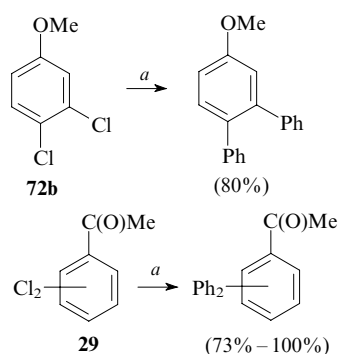


Isomers: 1,2,3 (**81a**, 94%); 1,2,4 (**81b**, ~ 100%); 1,3,5 (**81c**, ~ 100%); 1,2,3,4 (**82a**, 88%); 1,2,4,5 (**82b**, 94%).



Attempts to use this procedure for the synthesis of penta-phenylbenzene from C₆HCl₅ (**2**) and for the synthesis of hexaphenylbenzene from C₆Cl₆ (**5**) failed although the target products were detected by GLC-mass spectrometry in amounts up to 10%. After the introduction of four phenyl groups, the replacement of the chlorine atoms by hydrogen in the intermediates Ph₄C₆HCl and Ph₄C₆Cl₂ became the major reaction.

Polychloroarenes containing both electron-donating and electron-withdrawing substituents in the aromatic ring react with phenylboronic acid in the presence of the catalytic system Pd(OAc)₂–ligand. Under these conditions, all chlorine atoms were replaced in 3,4-dichloroanisole (**72b**) and isomeric dichloroacetophenones **29**.¹²⁵



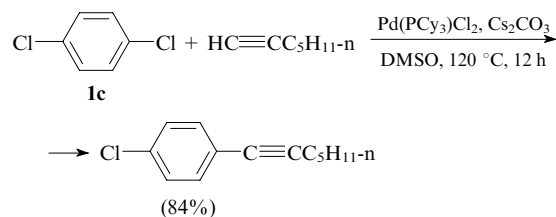
(a) PhB(OH)₂ (2.5 mol), Pd(OAc)₂, **46**, K₃PO₄, PhMe, 90 °C.

The use of palladium *N*-heterocyclic carbene complexes [prepared *in situ* from Pd(OAc)₂ and imidazolium salts]^{283, 288} and the ligand-free method²⁸⁹ for the cross-coupling of 1,2,4,5-tetrachlorobenzene (**10b**) and hexachlorobenzene (**5**) proved to be less efficient.

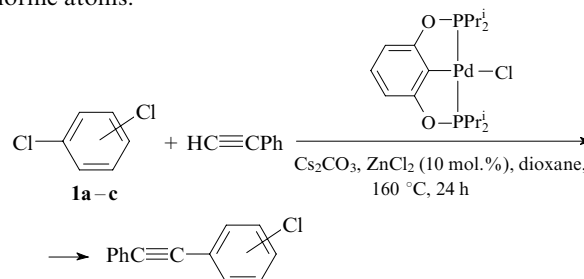
3. Reactions of polychloroarenes with terminal acetylenes

The reactions of di- and trichlorobenzenes with terminal acetylenes were carried out.^{290–293} The cross-coupling reaction of 1,4-dichlorobenzene (**1c**) with hept-1-yne in the presence of

Pd(PCy₃)₂Cl₂ affords the monosubstitution product in high yield.²⁹⁰

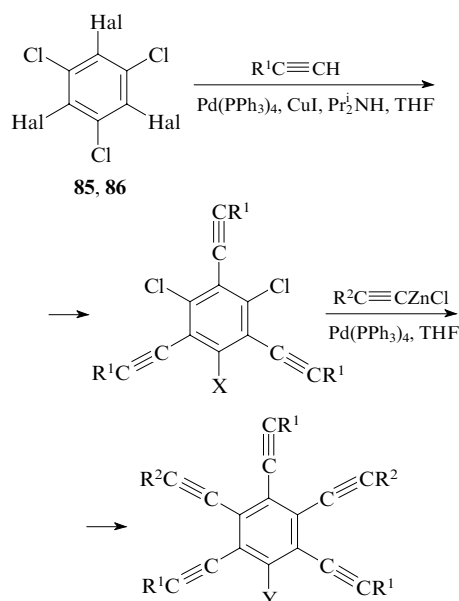


The reaction of isomeric dichlorobenzenes **1a–c** with phenylacetylene in the presence of a pincer palladium complex with additives of ZnCl₂ also gives monosubstitution products.²⁹¹ Their yields depend on the mutual arrangement of the chlorine atoms.



Isomers: 1,2 (36%), 1,3 (19%), 1,4 (80%).

Unexpected results were obtained in the reactions of alkynes with symmetrical tribromotrichloro- (**85**) and trichlorotriiodobenzenes (**86**).^{292, 293} For example, only bromine atoms are replaced in the Sonogashira reaction (75 °C, 30 h) of 1,3,5-tribromo-2,4,6-trichlorobenzene (**85**) with trimethylsilylacetylene. It has become possible to introduce six acetylene groups into the aromatic core only with the use of more reactive alkyne zinc derivatives.



Hal = Br (**85**): R¹ = Me₃Si, X = Cl (62%); R² = Ph, Y = C≡CR² (69%); Hal = I (**86**): R¹ = Ph (33%), R² = Me₃Si (51%), X = Y = C≡CR¹.

2,4,6-Trichloro-1,3,5-triiodobenzene (**86**) reacts with phenylacetylene to form 4,6-dichloro-1,2,3,5-tetrakis(phenylethynyl)benzene. To replace the remaining chlorine atoms, the

reaction with trimethylsilylethynylzinc was carried out at high temperature (90 °C) .

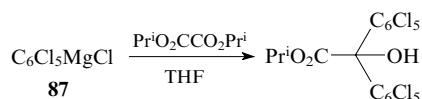
IX. Metallation

1. Grignard reagents based on polychloroarenes: synthesis and reactions with electrophiles

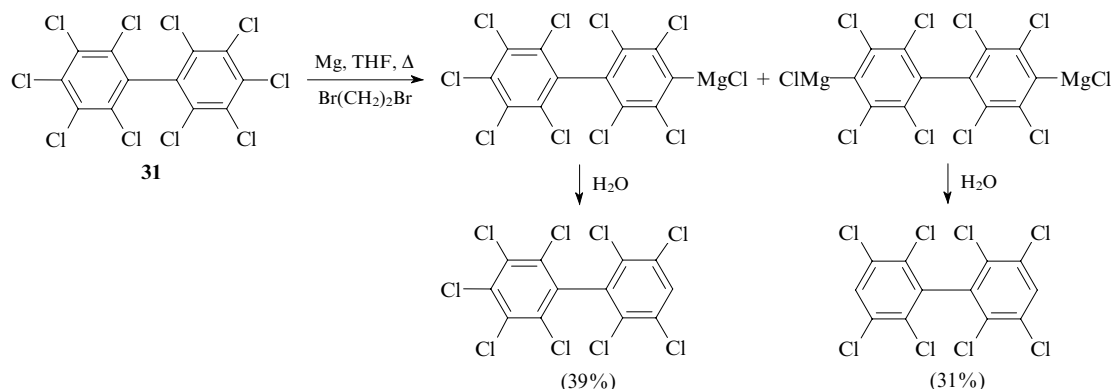
Polychloroarenes react with magnesium to form organomagnesium derivatives. The nature of the solvent is of considerable importance in the synthesis of polychloroarylmagnesium halides. Tetrahydrofuran and other cyclic ethers, such as tetrahydropyran, ethyl tetrahydrofurfuryl ether, 2-ethoxytetrahydropyran and dihydropyran are convenient solvents for this purpose. In these solvents, isomeric 1,3- and 1,4-dichlorobenzenes (**1b,c**) form the Grignard reagents in good yields.^{294, 295} The reaction of 1,2-dichlorobenzene (**1a**) and highly chlorinated PCA give the target products in low yields because of oligomerisation as the side process. An exception is hexachlorobenzene (**5**), which gives C_6Cl_5MgCl in THF in 77% yield.²⁹⁴ In diethyl ether, C_6Cl_5MgCl was prepared by slow (over 2 days) addition of 1,2-dibromoethane to a suspension of an excess of magnesium and hexachlorobenzene (**5**) in diethyl ether (the latter compound is very poorly soluble in diethyl ether).^{296, 297}

The reactions of these organomagnesium derivatives with a series of electrophiles were studied. For example, the reaction of the Grignard reagent prepared from C_6Cl_6 (**5**) with gaseous CO_2 affords pentachlorobenzoic acid in 77% yield,²⁹⁶ whereas the treatment of this Grignard reagent with acetic anhydride affords pentachloroacetophenone in 31% yield. These results are in contradiction with the data of the study,²⁹⁴ where it was noted that C_6Cl_5MgCl does not react with carbon dioxide in THF but reacts with more reactive $SiCl_4$ under analogous conditions.

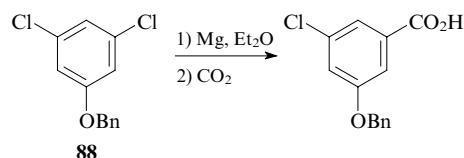
An α -hydroxy ester was synthesised by the reaction of C_6Cl_5MgCl (**87**) with diisopropyl oxalate in THF (the yield was not reported).²⁹⁸



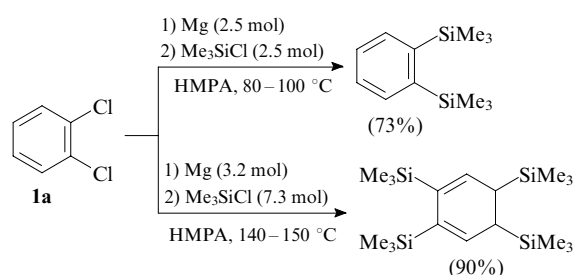
Decachlorobiphenyl (**31**), like hexachlorobenzene (**5**), forms the Grignard reagents in the reactions carried out in the presence of 1,2-dibromoethane.⁷⁵ The chlorine atoms at positions 4 and 4' are only involved in the reaction giving rise to mono- and dimetallated derivatives, and the latter can be transformed into nona- and octachlorobiphenyls by quenching with water (Scheme 2).



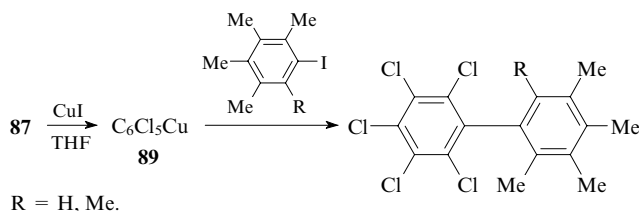
The one-pot synthesis of 3-benzyloxy-5-chlorobenzoic acid from 5-benzyloxy-1,3-dichlorobenzene (**88**) via the Grignard reagent was documented (the conditions and yields were not reported in detail).²⁹⁹



Slow (over 50 h) addition of 1,2-dichlorobenzene (**1a**) to a mixture of metallic magnesium and Me_3SiCl in HMPA at 80–100 °C resulted in 1,2-bis(trimethylsilyl)benzene as the major product.³⁰⁰ The reactions of other PCA containing from two to four chlorine atoms proceed analogously. 2,3,5,6-Tetrakis(trimethylsilyl)cyclohexa-1,3-diene was prepared from compound **1a** in high yield with the use of an excess of reagents at higher temperatures (140–150 °C).³⁰¹

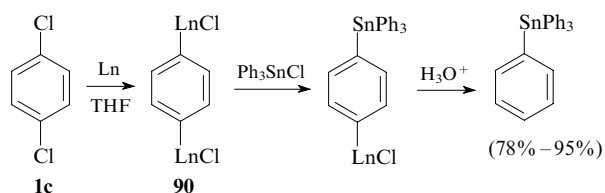


Transmetalation of compound **87** with CuI in THF produces organocopper compound **89**.³⁰² The corresponding biaryls were obtained in moderate yields (~25%) by the cross-coupling of compound **89** with tetra- and pentamethylphenyl iodides.



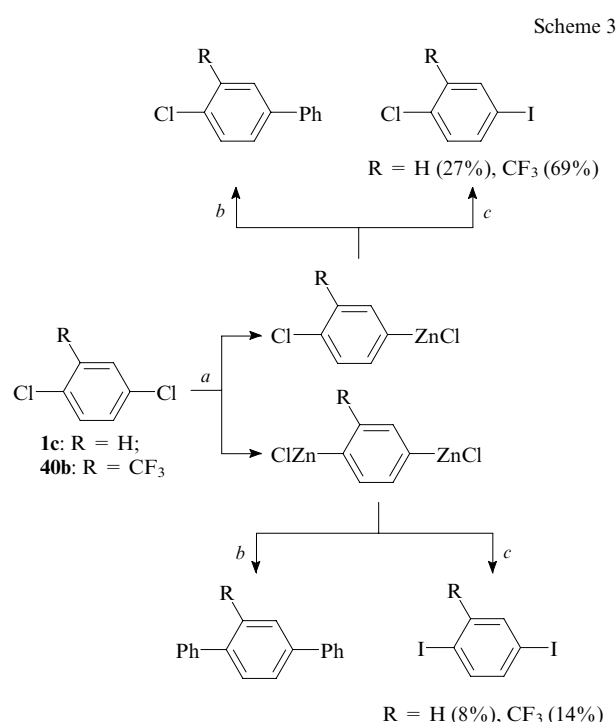
Organometallic reagents **90** analogous to the Grignard reagents were prepared by the reaction of 1,4-dichlorobenzene (**1c**) with yttrium and samarium.³⁰³ Their subsequent treatment with triphenyltin chloride and water in an acidic medium afforded tetraphenyltin in high yield.

Scheme 2



Ln = Yb, Sm.

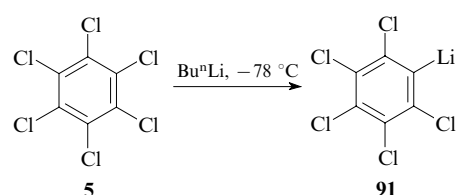
Organozinc derivatives of PCA were synthesised by electrolysis of 1,4-dichlorobenzene (**1c**) and 2,5-dichloro-1-trifluoromethylbenzenes (**40b**). The reactions were carried out in an undivided cell with a sacrificial zinc anode in a MeCN–pyridine mixture (9 : 1) in the presence of CoCl_2 and ZnBr_2 as the catalysts.³⁰⁴ The resulting organometallic compounds were transformed into the corresponding iodobenzenes or cross-coupling products with PhI in the presence of $\text{Pd}(\text{PPh}_3)_2\text{Cl}_2$ (Scheme 3).



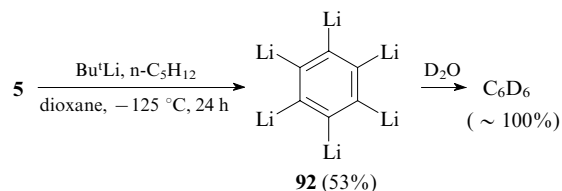
(a) e^- (2 F mol^{-1}); CoCl_2 (cat), ZnBr_2 (cat), Zn anode, MeCN–PyH (9 : 1); (b) PhI , $\text{Pd}(\text{PPh}_3)_4\text{Cl}_2$; (c) I_2 .

2. Synthesis and reactions of organolithium derivatives of polychloroarenes

Unlike aryl bromides and iodides, monochloroarenes do not, as a rule, react with alkyllithium reagents. However, the mutual activation of chlorine atoms in PCA favours the reactions with these organometallic compounds. For example, hexachlorobenzene (**5**) reacts with Bu^nLi in a THF–hexane mixture at -78°C to form pentachlorophenyllithium (**91**).³⁰⁵ In diethyl ether, this reaction proceeds at -10°C .³⁰⁶

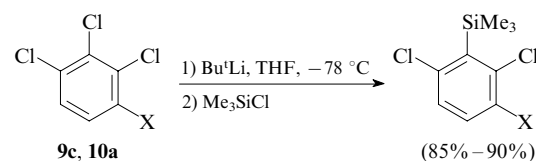


The reaction of hexachlorobenzene (**5**) with an excess of Bu^nLi gives a product, in which two Cl atoms in the *para* positions are replaced.³⁰⁷ Lithiation with *tert*-butyllithium at -125°C allows the replacement of all six Cl atoms. Upon treatment with D_2O , the resulting hexalithium derivative **92** gives benzene- d_6 in quantitative yield.³⁰⁸



In polychloroarenes containing aromatic C–H bonds, the hydrogen atom can selectively be replaced by lithium. For example, the reaction of 1,3,5-trichlorobenzene (**9a**) with Bu^nLi produces symmetrical trilithiotrichlorobenzene,³⁰⁷ whereas the reaction of 1,2,4,5-tetrachlorobenzene (**10b**) results in the replacement of one or two hydrogen atoms depending on the amount of the lithiating reagent.³⁰⁹ The reaction of pentachlorobenzene (**2**) with Bu^nLi also results in the replacement of the H atom by Li.^{307, 309}

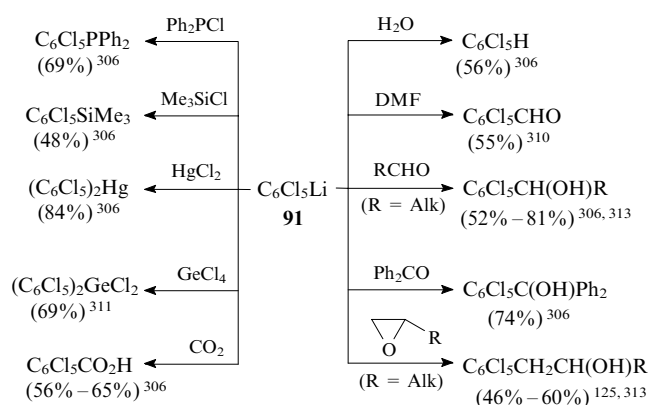
Under the lithiation conditions, 1,2,3-trichloro- (**9c**) and 1,2,3,4-tetrachlorobenzenes (**10a**) give mixtures of dechlorination and deprotonation products.³⁰⁷ High chemoselectivity was observed in the reaction with Bu^tLi . Thus treatment of the lithiation products with chlorotrimethylsilane affords the corresponding trimethylsilylarenes containing one less chlorine atom.



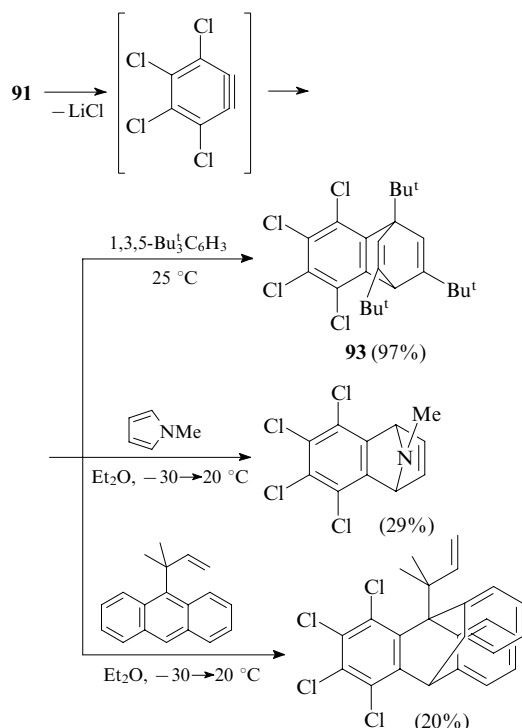
X = H (**9c**), Cl (**10a**).

The lithiation of decachlorobiphenyl (**31**), like the reaction with Mg, proceeds regioselectively at positions 4 and 4'.⁷⁵ Quenching of the lithiation products with water affords nona- and octachlorobiphenyls, and their reactions with dimethyl sulfate produce the corresponding 4-methyl- and 4,4'-dimethylperchlorobiphenyls.

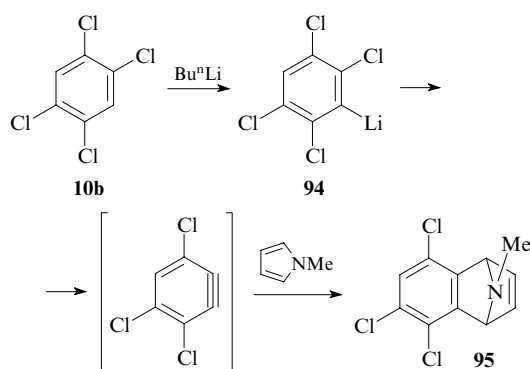
Lithium derivatives of PCA are valuable intermediates in the synthesis of various heteroorganic and functionalised arene derivatives.^{125, 306, 310–313} Selected reactions of pentachlorophenyllithium (**91**) with electrophiles with references to the original papers are given below.



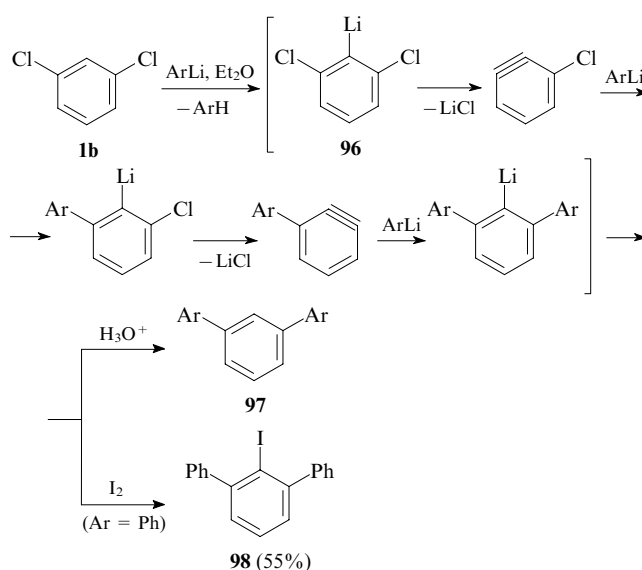
Although polychlorophenyllithium derivatives are rather stable (compound **91** is stable in diethyl ether at $-10\text{ }^{\circ}\text{C}$), in some cases these compounds eliminate LiCl to form the corresponding dehydrobenzenes.³¹⁴ For example, the reaction of compound **91** with 1,3,5-tri(*tert*-butyl)benzene affords the cycloaddition product **93**.³⁰⁵ The reactions of $\text{C}_6\text{Cl}_5\text{Li}$ (**91**) with *N*-methylpyrrole³¹⁵ and substituted anthracene proceed³¹⁶ analogously.



2,3,5,6-Tetrachlorophenyllithium (**94**) derived from 1,2,4,5-tetrachlorobenzene (**10b**) can be transformed into 3,4,6-trichlorobenzene, which was detected judging from the formation of the cycloaddition product with *N*-methylpyrrole, *viz.*, compound **95**.³¹⁵

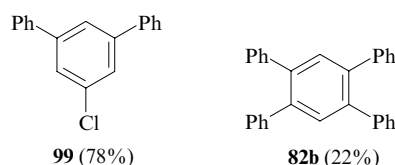


The reactions of 1,3-dichlorobenzene (**1b**) with an excess of ArLi were found³¹⁷ to proceed *via* 3-chlorobenzene, 1,3-dichloro-2-lithiobenzene (**96**) being a precursor of the latter. These reactions afford ultimately *m*-terphenyls **97**. The reaction of compound **1b** with phenyllithium followed by quenching of the reaction mixture with molecular iodine affords the iodo derivative of *m*-terphenyl **98**.

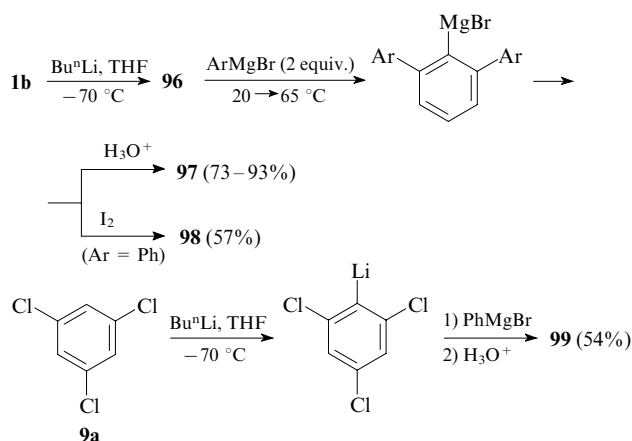


$\text{Ar} = \text{Ph}$ (73%), 4- PhC_6H_4 (65%), 2-MeOC₆H₄ (93%), 4-MeOC₆H₄ (80%).

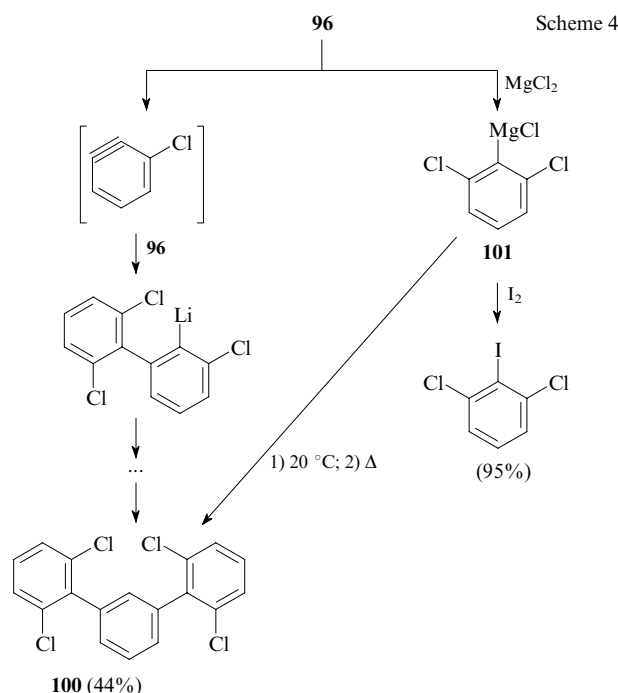
Compounds **99** and **82b** were prepared analogously from 1,3,5-trichloro- (**9a**) and 1,2,4,5-tetrachlorobenzenes (**10b**), respectively, by the reactions with PhLi .³¹⁷



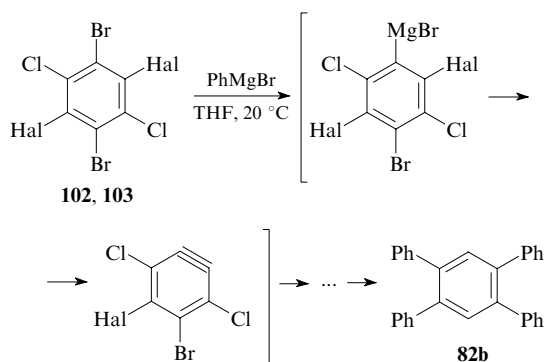
An efficient procedure for the synthesis of *m*-terphenyls is based on the lithiation of polychlorobenzenes **1b** or **9a** with *n*-butyllithium followed by treatment with ArMgBr . The mechanism of these transformations is analogous to that of the above-described reactions.³¹⁷



1,3-Dichloro-2-lithiobenzene (**96**) gives biphenyl and *m*-terphenyl derivatives as a result of the reaction with 3-chlorobenzene generated *in situ*.³¹⁸ The yield of 2,2',6,6'-tetrachloro-*m*-terphenyl (**100**) was increased to 44% by transforming the lithium derivative into organomagnesium compound **101**, which reacts more smoothly (Scheme 4).³¹⁷



The reactions of 1,2,4,5-tetrabromodichloro- (**102**) and 1,4-dibromotetrachlorobenzenes (**103**) with an excess of PhMgBr also proceed *via* the dihydrobenzene derivative to give 1,2,4,5-tetraphenylbenzene (**82b**).³¹⁹



Hal = Br (**102**, 65%); Cl (**103**, 36%).

* * *

As can be seen from the above data, polychloroarenes can serve as multifunctional synthons for the preparation of various classes of organic and heteroorganic compounds. Nucleophilic aromatic substitution and metallation reactions of PCA have been studied in sufficient detail, whereas transition metal-catalysed cross-coupling reactions have received less attention. A serious progress in the metal complex catalysis achieved in the past years allows the expectation of the development of new efficient methods for transformations of PCA into valuable aromatic compounds. Some of new catalytic systems have been successfully tested in the cross-coupling reactions of dichlorobenzenes and highly chlorinated arenes.

Investigations of the reactivity of PCA are of applied importance. The results of these investigations can substantially contribute to the solution of the problem of chemical utilisation of toxic organochlorine compounds, such as pesticides, waste transformer oil (see, for example, Refs 320–322), dioxins, *etc.*, including the processing of these compounds into new products and materials with practically useful properties.

This review has been written with the financial support of the INTAS (Grant No. 04-82-7271).

References

1. J B Hoke, G A Gramiccioni, E N Balko *Appl. Catal.*, **B** **1** 285 (1992)
2. F Murena, E Schioppa *Appl. Catal.*, **B** **27** 257 (2000)
3. Y Ukisu, S Iimura, R Uchida *Chemosphere* **33** 1523 (1996)
4. S Zinovyev, A Perosa, S Yufit, P Tundo *J. Catal.* **211** 347 (2002)
5. V V Lunin, E S Lokteva *Izv. Akad. Nauk, Ser. Khim.* 1609 (1996)^a
6. L N Zhanavskiy, V A Aver'yanov, Yu A Treger *Usp. Khim.* **65** 667 (1996) [*Russ. Chem. Rev.* **65** 617 (1996)]
7. F Alonso, I P Beletskaya, M Yus *Chem. Rev.* **102** 4009 (2002)
8. A R Pinder *Synthesis* 425 (1980)
9. E S Levin, Z I Fodiman *Zh. Fiz. Khim.* **28** 601 (1954)^b
10. M S Mubarak, D G Peters *J. Electroanal. Chem.* **435** 47 (1997)
11. *Polychloroaromatic Compounds* (Ed. H Suschitzky) (New York: Plenum, 1974)
12. M Ballester *Advances in Physical Organic Chemistry* Vol. 25 (Ed. D Bethel) (New York: Academic Press, 1989) p. 267
13. R D Chambers, S R James *Comprehensive Organic Chemistry* Vol. 1 (Oxford: Pergamon Press, 1979)
14. F Maiolo, L Testaferri, M Tiecco, M Tingoli *J. Org. Chem.* **46** 3070 (1981)
15. P Cogolli, F Maiolo, L Testaferri, M Tingoli, M Tiecco *J. Org. Chem.* **44** 2642 (1979)
16. M Tiecco, M Tingoli, L Testaferri, D Chianelli, F Maiolo *Synthesis* 478 (1982)
17. L Testaferri, M Tingoli, M Tiecco *J. Org. Chem.* **45** 4376 (1980)
18. M Evers *Chem. Scr.* **26** 585 (1986)
19. C W Dirk, S D Cox, D E Wellman, F Wudl *J. Org. Chem.* **50** 2395 (1985)
20. R Lapouyade, J-P Morand *J. Chem. Soc., Chem. Commun.* 223 (1987)
21. Z Chen, L R Sutton, D Moran, A Hirsch, W Thiel, P von R Schleyer *J. Org. Chem.* **68** 8808 (2003)
22. R Adams, A Ferretti *J. Am. Chem. Soc.* **81** 4927 (1959)
23. L Testaferri, M Tiecco, M Tingoli, D Chianelli, M Montanucci *Synthesis* 751 (1983)
24. T Nabeshima, N Furukawa, T Ishizawa, K Morihashi, O Kikuchi *Heterocycles* **31** 1575 (1990)
25. A M Richter, V Engels, N Beye, E Fanghaenel *Z. Chem.* **29** 444 (1989)
26. J Larsen, K Bechgaard *J. Org. Chem.* **52** 3285 (1987)
27. Å Bergman, C A Wachtmeister *Chemosphere* **7** 949 (1978)
28. J R Campbell *J. Org. Chem.* **29** 1830 (1964)
29. A Ueno, S Kanno, N Yamanaka *Jpn. Kokai Tokkyo Koho; Jpn. P.* 2001.172.254; *Chem. Abstr.* **135** 45984 (2001)
30. J H Uhlenbroek *Recl. Trav. Chim. Pays-Bas.* **80** 1057 (1961)
31. S D Pastor, E T Hessell *J. Org. Chem.* **50** 4812 (1985)
32. D D MacNicol, P R Mallison, A Murphy, G J Sym *Tetrahedron Lett.* **23** 4131 (1982)
33. J H R Tucker, M Gingras, H Brand, J-M Lehn *J. Chem. Soc., Perkin Trans. 2* 1303 (1997)
34. R Lang, R Mayer, D Decker, T Kniess *Z. Chem.* **30** 404 (1990)
35. M G Voronkov, E N Deryagina, L G Klochkova, A S Nakhmanovich *Zh. Org. Khim.* **12** 1515 (1976)^c
36. L F Shagun, E S Deriglazova, T V Kashik, E N Deryagina, M G Voronkov *Zh. Org. Khim.* **14** 187 (1978)^c
37. V Z Annenkov, L M Antonik, T I Vakul'skaya, M G Voronkov *Zh. Org. Khim.* **21** 2219 (1985)^c
38. M G Voronkov, E N Deryagina, E N Sukhomazova *Zh. Org. Khim.* **18** 1736 (1982)^c
39. V A Sergeev, V I Nedel'kin, A V Astankov *Izv. Akad. Nauk SSSR, Ser. Khim.* 1908 (1987)^a
40. E Klingsberg *Tetrahedron* **28** 963 (1972)
41. I Arai, T Yamaguchi, Y Koida *Jpn. Kokai Tokkyo Koho; Jpn. P.* 2000.07.649 (2000); *Chem. Abstr.* **132** 64054 (2000)
42. C Combellas, S Dellerue, G Mathey, A Thiebault *Tetrahedron Lett.* **38** 539 (1997)

43. M Tiecco, L Testaferri, M Tingoli, D Chianelli, M Montanucci *J. Org. Chem.* **48** 4289 (1983)
44. T Kemmitt, W Levason *Organometallics* **8** 1303 (1989)
45. J Nakayama, M Kashiwagi, R Yomoda, M Hoshino *Nippon Kagaku Kaishi* 1424 (1987); *Chem. Abstr.* **108** 150191 (1998)
46. T L Kachhee, V Gupta, D C Gautam, R R Gupta *Phosphorus, Sulfur Silicon Relat. Elem.* **178** 2671 (2003)
47. H Fiege, F Hagedorn *Eur. P.* 711754; *Chem. Abstr.* **125** 86296 (1996)
48. P Cogolli, L Testaferri, M Tingoli, M Tiecco *J. Org. Chem.* **44** 2636 (1979)
49. V Yu Orlov, A D Kotov, R S Begunov, G S Mironov *Azotistye Geterotsikly i Alkaloidy (Tez. Dokl. Mezhdunar. Konferentsii 'Khimiya i Biologicheskaya Aktivnost' Azotistykhet Geterotsiklov i Alkaloidov')*, Moskva, 2001 [Nitrogen Heterocycles and Alkaloids (Abstracts of Reports of the International Conference 'Chemistry and Biological Activity of Nitrogen Heterocycles and Alkaloids'), Moscow, 2001] Vol. 1, p. 452; *Chem. Abstr.* **141** 410846 (2004)
50. T S Safonova, M P Nemeryuk, M M Likhovidova, A L Sedov, N A Grineva, M A Keremov, N P Solov'eva, O S Anisimova, A S Sokolova *Khim.-Farm. Zh.* (6) 21 (2003)^d
51. Y Yoshida, D Barrett, H Azami, C Morinaga, S Matsumoto, Y Matsumoto, H Takasugi *Bioorg. Med. Chem.* **7** 2647 (1999)
52. J K Suzuki, A Zirnis, A A Manian *J. Heterocycl. Chem.* **16** 1227 (1979)
53. S Oya, S R Choi, H Coenen, H F Kung *J. Med. Chem.* **45** 4716 (2002)
54. H Takenaka, M Kiriha *Jpn. Kokai Tokkyo Koho*; *Jpn. P.* 2003.321.440; *Chem. Abstr.* **139** 364820 (2003)
55. T Ikemoto, T Ito, A Nishiguchi, K Tomimatsu *Tetrahedron* **60** 10851 (2004)
56. Y H Zhu, P Lu, H Lou, X M Zheng *Chinese Chem. Lett.* **14** 235 (2003); *Chem. Abstr.* **139** 149372 (2003)
57. M Tanemura, I Matsunaga, M Saitou *Eur. P.* 181526; *Chem. Abstr.* **105** 78667 (1986)
58. I Nasuno, S Tomita, M Shibata, H Yamamoto *WO PCT 97/08163*; *Chem. Abstr.* **126** 238301 (1997)
59. S Archer, L Pica-Mattoccia, D Cioli, A Seyed-Mozaffari, A H Zayed *J. Med. Chem.* **31** 254 (1988)
60. Z A Bayir, S Merey, E Hamuryudan *Monatsh. Chem.* **134** 1027 (2003)
61. D Wöhrle, M Eskes, K Shigehara, A Yamada *Synthesis* 194 (1993)
62. V Valenta, J Holubek, M Protiva *Collect. Czech. Chem. Commun.* **52** 1062 (1987)
63. S M Cramp *WO PCT 97/30026*; *Chem. Abstr.* **127** 205348 (1997)
64. J T Manka, V C McKenzie, P Kaszynski *J. Org. Chem.* **69** 1967 (2004)
65. T Hiyama, H Kano, S Nii *Jpn. Kokai Tokkyo Koho*; *Jpn. P.* 2001.302.616; *Chem. Abstr.* **135** 344275 (2001)
66. T Aoki, T Konoike *WO PCT 99/54296*; *Chem. Abstr.* **131** 286521 (1999)
67. D J Brunelle *J. Org. Chem.* **49** 1309 (1984)
68. D Landini, F Montanari, F Rolla *J. Org. Chem.* **48** 604 (1983)
69. J E Shaw *US P.* 5618981; *Chem. Abstr.* **126** 330492 (1997)
70. M Sakamoto, S Tomita, Y Takashima, H Koga *WO PCT 01/40176*; *Chem. Abstr.* **135** 19546 (2001)
71. U N Rao, J Maguire, E Biehl *ARKIVOC* (i) 88 (2004)
72. K Sukata, T Akagawa *J. Org. Chem.* **54** 1476 (1989)
73. J-E Ancel, G Perrin-Janet, P Leroy *WO PCT 00/69805*; *Chem. Abstr.* **133** 362614 (2000)
74. Y Liu, J Schwartz *Tetrahedron* **51** 4471 (1995)
75. F Binns, H Suschitzky *J. Chem. Soc., C* 1913 (1971)
76. L J Crane, M Anastassiadou, J-L Stigliani, G Baziard-Mouysset, M Payard *Tetrahedron* **60** 5325 (2004)
77. S-J Yan, J Lin, L-J Yang, R Huang, Z Zhang *Yunnan Daxue Xuebao, Ziran Kexueban* **25** 525 (2003); *Chem. Abstr.* **141** 156909 (2004)
78. H Hrenn, W Schwack, W Seilmeier, H Wieser *Tetrahedron Lett.* **44** 1911 (2003)
79. A A Lebedev, L I Mironova, M G Pleshakov, A K Matveeva, I A Timokhina *Khim.-Farm. Zh.* 1205 (1985)^d
80. A Magnano, S Sparapani, R Lucciarini, M Michela, C Amantini, G Santoni, I Antonini *Bioorg. Med. Chem.* **12** 5941 (2004)
81. D B Capps *Eur. P.* 138302; *Chem. Abstr.* **103** 196074 (1985)
82. J Romanowski, Z Eckstein *Pol. J. Chem.* **58** 263 (1984)
83. H Asakawa, M Matano *Chem. Pharm. Bull.* **27** 1287 (1979)
84. K Warning, G Folz *BRD P.* 3431827; *Chem. Abstr.* **104** 224685 (1986)
85. B Gong, F Hong, C Kohm, L Bonham, P Klein *Bioorg. Med. Chem. Lett.* **14** 1455 (2004)
86. Y-M Legrand, M Gray, G Cooke, V M Rotello *J. Am. Chem. Soc.* **125** 15789 (2003)
87. N Choy, K C Russell, J C Alvarez, A Fider *Tetrahedron Lett.* **41** 1515 (2000)
88. A Pawlik, A Ouart, S Kirstein, H-W Abraham, S Daehne *Eur. J. Org. Chem.* 3065 (2003)
89. S Özden, H Karatas, S Yildiz, H Göker *Arch. Pharm.* **337** 556 (2004)
90. T Ibata, M Shang, T Demura *Bull. Chem. Soc. Jpn.* **68** 2717 (1995)
91. T Ibata, Y Isogami, J Toyoda *Bull. Chem. Soc. Jpn.* **64** 42 (1991)
92. W Ried, G Sell *Chem. Ber.* **113** 2311 (1980)
93. G M Dubowchik, J A Michne, D Zuev, W Schwartz, P M Scola, C A James, E H Ruediger, S S Pin, K D Burris, L A Balanda, Q Gao, D Wu, L Fung, T Fiedler, K E Browman, M T Taber, J Zhang *Bioorg. Med. Chem. Lett.* **13** 3997 (2003)
94. J Fukunaga, T Ookuma, R Mita *Jpn. Kokai Tokkyo Koho*; *Jpn. P.* 1995.725.834; *Chem. Abstr.* **122** 265019 (1995)
95. T Ibata, X-Z Zou, T Demura *Bull. Chem. Soc. Jpn.* **68** 3227 (1995)
96. H-P Zhou, H-S Dong, Y Hao, M Huang *Hanneng Cailiao* **12** 107 (2004); *Chem. Abstr.* **142** 55938 (2005)
97. A Heaton, M G Hill, F G Drakesmith *J. Chem. Soc., Perkin Trans. 2* 1275 (1985)
98. G W Lawrence, H G Adolphz *Tetrahedron Lett.* **21** 1615 (1980)
99. C Yan, H Zhang, X Zhu, C Zhu, G Jing *Chin. P.* 1374291; *Chem. Abstr.* **140** 287161 (2004)
100. C Yan, X Li, X Zhu, C Zhu, Y Wang, H Zhang *Xiandai Nongyao* **2** (5) 5 (2003); *Chem. Abstr.* **140** 270575 (2004)
101. C Yan *Xiandai Nongyao* **2** (1) 13 (2003); *Chem. Abstr.* **140** 271168 (2004)
102. B Gallenkamp, O Schallner, E Klauke *BRD P.* 3447211; *Chem. Abstr.* **105** 152687 (1986)
103. X Kong, S Wang, G Wang, W Chai, W Yao, T Xu *Chin. P.* 1333205; *Chem. Abstr.* **138** 221344 (2003)
104. H Wu, C Yang, Y Huang, C Xie, Y Li, S Guan *Chin. P.* 1468838; *Chem. Abstr.* **142** 355035 (2005)
105. D Catarzi, V Colotta, F Varano, F R Calabrig, G Filacchioni, A Galli, C Costagli, V Carla *J. Med. Chem.* **47** 262 (2004)
106. T Haga, T Komyoji, T Nakajima, T Oshima, K Suzuki *Jpn. Kokai Tokkyo Koho*; *Jpn. P.* 61.72.755; *Chem. Abstr.* **105** 114927 (1986)
107. V N Boiko, I V Gogoman, G M Shchupak, L M Yagupol'skii *Zh. Org. Khim.* **23** 2586 (1987)^c
108. G A Selivanova, L M Pokrovskii, V D Shteingarts *Zh. Org. Khim.* **38** 1066 (2002)^c
109. T Shimomada, K Shimomiya, K Ueda, H Ono, S Furuhashi *Jpn. Kokai Tokkyo Koho*; *Jpn. P.* 63.130.567; *Chem. Abstr.* **109** 212817 (1988)
110. A Greiner *Synthesis* 312 (1989)
111. M L D Palacios, R F P Comdom *Synth. Commun.* **33** 1771 (2003)
112. H-S Mei, T-R Yan, Y-W Wu *Zhongguo Yiyao Gongye Zazhi* **31** 485 (2000); *Chem. Abstr.* **134** 326231 (2001)
113. S E Kitchen, Y Wang, A L Baumstark, W D Wilson, D W Boykin *J. Med. Chem.* **28** 940 (1985)
114. A A Joshi, S S Narkhede, C L Viswanathan *Bioorg. Med. Chem. Lett.* **15** 73 (2005)
115. T Papenfuhs, R Pfirmann, S Krause, D Neumann-Grimm *BRD P.* 19532054; *Chem. Abstr.* **126** 238655 (1997)
116. S Krause, D Neumann-Grimm, T Papenfuhs *BRD P.* 19624583; *Chem. Abstr.* **128** 102381 (1998)
117. T Kamiya, H Takehara, Y Inamoto, A Taniguchi, M Masumoto *WO PCT 97/24335*; *Chem. Abstr.* **127** 121747 (1997)

118. H Matsuda *Jpn. Kokai Tokkyo Koho*; Jpn. P. 2002.105.060; *Chem. Abstr.* **136** 294846 (2002)
119. S M Bech WO PCT 98/51685; *Chem. Abstr.* **130** 25071 (1999)
120. F Z Galin, R G Rakhimov, G A Tolstikov *Izv. Akad. Nauk, Ser. Khim.* 548 (1998)^a
121. L X Marill, R F P Comdom, U J Haza, M M Hernandez *Rev. CENIC, Cienc. Quim.* **30** 81 (1999); *Chem. Abstr.* **133** 176990 (2000)
122. E Brenner, R Schneider, Y Fort *Tetrahedron* **55** 12829 (1999)
123. J O Smith, M A Petruska, J J Longlet WO PCT 2004/054961; *Chem. Abstr.* **141** 90877 (2004)
124. J P Wolfe, H Tomori, J P Sadighi, J Yin, S L Buchwald *J. Org. Chem.* **65** 1158 (2000)
125. A S Burukin, Candidate Thesis in Chemical Sciences, Institute of Organic Chemistry, Russian Academy of Sciences, Moscow, 2006
126. A S Burukin, A A Vasil'ev, S G Zlotin *II Molodezhnaya Konferentsiya IOKh RAN (Tez. Dokl.)*, Moskva, 2006 [The IInd Youth Conference of the Institute of Organic Chemistry, Russian Academy of Sciences (Abstracts of Reports), Moscow, 2006] p. 91
127. H Geissler, S Haber, S Scherer, A Meudt *Eur. P.* 1083163; *Chem. Abstr.* **134** 222510 (2001)
128. I P Beletskaya, A D Averin, A A Borisenko, F Denat, R Guillard *Tetrahedron Lett.* **44** 1433 (2003)
129. I P Beletskaya, A D Averin, A G Bessmertnykh, R Guillard *Tetrahedron Lett.* **42** 4983 (2001)
130. I P Beletskaya, A D Averin, A G Bessmertnykh, R Guillard *Tetrahedron Lett.* **42** 4987 (2001)
131. I P Beletskaya, A G Bessmertnykh, A D Averin, F Denat, R Guillard *Eur. J. Org. Chem.* 281 (2005)
132. I P Beletskaya, A D Averin, A G Bessmertnykh, F Denat, R Guillard *Tetrahedron Lett.* **43** 1193 (2002)
133. G A Artamkina, A G Sergeev, M M Shtern, I P Beletskaya *Zh. Org. Khim.* **42** 1695 (2006)^c
134. L Testaferri, M Tiecco, M Tingoli, D Chianelli, M Montanucci *Tetrahedron* **39** 193 (1983)
135. Y Yoshida, Y Hamada, K Magaribuchi, H Takeuchi WO PCT 99/29699; *Chem. Abstr.* **131** 18836 (1999)
136. J A Chong, F Abdesaken, C C Wu *Jpn. Kokai Tokkyo Koho*; Jpn. P. 10.195.017; *Chem. Abstr.* **129** 161413 (1998)
137. J A Chong, F Abdesaken, C C Wu *Eur. P.* 831083; *Chem. Abstr.* **128** 230138 (1998)
138. J A Chong, F Abdesaken, L A Spangler, S R Joshi, C C Wu *Eur. P.* 941982; *Chem. Abstr.* **131** 214080 (1999)
139. T Much, H Weintritt, R Lantzs, W Huebschw WO PCT 01/83417; *Chem. Abstr.* **135** 344281 (2001)
140. K Yamaguchi, Y Yoshikawa, Y Tanabe, K Sugimoto, A Yamaguchi BRD P. 3429903 FRG; *Chem. Abstr.* **104** 33845 (1986)
141. M H Mach, J F Bunnett *J. Org. Chem.* **45** 4660 (1980)
142. J H Brady, B J Wakefield *Synthesis* 33 (1984)
143. A L Rocklin *J. Org. Chem.* **21** 1478 (1956)
144. F D Smith US P. 2449088; *Chem. Abstr.* **43** 813 (1949)
145. J H Brady, N Tahir, B J Wakefield *J. Chem. Soc., Perkin Trans. I* 2425 (1984)
146. T Humpi *Synthesis* 919 (1985)
147. S Gobbi, A Pampa, A Bisi, F Belluti, P Valenti, A Caputo, A Zampiron, M Carrara *J. Med. Chem.* **45** 4931 (2002)
148. C Corral, J Lissavetzky, A M Valdeolmillos *J. Heterocycl. Chem.* **22** 1349 (1985)
149. J Lu Chin. P. 1267663; *Chem. Abstr.* **134** 252145 (2001)
150. G B Eregowda, H N Kolpana, R Hegde, K N Thimmaiah *Indian J. Chem., Sect. B* **39** 243 (2000)
151. J Liu, Y Wang, Y Zhang, S Chen *Sichuan Daxue Xuebao, Ziran Kexueban* **38** 885 (2001); *Chem. Abstr.* **138** 55694 (2003)
152. R E Bozga, S P Cilianu-Bibianu, F I Cunesco, L Precup Roman. P. 88042; *Chem. Abstr.* **105** 114726 (1986)
153. R E Bozga, S Cilianu-Bibian, C E Sirbu, G Filip Roman. P. 86377; *Chem. Abstr.* **105** 114727 (1986)
154. T Yoshimoto, K Igarashi, K Oda, M Ura, N Safo BRD P. 2926829; *Chem. Abstr.* **93** 7835 (1980)
155. T M Shamsutdinov, Z M Poluektova, T A Kalistratova, A V Starkov *Zh. Prikl. Khim.* **59** 862 (1986)^c
156. E A Aly US P. 4548640; *Chem. Abstr.* **104** 168110 (1986)
157. M Osu, H Okabe, O Maruyama *Jpn. Kokai Tokkyo Koho*; Jpn. P. 61.27.950; *Chem. Abstr.* **105** 78643 (1986)
158. J T Gupton, G Hertel, G De Crescenzo, C Colon, D Baran, D Dukeshere, S Novick, D Liotta, J P Idoux *Can. J. Chem.* **63** 3037 (1985)
159. T L Siddall, M V M Edmonds, K L Krumel, J M Schomaker, M W Zettler, S L Shinkle, J D Webster WO PCT 98/42677; *Chem. Abstr.* **129** 290132 (1998)
160. T L Siddall, K L Krumel, M V M Emonds, J M Schomaker, M W Zettler US P. 6211403; *Chem. Abstr.* **134** 266305 (2001)
161. J Bakos, B Neil, L Kollar, S Toroes, G Eifert, F Bihari, L Sarosi, G P Durko, I Kuronya BRD P. 3539927; *Chem. Abstr.* **105** 74396 (1986)
162. K-H Linker, W Haas, O Schallner, K Findeisen, R Andree, M W Drewes BRD P. 19620992; *Chem. Abstr.* **128** 34579 (1998)
163. R Neidlein, R Leidholdt *Chem. Ber.* **119** 844 (1986)
164. G Soula *J. Org. Chem.* **50** 3717 (1985)
165. C Oniscu, V Bancila, S Toader, A Vlase, A Dumitrescu, J C Ionescu, M Bancila, C Musca, G Fagarasan Roman. P. 114785; *Chem. Abstr.* **134** 162818 (2001)
166. K Kunikata, K Nakamura *Jpn. Kokai Tokkyo Koho*; Jpn. P. 60.188.349; *Chem. Abstr.* **104** 88268 (1986)
167. M Watanabe, M Nihiyama, Y Koie *Tetrahedron Lett.* **40** 8837 (1999)
168. T A Di, W Hoelzl, D Reinehr, R Zink WO PCT 01/83418; *Chem. Abstr.* **135** 344278 (2001)
169. U Burckhardt, T A Di, W Hoelzl, D Reinehr, R Zink, H Sauter, U Gronde *Eur. P.* 857711; *Chem. Abstr.* **129** 161410 (1998)
170. I Okabayashi, N Iwata *Chem. Pharm. Bull.* **28** 2831 (1980)
171. Z-W Guo, G M Salamonczyk, K Han, K Machiya, C J Sih *J. Org. Chem.* **62** 6700 (1997)
172. C J Sih, I Malnar *Biocatal. Biotransform.* **18** 301 (2000)
173. I Malnar, C J Sih *Tetrahedron Lett.* **41** 1907 (2000)
174. G G Yakobson, V M Vlasov *Synthesis* 652 (1976)
175. *Reaktivnaya Sposobnost' Polifloraromaticheskikh Soedinenii* (Reactivity of Polyfluoroorganic Compounds) (Ed. G G Yakobson) (Novosibirsk: Nauka, 1983)
176. R D Chambers *Fluorine in Organic Chemistry* (Oxford: Blackwell, 2004)
177. E T McBee, V V Lindgren, W B Ligett *Ind. Eng. Chem.* **39** 378 (1947); *Chem. Abstr.* **41** 3435 (1947)
178. S Kumai, T Seki, M Sasabe, H Matsuo *Jpn. Kokai Tokkyo Koho*; Jpn. P. 60.246.326; *Chem. Abstr.* **104** 148470 (1986)
179. A Pleschke, A Marhold, M Schneider, A Kolomeitsev, G-V Rlschenthaler *J. Fluorine Chem.* **125** 1031 (2004)
180. N N Vorozhtsov, V E Platonov, G G Yakobson *Izv. Akad. Nauk SSSR, Ser. Khim.* 1524 (1963)^a
181. G G Yakobson, V E Platonov, N N Vorozhtsov *Zh. Obshch. Khim.* **35** 1158 (1965)^f
182. J Hitzke *J. Fluorine Chem.* **16** 103 (1980)
183. J Hitzke *J. Fluorine Chem.* **18** 101 (1981)
184. G G Yakobson, V D Shteingarts, N N Vorozhtsov *Izv. Akad. Nauk SSSR, Ser. Khim.* 1551 (1964)^a
185. R S Matthews *J. Fluorine Chem.* **50** 381 (1990)
186. R S Matthews *J. Fluorine Chem.* **48** 7 (1990)
187. J Russel, L Gilbert, J-P Maestro WO PCT 97/24318; *Chem. Abstr.* **127** 108776 (1997)
188. A Marhold, M Loehr, H Wamhoff *Eur. P.* 693466; *Chem. Abstr.* **124** 288972 (1996)
189. A Sivaprasad, P S Rao, K Radhakrishnan, B Narsaiah, V Revannuru, A V R Rao *Indian P.* 180493; *Chem. Abstr.* **140** 357049 (2004)
190. B Wang, J Wang Chin. P. 1357530; *Chem. Abstr.* **139** 100923 (2003)
191. W Xie Chin. P. 1515539; *Chem. Abstr.* **143** 7493 (2006)
192. W Xie Chin. P. 1515542; *Chem. Abstr.* **143** 7489 (2006)
193. K Kunikata *Jpn. Kokai Tokkyo Koho*; Jpn. P. 60.188.348; *Chem. Abstr.* **104** 88269 (1986)
194. H-M Becher BRD P. 3435889; *Chem. Abstr.* **104** 168101 (1986)
195. J M Birchall, R N Haszeldine, M E Jones *J. Chem. Soc., C* 1341 (1971)

196. K-i Ueda, T Hashiguchi *Bull. Chem. Soc. Jpn.* **40** 688 (1967)
197. E Klauk, U Peterson, K Grohe BRD P. 3420796; *Chem. Abstr.* **104** 168196 (1986)
198. J Lin, L-J Yang, S-J Yan, J-F Li, F-C Liu *Hecheng Huaxue* **12** 117 (2004); *Chem. Abstr.* **142** 155632 (2005)
199. J Lin, D-C Mao, R Xu, S-J Yan, L-J Yang, J-F Li, F-C Liu *Chem. Res. Chin. Univ.* **20** 429 (2004); *Chem. Abstr.* **142** 219027 (2005)
200. J Lin, R Xu, D Mao, S Yan, L Yang, F-C Liu Chin. P. 1465563; *Chem. Abstr.* **142** 336134 (2005)
201. M Kuwahara, Y Okumura. *Jpn. Kokai Tokkyo Koho*; Jpn. P. 2003.335.743; *Chem. Abstr.* **139** 364695 (2003)
202. A Takaoka, O Yokokohji, Y Yamaguchi, T Isono, M Motoyoshi, N Ishikawa *Nippon Kagaku Kaishi* 2155 (1985); *Chem. Abstr.* **105** 152649 (1986)
203. S Antons, A Marhold, B Beitzke Eur. P. 673912; *Chem. Abstr.* **124** 29419 (1996)
204. S Kumai, M Sasbe, H Matsuo *Jpn. Kokai Tokkyo Koho*; Jpn. P. 60.228.436; *Chem. Abstr.* **104** 148468 (1986)
205. S J Brown, J H Clark *J. Fluorine Chem.* **30** 251 (1985)
206. J H Clark, D Wails, C W Jones, H Smith, N Boechat, L U Mayer, J S Mendonca *J. Chem. Res. (S)* 478 (1994)
207. A I Shipilov, N G Fedoseev *Zh. Prikl. Khim.* **73** 522 (2000)^c
208. A I Shipilov, A B Bykova, L I Elokhoa, S M Igumnov *Izv. Akad. Nauk, Ser. Khim.* 464 (2003)^a
209. A I Shipilov, N N Karyukalova, S M Igumnov *Zh. Org. Khim.*, **38** 240 (2002)^c
210. V V Aksenov, V M Vlasov, I M Moryakina, P P Rodionov, V P Fadeeva, V S Chertok, G G Yakobson *J. Fluorine Chem.* **28** 73 (1985)
211. T Schach, T Papenfuhs Eur. P. 635481; *Chem. Abstr.* **122** 187106 (1995)
212. T Schach, T Papenfuhs, R Phirmann BRD P. 4324368; *Chem. Abstr.* **122** 187138 (1995)
213. T Schach, T Papenfuhs Eur. P. 635482; *Chem. Abstr.* **122** 187109 (1995)
214. B Wang, J Wang Chin. P. 1357524; *Chem. Abstr.* **139** 149411 (2003)
215. Y Liu, Y Wei *Nanjing Ligong Daxue Xuebao* **27** 188 (2003); *Chem. Abstr.* **139** 197202 (2003)
216. C Zhang, X Chen, M Wang, H Liu *Jingxi Huagong Zhongjianti* **33** 22 (2003); *Chem. Abstr.* **141** 331837 (2004)
217. C Zheng, H Zhao, J Xu Chin. P. 1468843; *Chem. Abstr.* **142** 316577 (2005)
218. M Henrich, A Marhold, A Kolomeitsev, G Roeschenthaler Eur. P. 1266904; *Chem. Abstr.* **138** 39405 (2003)
219. J J Maul, D Y Tang Eur. P. 180057; *Chem. Abstr.* **105** 97143 (1986)
220. J Luo, C Lm, C Cai, W Qm *J. Fluorine Chem.* **125** 701 (2004)
221. S Fujii, K Inukai *Nippon Kagaku Kaishi* 643 (1978); *Chem. Abstr.* **89** 42721 (1978)
222. T Tanabe *Gunma Daigaku Kyoyobu Kiyo* **19** 119 (1985); *Chem. Abstr.* **105** 190612 (1986)
223. S Cherkez, J Herzig, H Yellin *J. Med. Chem.* **29** 947 (1986)
224. P Trink, G Berecz, J Reiter *J. Prakt. Chem./Chem.-Ztg.* **338** 679 (1996)
225. K Sudo, M Kudo, K Yabutani *Jpn. Kokai Tokkyo Koho*; Jpn. P. 03.14.554; *Chem. Abstr.* **114** 206813 (1991)
226. M Gurjar, D S Reddy, A Murugaiah, S Murugaiah *Synthesis* 1659 (2000)
227. E A Kraynack, J E Dalgard, F C A Gaeta *Tetrahedron Lett.* **39** 7679 (1998)
228. N Selvakumar, A M Azhagan, D Srinivas, G G Krishna *Tetrahedron Lett.* **43** 9175 (2002)
229. R-X Feng, J Song, L Chen, Z J Mali, G-P Sun *Trans. Tianjin Univ.* **8** 40 (2002); *Chem. Abstr.* **138** 239646 (2003)
230. R A Kirchhoff US P. 4638078; *Chem. Abstr.* **106** 138879 (1987)
231. T V Shokol, Yu M Volovenko, F S Babichev *Khim. Geterotsikl. Soedin.* 1696 (1990)^g
232. C Combellas, H Marzouk, C Suba, A Thiebault *Synthesis* 788 (1993)
233. R A Alonso, R A Rossi *J. Org. Chem.* **45** 4760 (1980)
234. M Nakada, C Miura, H Nishiyama, F Higashi, T Mori, M Hirota, T Ishii *Bull. Chem. Soc. Jpn.* **62** 3122 (1989)
235. D G Gillespie, B J Walker, D Stevens, C A McAuliffe *J. Chem. Soc., Perkin Trans. 1* 1697 (1983)
236. E F Corsico, R A Rossi *Synlett* 227 (2000)
237. E F Corsico, R A Rossi *Synlett* 230 (2000)
238. C C Yammal, J C Podesta, R A Rossi *J. Org. Chem.* **57** 5720 (1992)
239. M T Lockhart, A B Chopra, R A Rossi *J. Organomet. Chem.* **582** 229 (1999)
240. T Kashimura, K Kudo, S Mori, N Sugita *Chem. Lett.* **15** 299 (1986)
241. T Kashimura, K Kudo, S Mori, N Sugita *Chem. Lett.* **15** 483 (1986)
242. T Kashimura, K Kudo, S Mori, N Sugita *Chem. Lett.* **15** 851 (1986)
243. K Kudo, T Shibata, T Kashimura, S Mori, N Sugita *Chem. Lett.* **16** 577 (1987)
244. Y Ben-David, M Portnoy, D Milstein *J. Am. Chem. Soc.* **111** 8742 (1989)
245. P Brungs, T Karcher, K Kuchlein, H Millauer, M Wildt Eur. P. 780371; *Chem. Abstr.* **127** 121564 (1997)
246. D Golinske, J Voss, G Adiwidjaja *Collect. Czech. Chem. Commun.* **65** 862 (2000)
247. J P Wolfe, R A Singer, B H Yang, S L Buchwald *J. Am. Chem. Soc.* **121** 9550 (1999)
248. A F Littke, C Dai, G C Fu *J. Am. Chem. Soc.* **122** 4020 (2000)
249. A F Littke, G C Fu *Angew. Chem., Int. Ed.* **41** 4176 (2002)
250. N Kataoka, Q Shelby, J P Stambuli, J F Hartwig *J. Org. Chem.* **67** 5553 (2002)
251. A Zapf, R Jackstell, F Rataboul, T Riermeier, A Monsees, C Fuhrmann, N Shaikh, U Dingerdissen, M Beller *Chem. Commun.* 38 (2004)
252. T E Barder, S D Walker, J R Martinelli, S L Buchwald *J. Am. Chem. Soc.* **127** 4685 (2005)
253. J E Milne, S L Buchwald *J. Am. Chem. Soc.* **126** 13028 (2004)
254. T J Colacot, H A Shea *Org. Lett.* **6** 3731 (2004)
255. B Liu, K K Moffett, R W Joseph, B D Dorsey *Tetrahedron Lett.* **46** 1779 (2005)
256. A Tewari, M Hein, A Zapf, M Beller *Tetrahedron* **61** 9705 (2005)
257. I P Beletskaya, A V Tsvetkov, G V Latyshev, N V Lukashev *Zh. Org. Khim.* **39** 1729 (2003)^c
258. C W K Gstöttmayr, V P W Böhm, E Herdtweck, M Grosche, W A Herrmann *Angew. Chem., Int. Ed.* **41** 1363 (2002)
259. O Navarro, H Kaur, P Mahjoor, S P Nolan *J. Org. Chem.* **69** 3173 (2004)
260. H Lebel, M K Janes, A B Charette, S P Nolan *J. Am. Chem. Soc.* **126** 5046 (2004)
261. K Arentsen, S Caddick, F G N Cloke, A P Herring, P B Hitchcock *Tetrahedron Lett.* **45** 3511 (2004)
262. A-E Wang, J Zhong, J-H Xie, K Li, Q-L Zhou *Adv. Synth. Catal.* **346** 595 (2004)
263. C Song, Y Ma, Q Chai, C Ma, W Jiang, M B Andrus *Tetrahedron* **61** 7438 (2005)
264. K Arentsen, S Caddick, F G N Cloke *Tetrahedron* **61** 9710 (2005)
265. O Navarro, N Marion, N M Scott, J González, D Amoroso, A Bell, S P Nolan *Tetrahedron* **61** 9716 (2005)
266. W Huang, J Guo, Y Xiao, M Zhu, G Zou, J Tang *Tetrahedron* **61** 9783 (2005)
267. B Tao, D W Boykin *Tetrahedron Lett.* **43** 4955 (2002)
268. L Ackermann, R Born *Angew. Chem., Int. Ed.* **44** 2444 (2005)
269. G Miao, P Ye, L Yu, C M Baldino *J. Org. Chem.* **70** 2332 (2005)
270. J-H Li, W-J Liu, Y-X Xie *J. Org. Chem.* **70** 5409 (2005)
271. A Corma, H Garcia, A Leyva *Tetrahedron* **61** 9848 (2005)
272. A K Gupta, C Y Rim, C H Oh *Synlett* 2227 (2004)
273. K Tamao, K Sumitani, Y Kiso, M Zembayashi, A Fujioka, S-i Kodama, I Nakajima, A Minato, M Kumada *Bull. Chem. Soc. Jpn.* **49** 1958 (1976)
274. M Rehahn, A-D Schlüter, W J Feast *Synthesis* 386 (1988)
275. M Kumada, K Tamao, K Sumitani *Org. Synth.* **58** 127 (1978)
276. T Katayama, M Umeno *Chem. Lett.* **20** 2073 (1991)
277. G S Reddy, W Tam *Organometallics* **3** 630 (1984)

278. T Katayama, Y Uchibori, M Umeno *Jpn. Kokai Tokkyo Koho*; *Jpn. P.* 04.356.431; *Chem. Abstr.* **118** 212648 (1993)
279. K C Eapen, S S Dua, C Tamborski *J. Org. Chem.* **49** 478 (1984)
280. G Kottirsch, G Szeimies *Chem. Ber.* **123** 1495 (1990)
281. N Yjshilai, H Mashima, E Nakamura *J. Am. Chem. Soc.* **127** 17978 (2005)
282. J Blum, O Berlin, D Milstein, Y Ben-David, B C Wassermann, S Schutle, H Schumann *Synthesis* 571 (2000)
283. A S Burukin, A A Vasil'ev, A O Chizhov, S G Zlotin *Izv. Akad. Nauk, Ser. Khim.* 947 (2005)^a
284. A F Indolese *Tetrahedron Lett.* **38** 3513 (1997)
285. K Inada, N Miyaure *Tetrahedron* **56** 8657 (2000)
286. M B Thathagar, J Beckers, G Rothenberg *J. Am. Chem. Soc.* **124** 11858 (2002)
287. M J Monteith WO PCT 98/16486; *Chem. Abstr.* **128** 294592 (1998)
288. A S Burukin, A A Vasil'ev, N L Merkulova, A O Chizhov, E A Mistryukov, S G Zlotin *Izv. Akad. Nauk, Ser. Khim.* 1414 (2007)^a
289. A S Burukin, A A Vasil'ev, N L Merkulova, M I Struchkova, S G Zlotin *Izv. Akad. Nauk, Ser. Khim.* 114 (2006)^a
290. C Yi, R Hua *J. Org. Chem.* **71** 2535 (2006)
291. M R Eberhard, Z Wang, C M Jensen *Chem. Commun.* 818 (2002)
292. M Sonoda, A Inaba, K Itahashi, Y Tobe *Org. Lett.* **3** 2419 (2001)
293. T Yoshimura, A Inaba, M Sonoda, K Tahara, Y Tobe, R V Williams *Org. Lett.* **8** 2933 (2006)
294. H E Ramsden, A E Balint, W R Whitford, J J Walburn, R Cserr *J. Org. Chem.* **22** 1202 (1957)
295. T Amano, T Ota, K Yoshikawa, T Sano, Y Ohuchi, F Sato, M Shiono, Y Fujita *Bull. Chem. Soc. Jpn.* **59** 1656 (1986)
296. D E Pearson, D Cowan, J D Beckler *J. Org. Chem.* **24** 504 (1959)
297. D E Pearson, D Cowan *Org. Synth.* **44** 78 (1964)
298. A F Hegarty, P O'Neill *Tetrahedron Lett.* **28** 901 (1987)
299. I M Bell, S N Gallicchio, M Abrams, L S Beese, D C Beshore, H Bhimnathwala, M J Bogusky, C A Buser, J C Culberson, J Davide, M Ellis-Hutchings, C Fernandes, J B Gibbs, S L Graham, K A Hamilton, G D Hartman, D C Heimbrook, C F Homnick, H E Huber, J R Huff, K Kassahun, K S Koblan, N E Kohl, R B Lobell, J J Lynch Jr, R Robinson, A D Rodrigues, J S Taylor, E S Walsh, T M Williams, C B Zartman *J. Med. Chem.* **45** 2388 (2002)
300. P Bourgeois, R Calas *J. Organomet. Chem.* **84** 165 (1975)
301. J Dunogues, D N Gabe, M Laguerre, N Duffaut, R Calas *Organometallics* **1** 1525 (1982)
302. H Suzuki, O Yagui, T Hanafusa *Bull. Chem. Soc. Jpn.* **47** 2260 (1974)
303. A F Rybakov, A V Garbar, E S Petrov *Dokl. Akad. Nauk SSSR* **291** 1386 (1986)^h
304. H Fillon, C Gosmini, J-Y Nédélec, J Périchon *Tetrahedron Lett.* **42** 3843 (2001)
305. N J Hales, H Heaney, J H Hollinshead, S M Lai, P Singh *Tetrahedron* **51** 7777 (1995)
306. M D Rauch, F E Tibbetts, H B Gordon *J. Organomet. Chem.* **5** 493 (1966)
307. I Haiduc, H Gilman *Rev. Roum. Chim.* **16** 907 (1971)
308. J R Baran Jr, C Hendrickson, D A Laude Jr, R J Lagow *J. Org. Chem.* **57** 3759 (1992)
309. C Tamborski, E J Soloski, C E Dills *Chem. Ind. (London)* 2067 (1965)
310. R P Polniaszek, S E Belmont, R Alvarez *J. Org. Chem.* **55** 215 (1990)
311. L Fajari, J Carilla, L Julia, J Riera, A Parraga, M Coll, X Solans *J. Organomet. Chem.* **474** 89 (1994)
312. P J Alonso, J Fornies, M A Garcia-Monforte, A Martin, B Menjon *Chem. Commun.* 728 (2002)
313. A S Burukin, A A Vasil'ev, M I Struchkova, V V Kachala, S G Zlotin *Izv. Akad. Nauk, Ser. Khim.* 941 (2005)^a
314. J M Vernon, M Ahmed, L J Kricka *J. Chem. Soc., Perkin Trans. I* 837 (1978)
315. G W Gribble, R W Allen, C S LeHoullier, J T Eaton, N R Easton Jr, R I Slayton, M P Sibi *J. Org. Chem.* **46** 1025 (1981)
316. M Oki, T Tanuma, Y Tanaka, G Yamamoto *Bull. Chem. Soc. Jpn.* **61** 4309 (1988)
317. A Saednya, H Hart *Synthesis* 1455 (1996)
318. T H Kress, M R Leanna *Synthesis* 803 (1988)
319. K Harada, H Hart, C-J F Du *J. Org. Chem.* **50** 5524 (1985)
320. T I Gorbunova, A Ya Zapevalov, V E Kirichenko, V I Saloutin, O N Chupakhin *Zh. Prikl. Khim.* **73** 610 (2000)^e
321. O N Zabelina, T I Gorbunova, M G Pervova, V E Kirichenko, A Ya Zapevalov, V I Saloutin, O N Chupakhin *Zh. Prikl. Khim.* **77** 1533 (2004)^e
322. O N Zabelina, V E Kirichenko, M G Pervova, Yu G Yaltuk, V I Saloutin *Zh. Prikl. Khim.* **79** 801 (2006)^e

^a — *Russ. Chem. Bull., Int. Ed. (Engl. Transl.)*

^b — *Russ. J. Phys. Chem. (Engl. Transl.)*

^c — *Russ. J. Org. Chem. (Engl. Transl.)*

^d — *Pharm. Chem. J. (Engl. Transl.)*

^e — *Russ. J. Appl. Chem. (Engl. Transl.)*

^f — *Russ. J. Gen. Chem. (Engl. Transl.)*

^g — *Chem. Heterocycl. Compd. (Engl. Transl.)*

^h — *Dokl. Chem. (Engl. Transl.)*

Outer-sphere association of calixarenes and other macrocyclic ligands with metal complexes as the basis for the design of molecular devices

A R Mustafina, V V Skripacheva, A I Konovalov

Contents

I. Introduction	917
II. The driving forces of outer-sphere association of transition metal complexes with various macrocycles, DNA and antibiotics	917
III. The thermodynamics of outer-sphere association of water-soluble calixarenes with charged complexes and organic ions in comparison with that of cyclodextrins and cucurbiturils	920
IV. Design of switchable systems on the basis of outer-sphere coordination of charged metal complexes and macrocycles	921
V. Outer-sphere association of metal complexes with macrocycles as a method of modifying physicochemical properties of a supramolecular system	924
VI. Conclusion	928

Abstract. The regular features of the formation of outer-sphere associates of water-soluble calixarenes with metal complexes in solutions and their structure in the solid state are analysed. A comparison with analogous data for other outer-sphere macrocyclic ligands is carried out. Some physicochemical properties of the outer-sphere associates are considered in regards to their potential use for the development of new processes and materials. The bibliography includes 150 references.

I. Introduction

Recent rise of the chemists' interest in transition metal complexes is caused, *inter alia*, by the important role of these complexes in biological processes and their possible application in the design of molecular and nano-devices (conductors,¹ switches,² sensors³ and molecular machines⁴). The transition metal ions are extremely important for living organisms.^{5,6} It is essential that most of 'metals of life' are present in an organism as complexes, that can be divided according to their biological functions into transporters (ionophores), accumulators, activators of inert molecules and bio-catalysts.⁷ The biochemical functioning of metal ions is related mainly to their outer-sphere coordination, which is also important in the design of switching systems based on transition metal complexes.^{1,4} Weak non-covalent interactions are the driving forces of the formation of outer-sphere complexes⁷ and therefore this is most efficient when a cooperative effect takes place. Such effect is especially pronounced in the case of many natural products (DNA molecules, natural ionophores, cyclodextrins) as well as artificial macrocycles. Calixarenes and their derivatives, which are receptors of various ions and molecules, belong to the latter

class of compounds.^{8,9} Calixarene complexes of ions and organic substrates are well documented. However, so far there are no reviews on calixarenes as outer-sphere ligands for metal complexes. The discussion of the chemistry of outer-sphere association of metal complexes with calixarene derivatives and comparison of these compounds with other similar natural and synthetic outer-sphere ligands, including macrocyclic ones, are the main objectives of the present review. The physicochemical properties of the resulting outer-sphere associates (super-complexes) and their potential application in advanced technological processes and design of new materials are also discussed.

II. The driving forces of outer-sphere association of transition metal complexes with various macrocycles, DNA and antibiotics

Many natural receptors, for example, DNA and antibiotics, are not macrocycles. However, their outer-sphere association with transition metal complexes follows the cooperative mechanism of 'host–guest' interactions. Numerous papers are devoted to complexation of DNA with transition metal complexes, many of them were discussed in a review.¹⁰ The interest is caused by the use of coordinatively saturated transition metal complexes for studying the DNA structure. Coordinatively saturated Co^{III} and Ru^{II} octahedral complexes (mainly, polypyridyl complexes) are used for cleavage of DNA molecules and for their direct molecular and/or enantiomeric recognition.^{10–12} It is known that charged phosphate fragments and hydrophobic grooves, formed by nitrogen-containing heterocycles, take part in binding of metal complex to the DNA molecule. Thus, in this case the electrostatic interactions, intermolecular hydrogen bonding and π – π interactions between heterocycles representing the ligands of metal ion and DNA heterocycles are the main driving forces of outer-sphere complex formation.

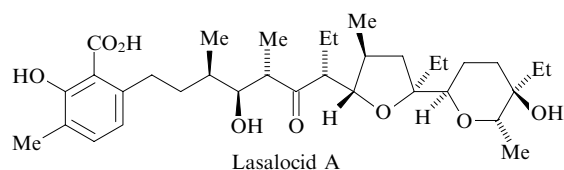
Some natural antibiotics are also devoid of macrocyclic cavities, but, nevertheless, they possess receptor properties towards transition metal complexes due to the cooperative effect of intermolecular hydrogen bonds and electrostatic interactions in the crown ether-like conformation of their

A R Mustafina, V V Skripacheva, A I Konovalov A E Arbuzov Institute of Organic and Physical Chemistry, Kazan Scientific Centre of the Russian Academy of Sciences, ul. Acad. Arbuzova 8, 420088 Kazan, Russian Federation. Fax (7-843) 273 22 53, tel. (7-843) 272 73 94, e-mail: asiya@iopc.knc.ru (A R Mustafina), vskripacheva@mail.ru (V V Skripacheva), tel. (7-843) 272 16 84, e-mail: konovalov@knc.ru (A I Konovalov)

Received 14 May 2007

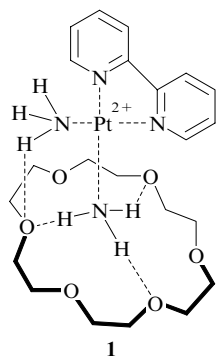
Uspekhi Khimii 76 (10) 979–993 (2007); translated by D S Yufit

molecules. Among the natural ionophores, lasalocid A is the most popular receptor of transition metal complexes.^{13, 14}



It is known that lasalocid A is an anionic ionophore capable of effective (outer-sphere) binding of positively charged ammine and amine complexes of transition metals $[Ct^{n+}]$ ($[Co(NH_3)_6]^{3+}$, $[Cr(NH_3)_6]^{3+}$, $[Co(NH_3)_5Cl]^{2+}$, Δ - and Λ - $[Co(en)_3]^{3+}$, $[Pt(NH_3)_6]^{4+}$) to the complexes $[Ct^{n+}][LAS^-]_n$. The lasalocid anion $[LAS^-]$ in the latter surrounds the metal complex and adopts a cyclic pseudo-crown-ether conformation.^{15–18}

Crown ethers represent a class of synthetic macrocyclic receptors modelling some intermolecular interactions ionophore–substrate.^{19–22} The same forces are responsible for binding of metal complexes to crown ethers and ionophores, because the spatially pre-arranged ether oxygen atoms can be involved in both hydrogen bonding and electrostatic interactions. The efficiency of electrostatic interactions of metal complexes with crown ethers is lower than that with ionophores, which results in the increase in the contribution of hydrogen bonding to the total bonding energy. Therefore, the presence of acidic hydrogens in ligands that surround the metal complex is prerequisite for the efficient outer-sphere coordination of metal complexes by crown ethers. Particularly, in the process of formation of outer-sphere complexes of metal ammine and ammine complexes with 18-crown-6 the hydrogen atoms of NH_3 or NH_2 ligands form hydrogen bonds with the oxygen atoms of the crown ether. Complex **1** is an example of such compounds.^{23, 24}

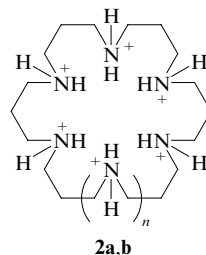


A great number of complexes of crown ethers with transition metal aqua complexes and with metal complexes containing acetonitrile ligands are known. Acetonitrile CH-protons are sufficiently acidic to form hydrogen bonds with the ether oxygen atoms of the macrocycle.²⁴

The structure modifications (*i.e.* introduction of various substituents) and enlargement of the crown-ether ring make possible π – π -interactions with ligands of metal complexes containing aromatic fragments.^{25, 26} Thus both NH_3 ligands take part in hydrogen bonding in the complex of dibenzo-18-crown-6 with $[Pt(bipy)(NH_3)_2]^{2+}$ (bipy is 2,2'-bipyridyl). The large and flexible crown-ether ring adopts a conformation favourable for the interactions of benzo-substituents with the bipy ligands in the inner coordination sphere of this platinum complex. The existence of these interactions was confirmed by

X-ray crystallography and UV-spectroscopy (judging from the presence of charge transfer bands). The recognition of natural siderophore ferrioxamine B ($FeHDFB^+$) by dicyclohexano-18-crown-6 is based upon the ability of the crown-ether ring to bind a primary ammonium group.^{20, 27, 28} However, lasalocid A binds $FeHDFB^+$ in a basic media more efficiently than benzo-18-crown-6 due to the possibility of ionisation and more flexible structure adjustable the structure of the 'guest' molecule. The charge neutralisation occurring simultaneously with hydrogen bonding with the deprotonated hydroxyl group and two ether oxygen atoms of the chain results in more efficient binding than that with the crown-ether oxygen atoms.^{27, 28}

In contrast to crown ethers possessing affinity to positively charged metal complexes, the polyaza-macrocycles in their protonated forms bind anionic complexes. For example, the macrocycles **2a, b** form outer-sphere associates (in the ratio 1:1) in water with transition metal anionic complexes $M(CN)_6^{4-}$, where $M = Fe, Ru, Co$.^{29, 30} In this case, the electrostatic interactions and hydrogen bonding are also the driving forces of formation of outer-sphere complex. The stability of such outer-sphere complexes being determined mainly by the number of protonated nitrogen atoms of the macrocyclic ligand rather than by the type of the metal in the complex anion.



$n = 1$ (**a**), 2 (**b**).

Thus, crown ethers and polyazamacrocycles may be regarded as macrocycles that efficiently bind the charged metal complexes due to electrostatic interactions and hydrogen bonds while hydrophobic interactions in this case are much less important.

Cyclodextrins (CD) is a class of natural macrocycles with a hydrophobic cavity owing to which they form inclusion compounds with metal complexes,^{31, 32} while the presence of hydrophilic outer surface provides good solubility in water.

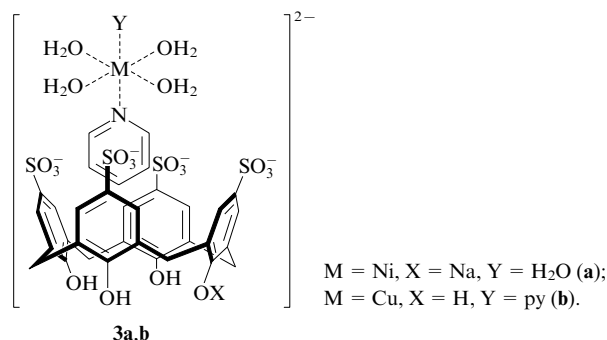
Cyclodextrins bind neutral and negatively charged species most efficiently, although many examples of the formation of inclusion complexes with positively charged metal complexes are documented.^{32–36} For instance, β -CD binds the oxidised and reduced forms of ferrocenes as well as ferrocenecarboxylate with approximately the same stability constants (10^3 – 10^4) (Ref. 35). Stability of inclusion complexes is determined mainly by the match between the cavity diameter and the hydrophobic fragment size of a 'guest' molecule,^{36–41} although intermolecular hydrogen bonds between a metal complex and hydroxyl groups of cyclodextrin may additionally stabilise the inclusion complexes.⁴² The 1:1 adducts of β - and γ -cyclodextrins with ferrocene are described in Ref. 36, the orientation of ferrocene molecule in β -CD adduct is axial and in γ -CD adduct is equatorial.

Cucurbit[n]urils and calix[n]arenes are the most intensively studied compounds among the synthetic macrocycles. They are widely used as molecular containers for metal complexes and the interest in these compounds increased significantly during the last decade.

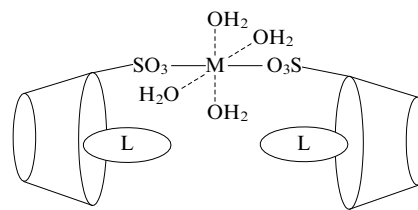
The size of internal cavities of cucurbit[*n*]urils with $n = 6-8$ is close to the size of cavities of the molecules of α -, β and γ -CD, respectively.⁴³ However, in contrast to the cyclodextrins, the oxygen atoms of carbonyl groups in cucurbituril portals are more polarised. As a result, the contribution of electrostatic interactions to the total binding energy of the 'host-guest' system is higher than that of CDs and the adducts with positively charged ions are more stable.⁴⁴ The adducts with metal aqua complexes are the most thoroughly studied. They are efficiently bound to carbonyl portals of cucurbiturils and do not form inclusion complexes.⁴⁵⁻⁴⁷ However, the inclusion complexes of cucurbiturils are also known. Particularly, such complexes are formed with a number of solvents and indicators.⁴⁸⁻⁵⁰ The cucurbit[8]uril is more suitable for the formation of inclusion complexes with positively charged metal complexes than cucurbit[6]- and cucurbit[7]urils due to the larger size of the molecular cavity. It was shown⁵¹⁻⁵⁴ that outer-sphere association of cobalt, copper and nickel complexes with ethylenediamine and cyclam results in the formation of inclusion complexes of cucurbit[8]uril.

Calixarenes represent an important class of synthetic receptors, which may exhibit all above-mentioned types of intermolecular interactions.^{8,9} Their spatial structure consists of clearly separated hydrophilic (rim) and hydrophobic (cavity) areas. Besides, the potential of rim modifications and cavity size variations for these molecules is higher than that for cyclodextrins and cucurbiturils.^{8,9} The present review mainly discusses the water-soluble receptors obtained by the introduction of ionised groups into the calixarene matrix, because compounds of this particular class are most comprehensively studied as outer-sphere ligands for charged metal complexes.⁵⁵⁻⁵⁹

For the first time, the possibility of outer-sphere coordination of nickel and copper complexes $[\text{Ni}(\text{H}_2\text{O})_5\text{py}]^{2+}$ and $[\text{Cu}(\text{H}_2\text{O})_4\text{py}_2]^{2+}$ with *p*-sulfonatocalix[4]arene was shown by X-ray analysis.⁵⁵ The pyridine moiety of the metal complexes is located inside the cavity (structures **3a,b**).



Later similar studies were performed for outer-sphere complexes of *p*-sulfonatocalix[4]arene with $[\text{Ni}(\text{phen})_3]^{2+}$ (phen is 1,10-phenanthroline) and $[\text{Co}(\text{diHOSar})]^{3+}$ [sar is 3,6,10,13,16,19-hexaazabicyclo[6.6.6]eicosane, diHOSar = 1,8-(OH)₂sar], and also its thia-analogue with $[\text{Co}(\text{bipy})_3]^{3+}$ (Refs 56-59). The structure of the outer-sphere associate depends on the composition of the solution when the outer-sphere coordination of a labile complex takes place or when free metal ions and ligands are present in the solution alongside with the complex. For example, the above-discussed outer-sphere complexes are not formed in slightly acidic aqueous solutions containing cobalt(II) or nickel(II) salts, pyridine *N*-oxide and *p*-sulfonatocalix[5]arene. Aqua-ions $[\text{Co}(\text{H}_2\text{O})_4]^{2+}$ or $[\text{Ni}(\text{H}_2\text{O})_4]^{2+}$ coordinate sulfo groups of two different calixarene units forming a bridge between them.⁶⁰ The cavities contain pyridine *N*-oxide molecule (L) non-coordinated to the metal.



M = Co, Ni.

Depending on the type of the metal, the system sulfonato-calix[5]arene-lanthanide ion-pyridine *N*-oxide yields, alongside with the complexes of the described type, complexes in which the molecules of pyridine *N*-oxide are coordinated by the metal atoms and complexes of the type **3** where the ligand is located inside the cavity.⁶¹ Thus, gadolinium forms complexes of the first type, while in Eu^{III} , Tb^{III} and Yb^{III} complexes, mixed inner- and outer-sphere coordination was observed. Hence, the presence of several binding centres (the cavity, substituents of the upper and lower rims) allows wide modification of a supra-molecular structure upon variation of the composition of a multi-component solution.⁶² Cucurbiturils also form such ternary complexes in which an organic molecule is incorporated into a macrocyclic cavity and a metal ion is linked to the donor groups of the rim. Particularly, such complexes with sodium ions and some solvents were described for cucurbit[6]uril.⁴⁷

It should be noted that the efficiency of the discussed classes of compounds including the macrocycles as the outer-sphere ligands is determined by cooperative effect of electrostatic and hydrophobic interactions as well as by hydrogen bonding, while the relative contribution of interactions of each type depends on the structure of the outer-sphere ligand. The presence of hydrophobic cavities and hydrophilic rims is a common feature of cyclodextrins, cucurbiturils and calixarenes. For this reason, we will restrict our discussion to the comparative analysis of these macrocycles. However, alongside with the common features, there is also a number of important differences between these compounds. Thus, in contrast to cyclodextrins, cucurbiturils, due to the presence of polar portals, are able to form non-inclusion outer-sphere associates with metal aqua complexes and ternary complexes where the solvent molecules are located inside the cavity and the metal ions are bound by the carbonyl groups of portals. Of numerous calix[*n*]arenes, the water-soluble derivatives, particularly *p*-sulfonatocalix[*n*]arenes, are of special interest as outer-sphere ligands for metal complexes. Such macrocycles can form outer-sphere associates with the charged metal complexes as well as bind metal ions (through inter-sphere coordination by donor groups of upper and lower rims) and, simultaneously ligands (through inclusion to the calixarene cavity). Yet another characteristic of calixarene molecules is their conformational flexibility, which distinguishes them from rigid molecules of cyclodextrins and cucurbiturils. The mobility of aromatic rings of even the most conformationally restricted *p*-sulfonatocalix[4]arenes allows the adjustment of the 'host' cavity to the 'guest' structure. The results of quantum chemical calculations⁶³ show that the inclusion of hydrophobic 'guest' fragment into the cavity of *p*-sulfonatocalix[4]arene decreases the conformational mobility of the cavity-forming rings; the inclusion of aliphatic fragments stabilises the C_{4v} conformation of the complex, the inclusion of aromatic fragments results in the C_{2v} conformation.⁶³ In all the known cases, inclusion of ligand fragments of Cu^{II} , Co^{II} , Co^{III} and Ni^{II} complexes into the cavity of *p*-sulfonatocalix[4]arene and its thia-analogue stabilises the flattened cone conformation (C_{2v}).^{56-59, 64} X-Ray structural analysis of the crystals obtained from the solution of *p*-sulfonatothiacalix[4]arene and tris(bipyridyl) nickel revealed⁶⁴ a conformational transition of the 'host' molecule

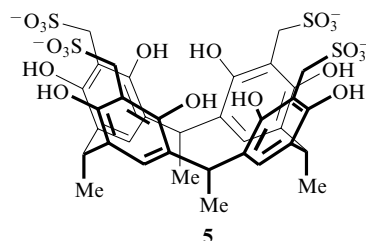
from the cone conformation into the so-called partial cone conformation due to the inclusion complex formation. However, it should be noted that the crystal was grown in an autoclave under high temperature and pressure.

III. The thermodynamics of outer-sphere association of water-soluble calixarenes with charged complexes and organic ions in comparison with that of cyclodextrins and cucurbiturils

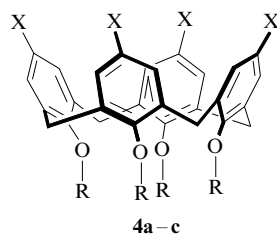
The data discussed in the previous Section provide a basis for the analysis of similarities and differences in the driving forces of the outer-sphere association of charged complex species with various macrocycles. As the number of papers on the thermodynamics of outer-sphere association of metal complexes with mentioned macrocycles in aqueous solutions is very limited, we compare the formation of complexes of calixarenes, cyclodextrins and cucurbiturils not only with metal complexes, but also with organic cations and neutral molecules. The main difference between cyclodextrins and water-soluble calixarenes is that the formation of cyclodextrin complexes with organic substrates is the entropy-favourable process, while the formation of complexes of water-soluble calix[4]resorcinarenes is entropy-unfavourable process.⁶⁵ In the case of cyclodextrins, the hydrophobic effect caused by water destructure due to the decrease in hydrophobic surface, is dominant and results in the entropy increase.⁶⁶ Meanwhile the multi-centred interactions of a guest molecule with the cyclodextrin cavity are usually not sufficiently effective to be a driving force of the formation of cyclodextrin complexes in aqueous solutions.⁶⁷ As it has already been mentioned, the presence of the polar portals in the cucurbituril molecules significantly increases the contribution of electrostatic interactions in comparison with that in the case of formation of cyclodextrin complexes. For instance, cucurbit[7]uril binds the methylviologen cation (MV^{2+}) more efficiently than β -CD of similar size due to the enthalpy contribution.⁶⁸ Cucurbit[7]uril is also more efficient in binding ferrocene and its alkylammonium derivatives: the corresponding binding constants of β -CD are in the range of 10^3 – 10^4 litre mol⁻¹, while for cucurbit[*n*]urils (*n* = 7, 8) the range is 10^9 – 10^{10} litre mol⁻¹. The value of the constant significantly increases (up to 10^{12} – 10^{13} litre mol⁻¹) for ammonium derivatives of ferrocene.⁶⁹ However, the entropy contribution in the binding of cucurbit[7]uril with MV^{2+} cation is positive, while the entropy changes in the interactions with ferrocene and its ammonium derivative are negative.³⁵ Thus, the presence of polar portals in the cucurbit[7]uril molecules makes the enthalpy contribution in the interactions with positively charged metal complexes favourable. At the same time, the entropy changes depend on a number of factors, the most important being desolvation of the guest species, which in turn is determined by its structure.

The presence of the ionised groups at the rims of water-soluble calix[*n*]arenes and calix[4]resorcinarenes significantly increases the contribution of electrostatic interactions to the total energy of formation of a 'host-guest' complex.⁶⁶ Such

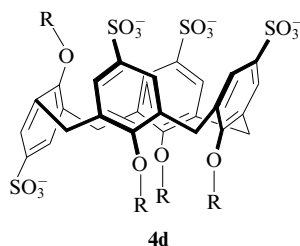
conclusion, for example, was made on the basis of a study of complexation properties of calixarenes **4a–c** and calixarene **4d**, which adopts a partial cone conformation.^{70–72} In particular, it was found that the efficiency of binding of tetramethylammonium cations by calixarene **4b** is an order of magnitude higher than that by calixarene **4c**. A comparison of the complexation ability of calixarenes with amino acids leads to the conclusion that the presence of sulfonate groups in the upper rim of calixarene is necessary for the binding of amino acids.⁷⁰ It should be noted that the binding constant of organic ions also depends on the conformational rigidity of sulfonate groups at the rim of the cyclophane receptor. For example, the binding constant of tetramethylammonium decreases by two orders of magnitude upon transition from calix[4]arene **4a** (Ref. 71) with fixed sulfonate groups in the upper rim of the molecule to sulfonatomethylcalix[4]resorcinarene (**5**)⁷³ with conformationally mobile sulfonate groups.^{70–73}



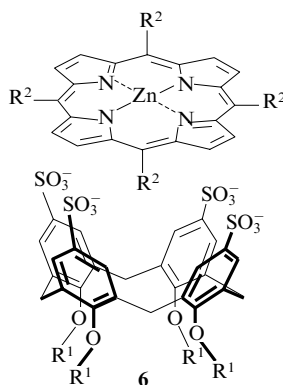
However, the contribution of the electrostatic interactions to the total energy of formation of inclusion complexes of water-soluble calixarenes and resorcinarenes is considerable, but not decisive. In particular, the analysis of ¹H NMR spectra and thermodynamic characteristics of inclusion complexes of water-soluble sulfonatocalix[4]resorcinarene with a number of organic molecules and ions⁶⁶ reveals that the complexation constant of a non-charged substrate with calixarene is determined mainly by the efficiency of interactions of CH-fragments of the guest molecule with the π -donor cavity of the host molecule. It was shown that the formation of inclusion complexes of water-soluble calix[4]resorcinarenes is an enthalpy-favourable process because CH- π -interactions make a significant contribution to the formation energy. As a result, the higher the CH-acidity of the substrate molecule and the higher the π -donor character of the calixarene cavity, the more efficient the binding.⁶⁶ Later⁷⁴ it was shown that benzene derivatives with electron-withdrawing substituents form more stable inclusion complexes with water-soluble calixarenes than their analogues with electron-donating substituents. This fact also indicates the importance of CH-acidity of the 'guest' molecule in the formation of 'host-guest' complexes. The process of binding of calix[4]arenes **4a** and **4b** with tetramethylammonium and tetramethylanilinium is also enthalpy favourable, while the change in entropy upon complexation is negative.⁷¹ However, when non-inclusion outer-sphere associates are formed, e.g., the associate **6** with a zinc porphyrin

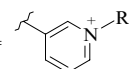
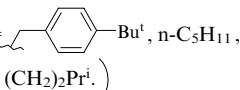


R = H, X = SO₃⁻ (**a**);
R = CH₂CO₂H; X = SO₃⁻ (**b**), (**c**).



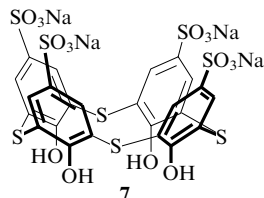
R = CH₂CO₂H.



R¹ = (CH₂)₂OEt,
R² = 
R³ = 

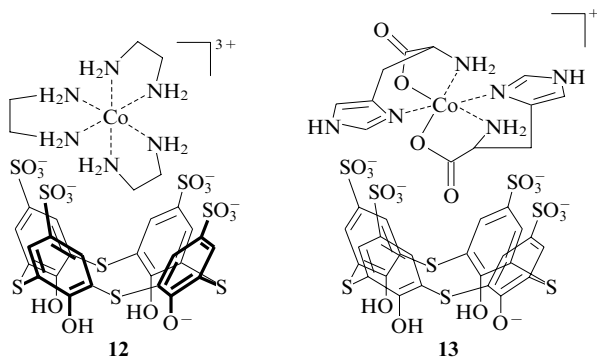
complex, the multi-centred interactions between charged rim and the guest molecule require their substantial desolvation. Probably, this is the reason for the positive entropy change in this process.⁷⁵

p-Sulfonatothiocalix[4]arene (**7**) is an analogue of *p*-sulfonatocalix[4]arene in which the methylene bridges are replaced by sulfur atoms.⁷⁶



It was suggested⁷⁷ that thiocalix[4]arene exceeds classical calixarene in its ability to form inclusion complexes due to the larger size of the cavity. However, the later results^{78–80} do not support this suggestion. In particular, a comparison of the values of ΔG , ΔH and ΔS of formation of pyridinium complexes with both receptors revealed that the binding with thiocalix[4]arene is less efficient due to smaller enthalpy contribution.⁷⁹ This was accounted for by the lesser π -donor character of thiocalixarene hydrophobic cavity in comparison with that of classic calixarene, which results in less efficient CH– π -interactions. Hence, thiocalixarene is more selective towards the aromatic fragment of toluene, while calixarene itself binds the methyl group and the aromatic ring with the same probability.⁷⁴

As already mentioned before, the thermodynamic characteristics of inclusion complexes of water-soluble calixarenes with metal complexes are little studied. However, it is natural to assume that the driving forces of the formation of such outer-sphere associates are also electrostatic interactions with the rim and CH– π -interactions with the hydrophobic cavity. The stability and the structure of outer-sphere associates of complexes $[\text{Co}(\text{en})_3]^{3+}$ (**8**), $[\text{Co}(\text{en})_2\text{ox}]^+$ (**9**), $[\text{Co}(\text{L-His})_2]^+$ (**10**), $[\text{Co}(\text{bipy})_3]^{3+}$ (**11**) (en is ethylenediamine, ox is oxalate, L-His is L-histidine) with *p*-sulfonatothiocalix[4]arene and sulfonatomethylcalix[4]resorcinarene (for example, associate **12**) were studied.⁸¹ It was shown that, similarly to the binding of organic cations, the larger the charge of the complex and the more compact its ligands, the higher the stability of outer-sphere associates. For both receptors, the association constant of compound **8** is the highest and the values of the constants decrease in the series **8** > **11** > **10** > **9**. Thus, the substitution of the oxalate anion for one of the en ligands as well as enlargement of the chelate ring on going from en to bipy results in the decrease in the calixarene complexation constant. Moreover, it was shown that the outer-sphere associate **13** containing cation **10** is not an inclusion complex and is formed as a result of multi-centred electrostatic interactions with the rim of the calixarene molecule.



Thus, the following conclusions may be drawn from the analysis of thermodynamic parameters of complexes of cyclodextrins, cucurbiturils and calixarenes with organic and metal-containing substrates:

1. Binding of substrates to cyclodextrins is usually the entropy-favourable process due to a hydrophobic effect, while the 'host–guest' interactions are not efficient enough for a favourable enthalpy contribution. The presence of polar portals in cucurbiturils and charge of rims in calixarenes increases their affinity towards positively charged metal complexes due to more favourable (in comparison with cyclodextrins) enthalpy contribution in the total interaction energy. The enthalpy contribution increases on going from cucurbiturils to water-soluble calixarenes. However, the favourable enthalpy contribution in the formation of 'host–guest' complexes of water-soluble calixarenes is the result of not only significant contribution of electrostatic interactions with charged groups of the rim but also of CH– π interactions with the calixarene cavity.

2. The hydrophobic effect is mainly responsible for the entropy change in the formation of 'host–guest' complexes of cyclodextrins. The entropy change in the cases of cucurbiturils and calixarenes is caused primarily by the guest molecule desolvation and therefore depends on the structure of the molecule as well as on the structure of the 'host–guest' complex.

3. In contrast to cyclodextrins and cucurbiturils, water-soluble calix[4]arenes form outer-sphere associates, where the charged metal complex only covers the charged rim and its ligands are not inserted into the macrocyclic cavity. Obviously, the efficiency of multi-centred electrostatic interactions with the ionised groups of the calixarene rim is responsible for the formation of such complexes of water-soluble calixarenes.

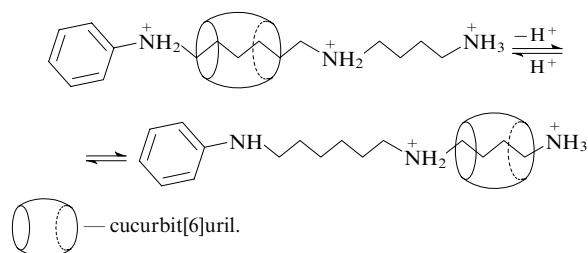
IV. Design of switchable systems on the basis of outer-sphere coordination of charged metal complexes and macrocycles

There is a growing interest in recent years in supramolecular systems in which an external action causes re-orientation of their fragments (components) and/or changes in their physicochemical properties as potential building blocks in the design of the so-called molecular devices and machines.^{82–84} In the present chapter, we discuss the possibility of changing the structure of outer-sphere associates of charged metal complexes and water-soluble macrocycles by varying pH and the electrochemical potential.

1. pH-Switchable systems

Obviously, the presence of ionisable groups in the macrocycle and/or in the guest molecule is a prerequisite for pH-switchable outer-sphere coordination of a metal complex to a macrocycle. Cucurbiturils are devoid of such groups and deprotonation of the hydroxyl groups of cyclodextrins is observed only under strongly basic conditions.⁴⁴ For that reason, the design of pH-switchable systems with these macrocycles is based on the processes of protonation–deprotonation of the guest species. For instance, it was shown⁸⁵ that the binding constants of novocaine with β -cyclodextrin in acidic and neutral media are almost identical in spite of the different degrees of protonation of novocaine (singly and doubly-charged cation, respectively). Only in the basic media, when a neutral form of novocaine is formed, was the fivefold increase in the binding constant was observed. Obviously, cucurbiturils with their additional sources of electrostatic interactions 'host–guest' (the polar portals) are more promising as potential pH-switchable systems than cyclodextrins. The system polyamine–cucurbit[6]uril is one of the first examples of pH-controllable translocation.⁸⁶ pH-In-

duced translocation in this system is caused by different basicity of the nitrogen containing fragments at the opposite ends of the guest molecule.



The protonation of amino groups also drives the polyrotaxane-based molecular machines.^{87, 88}

The carbonyl portals of cucurbiturils may be protonated in highly acidic media;⁴⁴ however, low basicity of the carbonyl groups seriously hinders the application of this process as the source of pH-induced translocation. As it has been mentioned above, the presence of ionised groups at the rim of water-soluble calixarenes results in much stronger dependence of the formation constant of a host–guest complex on the charge of the guest molecule, than in the case of cucurbiturils. However, there were no observations of threading of oxyethyl or polyrotaxane chains through the cavity in the case of water-soluble calix[4]arenes. It was shown⁸⁹ by ¹H NMR study in benzene that triphenylureidocalix[6]arene may form pseudorotaxanes due to the large size and conformational lability of the cavity. However, cyclodextrins and cucurbiturils are more widely used in the design of such molecular machines.

Yet another interesting feature of *p*-sulfonatocalix[4]arenes and their thia-analogues, namely the high acidity of their hydroxyl groups,⁹⁰ should be noted. It is caused by the presence of strong circular intramolecular hydrogen bonds between the phenolic OH-groups at the lower rim of the calixarene cavity. This in turn makes it possible to control the π -donor character of the cavity⁹¹ or the charge at the upper rim⁷³ of calixarenes by pH-induced deprotonation of hydroxyl groups. Alteration of the orientation of non-symmetrical organic cations inside calixarene cavity is one of interesting consequences of the pH dependence of water-soluble calixarene complexation. One of the first examples of pH-regulated relative orientation of a nonsymmetrical ‘guest’ (trimethylanilinium cation, TMA) and ‘host’ (*p*-sulfonatocalix[4]arene) was described.^{91, 92} The formation of inclusion complex in a wide range of pH values was proved on the basis of ¹H and ¹³C NMR spectroscopic data. The calixarene cavity contains mainly the aromatic fragment of TMA at high acidity (pD 0.4), while under neutral conditions (pD 7.3) trimethylammonium group and aromatic moiety are non-specifically bound by the ‘host’ molecule.

The differences in the binding modes may be caused,⁹¹ by changes in the electron-donating properties of an aromatic π -system due to dissociation of hydroxyl groups in the neutral media. The available data⁷¹ show that ditopic TMA is bound selectively through its aromatic fragment to all host molecules having fixed cone conformation and sulfonate groups at the upper rim (compounds **4a,b,d**). At the same time, calixarene **4c** recognises only polar alkylammonium group of TMA. Calixarene **4d**, which adopts a partial cone conformation binds TMA non-selectively like conformationally much more flexible receptor **4a**. Thus, the selectivity of inclusion of more hydrophobic (aromatic) or of more charged (trimethylammonium) fragments is determined by the efficiency of both electrostatic interactions at the rim and CH– π interactions with the calixarene cavity.

In the study of complexation of ditopic *N*-methylpyridinium cation with sulfonatomethylcalix[4]resorcinarene it was found⁷³ that in neutral and slightly acidic media the aromatic fragment is included into the resorcinarene cavity, while deprotonation of calix[4]resorcinarene hydroxyl groups predominantly results in inclusion of the *N*-methyl group into the cavity.

The use of a ditopic guest becomes even more interesting when there is a possibility of comparing the complexation that proceeds under kinetic or thermodynamic control (Fig. 1). Under kinetic conditions, in a multicomponent supramolecular system containing cucurbit[6]uril (CB[6]U), cucurbit[7]uril (CB[7]U), symmetrical cyclohexane-1,4-diammonium cation (**14**) and ditopic adamantyl(alkyl)ammonium ion (Alk = Buⁿ, n-C₆H₁₃, n-C₈H₁₇) (**15**), cation **14** is included into the cavity of cucurbit[7]uril and the alkyl chain of cation **15**, into the cavity of cucurbit[6]uril.⁹³ In equilibrium, the symmetrical cation **14** is included predominantly into the cavity of cucurbit[6]uril and the adamantyl fragment of ditopic cation **15**, into the cavity of cucurbit[7]uril.

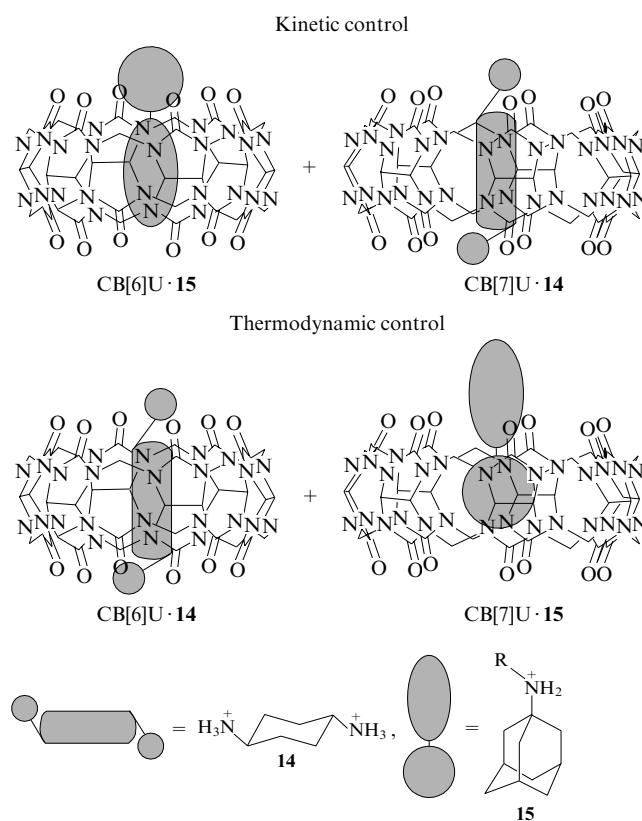
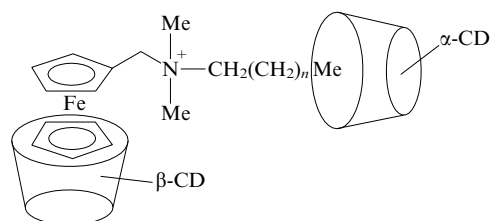
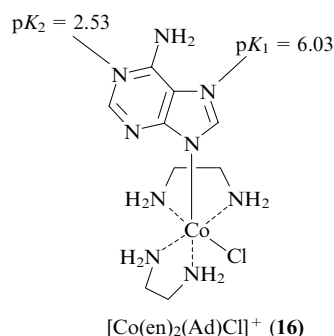


Figure 1. Kinetically and thermodynamically controlled complex formation of cucurbit[*n*]urils (*n* = 6, 7) with symmetrical cyclohexane-diammonium cation and ditopic adamantyl(alkyl)ammonium cation.

It is natural to suggest that the switchable complex formation may be based upon ditopic metal complexes, for instance, alkyldimethyl(ferrocenylmethyl)ammonium. It was shown⁹⁴ that the ferrocene fragment of this complex, in accordance with its size, is bound most efficiently to the cavity of β -CD, while the alkyl fragment, of α -CD. Thus, this ditopic ‘guest’ and α - and β -cyclodextrins are the basis for the construction of a multicomponent supramolecular system.

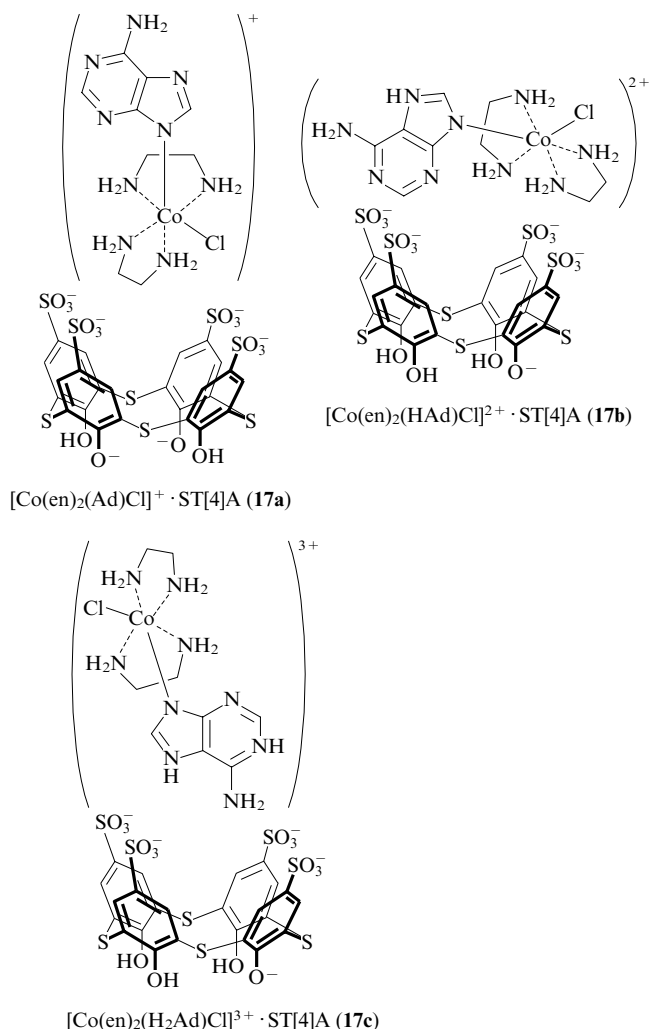


The mutual arrangement of guest and host molecules in the supramolecular complex formed can be changed by varying pH and hence, the charges on various parts of a metal complex. Adeninato-chloro-bis(ethylenediamine)cobalt(III) (**16**) has been chosen as a non-symmetrical guest. This complex undergoes two-stage protonation at the basic nitrogen atoms of adenine heterocycle in neutral and slightly acidic media.



Data from ^1H NMR spectroscopy show that the protonation of the adenine moiety of complex **16** upon decrease in pH from 9 to 6 results in structural changes of outer-sphere associate between *p*-sulfonatothiacalix[4]arene (ST[4]A) and cobalt complex (the structures **17a–c**) (Fig. 2) and in significant increase in its stability constant.⁹⁵ The decrease in pH brings about protonation of both the metal complex and the phenolate rim of *p*-sulfonatothiacalix[4]arene from hexa- to penta-anion. As mentioned above, the increase in π -donor character of the calixarene cavity induced by deprotonation of the phenolic groups results in more efficient $\text{CH}-\pi$ interactions. Therefore, in this case the neutralisation of the adenine fragment due to its protonation rather than the decrease in the π -donor character of the receptor cavity due to the protonation of the phenolate groups is the decisive factor that determines

the 'host–guest' binding constant and the orientation of metal complex relative the macrocycle cavity.



Thus, the presence of ionised and/or ionisable groups at both rims of calix[*n*]arenes is responsible for more efficient pH control of the complexation than in the case of cucurbiturils and cyclodextrins. However, the ability of the calixarene cavity to be 'threaded' by aliphatic and oxyethylene chains is much poorer than that of cyclodextrins and calixarenes, therefore the water-soluble calixarene-based molecular devices and machines should be designed differently.

2. Redox-switchable systems

The electrochemical properties of the inclusion complexes are crucial for the construction of redox-switchable systems. It is known that the redox potential of a redox-active species depends on the character of the solvent and the counter-ions. Naturally the outer-sphere association with macrocycles also should result in the modification of electrochemical properties. In other words, if the outer-sphere environment of a redox-active complex stabilises its reduced or oxidised form, the shift in the electrochemical potential of the pair is observed. Therefore, the larger the difference between the constants of outer-sphere association of macrocycle with reduced and oxidised forms of a metal complex, the larger the shift of the potential. As mentioned above, β -cyclodextrin binds the reduced form of ferrocene more efficiently, which results in a significant shift of potential of the pair $\text{Fe}^{\text{III}}/\text{Fe}^{\text{II}}$ into the anode region.³³

The opposite shift should be expected for macrocycles that contain polar or ionised groups and therefore form more stable outer-sphere associates with charged metal complexes. Indeed,

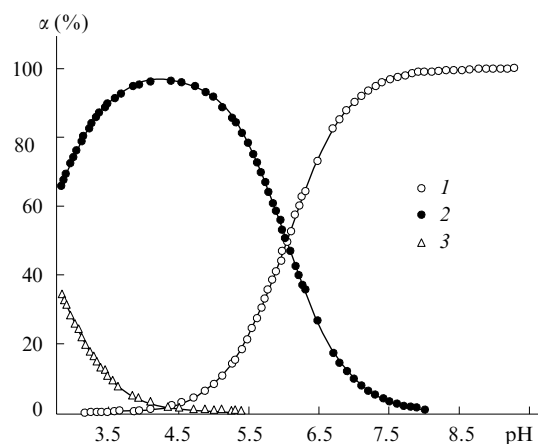


Figure 2. Percentage (α) of the adeninatochlorobis(ethylenediamine)-cobalt(III) forms with different degrees of protonation as a function of pH. (1) Form **17a**, (2) form **17b**, (3) form **17c**.

the outer-sphere association with *p*-sulfonatocalix[6]arene results in the cathodic shift of the redox potentials of Fe^{II} (ferrocene) and Co^{III} (cobaltocene) complexes due to stabilisation of oxidised forms with highest positive charge.^{96,97} Outer-sphere interaction of cobalt tris(bipyridyl) with sulfonate derivatives of thiocalix[4]arene and calix[4]resorcinarene⁵⁷ brings about analogous stabilisation of the oxidised form of the complex.

It is natural to expect that cucurbiturils should exhibit properties intermediate between these two extreme cases (sulfocalixarenes and cyclodextrins). Indeed, the inclusion of metal complexes and organic cations into the cavities of cucurbiturils may result in both the anodic and cathodic shifts of the reductive potential of a guest depending on the structure of the latter. Particularly, significant negative (cathodic) shift of the reductive potential of methylviologen ($\text{MV}^{2+}/\text{MV}^+$ and MV^+/MV^0) inserted into the cavity of cucurbit[8]uril indicates that the inclusion complex of the oxidised (charged) form of methylviologen is more stable than that of the reduced form.⁶⁸ However, the inclusion of copper cyclamate⁵⁴ and ferrocene⁶⁹ into the cucurbituril cavity causes a positive (anodic) shift of the potential of the pairs $\text{Cu}^{2+}/\text{Cu}^+$ and $\text{Fe}^{3+}/\text{Fe}^{2+}$. Probably, relative stabilisation of the reduced form in this case indicates a dominant hydrophobic contribution to the energy of host–guest binding. Thus, the cucurbiturils can stabilise preferably both oxidised and reduced forms of a guest molecule. Large cavity of cucurbit[8]uril may include two molecules of a partially reduced form MV^+ , which results in a redox-controlled stoichiometry of the complexation, because the oxidised form MV^{2+} produces a 1 : 1 complex.⁹⁸ Yet another very important difference between the electrochemical properties of inclusion complexes of cyclodextrins and cucurbiturils should be emphasised, namely, the different mechanism of redox processes. In the case of cucurbit[*n*]urils (*n* = 7, 8), the direct electron transfer to methylviologen or from cucurbit[*n*]uril-bound ferrocene takes place, which follows from the fact that the voltammograms recorded at the various scan rates are identical and that the difference in the reduction and oxidation potentials remains the same within the limits of

reversibility.^{68,69} At the same time the oxidation or reduction of cyclodextrin inclusion complexes takes place only upon their dissociation. This results in different cyclic voltammograms recorded at the different scan rates^{93,99} as well as in the increase in the difference of the reduction and oxidation potentials up to 70–80 mV, which is beyond the reversibility limits.

The combination of a redox-active metal complex and various macrocycles is of interest for the design of switchable systems. For example, the design of a molecular machine was based on the predominant inclusion of the oxidised form of cobaltocene into the cavity of sulfocalix[6]arene and of the reduced form, into the cyclodextrin cavity (Fig. 3).⁹⁷

V. Outer-sphere association of metal complexes with macrocycles as a method of modifying physicochemical properties of a supramolecular system

It was shown in the previous Section that it is possible to control the process of inclusion of a metal complex into the cavity of the macrocycles under consideration by an external action (variation of pH or electrochemical potential). The dependence of thermodynamic parameters of the complexation on the charge and structure of the metal complex is the basis for such control. Inclusion of metal complexes into macrocycles also results in changes of their electrochemical properties, which depend on the character of the macrocycle. Therefore, these macrocycles can be regarded as molecular containers, immersion of metal complexes into these containers modifies the physicochemical properties of the complexes. The modification of physicochemical properties of metal complexes induced by their outer-sphere association with macrocycles is discussed in the present Section.

1. Solubility modification

There are hydrophilic and lipophilic areas in molecules of all macrocycles under consideration, which enables modifying the solubility of metal complexes by formation of the corresponding outer-sphere associates. For instance, cyclodextrins and water-soluble calixarenes increase the solubility of water-insoluble species due to their inclusion into the hydrophobic cavity, while the hydrophilic outer surface of the molecule or the hydrophilic rim make the associate formed water-soluble. For this reason the cyclodextrins are used successfully for the transportation of lipophilic metal-containing catalysts into the aqueous phase.⁴¹ In the case of calixarenes, the outer-sphere association with charged metal complexes results in significant decrease in solubility mainly due to neutralisation of the macrocycle rim charge. On the contrary the formation of inclusion complexes of cucurbiturils with charged bis-chelate complexes of transition metals causes the increase in water solubility, while the macrocycle itself is soluble only in highly acidic aqueous media. Binding of charged metal complexes to the macrocycles possessing lipophilic outer surface and hydrophilic inner cavity (antibiotics,¹⁴ crown ethers,¹⁰⁰ calixarenes with hydrophobic substituents¹⁰¹), makes them lipophilic. It should be noted that the selectivity of metal ion–calixarene binding at the chloroform–water interface differs significantly from that in a one-phase system.¹⁰² It is caused by the increase in the contribution of solvation and dissolution energy to free energy of extraction. Similar effect is observed in the extraction of a series of charged copper and cobalt complexes by calix[4]resorcinarene derivatives from aqueous solutions into the chloroform layer.¹⁰¹ Identically measured degrees of extraction of various metal complexes by calix[4]resorcinarene derivatives do not correlate with the corresponding binding constants measured in water–alcohol media. The presence of

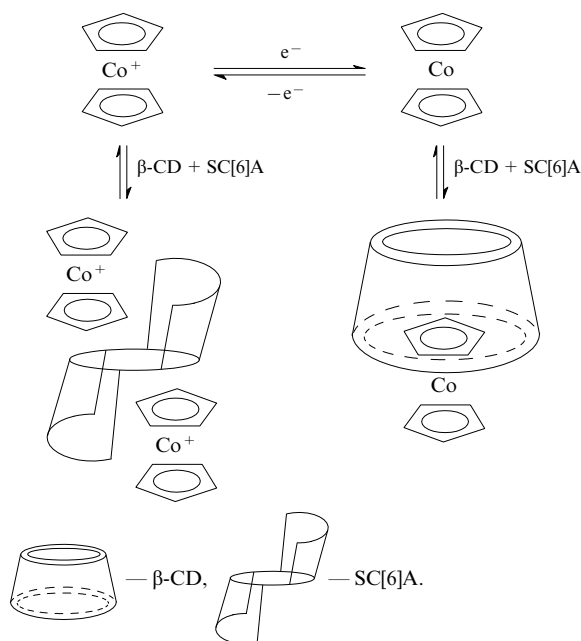
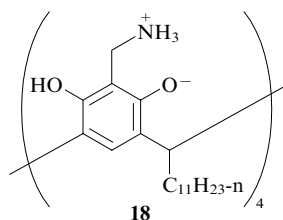


Figure 3. A scheme of the complexation of oxidised and reduced forms of cobaltocene with sulfonatocalix[6]arene (SC[6]A) and β-cyclodextrin, respectively.

ionisable groups, for example, hydroxyl groups in calix[4]resorcinarenes and lasalocid, determines the pH-dependence of extraction and transport of the corresponding metal complexes through the chloroform membrane.^{20, 101} We are not going to discuss this area in the present review as there is a number of other reviews on this subject (see, for example, Refs 102 and 103).

The case of calixarene functionalisation is a clear advantage over other macrocycles as it makes possible introduction of substituents required for the efficient binding of the ion to be extracted and the corresponding counter-ion as well as of groups ensuring the required lipophilicity of the extractant or the carrier.¹⁰³ For example, the effective transfer of charged metal complexes was achieved by the introduction of aminomethyl and alkyl (particularly, $n\text{-C}_{11}\text{H}_{23}$) groups in to the calix[4]resorcinarene matrix.¹⁰¹ Macrocycle **18** exists in a zwitter-ionic form due to intramolecular proton transfer from hydroxyl to aminomethyl group and its transportability depends on the presence of both anionic (phenolate) and cationic (ammonium) groups.



At the same time, the cyclodextrins increase the water solubility of lipophilic metal complexes more effectively than calixarenes and cucurbiturils.⁴¹ Probably, the reason is that cucurbiturils are less water-soluble than cyclodextrins while the cavity of calixarenes, in contrast to that of cyclodextrins, is not proper for deep embedding of a guest molecule.

2. Modification of spectral properties of metal complexes

a. NMR spectroscopy

It is known that the inclusion of a fragment of a guest molecule into the receptor cavity results in changes in chemical shifts of its protons in the ^1H NMR spectra.¹⁰⁴ These changes depend on the mutual arrangement of the guest protons in the host cavity and on the structure of the macrocycle. Taking into account the π -donor properties of the calixarene cavity, it is natural to assume that inclusion of a fragment of the inner sphere of the metal complex into the cavity will result in more substantial upfield shift of proton signals than in the case of cyclodextrins or cucurbiturils. From a comparison of single-crystal X-ray data for inclusion complexes of various macrocycles it is possible to conclude that metal complexes are embedded deeper in the cavities of cucurbiturils^{51–53} and cyclodextrins³⁹ than in the cavities of water-soluble calixarenes.^{55–59} However, the changes in the chemical shifts in ^1H NMR spectra are comparable with, or even less than, those in the case of calixarenes.^{35, 41, 51, 57} It should be noted that the calixarene cavity shielding effect provides additional possibilities for studying the structure of host–guest complexes due to more pronounced dependence of the chemical shifts of the guest protons on the position of the molecule in the cavity of the host.^{104–106}

The rate of exchange between free and macrocycle-bound guests is yet another important characteristic of the complexation process. The rate of such exchange for cucurbiturils and cyclodextrins depends on the nature of the guest. Particularly, the slow exchange rate was found for the complex of cucurbit[7]uril with methylviologen ($\sim 10^2 \text{ s}^{-1}$),⁶⁸ while the rate of exchange in the complexes of β -CD with ferrocenecarboxylate, cobaltocene and reduced forms of methylviologen is equal to

$\sim 10^4 \text{ s}^{-1}$. Fast (on the NMR time scale) exchange is typical of inclusion complexes of water-soluble calixarenes with organic cations and charged metal complexes.^{66, 71, 81} However, the exchange slows down significantly upon encapsulation of a guest molecule between two calixarene molecules.^{107–109}

Thus, the NMR spectra of the ‘guest’ and the ‘host’ change upon complexation with all three macrocycles. The shielding effect, which causes the upfield shift of signals of protons of the guest molecule is most pronounced for cucurbiturils (due to the presence of polar portals) and calix[4]arenes (due to the presence of ionised groups at the rim of the molecule and of the π -donating cavity).

b. Electronic absorption spectroscopy

Analysis of the changes in the spectra of metal complexes induced by interactions with macrocycles should be preceded by the analysis of similar changes in indicators because the spectral properties of molecules and ions of the indicators are extremely sensitive to the changes in the micro-environment polarity due to the presence of chromophore groups and an extended π -system. It is for this reason that many indicators are successfully used as probes in the studies of structural and thermodynamic parameters of micellar pseudophases in aqueous solutions.¹¹⁰ Thus the most long-wave absorption bands of some indicators (acridine red, acridine orange, pyronin) exhibit red shift in the formation of inclusion complexes with cyclodextrins and blue shift when placed into the cavity of sulfonated calix[6]arenes in aqueous solutions.¹¹¹ Using the known dependence of the shift of absorption bands of the indicator on the polarity of the solvent,¹¹⁰ one can conclude that the polarity of micro-environment decreases upon inclusion into the cyclodextrin cavity and increases in the cavities of water-soluble calixarenes.¹¹¹ This difference reveals significant dissimilarity between the cavities of these macrocycles. Unfortunately, the low solubility of cucurbiturils in neutral aqueous solutions prevents their comparison with their associates under analogous conditions. A comparison of the inclusion complex formation of β -CD and cucurbituril with a series of indicators in water–formic acid media⁴⁸ showed that the presence of carbonyl portals affects the ‘host–guest’ binding constant, but the changes in spectral characteristics of the indicator molecules upon inclusion into the cucurbituril cavity is analogous to those in the case of cyclodextrin.

The spectral properties of the transition metal complexes also may change as a result of outer-sphere association with macrocycles. It is known that outer-sphere coordination with crown ethers does not alter significantly the spectra of ruthenium amino and diimino complexes,^{112, 113} while the formation of intermolecular hydrogen bonds between hexacyano complexes of the transition metals and protonated polyazamacrocycles results in the shift of the charge transfer band metal–ligand or ligand–metal.¹¹⁴ Similar spectral changes were observed for ruthenium(II) and cobalt(III) tris(bipyridyl) complexes and were caused by intermolecular π – π -interactions with DNA.^{11, 12} Obviously, not merely the presence, but also some preorganisation of the aromatic fragments is required for the stacking interactions in the outer-sphere binding of metal tris(bipyridyl) complexes to macrocycles. For example, the inclusion of a bipyridyl fragment of tris(bipyridyl)cobalt(III) into the cavities of water-soluble calixarenes (sulfonatomethylcalix[4]resorcinarene and *p*-sulfonatocalix[4]arene) virtually does not affect the charge-transfer ligand–metal bands.⁵⁷ It should be noted that the contribution of stacking interactions increases as the conformation mobility of calixarenes increases with the enlargement of macrocycles on going from sulfonatocalix[4]arene to sulfonatocalix[*n*]arenes ($n = 6, 8$).¹¹⁵ The hypsochromic shift of the metal–ligand charge-transfer band observed upon inclusion of tris(bipyridyl)ruthenium(II)

into the cavity of *p*-sulfonatocalix[8]arene may also be explained by the contribution of stacking-interactions.¹¹⁶

The inclusion complex of cucurbit[8]uril with *trans*-dichlorobis(ethylenediamine)cobalt(III) is an example of a complex in which both chelate rings are significantly distorted upon inclusion in the cavity of cucurbit[8]uril.⁵¹ Particularly, one of the chelate rings contracts with the 0.06 Å shortening of the Co–N bonds while the second one expands and the corresponding bonds became 0.05 Å longer. Naturally, such a change in the geometry of the coordination polyhedron results in the variation of the ligand field and is confirmed by the corresponding spectral changes (by shifts and differences in the intensities of the bands of d–d-transitions).

It should be emphasised that the inclusion of Co^{III} bis- and tris(diethyldiamine) complexes into the cavity of water-soluble calixarenes does not affect the spectra in the region of d–d-transitions. This fact is in agreement with the abovementioned conformational mobility of the calixarene cavity, which adjusts itself to the guest molecule during inclusion complex formation.

Octahedral metal trischelates may exist as two chiral isomers (Δ and Λ),¹¹⁷ and spectropolarimetric properties of metal tris(ethylenediamine) complexes are a sensitive instrument for studying conformation of their flexible chelate rings. The conformation of chelate rings in [Co(en)₃]³⁺ in aqueous solution is a superposition of two limiting conformations: *lel* and *ob*. The C–C bond in the former is almost parallel and in the latter, orthogonal to the tris-chelate three-fold axis⁸¹ (Fig. 4). It is known that electrostatic interaction and two- or three-centred intermolecular hydrogen bond are the driving forces of outer-sphere coordination of [Co(en)₃]³⁺ to cyclic and acyclic polyanions.^{118, 119} As a result, the ethylenediamine chelate ring is distorted towards *lel*-conformation in which the NH-protons are the most accessible for the formation of intermolecular hydrogen bond. This, in turn, causes some changes in the CD spectrum of the complex corresponding to the increasing contribution of the *lel*-conformation (Fig. 5).¹²⁰ Interestingly, the outer-sphere association of [Co(en)₃]³⁺ complex with DNA results in changes in the CD spectrum similar to those in the case of association with such simple polyanions as tartrates, in spite of a much more complicated type of interactions.^{10, 121} Outer-sphere interaction with sulfonate derivatives of thiacalixarene and calix[4]resorcinarene results in the opposite effect, *i.e.* in the increase in the main rotational component and in the decrease in the additional component in the CD spectra. This suggests the *lel* → *ob* inversion of the chelate ring. As mentioned above, the CH– π interactions are the main driving force of interactions of hydrocarbon fragments with the hydrophobic cavity of cyclophanes.⁶⁵ Therefore, it is logical to assume that these interactions with the cavities of water-soluble receptors are responsible for the

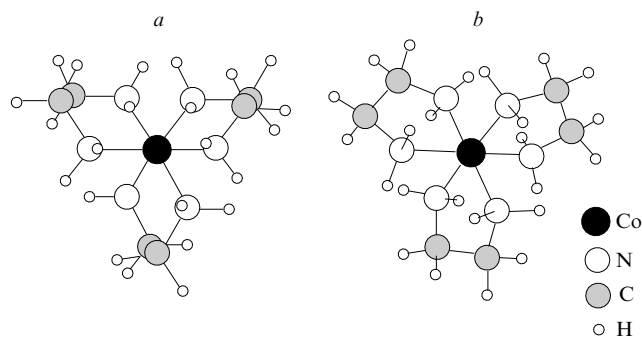


Figure 4. Limiting *lel*- (a) and *ob*-conformations (b) of ethylenediamine chelate rings in the complex [Co(en)₃]³⁺.

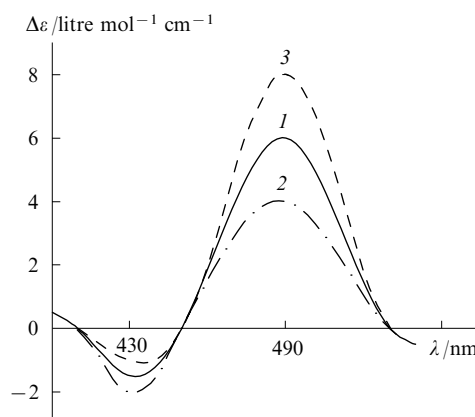


Figure 5. CD spectra of the complex [Co(en)₃]³⁺ without (1) and with outer-sphere coordination with tartrate ions (2) and *p*-sulfonatothiacalix[4]arene (3).

lel → *ob* inversion of the chelate ring as the *ob* conformation provides the best accessibility of CH-protons for the interactions with hydrophobic cavity.

Thus, the chiroptical properties of metal complexes are important for structural as well as chiral recognition and separation of macrocycles. Taking into account successful application of optical and chiroptical properties of cobalt and ruthenium trischelates for DNA recognition, application of chiral trischelates might be potentially useful for the synthesis of enantiomerically pure chiral synthetic macrocycles, such as oxazine derivatives of calix[4]resorcinarenes.¹²²

In conclusion of this Section, it should be noted that the spectral changes of the complexes reflect the types of interactions that emerge during the outer-sphere coordination of the complexes with various macrocycles. Particularly, the inclusion of complexes into rigid cavities of cyclodextrin and cucurbituril results in considerable distortion of the ligand environment of metal ion which, in turn, leads to more significant change in the spectral properties than in the case of non-rigid calixarenes. At the same time, the inclusion of a guest molecule into the calixarene cavity changes its spectral properties in a completely different way. CH– π interactions are typical of the most conformationally rigid *p*-sulfonatocalix[4]arene and its thia-analogue. These interactions cause distortion of the conformation of ethylenediamine chelate ring inside the cavity. The molecule of *p*-sulfonatocalix[8]arene better adjusts itself to the structure of included fragment due to higher conformational mobility. This makes possible, for example, the intermolecular π – π interactions between aromatic fragments of the ligand and one of the aromatic fragments of the 'host' molecule. These interactions cause the shift of metal–ligand or ligand–metal charge-transfer bands.¹¹⁹

c. Luminescent properties

Yet another practically important consequence of the inclusion of a complex into macrocyclic cavity is the change in its luminescent properties. Particularly, a significant increase in the quantum yield of luminescence and the change in the lifetime of the excited state of a lanthanide ion was observed upon inclusion of one of the ligands of the complexes Ln(NTA)₃·H₂O [Ln = Eu, Gd; NTA is 1-(2-naphthoyl)-3,3,3-trifluoroacetone] into the cyclodextrin cavity.^{123, 124} The alteration of photophysical properties of Ru^{II} polypyridyls upon their inclusion into the cavities of cyclodextrins^{125, 126} and into DNA grooves^{127, 128} is thoroughly studied. The increase in luminescence due to restricted deactivation of the emitting transition of Ru^{II} complex by water and oxygen

molecules was observed in both cases. The increase in intensity of luminescence was observed also upon addition of equimolar amount of *p*-sulfonatocalix[8]arene to the solution of tris(bipyridyl) ruthenium(II) in water.¹¹⁶ At the same time, the intensity of fluorescence of an outer-sphere associate of tris(bipyridyl) ruthenium(II) with *p*-sulfonatocalix[4]arene in methanol is considerably lower than that of the free complex. Slight (5 nm) bathochromic shift of the band in the emission spectrum of this associate was also observed.¹²⁹ These effects are presumably caused by interaction of *p*-sulfonatocalix[4]arene (counter-ion) with the dipole of tris(bipyridyl) ruthenium(II) in the excited state and possibly by photoinduced electron transfer as well. However, the possible influence of sulfonatocalix[4]arene on the photoinduced de-chelation caused by thermal transition from the emitting triplet level of bipyridyl to excited d-sublevels^{130, 131} was not taken into account. In turn, the photophysical properties of tris(bipyridyl) ruthenium(II) in aqueous solution are determined to a large extent by the efficiency of photoinduced de-chelation.¹³¹ Unfortunately, so far the number of similar papers on the changes in luminescent properties upon inclusion of complexes into the cucurbituril cavity is small.

3. Modification of reactivity and magnetic properties of metal complexes, stabilisation of unstable forms of complexes

It was already mentioned in Section II that the equilibrium of a complexation of a metal ion with ligands can be shifted upon formation of an outer-sphere associate with a macrocycle. It is very difficult to prove the existence of such stabilisation in solutions, which explains the scarcity of such studies. However, the X-ray studies of associates obtained from aqueous solutions of labile complexes under conditions of equilibrium between the metal ions, ligands and their complexes, show that the stabilisation of such complexes is possible by virtue of outer-sphere association with water-soluble derivatives of calix[*n*]arenes and calix[4]resorcinarenes.^{55, 59, 132} The structure of the complex in a crystal grown from a multicomponent solution is determined by stabilisation effects at both the molecular level (the host–guest interaction with the macrocycle) and the supramolecular level (the crystal packing effects). The selectivity of formation of inclusion complexes of cucurbit[8]uril with respect to the *trans*-isomer of bis(ethylenediamine)cobalt(III) in comparison with the *cis*-isomer is a striking example of the first type of stabilisation effects.⁵¹ Interestingly, the inclusion of the *trans*-isomer into the cavity of a macrocycle increases its thermal stability and inhibits its isomerisation into more thermodynamically stable *cis*-isomer in solutions..

As it has been mentioned in Section V.2.b, the inclusion of a molecule into the cavity of a macrocycle may result in changes in its spectra due to conformational and structural distortions of the chelate rings. The reactivity of the species inside the macrocycle cavity is also changed as a result of the change in the transition state energy upon inclusion complex formation. For example, the formation of a complex of the indicator Phenol Blue with sulfonatocalix[*n*]arenes (*n* = 4, 6, 8) inhibits its deamination in alkaline solutions.¹³³ Similarly, the inclusion of this indicator into the cavity of cucurbituril substantially inhibits its decomposition to *p*-benzoquinone and diamine in acidic media.⁵⁰

The kinetic parameters of redox reactions and the reactions of ligand exchange are the quantitative characteristics of the reactivity of transition metal complexes. There is a number of papers on the catalysis and inhibition of redox reactions, particularly on the changes in the rate of outer-sphere metal-to-metal electron transfer upon outer-sphere binding of one of the transition metal complexes to cyclodextrins, micellar pseudophase, polyazamacrocycles, DNA and polypepti-

des.^{134–141} The analysis of literature shows that there are two main factors determining the effect of outer-sphere association on the redox properties of a complex. The first one is a change in the interaction constant between metal complexes acting as reducing and oxidising agents. If a macrocycle is a counter-ion for one of these complexes, the outer-sphere association decreases the charge of the metal complex. If the oxidising and reducing agents bear opposite charges, inhibition of the redox process upon outer-sphere association of one of the reagents with a macrocycle may be related to the decrease in the constant of ion pair formation between the reactants. On the contrary, if the oxidising and reducing agents bear the same charge, the outer-sphere binding of one of the complexes with the macrocycle may result in more efficient interaction. For instance, it is possible to accelerate the reactions of hexacyanocobaltate and hexacyanoferrate with iodide ion upon outer-sphere association with a protonated polyazamacrocyle.¹¹⁴ Neutralisation of negative charges of the complexes $[\text{Co}(\text{CN})_6]^{3-}$ and $[\text{Fe}(\text{CN})_6]^{3-}$ results in more efficient reaction with iodide ion.

The second factor is the change in electrochemical potential or re-organisation energy. According to the Marcus–Hush theory, this may result in the change in a metal-to-metal electron transfer rate constant. The effect of *p*-sulfonatothiocalix[4]arene on the rate of outer-sphere electron transfer in the system $\text{Fe}^{\text{II}}-\text{Co}^{\text{III}}$ where the positively charged Co^{III} complex is included in the cavity of *p*-sulfonatothiocalix[4]arene and negatively charged Fe^{II} complex is not, was studied¹⁴² for the complexes $[\text{Co}(\text{en})_3]^{3+}$, $[\text{Co}(\text{en})_2\text{ox}]^+$, $[\text{Co}(\text{bipy})_3]^{3+}$, $[\text{Co}(\text{L-His})_2]^+$ and $[\text{Fe}(\text{CN})_6]^{4-}$. Kinetic data for the systems of *p*-sulfonatothiocalix[4]arene – $\text{Fe}^{\text{II}}-\text{Co}^{\text{III}}$ and for the corresponding binary systems indicate that the outer-sphere association with *p*-sulfonatothiocalix[4]arene results in the decrease in the formation constant of ion pair $\text{Fe}^{\text{II}}-\text{Co}^{\text{III}}$. This effect is particularly pronounced for the complex $[\text{Co}(\text{en})_2\text{ox}]^+$ because the inclusion of ethylenediamine chelate ring into the cavity leads to the conformation in which negatively charged oxalate ring is located outside the cavity. This ring prevents the formation of the ion pair with hexacyanoferrate, while the outer-sphere association of *p*-sulfonatothiocalix[4]arene with $[\text{Co}(\text{bipy})_3]^{3+}$ slightly decreases the association constant with hexacyanoferrate. It was noted in Chapter IV that outer-sphere association of tris(bipyridyl) cobalt(II) with *p*-sulfonatothiocalix[4]arene causes the shift of the reduction potential of the $\text{Co}^{\text{III}}/\text{Co}^{\text{II}}$ pair due to stabilisation of the oxidised form.⁵⁷ Irreversible decomposition of other Co^{III} complexes studied upon their reduction prevents obtaining similar data for them. However, it is likely that this effect should be observed for all Co^{III} complexes. According to the Marcus–Hush theory^{143, 144} the cathode shift of potential for the pair $\text{Co}^{\text{III}}/\text{Co}^{\text{II}}$ should cause the decrease in the $\text{Fe}^{\text{II}}-\text{Co}^{\text{III}}$ electron transfer constant on going from the binary system $\text{Fe}^{\text{II}}-\text{Co}^{\text{III}}$ to the ternary system $\text{Fe}^{\text{II}}-\text{Co}^{\text{III}}-p\text{-sulfonatothiocalix[4]arene}$. However, the values of the electron transfer constants in ternary systems calculated on the basis of experimental data are either close to, or even higher than, those in the binary systems. Therefore, other factors, for instance, the re-organisation energy, affect the value of the electron transfer constant on going from the binary to the ternary system. Interestingly, the increase in the rate constant is observed only in those complexes ($[\text{Co}(\text{en})_3]^{3+}$, $[\text{Co}(\text{en})_2\text{ox}]^+$) where the inclusion of a complex into *p*-sulfonatothiocalix[4]arene cavity results in the distortion of the chelate ring conformation. In conclusion, it should be emphasised that the mechanism of this unusual effect of calixarene on the electron transfer rate is unclear and requires further investigation.

The transition metal complexes are very interesting also due to their magnetic properties. It is known that the spin state of the transition metal complexes and accordingly their mag-

netic properties are determined mainly by the character of ligands in the first coordination sphere. However, there are several interesting examples of the influence of crystal lattice¹⁴⁴ and phase transition^{145, 146} on the spin state of Co^{II} and Fe^{II} complexes, respectively. One can assume that the distortions of the ligand environment due to inclusion of a metal complex into the macrocycle cavity may also cause admixture of the excited spin state of the complex to the ground state. This should result in a change in the spin state and accordingly of the spin transition temperature (high-spin–low-spin or *vice versa*). It is known, for example, that the increase in pressure destabilises the high-spin state and relatively stabilises the low-spin state of tris(ethylenediamine) cobalt(II), because the Co–N bond is longer in the high-spin state of Co^{II} than in the low-spin state.¹⁴⁷ It is of note that the internal pressure in a zeolite cavity exerts a similar effect of destabilisation of the high-spin state of tris(bipyridyl)cobalt(II).^{148–150} One can expect that similar effects will also be observed upon inclusion of metal complexes into cavities of macrocycles, but so far there are no such reports in literature.

VI. Conclusion

The formation of outer-sphere associates of the transition metal complexes with cyclodextrins, cucurbiturils and water-soluble calixarenes has much in common with the formation of the inclusion complexes with organic substrates, which serves as the basis for the development of new recognition methods. At the same time, the inclusion of transition metal complexes into the cavities of macrocycles is most perspective for the modification of their physicochemical properties and for the design of switchable systems as fragments of molecular devices and machines. The analysis of structural and thermodynamic parameters of outer-sphere associates of transition metal complexes with abovementioned macrocycles points to the following properties of water-soluble calix[n]arenes that make them unique as molecular containers for metal complexes.

1. π -Donor character of the calix[n]arene cavity determines both the type of 'host–guest' interactions (CH– π , π – π) and the polarity of microenvironment of a species included into the cavity or its fragment.

2. Due to conformational mobility of the cavity, calix[n]arenes adjust themselves to the structure of the guest molecule so that the type of the host–guest interactions depends on the value of n .

3. Polyfunctionality of calixarenes, in particular, the presence of substituents at the upper and lower rims and of the hydrophobic cavity as an additional binding centre, provides a great variety of complexes that are formed in a multicomponent system 'metal ion–ligand–calixarene'.

4. The predominant contribution of electrostatic interactions into the total Gibbs energy of the complexation of water-soluble calixarenes results in more pronounced dependence of the complexation on pH and on the electrochemical potential.

Thus, the accumulated data show that outer-sphere associates of water-soluble calixarenes with complexes of transition metals are a promising basis for the construction of supramolecular systems the properties of which can be switched by external action.

References

1. A Harriman, R Ziessel *Coord. Chem. Rev.* **171** 331 (1998)
2. F M Raymo *Adv. Mater.* **14** 401 (2002)
3. R Ballardini, V Balzani, A Credi, M T Gandolfi, M Venturi *Acc. Chem. Res.* **34** 445 (2001)
4. V Balzani, A Credi, M Venturi *Molecular Devices and Machines. A Journey into the Nanoworld* (Weinheim: Wiley-VCH, 2003)
5. B P Rosen *Top. Curr. Genet.* **14** 485 (2006)
6. A J Thomson, H B Gray *Curr. Opin. Chem. Biol.* **2** 155 (1998)
7. V E Mironov, I D Isaev *Vvedenie v Khimiyu Vneshnesferykh Kompleksnykh Soedinenii Metallov v Rastvorakh* (Introduction in the Chemistry of Outer-Sphere Complex Compounds of Metals in Solutions) (Krasnoyarsk: Krasnoyarsk University, 1986)
8. *Calixarenes in Action* (Eds L Mandolini, R Ungaro) (London: Imperial College Press, 2000)
9. *Calixarenes in the Nanoworld* (Eds J Vicens, J Harrowfield) (Dordrecht: Springer, 2007)
10. L-N Ji, X-H Zou, J-G Liu *Coord. Chem. Rev.* **216**–**217** 513 (2001)
11. X-L Wang, H Chao, H Li, X-L Hong, Y-J Liu, L-F Tan, L-N Ji *J. Inorg. Biochem.* **98** 1143 (2004)
12. C V Sastri, D Eswaramoorthy, L Giribabu, B G Maiya *J. Inorg. Biochem.* **94** 138 (2003)
13. L F Lindoy *Coord. Chem. Rev.* **148** 349 (1996)
14. Ch D Caldwell, A L Crumbliss *Inorg. Chem.* **37** 1906 (1998)
15. I Batinić-Haberle, I Spasojević, Y Jang, R A Bartsch, A L Crumbliss *Inorg. Chem.* **37** 1438 (1998)
16. J Shaw, G W Everett *Inorg. Chem.* **24** 1917 (1985)
17. F Takusagawa, J Shaw, G W Everett *Inorg. Chem.* **27** 3107 (1988)
18. P S K Chia, L F Lindoy, G W Walker, G W Everett *J. Am. Chem. Soc.* **113** 2533 (1991)
19. J H Fendler *Chem. Eng. News* **62** 25 (1984)
20. I Spasojević, I Batinić-Haberle, P L Choo, A L Crumbliss *J. Am. Chem. Soc.* **116** 5714 (1994)
21. J D Lamb, J J Christensen, S R Izatt, K Bedke, M S Astin, R M Izatt *J. Am. Chem. Soc.* **102** 3399 (1980)
22. J-M Lehn *Angew. Chem., Int. Ed. Engl.* **27** 90 (1988)
23. C J Pedersen *Angew. Chem., Int. Ed. Engl.* **27** 1021 (1988)
24. H M von Colquhoun, J F Stoddart, D J Williams *Angew. Chem., Int. Ed. Engl.* **27** 487 (1986)
25. H M von Colquhoun, J F Stoddart, D J Williams, J B Wolstenholme, R Zarzycki *Angew. Chem., Int. Ed. Engl.* **20** 1051 (1981)
26. R Ballardini, M T Gandolfi, V Balzani, F H Kohnke, J F Stoddart *Angew. Chem., Int. Ed. Engl.* **27** 692 (1988)
27. A L Crumbliss, I Batinić-Haberle, I Spasojević *Pure Appl. Chem.* **68** 1225 (1996)
28. I Batinić-Haberle, I Spasojević, A L Crumbliss *Inorg. Chem.* **35** 2352 (1996)
29. F Peter, M Gross, M W Hosseini, J-M Lehn, R B Sessions *J. Chem. Soc., Chem. Commun.* 1067 (1981)
30. B Dietrich, M W Hosseini, J M Lehn, R B Sessions *J. Am. Chem. Soc.* **103** 1282 (1981)
31. D R Alston, A M Z Slawin, J F Stoddart, D J Williams, R Zarzycki *Angew. Chem., Int. Ed. Engl.* **27** 1184 (1988)
32. D R Alston, A M Z Slawin, J F Stoddart, D J Williams *Angew. Chem., Int. Ed. Engl.* **24** 786 (1985)
33. T Matsue, T Kato, U Akiba, T Osa *Chem. Lett.* 1825 (1985)
34. A Mirzozian, A E Kaifer *Chem.–Eur. J.* **3** 1052 (1997)
35. W S Jeon, K Moon, S H Park, H Chun, Y H Ko, J Y Lee, E S Lee, S Samal, N Selvapalam, M V Rekharsky, V Sindelar, D Sobransingh, Y Inoue, A E Kaifer, K Kim *J. Am. Chem. Soc.* **127** 12984 (2005)
36. N Kobayashi, M Opallo *J. Chem. Soc., Chem. Commun.* 477 (1990)
37. A Harada, S Yamamoto, S Takahashi *Organometallics* **8** 2560 (1989)
38. E Zitha-Bovens, H van Bekkum, J A Peters, C F G C Gerales *Eur. J. Inorg. Chem.* 287 (1999)
39. L B Luo, Y Chen, H-L Chen, Z-Y Zhang, Z-Y Zhou, T C W Mak *Inorg. Chem.* **37** 6147 (1998)
40. F von Vögtle, W M Müller *Angew. Chem., Int. Ed. Engl.* **18** 623 (1979)
41. F Hapiot, S Tilloy, E Monlier *Chem. Rev.* **106** 767 (2006)
42. M D Johnson, J G Bernard *Chem. Commun.* 185 (1996)
43. J W Lee, S Samal, N Selvapalam, H-J Kim, K Kim *Acc. Chem. Res.* **36** 621 (2003)
44. O A Geras'ko, D G Samsonenko, V P Fedin *Usp. Khim.* **71** 840 (2002) [*Russ. Chem. Rev.* **71** 741 (2002)]

45. D Whang, J Heo, J H Park, K Kim *Angew. Chem., Int. Ed.* **37** 78 (1998)
46. M N Sokolov, A V Virovets, D N Dybtsev, O A Gerasko, V P Fedin, R Hernandez-Molina, W Clegg, A G Sykes *Angew. Chem., Int. Ed.* **39** 1659 (2000)
47. J Heo, J Kim, D Whang, K Kim *Inorg. Chim. Acta* **297** 307 (2000)
48. Y-M Jeon, J Kim, D Whang, K Kim *J. Am. Chem. Soc.* **118** 9790 (1996)
49. H-J Buschmann, E Schollmeyer *J. Inclusion Phenom. Mol. Recognit. Chem.* **29** 167 (1997)
50. H-J Buschmann, E Schollmeyer *J. Inclusion Phenom. Mol. Recognit. Chem.* **14** 91 (1992)
51. T V Mitkina, M N Sokolov, D Yu Naumov, N V Kuratieva, O A Gerasko, V P Fedin *Inorg. Chem.* **45** 6950 (2006)
52. T V Mitkina, D Yu Naumov, N V Kuratieva, O A Geras'ko, V P Fedin *Izv. Akad. Nauk, Ser. Khim.* **25** (2006)^a
53. T V Mitkina, D Yu Naumov, O A Geras'ko, F M Dolgushin, K Visent, R Yusar, M N Sokolov, V P Fedin *Izv. Akad. Nauk, Ser. Khim.* **2414** (2004)^a
54. S-Y Kim, I-S Jung, E Lee, J Kim, S Sakamoto, K Yamaguchi, K Kim *Angew. Chem., Int. Ed.* **40** 2119 (2001)
55. J L Atwood, G W Orr, F Hamada, R L Vincent, S G Bott, K D Robinson *J. Am. Chem. Soc.* **113** 2760 (1991)
56. P J Nichols, C L Raston, J W Steed *Chem. Commun.* 1062 (2001)
57. A R Mustafina, V V Skripacheva, A T Gubaidullin, Sh K Latipov, A V Toropchina, V V Yanilkin, S E Solovieva, I S Antipin, A I Konovalov *Inorg. Chem.* **44** 4017 (2005)
58. C B Smith, L J Barbour, M Makha, C L Raston, A N Sobolev *Chem. Commun.* 950 (2006)
59. Y Liu, D-S Guo, H-Y Zhang, S Kang, H-B Song *Cryst. Growth Des.* **6** 1399 (2006)
60. C P Johnson, J L Atwood, J W Steed, C B Bauer, R D Rogers *Inorg. Chem.* **35** 2602 (1996)
61. J W Steed, C P Johnson, C L Barnes, R K Juneja, J L Atwood, S Reilly, R L Hollis, P H Smith, L L Clark *J. Am. Chem. Soc.* **117** 11426 (1995)
62. S J Dalgarno, J L Atwood, C L Raston *Cryst. Growth Des.* **6** 174 (2006)
63. G Arena, A Casnati, A Contino, A Magri, F Sansone, D Sciotto, R Ungaro *Org. Biomol. Chem.* **4** 243 (2006)
64. Y Liu, D-S Guo, H-Y Zhang *J. Mol. Struct.* **734** 241 (2005)
65. T Fujimoto, R Yanagihara, K Kobayashi, Y Aoyama *Bull. Chem. Soc. Jpn.* **68** 2113 (1995)
66. C Reichardt *Solvents and Solvent Effects in Organic Chemistry* (Weinheim: VCH, 1990)
67. M V Rekharsky, Y Inoue *Chem. Rev.* **98** 1875 (1998)
68. H-J Kim, W S Jeon, Y H Ko, K Kim *Proc. Natl. Acad. Sci. USA* **99** 5007 (2002)
69. M V Rekharsky, Y Inoue *Encyclopedia of Supramolecular Chemistry* (Eds J L Atwood, J W Steed) (New York: Marcel Dekker, 2004)
70. G Arena, A Contino, F G Gulino, A Magri, F Sansone, D Sciotto, R Ungaro *Tetrahedron Lett.* **40** 1597 (1999)
71. G Arena, A Casnati, A Contino, F G Gulino, D Sciotto, R Ungaro *J. Chem. Soc., Perkin Trans. 2* 419 (2000)
72. G Arena, A Casnati, L Mirone, D Sciotto, R Ungaro *Tetrahedron Lett.* **38** 1999 (1997)
73. A R Mustafina, S V Fedorenko, N A Makarova, E Kh Kazakova, Z G Bazhanova, V E Kataev, A I Konovalov *J. Inclusion Phenom. Macrocycl. Chem.* **40** 73 (2001)
74. N Kon, N Iki, S Miyano *Org. Biomol. Chem.* **1** 751 (2003)
75. R Fiammengio, P Timmerman, F de Jong, D N Reinhoudt *Chem. Commun.* 2313 (2000)
76. N Iki, T Fujimoto, S Miyano *Chem. Lett.* 625 (1998)
77. N Iki, S Miyano *J. Inclusion Phenom. Macrocycl. Chem.* **41** 99 (2001)
78. R Amirov, Z McMillan, A Mustafina, I Chukurova, S Solovieva, I Antipin, A Konovalov *Inorg. Chem. Commun.* **8** 821 (2005)
79. Y Liu, E-C Yang, Y Chen, D-S Guo, F Ding *Eur. J. Org. Chem.* 4581 (2005)
80. Y Liu, D-S Guo, H-Y Zhang, Y-H Ma, E-C Yang *J. Phys. Chem. B* **110** 3428 (2006)
81. A R Mustafina, V V Skripacheva, V P Gubskaya, M Gryuner, S E Solov'eva, I S Antipin, E Kh Kazakova, A I Konovalov, V D Habikher *Izv. Akad. Nauk, Ser. Khim.* **1453** (2004)^a
82. V Balzani, A Credi, F M Raymo, J F Stoddart *Angew. Chem., Int. Ed.* **39** 3348 (2000)
83. B Schlicke, L de Cola, P Belser, V Balzani *Coord. Chem. Rev.* **208** 267 (2000)
84. A Harada *Acc. Chem. Res.* **34** 456 (2001)
85. E Iglesias *J. Org. Chem.* **71** 4383 (2006)
86. W L Mock, J Pierpont *J. Chem. Soc., Chem. Commun.* 1509 (1990)
87. J W Lee, Y H Ko, S-H Park, K Yamaguchi, K Kim *Angew. Chem., Int. Ed.* **40** 746 (2001)
88. K Kim *Chem. Soc. Rev.* **31** 96 (2002)
89. A Arduini, F Ciesca, M Fragassi, A Pochini, A Secchi *Angew. Chem., Int. Ed.* **44** 278 (2005)
90. H Matsumiya, Y Terazono, N Iki, S Miyano *J. Chem. Soc., Perkin Trans. 2* 1166 (2002)
91. M Takeshita, S Shinkai *Bull. Chem. Soc. Jpn.* **68** 1088 (1995)
92. S Shinkai, K Araki, T Matsuda, N Nishiyama, H Ikeda, I Takasu, M Iwamoto *J. Am. Chem. Soc.* **112** 9053 (1990)
93. P Mukhopadhyay, P Y Zavalij, L Isaacs *J. Am. Chem. Soc.* **128** 14093 (2006)
94. R Isnin, C Salam, A E Kaifer *J. Org. Chem.* **56** 35 (1991)
95. V V Skripacheva, A R Mustafina, V A Burilov, L F Galiullina, Sh K Latypov, S E Solov'eva, I S Antipin, A I Konovalov *J. Inclusion Phenom. Macrocycl. Chem.* **56** 369 (2006)
96. J Alvares, Y Wang, M Gomez-Kaifer, A E Kaifer *Chem. Commun.* 1455 (1998)
97. Y Wang, J Alvarez, A E Kaifer *Chem. Commun.* 1457 (1998)
98. W S Jeon, H-J Kim, C Lee, K Kim *Chem. Commun.* 1828 (2002)
99. T Matsue, D H Evans, T Osa, N Kobayashi *J. Am. Chem. Soc.* **107** 3411 (1985)
100. I Spasojević, A L Crumbliss *J. Chem. Soc., Dalton Trans.* 4021 (1998)
101. S V Fedorenko, A R Mustafina, A U Ziganshina, E Kh Kazakova, A I Konovalov *Mater. Sci. Eng., C* **18** 271 (2001)
102. J-P Behr, M Kirch, J-M Lehn *J. Am. Chem. Soc.* **107** 241 (1985)
103. H C Visser, D N Reinhoudt, F de Jong *Chem. Soc. Rev.* **23** 75 (1994)
104. M Pons, O Millet *Prog. Nucl. Magn. Reson. Spectrosc.* **38** 267 (2001)
105. *NMR in Supramolecular Chemistry* (Ed. M Pons) (Dordrecht: Kluwer Academic, 1999)
106. C A Hunter, M J Packer, C Zonta *Prog. Nucl. Magn. Reson. Spectrosc.* **47** 27 (2005)
107. A Shivanyuk, E F Paulus, V Böhmer *Angew. Chem., Int. Ed.* **38** 2906 (1999)
108. V Böhmer, M O Vysotsky *Aust. J. Chem.* **54** 671 (2001)
109. M H K Ebbing, M-J Villa, J-M Valpuesta, P Prados, J de Mendoza *Proc. Natl. Acad. Sci. USA* **99** 4962 (2002)
110. L P Novaki, O A El Seoud *Langmuir* **16** 35 (2000)
111. Y Liu, B-H Han, Y-T Chen *J. Phys. Chem. B* **106** 4678 (2002)
112. I Ando, D Ishimura, K Ujimoto, H Kurihara *Inorg. Chem.* **35** 3504 (1996)
113. I Ando, M Higashi, K Ujimoto, H Kurihara *Inorg. Chim. Acta* **282** 247 (1998)
114. F Pina, A J Parola *Coord. Chem. Rev.* **185–186** 149 (1999)
115. M Megyesi, L Biczok *Chem. Phys. Lett.* **424** 71 (2006)
116. C Li, T Hatano, M Takeuchi, S Shinkai *Tetrahedron* **60** 8037 (2004)
117. I Katsuki, Y Motoda, Y Sunatsuki, N Matsumoto, T Nakasima, M Kojima *J. Am. Chem. Soc.* **124** 629 (2002)
118. K Miyoshi, Yu Sakamoto, A Ohguni, H Yoneda *Bull. Chem. Soc. Jpn.* **58** 2239 (1985)
119. M Kinpara, W Kawamizu, A Tatehata *Inorg. Chem. Commun.* **3** 442 (2000)
120. T Nakashima, J Mishiro, M Ito, G Kura, Y Ikuta, N Matsumoto, K Nakajima, M Kojima *Inorg. Chem.* **42** 2323 (2003)
121. F Ascoli, M Branca, C Mancini, B Pispisa *J. Chem. Soc., Faraday Trans. 1* **23** 1213 (1972)

122. R Arnecke, V Böhmer, E F Paulus, W Vogt *J. Am. Chem. Soc.* **117** 3286 (1995)
123. S S Braga, R A Sa Ferreira, I S Goncalves, M Pillinger, J Rocha, J J C Teixeira-Dias, L D Carlos *J. Phys. Chem. B* **106** 11430 (2002)
124. J A Fernandes, S S Braga, R A Sa Ferreira, M Pillinger, L D Carlos, P Ribeiro-Claro, I S Goncalves *J. Inclusion Phenom. Macrocycl. Chem.* **55** 329 (2006)
125. J I Cline III, W J Dressick, J N Demas, B A DeGraff *J. Phys. Chem.* **89** 94 (1985)
126. W Y Xu, A Jain, B A Betts, J N Demas, B A DeGraff *J. Phys. Chem. A* **106** 251 (2002)
127. Q-X Zhen, B-H Ye, J-G Liu, Q-L Zhang, L-N Ji, L Wang *Inorg. Chim. Acta* **303** 141 (2000)
128. J-G Liu, B-H Ye, H Chao, Q-X Zhen, L-N Ji *Chem. Lett.* 1085 (1999)
129. M Chiba, H-B Kim, N Kitamura *J. Photochem. Photobiol., A* **151** 67 (2002)
130. J Van Houten, R J Watts *J. Am. Chem. Soc.* **98** 4853 (1976)
131. W J Vining, J V Caspar, T J Meyer *J. Phys. Chem.* **89** 1095 (1985)
132. A T Gubaidullin, Yu E Morozova, A R Mustafina, E Kh Kazakova, I A Litvinov, A I Kononov *Mendeleev Commun.* 9 (1999)
133. W Tao, M Barra *J. Org. Chem.* **66** 2158 (2001)
134. P Neto-Ponce, F Sánchez, F Pérez, A García-Santana, P Pérez-Tejeda *Langmuir* **17** 980 (2001)
135. M Morillo, C Denk, P Pérez, M López, A Sánchez, R Prado, F Sánchez *Coord. Chem. Rev.* **204** 173 (2000)
136. R Prado-Gotor, R Jimenez, P López, P Pérez, C Gomez-Herrera, F Sánchez *Langmuir* **14** 1539 (1998)
137. R Prado-Gotor, R Jimenez, P Pérez-Tejeda, M López-López, F Sánchez *Chem. Phys.* **263** 139 (2001)
138. P López-Cornejo, R Prado-Gotor, C Gomez-Herrera, R Jimenez, F Sánchez *Langmuir* **19** 5991 (2003)
139. R de la Vega, P Pérez-Tejeda, P López-Cornejo, F Sánchez *Langmuir* **20** 1558 (2004)
140. P López-Cornejo, P Pérez, F García, R de la Vega, F Sánchez *J. Am. Chem. Soc.* **124** 5154 (2002)
141. P López-Cornejo, R Prado-Gotor, A García-Santana, F Pérez, F Sánchez *Langmuir* **19** 3185 (2003)
142. A R Mustafina, V G Shtyrlin, L Ya Zakharova, V V Skripacheva, R R Zairov, S E Solov'eva, I S Antipin, A I Kononov *J. Inclusion Phenom. Macrocycl. Chem.* **59** 2532 (2007)
143. R A Marcus, N Sutin *Biochim. Biophys. Acta* **811** 265 (1985)
144. M D Newton *Chem. Rev.* **91** 767 (1991)
145. Sh Hayami, K Hashiguchi, G Juhász, M Ohba, H Ōkawa, Y Maeda, K Kato, K Osaka, M Takata, K Inoue *Inorg. Chem.* **43** 4124 (2004)
146. T Fujigaya, D-L Jiang, T Aida *J. Am. Chem. Soc.* **125** 14690 (2003)
147. Y Bodenthin, U Pietsch, H Möhwald, D G Kurth *J. Am. Chem. Soc.* **127** 3110 (2005)
148. W H Jolley, D R Stranks, T W Swaddle *Inorg. Chem.* **29** 385 (1990)
149. K Mizuno, J H Lunsford *Inorg. Chem.* **22** 3484 (1983)
150. S K Tiwary, S Vasudevan *Inorg. Chem.* **37** 5239 (1998)

^a — *Russ. Chem. Bull., Int. Ed. (Engl. Transl.)*

Spectroscopy and kinetics of germylene and digermene reactions photogenerated in the condensed phase

V F Plyusnin, M V Kaletina, T V Leshina

Contents

I. Introduction	931
II. Germylene precursors	932
III. Generation of transient species in the photolysis of germanium-containing compounds in low-temperature matrices	932
IV. Laser flash photolysis of germanium-containing compounds in solutions. Optical spectra of germylenes	933
V. Fluorescence of germylenes	936
VI. Electronic structure of germylenes and the nature of their optical absorption band	937
VII. Spectroscopy of germylene complexes	937
VIII. Vibrational spectra of germylenes	938
IX. Germylene reactions	939
X. Optical spectra, vibrational frequencies and kinetics of digermene decay	942
XI. Optical spectra of germyl radicals	943
XII. Stable germylenes	944
XIII. Comparison of the data obtained by chemically induced dynamic nuclear polarisation and laser flash photolysis methods	945
XIV. Conclusion	947

Abstract. The state of the art in the spectroscopic identification and kinetic analysis of condensed-phase reactions of bivalent germanium derivatives and their dimers is considered. Considerable attention is drawn to the comparison of results obtained by laser flash photolysis and spin chemistry methods. The bibliography includes 95 references.

I. Introduction

At present, the most important direction in chemistry and photochemistry of organometallic derivatives is devoted to the establishment of their reaction mechanisms. The wide use of modern physical research methods [optical, EPR and NMR spectroscopies, Chemically Induced Dynamic Nuclear Polarisation (CIDNP), flash photolysis, time-resolved luminescence, photolysis in cryogenic matrices] made it possible to identify short-lived species in many reactions of organosilicon and organogermanium derivatives. Keen attention of chemists to organometallic compounds containing the 14th Group elements is largely explained by their use in high technologies, first of all, in integrated microelectronics.

Laser flash photolysis and the methods of spin chemistry, namely, photochemically induced dynamic nuclear polarisation and the magnetic effect, play the decisive role in studying reactions that involve short-lived intermediates. The use of photogeneration makes it possible to produce transient species

in high concentrations, record their optical spectra and study the kinetics of their growth and decay.

The literature contains numerous publications devoted to the identification of transient species formed in the condensed-phase photolysis of different silicon and germanium compounds. Among these species, mention should be made of carbene analogues, namely, organylsilylenes and -germylenes, silyl and germyl free radicals and short-lived derivatives of tricoordinate silicon and germanium, namely, substituted silenes and germenes. Thus information on heavy analogues of carbenes can be found in a monograph¹ devoted to the carbene chemistry; results on the synthesis, structure, spectroscopy and reactivity of germylenes and stannylenes are summarised in several reviews^{2–8} and recently published collections^{9,10} of reviews. However, despite the abundance of reference literature on this issue, no comparative analysis of the kinetic data obtained by different spectroscopic techniques and by different authors was carried out.

From our viewpoint, a real assessment of the further development in this field of chemistry requires comparison of the results obtained by laser flash photolysis and CIDNP. Thus, to date, based on the results of spin chemistry methods, the detailed schemes of processes that occur in solutions, involving germylenes and digermenes and including their interconversions, were constructed and the mechanisms for the formation of germanium-containing biradicals were proposed. Note that, although the involvement of the latter in elementary steps was often postulated based on the analysis of reaction products, their presence has never been proved by physical methods with the exception of CIDNP. This is why it seems useful to compare the CIDNP data that contain information on the structure of paramagnetic intermediates (free radicals, carbene analogues, biradicals) as the precursors of products formed, on the one hand, with the kinetic data on the formation and decay of short-lived germanium derivatives obtained in laser flash photolysis techniques, on the other hand.

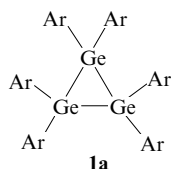
V F Plyusnin, M V Kaletina, T V Leshina Institute of Chemical Kinetics and Combustion, Siberian Branch of the Russian Academy of Sciences, ul. Institutskaya 3, 630090 Novosibirsk, Russian Federation.
Fax (7-383) 330 73 50, tel. (7-383) 333 23 85,
e-mail: plyusnin@ns.kinetics.nsc.ru (V F Plyusnin),
leshina@ns.kinetics.nsc.ru (T V Leshina),
tel. (7-383) 333 14 05, e-mail: kaletina@ns.kinetics.nsc.ru (M V Kaletina)

Received 27 February 2007

Uspekhi Khimii 76 (10) 994–1013 (2007); translated by T Ya Safonova

II. Germylene precursors

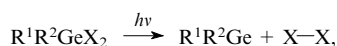
In this Section, we describe the organogermanium derivatives that generate diorganylgermylenes under radiation. Cyclic germanium compounds such as $(R^1R^2Ge)_n$ are the efficient sources of germynes.^{1, 11–20} In 1982, the first cyclotrimergermane, hexakis(2,6-dimethylphenyl)cyclotrimergermane (**1a**) was isolated and described.¹⁶ To date, other cyclic tri- and polygermanes were synthesised.



Ar = 2,6-Me₂C₆H₃.

The ring may also include atoms of other elements, *e.g.*, silicon or carbon.²¹

Linear germanes with alkyl and aryl substituents, the analogues of linear hydrocarbons, can also serve as germylene precursors.^{22, 23} The largest group of precursors is formed by germanes of the $R^1R^2GeX_2$ type, where R^1 , R^2 are alkyl or aryl groups and X is a weakly bound heteroatomic substituent.^{3, 24–28}

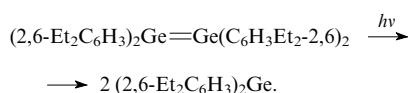


R^1 , R^2 = Alk, Ar; X = SiMe₃, SePh, N₃, *etc.*

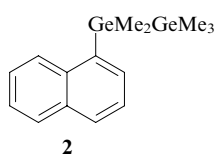
The possibility of generation of germynes from such compounds is often determined by the fact that a heteronuclear bond Ge–E (E = Si, Se, N) is less stable than a homonuclear bond E–E.

Stable digermenes with bulky substituents can serve as efficient sources of germynes. Digermenes with small substituents are short-lived species and are usually cyclised into cyclotetragermanes.

The formation of a germylene from tetraaryldigermene preliminarily synthesised by the photodecomposition of the corresponding trigermane was described.¹⁷

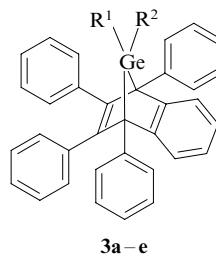


Aryl-substituted digermanes and silylgermanes $R^1R^2_2Ge-GeR^3_3$, $R^1R^2_2Ge-GeR^1R^2_2$ and $R^1R^2_2Ge-SiR^3_3$ (R^1 , R^2 = Ar) were synthesised and studied by laser flash photolysis and matrix-isolation methods.^{29–32} It was demonstrated that this kind of compounds are germylene precursors. Germanium-containing naphthalenes were distinguished as a separate class of precursors with properties similar to those of phenyl-substituted digermanes. Thus for photochemical reactions of 1-(pentamethyldigermanyl)naphthalene (PMDGN) (**2**), the transient species were identified and the composition of final products was determined using the methods of flash and steady-state photolyses.³³

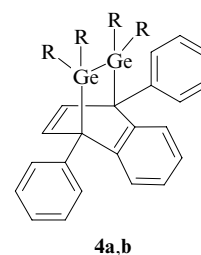


Among the most convenient and frequently used germylene sources, a special place belongs to bicyclic compounds that contain germanium atom(s) in their bridges, namely, 7,7-

dialkyl(diaryl or alkylaryl)-7-germanorbornadienes **3a–e** (see Refs 24, 25 and 34) and 7,8-digermbicyclo[2.2.2]octadienes **4a,b**. The latter serve as precursors of both germynes and digermenes.



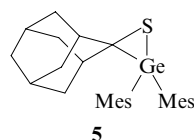
$R^1 = R^2$ = Me (**a**), Et (**b**), Buⁿ (**c**), Ph (**d**); R^1 = Me, R^2 = Ph (**e**).



R = Me (**a**), Et (**b**).

Photolysis of 7,7,8,8-tetramethyl-1,4-diphenyl-1,3-benzo-7,8-digermbicyclo[2.2.2]octa-2,5-diene (**4a**) was described for the first time by the authors of Ref. 35. Light-initiated reactions of these compounds were explored^{36, 37} by flash photolysis, matrix isolation and CIDNP methods.

The literature also contains a description of the photodecomposition of thiagermanes, for example, compound **5**, to afford the corresponding germylene and digermene.³⁸



Mes = 2,4,6-Me₃C₆H₂.

Thus, the precursors of reactive transient species of bivalent germanium are rather diverse. The wide choice of molecules with the desired and convenient spectroscopic and photochemical parameters makes it possible to carry out different pulse and steady-state experiments on the determination of properties of primary short-lived products.

III. Generation of transient species in the photolysis of germanium-containing compounds in low-temperature matrices

In chemistry and photochemistry of germanium-containing compounds, the identification of optical spectral bands of germynes and other transient species faces an essential problem associated with the strong dependence of the absorption band peak position (λ_{max}) on the experimental conditions. Moreover, both the method of species generation and the precursor type, on the one hand, and the solvent nature and temperature, on the other hand, are significant. According to modern concepts,⁴ one of the main reasons for this effect could be a trend of germynes towards complexation with Lewis acids and bases. The detection of active species involves either their stabilisation in low-temperature matrices or the use of methods with short detection times (time-resolved methods). Below, we consider the results of studies of short-lived germanium-containing intermediates that appear in the photolysis of different precursors in low-temperature matrices.

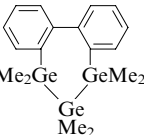
The first matrix-frozen germanium-containing compound subjected to the photolysis was (2,6-Et₂C₆H₃)₂Ge(SiMe₃)₂.¹⁷ The germylene formation was deduced solely from the analysis of final products obtained after the matrix was annealed.

Upon the photolysis (the excitation wavelength λ = 254 nm) of 7,7-dimethyl-1,4,5,6-tetraphenyl-2,3-benzo-7-germanorborna-2,5-diene (Me₂GNB) (**3a**) in 3-methylpentane (3-MP) glasses at 77 K, the optical spectra displayed absorp-

tion bands with maxima at 420 and 317 nm.^{24,25} The first band, which decayed above the matrix melting point, was assigned to dimethylgermylene (Me_2Ge). The second band, which remained in the spectrum after the sample was annealed, was attributed to 1,2,3,4-tetraphenyl-naphthalene (TPN) (**6**).

Photolysis of bis(trimethylsilyl)germane $\text{R}_2\text{Ge}(\text{SiMe}_3)_2$ derivatives ($\text{R} = 2,6\text{-Me}_2\text{C}_6\text{H}_3$, $2,6\text{-Et}_2\text{C}_6\text{H}_3$, $2,4,6\text{-Me}_3\text{C}_6\text{H}_2$) in 3-MP glasses made it possible to record optical spectra for a series of substituted germynes.²⁵ Table 1 shows spectral characteristics of germynes formed from different precursors. It is evident that the absorption maxima of observed bands fall in a range of 400–570 nm. (The nature of an electronic transition corresponding to germylene absorption bands is discussed below). It is noteworthy that the extinction coefficients of bands in low-temperature matrix spectra were not determined due to the absence of internal standards; the quantum yields of germynes described in the cited studies were also absent.

Table 1. Positions of absorption maxima for diorganylgermylenes in a 3-methylpentane matrix ($T = 77\text{ K}$).

Germylene	Precursor	$\lambda_{\text{max}}/\text{nm}$	Ref.
Me_2Ge	$\text{Me}_2\text{Ge}(\text{N}_3)_2$	405	28
	$\text{PhMe}_2\text{GeSiMe}_3$	418	29
	3a	420	24, 25
	$\text{Me}_2\text{Ge}(\text{SePh})_2$	420	27
	$\text{Me}_2\text{Ge}(\text{GePhMe}_2)_2$	422	12, 22, 23
		430	21
Et_2Ge	cyclo- $\text{Ge}_6\text{Me}_{12}$	430	11, 12
	$\text{Me}(\text{Me}_2\text{Ge})_5\text{Me}$	436	12
	cyclo- $\text{Ge}_5\text{Me}_{10}$	506	19
	3b	440	25
$\text{Bu}_2^{\text{n}}\text{Ge}$	3c	440	25
PhMeGe	3e	440	25
Ph_2Ge	$\text{PhMeGe}(\text{GeMe}_3)_2$	456	22
	3d	466	25
	$\text{Ph}_2\text{Ge}(\text{SiMe}_3)_2$	466	25
	$\text{Ph}_2\text{Ge}(\text{GeMe}_3)_2$	462	22
$(4\text{-MeC}_6\text{H}_4)_2\text{Ge}$	$(4\text{-MeC}_6\text{H}_4)_2\text{Ge}(\text{SiMe}_3)_2$	471	25
MesBu^tGe	$\text{MesBu}^t\text{Ge}(\text{SiMe}_3)_2$	508	25
$(2,6\text{-Me}_2\text{C}_6\text{H}_3)_2\text{Ge}$	$(2,6\text{-Me}_2\text{C}_6\text{H}_3)_2\text{Ge}(\text{SiMe}_3)_2$	543	25
$(2,6\text{-Et}_2\text{C}_6\text{H}_3)_2\text{Ge}$	$(2,6\text{-Et}_2\text{C}_6\text{H}_3)_2\text{Ge}(\text{SiMe}_3)_2$	544	25
Mes_2Ge	$\text{Mes}_2\text{Ge}(\text{SiMe}_3)_2$	550	25
$(2,4,6\text{-Pr}_3\text{C}_6\text{H}_2)_2\text{Ge}$	$(2,4,6\text{-Pr}_3\text{C}_6\text{H}_2)_2\text{Ge}(\text{SiMe}_3)_2$	558	25

In 'soft' matrices,[†] germylene molecules even those containing substituents move and gradually undergo dimerisation to digermenes. At liquid nitrogen temperature, this proceeds over tens and hundreds of minutes. Dimerised products exhibit absorption bands at shorter wavelengths. Thus digermene $(\text{Mes}_2\text{Ge})_2$ has an absorption band with the maximum at 406 nm, whereas the corresponding germylene (Mes_2Ge) absorbs at 550 nm (see Table 1). In 'soft' 3-MP–IP matrices, several germylene complexes with organic molecules were synthesised.²⁵ As a rule, complexation substantially shifts the optical absorption bands to shorter wavelengths.

Photolysis of Me_2GNB (**3a**) in a low-temperature toluene- d_8 matrix was observed³⁹ to give rise to an optical

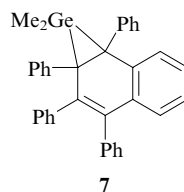
absorption band with the maximum at 420 nm, the same as for many other germanium-containing compounds (see Table 1). However, the authors of this study assigned this band not to a germylene but rather to a biradical $\text{TPN}^{\cdot-}\text{-GeMe}_2$ that appears on the cleavage of merely one $\text{Ge}-\text{C}$ bond. This assumption was based on the absence of noticeable decomposition of germanorbornadiene upon the annealing of the irradiated matrix. According to the authors, on heating of the matrix, the homolysis of the second $\text{Ge}-\text{C}$ bond proceeds much slower than the recombination of the first one. At higher temperatures, the rate constant for the second-bond homolysis may increase to the greater extent than the recombination rate constant. For this reason, in contrast to photolysis in matrices, photolysis in solutions leads to the decomposition of germanorbornadiene **3a**.

The data in Table 1 demonstrate that the position of the absorption band maximum (405–506 nm) in spectra of Me_2Ge formed in low-temperature matrices from different precursors varies over a wide range. One of the reasons for the band shift could be the different geometry of matrix-isolated germynes. As is seen from Table 1, the absorption band maxima of germynes with bulk substituents are shifted up to ~560 nm. As shown below, in such germynes, the $\text{C}-\text{Ge}-\text{C}$ angle is substantially larger due to the repulsion of substituents, which results in the long wavelength shift of the band. Apparently, in low-temperature matrices, too, Me_2Ge species generated from different precursors also have different $\text{C}-\text{Ge}-\text{C}$ angles.

IV. Laser flash photolysis of germanium-containing compounds in solutions. Optical spectra of germynes

Matrix isolation allows one to determine the spectroscopic parameters of reactive species but does not provide any kinetic information on their formation. The time resolution of an order of magnitude of 10 ns, which is typical of laser flash photolysis, offers a possibility for measuring rate constants for the fastest bimolecular reactions. At present, this method is widely used in photochemistry of germanium-containing compounds for studying transient species; this allowed optical spectra to be recorded and different reaction channels to be studied for many germynes.

One of the earliest studies³⁹ was devoted to the lamp flash photolysis of Me_2GNB (**3a**) solutions with 5 μs time resolution. Two absorption bands of transient species with maxima at 380 and 460 nm were observed. Experiments with the addition of dimethylgermylene acceptors into the solution have shown that this species is responsible for the first band. A comparison of absorbances at 380 nm (recorded immediately after the flash) and 320 nm (in 50 ms), *i.e.*, corresponding to the absorption range of TPN (**6**), the second stable product of norbornadiene decomposition, made it possible to determine the extinction coefficient of the dimethylgermylene band ($\epsilon^{380} = 1300\text{ litre mol}^{-1}\text{ cm}^{-1}$). The second band with the maximum at 460 nm in the original spectrum was assigned to germabenzonorcaradiene **7**, the product of the subsequent recovery of the broken $\text{Ge}-\text{C}$ bond.

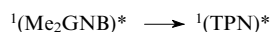


A later publication³⁴ described the results of laser flash photolysis (248 nm) of compound **3a** in methylcyclohexane

[†] At 77 K, the viscosity of 3-MP mixtures with isopentane (IP) is in the range of $10^{12}\text{--}10^7\text{ Ps (g s}^{-1}\text{ cm}^{-1})$,²⁵ which allows one to call them 'soft'.

with 10 ns time resolution. It was found that upon a laser pulse, two wide bands with maxima at 330 and 490 nm appeared, which were assigned to the triplet–triplet (T–T) absorption of a TPN (**6**) molecule. The same bands appeared when the solutions of tetraphenyl-naphthalene itself were subjected to flash photolysis. In both cases, the spectral bands decayed upon the addition of oxygen into the reaction mixture; moreover, these reactions were characterised by similarly high rate constants (1.5×10^9 litre mol⁻¹ s⁻¹). Note that such rate constants are typical of quenching of triplet states of molecules. Thus, no absorption that could have been assigned to dimethylgermylene was observed. This contradicts both the results of flash photolysis³⁹ and the data on the photolysis of Me₂GNB (**3a**) in low-temperature matrices²⁶ (see Table 1).

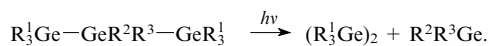
It was assumed³⁴ that, upon the germylene elimination, an excited **3a** molecule transforms into an excited TPN (**6**) molecule as a result of dissociation. The transient Me₂Ge was not detected because its lifetime is shorter than several hundreds of nanoseconds. The high quantum yield ($\phi \sim 0.4$) of the conversion



points to the fast (on the picosecond time scale) homolytic cleavage of two Ge–C bonds. In this case, the luminescence with a lifetime of 3 ns observed on the excitation of Me₂GNB (**3a**) can only be attributed to singlet-state ¹(TPN)* luminescence. It should be noted that this explanation is inconsistent with the CIDNP effects observed on the photolysis of compound **3a**, which will be discussed in Section XIII.

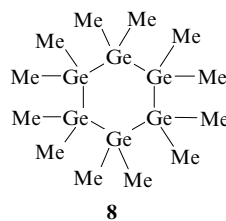
An attempt to obtain a spectrum of Ph₂Ge germylene on the flash photolysis (248 nm) of 7,7-diphenyl-7-germanorbornadiene **3d** in hexane was unsuccessful.⁴⁰ Strong T–T absorption of tetraphenyl-naphthalene **6**, which was present in the reaction mixture as an impurity (5%), prevented the detection of the weak germylene signal.

Photodissociation of many other compounds to generate germynes occurred without any complications associated with the formation of excited triplet molecules, in contrast to the case of compounds **3a,e**. Thus laser flash photolysis of aryl-substituted linear trigermynes R₃¹Ge–GeR²R³–GeR₃¹ (R¹–R³ = Me, Ph) led to the appearance of two absorption bands with maxima in the ranges of 320–330 and 420–450 nm in the spectra recorded after the pulse.^{22,23} Both bands decayed with second-order kinetics. The use of double-pulse excitation made it possible to prove that germylene forms upon extrusion from an excited molecule

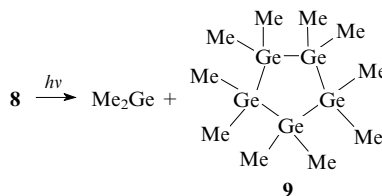


The analysis of kinetic data has shown that germynes possess long-wavelength absorption bands in the range of 420–450 nm. Short-wavelength bands (320–330 nm) might be associated with digermynes (R₃¹Ge)₂; however, these species have absorption bands in the range of 370–380 nm (see Section XI). Presumably,^{22,23} the homolytic cleavage of the Ge–Ge bond to form digermyl radicals that absorb in the range of 320–330 nm (see Section X) can occur simultaneously with the germylene extrusion. According to the results of laser flash photolysis, the positions of germylene absorption bands (420–450 nm) are well consistent with the results on the trigermine photolysis in low-temperature matrices,^{21,22} which demonstrated similar bands (see Table 1).

Laser flash photolysis (266 nm) of dodecamethylcyclohexagermane (**8**) in cyclohexane¹¹ led to the appearance of an absorption band with the maximum at 450 nm in the optical spectrum.



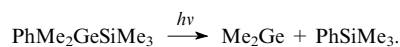
The decay of this band according to the second-order kinetics (the effective rate constant $k/\epsilon = 2.7 \times 10^7$ cm s⁻¹, where k is the reaction rate constant and ϵ is the extinction coefficient of the band) was accompanied by the appearance of a new band at 370 nm. The first band belongs to dimethylgermylene and the second one belongs to its dimerisation product, namely, digermene (Me₂Ge)₂. Photolysis of compound **8** in a low-temperature 3-MP matrix also resulted in the appearance of a germylene (identified by a band at 430 nm, see Table 1). Apparently, the shift of the band maximum to shorter wavelengths by 20 nm is explained by the changes in the reaction temperature and the solvent nature. Presumably,¹¹ dimethylgermylene is generated from the excited state of the parent molecule without the formation of transient germyl radicals.



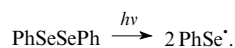
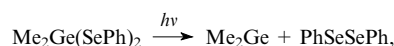
On excitation (266 nm) of decamethylcyclopentagermane (**9**) in cyclohexane,¹⁹ an absorption band with the maximum at 490 nm appeared in the spectrum immediately after the laser pulse and then decayed at a rate corresponding to the second-order kinetics ($k/\epsilon = 3.5 \times 10^7$ cm s⁻¹). As it decayed, a new band with the maximum at 370 nm grew and then also decayed by the second-order kinetics ($k/\epsilon = 4.8 \times 10^6$ cm s⁻¹). The former band belonged to dimethylgermylene and the latter corresponded to its dimerisation product (Me₂Ge)₂. Photolysis of compound **9** in a 3-MP matrix led to the appearance of a band with the maximum at 506 nm, which was also assigned to germylene. Thus, for unknown reasons, spectra of germynes formed from cyclopolygermanes **8** (Ref. 11) and **9** (Ref. 19) in cyclohexane solutions demonstrated absorption bands shifted with respect to one another by 40 nm. Moreover, for the germylene formed from compound **9**, the absorption band maximum in the low-temperature matrix shifted to long wavelengths.

Of considerable interest are experiments³³ on subjecting a solution of 1-(pentamethyldigermanyl)naphthalene (**2**) in cyclohexane to laser flash photolysis (308 and 337 nm). Two absorption bands with maxima at 440 and 400 nm appeared in the spectrum immediately after the flash, and a new band at 460 nm appeared in 10 μs. The band at 440 nm assigned to dimethylgermylene decayed with second-order kinetics ($k/\epsilon = 2.5 \times 10^7$ cm s⁻¹), which suggests the formation of a digermene (Me₂Ge)₂. The latter is presumably responsible for the band with the maximum at 400 nm. A comparison of the time of germylene appearance with the compound **2** fluorescence lifetime made it possible to conclude that dimethylgermylene forms from the parent molecule in the excited singlet state. The subsequent appearance of an additional band at 460 nm was explained by the T–T absorption of the parent molecule **2**. However, the 10 μs delay in the appearance of the triplet state ³(PMDGN), which forms from the same excited singlet state ¹(PMDGN) as dimethylgermylene, still remains unexplained.

A spectrum recorded on the laser flash photolysis (248 and 266 nm) of a solution of dimethylphenyl(trimethylsilyl)germane ($\text{PhMe}_2\text{Ge}-\text{SiMe}_3$) in cyclohexane demonstrated a broad absorption band with the maximum at 425 nm, which was explained by the appearance of dimethylgermylene.²⁹

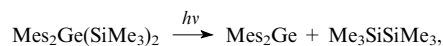


A similar intense absorption band with the maximum at 420 nm (together with two weaker bands at 330 and 490 nm and an additional shoulder in the vicinity of 380 nm) was observed upon a laser flash impact (308 nm) on a solution of dimethylbis(phenylseleno)germane [$\text{Me}_2\text{Ge}(\text{SePh})_2$] in cyclohexane.²⁷ To identify the absorption bands, $\text{Me}_2\text{Ge}(\text{SePh})_2$ was photolysed in 3-MP (77 K) and Ar (21 K) matrices. Upon irradiation (254 nm) of these matrices, similar spectra that contained the same bands as in flash photolysis experiments were observed. A band at 330 nm was assigned to a diphenyl diselenide molecule and the absorption at 490 nm was attributed to the radical PhSe^\bullet formed from this molecule.

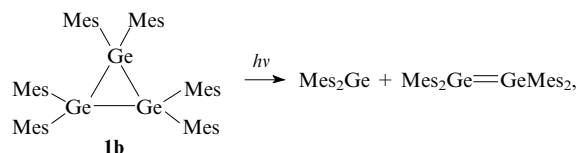


Thus, the remaining band (420 nm) might belong to dimethylgermylene. EPR spectra of irradiated matrices showed that the shoulder at 380 nm is related to the appearance of the radical PhSe^\bullet .

Germylene Me_2Ge represents a transient species that formed on the laser flash photolysis (248 nm) of dimethylbis(trimethylsilyl)germane [$\text{Me}_2\text{Ge}(\text{SiMe}_3)_2$] in hexane.¹³ After a flash, absorption bands at 550 and 320 nm were observed. A band at 550 nm decayed according to the second-order kinetics over *ca.* 10 μs with the simultaneous formation of a new band with the maximum at 405 nm. These spectral and kinetic transformations were explained by the following reaction sequence:



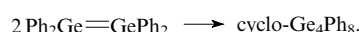
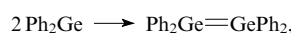
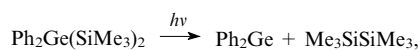
According to the data on the photolysis of organylgermanes in low-temperature matrices (see Table 1), the band at 550 nm was assigned to germylene Me_2Ge and the band at 405 nm was assigned to digermene $\text{Me}_2\text{Ge}=\text{GeMe}_2$. A band similar to the former was observed on the photolysis of hexamethylcyclotrigermene (cyclo- Ge_3Me_6 , **1b**).¹³ The absorbance in a band at 405 nm that appeared immediately after the pulse increased in the process. These data are well described by the following reaction scheme:



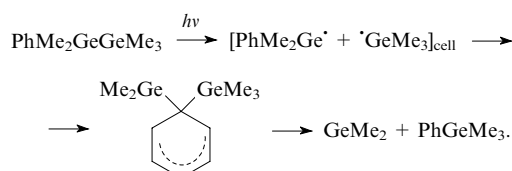
Flash photolysis (266 nm) of phenyl-substituted digermenes ($\text{Ph}_n\text{Me}_{3-n}\text{Ge}_2$), where $n = 1-3$, in tetrahydrofuran³⁰ also led to the appearance of two absorption bands in the optical spectrum, namely, in ranges of 440–470 and 315–330 nm. The long-wavelength absorption bands of germynes decayed with quasi-first-order kinetics, presumably, in their reaction with THF (for $n = 2$ and 3, the rate constants were 1.1×10^5 and $2.0 \times 10^5 \text{ s}^{-1}$, respectively). The short-

wavelength band assigned to germyl radicals $\text{Ph}_n\text{Me}_{3-n}\text{Ge}^\bullet$ decayed with second-order kinetics with the observed rate constants (k_{obs}) in the range of $(1.9-4.3) \times 10^5 \text{ s}^{-1}$.

The absorption band of germylene Ph_2Ge with the maximum at 445 nm was observed on the flash photolysis (266 nm) of a bis(trimethylsilyl)diphenylgermane [$\text{Ph}_2\text{Ge}(\text{SiMe}_3)_2$] solution in cyclohexane.⁴¹ The absorption decayed with second-order kinetics ($k_{\text{obs}} = 3.7 \times 10^5 \text{ s}^{-1}$) and was accompanied by growth of a new band at 320 nm. The latter corresponds to diphenyldigermene ($\text{Ph}_2\text{Ge}=\text{GePh}_2$) and also decayed with second-order kinetics ($k_{\text{obs}} = 1.5 \times 10^5 \text{ s}^{-1}$).



Studies of solutions of digermene $\text{PhMe}_2\text{GeGeMe}_3$ in cyclohexane revealed the appearance of two absorption bands with maxima at 430 and 320 nm 200 ns after a flash (266 nm).³¹ Presumably, the long wavelength band belongs to a dimethylgermylene formed in the following reactions:



This dimethylgermylene decayed with second order kinetics ($k/\epsilon = 3.2 \times 10^7 \text{ cm s}^{-1}$). The short-wavelength band at 320 nm corresponds to the germyl radical $\text{PhMe}_2\text{Ge}^\bullet$, which also dimerises ($k/\epsilon = 7.0 \times 10^7 \text{ cm s}^{-1}$).

Table 2 shows the positions of absorption band maxima for diorganylgermylenes revealed by the laser flash photolysis. The large number of molecular precursors used and the regular appearance of transient absorption bands in the range of 420–550 nm, and also the detection of similar bands on the photolysis of the same precursors in low-temperature matrices (see Table 1) allows one to conclude that these bands indeed belong to germynes. However, it should be noted that even in the same solvent, the position of a band maximum might considerably shift when a germylene was generated from different precursors. In matrices, the absorption band maxima for Me_2Ge were located in a narrower interval, 420–440 nm (see Table 1); the exception is the data of a study¹⁹ in which a band with the maximum at 506 nm was assigned to dimethylgermylene.

The position of absorption bands in solutions of germylene Me_2Ge (see Table 2) formed from different precursors varies in the interval of 420–470 nm. In this case, too, the position of the dimethylgermylene absorption band maximum (490 nm) given in Ref. 19 does not fit into this interval. Insofar as the majority of studies used cyclohexane as the solvent (see Table 2), the shift of the absorption band of germynes generated from different precursors cannot be explained by the solvent effect.

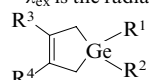
A recently published comprehensive review⁴⁴ on gas-phase reactions of germynes and dimethylstannylene points to a wide scatter of absorption band maxima assigned to dimethylgermylene. Presumably, this suggests that intermediates may have different structures including donor–acceptor complexes of this species.

It should be noted that in recent experiments on the flash photolysis with the better time resolution and the higher sensitivity (experiments with digital signal build-up), the absorption band maxima of germynes were shifted in the long-wavelength direction. It cannot be ruled out that in earlier

Table 2. Positions of absorption maxima for diorganylgermylenes in solutions observed on laser flash photolysis.

Germylene	Precursor	Solvent	$\lambda_{\text{ex}}/\text{nm}^a$	$\lambda_{\text{max}}/\text{nm}$	Ref.
Me ₂ Ge	3a	hexane	UV ^b	380	4, 39
	3a	methylcyclohexane	248	—	34
	Me ₂ Ge(SePh) ₂	cyclohexane	308	420	27
	PhMe ₂ GeGeMe ₂ GeMe ₂ Ph	"	266	420	22, 23
	PhMe ₂ GeSiMe ₃	"	248	425	29
	PhMe ₂ GeGeMe ₃	"	266	430	31
	(PhMe ₂ Ge) ₂	THF	266	440	30
	2	cyclohexane	308	440	33
	8	"	266	450	11
	9	"	266	490	19
	10a ^c	hexane	248	470	40
Et ₂ Ge	(Et ₂ Ge) _n (see ^d)	cyclohexane	266	430	14
Bu ₂ ⁿ Ge	(Bu ₂ ⁿ Ge) _n	"	266	450	14
PhMeGe	(PhMeGe) _n	"	266	440	14
	Me ₃ GeGePhMeGeMe ₃	"	266	440	22, 23
	10b ^c	hexane	248	490	42
	(Ph ₂ MeGe) ₂	THF	266	450	31
Ph ₂ Ge	Ph ₂ Ge(SiMe ₃) ₂	cyclohexane	266	445	41
	Me ₃ GeGePh ₂ GeMe ₃	"	266	450	22, 23
	(Ph ₂ Ge) ₂	THF	266	470	30
	10c ^c	hexane	248	500	43
(n-C ₆ H ₁₃) ₂ Ge	[(n-C ₆ H ₁₃) ₂ Ge] _n	cyclohexane	266	460	14
Mes ₂ Ge	Mes ₂ Ge(SiMe ₃) ₂	hexane	248	550	13
	cyclo-Ge ₃ Mes ₆	"	248	550	13
	cyclo-Ge ₃ Mes ₆	"	248	560	43

^a λ_{ex} is the radiation wavelength used for the precursor excitation; ^b measurements by lamp flash photolysis with time resolution of 5 μs ; ^c compounds **10**:

 [R³ = R⁴ = Me; R¹ = Ph, R² = H (**a**); R¹ = R² = Me; R³ = Ph, R⁴ = Me (**b**); R³ = R⁴ = Ph (**c**); ^d from hereon, the formula (R₂Ge)_n designates germanium-containing polymers ($\bar{M}_w \sim 10^3$).

studies, the shorter wavelength bands that belonged to digermenes were assigned to germynes due to insufficient resolution times and high recombination rates of intermediates. In the gas phase, the kinetics of reactions of dimethylgermylene formed from different precursors was studied by the absorption in a range of 450–510 nm.⁴⁴ The spectra represented a broad band with the maximum at 476.5 nm, which corresponds to the longest-wavelength absorption band observed for germylene in the liquid phase (see Table 2).

In solutions, germynes are almost always formed in a cage that contains the solvent and the residual precursor. Hence, the formation of germylene complexes with such residues may be assumed as the additional reason for the absorption band shift for germynes generated from different precursors.

In most cases, germynes are dimerised to form digermenes. The value $k/\varepsilon \sim (1-5) \times 10^7 \text{ cm s}^{-1}$ shows that the recombination occurs with a high rate constant. The rate constant for bimolecular recombination (k) is unknown because the extinction coefficient of the germylene band was determined in none of the cited studies. As was mentioned above, the value $\varepsilon^{380} = 1300 \text{ litre mol}^{-1} \text{ cm}^{-1}$ shown in Ref. 39 corresponds to a band with the maximum at 380 nm, which was revealed by the lamp flash photolysis method (time resolution $> 5 \mu\text{s}$). The position of this band strongly differs from those for germynes synthesised in later studies by laser flash photolysis. It is only in the past three years that the attempts were undertaken to determine the extinction coefficients of Me₂Ge and Ph₂Ge species. For dimethylgermylene, $\lambda_{\text{max}} = 470 \text{ nm}$, $\varepsilon = 730 \text{ litre mol}^{-1} \text{ cm}^{-1}$ (Ref. 40) and for diphenylgermylene, $\lambda_{\text{max}} = 500 \text{ nm}$, $\varepsilon = 1850 \text{ litre mol}^{-1} \text{ cm}^{-1}$ (Ref. 43). Therefore, assuming the extinction

coefficient equal to $10^3 \text{ litre mol}^{-1} \text{ cm}^{-1}$, the dimerisation of germynes proceeds with a rate constant in a range of $(1-5) \times 10^{10} \text{ litre mol}^{-1} \text{ cm}^{-1}$. This range virtually coincides with the diffusion rate constant of a bimolecular reaction in hexane [$2.1 \times 10^{10} \text{ litre mol}^{-1} \text{ cm}^{-1}$ (Ref. 40)].

V. Fluorescence of germynes

Photolysis of germanium-containing compounds in low-temperature matrices allows one to obtain not only optical absorption spectra, but also luminescence spectra of transient species. Luminescence of dimethylgermylene was first observed upon photolysis of dodecamethylcyclohexagermane (**8**) in a 3-MP matrix.¹¹ The spectrum represented a broad band with the maximum at 650 nm and was the mirror image of the dimethylgermylene absorption band with the Stokes shift of 7870 cm^{-1} . The fluorescence lifetime was 1–2 ns. Assuming that both the absorption and the fluorescence were due to the transitions between the ground (S_0) and the first excited (S_1) singlet states, the positions of band maxima allow one to determine the energy of the 0–0 transition (2.4 eV). The large Stokes shift was attributed to a considerable increase in the C–Ge–C angle in the first excited singlet state as compared with the ground state.

Fluorescence spectra of certain germynes synthesised from different molecular precursors can be found in Ref. 12. All germynes demonstrated an emission band with the maximum in the range of 620–650 nm (Table 3) and a considerable Stokes shift. Fluorescence excitation spectra coincided with the absorption spectra of these species. The energy of the 0–0 transition of germynes was 2.04–2.43 eV.

Table 3. Fluorescence maxima and the Stokes shift for diorganylgermylenes in 3-MP matrices ($T = 77$ K).

Germylene	Precursor	$\lambda_{\text{max}}/\text{nm}$	Stokes shift / cm^{-1}	Ref.
Me_2Ge	8	650	7870	11
	$\text{Me}(\text{Me}_2\text{Ge})_5\text{Me}$	628	7012	12
	$\text{Me}_2\text{Ge}(\text{GePhMe}_2)_2$	623	7645	12
	3a	620	7909	12
PhMeGe	$\text{PhMeGe}(\text{GeMe}_3)_2$	645	6426	12
Ph_2Ge	$\text{Ph}_2\text{Ge}(\text{GeMe}_3)_2$	651	6285	12

VI. Electronic structure of germynes and the nature of their optical absorption band

Whereas carbenes are characterised by the triplet ground state,^{45,46} the calculations by different quantum chemical methods have shown that the germylene ground state is singlet (Table 4). This was also confirmed by the absence of signals in the EPR spectra of matrices frozen at 77 and 10 K and containing a germylene accumulated on irradiation.¹¹ The singlet–triplet splitting in germynes X_2Ge substantially depends on the nature of substituent X ($\text{X} = \text{H}, \text{Me}, \text{F}, \text{Cl}, \text{Br}$) and lies in the range of 84–355 kJ mol^{-1} ($\sim 1\text{--}4$ eV).⁴⁵ As regards energy, the excited singlet state is higher than the ground state by $> 188\text{--}209$ kJ mol^{-1} .⁴⁶ On germylene excitation, the Ge–X bond distance changes insignificantly; however, the X–Ge–X angle between the bonds substantially increases. The results of quantum chemical calculations of the structure and electronic state energies for carbene heavy analogues including germynes were comprehensively surveyed in several studies.^{8,9} The calculations showed a slight decrease in the E–X bond distance ($\text{E} = \text{C}, \text{Si}, \text{Ge}$) and a substantial increase in the X–E–X angle upon the transition of all carbenes and their analogues into the excited states.

Table 4. Calculated energies ($E/\text{kJ mol}^{-1}$), bond lengths ($r_e/\text{\AA}$) and angles between X–Ge–X bonds (q_e/deg) for the ground ($^1\text{A}_1$) and electronically excited ($^3\text{B}_1$, $^1\text{B}_1$) electronic states of germynes.

Germylene	Parameter	Electronic state			Ref.
		$^1\text{A}_1$	$^3\text{B}_1$	$^1\text{B}_1$	
H_2Ge	E	0	43.5–123.1	182.9–199.3	47–55
	r_e	1.595 ± 0.018	1.543 ± 0.018	1.548 ± 0.005	
	q_e	92.3 ± 1.0	119.1 ± 0.5	122.7 ± 0.6	
Me_2Ge	E	0	57.3–128.3	213.1	45, 47, 53, 56
	r_e	2.022 ± 0.005	2.004 ± 0.004	2.021	
	q_e	97.1 ± 1.6	118.0 ± 0.5	122.0	
Ph_2Ge	E	0	—	—	57
	r_e	2.006	—	—	
	q_e	101.6	—	—	

The optical absorption bands of germynes shown in Tables 1 and 2 are attributed to the electronic transition from the binding $2a_1$ orbital of a germylene X_2Ge (a linear combination of the $4s$ and $4p_z$ orbitals of the germanium atom with the σ orbitals of the substituent X) to the non-bonding $1b_1$ orbital, which is the $4p_y$ orbital of the Ge atom. Presumably, germynes are characterised by the C_{2v} symmetry group. In this group, the $^1\text{A}_1 \rightarrow ^1\text{B}_1$ transition between the terms is permitted as regards the symmetry; however, the orbitals lie in different planes, which decreases their overlap and reduces the transition intensity. Apparently, for this reason the molar extinction coefficient of the germylene band does not substantially exceed 10^3 $\text{litre mol}^{-1} \text{cm}^{-1}$.

VII. Spectroscopy of germylene complexes

The presence of a vacant antibonding $4p_y$ orbital of the germanium atom in germynes makes possible the formation of donor–acceptor complexes of these species with different molecules. Spectroscopic studies of such complexes are often carried out in low-temperature matrices. The UV irradiation of a matrix containing a germanium precursor and a potential complexing agent leads to the accumulation of a germylene. Subsequent annealing and refreezing of the matrix makes it possible to obtain a germylene complex and record its spectrum. This procedure allowed the optical absorption bands of germylene complexes with organic molecules including those containing heteroatoms to be observed.²⁶

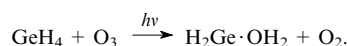
For instance, in the spectrum of a 3-MP–IP matrix in the presence of triethylamine, the absorption band of dimesitylgermylene (Mes_2Ge) with the maximum at 550 nm decayed upon annealing and a new band at 414 nm was formed.

Table 5 shows the positions of maxima of new bands that appeared upon the matrix refreezing and belong to germylene complexes. As is seen, the binding of a germylene into a complex shifts the absorption band to shorter wavelengths. Absorption bands of germylene complexes with molecules containing P, N, S and O atoms lie in the range of 306–376 nm. Apparently, this is explained by the interaction of the vacant $4p_y$ orbital of the germylene atom with orbitals of heteroatoms of organic molecules, which changes the energy of the corresponding $n \rightarrow \pi$ transition.^{3,25}

The studied germylene–heteroatomic compound complexes were unstable and dissociated as the matrix temperature increased so that germynes either dimerised to digermenes with the absorption bands in approximately the same spectrum range or were inserted into different bonds. Thus for a 3-MP–IP matrix, a band of the $\text{Bu}_3\text{P} \cdot \text{Ge}(\text{C}_6\text{H}_2\text{Pr}_2-2,4,6)_2$ complex at 334 nm was preserved at 153 K²⁵ but gradually decayed at 173 K with the appearance of the corresponding digermene signal. At 194 K, the lifetime of such a complex was 48 s. The germylene complex with dimethyl sulfide was stable only at 133 K. Certain complexes of this kind decomposed as the matrix melted. As was first observed in Ref. 12, a slight short-wavelength shift (~ 10 nm) of the germylene absorption band accompanies the formation of a germylene complex with aromatic molecules containing π -systems, namely, benzene and naphthalene (see Table 5).

At 77 K, the 3-MP–IP matrix is so ‘soft’ that germynes can diffuse in it. Upon the addition of ethanol into this matrix, the storage of an irradiated sample in it is accompanied by the decay of the germylene absorption band even at 77 K and the growth of a new absorption band with the maximum at 320–367 nm, which belongs to a germylene complex with ethanol (see Table 5).

An argon matrix containing germane (GeH_4) and ozone was studied at 14–18 K.⁵⁸ The analysis of numerous bands in the IR spectrum that appeared on irradiation in different spectral ranges allowed the identification of certain species including germylene complexes with a water molecule. Presumably, the complex was formed in the reaction



The IR spectrum of the complex $\text{H}_2\text{Ge} \cdot \text{OH}_2$ demonstrated absorption bands with frequencies of 1586, 3597, 3687 cm^{-1} , which are close to the vibrational frequencies of a free water molecule in an argon matrix (the matrix contained no water before excitation). Moreover, the H_2Ge fragment of this complex exhibited a triplet signal (1777, 1794, 1814 cm^{-1}) and a low-frequency line (898 cm^{-1}) that corresponded to vibrations of H–Ge–H bonds. A frequency of 1794 cm^{-1} is close to the double frequency of 898 cm^{-1} being its overtone.

Table 5. Absorption maxima for germylene complexes with complexing molecules in low-temperature ($T = 77$ K) matrices.

Complexing agent	$\lambda_{\text{max}}/\text{nm}$					Ref.
	Me ₂ Ge	Ph ₂ Ge	Mes ₂ Ge	(2,6-Et ₂ C ₆ H ₃) ₂ Ge	(2,4,6-Pr ₃ ⁱ C ₆ H ₂) ₂ Ge	
3-MP Matrix						
3-MP	420	466	550	544	558	25, 26
Bu ₃ ⁿ P	—	—	306	314	334	25, 26
1-Azabicyclo[2.2.2]octane	—	334	349	356	363	25, 26
Me ₂ S	—	326	348	357	357	25, 26
Thiophene	—	332	352	359	366	25, 26
2-Methyltetrahydrofuran	—	325	360	369	376	25, 26
cyclo-C ₆ H ₁₁ Cl	341	374	495	508	544	25, 26
PhCl	392	403	538	532	553	25, 26
Et ₃ N	—	—	414	—	445	25, 26
EtOH	—	320	333	332	—	25, 26
Bu ⁱ OH	—	332	363	367	—	25, 26
CH ₂ =CHCH ₂ Cl	—	—	530	—	—	25, 26
(CH ₂ =CHCH ₂) ₂ S	—	—	380	—	—	25, 26
Matrix 3-MP – IP (4 : 1)						
3-MP – IP	436	—	—	—	—	12
PhH	422	—	—	—	—	12
Haphthalene	422.5	—	—	—	—	12

Note. Precursors: for Me_2Ge , Me_2GeNB (**3a**)^{25, 26} and $\text{Me}(\text{GeMe}_2)_5\text{Me}$;¹² for Ph_2Ge , Ph_2GeNB (**3d**); for the rest germylenes, $\text{R}_2\text{Ge}(\text{SiMe}_3)_2$.

Moreover, the flash photolysis method allows one to detect germylene complexes with different molecules also in solutions. An optical spectrum of a dimethylgermylene complex with triphenylphosphine represented a broad band with the maximum at 370 nm and the extinction coefficient of 7.5×10^3 litre mol^{-1} cm^{-1} .^{4, 59}



The use of a competitive reaction of dimethylgermylene with CCl_4 made it possible to determine the rate constant of reaction (1), $k = 6.5 \times 10^8$ litre mol^{-1} s^{-1} . The $\text{Me}_2\text{Ge} \cdot \text{PPh}_3$ complex disappeared with the second-order kinetics presumably to form digermene (or a digermene complex with triphenylphosphine) with the rate constant $2k = 1.5 \times 10^9$ litre mol^{-1} s^{-1} . However, from our viewpoint, these results should be checked, because the earlier studies on the lamp flash photolysis of germanorbornadiene with the same time resolution (5 μs)³⁹ failed to correctly identify the transient absorption band at 380 nm.

An absorption band with the maximum at 325 nm was assigned to complexes $\text{R}_2\text{Ge} \cdot \text{NBu}^n\text{H}_2$ ($\text{R} = \text{Me}, \text{Ph}$).⁴³ Complexes $\text{PhMeGe} \cdot \text{NR}_2^1\text{R}^2$ ($\text{NR}_2^1\text{R}^2 = \text{NH}_2\text{Bu}^n$ and NEt_3) were characterised by bands at 330 nm.⁴² The absorption of germylene (PhMeGe) complexes with molecules that contain double bonds [isoprene, 2,3-dimethylbuta-1,3-diene (DMB), 4,4-dimethylpent-1-ene] was shifted to shorter wavelengths ($\lambda_{\text{max}} \sim 275$ nm).⁴² A comparison of these data with the position of absorption bands of complexes in low-temperature matrices (see Table 5) shows that in solutions, the spectrum substantially (by ~ 100 nm) shifts to shorter wavelengths. Provided the interpretation of the absorption band is correct, this shift may be associated with the different geometries of complexes in solutions and low-temperature matrices.

Thus, germylenes efficiently form complexes with organic molecules. In spectra of these complexes, the light absorption bands are substantially shifted as compared with germylene signals. For this reason, in the studies of optical spectra and kinetics of germylene reactions, the potent complexing agents should be removed from the solution. Data on germylene complexes are shown in a review.⁹

VIII. Vibrational spectra of germylenes

On irradiation of germane (GeH_4) isolated in an argon matrix at 4 K with visible and UV light the IR spectrum demonstrated lines that belonged to different photolysis products.⁶⁰ Among numerous signals, the lines of germylenes H_2Ge and D_2Ge with frequencies of 1887, 1864, 920 cm^{-1} and 1329, 1325, 662 cm^{-1} , respectively, were identified. These frequencies correspond to two stretching and one vibrations of $\text{Ge}-\text{H}(\text{D})$ bonds.

An IR spectrum of dimethylgermylene was recorded in a cryogenic (12 K) argon matrix under UV irradiation (254 or 248 nm) of diazodimethylgermane $[\text{Me}_2\text{Ge}(\text{N}_3)_2]$.²⁸ The preliminary irradiation of $\text{Me}_2\text{Ge}(\text{N}_3)_2$ in hydrocarbon matrices at 77 K in the presence of molecules-scavengers of germylenes and the analysis of trapping products showed that diazide is the source of Me_2Ge . In an argon matrix, the majority of bands observed in the IR range belonged to methyl group vibrations; however, in the 600–500 cm^{-1} range, bands corresponding to vibrations of $\text{Ge}-\text{C}$ bonds were observed (Table 6).

Table 6. Vibrational frequencies (ν/cm^{-1}) of argon matrix-isolated Me_2Ge at 12 K and stable $[(\text{Me}_3\text{Si})_2\text{CH}]_2\text{Ge}$ germylene in crystalline state.

Germylene	Vibration	Experiment		Calculation	
		ν	Ref.	ν	Ref.
Me_2Ge	$\nu(\text{Ge}-\text{C})$	541	28	560	47
	$\nu(\text{Ge}-\text{C})$	527	28	497	47
	$\delta(\text{C}-\text{Ge}-\text{C})$			288	47
$[(\text{Me}_3\text{Si})_2\text{CH}]_2\text{Ge}$	$\nu(\text{Ge}-\text{C})$	643	61	—	—
	$\nu(\text{Ge}-\text{C})$	613	61	—	—

Quantum chemical calculations of vibrational frequencies of $\text{Ge}-\text{C}$ bonds were carried out^{47, 50, 62–64} for the ground and excited states of two germylenes, namely, H_2Ge and Me_2Ge (Table 7). It was shown^{28, 60} that all frequencies calculated for the ground states of these species are well consistent with those measured in an argon matrix. Modern laser spectroscopic

Table 7. Calculated and experimental vibrational frequencies (ν/cm^{-1}) for ground and electronically excited states of germylene and dimethylgermylene.

Species	Method	Term	ν_1	ν_2	ν_3	Ref.
Calculation						
H ₂ Ge	CF-CI	¹ A ₁	1857	923	1866	50
		¹ A ₁	1887	958	2036	47
	CASSCF	³ B ₁	1855	924	2063	
		¹ B ₁	1864	860	2011	
		¹ A ₁	1840	913	1840	64
		³ B ₁	1998	801	2054	
		¹ B ₁	1809	783	1909	
		Me ₂ Ge	SCF	¹ A ₁	560	288
³ B ₁	576			203	611	
¹ B ₁	554			194	607	
Experiment						
H ₂ Ge	VUV photo-lysis in Ar matrix ^a	¹ A ₁	1887	920	1864	60
		LOS	¹ A ₁	1856	916	—
	Jet-cooled LIF	¹ B ₁	1798	783	—	64
^a VUV is Vacuum Ultra Violet.						

^a VUV is Vacuum Ultra Violet.

techniques, namely, Jet-cooled Laser Induced Fluorescence (Jet-cooled LIF) ⁶⁴ and Laser Optogalvanic Spectroscopy (LOS), ⁶⁵ made it possible to experimentally determine the vibrational frequencies of H_2Ge in the ground ⁶⁵ and singlet excited ⁶⁴ states (see Table 7). These results well agree with those obtained by the theoretical CFCI (Corrected Full Configuration Interaction) ⁵⁰ and CI (Configuration Interaction) ⁴⁷ methods and also with the recent quantum-chemical calculations using the CASSCF (Complete Active Space Self-Consistent Field) method. ⁶⁴ The bending vibrational frequency of the

C—Ge—C fragment was twice lower than the stretching vibrational frequency of the Ge—C bond (see Table 7), which is often observed in vibrational spectroscopy. Detailed information on vibrational frequencies of germynes and their complexes can be found in a review. ⁹

IX. Germylene reactions

As was noted above, in the absence of scavenging molecules, germynes disappear in a second-order reaction, *i.e.*, dimerise to form digermenes. A parameter k_{rec}/ϵ , where k_{rec} is the rate constant for bimolecular recombination, usually lies in the range of $(1-3) \times 10^7 \text{ cm s}^{-1}$ (Table 8). Although the exact extinction coefficient of the germylene band was not measured experimentally, it, as noted above, cannot substantially exceed $10^3 \text{ litre mol}^{-1} \text{ cm}^{-1}$, because the recombination constant would otherwise exceed the diffusion rate constant.

Germynes that contain bulky groups as substituents recombine with substantially lower rate constants as compared with dimethylgermylene. For example, k_{rec}/ϵ decreases by more than an order of magnitude (see Table 8) when the methyl group is replaced by an ethyl group and by two orders of magnitude for the butyl group substitution. Thus, the steric factor substantially affects the recombination rate.

Sometimes, germynes disappear in a first-order reaction. Thus the absorption band of diisopropylgermylene (Pr_2^iGe) with the maximum at 560 nm decays with first-order kinetics over 56 ns. ¹⁵ Presumably, Pr_2^iGe isomerises to 2-germapropene $\text{H}_2\text{C}=\text{CMeGeH}_2\text{Pr}^i$ so quickly that the dimerisation has no time to compete with this reaction. It was found ^{31,33} that germynes PhMeGe (the absorption band maximum at 450 nm) and Ph_2Ge (470 nm) disappear over *ca.* 5–10 μs in a first-order reaction (see Table 8) presumably with the solvent, namely, tetrahydrofuran. However, the same germynes were dimerised in cyclohexane. ^{22,23}

Laser flash photolysis studies have demonstrated that germynes quickly react with oxygen. For Me_2Ge , the rate constant for this reaction in cyclohexane lies in the range of

Table 8. Observed rate constants (k_{rec}/ϵ) for the germylene loss in recombination reactions ($T = 293 \text{ K}$).

Germylene	Precursor	Solvent	$\lambda_{\text{max}}/\text{nm}$	$k_{\text{rec}}/\epsilon/\text{cm s}^{-1}$	Ref.
Me_2Ge	$(\text{PhMe}_2\text{Ge})_2\text{GeMe}_2$	cyclohexane	420	2.5×10^7	22, 23
	8	"	450	2.7×10^7	11
	9	"	490	3.5×10^7	19
	2	"	440	2.5×10^7	33
	$\text{PhMe}_2\text{GeSiMe}_3$	"	430	1.0×10^7	31
	$\text{PhMe}_2\text{GeGeMe}_3$	"	430	3.2×10^7	31
	$(\text{PhMe}_2\text{Ge})_2$	THF	440	—	30, 32
	10a	hexane	470	5.0×10^7	40
	10d ^a	"	480	7.5×10^7	43
	$(\text{Et}_2\text{Ge})_n$	cyclohexane	430	1.1×10^6 (460 nm) ^b	14
Pr_2^iGe	cyclo- Ge_4Pr_8^i	hexane	560	1.8×10^7 (see ^c)	15
Bu_2^nGe	$(\text{Bu}_2^i\text{Ge})_n$	cyclohexane	450	2.4×10^5	14
$(n\text{-C}_6\text{H}_{13})_2\text{Ge}$	$[(n\text{-C}_6\text{H}_{13})_2\text{Ge}]_n$	"	460	1.5×10^5 (450 nm) ^b	14
PhMeGe	$\text{PhMeGe}(\text{GeMe}_3)_2$	"	440	2.2×10^7	22, 23
	$(\text{PhMeGe})_n$	"	440	4.1×10^5 (450 nm) ^b	14
	$(\text{Ph}_2\text{MeGe})_2$	THF	450	1.1×10^5 (see ^c)	30, 32
	$\text{Ph}_2\text{Ge}(\text{GeMe}_3)_2$	cyclohexane	450	3.0×10^6	22, 23
Ph_2Ge	$(\text{Ph}_3\text{Ge})_2$	THF	470	2.0×10^5 (see ^c)	30, 32
	$\text{Ph}_2\text{Ge}(\text{SiMe}_3)_2$	cyclohexane	445	~ 270 ^d	41
	10c	hexane	500	6.0×10^6	66
	cyclo- Ge_3Me_6	"	550	1.1×10^5 (see ^c)	13

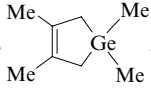
^a Compound **10d** is ; ^b wavelength of kinetic measurements is shown; in the other cases, λ_{max} ; ^c the first-order reaction rate constant is shown, in s^{-1} ; ^d the half-time of transformation (loss) is shown ($\tau_{1/2}$), in μs .

Table 9. Rate constants for germylene reactions with oxygen ($T = 293$ K).

Germyle- lene	Precursor	Solvent	$k /$ litre mol ⁻¹ s ⁻¹	Ref.
Me ₂ Ge	Me ₂ HGeGeMe ₃	see ^a	2.7×10^7	44
	3a	hexane	2.0×10^7	4, 39
	8	cyclohexane	9.7×10^8	11
	PhMe ₂ GeSiMe ₃	"	2.0×10^9	29
	PhMe ₂ GeSiMe ₃	"	2.1×10^9	31
	PhMe ₂ GeSiMe ₃	"	1.7×10^9	31
	9	"	1.6×10^9	19
	(PhMe ₂ Ge) ₂	THF	—	30, 32
	10a	hexane	9×10^7	40
PhMeGe	(Ph ₂ MeGe) ₂	THF	2.3×10^8	30, 32
	10b	hexane	6×10^7	42
Ph ₂ Ge	Ph ₂ Ge(SiMe ₃) ₂	cyclohexane	1.0×10^8	41
	(Ph ₃ Ge) ₂	THF	1.8×10^8	30, 32
	10c	hexane	2.7×10^7	66
Mes ₂ Ge	cyclo-Ge ₃ Mes ₆	"	7.3×10^6	13

^a In the gas phase.

$(1-2) \times 10^9$ litre mol⁻¹ s⁻¹ for different precursors (Table 9). These values are 10–20 times lower than the diffusion rate constant of the bimolecular reaction in cyclohexane, which is due to the steric effect and the spin prohibitions for the singlet germylene reaction with a triplet oxygen molecule. The steric effect is pronounced for germylenes with bulky substituents,

e.g., Ph₂Ge and Mes₂Ge, which react with oxygen, correspondingly, one- and two-orders-of-magnitude more slowly than dimethylgermylene. Note that the one-order-of-magnitude smaller rate constant obtained for Me₂Ge^{4,39} most probably belongs to the digermene reaction (see Section X).

In a solvent more polar than cyclohexane, namely, tetrahydrofuran, the rate constant decreased by an order of magnitude which was apparently associated with the formation of a Me₂Ge·THF complex that reacted with the oxygen molecule. In the gas phase, the rate constant for the dimethylgermylene reaction with oxygen (4.5×10^{14} cm³ mol⁻¹ s⁻¹ = 2.7×10^7 litre mol⁻¹ s⁻¹)⁴⁴ was two-orders-of-magnitude lower than the constants measured earlier in cyclohexane (see Table 9).

In recently published studies^{40,42,66} on the laser flash photolysis of solutions of germanium-containing compounds, the rate constants for reactions of germylenes Me₂Ge, PhMeGe and Ph₂Ge with oxygen were determined. These constants turned out to be one-order-of-magnitude smaller (see Table 9) than those measured earlier (e.g., see Refs 11, 19, 30–33, 41). These data additionally demonstrated the effect of complexation on the germylene reactivity. The structure of these complexes can be different in each particular case. It is noteworthy that high rate constants were obtained for reactions in cyclohexane, whereas lower rate constants were found in hexane. Probably, in hexane, oxygen forms complexes with solvent molecules, which lessens its diffusion mobility and, correspondingly, reactivity. Moreover, the presence of uncon-

Table 10. Rate constants for germylene reactions with unsaturated compounds ($T = 293$ K).

Germyle- lene	Precursor	Solvent	Reactant	$k /$ litre mol ⁻¹ s ⁻¹	Ref.
Me ₂ Ge	Me ₂ HGeGeMe ₃	see ^a	buta-1,3-diene	6.6×10^9	44
	Me ₂ HGeGeMe ₃	see ^a	3,3-dimethylbut-1-ene	5.9×10^9	44
	Me ₂ Ge(GePhMe ₂) ₂	cyclohexane	DMB	2.4×10^7	22, 23
	9	"	DMB	2.2×10^7	11
	PhMe ₂ GeSiMe ₃	"	DMB	1.7×10^7	29
	PhMe ₂ GeSiMe ₃	"	DMB	4.1×10^7	31
	PhMe ₂ GeSiMe ₃	"	buta-1,3-diene	1.24×10^7	29
	PhMe ₂ GeSiMe ₃	"	but-1-ene	$< 10^5$	29
	PhMe ₂ GeSiMe ₃	"	isoprene	1.63×10^7	29
	PhMe ₂ GeSiMe ₃	"	cis-piperylene	9.2×10^6	29
	PhMe ₂ GeSiMe ₃	"	trans-piperylene	2.9×10^6	29
	PhMe ₂ GeSiMe ₃	"	cis,cis-hexa-2,4-diene	1.2×10^6	29
	PhMe ₂ GeSiMe ₃	"	cis,trans-hexa-2,4-diene	3.5×10^6	29
	PhMe ₂ GeSiMe ₃	"	trans,trans-hexa-2,4-diene	$< 5 \times 10^5$	29
	PhMe ₂ GeSiMe ₃	"	hex-1-ene	$< 10^4$	29
	PhMe ₂ GeSiMe ₃	"	hex-1-ine	3.0×10^4	29
	PhMe ₂ GeSiMe ₃	"	prop-1-ine	$< 10^5$	29
	PhMe ₂ GeGeMe ₃	cyclohexane	DMB	2.1×10^7	31
	(PhMe ₂ Ge) ₂	THF	DMB	—	30, 32
	10d	hexane	DMB	12.5×10^9	40
	3a	"	11 ^b	5.0×10^8	4, 39
	3a	"	styrene	7×10^7	4, 39
Et ₂ Ge	(Et ₂ Ge) _n	cyclohexane	DMB	8.4×10^7	14
Bu ₂ ⁿ Ge	(Bu ₂ ⁿ Ge) _n	"	DMB	3.1×10^7	14
(n-C ₆ H ₁₃) ₂ Ge	[(n-C ₆ H ₁₃) ₂ Ge] _n	"	DMB	4.0×10^7	14
PhMeGe	(PhMeGe) _n	"	DMB	22.0×10^7	14
	(Ph ₂ MeGe) ₂	THF	DMB	4.5×10^6	30, 32
	PhMeGe(GeMe ₃) ₂	cyclohexane	DMB	2.2×10^6	22, 23
	10b	hexane	DMB	4×10^9	42
	(Ph ₃ Ge) ₂	THF	DMB	1.0×10^6	30, 32
Ph ₂ Ge	Ph ₂ Ge(GeMe ₃) ₂	cyclohexane	DMB	0.72×10^6	22, 23
	Ph ₂ Ge(SiMe ₃) ₂	"	DMB	2.75×10^4	41
	10c	hexane	isoprene	5.5×10^9	64

^a In the gas phase. ^b 3,3,6,6-Tetramethyl-1-thiacyclohept-4-yne (**11**).

Table 11. Rate constants of germylene reactions with carbon tetrachloride in cyclohexane ($T = 293$ K).

Germylene	Precursor	Solvent	k / litre mol ⁻¹ s ⁻¹	Ref.
Me ₂ Ge	3a	hexane	0.12×10^8	4, 39
	Me ₂ Ge(GePhMe ₂) ₂	cyclohexane	no reaction	22, 23
	8	"	4.9×10^8	11
	PhMe ₂ GeSiMe ₃	"	3.2×10^8	29
	10d	hexane	8×10^7	40
Et ₂ Ge	(Et ₂ Ge) _n	cyclohexane	10×10^8	14
Bu ₂ ⁿ Ge	(Bu ₂ ⁿ Ge) _n	"	9.2×10^8	14
(n-C ₆ H ₁₃) ₂ Ge	[(n-C ₆ H ₁₃) ₂ Ge] _n	"	13×10^8	14
PhMeGe	(PhMeGe) _n	"	1.6×10^8	14
	Me ₂ Ge(GePhMe ₂) ₂	"	0.65×10^8	22, 23
	10b	hexane	1.7×10^7	42
Ph ₂ Ge	Ph ₂ Ge(GeMe ₃) ₂	cyclohexane	1.5×10^8	22, 23
	10c	hexane	4.8×10^6	66

trolled impurities in cyclohexane, which bind germynes and accelerate their loss, is also possible.

One of the tests for the presence of a germylene in photochemical processes included its addition to the double bond of 2,3-dimethylbuta-1,3-diene to form the corresponding germa-cyclopentene. The rate constants for this reaction with Me₂Ge measured on flash photolysis of different molecular precursors lie in a range of $(1.7-4.1) \times 10^7$ litre mol⁻¹ s⁻¹ (Table 10).

Due to the fast reaction of Me₂Ge with the solvent, the rate constant of its reaction with DMB in tetrahydrofuran was not measured. In cyclohexane, the rate constant of the reaction of germynes Et₂Ge and PhMeGe with DMB increased 2- and

5-fold, respectively, as compared with rate constants for Me₂Ge (see Table 10). It should be noted that the rate constants for the reaction of PhMeGe with DMB measured in Refs 22 and 23 were exactly one-order-of-magnitude smaller than that found in Ref. 14 (both experiments were carried out in cyclohexane but used different precursors). For the reaction of Ph₂Ge with DMB in cyclohexane, the data on the rate constant considerably differed from one another, for instance, by a factor of 26 (see Refs 22, 23 and 41). Gas-phase measurements have shown⁴⁴ that in the limit (at high pressures), the rate constant for the addition of Me₂Ge to the double bonds of buta-1,3-diene and 3,3-dimethylbut-1-ene approaches the diffusion limit (1.1×10^{11} cm³ mol⁻¹ s⁻¹ = 6.6×10^9 cm³ mol⁻¹ s⁻¹) and exceeds the rate constant typical of this reaction in cyclohexane by two orders of magnitude (see Table 10). The rate constants for the germylene addition to unsaturated compounds found in recent studies^{40,42,66} exceed the earlier data by two orders of magnitude (see Table 10). Probably, the authors of earlier works observed reactions of digermenes rather than germynes. Thus, the development of instrumentation and methods for the detection of reactions in the liquid phase and also the use of new precursors bring the germylene rate constants measured in solutions closer to those measured in the gas phase.

Carbon tetrachloride is an efficient germylene scavenger. The rate constants for the germylene reaction with CCl₄ are $(1-10) \times 10^8$ litre mol⁻¹ s⁻¹ (Table 11). Studies of ¹H and ¹³C NMR spectra of the reaction products have shown²⁷ that germylene inserts into a CCl₄ molecule at a C-Cl bond.



For this reaction, the data on rate constants also vary depending on the precursor nature. However, the scatter (for the same germylene) is substantially weaker as compared with

Table 12. Rate constants for germylene reactions with some organic molecules ($T = 293$ K).

Germylene	Precursor	Solvent	Reagent	k /litre mol ⁻¹ s ⁻¹	Ref.
Me ₂ Ge	PhMe ₂ GeSiMe ₃	cyclohexane	DMSO	$< 10^7$	29
	PhMe ₂ GeSiMe ₃	"	THF	$< 10^4$	29
	PhMe ₂ GeSiMe ₃	"	Et ₃ SiH	$< 10^4$	29
	PhMe ₂ GeSiMe ₃	"	EtOH	1.86×10^4	29
	PhMe ₂ GeSiMe ₃	"	EtOH	no reaction	31
	PhMe ₂ GeGeMe ₃	"	EtOH	the same	31
	Me ₂ Ge(GePhMe ₂) ₂	"	Et ₃ SiH	4.2×10^6	22, 23
	Me ₂ Ge(GePhMe ₂) ₂	"	EtOH	no reaction	22, 23
	(PhMe ₂ Ge) ₂	THF	EtOH	the same	32
	3a	hexane	Me ₃ SnCl	3.5×10^8	4, 39
	3a	"	3a	1.2×10^7	4, 39
	3a	"	MeOH	3×10^7	4, 39
PhMeGe	PhMeGe(GeMe ₃) ₂	cyclohexane	Et ₃ SiH	4.1×10^6	22
	PhMeGe(GeMe ₃) ₂	"	Et ₃ SiH	6.5×10^7	23
	PhMeGe(GeMe ₃) ₂	"	EtOH	no reaction	22, 23
Ph ₂ Ge	Ph ₂ Ge(SiMe ₃) ₂	"	EtMe ₂ SiH	1.0×10^4	41
	Ph ₂ Ge(SiMe ₃) ₂	"	MeOH	no reaction	41
	Ph ₂ Ge(SiMe ₃) ₂	"	Me ₂ EtBr	1.0×10^4	41
	Ph ₂ Ge(SiMe ₃) ₂	"	Bu ^t Br	6.4×10^5	41
	Ph ₂ Ge(SiMe ₃) ₂	"	MeSSMe	5.0×10^6	41
	Ph ₂ Ge(SiMe ₃) ₂	"	Me ₂ EtBr	1.0×10^4	41
	Ph ₂ Ge(GeMe ₃) ₂	"	Et ₃ SiH	6.6×10^5	22, 23
	Ph ₂ Ge(GeMe ₃) ₂	"	EtOH	no reaction	22, 23
	10c	hexane	MeOH	6.1×10^9	66
	10c	"	Bu ^t OH	4.8×10^9	66
	(Ph ₃ Ge) ₂	cyclohexane	EtOH	no reaction	32
Me ₂ Ge	cyclo-Ge ₃ Me ₆	hexane	Et ₃ SiH	1.1×10^5	13
	cyclo-Ge ₃ Me ₆	"	EtOH	no reaction	13
	cyclo-Ge ₃ Me ₆	"	1-bromohexane	5.4×10^5	13

germylene reactions with DMB (see Tables 10 and 11). In the gas phase, the rate constant of the reaction of Me_2Ge with CCl_4 was not measured,⁴⁴ because the radiation (193 nm) used in the majority of studies was absorbed by carbon tetrachloride.

Reactions of insertion into $\text{H}-\text{X}$ bonds ($\text{X} = \text{C}, \text{N}, \text{O}, \text{F}, \text{Si}, \text{P}, \text{S}, \text{Cl}$) are typical of carbenes, silylenes and germylenes. According to quantum chemical calculations,^{45, 56, 67–69} the activation energies of such reactions are substantially higher for dimethylgermylene as compared with carbenes and silylenes. Nonetheless, such processes involving germylenes often proceed with high rate constants (Table 12).

X. Optical spectra, vibrational frequencies and kinetics of digermene decay

As was noted above, the annealing of low-temperature matrices containing an accumulated germylene and the flash photogeneration of germylenes in solutions lead in many cases to dimerisation of these species to form digermenes. Table 13 shows the position of absorption bands for certain digermenes formed from different precursors. The data obtained at 293 K pertain to laser flash photolysis experiments. A temperature of 77 K corresponds to experiments that involved annealing and refreezing of irradiated matrices. It is evident that digermene absorption bands are shifted to shorter wavelengths as compared with germylene bands (see Tables 1 and 2). Note that the extinction coefficients of digermene bands also remained unknown. The only extinction coefficient value was determined⁴³ for the $\text{Ph}_2\text{Ge}=\text{GePh}_2$ band with the maximum at 440 nm to be $5970 \text{ litre mol}^{-1} \text{ cm}^{-1}$.

On the photolysis (254 nm) of dimethyldiazidogermane [$\text{Me}_2\text{Ge}(\text{N}_3)_2$] in an argon matrix at 12–18 K, the IR spectrum of dimethylgermylene was recorded²⁹ (see Table 6). Matrix heating to 36 K led to changes in the spectrum, namely, the disappearance of Me_2Ge lines and the appearance of new signals assigned by the authors to tetramethyldigermene (Table 14). Similar results were obtained on the thermolysis of compound **3a** in the crystalline state with the isolation of gaseous products in argon or nitrogen matrices at 5 K.⁷⁰

In certain cases, the digermene absorption decayed with second-order kinetics, which implies the formation of cyclo-

Table 14. Calculated and experimental vibrational frequencies (cm^{-1}) of $\text{Ge}-\text{C}$ and $\text{Ge}-\text{Ge}$ bonds of tetramethyldigermene⁷⁰ recorded in argon (Ar) and nitrogen (N_2) matrices at 5 K.

Vibration	Raman spectra		IR Spectra		
	experiment		experiment		calculation
	Ar	N_2	Ar	Ar ^a	
$\nu(\text{Ge}-\text{C})$	591	589	588	598	594
	580	580	576	568	569
$\nu(\text{Ge}-\text{Ge})$	404	405	401	—	—
$\delta(\text{C}-\text{Ge}-\text{C})$	235	234	232	—	—
	200	198	206		

^a According to data of Ref. 28.

tetragermanes.¹¹ For this process, only the effective rate constant k/ϵ was determined (Table 15). Insofar as the changes in the absorbances at 450 (germylene) and 370 nm (digermene) were comparable,¹¹ the extinction coefficients of these species are close to one another and apparently equal to $\sim 10^3 \text{ litre mol}^{-1} \text{ cm}^{-1}$. Then, the rate constant for digermene dimerisation is approximately $k \sim 3.9 \times 10^6 \text{ s}^{-1} \sim 4 \times 10^9 \text{ litre mol}^{-1} \text{ cm}^{-1}$, i.e., fairly close to the diffusion limit. A constant that was found³⁷ for the $\text{Me}_2\text{Ge}=\text{GeMe}_2$ dimerisation in cyclohexane with compound **4a** used as the precursor turned out to be nearly six times smaller. Lower recombination rate constants were also found for digermenes containing more bulky substituents (Et and Ph groups) (see Table 15). Note that a digermene with mesityl groups¹³ disappeared with quasi-first-order kinetics ($\tau \sim 300 \mu\text{s}$) by a yet unclear mechanism.

Thus, the performed analysis shows that the dimerisation of, first, germylenes and, then, digermenes may lead to the formation of cyclic germanes. On steady-state photolysis of germanium organic derivatives, the formed germylenes and digermanes may react with cyclic products as the latter are accumulated, which ultimately leads to the appearance of germanium-containing polymers in solutions.

Table 13. Spectroscopic characteristics of digermenes in solutions ($T = 293 \text{ K}$) and low-temperature 3-MP matrices ($T = 77 \text{ K}$).

Digermene	Precursor	Solvent	$\lambda_{\text{max}}/\text{nm}$	Ref.
Solutions				
$\text{Me}_2\text{Ge}=\text{GeMe}_2$	8	cyclohexane	370	11
	4a	"	380	37
$\text{Et}_2\text{Ge}=\text{GeEt}_2$	4b	"	380	37
$\text{Pr}_2^i\text{Ge}=\text{GePr}_2^i$	cyclo- Ge_4Pr_8^i	"	390	15
$\text{Ph}_2\text{Ge}=\text{GePh}_2$	$\text{Ph}_2\text{Ge}(\text{SiMe}_3)_2$	"	320	41
	10c	hexane	440	43
$\text{Mes}_2\text{Ge}=\text{GeMes}_2$	cyclo- Ge_3Mes_6	"	405	13
	$\text{Mes}_2\text{Ge}(\text{SiMe}_3)_2$	"	405	13
$(2,6\text{-Me}_2\text{C}_6\text{H}_3)_2\text{Ge}=\text{Ge}(\text{C}_6\text{H}_3\text{Me}_2\text{-}2,6)_2$	cyclo- $\text{Ge}_3(\text{C}_6\text{H}_3\text{Me}_2\text{-}2,6)_6$	cyclohexane ^a	~ 410	16
Matrices				
$\text{Me}_2\text{Ge}=\text{GeMe}_2$	4a	—	370	37
$\text{Et}_2\text{Ge}=\text{GeEt}_2$	4b	—	380	37
$\text{Pr}_2^i\text{Ge}=\text{GePr}_2^i$	cyclo- Ge_4Pr_8^i	—	390	15
$\text{MesBu}^t\text{Ge}=\text{GeMesBu}^t$	$\text{MesBu}^t\text{Ge}(\text{SiMe}_3)_2$	—	378	25
$(2,6\text{-Me}_2\text{C}_6\text{H}_3)_2\text{Ge}=\text{Ge}(\text{C}_6\text{H}_3\text{Me}_2\text{-}2,6)_2$	$(2,6\text{-Me}_2\text{C}_6\text{H}_3)_2\text{Ge}(\text{SiMe}_3)_2$	—	406	25
$(2,6\text{-Et}_2\text{C}_6\text{H}_3)_2\text{Ge}=\text{Ge}(\text{C}_6\text{H}_3\text{Et}_2\text{-}2,6)_2$	$(2,6\text{-Et}_2\text{C}_6\text{H}_3)_2\text{Ge}(\text{SiMe}_3)_2$	—	400	25
$\text{Mes}_2\text{Ge}=\text{GeMes}_2$	$\text{Mes}_2\text{Ge}(\text{SiMe}_3)_2$	—	406	25
$\text{Mes}_2\text{Ge}=\text{GeMes}_2$	15	—	406	38
$(2,4,6\text{-Pr}^i\text{C}_6\text{H}_2)_2\text{Ge}=\text{Ge}(\text{C}_6\text{H}_2\text{Pr}^i\text{-}2,4,6)_2$	$(2,4,6\text{-Pr}^i\text{C}_6\text{H}_2)_2\text{Ge}(\text{SiMe}_3)_2$	—	416	25

^a Deuterated cyclohexane was used.

Table 15. Effective rate constants for second-order reactions (k/ϵ) of digermene loss ($T = 293$ K).

Digermene	Precursor	$\lambda_{\text{max}}/\text{nm}$	Solvent	$k/\epsilon/\text{cm s}^{-1}$	Ref.
$\text{Me}_2\text{Ge}=\text{GeMe}_2$	8	370	cyclohexane	3.9×10^6	11
	9	370	"	4.8×10^6	19
	4a	380	"	6.5×10^5	37
$\text{Et}_2\text{Ge}=\text{GeEt}_2$	4b	380	"	4.2×10^5	37
$\text{Ph}_2\text{Ge}=\text{GePh}_2$	$\text{Ph}_2\text{Ge}(\text{SiMe}_3)_2$	320	"	$\sim 8.0 \times 10^4$	41
	10c	440	hexane	$\sim 2.5 \times 10^4$ (see ^a)	43
$\text{Mes}_2\text{Ge}=\text{GeMes}_2$	cyclo- Ge_3Mes_6	405	cyclohexane	3.4×10^3 (see ^b)	13

^a Reaction of the first and second orders, k_{eff} is shown in s^{-1} ; ^b first-order reaction, k is shown in s^{-1} .

In addition to their loss in polymerisation, digermenes may disappear in competitive reactions with other molecules. Table 16 shows the rate constants for some of these processes. As seen, oxygen molecules are efficient scavengers of digermenes. However, literature provides the rate constant values for this reaction that differ by three orders of magnitude (see Table 16). Note that germynes react with oxygen and carbon tetrachloride at the rates nearly one-order-of-magnitude higher than digermenes. The reaction of a digermene with 2,3-dimethylbuta-1,3-diene is two-orders-of-magnitude slower than a similar reaction involving a germylene (compare the data in Tables 12 and 16). The rate constant for a digermene reaction with triethylsilane is also substantially lower as compared with a germylene. At the same time, the reactions of methyl-substituted digermenes with alcohols feature the opposite trend. Whereas germynes do not virtually react with alcohols, the rate constants for digermenes approach $\sim 5 \times 10^7 \text{ mol litre}^{-1} \text{ s}^{-1}$. Nonetheless, it can be concluded that by and large, digermenes exhibit considerably lower reactivity as compared with germynes.

XI. Optical spectra of germyl radicals

In addition to the heterolytic cleavage of the Ge—C bond on the photolysis and thermolysis of germanium-containing compounds, the homolytic processes to form germyl radicals may also occur. It was shown²² that the photolysis of tetramethylphenyldigermene $\text{PhMe}_2\text{GeGeHMe}_2$ in a low-temperature 3-MP matrix leads to the appearance of an absorption band with the maximum at 320 nm, which was assigned to a digermyl radical. The band decayed with the matrix melting.

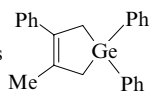
Laser flash photolysis of solutions of peraryltrigermenes $\text{R}_3^1\text{Ge}-\text{GeR}^2\text{R}^3-\text{GeR}_3^1$ ($\text{R}^1-\text{R}^3 = \text{Ar}$) also demonstrated^{22,23} absorption bands with maxima in the range of 320–330 nm, which were attributed to the formation of aryl-substituted digermyl radicals. Extinction coefficients of these bands were not determined. It was shown that the species responsible for this absorption did not react with 2,3-dimethylbuta-1,3-diene but reacted with carbon tetrachloride with high rate constants [$k = (1.3-7.2) \times 10^8 \text{ litre mol}^{-1} \text{ cm}^{-1}$].

Solutions of polygermanes (R_2Ge)_n in cyclohexane were subjected to laser flash photolysis.¹⁴ In addition to germylene absorption (430–460 nm), the spectrum showed bands in the

Table 16. Rate constants for digermene reactions ($T = 293$ K) in solutions.

Digermene	Precursor	Solvent	Reagent	$k/\text{litre mol}^{-1} \text{ s}^{-1}$	Ref.
$\text{Me}_2\text{Ge}=\text{GeMe}_2$	cyclo- Ge_4Me_8	cyclohexane	O_2	2.3×10^5	13
	8	"	O_2	2.8×10^8	11
	4a	"	O_2	4.0×10^8	37
	10e	hexane	O_2	5.0×10^7	40
	8	cyclohexane	CCl_4	$< 10^7$	11
	4a	"	CCl_4	1.2×10^7	37
	10c	hexane	CCl_4	2.3×10^7	40
	4a	cyclohexane	DMB	5.3×10^5	37
	4a	"	EtOH	4.9×10^7	37
	4a	"	EtOD	4.8×10^7	37
	4a	"	Pr^iOH	2.0×10^7	37
	4a	"	Bu^iOH	2.0×10^7	37
	10e	hexane	MeOH	2.7×10^6	71
	10e	cyclohexane	Bu^iOH	5.2×10^5	71
$\text{Et}_2\text{Ge}=\text{GeEt}_2$	4b	"	O_2	3.3×10^8	37
	4b	"	CCl_4	3.7×10^7	37
	4b	"	DMB	1.7×10^5	37
	4b	"	EtOH	9.4×10^7	37
$\text{Ph}_2\text{Ge}=\text{GePh}_2$	10c	hexane	O_2	4.8×10^6	40
	10c	"	CCl_4	2.0×10^6	40
	$\text{Ph}_2\text{Ge}(\text{SiMe}_3)_2$	cyclohexane	MeOH	7.1×10^3	41
	10c	hexane	MeOH	1.9×10^7	71
	10c	"	Bu^iOH	2.1×10^6	71
$\text{Mes}_2\text{Ge}=\text{GeMes}_2$	cyclo- Ge_3Mes_6	cyclohexane	O_2	2.3×10^5	13

^a Compound **10e** is



vicinity of 350–370 nm, which were assigned to polygermyl radicals $(R_2Ge)_m^\bullet$. The latter decayed as a result of recombination with effective rate constants in a range $k/\varepsilon = 2.3 \times 10^4$ – 5.1×10^5 litre mol⁻¹ cm⁻¹. It should be noted that the identification of bands assigned to germlyl radicals was complicated by the fact that digermenes exhibit absorption bands in the same spectral range (see Table 13) and disappear in a second-order reaction with very close k/ε parameters (see Table 15).

Laser flash photolysis of aryl-substituted digermenes $(Ph_nMe_{3-n}Ge)_2$ ($n = 1, 2$) led to the formation of germlylenes (absorption band maxima in the range of 440–470 nm) and germlyl radicals $Ph_nMe_{3-n}Ge^\bullet$ (315–330 nm).³⁰ The radicals disappeared through recombination with observed rate constants $k_{obs} = (1.9$ – $4.3) \times 10^5$ s⁻¹. The flash photolysis of a $PhMe_2GeGeMe_3$ solution made it possible to record³¹ the optical spectrum of a germlyl radical $PhMe_2Ge^\bullet$, which represented a band with the maximum at 320 nm. The radical dimerised with $k/\varepsilon = 7.0 \times 10^7$ cm s⁻¹.

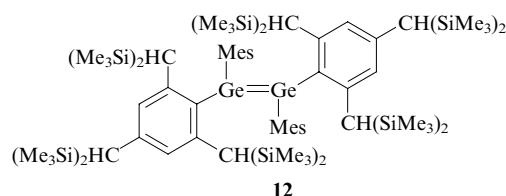
Thus, the available data on the laser flash photolysis of germanium-containing compounds show that germlyl and digermlyl radicals absorb in a range of 315–330 nm and disappear in recombination reactions with effective rate constants of the order of magnitude of 10^4 – 10^8 litre mol⁻¹ s⁻¹.

XII. Stable germlylenes

Diorganylgermylenes R_2Ge are usually short-lived reactive species; however, the introduction, into the precursor molecules, of bulky groups R (see Ref. 57) or ligands that are n or π donors able to transfer the electron density to the vacant orbital of the central germanium atom allows one to synthesise long-lived carbene analogues. At present, nearly 30 stable germlylenes are known.⁷² A comprehensive review⁷³ devoted to stable germanium analogues of carbenes, imines and thiones was published.

In certain cases, it is possible to isolate germlylenes in the crystalline form and study their structure. Crystals of stable germlylene $[(Me_3Si)_2CH]_2Ge$ were isolated and its solution in hexane was prepared.⁶¹ A spectrum of this solution demonstrated three light absorption bands with maxima at 414, 302 and 227 nm and extinction coefficients of 970, 1450 and 19 600 litre mol⁻¹ cm⁻¹, respectively. The position of the long-wavelength band (414 nm) well agrees with the absorption maxima of unstable germlylenes synthesised using laser flash photolysis (see Table 2). The extinction coefficient ($\varepsilon \sim 10^3$ litre mol⁻¹ cm⁻¹) assessed based on the recombination parameter for unstable germlylenes $2k_{rec}/\varepsilon$ was also close to the analogous characteristic of the long-wavelength band for $[(Me_3Si)_2CH]_2Ge$.

A sterically hindered stable digermene **12** was synthesised.^{74, 75}



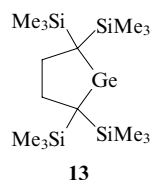
Repulsion of bulky groups led to a substantial increase in the Ge–Ge distance (2.416 Å) in this compound. In solution, as the temperature increased, digermene **12** reversibly dissociated to form two molecules of stable germlylene $\{2,4,6-[(Me_3Si)_2CH]_3C_6H_2\}MesGe$. Compound **12** exhibited

an absorption band with the maximum at 439 nm ($\varepsilon = 2 \times 10^4$ litre mol⁻¹ cm⁻¹), while germlylene $\{2,4,6-[(Me_3Si)_2CH]_3C_6H_2\}MesGe$ had a band at 575 nm ($\varepsilon = 1.6 \times 10^3$ litre mol⁻¹ cm⁻¹). Thermodynamic parameters of the reversible dissociation were $\Delta H = 61.5$ kJ mol⁻¹ and $\Delta S = 177.5$ J mol⁻¹ K⁻¹. The energy of the Ge–Ge bond (61.5 kJ mol⁻¹) was considerably lower[‡] due to the bond stretching as a result of repulsion of bulky substituents.

The extinction coefficient of the long-wavelength band of $MesBu^tGe$ germlylene was also consistent with the estimates for unstable germlylenes. The band itself was shifted to longer wavelengths similarly to the absorption bands of unstable germlylenes containing bulky substituents.

A stable germlylene $(2,4,6-Bu^t_3C_6H_2)_2Ge$ could be stored at -30 °C for several months.⁷⁷ At room temperature, it decomposed in several weeks to evolve 1,3,5-tri(*tert*-butyl)benzene. X-Ray diffraction analysis has shown that the spatial positions of two aryl groups were different and the Ge–C bond distance was 2.053 Å. The C–Ge–C angle was close to 108°, which substantially exceeded the estimates of 91–93° calculated for Me_2Ge (see Table 4). Despite its distorted geometry, germlylene $(2,4,6-Bu^t_3C_6H_2)_2Ge$ in solution exhibited an absorption band with the maximum at 430 nm, the position of which virtually coincided with that of the Me_2Ge band (see Tables 1, 2). A still wider C–Ge–C angle (111.3°) was observed for stable germlylene $(Me_3Si)_3CGeCH(SiMe_3)_2$ (Ref. 78) with Ge–C bond lengths equal to 2.012 and 2.067 Å. Unfortunately, the optical spectrum of this germlylene was not presented in the study.⁷⁸ Note that in germlylene $(2,6-Mes_2C_6H_3)_2Ge$ the C–Ge–C angle was equal to 114.4° and the Ge–C bond distance was 2.033 Å.⁷⁹

A stable cyclic dialkylgermylene, namely, 2,2,5,5-tetrakis(trimethylsilyl)-1-germacyclopentane-1,1-diyl (**13**), which is a monomer in the solid state with the averaged Ge–C bond length of 2.015 Å and the C–Ge–C angle of 91°, was described.⁸⁰



The absorption spectrum revealed a long-wavelength band of germlylene **13** at 450 nm with a small extinction coefficient. Its unstable analogue, 1-germacyclopent-3-ene-1,1-diyl in an argon matrix at 12 K demonstrated a broad absorption band with the maximum in the range of 400–410 nm; the Ge–C bond length was 2.017 Å and the C–Ge–C angle was 88.1° (Ref. 81). Table 17 shows the optical spectral parameters for certain stable germlylenes. It is noteworthy that a stable germlylene $(Bu^t_2N)_2Ge$ exhibits a long-wavelength absorption band with the maximum at 445 nm, the Ge–N bond length of 1.88 Å and the N–Ge–N angle of 111.4° (Ref. 80).

In a recent study,⁴³ the extinction coefficients of long wavelength spectral bands of different short-lived germlylenes were determined (see Table 17). As seen, the coefficients $\varepsilon \sim 1000$ – 2000 litre mol⁻¹ cm⁻¹ fall in the same range as those of stable germlylenes.

[‡] According to quantum chemical calculations,⁷⁶ for an unsubstituted digermene $(H_2Ge=GeH_2)$ the Ge–Ge bond energy is substantially higher (125.6–188.4 kJ mol⁻¹).

Table 17. Positions of maxima and extinction coefficients of bands in germylene spectra ($T = 293$ K).

Germylene	Solvent	$\lambda_{\text{max}} / \text{nm}$	$\epsilon / \text{mol litre}^{-1} \text{cm}^{-1}$	Ref.
Stable germylenes				
[2,4,6-(CF ₃) ₃ C ₆ H ₂] ₂ Ge	hexane	374	1300	72
MesBu ^t Ge	"	575	1600	74, 75
[(Me ₃ Si) ₂ CH] ₂ Ge	"	414	970	61, 82
	"	312	1450	61, 82
	"	227	19600	61, 82
(2,4,6-Bu ^t ₃ C ₆ H ₂) ₂ Ge	hexane, THF	430	520	77
(2,6-Mes ₂ C ₆ H ₃) ₂ Ge	Et ₂ O	578		79
(2,4,6-Pr ⁱ ₃ C ₆ H ₂)Bu ^t Ge	hexane, THF	580		83
13	"	450	320	80
	"	280	1300	80
(Bu ₂ N) ₂ Ge	cyclo-hexane	445	420	84
	"	310	shoulder	84
	"	227	7000	84
Unstable germylenes				
Ph ₂ Ge	hexane	500	1650	43
Mes ₂ Ge	"	550	1440	43

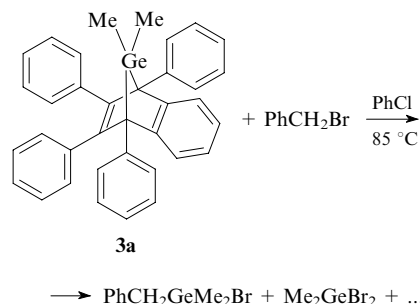
XIII. Comparison of the data obtained by chemically induced dynamic nuclear polarisation and laser flash photolysis methods

The analysis of chemically induced dynamic nuclear polarisation effects in thermal and photochemical reactions provides valuable information on the processes involving short-lived (with lifetimes varying from nano- to microsecond scales) radicals and biradicals. CIDNP measurements allow one to find the multiplicities of radical pairs, their precursors and also the reactive states of carbenes and their analogues, *viz.*, silylenes and germylenes.⁸⁵ Note that the nanosecond laser photolysis with the time resolution of an order of magnitude of 10 ns provides no way for the observation of intermediates with lifetimes of several nanoseconds.

Unfortunately, the literature contains no results of photochemical studies of germanium-containing compounds carried out in the pico- and nanosecond time resolution ranges. Apparently, this is associated with the low extinction coefficients of spectral bands of both the parent compounds and the transient species. Moreover, the studies on the photodissociation of germanium derivatives never used the time-resolved IR spectroscopy in the picosecond range. Hence, at present, CIDNP is the only method that allows one to acquire information on the processes involving species with lifetimes of nanoseconds. To date, the literature contains only one review⁸⁶ devoted to the application of spin chemistry methods to studies of short-lived intermediates of photochemical reactions of germanorbornadienes and digermabicyclooctadienes.

CIDNP effects were observed^{87,88} on the thermal decomposition of Me₂GeNB (**3a**). After heating (85 °C) of a chlorobenzene solution of this compound in the presence of benzyl bromide, two germanium-containing products were isolated.

It was assumed that the reaction produces a primary radical pair {PhCH₂· · · · · GeMe₂Br} the recombination of which affords a polarised molecule PhCH₂GeMe₂Br. Elimination of the bromine atom from PhCH₂GeMe₂Br by the radical ·GeMe₂Br results in the extrusion of a second germanium-containing product, Me₂GeBr₂, to the solution bulk. The analysis of CIDNP signs points to the singlet state of the radical pair and, hence, the



singlet ground state of the germylene, which is well consistent with quantum chemical calculations (see Table 4). Note that no CIDNP effects were observed for parent compound **3a** that could be associated with the synchronous cleavage of both Ge–C bonds during the thermal decomposition.

The NMR method was used^{89,90} to study the thermolysis of germanorbornadienes containing different substituents at the germanium atom and in the organic fragment. The authors of a study⁸⁹ assumed that the thermolysis includes two steps with the initial formation of a transient TPN' · · · · · GeR₂ biradical. Insofar as the authors^{89,90} did not study CIDNP effects, their conclusion on the involvement of a biradical in the reaction stemmed from enhanced thermal stability of germanorbornadienes with methyl substituents in the naphthalene fragment.

CIDNP effects were also observed⁹¹ in the photochemical decomposition of compound **3a**. The presence of CIDNP signals for methyl protons of the parent norbornadiene allowed the authors to assume the step-wise cleavage of Ge–C bonds to form a transient biradical. According to the proposed scheme, a singlet biradical produces the parent norbornadiene, whereas the triplet state serves as the source of the other products, namely, 1,2,3,4-tetraphenylnaphthalene (**6**) and dimethylgermylene. 3,3,6,6-Tetramethyl-1-thiacyclohept-4-yne (**11**) served as the dimethylgermylene scavenger. Based on the analysis of CIDNP signs for the dimethylgermylene adduct to the C≡C triple bond in compound **11**, it was concluded that germylene reacts in the triplet state. This was the first study that demonstrated the involvement of triplet dimethylgermylene in a chemical reaction.

Similar results were obtained with CCl₄ molecules used as the dimethylgermylene scavengers.⁸⁶ Photolysis of compound **3a** in a solution containing CCl₄ and C₆D₆ (in a ratio of 1 : 1 or 1 : 3) generated signals from polarised Me₂GeCl₂ and Me₂Cl-GeCCl₃ molecules that were formed from the primary radical pair ClMe₂Ge · · · · · CCl₃, as follows from NMR spectra recorded during the irradiation. The analysis of CIDNP signs showed that the radical pair was formed in the triplet dimethylgermylene reaction with carbon tetrachloride.

However, a later study³⁴ revealed no CIDNP effects for Me₂GNB (**3a**) and TPN (**6**), which allowed its authors to assume a single-step mechanism for the dimethylgermylene generation. In the latter study, an attempt was undertaken to detect transient species in the decomposition of compound **3a** in experiments with laser flash photolysis. It was shown that the excitation of a **3a** molecule leads to the formation of TPN (**6**) in the triplet excited state. Presumably, singlet germanorbornadiene **3a** undergoes one-step dissociation, which is accompanied by the cleavage of both Ge–C bonds over a picosecond time interval. A single TPN (**6**) molecule is formed and quickly converted into the triplet state (S₁ → T₁). Unfortunately, in the latter study,³⁴ no attempt was undertaken to measure the extinction coefficient for triplet–triplet transition band; hence, the relative yield of triplet TPN (**6**) was not determined. Therefore, there is a probability that the formation of TPN in the S₁ state followed by its transition into the

triplet state is not the main channel in the dissociation of Me_2GNB (**3a**).

A thorough analysis of the kinetics of transient absorption changes on the laser flash photolysis of compound **3a** in hexane was accomplished.⁹² A laser flash generated two transient species, which disappeared with substantially different rates. An absorption band in the range of 400–550 nm ($\lambda_{\text{max}} = 480$ nm), which decayed over 300 ns, was assigned to germylene Me_2Ge . Another wide band, which decayed much more slowly (over several microseconds), was assigned to the triplet–triplet absorption of TPN (**6**). This conclusion was substantiated by the measurements of the T–T absorption at the laser flash photolysis of a TPN solution in hexane.

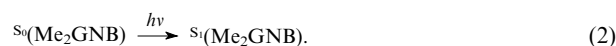
Photodecomposition of germanorbornadiene **3a** may produce TPN (**6**) molecules in the ground (S_0), and excited triplet (T_1) and singlet (S_1) states. The determination of relative yields (γ) of these states requires the knowledge of the extinction coefficient for T–T absorption and the quantum yield of intersystem crossing (ϕ_T for the $S_1 \rightarrow T_1$ process). To determine the extinction coefficient, the T–T energy transfer from a tetraphenylanthracene molecule to anthracene was considered and $\epsilon_{\text{TPN}}^{421} = 12\,700 \text{ litre mol}^{-1} \text{ cm}^{-1}$ was obtained.⁹² Measurements of the laser flash intensity on the photolysis of TPN solutions (excitation to the S_1 state) and the found ϵ_{TPN} value made it possible to determine the quantum yield of intersystem crossing $\phi_T = 0.13$. Note that the $S_1 \rightarrow S_0$ fluorescence quantum yield (ϕ_F) for TPN was found to be 0.09.³⁴ The use of these parameters and the kinetic curves measured on the flash photolysis of compound **3a** allowed the following yields of S_0 and T_1 states of TPN to be estimated: $\gamma_{S_0} = 0.66$ and $\gamma_{T_1} = 0.34$.⁹²

The value $\gamma_{S_0} = 0.66$ can be governed by both the TPN formation immediately in the ground state and the relaxation of the excited S_1 state ($S_1 \rightarrow S_0$). A parameter $\gamma_{T_1} = 0.34$ may also be due to both the direct formation of the triplet state and the intersystem crossing ($S_1 \rightarrow T_1$). According to the analysis, the direct triplet TNP yield on the photodissociation of compound **3a** falls in the range of 0.24–0.34. Thus, the formation of solely S_1 state as was proposed in Ref. 34 cannot provide the appearance of a considerable amount of triplet TNP molecules due to the low quantum yield of the intersystem crossing. A triplet TPN molecule cannot be formed in the photodissociation of a triplet molecule Me_2GNB (**3a**). It was shown³⁴ that the latter mechanism is unlikely because the sensitised photolysis (benzophenone and 9H-xanthen-2-one as triplet sensitizers) generated no transient absorption attributable to the triplet state of germanorbornadiene **3a**.

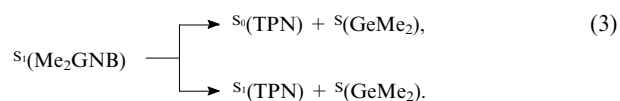
In the photodissociation of compound **3a** from the S_1 state, the appearance of a triplet TPN molecule can only be explained by the formation of a $^3(\text{TPN} \cdots \text{GeMe}_2)$ biradical with one Ge–C bond cleaved, which can transform from the initial singlet state to the triplet state $^3(\text{TPN} \cdots \text{GeMe}_2)$. In this case, upon the biradical decomposition (the cleavage of the second Ge–C bond), one of components (Me_2Ge or TPN) may find itself in the triplet state. The formation of triplet germylene was confirmed by the analysis of signs of ^1H CIDNP effects on the photolysis of compound **3a** in the presence of electron acceptors.^{90, 91, 93} Unfortunately, the CIDNP method gives no way for making quantitative estimates; hence, the relative yield of $^3(\text{Me}_2\text{Ge})$ species remains uncertain, although it is known to vary from 0% to 66%. The lower limit (0%) is reached in the dissociation of the triplet state $^3(\text{TPN} \cdots \text{GeMe}_2)$ to form the triplet state for only TPN. This is much unlikely because CIDNP confirms the existence of dimethylgermylene in the triplet state.^{86, 91, 93} The upper limit of the triplet Me_2Ge yield is restricted by $\gamma_{\text{Me}_2\text{Ge}} = 1 - \gamma_{T_1} = 0.66$.

Thus, in aggregate, the results of laser flash photolysis and CIDNP studies show that the photodissociation of dimethyl-

germanorborbadiene **3a** and the formation of dimethylgermylene may involve several competitive reactions. The primary process is the excitation of the molecule Me_2GNB (**3a**) into the first singlet excited state.

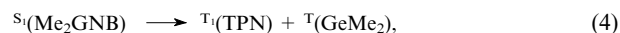


Insofar as the quantum yield of the photodissociation of compound **3a** is substantially lower than unity ($\phi \sim 0.4$ ³⁴) and fluorescence is virtually absent, the non-radiative relaxation into the ground state plays a considerable role for this molecule. From the excited state, $S_1(\text{Me}_2\text{GNB})$ can dissociate with the cleavage of two Ge–C bonds to form TPN and dimethylgermylene. In turn, TPN can be in either ground or excited singlet states.



The long-wavelength absorption band of compound **3a** lies in the vicinity of ~ 275 nm, which corresponds to the absorbed quantum energy of ~ 4.5 eV. The efficient thermal decomposition of Me_2GNB at approximately 100 °C showed^{87, 88} that the energy of the first Ge–C bond cleavage is 1.0–1.2 eV⁹⁴ (after this process, the break of the second bond consumes far less energy). Hence, the balance energy of ~ 3.3 –3.5 eV is indeed insufficient for the formation of an excited $S_1(\text{TPN})$ molecule, because the maximum of the long-wavelength absorption band of TPN is located at 300 nm [therefore, the energy of $S_1(\text{TPN}) \geq 4.1$ eV].

In the singlet-state dissociation, the appearance of one component (TPN or Me_2Ge) in the triplet state is forbidden in accordance with the total spin conservation law. Though this law does not forbid the simultaneous formation of two species in the triplet state

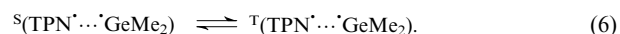


the probability of such a process is far lower (1 : 9) as compared with the appearance of singlet species. Moreover, in the former case, a problem of energy deficiency also exists, because the stored energy of 3.2–3.5 eV is obviously insufficient for the appearance of $T_1(\text{TPN})$ (with the energy of 2.8–3.0 eV) and $T_1(\text{GeMe}_2)$ (1.2 eV^{45, 53}).

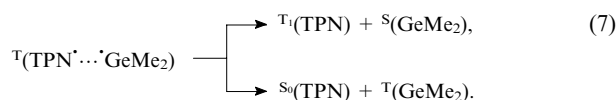
Above, we considered processes in which the photodissociation of Me_2GNB (**3a**) occurred in a single elementary event that included the cleavage of both Ge–C bonds. A reaction with products in singlet states would be more probable. The assumption on the elementary event means that the time lag between the cleavages of the first and second Ge–C bond is much shorter than the time resolution of the experimental method so that the short lifetime of the biradical (the cleavage of the first bond)



does not induce any substantial changes in the yields and electronic states of final products. However, measurements of CIDNP effects^{86, 91, 93} suggest that the biradical lifetime is sufficient for the transition into the triplet state



From this state, the biradical can dissociate to produce one component in the triplet state.



The S–T transition time of a biradical is determined by the intensity of hyperfine interaction (HFI) in radical centres, the difference of *g*-factors and the magnetic field intensity. For parameters characteristic of many radical pairs, the time of transition into the triplet state usually lies in a range of 1–10 ns. The nanosecond laser flash photolysis has the resolution time of 5–10 ns; hence, the optical spectrum of a biradical in both triplet and singlet states is yet unavailable.

The final product, TPN (6) in different electronic states, can appear in at least five of reactions shown above [see reactions (3), (4) and (7)]. The relative share of each channel remains unknown and only the value $\gamma_{\text{T}_1} = 0.34$ shows that the triplet biradical dissociation can contribute about 1/3 of the overall photoreaction yield. The use of the CIDNP method for the detection of reactions (4) and (7) provided evidence for the presence of $\text{T}(\text{GeMe}_2)$ species; however, the individual contribution of each product can be determined only after the determination of its relative yield. Disagreement on the photodissociation mechanism of Me_2GNB that exists in the literature^{34,91,93} can be due to the fact that each channel makes a substantial contribution into the overall yield of photoreaction products. The absence of quantitative measurements of yields led to different conclusions on the mechanism of phototransformations of dimethylgermanorbornadiene **3a**. The comprehensive quantitative characterisation of all processes will be possible only after the determination of the relative yield of dimethylgermylene in the triplet state.

Similar problems arise in the studies on the photochemistry of 7,7,8,8-tetramethyl-1,4-diphenyl-1,3-benzo-7,8-digermabicyclo[2.2.2]octa-1,5-diene (**4a**). This compound was studied by laser flash photolysis³⁷ and CIDNP³⁶ methods. After a laser pulse (in 300 ns), two absorption bands with maxima at 380 and 430 nm were observed in spectra of a cyclohexane solution of compound **4a**. The band at 430 nm, which decayed over 3 μs , was assigned³⁷ to the T–T absorption of diphenylnaphthalene [$\text{T}(\text{DPN})$, $\epsilon^{430} = 3.2 \times 10^4 \text{ litre mol}^{-1} \text{ cm}^{-1}$ (Ref. 95)]. The band at 380 nm, which was assigned to a digermene $\text{Me}_2\text{Ge}=\text{GeMe}_2$ (see Table 13), decayed with second-order kinetics ($k/\epsilon = 6.5 \times 10^5 \text{ cm s}^{-1}$).

Studying the CIDNP effects for methyl-group protons of the parent molecule **4a** and protons of the final product (DPN) made it possible to assume³⁶ that the cleavage of one Ge–C bond to form a singlet biradical $\text{DPN}-\text{Me}_2\text{Ge}^{\bullet}\cdots^{\bullet}\text{GeMe}_2$ is the primary process. The biradical reversible transition into the triplet state and the recovery of the broken bond led to the appearance of CIDNP for protons in parent compound **4a**. Two possible channels were discussed³⁶ for the triplet radical transformation. The first channel was the dissociation of the remaining Ge–C bond to form a digermene and a triplet DPN molecule. The second channel was the dissociation of the Ge–Ge bond to form dimethylgermylene and a triplet biradical ($\text{DPN}^{\bullet}\cdots^{\bullet}\text{GeMe}_2$). The latter could either pass into the singlet state and form a Ge–C bond with the remaining germanium atom (to afford germanorbornadiene) or dissociate to yield the triplet DPN and the second dimethylgermylene species. The analysis of CIDNP effects and the kinetic behaviour of the transient absorption gave no way for making the ultimate choice between these two mechanisms of the triplet 1,6-biradical transformation; however, its involvement in the formation of CIDNP signals is beyond any doubt.

Thus, to be completed, the description of photodissociation of compound **4a**^{36,37} requires the quantitative analysis of the relative yield of diphenylnaphthalene in the triplet and singlet states to be carried out. This information would be helpful in the determination of contributions of different

photodissociation channels for molecule **4a** (biradical dissociation from singlet and triplet states, dissociation without transient biradical formation with simultaneous cleavage of both Ge–C bonds to form a digermene). Insofar as the laser radiation used in Refs 36 and 37 was of different wavelengths (266 and 308 nm, respectively), it cannot be ruled out that the photolysis mechanisms were different. For example, on the excitation of compound **4a** with light with a wavelength of 266 nm, a single photoreaction channel was realised (the digermene $\text{Me}_2\text{Ge}=\text{GeMe}_2$ formation that involved no biradical),³⁷ whereas on the photolysis at longer wavelengths, only one Ge–C bond was cleaved to generate a biradical.³⁶

XIV. Conclusion

The analysis of literature data shows that the light absorption spectrum of dimethylgermylene has a band in the range of 420–490 nm. For this species in the gas phase, the band maximum lied at 480 nm. Apparently, the absorption observed at shorter wavelengths (405–420 nm) belongs to the donor–acceptor germylene complexes. Bands in the range of 370–380 nm are caused by the fast formation of digermenes due to the germylene dimerisation. The absorption of germylenes containing bulky substituents or groups with π -systems is shifted to longer wavelengths (450–550 nm), which is most probably due to widening of the C–Ge–C angle. The shift of germylene absorption bands in the spectra of low-temperature matrices as compared with the solution spectra can be explained by the effects of temperature, the solvent nature and the germylene geometry.

Germylenes usually disappear in dimerisation reactions to form digermenes. Determination of the recombination rate constants requires the knowledge of extinction coefficients of bands in spectra of unstable germylenes. To date, these parameters were measured only for two germylenes, namely, Ph_2Ge and Me_2Ge . The determination of the mentioned values for other germylenes is the burning problem of photochemistry of germanium-containing compounds. Digermenes also disappear in second-order reactions to form cyclic and eventually polymeric structures. Absorption bands of digermenes are shifted to shorter wavelengths by 40–50 nm as compared with germylene bands. For digermenes, the data on the extinction coefficients of bands are also absent. The wide scatter (sometimes up to 2–3 orders of magnitude) of literature data on the reaction rate constants for germylenes synthesised from different precursors presents an important problem. Most probably, the scatter is due to the incorrect assignment of transient absorption bands. Thus the bands earlier assigned to germylenes actually belong to digermenes or germanium-containing radicals. Moreover, this might also be due to the formation of germylene transition complexes with the decomposition products of germanium-containing compounds that appear simultaneously with germylenes.

The majority of studies on the photochemistry of germanium organic derivatives assumed that in the excited states of these molecules, the heterolytic break of Ge–C bonds occurs to form germylenes. However, presumably, in some cases, the competitive homolytic cleavage of a Ge–Ge bond takes place to form germyl radicals. The relative probability of these channels in photoreactions of germanium-containing compounds remains unknown, because for radicals with absorption bands located at still shorter wavelengths, the extinction coefficients are also unknown. The quantum yields of different transient species cannot be determined for the same reason.

The use of the CIDNP method that provides information on the short-lived species unobservable by even the laser flash photolysis method with the nanosecond time resolution is a very interesting trend in photochemistry. A more detailed photolysis mechanism with the formation of transient birad-

icals was first proposed in CIDNP studies of germanium-containing compounds. However, no studies were published to date that contain information on the quantitative relationship between the CIDNP data and the results of laser flash photolysis of germanium derivatives. For this purpose, the resolution time of the laser flash photolysis must be shifted in the pico- and femtosecond ranges. To detect short-lived transient biradicals, it seems promising to use nanosecond photolysis of cooled solutions and low-temperature matrices.

The publication was supported by the Russian Foundation for Basic Research (Project Nos 05-03-32474, 06-03-32110, 05-03-39007-GFEN, 06-03-90890-Mol, 07-02-91016-AF) and also by the Interdisciplinary and International Integration Grants of the Siberian Branch of the Russian Academy of Sciences (Project Nos 77 and 4.16).

References

- O M Nefedov, A I Ioffe, L G Menchikov *Khimiya Karbenov* (The Chemistry of Carbenes) (Moscow: Khimiya, 1990)
- J Barrau, J Escudie, J Satge *Chem. Rev.* **90** 283 (1990)
- W P Neumann *Chem. Rev.* **91** 311 (1991)
- M P Egorov, O M Nefedov *Metalloorg. Khim.* **5** 106 (1992)^a
- M B Taraban, O S Volkova, A I Kruppa, T V Leshina *The Chemistry of Organic Germanium, Tin and Lead Compounds* Vol. 2 (Ed. Z Rappoport) (New York: Wiley, 2002) p. 579
- A Sekiguchi, V Y Lee *Chem. Rev.* **103** 1429 (2003)
- M Driess, H Grützmacher *Angew. Chem., Int. Ed. Engl.* **35** 828 (1996)
- M Khargittai, T Shul'ts, I Khargittai *Izv. Akad. Nauk, Ser. Khim.* 1817 (2001)^b
- S E Boganov, M P Egorov, V I Faustov, O M Nefedov *The Chemistry of Organic Germanium, Tin and Lead Compounds* Vol. 2 (Ed. Z Rappoport) (New York: Wiley, 2002) p. 749
- C Long, M T Pryce *The Chemistry of Organic Germanium, Tin and Lead Compounds* Vol. 2 (Ed. Z Rappoport) (New York: Wiley, 2002) p. 1521
- K Mochida, N Kanno, R Kato, M Kotani, S Yamauchi, M Wakasa, H Hayashi *J. Organomet. Chem.* **415** 191 (1991)
- K Mochida, S Tokura, S Murata *J. Chem. Soc., Chem. Commun.* 250 (1992)
- N P Tötl, W J Leigh, G M Kollegger, W G Stibbs, K M Baines *Organometallics* **15** 3732 (1996)
- K Mochida, K Kimijima, H Chiba, M Wakasa, H Hayashi *Organometallics* **13** 404 (1994)
- K Mochida, S Tokura *Organometallics* **11** 2752 (1992)
- S Masamune, Y Hanzawa, D J Williams *J. Am. Chem. Soc.* **104** 6136 (1982)
- S Collins, S Murakami, J T Snow, S Masamune *Tetrahedron Lett.* **26** 1281 (1985)
- K M Baines, J A Cooke *Organometallics* **11** 3487 (1992)
- K Mochida, S Tokura *Bull. Chem. Soc. Jpn.* **65** 1642 (1992)
- T Tsumuraya, S A Batcheller, S Masamune *Angew. Chem., Int. Ed. Engl.* **30** 902 (1991)
- H Sakurai, K Sakamoto, M Kira *Chem. Lett.* **13** 1379 (1984)
- K Mochida, I Yoneda, M Wakasa *J. Organomet. Chem.* **399** 53 (1990)
- M Wakasa, I Yoneda, K Mochida *J. Organomet. Chem.* **366** C1 (1989)
- W Ando, T Tsumuraya, A Sekiguchi *Chem. Lett.* **16** 317 (1987)
- W Ando, H Itoh, T Tsumuraya *Organometallics* **8** 2759 (1989)
- W Ando, H Itoh, T Tsumuraya, H Yoshida *Organometallics* **7** 1880 (1988)
- S Tomoda, M Shimoda, Y Takeuchi, Y Kajii, K Obi, L Tanaka, K Honda *J. Chem. Soc., Chem. Commun.* 910 (1988)
- J Barrau, D L Bean, K M Welsh, R West, J Michl *Organometallics* **8** 2606 (1989)
- K L Bobbitt, V M Maloney, P P Gaspar *Organometallics* **10** 2772 (1991)
- K Mochida, M Wakasa, Y Nakadaira, Y Sakaguchi, H Hayashi *Organometallics* **7** 1869 (1988)
- K Mochida, H Kikkawa, Y Nakadaira *J. Organomet. Chem.* **412** 9 (1991)
- K Mochida, M Wakasa, Y Sakaguchi, H Hayashi *Bull. Chem. Soc. Jpn.* **64** 1889 (1991)
- K Mochida, H Ginyama, M Takahashi, M Kira *J. Organomet. Chem.* **553** 163 (1998)
- H Görner, M Lehnig, M Weisbeck *J. Photochem. Photobiol., A: Chem.* **94** 157 (1996)
- H Sakurai, Y Nakadaira, H Tobita *Chem. Lett.* **11** 1855 (1982)
- M B Taraban, O S Volkova, V F Plyusnin, Y V Ivanov, T V Leshina, M P Egorov, O M Nefedov, T Kayamori, K Mochida *J. Organomet. Chem.* **601** 324 (2000)
- K Mochida, T Kayamori, M Wakasa, H Hayashi, M P Egorov *Organometallics* **19** 3379 (2000)
- T Tsumuraya, S Sato, W Ando *Organometallics* **8** 161 (1989)
- S P Kolesnikov, M P Egorov, A S Dvornikov, V A Kuz'min, O M Nefedov *Metalloorg. Khim.* **2** 799 (1989)^a
- W J Leigh, F Lollmahomed, C R Harrington *Organometallics* **25** 2055 (2006)
- S Konieczny, S J Jacobs, J K Braddock-Wilking, P P Gaspar *J. Organomet. Chem.* **341** S17 (1988)
- W J Leigh, H G Dumbrava, F Lollmahomed *Can. J. Chem.* **84** 934 (2006)
- W J Leigh, C R Harrington, I Vargas-Baca *J. Am. Chem. Soc.* **126** 16105 (2004)
- S E Boganov, M P Egorov, V I Faustov, I V Krylova, O M Nefedov, R Beserra, R Uolsh *Izv. Akad. Nauk, Ser. Khim.* 477 (2005)^a
- M-D Su, S-Y Chu *J. Phys. Chem. A* **103** 11011 (1999)
- Y Apeloig, R Pauncz, M Karni, R West, W Steiner, D Chapman *Organometallics* **22** 3250 (2003)
- J C Barthelat, B S Roch, G Trinquier, J Satge *J. Am. Chem. Soc.* **102** 4080 (1980)
- G Olbrich *Chem. Phys. Lett.* **73** 110 (1980)
- K G Dyall *J. Chem. Phys.* **96** 1210 (1992)
- P R Bunker, R A Phillips, R J Buenker *Chem. Phys. Lett.* **110** 351 (1984)
- L G M Petterson, P E M Siegbahn *Chem. Phys.* **105** 355 (1986)
- A Selman, D R Salahub *J. Chem. Phys.* **89** 1529 (1988)
- M-D Su, S-Y Chu *J. Am. Chem. Soc.* **121** 4229 (1999)
- K Balasubramanian *J. Chem. Phys.* **89** 5731 (1988)
- C J Cramer, F J Dulles, J W Storer, S E Worthington *Chem. Phys. Lett.* **218** 387 (1994)
- M-D Su, S-Y Chu *J. Am. Chem. Soc.* **121** 11478 (1999)
- G L Wegner, R J F Berger, A Schier, H Schmidbaur *Organometallics* **20** 418 (2001)
- R Withnall, L Andrews *J. Phys. Chem.* **94** 2351 (1990)
- M P Egorov, A S Dvornikov, M B Ezhova, V A Kuz'min, S P Kolesnikov, O M Nefedov *Metalloorg. Khim.* **4** 1178 (1991)^a
- G R Smith, W A Guillory *J. Chem. Phys.* **56** 1423 (1972)
- P J Davidson, D H Harris, M F Lappert *J. Chem. Soc., Dalton Trans.* 2268 (1976)
- R C Binning Jr, L A Curtiss *J. Chem. Phys.* **92** 1860 (1990)
- R A Phillips, R J Buenker, R Beardsworth, P R Bunker, P Jensen, W P Kraemer *Chem. Phys. Lett.* **118** 60 (1985)
- J Karolczak, W W Harper, R S Grev, D J Clouthier *J. Chem. Phys.* **103** 2839 (1995)
- T C Smith, D J Clouthier, W Sha, A G Adam *J. Chem. Phys.* **113** 9567 (2000)
- W J Leigh, C R Harrington *J. Am. Chem. Soc.* **127** 5084 (2005)
- M W Heaven, G F Metha, M A Buntine *Aust. J. Chem.* **54** 185 (2001)
- M W Heaven, G F Metha, M A Buntine *J. Phys. Chem. A* **105** 1185 (2001)
- M-D Su, S-Y Chu *J. Chin. Chem. Soc.* **47** 135 (2000)
- P Bleckmann, R Minkwitz, W P Neumann, M Schriewer, M Thibud, B Watta *Tetrahedron Lett.* **25** 2467 (1984)
- W J Leigh, F Lollmahomed, C R Harrington, J M McDonald *Organometallics* **25** 5424 (2006)
- J E Bender IV, M M Banaszak Holl, J W Kampf *Organometallics* **16** 2743 (1997)
- J Barrau, G Rima *Coord. Chem. Rev.* **178–180** 593 (1998)
- K Kishikawa, N Tokitoh, R Okazaki *Chem. Lett.* **27** 239 (1998)

75. N Tokitoh, K Kishikawa, R Okazaki, T Sasamori, N Nakata, N Takeda *Polyhedron* **21** 563 (2002)
76. G Trinquier, J P Malrieu, P Riviere *J. Am. Chem. Soc.* **104** 4529 (1982)
77. P Jutzi, H Schmidt, B Neumann, H-G Stammler *Organometallics* **15** 741 (1996)
78. P Jutzi, A Becker, H-G Stammler, B Neumann *Organometallics* **10** 1647 (1991)
79. R S Simons, L Pu, M M Olmstead, P P Power *Organometallics* **16** 1920 (1997)
80. M Kira, S Ishida, T Iwamoto, M Ichinohe, C Kabuto, L Ignatovich, H Sakurai *Chem. Lett.* **28** 263 (1999)
81. V N Khabashesku, S E Boganov, D Antic, O M Nefedov, J Michl *Organometallics* **15** 4714 (1996)
82. D H Harris, M F Lappert, J B Pedley, G J Sharp *J. Chem. Soc., Dalton Trans.* 945 (1976)
83. N Tokitoh, K Manmaru, R Okazaki *Organometallics* **13** 167 (1994)
84. M F Lappert, M J Slade, J L Atwood, M J Zaworotko *J. Chem. Soc., Chem Commun.* 621 (1980)
85. K M Salikhov, Y N Molin, R Z Sagdeev, A I Buchachenko *Spin Polarization and Magnetic Effects in Radical Reactions* (Budapest: Akademiai Kiado, 1984)
86. T V Leshina, O S Volkova, M B Taraban *Izv. Akad. Nauk, Ser. Khim.* 1830 (2001)^a
87. J Kocher, M Lehnig *Organometallics* **3** 937 (1984)
88. J Kocher, M Lehnig, W P Neumann *Organometallics* **7** 1201 (1988)
89. W P Neumann, M Schriewer *Tetrahedron Lett.* **21** 3273 (1980)
90. G Billeb, W P Neumann, G Steinhoff *Tetrahedron Lett.* **29** 5245 (1988)
91. M P Egorov, M B Ezhova, S P Kolesnikov, O M Nefedov, M B Taraban, A I Kruppa, T V Leshina *Mendeleev Commun.* 143 (1991)
92. M V Kaletina, V F Plyusnin, V P Grivin, V V Korolev, T V Leshina *J. Phys. Chem. A* **110** 13341 (2006)
93. S P Kolesnikov, M P Egorov, A M Galminas, M B Ezhova, O M Nefedov, T V Leshina, M B Taraban, A I Kruppa, V I Maryasova *J. Organomet. Chem.* **391** C1 (1990)
94. A J Shusterman, B E Landrum, R L Miller *Organometallics* **8** 1851 (1989)
95. I Carmichael, W P Helman, G L Hug *J. Phys. Chem. Ref. Data* **16** 239 (1987)

^a— *Russ. J. Organomet. Chem. (Engl. Transl.)*

^b— *Russ. Chem. Bull., Int. Ed. (Engl. Transl.)*

Chirospecific analysis of plant volatiles

A V Tkachev

Contents

I. Introduction	951
II. Chiral gas-liquid chromatography	952
III. Two-dimensional gas-liquid chromatography	956
IV. Preparative enantiomeric resolution	957
V. Identification of enantiomers	958

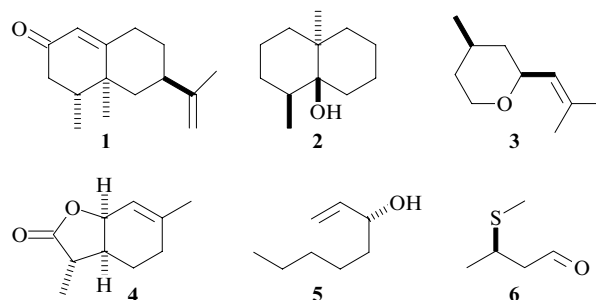
Abstract. Characteristic features of the analysis of plant volatiles by enantioselective gas (gas-liquid) chromatography and gas chromatography/mass spectrometry are discussed. The most recent advances in the design of enantioselective stationary phases are surveyed. Examples of the preparation of the most efficient phases based on modified cyclodextrins are given. Current knowledge on the successful analytical resolution of different types of plant volatiles (aliphatic and aromatic compounds and mono-, sesqui- and diterpene derivatives) into optical antipodes is systematically described. Chiral stationary phases used for these purposes, temperature conditions and enantiomer separation factors are summarised. Examples of the enantiomeric resolution of fragrance compounds and components of plant extracts, wines and essential oils are given. The bibliography includes 157 references.

I. Introduction

The enantiodifferentiation, *viz.*, the recognition of enantiomers (optical isomers), plays an important role in the functioning of living systems and the appearance of biological activity. Numerous examples concerning differences in biological activity of optical antipodes have been documented. An analysis of the optical purity is of great importance in chemistry of natural compounds, fine organic synthesis, pharmacognosy, drug technology, analytical chemistry and environmental analytical chemistry. Enantioselective gas (gas-liquid) chromatography and GLC-mass spectrometry are the main tools of investigation of enantiomeric composition of natural volatile compounds.

The differences in properties of optical isomers result in the difference in recognition at the molecular level. Many remarkable examples of the recognition of plant volatiles responsible for the characteristic aroma of plants and products of their processing can be given taking into account that the ability to perceive odours is also associated with the molecular recog-

nition of enantiomers as a result of their interaction with olfactory chemoreceptors. For example, the sesquiterpenoid (+)-nootkatone (**1**), which has the bitter taste of grapefruit, has the characteristic grapefruit flavour, which is 2200 times more intense than that of its (–) enantiomer.¹ (–)-Geosmin (**2**) isolated from grape wines has a much stronger flavour (at least ten times stronger) than (+)-geosmin. Grape wines produced from Cabernet Sauvignon grapes contain only (–)-geosmin.² Of four isomeric rose oxides, only (2*S*,4*R*)-rose oxide (**3**) has a pleasant strong rose aroma, whereas other stereoisomers have no flavour. Natural (3*S*,3*aS*,7*aR*)-lactone **4** has a sweat flavour with a coconut undertone, which is 25 million (!) times more intense than that of its (3*R*,3*aR*,7*aS*) isomer.^{3,4} Oct-1-en-3-ol is one of the major components responsible for the mushroom flavour, but only (*R*)-(–) enantiomer **5** has the intense mushroom aroma.⁵ (*R*)-3-Methylthiobutanol (**6**) has the characteristic aroma of potato products, whereas the (*S*) enantiomer has no flavour at all.⁶



The above-considered examples are not arbitrary because the development of methods of enantioselective analysis is to a large extent associated with investigations of fragrant substances; their enantiomeric composition often determines a particular characteristic flavour.

Different plants produce terpenes of different optical purity, whose enantiomeric composition depends on numerous factors. For example, studies on the essential oil of the dill herb *Anethum graveolens* L. showed that the enantiomeric ratio of the major components (dill ether,[†] limonene, α - and β -phellandrenes and carvone) changes with the age of plants and is

A V Tkachev N N Vorozhtsov Novosibirsk Institute of Organic Chemistry, Siberian Branch of the Russian Academy of Sciences, prosp. Akad. Lavrentieva 9, 630090 Novosibirsk, Russian Federation. Fax (7-383) 330 97 52, tel. (7-383) 330 88 52, (7-383) 330 98 55, e-mail: atkachev@nioch.nsc.ru

Received 16 May 2007

Uspekhi Khimii 76 (10) 1014–1033 (2007); translated by T N Safonova

[†] The systematic name is (3*S*,3*aS*,7*aS*)-3,6-dimethyl-2,3,3*a*,4,5,7*a*-hexahydrobenzo[*b*]furan.

different in different parts of the plants.⁷ The enantiomeric purity of camphor in essential oils from different plants of the Lamiaceae and Compositae families varies from 0% to 100%, with either the (+) or (−) enantiomer predominating in different plants.^{8,9} As was demonstrated with extracts from roots and seeds of angelica (*Angelica archangelica* L.), the enantiomeric excess of monoterpenes can vary depending on the place of vegetation.¹⁰ An analysis of the enantiomeric composition of the essential oil components allows the determination of the authenticity of essential oils available in the market, for example, of melissa (*Melissa officinalis* L.).^{11,12}

As a rule, sesquiterpene hydrocarbons are present in plant extracts in the optically active form, with a particular enantiomer predominating, whereas derivatives, which are artefacts and are produced in non-enzymatic secondary processes in the course of processing of plant materials, are detected in the optically inactive form (as racemates).¹³

The chirospecific analysis (analysis of the enantiomeric composition of the components) is of great importance in studies of foodstuff, as well as of flavour and fragrance compounds. For example, the quality of grape wines can be determined from the enantiomeric ratio of ethyl lactates.¹⁴ Only one of the enantiomers of octane-1,3-diol and some its derivatives were found in different varieties of apples.¹⁵ With a knowledge of the enantiomeric composition of the strawberry flavour components, it is possible to distinguish between products prepared from strawberry and those flavoured with synthetic strawberry flavourants.¹⁶ (*R*)-3-Mercapto-2-methylpropanol makes a major contribution to the flavour of red grape wines produced from Cabernet Sauvignon and Merlot grapes.¹⁷ Particular enantiomers of branched carboxylic acids are important contributors to the flavour of Parmesan cheese and the characteristic flavour of lamb meat.^{18,19}

Modern methods of chirospecific analysis allowed studies of racemic forms of compounds, which have long been used as fragrance compounds. For example, the characteristic lily flavour was demonstrated to be mainly due to the presence of the (*R*) isomer, which is hundred times more flavouring than the (*S*) isomer.²⁰ Numerous synthetic derivatives of campholenic and fencholenic aldehydes were investigated, which is associated with their unusual wood or sandal flavour.^{21,22} The enantioselective separation of enantiomers of α -ionone, which is an important fragrance compound, by gas chromatography was documented.²³

The analysis of the enantiomeric composition of plant metabolites has numerous applications. This method plays an important role in the determination of the origin of plant extracts and the authenticity of essential oils and flavour and taste components, as well as in the elucidation of the biosynthesis pathways of particular compounds.

Enantiomers of various chemical compounds can be separated by such methods as gas chromatography, high-performance liquid chromatography, capillary electrophoresis, supercritical fluid chromatography, capillary electrochromatography, thin-layer chromatography, *etc.*²⁴ Gas-liquid chromatography (GLC) is most often used for the analysis of the enantiomeric composition of plant volatiles and fragrance compounds.

Enantiomers can be resolved by GLC either directly or indirectly. The indirect approach is based on the preparation of derivatives of the analyte with an enantiomerically pure reagent^{25,26} to transform the enantiomeric pair into the diastereomeric pair and the subsequent separation of the diastereomers by GLC on a usual, *i.e.*, achiral, stationary phase. As an example, let us mention the enantiomeric resolution of (−)-menthol esters and hydroxy acids in the form of *O*-trifluoroacetyl derivatives.²⁷ As a rule, this method is used to analyse polar compounds (alcohols, amines, acids, amino

alcohols, *etc.*), because it is difficult, if at all possible, to study these compounds directly by gas chromatography.

The direct enantiomeric resolution on enantioselective stationary phase columns (chiral GLC) is a much more appealing method. In this case, there is no need to transform analytes into derivatives, and the separation is achieved due to the formation of diastereomeric associates between enantiomers of the analyte and a chiral selector[‡] of the stationary phase.

The history, advances and trends in the development of chiral GLC were covered in the reviews.^{28,29}

II. Chiral gas-liquid chromatography

1. Types of chiral stationary phases

In spite of a large variety of stationary phases used in gas chromatography, there are no universal phases for the separation of all types of compounds. The selectivity of each phase is limited to particular groups of compounds. However, though certain usual achiral stationary phases are suitable for the separation of several groups of organic compounds, no more or less universal chiral stationary phases are presently known.

Enantioselective stationary phases used in chiral GLC can be divided into three groups depending on the character of interactions between the analyte (selectand) and the chiral selector:

- derivatives of optically active amino acids (analytes form hydrogen bonds with the stationary phase);
- optically active metal complexes (analytes form coordination compounds with components of the stationary phase);
- natural and modified cyclodextrins, optically active crown ethers and calixarenes (analytes form inclusion compounds with components of the stationary phase³⁰).

The general methodology, the mechanism of separation, the scope and examples of the use of chiral GLC were considered in detail in the reviews.^{31–34} In the present review, only chiral selectors and stationary phases belonging to the third group, to be more precise, stationary phases based on modified cyclodextrins, will be considered. These stationary phases are most widely used in the analysis of natural volatile compounds, flavour and fragrance compounds, and they are employed in about 90% of examples of the successful enantiomeric resolution.³⁵ In particular, there are reviews on the use of such chiral stationary phases for the analysis of the enantiomeric composition of the components of essential oils and fragrance compounds,^{36–40} fragrant monocyclic monoterpenes⁴¹ and flavour components of cheeses.⁴²

Derivatives of natural amino acids suitable for the application in specific cases⁴³ and polysiloxane-based stationary phases containing optically active metal complexes[§] {for example, 3-(perfluoroacyl)camphorate complexes of metals [Ni(II), Co(II), Mn(II), Rh(I) and Eu(III)], which were used for the enantiomeric resolution of various compounds, including some terpenes³⁴} as chiral selectors are beyond the scope of the present review.

a. Cyclodextrins in enantioselective analysis

Cyclodextrins are cyclic oligomers consisting of α -D-glucopyranosyl residues, which are linked to each other by α -(1 \rightarrow 4) glycosidic bonds. Nowadays, α -, β - and γ -cyclodextrins containing 6, 7 and 8 α -D-glucopyranosyl residues, respectively,

‡ The chiral selector is an enantiomerically pure component of the stationary phase responsible for the recognition of optical isomers.

§ According to the data presented in the review,⁴³ phases containing chiral metal complexes are losing in popularity because of the universal use of cyclodextrin derivatives, as evidenced by a dramatic decrease (almost to zero in 2001–2004) in the number of publications on the use of phases based on chiral metal complexes.

are commercially available. Cyclodextrin molecules have a truncated cone shape. The outer surface of the molecules is hydrophilic, while the inner surface is hydrophobic. Due to this structural feature, cyclodextrins readily form inclusion complexes with organic molecules belonging to different classes of compounds.⁴⁴ It is the ability of cyclodextrins to form inclusion complexes that makes them attractive as agents in various applications[¶] associated with the molecular recognition.⁴⁶

The formation of host–guest complexes is believed to play a major role in the mechanism of recognition of enantiomeric molecules by cyclodextrins and their derivatives.⁴⁷ Complexes of hydrophobic molecules with cyclodextrins are formed through interactions between the substrate (selectand) and the hydrophobic cyclodextrin cavity; the complexation can lead to a change in the conformation of the guest molecule.⁴⁸ As a rule, less polar molecules form more stable complexes than higher-polarity molecules. Since the cavity volumes in α -, β - and γ -cyclodextrins are different, stability of complexes of hydrophobic molecules with a particular cyclodextrin depends on the matching of the size of the guest molecule to the cyclodextrin cavity size.⁴⁵ The formation of such complexes was detected by GLC analysis.⁴⁹

The mechanism of enantiomeric recognition with the use of cyclodextrin stationary phases remains unclear. An analysis of a wide range of model racemic mixtures revealed no relationship between the retention and the thermodynamic characteristics of interactions between selectands and chiral selectors.⁵⁰ However, in spite of the absence of detailed data on the recognition mechanism, cyclodextrin-based stationary phases are used with advantage for the enantiomeric resolution of various compounds. Enantioselective chromatography on cyclodextrin stationary phases plays an important role in the analysis of essential oils for the determination of their quality and authenticity,⁵¹ in the stereochemical analysis of terpenoids, in the determination of the absolute configurations and enantiomeric purity of components of complex natural mixtures,⁵² etc.

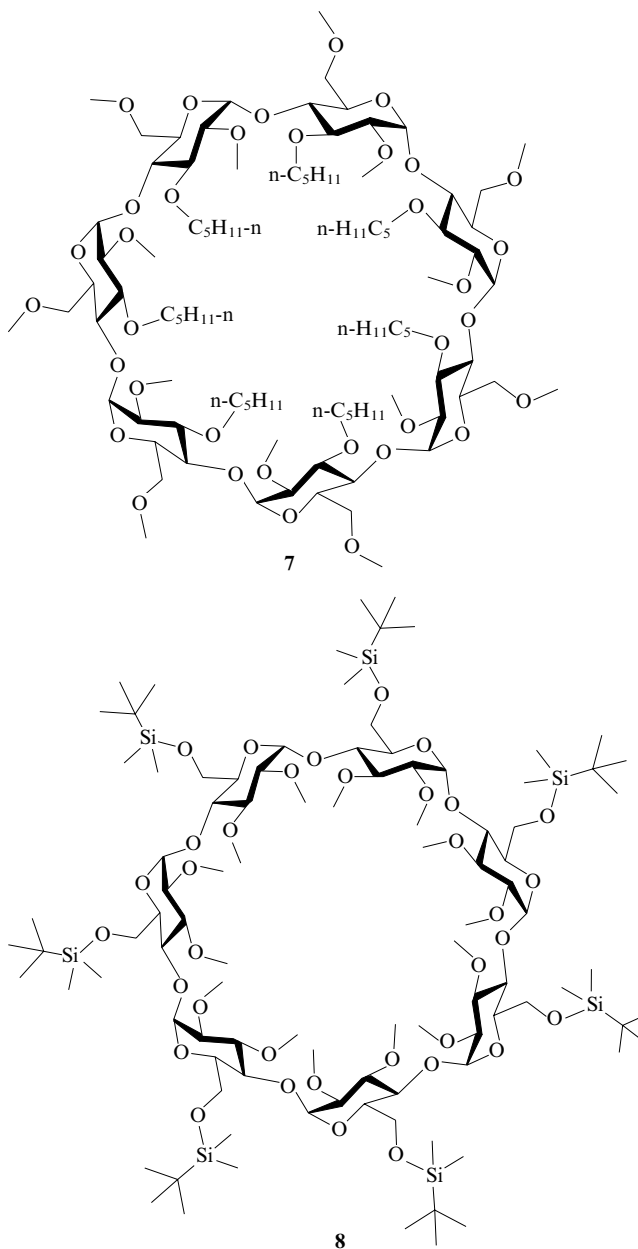
b. Chiral stationary phases based on modified cyclodextrins

Cyclodextrins and their simple derivatives have high melting points. Since cyclodextrins used as stationary phases in GLC should exist in the liquid (non-crystalline) state, the analysis should be performed at high temperatures. However, the enantioselectivity of chiral stationary phases, as a rule, sharply decreases with temperature. Hence, cyclodextrins and their simple derivatives are of little use in chiral capillary GLC because these compounds cannot serve as efficient chiral selectors at temperatures at which they are converted into the liquid state.

One way of solving this problem is to dilute high-melting-point cyclodextrin derivatives with polysiloxanes, with the result that the enantioselectivity of resolution is achieved at temperatures lower than the melting points of pure cyclodextrins,⁵³ the nature of polysiloxane having an effect on both the efficiency of the column and its enantioselectivity.^{54–56} However, the use of low-melting-point cyclodextrin derivatives is presently the approach of choice. This field of investigation

originated in 1988 in the research by König and co-workers,^{57–60} who synthesised liquid or wax-like (at room temperature) cyclodextrin derivatives, which had high thermal stability, were well soluble in low-polarity organic solvents and polysiloxanes and exhibited high enantioselectivity in the separation of a wide range of low-molecular-weight compounds. More recently, numerous such derivatives have been synthesised and many of these compounds proved to be very efficient in the enantioselective analysis of volatile plant substances.^{29, 61–66}

Of all available cyclodextrin derivatives, heptakis(2,6-di-*O*-methyl-3-*O*-*n*-pentyl)- (7) and heptakis(2,3-di-*O*-methyl-6-*O*-*tert*-butyl-dimethylsilyl)- β -cyclodextrins (8) are the most popular chiral selectors, which were employed in most of successful experiments on the separations of terpene compounds and essential oil components.



¶ Due to the ability of cyclodextrins to distinguish positional isomers, functional groups, homologues and enantiomers, these compounds are widely used for the separation of various compounds by different physicochemical methods. In particular, the review⁴⁵ presented data on new applications of cyclodextrins in gel electrophoresis, isotachopheresis, isoelectric focusing, preparative scale electrophoretic techniques, thin-layer chromatography, electrochemically modulated liquid chromatography, microdialysis, the separation on hollow fiber, liquid and composite membranes, foam floatation enrichment, solid- and liquid-phase extraction and counter-current chromatography.

Cyclodextrin derivatives containing the *tert*-butyldimethylsilyl group are of particular interest because these compounds are more easily mixed with various polysiloxanes (the latter are used as diluting agents and have gained wide acceptance in capillary gas chromatography), which facilitates the

preparation of chiral stationary phases. Although the polysiloxane component in these phases is called a diluting agent, it is not absolutely inert in chromatographic experiments. Thus, stationary phases prepared based on the same chiral selector but with the use of various polysiloxane diluting agents show somewhat different enantioselectivity (see, for example, the studies^{55, 56, 67–69}). The temperature of the analysis can be lowered and, as a consequence, the enantioselectivity of separation can be increased with the use of non-polar and low-polarity polysiloxanes as diluting agents for cyclodextrin derivatives.⁷⁰ The enantioselectivity of columns packed with chiral stationary phases depends also on the ratio of the cyclodextrin selector to the diluting agent. For example, for the phases containing 20%, 40% or 60% of octakis(2,6-di-*O*-*n*-pentyl-3-*O*-butanoyl)- γ -cyclodextrin, the maximum selectivity factor (R_s , α)[†] for different enantiomers is achieved with the use of mixtures containing either 60% or 40% of the selector.⁷¹

The enantioselectivity of cyclodextrin phases depends on both the cyclodextrin cavity size and the nature and number of substituents at positions 2, 3 and 6 of α -D-glucopyranosyl residues in the cyclodextrin molecule.^{31, 33} The elution order of enantiomers can change depending on the size of the cyclodextrin molecule.³⁸ For example, the relative retention times of oxygen-containing essential oil components on α -cyclodextrin-based phases are shorter than those on chiral stationary phases based on β -cyclodextrin derivatives.⁷² An investigation of 22 compounds showed that the retention times of analytes measured relative to *n*-undecane depend on their structures. This fact can be used in the preliminary analysis of unknown compounds to assign them to a particular structural group.

The type and position of substituents in cyclodextrin derivatives are apparently of equal importance.^{73, 74} Even small changes in the molecular structure of cyclodextrin derivatives can substantially influence the enantioselectivity of the phase. Consequently, all steps of the synthesis must be carefully controlled to obtain unambiguous results, because the substitution reactions, which are not brought to completion, often produce mixtures of cyclodextrin derivatives.⁷⁵ In addition, to achieve the reproducibility of the results of the subsequent enantioselective analysis, it is necessary to characterise the resulting products in detail.⁷⁶

In spite of the fact that capillary columns for chiral GLC are available in catalogues of many manufacturers and suppliers of gas-chromatographic systems, researchers prepare stationary phases and columns by themselves primarily with the aim of obtaining new, more selective and efficient, columns. Examples of the synthesis of cyclodextrin chiral selectors for chiral GLC are given below.

Mono-2-*O*-alkyl-substituted cyclodextrin derivatives can be synthesised by the treatment of cyclodextrins with dimethyl sulfate, diethyl sulfate or allyl bromide in a 0.37 M aqueous solution of sodium hydroxide.⁷⁷ The products are purified by fractional crystallisation from a water–toluene system followed by column chromatography. In the last step, the products are crystallised from water. 2-*O*-Propylcyclodextrins can be prepared by reduction of the corresponding allyl derivatives.⁷⁷ *O*-Pentyl derivatives of cyclodextrins have gained the widest acceptance.

It should be noted that the influence of the chain length of the alkyl substituent on the enantioselectivity of stationary phases is still debated. For example, the size of the alkyl substituent in 2,3-di-*O*-alkyl-6-*O*-*tert*-butyldimethylsilyl derivatives of cyclodextrins was found to have a substantial effect on the chromatographic characteristics of chiral phases. Accord-

ing to the data published in the study,⁷⁰ heptakis(2,3-di-*O*-ethyl-6-*O*-*tert*-butyldimethylsilyl)- β -cyclodextrin and octakis(2,3-di-*O*-ethyl-6-*O*-*tert*-butyldimethylsilyl)- γ -cyclodextrin are equally efficient in the separation of racemic mixtures of volatile compounds, whereas columns with the corresponding 2,3-di-*O*-methyl derivatives are less suitable for these purposes. The synthesis of cyclodextrin long-chain derivatives has been documented.⁷⁸

c. Optimisation of the selectivity of cyclodextrin chiral selectors

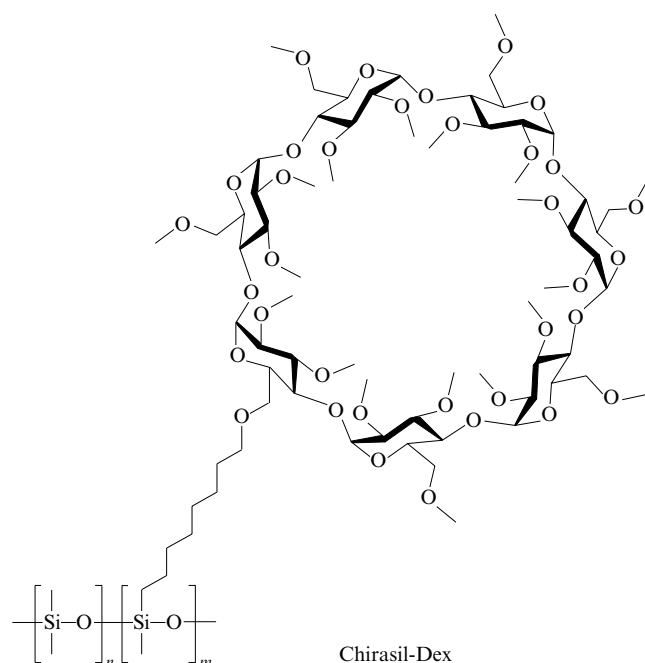
When analysing complex mixtures consisting of chiral compounds of different polarity with different functional groups, it is necessary to use simultaneously several chiral stationary phases with different enantioselectivity to separate all enantiomeric pairs. Several procedures for the preparation of mixed chiral stationary phases have been developed in recent years.^{73, 79–81} The simplest approach is based on the use of a mixture of cyclodextrin derivatives having mutually complementing enantioselectivities. This approach was used with advantage for the simultaneous (in one analysis) enantiomeric resolution of different classes of compounds (monoterpene hydrocarbons, alcohols, ketones and lactones).⁸⁰

Another procedure for optimisation of the properties of chiral cyclodextrin selectors is based on the selective replacement of some functional groups in D-glucopyranose rings. For example, the resolving properties of two cyclodextrins, *viz.*, compound **8** and its 2,3-di-*O*-acetyl analog, were combined in one compound by replacing the 3-*O*-methyl group with the acetyl group in one of the glucopyranosyl groups in compound **8**. The resulting β -cyclodextrin has the resolving properties of individual 2,3-di-*O*-methyl and 2,3-di-*O*-acetyl derivatives.⁷³ Analogously, the useful properties of octakis(2,3-di-*O*-methyl-6-*O*-*tert*-butyldimethylsilyl)- and octakis(2,3-di-*O*-acetyl-6-*O*-*tert*-butyldimethylsilyl)- γ -cyclodextrins were combined in octakis(3-*O*-acetyl-2-*O*-methyl-6-*O*-*tert*-butyldimethylsilyl)- and octakis(2-*O*-acetyl-3-*O*-methyl-6-*O*-*tert*-butyldimethylsilyl)- γ -cyclodextrins.⁷⁹

The enantioselectivity can be increased and more universal columns can be prepared also by mixing two chiral selectors of different nature. The addition of the chiral non-polymeric selector Lipodex E [octakis(3-*O*-butanoyl-2,6-di-*O*-*n*-pentyl)- γ -cyclodextrin] to an L-valine-based polymer was demonstrated⁸² to give a mixed stationary phase showing good enantioselectivity for a wider range of enantiomeric pairs compared to phases containing these individual chiral selectors, the selectivity factors for all the compounds under study in the enantiomeric resolution on the mixed phase having values averaged over these two phases. For examples, enantiomers of linalool cannot be resolved on a column with an L-valine-base stationary phase ($\alpha = 1.00$), but they can be resolved on a column with the Lipodex E phase ($\alpha = 1.05$). Enantiomers of linalool can also be resolved on the mixed stationary phase. In the latter case, the selectivity factor ($\alpha = 1.02$) is smaller than that on Lipodex E but is larger than that on the L-valine-based phase.

To improve cyclodextrin phases, they are chemically grafted to the polysiloxane backbone, which is, in turn, chemically attached to the inner surface of the column.⁸³ Due to strong retention of the chiral stationary phase, such columns are more durable and are characterised by high stability. In addition, these columns can easily be regenerated by washing with solvents.²⁹ The Chirasil-Dex phase consisting of a cyclodextrin-type selector based on mono-6-*O*-octamethylenepentyl- β -cyclodextrin, which is chemically grafted to polymethylpolysiloxane, is an example of such stationary phases.⁸⁴ This convenient and rather stable phase is widely used for the enantioselective analysis of various compounds.

[†] The selectivity factor is defined as the ratio of the retention times of enantiomers (as a rule, in isothermal conditions).



The Chirasil- γ -Dex phase is constructed analogously and consists of octakis(2,6-di-*O*-*n*-pentyl-3-*O*-butanoyl)- γ -cyclodextrin grafted to polymethylpolysiloxane through the octamethylene spacer.⁷¹

In recent years, efforts have been made to design universal phases for chiral GLC. In particular, combined (hybrid) phases (for example, the Chirasil-Calixval-Dex phase) belong to such phases. The Chirasil-Calixval-Dex phase consists of two chiral selectors, *viz.*, calixarene with pendant L-valine-based diamide groups and polymethylated β -cyclodextrin, chemically grafted to poly(hydromethyl)dimethylpolysiloxane. This combined phase retains the enantioselectivity of each chiral selector and combines their resolving properties. The selectand is bound to this phase both through hydrogen bonds with the calixarene fragments and due to the inclusion into the cyclodextrin cavity. These combined phases provide the separation of both non-polar compounds (hydrocarbons) and polar amino acid derivatives.⁸¹

2. Chromatography conditions

a. Temperature of the analysis

Modern commercially available capillary columns with chiral stationary phases based on substituted cyclodextrins allow operations in the temperature range from 10 to 250 °C, which is sufficient for the analysis of volatile aliphatic, alicyclic and aromatic compounds, mono- and sesquiterpenoids, diterpenes and some most volatile aldehydes, alcohols, ethers and esters of the diterpene series. Thermally labile compounds, for example, furan derivatives, can be separated on cyclodextrin phases by supercritical fluid chromatography at 45 °C and at a carbon dioxide pressure of 200 kg cm⁻².⁸⁵

As shown by numerous examples, the enantioselectivity of cyclodextrin selectors generally increases with decreasing temperature used for the gas chromatographic separation. Hence, to achieve better results, shorter chromatographic columns should be used. In this case, not only the temperature of the analysis can be lowered, thus improving the enantioselectivity of separation, but also the time of the analysis can be reduced.⁶⁸ Examples of the super-fast enantiomeric resolution were documented. For instance, less than 10 s were required to resolve enantiomers of bromochlorofluoromethane on a 50-cm column at ambient temperature (26 °C).⁸⁶

The enantiomeric resolution of the sesquiterpene erythrodiene can be offered as an example of the temperature depend-

ence of enantioselectivity. At 120 °C, the resolution was not achieved, whereas the α factor at 100 °C was 1.027.⁸⁷

b. Detection

Both conventional detection methods developed for achiral chromatography (for example, flame ionisation or chemiluminescence detectors for the determination of small amounts of sulfur-containing compounds⁸⁸) and specific methods based on special properties of optical isomers are used in the gas chromatographic resolution of enantiomeric mixtures. In spite of the fact that the measurement of the angle of rotation of the plane of polarised light is the simplest way of recognising enantiomers, polarimetric detectors have found no use in chiral gas chromatography. This is because the widely accepted separation on capillary columns requires high-sensitivity detectors, while polarimetric detectors are not sufficiently sensitive.

The olfactometric detection is used in studies of fragrance components. After the separation on a column with a chiral

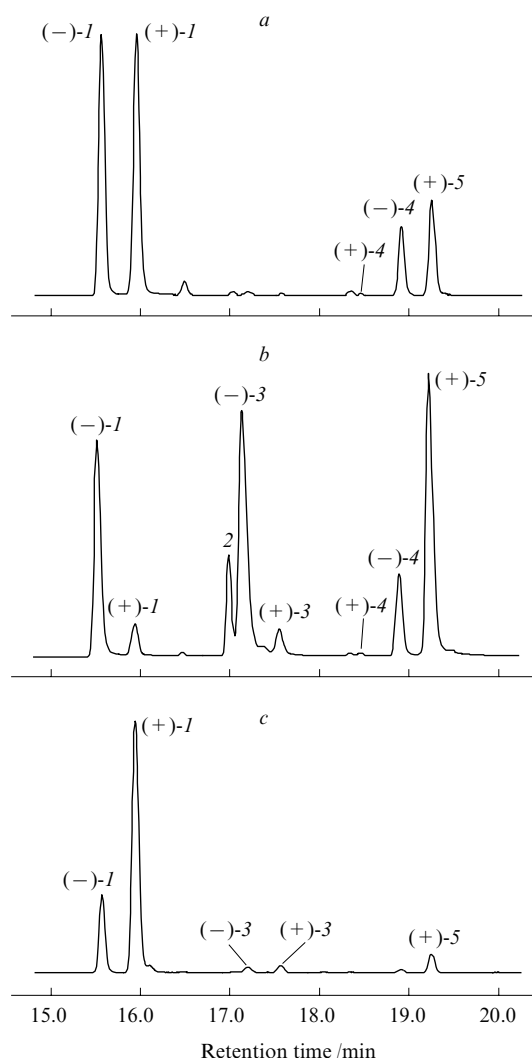


Figure 1. Chromatograms of monoterpene hydrocarbons from oleoresin of the Siberian stone pine (*Pinus sibirica* Du Tour.) (a), the Siberian spruce (*Picea obovata* Ledeb.) (b) and the Scots pine (*Pinus sylvestris* L.) (c) obtained by chiral gas chromatography/mass spectrometry on a 30 m \times 0.25 mm CycloSil-B column (0.25 μ m) at temperatures from 50 to 180 °C (the heating rate was 2 deg min⁻¹).

The peaks of compounds are identified by Arabic numerals: (1) α -pinene, (2) β -myrcene, (3) camphene, (4) β -pinene, (5) 3-carene.

stationary phase, the eluate is divided into two portions. One portion is delivered to a 'usual' (flame ionisation, mass selective, *etc.*) detector, and the odour of another portion of the eluate is evaluated by a human nose *via* a sniffing port.¹⁹ Studies of flavours characteristic of branched carboxylic acids that are present in Parmesan cheese and lamb meat can be referred to as examples.^{18, 19}

The olfactometric detection plays an important role in studies of flavour components of foodstuff because components present in large amounts not nearly always make a decisive contribution to a particular flavour. The analysis of the flavour of freshly squeezed orange juice showed that components that are hardly possible to identify reliably by conventional analysis because of their small amounts, play a great role in the flavour formation, and their true role can be revealed only by the olfactometric detection.⁸⁹

The enantioselective analysis of individual components in mixtures of compounds without their preliminary preparative separation can be performed with the use of mass-spectrometric detectors. However, due to some characteristic features of

mass-spectrometric detectors and the related substantial differences in the detector sensitivity to different groups of compounds, the quantitative analysis by gas chromatography/mass spectrometry presents difficulties. At the same time, the quantitative analysis of the enantiomeric composition of mixtures is very easy to perform by chiral gas chromatography/mass spectrometry, *i.e.*, by the direct method without the use of correction or the sensitivity factors, because enantiomers behave identically in mass spectrometric detectors. The chromatographic peak area ratio of enantiomers is equal to the enantiomeric ratio in the analyte.

Figure 1 shows chromatograms for the separation of mixtures of monoterpene hydrocarbons. It can be seen that pairs of overlapping peaks are absent in the chromatograms, *i.e.*, the separation was successful. The results of the more complex enantiomeric resolution by chromatography in the analysis of multicomponent mixtures containing limonene and β -phellandrene are presented in Fig. 2. These monoterpene hydrocarbons, which are present in many plants, are often found simultaneously and exist as pairs of compounds, which cause complications, because the peaks of these components are unseparable on many columns with widely used nonpolar polysiloxane phases. This pair of monoterpene hydrocarbons was successfully separated on the DB-1701 phase (Fig. 2*a*). However, researchers run into difficulty when attempting to resolve each compound into individual enantiomers on CycloSil-B columns (Fig. 2*b*) because the peak of (–)-limonene coincided with that of (+)- β -phellandrene.

In some cases, when the target components cannot be detected directly (for example in the analysis of labile compounds), their derivatives are synthesised. For instance, to detect (*R*)-3-mercapto-2-methylpropanol in red grape wines, compounds, which are present in the low-temperature vacuum distillation fraction, are subjected to acetylation, and the target compounds are determined as *O,S*-diacetyl derivatives.¹⁷ Enantiomers of some terpene alcohols are resolved as *O*-trifluoroacetyl derivatives.⁶²

III. Two-dimensional gas-liquid chromatography

In the analysis of plant volatiles and food extracts, researchers have, as a rule, to deal with very complex mixtures, which are impossible to separate on modern columns. Considerable progress in studies of such mixtures has been made only with the use of two-dimensional GLC.⁹⁰ This method is based on the successive separation of samples on two different columns. The analyte is delivered to column 1 (the so-called precolumn), where the preliminary separation of components is performed. Then the required fraction of the eluate is taken and divided into two portions. One portion is delivered to detector 1, and another portion is passed to column 2 (the so-called main column), in which the second separation is performed followed by the detection with detector 2. The precolumn is a usual 10–30 m capillary column with a low-polarity polysiloxane phase. This column is used to perform the rough separation of the starting complex mixture and isolate the required (narrow) fraction for the subsequent precision analysis on the main column. The main column is filled with a stationary phase containing a chiral selector, which offers considerable scope for the direct enantioselective analysis of components of complex mixtures of natural compounds.⁸⁷

The direct enantioselective analysis cannot be applied to most of mixtures of sesquiterpene compounds, unlike mixtures of monoterpenoids, because of a high 'density' of components in chromatograms and a large number of overlapping peaks. Only the use of the two-dimensional chromatographic techniques allows the direct analysis of such mixtures. Figure 3 presents the results of analysis of a mixture of sesquiterpene hydrocarbons isolated from oleoresin of the *Abies nephrolepis*

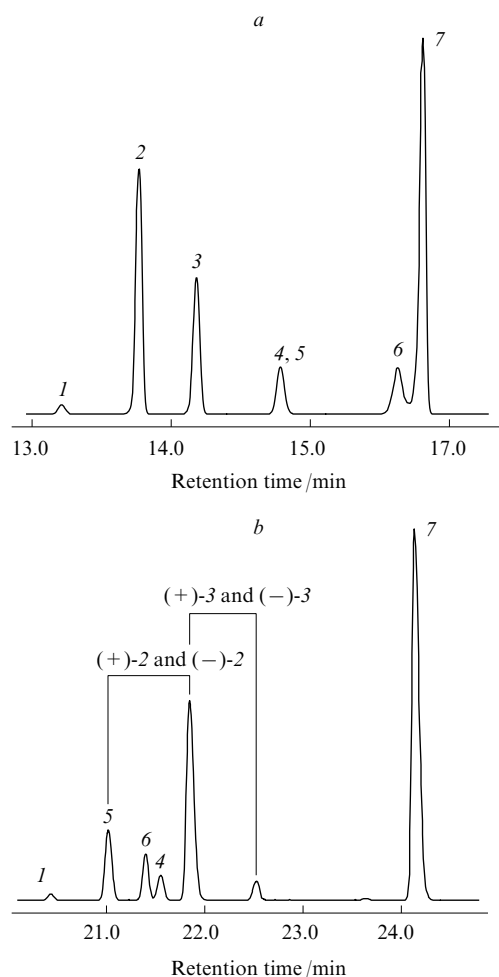


Figure 2. Fragments of chromatograms for the fractions of monoterpene hydrocarbons of essential oil from aerial parts of the *Seseli buchtormense* (Fischer ex Sprengel) W.Koch obtained on DB-1701 (a) and CycloSil-B (b) columns.

(a) 30 m \times 0.25 mm DB-1701 column (0.25 μ m), temperature 50–220 $^{\circ}$ C (the heating rate was 2 deg min^{–1}); (b) 30 m \times 0.25 mm CycloSil-B column (0.25 μ m), temperature 50–180 $^{\circ}$ C (the heating rate was 2 deg min^{–1}). The peaks of compounds are identified by Arabic numerals: (1) α -terpinene, (2) limonene, (3) β -phellandrene, (4) *p*-cymol, (5) *cis*- β -ocimene, (6) *trans*- β -ocimene, (7) γ -terpinene.

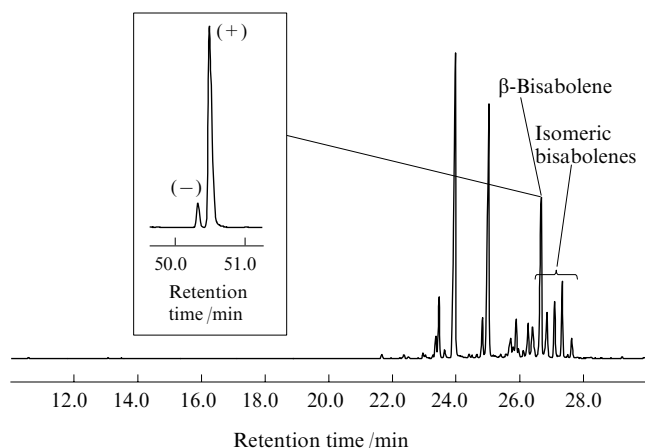
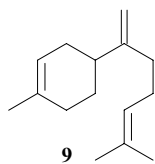


Figure 3. Determination of the optical purity of β -bisabolene in a mixture of sesquiterpene hydrocarbons from oleoresin of the *Abies nephrolepis* Maxim. by two-dimensional GLC.

Column 1: CPSil-5, 25 m \times 0.25 mm (0.25 μ m), temperature 50–200 $^{\circ}$ C (the heating rate was 4 deg min $^{-1}$); column 2: 30% heptakis(2,3-di-*O*-methyl-6-*O*-*tert*-butyldimethylsilyl)- β -cyclodextrin in OV-1701 (in the inset), 25 m \times 0.25 mm (0.125 μ m), temperature 50–180 $^{\circ}$ C (the heating rate was 2 deg min $^{-1}$).

followed by the determination of the optical purity of β -bisabolene (**9**) in a complex isomeric mixture.



The first chromatographic separation of a mixture of sesquiterpene hydrocarbons was performed on a column with a polysiloxane phase to isolate a fraction containing β -bisabolene (the retention time varies from 26.60 to 26.70 min). The resolution of this fraction into individual enantiomers was carried out on a column with a β -cyclodextrin-based phase. It should be noted that the direct analysis (using the one-dimensional technique) of the fraction of sesquiterpene hydrocarbons is of no use because the mixture contains, along with β -bisabolene, all other isomeric (*Z*)- α -, (*E*)- α -, (*Z*)- γ - and (*E*)- γ -bisabolenes, which hinder the analysis of enantiomers of β -bisabolene.

There are two radically different arrangements of the precolumn and the main column in two-dimensional chiral GLC (in one or two different thermostats). Manufacturers of gas-chromatographic systems suggest simple solutions for two-dimensional chromatography as instruments in which both columns are placed in a single thermostat. However, this instrumental simplicity, despite a price benefit, offers less possibilities for tuning. In the overwhelming majority of cases, to achieve the most efficient resolution by two-dimensional chiral GLC, the precolumn and the main column with a chiral stationary phase should operate under different temperature conditions, which cannot be provided in instruments, in which both columns are placed in a single thermostat.

A quick technique was developed for the analysis of the enantiomeric composition of mixtures by two-dimensional chiral GLC with the use of a short (1 m) column packed with a cyclodextrin phase. The satisfactory enantiomeric resolution of limonene according to this procedure took only 8 s (!), and the enantiomeric composition of all monoterpene compounds isolated from bergamot oil was determined within 8–9 min.⁹¹

A combination of liquid and gas chromatography (LC-GC) is another efficient combined method for the determination of the enantiomeric composition of mixtures. However, only a few examples of the successful application of this method were documented.⁴⁰

IV. Preparative enantiomeric resolution

The preparative enantiomeric resolution of volatile natural compounds by chiral GLC with the use of cyclodextrin stationary phases is performed on packed columns filled with a solid support coated with modified cyclodextrin as the stationary phase. This method allows the isolation of milligram amounts of individual enantiomers.⁹²

The characteristic feature of preparative chiral GLC is that the best enantiomeric resolution is, as a rule, achieved at the minimum temperatures of the analysis because a lowering of the temperature leads to an increase in the retention times of the components. To decrease the temperature of the analysis, rather short columns and a packing material with a small (compared to usual preparative columns) amount of a stationary phase are used. In addition, the separation is performed at carrier gas flow rates 3–4 times higher than the optimal rates. An increase in the carrier gas flow rate leads to a slight decrease in the efficiency of the column. However, this drawback is compensated, on the whole, by the gain in enantioselectivity of resolution due to lowering of the temperature.

Preparative chiral GLC is generally carried out on a 1.8–2.0-m steel column with a diameter of 4–5 mm filled with a solid support (for example, with the Chromosorb W/HP sorbent with a grain size of 100–120 mesh) coated with a 20%–50% solution of modified cyclodextrin [heptakis(2,6-di-*O*-methyl-3-*O*-*n*-pentyl)- β -cyclodextrin,⁹³ heptakis(2,3-di-*O*-methyl-6-*O*-*n*-hexyl)- β -cyclodextrin,⁹⁴ octakis(2,3-di-*O*-*n*-pentyl-6-*O*-methyl)- γ -cyclodextrin,⁹⁵ octakis(2,6-di-*O*-methyl-3-*O*-*n*-pentyl)- γ -cyclodextrin⁹⁶ or heptakis(2,3-di-*O*-methyl-6-*O*-*tert*-butyldimethylsilyl)- β -cyclodextrin⁹⁶] in polysiloxane [OV-1701,⁹⁷ PS-086⁹⁵ or SE-52 (Ref. 96)] as the stationary phase (2%–6%). The carrier gas flow rate is 200–400 ml min $^{-1}$; the temperature is chosen depending on the nature of the compounds and is varied from 35–45 $^{\circ}$ C (for monoterpene hydrocarbons) to 100–120 $^{\circ}$ C (for sesquiterpenes). The temperature of the chromatographic analysis should be chosen so as to achieve the selectivity factor of ≥ 1.1 . In this case, enantiomers of an optical purity of no less than 90% can be obtained.

Under these conditions, 1–2 mg of racemic compounds can be separated in a single chromatographic run. Milligram amounts of pure enantiomers (up to 97% *ee*) can be obtained by repeated chromatographic steps, these amounts being sufficient for the determination of the sign of optical rotation and, consequently, for the determination of the elution order of enantiomers, as well as for biological assays and pharmacokinetic studies.⁹²

The preparative enantiomeric resolution with the use of capillary columns with a large inner diameter (0.53 mm) and a larger layer thickness of the stationary phase was documented.^{98,99} Such columns provide better resolution compared to packed columns. However, this approach has found little application apparently because of rather complex technical equipment and labour-consuming experiments associated with a low capacity of capillary columns compared to packed columns.

Some plant volatiles exist in the gaseous state. However, no examples of the enantioselective analysis of gaseous plant metabolites have yet been reported, although a procedure for the preparative resolution of chiral gaseous compounds on

cyclodextrin phases at room temperature was elaborated for bromochlorofluoromethane.¹⁰⁰

V. Identification of enantiomers

The reliable assignment of peaks of optical isomers plays a decisive role in chiral chromatography. Since the mechanism of enantiodifferentiation based on interactions of a chiral selector with an enantiomeric pair remains to be elucidated, it is impossible to predict the elution order of enantiomers. Taking into account the fact that the selectivity of columns depends, among other factors, on the chromatographic conditions, it can be concluded that the identification of enantiomers is a complex problem. Generally, at least two model samples are required for the reliable assignment of peaks. One sample should contain both enantiomers (the presence of a racemic mixture is preferable). This sample is used for choosing the optimal chromatographic conditions. Another sample should be enriched in a particular enantiomer with the aim that the elution order of optical isomers can be determined under the optimised conditions.

Many of the most widespread monoterpene compounds are commercially available both as racemic mixtures and individual enantiomers. The situation is more difficult with less widespread compounds. Researchers often have to synthesise such compounds or isolate them from natural mixtures. This is particularly true for sesquiterpene compounds because only a few of them are present in catalogues of manufacturers of chemicals. Moreover, natural sources, from which the target compound can easily be isolated in required amounts, are unknown for many sesquiterpenoids. In this connection, studies aimed at preparing individual sesquiterpenoids or their mixtures of known composition for the use as reference samples in chiral GLC deserve particular notice. For example, the easily available natural sesquiterpene hydrocarbon germacrene D was transformed¹⁰¹ into mixtures of sesquiterpenoids of known composition containing selinane-, cadalene-, eudesmane- and oppositane-type sesquiterpenoids and other

related compounds belonging to the biogenetic tree of germacrane by acid-catalysed, photoinduced or thermally induced rearrangements. However, far not all important sesquiterpenes required as reference compounds can be synthesised from known precursors by rearrangements. Extracts of some lower plants and fungi can be mentioned as sources of 'unusual' enantiomers of plant sesquiterpenoids.⁹⁵

Extensive experimental data on the enantiomeric resolution of plant volatiles, fragrance and flavour compounds by chiral GLC on capillary columns with stationary phases based on chiral selectors are available. Data on the separation factors of enantiomers of various compounds, including plant compounds, were published. In particular, enantiomers were analysed on capillary columns with phases based on octakis(6-*O*-methyl-2,3-di-*O*-*n*-pentyl)- γ -cyclodextrin,¹⁰² heptakis(2,6-di-*O*-methyl-3-*O*-*n*-pentyl)- β -cyclodextrin (Ref. 103) and octakis(3-*O*-butyryl-2,6-di-*O*-*n*-pentyl)- γ -cyclo-dextrin.¹⁰⁴ The enantiomeric separation of octane-1,3-diol, (5*Z*)-octene-1,3-diol, ethyl 3-hydroxyoctanoate and ethyl (5*Z*)-3-hydroxyoctenoate on a column with heptakis(2,3-*O*-acetyl-6-*O*-*tert*-butyldimethylsilyl)- β -cyclodextrin was documented.^{15, 105} However, the published data summaries are not always useful in practice because they contain no information on the elution order of enantiomers. Data on the resolution of 260 enantiomeric pairs of cyclopropane derivatives were presented in the review,¹⁰⁶ where the selectivity factors were reported without mentioning the conditions of resolution. The successful enantiomeric resolution of γ - and δ -thiolactones of the fatty acid series (C₆, C₈, C₁₀, C₁₂),¹⁰⁷ optical isomers of various natural and synthetic compounds,¹⁰⁸ trifluoroacetates of terpene and nonterpene alcohols⁶² and β - and γ -lactones of the fatty acid series was documented.⁶² However, the elution orders of these enantiomers were also not reported, although the selectivity factors were published.

The aim of the present review was to provide the most detailed information on the chirospecific analysis of plant volatiles. Tables 1–4 summarise data on the enantiomeric resolution of natural plant compounds and selected important

Table 1. Enantiomeric resolution of mono- and sesquiterpenoids and related compounds by chiral GLC on stationary phases containing cyclodextrin derivatives as chiral selectors.

Selectand	Chiral selector ^a	Column temperature (°C) or the temperature conditions (see comments in the text)	α	First-eluted enantiomer	Ref.
Borneol	β -(2,3-Ac-6-TBS)	80°	1.032		108
Borneol ^b	γ -(2,6-Pe-3-But)	90°		(+)	62
Isoborneol	β			(-)	109
	β -(2,3-Ac-6-TBS)	90°	1.038		108
Isoborneol ^b	γ -(2,6-Pe-3-But)	90°		(-)	62
Verbenone	γ -(2,6-Pe-3-But)	60°(2)–200°(4°)		(+)	110
Vitispirane I	β -(2,6-Me-3-Pe)	60°(25)–240°(1.5°)		(2 <i>R</i> ,5 <i>R</i>)	111
Vitispirane II	β -(2,6-Me-3-Pe)	60°(25)–240°(1.5°)		(2 <i>R</i> ,5 <i>S</i>)	111
Dill ether	γ -(2,3-But-6-TBS)	60°–200°(2.5°)	1.014	(3 <i>R</i> ,3 <i>aR</i> ,7 <i>aS</i>)	112
Dill ether (<i>cis</i> isomer)	γ -(2,3-But-6-TBS)	60°–200°(2.5°)	1.018	(3 <i>S</i> ,3 <i>aR</i> ,7 <i>aS</i>)	112
Camphene	β -(2,3-Pe-6-Me)	35°	1.074	(-)	113
	β -(2,3-Pe-6-Me)	70°–220°(6°)	1.04	(-)	10
	β -(2,6-Pe-3-Me)	60°		(-)	114
	γ -(2,3-Pe-6-Me)	35°	1.000 ^c		113
	γ -(2,3-Pe-6-Me)	45°	1.000 ^c		113
	α (see ^d)	70°	2.31	(-)	49
α -Campholenal	β -(2,3,6-Me)	110°		(<i>R</i>)	21
Camphor	γ -(2,6-Pe-3-But)	100°–160°(2°)		(+)	62
	β -(2,3-Ac-6-TBS)	100°	1.054	(<i>S</i>)	108
	γ -(2,6-Pe-3-But)			(+)	114
	γ -(2,6-Pe-3-But)	50°(2)–100°(1°)		(1 <i>R</i>)-(+))	8
	β -(2,3-Ac-6-TBS)	60°(18)–120°(1°)–200°(10°)		(1 <i>S</i>)	115
	β -(2,3-Et-6-TBS)	60°(10)–120°(3°)		(-)	9

Table 1 (continued).

Selectand	Chiral selector ^a	Column temperature (°C) or the temperature conditions (see comments in the text)	α	First-eluted enantiomer	Ref.
<i>trans</i> -Carveol	γ -(2,3-Pe-6-Me)	50°(1.5)–110°(2°)(8)–200°(20°)(6)	1.014	(+)	116
<i>cis</i> -Carveol	γ -(2,3-Pe-6-Me)	50°(1.5)–110°(2°)(8)–200°(20°)(6)	1.022	(–)	116
Carvone	α (see ^d)	70°	1.11	(+)	49
	β -(2,3-Ac-6-TBS)	110°	1.05	(<i>R</i>)-(–)	108
	α -(2,3,6-Pe)	100°		(–)	114
	β -(2,3-Me-6-TBS)	100°	1.018	(+)	73
	β -(2,3-Ac-6-TBS)	100°	1.065	(–)	73
	γ -(2,3-Pe-6-Me)	50°(1.5)–110°(2°)(8)–200°(20°)(6)	1.015	(+)	116
3-Carene	β -(2,3-Pe-6-Me)	35°	1.040	(+)	113
	β -(2,3-Pe-6-Me)	70°–220°(6°)	1.03	(+)	10
	γ -(2,3-Pe-6-Me)	35°	1.000 ^c		113
	γ -(2,3-Pe-6-Me)	45°	1.388	(+)	113
	β -(2,6-Pe-3-AcF)			(–)	37
Lavandulol	β -(2,3-Ac-6-TBS)	60°(18)–120°(1°)–200°(10°)		(<i>R</i>)	115
	β -(2,3-Ac-6-TBS)	80°	1.022	(<i>R</i>)	108
Limonene	β -(2,3-Pe-6-Me)	35°	1.026	(–)	113
	β -(2,3-Pe-6-Me)	70°–220°(6°)	1.01	(–)	10
	β -(2,6-Pe-3-Me)	60°		(–)	114
	β -(2,3-Et-6-TBS)	45°(6)–180°(2°)		(–)	117
	γ -(2,3-Pe-6-Me)	35°	1.261	(+)	113
	γ -(2,3-Pe-6-Me)	45°	1.180	(+)	113
	γ -(2,3-Pe-6-Me)	55°		(+)	118
	β (see ^c)	40°(8)–200°(2°)		(–)	119
	β -(2,3,6-Me)			(–)	37
	γ -(2,3,6-Me)	50°	1.03	(+)	120
	α (see ^d)	70°	1.11	(+)	49
	γ -(2,3-Pe-6-Me)	50°(1.5)–110°(2°)(8)–200°(20°)(6)	1.044	(+)	116
<i>trans</i> -Limonene 1,2-epoxide	γ -(2,3,6-Me)	50°	1.01	(+)	120
<i>cis</i> -Limonene 1,2-epoxide	γ -(2,3,6-Me)	50°	1.04	(–)	120
Linalyl acetate	β -(2,3-Ac-6-TBS)	60°(18)–120°(1°)–200°(10°)		(<i>R</i>)	115
	β -(2,3-Ac-6-TBS)	80°	1.021	(<i>R</i>)	108
Linalool	β -(2,3-Ac-6-TBS)	60°(18)–120°(1°)–200°(10°)		(<i>R</i>)	115
	β -(2,3-Ac-6-TBS)	80°	1.08	(<i>R</i>)-(–)	108
	β -(2,3-Ac-6-TBS)	60°(20)–120°(1.3°)		(<i>R</i>)-(–)	11
	β -(2,3-Et-6-TBS)	45°(6)–180°(2°)		(–)	117
	β -(2,3,6-Pe)	80°		(–)	114
	α (see ^d)	70°	1.000 ^c		49
	β -(2,3,6-Me)			(–)	37
(<i>E</i>)-3,7-Dimethylocta-1,5-diene-3,7-diol	β -(2,3-Me-6-TBS)	60°(25)–200°(2°)		(3 <i>R</i>)	121
	β -(2,3-Ac-6-TBS)	60°(30)–200°(2°)	1.000 ^c		121
3,7-Dimethylocta-1,7-diene-3,6-diol (I)	β -(2,3-Me-6-TBS)	60°(25)–200°(2°)		(3 <i>R</i> ,6 <i>S</i>)	121
	β -(2,3-Ac-6-TBS)	60°(30)–200°(2°)		(3 <i>R</i> ,6 <i>S</i>)	121
3,7-Dimethylocta-1,7-diene-3,6-diol (II)	β -(2,3-Me-6-TBS)	60°(25)–200°(2°)		(3 <i>R</i> ,6 <i>R</i>)	121
	β -(2,3-Ac-6-TBS)	60°(30)–200°(2°)		(3 <i>S</i> ,6 <i>S</i>)	121
(<i>E</i>)-3,7-Dimethylocta-1,6-diene-3,8-diol	β -(2,3-Me-6-TBS)	60°(25)–200°(2°)	1.000 ^c		121
	β -(2,3-Ac-6-TBS)	60°(30)–200°(2°)		(6 <i>S</i>)	121
(<i>Z</i>)-3,7-Dimethylocta-2,7-diene-1,6-diol	β -(2,3-Me-6-TBS)	60°(25)–200°(2°)		(3 <i>R</i>)	121
	β -(2,3-Ac-6-TBS)	60°(30)–200°(2°)	1.000 ^c		121
(<i>E</i>)-3,7-Dimethylocta-2,7-diene-1,6-diol	β -(2,3-Me-6-TBS)	60°(25)–200°(2°)		(3 <i>R</i>)	121
	β -(2,3-Ac-6-TBS)	60°(30)–200°(2°)	1.000 ^c		121
<i>trans</i> -Linalool oxide (pyranoid)	β -(2,3,6-Me)			(2 <i>S</i>)	41
	β -(2,3,6-Et)			(2 <i>S</i>)	41
	β -(2,3-Ac-6-TBS)			(2 <i>R</i>)	41
	β -(2,3-Me-6-TBS)			(2 <i>S</i>)	41
<i>cis</i> -Linalool oxide (pyranoid)	β -(2,3,6-Me)			(2 <i>S</i>)	41
	β -(2,3,6-Et)			(2 <i>S</i>)	41
	β -(2,3-Ac-6-TBS)			(2 <i>S</i>)	41
	β -(2,3-Me-6-TBS)			(2 <i>S</i>)	41

Table 1 (continued).

Selectand	Chiral selector ^a	Column temperature (°C) or the temperature conditions (see comments in the text)	α	First-eluted enantiomer	Ref.
<i>trans</i> -Linalool oxide (furanoid)	β -(2,3,6-Me)			(2 <i>R</i>)	41
	β -(2,3,6-Et)			(2 <i>R</i>)	41
	β -(2,3-Pe-6-Me)			(2 <i>R</i>)	41
	β -(2,3-Ac-6-TBS)			(2 <i>S</i>)	41
	β -(2,3-Me-6-TBS)			(2 <i>R</i>)	41
<i>cis</i> -Linalool oxide (furanoid)	β -(2,3,6-Me)			(2 <i>R</i>)	41
	β -(2,3,6-Et)			(2 <i>R</i>)	41
	β -(2,3-Pe-6-Me)			(2 <i>R</i>)	41
	β -(2,3-Ac-6-TBS)			(2 <i>R</i>)	41
	β -(2,3-Me-6-TBS)			(2 <i>R</i>)	41
<i>p</i> -Menth-1-ene-8-thiol	β -(2,3-Me-6-TBS)			(<i>S</i>)	38
<i>trans</i> -8-Mercapto- <i>p</i> -menth-3-one	β -(2,3,6-Me)	110°		(1 <i>R</i> ,4 <i>R</i>)	122
<i>trans</i> -8-Mercapto- <i>p</i> -menth-3-one	γ -(2,3-Ac-6-TBS)	80° – 125°(1.5°)(40) – 190°(3°)		(1 <i>R</i> ,4 <i>R</i>)	123
<i>cis</i> -8-Mercapto- <i>p</i> -menth-3-one	β -(2,3,6-Me)	110°		(1 <i>R</i> ,4 <i>S</i>)	122
<i>cis</i> -8-Mercapto- <i>p</i> -menth-3-one	γ -(2,3-Ac-6-TBS)	80° – 125°(1.5°)(40) – 190°(3°)		(1 <i>S</i> ,4 <i>R</i>)	123
<i>trans</i> -8-Acetylmercapto- <i>p</i> -menth-3-one	γ -(2,3-Ac-6-TBS)	80° – 125°(1.5°)(40) – 190°(3°)		(1 <i>R</i> ,4 <i>R</i>)	123
<i>cis</i> -8-Acetylmercapto- <i>p</i> -menth-3-one	γ -(2,3-Ac-6-TBS)	80° – 125°(1.5°)(40) – 190°(3°)		(1 <i>S</i> ,4 <i>R</i>)	123
Menthyl acetate	γ -(2,3-Pe-6-Me)	85°		(–)	118
	β -(2,3-Ac-6-TBS)	90°	1.035		108
	β -(2,3,6-Me)			(–)	37
Menthol	β -(2,3-Me-6-TBS)	47°(19) – 70°(20°)(15) – 210°(1.5°)		(–)	124
	γ -(2,3-Pe-6-Me)	75°(15) – 150°(2°)		(+)	118
	β -(2,3-Ac-6-TBS)	90°	1.048		108
	α (see ^d)	70°	1.000 ^c		49
	β -(2,3-Me-6-TBS)	47°(19) – 70°(20°)(15) – 210°(1.5°)		(+)	124
Isomenthol	β -(2,3-Ac-6-TBS)	100°	1.043		108
Neomenthol	β -(2,3-Me-6-TBS)	47°(19) – 70°(20°)(15) – 210°(1.5°)		(+)	124
	β -(2,3-Ac-6-TBS)	100°	1.039		108
	α (see ^d)	70°	1.000 ^c		49
Neoisomenthol	β -(2,3-Me-6-TBS)	47°(19) – 70°(20°)(15) – 210°(1.5°)		(–)	124
Menthone	γ -(2,3-Pe-6-Me)	75°(15) – 150°(2°)		(+)	118
	β -(2,3-Ac-6-TBS)	75°	1.073		108
	α (see ^d)	70°	1.10	(+)	49
	β -(2,3-Me-6-TBS)	47°(19) – 70°(20°)(15) – 210°(1.5°)		(–)	124
	γ -(2,6-Pe-3-But) ^f	80°	1.088 – 1.164	(2 <i>R</i> ,5 <i>S</i>)-(+)	71
	γ -(2,6-Pe-3-But)	100° – 160°(2°)		(+)	62
	γ -(2,6-Pe-3-AcF)			(+)	37
	β -(2,3,6-Me)		1.000 ^c		37
	γ -(2,3-Pe-6-Me)	75°(15) – 150°(2°)		(+)	118
	β -(2,3-Ac-6-TBS)	75°	1.059		108
Isomenthone	α (see ^d)	70°	1.21	(–)	49
	γ -(2,6-Pe-3-But)			(+)	31
	γ -(2,6-Pe-3-But)	100° – 160°(2°)		(+)	62
	γ -(2,6-Pe-3-AcF)		1.000 ^c		37
	β -(2,3,6-Me)			(+)	37
	β -(2,3-Me-6-TBS)	47°(19) – 70°(20°)(15) – 210°(1.5°)		(+)	124
	β -(2,3,6-Me)			(<i>R</i>)	37
Menthofuran	β -(2,3-Ac-6-TBS)	60°(13) – 85°(0.4°)		(<i>R</i>)-(+)	11
Methyl citronellate	β -(2,6-Pe-3-AcF)			(6 <i>R</i> ,7 <i>aR</i>)-(–)	37
Mintlactone	β -(2,6-Pe-3-AcF)			(<i>S</i>)-(–)	37
Mintlactone, dehydromyrtanal	γ -(2,6-Pe-3-But)	120°		(+)	114
Myrtenol ^b	β -(2,6-Pe-3-Me)	100°		(–)	114
Nerol oxide	γ -(2,3-But-6-TBS)			(<i>R</i>)-(+)	41
<i>cis</i> -Pinane	β (see ^c)	40°(8) – 200°(2°)		(–)	119
<i>trans</i> -Pinane	γ -(2,6-Pe-3-But) ^f	26°	1.018 – 1.044	(1 <i>R</i>)-(+)	71
α -Pinene	β -(2,3-Pe-6-Me)	35°	1.054	(–)	113
	γ -(2,6-Pe-3-But) ^f	26°	1.032 – 1.068	(1 <i>R</i>)-(+)	71
	β -(2,3-Pe-6-Me)	70° – 220°(6°)	1.04	(–)	10
	γ -(2,3-Pe-6-Me)	35°	1.053	(+)	113
	γ -(2,3-Pe-6-Me)	45°	1.000 ^c		113
	β (see ^c)	40°(8) – 200°(2°)		(–)	119
	γ -(2,3-Pe-6-Me)	55°		(+)	118

Table 1 (continued).

Selectand	Chiral selector ^a	Column temperature (°C) or the temperature conditions (see comments in the text)	α	First-eluted enantiomer	Ref.
α -Pinene	α (see ^d)	70°	2.22	(–)	49
	γ -(2,6-Pe-3-But) ^f	26°	1.03–1.07	(+)	71
	β -(2,3,6-Me)			(–)	37
β -Pinene	β -(2,6-Pe-3-Me)	60°		(–)	114
	β -(2,3-Pe-6-Me)	35°	1.034	(–)	113
	β -(2,3-Pe-6-Me)	70°–220°(6°)	1.008	(–)	10
	β -(2,3-Et-6-TBS)	45°(6)–180°(2°)		(+)	117
	γ -(2,3-Pe-6-Me)	35°	1.060	(+)	113
	γ -(2,3-Pe-6-Me)	45°	1.043	(+)	113
	γ -(2,3-Pe-6-Me)	55°		(+)	118
	α (see ^d)	70°	1.86	(–)	49
	β -(2,3,6-Me)			(+)	37
	β -(2,3,6-Me)	100°		(–)	21
α -Pinene epoxide	α (see ^d)	70°	1.15	(–)	49
Isopinocampheol	β -(2,6-Pe-3-Me)	100°		(–)	114
<i>trans</i> -Pinocarveol ^b	γ -(2,3-Pe-6-Me)	75°(15)–150°(2°)		(–)	118
Piperitone	β -(2,3-Ac-6-TBS)	90°	1.037		108
	γ -(2,6-Pe-3-But)	100°–160°(2°)		(–)	114
	α (see ^d)	70°	1.000 ^c		49
Pulegone	β -(2,3,6-Me)	130°		(<i>R</i>)	122
	γ -(2,6-Me-3-Pe)			(2 <i>S</i>)	41
<i>trans</i> -Rose oxide	β -(2,3-Ac-6-TBS)	70°	1.040	(2 <i>R</i> ,4 <i>R</i>)	108
	γ -(2,6-Pe-3-AcF)			(2 <i>S</i>)	41
	γ -(2,6-Pe-3-AcF)			(+)	37
	β -(2,3-Ac-6-TBS)			(2 <i>R</i>)	41
	β -(2,3-Ac-6-TBS)	60°(20)–120°(1.3°)		(2 <i>R</i> ,4 <i>R</i>)-(–)	11
	γ -(2,3-Ac-6-TBS)			(2 <i>R</i>)	41
	α -(2,3,6-Me)		1.000 ^c		37
	γ -(2,3,6-Me)		1.000 ^c		37
	γ -(2,6-Pe-3-But)			(+)	37
	γ -(2,6-Me-3-Pe)			(2 <i>S</i>)	41
<i>cis</i> -Rose oxide	β -(2,3-Ac-6-TBS)	70°	1.039	(2 <i>R</i> ,4 <i>S</i>)	108
	γ -(2,6-Pe-3-AcF)			(2 <i>S</i>)	41
	β -(2,3-Ac-6-TBS)			(2 <i>R</i>)	41
	β -(2,3-Ac-6-TBS)	60°(20)–120°(1.3°)		(2 <i>R</i> ,4 <i>S</i>)-(+)	11
	γ -(2,3-Ac-6-TBS)			(2 <i>R</i>)	35
	α -(2,3,6-Me)			(–)	37
	γ -(2,3,6-Me)			(–)	37
	γ -(2,6-Pe-3-But)		1.000 ^c		37
	γ -(2,6-Pe-3-AcF)			(–)	37
	β -(2,3-Ac-6-TBS)			(2 <i>S</i>)	41
<i>trans</i> -Rose oxide ketone	β -(2,3-Ac-6-TBS)			(2 <i>R</i>)	41
<i>cis</i> -Rose oxide ketone	β -(2,3-Ac-6-TBS)				
Sabinene	β -(2,3-Pe-6-Me)	35°	1.063	(+)	113
	β -(2,3-Pe-6-Me)	70°–220°(6°)	1.02	(+)	10
	γ -(2,3-Pe-6-Me)	35°	1.124	(–)	113
	γ -(2,3-Pe-6-Me)	45°	1.093	(–)	113
	β -(2,3-Et-6-TBS)	45°(6)–180°(2°)		(+)	117
	β -(2,3-Ac-6-TBS)	60°(18)–120°(1°)–200°(10°)		(<i>R</i>)	115
	β -(2,3-Ac-6-TBS)	110°	1.042	(<i>R</i>)	108
Terpinen-4-ol	β -(2,3-Et-6-TBS)	45°(6)–180°(2°)		(+)	117
	α (see ^d)	70°	1.000 ^c		49
	β -(2,3,6-Me)			(+)	37
	α (see ^d)	70°	1.000 ^c		49
α -Terpineol	β -(2,3-Ac-6-TBS)	80°	1.059		108
	β -(2,3,6-Me)			(–)	37
	β -(2,3-Et-6-TBS)	45°(6)–180°(2°)		(–)	117
α -Tujene	β -(2,3-Pe-6-Me)	35°	1.045	(+)	113
	γ -(2,3-Pe-6-Me)	35°	1.040	(–)	113
	γ -(2,3-Pe-6-Me)	45°	1.000 ^c		113
Fencholenal	β -(2,3,6-Me)	115°		(<i>R</i>)	21

Table 1 (continued).

Selectand	Chiral selector ^a	Column temperature (°C) or the temperature conditions (see comments in the text)	α	First-eluted enantiomer	Ref.
Fenchone	α (see ^d)	70°	2.01	(–)	49
	γ -(2,6-Pe-3-But)	100°–160°(2°)		(–)	62
	γ -(2,6-Pe-3-But) ^f	70°	1.083–1.131	(1 <i>R</i>)-(–)	71
α -Phellandrene	β -(2,3-Pe-6-Me)	35°	1.020	(–)	113
	γ -(2,3-Pe-6-Me)	35°	1.248	(+)	113
	γ -(2,3-Pe-6-Me)	45°	1.202	(+)	113
	γ -(2,3,6-Pe)	80°		(+)	114
	α (see ^d)	70°	1.24	(–)	49
β -Phellandrene	β -(2,3-Pe-6-Me)	35°	1.030	(–)	113
	β -(2,3-Pe-6-Me)	70°–220°(6°)	1.000 ^c		10
	γ -(2,3-Pe-6-Me)	35°	1.000 ^c		113
	γ -(2,3-Pe-6-Me)	45°	1.000 ^c		113
Ho-trienol	β -(2,3-Me-6-TBS)	60°(25)–200°(2°)		(3 <i>R</i>)	121
	β -(2,3-Ac-6-TBS)	60°(30)–200°(2°)		(3 <i>R</i>)	121
Citronellal	β -(2,3-Ac-6-TBS)	60°(20)–120°(1.3°)		(<i>S</i>)-(–)	11
	β -(2,3-Ac-6-TBS)	90°	1.036		108
	β -(2,6-Pe-3-Ac)			(–)	37
	α (see ^d)	70°	1.000 ^c		49
Citron	α (see ^d)	70°	1.000 ^c		49
Citronellol	β -(2,3-Ac-6-TBS)	60°(20)–120°(1.3°)		(<i>S</i>)-(–)	11
	β -(2,3-Ac-6-TBS)	80°	1.022	(<i>S</i>)-(–)	108
Citronellol ^b	γ -(2,6-Pe-3-But)	110°		(+)	62
α -Ionone	β -(2,3,6-Me)	120°		(–)	23
	β -(2,3-Ac-6-TBS)	135°	1.029		108
	γ -(2,6-Pe-3-AcF)	120°		(–)	23
	γ -(2,6-Pe-3-But)	75°		(–)	23
	β -(2,3-Me-6-TBS)	60–200°		(<i>S</i>)	16
	β -(2,3,6-Me)			(–)	37
α -Irone (I)	β -(2,3-Ac-6-TBS)	125°	1.049		108
α -Irone (II)	β -(2,3-Ac-6-TBS)	125°	1.238		108
2,3-Dehydro- α -ionol I [(2,6,6-trimethylcyclohexa-2,4-dienyl)but-3-ene-2-ol]	β -(2,6-Me-3-Pe)	100°(60)–200°(2°)	1.003	(2 <i>R</i> ,1' <i>S</i>)	125
3,4-Dehydro- γ -ionol I	β -(2,6-Me-3-Pe)	100°(60)–200°(2°)	1.004	(2 <i>S</i> ,1' <i>S</i>)	125
3,4-Dehydro- γ -ionol I	β -(2,6-Me-3-Pe)	100°(95)–200°(1°)	1.003	(2 <i>R</i> ,1' <i>R</i>)	125
3,4-Dehydro- γ -ionol II	β -(2,6-Me-3-Pe)	100°(60)–200°(2°)	1.002	(2 <i>S</i> ,1' <i>R</i>)	125
Riesling acetal	β -(2,3,6-Me)	60°(15)–220°(2°)		(5 <i>R</i> ,6 <i>S</i> ,9 <i>S</i>)	126
Theaspirane A	β -(2,3,6-Me)			(2 <i>R</i> ,5 <i>R</i>)-(–)	37
	β -(2,3,6-Me)	80°(20)–220°(2°)	1.016	(2 <i>R</i> ,5 <i>R</i>)	127
Theaspirane B	β -(2,3,6-Me)			(2 <i>S</i> ,5 <i>R</i>)-(+)	37
	β -(2,3,6-Me)	80°(20)–220°(2°)	1.010	(2 <i>S</i> ,5 <i>R</i>)	127
Theaspirone A	β -(2,3,6-Me)	80°(20)–220°(2°)	1.007	(2 <i>R</i> ,5 <i>R</i>)	127
	β -(2,3,6-Me)			(2 <i>R</i> ,5 <i>R</i>)-(+)	37
	β -(2,6-Me-3-Pe)	60°(25)–240°(1.5°)		(2 <i>R</i> ,5 <i>R</i>)	111
Theaspirone B	β -(2,3,6-Me)	80°(20)–220°(2°)	1.006	(2 <i>S</i> ,5 <i>R</i>)	127
	β -(2,3,6-Me)			(2 <i>S</i> ,5 <i>R</i>)-(+)	37
	β -(2,6-Me-3-Pe)	60°(25)–240°(1.5°)		(2 <i>S</i> ,5 <i>R</i>)	111
<i>trans</i> -Edulan I	β -(2,6-Me-3-Pe)	60°(20)–200°(2°)		(2 <i>S</i> ,8 <i>aR</i>)	128
<i>cis</i> -Edulan II	β -(2,6-Me-3-Pe)	60°(20)–200°(2°)		(2 <i>R</i> ,8 <i>aR</i>)	128
<i>trans</i> -3,4-Dihydro-3-oxoedulan	β -(2,6-Me-3-Pe)	60°(20)–200°(2°)	1.003	(2 <i>S</i> ,8 <i>aR</i>)	129
<i>cis</i> -3,4-Dihydro-3-oxoedulan	β -(2,6-Me-3-Pe)	60°(20)–200°(2°)	1.016	(2 <i>S</i> ,8 <i>aS</i>)	129
(<i>E</i>)-2,3-Dihydrofarnesal	β -(2,3-Ac-6-TBS)	110°(40)–160°(1°)		(3 <i>S</i>)	130
(<i>Z</i>)-2,3-Dihydrofarnesal	β -(2,3-Ac-6-TBS)	110°(40)–160°(1°)		(3 <i>S</i>)	130
(<i>E</i>)-2,3-Dihydrofarnesoic acid	β -(2,3-Me-6-TBS)	130°(5)–155°(1.5°)(5)–162°(0.5°)–200°(2°)(20)	1.000 ^c		130
(<i>Z</i>)-2,3-Dihydrofarnesoic acid	β -(2,3-Me-6-TBS)	130°(5)–155°(1.5°)(5)–162°(0.5°)–200°(2°)(20)		(3 <i>S</i>)	130

^a The following abbreviations are used: AcF is trifluoroacetyl, Bu is n-butyl, But is butyryl (butanoyl), Pe is n-pentyl and TBS is *tert*-butyldimethylsilyl;

^b determined as trifluoroacetate; ^c enantiomers are not resolved; ^d A 0.162 M solution of α -cyclodextrin in glycerol; ^e 10% β -cyclodextrin in polysiloxane SPB-35; ^f Chirasil- γ -Dex phase: the chiral selector γ -(2,6-Pe-3-But) is grafted to polymethylpolysiloxane through the octamethylene spacer.

Table 2. Enantiomeric resolution of sesquiterpene hydrocarbons by chiral GLC under isothermal conditions on stationary phases containing cyclodextrin derivatives as chiral selectors.

Selectand	Column 1 ^a			Column 2 ^b			Ref.
	α	column temperature /°C	first-eluted enantiomer	α	column temperature /°C	first-eluted enantiomer	
α -Amorphene	1.385	120	(−)	1.193	120	(−)	87
γ -Amorphene	1.895	115	(+)	1.218	115	(+)	87
δ -Amorphene	1.394	120	(+)				131
ε -Amorphene				1.093	115	(+)	87
Aristolene	1.078	90 ^c	(−)				87
Aristolochene	1.120	110	(+)				132
Aromadendrene	1.170	120	(−)	1.437	120	(−)	87
Alloaromadendrene	1.233	110	(−)	1.379	110	(−)	87
α -Barbatene	1.025	90	(−)				97
β -Barbatene	1.057	90	(−)				97
<i>cis</i> - α -Bergamotene	1.070	100	(−)				132
<i>trans</i> - α -Bisabolene	1.036	85 ^c	(−)				93
β -Bisabolene	1.018	85 ^c	(−)	1.050	115	(−)	93
Bicyclogermacrene	1.000 ^d			1.078	100	(+)	93
Bicycloelemene	1.100	80 ^c	(+)	1.143	110		87
α -Bourbonene				1.152	105	(+)	87
β -Bourbonene	1.068	105 ^c	(+)	1.081	105	(−)	87
Valencene	1.120	110 ^c	(−)	1.075	125	(−)	87
Geijerene				1.071	115		87
Germacrene D	1.11	110 ^c	(+)	1.074	115	(+)	133
α -Gurjunene	1.000 ^d			1.344	110	(−)	87
γ -Gurjunene	1.000 ^d			1.150	100	(+)	134
Zonarene				1.170	120	(−)	87
Epizonarene				1.437	120	(−)	87
Isobarbatene	1.032	90 ^c	(+)				97
Isobicyclogermacrene	1.037	105 ^c	(+)				87
Isolongifolene	1.120	85 ^c	(+)				87
Isosativene	1.049	105 ^c	(+)				87
α -Ylangene	1.220	90	(+)				87
β -Ylangene	1.088	120	(+)	1.064	115	(−)	87
Cadina-1,4-diene	1.038	115	(−)	1.249	120	(+)	87
α -Cadinene				1.140	120	(−)	87
β -Cadinene				1.145	120	(−)	87
γ -Cadinene	1.257	115	(−)	1.249	115	(−)	87
δ -Cadinene	1.680	115 ^c	(−)	1.260	115	(−)	93
ε -Cadinene	1.230	120	(+)				87
α -Calocorene	1.084	120 ^c	(+)				13
<i>trans</i> -Calamenene				1.257	120	(−)	93
<i>cis</i> -Calamenene				1.272	120	(−)	93
Calarene	1.045	90 ^c	(+)	1.026	100	(+)	135
Caryophyllene	1.131	95 ^c	(+)	1.065	100	(+)	95
Clovene	1.039	80 ^c	(−)				87
α -Copaene	1.084	90 ^c	(+)	1.015	90 ^c		93
β -Copaene				1.052	115	(−)	87
α -Cubebene	1.173	90 ^c	(+)	1.030	100	(+)	135
β -Cubebene	1.000 ^d			1.028	90 ^c	(−)	135
Cuparene	1.027	105 ^c	(−)	1.048	120	(−)	135
α -Cuprenene	1.029	95 ^c	(−)				87
Iso- <i>ar</i> -curcumene	1.031	110		1.041	110		87
<i>ar</i> -Curcumene	1.030	85	(+)	1.030	115	(+)	93
Ledene	1.05	105 ^c	(−)				135
Longifolene	1.048	80 ^c	(−)				87
α -Longipinene	1.030	80 ^c	(+)	1.028	105	(−)	87
α -Microbiotene	1.020	110	(−)				136
β -Microbiotene	1.022	110	(+)				136
<i>cis</i> -Muuro-4-ene		110 ^c	(1R)				137
<i>cis</i> -Muuro-4-ene		110 ^c	(1R)				137
α -Muuro-4-ene	1.206	105 ^c	(−)	1.056	125	(−)	87

Table 2 (continued).

Selectand	Column 1 ^a			Column 2 ^b			Ref.
	α	column temperature /°C	first-eluted enantiomer	α	column temperature /°C	first-eluted enantiomer	
γ -Muurolene	1.146	115 ^c	(–)	1.163	115	(+)	87
ϵ -Muurolene				1.124	115	(–)	87
α -Neocallitropsene	1.066	110	(–)				87
α -Selinene	1.110	110 ^c	(–)				87
α -7- <i>epi</i> -Selinene	1.060	105	(+)	1.085	105	(–)	132
δ -Selinene	1.148	110 ^c	(+)	1.136	115	(+)	135
δ -Selinene	1.133	120	(+)	1.073	120	(+)	138
Thujopsene	1.048	110	(+)				135
α -Cedrene	1.079	110 ^c	(+)	1.076	110	(+)	135
β -Elemene	1.000 ^d			1.024	90	(+)	95
γ -Elemene	1.023	110	(+)				135
δ -Elemene	1.026	80 ^c		1.063	90 ^c		93
Eremophyllene	1.063	100 ^c	(–)	1.024	100 ^c	(–)	87
Erythrodiene	1.027	100					87

^a 50% β -(2,6-Me-3-Pe) in polysiloxane OV-1701; ^b 50% β -(2,3-Me-6-TBS) in polysiloxane OV-1701; ^c the corresponding cyclodextrin was taken in an amount of 20%; ^d enantiomers are not resolved.

Table 3. Enantiomeric resolution of diterpenoids by chiral GLC under isothermal conditions on stationary phases containing cyclodextrin derivatives as chiral selectors.

Selectand	Chiral selector	Column temperature /°C	α	First-eluted enantiomer	Ref.
Abieta-7,13-diene	β -(2,3-Me-6-TNS)	150	1.02	(+)	139
15-Beyerene	β -(2,6-Me-3-Pe)	145	1.03	(+)	139
Dolabradiene	γ -(2,6-Me-3-Pe)	120		(–)	140
15-Kaurene	β -(2,6-Me-3-Pe)	145	1.04	(–)	139
16-Kaurene	β -(2,6-Me-3-Pe)	145	1.08	(–)	139
Isopimara-8,15-diene	β -(2,3-Me-6-TBS)	150		(–)	141
13- <i>epi</i> -Manoyl oxide	β -(2,3-Me-6-TBS)	140		(+)	140
Pimara-8,15-diene	β -(2,3-Me-6-TBS)	150		(+)	141
Pimara-8(14),15-diene	γ -(2,6-Me-3-Pe)	120		(+)	140
Rosa-5,15-diene	γ -(2,6-Me-3-Pe)	120		(+)	140
Sclarene	γ -(2,6-Me-3-Pe)	150		(–)	140
Sclareol	β -(2,3-Me-6-TBS)	175		(–)	140

Table 4. Enantiomeric resolution of non-terpene flavour and fragrance compounds by chiral GLC on stationary phases containing cyclodextrin derivatives as chiral selectors.

Selectand	Chiral selector	Column temperature (°C) or the temperature conditions	α	First-eluted enantiomer	Ref.
2-Methylbutanal	β -(2,3-Ac-6-TBS)	40°(5)–220°(1.5°)		(<i>R</i>)	142
Filbertone	β -(2,3-Ac-6-TBS)	80°	1.108		108
Alk-1-en-3-ols (C ₅ –C ₉)	γ -(2,3-Bu-6-TBS)	40°(5)–220°(1°)		(<i>R</i>)	142
Alkan-3-ols (C ₆ –C ₈)	γ -(2,3-Bu-6-TBS)	40°(5)–220°(1°)		(<i>R</i>)	142
Alkan-2-ols (C ₅ –C ₁₀)	γ -(2,3-Bu-6-TBS)	40°(5)–220°(1°)		(<i>S</i>)	142
Oct-1-en-3-ol	β -(2,3-Ac-6-TBS)	80°	1.044	(<i>S</i>)	108
	β -(2,3-Ac-6-TBS)	60°(18)–120°(1°)–200°(10°)		(<i>S</i>)	115
	β -(2,3-Ac-6-TBS)	60°(20)–120°(1.3°)		(<i>S</i>)-(+))	11
Octan-3-ol	β -(2,3-Ac-6-TBS)	60°(18)–120°(1°)–200°(10°)		(<i>R</i>)	115
	β -(2,3-Ac-6-TBS)	60°(20)–120°(1.3°)		(<i>R</i>)-(–)	11
	β -(2,3-Ac-6-TBS)	80°	1.013	(<i>R</i>)	108
Octane-1,3-diol	β -(2,3-Ac-6-TBS)				105
1,3-Dioxanes	β -(2,3-Ac-6-TBS)				143
2-Methylbutan-1-ol	β -(2,3-Me-6-TBS)	70°(5)–200°(1.5°)		(<i>R</i>)	38
	β -(2,3-Ac-6-TBS)	50°	1.064	(<i>R</i>)	108
2-Methylpentan-1-ol	β -(2,3-Ac-6-TBS)	70°	1.065	(<i>R</i>)	108
2-Methylhexan-1-ol	β -(2,3-Ac-6-TBS)	70°	1.071	(<i>R</i>)	108
2-Ethylhexan-1-ol	β -(2,3-Ac-6-TBS)	70°	1.075	(<i>R</i>)	108
2-Methylbutyl acetate	β -(2,3-Me-6-TBS)	70°(5)–200°(1.5°)		(<i>S</i>)	32
3-Butyl-4-vinylcyclopentene	CP-Cyclodex 236 M	30°(4)–215°(1°)	1.009	(3 <i>S</i> ,4 <i>S</i>)-(+))	144

Table 4 (continued).

Selectand	Chiral selector	Column temperature (°C) or the temperature conditions	α	First-eluted enantiomer	Ref.
Ethyl 2-methylbutanoate	β -(2,3-Me-6-TBS)	70°(5)–200°(1.5°)		(R)	38
	β -(2,3,6-Me)			(R)-(–)	37
Propyl 2-methylbutanoate	β -(2,3-Ac-6-TBS)	55°	1.033	(S)	108
Methyl 2-methylbutanoate	β -(2,3-Me-6-TBS)	60°(13)–108°(1.5°)–200°(2.5°)		(R)	16
Methyl jasmonate	β -(2,3,6-Me)			(1R,2R)-(–)	31
	β -(2,6-Me-3-Pe)	120°		(–)	92
Methyl <i>epi</i> -jasmonate	β -(2,6-Pe-3-AcF)			(1R,2S)-(+)	37
Methyl 2-hydroxypropanoate (methyl lactate)	γ -(2,6-Pe-3-But) ^a	80°	1.198–1.236	(S)-(–)	71
Ethyl 2-hydroxypropanoate (ethyl lactate)	β -(2,3-Me-6-TBS)	80°(7)–200°(2°)		(R)	14
Ethyl 4-hydroxy-5-oxohexanoate	β -(2,6-Me-3-Pe)	100°(20)–200°(2°)		(R)	145
Methyl lipolate	β -(2,6-Pe-3-Ac)	180°		(R)	118
α -Hydroxy acid methyl esters (C ₁₀ –C ₂₂)	β -(2,3-Me-6-TBS)	110°–175°(1.5°)–190°(0.5°)		(R)	123
Methyl 2-methylcarboxylates (C ₄ –C ₇)	β -(2,3-Me-6-TBS)	40°–230°(1.5°)		(R)	123
Methyl 2-ethylhexanoate	β -(2,3-Me-6-TBS)	40°–230°(1.5°)		(R)	123
Methyl 4-methylcarboxylates (C ₆ –C ₉)	β -(2,3-Me-6-TBS)	40°–230°(1.5°)		(S)	123
2-Methylbutyric acid	β -(2,3-Me-6-TBS)	70°(5)–200°(1.5°)		(S)	38
	β -(2,3,6-Me)			(S)-(+)	37
2-Methylcarboxylic acids (C ₄ –C ₇)	β -(2,3-Me-6-TBS)	90°(5)–230°(1.5°)		(S)	123
	γ -(2,3-Me-6-TBS)	80°(5)–230°(1.5°)		(S)	123
2-Methylbutanoic acid	β -(2,3-Me-6-TBS)	40°(5)–85°(5°)–140°(1.5°)–230°(4°)		(2S)	18
2-Methylpentanoic acid	γ -(2,3-Me-6-TBS)	40°(5)–100°(10°)–130°(1°)–235°(3°)		(2S)	19
	β -(2,3-Me-6-TBS)	40°(5)–85°(5°)–140°(1.5°)–230°(4°)		(2S)	18
2-Methylhexanoic acid	γ -(2,3-Me-6-TBS)	40°(5)–100°(10°)–130°(1°)–235°(3°)		(2S)	19
	β -(2,3-Me-6-TBS)	40°(5)–85°(5°)–140°(1.5°)–230°(4°)		(2S)	18
2-Methylheptanoic acid	γ -(2,3-Me-6-TBS)	40°(5)–100°(10°)–130°(1°)–235°(3°)		(2S)	19
	β -(2,3-Me-6-TBS)	40°(5)–85°(5°)–140°(1.5°)–230°(4°)		(2S)	18
2-Methyloctanoic acid	γ -(2,3-Me-6-TBS)	40°(5)–100°(10°)–130°(1°)–235°(3°)		(2R)	19
2-Ethylhexanoic acid	β -(2,3-Me-6-TBS)	90°(5)–230°(1.5°)		(S)	123
	γ -(2,3-Me-6-TBS)	40°(5)–100°(10°)–130°(1°)–235°(3°)		(2S)	19
	γ -(2,3-Me-6-TBS)	80°(5)–230°(1.5°)		(S)	123
3-Methylcarboxylic acids (C ₅ –C ₇)	β -(2,3-Me-6-TBS)	90°(5)–230°(1.5°)		(S)	123
3-Methylcarboxylic acids (C ₅ , C ₈ –C ₁₀)	γ -(2,3-Me-6-TBS)	80°(5)–230°(1.5°)	1.000 ^d		123
3-Methylenanthic acid	γ -(2,3-Me-6-TBS)	80°(5)–230°(1.5°)		(S)	123
4-Methylcarboxylic acids (C ₆ –C ₉)	β -(2,3-Me-6-TBS)	90°(5)–230°(1.5°)		(R)	123
4-Methylhexanoic acid	γ -(2,3-Me-6-TBS)	80°(5)–230°(1.5°)	1.000 ^d		123
	β -(2,3-Me-6-TBS)	90°(5)–190°(1.5°)(20)		(4R)	130
4-Methylcarboxylic acids (C ₈ , C ₉)	γ -(2,3-Me-6-TBS)	80°(5)–230°(1.5°)		(R)	123
4-Ethyl octanoic acid	β -(2,3-Me-6-TBS)	90°(5)–230°(1.5°)		(4R)	18, 19
	γ -(2,3-Me-6-TBS)	40°(5)–100°(10°)–130°(1°)–235°(3°)		(4R)	19
4-Pentanolide	β -(2,3-Ac-6-TBS)	140°	1.422		108
4-Hexanolide	β -(2,3-Ac-6-TBS)	140°	1.221	(R)	108
4-Heptanolide	β -(2,3-Ac-6-TBS)	140°	1.061	(R)	108
4-Octanolide	β -(2,3-Ac-6-TBS)	155°	1.056	(R)	108
	β -(2,3-Me-6-TBS)	60°(13)–108°(1.5°)–200°(2.5°)		(R)	16
4-Nonanolide	β -(2,3-Ac-6-TBS)	160°	1.047	(R)	108
4-Decanolide	β -(2,3-Me-6-TBS)	60°(13)–108°(1.5°)–200°(2.5°)		(R)	16
	β -(2,3-Ac-6-TBS)	165°	1.043	(R)	108
4-Undecanolide	β -(2,3-Ac-6-TBS)	170°	1.042	(R)	108
4-Dodecanolide	β -(2,3-Ac-6-TBS)	175°	1.038	(R)	108
	β -(2,3-Me-6-TBS)	60°(13)–108°(1.5°)–200°(2.5°)		(R)	16
γ -Lactones (C ₇ –C ₁₂)	β -(2,6-Pe-3-Ac)			(R)-(+)	37
5-Hexanolide	β -(2,3-Ac-6-TBS)	140°	1.121	(R)	108
5-Octanolide	β -(2,3-Ac-6-TBS)	145°	1.070	(S)	108
5-Nonanolide	β -(2,3-Ac-6-TBS)	140°	1.039	(S)	108
5-Decanolide	β -(2,3-Ac-6-TBS)	155°	1.030	(S)	108
5-Undecanolide	β -(2,3-Ac-6-TBS)	170°	1.023	(S)	108
5-Dodecanolide	β -(2,3-Ac-6-TBS)	175°	1.022	(S)	108
δ -Lactones (C ₈ –C ₁₂)	β -(2,3-Ac-6-TBS)	45°(2)–120°(20°)(15)–125°(3°)–175°(1.5°)		(S)	146
δ -Lactones (C ₈ –C ₁₄)	γ -(2,6-Pe-3-AcF)			(S)-(–)	37
δ -Lactones (C ₁₃ –C ₁₈)	β -(2,3-Ac-6-TBS)	45°(2)–120°(20°)(35)–160°(2°)–200°(1°)		(S)	146
	β -(2,3-Ac-6-TBS)	120°(15)–220°(1.5°)		(S)	123

Table 4 (continued).

Selectand	Chiral selector	Column temperature (°C) or the temperature conditions	α	First-eluted enantiomer	Ref.
Dec-2-en-5-olide (massoilactone)	α -(2,6-Pe-3-Ac)	80°–160°(1°)		(S)-(+)	147
4-Methyl-5-decanolide	β -(2,3-Me-6-TBS)	60°(13)–108°(1.5°)–200°(2.5°)		(R)	148
γ -Jasmine lactone	β -(2,6-Pe-3-Ac)			(+)	37
δ -Jasmine lactone	β -(2,6-Pe-3-Ac)			(R)-(–)	37
Sherry lactone	γ -(2,6-Pe-3-Bu)				149
Furaneol	β -(2,3-Me-6-TBS)	35°(2)–80°(20°)(5)–230°(1°)		(–)	150
2-Methyl-4-pentyl-1,3-dioxane	β -(2,3-Ac-6-TBS)	50°(30)–220°(1°)		(2S,4R)	143
3-Mercapto-2-methylpropan-1-ol diacetate	β -(2,3-Me-6-TBS)	50°–210°(1°)		(–)	17
<i>trans</i> -2-Methyl-4-propyl-1,3-oxathiane	β -(2,3,6-Me)			(2R,4R)-(+)	37
	β -(2,3-Ac-6-TBS)	100°	1.100	(2R,4S)	108
	γ -(2,3-But-6-TBS)	40°(5)–105°(5°)(22)–150°(1.5°)–220°(1.5°)(30)		(2R,4R)	151
<i>cis</i> -2-Methyl-4-propyl-1,3-oxathiane	β -(2,3,6-Me)			(2R,4S)-(–)	37
	β -(2,3-Ac-6-TBS)	100°	1.227	(2R,4R)	108
	γ -(2,3-But-6-TBS)	40°(5)–105°(5°)(22)–150°(1.5°)–220°(1.5°)(30)		(2R,4S)	151
2,2-Dimethyl-4-propyl-1,3-oxathiane	γ -(2,3-But-6-TBS)	40°(5)–105°(5°)(22)–150°(1.5°)–220°(1.5°)(30)		(4S)	151
	β -(2,3-Ac-6-TBS)	80°	1.043		108
3-(Methylthio)hexan-1-ol	β -(2,3,6-Me)			(R)-(–)	37
	β -(2,3-Ac-6-TBS)	95°	1.035	(S)	108
2-Mercapto-3-pentanone	β -(2,3,6-Me)			(+)	37
3-(Methylthio)butanal	γ -(2,3-But-6-TBS)	50°(5)–220°(1.5°)(30)		(S)	6
3-(Methylthio)butan-1-ol	γ -(2,3-But-6-TBS)	50°(5)–220°(1.5°)(30)		(S)	6
3-Mercaptobutan-1-ol	γ -(2,3-But-6-TBS)	50°(5)–220°(1.5°)(30)		(S)	6
3-Mercaptohexan-1-ol	β -(2,3-Ac-6-TBS)	95°	1.164	(S)	108
3-Mercaptohexyl acetate	γ -(2,3-But-6-TBS)	40°(5)–105°(5°)(22)–150°(1.5°)–220°(1.5°)(30)		(R)	151
3-Mercaptohexyl propanoate	γ -(2,3-But-6-TBS)	40°(5)–105°(5°)(22)–150°(1.5°)–220°(1.5°)(30)		(R)	151
3-Mercaptohexyl butanoate	γ -(2,3-But-6-TBS)	40°(5)–105°(5°)(22)–150°(1.5°)–220°(1.5°)(30)		(R)	151
3-Butylhexahydrophthalide I	β -(2,3-Ac-6-TBS)	110°(120)–120°(1.5°)(5)–180°(1°)	1.037	(3S,3aS,7aR)	152
	β -(2,3-Ac-6-TBS)	40°(5)–140°(60°)(25)–180°(1.5°)	1.032	(3S,3aS,7aR)	152
3-Butylhexahydrophthalide II	β -(2,3-Ac-6-TBS)	110°(120)–120°(1.5°)(5)–180°(1°)	1.014	(3S,3aR,7aS)	152
	β -(2,3-Ac-6-TBS)	40°(5)–120°(60°)(70)–180°(1°)	1.018	(3S,3aR,7aS)	152
3-Butylhexahydrophthalide III	β -(2,3-Ac-6-TBS)	110°(120)–120°(1.5°)(5)–180°(1°)	1.010	(3S,3aR,7aR)	152
	β -(2,3-Ac-6-TBS)	40°(5)–105°(60°)(120)–125°(1.5°)(30)	1.009	(3S,3aR,7aS)	152
3-Butylhexahydrophthalide IV	β -(2,3-Ac-6-TBS)	110°(120)–120°(1.5°)(5)–180°(1°)	1.023	(3S,3aS,7aS)	152
	β -(2,3-Ac-6-TBS)	40°(5)–140°(60°)(25)–180°(1.5°)	1.031	(3S,3aS,7aS)	152
3-Butylphthalide	γ -(2,3-TBS)	140°(5)–180°(2°)		(3S)	153
	β -(2,3-Ac-6-TBS)	95°(25)–109°(2.5°)(160)–150°(1.2°)(30)		(3S)	154
3a,7a- <i>trans</i> -3-Butylhexahydrophthalide	β -(2,3-Ac-6-TBS)	95°(25)–109°(2.5°)(160)–150°(1.2°)(30)		(3S,3aR,7aR)	154
				(3S,3aS,7aS)	154
3a,7a- <i>cis</i> -3-Butylhexahydrophthalide	β -TBS ^b	140°(1)–160°(1°)(1)–200°(20°)(10)			155
	β -(2,3-Ac-6-TBS)	95°(25)–109°(2.5°)(160)–150°(1.2°)(30)		(3S,3aS,7aR)	154
3-Methylalkane-1-thiols	β -(2,3-Me-6-TBS)				6
Pentane-2-thiol	β -(2,3-Et-6-TBS)	40°	1.04	(S)	88
Solerole I	β -(2,3-Ac-6-TBS)	100°(20)–200°(2°)		(4S,5S)	156
	γ -(2,6-Me-3-Pe)	110°(30)–200°(1°)		(4S,5S)	156
Solerole II	β -(2,6-Me-3-Pe)	100°(20)–200°(2°)		(4R,5S)	156
	γ -(2,6-Me-3-Pe)	110°(30)–200°(1°)		(4S,5R)	156
Solerone	β -(2,3-Ac-6-TBS)	100°(20)–200°(3°)		(R)	145
Lilial aldehyde	β -(2,3-Ac-6-TBS)	40°(5)–110°(60°)(35)–140°(1.5°)		(S)	20
2-Phenylpropanal	β -(2,3-Ac-6-TBS)	40°(5)–100°(60°)(30)		(R)	157
2-Phenylpropanol	β -(2,3-Ac-6-TBS)	40°(5)–100°(60°)(30)		(R)	157
2-Phenylpropanal dimethylacetal	β -(2,3-Ac-6-TBS)	40°(4)–100°(60°)(10)–140°(1.5°)		(R)	157
Arabinitol ^c	α -(2,3,6-Pe)	110°		(D)	118
Geosmin	β -(2,3-Me-6-TBS)	60°(35)–200°(1.5°)		(+)	2

^a The Chirasil- γ -Dex phase: the chiral selector γ -(2,6-Pe-3-But) is grafted to polymethylpolysiloxane through the octamethylene spacer; ^b 6-*tert*-butyldimethylsilyl- β -cyclodextrin in polysiloxane; ^c as pentakis(trifluoroacetyl) derivatives; ^d enantiomers are not resolved.

flavour compounds, such as mono- and sesquiterpenoids and related compounds (Table 1), sesquiterpene hydrocarbons (Table 2), diterpenoids (Table 3) and various aliphatic and alicyclic compounds (Table 4). These data include the types of chiral selectors (modified cyclodextrin), the temperature con-

ditions of chromatography, the selectivity factors and the elution orders of enantiomers.

The following abbreviations are used in the tables to denote chiral cyclodextrin selectors involved in stationary phases: the nature of the starting cyclodextrin (α , β or γ) followed

(in parentheses) by the position and the nature of substituents in modified cyclodextrin molecules. For example, the notation β -(2,6-Me-3-Pe) means that the stationary phase for chiral GLC was prepared based on heptakis(2,6-di-*O*-methyl-3-*O*-*n*-pentyl)- β -cyclodextrin. For the temperature conditions, the following abbreviations are used: 60°(18)–120°(1°)(10)–200°(10°)(5). This means that heating is performed for 18 min at 60 °C followed by the rise of the temperature to 120 °C at a rate of 1 deg min^{−1}, storage at 120 °C for 10 min, the rise of the temperature to 200 °C at a rate of 10 deg min^{−1} and storage at 200 °C for 5 min. For many enantiomeric pairs, the selectivity factors (α) and first-eluted enantiomer are given.

This review has been written with the financial support of the Russian Foundation for Basic Research (Project No. 07-03-00 620-a). I thank N I Tkacheva (N N Vorozhtsov Novosibirsk Institute of Organic Chemistry, Siberian Branch of the Russian Academy of Sciences) for help in the literature search.

References

- H G Haring, F Rijkens, H Boelens, A Van der Gen *J. Agric. Food Chem.* **20** 1018 (1972)
- P Darriet, S Lamy, S La Guerche, M Pons, D Dubourdieu, D Blancard, P Steliopoulos, A Mosandl *Eur. Food Res. Technol.* **213** 122 (2001)
- H Guth *Helv. Chim. Acta* **76** 1559 (1996)
- E Brenna, C Fuganti, S Serra *Tetrahedron: Asymmetry* **14** 1 (2003)
- R Zawirska-Wojtasiak *Food Chem.* **86** 113 (2004)
- B Weber, A Mosandl *Z. Lebensm.-Unters.-Forsch. A* **204** 194 (1997)
- B Faber, K Bangert, A Mosandl *Flavour Fragr. J.* **12** 305 (1997)
- U Ravid, E Putievsky, I Katzir *Flavour Fragr. J.* **8** 225 (1993)
- F Tateo, M Bononi, E D Dominicus, V Fumagalli *Anal. Commun.* **36** 149 (1999)
- Y Holm, P Vuorela, R Hiltunen *Flavour Fragr. J.* **12** 397 (1997)
- P Kreis, A Mosandl *Flavour Fragr. J.* **9** 249 (1994)
- U Hener, S Faulhaber, P Kreis, A Mosandl *Pharmazie* **50** 60 (1995)
- I H Hardt, A Reick, C Fricke, W A König *Flavour Fragr. J.* **10** 165 (1995)
- A Kaunzinger, M Wüst, H Grobmiller, S Burow, U Hemmrich, A Dietrich, T Beck, U Hener, A Mosandl, A Rapp *Z. Lebensm.-Unters.-Forsch. A* **203** 499 (1996)
- T Beuerle, P Schreier, P Brunerie, C Bicchì, W Schwab *Phytochemistry* **43** 145 (1996)
- M Kreck, A Scharrer, S Bilke, A Mosandl *Eur. Food Res. Technol.* **213** 389 (2001)
- P Bouchilloux, P Darriet, D Dubourdieu, R Henry, S Reichert, A Mosandl *Eur. Food Res. Technol.* **210** 349 (2001)
- V Karl, A Kaunzinger, J Gutser, P Steuer, J Angles-Angel, A Mosandl *Chirality* **6** 420 (1994)
- V Karl, J Gutser, A Dietrich, B Maas, A Mosandl *Chirality* **6** 427 (1994)
- D Bartschat, S Börner, A Mosandl, J W Bats *Z. Lebensm.-Unters.-Forsch. A* **205** 76 (1997)
- R Reinhardt, A Steinborn, W Engewald, K Anhalt, K Schulze *J. Chromatogr., A* **697** 475 (1995)
- A Steinborn, R Reinhardt, W Engewald, K Wyssuwa, K Schulze *J. Chromatogr., A* **697** 485 (1995)
- F Quattrini, G Biressi, M Juza, M Mazzotti, C Fuganti, M Morbidelli *J. Chromatogr., A* **865** 201 (1999)
- T J Ward *Anal. Chem.* **74** 2863 (2002)
- N R Srinivas, W C Shyu, R H Barbhaiya *Biomed. Chromatogr.* **9** 1 (1995)
- G Sándor *Fresenius' J. Anal. Chem.* **362** 4 (1998)
- K-R Kim, J Lee, D Ha, J H Kim *J. Chromatogr., A* **891** 257 (2000)
- W A König *TrAC — Trends Anal. Chem.* **12** 130 (1993)
- V Schurig *TrAC — Trends Anal. Chem.* **21** 647 (2002)
- L A Kartsova *Molekulyarnoe Raspoznavanie v Khromatografii: Ispol'zovanie Makrotsiklov v Sostave Khromatograficheskikh Faz* (Molecular Recognition in Chromatography: The Use of Macrocycles in Chromatographic Phases) (St Petersburg: St Petersburg State University, 2004)
- Z Juvancz, P Petersson *J. Microcolumn Sep.* **8** 99 (1996)
- B Feibush *Chirality* **10** 382 (1998)
- V Schurig *J. Chromatogr., A* **906** 275 (2001)
- V Schurig *J. Chromatogr., A* **965** 315 (2002)
- W A König *Gas Chromatographic Enantiomer Separation with Modified Cyclodextrins* (Heidelberg: Hüthig, 1992)
- A Mosandl *J. Chromatogr., A* **624** 267 (1992)
- P Werkhoff, S Brennecke, W Bretschneider, M Güntert, R Hopp, H Surburg *Z. Lebensm.-Unters.-Forsch. A* **196** 307 (1993)
- A Mosandl *Food Res. Int.* **11** 597 (1995)
- C Bicchì, V Manzin, A D'Amato, P Rubiolo *Flavour Fragr. J.* **10** 127 (1995)
- C Bicchì, A D'Amato, P Rubiolo *J. Chromatogr., A* **843** 99 (1999)
- M Wmst, A Mosandl *Eur. Food Res. Technol.* **209** 3 (1999)
- R G Mariaca, M I Imhof, J O Bosset *Eur. Food Res. Technol.* **212** 253 (2001)
- L He, T E Beesley *J. Liq. Chromatogr. Relat. Technol.* **28** 1075 (2005)
- M V Rekharsky, Y Inoue *Chem. Rev.* **98** 1875 (1998)
- E Schneiderman, A M Stalcup *J. Chromatogr., B* **745** 83 (2000)
- J Szejtli *Chem. Rev.* **98** 1743 (1998)
- W A König, R Krebber, G Wenz *J. High Resolut. Chromatogr.* **12** 641 (1989)
- Yu A Zhdanov, Yu E Alekseev, E V Kompantseva, E N Vergeichik *Usp. Khim.* **61** 1025 (1992) [*Russ. Chem. Rev.* **61** 563 (1992)]
- M Asztemborska, D Sybilska, R Nowakowski, G Perez *J. Chromatogr., A* **1010** 233 (2003)
- R Reinhardt, W Engewald, U Himmelreich, B Christian, B Koppenhoefer *J. Chromatogr. Sci.* **33** 236 (1995)
- W A König, C Fricke, Y Saritas, B Momeni, G Hohenfeld *J. High Resolut. Chromatogr.* **20** 55 (1997)
- W A König *Chirality* **10** 499 (1998)
- V Schurig, H-P Nowotny *J. Chromatogr., A* **441** 155 (1988)
- H-G Schmarr, A Mosandl, A Kaunzinger *J. Microcolumn Sep.* **3** 395 (1991)
- A Dietrich, B Maas, G Brand, V Karl, A Kaunzinger, A Mosandl *J. High Resolut. Chromatogr.* **15** 769 (1992)
- A Dietrich, B Maas, A Mosandl *J. Microcolumn Sep.* **6** 33 (1994)
- W A König, S Lutz, P Mischnick-Lübbecke, B Brassat, G Wenz *J. Chromatogr.* **447** 193 (1988)
- W A König, S Lutz, G Wenz *Angew. Chem., Int. Ed. Engl.* **27** 979 (1988)
- W A König, S Lutz, G Wenz, E von der Bey *J. High Resolut. Chromatogr.* **11** 506 (1988)
- W A König, S Lutz, C Colberg, N Schmidt, G Wenz, E von der Bey, A Mosandl, C Günther, A Kustermann *J. High Resolut. Chromatogr.* **11** 621 (1988)
- W A König, S Lutz, M Hagen, R Krebber, G Wenz, K Baldenius, J Ehlers, H T Dieck *J. High Resolut. Chromatogr.* **12** 35 (1989)
- W A König, R Krebber, P Mischnick *J. High Resolut. Chromatogr.* **12** 732 (1989)
- W A König, R Krebber, G Wenz *J. High Resolut. Chromatogr.* **12** 641 (1989)
- W A König, D Icheln, T Runge, I Pforr, A Krebs *J. High Resolut. Chromatogr.* **13** 702 (1990)
- G Wenz, P Mischnick, R Krebber, M Richters, W A König *J. High Resolut. Chromatogr.* **13** 724 (1990)
- W A König, B Gehrcke, D Icheln, P Evers, J Dönnecke, W Wang *J. High Resolut. Chromatogr.* **15** 367 (1992)
- C Bicchì, G Artuffo, A D'Amato, V Manzin, A Galli, M Galli *J. High Resolut. Chromatogr.* **16** 209 (1993)
- I H Hardt, W A König *J. Microcolumn Sep.* **5** 35 (1993)
- C Bicchì, A D'Amato, V Manzin, A Galli, M Galli *J. Microcolumn Sep.* **7** 327 (1995)

70. C Bicchi, A D'Amato, V Manzin, A Galli, M Galli *J. Chromatogr.*, **A 742** 161 (1996)
71. H Grosenick, V Schurig *J. Chromatogr.*, **A 761** 181 (1997)
72. T J Betts *J. Chromatogr.*, **A 724** 403 (1996)
73. M Junge, W A König *J. Sep. Sci.* **26** 1607 (2003)
74. G Chen, X Shi *Anal. Chim. Acta* **498** 39 (2003)
75. H Cousin, O Trapp, V Peulon-Agasse, X Pannecoucke, L Banspach, G Trapp, Z Jiang, J C Combret, V Schurig *Eur. J. Org. Chem.* 3273 (2003)
76. A Jaus, M Oehme *J. Chromatogr.*, **A 905** 59 (2001)
77. J Jindrich, J Pitha, B Lindberg, P Seffers, K Harata *Carbohydr. Res.* **266** 75 (1995)
78. M-Y Nie, L-M Zhou, X-L Liu, Q-H Wang, D-Q Zhu *Anal. Chim. Acta* **408** 279 (2000)
79. C Bicchi, G Brunelli, G Cravotto, P Rubiolo, M Galli *J. Sep. Sci.* **25** 125 (2002)
80. S Tamogami, K-i Awano, M Amaike, Y Takagi, T Kitahara *Flavour Fragr. J.* **16** 349 (2001)
81. A Ruderisch, J Pfeiffer, V Schurig *J. Chromatogr.*, **A 994** 127 (2003)
82. P A Levkin, A Levkina, H Czesla, S Nazzi, V Schurig *J. Sep. Sci.* **30** 98 (2007)
83. J Dönnecke, W A König, O Gyllenhaal, J Vessman, C Schulze *J. High Resolut. Chromatogr.* **17** 779 (1994)
84. V Schurig, M Jung, S Mayer, M Fluck, H Negura, H Jakubetz *J. Chromatogr.*, **A 694** 119 (1995)
85. H F Kasai, M Tsubuki, K Takahashi, M Shirao, Y Matsumoto, T Honda, Y Seyama *J. Chromatogr.*, **A 977** 125 (2002)
86. H Grosenick, V Schurig, J Costante, A Collet *Tetrahedron: Asymmetry* **6** 87 (1995)
87. W A König, N Bülow, Y Saritas *Flavour Fragr. J.* **14** 367 (1999)
88. T König, C Ruff, M Kleinschnitz, P Schreier, N Fischer, W Neugebauer *J. High Resolut. Chromatogr.* **21** 371 (1998)
89. A Hinterholzer, P Schieberle *Flavour Fragr. J.* **13** 49 (1998)
90. J Beens, U A T Brinkman *Analyst (Cambridge, UK)* **130** 123 (2005)
91. R Shellie, P J Marriott *Anal. Chem.* **74** 5426 (2002)
92. I Hardt, W A König *J. Chromatogr.*, **A 666** 611 (1994)
93. W A König, A Reick, I Hardt, B Gehrcke, K-H Kubiczka, H Muhle *J. High Resolut. Chromatogr.* **17** 315 (1994)
94. M M Sonwa, W A König, K-H Kubiczka, O Motl *Phytochemistry* **45** 1435 (1997)
95. C Fricke, A Reick, I H Hardt, W A König, H Muhle *Phytochemistry* **39** 1119 (1995)
96. A M Adio, C Paul, P Kloth, W A König *Phytochemistry* **65** 199 (2004)
97. W A König, A Reick, Y Saritas, I H Hardt, K-H Kubiczka *Phytochemistry* **42** 461 (1996)
98. C Bicchi, A D'Amato, V Manzin, A Galli, M Galli *J. High Resolut. Chromatogr.* **20** 493 (1997)
99. C Bicchi, C Balbo, A D'Amato, V Manzin, P Schreier, A Rozenblum, P Brunerie *J. High Resolut. Chromatogr.* **21** 103 (1998)
100. M Juza, E Braun, V Schurig *J. Chromatogr.*, **A 769** 119 (1997)
101. N Bülow, W A König *Phytochemistry* **55** 141 (2000)
102. *J. High Resolut. Chromatogr.* **16** 312 (1993)
103. W A König *J. High Resolut. Chromatogr.* **16** 338 (1993)
104. W A König *J. High Resolut. Chromatogr.* **16** 569 (1993)
105. T Beuerle, W Schwab *Z. Lebensm.-Unters.-Forsch. A* **205** 215 (1997)
106. B Koppenhoefer, U Epperlein *J. Chromatogr. Sci.* **33** 244 (1995)
107. I Roling, H-G Schmarr, W Eisenreich, K-H Engel *J. Agric. Food Chem.* **46** 668 (1998)
108. B Maas, A Dietrich, A Mosandl *J. High Resolut. Chromatogr.* **17** 169 (1994)
109. P Kreis, A Dietrich, A Mosandl *Pharmazie* **49** 761 (1994)
110. U Ravid, E Putievsky, I Katzir, E Lewinsohn, N Dudai *Flavour Fragr. J.* **12** 109 (1997)
111. P Herion, G Full, P Winterhalter, P Schreier, C Bicchi *Phytochem. Anal.* **4** 235 (1993)
112. S Reichert, M Wüst, T Beck, A Mosandl *J. High Resolut. Chromatogr.* **21** 185 (1998)
113. W A König, A Krüger, D Icheln, T Runge *J. High Resolut. Chromatogr.* **15** 184 (1992)
114. W A König, R Krebber, P Evers, G Bruhn *J. High Resolut. Chromatogr.* **13** 328 (1990)
115. P Kreis, A Mosandl *Flavour Fragr. J.* **7** 187 (1992)
116. H J Bouwmeester, J A R Davies, H Toxopeus *J. Agric. Food Chem.* **43** 3057 (1995)
117. L Mondello, M Catalfamo, C Dugo, P Dugo *J. Microcolumn Sep.* **10** 203 (1998)
118. W A König *Drug Stereochemistry. Analytical Methods and Pharmacology* (Ed. I W Wainer) (New York: Marcel Dekker, 1993) p. 107
119. N Yassaa, B Y Meklati, A Cecinato *Atmos. Environ.* **34** 2809 (2000)
120. G P Blanch, G J Nicholson *J. Chromatogr. Sci.* **36** 37 (1998)
121. F Luan, D Hampel, A Mosandl, M Wüst *J. Agric. Food Chem.* **52** 2036 (2004)
122. T Köpke, A Mosandl *Z. Lebensm.-Unters.-Forsch. A* **194** 372 (1992)
123. B Maas, A Dietrich, V Karl, A Kaunzinger, D Lehmann, T Köpke, A Mosandl *J. Microcolumn Sep.* **5** 421 (1993)
124. B Faber, A Dietrich, A Mosandl *J. Chromatogr.*, **A 666** 161 (1994)
125. W Neugebauer, P Schreier *J. Agric. Food Chem.* **43** 1647 (1995)
126. B Dollman, G Full, P Schreier, P Winterhalter, M Güntert, H Sommer *Phytochem. Anal.* **6** 106 (1995)
127. G Full, P Winterhalter, G Schmidt, P Herion, P Schreier *J. High Resolut. Chromatogr.* **16** 642 (1993)
128. G Schmidt, G Full, P Winterhalter, P Schreier *J. Agric. Food Chem.* **43** 185 (1995)
129. G Schmidt, W Neugebauer, P Winterhalter, P Schreier *J. Agric. Food Chem.* **43** 1898 (1995)
130. D Bartschat, C Kuntzsch, M Heil, A Schittigkeit, K Schumacher, M Mang, A Mosandl, R Kaiser *Phytochem. Anal.* **8** 159 (1997)
131. S Melching, N Bülow, K Wihstutz, S Jung, W A König *Phytochemistry* **44** 1291 (1997)
132. Y Saritas, N Bülow, C Fricke, W A König, H Muhle *Phytochemistry* **48** 1019 (1998)
133. C O Schmidt, H J Bouwmeester, J-W de Kraker, W A König *Angew. Chem., Int. Ed.* **37** 1400 (1998)
134. M M Sonwa, W A König *Phytochemistry* **58** 799 (2001)
135. W A König, A Reick, C Fricke, S Melching, Y Saritas, I H Hardt *Proceedings of the 13th International Congress of Flavours, Fragrances and Essential Oils* (Ed. K-H C Baser) (Istanbul: AREP Publ., 1995) p. 169
136. S Melching, A Blume, W A König, H Muhle *Phytochemistry* **48** 661 (1998)
137. Y Saritas, M M Sonwa, H Iznaguen, W A König, H Muhle, R Mues *Phytochemistry* **57** 443 (2001)
138. W A König, N Bülow, C Fricke, S Melching, A Reick, H Muhle *Phytochemistry* **43** 629 (1996)
139. M Pietsch, W A König *J. High Resolut. Chromatogr.* **20** 257 (1997)
140. M Pietsch, W A König *Phytochem. Anal.* **11** 99 (2000)
141. H Oikawa, H Toshima, S Ohashi, W A König, H Kenmoku, T Sassa *Tetrahedron Lett.* **42** 2329 (2001)
142. B Maas, A Dietrich, D Bartschat, A Mosandl *J. Chromatogr. Sci.* **33** 223 (1995)
143. C Dietrich, T Beuerle, B Withopf, P Schreier, P Brunerie, C Bicchi, W Schwab *J. Agric. Food Chem.* **45** 3178 (1997)
144. T Kajiwarra, Y Akakabe, K Matsui, K Kodama, H Koga, T Nagakura *Phytochemistry* **45** 529 (1997)
145. D Häring, T König, B Withopf, M Herderich, P Schreier *J. High Resolut. Chromatogr.* **20** 351 (1997)
146. D Lehmann, B Maas, A Mosandl *Z. Lebensm.-Unters.-Forsch. A* **201** 55 (1995)
147. A Bernreuther, V Lander, M Huffer, P Schreier *Flavour Fragr. J.* **5** 71 (1990)
148. D Bartschat, D Lehmann, A Dietrich, A Mosandl, R Kaiser *Phytochem. Anal.* **6** 130 (1995)
149. R Näf, A Jaquier, A F Boschung, M Lindström *Flavour Fragr. J.* **10** 243 (1995)

150. G Bruche, A Dietrich, A Mosandl *Z. Lebensm.-Unters.-Forsch. A* **201** 249 (1995)
151. B Weber, B Maas, A Mosandl *J. Agric. Food Chem.* **43** 2438 (1995)
152. D Bartschat, M Wüst, A Mosandl, H Hanssum *J. High Resolut. Chromatogr.* **20** 251 (1997)
153. D Bartschat, B Maas, S Smietana, A Mosandl *Phytochem. Anal.* **7** 131 (1996)
154. D Bartschat, T Beck, A Mosandl *J. Agric. Food Chem.* **45** 4554 (1997)
155. G G G Manzardo, S Kürsteiner-Laube, D Perrin *Z. Lebensm.-Unters.-Forsch. A* **203** 501 (1996)
156. D Krajewski, W Neugebauer, I K Amajoyi, P Schreier, C Bicchi *Z. Lebensm.-Unters.-Forsch. A* **201** 378 (1995)
157. D Bartschat, A Mosandl *Z. Lebensm.-Unters.-Forsch. A* **202** 266 (1996)

Physicochemical methods for enhancing oil recovery from oil fields

L K Altunina, V A Kuvshinov

Contents

I. Introduction	971
II. Trends in the development of enhanced oil recovery methods	971
III. Compositions of surfactants and alkaline buffer systems used for enhancing oil recovery of low-permeability reservoirs	973
IV. Surfactant compositions generating carbon dioxide and an alkaline buffer system in the reservoir	977
V. Thermotropic gel-forming systems for increasing sweep efficiency in water flooding and thermal steam treatment	979

Abstract. Physicochemical methods for enhancing oil recovery from oil fields that are developed using water flooding and thermal steam treatment are considered. The results of pilot testing of processes based on these methods carried out at West Siberian and Chinese oil fields are analysed. The attention is focused on the processes that make use of surfactant blends and alkaline buffer solutions and thermotropic gel-forming systems. The bibliography includes 123 references.

I. Introduction

Currently, Russia is a prominent supplier of hydrocarbon raw materials to the world market. Russia fully satisfies the internal requirements in crude oil and remains simultaneously among the main exporting countries. During the period from 2000 to 2006, crude oil production has steadily increased from 323 to 480 mln t.¹ These are the highest values over the last 20 years. According to data of oil companies, the increase in oil production in Russia due to implementation of enhanced oil recovery (EOR) techniques was ~43–45 mln t per year in 2002–2006.¹

The key method for oil field development in Russia is water flooding used to produce ~95% of crude oil. Most of large oil fields are now at a late stage of development, the current water cut being more than 80%. The flooded reservoir rocks contain residual oil reserves. The newly developed oil fields are characterised, most often, by low rock permeability, high oil viscosity and complex geological structures; therefore, these reserves are difficult to recover. In Russia, the fraction of this type of oil reserves constantly increases. Calculations have shown that an increase in final oil recovery by only 1% would increase the annual production by 20–30 mln t. Therefore, the possibility of increasing oil reserves by enhancing the oil recovery of water-flooded reservoirs appears significant. According to expert estimates, the oil reserves difficult to recover exceed 10¹² tons all over the world, and in mature

economies, these are regarded not only as an inventory for crude oil production, but also as a main source for its intensification in the near future. Effective development of difficult-to-recover oil reserves and further buildup of production requires the design and wide-scale application of new integrated EOR techniques.^{2,3}

II. Trends in the development of enhanced oil recovery methods

In oil field development by water flooding, water is injected into an oil deposit through a network of injection wells. The injection of water makes up for the decrease in the formation pressure caused by oil withdrawal through producing wells. Water flooding is interpreted as displacement of oil from the fractured-porous medium by water with the formation pressure remaining the same and with full compensation of the produced oil volume by the injected water volume. In the initial stage of development, producing wells give anhydrous crude oil and later, a fluid comprising an oil–water mixture. The ratio of the amount of the produced water to the amount of the produced fluid is called water cut.

The oil recovery factor (ORF) is the ratio of the produced oil volume to the initial oil reserves. The development target is one or several oil formations developed together. The ORF value can be represented as the product of oil displacement efficiency (K_d) by the sweep efficiency (K_c) of the target by the given treatment method

$$\text{ORF} = K_d K_c.$$

Even in the favourable case where water has penetrated through 70% of the formation volume ($K_c = 0.7$) and has displaced 70% of oil from the penetrated areas ($K_d = 0.7$), the final ORF would not exceed 50%:

$$\text{ORF} = K_d K_c = 0.7 \times 0.7 = 0.49.$$

Computer simulation of oil field development does not imply explicit use of the coefficients K_d and K_c in design documents. Nevertheless, these values are useful as they allow one to distinguish contributions of K_d and K_c to the ORF.

There are several reasons for incomplete oil recovery on water flooding.^{4–10} They can be divided into three groups. The first group is related to the capillary-porous structure of the reservoir rock and to the enormous overall oil–rock contact

L K Altunina, V A Kuvshinov Institute of Petroleum Chemistry, Siberian Branch of the Russian Academy of Sciences, Akademichesky prosp. 3, 634021 Tomsk, Russian Federation. Fax (7-3822) 49 14 57, tel. (7-3822) 49 16 23, e-mail: alk@ipc.tsc.ru (L K Altunina), tel. (7-3822) 49 24 11, e-mail: vak@ipc.tsc.ru (V A Kuvshinov)

Received 23 April 2007

Uspekhi Khimii 76 (10) 1034–1052 (2007); translated by Z P Bobkova

area. The rock surface is always coated with an oil film that is not displaced by water. The film oil can account for 10%–20% of the total oil volume in the reservoir rock. In addition, ~10% of oil remains in the formation as drops entrapped in narrow sections of capillary pores and rock cracks. The displacement of drops is hampered by the capillary pressure gradient, which may be hundreds (or even thousands) times higher than practicable pressure gradients of oil displacement with water. Therefore, the highest K_d value usually does not exceed 0.7. Thus, the first group of reasons is associated with adverse influence of the ion-molecular surface forces at interfaces in the oil–water–rock system.

The second group is related to the difference between oil and water parameters, *viz.*, density and viscosity, resulting in uneven migration of the displacement front of oil by water.

The third group is related to geological and physical heterogeneity of the reservoir (mainly, heterogeneous structure and properties of the reservoir rock at macro- and micro-levels) and is manifested as incomplete sweep of the rock by water flooding, *i.e.*, K_c is < 1 . Finally, this enhances the variance of hydrodynamic and energy and mass exchange processes in the formation.

Enhanced oil recovery can be attained by using physicochemical methods of productive formation treatment, in particular, by introducing chemical reagents, which (*e.g.*, surfactants, solvents, carbon dioxide) eliminate partially or fully the adverse influence of capillary forces. Other materials (polymer solutions, gels, emulsions and foams) change the rheological properties and structure of the filtration flows of the formation fluids (oil, water or emulsions with dissolved gases) and decrease the hydrodynamic anisotropy of the oil formation.

The long experience of using diversified methods for enhancing oil recovery at West Siberia oil fields has shown that methods that increase the sweep efficiency of the injected water are most promising. This is due to the fact that in many deposits progressive increase in the water content in the produced oil (water cut $> 70\%$) is observed even at early stage of development due to the low sweep efficiency ($K_c \approx 0.1–0.2$). Meanwhile, the K_d value for high-permeability, flooded-out formation zones is close to the maximum attainable value, oil displacement by water is close to the frontal drive and $K_c \approx 0.6–0.7$.

The EOR methods that increase K_d (for example, injection of dilute surfactant and polymer solutions) proved to be of low efficiency under field conditions. Meanwhile, the methods that increase K_c (or both coefficients) provided engineering and economic benefits irrespective of the particular impact mechanism.^{11–18} These methods include the following:

- hydrodynamic methods changing the direction of filtration flows (various versions of non-stationary cyclic water flooding);¹⁹

- physicochemical methods for the control of filtration flows: injection of concentrated solutions of surfactants, oil-displacement compositions, cross-linked polymeric and polymer-dispersion systems, viscoelastic and gel-forming systems, gas, emulsions and foam and generation of such systems *in situ*, directly within the oil formation, by using thermotropic gel-forming compositions, organosilicate systems, *etc.*^{5, 8, 9, 20}

From the standpoint of subsurface gas- and hydrodynamics, the problem of coverage of an oil-bearing formation with water flooding is reduced to the control of the filtration flows of formation fluids.²¹ Currently, the predominant view considers EOR methods as efficient means for the control of filtration flows, increase in the sweep efficiency of water-flooding or another active treatment. The same goal is pursued in using hydraulic fracturing of the formation, horizontal drilling and branch wellbore drilling.^{22–24} These methods give rise to a fracture crack network and enhance oil produc-

tion. However, after that, the water cut of producing well fluid rapidly increases. This also suggests using physicochemical methods to control the sweep efficiency and intensify the capillary counter-current impregnation of low-permeability blocks of the fractured reservoir matrix. Physicochemical methods for the control of filtration flows by creating gel barriers in the formation are promising.

The oil remaining in the reservoir after water flooding is called residual. On the basis of expert estimates, the residual oil reserves are classified in the following way:⁴

- oil remaining in low-permeability interlayers and sections not swept by water, 27%;

- oil in stagnant pockets of uniform formations, 19%;

- oil remaining in lenses and at impermeable barriers not exposed by wells, 24%;

- oil retained in capillaries and films, 30%.

Thus, the oil not swept by water flooding due to reservoir heterogeneity accounts for 70% of all residual reserves and represents the main source for enhancing oil recovery. For the production of residual oil, it is important to systematically select the EOR method and to schedule various types of stimulation of producing and injection wells in a definite order with time matching.^{25, 26}

In recent years, the fraction of high-viscosity oils in the total amount of crude oil produced in the world has increased. The reserves of high-viscosity oils exceed ~5 times the recoverable reserves of low- and medium-viscosity oils (according to estimates, 810 and 162 bln t, respectively).²⁷ Large reserves of high-viscosity oils are found in Canada, Venezuela, Mexico, USA, Russia, Kuwait and China.

Of the modern methods for production of high-viscosity oils, thermal steam treatment of formation by stationary or cyclic (huff-and-puff) steam injection is most efficient.^{28–30} Most often, the injected steam has a temperature of 310 to 320 °C at the wellhead and dryness of 70%–80%. The injection pressure usually does not exceed 15–18 MPa. Combustion of 1 t of oil in a steam generation plant gives from 10 to 15 t of steam. The treatment is considered efficient if this gives 1 t of additional produced oil per 3–4 t of steam. The stationary steam injection is accomplished continuously through a network of steam injection wells, while oil is produced through a network of producing wells. The cyclic (huff-and-puff) stimulation consists of three stages: first, steam is injected into producing well, then the well is closed and kept for some period for formation warming up, and after that, oil production is resumed. When oil no longer enters the well, the huff-and-puff cycle is repeated. In this case, the first cycle is most effective, the efficiency of subsequent cycles being lower.

The efficiency of thermal steam treatment can be increased by combining it with physicochemical methods that use gel-forming and oil-displacing compositions. The use of gels increases the sweep efficiency of steam injection, while the use of oil-displacing compositions ensures additional oil recovery. Integrated methods that combine thermal steam and physicochemical treatment of formation are at an early stage of development (the number of these projects is small but they arouse considerable interest).

In 1981, works on enhancing oil recovery by using physicochemical methods were started at the Institute of Petroleum Chemistry of the Siberian Branch of the RAS (IPC SB RAS). A new approach to the development of efficient oil-displacing compositions based on surfactants and alkaline buffer systems has been proposed. A set of original devices and methods for investigation of the physicochemical and rheological properties of the surface and bulk phases in the oil–rock–surfactant solution system have been developed. A promising concept of using the reservoir or injected heat carrier energy for *in situ* generation of oil-displacing fluids, gels and sols directly in the reservoir has been proposed. The physicochemical grounds for

EOR methods making use of gel-forming systems and surfactant compositions were proposed. The principles of selection of oil recovery-enhancing compositions were implemented within the concept considering oil-displacing liquids as physicochemical systems with negative feedback, which maintain self-adjusting properties optimal for oil recovery in the producing formation for a long period of time. In recent years, development of new techniques using inorganic and polymeric gel-forming systems capable of generating gels directly in the formation has been in progress. By using these techniques, it is possible to create diverting barriers and control filtration flows, which would increase oil production and decrease water cut in the producing well product.

The chemical reagents used in industrial oil production should be relatively cheap, environmentally safe and commercially available on a large scale. Their application should not induce irreversible changes in the environmental situation in oil producing regions. The search for new cheap raw material sources for the use in EOR techniques is of special value. In this respect, good promise is given by the joint work of the Institute of Petroleum Chemistry and the Institute of Solid State Chemistry and Mechanochemistry of the Siberian Branch of the RAS dealing with the preparation of soluble compounds from plant stock (cellulose, rice hulls and so on) using mechanochemical treatment and coordinating solvents³¹ and with the use of large-scale industrial products manufactured in Russia, wastes from chemical and petrochemical plants and Kuznetsk Basin coal industry and so on.³²

The specialists of the IPC have developed eight EOR techniques, which are used at West Siberian and other oil deposits. Annually, 150–200 wells are treated according to these techniques. The additional oil production is on average 1–3 th t per treated well and the payback period is 5–10 months. Due to the use of the developed technologies at the West Siberia oil fields, >1.5 mln t of oil were additionally produced during the last 5 years alone. These technologies are cost effective and environmentally safe; they make use of large-scale products available as wastes of various industrial processes in Russia. The pilot tests of gel technologies were successfully carried out in the White Tiger offshore field in South China Sea (Vietnam).

Currently, new technologies for enhancing oil recovery, in particular, for high-viscosity oil fields, are developed. For increasing the efficiency of cyclic steam treatment of high-viscosity oil reservoirs, it was proposed to combine this method with physicochemical methods, in particular, those using polymeric and inorganic gels (for water shutoff) and surfactant compositions and generating, on thermal treatment, carbon dioxide and alkaline buffer system (for decreasing oil viscosity and for additional oil displacement). A set of laboratory studies has been performed. The first field tests of thermotropic gel-forming compositions for water shutoff and surfactant-based oil-displacing compositions were carried out between 2003 and 2006 as applied to cyclic steam treatment of high-viscosity oil reservoirs of the Usinskoye oil field (Komi Republic) and Liaohe and Gaosheng oil fields in China.

III. Compositions of surfactants and alkaline buffer systems used for enhancing oil recovery of low-permeability reservoirs

1. Effect of pH on oil displacement by water

A key factor hampering oil displacement by water is structuring of the adsorption layers in the oil–rock–formation water system. These layers contain tars, asphaltenes, heteroatomic compounds, high-molecular-mass paraffins, mineral colloidal particles.^{33–42} As a result, gel-like layers (films), possibly microemulsions, having high viscosity are formed at the inter-

face. These layers (films) create a structure-mechanical barrier, which accounts for the kinetic stability of the disperse system and prevents thermodynamically favourable processes.⁴³ Therefore, of interest are investigations of boundary layers in the oil–water–surfactant system, especially those carried out by low-frequency vibration methods.^{44–46} These methods allow one to measure rheological parameters of contacting bulky and surface phases under conditions of continuous deformation with small amplitude (this type of deformation occurs in an oil drop or film on filtration through a water-saturated capillary-porous formation material).

For enhancing oil recovery, it is insufficient to ensure low oil–water interfacial tension. The interfacial tension is a thermodynamic value equal to the free energy of the interface; the lower the interfacial tension, the thermodynamically more favourable the oil displacement process.^{47,48} However, thermodynamically favourable process often cannot be accomplished due to its too long duration. In the case we consider, adsorption layers rearrange slowly upon mechanical impact due to the sharp increase in the structural viscosity or, what is the same, due to the appearance of relaxing shear elasticity following a decrease in the layer thickness. Consequently, during water flooding at the formation pressure gradients, the structured adsorption layers behave as non-thixotropic mechanically strong films, which deteriorate filtration of formation fluids and reduce oil recovery.^{33–42,49,50} Thus, to enhance the oil recovery, it is necessary to find practicable ways for destructuring of the adsorption layers and decreasing the interfacial tension.

When aqueous solutions immiscible with oil are used for oil displacement, the interfacial films can be destructured by chemical reagents, namely, by surfactants and/or low-molecular-mass inorganic compounds dissolved in the injected water that are able to destroy hydrogen bonds and weaken hydrophobic interactions between the oil components constituting these films.^{51–55} The surface activity of surfactants should be higher than that of oil components to provide the possibility of displacing them from the adsorption layers. However, surfactants should not form structured interfacial films. None of the commercially manufactured surfactants fully meets these requirements. The properties of the colloidal surfactants used can be improved by adding low-molecular-weight organic co-surfactants and by forming surfactant compositions with low-molecular-mass inorganic chemicals that ensure destructuring (fluidisation) of adsorption layers.

In the oil–water–rock system, the key role in structuring (strengthening) of interfacial layers belongs to hydrogen bonds, although hydrophobic interaction also plays a role at high formation temperatures. The interfacial layers can be destructured most readily and efficiently using alkaline chemicals as parts of oil-displacing compositions to destroy hydrogen bonds and weaken hydrophobic interactions between the oil components of these layers.^{56,57}

The destructuring of interfacial layers by solutions of alkaline reagents is caused by various chemical reactions involving hydroxyl ions, specifically, neutralisation of acid groups (carboxy, phenolic and thiol); saponification of ester bonds; deprotonation of donor heteroatoms (nitrogen, sulfur); association of hydroxyl ions with aromatic fragments of the oil components; and influence on the structure of water and thus on hydrophobic bonding, the conformational mobility of hydrophobic parts of surfactants, *etc.* These reactions involving hydroxyl ions reduce the oil–water interfacial tension (Fig. 1),^{58–60} change the electric double layer,^{61–63} decrease the viscosity of interfacial layers^{58,64} and increase the wettability of the reservoir rock and oil phase by water.^{65–69}

Among all anions, the hydroxyl ion has the highest adsorption potential with respect to the rock oxide minerals in an aqueous medium and the highest mobility and exerts the

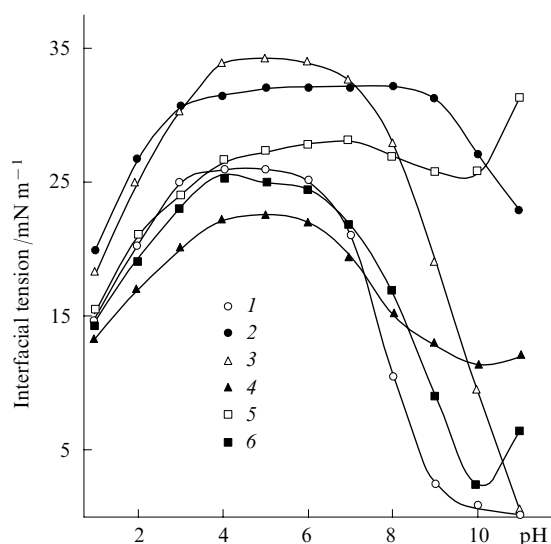


Figure 1. Oil interfacial tension for the AV₁ formation of the Sovetskoye (1, 4), D₁ formation of the Romashkinskoye (2, 5) and PK₁₋₂ formation of the Russkoye deposits (3, 6) vs. pH of the aqueous phase of different compositions.⁵

Aqueous solution: (1–3) 0.1 M HCl + NaOH; (4–6) 0.1 M HNO₃ + NH₃.

most pronounced ordering effect on water. In an alkaline solution, the initially hydrophobic sections of the rock become hydrophilic and the thickness of the stable aqueous interlayer between the rock and oil increases. The adsorption of hydroxyl ions increases the surface density of the negative charge of the rock and decreases the number of adsorption sites able to form hydrogen bonds.^{65, 70} This is favourable for improving rock wetting by water and for decreasing adsorption of both anionic and non-ionic surfactants.^{71–75} When surfactants are adsorbed from alkaline solutions onto a negatively charged rock surface, the orientation of surfactant molecules in the adsorption layer is such that the hydrophilic character of the rock does not change. For alkaline solutions of non-ionic and anionic surfactants, a low interfacial tension and neutral wetting in the rock–oil–aqueous phase system can be implemented simultaneously, which is confirmed by the results of testing of selective wetting in a model system with controlled properties of interfaces.^{76–78} This results in high capillary numbers so that the oil-displacing ability of surfactant solutions increases.^{5, 79, 80}

In view of the foregoing, it appears promising to develop compositions containing surfactants and alkaline chemicals and combining the useful features of alkaline water flooding and water flooding using surfactant solutions.^{4, 47, 48, 81, 82} Analysis of the features of oil displacement process by alkaline solutions of surfactants⁵ attests to the presence of an optimal alkalinity range (pH 9.0–10.5) in which the surfactants are chemically stable and have the highest oil-sweeping ability.⁷⁹ In addition, it is in the range of pH 9.0–10.5 that suspensions of clay minerals have the lowest viscosity and adhesion to the reservoir rock,⁸³ which is important for water flooding of low-permeability reservoirs. In this pH range, no noticeable dissolution of rock minerals and precipitation of alkaline-earth metal hydroxides from formation or injected water are observed, whereas at pH > 10.5, calcium and magnesium hydroxides can precipitate and rock minerals dissolve. In highly alkaline media, non-ionic surfactants like hydroxyethylated phenols undergo denaturation resulting in a sharp increase in the critical micelle concentration.⁷¹

Thus, selection of an appropriate alkaline reagent is crucial for the development of effective oil-displacing compositions

based on surfactants. A self-maintained, self-adjusted pH value in the range from 9.0 to 10.5 can be ensured by using buffer systems with maximum buffer capacity in this pH range. In terms of more general views on an oil-displacing composition as a physicochemical system, the presence of an alkaline buffer solution generates a negative feedback and thus imparts the composition with self-adjustment property, *i.e.*, maintenance of its functions in the formation for a long period of time. In physicochemical systems, self-adjustment is necessarily accompanied by a change in the component concentrations and has natural concentration limits within which the parameter characterising the self-adjustment efficiency reaches a maximum. For buffer solutions, the buffer capacity is such a parameter. The condition for maximum capacity is met if the concentrations of the acid (base) and salt composing the buffer system are equal. The thermodynamics of buffer solutions was considered previously.^{84, 85} The effects of dilution, neutral electrolyte and non-electrolyte additives, temperature and pressure on the buffer capacity have been described in detail in a monograph.⁸⁶

Despite the enormous number of substances capable of forming buffer solutions, only some organic and only four inorganic buffer systems are suitable for the required pH range (9 to 10.5): phosphate (tripolyphosphate), silicate, ammonia and borate systems. The tripolyphosphate system can be used to enhance oil recovery of high-permeability reservoirs with low temperature. In the case of low-permeability reservoirs of the West Siberia oil fields, its use is problematic, because sodium tripolyphosphate rapidly hydrolyses above 323 K being converted into trisodium phosphate, which forms insoluble salts with calcium, magnesium and iron ions present in injected and formation waters. The use of silicate systems (specifically, their field preparation) is faced with technical difficulties caused by the tendency of sodium silicate to hydrolytic polycondensation and poor compatibility with oil field brine. It is noteworthy that phosphate and silicate systems are used in the techniques implementing the precipitation and gelation effects for selective isolation of highly permeable zones of the reservoir.

Ammonia, borate and mixed ammonia–borate systems are the systems of choice. They are prepared from ammonia, ammonium nitrate, sodium tetraborate and boric acid. These compounds are rather cheap commercial chemicals manufactured on a large scale.

The use of compositions of non-ionic surfactants with an alkaline reagent at high formation temperatures requires that they contain anionic components, which increase the cloud point of the non-ionic surfactant.⁸⁷ Additionally, in order to enhance the oil-sweeping ability and improve the compatibility with oil field brine and injected water, it is desirable to introduce low-molecular-mass organic compounds that combine the functions of a non-colloidal co-surfactant and a precipitation inhibitor for hydroxides and hardness calcium or magnesium salts. Taking into account the above requirements, a number of compositions based on ionic and non-ionic surfactants (oxyethylated alkylphenols: OP-10, Neonol AF 9-12 and its analogues) were developed and laboratory tested.⁵

2. IPC compositions based on surfactants and alkaline buffer systems

Analysis of the development of physicochemical methods for enhancing oil recovery reveals a clear tendency to impart self-adjustment feature to the oil-displacing fluid, which allow the fluid to maintain its functions in the reservoir rock for a long period of time.⁸⁸ The development of physicochemical principles for selection of surfactant compositions taking into account the thermodynamic and kinetic parameters of the oil–rock–aqueous phase system, which affect the oil displace-

ment from the porous rock, carried out at the IPC SB RAS is based on the concept of an oil-displacing fluid as an above-mentioned physicochemical system with negative feedback. It was proposed that alkaline buffer systems with a highest buffer capacity in the pH range of 9.0–10.5 would be used in the oil-displacing compositions of the IPC series.

Systematic studies of the effect of pH and the ionic strength of aqueous electrolyte solutions on the interfacial tension of oils showed that the pH dependence of the interfacial tension (see Fig. 1) has extreme points: a maximum in the pH range from 4.5 to 5.5 and a minimum at pH 9–10. The maximum is due to the presence of natural surfactants in oil.⁵ These are heteroatomic compounds present as parts of tars and asphaltenes, the most high-molecular-mass oil components. The functional groups of the cationic surfactants present in oil include pyridine, quinoline and other, mainly heterocyclic, basic groups and also tetrapyrrole fragments of oil metal porphyrins. The anionic surfactants present in oil typically contain carboxy, phenolic and thiol functional groups. The decrease in the interfacial tension upon the shift of the aqueous phase pH to the acidic region with respect to the maximum is due to protonation of functional groups of cationic surfactants in the interfacial layer, while that upon the shift of pH to the alkaline region from the maximum is due to neutralisation of the carboxy, phenolic and thiol groups of anionic surfactants. The pH dependences of the interfacial tension for crude oils of West Siberia and the Ural–Volga region are different. In the alkaline region, the interfacial tension decreases substantially for West Siberian crudes, whereas for the sour crudes of the Ural–Volga region, this decrease is slight, which may be attributed to the presence of saturated sulfides having weakly basic properties. For all crudes studied, the interfacial tension varied inversely to the ionic strength of the aqueous phase.

At the oil–aqueous phase interface, the natural surfactants of oil form an amphoteric adsorption layer. The ionisation of the polar ionic groups in the oil natural surfactants in acidic or alkaline medium gives rise to an electric double layer at the interface. The maximum in the dependence of the interfacial tension of oil at the interface with the aqueous phase vs. pH of the aqueous phase corresponds to the isoionic state of the adsorption layer. The maximum pH value corresponds to the isoionic point of the layer (pH_i); it can be calculated as the half-sum of the acid constant indexes (pK_a) of the strongest acidic and basic functional groups in the adsorbed molecules. The strongest acidic groups present in oil surfactants are carboxy groups (pK_a = 5.6), while the strongest basic groups are pyridine (pK_a = 4.6) or quinoline groups (pK_a = 4.9). The calculated pH_i value equal to 5.3 virtually coincides with the experimental pH_i 5.2.

Taking into account the experimental dependences of the interfacial tension on pH and the ionic strength of the aqueous phase, an electrocapillary model of the interfacial layer has been developed.^{5,89} According to this model, the interfacial layer (amphoteric adsorption layer of the natural surfactants present in oil) has the properties of ion exchange membrane. The extremal pattern of dependence of the interfacial tension of oils on pH of the aqueous phase is caused by the presence of an electric double layer arising due to ionisation of the ionisable groups in natural surfactants of oil. The model establishes relationship between the oil composition and the physicochemical parameters of the interfacial layer, which dictates the mechanism of oil displacement by aqueous solutions (due to the change in the interfacial tension, adsorption of the natural surfactants of oil, the composition and concentration of electrolytes in the aqueous phase). In terms of this model, the dependence of the interfacial tension of oil (σ) on the aqueous phase pH is given by the equation

$$\sigma = \sigma_i - b\vartheta^2[-\log(a_{H^+} + KI) - \text{pH}_i]^2 + c\vartheta^4[-\log(a_{H^+} + KI) - \text{pH}_i]^4 - 2.303\Gamma_0 RT \log(1 + K_a I),$$

where σ_i is the interfacial tension in the isoionic point; b is the integral capacity of the electric double layer; $\vartheta = 2.303RT/F$, R is the universal gas constant, T is temperature, F is the Faraday number; a_{H^+} is the proton activity in the aqueous phase; K is the ion exchange constant for the interfacial membrane; I is the ionic strength of the aqueous phase; c is a parameter characterising the dependence of the integral capacity of the electric double layer on its potential; Γ_0 is the limiting adsorption of electrolyte ions in the interfacial layer; K_a is the adsorption constant for electrolyte ions in the interfacial layer.

As an example, Fig. 2 shows the dependences of the interfacial tension on pH, one calculated using the above equation (line) and one experimental (dots) for the crude of the Sovetskoye oil field (AV_{1–2} formation) at the interface with an aqueous electrolyte solution with a constant ionic strength.

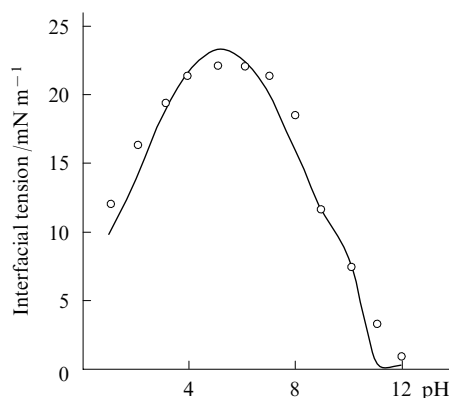


Figure 2. Oil interfacial tension vs. pH for the oil of Sovetskoye field (AV_{1–2} formation) at the interface with an aqueous solution of a 1:1 electrolyte with a constant ionic strength $I = 0.1$ mol per kg of water.⁶⁰

On the basis of investigation of the thermodynamic and kinetic parameters of the oil–rock–water–surfactant systems, the most promising IPC compositions involving surfactants and ammonia buffer based on ammonia and ammonium nitrate (cheap commercial products) were proposed for the industrial use at the oil fields of West Siberia. These compositions combine the advantages of alkaline water flooding and water flooding with surfactant solutions.

A distinctive feature of IPC compositions is the fact that they contain constituents of the geochemical nitrogen, carbon or oxygen cycles. This accounts for their environmental acceptability and multifunctionality: the components serve as the nutrition sources for the reservoir microflora, natural indicators (tracer agents) of the filtration flows in the oil accumulation, etc.

Waxy IPC compositions IHN-60 and IHN-100, low-viscosity non-combustible liquids with freezing points ranging from -33 to -55 °C were proposed for winter injection in Northern regions. The use of IPC compositions increases the oil displacement efficiency by 10%–20%. They can be employed over broad ranges of formation temperatures and compositions of formation water and for the development of low-permeability and heterogeneous reservoirs. Upon oil displacement by IPC compositions, the mobility of filtered fluid increases 3–7-fold, which attests to the possibility of appreci-

able increase in the injectivity of injection wells on treatment of the bottomhole formation zone.⁹⁰ The specific loss of the surfactant caused mainly by adsorption on the core material during oil displacement equals 0.2–0.6 mg g⁻¹.

3. Pilot testing of EOR processes using IPC compositions

Two processes making use of IPC compositions have been developed: treatment of the bottomhole zones with small volumes of the compositions; injection of large-volume slugs (portions) of compositions in order to affect the interwell space of the formation.

From 1984 to 2006, treatment of the bottomhole zones of more than 150 injection wells was carried out under different geological conditions in the oil fields of the Tomsk and Tyumen Regions. This process increases the well injectivity 1.5–2.5-fold, decreases the injection pressure by 30%–40%, increases the efficiency of the producing wells that are hydrodynamically connected to injection wells. The duration of the effect is 6 to 16 months. The additional oil production is 20–30 t per t of the injected composition. The technology is cost effective, the payback time being 4–9 months; it is applicable to formations with temperatures of 10–130 °C and permeability of 0.005–0.500 μm², the effect being most pronounced for low-permeable heterogeneous reservoirs of Jurassic and Cretaceous deposits typical of West Siberia.⁵

The pilot testing of technology with injection of large-volume slugs of IPC compositions with controlled alkalinity was carried out from 1985 to 1989 under different geological conditions in the pilot sites of oil fields of West Siberia: AV₁ formation of the Sovetskoye field, YuV₁ formation of the Vakhskoye field, AV₁₋₃, AV₂₋₃, and BV₁₀ formations of the Samotlorskoye field, BV₁₀ formation of the Lor-Yeganskoye field, Yu₁ formation of the Malo-Chernogorskoye field, and AS₄ formation of the Mamontovskoye field (Table 1), and in pilot sites of the V₃ formation of the Severo-Savinoborskoye field (Komi Republic). Altogether > 30 th t of IPC compositions was injected. The slug volume was 0.2%–0.4% of the oil-saturated pore volume of the pilot site formation.^{5, 18}

Analysis of the state of the art of development of the pilot sites resorting to the results of geophysical, hydrodynamic and physicochemical studies showed that IPC compositions improve the water flooding process: the water cut of producing wells decreases, remains constant or increases at a lower rate; the parameters of the bottomhole zone of injection wells and the reservoir (productivity, hydroconductivity, piezoconductivity and permeability) are improved; the dynamic liquid levels in producing wells increase; the residual oil saturation decreases; oil displacement parameters are improved; and the effective formation thickness either increases or remains the same. The injectivity of the injection wells increases, resulting in more intense development. The IPC compositions move

along the formation as a whole entity, being gradually diluted with the formation water. The migration of the composition front is accompanied by a decrease in the water cut of oil, to the utmost, by 30%–40% and a pH increase from 6–7 to 8–10. Some components of the IPC composition can be found in reliably determinable concentrations (0.001%–0.1%) in the producing well product for long periods of time, up to 2–3 years, the highest surfactant and ammonium nitrate concentrations being 0.2%–1.0%. The production of the components from different wells occurs in comparable amounts, which indicates that the formation has been swept throughout the whole pilot site. The diagrams of the space distribution of surfactant and the oil production according to wells are similar, *i.e.*, an increase in the surfactant production is accompanied by an increase in the specific oil production.^{5, 18}

The produced water is less corrosive in the presence of IPC compositions than the injected water. Thus the rate of corrosion of the test samples mounted in the oil-gathering systems in the pilot sites of the Lor-Yeganskoye field was 0.1 mm per year. The IPC compositions present in produced water in concentrations of 0.5% enhance oil dehydration processes.

The engineering and cost efficiency of using IPC compositions at the West Siberia oil fields was evaluated (see Table 1). The increase in the oil recovery was from 2.8% to 27.5% (on average, 8.2%). This technology provides from 9.8 to 68 t (on average, 26.2 t) of oil produced additionally per t of the composition or 183 t of oil per t of the surfactant. A computer model of the process was designed.⁵ The industrial production of the IPC compositions IHN-60 and IHN-100 was organised in Russia (at the CJSC KHIMEKO-GANG and CJSC Polyex plants).

The field tests revealed the stimulating effect of IPC compositions on the development of the reservoir microflora.^{91–93} The components of the ammonia buffer system are involved in the geochemical nitrogen cycle and serve as additional nitrogen nutrition for anaerobic and aerobic bacteria in trophic chains of the microbial biocenosis of the oil-bearing formation. Microbiological studies carried out in injection areas of IPC compositions IHN-60 and IHN-100 into the AV₁ formation of the Sovetskoye oil field, AV₁, AV₂₋₃ and BV₁₀ formations of the Samotlorskoye oil field, YuV₁ formation of the Vakhskoye and BV₁₀ formation of the Lor-Yeganskoye oil fields have shown that the amount of denitrifying and heterotrophic bacteria, including *Pseudomonas* and *Actinomyces*, is much higher than in reference sites. The count of sulfate-reducing bacteria in the produced water in the pilot sites was much lower than that in the injected water or in the produced water in the reference sites. The geochemical activity of the denitrifying bacteria is directed at the oxidation of organic compounds present in oil to give carbon dioxide, bio-surfactants and other substances enhancing the oil recovery.

Table 1. Oil production with the use of IPC compositions on the pilot sites of West Siberia oil fields.¹⁸

Oil field			Oil in place reserves/th t	Amount of the injected IPC composition/th t	Gain in ORF (%)	Additional oil production	
name	formation	number of the injection well				th t	t per t of the IPC composition
Samotlorskoye	AV ₁₋₃	4110	1576.0	5.0	12.8	201.7	40.3
	BV ₁₀	12168	369.0	2.3	27.5	101.5	44.1
	BV ₁₀	12162	403.9	1.6	3.9	15.8	9.9
	AV ₁ ¹⁺²	15 930	582.9	1.7	5.3	30.9	18.2
	AV ₁ ³	15 618	589.0	1.5	2.8	16.5	11.0
Lor Yeganskoye	BV ₁₀	site 1 (wells 129, 132 133, 134)	706.9	2.1	2.9	20.5	9.8
	BV ₁₀	site 3 (wells 85, 86 87, 88)	901.2	4.2	8.3	74.8	17.8
Malo-Chernogorskoye	Yu ₁ ¹	239	551.6	1.8	3.7	20.4	11.3
Sovetskoye	AV ₁	644	2458.0	5.8	7.5	184.4	31.8
Mamontovskoye	AC ₄	2054	768.0	0.8	7.1	54.5	68.1

IV. Surfactant compositions generating carbon dioxide and an alkaline buffer system in the reservoir

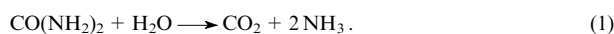
It was noted above that development of high-viscosity oil fields involves thermal treatment techniques. Steam is used most often as the heat carrier. Many researchers have attempted to find chemicals for the addition to steam to improve its action.^{28,30,94} Theoretically, the use of such additives may decrease the temperature of steam condensation, for example, by formation of an azeotropic mixture or water solubility in compressed gases, increase the reservoir permeability for a steam – gas mixture and so on. Carbon dioxide is the additive of choice. The grounds for the beneficial effect of CO₂ are well-known; they include the increase in the reservoir rock permeability for oil, the decrease in the oil viscosity, *i.e.*, a favourable change in the mobility ratio of oil and the aqueous phase, and so on.⁴⁸

For a number of years, the concept of high-viscosity oil formation stimulation by a surfactant-based compositions, which form CO₂ and an ammonia buffer system under the action of formation temperature, has been developed at the IPC SB RAS.^{5,95} Prior to steam injection, a slug of a composition representing an aqueous solution of a blend of non-ionic and anionic surfactants, carbamide and ammonium salts, are introduced into the well. In the oil-bearing formation, carbamide is hydrolysed under the action of high steam temperature to give carbon dioxide and ammonia. Unlike ammonia, carbon dioxide is soluble in oil much better than in water. The partition coefficient for carbon dioxide in the oil – water system in the temperature range of 35–100 °C and the pressure range of 10–40 MPa is between 4 and 10, whereas this value for ammonia does not exceed 6×10^{-4} . Therefore, in the oil – water system, the oil phase is enriched in carbon dioxide and the aqueous phase is enriched in ammonia, which forms, together with the ammonium salt, an alkaline system with the maximum buffer capacity at pH 9.0–10.5, as in IPC compositions. This gives rise to several useful effects. The dissolution of carbon dioxide in oil decreases oil viscosity. In the vapour phase, carbon dioxide and ammonia help to maintain vapor – gas mixture at a temperature below the vapour condensation point; therefore, the efficiency of transfer of oil components by the distillation mechanism increases. Carbon dioxide and ammonia reduce swelling of clay minerals of the reservoir rock and thus help maintaining the initial reservoir permeability. The same role is played by the ammonia buffer system, which is formed upon dissolution of ammonia in an aqueous solution of ammonium salts. In addition, owing to its alkalinity (pH 9–10) and the presence of surfactants, it promotes intensification of the counter-current impregnation of the formation and oil displacement.

1. Kinetics of carbamide hydrolysis in water and surfactant-based compositions

The physicochemical mechanism of action of oil-displacing compositions comprising surfactants and alkaline buffer solutions producing CO₂ *in situ* is based on the kinetics of carbamide (urea) hydrolysis in water and compositions at 80–250 °C.

Carbamide dissolved in water is rather stable up to 80 °C. Above this temperature, it is hydrolysed to give ammonia and carbon dioxide according to the overall reaction

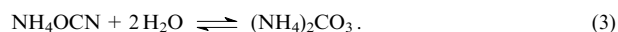


Detailed information about the physicochemical properties of components, phase equilibria and reaction kinetics in the carbamide – water – ammonia – carbon dioxide system have been reported;^{96,97} the kinetics of carbamide hydrolysis has

been described.⁹⁶ The hydrolysis takes place in two steps. The first step is isomerisation of carbamide to ammonium isocyanate



The second step is hydrolysis of ammonium isocyanate to give ammonium carbonate



A kinetic study of carbamide hydrolysis in water and in compositions has shown that the reaction follows the first order kinetics with respect to carbamide in the carbamide concentration range from 0.5% to 20% at 80–100 °C. The average temperature coefficient was 2.4, *i.e.*, the Van't Hoff rule was fulfilled.

For the temperature range of 100–250 °C, the following kinetic parameters were found: the activation energy and the pre-exponential factor for the Arrhenius equation for carbamide hydrolysis in water are 44.6 kJ mol⁻¹ and $4.01 \times 10^4 \text{ h}^{-1}$; for hydrolysis in compositions, $50.8 \pm 1.5 \text{ kJ mol}^{-1}$ and $10.9 \times 10^4 \text{ h}^{-1}$, respectively.⁹⁸ The increase in the activation energy in the latter case is due to the effect of the ammonium salt.

The activation energy for carbamide hydrolysis in the temperature range of 80–100 °C is twice as high as that in the 100–250 °C range. In the 80–250 °C range, the rate-limiting step of the reaction changes, as indicated by a change in the slope of the temperature dependence of the reaction rate constant (Fig. 3). At 80–100 °C, the rate-limiting step is carbamide isomerisation (2), which has a higher activation energy than reaction (3). At 150–250 °C, the rate of carbamide decomposition increases and the solution pH reaches 9–10.5 where reaction (3) becomes the rate-limiting step.

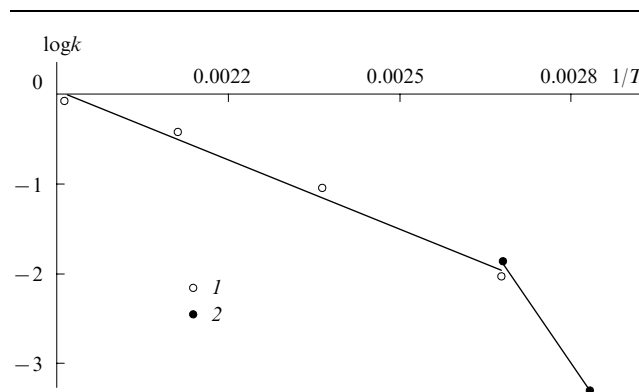


Figure 3. Temperature dependence of the rate constant for hydrolysis of carbamide in a surfactant-based composition at 80–250 °C.⁹⁵ Temperature range /°C: (1) 100–250, (2) 80–100.

As a result of carbamide hydrolysis at 80–250 °C, solutions of carbamide and oil-displacing compositions acquire high buffer capacity with a maximum at pH 9.0–10.5 (Fig. 4).⁹⁸ In water, the rate of carbamide hydrolysis is higher and the time it takes to attain the maximum pH is shorter than in solutions containing ammonium salt; however, the highest buffer capacity is observed only in the presence of the ammonium salt. Indeed, at 100 °C, the highest buffer capacity of the composition is 14.4 g-equiv. litre⁻¹ (pH unit)⁻¹, while that of a carbamide solution is 5.3 g-equiv. litre⁻¹ (pH unit)⁻¹. At 250 °C, the buffer capacities of the composition and carbamide solutions are 22.3 and 7.22 g-equiv. litre⁻¹ (pH unit)⁻¹, respectively. The buffer capacity of compositions is 2–4

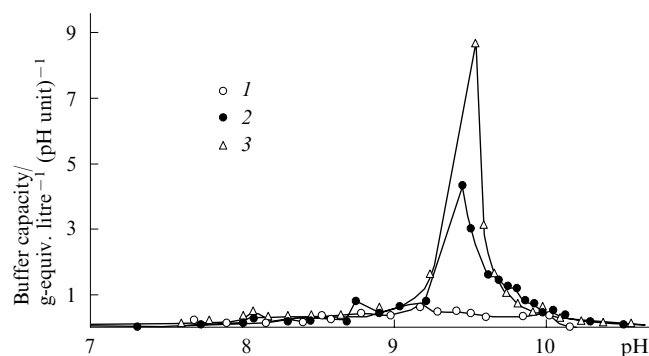


Figure 4. Buffer capacity of the surfactant-based composition vs. pH.⁹⁸ (1) Before heating; (2, 3) after heating at 150 °C for 7 and 10 h, respectively.

times higher than that of carbamide solutions in water under the same conditions. Due to the high buffer capacity, 10–100-fold dilution of the hydrolysed composition with water results in only a slight change in pH (0.2–0.5 pH units).

2. Rheological and filtration properties of high-viscosity oil systems with various surfactant compositions generating carbon dioxide and an alkaline buffer system in the oil formation

The alternating thermal steam treatment and physicochemical treatment with surfactant compositions of a high-viscosity oil formation is based on the changes in the rheological properties and a decrease in the viscosity of oil.^{28–30, 48} The features of such alternating treatment were revealed by rheokinetic studies of high-viscosity oils of the Usinskoye and Yaregskoye oil fields in Russia and the Liaohe and Fluarti oil fields in China. The effects of time and temperature of oil autoclaving with compositions on the temperature dependence of oil viscosity during the consecutive heating and cooling were investigated by vibrational and rotational viscometry^{44, 45} in the temperature range of 150–250 °C. For oil:composition ratios varying from 4:1 to 1:1, heating at 150–250 °C for 4–24 h results in a 3–6-fold decrease in oil viscosity in the temperature range of 20–50 °C (Fig. 5). Moreover, the higher the autoclaving temperature the lower the oil viscosity and the broader the composition concentration range in which the viscosity drop takes place. For autoclaving temperature of >200 °C, the viscosity almost does not decrease. The most pronounced decrease in the viscosity of the oils from the Usinskoye and

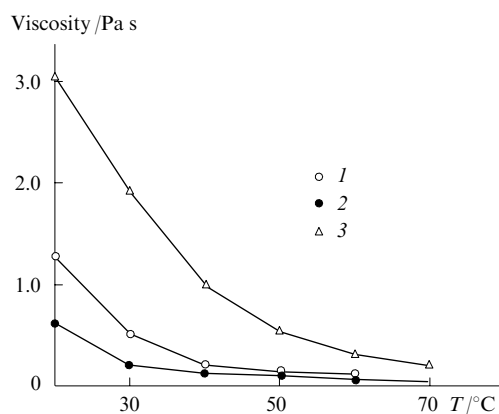


Figure 5. Temperature dependences of the oil viscosity of the Usinskoye field after maintenance at 200 °C for 6 h with the IHN-KA (1) and NINKA (2) compositions and water (3).⁹⁸

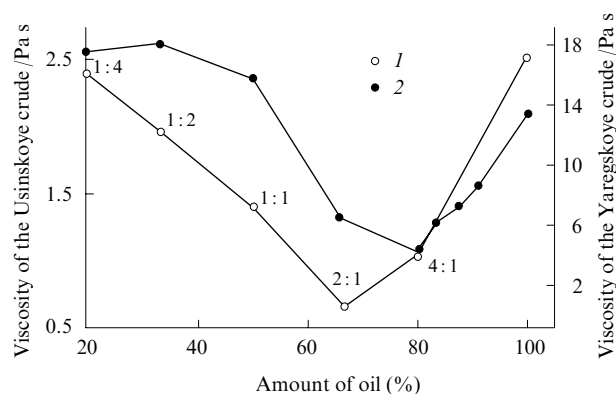


Figure 6. Viscosities of the oil from Usinskoye (1) and Yaregskoye (2) oil fields at 20 °C after maintenance at 150 °C vs. oil to surfactant composition ratio.⁹⁸

Yaregskoye fields occurs at the oil to composition ratio of 2:1 and 4:1, respectively (Fig. 6). As the fraction of the composition heated with oil increases further, the oil viscosity increases due to the formation of high-viscosity emulsions, which was confirmed by ¹H NMR.⁹⁵ These regularities hold most clearly for small shearing stresses corresponding to the filtration conditions of the formation fluids in the reservoir rock and are retained under thermobaric conditions similar to those in the formation, which was confirmed by studies of these systems with a high-pressure viscometer.⁹⁵

Laboratory studies on a high-pressure filtration setup have shown that alternation of steam and composition slugs allows one to enhance oil displacement efficiency compared to thermal steam treatment. The major contribution to the gain in oil displacement efficiency comes from the injection of the first composition slug. A computer model for such process was designed.⁹⁹

3. Pilot-plant testing of the technology using the NINKA compositions

The pilot tests of the technology using surfactant compositions generating *in situ* CO₂ and alkaline buffer system (the NINKA compositions) were carried out in the Permo-Carboniferous high-viscosity oil formation region of the Usinskoye field occurring at a late stage of development. The process was designed to increase the efficiency of thermal steam treatment.^{100, 101} In 2002, injection of 264 m³ of the NINKA composition into three steam injection wells was carried out. The use of this process in long-term steam injection decreases the water cut of the product by 10%–20% and increases the oil production rate by 40% on average with increasing the liquid production rate by 5%–10% on average. The total additional oil production from October 2002 to February 2004 in three pilot sites was 44.3 th t (Table 2) or 14.7 th t of additional oil production per treated well. The process was recommended for use in high-viscosity oil deposits developed using thermal steam treatment.

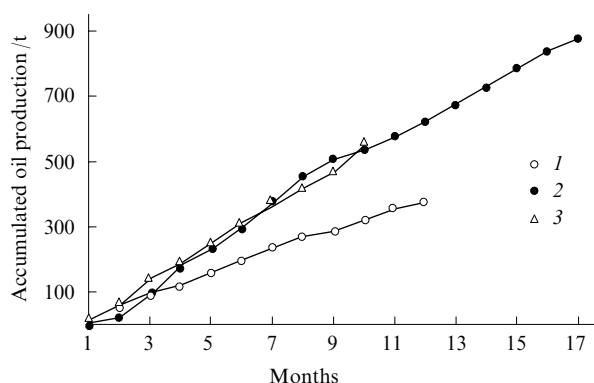
A promising way is the integrated use of gel-forming and oil-displacing compositions in the high-viscosity oil pool development by means of thermal steam treatment. As a result, it is possible to increase both the sweep efficiency and the oil displacement efficiency with simultaneous intensification of the development.

In 2003, pilot tests of the process involving alternating physicochemical treatment and cyclic steam treatment of the high-viscosity oil pool of the Liaohe field (China) using the NINKA composition were successfully carried out.¹⁰⁰ Thirty and forty tons of the composition and 2.5 th t of steam were injected into each of two wells as several slugs. This provided a

Table 2. Additional oil production from October 2002 to February 2004 for injection of the NINKA composition in the pilot sites of the Usinskoye field.¹⁰⁰

Number of the injection well	Target	Additional oil production /th t	Gain in the month average oil production rate for producing wells (%)
4029	lower	11.2	31
4040	lower	14.0	41
4596	upper	19.1	49
Total		44.3	on average, by 40%

1.8–2.3-fold increase in oil production with respect to steam injection alone, the oil production time increased by 3–5 months; oil viscosity decreased three-fold and the oil pour point decreased from (6–10) to –(4–16) °C. For example, oil production from well 3-2 was 874 t between October 2003 and March 2005, while in the previous cycle with steam injection alone, this was 375 t (Fig. 7). In 2005, the works on using the NINKA composition were continued; injection into five cyclic steam wells was carried out, and monitoring of their operation was completed in 2006. Note that in 2005, repeated injection of the NINKA composition into well 3-2 was carried out (see Fig. 7). Oil production in this cycle was nearly the same as in previous cycle. The alternating injection of steam and the composition is more efficient than steam injection alone.

**Figure 7.** Dynamics of the accumulated oil production from well 3-2 of the Huanxiling region of the Liaohe field (China) in the steam injection cycle in 2001 (1) and the subsequent steam injection cycles with the NINKA composition in 2003 and 2005 (2, 3).¹⁰¹

The pilot tests of using the NINKA composition with thermal steam and cyclic steam treatment of high-viscosity oil pools of Russian and Chinese fields demonstrated the engineering efficiency and environmental safety of the composition.

In China, industrial manufacture of the solid commercial form of the NINKA-1 oil-displacing composition was organized.

V. Thermotropic gel-forming systems for increasing sweep efficiency in water flooding and thermal steam treatment

The increase in the formation sweep efficiency in water flooding is especially topical for oil pools consisting of formations not connected hydrodynamically. In this case, the mechanism of alignment of the displacement front due to capillary and

hydrodynamic cross-flows is not effective. The producing wells are water-flooded even at an early stage of development; it is desirable that the EOR methods that increase the sweep efficiency be used prior to the methods that increase the oil displacement efficiency.

A promising way of solving the problem is gel generation *in situ*. A number of methods for gel generation differing in the type of gel-formation reaction are known. The most widely used reactions are hydrolytic polycondensation ending in the formation of inorganic gels (for example, metal hydroxide and silicic acid gels),^{4,8} the formation of three-dimensional polymeric structures through cross-linking of the macromolecules of natural and synthetic polymers in solutions (polyacrylamide cross-linked by chromium salts, *etc.*),^{8,9,12,13} and solution–gel phase transitions in systems involving polymers with either upper or lower critical solution temperature and water (ethers, cellulose, polyvinyl alcohol, *etc.*).^{102,103}

In the IPC SB RAS, new methods were developed for enhancing oil recovery using thermotropic inorganic and polymeric gel-forming systems that generate gels *in situ* and are designed for increasing sweep efficiency of water flooding or thermal steam treatment.^{95,102–106}

Each oil deposit has its geological and physical characteristics. The composition of oil and the reservoir rock, the oil viscosity, water salinity and the formation temperature and pressure vary over broad ranges. Thus the formation temperature is 8–12 °C in Yakutia oil fields, 20–40 °C in Tatarstan fields, 50–100 °C in West Siberia and 110–170 °C in the South China sea offshore deposits in Vietnam. Water salinity can vary from 0 to 300–400 g litre^{–1}. Therefore, gel-forming systems with controllable properties should be used for enhancing oil recovery.

A study of the physicochemistry and hydrodynamics of the *in situ* gel generation has shown that gel-forming systems are low-viscosity aqueous solutions under surface conditions, while under reservoir conditions, they are converted into gels. Gelation is induced by the thermal energy of the formation or an injected heat carrier, or by the interaction of the injected system with the formation fluids and reservoir rock. The gel formation kinetics and the rheological and filtration characteristics of various types of gels for heterogeneous formations with permeability ranging from 0.01 to 10 μm² were studied. Gel-forming systems with different gel-generation times (ranging from several minutes to several days) in the temperature range of 30–320 °C were proposed. Using these systems, five gel processes for enhancing oil recovery of highly heterogeneous formations were developed at the IPC SB RAS; these processes are used at oil fields of West Siberia and the Komi Republic.^{95,102–107} The environmental safety of reagents accounts for the extensive use of gel processes at oil fields in Russia and abroad.

1. Thermally reversible polymeric gels

A new method for enhancing oil recovery from highly heterogeneous formations based on control of filtration flows and increase in the sweep efficiency by thermally reversible polymeric gels during water flooding has been developed. The gels are formed from polymer solutions with a lower critical solution temperature (LCST).^{103,108,109} The gelation is induced by the thermal energy of the formation or injected heat carrier. Solutions of LCST polymers can form gel *in situ*: at low temperatures, the solutions have low viscosity, while at high temperatures they are converted into gels. The process is reversible: on cooling, the gel is liquefied and becomes again a low-viscosity solution and on repeated heating, the gel is restored. The gelation temperature in the range from 30 to 120 °C and the gelation time can be controlled by inorganic and organic additives, thus adjusting the systems to particular formation conditions, *viz.*, temperature and water salinity. The

gels can be used as effective means for controlling the water influx, preventing gas breakthrough, elimination of gas cones, etc.

At temperatures below LCST, an aqueous solution of the polymer represents a homogeneous system, which splits into two phases above LCST:^{103–109} one phase is a highly dilute and the other phase is a concentrated polymer solution. Due to high viscosity of the latter, decomposition is hindered and non-equilibrium. This gives rise to a microheterogeneous kinetically stable structure, *viz.*, a thermally reversible polymeric gel. In the concentrated phase, a three-dimensional framework is formed, the dilute polymer phase being situated in its cells.

The ability of LCST polymer–water systems to form gels with an increase in temperature allows one to use them in EOR processes aimed at increasing the formation sweep efficiency in water flooding by selective isolation of the swept highly permeable areas of the formation. Cellulose ethers (CE) are the LCST polymers of choice.

The gelation kinetics and rheological characteristics in the CE–aqueous phase system have been studied^{102, 106} in order to establish the possibility of using CE gels under various geological deposit conditions. A typical example of LCST CE is methylcellulose (MC). The properties and structure of MC solutions and gels have been considered in the literature.^{110–114} The temperature dependence of the viscosity of MC solutions passes through a minimum: on heating, the viscosity first gradually decreases from 40–70 to 5–20 MPa s, *i.e.*, 2–14-fold and, after the gelation point has been reached, sharply increases to 100–2000 MPa s (20–100-fold), which is due to a phase transition (Fig. 8). The process is reversible: on cooling, the gel is converted again into a liquid. The temperature where the viscosity is minimum corresponds to the LCST. In cycling (alternation of heating and cooling processes), the rheological parameters of the gel are reproduced.

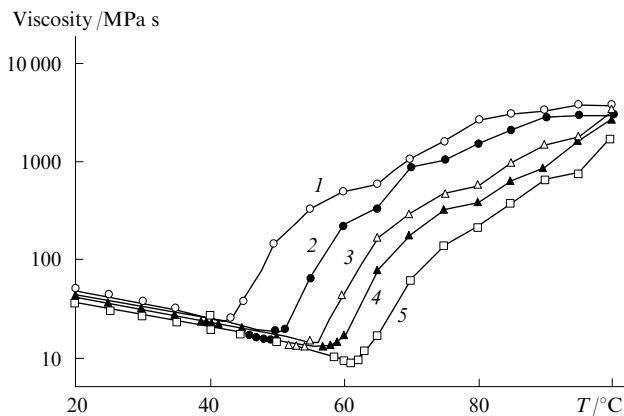


Figure 8. Viscosities of the aqueous solutions of methylcellulose (1 mass %) vs. temperature at different formation water salinity.⁹⁵ Salinity / g litre⁻¹: (1) 60, (2) 30, (3) 15, (4) 7.5, (5) 0.

The effect of electrolytes and non-electrolytes that change the hydrophobic interactions in the system on phase equilibria and gelation kinetics in MC solutions has been studied experimentally (Fig. 9 and 10). The change in the gelation point of CE solutions is affected most appreciably by anions, the effect being correlated with positions of the anions in the lyotropic series.⁹⁵ The greatest decrease in the LCST is induced by chlorides. The opposite effect, *i.e.*, an increase in the LCST, is exerted by salts with the CNS⁻ anion, and the effect of salts with NO₃⁻ is intermediate: the LCST somewhat increases on a decrease in the gelation point depending on the cation nature. The effect of cations is much less pronounced. For salts with

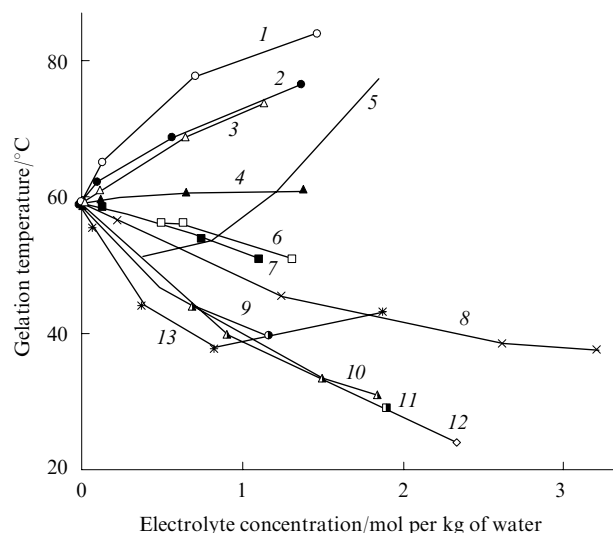


Figure 9. Effect of the electrolyte nature on the gelation temperature of solutions with a methylcellulose concentration of 1 mass %.⁹⁵ (1) NH₄CNS, (2) NaCNS, (3) KCNS, (4) NH₄NO₃, (5) ZnCl₂, (6) NaNO₃, (7) KNO₃, (8) LiCl, (9) MgCl₂, (10) CaCl₂, (11) KCl, (12) NaCl, (13) AlCl₃.

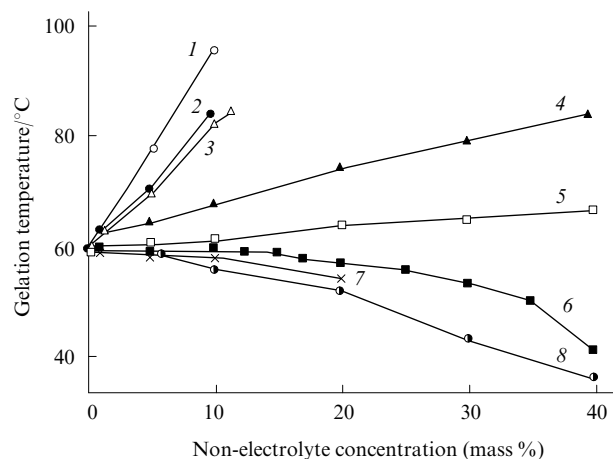


Figure 10. Effect of the electrolyte nature on the gelation temperature of methylcellulose solutions (1 mass %).⁹⁵ (1) Thiourea, (2) isopropyl alcohol, (3) ethyl alcohol, (4) carbamide, (5) triethanolamine, (6) ethylene glycol, (7) polyglycol, (8) glycerol.

Cl⁻ or CNS⁻ anions, cations play a noticeable role but are unable to change the pattern of anion effect. The most pronounced decrease in the gelation point is induced by 1:1 electrolytes, while the action of 2:1 or 3:1 electrolytes is weaker and almost equivalent. An exception is provided by zinc chloride [a ZnCl₂ concentration above 0.4 mol per kg of water changes the character of effect on the gelation point, which increases (see Fig. 9)] and aluminium chloride (when present in a concentration of >0.8 mol per kg of water). At these concentration, solutions of these chlorides are coordinating solvents. Thiourea, ethyl alcohol and isopropyl alcohol also substantially increase the LCST. The action of electrolyte and non-electrolyte agents is additive.

In view of geological parameters of oil fields, in particular, the formation temperature, salinity of the formation and injected water, it is possible to select gel-forming compositions

optimal for particular conditions to control the filtration flows and increase the sweep efficiency during water flooding.

The rheological measurements carried out using a Haake RheoStress 600 rotational viscometer at temperatures from 20 to 150 °C and pressures of up to 50 atm have shown that joint addition of carbamide and ammonium thiocyanate into CE solutions may give solutions with gelation points of > 100 °C (Fig. 11).¹⁰⁰ The gels retain their rheological characteristics at high temperatures, up to 150–220 °C. In the range of shear rates of $0.5\text{--}5\text{ s}^{-1}$, the gel is a solid-like body exhibiting (judging by the rheological curves) viscoelastic properties. Therefore, gel-forming compositions can be used to control the steam injection profile in cyclic steam wells.

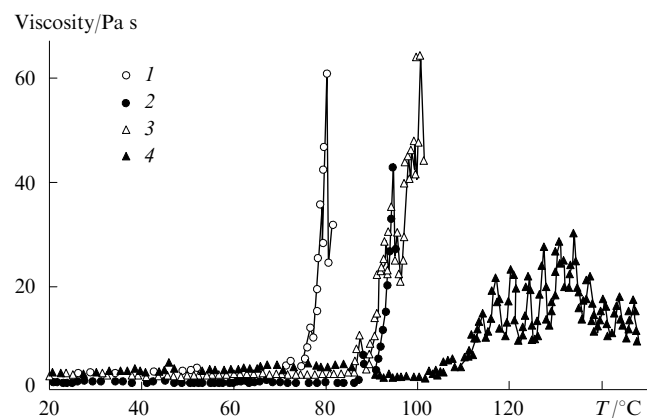


Figure 11. Change in the gelation point of an MC solution upon the addition of ammonium thiocyanate and carbamide (viscosity measurement at a shear rate of 3 s^{-1}).¹⁰⁰

Solution: (1) 1 mass % MC; (2) 1 mass % MC + 5 mass % NH_4CNS ; (3) 1 mass % MC + 20 mass % carbamide; (4) 1 mass % MC + 5 mass % NH_4CNS + 20 mass % carbamide.

The LCST polymer–water systems typically exhibit a temperature hysteresis for the solution–gel phase transition. The hysteresis in the MC–aqueous phase system was studied by determining the gelation point during heating and the liquefaction point during cooling.¹⁰⁰ The effect of additives increasing the gelation point (ethanol, ammonium thiocyanate, thiourea and carbamide) on the hysteresis was studied. The gelation points in these systems were found to almost coincide with the LCST values of polymers found by vibrational viscometry.⁹⁵ The liquefaction point was $30\text{--}50^\circ$ below the gelation point (Fig. 12). The gelation and liquefaction points increase almost linearly with the reagent concentrations, these dependences being parallel for all reagents studied except for carbamide.

The reversibility of the solution–gel phase transition was established experimentally in a study of water filtration through a heterogeneous reservoir model under simulated formation conditions. The studies were carried out in a setup for filtration measurements at a constant water flow rate through the model, which consisted of two parallel columns with different permeabilities to simulate a heterogeneous reservoir. Reservoir rock cores from oil field, various crude oils and formation waters were used in the experiments. After injection of the gel-forming solution into the reservoir model and heating to 60°C , redistribution of the filtration flows took place and was retained on temperature increase up to 220°C . As the temperature was decreased from 220 to 20°C and during the subsequent water filtration, the initial flow distribution was restored.

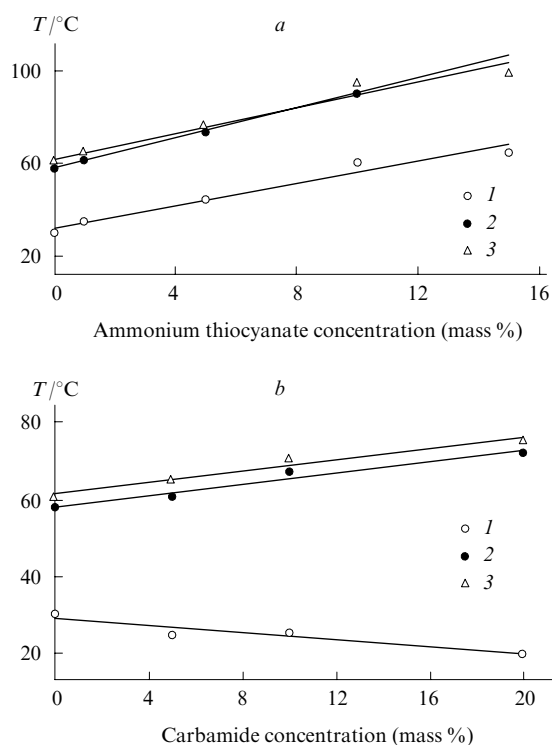


Figure 12. Effect of ammonium thiocyanate (a) and carbamide (b) on gel formation and liquefaction temperatures in solutions with MC concentration of 1 mass %.

$T/^\circ\text{C}$: (1) liquefaction, (2) LCST, (3) gelation.

The gel formation in the reservoir rock results in a selective decrease in the phase permeability of the rock with respect to water (Fig. 13): the pressure gradient for water filtration through the gel is 2–3 times higher than that for oil filtration.¹⁰⁰

The filtration characteristics and the oil-displacing properties of gel-forming compositions based on MC were studied experimentally as applied to heterogeneous reservoirs of West Siberia oil fields.^{115, 116} It was found that injection of a slug of the gel-forming solution into a heterogeneous reservoir model results in redistribution of the filtration flows where the liquid mobility in the highly permeable part sharply decreases, while

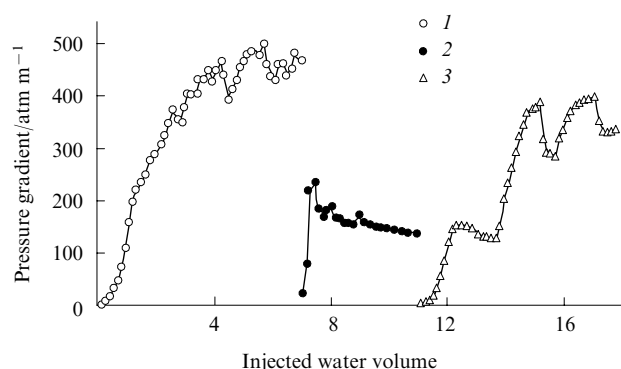


Figure 13. Selective increase in the phase permeability for water after the formation of the MC gel in the reservoir rock with a permeability of $11\text{ }\mu\text{m}^2$.

(1) Water injection, (2) oil injection, (3) repeated water injection. The volume of the injected water is determined by the number of pore volumes.

that in the low-permeability part most often remains the same. The redistribution of filtration flows is accompanied by after-sweeping of the residual oil, which is especially pronounced in the case of low-permeability model. Gel-forming compositions have shown high efficiency in increasing the sweep efficiency on heterogeneous reservoir models with interlayer permeability differing by factors of 3–20. Therefore, these compositions were recommended for the control of filtration flows of formation fluids and water shutoff in highly heterogeneous reservoirs. Ammonium thiocyanate and carbamide present in gel-forming compositions are simultaneously trace indicators.

At a temperature of 200 °C under simulated formation conditions, the filtration characteristics and oil displacement efficiency upon physicochemical action of a gel-forming composition on the high-viscosity oil pool were studied. The use of gel-forming composition ensured equalisation of filtration flows due to a decrease in the liquid phase mobility in high-permeability interlayers, which is accompanied by oil after-sweeping from both low- and high-permeability zones of the reservoir model. For example, after injection of the composition into the heterogeneous reservoir model with permeabilities of the columns differing by a factor of 5.4 (0.397 and 2.123 μm^2), redistribution of the filtration flows took place and the ratio of liquid mobilities in the reservoir model changed from 1:4.3 to 50:1. When water was pumped in the opposite direction (simulation of the operation conditions of a cyclic steam well), the filtration pattern was retained. The oil displacement efficiency increased by 12%–13% compared to that observed with steam injection.¹¹⁵

The investigations resulted in the selection of the optimal gel-forming blends for enhancing oil recovery by water influx control during water flooding or thermal treatment of the formation. In particular, gel-forming METKA compositions were developed. A low-viscosity aqueous solution capable of forming gels under formation conditions is injected into the formation at 30–120 °C. A gel screen is formed in the high-permeability formation part into which the main bulk of the composition gets; this results in redistribution of filtration flows. Upon pumping of the METKA composition into injection wells, their input profiles are equalised, water production decreases and the oil production rates of the producing

wells that are hydrodynamically connected to injection wells increase. The METKA compositions are easy to handle; the best water solubility of the polymer is attained in the temperature range of 0–10 °C. The processes are cost effective and environmentally safe and are implemented by means of standard oil field equipment.

Successive large-scale pilot tests of EOR processes based on the use of thermally reversible gels in the West Siberia oil fields were carried out from 1996 to 1997. In 1996, the METKA composition was injected into 11 wells and in 1997, into 47 injection wells (50–100 m^3 per well). In 2–3 months after injection, the producing wells hydrodynamically connected to injection wells showed lower water production and higher oil production rates. This process has been used on an industrial scale at the West Siberia oil fields since 1998 (Lukoil company). An industrial mobile unit for the preparation and injection of the composition was designed (designer the OJSC OTO). Between 1998 and 2003, the METKA composition was injected into 382 wells. The additional oil production amounted to 480 th t ; the payback period was 5–9 months; the process efficiency was on average 1300 t of additionally produced oil per treated well. All reagents are large-scale commercial chemicals.

On combined treatment of both hydrodynamically connected injection wells and producing wells, the process efficiency increases. In 2001, pilot testing of the water shutoff process by simultaneous treatment of the bottomhole zones of the injection and producing wells with gel-forming compositions was carried out in two pilot sites of the AB_1 formation of the Urievskoye oil field.^{107, 117} The injected volume of the composition per well was from 50 to 200 m^3 ; altogether 620 m^3 were injected. This resulted in redistribution of the filtration flows and decrease in water influx, which was manifested in lower water production and higher oil production rates of the producing wells (Fig. 14). The additional oil production was 6542 t over 7 months.

Thermally reversible polymer gels are used in a number of technologies.

A technology for elimination of the behind-the-casing water flow was tested in gas wells of the Myldzhinskoye gas condensate field.¹¹⁸ For example, well No. 133 produced gas

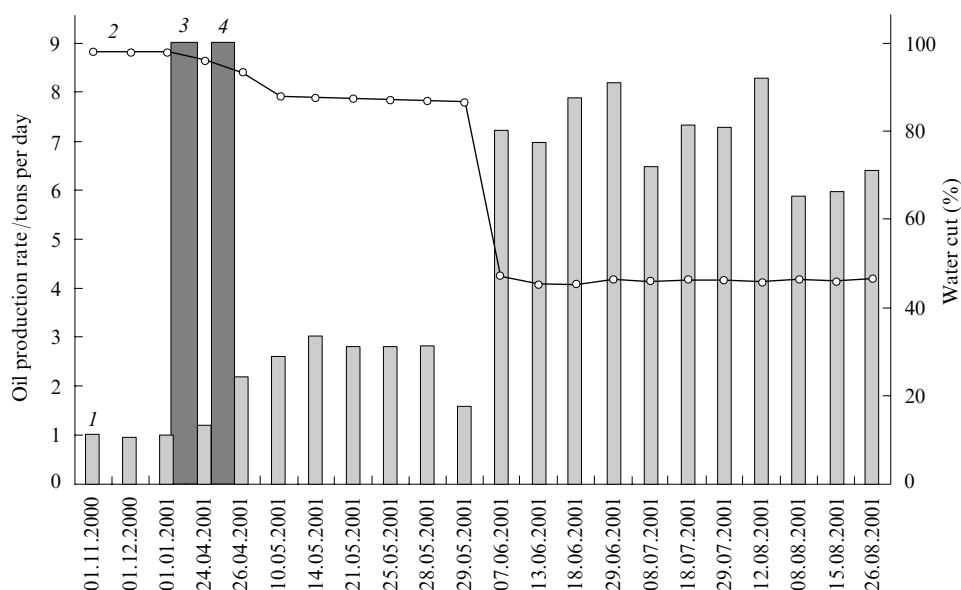


Figure 14. Increase in the oil production (1) and decrease in the water cut (2) for the producing well 1438 after pumping of the gel-forming composition into injection well 1810 (3) and producing well 1438 (4) in the Urievskoye field, formation AV_1 .¹¹⁷

containing formation water; at a gas production rate of 300 th m³ per day, water content was 30 t, which is much higher than the allowable value. After injection of the METKA gel-forming composition together with the installation of a cement bridging, the gas production rate was 430 th m³ per day with only traces of water; the well has operated at such production rate for three years.

In 2002–2003, the Institute of Petroleum Chemistry of the Siberian Branch of the RAS, together with the Institute of Mining of the Siberian Branch of the RAS carried out successful pilot testing of integrated vibroseismic and physicochemical treatment of the BV₈ formation of the Pokachevskoye oil field using the METKA composition.¹⁰⁷

In 2005–2006, processes of increasing the efficiency of cyclic steam treatment of a high-viscosity oil pool using the METKA composition for water shutoff were successfully tested at two wells of the Liaohe deposit (China).¹⁰⁰ After injection of the gel-forming composition, the oil water cut in producing wells decreased and oil production rate increased.

2. Methods for enhancing oil recovery using inorganic gel-forming systems

The ability of the aluminium salt–carbamide–water–surfactant system to generate inorganic gel and CO₂ *in situ* at temperatures 40–320 °C underlies the technology where inorganic gel-forming compositions are used to increase the sweep efficiency of water or steam injection.^{105, 107, 119–121}

The free or bound disperse systems (sols and gels) may be generated in the oil formation by the condensation mechanism, in particular, based on the ‘arising reactants’ (homogeneous precipitation) principle known in analytical chemistry.⁵ Within the framework of this principle, a new physicochemical method for enhancing oil recovery was proposed. A homogeneous aqueous solution containing a gel-forming system is injected into the oil formation. Due to the thermal energy of the formation or an injected heat carrier, one component of the system is gradually hydrolysed, the hydrolysis products inducing a shift of the protolytic equilibrium of another component. This triggers hydrolytic polycondensation of monomer units, and, after a definite period of time, a gel is formed almost instantaneously throughout the whole solution volume. The ‘arising reactants’ principle was implemented in the development of the reported physicochemical EOR method.^{122, 123}

Liquid aluminium salt–carbamide–water–surfactant gel-forming systems are low-viscosity solutions with pH 2.5–3.5. They are able to dissolve carbonate minerals in the reservoir rock and decrease (suppress) clay swelling. The solutions can be prepared using water with any salinity. They are injected into the oil-bearing formation through injection wells using standard equipment.

Carbamide is hydrolysed in the formation to give ammonia and carbon dioxide, which leads to gradual increase in the solution pH. When pH becomes 3.8–4.2, hydrolysis of aluminium ions takes place, and, as a consequence, after some period of time, aluminium hydroxide gel is formed almost instantaneously throughout the whole solution bulk (Figs 15, 16). The time required for gelation depends on the formation temperature and the component ratio in the gel-forming system. After gel generation, the reservoir rock permeability for water decreases 4–35-fold. The greater the initial water saturation and permeability of the reservoir rock the higher the degree of permeability decrease. The static shear stress of the gel is within 3–40 Pa. In the presence of surfactants, wetting of the oil reservoir rock by the gel-forming solution is enhanced and the penetrating and oil-displacing ability of the solution increases. In addition, the surfactant exerts a plasticising action on the aluminium hydroxide gel and can form a foam with carbon dioxide and ammonia evolved upon carbamide hydrolysis.⁵

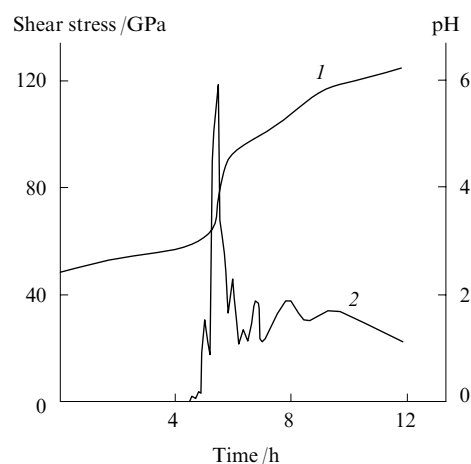


Figure 15. Change in the pH (1) and shear stress (2) in the aluminium salt–carbamide–water system upon gel formation during maintenance at 97 °C.¹⁰⁷

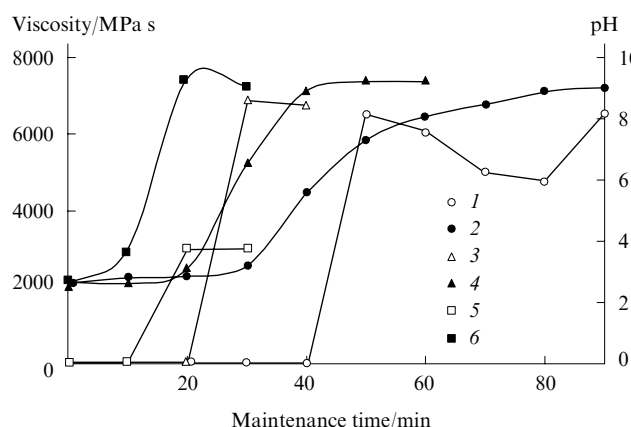


Figure 16. Viscosity (1–5) and pH (6) change in the aluminium salt–carbamide–water system upon gel formation during maintenance at 150 °C (1, 2), 200 °C (3, 4) and 250 °C (5, 6).¹⁰⁶

The rheological properties of the gel correspond to the properties of a thixotropic pseudoplastic body with the coagulation structure. A distinctive feature of the gel is the permeability for the aqueous phase at shear stresses lower than the static shear stress of the gel itself. Gelation results in redistribution of filtration flows, equalisation of input profiles of injection wells, and a decrease in water cut of the oil from producing wells. Gel-forming systems are designed for the development of oil pools with high formation temperature and heterogeneity, which is typical of West Siberia oil fields and high-viscosity oil pools developed by thermal methods.

In the temperature range of 70–100 °C, the gelation kinetics is determined by the hydrolysis of carbamide, which is much slower than the formation of aluminium hydroxide gel by the coagulation mechanism representing is a cooperative process. The pre-exponential factor ($1.1 \times 10^{12} \text{ s}^{-1}$) in the Arrhenius equation and the activation energy (115 kJ mol^{-1}) for carbamide hydrolysis in the gel-forming solution were estimated. The results are consistent with published values.⁹⁶ However, the activation energy found is lower than the activation energy for carbamide hydrolysis in the absence of aluminium salt (134 kJ mol^{-1}), which is indicative of catalysis by the acid resulting from hydrolysis of the aluminium salt. The effect of temperature on the gelation time (t_g) obeys the Van't

Hoff rule: upon temperature increase by each 10°, the gelation time increases 3.5-fold.

In the temperature range of 100–250 °C the Arrhenius dependence for the solution–gel transition is described analytically by the following regression:

$$\log \frac{1}{t_g} = 0.8322 - 3999.9 \frac{1}{T}.$$

The activation energy and the pre-exponential factor in the Arrhenius equation for the solution–gel transition are equal to 33.3 kJ mol^{−1} and 2.3 s^{−1}, respectively, which is much lower than for the temperature below 100 °C. In addition, in the 100–250 °C range, the effect of temperature on the gelation time does not obey the Van't Hoff rule: an increase in temperature by each 10° results in a 1.2-fold increase in the gelation time. These results provide the conclusion that in the temperature range of 100–250 °C the gelation kinetics in the aluminium salt–carbamide–water system is determined by the coagulation type formation of the aluminium hydroxide gel. The S-shape of the curves shown in Fig. 16 and the low activation energy attest to a cooperative mechanism of the coagulation process similar to the mechanism of phase transition or branching chain reaction.

At 70–100 °C, the gelation time depends on the concentrations and the concentration ratio of aluminium chloride and carbamide in solution; at a temperature above 150 °C this dependence is smoothened down. The lower the carbamide concentration the longer the gel formation. By varying the ratio of the aluminium salt and carbamide, one can control the gelation time, thus adjusting it to a particular formation temperature.^{119, 120}

In the range of 100–250 °C, the gel viscosity depends most appreciably on the aluminium chloride concentration. The effect of the component ratio and temperature is insignificant. The viscosity of solutions with aluminium chloride concentration of 4.0 mass % and 8.0 mass % increases during gel formation by the coagulation mechanism from 1.2–1.6 to 300–3500 MPa s and from 1.8–2.5 to 1800–7500 MPa s, respectively.

On the basis of the results of studies on the gelation kinetics and the rheological characteristics of the aluminium salt–carbamide–water–surfactant systems, gel-forming GALKa compositions and GALKa–surfactant systems were designed. During the period from 1989 to 1995, pilot testing of the EOR technology using inorganic gel-forming GALKa compositions was successfully carried out at West Siberia oil fields; since 1996, this method has been industrially used. This results in redistribution of filtration flows, an increase in the sweep efficiency of water flooding, and, hence, an increase in the ultimate oil recovery by 5%–8%. The additional oil production was 400 to 3000 t per treated well. The pilot testing of gel-processes was successfully carried out at the White Tiger oil field (Vietnam).

In 1996, the IPC SB RAS organised, in cooperation with the OJSC Nefteotdacha, the manufacture of the GALKa composition as a liquid commercial product using aluminium-containing industrial wastes. In 2000, the IPC SB RAS organised, in cooperation with the OJSC AURAT, the manufacture of solid commercial products including the GALKa composition, *viz.*, GALKa–thermogel-S for formation temperatures of 70–320 °C, GALKa–thermogel-U for temperatures of 40–70 °C, GALKa–thermogel-NT for temperatures of 20–40 °C. The advantages of the GALKa–thermogel systems include: controlled gelation temperature, homogeneity and low viscosity of aqueous solutions, low pour points of solutions, and availability of a solid commercial product. This allows them to be used over a broad temperature range (from 20 to 320 °C); they are applicable to low-permeability reservoirs; the composition can be injected into a well by batching directly into the water pipe without preliminary dissolution (this process can be used in the winter season).

The inorganic gels GALKa withstand the temperatures of 300–320 °C; hence, they can be used to increase the sweep efficiency in the thermal steam treatment for the development of high-viscosity oil pools.¹⁰⁷ In 2002, pilot testing of the process using the composition as the commercial solid product was carried out on the thermal steam treatment site PTV-3 of the Permo-Carboniferous pool of the Usinskoye field; 600 m³ of the GALKa–thermogel-S composition were injected into four steam injection wells. The composition showed good field

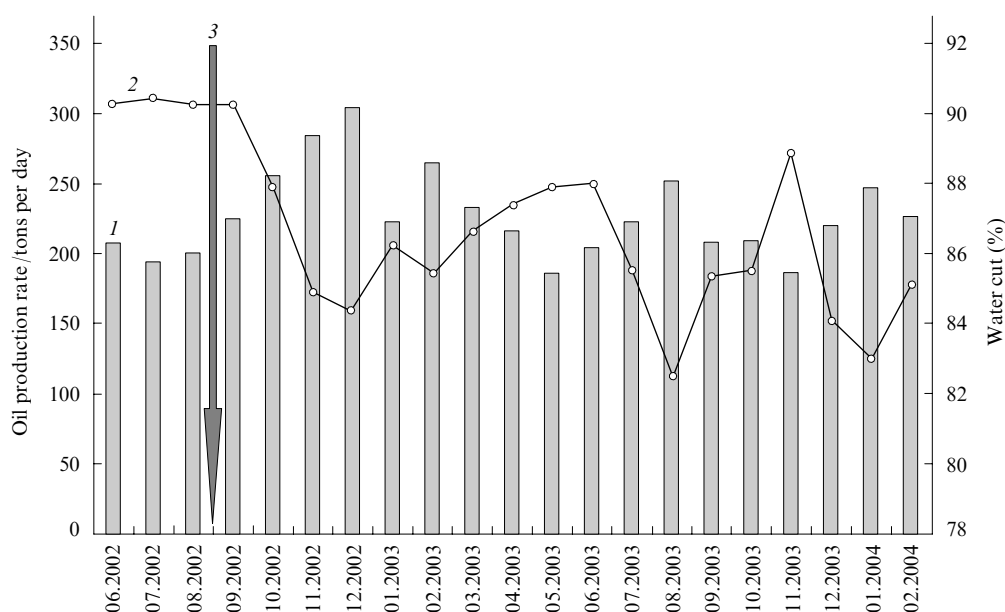


Figure 17. Monthly oil production (1) and water cut (2) dynamics for 29 wells of the pilot site after injection of the GALKa–thermogel-S composition (3) in the Usinskoye field (observation period from June 2002 to February 2004).¹⁰⁷

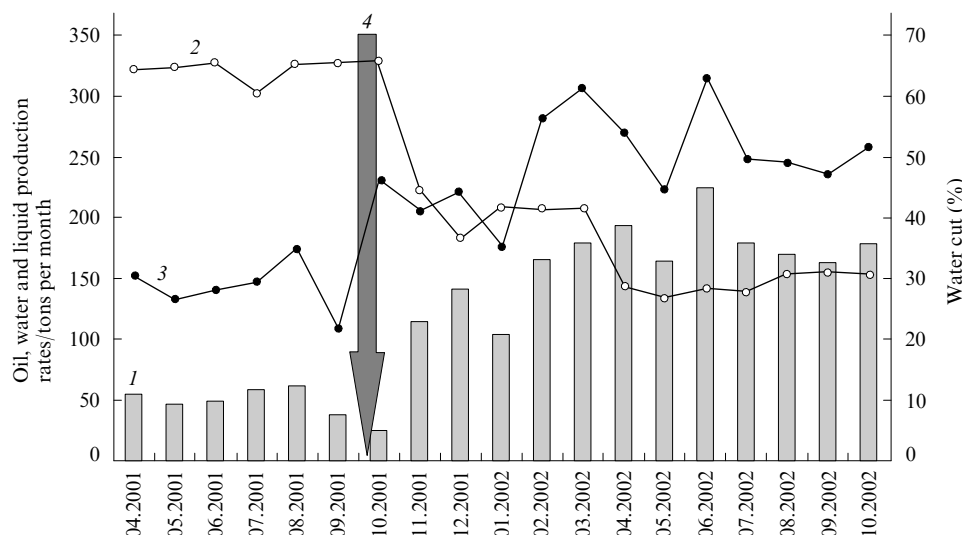


Figure 18. Results of the use of the integrated EOR technology including injection of the gel-forming GALKa composition and an oil-displacing composition IHN-100 on the pilot site of the YuV₁ formation of the Las-Yeganskoye field (injection well 9066, producing well 152p).¹⁰⁷ (1) Oil production rate, (2) water cut (%), (3) liquid production rate, (4) injection of compositions.

handling properties and environmental safety. The 29 producing wells of the pilot site produced additionally 33 th t of oil from October 2002 to February 2004. The engineering efficiency amounts to 275 t of additional oil production per t of the solid commercial GALKa – thermogel-S composition. The water production of the producing wells decreased by 3%–45% and the oil production rate increased by 23% on average (Fig. 17); the decrease of the monthly liquid production rate was 19.8% on average.

3. Integrated EOR process using gel-forming and oil-displacing compositions

For enhancing the oil recovery of fields with highly heterogeneous reservoirs at a later stage of development, the isolation of high-permeability watered formations by their blocking should be followed by intensification of liquid filtration in low-permeability formations. This requires an integrated technology: first, a gel-forming composition is used to increase the sweep efficiency of water flooding and then an oil-displacing composition is employed to intensify the development of a low-permeability formation. This combined action on the oil pool allows one to efficiently redistribute the filtration flows of formation fluids and to develop the formations not swept previously by water flooding; this method is efficient for enhancing the oil recovery of low-permeability highly heterogeneous oil pools at both early and late stages of field development.

For the development of oil reserves difficult to recover of the Jurassic deposits of West Siberia, an integrated process was proposed wherein GALKa – thermogel was used as the gel-forming composition and IHN-100 was used as the oil-displacing composition. Unlike the known compositions, these gel-forming and oil-displacing compositions possess complementary physicochemical properties, resulting in synergistic action.

In 2001, pilot testing of the integrated process was carried out in the Las-Yeganskoye field (YuV₁ formation). The GALKa – thermogel-U composition (6, 10 and 18 t) and IHN-100 composition (30, 50 and 48 t) were pumped into injection wells. Analysis of the field data showed that the combined action of these compositions resulted in redistribution of the filtration flows in the formation, involvement of low-permeability interlayers and intensification of their development, which is manifested in lower water cut of the products

and higher oil and liquid production rates from the producing wells hydrodynamically connected to the injection wells (Fig. 18). The additional oil production over the site from January 2001 to October 2002 was 4.4 th t.¹⁰⁷ The process was recommended for industrial use in West Siberia fields.

Currently, development of other integrated methods is in progress, for example, the pulse explosive stimulation of the formation combined with using oil-displacing and gel-forming compositions, physicochemical and microbiological EOR methods.

The development of the physicochemical methods for enhancing oil recovery and increase in the extent of their application may provide, even in the near future, a significant gain in the recoverable reserves and current oil production both on operating and newly explored oil fields in Russia.

References

1. A Varlamov *Nef. Rossii* **1** 106 (2007)
2. A Bokserman, I Mishchenko *Tekhnol. TEK* **8** 30 (2006)
3. Kh Kh Gumerskii, S A Zhdanov, V K Gomzikov *Neftyanoe Khozyaistvo* **5** 38 (2000)
4. M L Surguchev, A T Gorbunov, D P Zabrodin, E A Ziskin, G S Malyutina *Metody Izvlecheniya Ostatochnoi Nefti* (The Methods of Residual Oil Recovery) (Moscow: Nedra, 1991)
5. L K Altunina, V A Kuvshinov *Uvelichenie Nefteotdachi Plastov Kompozitsiyami PAV* (Enhancing Oil Recovery by Surfactant Blends) (Novosibirsk: Nauka, 1995)
6. V D Lysenko *Geol. Geofiz. Razrab. Nef. Gaz. Mestorozh.* **6** 37 (1996)
7. L W Lake *Enhanced Oil Recovery* (New York: Prentice-Hall, 1996)
8. V N Manyrin, I A Shvetsov *Fiziko-khimicheskie Metody Uvelicheniya Nefteotdachi pri Zavodnenii* (Physicochemical Methods for Enhanced Oil Recovery using Water Flooding) (Samara: Samarskii Dom Pechati, 2002)
9. A A Gazizov *Uvelichenie Nefteotdachi Neodnorodnykh Plastov na Pozdnei Stadii Razrabotki* (Enhanced Oil Recovery from Heterogeneous Formations in Late Stages of Development) (Moscow: Nedra-Biznestsentr, 2002)
10. A Ya Khavkin *Geologo-fizicheskie Faktory Effektivnoi Razrabotki Mestorozhdenii Uglevodorodov* (Geological and Physical Factors of Effective Hydrocarbon Field Development) (Moscow: Sputnik +, 2005)

11. A I Shvetsov, G N Bakaev, V Ya Kabo, V V Perunov, Yu V Solyakov *Neftyanoe Khozyaistvo* (4) 37 (1994)
12. A Sh Gazizov, L A Galaktionova, V S Adagymov, A A Gazizov *Neftyanoe Khozyaistvo* (2) 12 (1998)
13. V V Devyatov, R Kh Almaev, P I Pastukh, V M Sankin *Primenenie Vodoizoliruyushchikh Khimreagentov na Obvodnennykh Mestorozhdeniyakh Shaimskogo Raiona* (The Use of Water-Shutoff Agents in the Flooded Fields of the Shaimsky Region) (Moscow: VNIOENG, 1995)
14. A G Dyabin, A Ya Sorkin, V E Stupochenko, V A Kan, I A Sidorov, A B Pogoyan, Yu M Smirnov *Neftyanoe Khozyaistvo* (12) 16 (2000)
15. S V Ivanov, L S Brilliant *Neftyanoe Khozyaistvo* (9) 47 (2000)
16. E V Lozin, O G Gafurov, Ya G Mukhtarov, R G Shirgazin *Neftyanoe khozyaistvo* (2) 39 (1996)
17. N A Lebedev *Neftyanoe Khozyaistvo* (7) 16 (1997)
18. L K Altunina, V A Kuvshinov *Ros. Khim. Zh.* (5) 16 (1994)^a
19. O E Tsinkova, N A Myasnikova, B T Baishev *Gidrodinamicheskie Metody Uvelicheniya Nefteotdachi* (Hydrodynamic Methods of Enhanced Oil Recovery) (Moscow: Nedra, 1993)
20. R R Ibatullin, N G Ibragimov, Sh F Takhautdinov, R S Khisamov *Uvelichenie Nefteotdachi na Pozdnei Stadii Razrabotki Mestorozhdenii* (Enhanced Oil Recovery in the Late Stages of Oil Field Development) (Moscow: Nedra, 2004)
21. V N Martos, T M Umariev *Geol. Geofiz. Razrab. Nef. Gaz. Mestorozh.* 2 37 (1994)
22. R D Kanevskaya *Matematicheskoe Modelirovanie Razrabotki Mestorozhdenii Nefti i Gaza s Primeneniem Gidravlicheskogo Razryva Plasta* (Mathematical Modelling of Oil and Gas Field Development using Hydrofracturing) (Moscow: Nedra-Bizness-sentr, 1999)
23. B M Suchkov *Gorizontal'nye Skvazhiny* (Horizontal Wells) (Izhevsk: RKhD, 2006)
24. M M Khasanov *Neftyanoe Khozyaistvo* (3) 43 (2007)
25. Kh Kh Gumerskii, A T Gorbunov, S A Zhdanov, A M Petrakov *Neftyanoe Khozyaistvo* (12) 12 (2000)
26. S A Zhdanov, D Yu Kryanev, A M Petrakov *Neftyanoe Khozyaistvo* (5) 39 (2005)
27. R Maksutov, G Orlov, A Osipov *Tekhnologii TEK* (6) 23 (2005)
28. Zh Burzhe, P Surio, M Kombarnu *Termicheskie Metody Povysheniya Nefteotdachi Plastov* (Thermal Methods of Enhanced Oil Recovery) (Moscow: Nedra, 1988)
29. N K Baibakov, A R Garushev, D G Antoniadi, V G Ishkhanov *Termicheskie Metody Dobychi Nefti v Rossii i za Rubezhom* (Thermal Methods of Oil Production in Russia and Abroad) (Moscow: VNIOENG, 1995)
30. D G Antoniadi *Uvelichenie Nefteotdachi Plastov Gazovymi i Parogazovymi Metodami* (Enhanced Oil Recovery by Gas and Steam-and-Gas Methods) (Moscow: Nedra, 1998)
31. L K Altunina, L P Gossen, L D Tikhonova, E G Yarmukhametova *Zh. Prikl. Khim.* 75 166 (2002)^b
32. L K Altunina, V A Kuvshinov, A I Gyngazov, V P Dorokhov *Ekonomicheskaya Nauka na Sluzhbe Proizvodstva (Tezisy Dokladov Nauchno-prakticheskoi Konferentsii MINIEKO TEK), Perm', 1998* [Economic Science for Production (Abstracts of Reports of the Scientific and Practice Conference MINIEKO TEK), Perm, 1998] p. 51
33. S S Sergienko, B A Taimova, E I Talalaev *Vysokomolekulyarnye Neuglevodorodnye Soedineniya Nefti* (High-molecular Non-hydrocarbon Oil Compounds) (Moscow: Nauka, 1979)
34. V F Kam'yanov, V S Aksenov, V I Titov *Geteroatomnye Komponenty Neftei* (Heteroatomic Oil Components) (Novosibirsk: Nauka, 1983)
35. O K Kimbler, R L Reed, I H Silberberg *Soc. Petrol. Eng. J.* 6 153 (1966)
36. D D Eley, V L Hey, M A Lee *Colloids Surf.* 24 173 (1987)
37. I L Markhasin *Fiziko-khimicheskaya Mekhanika Neftyanogo Plasta* (Physicochemical Mechanics of Oil Formation) (Moscow: Nedra, 1977)
38. N M Baikov, G N Pozdnyshev, R I Mansurov *Sbor i Promyslovaya Podgotovka Nefti, Gaza i Vody* (Collection and Field Treatment of Oil, Gas and Water) (Moscow: Nedra, 1981)
39. B P Singh, B P Pandey *Indian J. Technol.* 29 443 (1991)
40. S Acevedo, G Escobar, L Gutierrez, H Rivas *Fuel* 71 619 (1992)
41. E J Shen, M M De Tar, D Storm *Fuel* 71 1277 (1992)
42. S Acevedo, M A Ranaudo, G Escobar, G Gutierrez *Fuel* 78 308 (1999)
43. V N Izmailova, G P Yampol'skaya *Uspekhi Kolloidnoi Khimii i Fiziko-khimicheskoi Mekhaniki* (Progress in Colloid Chemistry and Physicochemical Mechanics) (Moscow: Nauka, 1992) p. 103
44. A V Bogoslovskii, L K Altunina *Molekulyarnye Vzaimodeistviya i Elektronnye Protsessy v Rastvorakh* (Molecular Interactions and Electronic Processes in Solutions) (Novosibirsk: Nauka, 1987) p. 55
45. Russ. P. 1229647; *Byull. Izobret.* (17) 179 (1985)
46. N Aske, R Orr, J Sjoblom, H Kallevik, G pye *J. Dispersion Sci. Technol.* 25 263 (2004)
47. G A Babalyan, I I Kravchenko, I L Markhasin, G V Rudakov *Fiziko-khimicheskie Osnovy Primeneniya Poverkhnostno-aktivnykh Veshchestv pri Razrabotke Neftnykh Plastov* (Physicochemical Foundations of Application of Surfactants for Oil Formation Development) (Moscow: Nedra, 1962)
48. M L Surguchev *Vtorichnye i Tretichnye Metody Uvelicheniya Nefteotdachi Plastov* (Secondary and Tertiary Methods of Enhancing Oil Recovery) (Moscow: Nedra, 1985)
49. R M Giordano, J C Slattery *AIChE J.* 33 1592 (1987)
50. M Li, M Xu, Y Ma, Z Wu, A A Christy *Fuel* 81 1847 (2002)
51. L K Altunina, V A Kuvshinov, I F Efremov, V V Novgorodov *Proceedings of the Third Symposium on Mining Chemistry, Siofok, Hungary, 1990* p. 211
52. V V Nauchitel', I V Golovanov, M V Vol'kenshtein *Dokl. Akad. Nauk SSSR* 392 1144 (1988)^c
53. A L Nicholls, L R Pratt *J. Chem. Phys.* 81 579 (1984)
54. J Monin, A Vignat *Rev. Inst. Fr. Petrol.* 39 821 (1984)
55. J Murgich *Petrol. Sci. Technol.* 20 983 (2002)
56. N Siddiqui *Petrol. Sci. Technol.* 21 1601 (2003)
57. L K Altunina, V A Kuvshinov *Problemy i Dostizheniya v Issledovanii Nefti* (The Problems and Achievements in Oil Investigation) (Tomsk: Tomsk Scientific Centre, Siberian Branch of Academy of Sciences of the USSR, 1990) p. 221
58. J Reisberg, T M Doscher *Producers Mon.* 21 43 (1956)
59. V A Kuvshinov, L K Altunina, L F Genkina *Zh. Prikl. Khim.* 63 926 (1990)^b
60. L K Altunina, V A Kuvshinov *Eurasian Chem.-Technol. J., Kazakhstan* 3 (3) 179 (2001)
61. A Watanabe *Surface Coll. Sci.* 13 1 (1984)
62. M I Gugeshashvili, A V Indenbom, L I Boguslavskii *Elektrokhimiya (Itogi Nauki i Tekhniki. Ser.)* [Electrochemistry (Advances in Science and Engineering Series)] (Moscow: Izd. VINITI, 1988) No. 28, p. 172
63. M Senda, T Kakiushi, T Osakai, T Kakutani *Elektrokhimiya (Itogi Nauki i Tekhniki. Ser.)* [Electrochemistry (Advances in Science and Engineering Series)] (Moscow: Izd. VINITI, 1988) No. 28, p. 248
64. I V Pisareva, A V Bogoslovskii, L K Altunina *Fiziko-khimicheskie Svoistva Rastvorov i Dispersii* (Physicochemical Properties of Solutions and Dispersions) (Novosibirsk: Nauka, 1992) p. 30
65. V A Kuvshinov, L K Altunina, L F Genkina *Kolloid. Zh.* 47 279 (1985)^d
66. B V Deryagin, N V Churaev *Smachivanie Plenki* (Watering Film) (Moscow: Nauka, 1984)
67. N P Tantsura, O G Us'yarov *Kolloid. Zh.* 43 375 (1981)^d
68. N R Morrow *J. Petrol. Technol.* 42 1476 (1990)
69. S Y Yang, G J Hirasaki, S Basu, R Vaidya *J. Petrol. Sci. Eng.* 33 203 (2002)
70. V A Kuvshinov, L K Altunina, N A Marchenko *Kolloid. Zh.* 50 1184 (1987)^d
71. V V Pushkarev, D I Trofimov *Fiziko-khimicheskie Osobennosti Ochistki Stochnykh Vod ot Poverkhnostno-aktivnykh Veshchestv* (Physicochemical Features of Waste Water Purification from Surfactants) (Moscow: Khimiya, 1975)
72. I V Sheveleva, A V Voit, A V Zryanina *Zh. Fiz. Khim.* 67 1654 (1993)^c

73. A M Koganovskii, N A Klimenko, T M Levchenko, I G Roda *Adsorbtsiya Organicheskikh Veshchestv iz Vody* (Adsorption of Organic Substances from Water) (Leningrad: Khimiya, 1990)
74. L K Altunina, V A Kuvshinov, I F Efremov *Sovremennye Metody Uvelicheniya Nefteotdachi Plastov* (Modern Methods for Enhancing Oil Recovery) (Moscow: Nauka, 1992) p. 121
75. T S Ramakrishnan, D T Wasan *AIChE J.* **36** 725 (1990)
76. V A Kuvshinov, L K Altunina, L F Genkina *Instrumental'nye Metody Issledovaniya Neftei* (Instrumental Methods of Investigation of Oil) (Novosibirsk: Nauka, 1987) p. 116
77. V A Kuvshinov, L K Altunina, N A Marchenko *Izucheniye Sostava i Svoistv Neftei Nizhnevartovskogo Svoda* (Study of the Composition and Properties of Nizhnevartovsk Oil Field) (Tomsk: TF SO RAN SSSR, 1984) p. 132
78. N V Churaev *Uspekhi Kolloidnoi Khimii* (Progress in Colloid Chemistry) (Kiev: Naukova Dumka, 1983) p. 24
79. G Shtyupel' *Sinteticheskie Moyushchie i Ochishchayushchie Sredstva* (Synthetic Detergents) (Moscow: Goskhimizdat, 1960)
80. M I Shakparonov, V V Devlikamov, A B Tumasyan, A L Shtangeev, E V Lozin, T N Maksimova, T M Usacheva *Issledovaniya Stroeniya, Teplovogo Dvizheniya i Svoistv Zhidkostei* (Investigation of the Structure, Thermal Motion and Properties of Liquids) (Moscow: Moscow State University, 1986) p. 5
81. A T Gorbunov, L N Buchenkov *Shchelochnoe Zavodnenie* (Alkaline Water Flooding) (Moscow: Nedra, 1989)
82. R V Smith *Petrol. Eng. Int.* **61** 44 (1989)
83. G I Fuks, Ya Buribaev *Issledovaniya po Fizikokhimiі Kontakt-nykh Vzaimodeistvii* (Investigations in the Physical Chemistry of Contact Interactions) (Ufa: Bashkirkoe Knizhnoe Izd., 1971)
84. A A Bugaevskii *Matematicheskie Zadachi Khimicheskoi Termodinamiki* (Mathematical Problems in Chemical Thermodynamics) (Novosibirsk: Nauka, 1985) p. 42
85. Yu A Kokotov *Matematicheskie Zadachi Khimicheskoi Termodinamiki* (Mathematical Problems in Chemical Thermodynamics) (Novosibirsk: Nauka, 1985) p. 49
86. R Beits *Opreделение pH. Teoriya i Praktika* (Determination of pH. Theory and Practice) (Leningrad: Khimiya, 1968)
87. S Outubuddin, C A Miller, T Fort *J. Colloid Interface Sci.* **101** 46 (1984)
88. L K Altunina, V A Kuvshinov *Proceedings of EUROPEC European Petroleum Conference Integrated Reservoir Management, Paris, 2000* p. 515
89. L K Altunina, V A Kuvshinov *Fiziko-khimicheskie Svoistva Rastvorov i Dispersii* (Physicochemical Properties of Solutions and Dispersions) (Novosibirsk: Nauka, 1992) p. 3
90. L Altunina, V Kuvshinov *Vestn. Inzhiniring. Tsentra YuKOS* **4** 49 (2002)
91. L I Svarovskaya, L K Altunina *Neftekhimiya* **39** 148 (1999)^f
92. V S Ovsyannikova, L K Altunina, L I Svarovskaya, G S Peveva, L D Stakhina *Trudy 12 Evropeiskogo Simpoziuma 'Povyshenie Nefteotdachi Plastov', Kazan', 2003* (Proceedings of the 12th European Symposium 'Enhancing Oil Recovery', Kazan, 2003) p. 169
93. L K Altunina, L I Svarovskaya, O P Boeva *Sovremennye Metody Uvelicheniya Nefteotdachi Plastov* (Modern Methods for Enhancing Oil Recovery) (Moscow: Nauka, 1992) p. 124
94. M Metwally *J. Can. Petrol. Technol.* **29** 26 (1990)
95. L K Altunina, V A Kuvshinov *Khim. Inter. Ustoich. Razvitiya* **9** 331 (2001)^g
96. V I Kucheryavii, V V Lebedev *Sintez i Primenenie Karbamida* (Synthesis and Applications of Carbamide) (Leningrad: Khimiya, 1970)
97. D M Gorlovskii, L N Al'tshuler, V I Kucheryavii *Tekhnologiya Karbamida* (Technology of Carbamide) (Leningrad: Khimiya, 1981)
98. L K Altunina, V A Kuvshinov, L A Stasyeva *Progress in Mining and Oilfield Chemistry. Novelties in Enhanced Oil and Gas Recovery* Vol. 5 (Ed. I Lakatos) (Budapest: Akademiai Kiado, 2003) p. 123
99. V A Kuvshinov, V V Kuvshinov, L K Altunina *Proceeding of the 11th Symposium on Improved Oil Recovery, Amsterdam, 2001*
100. L K Altunina, V A Kuvshinov *Tekhnol. TEK* **2** 41 (2007)
101. L K Altunina, V A Kuvshinov, L A Stasyeva *Progress in Oilfield Chemistry. Managing Matured Fields and Wells* Vol. 6 (Ed. I Lakatos) (Budapest: Akademiai Kiado, 2005) p. 81
102. L K Altunina, V A Kuvshinov, L A Stas'eva, V V Gusev *Neftekhimiya* **39** 42 (1999)^f
103. I Yu Galaev *Usp. Khim.* **64** 505 (1995) [*Russ. Chem. Rev.* **64** 471 (1995)]
104. L K Altunina, V A Kuvshinov *Nefteotdacha* **5** 28 (2002)
105. L K Altunina, A A Bokserman, V A Kuvshinov, V V Polkovnikov *Geol. Soc. Spec. Publ.* **84** 219 (1995)
106. L K Altunina, V A Kuvshinov *Progress in Mining and Oilfield Chemistry. Novelties in Enhanced Oil and Gas Recovery* Vol. 5 (Ed. I Lakatos) (Budapest: Akademiai Kiado, 2003) p. 115
107. L K Altunina, V A Kuvshinov *Tekhnologii TEK* (6) 44 (2004)
108. R A Rehinder *Izbrannye Trudy. Poverkhnostnye Yavleniya v Dispersnykh Sistemakh. Kolloidnaya Khimiya* (Selected Works. Surface Effects in Dispersion Systems. Colloid Chemistry) (Moscow: Nauka, 1978)
109. S P Papkov *Fiziko-khimicheskie Osnovy Pererabotki Rastvorov Polimerov* (Physicochemical Foundations of Processing of Polymer Solutions) (Moscow: Khimiya, 1971)
110. G A Petropavlovskii *Gidrofil'nye Chastichno Zameshchennye Efirny Tselyulozy i ikh Modifikatsiya Putem Khimicheskogo Sshivaniya* (Hydrophilic Partially Substituted Cellulose Esters and Their Modification by Chemical Cross-linking) (Leningrad: Nauka, 1988)
111. A M Bochek, G A Petropavlovskii, O V Kallistov *Zh. Prikl. Khim.* **69** 1363 (1996)^b
112. O V Alekseev, O V Rozhkova, A N Prusov, V A Padokhin, Ya A Anikin *Zh. Prikl. Khim.* **77** 483 (2004)^b
113. M A V Axelos, J Desbrieres, M Rinaudo, M Hirrien, C Chevallard *Polymer* **39** 6251 (1998)
114. S B Ross-Murphy, M Hirrien, J Desbrieres *Polymer* **41** 2451 (2000)
115. L K Altunina, V A Kuvshinov, L A Stas'eva *Bashk. Khim. Zh.* **8** 53 (2001)
116. L K Altunina, V A Kuvshinov, L A Stasyeva *Progress in Mining and Oilfield Chemistry. Recent Advances in Enhanced Oil and Gas Recovery* Vol. 3 (Ed. I Lakatos) (Budapest: Akademiai Kiado, 2001) p. 67
117. L K Altunina, V A Kuvshinov, L A Stasyeva *Progress in Mining and Oilfield Chemistry. Focus on Remaining Oil and Gas Reserves* Vol. 4 (Ed. I Lakatos) (Budapest: Akademiai Kiado, 2003) p. 117
118. V A Kuvshinov, L K Altunina, V V Shevlyuk, V V Varaksin, S L Legeza, O A Ostapenko *Interval. Peredovye Neftegaz. Tekhnol.* **2** 72 (2003)
119. L K Altunina, A A Bokserman, V A Kuvshinov, V V Polkovnikov *Neftyanoe Khozyaistvo* (4) 45 (1994)
120. L K Altunina, V A Kuvshinov *Neftyanoe Khozyaistvo* (4) 36 (1995)
121. L K Altunina, V A Kuvshinov, A A Bokserman, V V Polkovnikov *Povyshenie Effektivnosti Razrabotki Trudnoizvlekaemykh Zapasov Nefti* (Increase in the Efficiency of the Development of Hard-to-Recover Oil Reserves) (Moscow: All-Russian Oil and Gas Research Institute, 1997) p. 222
122. L K Altunina, V A Kuvshinov, L A Stas'eva *Fiziko-khimicheskie Svoistva Rastvorov i Dispersii* (Physicochemical Properties of Solutions and Dispersions) (Novosibirsk: Nauka, 1992) p. 18
123. V A Kuvshinov, V N Manzhai, L K Altunina *Fiziko-khimicheskie Svoistva Rastvorov i Dispersii* (Physicochemical Properties of Solutions and Dispersions) (Novosibirsk: Nauka, 1992) p. 24

^a — *Mendeleev Chem. J. (Engl. Transl.)*^b — *Russ. J. Appl. Chem. (Engl. Transl.)*^c — *Dokl. Chem. (Engl. Transl.)*^d — *Colloid. J. (Engl. Transl.)*^e — *Russ. J. Phys. Chem. (Engl. Transl.)*^f — *Petrol. Chem. (Engl. Transl.)*^g — *Chem. Sust. Develop. (Engl. Transl.)*

Electronic mechanisms of molecular oxygen activation

B F Minaev

Contents

I. Introduction	988
II. Mechanisms of triplet – singlet transitions in the oxygen molecule	989
III. Influence of collisions of oxygen molecule on intensities of forbidden transitions	993
IV. Quenching of the $O_2(a^1\Delta_g)$ molecule	1002
V. Biochemical activation of the molecular oxygen	1004
VI. Conclusion	1008

Abstract. Theoretical views on the mechanisms of overcoming spin prohibitions in photoprocesses and in enzymatic activation of the O_2 molecule are considered. The electronic structures of various quantum states of this molecule and collision complexes of oxygen with other molecules are given. The patterns of biochemical activation of O_2 through T–S transitions in enzymatic complexes are proposed. It is noted that the enhancement mechanisms for specific exchange interactions in enzymatic complexes have common features with mechanisms of physical photoactivation of oxygen. The bibliography includes 164 references.

I. Introduction

Specific physicochemical properties of the diatomic oxygen molecule are due to incompleteness of the outer π_g -electron shell.^{1–9} Oxygen is paramagnetic⁴ and can both quench and sensitise luminescence of organic compounds,^{1,2} acts as a catalyst of some chemical transformations⁶ and as an oxidant in many processes, in particular, breath, combustion and putrefaction, which occur at different rates and by different mechanisms.^{5–7} Molecular oxygen is basic to life on Earth.⁶ Indeed, it protects living organisms from hard solar radiation, absorbs the most part of UV radiation in upper atmosphere, generates the ozone layer that absorbs softer UV radiation in the stratosphere and, finally, provides the aerobic life with the energy of breath. However, since Lavoisier, who discovered the ability of the oxygen molecule to maintain breath and combustion, there is no clear understanding of the mechanisms of enzymatic activation of O_2 , their relation to the electronic structure and spin of the molecule, to the fine structure of spin multiplet states of oxygen and to other physical (optical and magnetic) properties of this molecule.^{3–21}

The present review is concerned with many aspects of photophysical and biochemical activation of O_2 associated with overcoming spin prohibitions. Photochemistry of singlet

oxygen is only briefly outlined, because it was considered in recent reviews.^{17–21}

Almost all reactions of oxygen molecule with chemically stable diamagnetic compounds are exothermic and require specific activation.^{5–8} Combustion requires initial high-temperature activation of O_2 in the form of ignition (generation of primary radicals),⁸ breath requires biochemical enzymatic activation;⁵ in the case of autooxidation the activation is inefficient and slow.⁶ Exothermicity of the oxidation reactions of organic substances is usually explained by high electronegativity of oxygen and by additional stabilisation of C–O and O–H bonds due to their higher polarity⁶ compared to C–C and C–H bonds. It is believed^{5,6} that, owing to high strength of the O–O bond in the O_2 molecule, the activation energies for reactions involving oxygen are too high for them to proceed at sufficiently high rates under normal conditions. However, the chemical inertness of the oxygen molecule is not due only to high bond energy, but also to spin restrictions.^{3–5,12}

Clearly, aerobic life has appeared and exists due to specific kinetic prohibitions to reactions of paramagnetic oxygen with diamagnetic organic substances.^{3,12} The main source of slowing down of the O_2 reactions is the spin prohibition, namely, the reactants have two unpaired spins (from O_2 molecule; electrons in substrate are paired), while in diamagnetic oxidation products all spins are always paired. The overcoming of this prohibition by introducing (generating) radicals to react with oxygen (burn) is inadmissible to living matter. Enzymes of a living cell find another way to overcome the spin prohibition to reactions of oxygen ‘insertion’ into diamagnetic organic substances. Therefore, establishment of the mechanisms of enzymatic bio-activation of oxygen requires investigations of spin effects.^{3,12}

Nearly three decades ago the author of this review first explained intensity borrowing mechanism of magnetic dipole transitions^{22–24} responsible for the known atmospheric absorption bands of oxygen.¹¹ Calculations of the structure of collision complexes of O_2 with diamagnetic substances^{25–28} and their chemical reactions with account of spin–orbit coupling^{29–33} underlie the theory that made it possible to find the ways of overcoming spin prohibitions in the case of weak intermolecular interactions and in the course of chemical reactions.^{12,29,34–38} Recently, this theory has found numerous supports.^{1,3,35–37,39–43}

B F Minaev Bogdan Khmelnskiy National University in Cherkassy, bul. Shevchenko 81, 18031 Cherkassy, Ukraine. Fax (38-0472) 35 44 63, tel. (38-0472) 37 65 76, e-mail: bfin@rambler.ru

Received 16 April 2007

Uspekhi Khimii 76 (11) 1059–1083 (2007); translated by A M Raevskiy

This review considers the electronic mechanisms of over-coming spin prohibitions to the reactions of O₂ and oxygen complexes with other molecules including solvent molecules and active sites of enzymes. Processes leading to acceleration of radiative and non-radiative triplet–singlet (T–S) transitions in O₂ molecule induced by collisions in the gas phase and in solution including sensitisation of singlet oxygen are generally termed ‘photophysical activation’. We will also consider mechanisms of singlet oxygen luminescence and quenching, although these processes are in essence deactivation. The possibility of removal of spin prohibition in photophysical processes is treated as the first step towards understanding of biochemical enzymatic reactions of oxygen.^{3,24–37} In the review we also analyse the physical (mainly spectral) and chemical properties of O₂ molecule and the properties of other active forms of oxygen in relation to photosynthesis of atmosphere, combustion, catalysis and bio-oxidation.

II. Mechanisms of triplet – singlet transitions in the oxygen molecule

1. Energy characteristics of pure spin states of the oxygen molecule

Let us consider the ground- and excited-state electronic structure of O₂ molecule and factors determining the probability of T–S-transitions in free the oxygen molecule.

Back in 1848, Faraday weighed various gases with a magnetic balance and established that, unlike many other elements, molecular oxygen is paramagnetic.⁶ An explanation for this amazing fact was reported much later.⁴ Mulliken explained paramagnetism of molecular oxygen by considering the ground-state configuration in which the highest occupied molecular orbital (MO) is a doubly degenerate π_g orbital occupied by two electrons.⁴ In this case the inclusion of a ‘molecular’ analogue of Hund’s rule leads to parallel electron spin orientations in the lowest-energy state. Thus, atmospheric oxygen contains O₂ molecules in the triplet ground state corresponding to the following electronic configuration^{4,22}

$$\Psi = (1\sigma_g)^2(1\sigma_u)^2(2\sigma_g)^2(2\sigma_u)^2(3\sigma_g)^2(1\pi_u)^4(1\pi_g)^2. \quad (1)$$

There are four possible quantum states of the molecule with particular values of the spin (S) and orbital (L_z) angular momenta⁴ depending on arrangement of two outer electrons in two degenerate $1\pi_g$ -MOs. Using complex wave functions of MO in the form¹⁵

$$\pi_g^\pm = \psi(r, \theta) e^{\pm i\phi}, \quad (1a)$$

where θ is the angle between the z axis and the radius vector \mathbf{r} , ϕ is the angle of rotation of the radius vector \mathbf{r} about the molecular axis z , these states can be represented by the following qualitative models:

$$\begin{array}{cccc} [\uparrow\uparrow][\uparrow\uparrow] & [\uparrow\downarrow][\uparrow\downarrow] & [\uparrow\uparrow][\downarrow\downarrow] & [\uparrow\downarrow][\downarrow\uparrow] \\ |^3\Sigma_g^- \rangle & |^1\Delta_g \rangle & |^1\Delta_g \rangle & |^1\Sigma_g^+ \rangle \end{array} \quad (2)$$

Here the quantum cells $[\uparrow\uparrow]$ denote degenerate π_g^\pm -orbitals. The respective complex determinant wave functions for the open shells of the states (2) have the form^{4,10}

$$|^3\Sigma_g^- \rangle = \frac{1}{\sqrt{2}} (|\pi^+\pi^-| - |\pi^-\pi^+|), \quad (2a)$$

$$|^1\Delta_g \rangle = |\pi^+\pi^+|,$$

$$|^1\Delta_g \rangle = |\pi^-\pi^-|,$$

$$|^1\Sigma_g^+ \rangle = \frac{1}{\sqrt{2}} (|\pi^+\pi^-| + |\pi^-\pi^+|).$$

Here $|\cdot|$ is the conventional notation of the determinant wave functions,¹⁰ π^+ denotes the α -spin MO (spin-up MO) and π^- denotes the β -spin π_g^\pm -MO (spin-down MO). The functions (2a) are eigenfunctions of the operator of the orbital angular momentum projection (L_z) with the quantum number $\Lambda = 0$ (for the states Σ_g^\pm) and 2 (for the states $^1\Delta_g$)^{4,10–16} in $\hbar = h/2\pi$ units (h is the Planck constant). With allowance for exchange interaction between two π_g -electrons, the triplet state $^3\Sigma_g^-$ has the lowest energy, thus being the ground state; the next is the doubly degenerate singlet state $^1\Delta_g$, while the singlet state $^1\Sigma_g^+$ has the highest energy.^{4,9}

The total spin quantum number (S) in the expression for the eigenfunctions of the operator S^2

$$S^2\Psi = S(S+1)\hbar^2\Psi \quad (3)$$

is equal to zero for singlets and to unity, for triplets.¹⁵ Functions (2a) obey relation (3), their multiplicity (left superscript) is $2S+1$. Qualitative description of energy characteristics of O₂ can be obtained²² using simple semiempirical quantum chemical methods, e.g., INDO.¹⁵ The inclusion of configuration interaction (CI) with the basis set (2) leads to the same splitting between the three states $^3\Sigma_g^-$, $^1\Delta_g$, $^1\Sigma_g^+$, equal to the atomic exchange integral:¹³ $\langle p_x p_y | p_x p_y \rangle = 0.8$ eV. The energies of the singlet states $^1\Delta_g$ and $^1\Sigma_g^+$ calculated relative to the triplet ground-state energy are 0.8 and 1.6 eV, respectively,²² which agrees with experimental data (0.98 and 1.63 eV, respectively).⁹ The agreement is improved by inclusion of configuration interaction and the ... $(1\pi_u)^2(1\pi_g)^4$ configuration, however the pattern of the wave functions remains essentially the same.¹² The following is quite important. Computational quantum chemistry methods usually employ real wave functions for the atomic basis set p_x , p_y and p_z .¹⁵ The singlet states are described by the following combinations of the wave functions:^{10,22}

$$|^1\Delta_g \rangle = ^1\Phi_1 = \frac{1}{\sqrt{2}} (|\pi_x\bar{\pi}_x| - |\pi_y\bar{\pi}_y|), \quad (4)$$

$$|^1\Delta_g \rangle = ^1\Phi_2 = \frac{1}{\sqrt{2}} (|\pi_x\bar{\pi}_y| + |\pi_y\bar{\pi}_x|), \quad (4a)$$

$$|^1\Sigma_g^+ \rangle = ^1\Phi_3 = \frac{1}{\sqrt{2}} (|\pi_x\bar{\pi}_x| + |\pi_y\bar{\pi}_y|), \quad (5)$$

$$|^3\Sigma_g^- \rangle = ^3\Phi_0 = \frac{1}{\sqrt{2}} (|\pi_x\bar{\pi}_y| - |\pi_y\bar{\pi}_x|),$$

where π_x denotes the spin-up (α -spin) $1\pi_{gx}$ -MO and $\bar{\pi}_x$ denotes the spin-down (β -spin) $1\pi_{gx}$ -MO. The real π_g -MO functions in the INDO approximation have a simple form²²

$$\pi_x = \frac{1}{\sqrt{2}} (p_x^A - p_x^B), \quad (6)$$

$$\pi_y = \frac{1}{\sqrt{2}} (p_y^A - p_y^B),$$

where p_x^A denotes the real 2p-AO of the atom A, oriented along the x axis and the symbols ‘A’ and ‘B’ denote the two oxygen atoms. Electrons of the closed shell in Eqns (4) and (5) are omitted because they do not affect the matrix elements of the one-electron operators [dipole moment, angular momentum, spin–orbit coupling (SOC)]. For the triplet ground state $^3\Sigma_g^-$, the form of the determinant functions (2) and (5) remains unchanged, whereas the functions for the singlet states (2) in

the real basis set (6) have another form. This feature should be taken into account¹² in calculations of (i) collision complexes of oxygen molecule with other molecules and (ii) chemical reactions involving this molecule.

The complex functions (1a) and (2) are only convenient in the case of isolated O₂ molecule. By expanding determinants in relationships (5), one can separate the orbital and spin contributions; then the singlet and triplet Σ -states have the form

$$|{}^1\Sigma_g^+\rangle = {}^1\Phi_3 = \frac{1}{\sqrt{2}} [\pi_x(1)\pi_x(2) + \pi_y(2)\pi_y(1)] \frac{1}{\sqrt{2}} [\alpha(1)\beta(2) - \alpha(2)\beta(1)], \quad (5a)$$

$$|{}^3\Sigma_g^-\rangle = {}^3\Phi_0 = \frac{1}{\sqrt{2}} [\pi_x(1)\pi_y(2) - \pi_x(2)\pi_y(1)] \frac{1}{\sqrt{2}} [\alpha(1)\beta(2) + \alpha(2)\beta(1)]. \quad (5b)$$

The '+' and '-' signs at the term ' Σ ' denote mirror symmetry relative to any plane containing the molecular axis, *e.g.*, the *yz* plane. Reflection in this plane causes the π_x -MO to change its sign while the sign of the π_y -MO remains unchanged. Because of this, both components in the orbital part of the wave function (5b) change their signs; *i.e.*, this function is antisymmetrical with respect to reflection in plane, while the wave function (5a) is symmetrical. The same conclusions can be drawn by considering the *xz* plane. As to the complex functions (1a) and (2a), these conclusions are valid for any plane containing the molecular axis,¹⁵ because reflection in plane causes replacement of ϕ by $-\phi$ and, hence, replacement of π^+ by π^- in relation (1a).

Thus, for planar collision complexes of O₂ the real wave functions (5) characterise the key symmetry properties of the low-lying electronic states of this molecule. Selection rules for functions (1) and (2) are also valid for functions (4)–(6). Collision complexes have no inversion point. This formally breaks quantisation of the projection of the orbital angular momentum and in polyatomic molecules the quantum number of the operator L_z is no longer a 'good quantum number'.¹³ However, calculations^{27–31} revealed only minor changes in the structure of the wave functions (4) and (5) and in the energies of corresponding states of collision complexes. Therefore, the collision complexes can be treated using the same notations of terms (4) and (5) as those of free O₂ molecule.

Specific behaviour of O₂ molecule in animated nature is mainly due to the presence of low-energy excited singlet states and the intrinsic magnetic moment (spin) in the ground state (paramagnetism of O₂).^{12, 27} Figure 1 presents the potential curves for certain states of the O₂ molecule, obtained from multiconfiguration self-consistent field (MC SCF) calculations with subsequent inclusion of configuration interaction.^{30, 40} High-energy excited states ${}^3\Sigma_u^-$ and ${}^3\Delta_u$, ${}^3\Sigma_u^+$ responsible for UV emission of oxygen (Herzberg bands) are of great interest for atmosphere photochemistry and gas discharge spectroscopy.^{9, 39–42} When discussing the photochemistry of singlet oxygen (${}^1\Delta_g$), these states are usually left out of consideration, although from the standpoint of spin catalysis theory^{32–34} they should also be taken into account. The triplet state $B^3\Sigma_u^-$ gives an allowed electric dipole transition $B^3\Sigma_u^- \leftarrow X^3\Sigma_g^-$ (Ref. 9) responsible for the Schumann–Runge absorption band. Due to this intense absorption in upper atmosphere, hard solar UV radiation (135–190 nm) does not arrive to the Earth's surface. Since minima on the potential curves for the *B*- and *X*-states are strongly shifted relative to one another

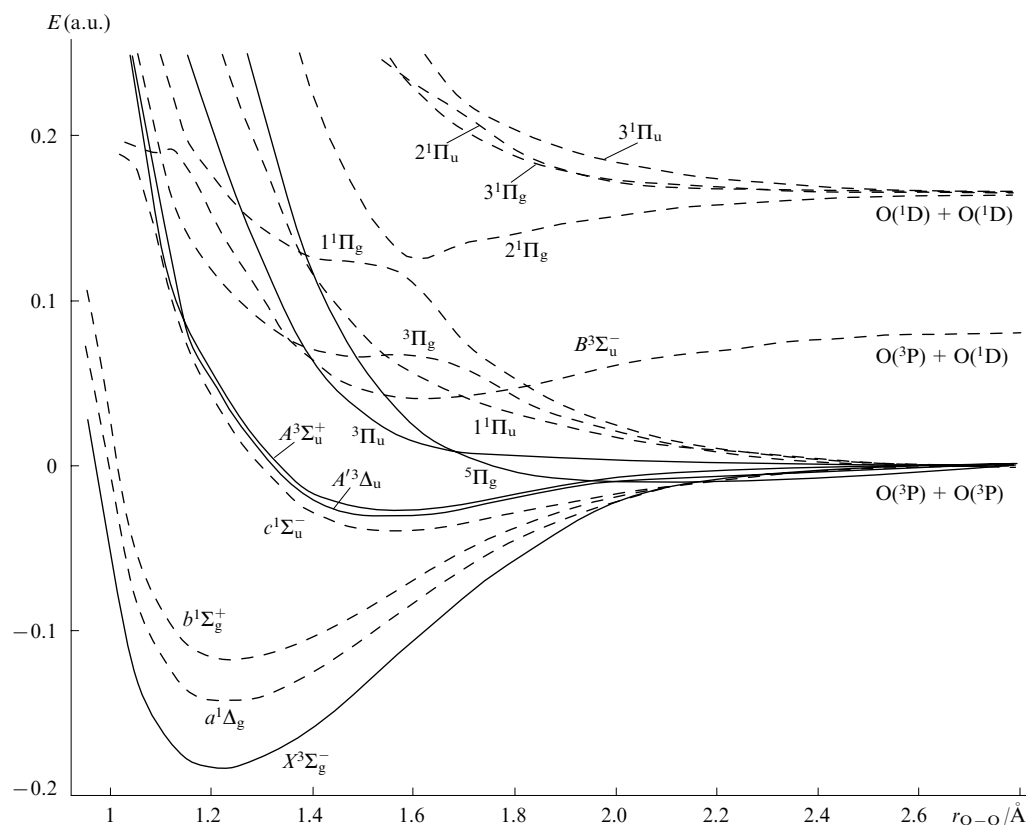


Figure 1. Potential curves for certain quantum states of O₂ molecule obtained from *ab initio* calculations.^{30, 31}

Literary notations of terms used here and in Fig. 2 are common to molecular spectroscopy. Main multiplet states: singlet (*a*, *b*, *c*) and triplet (*A*, *B*).

(see Fig. 1), the vertical transition $B^3\Sigma_u^-/X^3\Sigma_g^-$ leads to dissociation of O_2 molecule. In addition, pre-dissociation of bound vibrational states of the upper term is also possible due to crossing with the potential curves of the Π_u -states.⁹

Various glow phenomena in the night sky including auroral ones are due to decomposition of oxygen molecule to atoms and subsequent recombination of oxygen atoms with the formation of excited O_2 molecules.⁹ In this review, we will leave these interesting phenomena out of consideration. Mention may only be made that theory of forbidden transitions from the $c^1\Sigma_u^-$, $A'^3\Delta_u$ and $A^3\Sigma_u^+$ excited states provides a great body of valuable information on the SOC mechanisms¹² that are important for understanding of the enzymatic activation of oxygen. In addition to the Herzberg bands, red atmospheric bands of oxygen [transition $b^1\Sigma_g^+ \rightarrow X^3\Sigma_g^-$ (762 nm)] and IR radiation (transition $a^1\Delta_g \rightarrow X^3\Sigma_g^-$ at 1270 nm) were detected.⁹ Long optical path in the atmosphere also allows these bands to be clearly defined in absorption (the red band represents a combination of certain Fraunhofer lines) in spite of the forbiddenness and low probability of these transitions.

Until recently, the singlet state of oxygen was of interest only for researchers working in atmosphere optics.^{10,11} In 1976, Krasnovsky¹⁴ first detected luminescence of singlet oxygen ($a^1\Delta_g$) in solution. At present, singlet oxygen is used in technics,^{1,17,18} chemistry^{17–21} and medicine.^{1,19,43} Singlet oxygen molecule $O_2(a^1\Delta_g)$ is known as oxidant in chemical and biological processes, because the spin prohibition is removed and the species is more reactive than the triplet atmospheric oxygen molecule $O_2(X^3\Sigma_g^-)$.^{1–7,19–21} Taking into account four quantum states (2) of oxygen molecule is required for not only understanding of oxygen photochemistry, but also development of theory of the dark chemical reactions,^{12,29,32} in particular, for studies of enzymatic oxidation processes.³⁷

2. Intensities of singlet–triplet transitions in optical spectra of the oxygen molecule

To understand the mechanism of removal of spin prohibitions in chemical reactions involving oxygen, one should consider a theory of intensity of singlet–triplet transitions in isolated O_2 molecule and the effect of solvent on these transitions.^{22–96} Radiative transitions between all states (2) are strictly forbidden in the electric dipole approximation,^{11,43} because all of them have the same parity (gerade symmetry relative to inversion point), whereas the selection rules require a change in parity upon transitions. For electric dipole transitions the projection of the orbital angular momentum on the molecular axis (Λ) should vary by $\Delta\Lambda = \pm 1, 0$. The $^1\Delta - ^1\Sigma^+$ transition is also forbidden due to the selection rule for the projection of the orbital angular momentum ($\Delta\Lambda = 2$). In free O_2 molecule, this transition is detected as a weak quadrupole transition because in the quadrupole approximation the prohibition for $\Delta\Lambda = 2$ is removed.^{12,26} Singlet–triplet transitions between terms (2) are additionally forbidden by the spin selection rule, $\Delta S = 1$. Transition between states (5) is also forbidden by the $\Sigma^- - \Sigma^+$ rule, *i.e.*, we deal with the triple prohibition.

All the prohibitions mentioned above are strict.⁴⁹ The more long-wavelength singlet–triplet transition $^1\Delta_g - ^3\Sigma_g^-$ is additionally forbidden by the selection rule for the orbital angular momentum ($\Delta\Lambda = 2$) and thus characterised by triple prohibition [with respect to spin, parity (gerade–gerade) and orbital angular momentum, that is, $\Delta\Lambda = 2$] in the electric dipole approximation. A diagram of different quantum states (4), (5) and transitions between them for the collision complex of O_2 molecule and a dye is shown in Fig. 2. Both singlet–triplet transitions, $a \rightarrow X$ and $b \rightarrow X$, should be very weak due to the triple prohibition on emission in the dipole approximation.

The potential curves (see Fig. 1) for all the three states (X , a and b) are only slightly shifted relative to one another, the

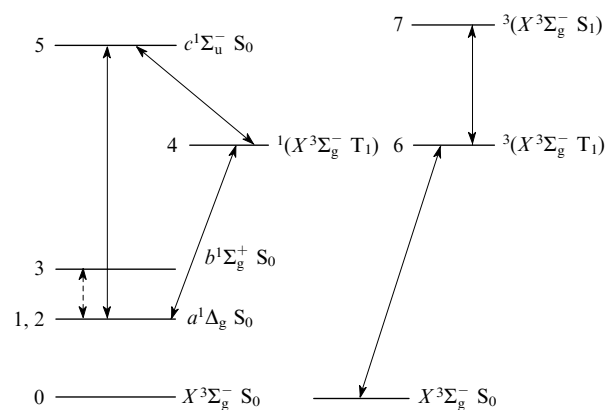


Figure 2. Scheme of quantum states in a collision complex of O_2 with a dye.

equilibrium internuclear distances (r) being respectively equal to 1.207, 1.216 and 1.227 Å (see Ref. 9). Therefore, only the 0–0 bands corresponding to electronic vibrational transitions between these states are intense in optical spectra.^{9,42,46} The rate constant (k) for spontaneous emission $a \rightarrow X$ obtained by interpolation to zero oxygen pressure (no collisions; intermolecularly unperturbed O_2 molecule) was found to be record-low ($k_{a \rightarrow X} = 2.6 \times 10^{-4} \text{ s}^{-1}$).¹⁷ The $b \rightarrow X$ transition is much more intense ($k_{b \rightarrow X} = 8.9 \times 10^{-2} \text{ s}^{-1}$). The radiative lifetimes¹⁷ of the a and b states are 4600 and 12 s, respectively. The $a \rightarrow X$ and $b \rightarrow X$ transition intensities were first calculated in Ref. 22. In spite of semiempirical character of the wave functions used in the INDO method, the results of calculations²² correctly describe the mechanisms of overcoming spin prohibitions, as was confirmed later by the results of *ab initio* calculations.^{42,50,57} To understand the spin mechanisms of photo- and bio-activation of oxygen, we will consider the key points of the semiempirical theory.²²

Symmetry analysis of the wave functions revealed the possibility of mixing of the singlet and triplet states (5) due to the SOC operator.⁴⁹ For simplicity, we will write this operator in the effective one-electron form^{12,23}

$$H_{so} = \sum_A \zeta_A \sum_i \vec{l}_{i,A} \vec{s}_i = \sum_i \vec{B}_i \vec{s}_i = \sum_i (B_{i,x} s_{i,x} + B_{i,y} s_{i,y} + B_{i,z} s_{i,z}), \quad (7)$$

where ζ_A is the SOC constant for the atom A ($\zeta_O = 153 \text{ cm}^{-1}$), $\vec{l}_{i,A}$ and \vec{s}_i are respectively the operators of the orbital angular momentum and spin angular momentum of the i th electron.¹² The one-electron SOC operator (7) with inclusion of the constants ζ_A determined from atomic spectra gives quite reliable results suitable for explanation of numerous SOC effects in molecules.^{12,13,49} The spin–orbit coupling between the singlet and triplet ($b^1\Sigma_g^+ - X^3\Sigma_{g,0}^-$) states [see relations (5)] is given by²²

$$\begin{aligned} \langle ^3\Sigma_g^- | H_{so} | ^1\Sigma_g^+ \rangle &= \langle ^3\Phi_0 | H_{so}^Z | ^1\Phi_3 \rangle = \\ &= \langle \pi_x | B_z | \pi_y \rangle = -i\zeta_O = -153i \text{ cm}^{-1}. \end{aligned} \quad (8)$$

Equation (5) was written for the triplet state with the zero projection of the total spin on the molecular axis (z axis).²² In the text below this spin sublevel with the quantum number $M_S = 0$ will be designated by $|^3\Sigma_{g,0}^- \rangle$ (for the frame of reference associated with the O_2 molecule) and t_z (if the z axis of the frame of reference in the collision complexes of O_2 with organic reactant molecules matches the line of the O–O bond). The

other two spin sublevels of the triplet state with the quantum numbers $M_S = \pm 1$ in the oxygen molecule are degenerate; we will denote them $|^3\Sigma_{g,1}^- \rangle$. The separation between them and the $M_S = 0$ level equals the zero-field splitting (ZFS) energy,^{9, 22} which for the oxygen molecule is rather high (3.97 cm^{-1} ; cf. a conventional value of 0.1 cm^{-1} for the triplet-excited states of aromatic molecules¹³). The ZFS is due to the dipole–dipole magnetic interaction between two unpaired spins.⁴⁹ In the case of O_2 molecule the SOC also contributes largely to the ZFS at the second-order level of perturbation theory.⁴⁸ Recently, correct *ab initio* calculations of the ZFS energy for oxygen molecule have been reported.⁴⁶ Among previous calculations presented in Refs 47–49, a number of errors are found, whereas semiempirical estimates^{22, 59} appeared to be more reliable.^{13, 46} Seemingly, the results of *ab initio* calculations⁴⁷ are in good agreement with the observed ZFS; however, this is a random coincidence. Indeed, the SOC contribution to ZFS is overestimated (doubled) owing to incorrect value of a factor. Correct calculation of magnetic perturbations in the ZFS is important for understanding of the mechanism of removal of spin prohibition for the singlet–triplet transitions in oxygen.

The matrix element of the operator of the SOC between the $\Sigma^- - \Sigma^+$ triplet and singlet states differs from zero only for the states (5) characterised by the quantum number $M_S = 0$. At the first-order level of perturbation theory, the wave functions of these states are mixed due to SOC²²

$$\Psi_b = |b^1\Sigma_g^+\rangle + c|X^3\Sigma_{g,0}^-\rangle, \quad (9)$$

$$\Psi_{X,0} = |X^3\Sigma_{g,0}^-\rangle - c^*|b^1\Sigma_g^+\rangle, \quad (10)$$

where the mixing coefficient

$$c = \frac{\langle X^3\Sigma_{g,0}^- | H_{\text{so}} | b^1\Sigma_g^+ \rangle}{E(b^1\Sigma_g^+) - E(X^3\Sigma_{g,0}^-)} \quad (11)$$

is small (E is the energy of the corresponding state). With allowance for the semiempirical estimate of the SOC using Eqn (8) and energy difference⁹ in the denominator of Eqn (11) ($13\,195 \text{ cm}^{-1}$), one gets²² $c = -0.0116i$. The small value of the coefficient c provides an excellent substantiation of the applicability of perturbation theory and the wave functions (9) and (10) are characterised by rather high accuracy and correct normalisation. According to *ab initio* calculations,^{42, 50} the SOC matrix element [numerator in Eqn (11)] equals $-178i \text{ cm}^{-1}$, the absolute value of coefficient c being somewhat increased: $|c| = 0.0135$. This coefficient plays a key role in the theory of singlet–triplet transitions of oxygen molecule in the gas phase at low and high pressures and in O_2 solutions in organic compounds and biopolymers.^{22–31}

Let us consider a magnetic dipole transition from the state (9) to the state $|^3\Sigma_{g,1}^- \rangle$ with the quantum number $M_S = \pm 1$. Unlike the spin sublevel $|^3\Sigma_{g,0}^- \rangle$, the $|^3\Sigma_{g,1}^- \rangle$ state is almost ‘pure’, i.e., it contains minor contributions of singlet states. (Actually, it has a small contribution of the $^1\Pi_g$ state, but this is of no concern for the simplified treatment²² of the $b-X$ transition.) The magnetic dipole moment operator

$$\mathbf{M} = \mu_B(\mathbf{L} + 2\mathbf{S}),$$

where μ_B is the Bohr magneton, contains the orbital (\mathbf{L}) and spin (\mathbf{S}) contributions. According to calculations,^{22, 42, 50} the orbital contribution to the moment of the $b^1\Sigma_g^+ - X^3\Sigma_{g,1}^-$ transition is negligible. The major contribution to the $b-X$ transition intensity comes from the spin component²² with the magnetic moment polarisation vector directed perpendicular to the molecular axis. Taking into account expression (9), one has²²

$$\mathbf{M}_{b-X,1} = \mu_B \langle \Psi_b | 2\mathbf{S} | \Psi_{X,1} \rangle = \quad (12)$$

$$= \mu_B \sqrt{2} c \langle X^3\Sigma_{g,0}^- | S_x \pm iS_y | X^3\Sigma_{g,1}^- \rangle = -2\mu_B c.$$

Thus, the $b^1\Sigma_g^+ - X^3\Sigma_{g,1}^-$ transition in the visible region (red atmospheric band of oxygen at 760 nm) in fact ‘borrows’ its intensity from the microwave transition between the spin sublevels $^3\Sigma_{g,0}^- - ^3\Sigma_{g,1}^-$ (magnetic dipole EPR transition induced by the spin operator). The calculated transition moment $\mathbf{M}_{b-X,1} = -0.027 \mu_B$ is almost equal to the value obtained from intensity measurements.⁹ This is a unique example in molecular spectroscopy; here the intensity of an optical electronic transition is determined by the EPR spin current intensity. This provides an explanation for a higher probability of the $b-X$ transition compared to that of the $a-X$ transition. In the latter case there is only a small orbital contribution to the magnetic dipole moment of the transition, due to the SOC-induced mixing of the a , X and $^3, ^1\Pi_g$ states.²² Owing to large energy differences between these states

$$E(^1\Pi_g) - E_X = 78\,000 \text{ cm}^{-1},$$

$$E(^3\Pi_g) - E_a = 48\,000 \text{ cm}^{-1},$$

mixing of the singlets and triplets is negligible and the spin prohibition to the $a-X$ transition remains strict.

One should also consider the probability of the $b-a$ transition, which plays an important role in analysis of the solvent effect on the oxygen spectra. The $b-a$ transition of a free O_2 molecule is responsible for the appearance of a weak Noxon band, which is a quadrupole^{26, 89} with the maximum possible quadrupole moment.²⁶ However, the rate constant for spontaneous emission $b \rightarrow a$ obtained by interpolation to zero pressure is very small ($k_{b \rightarrow a} = 1.7 \times 10^{-3} \text{ s}^{-1}$).⁹ Theoretical studies^{25–28} revealed that this transition should be dramatically enhanced upon collision of O_2 molecule with any diamagnetic molecule. Later on, this conclusion was confirmed experimentally for the gas,³⁹ solid^{51, 52} and liquid phases.^{1, 17, 43, 56}

With allowance for the SOC in the framework of perturbation theory one can explain the intensities of many UV bands of oxygen molecule.^{30, 31, 59, 65, 67, 91–96} In addition to calculations of well-known Herzberg bands,^{9, 30, 49, 65, 67} a reliable explanation was obtained for the intensities of some new bands originated from recently detected new electronic transitions from the metastable state (9), namely, $b^1\Sigma_g^+ - B^3\Sigma_u^-$ and $b^1\Sigma_g^+ - c^1\Sigma_u^-$ (Refs 31, 91–95). The $b^1\Sigma_g^+ - B^3\Sigma_u^-$ transition proceeds by the mechanism of intensity ‘stealing’ from the Schumann–Runge band ($X-B$) due to the SOC (9); the coefficient c [see Eqn (11)] gives a correct order of magnitude^{31, 92} for the electric dipole moment of this transition. The $b^1\Sigma_g^+ - c^1\Sigma_u^-$ transition is also electric dipole in nature; removal of the $\Sigma^- - \Sigma^+$ -type prohibition for the singlet–singlet transition is due to electronic-rotational coupling⁹⁵

$$\begin{aligned} & \left\langle \tilde{c}^1\Sigma_u^- \left| \sum_i \mathbf{er}_i \right| b^1\Sigma_g^+ \right\rangle = \\ & = \sum_n \frac{\langle n^1\Pi_g | B L_+ | b^1\Sigma_g^+ \rangle}{E(b^1\Sigma_g^+) - E(n^1\Pi_g)} \left\langle c^1\Sigma_u^- \left| \sum_i \mathbf{er}_i \right| n^1\Pi_g \right\rangle + \\ & + \sum_k \frac{\langle k^1\Pi_u | B L_+ | c^1\Sigma_u^- \rangle^*}{E(c^1\Sigma_u^-) - E(k^1\Pi_u)} \left\langle k^1\Pi_u \left| \sum_i \mathbf{er}_i \right| b^1\Sigma_g^+ \right\rangle. \end{aligned}$$

Here \mathbf{er}_i is the dipole moment of the i th electron and B is the rotational constant.

Detection⁹⁴ and theoretical identification⁹⁵ of the $b^1\Sigma_g^+ - c^1\Sigma_u^-$ transition bands opens new prospects for atmosphere photochemistry studies. However, no $A^3\Sigma_u^+ - c^1\Sigma_u^-$ electronic transition in the IR region (2400 cm^{-1}) was detected so far, although the corresponding intensity stealing mechanism was developed two decades ago.¹² The magnetic dipole moment of this transition ($M_{A-c} = 0.12\mu_B$) is about five times larger than that of the $b-X$ transition [see Eqn (12)]. The intensity stealing and the spin-prohibition removal mechanisms are very similar to those described by relations (9)–(12); however, this only concerns the $A^3\Sigma_u^+$ and $c^1\Sigma_u^-$ states. The SOC matrix element between these states is equal to the integral (8) while the energy difference in the denominator is very small (2400 cm^{-1}); this is the reason for high extent of intensity stealing from the transitions between spin sublevels of the $A^3\Sigma_u^+$ state (see Refs 12 and 91). The aforesaid is valid for a free O_2 molecule in a highly rarefied gas (upper atmosphere), when collisions can be ignored. Under normal pressure at Earth's surface, collisions with other molecules (O_2 , N_2 , water vapour) significantly affect the intensities of certain absorption bands of oxygen.^{25–43, 51–56}

III. Influence of collisions of oxygen molecule on intensities of forbidden transitions

1. The Noxon transition

Let us consider simple models for collision complexes of O_2 with diamagnetic molecules.^{1, 28, 39, 51, 58, 89, 97–109} Changes in the orbitals of the open π_g -shell of oxygen molecule upon its collision with the nitrogen molecule are shown in Fig. 3. For simplicity, we assume that the collision complex has a planar geometry and lies in the xz plane. All subsequent conclusions are also valid for arbitrary geometry of the complex. The moment of the Noxon transition $a^1\Delta_g - b^1\Sigma_g^+$ of the collision complex radically changes its nature, following the changes in the nature of orbitals of the open π_g -shell. In addition to the pure quadrupole component $\langle^1\Delta_g|Q|^1\Sigma_g^+\rangle$, which is the same for both terms (4) and (4a), the electric dipole component $\langle^1\Delta_g|D|^1\Sigma_g^+\rangle$ appears, which can differ for the two quasi-degenerate components of the singlet state a . The matrix elements of the dipole moment operator

$$D = e \sum_i r_i = \sum_i d_i$$

for the singlet–singlet ($a^1\Delta_g - b^1\Sigma_g^+$) transition [see Eqns (4) and (5)] are equal to the dipole moment difference between two π_g -MOs (see Ref. 28)

$$\langle^1\Phi_1|D|^1\Phi_3\rangle = \langle\pi_x|d|\pi_x\rangle - \langle\pi_y|d|\pi_y\rangle. \quad (13)$$

For the second component of the $a^1\Delta_g$ state [see Eqn. (4a)] the dipole moment of the $a-b$ transition is

$$\langle^1\Phi_2|D|^1\Phi_3\rangle = \langle\pi_y|d|\pi_x\rangle + \langle\pi_x|d|\pi_y\rangle. \quad (14)$$

For the planar collision complex $O_2 + N_2$ (see Fig. 3), the dipole moment difference between two oxygen π_g -MOs differs from zero. Spin-restricted Hartree–Fock⁸⁷ calculations of the triplet ground state of the complex $O_2 + N_2$ (see Fig. 2) revealed significant deformation of the $\pi_{g,x}$ -orbital of the O_2 molecule due to mixing with orbitals of the nitrogen molecule (see Fig. 3b), whereas the $\pi_{g,x}$ -MO remains almost unchanged (see Fig. 3a).^{12, 27} The overlap of the π_x -orbitals of the two molecules (σ -type overlap, see Fig. 3b) is much larger than that of the π_y orbitals (π -type overlap).

The structures of the states (4) and (5) determined with allowance for configuration interaction remain almost unchanged.¹² The dipole moment of the $\pi_{g,x}$ -orbital differs from zero, because it includes quite large contributions of nitrogen atoms; despite small coefficients in the LCAO expansions for these atoms, the dipole moment $\langle\pi_x|d|\pi_x\rangle$ of the $\pi_{g,x}$ -orbital is of great importance because of the long intermolecular distance ($R = 2.8\text{ \AA}$). The moment of the transition (13) reaches a value of 0.1 D, the transition intensity being four orders of magnitude higher than the intensity of the pure quadrupole transition $a^1\Delta_g - b^1\Sigma_g^+$ of free O_2 molecule.¹² This example (see Fig. 3) provides the simplest illustration of the Noxon band (transition $a^1\Delta_g - b^1\Sigma_g^+$) enhancement mechanism in the collision complex due to the appearance of the electric dipole moment of the transition. At arbitrary collision geometry, both terms on the right side of Eqns (13) and (14) differ from zero, but the total intensity of the Noxon band mainly depends on R . The off-diagonal matrix elements of the one-electron operator of the dipole moment between the π_g -orbitals of the open shell of oxygen [see Eqn (14)] depend on the extent of deviation of the collision complex geometry from planar one (see Fig. 3). This is also characteristic of most molecules having more complex structures compared to N_2 . For instance, an oxygen–butadiene collision complex cannot have planes among symmetry elements (only the most probable non-planar π -complex is considered here); in this case the integrals (13) and (14) are commensurable.⁸⁷

The extent of the Noxon band enhancement depends on the polarisability (α_{cp}) of the partner in collision.^{1, 17, 87, 98} This was revealed by the first MINDO/3 calculations with inclusion of configuration interaction for singly and doubly excited configurations.²⁸ Qualitative correlation between the Noxon band enhancement and an increase in the ionisation potential of the partner in collision (molecular polarisability increases as the ionisation potential decreases) was pointed out.¹³ The dipole moment $\langle\pi_x|d|\pi_x\rangle$ of the oxygen $\pi_{g,x}$ -orbital in the complex with nitrogen (see Fig. 3) depends on the contribution of the vacant nitrogen π_g -MO, which is in turn determined by the polarisability of this molecule.^{87, 98} Enhancement of the Noxon band with an increase in the collision-partner polarisability^{28, 87, 98–101} was even better demonstrated in analysis of the results of CI calculations^{12, 97, 98} in the oxygen complexes with helium and hydrogen.

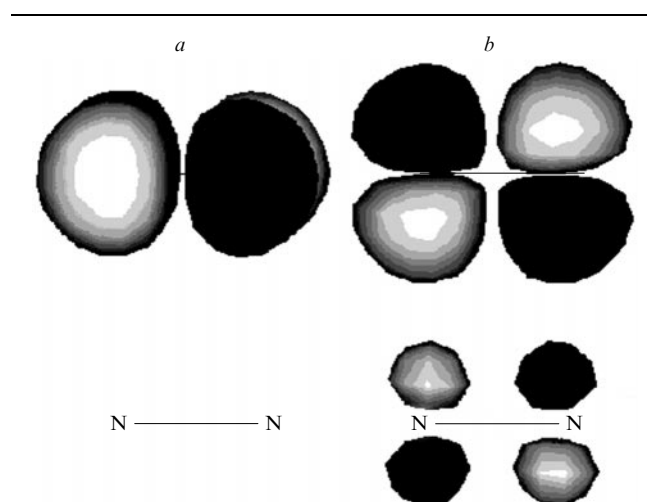


Figure 3. Molecular orbitals, $\pi_{g,y}$ (a) and $\pi_{g,x}$ (b), of O_2 in collision complex of oxygen and nitrogen molecules.

The z axis matches the N_2 molecular axis; the y axis is normal to the xz plane of the complex. White and dark background corresponds to the positive and negative signs of the wave functions.

2. Effect of collisions on intensities of singlet–triplet transitions of oxygen in the visible and near IR optical spectra

Singlet molecular oxygen in the $a^1\Delta_g$ state is produced by photosensitisation of dye solutions.^{1,28} This species plays a key role in some photochemical and photobiological processes.^{53–56} Such diseases as skin cancer and cataract as well as ageing are associated with reactions involving $O_2(a^1\Delta_g)$.^{17–21} Recently, this form of oxygen has been used in organic synthesis, in bleaching, in medicine for treatment of malignant tissues (photodynamic therapy),^{1,18,19} as an air pressure gauge in aerodynamics,^{17,105} as fixing agent in high-spatial and high-temporal resolution microscopes^{56,82,83} and as a microscopic luminescing detector.^{1,17}

Wide use of singlet oxygen is due to unique properties of the singlet–triplet transition $a^1\Delta_g \rightarrow X^3\Sigma_g^-$. As mentioned above, this transition of free O_2 molecule (at zero pressure) is characterised by very low emission (rate constant for spontaneous emission is $2.6 \times 10^{-4} \text{ s}^{-1}$).⁹ In compressed gas and in solution the transition probability increases by 3–4 orders of magnitude; luminescence is detected using sensitive photomultipliers.^{14,17,53,56} Such a luminescence was first detected in solutions of biological pigments (photosensitisers of 1O_2) using an improved phosphoroscope under steady-state excitation.^{14,60} Later on, the characteristic narrow band at 1270 nm corresponding to the $a^1\Delta_g \rightarrow X^3\Sigma_g^-$ transition of oxygen molecule in solution was observed in numerous studies using pulsed excitations of photosensitisers.^{1,17,58,61–64,73–77} Good temporal resolution obtained with a germanium detector was reported.^{61–63,75} The quantum yield (Q_a) of luminescence ($a \rightarrow X$ transition) and the lifetime of singlet oxygen (τ_a) in some solutions of saturated hydrocarbons and their halo derivatives were measured.⁶³ Measurements of Q_a in the near IR region are complicated by the lack of appropriate references, because the quantum yield of singlet oxygen (Q_a) should be measured for each solution with a given sensitiser. The radiative rate constant for the $a^1\Delta_g \rightarrow X^3\Sigma_g^-$ transition⁶³

$$k_{a-X} = \frac{Q_a}{\tau_a Q_a}, \quad (15)$$

determined for a series of saturated solvents falls in the range $\sim 0.1–0.2 \text{ s}^{-1}$. The conclusion about independence of k_{a-X} on the solvent is only valid for this series of solutions.⁶³

The author of this review developed^{12,27,28} a simple scheme of stealing the emission intensity of the $a \rightarrow X$ transition of collision complexes of O_2 with diamagnetic molecules starting from calculations of a model complex $O_2 + H_2$. Using a program of configurational interaction calculations^{12,97} for single and double excitations debugged for the modified¹² MINDO/3 method,¹⁵ qualitatively correct description of the spectrum of the complex was obtained and the collision-induced electric dipole moments of transitions were calculated.^{27,28} It was established that the $b-a$ transition of the collision complex acquires a relatively large dipole moment [see Eqn (13)]. As mentioned above, this is characteristic of all collisions of the O_2 molecule with diamagnetic molecules; this also follows from Eqns (13) and (14). In the case of a planar symmetric complex similar to that shown in Fig. 3, relation (13) predicts that the intensity of the $b-a$ transition of the O_2 molecule in the collision complex should dramatically increase due to deformation of the $\pi_{g,x}$ -orbital electron cloud. Even small contributions of the collision-partner (H_2 , N_2 , C_2H_4 , C_6H_6) orbitals induce a large dipole moment of the $b-a$ transition. With allowance for the abnormally strong spin–orbit coupling of the $b^1\Sigma_g^+$ and $X^3\Sigma_{g,0}^-$ states [see Eqn (8)] and for the contribution of the $|b^1\Sigma_g^+\rangle$ state to the wave function $\Psi_{X,0}$ of the ground-state term [see Eqn (10)] one gets that the $a^1\Delta_g \rightarrow X^3\Sigma_{g,0}^-$ transition ‘steals’ the intensity¹² from the $a-b$ transition

$$\langle a^1\Delta_g | D | \Psi_{X,0} \rangle = -c \langle a^1\Delta_g | D | b^1\Sigma_g^+ \rangle. \quad (16)$$

Since the spin–orbit coupling (8) in the oxygen molecule is still the strongest and the coefficient c only depends on the properties of the O_2 molecule, the $|c|$ value in the collision complex remains almost unchanged.^{27,98} The electric dipole moment of the $a^1\Delta_g-b^1\Sigma_g^+$ transition of the collision complex $O_2 + H_2$ at $R = 2.4 \text{ \AA}$ is²⁸

$$\langle a^1\Delta_g | D | b^1\Sigma_g^+ \rangle = 0.0113 \text{ e \AA}.$$

The moment of the $O_2 + H_2$ -collision induced transition $a^1\Delta_g \rightarrow X^3\Sigma_{g,0}^-$ determined using relation (16) is

$$\langle a^1\Delta_g | D | \Psi_{X,0} \rangle = 1.5 \times 10^{-4} \text{ e \AA},$$

which corresponds to an absorption oscillator strength f of 2×10^{-9} and a radiative rate constant of $k_{a-X} = 0.08 \text{ s}^{-1}$. This coincides in order of magnitude with the results obtained by Krasnovsky⁶³ ($k_{a-X} \approx 0.1 \text{ s}^{-1}$). The electron shell of the H_2 molecule provides a simple example of the closed electron shell of the molecule of a saturated compound; therefore, the model for the $O_2 + H_2$ complex chosen here is quite reliable.^{12,28} This was confirmed in calculations of O_2 complexes with other molecules.^{43,53,54,71,84–88,109}

As mentioned above, the Noxon band enhancement depends on the polarisability of the collision partner, which leads to the same dependence for the luminescence band $a^1\Delta_g \rightarrow X^3\Sigma_g^-$. The dependence of the radiative rate constant k_{a-X} on solvent properties has been a subject of discussion initiated by the contradictory results of measurements using different luminescent standards for calibration.^{1,17,35,36,60–64,73–77,101–106} Ogilby *et al.*^{17,77,104} showed that the relative rate constant k_{a-X} changes by an order of magnitude on going from trifluoroethanol to carbon disulfide. These discussions outcompeted a problem of paramount importance, namely, why the intensity of the spin-forbidden transition $a^1\Delta_g \rightarrow X^3\Sigma_g^-$ increases by 3–4 orders of magnitude upon collisions in solutions, gases and solid matrices compared to the intensities of the transitions of free oxygen molecule.²⁷ The mechanism of stealing the intensity of this transition from the $a^1\Delta_g-b^1\Sigma_g^+$ transition of collision complexes was proposed more than two decades ago;^{12,28} however, until recently^{1,17,43,56} it attracted no attention of specialists in singlet oxygen photophysics. From relation (16) it follows^{12,28} that the ratio of the rate constants for oxygen–solvent collision induced transitions,

$$\begin{aligned} \frac{k_{a-X}}{k_{b-a}} &= \frac{\omega_{a-X}^3 D_{a-X}^2 g_X g_b}{\omega_{b-a} D_{b-a}^2 g_a^2} = \frac{3\omega_{a-X}^3 |c|^2}{4\omega_{b-a}^3} = \\ &= \frac{3(7882 \text{ cm}^{-1})^3 |0.0134i|^2}{4(5239 \text{ cm}^{-1})^3} = 0.00045 \end{aligned} \quad (17)$$

(ω is the transition frequency) should be constant for any solvent, because collisions do not affect mixing of the states (10) and (11) due to SOC. Here, we accounted for equality

$$\langle a^1\Delta_g | D | b^1\Sigma_g^+ \rangle = D_{a-b} = D_{b-a}$$

and used the statistical weights ($g_X = 3$, $g_a = 2$, $g_b = 1$). The matrix element of SOC (11) in oxygen molecule reaches the maximum possible value; its magnitude is large *per se* and does not need an increase through symmetry reduction upon collision. The latter is necessary for the singlet–singlet transition $a^1\Delta_g-b^1\Sigma_g^+$, which is symmetry-forbidden for isolated O_2 molecule in the dipole approximation; this prohibition is

effectively removed in collision complexes. Thus, the spin prohibition to the $a \rightarrow X$ transition is removed due to the SOC in the O_2 molecule itself. This provides an explanation for an increase in the $a \rightarrow X$ transition probability by three and more orders of magnitude in almost any solvent (in proportion to an increase in the $b \rightarrow a$ transition probability).¹²

Pioneering studies^{12,28} in this field were devoted to explanation of the results obtained by Krasnovsky,⁶³ who investigated the luminescence of singlet oxygen in solutions. These studies attracted the attention of researchers who studied the spectra of O_2 in crystals of noble gases^{51,52} and in buffer gas mixtures.³⁹ Considerable enhancement of the $b \rightarrow a$ and $a \rightarrow X$ transitions was found for oxygen present in Ne, Ar, Kr and Xe matrices. The intensity increased with an increase in the atomic number of the noble gas.^{51,52} Gas-phase experiments gave the following values of the ratio (17): 0.00032 (Ne), 0.00037 (Ar), 0.00042 (Kr) and 0.00083 (Xe).³⁹ (The last value for Xe can be easily explained by additional enhancement of the singlet–triplet transition $a \rightarrow X$ due to the effect of the external heavy atom.^{25,98}) Similar values of the ratio (17) confirmed predictions of theoretical studies^{12,27,28,98} while a slight increase in this ratio with the noble gas atomic number was explained by the strengthening of the SOC and by the effect of the external heavy atom.^{24,25}

The ratio of the statistical weights of all states (17) was taken to be unity,⁸⁸ because the collision model chosen assumed only one sublevel of the a and X states is active in transitions. Indeed, only the sublevel (10) of the $X^3\Sigma^-$ state with the quantum number $M_S = 0$ is involved in the formation of the intensity of collision-induced transition $a \rightarrow X$ through ‘mixing’ with the $b^1\Sigma_g^+$ state and stealing of the dipole moment of the Noxon transition [see Eqn (16)]. Both components of the degenerate state $a^1\Delta_g$ can participate in the Noxon band enhancement [see Eqns (13) and (14)]; however, the total intensity corresponds to involvement of only one component (at least for most calculated models for complexes).^{12,27,87,88} Therefore, for the $b \rightarrow a$ transition the statistical weights of the states participating in the transition are equal to unity. Irrespective of the type of the system (gas or solution) and $O_2(a^1\Delta_g)$ generation procedure (gas discharge or sensitisation) both components of the Δ_g state are populated before light emission. Therefore, the statistical weight ratio of the lower-to-upper term for the $a \rightarrow X$ collision-induced transition is 1:2. Thus, the actual ratio of these quantities in relation (17) is 1/2 rather than 3/4 and theory predicts⁸⁸ that

$$\frac{k_{a-X}}{k_{b-a}} = \frac{\omega_{a-X}^3 D_{a-X}^2}{\omega_{b-a} D_{b-a}^2 g_a} = \frac{\omega_{a-X}^3 |c|^2}{2\omega_{b-a}^3} = 0.0003, \quad (17a)$$

which corresponds to the results of measurements in gases,³⁹ solutions^{1,17,64,106} and cryogenic matrices.⁵¹

Analysis of the electronic emission spectrum of NCl molecule in Ar matrix⁶⁸ gave a clear substantiation of the theoretical model (9)–(14), (16). This molecule is a valence-isoelectronic analogue of oxygen molecule; it has a triplet ground state $X^3\Sigma^-$ and the same set of excited singlet states, $a^1\Delta$ and $b^1\Sigma^+$, as the O_2 molecule.⁹ Nitrogen chloride molecule only possesses no inversion symmetry; therefore, electric dipole transitions $b \rightarrow X$ and $a \rightarrow X$ with inclusion of the SOC are allowed.^{12,42} In particular, the $a \rightarrow X,1$ transition is allowed for the sublevels with $M_S = \pm 1$, while transition to the $M_S = 0$ sublevel is forbidden, as well as the corresponding magnetic dipole transitions of free oxygen molecule.¹² The scheme of the $b \rightarrow a$ and $a \rightarrow X$ transition enhancement for the complex with Ar atom in an inert matrix is the same as that proposed for the O_2 collision complexes considered above [see Eqns (9)–(14)]. Only transition to the sublevel with $M_S = 0$ is enhanced, as

follows from relation (16). The NCl molecule is convenient in that the zero-field splitting for sublevels of the $X^3\Sigma^-$ state is clearly seen⁶⁸ in the $a \rightarrow X$ emission spectrum. In addition to the allowed transition $a \rightarrow X,1$ the spectrum of NCl in Ar matrix (1091.2 nm) exhibits a weak band of the $a \rightarrow X,0$ transition (1090.7 nm), which is strictly forbidden for free molecule.⁶⁸ The change in the intensity of this band obeys relation (16) with the coefficient $c = 0.026$ for the NCl molecule (obtained by the author of this review from configurational interaction calculations with inclusion of SOC and with allowance for the measured probability of the $b \rightarrow a$ transition in the Ar matrix).⁶⁸

The intensities of the $a \rightarrow X,0$ transitions of isovalent molecules NBr and NI in solid argon are also in agreement with the model (16). Analysis of the relative intensities in the fine structure of the $a^1\Delta \rightarrow X^3\Sigma^-$ bands of the isoelectronic molecules NCl, NBr and NI in solid argon⁶⁸ confirmed the validity of the intensity borrowing theory for this band [see Eqns (8)–(13)], considered taking oxygen as an example. These data, which were obtained long before the results of direct intensity measurements for the $b \rightarrow a$ and $a \rightarrow X$ transitions of oxygen in solutions,^{17,64} provided strong arguments in favour of correctness of the model (8)–(13), (17a). However, for a decade did these data remain uncalled by researchers who studied photophysics of the singlet state of oxygen in organic and biological systems.^{43,61–64}

In the late 1990s Schmidt *et al.*,^{1,64} and Ogilby¹⁷ carried out direct experimental evaluation of theoretical predictions made using relation (17) for certain solutions. For liquid CCl_4 at room temperature the ratio of the rate constants $k_{a-X} = 1.1 \text{ s}^{-1}$ and $k_{b-a} = 3400 \text{ s}^{-1}$ is 0.000325, which is similar to the value 0.00317 obtained in the argon matrix ($k_{a-X} = 0.013 \text{ s}^{-1}$ and $k_{b-a} = 41 \text{ s}^{-1}$ at 5 K).^{1,51,64,106} In spite of large differences between the rate constants, the ratio (17a) also remains constant for some other solutions.^{17,64} This ratio was measured⁸² for the absorption of singlet and triplet oxygen molecules in deuterated water, where $O_2(a^1\Delta_g)$ has a relatively long lifetime. In all cases including homogeneous mixtures of solvents the $a \rightarrow X$ and $b \rightarrow a$ transition probabilities changed in parallel, as predicted by theory.^{12,27}

Knowledge of the enhancement mechanism of the radiating capacity of singlet oxygen is crucially important for progress in photobiology and medicine. Detection of $O_2(a^1\Delta_g)$ in various biological media is difficult owing to weak intensity and low temporal resolution of the $a \rightarrow X$ phosphorescence signals [this is determined by the radiative rate constant that strongly depends on the structure of (i) biopolymers in the oxygen environment and (ii) entire solution]. Singlet oxygen plays an important role in photobiological processes and photodynamic therapy;^{1,17,18} therefore, one can expect that *in vivo* detection of $O_2(a^1\Delta_g)$ will become a tool of medical practice in the near future. The widely used procedure for $O_2(a^1\Delta_g)$ detection with cryogenic germanium diodes is still far from meeting these requirements. The use of modern photomultipliers for the near IR region (sensitivity of these devices at 1270 nm is ten times higher than that of germanium diodes) allowed the lifetime of $O_2(a^1\Delta_g)$ to be measured ($\tau_\Delta = 40 \text{ ns}$, $Q_\Delta = 0.005$) *in vivo* in rat liver studies.¹ Biological media are highly inhomogeneous and the observed lifetime of singlet oxygen is the average result of various quenching processes. Note that the τ_Δ values are many orders of magnitude smaller than the radiative lifetimes τ_Δ^r determined from the rate constants $k_{a-X} = 1/\tau_\Delta^r$. However, understanding of the mechanisms of intermolecular interactions responsible for the τ_Δ^r values is at least equally important for progress in theory and strategy of $O_2(a^1\Delta_g)$ detection compared to the understanding of quenching mechanisms.

As mentioned above, the rate constant k_{a-X} increases in proportion to the increase in the rate constant k_{b-a} upon

collision of O₂ with the solvent molecule M.[†] The latter constant depends on the difference between the induced dipole moments of two degenerate MOs, $\pi_{g,x}$ and $\pi_{g,y}$ [see Eqn (13)] and, hence, on the polarisability of the solvent molecule α_s . Such an asymmetry of charge transfer to these orbitals of oxygen molecule appears in the case of a ‘planar’ collision, where the O₂ and M molecules lie in the same plane or where the atomic orbitals of the nearest atoms in the O₂ and M molecules overlap to the greatest extent and share the nodal plane. Deviation from this ‘planar’ structure causes mutual cancellation of both terms in relationship (13), but this is accompanied by an increase in the summands in expression (14). All summands in Eqns (13) and (14) depend on the overlap of the O₂ and M molecular orbitals and on the orbital mixing. Intermolecular interaction responsible for an increase in the rate constant k_{a-X} is essentially dispersion interaction,^{12,88} and depends on R^{-6} . The polarisability of the solvent molecule can be expressed through molar refraction:⁶⁴

$$R_m = \frac{4\pi}{3} N_A \alpha_s,$$

where N_A is the Avogadro constant.

If the interaction responsible for acceleration of the $a \rightarrow X$ transition is bimolecular in character, the second-order rate constant

$$k_{a-X}^c = \frac{k_{a-X}}{[S]} \quad (18)$$

should be related to the molar refraction ($[S]$ is the molar concentration of solvent). Actually, linear correlations between $\log k_{a-X}^c$ and $\log R_m$ were observed for a large number of solutions.⁶⁴ The radiative rate constants for $a \rightarrow X$ phosphorescence corresponding to neat liquids are listed in Table 1. The k_{a-X} vary over a wide range from 0.209 s⁻¹ for water to 3.14 s⁻¹ for CS₂.

The first-order rate constants k_{a-X} were calculated assuming^{12,27} that the whole solvent is represented by the nearest collision-partner and the lifetime of such a complex in the solvation shell is sufficiently long to determine the rate constant.

The effect of solvent was also included in other models.^{12,27,54,71,85,86,99} For instance, a loosely bound collision complex O₂ + M was placed in a solvent cavity; the solvent was treated as dielectric continuum (semi-continuum model).⁷¹ Short-range interactions in the O₂ + M pair are fundamentally important for the description of quantum exchange and dispersion interactions responsible for the enhancement of quantum transitions and shifts of energy levels. The semi-continuum model allows for small additional corrections to transition energies, which leads to better agreement between experimental data and results of bathochromic shift calculations[‡] for the $a \rightarrow X$ transition band in solutions; however, the effect of continuum on the emission intensity is negligible.^{54,71} The 0–0 transition band in the gas phase (7882 cm⁻¹, see Ref. 9) is slightly shifted in trifluoroacetic acid (7873 cm⁻¹), the shift being more pronounced in other solvents (e.g., CH₂I₂: 7824 cm⁻¹).¹ A bathochromic shift of the $a \rightarrow X$ transition band within 100 cm⁻¹ was predicted in the first calculations of O₂ + M complexes with M = H₂, C₂H₄, C₆H₆, C₁₀H₈.^{12,103} *Ab initio* calculations⁷¹ gave a 45 cm⁻¹ shift (see Table 3 in Ref. 71) for the 0–0 band of the $a^1\Delta_g \rightarrow X^3\Sigma_g^-$ transition of oxygen in benzene, which is in agreement with experimental

Table 1. Radiative rate constants for singlet–triplet transition $a^1\Delta_g \rightarrow X^3\Sigma_g^-$ of oxygen molecule in different solvents.^{17,64,76,74,104}

Solvent	k_{a-X}/s^{-1}	$k_{a-X}^c/\text{litre mol}^{-1} \text{s}^{-1}$
Water	0.209	0.0038
Methanol	0.390	0.0159
Acetonitrile	0.45	0.0234
Acetone	0.543	0.040
Ethanol	0.55	0.032
Cyclohexane	0.66	0.071
Chloroform	0.962	0.077
Tetrachloromethane	1.17, ^a 0.8, ^b 0.25 ^c	0.113
Toluene	1.44	0.153
Benzene	1.50 ^a	0.133
Chlorobenzene	1.68	0.171
Tetrachloroethylene	1.89	0.193
Iodobenzene	2.61	0.291
Diphenyl sulfide	2.66	0.442
1,3-Dibromobenzene	2.72	0.328
1-Methylnaphthalene	2.96	0.420
1-Bromobenzene	3.11	0.432
Carbon disulfide	3.14	0.189

Note. k_{a-X} and k_{a-X}^c are the mono- and bimolecular rate constants, respectively. For free O₂ molecule (*in vacuo*),^{1,9} $k_{a-X} = 0.00023 \text{ s}^{-1}$. For

a homogeneous mixture of solvents $k_{a-X} = \sum_i k_{a-X,i}^c [i]$, where $[i]$ is the

molar concentration of the i th component of the system and $k_{a-X,i}^c$ is the corresponding second-order rate constant.

^a Measured using three different sensitizers with their fluorescence as luminescence standards.⁶⁴

^b With Li–Nd phosphate glass as luminescence standard.¹⁰¹

^c With fluorescence of tetraphenylporphine as luminescence standard.⁶³

data.^{1,54} The calculated dependence of the bathochromic shift of the $a \rightarrow X$ transition band in the collision complex O₂ + Ar on the interparticle distance was reported;⁹⁸ the shift is very small ($\Delta\nu = 2.1 \text{ cm}^{-1}$) near the potential curve minimum ($R = 3.6 \text{ \AA}$) and rapidly increases as R decreases. At $R = 3.25$ and 3 \AA , where the repulsive potential considerably increases, one gets $\Delta\nu = 13.2$ and 39 cm^{-1} , respectively. The continuum model of self-consistent reactive field of the solvent gives poorer results.⁷¹ This model ignores the overlap and orbital mixing between the collision partners, which precludes correct calculations of not only enhancement of the radiating capacity of the $a \rightarrow X$ transition, but also the solvatochromic shift.

Knowledge of the enhancement mechanism of singlet oxygen radiating capacity is also basic to understanding of the nature of solvatochromic shift of the $a-X$ band. In all solutions studied the maximum of the 0–0 phosphorescence band of O₂ (7882.4 cm⁻¹) is shifted by 20–50 cm⁻¹ towards the long-wavelength region, the shift increasing with the solvent polarisability.

Taking into account the fact that the major contribution to the shift of energy levels comes from dispersion interaction, Schmidt^{1,35} proposed a theory of solvatochromic shift of the $a-X$ band. The theory assumes that the shift of the maximum of the 0–0 band ($\Delta\nu$) depends on the polarisability difference between the $a^1\Delta_g$ and $X^3\Sigma_g^-$ states (*i.e.*, on α_Δ and α_Σ)

$$\Delta\nu = -\frac{3\alpha_s}{2d_c^6} \left(\frac{\alpha_\Delta I_\Delta I_s}{I_\Delta + I_s} - \frac{\alpha_\Sigma I_\Sigma I_s}{I_\Sigma + I_s} \right),$$

where I_Σ , I_Δ and I_s are the ionisation potentials of the O₂ and solvent molecules, $d_c = (d_\Sigma + d_s)/2$ is the distance between spherical molecules, d_s is determined from the molar volume of

[†] Notations: M is the solvent molecule involved in the collision complexes and S are other solvent molecules.

[‡] Shift towards long-wavelength region.

the solvent and d_Σ is determined from the van der Waals volume of the O_2 molecule. The solvent polarisability

$$\alpha_s = \frac{3R_m}{4\pi N_A}$$

was determined through the refraction

$$R_m = V_m P_n,$$

where V_m is the molar volume of the solvent,

$$P_n = \frac{n^2 - 1}{n^2 + 2},$$

(n is the refractive index). To explain the bathochromic shift of the $a-X$ band, Schmidt assumed³⁵ that $\alpha_\Delta > \alpha_\Sigma$, as is the case for the excited-state and ground-state polarisabilities. However, the characteristics of the open-shell oxygen molecule [see Eqns (1)–(3)] and the paramagnetic ground state are basically different from those of conventional diamagnetic molecules with closed shells in the ground state. This also concerns the polarisability tensor. For instance, the diagonal elements of this tensor for the x axis are defined as follows:

$$\alpha_{xx} = \sum_n \frac{\langle 0|ex|n\rangle\langle n|ex|0\rangle}{E_n - E_0}, \quad (18a)$$

where ex is the projection of the dipole moment on the x axis; $|n\rangle$ and E_n are respectively the wave function and energy of the n th excited state; the case $|n\rangle = 0$ (not included in the sum) corresponds to the ground state for which the tensor is calculated.¹³ Expressions for other components of the tensor are similar. The excited-state polarisability of a conventional organic molecule should be higher than that of the singlet ground-state, because the energies of transitions between excited states are always lower than the energy of excitation from the closed shell at a sufficiently large number of intense transitions in both cases.

Schmidt's assumption³⁵ $\alpha_\Delta > \alpha_\Sigma$ was rejected based on the results of *ab initio* calculations of O_2 molecule (see Refs 40, 53 and 93), which also cast some doubt⁵³ on his theory of red solvatochromic shift of the $a-X$ band. At all values of the internuclear distance in the O_2 molecule, the polarisability in the $a^1\Delta_g$ state is lower than in the $X^3\Sigma_g^-$ state,⁹⁸ which contradicts the Schmidt hypothesis. Thus, even averaging over vibrational states does not change the conclusion, namely, $\alpha_\Delta < \alpha_\Sigma$. This result can be explained as follows. The polarisability α_Σ of the triplet ground state is mainly determined by the electric dipole moment of the Schumann–Runge transition (D_{SR}^2 , divided by the transition energy), whereas that of the singlet state $a^1\Delta_g$ is determined by the electric dipole moment of the $a^1\Delta_g - ^1\Delta_u$ transition, which is much smaller than D_{SR} (Schumann–Runge transition energy is also lower, especially at $r > 1.23$ Å).^{30, 66} Here the case in point are the components of the tensor α_{zz} , since these transitions are polarised along the molecular axis. It is these transitions that make the major contributions to the average polarisability

$$\alpha_{cp} = \frac{2\alpha_{xx} + \alpha_{zz}}{3}.$$

The perpendicular component is determined by the dipole moments of transitions to the $^1,^3\Pi_u$ states, which are nearly equal for the triplet and singlet transitions. The α_{xx} and α_{zz} values we have obtained are respectively 8.16 and 15.48 a_0^3 for the $X^3\Sigma_g^-$ state and 8.15 and 14.12 a_0^3 , respectively, for the singlet state $a^1\Delta_g$. Here $\alpha_{cp} = 10.6 a_0^3$ for $X^3\Sigma_g^-$ and $\alpha_{cp} = 10.14 a_0^3$ for $a^1\Delta_g$, $\alpha_\Delta - \alpha_\Sigma = -0.46 a_0^3$.

The relation $\alpha_\Delta < \alpha_\Sigma$ is valid for free O_2 molecule in vacuum,⁵³ but will it hold for oxygen in solution? To clarify the issue, we carried out polarisability calculations for collision complexes of O_2 with diamagnetic molecules.⁹⁸ As an example we will consider a collision complex $O_2 + He$, where the He atom serves a model for a simplest closed-shell species.⁹⁸ In this case the average polarisabilities of the triplet and singlet states somewhat increase to $\alpha_{cp} = 11.72 a_0^3$ for $X^3\Sigma_g^-$, $\alpha_{cp} = 12.69 a_0^3$ for $a^1\Delta_g$, i.e., $\alpha_\Delta > \alpha_\Sigma$. The reason consists in the appearance of additional contribution to polarisability due to the induced $a-b$ -transition [see Eqns (13) and (14)] and the contributions of charge transfer transitions for the $a^1\Delta_g$ state. The charge transfer transitions are more intense for the $a^1\Delta_g$ state rather than $X^3\Sigma_g^-$ ground state.^{12, 27, 70} The singlet and triplet charge transfer states are almost degenerate;²⁷ therefore, the energies of the charge transfer transitions from the singlet state $a^1\Delta_g$ are nearly 1 eV lower than those of similar transitions from the triplet ground state $X^3\Sigma_g^-$. The mixing coefficients of the triplet and singlet ground-state wave function (2) with the wave functions of the charge transfer states due to configurational interaction are noticeably larger for the $a^1\Delta_g$ state than for the $X^3\Sigma_g^-$ state,^{12, 27} which predetermines higher intensities of dipole transitions and their greater contribution to polarisability.⁹⁸ The calculated polarisability difference

$$\alpha_\Delta - \alpha_\Sigma = 0.97 a_0^3$$

is in qualitative agreement with the predicted value.³⁵ Using the results of such calculations, one can explain the red solvatochromic shift of the $a-X$ transition band in the framework of the Schmidt theory.

Thermal motion of molecules in solutions is reduced to random jumpwise translational motions from one metastable position to another. O_2 -Type gas molecules are known to exist in solutions in cavities, with rather long lifetimes that are much longer than the jump time. An important contribution to stimulation of the radiative transition $a^1\Delta_g \rightarrow X^3\Sigma_g^-$ of oxygen molecule comes from asymmetrical intermolecular vibrations in those cavities that are included in modelling as the effect of nearest neighbours only. The inclusion of a few solvent molecules in the nearest solvation shell leads to non-additive enhancement of the $a \rightarrow X$ transition.⁹⁸ Model ternary complexes $O_2 + C_2H_4 + H_2$ were calculated¹⁰⁰ at different collision geometries and co-operative effects of a complex solvation shell on the intensities of the $b \rightarrow a$ and $a \rightarrow X$ transition bands were studied in detail. It was shown that both an increase and a decrease in the probability of the radiative transition $a \rightarrow X$ are possible depending on the mutual position of the collision partners. By and large, calculations^{98, 100} revealed the possibility of co-operative effect of a few solvent molecules on the moment of the $a \rightarrow X$ transition, which explains a large enhancement of singlet oxygen emission in solution compared to that observed in the gas phase.

Fink *et al.*³⁹ studied the intensity of the Noxon band in the microwave discharge spectra of O_2 mixtures with noble and other gases at a reduced pressure. Using a FT IR spectrometer, they obtained a high resolution for the $b \rightarrow a$ transition band at 1.91 μm and found that raising the pressure causes the appearance of a continuum against the background of discrete lines of rotational branches of the $b^1\Sigma_g^+ \rightarrow a^1\Delta_g$ quadrupole transition. The discrete spectrum was assigned³⁹ to unperturbed $O_2(b^1\Sigma_g^+)$ molecule, while the continuum was attributed to collision-induced emission. Metastable molecules $O_2(b^1\Sigma_g^+)$ generated in discharge also give rise to an emission band $b^1\Sigma_g^+ \rightarrow X^3\Sigma_g^-$ the intensity of which depends only slightly on collisions.³⁹ This follows from the old semiempirical theory^{12, 25} and is confirmed by *ab initio* calculations,⁸⁷ namely, with allowance for the SOC [see Eqns (9) and (10)] the electric dipole moment of the $b \rightarrow X$ transition is proportional to the dipole moment

Table 2. Radiative rate constants for singlet–singlet transition $b^1\Sigma_g^+ \rightarrow a^1\Delta_g$ of O_2 molecule induced by collisions with various buffer gas molecules.³⁹

Buffer gas	k_{b-a}^c /litre mol ⁻¹ s ⁻¹	R_m /ml mol ⁻¹
He	≤ 0.6	—
Ne	~ 0.6	1.00
N ₂	7.8	4.34
O ₂	9.0	4.00
Ar	10.2	4.13
Kr	21.6	6.22
Xe	46.8	10.10
SF ₆	26.4	11.34
SO ₂	31.8	9.71
PCl ₃	252.0	25.0

Note. Bimolecular constants k_{a-X}^c were determined from the integral intensity ratio of discrete lines and broad bands corresponding to collision-induced transitions. The rate constant for the $b^1\Sigma_g^+ \rightarrow a^1\Delta_g$ transition of free O_2 molecule was taken to be $k_{b-a} = 0.0014$ s⁻¹ (Ref. 39).

difference between the $b^1\Sigma_g^+$ and $X^3\Sigma_g^-$ states. For some calculated collision complexes this difference is negligible and no $b \rightarrow X$ transition enhancement is observed.

Once measured the intensity ratios of the $b \rightarrow X$ and $b \rightarrow a$ transition bands as functions of pressure of various gases, the second-order rate constants for collision-induced singlet–singlet transition $b \rightarrow a$ (Table 2) were determined.³⁹ For neon, one has $k_{b-a}^c = 0.9 \times 10^{-21}$ cm³ s⁻¹, whereas for PCl₃ this rate constant increases by a factor of 467 ($k_{b-a}^c = 42 \times 10^{-20}$ cm³ s⁻¹).³⁹ In Table 2 the rate constants taken from Ref. 39 are given per mole in order to compare with the results of measurements in solutions.¹ The rate constants for quenching of excited $O_2(b^1\Sigma_g^+)$ molecules are 2–3 orders of magnitude higher than the radiative rate constants in the gas phase.^{1,39} In the condensed phase quenching is even more efficient; therefore, luminescence measurements for the $b \rightarrow a$ transition in solutions are difficult.^{1,17,58,64} Chou and Frei⁵⁸ first discovered this emission in CCl₄ solution using triplet benzophenone as sensitizer of the $O_2(b^1\Sigma_g^+)$ state. This result could not be reproduced for long.¹⁰⁶ Taking into account the low rate constant for the Noxon band in free O_2 molecule ($k_{b-a} = 1.4 \times 10^{-3}$ s⁻¹), the observation of a narrow band at 1.92 μ m indicated⁵⁸ a giant enhancement of the $b \rightarrow a$ transition in solution. According to Schmidt *et al.*,^{1,106} the quantum yield of luminescence for the $b \rightarrow a$ transition in CCl₄ solution is 0.00045. Using the observed lifetime of $O_2(b^1\Sigma_g^+)$ molecules, he determined the radiative rate constant for the Noxon band in CCl₄ solution ($k_{b-a} = 3.45 \times 10^3$ s⁻¹); this is six orders of magnitude higher than the rate constant for free O_2 molecule. The calculated moment of the $b \rightarrow a$ transition in the collision complex $O_2 + CCl_4$ depends strongly on the intermolecular distance, being almost independent of collision angles.¹² The average value of R is governed by the molecular velocity in the vicinity of the nearest solvation shell. Assuming that $R_{av} = 2.87$ Å at room temperature, one can obtain the observed enhancement of the $b \rightarrow a$ transition. Tetrachloromethane is not a ‘champion’ with respect to enhancement of the $a \rightarrow X$ and $b \rightarrow a$ transitions in solutions, as follows from calculations^{12,24–28,85–88,98–100} and from the data listed in Table 1.

3. Inclusion of vibrations and vibronic interactions

Enhancement of forbidden transitions in oxygen molecule trapped in a low-temperature inert gas matrix is much less pronounced.^{98–123} Taking into account the symmetry of the nearest environment of an impurity O_2 -centre in the crystal

lattice, one can conclude that the $b \rightarrow a$ transition remains forbidden ignoring lattice vibrations.^{113,123} Transitions become allowed only when assisted by electron–phonon interactions.¹²³ In argon matrix at 5 K, the $b \rightarrow a$ transition is characterised by a radiative lifetime of 24.5 ms, or a rate constant $k_{b-a} = 41$ s⁻¹ (Refs 51 and 52), which is nearly two orders of magnitude lower than in CCl₄ solution. In this matrix the electric dipole moment of the $b \rightarrow a$ transition is induced by each neighbouring argon atom, in the direction from O_2 towards Ar, so the resultant moment of the transition is zero. Thus, enhancement of the $b \rightarrow a$ transition can be due to asymmetrical lattice vibrations. With allowance for nuclear displacements

$$q = R - R_0$$

from the equilibrium position R_0 (change in the intermolecular distance) in the adiabatic approximation, the dipole moment of a vibronic transition $a \rightarrow X$ can be written in the form¹¹³

$$\langle a^1\Delta_g\chi_0 | D | \Psi_{X,0}\chi_v \rangle = -c \left(\frac{\partial D_{b-a}}{\partial q} \right)_{R_0} \langle \chi_0 | q | \chi_v \rangle, \quad (19)$$

where χ_0 and χ_v are the vibrational functions with quantum numbers 0 and v , respectively; for the coefficient c , see Eqn (11). By analogy, for the $b \rightarrow a$ transition one gets

$$\langle b^1\Sigma_g^+\chi_0 | D | a^1\Delta_g\chi_v \rangle = \left(\frac{\partial D_{b-a}}{\partial q} \right)_{R_0} \langle \chi_0 | q | \chi_v \rangle.$$

The equilibrium positions and vibrational functions for the states b , a and X are thought to be the same, which is quite realistic.^{9,98} For many models the calculated moment of the D_{b-a} transition depends strongly on q near the equilibrium complex $O_2 + M$.^{12,98,99,113} The radiative rate constants for the $a \rightarrow X$ and $b \rightarrow a$ transitions determined with allowance for asymmetrical vibrations in the octahedral model of impurity centre $O_2 \cdot Ar_6$ are similar to the observed ones.^{12,51,98}

The 0–0-bands of the $a \rightarrow X$, $b \rightarrow a$ and $b \rightarrow X$ transitions are the most intense because the potential curves for these states are characterised by nearly equal equilibrium distances (see Fig. 1). The Franck–Condon (FC) factors for these bands approach unity, whereas for vibronic overtones they are negligible. For O_2 in the gas phase, even the 0–1 bands have low intensities. In addition to the FC factors, here the dependence of the transition moment on the interatomic distance r should also be taken into account. The magnetic moment of the transition [see expression (12)] rapidly increases with the distance r , because the energy difference in the denominator of Eqn (11) decreases to zero in the limit $r \rightarrow \infty$. The Einstein coefficients for spontaneous emission of this transition determined by integration over r for the magnetic moment of the $b \rightarrow X$ transition of O_2 molecule are equal to 0.0047, 0.0064 and 0.0003 s⁻¹ for the 0–1, 1–0 and 2–0 bands, respectively.⁵⁰ These values are similar to measured ones⁹ and their ratios differ from the FC factor ratios.

Deviations from the FC effects were also obtained for the $a \rightarrow X$ transition.^{12,86} In addition to the 0–0-band of the $a \rightarrow X$ transition (1.27 μ m), Chou and Khan¹¹⁴ found a new, very weak emission band near 1.4 μ m in spectra of chlorine-containing organic solvents ($C_2H_4Cl_2$, $C_3H_5Cl_3$, *etc.*). The band is red-shifted relative to the 0–0-band, the shift being equal to the C–Cl vibrational frequency. Similar weak bands were also detected for other halogen-containing solutions.¹¹⁴ They correspond to the $a \rightarrow X$ transition of O_2 and simultaneous vibrational excitation of the solvent molecule.

Understanding of the nature of these co-operative vibronic transitions is of fundamental importance for theory of singlet state ($a^1\Delta_g$) of oxygen in solutions. Having included these transitions, one can obtain direct substantiation of relations

(11) and (16) and the bimolecular model for oxygen complex with solvent as the primary source of stimulation of emission of the forbidden transition $a^1\Delta_g \rightarrow X^3\Sigma_g^-$ (Ref. 113).

A model for the complex of O_2 with CH_3Cl used in calculations¹¹³ of the transition moment D_{b-a} and its derivative [see Eqn (19)] is shown in Fig. 4. The dipole moment of co-operative vibronic transition $a \rightarrow X$ with simultaneous vibrational excitation of the C–Cl bond in CH_3Cl molecule can be calculated using expression (19) and the standard integral

$$\langle \chi_0 | q | \chi_{v=1} \rangle = \sqrt{\frac{\hbar}{2\mu\omega}},$$

where μ is the reduced mass and ω is the vibration frequency.

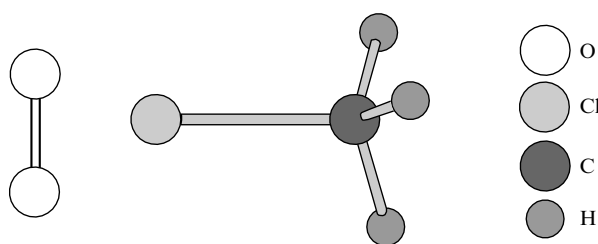


Figure 4. Structure of a collision complex $O_2 + CH_3Cl$. C–Cl vibration modulates the intermolecular distance in the equilibrium complex.

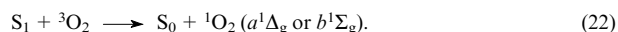
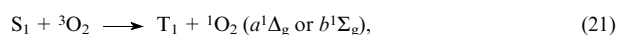
Vibrations of the C–Cl bond in the equilibrium complex modulate the intermolecular distance, which in turn strongly affects the moment of the $a \rightarrow X$ electronic transition, induced by intermolecular interactions. The dipole moment of co-operative vibronic transition [see Eqn (19)] was estimated to be equal to 1.42×10^{-5} e Å.¹¹³ This leads to a radiative rate constant of 0.0056 s⁻¹, which is nearly 100 times lower than typical rate constants for the $a \rightarrow X$ transition of the O_2 molecule in related solvents (see Table 1). This estimate is in good agreement with the results reported by Chou and Khan:¹¹⁴ the new emission band is about 100 times less intense than the 0–0-band of the $a \rightarrow X$ transition.

Absorption of thermal IR radiation by homonuclear molecules O_2 and N_2 is strictly forbidden by selection rules. However, weak absorption of IR radiation by air at 6.4 μ m is known. Theory of intensity of vibrational transitions is intimately connected with the theory of enhancement of absorption bands of oxygen in electronic spectra. Geometry optimisation of $O_2 + Ar$ complexes allowed the shifts of the IR bands in different excited states of the O_2 molecule and the corresponding band intensities to be calculated. Of particular importance is the theoretical prediction,⁹⁸ according to which intermolecular interaction affects the $O_2(^5\Pi_g)$ metastable state and its IR absorption spectrum. This state is formed upon recombination of $O(^3P)$ atoms in atmosphere and corresponds to a loosely bound complex or a biradical pair $O(^3P)\cdots O(^3P)$ with a long internuclear distance (2.2 Å). The bond energy (0.12 eV) and vibrational frequency (113 cm⁻¹) of this species are unexpectedly low for diatomic molecule.⁹⁸ Recently,⁹⁴ this associate was detected by the quintet–quintet transition to the ion-pair state. According to calculations of the complex $O_2 + Ar$, it is the $^5\Pi_g$ state that is characterised by the greatest enhancement of IR absorption.⁹⁸ Loosely bound molecules O_2^+ can ‘stick’ to inert gases or aerosol particles, which should manifest itself in the IR spectra. Recombination of $O(^3P)$ atoms also leads to formation of more stable states $^1\Sigma_u^+$, $^3\Delta_u$, $^3\Sigma_u^+$ of O_2^+ molecules; this is accompanied by release of energy and subsequent decomposition of the complex of oxygen with aerosol. Only metastable quintets can readily relax, being at the

same time bound to the third particle (aerosol). Check-up of these predictions seems to be important for remote control in atmospheric photochemistry.

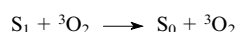
4. Optical effects stimulated by collisions of oxygen and organic dye molecules

Among numerous optical effects,^{1,2} we will consider the enhancement of absorption intensity upon $S_0 \rightarrow T_1$ transition of dye, quenching of dye luminescence and a number of co-operative transitions.^{27, 69–71, 73–88, 98–122} Organic dye molecules typically contain an extended π -conjugation chain and readily excitable π -electrons and have low triplet-state energies and high polarisabilities.^{2, 7} Therefore, the effects of intermolecular interaction manifest themselves most pronouncedly when they influence the optical properties of both oxygen and dye molecules. A collision between excited dye molecule and $O_2(^3\Sigma_g^-)$ produces a short-lived collision complex with a nearly zero equilibrium constant.^{7, 13} Mixing of excited states of the complex and electronic-vibrational relaxation can lead to quenching of fluorescence of the $S_1 \rightarrow S_0$ transition of the dye molecule.^{2, 7, 13}



Here S_0 and S_1 are the ground and excited singlet state of the dye molecule, respectively.

Measurements of the yield of T_1 triplet states of pyrene and anthracene molecules and its perfluoro analogues showed² that quenching of fluorescence proceeds by reaction (20); no energy-transfer products [see Eqn (21)] were detected. It has long been known² that the rate of fluorescence quenching by oxygen varies insignificantly on going from organic molecules [in this case the S_1 – T_1 splitting is such that reaction (21) is exothermic] to molecules for which reaction (21) is highly endothermic. Reaction (22) is spin forbidden. Immediate quenching



is independent of specific features of intermolecular interaction associated with paramagnetism of the oxygen, because there is no need of spin changes in individual molecules; this process should not differ from the quenching by conventional diamagnetic molecules and is therefore of low efficiency. At present, it is commonly accepted that quenching of dye fluorescence by oxygen is mainly due to stimulation of intersystem crossing (ISC) with the transition from the S_1 to the T_1 state.^{1, 2, 13} Theoretical explanation for the high efficiency of ISC (20) is based on quantum chemical calculations of collision complexes.^{27, 70, 71, 103, 109} Now we will give some examples including the results of recent calculations.¹⁰⁷

First, we will consider a collision complex with ethylene as a simplified model. This unsaturated hydrocarbon is not a dye, but has the S_1 - and T_1 -states of the $\pi\pi^*$ -type; calculations of the collision complex of ethylene with oxygen simulate the characteristic features of the intermolecular interaction of O_2 with the π -system. In this model the O_2 molecule is above the ethylene plane at the distance R between the centres of the molecules; the oxygen and carbon atoms form an equilateral trapezoid O–O–C–C similar to that formed by the oxygen and nitrogen atoms in the collision complex $O_2 + N_2$ (see Fig. 3). The complex was calculated¹⁰⁷ using the spin-restricted Hartree–Fock method for open-shell systems with inclusion of configuration interaction in the 6-311G** basis set. The active space of configuration interaction included the most important orbitals of oxygen (from $3\sigma_g$ -MO to vacant

$3\sigma_u$ -MO). Six ethylene orbitals were also included in the CI calculations.¹⁰⁷ The use of extended AO and CI basis sets made it possible to reach¹⁰⁷ a better accuracy compared to that reported earlier,¹⁰⁹ although the models of the complexes were identical.

Comparison of the results obtained by this method (Fig. 5) with the results of calculations of the moments of singlet–singlet transitions¹⁰⁹ showed that extension of the CI basis set leads to enhancement of certain collision-induced transitions. This first of all concerns the 1–4 transition (see Fig. 2), *i.e.*, the co-operative singlet–triplet transition of ethylene with simultaneous excitation of the oxygen $a^1\Delta_g$ state. This transition could be observed in emission as dye phosphorescence whose band is shifted towards the red spectral region by the energy of the $a^1\Delta_g - X^3\Sigma_g^-$ transition.¹⁰⁹ Simultaneously, collisions between oxygen and dye molecules cause quenching of dye phosphorescence; therefore, observation of this co-operative emission is difficult. In principle, it cannot be ruled out that appropriate choice of the dye and the solution concentration will allow one to detect this co-operative emission.

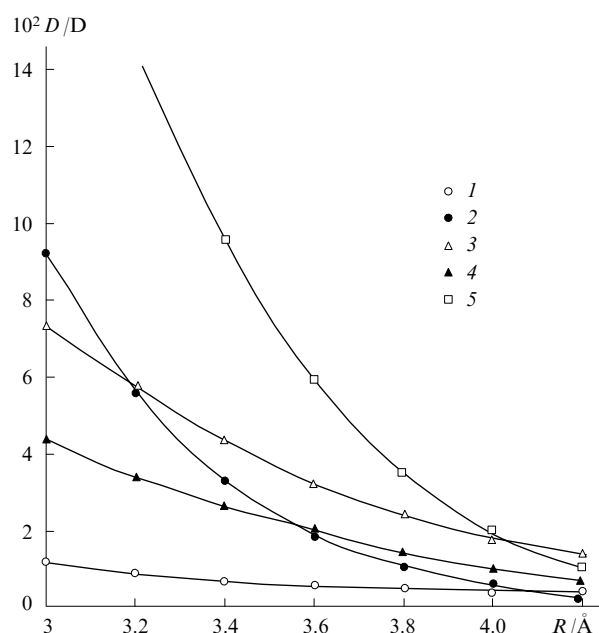


Figure 5. Dipole moments of singlet–singlet transitions (D) induced by collisions between oxygen and ethylene molecules plotted vs. intermolecular distance (R).

Calculations of configuration interaction with the 6-311G** basis set and molecular orbitals using the spin-restricted Hartree–Fock method. Transition (see Fig. 2): 3–1 (1), 1–4 (2), 1–5 (3), 3–2 (4) and 4–5 (5).

The dipole moment of the 1–4 transition rapidly decreases as R increases (see Fig. 5) and becomes the smallest among all dipole moments of the collision induced transitions at $R = 4.2$ Å. It is interesting to compare it with the dipole moment of the 1–5 transition ($a^1\Delta_g - c^1\Sigma_u^-$ transition of oxygen molecule, the frequency of which is similar to the frequency of the Chamberlain band $a^1\Delta_g - A'^3\Delta_u$).⁹⁴ The $a^1\Delta_g - c^1\Sigma_u^-$ transition with intensity strongly enhanced compared to those of the transitions of free oxygen molecule has been revealed in argon matrix;¹⁰⁸ this was explained by strong effect of intermolecular interaction on the electric dipole moment of this transition.^{98, 107, 109} Figure 5 shows that the dipole moment of the 1–5 transition is large even at long intermolecular distances, being the largest among all calculated dipole moments at $R = 4.2$ Å. Enhancement of transitions for oxygen in inert

gas matrix is determined by asymmetrical lattice vibrations relative to O_2 ; it depends on the difference between the distances to nearest neighbours rather than R . Therefore, enhancement of the $a^1\Delta_g - c^1\Sigma_u^-$ transition intensity at long intermolecular distances is of particular importance for explanation of the matrix effect on this transition.¹⁰⁹

Comparison of two transitions, 1–5 and 1–4, shows that the latter becomes more intense at $R < 3.2$ Å (see Fig. 5). It was reported¹⁰⁹ that the dipole moments of the transitions increased not so rapidly, as shown in Fig. 5, as the molecules approached each other. This can be explained by lesser ‘flexibility’ of the 6-31G basis set (see Ref. 97) and poorer inclusion of electron correlation in the configuration interaction method compared to more recent calculations that provide (see Fig. 5) better agreement with experimental data on the radiative lifetimes of emission $c^1\Sigma_u^- \rightarrow a^1\Delta_g$; they also predict a higher probability of the co-operative transition 1–4. This gives grounds to hope that at a sufficiently high concentration of $O_2(a^1\Delta_g)$ in solution this transition can also be detected in absorption.

For the transition $b^1\Sigma_g^+ - a^1\Delta_g$ the component (4) is more active (transition 3–2) than the other quasi-degenerate component (4a) of the $a^1\Delta_g$ state (transition 3–1). This agrees with the results of the simplified analysis of relations (13) and (14) and with Fig. 3. The $b^1\Sigma_g^+ - a^1\Delta_g$ (3–2) transition is relatively intense at long R (3.8–4.2 Å), while at smaller R values the other, shorter-wavelength transitions are enhanced to a much greater extent (see Fig. 5). This is due to an increase in the contributions of charge transfer states to higher-energy terms.¹⁰⁹

Curve 5 in Fig. 5 shows a rapid increase in the probability of the 4–5 transition as the molecules approach each other. This is a co-operative transition from the triplet state to the ground singlet state of ethylene with simultaneous excitation of the oxygen $c^1\Sigma_u^-$ state. At $R = 3$ Å, the dipole moment of this transition is 0.2 D, being commensurable with the dipole moments of the allowed optical transitions.¹³ For many dyes the wavelength of this co-operative transition falls in the visible region; observation of this transition in electric discharge may appear to be useful in studies of the concentration of the $c^1\Sigma_u^-$ states of the oxygen molecule and in the design of new chemical lasers.

The $S_0 - T_1$ transition of ethylene becomes an allowed triplet–triplet transition of the collision complex with oxygen (transition 0–6 in Fig. 2).^{2, 12, 27, 70, 110} Formally, the dipole moment of the transition between the pure configurations, $X^3\Sigma_g^- \times S_0 - X^3\Sigma_g^- \times T_1$, equals to zero; however as configurational interaction causes the triplet states to mix and thus the contributions of charge transfer states and triplet states of the type $X^3\Sigma_g^- \times S_1$ appear, the 0–6 transition is collision induced.^{70, 109} The $S_0 - T_1$ transitions of ethylene were observed upon adding oxygen at high pressure¹¹¹ and in many dye solutions.² The theoretical intensity¹⁰⁹ of the 0–6 transition matches experimental data;¹¹¹ this gives grounds to believe that calculations¹⁰⁹ are suitable for comparative predictions of the probabilities of some other triplet–triplet transitions including co-operative excitations. New intense transitions induced by oxygen–dye collisions were predicted.^{12, 27, 109}

Of particular interest is the singlet–triplet transition 6–7 between two excited states, S_1 and T_1 , of the dye. As the dye molecule contacts the triplet oxygen ($X^3\Sigma_g^-$), this transition not only becomes a dipole-allowed triplet–triplet transition, but also acquires the maximum intensity, which is due to comparatively large contribution of charge transfer states.^{12, 70, 86, 99, 109} Indeed, the S_1 state of the dye has a relatively high energy (1.5–2 eV higher than that of the T_1 state) and stronger mixes with the charge transfer states. In the complex of O_2 with ethylene the dipole moment of the

$X^3\Sigma_g^- \times S_1 - X^3\Sigma_g^- \times T_1$ transition is 0.38 D at an intermolecular distance R of 3.6 Å which is similar to equilibrium one.⁹⁹ Commensurable, although smaller, values were obtained for the O_2 complexes with naphthalene and conventional dyes.¹⁰³ This 'colossal' enhancement of the $S_1 - T_1$ radiative transition, which is forbidden for free dye molecule, provides an explanation for the high rate of quenching of dye fluorescence.²⁷

Analysis of calculations^{99,109} also made it possible to explain the known enhancement of the Herzberg(III) band ($X^3\Sigma_g^- - A'^3\Delta_u$) at high pressure of oxygen or buffer gas and in inert gas matrices.^{9,93,103} High intensity of the Herzberg(III) band and the $c^1\Sigma_u^- - a^1\Delta_g$ transition, as well as co-operative transitions involving the Herzberg state¹⁰⁴ is due to much more efficient mixing of π_u -MOs with the solvent orbitals rather than π_g -orbitals.¹² All features of the interaction between oxygen open shells and solvent molecules are clearly related to enhancement of radiative transitions. Taking account of this fact makes understandable numerous optical effects due to collisions between oxygen and organic dye molecules.^{12,86}

5. Relation between enhancement of radiative transitions and quenching of dye fluorescence

The mechanism of enhancement of collision-induced radiative singlet-triplet transitions of oxygen is intimately related to the acceleration mechanism of non-radiative deactivation of $O_2(a^1\Delta_g)$ (Refs 26, 27, 81) and other quenching processes in the contact complex $O_2 + M$.^{2,13,112-137} Within the framework of the model for dispersion forces the collision induced electric dipole moment of transition of the oxygen molecule can interact with the moments of transitions in solvent. Recall that the dipole-dipole interaction between all virtual transitions in two closely spaced molecules determines the attractive forces acting between them; this interaction is responsible for the dipole-dipole non-radiative energy transfer and (partially) for quenching of singlet oxygen.^{1,2,27,71,115}

An explanation for various types of generation of singlet oxygen due to dipole-dipole energy transfer and CI-calculated transition moments in collision complexes is available.²⁷ Collision-induced dipole moments of $S - T$ -transitions (forbidden in isolated molecules) are mainly due to exchange interaction; therefore, this type of energy transfer can be treated as exchange-resonant one.¹⁰⁷ However, in this case²⁷ its rate should be calculated using the expression for the dipole-dipole interaction between the moments of induced transitions. For instance, quenching of dye fluorescence can be explained by enhancement of non-radiative collision-induced $S_1 - T_1$ -transition with $O_2(X^3\Sigma_g^-)$. Namely, a relatively large dipole moment of the $S_1 - T_1$ -transition (D_{S-T}) induced by collisions between dye and oxygen molecules strongly interacts, by the dipole-dipole mechanism, with the moments of $T_{1,0} - T_{1,v}$ resonant transitions between vibrational sublevels of high-frequency C-H (O-H) vibrations and their overtones of the dye molecule.^{2,27} This also makes understandable the contribution of charge transfer states to the quenching mechanism, because the D_{S-T} strongly depends on them.²⁷ Quenching of T_1 states through energy transfer to singlet oxygen depends on the intensity enhancement of the 0-6 and 1-3 (2-3) transitions and the $a-X$ transition; all of them become dipole-allowed transitions upon collision.²⁷ The applicability of the dipole-dipole mechanism is substantiated by the fact that the distance between the 'emitting' oscillator (induced dipole moment of the $S_1 - T_1$ -transition) and 'absorbing' oscillators (overtones) is noticeably longer than the oscillator size, namely,² both 'dipoles' are at most 0.1 Å long.

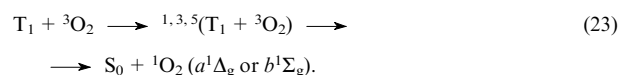
The dipole moments of the $S_1 - T_1$ -transitions in the O_2 complexes with ethylene²⁷ and naphthalene,¹⁰³ obtained from MINDO calculations with inclusion of configurational interaction are equal to 0.02 and 0.01 D, respectively, at an

intermolecular distance of 3.2 Å. The D_{S-T} value rapidly increases as the molecules approach each other;^{27,87} however, this is hard to reach in the gas phase under normal pressure. The vector of the dipole D_{S-T} connects the centres of the molecules, being distant from the C-H oscillators. The size and orientations of these oscillators are comparable with analogous parameters of H atom displacements.^{2,86} Theory of non-radiative transitions in the case of non-adiabatic perturbation was considered in Ref. 2. Calculations of the rate of quenching of dye fluorescence by oxygen due to enhancement of non-radiative $S_1 - T_1$ -transition give the rate constants of the order of 10^{13} litre mol⁻¹ s⁻¹, which is much higher than the diffusion constants.²⁷

6. Sensitisation of $O_2(a^1\Delta_g)$ molecule

Singlet oxygen is most often generated using photosensitisation, *i.e.*, energy transfer from excited state of sensitizer to $O_2(^3\Sigma_g^-)$ state. Possible sensitizers include many dyes absorbing visible light, in particular, widely abundant natural compounds, such as chlorophyll, haem, protoporphyrin and other porphyrin derivatives. Therefore, singlet oxygen plays an important role in many photobiological processes.

Excited singlet state of a dye sensitizer (S_1) formed upon absorption of a light quantum is efficiently quenched through oxygen-induced ISC [see Eqn (20)] or due to fast monomolecular transition to the T_1 state. Upon collision with $O_2(^3\Sigma_g^-)$, the long-lived state T_1 generates the quintet, triplet and singlet states of the collision complex. Decomposition of the singlet state into products is spin allowed



Quenching of phosphorescence of tripaflavin adsorbed on silica gel [reaction (23)], was proposed by Kautsky in 1931.^{2,7} Experiments were carried out in a sealed vessel at low concentration of the oxygen added. Quenching was explained by the formation of active oxygen in the singlet state. According to Kautsky's hypothesis, 1O_2 reaches the oppositely lying surface of a silica gel bead containing adsorbed dye and transforms it to the coloured form. This hypothesis was soon forgotten and quenching of the T_1 states of organic molecules was explained by formation of unstable peroxide intermediates (moleoxides).⁷ Only three decades ago Kautsky's ideas were completely substantiated.^{1,2,7} Oxygen efficiently quenches the T_1 states of all organic molecules studied in vapours, liquid solutions, adsorbates and polymers (where diffusion of O_2 is possible).^{1,2} The rate constant for quenching of triplets with oxygen ($k_T^{O_2}$) is about an order of magnitude lower than the rate constant for diffusion (k_d).

Since the quintet, triplet and singlet states of the collision complex are equiprobable, nine collisions on the average produce five quintets, three triplets and one singlet; only in the last-mentioned case reaction (23) is spin-allowed and only in this case singlet oxygen can be generated. Then one has $k_T^{O_2} \leq (1/9)k_d$, which is in agreement with many (not all) experimental data.^{1,2} Complete quenching



can start from the triplet state of the complex;²⁷ it also contributes to $k_T^{O_2}$. Quantum yield measurements confirmed the importance of this quenching channel.¹³¹ Rate constant measurements for quenching of T_1 states of carotenoids gave $k_T^{O_2} \approx 10^9$ litre mol⁻¹ s⁻¹. In this case the formation of $O_2(a^1\Delta_g)$ is impossible, because its energy exceeds that of the T_1 -state,^{1,131} which also points to important role of this channel of complete quenching.

IV. Quenching of the $O_2(a^1\Delta_g)$ molecule

The main mechanism of quenching of singlet oxygen in the gas and liquid phases involves transfer of electronic excitation energy of the $O_2(a^1\Delta_g)$ to the vibrational degree of freedom of the collision partner.^{2, 12, 26, 78, 116–122} In its pure form this mechanism occurs for quenchers with molecules having high oxidation potentials or high energies of triplet-excited states: here the mechanism of charge transfer¹¹⁹ or quenching by transfer of electronic energy to triplet state is impossible.¹ The electronic excitation energy of the $O_2(a^1\Delta_g)$ is transformed to vibrational, rotational or kinetic energy of quencher. Noble gases are the poorest quenchers of singlet oxygen¹ (for argon, the second-order rate constant for quenching is $k_Q^\Delta = 5 \text{ litre mol}^{-1} \text{ s}^{-1}$) because in the gas phase their atoms have no vibrational degrees of freedom and cannot efficiently transform the electronic excitation energy of $O_2(a^1\Delta_g)$ to heat. However such gases as H_2 ($k_Q^\Delta = 2800 \text{ litre mol}^{-1} \text{ s}^{-1}$), NH_3 ($k_Q^\Delta = 2600 \text{ litre mol}^{-1} \text{ s}^{-1}$), C_6H_6 vapour ($k_Q^\Delta = 3200 \text{ litre mol}^{-1} \text{ s}^{-1}$) and water vapour ($k_Q^\Delta = 4900 \text{ litre mol}^{-1} \text{ s}^{-1}$) are the most efficient scavengers.^{1, 118} All hydrides have high-frequency X–H bond vibrations (e.g., $\omega_{\text{sym}} = 2916 \text{ cm}^{-1}$ for CH_4 molecule, $\omega_{\text{asym}} = 3939 \text{ cm}^{-1}$ for H_2O molecule, $\omega_e = 4401 \text{ cm}^{-1}$ for H_2 molecule);^{2, 9} here two or three vibrational quanta are sufficient to absorb the energy of singlet oxygen (7918 cm^{-1}). Molecules containing no C–H or O–H bonds (e.g., CS_2 , CCl_4) are much poorer quenchers of singlet oxygen.^{1, 78}

Initially, lifetime measurements of singlet oxygen in solutions were carried out by indirect chemical methods.^{78, 120–122} By conducting steady-state photo-oxidation of benzofuran in solution with variable concentration of β -carotene, which physically quenches $O_2(a^1\Delta_g)$,¹²² one can determine the product $\tau_\Delta k_Q^\Delta$. Assuming that the rate constant k_Q^Δ for β -carotene is diffusion controlled,¹²⁰ Young *et al.*¹²² determined $\tau_\Delta = 5.5 \text{ }\mu\text{s}$ in methanol.¹²² Later on,^{77, 78, 121} direct lifetime measurements of singlet oxygen in solutions were carried out using pulsed lasers (a greater value was obtained in methanol, $\tau_\Delta = 9.5 \text{ }\mu\text{s}$).^{1, 106} Merkel and Kearns⁷⁸ were the first who noticed significant changes in τ_Δ for different solutions and applied the theory of transfer of the energy of oxygen $a^1\Delta_g$ electronic excitation to solvent vibrations. Later on, these results were repeatedly refined.^{1, 73–77, 101–106, 116–118} According to recent data,^{1, 102} the time τ_Δ varies from $3.1 \text{ }\mu\text{s}$ (H_2O) to 128 ms (CCl_4) and 309 ms ($C_{10}F_{18}$), *i.e.*, within five orders of magnitude.

A number of quantitative theories of $O_2(a^1\Delta_g)$ quenching through transfer of electronic excitation energy to solvent vibrations were put forward.^{1, 26, 78, 116, 118} (This energy transfer is called e–v-deactivation.^{1, 76}) Merkel and Kearns⁷⁸ used the theory of dipole–dipole energy transfer and related τ_Δ to the optical density (OD) of IR absorption of the solvent at the 0–0 and 0–1 vibronic band wavelengths of the $a^1\Delta_g \rightarrow X^3\Sigma_g^-$ transition (1270 and 1592 nm, respectively)

$$\frac{1}{\tau_\Delta} = 0.5(OD_{1270}) + 0.05(OD_{1592}) + \quad (24)$$

+ higher-order corrections.

Rodgers¹¹⁷ measured τ_Δ for a number of solvents and determined the second-order rate constants for quenching of $O_2(a^1\Delta_g)$ by the solvent molecules A ($1/\tau_\Delta = k_{Q,A}^\Delta[A]$); then he measured the τ_Δ values in binary mixtures of solvents A and B and showed the validity of the following equation:

$$\frac{1}{\tau_\Delta} = k_{Q,A}^\Delta[A] + k_{Q,B}^\Delta[B]. \quad (25)$$

The study¹¹⁷ not only appeared to be useful for practical purposes, but also confirmed that quenching of singlet oxygen in the liquid phase is also bimolecular in character. An important contribution of Hurst and Schuster¹¹⁶ consists in thorough choice of solvents. A linear correlation between $1/\tau_\Delta$ and concentration of hydrogen per mole found for a series of aromatic compounds $C_6H_nF_{6-n}$ ($n = 1–5$) made it possible to introduce the second-order rate constants for quenching k_{CH}^Δ per C–H bond (irrespective of the number of fluorine atoms in the molecule). It follows that the quenching ability of the solvent is governed by a certain specific feature of C–H-bonds and that donor–acceptor interactions in these solutions are of no concern (since the fluorobenzenes studied possess the properties of donors). However, this does not mean that the interactions in question are insignificant for quenching of $O_2(a^1\Delta_g)$ in other media (e.g., porphyrin solutions).

The dependences of $1/\tau_\Delta$ on the concentration of C–H bonds and on the OD-containing terms in expression (24) were compared.¹¹⁶ It was found that the dependence on $[CH]$ accounts more correctly for the solvent effect on the quenching rate and that the results of calculations using relation (24) are in poor agreement with experimental values of $1/\tau_\Delta$. Both parameters are interrelated (the higher $[CH]$ the higher OD); however, the optical density of IR absorption explicitly depends on the dipole moment of the transition, so the results¹¹⁶ cast some doubt on the dipole–dipole mechanism of energy transfer. Apparently, the exchange mechanism as well as the dipole–quadrupole one²⁶ also contribute to the quenching through e–v-deactivation.

Hurst and Schuster¹¹⁶ proposed an expression for the second-order rate constant for quenching (k_{XY}^Δ) involving the X–Y bond in the solvent molecule

$$k_{XY}^\Delta = C_\Delta \sum_{mn} F_m F'_n R_{mn}. \quad (26)$$

Here C_Δ is the matrix element of electronic interaction, which includes the type-(11) term and is independent of the solvent; F_m and F'_n are the Franck–Condon factors for the (0– m) vibronic band of the $a \rightarrow X$ transition and for the (0– n) vibrational transition of the X–Y bond, respectively; and the factor R_{mn} characterises the resonance detuning between these two transitions. Table 3 lists a number of rate constants for quenching of singlet oxygen k_{XY}^Δ reported by Hurst and Schuster;¹¹⁶ the data exhibit a large scatter.

Table 3. Second-order rate constants k_{XY}^Δ for quenching of $O_2(a^1\Delta_g)$ involving stretching vibrations of X–Y bonds in the solvent molecule.¹¹⁶

X–Y bond	Wave number / cm^{-1}	k_{XY}^Δ / $\text{litre mol}^{-1} \text{ s}^{-1}$
O–H	3500	2000
O–D	2550	150
C–H	3050	420
C–D	2240	17

Schmidt and Brauer¹¹⁸ studied solvents possessing poor quenching ability, the isotopomer $^{18}O_2$, and improved the Hurst and Schuster theory. For a large number of solvents the measured rate constants for quenching of singlet oxygen are reasonably well described by the relation^{1, 116, 118}

$$k_Q^\Delta = \sum_{XY} N_{XY} k_{XY}^\Delta, \quad (26a)$$

where N_{XY} is the number of X–Y bonds in peripheric regions of the solvent molecule that are accessible to the interaction with molecular oxygen.

Quenching of singlet oxygen can be due to not only the dipole-dipole interaction, but also dipole-quadrupole interactions.^{2,26} The first estimation of the quadrupole moment of the $a-X$ transition showed²⁶ that it is stolen from the quadrupole moment of the spin-allowed $b^1\Sigma_g^+ - a^1\Delta_g$ transition. The stealing mechanism is identical to that described by relation (16) and is due to SOC-induced mixing of the X - and b -states (9) and (10). In addition, the dipole moment operator (D) in relation (16) should be replaced by the quadrupole moment operator (Q). The quadrupole moment of the $a-X$ transition is

$$Q_{a-X} = -cQ_{a-b} = 0.0038 \text{ e } \text{\AA}^2.$$

It contributes negligibly to the radiating capacity¹² but largely to quenching of the $O_2(a^1\Delta_g)$ state through the dipole-quadrupole interaction.²⁶

Collision-induced dipole moment of the $a-X$ transition of oxygen also interacts with the moments of weak overtone IR transitions of solvent and quenches the phosphorescence of O_2 .²⁷ In both cases the rate constant for quenching should depend on the overlap of the emission spectra of singlet oxygen and IR absorption overtones of the solvent. Both predictions are in semiquantitative agreement with the results of indirect measurements $\tau_\Delta^{-2,26,78}$. However, direct (more accurate) measurements of $O_2(a^1\Delta_g)$ lifetime^{116–118} did not confirm this correlation, probably, due to additional (undiscussed) contributions to the quenching mechanism.

As mentioned above, a unique spectral phenomenon, namely, observation of co-operative vibronic emission of singlet oxygen in solutions of halogenated hydrocarbons was explained.^{28,113} The $a-X$ wavelength experienced a bathochromic shift by the energy of the vibrational quantum of the solvent.¹¹⁴ The dipole moment of the $a-X$ transition of oxygen in solution is induced by the collision of O_2 with the solvent molecule (M) and strongly depends on the intermolecular distance (R). Vibrations of the C–Cl bond in the molecule M upon collision of O_2 with the solvent molecule (see Fig. 4) strongly affect the R magnitude and give rise to the derivative of the dipole moment of the $a-X$ transition with respect to R . It is this derivative that determines the probability of co-operative vibronic emission of singlet oxygen accompanied by the bathochromic shift on the C–Cl vibrational frequency.^{28,113} The $a \rightarrow X$ transition of oxygen is accompanied by simultaneous excitation of C–Cl vibrations in the solvent molecule. Calculations of the derivative in Eqn (19) give a correct estimate of the intensity of this synchronised transition in the two molecules.^{28,113} The transition is two orders of magnitude less intense than the $a-X$ transition,²⁸ which agrees with experimental data.¹¹⁴

The theory¹¹³ is important for not only understanding of weak co-operative emission,¹¹⁴ but also explanation of deviations in the rate of $O_2(a^1\Delta_g)$ quenching from the values calculated using the simple theory of inductive-resonant energy transfer to solvent vibrations.^{1,2,26,60,78} The rate of quenching of singlet oxygen is not always related to the overlap integral between the $a \rightarrow X$ emission spectrum and IR absorption spectrum of solvent overtones.^{1,60,78} The frequency of the co-operative vibronic transition differs from the eigenfrequencies of oxygen appearing in Eqn (24), and the moment of this transition efficiently interacts with molecular vibrations of the solvent. In essence, the driving force of energy transfer is reduced to the coupling of the molecular vibrations of the solvent and the motion of electrons in the O_2 molecule with allowance for SOC [see Eqn (11)]. Electronic-vibrational interaction in the contact complex $O_2 + M$ directly relates the electronic wave function of the $O_2(a^1\Delta_g)$ state to the intermolecular and internal vibrations in the molecule M . The intermolecular distance q in expression (19) determines not only the electronic-vibrational contribution to the dipole moment of

the co-operative transition, but also the mixing with the molecular vibrations of the solvent. The intensity of the co-operative transition is very low; however, owing to direct character of energy exchange with the solvent vibrations it can contribute largely to quenching of singlet oxygen. Note that the results obtained using the simple theory of inductive-resonant energy transfer to solvent vibrations show the largest deviation from the experimental data for halogen-containing solvents.²⁶

Yet another important mechanism of quenching of $O_2(a^1\Delta_g)$ is the inclusion of configuration interaction and SOC in the mixing with charge transfer states.¹¹⁵ Unlike the universal mechanism of $e-v$ -deactivation, the charge transfer mechanism manifests itself only for molecules with low oxidation potential ($\leq 1.9 \text{ V vs. s.c.e.}$).¹ It is important to distinguish between this mechanism and actual charge transfer that occurs as the kinetic stage of quenching.^{1,115} We believe that this confusion^{119,121} often occurs in discussing the mechanism of quenching of $O_2(a^1\Delta_g)$. The dependence of the rate constant for quenching ($k_Q^\Delta = 1/\tau_\Delta$) on the ionisation potential (IP) of the quencher was found long ago.^{119–122} Aliphatic amines do not react with $O_2(a^1\Delta_g)$, but efficiently inhibit the oxidation of other compounds possessing high reactivity towards singlet oxygen.^{2,119} Taking into account the increase in $\log k_Q^\Delta$ with a decrease in the amine IP, one can assume¹¹⁹ that the charge transfer configurations (CTC) are mixed with the $a^1\Delta_g$ and $^3\Sigma_g^-$ states and somehow enhance the SOC between them. Explanation for this mechanism (also important for understanding of biochemical activation of oxygen) was reported.¹¹⁵

Now we will write the wave functions of the $a^1\Delta_g$ and $^3\Sigma_g^-$ states in a collision complex with amine molecule in the form^{12,115}

$$^3\Psi_0 = |S_0^3\Sigma_{g,0}^- \rangle = \frac{1}{\sqrt{2}}(|a\bar{a}\pi_x\bar{\pi}_y| - |a\bar{a}\pi_y\bar{\pi}_x|), \quad (27)$$

$$^1\Psi_1 = |S_0^1\Delta_g \rangle = \frac{1}{\sqrt{2}}(|a\bar{a}\pi_x\bar{\pi}_x| - |a\bar{a}\pi_y\bar{\pi}_y|). \quad (28)$$

Here a denotes the highest occupied molecular orbital (HOMO) of the aliphatic amine in the singlet ground state S_0 , i.e., the lone pair orbital of the nitrogen atom. Electrons of inner shells are left out of consideration. Note that the wave function (27) differs from that reported in Ref. 115 in permutation of two MOs and, hence, the sign of the determinant. Charge transfer from amine to the degenerate orbitals, $\pi_{g,x}$ and $\pi_{g,y}$, of the oxygen molecule gives four CTC, namely, two degenerate singlet and two triplet states in the radical pair $\{D^+\cdot O_2^-\}$ produced upon charge transfer (D denotes the electron donor).¹¹⁵ We will consider only those configurations that are important for the explanation of the quenching mechanism,

$$^3\Psi_{ct_y} = |D^+\cdot O_2^-\rangle = \frac{1}{\sqrt{2}}(|\pi_y\bar{a}\pi_x\bar{\pi}_y| - |a\bar{\pi}_y\pi_y\bar{\pi}_x|), \quad (29)$$

$$^1\Psi_{ct_x} = |D^+\cdot O_2^-\rangle = \frac{1}{\sqrt{2}}(|a\bar{\pi}_x\pi_x\bar{\pi}_y| + |\pi_x\bar{a}\pi_y\bar{\pi}_x|). \quad (30)$$

Analysis of intermolecular interaction using the CI method revealed an effective mixing of the triplet configurations (27) and (29) in the collision complex. The singlet states (28) and (30) possess different symmetry with respect to reflection in the O–O–N plane, also being effectively mixed with each other due to CI. Mixing of the second singlet component (4a) with the CTC (30) is impossible. The inclusion of intermolecular interaction in the framework of the CI method gives the $^3\Psi_0 + \varepsilon^3\Psi_{ct_y}$ and $^1\Psi_1 + \delta^1\Psi_{ct_x}$ states which strongly interact

with each other due to SOC.¹¹⁵ The matrix element of the SOC operator between these states includes the integral

$$\varepsilon\delta^* \langle {}^3\Psi_{\text{ct},r} | H_{\text{so}} | {}^1\Psi_{\text{ct},x} \rangle = \frac{\varepsilon\delta^*}{2} \langle \pi_y | B_z | \pi_x \rangle = \frac{\varepsilon\delta^*}{2} \zeta_{\text{O}}, \quad (31)$$

where ε and δ are the admixture coefficients to the $a^1\Delta_{\text{g}}$ and $X^3\Sigma_{\text{g}}^-$ states, respectively.

Relations (27), (29) and (31) include the wave functions of the triplet states with the zero projection of the total spin on the z axis. Comparison with expression (8) shows that the SOC between the CTC (29) and (30) is reduced to the same integral between the degenerate orbitals, $\pi_{\text{g},x}$ and $\pi_{\text{g},y}$, of the oxygen molecule, as that appearing in the matrix element of the SOC between the states (5). Thus, the presence of CTC admixtures always gives rise to the SOC between the $a^1\Delta_{\text{g}}$ and $X^3\Sigma_{\text{g}}^-$ states, which accelerates the non-radiative transition and quenching of singlet oxygen.¹¹⁵ The admixture coefficients ε and δ to the states become significant only for the quencher molecules having low oxidation potentials (≤ 1.9 V v.s. s.c.e.). Otherwise, the CTC energy is too high while the CTC admixture coefficients in Eqn (31) are negligible. According to calculations,^{12, 27, 34, 70, 99, 103} for molecules with ionisation potentials higher than 10.5 eV the ε and δ values are at most 0.01, the integrals (31) being negligible.

Charge transfer configurations (29) and (30) differ in spin and population of the $\pi_{\text{g},x}$ and $\pi_{\text{g},y}$ orbitals. The matrix element of the SOC operator between them can be treated as an electron ‘jump’ from the $\pi_{\text{g},y}$ -MO to the $\pi_{\text{g},x}$ -orbital with a spin flip. This ‘jump’ is identical to rotation of the orbital, *i.e.*, the appearance of an orbital angular momentum or ring current, which induces the magnetic moment interacting with the spin. Since the case in point is the quantum singlet–triplet transition, visual interpretation of this effect is, strictly speaking, inadmissible.¹⁵ However, the simplified ideas of an electron ‘jump’ and orbital rotation are useful in revealing the essence of the mechanism of quenching of singlet oxygen by amines due to admixtures of charge transfer states.

Strengthening of the SOC (to some extent) between the $a^1\Delta_{\text{g}}$ and ${}^3\Sigma_{\text{g}}^-$ states of the O_2 molecule due to CTC contributions always occurs in collision complexes. It is determined by the weight factors of the admixtures ε and δ , which are large only for donor lone electron pairs with low ionisation potential provided a local character of donor–acceptor interaction.¹¹⁵ At present, exact determination of the contributions of different mechanisms to the rate constant for quenching k_{Q}^{A} is impossible owing to the difficulties in the inclusion of vibrational modes of the solvent molecules in the nearest environment of the $\text{O}_2(a^1\Delta_{\text{g}})$ molecule. The concept of admixtures of the charge transfer states [see Eqns (29)–(31)] is fundamentally important for analysis of the mechanisms of biochemical activation of oxygen by oxidases.

V. Biochemical activation of the molecular oxygen

Nearly 100 years ago Academician A N Bach first studied breath from the standpoint of oxygen activation.^{137–139} Based on the concepts of classical chemistry, he assumed the necessity of cleaving a bond in divalent oxygen and release of a chemical valence for addition of other compounds. According to Bach, the corresponding activation energy should be supplied from readily oxidisable unsaturated compounds; O_2 adds to them to give peroxides that degrade under the action of enzymes, and oxygen is transferred to other substrates that are incapable of immediately adding to atmospheric oxygen.¹³⁷ Clearly, at that time it was impossible to allow for specific quantum features of microparticles constituting the molecule, in particular, the spin. The energy of spin-related magnetic interactions is low, however it should be taken into account when studying not only

line splitting in atomic optical spectra and in EPR spectra of radicals,^{13, 38, 46–49, 84, 138, 139} but also the mechanisms of certain chemical reactions.^{12, 37, 140–149} In spite of rapid progress in biochemistry and detailed knowledge of molecular mechanisms of the action of many enzymes, the nature of bio-activation of oxygen is still unclear.^{5, 6, 150, 151} Below we will show that it is the magnetic and exchange spin effects that are often responsible for activation of molecular oxygen by oxidase co-enzymes. The nature of these effects has much in common with the mechanisms considered above when we analysed the photophysical properties of oxygen.

1. Role of spin in chemical reactions involving oxygen

Two unpaired electrons in antibonding π_{g} -MOs are responsible for specific character of the interaction of molecular oxygen with radicals (combustion) and chemically stable diamagnetic compounds (slow oxidation). Two antibonding π_{g} -vacancies make it possible to transform O_2 to O_2^- and O_2^{2-} anions, the formation of the latter being strongly dependent on the presence of electron donors (enzymes) and magnetic perturbations that affect the spin prohibitions.

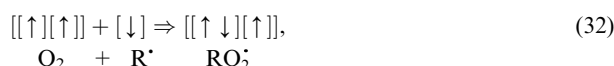
In 1937, Pauling established that the magnetic moments of hemoproteins decrease as the pH values of solutions increase. The effect was explained by the iron ion spin flip owing to small changes in the coordination of ligands.⁵ The total spin of the Fe^{3+} ion is determined by the number of unpaired electrons in the 3d-shell of the metal. The low-spin state ($S = 3/2$) becomes more stable than the state with $S = 5/2$ as the pH value increases; the transition between these states is induced by the spin–orbit coupling in the 3d-shell of the metal. In weak ligand field the unfilled 3d-shell has degenerate orbitals and the states with different spins have similar energies. Recall that the spin quantum number of one electron ($S = 1/2$) determines the absolute value of the momentum vector

$$\sqrt{S^2} = \sqrt{S(S+1)}\hbar = \frac{\sqrt{3}}{2}\hbar.$$

The summation of electron spins obeys the quantum addition rules,¹⁵ so the total spin of the molecule is zero at ‘antiparallel spins (all spins are paired); such state is called a singlet state. Most chemically stable organic compounds and corresponding oxidation products are diamagnetic, *i.e.*, they have no intrinsic magnetic moment (all spins are paired due to saturation of valences; the total spin of the molecule $S = 0$). Spins can undergo ‘depairing’ when exposed to light; here an electron goes to a vacant MO; according to the Pauli principle, both spins can be parallel (total spin $S = 1$). This excited state is called a triplet state because of three possible orientations of the total spin vector $M_{\text{S}} = \pm\hbar, 0$.

Singlet–triplet transitions are spin-forbidden;¹⁵ this is a strict prohibition, because it can be removed only in the presence of magnetic interactions that are much weaker than electric ones.¹³ The latter determine the energies of chemical bonds and excited states and the pathways of chemical reactions. The spin affects the energy through exchange interaction.¹⁵ A weak SOC slightly mixes the singlet and triplet states of molecules, which gives a nonzero rate of S–T transitions that are observed in the form of phosphorescence and are well known in photochemistry.^{2, 7, 13} Non-radiative S–T transitions also play an important role in the dark reactions, in particular, in catalysis.^{12, 32} Weak SOC acts as a ‘key’ needed to open a ‘heavy door’, that is, the system chooses a pathway of chemical reaction with low activation barrier in the triplet state instead of overcoming a high activation barrier in the singlet state. Recall that the exchange integral appears with different signs in the energies of the S and T states, namely, two radicals form a chemical bond in the S state and repel in the T-state.¹⁵

Unlike most chemically stable organic compounds the O_2 molecule has the triplet ground state. According to Hund's rule, two unpaired electrons in two degenerate $\pi_{g,x}$ and $\pi_{g,y}$ orbitals (configurations π_g^2) have a lower repulsive energy in the triplet state [see Eqn (5b)] compared to the singlet state [see Eqn (5a)]. Because of this oxygen is paramagnetic (it has intrinsic magnetic moment due to spins of two unpaired electrons) and its addition to organic compounds is spin forbidden: starting reactants have the total spin $S = 1$, whereas the oxidation products are diamagnetic ($S = 0$).⁶ Because of spin prohibition, combustion of organic fuels requires activation in the form of high-temperature ignition stage, *i.e.*, generation of primary radicals.^{6–8} Reaction of R^\bullet radical (one unpaired electron, $S = 1/2$, doublet state) with O_2 molecule is spin-allowed, because the starting reactants ($O_2 + R^\bullet$) and product (RO_2^\bullet) have doublet states, which provides the chain character of radical reactions

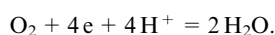


Here the quantum cell denotes the MO (see above).

Radical RO_2^\bullet can decompose into radicals RO^\bullet and $^\bullet O$, thus making chain branching possible. In radical chain oxidation (combustion) processes the energy is released uncontrollably in the form of heat and light.⁸ Clearly, this mechanism of oxidation with molecular oxygen cannot take place in living cells. However, cells meet their energy needs in the course of metabolic processes using the energy of oxidation of organic compounds under the action of oxygen.⁵ Since cells cannot resist large temperature gradients, they should transform the energy released through oxidation to some kind of chemical energy prior to dissipation in the form of heat. This occurs by combining oxidation with the synthesis of adenosine triphosphate (ATP).^{5, 139} In turn, the cell uses the ATP energy to carry out all endogenic processes, such as chemical syntheses of DNA and proteins, ion transport and mechanical work.¹³⁹ All versatile energy-supplying metabolic processes and reactions occur under subtle enzymatic regulation.⁵ Is it spin-dependent? Despite the fact that to date many reactions of enzymes and metabolic pathways have been studied in detail,^{143–147} the role of spin in biological oxidation of molecular oxygen is still unclear.^{148–158}

2. Cytochrome oxidase

The simplest type of oxygen activation by enzymes containing metal cations involves the formation of intermediate peroxide ions O_2^{2-} . Reduction of O_2 by direct insertion of an electron pair into the filled π_g -orbitals requires spin changes, because the π_g^4 configuration can only be a singlet. Intermediates containing O_2^{2-} are formed in, *e.g.*, cytochromes.^{5, 139} The $Fe^{3+} - O - O - Cu^{2+}$ structure, where the peroxide group is formed from the triplet oxygen and stabilised at its position until introduction of the second electron pair, is quite possible intermediate.¹⁴³ Apparently, electron transfer and formation of O_2^{2-} involves a triplet–singlet quantum transition called spin inversion.^{145, 148} Cytochrome oxidase catalyses four-electron reduction of oxygen molecule to water. No intermediates were detected in the reaction



However, experimental measurements^{5, 158} proved the formation of O_2^{2-} . The reaction centre of cytochrome oxidase includes one haem iron atom and one copper atom. The oxygen molecule binds to the haem Fe^{2+} cation and to Cu^+ ion that donate one electron each to form an O_2^{2-} anion. This provides a way to overcome the major obstacle to oxygen activation, that is, spin inversion (T–S transition).¹⁴⁵ Since the O_2^{2-} dianion has a filled electron shell, the ground state of this species is

totally symmetrical and characterised by the term $|^1\Sigma_g^+ \rangle$. Transfer of two electrons causes the ground-state term, $|X^3\Sigma_g^- \rangle$, of the O_2 molecule to smoothly transform to the term $|^1\Sigma_g^+ \rangle$ of the dianion. The spin–orbit coupling between the states $|^3\Sigma_g^- \rangle$ and $|^1\Sigma_g^+ \rangle$ is symmetry-allowed [see Eqn (8)]; therefore, the reduction

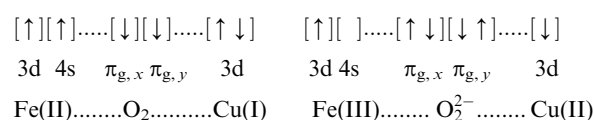


is also symmetry allowed with inclusion of the SOC. Since the SOC integral [see Eqns (8) and (11)] reaches its maximum value owing to symmetry of the oxygen MOs, one can expect that reduction of the oxygen molecule to the dianion should be accelerated due to effective removal of spin prohibition. These qualitative considerations should be complemented by analysis of the structure of the 3d-shells of the metal ions.¹⁴⁸

Transition of the active site of cytochrome oxidase to the singlet state removes spin prohibition to subsequent fast chemical reactions up to formation of stable diamagnetic products.⁵ According to calculations, the spin–orbit coupling that induces the T–S transition involves not only oxygen π_g -MOs, but also electronic changes in the 3d-shell of the iron ion.^{133, 148}

The SOC mechanism can be represented as follows.^{145, 148} Activation upon electron transfer to O_2 first involves excitation of Fe^{2+} ion ($3d \rightarrow 4s$) to form the $1,^3D$ terms. Combination of two triplet states (iron and oxygen) gives the singlet, triplet and quintet states similarly to the case for collision of triplet oxygen and ethylene molecules (states 4 and 6, see Fig. 2). A singlet combination of two triplet states in the initial structure of cytochrome-*c* oxidase is shown in Scheme 1. The T–S transition in this quasi-degenerate pair is formed in the electron shell of the iron ion. The SOC is relatively weak and spin inversion is a relatively slow process. This is the reason for much lower (compared to the expected⁵) reactivity of O_2 towards certain ligands present in cytochromes. The singlet state formed upon T–S transition is shown on the left side of Scheme 1. Transition from this state to the peroxide form O_2^{2-} owing to transfer of two electrons from the metal ions is now spin allowed. This and subsequent processes occur in the singlet states.

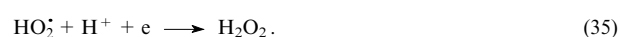
Scheme 1



This mechanism of spin inversion occurs in hemerythrin and hemocyanin.¹⁴⁴ Cytochromes containing different protein residues coordinated to the iron ion can include $Fe(II)$ ions in different spin states. Particular cytochromes have iron ions in the triplet ground spin state.¹⁴⁴ In this case reduction of the oxygen molecule to the dianion should occur in accordance with Scheme 1 (see above) with a very high probability without involving SOC.

3. Flavoproteins

Usually,^{5, 139, 148–153} it is assumed that one can overcome the spin prohibition to oxidation of organic substrates with atmospheric oxygen by successive addition of single electrons in the reduction of O_2



Further reactions of diamagnetic hydrogen peroxide are spin allowed. It is assumed⁵ that removal of spin prohibition in

reactions (33)–(35) proceeds as in the case of radical-chain oxidation where the spin prohibition can be removed upon formation of primary radicals. The author of this review found no clear discussion of the issue in biochemical literature (see, e.g., Refs 5, 6, 152 and 153). A fundamental difference between the enzymatic reactions (33)–(35) involving radicals and the radical reactions of the type (32) in chain oxidation processes should be emphasised. In the latter case radicals go to the bulk of gas plasma flame (or in the solution bulk) and do not longer retain the ‘spin memory’ about precursors. All participants of biochemical oxidation reactions (33) and (35), *i.e.*, oxygen and electron transfer agents, are confined within the same active site of enzyme. If an electron is transferred to the oxygen molecule from diamagnetic enzyme, reaction (33) produces a radical ion pair [see Eqn (29)], all spins remain correlated, the ‘spin memory’ is retained and the spin prohibition to subsequent reactions (34) and (35) of a radical ion pair (triplet precursor) thus generated remains valid.

Many researchers believe that the oxygen molecule is very stable and can hardly add one more electron to give a radical anion $O_2^{\cdot-}$; as a consequence, they emphasise that stage (33) is the limiting one.^{5, 139} Further addition of electrons is facilitated and subsequent reduction occurs readily.^{5, 139} The bottleneck of this commonly accepted scheme is that the difficulty of electron addition to O_2 contradicts experimental data, namely, the process is exothermic and occurs with energy release (42 kJ mol^{-1} , see Refs 9 and 55). Enzyme molecules are designed in such a fashion that electron transfer in the respiratory chain be easy.⁵ Indeed, reduced flavoproteins have very low ionisation potentials and are readily oxidisable.¹³⁹ If an O_2 molecule is delivered to the active site of an oxidase and interacts with flavoprotein, there are no physical prerequisites to assume that electron transfer to the oxygen molecule should proceed with difficulty.¹⁴⁹ The obstacle consists in the need of spin flip in the electron transfer stage (33) and formation of a triplet radical ion pair rather than addition of an electron to O_2 .

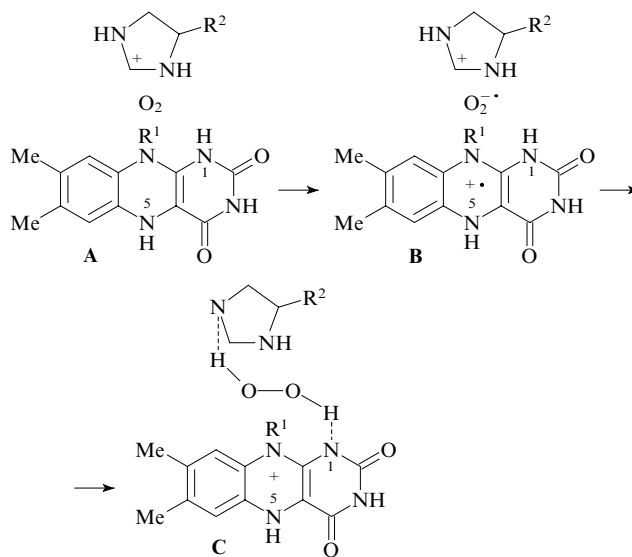
To clarify the situation, we will consider glucose oxidase as an example.^{3, 37, 148} Reaction (33) in glucose oxidase involves flavine adenine dinucleotide (FAD). Such compounds (flavoproteins) are typical of many co-enzymes; they were discovered in 1932 (‘yellow enzyme’ capable of catalysing the oxidation of nicotinamide nucleotides was isolated from yeasts).⁵ Flavoproteins transfer electrons, as constituents of hydrogen atoms, from organic substrate to the riboflavin component of the enzyme using nicotinamide adenine dinucleotide (NAD^+) and its reduced form ($NADH$).^{5, 139} The structures of these molecules were undoubtedly ‘selected’ by Nature to impart corresponding redox potentials to the co-enzymes.¹⁵⁰ NAD^+ exists in individual form and diffusively moves from one enzyme to another, whereas FAD is tightly bound to protein. Flavoproteins tend to attach H atoms from one substrate and then transfer them to the other (O_2), being added to the same enzyme.⁵ A covalent or hydrogen bond connects FAD to the residue of the polypeptide protein chain; therefore, FAD remains bound to a particular amino acid after proteolysis.

The action of glucose oxidase involves two stages, namely,^{5, 155} glucose oxidation to gluconolactone with reduction of FAD to $FADH_2$ and the reverse cycle, $FADH_2 \rightarrow FAD$, with reduction of O_2 to H_2O_2 . From the standpoint of oxygen activation it is of interest to consider the second stage.

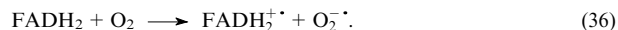
The active site of glucose oxidase from *Aspergillus Niger* has a histidine residue (His516) near the flavin ring of FAD; the distance between the protonated nitrogen atom N^e of histidine and the N(1) atom of $FADH_2$ is about 4 \AA (see Ref. 152). Scheme 2 presents a model for the active site of glucose oxidase. The first phase of the catalytic cycle involves reduction of FAD to $FADH_2$. The initial model A illustrates the O_2 insertion into the active site between the histidine residue of the

protein chain and the N(1) atom; model B illustrates transfer of an electron from $FADH_2$ and formation of a radical pair; and C is the second to the last phase of the catalytic cycle accompanied by the formation of hydrogen peroxide. The last-mentioned stage involves abstraction of a proton from the N(5) atom and its transfer to histidine across the system of H-bonds in the protein and aqueous environments.

Scheme 2



When entering the active site, the O_2 molecule occupies the cavity between these atoms and then transfer of an electron from $FADH_2$ to the oxygen molecule occurs.¹⁴⁸



This results in the formation of a triplet radical pair $\{FADH_2^{\cdot+} \cdots O_2^{\cdot-}\}$ in the active site of glucose oxidase, because the precursor of O_2 is in the triplet state, whereas that of $FADH_2$ is in the singlet state. According to density functional calculations (B3LYP/6-31G*),³ electron transfer is almost thermally neutral (thermal effect of reaction is 0.6 kJ mol^{-1}).

In glucose oxidase, the O_2 molecule is transformed to superoxide ion $O_2^{\cdot-}$ upon addition of an electron, thus being activated.^{3, 148} This slow stage is followed by fast proton transfer from the protonated histidine residue and simultaneous transfer of hydrogen atom from semi-oxidised radical $FADH_2^{\cdot+}$, which results in the formation of hydrogen peroxide.^{148, 150}

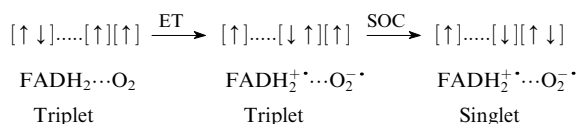
4. Electron transfer in glucose oxidase and the spin flip

Now we will return to the key issue, namely, why the electron transfer stage (36) is slow ($k < 10^{-3} \text{ s}^{-1}$). According to calculations, electron transfer to the active site of glucose oxidase should occur spontaneously and rapidly ($k = 10^{-9} \text{ s}^{-1}$), just as O_2 will enter the active site. The O_2 molecule is characterised by a positive electron affinity (0.45 eV), *i.e.*, the addition of an electron is energetically favourable.^{9, 44, 55, 154} Reduced FAD readily donates an electron; indeed, $FADH_2$ has a relatively low ionisation potential.³ The reason is clear. The lowest occupied MO (LUMO) of the FAD molecule is the π^* -orbital of the isoalloxazine ring. In spite of the non-planar structure of this nucleus in $FADH_2$, its highest occupied molecular orbital is similar to the LUMO of the FAD molecule. Both orbitals are mainly localised on the central ring of the flavin nucleus.¹⁵⁰ This confirms a simple MO pattern obtained in the Hückel calculations, namely, the FAD LUMO is identical to the $FADH_2$ HOMO. Namely, the addition of two hydrogen atoms to the N(1) and N(5) atoms

is similar to attachment of two π -electrons to the ring π -system. From this a considerable decrease in the ionisation potential on going from FAD to FADH₂ becomes clear. The electron affinity of the O₂ molecule is much lower than the ionisation potential of FADH₂; however, when O₂ contacts protonated histidine, electron transfer becomes energetically favourable. Electrostatic attraction between the histidine cation and newly formed superoxide O₂^{•−} is the primary driving force of electron transfer and reduction of corresponding activation energy. It also facilitates strengthening of the SOC.

Thus, the active site of glucose oxidase is 'tuned for oxygen activation through electron transfer followed by spin flip according to Scheme 3.

Scheme 3



TE is transfer of an electron.¹⁴⁵

Simultaneous occurrence of reactions (34) and (35) resulting in diamagnetic products requires flip of one spin in the radical pair stage, *i.e.*, a triplet–singlet quantum transition. Such a transition is induced by the spin–orbit coupling, *i.e.*, magnetic interactions due to the orbital and spin motions of electrons (see Scheme 3).³

Spin flip is actually due to relatively strong SOC characteristic of radical pairs including superoxide ions.³ In Scheme 3 the quantum cells denote the HOMOs of both molecules, that is, FADH₂ and O₂. As in the case of quenching of singlet oxygen by amines, where the role of CTC was shown [see Eqns (29), (30)], Scheme 3 presents different orbital structures of the triplet and singlet CTC. The starting triplet radical pair corresponds to a CTC described by Eqn (29), that is, transfer of an electron to the $\pi_{g,y}$ -MO of O₂ molecule, whereas the singlet radical pair corresponds to a CTC described by Eqn (30), namely, transfer of an electron to another degenerate orbital of oxygen, $\pi_{g,x}$. The SOC arises between these CTC and is maximum possible for a system comprised of light (oxygen, nitrogen and carbon) atoms.

Actually, the formation of superoxide is not difficult. Indeed, a triplet radical pair is easily formed just after transfer of H atoms and reduction of FAD to FADH₂. The problem is to carry out a triplet–singlet transition in the radical pair {FADH₂^{•+}...O₂^{•−}} generated in reaction (36), because only the singlet pair can produce peroxide: reactions (34) and (35) involving protonated histidine and radical FADH₂^{•+} proceed concertedly.^{3, 148} Reaction (34) has no effect on electron spins and in reaction (35) the spins remain correlated as in the initial state. Therefore, the initial steps of chemical reactions (34) and (35) should involve a spin flip (T → S transition from the triplet radical pair created upon electron transfer). In accordance with Scheme 3 the SOC integral includes the same components as the integrals (8) and (31)^{3, 37, 148}

$$\langle {}^3\Psi_{\text{ct}_y} | H_{\text{so}}^Z | {}^1\Psi_{\text{ct}_x} \rangle = \langle \pi_y | B_z | \pi_x \rangle = \frac{1}{2} \zeta_{\text{O}} = 76.5 \text{ i cm}^{-1}. \quad (37)$$

The absolute value of this integral equals half the splitting between the ground-state terms $\Omega = 1/2$ and $\Omega = 3/2$ of the superoxide ion $X^2\Pi_g$ (*cf.* experimental value of 160 cm^{−1} (Ref. 9), which is in good agreement with our estimate¹⁵⁴). The rate constant for the triplet–singlet transition can be estimated using the Fermi golden rule¹³

$$k_{\text{T} \rightarrow \text{S}} = \frac{2\pi\rho}{\hbar} |\langle {}^3\Psi_{\text{ct}_y} | H_{\text{so}}^Z | {}^1\Psi_{\text{ct}_x} \rangle|^2 \text{FC}, \quad (38)$$

where FC is the Franck–Condon factor and ρ is the density of final states.

The SOC integral (37) is relatively large; usually,^{12, 13} the matrix elements of the SOC operator for the molecules comprised of the first or second row elements are of the order of 1–10 cm^{−1}. These SOC integrals provide the rate constants for triplet–singlet transitions that are 10⁶–10⁴ times lower than the rate constants for spin-allowed transitions.¹³ The SOC integral (37) provides the rate constant $k_{\text{T} \rightarrow \text{S}}$ that can be compared with the rates of other chemical reactions that are, in principle, possible during existence of the triplet radical pair {FADH₂^{•+}...O₂^{•−}} (back electron transfer, decomposition to new radicals). Despite the fact that the T → S transition in the {FADH₂^{•+}...O₂^{•−}} pair is relatively slow, it is much more efficient than typical T → S transitions in organic molecules and undoubtedly occurs in the active site of glucose oxidase. Subsequent reactions (34) and (35) in the singlet state of the entire flavoprotein system have low activation energies³ and proceed rapidly. Transfer of a proton from the N^ε atom of the histidine fragment [see reaction (34)] is accompanied by proton transfer from the N(1) atom of FADH₂ to give hydrogen peroxide [see reaction (35)] with an the activation energy of only 29 kJ mol^{−1} (see Ref. 3).

Since the SOC integral (37) is only determined by the specific character of O₂^{•−} anion and does not depend on the co-enzyme cation (K), effective T–S transitions in radical pairs {K⁺...O₂^{•−}} should occur in the activation of oxygen by flavoproteins and other oxidases following reactions (33)–(35). This mechanism of the T–S-transition in the radical pair is similar to spin relaxation in the superoxide ion.^{145, 148}

5. Other examples of biochemical activation of oxygen

An important mechanism of enzymatic spin catalysis is characteristic of oxidases containing paramagnetic metal ions.^{37, 145, 149, 156–158} Let us consider the exchange mechanism of acceleration of T → S transitions in radical pairs {K⁺...O₂^{•−}} taking copper amine oxidase as an example. This enzyme contains a bound quinonoid cofactor (topaquinone) near the Cu(II) ion coordinated to the ligands.¹⁴⁹ Consider the limiting stage of the operation of this enzyme, which can also be represented by the common processes (33)–(35). A radical pair {K⁺...O₂^{•−}} in the T-state is formed in the reaction of the type (36). The T → S transition is activated by exchange interactions with the copper ion following the scheme



Exchange interaction with copper ion for the superoxide ion is much stronger than for the co-enzyme (K⁺) radical cation; therefore, the T → S transition of the radical pair is rather fast.³⁷ Measurements of kinetic isotope effects showed that replacement of the ¹⁶O isotope by ¹⁸O significantly slows down the limiting stage of oxygen reduction to peroxide for all enzymes studied.¹⁵² In this case the Franck–Condon factor decreases; therefore, the proposed scheme of enzymatic spin-catalysis^{3, 37, 148–150} provides a complete explanation for all results obtained in the kinetic studies on molecular oxygen activation by the enzymes mentioned above.^{3, 152}

We will complete our comparative analysis of oxygen activation mechanisms taking cytochrome oxidase as an example; this compound catalyses four-electron reduction of O₂ to water in the final reactions of aerobic metabolism.⁵ This is a very important process in the chain of continuous redox reactions involving proton transfer across membranes and creation of chemiosmotic gradient for ATP synthesis.^{139, 157}

Cleavage of the O–O bond in cytochrome oxidase is a related to transfer of electrons and protons across mitochondrial membranes and to the formation of Fe(IV)=O groups in

a complex manner.¹⁵⁸ Note that the O—O bond dissociation, which continuously occurs in upper atmosphere, produces two highly reactive biradicals $O(^3P) + O(^3P)$ having four unpaired electron spins. (The process is spin allowed and can occur in the dark.) These species possess extremely high reactivity, but at low gas concentration the reactivity ‘dissipates’ into recombination, atmospheric emission and particularly, ozone synthesis. The O—O bond dissociation in cytochrome oxidase also causes ‘depairing’ of four spins and could produce two biradicals. Would these biradicals escape from the active site of enzyme to the bulk of proteins, they would ‘burn out’ mitochondria and cytoplasm. It is of great importance to cleave the O—O bond in cytochrome oxidase using the concerted mechanism consistent with other reactions, and thus chemically bind oxygen atoms and simultaneously ‘quench’ the spin. As shown above, in such enzymes chemical reactions are governed by the SOC and weak exchange interactions involving spins of paramagnetic iron and copper ions.⁵ Spin catalysis favours fast and efficient (with small energy expenditure) dissociation of the O—O bond in the oxygen molecule.

Quantum chemistry is a unique tool for understanding of vitally important processes.^{156–160} Similarly to quantum mechanics, which provides explanation for very subtle effects of spin interaction in solids,^{161–164} quantum chemistry makes it possible to study electron-spin dependent properties of living matter.

VI. Conclusion

Removal of spin prohibition on singlet–triplet transitions in oxygen molecule interacting with buffer gas, solvent or co-enzyme molecules in complex biopolymers is in some cases determined by certain common mechanisms. Physical substantiation of the mechanisms of bio-activation of oxygen is impossible if simpler mechanisms of O_2 photo-activation in solutions of organic dyes or upon collisions with other molecules in the gas phase remain unclear. In this review the term ‘photo-activation’ means acceleration of radiative and non-radiative triplet–singlet transitions in oxygen molecule induced by collisions with the solvent molecule, including sensitisation of singlet oxygen.

Analysis of the mechanisms of $O_2(a^1\Delta_g)$ quenching is closely related to these problems, being very important for understanding of the mechanism of bio-activation of oxygen. We considered the electronic structures and energies of various low-lying states of the O_2 molecule and the collision complexes of oxygen with simple (H_2 , N_2 , CH_3Cl , C_2H_4) and more complex molecules (benzene, naphthalene, dyes). The inclusion of specific spin–orbit coupling in the open π_g -shell of oxygen makes it possible to explain the intensities of the T–S transitions of the O_2 molecule and collision complexes. Selective enhancement of the intensity of the $a^1\Delta_g \rightarrow X^3\Sigma_g^-$ radiative transition upon collisions and its quenching in various solvents (M) was explained. The contribution of $M^+ - O_2^-$ charge transfer causes the SOC between the T–S states of oxygen to strengthen, which enhances the quenching of $O_2(a^1\Delta_g)$. Enzymatic activation of oxygen by, e.g., glucose oxidase proceeds by a similar mechanism of T–S-transitions.

The mechanisms of activation and quenching of singlet oxygen involve energy transfer, which depends on exchange interactions, SOC, charge transfer, intra- and intermolecular vibrations. Based on analysis of the physical mechanisms of photo-activation, three types of oxygen activation by oxidase enzymes were proposed. They involve intermediate formation of the superoxide ion, O_2^- , and peroxide ion, O_2^{2-} . Elucidation of O_2 activation mechanisms due to T–S transitions in oxygen-binding enzymatic complexes opens new fields of investigations in biotechnology, namely, research on magnetic biopolymers and the effect of magnetic and microwave fields

on the rate of spin inversion in these complexes,^{13,142} on the yield of O_2^- and OOH radicals and on other important biochemical processes.¹⁶⁰

References

1. C Schweitzer, R Schmidt *Chem. Rev.* **103** 1685 (2003)
2. V L Ermolaev, E N Bodunov, E B Sveshnikova, T A Shakhverdov *Bezyzluchatel'nyi Perenos Energii Elektronogo Vozbuzhdeniya* (Non-radiative Transfer of Electronic Excitation Energy) (Leningrad: Nauka, 1977)
3. R Prabhakar, P Siegbahn, B F Minaev, H Agren *J. Phys. Chem. B* **106** 3742 (2002)
4. R S Mulliken *Phys. Rev.* **32** 186 (1928)
5. A White, Ph Handler, E Smith *Principles of Biochemistry* (New York: McGraw-Hill, 1978)
6. D T Sawyer *Oxygen Chemistry* (Oxford: Oxford University Press, 1991)
7. A N Terenin *Fotonika Molekul Krasitelei i Rodstvennykh Organicheskikh Soedinenii* (Photonics of Dye Molecules and Related Organic Compounds) (Leningrad: Nauka, 1967)
8. N N Semenov *O Nekotorykh Problemakh Khimicheskoi Kinetiki i Reaktsionnoi Sposobnosti* (Some Problems of Chemical Kinetics and Reactivity) (Moscow: Academy of Sciences of the USSR, 1958)
9. K-P Huber, G Herzberg *Molecular Spectra and Molecular Structure* (New York: Van Nostrand, 1979)
10. M Kasha, D E Brabham *Singlet Oxygen* (Eds H H Wasserman, R W Murray) (New York: Academic Press, 1979) p. 1
11. J H Van Vleck *Astrophys. J.* **80** 161 (1934)
12. B F Minaev, Doctoral Thesis in Chemical Sciences, Institute of Chemical Physics, Academy of Sciences of the USSR, Moscow, 1983
13. Z M Muldakhmetov, B F Minaev, G A Ketsle *Opticheskie i Magnitnye Svoistva Tripletного Sostoyaniya* (Optical and Magnetic Properties of the Triplet State) (Alma-Ata: Nauka, 1983) p. 263
14. A A Krasnovskii Jr *Biofizika* **21** 748 (1976)^a
15. J Murrell, S Kettle, J Tedder *Valence Theory* (London: Wiley, 1966)
16. R N Zare *Angular Momentum* (New York: Wiley, 1988)
17. P R Ogilby *Acc. Chem. Res.* **32** 512 (1999)
18. D Datta, N Vaidehi, X Xu, W A Goddard *Proc. Natl. Acad. Sci. USA* **99** 2636 (2002)
19. E L Clennan *Acc. Chem. Res.* **34** 875 (2001)
20. R W Redmond, J N Gamlin *Photochem. Photobiol.* **70** 391 (1999)
21. A A Gorman *Adv. Photochem.* **17** 217 (1992)
22. B F Minaev *Izv. Vyssh. Uchebn. Zaved., Fiz.* (9) 115 (1978)^b
23. B F Minaev *Opt. Spektroskop.* **32** 22 (1972)^c
24. B F Minaev *Opt. Spektroskop.* **45** 936 (1978)^c
25. B F Minaev *Int. J. Quant. Chem.* **89** 367 (1980)
26. E V Sveshnikova, B F Minaev *Opt. Spektroskop.* **54** 542 (1983)^c
27. B F Minaev *Zh. Prikl. Spektroskop.* **42** 766 (1985)^d
28. B F Minaev *Opt. Spektroskop.* **58** 1238 (1985)^c
29. B F Minaev *Zh. Strukt. Khim.* **23** 7 (1982)^e
30. B F Minaev, V A Minaeva *Phys. Chem. Chem. Phys.* **3** 720 (2001)
31. B F Minaev *Phys. Chem. Chem. Phys.* **1** 3403 (1999)
32. B F Minaev, H Agren *Collect. Czech. Chem. Commun.* **60** 339 (1995)
33. B F Minaev, H Agren *Int. J. Quant. Chem.* **57** 519 (1996)
34. B F Minaev *Bull. Pol. Acad. Sci. Chem.* **49** 27 (2001)
35. R Schmidt *Chem. Phys.* **304** 315 (2004)
36. N Dam, T Keszthelyi, L K Andersen, K V Mikkelsen, P Ogilby *J. Phys. Chem. A* **106** 5263 (2002)
37. B F Minaev *RIKEN Rev.* **44** 147 (2002)
38. B F Minaev *Opt. Spektroskop.* **36** 275 (1974)^c
39. E H Fink, K D Setzer, J Wildt, D A Ramsay, M Vervloet *Int. J. Quant. Chem.* **39** 287 (1991)
40. B F Minaev *Spectrochim. Acta, A* **60** 1027 (2004)

41. O Vahtras, B F Minaev, H Ågren *Chem. Phys. Lett.* **281** 186 (1997)
42. B A Hess, C M Marian, S D Peyerimhoff *Modern Electronic Structure Theory Pt I* (Ed. D R Yarkoney) (Singapore: World Scientist, 1995) p. 152
43. M J Paterson, O Christiansen, F Jensen, P Ogilby *Photochem. Photobiol.* **82** 1136 (2006)
44. U Freichs-Deeken, K Rangelova, R Kappl *Biochemistry* **43** 14485 (2004)
45. R Prabhakar, P Siegbahn, B F Minaev, H Ågren *J. Phys. Chem. B* **108** 13882 (2004)
46. O Vahtras, O Loboda, B F Minaev, H Ågren *Chem. Phys.* **279** 133 (2002)
47. S R Langhoff *J. Chem. Phys.* **61** 1708 (1974)
48. O Zamani-Khamiri, H F Hameka *J. Chem. Phys.* **55** 2191 (1971)
49. H Lefebvre-Brion, R Field *Perturbation in the Spectra of Diatomic Molecules* (Orlando: Academic Press, 1986)
50. B F Minaev, O Vahtras, H Ågren *Chem. Phys.* **208** 299 (1996)
51. A C Becker, U Schurath, H Dubost, J P Galaup *Chem. Phys.* **125** 321 (1988)
52. G Tuzzkowski, U Schurath, M Bodenbinde, H Willner *Chem. Phys.* **215** 379 (1997)
53. T D Poulsen, P R Ogilby, K V Mikkelsen *J. Phys. Chem. A* **102** 8970 (1998)
54. T D Poulsen, P R Ogilby, K V Mikkelsen *J. Phys. Chem. A* **103** 3418 (1999)
55. K M Ervin, W Anusiewicz, P Skurski *J. Phys. Chem. A* **107** 8521 (2003)
56. L K Andersen, P Ogilby *Photochem. Photobiol.* **73** 489 (2001)
57. R Klotz, C M Marian, S D Peyerimhoff, B A Hess, R J Buenker *Chem. Phys.* **89** 223 (1984)
58. P-T Chou, H Frei *Chem. Phys. Lett.* **122** 87 (1985)
59. B F Minaev, Candidate Thesis in Physical and Mathematical Sciences, Tomsk State University, Tomsk, 1973
60. A A Krasnovsky Jr. *Photochem. Photobiol.* **29** 29 (1979)
61. I M Byteva, G P Gurinovich, S P Izbavitelev *Zh. Prikl. Spektroskop.* **23** 285 (1978)^d
62. K I Salokhiddinov, I M Byteva, G P Gurinovich *Zh. Prikl. Spektroskop.* **34** 92 (1981)^d
63. A A Krasnovsky Jr *Chem. Phys. Lett.* **81** 443 (1981)
64. M Hild, R Schmidt *J. Phys. Chem. A* **103** 6091 (1999)
65. R Klotz, S D Peyerimhoff *Mol. Phys.* **57** 573 (1986)
66. B F Minaev, L G Telyatnik *Opt. Spektroskop.* **91** 883 (2001)^c
67. B F Minaev, Z M Muldakhmetov *Opt. Spektroskop.* **56** 48 (1984)^c
68. A C Becker, U Schurath *Chem. Phys. Lett.* **160** 586 (1989)
69. A U Khan, M Kasha *Proc. Natl. Acad. Sci. USA* **76** 6047 (1979)
70. B F Minaev, V S Cherkasov *Opt. Spektroskop.* **45** 264 (1978)^c
71. B F Minaev, K V Mikkelsen, H Ågren *Chem. Phys. Lett.* **220** 79 (1997)
72. R P Saxon, B Liu *J. Chem. Phys.* **67** 5432 (1977)
73. A P Darmanyan *Chem. Phys. Lett.* **215** 477 (1993)
74. A P Darmanyan *J. Phys. Chem. A* **102** 9833 (1998)
75. K I Salokhiddinov, B M Dzaghárov, I M Byteva, G P Gurinovich *Chem. Phys. Lett.* **76** 85 (1980)
76. J R Hurst, J D McDonald, G B Schuster *J. Am. Chem. Soc.* **104** 2065 (1982)
77. P R Ogilby, C S Foote *J. Am. Chem. Soc.* **105** 3423 (1983)
78. P B Merkel, D R Kearns *J. Am. Chem. Soc.* **94** 7244 (1972)
79. B F Minaev *Mol. Eng.* **6** 261 (1996)
80. J N Murrell *Mol. Phys.* **3** 319 (1960)
81. G J Hoijtink *Mol. Phys.* **3** 60 (1960)
82. L K Andersen, P Ogilby *J. Phys. Chem. A* **106** 11064 (2002)
83. L K Andersen, P Ogilby *Rev. Sci. Instrum.* **73** 4313 (2002)
84. H Ågren, O Vahtras, B F Minaev *Adv. Quant. Chem.* **27** 71 (1996)
85. B F Minaev, S Lunell, G I Kobzev *Int. J. Quant. Chem.* **50** 279 (1994)
86. B F Minaev *J. Mol. Struct. (THEOCHEM)* **183** 207 (1989)
87. B F Minaev, H Ågren *J. Chem. Soc., Faraday Trans.* **93** 223 (1997)
88. B F Minaev, S Lunell, G I Kobzev *J. Mol. Struct. (THEOCHEM)* **284** 1 (1993)
89. J F Noxon *Can. J. Phys.* **39** 1110 (1961)
90. C Long, D R Kearns *J. Chem. Phys.* **59** 5729 (1973)
91. B F Minaev *Chem. Phys.* **252** 25 (2000)
92. B R Lewis, S T Gibson, T G Slanger, D L Huestis *J. Chem. Phys.* **110** 11129 (1999)
93. Y Luo, H Ågren, B F Minaev, P Jorgenson *J. Mol. Struct. (THEOCHEM)* **336** 61 (1995)
94. T G Slanger, R A Copeland *Chem. Rev.* **104** 1229 (2004)
95. B F Minaev, L B Yashchuk *Khim. Vys. Energ.* **38** 243 (2004)^f
96. M C G N van Vroonhoven, G C Groenenboom *J. Chem. Phys.* **117** 5240 (2002)
97. S Langhoff, C Kern *Methods of Electronic Structure Theory Vol. 4* (Ed. H Schaeffer) (New York: Plenum Press, 1977)
98. B F Minaev, G I Kobzev *Spectrochim. Acta, A* **59** 3387 (2003)
99. B F Minaev *Zh. Fiz. Khim.* **68** 1228 (1994)^g
100. B F Minaev, E I Fedulova, N M Ivanova, G I Kobzev, Z M Muldakhmetov *Zh. Prikl. Spektroskop.* **67** 453 (2000)^d
101. A P Losev, I M Byteva, G P Gurinovich *Chem. Phys. Lett.* **143** 127 (1988)
102. S Y Egorov, V F Kamalov, N I Koroteev, A A Krasnovsky Jr, B N Toleutaev *Chem. Phys. Lett.* **163** 421 (1989)
103. B F Minaev, G K Mambeterzina *Fotoprotsessy v Atomnykh i Molekulyarnykh Sistemakh* (Photoprocesses in Atomic and Molecular Systems) (Karaganda: Karaganda State University, 1984) p. 35
104. R D Schurlock, P Ogilby *J. Phys. Chem.* **91** 4599 (1987)
105. A A Krasnovsky Jr, C Schweitzer, H Leismann, C Tanielian, E A Luk'yanets *Quant. Electron.* **30** 445 (2000)
106. R Schmidt, M Bodesheim *J. Phys. Chem.* **99** 15919 (1995)
107. B F Minaev, L B Yashchuk *Biopolim. Kletka* **22** 231 (2006)
108. F Okada, H Kajihara, S Koda *Chem. Phys. Lett.* **192** 357 (1992)
109. B F Minaev, V V Kukueva, H Ågren *J. Chem. Soc., Faraday Trans.* **90** 1479 (1994)
110. V K Mikhalko, G M Zhidomirov, O L Lebedev *Zh. Fiz. Khim.* **58** 1857 (1984)^g
111. D F Evans *J. Chem. Soc.* 1351 (1957)
112. D L Dexter *J. Chem. Phys.* **21** 836 (1953)
113. B F Minaev *Teor. Eksp. Khim.* **21** 594 (1985)^h
114. P T Chou, A U Khan *Chem. Phys. Lett.* **103** 281 (1984)
115. B F Minaev *Teor. Eksp. Khim.* **20** 209 (1984)^h
116. J R Hurst, G B Schuster *J. Am. Chem. Soc.* **105** 5756 (1983)
117. M A J Rodgers *J. Am. Chem. Soc.* **105** 6201 (1983)
118. R Schmidt, H-D Brauer *J. Am. Chem. Soc.* **109** 6976 (1987)
119. E A Ogryzlo, C W Tang *J. Am. Chem. Soc.* **92** 5034 (1970)
120. C S Foot, Y C Chang, R W Denny *J. Am. Chem. Soc.* **92** 5216 (1970)
121. R H Young, D Brewer, R A Keller *J. Am. Chem. Soc.* **95** 375 (1973)
122. R H Young, K Wehrly, R L Martin *J. Am. Chem. Soc.* **93** 5774 (1971)
123. R Boehling, A C Becker, B F Minaev, K Seranski, U Schurath *Chem. Phys.* **142** 445 (1990)
124. B F Minaev, E Jansson, M Lindgren *J. Chem. Phys.* **125** 094306 (2006)
125. T G Slanger, P C Cosby, D L Huestis, D E Osterbrock *J. Geophys. Res.* **105** 20557 (2000)
126. A A Krasnovsky Jr, M E Bashtanov, N N Drozdova *Quant. Electron.* **32** 83 (2002)
127. B F Minaev, L B Yashchuk *Opt. Spektroskop.* **95** 553 (2003)^c
128. D Weldon, T D Poulsen, K V Mikkelsen, P R Ogilby *Photochem. Photobiol.* **70** 369 (1999)
129. B F Minaev *Zh. Fiz. Khim.* **68** 1432 (1994)^g
130. C Schweitzer, Z Mehrdad, F Shafii, R Schmidt *Phys. Chem. Chem. Phys.* **3** 3095 (2001)
131. C Schweitzer, Z Mehrdad, A Noll, E-W Grabner, R Schmidt *J. Phys. Chem. A* **107** 2192 (2003)
132. B F Minaev *Khim. Fiz.* **3** 983 (1984)ⁱ
133. G I Kobzev, Doctoral Thesis in Chemical Sciences, Bashkir State University, Ufa, 2006
134. G I Kobzev, B F Minaev *Zh. Fiz. Khim.* **79** 152 (2005)^g
135. B F Minaev, V A Tikhomirov *Zh. Fiz. Khim.* **58** 646 (1984)^g
136. B F Minaev, V A Tikhomirov, Zh K Dausheev *Khim. Fiz.* **3** 615 (1984)ⁱ
137. B F Minaev, L B Yashchuk *Visn. Odes. Nats. Univ., Ser. Khim.* **9** 52 (2004)
138. B F Minaev *Zh. Fiz. Khim.* **66** 2992 (1992)ⁱ

139. I V Savitskii *Biologicheskaya Khimiya* (Biological Chemistry) (Kiev: Vishcha Shkola, 1982)
140. M Engstrom, B F Minaev, O Vahtras, H Ågren *Chem. Phys.* **237** 149 (1998)
141. G Herzberg *Science* **177** 123 (1972)
142. Yu A Serebrennikov, B F Minaev, B Abdrakhmanov *Khim. Fiz.* **5** 878 (1986)ⁱ
143. T C Brunold, E I Solomon *J. Am. Chem. Soc.* **121** 8277 (1999)
144. T C Brunold, E I Solomon *J. Am. Chem. Soc.* **121** 8288 (1999)
145. B F Minaev *Ukr. Biokhim. Zh.* **74** 11 (2002)ⁱ
146. A Bassan, M R Blomberg, P Siegbahn *Eur. J. Chem. A* **9** 106 (2003)
147. J N Harvey *Faraday Disc.* **127** 165 (2004)
148. B F Minaev *Visn. Cherkas. Inzh.-Tekhnol. In-tu* (3) 6 (2001)
149. R Prabhakar, P Siegbahn, B Minaev *Biochim. Biophys. Acta Proteins Proteomics* **1647** 173 (2003)
150. B F Minaev, V A Minaeva, V N Leshchenko *Biopolim. Kletka* **20** 1 (2004)
151. V A Belyakov, R F Vasil'ev, N M Ivanova, B F Minaev *Izv. Akad. Nauk SSSR, Ser. Fiz.* **51** 540 (1987)^k
152. J P Klinman *J. Biol. Inorg. Chem.* **6** 1 (2001)
153. J P Roth, J P Klinman *Proc. Natl. Acad. Sci. USA* **100** 62 (2003)
154. B F Minaev *Opt. Spektroskop.* **80** 407 (1996)^c
155. M F Gulyi, V I Bilai, N M Pidoplichko, R G Degtyar', E A Nikol'skaya *Ferment Glyukozooksidaza i Ego Primenenie* (The Glucose Oxidase Enzyme and Its Applications) (Kiev: Naukova Dumka, 1964)
156. P E M Siegbahn *Inorg. Chem.* **38** 2880 (1999)
157. P E M Siegbahn *J. Comput. Chem.* **22** 1634 (2001)
158. P E M Siegbahn, M R A Blomberg *Chem. Rev.* **100** 421 (2000)
159. S Shaik, M Filatov, D Schroder, H Schwarz *Chem. – Eur. J.* **4** 193 (1998)
160. L A Buchachenko, R Z Sagdeev, K M Salikhov *Magnitnye i Spinovye Effekty v Khimicheskikh Reaktsiyakh* (Magnetic and Spin Effects in Chemical Reactions) (Novosibirsk: Nauka, 1978)
161. Yu A Serebrennikov, B F Minaev, B Abdrakhmanov *Khim. Fiz.* **6** 799 (1987)ⁱ
162. L A Buchachenko *Usp. Khim.* **59** 529 (1990) [*Russ. Chem. Rev.* **59** 307 (1990)]
163. S V Vonsovskii *Magnetizm* (Magnetism) (Moscow: Nauka, 1971)
164. R White *Quantum Theory of Magnetism* (New York: McGraw-Hill, 1970)

^a — *Biophysics* (Engl. Transl.)

^b — *Russ. Phys. J.* (Engl. Transl.)

^c — *Opt. Spectroscop.* (Engl. Transl.)

^d — *J. Appl. Spectroscop.* (Engl. Transl.)

^e — *J. Struct. Chem.* (Engl. Transl.)

^f — *High Energ. Chem.* (Engl. Transl.)

^g — *Russ. J. Phys. Chem.* (Engl. Transl.)

^h — *Theor. Exp. Chem.* (Engl. Transl.)

ⁱ — *Chem. Phys. Rep.* (Engl. Transl.)

^j — *Ukr. Biochem. J.* (Engl. Transl.)

^k — *Bull. Russ. Acad. Sci., Phys.* (Engl. Transl.)

Nanomaterials for sensors

V E Bochenkov, G B Sergeev

Contents

I. Introduction	1011
II. Physicochemical properties of nanomaterials for sensors	1011
III. Certain application fields of sensors based on nanomaterials	1015
IV. Conclusion	1018

Abstract. Publications of the past five years dealing with nanomaterials used as sensors for determination of gases are analysed. Peculiarities of the production of chemoresistive nanosensors based on semiconducting oxides, carbon nanotubes and polyaniline are outlined. The main application fields of gas sensors are considered. Prospects for the use of quasi-one-dimensional nanomaterials such as nanorods, nanotubes and nanobelts as the materials in sensor units are discussed. The bibliography includes 114 references.

I. Introduction

Nanoscience deals with fundamental problems of natural science on the nanoscale; its results are implemented in nanotechnologies as nanodevices, nanosystems, new substances and nanomaterials.^{1,2}

Nanoparticles are highly reactive; this is why, in the absence of stabilising media, they are studied in high vacuum or at low temperatures. Under conditions of ultralow temperatures, unusual chemical reactions were carried out and different reactivity of metal atoms, clusters and nanoparticles of different sizes was demonstrated.³ The use of low temperatures and the joint condensation of vapours of different compounds led to the development of methods for the cryogenic formation of nanosystems with the gas-sensitive and sensor properties.⁴ Studies in the field of cryochemistry play the important role in the development of nanochemistry.⁵ Nanotechnologies are also beginning to use cryogenic freeze-drying.⁶

Preparation of materials with sensor properties and the development of the corresponding instruments based on these materials is an important problem. After the terrorist act of September 11, 2001, the USA sharply raised financing of the field of nanoscience devoted to sensors and correspondingly reoriented their research policy. New sensor materials are of great social and economic importance. According to the Business Corporation Company, the total sum obtained by the

USA from nanosensors sold in 2004 was ~\$ 190 million. The annual increase in the sale volume of nanomaterial-based sensors is 26% and the total sum from their sale will reach 592 million to 2010. The annual gain in the sale volume was 53% for gas sensors and 32% for biosensors. According to the 'Nanomaterials Research' Journal, the total sale of all types of sensors will reach \$ 2.5 billion in 2010.

The diversity of sensors developed for different fields of science, technology, and industry as well as their properties, preparation techniques and application areas were surveyed in the monograph⁷ and the following review papers:

- control over volatile combustion products in industry,⁸
- analysis of exhaust gases of cars,⁹
- quality inspection of foodstuffs,¹⁰
- peculiarities of using the polyaniline gas sensors,¹¹
- using the plasmon resonance in biosensorics,¹²
- sensors for ammonia detection,¹³
- preparation and chemoresistive properties of nanostructured materials,⁴
- materials for environmental monitoring.¹⁴

In this study, attention is focused on the materials and sensors used in the determination of combustible and toxic gases, volatile organic compounds and in the diagnostics of certain diseases. In our opinion, at present the demand for such sensors is the highest. They are required for the prevention of technological disasters and terrorist attacks, in the environmental protection and the human health care. All these problems are currently central in Russia.

This review considers the problems associated with the use of low temperatures in the synthesis of new gas-sensitive nanomaterials for sensors. Physical and chemical methods of the formation of sensor systems and certain general properties of gas-sensitive materials are discussed. For the most part, chemoresistive sensor materials that change their properties upon adsorption of a particular substance are considered. In contrast to other reviews on the related subjects (*e.g.*, see Refs 4, 15), in the analysis of properties of nanomaterials for sensors special attention is paid to the peculiarities of their synthetic methods of their synthesis, and certain general problems of nanosensors are discussed in relation to the detection of ammonia.

II. Physicochemical properties of nanomaterials for sensors

Nowadays, nanoparticles and nanomaterials are coming into extensive use in the development of sensors.^{4,8–14} However,

V E Bochenkov, G B Sergeev

Department of Chemistry, M V Lomonosov Moscow State University, Leninskie Gory, 119992 Moscow, Russian Federation.

Fax (7-495) 932 88 46, tel. (7-495) 939 54 42,

e-mail: boch@kinet.chem.msu.ru (V E Bochenkov),

gbs@kinet.chem.msu.ru (G B Sergeev)

Received 25 June 2007

Uspekhi Khimii 76 (11) 1084–1093 (2007); translated by T Ya Safonova

recently published monographs on sensors^{16,17} described the use of nanomaterials only briefly and fragmentarily.

Nanomaterials to be used as sensors should exhibit sensitivity, selectivity and stability. The size dependence of nanoparticle properties forms the basis for the development of highly sensitive sensor devices. Certain problems associated with the dependence of the sensitivity of sensors on the size and shape of nanosystems, the ligand type and the response mechanism were considered in several reviews.^{4,15}

In this review, the methods of preparation of gas-sensitive nanomaterials are conditionally divided into physical and chemical. A method used for the formation of nanoheterogeneities in materials at low temperatures, *i.e.*, cryosynthesis, is considered separately.

1. Physical and chemical methods of synthesis of sensor nanomaterials

Physical methods of preparation of gas-sensitive nanomaterials include, *inter alia*, different versions of vacuum deposition that employ the resistive, laser and electron-beam evaporation and magnetron sputtering. As a rule, these methods are used in the preparation of metal-oxide semiconducting nanosystems and metal nanoparticles deposited on different substrates.

Operation of gas sensors is based on the variations in the resistance (conductivity) of chemoresistive materials under the effect of the analysed gas. At present, the majority of sensors for the gas analysis employ semiconducting materials. As a rule, the operation of these materials requires elevated temperatures.

Metal-oxide semiconducting nanomaterials are the most thoroughly studied sensor materials — they were the subject of a considerable number of publications devoted to methods of synthesis^{18–20} and mechanisms of sensor response.^{18,21,22} This is why we do not consider in detail metal-oxide nanomaterials (with the exception of new types of sensors based on nanowires, nanobelts and nanotubes).

Chemical methods of synthesis of sensor nanosystems include their conventional synthesis in solutions and the chemical synthesis in the gas phase. The former is used in the production of materials based on self-assembled nanoparticles of noble metals coated with alkanethiols and in the preparation of gas-sensitive polymeric films. The latter method is actively employed in the synthesis of materials based of carbon nanotubes.

Metal nanoparticles stabilised with organic molecules and the materials based on them are interesting due to their unique properties and the possibility of their application as gas sensors. Metal nanoparticles are stabilised by monolayers of alkanethiol derivatives.^{23,24} The organic coating prevents aggregation of particles and affects their physicochemical properties.²⁵

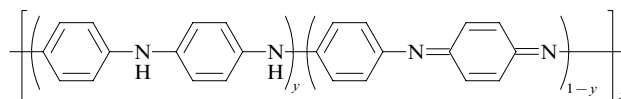
One of the first studies that employed gold nanoparticles coated with a thin octanethiol film as the sensor[†] units considered the effect of vapours of volatile organic substances on the film conductivity. It was found that the film conductivity remained virtually unchanged under the action of propanol and water vapours and decreased when subjected to action of toluene and trichloroethylene vapours.²⁶ For toluene, the detection limit was several molecules per million. Later, materials sensitive with respect to vapours of polar solvents were synthesised.²⁷ The conductivity in such systems was discussed in terms of two possible mechanisms, namely, the electron tunnelling between metal nuclei and the hopping mechanism of conduction *via* thiol molecules. Changes in the charge distribution in a system with the adsorption of vapours

of volatile substances give rise to the sensor response. Moreover, it was assumed that the swelling of organic matrices upon adsorption of a solvent vapour may influence the film conductivity that is related to the variations in the distance between metal particles.²⁸

When manufacturing chemoresistive thin films based on metal nanoparticles coated with thiol derivatives, it is necessary to know the dependences of the material conductivity on the particle radius, the distance between particles and the dielectric permittivity of the medium. The effect of the distance between nanoparticles of gold and a gold–silver alloy on the conductivity and sensitivity of films was studied.²⁹ For the first time, certain α,ω -dithiols and dicarboxylic acids with different numbers of CH_2 units ($n = 3–18$) were used in addition to decanethiol for the fixation of interparticle distances. It was shown that the sensitivity of samples with respect to vapours of hexane, toluene and benzene depends on the number n of CH_2 units in the spacer chain. This dependence has a sigmoid form, where the largest changes in the sensitivity fall to the n range from 9 to 13.

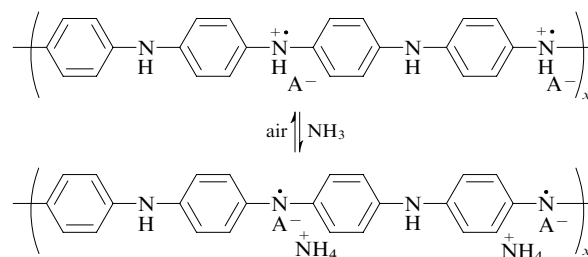
Conducting polymeric films³⁰ synthesised by chemical methods display the following advantages over metal-oxide sensors: the possibility of operation at room temperature, high sensitivity and short response times. Conducting polymers can be synthesised by chemical and electrochemical reactions, their molecular structure is changed by co-polymerisation or modification of functional groups.³⁰

Attention of scientists was always attracted to the development of the so-called synthetic metals, *i.e.*, conducting materials based on organic compounds. The interest in such compounds increased with the discovery of conduction in polymers.[‡] Different modifications of polyaniline were used most extensively as the sensor materials.



Polyaniline samples can have different shapes and acquire different colours depending on the y value. This makes it difficult to carry out their reproducible synthesis and measure their conductivity. Protonated forms (or salts) of polyaniline have the highest conductivity that reaches $15 \Omega^{-1} \text{cm}^{-1}$ (Ref. 31), which is much lower than the metal conductivity ($10^3 \Omega^{-1} \text{cm}^{-1}$).

The methods of preparation of polyaniline films, the mechanism and features of their modification with different inorganic and organic compounds were analysed.¹¹ Their modification involved the use of acids (HA), where $\text{A} = \text{Cl}, \text{HSO}_4, \text{ClO}_4$. The sensitivity of modified polyaniline films placed, *e.g.*, in the ammonia atmosphere changed as a result of protonation and deprotonation.^{32,33}



[†] Nowadays, solutions containing alkanethiol-stabilised gold and silver nanoparticles can be purchased from suppliers of chemicals.

[‡] For this discovery, A J Heeger, A D MacDiarmid and H Shirakawa were awarded the Nobel Prize-2000 in chemistry.

Table 1. Sensitivity of polyaniline films with respect to different gases depending on the preparation method.

NO ₂	H ₂ S	SO ₂
Spin-coating		
++ (4 ppm)	+++ (4 ppm)	++ (2 ppm)
Thermal deposition		
++ (2 ppm)	+(10 ppm) irreversible	+(10 ppm)

Note. In parentheses, the gas concentration is shown. Symbols +, ++ and +++ designate the relative value of response.

Table 1 shows the sensitivity of non-modified polyaniline films synthesised by different methods with respect to different gases.

It was noted³⁴ that polyaniline is insensitive with respect to carbon dioxide or methane; the same paper reports the results of studies of the polyaniline film conductivity (in nitrogen atmosphere, at room temperature) as a function of its thickness and the method of preparation. The conductivity of polyaniline synthesised by thermal evaporation was $10^{-10} \Omega^{-1} \text{ cm}^{-1}$. This was higher as compared with samples synthesised by the spin-coating method. The higher conductivity of films obtained by the thermal deposition was associated with the predominant presence of *N*-phenyl-*p*-phenylenediamine blocks in the sample. The other method produced a mixture of *N*-phenyl-*p*-phenylenediamine and quinonediimine blocks, which interrupted the sequence of conjugated double bonds. It was demonstrated³⁵ that polyaniline films containing polyvinyl alcohol may be used in the analysis for carbon dioxide. Composites based on polyaniline and copper particles were used in the analysis for chloroform.³⁶

Incorporation of palladium particles into polyaniline was accomplished.³⁷ Examination of the ability of different surfaces to change the conductivity of deposited polyaniline films has shown that the deposition rate of polyaniline on a hydrophobic surface was higher as compared with hydrophilic films. Similar dependences were obtained^{38,39} for thiol-modified silicon and gold surfaces, respectively. The conductivity of films on hydrophobic surface was higher; however, the adhesion of films to hydrophilic surfaces was stronger. The use of polyaniline as the material chemoresistive towards different gases faces the problems associated with stability, selectivity and response times that are typical of all gas sensors.

Carbon nanotubes are the promising material for gas sensors. They are synthesised by several methods, which can be classified into two groups associated with the use of either high or moderate temperatures. The former group includes the methods that employ arc discharge, the second group comprises the catalytic chemical vapour deposition.⁴⁰

One of the first gas sensors based on carbon nanotubes could detect low concentrations of NO₂ and NH₃ at room temperature.⁴¹ This result served as an impetus for the further experimental^{42,43} and theoretical^{43,44} studies of the sensitivity of carbon nanotubes with respect to gases. Particularly, it was shown⁴⁵ that materials synthesised upon the deposition of carbon nanotubes on tin(IV) oxide substrates were chemoresistive with respect to NO₂. For multi-walled carbon nanotubes with external diameters of ~30 nm, a linear dependence of their response on the ammonia concentration in the range of 5–200 ppm at 25 °C was revealed.⁴² The response time was 3 min; however, to recover its performance, a sensor should be annealed at 250 °C for 6 h.

To enhance the sensitivity of carbon nanotubes, their surface was modified with metal particles,^{46,47} covalently bound functional groups, polymers and even DNA mole-

cules.⁴⁸ This provided an increase in the selective adsorption of particles of a certain kind due to their interaction with functional groups or as a result of acceleration of catalytic processes on the surface of metal nanoparticles. Carbon nanotubes modified with palladium nanoparticles exhibited sensitivity with respect to hydrogen for its content in the range from 50 to 10 000 ppm at room temperature.⁴⁹

Single-walled nanotubes functionalised with poly(*m*-aminobenzenesulfonic acid) demonstrated the detection limit at a level of 5 ppm (Ref. 50). The use of a polyaniline coating allowed the record-breaking detection limit for ammonia of 50 ppb to be reached.⁵¹

In the gas detection, it was proposed^{52,53} to use carbon nanotubes as the anode in ionisation detectors. Due to the high field intensity, vertically aligned carbon nanotubes allowed the breakdown potential to be substantially reduced. This made it possible to use such detectors in portable gas analysers and gas chromatographs. The advance in the synthesis of vertical carbon nanotube forests promotes the development in this field.⁵⁴

2. Cryosynthesis

The use of low temperatures in the production of nanostructured materials is first of all associated with the possibility of limiting the diffusion mobility of particles and, as a consequence, decreasing the sizes of growing aggregates.

Cryochemical technologies were successfully employed in the preparation of small-size particles⁶ that can be used in the production of gas-sensitive materials. Thus samples of nanograin tin(IV) oxide synthesised by chemical deposition followed by cryogenic freeze-drying were chemoresistive with respect to carbon monoxide.⁵⁵

Based on fundamental studies in the field of low-temperature chemistry,⁵⁶ a new approach to the synthesis of nanostructured gas-sensitive materials has been developed, namely, the low temperature deposition of metal vapour in vacuum followed by oxidation.⁵⁷

Figure 1 illustrates the essence of this method, which consists of the vacuum condensation of metal vapour on a substrate kept at a temperature from 80 to 300 K. Cooling of the substrate considerably decreases the diffusion mobility in the deposition. As a result, columnar structures can be formed in the moment of condensation as a result of the attraction of the approaching atoms to the already deposited clusters. The subsequent controlled annealing destroys the structure to afford spherical particles on the oxide substrate non-wettable by the metal.

The introduction of oxygen makes it possible to form materials with certain nanostructures and chemical compositions, particularly, with nanograins of the core-shell structure that are connected with bridges. The control over the deposition parameters such as the rate and the temperatures of the substrate and the evaporator allows one to govern the structure of synthesised condensates and chemically modify the surface of grains. Low-temperature deposition made it possible to synthesise lead nanoparticles sensitive with respect to ammonia and water vapours.^{58,59} From our viewpoint, the sensitivity of such systems is due to the formation of a percolation structure of lead nanoparticles with the size of ~50 nm coated with semiconducting oxides. Oxide bridges between the metal particles are responsible for the overall conductivity of the material and the manifestation of the chemoresistive effect.

The chemoresistive properties of materials also depend on the changes in their microstructure and porosity. This was taken into account in a method of low-temperature co-condensation with an additional component (e.g., an inert gas), which is removed from the system on annealing. Thus the structure of thin lead films was affected by its co-condensation with carbon dioxide.⁶⁰ It was shown that the roughness of the

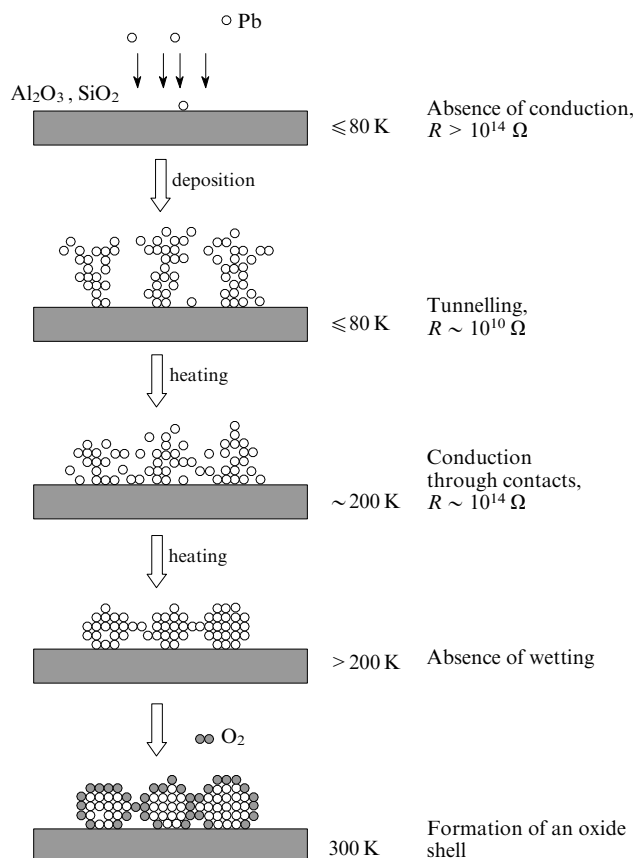


Figure 1. A model of cryogenic formation of gas-sensitive metal condensates on non-wettable substrates.⁵⁷

resulting films was higher as compared with lead films untreated with carbon dioxide. The noted fact allows one to consider the co-condensation – annealing method as promising for the preparation of materials with well-developed surface areas.

3. Sensitivity and selectivity

The sensitivity of semiconducting nanomaterials is determined by two basic factors, namely, the ratio of the surface area (S) to the volume (V) and the ratio of the Debye screening length (L_D) to the effective radius of conducting channels (R). All other conditions being the same, the larger the S/V and L_D/R ratios the higher the material sensitivity.

Numerous studies of thin nanostructured SnO_2 films showed that the sensitivity of samples with respect to detected gases dramatically increased as the grain size decreased to several nanometers.^{61–64} A systematic analysis of the size dependence of the sensitivity of SnO_2 samples can be found in Ref. 65. Problems of the selectivity of nanostructured gas-sensitive materials and the possibility of their use in the analysis of multicomponent gas mixtures.⁶⁶

A conventional method aimed at the enhancement of sensitivity and selectivity of semiconducting metal-oxide nanomaterials consists of doping samples with metal nanoparticles, *e.g.*, palladium,⁶⁷ platinum,⁶⁸ gold,^{69,70} silver.^{65,71} Thus the deposition of palladium nanoparticles on the surface of tin dioxide nanowires led to the increase in the sensitivity of such a system with respect to oxygen and hydrogen. This is explained by the increase in the concentration of O^- anions due to the acceleration of dissociation of oxygen molecules on palladium particles.⁷² In turn, the size of dopant nanoparticles also affects the sensitivity of nanomaterials with respect to gases. It was

shown that with a decrease in the size of silver particles deposited on tin dioxide particles, the sensitivity of this system with respect to ethanol vapours increased.⁷³

Recently, to enhance the sensitivity of chemoresistive materials, quasi-one-dimensional nanomaterials such as nanowires, nanorods and nanobelts came into use in addition to films.^{15,74–77} To a certain degree, this was associated with the development and investigation of such structures.^{78,79} Their use allows one to substantially lower the detection limits, because as compared with films, the conductivity of a one-dimensional nanosample responds to a smaller amount of the adsorbate.

As an example, we consider the mechanism of the sensor response of silver oxide nanowires to ammonia and hydrogen chloride vapours (Fig. 2).

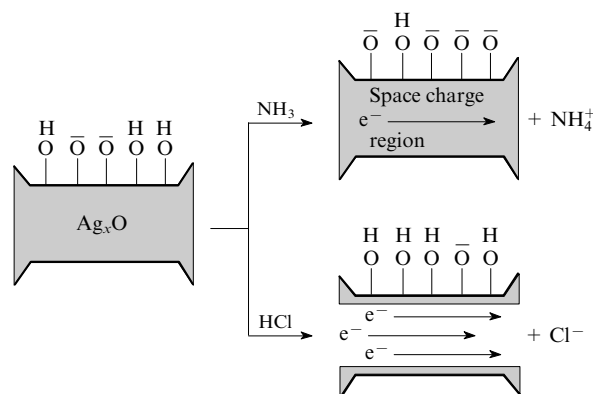


Figure 2. Scheme of a presumed mechanism of the Ag_2O response to ammonia and hydrogen chloride at room temperature.⁸⁰

The proposed mechanism takes into account that, at room temperature, the oxide surface is coated by hydroxyl groups.⁸⁰ With the adsorption of ammonia and amines, these groups are deprotonated to form a negatively charged surface layer, which prevents the transport of electrons and favours an increase in the wire resistance. The effect of acid vapour leads to protonation of surface hydroxyl groups and, as a consequence, reduces the resistance.

A comparison of properties of nanowires and thin granulated films formed by silver particles connected with oxide bridges has evidenced the higher sensitivity of nanowires.⁸¹ A qualitative model explaining this effect is shown in Fig. 3.

The adsorption of ammonia molecules increases the resistance of contacts between silver nanoparticles. For films, a change in the resistance of several contacts merely changes the route of electron transport (Fig. 3*a*). For nanowires, ‘blocking’ of a single contact can substantially decrease the conductivity of the whole wire (Fig. 3*b*). Thus, the adsorption of the same amount of substance will induce a greater change in the nanowire conductivity as compared with a thin film, which is the case in practice. It was shown^{82–84} that tin dioxide nanowires exhibit sensitivity with respect to low concentrations of CO.

New types of nanomaterials for sensors were discussed in a review.⁸⁵

Sensitivity of sensors can additionally be increased by designing one-dimensional objects connected with bridges that control the conductivity of the whole nanosystem. A comparative study of how straight SnO_2 nanowires ~ 100 nm thick and segmented nanowires with a diameter of ~ 500 nm formed by segments ~ 80 nm long and 10 nm thick respond to the addition of 0.4 ppm hydrogen have shown that the signal was higher for segmented wires although their

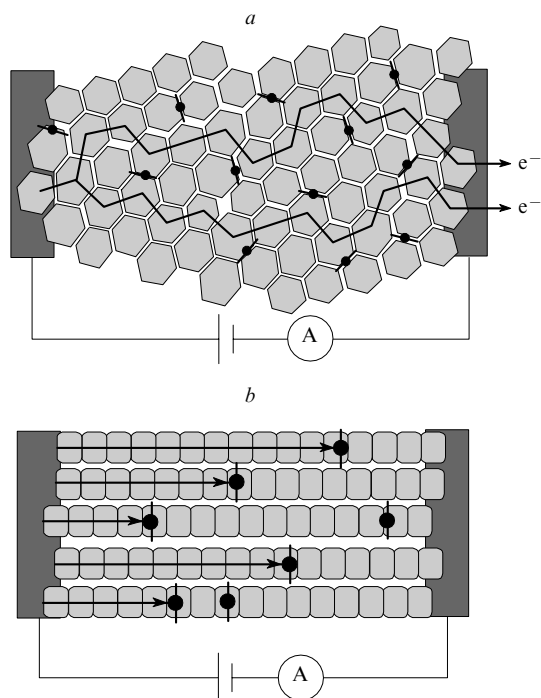


Figure 3. Model illustrating the changes in conductivity upon adsorption of ammonia on oxidised surface of silver particles (a) thin films and (b) nanowires.⁸¹

average radius several times exceeded that of straight nanowires.⁸⁶

Highly ordered arrays of core-shell nanoparticles with metal cores and semiconductor shells was proposed as a new type of sensor materials.⁸⁷

The increase in the sensitivity and selectivity of sensor nanosystems is the prime objective of scientists. The application field of sensors (especially oxide-based) can be extended by lowering the working temperature of gas-sensitive materials to room temperature. One of the ways to solve this problem may be the use of metal oxides in the form of quasi-one-dimensional materials. From our viewpoint, the development of systems with the higher selectivity should be based on the targeted synthesis of ligands capable of the selective interaction with the determined gases.

III. Certain application fields of sensors based on nanomaterials

Chemoresistive sensors are used in different fields of science and technology and in industry for the control over technological processes and the contents of toxic substances in air, water and soil. Below, certain fields of practical application of sensors are considered by the example of ammonia and several other gases and volatile organic substances. Attention is focused on the use of sensors in medicine.

1. Environmental monitoring

The environmental air and water contain large (and permanently growing) amounts of different impurities with wide concentration ranges. This stimulates the search for new versions of the use of metal oxides, which form the basis of conventional sensor materials. For example, a system comprising SnO_2 , ZnO , WO_3 , CuO and In_2O_3 was proposed for flow-through determinations of CH_4 , CO , NO , NO_2 , NH_3 , SO_2 and H_2S at temperatures in the range of 200–400 °C.⁸⁸

The environmental monitoring requires the knowledge of temperature dependence of the sensitivity with respect to the determined gas. The effect of temperature on the sensitivity of thin tin dioxide films manufactured by electron beam evaporation was explored for the determination of different concentrations of hydrogen, carbon oxide and ethylene, and the kinetics of their response was simulated.⁸⁹ It was shown that the minimum sensitivity and temperature are related to the energies of adsorption (E_{ads}) and activation (E_a). Being dependent on the nature of a gas, the adsorption energy determines the strength of its bonding with the oxide surface, whereas the activation energy determines a barrier that should be overcome to induce the surface oxidation. In turn, the quantities E_{ads} and E_a depend on the concentration of the analysed gas.

A cheap and relatively sensitive sensor for hydrogen was developed based on palladium nanowires deposited on the surface of highly oriented pyrolytic graphite.⁹⁰ The sensor operates at room temperature; its conductivity is two orders of magnitude higher in the presence of hydrogen than in its absence.

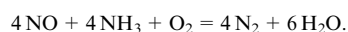
New sensors for ammonia and amines were developed. A new sensor based on V_2O_5 nanowires with extremely high sensitivity with respect to amines was described.⁹¹ The high conductivity of wires makes it possible to use this sensor at room temperature. The limiting sensitivity, which was defined as a concentration at which the signal exceeds the noise by a factor of three, was <30 ppb for *tert*-butylamine. Sensitivity with respect to amines increased linearly as the humidity of the carrier gas increased to 60%. The conductivity depended on the position of the amine contact with vanadium wires. The selectivity of the sensor was determined by comparing its response to amine, ammonia, propanol and toluene following 5-min contacts. The highest sensitivity was exhibited towards ammonia and amine.

In air, sulfuric and nitric acids react with ammonia to form particles of ammonium sulfate and nitrate. These particles serve as nuclei for the formation of aerosols and smog in air over large cities. With the appearance of smog, the air temperature decreases due to the sunlight screening.

The ammonia content in air is usually 10–100 ppb and falls to several molecules per billion over the ocean. In the vicinity of livestock farms, the ammonia concentration can reach 10 ppm (Ref. 92). To determine ammonia in the atmosphere, response times of about a minute are sufficient; air is delivered to the sensitive material by jet systems.

A different situation is observed in the determination of ammonia in exhaust gases of vehicles or in air-conditioned passenger compartments. The ammonia content in exhaust gases should be determined at a level of ~8 ppm (Ref. 93). To prevent the appearance of odour in the passenger compartment, the ammonia concentration should be detectable at a level of no higher than 50 ppm with the sensor response time of several seconds.

Exhaust gases of engines operating on diesel oil contain high concentrations of NO and NO_2 (NO_x).^{94,95} The amount of toxic nitrogen oxides can be reduced by their selective catalytic reduction⁹⁶



The reaction is carried out by the injection of a controlled amount of ammonia into the exhaust system. In this process, the ammonia sensor should measure its concentrations of an order of magnitude of several molecules per million, have the response time within 1 minute and operate at elevated temperatures.⁹⁴

Sensors based on zinc oxide nanorods with palladium particles deposited on the surface have demonstrated high

sensitivity with respect to hydrogen.⁹⁷ In a nitrogen flow with the hydrogen concentration varied from 10 to 500 ppm, the sensor determined concentrations < 10 ppm, was easily recoverable and did not respond to the presence of oxygen.

Nanorods of molybdenum oxide with the diameter from 50 to 300 nm and the length of 2–4 μm were used in sensors for the detection of carbon monoxide and ethanol at 200 °C. Carbon oxide was determined in amounts < 30 ppm (Ref. 98).

2. Sensors in chemical industry

The use of sensors in chemical industry is discussed by the example of ammonia. Ammonia is synthesised from molecular nitrogen and hydrogen at high temperatures and pressures in

the presence of catalysts. For the most part, it is used in the production of fertilisers and in certain chemical processes; large amounts of ammonia are still used in refrigerating units for foodstuff storage at temperatures below 0 °C.^{99,100} At ammonia utilising plants, its leakage is possible; this is why such plants should be equipped with appropriate detection systems that allow one to prevent environmental contamination with ammonia. The maximum allowable amount of ammonia in the surrounding air should not exceed 20 ppm. Such a concentration is allowed to hold for a long time; for its detection, sensors with the response times of an order of magnitude of one minute may be used. The ammonia production is a high-temperature process; hence, sensors should withstand temperatures of up to 500 °C.

In recent years, keen attention has been paid to the development of new sensors for ammonia. Sensors based on silver oxide microwires were developed.⁸⁰ Nanowires of zinc oxide were prepared and their sensitivity with respect to ammonia at room temperature was studied (using quartz crystal microbalance).¹⁰¹ The nanowires were synthesised by evaporation of zinc granules at 900 °C in air and then deposited onto the quartz crystal surface. It was found that with the increase in the thickness of layers, the absolute magnitude of response towards ammonia linearly increased. Samples were sensitive to ammonia in the concentration range from 40 to 1000 ppm. The response time was ~5 s. Sensors based on ZnO nanowires were stable and provided reproducible results.

Semiconducting oxides underlie the majority of sensors for ammonia used in the chemical industry. In such sensors, the signal is determined by the conductivity variations caused by the reaction of negatively charged oxygen species (O^- , O^{2-}) with the reducing gas on the sensor surface. To enhance the selectivity of oxide sensors, different doping additives were used, particularly, transition metals.

Figure 4 illustrates the dependence of the sensitivity of tungsten oxide with respect to NH_3 and NO on the addition of different metals.¹⁰² These data were obtained at 350 °C in the analysis of exhaust gases of vehicles. The sensor systems, which in addition to SnO_2 , employed WO_3 doped with gold and MoO_3 , were capable of detecting ammonia in the concentration range from 1 to 1000 ppm.¹⁰³ Such sensors were used in the detection of ammonia losses in refrigerating units¹⁰⁴ and in the combustion of gases.⁸⁸

Sensors for the determination of hydrogen, methane, carbon monoxide and hydrogen sulfide were developed by the deposition of metal particles with different catalytic activity on the surface of carbon nanotubes. The selective determination of these gases involved the use of a pattern-recognition method.⁴⁷

3. Sensors in biology and medicine

Nowadays, active studies are carried out aimed at the use of nanoparticles in biology and medicine. The problems to be solved in these fields of knowledge are closely interrelated; this is why they are often considered together. For biological and medicinal applications, nanoparticles that as a rule have hydrophobic stabilising shells should be transferred to aqueous solutions where the hydrophobic ligands are replaced by hydrophilic. For this purpose, it is necessary to use molecules that contain several functional groups of which some groups can be used for stabilisation of nanoparticles and the other should promote their modification and functionalisation.

As such molecules, amphiphilic polymeric molecules that are capable of transferring virtually any particle into aqueous media are used.¹⁰⁵ Their relative drawback is associated with the increase in the nanoparticle volume due to the formation of several stabilising layers. At the same time, the diversity of amphiphilic polymers makes it possible to introduce different

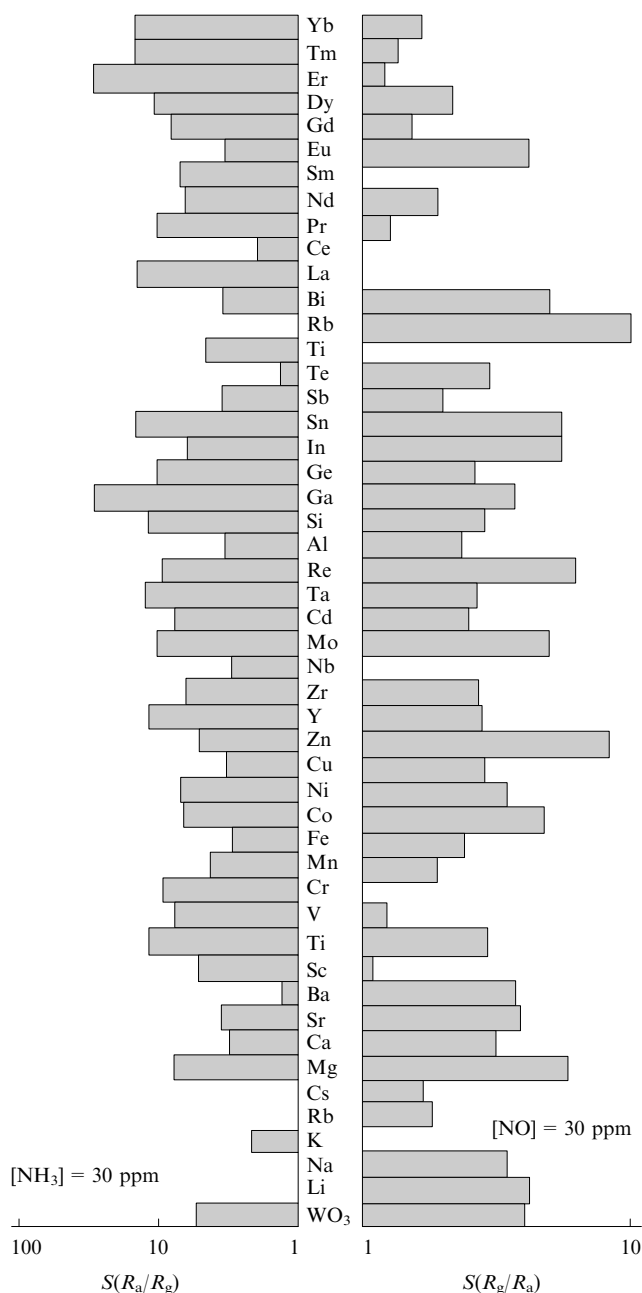


Figure 4. The effect of the introduction of 1 mass % of different dopants on the sensitivity of a gas sensor based on tungsten oxide with respect to ammonia and nitrogen monoxide.¹⁰² S is sensor response, R_a and R_g are the sample resistance in air and in the analysed gas atmosphere, respectively.

functional groups into shells of nanoparticles, bind the latter with bioactive molecules and use them as sensors.

When using nanoparticles, attention should be paid to the toxicity of nanosystems. Substances utilised in biology and medicine even if safe on the microlevel can become toxic on the nanoscale. Bearing this in mind, it is important to study the particle–cell interactions.² The adverse effect of nanoparticles on a cell can manifest itself as follows:

- a nanoparticle may oxidise the cell membrane; finding itself in the cell environment, a nanoparticle can behave as a toxic chemical that causes apoptosis,⁸ *i.e.*, the cell death;
- a nanoparticle captured by the cell membrane or adsorbed on its surface can become the reason for the impaired cell functions;
- a toxic effect can appear in the interaction of nanoparticles of different shapes (*e.g.*, spherical and fibre) in a cell.

Studies of the properties of CdSe nanoparticles and the CdSe/ZnS nanosystem have shown that the toxicity depends on the nanoparticle size, its surface coverage and the nature of functional groups bound with its surface.¹⁰⁶ Toxicity of CdSe particles was found in yet another study.¹⁰⁷

Studies on the use of different types of quantum dots[¶] as the markers for cells, tissues, bacteria and viruses are actively progressing. As compared with organic dyes, quantum dots exhibit the higher photostability and sensitivity.

The ambiguity of views of scientists on the toxicity of nanoparticles does not reduce the number of publications on the use of these materials as the sensitive tags for sensors. Nanocrystals and especially quantum dots are the convenient markers that are unsusceptible to light bleaching and sufficiently biocompatible. Moreover, in cell fission, nanoparticles get to both new cells preventing the loss of the label. Particles CdS that exhibit fluorescence properties were grown on magnetic FePt nanoparticles. Such nanoformations can be delivered to any internal organ to follow the state of the latter.

For the same purpose, hybri nanoparticles and quantum dots covered with phospholipid bilayers (phospholipids are also parts of the membrane) were used.¹⁰⁸ Such nanosystems exhibit good luminescence properties, biocompatibility and can be used in the monitoring of cell transformations. For example, similar particles were introduced into frog's embryonal cells, which allowed scientists to follow the foetus development.[†]

Metal nanoparticles can be used in enhancing the sensitivity of a sensor for the determination of DNA. Thus detection of 5–10 DNA chains¹⁰⁹ involved the use of magnetic iron oxide nanoparticles and citrate-stabilised gold nanoparticles, which allowed the DNA detection with sufficiently high sensitivity. Figure 5 illustrates this process. In addition to using two metals, silver-coated electrodes were employed for the amplification of the signal from gold-modified DNA. Such a trick increased the light scattering (outlet signal), which allowed 10 chains or 500 zeptomoles ($1 \text{ zmol litre}^{-1} = 10^{-21} \text{ mol litre}^{-1}$) to be detected. This method requires neither the use of enzymes nor great times and is relatively cheap. It also allows one to distinguish DNA molecules containing individual bases with the sensitivity of up to $10^{-18} \text{ mol litre}^{-1}$. The elaborated method was used in the detection of anthrax DNA.

§ Apoptosis is a phenomenon of programmed cell death accompanied by the appearance of typical cytological evidence (apoptosis markers) and molecular processes.

¶ Quantum dots are crystals of, as a rule, nanosize inorganic semiconductors that exhibit unique physical and chemical properties untypical of the same substances on the macroscale. Quantum dots may be bound to biological molecules by chemical bonds.

† In contrast to other studies, no mention was made on the toxicity of CdSe.¹⁰⁸

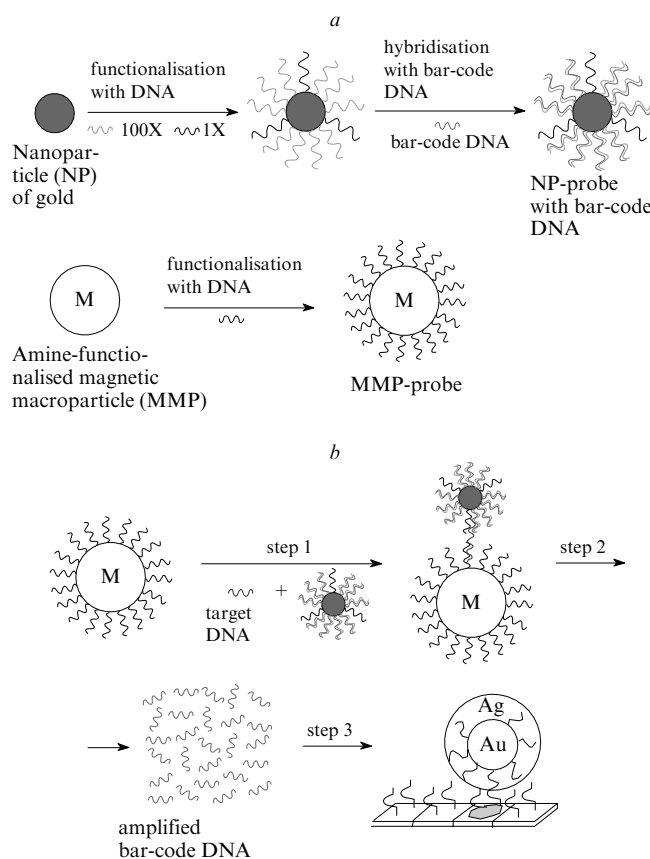


Figure 5. Scheme of operation of metal nanoparticles used in DNA detection.¹⁰⁹

(a) Scheme of synthesis of probes based on nanoparticles and magnetic microparticles; (b) DNA amplification scheme: step 1 is the binding of the target DNA to functionalised DNA-NP and MMP probes, step 2 is the magnetic separation and decomposition of duplexes of bar-code DNA; step 3 is the determination and analysis of bar-code DNA. Target DNA (anthrax): 5'GGATTATTGTTAAATATTGATAAGGAT3', bar code DNA: 5'AGCTACGAGTTGAGAATCCTGAATGAATGCGACG3'.

The development of the similarly fast and high-sensitive sensors is the burning problem for the prevention of terrorist attacks.

The requirements imposed upon the selectivity, precision and reliability of methods for the determination of clinically important metabolites as the indicators of the state of human health are gradually becoming more stringent. New versions of the detection of compounds associated with different diseases are being actively developed. One of such methods was used in the creatinine determination.¹¹⁰ Creatinine, a common urine component, is also present in blood and muscles. Blood of a healthy person contains creatinine at a level of 35–140 $\mu\text{mol litre}^{-1}$. In kidney diseases or their transplantation, the creatinine concentration in blood serum and plasma may reach 1 mmol litre^{-1} .

Figure 6 illustrates the operation of a sensor by the example of creatinine determination. The main components of this system include the enzyme creatinase deaminase and a polyacrylamide hydrogel that contains spheres of polystyrene latex with diameter of 120 nm.

Under the action of the enzyme, creatinine is quickly hydrolysed to form hydroxide ion OH^- . In the second stage, 2-nitrophenol is added to the system by titration, which changes pH of the medium. Phenol deprotonation leads to hydrogel swelling due to an increase in the phenol solubility. As

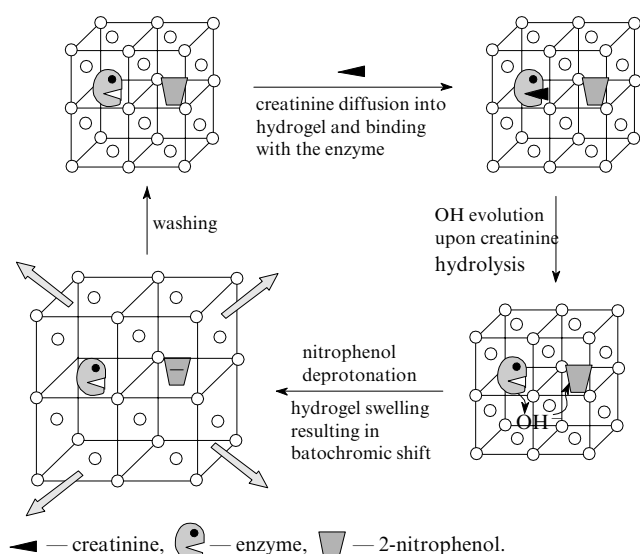


Figure 6. Illustration of operation of a sensor for creatinine.¹¹⁰

a result, with the increase in the creatinine concentration, the luminescence lines shift to lower energies, *i.e.*, the bathochromic shift is observed.

The spectral sensitivity of a sensor allows one to reliably determine creatinine concentrations in the range of $0.1 - 1 \text{ mmol litre}^{-1}$. With the aim of simplifying the creatinine determination, coloured calibration charts were proposed.¹¹⁰ Such charts will allow patients to obtain information without using special instruments, which is of vital importance for those suffering kidney diseases.

The approach developed for the creatinine determination was used in designing a sensor for glucose.¹¹¹ Clinical tests have shown that such a sensor makes it possible to determine up to $0.15 \text{ mmol litre}^{-1}$ glucose in solutions at 37°C . The elaboration of such sensors is of great importance for diabetic patients.

Inhalation of air containing high ammonia concentrations can lead to pulmonary edema; once the ammonia concentration reaches $5000 - 10\,000 \text{ ppm}$, death occurs in $5 - 10 \text{ min}$. Prolonged exposure in an atmosphere containing small ammonia concentration does not harm the health. This is due to the fact that ammonia is not accumulated in organisms. It is the metabolite of proteins and nucleic acids. Ammonia is removed from organisms with urine in the form of urea and ammonium salts. A small amount of ammonia is secreted by sweat glands.

In certain diseases, the organism contains an enhanced amount of ammonia, which can be found by the analysis of the exhaled air.¹¹² Such a test makes it possible to quickly diagnose stomach ulcer induced by the presence of bacteria *Helicobacter pylori*¹¹³ or the urea imbalance inherent of kidney diseases. As little as several cubic centimetres of exhaled air are sufficient for the analysis with gas-sensitive sensors.¹¹⁴

Diagnosing of *Helicobacter pylori* is based on the urea conversion to ammonia and bicarbonate. Laying aside the complex processes that involve bacteria and lead to the ammonia synthesis, it should be noted that such analyses require sensors capable of the detection of $< 50 \text{ ppb}$ ammonia in the exhaled air in the presence of carbon dioxide in concentrations up to 3% .¹¹² The response time of such sensors should not exceed several minutes. To date, this problem is still unsolved. This example of the ammonia determination for the identification of *Helicobacter pylori* demonstrates all the complexity of problems faced by a designer of sensors for diagnosing diseases.

IV. Conclusion

The analysis of studies published in the recent years allows one to draw several general conclusions on the synthesis and application of nanomaterials in the development of new gas sensors. Two trends are clear, *viz.*, the development of sensors to be employed at room temperature and the use of new quasi-one-dimensional nanostructures (such as nanotubes, nanorods, nanobelts, nanowires, *etc.*) as the sensors.

Studies of size effects typical of substances in the nanostate should stimulate the further investigations of the sensor activity that depends on the surface-to-volume ratio, porosity, sample size and possible reactions with different oxygen forms on the sensor surface.

The use of quasi-one-dimensional materials and the production of hybrid systems require the refinement of mechanisms of the sensor sensitivity. Understanding of these mechanisms determines the successful use of new sensor materials. The following general requirements can be imposed upon virtually all sensor materials: the high sensitivity, selectivity, stability and safety. The other requirements to sensors differ depending on application fields and conditions. The development of nanoscience opens up new directions in the use of sensors, particularly, in the analysis of operation, identification, and safe performance of instruments and materials produced by nanotechnologies.

This review was written at partial financial support of the Russian Foundation for Basic Research (Project No 05-03-32 293) and the Grant of President of the Russian Federation for young Russian scientists, namely, candidates of sciences and their supervisors, (No. MK-4996.2006.3).

References

1. M S Roco *Nanotechnology Research Directions: IWGN Workshop Report. Vision for Nanotechnology R&D in the Next Decade* (Dordrecht: Kluwer Academic, 2000)
2. G A Ozin, A C Arsenault *Nanochemistry. A Chemical Approach to Nanomaterials* (London: Royal Society of Chemistry, 2005)
3. G B Sergeev *Nanochemistry* (Amsterdam: Elsevier, 2006)
4. V E Bochenkov, G B Sergeev *Adv. Coll. Int. Sci.* **116** 245 (2005)
5. *The Vth International Conference on Low Temperature Chemistry (Book of Abstracts)* Moscow, 2006
6. C G Wang, W Wang *Drying Technol.* **25** 29 (2007)
7. B Eggers *Khimicheskie i Biologicheskie Sensory* (Chemical and Biological Sensors) (Moscow: Tekhnosfera, 2005)
8. D Kohl *J. Phys. D* **34** R125 (2001)
9. N Docquier, S Candel *Prog. Energy Combust. Sci.* **28** 107 (2002)
10. S Ampuero, J O Bosset *Sens. Actuators, B* **94** 1 (2003)
11. D Nicolas-Debarnot, F Poncin-Epaillard *Anal. Chim. Acta* **475** 1 (2003)
12. A J Haes, R P Van Duyne *Anal. Bioanal. Chem.* **379** 920 (2004)
13. B Timmer, W Olthuis, A van den Berg *Sens. Actuators, B* **107** 666 (2005)
14. J Riu, A Maroto, F X Rius *Talanta* **69** 288 (2006)
15. X-J Huang, Y-K Choi *Sens. Actuators, B* **122** 659 (2007)
16. J Fraden *Handbook of Modern Sensors: Physics, Design and Applications* (Berlin: Springer, 2003)
17. J Wilson *Sensor Technology Handbook* (Burlington: Elsevier, 2004)
18. R B Vasiliev, L I Ryabova, M N Rumyantseva, A M Gaskov *Usp. Khim.* **73** 1019 (2004) [*Russ. Chem. Rev.* **73** 939 (2004)]
19. M Graf, A Gurlo, N Barsan, U Weimar, A Hierlemann *J. Nanopart. Res.* **8** 823 (2005)
20. N Barsan, D Koziej, U Weimar *Sens. Actuators, B* **121** 18 (2007)
21. N Barsan, U Weimar *J. Electroceram.* **7** 143 (2001)
22. N Barsan, U Weimar *J. Phys., Condens. Matter* **15** R813 (2003)
23. J C Love, L A Estroff, J K Kriebel, R G Nuzzo, G M Whitesides *Chem. Rev.* **105** 1103 (2005)
24. M-C Daniel, D Astruc *Chem. Rev.* **104** 293 (2004)

25. A C Templeton, W Wuelfing, R Murray *Acc. Chem. Res.* **33** 27 (2000)
26. H Wohltjen, A Snow *Anal. Chem.* **70** 2856 (1998)
27. E E Foos, A W Snow, M E Twigg, M G Ancona *Chem. Mater.* **14** 2401 (2002)
28. H-L Zhang, S D Evans, J R Henderson, R E Miles, T-H Shen *Nanotechnology* **13** 439 (2002)
29. L Wang, X Shi, N Kariukim, M Schadt, Q Renger, J Choi, J Luo, S Lu, C-J Zhong *J. Am. Chem. Soc.* **129** 2161 (2007)
30. H Bai, G Shi *Sensors* **7** 267 (2007)
31. J Stejskal, J Zemek, J Prokes, I Sapurina *Synth. Met.* **105** 195 (1999)
32. V Chabukswar, S Pethkar, A Athawale *Sens. Actuators, B* **77** 657 (2001)
33. A Kukla, Y Shirshov, S Piletsky *Sens. Actuators, B* **37** 135 (1996)
34. N Agbor, M Petty, A Monkman *Sens. Actuators, B* **41** 137 (1997)
35. K Ogura, H Shiigi, T Oho, T Tonosaki *J. Electrochem. Soc.* **147** 4351 (2000)
36. S Sharma, C Nirkhe, S Pethkar, A Athawale *Sens. Actuators, B* **85** 131 (2002)
37. A A Athawale, S V Bhaqwat, P P Katre *Sens. Actuators, B* **114** 263 (2006)
38. Z Huang, P-C Wang, A G MacDiarmid, Y Xia, G Whitesides *Langmuir* **13** 6480 (1997)
39. M Mazur, P Kryszinski *Thin Solid Films* **396** 131 (2001)
40. A Loiseau *Synthesis Methods and Growth Mechanisms* Vol. 677 (Berlin, Heidelberg: Springer, 2006) p. 49
41. J Kong, N Franklin, C Zhou, M Chapline, S Peng, K Cho, H Dai *Science* **287** 622 (2000)
42. S G Wang, Q Zhang, D J Yang, P J Sellin, G F Zhong *Diamond Relat. Mater.* **13** 1327 (2004)
43. X Feng, S Irle, H Witek, K Morokuma, R Vidic, E Borguet *J. Am. Chem. Soc.* **127** 10533 (2005)
44. S Peng, K Cho, P Qi, H Dai *Chem. Phys. Lett.* **387** 271 (2004)
45. B-Y Wei, M-C Hsu, P-G Su, H-M Lin, R-J Wu, H-J Lai *Sens. Actuators, B* **101** 81 (2004)
46. Q Zhao, M Buongiorno Nardelli, J Bernholc *Nano Lett.* **5** 847 (2005)
47. A Star, V Joshi, S Skapuro, D Thomas, J-C P Gabriel *J. Phys. Chem. B* **110** 21014 (2006)
48. C Staii, A T Johnson *Nano Lett.* **5** 1774 (2005)
49. Y Sun, H H Wang *Appl. Phys. Lett.* **90** 213107 (2007)
50. E Bekyarova, M Davis, T Burch, M E Itkis, B Zhao, S Sunshine, R C'Haddon *J. Phys. Chem.* **108** 19717 (2004)
51. T Zhang, M B Nix, B-Y Yoo, M A Deshusses, N V Myung *Electroanalysis* **18** 1153 (2006)
52. A Modi, N Koratkar, E Lass, B Wei, P M Ajayan *Nature (London)* **424** 171 (2003)
53. N Koratkar *Int. J. Nanosci.* **4** 945 (2005)
54. S Noda, K Hasegawa, H Sugime, K Kakehi, Z Zhang, S Maruyama, Y Yamaguchi *Jpn. J. Appl. Phys.* **46** L399 (2007)
55. O Dos Santos, M L Weiller, D Q Junior, A N Medina *Sens. Actuators, B* **75** 83 (2001)
56. G B Sergeev *Nanokhimiya (Nanotechnology)* (Moscow: Moscow State University, 2003)
57. V E Bochenkov, Candidate Thesis in Physical and Mathematical Sciences, Moscow State University, Moscow, 2004
58. V E Bochenkov, V V Zagorskii, G B Sergeev *Sens. Actuators, B* **103** 375 (2004)
59. V E Bochenkov, P Karageorgiev, L Brehmer, G B Sergeev *Thin Solid Films* **458** 304 (2004)
60. E V Shmanova, V E Bochenkov, V V Zagorskii, G B Sergeev *Mendeleev Commun.* (1) (2008) (in the press)
61. N Yamazoe, N Miura *Some Basic Aspects of Semiconductor Gas Sensors (Chemical Sensor Technology)* (Tokyo: Kodansha, 1992) Vol. 4, p. 19
62. R C Aiyer, S G Ansari, P Borojerdian, R N Karekar, S K Kulkarni, S R Sainkar *Thin Solid Films* **295** 271 (1997)
63. A Gurlo, M Ivanovskaya, N Barsan, M Schweizer-Berberich, U Weimar, W Gopel, A Dieguez *Sens. Actuators, B* **44** 327 (1997)
64. O K Tan, W Zhu, Q Yan, L B Kong *Sens. Actuators, B* **65** 361 (2000)
65. M K Kennedy, F E Kruis, H Fissan, B R Mentha, S Stappert, G Dumpich *J. Appl. Phys.* **93** 551 (2003)
66. L Yu Kupriyanov *Nanotekhnika* **1** 30 (2004)
67. A N Shatokhin, S I Kudryashov, O V Safonova, A M Gas'kov, A V Demidov, F N Putilin *Khim. Vys. Energ.* **34** 219 (2006)^a
68. L Madler, A Roessler, S E Pratsinis, T Sahm, A Gurlo, N Barsan, U Weimar *Sens. Actuators, B* **114** 283 (2006)
69. U-S Choi, G Sakai, K Shimano, N Yamazoe *Sens. Actuators, B* **107** 397 (2006)
70. O Wurzing, G Reinhardt *Sens. Actuators, B* **103** 104 (2006)
71. R K Joshi, F E Kruis, O Dmitrieva *J. Nanopart. Res.* **8** 797 (2006)
72. A Kolmakov, D O Klenov, Y Lilach, M Moskovits *Nano Lett.* **5** 667 (2005)
73. R K Joshi, F E Kruis *Appl. Phys. Lett.* **89** 153116 (2006)
74. E Comini, G Faglia, G Sberveglieri, Z Pan, Z L Wang *Appl. Phys. Lett.* **81** 1869 (2002)
75. I Z Rahman, K M Razeed, M A Rahman, M Kamruzzaman *J. Magn. Magn. Mater.* **262** 166 (2003)
76. E Comini, V Guidi, C Malagu, G Martinelli, Z Pan, G Sberveglieri, Z Wang *J. Phys. Chem.* **108** 1882 (2004)
77. A Kolmakov, M Moskovits *Annu. Rev. Mater. Res.* **34** 151 (2004)
78. Y Xia, Y Yang P Sun, Y Wu, B Mayers, B Gates, Y Yin, F Kim, H Yan *Adv. Mater.* **15** 353 (2003)
79. W Gu, H Choi, K Kim *Appl. Phys. Lett.* **89** 253102 (2006)
80. B J Murray, Q Li, J T Newberg, J C'Hemmeringer, R M Penner *Chem. Mater.* **17** 6611 (2005)
81. B J Murray, E C'Walter, R M Penner *Nano Lett.* **4** 665 (2004)
82. A Kolmakov, Y X Zhang, G S Cheng, M Moskovits *Adv. Mater.* **15** 997 (2003)
83. Y L Wang, X C'Jiang, Y N Xia *J. Am. Chem. Soc.* **125** 16176 (2003)
84. F Fernandez-Ramirez, A Tarancon, O Casals, J Arbiol, A Romano-Rodriguez, J R Morante *Sens. Actuators, B* **121** 3 (2007)
85. Z L Wang *Annu. Rev. Phys. Chem.* **55** 159 (2004)
86. S Dmitriev, Y Lilach, B Button, M Moskovits, A Kolmakov *Nanotechnology* **18** 1 (2007)
87. Y Lei, W-K Chim *J. Am. Chem. Soc.* **127** 1487 (2005)
88. A Tomchenko, G Harmer, B Marquis, J Allen *Sens. Actuators, B* **93** 126 (2003)
89. S Ahlers, G Muller, T Doll *Sens. Actuators, B* **107** 587 (2005)
90. M Z Atashbar, S Singamaneni *Sens. Actuators, B* **111** – **112** 13 (2005)
91. I Raible, M Burghard, U Schlecht, A Yasuda, T Vossmeier *Sens. Actuators, B* **106** 730 (2005)
92. G Mount, B Rumburg, J Havig, B Lamb, H Westberg, D Yonge, K Johnson, R Kincaid *Atmos. Environ.* **36** 1799 (2002)
93. R Moos, R Muller, C Plog, H Leye, E Irion, T Braun, K-J Marquardt, K Binder *Sens. Actuators, B* **83** 181 (2002)
94. M Wallin, C-J Karlsson, M Skoglundha, A Palmqvist *J. Catal.* **218** 354 (2003)
95. X Xuan, C Yue, S Li, Q Yao *Fuel* **82** 575 (2003)
96. S G Buckley, C J Damm, W M Vitovec, L A Sgro, R F Sawyer, C P Koshland, D Lucas *Appl. Opt.* **37** 8382 (2003)
97. H T Wang, B S Kang, F Ren, L C Tien, P W Sadik, D P Norton, S J Pearton, J Lin *Appl. Phys. Lett.* **86** 243503 (2005)
98. E Comini, L Yubao, Y Brando, G Sberveglieri *Chem. Phys. Lett.* **407** 368 (2005)
99. P Colonna, S Gabrielli *Appl. Thermal. Eng.* **23** 381 (2003)
100. J Fernandez-Seara, J Sieres, M Vazquez *Int. J. Refrig.* **26** 28 (2003)
101. X Wang, J Zhang, Z Zhu *Appl. Surf. Sci.* **252** 2404 (2006)
102. X Wang, N Miura, N Yamazoe *Sens. Actuators, B* **66** 74 (2000)
103. C Xu, N Miura, Y Ishida, K Matsuda, N Yamazoe *Sens. Actuators, B* **65** 163 (2000)
104. A Jerger, H Kohler, F Becker, H Keller, R Seifert *Sens. Actuators, B* **81** 301 (2000)
105. M A Petrushka, A P Bartko, V I Klimov *J. Am. Chem. Soc.* **126** 714 (2004)

106. C Kirchner, T Liedl, S Kudera, T Pellegrino, A M Javier, H E Gaub, S Stolzle, N Fertig, W J Parak *Nano Lett.* **5** 331 (2005)
107. A M Derfus, W C W Chan, S N Bhatia *Nano Lett.* **4** 11 (2005)
108. B Dubertret, P Skourides, D J Norris, V Noireaux, A H Brivanlou, A Libchaber *Science* **298** 1759 (2002)
109. J-M Nam, S I Stoeva, C A Mirkin *J. Am. Chem. Soc.* **126** 5932 (2004)
110. A C Sharma, T Jana, R Kesavamoorthy, L Shi, M A Virji, D N Finegold, S A Asher *J. Am. Chem. Soc.* **126** 2971 (2004)
111. M Ben-Moshe, V L Alexeev, S A Asher *Anal. Chem.* **78** 5149 (2006)
112. W Ament, J R Huizenga, E Kort, T W van der Mark, R G Grevink, G J Verkerke *Int. J. Sports Med.* **20** 71 (1999)
113. L R Narasimhan, W Goodman, C K N Patel *PNAS* **98** 4617 (2001)
114. E Verpoorte *Electrophoresis* **23** 677 (2002)

^a — *High Energ. Chem. (Engl. Transl.)*

The chemistry of combustion of organophosphorus compounds

O P Korobeinichev, V M Shvartsberg, A G Shmakov

Contents

I. Introduction	1021
II. Methods and approaches to investigation of the combustion mechanism of organophosphorus compounds	1022
III. The mechanism of destruction of organophosphorus compounds in the flame	1024
IV. Mechanism of promotion and inhibition of the H_2/O_2 flames by addition of organophosphorus compounds	1031
V. Studies of the mechanism of inhibition and quenching of hydrocarbon flames by organophosphorus additives	1034
VI. Toxicity and environmental impact of organophosphorus compounds	1044

Abstract. The state of the art of studies on combustion of organophosphorus compounds (OPC) is presented. The chemical processes occurring in flames upon introduction of OPC additives, the mechanisms of OPC transformations and effect on the combustion rate and the structure and propagation limits of hydrogen and hydrocarbon flames are considered. The key results of experimental and theoretical studies and simulation of the combustion chemistry of hydrogen and hydrocarbon mixed and diffusion flames with and without OPC are described. The mechanism of flame promotion and inhibition by OPC is analysed. The prospects of practical applications of phosphorus compounds as flame promoters and suppressants are evaluated. The toxicity and environmental impact of OPC are discussed. The bibliography includes 124 references.

I. Introduction

The chemistry of phosphorus compounds is very extensive and diversified. Phosphorus and its compounds are common in nature ranging from Earth crust minerals to living organisms where phosphorus is vitally important.

The first mention on the investigation into combustion of phosphorus dates back to the 17th century. In 1680, R Boyle¹ burned phosphorus in air and obtained white vapour, which turned into a white powder on cooling. On treating this powder with water, he obtained a liquid with acid properties. Later in has been found that during combustion of phosphorus and its compounds, a large number of phosphorus-containing species are present in the flame. The mechanism of phosphine combustion proposed in 1993 included about 20 phosphorus oxides and phosphorus-containing acids.² The existence of numerous phosphorus derivatives in the flames attest to a

complex chemical mechanism of transformations of phosphorus and its compounds.

The interest in the combustion chemistry of organophosphorus compounds (OPC) first arose in relation to the problem of destruction of chemical weapons (first of all, nerve agents), which present a serious hazard for both the environment and human life. The combustion of war gases in furnaces formed the basis of an advanced process for the destruction of chemical agent stockpiles. This process was implemented in the USA in the Johnston atoll.^{3,4} At that stage, researchers were mainly interested in the mechanism of destruction of complex organophosphorus molecules that simulate chemical agents in a flame.

The term ‘destruction’ is used to mean the transformation of a compound upon reactions with other flame components or upon pyrolysis rather than its thermal decomposition. The intermediate and final products of OPC destruction in the flame were identified using dimethyl methylphosphonate [DMMP, $CH_3PO(OCH_3)_2$], trimethyl phosphate [TMP, $(CH_3O)_3PO$] and diisopropyl methylphosphonate [DIMP, $CH_3PO(iso-OC_3H_7)_2$] as models. On the basis of obtained results, reactions of H and OH radicals with OPC molecules were proposed, their rate constants were estimated and a number of kinetic mechanisms of OPC combustion were developed. Subsequently, OPC aroused interest as compounds able to retard (inhibit) combustion.

For many years, halo-substituted, mainly bromo-substituted hydrocarbons (halons) such as CF_3Br have been employed as flame suppressants. However, after these compounds were found to deplete the Earth ozone screen, the production of environmentally hazardous halons ceased in industrially developed countries in conformity with the Montreal convention (1990).⁵ Environmentally safe halons like CF_3H and C_2F_5H had low flame suppression efficiency compared to bromine-containing halons; therefore, search for a substitute for halons among other classes of compounds was started. The search led to the OPC family having good prospects as combustion inhibitors.^{6–8}

It is noteworthy that OPC do not merely dilute flames (thermophysical flame suppression effect), but rather change the concentration of the most reactive atoms and radicals in the flame, first of all, H, O and OH (chemical suppression of flame by additives), thus having considerable effect on combustion parameters even at low additive concentration (0.03 vol.%).

O P Korobeinichev, V M Shvartsberg, A G Shmakov Institute of Chemical Kinetics and Combustion, Siberian Branch of the Russian Academy of Sciences, ul. Institutskaya 3, 630090 Novosibirsk, Russian Federation. Fax (7-383) 330 73 50, tel. (7-383) 333 28 52, e-mail: korobein@kinetics.nsc.ru (O P Korobeinichev), tel. (7-383) 33 33 46, e-mail: vshvarts@kinetics.nsc.ru (V M Shvartsberg), shmakov@kinetics.nsc.ru (A G Shmakov)

Received 4 April 2007

Uspekhi Khimii 76 (11) 1094–1121 (2007); translated by Z P Bobkova

The purpose of this review is to generalise the data on the chemistry and mechanism of OPC transformations in the flames and non-thermal plasma published in the last decades. The review considers in detail the mechanisms of flame promotion, inhibition and suppression by OPC additives. The specific features of inhibition processes for different types of flames are analysed and the dependences of the efficiency of these processes on their conditions (pressure, fuel type, and fuel excess or deficiency) were found. The unique properties of OPC (in particular, physicochemical and toxicological) that distinguish them from other inhibitors were revealed, the effect of OPC on the Earth ozone layer was estimated. On the basis of all the available published data, the prospects for practical applications of phosphorus-containing inhibitors were evaluated.

II. Methods and approaches to investigation of the combustion mechanism of organophosphorus compounds

The chemistry of combustion of organophosphorus compounds has been studied using special experimental and computational methods. Since these processes occur under extreme conditions, many of these methods are actually unique and often poorly known; therefore, below they are described in brief.

1. Experimental methods for investigation of combustion mechanism of organophosphorus compounds

a. Study of the chemical structure of flames by molecular-beam mass spectrometry

The understanding of the essence of chemical kinetic processes taking place in the flames requires knowledge of gas composition in the flames and distribution of combustion product concentrations over the combustion zone. The identification of compounds in the flames and measurement of their concentrations and concentration profiles are usually performed by probe sampling followed by mass spectrometric^{9, 10} or optical spectroscopic analysis. Each of the procedures has its advantages; they have repeatedly been used in the research of flames.

Some species found in the flames (atoms, free radicals and ions) are too reactive and unstable to be sampled and analysed by conventional methods; therefore, the sample was introduced into the ionisation chamber of a mass spectrometer as a molecular beam in which molecules did not collide with either one another or the vacuum chamber walls. The profiled probe nozzle and a large pressure differential promote efficient freezing of reactions that occur in the flame, so that quite a robust sample enters the analyser.

Probe molecular beam mass spectrometry (MBMS) is now the only method to detect all species present in the flame (including reactive species), measure their concentrations and spatial distribution, *i.e.*, determine the chemical structure of the flame.¹¹ However, this method requires additional measures for the separation of substances having similar mass spectra. One of such measures is selective (or so-called soft) ionisation of species in the sample by photoionisation^{12, 13} or electron impact.^{14, 15} For this purpose, a setup with an advanced ion source with a small energy scatter of electrons (± 0.25 eV) corresponding to thermal scatter was designed at the Institute of Chemical Kinetic and Combustion of the Siberian Branch of the RAS.

Owing to soft ionisation, analysis can be carried out at low ionisation energies close to the ionisation potentials of atoms, radicals and molecules and thus it serves for mitigation (or elimination) of molecular ion fragmentation upon electron impact and, hence, facilitates identification of compounds based on their mass spectra.^{14, 15} Table 1 presents ionisation

Table 1. Ionisation potentials and ionisation electron energies for major components of the flame with OPC additives.

Compound or species	<i>m/z</i>	Ionisation potential/eV	Ionisation electron energy in the experiment /eV
PO	47	8.3 ± 0.3	12.8
PO ₂	63	11.0 ± 0.5	12.8
HOPO	64	10.7 ± 0.3	12.8
HOPO ₂	80	12.4 ± 0.2	14.5
(HO) ₃ PO	98	11.5 ± 0.5	17.5
(CH ₃ O) ₂ (CH ₃)PO	124	9.9 ± 0.5	20.0
(CH ₃ O) ₃ PO	140	9.9 ± 0.5	20.0
H	1	13.3 ± 0.5	16.2
O	16	13.6 ± 0.2	16.2
OH	17	13.2 ± 0.2	16.2

potentials and ionisation voltages (ionisation energies, IE) used to measure the major components of flames with OPC additives: atoms, free radicals and key phosphorus-containing compounds. The ionisation potentials of compounds such as PO, PO₂, HOPO, HOPO₂ and (HO)₃PO were determined by measuring the ionisation efficiency curves upon direct sampling of flames with OPC additives. The relative error of measurement of the concentrations of stable compounds in the flame by this method is $< 10\%$, that for radicals is $< 30\% - 50\%$. The perturbing effect of the sampler during flame probing is an important aspect influencing correct interpretation of the experimental results. In recent years, a number of experimental and computational studies dealing with the flame perturbation by the probe were published (see, for example, Refs 16, 17). The results obtained in these studies substantiate the efficiency of using the experimental temperature profile for simulation of the concentration profiles of compounds in the flame.

b. Measurement of flame temperature using thermocouples

The temperature distribution across the combustion zone is usually measured by microthermocouples [Pt/(Pt + 10% Rh) and so on] with different diameters. For preventing catalytic processes, the thermocouple surface is coated by SiO₂ or ceramics.¹⁸ The emission corrections were estimated by the Kaskan formula¹⁹ or excluded by using compensation measurements.²⁰ The agreement between the temperature and concentration profiles across the zone was attained by shifting the concentration profiles with respect to the temperature profile.²¹ The error of temperature measurement usually did not exceed ± 30 K.

c. Methods of measurement of normal flame propagation speed

Several methods exist for measuring of the normal propagation speed of the flame front in laminar pre-mixed gas mixtures. One method is based on the use of the Mache–Hebra burner,²² which provides the contour of the visible image of the flame as a regular cone. The accuracy of measurement of the flame speed by this method is $\pm 5\%$. This method for flame propagation speed measurement is very convenient due to its simplicity and availability but is considered to be least accurate.

The technique of zero heat flux to the burner, which has found wide use in recent years, is more accurate.^{23, 24} This method makes use of a flat burner consisting of a copper disc with evenly distributed holes and the side surface cooled by tap water. The radial temperature distribution over the burner surface is measured by insertion of thermocouples into its holes at different distances from the burner centre. When temperature is evenly distributed over the burner disc surface, a heat flux from the flame to the burner is absent, the flame existing

under nearly adiabatic conditions. This means that the flow rate of the combustible mixture is equal to the free distribution speed of the flame.

The method of measurement of the normal speed of flame propagation using a constant volume bomb also deserves attention.²⁵ This measurement requires a special high-pressure chamber, as ignition of the combustible mixture results in substantial pressure rise in a closed vessel.

d. Methods of determination of the minimum quenching concentrations of flame suppressants

The minimum quenching concentration (MQC) is a concentration of a substance in the flame such that the flame is quenched when this concentration has been attained. This is an important characteristics for evaluating the prospects of using a particular compound as a flame suppressant. A standard method for determining the MQCs of flame suppressants^{26, 27} is the cup burner method. It consists of suppression of the diffusion methane–air or n-heptane–air flame by introducing flame suppressant vapour into the air stream.²⁷ Poorly volatile (liquid) compounds are injected into the air stream by means of a nebulizer. Air is heated to enhance evaporation rate of the aerosol of the liquid compound. Yet another, alternative method for determination of MQC is the ‘cylinder’ method described by Baratov *et al.*^{28, 29} Whereas the cup burner method implements a scenario of extinguishing a local ignition source by an air stream with admixed flame suppressants, the ‘cylinder’ method is based on a fire extinguishing scenario in an indoor area.

One more method, the fire chamber method, is used to determine the MQC of flame suppressants under nearly natural conditions. These measurements require a large amount of flame suppressant; therefore, this method cannot be used for screening.

A special setup was designed to study the quenching efficiency of a turbulent[†] flame upon short-term supply of a flame suppressant.³⁰ Using this setup, the dependence of MQC on the supply time of the flame suppressant and the fuel volumetric flow rate was studied. For the study of turbulent flame quenching by poorly volatile liquid OPC, a setup similar to that described previously³⁰ was manufactured.³¹ Both simulate aircraft engine fire extinguishing. Liquid flame suppressants were supplied by a highly dispersed aerosol generator (particle size < 1 µm) of an original design.³¹

2. Numerical simulation and quantum chemical calculations

a. Simulation software

The chemistry of OPC combustion is often studied by numerical simulation, which allows one to calculate the propagation speed and the chemical and thermal structures of multicomponent laminar and diffusion flames. Model calculations use thermochemical and transport characteristics of flame components, detailed chemical mechanism of the combustion process as a set of elementary steps with indicated rate constants for each step. These calculations were carried out using PREMIX and CHEMKIN softwares.^{32, 33} The PREMIX programme calculates (for a unidimensional case) the flame propagation speed and the temperature and component concentration profiles in a freely propagating flame or a flame stabilised on a flat burner. The CHEMKIN-II programme and later versions CHEMKIN-III and CHEMKIN-IV softwares choose the required thermochemical, kinetic and transport characteristics of flame components from the databases included in the program package. All calculations are based on solution of the energy conservation equation with allowance for diffusion.

[†] A turbulent flame site above a tank with liquid fuel is most difficult for extinguishing, especially if the tank is located behind a wedge-like barrier.

One can also use the HCT programme (Hydrodynamics, Chemistry and Transport)³⁴ developed at the Lawrence Livermore National Laboratory (USA) and the OPPDIF programme,³⁵ which is a part of the CHEMKIN package. The latter programme was used to calculate the temperature and component concentration profiles, the radial and axial constituents of the flow velocities along the burner axis in the diffusion flame stabilised at the counterflow of the fuel and the oxidant (the Potter burner^{36, 37}).

b. Kinetic mechanisms

Although the kinetic models of hydrogen and hydrocarbon combustion bear only an indirect relation to the OPC combustion chemistry, the results of simulation of the structure or propagation speed of OPC-doped flames still depend appreciably on the selected mechanism for hydrogen and hydrocarbons. In this connection, we considered it necessary to present brief information on the most often encountered mechanisms of combustion of these compounds.

The rate constants for reactions that describe the hydrogen combustion process have been reported.^{38–40} The H₂ combustion was studied in detail by Dixon-Lewis *et al.*,⁴¹ Tsang and Hampson⁴² and Yetter *et al.*⁴³ A kinetic scheme of hydrogen combustion that includes 40 most important elementary steps involving 8 species has been described.⁴⁴ Although this process has been well studied, a large number of models that differ from one another in both the set of reactions and the rate constants for these reactions can be found in the literature. The latest model of hydrogen oxidation under atmospheric pressure was developed in 2004.⁴⁵

Hydrocarbon flames can be simulated using the GRI-Mech mechanism⁴⁶ describing the combustion of natural gas in the presence of nitrogen. A version of this mechanism, namely, GRI-Mech 3.0 comprises 325 reactions involving 53 components (including argon). One more, Konnov's mechanism⁴⁷ includes 1207 reactions involving 127 components. This is used to describe the combustion of hydrocarbons (≤C₃) and their derivatives. The last-mentioned mechanism was successfully used to calculate the speed of free propagation of propane–air flames.⁴⁷ The results are in good agreement with experimental results.^{48, 49} The kinetic mechanism of propane combustion proposed by Conaire *et al.*⁵⁰ and upgraded by Curran *et al.*⁵¹ was used to describe the structure of propane–oxygen flames with OPC additives stabilised on a flat burner⁵² and to calculate the propagation speed of propane–air flames.⁵³ The mechanism includes 469 steps which involve 77 components.

c. Quantum chemical calculations

The thermochemistry of phosphorus-containing compounds has little been studied until recently. Only recently, was this field of OPC chemistry developed owing to quantum chemical calculations,^{54–56} which became much more precise. This is especially important, as phosphorus oxides are unavailable as commercial chemicals due to their low stability. Table 2 presents the formation enthalpies of PO, PO₂, PO₃, HOPO, HOPO₂, (HO)₂PO, HPO, HPO₂, P₂O₃, P₂O₄ and P₂O₅(gas). Not only thermochemical parameters of OPC (enthalpy, entropy), but also the rate constants for some key reactions of phosphorus-containing species with atoms (H, O, C, N) and radicals were calculated.^{52, 53}

As shown below, these calculations identify more precisely the previously developed kinetic mechanisms and provide better agreement between the experimental data and the results of simulation of the flame propagation speed and chemical structure.

A considerable contribution to the development of OPC combustion mechanism and the kinetic model of the process was made by theoretical works carried out at the Lawrence

Table 2. Formation enthalpies ($\Delta H_f^\circ/\text{kJ mol}^{-1}$) of phosphorus-containing compounds calculated by various methods.

Compound	BAC-MP4 (Ref. 54)	CBS (Ref. 56)	BAC-G2 (Ref. 52)	G3X2 (Ref. 55)
PO	−12.6	−33	−37	−38
PO ₂	−283	−294.9	−298	−291
PO ₃	−430	−450	−450	
HOPO	−452	−470	−468	−470
HOPO ₂	−690	−717	−719	−713
(HO) ₂ PO	−647		−661	−664
HPO	−75	−95	−96	
HPO ₂	−406		−425	
P ₂ O ₃	−616		−658	
P ₂ O ₄	−855		−908	
P ₂ O ₅	−1072		−1135	

Livermore National Laboratory (USA). The OPC combustion model proposed at this laboratory was based on quantum chemical calculations of the thermochemical properties of phosphorus-containing molecules and transition states and reaction rate constants. This approach is more substantiated from the kinetic standpoint as compared with mere variation of the rate constants, as was done in the early investigations. The thermochemical data (enthalpy, entropy and heat capacity) were calculated for 25 compounds of pentavalent phosphorus in which the phosphorus atom is bound to hydrogen, carbon, nitrogen or sulfur atoms.

3. Integrated approach to elucidation of the combustion mechanism of organophosphorus compounds

An efficient approach to investigation of the OPC combustion chemistry is a comparison of experimental and simulated data. The larger the number of combustion characteristics being compared (propagation speed and chemical structure of the flame, propagation limits, minimum quenching concentrations and so on) the more thorough the verification of the proposed kinetic model and the more reliable the model. A problem of many (almost all) kinetic mechanisms is that they have been validated against a limited number of data.

It is noteworthy that the combustion mechanism depends on the stoichiometric composition of the fuel mixture. In the fuel-rich flames, the processes are complicated due to the formation of heavy hydrocarbons, soot precursors. These flames are most often difficult to study, and general hydrocarbon combustion models often poorly predict the characteristics of these flames.

The most thorough verification for any mechanism is a comparison of the calculated and measured flame structures, first of all, a comparison of the concentration profiles of atoms, radicals and other unstable species. This approach was used to study the chemistry of OPC combustion and especially to study the mechanism of inhibition of hydrocarbon flames by TMP.

III. The mechanism of destruction of organophosphorus compounds in the flame

The first soft ionisation MBMS study⁵⁷ devoted to the OPC transformations in the flames (1994) reported the mass spectra of samples taken from the flame and the intensity profiles for ion peaks with m/z corresponding to the initial compounds and intermediate and final products of TMP and tributyl phosphate (TBP) combustion in a hydrogen–oxygen flame at a pressure of 80 Torr. When measuring the TMP and TBP concentration in the flame, it was shown that OPC in a low-pressure hydrogen–oxygen flame are consumed faster than the major flame components (H₂ and O₂). Systematic research into the mechanism of destruction of DMMP, TMP, DIMP, and some other OPC was carried out in the subsequent studies.

1. Mechanism of destruction of dimethyl methylphosphonate

In a study of the structure of a hydrogen–oxygen flame doped with DMMP at 47 and 76 Torr, key intermediates of DMMP destruction with masses of 110 and 94 were detected and identified as methyl methylphosphonate and methylphosphonic acid, respectively. The final phosphorus-containing products of DMMP combustion with m/z 47, 63, 64 and 80 were identified as (PO), (PO₂), (HOPO) and (HOPO₂).^{14, 58, 59}

a. Intensity profiles of the mass peaks of the starting dimethyl methylphosphonate and the intermediate and final products of its destruction

In order to analyse the possible intermediates of DMMP destruction, mass spectra of samples taken from the H₂/O₂/Ar flame ($P = 47$ Torr) doped with 0.2 vol.% DMMP were recorded. The flame samples were taken at distances of ≤ 4 mm from the burner (within the DMMP destruction zone in the flame).¹⁴ The ion peaks with m/z 79, 80, 81, 93, 94, 95, 96, 98, 109, 110 were found in the mass spectra of the samples. The contributions of the fragment ions resulting from ionisation of the DMMP molecule to these peaks were eliminated using a mass spectrum of DMMP recorded in an argon flow. Note that the mass spectrum of DMMP recorded in this way does not contain ion peaks with m/z 110 or 80.

Figure 1 shows the intensity profiles of the peaks of DMMP with m/z 124 and ions with m/z 110, 94 and 80 (with subtracting the contributions of fragment ion peaks) depending on the distance (l) from the burner surface to the probe at $P = 43$ Torr and IE = 12.1 eV. The intensity profiles of ion peaks with m/z 110, 94 and 80 pass through maxima; the intensity maxima of the peaks with m/z 110 and 80 are located at a 1.5 mm distance from the burner, while that for the peak with m/z 94 is at a 2.5 mm distance from the burner. Figure 2 shows the intensity profiles of the peaks of DMMP and ions with m/z 95, 96, 98 and 110 (with subtracting the small contributions of fragment ion peaks) depending on the distance l for $P = 47$ Torr and IE = 20 eV. The presence of maxima in the intensity curves for ion peaks with m/z 80, 94, 95, 96, 98 and 110 indicates that these peaks may correspond to intermediates.

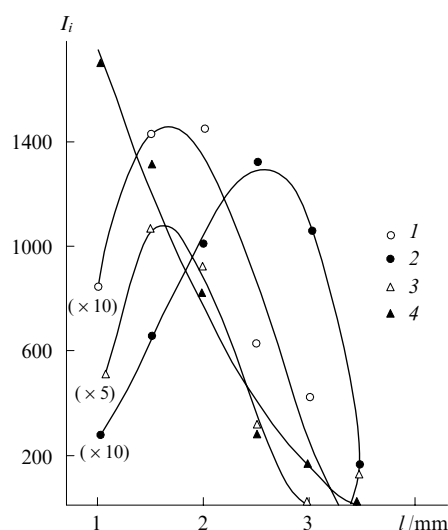


Figure 1. Intensity profiles of ion peaks with m/z 80 (curve 1), 94 (2), 110 (3) and 124 (4) in the H₂/O₂/Ar flame with 0.2 vol.% DMMP at $P = 43$ Torr and IE = 12.1 eV.¹⁴

There are two intermediates with the mass 110: dimethyl phosphonate [HPO(OCH₃)₂] and methyl methylphosphonate [HOPO(OCH₃)(CH₃)]. Under electron impact, both com-

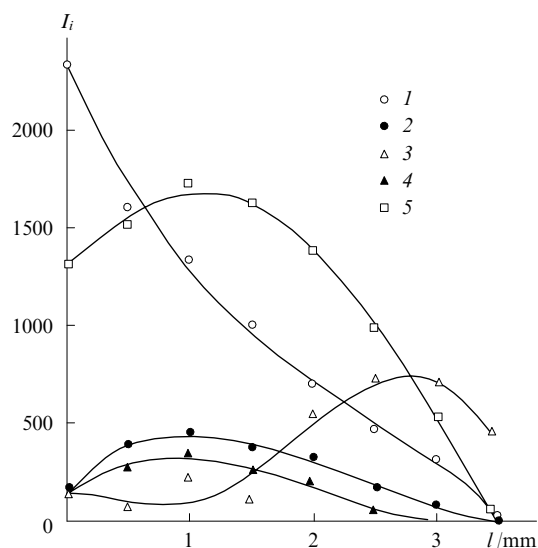


Figure 2. Intensity profiles of the peaks of initial DMMP (curve 1) and ions with m/z 110 (curve 2), 98 (3), 96 (4) and 95 (5) in the $\text{H}_2/\text{O}_2/\text{Ar}$ flame with 0.2 vol.% DMMP at $P = 47$ Torr and $\text{IE} = 20$ eV.¹⁴

pounds give species with masses of 95 and 80;⁶⁰ therefore, ion peaks with m/z 95 and 80 correspond to intermediate fragment compounds (presumably, decomposition products of methyl methylphosphonate¹⁴). The peak with m/z 96 corresponds to methylphosphonic acid $[(\text{HO})_2\text{PO}(\text{CH}_3)]$. The intensity of the ion peak with m/z 81 is approximately twice as high as the intensity of the m/z 98 peak, and the behaviour of the intensity curve of the m/z 81 peak fully reproduces that for the ion peak with m/z 98. The ion with mass 81 may thus be a fragment ion of a compound with mass 98 (this compound was identified as orthophosphoric acid). The ion with mass 94 was identified as the $\text{PO}_2(\text{OCH}_3)$ molecular ion. The ion peaks with m/z 79, 93 and 109 correspond to the fragment ions formed upon bombardment of DMMP with electrons. The mass spectra of samples taken from flames were also found to contain peaks corresponding to species with m/z 28 (CO), 44 (CO_2), 47 (PO), 63 (PO_2) and 64 (HOPO).

The intensity profiles of ion peaks with m/z 47, 63, 64, 80 and 98 recorded for flames doped by 0.2 vol.% DMMP at $P = 47$ Torr are presented in Fig. 3. The ion peak with mass 80 has a maximum at a ~ 1 mm distance from the burner surface. It was found that different substances are responsible for contributions to the ion peak with m/z 80 at different distances from the burner surface. Thus analysis of the curve of DMMP ionisation efficiency has shown that the peak with m/z 80 recorded in the flame at a 1 mm distance from the burner surface has the appearance potential $AP = 11.5 \pm 0.3$ eV, while the ion peak with the same mass detected at a distance of 7–10 mm has $AP = 13.5 \pm 0.5$ eV. Analysis of the mass spectra⁶⁰ of the presumed intermediate product, *viz.*, methyl methylphosphonate (mass 110), indicates that it is fragmented upon electron impact to give an ion with mass 80. Thus, at distances of up to 3 mm (where the ion with m/z 110 was detected as an intermediate), the major contribution to the intensity of the peak with m/z 80 is due to the methyl methylphosphonate fragment ion. At distances $l > 3$ –4 mm from the burner surface (*i.e.*, in the final products of DMMP destruction), the molecular ion of HOPO_2 with the same mass appears in the flame.

Analysis of the concentration profiles of intermediates recorded in the $\text{H}_2/\text{O}_2/\text{Ar}$ flame doped with 0.2 vol.% DMMP suggests the following sequence of DMMP transformations in the flames (possible compounds corresponding to these masses are given in brackets):

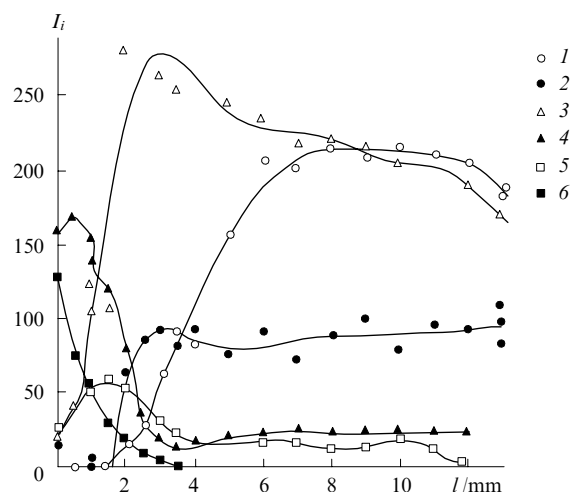
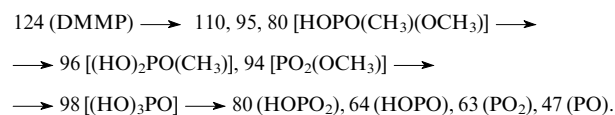


Figure 3. Intensity profiles of ion peaks with m/z 47 (PO, curve 1), 63 (PO_2 , curve 2), 64 (HOPO, curve 3), 80 (curve 4), 98 $[(\text{HO})_3\text{PO}]$, curve 5] and 124 (DMMP, curve 6) in the $\text{H}_2/\text{O}_2/\text{Ar}$ flame with 0.2 vol.% DMMP at $P = 47$ Torr and $\text{IE} = 13.4$ eV.¹⁴



For interpreting the obtained experimental results, the possible fragmentation routes of DMMP (subsequently, also TMP) in the $\text{H}_2/\text{O}_2/\text{Ar}$ flame were analysed. The following types of reactions were considered:

- (i) unimolecular decomposition and four-centre reactions;
- (ii) bimolecular elimination of H, CH_3 and OCH_3 from the DMMP molecule by H, O and OH radicals and the substitution of alkyl and alkoxy groups;
- (iii) bi- and trimolecular recombination reactions.

The enthalpies of the reactions were calculated using the enthalpies of formation of some OPC estimated by Melius.[‡] On the basis of these data, a detailed kinetic mechanism of DMMP destruction in the flame was proposed.⁵⁸ Subsequently, this mechanism was upgraded (reactions from the mechanism proposed by Twarowski^{61–63} were also included).

b. The Twarowski mechanism

An important step towards the understanding of the mechanism of OPC effect on flames was made after they were found to be applicable for increasing the efficiency of a ramjet fueled by hydrogen. It was found that combustion of hydrogen at high altitudes and, hence, at low pressures gives H and OH radicals in super equilibrium concentrations in the combustion chamber. These radicals have no time to recombine in the combustion chamber and are carried away to atmosphere, resulting in a loss in the engine power. For increasing the completeness of combustion, it was proposed to add phosphine to the fuel; this additive ensured an additional kinetic channel of recombination of H and OH radicals to give water. Twarowski^{2, 61–63} carried out a series of studies dealing with the effect of phosphine additive on the H and OH radical recombination rate in the flame. On measuring the variation of the concentrations of OH radicals formed upon combustion of a diffusion hydrogen–oxygen flame in the presence of phosphine vapour by laser-induced fluorescence, Twarowski²

[‡] Private communication (1996, the Lawrence Livermore National Laboratory, USA).

assumed that recombination of OH radicals is catalysed by phosphorus oxides and phosphorus-containing acids: PO, PO₂, HOPO and HOPO₂. He proposed a mechanism for catalytic recombination of H and OH radicals with participation of these phosphorus compounds; in more recent works,^{61–63} he supplemented this mechanism by new reactions with modified rate constants.

c. Analysis of the destruction mechanism

In a study¹⁴ devoted to determination of the general mechanism of OPC transformations in the flame, it was shown that destruction of OPC takes place through replacement of CH₃ and CH₃O groups by H and OH radicals. The full spectrum of the final phosphorus-containing products of OPC combustion was also identified. The obtained results served as the prerequisite for the design of other models for OPC destruction in flames on the basis of detailed kinetics and calculations of structures and propagation velocities of OPC-doped flames.

An essential contribution to the study of chemistry and mechanism of OPC destruction in flames was made by Werner and Cool,¹³ who investigated the chemical structure of rich hydrogen–oxygen flames doped with 0.1 vol.% DMMP.[§] On the basis of the obtained results, they developed a kinetic model for DMMP destruction in the flames. Using soft UV ionisation MBMS, they identified a number of intermediates of DMMP destruction in the flame such as (CH₃)PO₂ (78), (CH₃O)PO (78), (CH₃)(CH₃O)(OCH₂)PO (123), (HO)₂PO(CH₃) (94) and HOPO(CH₃)(OCH₃) (110) (the values in parentheses are the molecular masses of the products). It was shown experimentally¹³ that the destruction occurs upon the reaction of DMMP molecule with H and OH radicals (mainly, with replacement of alkyl and alkoxy substituents by OH groups).

Werner and Cool¹³ also calculated the rate constant for the thermal decomposition of DMMP. According to their data, the activation energy of the reaction of DMMP with OH equals 365 kJ mol^{−1}, indicating a negligibly low contribution of DMMP pyrolysis during combustion. On the basis of their own experimental results¹³ and earlier data¹⁴ and resorting to quantum chemical calculation data obtained by Melius, Werner and Cool¹³ proposed the first detailed mechanism of DMMP destruction in the flame. Using this mechanism, the flame structure was simulated and the results were compared with the experiment. Unfortunately, the researchers did not measure the concentrations of final and intermediate phosphorus-containing combustion products (including stable ones); therefore, the concentration intensity profiles across the combustion zone were equated (in the maximum) to the maximum concentrations of these compounds found by simulation. This somewhat decreases the significance of the work,¹³ as the lack of quantitative experimental results did not allow them to verify whether the model can correctly predict the distribution of combustion product concentrations across the flame zone.

The knowledge of the presence of the above-listed compounds in DMMP-doped flames was used by some researchers to design their own models for DMMP destruction in the flames and to calculate the chemical structure and the free propagation speed of a flame with DMMP additive (see, for example, Refs 64 and 65).

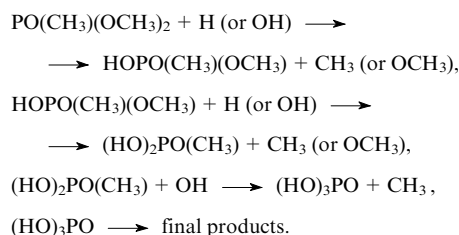
Quantitative measurement of the concentrations of combustion products was the next step towards the understanding of the OPC combustion chemistry.⁶⁶ Thus the proposed mechanisms of OPC destruction were verified by comparing the simulation data with experimental results on the flame structure, and this allowed the researchers to perfect the mechanisms. Since direct calibration of a MBMS unit used to

study the OPC transformations in the flame with respect to PO, PO₂, HOPO or HOPO₂ is impossible due to their instability and, hence, the lack of these compounds, their calibration coefficients were determined from the phosphorus material balance in the flame. Metaphosphoric acid HOPO₂, which exists as the crystals (P₂O₅)_x(H₂O)_y, where $x:y \approx 1:1$, can be considered an exception. However, the extremely low saturated vapour pressure of this acid precludes direct calibration of the unit with respect to this compound.

The calibration factors of phosphorus oxides and phosphorus-containing acids were determined by measuring the intensities of peaks of ions with m/z 40 (Ar), 47 (PO), 63 (PO₂), 64 (HOPO) and 80 (HOPO₂), *i.e.*, the final products of DMMP and TMP combustion in hydrogen–oxygen flames with different composition. The introduction of knowingly larger number of equations than variables into the set of phosphorus balance equations (the set of equations was overdetermined) owing to the large number of peak intensity measurements in the flames with different composition increased the calculation accuracy. The calculated calibration coefficients were used to determine the concentration profiles for PO, PO₂, HOPO and HOPO₂ in a hydrogen–oxygen flame with OPC additive.

The structure simulation of burner-stabilised flames used, as the input data, the temperature profiles measured by a thermocouple with a junction located near the probe orifice. Simulation of the structure of the H₂/O₂/Ar flames in the presence of DMMP⁵⁸ in terms of the Twarowski mechanism² demonstrated that with reaction rate constants proposed by Twarowski, the model predicts incorrectly the concentrations of these components. Analysis of the sensitivity of the rate constants of reactions comprised in the Twarowski kinetic mechanism (Table 3) to the concentrations of phosphorus oxides and phosphorus-containing acids showed that agreement between the simulation and measurement results can be attained by increasing the rate constants for trimolecular reactions 3, 5, 10 and 13 and simultaneously decreasing the rate constants for bimolecular reactions 2, 4, 7, 8, 9, 11, 12 and 14. Such changes in the rate constants resulted in an increase in the calculated HOPO₂ concentration and a decrease in the PO concentration. As a result, the concentration ratio [HOPO]/[PO₂] approached the experimental value.

Previously, incorporation of a number of primary steps giving rise to HOPO(CH₃)(OCH₃) (m/z 110), HOPO(OCH₃)₂ (126), HOP(CH₃)(OCH₃)₂ (125) and PO(CH₃)(OCH₃)(OCH₂) (123) into the DMMP destruction mechanism has been proposed.^{13,14} In the study considered,⁵⁸ reactions involving HOP(CH₃)(OCH₃)₂ (m/z 125) were not included in the final DMMP destruction model, as sensitivity analysis of the consumption rate of DMMP revealed a negligibly low influence of these steps on the kinetics of DMMP consumption. The measurements also showed that only HOPO(CH₃)(OCH₃) was present in the flame in considerable amounts, while HOPO(OCH₃)₂ and PO(CH₃)(OCH₃)(OCH₂) were not detected at all. Thus, the following route of DMMP destruction in the flame was proposed:⁵⁸



The assumption that the reactions of DMMP with hydroxyl yield preferably methyl methylphosphonate rather than dimethyl phosphate is supported by the fact that the C–O bond energy is lower than the C–P bond energy. The mechanism of DMMP destruction proposed by

[§] The same authors published a special study dealing with determination of the ionisation potentials of compounds (CH₃)PO₂ and (CH₃O)PO₂.¹²

Table 3. Reactions included in the Twarowski mechanism² and measured⁵⁸ parameters A , n and E of the equation $k = AT^n \exp(-E/RT)$.

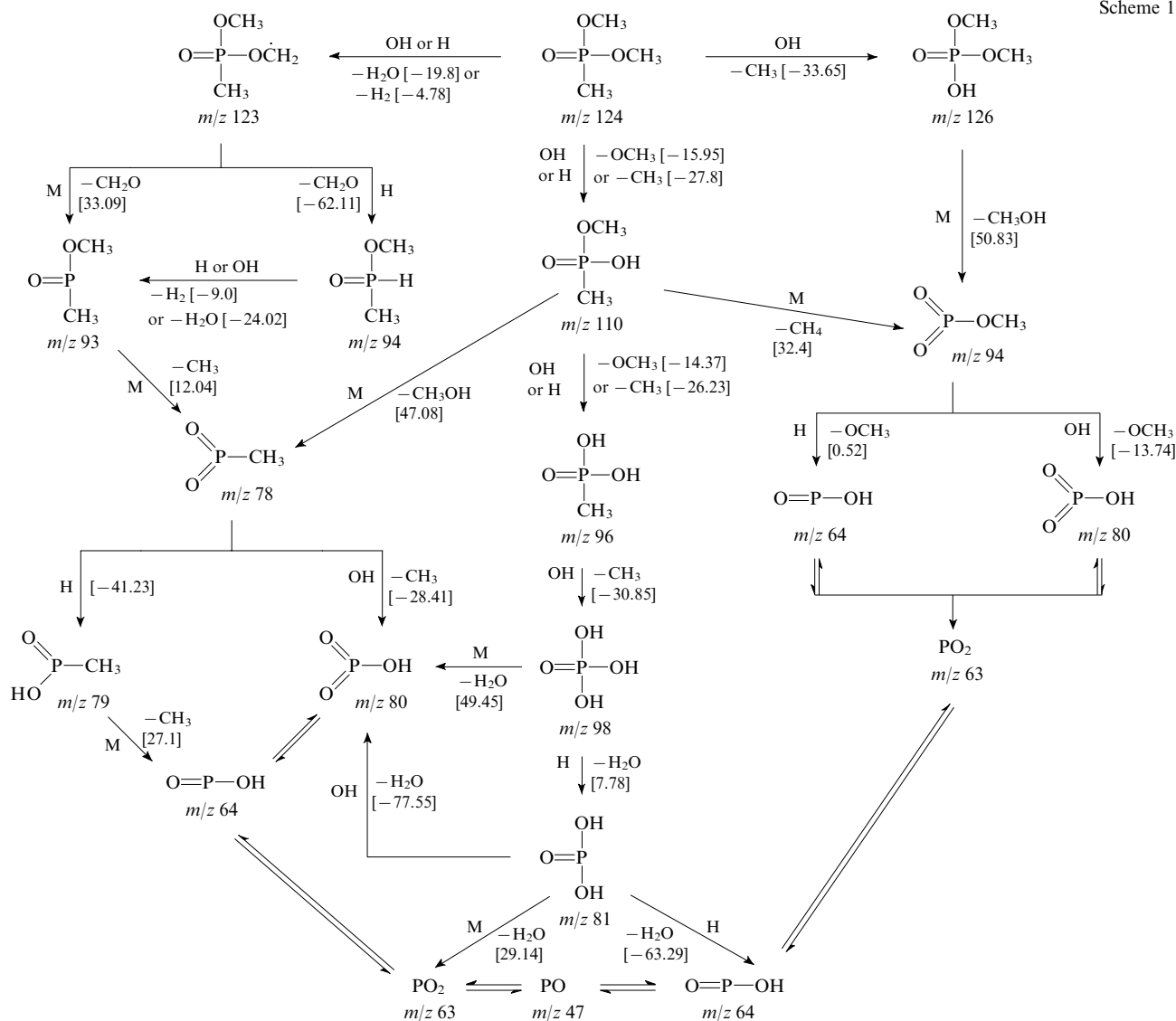
Number of the reaction	Reaction	A (from data of Ref. 2) ^a	A (from data of Ref. 58) ^a	n	$E/\text{kJ mol}^{-1}$
1	$\text{OH} + \text{PO} + \text{M} = \text{HOPO} + \text{M}$	1.196×10^{20}	1.19×10^{20}	-1.8	5.81
2	$\text{H} + \text{HOPO} = \text{H}_2\text{O} + \text{PO}$	3.16×10^{13}	6.32×10^{11}	0	49.87
3	$\text{OH} + \text{PO}_2 + \text{M} = \text{HOPO}_2 + \text{M}$	1.60×10^{24}	1.60×10^{25}	-2.3	1.19
4	$\text{H} + \text{HOPO}_2 = \text{H}_2\text{O} + \text{PO}_2$	3.16×10^{13}	6.32×10^{11}	0	49.87
5	$\text{H} + \text{PO}_2 + \text{M} = \text{HOPO} + \text{M}$	9.73×10^{23}	9.73×10^{24}	-2.0	2.7
6	$\text{OH} + \text{HOPO} = \text{H}_2\text{O} + \text{PO}_2$	3.16×10^{11}	3.16×10^{11}	0	0
7	$\text{H} + \text{HOPO} = \text{H}_2 + \text{PO}_2$	3.16×10^{13}	7.90×10^{11}	0	0.18
8	$\text{O} + \text{HOPO} = \text{OH} + \text{PO}_2$	3.16×10^{13}	1.58×10^{12}	0	0
9	$\text{OH} + \text{PO} = \text{H} + \text{PO}_2$	3.16×10^{11}	6.32×10^{10}	0	2.49
10	$\text{O} + \text{PO} + \text{M} = \text{PO}_2 + \text{M}$	2.36×10^{23}	2.36×10^{24}	-2.1	1.62
11	$\text{O}_2 + \text{PO} = \text{O} + \text{PO}_2$	3.16×10^{11}	3.16×10^{10}	0	23.91
12	$\text{OH} + \text{HOPO} = \text{H} + \text{HOPO}_2$	3.16×10^{11}	6.32×10^{10}	0	40.63
13	$\text{O} + \text{HOPO} + \text{M} = \text{HOPO}_2 + \text{M}$	1.59×10^{24}	7.95×10^{24}	-2.1	4.16
14	$\text{O} + \text{HOPO}_2 = \text{O}_2 + \text{HOPO}$	3.16×10^{13}	6.23×10^{11}	0	34.43
15	$\text{PO} + \text{HOPO}_2 = \text{PO}_2 + \text{HOPO}$	3.16×10^{11}	3.16×10^{11}	0	40.71

^a The dimensionality of the pre-exponential factor A in the equation for the rate constant is s^{-1} for a unimolecular reaction, $\text{cm}^3 \text{mol}^{-1} \text{s}^{-1}$ for a bimolecular reaction and $\text{cm}^6 \text{mol}^{-2} \text{s}^{-1}$ for a trimolecular reaction.

Korobeinichev *et al.*⁵⁸ is presented in Scheme 1 (the corresponding reaction enthalpies are given in brackets).

The proposed mechanism of DMMP destruction in the flame was used to calculate the structure of a flame doped with 0.2 vol.% DMMP and the results of calculations were com-

Scheme 1



pared with the results of measurements. The agreement was satisfactory for almost all flame components. The concentration profiles of the following intermediates of DMMP destruction in the flame were reported:⁵⁸ methyl metaphosphate ($(\text{CH}_3\text{O})\text{PO}_2$), methyl methylphosphonate, methylphosphonic acid and orthophosphoric acid.

No direct calibration of an MBMS unit with respect to intermediate organophosphorus products of DMMP destruction was carried out, as these compounds are lacking, unstable or non-volatile (as, for example, methylphosphonic acid), and calibration with respect to orthophosphoric acid proved to be impossible, because this acid decomposed above 100 °C to give water and pyrophosphoric acid. Therefore, the calibration coefficients of the intermediate organophosphorus compounds in the flame were found using the procedure of equating the maximum measured and calculated concentrations, as this was done before (see Ref. 13).

It should be borne in mind that PO , PO_2 , HOPO and HOPO_2 are formed in the flame at high temperature, while after cooling, the composition of combustion products may change appreciably (apparently, various phosphorus-containing acids may form).

2. Mechanism of trimethyl phosphate destruction

The mechanism of destruction of TMP in the flame, unlike that of DMMP, has been studied in detail.^{15, 58, 64, 67–69} Mass spectra of the samples taken from the $\text{H}_2/\text{O}_2/\text{Ar}$ flame doped with TMP exhibited peaks for the intermediate and final products of TMP destruction with m/z 80, 95, 96, 109, 110, 111, 112 and 126. The intensity profiles of some of these peaks and the TMP peak with m/z 140, recorded with $\text{IE} = 21$ eV, are presented in Fig. 4. Since the ion peak with m/z 126 is missing from the mass spectrum of TMP and its intensity profile passes through a maximum, this peak may be related to an intermediate of TMP destruction identified as dimethyl phosphate $\text{HOPO}(\text{OCH}_3)_2$ (DMP).

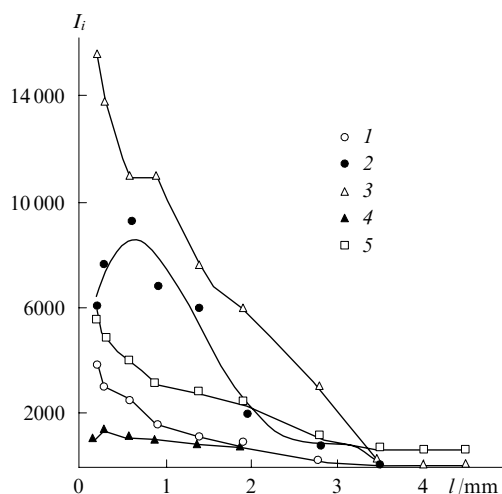


Figure 4. Intensity profiles of peaks of initial TMP (m/z 140) (curve 1) and ions with m/z 126 (2), 110 (3), 109 (4) and 80 (5) in the $\text{H}_2/\text{O}_2/\text{Ar}$ flame with 0.2 vol.% TMP at $P = 47$ Torr, $\text{IE} = 21$ eV.¹⁴

The mass spectra of tri- and dimethyl phosphates exhibit ion peaks with m/z 80, 95, 96, 109, 110, 111 and 112. Figures 5 and 6 present the intensity profiles of these peaks in the flame with subtracting the contributions of TMP and DMP. It can be seen from Fig. 6 that the profile of the ion peak with m/z 110 has three maxima, the third one being feebly pronounced and may be the result of overlap of two curves with maxima at

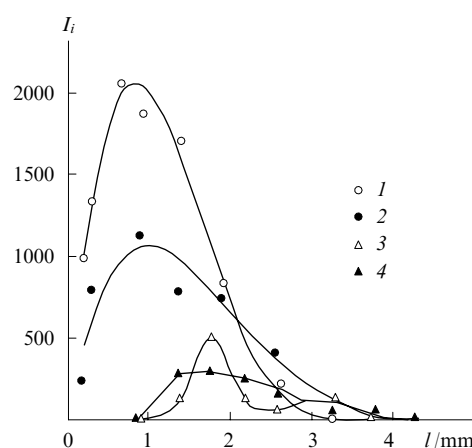


Figure 5. Intensity profiles of ion peaks with m/z 96 (curve 1), 95 (2), 111 (3), 112 (4) with allowance for contributions of TMP and DMP fragment ions at $P = 47$ Torr in the $\text{H}_2/\text{O}_2/\text{Ar}$ flame with 0.2 vol.% TMP.

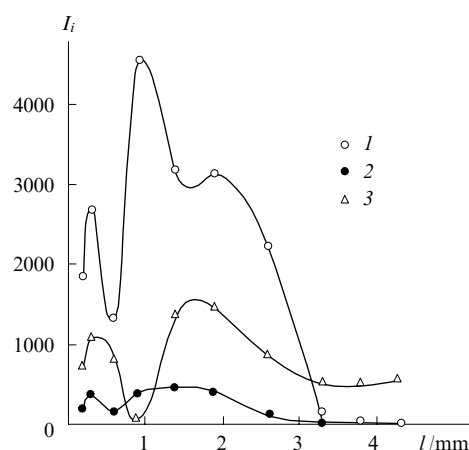


Figure 6. Intensity profiles of ion peaks with m/z 110 (curve 1), 109 (2), 80 (3) with allowance for contributions of TMP and DMP fragment ions at $P = 47$ Torr in the $\text{H}_2/\text{O}_2/\text{Ar}$ flame with 0.2 vol.% TMP.¹⁴

$l = 1.1$ and 1.9 mm. The ion with m/z 110 can be identified either as the molecular ion of dimethyl phosphonate $\text{HPO}(\text{OCH}_3)_2$ or dimethyl phosphite $\text{HOP}(\text{OCH}_3)_2$ or as the fragment ion formed from monomethyl phosphate $(\text{HO})_2\text{PO}(\text{OCH}_3)$ (molecular mass 112). It can be seen from Figs 5 and 6 that the maximum of the ion peak with m/z 112 coincides with the third maximum of the m/z 110 peak. This prompted the conclusion that the third maximum of the m/z 110 peak corresponds to monomethyl phosphite, while the first one is due to dimethyl phosphite. The second maximum has not yet been interpreted. The peaks with m/z 80 and 109 were attributed to fragment ions formed from monomethyl phosphate and dimethyl phosphite. The ion peak with m/z 96 belongs apparently to monomethyl phosphite (the m/z 95 peak is due to a product of its fragmentation). The intensity profiles of ion peaks with m/z 47 (PO), 63 (PO_2), 64 (HOPO) and 80 (HOPO_2) in the flames with TMP and DMMP additives follow the same pattern.

On the basis of these data, possible reactions for TMP destruction in the flame were proposed. The kinetic model of TMP destruction based on these studies was verified in relation to different flames. The concentration profiles of the organophosphorus products of TMP destruction were constructed by

carrying out direct calibrations of an MBMS unit with respect to TMP, DMP and dimethyl phosphite.⁶⁴ Pure monomethyl phosphate was not obtained; therefore, its concentration was estimated from the phosphorus material balance for the flames. Apart from the transformation steps of TMP and the intermediate products of its combustion, which logically follow from analysis of the composition of the combustion products, the reactions of TMP with the OH radical were also considered. It was found that this reaction does not give dimethyl phosphate and methyl alcohol, as was considered previously, but gives water and organophosphorus radical resulting from elimination of the H atom from a TMP molecule.⁷⁰



$$(\Delta H_{298}^\circ = -79.09 \text{ kJ mol}^{-1}).$$

The rate constant for this reaction was measured at a temperature of 300 K, and no activation energy was determined.⁷⁰ This was taken to be equal to the activation energy of a similar reaction of DMMP with OH,¹³ i.e., 16.7 kJ mol⁻¹. The pre-exponential factor in the Arrhenius equation was calculated proceeding from the accepted activation energy and the measured rate constant.⁷⁰ Thus, this reaction was included in the mechanism as a possible primary step of TMP destruction in the flame.

The mechanism of TMP destruction is presented in Scheme 2.^{58, 64} It is of interest to carry out the integral analysis of the transformation routes of TMP and some products of its incomplete destruction to elucidate the role of each step. Analysis showed that the ($\cdot\text{CH}_2\text{O}$)(CH₃O)₂PO radical formation is a key step (consuming more than 70% of TMP), the

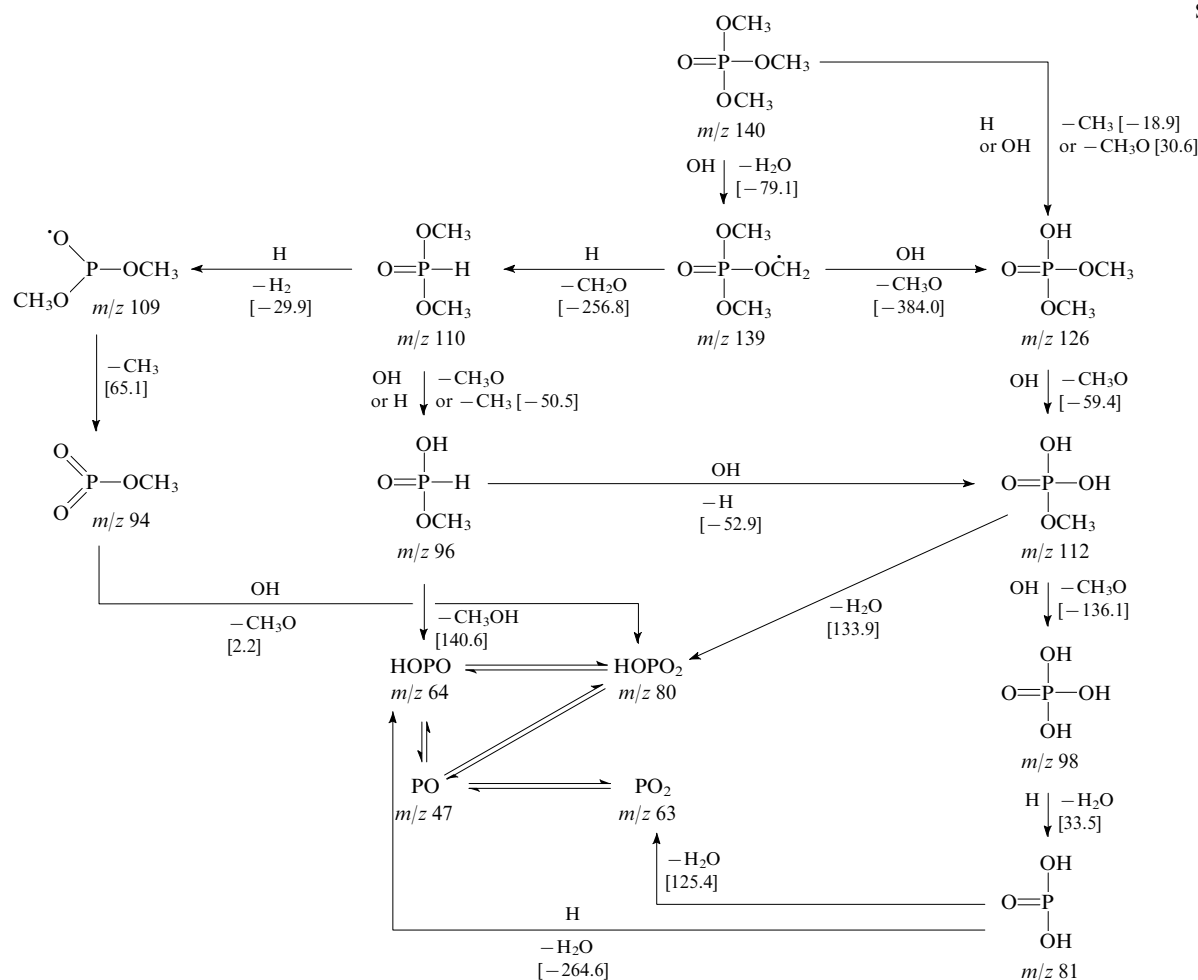
main bulk of products being formed *via* this step. The proposed mechanism of TMP destruction was used to model the structure of the H₂/O₂/Ar flame with a TMP additive.

Figure 7 presents the measured and calculated concentration profiles for TMP and intermediate organophosphorus products of its decomposition in the H₂/O₂/Ar flame at low temperature. It can be seen from comparison of the calculated and experimental data that, despite certain discrepancies, the proposed⁵⁸ model predicts with a satisfactory accuracy the concentration profiles of intermediate organophosphorus products of the destruction of the starting compound. Figure 8 shows the calculated and measured concentration profiles of the final phosphorus-containing products of TMP combustion, namely, PO, PO₂, HOPO, HOPO₂ and (HO)₃PO. Satisfactory agreement between the simulated and experimental results was obtained. [The experimental and simulated results for stable substances (H₂, O₂, H₂O) are compared in Section IV.]

It follows from the series of studies devoted to the OPC combustion chemistry that predicting the concentration profiles of the combustion products PO, PO₂, HOPO and HOPO₂ using the kinetic model is the most complicated task, but these concentration profiles, in addition to the concentration profiles of the H and O atoms and OH radicals, allow one to find whether the mechanism correctly describes the OPC combustion, which is especially important for the description of OPC as combustion inhibitors (or promoters).

Original mechanisms for DMMP and TMP destruction in the flames based on quantum chemical calculations of thermochemical data and on the estimation of rate constants for separate steps were proposed almost simultaneously by two

Scheme 2



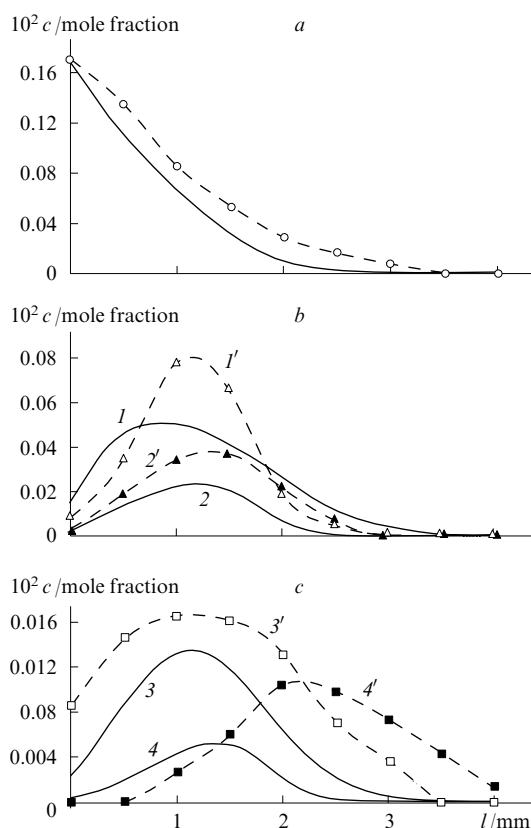


Figure 7. Concentration profiles of TMP (a) and intermediate products of its destruction: phosphites (b) and phosphates (c) in the $\text{H}_2/\text{O}_2/\text{Ar}$ flame.⁵⁸

The dots show the experimental values and the continuous lines correspond to calculations;

(b) (1, 1') dimethyl phosphite; (2, 2') monomethyl phosphite;
(c) (3, 3') dimethyl phosphate; (4, 4') monomethyl phosphate.

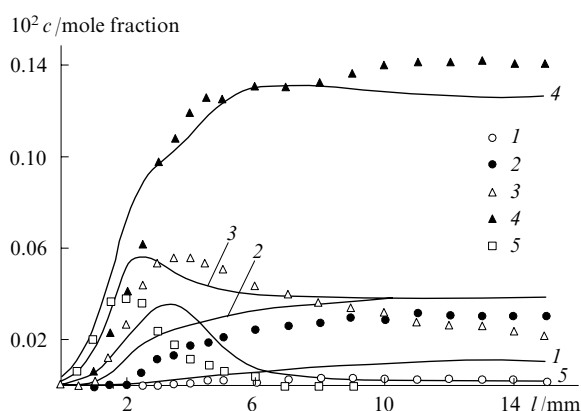


Figure 8. Concentration profiles of phosphorus-containing products of TMP combustion in the $\text{H}_2/\text{O}_2/\text{Ar}$ flame.⁵⁸

Phosphorus-containing products: PO (curve 1), PO_2 (2), HOPO (3), HOPO_2 (4), $(\text{HO})_3\text{PO}$ (5). The dots show the experimental values and the continuous lines correspond to calculations.

research groups.^{52, 54} (Glaude *et al.*⁵⁴ took into account all the possible intermediates of destruction of these OPC.) The developed mechanisms were used to simulate the structure of the low-pressure hydrogen–oxygen flame doped with 0.2 vol.% DMMP or TMP. A comparison of the calculation results⁵⁴ with earlier experimental results^{64, 69} demonstrated

good agreement between them as regards both the concentrations of stable components in the flame (H_2 , O_2 and H_2O) and the concentrations of PO, PO_2 , HOPO, HOPO_2 and $(\text{HO})_3\text{PO}$, which is the most difficult-to-attain fitting criterion. At that time, the developed mechanism was the most complete (it included 202 reactions involving 41 phosphorus compounds). This mechanism served as the basis for the development of the mechanism of inhibition of methane and propane flames by OPC additives under atmospheric pressure (see below).

3. Mechanism of destruction of diisopropyl methylphosphonate and sarin

The chemistry of DIMP combustion in the H_2/O_2 flame at low pressure has been studied.⁷¹ Diisopropyl methylphosphonate decomposes rather readily, unlike TMP or DMMP, when heated in an inert gas flow; therefore the thermal decomposition reactions were included in the mechanism of DIMP destruction in the flame. The kinetics and the products of DIMP pyrolysis in a flow type reactor were studied by Zegers and Fisher;⁷² the results are presented below.



$$k = 10^{12} \exp\left(\frac{-153.4 \pm 20}{RT}\right) \text{ cm}^3 \text{ mol}^{-1} \text{ s}^{-1}.$$

While estimating the contribution of thermal decomposition of DIMP to the overall destruction rate of the substance in the flame, it was concluded⁷² that thermal decomposition plays a minor role in the total mechanism of DIMP destruction. As in the case of other OPC, the major steps of DIMP destruction include the reactions of the OPC molecule with the H atom and OH radical, resulting in replacement or elimination of the CH_3 and $\text{C}_3\text{H}_7\text{O}$ groups, respectively.

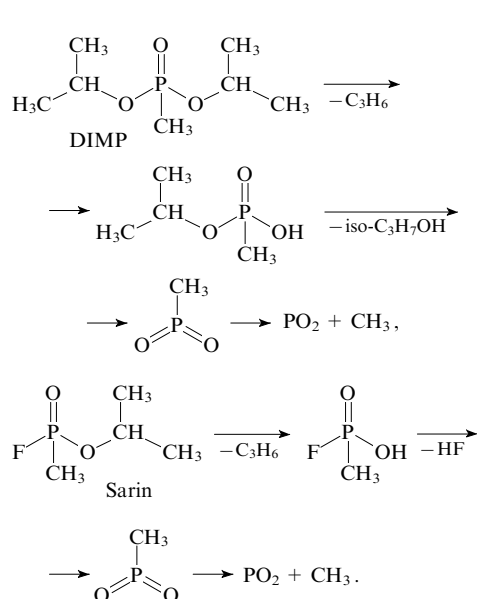
By analogy with the DIMP destruction steps, Korobeinichev *et al.*⁷¹ proposed also the possible steps of sarin destruction. They carried out altogether 10 reactions and calculated the heats of reactions based on the Melius thermochemical data (the Lawrence Livermore National Laboratory).

The rate constants for unimolecular decomposition of dimethyl ethylphosphonate, triethyl phosphate and DIMP were calculated.⁵⁴ The correctness of calculations was verified by comparing the simulation data with the experimental results on the pyrolysis of the above-mentioned OPC in a flow type reactor.

As a continuation of their research, the same group⁷³ developed the destruction mechanisms for a number of fluorinated OPC and TMP, DMMP, DIMP and sarin. The hierarchical schemes of reactions were based on previously proposed mechanisms of OPC destruction using the principle of chemical bond additivity. The kinetic models of combustion of the above-listed OPC and sarin were used in the calculations predicting their consumption rates during the combustion of natural gas (94% of methane and 6% of ethane) with air in a perfect-mixing reactor.[¶] A comparison of the dependences of concentrations of various OPC in the combustion on temperature and residence time has shown that TMP and DMMP consumption follow identical kinetics; the same is true for DIMP and sarin. The researchers concluded that only DIMP is a true mimic of sarin.

Scheme 3 shows simplified patterns of the thermal destruction of DIMP and sarin at high temperature in a perfect-mixing

¶ This process simulates disposal of these compounds by incineration in a furnace.



reactor. It is noteworthy that both DIMP and sarin destruction mechanisms include not only thermal decomposition steps. A full mechanism of sarin combustion that includes 24 steps most of which are reactions of sarin with H and OH radicals has been reported.⁷³

Comparative analysis of the mechanisms of destruction of various OPC carried out by the researchers cited has shown that the six-centred elimination of C_3H_6 present in the destruction mechanisms of DIMP and sarin is responsible for their higher reactivity compared to that of TMP or DMMP. This means that C—C bonds are most susceptible to cleavage in the OPC molecule.

It is noteworthy that the conclusions drawn⁷³ are at variance with the conclusions of an earlier publication.⁷¹ As noted above, experimental study and numerical simulation of the DIMP destruction mechanism in the low-pressure hydrogen—oxygen flame⁷¹ led to the conclusion that the thermal decomposition of DIMP gives a minor contribution to the overall destruction rate. Apparently, these discrepancies can be interpreted in the following way. The concentrations of H, O and OH atoms and radicals in the hydrogen—oxygen flame at low pressure are very high (according to a publication,⁷⁴ the $\text{H} + \text{O} + \text{OH}$ molar concentration is about 10%). This suggests that the role of thermal decomposition of even thermally unstable compounds is negligibly low against the high rate of DIMP consumption in reactions with the H, O and OH radicals. In hydrocarbon flames, the total molar concentration of active species was reported⁷⁵ to be two orders of magnitude lower. In this case, the role of thermal decomposition markedly increases.

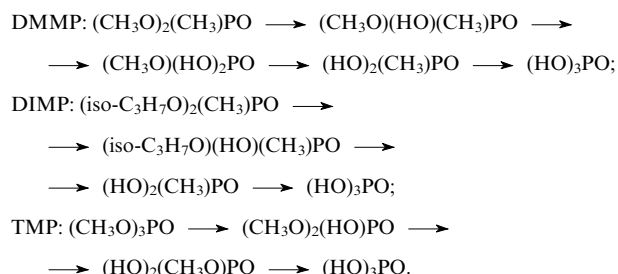
4. Mechanism of destruction of organophosphorus compounds in a non-thermal plasma

The mechanisms of OPC destruction in the flame and non-thermal plasma have much in common. Therefore, it is pertinent to consider briefly the works devoted to the chemistry of OPC destruction in corona discharge plasma. From the practical standpoint, the non-thermal plasma attracts attention of researchers as a medium for effective destruction of toxic or hazardous compounds in low concentrations.

The identification of the OPC destruction products in a non-thermal plasma^{76–78} made it possible to propose the mechanism of their destruction. Among the stable intermediate products of DMMP destruction in the corona discharge plasma, methyl methylphosphonate and monomethyl phosphate were detected; methylphosphonic and orthophosphoric

acids were formed as the final products of DMMP destruction. The same species are also the final products of DIMP destruction, whereas isopropyl methylphosphonate is an intermediate product. The destruction of TMP yields dimethyl and monomethyl phosphates (intermediates) and orthophosphoric acid (final product).

Thus, in a non-thermal plasma, DMMP, DIMP and TMP undergo the following transformations:



The identification of the OPC decomposition products in a non-thermal plasma showed that they are the same as many OPC destruction products in the flame. Apparently, in a corona discharge, as in the flame, the alkoxy and alkyl groups are replaced successively by H or OH. Two possible mechanisms of OPC destruction in the nonthermal plasma, radical and ionic ones, have been described. According to the radical mechanism, OPC destruction occurs upon the reaction of the atoms and radicals formed in the discharge with OPC, similarly to the situation in the flame. The discussion of the ionic mechanism in the OPC destruction in the nonthermal plasma is beyond the scope of this review. It should be noted that no unambiguous evidence supporting either of these two mechanisms is currently available.

IV. Mechanism of promotion and inhibition of the H_2/O_2 flames by addition of organophosphorus compounds

Korobeinichev *et al.*^{14, 57, 64} first demonstrated experimentally that the addition of 0.2 vol.% OPC to the $\text{H}_2/\text{O}_2/\text{Ar}$ flames at low pressure results in an increase in the final temperature of the flame and the degree of combustion and in a decrease in the combustion zone width. Figure 9 shows the measured and calculated (at a 15 mm distance from the burner) final temperatures of the $\text{H}_2/\text{O}_2/\text{Ar}$ flame stabilised on a flat burner at 47 Torr, depending on the initial concentration of the TMP additive.⁷⁹ Under these conditions, the increase in temperature

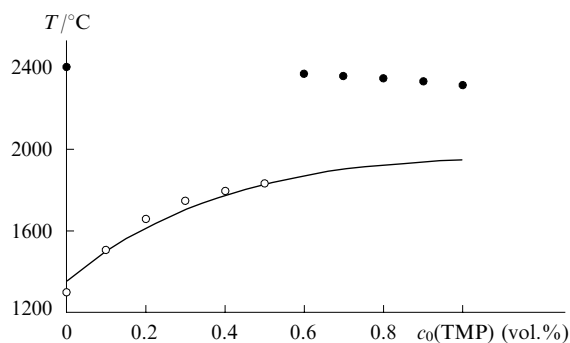


Figure 9. Maximum temperature of the $\text{H}_2/\text{O}_2/\text{Ar}$ flame stabilised on a flat burner at a pressure of 47 Torr vs. TMP concentration.⁷⁹ The continuous line shows the calculated values; the light dots are experimental values and the dark dots show the change in the adiabatic equilibrium temperature.

of the stabilised flame is not related to lower heat loss in the burner, as is usually the case upon the addition of inhibitors; conversely, on the addition of TMP, the flame temperature increases simultaneously with the increase in the temperature gradient at the burner surface, *i.e.*, with an increase in the heat loss. Thus, the increase in the flame temperature with an increase in the TMP concentration is due not to the introduction of additional fuel into the flame but to more complete combustion of the fuel already present as a result of the ability of OPC combustion products to catalyse recombination of the H and OH radicals to give water, *i.e.*, to promote combustion.

The experimental and simulation results are in satisfactory agreement, which confirms the consistency of the kinetic model. For comparison, Fig. 9 shows also the equilibrium temperatures of the adiabatic flames with the same composition. The difference between the adiabatic flames and flames stabilised on a flat burner (cooled) is that in the latter case, a large portion of heat is absorbed by the burner.

Figure 10 shows the concentration profiles of the stable components H_2 , O_2 and H_2O in the $H_2/O_2/Ar$ flame stabilised on a flat burner at a reduced pressure of 47 Torr without additives or with 0.2 vol.% TMP.⁶⁶ The narrowing of the combustion zone (the final composition of the combustion products is attained at a shorter distance from the burner surface) and fuller combustion of the H_2 and O_2 components attest to a promoting effect of TMP on the flame.

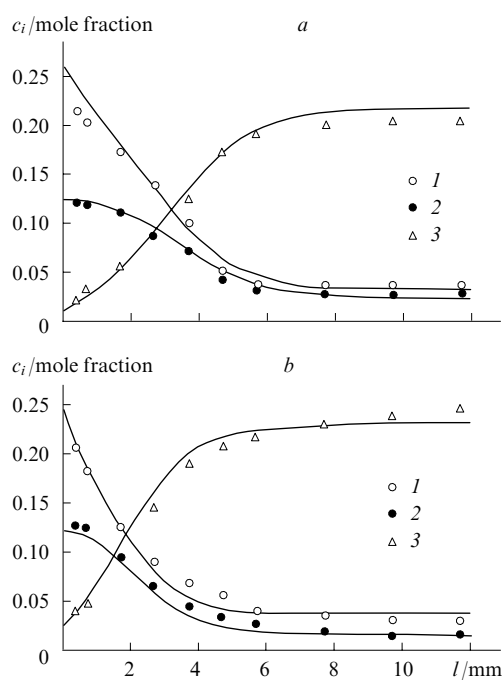


Figure 10. Concentration (c_i) profiles of stable components H_2 (1), O_2 (2) and H_2O (3) in the $H_2/O_2/Ar$ flame stabilised on a flat burner at $P = 47$ Torr without additives (a) and with 0.2 vol.% TMP (b).⁶⁶ The dots show experimental values and the lines correspond to simulation results.

The observed promoting effect was confirmed by comparing experimental data with simulation results obtained using the mechanism proposed by Glaude *et al.*⁵⁴ The promoting effect of OPC increases with an increase in the concentration and reaches a maximum at an OPC concentration of ~ 0.6 vol.%. This can be seen from the computational data presented in Fig. 11, which shows the dependence of the free propagation speed of the hydrogen–oxygen flame on the additive concentration at a reduced pressure (47 Torr). In the

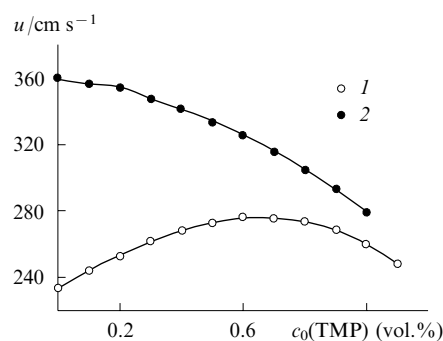


Figure 11. Normal propagation speed of the H_2/O_2 flames vs. the concentration of TMP additive at pressures of 47 (curve 1) and 760 Torr (curve 2).

TMP concentration range from 0 vol.% to 0.6 vol.%, this additive acts as a promoter. On further increase in the TMP concentration, the flame propagation speed decreases. At a pressure of 760 Torr (1 atm), OPC acts only as an inhibitor.

The effect of OPC on the concentration of the H, O and OH radicals in the flame is shown in Fig. 12, which gives the calculated and measured concentrations of these radicals in the $H_2/O_2/Ar$ flame without additives and with 0.2 vol.% TMP.⁶⁶ The introduction of OPC results in a decrease in the concentration of hydrogen and oxygen atoms and an increase in the hydroxyl concentration. It can be seen

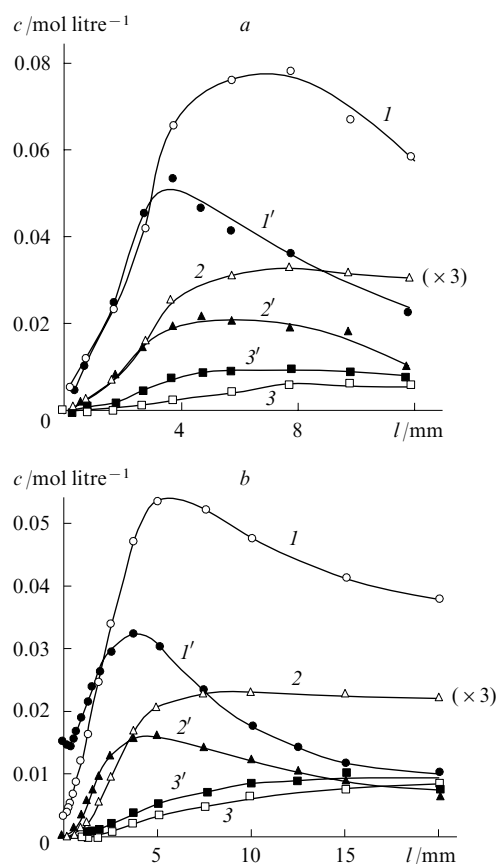
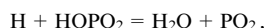
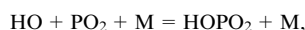


Figure 12. Concentration profiles of radicals H (curves 1, 1'), O (2, 2') and OH (3, 3') in the $H_2/O_2/Ar$ flame stabilised on a flat burner at $P = 47$ Torr without an additive (light dots) and with 0.2 vol.% TMP (black dots).⁶⁶ (a) experimental data, (b) simulation results.

from comparison of the concentration profiles that the computation and experimental results are in satisfactory agreement. The effect of OPC on the concentrations of H, O, and OH radicals is an important feature of these compounds, which accounts for their possible practical application as combustion inhibitors and flame suppressants.

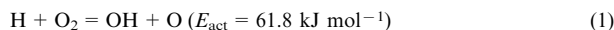
It was shown⁶⁹ that the addition of OPC to a methane–oxygen flame at a pressure of 0.1 bar decreases the flame propagation speed. Thus, OPC are combustion promoters only for low-pressure hydrogen flames. Note that an increase in the propagation speed of flames with an increase in the concentration of the inhibitor (bromoethane, dibromotetrafluoroethane, bromine, diethylamine, methane, and methanol) in lean and rich hydrogen–air flames at high pressures was described previously.⁸⁰ However, the mechanism of this effect is different and is related, in the authors' opinion, to the fact that active additives can function as additional fuel or oxidant.

The additional heat release caused by combustion of the additive (at a definite concentration) can counterbalance its inhibiting action. However, the action of OPC is due to a kinetic rather than thermophysical effect. The H and OH radical recombination in the flame catalysed by OPC destruction products is yet another channel for water formation



which provides heat release. The evolved heat increases the temperature and accelerates recombination of active species, despite the decrease in their concentration in the flame.

A detailed interpretation of the promoting effect of OPC based on the analysis of the kinetic model of OPC destruction (see Ref. 58) has been proposed.^{79, 81} The calculations of the quadratic branching rate



for the combustion zone of a hydrogen–oxygen flame at low pressure showed that the rate of this reaction considerably increases with an increase in the TMP concentration and reaches a maximum at $c_{\text{TMP}} = 0.5 \text{ vol.}\% - 0.6 \text{ vol.}\%$. This increase in the reaction rate is mainly due to an increase in the flame temperature[†] as a result of increase in the recombination rate of H, O and OH atoms and radicals. The quadratic branching rate stops to grow following an increase in the TMP concentration where the flame temperature reaches an equilibrium.

A comparison of contributions of various reactions to the flame propagation speed demonstrated that with an increase in the TMP concentration, the contribution of branching exceeds considerably the contributions of reactions (2)–(5) contained in the hydrogen oxidation mechanism (Fig. 13).



The increase in the branching rate with an increase in the TMP concentration and saturation of this effect as the flame temperature approaches the equilibrium value is shown in Fig. 14. Among reactions involving phosphorus-containing

[†] The rate of branching reaction, which is proportional to the product of H atom concentration by the rate constant for the reaction, increases with an increase in the TMP concentration owing to the fact that the reaction rate constant grows (with an increase in temperature) faster than the H concentration drops.

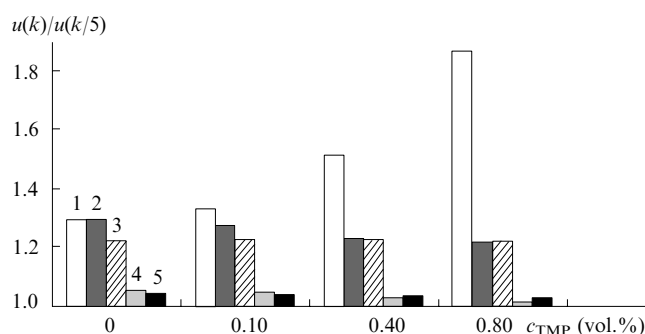


Figure 13. Sensitivity coefficients $[u(k)/u(k/5)]$ of reactions (1)–(5) taking place in the flame comprising 26% H_2 + 13% O_2 + 61% Ar at $P = 47.5$ Torr and $T_0 = 370$ K for different TMP concentrations;⁸¹ $u(k)$ is the flame propagation speed calculated with the standard rate constant for the reaction; $u(k/5)$ is the rate calculated with the rate constant decreased fivefold.

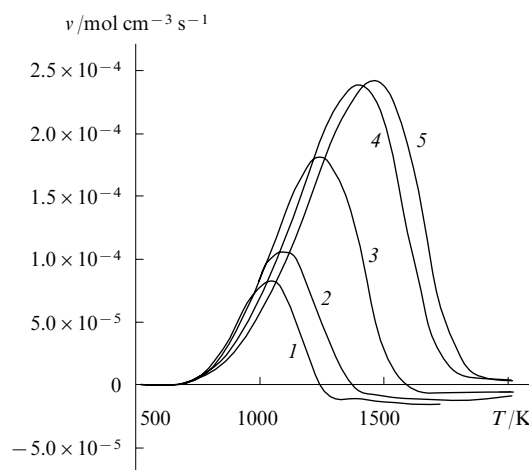
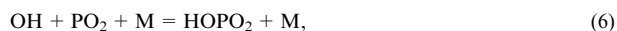


Figure 14. Rate constant for quadratic branching $\text{H} + \text{O}_2 = \text{OH} + \text{O}$ as a function of temperature of the flame comprising 26% H_2 + 13% O_2 + 61% Ar without additives (curve 1) and with TMP (curves 2–5) added in different concentrations at $P = 47.5$ Torr and $T_0 = 370$ K.⁸¹ c_{TMP} (%): 0.1 (2), 0.4 (3), 0.8 (4), 1.0 (5).

compounds to which the flame propagation speed is most sensitive (according to Ref. 81), the following reactions should first be noted:



These reactions result in chain termination and play an important role in the catalytic radical recombination cycle. The calculation of the sensitivity coefficients of the flame propagation speed to the reaction rate constants for flames with different OPC concentrations has shown that in the additive concentration range from 0 vol.% to 0.5 vol.%, these coefficients are positive, *i.e.*, recombination reactions increase the flame propagation speed. When the TMP concentration is $> 0.5 \text{ vol.}\%$, the coefficients are negative and decrease with an increase in the OPC concentration in the flame, *i.e.*, the

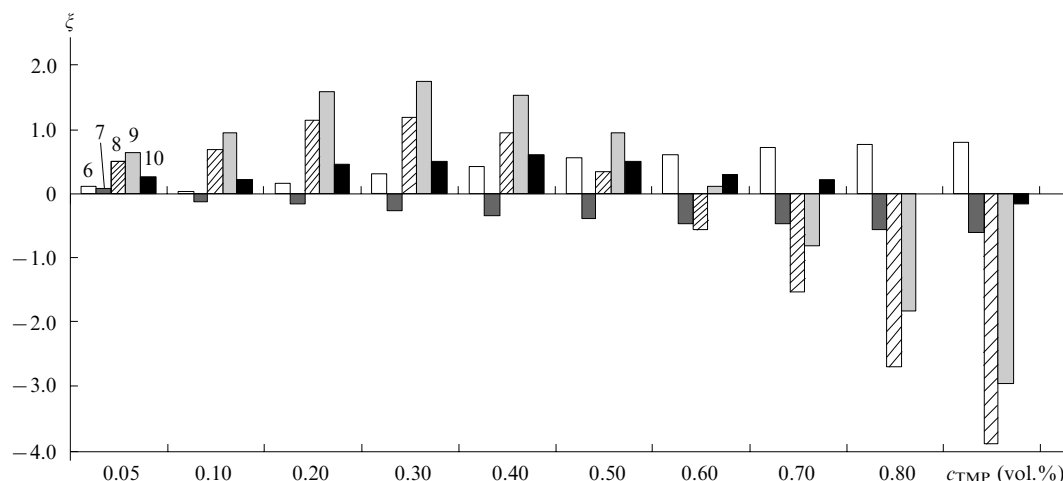


Figure 15. Sensitivity coefficients of key reactions (6)–(10) taking place in the $\text{H}_2/\text{O}_2/\text{Ar}$ flame with participation of OPC for different TMP concentrations.⁸¹

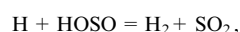
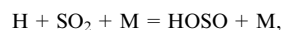
hydrogen combustion is retarded. Thus, transition from promotion to inhibition with the same reactions being responsible for this attests to unique properties of phosphorus compounds. Figure 15 presents the sensitivity coefficients (ξ) for the key reactions that take place in the flame and involve phosphorus-containing compounds at different TMP concentrations. The sensitivity coefficients were determined from the relation

$$\xi = \frac{u(k) - u(k/5)}{u(k)} 100\%,$$

where $u(k)$ is the free propagation speed of the $\text{H}_2/\text{O}_2/\text{Ar}$ flame with a TMP additive at a pressure of 47.5 Torr; $u(k/5)$ is the free propagation speed of the flame calculated using the reaction rate constant reduced fivefold.

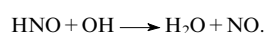
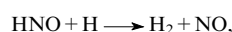
Under atmospheric pressure, the concentration of active species in the flame is two orders of magnitude lower than under reduced pressure, and the temperature of the adiabatic flame is close to thermodynamic equilibrium; therefore, even a minor additive of phosphorus compounds results only in flame inhibition.

The chemistry of combustion of sulfur and nitrogen compounds is similar to the phosphorus combustion chemistry. The inhibiting action of SO_2 on the hydrogen–oxygen flame stabilised on a flat burner has been studied.⁸² The reactions



which play the key role in the inhibition mechanism and form the inhibition cycle, are similar to the reactions of phosphorus oxides and phosphorus-containing acids. However, the inhibiting efficiency of sulfur compounds is much lower compared to phosphorus. This can be attributed to the lower rates of catalytic reactions.

A computational theoretic analysis of the effect of nitrogen oxide admixture on the ignition delay in a hydrogen–air mixture has been carried out.⁸³ The calculations showed that at temperatures above 1200 K, the addition of NO to a hydrogen–air mixture somewhat decreases the ignition delay, *i.e.*, NO functions as a promoter. However, at lower temperature, the ignition delay increases, *i.e.*, the NO admixture functions as an inhibitor. The researchers believe that the effect of nitrogen oxide on the hydrogen oxidation kinetics is due to its ability to catalyse radical recombination



These reactions are analogous to those presented for OPC.

V. Studies of the mechanism of inhibition and quenching of hydrocarbon flames by organophosphorus additives

1. Premixed laminar flames

a. The structure of flames with organophosphorus additives

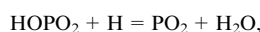
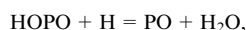
The work of Hastie and Bonnell,⁶ who studied the effect of the classical inhibitor CF_3Br and of TMP on the methane–oxygen and hydrogen–oxygen flames of various types and compositions by molecular-beam mass spectrometry and optical methods, should be considered the pioneering study dealing with the effect of OPC on the combustion processes under atmospheric pressure. The visual monitoring of the height of the flame cone stabilised on the Bunsen burner allowed them to draw the first conclusion that the introduction of a TMP additive resulted in a decrease in the normal free propagation speed of the methane–oxygen flame, *i.e.*, they demonstrated that TMP is a combustion inhibitor. Hastie and Bonnell⁶ were the first to propose a series of reactions involving phosphorus compounds (phosphorus oxides and phosphorus-containing acids), which described recombination of H and OH radicals. This was actually the first interpretation of the mechanism of flame inhibition by OPC.

Numerous experimental data collected by these researchers are unique and highly important. The key result of their studies is the discovery of the change in the concentrations of H, O and OH radicals upon the introduction of TMP into the flame. Hastie and Bonnell⁶ obtained the first experimental proof for the existence of a relationship between the addition of TMP and the decrease in the concentration of active species in the flame. They measured the intensity profiles for ion peaks of PO, PO_2 and HPO_2 in the mass spectra. Noteworthy also is Hastie's contribution to the molecular-beam mass spectrometry studies of the behaviour of PO, PO_2 and HOPO_2 in the flames.⁸⁴ However, his paper⁸⁴ presents no consistent quantitative experimental data that could be compared with simulation results to verify the proposed inhibition mechanism. This study seems not to be completed as yet, because the results

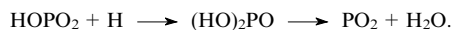
were presented only in a report⁶ and were not published in refereed editions.

Korobeinichev *et al.*⁸⁵ measured experimentally the concentration profiles of phosphorus oxides and phosphorus-containing acids in the methane–oxygen flames with TMP additive at a pressure of 1 atm and determined the dependences of the flame propagation speed on the additive concentration. A comparison of the results thus obtained with the data of simulation of the flame structure and propagation speed in terms of the mechanism proposed for the low-pressure flame⁵⁸ showed a discrepancy between the simulation and experimental results. Analysis of the sensitivity of flame propagation speeds to the change in the rate constants for PO-, PO₂-, HOPO- and HOPO₂-involving reactions and the effect of these reactions on the concentrations of phosphorus-containing products in the flame prompted the necessity of changing the pre-exponential factor in the expression for the rate constants for some key steps in the mechanism proposed by Korobeinichev *et al.*⁵⁸

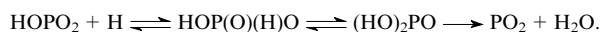
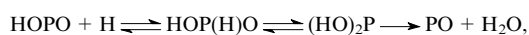
Considerable progress in the understanding of processes that take place in the flames with OPC additives was attained owing to quantum chemical calculations,⁵⁵ which resulted in upgrading of the Twarowski mechanism of flame inhibition by organophosphorus compounds. By computation of the potential energy surfaces for the transformations



which were earlier regarded as elementary steps,⁵⁴ Mackie *et al.*⁵⁵ demonstrated that actually these reactions occur in two steps:



The subsequent calculation of the potential energy surfaces using more advanced methods^{52, 53} demonstrated that these reactions may include even more steps:



According to the calculation,⁵³ the rate constant for the latter reaction at a temperature of 1500 K was 10 times higher than the value proposed previously.⁵⁴ Figure 16 shows the potential energy surfaces for the possible paths of the HOPO₂ + H reaction. On the basis of quantum chemical calculations of the rate constants for some reactions and calculation of the thermochemical properties of phosphorus-containing molecules and transition states, the most complete and currently substantiated mechanism of flame inhibition by OPC additives under atmospheric pressure was developed at the Lawrence Livermore National Laboratory.⁸⁶ This mechanism includes

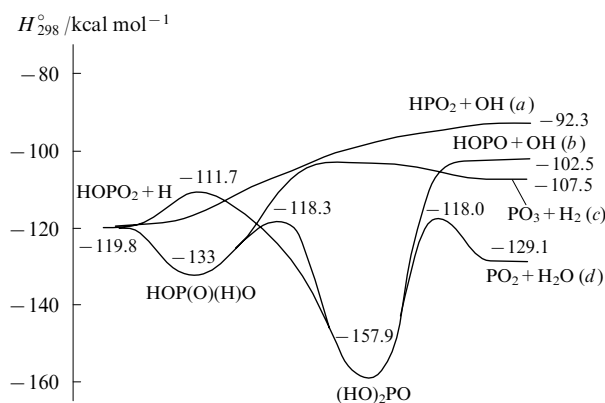


Figure 16. Potential surfaces of the possible transformation paths of the system HOPO₂ + H (paths a–d) and the reaction products of HOPO₂ with H.⁵³

The enthalpies of formation (in kcal mol^{–1}) for compounds and transition states are given.

210 steps involving 43 compounds. Apart from the above-considered steps, the steps involving compounds like P₂O_n and reactions of phosphorus oxides with alkyl radicals such as CH₃ and C₂H₅ were also included. The subsequent analysis showed that these steps do not have a significant effect on the results of flame simulation over a wide range of equivalence ratio. Thus, this mechanism can be considered even somewhat excessive.

The mechanism of flame inhibition by OPC additives can conventionally be divided into two parts. The first part includes destruction of OPC (TMP and DMMP) to ‘light’ phosphorus-containing compounds like H_xP_yO_z; the second one includes reactions of H_xP_yO_z with the H, O and OH radicals, which ensure their removal from the flame through their catalytic recombination. This part of the mechanism is crucial in the description of flame inhibition phenomena by OPC additives. Table 4 presents the reactions from the second part of the mechanism and the corresponding rate constants. The notes to the Table outline the methods used to estimate the rate constants.

Note that Jayaweera *et al.*⁵³ made considerable advances not only in the development of the proper mechanism but in the in-depth understanding of processes taking place in the flames with OPC additives. They estimated the efficiency of action of inhibitors on the premixed flames using two parameters: the change in the concentrations of the H and OH radicals and the flame propagation speed. Both parameters were discussed for lean and rich flames with equivalence ratio $\phi = 0.8$ and 1.3, respectively.

It was mentioned above that the addition of OPC inhibits flame propagation by accelerating the recombination of H and OH radicals; therefore, the distribution of concentrations of

Table 4. Reactions of the key components in the flame with ‘light’ phosphorus-containing compounds H_xP_yO_z and their rate constants [the rate constant is presented as $AT^n \exp(-E_a/RT)$, the pre-exponential factor A is expressed in s^{–1}, litre mol^{–1} s^{–1} or litre² mol^{–2} s^{–1}].

Number of the reaction	Reaction	A	n	$E_a/\text{J mol}^{-1}$	Notes
1	PO ₂ + PO + M = P ₂ O ₃ + M				calculation data
	high pressure	4.00×10^{14}	–1.00	0	
2	PO ₂ + PO ₂ + M = P ₂ O ₄ + M				the same
	high pressure	6.00×10^{14}	–1	0	
	low pressure	2.00×10^{20}	–2	0	
3	PO ₂ + PO ₃ + M = P ₂ O ₅ + M				"
	high pressure	6.00×10^{14}	–1	0	
	low pressure	5.00×10^{20}	–2	0	

Table 4 (continued).

Number of the reaction	Reaction	A	n	$E_a/\text{J mol}^{-1}$	Notes
4	$\text{PO}_2 + \text{OH} + \text{M} = \text{HOPO}_2 + \text{M}$ (low pressure) ^b	1.60×10^{24}	-2.28	1193.8	see ^a
5	$\text{PO}_3 + \text{H} + \text{M} = \text{HOPO}_2 + \text{M}$ (high pressure) ^b	4.80×10^{24}	-2.37	5977.4	"
6	$\text{HOPO} + \text{O} + \text{M} = \text{HOPO}_2 + \text{M}$ (high pressure) ^b	1.20×10^{27}	-2.99	8527.2	see ^a
7	$\text{PO}_3 + \text{H}_2 = \text{HOPO}_2 + \text{H}$	2.00×10^{12}	0	0	see ^c
8	$\text{HOPO} + \text{OH} = \text{PO}_2 + \text{H}_2\text{O}$	3.72×10^{13}	-0.22	13401.08	see ^d (date from Ref. 55)
9	$\text{HOPO}_2 + \text{H} = \text{PO}(\text{OH})_2$	1.27×10^{32}	-6.10	36391.08	see ^c
10	$\text{HOPO}_2 + \text{H} = \text{PO}_2 + \text{H}_2\text{O}$	5.16×10^{19}	-1.83	44726	"
11	$\text{PO}(\text{OH})_2 = \text{PO}_2 + \text{H}_2\text{O}$	1.45×10^{28}	-4.97	186678.8	"
12	$\text{HPO}_2 + \text{OH} = \text{PO}(\text{OH})_2\text{O}$	1.00×10^{19}	-2	0	calculation data
13	$\text{PO}(\text{OH})_2\text{O} + \text{H} = \text{HOPO}_2 + \text{H}_2\text{O}$	2.00×10^{13}	0	0	the same
14	$\text{PO}(\text{OH})_2 + \text{H} = \text{HPO}_2 + \text{H}_2\text{O}$	4.00×10^{19}	-2	0	estimated by Glaude <i>et al.</i> ⁵⁴
15	$\text{PO}(\text{OH})_2 + \text{OH} = \text{HOPO}_2 + \text{H}_2\text{O}$	2.00×10^{13}	0	0	calculation data
16	$\text{PO}(\text{OH})_2 + \text{H} = \text{HOPO}_2 + \text{H}_2$	5.00×10^{12}	0	0	the same
17	$\text{PO}(\text{OH})_2 + \text{OH} = \text{PO}(\text{OH})_3$	1.00×10^{13}	0	0	estimated by Glaude <i>et al.</i> ⁵⁴
18	$\text{PO}(\text{OH})_2 + \text{O} = \text{HOPO}_2 + \text{OH}$	5.00×10^{13}	0	0	the same
19	$\text{P}_2\text{O}_4 + \text{H}_2\text{O} = \text{HOPO} + \text{HOPO}_2$	1.00×10^{11}	0	0	calculation data
20	$\text{P}_2\text{O}_5 + \text{H}_2\text{O} = \text{HOPO}_2 + \text{HOPO}_2$	1.00×10^{11}	0	0	the same
21	$\text{HOPO}_2 + \text{O} = \text{OH} + \text{PO}_3$	1.00×10^{13}	0	51664.8	see ^f
22	$\text{HOPO}_2 + \text{OH} = \text{H}_2\text{O} + \text{PO}_3$	1.20×10^6	2	8360	see ^g
23	$\text{HOPO} + \text{HO}_2 = \text{HOPO}_2 + \text{OH}$	1.50×10^{14}	0	98648	see ^h
24	$\text{HOPO}_2 + \text{HO}_2 = \text{H}_2\text{O}_2 + \text{PO}_3$	2.50×10^{12}	0	103078.8	see ⁱ
25	$\text{HOPO}_2 + \text{O}_2 = \text{HO}_2 + \text{PO}_3$	7.00×10^{12}	0	276130.8	see ^j
26	$\text{HOPO}_2 + \text{CH}_3 = \text{CH}_4 + \text{PO}_3$	1.50×10^{12}	0	54758	see ^k
27	$\text{PO} + \text{OH} + \text{M} = \text{HOPO} + \text{M}$ (low pressure) ^b	1.00×10^{21}	-2.09	6646.2	see ^a
28	$\text{PO}_2 + \text{H} + \text{M} = \text{HOPO} + \text{M}$ (low pressure) ^b	4.87×10^{24}	-2.04	2698.6	see ^{a, d, l}
29	$\text{HOPO} + \text{H} = \text{H}_2 + \text{PO}_2$	1.00×10^{13}	0	45980	calculation data
30	$\text{HOPO} + \text{O} = \text{OH} + \text{PO}_2$	1.00×10^{13}	0	0	estimated by Glaude <i>et al.</i> ⁵⁴
31	$\text{HOPO} + \text{O} = \text{H} + \text{PO}_3$	1.00×10^{12}	0	62700	the same
32	$\text{HOPO} + \text{HO} = \text{PO}_2 + \text{H}_2\text{O}$	1.20×10^6	2	-6270	see ^{d, m}
33	$\text{HOPO} + \text{HO}_2 = \text{H}_2\text{O}_2 + \text{PO}_2$	2.50×10^{12}	0	97394	estimated by Glaude <i>et al.</i> ⁵⁴
34	$\text{HOPO} + \text{O}_2 = \text{HO}_2 + \text{PO}_2$	7.00×10^{12}	0	189354	see ^j
35	$\text{HOPO} + \text{CH}_3 = \text{CH}_4 + \text{PO}_2$	1.50×10^{12}	0	54758	estimated by Glaude <i>et al.</i> ⁵⁴
36	$\text{PO} + \text{O} + \text{M} = \text{PO}_2 + \text{M}$ (low pressure) ^b	1.60×10^{25}	-2.63	7189.6	see ^a
37	$\text{PO} + \text{OH} = \text{H} + \text{PO}_2$	1.00×10^{13}	0	0	see ⁿ
38	$\text{PO} + \text{HO}_2 = \text{PO}_2 + \text{OH}$	2.10×10^{12}	0	-2090	see ^o
39	$\text{PO} + \text{O}_2 = \text{PO}_2 + \text{O}$	1.00×10^{12}	0	0	see ^p
40	$\text{PO} + \text{CH}_3 = \text{CH}_3\text{PO}$	1.00×10^{13}	0	0	estimated by Glaude <i>et al.</i> ⁵⁴
41	$\text{PO}_2 + \text{O} + \text{M} = \text{PO}_3 + \text{M}$ (low pressure) ^b	1.30×10^{27}	-3.15	7858.4	see ^a
42	$\text{PO}_3 + \text{H} = \text{PO}_2 + \text{OH}$	3.16×10^{13}	0	167.2	date from Ref. 62
43	$\text{PO}_2 + \text{HO}_2 = \text{OH} + \text{PO}_3$	5.00×10^{11}	0	0	estimated by Glaude <i>et al.</i> ⁵⁴
44	$\text{PO}_2 + \text{O}_2 = \text{O} + \text{PO}_3$	1.00×10^{12}	0	125400	the same
45	$\text{PO}_2 + \text{CH}_3 = \text{CH}_3\text{PO}_2$	6.30×10^{14}	-0.60	0	the same ^q
46	$\text{PO}_2 + \text{CH}_3 = \text{CH}_3\text{OPO}$	2.10×10^{12}	-0.60	0	the same ^r
47	$\text{PO}_2 + \text{CH}_3 = \text{CH}_3\text{O} + \text{PO}$	5.00×10^{11}	0	180994	the same
48	$\text{PO}_2 + \text{CH}_3\text{O} = \text{CH}_2\text{O} + \text{HOPO}$	1.00×10^{13}	0	0	"
49	$\text{HOPO} + \text{PO}_3 = \text{PO}_2 + \text{HOPO}_2$	5.00×10^{11}	0	0	"
50	$\text{PO}_3 + \text{PO} = \text{PO}_2 + \text{PO}_2$	5.00×10^{11}	0	0	"
51	$\text{PO}_3 + \text{CH}_3 = \text{CH}_3\text{OPO}_2$	5.00×10^{11}	0	0	"
52	$\text{PO}_3 + \text{CH}_3 = \text{PO}_2 + \text{CH}_3\text{O}$	5.00×10^{11}	0	63954	"
	$\text{PO}_2 + \text{CH}_3\text{O} = \text{PO}_3 + \text{CH}_3$	5.00×10^{11}	0	45980	"

Table 4 (continued).

Number of the reaction	Reaction	<i>A</i>	<i>n</i>	<i>E_a</i> / J mol ⁻¹	Notes
53	PO ₃ + CH ₃ O = CH ₂ O + HOPO ₂	1.00 × 10 ¹³	0	0	estimated by Glaude <i>et al.</i> ⁵⁴
54	CH ₃ + H = CH ₃ + HPO	1.00 × 10 ¹³	0	25080	the same
55	CH ₃ PO + O = CH ₃ + PO ₂	1.00 × 10 ¹³	0	0	"
56	CH ₃ PO ₂ = CH ₃ PO + O	1.00 × 10 ¹⁴	0	555940	"
57	PO + H + M = HPO + M (low pressure) ^b	1.80 × 10 ²²	-1.95	5559.4	see ^a
58	HPO + H = H ₂ + PO	2.40 × 10 ⁸	1.50	0	estimated by Glaude <i>et al.</i> ⁵⁴
59	HPO + O = OH + PO	1.70 × 10 ⁸	1.50	0	the same
60	HPO + O = PO ₂ + H	1.00 × 10 ¹³	0.00	12540	"
61	HPO + O ₂ = PO + HO ₂	7.00 × 10 ¹²	0.00	83600	"
62	HPO + OH = PO + H ₂ O	1.20 × 10 ⁶	2.00	-8360	"
63	HPO + OH = PO(H)(OH)	1.40 × 10 ¹²	0	0	estimated by Glaude <i>et al.</i> ⁵⁴
64	HOPO + H = H ₂ O + PO	3.00 × 10 ¹²	0	34694	see ^s
65	PO(H)(OH) + H = HOPO + H ₂	5.00 × 10 ¹³	0	0	estimated by Glaude <i>et al.</i> ⁵⁴
66	PO(H)(OH) + OH = HOPO + H ₂ O	1.00 × 10 ¹³	0	0	the same
67	PO(H)(OH) + O = HOPO + OH	5.00 × 10 ¹³	0	0	"
68	HPO + HO ₂ = PO + H ₂ O ₂	2.00 × 10 ¹¹	0	20900	"
69	HPO + PO ₂ = PO + HOPO	2.00 × 10 ¹¹	0	0	"
70	HPO + PO ₃ = PO + HOPO ₂	2.00 × 10 ¹¹	0	0	"
71	HPO + CH ₃ = PO + CH ₄	8.10 × 10 ⁵	1.87	0	"
72	PO ₂ + H + M = HPO ₂ + M (low pressure) ^b	4.87 × 10 ²¹	-2.04	2696.1	see ^{d, t}
73	PO ₂ + H + M = HOPO + M (low pressure) ^b	4.87 × 10 ²³	-2.04	2696.1	see ^{d, u}
74	HPO ₂ = HOPO	2.35 × 10 ¹⁴	0	193952	see ^v
75	HPO ₂ + H = H ₂ + PO ₂	2.40 × 10 ⁸	1.50	20900	estimated by Glaude <i>et al.</i> ⁵⁴
76	HPO ₂ + H = PO(H)(OH)	5.00 × 10 ¹²	0	20900	the same
77	HPO ₂ + O = OH + PO ₂	1.70 × 10 ⁸	1.50	10450	"
78	HPO ₂ + O ₂ = PO ₂ + HO ₂	7.00 × 10 ¹²	0	143792	"
79	HPO ₂ + OH = H ₂ O + PO ₂	1.20 × 10 ⁶	2	-8360	"
80	HPO ₂ + OH = H + HOPO ₂	1.00 × 10 ¹²	0	8360	"
81	HPO ₂ + HO ₂ = H ₂ O ₂ + PO ₂	2.00 × 10 ¹¹	0	41800	"
82	HPO ₂ + CH ₃ = CH ₄ + PO ₂	8.10 × 10 ⁵	1.87	29260	"
83	HPO + PO ₂ = HPO ₂ + PO	1.00 × 10 ¹¹	6.00	0	"
84	HPO ₂ + PO ₂ = HOPO + PO ₂	5.00 × 10 ¹¹	0	0	"
85	HPO ₂ + PO ₃ = HOPO ₂ + PO ₂	5.00 × 10 ¹¹	0	0	"

^a The rate constant was taken from Ref. 62 (the expression for the rate constant was converted into the Arrhenius form). ^b The efficiency coefficients for a third body M (H₂O or H₂) are referred to N₂ (the efficiency factor of H₂O is 16, that of H₂ is 2.5). ^c The pre-exponential factor present in the equation for the rate constant for forward reaction was calculated using the pre-exponential factor from the equation for the rate constant for the reverse reaction taking into account partial equilibrium. The activation energy of the forward reaction CH₃OH + H = CH₃O + H₂ (elimination of the hydrogen atom) was equal to zero according to calculations. Estimated by Glaude *et al.*⁵⁴ ^d The proposed mechanism includes several reactions with identical initial compounds and products but following different channels (for example, elimination and addition reactions). ^e The rate constant was adjusted to the temperature range of 300–2400 K and *P* = 1 atm (see the text). ^f Estimated by Glaude *et al.*⁵⁴ ^g The pre-exponential factor of the forward reaction was taken from reaction CH₃OH + O = CH₃O + OH.⁸⁷ The activation energy of the forward reaction was calculated from the activation energy of reverse reaction taking into account the partial equilibrium. The activation energy of reverse reaction is equal to zero (from the Evans–Polanyi diagramme⁸⁸). ^h According to calculation, the rate constant for reaction (22) is the same as that for H₂O + OH = H₂O + OH, estimated by Glaude *et al.*⁵⁴ ⁱ Calculated by analogy with the reaction CO + HO₂ = CO₂ + OH (Ref. 42). Estimated by Glaude *et al.*⁵⁴ ^j Calculated by analogy with the reaction C₂H₅OH + HO₂ = C₂H₅O + H₂O₂ (Ref. 89). Estimated by Glaude *et al.*⁵⁴ ^k Based on Walker's recommendation for the reactions RH + O₂ = R + HO₂ (Ref. 90). Estimated by Glaude *et al.*⁵⁴ ^l Calculated by analogy with the reaction CH₃OH + CH₃ = CH₃O + CH₄ (Ref. 91). Estimated by Glaude *et al.*⁵⁴ ^m Addition of the H atoms to the O atom in PO₂. Rate constant calculated by Twarowski and increased threefold.⁶⁵ ⁿ By analogy with the reaction ROH + OH = RO + H₂O (Ref. 92). The activation energy was taken to be equal to the bond energy H–C (tertiary carbon atom), which corresponds approximately to the H–O bond energy in HOPO. ^o Calculated on the basis of the radical recombination rate. ^p Based on the reaction NO + HO₂ = NO₂ + OH (Ref. 93). Estimated by Glaude *et al.*⁵⁴ ^q Calculated on the basis of compact transition state with a zero activation barrier. ^r By analogy with the reaction CH₃ + NO₂ = CH₃NO₂ (Ref. 94). ^s By analogy with the reaction CH₃ + NO₂ = CH₃ONO (Ref. 95). ^t The Mackie addition reaction,⁵⁵ the pre-exponential factor was decreased. ^u Addition of an H atom to the P atom in PO₂. It is assumed that 1% of all reaction products is HPO₂. ^v Addition of the H atoms to the P atom in PO₂. It is assumed that virtually the whole reaction gives HOPO. The rate constant was taken from Ref. 65. ^w The rate constant was calculated from the BAC MP4 data. The *cis* transition state was used.^{96,97}

these two radicals over the flame zone with and without OPC is an important characteristics. As follows from computation results,⁵³ DMMP decreases considerably the concentrations of these radicals in both types of flame; the concentration of the H radical decreases faster in the rich flame than in the lean flame. On the basis of foregoing, the authors concluded that there is a difference between the inhibition efficiency of lean and rich flames by OPC [the inhibition efficiency is the difference between the flame propagation speed without an additive (u_0) and with DMMP additive (u) normalised to the flame propagation speed without DMMP: $(u_0 - u)/u_0$]. The experimental and computation results were used to plot the dependence of the inhibition efficiency on the equivalence ratio (ϕ). This value proved to be very sensitive to the accuracy of measurement of the combustion rate.[‡] The mechanism of flame inhibition by OPC additives developed at the Livermore National Laboratory describes well the dependence of the inhibition efficiency on the equivalence ratio.

According to simulation data,⁹⁸ the efficiency of flame propagation inhibition by the addition of DMMP increases monotonically with an increase in the equivalence ratio from 0.8 to 1.3. However, when experimenting with rich and lean flames, Jayaweera *et al.*⁵³ did not find any significant difference between the DMMP action on these flames, and only calculations did show a slight difference in the inhibition efficiency. To gain an understanding of how OPC inhibit lean and rich flames, the inhibition cycles of these flames were studied in detail.⁵³ Using PREMIX software,⁹⁹ the authors simulated the concentration profiles of OPC involved in the recombination of H and OH radicals in freely propagating propane–air flame with DMMP additive at $P = 1$ atm and calculated the profiles for the formation rates of PO_2 in lean and rich flames (Fig. 17 *a* and *b*, respectively). It follows from the obtained data that the major reaction of PO_2 formation in both types of flames is as follows:



This path to PO_2 is reasonable for a lean flame characterised by high concentrations of OH radicals but for a rich flame characterised by high concentrations of H radicals, it was more reasonable to assume that reaction (10) would be the major path to PO_2 .

However, it was found that reaction (10) makes a minor contribution to the formation of PO_2 due to its high activation energy (11 kcal mol⁻¹) [for comparison, the activation energy of reaction (11) equals 1.5 kcal mol⁻¹]. The major path of PO_2 consumption in both flames is reaction (7). Reactions (7) and (11) form together the catalytic cycle $\text{HOPO} \rightleftharpoons \text{PO}_2$ in which the H and OH radicals recombine to give H_2O .

The sensitivity coefficients (ξ) of reactions (6)–(11) to the concentrations of H atoms were analysed⁵³ to determine those having the most pronounced effect on the concentration of hydrogen atoms and to identify the key inhibitor. The sensitivity coefficients of particular reactions to the concentrations of H atoms were determined as derivatives of the mass fractions of H atoms with respect to the pre-exponential factor present in the equation for the rate constant (Fig. 18). A negative sensitivity coefficient means that an increase in the reaction rate results in a decrease in the H atom concentration, *i.e.*, inhibition, while a positive coefficient means that an increase in the reaction rate results in an increase in the H atom concentration. Only reactions involving compounds like H_xPO_y were taken into account. It was noted⁵³ that the sensitivity coefficient of key reaction (1) to the H atom

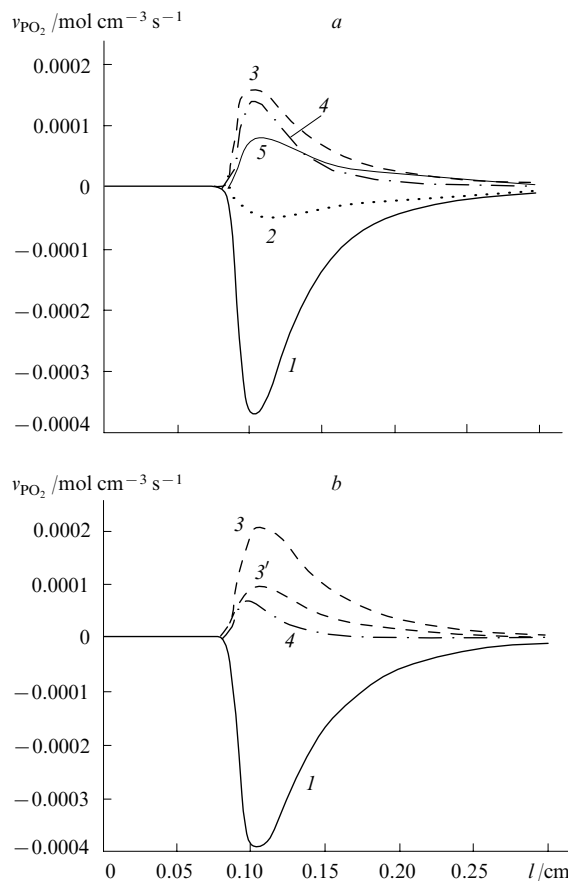


Figure 17. Rates of PO_2 formation and consumption (v_{PO_2}) along reactions (6)–(9) and (11) in lean (*a*) and rich (*b*) flames.⁵³ (1, 2) PO_2 consumption by reactions (7) and (6), respectively, (3–5) PO_2 formation by reactions (11), (8) and (9), respectively (3, through H elimination, 3', through adduct formation).

concentration markedly exceeds in magnitude the sensitivity coefficients of other reactions.

It was found⁵³ that the highest sensitivity of reactions involving H_xPO_y to the H atom concentration in the flame is observed in the post-flame zone. Reaction (7) and, for lean flames, also reaction (9) are most sensitive to the H atom concentration (the rate constant for the latter reaction increases owing to the appearance of a new reaction channel, which was described above).

A curious fact is the increase in the rate of reaction (6) in the lean flame upon an increase in the concentration of H atoms (in the rich flame, the sensitivity of this reaction to the concentration of H atoms is insignificant). The authors believe⁵³ that the sign of the sensitivity coefficient of reaction (6) to the concentration of H atoms changes owing to the fact that the concentrations of H and OH radicals in the cycle $\text{HOPO} \rightleftharpoons \text{PO}_2$ decrease faster than in the cycle $\text{HOPO}_2 \rightleftharpoons \text{PO}_2$. The formation of HOPO_2 by reaction (6) results in a decrease in the PO_2 concentration and a decrease in the rate of reaction (7); as a consequence, smaller amounts of H and OH radicals recombine. This suggests that HOPO is a better catalyst than HOPO_2 . In a lean flame where the HOPO_2 concentration is higher than in a rich flame, a lower inhibition efficiency should be expected. The data of calculation of the relative change in the flame propagation speed (see below) also demonstrate that phosphorus inhibits flame less efficiently in lean mixtures than in rich mixtures.

[‡] Note that the accuracy of measurements of propagation speeds of rich flames is relatively low. This hampers comparison of the experimental and calculation data.

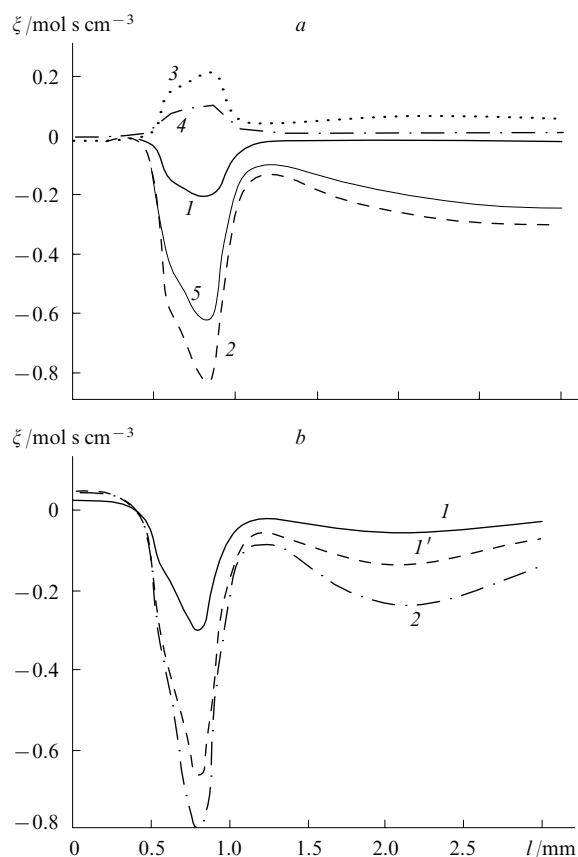


Figure 18. Sensitivity of reactions involving H_3PO_3 taking place in lean (a) and rich (b) flames to H atom concentration:⁵³ (1, 1') reactions (11) (1, through adduct formation, 1', through H atom elimination); (2) reactions (7); (3) reactions (6); (4) reactions (12); (5) reactions (9).

The sensitivity of other reactions was interpreted⁵³ proceeding from the fact that recombination of the H and OH atoms is more efficient in the catalytic cycle $\text{HOPO} \rightleftharpoons \text{PO}_2$ than in the cycle $\text{HOPO}_2 \rightleftharpoons \text{PO}_2$. The increase in the rate constants of reactions that direct the reaction stream along the more efficient cycle $\text{HOPO} \rightleftharpoons \text{PO}_2$ leads to a decrease in the concentrations of the H and OH radicals (flame inhibition), while the increase in the rate constants for reactions that direct the reaction stream through the cycle $\text{HOPO}_2 \rightleftharpoons \text{PO}_2$ decreases the overall recombination rate of the H and OH radicals and, hence, increases their concentration in the flame.

The reaction



that directs the reaction stream along the less efficient cycle accelerates the formation of the H and OH radicals. The same is true for reaction (6). Both reactions have positive sensitivity coefficients to the concentrations of H atoms. Meanwhile, an increase in the rate constant for reaction (9) returns the reaction stream to the more efficient cycle $\text{HOPO} \rightleftharpoons \text{PO}_2$ and inhibits the formation of the H and OH radicals. The transformation paths of the initial components and final and intermediate products in lean and rich flames are sketched in Figs 19 a,b, respectively [only reactions with the rates of $> 2 \times 10^{-6} \text{ mol cm}^{-3} \text{ s}^{-1}$, which make the greatest contributions to the formation and consumption of the H and OH radicals (given in brackets⁸), are given].

§ The reaction rates are given for the distance of 1.07 mm from the burner surface where the PO_2 formation rate is maximum.

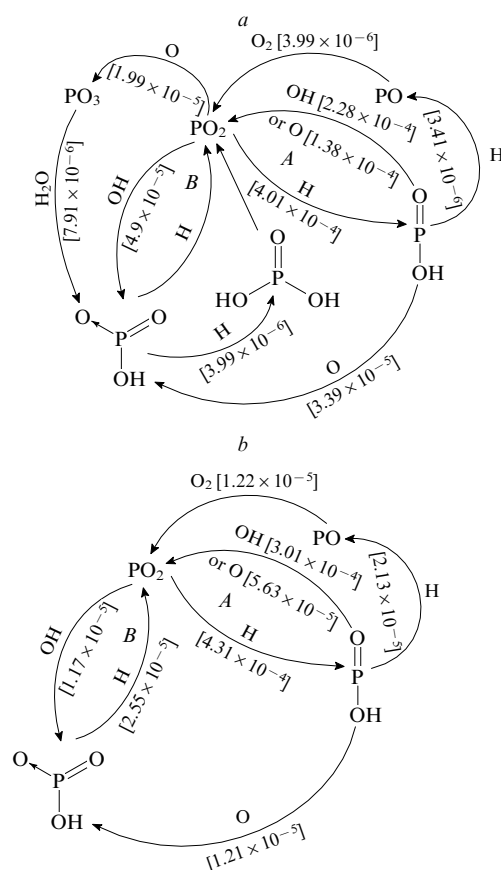


Figure 19. Transformation paths of PO_2 in lean (a) and rich (b) flames.⁵³

It can be seen from Fig. 19 that $\text{HOPO} \rightleftharpoons \text{PO}_2$ (cycle A) and $\text{HOPO}_2 \rightleftharpoons \text{PO}_2$ (cycle B) are the key inhibition cycles. In both cycles, phosphorus compounds act as catalysts of recombination of H and OH radicals to give H_2O . Reaction (12) also takes place being a part of a large cycle. MacDonald *et al.*¹⁰⁰ observed also the recombination of two H atoms with participation of PO_2 and HOPO in diffusion flames. Analysis has shown that recombinations $\text{H} + \text{OH}$ and $\text{H} + \text{O}$ predominate over the reaction $\text{H} + \text{H}$.

To understand how the two inhibition cycles change with the variation of the equivalence ratio, the extent of oxidation of key phosphorus-containing compounds in lean and rich flames were studied. It could be expected (as was actually shown⁵²) that in a lean flame, compounds with a higher oxidation state (for example, HOPO_2) would be present in higher concentrations than compounds with lower oxidation state (for example, HOPO). The opposite is true for a rich flame: the HOPO concentration is higher than the HOPO_2 concentration. The concentration of HPO is insignificant in both types of flame and has no influence on the reaction rates. As a result of the difference between the HOPO and HOPO_2 concentrations, *i.e.*, depending on the equivalence ratio, the directions of the reaction streams change. In both types of flame, the cycle $\text{HOPO} \rightleftharpoons \text{PO}_2$ is more efficient but in the rich flame where the HOPO concentration is higher than in the lean flame, it is 30% more efficient than the cycle $\text{HOPO}_2 \rightleftharpoons \text{PO}_2$. In a rich flame, the species PO plays a significant role in the inhibition, while in lean flame, PO_3 is such a species. In the lean flame, the cycle $\text{HOPO}_2 \rightleftharpoons \text{PO}_2$ is approximately 5 times as significant as in the rich flame owing to the much higher concentration of HOPO_2 . For this reason, the inhibition path involving $(\text{HO})_2\text{PO}$ becomes important.

It should be noted that, although the inhibition efficiencies of the flame involving the catalytic cycles $\text{HOPO}_2 \rightleftharpoons \text{PO}_2$ and $\text{HOPO} \rightleftharpoons \text{PO}_2$ are different in lean and rich flames, their total efficiency is comparable in these two cases, *i.e.*, phosphorus ‘finds’ the most efficient route for flame inhibition. Thus, the ability of phosphorus compound to inhibit flame is unique.

Yet another interesting issue is that the reactions of flame inhibition by phosphorus-containing compounds are most efficient in rather high-temperature regions of the flame at $T > 1600$ K (this corresponds to a distance of 0.9 mm from the burner surface). This is due to the fact that at $T < 1300$ K, the concentrations of all key phosphorus-containing radicals are low (the temperature of 1300 K, which was taken as the reference point, corresponds to consumption of a half of DMMP). The compound $(\text{HO})_2\text{PO}$ formed in the beginning of the combustion zone, which is also an inhibitor, is consumed at higher temperature.

The authors⁵³ pointed to a certain similarity between OPC and the ‘ideal’ inhibitor described by Rumminger *et al.*,¹⁰¹ who showed, using a stoichiometric methane–air flame as an example, that at 1 atm an efficient inhibitor starts to operate at $T > 1700$ K and does not lose activity at least up to 2150 K. In the opinion of the researchers cited,¹⁰¹ the inhibitor that is active at low temperatures is inefficient. This conclusion is based on numerical calculations of the flame propagation speed and structure and on the calculation of the rate of formation and consumption of radicals over the flame zone. Calculations¹⁰¹ showed that inhibition is most efficient in the case where the maximum chain termination rate in catalytic recombination of H and OH radicals involving the inhibitor coincides with the maximum concentrations of these radicals. Analysis of the model has shown that spatial coincidence of the maximum rates of formation of H atoms according to the quadratic chain branching reaction (1) with the maximum rate of consumption of H atoms in catalytic recombination is the actual criterion.

The studies,^{75,102} which partly confirm the conclusions drawn by Jayaweera *et al.*,⁵³ are devoted to the structure of methane–oxygen flames with TMP additives stabilised on a flat burner under atmospheric pressure. Figures 20 *a–d* show the concentration profiles of the H and OH radicals in lean

($\phi = 0.8$, Fig. 20 *a,b*) and rich ($\phi = 1.2$, Fig. 20 *c,d*) flames without an additive and with 0.22 vol.% TMP. Note that in the study cited,¹⁰² the concentration profiles of the hydrogen atom in the flame under atmospheric pressure were measured for the first time. It was found that the introduction of the inhibitor results in a sharper decrease in the concentrations of H and OH radicals in a rich flame compared to the lean flame; the most pronounced decrease in the concentrations of H and OH radicals occurs in the zone of chemical reactions rather than in the zone of formation of the final combustion products (which is consistent with the simulation results⁵³).

It was found^{75,102} that the concentrations of radicals and key phosphorus-containing compounds in the zone of combustion products in inhibited flames under atmospheric pressure are close to equilibrium values. A comparison of experimental data with the results of calculation of the flame structure using the inhibition mechanism⁵³ shows that in the case of lean flames they are in satisfactory agreement. For rich hydrocarbon flames, the agreement is less satisfactory, which is apparently due to the fact that the inhibition mechanism of rich flames needs to be further developed. This is also indicated by the results of another work¹⁰³ dealing with the structure of rich and stoichiometric methane–oxygen flames without additives and with ~ 0.05 vol.% DMMP at a pressure of 660–670 Torr. The experimental procedure used in the study cited¹⁰³ included microprobe sampling of the flame followed by analysis of gaseous products by FT IR spectroscopy. Although the sampling procedure used precluded measurement of the concentrations of labile components, the researchers measured the concentration profiles for formaldehyde, methanol, all C_2 hydrocarbons and the oxides CO and CO_2 in the flame.

It was found that the addition of DMMP into rich flame results in an almost sevenfold increase in the concentration of methanol and a twofold increase in the concentration of acetylene, the ethylene concentration being somewhat decreased. Since the transformation of the CH_3 radical into CH_3OH requires an oxygen atom, while the transformation of CH_3 into C_2 hydrocarbons requires only CH_3 , the increase in the CH_3OH concentration may be indicative of the change in the concentration of oxygen atoms in the flame upon the introduction of an inhibitor.

The simulation of the flame structure¹⁰³ using two different inhibition mechanisms by OPC additives proposed by Glaude *et al.*^{54,65} showed that neither of these mechanisms predicts correctly the variation of the concentrations of CH_2O , CH_3OH and C_2 hydrocarbons caused by introduction of the inhibitor. The disagreement between the experimental and simulation results indicates that none of the models used in calculations takes into account the most important processes of the chemistry of inhibition of rich flames by OPC. Thus, a mechanism of inhibition of rich flames by OPC additives that would take into account the reactions of phosphorus-containing products with carbon-containing flame components has not been developed so far, which is due to some extent to the lack of understanding of the chemistry of hydrocarbon combustion under conditions of excess fuel and to the lack of the model describing the combustion of rich flames.

b. Propagation speed of flames with organophosphorus additives

The dependence of the speed of free propagation of a 4:96 propane–air flame on the concentration of the OPC additive at an initial temperature of 95 °C has been studied.¹⁰⁴ The results of measurements of flame burning velocities with addition of nineteen OPC, including fluorinated OPC, are summarised in Fig. 21. The calculation results for TMP are also presented. The compounds demonstrated similar efficiencies (to within the error of measurements).¹⁰⁴ The OPC used and their boiling points are summarised in Table 5.

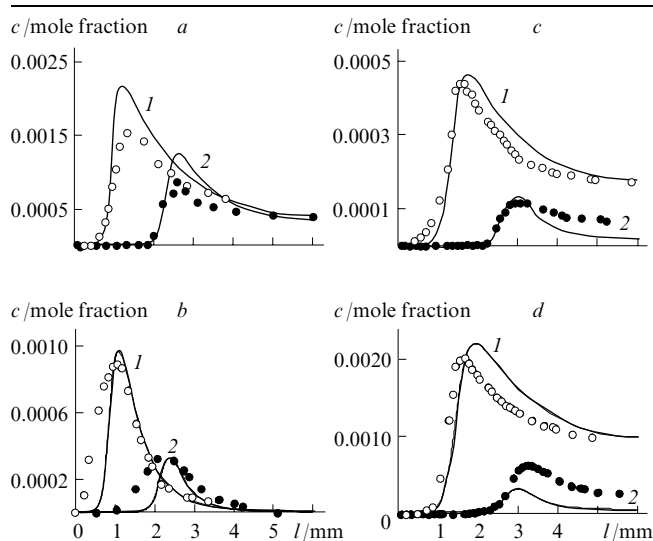


Figure 20. Concentration profiles of H (*b, d*) and OH (*a, c*) radicals in lean (*a, b*) and rich (*c, d*) flames without additives (light dots and curves 1) and with 0.22 vol.% TMP (dark dots and curves 2).¹⁰²

The dots show experimental values and the lines correspond to simulation results.

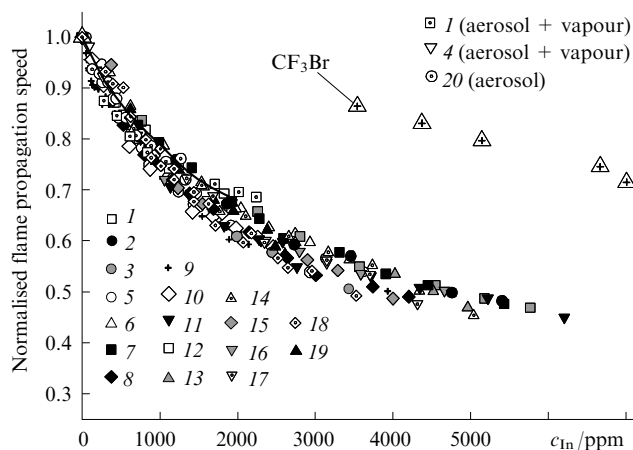


Figure 21. Propagation speed of the $C_3H_8/O_2/N_2$ flame vs. inhibitor concentration (c_{in}).¹⁰⁴ The inhibitors were a number of OPC (presented in Table 5) and CF_3Br . The dots show experimental values and the lines correspond to simulation results with addition of TMP.

The decrease in the normal propagation speed of the flame upon injection of an inhibitor is due to two factors: chemical (radical decay) and thermal (dilution of the flame with the inhibitor and introduction of additional fuel). The contributions of each factor were identified by analysing the curve for the flame propagation speed vs. the limiting concentration of the inhibitor.¹⁰⁵ (This method has been already successfully used to compare the chemical efficiencies of the additives.¹⁰⁶) After introduction of OPC in low concentrations ($<0.3\%–0.4\%$) into the flame, the decay of radicals in recombination reactions involving these OPC becomes the major factor responsible for the decrease in the combustion rate. Therefore, all compounds show similar efficiencies (see Fig. 21), which almost do not depend on their chemical structure and are determined by the presence of a phosphorus atom in their molecules.

Table 5. Flame suppressants and their boiling points.

Number of the compound	OPC	Boiling point / °C	Pressure / Torr
1	$(CH_3O)_3PO$ (TMP)	180	760
2	$(C_2H_5O)_3PO$	215	760
3	$(CF_3CH_2O)_3PO$	187	760
4	$(HCF_2CF_2CH_2O)_3PO$	90	0.5
5	$(C_3F_7CH_2O)_3PO$	97	2.5
6	$(CH_3O)_2P(O)CH_3$ (DMMP)	181	760
7	$(C_2H_5O)_2P(O)CH_3$	194	760
8	$(CF_3CH_2O)_2P(O)CH_3$	193	760
9	$(C_3F_7CH_2O)_2P(O)CH_3$	92	9
10	$(C_3F_7)_3PO$	144	760
11	$(CH_3O)_3P$	111	760
12	$(C_2H_5O)_2P(O)H$	204	760
13	$(CF_3CH_2O)_2P(O)H$	194	760
14	$(C_2H_5O)_3P$	158	760
15	$(CF_3CH_2O)_3P$	131	760
16	$(HCF_2CF_2CH_2O)_3P$	95	3
17	$(CF_3CH_2O)_2P(O)CF_3$	147	760
18	$(CF_3CH_2O)_2PO(OCH(CF_3)_2)$	83	10
19	$POCl_3$	105	760
20	H_3PO_4 (60% aq. solution)	—	—
21	$(HCF_2CF_2CH_2O)_2P(O)CH_3$	115	6

The effect of TMP (0.06 vol.%) on the propagation speed of methane–air flames at a mixture temperature of $35^\circ C$ has been studied as a function of the composition of the mixture (the ϕ value varied from 0.75 to 1.45).⁷⁵ The flame propagation speed was measured by measuring the heat flux to the burner^{23,24} and calculated in terms of the mechanism of flame inhibition by phosphorus compounds described by Jayaweera *et al.*^{53,86} and two mechanisms of methane oxidation, namely, the GRI⁴⁶ and the Curran^{50,51} mechanisms (Fig. 22).

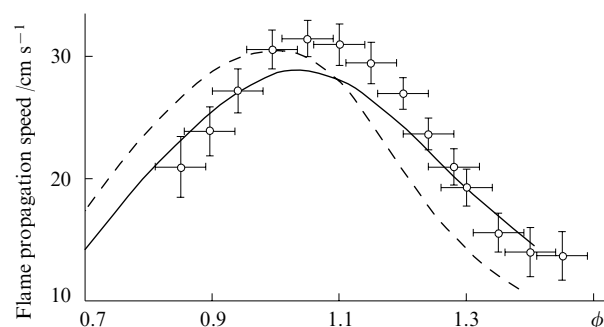


Figure 22. Propagation speed of methane–air flames with 0.06 vol.% TMP vs. ϕ .⁷⁵ The dots show experimental values, the continuous line corresponds to simulation results in terms of the GRI mechanism,⁴⁶ and the dashed line corresponds to simulation in terms of the Curran mechanism.^{50,51}

The calculated flame propagation speeds depended on the selected mechanism of methane oxidation; none of the mechanisms used provided a satisfactory description for the measured dependence of the combustion rate on the equivalence ratio over the whole range (this is one more piece of evidence pointing to imperfection of the proposed multistage kinetic models for hydrocarbon combustion).

Figure 23 shows the efficiency of flame inhibition (E_f) vs. ϕ . The value

$$E_f = \frac{u_0 - u}{u_0}$$

was determined from the experimental and simulated data. All curves (both those calculated from experimental data and those obtained by simulation) had a maximum at $\phi = 1.1–1.3$. The calculation data predict an increase in the inhibition efficiency in the range $\phi = 0.7–1.2$, which is attrib-

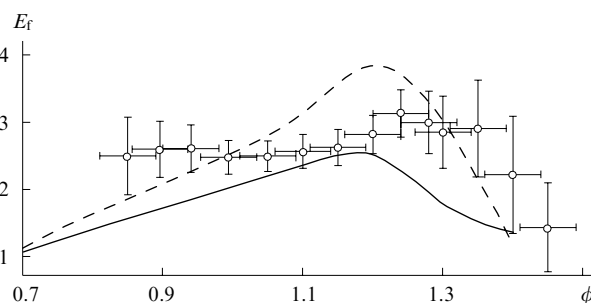


Figure 23. Inhibition efficiency (E_f) vs. ϕ .¹⁰⁴ The dots show experimental values, the continuous line corresponds to simulation results in terms of the GRI mechanism,⁴⁶ and the dashed line corresponds to simulation in terms of the Curran mechanism.^{50,51}

utable to higher efficiency of the cycle $\text{PO}_2 \rightleftharpoons \text{HOPO}$ compared to $\text{PO}_2 \rightleftharpoons \text{HOPO}_2$. The inhibition efficiency calculated from experimental data is almost invariable over this range of ϕ . The decrease in the inhibition efficiency in rich flames was attributed⁷⁴ to incomplete destruction of phosphorus-containing products of TMP destruction into active inhibitors, *viz.*, phosphorus oxides and phosphorus-containing acids. The results indicate that further studies of the OPC combustion chemistry are required in order to elucidate the inhibition mechanism of flames with a large excess of fuel.

2. Diffusion flames formed at the counterflows of the fuel and the oxidant

Diffusion flames have aroused enhanced interest in recent years. The diffusion flame formed at the counterflows of the fuel and the oxidant is a convenient investigation object for the following reasons. This flame is stabilised in space between the nozzles at a certain distance from them under nearly adiabatic conditions. Although the diffusion flame is two-dimensional, the simulation of its structure can be reduced to a one-dimensional problem, which is implemented in the readily available OPDIFF programme.³⁵ This allows one to compare experimental data on the flame structure with simulation results and make counterflow flames a convenient investigation object in the OPC combustion chemistry.

Consider the series of papers^{36,37,107} devoted to the effect of OPC on diffusion flames stabilised on the Potter burner with fuel and oxidant counterflows. Diffusion flames are 'stretched'. An important parameter of such flames is the stretch ratio (a , s^{-1}), which is calculated from the relation

$$a = \frac{2V}{L} \left(1 + \frac{V_f}{V_{\text{ox}}} \sqrt{\frac{\rho_f}{\rho_{\text{ox}}}} \right),$$

where V is the gas linear velocity, L is the distance between the nozzles, ρ is the density (the subscripts f and ox refer to the fuel and the oxidant, respectively). The stretch ratio is actually inversely proportional to the residence time of the reaction mixture in the flame. This value is also called the velocity gradient (the change in the gas flow velocity in the space between two nozzles).

Typical stretch ratio values for counterflow flames are 100 to 800 s^{-1} . The higher the fuel and oxidant feed rates, the greater the flame stretch ratio. Finally, at a certain stretch ratio (quenching stretch ratio), the flame is quenched. The inhibitor (flame suppressant) decreases the stretch ratio needed to quench the flame; therefore, the efficiency of flame suppressants can be conveniently determined from the dependence of the quenching stretch ratio of a flame on the flame suppressant concentration.

The parameter E_q calculated from the formula

$$E_q = \frac{a_{q0} - a_q}{a_{q0}},$$

where a_{q0} is the quenching stretch ratio for a pure flame, a_q in the quenching stretch ratio for an inhibited flame, has been proposed¹⁰⁰ for comparison of the efficiency of counterflow flame quenching by various inhibitors. The subscript q (quenching) implies that all parameters correspond to the instant of quenching. It was found that DMMP and TMP are 2–4 times more efficient suppressants than CF_3Br .^{7,63,108,109} The introduction of a phosphorus-containing compound (1500 ppm) decreases the quenching stretch ratio of the flame by 35%. The injection of the additive into the oxidant flow in a diffusion methane – air flame was found to be 2–4 times more efficient than injection into the fuel flow (in this case, a region with excess fuel is formed on the fuel injection side in the

diffusion flames).¹⁰⁹ This is attributable to low inhibition efficiency of rich flames ($\phi > 1.2$) by phosphorus compounds.⁷⁵

The efficiency of quenching of the counterflow $\text{CH}_4/\text{O}_2 - \text{O}_2/\text{N}_2$ flame (0.2/0.8–0.4/0.6) by fourteen OPC and CF_3Br was studied (Fig. 24, the OPC numbering is the same as in Table 5).¹⁰⁴ The additives were injected into the oxidant flow whose temperature was 100°C . The plots for the quenching stretch ratio *vs.* the inhibitor concentration were compared with the quenching stretch ratios obtained with one of the most effective inhibitors, *viz.*, iron pentacarbonyl $\text{Fe}(\text{CO})_5$ (curve 2 in Fig. 24).¹¹⁰

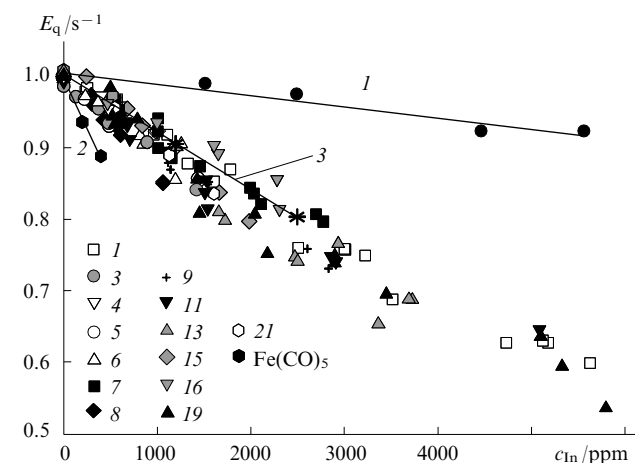


Figure 24. Quenching stretch ratio (E_q) of counterflow flames *vs.* initial concentration of the inhibitor (c_{in}).¹⁰⁴ Inhibitor: OPC (compound numbering is the same as in Table 5), CF_3Br (curve 1), $\text{Fe}(\text{CO})_5$ (curve 2); (3) calculation results for TMP.

According to the measurement results, at $c_{\text{in}} < 0.1$ vol.%, all of the OPC had equal efficiency, which was 7 times higher than that of CF_3Br but 3 times lower than that of iron pentacarbonyl. These results indicate that the efficiency of OPC depends on the concentrations of phosphorus oxides and phosphorus acids and hardly depends on the structure of the initial molecule. The quenching stretch ratios (curve 3 in Fig. 24) for the flames with 0.12 vol.% and 0.25 vol.% TMP (designated by * in Fig. 24) calculated in terms of the mechanism of inhibition by OPC proposed by Korobeinichev *et al.*^{58,85} were compared with the experimental data. It was found experimentally that the quenching stretch ratio decreases by 10% and 20% in the presence of 0.12 vol.% and 0.25 vol.% TMP, respectively. The values predicted by numerical simulation are 9.4% and 18.8%. Thus, the results of measurements are in good agreement with the computation data.

The chemical structure of counterflow flames (diffusion or premixed) was studied by laser-induced fluorescence^{7,8,111,112} and probe mass spectrometry techniques.^{113–115} The molecular-beam mass spectrometry was first applied to probing of a counterflow diffusion flame by Marinov *et al.*¹¹⁶ The concentration profiles of stable components and phosphorus compounds were obtained and the concentration profile of the OH radical in the flame without additives and with 0.12 vol.% TMP was measured.^{113–118}

Analysis of the concentration profiles of phosphorus oxides and phosphorus acids shows that the composition of these compounds in the 'lean' region of the diffusion flame (where excess oxygen is present) is the same as their composition in a lean premixed flame in which HOPO_2 predominates.^{75,102} In the 'rich' region of the diffusion flame, the

HOPO is the main phosphorus-containing component, which is typical of rich premixed flames.^{75, 102} The numerical calculation of the flame temperature and comparison of the obtained data with the results of measurements have shown that the temperature measurement by a thermocouple arranged on the burner axis gives results that best coincide with the computation results.

The flame structure was also calculated upon simulation in terms of the mechanism of inhibition by OPC.^{53, 85} The calculated concentration profiles describe experimental data with a satisfactory accuracy; however, the experimental concentration profiles of compounds in the flame are somewhat broadened compared to calculated profiles, which is due to imperfection of the model used in the OPPDIF programme (the model neglects the edge effects).

3. Air co-flow diffusion flames

The studies of air co-flow diffusion flames were aimed first of all at determining the minimum quenching concentrations of flame suppressants by the cup burner method. Studies of OPC containing no fluorine atoms showed that they are combustible and useless as flame suppressant; therefore, fluorine-substituted OPC were chosen. The MQC values for fluorine-containing organophosphorus inhibitors were measured by the cup burner method independently by Russian³¹ and American¹¹⁹ research groups. In both cases, almost identical cup burners were used, the flame suppressant was supplied through a nebulizer, and the only difference was in the air flow temperature: in one study,¹¹⁹ the measurements were carried out at 55 °C and in the other study,³¹ at 75 °C. In the latter work,³¹ five fluorine-containing OPC and CF₃Br were additionally studied (note that organofluorine compounds proved to be less effective than OPC). The measured MQC values are summarised in Table 6. The minimum quenching concentrations are usually expressed as volume fractions or percent, but for practical purposes it is required to know the mass MQC. Analysis of the data presented in Table 6 shows that many fluorine-containing OPC are capable of flame quenching when present in low volume concentrations; however, owing to high molecular masses, their weight consumption exceeds that of

Table 6. Minimum quenching concentrations of fluorine-substituted OPC and CF₃Br.³¹

Compound	Minimum quenching concentration	
	vol. %	g m ⁻³
[(CF ₃) ₂ CHO] ₂ PO(C ₂ H ₅)	2.0 ± 0.2	366
[(CF ₃) ₂ CHO] ₃ P	2.2 ± 0.2	523
(CF ₃ CH ₂ O) ₂ PO(CF ₃)	2.3 ± 0.2	322
(CF ₃ CH ₂ O) ₃ P	2.6 ± 0.2 (3.1) ^a	381
(CF ₃ CH ₂ O) ₂ PO[OCH(CF ₃) ₂]	no quenching at 3% concentration	—
(CF ₃ CH ₂ O)PO[OCH(CF ₃) ₂] ₂	burns	—
(CF ₃ CH ₂ O) ₂ PO(C ₂ H ₅)	"	—
[(CF ₃) ₂ CHO] ₂ PO(CH ₃)	3.0 ± 0.2	530
[(CF ₃) ₂ CHO] ₂ PO(CF ₃)	2.0 ± 0.2	400
(CF ₃) ₃ PO	no quenching at 5% concentration (see ^a)	—
(CF ₃) ₂ (CH ₃)OP	ignites in air ^a	—
(CF ₃ CH ₂ O) ₂ P(CF ₃)	3.0 ^a	400
(CH ₃ O)PO(CF ₃) ₂	4.6 ^a	443
(CF ₃ CH ₂ O)P(CF ₃) ₂	1.8 ^a	215
(CF ₃ CH ₂ O)PO(CF ₃) ₂	no quenching at 5% concentration (see ^a)	—
CF ₃ Br	4.6	306

^a Data from Ref. 119.

less effective CF₃Br. Unfortunately, it was impossible to extinguish the flame with (CF₃)₃PO, which has low molecular mass,¹¹⁹ apparently due to its combustibility.

The results of cup burner experiments give not only the MQC values, but also the dependence of the quenching concentration of one flame suppressant (often an inert diluent, for example, CO₂) on the quenching concentration of the other one, often an active agent. Figure 25 shows the dependences of the quenching concentration of CO₂ on the quenching concentration of fluorine-containing OPC, organofluorine compounds and CF₃Br. It can be seen from the presented data that despite the different MQC values, all phosphorus-containing flame suppressants have similar efficiencies (when present in concentration of ~0.5%). Note that the quenching concentration of CO₂ ceases to decrease with an increase in the quenching concentration of some OPC [for example, (CF₃CH₂O)₂(C₂H₅)PO], which is indicative of combustibility of these compounds under these conditions (the heat evolved upon their combustion counterbalances the inhibitory effect).

British researchers^{120, 121} used an advanced flame ionisation detector (FID) of a chromatograph to study quenching of air co-flow diffusion flames (hydrogen–air and methane–air) by flame suppressants. They tested a large number of OPC. When methane–air flame was used, the MQC values of flame suppressants determined by this and by the cup burner techniques coincided with satisfactory accuracy. The advantage of the FID method^{120, 121} is the possibility of using a small amount of a flame suppressant for determining its MQC. Despite the encouraging results and the simple design, the FID method has not yet found extensive use.

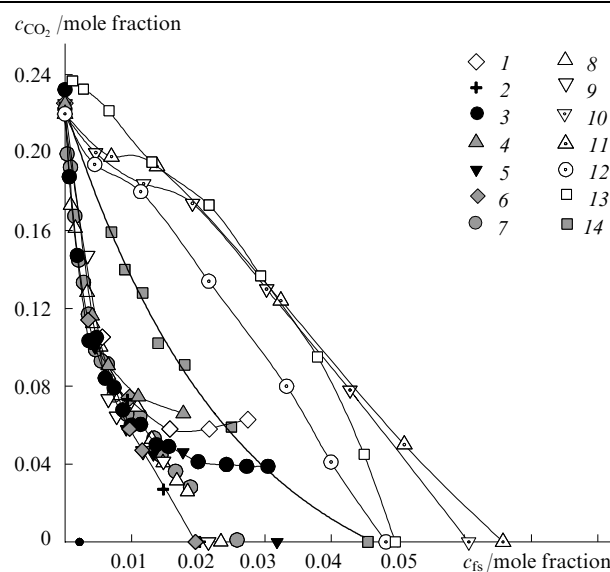


Figure 25. Quenching concentration of CO₂ vs. quenching concentration (*c_{RS}*) of fluorine-substituted OPC (curves 1–9), organofluorine compounds (curves 10–13) and CF₃Br (curve 14).³¹

Compounds: (1) (CF₃CH₂O)₂PO(C₂H₅), (2) [(CF₃)₂CHO]₂PO(C₂H₅), (3) (CF₃CH₂O)₂PO[OCH(CF₃)₂], (4) (CF₃CH₂O)PO[OCH(CF₃)₂]₂, (5) [(CF₃)₂CHO]₂PO(CH₃), (6) [(CF₃)₂CHO]₂PO(CF₃), (7) (CF₃CH₂O)₃P, (8) (CF₃CH₂O)₂PO(CF₃), (9) [(CF₃)₂CHO]₃P, (10) HCF₂CF₂CH₂OCF₂CHF₂CF₃, (11) CF₃CF₂CF₂OCH₂CF₃, (12) (CF₃)₂C=CFCF₂CF₃, (13) (CF₃)₂CFCF=CFCF₃, (14) CF₃Br.

4. Turbulent flames

The efficiency of quenching turbulent flames by short-term injection of (CF₃CH₂O)₃P and CF₃Br into the air stream was determined³¹ on a test bench analogous to that described in

Table 7. Parameters GWP and HGWP calculated for different time ranges characterising the effect of OPC on climatic changes.

Compound	HGWP				GWP			
	20 years	100 years	500 years	∞	20 years	100 years	500 years	∞
$P_3N_3F_6$	0.1	43.5	12.9	4.0	6.9×10^{-3}	2.8×10^{-3}	2.5×10^{-3}	0
$(CF_3CH_2O)_3P$	7.56×10^{-4}	3.1×10^{-4}	2.74×10^{-4}	2.71×10^{-4}	4.8	0.43	0.426	0.426

Ref. 30. A study of the temperature dependence of the MQC of the phosphite $(CF_3CH_2O)_3P$ in the air temperature range of 35 to 86 °C showed³¹ that at $T < 60$ °C some of the flame suppressant occurs as an aerosol and some as vapour; therefore MQC is the sum of concentrations. When $T > 60$ °C, MQC corresponds only to the concentration of flame suppressant vapour.

For $T = 75$ °C, the MQC measured for the turbulent flame equals 4 vol.%, which is approximately 1.5 times higher than the concentration measured for the diffusion flame by the cup burner technique. The difference may be related to either the loss of $(CF_3CH_2O)_3P$ during its supply to the flame or to the fact that quenching of the turbulent flame differs appreciably from quenching of the laminar flame. No such difference was observed in determination of the MQC of CF_3Br ;³¹ however, the coincidence of its MQC values may be accidental.

It was impossible to determine the MQC of trimethyl phosphite,³¹ because after the flame quenching, the mixture of TMP vapour with air and combustion products self-ignited.[¶] It was found that at an air temperature of 90 °C and a TMP concentration of 8.5 vol.%, no repeated ignition of TMP vapour takes place; however, this quenching concentration can hardly be considered minimum.

VI. Toxicity and environmental impact of organophosphorus compounds

1. Determination of toxicity

In order to evaluate the prospects of using OPC as flame suppressants, the toxicity of a number of OPC was studied. For example, the toxicities of TMP, DMMP, DEMP, tris(2,2,2-trifluoroethyl) phosphate, trimethyl phosphite and tris(2,2,2-trifluoroethyl) phosphite were assessed.¹²³ The toxicological parameters were measured for laboratory mice upon intragastric administration of the tested compounds in various doses. Dimethyl and diethyl methylphosphonates were dissolved in water prior to the measurements and $(CF_3CH_2O)_3PO$, which is almost insoluble in water, was used as an emulsion in olive oil. Each test series was carried out for 4–8 mice.

The toxicity (LD_{50}) of the OPC upon intragastric administration was relatively low ranging from 0.27 to 10.5 ± 0.09 ml per kg of live weight.¹²³ DMMP was least toxic, while tris(2,2,2-trifluoroethyl) phosphite was the most toxic. No action of these compounds to skin or mucous membranes was observed.

The toxicity of tris(2,2,2-trifluoroethyl) phosphite vapour upon inhalation was also assessed. The concentration of tris(2,2,2-trifluoroethyl) phosphite vapour at 25 °C is 0.4 vol.% (59 mg litre⁻¹). This concentration was not lethal for mice, which have spent 15 min in a chamber with atmosphere saturated with the phosphite vapour. They all survived for 5 weeks. However, when the temperature in the chamber was raised to 30–35 °C and the OPC concentration increased to 0.68 vol.% (100 mg litre⁻¹), one mice died within 15 min

after inhalation of $(CF_3CH_2O)_3P$ vapour and the other four mice died after 2 days. The animal death was due to lung damage. Although the toxicological parameters (LC_{50}) of the tris(2,2,2-trifluoroethyl) phosphite vapour could not be determined, it is obvious that the vapour toxicity is much higher than that of intragastrically administered liquid compound.

2. Environmental impact of organophosphorus compounds

When assessing the impact of various compounds on the environment, two key factors are considered first of all: their impact on the Earth ozone layer and the contribution to the global warming. The impact on the ozone layer is determined by the dimensionless parameter ODP (ozone depletion potential). Trichlorofluoromethane was used as the reference, its ODP being taken to be unity. The efficient flame suppressant CF_3Br (halon 13B1) the production of which was forbidden by the Montreal Convention efficiently depletes the ozone layer, its ODP being 10.

The effect of $(CF_3CH_2O)_3P$ as a representative of OPC on the environment was studied at the laboratory of the Chemical Physics of Atmosphere of the Institute of Energy Problems of Chemical Physics of the RAS.¹²⁴ The calculations showed that ODP of this OPC can be considered to be zero. The presence of $(CF_3CH_2O)_3P$ in the atmosphere in a practically infinite amount does not deplete the ozone layer. According to calculation data, the existence time of $(CF_3CH_2O)_3P$ in the atmosphere is 0.019 years.

The contributions of compounds to the global warming (enhancement of the greenhouse effect) are characterised by two dimensionless parameters, the main parameter GWP (Global Warming Potential) and additional parameter HGWP (Halocarbon Global Warming Potential), which is calculated with respect to the GWP of trichlorofluoromethane. The GWP and HGWP parameters are calculated for particular time intervals. The GWP of carbon dioxide for the interval $t = \infty$ is taken to be unity. The GWP and HGWP values for two OPC, *viz.*, phosphazene $P_3N_3F_6$ and tris(2,2,2-trifluoroethyl) phosphite, were calculated.¹²⁴ The calculation results are presented in Table 7. The data indicate that these OPC do not possess properties of greenhouse gases and have almost no impact on the Earth climate warming.

* * *

The information summarised in this review shows that considerable progress in the understanding of OPC combustion chemistry has been achieved in the last decade. However, a number of problems still remain unsolved. First of all, this refers to the chemistry of combustion of rich hydrocarbon flames. No data on the combustion chemistry and the mechanism of inhibition of atmospheric hydrogen–oxygen flames, especially rich ones, by organophosphorus compounds are available either, although they are much simpler as regards possible combustion intermediates and final products than hydrocarbon flames.

This review was written with the financial support of the Russian Foundation for Basic Research (Project No. 07-03-11 005-ano).

[¶] Previously, it has been shown¹²² that TMP vapour burns at elevated temperature.

References

1. R Boyle *Philos. Trans. R. Soc. London* **13** 196 (1680)
2. A Twarowski *Combust. Flame* **94** 91 (1993)
3. Johnston Atoll Chemical Agent Disposal System. (JACADS). *Final Second Supplemental Environmental Impact Statement for the Storage and Ultimate Disposal of the European Chemical Munitions Stockpile*, Edgewood, MD, 1990
4. Demilitarization and Disposal of U.S. Chemical Warfare Agent and Munitions. *Conference on Disarmament*. Ad Hoc Committee on Chemical Weapons. CD/CW/WP. 265 (1989)
5. World Meteorological Organization Global Ozone Research and Monitoring Project. *Scientific Assessment of Stratospheric Ozone*, Geneva, 1989 Vol. 1, Report 20
6. J W Hastie, D W Bonnell *Molecular Chemistry of Inhibited Combustion Systems* National Bureau of Standards, NBSIR, 80-2169, 1980
7. M A MacDonald, T M Jayaweera, E M Fisher, F C Gouldin *Combust. Flame* **116** 166 (1999)
8. J E Siow, N M Laurendeau *Combust. Flame* **136** 16 (2004)
9. R M Fristrom, A A Vestenberg *Struktura Plameni* (The Structure of Flame) (Moscow: Metallurgiya, 1969)
10. R M Fristrom, C Grunfelder, S Favin *J. Phys. Chem.* **64** 1386 (1960)
11. O P Korobeinichev, A G Tereshchenko, I D Emel'yanov, L V Kuibida, R A Mavliev, K P Kutsenogii, A L Rudnitskii, S Yu Fedorov, N E Ermolin, V M Fomin *Obosnovanie Metoda Mass-spektrometricheskogo Zondirovaniya Plamen Kondensirovannykh Sistem s Uzkimi Zonami Goreniiya* (Substantiation of the Method of Mass-spectrometric Probe for Flames of Condensed Systems with Narrow Combustion Zones) (Novosibirsk: Siberian Branch, Academy of Sciences of the USSR, 1985) Preprint No. 14
12. J H Werner, T A Cool *Chem. Phys. Lett.* **275** 278 (1997)
13. J H Werner, T A Cool *Combust. Flame* **117** 78 (1999)
14. O P Korobeinichev, S B Ilyin, V V Mokrushin, A G Shmakov *Combust. Sci. Technol.* **116** 51 (1996)
15. O P Korobeinichev, V M Shvartsberg, A A Chernov, V V Mokrushin *Proc. Combust. Institute* **26** 1035 (1996)
16. P A Skovorodko, A G Tereshchenko, O P Korobeinichev, D A Knyazkov, A G Shmakov *Khim. Fiz.* **25** 23 (2006)^a
17. P A Skovorodko, A G Tereshchenko, O P Korobeinichev, D A Knyazkov, A G Shmakov *Khim. Fiz.* **25** 33 (2006)^a
18. K A Burton, H D Ladouceur, J W Fleming *Combust. Sci. Technol.* **81** 141 (1992)
19. W E Kaskan *Proc. Combust. Institute* **6** 134 (1957)
20. A N Hayhurst, D B Kittelson *Combust. Flame* **28** 301 (1977)
21. O P Korobeinichev, V M Shvartsberg, T A Bolshova, A G Shmakov, D A Knyazkov *Fiz. Goreniya i Vzryva* **38** (2) 3 (2002)^b
22. G T Linteris, L Truett *Combust. Flame* **105** 15 (1996)
23. L P H de Goey, A van Maaren, R M Quax *Combust. Sci. Technol.* **92** 1 (1993)
24. A van Maaren, D S Thung, L P H de Goey *Combust. Sci. Technol.* **96** 327 (1994)
25. B Lewiss, G von Elbe *Combustion, Flames and Explosions of Gases* (New York: Academic Press, 1961)
26. NFPA 2001: *Standard on 'Clean Agents Fire Extinguishing Systems'*, USA, 1994
27. J D Mather, R E Tapscott, T A Moore *Proceedings of Halon Options Technical Working Conference 1998* CD-ROM NIST SP 948-3, National Institute of Standards and Technology, Gaithersburg, MD, 2005
28. A N Baratov, N P Kopylov, E V Timofeev *Proceedings of Halon Options Technical Working Conference, 2002* CD-ROM NIST SP 948-3, National Institute of Standards and Technology, Gaithersburg, MD, 2005
29. A N Baratov, S G Tsarichenko, A F Zhevlakov, E V Timofeev, R A Yajliyan *Proceedings of the Fourth Asia-Pacific Symposium on Fire Science and Technology*, Tokyo, 2000 p. 351
30. W Grosshandler, A Hamins, K McGrattan, C Presser *Transient Application, Recirculating Pool Fire, Agent Effectiveness Screen, Final Report* NGP Project 3A/2/890, National Institute of Standards and Technology, Gaithersburg, MD, 2001
31. A G Shmakov, O P Korobeinichev, V M Shvartsberg, S A Yakimov, D A Knyazkov, V F Komarov, G V Sakovich *Fiz. Goreniya i Vzryva* **42** (6) 64 (2006)^b
32. R J Kee, J F Grcar, M D Smooke, J A Miller *Sandia National Laboratories Report*, 1990 SAND85-8240
33. R J Kee, F M Rupley, J A Miller *CHEMKIN-II: A Fortran Chemical Kinetics Package for the Analysis of Gas Phase Chemical Kinetics*. Sandia National Laboratories Report New Mexico, CA, 1989, SAND89-8009B
34. C M Lund *HCT—A General Computer Program for Calculating Time-Dependent Phenomena Involving One-Dimensional Hydrodynamics, Transport, and Detailed Chemical Kinetics* Lawrence Livermore National Laboratory, Livermore, CA, 1978, Report UCRL-52504
35. A E Lutz, R J Kee, J F Grcar, F M Rupley *Chemkin Collection, Unlimited Release* Sandia National Laboratories, Livermore, CA, 1997
36. A E Potter, J N Butler *Int. ARS J.* **50** (1959)
37. A E Potter, S Heimel, J N Butler *Proc. Combust. Institute* **9** 1027 (1962)
38. J Warnatz *Combustion Chemistry* (Ed. W C Gardiner) (New York: Springer, 1984)
39. G Dixon-Lewis *Arch. Combust.* **4** 279 (1984)
40. J A Miller, M D Smoke, R M Green, R J Kee *Combust. Sci. Technol.* **34** 149 (1983)
41. G Dixon-Lewis, M M Sutton, A Willams *Proc. R. Soc. London, Ser. A* **317** 227 (1970)
42. W Tsang, J Hampson *J. Phys. Chem. Ref. Data* **15** 1087 (1986)
43. R A Yetter, F L Dryer, H Rabitz *Combust. Sci. Technol.* **79** 97 (1991)
44. D L Baulch, D D Drysdale, D G Horne *Evaluated Kinetic Data for High Temperature Reactions. Homogeneous Gas Phase Reactions of the H₂–O₂ System* (London: Butterworths, 1976) Vol. 1
45. M Ó Connaire, H J Curran, J M Simmie, W J Pitz, C K Westbrook *Int. J. Chem. Kinet.* **36** 603 (2004)
46. G P Smith, D M Golden, M Frenklach, N W Moriarty, B Eiteneer, M Goldenberg, C T Bowman, R K Hanson, S Song, W C Gardiner Jr, V V Lissianski, Z Qin *GRI Mech 3.0* 1999; http://www.me.berkeley.edu/gri_mech
47. A Konnov *Detailed Reaction Mechanism for Small Hydrocarbons* Combustion Release 0.5, <http://homepages.vub.ac.be/~akonnov>
48. A van Maaren, L P H de Goey *Combust. Sci. Technol.* **102** 309 (1994)
49. C M Vagelopoulos, F N Egolfopoulos, C K Law *Proc. Combust. Institute* **25** 1341 (1994)
50. M Ó Connaire, H J Curran, J M Simmie *Proceedings of the European Combustion Meeting, Orléans, France, 2003*
51. H J Curran, T M Jayaweera, W J Pitz, C K Westbrook *Western States Section of the Combustion Institute, Davis, CA, 2004* Paper 04S-58
52. O P Korobeinichev, V M Shvartsberg, A G Shmakov, T A Bolshova, T M Jayaweera, C F Melius, W J Pitz, C K Westbrook, H Curran *Proc. Combust. Institute* **30** 2353 (2005)
53. T M Jayaweera, C F Melius, W J Pitz, C K Westbrook, O P Korobeinichev, V M Shvartsberg, A G Shmakov, I V Rybitskaya, H J Curran *Combust. Flame* **140** 103 (2005)
54. P A Glaude, H J Curran, J W Pitz, C K Westbrook *Proc. Combust. Institute* **28** 1749 (2000)
55. J C Mackie, G B Bacskay, N L Haworth *J. Phys. Chem. A* **106** 10825 (2002)
56. C W Bauschlicher *J. Phys. Chem. A* **103** 11126 (1999)
57. O P Korobeinichev, A A Chernov, V M Shvartsberg *Prepr. Pap. Am. Chem. Soc., Div. Fuel Chem.* **39** (1) 193 (1994)
58. O P Korobeinichev, S B Ilyin, T A Bolshova, V M Shvartsberg, A A Chernov *Combust. Flame* **121** 593 (2000)
59. S B Il'in, Candidate Thesis in Physical and Mathematical Sciences, Institute of Chemical Kinetics and Combustion, Siberian Branch of the Russian Academy of Sciences, Novosibirsk, 1998
60. E R Wils *Fresenius' J. Anal. Chem.* **338** 22 (1990)
61. A Twarowski *Combust. Flame* **94** 341 (1993)
62. A Twarowski *Combust. Flame* **102** 41 (1995)
63. A Twarowski *Combust. Flame* **105** 407 (1996)

64. O P Korobeinichev, V M Shvartsberg, A A Chernov *Combust. Flame* **118** 727 (1999)
65. R T Wainner, K L McNesby, A W Daniel, A W Miziolek, V I Babushok *Proceedings of Halon Options Technical Working Conference, 2000* CD-ROM NIST SP 948-3, National Institute of Standards and Technology, Gaithersburg, MD, 2005
66. O P Korobeinichev, S B Ilyin, V M Shvartsberg, A A Chernov *Combust. Flame* **118** 718 (1999)
67. V M Shvartsberg, Candidate Thesis in Chemical Sciences, Institute of Chemical Kinetics and Combustion, Siberian Branch of the Russian Academy of Sciences, Novosibirsk, 2000
68. O P Korobeinichev, V M Shvartsberg, S B Il'in *Fiz. Goren. Vzryva* **33** (3) 32 (1997)^b
69. O P Korobeinichev, T A Bolshova, V M Shvartsberg, A A Chernov *Combust. Flame* **125** 744 (2001)
70. R Atkinson *J. Chem. Phys. Ref. Data (Monograph I)* 201 (1989)
71. O P Korobeinichev, A A Chernov, T A Bolshova *Combust. Flame* **123** 412 (2000)
72. E J P Zegers, E M Fisher *Combust. Flame* **115** 230 (1998)
73. P A Glaude, C F Melius, W J Pitz, C K Westbrook *Proc. Combust. Institute* **29** 2469 (2002)
74. O P Korobeinichev, V M Shvartsberg, S B Il'in, A A Chernov, T A Bolshova *Fiz. Goren. Vzryva* **35** (3) 29 (1999)^b
75. O P Korobeinichev, V M Shvartsberg, A G Shmakov, D A Knyazkov, I V Rybitskaya *Proc. Combust. Institute* **31** 2741 (2007)
76. O P Korobeinichev, A A Chernov, L N Krasnoperov *Proceedings of International CWA Destruction Symposium, Munster, Germany, 1998* p. 225
77. O P Korobeinichev, A A Chernov, V V Sokolov, L N Krasnoperov *Int. J. Chem. Kinet.* **34** 331 (2002)
78. O P Korobeinichev, A A Chernov, V V Sokolov, L N Krasnoperov *Khim. Fiz.* **21** (12) 27 (2002)^a
79. T A Bolshova, Candidate Thesis in Physical and Mathematical Sciences, Institute of Chemical Kinetics and Combustion, Siberian Branch of the Russian Academy of Sciences, Novosibirsk, 2006
80. V S Babkin, A V V'yun *Fiz. Goren. Vzryva* **17** (5) 8 (1981)^b
81. T A Bolshova, O P Korobeinichev *Fiz. Goren. Vzryva* **42** (5) 3 (2006)^b
82. M R Zachariah, O I Smith *Combust. Flame* **69** 125 (1987)
83. V N Stokin, V M Khailov *Fiz. Goren. Vzryva* **10** (2) 230 (1974)^b
84. J W Hastie *Int. J. Mass Spectrom. Ion Processes* **16** 89 (1975)
85. O P Korobeinichev, A L Mamaev, V V Sokolov, T A Bolshova; V M Shvartsberg, L Zakharov, I Yu Kudryavtsev *Proceedings Halon Options Technical Working Conference, 2001* CD-ROM NIST SP 948-3, National Institute of Standards and Technology, Gaithersburg, MD, 2005
86. http://www.kinetics.nsc.ru/labor/kcp_en/opc_mech.html
87. J Warnatz *Gas-Phase Combustion Chemistry* (Ed. W C Gardiner) (New York: Springer, 2000)
88. M G Evans, M Polanyi *Trans. Faraday Soc.* **34** 11 (1938)
89. N Marinov *Int. J. Chem. Kinet.* **31** 183 (1999)
90. T Ingham, R W Walker, R E Woolford *Proc. Combust. Institute* **25** 767 (1994)
91. W Tsang *J. Phys. Chem. Ref. Data* **16** 471 (1987)
92. R Atkinson *Int. J. Chem. Kinet.* **18** 555 (1986)
93. W B DeMore, S P Sander, D M Golden, R F Hampson, M J Kurylo, C J Howard, A R Ravishankara, C E Kolb, M J Molina *Chemical Kinetics and Photochemical Data for Use in Stratospheric Modeling (Evaluation Number 12), Jet Propulsion Laboratory, California Institute of Technology, Pasadena, CA, 1997* Publication 97-4
94. K Glaenger, J Troe *Ber. Bunsen-Ges. Phys. Chem.* **78** 182 (1974)
95. C Canosa, R-D Penzhorn, C von Sonntag *Ber. Bunsen-Ges. Phys. Chem.* **83** 217 (1979)
96. C F Melius, M D Allendorf *J. Phys. Chem. A* **104** 2168 (2000)
97. C F Melius *Chemistry and Physics of Energetic Materials* (Ed. S N Bulusu) (Dordrecht: Kluwer Academic, 1990) p. 21
98. T M Jayaweera, C F Melius, W J Pitz, C K Westbrook, O P Korobeinichev, V M Shvartsberg, A G Shmakov, I V Rybitskaya, H Curran *Western States Section of the Combustion Institute, Davis, CA, 2004* Paper 042-43
99. R J Kee, F M Rupley, J A Miller, M E Coltrin, J F Grear, E Meeks, H K Moffat, A E Lutz, G Dixon-Lewis, M D Smooke, J Warnatz, G H Evans, R S Larson, R E Mitchell, L R Petzold, W C Reynolds, M Caracotsios, W E Stewart, P Glarborg, C Wang, O Adigun, W G Houf, C P Chou, S F Miller *Chemkin Collection. Release 3.7.1, Reaction Design, San Diego, CA, 2003*
100. M A MacDonald, F C Gouldin, E M Fisher *Combust. Flame* **124** 668 (2001)
101. M D Rumminger, V I Babushok, G T Linteris *Proc. Combust. Institute* **29** 329 (2002)
102. D A Knyazkov, V M Shvartsberg, A G Shmakov, O P Korobeinichev *Fiz. Goren. Vzryva* **43** (2) 23 (2007)^b
103. M F M Nogueira, E M Fisher *Combust. Flame* **132** 352 (2003)
104. A G Shmakov, O P Korobeinichev, V M Shvartsberg, D A Knyazkov, T A Bolshova, I V Rybitskaya *Proc. Combust. Institute* **30** 2345 (2005)
105. V V Zamashchikov, V A Bunev *Fiz. Goren. Vzryva* **37** (1) 15 (2001)^b
106. V V Zamashchikov, V A Bunev *Fiz. Goren. Vzryva* **38** (5) 3 (2002)^b
107. D A Knyazkov, Candidate Thesis in Physical and Mathematical Sciences, Institute of Chemical Kinetics and Combustion, Siberian Branch of the Russian Academy of Sciences, Novosibirsk, 2006
108. M A MacDonald, T M Jayaweera, E M Fisher, F C Gouldin *Technical Meeting 'Central States Section of The Combustion Institute', Point Clear, AL, 1997*
109. M A MacDonald, T M Jayaweera, E M Fisher, F C Gouldin *Proc. Combust. Institute* **27** 2749 (1998)
110. D Reinelt, G T Linteris *Proc. Combust. Institute* **26** 1421 (1996)
111. R R Skaggs, R G Daniel, A W Miziolek, K L McNesby *Proceedings of the First Joint Meeting of the US Sections of the Combustion Institute, Washington, DC, 1999* p. 575
112. D D Thomsen, N M Laurendeau *Combust. Flame* **124** 350 (2001)
113. S C Li, F A Williams *Proc. Combust. Institute* **28** 1031 (2000)
114. M M Y Waly, F A Williams *Proc. Combust. Institute* **28** 2005 (2000)
115. R Seiser, L Truett, D Trees, K Seshadri *Proc. Combust. Institute* **27** 649 (1998)
116. N M Marinov, W J Pitz, C K Westbrook, A E Lutz, A M Vincitore, S M Senkan *Proc. Combust. Institute* **27** 605 (1998)
117. D A Knyazkov, O P Korobeinichev, A G Shmakov *Fiz. Goren. Vzryva* **42** (4) 26 (2006)^b
118. D A Knyazkov, A G Shmakov, O P Korobeinichev *Proceedings of the 5th International Seminar on Flame Structure, Novosibirsk, 2005* (Ed. O P Korobeinichev) Paper OP-03 (CD)
119. J D Mather, R E Tapscott, J M Shreeve, R P Singh *Proceedings of Halon Options Technical Working Conferences, 2003* CD-ROM NIST SP 984-4, National Institute of Standards and Technology, Gaithersburg, MD, 2006
120. J Riches, L Knutsen, E Morrey, K Grant *Proceedings of Halon Options Technical Working Conferences, 2000* CD-ROM NIST SP 984-4, National Institute of Standards and Technology, Gaithersburg, MD, 2006
121. L Knutsen, E Morrey, J Riches *Proceedings of Halon Options Technical Working Conferences, 2002* CD-ROM NIST SP 984-4, National Institute of Standards and Technology, Gaithersburg, MD, 2006
122. O P Korobeinichev, A G Shmakov, V M Shvartsberg, D A Knyazkov, K P Kutsenogii, V I Makarov, Y M Samsonov, E E Nifantiev, I Yu Kudryavtsev, E I Goryunov, V P Nikolin, B I Kaledin *Proceedings of Halon Options Technical Working Conferences, 2003* CD-ROM NIST SP 984-4, National Institute of Standards and Technology, Gaithersburg, MD, 2006

123. O P Korobeinichev, A G Shmakov, A A Chernov, V M Shvartsberg, I V Rybitskaya, V I Makarov, E E Nifantev, I Y Kudryavtsev, E I Goryunov, V P Nikolin *Proceedings of Halon Options Technical Working Conferences, 2004* CD-ROM NIST SP 984-4, National Institute of Standards and Technology Gaithersburg, MD, 2006
124. A G Shmakov, O P Korobeinichev, D A Knyazkov, V M Shvartsberg, S A Yakimov, A N Baratov, S N Kopylov, D B Zhiganov, I K Larin *Proceedings of Halon Options Technical Working Conferences, 2006* CD-ROM NIST SP 984-4, National Institute of Standards and Technology Gaithersburg, MD, 2006

^a — *Chem. Phys. Rep. (Engl. Transl.)*

^b — *Combust. Explos. Shock Waves (Engl. Transl.)*

Non-metallocene rare-earth organometallic derivatives: synthesis, structure and application in the catalysis of transformations of unsaturated substrates[†]

A A Trifonov

Contents

I. Introduction	1049
II. Neutral alkyl and aryl complexes	1050
III. Cationic alkyl complexes	1062
IV. Hydride complexes	1064
V. Non-metallocene rare-earth organometallic derivatives in catalysis of transformations of unsaturated substrates	1065

Abstract. The review summarises advances in the post-metallocene chemistry of rare-earth organometallic compounds. The synthesis, structures and reactivities of complexes containing metal–carbon and metal–hydrogen bonds and stabilised by N-, P- or O-donor ligands are considered. The catalytic activities of these compounds in alkene polymerisation, hydroamination, hydrosilylation and hydroboration are discussed. The bibliography includes 139 references.

I. Introduction

Organic derivatives of rare-earth metals (rare-earth elements, REE) have a unique combination of properties and are of considerable interest as catalysts for different reactions. Due to large ionic radii of rare-earth elements^{1,2} combined with Lewis acidity and the presence of unoccupied 5d and 6s orbitals (for Ln^{3+} ions), these compounds have a pronounced tendency to form complexes and exhibit high coordination numbers.³ An insignificant contribution of the covalent component to rare-earth metal–ligand interactions removes restrictions associated with the compatibility of the orbitals in symmetry. This can give rise to radically new types of compounds the reactivity of which differs from that of d element derivatives. Due to the similarity of the redox and chemical properties of rare-earth elements combined with a substantial variation in the ionic radii in the series of these compounds (from 0.885 Å for Sc to 1.172 Å for La),² there is a unique possibility for optimising the reactivity of metal complexes by constructing the metal coordination sphere and choosing the appropriate radius of the central atom in accordance with specific features of the catalysed reaction. The fact that metallocene-type rare-earth metal alkyl and hydride complexes are efficient catalysts (or their precursors) for hydrogenation,^{4–7} polymerisation,^{8–10} hydrosilylation,¹¹ hydroboration,^{12,13} hydroamination^{14–16} and hydrophosphination^{17–19} of alkenes clearly demonstrates that these compounds have a high catalytic potential.

Since rare-earth metals are electropositive and the metal–ligand interactions in their organic derivatives are predominantly ionic in character, ligands capable of forming stable anions were traditionally used in this field of chemistry. This is why cyclopentadienyl complexes have prevailed among known organic derivatives of REE until recent years.²⁰ The stability and reactivity of rare-earth organometallic compounds are largely determined by the degree of steric saturation of their coordination spheres with the result that certain requirements are imposed on the ligands. The latter should be rather bulky and fill the metal coordination sphere at low coordination numbers of metal atoms, resulting in the kinetic stability of metal complexes. The synthesis of complexes soluble in non-polar non-coordinating solvents is an important problem, the solution of which would allow the synthesis of derivatives containing no coordinated Lewis bases and bearing the central atoms with low coordination numbers. This would lead to an increase in the catalytic activity of complexes as a result of the exclusion of the competition between the Lewis base and the substrate for a site in the metal coordination sphere.

In recent years, the trend has been toward the design of new non-cyclopentadienyl ligand systems allowing for stabilisation of rare-earth metal alkyl[‡] and hydride complexes.^{21–23} The aims of the replacement of ligands are to enhance stability of REE derivatives with retention of high catalytic activity, to increase the catalyst tolerance to functional groups of monomers, to extend the scope of the design and control of the geometry of the metal coordination sphere in complexes and to control the catalytic activity of metal complexes and the selectivity of the reactions. At the same time, studies of the influence of the coordination environment of rare-earth metal atoms on the reactivities of M–C and M–H bonds and the catalytic activity of compounds are of considerable interest. A comparison of the catalytic activities of rare-earth metal complexes containing anionic non-carbocyclic-type ligands with those of metallocene-type analogues would allow the determination of the relationship between the properties of metal complexes (structure, effective positive charges on metal

A A Trifonov G A Razuvaev Institute of Organometallic Chemistry, Russian Academy of Sciences, ul. Tropinina 49, 603950 Nizhniy Novgorod, Russian Federation. Fax (7-831) 462 74 97, tel. (7-831) 462 66 52, e-mail: trif@iomc.ras.ru

Received 9 January 2007

Uspekhi Khimii 76 (11) 1122–1144 (2007); translated by T N Safonova

[†] Dedicated to Academician G A Abakumov on the occasion of his 70th birthday.

[‡] Hereinafter, the term alkyl complexes is used in reference to complexes containing alkyl or substituted alkyl ligands (for example, CH_2SiMe_3 , etc.).

atoms and Lewis acidity) and their activity in the catalysis of transformations of alkenes.

The present review summarises methods for the synthesis, structures, reactivities and catalytic activities of rare-earth metal complexes (alkyl, cationic alkyl, hydride, *etc.*) stabilised by N-, O- or P-donor ligands.

II. Neutral alkyl and aryl complexes

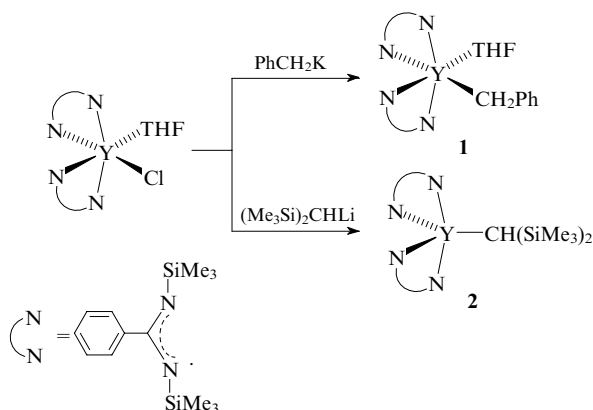
1. Monoalkyl and -aryl complexes

a. Complexes with monoanionic N-containing ligands

The bidentate amidinate anions $[R^1C(NR^2)_2]^-$ are among the first non-cyclopentadienyl ligands, which have been successfully used for stabilisation of rare-earth metal alkyl complexes. The monomeric yttrium derivatives $L_2YR(THF)$ [$L = PhC(NSiMe_3)_2$, $R = CH_2Ph$ (**1**)] and L_2YR [$L = PhC(NSiMe_3)_2$, $R = CH(SiMe_3)_2$ (**2**), $L = p\text{-MeOC}_6\text{H}_4C(NSiMe_3)_2$; $R = CH(SiMe_3)_2$ (**3**)] were synthesised.²⁴

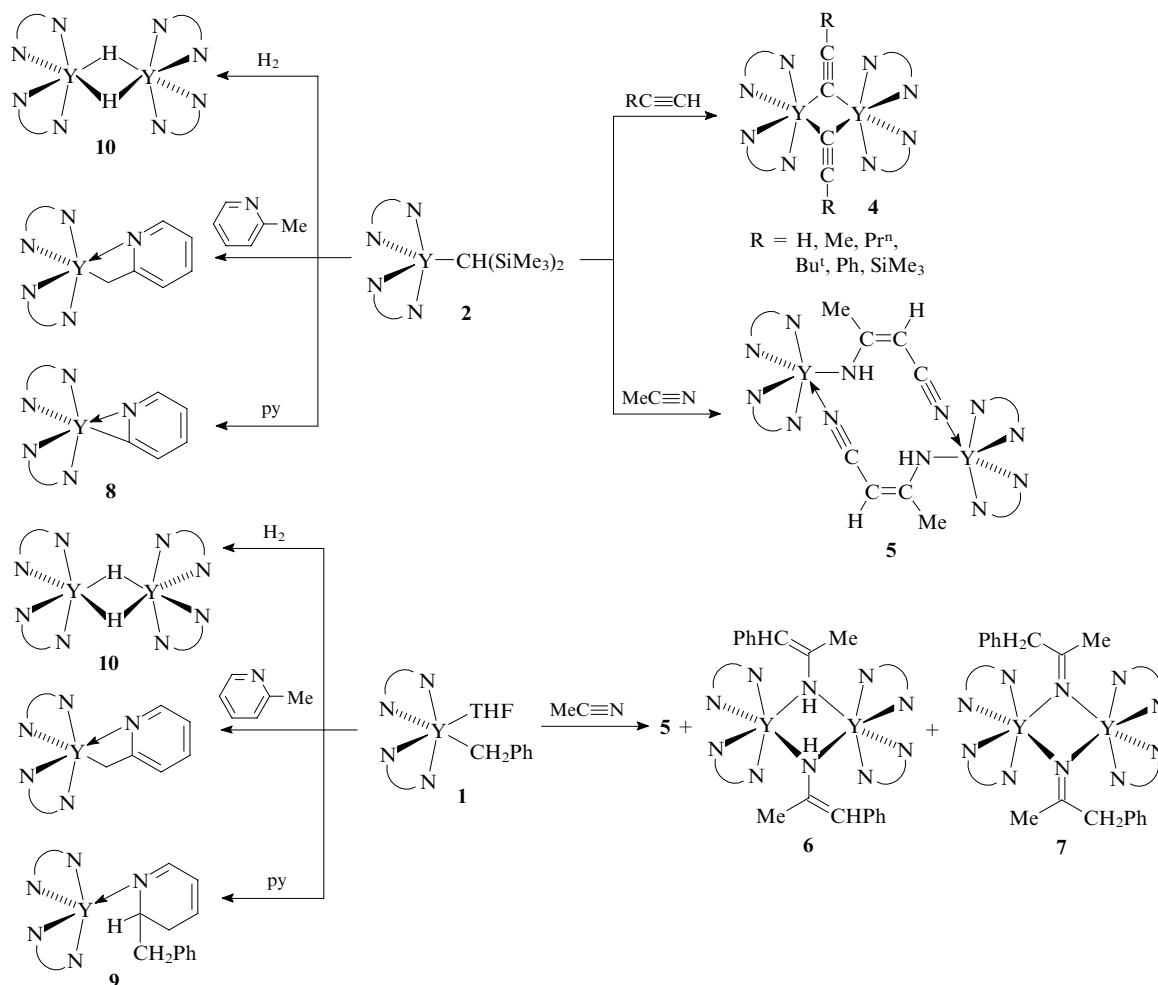
Complexes **1–3** are thermally stable in deuteriocyclohexane or deuteriobenzene. No evidence of the H/D exchange, metallation of the solvent or thermal decomposition of the complexes was observed upon heating of these solutions at 100 °C for several hours. The X-ray diffraction study of complex **3** showed that this complex is monomeric. The steric parameters of the amidinate fragments are similar to those of the pentamethylcyclopentadienyl ligands, whereas their electronic properties are substantially different. Based on semi-empirical INDO/1 calculations for the model $[HC(NH)_2]_2YMe$ and $(\eta^5\text{-Cp})_2YMe$ complexes, it was concluded that the higher electron-withdrawing ability of amidinate ligands results in an increase in the positive charge on the

yttrium atom in bis(amidinate) derivatives compared to metallocene-type analogues. The charge separation for the $Y-C$ bond in the $[HC(NH)_2]_2YMe$ and $(\eta^5\text{-Cp})_2YMe$ complexes is 1.06 and 0.75e, respectively, *i.e.*, the bond in the former compound is much more polar. In the authors' opinion, the larger positive charge on the yttrium atom in $[HC(NH)_2]_2YMe$ leads to a larger orbital contraction, thus hindering interactions between the metal and the substrate (for example, H_2) and resulting in the absence of the H/D exchange and in lower hydrogenolysis rates compared to cyclopentadienyl derivatives.²⁴



Compound **2** reacts with terminal alkynes to form dimeric acetylide complexes **4** and activates C–H bonds in acetonitrile to give dimeric complex **5** (Scheme 1). The reaction of

Scheme 1

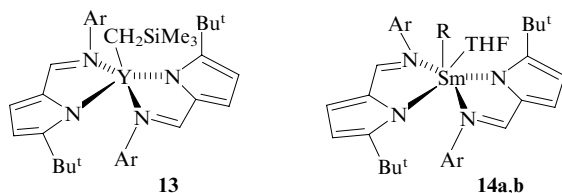


complex **1** affords, in addition to C–H bond activation product **5**, compounds **6** and **7** as a result of the insertion at the nitrogen–carbon double bond. The reaction of compound **2** with pyridine involves the metallation of the pyridine ring at the α position with respect to the nitrogen atom to give complex **8**. The reaction of compound **1** affords the addition product at the double bond of the heterocycle (compound **9**). The hydrogenolysis of compounds **1** and **2** gives rise to dimeric hydride **10** (see Scheme 1).^{25,26}

Alkyl and aryl derivatives of scandium stabilised by amidinate ions $\{[\text{PhC}(\text{NSiMe}_3)_2]_2\text{ScR}, \text{R} = \text{CH}_2\text{SiMe}_3 \text{ (11), Mes; } [\text{PhC}(\text{NSiMe}_3)_2]_2\text{ScMe}(\text{THF})\}$ were synthesised by the exchange reaction of the chloride complex $[\text{PhC}(\text{NSiMe}_3)_2]_2\text{ScCl}(\text{THF})$ with the corresponding alkyllithium reagents.²⁷ The reactions of complex **11** with $\text{Me}_3\text{SiC}\equiv\text{CH}$ and H_2 produce monomeric acetylenide $[\text{PhC}(\text{NSiMe}_3)_2]_2\text{Sc}(\text{C}\equiv\text{CSiMe}_3)$ and dimeric hydride $\{[\text{PhC}(\text{NSiMe}_3)_2]_2\text{Sc}(\mu\text{-H})\}_2$ (**11a**), respectively.

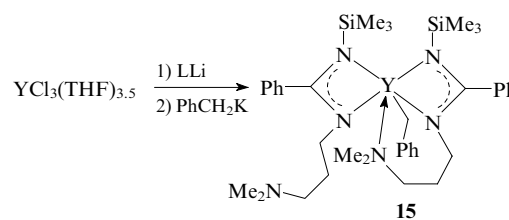
The tetrasubstituted guanidinate ligands $[\text{R}_2\text{NC}(\text{NR}')_2]^-$, like the amidinate anions, are N,N-chelating singly charged ligands and are of interest because of the simplicity of their synthesis, the diversity of coordination abilities and the ease of modifications of their electronic and steric characteristics.²⁸ Monomeric alkyl derivatives of yttrium with diisopropyl-substituted guanidinate ligands $[(\text{Me}_3\text{Si})_2\text{NC}(\text{NPr}^i)_2]_2\text{YR}$ [$\text{R} = \text{Bu}^t$ or $\text{CH}(\text{SiMe}_3)_2$] were synthesised and structurally characterised.²⁹ These compounds contain no coordinated Lewis bases, resulting in low coordination numbers of the central atom. Bulkier dicyclohexyl-substituted guanidinate ligands were also successfully used for the synthesis of alkyl and aryl derivatives of yttrium and samarium, *viz.*, L_2YBu^t (**12**), $\text{L}_2\text{YPh}(\text{THF})$ ³⁰ and $\text{L}_2\text{SmCH}(\text{SiMe}_3)_2$ ³¹ [$\text{L} = (\text{Me}_3\text{Si})_2\text{NC}(\text{NCy})_2$, Cy is cyclohexyl]. It should be noted that the yttrium atom in complex **12** is coordinatively saturated, resulting in the agostic interaction between the metal atom and two methyl groups of the *tert*-butyl substituent, which is responsible for short Y–C contacts and substantial deviations of the bond angles at the central carbon atom of the Bu^t group from the tetrahedral value.³⁰ X-Ray diffraction and ¹³C NMR spectroscopic studies showed that agostic interactions exist not only in the crystalline state, but also in deuterobenzene.

Monoanionic bidentate pyrrolocarbaldiminate ligands (L) were successfully used in the synthesis of yttrium (**13**) and samarium (**14a,b**) complexes by the reactions of chlorides $\text{L}_2\text{LnCl}(\text{THF})$ ($\text{Ln} = \text{Y}$ or Sm) with the corresponding alkyllithium reagents in toluene.³² Attempts to synthesise the methyl derivative of yttrium according to an analogous procedure failed. The monomeric structure of complex **14a** and the bidentate coordination of the ligands L were confirmed by X-ray diffraction.



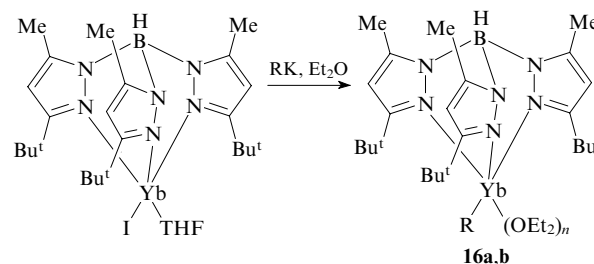
Ar = 2,6- $\text{Pr}_2\text{C}_6\text{H}_3$; R = CH_2SiMe_3 (a), Me (b).

A tridentate amidinate ligand containing an additional donor group in the side chain was used for the synthesis of the corresponding benzyl derivatives of yttrium **15**.³³ The X-ray diffraction study showed that in the crystalline state, only one of the amino groups of the amidinate ligands is coordinated to the metal atom.



L = $\text{PhC}(\text{NSiMe}_3)\text{N}(\text{CH}_2)_3\text{NMe}_2$.

The monoanionic tridentate hydridotris(3-*tert*-butyl-5-methylpyrazolyl)borate ligand (TPB-Me, Bu^t) belongs to a few ligand systems allowing the synthesis of organometallic derivatives of divalent ytterbium (**16a,b**).



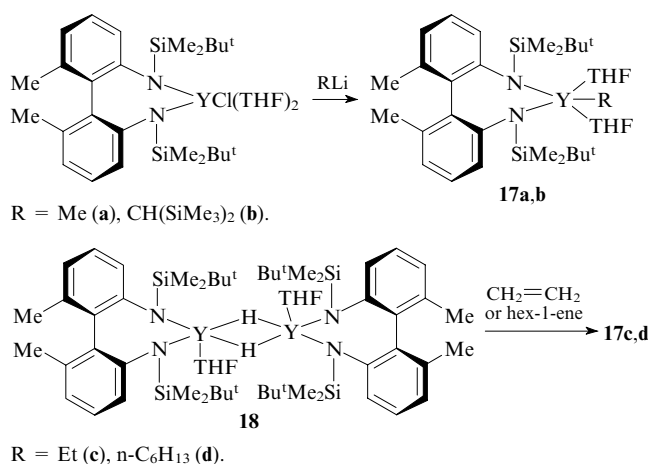
R = CH_2SiMe_3 , $n = 1$ (a); R = $\text{CH}(\text{SiMe}_3)_2$, $n = 0$ (b).

Complex **16b** was studied by X-ray diffraction, which confirmed its monomeric structure. This compound readily reacts with phenylacetylene to form the corresponding acetylenide $\text{LYb}(\text{C}\equiv\text{CPh})$.³⁴

Complexes with dianionic N-containing ligands

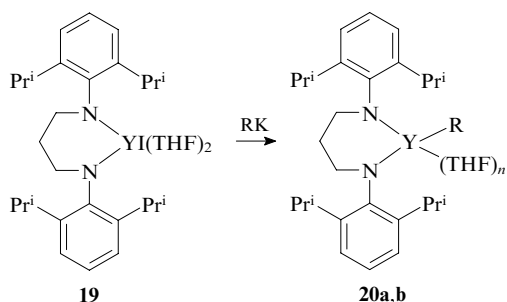
Diamide ligands, which differ in the number of donor groups, as well as in the nature and length of the bridge between the functional groups, are among the most widely used ligands in chemistry of rare-earth non-cyclopentadienyl ligands. The sterically rigid dianionic ligand 2,2'-bis(*tert*-butyldimethylsilylamido)-6,6'-dimethylbiphenyl (DADMB) was used for the synthesis of alkyl derivatives of yttrium. The coordination of this ligand to the metal atom gives rise to the seven-membered metallacycle. Compounds **17a,b** were synthesised by the exchange reactions of the starting chloride $(\text{DADMB})\text{YCl}(\text{THF})_2$ with MeLi and $(\text{Me}_3\text{Si})_2\text{CHLi}$, respectively (Scheme 2). Analogous ethyl and *n*-hexyl complexes **17c,d** were prepared by the addition of hydride **18** at the double bonds of ethylene and hex-1-ene, respectively, in THF.³⁵ The structure of compound **17c** was established by X-ray diffraction.

Scheme 2



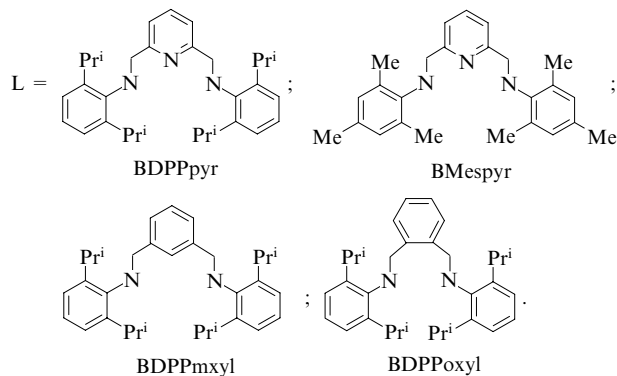
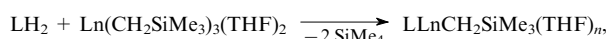
tion. This study demonstrated that complex **17c** is monomeric, and the yttrium atom is additionally coordinated by two THF molecules.

The use of a sterically less rigid ligand (L), in which two amide groups are linked by the propylene bridge, allowed the synthesis of more strained six-membered metallacyclic derivatives of yttrium. The reactions of iodo derivative **19** with PhCH₂K and (Me₃Si)₂CHK afforded complexes **20a,b**; their structures were established by X-ray diffraction.^{36,37} Both complexes proved to be rather stable in deuterobenzene at room temperature and are inert to hex-1-ene and ethylene.



R = CH₂Ph, *n* = 2 (a); R = CH(SiMe₃)₂, *n* = 1 (b).

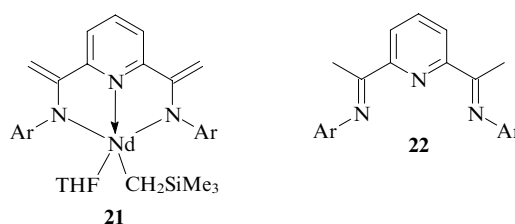
Diamino-substituted pyridines and benzenes (LH₂), which can act as bi- and tridentate ligands, were used for the synthesis of scandium, yttrium and lutetium derivatives by the elimination of tetramethylsilane from the tris(trimethylsilylmethyl) derivatives Ln(CH₂SiMe₃)₃(THF)₂ (Ln = Sc, Y or Lu) in the reactions with LH₂.



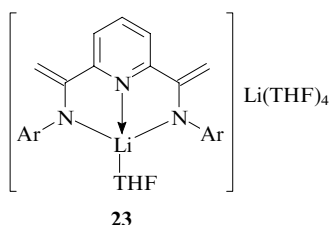
The monomeric complexes (BDPPpyr)LnCH₂SiMe₃.(THF)_{*n*} (*n* = 1, Ln = Sc or Lu; *n* = 2, Ln = Y) proved to be

rather stable at room temperature in hexane; their stability was found to decrease with increasing ionic radius of the metal atom. Derivatives of the sterically less hindered pyridine-containing analogue BMespyr, for example, (BMespyr).LnCH₂SiMe₃(THF)_{*n*} (*n* = 1, Ln = Sc; *n* = 2, Ln = Lu), appeared to be less stable under analogous conditions (hexane, 20 °C), the yttrium compound being unstable to an extent that attempts to isolate this compound at room temperature failed. Alkyl derivatives (BDPPoxyl)LnCH₂SiMe₃(THF) (Ln = Sc, Lu or Y) were synthesised in good yields with the use of diamino-substituted benzene BDPPoxyl, which, unlike pyridine-containing ligands, cannot be intramolecularly stabilised by the coordination of the nitrogen atom to metal but which contains the bulky isopropyl substituents in the aniline fragments.³⁸

An unusual approach to the synthesis of trimethylsilylmethyl derivative of neodymium **21** containing the tridentate 2,6-diiminopyridine ligand was proposed.³⁹ The partial alkylation of the starting NdCl₃(THF)₃ with RLi (R = CH₂SiMe₃) is followed by the reaction with diimine **22** or lithium salt **23** depending on the Nd : R ratio (1 : 4 or 1 : 2, respectively). The dianion is formed as a result of C–H bond activation in the methyl groups at the imine carbon atoms of the 2,6-diiminopyridine fragment of 2,6-(2,6-Pr₂C₆H₃N=CMe)₂C₅H₃N. The structure of complex **21** was established by X-ray diffraction.



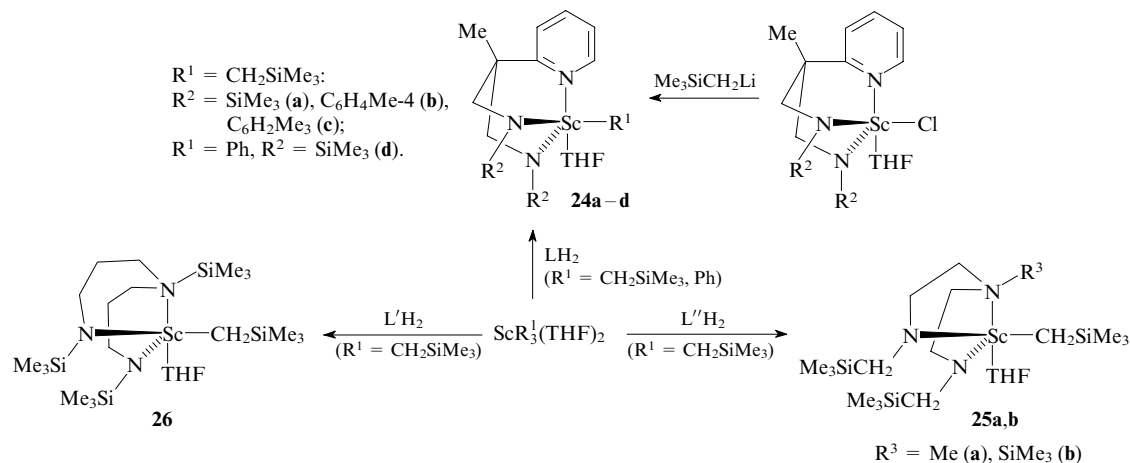
Ar = 2,6-Pr₂C₆H₃.



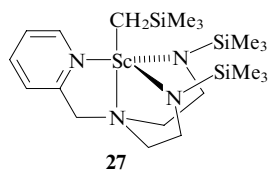
Ar = 2,6-Pr₂C₆H₃.

Diamido-pyridine- and diamido-amine-type tridentate dianionic ligands (LH₂) have also found use in recent years. For example, five-coordinate scandium alkyl and aryl complexes **24a–d**, **25a,b**, **26** (Scheme 3) and **27** were synthesised starting

Scheme 3

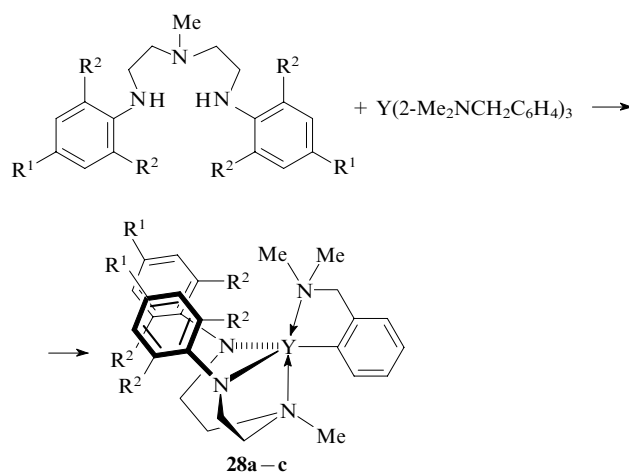


from anhydrous chloride ScCl_3 by two successive exchange reactions or by the protolysis of the corresponding $\text{R}_3\text{Sc}(\text{THF})_2$ derivatives ($\text{R} = \text{CH}_2\text{SiMe}_3$ or Ph) with an equimolar amount of a neutral ligand.^{40–42}



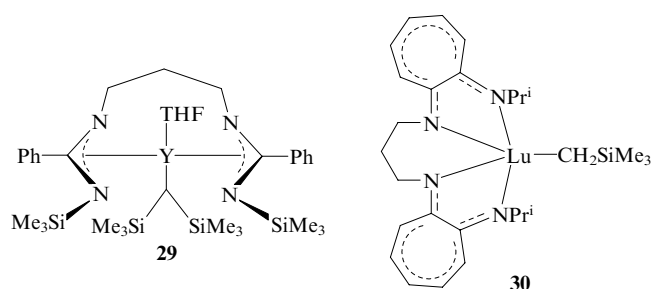
The X-ray diffraction study showed that five-coordinate compounds **24c** and **27** are monomeric, whereas the four-coordinate complex $[(\text{MeC}(2\text{-C}_5\text{H}_4\text{N})(\text{CH}_2\text{NC}_6\text{H}_4\text{Me-4})_2)_2\text{ScCH}_2\text{SiMe}_3]_2$, which contains no coordinated THF molecules, has (in the crystalline state) the dimeric structure due to the presence of two bridging amide groups.

Yttrium complexes **28a–c** with σ -bonded aryl ligands containing an additional donor group were synthesised⁴³ by the elimination of arene in the reactions of the corresponding amines with the triaryl derivative. Compound **28a** decomposes at 25 °C, whereas complexes **28b,c** are much more stable.



$\text{R}^1 = \text{R}^2 = \text{Me}$ (**a**); $\text{R}^1 = \text{H}$; $\text{R}^2 = \text{Et}$ (**b**), Cl (**c**).

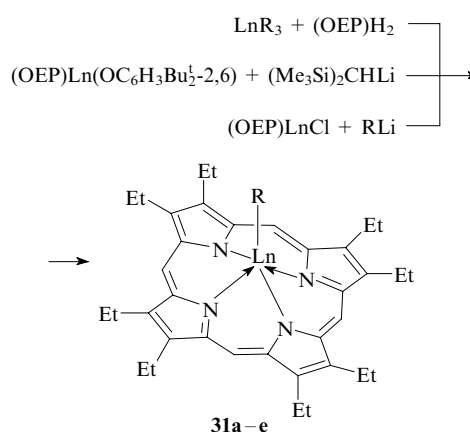
Alkyl complexes with tetradentate dianionic ligands are represented by bis(amidinate) (**29**)⁴⁴ and aminotropone imine (**30**)⁴⁵ derivatives.



c. Complexes with dianionic N-containing macrocyclic ligands

Rare-earth metal complexes with macrocyclic ligands have attracted attention due mainly to their luminescence and magnetic properties.⁴⁶ However, examples of the use of N-containing macrocyclic ligands as the stabilising coordination environment for alkyl derivatives of rare-earth elements are scarce. The doubly deprotonated octaethylporphyrin (OEP) macrocycle was successfully used for the synthesis of alkyl derivatives of yttrium (**31a**), lutetium (**31b**)⁴⁷ and scandium (**31c–e**).⁴⁸ Complexes **31a,b** were synthesised in 70%–80%

yields by the reactions of octaethylporphyrin (OEP) H_2 with the $\text{Ln}[\text{CH}(\text{SiMe}_3)_2]_3$ derivatives ($\text{Ln} = \text{Y}$ or Lu) involving elimination of alkane and by the exchange reactions of the corresponding phenoxides $(\text{OEP})\text{Ln}(\text{OC}_6\text{H}_3\text{Bu}_2^1\text{-2,6})$ ($\text{Ln} = \text{Y}$ or Lu) with $(\text{Me}_3\text{Si})_2\text{CHLi}$. The resulting compounds proved to be thermally rather stable and withstand heating in toluene at 60 °C for 6 h. The structure of complex **31b** was established by X-ray diffraction. The coordination sphere of the lutetium atom can be described as a square pyramid formed by the coordinated slightly curved OEP ligand and the $\text{CH}(\text{SiMe}_3)_2$ group. Scandium compounds **31c–e** were prepared by the reactions of chloride $(\text{OEP})\text{ScCl}$ with the corresponding alkyl-lithium reagents. According to the X-ray diffraction study, complexes **31c,d** are structurally similar to lutetium complex **31b**.

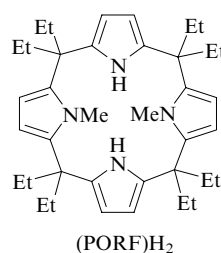


$\text{Ln} = \text{Y}$, $\text{R} = \text{CH}(\text{SiMe}_3)_2$ (**a**); $\text{Ln} = \text{Lu}$, $\text{R} = \text{CH}(\text{SiMe}_3)_2$ (**b**);

$\text{Ln} = \text{Sc}$: $\text{R} = \text{Me}$ (**c**), CH_2SiMe_3 (**d**), $\text{CH}(\text{SiMe}_3)_2$ (**e**).

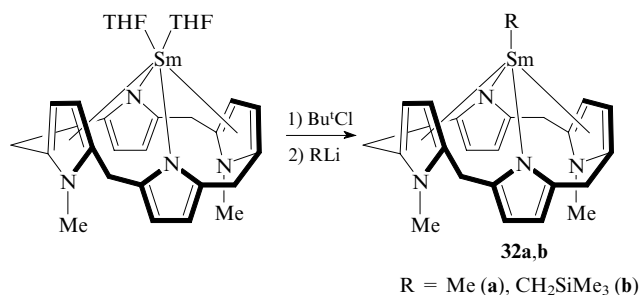
Derivatives **31a,b** readily react with $\text{HOC}_6\text{H}_3\text{Bu}_2^1\text{-2,6}$, $\text{Bu}^t\text{C}\equiv\text{CH}$ and H_2O to give monomeric phenoxide $(\text{OEP})\text{Ln}(\text{OC}_6\text{H}_3\text{Bu}_2^1\text{-2,6})$, dimeric acetylide $[(\text{OEP})\text{Ln}(\mu\text{-C}\equiv\text{CBu}^t)]_2$ and dimeric hydroxide $[(\text{OEP})\text{Ln}(\mu\text{-OH})]_2$, respectively. Unlike compounds **2** and **17a,b**, complexes **31a,b** do not react with hydrogen even under a pressure of 25 atm (25 °C).⁴⁷ Scandium derivatives **31c–e** readily bind at the $\text{C}=\text{O}$ double bond of carbon monoxide and at the $\text{C}=\text{N}$ double bond of xylil isocyanate; however, the reactions afford inseparable mixtures of products. The reactions of methyl derivative **31c** with CO_2 and acetone also readily proceed at room temperature to give, respectively, the acetate and *tert*-butoxide complexes.⁴⁸

trans-*N,N*-Dimethylated porphyrinogen (PORF) was used as a convenient polydentate ligand, which allowed the synthesis of monomeric alkyl complexes of trivalent samarium **32a,b** containing no coordinated solvent molecules, halide ions or alkali metals.⁴⁹



The divalent samarium derivative $(\text{PORF})\text{Sm}(\text{THF})_2$ was used as the starting compound. The oxidation of this compound with *tert*-butyl chloride followed by the treatment with the corresponding derivative RLi afforded complexes **32a,b**,

their structures were confirmed by X-ray diffraction (the ethyl groups are omitted for simplicity).



Unlike metallocene-type samarium methyl complexes, complex **32a** appeared to be rather inert. This compound does not activate C–H bonds in benzene, alkenes or diethyl ether.

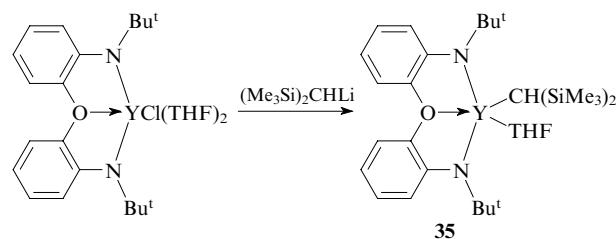
d. Complexes with monoanionic N,O-containing amide ligands

Bidentate monoanionic amide ligands containing an additional donor group, [Me₂Si(NBu^t)(OBu^t)][−] (L), have been proposed for the first time as an alternative to cyclopentadienyl ligands.^{50, 51} The monomeric five-coordinate yttrium complex L₂YCH(SiMe₃)₂ (**33**) was synthesised by the exchange reaction of chloride L₂Y(μ-Cl)₂Li(THF)₂ with (Me₃Si)₂CHLi. Compound **33** reacts with hydrogen in THF to give unstable hydride [L₂Y(μ-H)]₂, which was characterised in solution by ¹H and ¹³C NMR spectroscopy. The reactions of complex **33** with alkynes RC≡CH (R = Me₃Si or Bu^t) are accompanied by the Y–C and Y–N bond cleavage to form acetylenides (RC≡C)₃Y; however, PhC≡CH undergoes polymerisation in this reaction. The reaction of derivative **33** with excess of MeC≡N is accompanied by the C–H bond activation and elimination of bis(trimethylsilyl)methane. The subsequent insertion of one equivalent of MeC≡N at the Y–C bond and the 1,3-proton shift give rise to complex **34** (Scheme 4). The C–H bond activation was observed also in the reactions of complex **33** with pyridine, methylpyridine and ethylpyridine. The X-ray diffraction study of complexes **33** and **34** showed that this ligand system is bulkier than the η⁵-C₅Me₅ ligand.

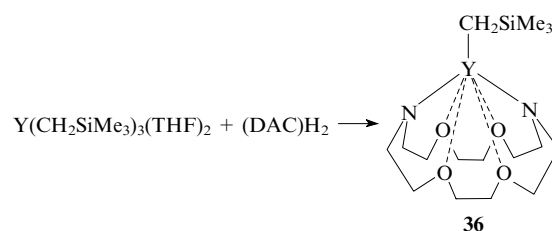
e. Complexes with dianionic N,O-containing diamide ligands

The tridentate dianionic ligand containing two oxygen-bridged amido-containing fragments, [2-Bu^tNC₆H₄)₂O]^{2−}, was used⁵²

for the synthesis of five-coordinate yttrium complex **35**. The structure of the latter was determined by X-ray diffraction.



Doubly deprotonated 4,13-diaza-18-crown-6 (DAC) proved to be suitable coordination environment for the synthesis of the yttrium derivative (DAC)YCH₂SiMe₃ (**36**).^{53, 54}



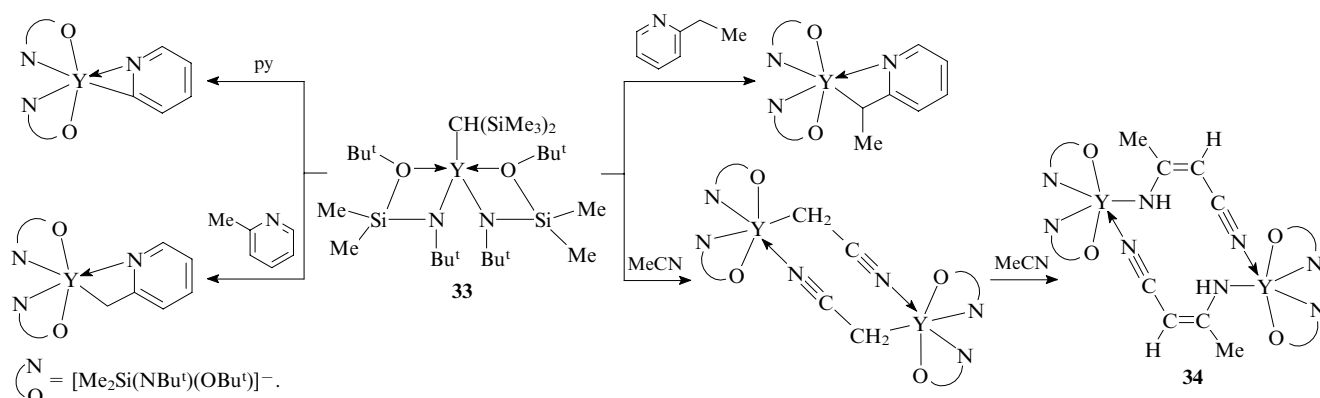
The reaction of complex **36** with phenylacetylene produces an equilibrium mixture of butatrienediyl {[(DAC)Y]₂Y. (μ-PhC=C=C=CPh)} and dimeric acetylenide {[(DAC)Y(μ-C≡CPh)]₂} complexes.

f. Complexes with monoanionic N,P-containing amide ligands

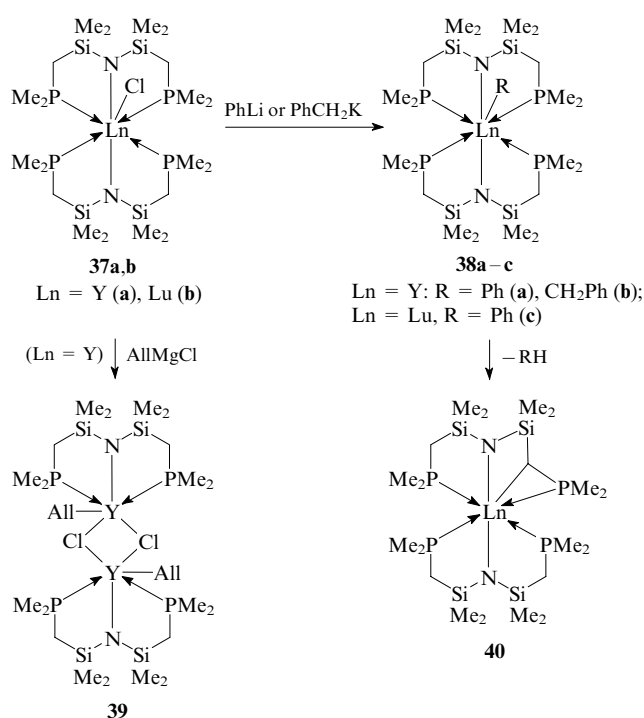
Being soft Lewis bases, neutral phosphines are considered as unsuitable ligands for coordination to hard rare-earth metal ions.⁵⁵ The coordination of the phosphine groups to rare-earth metal atoms was achieved with the use of the monoanionic amide ligand [N(SiMe₂CH₂PMe₂)₂][−] containing two PMe₂ fragments in the side chains (Scheme 5).

The exchange reaction involving yttrium or lutetium chloro complexes (**37**) and phenyllithium or benzylpotassium produced^{56, 57} the corresponding derivatives **38a–c**. An attempt to synthesise⁵⁸ allyl derivatives of yttrium by the reaction of complex **37a** with AlIMgCl led to the replacement of one of the amide ligands to form compound **39**, rather than to the expected substitution of the chlorine atom. Complexes **38a–c** are thermally unstable and are involved in cyclometallation at the methylene group to give metallacyclic derivative **40**.⁵⁹

Scheme 4



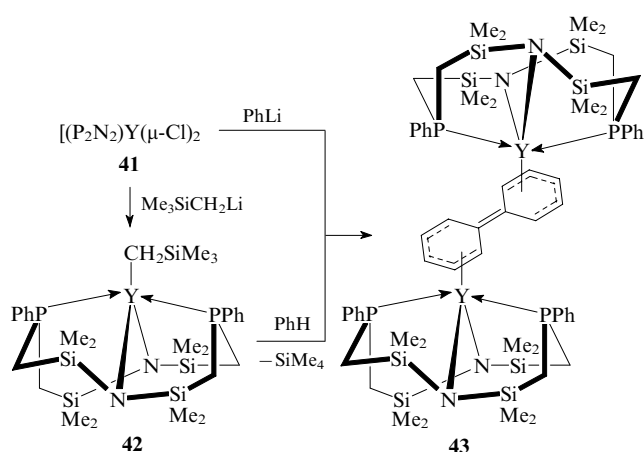
Scheme 5



g. Complexes with dianionic N,P-containing amide ligands

The macrocyclic dianionic bis(amidophosphine) ligand $[\text{PhP}(\text{CH}_2\text{SiMe}_2\text{NSiMe}_2\text{CH}_2)_2\text{PPh}]^{2-}$ (P_2N_2) was used for the synthesis of rare-earth metal alkyl and aryl complexes. The reactions of $[(\text{P}_2\text{N}_2)\text{Ln}(\mu\text{-Cl})_2]$ (Ln = Y (**41**), Ho, Yb or Lu) with $(\text{Me}_3\text{Si})_2\text{CHLi}$ and $\text{Me}_3\text{SiCH}_2\text{Li}$ in toluene produce the corresponding derivatives $(\text{P}_2\text{N}_2)\text{LnR}$ [Ln = Y, R = $\text{CH}(\text{SiMe}_3)_2$, CH_2SiMe_3 (**42**); Ln = Ho, R = CH_2SiMe_3 ; Ln = Yb, R = CH_2SiMe_3 ; Ln = Lu, R = CH_2SiMe_3], whereas the arylation of these complexes strongly depends on the ionic radius of the metal atom.^{60, 61} For example, the reactions of Y and Ho complexes with phenyllithium and biphenyllithium are accompanied by the dimerisation of aryl radicals to form the dinuclear complexes $[(\text{P}_2\text{N}_2)_2\text{Ln}]_2 \cdot (\mu\text{-}\eta^6\text{:}\eta^6\text{-Ph}_2)$ [Ln = Y (**43**) or Ho] and $[(\text{P}_2\text{N}_2)_2\text{Y}]_2[\mu\text{-}\eta^6\text{:}\eta^6\text{-(C}_6\text{H}_4\text{-Ph-}p)_2]$ containing the biphenyl or quaterphenyl dianion, respectively (Scheme 6).

Scheme 6

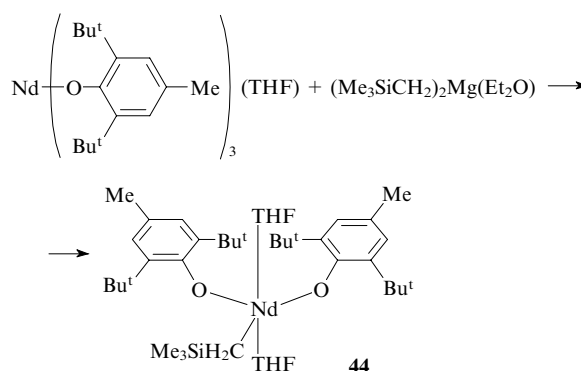


The slow transformation of complex **42** into dimer **43** in benzene at room temperature accompanied by elimination of tetramethylsilane was observed. For ytterbium having a

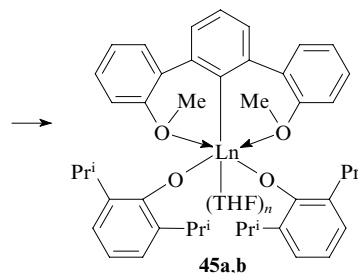
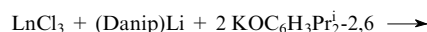
smaller ionic radius, the phenyl derivative $(\text{P}_2\text{N}_2)_2\text{YbPh}$ was isolated and characterised by X-ray diffraction. The presence of THF appeared to be the decisive factor for the suppression of the dimerisation of the aryl radicals. For example, the yttrium aryl complex was isolated as the adduct with THF, $(\text{P}_2\text{N}_2)\text{Y}(\text{C}_6\text{H}_4\text{Me-4})(\text{THF})$, in the reaction of $[(\text{P}_2\text{N}_2)\text{Y} \cdot (\mu\text{-Cl})_2]$ with *p*-tolyllithium in a toluene–THF mixture.⁶¹

h. Complexes with monoanionic alkoxide ligands

The five-coordinate neodymium alkyl complex $\text{L}_2\text{Nd} \cdot (\text{CH}_2\text{SiMe}_3)(\text{THF})_2$ (**44**) containing two sterically hindered phenoxide ligands L was obtained in a mixture with the derivative $\text{LNd}(\text{CH}_2\text{SiMe}_3)_2$ by the reaction of neodymium tris(phenoxide) with the corresponding magnesium derivative in a toluene–THF mixture.⁶² The structure of complex **44** was confirmed by X-ray diffraction.



Yttrium compound **45a** and ytterbium compound **45b** with the Danip ligand containing two *o*-anisole fragments were synthesised by the successive exchange reactions of LnCl_3 with one equivalent of $(\text{Danip})\text{Li}$ and two equivalents of $\text{KOC}_6\text{H}_3\text{Pr}_2\text{-2,6}$ in THF.⁶³ In complex **45b**, the ytterbium coordination sphere involves one carbon atom and two oxygen atoms of the 2,6-di(*o*-anisyl)phenyl fragment and two oxygen atoms of the 2,6-diisopropylphenoxide ligands, *i.e.*, the coordination number is 5. The compound of yttrium having a larger ionic radius⁶⁴ was isolated as the adduct with THF (**45a**); the coordination number of the metal atom in this adduct is 6.



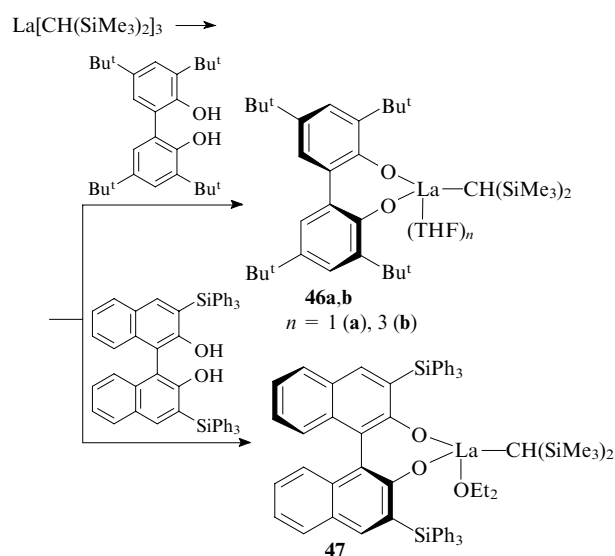
Ln = Y, *n* = 1 (a); Ln = Yb, *n* = 0 (b).

i. Complexes with dianionic alkoxide ligands

Derivatives containing biphenyl-2,2'-diolate and 1,1'-binaphthyl-2,2'-diolate anions represent complexes with dianionic alkoxide ligands. Compounds **46** and **47** were synthesised for the first time⁶⁵ by the reaction of substituted biphenyldiol or binaphthyldiol with the $\text{La}[\text{CH}(\text{SiMe}_3)_2]_3$ complex (Scheme 7).

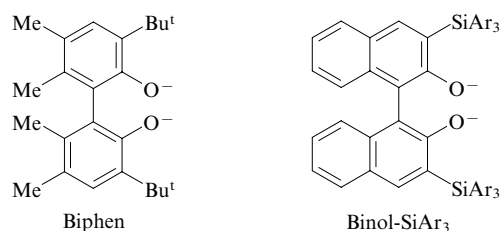
The reaction of complex **47** with CO is accompanied by the insertion of the latter at the La–C bond followed by the 1,2-

Scheme 7

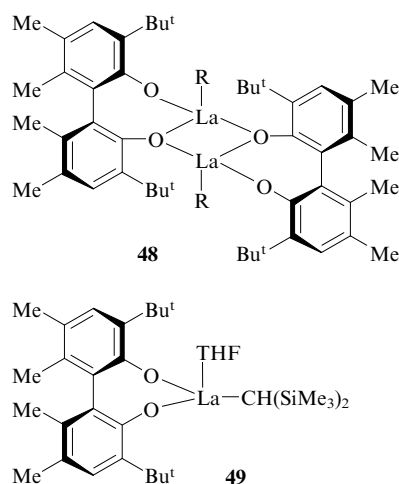


migration of the SiMe_3 group to form enolate $[1,1'-(2\text{-OC}_{10}\text{H}_5\text{.SiPh}_3\text{-3})_2]\text{La}[\text{OC}(\text{SiMe}_3)=\text{CHSiMe}_3]$.⁶⁵

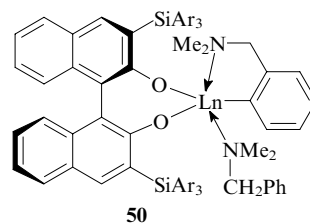
An analogous approach was used for the preparation of rare-earth metal alkyl and aryl complexes containing the enantiomerically pure (*R*)-Biphen⁶⁶ and (*R*)-Binol- SiAr_3 ligands.^{67,68}



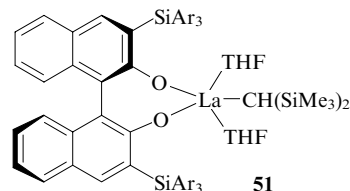
Complex **48** was isolated⁶⁶ as the dimer formed by two bridging aryloxy groups. The treatment of this complex with excess THF leads to dissociation of the dimer and the formation of adduct **49**.⁶⁶



The Binol- SiAr_3 derivatives are monomeric.^{67,68} Compounds **50** and **51** can be given as examples.



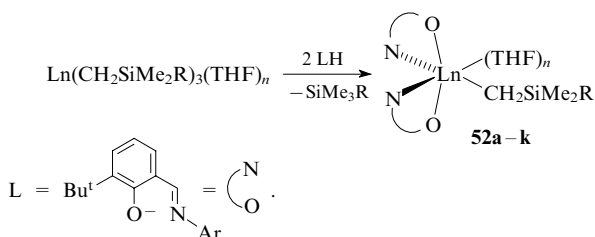
$\text{Ln} = \text{Sc, Y, Lu}$; $\text{Ar} = \text{Ph, 3,5-Me}_2\text{C}_6\text{H}_3$.



$\text{Ar} = \text{Ph, 3,5-Me}_2\text{C}_6\text{H}_3$.

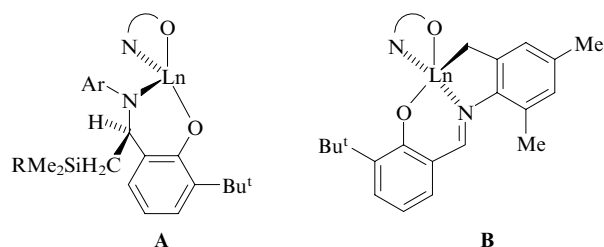
j. Complexes with monoanionic N,O-alkoxide ligands

Among bidentate N,O-alkoxide ligands, salicylaldiminate ligands are most widely used in the synthesis of alkyl derivatives. The elimination of substituted alkane in the reactions of 2-iminomethylphenols with trialkyl derivatives was demonstrated^{69–71} to be a convenient procedure for the preparation of such complexes, whereas the exchange reactions do not produce the target compounds in good yield. The reactions of the $\text{Ln}(\text{CH}_2\text{SiMe}_2\text{R})_3(\text{THF})_n$ compounds ($\text{Ln} = \text{Sc}$ or Y ; $\text{R} = \text{Me}$ or Ph ; $n = 1$ or 2) with two equivalents of 2-iminomethylphenol LH afford complexes **52a–k** in high yields.^{69–71}



Compound 52	Ln	Ar	R	n
a	Sc	Ph	Ph	1
b	Y	Ph	Ph	2
c	Sc	2- $\text{Pr}^i\text{C}_6\text{H}_4$	Ph	1
d	Y	2- $\text{Pr}^i\text{C}_6\text{H}_4$	Ph	1
e	Sc	Mes	Me	0
f	Y	Mes	Ph	1
g	Y	Mes	Me	0
h	Sc	2,6- $\text{Pr}_2\text{C}_6\text{H}_3$	Me	0
i	Sc	2,6- $\text{Pr}_2\text{C}_6\text{H}_3$	Ph	0
j	Y	2,6- $\text{Pr}_2\text{C}_6\text{H}_3$	Ph	0
k	Y	2,6- $\text{Pr}_2\text{C}_6\text{H}_3$	Me	0

Thermal stability of the reaction products substantially depends on the bulkiness of the substituent at the nitrogen atom. The complexes with the substituents $\text{Ar} = \text{Ph, 2-Pr}^i\text{C}_6\text{H}_4$ or Mes are unstable and slowly decompose in the temperature range from -20 to $+20$ °C, in the case of $\text{Ar} = \text{Ph}$ or $2\text{-Pr}^i\text{C}_6\text{H}_4$ the decomposition being accompanied by the migration of the $\text{CH}_2\text{SiMe}_2\text{R}$ group to the aldimine carbon atom (structure **A**), whereas the *ortho*-methyl substituents of the aryl group are metallated in the case of $\text{Ar} = \text{Mes}$ (structure **B**).⁷⁰

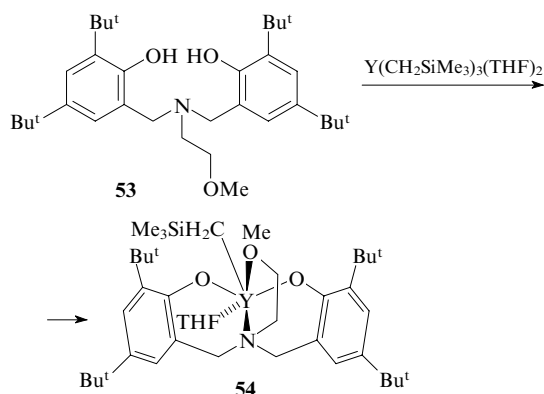


On the contrary, five-coordinate derivatives of the bulkiest ligand with $\text{Ar} = 2,6\text{-Pr}_i^2\text{C}_6\text{H}_3$ (compounds **52h–k**) are characterised by high thermal stability and decompose in the toluene solvent only upon prolonged heating at 140°C . This reaction is accompanied by metallation of one methyl group of the isopropyl substituent.⁷¹

The reaction of the trialkyl complex $\text{Y}(\text{CH}_2\text{SiMe}_3)_3(\text{THF})$ with iminomethylphenol 2-($\text{CyN}=\text{CH}$)-6- $\text{Bu}^t\text{C}_6\text{H}_3\text{OH}$ (LH) produced the monoalkyl yttrium derivative $\text{L}_2\text{Y}(\text{CH}_2\text{SiMe}_3)(\text{THF})$ even when the starting compounds were taken in equimolar amounts.⁷²

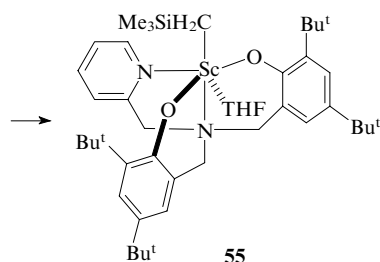
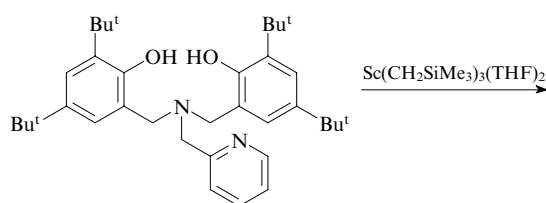
k. Complexes with dianionic N,O-alkoxide ligands

In recent years, sterically hindered polydentate bis(phenoxide) ligands containing additional donor groups capable of coordinating to metal atoms have found wide use in the chemistry of rare-earth organometallic compounds. The reaction of $\text{Y}(\text{CH}_2\text{SiMe}_3)_3(\text{THF})_2$ with bis(phenol) **53** was demonstrated⁷³ to proceed selectively to give six-coordinate yttrium complex **54** in good yield.

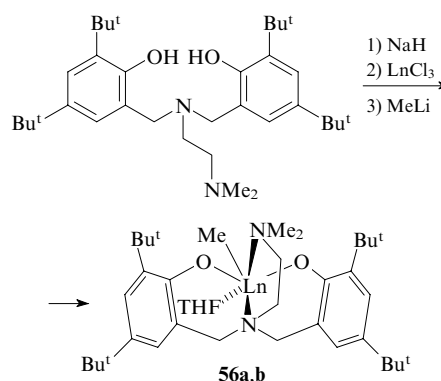


The X-ray diffraction and NMR spectroscopic data provide evidence that the methoxy group is coordinated to the metal atom in complex **54** both in the crystalline state and in nonpolar solvents. It should be noted that complex **54** is inactive in the ethylene polymerisation.

An analogous approach was used⁷⁴ for the synthesis of scandium complex **55** with the bis(phenoxide) ligand containing the tertiary amine and pyridine groups.

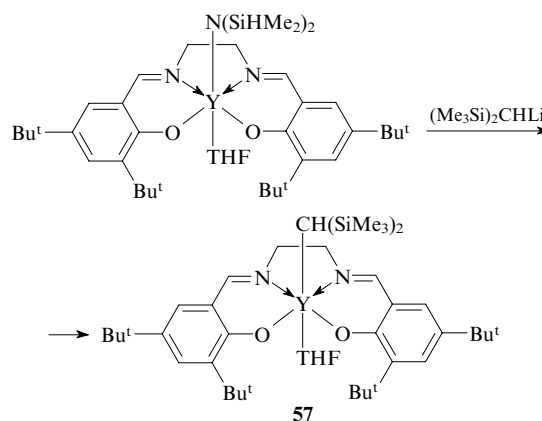


Erbium and ytterbium complexes (**56a,b**) with the related bis(phenoxide) ligand containing two amino groups were synthesised from metal trichlorides by the successive exchange reactions. The structure of compound **56b** was established by X-ray diffraction.⁷⁵



$\text{Ln} = \text{Er (a)}, \text{Yb (b)}$.

Yttrium alkyl complex **57** stabilised by the substituted tetradentate N,N' -ethylenebis(salicylaldimine) ligand was also prepared by the exchange reaction; however, the bis(dimethylsilyl)amide fragment was used in the latter case as the leaving group.⁷⁶

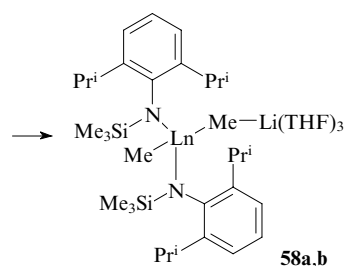
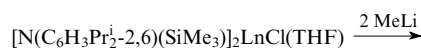


2. Heterobimetallic alkyl complexes

a. Complexes with monoanionic N-containing ligands

Monoanionic monodentate amide ligands have found little use in the synthesis of alkyl derivatives of rare-earth elements. The sterically hindered N -(2,6-diisopropylphenyl)trimethylsilylamide ligand was used⁷⁷ for the first time for the preparation of the bis(arylamido) chloride complexes $[\text{N}(\text{C}_6\text{H}_3\text{Pr}_i^2-2,6)(\text{SiMe}_3)_2\text{LnCl}(\text{THF})]$ ($\text{Ln} = \text{Nd}$ or Yb). The reactions of these compounds with methyl lithium (in a molar ratio of 1 : 2) in a toluene–diethyl ether mixture produce ate complexes **58a,b**.⁷⁸ The X-ray diffraction study showed that only one of

two methyl groups serves as a bridge between the lanthanide and lithium atoms.



Ln = Nd (a), Yb (b).

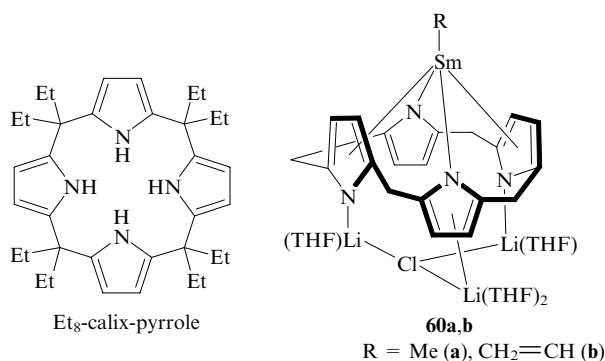
Ate complexes containing monoanionic bidentate amidinate and guanidinate ligands, $L_2Ln(\mu-Me)_2Li(TMEDA)$ [$L = PhC(NSiMe_3)_2$, $Ln = Y$ (**59a**);²⁶ $L = (Me_3Si)_2NC(NPr^i)_2$, $Ln = Y$,²⁹ Nd (**59b**), Yb (**59c**);^{79, 80} $L = (Me_3Si)_2NC(NCy)_2$, $Ln = Y$,³⁰ TMEDA is N,N,N',N' -tetramethylethylenediamine], were synthesised by the reactions of the corresponding chlorides $[L_2Ln(\mu-Cl)]_2$ or $L_2Ln(\mu-Cl)_2Li(B)_n$ ($B = THF$, DME or Et_2O) with two equivalents of MeLi in the presence of excess TMEDA. The reaction of complex **59a** with $Bu^tC\equiv CH$ afforded the corresponding heterobimetallic acetylenide $L_2Y(\mu-C\equiv CBu^t)_2Li(TMEDA)$.

b. Complexes with dianionic amide ligands and N-containing macrocycles

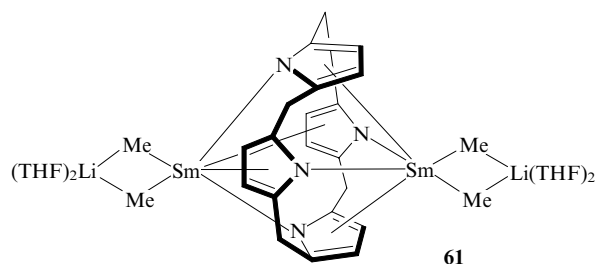
The synthesis of derivatives of the dianionic tridentate 2,6-diiminopyridine ligand, in which the neodymium and lithium atoms are linked by two bridging methyl ligands or one methyl ligand and one chloride ligand, respectively, $[2,6-(2,6-Pr^i_2C_6H_3NC(=CH_2))_2C_5H_3N]Nd(\mu-Me)(\mu-X)[Li(THF)_2]$ ($X = Me$ or Cl), was documented.³⁹

The octaethylporphyrin derivative of yttrium (OEP)Y. $(\mu-Me)_2Li(OEt_2)$, which was synthesised^{47, 81} by the reaction of phenoxide (OEP)Y($OC_6H_3Bu^t_{2-6}$) with MeLi (in a ratio of 1:2), belongs to heterobimetallic alkyl complexes with dianionic N-containing ligands.

Trivalent samarium methyl and vinyl complexes **60a,b** with the octaethylcalix-tetrapyrrole ligand (Et_8 -calix-pyrrole) were synthesised⁸² by the reactions of chloride (Et_8 -calix-pyrrole). $SmCl[Li_2(THF)_3]$ with the corresponding lithium reagents RLi ($R = Me$, $CH_2=CH$). The alkylation of the dinuclear complex $(Et_8$ -calix-pyrrole) $Sm_2\{(\mu-Cl)_2[Li(THF)_2]\}_2$ affords tetramethyl complex **61**.⁸³ (The ethyl groups in structures **60** and **61** are omitted for clarity.)

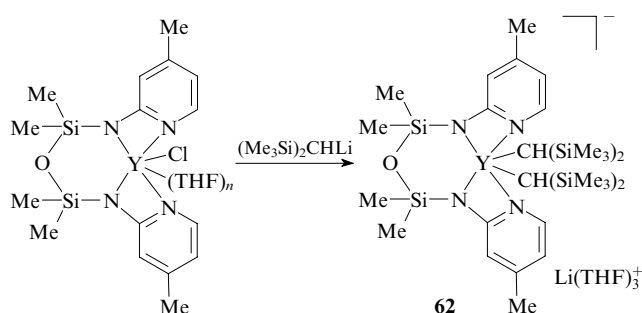


R = Me (a), $CH_2=CH$ (b)

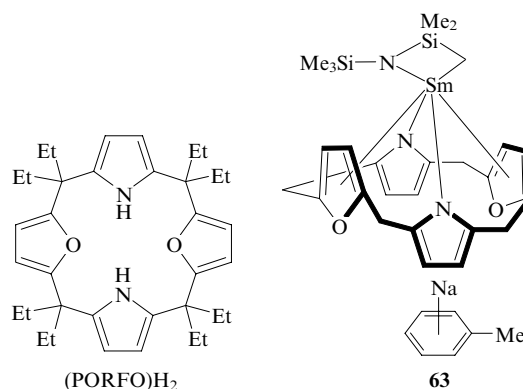


c. Complexes with dianionic N,O-containing diamide ligands

The tetradentate ligand, in which two 2-amino-4-methylpyridine (Ap) fragments are linked by the siloxane bridge $O(SiMe_2)_2$, was used⁸⁴ for the synthesis of heterobimetallic yttrium complex **62**.

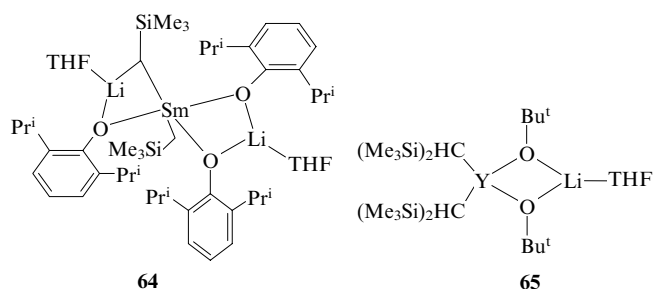


In the study of the reaction of the Sm^{III} bis(trimethylsilyl)-amide complex containing the *trans*-dioxaporphyrinogen ligand (PORFO) with amide $NaN(SiMe_3)_2$,⁸⁵ the process was found to be accompanied by activation of one C—H bond of the trimethylsilylamide group and produces metallacyclic γ -alkylamide complex **63** (the ethyl groups are omitted).

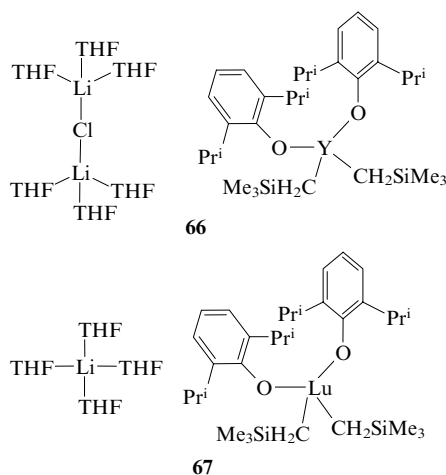


d. Complexes with alkyl- and aryloxy ligands

The reaction of $Sm(OC_6H_3Pr^i_{2-6})_3$ with three equivalents of Me_3SiCH_2Li in toluene produced heterobimetallic trinuclear samarium complex **64**,⁸⁶ in which the metal atom is coordinated by one terminal CH_2SiMe_3 group, one bridging CH_2SiMe_3 group and three bridging aryloxy ligands (coordination number of Sm is 5).



Bimetallic four-coordinate yttrium complex **65** was synthesised⁸⁷ by two successive exchange reactions of YCl_3 with two equivalents of $(\text{Me}_3\text{Si})_2\text{CHLi}$ and two equivalents of LiOBu^t . The structures of complexes **64** and **65** were established by X-ray diffraction. The coordination environment of the yttrium atom can be described as a distorted tetrahedron formed by two terminal $\text{CH}(\text{SiMe}_3)_2$ groups and two bridging *tert*-butoxide groups. The formation of yttrium ate complex **66**, which is a separated ion pair, was observed⁸⁸ in the reaction of YCl_3 with $\text{Me}_3\text{SiCH}_2\text{Li}$ and $\text{LiOC}_6\text{H}_3\text{Pr}_2^1\text{-2,6}$ (in a ratio of 1 : 2 : 2). The analogous reaction of the lutetium complex also produced ionic complex **67** consisting of the discrete cation and anion; however, this complex does not contain LiCl . It should be noted that complex **66** contains the unusual $[\text{Li}(\text{THF})_3]_2\text{Cl}]^+$ cation.



The formation of the heterodinuclear complex $\text{Li}[\text{Y}(\text{OSiBu}^t\text{Ar}_2)(\text{OC}_6\text{H}_3\text{Bu}_2^1\text{-2,6})(\text{CH}_2\text{SiMe}_3)_2]$ ($\text{Ar} = \text{C}_6\text{H}_4$, CH_2NMe_2) by the reaction of the derivative $\text{Y}(\text{OSiBu}^t\text{Ar}_2)(\text{OC}_6\text{H}_3\text{Bu}_2^1\text{-2,6})_2$ with two equivalents of $\text{Me}_3\text{SiCH}_2\text{Li}$ was documented.⁸⁹

e. Adducts of rare-earth metal complexes with trialkylaluminium

Due to the catalytic activity of the Ziegler–Natta systems based on rare-earth metal complexes in the alkene and diene polymerisation, considerable attention has been given to the reactions of their tris(amides) and tris(alkoxides) with various trialkyl derivatives of aluminium. These reactions produce heterobimetallic complexes containing the $\text{Ln}-\text{C}$ bond. The reaction of $\text{Nd}(\text{NPr}_2)_3(\text{THF})$ with 3 equivalents of AlMe_3 was found⁹⁰ to be accompanied by the $\text{Nd}-\text{C}$ bond formation to give the heterobimetallic trinuclear complex with three bridging methyl groups, $\text{Nd}(\text{NPr}_2)[(\mu\text{-Me})\text{AlMe}_2][(\mu\text{-Me})_2\text{AlMe}_2]$. The seven-coordinate neodymium complex $[\{\text{Me}_2\text{Al}(\mu\text{-Me})\}_2\text{Nd}(\mu_3\text{-NPh})(\mu\text{-Me})\text{AlMe}_2]$ containing the μ_3 -imide ligand was synthesised⁹¹ by the reaction of $[\text{Nd}(\text{NPh})_3(\text{KCl})_3]$ with Al_2Me_6 . Four sites in the neodymium coordination sphere are occupied by two chelating anions $[(\mu\text{-Me})\text{AlMe}_2]^-$, and three sites are occupied by the tridentate group $(\mu_3\text{-NPh})(\mu\text{-Me})\text{AlMe}$. The yttrium octaethylporphyrin complex $(\text{OEP})\text{Y}$.

$(\mu\text{-Me})_2\text{AlMe}_2$ was synthesised^{47, 81} by the reaction of 2 equivalents of AlMe_3 with $(\text{OEP})\text{Y}(\mu\text{-Me})_2\text{Li}(\text{OEt}_2)$.

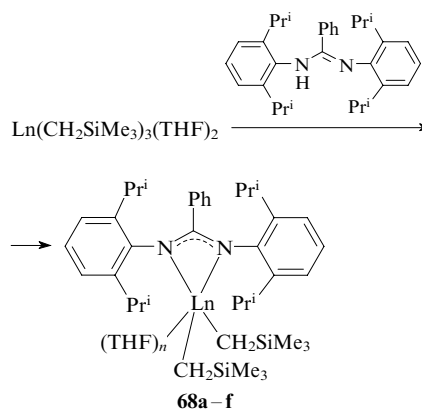
Studies of the reactions of lanthanide aryloxides with AlR_3 showed that they can produce adducts of different composition depending on the bulkiness of the ArO group and the ionic radius of the lanthanide atom. For example, the reaction of $\text{Ln}(\text{OC}_6\text{H}_3\text{Pr}_2^1\text{-2,6})_3$ with AlR_3 (in a ratio of 1 : 4) produced the trinuclear complexes $\text{Ln}(\text{OC}_6\text{H}_3\text{Pr}_2^1\text{-2,6})[(\mu\text{-OC}_6\text{H}_3\text{Pr}_2^1\text{-2,6})\cdot(\mu\text{-R})\text{AlR}_2]_2$ [$\text{Ln} = \text{La}$ or Sm ; $\text{R} = \text{Me}$ or Et ;^{92, 93} $\text{Ln} = \text{Y}$, $\text{R} = \text{Me}$ (Ref. 94)]. Lanthanum aryloxide containing the bulkier 2,6-di-(*tert*-butyl)phenoxide groups OAr ($\text{Ar} = \text{C}_6\text{H}_3\text{Bu}_2^1\text{-2,6}$ or $\text{C}_6\text{H}_2\text{Bu}_2^1\text{-2,6-Me-4}$) reacts with AlMe_3 to form the dinuclear complex $\text{La}(\text{OAr})_3(\text{AlMe}_3)$.⁹⁴ The reactions of aryloxides of rare-earth metals having a smaller ionic radius produce the monotetramethylaluminate complexes $\text{Ln}(\text{OAr})_2\cdot[(\mu\text{-Me})_2\text{AlMe}_2]$ ($\text{Ln} = \text{Y}$ or Lu ; $\text{Ar} = \text{C}_6\text{H}_3\text{Bu}_2^1\text{-2,6}$, $\text{C}_6\text{H}_2\text{Bu}_2^1\text{-2,6-Me-4}$ or $\text{C}_6\text{H}_2\text{Bu}_3^1\text{-2,4,6}$).⁹⁴ The reaction of the trinuclear complex $\text{Y}_3(\text{OBu}^t)_7\text{Cl}_2(\text{THF})_2$ with AlMe_3 in hexane afforded⁹⁵ bimetallic complexes, in which the yttrium and aluminium atoms are linked by the bridging methyl ligands $\text{Y}[(\mu\text{-OBu}^t)(\mu\text{-Me})\text{AlMe}_2]_3$ or $(\text{Bu}^t\text{O})(\text{THF})\text{Y}[(\mu\text{-OBu}^t)(\mu\text{-Me})\cdot\text{AlMe}_2]_2$. The mono- and bis(tetraalkylaluminate) complexes $[\text{Me}_2\text{Al}(\text{O}_2\text{CC}_6\text{H}_2\text{Pr}_3^1\text{-2,4,6})_2\text{Ln}[(\mu\text{-Me})_2\text{AlMe}_2]]$ and $\{\text{Ln}(\text{O}_2\text{CC}_6\text{H}_2\text{Bu}_3^1\text{-2,4,6})[(\mu\text{-Me})_2\text{AlMe}_2]_2\}_2$ were synthesised^{96, 97} by the alkylation of rare-earth carboxylates $[\text{Ln}(\text{O}_2\text{CC}_6\text{H}_2\text{R}_3\text{-2,4,6})_3]_n$ ($\text{R} = \text{Me}$, Pr^i or Bu^t ; $\text{Ln} = \text{Y}$, La or Nd) with trialkylaluminium AlR_3 ($\text{R} = \text{Me}$ or Et).

3. Dialkyl and diaryl complexes

Rare-earth metal dialkyl complexes have attracted increasing attention as the starting compounds for the synthesis of cationic alkyl derivatives serving as active alkene polymerisation and co-polymerisation catalysts.^{98, 99} Half-sandwich dialkyl complexes were considered in special sections of recent reviews.^{100, 101}

a. Complexes with monoanionic N-containing ligands

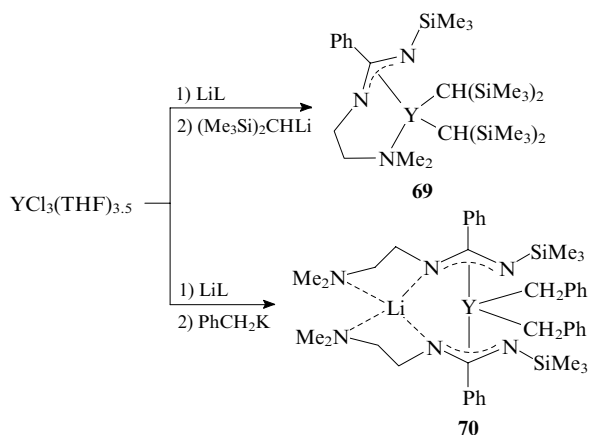
The synthesis, structures and reactivities of yttrium, scandium and lanthanide dialkyl complexes (**68a–f**) stabilised by bulky benzamidinate ligands were documented.^{102, 103} The complexes were synthesised by elimination of tetramethylsilane in the reactions of amidine with the trialkyl compounds $\text{Ln}(\text{CH}_2\text{SiMe}_3)_3(\text{THF})_2$. Derivatives of metals having a smaller ionic radius contain one coordinated THF molecule (compounds **68b, f**), whereas the coordination number of the central atom in complexes of metals with larger ionic radii (**68a, c–e**) increases to 6 as a result of coordination of an additional THF molecule.



$\text{Ln} = \text{Y}$ (**a**), Sc (**b**), La (**c**), Nd (**d**), Gd (**e**), Lu (**f**); $n = 1$ (**b, f**), 2 (**a, c–e**).

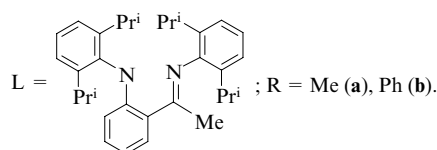
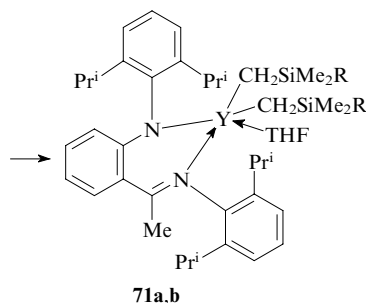
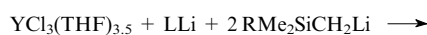
Yttrium dialkyl complex **69** can also be prepared by the exchange reaction with a less bulky tridentate amidinate ligand containing an additional amino group in the substituent.³³ An

attempt to apply this procedure to the synthesis of the dibenzyl derivative led to the formation of ate complex **70**, in which the Y and Li atoms have the coordination numbers 6 and 4, respectively. Therefore, a decrease in the volume of the σ -bonded ligand (CH_2Ph instead of $\text{CH}(\text{SiMe}_3)_2$) leads to substantial changes in the coordination environment of the Y atom. Thus, the amidinate ligands are coordinated only by two N atoms, whereas the nitrogen atom of the amino group is coordinated to the lithium ion.

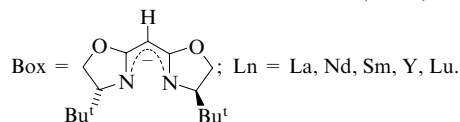
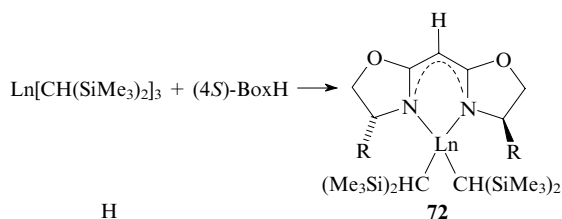


$\text{L} = \text{PhC}(\text{NSiMe}_3)\text{N}(\text{CH}_2)_2\text{NMe}_2$.

A bidentate anilido-imine ligand was used¹⁰⁴ for the synthesis of yttrium dialkyl complexes **71a,b**.



A series of lanthanide dialkyl complexes **72** containing the chiral bidentate bis(oxazoline) ligands (Box) were synthesised *in situ* by elimination of alkane from the corresponding derivatives $\text{Ln}[\text{CH}(\text{SiMe}_3)_2]_3$ in the reactions with BoxH. The lutetium complex was isolated from the reaction mixture and its structure was established by X-ray diffraction.¹⁰⁵

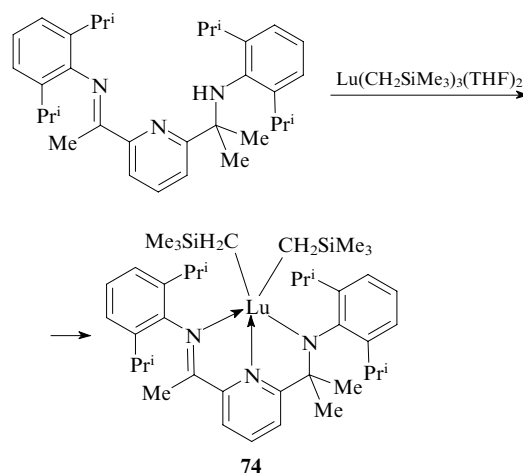


β -Diketiminato ligands have found wide use in the synthesis of four-coordinate scandium dialkyl complexes. The $[\text{ArNC}(\text{R}^1)\text{CHC}(\text{R}^1)\text{NAr}]\text{ScR}_2^2(\text{THF})_n$ complexes (**73a–i**) ($\text{Ar} = 2,6\text{-Pr}_2^i\text{C}_6\text{H}_3$) were synthesised^{106,107} by the alkylation of the corresponding dichlorides $[\text{ArNC}(\text{R}^1)\text{CHC}(\text{R}^1)\text{NAr}]\text{ScCl}_2(\text{THF})_n$ ($n = 0$ or 1).

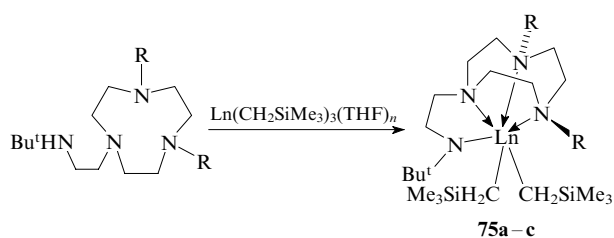
Compound 73	R ¹	R ²	Compound 73	R ¹	R ²
a	Me	Me	f	Me	CH_2Bu^t
b	Me	CH_2Ph	g	Bu^t	CH_2Bu^t
c	Bu^t	Me	h	Me	CH_2SiMe_3
d	Bu^t	Et	i	Bu^t	CH_2SiMe_3
e	Bu^t	CH_2Ph			

It should be noted that only derivative **73a** ($\text{R}^1 = \text{R}^2 = \text{Me}$) contains one coordinated THF molecule. For derivatives bearing larger substituents R^1 and R^2 , $n = 0$. This synthetic approach allows the preparation of the mixed alkyl derivatives $[\text{ArNC}(\text{Bu}^t)\text{CHC}(\text{Bu}^t)\text{NAr}]\text{ScMe}(\text{CH}_2\text{SiMe}_3)$ and dialkyl derivatives containing no coordinated Lewis bases. The high potential of these ligands in stabilisation of rare-earth organometallic compounds is demonstrated by the fact that even diethyl derivatives, which are generally very unstable because of the tendency to undergo β -hydride elimination, can be isolated in the presence of β -diketiminato ligands. The structures of complexes **73a,c,e,h,i** were established by X-ray diffraction. The dimeric dimethyl complex $[\{\text{ArNC}(\text{Me})\text{CHC}(\text{Me})\text{NAr}\}\text{ScMe}_2]_2$ is involved in the disproportionation with dichloride $[\{\text{ArNC}(\text{Me})\text{CHC}(\text{Me})\text{NAr}\}\text{ScCl}_2]_2$ to give the alkyl chloride derivative $[\{\text{ArNC}(\text{Me})\text{CHC}(\text{Me})\text{NAr}\}\text{ScClMe}]_2$.¹⁰⁸ The reactions of complexes **73h,i** with $\text{Bu}^n\text{P}=\text{Te}$ are accompanied by the insertion of the tellurium atom at the $\text{Ln}-\text{C}$ bond to form the corresponding tellurolates $[\text{ArNC}(\text{Me})\text{CHC}(\text{Me})\text{NAr}]\text{Sc}(\text{TeCH}_2\text{SiMe}_3)_2$.¹⁰⁹

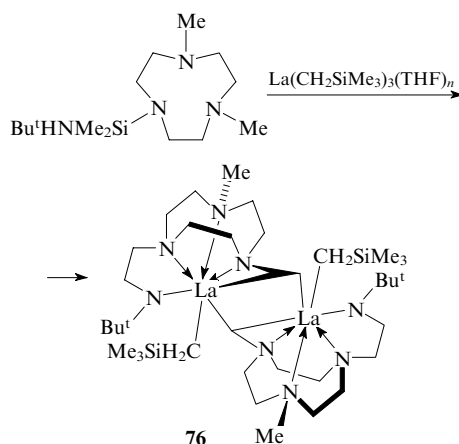
The synthesis and structure of lutetium complex **74** containing the tridentate anilido-pyridine-imine ligand were documented.¹¹⁰



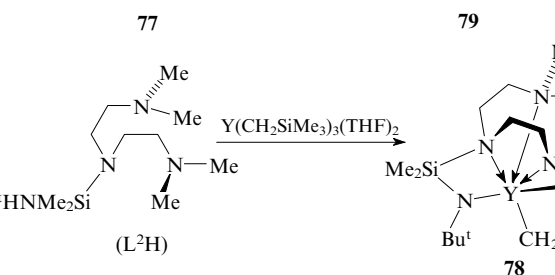
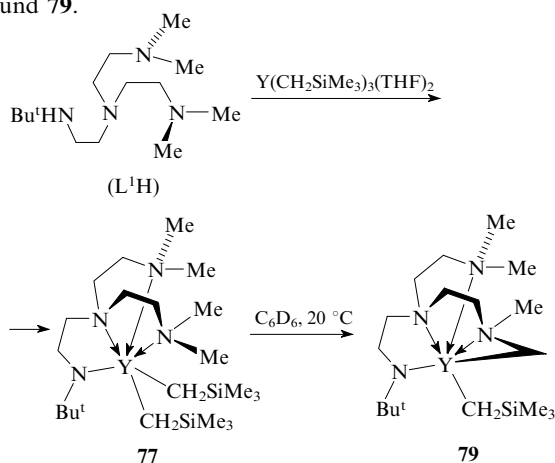
Recently, monoanionic tetradentate amide ligands have been designed^{111,112} and used in the synthesis of yttrium (**75a,b**) and lanthanum (**75c**) dialkyl complexes. It should be noted that the use of a ligand in which the 1,4,7-triazacyclononane and amide fragments are dimethylene-bridged allows the isolation of the lanthanum dialkyl complex. In the case of the ligand containing the shorter silylene (SiMe_2) bridge, the reaction is accompanied by the metallation of one methyl group resulting in the formation of dimer **76**.



$\text{Ln} = \text{Y}$; $\text{R} = \text{Me}$ (**a**), Pr^i (**b**); $\text{Ln} = \text{La}$, $\text{R} = \text{Me}$ (**c**).

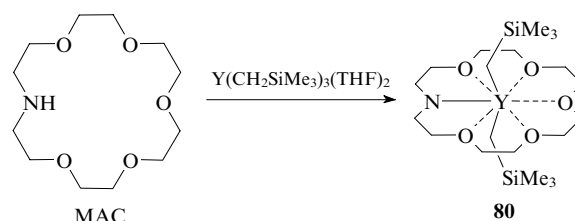


The monoanionic tetradentate ligands $[(\text{Me}_2\text{NCH}_2\text{CH}_2)_2\text{N}-\text{X}-\text{NBu}^t]^-$ [$\text{X} = (\text{CH}_2)_2$ (L^1) or SiMe_2 (L^2)], in which three neutral amine fragments are not linked together to form a rigid ring, were used¹¹³ for the synthesis of yttrium derivatives. The reaction of L^1H with $\text{Y}(\text{CH}_2\text{SiMe}_3)_3(\text{THF})_2$ produces complex **77**, whereas the reaction of this starting compound with L^2H is accompanied by the rapid metallation of one methyl group to form metal-lacyclic product **78**. The C–H bond activation was observed also upon storage of compound **77** in deuterobenzene at room temperature for 8 h resulting in the formation of compound **79**.



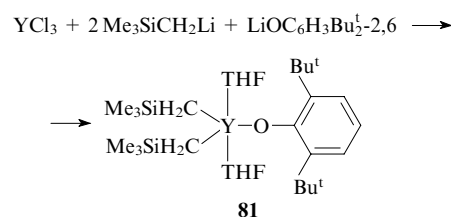
The synthesis of yttrium dialkyl and diphenyl complexes containing the dimethyl tris(pyrazolyl)borate ligands TPB-Me_2 and $(\text{TPB-Me}_2)\text{YR}_2(\text{THF})$ ($\text{R} = \text{Me}$, Bu^t , CH_2SiMe_3 or Ph) was documented.¹¹⁴ Unfortunately, these compounds were characterised only by spectroscopic methods and elemental analysis.

The deprotonation of aza-18-crown-6 (MAC) with the yttrium derivative $\text{Y}(\text{CH}_2\text{SiMe}_3)_3(\text{THF})_2$ affords complex **80** in which the metal atom is located in the centre of the cavity of the hexadentate macrocyclic ligand, and the CH_2SiMe_3 groups are in axial positions.¹¹⁵



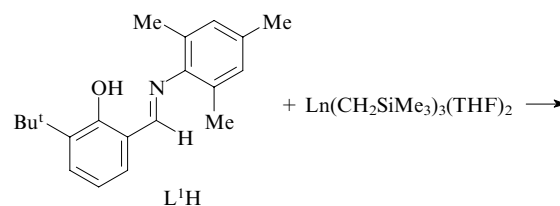
b. Complexes with monoanionic O-containing ligands

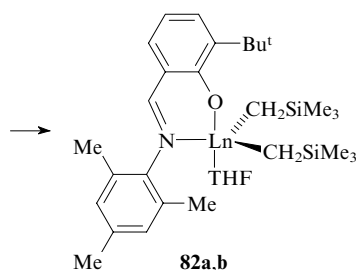
The only dialkyl derivative containing an aryloxy ligand is known. An X-ray diffraction study showed⁸⁷ that compound **81** exists as a monomer in the crystalline state.



c. Complexes with monoanionic N,O-containing aryloxy ligands

Salicylaldimine ligands containing substituents of different bulkiness in the aromatic rings of the phenol and imine fragments were used for the synthesis of scandium and yttrium dialkyl complexes. The reactions of equimolar amounts of the $\text{Ln}(\text{CH}_2\text{SiMe}_3)_3(\text{THF})_2$ compounds ($\text{Ln} = \text{Sc}$ or Y) with the 2-($\text{MesN}=\text{CH}$)-6- $\text{Bu}^t\text{C}_6\text{H}_3\text{OH}$ (L^1H) ligand produce trigonal-bipyramidal five-coordinate complexes **82a,b**. Scandium compound **82a** is stable in a toluene solution at room temperature, whereas yttrium analogue **82b** undergoes disproportionation to form the homoligand complex L_3Y . The scandium derivative $\text{L}^2\text{Sc}(\text{CH}_2\text{SiMe}_3)_2(\text{THF})$ was isolated also in the reaction with the iminomethylphenol 2-($\text{CyN}=\text{CH}$)-6- $\text{Bu}^t\text{C}_6\text{H}_3\text{OH}$ (L^2H).⁷² The reaction of L^2H with the yttrium compound produces the six-coordinate complex $\text{L}_2^2\text{Y}(\text{CH}_2\text{SiMe}_3)(\text{THF})$ containing two phenoxy-imine ligands and one CH_2SiMe_3 group regardless of the reactant molar ratio.

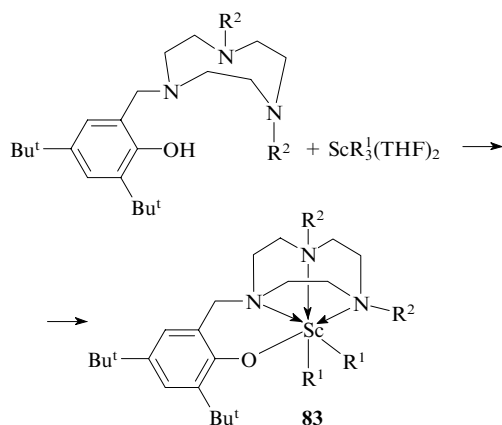




Ln = Sc (**a**), Y (**b**).

The related ligand with the bulkier diisopropylphenyl substituent at the nitrogen atom, 2-(2,6-Prⁱ₂C₆H₃N=CH)-6-Bu^tC₆H₃OH (L³H), was used in the study.⁷¹ An analogous synthetic approach allowed the synthesis of the yttrium alkyl complexes L³Y(CH₂SiMe₂R)₂(THF)_n (R = Me or Ph; n = 1 or 2); however, a mixture of products was obtained in the case of the scandium complex.

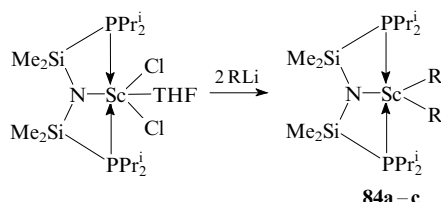
Phenols containing the 1,3,5-triazacyclononane fragment as the substituent were used¹¹⁶ as polydentate ligands in the synthesis of scandium derivatives **83**.



R¹ = CH₂SiMe₃; R² = Me, Prⁱ; R¹ = Ph, R² = Me.

d. Complexes with monoanionic N,P-containing amide ligands

A series of scandium dialkyl complexes **84a–c** containing the amidodiphosphine ligand were synthesised¹¹⁷ by the exchange reaction of the dichloride [N(SiMe₂CH₂PPRⁱ₂)₂]ScCl₂(THF) with 2 equivalents of the corresponding alkyllithium reagents. An X-ray diffraction study of compounds **84b,c** showed that the complexes are monomeric in the crystalline state and have a distorted trigonal-bipyramidal structure. In the cited study, the reactions of complexes **84** with CO, H₂, CH₃I, nitriles, isocyanides and silanes were investigated; however, all these reactions are accompanied by decomposition of the starting compound and give complex mixtures of products.



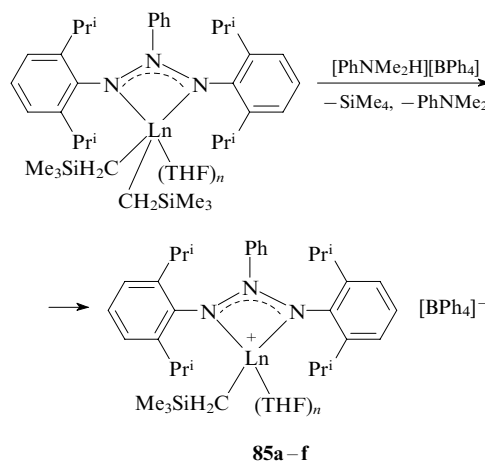
R = Me (**a**), Et (**b**), CH₂SiMe₃ (**c**).

III. Cationic alkyl complexes

The first cationic rare-earth metal complex containing the substituted alkyl group, [La(η⁵-C₅Me₅){CH(SiMe₃)₂}.(THF)_n]⁺[BPh₄][−], was synthesised in 1992.¹¹⁸ This class of

compounds has attracted considerable interest after the discovery¹¹⁹ of the catalytic activity of cationic scandium complexes in the ethylene polymerisation.

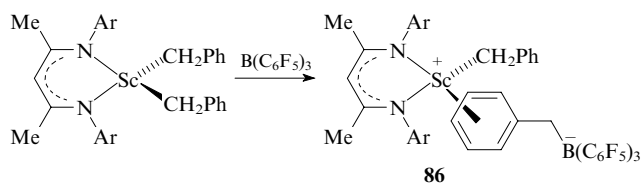
Cationic complexes **85a–f** with bulky benzamidinate ligands were synthesised^{102,103} by the reactions of the corresponding dialkyl derivatives with the Brønsted acid [PhNMe₂H]⁺[BPh₄][−] in THF. The structures of compounds **85a–e** were established by X-ray diffraction.



Ln = Sc, n = 2 (**a**); Ln = Y, n = 3 (**b**); Ln = La, n = 4 (**c**);

Ln = Nd, n = 4 (**d**); Ln = Gd, n = 4 (**e**); Ln = Lu, n = 3 (**f**).

Cationic derivatives can also be prepared by the transfer of one organic ligand, which is coordinated to the metal atom through the M–C σ-bond, to a strong electrophile. For example, the reaction of the scandium dibenzyl complex containing the β-diketiminato ligand with the Lewis acid B(C₆F₅)₃ produces cationic compound **86**.¹⁰⁶ Unlike complexes **85a–f**, compound **86** exists as a contact ion pair, in which the aromatic ring of the benzyl group is η⁶-coordinated to the metal atom.

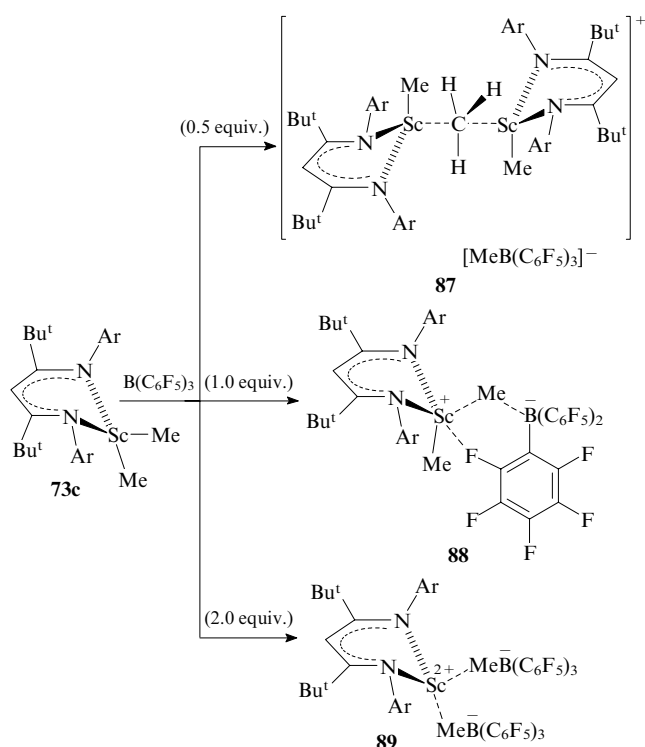


Ar = 2,6-Prⁱ₂C₆H₃.

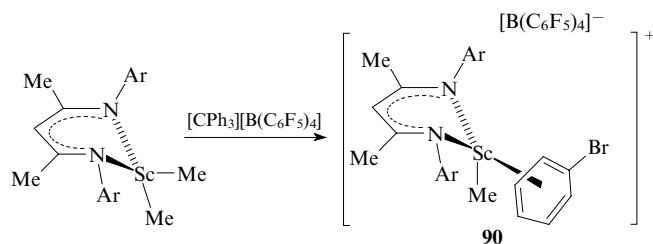
The reactions of rare-earth metal dialkyl complexes with Lewis acids can produce different cationic complexes depending on the reactant ratio (Scheme 8), as was exemplified¹²⁰ by scandium dimethyl complex **73c** containing the β-diketiminato ligand with the bulkier *tert*-butyl substituents at the imine carbon atoms.

For example, the reaction of **73c** with B(C₆F₅)₃ in a molar ratio of 1 : 0.5 affords dinuclear cationic complex **87**, in which two metal atoms are linked by the bridging methyl group. This complex is unstable and decomposes with the evolution of methane. If the reactants are used in a ratio of 1 : 1, the reaction produces monomeric compound **88** existing as an ion pair in which the counterions are linked together by the bridging methyl ligand and by a weak interaction between the scandium atom and the fluorine atom in the *ortho* position of one of the C₆F₅ rings. This compound is stable in the solid state at −30 °C; however, in solution it undergoes decomposition accompanied by the evolution of methane and the metallation of the isopropyl group. ¹H NMR spectroscopic studies showed that the ion pair is not dissociated in solution. The treatment of complex **73c** with two equivalents of B(C₆F₅)₃ affords doubly charged cationic derivative **89**.

Scheme 8

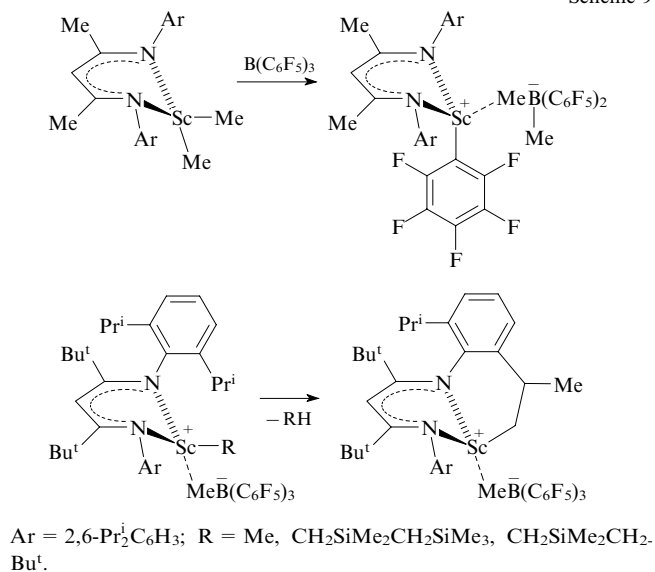


Cationic scandium alkyl complex **90**, which exists as a solvent-separated ion pair and contains the bromobenzene molecule η^6 -coordinated to the metal atom in the cationic moiety, was synthesised¹²¹ by the reaction of [ArNC(Me).CHC(Me)NAr]ScMe₂ with [Ph₃C][B(C₆F₅)₄] in bromobenzene. In the reactions of complex **90** with arenes having a higher basicity (C₆H₆, C₆H₅Me or C₆H₃Me₃) compared to bromobenzene, the arenes replace the PhBr molecule in the metal coordination sphere.

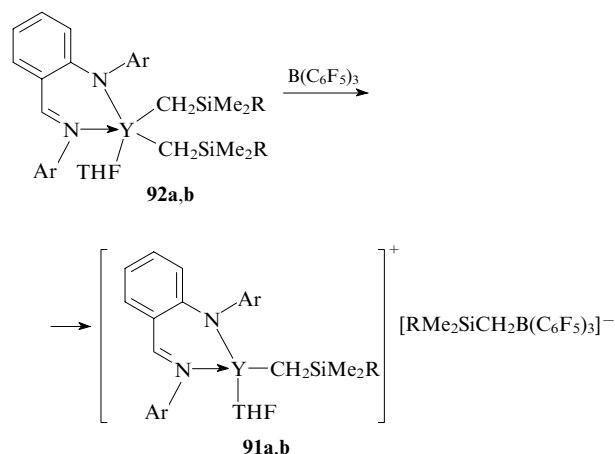


The reactions of the scandium dialkyl complexes [ArNC(R¹)CHC(R¹)NAr]ScR₂ (R¹ = Me or Bu^t; R² = Me, CH₂SiMe₃ or CH₂Bu^t) with B(C₆F₅)₃ and B(C₆F₅)(BPF) (BPF is perfluorinated biphenyl-2,2'-diyl, C₁₂F₈), the properties of the resulting cationic complexes and the dynamics of the constituent contact ion pairs were described.¹²² It was found that cationic derivatives of less bulky β -diketiminate ligands containing methyl substituents at the imine carbon atoms are less stable, and the migration of one C₆F₅ group from the boron atom to the metal atom is observed in a toluene solution (Scheme 9). For complexes containing Bu^t-substituted β -diketiminate ligands, this migration is not typical. At room temperature, these compounds are rather stable. However, the metallation of the methyl group of the isopropyl fragment occurs at high temperatures (308–323 K).

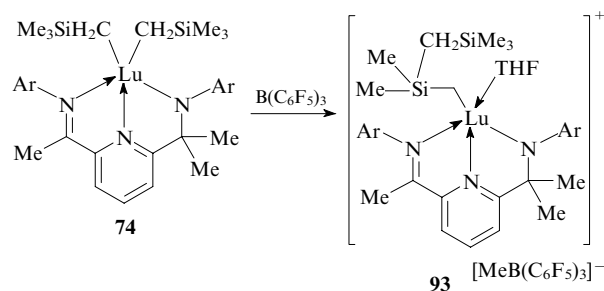
Scheme 9



Cationic yttrium organometallic derivatives **91** containing the anilido-imine ligand were synthesised as a result of the migration of one CH₂SiMe₂R group (R = Me or Ph) in complexes **92** to B(C₆F₅)₃.¹⁰⁴



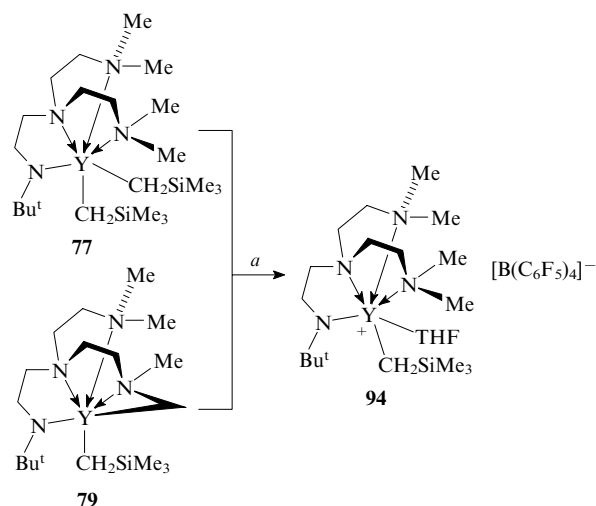
It was demonstrated¹¹⁰ that the reactions of compounds containing two M–C bonds with Lewis acids can have a more complex mechanism. For example, the reaction of lutetium complex **74** with B(C₆F₅)₃ in THF is accompanied by elimination of one methyl group from the SiMe₃ fragment to form a new Si–C bond, resulting in the formation of the fragment CH₂SiMe₂CH₂SiMe₃ in complex **93**.¹¹⁰



The fact that the reaction of B(C₆F₅)₃ with complex **80** in THF produces the cationic derivative [(MAC)YCH₂SiMe₃].

$[\text{B}(\text{C}_6\text{F}_5)_3\text{CH}_2\text{SiMe}_3]$ was confirmed by multinuclear NMR spectroscopy. This compound is very unstable at room temperature and decomposes within a few minutes to give tetramethylsilane.¹¹⁵

It was found¹¹³ that the protonation in the reactions of the Brønsted acid $[\text{PhNMe}_2\text{H}][\text{B}(\text{C}_6\text{F}_5)_4]$ with complexes **77** and **79** proceeds differently (at the $\text{Y}-\text{CH}_2\text{SiMe}_3$ or $\text{Y}-\text{CH}_2\text{N}$ bond for compounds **77** and **79**, respectively) but gives the same cationic derivative **94**.



(a) $[\text{PhNMe}_2\text{H}][\text{B}(\text{C}_6\text{F}_5)_4]$.

IV. Hydride complexes

Metallocene-type rare-earth metal hydride complexes exhibit unique reactivity¹²³ and still remain among the most promising catalysts. Most of the known rare-earth metal hydride complexes are dimeric.^{3, 123} The only reliably characterised monomeric hydride $[\text{1,3,4-Bu}_3\text{C}_5\text{H}_2]_2\text{CeH}$ containing the bulky cyclopentadienyl ligands was described as late as in 2005.¹²⁴ Hydride complexes are most often synthesised by the $\text{Ln}-\text{C}$ σ -bond cleavage with molecular hydrogen^{125, 126} or phenylsilane.¹²⁷

The development of post-metallocene chemistry of rare-earth metal hydride complexes has started in recent years. Benzamidinate complex **10**, which was prepared by the hydrogenolysis of compound **2** at 3 atm and 40 °C in benzene (see Scheme 1), was the first and, for many years, the only hydride complex containing no cyclopentadienyl ligands.

Complex **10** is rather stable in hydrocarbon solvents up to 100 °C; however, it reacts with the $\text{C}-\text{O}$ bond of THF and also binds to the $\text{C}-\text{N}$ bonds of acetonitrile and pyridine to form the $\{[\text{PhC}(\text{NSiMe}_3)_2]_2\text{Y}(\mu-\text{N}=\text{C}(\text{H})\text{Me})_2$ and $[\text{PhC}(\text{NSiMe}_3)_2]_2\text{Y}(\text{py})$ compounds, respectively. The reaction of compound **10** with α -picoline is accompanied by the $\text{C}-\text{H}$ bond activation to give the $[\text{PhC}(\text{NSiMe}_3)_2]_2\text{Y}(\eta^2-(\text{C},\text{N})-2-\text{CH}_2\text{NC}_5\text{H}_4)$ complex.²⁶ The reaction of complex **10** with acetylene is accompanied by hydrogen elimination to form dimeric acetylenide $\{[\text{PhC}(\text{NSiMe}_3)_2]_2\text{Y}(\mu-\text{C}\equiv\text{CH})_2\}$. The scandium analogue $\{[\text{PhC}(\text{NSiMe}_3)_2]_2\text{Sc}(\mu-\text{H})_2$ (**11a**) was synthesised²⁷ by the reaction of the corresponding alkyl complex **11** with H_2 (benzene or hexane, 1 atm, 20 °C). The $[\text{PhC}(\text{NSiMe}_3)_2]_2\text{ScMe}(\text{THF})$ and $[\text{PhC}(\text{NSiMe}_3)_2]_2\text{ScMes}$ compounds react with H_2 to give hydride **11a** only at high temperature (70 °C). Complex **11a** is stable in deuteriobenzene; no evidence of decomposition was observed even upon heating at 60 °C overnight. Compound **11a** is not involved in the exchange reaction with D_2 . The dimeric structure of this

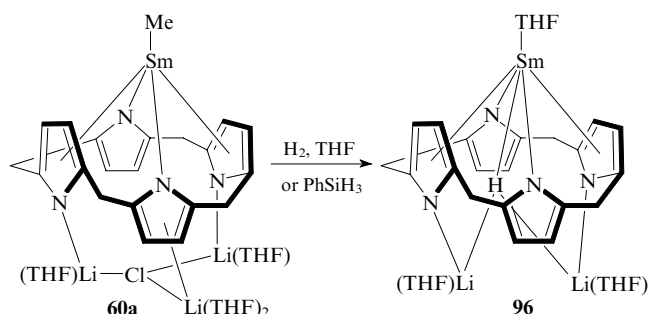
complex is rather stable, and dissociation was not observed even after the treatment with THF. The addition of complex **11a** at the triple bond of tolane affords the $[\text{PhC}(\text{NSiMe}_3)_2]_2\text{ScC}(\text{Ph})=\text{CHPh}$ compound.

Lutetium hydride $\{[(\text{Me}_3\text{Si})_2\text{NC}(\text{NPr}^i)_2]_2\text{Lu}(\mu-\text{H})_2$ (**95**) stabilised by the guanidinate ligands and containing no coordinated Lewis bases was synthesised¹²⁸ by the reaction of the $[(\text{Me}_3\text{Si})_2\text{NC}(\text{NPr}^i)_2]_2\text{LuCH}_2\text{SiMe}_3$ complex with PhSiH_3 (in a ratio of 1 : 1) in hexane. This compound differs from other bis(guanidinate)-type derivatives by the asymmetric coordination of the guanidinate ligands in two $[(\text{Me}_3\text{Si})_2\text{NC}(\text{NPr}^i)_2]_2\text{Lu}$ fragments.

Yttrium alkyl complexes **17a,b** readily react with phenylsilane in benzene at room temperature to form hydride **18**. This hydride can also be prepared by the hydrogenolysis of compounds **17a,b** under high pressure at room temperature in deuterobenzene. The exchange of the hydride ligands for deuterium from the solvent was observed upon storage of hydride **18** in THF-d_8 . In THF, complex **18** binds to the $\text{C}=\text{C}$ bonds of ethylene and hex-1-ene to give the corresponding alkyl complexes (see Scheme 2).

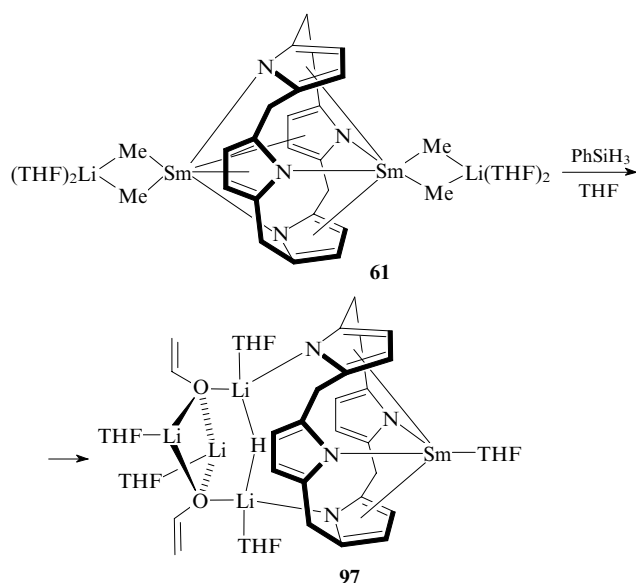
It was reported³⁷ that the hydrogenolysis of the $[2,6-\text{Pr}^i_2\text{C}_6\text{H}_3\text{N}(\text{CH}_2)_2\text{NC}_6\text{H}_3\text{Pr}^i_2-2,6]\text{YCH}(\text{SiMe}_3)_2(\text{THF})$ complex in toluene under an H_2 pressure of 1.5 atm proceeds very slowly. The hydrogenation of the $\text{Y}-\text{C}$ bonds was accompanied by the insertion of H_2 at one of the two $\text{Y}-\text{N}$ bonds of two diamide ligands to form the trinuclear $[\text{Y}_3\{2,6-\text{Pr}^i_2\text{C}_6\text{H}_3\text{NH}(\text{CH}_2)_2\text{NC}_6\text{H}_3\text{Pr}^i_2-2,6\}_2\{2,6-\text{Pr}^i_2\text{C}_6\text{H}_3\text{N}(\text{CH}_2)_2\text{N}(\text{C}_6\text{H}_3\text{Pr}^i_2-2,6\}(\mu-\text{H})_3(\mu_3-\text{H})_2(\text{THF})]$ complex.

The μ_3 -bridging coordination of the hydride ligand linking together the samarium atom and two lithium atoms was observed⁸² also in hydride complex **96** containing the calixpyrrole ligand. Complex **96** can be synthesised from methyl derivative **60a** by either the hydrogenolysis in THF at room temperature or the treatment with phenylsilane.

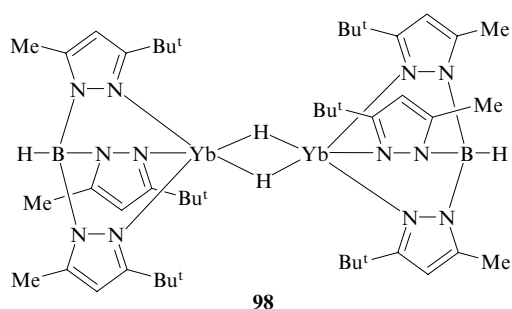


The $\text{Sm}-\text{H}$ distance in complex **96** is 2.25(7) Å, which is substantially larger than the bond lengths in known dimeric metallocene-type samarium hydrides (2.05 Å).¹²⁹ Complex **96** is stable in THF at room temperature for several weeks or at 60 °C for several hours. Compound **96** rapidly reacts with ethylene at room temperature and under atmospheric pressure to form the vinyl derivative accompanied by hydrogen elimination.

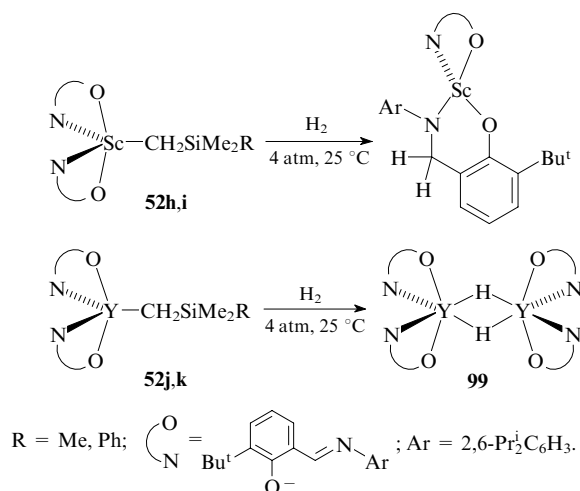
Heterobimetallic five-coordinate hydride complex **97** was prepared in 10% yield by the treatment of samarium methyl complex **61** with phenylsilane in THF at room temperature. The structure of complex **97** was established by X-ray diffraction. The complex contains two $\text{LiOCH}=\text{CH}_2$ fragments, which are formed, apparently, as a result of the cleavage of the THF molecule under the action of two MeLi molecules.⁸³ The second hydride-containing product, $(\text{Et}_3\text{-calix-pyrrole})\cdot\text{Sm}(\text{H})\text{Li}_2(\text{THF})_6$, was also isolated from the reaction mixture; however, the latter product was not reliably characterised.



The only hydride complex of lanthanides in the oxidation state +2 (compound **98**) was described. This complex was synthesised¹³⁰ with the use of the tris(pyrazolyl)borate ligands (TPB-Me,Bu^t) as the stabilising coordination environment.



The hydrogenolysis of alkyl complexes **52h–k** stabilised by the salicylaldiminate ligands **L** was found^{69,71} to proceed differently depending on the nature of the metal. For example, the hydride compound that is formed in the case of scandium immediately binds to the C=N bond of one of the ligands **L**, whereas dimeric hydride **99** was isolated in the case of yttrium. The latter complex is inert to ethylene.



The reaction of complex **34** with hydrogen was demonstrated to produce centrosymmetric dimeric hydride $[\{\text{Me}_2\text{Si}(\text{NBu}^t)(\text{OBu}^t)\}_2\text{Y}(\mu\text{-H})_2]$, which was detected⁵⁰ in the

reaction mixture by ¹H NMR spectroscopy. However, attempts to isolate the hydride complex failed because this complex undergoes disproportionation in solution to give the $[\text{Me}_2\text{Si}(\text{NBu}^t)(\text{OBu}^t)]_3\text{Y}$ compound.

The reactions of complexes **84b,c** with hydrogen are accompanied by elimination of the corresponding alkanes; however, hydrides were not detected in the reaction mixtures, and the ³¹P NMR spectra provided evidence for the presence of a complex mixture of products.¹¹⁷

An attempt to synthesise the yttrium dihydride complex by the reaction of the dimethyl derivative (TPB-Me₂)YMe₂(THF) with H₂ under a pressure of 8 atm at 0 °C led to the formation of a thermally unstable complex, which was characterised by IR spectroscopy.¹¹⁴

V. Non-metallocene rare-earth organometallic derivatives in catalysis of transformations of unsaturated substrates

1. Catalysis of alkene and diene polymerisation

Yttrium dihydride complex **10** catalyses the ethylene polymerisation under a pressure of 4 atm at 65 °C in deuteriobenzene.^{25,26} An increase in the monomer pressure to 70 atm improves the efficiency of the reaction, but the activity, on the whole, remains low $[4 \text{ (g PE) (mmol catalyst)}^{-1} \text{ h}^{-1}]$. The resulting polyethylene has a molecular mass $M_w = 2.399 \times 10^5$, $M_n = 4.63 \times 10^4$ and a high polydispersity ($M_w/M_n = 5.2$). It should be noted that no yttrium organometallic derivatives, except for complex **10**, were detected in the reaction mixture by ¹H NMR spectroscopy. Yttrium benzyl complex **1** also initiates the ethylene polymerisation, but the activity of this complex is even lower than that of hydride **10**. Both complexes do not catalyse the propylene and hex-1-ene polymerisation. No traces of oligomerisation products or allyl complexes were found even at 80 °C. Scandium analogue **11a** proved to be²⁷ virtually inactive in the ethylene and propylene polymerisation.

Yttrium dialkyl complex **68a** with the bulky amidinate ligand initiates the ethylene polymerisation in the presence of the activator $[\text{PhNMe}_2\text{H}][\text{B}(\text{C}_6\text{F}_5)_4]$ at 50 °C and a monomer pressure of 5 atm at a high rate.¹⁰² After a polymerisation time of 5 min, the molecular mass M_w of the polymer was 4.3×10^5 ; after 30 min, M_w was 1.211×10^6 , the polydispersity being very low ($M_w/M_n = 1.2$). Calculations demonstrated that there is one yttrium centre per 1.1 polymer chain in the course of polymerisation, which is indicative of the living polymerisation and a low probability of the chain transfer through β -elimination. It was noted that the efficiency of the catalyst decreases with time. The catalyst efficiency was $1037 \text{ (kg PE) mol}^{-1} \text{ h}^{-1} \text{ atm}^{-1}$ at a reaction time of 5 min, and it was only $400 \text{ (kg PE) mol}^{-1} \text{ h}^{-1} \text{ atm}^{-1}$ after 30 min. It should be noted that the six-coordinate analogue of compound **68a** containing an additional THF molecule in the metal coordination sphere is absolutely inactive in the ethylene polymerisation under analogous conditions. However, the addition of partially hydrogenated AlBu_3 (TIBAO) to a mixture of compound **68a** and $[\text{PhNMe}_2\text{H}][\text{B}(\text{C}_6\text{F}_5)_4]$ results in the formation of catalytic systems active in the ethylene polymerisation [the efficiency is $2670 \text{ (kg PE) mol}^{-1} \text{ h}^{-1} \text{ atm}^{-1}$, $M_w/M_n = 2.1$]. In the presence of TIBAO, M_w of the polymer is somewhat lower and the polydispersity is higher (~ 2) than the corresponding characteristics in the absence of this additive.

The catalytic activity of dialkyl amidinate complexes **68b–f** in the ethylene polymerisation in the presence of $[\text{PhNMe}_2\text{H}][\text{B}(\text{C}_6\text{F}_5)_4]$ and TIBAO at 30 °C and a monomer pressure of 5 atm was investigated.¹⁰³ It was found that the catalytic activity of the systems substantially depends on the ionic radius of the metal atom. Scandium having the smallest

ionic radius among the rare-earth elements, as does lanthanum having the largest ionic radius, show low activities. The activities of about $3000 \text{ (kg PE) mol}^{-1} \text{ h}^{-1} \text{ atm}^{-1}$ were observed for metals having intermediate ionic radii (Y and Gd). The polyethylene prepared in the presence of these catalysts is characterised by a high molecular mass ($M_w = 1.5 \times 10^6$) and the polydispersity $M_w/M_n \approx 2$. The conclusion was drawn that the main mechanism of the chain transfer in this system involves the transfer of the alkyl radical to the Al atom. It should be noted that the lutetium complex having a small ionic radius showed a moderate activity [$342 \text{ (kg PE) mol}^{-1} \text{ h}^{-1} \text{ atm}^{-1}$] and gave rise to the product with a low polydispersity ($M_w/M_n = 1.4$), which is indicative of the absence of the chain transfer, as opposed to systems with complexes of metals with larger ionic radii.

Lutetium hydride **95** stabilised by guanidinate ligands catalyses¹²⁸ the ethylene polymerisation; however, its efficiency is low. Complex **95** belongs to a few rare-earth metal derivatives initiating the propylene polymerisation [the activity was $3.9 \text{ (kg PE) mol}^{-1} \text{ h}^{-1} \text{ atm}^{-1}$]. Compound **95** is also efficient in the styrene polymerisation at room temperature and allows the preparation of polymers with a high molecular mass $M_w = 1.25 \times 10^6$ and a rather low polydispersity $M_w/M_n = 1.54$.

Heterobimetallic bis(guanidinato)alkyl complexes **59b,c** initiate the styrene polymerisation⁷⁹ in the temperature range of $70\text{--}100^\circ\text{C}$. It should be noted that the reaction does not proceed at 55°C ; at 100°C , the yield of the polymer is substantially lower, which was accounted for by the deactivation of the catalysts at high temperatures. The polystyrene samples have molecular masses in a range of $(1.72\text{--}5.89) \times 10^4$ and rather low polydispersities (~ 2), which increase with temperature. Studies of the microstructures of the resulting polymer samples showed that they are predominantly atactic. However, the macromolecules contain from 53% (70°C) to 28% (85°C) of syndiotactic fragments depending on the polymerisation temperature.

In spite of numerous investigations on the synthesis of rare-earth metal complexes with β -diketiminate ligands, data on their catalytic activity are scarce. Scandium dimethyl complex **73c** showed high catalytic activity in the ethylene polymerisation [$300\text{--}1200 \text{ (kg PE) mol}^{-1} \text{ h}^{-1} \text{ atm}^{-1}$] in the presence of $\text{B}(\text{C}_6\text{F}_5)_3$ or $[\text{Ph}_3\text{C}][\text{B}(\text{C}_6\text{F}_5)_4]$ as the activator and poly-(methylalumoxane) (MAO) as the cocatalyst at 50°C .¹²⁰ This complex allows the preparation of polyethylene with a high molecular mass [$(0.851\text{--}1.866) \times 10^6$] and a rather narrow molecular mass distribution (MMD) ($M_w/M_n = 1.7\text{--}2.2$). The use of an analogous complex containing Cl ligands instead of Me groups in the presence of MAO leads to a decrease in the catalytic activity of the system to $9.9 \times 10^4 \text{ (kg PE) mol}^{-1} \text{ h}^{-1} \text{ atm}^{-1}$ (polyethylene has $M_w = 1.357 \times 10^6$, $M_w/M_n = 2.2$).

Yttrium alkyl and hydride complexes **17a,b** and **18** containing the dianionic ligand DADB proved to be poorly active in the ethylene polymerisation.³⁵

A study of yttrium dialkyl complexes stabilised by the monoanionic tetradentate N-donor ligands (L) in the ethylene polymerisation showed¹¹¹ that the nature of the ligand has a decisive effect on the catalytic activity of the complexes generated in the $\text{LY}(\text{CH}_2\text{SiMe}_3)_2\text{--}[\text{PhNMe}_2\text{H}][\text{B}(\text{C}_6\text{F}_5)_4]$ systems. For example, complexes **75a,b** containing the 1,4,7-triazacyclononane ligand proved¹¹¹ to be active catalysts for the ethylene polymerisation in the presence of $[\text{PhNMe}_2\text{H}][\text{B}(\text{C}_6\text{F}_5)_4]$ (toluene, $30\text{--}80^\circ\text{C}$, 5 atm). Their efficiency was $(0.70\text{--}1.79) \times 10^3 \text{ (kg PE) mol}^{-1} \text{ h}^{-1} \text{ atm}^{-1}$. The polyethylene samples had a high polydispersity ($M_w/M_n = 4.0\text{--}6.0$). In addition, catalysts lost 5%–30% of the initial activity during a rather short period of time (10–15 min). Unlike complexes **75a,b**, compound **77**, in which the yttrium

atom is in an analogous coordination environment but which contains the structurally different N,N-donor ligand, is inert to ethylene in the presence of $[\text{PhNMe}_2\text{H}][\text{B}(\text{C}_6\text{F}_5)_4]$ as the activator. In the presence of $[\text{Ph}_3\text{C}][\text{B}(\text{C}_6\text{F}_5)_4]$ as the activator, which does not form the free Lewis base PhNMe_2 in the reactions with dialkyl complexes, complex **77** catalyses the ethylene polymerisation (toluene, 50°C , 5 atm) but it loses catalytic activity during 4 min.¹¹³

Yttrium dialkyl and diaryl complexes containing the dimethyl tris(pyrzoly)borate ligands (TPB-Me_2) or $(\text{TPB-Me}_2)\text{YR}_2(\text{THF})$ ($\text{R} = \text{Me}$, Bu^t , CH_2SiMe_3 or Ph) catalyse the ethylene polymerisation giving a linear polymer with a high molecular mass (up to 2×10^6) and a high polydispersity (2.50–4.14).¹¹⁴ The complex with $\text{R} = \text{Bu}^t$ proved to be more active (the total turnover number was 1932).

Yttrium dialkyl complex **81** initiates the ethylene polymerisation but it is inert to propylene and butadiene.⁸⁷

The treatment of neodymium alkoxide $\text{Nd}_3(\mu_3\text{-OBU}^t)_2 \cdot (\mu_2\text{-OBU}^t)_3(\text{OBU}^t)_4(\text{THF})_2$ (Refs 62 and 131) with dialkylmagnesium compounds affords systems, which can catalyse the ethylene polymerisation. The polymerisation at 0°C and a monomer pressure of 1 atm in the presence of these catalysts and phenylsilane or H_2 gives low-molecular-mass polyolefins [the activity is $5\text{--}20 \text{ (kg PE) mol}^{-1} \text{ h}^{-1} \text{ atm}^{-1}$].¹³¹

Complexes **32a,b**,⁴⁹ **35** (Ref. 52) and **54** (Ref. 73) proved to be inactive as initiators for the ethylene polymerisation.

The heterobimetallic diiminopyridine complex $[\text{2,6-}\{\text{2,6-Pr}^i\text{C}_6\text{H}_3\text{NC}(\text{=CH}_2)\}_2\text{C}_5\text{H}_3\text{N}\}\text{Nd}(\mu\text{-Me})(\mu\text{-Cl})[\text{Li}(\text{THF})_2]$ containing the bridging methyl and chloride ligands, which link together the neodymium and lithium atoms, proved to be a highly efficient catalyst for the synthesis of *cis*-polybutadiene, whereas the activity of the fully methylated analogue (containing the Me group instead of the Cl atom) was unexpectedly much lower.³⁹

The catalytic system, which was prepared by the treatment of neodymium alkoxide $\text{Nd}_3(\text{OBU}^t)_9(\text{THF})_2$ with dialkylmagnesium reagents, proved to be inefficient in the butadiene polymerisation, whereas systems based on tris(phenoxides) $\text{Nd}(\text{OC}_6\text{H}_4\text{Bu}^t\text{-2,6-Me-4})_3(\text{THF})_n$ ($n = 0$ or 1) are suitable for the living polymerisation of butadiene and the preparation of polymers with a low polydispersity ($M_w/M_n = 1.3$) containing up to 95% of *trans* units.¹³² These systems allow also the synthesis of butadiene–styrene copolymers with a molecular mass M_n up to 5×10^4 and a styrene content of 3%–15%.

2. Catalysis of polymerisation of polar monomers

a. Acrylic monomers

Yttrium and samarium alkyl complexes **13** and **14a,b** were studied³² as initiators for the methyl methacrylate (MMA) polymerisation. Compounds **13** and **14a** exhibit high catalytic activity and isospecificity in both the block and solution polymerisation of MMA. Compound **14a** showed good results as regards the stereoregularity of polymer products in a wide temperature range (from -40 to $+65^\circ\text{C}$); however, the isotacticity of poly(methyl methacrylate) (PMMA) samples somewhat decreases with temperature. The block copolymerisation initiated by complex **14a** affords a isotactic polymer with a very high molecular mass ($M_n = 1.41 \times 10^6$) and a low polydispersity ($M_w/M_n = 1.31$). Yttrium complex **13** provided much lower selectivity but the molecular mass distribution remained rather narrow (1.24–1.98). It should be noted that methyl complex **14b** appeared to be absolutely inactive in the MMA polymerisation.

The scandium complex $(\text{BDPPpyr})\text{ScCH}_2\text{SiMe}_3(\text{THF})$ with the tridentate diamino-substituted pyridine ligand (see Section II.1.b) catalyses³⁸ the MMA polymerisation at 40°C in toluene at a high rate to give PMMA with molecular masses $M_w = 1.29 \times 10^5$, $M_n = 8.1 \times 10^4$ and a low polydispersity ($M_w/M_n = 1.6$). Analogous yttrium and lutetium complexes

with large ionic radii exhibited very low activity, whereas derivatives of other ligands examined in the study³⁸ proved to be inactive.

Heterobimetallic neodymium and ytterbium complexes **58a,b** initiate the MMA polymerisation⁷⁸ at good rates even at $-78\text{ }^{\circ}\text{C}$. The PMMA samples have predominantly syndiotactic structures, high molecular masses ($>10^4$) and polydispersities varying from 1.61 to 1.93.

Neodymium bis(guanidinate) complex **59b** proved to be an efficient catalyst for the MMA polymerisation at $40\text{ }^{\circ}\text{C}$. The resulting polymer⁸⁰ had a molecular mass of 10.8×10^4 and a polydispersity of 2.16.

The use of the $\text{Nd}_3(\mu_3\text{-O}^t\text{Bu})(\mu_2\text{-O}^t\text{Bu})_3(\text{O}^t\text{Bu})_4 \cdot (\text{THF})_2 - (\text{n-C}_6\text{H}_{13})_2\text{Mg}$ systems allows the synthesis of polyethylene–PMMA block-copolymers.¹³¹ The $\text{Nd}(\text{OC}_6\text{H}_2 \cdot \text{Bu}^t\text{-2,6-Me-4})_3(\text{THF})$ and $\text{Nd}(\text{OC}_6\text{H}_2\text{Bu}^t\text{-2,6-Me-4})_3 - (\text{n-C}_6\text{H}_{13})_2\text{Mg}$ systems¹³² catalyse copolymerisation of butadiene with glycidyl methacrylate, resulting in the formation of block polymers.

b. ϵ -Caprolactone and lactides

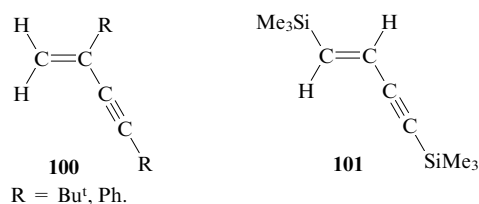
Bis(guanidinate) complexes **59b,c** are efficient catalysts for the ϵ -caprolactone polymerisation.⁸⁰ In the case of neodymium complex **59b**, the conversion achieved 100% at $20\text{ }^{\circ}\text{C}$ during 15 min even at the monomer: initiator ratio of 1000:1; ytterbium derivative **59c** proved to be somewhat less active. The resulting polymer has a high molecular mass [$M_n = (7.44\text{--}11.03) \times 10^4$] but a rather wide MMD ($M_w/M_n = 1.92\text{--}2.96$).

Yttrium alkyl complexes **66** and **81** and lutetium alkyl complex **67** containing the phenoxide ligands were demonstrated⁸⁷ to initiate ϵ -caprolactone polymerisation. However, data on the activity of the catalysts and the properties of the polymers were not reported.

The use of scandium complex **82a** with the phenoxy-imine ligand allows the polymerisation of ϵ -caprolactone with a quantitative conversion at $0\text{ }^{\circ}\text{C}$ during 1 min. The molecular mass of the polymer was 7.1×10^4 , and the polydispersity was 2.9.⁷² Complex **56b** exhibited somewhat lower activity;⁷⁵ however, the resulting polyester had a much lower polydispersity ($M_w/M_n = 1.49$) and a lower molecular mass ($M_n = 5.05 \times 10^4$). Related bis(phenoxide) complex **54** initiates the living polymerisation of racemic lactide at a high rate, which gives predominantly a heterotactic polymer.¹³³

3. Catalytic C–C bond formation (dimerisation of alkynes)

An investigation of the catalytic activity of yttrium complexes **1**, **2** and **10** in the dimerisation of terminal alkynes showed²⁶ that, as opposed to systems with metallocene-type catalysts,^{134,135} the reaction pathway in the presence of these complexes substantially depends on the size of the substituent at the triple bond of the substrate. For example, dimerisation of alkynes $\text{RC}\equiv\text{CH}$ with small substituents ($\text{R} = \text{H}$, Me or Pr^{*t*}) was not observed even upon prolonged heating ($80\text{ }^{\circ}\text{C}$), whereas alkynes with bulky substituents ($\text{R} = \text{Ph}$, SiMe_3 or Bu^t) do undergo dimerisation under analogous conditions. It should be noted that the rate of alkyne dimerisation catalysed by amidinate complexes **1**, **2** and **10** is much lower than that in the presence of bis(cyclopentadienyl)-type complexes.¹³⁴ The regioselectivity of the reaction depends also on the nature of alkyne. Thus, the $\text{PhC}\equiv\text{CH}$ and $\text{Bu}^t\text{C}\equiv\text{CH}$ compounds undergo the selective head-to-tail dimerisation to form 2,4-disubstituted but-1-en-3-yne **100**, whereas the reverse selectivity is observed for $\text{Me}_3\text{SiC}\equiv\text{CH}$, and the reaction affords exclusively the 1,4-substituted head-to-head addition product, viz., *trans*- $\text{Me}_3\text{SiC}(\text{H})=\text{C}(\text{H})\text{C}\equiv\text{CSiMe}_3$ (**101**).

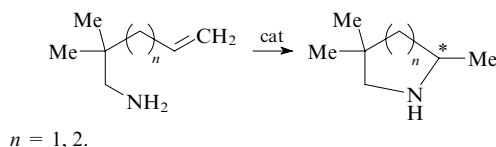


The cationic complex $[\text{LLa}(\text{CH}_2\text{SiMe}_3)]^+[\text{B}(\text{C}_6\text{F}_5)_4]^-$, which was prepared by the reaction of $[\text{PhNMe}_2\text{H}][\text{B}(\text{C}_6\text{F}_5)_4]$ with the $\text{LLa}(\text{CH}_2\text{SiMe}_3)_2$ complex (**75c**), was used *in situ* in the catalysis of the phenylacetylene dimerisation. At $50\text{ }^{\circ}\text{C}$, the reaction proceeds at a high rate and a very high selectivity to give *cis*-1,4-diphenylbut-1-en-3-yne in 99% yield.¹¹²

4. Catalytic C–N bond formation (hydroamination of alkenes)

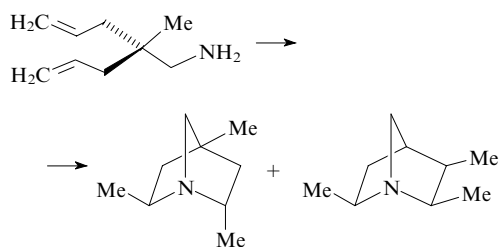
The catalytic hydroamination of alkenes and alkynes resulting in the addition of amines at multiple bonds of unsaturated substrates is a very convenient, efficient and environmentally safe procedure for the synthesis of nitrogen-containing compounds.^{14, 136, 137} Organic rare-earth metal derivatives are among the most promising catalysts for the hydroamination–cyclisation of unsaturated compounds with unactivated double bonds proceeding under mild conditions at a high rate and a high enantioselectivity, which allows the synthesis of nitrogen-containing heterocyclic, including biologically active, compounds.^{15, 16}

Lanthanum alkyl complexes **48** and **49** containing the chiral Biphen ligand proved to be efficient catalysts for the hydroamination–cyclisation of 2,2'-dimethylpent-4-enylamine and hex-5-enylamine at room temperature, the activity of monomeric complex **49** being almost twice as high as that of dimer **48**.⁶⁶



Unfortunately, the enantioselectivity of complexes **48** and **49** is low, and the reactions produce racemic mixtures of heterocycles. The use of the Binol-SiAr₃ ligands with the bulky Ar₃Si substituents at positions 3 and 3' (complexes **50** and **51**) allows not only the retention of high activity in the hydroamination, but also a substantial enhancement of the enantioselectivity of the reaction (to 95%).^{67, 68} In the presence of these complexes, the cyclisation of aminopentenes proceeds at a high rate even at room temperature, whereas the reaction of aminohexenes requires high temperature ($60\text{--}100\text{ }^{\circ}\text{C}$). The catalytic activity of these complexes increases with increasing ionic radius of metal. Compound **51** catalyses the hydroamination of styrene with propylamine at $60\text{ }^{\circ}\text{C}$, the addition being anti-Markovnikov.⁶⁸

Yttrium complexes **28a–c** also exhibited high activity in the catalysis of the hydroamination–cyclisation of various aminoalkenes and aminoalkynes.⁴³ The electron-withdrawing effect of the dichlorophenyl substituents (compound **28c**) enhances the stability of the catalyst to degradation as a result of protonolysis, which is manifested in its high activity in the cyclisation of pent-4-enylamine and 5-phenylpent-4-enylamine. The double cyclisation of 2-allyl-2-methylpent-4-enylamine can be performed at $60\text{ }^{\circ}\text{C}$ with the use of complexes **28a** and **28c**; this reaction affords 2,4,6-trimethyl-1-azabicyclo[2.2.1]heptane as a mixture of *endo,endo* and *exo,exo* isomers.



The use of scandium organometallic complexes with salicylaldimine and β -ketimine ligands for the initiation of the hydroamination–cyclisation of aminoalkynes and aminoalkenes was documented.¹³⁸ In the cited study, the first cationic system (compound **88**) initiating the intramolecular hydroamination was described.

Complexes **52i**, **73c** and **52l** ($L = \text{Sn}$, $\text{Ar} = \text{Mes}$, $R = \text{Ph}$) catalyse the hydroamination–cyclisation of 5-phenylpent-4-ynylamine (25 °C for complexes **52i**, **l** and 65 °C for complex **73c**) giving substituted pyrrolidine in quantitative yield. However, these complexes are inactive in the catalysis of the intermolecular hydroamination of hex-1-yne with aliphatic amines. Complex **52i** containing ligands with the bulky diisopropylphenyl substituent at the imine nitrogen atom is inactive in the hydroamination of 2,2-diphenylpent-4-enylamine. However, the use of a less bulky ligand containing the mesityl substituent (complex **52l**) results in the appearance of the catalytic activity; the complete conversion is achieved at 65 °C for 2 h. β -Diketimine complex **73c** catalyses the hydroamination of 2,2-diphenylpent-4-enylamine at room temperature but at a low rate. The activity of the catalyst was increased by a factor of ~ 60 and the amount of the catalyst charge was halved with the use of cationic derivative **88**. The use of this cationic complex makes it also possible to perform the cyclisation of aminoalkenes, which is, as a rule, a more complex process compared to aminopentenes.

5. Catalytic C–Si bond formation (hydrosilylation of alkenes)

Yttrium methyl and hydride complexes **17a** and **18** can catalyse the formation of ethylphenylsilane from ethylene and PhSiH_3 at room temperature and an ethylene pressure of 0.35 atm.¹³⁹ The hydrosilylation of hex-1-ene, styrene and norbornene with PhSiH_3 proceeds in the presence of complex **17a**, whereas cyclohexene, α -methylstyrene and *trans*-stilbene are not involved in this reaction. In the presence of this complex, secondary silane PhMeSiH_2 is involved in the addition reaction only with hex-1-ene and styrene. It should be noted that aliphatic alkenes give predominantly anti-Markovnikov addition products, whereas the hydrosilylation of styrene affords benzyldisilane derivatives as the major products. Complex **17a** containing the enantiomerically pure (*S*)-biphenyl ligand showed a high enantioselectivity in the catalysis of the hydrosilylation of norbornene with phenylsilane (*ee* 90.4%).

Lanthanum complexes **48** and **49** (Ref. 66) catalyse the hydrosilylation of hex-1-ene, styrene and norbornene with ethylphenylsilane at 60 °C, the catalytic activity of monomeric complex **49** is, as a rule, lower than the activity of dimeric complex **48** containing no coordinated THF molecules. The hydrosilylation of styrene proceeds at a high rate and a high selectivity to give predominantly the Markovnikov addition product. Unexpectedly, the rates of hydrosilylation of hex-1-ene and norbornene appeared to be substantially lower than that of styrene. Both reactions are stereoselective and give exclusively the 1,2-addition product and the *exo* adduct for hex-1-ene and norbornene, respectively.

6. Catalytic C–B bond formation (hydroboration of alkenes)

Yttrium bis(amidinate) complexes **1**, **2** and **10** (Refs 12 and 26) catalyse the hydroboration of hex-1-ene with catecholborane. However, the activity of these complexes is substantially lower than that of the $(\eta^5\text{-C}_5\text{Me}_5)_2\text{LaCH}(\text{SiMe}_3)_2$ complex.¹³ In all reactions, the catalyst deactivation was observed, which is apparently due to the reaction of catecholborane with the benzamidinate ligands. The catalytic activity of complexes **1**, **2** and **10** is substantially higher than that of metallocene-type yttrium catalysts.

* * *

The data summarised in the present review clearly show that the last decade witnessed considerable advances in the search for new ligand systems alternative to the cyclopentadienyl ligand and capable of stabilising highly reactive rare-earth organometallic derivatives. The progress achieved in this field confirms great possibilities for manipulating the reactivity of rare-earth metal complexes containing M–C and M–H bonds by the design of ligand systems and the coordination sphere of the central atom and a considerable potential of these compounds in the catalysis of various transformations of unsaturated substrates. The further progress in the catalytic applications of rare-earth organometallic compounds would be expected to be determined by advances in the chemistry of their hydride and cationic complexes.

This review has been written with the financial support of the Russian Foundation for Basic Research (Project No. 05-03-32390), the Russian Science Support Foundation and the Federal Agency for Science and Innovations of the Russian Federation (Contract No. 02.513.11.3029).

References

1. F A Cotton, G Wilkinson *Advanced Inorganic Chemistry* (IVth Ed.) (New York: Wiley, 1980) p. 23
2. R D Shannon *Acta Crystallogr., Sect. A* **32** 751 (1976)
3. M N Bochkarev, L N Zakharov, G S Kalinina *Organoderivatives of Rare Earth Elements* (Dordrecht: Kluwer Academic, 1995)
4. V P Conticello, L Brard, M A Giardello, Y Tsuji, M Sabat, C L Stern, T J Marks *J. Am. Chem. Soc.* **114** 2761 (1992)
5. D Stern, M Sabat, T J Marks *J. Am. Chem. Soc.* **112** 9558 (1990)
6. G Jeske, H Lauke, H Mauermann, H Schumann, T J Marks *J. Am. Chem. Soc.* **107** 8111 (1985)
7. W J Evans, I Bloom, W E Hunter, J L Atwood *J. Am. Chem. Soc.* **105** 1401 (1983)
8. Z M Hou, Y Wakatsuki *Coord. Chem. Rev.* **231** 1 (2002)
9. H Yasuda *J. Organomet. Chem.* **647** 128 (2002)
10. Y Nakayama, H Yasuda *J. Organomet. Chem.* **689** 4489 (2004)
11. G A Molander, J A C Romero *Chem. Rev.* **102** 2161 (2002)
12. E A Bijpost, R Duchateau, J H Teuben *J. Mol. Catal. A: Chem.* **95** 121 (1995)
13. K N Harrison, T J Marks *J. Am. Chem. Soc.* **114** 9220 (1992)
14. T E Müller, M Beller *Chem. Rev.* **98** 675 (1998)
15. K C Hultsch *Adv. Synth. Catal.* **347** 367 (2005)
16. S Hong, T J Marks *Acc. Chem. Res.* **37** 673 (2004)
17. A N Kawaoka, T J Marks *J. Am. Chem. Soc.* **127** 6311 (2005)
18. A N Kawaoka, T J Marks *J. Am. Chem. Soc.* **126** 12764 (2004)
19. M R Douglass, T J Marks *J. Am. Chem. Soc.* **122** 1824 (2000)
20. H Schumann, J A Meese-Marktscheffel, L Esser *Chem. Rev.* **95** 865 (1995)
21. F T Edelman, D M M Freckmann, H Schumann *Chem. Rev.* **102** 1851 (2002)
22. W E Piers, D J H Emslie *Coord. Chem. Rev.* **233–234** 131 (2002)
23. P Mountford, B D Ward *Chem. Commun.* 1797 (2003)
24. R Duchateau, C T van Wee, A Meetsma, P T van Duijnen, J H Teuben *Organometallics* **15** 2279 (1996)

25. R Duchateau, C T van Wee, A Meetsma, J H Teuben *J. Am. Chem. Soc.* **115** 4931 (1993)
26. R Duchateau, C T van Wee, J H Teuben *Organometallics* **15** 2291 (1996)
27. J R Hagadorn, J Arnold *Organometallics* **15** 984 (1996)
28. P J Bailey, S Pace *Coord. Chem. Rev.* **214** 91 (2001)
29. Z Lu, G P A Yap, D S Richeson *Organometallics* **20** 706 (2001)
30. A A Trifonov, D M Lyubov, E A Fedorova, G K Fukin, H Schumann, S Muhle, M Hummert, M N Bochkarev *Eur. J. Inorg. Chem.* 747 (2006)
31. Y Zhou, G P A Yap, D S Richeson *Organometallics* **17** 4387 (1998)
32. C Cui, A Shafir, C L Reeder, J Arnold *Organometallics* **22** 3357 (2003)
33. S Bambirra, M J R Brandsma, E A C Brussee, A Meetsma, B Hessen, J H Teuben *Organometallics* **19** 3197 (2000)
34. L Hasinoff, J Takats, X W Zhang *J. Am. Chem. Soc.* **116** 8833 (1994)
35. T I Gountchev, T Don Tilley *Organometallics* **18** 2896 (1999)
36. F G N Cloke, B R Elvidge, P B Hitchcock, V M E Lamarche *J. Chem. Soc., Dalton Trans.* 2413 (2002)
37. A G Avent, F G N Cloke, B R Elvidge, P B Hitchcock *Dalton Trans.* 1083 (2004)
38. F Elster, G Eickerling, E Herdtweck, R Anwender *Organometallics* **22** 1212 (2003)
39. H Sugiyama, S Gambarotta, G P A Yap, D R Wilson, S K-H Thiele *Organometallics* **23** 5054 (2004)
40. B D Ward, S R Dubberley, A Maisse-François, L H Gade, P Mountford *J. Chem. Soc., Dalton Trans.* 4649 (2002)
41. M E G Skinner, P Mountford *J. Chem. Soc., Dalton Trans.* 1694 (2002)
42. M E G Skinner, B R Tyrrell, B D Ward, P Mountford *J. Organomet. Chem.* **647** 145 (2002)
43. K C Hultsch, F Hampel, T Wagher *Organometallics* **23** 2601 (2004)
44. S Bambirra, A Meetsma, B Hessen, J H Teuben *Organometallics* **20** 782 (2001)
45. P W Roesky *J. Organomet. Chem.* 603 161 (2000)
46. F Arnaud-Neu *Chem. Soc. Rev.* 235 (1994)
47. C J Schaverien, A G Orpen *Inorg. Chem.* **30** 4968 (1991)
48. J Arnold, C G Hoffman, D Y Dawson, F J Hollander *Organometallics* **12** 3645 (1993)
49. J Wang, M G Gardiner, B W Skelton, A H White *Organometallics* **24** 815 (2005)
50. R Duchateau, T Tuinstra, E A C Brussee, A Meetsma, P T van Duijn, J H Teuben *Organometallics* **16** 3511 (1997)
51. R Duchateau, E A C Brussee, A Meetsma, J H Teuben *Organometallics* **16** 5506 (1997)
52. D D Graf, W M Davis, R R Schrock *Organometallics* **17** 5820 (1998)
53. L Lee, D J Berg, G W Bushnell *Organometallics* **14** 8 (1995)
54. L Lee, D J Berg, G W Bushnell *Organometallics* **14** 5021 (1995)
55. M D Fryzuk, T S Haddad, D J Berg *Coord. Chem. Rev.* **99** 137 (1990)
56. M D Fryzuk, T S Haddad *J. Am. Chem. Soc.* **110** 8263 (1988)
57. M D Fryzuk, T S Haddad *J. Chem. Soc., Chem. Commun.* 1088 (1990)
58. M D Fryzuk, T S Haddad, S J Rettig *Organometallics* **11** 2967 (1992)
59. M D Fryzuk, T S Haddad, S J Rettig *Organometallics* **10** 2026 (1991)
60. M D Fryzuk, J B Love, S J Rettig *J. Am. Chem. Soc.* **119** 9071 (1997)
61. M D Fryzuk, L Jafarpour, F M Kerton, J B Love, B O Patrick, S J Rettig *Organometallics* **20** 1387 (2001)
62. J Gromada, A Mortreux, G Nowogrocki, F Leising, T Mathivet, J-F Crapentier *Eur. J. Inorg. Chem.* 3247 (2004)
63. G W Rabe, M Zhang-Presse, F A Riederer, G P A Yapp *Inorg. Chem.* **42** 3527 (2003)
64. F A Allen, O Konnard, D G Watson, L Brammer, A G Orpen, R Taylor *J. Chem. Soc., Perkin Trans. 2* S1 (1987)
65. C J Schaverien, N Meijboom, A G Orpen *J. Chem. Soc., Chem. Commun.* 124 (1992)
66. D V Gribkov, F Hampel, K C Hultsch *Eur. J. Inorg. Chem.* 4091 (2004)
67. D V Gribkov, K C Hultsch *Chem. Commun.* 730 (2004)
68. D V Gribkov, K C Hultsch, F Hampel *J. Am. Chem. Soc.* **128** 3748 (2006)
69. D J H Emslie, W E Piers, R McDonald *J. Chem. Soc., Dalton Trans.* 293 (2002)
70. D J H Emslie, W E Piers, M Parvez *Dalton Trans.* 2615 (2003)
71. D J H Emslie, W E Piers, M Parvez, R McDonald *Organometallics* **21** 4226 (2002)
72. A Lara-Sanchez, A Rodriguez, D L Hughes, M Schormann, M Bochmann *J. Organomet. Chem.* **663** 63 (2002)
73. C-X Cai, L Toupet, C W Lehmann, J-F Carpentier *J. Organomet. Chem.* **683** 131 (2003)
74. F Bonnet, A C Hillier, A Collins, S R Dubberley, P Mountford *Dalton Trans.* 421 (2005)
75. Y Yao, M Ma, X Xu, Y Zhang, Q Shen, W-T Wong *Organometallics* **24** 4014 (2005)
76. O Runte, T Priermeier, R Anwender *Chem. Commun.* 1385 (1996)
77. H Schumann, J Winterfeld, E C E Rosenthal, H Hemling, L Esser *Z. Anorg. Allg. Chem.* **621** 122 (1995)
78. Y Luo, Y Yao, W Li, J Chen, Z Zhang, Y Zhang, Q Shen *J. Organomet. Chem.* **679** 125 (2003)
79. Y Luo, Y Yao, Q Shen *Macromolecules* **35** 8670 (2002)
80. X Y Luo, Y M Yao, Q Shen, K B Yu, L H Weng *Eur. J. Inorg. Chem.* 318 (2003)
81. C J Schaverien *J. Chem. Soc., Chem. Commun.* 458 (1991)
82. T Dubé, S Gambarotta, G P A Yap *Organometallics* **19** 121 (2000)
83. T Dubé, S Gambarotta, G P A Yap *Organometallics* **19** 817 (2000)
84. H Noss, M Oberthür, C Fischer, W P Kretschmer, R Kempe *Eur. J. Inorg. Chem.*, 2283 (1999)
85. J Wang, M G Gardiner *Chem. Commun.* 1589 (2005)
86. D L Clark, J C Gordon, J C Huffmann, J G Watkin, B D Zwick *Organometallics* **13** 4266 (1994)
87. W J Evans, R N R Broomhall-Dillard, J W Ziller *Organometallics* **15** 1351 (1996)
88. W J Evans, R N R Broomhall-Dillard, J W Ziller *J. Organomet. Chem.* **569** 89 (1998)
89. P Shao, D J Berg, G W Bushnell *Inorg. Chem.* **33** 6334 (1994)
90. W J Evans, R Anwender, J W Ziller, S I Kraw *Inorg. Chem.* **34** 5927 (1995)
91. W J Evans, M A Ansari, J W Ziller, S I Khan *Inorg. Chem.* **35** 5435 (1996)
92. J C Gordon, G R Giesbrecht, J T Brady, D L Clark, D Webster Keogh, B L Scott, J G Watkin *Organometallics* **21** 127 (2002)
93. G R Giesbrecht, J C Gordon, J T Brady, D L Clark, D Webster Keogh, R Michalczyk, B L Scott, J G Watkin *Eur. J. Inorg. Chem.* 723 (2002)
94. A Fischbach, E Herdtweck, R Anwender, G Eikerling, W Scherer *Organometallics* **22** 499 (2003)
95. W J Evans, T J Boyle, J W Ziller *J. Am. Chem. Soc.* **115** 5084 (1993)
96. A Fischbach, F Perdih, P Sirsch, W Scherer, R Anwender *Organometallics* **21** 4569 (2002)
97. A Fischbach, F Perdih, E Herdtweck, R Anwender *Organometallics* **25** 1626 (2006)
98. Y Luo, J Baldamus, Z Hou *J. Am. Chem. Soc.* **126** 13910 (2004)
99. X Li, J Baldamus, Z Hou *Angew. Chem., Int. Ed.* 962 (2005)
100. S Arndt, J Okuda *Chem. Rev.* **102** 1953 (2002)
101. H Schumann, I L Fedushkin *Encyclopedia of Inorganic Chemistry* (Ed. B R King) (Oxford: Wiley, 2005) p. 4878
102. S Bambirra, D van Leusen, A Meetsma, B Hessen, J H Teuben *Chem. Commun.* 522 (2003)
103. S Bambirra, M W Bouwkamp, A Meetsma, B Hessen *J. Am. Chem. Soc.* **126** 9182 (2004)
104. P G Hayes, G C Welch, D J H Emslie, C L Noack, W E Piers, M Parvez *Organometallics* **22** 1577 (2003)

105. S Hong, S Tian, M V Metz, T J Marks *J. Am. Chem. Soc.* **125** 14768 (2003)
106. L W M Lee, W E Piers, M R J Elsegood, W Clegg, M Parvez *Organometallics* **18** 2947 (1999)
107. P G Hayes, W E Piers, L W M Lee, L K Knight, M Parvez, M R J Elsegood, W Clegg *Organometallics* **20** 2533 (2001)
108. L K Knight, W E Piers, P Fleurat-Lessard, M Parvez, R McDonald *Organometallics* **23** 2087 (2004)
109. L K Knight, W E Piers, R McDonald *Chem. – Eur. J.* **6** 4322 (2000)
110. T M Cameron, J C Gordon, R Michalczyk, B L Scott *Chem. Commun.* 2282 (2003)
111. S Bambirra, D van Leusen, A Meetsma, B Hessen, J H Teuben *Chem. Commun.* 637 (2001)
112. C G J Tazelaar, S Bambirra, D van Leusen, A Meetsma, B Hessen, J H Teuben *Organometallics* **23** 936 (2004)
113. S Bambirra, S J Boot, D van Leusen, A Meetsma, B Hessen *Organometallics* **23** 1891 (2004)
114. D P Long, P A Bianconi *J. Am. Chem. Soc.* **118** 12453 (1996)
115. L Lee, D J Berg, F W Einstein, R J Batchelor *Organometallics* **16** 1819 (1997)
116. C S Tredget, S C Lawrence, B D Ward, R G Howe, A R Cowley, P Mountford *Organometallics* **24** 3136 (2005)
117. M D Fryzuk, G Giesbrecht, S J Rettig *Organometallics* **15** 3329 (1996)
118. C J Schaverien *Organometallics* **11** 3476 (1992)
119. S Hajela, W P Schaefer, J E Bercaw *J. Organomet. Chem.* **532** 45 (1997)
120. P G Hayes, W E Piers, R McDonald *J. Am. Chem. Soc.* **124** 2132 (2002)
121. P G Hayes, W E Piers, M Parvez *J. Am. Chem. Soc.* **125** 5622 (2003)
122. P G Hayes, W E Piers, M Parvez *Organometallics* **24** 1173 (2005)
123. M Ephritikhine *Chem. Rev.* **97** 2193 (1997)
124. L Maron, E L Werkema, L Perrin, O Eisenstein, R A Andersen *J. Am. Chem. Soc.* **127** 279 (2005)
125. G Jeske, H Lauke, H Mauermann, P N Swebston, H Schumann, T J Marks *J. Am. Chem. Soc.* **107** 8091 (1985)
126. G Jeske, L E Schock, P N Swebston, H Schumann, T J Marks *J. Am. Chem. Soc.* **107** 8103 (1985)
127. A Z Voskoboinikov, I N Parshina, A K Shestakova, K P Butin, I P Beletskaya, L G Kuzmina, J A K Howard *Organometallics* **16** 4041 (1997)
128. A A Trifonov, E A Fedorova, G K Fukin, M N Bochkarev *Eur. J. Inorg. Chem.* 4396 (2004)
129. Y K Gunko, B M Bulychev, G L Soloveichik, V K Belsky *J. Organomet. Chem.* **424** 289 (1992)
130. G M Ferrence, J Takats *J. Organomet. Chem.* **647** 84 (2002)
131. J Gromada, T Chenal, A Mortreux, F Leising, J-F Carpentier *J. Mol. Catal. A: Chem.* **182** 525 (2002)
132. J Gromada, L le Pichon, A Mortreux, F Leising, J-F Carpentier *J. Organomet. Chem.* **683** 44 (2003)
133. C-X Cai, A Amgoune, C W Lehmann, J-F Carpentier *Chem. Commun.* 330 (2004)
134. H J Heeres, J Nijhof, J H Teuben, R D Rogers *Organometallics* **12** 2609 (1993)
135. A D Horton *J. Chem. Soc., Chem. Commun.* 185 (1992)
136. M Nobis, B Driessen-Hölscher *Angew. Chem., Int. Ed.* **40** 3983 (2001)
137. F Pohlki, S Doye *Chem. Soc. Rev.* **32** 104 (2003)
138. F Lauterwasser, P G Hayes, S Bräse, W E Piers, L L Schafer *Organometallics* **23** 2234 (2004)
139. T I Gountchev, T Don Tilley *Organometallics* **18** 5661 (1999)

Synthesis of polymers with protogenic groups by polymer-analogous transformations

A L Rusanov, E A Solodova, E G Bulycheva, M Abadie, V Voitekunas

Contents

I. Introduction	1071
II. Transformations of metallated polymers	1071
III. Transformations of polymers without preliminary metallation	1077

Abstract. The progress in the synthesis of polymers containing sulfonic and phosphonic acid groups by polymer-analogous transformations is analysed. Two key methods for the introduction of these groups are considered, namely, metallation of the original polymers followed by functionalisation and modification of reactive fragments of macromolecular chains. Special concern is focused on the properties of polymeric materials obtained. The bibliography includes 71 references.

I. Introduction

Permanently growing interest in fuel cells and their key components, proton-conducting membranes,^{1–10} is the challenge for the search for new methods of the synthesis of polymeric electrolytes containing protogenic (sulfonic and phosphonic acid) groups. Despite significant progress in the creation of proton-conducting membranes based on basic polymer–acid complexes,¹¹ the membranes based on solid polymeric electrolytes in which the protogenic groups are linked to macromolecules by covalent bonds are the most interesting. These systems are usually prepared by functionalisation (for example, sulfonation or phosphorylation) of polymeric compounds or by polymerisation of monomers containing sulfonic and phosphonic acid groups.^{1–10}

Each approach has its advantages and drawbacks. Thus, many aromatic polymers can readily be sulfonated at fragments with the highest electron density. However, sulfonic groups located at these positions can be substituted under the action of H^+ , which decreases hydrolytic stability of sulfonated polymers in highly acidic media. The synthesis of polymers from monomers containing protogenic groups is complicated due to reduced reactivity and labourious procedure for purification of the starting compounds.

A L Rusanov, E A Solodova, E G Bulycheva A N Nesmeyanov Institute of Organoelement Compounds, Russian Academy of Sciences, ul. Vavilova 28, 119991 Moscow, Russian Federation. Fax (7-499) 135 50 85, tel. (7-499) 135 63 72, e-mail: alrus@ineos.ac.ru (A L Rusanov), tel. (7-499) 135 93 17, e-mail: elena-solodova@bk.ru (E A Solodova), bulychev@ineos.ac.ru (E G Bulycheva)
M Abadie, V Voitekunas University of Montpellier 2, Place Eugene Bataillon, 34095 Montpellier, Cedex 5, France. Fax (33-46) 714 93 02, e-mail: abadie@univ-montp2.fr (M Abadie), voytekunas@univ-montp2.fr (V Voitekunas)

Received 26 April 2007

Uspekhi Khimii 76 (11) 1145–1156 (2007); translated by M G Esernitskaya

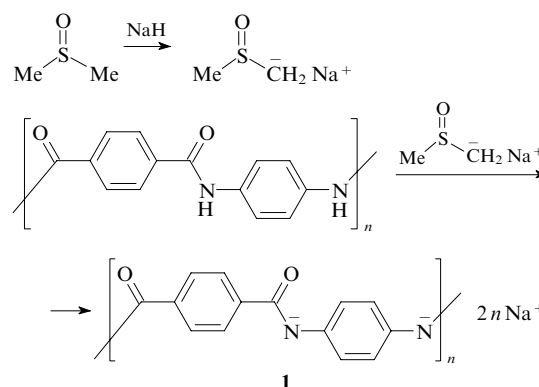
Currently, an alternative approach to the synthesis of polymers containing sulfonic and phosphonic acid groups is being developed, namely, polymer-analogous transformations of compounds containing protogenic groups in an explicit or latent form. In the present review, progress in development of this promising field of polymer chemistry is analysed.

II. Transformations of metallated polymers

Introduction of sulfonic acid groups into macromolecules usually includes preliminary metallation of polymers followed by the treatment of polyanions with compounds containing sulfonic acid groups in an explicit or latent form. Most researchers apply this method for the preparation of sulfonylated polyamides and polybenzimidazoles.

1. Polyamides and polybenzimidazoles containing sulfonic and phosphoric acid groups

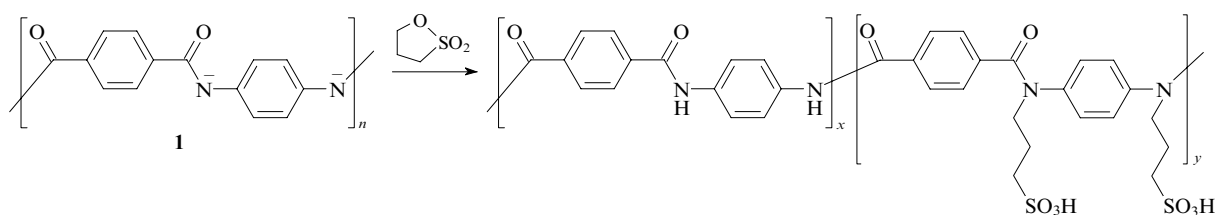
Metallation of aromatic polyamides, primarily poly(*p*-phenyleneterephthalamide) (PPPTA), is discussed by Takayanagi *et al.*^{12–22} and by other researchers.^{23–27} Treatment of PPPTA with sodium hydride in DMSO results in deprotonation of the amide groups of PPPTA to yield polyanion **1**.



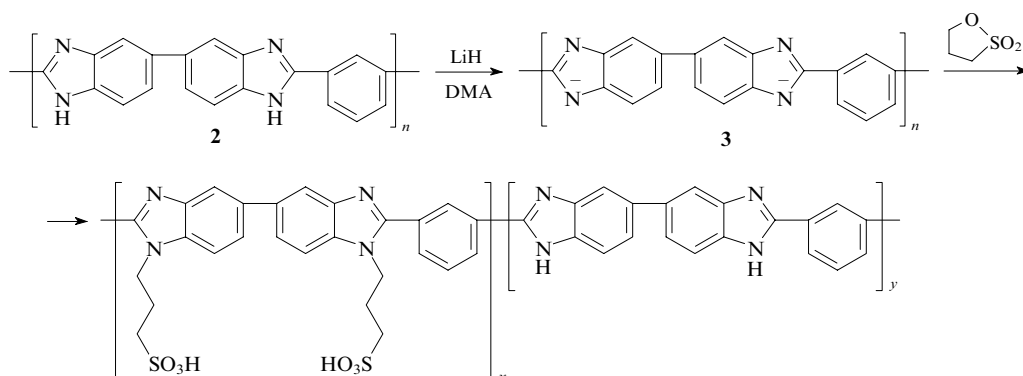
Subsequent reaction of polyanion **1** with propane 1,3-sultone gives a copolymer of *p*-phenyleneterephthalamide and 3-(*p*-phenyleneterephthalamido)propanesulfonic acid (Scheme 1).²⁸

Transformation of poly(2,2'-*m*-phenylene-5,5'-dibenzimidazole) **2** was carried out in a similar way.^{29–36} The corresponding polyanion **3** was prepared by the reaction of the initial polymer with lithium hydride in dimethylacetamide (DMA) (Scheme 2). The final reaction product is polybenz-

Scheme 1



Scheme 2



imidazole (PBI) containing propanesulfonic acid residues (PBI-PS).

Polymers with butanesulfonic acid (PBI-BS) and methylpropanesulfonic acid (PBI-MPS) residues were synthesised from polybenzimidazole and butane 1,4-sultone and butane 2,4-sultone, respectively, using the same procedure.

The degree of substitution (α) of sulfoalkyl groups for the hydrogen atoms at the nitrogen atom in polybenzamide was estimated from the ^1H NMR and elemental analysis data; α appeared to depend on the reactant ratio. For instance, α reaches 60% at a propane-1,3-sultone:PBI ratio equal to 5. PBI modified with these groups are better soluble in polar organic solvents (for example, in DMA or DMSO) than the initial polymers, solubility also depending on the α value.

Introduction of sulfoalkyl substituents into aromatic macromolecules gives heat-resistant proton conducting polymeric electrolytes having electrochemical characteristics that can be controlled by changing the amount of protogenic groups and the length of alkyl chains. These polymers exhibit good moisture absorption and proton conductivity, close to those observed for sulfonic groups, but they retain such important characteristics as heat resistance, chemical stability, and mechanical strength.

Heat resistance of PPPTA and PBI, as well as of their sulfoalkyl derivatives have been compared in a number of publications (see, for example, Ref. 32). It was found that no destruction of PPPTA occurs in a nitrogen atmosphere up to 550 °C, whereas fast mass loss (up to 50% of the initial mass) starts at 600 °C. Polymers modified with sulfopropyl side groups ($\alpha = 66\%$) are stable to 400 °C; at 800 °C 40% of the initial mass is retained.

Heat resistance of anhydrous copolymer PBI-PS was studied by thermogravimetric analysis (TGA) in a nitrogen atmosphere.⁵ Destruction of PBI-PS occurred in the temperature range of 400–450 °C, that is, at significantly lower temperatures than that of the initial PBI.

In spite of the fact that for copolymer PBI-PS, destruction temperature decreases to 400 °C with increasing α , it is nevertheless higher than destruction temperature for perfluorinated polymeric electrolytes (280 °C).

Elemental analysis and FTIR studies of destruction of copolymer PBI-PS showed that the sulfur content and the

intensity of the S–O absorption band decrease following heating of the samples at the temperature above 400 °C for 1 h. This result is similar to that obtained by Gieselmann and Reynolds,³² who have found that destruction of PBI-PS was connected with desulfonation processes. Destruction temperatures for sulfonated aromatic polymeric electrolytes lie within the range of 200–350 °C. Thus, polybenzimidazoles containing sulfoalkyl groups are more heat resistant. Heat resistance of sulfoalkyl polymers is the result of strong chemical bond between alkyl and sulfonic acid groups. Introduction of sulfoalkyl groups into the polymer with the use of alkane sultones is one of the most common methods for the synthesis of heat-resistant proton-conducting polymeric electrolytes.

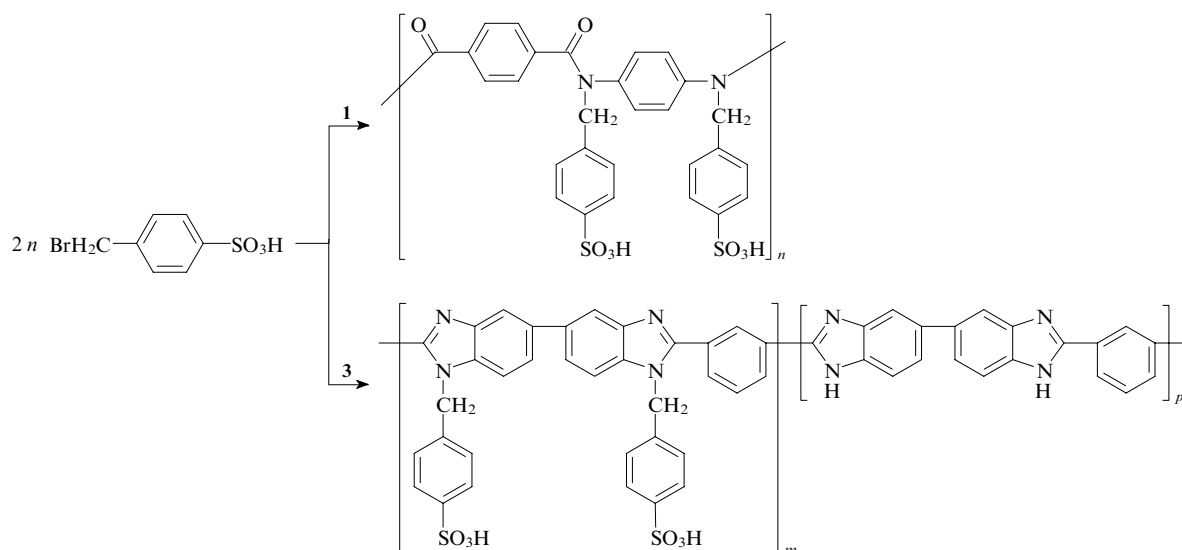
Arenesulfonic acid fragments can also be introduced into aromatic condensation polymers. Thus polyanions **1** and **3** prepared from PPPTA and poly(2,2'-*m*-phenylene-5,5'-dibenzimidazole), respectively, readily react with *p*-bromomethylbenzenesulfonic acid (Scheme 3).^{28–36}

The peripheral sulfoalkyl substituent is detached from the polymeric chain under more drastic conditions than the sulfopropyl group, this being independent of the polymer type.

The above-considered polymers were studied by TGA in inert and oxidative (in the presence of oxygen) environments.³³ The initial PBI is a heat-resistant polymer: in an inert atmosphere, the mass loss begins at 650 °C, 5% mass loss is observed at 700 °C and at 800 °C, > 80% of the initial mass is retained. Mass loss for substituted polymers in an inert environment starts at lower temperatures, as could be expected upon introduction of substituents non-conjugated with the polymer backbones. Destruction of poly(2,2'-*m*-phenylene-1,1'-(4-sulfoalkyl)-5,5'-dibenzimidazole) with $\alpha = 22\%$ starts at 480 °C, while that with $\alpha = 54\%$ starts at 450 °C. After elimination of all substituents from the polymer, the process slows down; at 800 °C, 50%–60% of the initial mass is retained.

In dry air, the mass loss of polybenzimidazole starts at 520 °C, whereas its destruction in an inert environment starts at a temperature about 100 °C lower. Substituted PBI demonstrate insignificant difference in destruction temperatures in oxidative environments. The main difference in the behaviour of polymers in air and in a nitrogen atmosphere is that in air the mass losses are markedly higher, but the amount of the residual

Scheme 3



coke at high temperatures is much less. This effect originates first from the lower stability of PBI in dry air and only then from the influence of substituents.

Introduction of sulfoaryl and sulfoalkyl groups into aromatic polymers increases moisture absorption, in other words, polymers become more hygroscopic. Moisture absorption of polymers is defined as a change in the polymer mass prior and after hydration and depends on the relative humidity of the medium. Equilibrium moisture absorption for the copolymer PBI-PS increases with an increase in relative air humidity and degree of sulfoalkylation. For example, moisture absorption of PBI-PS with $\alpha = 73.1\%$ is $11.3 \text{ mol H}_2\text{O (g-mol SO}_3\text{H)}^{-1}$ (see[†]) at a relative humidity of 90% and room temperature, whereas polymeric membrane Nafion 117 (perfluorinated polymer containing a small amount of sulfonate groups) has a moisture absorption of $11.0 \text{ mol H}_2\text{O (g-mol SO}_3\text{H)}^{-1}$ under the same conditions. Moisture absorption values for copolymers PBI-BS and PBI-MPS at a relative air humidity of 90% are 19.5 and $27.5 \text{ mol H}_2\text{O (g-mol SO}_3\text{H)}^{-1}$, respectively. These high dehumidification values for sulfoalkylated PBI result from a larger length and branching of alkyl chains. This seems to be associated with larger flexibility of long alkyl chains and larger water amount capable of being absorbed in cavities formed by branched substituents.

Studies of proton conductivity of polymers under consideration show that hydrated copolymers PBI-PS demonstrate high proton conductivity at room temperature. Conductivity of PBI-PS containing $3.1 \text{ mol H}_2\text{O (g-mol SO}_3\text{H)}^{-1}$ reaches $10^{-5} \text{ S cm}^{-1}$ at 80°C and somewhat decreases at higher temperatures due to moderate (about 10 mass %) loss of water. Conductivity of the PBI-PS film containing $> 5.2 \text{ mol H}_2\text{O (g-mol SO}_3\text{H)}^{-1}$ increases with increase in temperature and reaches a value of $10^{-3} \text{ S cm}^{-1}$ at temperatures above 100°C . The PBI-PS film containing more water [moisture absorption $11.3 \text{ mol H}_2\text{O (g-mol SO}_3\text{H)}^{-1}$] also demonstrates high proton conductivity ($\sim 10^{-3} \text{ S cm}^{-1}$).

Moisture absorption values for membranes prepared from copolymers PBI-PS at a relative air humidity of 90% are comparable with that for Nafion.

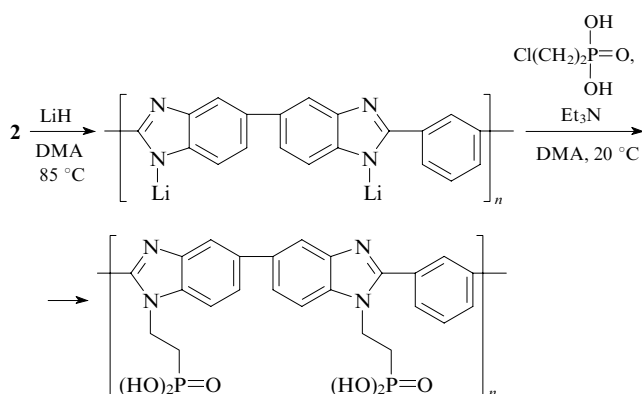
Proton conductivity of the membrane Nafion reaches $10^{-3} \text{ S cm}^{-1}$ at room temperature, but it decreases at temper-

atures $> 100^\circ\text{C}$ due to a loss of absorbed moisture.³⁷ In contrast, high proton conductivity of hydrated PBI-PS is retained at temperatures above 100°C . High values of moisture absorption and proton conductivity for copolymers PBI-PS at elevated temperatures are associated with peculiar behaviour and physical state of absorbed water.

The above results give reasons to conclude that sulfoalkyl aromatic polymeric electrolytes possess sufficient heat resistance to be used in fuel elements at 80°C , that is, at the temperature that is optimal for the work of membranes based on perfluorinated polymeric electrolytes.

Study of proton conductivity of sulfoalkylated PBI at various relative humidity values showed³⁸ that conductivity increases with an increase in degree of substitution. Sulfoalkylated polybenzimidazole with $\alpha = 75\%$ demonstrates high conductivity (about $10^{-2} \text{ S cm}^{-1}$) at 40°C and 100% relative humidity.

Phosphoalkylated polymer was obtained by metallation of PBI 2 followed by introduction of the phosphoethyl groups.⁵

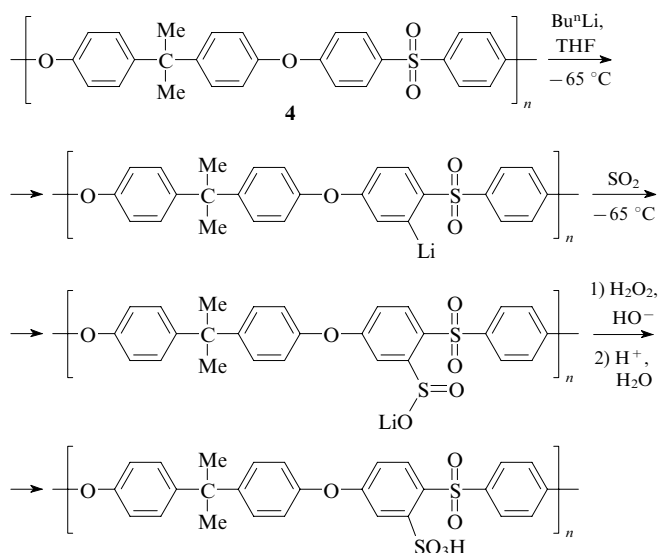


N-Substitution of the benzimidazole ring occurs readily. However, the polymer formed is insoluble in organic solvents, probably, due to self-aggregation of the phosphonate groups in the course of substitution. Phosphoethylated PBI demonstrates high proton conductivity ($10^{-3} \text{ S cm}^{-1}$) even in the form of a pellet. Thus, it can be stated that introduction of polar phosphonic acid groups is an efficient method for the preparation of novel proton-conducting polymeric electrolytes.

[†] Hereinafter moisture absorption is expressed as moles of H_2O per 1 g-mol of SO_3H .

2. Poly(ether sulfones) containing sulfonic and phosphoric acid groups

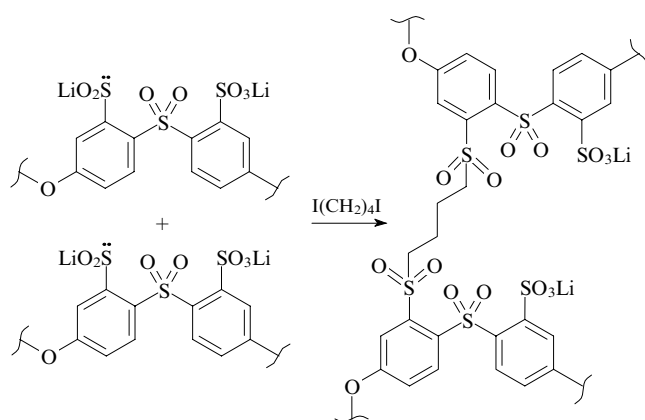
Metallation of polymers was also used for the introduction of protogenic groups into poly(ether sulfone)s (PES).^{39–41} Synthesis of sulfonated PES based on commercially produced poly(ether sulfone) Udel (**4**) was reported.³⁹ The process includes lithiation of the polymer, treatment of the product with sulfur dioxide, oxidation of lithium sulfinates formed to lithium sulfonate, and transformation of the latter into corresponding polysulfonic acid under the action of HCl.



This approach allows the introduction of sulfonic acid groups into positions that determine high hydrolytic stability of the target polymers.³⁹

Sulfonated PES prepared in this way exhibit ion exchange capacity of $(0.5–3.2) \times 10^{-3}$ g-mol SO_3H per 1 g of polymer. Membranes based on these polymers are characterised by high conductivity and hydrolytic stability in 1 N HCl and in water at temperatures up to $80^\circ C$.

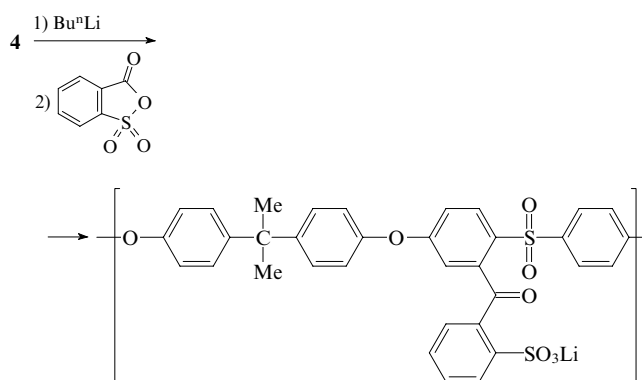
In continuation of this study, partial oxidation of lithium sulfinates groups of PES formed to lithium sulfonate groups was carried out,⁴⁰ and the residual lithium sulfinates groups were alkylated with α,ω -diiodoalkanes. This alkylation gave cross-linked polymers, which were transformed into the acidic form by the action of 1 N HCl.



Membranes from polymers obtained in this way with optimum degree of cross-linking and the length of alkylene cross-linking bridges demonstrate low ionic resistance and high heat resistance.

Lithiation of PES is also used for the preparation of sulfophenylated systems.⁴¹ In this case, a metallated polymer

reacts with cyclic anhydride of 2-sulfobenzoic acid, which followed by ion exchange under the action of 0.5 N HCl.

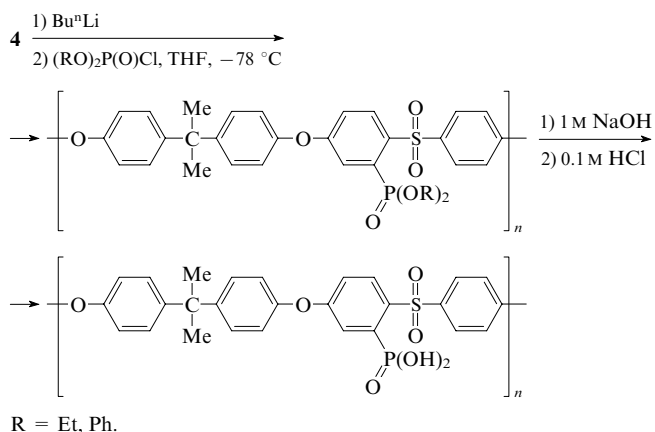


The values of proton conductivity for these polymeric membranes determined by impedance spectroscopy at $60^\circ C$ are $(14–32) \times 10^{-3}$ S cm^{-1} , which, in principle, demonstrates a possibility to use them as promising proton-conducting materials. For a detailed description of electrochemical characteristics of membranes obtained, see Ref. 42.

PES with short alkyl chains in sulfoalkyl substituents have been synthesised.⁴³ In this case, the polymers containing lithium sulfinates groups reacted with sodium ω -bromoalkane-sulfonates and butane-1,4-sultone (Scheme 4).

Thermogravimetric analysis of PES-based membranes containing sulfoethyl, -propyl, and -butyl groups showed that these materials are stable up to $300^\circ C$ in a nitrogen atmosphere. Calorimetry studies show that these modified polymers absorb more moisture [moisture absorption values are from 11 to 14 mol H_2O (g-mol SO_3H) $^{-1}$]. The proton conductivity value for membranes containing 0.9 sulfopropyl substituents per elementary unit of poly(ether sulfone) is 77 mS cm^{-1} at $70^\circ C$.

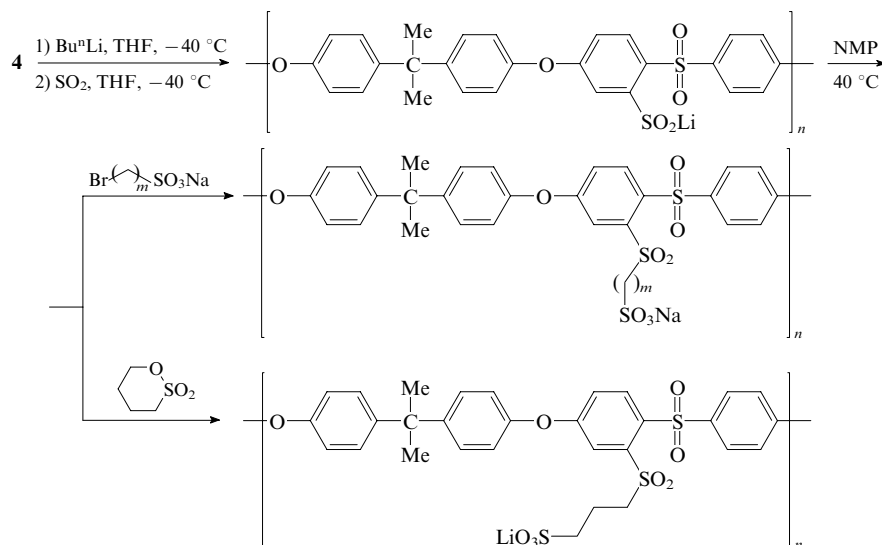
Lithiated PES were used for the preparation of phosphorylated polymers. In particular, the synthesis of poly(ether sulfones) containing phosphonate groups in the *ortho*-positions relative to sulfo groups of the macromolecular backbone is reported⁴⁴ which is based on $S_nP(V)$ nucleophilic substitution.⁴⁵ The reaction of metallated PES **4** with dialkyl and diaryl phosphochloridates occurs without catalysts.



According to Guiver *et al.*,⁴⁶ lithiation and subsequent reaction of polyanions with electrophiles do not lead to destruction of macromolecules of poly(ether sulfones).

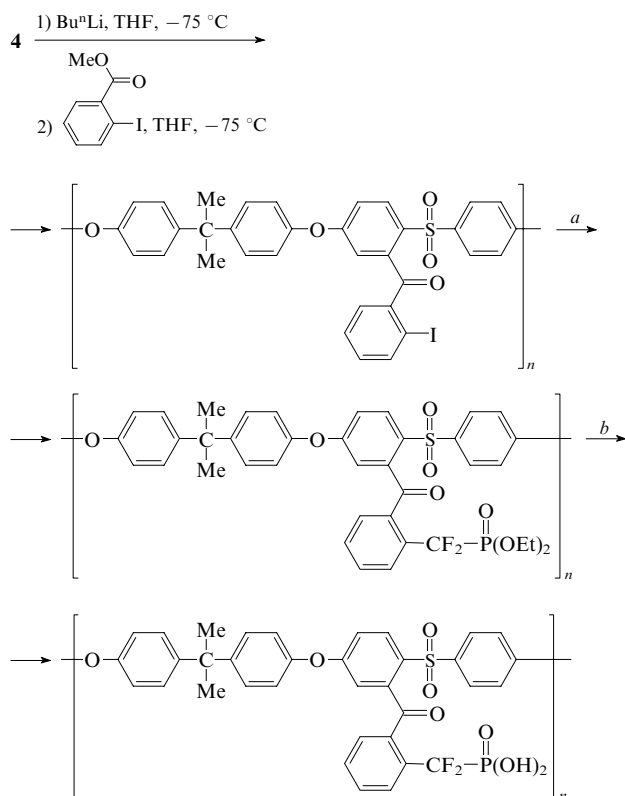
Polymer containing $P(O)(OH)$ groups bound to the benzene ring through a difluoromethylene bridge was prepared by the following route: lithiation of PES **4**, its transformation into iodobenzoyl derivative, phosphorylation of the intermediate

Scheme 4



NMP is *N*-methylpyrrolidone.

under the action of diethyl (bromodifluoromethyl)phosphonate in the presence of zinc and dealkylation of the polymer formed with bromotrimethylsilane.⁴⁷ This polymer exhibits enhanced acidity.

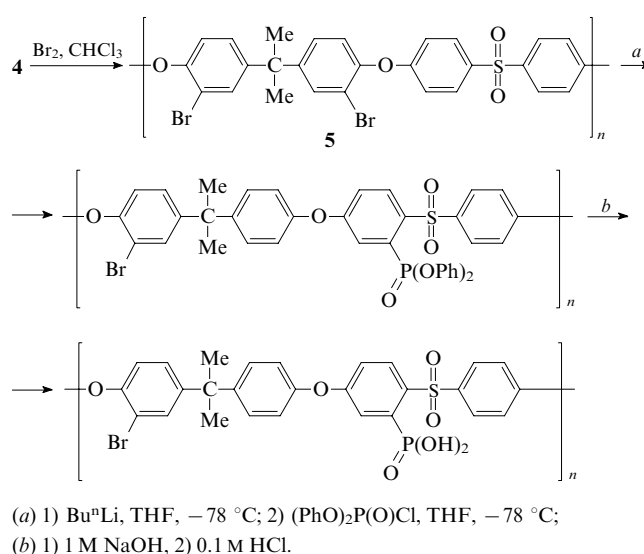


(a) Zn, BrCF₂P(O)(OEt)₂, CuBr, DMF, sonication, 25 °C;
(b) 1) BrSiMe₃, CHCl₃, 40 °C; 2) 5% 1 M HCl in MeOH.

Proton conductivity of membranes based on this polysulfone reached 5 mS cm⁻¹ at 100 °C; according to TGA, destruction started at ~230 °C and was accompanied by the cleavage of the C–P bond.⁴⁷

A more convenient approach to phosphorylated PES is based on lithiation of the brominated polymer **5**,⁴⁸ because substitution of lithium for the halogen atom occurs easier than for the hydrogen atom. The synthesis of phosphorylated PES

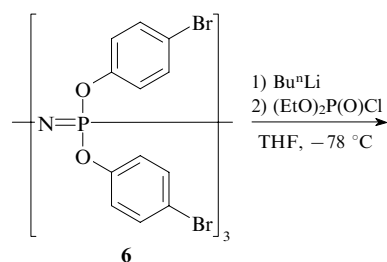
after the stages of bromination and lithiation of the initial polymer **4** includes the reaction of the intermediate with diphenyl phosphochloridate followed by hydrolysis of the phenoxy groups.

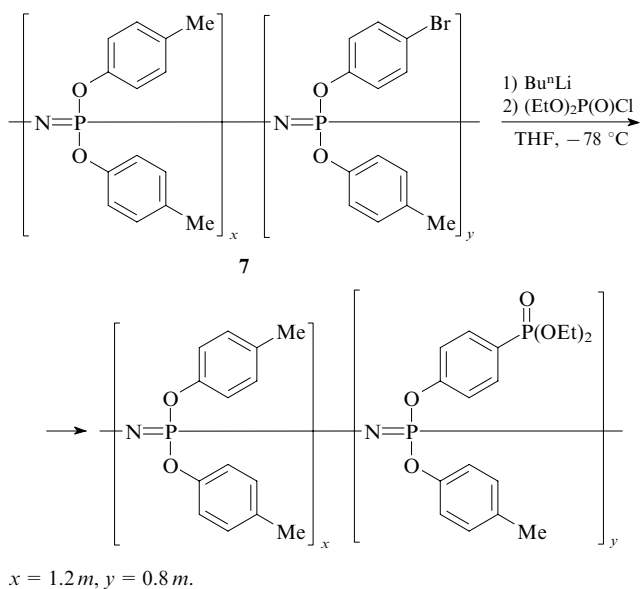
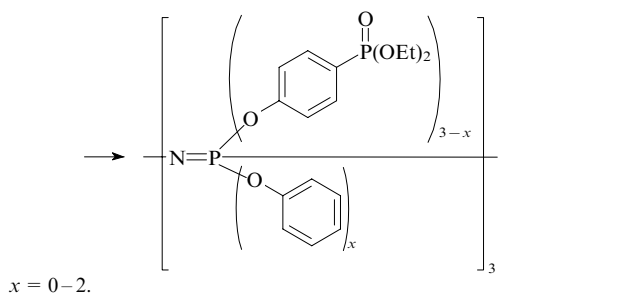


In this case, the degree of phosphorylation reached 50%.

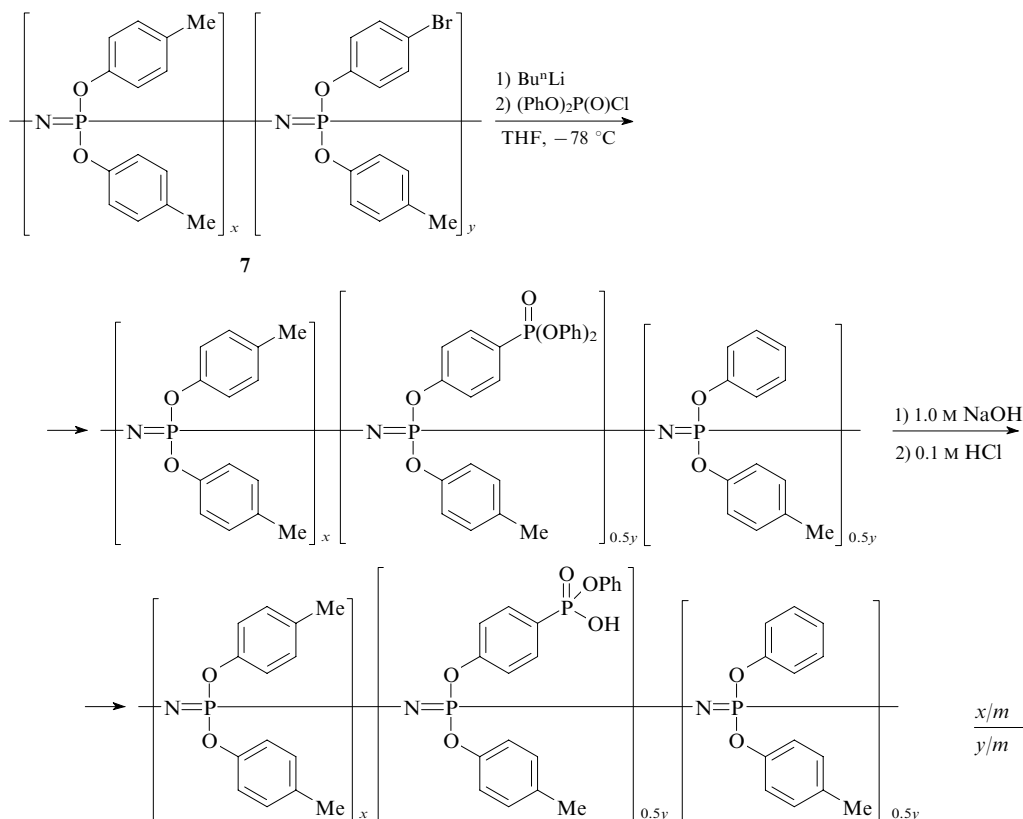
3. Poly(aryloxyposphazenes) with phosphonic acid groups

Cyclic (**6**) and polymeric phosphazenes (**7**) containing *p*-bromophenoxy side groups are used for the synthesis of phosphorylated poly(aryloxyposphazenes). Compounds **6** and **7** were treated with butyllithium and then with diethyl phosphochloridate.^{49, 50}



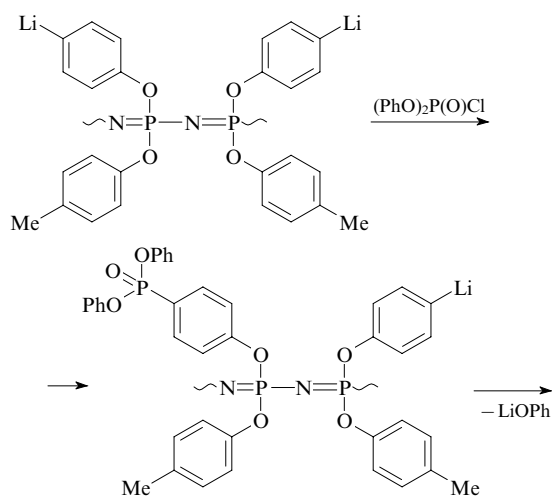


Poly(aryloxyphosphazenes) functionalised by phenylphosphonic acid are formed⁵¹ from the polymers **7** in accordance

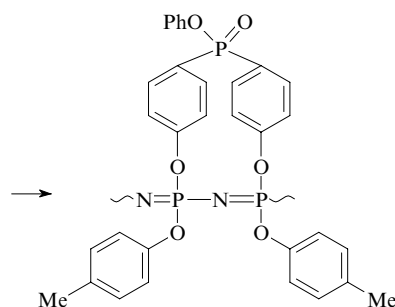


with Scheme 5. *tert*-Butyllithium is added to a solution of poly(aryloxyphosphazenes) **7** with different numbers of brominated benzene rings in THF at -75°C , lithium phenoxide intermediates obtained are treated with diphenyl phosphochloridate. Subsequent alkaline hydrolysis and treatment with an acid give polymers with phenylphosphonate groups.

Attempts to phosphorylate lithiated polymers by gradual addition of diphenyl phosphochloridate to the reaction mixture resulted in precipitation of the polymer and formation of an insoluble product. If the reagent was added quickly, a soluble polymer was obtained. ^{31}P NMR studies showed that in the latter case, intramolecular reaction of diphenyl phosphonate groups with the lithium phenoxide fragments of the same polymeric chains takes place, thus promoting the formation of the phosphorus-containing 'bridge' between two aryloxide side groups.



Scheme 5



Phosphorylation of polymers *via* lithium phenoxide intermediates usually occurs with 50% conversion of bromophenoxy substituents into diphenyl phosphonates. The overall amount of lithium phenoxide intermediates that react with diphenyl phosphochloridate is about 70%; however, only half of the metallated groups is converted into the diphenyl phosphonate groups. According to elemental analysis, more than 90% of the bromine atoms of the initial polymer were lithiated. Thus, it is side reactions of reactive lithium phenoxide intermediates formed upon reaction with diphenyl phosphochloridate that is the limiting factor of the overall transformation rather than incomplete lithiation. These results are in accord with the data obtained for diethyl chlorophosphate.⁵⁰

Hydrolysis of phenyl esters was performed by treatment of a polymer solution in THF with 1.0 N NaOH for 24 h. In the course of the reaction, the polymer precipitates from the solution, after that hydrolysis continues, but to an insignificant extent. No changes in the molecular mass of the polymer were observed, thus proving the known fact that polyphosphazene macromolecules are stable against basic hydrolysis.

The advantage of this method for the synthesis consists of the possibility of varying the polymer composition by changing the ratio of the initial side aryloxy groups, degree of lithiation and the degree of hydrolysis of the ester groups.

The polymers obtained were tested as membranes for fuel elements.^{52,53} These membranes are characterised by a low

coefficient of methanol diffusion. This coefficient for membranes based on phosphorylated polymers appeared to be 12 times smaller than that for membrane Nafion 117 and 6 times smaller than that for membrane made of cross-linked sulfonated polyphosphazenes.^{52,53} Ion-exchange capacity values for membranes from phosphorylated polymers are in the range of $(1.17-1.47) \times 10^{-3}$ equiv g⁻¹, proton conductivity values lie in the range of $10^{-2}-10^{-1}$ S cm⁻¹. Thus, membranes under consideration exceed in some characteristics the analogues based on sulfonated polyphosphazenes.^{52,53}

III. Transformations of polymers without preliminary metallation

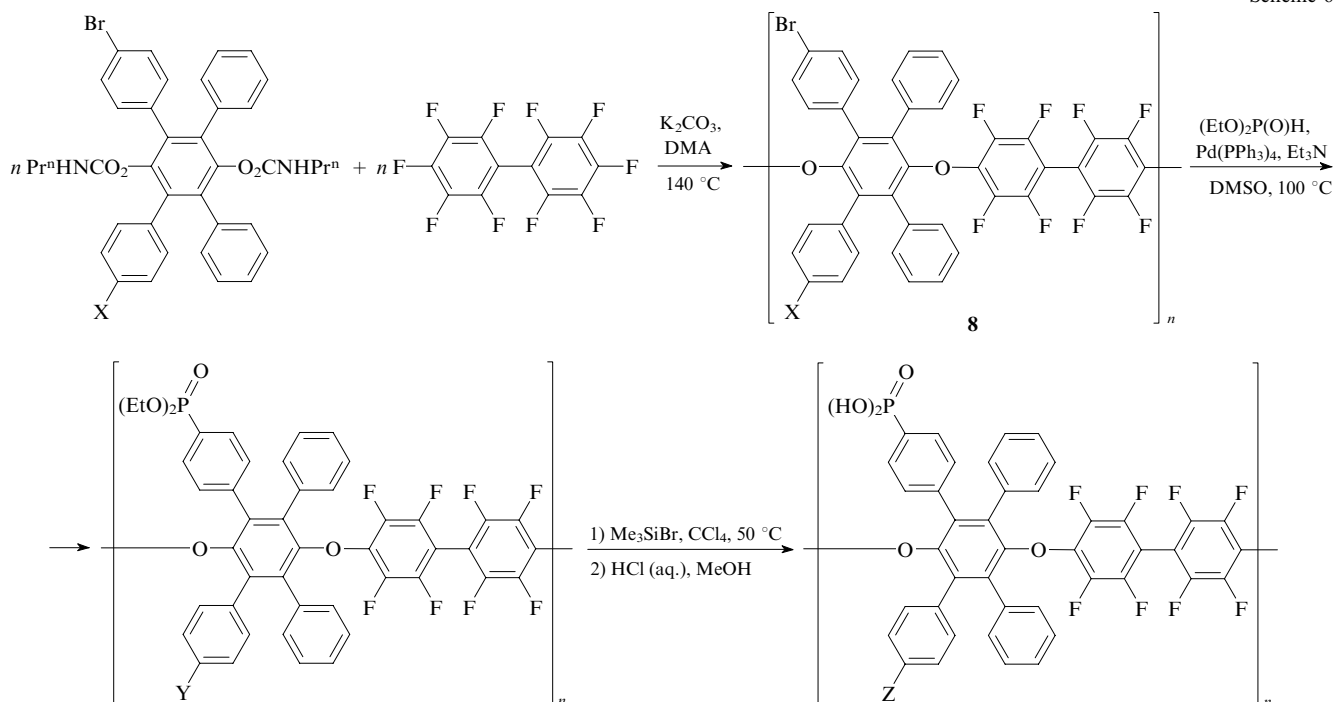
Along with the introduction of protogenic groups into metallated polymers, the method based on transformations of reactive groups of macromolecular chains without preliminary metallation is also widespread.⁵⁴⁻⁶⁴ Bromine and fluorine atoms, NH fragment of the benzimidazole ring, and carboxy groups could be distinguished as reactive groups in polymers.

Bromination⁵⁴ of aromatic polyethers **8** obtained from bis(propylcarbamate) derivatives of mono- and dibromotetra-phenylhydroquinone (Scheme 6) was among the first attempts to use substitution of bromine atoms in polymers for the introduction of phosphonic acid groups.

Treatment of polymers **8** with diethyl phosphite in the presence of triethylamine and tetrakis(triphenylphosphine)-palladium as a catalyst results in polymers containing diethyl phosphonate groups. Dealkylation of the latter is performed with an excess of bromotrimethylsilane in CCl₄. Bis(trimethylsilylated) intermediate is hydrolysed with HCl in methanol. The target polymers are well soluble in DMSO; flexible and strong films were cast from these solutions. Thermal, chemical and hydrophilic properties of the films suggest that they can be used as polymeric electrolyte membranes for fuel elements.⁵⁴

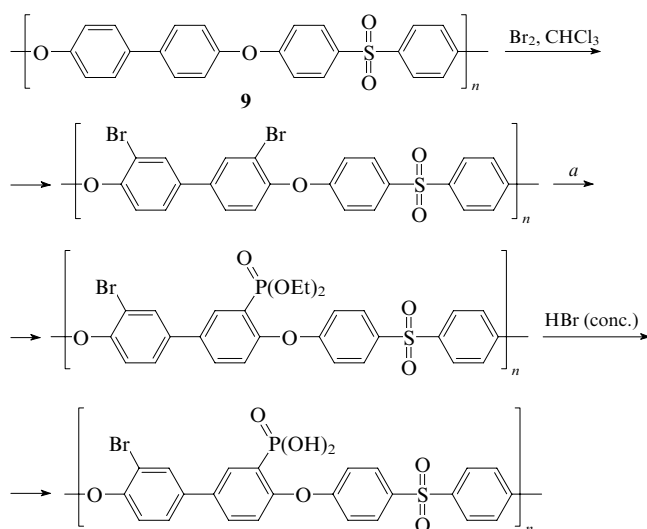
Brominated poly(ether sulfones) can be transformed into phosphorylated polymeric systems using Pd-catalysed formation of the P-C bond. Bromination of PES **9** followed by

Scheme 6



X = Y = Z = H; X = Br, Y = (EtO)₂P(O), Z = P(O)(OH)₂.

phosphorylation of the bromine-containing product is described.⁵⁵

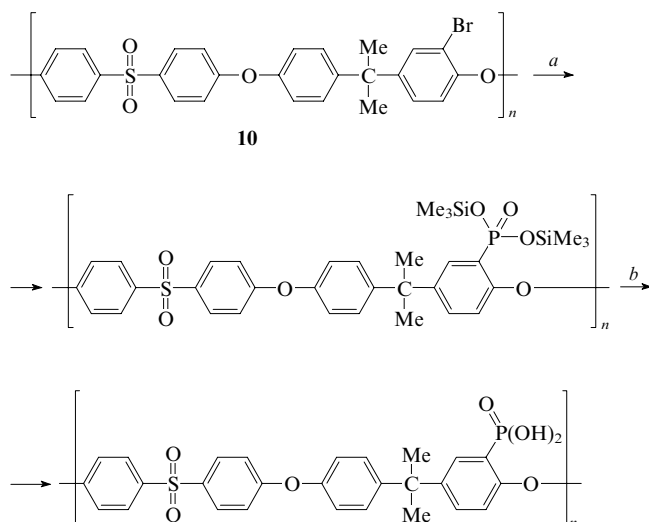


(a) $(\text{EtO})_2\text{P}(\text{O})\text{H}$, Et_3N , $\text{Pd}(\text{Ph}_3\text{P})_4$ or $\text{Pd}(\text{dba})_2$.

Complexes of $\text{Pd}(0)$ with triphenylphosphine and dibenzylideneacetone (dba) were used as catalysts for phosphorylation. Triethylamine was added to the reaction mixture to bind the evolving HBr . It is known^{56, 57} that the molar ratio of the components and the reaction temperature markedly influence the yield, therefore, the effect of all these parameters on phosphorylation of polymers was comprehensively studied.

In particular, it was shown that an increase in temperature from 90 to 120 °C results in an increase in degree of phosphorylation, whereas further temperature increase to 140 °C causes destruction of the polymer. The Pd catalyst was found to be more active in the absence of triphenylphosphine ligands. The highest degree of phosphorylation ($\alpha = 88\%$) was achieved with diphenyl oxide as a solvent. The optimum aryl bromide : diethyl phosphite : triethylamine ratio was found to be 1 : 22 : 4, which is close to the values reported.⁵⁸

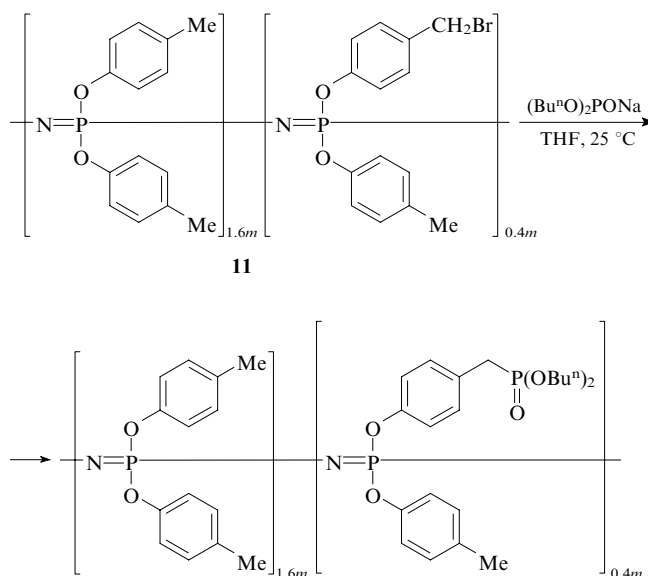
Transformation of brominated PES into phosphorylated PES also occurs in the presence of nickel catalysts. The reaction of brominated PES **10** with tris(trimethylsilyl) phosphite (TMSP) catalysed by NiCl_2 is reported.⁵⁹ Subsequent methanolysis results in removal of the trimethylsilyl groups to give phosphorylated product.



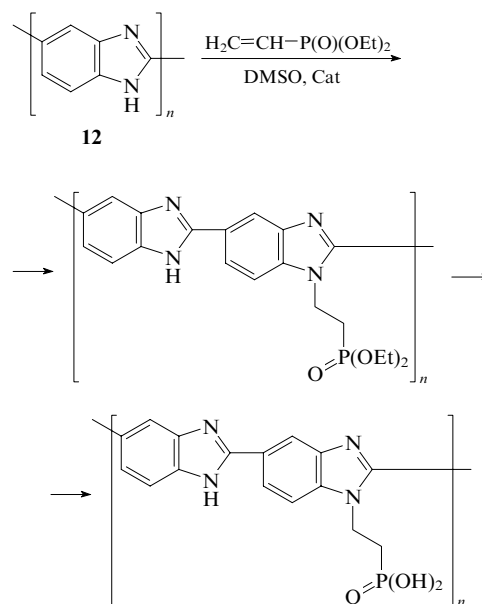
(a) NiCl_2 , TMSP, PhOPh , 200 °C; (b) MeOH .

The polymers obtained are soluble in *N*-methylpyrrolidone as such or in the presence of 2 vol.% – 5 vol.% concentrated HCl . According to TGA, destruction of polymers with arylphosphonic groups starts at temperatures > 325 °C, whereas similar polymer with sulfonic acid groups decomposes at temperatures > 200 °C. Depending on the degree of acidic group substitution, proton conductivity values for PES with arylphosphonate groups at 25 °C are $1.2\text{--}8.7\text{ mS cm}^{-1}$, which is less than proton conductivity of the polymer with sulfonic acid groups (20 mS cm^{-1}).

Polyaryloxyphosphazenes **11** containing bromomethyl groups are phosphorylated under the action of sodium organophosphites, in particular, sodium dibutyl phosphite.⁵⁰ The reaction proceeds in THF at 25 °C and results in the product in a quantitative yield. Studies of the routes for transformation of the ester fragments into phosphonic acid fragments are in progress.

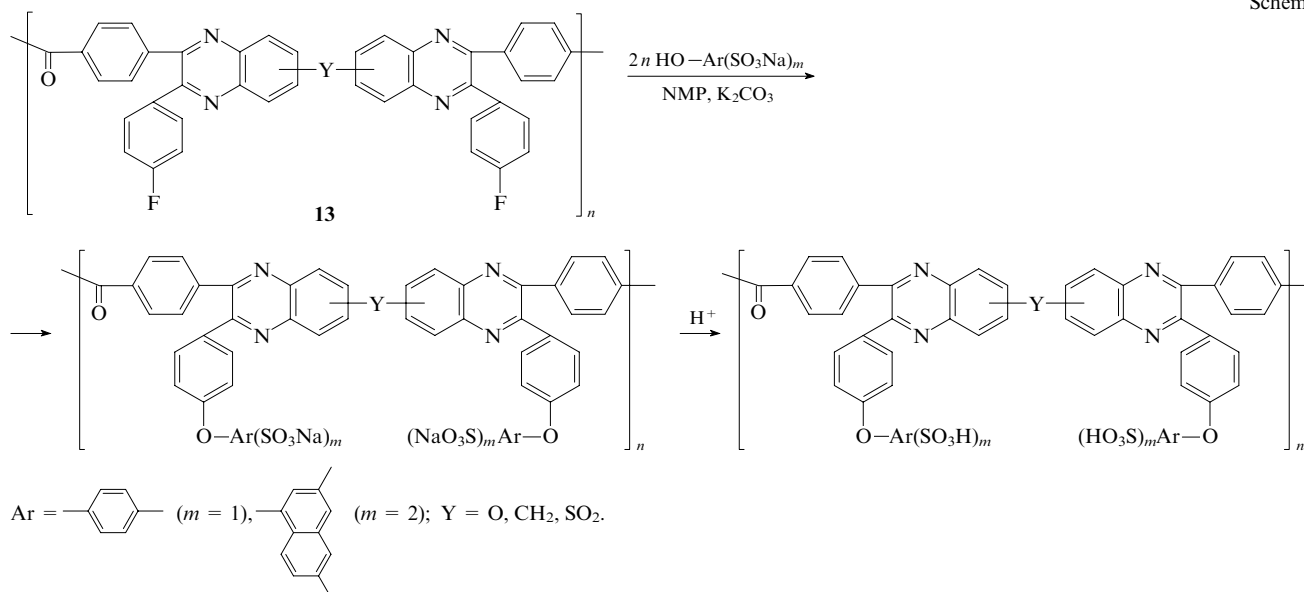


N-Substituted polybenzimidazoles containing the $\text{P}(\text{O})(\text{OH})$ groups bound to the benzimidazole rings through the ethylene bridge were prepared by the reaction of polybenzimidazoles **12** with diethyl vinylphosphonate.⁶⁰



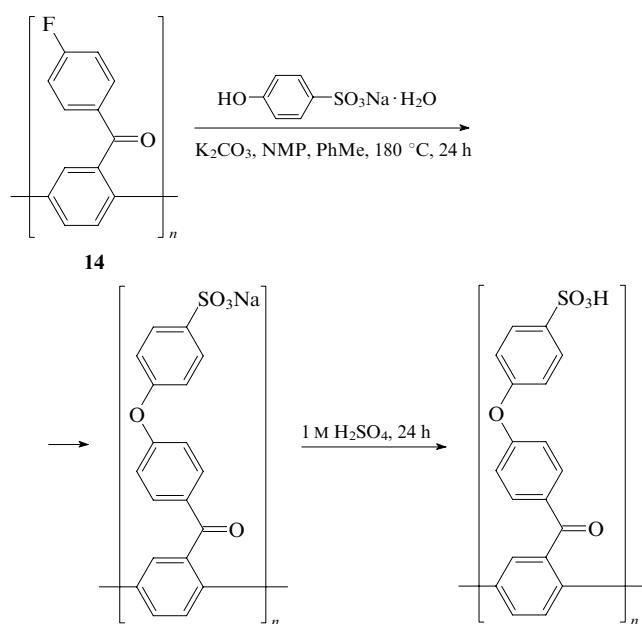
Currently, hetero- and carbocyclic polymers with activated fluorine atoms in aromatic rings have attracted significant

Scheme 7



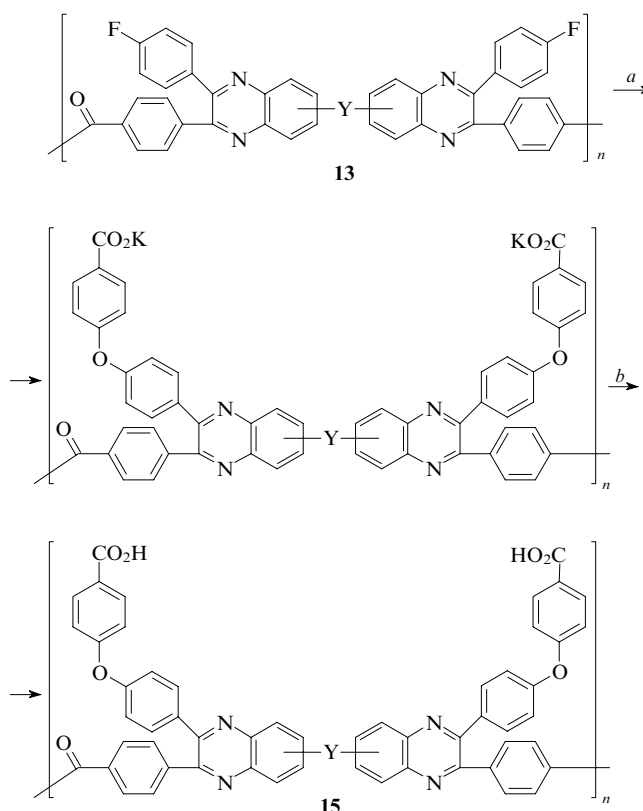
attention. These polymers can undergo aromatic nucleophilic substitution with various nucleophiles, for example, with phenols containing acidic groups.^{59–62} In particular, *p*-fluorophenyl-substituted polyquinoxalines **13** were involved into the reactions with phenol- and naphtholsulfonic acids.^{61–64} The reaction was carried out in NMP in the presence of potassium carbonate (Scheme 7). The polymers obtained in this way are well soluble in *m*-cresol, NMP, and possess film-forming properties.

Similar approach was used by Ghassemi and McGrath,⁶⁴ who performed the reaction of fluorinated polybenzophenone **14** with sodium *p*-phenolsulfonate. According to the ¹⁹F and ¹³C NMR data, about 50% of all fluorine atoms are substituted under these conditions. The authors believe that a relatively low degree of substitution is associated with deactivating effect of the sulfonate group on the phenoxide fragment. Another factor affecting the degree of transformation is partial precipitation of the sulfonated polymer.



Poly[(4-carboxy)phenoxy]phenylquinoxalines **15** were synthesised by the treatment of *p*-fluorophenyl-substituted poly-

quinoxalines **13** by *p*-hydroxybenzoic acid under the conditions of aromatic nucleophilic substitution (NMP, K₂CO₃).⁶³

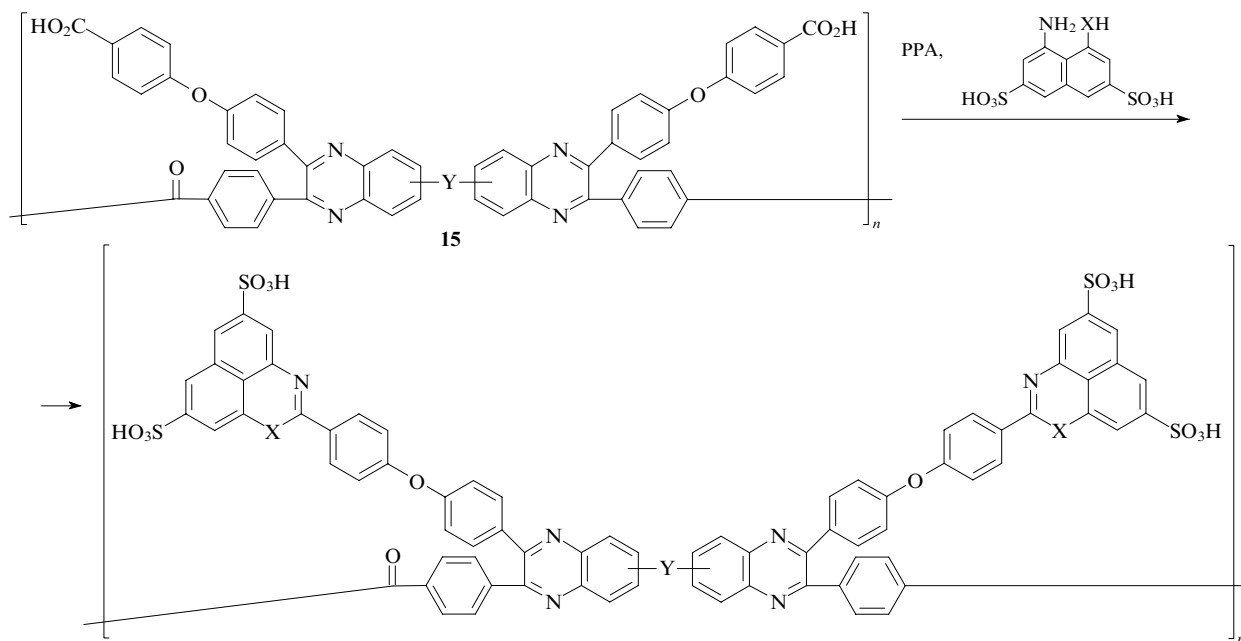


Y is O, CH₂, SO₂ or none;

(a) n HO-C₆H₄-CO₂H, NMP, K₂CO₃; (b) CF₃CO₂H.

Then poly[(4-carboxy)phenoxy]phenylquinoxalines **15** were involved into the reactions with 8-aminonaphth-1-ol-3,6-disulfonic acid and 1,8-diaminonaphthalene-3,6-disulfonic acid (Scheme 8)⁶² in polyphosphoric acid. High-molecular-mass polymers containing naphthoxazine- and pyrimidinedisulfonic acid substituents were formed as products.

Scheme 8



This approach to the creation of polymers with sulfonic acid groups has a general character. Any polymers containing carboxy groups or their derivatives can be involved in the reaction. Moreover, introduction of two sulfonic acid groups into the same aromatic ring of the substituent leads not only to increasing proton conductivity of the membrane, but also to an increase in its heat resistance, because in this case sulfonic acid groups stabilise one another.

* * *

The method for the synthesis of polymers by polymer-analogous transformations, which has been recently developed, is a promising approach to polymers with protogenic, sulfonic and phosphonic acid groups. It is remarkable that this method is especially efficient for the preparation of polymers with phosphonic acid groups, because the latter show higher heat resistance and hydrolytic stability than sulfonic acid groups.⁶⁵ This method allows preparation of polymers containing protogenic groups not only in backbones the of macromolecules, but also in peripheral fragments, which, according to Refs 66–71, favours the increase in the resistance of these polymers against high temperatures, oxidation, and hydrolysis. Stability of polymers is a factor determining potentialities of this method for creation of novel proton-conducting membranes with valuable properties.

The review was written with a financial support of the Russian Foundation for Basic Research (Project No. 05-03-33-181).

References

1. J C Lasseques *Proton Conductors: Solids, Membranes and Gels* (Ed. P Colombon) (Cambridge: Cambridge University Press, 1992) p. 311
2. S Watkins *Fuel Cell Systems* (Eds L G Blumen, M M Mugerwa) (New York: Plenum, 1993) p. 493
3. T A Zawodzinski, C Deraum, S Rodzinski, R J Sherman, U T Smith, T E Springer, S Gottesfeld *J. Electrochem. Soc.* **140** 1041 (1993)
4. O Savadogo *J. New Mater. Electrochem. Syst.* **1** 66 (1998)
5. M Rikukawa, K Sanui *Prog. Polym. Sci.* **25** 1463 (2000)
6. J A Kerres *J. Membr. Sci.* **185** 3 (2001)
7. A L Rusanov, D Yu Likhatchev, K Müllen *Usp. Khim.* **71** 862 (2002) [*Russ. Chem. Rev.* **71** 761 (2002)]
8. A L Rusanov, D Y Likhatchev, P V Kostoglodov, K Müllen, M Klapper, M Schmidt *Inorganic Polymeric Nanocomposites and Membranes (Advances in Polymer Sciences)* (Berlin, Heidelberg: Springer, 2005) Vol. 179, p. 83
9. M A Hickner, H Ghassemi, Y S Kim, B R Einsla, J E McGrath *Chem. Rev.* **104** 4587 (2004)
10. P Jannasch *Curr. Opin. Coll. Interface Sci.* **8** 96 (2003)
11. A Yu Leikin, E G Bulycheva, A L Rusanov, D Yu Likhatchev *Vysokomol. Soedin., Ser. B* **48** 1031 (2006)^a
12. M Takayanagi, T Katayose *J. Polym. Sci., Polym. Chem. Ed.* **19** 1133 (1981)
13. M Takayanagi, T Kagiya, T Katayose *J. Appl. Polym. Sci.* **27** 3903 (1982)
14. M Takayanagi, T Katayose *J. Polym. Sci., Polym. Chem. Ed.* **21** 31 (1983)
15. M Takayanagi *Pure Appl. Chem.* **55** 819 (1983)
16. M Takayanagi, T Katayose *J. Appl. Polym. Sci.* **29** 141 (1984)
17. M Takayanagi, K Goto *J. Appl. Polym. Sci.* **29** 2057 (1984)
18. M Takayanagi, K Goto *J. Appl. Polym. Sci.* **29** 2547 (1984)
19. M Takayanagi, K Goto *Polym. Bull. (Berlin)* **13** 35 (1985)
20. M Takayanagi, S Ueta, W-Y Lei, K Koga *Polym. J.* **19** 467 (1987)
21. K Koga, S Ueta, M Takayanagi *Polym. J.* **20** 639 (1988)
22. M-L Chen, S Ueta, M Takayanagi *Polym. J.* **20** 673 (1988)
23. D R Moore, L J Mathias *J. Appl. Polym. Sci.* **32** 6299 (1986)
24. D R Moore, L J Mathias *Polym. Prepr. (Am. Chem. Soc., Div. Polym. Chem.)* **28** 52 (1982)
25. N Ogata, K Sanui, S Kitayama *J. Polym. Sci., Polym. Chem. Ed.* **22** 865 (1984)
26. H G Rogers, R A Gaudiana, R A Minns, D M Spero *J. Macromol. Sci., Part A: Pure Appl. Chem.* **23** 905 (1986)
27. R R Burch, W Sweeny, H-W Schmidt, Y H Kim *Macromolecules* **23** 1065 (1990)
28. M B Gieselman, J R Reynolds *Macromolecules* **23** 3118 (1990)
29. M J Sansone, B Gupta, R W Stackman US P 4814399 (1987)
30. T D Dong, F E Arnold *Polym. Prepr. (Am. Chem. Soc., Div. Polym. Chem.)* **33** 912 (1992)
31. M B Gieselman, J R Reynolds *Macromolecules* **25** 4832 (1992)
32. M B Gieselman, J R Reynolds *Macromolecules* **26** 5633 (1993)

33. X Clipa, M El Haddad, D J Jones, J Roziere *Solid State Ionics* **97** 323 (1997)
34. K Tsuruhara, K Hara, M Kawahara, M Rikukawa, K Sanui, N Ogata *Electrochim. Acta* **45** 1223 (2000)
35. M Kawahara, M Rikukawa, K Sanui *Polym. Adv. Technol.* **11** 544 (2000)
36. M Kawahara, M Rikukawa, K Sanui, N Ogata *Proceedings of the 6th International Symposium on Polymer Electrolytes. (Extended Abstracts of Papers)*, Montreal, 1998 p. 98
37. H Yoshida, T Hatakeyama, H Hatakeyama *Polymer* **31** 693 (1990)
38. M Folk *Can. J. Chem.* **58** 1495 (1980)
39. J Kerres, W Cui, S Reichle *J. Polym. Sci., Part A: Polym. Chem.* **34** 2421 (1996)
40. J Kerres, W Zhang, W Cui *J. Polym. Sci., Part A: Polym. Chem.* **36** 1441 (1998)
41. B Lafitte, L E Karlsson, P Jannasch *Macromol. Rapid Commun.* **23** 896 (2002)
42. L E Karlsson, P Jannasch *Electrochim. Acta* **50** 1939 (2003)
43. L E Karlsson, P Jannasch *J. Membr. Sci.* **230** 61 (2004)
44. B Lafitte, P Jannasch *J. Polym. Sci., Part A: Polym. Chem.* **43** 273 (2005)
45. F Eymery, B Jorga, P Savignac *Tetrahedron* **55** 13109 (1999)
46. M D Guiver, G P Robertson, M Yoshikawa, C M Tom *ACS Symp. Ser.* **744** 137 (2000)
47. B Lafitte, P Jannasch *J. Polym. Sci., Part A: Polym. Chem.* **45** 269 (2007)
48. M D Guiver, O Kutowy, J W ApSimon *Polymer* **30** 1137 (1989)
49. H R Allcock, J P Taylor *Polym. Eng. Sci.* **40** 1177 (2000)
50. H R Allcock, M A Hofmann, R M Wood *Macromolecules* **34** 6915 (2001)
51. H R Allcock, M A Hofmann, C M Ambler, R V Morford *Macromolecules* **35** 3484 (2002)
52. M U Fedkin, X Y Zhou, M A Hofmann, E Chalkova, J A Weston, H R Allcock, S N Lvov *Mater. Lett.* **52** 192 (2002)
53. H C Yang *Nengyuan Jikan* **33** 127 (2003)
54. K Miyatake, A S Hay *J. Polym. Sci., Part A: Polym. Chem.* **39** 3770 (2001)
55. K Jacoby, K V Peinemann, S P Nunes *Macromol. Chem. Phys.* **204** 61 (2003)
56. J Park, J H Lee *Bull. Korean Chem. Soc.* **18** 1130 (1997)
57. F Skoda-Foldes, L Kollar, J Horvach, Z Tuba *Steroids* **60** 791 (1995)
58. T Hirao, S Kohno, Y Ohshiro, T Agawa *Bull. Chem. Soc. Jpn.* **56** 1881 (1983)
59. T Bock, R Mülhaupt, H Möhwald *Macromol. Rapid Commun.* **27** 2065 (2006)
60. Yu Yu Rybkin, Candidate Thesis in Chemical Sciences, Institute of Organoelement Compounds, Russian Academy of Sciences, Moscow, 2005
61. A L Rusanov, N M Belomoina, N A Yanul, D Y Likhatchev *Advances in Materials for Proton Exchange Membrane Fuel Cell Systems (Preprints of Conference)*, Asilomar, CA, 2003 Pr. 15
62. A L Rusanov, E G Bulycheva, D Y Likhatchev, A Y Leikin *Proceedings of the 7th European Technical Symposium on Polyimides and Other High Performance Functional Polymers (STEPI-7)*, Montpellier, France, 2005 p. 113
63. A L Rusanov, M L Keshtov, N M Belomoina, D Y Likhatchev *High Perform. Polym.* **17** 449 (2005)
64. M Ghassemi, J E McGrath *Polymer* **45** 5847 (2004)
65. B Lafitte, P Jannasch *Advances in Fuel Cells* (Eds T Zhao, K-D Krener) (Amsterdam: Elsevier, 2007) Vol. 1, Ch. 3
66. K Miyatake, K Oyaizu, E Tsuchida, A S Hay *Macromolecules* **34** 2065 (2001)
67. K Miyatake, A S Hay *J. Polym. Sci., Part A: Polym. Chem.* **39** 3211 (2001)
68. B Liu, G P Robertson, D-S Kim, M D Guiver, W Ho, Z Jiang *Macromolecules* **40** 1934 (2007)
69. Y Yin, O Yamada, Y Suto, T Mishima, K Tanaka, H Kita, K-i Okamoto *J. Polym. Sci., Part A: Polym. Chem.* **43** 1545 (2005)
70. S Chen, Y Yin, K Tanaka, H Kita, K-i Okamoto *Polymer* **47** 2660 (2006)
71. T Yasuda, Y Li, K Miyatake, M Hirai, M Nanusawa, M Watanabe *J. Polym. Sci., Part A: Polym. Chem.* **44** 3995 (2006)
- ^a — *Polym. Sci. (Engl. Transl.)*

Investigation of matrix-isolated species: spectroscopy and molecular modelling

A V Nemukhin, L Yu Khriachtchev, B L Grigorenko, A V Bochenkova, M Räsänen

Contents

I. Introduction	1085
II. Matrix effects in the spectroscopy of SH radicals in krypton matrices	1085
III. Structure and spectra of the HArF molecule in argon matrices	1088
IV. Structure and dynamics of HXeOH in water clusters	1089
V. Conclusion	1090

Abstract. The results of experimental and theoretical approaches to the study of some stable and unstable chemical species in low-temperature noble gas matrices are considered. The characteristic features of matrix effects manifested in the spectra of the SH radicals in krypton matrices are discussed. The structure and the spectra of HArF in argon matrices and the structure and dynamics of the intermolecular complexes HXeOH with water are analysed. The bibliography includes 55 references.

I. Introduction

Cryochemistry is concerned with the structure and properties of substances at low temperatures.¹ Using methods of cryochemistry, it is possible to obtain and stabilise chemically unstable species and compounds; to this end, the species are isolated from one another in inert matrices (most often, in solid noble gases) at temperatures that preclude thermal diffusion. Matrix-isolated chemical species are traditionally studied using various spectroscopic methods.² (The term ‘chemical species’ usually refers to any molecular system: atoms, molecules, ions, radicals or intermolecular complexes.)

In recent years, studies dealing with matrix-isolated species have been carried out in a number of laboratories all over the world. One trend of such studies is the synthesis of chemical compounds of noble gases.^{3–5} One more important trend is the study of photodissociation of small molecules in solid noble gas matrices.⁶ These two trends are closely interrelated,

because, on the one hand, the synthesis of inert gas compounds always includes the step of photolysis and, on the other hand, studies of compounds formed upon insertion of chemical species into a noble gas matrix provide important information concerning the dynamics of a photochemical process.^{7,8}

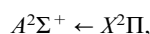
Identification of matrix-isolated species based on their low-temperature vibrational and/or electronic spectra is a challenge. The solution of this problem requires advanced experimental equipment, reliable procedures, experienced researchers and often good fortune. Molecular modelling techniques based on quantum theory form an essential part of these studies.

This review presents several examples of experimental and theoretical studies of stable and unstable chemical species isolated in low-temperature noble gas matrices: SH radicals in krypton matrices, HArF species in argon matrices and intermolecular complexes HXeOH in water clusters. These studies have recently been carried out at the Departments of Chemistry of the M V Lomonosov Moscow State University and the University of Helsinki.

II. Matrix effects in the spectroscopy of SH radicals in krypton matrices

The interest in the photochemistry of SH radicals, close analogues of OH radicals, is due first of all to the topicality of studies of photochemical processes taking place in the atmosphere.⁹ Free OH and SH radicals are investigated most often by spectroscopic methods. The spectra of the SH radical in the gas phase and in the van der Waals clusters SH·Rg (Rg is a noble gas: Ne, Ar, Kr) have been reported.¹⁰ However, spectroscopic studies in condensed media, in particular, in low-temperature noble gas matrices, are required to obtain a more comprehensive picture of the properties of this species. Yet another reason for the interest in matrix-isolated SH radicals is related to noble gas chemistry. For example, upon annealing of a xenon matrix containing SH and H species, the formation of the HXeSH molecule was detected.¹¹

The luminescence spectra of SH corresponding to the transition between the ground ($X^2\Pi$) and the first excited ($A^2\Sigma^+$) states



were recorded in various low-temperature matrices.¹² (In the interpretation of these spectra, differences between OH and SH radicals were taken into account.) However, the spectra

A V Nemukhin, B L Grigorenko, A V Bochenkova Department of Chemistry, M V Lomonosov Moscow State University, Leninskie Gory, 119992 Moscow, Russian Federation. Fax (7-495) 939 02 83, tel. (7-495) 939 10 96, e-mail: anem@lcc.chem.msu.ru, anemukhin@yahoo.com (A V Nemukhin), bella@lcc.chem.msu.ru, bell_grig@yahoo.com (B L Grigorenko), tel. (7-495) 939 48 40, e-mail: anastasia.bochenkova@gmail.com (A V Bochenkova)

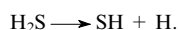
L Yu Khriachtchev, M Räsänen Department of Chemistry, University of Helsinki, A I Virtasen 1, FIN-00014 Helsinki, Finland. Fax (35-89) 191 50279, tel. (35-89) 191 50310, e-mail: leonid.hriachtchev@helsinki.fi (L Yu Khriachtchev), tel. (35-89) 191 50281, e-mail: markku.rasanen@helsinki.fi (M Räsänen)

Received 4 June 2007

Uspekhi Khimii 76 (12) 1163–1170 (2007); translated by Z P Bobkova

recorded in a krypton matrix differed from the spectra recorded in other matrices.¹³ Detailed investigation of the luminescence spectra of SH in krypton led to a conclusion that the specific behaviour of the species isolated in a solid matrix is a result of a change in the electronically excited state of the species caused by the interaction with the matrix Kr atoms.^{14,15} Thus, in this case, we are dealing with the so-called 'matrix effect'.

Figure 1 shows the characteristic luminescence spectrum of SH radicals in solid krypton at 7.5 K.¹³ The SH species were generated by photolysis of H₂S induced by an excimer laser ($\lambda = 193$ nm) mainly according to the reaction



After electronic excitation of the photolysis products, the luminescence spectra were recorded on a Spec 270M spectrophotometer with a resolution of 0.3 nm. A specific feature of the spectra is the presence of two peaks, at 375 (hereinafter referred to as peak *I*) and 413 nm (peak *II*) corresponding to excited states of the molecule with different lifetimes. It was found experimentally that peaks *I* and *II* refer to the transition between the first excited $A^2\Sigma^+$ ($v' = 0$) and the ground $X^2\Pi$ (v'') electronic states of the SH radical. By processing the kinetic data, the lifetimes of the states for both peaks were estimated as 350 (peak *I*) and 750 ns (peak *II*).

On the basis of the results of spectroscopic studies, it was suggested that the presence of two peaks in the SH luminescence spectra in a krypton matrix is due to different trapping sites of this radical by the matrix.¹³ Molecular modelling of the dynamics of the SH radical in solid krypton made it possible to substantiate this statement and identify the trapping sites.

The general strategy of modelling of matrix effects is as follows. A heterogeneous cluster of a specified size representing

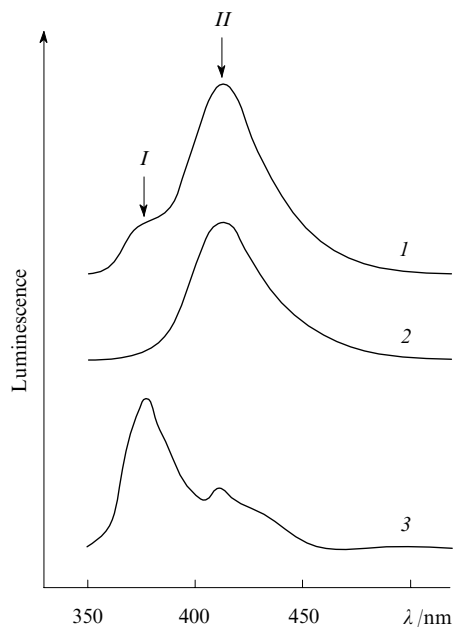


Figure 1. Experimental luminescence spectra of the SH radical in a krypton matrix at short (30 ns, curve 1) and long (1300 ns, 2) delay times and their difference (3). [Curve 3 shows the dependence of the short-lived component *I* on the wavelength; two bands can clearly be seen, which correspond to 0–0 and 0–1 transitions separated by a distance (~ 2500 cm⁻¹) comparable with the SH vibration frequency in the ground electronic state.]

a fragment of the inert gas crystal lattice (face-centred cubic, fcc) with a cavity accommodating the SH species is used as the model. Construction of the potential energy surface (PES) of such heterocluster is a challenge. Combination of *ab initio* and semiempirical quantum chemistry methods is most reasonable. The former are used to describe the structure and dynamics of the embedded molecule, while the latter are used to calculate the interactions of the embedded molecule with the matrix atoms. On the basis of the chosen interaction potentials, characteristics of this heterocluster system are calculated, and the results of calculations serve as the basis for interpretation of experimental data.

The behaviour of the SH radical in krypton matrices has been simulated.¹⁴ The potential energy surfaces of the heteroclusters SH@Kr_{*n*} ($n \leq 56$) correlated with either ground [SH($X^2\Pi$) + *n* Kr] or excited [SH($A^2\Sigma^+$) + *n* Kr] states of the system were constructed by combining an *ab initio* quantum chemical method to describe the SH species and the semiempirical method using diatomic fragments in molecules (diatomics-in-molecules, DIM) for SH interaction potentials ($X^2\Pi$ or $A^2\Sigma^+$) with the Kr atoms¹⁶ and Kr...Kr pair interaction potentials. The DIM method (see, for example, Ref. 17) is, on the one hand, an extension of the pair interaction potentials algorithm and, on the other hand, this is a semiempirical version of the valence bond theory, which allows effective inclusion of energy contributions of diatomic fragments in various electronic states to the total energy of a polyatomic molecular system.

The reliability of the potential energy surfaces of the triatomic complex SH...Kr in the ground and electronically excited states calculated by the DIM method was verified by thorough comparison of these surfaces with empirical approximations¹⁰ of the SH($X^2\Pi$)...Kr and SH($A^2\Sigma^+$)...Kr surfaces derived from high-resolution spectroscopy data of the van der Waals clusters. According to these results,¹⁰ in the ground electronic state the triatomic complex is weakly bound, the energy of its dissociation into SH in the ground state $X^2\Pi$ and a Kr atom in the ¹S state is about 100 cm⁻¹. The equilibrium geometry structure of the complex is linear with a distance (R_e) from the SH centre of mass to the Kr atom equal to 4.28 Å and an S–H bond length of 1.35 Å. The PES of the SH($A^2\Sigma^+$) + Kr(¹S) system in the electronically excited state has two minima separated by a saddle point. The deepest minimum with the energy of 1706 cm⁻¹ corresponds to linear SH...Kr with $R_e = 3.26$ Å and $\theta = 0^\circ$ (θ is the angle formed by the S–H bond and the straight line from the centre of mass of the SH radical to the Kr atom), while the other minimum (with the energy of ~ 1400 cm⁻¹) corresponds to the position of the krypton atom near the SH radical on the side of the sulfur atom (Kr...SH) with $R_e = 2.6$ Å and $\theta = 180^\circ$. The saddle point is characterised by $R_e = 4.02$ Å and $\theta = 64^\circ$. Substantial differences in the interaction energies of the krypton atom with the SH radical occurring in the electronically excited state in different parts of the krypton matrix are responsible for the features of low-temperature spectra of SH, namely, the presence of two peaks in the luminescence spectrum (see Fig. 1). Figure 2 shows the plots for the DIM-calculated potentials of the ground (*a*) and excited (*b*) states of the triatomic complex.

It is noteworthy that representing the interaction potentials of species in the SH@Kr_{*n*} clusters in terms of the DIM approximation calculated for each group of three atoms SHKr_{*i*} ($i = 1, \dots, n$) and the Kr_{*i*} – Kr_{*j*} pair potentials allows one to estimate the energies and forces acting on atoms and use them for calculating the molecular dynamic (MD) trajectories of species.

Firsov *et al.*¹⁵ simulated the spectrum of the SH radical in the krypton matrix corresponding to the electronic transition $A^2\Sigma^+$ ($v' = 0$) \rightarrow $X^2\Pi$ (v'') using a version of mixed quantum

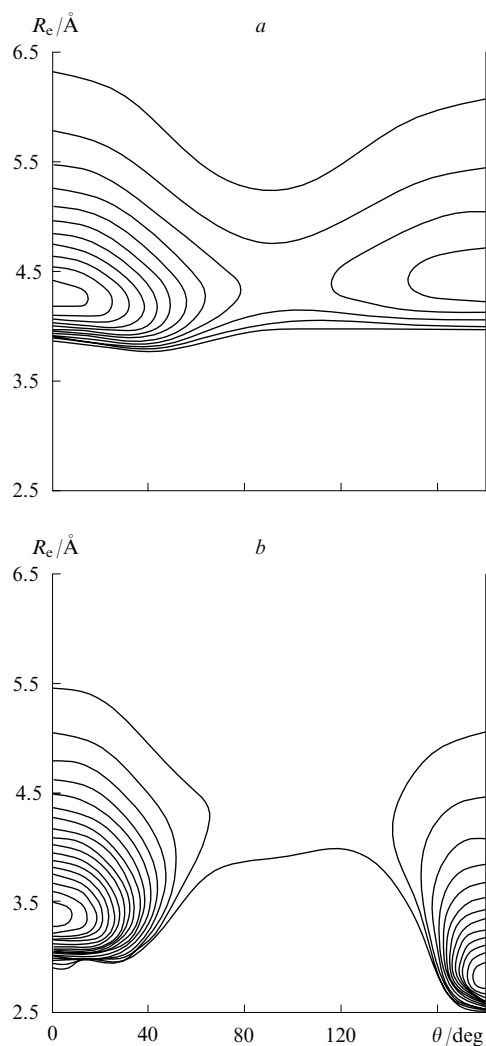


Figure 2. Potential energy surfaces of the ground (*a*) and electronically excited (*b*) states of the triatomic complex SH...Kr. The contour lines for the ground state are drawn every 10 cm^{−1}, those for the excited state are drawn every 100 cm^{−1}.

and classical molecular dynamics.[†] In this approximation, the SH radical with a random orientation of the S–H bond was placed on a random site in the central part of the fcc lattice composed of 256 Kr atoms (the lattice parameter was 5.67 Å). Then the Kr atoms located closely to S or H atom were removed; as the closeness criterion, distances of 2.9 Å on the side of sulfur and of 2.5 Å on the side of hydrogen were used. Then MD trajectories were calculated in two stages. In the first stage, which was 1 ps long, the system temperature was maintained at 7 K by correcting (scaling) the species velocities on the PES of the ground state of the SH(*X*²@)Kr_{*n*} cluster. In the second stage, the calculation was carried out for the PES of the excited state of the SH(*A*²Σ⁺)@Kr_{*n*} cluster with the system energy being maintained constant. The second stage of about 10 ps long was split into 20 000 steps. Every 10 steps (2000 times over the trajectory), the electron transition wavelengths and intensities (the Franck–Condon factors), radial distribution functions and particle lifetimes (τ) were found by the numerical solution of the one-dimensional Schrödinger equa-

tion along the variable corresponding to the S–H distance, and the positions of the Kr atoms located most closely to the S and H atoms were recorded for subsequent averaging. After the calculation, the average spectrum over the trajectory, the average lifetime and the average radial distribution function were estimated and the probability map for the Kr atoms to occur in various positions near the H atom was constructed. The lifetime was estimated from the formula¹⁹ for each discrete vibrational state of the electronically excited state:

$$\tau_{v''}^{-1} = \frac{4}{3c^2} \langle v' | \Delta U^3 D^2 | v' \rangle, \quad (1)$$

where c is the velocity of light, v' is the wave function of the lower vibrational level of the electronically excited state, ΔU is the energy difference between the ground and electronically excited states, D is the transition dipole moment of the SH radical from the ground to excited state. For calculation of the corresponding matrix elements, it was necessary to calculate the dependence of the transition dipole moment between the electronic states on the internuclear distance in SH.

Analysis of the calculated trajectories and spectra led to the conclusion that both peaks observed in the experiments (*I* and *II*, see Fig. 1) refer to two different trapping sites of the SH radical by the krypton cluster. The peak with a lower wavelength (peak *I*) corresponds to the trajectories along which the SH radical freely moves within the krypton cluster. The peak at greater wavelength (peak *II*) refers to the trajectories characterised by the formation of the triatomic complex SH...Kr, *i.e.*, the radical is bound to one atom of the Kr lattice. The calculated lifetimes of SH excited states for both types of trajectories also correlate with experimental characteristics of the luminescence spectra (Table 1).

Table 1. Experimental and theoretical characteristics of peaks in the luminescence spectra of the SH radical in the Kr matrix.

Characteristics	Peak <i>I</i>		Peak <i>II</i>	
	experiment	calculation	experiment	calculation
Peak position/nm	375	340–350	413	390–400
Lifetime/ns	350	550–600	750	800–840
Features of MD trajectories	—	free rotation of SH in Kr	—	complex SH...Kr

A more comprehensive picture of the spatial distribution of Kr atoms around the SH radical is provided by Fig. 3. Different colour intensity shows the configuration space areas corresponding to different positions of the inert gas atom located most closely (this is determined in every integration step) to the hydrogen atom. The maps are constructed in a relative coordinate system in which the H atom is always located in the origin of coordinates and the x -axis is directed along the S→H bond. The results validate the assumption concerning the presence of different trapping sites of the SH molecule by the krypton matrix, which is reflected in the observed experimental spectra.

In addition to providing new information on the spectroscopy of SH radicals, Refs 14 and 15 considerably contributed to the investigations into structure and dynamics of solids doped with small molecules. These studies demonstrate the possibility of observing and interpreting the trapping sites of a molecule occurring in the electronically excited state in a low-temperature krypton matrix. Previously, such effects in cryochemistry have not been reported.

[†] This method was first applied to describe the spectra of the Cl₂ molecule in solid neon.¹⁸

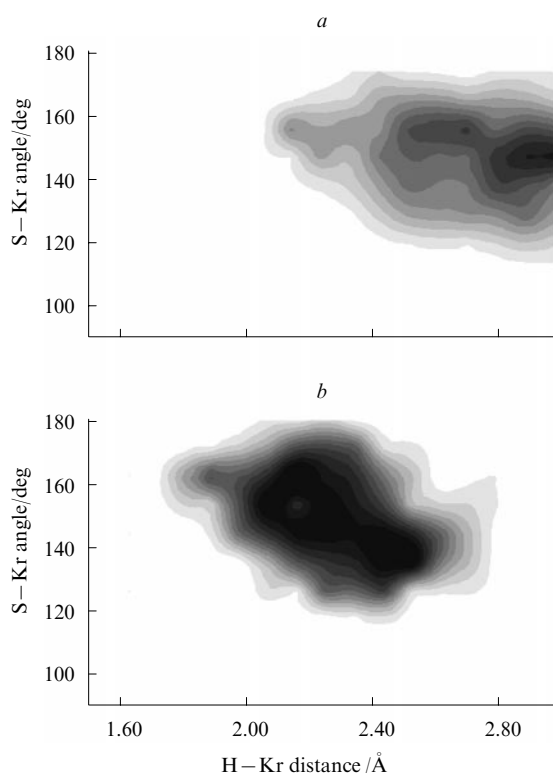
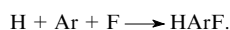


Figure 3. Distribution of the probability density for the occurrence of Kr atoms around the SH radical in the SH@Kr_n clusters; (a) trajectories describing free rotation of SH in the Kr matrix (peak I in the luminescence spectrum of matrix isolated SH radicals); (b) trajectories that tend to give SH · Kr complexes (peak II).

III. Structure and spectra of the HArF molecule in argon matrices

As a continuation of molecular dynamics studies for interstitial compounds in low-temperature noble gas matrices, the trapping sites of the exotic HArF molecule in the ground electronic state by an argon matrix were determined. The HArF species discovered in 2000 is the first electrically neutral chemical compound of argon.^{3–5} It is formed upon photodissociation of HF in solid argon at 7 K followed by matrix annealing at temperatures up to ~20 K:



Initially, the formation of this compound was established by IR spectroscopy.^{3–5} Subsequently, it has been shown¹⁴ that IR spectroscopy provides knowledge also on the molecular structure and dynamics in a doped matrix.

Figure 4 shows the spectra of HArF in solid argon in the region of H–Ar stretching vibrations. Curves 1 and 2 were recorded at different matrix annealing temperatures, 20 and 33 K. The characteristic triplet of the spectral lines (1965.7, 1969.4 and 1972.3 cm^{–1}) is observed only for low annealing temperature and completely disappears at higher temperature. The doublet shifted towards larger wavenumbers (2016.3 and 2020.8 cm^{–1}) predominates, conversely, at higher annealing temperatures up to matrix destruction at 40 K. On the basis of the obtained experimental results, it was hypothesised that the triplet of the spectral lines corresponds to a thermally unstable trapping site of HArF in the argon matrix, while the doublet shifted to the blue spectral region is due to another, more stable (or thermally relaxed) trapping site of the HArF molecule in the solid argon matrix.^{20–22} The use of molecular modelling

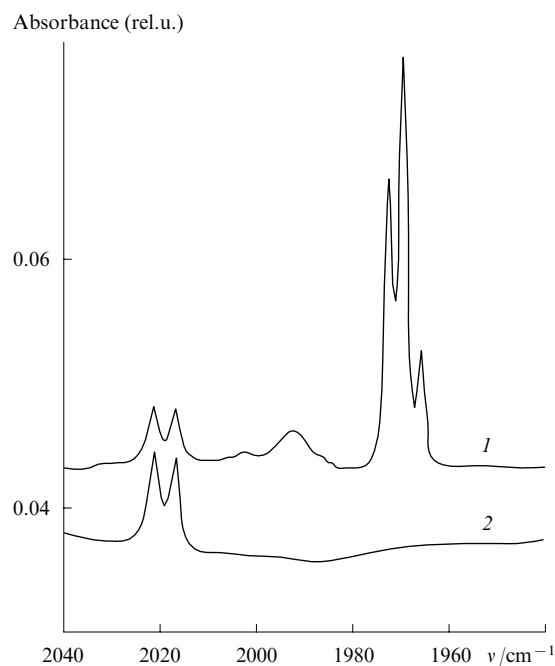


Figure 4. Spectra of the HArF molecule in solid argon recorded at matrix annealing temperatures of 20 (1) and 33 K (2). The measurements were carried out at 7 K.

confirmed this assumption and identified the trapping sites of the guest species.^{23–25}

An original hybrid procedure for calculation of the PES of HArF@Ar_n heteroclusters ($n = 363$ or 364) has been reported.²³ The energy of the embedded molecule (HArF) and its first and second derivatives with respect to nuclear coordinates were calculated by the high-precision *ab initio* method MP2/6-311++G(2d,2p) using PC GAMESS software.²⁶ The interactions of argon atoms with one another were described by pair potentials well parametrised to many properties of this gas.²⁷ The interaction of HArF with each atom of the matrix was calculated in the DIM approximation taking into account contributions of ionic and neutral pair potentials. This calculation algorithm proved to be useful for modelling the properties of the HF@Ar_n clusters.²⁸ This combined procedure, that is, quantum mechanics with diatomics-in-molecules approximation (QM/DIM), was also successfully tested in the simulation of the spectra of gas-phase mixed Ar_n(HCl)_m and Ar_n(HF)_m clusters.²⁹

The calculated PES for the HArF@Ar_n system was used to find the stationary points on the surface and calculate the harmonic vibration frequencies. The atom sites in the fcc lattice of the argon matrix served as the initial coordinates. Figure 5 shows two optimised structures corresponding to the trapping sites of the HArF molecule by solid argon. According to the calculation results, the structure presented in Fig. 5a refers to a thermally unstable trapping site; it is responsible for characteristic spectral bands at 1970 cm^{–1} (see Fig. 4). The structure shown in Fig. 5b was assigned to the stable trapping site characterised by bands at 2120 cm^{–1}.

This assignment was based on the following computation data. First, the H–Ar vibrations in the unstable structure (see Fig. 5a) are responsible for a triplet of harmonic frequencies of 2203, 2204 and 2207 cm^{–1} (depending on the vacancy position in the lattice), and the harmonic frequency of 2246 cm^{–1} assigned to the stable structure (see Fig. 5b) is shifted to the blue region by almost the same distance as in the experimental spectrum. Second, the energy of the unstable structure is

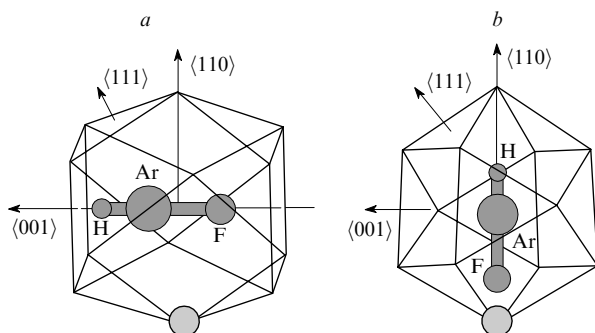


Figure 5. First solvation shells of two possible structures formed upon trapping of the HArF molecule by solid argon. Trapping site: (a) unstable, (b) stable.

4–5 kJ mol^{−1} higher than that of the stable structure and with the possibility of matrix relaxation (*i.e.*, at higher temperature), the structure with lower energy should predominate, which was actually observed in experiments. Thus, the trapping sites of the HArF molecule by solid argon can be considered to be established. However, the thermal relaxation mechanism of the unstable configuration still remains unknown, which requires further theoretical analysis.

IV. Structure and dynamics of HXeOH in water clusters

Matrix cryochemistry methods are widely used at the University of Helsinki to study the properties of chemical compounds containing noble gas atoms.^{3–5} In particular, the HXeOH species formed upon laser irradiation of a low-temperature water–xenon mixture followed by matrix annealing was detected experimentally.^{30–32} The metastable species HXeOH is responsible for a local minimum in the PES of the Xe + H₂O system, whereas the complex Xe · H₂O is the major compound (having the lowest energy). It was suggested that complexes of HXeOH with water molecules may exist. This was of interest, in particular, in relation to the geochemical problem of xenon deficiency.^{33, 34}

Figure 6*a,b* shows the IR spectra of a water molecule in solid xenon near the bending mode of the H₂O molecule. It can be seen that the spectra of the Xe + H₂O system with a low water content (see Fig. 6*a*) vary with an increase in the H₂O concentration (see Fig. 6*b*). After photolysis at 193 nm, which results in decomposition of the water molecule in the xenon matrix, and matrix annealing, which increases the mobility of the active species, the spectra exhibit the bands for HXeOH (at 1578 cm^{−1}) and two additional peaks designated in curve 3 by C₁ and C₂ (see Fig. 6*b*). It was suggested that these peaks correspond to H–Xe vibrations in the complexes HXeOH · H₂O and HXeOH · (H₂O)₂, respectively. Later this hypothesis was confirmed in a theoretical study³⁵ dealing with molecular modelling of the intermolecular complexes of HXeOH with water. Previously, similar complexes of noble gas hydrides with nitrogen have been observed experimentally (for example, HArF · N₂ in Ref. 36) and studied by computational chemistry.³⁷

The first stage of modelling included the use³⁵ of the combined quantum and molecular mechanics (QM/MM) method, specifically, the embedded species (HXeOH) was described by quantum chemistry methods and the surrounding water molecules were described by molecular mechanics in the effective fragment (EF) potential approximation.³⁸ The calculations were carried out using PC GAMESS software.²⁶ The computation showed that water molecules of a specified

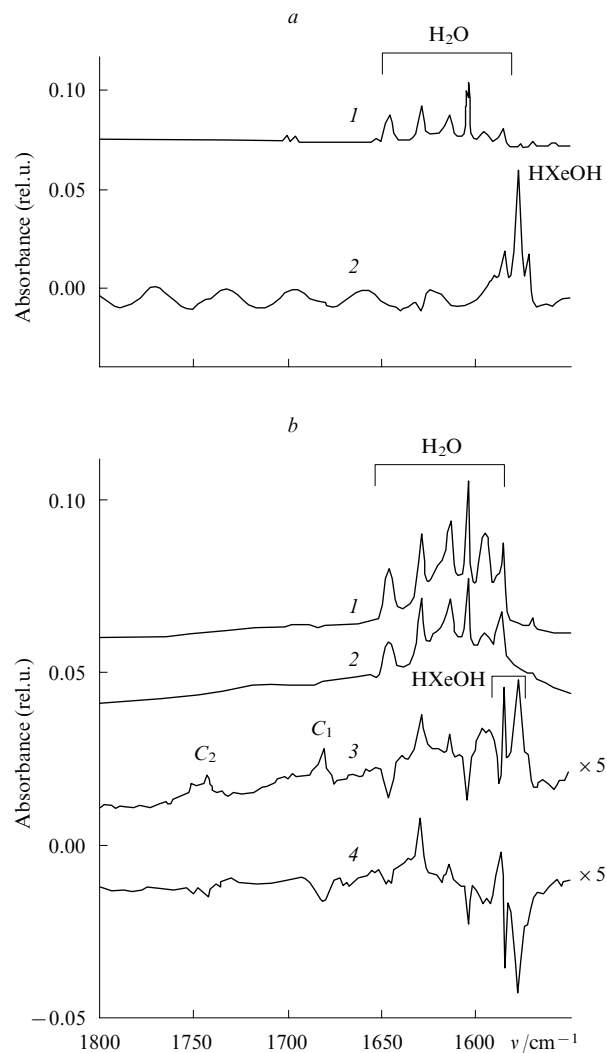


Figure 6. IR spectra of water in solid xenon recorded at low (a) and higher (b) concentrations of water; (a): (1) spectrum recorded after condensation, (2) after matrix annealing; (b): (1) spectrum recorded after condensation; (2) after photolysis; (3) after matrix annealing; (4) after short-term photolysis of the annealed matrix.

geometry configuration (*i.e.*, effective fragments) can form cages that completely trap HXeOH. However, these local minima in the PES proved to be artifacts of this computational procedure; on passing to a higher modelling level (by quantum chemistry techniques), the clusters containing > 3 water molecules were destroyed. In particular, the use of MP2 method with aug-cc-pVTZ basis functions on the oxygen and hydrogen atoms, Stuttgart pseudopotential³⁹ and the appropriate basis set (6s6p1d)/[4s4p1d] on xenon resulted in configurations of the local and global minima in the PES of the HXeOH complexes containing from one to three water molecules. Thus, it was established that the PES local minima correspond to the bound states of the HXeOH · (H₂O)_n systems (*n* = 0–3). Figure 7 shows the calculated equilibrium structures for the complexes HXeOH · (H₂O)_n. These complexes may decompose through potential barriers ranging from 0.4 (for *n* = 3) to 39.6 kcal mol^{−1} (*n* = 0) to give xenon complexes with water clusters: Xe · (H₂O)_{n+1}, which account for the PES global minima.

Table 2 summarises the computation results for the parameters of the HXeOH · (H₂O)_n complexes.

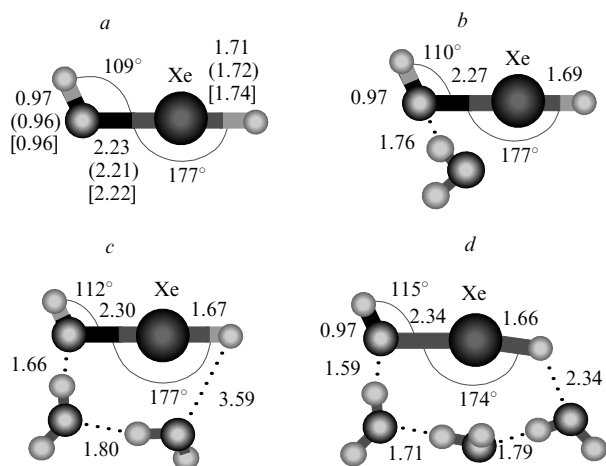


Figure 7. Equilibrium geometry configurations of the complexes $\text{HXeOH} \cdot (\text{H}_2\text{O})_n$ for $n = 0$ (a), 1 (b), 2 (c), 3 (d) corresponding to the local minima in PES. The distances are given in Å.

[For the HXeOH molecule (a) the results of various *ab initio* calculations taken from Ref. 32 are given in brackets.³²]

The use of a conventional scaling procedure for the vibration frequencies calculated in the harmonic approximation permits direct comparison of the theoretically calculated frequencies and experimental positions of bands in the vibrational spectrum. If a scaling factor has been selected (e.g., 0.88 based on the H–Xe stretching band in the HXeOH molecule), the theoretical estimates of the bands for the complexes $\text{HXeOH} \cdot \text{H}_2\text{O}$ and $\text{HXeOH} \cdot (\text{H}_2\text{O})_2$ (1669 and 1735 cm^{-1} , respectively) are in good agreement with experimental data (1681 and 1742 cm^{-1}). Thus, peaks C_1 and C_2 in the spectra of matrix isolated species (see Fig. 6b) are due to the HXeOH complexes with one and two water molecules. In the spectra of systems containing hydrogen bonds, the signals are shifted to the blue (short-wavelength) region with respect to the initial spectrum. Currently, such systems are under vigorous research.⁴⁰ In the case of HXeOH , the blue shift of the H–Xe frequency is attributable to additional charge transfer between the HXe and OH fragments induced by complexation with a water molecule.

Interesting results were obtained in the modelling of decomposition pathways of the $\text{HXeOH} \cdot (\text{H}_2\text{O})_n$ complexes, i.e., upon system transition from local to global minima along the reaction coordinate. To this end, configurations of the transition states as saddle points with the only vibration frequency were found. On both sides from these points, minimum energy paths to the reactant and product valleys were constructed. Figure 8 shows the calculated energy profile corresponding to decomposition of the $\text{HXeOH} \cdot (\text{H}_2\text{O})_2$ complex. The local minimum in the beginning of the reaction path

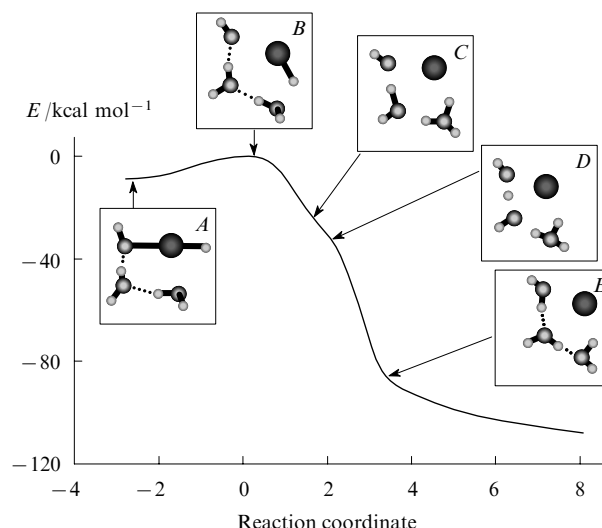


Figure 8. MP2 calculated decomposition pathway of the complex $\text{HXeOH} \cdot (\text{H}_2\text{O})_2 \rightarrow \text{Xe} \cdot (\text{H}_2\text{O})_3$. The insets show configurations of the metastable state of the initial complex (A), transition state (B), reaction product (E) and two intermediate structures along the proton transfer path (C and D).

corresponds to the metastable state of the $\text{HXeOH} \cdot (\text{H}_2\text{O})_2$ complex (A), transition state B is shown on the top of the barrier and the decomposition product $\text{Xe} \cdot (\text{H}_2\text{O})_3$ (E) occurs at the end of the path. Intermediate structures C and D illustrate the proton migration along the hydrogen bond system. As the system moves from left to right, immediately after transition state B has been reached, the proton from the XeH^+ fragment migrates to the nearest water molecule (structure C). The proton from the resulting H_3O^+ species migrates to the next water molecule from which one more proton moves to the hydroxyl ion OH^- (structure D).

This mechanism of proton transfer along the oriented chains of water molecules illustrates the molecular scheme usually referred to as water (or proton) conductor.

V. Conclusion

Despite the obvious priority of experimental works in modern chemistry and physics, the contribution of computer molecular modelling of the physicochemical properties of compounds has become rather weighty in recent years. This is due to fast progress in the computer technology, development of new effective theoretical approaches to this problem and the accumulated experience in the study of particular systems. The examples of solution of complicated problems dealing with structure determination of unstable chemical species, HArF and HXeOH , isolated in low-temperature inert gas matrices demonstrate the advantages of combined effort of experimentalists and theorists. We focused on the theoretical aspect of the studies dealing with the structures, spectra and transformation dynamics of noble gas compounds, because the experimental studies of these compounds have been the subject of recent comprehensive reviews.^{4,5}

The examples we considered are fairly typical, although they represent only a minor portion of the studies of matrix-isolated species by combinations of spectroscopic and molecular modelling methods. Consider briefly other achievements in this field of chemistry. Thus Frenking and co-workers^{41,42} predicted the structure of the stable neutral noble gas compound HeBeO using quantum chemical calculations before the experimental proof for the existence of HArF molecule was

Table 2. Calculated parameters of the $\text{HXeOH} \cdot (\text{H}_2\text{O})_n$ complexes.

Parameter	$n = 0$	$n = 1$	$n = 2$	$n = 3$
Harmonic frequencies of Xe–H vibrations/ cm^{-1}	1790	1897	1972	2066
(relative intensities of the IR bands)	(1.00)	(0.77)	(0.58)	(0.15)
Energies of complexes (kcal mol^{-1}) with respect to the $\text{Xe} + (n+1) \text{H}_2\text{O}$ system	109.5	98.7	87.7	76.4

obtained.³ Significant for further development of this field of science are also studies by Feldman *et al.*^{43–46} and Misochko *et al.*,^{47–49} who analysed active species in noble gas matrices using both experimental and theoretical approaches. Chaban and co-workers^{50–52} performed a number of important theoretical investigations of noble gas compounds, and the review by Gerber⁵³ presents a detailed discussion of the works on the structure and dynamics of these compounds. The review by McDowell³⁷ covers both published and author's results of quantum chemical calculations of molecules containing noble gas atoms. Finally, special mention should be made of two theoretical works^{54,55} predicting the possibility of existence of biomolecules with an inserted xenon atom on the basis of quantum chemical calculations.

Low-temperature matrix isolation has been developed as an experimental technique that allowed investigation of the properties of stable and unstable molecules isolated as fully as possible from the influence of other species. However, the progress in the instrumental equipment enabled detection of the interaction of matrix isolated compounds with the matrix material. The obtained experimental data are of interest for the development of the theory of intermolecular interactions; however, interpretation of the experimental results requires much effort.

Modern *ab initio* quantum chemistry methods provide virtually exact description of the structures and spectra of small (comprising up to 10 atoms) molecules in vacuum, *i.e.*, under conditions where they are separated from other species. Accurate calculations for intermolecular complexes, especially weakly bound complexes with noble gas atoms, are very difficult. The studies discussed in this review used the approach in which the theoretical problem was split into two levels: a matrix-isolated species was modelled by *ab initio* quantum chemistry methods, while its interaction with the matrix species was described by well parametrised semiempirical potentials, in particular, by diatomics-in-molecules potentials. Direct comparison of the calculation results obtained by this combined approach with experimental results often demonstrates the success of this strategy.

Apparently, the future development of the modelling techniques for matrix-isolated species would be related to more active use of molecular dynamics combined with *ab initio* quantum chemical calculations. This would allow direct calculation of the temperature dependences of spectra of matrix isolated species.

The authors are grateful to co-authors of their publications A A Granovskii, D A Firsov, M Pettersson, E Isoniemi, H Tanskanen and A Lignell for fruitful discussion during the research and to Professor G B Sergeev for steady interest and attention to our work. This review was written with partial financial support of the Federal Target Science and Technology Programme of the RF (Project No. 2006-RF-112.0/001/052) and of the Academy of Sciences of Finland (Project CoE CMS).

References

1. G B Sergeev, V A Batyuk *Kriokhimiya* (Cryochemistry) (Moscow: Khimiya, 1978)
2. *Chemistry and Physics of Matrix-Isolated Species* (Eds L Andrews, M Moskovits) (Amsterdam: North Holland, 1989)
3. L Khriachtchev, M Pettersson, N Runeberg, J Lundell, M Räsänen *Nature (London)* **406** 874 (2000)
4. J Lundell, L Khriachtchev, M Pettersson, M Räsänen *Low Temp. Phys.* **26** 680 (2000)
5. M Pettersson, L Khriachtchev, J Lundell, M Räsänen *Inorganic Chemistry in Focus II* (Eds G Meyer, D Naumann, L Wesemann) (Weinheim: Wiley-VCH, 2005) p. 15
6. V A Apkarian, N Schwentner *Chem. Rev.* **99** 1481 (1999)
7. L Khriachtchev, M Pettersson, M Räsänen *Chem. Phys. Lett.* **288** 727 (1998)
8. L Khriachtchev, M Pettersson, J Lundell, M Räsänen *J. Chem. Phys.* **114** 7727 (2001)
9. R P Wayne *Chemistry of Atmospheres* (2nd Ed.) (Oxford: Clarendon Press, 1991)
10. P P Korambath, X T Wu, E F Hayes, C C Carter, T A Miller *J. Chem. Phys.* **107** 3460 (1997)
11. M Pettersson, J Lundell, L Khriachtchev, E Isoniemi, M Räsänen *J. Am. Chem. Soc.* **120** 7979 (1998)
12. J Zoval, D Imre, P Ashjian, V A Apkarian *Chem. Phys. Lett.* **197** 549 (1992)
13. L Khriachtchev, M Pettersson, E Isoniemi, M Räsänen *J. Chem. Phys.* **108** 5747 (1998)
14. B L Grigorenko, L Khriachtchev, A V Nemukhin, M Pettersson, E Isoniemi, M Räsänen *J. Chem. Phys.* **110** 5836 (1999)
15. D A Firsov, B L Grigorenko, A V Nemukhin, L Y Khriachtchev, M Räsänen *Chem. Phys. Lett.* **338** 317 (2001)
16. A V Nemukhin, B L Grigorenko, A A Granovsky *Chem. Phys. Lett.* **301** 287 (1999)
17. B L Grigorenko, A V Nemukhin, V A Apkarian *J. Chem. Phys.* **108** 4413 (1998)
18. B L Grigorenko, A V Nemukhin, N V Ozhegova *Chem. Phys. Lett.* **296** 84 (1998)
19. V I Pupyshev *Opt. Spektrosk.* **63** 570 (1987)^a
20. L Khriachtchev, M Pettersson, A Lignell, M Räsänen *J. Am. Chem. Soc.* **123** 8610 (2001)
21. L Khriachtchev, A Lignell, M Räsänen *J. Chem. Phys.* **120** 3353 (2004)
22. L Khriachtchev, A Lignell, M Räsänen *J. Chem. Phys.* **123** 64507 (2005)
23. A V Bochenkova, D A Firsov, A V Nemukhin *Chem. Phys. Lett.* **405** 165 (2005)
24. Z Bihary, G M Chaban, R B Gerber *J. Chem. Phys.* **116** 5521 (2002)
25. S Jolkkonen, M Pettersson, J Lundell *J. Chem. Phys.* **119** 7356 (2003)
26. A V Nemukhin, B L Grigorenko, A A Granovsky *Vest. Mosk. Univ., Ser. 2, Khim.* **45** 75 (2004)^b
27. R A Aziz, H H Chen *J. Chem. Phys.* **67** 5719 (1977)
28. B L Grigorenko, A V Nemukhin, V A Apkarian *J. Chem. Phys.* **104** 5510 (1996)
29. A V Bochenkova, M A Suhm, A A Granovsky, A V Nemukhin *J. Chem. Phys.* **120** 3732 (2004)
30. L Khriachtchev, H Tanskanen, M Pettersson, M Räsänen, J Ahokas, H Kunttu, V Feldman *J. Chem. Phys.* **116** 5649 (2002)
31. L Khriachtchev, J Lundell, M Pettersson, H Tanskanen, M Räsänen *J. Chem. Phys.* **116** 4758 (2002)
32. M Pettersson, L Khriachtchev, J Lundell, M Räsänen *J. Am. Chem. Soc.* **121** 11904 (1999)
33. W A Caldwell, J H Nguyen, B G Pfrommer, F Mauri, S G Louie, R Jeanloz *Science* **277** 930 (1997)
34. C Sanloup, B C Schmidt, E M C Perez, A Jambon, E Gregoryanz, M Mezouar *Science* **310** 1174 (2005)
35. A V Nemukhin, B L Grigorenko, L Khriachtchev, H Tanskanen, M Pettersson, M Räsänen *J. Am. Chem. Soc.* **124** 10706 (2002)
36. A Lignell, L Khriachtchev, M Pettersson, M Räsänen *J. Chem. Phys.* **118** 11120 (2003)
37. S A C McDowell *Cur. Org. Chem.* **10** 791 (2006)
38. J Joseph, E D Jemmis *J. Am. Chem. Soc.* **129** 4620 (2007)
39. M S Gordon, M A Freitag, P Bandyopadhyay, J H Jensen, V Kairys, W Stevens *J. Phys. Chem. A* **105** 293 (2001)
40. A Nicklass, M Dolg, H Stoll, H Preuss *J. Chem. Phys.* **102** 8942 (1995)
41. G Frenking, D Cremer *Struct. Bonding* **73** 17 (1990)
42. M Lein, J Frunzke, G Frenking *Struct. Bonding* **106** 181 (2004)
43. V I Feldman, F F Sukhov *Chem. Phys. Lett.* **255** 425 (1996)
44. V I Feldman, F F Sukhov, A Y Orlov *Chem. Phys. Lett.* **280** 507 (1997)

45. V I Feldman, F F Sukhov, A Y Orlov, I V Tyulpina *J. Am. Chem. Soc.* **125** 4698 (2003)
46. V I Fel'dman, F F Sukhov, A Yu Orlov, I V Tyul'pina, E A Logacheva, D A Tyurin *Izv. Akad. Nauk, Ser. Khim.* 1415 (2005)^c
47. E Y Misochko, I U Goldschleger, A V Akimov, C A Wight *J. Am. Chem. Soc.* **123** 5156 (2001)
48. A V Akimov, I U Goldschleger, E Y Misochko, C A Wight *J. Phys. Chem. A* **106** 9756 (2002)
49. E Y Misochko, A V Akimov, I U Goldschleger, D A Tyurin, D N Laikov *J. Chem. Phys.* **122** 034503 (2005)
50. G M Chaban, J Lundell, R B Gerber *J. Chem. Phys.* **115** 7341 (2001)
51. Z Bihary, G M Chaban, R B Gerber *J. Chem. Phys.* **119** 11278 (2003)
52. G M Chaban *Chem. Phys. Lett.* **395** 182 (2004)
53. R B Gerber *Annu. Rev. Phys. Chem.* **55** 55 (2004)
54. J Lundell, M Pettersson, M Räsänen *Comput. Chem.* **24** 325 (2000)
55. G M Chaban *Chem. Phys. Lett.* **401** 318 (2005)

^a — *Opt. Spectrosc. (Engl. Transl.)*

^b — *Moscow Univ. Chem. Bull. (Engl. Transl.)*

^c — *Russ. Chem. Bull, Int. Ed. (Engl. Transl.)*

Gas phase reaction kinetics at very low temperatures: recent advances on carbon chemistry using the CRESU technique

A Canosa

Contents

I. Introduction	1093
II. Neutral–neutral reactions in interstellar chemistry	1095
III. Obtaining rate coefficients at very low temperatures	1096
IV. Recent results on the carbon chemistry at very low temperatures	1097
V. Perspectives	1102

Abstract. The review describes briefly the chemistry of interstellar clouds and focusses on how bimolecular neutral–neutral reactions may influence its evolution. Experimental techniques that give information on the reactivity and the dynamics of these processes are presented with a special attention to the CRESU (Cinétique de Réaction en Ecoulement Supersonique Uniforme) technique, which is the only one able to deliver rate coefficients at very low temperatures for reactions between two neutral partners. Recent advances concerning the reactivity of carbon-bearing molecules are described in more detail with a special attention to the reaction kinetics of C_2 and C_4H with small stable hydrocarbons. The bibliography includes 161 references.

I. Introduction

For many years, the field of gas phase reaction kinetics involving neutral partners has been restricted to experimental studies which were carried out essentially at temperatures greater or equal to room temperature. The interest in the chemistry of the Earth stratosphere that arose in the early 1970s stimulated the adaptation of experimental equipment to extend the study of kinetics down to 200 K. This led to a significant increase, although still limited, in the number of available rate coefficients at sub-ambient temperatures.^{1–3} For reasons that will be explained further, only in some very specific cases experimental data had been obtained down to 77 K.^{4–7} In the last twenty years, however, the development and adjustment of new technologies opened the possibility of exploring much colder temperature areas leading to a significant amount of reaction rate constant measurements down to 13 K.^{8,9} Although some experiments were also carried out at 7 K,⁸ these dealt with inelastic collisions and focussed on energy transfer processes only. In the solid state, it is worth mentioning however that this record was beaten and an

abundant research field on autowave chemical transformations near 4 K has been developed within the last 20 years.^{10–13}

From the fundamental point of view, the new obtained data in the gas phase were like a revolution for chemical physics science as they revealed that the Arrhenius equation does not hold for a large number of neutral–neutral reactions including those for which a saturated molecule was involved. Barrierless reactions, indeed, were found to be much more frequent than suspected. Furthermore, these new experiments stimulated the development of new theories of reactive collisions.^{14–31} A comparison between experiment and theory at such low energies (let us remember that 13 K corresponds to about 1 meV) was actually a decisive test of the quality of potential energy surfaces required for a correct description of chemical processes. A large number of theoretical studies was then undertaken in order to reproduce the experiments but till now, most of these works were carried out on a case-by-case basis (see for example^{14, 18, 24, 26}) and no general trends are presently known to quantify the effectiveness of a chemical process at very low temperature although some very recent attempts are shedding interesting light in this difficult task.^{9, 21, 30–32}

Beside these fundamental considerations, studying reactivity at temperatures as low as 10 K is of major importance for the understanding of a large number of (very) cold natural environments in which a rich chemistry is taking place. Whereas the mean surface temperature of the Earth is presently about 288 K, much lower temperatures can be found as, for example, in the area of Verkhoyansk in Siberia (Russia) where the thermometer can go down to 200 K. In our own atmosphere, recent observations indicate that the temperature at the mesopause can be lower than 150 K at high latitudes.³³ Thanks to the development of space missions, ground telescopes and satellites, new horizons were revealed to our knowledge and demonstrated the existence of even colder extraterrestrial environments. The atmosphere of Giant Planets or their satellites is only several tens of a Kelvin: 70 K at the tropopause of the now well known Saturn's satellite Titan,³⁴ 50 K in the atmosphere of Neptune³⁵ or Pluto.³⁶ In the coma of comets, temperatures ranging from 10 K to 200 K³⁷ have been determined according to the distance to the Sun and the position with respect to the nucleus. Beyond the solar system, we penetrate in the so-called interstellar medium, an apparently empty space which separates stars from each other. This very tenuous environment (mean density ~ 1 atom cm^{-3}) is actually quite heterogeneous containing for example very

A Canosa Université de Rennes 1, Laboratoire PALMS, UMR 6627 CNRS-Université, Bâtiment 11 C, Campus de Beaulieu, Université de Rennes 1, 35042 RENNES Cedex, France. Fax (33-223) 23 67 86, tel. (33-223) 23 69 96, e-mail: andre.canosa@univ-rennes1.fr

Table 1. List of interstellar molecules ordered by their number of atoms.^{39,40}

Number of atoms (<i>N</i>)									
<i>N</i> = 2	<i>N</i> = 3			<i>N</i> = 4	<i>N</i> = 5	<i>N</i> = 6	<i>N</i> = 7	<i>N</i> = 8	<i>N</i> = 9
CH (1937)	CN (1940)	H ₂ O (1969)	HCO ⁺ (1970)	NH ₃ (1968)	HCO ₂ H (1971)	CH ₃ OH (1970)	CH ₃ CHO (1973)	HCO ₂ CH ₃ (1975)	CH ₃ OCH ₃ (1974)
CH ⁺ (1941)	OH (1963)	OCS (1971)	HCN (1971)	H ₂ CO (1969)	HC ₃ N (1971)	CH ₃ CN (1971)	CH ₃ CCH (1973)	CH ₃ C ₃ N (1984)	CH ₃ CH ₂ OH (1975)
H ₂ (1970)	CO (1970)	H ₂ S (1972)	HNC (1973)	HNCO (1972)	CH ₂ NH (1973)	NH ₂ CHO (1971)	CH ₃ NH ₂ (1974)	CH ₃ CO ₂ H (1997)	CH ₃ CH ₂ CN (1977)
CS (1971)	SiO (1971)	C ₂ H (1974)	N ₂ H ⁺ (1974)	H ₂ CS (1973)	NH ₂ CN (1975)	CH ₃ SH (1979)	CH ₂ CHCN (1975)	C ₇ H (1997)	HC ₇ N (1978)
SO (1973)	NS (1975)	HDO (1975)	SO ₂ (1975)	C ₃ N (1977)	H ₂ CCO (1977)	C ₂ H ₄ (1983)	HC ₅ N (1978)	HOCH ₂ CHO (2000)	HC ₉ N (1978)
SiS (1975)	C ₂ (1977)	HCO (1976)	HNO (1977)	HNCS (1979)	C ₄ H (1978)	C ₅ H (1986)	C ₆ H (1986)	C ₆ H ₂ (2001)	CH ₃ C ₄ H (1984)
NO (1978)	HCl (1985)	HCS ⁺ (1981)	HOC ⁺ (1983)	HOCO ⁺ (1981)	SiH ₄ (1984)	CH ₃ NC (1988)	c-C ₂ H ₄ O (1997)	CH ₂ CHCHO (2004)	(CH ₃) ₂ CO (1987)
AlCl (1987)	AlF (1987)	c-SiC ₂ (1984)	MgNC (1986)	C ₃ H (1985)	c-C ₃ H ₂ (1985)	HC ₂ CHO (1988)	CH ₂ CHOH (2001)	CH ₂ CCHCN (2006)	C ₈ H (1996)
KCl (1987)	NaCl (1987)	C ₂ S (1987)	C ₃ (1988)	C ₃ O (1985)	CH ₂ CN (1988)	HC ₃ NH ⁺ (1994)	C ₆ H ⁻ (2006)		HC ₁₁ N (1997)
PN (1987)	SiC (1989)	CO ₂ (1989)	CH ₂ (1989)	H ₃ O ⁺ (1986)	C ₅ (1989)	C ₅ N (1998)			C ₆ H ₆ (2001)
CP (1990)	NH (1991)	C ₂ O (1991)	NH ₂ (1993)	HCNH ⁺ (1986)	SiC ₄ (1989)	C ₄ H ₂ (2001)			(CH ₂ OH) ₂ (2002)
SiN (1992)	SO ⁺ (1992)	N ₂ O (1994)	NaCN (1994)	c-C ₃ H (1987)	CH ₄ (1991)	HC ₄ N (2004)			NH ₂ CH ₂ CO ₂ H (2003) ^a
CO ⁺ (1993)	HF (1997)	MgCN (1995)	H ₃ ⁺ (1996)	C ₃ S (1987)	C ₃ H ₂ (1991)	CH ₂ CNH (2006)			CH ₃ CH ₂ CHO (2004)
LiH (1998) ^a	SH (2000)	SiCN (2000)	AINC (2002)	C ₂ H ₂ (1989)	HCCNC (1992)	c-H ₂ C ₃ O (2006)			CO(CH ₂ OH) ₂ (2005) ^a
FeO (2002)	N ₂ (2004)	SiNC (2004)		HC ₂ N (1991)	HNCCC (1992)				CH ₃ C ₅ N (2006)
CF ⁺ (2006)	O ₂ (2007)			H ₂ CN (1994)	H ₂ COH ⁺ (1996)				CH ₃ C ₆ H (2006)
PO (2007)				SiC ₃ (1999)	C ₄ H ⁻ (2007)				CH ₃ CONH ₂ (2006)
				CH ₃ (2000)					C ₈ H ⁻ (2007)
									CH ₂ CHCH ₃ (2007)

Note. The year of their discovery is also included in parentheses; ‘c’ stands for cyclic species. ^a Tentative or still controversial detections.

diluted (< 0.01 atom cm^{-3}) and hot ($\sim 10^6$ K) areas, remnants of super novae explosions where atoms have lost several of their electrons and much colder (10 K) and denser (10^4 molecules cm^{-3}) zones where an amazingly rich chemistry is now identified. The latter are called molecular clouds (or dark clouds) because most of the molecules identified in the interstellar medium were discovered in these dense enough media so that the UV light coming from neighbouring stars cannot penetrate deep inside.³⁸ To date, thanks to radioastronomy and satellites such as ISO (Infrared Space Observatory) or orbiting telescopes such as HST (Hubble Space Telescope), about 150 different molecules have been identified in the interstellar medium (230 including isotopomers).^{39, 40} This number is permanently growing and the development of the ALMA interferometer in Chile and the future space telescope Herschel (launching July 31st, 2008) will certainly considerably enrich the list. A compilation of the presently known molecules in the interstellar and circumstellar media is presented in Table 1 which also includes the year of the first detection of each molecule. More details, and particularly the references announcing the first discovery of each species, can be found at the website held by Woon.³⁹ How such a variety of molecules, among which a large number are organic, can be produced and survive in such harsh environments is a fundamental question that gave birth to a new field in astronomy about 40 years ago: astrochemistry.

In the present review, I will essentially focus the discussion on interstellar molecular clouds and experimental techniques that could be employed for the study of gas phase neutral–neutral reaction kinetics at very low temperature.

II. Neutral–neutral reactions in interstellar chemistry

Understanding how stars and their associated planetary system form is one of the major challenges of modern astrophysics. It is now largely accepted that molecular clouds are the cradle of stars which are generated by local gravitational collapses inside the cloud leading to a strong pressure increase which eventually will start thermonuclear reactions. In this frame, molecules play a critical role in the dynamical stability of the cloud and act as a cooling reservoir.⁴¹ Inelastic collisions with other species, and more particularly H_2 , which is by far the more abundant molecule, enable conversion of kinetic energy into radio or mm radiations which eventually can escape from the cloud which is optically thin in this wavelength range. As a consequence of molecular cooling, the thermal pressure inside the cloud is reduced and eventually will not be able to counterbalance gravitation any more leading to the collapse of the cloud.⁴²

It is then essential to clearly understand the fate of interstellar molecules. With this objective in mind, astronomers started to develop gas phase photochemical models of interstellar clouds in the mid-seventies.^{43–48} Their aim was to reproduce the observed abundances of these molecules taking into account all chemical and physical processes that were expected to play a role in their formation and destruction. Knowledge of a large number of parameters was required including the photon and cosmic ray fluxes coming from outside the cloud, the rate constants for reactive and inelastic collisions and the branching ratios of reactions. The most elaborated interstellar models are presently taking into account about 400 species (neutral and charged) and 4000 processes.^{49, 50} It is worth mentioning here that the most recent models are now starting to include gas surface processes, as the presence of important molecules such as H_2 cannot be explained by chemical schemes simply based on gas phase chemistry. The physical conditions reigning in molecular clouds (low temperatures, low pressures) restrict however the

Table 2. Classes of chemical reactions that are included in chemical models of interstellar clouds.

Reaction	Reaction scheme
Ion–molecule reactions	
Charge transfer	$\text{A}^+ + \text{B} \rightarrow \text{B}^+ + \text{A}$
Radiative association	$\text{A}^+ + \text{B} \rightarrow \text{AB}^+ + h\nu$
Atomic transfer	$\text{AB}^+ + \text{C} \rightarrow \text{A}^+ + \text{BC}$
Electronic recombination reactions	
Radiative	$\text{A}^+ + \text{e}^- \rightarrow \text{A} + h\nu$
Dissociative	$\text{AB}^+ + \text{e}^- \rightarrow \text{A} + \text{B}$
Photochemical processes	
Photodissociation	$\text{AB} + h\nu \rightarrow \text{A} + \text{B}$
Photoionisation	$\text{AB} + h\nu \rightarrow \text{AB}^+ + \text{e}^-$
Neutral neutral reactions	
Atomic transfer	$\text{A} + \text{BC} \rightarrow \text{AB} + \text{C}$
Radiative association	$\text{A} + \text{B} \rightarrow \text{AB} + h\nu$
Other reactions	
Ion–ion neutralisation	$\text{A}^+ + \text{B}^- \rightarrow \text{AB}$
Neutral–negative ion reactions	$\text{A}^- + \text{B} \rightarrow \text{AB} + \text{e}^-$
	$\text{A}^- + \text{BC} \rightarrow \text{AB}^- + \text{C}$
Electron attachment	$\text{A} + \text{e}^- \rightarrow \text{A}^- \text{ or }$
	$\text{AB} + \text{e}^- \rightarrow \text{A}^- + \text{B}$

chemistry to two-body, exothermic and barrierless processes. The different families of reactions that are considered in interstellar models are listed in Table 2.

Chemistry is initiated by ionisation of molecular and atomic hydrogen, helium and carbon atoms by the VUV radiation of stars in the outer part of the cloud and cosmic rays in its inner part, which is opaque to VUV photons. A series of ion–atom (H) and ion–molecule (H_2) reactions lead to the production of bigger polyatomic ion molecules, which eventually will recombine dissociatively thus producing neutral molecules. These can also be generated by radiative association processes and neutral–neutral reactions, which is the scope of this paper. Then, although detected cations in the interstellar medium represent only about 10% of the presently known species, they play a central role in the increase of chemical complexity. Very recently, it is worth stressing that the first negative ion molecules C_8H^- (Refs 51, 52), C_6H^- (Ref. 53) and C_4H^- (Ref. 54) have been discovered in the molecular envelope of IRC + 10 216 and in the dense molecular cloud TMC-1, which will certainly focus the interest of modellers on the anion chemistry in a very close future.

For about twenty years and up to the early nineties, interstellar cloud chemistry was thought to be essentially driven by ion–molecule reactions because, due to the strong attractive forces between an ion and the permanent or induced dipole on the neutral reagent, these processes were generally barrierless and very fast ($> 10^{-9}$ $\text{cm}^3 \text{ s}^{-1}$ molecules $^{-1}$). On the other hand, for many years, neutral–neutral reactions were expected to be inefficient at the very low temperature of molecular clouds as they were thought to proceed with positive activation energy barrier (E_a). The temperature dependence of the rate coefficient k was then usually described by the Arrhenius equation $k = k_0 \exp(-E_a/k_B T)$ which leads to insignificantly small rate coefficients at temperature of *ca* 10 K. Only a few radical–radical reactions such as $\text{O} + \text{OH} \rightarrow \text{O}_2 + \text{H}$ were considered in models because this class of processes could be expected to have no barrier.⁴⁷ Furthermore, at that time very few data were available at temperatures below 200 K because experimental techniques were not suited for this kind of measurements (see below). In the early nineties, as

explained further, the adaptation of the CRESU technique to the study of radical–neutral reactions shed a new light on the field and demonstrated that a large number of these processes, and more particularly those involving a saturated molecular partner, can be very efficient at temperatures as low as 13 K. This discovery was carefully considered by interstellar cloud modellers who then published dedicated articles analysing the impact of these new views.^{49,55,56} The number of neutral–neutral processes included in models was significantly increased and rate coefficients were re-evaluated on the bases of the new experimental data (initially concerning the reactivity of the CN and CH radicals). The main consequence of this upgrading was to reduce the rate of formation of complex species because of a prompt destruction of small radicals which initiate the chemical scheme leading to complex molecules.⁵⁵

Although a significant number of binary neutral–neutral reactions have been studied at very low temperatures now, much more data are still required. In the following section I will discuss the main difficulties faced by this kind of studies and I will show how the CRESU technique can resolve a large part of them.

III. Obtaining rate coefficients at very low temperatures

As mentioned previously, for a long time low temperature experimental rate coefficients were not available. Modellers had then to estimate or evaluate these parameters and therefore the results of simulations of the interstellar cloud chemistry were subject to very large uncertainties although they were able to reproduce some general aspects. To obtain low temperature data, one common practice (still in use nowadays) was to extrapolate the temperature dependence of a reaction for which rate coefficients were measured at room temperature and higher. As illustrated in Figure 1a and 1b, this can lead to dramatic errors at temperatures as low as 20 K. In this example, the reaction $\text{CN} + \text{C}_2\text{H}_6$ was initially studied by Herbert *et al.*⁵⁷ in the temperature range 297–694 K. Data are shown in Fig. 1a on an Arrhenius plot and seem to fit an Arrhenius dependence with modest activation energy. Figure 1b shows the attempt to extrapolate these measurements down to interstellar temperatures. As it can be seen, the extrapolated rate coefficient decreases impressively by almost 7 orders of magnitude from room temperature down to 20 K. However, experimental results obtained by Sims *et al.*⁵⁸ one year after the study by Herbert *et al.* show that the rate coefficient behaviour changes completely since a minimum was reached at about 200 K and then the rate starts again to increase leading to a difference of 6 orders of magnitude at 25 K between experiment and extrapolation. Fortunately, all situations are not as critical as this one, but this example clearly indicates that experimental data are definitely required to strongly and correctly constrain interstellar cloud models.

It is then necessary to generate a cool environment in which reaction kinetics could be studied. The simplest idea is to cryogenically cool down a slow-flow reactor cell. In that case, however, one is immediately faced with the decay of the saturated vapour pressure of gases when the temperature is reduced and, as a consequence, condensation to the refrigerated walls of the cooled vessel. The solution to prevent condensation is to limit the total concentration of the reagents in the cell to keep them at partial pressures that are below their vapour pressure at the wall temperature. However, the concentration must be high enough to perform kinetic experiments, and only gases with a significant vapour pressure at the wall temperature are then suitable. This method therefore becomes more and more limited at temperatures lower than 200 K and was never applied below the liquid nitrogen temper-

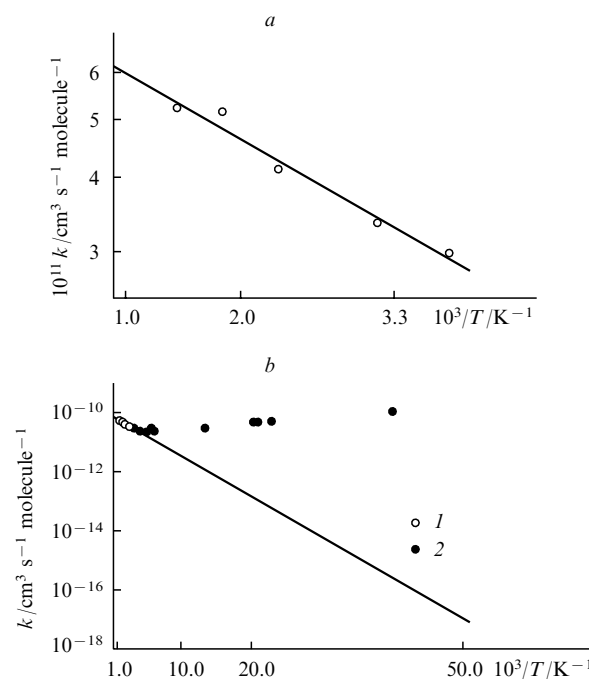


Figure 1. Arrhenius plot of the rate constant for the reaction $\text{CN} + \text{C}_2\text{H}_6$ in the temperature range 297–694 K (a)⁵⁷ and Arrhenius plot of the rate constant for the reaction $\text{CN} + \text{C}_2\text{H}_6$ in the temperature range 25–694 K (b) (1),⁵⁷ (2).⁵⁸ The straight line is an Arrhenius extrapolation to low temperature of the data obtained by Herbert *et al.* at temperature greater than 297 K.

ature of 77 K. At this temperature, only a few experiments have been conducted for a limited number of reactions involving gases such as CO (Refs 6, 7) and H_2 (Refs 4, 5) which have high enough vapour pressures at such temperatures. More details and references in relation to these techniques can be found in Ref. 3.

Generating low temperatures can also be achieved using supersonic expansions. The fundamentals of the technique here is to convert part of the internal energy of a quasi static flow into kinetic energy. There are several kinds of supersonic expansions.

The simplest is the so-called free jet, which is formed by expanding a gas from a high-pressure reservoir (typically ~ 1 bar) into a high-vacuum chamber through a small orifice or a nozzle. The temperatures obtained with this method can be extremely low down to 0.1 K but cannot generally exceed 20 K. The density is typically less than 10^{15} cm^{-3} in most of the useable areas of the jet.^{59,60} However, the expansion is inhomogeneous, with strong spatial density and temperature gradients.^{61,62} As the expansion evolves the collision frequency decreases and therefore the different temperature moments (translation, rotation and vibration) cannot reach equilibrium.⁶³ The gradients of temperature and density, the low frequency of collisions and the short useable area of the jet make it difficult to perform kinetic experiments in these free-jet expansions although some ion–molecule reactions have been studied⁶⁰ because for this class of processes the long-range electrostatic forces are strong enough to attract together reagents travelling with virtually no translational velocity. Nevertheless, free jet expansions are widely employed in spectroscopy⁶⁴ for which problems of disequilibrium in the flow are not important.

A molecular beam is an extension of the free jet technique as it is obtained by extracting the centreline beam of the free jet by skimming and pumping away the excess gas. The skimming

action prevents supersonic waves from spreading back into the gas and increasing the translational temperature, and at the same time, enables one to obtain a well-collimated flow with a narrow velocity distribution. Molecular beams are very useful in studies of collisional dynamics.^{65,66} As the frequency of collisions is very small in a molecular beam, data are obtained from experiments in which two collimated reagent beams intersect at fixed angle in a scattering region where single reactive or inelastic collisions occur between the components of the beams.^{65–72} The species of each beam are characterised by a well-defined velocity and usually also internal quantum states. By varying the velocity of the molecular beams and their intersection angle, differential cross sections (product angular and velocity distributions) can be measured at different collisional energies. The technique provides valuable information on the nature of the products of the reaction and its mechanism.⁷² Most of these so-called crossed molecular beam machines, however, work with beams at right angle and therefore the usual collisional energies are rather high with respect to those encountered in the molecular rich interstellar medium. Some devices are designed to vary the beam intersection angle which enables some reduction in the relative collision energy.^{73–77} The lowest collision energy presently available was obtained by Naulin and Costes⁷⁶ who can make experiments using an apparatus for which the intersection angle can be varied from 90° down to 22°, the latter corresponding to a collision energy of 0.35 kJ mol^{−1} (*i.e.* ~30 K). In this experiment, relative total cross sections (also referred as excitation function in the literature) can be integrated assuming a Maxwell distribution of relative velocities at temperature T and a Boltzmann distribution of reactant internal energies to extract a thermal rate coefficient, $k(T)$. This, however, is a relative value and has to be normalised using data obtained from other techniques. More interestingly, the technique provides the temperature dependence of the calculated rate coefficient which can be directly compared with other experimental methods.^{76,78}

Absolute rate coefficients can be obtained as a function of temperature using ‘collimated’ supersonic flows generated by the isentropic expansion of a buffer gas through an axisymmetric convergent–divergent Laval nozzle.⁷⁹ At the exit of the nozzle, the supersonic flow, typically 10 to 20 mm in diameter, moves with a bulk velocity which is parallel to the axis of the nozzle and uniform for several tens of centimetres which is also the case for temperature, pressure and hence density. The diffusion velocity is always negligible with respect to the bulk velocity, thus avoiding the major problem of condensation associated with the use of cryogenically cooled cells. As a consequence, in such expansions, heavily supersaturated conditions prevail and as a matter of example condensable species such as water, ammonia⁸⁰ or even polycyclic aromatic hydrocarbons^{81,82} can be maintained in the gas phase at very low temperatures. In contrast to free jet expansions and molecular beams where the concept of temperature is not really valid, the relatively high gas density (10^{16} – 10^{17} molecule cm^{−3}) in the uniform supersonic flow ensures that frequent collisions take place during the expansion and subsequent flow, maintaining thermal equilibrium. It is worth stressing here that the temperature of the supersonic flow is not a tuneable parameter as it is constrained by the divergent profile of the Laval nozzle which is specifically designed to obtain a given temperature and pressure in the supersonic flow.[†] Hence, a series of Laval nozzles are required to match

the range of temperature that needs to be explored. Clearly, uniform supersonic flows are ideal chemical reactors.^{8,79,83}

Uniform supersonic flows were initially developed in a continuous flow version for the study of ion–molecule reactions by Rowe and co-workers⁷⁹ in the early eighties in the laboratoire d’Aérothermique in Meudon (France). The technique was christened as CRESU, a French acronym meaning Cinétique de Réaction en Ecoulement Supersonique Uniforme which can be translated in English by Reaction Kinetics in a Uniform Supersonic Flow. About ten years later, the methodology was adapted to the study of neutral–neutral reactions⁸³ at the Université de Rennes 1 (France) and in the mid-nineties mimicked at the University of Birmingham (United Kingdom).⁸⁴

The typical temperatures than can be achieved are usually in the range 15–300 K.^{8,9} However, the reservoir of the nozzle and the nozzle itself can be pre-cooled using for example liquid nitrogen. In these conditions, supersonic flows with a temperature as low as 7 K (see Refs 85, 86) can be achieved. The choice of the reactant, however, is then limited to those having a vapour pressure high enough to avoid condensation on the walls of the reservoir of the nozzle in which the flow is almost stagnant.

With respect to the determination of rate coefficients, a limitation of the CRESU technique lies in the supersonic nature of the flow which restricts the available hydrodynamic time to a few hundreds of microseconds. As a consequence, only rate coefficients greater than 5×10^{-13} cm³ s^{−1} molecule^{−1} can usually be measured. Another aspect that is worth mentioning concerns the size of the apparatus. The supersonic flow is made of an inner isentropic core embedded into a boundary layer resulting from the viscosity of the gas. Minimising this boundary layer (and hence optimising the length of the supersonic flow) requires introducing large gas flow rates into the reservoir (typically 50 standard litres per minute). Since Laval nozzles are usually designed to obtain a low pressure into the supersonic flow (typically a fraction of a mbar) in order to avoid possible clustering, large pumping capacities are necessary for the apparatus (typically 25 000 m³ h^{−1}). The size of pumps directly determines the size of the chamber which is 3 m long and 50 cm in diameter.

If pressures of about 1 mbar are however acceptable in the supersonic flow for the study of a given process, then a significant reduction in pumping capacities can be accepted as it is the case for the mini-CRESU that has been constructed in the Université de Bordeaux 1 by Costes and co-workers.⁸⁷ This apparatus however cannot reproduce temperatures lower than 50 K in the supersonic flow because of its limited pumping capacities. In order to reduce the cost required for the development of a CRESU continuous supersonic flow, another alternative can be to pulse the supersonic flow so that large flow rates are only introduced during a few milliseconds and therefore pumping capacities are significantly diminished. The pulsed CRESU technique was first developed at the University of Arizona (USA) by Smith and co-workers⁸⁸ and it is now also in use at the University of Berkeley (USA) in Leone’s group⁸⁹ and at the University of Goettingen (Germany) in Troe’s team.^{90–92} Another apparatus is under development at the University of Leeds (United Kingdom) in Pilling’s group. Due to their small pumping capacities, the pulsed CRESU supersonic flows are limited to temperatures greater than 50 K.

Table 3 lists the two-body neutral–neutral reactions that were experimentally studied using the continuous or pulsed version of the CRESU method.

IV. Recent results on the carbon chemistry at very low temperatures

In this section, I will discuss recent results that were obtained concerning the reactivity of neutral carbon-bearing radicals,

[†] It is worth mentioning here that originally, Laval nozzles were developed in the aeronautics area for their ability in maintaining a collimated gas at their exit. They are used as exhausts for the burnt gases of rockets because their design optimises the thrust when the spacecraft takes off.

Table 3. Bimolecular reactions studied using the continuous and pulsed versions of the CRESU apparatus.

Reactant	Radical	T_{\min}/K^a	Ref.	Reactant	Radical	T_{\min}/K^a	Ref.
O(³ P _J)	OH	39	93	C ₂ H ₆	CN	25	58
O ₂	CN	13	83, 94		CH ($v = 0$)	23	110
	CH ($v = 0$)	13	95		NH	53	105
	C ₂ H	15	96		C ₂ H	96	116
	C ₂ (¹ Σ _g ⁺)	145	97		C ₂ (¹ Σ _g ⁺)	24	111
	C(³ P _J)	15	18, 98, 99		C ₂ (³ Π _u)	200	113
	Al(² P _J)	23	24, 100		C ₄ H	39	112
	Si(³ P _J)	15	101, 102	MeC≡CH	CN	15	117
	B(² P _J)	24	103		CH ($v = 0$)	77	87
D ₂	CH ($v = 0$)	13	104		C ₂ H	63	117
NO	CH ($v = 0$)	13	95		C ₄ H	39	112
	NH	53	105		C(³ P _J)	15	118
	C ₂ (¹ Σ _g ⁺)	24	97	CH ₂ =C=CH ₂	CN	15	117
	C ₂ (³ Π _u)	24	97		CH ($v = 0$)	77	87
	C(³ P _J)	15	18, 99		C ₂ H	63	117
	Si(³ P _J)	15	101		C ₄ H	39	see ^c
H ₂ O ₂	OH	96	106		C(³ P _J)	15	118
HBr	OH	23	107, 108	MeCH=CH ₂	CH ($v = 0$)	77	87
NH ₃	CN	25	83		NH ^b	53	105
	CH ($v = 0$)	23	95		C ₂ H	15	96
	C ₂ H	104	109		C ₄ H	39	see ^c
CH ₄	CH ($v = 0$)	23	110		C(³ P _J)	15	98
	NH	53	105		O(³ P _J)	23	31
	C ₂ (¹ Σ _g ⁺)	24	111	C ₃ H ₈	C ₂ H	96	116
	C ₄ H	200	112		C ₂ (¹ Σ _g ⁺)	24	111
C ₂ H ₂	CN	25	58		C ₂ (³ Π _u)	36	113
	CH ($v = 0$)	23	110		C ₄ H	39	112
	NH ^b	53	105	C ₄ H ₂	NH ^b	53	105
	C ₂ H	15	96	but-1-yne	C ₄ H	39	see ^c
	C ₂ (¹ Σ _g ⁺)	24	111	buta-1,3-diene	C ₂ H	104	119
	C ₂ (³ Π _u)	24	113		C ₄ H	39	see ^c
	C ₄ H	39	112	<i>cis</i> -but-2-ene	O(³ P _J)	23	31
	C(³ P _J)	15	14, 98	but-1-ene	CH ($v = 0$)	23	110
	Si(³ P _J)	15	114		C ₂ H	103	119, 120
	B(² P _J)	23	78		C ₄ H	39	see ^c
C ₂ H ₄	CN	25	58		O(³ P _J)	23	31
	CH ($v = 0$)	23	110	Me ₂ C=CH ₂	C ₂ H	104	119
	NH ^b	53	105		O(³ P _J)	23	31
	C ₂ H	15	96	<i>trans</i> -But-2-ene	O(³ P _J)	23	31
	C ₂ (¹ Σ _g ⁺)	24	111	<i>n</i> -Butane	C ₂ H	96	116
	C ₂ (³ Π _u)	24	113		C ₄ H	39	see ^c
	C ₄ H	39	112		O(³ P _J)	23	31
	C(³ P _J)	15	98	isobutane	C ₂ H	104	119
	Si(³ P _J)	15	114	benzene	C ₂ H	105	121
	B(² P _J)	23	115	anthracene	CH ($v = 0$)	58	82
	O(³ P _J)	39	31	MeCN	C ₂ H	165	119
				EtCN	C ₂ H	104	119
				Pr ⁿ CN	C ₂ H	104	119

^a T_{\min} is the minimum temperature at which the experiment has been carried out. ^b For these reactions, the binary nature is not firmly established. ^c Personal unpublished data.

and more particularly C₂ and C₄H, in the presence of hydrocarbon reactants. One of the main motivations for these studies lay in the involvement of these species in the photochemical cycle of diacetylene C₄H₂ in the atmosphere of Titan, a molecule considered to be an important step through the production of polyacetylene polymers and eventually the observed hazes.¹²² Furthermore, both radicals have been identified in the interstellar medium^{123–129} as well and can contribute to the production of more complex molecules by reacting with other hydrocarbons.

Rate coefficients were measured using the continuous CRESU apparatus available in Rennes in the temperature

range 24–300 K for reactions involving C₂ (Refs 111, 113) and 39–300 K for those concerning C₄H.¹¹² The CRESU supersonic flow was associated to laser techniques to produce and detect the radicals *in situ* using the time resolved Pulsed Laser Photolysis–Laser Induced Fluorescence (PLP-LIF) technique. The fundamentals of the method have been described in detail elsewhere⁸³ and therefore a brief summary will be presented here focussing only on the specificities connected to the present studies. The PLP-LIF technique uses two pulsed lasers which are combined and co-propagate along the axis of the supersonic flow as it can be shown in Fig. 2. The first laser produces a homogeneous concentration of the

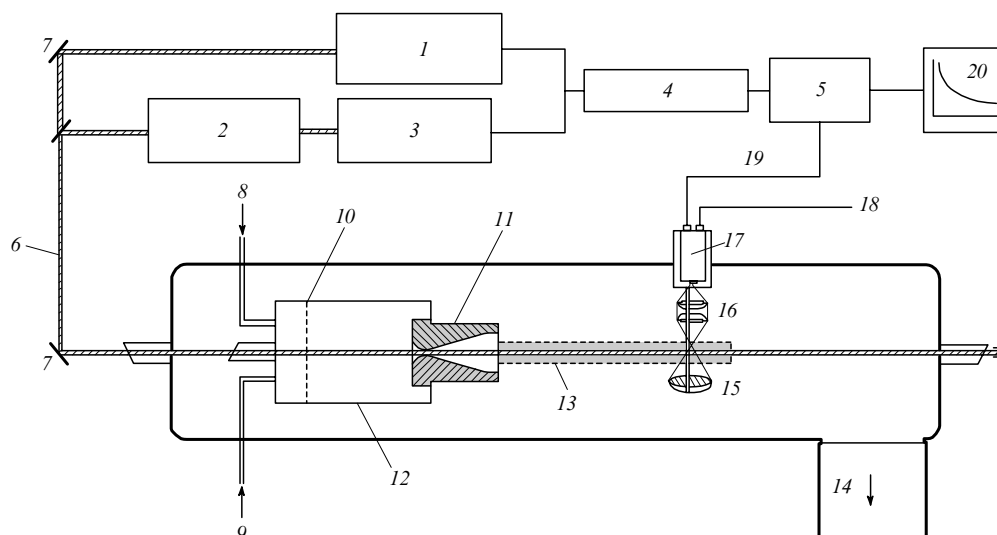


Figure 2. Sketch of the CRESU apparatus.

(1) Nd:YAG 266 nm or excimer 193 or 248 nm; (2) MOPO 730 or dye laser; (3) Nd:YAG 355 nm; (4) delay-generator; (5) computer interface; (6) laser beams; (7) combining optics; (8) precursor; (9) carrier/reagent gas main flow; (10) diffuser; (11) Laval nozzle; (12) moveable reservoir; (13) supersonic flow; (14) to pumps; (15) mirror; (16) telescope; (17) photomultiplier; (18) high voltage; (19) signal; (20) computer.

desired radical by photolysis of a suitable precursor. Then, after a variable and controlled time delay, the radical is excited to an upper electronic state by a tuneable laser acting as a probe and its fluorescence is collected by means of an optically fast telescope – mirror combination mounted within the main vacuum chamber in which it is set at right angle of the supersonic flow. Photons are then directed onto a fixed photomultiplier tube through an interference filter. Production and detection conditions for $C_2(X^1\Sigma_g^+)$, $C_2(a^3\Pi_u)$ and $C_4H(\tilde{B}^2\Pi_i)$ are specified in Table 4.

For a given concentration of the reactant, the rate of loss of the radical along the flow axis is observed by scanning the delay time between the pulses from the photolysis and probe lasers using a delay generator. As the time delay between lasers increases the fluorescence signal decreases because radicals have been consumed in the reaction during their transit along the flow. A typical trace of the LIF decay can be seen in Fig 3 as well as the exponential fit which allows one to determine a first-order rate coefficient. Plotting this rate as a function of the reactant concentration, which can be varied by means of flow controllers, leads to a straight line whose slope gives the requested second-order rate coefficient. A typical second-order plot is shown in Fig. 4 as an illustration. It is worth

stressing that this kind of study only scans the destruction of the reagent radical, hence no information can be extracted about the nature of the products and the branching ratios when several exit channels are open.

The C_2 radical is a peculiar molecule in the sense that its first excited electronic state $a^3\Pi_u$ ($v = 0$) is only separated from the ground state $X^1\Sigma_g^+$ ($v = 0$) by 610 cm^{-1} ($\sim 880\text{ K}$).¹³⁰ In our experimental protocol,⁹⁷ photolysis of the precursor tetrachloroethylene at 193 nm produces mainly the triplet state which then can relax to the ground state when suitable conditions exist in the flow. Using He, Ar or N_2 as the buffer gas of the supersonic flow results in the presence of both states out of Boltzmann equilibrium in the flow. This is an uncomfortable situation for the study of the reactivity of the singlet state because introducing a reagent may result in a partial relaxation of the triplet state to the ground state in characteristic times of the same order of magnitude than the reaction of the ground state with that reagent. The LIF signal of the ground state will then be sustained by this source involving the measurement of an underestimated rate coefficient. To get rid of this complex situation, molecular oxygen was introduced in the reservoir of the nozzle at a fixed flow rate in addition to the studied reagent. We have demonstrated in a previous work⁹⁷

Table 4. Production and detection conditions for the study of C_2 and C_4H radicals.

Radical	Precursor	Production laser	Excitation radiation, ^a dye	Collection radiation ^a	Interference filter
$C_2(X^1\Sigma_g^+)$	C_2Cl_4	excimer laser Lambda Physik LPX 210i 193 nm	231 nm ($D^1\Sigma_u^+ \leftarrow X^1\Sigma_g^+(0,0)$) coumarin 460	231 nm ($D^1\Sigma_u^+ \leftarrow X^1\Sigma_g^+(0,0)$)	228 nm 11 nm fwhm
$C_2(a^3\Pi_u)$	C_2Cl_4	excimer laser Lambda Physik LPX 210i 193 nm	516 nm ($d^3\Pi_g \leftarrow a^3\Pi_u(0,0)$) coumarin 307	563 nm ($d^3\Pi_g \leftarrow a^3\Pi_u(0,1)$)	561.4 nm 9 nm fwhm
C_4H	C_4H_2	excimer laser Lambda Physik LPX 210i 248 nm	408 nm $\tilde{B}^2\Pi_i - \tilde{X}^2\Sigma^+$ $2\Sigma^+ - 2\Sigma^+$ styryl 9M (frequency doubling)	$> 430\text{ nm}$ $\tilde{B}^2\Pi_i - \tilde{X}^2\Sigma^+$ $2\Sigma^+ - 2\Sigma^+$	low pass band filter GG435

^a Wavelengths and the corresponding transitions (see text for details).

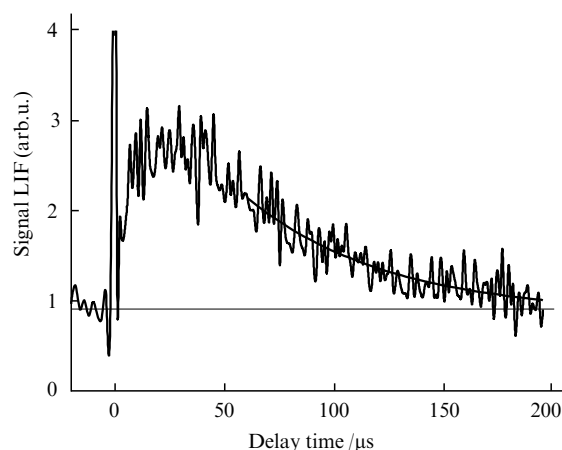


Figure 3. Decay of $C_2(X^1\Sigma_g^+)$ LIF signal at 36 K in the presence of C_2H_2 ($[C_2H_2] = 3.8 \times 10^{13}$ molecules cm^{-3}) and He buffer gas ($[He] = 5.3 \times 10^{16}$ atoms cm^{-3}), fit to a single exponential function.

that O_2 was an efficient scavenger for the triplet state in the temperature range 50–200 K and therefore in this range, experiments were carried out with the singlet ground state only present in the reactor. At temperatures below 50 K, a mixture of both states was, however, present and consequences will be discussed in a further paragraph. At room temperature, oxygen was also introduced to generate an equilibrated population of triplet and singlet states before reaction with the reagent took place. The study of the removal of the triplet state was obviously made without introducing oxygen.

As mentioned in Table 4, the ground state was detected using the Mulliken bands at *ca.* 231 nm whereas the triplet state was identified through the Swan bands at about 516 nm. Five hydrocarbons were studied: CH_4 , C_2H_2 , C_2H_4 , C_2H_6 and C_3H_8 . The whole results are presented in Figs 5 to 9 where data are gathered by reactant for both singlet and triplet states. In the case of CH_4 , the triplet state however is non reactive and therefore Fig. 5 contains data for the singlet state only.

As it can be observed, the reactivity of the triplet state is always lower than that of the ground state. The former is poorly removed by saturated hydrocarbons. For C_2H_6 measurements were only carried out at 200 K and 300 K because the process was not efficient enough at lower temperatures to be measurable by the CRESU apparatus. It seems however that destruction of $C_2(a^3\Pi_u)$ increases with the complexity of the hydrocarbon because measurement for propane showed a

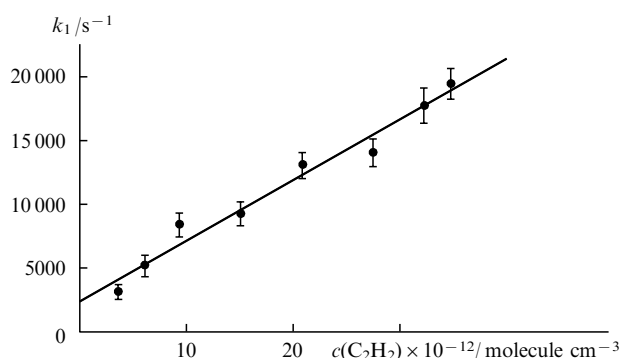


Figure 4. Plot for the removal of $C_2(X^1\Sigma_g^+)$ by C_2H_2 at 36 K in He, yielding a value for the second-order rate coefficient of $k = 4.7 \times 10^{-10}$ cm^3 s^{-1} molecule $^{-1}$.

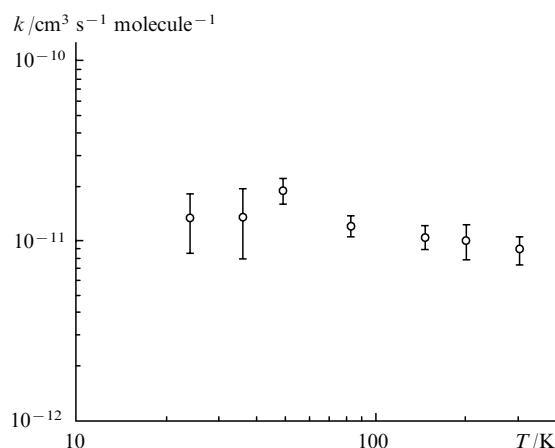


Figure 5. Second-order rate coefficients k for the removal of $C_2(X^1\Sigma_g^+)$ by CH_4 measured as a function of the temperature.

rate coefficient that is one order of magnitude greater than for C_2H_6 . At the lowest temperature of the experiment however the rate coefficient was also unquantifiable. Although measurable, the removal of the triplet state with propane was still an order of magnitude lower than the reactivity of the singlet state. For unsaturated hydrocarbons, the triplet state is significantly more destroyed, but still in a less efficient way than the singlet state (about a factor of 2 to 3). Finally, it is important to stress that it is not possible in this experiment to discriminate between the pure reactivity and the possible relaxation of the triplet state to the ground state. It is then more appropriate to talk about the total removal of the triplet state rather than about the reactivity with reactants. More details can be found in Ref. 113.

With respect to the singlet ground state, the determined rate coefficients were always found to be very fast over the whole temperature range (greater than 10^{-10} cm^3 s^{-1} molecule $^{-1}$) except for methane for which the rate coefficient was measured to be about constant and at least one order of magnitude lower than for C_2 - and C_3 -based hydrocarbons. The temperature dependence is usually rather weak although a shallow maximum can be identified at about 50–70 K. Values are very close to the collisional limit and this is more particularly true for C_2H_2 and C_2H_4 .

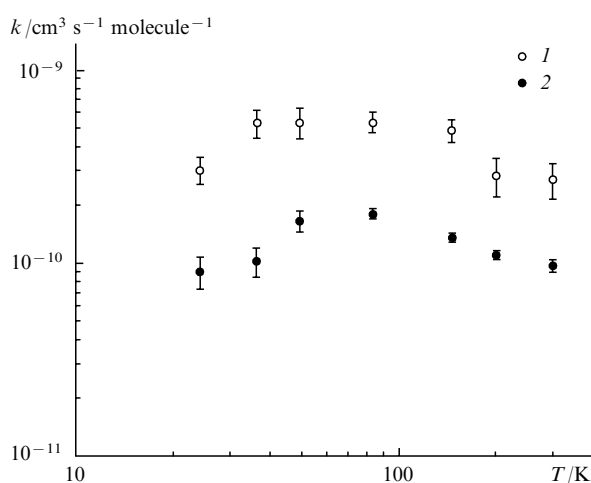


Figure 6. Second-order rate coefficients k for the removal of $C_2(X^1\Sigma_g^+)$ (1) and $C_2(a^3\Pi_u)$ (2) by C_2H_2 measured as a function of the temperature.

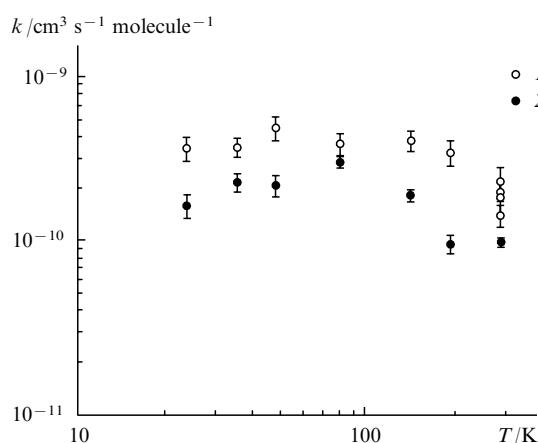


Figure 7. Second-order rate coefficients k for the removal of $C_2(X^1\Sigma_g^+)$ (1) and $C_2(a^3\Pi_u)$ (2) by C_2H_4 measured as a function of the temperature.

Concerning data obtained for the singlet state at temperatures below 50 K the analysis shows that the removal of the singlet state by the three saturated hydrocarbons only results from pure reactivity with these species because the removal of the triplet state is very small or immeasurable below 50 K. For unsaturated hydrocarbons the situation is more complex because the removal of the triplet and the singlet states are found to be very fast. Then the observed decay of the rate coefficient below 50 K could come from underestimated values of the rate coefficient due to relaxation of the triplet state. Since this latter process cannot be clearly evaluated, we prefer to maintain a cautious analysis and claim that these results are lower-limit rate coefficients for the reactivity of $C_2(X^1\Sigma_g^+)$ with C_2H_2 and C_2H_4 . It is worth stressing however that this behaviour was already observed at low temperature for several reactions as for example those involving boron⁷⁸ or silicon^{101,114} atoms with hydrocarbons. As for the reaction $B + C_2H_2$,⁷⁸ a very small activation barrier can also be responsible for the observed decay.

More details concerning these studies can be found elsewhere¹¹¹ and more particularly a discussion concerning the possible consequences of these high rate coefficients for the photochemistry of Titan and Giant Planets. Briefly, these results show that reactions of C_2 with C_2H_2 , C_2H_4 and C_2H_6 are significant destruction routes of the dicarbon radical which are presently not taken into account in the photochemical models of the atmospheres of these bodies. Moreover, in the

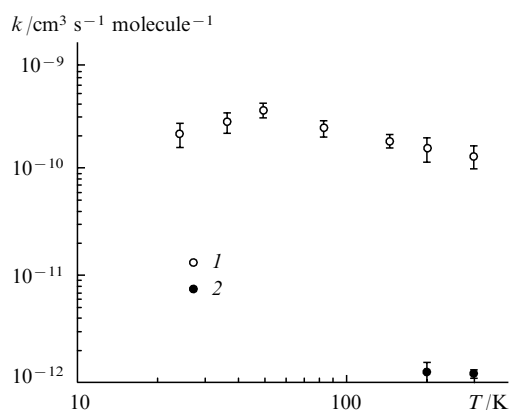


Figure 8. Second-order rate coefficients k for the removal of $C_2(X^1\Sigma_g^+)$ (1) and $C_2(a^3\Pi_u)$ (2) by C_2H_6 measured as a function of the temperature.

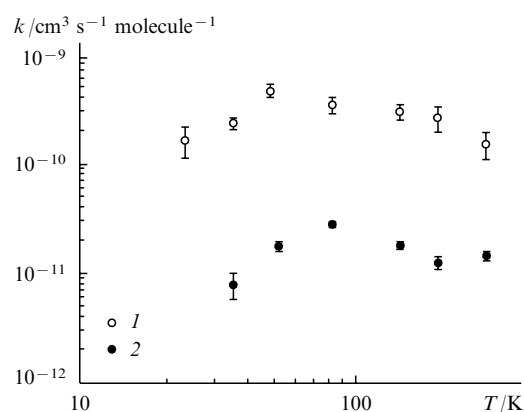


Figure 9. Second-order rate coefficients k for the removal of $C_2(X^1\Sigma_g^+)$ (1) and $C_2(a^3\Pi_u)$ (2) by C_3H_8 measured as a function of the temperature.

chemistry of circumstellar envelopes,¹³¹ the reactivity of C_2 with C_2H_2 , which is a potential source of C_4H , has been recently updated using our new measurements because the rate coefficient which was in use was underestimated by at least a factor of four⁵⁰ (and associated website <http://www.udfa.net/>). Reactions with C_2H_4 and CH_4 which were absent in the chemical scheme have also been added.

Finally, it is interesting to note that the kinetic behaviour of $C_2(X^1\Sigma_g^+)$ with C_2H_2 , C_2H_4 , C_2H_6 and C_3H_8 is quite similar to that observed for CH with the same reactants¹¹⁰ indicating that the reactive mechanisms might be similar *i.e.*, insertion or addition of the radical followed by a hydrogen elimination. Regarding to the products, little information can be found in the literature. The reaction of the ground state of C_2 with CH_4 is expected to proceed *via* insertion of C_2 in the C–H bond.^{132,133} Kaiser *et al.*^{134,135} performed crossed molecular beam experiments to study the dynamics of $C_2(X^1\Sigma_g^+)$ and $C_2(a^3\Pi_u)$ with C_2H_2 (see Ref. 135) and C_2H_4 (see Ref. 134) at collision energies in the range 14.7–28.9 kJ mol^{−1} (*i.e.* ~1100–2300 K) and combined them with *ab initio* electronic structure calculations. They concluded that one exit channel was available and leads to 1 hydrogen atom elimination.

The C_4H radical is produced in the laboratory by photodissociation of diacetylene, C_4H_2 , using UV or VUV light. One of the major difficulties concerning the study of the reactivity of this radical with hydrocarbons lies in the synthesis of diacetylene which cannot be bought from private companies. This very unstable molecule was made in our laboratory from the dehydrochlorination of 1,4-dichloro-2-butyne ($C_4H_4Cl_2$). It was then stored into a 20-litre glass vessel buffered with helium under a total pressure of 1.2 bar. This mixture was then introduced in the reservoir of the Laval nozzle using a micro-metric valve. The C_4H radical was produced by photolysis of C_4H_2 using an excimer laser working at 248 nm. The pencil of radicals generated all along the flow axis was detected by LIF exciting a $^2\Sigma^+ \rightarrow ^2\Sigma^+$ vibronic band of the $\tilde{B}^2\Pi_i - \tilde{X}^2\Sigma^+$ electronic system at a wavelength of *ca.* 408 nm. Fluorescence was collected with a photomultiplier tube through a low-pass glass filter (see Table 4).

Twelve hydrocarbons were studied including CH_4 , C_2H_2 , C_2H_4 , C_2H_6 , C_3H_4 (propyne and propadiene), C_3H_6 , C_3H_8 , C_4H_6 (butyne and butadiene), C_4H_8 and C_4H_{10} . This work was limited to temperatures greater than 39 K because below that value rotational relaxation of C_4H was not fast enough to be completed within the available hydrodynamic time of the experiment. A sample of our results limited to CH_4 , C_2H_2 , C_2H_4 , C_2H_6 , C_3H_4 (propyne) and C_3H_8 is presented in Figures 10 and 11. In all cases, reactivity increases when the temperature is lowered and, as for C_2 , the rate coefficient reaches a

shallow maximum before starting to slightly decrease in some cases. It is worth noting that the rate coefficient increases with the number of carbon atoms in the molecule when considering the reagents by family (alkanes, alkenes, alkynes and dienes). As for $C_2(X^1\Sigma_g^+)$, the rate coefficients are very fast and close to the collision limit indicating that these processes are certainly barrierless. More details concerning these measurements can be found elsewhere.¹¹²

Among the studied hydrocarbons, six have been detected in the atmosphere of Titan (CH_4 , C_2H_2 , C_2H_4 , C_2H_6 , C_3H_4 : propyne and C_3H_8). In photochemical models of this Saturn's moon, only reactions of C_4H with the first four reagents are taken into account probably because the abundance of propyne and propane are too small. We have compared our measurements with the values of the rate coefficients included in these models^{136–140} and realised that the chosen rates were always underestimated, sometimes by more than one order of magnitude. The closest estimations were proposed in a recent model by Wilson and Atreya¹⁴⁰ who used rate coefficients comparable with those measured recently for reactions of C_2H with CH_4 , C_2H_2 , C_2H_4 and C_2H_6 (see references in Table 3). These aspects clearly show that the photochemical models should be revised. In particular, these new experimental data may affect the formation of polyaromatic polymers which are

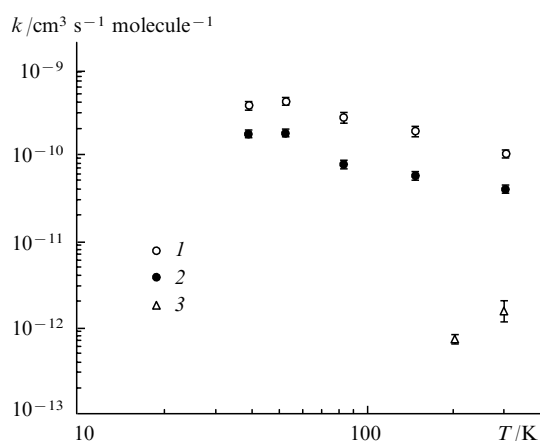


Figure 10. Second-order rate coefficients k for the reaction of C_4H with alkanes [C_3H_8 (1), C_2H_6 (2), CH_4 (3)] measured as a function of the temperature.

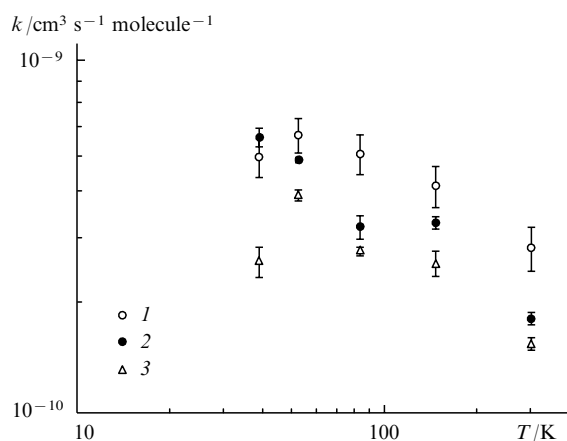


Figure 11. Second-order rate coefficients k for the reaction of C_4H with C_3H_4 (propyne) (1), C_2H_4 (2), and C_2H_2 (3) measured as a function of the temperature.

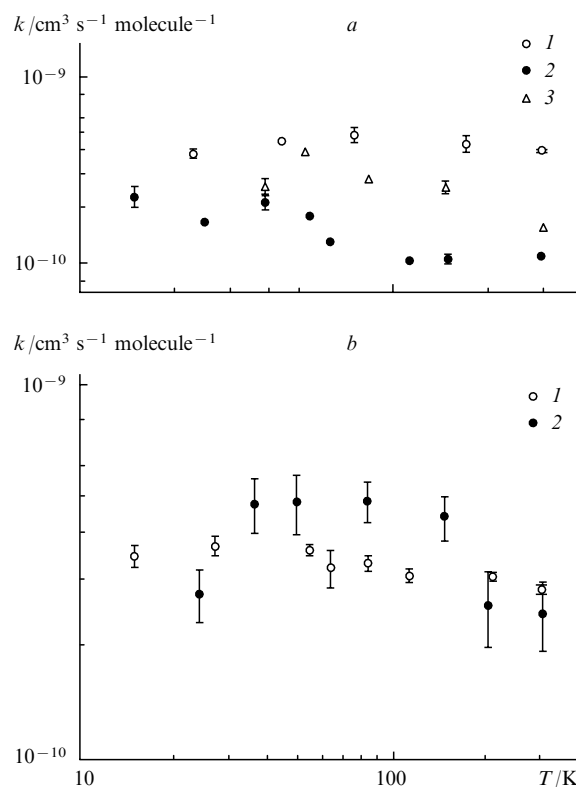


Figure 12. Second-order rate coefficients k for the reaction of C_2H_2 with CH (1),¹¹⁰ C_2H (2)⁹⁶ and C_4H (3)¹¹² measured as a function of the temperature (a). Second-order rate coefficients k for the reaction of C_2H_2 with $C(^3P)$ (1)⁹⁸ and $C_2(X^1\Sigma_g^+)$ (2)¹¹¹ measured as a function of the temperature (b).

one possible route for the production of the thick haze that is present in the upper atmosphere of Titan.^{122, 141}

At this stage of our knowledge, it is rather interesting to start comparisons of the known rate coefficients that were measured within the last 15 years at very low temperature. More particularly, some stable reagents have now been studied in the presence of a large number of differing radicals. Concerning carbon-based species the reactivity of acetylene has been studied in flow gases containing radicals such as $C(^3P)$, CH , C_2 , C_2H and C_4H (see references in Table 3). The temperature evolution of the rate coefficients for these five reactions is presented in Fig. 12a and 12b. As it can be seen, rates are all fast and present temperature dependences that are rather similar. These observations may help in the estimation of rate coefficients for which the measurement is not experimentally possible and may suggest new theoretical routes to explore.

V. Perspectives

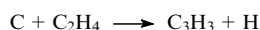
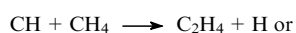
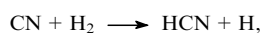
Although a lot of studies have been carried out on the experimental determination of rate coefficients at very low temperature within the last 15 years, there is still a considerable amount of work to be achieved. Beside carbon chemistry, there are several directions that are of particular interest.

Most of the present available studies concern small systems *i.e.*, atomic radicals or simple molecular radicals and reagents (see Table 3). There are still several aspects that remain unexplored however. As a matter of example, the chemistry of sulfur is completely unknown at very low temperature although molecules such as SO or SO_2 are routinely used to trace shock areas in the interstellar medium.^{142, 143} The reac-

tivity of sulfur atoms is certainly of interest in the production of more complex sulfur-bearing molecules. The chemistry of metastable atoms is also important in our atmosphere and in planetary atmospheres as well. Only a few data concerning the reactivity of $O(^1D)$ are available at temperatures close to 200 K.^{144–146} Extension to the lower temperatures of Titan should be valuable as well as determining rate coefficients for other atoms such as $N(^2D)$, $C(^1D)$ or $S(^1D)$. A much more difficult task resides on the experimental study of radical–radical reactions because in that case one of the partners must be produced in a large and well-defined quantity (typically 10^{13} molecules cm^{-3}) so that the characteristic time of the reaction is small enough to be measured by experimental setups such as supersonic flows. It is worth mentioning here the very recent study concerning $O + OH$ which was conducted at temperatures as low as 39 K.⁹³ Future work may focus on reactions such as $N + OH$, $O + CN$, $O + CH$ or a simpler one $N + NO$ which are all of particular interest in interstellar chemistry.

Another important aspect that modern astrophysics revealed is the complexity of the existing interstellar molecules as illustrated by Table 1. It is important to understand how this complexity may be generated and to which level it can be brought. Although polycyclic aromatic hydrocarbons have not yet been directly observed in the interstellar medium, it is now largely accepted that they are mostly present. Their reactivity with other molecules is then of particular interest because insertion mechanisms could contribute to the building up of new species containing an increasing number of aromatic cycles. The study of dimerisation and eventually nucleation of PAHs can also give new insights in the generation of nanoparticles by extension of interstellar dust. Finally, reactions of simple stable C_2 , C_3 and C_4 -based hydrocarbons with radicals should also be completed although it is rather well documented now.

Measuring rate coefficients, although being of crucial importance, is only a partial answer to the understanding of a chemical process. Obviously, the identification of the products and the quantification of the branching ratios are vital as well. This aspect is much more difficult with the available experimental techniques dedicated worldwide to the investigation of gas phase kinetics. Although products can be identified by several methods such as LIF or mass spectrometry, the determination of their concentration is usually not possible. Some recent works are noteworthy however. Reactions for which only one exit channel is open can be used as references to determine the quantity of products of another process. This idea was used by the group of Seakins in Leeds (UK)^{147, 148} and Loison in Bordeaux (France)^{149–153} to obtain the branching ratio of channels containing hydrogen atoms. Calibration reactions such as



can be used whereas H atoms are detected by VUV-LIF. These studies however are only available at room temperature and it would be worth to extend them at interstellar temperatures. The development of infrared lasers opens new possibilities for the determination of branching ratios. Multipass cells can be coupled to infrared light to detect molecular radicals by absorption techniques and quantify their concentration. Using this method, Herschberger and co-workers^{154–159} obtained a significant amount of results at room temperature and above. One of the major problems here lies in the vibrational population of the produced molecules which may not be in equilibrium and therefore relaxation processes could inter-

fere in the measurements. This was solved by the authors using SF_6 as a buffer gas,¹⁶⁰ a technique which is inapplicable to CRESU supersonic flows because of potential polymerisation of large concentrations of SF_6 during the expansion. A more promising technique lies on the photoionisation of products at threshold using VUV light and collection of the ions by a time-of-flight mass spectrometer. VUV can be generated by wave mixing laser techniques. This however is rather limited because of the restricted accordability of the generated light. Furthermore, the quantity of photons is generally rather small. A more appropriate tool for this kind of study is light produced from a synchrotron. Recent works have been undertaken at room temperature coupling a slow flow cell reactor to the ALS synchrotron in Berkeley.¹⁶¹ By scanning the VUV light it is possible to detect products according to their ionisation potential which allows one to separate isomers. Provided that ionisation cross sections are known, the concentration of the products can be extracted from the experiment. Using a reduced version of the CRESU apparatus, it could be possible to couple it to a synchrotron (SOLEIL in France) and then make this kind of experiments at low temperatures.

Another challenge of experimental gas kinetics would be to be able to study the reactivity of molecules at even colder temperatures. The CRESU technique is well designed for this kind of task although the continuous version will request considerable pumping capacities to reach temperatures as low as a few Kelvin. Let's remind that the technique is presently limited to temperatures greater than 15 K for a reservoir kept at room temperature. Using a pulsed version of the CRESU apparatus coupled to the pumping capacities which are available in Rennes will make it possible however to obtain temperatures lower than 5 K reducing by a factor of 3 the present limit. This idea is in development in our lab and would open new horizons. More particularly it would allow one to compare theory and experiments in these extreme conditions. Indeed, theoretical predictions indicate that peculiar behaviours of the rate coefficients below 10 K should occur. As a matter of example, capture theories are expecting a maximum of the rate coefficient close to that temperature and then a significant decrease for colder conditions.

As it can be seen through these pages, the field of gas kinetics at low temperature is very active and has still unexplored areas. The development of new technologies however should allow experimentalists to push the limits even further and exciting results are expected in the future.

The present work was made possible thanks to the very efficient collaboration of my colleagues in Rennes: C Berteloite, P Birza, S Le Picard, A Páramo, B R Rowe, I R Sims and D Travers. I am particularly grateful to B R Rowe and I W M Smith, whose association made possible the development and success of the studies of neutral–neutral reactions at very low temperatures. The work is funded through two French national programmes: Physique et Chimie du Milieu Interstellaire (PCMI) et Planétologie (PNP); the European commission through the 'Molecular Universe' network; the Region of Brittany and Rennes Metropole to which I express my deep thanks.

References

1. R Atkinson, D L Baulch, R A Cox, J N Crowley, R F Hampson, R G Hynes, M E Jenkin, M J Rossi, J Troe *Atmos. Chem. Phys.* **6** 3625 (2006)
2. R Atkinson, D L Baulch, R A Cox, J N Crowley, R F Hampson, R G Hynes, M E Jenkin, M J Rossi, J Troe *Atmos. Chem. Phys.* **4** 1461 (2004)
3. I W M Smith *Chem. Rev.* **103** 4549 (2003)

4. D W Trainor, D O Ham, F Kaufman *J. Chem. Phys.* **58** 4599 (1973)
5. D O Ham, D W Trainor, F Kaufman *J. Chem. Phys.* **53** 4395 (1970)
6. M J Frost, P Sharkey, I W M Smith *J. Phys. Chem.* **97** 12254 (1993)
7. M J Frost, P Sharkey, I W M Smith *Faraday Discuss.* **91** 305 (1991)
8. I W M Smith, B R Rowe *Acc. Chem. Res.* **33** 261 (2000)
9. I W M Smith *Angew. Chem., Int. Ed.* **45** 2842 (2006)
10. V V Barelko, I M Barkalov, V I Goldanskii, D P Kiryukhin, A M Zanin *Adv. Chem. Phys.* **74** 339 (1988)
11. V V Barelko, I M Barkalov, V I Goldanskii, A M Zanin, D P Kiryukhin *Usp. Khim.* **59** 353 (1990) [*Russ. Chem. Rev.* **59** 205 (1990)]
12. D P Kiryukhin, I M Barkalov *Vysokomol. Soedin., Ser. B* **42** 244 (2000)^a
13. D P Kiryukhin, I M Barkalov *Usp. Khim.* **72** 245 (2003) [*Russ. Chem. Rev.* **72** 217 (2003)]
14. D C Clary, E Buonomo, I R Sims, I W M Smith, W D Geppert, C Naulin, M Costes, L Cartechini, P Casavecchia *J. Phys. Chem. A* **106** 5541 (2002)
15. A I Maergoiz, E E Nikitin, J Troe, V G Ushakov *J. Chem. Phys.* **105** 6277 (1996)
16. A I Maergoiz, E E Nikitin, J Troe, V G Ushakov *J. Chem. Phys.* **108** 5265 (1998)
17. A I Maergoiz, E E Nikitin, J Troe, V G Ushakov *J. Chem. Phys.* **108** 9987 (1998)
18. W D Geppert, D Reignier, T Stoecklin, C Naulin, M Costes, D Chastaing, S D Le Picard, I R Sims, I W M Smith *Phys. Chem. Chem. Phys.* **2** 2873 (2000)
19. D C Clary *Annu. Rev. Phys. Chem.* **41** 61 (1990)
20. J Troe *Z. Phys. Chem.-Int. J. Res. Phys. Chem. Chem. Phys.* **218** 457 (2004)
21. Y Georgievskii, S J Klippenstein *J. Chem. Phys.* **122** 194103 (2005)
22. E I Dashevskaya, A I Maergoiz, J Troe, I Litvin, E E Nikitin *J. Chem. Phys.* **118** 7313 (2003)
23. T Stoecklin, C E Dateo, D C Clary *J. Chem. Soc., Faraday Trans.* **87** 1667 (1991)
24. D Reignier, T Stoecklin, S D Le Picard, A Canosa, B R Rowe *J. Chem. Soc., Faraday Trans.* **94** 1681 (1998)
25. J Troe, J C Lorquet, J Manz, R A Marcus, M Herman *Advances in Chemical Physics. Chemical Reactions and their Control on the Femtosecond Time Scale. The 20th Solvay Conference on Chemistry* (New York: Wiley, 1997) Vol. 101, p. 819
26. L B Harding, A I Maergoiz, J Troe, V G Ushakov *J. Chem. Phys.* **113** 11019 (2000)
27. A Faure, L Wiesenfeld, P Valiron *Chem. Phys.* **254** 49 (2000)
28. J Troe *J. Chem. Soc., Faraday Trans.* **90** 2303 (1994)
29. J Troe, V G Ushakov *J. Chem. Phys.* **115** 3621 (2001)
30. A Fernandez-Ramos, J A Miller, S J Klippenstein, D G Truhlar *Chem. Rev.* **106** 4518 (2006)
31. H Sabbah, L Biennier, I R Sims, Y Georgievskii, S J Klippenstein, I W M Smith *Science* **317** 102 (2007)
32. I W M Smith, A M Sage, N M Donahue, E Herbst, D Quan *Faraday Discuss.* **133** 137 (2006)
33. O Gusev, M Kaufmann, K U Grossmann, F J Schmidlin, M G Shepherd *J. Atmos. Solar-Terr. Phys.* **68** 1684 (2006)
34. M Fulchignoni, F Ferri, F Angrilli, A J Ball, A Bar-Nun, M A Barucci, C Bettanini, G Bianchini, W Borucki, G Colombatti, M Coradini, A Coustenis, S Debei, P Falkner, G Fanti, E Flamini, V Gaborit, R Grard, M Hamelin, A M Harri, B Hathi, I Jernej, M R Leese, A Lehto, P F L Stoppato, J J Lopez-Moreno, T Mäkinen, J A M McDonnell, C P McKay, G Molina-Cuberos, F M Neubauer, V Pirronello, R Rodrigo, B Saggin, K Schwingenschuh, A Seiff, F Simoes, H Svedhem, T Tokano, M C Towner, R Trautner, P Withers, J C Zarnecki *Nature (London)* **438** 785 (2005)
35. R V Yelle, F Herbert, B R Sandel, R J Vervack, T M Wentzel *Icarus* **104** 38 (1993)
36. D F Strobel, X Zhu, M E Summers, M H Stevens *Icarus* **120** 266 (1996)
37. S D Rodgers, S B Charnley, W F Huebner, D C Boice *Comets II*. (Eds M Festou, H U Keller, H A Weaver) (Tucson: University Arizona Press, 2005) p. 505
38. J Lequeux, E Falgarone, C Rytter *The Interstellar Medium* (Berlin, Heidelberg: Springer, 2005)
39. D E Woon www.astrochymist.org/astrochymist_ism.html (2007)
40. www.astrochemistry.net (2007)
41. P F Goldsmith, W D Langer *Astrophys. J.* **222** 881 (1978)
42. J Rawlings *Astrophys. Space Sci.* **285** 777 (2003)
43. W D Watson *Rev. Mod. Phys.* **48** 513 (1976)
44. Y P Viala, C M Walmsley *Astron. Astrophys.* **50** 1 (1976)
45. G F Mitchell, J L Ginsburg, P J Kuntz *Astrophys. J.* **212** 71 (1977)
46. J H Black, A Dalgarno *Astron. Astrophys., Suppl. Ser.* **34** 405 (1977)
47. E Herbst, W Klemperer *Astrophys. J.* **185** 505 (1973)
48. T J Millar, D A Williams *Astron. Astrophys.* **173** 527 (1975)
49. I W M Smith, E Herbst, Q Chang *Astron. Astrophys.* **350** 323 (2004)
50. J Woodall, M Agúndez, A J Markwick-Kemper, T J Millar *Astron. Astrophys.* **466** 1197 (2007)
51. S Brünken, H Gupta, C A Gottlieb, M C McCarthy, P Thaddeus *Astrophys. J.* **664** L43 (2007)
52. A J Remijan, J M Hollis, F J Lovas, M A Cordiner, T J Millar, A J Markwick-Kemper, P R Jewell *Astrophys. J.* **664** L47 (2007)
53. M C McCarthy, C A Gottlieb, H Gupta, P Thaddeus *Astrophys. J.* **652** L141 (2006)
54. J Cernicharo, M Guélin, M Agúndez, K Kawaguchi, M C McCarthy, P Thaddeus *Astron. Astrophys.* **467** L37 (2007)
55. E Herbst, H H Lee, D A Howe, T J Millar *Astron. Astrophys.* **268** 335 (1994)
56. R P A Bettens, H H Lee, E Herbst *Astrophys. J.* **443** 664 (1995)
57. L Herbert, I W M Smith, R D Spencer-Smith *Int. J. Chem. Kinet.* **24** 791 (1992)
58. I R Sims, J L Queffelec, D Travers, B R Rowe, L B Herbert, J Karthäuser, I W M Smith *Chem. Phys. Lett.* **211** 461 (1993)
59. M A Smith, M Hawley *Advances in Gas Phase Ion Chemistry* (Amsterdam: Elsevier, 1992) Vol. 1, p. 167
60. M A Smith *Unimolecular and Bimolecular Reaction Dynamics* (Eds C Y Ng, T Baer, I Powis) (New York: Wiley, 1994) p. 183
61. B Maté, A Graur, T Elizarova, I Chirokov, G Tejeda, J M Fernández, S Montero *J. Fluid Mech.* **426** 177 (2001)
62. T L Mazely, M A Smith *J. Chem. Phys.* **89** 2048 (1988)
63. L K Randeniya, M A Smith *J. Chem. Phys.* **93** 661 (1990)
64. M Herman, R Georges, M Hepp, D Hurtmans *Int. Rev. Phys. Chem.* **19** 277 (2000)
65. P Casavecchia *Rep. Prog. Phys.* **63** 355 (2000)
66. R D Levine *Molecular Reaction Dynamics* (Cambridge: Cambridge University Press, 2005)
67. Y T Lee, J D McDonald, P R Le Breton, D R Herschbach *Rev. Sci. Instrum.* **40** 1402 (1969)
68. Y T Lee *Atomic and Molecular Beam Methods* (Ed. G Scoles) (New York: Oxford University Press, 1988) p. 553
69. K P Liu *Int. Rev. Phys. Chem.* **20** 189 (2001)
70. K P Liu *Annu. Rev. Phys. Chem.* **52** 139 (2001)
71. R I Kaiser *Chem. Rev.* **102** 1309 (2002)
72. N Balucani, G Capozza, F Leonori, E Segoloni, P Casavecchia *Int. Rev. Phys. Chem.* **25** 109 (2006)
73. G Hall, K Liu, M J McAuliffe, C F Giese, W R Gentry *J. Chem. Phys.* **81** 5577 (1984)
74. W R Gentry *Atomic and Molecular Beam Methods* (Ed. G Scoles) (New York: Oxford University Press, 1988) p. 54
75. R G Macdonald, K Liu *J. Chem. Phys.* **91** 821 (1989)
76. C Naulin, M Costes *Chem. Phys. Lett.* **310** 231 (1999)
77. P Casavecchia, G Capozza, E Segoloni *Modern Trends in Chemical Reaction Dynamics: Experiment and Theory Pt II* (Eds X Yang, K Liu) (Singapore: World Sci., 2004) p. 329
78. W D Geppert, F Goulay, C Naulin, M Costes, A Canosa, S D Le Picard, B R Rowe *Phys. Chem. Chem. Phys.* **6** 566 (2004)

79. G Dupeyrat, J B Marquette, B R Rowe *Phys. Fluids* **28** 1273 (1985)
80. J B Marquette, B R Rowe, G Dupeyrat, G Poissant, C Rebrion *Chem. Phys. Lett.* **122** 431 (1985)
81. F Goulay, C Rebrion-Rowe, J L Le Garrec, S D Le Picard, A Canosa, B R Rowe *J. Chem. Phys.* **122** 104308 (2005)
82. F Goulay, C Rebrion-Rowe, L Biennier, S D Le Picard, A Canosa, B R Rowe *J. Phys. Chem. A* **110** 3132 (2006)
83. I R Sims, J-L Queffelec, A Defrance, C Rebrion-Rowe, D Travers, P Bocherel, B R Rowe, I W M Smith *J. Chem. Phys.* **100** 4229 (1994)
84. P L James, I R Sims, I W M Smith *Chem. Phys. Lett.* **272** 412 (1997)
85. P L James, I R Sims, I W M Smith *Chem. Phys. Lett.* **276** 423 (1997)
86. P L James, I R Sims, I W M Smith, M H Alexander, M Yang *J. Chem. Phys.* **109** 3882 (1998)
87. N Daugey, P Caubet, B Retail, M Costes, A Bergeat, G Dorthé *Phys. Chem. Chem. Phys.* **7** 2921 (2005)
88. D B Atkinson, M A Smith *Rev. Sci. Instrum.* **66** 4434 (1995)
89. S Lee, R J Hoobler, S R Leone *Rev. Sci. Instrum.* **71** 1816 (2000)
90. E Vohringer-Martinez, B Hansmann, H Hernandez, J S Francisco, J Troe, B Abel *Science* **315** 497 (2007)
91. T Spangenberg, S Köhler, B Hansmann, U Wachsmuth, B Abel, M A Smith *J. Phys. Chem. A* **108** 7527 (2004)
92. B Hansmann, B Abel *ChemPhysChem* **8** 343 (2007)
93. D Carty, A Goddard, S Köhler, I R Sims, I W M Smith *J. Phys. Chem. A* **110** 3101 (2006)
94. I R Sims, J L Queffelec, A Defrance, C Rebrion-Rowe, D Travers, B R Rowe, I W M Smith *J. Chem. Phys.* **97** 8798 (1992)
95. P Bocherel, L B Herbert, B R Rowe, I R Sims, I W M Smith, D Travers *J. Phys. Chem.* **100** 3063 (1996)
96. D Chastaing, P L James, I R Sims, I W M Smith *Faraday Discuss.* **109** 165 (1998)
97. A Páramo, A Canosa, S D Le Picard, I R Sims *J. Phys. Chem. A* **110** 3121 (2006)
98. D Chastaing, P L James, I R Sims, I W M Smith *Phys. Chem. Chem. Phys.* **1** 2247 (1999)
99. D Chastaing, S D Le Picard, I R Sims *J. Chem. Phys.* **112** 8466 (2000)
100. S D Le Picard, A Canosa, D Travers, D Chastaing, B R Rowe, T Stoeklin *J. Phys. Chem. A* **101** 9988 (1997)
101. S D Le Picard, A Canosa, D Reignier, T Stoeklin *Phys. Chem. Chem. Phys.* **4** 3659 (2002)
102. S D Le Picard, A Canosa, G Pineau des Forêts, C Rebrion-Rowe, B R Rowe *Astron. Astrophys.* **372** 1064 (2001)
103. S D Le Picard, A Canosa, W D Geppert, T Stoeklin *Chem. Phys. Lett.* **385** 502 (2004)
104. R A Brownsword, A Canosa, B R Rowe, I R Sims, I W M Smith, D W A Stewart, A C Symonds, D Travers *J. Chem. Phys.* **106** 7662 (1997)
105. C Mullen, M A Smith *J. Phys. Chem. A* **109** 1391 (2005)
106. A B Vakhtin, D C McCabe, A R Ravishankara, S R Leone *J. Phys. Chem. A* **107** 10642 (2003)
107. V Jaramillo, S Gougeon, S D Le Picard, A Canosa, M Smith, B R Rowe *Int. J. Chem. Kinet.* **34** 339 (2002)
108. I R Sims, I W M Smith, D C Clary, P Bocherel, B R Rowe *J. Chem. Phys.* **101** 1748 (1994)
109. B Nizamov, S R Leone *J. Phys. Chem. A* **108** 3766 (2004)
110. A Canosa, I R Sims, D Travers, I W M Smith, B R Rowe *Astron. Astrophys.* **323** 644 (1997)
111. A Canosa, A Páramo, S D Le Picard, I R Sims *Icarus* **187** 558 (2007)
112. C Berteloite, S D Le Picard, P Birza, M C Gazeau, A Canosa, Y Benilan, I R Sims *Icarus* (2008) (in the press)
113. M A Páramo-Martínez, Ph.D. School of Chemistry, University of Birmingham, Birmingham, UK, 2005
114. A Canosa, S D Le Picard, S Gougeon, C Rebrion-Rowe, D Travers, B R Rowe *J. Chem. Phys.* **115** 6495 (2001)
115. A Canosa, S D Le Picard, W D Geppert *J. Phys. Chem. A* **108** 6183 (2004)
116. J E Murphy, A B Vakhtin, S R Leone *Icarus* **163** 175 (2003)
117. D Carty, V Le Page, I R Sims, I W M Smith *Chem. Phys. Lett.* **344** 310 (2001)
118. D Chastaing, S D Le Picard, I R Sims, I W M Smith, W D Geppert, C Naulin, M Costes *Chem. Phys. Lett.* **331** 170 (2000)
119. B Nizamov, S R Leone *J. Phys. Chem. A* **108** 1746 (2004)
120. A B Vakhtin, D E Heard, I W M Smith, S R Leone *Chem. Phys. Lett.* **348** 21 (2001)
121. F Goulay, S R Leone *J. Phys. Chem. A* **110** 1875 (2006)
122. E H Wilson, S K Atreya *Planet. Space Sci.* **51** 1017 (2003)
123. E J Bakker, E F van Dishoeck, L B F M Waters, T Schoenmaker *Astron. Astrophys.* **323** 469 (1997)
124. C Cecchi-Pestellini, A Dalgarno *Mon. Not. R. Astron. Soc.* **331** L31 (2002)
125. T Oka, J A Thorburn, B J McCall, S D Friedman, L M Hobbs, P Sonnentrucker, D E Welty, D G York *Astrophys. J.* **582** 823 (2003)
126. S P Souza, B L Lutz *Astrophys. J.* **216** L49 (1977)
127. M Guelin, S Green, P Thaddeus *Astrophys. J.* **224** L27 (1978)
128. M B Bell, T J Sears, H E Matthews *Astrophys. J.* **255** L75 (1982)
129. M B Bell, P A Feldman, H E Matthews *Astrophys. J.* **273** L35 (1983)
130. E A Ballick, D A Ramsay *Astrophys. J.* **137** 84 (1963)
131. T J Millar, E Herbst *Astron. Astrophys.* **288** 561 (1994)
132. W M Pitts, L Pasternack, J R McDonald *Chem. Phys.* **68** 417 (1982)
133. D A Horner, L A Curtiss, D M Dieter *Chem. Phys. Lett.* **233** 243 (1995)
134. R I Kaiser, T N Le, T L Nguyen, A M Mebel, N Balucani, Y T Lee, F Stahl, P V Schleyer, H F Schaefer *Faraday Discuss.* **119** 51 (2001)
135. R I Kaiser, N Balucani, D O Charkin, A M Mebel *Chem. Phys. Lett.* **382** 112 (2003)
136. Y L Yung, M Allen, J P Pinto *Astrophys. J., Suppl. Ser.* **55** 465 (1984)
137. D Toubanc, J P Parisot, J Brillet, D Gautier, F Raulin, C P McKay *Icarus* **113** 2 (1995)
138. L M Lara, E Lellouch, J J López-Moreno, R Rodrigo *J. Geophys. Res.* **101** 23261 (1996)
139. S Lebonnois, D Toubanc, F Hourdin, P Rannou *Icarus* **152** 384 (2001)
140. E H Wilson, S K Atreya *J. Geophys. Res. Planet.* **109** E06002 (2004)
141. S K Atreya, E Y Adams, H B Niemann, J E Mick-Montelara, T C Owen, M Fulchignoni, F Ferri, E H Wilson *Planet. Space Sci.* **54** 1177 (2006)
142. G Pineau des Forêts, E Roueff, P Schilke, D R Flower *Mon. Not. R. Astron. Soc.* **262** 915 (1993)
143. F F S van der Tak, A M S Boonman, R Braakman, E F van Dishoeck *Astron. Astrophys.* **412** 133 (2003)
144. E J Dunlea, A R Ravishankara *Phys. Chem. Chem. Phys.* **6** 2152 (2004)
145. E J Dunlea, A R Ravishankara *Phys. Chem. Chem. Phys.* **6** 3333 (2004)
146. M A Blitz, T J Dillon, D E Heard, M J Pilling, I D Trought *Phys. Chem. Chem. Phys.* **6** 2162 (2004)
147. N Choi, M A Blitz, K McKee, M J Pilling, P W Seakins *Chem. Phys. Lett.* **384** 68 (2004)
148. K McKee, M A Blitz, K J Hughes, M J Pilling, H -B Qian, A Taylor, P W Seakins *J. Phys. Chem. A* **107** 5710 (2003)
149. J C Loison, A Bergeat *Phys. Chem. Chem. Phys.* **6** 5396 (2004)
150. N Galland, F Caralp, Y Hannachi, A Bergeat, J-C Loison *J. Phys. Chem. A* **107** 5419 (2003)
151. P Fleurat-Lessard, J C Rayez, A Bergeat, J-C Loison *Chem. Phys.* **279** 87 (2002)
152. A Bergeat, J C Loison *Phys. Chem. Chem. Phys.* **3** 2038 (2001)
153. A Bergeat, T Calvo, F Caralp, J H Fillion, G Dorthé, J C Loison *Faraday Discuss.* **119** 67 (2001)
154. C A Taatjes, J F Hershberger *Annu. Rev. Phys. Chem.* **52** 41 (2001)

155. W D Thweatt, M A Erickson, J F Hershberger *J. Phys. Chem. A* **108** 74 (2004)
156. J P Meyer, J F Hershberger *J. Phys. Chem. B* **109** 8363 (2005)
157. J P Meyer, J F Hershberger *J. Phys. Chem. A* **109** 4772 (2005)
158. W Feng, J P Meyer, J F Hershberger *J. Phys. Chem. A* **110** 4458 (2006)
159. W Feng, J F Hershberger *J. Phys. Chem. A* **110** 12184 (2006)
160. W F Cooper, J F Hershberger *J. Phys. Chem.* **96** 771 (1992)
161. G Meloni, P Zou, S J Klippenstein, M Ahmed, S R Leone, C A Taatjes, D L Osborn *J. Am. Chem. Soc.* **128** 13559 (2006)

^a — *Polym. Sci. (Engl. Transl.)*

Tunnelling chemical reactions of hydrogen isotopes in quantum solids

V V Khmelenko, E P Bernard, S Vasiliev, D M Lee

Contents

I. Introduction	1107
II. Historical background	1107
III. Studies of exchange tunnelling reactions of hydrogen isotopes in clusters forming impurity – helium solids	1109
IV. Studies of H atoms in solid H ₂ films at ultralow temperatures	1117
V. Conclusions and future work	1120

Abstract. The kinetics of tunnelling reactions of hydrogen isotopes in solid molecular nanoclusters immersed in superfluid helium and the changes in the environment of the atoms during the course of these reactions are reviewed. Results of pulsed electron spin resonance show that a very large fraction (50%–60%) of the stabilised atoms reside on the surfaces of the nanoclusters. The results of studies of the recombination and the exotic behaviour of hydrogen atoms in a solid molecular hydrogen matrix at ultralow temperatures (0.15–0.9 K) are also discussed. The bibliography includes 68 references.

I. Introduction

In this paper we review recent experimental and, briefly, theoretical studies of quantum chemical reactions of atomic hydrogen isotopes in solid molecular matrices at low and ultralow temperatures. We put our main emphasis on the experimental work utilising the magnetic resonance methods of electron spin resonance (ESR), nuclear magnetic resonance (NMR) and electron – nuclear double resonance (ENDOR).

We begin in Section II with a brief historical background of the research on the physical processes and chemical reactions which occur with atomic hydrogen isotopes trapped inside solid hydrogen and/or deuterium molecular matrices. In Section III, we present in more detail a description of the experimental procedure for the preparation of the nanoclusters in superfluid helium and the ESR methods (9 GHz continuous

wave and pulsed spectrometers) used for these studies. We also discuss the studies of the kinetics of exchange tunnelling reactions of hydrogen isotopes at $T \sim 1.35$ K in nanoclusters of impurity – helium (Im – He) solids. The changes of the environment of the atoms during the course of these reactions and the trapping sites of atoms in nanoclusters are also reviewed. In Section IV we discuss the experimental techniques for studies of H atoms in solid H₂ films at ultralow (0.15–0.9 K) temperatures. We present the results of studies of the recombination and the exotic behaviour of H atoms in thin (~ 50 nm) H₂ films in this temperature range. Section V contains a summary, some conclusions and future prospects for investigations of tunnelling reactions of hydrogen isotopes.

II. Historical background

Studies of hydrogen atoms trapped in solid molecular matrices have a long history, starting in the mid-1950s. Jen *et al.*,^{1,2} Wall *et al.*,³ and Pietter *et al.*⁴ performed the first investigations of H atoms in solid H₂. The main motivation for these studies was the achievement of high concentrations of stabilised H atoms for possible application as a rocket fuel. An advantage as compared to existing chemical fuels would be realised only if concentrations of H atoms in solid H₂ of order 7.5% could be achieved.⁵ Various methods were employed for producing H atoms, such as electron and γ -ray bombardment of solid H₂, deposition of the products of electrical discharges in gaseous H₂ on cold surfaces, and the addition of low concentrations of radioactive T₂ to solid H₂. Electron spin resonance (ESR) was used to measure the H atom concentrations. It was found that the average concentrations of H atoms were very small (less than 0.01%). This fact made impossible any practical applications of H – H₂ solid mixtures. Moreover, the amounts of H atoms were found to decrease gradually due to their recombination:



A revival of interest in this system occurred only after three decades because it provided a unique opportunity to study the processes of quantum physical diffusion and quantum tunnelling reactions. The influence of isotopic effects on these processes could also be studied. According to the idea of Andreev and Lifshits,⁶ at low enough temperatures, any impurity inside a crystal becomes delocalised and may freely move within certain energy bands in a fashion similar to the

V V Khmelenko Department of Physics, Cornell University, 14853 Ithaca, NY, USA. Fax (1-607) 255 64 28, tel. (1-607) 255 06 70, e-mail: khmel@ccmr.cornell.edu; Institute of Energy Problems for Chemical Physics (Branch), Russian Academy of Sciences, 142432 Chernogolovka, Moscow Region, Russian Federation. Fax (7-496) 680 35 73

E P Bernard, D M Lee Department of Physics, Cornell University, 14853 Ithaca, NY, USA. Fax (1-607) 255 64 28, tel. (1-607) 255 06 70, e-mail: epb22@cornell.edu (E P Bernard), tel. (1-607) 255 06 71, e-mail: dml20@cornell.edu (D M Lee)

S Vasiliev Department of Physics, University of Turku, 20014 Turku, Finland. Fax (358-2) 333 63 70, tel. (358-2) 333 59 39, e-mail: servas@utu.fi

Received 29 May 2007

Uspekhi Khimii 76 (12) 1185–1201 (2007)

conduction of electrons in metals. This proposal was followed by detailed theoretical studies by Kagan *et al.*⁷ They suggested a phonon assisted mechanism for the physical diffusion of H atoms through the potential barriers in H₂ crystal lattices. The dependence of the recombination rate of H atoms in solid H₂ on temperature according to this mechanism was determined to be linear, as given by

$$k_H(T) = AT.$$

At the same time Ivliev *et al.*⁸ experimentally studied the diffusion of H atoms in solid H₂. The main method for studying the process of quantum diffusion was to measure the rate of recombination of the atoms. However, before recombining, the atoms need to approach each other within a lattice constant. At close enough spacing between the atoms, they distort the lattice potential, and their motion may become severely impeded by the energy level mismatch between the neighbouring sites. Therefore, such 'recombinational' diffusion appears to be much slower than the actual spatial diffusion in an ideal crystal. The studies of the latter still remain an important and challenging task in this research field. It was found that at temperatures above 4.3 K the recombination rate of H atoms follows the Arrhenius law,

$$k_H(T) \sim \exp\left(-\frac{E_a}{kT}\right),$$

where $E_a \sim 103$ K and k is the Boltzmann constant. However, in the temperature range 1.3–4.2 K a linear dependence of k_H on temperature was observed. The latter result was explained by the quantum diffusion mechanism discussed by Kagan *et al.*⁷ From the measurements of the concentration of H atoms in these experiments it was possible to calculate the absolute rate constants and the value of the coefficient A in the formula $k_H(T) = AT$, which was found to be equal to $(2 \pm 1) \times 10^{-24} \text{ cm}^3 \text{ s}^{-1} \text{ K}^{-1}$. These results suggested that the physical quantum diffusion of H atoms in solid H₂ was an important process leading to recombination. In contrast, the Nagoya group led by Miyazaki⁹ and the Chernogolovka group led by Gordon¹⁰ suggested that the dominant process for the migration of H atoms in solid H₂ is the tunnelling exchange chemical reaction:



which provides a chemical diffusion mechanism for the motion of the H atoms from one trapping site to another. Matrix isolated H atoms are confined to potential wells in a molecular H₂ matrix. These wells are not infinitely deep so it is possible for the H atom to tunnel *via* chemical reactions (1) through the matrix. For substitutional sites, tunnelling would correspond to a change in position of the atom by one lattice spacing, so the position of the atom and the neighbouring molecule are interchanged. This process could be repeated many times, thus providing a mechanism for an atom to move through the matrix. The barrier for this reaction is known¹¹ to be 4600 K, which is significantly larger than that for the physical diffusion of H atoms in solid H₂ (~ 100 K). On the other hand the potential barrier for exchange tunnelling is significantly narrower. Takayanagi *et al.*¹² performed theoretical calculations of rate constants for exchange tunnelling reactions of hydrogen isotopes. The theoretical prediction gives a very fast rate constant for reaction (1). Additionally, recent measurements of the recombination rates at different pressures up to 13 MPa show the independence of k_H on pressure.¹³ This important finding could not be explained by physical diffusion, which should be suppressed with increasing pressure, thus supporting the hypothesis of chemical exchange tunnelling of H atoms.

The exchange chemical reaction:



is expected to be much slower because of the larger mass. The experimental results obtained by studying D atom recombination decay are in good qualitative agreement with theoretical predictions by Takayanagi *et al.*¹² Experimental studies of D atoms in bulk D₂ solids were performed by Sharnoff and Pound,¹⁴ Iskovskikh *et al.*¹⁵ and Miyazaki *et al.*^{16–18} Deuterium atoms in D₂ nanoclusters were studied by Gordon *et al.*^{10,19} and Bernard *et al.*^{20,21} Iskovskikh *et al.* found that thermally activated diffusion is responsible for recombination of atoms at temperatures higher than 7 K, but at lower temperatures the two-phonon quantum physical diffusion of D atoms was suggested.¹⁵ The latter mechanism explained the temperature dependence obtained for the rate constant, $k_D \sim T^9$. In contrast, Miyazaki *et al.*^{16,17} and Gordon *et al.*¹⁰ considered that the migration of D atoms through D₂ crystals occurred due to the tunnelling exchange chemical reactions similar to the case of H atoms in solid H₂.

Two important tunnelling exchange reactions that have also been studied experimentally are:



Exchange tunnelling reactions between atoms and molecules of hydrogen isotopes in solid mixtures were discovered by Gordon *et al.*¹⁰ during studies of the stabilisation of nanoclusters containing H and D atoms produced by injection of a gaseous mixture into superfluid ⁴He (at $T \sim 1.8$ K) after it had passed through a radiofrequency (RF) discharge. They found a large enhancement of the concentration of hydrogen atoms in hydrogen–deuterium solid samples so obtained, as compared with the content of hydrogen atoms in the initial gas jets. For example, for a gas content ratio $[\text{H}_2]/[\text{D}_2]$ equal to unity, they observed only ESR signals from hydrogen atoms, indicating an absence of D atoms. Considering all possible exchange chemical reactions between atoms and molecules of hydrogen isotopes, they concluded that due to differences in the zero-point energies of H₂, HD and D₂ molecules, only reactions (1)–(4) and reactions



can occur, leading to a depletion of D atoms and a growth in the H atom population. Reactions:



are endothermic and cannot proceed at the temperature of experiment. As a result of reactions (1)–(6), which occur at these temperatures mainly by tunnelling, H atoms tend to migrate through the matrix until they are surrounded by a shell of deuterium molecules or they recombine with other H atoms.

A few month later, Ivliev *et al.*²² in Moscow and Tsuruta *et al.*⁹ in Nagoya, Japan, using different experimental approaches, studied the evolution of concentrations of hydrogen and deuterium atoms in solid molecular hydrogen–deuterium mixtures, providing direct confirmation of exchange tunnelling reactions at low temperatures. The Nagoya group performed comprehensive quantitative studies of atoms in solid molecular matrices of hydrogen isotopes. They studied the rates of different tunnelling reactions,^{9,16–18,23} the influence of *o*-H₂ in solid H₂ on the rate constant for reactions of H atoms,^{24–26} the temperature effect on the reaction of atoms²⁷ and the trapping sites of the atoms in molecular matrices.^{28–32}

These results were summarised in the monograph edited by Miyazaki.³³

Ivanov *et al.*³⁴ have modeled the temperature dependence of the rate constant for tunnelling reaction (4) in the solid phase. Their model describes the rate constant K at lowest temperatures by the formula

$$\ln k = \ln k_0 + C_4 T^4 + C_5 T^5 + C_6 T^6 + C_8 T^8.$$

The coefficients in this formula were obtained from comparison with the experimental measurements of rate constants in the temperature range 2.6–6.5 K by Miyazaki *et al.*²⁷ The formula predicted that at the lowest temperatures $\ln k$ would be almost independent of temperature. Further studies of this reaction in the solid phase at lower temperatures would be desirable.

The exchange reactions between atoms and molecules of hydrogen isotopes have also been studied in cross beam experiments in gas phase at room temperature. Zhang and Miller³⁵ performed theoretical calculations of the rate constants for these reactions and obtained very good agreement with the experimental results.

During the past five years, the kinetics of exchange tunnelling reactions have been studied at Cornell in samples created by the method that originated in Chernogolovka.^{36,37} The gel-like solids created in superfluid helium are now known as impurity–helium solids or alternatively as impurity–helium condensates.^{38,39} Impurity–helium solids are highly porous gel-like nanomaterials consisting of interconnecting clusters of impurities with a characteristic size 5–9 nm and an average density over the entire sample volume as low as 10^{20} atoms (molecules) cm^{-3} . Each cluster contains approximately 10^4 atoms and molecules. This means that the concentration of the clusters in the impurity–helium solids is of order 10^{16} cm^{-3} . Tunnelling exchange reactions between atoms and molecules of hydrogen isotopes could then be investigated in the collection of nanoclusters and the results could be compared with those obtained earlier in bulk solids. Reactions among chemically active atoms and molecules within nanoclusters are predicted to be more efficient and selective than analogous reactions in bulk material.⁴⁰

Although most studies of H atoms in solid H_2 were performed at temperatures above 1 K, Webeler⁴¹ studied the recombination heating in solid H_2 containing 0.03% radioactive T_2 in the temperature range $0.16 \text{ K} \leq T \leq 0.8 \text{ K}$. The β -decay led to the dissociation of H_2 molecules, thus providing a population of H atoms. Results show an increase of H atom concentration with time, followed by spontaneous decay. Lowering the temperature led to an increase in the energy release from the recombination of H atoms during spontaneous decay. The first studies of recombination rates of H atoms in solid H_2 in the temperature range 0.15–0.9 K were performed very recently by Ahokas *et al.*⁴² A high-field ESR spectrometer,⁴³ in combination with a ^3He – ^4He dilution refrigerator cryostat, was employed in these investigations.

III. Studies of exchange tunnelling reactions of hydrogen isotopes in clusters forming impurity–helium solids

1. A setup for studies of tunnelling reactions in nanoclusters

The experimental setup for investigating exchange tunnelling chemical reactions in nanoclusters at low temperatures at Cornell University is described in more detail elsewhere.⁴⁴ The experiments were performed in a specially designed Janis cryostat with a variable temperature insert (VTI), which is a thermally insulated chamber, separated from the main 4 K helium bath. A needle valve connects the main helium bath of

the cryostat to the VTI. Continuously pumping the VTI while supplying helium from the main bath permits long-term investigations of impurity–helium solids well below the lambda temperature (2.17 K) of liquid helium. The lower part of the cryostat was placed between the pole pieces of a homogeneous Varian electromagnet for CW and pulsed ESR investigations. Impurity–helium solids with stabilised H and D atoms for ESR investigations were prepared *in situ* in the Janis cryostat. The homemade insert for formation and investigation of atoms contained in Im–He solids is shown in Fig. 1. For sample preparation, a gas mixture of H_2 and/or D_2 and He was transported from a room temperature gas handling system to the cryogenic region. To provide H and D atoms *via* dissociation of the gas molecules, high-power radio-frequency ($f \sim 50 \text{ MHz}$, $P \sim 70 \text{ W}$) was applied to electrodes around the quartz capillary carrying the mixed gases. The resulting jet of helium gas with a small fraction (1%–4%) of impurity atoms and molecules emerging from the quartz capillary was directed onto the surface of superfluid ^4He

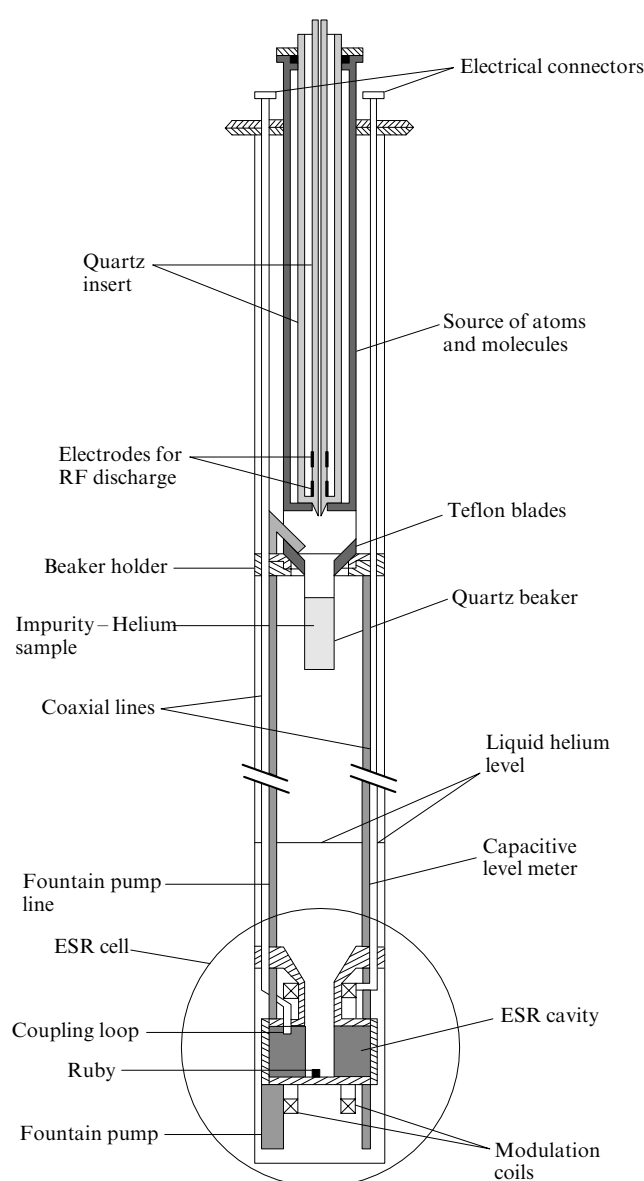


Figure 1. Low temperature insert used in the ESR investigation of Im–He solids.⁴⁴ The quartz beaker is lowered into ESR resonant cavity for measurements after sample preparation.

contained in a small beaker suspended above the VTI helium bath. The addition of helium gas increased the efficiency of dissociations of impurity molecules in the discharge due to interactions between the impurity and metastable He atoms and also retarded agglomeration of impurity atoms and molecules in the gas jet. The jet penetrated the surface of the liquid helium and a macroscopic snow-like translucent material was created. This material fell down through the liquid ^4He to form a porous solid at the bottom of the beaker. A fountain pump connected to the bottom of the helium bath in the VTI maintained a constant liquid helium level in the beaker. The temperature during sample preparation was 1.5 K. At the top of the beaker was a funnel that caught the sample as it condensed below the helium surface, which was 2 cm below the end of the quartz capillary. A set of teflon blades scraped the sample from the funnel while the beaker was rotated so that the sample could fall to the bottom of the cylindrical part of the beaker. A jet with a flux of $\sim 5 \times 10^{19}$ atoms and molecules per second yielded $\sim 0.3\text{--}0.4\text{ cm}^3$ of sample in 10 minutes.

In independent X-ray scattering studies of the $\text{D}_2\text{--He}$ and $\text{D}_2\text{--Ne--He}$ samples, it was shown that these samples consisted of nanoclusters of D_2 molecules, each surrounded by thin layers of solid helium.^{20,21} The typical deuterium cluster size is estimated to be $\sim 5\text{--}9\text{ nm}$. These nanoclusters assemble into a porous gel-like structure. From the comparison of the intensity of the D_2 cluster peak with the intensity of the scattering from liquid helium, the molecular deuterium densities in these samples were found to be of order 10^{20} cm^{-3} . It was difficult to carry out structural studies of $\text{H}_2\text{--He}$ solids because solid hydrogen tends to float to the surface of the collection beaker filled with superfluid helium. Actual studies of hydrogen clusters in this research were performed with $\text{H}_2\text{--Ne--He}$ solids prepared with a mixture of hydrogen and neon make-up gas. The heavier neon clusters allowed the mixture to accumulate in the sample cell. An X-ray investigation of similar $\text{D}_2\text{--Ne--He}$ solids provided evidence that neon and deuterium existed in separate clusters in the sample. The result justifies the assumption that H_2 and Ne mainly occurred in separate nanoclusters in these experiments.

After sample preparation, the beaker containing the sample was lowered into the ESR cavity, which was situated at the bottom of the cryostat in the homogeneous field region of the Varian 7800 electromagnet. The volume occupied by the sample inside the cavity was 0.35 cm^3 . The homemade cylindrical cavity was operated in the TE_{011} mode. The cavity has an axial hole to provide access for the sample to be introduced. Two different inserts were used in the experiments, one for detection of CW ESR signals by an X-band homodyne spectrometer and the other for detection of electron spin echo signals by a pulsed X-band homodyne spectrometer. Only the microwave cavities were different in these inserts. A high quality factor cavity ($Q \sim 3000$) was used in the CW ESR experiments, while in the pulsed ESR experiments a low quality factor cavity ($Q \sim 700$) was employed to avoid a long cavity ring-down time. CW and pulsed ESR signals were obtained for samples immersed in liquid helium at temperatures $\sim 1.35\text{ K}$. CW ESR signals were recorded by using a continuous wave reflection homodyne spectrometer (Varian E-4) operating near 9.1 GHz. Derivatives of the ESR absorption lines were detected at $\sim 0.32\text{ T}$ by lock-in amplification using an additional small amplitude modulation field oscillating at 100 kHz. Atomic concentrations were measured by comparing the intensity of the atomic signals with the intensity of a signal from a small ruby crystal that was used as a secondary standard. The ruby crystal was attached permanently to the bottom of the microwave cavity. The calibration of the absolute value of the number of spins in the ruby crystal was made by using a standard organic diphenyl-picrylhydrazyl (DPPH) sample with a known number $\sim 2.4 \times 10^{17}$ of spins. The measurements

were carried out at $T = 1.35\text{ K}$. A nuclear magnetic resonance (NMR) magnetometer was used for precise measurements of the applied magnetic field.

For pulsed ESR studies of atoms in Im--He solids, a special homodyne detection spectrometer was designed.⁴⁵ The spectrometer operates in the X-band region with a microwave frequency of 8930 MHz. Figure 2 shows a simplified block scheme of the pulsed ESR spectrometer. A 12-channel programmable pulse generator, operating at a 125-MHz clock frequency, provides logic signals to the P–I–N diode switch, bi-phase modulator, oscilloscope trigger and traveling wave tube (TWT) grid modulator. Microwaves from the tunable oscillator are amplified and split into pulse and reference paths. The pulses are amplified by a 1 kW, 50 dB TWT amplifier operating in the saturated regime. The amplified pulses pass through a circulator before transitioning to a 20 cm length of stainless steel coax at the entrance to the cryostat. (A similar arrangement was used in the CW spectrometer). This prevents excessive heat conduction into the cryostat. A low loss coax traverses the remaining 107 cm to the resonant cavity at the bottom of the cryostat, which is situated between the poles of the Varian electromagnet. Echo signals return through the same cabling to the circulator, which routes them to a low noise amplifier (LNA) that is protected by a diode limiter from the powerful microwave pulses. After amplification, a quadrature mixer provides homodyne detection by referencing the echo signals to the microwave oscillator. The resulting in-phase and quadrature signals are sampled by a digital oscilloscope and transferred *via* GPIB to a computer. The spectrometer design differs from other machines used to acquire electron spin echo data at cryogenic temperatures in three significant ways.⁴⁶ First, space constraints in our cryostat require the use of a coax rather than a waveguide connection to our cavity-type resonator. Second, our resonant cavity is a modified CW ESR

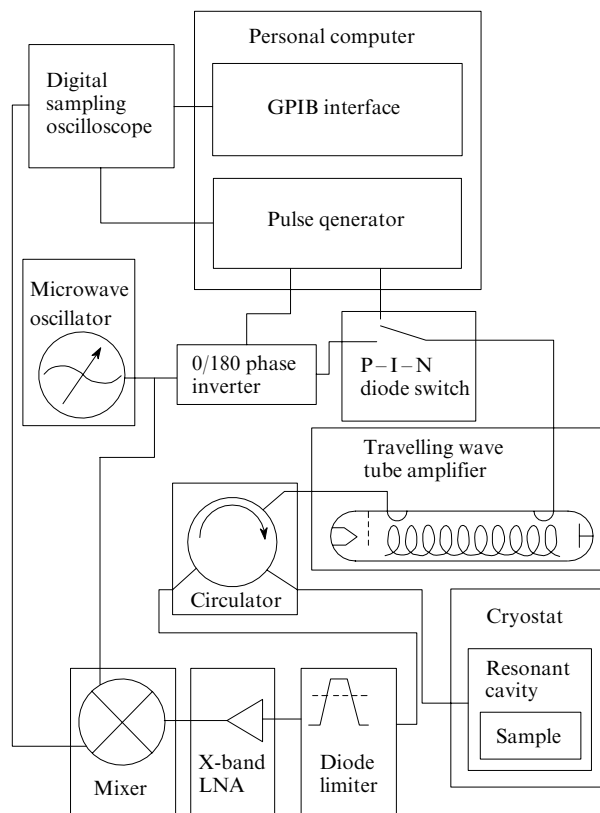


Figure 2. Block diagram of pulsed ESR spectrometer.

quartz-filled cavity designed to admit a funnel containing Im–He solid samples. To facilitate broadband excitation by short pulses, a chromium coated quartz ring is bonded with epoxy to thin fingers protruding from a brass pedestal. Adjusting the pedestal position then adjusts the Q factor of the cavity; we have found a Q of ~ 700 to be effective for detecting electron spin echo envelope modulation (ESEEM) due to deuterium nuclei. Further details of this method will be provided in a later section. For this apparatus, a 90° pulse has duration 40 ns. Finally, the spectrometer output is sampled by a sampling oscilloscope, not a boxcar integrator. Integrating a narrow section of the echo peak recovers standard boxcar ESEEM data. Alternatively, for two-pulse ESEEM experiments the echo can be sectioned in time and the phase correction algorithm of Astashkin *et al.* applied.⁴⁷ This corrects for the fact that the phase of the modulation harmonics varies within each echo, and therefore allows the entire echo to contribute to the signal, thus improving the signal/noise ratio.

2. CW ESR studies of tunnelling exchange reactions of hydrogen isotopes in clusters forming impurity–helium solids

The Im–He solids formed by injection of hydrogen isotopes into He II are of special interest due to their potential to manifest various quantum phenomena. The observation of tunnelling exchange chemical reactions between atoms and molecules of hydrogen isotopes at low temperatures in Im–He solids represents an important example of such a quantum phenomenon. Investigations of tunnelling reactions in Im–He solids were first performed by the Chernogolovka group.^{10, 19} By using the CW ESR method, they studied the efficiency of the stabilisation of hydrogen and deuterium atoms in Im–He solids using hydrogen–neon–helium, deuterium–helium, or hydrogen–deuterium–helium gas mixtures. In contrast with earlier work, it was found that maximum local concentrations of H and D atoms as high as 1% could be easily achieved in Im–He solids. However, they were not able to study the time evolution of the concentration of stabilised atoms.

Recently, studies of the kinetics of tunnelling exchange reactions between atoms and molecules of hydrogen isotopes in nanoclusters have been performed by the Cornell group.^{44, 48–51} The X-band CW ESR method was used in these studies. This method allows a determination of the time dependence of the hydrogen and deuterium atom concentrations during the tunnelling exchange reaction and it also provides information concerning changes in the environment of these atoms as the reactions proceed.

Initially the kinetics of tunnelling reactions were studied in each of the two pure hydrogen isotopes. The main features of the atomic hydrogen and atomic deuterium spectra recorded from a sample with initial gas mixtures in the ratios $\text{H}_2:\text{Ne}:\text{He} = 1:4:100$ and $\text{D}_2:\text{He} = 1:20$ are shown in Fig. 3. The hydrogen ESR lines are accompanied by two satellite lines, one on either side of the main line. The satellite lines are assigned to forbidden transitions involving an electron spin flip and a simultaneous spin flip of a proton on a neighbouring ortho-hydrogen molecule. Each of the ESR signals of H atoms was fitted with a sum of three Gaussians (one central line plus two symmetric satellites). From these fits the ratio of the intensities of the satellite and main lines is found to be 0.2. The splittings observed between the main and satellite lines (4.5 ± 0.1 G) are consistent with a proton spin flip in the 3 kG field. Because of the small nuclear magnetic moment of the deuteron, the corresponding splitting for electron spin–deuteron spin interactions is only 0.7 G. This is unobservable in these experiments because the ESR linewidths of the main lines are about 2 G and thus the small satellite lines are hidden by the broad main lines.

In the mixed samples, which contain both H and D atoms, the observation of satellite lines provides strong evidence that a

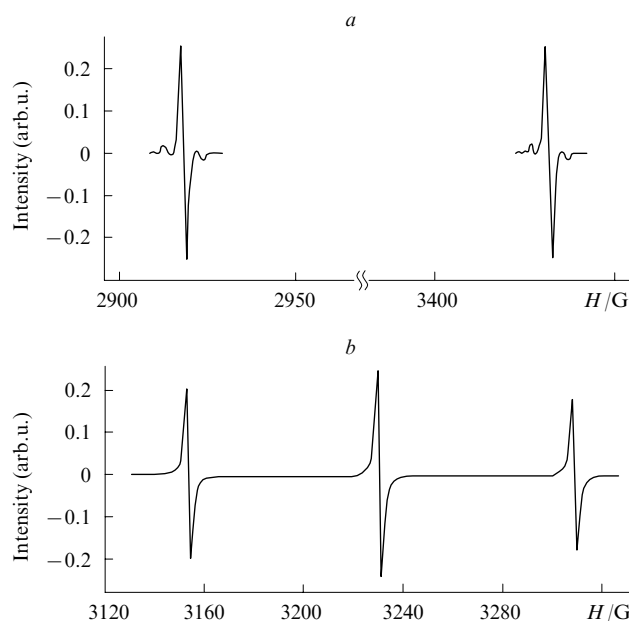


Figure 3. CW ESR derivative signals of atomic hydrogen in Im–He solid prepared from $\text{H}_2:\text{Ne}:\text{He} = 1:4:100$ gas mixture (a) and of atomic deuterium in Im–He solid prepared from a $\text{D}_2:\text{He} = 1:20$ gas mixture (b). ESR spectra were obtained at $T = 1.35$ K.

large fraction of the hydrogen and deuterium atoms are found in clusters of molecular hydrogen and/or molecular HD. In other words, they are not isolated as individual atoms separated by layers of solid helium. Therefore the solid samples provide a unique opportunity to carry out quantitative studies of the kinetics of tunnelling reactions of hydrogen isotopes in nanoclusters. The results of such experiments can then be compared with analogous studies performed in bulk solid mixtures of hydrogen isotopes. Different behaviour can be expected as a result of the large surface areas of the clusters.

According to Trammel *et al.*⁵² the intensity ratio between the satellite lines and their respective main lines is proportional to the number of protons surrounding a stabilised atom and is strongly dependent on their positions:

$$\frac{I_{\text{sat}}}{I_{\text{main}}} = \frac{3}{20} \left(g_e \frac{\beta_e}{H_0} \right)^2 \langle r^{-6} \rangle N. \quad (9)$$

In the above equation g_e is the electron g factor, β_e is the Bohr magneton, H_0 is the applied magnetic field, r is the distance from an atom to a proton belonging to a neighbouring molecule, and N is the number of these protons. If a reasonable assumption can be made for the number of protons in molecules surrounding the atom, then the average distance between the atom and molecules can be found. Moreover, from the time dependence of this ratio during the course of the chemical reactions, it is possible to obtain the changes in the number of ortho-hydrogen molecules surrounding the atoms.

The time dependence at $T = 1.35$ K of the average concentration of H atoms in a $\text{H}-\text{H}_2-\text{Ne}-\text{He}$ sample and that of D atoms in a $\text{D}-\text{D}_2-\text{He}$ sample are displayed in Fig. 4. The addition of neon was required in the former sample because, unlike the D_2-He sample, the H_2-He solid does not sink to the bottom of the cell, due to its small density. As mentioned earlier, the tunnelling exchange reactions drive the migration of isolated atoms. The relatively fast migration of a hydrogen atom due to the tunnelling reaction (1) leads to recombination with another H atom ($\text{H} + \text{H} \rightarrow \text{H}_2$), and thus explains the

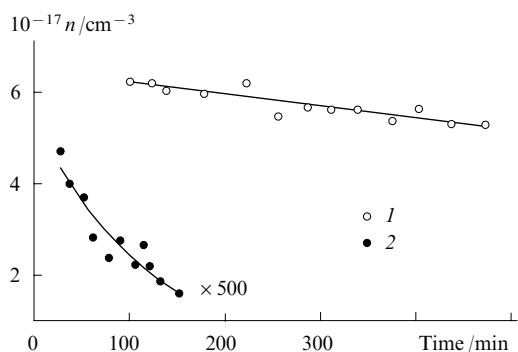


Figure 4. Time dependence of concentrations of atomic deuterium prepared from a D_2 :He = 1:20 gas mixture (1) and atomic hydrogen prepared from H_2 :Ne:He = 1:4:100 gas mixture (2) in Im-He solids stored at $T = 1.35$ K.⁴⁹

rapid decay of the number of hydrogen atoms in the sample at $T = 1.35$ K.

The equation

$$\frac{dn}{dt} = -2k_H(T)n^2. \quad (10)$$

describes the decrease of the concentration of H atoms (n) with time (t) when the temperature of the sample is kept constant.¹⁵ The experimental dependence of the variable $1/n$ on t should thus be linear, with the slope equal to $2k_H(T)$. The characteristic time (the half life) for the concentration to drop by 50% is

$$\tau_{1/2} = [2k_H(T)n_{H,loc}]^{-1}, \quad (11)$$

where $n_{H,loc}$ is the initial local concentration of H atoms. The average concentration of H atoms at the beginning of the measurements is $n_{H,av} = 10^{15} \text{ cm}^{-3}$ according to Fig. 4. As indicated earlier the H_2 clusters and Ne clusters form separately. We shall make the reasonable assumption that the density of H_2 molecules in the H- H_2 -Ne-He samples is roughly similar to the density of D_2 in D_2 -He samples,²¹ which is equal to $\sim 10^{20} \text{ cm}^{-3}$. This is more than two orders of magnitude lower than the density of the solid molecular hydrogen, which is equal to $2.4 \times 10^{22} \text{ cm}^{-3}$. This means that the local concentration of H atoms in the clusters constituting the sample is two orders magnitude larger than the average concentration, giving $n_{H,loc} = 10^{17} \text{ cm}^{-3}$. The decay time of H atoms, $\tau_{1/2}$, shown in Fig. 4 is 150 ± 20 min. From Eqn (11), the rate constant for recombination of H atoms in solid H_2 was found to be $k_H(1.35) = 5.5 \times 10^{-22} \text{ cm}^3 \text{ s}^{-1}$. This value is much larger than those obtained in bulk H_2 solids by the Nagoya group,¹⁸ $k_H(1.9-4.2) = (4.4-5.9) \times 10^{-23} \text{ cm}^3 \text{ s}^{-1}$, and the Moscow group,^{8,15} $k_H(1.35) = 2.7 \times 10^{-24} \text{ cm}^3 \text{ s}^{-1}$. This result may be due to a higher mobility of H atoms on the surfaces of the clusters or due to an inhomogeneous distribution of H atoms within the clusters.

The significantly slower decay of D atoms is attributed to the much slower migration of deuterium atoms through molecular deuterium due to the reaction (2). The same Eqn (10) describes the decrease of the concentration of D atoms with time. The initial local concentration of D atoms, $n_{D,loc}$, is equal to $6.25 \times 10^{19} \text{ cm}^{-3}$ and the characteristic decay time of D atoms is 2500 ± 500 min. From the relation

$$k_D = \frac{1}{2} \tau_{1/2} n_{D,loc},$$

it is found that

$$k_D(1.35 \text{ K}) = 5 \times 10^{-26} \text{ cm}^3 \text{ s}^{-1}.$$

This value is in qualitative agreement with value $k_D(4.2) = 4 \times 10^{-26} \text{ cm}^3 \text{ s}^{-1}$, obtained by Iskovskikh *et al.*¹⁵ in solid D_2 at $T = 4.2$ K, but significantly larger than value $k_D = 3.3 \times 10^{-27} \text{ cm}^3 \text{ s}^{-1}$ obtained by Miyazaki *et al.*¹⁷

A completely different behaviour of hydrogen and deuterium atoms was observed in impurity-helium solids containing hydrogen and deuterium atoms along with hydrogen and deuterium molecules.⁴⁹ The main features of atomic hydrogen and deuterium spectra recorded from a sample with an initial gas mixture in the ratio $H_2:D_2:He = 1:4:100$ are shown in Fig. 5. Both the deuterium and the hydrogen ESR lines are

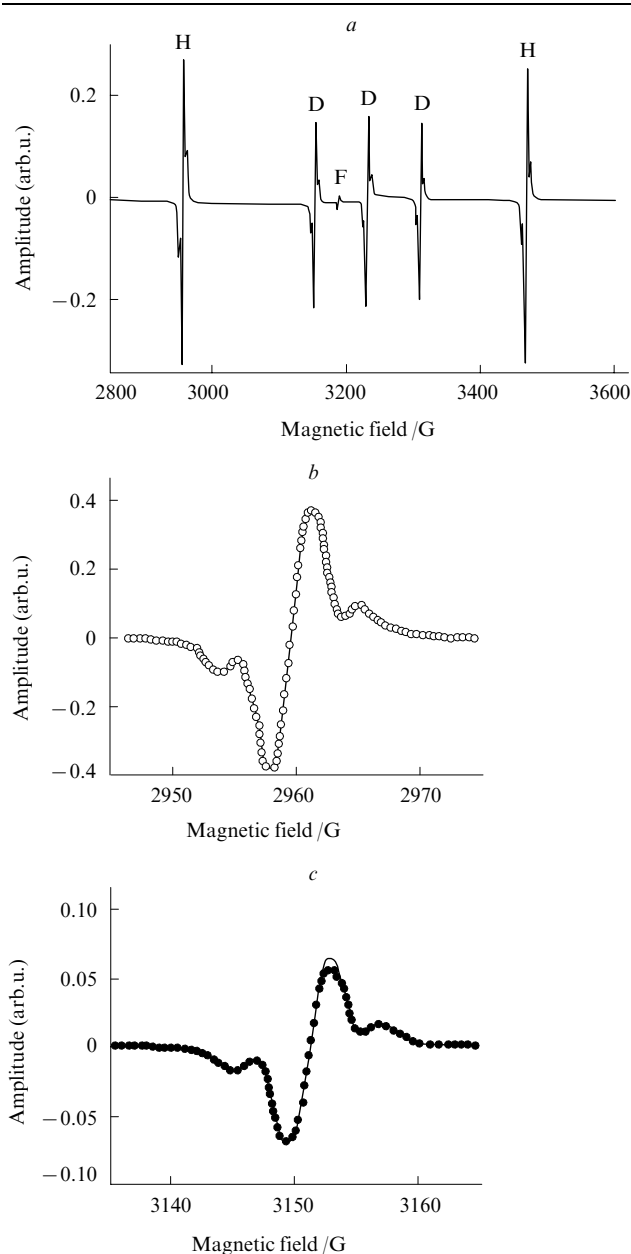


Figure 5. CW ESR derivative signal from Im-He sample prepared from gas mixture $H_2:D_2:He = 1:4:100$ (a). 'H' marks the allowed ESR transitions between the hyperfine levels of atomic H; 'D' indicates the hyperfine transitions of atomic D, and 'F' indicates the forbidden ESR transition of H atoms. Typical derivative signals for low field hyperfine line of hydrogen atoms (b) and deuterium atoms (c) show, at an expanded scale, both the allowed and the accompanying satellite lines. The lines in figures (b) and (c) represent simulations of the signals as the sum of three Gaussians.⁴⁹

accompanied by two satellite lines symmetrically positioned about the main line. The satellite lines are assigned to forbidden transitions involving an electron spin flip and a simultaneous spin flip of a proton on a neighbouring HD or on an ortho-hydrogen molecule. The forbidden transition associated with the hyperfine levels of H atoms is also shown.

A large number of different initial gas mixtures were used for preparation of $\text{H}_2\text{--D}_2\text{--He}$ solids.^{44,49} Immediately after preparation of all Im–He solids, a large enhancement of the H atom concentration relative to that of D atoms was observed, as compared to the ratio of H_2 to D_2 in the original gas mixtures. The fraction of H and D atoms as a function of the relative H_2 concentration in the condensed $\text{H}_2\text{--D}_2$ gas mixtures is shown in Fig. 6. The enhancement of the H atom concentrations at the earliest stage of sample preparation is attributed to the fast exchange tunnelling reaction (3), which leads to a large reduction in the number of D atoms and a corresponding increase in the number of H atoms with a time constant of order 1 min. During this reaction, most of the H_2 molecules that have neighbouring D atoms in the sample are converted into HD molecules. The rate constant for this reaction is calculated theoretically to be $3.56 \times 10^{-25} \text{ cm}^3 \text{ s}^{-1}$ (Ref. 12). Recently, this tunnelling reaction was studied experimentally by Kumada⁵³ in bulk HD--D_2 and $\text{D}_2\text{--H}_2$ solid mixtures in the temperature range between 4 and 8 K. The reactions were initiated by UV photolysis of DI molecules doped in these solids for 30 s, followed by measuring the time variation of the ESR intensities of H and D atoms. The ESR intensity of D atoms produced by photolysis decreases but that of H atoms increases with time. The variation of the concentrations of the D and H atoms with time can be described in terms of a fast and a slow processes. The fast process, which was essentially complete within 300 s after photolysis, is assigned to the reaction (3). The rate constant for this reaction was determined to be $(2.9 \pm 0.3) \times 10^{-25} \text{ cm}^3 \text{ s}^{-1}$ in solid HD--H_2 and $(5.0 \pm 1.1) \times 10^{-25} \text{ cm}^3 \text{ s}^{-1}$ in solid $\text{D}_2\text{--H}_2$ mixtures at $T = 4.1 \text{ K}$, which is very close to the theoretical calculations by Takayanagi *et al.*¹² These results provide very strong evidence favouring the role of tunnelling exchange reactions in the solid hydrogen isotopes.

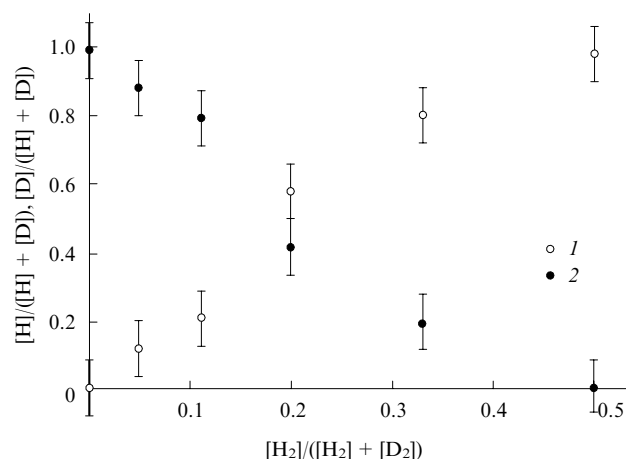


Figure 6. The dependence of the fractional concentrations of H (1) and D (2) atoms in the $\text{HD--D}_2\text{--He}$ samples as a function of H_2 content in the $\text{H}_2\text{--D}_2$ gas mixtures used for sample preparation. For each point the concentrations were determined just after sample preparation.

For the case of Im–He solids, the time dependence of the concentration of H and D atoms on a longer time scale (2–40 h) showed a further increase in the concentration of H

atoms. The simultaneous presence of deuterium and hydrogen molecules in the make up gas allows us to form impurity helium solids containing hydrogen atoms and deuterium atoms as well as hydrogen, deuterium, and hydrogen deuteride molecules. In Fig. 7a–c we show the results obtained at Cornell, which dramatically illustrate the time dependence of the hydrogen and deuterium atom concentrations for different initial make-up gas mixtures.⁴⁹ In spite of the higher concentration of D_2 compared with that of H_2 in the sample produced from the initial gaseous mixture $\text{H}_2:\text{D}_2:\text{He} = 1:2:60$, the concentration of deuterium atoms is about two orders of magnitude smaller than the hydrogen atom concentration and it decays more rapidly (Fig. 7a). These results are in sharp contrast to the Cornell studies of $\text{H}_2\text{--Ne--He}$ impurity solids, with no deuterium present, in which the decay of hydrogen atoms due to recombination was much more rapid. This can be explained by the presence of many D_2 and HD molecules in the sample, which lead to anomalously slow diffusion of the H atoms through the clusters, and by the partial replenishment of hydrogen atoms through the chemical reactions (3) and (4).

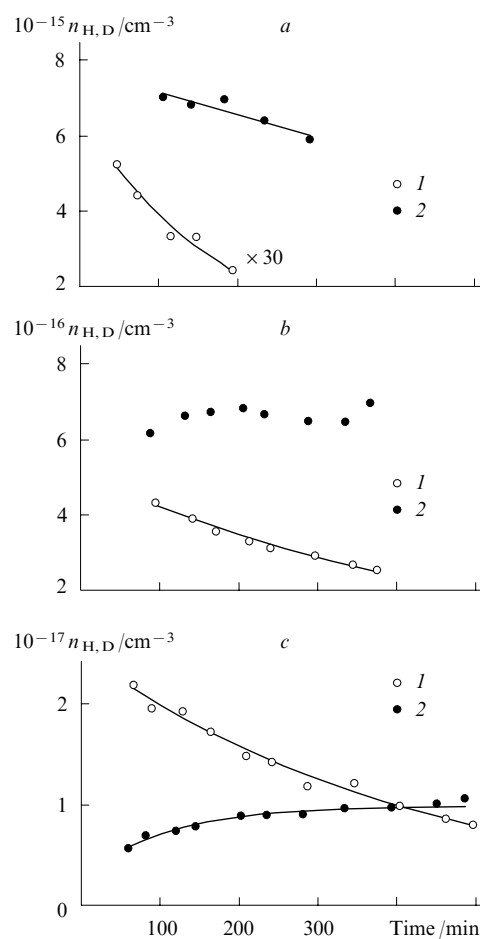


Figure 7. Time dependence of concentrations of atomic deuterium (1) and atomic hydrogen (2) in different Im–He solids at $T = 1.35 \text{ K}$.⁴⁹ $\text{H}_2:\text{D}_2:\text{He}$ mixture: 1:2:60 (a), 1:4:100 (b), 1:8:180 (c).

Furthermore, these reactions also explain the faster decrease of the deuterium atom concentration as compared with that in the $\text{D--D}_2\text{--He}$ sample (see Fig. 4). In Fig. 7b the population of hydrogen atoms remains almost constant, meaning that the production is almost in balance with recombinational decay in the sample produced from an $\text{H}_2:\text{D}_2:\text{He} = 1:4:100$ mixture. In Fig. 7c the population of hydrogen

atoms actually shows an increase that is driven by the chemical reactions as time evolves. The large initial supply of deuterium molecules in the gas mixture $\text{H}_2:\text{D}_2:\text{He} = 1:8:180$ means that a copious supply of deuterium atoms is available in the sample, leading to a higher production of hydrogen atoms.

The exchange tunnelling reactions can be used to produce very large concentrations of atomic hydrogen in these mixed solids. In the Cornell studies samples obtained from a variety of initial gas mixtures have been investigated in order to determine the one which yields the highest hydrogen atom concentration.⁴⁴ The experimental plot shown in Fig. 8 gives the H and D average concentrations after a storage time ~ 500 min following initial sample preparation. The largest concentration, of order $(7.5 \pm 3.0) \times 10^{17} \text{ cm}^{-3}$, was obtained by using the gas mixture $\text{H}_2:\text{D}_2:\text{He} = 1:4:100$.

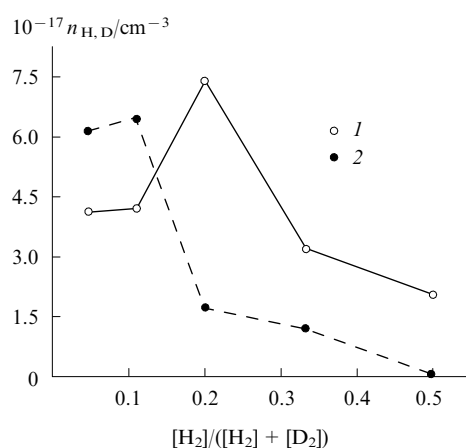


Figure 8. The dependence of the average concentrations of H atoms (1) and D atoms (2) in Im-He solids on the fraction of hydrogen gas in the make up gas mixture.⁴⁴ For each point the concentrations were determined after a waiting period of 500 minutes following sample collection.

The very long term stability of the sample obtained from this gas mixture at a temperature of $T = 1.35 \text{ K}$ has also been studied in these investigations.⁵¹ The time dependence of the logarithm of the average concentrations of H and D atoms in the sample produced from an initial gas mixture $\text{H}_2:\text{D}_2:\text{He} = 1:4:100$ is displayed in Fig. 9. The concentration of H atoms remained constant throughout the 40-h experiment. During the same period of time, the concentration of D atoms decreased from its initial value of 10^{17} cm^{-3} by 2.5 orders of magnitude. The reaction (4) continued to eliminate D atoms and generate H atoms in the $\text{HD}-\text{D}_2-\text{He}$ solid during the long-term experiment. From the decay rate of the D atoms, one can estimate a rate constant, $k_{\text{D-HD}}$, for this reaction from the equation

$$\frac{d[\text{D}]}{dt} = -k_{\text{D-HD}}[\text{HD}][\text{D}].$$

The decay time of D atoms was determined from the slope of the line presented in Fig. 9; $k_{\text{D-HD}} = 2.9 \times 10^4 \text{ s}$. Assuming the impurity cluster density is close to that of solid D_2 , one finds an initial HD concentration equal to $9.3 \times 10^{21} \text{ cm}^{-3}$ and a rate constant $k_{\text{D-HD}} = 3.6 \times 10^{-27} \text{ cm}^3 \text{ s}^{-1}$, which agrees with the value found by Kumada *et al.*²⁷ in bulk samples.

The time dependence of the ratio of the satellite line to the main line for hydrogen and deuterium atoms was studied for a $\text{HD}-\text{D}_2-\text{He}$ sample, while the tunnelling reaction (4) was occurring. The time dependence of these ratios for H and D

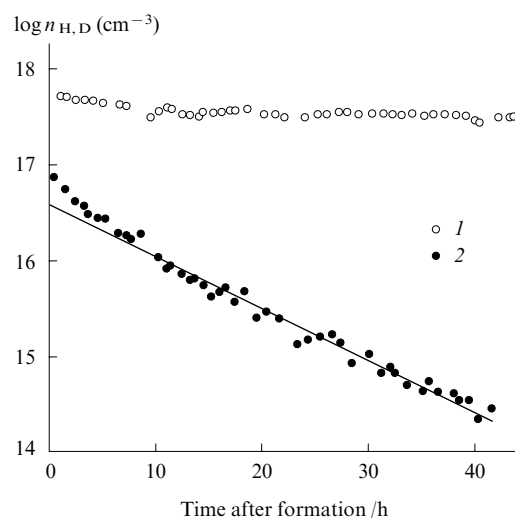


Figure 9. Time dependence of the logarithms of the average concentration of H atoms (1) and D atoms (2) in $\text{HD}-\text{D}_2-\text{He}$ solids immersed in superfluid helium at $T = 1.35 \text{ K}$.⁵¹ Sample was prepared from $\text{H}_2:\text{D}_2:\text{He} = 1:4:100$ gas mixture.

atoms is shown in Fig. 10. It was found that for H atoms, the ratio is equal to 0.11 and this value remains essentially constant during the course of the reaction. Thus, by Eqn (9), the average number of HD molecules surrounding H atoms in the sample does not change during the experiment. Due to the tunnelling reaction (5), a hydrogen atom might migrate to the next site in the solid matrix and possibly meet another hydrogen atom, which could lead to recombination and decay of the hydrogen atom concentration. However, this process is predicted to be ~ 200 times slower than the diffusion of H through H_2 by tunnelling.¹² The observed stability of hydrogen atoms in the sample being discussed is not yet completely understood. Additional studies of the immediate environment of the stabilised atoms are needed for further elucidation of the nature of the tunnelling reactions.

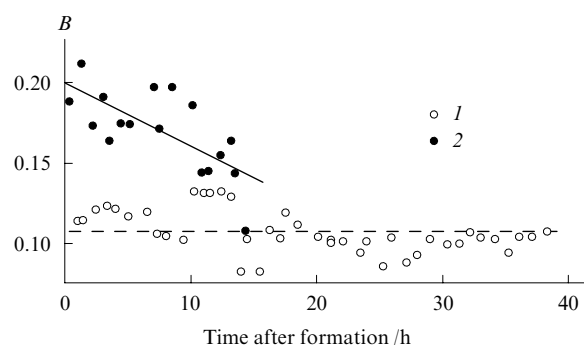


Figure 10. Time dependence of the ratio of the intensities of the satellite and the main lines (B) for hydrogen atoms (1) and deuterium atoms (2) in $\text{HD}-\text{D}_2-\text{He}$ solids stored at $T = 1.35 \text{ K}$.⁵¹

In contrast, for D atoms the ratio was reduced from 0.2 to 0.14 in 14 h, showing that the number of HD molecules surrounding D atoms is decreased by 30%. The D atoms consume HD and release H atoms. The rate process is complicated by the fact that the D atoms exist in a variety of sites having between zero and twelve neighbouring HD molecules. The population of these sites initially follows a binomial distribution, with 40% of the neighbours of the D atoms being

HD and the remainder being D₂. The lifetime of a D atom in a given site is inversely proportional to the number of HD neighbours, so that over time the distribution of sites becomes skewed toward D atoms occupying sites with fewer HD nearest neighbours that show smaller satellite line ratios.

3. Pulsed ESR studies of H and D atoms in clusters forming Im–He solids

The CW method suffers from a high degree of inhomogeneous line broadening due to the neighbouring nuclei and atomic radicals. As we mentioned earlier, this broadening obscures the observation of satellite lines associated with transitions involving the spin flip of an electron and a simultaneous spin flip of a deuteron on a neighbouring HD or D₂ molecule. The standard pulsed ESR method of echo refocusing provides a means to study these weak couplings within inhomogeneously broadened systems. As discussed earlier, a homemade pulsed homodyne X-band spectrometer, designed for the study of atoms in Im–He solids, was used in the experiments at Cornell.⁴⁵ A primary echo sequence of 90°–τ–180°–τ–echo with a 90° pulse length of 40 ns was used. To obtain the dependence of the amplitude of spin echo signals on the time between subsequent pulse pairs, τ was varied from 460 ns to 12 μs, while the recovery time *t* between successive pulse sequences was held constant at 400 ms. The method of ESEEM proved to be a powerful technique for observing spin flips on neighbouring deuterons. The first experiments were performed on D–D₂–He samples prepared from a gas mixture with a ratio D₂:He = 1:20. Figure 11 displays the experimental electron spin echo amplitude vs. τ, giving the ESEEM trace along with the simulated one for the low field hyperfine line of

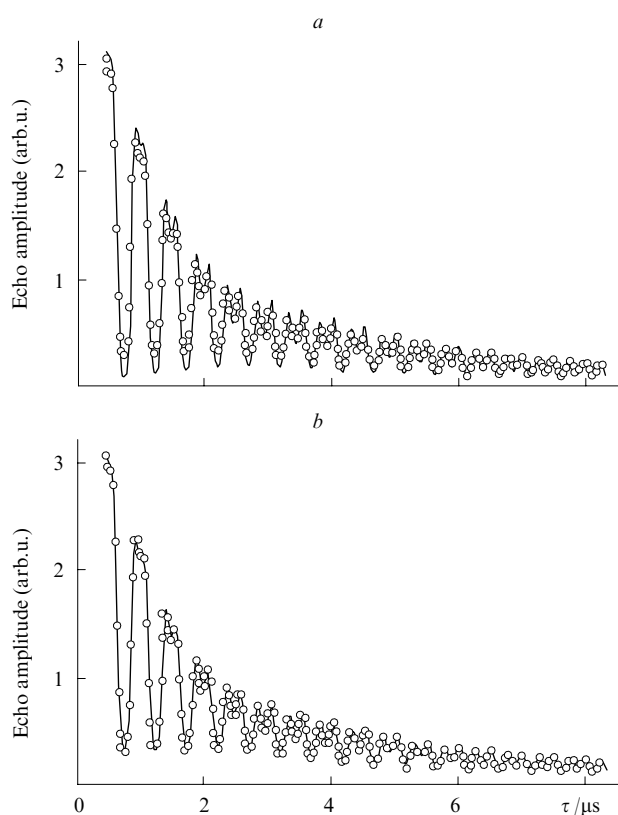


Figure 11. Two-pulse ESEEM trace of the low field hyperfine line of D in D₂–He sample.⁵⁴ (a) The circles show every fourth data point. The line shows the best fit of the bulk population model. (b) The circles show every fourth data point. The line shows the best fit of the two population (bulk and surface) model $E(\tau)$.

the D atom. The echo signal intensity decreased monotonically and was strongly modulated by the first and second harmonics of the Larmor frequency of deuterons in the molecules near the D atoms. The applied magnetic field couples to the deuterons much more strongly than the field due to the electron spins, so the applied magnetic field determines the ~2 MHz Larmor frequency of the deuterons. The amplitude of the modulation depends on the number of deuterons surrounding the D atoms and their proximity to those atoms. The amplitude of modulation is also proportional to $I(I+1)$, where *I* is the nuclear spin quantum number of the molecule interacting with the D atom. Therefore the amplitude of modulation of ESEEM signals for atoms surrounded by D₂ molecules with *I* = 2 and *I* = 1 should be much larger than for the case of atoms surrounded by protons (as a constituent of HD) with *I* = 1/2. This difference is especially pronounced at low temperatures because the ground state of D₂ is predominantly of the *I* = 2 form and conversion to the ground state occurs rapidly in the vicinity of the unpaired electron spins of the hydrogen and deuterium atoms. The ESEEM signal associated with the proton moment has not been observed in our experiments.

For analysis of the experimental ESEEM data the model used initially was that developed by Kumada *et al.*³¹ to study D atoms in bulk D₂. They simulated their ESEEM signals with the standard theoretical results for orientationally disordered crystalline systems.⁵⁵ This model assumes that all possible orientations of the face centred cubic (fcc) deuterium crystal axis with respect to the applied magnetic field are equally represented within the sample. The Hamiltonian includes terms representing electron–nuclear interactions through dipolar magnetic coupling and an isotropic superhyperfine coupling due to the contact interaction of the electronic wave function with the nuclear wave function of the nearest neighbouring molecules. No internuclear couplings are included; as a result, the echo modulation due to the presence of several nuclei surrounding the electron spin is simply the product of the modulation due to each individual nucleus.

The echo signal as a function of the interpulse time τ was modeled as:

$$E(\tau) = E_{\text{dec}}(\tau)E_{\text{b}}(\tau),$$

$$E_{\text{b}}(\tau) = \prod_{i=1}^5 \langle E_i(\tau) \rangle_{\theta}^{N_i},$$

$$E_{\text{dec}}(\tau) = Ae^{-\tau/T_2},$$

where $E_{\text{dec}}(\tau)$ contains the characteristic exponential decay time T_2 of the electron spin echo and $E_{\text{b}}(\tau)$ represents the modulation of the echo due to the N_i molecules populating the closest five coordination shells $i = 1-5$ around the electron spin. The modulation functions $E_i(\tau)$ due to each individual molecule are averaged over all orientations before they are multiplied. This unphysical feature of the model is computationally expedient and causes only slight changes in the predicted echo signals for systems with weak electron–nuclear couplings such as hydrogen or deuterium atoms substitutionally positioned within a deuterium matrix.⁵⁶

At liquid helium temperatures D₂ can exist in ortho- and para-states corresponding respectively to the *J* = 0 and *J* = 1 rotational states of the molecule. The para state is 85 K more energetic than the ortho-state but its conversion to the ortho-state is highly forbidden. Deuterons are bosons, so the product of the spatial and spin wave functions of the deuterons must be symmetric under particle exchange. The allowed molecular spin states are then *I* = 0 and *I* = 2 for ortho-deuterium and *I* = 1 for para-deuterium. The energy difference between the *I* = 0 and *I* = 2 states is extremely small compared to the

thermal energy, so the populations of the states are determined by their degeneracy. As there are five orientations of the $I = 2$ state and one orientation of the $I = 0$ state, 5/6 of the ortho-deuterium molecules are in the $I = 2$ spin state, while 1/6 of the ortho-deuterium molecules are in $I = 0$ spin state. The para-to-ortho relaxation of deuterium is catalysed by the magnetic field gradients produced by paramagnetic species, so that all of the deuterium molecules in the nearby coordination shells around a D atom can be assumed to be of the ortho-form. As the $I = 0$ molecules are not magnetically active, the number of molecules in each coordination shell must be adjusted accordingly. For example, for an atom substitutionally positioned in D_2 fcc, the first shell of twelve nearest neighbours is modelled with ten spin-2 particles, each possessing the Larmor frequency of the deuteron.

Ponti⁵⁷ has shown that Chebyshev polynomials of the second kind relate the ESEEM modulation function due to a particle of any spin to the modulation function that would result if that particle were spin 1/2. Specifically,

$$E_i(\tau) = \frac{1}{2I+1} U_{2I}[V_i(\tau)],$$

where U_n is the n th Chebyshev polynomial of the second kind and $V_i(\tau)$ is the spin 1/2 modulation function. Finally, the explicit form of $V_i(\tau)$ is

$$V_i(\tau) = \frac{K}{2} \left[1 - \cos(\omega_\alpha \tau) \right] \left[1 - \cos(\omega_\beta \tau) \right],$$

$$K = \left(\frac{B\omega_L}{\omega_\alpha \omega_\beta} \right)^2,$$

$$B = 3g_n \beta_n g_e \beta_e \frac{\cos \theta \sin \theta}{\hbar(r_i)^3},$$

$$\omega_L = g_n \beta_n H_0,$$

$$\omega_\alpha = \left[\left(\frac{A}{2} + \omega_L \right)^2 + \left(\frac{B}{2} \right)^2 \right]^{1/2},$$

$$\omega_\beta = \left[\left(\frac{A}{2} - \omega_L \right)^2 + \left(\frac{B}{2} \right)^2 \right]^{1/2},$$

$$A = g_n \beta_n g_e \beta_e \frac{3 \cos^2 \theta - 1}{\hbar(r_i)^3} + 2\pi a_{\text{sup}},$$

where r_i is the distance from the electron to coordination shell i , θ is the angle between the applied field H_0 and the vector pointing from the radical to the molecule, g_e and g_n are the g -factors of the electron and nuclear spins, β_e and β_n are the Bohr and nuclear magnetons, and a_{sup} is the isotropic superhyperfine coupling.

Kumada *et al.*³¹ fitted a_{sup} and r_i to their data obtained from pure irradiated solid deuterium for two sets of N_i and r_i . One set corresponded to the environment around substitutional sites in the D_2 fcc lattice and the other set corresponded to the environment around interstitial sites. The predicted modulation functions were radically different (the interstitial sites have much deeper modulation due to the smaller nearest neighbour distances) and it was immediately clear that the D atoms reside in the substitutional sites. Numerical fitting gave $r_i = 3.6$ Å, corresponding to the nearest neighbour spacing of the unstrained molecular lattice, and $a_{\text{sup}} = 70$ kHz.

Applying the above model to our Im–He solid gave poor agreement with the data obtained for the D– D_2 –He sample

as presented in Fig. 11 *a*. For Im–He solids it is reasonable to suggest that atoms are stabilised not only inside molecular clusters, but also on the surfaces of these clusters. Following this suggestion, the experimental ESEEM data were fitted with two decaying exponentials multiplied with two oscillatory modulation terms:

$$E(\tau) = A \left[Q e^{-\tau/T_{2Q}} + (1-Q) e^{-\tau/T_{2L}} \right] \left[b E_b(\tau) + (1-b) E_s(\tau) \right],$$

where A , Q , T_{2Q} and T_{2L} parameterise the echo decay and b weights the modulation functions E_b and E_s .⁵⁴ The function E_b simulates the ESEEM signal of D atoms within the solid clusters by assuming they are substituted into an fcc lattice composed of D_2 molecules. The modulation signal E_b produced by atoms positioned within deuterium nanoclusters was identical to that described above for atoms substituted in bulk deuterium. The function E_s is produced by the same model, but with the population of each coordination shell around the atom reduced by one-half. This simulates D atoms at the surfaces of the clusters in contact with the helium. We fixed r_i and a_{sup} to the values found to describe bulk deuterium so that our modulation function contained only one free parameter, the ratio of atoms within the deuterium nanoclusters to atoms at the cluster–helium interface. The functional form of the echo decay was found empirically to fit the data well with a small number of parameters. Notably, modelling the data with separate decay functions for the bulk and surface terms results does not improve the fits.

As a result of applying the modified model, the two-pulse ESEEM measurements presented in Fig. 11 *b* were well described by fits that placed 50%–60% of the deuterium atoms at the interface between the molecular deuterium nanoclusters and the superfluid liquid helium.⁵⁴ The rest of the atoms occupy substitutional sites within the nanoclusters. These pulsed ESR measurements provide the first direct indication that a large fraction of the atomic radicals within impurity–helium solids reside on the cluster–helium interfaces, as first suggested by Gordon.⁵⁸ This result implies that some mechanism causes the deuterium atoms to preferentially occupy the nanocluster surfaces, whereas a random substitution of the deuterium molecules of the clusters would only place 10%–20% of the atoms at the cluster–helium interface, depending on the cluster size.

The measurements of ESEEM signals by pulsed ESR provide complementary information about deuterons surrounding H and D atoms in solid mixtures of hydrogen isotopes that cannot be provided by CW ESR due to the small deuteron magnetic moment. The ESEEM signal associated with ESR studies of H atoms in a HD– D_2 –He solid produced from an initial gaseous mixture $H_2:D_2:He = 1:4:100$ is shown in Fig. 12 *a*. For the analysis of the ESEEM data, the model applied for D– D_2 –He solid was modified to account for the presence of D_2 and HD molecules surrounding the atoms, with the ratio of HD and D_2 molecules allowed to vary as a fitting parameter. The fraction of atoms at the surface was assumed to be 55%, the same as was found in the D_2 –He solid.⁵⁴ The best fit in a model calculation of the ESEEM signal of the H atoms, which is represented as a solid line in Fig. 12 *a*, was obtained for a configuration in which ten deuterium and two HD molecules surrounded the H atoms.⁵⁹ The ESEEM signals for H atoms recorded at the beginning of the experiment and 6 hours later were identical, showing that the number of D_2 and HD molecules surrounding the H atoms did not change as the reaction proceeded. This result was in agreement with previously described CW experiments in which the satellite amplitudes remained unchanged throughout the experiment.⁵¹

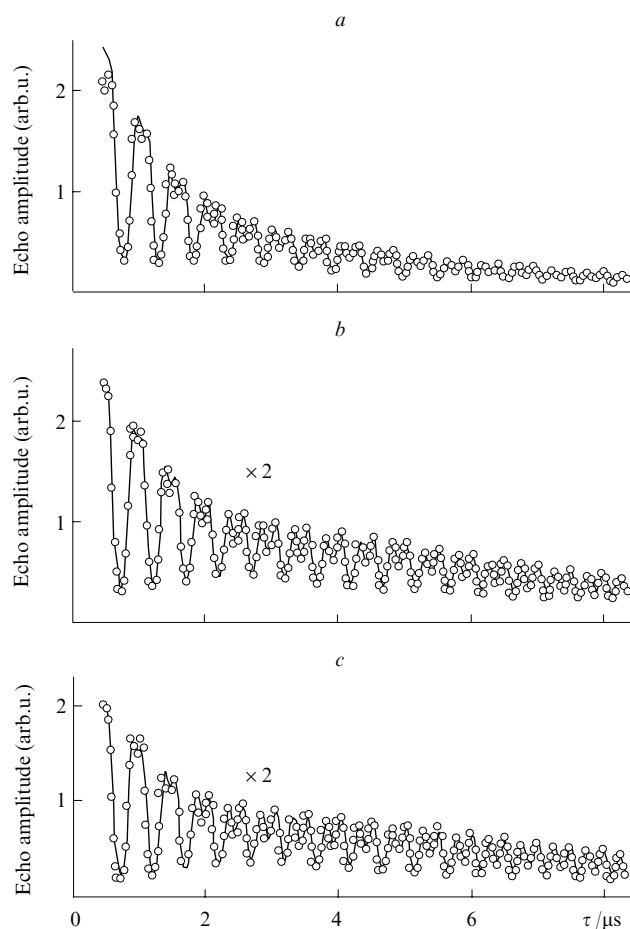


Figure 12. Two pulse ESEEM signals (circles) for the H and D atoms in HD–D₂–He solid at 1.35 K taken at 8.93 GHz: (a) low field hyperfine component of H atoms at 2910.1 G; (b, c) low field hyperfine components for D atoms at 3105.5 G at the beginning of the experiment and six hours later, respectively. Solid lines are the best fits of model calculations to the experimental data (see text).⁵⁹

The ESEEM data for D atoms show that their number decreases over the course of the tunnelling reaction (see Figs 12 *b* and 12 *c*). Modelling of the ESEEM signals for D atoms in the HD–D₂–He solid obtained at the beginning of the experiment (solid line in Fig. 12 *b*) shows that nine D₂ and three HD molecules surrounded a typical D atom within the bulk of the cluster. The same model shows that six hours later (see Fig. 12 *c*) ten D₂ and two HD molecules surrounded a typical D atom. This result is also in good agreement with the results obtained from CW ESR measurements discussed earlier, which suggested that the number of protons (and thus the number of HD molecules) surrounding the D atoms decreases by about 30% in the first six hours following the formation of the sample obtained from the H₂:D₂:He = 1:4:100 gas mixture.

In conclusion, the CW and pulsed ESR methods provide complementary information about the trapping sites and the changing environment of atoms participating in low temperature tunnelling reactions. This information is particularly important for elucidation of the mechanisms of tunnelling reactions of hydrogen atoms.

IV. Studies of H atoms in solid H₂ films at ultralow temperatures

The methods for creating systems of matrix isolated hydrogen atoms mentioned above led to the formation of highly inhomogeneous solids with many defects. In all of these methods one gets quite irregular solids, where the diffusion of the atoms is mediated by inhomogeneities of the crystalline field.

A novel method of ultra-slow deposition of films of solid H₂ with embedded hydrogen atoms has been recently discovered in experiments with spin polarised atomic hydrogen gas.⁴² It is well known that spin-polarised atomic hydrogen gas can be stabilised at temperatures approaching absolute zero (see Ref. 60 and references therein). Atoms are stabilised by applying a strong magnetic field and lining the walls of the experimental cell with a superfluid helium film, thus preventing adsorption of the atoms. The schematic of a typical experimental setup for studies of spin-polarised H gas (H↓) is presented in Fig. 13. Atomic hydrogen gas is produced in a cryogenic radiofrequency dissociator, and the high field-seeking fraction (H↓) is pulled into the sample cell located in a 4.6 T magnetic field. The typical flux of atoms entering the sample chamber (SC) (see also Fig. 14 *a*) is $\sim 2 \times 10^{13} \text{ s}^{-1}$. With the continuously operating dissociator, bulk gas densities up to $2 \times 10^{15} \text{ cm}^{-3}$ can be accumulated in the SC at a temperature of $\sim 350 \text{ mK}$. H↓ atoms of both lowest hyperfine states *a* and *b* (Fig. 14 *b*) are accumulated in equal amounts. The H↓ samples were not perfectly stable against recombination of the atoms into H₂ even in very strong ($> 10 \text{ T}$) magnetic fields due to the unavoidable three-body recombination channel. The molecules resulting from recombination stick to the walls of the experimental chamber and slowly form a layer of solid H₂. This layer in the experiments with H↓ helps to reduce the decay rate of the sample due to one-body nuclear relaxation. A typical rate for solid H₂ film growth is very slow, 0.5–1 molecular layer per hour, which is mainly limited by the efficiency of the radiofrequency dissociator.

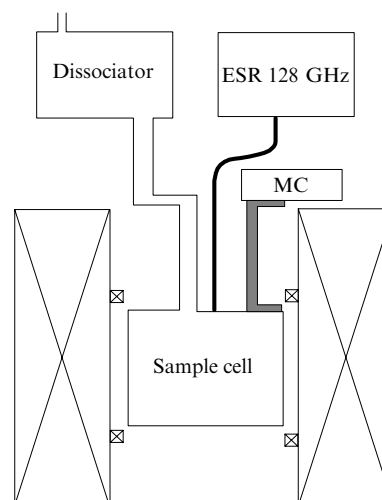


Figure 13. Block diagram of the setup for investigations of H atoms in solid H₂ at ultralow temperatures. The label MC denotes the mixing chamber of the ³He–⁴He dilution refrigerator.

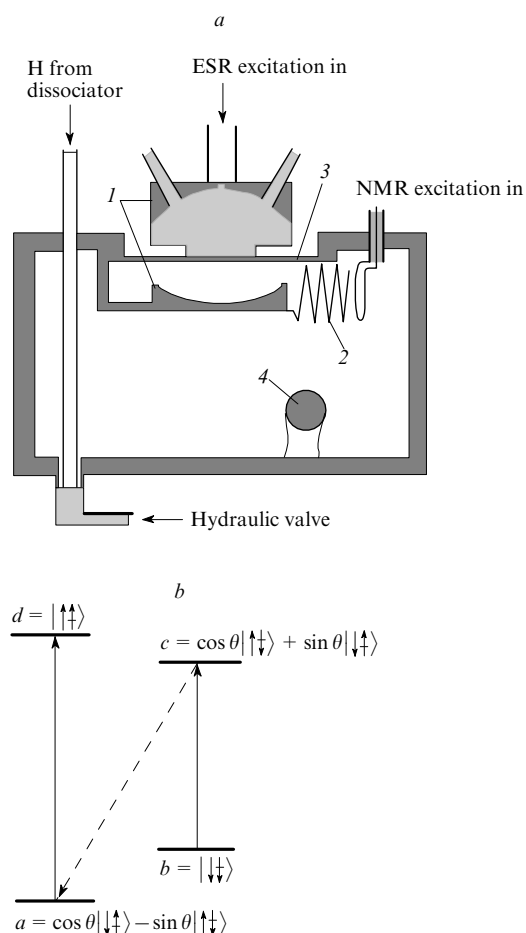


Figure 14. Schematic drawing of the sample cell (a); hyperfine level diagram for hydrogen atom in a strong magnetic field (b).⁴²

(a) Fabry–Perot ESR resonator (1), helical NMR resonator (2), Mylar foil (3), quartz microbalance crystal (4). (b) Arrows denote electron and nuclear spin projections. The values of the angles θ are determined from the equation $\tan 2\theta = a/[h(\gamma_e + \gamma_p)H]$, where a is the hyperfine constant, H is the magnetic field and γ_e , γ_p are the electron and proton gyromagnetic ratios, respectively.

It has been found that H atoms are captured inside the solid H_2 films covering the SC walls.⁴² The mechanism of this process is not known. One of the possibilities is that the molecules appear in the gas phase in one of the highest rovibrational states⁶¹ and may transfer their energy to the atoms in binary collisions. The energy acquired by the atom in such an event can exceed the potential barrier for the atoms to penetrate into the helium film (~ 40 K), and therefore the atom can punch through the film and stick to the solid H_2 . It has been verified that the atoms do not appear in the sample cell as a result of diffusion from the dissociator along the solid H_2 film covering the surface of the fill line. Closing the hydraulic valve at the cell bottom stopped the growth of the atomic ESR signal. Although very slow, this method of deposition of films of H_2 with embedded H atoms has a number of advantages in comparison with the traditional methods of creating such systems employed earlier. The system is absolutely free of any possible impurities, since no other gas, except H_2 can exist at temperatures below 1 K. Although some small admixtures ($< 10^{-4}$) of spin-polarised deuterium can be generated in the dissociator, they cannot reach the sample cell passing through the 0.5 m long filling line, since the recombination rates for D are $> 10^3$ times larger than for H. Another advantage of this method is that the deposition rate and

average energy flux into the system is so slow that one may expect to obtain solid crystals with the least amount of internal crystalline defects, thus making this system very close to ideal for studies of quantum diffusion and tunnelling chemical reactions.

Due to the strong magnetic fields needed for the stabilisation of H_2 , high frequency (128 GHz) ESR and 910 MHz NMR and ENDOR methods were used to characterise the samples. The H_2 films containing H atoms were situated on the surface of the Mylar foil and on the lower spherical mirror (see Fig. 14 a), both located at antinodes of the Fabry–Perot resonator (FPR) operating in the TEM_{005} mode (see Refs 43 and 60 for more details of the experimental setup).

The ESR spectrum of H atoms in solid H_2 in the applied magnetic field of 4.6 T basically consists of two lines separated by 507 G due to the hyperfine interaction. In Fig. 15 (upper trace) the ESR spectra of the lower field line of H atoms in solid H_2 are presented together with the corresponding line originating from the atoms of the gas phase above the film obtained at $T \sim 350$ mK. Special shim coils were used to minimise the magnetic field inhomogeneity, or *vice versa*, to increase the gradient and resolve the absorption lines originating from the atoms located on the Mylar foil and the lower mirror. Integrals of these lines were equal to each other, which indicates a homogeneous film coating over the sample cell walls. Having the possibility to resolve the lines from the free atoms in the gas phase and the matrix isolated ones, one can obtain useful information about the influence of the crystal environment on the g -factor and the hyperfine constants. The ESR lines of H atoms in solid H_2 were found to be shifted by ~ 0.28 G towards the centre of the spectrum compared with those of free atoms (see Fig. 15) with the magnitude of the shift being the same for both ESR lines. Therefore, the atoms in the solid have the same value of the g -factor and a somewhat reduced hyperfine interaction.

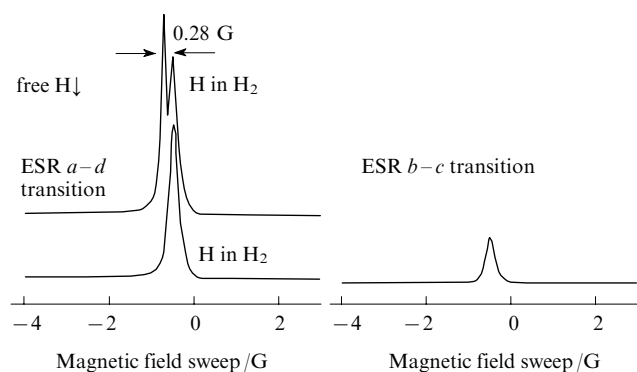


Figure 15. ESR spectra of the H_2 gas and of H atoms in the solid H_2 matrix observed in the measurements: upper left trace is small H_2 density $\sim 2 \times 10^{13} \text{ cm}^{-3}$ (left peak) together with the H in solid H_2 line (right peak); bottom traces are H in solid H_2 spectrum.⁴² Note that the $a-d$ transition signal is larger than the $b-c$ transition signal.

To manipulate the populations of the states a and b , nuclear spin transitions were induced by applying resonant excitation to the helical 910 MHz resonator (HR) located on the side of the FPR (see Fig. 14 a). Due to the small number of atoms in the sample and the poor sensitivity of NMR, it is not possible to detect the NMR absorption directly. However, one can detect it through the change of the ESR signal associated with the change of the populations of hyperfine states. For observation of such double resonance spectra, the allowed

electron $b \rightarrow c$ transition was saturated with high excitation power while the ESR sweep was stopped in the middle of the H in H_2 line. Then a radiofrequency signal was applied to the helical NMR resonator (HR) with its frequency swept through the position of the nuclear $a \rightarrow b$ transition (near 909 MHz). The power absorbed by the ESR is increased once the nuclear resonance condition is reached, since the atoms are transferred from the a to the b state (Fig. 16). The position of the ENDOR line relative to that of the free atoms gives the value of the hyperfine constant change $-1320(10)$ kHz. This reduction of the hyperfine constant with respect to the free atoms implies that the atoms are situated in substitutional sites. In this case the effects of van-der-Waals attraction to the neighbouring molecules dominate over the Pauli repulsion.⁶² A similar conclusion has been made in the ENDOR studies of Nagoya group³⁰ for the H in H_2 samples obtained by a different method. A remarkable feature of the ENDOR spectra observed in the films of H in H_2 created by the slow deposition method⁴² is the unusually small width of the NMR transition (~ 15 kHz). This provides good evidence of the high quality of the H_2 crystals obtained by this method.

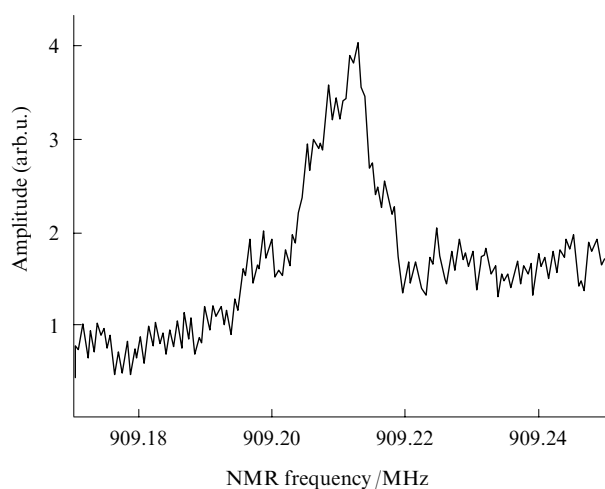


Figure 16. ENDOR spectrum of hydrogen atoms in solid H_2 .⁴²

Another interesting feature found in the experiments with the H in H_2 films⁴² was the very high stability of the atoms to recombination (Fig. 17) at temperatures below 150 mK. For this temperature range no decay of H atoms was detected over a period of at least two weeks. A slow decrease of H atom concentration has been observed at 300 mK and 480 mK. Figure 18 shows the values of the recombination rate constants obtained in these experiments compared with the previous higher temperature results and with the theoretical predictions. It has been found that for temperatures below 0.9 K the recombination rate constants, $k_H(300 \text{ mK}) = 1.5 \times 10^{-25} \text{ cm}^{-3} \text{ s}^{-1}$ and $k_H(480 \text{ mK}) = 3 \times 10^{-25} \text{ cm}^{-3} \text{ s}^{-1}$ are much smaller than predicted theoretically^{7,63} and found in previous experiments⁸ at $1.35 < T < 4.2$ K. However, at the highest temperatures (900 mK) used in the studies of the H in H_2 films⁴² the rate constant increased substantially and came into close agreement with extrapolation of the previous results. The vanishingly small recombination at the lowest temperatures makes it promising to achieve extremely low temperatures for this metastable system in future experiments, since recombination heating would not be a factor.

Populations of the lower hyperfine states can be manipulated by saturation of the ESR or NMR transitions. Saturating the $b \rightarrow c$ transition leads to the pumping of the atoms from the state b to a (via the Overhauser effect) through the relaxation of

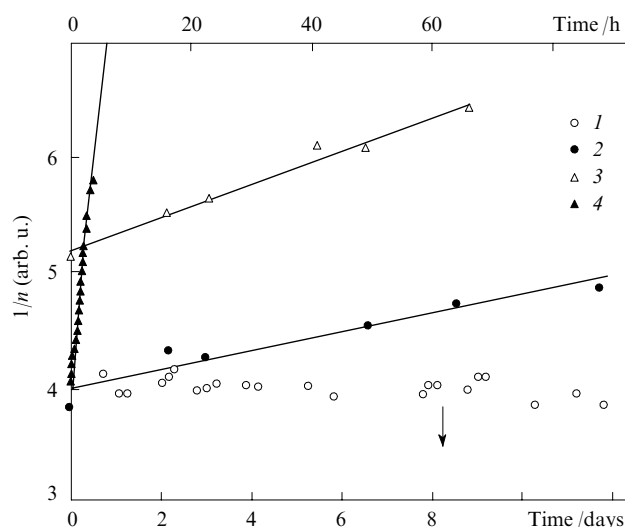


Figure 17. Decay of H in H_2 sample at different temperatures.⁴² T/mK : (1) 150 (lower time scale), (2) 300, (3) 480, (4) 900 (all upper time scale).

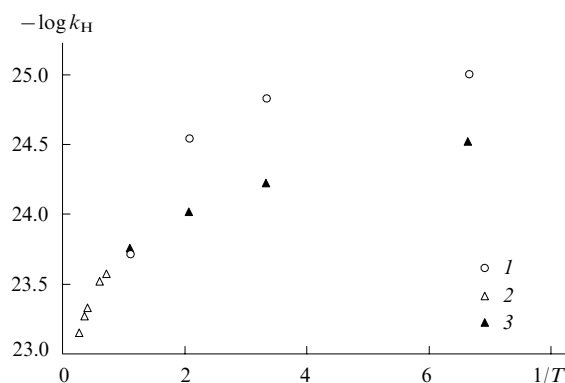


Figure 18. Temperature dependence of logarithm of rate constant for recombination of H atoms in solid H_2 : our experimental results at $T < 1$ K (1), experimental results⁸ for the temperature range $1.3 < T < 4.2$ K (2) and theoretical prediction for $T < 1$ K (3).⁷

the partially forbidden $a \rightarrow c$ transition. The relaxation time of the $a \rightarrow c$ transition of H atoms inside H_2 films is about 3 s. Using the Overhauser effect, one can transfer the entire population to the a state within several seconds. Then the a and b populations can again be equalised by applying resonance power to the $a \rightarrow b$ transition. Recovery of the population ratio n_a/n_b or the polarisation

$$p = \frac{n_a - n_b}{n_a + n_b}$$

to the equilibrium value is controlled by the nuclear relaxation process which turns out to be very slow, $t_{b \rightarrow a} \sim 60\text{--}80$ h at 150 mK (Fig. 19). A most intriguing observation in the experiment of Ref. 42 was the non-Boltzmann population of the hyperfine states b and a in the steady state. The populations ratio is typically characterised by the value of nuclear polarisation. The value of $p(t \rightarrow \infty) = 0.5(1)$ observed at $T = 150$ mK was much larger than $p \approx 0.14$ dictated by the Boltzmann statistics with $n_a/n_b = \exp(E_{a-b}/T)$, with $E_{a-b} \approx 43$ mK being the energy difference between the a and b states. The

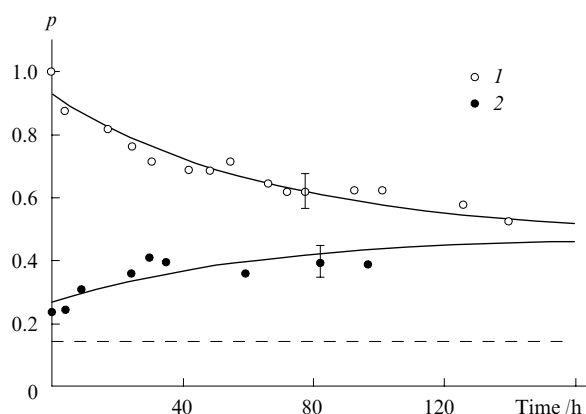


Figure 19. Evolution of the nuclear polarisation $p = (n_a - n_b)/(n_a + n_b)$ at $T = 150$ mK after saturation of the $b-c$ transition (1) and after partial saturation of the $a-b$ transition (2). The horizontal dashed line marks the nuclear polarisation corresponding to a thermal (Boltzmann) ratio $n_a/n_b = \exp(E_{a-b}/T)$ with $T = 150$ mK.⁴²

non-equilibrium population ratio observed in these experiments can be explained by the possible formation of a Bose–Einstein condensate (BEC) in the ensemble of atoms. This cannot occur if the atoms are evenly distributed over the crystal because the average density is not high enough to reach quantum degeneracy. If however, there are regions in the crystal with much higher local concentrations, the condensation may happen there and the system should then consist of two kinds of atoms, those in the high concentration regions and those in the rest of the crystal.

A powerful concentrating mechanism such as the phase separation seen in solid ^3He – ^4He mixtures^{64,65} and potentially in ortho-para solid H_2 mixtures^{66,67} is required to reach a concentration of $\sim 5 \times 10^{20} \text{ cm}^{-3}$, which corresponds to a BEC onset temperature of 0.2 K for H atoms with effective mass $3.5 m_{\text{H}}$ as calculated from the experimental n_a/n_b population ratio. Diffusion of the H atoms *via* exchange tunnelling can be considered as a motion of ‘quasivacancies’, leading to a broad energy band and low effective mass.⁶⁸ One might imagine that the H atom rich phase exists in small bubbles or layers surrounded by the H atom starved phase.

V. Conclusions and future work

Impurity–helium solids are highly porous gel-like nanomaterials consisting of interconnecting clusters of impurities with a characteristic size 5–9 nm and an average density over the entire sample volume as low as 10^{20} atoms (molecules) cm^{-3} . In fact, Im–He solids are a collection of nanoclusters. One cubic centimeter of a typical Im–He sample contains a large number ($\sim 10^{16}$) of clusters, each consisting of $\sim 10^4$ molecules and 10–100 or more stabilised atoms. Therefore, it is possible to study simultaneously a large collection of nanoreactors, in which low temperature chemical reactions can be investigated.

The kinetics of exchange tunnelling reactions of hydrogen isotopes were studied in nanoclusters immersed in superfluid helium at $T = 1.35$ K. The rate constants for different reactions have been determined and the changes of the environments of hydrogen and deuterium atoms in the course of these reactions have been studied. The rate constants for reactions (2) and (4) in nanoclusters were found to be similar to those obtained in bulk solids. In contrast, the rate constant for the reaction (1) in nanoclusters is an order of magnitude higher as compared to that obtained in bulk solid hydrogen. Possibly the recombination of H atoms occurs primarily on the surfaces of

the nanoclusters. The analysis of the pulsed ESR data shows that 50%–60% of all stabilised atoms reside on the surfaces of the nanoclusters.

Reactions between hydrogen atom isotopes might be studied at even lower temperatures. This would shed more light on the details of tunnelling processes in chemical reactions occurring in the solid phase. The study of Im–He solids at ultralow (10–20 mK) temperatures should be pursued. Obviously, such a program will encounter major technological challenges to adapt methods of preparation of Im–He solids with high concentrations of stabilised atoms to the restrictions existing in a dilution refrigerator cryostat. Nevertheless, such investigations could show great promise. Cooling down the H– H_2 –He samples with high concentrations of stabilised H atoms to the temperature region of 10–20 mK could lead to the observation of Bose–Einstein condensation of H atoms.

Another approach to studies of the kinetics of recombination of H atoms in H_2 solids at ultralow temperatures was demonstrated. The technique usually used for studies of spin-polarised hydrogen gas also provided the opportunity to prepare and investigate H atoms in thin molecular films of solid H_2 . For the first time, the recombination rates of H atoms in solid H_2 were studied in the temperature range 0.15–0.9 K. It was found that recombination rate constants are significantly smaller at these temperatures than was predicted theoretically. Moreover, at $T = 0.15$ K, H atoms were very stable during two weeks of observations. At this temperature the population of the lowest hyperfine state of atomic hydrogen was found to be much larger than that expected from the Boltzmann distribution. A possible explanation for this observation is achievement of the Bose–Einstein condensation of H atoms in solid H_2 . This might be possible if regions of high local concentration of H atoms can be created in solid H_2 . Additional studies of the temperature dependence of the populations of the lowest energy levels of H atoms are necessary to confirm whether BEC is actually occurring in this system. Alternative explanations should also be explored in future experiments and theoretical work.

We would like to thank the National Science Foundation (Grant No. DMR-0504683), NASA (Grant No. NAG3-2871) and CRDF (Grant No. RUP1-2841-CG-06) for support prior to and during the preparation of this review. We also are grateful to the Academy of Finland (Grant No. 206109) and the Wihuri Foundation for supporting the research program at Turku University. One of us (D M Lee) would like to thank the Aspen Center for physics, which provided a forum for interesting discussions. The authors take this opportunity to express their gratitude to R Boltnev, S Kiselev, P Borbat, J Freed, E Müller, V Kiryukhin, J Jarvinen, J Ahokas and E Vehmanen for stimulating and useful discussions.

References

1. C K Jen, S N Foner, E L Cochran, V A Bowers *Phys. Rev.* **104** 846 (1956)
2. C K Jen, S N Foner, E L Cochran, V A Bowers *Phys. Rev.* **112** 1169 (1958)
3. L A Wall, D W Brown, R E Florin *J. Phys. Chem.* **63** 1762 (1959)
4. L H Piette, R C Rempel, H E Weaver, J M Flournoy *J. Chem. Phys.* **30** 1623 (1959)
5. A M Bass, H P Broida *Formation and Trapping of Free Radicals* (New York, London: Academic Press, 1960)
6. A F Andreev, I M Lifshits *Zh. Eksp. Teor. Fiz.* **29** 1107 (1969)^a
7. Yu Kagan, L A Maksimov, N V Prokofev *Pisma Zh. Eksp. Teor. Fiz.* **36** 204 (1982)^b
8. A V Ivliev, A Ya Katunin, I I Lukashevich, V V Sklyarevskii, V V Suraev, V V Filippov, N I Filippov, V A Shevtsov *Pisma Zh. Eksp. Teor. Fiz.* **36** 391 (1982)^b

9. H Tsuruta, T Miyazaki, K Fueki, N Azuma *J. Phys. Chem.* **87** 5422 (1983)
10. E B Gordon, A A Pel'menev, O F Pugachev, V V Khmelenko *Pisma Zh. Eksp. Teor. Fiz.* **37** 282 (1983)^b
11. R N Porter, M Karplus *J. Chem. Phys.* **40** 1105 (1964)
12. T Takayanagi, K Nakamura, S Sato *J. Chem. Phys.* **90** 1641 (1989)
13. T Kumada *Phys. Rev. B* **68** 052301 (2003)
14. M Sharnoff, R V Pound *Phys. Rev.* **132** 1003 (1963)
15. A S Iskovskikh, A Ya Katunin, I I Lukashevich, V V Sklyarevskii, V V Suraev, V V Filippov, N I Filippov, V A Shvetsov *Zh. Eksp. Teor. Fiz.* **64** 1085 (1986)^a
16. T Miyazaki, K-P Lee, K Fueki, A Takeuchi *J. Phys. Chem.* **88** 4959 (1984)
17. K-P Lee, T Miyazaki, K Fueki, K Gotoh *J. Phys. Chem.* **91** 180 (1987)
18. T Miyazaki, N Iwata, K-P Lee, K Fueki *J. Phys. Chem.* **93** 3352 (1989)
19. E B Gordon, A A Pel'menev, O F Pugachev, V V Khmelenko *Fiz. Nizk. Temp.* **11** 307 (1985)^c
20. E P Bernard, R E Boltnev, V V Khmelenko, V Kiryukhin, S I Kiselev, D M Lee *J. Low Temp. Phys.* **134** 169 (2004)
21. E P Bernard, R E Boltnev, V V Khmelenko, V Kiryukhin, S I Kiselev, D M Lee *Phys. Rev. B* **69** 104201 (2004)
22. A V Ivliev, A S Iskovskikh, A Ya Katunin, I I Lukashevich, V V Sklyarevskii, V V Suraev, V V Filippov, N I Filippov, V A Shvetsov *Pisma Zh. Eksp. Teor. Fiz.* **38** 317 (1983)^b
23. T Miyazaki, K-P Lee *J. Phys. Chem.* **90** 400 (1986)
24. T Miyazaki, S Mori, T Nagasaka, J Kumagai, Y Aratono, T Kumada *J. Phys. Chem. A* **104** 9403 (2000)
25. T Kumada, S Mori, T Nagasaka, J Kumagai, T Miyazaki *J. Low Temp. Phys.* **122** 265 (2001)
26. T Kumada, M Sakakibara, T Nagasaka, H Fukuta, J Kumagai, T Miyazaki *J. Chem. Phys.* **116** 1109 (2002)
27. T Kumada, K Komaguchi, Y Aratono, T Miyazaki *Chem. Phys. Lett.* **261** 463 (1996)
28. T Miyazaki, N Iwata, K Fueki, H Hase *J. Phys. Chem.* **94** 1702 (1990)
29. T Miyazaki *Chem. Phys. Lett.* **176** 99 (1991)
30. T Kumada, N Kitagawa, T Noda, J Kumagai, Y Aratono, T Miyazaki *Chem. Phys. Lett.* **288** 755 (1998)
31. T Kumada, T Noda, J Kumagai, Y Aratono, T Miyazaki *J. Chem. Phys.* **111** 10974 (1999)
32. J Kumagai, T Noda, T Miyazaki *Chem. Phys. Lett.* **321** 8 (2000)
33. *Atom Tunnelling Phenomena in Physics, Chemistry and Biology* (Ed. T Miyazaki) (Berlin: Springer, 2004)
34. G K Ivanov, M A Kozhushner, L I Trakhtenberg *J. Chem. Phys.* **113** 1992 (2000)
35. J Z H Zhang, W H Miller *J. Chem. Phys.* **91** 1528 (1989)
36. E B Gordon, L P Mezhev-Deglin, O F Pugachev *Pisma Zh. Eksp. Teor. Fiz.* **19** 103 (1974)^b
37. E B Gordon, V V Khmelenko, E A Popov, A A Pel'menev, O F Pugachev *Chem. Phys. Lett.* **155** 301 (1989)
38. V Kiryukhin, B Keimer, R E Boltnev, V V Khmelenko, E B Gordon *Phys. Rev. Lett.* **79** 1774 (1997)
39. S I Kiselev, V V Khmelenko, D M Lee, V Kiryukhin, R E Boltnev, E B Gordon, B Keimer *Phys. Rev. B* **65** 024517 (2002)
40. E B Gordon *Dokl. Akad. Nauk* **378** 156 (2001)^d
41. R W H Webeler *J. Chem. Phys.* **64** 2253 (1976)
42. J Ahokas, J Jarvinen, V V Khmelenko, D M Lee, S Vasiliev *Phys. Rev. Lett.* **97** 095301 (2006)
43. S Vasiliev, J Jarvinen, E Tjukanov, A Kharitonov, S Jaakola *Rev. Sci. Instrum.* **75** 94 (2004)
44. S I Kiselev, V V Khmelenko, E P Bernard, D M Lee *Fiz. Nizk. Temp.* **29** 505 (2003)^c
45. E P Bernard, V V Khmelenko, E Vehmanen, P P Borbat, J H Freed, D M Lee *AIP Conference Proceedings 850: The 24th International Conference on Low Temperature Physics, Orlando, FL, 2005* p. 1659
46. W E Blumberg, W B Mims, D Zuckerman *Rev. Sci. Instrum.* **44** 546 (1973)
47. A V Astashkin, V V Kozlyuk, A M Raitsimring *J. Magn. Reson.* **145** 357 (2000)
48. S I Kiselev, V V Khmelenko, C Y Lee, D M Lee *J. Low Temp. Phys.* **128** 37 (2002)
49. S I Kiselev, V V Khmelenko, D M Lee *Phys. Rev. Lett.* **89** 175301 (2002)
50. V V Khmelenko, S I Kiselev, D M Lee, C Y Lee *Phys. Scr.* **T102** 118 (2002)
51. E P Bernard, R E Boltnev, V V Khmelenko, D M Lee *J. Low Temp. Phys.* **138** 829 (2005)
52. G T Trammell, H Zeldes, R Livingston *Phys. Rev.* **110** 630 (1958)
53. T Kumada *J. Chem. Phys.* **124** 094504 (2006)
54. E P Bernard, V V Khmelenko, E Vehmanen, P P Borbat, J H Freed, D M Lee *AIP Conference Proceedings 850: The 24th International Conference on Low Temperature Physics, Orlando, FL, 2005* p. 372
55. W B Mims, J Peisach, J L Davis *J. Chem. Phys.* **66** 5536 (1977)
56. M Iwasaki, K Toriyama, K Nunome *J. Chem. Phys.* **86** 5971 (1987)
57. A Ponti *J. Magn. Reson.* **127** 87 (1997)
58. E B Gordon *Fiz. Nizk. Temp.* **30** 756 (2004)^c
59. V V Khmelenko, E P Bernard, E Vehmanen, D M Lee *AIP Conference Proceedings 850: The 24th International Conference on Low Temperature Physics, Orlando, FL, 2005* p. 376
60. J Järvinen, J Ahokas, S Jaakkola, S Vasilyev *Phys. Rev. A* **72** 052713 (2005)
61. Y M Xiao, S Buchman, L Pollack, D Kleppner, T J Greytak *Phys. Rev. B* **48** 15744 (1993)
62. S N Foner, E L Cochran, V A Bowers, C K Jen *J. Chem. Phys.* **32** 963 (1960)
63. Yu Kagan, A J Leggett *Quantum Tunnelling in Condensed Media* (Amsterdam: North-Holland, 1992)
64. D O Edwards, A S McWilliams, J G Daunt *Phys. Rev. Lett.* **9** 195 (1962)
65. V Maidanov, A Ganshin, V Grigor'ev, A Penzev, E Rudavskii, A Rybalko, Ye Syrnikov *J. Low Temp. Phys.* **126** 133 (2002)
66. H Meyer *Can. J. Phys.* **65** 1453 (1987)
67. H Meyer *Fiz. Nizk. Temp.* **24** 507 (1998)^c
68. D I Pushkarev *Centr. Eur. J. Phys.* **2** 420 (2004)

^a — *J. Exp. Theor. Phys. (Engl. Transl.)*

^b — *J. Exp. Theor. Phys. Lett. (Engl. Transl.)*

^c — *Low Temp. Phys. (Engl. Transl.)*

^d — *Dokl. Phys. Chem. (Engl. Transl.)*

Competitive cryochemical reactions of transition metal atoms, clusters and nanosized particles

T I Shabatina, J Mascetti, J S Ogden, G B Sergeev

Contents

I. Introduction	1123
II. Size effects in reactions of atoms and small clusters of transition metals (Sc, Ti, Cr, Fe, Co, Ni, Cu) with organic and inorganic molecules in inert matrices at low temperatures	1124
III. Formation of metal nanoparticles in active matrices	1126
IV. Thermal transformations of metastable complexes of lanthanide atoms and clusters	1128
V. Competitive reactions of silver and gold particles of different sizes and shapes with model reagents	1131
VI. Conclusion	1134

Abstract. Specific features of cryochemical reactions of transition metal atoms, small clusters, complexes and nanoparticles are considered. New phenomena that arise in nano- and subnanoscale systems at low temperatures are analysed. It is shown that the competition between self-assembly processes of metal atoms and reactions of metal aggregates of different size with organic and inorganic reagents determines the chemical nature and properties of the intermediate and final products. Special attention is paid to the analysis of size effects caused by the dependence of the reactivity of metal clusters and nanoparticles on the number of constituent atoms. Prospects for the use of competitive cryochemical reactions are discussed. The bibliography includes 185 references.

I. Introduction

Recent progress in cryochemistry was largely associated with the development of methods for synthesis and stabilisation of atoms, small clusters and nanoparticles incorporating from just a few metal atoms to hundreds and thousands.^{1–5} At present, studies of these systems form the basis of a new direction of chemistry, namely, cryonanochemistry. In cryonanochemistry, attention is focused on the size effects associated with the dependence of the reactivity of clusters and nanoparticles on the number of constituting atoms.¹ Atoms and clusters that emerge in the thermal evaporation of metals in vacuum are much more reactive than bulk metals.⁵ At low

temperatures, these high-energy and extremely reactive particles undergo consecutive and competitive chemical reactions with different organic and inorganic molecules. Low-temperature covalent and non-covalent interactions lead to the formation of new chemical compounds of metals in the zero or lower oxidation states and to the stabilisation of unstable structures and labile coordinatively unsaturated complexes, radicals and unusual molecules. Such systems are of interest for coordination chemistry, chemistry of clusters and organometallic compounds, atmosphere and space chemistry. They may also be used in the development of new metal-containing nanomaterials and in the elaboration of new nanotechnologies.

This review analyses the experimental and theoretical data on competitive cryochemical reactions of metal atoms and small clusters in condensed media, namely, in solid matrices of inert gases (in the presence of one or two active reagents) and in low-temperature co-condensates containing reactive components, for the metals of the first, second and third transition rows. Special sections are devoted to thermal transformations of metastable mono- and polynuclear lanthanide complexes and to chemical reactions of silver and gold atoms, clusters and nanoparticles as the systems most promising for nanochemical and nanocatalytic applications. Attention is focused on the kinetic analysis of competitive chemical reactions that involve metal particles of different sizes and shapes with different ligands. Processes of formation and stabilisation of nanoparticles in low-temperature matrices and co-condensates are considered; mechanisms of their reactions with certain organic and inorganic reagents are discussed and manifestations of size effects typical of reactions of these small-scale chemical entities are analysed. In this review, almost no attention is paid to the problems associated with the development of a new promising research direction, *viz.*, spectroscopic studies of metal clusters and their reactions in solid hydrogen matrices and liquid helium nanodroplets as condensed quantum systems. This is explained by the fact that these problems are of their own, independent importance.

The authors of this review are united by long-term collaboration within the framework of INTAS projects. The material of this review was partly presented as the plenary lectures at the VIth International Conference on Low Temperature Chemistry (Chernogolovka, 2006).

T I Shabatina, G B Sergeev Department of Chemistry, M V Lomonosov Moscow State University, Leninskie Gory, 119992 Moscow, Russian Federation. Fax/tel. (7-495) 939 54 42, e-mail: tsh@kinet.chem.msu.ru (T I Shabatina), gbs@kinet.chem.msu.ru (G B Sergeev)

J Mascetti Université Bordeaux I, Institut des Sciences Moléculaires, CNRS, 33405 Talence Cedex, France. Fax (33-540) 00 84 02, tel. (33-540) 00 63 60, e-mail: j.mascetti@ism.u-bordeaux1.fr

J S Ogden Department of Chemistry, University of Southampton, Highfield, SO17 1BJ Southampton, UK. Fax (44-2380) 59 37 81, tel. (44-2380) 59 23 54, e-mail: js.ogden@soton.ac.uk

Received 6 August 2007

Uspekhi Khimii 76 (12) 1202–1217 (2007); translated by T Ya Safonova

II. Size effects in reactions of atoms and small clusters of transition metals (Sc, Ti, Cr, Fe, Co, Ni, Cu) with organic and inorganic molecules in inert matrices at low temperatures

Reactions of transition metal atoms and clusters with organic and inorganic molecules attract keen attention. Indeed, such processes model the reactions of molecules of various reagents with the active sites on the metal catalyst surface, which allows study of unusual chemical processes including the activation of small molecules such as carbon dioxide and nitrogen.^{6–8} Coordination of CO₂ to metal sites is the key stage of its catalytic and electrochemical reduction.^{9–11} The method of matrix spectroscopy makes it possible to identify intermediate products of various reactions and elucidate the mechanism of metal coordination with ligand molecules.

The reactions of atoms of the 1st transition series elements (Sc, Ti, Cr, Fe, Co, Ni, Cu) with carbon dioxide were studied systematically by matrix Fourier transform IR spectroscopy (FT IR) using isotopically labelled molecules ¹³CO₂ and C¹⁸O₂.^{12–15} The obtained results together with density functional theory calculations made it possible to determine the equilibrium parameters of formed complexes and elucidate the coordination type of a metal. It was shown that in a carbon dioxide matrix at 10 K, metal atoms of the first transition rows (Fe, Co, Ni and Cu) form 1 : 1 complexes with CO₂ molecules. In these complexes, the coordination of these molecules to metal atoms was of the ‘side-on’ ($\eta^2_{O,O}$) type for nickel, the ‘end-on’ ($\eta^1_{C,O}$) type for copper and the C type (η^1_C) for iron (Fig. 1). The energy of a bond formed by a nickel atom with CO₂ was 17.5 kcal mol^{–1}, which is comparable with the binding energies of this atom in its complexes with similar molecules, namely Ni(C₂H₄), Ni(C₂H₄)₂ and NiCO.^{16–20} On the other hand, atoms of elements situated in the beginning of this period (Ti, V and Cr) effectively inserted into C–O bonds of CO₂ molecules to form oxocarbonyl derivatives (O)M(CO)(CO₂). According to calculations, the insertion of a titanium atom into a C–O bond of the CO₂ molecule proceeded virtually without activation and the thermodynamic stability of a (O)Ti(CO) molecule substantially exceeded the stability of possible complexes Ti(CO₂) (Fig. 2). The interaction of a titanium atom with the second CO₂ molecule resulted in the formation of an even more stable (O)Ti(CO)(CO₂) complex [$D_e(\text{CO}_2) = 28 \text{ kcal mol}^{-1}$, D_e is the energy of ligand bonding] in which the CO₂ molecule turned out to be in the ‘side-on’ coordination with respect to the titanium atom and the fragments (O)Ti(CO) and Ti(CO₂) were located in perpendicular planes.

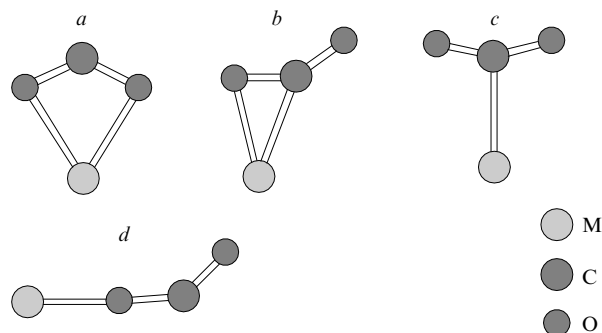


Figure 1. Types of complexes formed in the reaction of transition metals with CO₂.

Type: (a) $\eta^2_{O,O}$, (b) $\eta^1_{C,O}$, (c) η^1_C , (d) η^1_O .

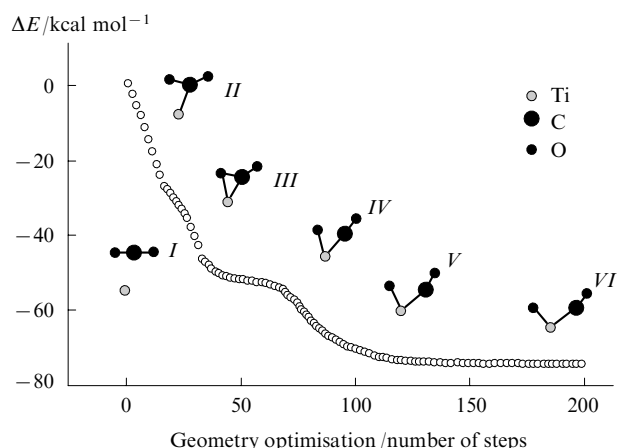


Figure 2. Possible structures of complexes formed in the titanium reaction with CO₂.¹²

(I–VI) are the types of structures corresponding to different steps of optimisation.

It was found²¹ that excited titanium atoms insert into C–H bonds of ethylene molecules in argon matrices at 10 K upon irradiation of samples with light with a wavelength > 400 nm. The TT IR method using isotopically labelled ethylene molecules ¹²C₂H₄, ¹³C₂H₄, C₂D₄, CH₂CD₂ and natural titanium isotopes revealed the formation of compounds containing Ti–C bonds, namely, titanacyclopentene H₂Ti(C₂H₂) and vinyltitanium monohydride. The appearance of monoligand titanium π -complexes Ti(C₂H₄) was not confirmed experimentally, although model calculations carried out within the framework of the density functional theory (DFT) predicted the presence of strong bonding in this case. Titanium hydrides and carbonyls were obtained in the co-condensation of metal atoms with ligand molecules at superlow temperatures in inert matrices.^{22–25}

In argon-diluted systems at low temperatures (10–30 K), virtually no interaction of atoms of the metal group under consideration with CO₂ was observed. The competitive interaction of nickel simultaneously with two ligands (N₂ and CO₂) in dilute argon matrices led to an unexpected result, the cooperative effect of co-ligands.¹² The binding of CO₂ molecules into a complex was substantially intensified when N₂ molecules were added to the argon matrix. The preliminary coordination of a nitrogen molecule into transient Ni(N₂) species induced the hybridisation of 4s and 3d orbitals of the nickel atom, which intensified the Ni → CO₂ charge transfer in a mixed-ligand complex Ni(CO₂)(N₂) as compared with a monoligand Ni(CO₂) complex. The obtained data are well described by a model ‘electron donation L → M/back donation M → L’ (the Chatt–Dewar–Duncanson model), which was used for the description of these systems.^{26–28} A comparison of potential energy curves of these interactions have shown that the binding energy of a nickel atom with the CO₂ molecule is 17.5 kcal mol^{–1}, whereas the binding energy of a Ni(N₂) complex with the CO₂ molecule is almost twice as high, namely, 32 kcal mol^{–1}.

A reaction of copper with molecular nitrogen was studied in nitrogen and argon matrices by the FT IR and UV-Vis spectroscopic techniques.²⁹ In argon matrices with a constant ratio metal : matrix = 1 : 1000, the aggregation of metal atoms was determined by the nitrogen content. The Cu₂ : Cu ratio in a nitrogen matrix was larger than in an argon matrix and decreased upon dilution with argon. The co-condensation led to the formation of two complexes of copper dimers with the ‘end-on’ coordination of ligands, namely, mono- [Cu₂(N₂)]

and bisligand $[\text{Cu}_2(\text{N}_2)_2]$ complexes with binding energies of 7.9 and 12.8 kcal mol⁻¹, respectively.

No complexes were formed in argon-diluted systems with a ratio $\text{N}_2:\text{Ar} < 0.5$ that contained infinitesimal amounts of copper aggregates.²⁹ The interaction of copper atoms with nitrogen molecules started with the addition of a second ligand, CO, into the system. This was manifested by the formation of mixed complexes of copper atoms $\text{Cu}(\text{N}_2)\text{CO}$ for which the energies of ligand bonding [$D_e(\text{Cu}-\text{CO}) = 17.2$ and $D_e(\text{Cu}-\text{N}_2) = 7.5$ kcal mol⁻¹] were substantially higher as compared with the corresponding monoligand complexes, namely, 9.5 kcal mol⁻¹ for $\text{Cu}-\text{CO}$ and -0.1 kcal mol⁻¹ for $\text{Cu}-\text{N}_2$. The strong polarisation of 4s orbitals in a dimer Cu_2 substantially weakened the σ -repulsion between the lone electron pair of a ligand and the $4s^1 3d^{10}$ electron shells of a copper atom in Cu_2L complexes. Thus, in the systems under consideration, dimeric nitrogen complexes $\text{Cu}_2(\text{N}_2)$ were preferentially formed.

Co-condensation of thermally evaporated copper atoms with carbon dioxide and an excess of argon afforded no reaction products. Co-condensation of copper vapour with an excess of carbon dioxide in the absence of matrix components led to the formation of 'end-on' monoligand complexes.¹² Density functional theory calculations using the 'Gaussian 03' computational package and the B3LYP functional were aimed at the comparison of reactivities of Cu atoms and Cu_2 dimers with respect to carbon dioxide and carbon disulfide.^{30–32} The potential energy surface of the $\text{Cu}-\text{CO}_2$ system demonstrated a single minimum, which corresponded to the OCuCO insertion product with a potential barrier of 63 kcal mol⁻¹ (Fig. 3). At the same time, a copper dimer Cu_2 in the singlet state underwent an activationless transformation into an 'end-on' complex $\text{Cu}_2(\text{OCO})$ with the energy 2.1 kcal mol⁻¹ lower than that of the starting reactants Cu_2 and CO_2 . Based on the performed calculations, several insertion products into the C–O bond of carbon dioxide were proposed as other putative intermediate products (Fig. 4). As in the case of copper reaction with nitrogen molecules, the reactivity of a copper dimer turned out to be higher than that of a copper atom.

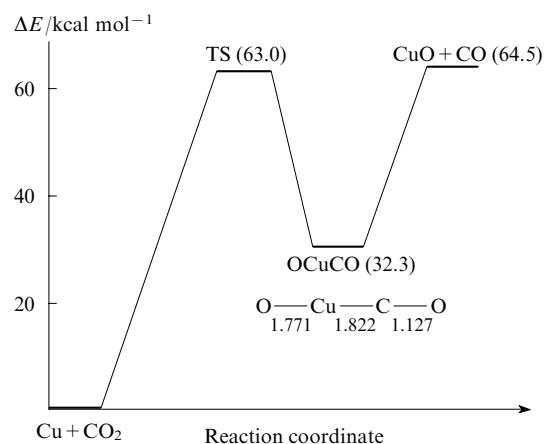


Figure 3. Potential energy variations in the $\text{Cu} + \text{CO}_2$ reaction and the structure of an intermediate product corresponding to the energy minimum (bond distances are shown in Å).³¹ TS is the transition state.

A series of $\text{Fe}_x(\text{N}_2)_y$ complexes were obtained in the reaction of mass-selected iron clusters with an excess of molecular nitrogen.³³ An IR spectroscopic study coupled with the Fourier analysis using isotopically labelled ligand molecules and the results of DFT simulations have shown 'end-on' $\text{Fe}(\text{N}_2)_5$ complexes to be the main reaction products of iron atoms with nitrogen molecules. Furthermore, cluster complexes $\text{Fe}_2(\text{N}_2)_x$ and $\text{Fe}_3(\text{N}_2)_x$ were observed. The early formation of $\text{Fe}_2(\text{N}_2)_x$ complexes ($x = 1–5$) in argon matrices was revealed by UV-Vis and IR spectroscopic techniques.³⁴ As in the case of copper, the ratio between the matrix-stabilised metal atoms and clusters $\text{Fe}:\text{Fe}_x$ was determined by the content of additionally introduced nitrogen. The maximum content of Fe_2 dimers was observed for the 0.05% nitrogen concentration in the argon matrix. For the higher nitrogen concentrations, iron dimers efficiently reacted with nitrogen

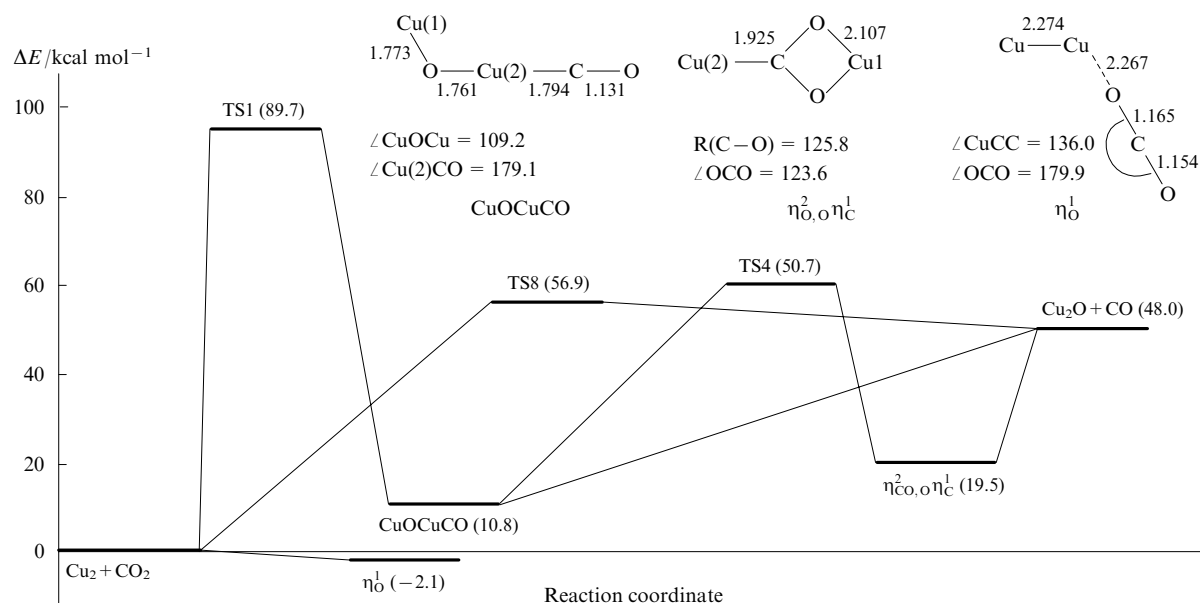


Figure 4. Potential energy variations in the reaction of a copper dimer Cu_2 (singlet state) with CO_2 and the structure of intermediate products corresponding to the energy minima (bond distances are shown in Å, angles are shown in degrees).^{31, 32}

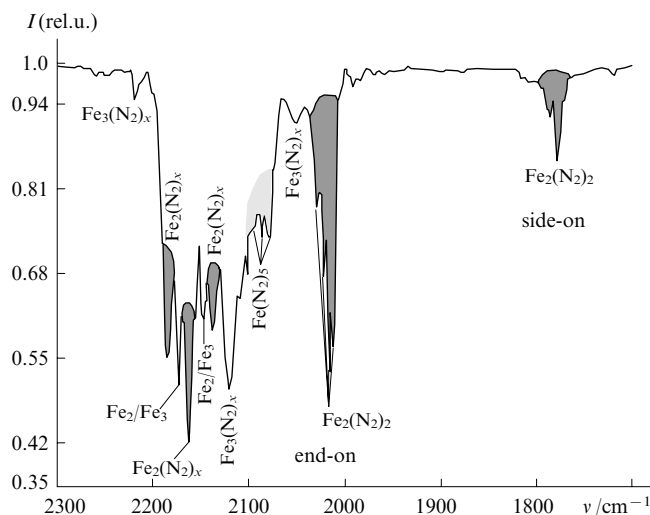
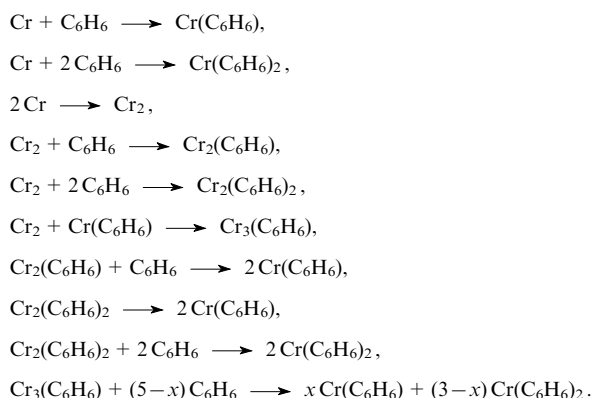


Figure 5. IR spectra of co-condensates of vapour of heat-evaporated iron and molecular nitrogen ($T = 12$ K, $\text{Fe}:\text{N}_2 = 1:1000$).³⁴ Complex $\text{Fe}_2(\text{N}_2)_2$ exists in two forms, namely, 'end-on' and 'side-on'.

molecules to form diverse complexes with different coordination types (Fig. 5).

Co-condensation of nitrogen with certain metallocenes $\text{M}(\text{Cp})_2$ ($\text{Cp} = \eta^5\text{-C}_5\text{H}_5$; $\text{M} = \text{Fe}, \text{Co}, \text{Ni}, \text{Mn}, \text{V}$) at 12–20 K afforded mixed-ligand complexes in which a nitrogen molecule was coordinated to a metal atom.^{35–37} The reaction of iron porphyrin complexes with NO produced nitrosyl adducts of porphyrins that may be considered as a heme model.³⁸

Co-condensates of transition metal vapours and aromatic hydrocarbons represent very reactive systems that produced mono- and bisarene complexes of transition metals and clusters and their more intricate complexes.³⁹ The reactions of chromium atoms and small clusters with benzene in argon matrices at 12 K were studied by FT IR, UV-Vis and resonance Raman spectroscopic methods.³⁹ The following chromium compounds were identified: $\text{Cr}(\text{C}_6\text{H}_6)$, $\text{Cr}(\text{C}_6\text{H}_6)_2$, Cr_2 , $\text{Cr}_2(\text{C}_6\text{H}_6)$, $\text{Cr}_2(\text{C}_6\text{H}_6)_2$ and $\text{Cr}_3(\text{C}_6\text{H}_6)$. The use of selective photoexcitation of certain species allowed the authors to carry out a series of competitive chemical reactions of chromium atoms and dimers and their complexes



Exothermic reactions at low and ultralow temperatures (1.3–30 K) can also occur in the space on cosmic dust particles under the action of radiation.^{40–47} The reactions of transition metals with polycyclic aromatic hydrocarbons are of undeniable interest for astrochemistry and astrophysics. It was assumed that such reaction products might be a source of

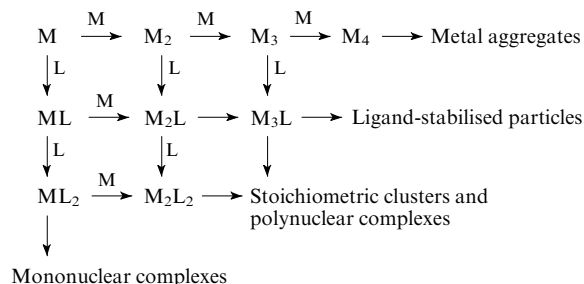
certain unidentified radiation types observed in the interplanetary space.⁴⁸

The possibility of these reactions was demonstrated by the FT IR spectroscopy in reactions of iron with pyrene and coronene in argon matrices at 4–10 K as an example.⁴⁹ It was found that pyrene forms unstable complexes with iron atoms, whereas coronene preferentially reacts with Fe_2 dimers to form mono- and bisligand complexes $\text{Fe}_2(\text{C}_{24}\text{H}_{12})_n$, where $n = 1$ or 2. These complexes were thermally stable up to 40 K and resistant to irradiation in the near UV and visible ranges (200–700 nm). Iron aggregates were easily formed in argon matrices with an increase in the metal concentration and exhibited the higher electron affinity (0.9 eV for Fe_2) as compared with an iron atom (0.15 eV); this explains the higher stability of their complexes. It is interesting that Fe_2 and Fe_3 clusters readily formed complexes with nitrogen molecules in binary $\text{Fe}-\text{N}_2$ systems, whereas no coronene complexes were detected in ternary $\text{Fe}-\text{coronene}-\text{N}_2$ co-condensates. This can serve as an indirect confirmation of the fact that coronene preferentially reacts with iron dimers. It is noteworthy that no coronene complexes were observed for nickel and titanium that do not form any aggregates under similar conditions.

III. Formation of metal nanoparticles in active matrices

The interaction of metal atoms with active ligand molecules in low-temperature co-condensates can be described as a sequence of competitive processes of aggregation of metal atoms and reactions of metal aggregates containing different numbers of nuclei with ligand molecules (Scheme 1).

Scheme 1



M is metal, L is ligand

The active-matrix molecules can play the role of ligands and form donor–acceptor or charge-transfer complexes with atoms and clusters. Depending on the temperature of the system and the concentrations of metal atoms and clusters, this may lead to the formation of mono- or polynuclear complexes and of nano- or subnanosized metal particles solvated with matrix molecules. Silver and copper feature the formation of different-sized clusters and nanoparticles in which a metal formally exists in the zero-valent state. Studying particles of different sizes makes it possible to follow the formation of the electronic and crystal structures of metals.

Silver and copper clusters and nanoparticles are easily formed at low temperature by the condensation of their vapours with the excess of an inert component,⁵⁰ thermo- and photo-aggregation of atoms⁵¹ and by mass-spectral selection of clusters followed by their condensation in inert matrices.² Nanoparticles can be stabilised at room temperature provided the metal vapour is co-condensed with certain organic substances that are capable of specific non-covalent interactions and can form donor–acceptor complexes with transition metal atoms, clusters and nanoparticles.⁵²

Metal particles measuring up to 10 nm were synthesised by low-temperature co-condensation of vapour of silver, copper, gold and other transition metals with acetone, ethanol, tol-

uene, trimethylamine, dimethylformamide, dimethyl sulfoxide and other compounds.⁵ Heating of the co-condensate to room temperature afforded colloid solutions of nanoparticles with different stability that could be sputtered on different surfaces to form film coatings of various thickness.^{52, 53}

Acrylic acid (AA), methyl acrylate (MA) and dimethylaminomethyl acrylate were also used for the stabilisation of silver nanoparticles.^{54, 55} Low-temperature co-condensation of the metal vapour with MA followed by heating of the system to room temperature afforded stable silver organosols with 15 nm particles. Co-condensation with lead vapour produced bimetallic particles measuring < 5 nm. The transition from binary Ag/MA and Pb/MA systems to the ternary Ag/Pb/MA system was accompanied by non-additive changes in the properties. Polymerisation of MA was inhibited by lead and initiated by silver and the competition of these processes led to the formation of smaller bimetallic particles.⁵⁴ Co-condensation of silver vapour with 2-methylaminoethyl methacrylate afforded silver particles with diameters of 15–20 nm and their aggregates. Such cryochemical methods made it possible to synthesise silver particles dispersed in water, acetone and toluene, which were stabilised in the presence of poly(2-methylaminoethyl methacrylate).⁵⁵

A method of stabilisation of copper nanoparticles in polyethylene was developed.⁵⁶ According to EXAFS and electron microscope studies, the average size of stabilised particles (copper nanocrystals) was 17 nm. A highly dispersed phase was formed upon decomposition of copper diacetate.

Low-temperature co-condensation of vapour of silver and copper and of Cd, Pb, Sn, Mn, Sm, Zn with the *p*-xylylene monomer, which undergoes easy polymerisation even at 100–120 K, was used in the synthesis of nanosized metal particles encapsulated in polymeric films.^{57–59} The particle size determined by the transmission electron microscopy was 3–8 nm. The resulting films exhibited sensor and chemoresistive properties with respect to water and ammonia vapour.^{60, 61}

Copper nanoparticles incorporated into poly(*p*-xylylene) in the course of low-temperature co-condensation of components were observed to exhibit high catalytic activity with respect to isomerisation of chlorine-containing compounds.^{62, 63} The activity of these particles was two orders of magnitude higher than that of highly dispersed copper supported on silica gel.

Cryoformation of nanosized silver and copper particles in mesogenic alkylcyanobiphenyl matrices was studied in detail.^{64–68} In co-condensates of silver and copper vapour with alkylcyanobiphenyl molecules at 80–90 K, low-temperature complexes of metal atoms were revealed.^{69, 70} IR spectra of co-condensates demonstrated two new bands in the range of stretching vibrations. The characteristic bands of the CN group were shifted by –150 and –200 cm^{–1}, which pointed to the formation of silver and copper π -complexes with the cyanobiphenyl fragments of the matrix molecules. Indeed, the electron density shift from the binding orbital and the partial population of the antibonding orbital of the ligand should lead to loosening of the multiple bond in the complex, *i.e.*, to a decrease in the vibration frequency of the corresponding bond in the π -complex. Spectra of Ag/5CB and Ag/5CB/C₁₀H₂₂ (5CB is 4-*n*-pentyl-4'-cyanobiphenyl) co-condensates also exhibited new bands in the range of 650–660 cm^{–1}, which were attributed to the metal–ligand vibrations in π -complexes. The formation of π -complexes was confirmed by quantum chemical calculations performed for 4-*n*-pentyl-4'-cyanobiphenyl and its central cyanobiphenyl fragment.^{71, 72} The structure of this complex includes two cyanobiphenyl fragments antiparallel to one another and a silver atom sandwiched between the CN fragment of ligand 1 and the centre of a benzene ring of ligand 2 (Fig. 6). In the ground state, the complex may acquire two electronic configurations, namely, a

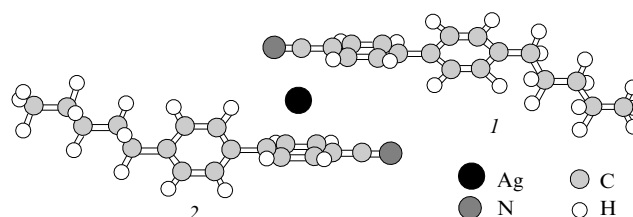


Figure 6. The structure of a bisligand silver complex with alkylcyanobiphenyl ligands Ag(5CB)₂; (1, 2) see text.

neutral complex Ag(5CB)₂ and a charge-transfer complex Ag⁺(5CB)₂[–]. For an interligand distance of 4.4 Å (the charge-transfer complex configuration), the calculated vibration frequency shifts of the C≡N bond in this complex as compared with this bond in the ligand molecule were –150 and –175 cm^{–1}, which were consistent with the experimentally observed values of –150 and –200 cm^{–1} for Ag/5CB films at 90 K.

EPR spectra of Ag/5CB samples contained a doublet of doublets (*A* and *B*, low-field and high-field spectrum components) with *g*-factors of 2.001, 2.003 and hyperfine coupling (HFC) constants of 48.5 and 55.7 mT, respectively (Fig. 7).⁷⁰ The analysis of literature data^{73, 74} suggests that the appearance of components *A* and *B* in the EPR spectrum is the result of the formation of π -complexes of silver atoms (¹⁰⁷Ag and ¹⁰⁹Ag) with cyanobiphenyl molecules. A comparison of HFC constants of silver atoms in the obtained samples with those of atoms stabilised in an inert hydrocarbon matrix (63.22 and 72.75 mT for ¹⁰⁷Ag and ¹⁰⁹Ag, respectively) allowed assessment of the spin density on the Ag atom as 0.89. This value is typical of π -complexes with metal atoms and points to the partial donation of the electron density from occupied orbitals of a metal atom to the antibonding π^* -molecular orbital of a ligand.

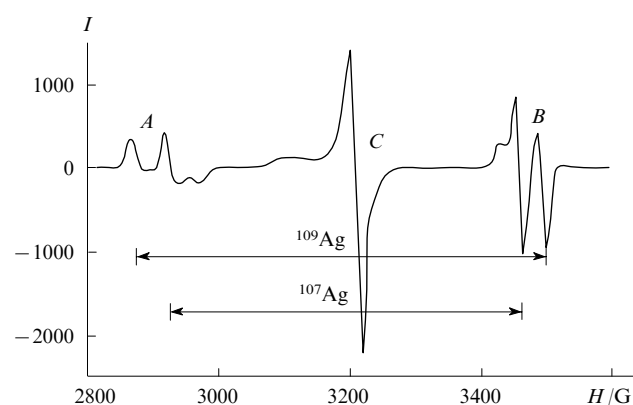


Figure 7. EPR spectrum of an Ag/5CB co-condensate at 80 K.⁶⁸

In EPR spectra of Cu/5CB co-condensates, an anisotropic quartet signal of a cyanobiphenyl complex of a copper atom was detected ($J = 3/2$).^{66, 75} Spin-resonance parameters of complexes were as follows: $g_{xx} = g_{yy} = 2.007$, $g_{zz} = 1.981$, $A_{iso} = 19$ mT; HFC on ⁶³Cu and ⁶⁵Cu isotopes were unresolved due to the close *g*-factors of their nuclei. The relatively low HFC constants for copper together with the highly anisotropic signal suggested that the highest occupied molecular orbital in a complex that contained a lone localised electron was of the hybrid nature and that the electron density

was shifted from a metal atom to ligand molecules. The spin density on the metal atom did not exceed 0.1.

The EPR spectra of co-condensates also revealed a central signal *C* (see Fig. 7) with a *g*-factor close to that of a free electron (2.003). The signal could be caused by the conducting electrons spin resonance (CESR) from a set of nanosized metal clusters and their complexes stabilised in the 5CB matrix. Similar signals were also observed for sufficiently concentrated silver and copper co-condensates with saturated hydrocarbons and inert gases.^{76,77} This signal represented a superposition of several isotropic lines of Lorentzian shape. The *g*-factor and the widths of signal line depended on the size of metal particles due to the difference in the spin–lattice relaxation times (*T*₁). Taking into account the presence of experimental *g*-factor shifts, the average size of metal particles stabilised in cyanobiphenyl matrices at 90–120 K was assumed to be 1–2 nm. An increase in the Ag to 5CB ratio led to the domination of processes of silver aggregation in the system, which substantially decreased the yield of this complex. On heating of co-condensates from 90 to 150 K, the relative intensity of doublet lines of silver complexes (quartet lines for copper complexes) decreased and the relative intensity of the central component increased, which pointed to the thermal decomposition of metastable complexes and the increase in the concentration of nanosized metal clusters due to the spontaneous aggregation of metal atoms that emerge in the system.

Studies of electron absorption spectra for the Ag/5CB and Ag/5CB/decane systems confirmed the results obtained by IR and EPR spectroscopic techniques. UV-Vis spectra of Ag/5CB co-condensates at 80 K (Fig. 8, curve 1) revealed a structured absorption band of a silver complex with a peak at 360 nm, which corresponded to light-yellow co-condensate films. Quantum chemical simulation of excited states of this complex pointed to the presence of several intense charge-transfer transitions metal–ligand and ligand–ligand in the range of 360–400 nm.⁷⁸ The absorption at 360 nm disappeared as the co-condensate film was annealed to 200–300 K. A broad band with the peak at 420 nm that appeared at these temperatures (see Fig. 8, curves 2, 3) was probably due to the absorption of surface plasmons of nanosized silver particles⁷⁹ formed as a result of aggregation of silver atoms and small clusters during the thermal decomposition of the complex. According to the data of transmission electron spectroscopy, depending on the phase state of the Ag/5CB system, two types of particles were formed, namely, globular with the average diameter of 15 nm and anisotropic rod-like particles ~200 nm long. The increase in the metal concentration and aggregation in an orientation-

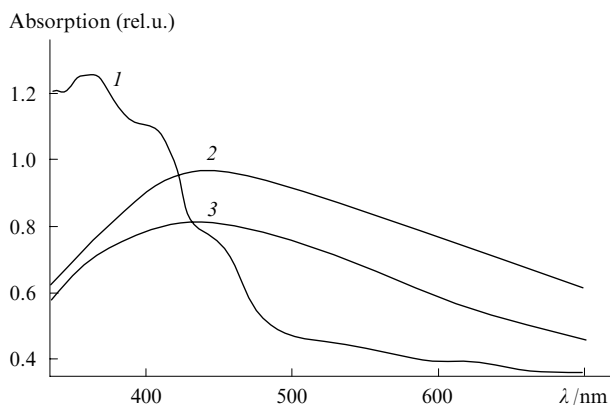


Figure 8. Optical spectra of silver co-condensates with 4-n-pentyl-4'-cyanobiphenyl at different temperatures.⁶⁹
T/K: (1) 80, (2) 200, (3) 300.

ordered mesophase favoured the formation of rod-like metal particles.^{80,81}

Thus, metal complexes appear in the course of low-temperature co-condensation of metal vapour and reactive organic components containing functional complexing groups. Annealing of this system leads to the thermally induced decomposition of unstable complexes and the matrix-controlled aggregation of metal atoms and small clusters of different sizes and shapes. The chemical nature and properties of the resulting reaction products are determined by the competition between self-assembling processes and the reactions of different-sized metal aggregates with molecules of reagents added to the system.

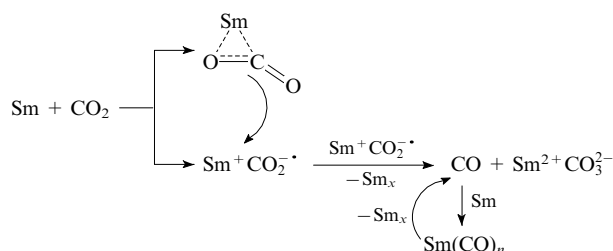
IV. Thermal transformations of metastable complexes of lanthanide atoms and clusters

As was shown above, cryochemical synthesis allows one to obtain new compounds and complexes for a series of d-metals in unusual oxidation states and with unusual coordination of ligand molecules. Competitive cryochemical reactions of lanthanide atoms with certain organic and inorganic ligands also lead to unusual products, where both the changes in the oxidation state and the formation of complexes between zero-valent lanthanides and CO, ethylene, tri(*tert*-butyl)benzene and its derivatives can be expected.^{81–84}

The majority of reactions of lanthanide atoms lead to the changes in the metal oxidation state. Their reactions with oxygen were studied by the example of cerium, praseodymium, terbium and europium. Europium formed several oxides and peroxides with different compositions, namely, EuO₂, Eu₂O₄, Eu₂O₃, EuO₂·Eu₂O₂.⁸⁵ Cerium, praseodymium and terbium produced mixtures of oxides LnO and peroxides LnO₂.⁸⁶ The reaction of gadolinium with chlorine in argon matrices afforded GdCl₃. In the case of holmium, this reaction produced a mixture of comparable amounts of metal dichloride and trichloride and the monochloride HoCl; for ytterbium, a mixture of dichloride and trichloride was formed. Europium formed a mixture of dichloride and trichloride, where the former prevailed. No formation of europium monochloride was detected. All the products were identified by IR spectroscopy.⁸⁷ Under similar conditions, reactions of holmium and europium with bromine and iodine were carried out. It was shown that with bromine, both lanthanides produce di- and tribromides in comparable amounts. Their reaction with iodine also afforded di- and triiodides, where diiodide dominated for europium and triiodide prevailed for holmium. IR spectra of iodine co-condensates with holmium and europium also contained bands that could be assigned to polymeric iodides.⁸⁸

The reaction of samarium with alkyl halides was studied under conditions of matrix isolation in the temperature range of 12–30 K.⁸⁹ IR spectroscopic data revealed the formation of methane in this reaction. Under conditions of matrix isolation, a reaction of samarium with CO₂ was studied.^{89,90} Based on the IR and UV spectroscopic data, the reaction sequence shown in Scheme 2 was proposed.

Scheme 2

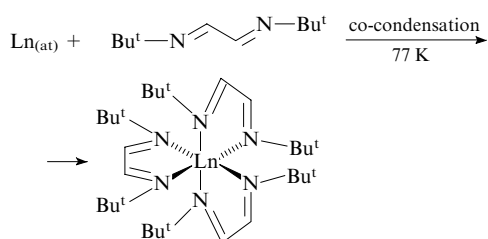


Straight lines mean that the corresponding reaction occurs at the condensation temperature (12 K); curved lines correspond to the reaction on heating (30 K)

The reactions of samarium with alcohols (ROH) were studied.^{91–94} These reactions afforded the corresponding hydrocarbons RH and samarium alkoxides $\text{Sm}(\text{OR})_x(\text{OH})_{3-x}$. The reaction products contained insignificant amounts of doubled alkanes R–R, which pointed to the radical mechanism of this process. In the first stage, samarium atom was inserted into the C–O bond of an alcohol molecule to form RSmOH and trivalent samarium alkoxide $\text{Sm}(\text{OR})_3$. For isopropyl alcohol, a cluster compound $\text{Sm}_5\text{O}(\text{OR})_{13}$ could also be formed.⁹⁴ The composition of this compound was revealed by elemental analysis and NMR spectroscopy.

Cryocondensation of samarium with acetone followed by annealing of the co-condensate and hydrolysis led to a set of saturated and unsaturated hydrocarbons and alcohols, namely, $\text{CH}_3\text{CH}=\text{CH}_2$, C_3H_8 , $(\text{CH}_3)_2\text{CHCH}(\text{CH}_3)_2$, $(\text{CH}_3)_2\text{C}=\text{C}(\text{CH}_3)_2$, $(\text{CH}_3)_2\text{CHOH}$ and samarium hydroxide.⁹⁵ A samarium cryocolloid produced in the co-condensation of samarium atoms with an unsaturated hydrocarbon reacted with acetone and the co-condensate was heated to its melting point. Co-condensation of metals with acetylacetone also produced samarium, holmium, erbium and dysprosium acetylacetonates.⁹⁶ Furthermore, the co-condensation of samarium, acetylacetone and dimethyl sulfoxide afforded a samarium acetylacetonate adduct to dimethyl sulfoxide.⁹⁶

Co-condensation of lanthanide atoms with substituted diazabutadiene $\text{Bu}^t\text{N}=\text{CHCH}=\text{NBu}^t$ (Bu^tDAB) led to the formation of a chelate complex containing three ligand molecules (Scheme 3).^{97,98}

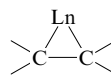


$\text{Ln} = \text{Y}, \text{Nd}, \text{Sm}, \text{Eu}, \text{Gd}, \text{Ho}, \text{Yb}$.

The structure of the samarium complex was studied by X-ray diffraction analysis. It was shown that five-membered rings $\text{Sm}-\text{N}-\text{C}-\text{C}-\text{N}-\text{Sm}$ are virtually planar, deviating by 0.051 \AA from the plane. The $\text{C}=\text{N}$ bond distance was $1.35(3) \text{ \AA}$, which is much longer as compared with the free ligand [$1.283(6) \text{ \AA}$]. This may be due to the electron density transfer from a metal atom to the lowest unoccupied molecular orbitals (LUMO) of the ligand to form Ln^{2+} and Ln^{3+} ions. This is why it is more correct to represent the samarium complex and analogous compounds of the lanthanides as the complexes formed by trivalent metals with radical anions, *i.e.*, $[\text{Ln}^{3+}(\text{Bu}^t\text{DAB}^{\cdot-})_3]$. The analogous ytterbium compound $[\text{Yb}^{3+}(\text{Bu}^t\text{DAB}^{\cdot-})_3]$ had a magnetic moment of $5.9 \mu_{\text{B}}$ in the solid state at room temperature and $2.4 \mu_{\text{B}}$ at $T < 100 \text{ K}$. A model was proposed according to which this compound exists in two forms, namely, as $[\text{Yb}^{3+}(\text{Bu}^t\text{DAB}^{\cdot-})_3]$ at temperatures above 100 K and $[\text{Yb}^{2+}(\text{Bu}^t\text{DAB}^{\cdot-})_2(\text{Bu}^t\text{DAB})]$ at lower temperatures. The calculated magnetic moments of these species were 5.5 and $2.45 \mu_{\text{B}}$, respectively, which was consistent with the experimental data. Erbium, neodymium and samarium co-condensation with buta-1,3-diene produced analogous products, namely, $\text{Ln}(\text{C}_4\text{H}_6)_3$.⁹⁹ The introduction of dimethylbutadiene into this reaction resulted in the formation of complexes with the composition $\text{Ln}[(\text{CH}_3)_2\text{C}_4\text{H}_4]_2$. The magnetic susceptibility measurements have shown that

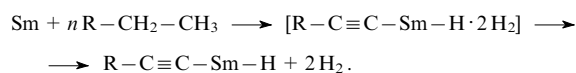
in all the cases, the degree of oxidation of lanthanide atoms was $3+$.

Co-condensation of samarium, erbium and ytterbium vapours with hydrocarbons containing double bonds, namely, ethylene, propylene and allene, led to the formation of products that afforded a mixture of saturated and unsaturated hydrocarbons from C_1 to C_6 upon hydrolysis. This suggests that the reaction mechanism is rather complex and involves the insertion of lanthanide atoms into the C–C bond to form a ring



or a chain $\text{Ln}-\text{C}-\text{C}-\text{Ln}$.¹⁰⁰

Low-temperature reactions of ytterbium, erbium and samarium with terminal alkynes afforded products with absorptions in the range of $2020\text{--}2060 \text{ cm}^{-1}$ (triple bond vibrations), namely, $(\text{YbC}_9\text{H}_{14})_n$, $(\text{ErC}_{12}\text{H}_{19})_n$ and $(\text{SmC}_{12}\text{H}_{19})_n$.¹⁰¹ Co-condensation of samarium atoms with hexane gave rise to the evolution of hydrogen; hydrolysis of the co-condensate produced hex-1-yne and insignificant amounts of destruction products.¹⁰² Experimental data suggest the following reaction sequence:



$\text{R} = n\text{-C}_4\text{H}_9$.

Co-condensation of samarium vapour with 1-bromopentane at 80 K afforded green films. On heating, a mixture of saturated and unsaturated hydrocarbons, namely, pentane, decane and pentene, was obtained. Results of EPR studies gave grounds for assuming the radical mechanism of this process.¹⁰³

At present, several reactions of lanthanide atoms and clusters are known to involve no changes in oxidation state. It was assumed that for efficient complexation a lanthanide atom should acquire the $4f^{n-1}5d^16s^2$ configuration as a result of the transition of one f electron to the d shell.¹⁰² The energy of excitation of an f electron to the d sublevel is of crucial importance for this process. Figure 9 illustrates the dependence of this energy on the degree of population of the f shell. The interaction of lanthanide atoms with CO molecules was studied for a series of metals, namely, Pr, Nd, Sm, Eu, Gd, Ho and Yb, in an argon matrix at $10\text{--}40 \text{ K}$ using the electronic and IR spectroscopic methods.^{104–106} In the majority of cases, carbonyls $\text{Ln}(\text{CO})_x$ were formed ($x = 1\text{--}6$). Heating of the

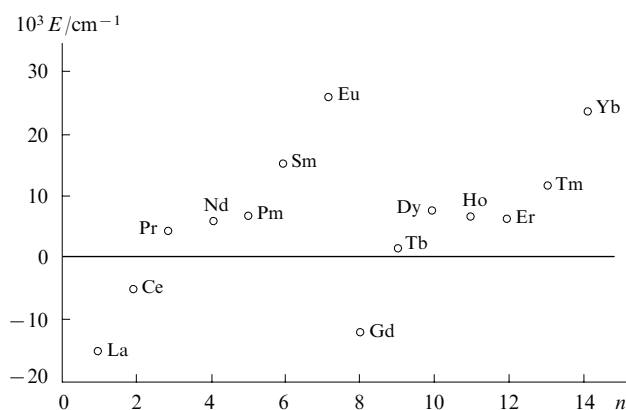


Figure 9. Calculated excitation energy $[f^n s^2] \rightarrow [f^{n-1} d^1 s^2]$ as a function of the degree of population of the f orbital of a non-excited lanthanide atom.⁸²

system to 15–40 K transformed the lower carbonyls to the higher, $\text{Ln}(\text{CO})_6$. In a range >40 K, carbonyls of all metals underwent destruction, where the destruction temperature corresponded to the matrix melting point. The distinguishing feature of samarium and europium is that they did not form carbonyls at $x = 1-3$ for Sm and $x = 1, 3$ for Eu. It should be mentioned that the decomposition temperature of the higher samarium carbonyl (30 K) was lower as compared with the higher europium carbonyl (40 K), which is in conflict with their excitation energies (see Fig. 9). Gadolinium carbonyl that has a d electron in the ground state also proved to be unstable. The most stable carbonyls were formed by metals with the larger number of d-electrons, *e.g.*, by Cr, Mn, Fe, Co, Ni.

Reactions with ethylene were studied in detail for europium and samarium atoms and clusters in argon matrices and also for samarium co-condensates with ethylene.^{89,107} It was found that two complexes, $\text{Ln}(\text{C}_2\text{H}_4)$ and $\text{Ln}(\text{C}_2\text{H}_4)_2$, are formed. On gentle heating, the monoligand complex was transformed to the biligand complex. Taking into account the presence of free samarium atoms even in non-dilute ethylene, it can be assumed that the formation of a $\text{Ln}\cdot\text{L}$ complex and its subsequent transformation to $\text{Ln}\cdot 2\text{L}$ are limited by the rotational diffusion. The decomposition temperature of the higher europium complex (~ 60 K) exceeded that of the higher samarium complex (~ 40 K). The structure of the monoligand samarium complex with ethylene was studied.¹⁰⁷ It was assumed that this complex is stabilised due to weak direct interaction of half-occupied metal f orbitals with σ and π orbitals of their ligand.

Reactions of lanthanides with aromatic ligands, namely, 1,3,5-tri(*tert*-butyl)benzene (TTB), 2,4,6-tri(*tert*-butyl)pyridine (TTPy) and 2,4,6-tri(*tert*-butyl)phosphorine (TTP), were studied in their co-condensates in the temperature range of 80–373 K.^{82,83,108,109} The structure of a single crystal of the gadolinium TTB complex was determined by X-ray diffraction analysis. The molecules of the complex had a sandwich structure with a metal atom located between two benzene rings in the staggered conformation. The LUMO energy of heteroaromatic ligands is lower than the LUMO energy of benzene, which leads to the stronger interaction of ligands with the metal d orbitals. As a result, on going to analogous heteroaromatic complexes of lanthanides, the bond becomes stronger and the decomposition temperature increases (Table 1). The bond strength in lanthanide complexes with aromatic ligands increased with the decrease in the metal atom radius, the reduction of the energy of f electron excitation and the lowering of the LUMO energy of the ligand.^{82,109}

Samarium complexes with 4-n-pentyl-4'-cyanobiphenyl were detected in an argon matrix at 6–10 K and in Sm co-condensates with 5CB at 80–240 K.^{110,111} The formation of

such complexes was revealed by the appearance of new absorption bands in the IR spectra, namely, a triplet band at 2170 cm^{-1} (complex I) and 2060 cm^{-1} (complex II) (Fig. 10). The bands were shifted to lower frequencies as compared with vibrations of the CN group of the ligand (2230 cm^{-1}). This made it possible to assign new bands to CN vibrations in π -complexes. Splitting of a band at 2170 cm^{-1} to three components can be associated with the stabilisation of different complex configurations in a low-temperature argon matrix and also with different local environment. The activation energy of the formation of complexes was close to zero, which confirmed their formation at 6–10 K. The first complex was formed at 6–10 K in a molar ratio $\text{Sm}:5\text{CB}:\text{Ar} = 1:33:10\,000$. At such dilution, the aggregation of metal atoms was absent, and the complex was formed from samarium atoms. The composition was determined by a modified method of multiple ratios in a series of experiments on the joint condensation of samarium and 5CB with a 100–1000-fold excess of decane. The stoichiometric composition was $\text{M}\cdot 2\text{L}$ for complex I and $\text{M}\cdot\text{L}$ for complex II. Bearing in mind the tendency of lanthanide atoms for the formation of bisligand sandwich complexes and the susceptibility of cyanobiphenyl molecules to dimerisation at low temperatures,¹¹² the second complex was also considered as a bisligand binuclear $2\text{M}\cdot 2\text{L}$ complex.

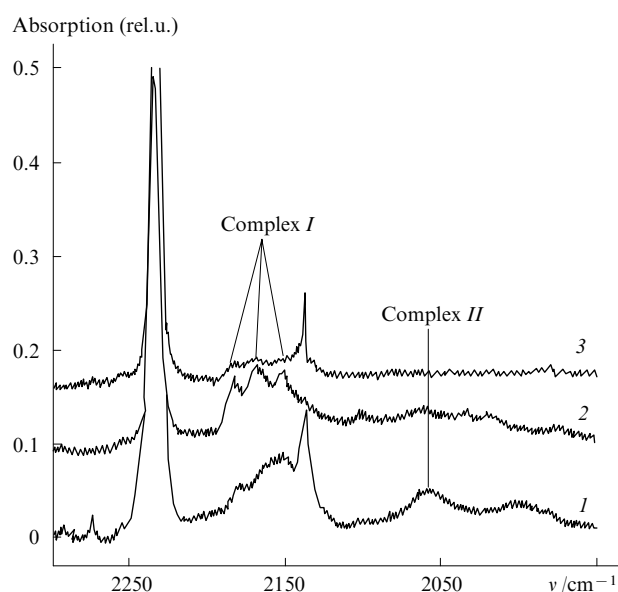


Figure 10. IR spectra of complexes $\text{Sm}\cdot 5\text{CB}$ isolated in an argon matrix.¹¹⁰

(I) Molar ratio $\text{Sm}:5\text{CB}:\text{Ar} = 1:10:400$, $T = 6.5$ K; (2) $1:24:5000$, $T = 10.5$ K; (3) $1:33:10\,000$, $T = 10.5$ K.

Table 1. Decomposition temperatures (K) of lanthanide complexes with different ligands.

Ln	Ground state	TTB	TTPy	TTP
La	d^1s^2	263	—	283
Ce	$f^1d^1s^2$	—	—	—
Pr	f^3s^2	318	—	—
Nd	f^4s^2	> 373	—	—
Sm	f^6s^2	213	223	223
Eu	f^7s^2	190	225	—
Gd	$f^7s^2d^1s^2$	> 373	—	—
Tb	f^9s^2	> 373	—	—
Dy	$f^{10}s^2$	> 373	—	—
Ho	$f^{11}s^2$	> 373	—	> 443
Er	$f^{12}s^2$	> 373	—	—
Tm	$f^{13}s^2$	—	—	—
Yb	$f^{14}s^2$	—	—	—
Lu	$f^{14}d^1s^2$	> 373	—	—

In the temperature range of 80–95 K, samarium co-condensates with 4-n-pentyl-4'-cyanobiphenyl in a molar ratio $\text{M}:\text{L} = 1:10$ contained only the complex $\text{M}\cdot 2\text{L}$.^{113,114} As the sample was heated to 210 K, the absorption band of the complex $\text{M}\cdot 2\text{L}$ disappeared and a band of the complex $2\text{M}\cdot 2\text{L}$ emerged. Heating above 210 K led to the decomposition of both complexes. The complex $\text{M}\cdot 2\text{L}$ absorbed in the visible range at 400 nm, while the complex $2\text{M}\cdot 2\text{L}$ absorbed at 420 nm. The UV spectrum of the $\text{Sm}/5\text{CB}$ co-condensate contained an absorption band of the complex $\text{M}\cdot 2\text{L}$ at 400 nm at 95 K. As the temperature increased, a shoulder at 420 nm appeared, which corresponded to the complex $2\text{M}\cdot 2\text{L}$. Electronic spectra of co-condensates demonstrated a broad long-wavelength absorption band with a peak at

~ 600 nm, which can be assigned to the absorption of metal nanoparticles. An increase in the length of the hydrocarbon substituent chain in the ligand molecule had no effect on the stability of complexes. On going from 5CB to its heteroaromatic analogue, 4-n-pentyl-4'-cyanophenylpyridine (5Py), the stability of complexes increased.¹¹⁴ The IR spectrum of the co-condensate at liquid nitrogen temperature contained a single band at 2150 cm⁻¹, which corresponded to the complex Sm·2(5Py). As the temperature increased to 230 K, a new band at 2100 cm⁻¹ appeared (Sm·5Py). The thermal decomposition of complexes occurred above 230 K, *i.e.*, 20 K higher as compared with the Sm/5CB system. This can be associated with the stronger metal–ligand bonding in complexes Sm·5Py. On going from samarium to europium, the thermal stability of the complex Ln(5CB)₂ also increased.

Model calculations of structures of complexes were carried out in terms of the density functional theory with the B3LYP exchange-correlation potential using the NWChem programme.^{115, 116} Only the ligand part involved in the complexation was considered. The optimised structures had the form of sandwiches (Fig. 11). The most stable state was reached at multiplicity 10 for complex *I* and multiplicity 15 for complex *II*; the binding energies were 10.6 and 31.3 kcal mol⁻¹, respectively. Multiplicity substantially affected the values of a torsion angle between the benzene ring planes of one ligand (φ_1), an angle between benzene ring planes of two ligands (φ_2) and an angle formed by axes of ligands (φ_3). In the complexation, the stretching frequency of the cyanobiphenyl CN group in both complexes shifted to lower values, which was consistent with the experimental data.

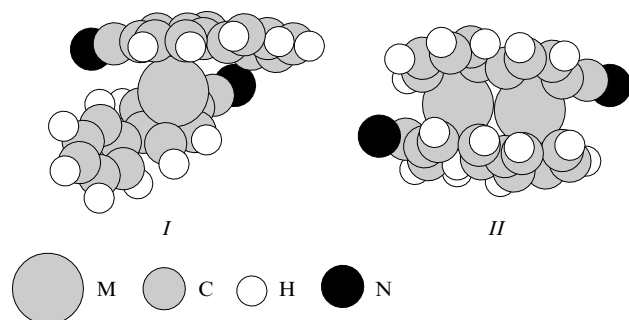


Figure 11. Optimised structures of complexes M(CB)₂ (*I*) and M₂(CB)₂ (*II*).¹¹⁵

The equilibrium structures and complexes formed by europium atoms and their dimers with non-substituted cyanophenylpyridyl ligands were simulated using quantum chemical methods.¹¹⁷ For mononuclear complexes, the competition between two mechanisms of metal atom coordination was observed, namely, between the formation of sandwich π -complexes, which is caused by the interaction with π orbitals of the ligand, and the σ -coordination to the nitrogen atom of the pyridine ring. Sandwich structures of alkylcyanophenylpyridyl ligands were stabilised as a result of intermolecular N...H contacts between the nitrogen atom of the cyano group and the terminal hydrogen atom of the ethyl group. The higher thermal stability of the binuclear complex was demonstrated.

As the temperature of Sm/5CB and Sm/5Py co-condensates increased from 183 to 223 K, simultaneous decay of SmL₂ signals and growth of Sm₂L₂ signals were observed in the IR spectra (Fig. 12). This pointed to the transformation of mononuclear complexes ML₂ to binuclear complexes M₂L₂.^{118, 119} The following kinetic scheme, which includes the competition between processes of metal atom aggregation and their interaction with ligand molecules, was proposed:

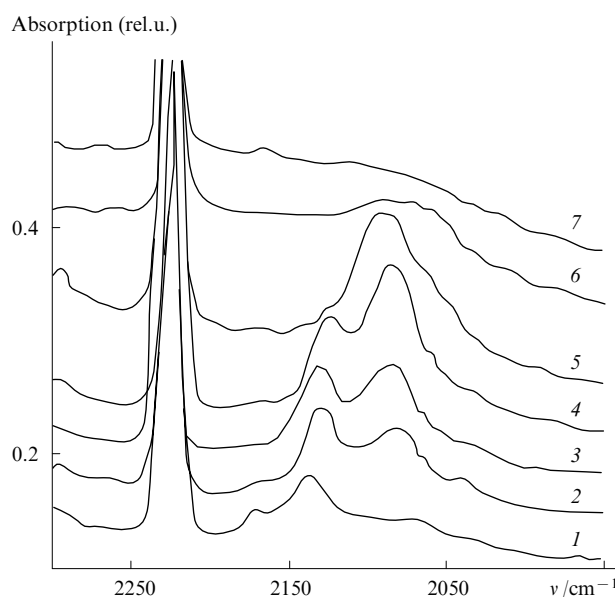
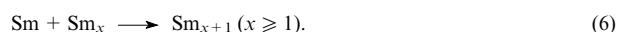
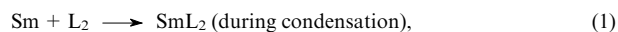


Figure 12. IR spectrum of a Sm/5CB co-condensate at different temperatures.¹¹¹

T/K: (1) 8, (2) 163, (3) 183, (4) 203, (5) 223, (6) 243, (7) 273.



The consumption of a complex ML₂ at this temperature did not reach zero but stopped at a certain degree of transformation, which is typical of multistep chemical reactions in the solid phase.¹²⁰ As the temperature increased, the degree of transformation increased. The effective activation energies were 17.5 and 18.5 kJ mol⁻¹ for 5CB and 5Py, respectively. The results of experimental and theoretical studies^{113–119} have demonstrated the importance of taking into account the competitive reactions of metal atoms and aggregates when analysing the thermal transformations of complexes in low-temperature co-condensates.

V. Competitive reactions of silver and gold particles of different sizes and shapes with model reagents

Studies of competitive chemical reactions of metal particles in different degrees of aggregation with model chemical reagents attracted special attention.^{121, 122}

Competitive reactions of silver and copper atoms and clusters, which were stabilised in a nanostructured 4-n-pentyl-4'-cyanobiphenyl matrix, with carbon tetrachloride as a model reagent, were studied by EPR and UV-Vis spectroscopic techniques.^{122–125} EPR spectra of ternary co-condensates of silver with carbon tetrachloride and 4-n-pentyl-4'-cyanobiphenyl, which contained CCl₄ in a concentration varying from 0 mol % to 10 mol % with respect to cyanobiphenyl, were studied at 80–300 K. For systems with [CCl₄]:[5CB] ≤ 0.03, only doublet signals of π -complexes formed by silver atoms with cyanobiphenyl ligands Ag(5CB)₂

were observed. The addition of carbon tetrachloride to the system led to the formation of several paramagnetic products of competitive reactions of silver atoms and clusters with 5CB matrix molecules and added CCl_4 . Heating-cooling cycling of samples and computer simulations of spectra corresponding to different temperatures and different component concentrations made it possible to reveal several paramagnetic species, namely, nanosized metal particles, a σ -complex of a silver atom with two ligands (5CB and CCl_4) and an adduct of trichloromethyl radical to silver chloride $\text{AgCl}-\text{CCl}_3$ (Ref. 125).

Annealing of co-condensates at 90–200 K changed relative intensities of signals under consideration. Figure 13 shows the temperature dependences of yields of paramagnetic products formed in the reactions of silver atoms and nanosized clusters with carbon tetrachloride and matrix (5CB) molecules for co-condensates with different ratios of reagents (Ag, CCl_4 and 5CB). In the temperature range of 90–120 K, the doublet signals of a π -complex formed by silver atoms with 5CB matrix molecules, which could be detected in systems with low CCl_4 concentrations, were observed to decay. This was caused by the thermal decomposition of the π -complex. Simultaneously, for samples with low carbon tetrachloride concentrations, an increase in the intensity of signals of silver nanoclusters was observed (see Fig. 13 *a*). At the same time, samples with higher CCl_4 concentrations demonstrated no increase in intensity of signals of silver nanoclusters (see Fig. 13 *b*).

These changes were attributed to the reactions of silver atoms, which emerge in the decomposition of π -complexes, with carbon tetrachloride and metal clusters formed in the system. At substantially lower CCl_4 concentrations, the

decomposition of π -complexes was accompanied by the preferential aggregation of atoms to form nanosized silver clusters, which were stabilised in the matrix up to a temperature corresponding to the system restructuring, *i.e.*, 210–230 K. It is noteworthy that the CESR signals of nanosized silver clusters were more symmetric for ternary co-condensates $\text{Ag}/5\text{CB}/\text{CCl}_4$ as compared with the binary $\text{Ag}/5\text{CB}$ system. This may serve as evidence for the narrowing of the size distribution of metal clusters. Apparently, the observed effect was caused by the fact that the least stable and most reactive clusters were the first to react; the most stable and highly symmetrical icosahedral clusters (Ag_{13} , Ag_{55} , *etc.*) were stabilised in the 5CB matrix and accumulated at this temperature. Thus, at low temperatures, the role of active species in the reaction with CCl_4 was played by silver atoms; on heating of the co-condensate, the nanosized clusters, which were formed in the aggregation of the silver atoms emerged in the thermal decomposition of complexes, also became reactive.

Gold is conventionally classified with the most stable and least reactive metals the surface of which is inert with respect to chemisorption of molecules of most gases.¹²⁶ Gold is the only transition metal that does not have a stable oxide (its most stable oxide, Au_2O_3 , is actually metastable). Gold exhibits the maximum electronegativity among all metals, being only slightly more positive as compared with typical non-metals such as sulfur or iodine; gold has the record-breaking electron affinity (2.31 eV) and ionisation potential (9.22 eV).¹²⁷

In the past decade, gold particles measuring <5 nm attracted attention due to their unique catalytic properties.^{128–133} It was shown that gold clusters and nanoparticles are efficient catalysts in low-temperature CO oxidation,^{131, 132} selective propene oxidation to propene oxide,¹³⁴ NO reduction,¹³⁵ selective hydrogenation of acetylene and butadiene,¹³⁶ reduction of nitrogen oxides,¹³⁷ hydrochlorination of acetylene to vinyl chloride,^{138, 139} vinyl acetate synthesis¹⁴⁰ and some other reactions.^{141, 142}

Low-temperature (10 K) co-condensation of gold atoms with a CO and O_2 mixture (1 : 1) was found to produce gold(II) carbonyl peroxyformate. The latter underwent decomposition to two CO_2 molecules when heated to 30–40 K.¹⁴³ Thus, it can be concluded that the carbon monoxide oxidation to dioxide CO_2 is catalysed by individual gold atoms.

It was stated that Au_2 dimers react with CO, NH_3 and ethylene.¹⁴⁴ In contrast to silver and copper dimers, gold dimers reacted with molecular hydrogen, which may be associated with the relativistic nature of gold. This determines the contraction of s orbitals to make the resulting Au–H bond more stable.

Using a mass-selection technique and jet reactors, the molecular adsorption of different molecules on neutral and charged gold clusters Au_x , Au_x^- , Au_x^+ ($x = 2–20$) was studied.^{145–147} For anionic clusters involving up to 20 atoms, a ‘saw-tooth’ size dependence of oxygen adsorption with a clearly pronounced even-odd alternation was observed.^{147, 148} Clusters containing even numbers of atoms readily adsorbed oxygen, whereas those with odd number of atoms were inert. This effect was due to the strong alternation of the electron affinity with the varied cluster size. The higher electron affinity for clusters with odd numbers of atoms¹⁴⁶ prevented the adsorption of oxygen molecules that occurs due to the electron density transfer from a gold cluster to the antibonding π^* orbital of the oxygen molecule.¹⁴⁸ Gold species with the number of atoms > 20 were far less reactive.

The chemisorption of carbon monoxide on anionic gold clusters led to preferential formation of mono- and dicarbonyl clusters with odd numbers of gold atoms, namely, Au_5CO , Au_{11}CO , Au_{15}CO , $\text{Au}_{15}(\text{CO})_2$.^{149, 150} Even the long-term exposure of this system at high CO concentrations did not lead to the formation of higher carbonyls. This agrees with the

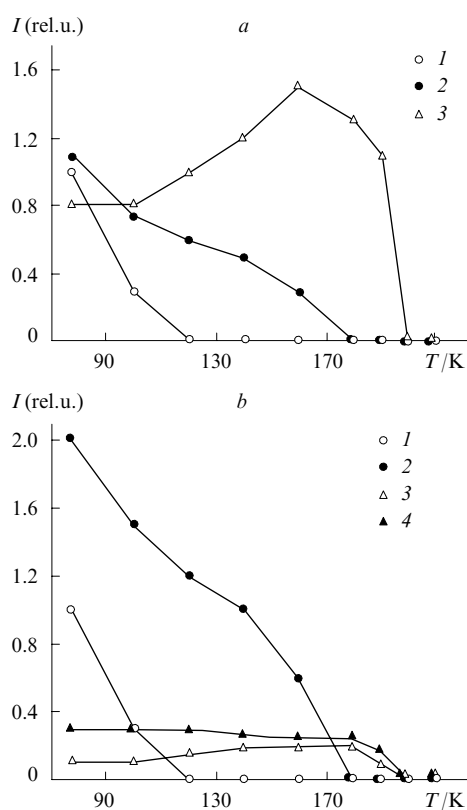
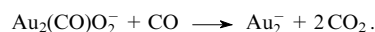


Figure 13. Temperature dependences of relative intensities of paramagnetic signals of the reaction products of silver atoms and clusters with carbon tetrachloride and matrix (5CB) molecules for co-condensates with reactant ratios (a) $\text{Ag} : \text{CCl}_4 : 5\text{CB} = 1 : 3 : 100$ and (b) $1 : 10 : 100$.¹²⁵ (1) $\text{Ag}(5\text{CB})_2$, (2) ClAgCCl_3 , (3) Ag_x , (4) $\text{Ag}(5\text{CB})\text{CCl}_4$.

earlier data on the CO adsorption on the surface of gold single crystals for which the adsorption curves reached saturation at small surface coverages. It is interesting that a single-atom gold anion did not virtually react with CO, whereas one or two CO molecules reacted with dimeric (Au_2^-) and trimeric (Au_3^-) gold anions to preferentially afford $\text{Au}_3(\text{CO})_2$ dicarbonyl in a stable 8-electron configuration.¹⁵¹ This also involved a shift of s and d orbitals of a gold atom as a manifestation of the relativistic effects.

Studies of oxygen and CO chemisorption play an important role for efficient CO oxidation to CO_2 . Co-chemisorption of oxygen and CO was successfully performed on anions of gold dimers (Au_2^-) and trimers (Au_3^-); no adsorption was observed on monomeric anions Au^- (see Ref. 152). No formation of gold carbonyls was detected in the reaction with oxygen that proceeded an order of magnitude faster than the CO adsorption. Among intermediate products, $\text{Au}_3(\text{CO})\text{O}_2$ and $\text{Au}_3(\text{CO})(\text{O}_2)$ were detected, which confirmed the co-adsorption. The initial CO adsorption on Au_6^- clusters led to the formation of several carbonyls $\text{Au}_6(\text{CO})_n$. Subsequent treatment of these clusters with oxygen resulted in the ligand substitution to form $\text{Au}_6(\text{CO})_{n-1}\text{O}_2^-$, where one CO molecule underwent oxidation to CO_2 . For gold clusters, the reaction rate exceeded that observed on common gold catalysts by at least two orders of magnitude. The disadvantage of using such small particles concerns the impossibility of recycling this catalytic system.¹⁵³

The reaction of gold dimer anion Au_2^- with CO and O_2 led to the formation of Au_2O_2^- and $\text{Au}_2(\text{CO})\text{O}_2^-$; the final system contained also Au_2^- species.¹⁵⁴ The following scheme of oxidation was assumed:



Density functional theory calculations pointed to a possibility of the existence of an intermediate species $\text{Au}_2(\text{CO})\text{O}_2^-$ both as the product of CO insertion into the O—O bond (Fig. 14a) and in the form of gold dimer peroxyformate (Fig. 14b), which opens up a virtually activationless route of Au_2O_2^- reaction with CO.^{153, 154}

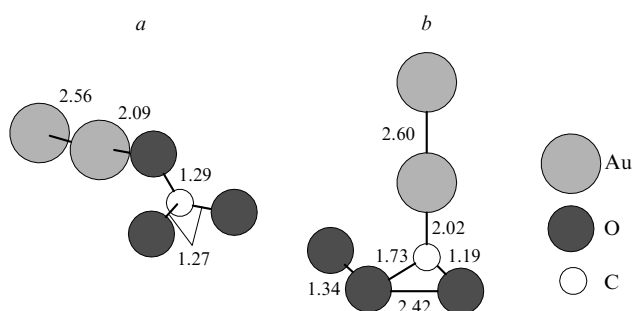


Figure 14. Reaction products of CO and O_2 with gold clusters (bond distances are shown in Å); (a, b) see text.¹⁵⁴

Fourier-transform mass spectrometry and ion-cyclotron resonance studies of the O_2 and CO co-chemisorption on gold nanoclusters have unambiguously demonstrated that the preliminary treatment with CO considerably accelerated the reaction of the cluster with O_2 . This pointed to the cooperative

effect of two ligands on the CO oxidation.¹⁵⁵ In this process, both the reaction with Au_n^- gold anions and the oxidation of preliminarily formed carbonyl complexes $\text{Au}_n(\text{CO})_m$ were size-sensitive. Carbon dioxide was the product of both reactions.

The presence of water vapour had a considerable effect on the reactivity of gold clusters Au_n . As compared with the original clusters, the hydroxylated Au_nOH^- clusters formed upon oxidation exhibited the inverse reactivity, namely, clusters with an even number n were inert and those with an odd numbers easily chemisorbed oxygen.¹⁵⁶

The reactivity of Au_n^+ ($n = 1-12$) clusters in their reactions with H_2S was studied.¹⁵⁷ Cations Au^+ and Au_2^+ were virtually inert; among larger species, clusters with even n were more reactive. The reaction led to the liberation of hydrogen and formation of sulfur-containing products. Cationic clusters with the number of gold atoms up to 10 efficiently chemisorbed hydrogen.

The reactivity of large gold clusters ($n \geq 10$) depended on their structure and shape.^{158, 159} Modelling of structures of nanosized gold clusters both anionic and neutral has shown¹⁶⁰⁻¹⁶² that due to the contribution of relativistic factors, gold species (containing up to 13 atoms) had the shape of a plane or a plate. Moreover, the ionisation potential, the electron affinity, the difference in energies of the highest occupied and the lowest unoccupied molecular orbitals, and the ability to selectively chemisorb molecules of O_2 , CO, etc. are all the size-dependent quantities that exhibit the typical alternation for clusters containing even and odd numbers of metal atoms.^{163, 164} For planar gold species, substantial anisotropy of polarisability was observed.¹⁶⁵ In the lateral direction, the polarisability was high (close to that of metals), whereas in the normal direction, the polarisability value approached that of semiconducting silicon. The theoretical prediction of structures for species with $n = 30-10000$ has demonstrated the possibility of formation of different types of disordered,¹⁶⁶ edged cuboctahedral and icosahedral clusters¹⁶⁷⁻¹⁶⁹ that could be transformed to one another¹⁷⁰ due to small difference in stabilisation energies.¹⁶⁶

In catalysis, nanosized gold clusters and particles deposited on metal-oxide supports were used.¹⁷¹⁻¹⁷⁴ Several studies were devoted to the formation of gold nanoparticles in the vapour deposition from the gas phase to afford two- and three-dimensional aggregates.¹⁷⁵⁻¹⁷⁷ It was shown that the activity of deposited nanodispersed gold particles is largely determined by the interaction of metal particles with the substrate, the presence of adsorbed and covalently bound functional groups, the electron-donating or -withdrawing properties of the surface, the size of deposited particles and the presence of low-coordinated gold atoms in their structure as well as by the degree of charge transfer in the chemisorption of a reagent molecule.¹⁷⁸⁻¹⁸⁰ A strong size effect was observed in the CO oxidation to CO_2 on the exposure of a $\text{CO}:\text{O}_2 = 1:5$ mixture over deposited Au/TiO₂ clusters at room temperature. The maximum activity was observed for gold particles measuring 2.8–3.2 nm (Fig. 15). This was associated with the transformation of particles that exhibit non-metal properties into particles with metallic properties.¹⁸¹ A detailed analysis of the effect of the size and the shape of gold particles deposited on different substrates was performed.¹⁸² The properties of deposited gold nanoparticles were observed to widely deviate from those of bulk gold samples, e.g., the activity deviated by more than an order of magnitude.^{183, 184} Highly symmetric (with a fifth-order symmetry axis) gold clusters with ‘magic’ numbers of atoms, namely, 13, 55, 147, etc., proved to be more stable and less reactive. Thus an Au_{55} cluster ($d = 1.4$ nm) was unsusceptible to oxidation under the action of oxygen plasma, whereas smaller clusters (< 1 nm) underwent oxidation under these conditions.¹⁸⁵

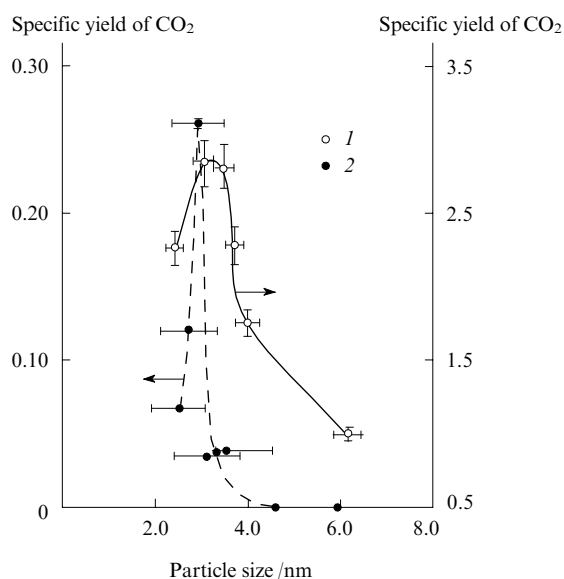


Figure 15. Activity of gold particles deposited on TiO₂ by (1) vacuum condensation and (2) chemical deposition as a function of their size.¹²⁹

VI. Conclusion

This survey of the literature data and of the results obtained by the authors of this review shows that the methods of cryochemistry and nanochemistry make it possible to carry out and control self-assembling processes of metal atoms to form nano- and subnanosized aggregates, perform competitive chemical reactions of atoms, small clusters and nanosized particles of transition metals with different organic and inorganic substances, study the kinetics of cryochemical process and simulate their individual stages, and acquire information on the mechanisms of uncommon chemical reactions in low-temperature co-condensates.

At present, effective low-temperature methods are being developed aimed at the stabilisation of small clusters and nanosized metal particles in the matrices formed by inert gases and certain organic and inorganic substances and on the surfaces of different substrates and at carrying out selective chemical reactions of particles of different sizes and shapes with reagents added to the systems. The accumulation of data on the reactions of nanosized particles of different metals for a wide range of temperatures in the gas phase and in condensed systems, namely, liquid and solid co-condensates, as well as their kinetic analysis will allow one to reveal the fundamental trends in the manifestation of size effects in nanochemistry of metals and the periodicity in the variation of reactivity of these particles. This information together with the comparative analysis of characteristics of ligand-free and ligand-stabilised clusters makes it possible to separate the effect of the metal core size and the stabilising effect of the ligand shell and the effects of the phase state of the system and its temperature. This approach coupled with the quantum chemical modelling of the studied systems will allow one to pass from documentation of separate cases of the dependence of the particle reactivity on the number of the constituent atoms to the development of the general kinetic theory that would relate the particle size in the studied substances to their chemical properties. Cryonanochemistry is used in the elaboration of new methods for the synthesis of nanostructured materials with unique optical, magnetic, electrophysical and mechanical characteristics.

It is also necessary to mention certain general problems that challenge modern cryonanochemistry. First of all, this is the development of methods of synthesis of metal particles with

controlled sizes and narrow size distributions in the range of 1–5 nm. The synthesis of highly reactive nanoparticles requires the elaboration of special effective methods for their stabilisation.

Second, it is necessary to develop methods for carrying out highly selective catalytic, photochemical and thermal processes based on competitive reactions of small metal particles to be used as the basis in the production of nanodevices and nanomaterials. The quest for promising applications is associated with the development of methods for the formation of ordered ensembles of metal particles of definite sizes and shapes incorporated into the structured matrices based on polymers, liquid crystals, carbonaceous and biological systems. The use of low temperatures offers a possibility of the direct introduction of metal atoms and clusters into organic and inorganic matrices without using additional chemical reagents and solvents. This can result in the development of environmentally clean and safe methods for the synthesis of nanostructured materials.

Third, the carrying out of cryonanochemical processes and the synthesis of nanoparticles and nanostructured materials to be used in practice should be accompanied by scaling of synthetic methods to obtain the required macroamounts of target products and by the development of procedures for maintaining long-term stability of their physical and chemical properties.

Wide prospects are opened up for the use of cryochemical methods in the production of metal-containing nanostructures on cooled surfaces of organic, inorganic and polymeric substances. The use of low temperatures and the controlled condensation of reagent vapour allow one to synthesise and stabilise particles measuring 1 nm and smaller. Such hybrid materials may find their application in catalysis and as chemical sensors.

Of undeniable interest is the development of multifunctional hybrid nanosystems based on chemically modified metal particles and biologically active substances, which includes the development of new systems for medicinal diagnostics and the target delivery of medicinal drugs.

This review was financially supported by the Russian Foundation of Basic Research (Project Nos 04-03-32 748 and 05-03-32 293) and the INTAS programme (Grant No. 2000-00 911).

References

1. G B Sergeev *Nanochemistry* (Amsterdam, Boston, Heidelberg, London, New York, Oxford, Paris, San Diego, San Francisco, Singapore, Sydney, Tokyo: Elsevier, 2006)
2. G B Sergeev *J. Nanopart. Res.* **5** 529 (2003)
3. T I Shabatina, G B Sergeev *Usp. Khim.* **72** 643 (2003) [*Russ. Chem. Rev.* **72** 571 (2003)]
4. G B Sergeev, T I Shabatina *Surf. Sci.* **500** 628 (2002)
5. K J Klabunde *Free Atoms, Clusters and Nanoscale Particles* (San Diego, New York, Boston, London, Sydney, Tokyo: Academic Press, 1994)
6. G B Sergeev *Usp. Khim.* **70** 915 (2001) [*Russ. Chem. Rev.* **70** 809 (2001)]
7. W Leitner *Coord. Chem. Rev.* **153** 257 (1996)
8. D H Gibson *Chem. Rev.* **96** 2063 (1996)
9. A Behr *Carbon Dioxide Activation by Metal Complexes* (Weinheim: VCH, 1988)
10. M Aresta, E Quaranta, I Tomassi *New J. Chem.* **18** 133 (1994)
11. P Brounstein, D Matt, D Nobel *Chem. Rev.* **88** 747 (1988)
12. J Mascetti, F Galan, I Papai *Coord. Chem. Rev.* **190–192** 557 (1999)
13. F Galan, M Fouassier, M Tranquille, J Mascetti, I Papai *J. Phys. Chem. A* **101** 2626 (1997)
14. J Mascetti, R Fournier, I Papai *J. Phys. Chem. A* **101** 4465 (1997)

15. C Jegat, J Mascetti *New J. Chem.* **15** 17 (1991)
16. Y K Lee, Y Hannachi, C Xu, L Andrews, L Manceron *J. Phys. Chem.* **100** 11228 (1996)
17. F Bernardi, A Bottoni, M Calcinari, I Rossi, M A Robb *J. Phys. Chem.* **101** 6316 (1997)
18. K Pierloot, B J Persson, B O Roos *J. Phys. Chem.* **99** 3465 (1995)
19. T H Upton, W A Goodbart *J. Am. Chem. Soc.* **100** 321 (1978)
20. T Merle-Mejean, C Cosse-Merteas, S Bouchareb, F Galan, J Mascetti, M Tranquille *J. Phys. Chem.* **96** 9148 (1992)
21. Yu K Lee, L Manceron, I Papai *J. Phys. Chem. A* **101** 9650 (1997)
22. G V Chertihin, L Andrews *J. Am. Chem. Soc.* **116** 8322 (1994)
23. Z Xiao, R H Hauge, J L Margrave *J. Phys. Chem.* **95** 2696 (1991)
24. J Mascetti, M Tranquille *J. Phys. Chem.* **92** 2177 (1988)
25. G V Chertihin, L Andrews *J. Am. Chem. Soc.* **117** 1595 (1995)
26. C Jegat, M Fouassier, M Tranquille, J Mascetti *Inorg. Chem.* **30** 1529 (1991)
27. C Jegat, M Fouassier, J Mascetti, M Tranquille, I Tomassi, M Aresta, F Ingold, A Dendieu *Inorg. Chem.* **35** 4254 (1996)
28. Y Hannachi, J Mascetti, A Stirling, I Papai *J. Phys. Chem. A* **107** 6708 (2003)
29. F Elustondo, J Mascetti, I Papai *J. Phys. Chem. A* **104** 3572 (2000)
30. Y Dobrogorskaya, J Mascetti, I Papai, A Nemukhin, Y Hannachi *J. Phys. Chem. A* **107** 2711 (2003)
31. Y Dobrogorskaya, J Mascetti, A Nemukhin, I Papai, Y Hannachi *J. Phys. Chem. A* **109** 7932 (2005)
32. Y Dobrogorskaya, J Mascetti, Y Hannachi *J. Phys. Chem. A* **111** (2008) (in the press)
33. T L Haslett, S Fedrigo, K Bosnick, M Moskovits, H A Duarte, D Salahub *J. Am. Chem. Soc.* **122** 6039 (2000)
34. F Elustondo, Ph.D. Thesis Université Bordeaux I, Bordeaux, 1997
35. V T Aleksanyan, B V Lokshin *Stroenie Molekul i Khimicheskaya Svyaz' (Itogi Nauki i Tekhniki)* [Structure of Molecules and Chemical Bond (Advances in Sciences and Engineering)] (Moscow: Izd. VINITI, 1976) Vol. 5, p. 178
36. B V Lokshin *Proceedings of the 6th International Conference on Low Temperature Chemistry, Chernogolovka, 2006* p. 45
37. B V Lokshin, I I Greenwald *J. Mol. Struct.* **220** 11 (1990)
38. T S Kurtikyan, G M Gulyan, A A Hovhannisyan, N A Gabrielyan *Proceedings of the 6th International Conference on Low Temperature Chemistry, Chernogolovka, 2006* p. 44
39. M Dalibart, J Derouault *J. Mol. Struct.* **218** 1 (1990)
40. T R Gebale, T Oka *Nature (London)* **384** 334 (1996)
41. T R Geballe, B J Mc Call, K H Hinkle, T Oka *Astrophys. J.* **510** 251 (1999)
42. M Cordonier, D Uy, R M Dickson, K E Kerr, Y Zang, T Oka *J. Chem. Phys.* **113** 318 (2000)
43. S Tam, M E Fajardo, H Katsuki, H Hoshina, T Wakabayashi, T Momose *J. Chem. Phys.* **111** 4191 (1999)
44. T Momose, M Miki, T Wakabayashi, T Shida, M C Chan, S S Lee, T Oka *J. Chem. Phys.* **107** 7707 (1997)
45. R J Hinde, D T Anderson, S Tam, M E Fajardo *Chem. Phys. Lett.* **356** 355 (2002)
46. S I Kiselev, V V Khmelenko, D M Lee, V Kiryuhin, R E Boltnev, E B Gordon, B Keimer *Phys. Rev. B* **65** 024517 (2002)
47. S I Kiselev, V V Khmelenko, C Y Lee, D M Lee *J. Low Temp. Phys.* **128** (2002)
48. E G Kisvarsanyi, N S Sullivan *Phys. Rev. B* **48** 16577 (1993)
49. F Elustondo, M Dalibart, J Derouault, J Mascetti *Phys. Chem. Earth* **24** 583 (1999)
50. M Moskovits, G Ozin *Cryochemistry* (New York: Wiley, 1976)
51. W Harbig, S Fedrigo, S Buttet, D Lindsay *J. Chem. Phys.* **96** 8104 (1992)
52. G A Ozin, A C Arsenault *Nanochemistry. A Chemical Approach to Nanochemistry* (Cambridge: RSC, 2005)
53. *Nanoparticles from Theory to Applications* (Ed. G Schmid) (Weinheim: VCH, Wiley, 2005)
54. B M Sergeev, G B Sergeev, A N Prusov *Mendeleev Commun.* **68** (2001)
55. B M Sergeev, G B Sergeev, V A Kasaikin, E A Litmanovich, A N Prusov *Mol. Cryst. Liq. Cryst.* **356** 121 (2001)
56. G Yu Yurkov, A V Kozinkin, T I Nedoseikina, A T Shuvaev, V G Vlasenko, S P Gubin, I D Kosobudskii *Neorg. Mater.* **37** 1175 (2001)^a
57. G B Sergeev, V V Zagorskii, M A Petrukhina *J. Mater. Chem.* **5** 31 (1995)
58. G B Sergeev, M A Petrukhina *Prog. Solid State Chem.* **24** 183 (1996)
59. L I Trahtenberg, G N Gerasimov *Metal-Polymer Nanocomposites* (Eds L Nicolais, G Carotenuto) (New York: Wiley, 2005) p. 37
60. G B Sergeev, V V Zagorskii, M A Petrukhina, S Zaviyalov, E Grigoriev, L Trachtenberg *Anal. Commun.* **34** 113 (1997)
61. V E Bochenkov, N Stephan, L Brehmer, V V Zagorskii, G B Sergeev *Colloids Surf. A* **198–200** 911 (2002)
62. V M Kozhevnikov, D A Yavsin, S A Gurevich, T N Rostovshikova, V V Smirnov *Ros. Nanotekhnol.* **2** 47 (2007)^b
63. P S Vorontsov, E I Grigor'ev, S A Zav'yalov, L M Zav'yalo, T N Rostovshchikova, O V Zagorskaya *Khim. Fiz.* **21** 45 (2002)^c
64. T I Shabatina *Vestn. Mosk. Univ., Ser. 2, Khim.* **43** 273 (2002)^d
65. T I Shabatina, E V Vovk, V A Timoshenko, Yu N Morosov, G B Sergeev *Colloids Surf. A* **198–200** 255 (2002)
66. T I Shabatina, V A Timoshenko, A A Belyaev, Yu N Morozov, G B Sergeev *Dokl. Akad. Nauk* **387** 219 (2002)^e
67. T I Shabatina *Struct. Chem.* **18** 511 (2007)
68. T I Shabatina, V A Timoshenko, Yu N Morosov, G B Sergeev *Mater. Sci. Eng., C* **22** 193 (2002)
69. T I Shabatina, E V Vovk, Yu N Morosov, V A Timoshenko, G B Sergeev *Mol. Cryst. Liq. Cryst.* **356** 143 (2001)
70. T I Shabatina, V A Timoshenko, Yu N Morosov, G B Sergeev *Mol. Cryst. Liq. Cryst.* **390** 43 (2003)
71. N V Ozhegova, T I Shabatina, A V Nemukhin, G B Sergeev *Mendeleev Commun.* **218** (1998)
72. T I Shabatina, E V Vovk, N V Ozhegova, Yu N Morosov, A V Nemukhin, G B Sergeev *Mater. Sci. Eng.* **8–9** 53 (1999)
73. J A Howard, H A Joly, D Mile *J. Phys. Chem.* **94** 1275 (1990)
74. A J Buck, B Mile, J A Howard *J. Am. Chem. Soc.* **105** 3381 (1983)
75. V A Timoshenko, A A Belyaev, Yu N Morosov, T I Shabatina, G B Sergeev *Mol. Cryst. Liq. Cryst.* **440** 79 (2005)
76. J H Michalik, D Yamada, R Brown, L Kevan *J. Phys. Chem.* **100** 4213 (1996)
77. G Mitrikas, Y Deligiannakis, C C Trapalis, N Boukos, G Kordas *J. Sol-Gel Sci. Technol.* **13** 503 (1998)
78. E V Polikarpov, T I Shabatina, G B Sergeev, A V Nemukhin *Vestn. Mosk. Univ., Ser. 2, Khim.* **41** 283 (2000)^d
79. U Kreibitz, M Volmer *Optical Properties of Metal Clusters* (Berlin: Springer, 1995) p. 532
80. T I Shabatina *Zhidkie Kristally i Ikh Prakticheskoe Ispol'zovanie* (Liquid Crystals and Their Practical Use) (Ivanovo: Ivanovo State University, 2002) Vol. 1, p. 58
81. T I Shabatina, G B Sergeev *Fizikokhimiya Ul'tradispersnykh Nanosistem* (Physical Chemistry of Ultradisperse Nanosystems) (Moscow: Moscow Engineering Physical Institute, 2005) p. 108
82. F G N Cloke *Chem. Soc. Rev.* **17** (1993)
83. P L Arnold, M A Petrukhina, V E Bochenkov, T I Shabatina, V V Zagorskii, G B Sergeev, F G N Cloke *J. Organomet. Chem.* **688** 49 (2003)
84. L Maron, O Eisenstein *J. Phys. Chem. A* **104** 7140 (2000)
85. S A Konnov, L V Serebrennikov, A A Mal'tsev *Zh. Neorg. Khim.* **27** 654 (1982)^f
86. R L DeKock, W Weltner Jr *J. Phys. Chem.* **75** 514 (1971)
87. N S Loktyushina, S B Osin, A A Mal'tsev *Zh. Neorg. Khim.* **29** 1718 (1984)^f
88. N S Loktyushina, S B Osin *Zh. Neorg. Khim.* **32** 2918 (1987)^f
89. V N Solov'ev, Candidate Thesis in Chemical Sciences, Moscow State University, Moscow, 1998
90. G B Sergeev, T I Shabatina, V N Solov'ev, A V Nemukhin *Spectrochim. Acta, A* **56** 2527 (2000)
91. G B Sergeev, V V Zagorskii, M V Grishechkina *Vestn. Mosk. Univ., Ser. 2, Khim.* **29** 583 (1988)^d
92. G B Sergeev, V V Zagorskii, M V Grishechkina *Metalloorg. Khim.* **1** 820 (1988)^g
93. V V Zagorsky, G B Sergeev *Mol. Cryst. Liq. Cryst.* **186** 81 (1990)
94. J M Carretas, A Pires de Matos *Mater. Chem. Phys.* **31** 123 (1992)

95. V V Zagorskii, S E Kondakov, A M Kosolapov, G B Sergeev, V N Solov'ev *Metalloorg. Khim.* **5** 533 (1992)^g
96. G B Sergeev, V V Zagorskii, A M Kosolapov, S E Kondakov *Metalloorg. Khim.* **8** 3212 (1995)^g
97. F G N Cloke, H C de Lemos, A A Sameh *J. Chem. Soc., Chem. Commun.* 1344 (1986)
98. W J Evans, S C Engerer, A C Neville *J. Am. Chem. Soc.* **331** (1978)
99. W J Evans, K M Coleson, S C Engerer *Inorg. Chem.* **20** 4320 (1981)
100. W J Evans, S C Engerer, K M Coleson *J. Am. Chem. Soc.* **103** 6672 (1981)
101. W J Evans *Polyhedron* **6** 803 (1987)
102. I G Tarkhanova, Candidate Thesis in Chemical Sciences, Moscow State University, Moscow, 1990
103. V V Zagorskii, S E Kondakov, A M Kosolapov *Vestn. Mosk. Univ., Ser. 2, Khim.* **33** 249 (1992)^d
104. J L Slater, T C De Vore, V Calder *Inorg. Chem.* **13** 1808 (1974)
105. J L Slater, T C De Vore, V Calder *Inorg. Chem.* **12** 1918 (1973)
106. W E Klotzbucher, M A Petrukchina, G B Sergeev *Mendeleev Commun.* **5** (1994)
107. M P Andrews, A L Wayda *Organometallics* **7** 743 (1988)
108. V E Bochenkov, V V Zagorskii, G B Sergeev *Vestn. Mosk. Univ., Ser. 2, Khim.* **41** 327 (2000)^d
109. W A King, T J Marks, D M Anderson, D J Duncalf, F G N Cloke *J. Am. Chem. Soc.* **114** 9221 (1992)
110. A V Vlasov, T I Shabatina, A Yu Ivanov, G G Sheina, A V Nemukhin, G B Sergeev *Mendeleev Commun.* **10** (2005)
111. T I Shabatina, A V Vlasov, G B Sergeev *Mol. Cryst. Liq. Cryst.* **356** 149 (2001)
112. T I Shabatina, A V Vlasov, E V Vovk, D J Stufkens, G B Sergeev *Spectrochim. Acta, A* **56** 2539 (2000)
113. T I Shabatina, A V Vlasov, G B Sergeev *Mater. Sci. Eng., C* **22** 373 (2002)
114. A V Vlasov, I N Zelikov, T I Shabatina, G B Sergeev *Mol. Cryst. Liq. Cryst.* **390** 35 (2003)
115. A V Vlasov, T I Shabatina, S V Konyukhov, A Yu Ermilov, A V Nemukhin, G B Sergeev *Zh. Strukt. Khim.* **45** 406 (2004)^h
116. T I Shabatina, A V Vlasov, S V Konyukhov, A Yu Ermilov, A V Nemukhin, G B Sergeev *Mol. Cryst. Liq. Cryst.* **440** 317 (2005)
117. T I Shabatina, A V Vlasov, A Yu Ermilov, S V Konyukhov, A V Nemukhin, G B Sergeev *Zh. Strukt. Khim.* **48** 814 (2007)^h
118. A V Vlasov, T I Shabatina, G B Sergeev *Zh. Fiz. Khim.* **76** 1965 (2002)ⁱ
119. A V Vlasov, Candidate Thesis in Chemical Sciences, Moscow State University, Moscow, 2006
120. N M Emanuel', A L Buchachenko *Khimicheskaya Fizika Razrusheniya i Stabilizatsii Polimerov* (Chemical Physics of Destruction and Stabilisation of Polymers) (Moscow: Nauka, 1988) p. 368
121. G B Sergeev *Mol. Cryst. Liq. Cryst.* **440** 85 (2005)
122. G B Sergeev, T I Shabatina *Colloids Surf. A* (2008) (in the press)
123. V A Timoshenko, T I Shabatina, Yu N Morosov, G B Sergeev *Appl. Surf. Sci.* **246** 420 (2005)
124. T I Shabatina, Yu N Morosov, V A Timoshenko, G B Sergeev *Mol. Cryst. Liq. Cryst.* **440** 325 (2005)
125. V A Timoshenko, T I Shabatina, Yu N Morozova, G B Sergeev *Zh. Strukt. Khim.* **47** 146 (2006)^h
126. M Haruta *Catal. Today* **36** 153 (1997)
127. D F Shriver, P A Atkins *Inorganic Chemistry* (Oxford: Oxford University Press, 1999)
128. M-C Daniel, D Astruc *Chem. Rev.* **104** 293 (2004)
129. R Meyer, C Lemire, Sh K Shaikhutdinov, H-J Freund *Gold Bull.* **37** 72 (2004)
130. S Schimpf, M Lucas, C Mohr, U Rodemerk, A Brukner, J Radnik, H Hofmeister, P Claus *Catal. Today* **72** 63 (2002)
131. D T Thompson *Appl. Catal., A* **243** 201 (2003)
132. M M Schubert, S Hacjenberg, A C Van Vee, M Muhler, V Plzak, R Behm *J. Catal.* **197** 113 (2001)
133. L Fan, N Ichikuni, S Shimadzu, T Uematsu *Appl. Catal.* **246** 87 (2003)
134. T Hayashi, K Tanaka, M Haruta *J. Catal.* **178** 566 (1998)
135. M A Banares *Catal. Today* **100** 71 (2005)
136. A Ueda, M Haruta *Gold Bull.* **32** 3 (1999)
137. H Sakuri, M Haruta *Catal. Today* **29** 361 (1996)
138. A Ueda, T Oshima, M Haruta *Appl. Catal., B* **12** 81 (1997)
139. G Hutchings *Catal. Today* **72** 11 (2002)
140. T V Choudhary, D W Goodman *Catal. Today* **77** 65 (2002)
141. A S K Hashimi *Gold Bull.* **36** 3 (2003)
142. V V Smirnov, S N Lanin, A Yu Vasil'kov, S A Nikolaev, G P Murav'eva, L A Tyurina, E V Vlasenko *Izv. Akad. Nauk, Ser. Khim.* 2215 (2005)^j
143. L Lian, P A Hackett, D M Rayner *J. Phys. Chem.* **99** 2583 (1993)
144. J Li, X Li, H J Zhai, L S Wang *Science* **299** 864 (2003)
145. B E Salisbury, W T Wallace, R L Whetten *Chem. Phys.* **262** 131 (2000)
146. D Stolcic, M Fisher, G Gantefor, Y D Kim, Q Sun, P Jena *J. Am. Chem. Soc.* **125** 2848 (2003)
147. Y D Kim, M Fisher, G Gantefor *Chem. Phys. Lett.* **377** 170 (2003).
148. S A C Carabineiro, D T Thompson *Nanocatalysis* (Eds U Heinz, U Landman) (Berlin: Springer, 2007) p. 37
149. W T Wallace, R L Whetten *J. Phys. Chem. B* **104** 10964 (2000)
150. W T Wallace, R L Whetten *Eur. Phys. J. D* **16** 123 (2001)
151. J Hagen, L D Socaciu, U Heiz, T M Bemhardt, L Woste *Eur. Phys. J. D* **24** 327 (2003)
152. J Hagen, L D Socaciu, M Elijażyfer, U Heiz, T M Bemhardt, L Woste *Phys. Chem. Chem. Phys.* **4** 1707 (2002)
153. W T Wallace, R L Whetten *J. Am. Chem. Soc.* **124** 7499 (2002)
154. L D Socaciu, J Hagen, T M Bemhardt, L Woste, U Heiz, H Hakkinen, U Landman *J. Am. Chem. Soc.* **125** 10437 (2003)
155. I Balteanu, O P Balaj, B S Fox, M K Beyer, Z Bastl, V E Bondybey *Phys. Chem. Chem. Phys.* **5** 1213 (2003)
156. W T Wallace, R B Wrywas, R L Whetten, R Mitric, V Bonacic *J. Am. Chem. Soc.* **125** 8408 (2003)
157. K Sugawa, F Sobbot, A V Vakhtin *J. Chem. Phys.* **118** 7808 (2003)
158. B Hammer, J Norskov *Nature (London)* **376** 238 (1995)
159. M Mavrikakis, P Stoltze, J Norskov *Catal. Lett.* **64** 101 (2001)
160. H Hakkinen, B Yoon, U Landman, X Li, H J Zhai, L S Wang *J. Phys. Chem. A* **107** 6168 (2003)
161. J Wang, G Wang, J Zhao *Phys. Rev., B* **66** 035418 (2002)
162. N Lopez, J K Norskov *J. Am. Chem. Soc.* **124** 11262 (2002)
163. B Yoon, H Hakkinen, U Landman *J. Phys. Chem. A* **107** 4066 (2003)
164. H Gronbek, W Andreoni *Chem. Phys.* **262** 1 (2000)
165. I L Garzon, K Michaelian, M R Beltrán, A Posada-Amarillias, P Ordejón, E Artacho, D Sanchez-Portal, J M Soler *Eur. Phys. J. D* **9** 211 (1999).
166. C L Cleveland, U Landman, M N Shafigullin, P W Stephens, R L Whetten *Z. Phys. D: At., Mol. Clusters* **40** 503 (1997)
167. C L Cleveland, U Landman, T G Schaff, M N Shafigullin, P W Stephens, R L Whetten *Phys. Rev. Lett.* **79** 1873 (1997)
168. G Mills, M S Gordon, H Metiu *Chem. Phys. Lett.* **359** 493 (2002)
169. S A Varganov, R M Olson, M S Gordon, H Metiu *J. Chem. Phys.* **119** 2531 (2003)
170. P Gunter, J W Niemantsverdriet, F Ribiero, G Somorjai *Catal. Rev. Sci. Eng.* **38** 77 (1997)
171. H J Freund, M Baumer, H Kühlenbeck *Adv. Catal.* **45** 333 (2000)
172. H J Freund *Surface Sci.* **500** 271 (2002)
173. U Diebold *Surface Sci. Rep.* **48** 53 (2003)
174. L Zhang, R Persaud, T E Madey *Phys. Rev. B* **56** 10549 (1997)
175. T Bredow, G Pacchioni *Chem. Phys. Lett.* **355** 417 (2002)
176. X Lai, T P S Lclair, M Valden, D W Goodman *Prog. Surf. Sci.* **59** 25 (1998)
177. N Lopez, T V W Janssens, B S Clausen, Y Xu, M Mavrikakis, T Bligaard, J K Norskov *J. Catal.* **223** 232 (2004)
178. J A Rodriguez, M Perez, T G Jirsak, J Evans *J. Chem. Phys. Lett.* **378** 526 (2003)
179. C L Bianchi, S Biella, A Gervasini, L Prati, M Rossi *Catal. Lett.* **85** 91 (2003)

180. A K Santra, D W Goodman *J. Phys.: Condens. Matter* **14** R31 (2002)
181. T V W Janssens, A Carlsson, A Puig-Molina, B S Clausen *J. Catal.* **240** 108 (2006)
182. B Hvolback, T V W Janssens, B S Clausen, C H Christensen, J K Nørskov *Nano Today* **2** 14 (2007)
183. Y J Zhu, A Schnieders, J D Alexander, T P Beebe *Langmuir* **18** 5728 (2002).
184. H G Boyen, G Kastle, F Wieg, B Kozłowski, C Dietrich, P Ziemann, J P Spatz, S Riethmüller, C Hartmann, M Moeller, G Schmid, M C Garnier, P Oelhafen *Science* **297** 1533 (2002)
185. H Zhang, G Schmid, U Hartmann *Nano Lett.* **3** 305 (2003)

^a — *Inorg. Mater. (Engl. Transl.)*

^b — *Nanotechnol. Russ. (Engl. Transl.)*

^c — *Chem. Phys. Rep. (Engl. Transl.)*

^d — *Bull. Moscow Univ., Chem. (Engl. Transl.)*

^e — *Dokl. Phys. Chem. (Engl. Transl.)*

^f — *Russ. J. Inorg. Chem. (Engl. Transl.)*

^g — *Russ. J. Organomet. (Engl. Transl.)*

^h — *J. Struct. Chem. (Engl. Transl.)*

ⁱ — *Russ. J. Phys. Chem. (Engl. Transl.)*

^j — *Russ. Chem. Bull., Int. Ed. (Engl. Transl.)*

Study of photochemical transformations of organic azides by matrix isolation techniques and quantum chemistry

N P Gritsan

Contents

I. Introduction	1139
II. Detection and properties of the simplest nitrene NH	1140
III. Photochemical transformations of alkyl azides	1141
IV. Photochemical transformations of acyl azides	1143
V. Photochemical transformations of aryl azides	1146
VI. Reactions of triplet nitrenes with oxygen	1153
VII. Conclusion	1157

Abstract. Results of investigations of organic azide photochemistry in inert gas matrices and the most important spectroscopic studies of the last decade, which formed the basis for the modern views on the photochemistry of azides, are analysed. The unique potential of the matrix isolation technique for the reliable identification of reaction intermediates is demonstrated. The bibliography includes 226 references.

I. Introduction

The term ‘matrix isolation’ was introduced by Pimentel^{1,2} and Porter³ in 1954 to describe the technique in which the substrate in a mixture with an inert gas is deposited onto a rather cold surface providing rapid freezing of the mixture. This gives rise to solid samples in which (in the ideal case) each substrate molecule is surrounded by one or several layers of the inert gas and is thus isolated from other substrate molecules. Argon, neon, nitrogen, their mixtures and xenon are most commonly used as inert gases. The technical details of the method and its numerous applications have been considered in a series of monographs and reviews.^{4–10}

In the course of time, the term ‘matrix isolation’ came to be applied in a more general sense, encompassing a range of techniques where substrate (guest) molecules are trapped in a solid inert material (host). Crystals, zeolites, polymers, *etc.* can serve as such materials. Numerous studies of reaction intermediates were carried out in frozen glassy organic solvents. This method of investigation is also sometimes referred to as the matrix isolation. However, in the present review the term matrix isolation will be used only in its original sense.

Two presently available methods for the detection and investigation of reaction intermediates are based on either time-resolved spectroscopic techniques or the stabilisation of intermediates in different matrices at low temperatures and

their studies by conventional spectroscopic methods. In the former case, not only spectroscopic but also kinetic data can be obtained. In the latter case, the structures of possible intermediates can be more reliably predicted due to more detailed spectroscopic information. The use of the matrix isolation techniques is particularly promising in combination with IR spectroscopy of intermediates, because well-resolved IR spectra with a linewidth of $\sim 1\text{--}3\text{ cm}^{-1}$ can be recorded in inert gas matrices at very low temperatures even for rather complex species in a very wide spectral range.

In early studies on the matrix isolation, the assignment of bands in IR spectra of intermediates was based primarily on the record of the characteristic absorption bands with a wide use of the isotopic substitution, reactions of primary intermediates, *etc.* The interpretation of experimental IR and electronic absorption spectra was greatly simplified due to the development of accurate theoretical methods for their calculation. For example, good agreement between calculated and experimental IR spectra can be achieved with the use of the density functional theory (DFT). The hybrid B3LYP method^{11,12} with the 6-31G* basis set is most widely used for this purpose. In these calculations, the vibrational frequencies are somewhat overestimated, which is accounted for by introducing the correction coefficient of 0.9614.¹³

The positions of maxima in electronic absorption spectra and the oscillator strengths for transitions can also be calculated by quantum chemical methods with good accuracy. The CASSCF/CASPT2 approach,^{14,15} which is implemented, for example, in the MOLCAS programme package,¹⁶ provides the most accurate results. The time-dependent DFT method^{17,18} also gives reliable results, particularly, for systems with closed-shell electronic configurations.

The aim of the present review is to analyse the role of the matrix isolation technique in revealing the mechanisms of photolysis of certain classes of organic azides. Organic azides have found use as photoresists in lithography,¹⁹ in the design of conducting polymers,²⁰ organic synthesis,²¹ photoaffinity labelling of biopolymers²² and covalent labelling of the polymer surface.^{23–25} Numerous spectroscopic studies of the intermediates of the organic azides photolysis were performed in the gas phase, in low-temperature glasses and inert gas matrices, and in solutions using time-resolved methods. The results of early studies were summarised in reviews (see, for

N P Gritsan Institute of Chemical Kinetics and Combustion, Siberian Branch of the Russian Academy of Sciences, ul. Institutskaya 3, 630090 Novosibirsk, Russian Federation. Fax (7-383) 330 73 50, tel. (7-383) 333 30 53, e-mail: gritsan@kinetics.nsc.ru

Received 27 February 2007

Uspekhi Khimii 76 (12) 1218–1240 (2007); translated by T N Safonova

example, Refs 26–31). The data obtained by the matrix isolation technique were considered in reviews.^{32, 33}

In the last decade, there has been dramatic progress in the understanding of the mechanisms of photochemical transformations of alkyl, acyl and aryl azides. The successful use of time-resolved spectroscopic methods for the detection of singlet aryl nitrenes (primary photolysis products of aryl azides) and high-level quantum chemical calculations for the analysis of the spectra and reactivity of these compounds provided a detailed understanding of the complex mechanism of the phototransformations of aryl azides.^{34–37} A considerable progress in the elucidation of the unusual nature of singlet acyl nitrenes was achieved due to the use of the matrix isolation technique combined with high-level quantum chemical calculations.^{38–40}

In the present review, the results of studies on photochemistry of alkyl, aryl and acyl azides in inert gas matrices are analysed. The most interesting recent data obtained with the use of time-resolved methods and the most important spectroscopic and theoretical results underlying the modern views on the photochemistry of azides are considered.

II. Detection and properties of the simplest nitrene NH

Singlet nitrenes are the primary photolysis products of most of azides.^{36, 37} Almost all nitrenes exist in the triplet ground state.^{29–31, 35–37} (Acyl nitrenes considered in Section IV are exceptions.)

The imino radical NH generated in the photolysis,^{41–46} thermolysis⁴⁷ or the multiphoton dissociation^{48, 49} of hydrazoic acid is the simplest nitrene.

Pimentel and co-workers⁵⁰ were the first to study the photolysis of HN₃ by the matrix isolation technique. The IR spectrum of the photolysis products was recorded in an argon and nitrogen matrices, and a series of lines in the spectrum were assigned to nitrene NH and the radical NH₂. This publication was followed by a number of investigations of matrix-isolated nitrene NH and its deuterium-substituted analogue (ND) both in the triplet ground state $^3\Sigma^-$ and the excited metastable state $^1\Delta$ by UV and luminescence spectroscopy.^{51–55} The spectroscopic characteristics and the relaxation of the lowest excited singlet state of nitrene NH (or ND) ($^1\Delta$) in Ne, Ar, Kr and Xe matrices were studied in detail.^{54, 55} The diagram of the lowest energy levels of the NH radical (Fig. 1) can be constructed based on the results of spectroscopic investigations in matrices^{54, 55} and in the gas phase.^{41–46}

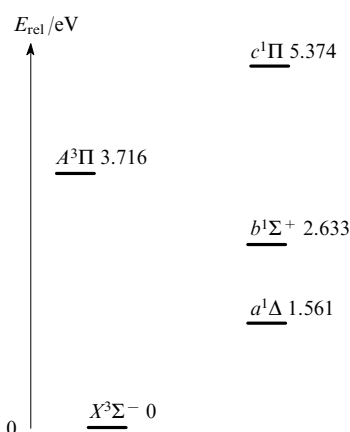


Figure 1. Energy level diagram for nitrene NH based on experimental data.^{41–46, 54, 55}

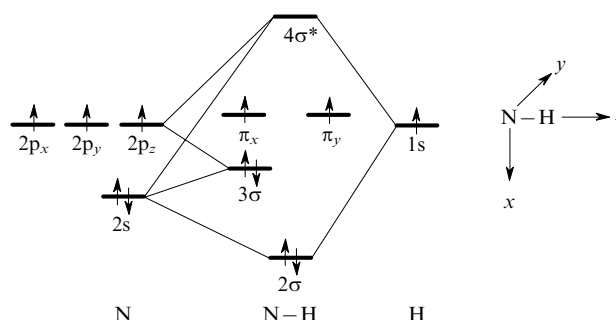


Figure 2. Molecular orbitals of nitrene NH. (The 1σ orbital, the $1s$ atomic orbital of the nitrogen atom, is omitted.)

A knowledge of the electronic structure and the spectra of the simplest nitrene is very useful in the analysis of more complex nitrenes formed by the photolysis of alkyl, acyl and aryl azides. In the NH species, the molecular orbital (MO) corresponding to the N–H bond (2σ) and the MO of the nitrogen lone pair (3σ) are occupied by electron pairs (Fig. 2). Two valence electrons should be distributed between two degenerate antibonding MO, π_x and π_y . This electronic configuration gives rise to three lowest electronic states (terms) of NH, $^3\Sigma^-$, $^1\Delta$ and $^1\Sigma^+$; the triplet state $^3\Sigma^-$ is the ground state (Fig. 3). This figure gives also components of the doubly degenerate lowest singlet state $^1\Delta$ with the closed- and open-shell electronic configurations and the electronic state $^1\Sigma^+$. Two configurations, which are mixed in the lowest singlet state $^1\Delta$ with a minus sign, are mixed with a plus sign in the state $^1\Sigma^+$. It can easily be demonstrated that in this state the probability of finding two non-bonding electrons at a single point in the space is much higher compared to the state $^1\Delta$ and consequently the energy of the state $^1\Sigma^+$ is substantially higher.

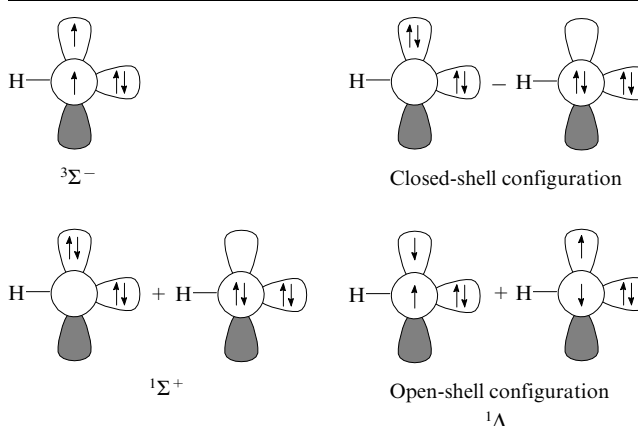


Figure 3. Schematic representation of the electronic states of nitrene NH: one of three spin components of the lowest triplet state $^3\Sigma^-$, two components of the lowest singlet state $^1\Delta$ (having the closed- and open-shell electronic configurations) and the second singlet state $^1\Sigma^+$.

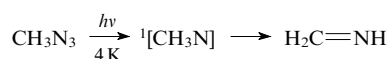
The electronic absorption spectra of NH both in the triplet ground state ($^3\Sigma^-$) and the lowest singlet state ($^1\Delta$) show intense lines in the near-UV region with maxima at 336 and 324 nm, respectively.^{41, 46} Both transitions are associated with the electron excitation from the lone pair (3σ) to the π orbital occupied by one electron (π_x or π_y in Fig. 2). This transition is

observed also in the electronic absorption spectra of other organic nitrenes (see Sections III and V).

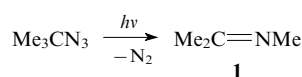
III. Photochemical transformations of alkyl azides

Photolysis of alkyl azides, including those in which the azido group is bound to the tertiary carbon atom, in solution at room temperature affords the corresponding imines or their further transformations products in quantitative yields.^{56,57} No reaction products of alkyl nitrenes with solvents or active additives could be detected.⁵⁷

The photochemistry of the simplest alkyl azide, *viz.*, methyl azide, was studied in sufficient detail,^{57–60} including the use of the matrix isolation technique.^{61,62} According to the IR spectroscopic data, the photolysis of methyl azide and its different isotopically substituted analogues in Ar, N₂ and CO₂ matrices at 4 and 14 K gives methyleneimine as the only product.^{61,62} It cannot be ruled out that singlet methylnitrene is the primary species formed in the photolysis of methyl azide; however, this species readily undergoes isomerisation to methanimine even at cryogenic temperatures and has no time to relax to the triplet ground state.

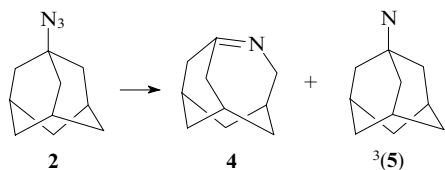


In subsequent studies, emphasis was given to the matrix photochemistry of alkyl azides in which the azide group is bound to the tertiary carbon atom. The absence of the α -H atom gave promise that the rate of isomerisation of singlet alkyl nitrene to imine would be lower, thus making possible the relaxation of singlet alkyl nitrene to the triplet ground state. The photolysis of *tert*-butyl azide in a nitrogen matrix was performed at 12 K.⁶³ Imine **1** was detected by IR spectroscopy as the only reaction product.



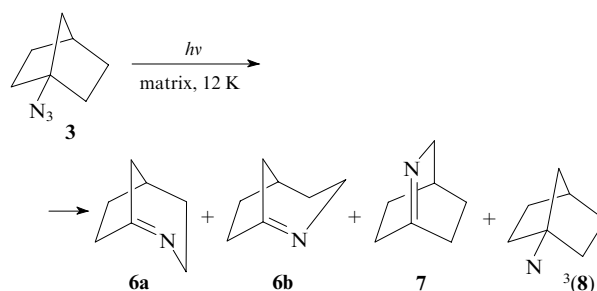
The formation of strained bridgehead imines was observed in the photolysis of matrix-isolated bridgehead azides, for example, of adamantyl, bicyclo[2.2.2]octyl, bicyclo[3.2.1]heptyl and norbornyl azides.^{64–68} The matrix photochemistry of 1-azidoadamantane (**2**)⁶⁷ and 1-azidonorbornane (**3**)⁶⁸ was studied in most detail.

The low-temperature photolysis of azide **2** in argon and nitrogen matrices, 3-methylpentane glasses, a polyethylene matrix and the solid state afforded strained imine **4**, which was characterised by IR, electronic absorption, Raman and circular dichroism spectra, along with trace amounts of triplet 1-adamantyl nitrene **3**(**5**), which was identified from the ESR spectrum at 8210 G ($E = 0$, $|D/hc| = 1.69 \text{ cm}^{-1}$) and based on the reaction with CO.⁶⁷ Heating of the matrices (for example, to 36 K in the case of an argon matrix) led to dimerisation of imine **4**.



1-Azidonorbornane (**3**) was irradiated in an argon or polyethylene matrix at 12 K using monochromatic radiation with different wavelengths, and the reaction products were identified by IR, UV and ESR spectroscopy method, as well as based on the reaction with methanol or CO.⁶⁸ The photolysis of azide **3** is a more complex process compared to the photolysis of

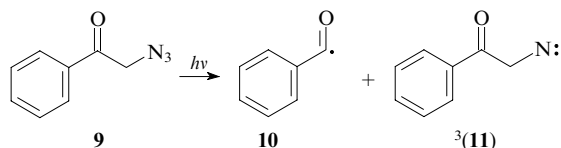
azide **2**. Three types of imines (**6a**, **b** and **7**) and trace amounts of triplet nitrene **8** were detected.⁶⁸ Imines **6** and **7** are light-sensitive, undergo interconversions and are decomposed to unidentified products.



Triplet nitrene **8** was identified based on the ESR signal at 8124 G ($E = 0$, $|D/hc| = 1.65 \text{ cm}^{-1}$), the narrow band in the electronic absorption spectrum at 298 nm and its reaction with CO in an argon matrix at 36 K.⁶⁸

Since the photolysis of alkyl azides in solution, low-temperature glasses and inert gas matrices affords the corresponding imines as the major primary products, it was hypothesised⁵⁷ that the elimination of molecular nitrogen from alkyl azides in the excited singlet state and the formation of imine are concerted processes and occur without the involvement of singlet alkyl nitrene as an intermediate. This hypothesis has been neither confirmed nor denied experimentally.

Since the irradiation of alkyl azides in inert gas matrices and low-temperature glasses affords triplet alkyl nitrenes only in trace amounts, the sensitised photolysis was proposed as a method for the detection of these species.^{58,69,70} More recently, a series of alkyl nitrenes have been generated by intramolecular sensitisation,^{71–73} including that in an argon matrix.⁷³ For example, the irradiation of α -azidoacetophenone (**9**) and its derivatives gives benzoyl radical (**10**) (through the α -C–C bond cleavage) and triplet nitrene **11**. In solution at room temperature, the main reaction involves the C–C bond cleavage.⁷³ In an argon matrix, only nitrene **11** was detected at 12 K based on the absorption band in the near-UV region with a maximum at 280 nm.⁷³



As mentioned above, the photochemistry of methyl azide was studied in most detail. Triplet methylnitrene was detected in numerous studies both in the condensed phase by the triplet sensitisation^{58,60} and in the gas phase in the corona discharge.^{74–77} The zero-field splitting parameters ($|D/hc| = 1.595 \text{ cm}^{-1}$), which have been initially determined^{58,60} based on the results of experiments in low-temperature glasses, were doubted.⁷⁵ The commonly accepted value $|D/hc| = 1.720 \text{ cm}^{-1}$ was determined by gas-phase spectroscopy.⁷⁸

The electronic absorption spectrum^{79–82} and the luminescence spectrum^{74–77,78–82} of triplet methylnitrene were recorded many times. The 0–0 transition in its electronic absorption spectrum is observed at 316.9 nm in a nitrogen matrix⁸⁰ and at 314.3 nm in the gas phase,⁸¹ which is close to the maximum observed in the electronic absorption spectrum of the NH radical (336 nm).^{41,42} The singlet–triplet splitting in methylnitrene ($\Delta E_{\text{ST}} = 1.352 \pm 0.011 \text{ eV}$ or $130.7 \pm 1.3 \text{ kJ mol}^{-1}$) was determined from the photoelectron spectrum of the CH_3N^- anion.⁸³ This parameter appeared to

be somewhat smaller than that for the NH radical (1.561 eV, see Fig. 1).

Therefore, it is impossible to decide between two probable mechanisms of photolysis of methyl azide based on the published data. According to one mechanism, singlet methylnitrene is formed as the primary intermediate, but its lifetime, even in cryogenic matrices, is too short (due to the isomerisation to methyleneimine) for the relaxation of this species to the triplet ground state. According to another mechanism, the elimination of molecular nitrogen from methyl azide in the excited singlet state and the formation of imine are concerted and proceed without the involvement of singlet nitrene as an intermediate. To understand whether $^1[\text{CH}_3\text{N}]$ is the real intermediate, *i.e.*, whether it is characterised by a minimum on the potential energy surface (PES), the properties of this species were calculated by quantum chemical methods.^{84–93}

Based on the results of earlier studies,^{84–88} it was concluded that no minima on the PES correspond to singlet methylnitrene. However, these calculations were carried out at a low level of theory with the use of small basis sets. Because of this, quantum chemical calculations were repeated in 1990s.^{89–93}

As in the case of the NH radical, the components of the lowest singlet state with the closed- and open-shell electronic configurations in singlet methylnitrene having the C_{3v} symmetry form the doubly degenerate state 1E . The latter undergoes a Jahn–Teller distortion to give the states $^1A'$ and $^1A''$ (C_s symmetry) with the energy difference smaller than 0.04 kJ mol^{−1}.^{86,93} The isomerisation of $^1[\text{CH}_3\text{N}]$ in the state $^1A'$ was studied⁸⁹ at the TC-CISD+Q level of theory (the configuration interaction with single and double excitations based on two-configuration wavefunctions) with a rather large basis set (TZ2P+f). The maximum with a barrier height of ~ 4 kJ mol^{−1} was found on the PES. Nevertheless, the authors of this study suggested that lowering of the symmetry of the system and a more accurate account of the electronic correlation would lead to the disappearance of the barrier in accordance with the results of earlier calculations.^{85,86}

In 2000, a new attempt was made⁹³ to establish the presence of a barrier between the positions $^1[\text{CH}_3\text{N}]$ and $\text{H}_2\text{C}=\text{NH}$ on the PES. The calculations were carried out by the CASSCF(12/11) and CASPT2 methods with the cc-pVDZ and cc-pVTZ basis sets. As in the earlier study,⁸⁹ the maximum on the PES was found, and its energy appeared to be higher than that of the reagent by ~ 2 kJ mol^{−1} (CASSCF calculations) and 16 kJ mol^{−1} (CASPT2 calculations). An analysis of vibrations calculated by the CASSCF(12/11) method showed that the maximum with the C_s symmetry corresponds to the true transition state. Since the electronic correlation is generally overestimated by the CASPT2 method, it was suggested that the barrier height for the isomerisation of $^1[\text{CH}_3\text{N}]$ to $\text{H}_2\text{C}=\text{NH}$ is in the range of 11 ± 4 kJ mol^{−1}.⁹³ Since the reaction is highly exothermic ($\Delta H = -348$ kJ mol^{−1}, the CASPT2 method), the transition state is early, the C–H bond in this state is elongated by only 0.01 Å, and the C–N bond is shortened by 0.016 Å.⁹³ Therefore, according to the results of calculations at the highest levels of theory, singlet methylnitrene does correspond to a minimum on the PES, but its formation was not detected even by femtosecond spectroscopy.⁵⁹

Recently, the photolysis of trifluoromethyl azide (**12**) has been studied⁹⁴ by IR and UV spectroscopy in an argon matrix at 12 K and by the ESR method in polycrystalline pentane. After irradiation of a solution of azide **12** in polycrystalline pentane at 6–10 K with light with a wavelength of 254 nm, the ESR signal centered at 8620 G was observed. This signal was assigned to triplet trifluoromethylnitrene (**13**). The parameters

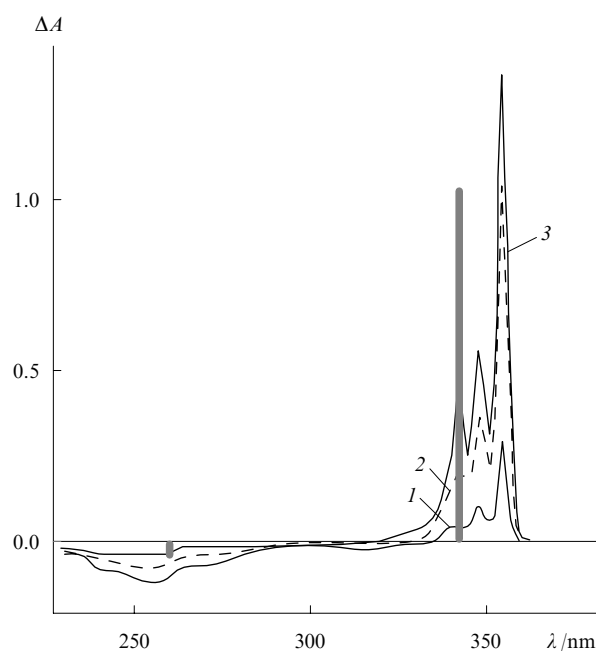
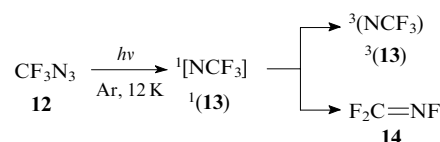


Figure 4. Difference electronic absorption spectra recorded after irradiation of trifluoromethyl azide in an argon matrix at 12 K for 5 (1), 25 (2) and 45 min (3).⁹⁴

The positions and relative intensities of the absorption bands in the spectra of triplet nitrene **13** (positive peak) and azide **12** (negative peak) calculated at the TD-B3LYP/6-31G* level of theory are indicated by vertical bars.

of this spectrum ($|D/hc| = 1.736$ cm^{−1}) are similar to those for nitrenes $^3(\text{NH})$ ($|D/hc| = 1.863$ cm^{−1})⁹⁵ and $^3(\text{CH}_3\text{N})$ ($|D/hc| = 1.720$ cm^{−1}).⁷⁸

Upon irradiation of azide **12** in an argon matrix at 12 K with a wavelength of 254 nm, its absorption ($\lambda_{\text{max}} = 257$ nm) decreased and an intense absorption band with a pronounced vibrational structure ($\lambda_{\text{max}} = 342, 347.5$ and 354 nm) appeared (Fig. 4).⁹⁴ The latter band was assigned to triplet nitrene **13** based on the similarity to the spectrum of $^3(\text{CH}_3\text{N})$ and agreement with the results of calculations. The IR spectrum showed new bands, one of which (1185 cm^{−1}) was assigned to nitrene $^3(\text{13})$; a series of bands (929, 1015, 1379 and 1735 cm^{−1}) were assigned to perfluoromethyleneimine (**14**) (Fig. 5). A comparison of the experimental and calculated IR spectra shows that nitrene $^3(\text{13})$ and imine **14** are produced in comparable amounts. The formation of $^3(\text{NCF}_3)$ upon irradiation of azide **12** is indicative of the formation of singlet nitrene $^1(\text{13})$ as an intermediate, and a minimum on the PES corresponds to this species.



According to the results of CASSCF (8,8)/6-31G* calculations, the isomerisation of $^1[\text{NCF}_3]$ to imine **14** is exothermic ($\Delta H = -193$ kJ mol^{−1}).⁹⁴ However, it is substantially less exothermic than the presumed isomerisation of singlet methylnitrene ($\Delta H = -348$ kJ mol^{−1}),⁹³ which is indicative of the presence of a much higher barrier to the isomerisation of nitrene $^1(\text{13})$ compared to methylnitrene.

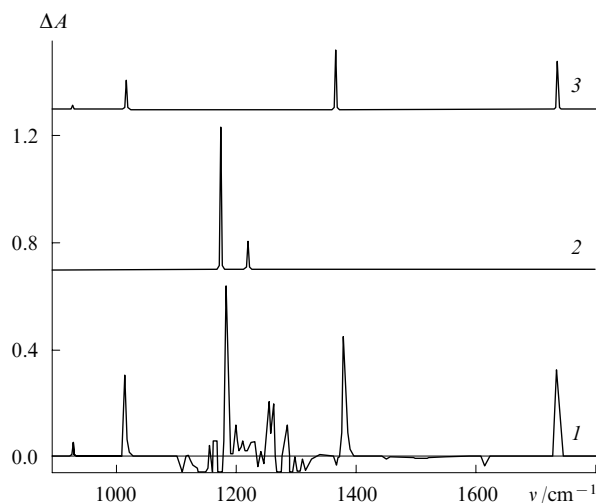
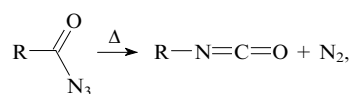


Figure 5. IR difference spectrum recorded after irradiation of azide **12** in an argon matrix at 12 K for 25 min (*I*). The IR spectra of triplet nitrene **13** (*2*) and imine **14** (*3*) calculated at the B3LYP/6-31G* level of theory (the calibration factor is 0.97) (data of the author of the present review).

IV. Photochemical transformations of acyl azides

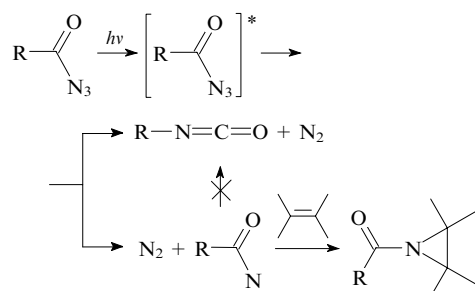
The thermal rearrangement of acyl azides RC(O)N_3 (the Curtius rearrangement) giving isocyanates in quantitative yields at 60–80 °C has been known over the years and has been studied in detail.^{39, 96–99}



R = Alk, Ar.

The photolysis of acyl azides in solution affords two types of products, *viz.*, isocyanates (the photo-Curtius rearrangement) and products derived from capture of the carbonyl nitrenes $[\text{RC(O)N}]$ by solvent molecules.⁹⁸ For example, the thermolysis of pivaloyl azide $[\text{Bu}^t\text{C(O)N}_3]$ in cyclohexane produces the corresponding isocyanate in 99.4% yield.^{100, 101} The photolysis of $\text{Bu}^t\text{C(O)N}_3$ gives isocyanate in a yield of only 40% both in inert solvents and alkenes, which react with acylnitrenes to form the corresponding aziridines.^{100, 101} The photolysis of benzoyl azide and a series of its derivatives in both inert solvents and solvents giving adducts with acylnitrenes affords isocyanates in similar yields (40%–50%).^{102, 103}

Based on these facts, it was concluded that isocyanates and acylnitrenes are independently formed in the photolysis of acyl azides and that acylnitrenes do not undergo isomerisation to isocyanates.^{98, 100–103}

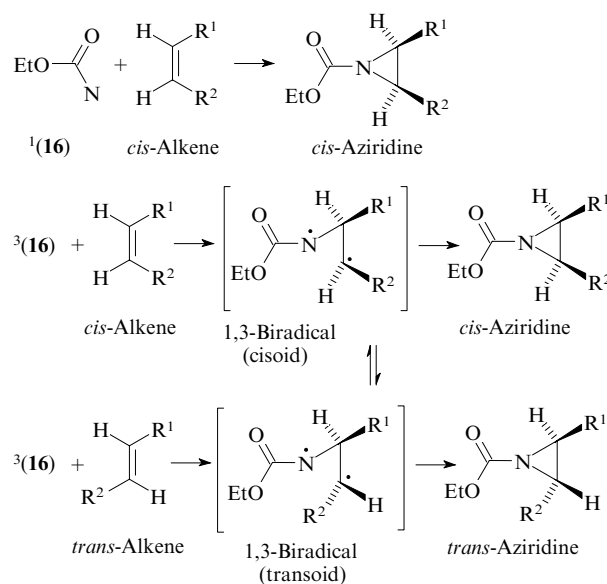


R = Alk, Ar.

The photolysis and thermolysis of alkoxy carbonyl and aryloxy carbonyl azides $[\text{ROC(O)N}_3]$ afford mainly products derived from the corresponding nitrenes $[\text{ROC(O)N}]$ as precursors.⁹⁸ The yields of isocyanates and their transformation products are generally low.

Ethoxycarbonyl azide **15** has received the most attention in the literature. The analysis of the reaction products led to the conclusion that the thermolysis of azide **15** affords ethoxycarbonylnitrene (**16**) in the singlet state, which stereospecifically reacts with alkenes to give the corresponding aziridines (Scheme 1) and undergoes the relaxation to the triplet ground state $^3(\text{16})$.^{98, 104, 105} Triplet nitrene $^3(\text{16})$ also reacts with alkenes, but this reaction is not stereospecific (apparently, the reaction proceeds *via* the intermediate biradical) (see Scheme 1).⁹⁸

Scheme 1

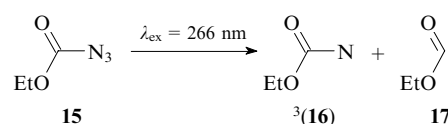


R = Alk, Ar.

In the photolysis of azide **15**, the yield of the products generated in the reaction of nitrenes was ~70%.^{104, 105} The analysis of aziridines showed that singlet $^1(\text{16})$ and triplet $^3(\text{16})$ nitrenes are simultaneously formed in the primary process in a ratio of 2 : 1.^{98, 105} Singlet nitrene $^1(\text{16})$ is also inserted into the C–H bonds of alkanes and O–H bonds of alcohols and is captured by alkynes and benzene to form azepine.⁹⁸

The triplet nature of the ground state of nitrene **16** was confirmed by the observation of the ESR spectrum in low-temperature glasses ($|D/hc| = 1.603 \text{ cm}^{-1}$, $|E/hc| = 0.0215 \text{ cm}^{-1}$).⁶⁰ A similar spectrum ($|D/hc| = 1.65 \text{ cm}^{-1}$, $|E/hc| = 0.024 \text{ cm}^{-1}$) was recorded for triplet (4-acetylphenoxy)carbonylnitrene.^{106, 107}

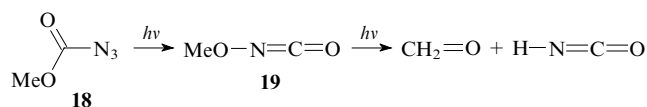
Recently, the photochemistry of azide **15** has been studied¹⁰⁸ by laser flash photolysis ($\lambda_{\text{ex}} = 266 \text{ nm}$) in Freon ($\text{CF}_2\text{ClCFCl}_2$) at room temperature. The formation of at least two intermediates, *viz.*, triplet nitrene **16** ($\lambda_{\text{max}} = 400 \text{ nm}$, the lifetime was $\tau = 1.5 \text{ }\mu\text{s}$) and ethoxycarbonyl radical **17** ($\lambda_{\text{max}} = 333 \text{ nm}$, $\tau = 0.4 \text{ }\mu\text{s}$), was observed. Triplet nitrene **16** reacted with tetramethylethylene ($k = 3 \times 10^8 \text{ litre mol}^{-1} \text{ s}^{-1}$) and triethylsilane ($k = 1 \times 10^6 \text{ litre mol}^{-1} \text{ s}^{-1}$).¹⁰⁸



The photolysis of (4-acetylphenoxy)carbonyl azide was also studied.^{106, 107} Only the reaction products of the corre-

sponding nitrene were found, whereas isocyanate and its transformation products were not detected.¹⁰⁷

The photochemistry of methoxycarbonyl azide (**18**) and its deuterium derivative was studied in inert gas matrices at 4 and 10 K.^{109, 110} The IR spectrum of the reaction products shows characteristic lines assigned to methoxy isocyanate (**19**) and its further transformations products, *viz.*, formaldehyde and isocyanic acid.



Triplet methoxycarbonylnitrene was not detected.¹¹⁰ This is apparently due to the photochemical transformation of the latter into isocyanate.

Thus, the photochemical reactions of azides $\text{ROC}(\text{O})\text{N}_3$ ($\text{R} = \text{Alk}$ or Ar) have not been adequately studied, and it is necessary to study these reactions in more detail by the matrix isolation technique. However, the analysis of the reaction products showed that the photolysis and thermolysis of these azides produce the corresponding nitrenes having the triplet ground state^{60, 106–108} in high yields.^{98, 101, 102, 104–108}

As was mentioned in the beginning of this Section, the photolysis of acyl azides $\text{RC}(\text{O})\text{N}_3$ ($\text{R} = \text{Alk}$ or Ar) affords isocyanates in rather high yields.⁹⁸ The ESR spectra of acylnitrenes in the triplet state were not observed after the photolysis of azides $\text{RC}(\text{O})\text{N}_3$, as opposed to the photolysis of azides $\text{ROC}(\text{O})\text{N}_3$. The characteristic features of the photolysis of carbonyl azides were revealed and the unusual properties of the corresponding nitrenes were explained with the use of the matrix isolation techniques^{38, 40} combined with the results of quantum chemical calculations.^{38–40, 99, 111, 112}

Among acyl azides, benzoyl azide (**20**) has received most attention.^{38–40, 102, 103, 113–116} In early studies,^{102, 103, 113–116} the photolysis of this compound was demonstrated to give the photo-Curtius rearrangement product (phenyl isocyanate **21**, ~40% yield) along with the reaction products of singlet benzoylnitrene (**22**) with alkenes, sulfides, *etc.* The direct and triplet-sensitised photolysis of benzoyl azide in alkenes affords the same products characteristic of the reactions of nitrene **1**(**22**).^{115, 116} No ESR spectra of triplet benzoylnitrene were observed upon the photolysis of benzoyl azide in glassy solvents.^{60, 70}

To reveal the multiplicity of the ground state of aroylnitrenes, the photochemistry of 2-naphthoyl azide (**23**) and a series of acetyl and nitro derivatives of benzoyl azide was studied in detail,^{106, 107, 117, 118} including investigations by the laser flash photolysis technique. As in the case of benzoyl azide, the corresponding isocyanate (~50%) and the reaction products of singlet 2-naphthoylnitrene (**24**) with alkenes and cyclohexane (~45%) were detected upon irradiation of azide **23**. The triplet sensitisation also affords products typical of the reactions of nitrene **1**(**24**).¹⁰⁶ The ESR spectrum of triplet nitrene **24** was not observed. Analogous results were obtained in studies of the photolysis of acetyl and nitro derivatives of benzoyl azide. Although the authors failed to detect singlet aroylnitrenes by spectroscopic methods, their data leave little doubt that the ground state of aroylnitrenes is singlet.^{106, 107, 117, 118} However, this unusual fact remained unexplained.

To understand why aroylnitrenes can have the singlet ground state, we calculated the singlet–triplet splitting (ΔE_{ST}) for nitrenes **22** and **24** by the B3LYP method.¹¹¹ The calculated ΔE_{ST} is small (~21 kJ mol⁻¹); however, according to the calculations, the triplet state is the ground state. Recall

that $\Delta E_{\text{ST}} = 150.6$ kJ mol⁻¹ for the simplest nitrene NH and 130.7 kJ mol⁻¹ for CH₃N. The significant stabilisation of the singlet state compared to the triplet state in aroylnitrenes is attributed to the special bonding between the nitrogen and oxygen atoms, due to which the structure of the singlet nitrenoid species is intermediate between the nitrene and oxazirine structures.¹¹¹

Having understood the nature of the singlet nitrenoid species, we studied the photolysis of benzoyl azide by the matrix isolation technique with the aim of detecting this species by spectroscopic methods.³⁸ After irradiation for 2 min in an argon matrix with light with the wavelength of 254 nm, the electronic absorption spectrum of azide **20** disappeared and a new band with a maximum at 300 nm appeared (Fig. 6, spectrum 1). Simultaneously, absorption bands of azide **20** virtually completely disappeared in the IR spectrum, and new bands appeared, among which the intense absorption at ~2270 cm⁻¹ was assigned to phenyl isocyanate.³⁸ The subsequent irradiation with light with the wavelength of 313 nm led to the disappearance of the absorption band in the UV spectrum (see Fig. 6, spectrum 2). At the same time, the intensity of some bands in the IR spectrum substantially decreased, whereas the intensity of other bands increased (Fig. 7, spectrum 1).

Thus, the photolysis of benzoyl azide affords at least two products. One of these products is characterised by absorption with a maximum at ~300 nm and it is transformed into another product upon irradiation with light with the wavelength of 313 nm. Most of the lines in the experimental IR spectrum recorded 8 min after irradiation are in good agreement with the calculated spectrum of isocyanate (see Fig. 7, spectrum 2), except for one rather intense band at 1193 cm⁻¹, which is absent in the calculated spectrum.³⁸ The results of our investigations^{38, 40} were reproduced in the study,¹¹⁹ and the previously unidentified band was assigned to phenyl cyanate (**25**) produced in a small amount. Therefore, isocyanate **21** and trace amounts of cyanate **25** are the final products.^{40, 119}

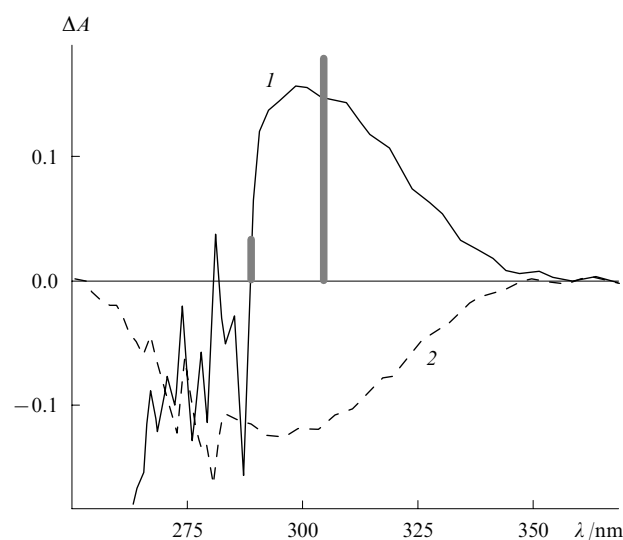


Figure 6. Difference electronic absorption spectra recorded upon irradiation of compound **20** at 254 nm for 2 min in an argon matrix at 12 K (**1**) and of the same sample irradiated at 313 nm for 8 min (**2**).³⁸ The positions and relative intensities of the absorption bands of nitrene **1**(**22**) calculated at the CASSCF/CASPT2 level of theory are indicated by vertical bars.

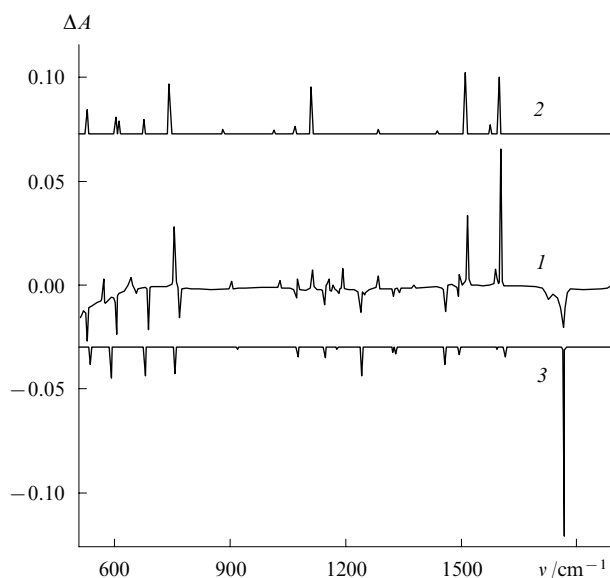
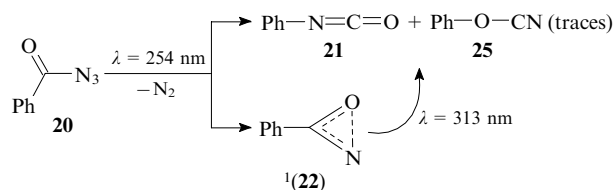


Figure 7. IR difference spectrum of the photolysis products of benzoyl azide upon irradiation with light with $\lambda = 254$ nm for 2 min followed by irradiation for 8 min with light with $\lambda = 313$ nm in an argon matrix at 12 K (*I*).

Positions and relative intensities of the bands in the IR absorption spectrum of isocyanate **21** (**2**) and nitrene $^1(\mathbf{22})$ (**3**) calculated at the B3LYP/6-31G(d) level (the correction factor is 0.97).^{38, 40}



The band in the electronic absorption spectrum at 300 nm (see Fig. 6, spectrum *I*) belongs to the singlet nitrenoid species $^1(\mathbf{22})$, which has the structure intermediate between the nitrene and oxazirine structures. According to CASSCF/CASPT2 calculations, two most intense transitions in the optical absorption spectrum of the species $^1(\mathbf{22})$ have maxima at 306 and 290 nm (see Fig. 6). In addition, the calculated spectrum shows a band corresponding to the transition to the first excited state with a maximum at 513 nm and a very low intensity. This band is associated with the electron excitation from the allyl-type π orbital to the σ^* orbital of a very weak N–O bond.

The calculated IR spectrum of the species $^1(\mathbf{22})$ is also in excellent agreement with the experimental IR spectrum of an intermediate species having an absorption maximum at 300 nm (see Fig. 7, spectrum *I*, negative peaks).

The ratio of the yields of **21** and $^1(\mathbf{22})$ in the primary process is estimated as 64 : 36 from the initial slope of the kinetic curves of the formation of these products upon irradiation ($\lambda = 254$ nm).³⁸

Thus, the use of the matrix isolation techniques combined with quantum chemical calculations provided an insight into the unusual nature of singlet aroylnitrenes.

It should be noted that the calculations of the properties of the simplest acylnitrenes HC(O)N and HOC(O)N were carried out in numerous studies.^{38–40, 99, 111, 112, 120–127} In early studies,^{120–124} quantum chemical calculations were performed at a rather low level of theory, and, as a consequence, the results of these calculations are inconsistent with the modern views of the electronic and geometric structures of acylnitrenes. In 1999,

the potential energy surfaces for the model systems CHNO¹²⁵ and CH₂NO¹²⁶ were studied in detail by the high-level G2, CASSCF, CASPT2 and QCISD(T) methods. Numerous local minima and transition states between these minima were found, and structures of triplet formylnitrene and singlet cyclic oxazirine with a very long N–O bond (1.73 Å) were located. According to calculations by the G2 method, the energy of the singlet species is lower than that of the triplet species by 12 kJ mol^{−1}.¹²⁶ In turn, according to CASPT2/cc-pVTZ and QCISD(T)/cc-pVTZ calculations (with the CASSCF/cc-pVTZ geometry), the energy of the triplet state is lower than that of the singlet state by 16 and 3 kJ mol^{−1}, respectively.¹²⁶ It is known^{127–129} that the CASPT2 method underestimates the energy of systems with open-shell electronic configurations (in the case under consideration, of the triplet state) compared to those with closed-shell electronic configurations (the singlet species) by 13–17 kJ mol^{−1}. Our calculations by the CCSD(T) method with an extrapolation to the infinite basis-set limit³⁸ predicted that the singlet state lies 3 kJ mol^{−1} lower in energy than the triplet state. For acetylnitrene [MeC(O)N], according to the recent calculations by the high-level CBS-QB3 method, the singlet state is lower in energy than the triplet state by ~ 17 kJ mol^{−1} (Ref. 39).

In addition, the energy of the singlet species calculated by the B3LYP method was demonstrated^{38–40} to be substantially overestimated (by ~ 38 kJ mol^{−1}) compared to the energy of the triplet nitrene. Hence, the energy of the singlet nitrenoid species $^1(\mathbf{22})$ should be ~ 17 kJ mol^{−1} lower than that of the triplet species $^3(\mathbf{22})$, which is consistent with its detection in an argon matrix.

The CCSD(T) calculations with an extrapolation to the infinite basis-set limit for the simplest nitrene HOC(O)N⁴⁰ showed that the triplet state for both the *syn* and *anti* rotamers is the ground state, and the singlet nitrenoid species lies higher in energy by 26 and 16 kJ mol^{−1}, respectively. For methoxycarbonylnitrene, the ground state is also the triplet. According to CBS-QB3 calculations, the singlet state is higher in energy by 23.8 kJ mol^{−1} (Ref. 39).

The singlet–triplet splittings for nitrenes ROC(O)N and RC(O)N are different due to the weaker bonding between the nitrogen and oxygen atoms in the $^1A'$ state of the former, which manifests itself in lengthening of the N–O bond. It is unlikely that the oxygen atom of the alkoxy or aryloxy group can hinder the σ bonding between the nitrogen and oxygen atoms in the CON fragment. Presumably, the π bonding between these atoms is weaker due to an extension of the π system in the presence of the OR group.

The commonly accepted view (presented in many handbooks and reviews^{21, 22, 26–33}) is that the addition at double bonds and the insertion into the C–H, O–H and N–H bonds are typical of singlet nitrenes. However, these reaction products were detected only for acylnitrenes and, as will be demonstrated in the next section, for perfluoro-substituted phenylnitrenes. However, these singlet nitrenes do not belong to ‘usual’ nitrenes. The electronic and geometric structures of these nitrenoid species are characteristic of oxazirines, although the N–O bond in these species (1.7–1.8 Å) is substantially longer than the typical single bond (~ 1.5 Å).

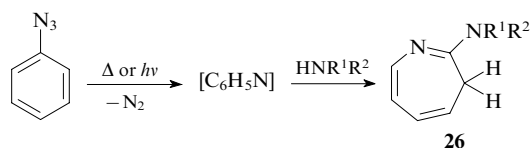
The calculations demonstrated^{39, 40} that the above-considered reactions (the addition at double bonds and the insertion into the bonds) of nitrenoid species with an unusual structure proceed with a low or even zero activation energy. Recently, the temperature dependence of the rate constant for the reaction of nitrene $^1(\mathbf{22})$ with hex-1-ene in Freon has been experimentally studied.³⁹ It appeared that the rate of this reaction is virtually temperature independent, and even a small negative activation energy ($E_a = -0.25$ kJ mol^{−1}) was measured.

V. Photochemical transformations of aryl azides

As mentioned in the Introduction, considerable progress in understanding the photochemical transformations of aryl azides was achieved in the last decade. This is mainly due to the fact that the primary products of their photolysis, *viz.*, singlet arylnitrenes, were detected and their reactivity was studied.^{34–37} The spectroscopic and kinetic data were analysed using high-level quantum chemical calculations (CASSCF/CASPT2).^{34–37} Combined theoretical and experimental studies of the properties of phenylnitrene and its simple derivatives were covered in reviews.^{34, 36} The kinetic and spectroscopic properties of short-lived (~ 100 ps – 100 ns) singlet arylnitrenes were examined in detail.^{35, 37} However, investigations by the matrix isolation techniques have received little attention. In addition, a series of very recent studies^{130–133} dealt with the photolysis of aryl and heteroaryl azides by the matrix isolation techniques, which provided deeper insight into the characteristic features of these processes.

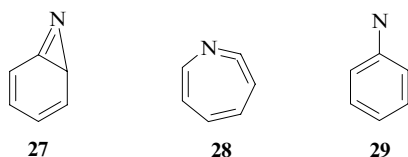
1. Photochemistry of phenyl azide

The photochemistry of the simplest aryl azide, *viz.*, phenyl azide, has attracted most attention. For many years, only polymeric tars have been detected upon the photolysis and thermolysis of this compound.^{21, 27} However, the thermolysis¹³⁴ and photolysis¹³⁵ of phenyl azide in the presence of aniline or diethylamine (DEA) afforded the corresponding azepines **26** in high yield (no lower than 70%). It was postulated that the thermolysis and photolysis of phenyl azide lead to the elimination of molecular nitrogen and the formation of the $[C_6H_5N]$ intermediate.^{134, 135}



$R^1 = R^2 = Et$; $R^1 = H$, $R^2 = Ph$.

It was hypothesised that either benzoazirine (**27**) or cyclic ketene imine (1-azacyclohepta-1,2,4,6-tetraene or 1,2-didehydroazepine, **28**) is a species reacting with amines.^{134, 135} It was not ruled out that singlet phenylnitrene (**29**) can be the precursor of these compounds.



An analysis of the photolysis products of phenyl azide under different conditions is indicative of the formation of all the above-mentioned intermediates. At lower concentrations of solutions of phenyl azide, tarring decreases and the reaction produces azobenzene.^{136, 137} This indicates that singlet intermediates [compounds **27** and/or **28**] serve as a reservoir for triplet nitrenes $^3(29)$, which either undergo dimerisation or react with the starting azide to give azobenzene as the final product. Unfortunately, the formation of azobenzene was not studied by direct methods, for example, by the laser flash photolysis.

In 1962, the ESR spectrum of triplet nitrene $^3(29)$ was recorded in a glassy matrix at 77 K ($|D/hc| = 0.998$ cm⁻¹), and the triplet state of this nitrene was demonstrated to be the ground state.⁶⁹ Shortly thereafter, the low-temperature electronic absorption spectrum of nitrene $^3(29)$ was recorded in a glassy matrix.¹³⁸ More recent studies¹³⁹ showed that this

nitrene readily undergoes isomerisation to ketene imine **28** upon irradiation.

It was hypothesised that the nucleophilic addition of amines to benzoazirine **27** affords substituted 3*H*-azepines **26** as the major products.^{134, 140–142} The transient absorption spectrum observed in experiments on the laser flash photolysis was also assigned to compound **27**.^{140–142}

The situation changed when ketene imine **28** was detected upon the photolysis of phenyl azide in an argon matrix.¹⁴³ The irradiation of phenyl azide in an argon matrix at 8 K with light at $\lambda > 360$ nm (or $\lambda > 216$ nm) led to the formation of a product giving an intense band in the IR spectrum at 1895 cm⁻¹ characteristic of heterocumulene structures ($-N=C=C-$).

It appeared that ketene imine **28** is unstable upon further irradiation ($\lambda > 360$ nm); however, the formation of benzoazirine **27** was not observed.¹⁴³ In a more thorough investigation¹⁴⁴ of the photolysis of phenyl azide and its ¹⁵N-labelled analogue in argon and neon matrices at 12 K, at least 40 new bands were found in the IR spectrum, and 11 bands were assigned to compound **28**.¹⁴⁴ The assignment of the other bands was not made; however, the authors hypothesised that these bands belong to photolysis products of ketene imine. In addition, the ESR spectrum characteristic of nitrene $^3(29)$ ($|D/hc| = 1.027$ cm⁻¹, $E = 0$ cm⁻¹) was observed upon irradiation ($\lambda > 216$ nm) of phenyl azide in an argon matrix at 12 K.¹⁴⁵

Detailed study of the photolysis products of phenyl azide in organic solvents in a wide temperature range (77–293 K) combined with the measurements of their electronic absorption and luminescence spectra led to the conclusion¹³⁹ that triplet nitrene **29** is the major product at 77 K.

Studies by time-resolved IR spectroscopy and the laser flash photolysis convincingly demonstrated^{146, 147} that ketene imine **28** ($\lambda_{max} \approx 350$ nm, $\nu_{max} = 1889$ cm⁻¹) is the intermediate detected in time-resolved experiments at room temperature. This ketene imine reacts with DEA to give intermediate 1*H*-azepine, which is transformed into 3*H*-azepine (**26**) as the final product.^{146, 147}

Thus, the results obtained in solutions and inert gas matrices differ substantially from those obtained in low-temperature glasses. In glasses, triplet nitrene **29** is formed as the major product, whereas ketene imine **28** is the major reaction product in solution at room temperature and in inert gas matrices at ~ 10 K. Two hypotheses were put forward to explain this contradiction.¹³⁹ According to one hypothesis, the secondary photolysis of nitrene $^3(29)$ proceeds in inert gas matrices to give ketene imine **28**. According to another hypothesis, the primary intermediate, *viz.*, vibrationally excited singlet nitrene $^1(29)$, has no time to relax to the ground vibrational state and undergoes rapid isomerisation to ketene imine.

To find an explanation for this contradiction, new investigations of the photolysis of phenyl azide in the inert gas matrices and low-temperature glasses were carried out.^{148, 149} The irradiation in nitrogen or argon matrices at 12 K with light with the wavelength of 334 nm afforded compound **28** in a small amount, whereas another species was generated as the major product. The IR spectrum of the latter was assigned to nitrene $^3(29)$.¹⁴⁸ The irradiation of nitrene $^3(29)$ with long-wavelength light (485 nm or > 450 nm) caused its transformation into ketene imine **28**, which, in turn, could be transformed into nitrene $^3(29)$ under irradiation with light with $\lambda = 334$ nm. The ratio between the concentrations of the nitrene and the ketene imine in the initial steps of irradiation ($\lambda = 334$ nm) was found¹⁴⁸ to be $\sim 4:1$ in all matrices (nitrogen, argon and glassy 2-methylbutane). It was hypothesised¹⁴⁸ that ketene imine **28** is generated from the vibrationally or electronically excited state of singlet nitrene $^1(29)$.

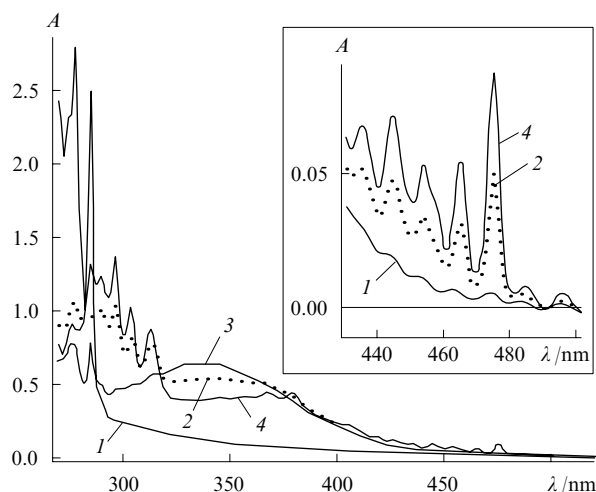


Figure 8. Electronic absorption spectra of the starting phenyl azide in an argon matrix (with an addition of 10% nitrogen for the improvement of the optical properties) at 12 K (1) and of a sample after irradiation: $\lambda = 254$ nm, 10 min (2); visible light ($\lambda > 455$ nm), 15 min (3); UV irradiation ($\lambda = 334$ nm), 130 min (4).

The influence of the nature of the matrix (Ar, CH₄ or 3-methylpentane) on the photolysis of phenyl azide was studied¹⁴⁹ but the irradiation was performed with shorter-wavelength light ($\lambda = 280 \pm 5$ nm). A conclusion was reached that the formation of nitrene **3**(**29**) is more preferable in CH₄ and 3-methylpentane matrices than in an argon matrix. This effect was attributed to the faster relaxation of vibrationally excited singlet nitrene **1**(**29**) in polyatomic solvents compared to that in a one-atom argon matrix.

The spectra, which we recorded upon irradiation of phenyl azide in an argon matrix, are given as examples in Figs 8 and 9. The short-wavelength irradiation ($\lambda = 254$ nm) affords a mixture of nitrene **3**(**29**), which gives a well-resolved spectrum at 290–320 and 430–480 nm, and ketene imine **28** with a characteristic broad band at $\lambda_{\text{max}} = 340$ nm (Fig. 8, spectrum 2). The further irradiation with visible light ($\lambda > 455$ nm, 15 min) leads to the virtually complete disappearance of the absorption of nitrene **3**(**29**) and an increase in the intensity of the absorption of ketene imine **28** (Fig. 8, spectrum 3). The subsequent irradiation with light with $\lambda = 334$ nm leads to an increase in the intensity of the absorption of nitrene **3**(**29**) (Fig. 8, spectrum 4).

As can be seen from Fig. 9, all lines in the experimental IR spectra of the photolysis products can be assigned to nitrene **3**(**29**) and ketene imine **28**, and there is a good agreement between the calculated and experimental IR spectra of both intermediates. It can also be seen from this Figure that nitrene **3**(**29**) is transformed into ketene imine upon irradiation with visible light (spectrum 1), whereas the irradiation with UV light causes the transformation of ketene imine **28** into nitrene **3**(**29**).

Assuming that the photolysis affords only products **27** and **3**(**29**), which is consistent with the observed IR spectrum, the individual electronic absorption spectra of these compounds can be obtained (Fig. 10). The calculated electronic absorption spectra of these intermediates are in good agreement with experimental data. It should be noted that transitions of an electron of the lone pair to the π -type singly occupied molecular orbital (SOMO) ($\lambda_{\text{calc}} = 289$ nm) and the p_x -type SOMO lying in the plane of the ring ($\lambda_{\text{calc}} = 287$ nm) make a considerable contribution to the absorption band of triplet phenyl-nitrene at 270–320 nm. The spectra of the simplest nitrenes **3**(NH) ($\lambda_{\text{max}} = 336$ nm)^{41,42} and **3**(CH₃N) (316.9 nm) are also associated with analogous transitions.⁸⁰

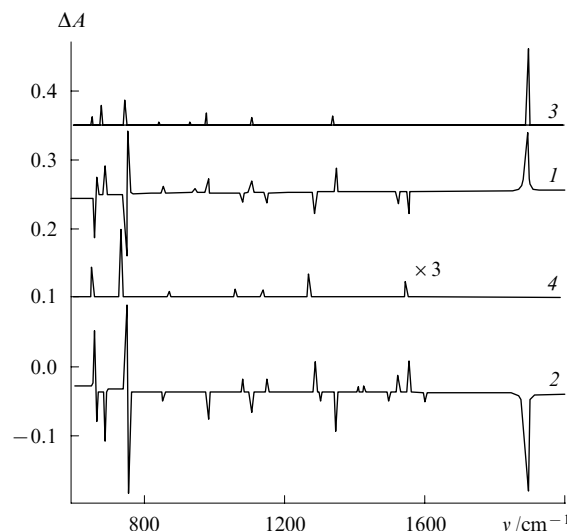


Figure 9. IR difference spectra of preirradiated ($\lambda = 254$ nm, 10 min) matrix-isolated phenyl azide (an argon matrix with 10% nitrogen, 12 K) after irradiation with visible light ($\lambda > 455$ nm) for 15 min (1) and after UV irradiation ($\lambda = 334$ nm) for 130 min (2).

The IR spectra of ketene imine **28** (3) and triplet nitrene **29** (4) calculated at the B3LYP/6-31G* level of theory (the correction factor is 0.9614).

As opposed to the results of the study,¹⁴⁸ according to which irradiation of phenyl azide at 334 nm affords compounds **3**(**29**) and **28** as the primary products in a ratio of 4 : 1, our investigation showed that the irradiation with shorter-wavelength light ($\lambda = 254$ nm) gives primary products in a yield of $\sim 0.5 : 1$, i.e., the formation of ketene imine **28** is more preferable. This fact indicates that the latter is actually formed in the course of isomerisation of vibrationally excited singlet nitrene **29** and is consistent with the results of the recent studies

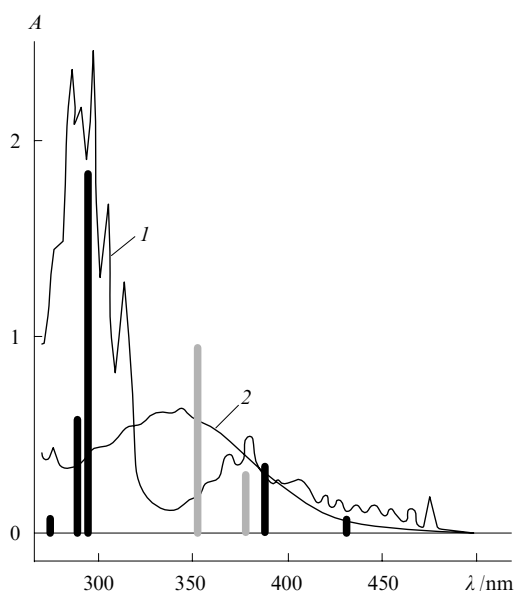


Figure 10. Electronic absorption spectra of triplet nitrene **29** (1) and ketene imine **28** (2). The calculated positions and relative intensities of the absorption bands of nitrene **3**(**29**) [solid bars, CASSCF(12,12)/CASPT2//CASSCF(8,8)/6-31G* calculations]¹⁵⁰ and ketene imine **28** (dotted bars, B3LYP/6-31+G* calculations) are indicated by vertical bars.

on the photolysis of phenyl azide and a series of its derivatives in solution at room temperature by femtosecond electronic absorption spectroscopy^{151–154} and femtosecond IR spectroscopy.¹⁵⁵ It was found that the N–N bond dissociation in aryl azides under study proceeds on the femtosecond time scale (*ca.* 100–500 fs).^{151–154} For example, the time of formation of singlet biphenyl-4-yl nitrene in the photodissociation of biphenyl-4-yl azide ($\lambda_{\text{ex}} = 266$ nm) in acetonitrile is ~ 100 fs, and the time of formation of the corresponding nitrene from biphenyl-2-yl azide is 280 ± 150 fs.^{152, 153} The resulting singlet aryl nitrenes [including nitrene **1(29)**] are vibrationally excited, and the shorter the wavelength of the photoexcitation the larger the excess of vibrational energy. The vibrational relaxation in acetonitrile proceeds within 10 ps (for singlet biphenyl-4-yl nitrene^{152, 153} and 3,5-dichlorobiphenyl-2-yl nitrene in cyclohexane,¹⁵¹ the relaxation time is 11 ps).

The theoretical analysis¹⁵³ of the PES section along the reaction coordinate corresponding to the elimination of molecular nitrogen for the ground (S_0) and two excited singlet states (S_1 and S_2) of aryl azides suggests that the first excited state (S_1) is apparently dissociative. The second excited state (S_2) is the bound state, and its geometry is similar to that of the state S_0 . Upon absorption of UV irradiation, the excitation to the state S_2 takes place. The time of formation of vibrationally excited singlet aryl nitrene (< 500 fs) corresponds to the time of internal conversion into the dissociative state S_1 . It was also found¹⁵³ that the surfaces for S_1 and S_0 intersect each other. Consequently, the S_1 state of aryl nitrenes can be deactivated to the ground state. This explains why, in spite of a high rate of formation of aryl nitrenes, the quantum yield of photodissociation can be substantially smaller than unity; for example, the quantum yield for phenyl nitrene is close to 0.5 and is temperature independent (300 and 77 K).³¹

Singlet aryl nitrene [for example, **1(29)**], which is formed upon dissociation of aryl azide, has a considerable excess of vibrational energy and can easily overcome the potential barrier. Actually, studies by femtosecond time-resolved IR spectroscopy showed that a part of ketene imine **28** is very rapidly formed in acetonitrile at room temperature (also in the vibrationally excited state).¹⁵⁵ The formation of ketene imine and its vibrational relaxation proceed on the time scale of 10–50 ps. Unfortunately, attempts to separate these two processes and determine the time of formation of ketene imine failed.¹⁵⁵

Although the hypothesis about the possible involvement of vibrationally excited singlet phenyl nitrene **1(29)**[#] in the isomerisation was made^{139, 148} many years ago, it was confirmed only very recently.¹⁵⁵ However, the isomerisation of nitrene **1(29)**[#] to ketene imine **28** competes with its vibrational relaxation to the ground vibrational state **1(29)**, in which this species also undergoes the thermally activated isomerisation to form ketene imine **28**.^{34–37}

In 1997, the spectrum of singlet nitrene **1(29)** ($\lambda_{\text{max}} = 350$ nm, Fig. 11) with a lifetime of ~ 1 ns at room temperature was recorded for the first time.^{156, 157} The kinetics of transformations of this species was studied in detail in a wide temperature range (170–270 K), which allowed the simultaneous determination of the rate constant of its intersystem crossing to the triplet ground state and the activation parameters of the isomerisation (A and E_a).¹⁵⁰ The observed rate constant (k_{obs}) decreases as the temperature is lowered to ~ 170 K, and then reaches the constant value of $\sim 3.2 \times 10^6 \text{ s}^{-1}$, which was assigned¹⁵⁰ to the rate constant of the intersystem crossing (k_{isc}) of singlet nitrene **29** to the triplet ground state. The temperature dependence of the rate constant of isomerisation $k_R = k_{\text{obs}} - k_{\text{isc}}$ obeys the Arrhenius law (Fig. 12). The activation energies ($E_a = 23.4 \pm 1.3 \text{ kJ mol}^{-1}$) and the preexponential factors ($A = 10^{13.1 \pm 0.3} \text{ s}^{-1}$) were determined.¹⁵⁰

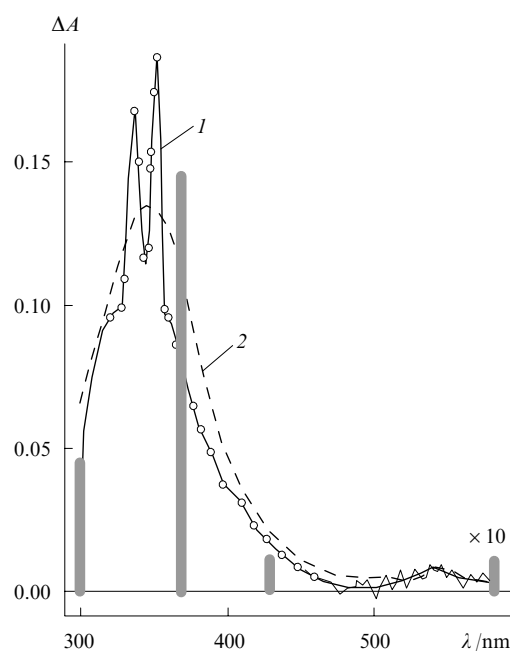


Figure 11. Electronic absorption spectra recorded after the laser excitation (266 nm, 35 ps) of phenyl azide in pentane: after 2 ns at 233 K (1) and after 10 ns at 295 K (2).^{150, 156}

The calculated positions and relative intensities of transitions in nitrene **1(29)** [at the CASSCF(12,12)/CASPT2 level of theory with the geometry calculated at the CASSCF(8,8)/6-31G* level]¹⁵⁰ are indicated by vertical bars.

The rate constants of the intersystem crossing estimated from the data obtained in solution [$(3.2 \pm 0.3) \times 10^6 \text{ s}^{-1}$]¹⁵⁰ and in glassy methylcyclohexane at 77 K [$(3.8 \pm 0.3) \times 10^6 \text{ s}^{-1}$]¹⁵⁸ have similar values, thus confirming the hypothesis that the constant k_{isc} is temperature independent.¹⁵⁰

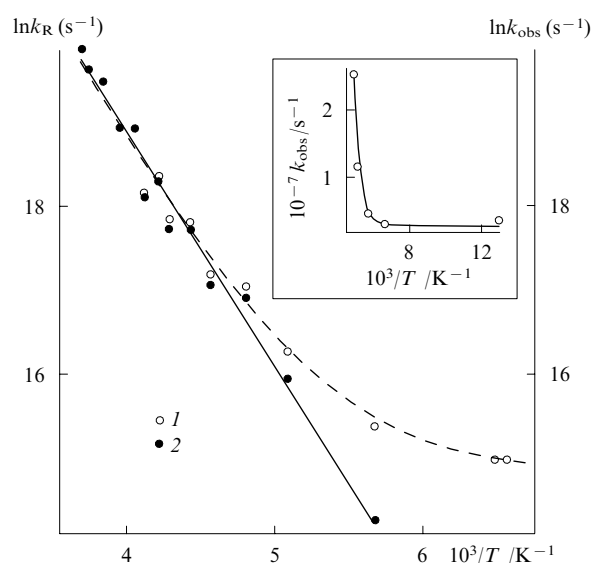


Figure 12. Temperature dependences of the observed rate constant for the decay of singlet nitrene **1(29)** (k_{obs}) (1) and the rate constant for the isomerisation k_R ($k_R = k_{\text{obs}} - k_{\text{isc}}$) (2) in the Arrhenius coordinates.¹⁵⁰ The inset shows the temperature dependence of the rate constant k_{obs} .

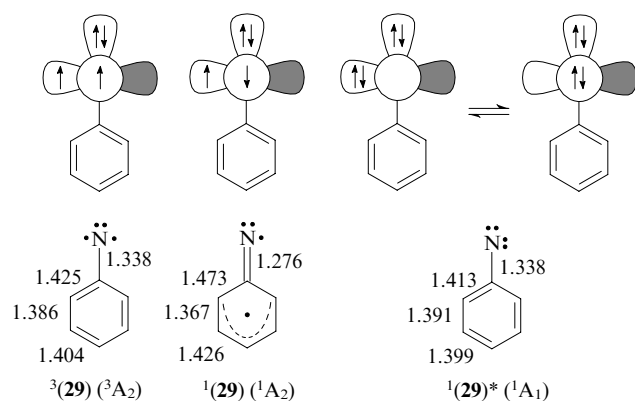
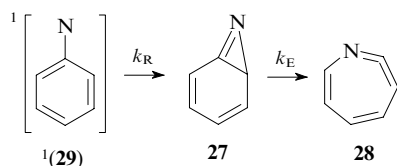


Figure 13. Occupation of the orbitals in nitrene **29** by non-bonding electrons and the bond lengths (in Å) for the lowest states calculated at the CASSCF/6-31G* level.¹²⁹

It has long been commonly accepted that singlet phenylnitrene, like other singlet arylnitrenes, has a closed-shell electronic configuration (1A_1).^{21, 26–30} However, relatively recently it has been shown that the lowest singlet state of nitrene **29** (1A_2) has an open-shell electronic configuration, *i.e.*, two electrons with opposite spins occupy two different orbitals, *viz.*, the π -type orbital and the p_x orbital located on the nitrogen atom and lying in the ring plane.^{159–161} The excited singlet state 1A_1 lies higher in energy by ~ 60 kJ mol⁻¹ (Ref. 162). The orbital populations and the bond lengths for three lowest spin states of nitrene **29** are shown in Fig. 13.

The singlet–triplet splittings ($\Delta E_{ST} = 73–76$ kJ mol⁻¹) calculated at high levels of theory^{129, 160, 161, 163} are in good agreement with the experimental values estimated by photoelectron spectroscopy (75 ± 8 kJ mol⁻¹)¹⁶² and photoionisation spectroscopy (77 ± 3 kJ mol⁻¹).¹⁶⁴

In 1997, quantum chemical calculations at the CASSCF/CASPT2 level of theory showed that the isomerisation of nitrene **1(29)** to ketene imine **28** proceeds in two steps.¹²⁹ In the first rate-limiting step, the nitrene undergoes isomerisation to azirine **27**. The second step involves the three-membered ring opening to form compound **28**.



The barrier for the cyclisation reaction evaluated at the CASPT2 level is 39 kJ mol⁻¹ (Ref. 129). However, this method generally overestimates the stabilisation of systems having an open-shell electronic configuration compared to species containing paired electrons¹²⁷ [for an analogous system, the error was 14 kJ mol⁻¹ (Ref. 129)]. Taking into account this error, the barrier for the cyclisation of nitrene **1(29)** is 25 kJ mol⁻¹, which is in excellent agreement with the measured activation energy of isomerisation (23.4 ± 1.4 kJ mol⁻¹).¹⁵⁰

According to calculations,¹²⁹ the barrier for the second step (**27** \rightarrow **28**) is as low as 13 kJ mol⁻¹ (Fig. 14). This result is consistent with the fact that azirine **27** was not detected in time-resolved experiments.^{139, 146, 147, 150, 156, 157} Although the lifetime of this intermediate is very short, the formation of the reaction product of this species with ethanethiol, *viz.*, the

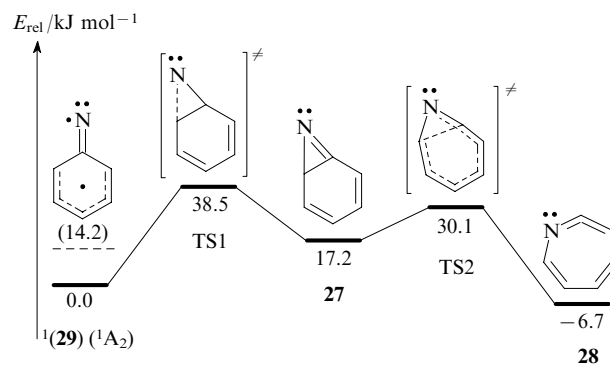
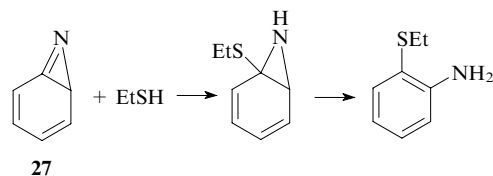


Figure 14. Energetics of the isomerisation of singlet phenylnitrene **1(29)** calculated at the CASPT2(8,8)/6-311G(2d,p)//CASSCF/6-31G(d) level.¹²⁹ TS is the transition state.

corresponding *ortho*-substituted aniline (in 39% yield), in the photolysis of phenyl azide in ethanethiol was documented.¹⁶⁵



The mechanism of photolysis of phenyl azide taking into account the results of the very recent studies^{150, 155–158} is presented in Scheme 2.

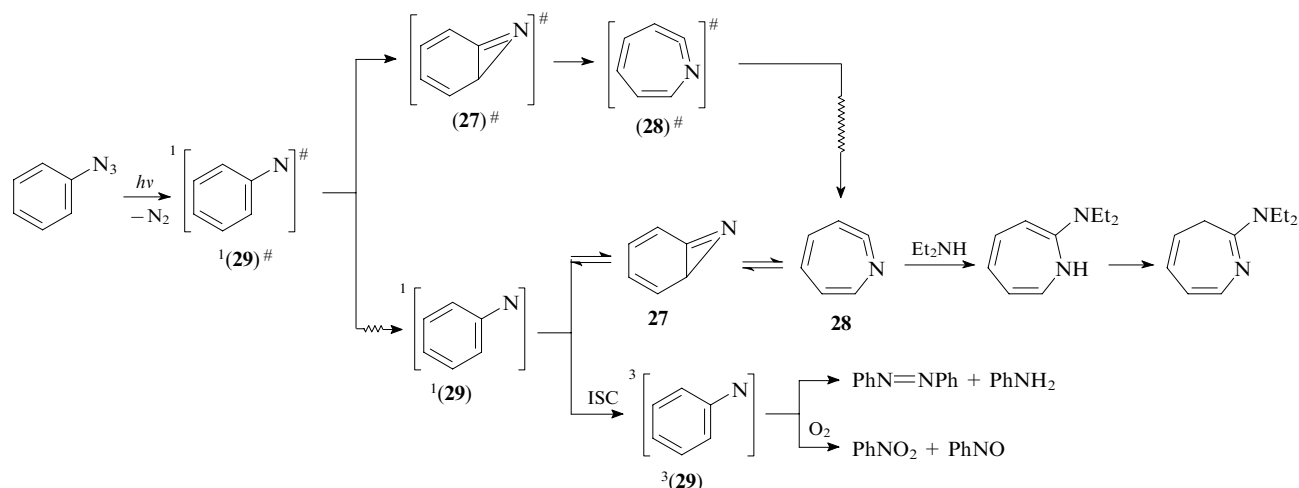
The above-considered data can be briefly summarised as follows. The photodissociation of phenyl azide proceeds on the femtosecond time scale (< 500 fs) to form singlet phenylnitrene in the vibrationally excited state **1(29)[#]**. The vibrational relaxation of the latter competes with the isomerisation to azepine, which is also formed in the vibrationally excited state. Singlet phenylnitrene in the ground vibrational state **1(29)** can undergo relaxation to the triplet ground state $3(29)$ (the intersystem crossing, ISC) or, by overcoming the barrier, transformed into benzoazirine **27**, which, in turn, is transformed into azepine **28**. At room temperature, the isomerisation is the major process. The contribution of the intersystem crossing increases as the temperature is lowered; it becomes the major process at temperatures below 170 K.

2. Photochemistry of phenyl azide derivatives

The photochemistry of simple derivatives of phenyl azide has been studied in sufficient detail, including investigations by the matrix isolation technique.^{144, 166–170} The spectroscopy and kinetics of the reactions of substituted singlet phenylnitrenes in solution in a wide temperature range (150–300 K) have been investigated recently.^{151, 158, 171–178} The influence of substituents was considered in detail in the reviews.^{35, 37} It should be noted that the influence of substituents on the rate constant for the cyclisation of phenylnitrene to azirine is not very significant. For example, the presence of two methyl substituents in the *ortho* position with respect to the nitrogen atom leads to an increase in the reaction barrier due to the steric effect and an increase in the lifetime of nitrene at room temperature by approximately an order of magnitude.¹⁷³ Such substituents as the cyano and phenyl groups in the *para* position also increase the lifetime by approximately an order of magnitude.^{176, 178}

The introduction of two fluorine atoms at the *ortho* position with respect to the nitrogen atom has the maximum effect on the rate constant for the cyclisation.^{175, 177} For

Scheme 2



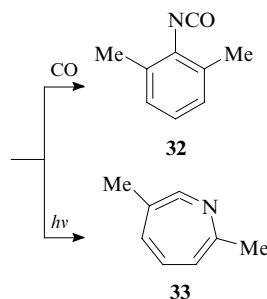
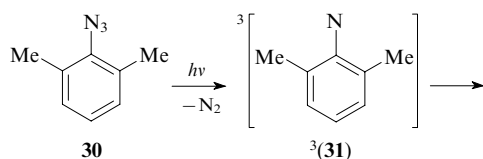
ISC is the intersystem crossing; \rightsquigarrow is the vibrational relaxation.

example, the lifetime of singlet 2,6-difluorophenylnitrene at room temperature increases by two orders of magnitude. This is due to the high electronegativity of the fluorine atom.^{37, 177} Due to rather long lifetimes, polyfluorinated singlet arylnitrenes can be involved in bimolecular reactions, including the insertion into C–H bonds and the addition at double bonds.^{179–185} Hence, polyfluorinated aryl azides are the most promising reagents for photoaffinity labelling of biopolymers^{186–192} and covalent modification of the surface of polymer coatings.^{23–25}

The introduction of substituents can lead also to changes in the relative reaction rates of the two-step isomerisation of singlet nitrene to the corresponding ketene imine. For example, the second step (the ring opening) is the rate-limiting step for biphenyl-2-yl nitrene and 2,4,6-tri-(*tert*-butyl)phenyl nitrene, and it is possible to detect the derivative of azirine **27**.^{158, 178} All these effects have been analysed in detail earlier³⁷ and are beyond the scope of the present review.

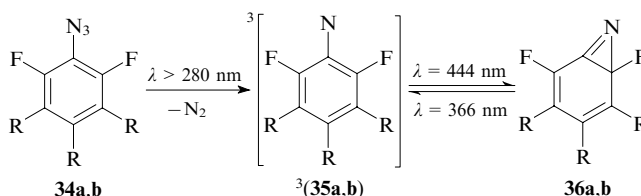
In the study,¹⁴⁴ the photolysis of phenyl azide was investigated (along with the photolysis of ten its *para* and *meta* derivatives containing F, Cl, CN, Me or MeO substituents) in nitrogen and argon matrices. In all cases, the IR spectra of the photolysis products in the matrices at 12 K show the most intense band (or a series of bands) at 1890–1906 cm^{−1}. Consequently, it was concluded that the corresponding ketene imine derivatives **28** are the major products in all reactions.

Unlike the photolysis of *para*- and *meta*-methyl derivatives of phenyl azide,¹⁴⁴ the photolysis of 2,6-dimethylphenyl azide (**30**) in a nitrogen matrix at 12 K affords the corresponding triplet nitrene ³(**31**) as the major product. In the presence of CO, the latter gives 2,6-dimethylphenyl isocyanate (**32**).¹⁶⁷ Insignificant amounts of the corresponding ketene imine **33** were found upon UV irradiation of triplet nitrene.



Analogous results were obtained¹⁶⁶ in the study of the photolysis of perfluorophenyl azide (**34a**) in a nitrogen matrix. The major primary product, *viz.*, perfluorophenyl nitrene (**35a**) in the triplet state, was involved in the photochemical reaction with CO to give the corresponding isocyanate. Azirine and ketene imine were not found.¹⁶⁶

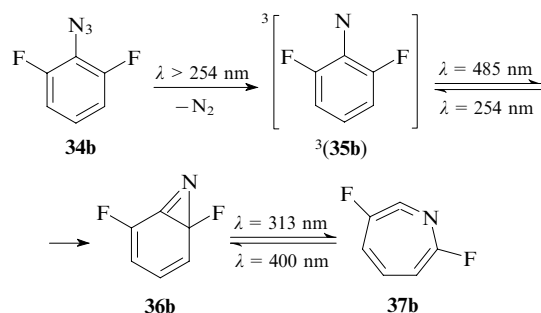
More recently, it was confirmed¹⁶⁸ that the photolysis of perfluorophenyl azide (**34a**) and 2,6-difluorophenyl azide (**34b**) in an argon matrix affords the corresponding triplet nitrenes **35a,b** as the major products. However, as opposed to the previous study,¹⁶⁶ the irradiation of nitrenes ³(**35a,b**) with visible light ($\lambda = 444$ nm) was found to give the corresponding azirines **36a,b**. This process is reversible, and the irradiation of azirines **36** with light with $\lambda = 366$ nm leads to their transformation into the corresponding triplet nitrenes **35**.¹⁶⁸



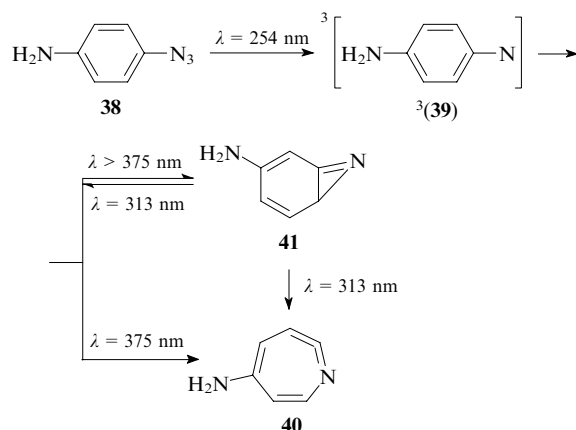
R = F (a), H (b).

In the very recent past, the photolysis of azide **34b** in an argon matrix at 12 K has been more thoroughly studied by IR and electronic absorption spectroscopy combined with quantum chemical calculations.¹⁶⁹ As opposed to the earlier studies,^{166, 168} the interconversions of benzazirine **36b** and ketene imine **37b** were also observed. The complete scheme of the

phototransformations of azide **34b** can be represented as follows.



The formation not only of the corresponding triplet nitrene and ketene imine but also of azirine was observed¹⁷⁰ in the photolysis of *p*-azidoaniline (**38**) in an argon matrix at 12 K. The irradiation of triplet nitrene **39** was found to give not only ketene imine **40** but also azirine **41**, which, in turn, disappears upon irradiation at 313 nm.



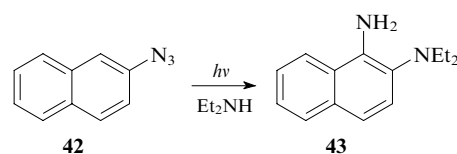
Therefore, the photolysis of phenyl azide and a series of its *meta* and *para* derivatives in nitrogen and argon matrices at ~ 10 K affords the corresponding ketene imines in high yield. The latter are, most likely, generated from vibrationally excited singlet nitrene, as well as in the course of the secondary photolysis of the corresponding triplet nitrenes.

The photolysis of phenyl azide derivatives containing two substituents in the *ortho* position (azides **30** and **34a,b**) or a strong electron-donating substituent in the *para* position (azide **38**) gives the corresponding triplet nitrene, $^3(31)$, $^3(35)$ or $^3(39)$, as the only primary photolysis product.^{166–170, 193} This result correlates with a substantial increase in the barrier for the cyclisation of the corresponding singlet nitrenes [$^1(31)$, $^1(35)$ or $^1(39)$] to azirines.^{37, 194} In some cases, azirines (**36a,b** and **41**) were detected. According to calculations,^{37, 177, 194} the barriers for the isomerisation of the latter azirines to the corresponding ketene imines (**37a,b** and **40**) are rather high.

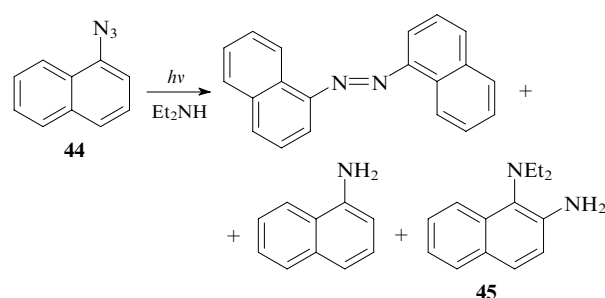
3. Photochemistry of polycyclic aryl azides

As in the case of phenyl azide and its derivatives, the formation of polycyclic aryl nitrenes in the triplet ground state giving characteristic ESR spectra was observed upon irradiation of polycyclic aryl azides in glassy matrices at 77 K.^{60, 195–198} The photochemistry of 1- and 2-naphthyl azides was studied in most detail, including investigations by the matrix isolation technique.^{131, 198, 199}

The photolysis of 2-naphthyl azide (**42**) in solution in the presence of diethylamine affords the corresponding diamino derivative **43** in high yield.²⁰⁰

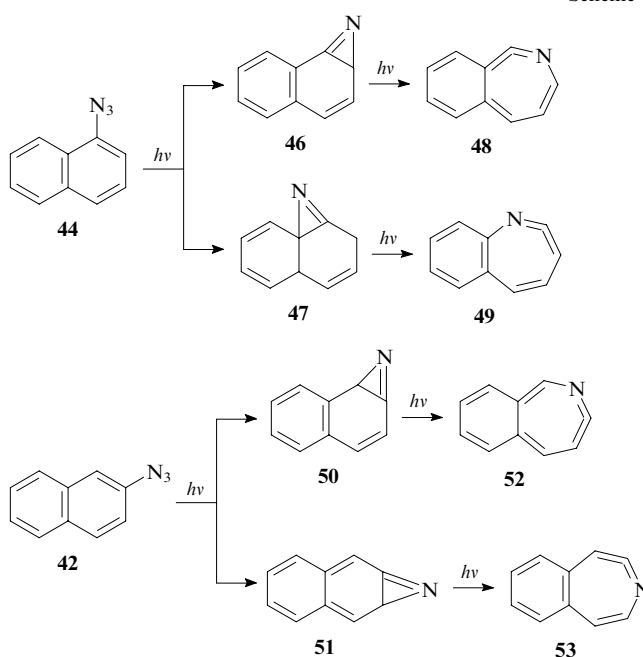


However, the photolysis of 1-naphthyl azide (**44**) in the presence of DEA gives mainly azanaphthalene²⁰⁰ along with small amounts of 1-aminonaphthalene²⁰⁰ and diamino derivative **45**.²⁰¹ The yield of compound **45** increases as the temperature decreases.²⁰¹

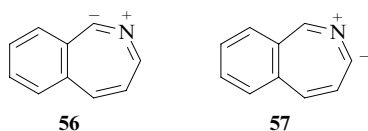


The formation of products **43** and **45** suggests that the corresponding tricyclic azirines are involved as intermediates of the photolysis of azides **42** and **44**. The spectrum of the products recorded in the photolysis ($\lambda > 330$ nm) of these azides in nitrogen and argon matrices at 12 K showed characteristic bands, which can be assigned to the corresponding azirines and ketene imines.¹⁹⁹ In the case of azide **44**, the band that appeared at 1730 cm^{-1} was assigned to tricyclic azirines **46** and(or) **47**. Upon prolonged photolysis, the spectrum showed bands at 1926 and 1912 cm^{-1} assigned to the corresponding dihydroazepines **48** and(or) **49**. Analogously, bands with maxima at 1708 , 1723 and 1736 cm^{-1} were initially observed in the IR spectrum recorded in the photolysis of azide **42**; these bands can be assigned to azirines **50** and(or) **51**. The secondary photolysis was accompanied by the appearance of bands at 1911 and 1923 cm^{-1} assigned to dihydroazepines **52** and(or) **53** (Scheme 3). Unfortunately, it was impossible to make a more precise assignment at that time.

Scheme 3



As mentioned above, the development of more precise methods for calculations of IR and electronic absorption spectra of possible products allowed a more reliable and comprehensive analysis of the results obtained by the matrix isolation technique. Recently, the photolysis of azides **42** and **44** in an argon matrix has been reinvestigated,¹³² and the new assignment of the bands in experimental electronic absorption and IR spectra was carried out based on detailed theoretical calculations. In the experimental IR and electronic absorption spectra, bands of triplet nitrenes **54** and **55**, azirines **46** and **50**, ketene imines **49** and **53** (Figs 15 and 16) and cyclic ylides **56** and **57** were identified.



Detailed calculations of PES, on which interconversions of the species under consideration proceed (see Figs 15 and 16), were performed in the study.¹³² According to the calculations, singlet nitrene ¹(**55**) undergoes cyclisation to form exclusively azirine **46**, whereas nitrene ¹(**54**) gives azirine **50**. Azirines **47** and **51**, being highly energetic, are not formed.

The photolysis of 1- and 2-naphthyl azides with light with $\lambda = 313$ nm initially affords singlet nitrenes ¹(**55**) and ¹(**54**), whose relaxation to the triplet ground state competes with the cyclisation to azirines **46** and **50**. The latter are generated also in the secondary photolysis of triplet nitrenes ³(**55**) and ³(**54**).¹³⁴ The prolonged irradiation of the triplet nitrenes can lead to their transformations into cyclic ketene imines **49** and **53**, respectively, which have been observed earlier.¹⁹⁹

The photolysis of azirines **46** and **50** affords new previously unknown isomers **56** and **57** instead of the expected ketene imines **48** and **52**. These compounds can formally be assigned to cyclic nitrile ylides the existence of which has been predicted.²⁰²

Recently, the photolysis of naphthyl azides has been studied in solution at room temperature by IR spectroscopy with a time resolution of ~ 200 ns and by the laser flash photolysis technique in glassy 3-methylpentane at 77 K.²⁰³ Upon the laser excitation of azide **44** at 77 K, singlet nitrene ¹(**55**) was found, and this compound relaxed to the triplet ground state ³(**55**) with a rate constant of $k_{isc} = (1.1 \pm 0.1) \times 10^7$ s⁻¹. In turn, azirine **46** having a lifetime of 3.2 ± 0.6 μ s in acetonitrile at room temperature was detected by time-resolved IR spectroscopy.²⁰³ The rate constant of the reaction of **46** with DEA was estimated at $\sim 1.4 \times 10^5$ litre mol⁻¹ s⁻¹. The low rate constant is consistent with low yields of diamine **45** in steady-state experiments.

As opposed to the photolysis of azide **44**, no intermediates having absorption at > 320 nm were observed upon the laser excitation of azide **42** in glasses at 77 K. Under steady-state conditions, the formation of triplet nitrene **54** was also not observed. These data are in contradiction with the fact that triplet nitrene **54** was obtained as the major primary photolysis product of azide **42** in an argon matrix.¹³² Two explanations were given for this contradiction.²⁰³ First, nitrene ³(**54**) could be the product of the secondary photolysis of azirine **50** in an argon matrix. According to an alternative hypothesis, $k_R \gg k_{isc}$ for singlet nitrene ¹(**54**) at 77 K, but $k_{isc} \gg k_R$ at 12 K (k_R is the rate constant for the cyclisation of singlet nitrene, and k_{isc} is the rate constant for the intersystem crossing to the triplet ground state). For the fulfillment of these conditions, the barrier for the cyclisation of nitrene ¹(**54**) (E_a)

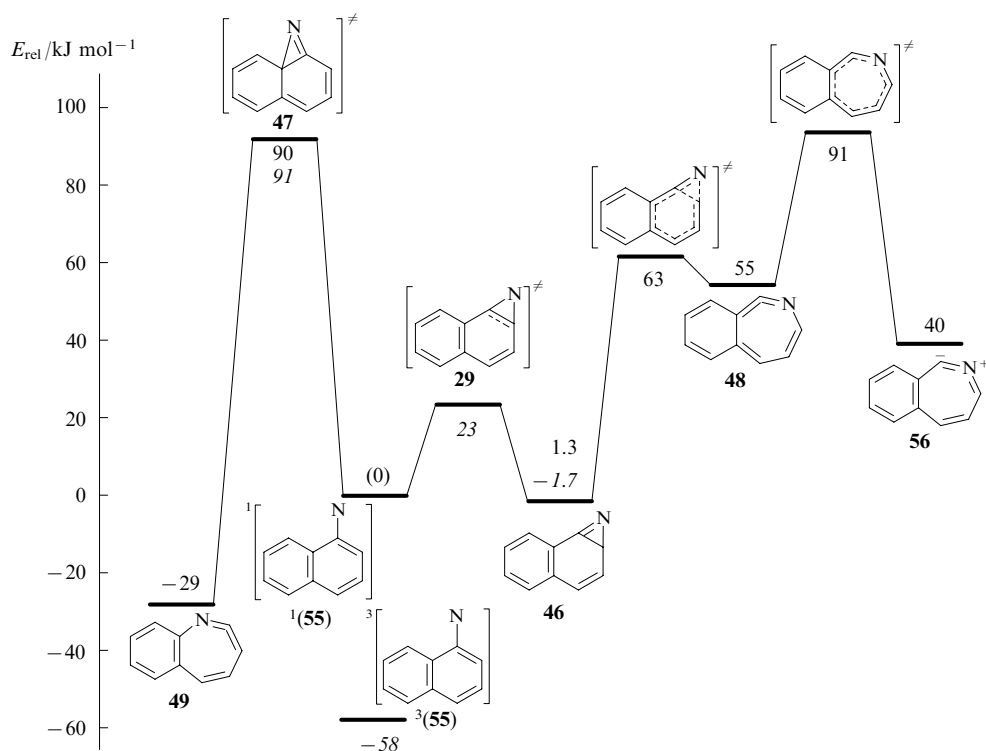


Figure 15. Relative energies of isomers of 1-naphthyl nitrene and the transition states of their transformations.¹³²

The CASPT2//CASSCF(12,12)/6-31G* calculations relative to the energy of ¹(**55**) (italic) and the B3LYP/6-311 + G(2d,p)//B3LYP/6-31G* calculations relative to the energy of ³(**55**) and taking into account the singlet–triplet splitting for nitrene **55** calculated at the CASPT2 level (normal font). In all cases, the zero-point energy was taken into account. Structure **47** corresponds to the transition state in the DFT calculations and a shallow minimum in the CASSCF calculations.

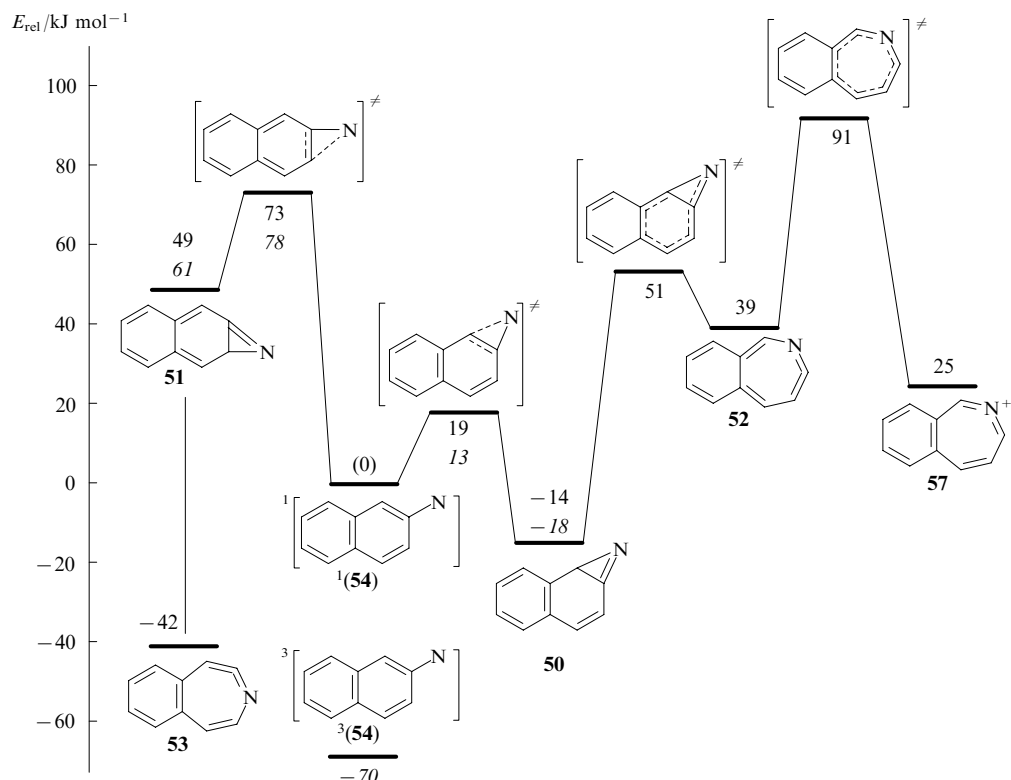


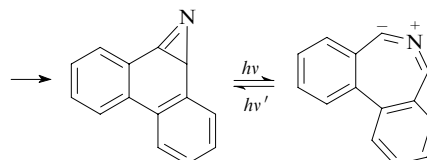
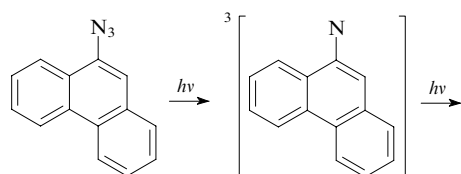
Figure 16. Relative energies of isomers of 2-naphthyl nitrene and the transition states of their transformations.¹³²

The CASPT2//CASSCF(12,12)/6-31G* calculations relative to the energy of ¹(54) (italic) and the B3LYP/6-311 + G(2d,p)//B3LYP/6-31G* calculations relative to the energy of ³(54) and taking into account the singlet – triplet splitting for nitrene 54 calculated at the CASPT2 level (normal font). In all cases, the zero-point energy was taken into account.

should be in the range of $1.26 < E_a < 8.80 \text{ kJ mol}^{-1}$, which is consistent with the calculated data (see Fig. 16).¹³²

Azirine **50** was also detected as the photolysis product of 2-naphthyl azide in acetonitrile at room temperature by time-resolved IR spectroscopy. The lifetime of this compound appeared to be substantially longer ($150 \pm 10 \text{ }\mu\text{s}$) than that of azirine **46**, which is consistent with the theoretical calculations (see Figs 15 and 16).²⁰³ The rate constant of the reaction of azirine **50** with DEA ($\sim 2.5 \times 10^5 \text{ litre mol}^{-1} \text{ s}^{-1}$) is almost twice as high as that for azirine **46** ($\sim 1.4 \times 10^5 \text{ litre mol}^{-1} \text{ s}^{-1}$). The substantially higher yield of diamine **43** is attributed to the longer lifetime of azirine **50** compared to azirine **46**.

The photolysis ($\lambda = 308$ and 313 nm) of phenanthren-9-yl azide in an argon matrix has been studied recently,¹⁹⁸ and the corresponding azirine was detected. Under irradiation, the latter (like 1- and 2-naphthyl azides, see Figs 15 and 16) was transformed into the corresponding cyclic ylide. The ESR spectrum of triplet phenanthren-9-yl nitrene was also observed. The following scheme of the phototransformations of this azide was proposed.



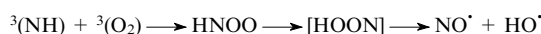
Therefore, the difference in the photochemistry of phenyl azide (and its simple derivatives) and polycyclic aryl azides (1- and 2-naphthyl azides, phenanthren-9-yl azide, *etc.*) is associated mainly with the differences in the thermodynamics of the isomerisation of the corresponding singlet aryl nitrenes. As can be seen from the PES for the transformations of singlet phenyl nitrene ¹(29) (and a series of its derivatives),^{35, 37} ketene imine is thermodynamically more favourable than azirine (see Fig. 14, $\Delta H = -10.5 \text{ kJ mol}^{-1}$). This is why ketene imine is involved in the reactions with nucleophiles. The introduction of one more phenyl ring into the molecule substantially stabilises one of isomeric azirines and destabilises another isomer (see Figs 15 and 16). For energy reasons, only one azirine can be formed, the isomerisation of which to the corresponding ketene imine is thermodynamically impossible. As a result, the photolysis of naphthyl azides and some other polycyclic azides in the presence of amines affords the corresponding diamines.^{200, 201}

VI. Reactions of triplet nitrenes with oxygen

As mentioned in Section V.2, triplet aryl nitrenes can react with a CO molecule either upon slight heating of a matrix or under the photochemical conditions.^{166, 167} The present Section deals with reactions of nitrenes in the triplet ground state with

molecular oxygen. For aryl nitrenes, this reaction was studied primarily in glasses at 77 K (Refs 159 and 204–207) and in solutions at room temperature by the flash photolysis technique.^{159, 206–212} The reactions of triplet *p*-aminophenyl nitrene **3**(**39**) with oxygen was studied by the matrix isolation technique.¹⁷⁰ This reaction was studied also for the simplest triplet nitrene ³(NH) in the gas phase^{213, 214} and in xenon and argon matrices.²¹⁵

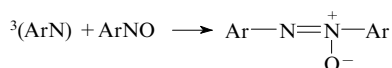
The NO[•] and HO[•] radicals are generated as the major reaction products of the ³(NH) species with molecular oxygen in the gas phase.^{213, 214} Based on the results of quantum chemical calculations,^{214, 216} it was hypothesised that the primary event affords imine peroxide HNOO; the isomerisation of the latter (the 1,3-hydrogen shift) gives rise to hydroperoxynitrene HOON, which is rapidly decomposes to radicals.



The IR spectrum of imine peroxide and its ¹⁸O-isotopically substituted analogue was recorded in the course of the photolysis of HN₃ followed by heating of an oxygen-containing xenon matrix.²¹⁵ After irradiation of an HN₃–O₂–Xe mixture (in a ratio of 1 : 5 : 550), *cis*- and *trans*-HONO, NH₂OH, N₂H₂ and ³(NH) were obtained. After heating of the preirradiated sample to 50 K followed by cooling to 12 K, a group of lines in the IR spectrum (3132.2, 3120.5 and 3109.8 cm^{–1}) assigned to nitrene ³(NH) completely disappeared and five new intense lines assigned to imine peroxide HNOO appeared.

Analogous results were obtained upon irradiation of HN₃ in an O₂-containing argon matrix. However, in this case, HNOO is formed without heating upon storage of a sample at 12 K for several hours. Based on a comparison of the calculated and experimental IR spectra, it was concluded that only one isomer (most likely, *trans*-HNOO) is formed.²¹⁵ Unfortunately, the electronic absorption spectra were not measured in the study.²¹⁵ However, it is evident that HNOO has absorption in the visible spectral region, because the irradiation with light with 400–600 nm led to the disappearance of peroxide and the appearance of an additional amount of nitrous acid (HONO).

The reaction of triplet aryl nitrenes with oxygen has received much more attention. It has long been believed that the corresponding nitro compounds (ArNO₂) are the major oxygen-containing photolysis products of aryl azides (ArN₃) in the presence of oxygen.^{193, 204, 217–219} Later, the formation of small amounts of nitroso compounds (ArNO)^{220, 221} and azoxy compounds that are formed apparently, by the reaction of triplet aryl nitrenes with ArNO has been documented.^{137, 218}

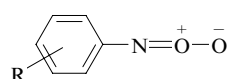


It was stated²²² that PhNO is the primary photolysis product of phenyl azide in acetonitrile in the presence of oxygen, and only this compound is formed at a low concentration (10^{–4} mol litre^{–1}) of the irradiated solution. Nitrobenzene becomes the major reaction product upon irradiation of a concentrated (~10^{–2} mol litre^{–1}) solution of phenyl azide.²²²

More recently, it has been shown^{159, 206, 207} that the corresponding nitro and nitroso compounds are the primary photolysis products of *p*-amino-, *p*-nitro- and *p*-methylphenyl azides. It should be noted that in these studies, small volumes of solutions containing azides at low concentrations (~10^{–4} mol litre^{–1}) were irradiated, thus excluding the secondary phototransformations of the initially formed products. The photolysis of all azides under study in alkanes affords nitro compounds in higher yields.

In the case of *p*-azidoaniline, the influence of the medium on the ratio of the yields of *p*-nitro- to *p*-nitrosoanilines was investigated, and this ratio was demonstrated to decrease on going from hexane (2.4) to acetonitrile (0.53).^{205, 206} Recently, the kinetics of the consumption of phenyl azide and the accumulation of the photolysis products in acetonitrile (2.5 × 10^{–4} mol litre^{–1}) has been studied.²¹⁰ It was demonstrated that during irradiation of phenyl azide, the concentration of PhNO₂ monotonically increased, and the concentration of PhNO first increased and then decreased virtually to zero, the yield of PhNO being substantially higher than that of PhNO₂ in the initial step of irradiation, as in the irradiation of *p*-azidoaniline.^{206, 207}

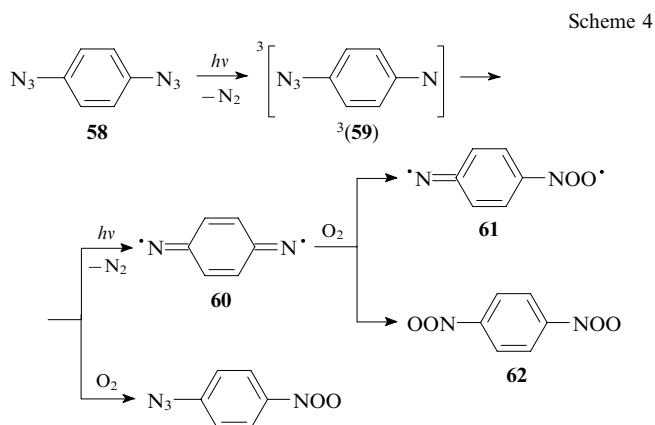
Heating of glassy matrices containing triplet aryl nitrenes and dissolved O₂ to temperatures, at which the mobility of the latter substantially increases (90–110 K), affords diamagnetic adducts giving an intense absorption band in the near-UV or visible spectral region.^{159, 204–207} The structures of aryl nitroso oxides were assigned to these adducts.



In the pioneering study,²⁰⁴ emphasis was given to diazide **58**, photolysis of which can afford triplet nitrene **3**(**59**) and dinitrene **3**(**60**). Upon prolonged storage of the irradiated sample, both diamagnetic and paramagnetic products were obtained, and both these products were assigned to adducts of mononitrene **3**(**59**) with oxygen. In the study,²⁰⁴ based on the fact that the intensity of the ESR spectrum assigned to dinitrene **60** remains unchanged, it was stated that dinitrene does not react with O₂. However, the accuracy of the ESR method is low. Hence, these results cannot completely exclude the formation of adducts **61** and **62**, among which paramagnetic compounds can be present (Scheme 4).

Although the assignment of the paramagnetic species to the adduct of mononitrene **59** with oxygen was erroneous,²⁰⁴ it has long been commonly accepted that the reaction of triplet aryl nitrenes produces both diamagnetic aryl nitroso oxides and paramagnetic aryliminodioxo biradicals.

Recently, the reaction of triplet *p*-aminophenyl nitrene **3**(**39**) with oxygen in a matrix consisting of 86% argon, 10% N₂ and 4% O₂ has been studied.¹⁷⁰ The irradiation of azide **38** in this matrix with light with λ = 254 nm, as well as in the absence of O₂, gave triplet nitrene **39** (Fig. 17, spectrum 1). After slow heating of the matrix to 30 K followed by the storage at this temperature for 5 min and the subsequent cooling to 12 K, the intensity of the bands of nitrene **3**(**39**) in the electronic absorption spectrum slightly decreased, a band characteristic of aryl nitroso oxides appeared in the visible spectral region at λ_{max} = 445 nm (Fig. 17, spectrum 2), and



Scheme 4

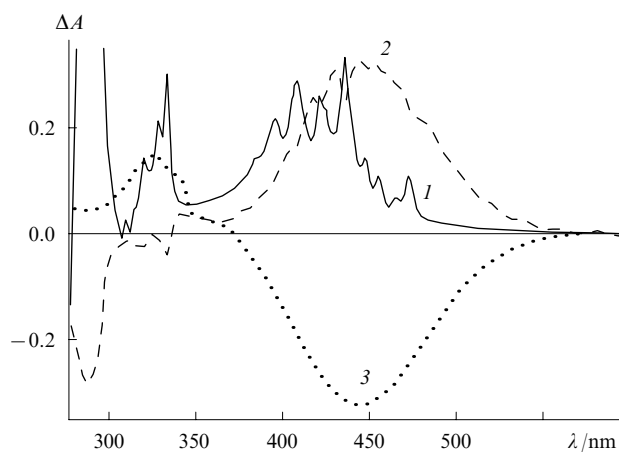


Figure 17. Difference electronic absorption spectra recorded in an argon matrix containing 4% O₂ at 12 K after irradiation of azide **38** with light at $\lambda = 254$ nm (*1*), after annealing of a sample at 30 K (*2*) and after irradiation with light at $\lambda > 515$ nm for 5 min (*3*).¹⁷⁰

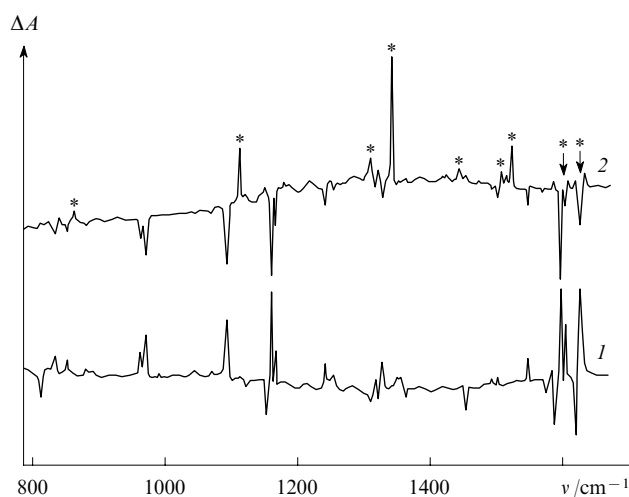


Figure 18. IR difference spectra recorded after annealing of a preirradiated sample of azide **38** at 30 K (*1*) and after irradiation with light at $\lambda > 515$ nm for 5 min (*2*).¹⁷⁰ The signals of *p*-nitroaniline are marked with asterisks.

the IR spectrum showed a series of new bands (Fig. 18, spectrum *1*). It should be noted that the reaction of nitrene **3**(**39**) with oxygen has been studied earlier in a glassy mixture of tetrahydrofuran and toluene (1 : 1) at 95 K; the formation of the adduct giving a band at $\lambda_{\text{max}} = 495$ nm was observed.^{207, 208}

The irradiation of a sample with visible light ($\lambda > 515$ nm) leads to the disappearance of the absorption band of nitroso oxide **63** and the appearance of a new band in the near-UV region at $\lambda_{\text{max}} = 326$ nm (Fig. 17, spectrum *3*) and a series of bands in the IR spectrum (Fig. 18, spectrum *2*), which are identical to the bands in the IR spectrum of *p*-nitroaniline (**64**) (marked with asterisks in Fig. 18).

It appeared¹⁷⁰ that two isomers of nitroso oxide (*cis*- and *trans*-**63**) are formed. One of them disappears after irradiation for 30 s ($\lambda > 515$ nm) being transformed into *p*-nitroaniline. This isomer is characterised by a long-wavelength band at $\lambda_{\text{max}} = 460$ nm (Fig. 19, spectrum *1*) and a series of bands in the IR spectrum (Fig. 20, spectrum *1*, the negative differential

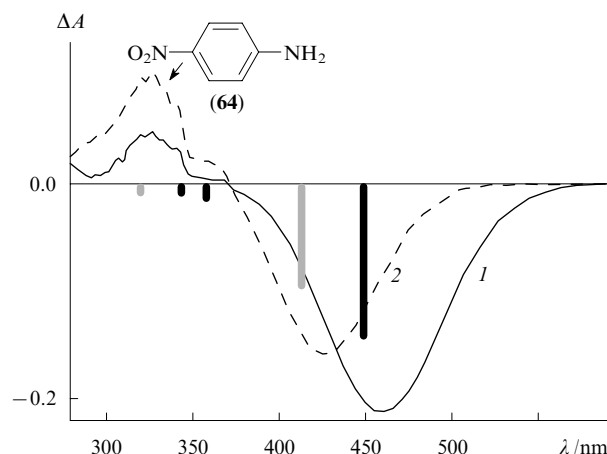


Figure 19. Difference electronic absorption spectra recorded in an argon matrix at 12 K after irradiation of the adduct of triplet nitrene **39** with O₂ with light at $\lambda > 515$ nm for 30 s (*1*) and after additional irradiation for 5 min (*2*).

The positions and relative intensities of electron transitions in the spectrum of the *trans* isomer of nitroso oxide **63** (black bars) and its *cis* isomer (gray bars) calculated at the CASSCF/CASPT2 level with the geometry optimised at the CASSCF level¹⁷⁰ are indicated by vertical bars.

absorption). Another isomer, the absorption spectrum of which is shifted to shorter wavelengths ($\lambda_{\text{max}} = 425$ nm), is also transformed into *p*-nitroaniline upon further irradiation (see Figs 19 and 20, difference spectra *2*).¹⁷⁰

The validity of the assignment of the adducts of nitrene **3**(**39**) with oxygen to the *cis* and *trans* isomers of nitroso oxide **63** was confirmed by a good agreement between the experimental and calculated electronic absorption spectra (see Fig. 19) and IR spectra (see Fig. 20). The agreement between the calculated and experimental electronic absorption spectra is much poorer when the geometry calculated by the density functional theory is used.¹⁷⁰ The agreement between the IR spectra calculated by the DFT method and the experimental spectra of the *cis* and *trans* isomers of nitroso oxide **63** is

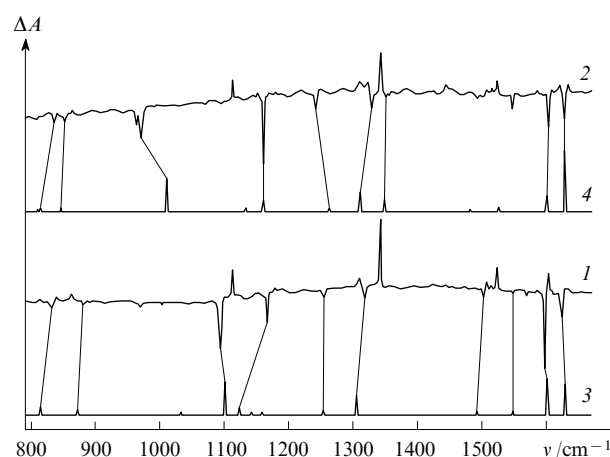


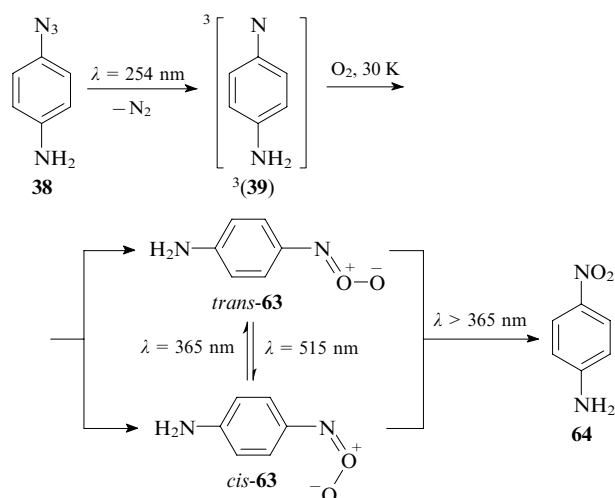
Figure 20. IR difference spectra recorded in an argon matrix at 12 K after irradiation of the adduct of triplet nitrene **39** with O₂ with light at $\lambda > 515$ nm for 30 s (*1*) and after additional irradiation for 5 min (*2*). IR spectra of the *cis* isomer of nitroso oxide **63** (*3*) and its *trans* isomer (*4*) calculated at the B3LYP/6-31G* level (the correction factor is 0.9614).¹⁷⁰

satisfactory (see Fig. 20) but it is noticeably poorer than that for triplet nitrene **39**. Hence, it is incorrect to describe nitroso oxides by single-determinant wavefunctions. For example, the contribution of the ground state configuration to the wave function of the *cis* and *trans* isomers of nitroso oxide **63** estimated at the CASSCF level of theory is $\sim 82\%$, and the contribution of the doubly excited configurations is $\sim 18\%$.¹⁷⁰

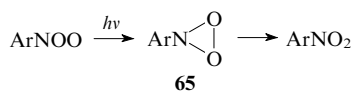
However, the population numbers of the CASSCF natural orbitals only slightly differ from 0 and 2 (the largest deviation is 0.13 for HOMO and LUMO), and this fact contradicts the statement^{220, 221, 223} that arylnitroso oxides are essentially biradical in character.

The use of low-intensity monochromatic radiation allows the observation of interconversions of the *cis* and *trans* isomers of compound **63** along with their transformation into *p*-nitroaniline (Scheme 5).

Scheme 5



It is commonly accepted^{2204, 210, 212, 220, 221, 224, 225} that the photolysis of arylnitroso oxides (ArNOO) affords cyclic dioxaziridines **65**, which are transformed into nitro compounds through the ring opening. Actually, intermediate species were observed²²⁴ in the photolysis of a series of nitroso oxides of stilbene and *p*-biphenyl in glassy tetrahydrofuran at 77 K. These species were transformed into the corresponding nitro derivatives in the dark at a rate constant of $3 \times 10^{-3} \text{ s}^{-1}$. It was hypothesised that these species can be assigned to the corresponding dioxaziridines **65**. Unfortunately, we failed to detect intermediate species in the photolysis of nitroso oxide **63**.¹⁷⁰



The formation of nitroso oxides in cryogenic matrices is evidence for a low activation energy of the reaction of triplet nitrenes with molecular oxygen. The rate constants for this reaction were measured for triplet phenylnitrene,²¹⁰ a series of its derivatives^{159, 206, 207} and pyren-1-yl nitrene.¹⁹³ It appeared that the rate constant is substantially lower than the diffusion limit and is in a range of $(0.8-8) \times 10^6 \text{ litre mol}^{-1} \text{ s}^{-1}$ for all aryl nitrenes under study. For phenylnitrene, the temperature dependence of the rate constant was studied and the activation parameters were estimated ($A = 10^{9.6 \pm 0.4} \text{ litre mol}^{-1} \text{ s}^{-1}$ and $E_a = 18 \pm 2 \text{ kJ mol}^{-1}$).²¹⁰

Numerous attempts were made to calculate the thermodynamics of the reaction of triplet nitrenes with oxygen.^{170, 207, 216, 224-226} The results obtained^{170, 226} with the use of the CBS-QB3 approach, which is one of the most accurate multi-level techniques, are presented in Fig. 21. According to

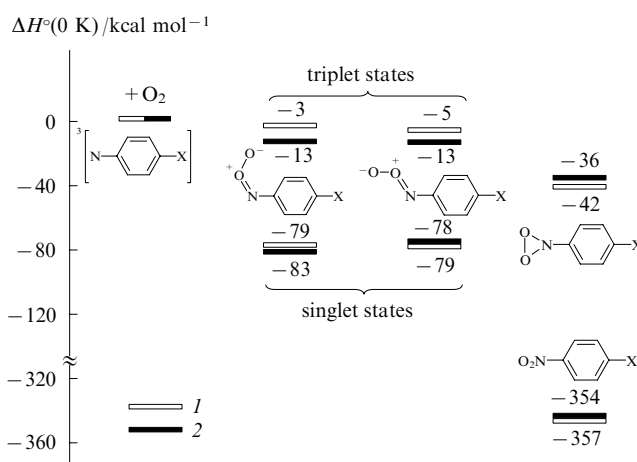
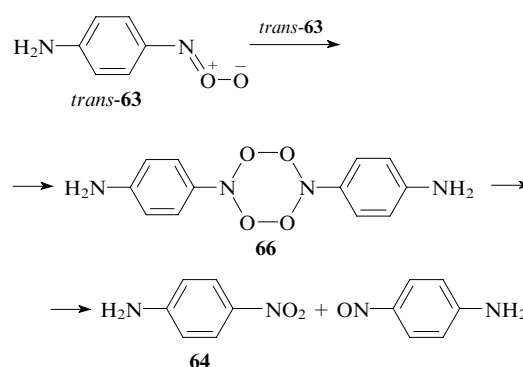


Figure 21. Relative enthalpies (at 0 K) of species involved in the formation and transformations of phenyl- (**1**, X = H) and *p*-aminophenyl nitroso oxides (**2**, X = NH₂) calculated by the CBS-QB3 method.^{170, 226}

the Wigner rule, the reaction of triplet nitrene with a triplet oxygen molecule can, in principle, produce nitroso oxide both in the singlet and triplet states. The reaction giving nitroso oxides in the triplet state is virtually thermoneutral and, according to calculations,²²⁶ its activation energy is rather high ($45-55 \text{ kJ mol}^{-1}$). The reaction producing arylnitroso oxides in the singlet ground state is exothermic ($\Delta H \approx -80 \text{ kJ mol}^{-1}$). However, the transition state on the singlet PES was not located.²²⁶

The mechanism of the transformation of arylnitroso oxides into the final nitro and nitro compounds remains obscure. Only in the case of arylnitroso oxide **63**, the flash photolysis study showed that the decay kinetics of this compound is described by the second-order reaction with a rate constant close to the diffusion limit.^{206, 208} The electronic absorption spectrum of the intermediate, the precursor of the final products (ArNO and ArNO₂), was recorded, and the structure of dimeric peroxide **66** was assigned to this intermediate. The formation of the final nitro and nitroso compounds from this intermediate can easily be conceived.



The decay kinetics of all other nitroso oxides under study (PhNOO and its *p*-Me, *p*-NO₂, *p*-Br, *p*-OMe and *p*-NMe₂ derivatives) is not described by the second-order reaction and is either exponential or biexponential.^{159, 207, 209-212} The biexponential character of the decay kinetic curves is associated with the formation of the *cis* and *trans* isomers of arylnitroso oxides having different reactivities.^{211, 212}

It was hypothesised that thermal transformations of arylnitroso oxides (like photochemical transformations) proceed through the formation of intermediate dioxaziridine **65**.^{209-214, 225} However, this reaction cannot explain the for-

mation of ArNO. The assumption of the possible formation of ArNO in the reaction of aryl azide in the triplet excited state $^3(\text{ArN}_3)^*$ with oxygen is invalid because the dissociation of the azido group in the singlet excited state of aryl azides proceeds on a hundred femtosecond time scale.^{152–155} The intersystem crossing to the triplet state cannot proceed on such a short time scale.

The possibility of the formation of ArNO in the reaction with solvents cannot be ruled out. For example, the irradiation of phenyl azide in the presence of O₂ in acetonitrile with 10% benzene additive was found^{220, 221} to give phenol in 15% yield. The irradiation of phenyl azide in acetonitrile in the presence of 10% toluene afforded kresol (in 12% yield) and benzaldehyde (in 5% yield). The addition of cyclohexane to the solution resulted in the isolation of cyclohexanone (5%) and cyclohexanol (17%).

Thus, both the simplest triplet nitrene $^3(\text{NH})$ and triplet aryl nitrenes react with molecular oxygen in cryogenic matrices to form the corresponding nitroso oxides. In the case of imino peroxide HNOO, only the *trans* isomer was detected, whereas the formation of both the *cis* and *trans* isomers was observed for aryl nitroso oxides. Nitrous acid (HONO) is formed in the course of photolysis of imino peroxide HNOO. Upon irradiation of aryl nitroso oxides (ArNOO), the reversible *cis*–*trans* isomerisation and the irreversible transformation into the nitro compounds (ArNO₂) were observed. The formation of intermediates, viz., dioxaziridines, in the course of photolysis was not reliably confirmed. The mechanism of dark transformations of aryl nitroso oxides into the final nitro and nitroso compounds was not ultimately established as well.

VII. Conclusion

Before the modern physicochemical methods were developed, knowledge about intermediate species could be obtained solely based on the analysis of the reaction products. Only in the mid-20th century, when two powerful tools of investigation (the flash photolysis and matrix isolation techniques) were devised, the direct observation and studies of the properties of the reaction intermediates became possible. Considerable progress has been achieved in the development of the flash photolysis techniques allowing experiments to be performed with femtosecond and even attosecond time resolution. Although the progress in the matrix isolation techniques is less impressive, it remains one of the main methods of obtaining the most complete spectroscopic information on the reaction intermediates, which allows their reliable identification. The matrix isolation technique is particularly promising in combination with IR spectroscopy of intermediates, because well-resolved IR spectra with a linewidth of $\sim 1 \text{ cm}^{-1}$ can be recorded in a very wide spectral range in inert gas matrices at very low temperatures ($\sim 10 \text{ K}$). In the last decade, the procedure of the assignment of bands in the experimental electronic absorption and IR spectra of intermediates has been substantially simplified and it has become more reliable due to the development of rather precise theoretical calculation methods.

Investigations of the photolysis of azides by the matrix isolation technique made a considerable contribution to the elucidation of the rather complex mechanism of this important photochemical reaction. For example, the detection of ketene imine in the course of photolysis of phenyl azide in an argon matrix had a considerable effect on the interpretation of the results obtained by alternative methods, including the flash photolysis technique. The hypothesis about the possibility of the formation and isomerisation of singlet aryl nitrenes in the vibrationally excited state, which has been made for the first time to interpret the results obtained in cryogenic matrices, has been confirmed very recently in femtosecond studies.^{151–155} In very recent years, the use of the matrix isolation technique

combined with high-level quantum chemical calculations allowed the elucidation of the unusual nature of singlet acyl nitrenes,^{38–40} which are promising for the photoaffinity labelling of biopolymers, and provided an insight into the detailed mechanism of photolysis of polycyclic aryl azides.¹³²

My studies included in the present review were carried out with the financial support of the Russian Foundation for Basic Research (Project Nos 95-03-08920, 98-03-32021 and 01-03-32864), the Ministry of Education of the Russian Federation (Grant E02-5.0-27), the Division of Chemistry and Materials Science of the Russian Academy of Sciences, the US National Science Foundation (Grants CHE-8814950 and CHE-9613861) and the Swiss National Science Foundation (SCOPES2000, Grant No. 7SUPJ062336).

References

1. E Whittle, D A Dows, G C Pimentel *J. Chem. Phys.* **22** 1943 (1954)
2. E D Becker, G C Pimentel *J. Chem. Phys.* **25** 224 (1956)
3. I Norman, G Porter *Nature (London)* **174** 58 (1954)
4. M Moskovits, G A Ozin *Crychochemistry* (New York: Wiley-Interscience, 1976)
5. *Matrix Isolation Spectroscopy (NATO Advanced Study Institute, Ser. C Vol. 76)* (Eds J Barnes, W J Orville-Thomas, A Muller, R Gaudes) (Dordrecht: Reidel, 1981)
6. *Chemistry and Physics of Matrix Isolated Species* (Eds L Andrews, M Moskovits) (Amsterdam: North-Holland, 1988)
7. M J Almond, A J Downs *Spectroscopy of Matrix Isolated Species* (Chichester: Wiley, 1989)
8. R Dunkin *Matrix Isolation Techniques: a Practical Approach* (Oxford: Oxford University Press, 1998)
9. V E Bondybey, A M Smith, J Agreiter *Chem. Rev.* **96** 2113 (1996)
10. T Bally *Reactive Intermediate Chemistry* (Eds R A Moss, M S Platz M.Jones) (Hoboken, NJ: Wiley, 2004) p. 797
11. A D Becke *J. Chem. Phys.* **98** 5648 (1993)
12. C Lee, W Yang, R G Parr *Phys. Rev. B* **37** 785 (1988)
13. C Cramer *Essentials of Computational Chemistry* (Chichester: Wiley, 2002) p. 305
14. B O Roos *Adv. Chem. Phys.* **69** 399 (1987)
15. K Andersson, B O Roos *Modern Electronic Structure Theory* (Singapore: World Scientific, 1995) Pt 2 P. 55
16. K Andersson, M R A Blomberg, M P Fülcher, V Kelll, R Lindh, P Å Malmqvist, J Noga, J Olson, B O Roos, A Sadlej, P E M Siegbahn, M Urban, P-O Widmark *MOLCAS, Version 5* (Lund: University of Lund, 2002)
17. E K U Gross, W Kohn *Adv. Quantum Chem.* **21** 255 (1990)
18. K B Wiberg, R E Stratmann, M J Frisch *Chem. Phys. Lett.* **297** 60 (1998)
19. D S Breslow *Azides and Nitrenes; Reactivity and Utility* (Ed. E F V Scriven) (New York: Academic Press, 1984) p. 491
20. E W Meijer, S Nijhuis, F C B M Von Vroonhoven *J. Am. Chem. Soc.* **110** 7209 (1988)
21. P A S Smith *Nitrenes* (Ed. W Lwowski) (New York: Wiley-Interscience, 1970)
22. H Bayley *Photogenerated Reagents in Biochemistry and Molecular Biology* (New York: Elsevier, 1983)
23. S X Cai, D J Glenn, J F W Keana *J. Org. Chem.* **57** 1299 (1992)
24. H Niino, Y Koga, A Yabe *J. Photochem. Photobiol. A: Chem.* **106** 9 (1997)
25. H Niino, T Sato, A Yabe *Appl. Phys. A* **69** 605 (1999)
26. E F V Scriven *Reactive Intermediates Vol. 2* (Ed. R A Abramovitch) (New York: Plenum, 1982)
27. P A S Smith *Azides and Nitrenes; Reactivity and Utility* (Ed. E F V Scriven) (New York: Academic Press, 1984) p. 95
28. M S Platz, V M Maloney *Kinetics and Spectroscopy of Carbenes and Biradicals* (Ed. M S Platz) (New York: Plenum, 1990)
29. G B Schuster, M S Platz *Adv. Photochem.* **17** 69 (1992)

30. M F Budyka, M M Kantor, M V Alfimov *Usp. Khim.* **61** 48 (1992) [*Russ. Chem. Rev.* **61** 25 (1992)]
31. N P Gritsan, E A Pritchina *Usp. Khim.* **61** 910 (1992) [*Russ. Chem. Rev.* **61** 500 (1992)]
32. C Wentrup *Reactive Molecules. The Neutral Reactive Intermediates in Organic Chemistry* (New York: Wiley-Interscience, 1984)
33. C Wentrup *Azides and Nitrenes; Reactivity and Utility* (Ed. E F V Scriven) (New York: Academic Press, 1984) p. 395
34. W T Borden, N P Gritsan, C M Hadad, W L Karney, C R Kemnitz, M S Platz *Acc. Chem. Res.* **33** 765 (2000)
35. N P Gritsan, M S Platz *Adv. Phys. Org. Chem.* **36** 255 (2001)
36. N P Gritsan, M S Platz, W T Borden *Computational Methods in Photochemistry*. (Ed. A G Kutateladze) (Boca Raton, FL: CRC, 2005) p. 235
37. N P Gritsan, M S Platz *Chem. Rev.* **106** 3844 (2006)
38. E A Pritchina, N P Gritsan, A Maltsev, T Bally, T Autrey, Y Liu, Y H Wang, J P Toscano *Phys. Chem. Chem. Phys.* **5** 1010 (2003)
39. J Liu, S Mandel, C M Hadad, M S Platz *J. Org. Chem.* **69** 8583 (2004)
40. E A Pritchina, N P Gritsan, T Balli *Izv. Akad. Nauk, Ser. Khim.* 519 (2005)^a
41. H Okabe *J. Chem. Phys.* **49** 2726 (1968)
42. H Okabe *Photochemistry of Small Molecules* (New York: Wiley, 1978)
43. J R McDonald, R G Miller, A P Baronavski *Chem. Phys. Lett.* **51** 57 (1977)
44. A P Baronavski, R G Miller, J R McDonald *Chem. Phys.* **30** 119 (1978)
45. F Rohrer, F Stuhl *J. Chem. Phys.* **88** 4788 (1988)
46. J Masanet, A Gilles, C Vermeil *J. Photochem.* **3** 417 (1974/75)
47. O Kajimoto, T Yamamoto, T Fueno *J. Phys. Chem.* **83** 429 (1979)
48. J C Stephenson, M P Casassa, D S King *J. Phys. Chem.* **89** 1378 (1988)
49. M H Alexander, H-J Werner, P J Dagdigian *J. Chem. Phys.* **89** 1388 (1988)
50. E D Becker, G C Pimentel, M Van Thiel *J. Chem. Phys.* **26** 145 (1957)
51. M McCarty, G W Robinson *J. Am. Chem. Soc.* **81** 4472 (1959)
52. V E Bondybey, L E Brus *J. Chem. Phys.* **63** 794 (1975)
53. H Esser, J Langen, U Schurath *Ber. Bunsen-Ges. Phys. Chem.* **87** 636 (1983)
54. A Ramsthaler-Sommer, K E Eberhardt, U Schurath *J. Chem. Phys.* **85** 3760 (1986)
55. C Blindauer, N van Riesenbeck, K Seranski, M Winter, A C Backer, U Schurath *Chem. Phys.* **150** 93 (1991)
56. E P Kyba, R A Abramovitch *J. Am. Chem. Soc.* **102** 735 (1980)
57. E P Kyba *Azides and Nitrenes; Reactivity and Utility* (Ed. E F V Scriven) (New York: Academic Press, 1984) p. 2
58. L Barash, E Wasserman, W A Jager *J. Am. Chem. Soc.* **89** 3931 (1967)
59. J H Glowina, J Misewich, P P Sorokin *Supercontinuum Laser Sources* (Ed. R R Alfano) (New York: Springer, 1989)
60. E Wasserman *Prog. Phys. Org. Chem.* **8** 319 (1971)
61. D E Milligan *J. Chem. Phys.* **35** 1491 (1961)
62. M E Jacox, D E Milligan *J. Mol. Spectrosc.* **56** 333 (1975)
63. I R Dunkin, P C P Thomson *Tetrahedron Lett.* **21** 3813 (1980)
64. J Michl, J G Radziszewski, J W Downing, K B Wiberg, F H Walker, R D Miller, P Kovacic, M Jawdosiuk, V Bonacic-Koutecky *Pure Appl. Chem.* **55** 315 (1983)
65. I R Dunkin, C J Shields, H Quasi, B Seiferling *Tetrahedron Lett.* **24** 3887 (1983)
66. R S Sheridan, G A Ganzer *J. Am. Chem. Soc.* **105** 6158 (1983)
67. J G Radziszewski, J W Downing, M Jawdosiuk, P Kovacic, J Michl *J. Am. Chem. Soc.* **107** 594 (1985)
68. J G Radziszewski, J W Downing, C Wentrup, P Kaszynski, M Jawdosiuk, P Kovacic, J Michl *J. Am. Chem. Soc.* **107** 2799 (1985)
69. G Smolinsky, E Wasserman, W A Yager *J. Am. Chem. Soc.* **84** 3220 (1962)
70. E Wasserman, E Smolinsky, W A Yager *J. Am. Chem. Soc.* **86** 3166 (1964)
71. P J Wagner, B J Scheve *J. Am. Chem. Soc.* **101** 378 (1979)
72. S M Mandel, J A K Bauer, A D Gudmundsdóttir *Org. Lett.* **3** 523 (2001)
73. P N D Singh, S M Mandel, R M Robinson, Z Zhu, R Franz, B S Ault, A D Gudmundsdóttir *J. Org. Chem.* **68** 7951 (2003)
74. P G Carrick, P C Engelking *J. Chem. Phys.* **81** 1661 (1984)
75. P G Carrick, C R Brazier, P F Bernath, P C Engelking *J. Am. Chem. Soc.* **109** 5100 (1987)
76. E L Chappell, P C Engelking *J. Chem. Phys.* **89** 6007 (1988)
77. C R Brazier, P G Carrick, P F Bernath *J. Chem. Phys.* **96** 919 (1992)
78. R F Ferrante *J. Chem. Phys.* **86** 25 (1987)
79. T Franken, D Perner, M W Bosnali *Z. Naturforsch., A* **25** 151 (1970)
80. R F Ferrante *J. Chem. Phys.* **94** 4678 (1991)
81. H Shang, C Yu, L Ying, X Zhao *J. Chem. Phys.* **103** 4418 (1995)
82. L Ying, Y Xia, H Shang, X Zhao, Y Tang *J. Chem. Phys.* **105** 5798 (1996)
83. M J Travers, D C Cowles, E P Clifford, G B Ellison, P C Engelking *J. Phys. Chem.* **111** 5349 (1999)
84. D R Yarkony, H F Schaefer, S Rothenberg *J. Am. Chem. Soc.* **96** 5974 (1974)
85. J Demuyne, D J Fox, Y Yamaguchi, H F Schaefer III *J. Am. Chem. Soc.* **102** 6204 (1980)
86. J A Pople, K Raghavachari, M J Frisch, J S Binckley, P v R Schleyer *J. Am. Chem. Soc.* **105** 6389 (1983)
87. M T Nguyen *Chem. Phys. Lett.* **117** 290 (1985)
88. Y Xie, G E Scuseria, B F Yates, Y Yamaguchi, H F Schaefer III *J. Am. Chem. Soc.* **111** 5181 (1989)
89. C Richards Jr, C Meredith, S-J Kim, G E Quench, H F Schaefer III *J. Chem. Phys.* **100** 481 (1994)
90. M T Nguyen, D Sengupta, T-K Ha *J. Phys. Chem.* **100** 6499 (1996)
91. J F Arenas, J C Otero, A Sánchez-Gálvez, J Soto, P Viruela *J. Phys. Chem.* **102** 1146 (1998)
92. J F Arenas, J I Marcos, J C Otero, A Sánchez-Gálvez, J Soto *J. Chem. Phys.* **111** 551 (1999)
93. C R Kemnitz, G B Ellison, W L Karney, W T Borden *J. Am. Chem. Soc.* **122** 1098 (2000)
94. N P Gritsan, I Likhovotvorik, Z D Zhu, M S Platz *J. Phys. Chem. A* **105** 3039 (2001)
95. F D Wayne, H E Radford *Mol. Phys.* **32** 1407 (1976)
96. W Lwowski, G T Tissue *J. Am. Chem. Soc.* **87** 4022 (1965)
97. G M Nazin *Usp. Khim.* **41** 1537 (1972) [*Russ. Chem. Rev.* **41** 711 (1972)]
98. W Lwowski *Azides and Nitrenes; Reactivity and Utility* (Ed. E F V Scriven) (New York: Academic Press, 1984) p. 205
99. M V Zabalov, R P Tiger *Izv. Akad. Nauk, Ser. Khim.* 2200 (2005)^a
100. G T Tissue, S Linke, W Lwowski *J. Am. Chem. Soc.* **89** 6303 (1967)
101. S Linke, G T Tissue, W Lwowski *J. Am. Chem. Soc.* **89** 6308 (1967)
102. E Eibler, J Sauer *Tetrahedron Lett.* 2569 (1974)
103. V P Semenov, A N Studenikov, A D Bepalov, K A Ogloblin *Zh. Org. Khim.* **13** 2202 (1977)^b
104. W Lwowski, F P Woerner *J. Am. Chem. Soc.* **87** 5491 (1965)
105. J S McConaghy, W Lwowski *J. Am. Chem. Soc.* **89** 4450 (1967)
106. T Autrey, G B Schuster *J. Am. Chem. Soc.* **109** 5814 (1987)
107. M E Sigman, T Autrey, G B Schuster *J. Am. Chem. Soc.* **110** 4297 (1988)
108. C Buron, M S Platz *Org. Lett.* **5** 3383 (2003)
109. R E Wilde, T K K Srinivasan, W Lwowski *J. Am. Chem. Soc.* **93** 860 (1971)
110. J H Teles, G Maier *Chem. Ber.* **122** 745 (1989)
111. N P Gritsan, E A Pritchina *Mendeleev Commun.* 94 (2001)
112. V I Faustov, E G Baskir, A A Biryukov *Izv. Akad. Nauk, Ser. Khim.* 2203 (2003)^a
113. R Puttner, K Hafner *Tetrahedron Lett.* 3119 (1964)
114. Y Hayashi, D Swern *J. Am. Chem. Soc.* **95** 5205 (1973)
115. M Inagaki, T Shingaki, T Nagai *Chem. Lett.* **10** 1419 (1981)
116. M Inagaki, T Shingaki, T Nagai *Chem. Lett.* **11** 9 (1982)
117. I Woelfle, B Sauerwein, T Autrey, G B Schuster *Photochem. Photobiol.* **47** 497 (1988)

118. T Melvin, G B Schuster *Photochem. Photobiol.* **51** 155 (1990)
119. C Wentrup, H Bornemann *Eur. J. Org. Chem.* 4521 (2005)
120. P F Alewood, P M Kazmaier, A Rauk *J. Am. Chem. Soc.* **95** 5466 (1973)
121. J F Harrison, G Shalhoub *J. Am. Chem. Soc.* **97** 4172 (1975)
122. A Rauk, P F Alewood *Can. J. Chem.* **55** 1498 (1977)
123. D Poppinger, L Radom *J. Am. Chem. Soc.* **100** 3674 (1978)
124. A Mavridis, J F Harrison *J. Am. Chem. Soc.* **99** 7651 (1980)
125. W A Shapley, G B Bacskay *J. Phys. Chem. A* **103** 4514 (1999)
126. W A Shapley, G B Bacskay *J. Phys. Chem. A* **103** 6624 (1999)
127. K Anderson *Theor. Chim. Acta* **91** 31 (1995)
128. V Parasuk, C J Cramer *Chem. Phys. Lett.* **260** 7 (1996)
129. W L Karney, W T Borden *J. Am. Chem. Soc.* **119** 1378 (1997)
130. C Addicott, M W Wong, C Wentrup *J. Org. Chem.* **67** 8538 (2002)
131. B T Hill, M S Platz *Phys. Chem. Chem. Phys.* **5** 1051 (2003)
132. A Maltsev, T Bally, M-L Tsao, M S Platz, A Kuhn, M Vosswinkel, C Wentrup *J. Am. Chem. Soc.* **126** 237 (2004)
133. C Carra, R Nussbaum, T Bally *ChemPhysChem* **7** 1268 (2006)
134. R Huisgen *Angew. Chem.* **67** 756 (1955)
135. W E Doering, R A Odum *Tetrahedron* **22** 93 (1966)
136. A K Schrock, G B Schuster *J. Am. Chem. Soc.* **106** 5228 (1984)
137. T Y Liang, G B Schuster *J. Am. Chem. Soc.* **109** 7803 (1987)
138. A Reiser, G Bowes, R Horne *Trans. Faraday Soc.* **62** 3162 (1966)
139. E Leyva, M S Platz, G Persy, J Wirz *J. Am. Chem. Soc.* **108** 3783 (1986)
140. B A DeGraff, D W Gillespie, R J Sundberg *J. Am. Chem. Soc.* **96** 7491 (1974)
141. R J Sundberg, M Brenner, S R Suter, B P Das *Tetrahedron Lett.* 2715 (1970)
142. R J Sundberg, S R Suter, M Brenner *J. Am. Chem. Soc.* **94** 513 (1972)
143. O L Chapman, J P Le Roux *J. Am. Chem. Soc.* **100** 282 (1978)
144. T Donnelly, I R Dunkin, D S D Norwood, A Prentice, C J Shields, P C P Thomson *J. Chem. Soc., Perkin Trans. 2* 305 (1985)
145. O L Chapman, R S Sheridan, J P Le Roux *J. Am. Chem. Soc.* **100** 6245 (1978)
146. C J Shields, D R Chrisope, G B Schuster, A J Dixon, M Popiakoff, J J Turner *J. Am. Chem. Soc.* **109** 4723 (1987)
147. Y Z Li, J P Kirby, M W George, M Poliakoff, G B Schuster *J. Am. Chem. Soc.* **110** 8092 (1988)
148. J C Hayes, R S Sheridan *J. Am. Chem. Soc.* **112** 5879 (1990)
149. I R Dunkin, M A Lynch, F McAlpine, D Sweeney *J. Photochem. Photobiol. A: Chem.* **102** 207 (1997)
150. N P Gritsan, Z Zhu, C M Hadad, M S Platz *J. Am. Chem. Soc.* **121** 1202 (1999)
151. N P Gritsan, D Polshakov, M-L Tsao, M S Platz *Photochem. Photobiol. Sci.* **4** 23 (2005)
152. G T Burdzinski, T L Gustafson, J C Hackett, C M Hadad, M S Platz *J. Am. Chem. Soc.* **127** 13764 (2005)
153. G T Burdzinski, J C Hackett, J Wang, T L Gustafson, M C Hadad, M S Platz *J. Am. Chem. Soc.* **128** 13402 (2006)
154. R D McCulla, G T Burdzinski, M S Platz *Org. Lett.* **8** 1637 (2006)
155. G T Burdzinski, C T Middleton, T L Gustafson, M S Platz *J. Am. Chem. Soc.* **128** 14804 (2006)
156. N P Gritsan, T Yuzawa, M S Platz *J. Am. Chem. Soc.* **119** 5059 (1997)
157. R Born, C Burda, P Senn, J Wirz *J. Am. Chem. Soc.* **119** 5061 (1997)
158. M-L Tsao, M S Platz *J. Am. Chem. Soc.* **125** 12014 (2003)
159. N P Gritsan, E A, Pritchina *J. Inform. Rec. Mater.* **17** 391 (1989)
160. S J I Kim, T P Hamilton, H F Schaefer III *J. Am. Chem. Soc.* **114** 5349 (1992)
161. D A Hrovat, E E Waali, W T Borden *J. Am. Chem. Soc.* **114** 8698 (1992)
162. M J Travers, D C Cowles, E P Clifford, G B Ellison *J. Am. Chem. Soc.* **114** 8699 (1992)
163. O Castell, V M Carefa, C Bo, R Caballol *J. Comput. Chem.* **17** 42 (1996)
164. R N McDonald, S J Davidson *J. Am. Chem. Soc.* **115** 10857 (1993)
165. S E Carroll, B Nay, E F V Scriven, H Suschitzky, D R Thomas *Tetrahedron Lett.* 3175 (1977)
166. I R Dunkin, P C P Thomson *J. Chem. Soc., Chem. Commun.* 1192 (1982)
167. I R Dunkin, T Donnelly, T S Lockhart *Tetrahedron Lett.* **26** 359 (1985)
168. J Morawietz, W Sander *J. Org. Chem.* **61** 4351 (1996)
169. C Carra, R Nussbaum, T Bally *ChemPhysChem* **7** 1268 (2006)
170. E A Pritchina, N P Gritsan, T Bally *Phys. Chem. Chem. Phys.* **8** 719 (2006)
171. N P Gritsan, H B Zhai, T Yuzawa, D Karweik, J Brooke, M S Platz *J. Phys. Chem. A* **101** 2833 (1997)
172. N P Gritsan, D Tigelaar, M S Platz *J. Phys. Chem. A* **103** 4465 (1999)
173. N P Gritsan, A D Gudmundsdottir, D Tigelaar, M S Platz *J. Phys. Chem. A* **103** 3458 (1999)
174. M Cerro-Lopez, N P Gritsan, Z Zhu, M S Platz *J. Phys. Chem. A* **104** 9681 (2000)
175. D A Pol'shakov, Yu P Tsentalovich, N P Gritsan *Kinet. Katal.* **42** 664 (2001)^c
176. N P Gritsan, I Likhovotvorik, M-L Tsao, N Telebi, M S Platz, W L Karney, C R Kemnitz, W T Borden *J. Am. Chem. Soc.* **123** 1425 (2001)
177. N P Gritsan, A D Gudmundsdottir, D Tigelaar, Z Zhu, W L Karney, C M Hadad, M S Platz *J. Am. Chem. Soc.* **123** 1951 (2001)
178. M-L Tsao, N P Gritsan, T R James, M S Platz, D A Hrovat, W T Borden *J. Am. Chem. Soc.* **125** 9343 (2003)
179. R A Abramovitch, S R Challand, E F V Scriven *J. Am. Chem. Soc.* **94** 1374 (1972)
180. R A Abramovitch, S R Challand, Y Yamada *J. Org. Chem.* **40** 1541 (1975)
181. R E Banks, G R Sparkes *J. Chem. Soc., Perkin Trans. 1* 1964 (1972)
182. R E Banks, A Prakash *Tetrahedron Lett.* 99 (1973)
183. R E Banks, A Prakash *J. Chem. Soc., Perkin Trans. 1* 1365 (1974)
184. R E Banks, N D Venayak *J. Chem. Soc., Chem. Commun.* 900 (1980)
185. R E Banks, I M Madany *J. Fluorine Chem.* **30** 211 (1985)
186. P J Crocker, N Imai, K Rajagopalan, M A Boggess, S Kwiatkowski, L D Dwyer, T C Vanaman, D C Watt *Bioconjugate Chem.* **1** 419 (1990)
187. R R Drake, J T Slama, K A Wall, M Abramova, C D'Souza, A D Elbein, P J Crocker, D S Watt *Bioconjugate Chem.* **3** 69 (1992)
188. K C Pinney, J A Katzenellenbogen *J. Org. Chem.* **56** 3125 (1991)
189. K C Pinney, K E Carlson, S B Katzenellenbogen, J A Katzenellenbogen *Biochemistry* **30** 2421 (1991)
190. M W Reed, D Fraga, D E Schwartz, J Scholler, R D Hinrichsen *Bioconjugate Chem.* **6** 101 (1995)
191. I Kapfer, J E Hawkinson, J E Casida, M P Goeldner *J. Med. Chem.* **37** 133 (1994)
192. I Kapfer, P Jacques, H Toubal, M P Goeldner *Bioconjugate Chem.* **6** 109 (1995)
193. T Yamaoka, H Kashiwagi, S Nagakura *Bull. Chem. Soc. Jpn.* **45** 361 (1972)
194. W T G Johnson, M B Sullivan, C J Cramer *Int. J. Quantum Chem.* **85** 492 (2001)
195. J A R Coope, J B Farmer, C L Gardner, C A McDowell *J. Chem. Phys.* **42** 54 (1965).
196. M Kazaj, H Luerksen, C Wentrup *Angew. Chem., Int. Ed. Engl.* **25** 480 (1986)
197. R Alvarado, J-P Grivet, C Igier, J Barcelo, J Rigaudy *J. Chem. Soc., Faraday Trans. 2* 844 (1977)
198. D Kvaskoff, P Bednarek, L George, S Pankajakshan, C Wentrup *J. Org. Chem.* **70** 7947 (2005)
199. I R Dunkin, P C P Thomson *J. Chem. Soc., Chem. Commun.* 499 (1980)
200. S E Hilton, E F V Scriven, H Suschitzky *J. Chem. Soc., Chem. Commun.* 853 (1974)
201. E Leyva, M S Platz *Tetrahedron Lett.* **28** 11 (1987)

202. A Kuhn, M Vosswinkel, C Wentrup *J. Org. Chem.* **67** 9023 (2002)
203. M-L Tsao, M S Platz *J. Phys. Chem. A* **108** 1169 (2004)
204. J C Brinen, B Singh *J. Am. Chem. Soc.* **93** 6623 (1971)
205. E A Pritchina, N P Gritsan, N M Bazhin *Izv. AN. Ser. khim.* 1749 (1986)
206. E A Pritchina, N P Gritsan *J. Photochem. Photobiol. A: Chem.* **43** 165 (1988)
207. E A Kuklina (E A Pritchina) Candidate Thesis in Chemical Sciences, Institute of Chemical Kinetics and Combustion, Siberian Branch of the Russian Academy of Sciences, Novosibirsk, 1989
208. E A Pritchina, N P Gritsan *Kinet. Katal.* **28** 1044 (1987)^c
209. E M Chainikova, S L Khursan, R L Safiullin *Dokl. Akad. Nauk* **396** 793 (2004)^d
210. R L Safiullin, S L Khursan, E M Chainikova *Kinet. Katal.* **45** 680 (2004)^c
211. E M Chainikova, S L Khursan, R L Safiullin *Dokl. Akad. Nauk* **403** 358 (2005)^d
212. E M Chainikova, S L Khursan, R L Safiullin *Kinet. Katal.* **47** 566 (2006)^c
213. C Zetzsch, I Hansen *Ber. Bunsen-Ges. Phys. Chem.* **82** 830 (1978)
214. W Hack, H Kurzke, H G Wagner *J. Chem. Soc., Faraday Trans.* 2 949 (1985)
215. S L Laursen, J E Grace Jr, R L DeKock, S A Spronk *J. Am. Chem. Soc.* **120** 12583 (1998)
216. T Fueno, K Yokoyama, S Takane *Theor. Chim. Acta* **82** 299 (1992)
217. R A Abramovitch, C J Azogu *J. Chem. Soc., Chem. Commun.* 134 (1971)
218. R A Abramovitch, S R Challand *J. Chem. Soc., Chem. Commun.* 964 (1972)
219. P E Nielsen, O Buchardt *Photochem. Photobiol.* **35** 317 (1982)
220. Y Sawaki, S Ishikawa *J. Am. Chem. Soc.* **109** 584 (1987)
221. S Ishikawa, S Tsuji, Y Sawaki *J. Am. Chem. Soc.* **113** 4282 (1991)
222. C L Go, W H Waddell *J. Org. Chem.* **48** 2897 (1983)
223. M P Talipov, A B Ryzhkov, L S Khursan, R L Safiullin *Zh. Strukt. Khim.* **47** 1054 (2006)^e
224. T Harder, P Wessig, J Bendig, R Stösser *J. Am. Chem. Soc.* **121** 6580 (1999)
225. A A Shchepalov, S V Zelentsov, A G Razuvaev *Izv. Akad. Nauk, Ser. Khim.* 2239 (2001)^a
226. J Liu, C M Hadad, M S Platz *Org. Lett.* **7** 549 (2005)

^a — *Russ. Chem. Bull., Int. Ed. (Engl. Transl.)*

^b — *Russ. J. Org. Chem. (Engl. Transl.)*

^c — *Kinet. Catal. (Engl. Transl.)*

^d — *Dokl. Phys. Chem. (Engl. Transl.)*

^e — *J. Struct. Chem. (Engl. Transl.)*